ChemComm
FEATURE ARTICLE

Superstructural diversity in two dimensions: crystal engineering of laminated solids

Michael J. Zaworotko

Department of Chemistry, University of South Florida, 4202 E. Fowler Avenue, SCA 400, Tampa, Florida, 33620, USA. E-mail: zaworo@chuma1.cas.usf.edu

Received (in Cambridge, UK) 4th September 2000, Accepted 15th November 2000
First published as an Advance Article on the web 13th December 2000

The application of supramolecular concepts such as self-assembly to the solid state offers an approach to crystal design and crystal engineering, namely supramolecular synthesis of solids, that is based upon the design of infinite networks. Self-assembly of more than one molecular component, modular self-assembly, is particularly attractive since it can be accomplished in one-pot reactions with existing molecular components and allows for facile fine-tuning of structural and functional features. The challenges and opportunities that face crystal engineering are illustrated by concentrating on the superstructural diversity that has been exhibited in 2D network structures. Despite the observed superstructural diversity, which can manifest itself in the form of supramolecular isomerism, and the range of molecular components that have been utilized, these structures have in common an inherent ability to mimic clays by intercalation of guest molecules.

From molecules to crystal engineering and design

That the physical and chemical properties of crystalline solids are as critically dependent upon the distribution of molecular components within the crystal lattice as the properties of its individual molecular components has provided impetus for research into crystal design and engineering. In such a context, it is probably more than coincidental that the late 1980s represents a watershed for research in this area. A provocative statement by Maddox[1] highlighted the issue as follows: '*One of the continuing scandals in the physical sciences is that it remains in general impossible to predict the structure of even the simplest crystalline solids from a knowledge of their chemical composition*'. It is reasonable to assert that Maddox's statement still holds true, especially for organic solids. Nevertheless, it has not precluded a seemingly exponential growth in research activity devoted to the subjects of crystal design and crystal engineering. This should be unsurprising since the implications of crystal engineering go beyond materials science. Indeed, the term crystal engineering was first coined in a contribution by G. M. J. Schmidt concerning the subject of organic solid-state photochemistry.[2] An important consequence of Schmidt's research into solid-state reactions is that it is implicit by use of the term crystal engineering that crystals can be thought of as the sum of a series of molecular recognition events, self-assembly, rather than the result of the need to 'avoid a vacuum'. In other words, crystal engineering uses the concepts of supramolecular chemistry. It is now evident that supramolecular chemistry, defined by Lehn as chemistry beyond the molecule,[3] and 'supramolecular assemblies' are inherently linked to the concepts of crystal engineering. Therefore, crystal engineering has implications that extend into areas as diverse as pharmaceutical development and synthetic chemistry. In the context of the former, there are important processes and intellectual property implications related to polymorphism.[4,5] In the context of synthetic chemistry, solid-phase organic synthesis can be solvent free and offer significant yield and regioselectivity advantages over solution phase reactions,[6] including some that cannot be effected in solution.[7–9]

The field of crystal engineering developed further in the 1980s thanks to a series of papers and monographs by Desiraju[10,11] and Etter[12] that concentrated upon applying the Cambridge Structural Database for analysis, interpretation and design of noncovalent bonding patterns in organic solids. In this contribution, we focus upon how these supramolecular concepts have been exploited to rationally generate laminated architectures in the solid state. Particular emphasis is placed upon supramolecular isomerism and how it affords superstructural diversity in two classes of compound: coordination polymers and organic networks.

Coordination polymers: networks from first principles

Coordination polymers exemplify how crystal engineering has become a paradigm for the design of new supramolecular architectures. In this context, the work of Wells[13,14] serves as an excellent reference point. Wells defined crystal structures in terms of their topology by reducing them to a series of points (nodes) of a certain geometry (tetrahedral, trigonal planar, *etc.*) that are connected to a fixed number of other points. The resulting structures, which can also be calculated mathematically, can be either discreet (zero-dimensional) polyhedra or infinite (one-, two-, and three-dimensional) periodic nets. It is perhaps surprising that it was not until the 1990s that the

Michael John Zaworotko was born in South Wales in 1956 and attended Bedwellty Grammar School and Imperial College, where he received a B.Sc. in 1977. His doctoral research was conducted at the University of Alabama under the supervision of Prof. Jerry L. Atwood and the Ph.D. was granted in 1982. This was followed by post-doctoral research in structural and organometallic chemistry with Prof. S. R. Stobart at University of Victoria, Canada. He joined the faculty at Saint Mary's University, Halifax, Canada in 1985, where he remained until 1998. His interest in crystal engineering was developed during a sabbatical leave at the Frank J. Seiler Research Laboratory at the United States Air Force Academy in Colorado Springs, USA. He moved to the University of Winnipeg, Canada in 1998, where he served as Dean of Arts and Science and to the University of South Florida, Tampa, USA in September 1999, where he currently serves as Chairperson of the Department of Chemistry. His current interests focus upon expanding the field of crystal engineering further into the nanoscale by concentrating upon biological and synthetic supermolecules.

DOI: 10.1039/b007127g

approach of Wells began to bear fruit in the laboratory. Discrete coordination compounds that are based upon Platonic or Archimedean polyhedra have attracted considerable interest in recent years[15–17] and are conceptually related to the 'Wellsian' approach. However, we shall focus upon infinite architectures, for which Robson and coworkers[18] delineated principles that facilitated rapid development of the field of coordination polymers. In effect, Robson extrapolated Wells' work on inorganic network structures into the realm of metal–organic compounds and coordination polymers. In this context, the 'node and spacer' approach has been remarkably successful at producing predictable network architectures. Scheme 1 illustrates some of the simplest architectures that can be generated by using commonly available metal moieties and linking them with linear 'spacer' ligands.

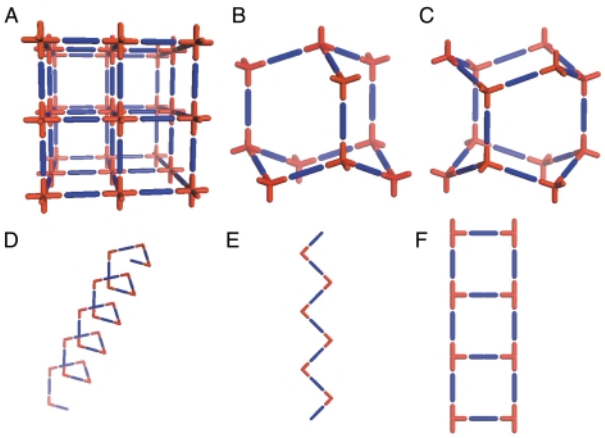

Scheme 1 A schematic representation of some of the simple 3D and 1D network architectures that have been structurally characterized for metal–organic polymers: A. octahedral; B. cubic diamondoid; C. hexagonal diamondoid; D. helix; E. zigzag chain; F. molecular ladder.

These network structures are salient from a design perspective as follows:

- Each of the networks illustrated in Scheme 1 is based upon at least two components (*i.e.* the metal node and the ligand spacer) and the components can be pre-selected for their inherent ability to self-assemble. These network structures can therefore be regarded as blueprints for the construction of networks that, in principle, can be generated from a diverse range of chemical components, *i.e.* they are prototypal examples of modular frameworks. It should be noted that the construction of networks from single component systems also represents an important area of activity but that there are conceptual differences between the two approaches.
- The architecture alone often affords information that allows the chemist to predict some of the bulk properties. For example, most of the structures in Scheme 1 inherently generate cavities that are based upon the size and length of the spacer ligand. The 3D architectures A–C represent in some ways the ultimate challenge in terms of crystal engineering since they lead directly to crystal structure prediction. It should therefore be unsurprising that diamondoid[19] and octahedral[20–22] frameworks have attracted considerable attention. In general, for 3D architectures one would expect rigidity to be coupled with porosity, *i.e.* analogies to zeolites may be drawn. In the case of 1D structures one would normally expect close-packing variability in the context of how adjacent networks pack with respect to one another.
- We have coined the term 'supramolecular isomerism'[23] to define the existence of more than one superstructure for a given set of molecular components. This concept is illustrated by structures B and C, which represent cubic and hexagonal diamondoid structures, respectively, and structures D and E, which are also supramolecular isomers of one another. It is important to note that, although supramolecular isomerism affords superstructural diversity, it also limits the number of possible architectures to those that can be generated rationally from the molecular components that are present in a network.

The diversity of network structures that can result from supramolecular isomerism is the focus of this article. In the case of 2D architectures, one would anticipate that networks would possess an inherent ability to intercalate guest molecules, *i.e.* clay-like properties will be expected. As revealed herein, this is indeed the case for many of the 2D networks that have been studied by us and other groups. We also highlight the surprising degree of diversity that can exist in 2D structures.

Square-grid coordination polymers

Square-grid networks exemplify a particularly simple and commonly reported example of a predictable 2D metal–organic network. Square grid coordination polymers are based upon 1 : 2 metal:ligand complexes with linear bifunctional spacer ligands. They were first reported using cyano ligands[24–26] and have recently been expanded in terms of chemical type and cavity size to include pyrazines,[27–30] 4,4′-bipyridine(bipy)[30–35] and longer analogues of bipy.[23,36] These compounds can indeed be regarded as being analogues of clay minerals since they also have an ability to intercalate guest molecules. However, they have added features that are not likely to be present in clays and they are complementary to 'organoclays',[37] which are chemically modified inorganic clays or calixarene 'organic clay mimics',[38,39] that are based upon calix[4]arenesulfonate salts that form alternating hydrophobic and hydrophilic layers. For example, cavities lie within the plane of the structure and they are suitable for either interpenetration or enclathration of a wide range of organic guest molecules. Furthermore, since they are designed from first principles, it is possible to design the cavities to be inherently hydrophobic or hydrophilic and to tune their dimensions, although interpenetration can mitigate against the existence of frameworks with very large cavities.[40] Finally, it should be noted that the metal sites can possess chemical as well as structural properties. Indeed, catalytically active sites have been incorporated into square-grid structures.[32]

Square-grid networks generated with bipy spacer ligands were first reported by Fujita *et al.*[32] Fujita's compounds are based on Cd(II) and related structures were subsequently reported for other transition metals, including Co(II) and Ni(II) and Zn(II). Although these 2D coordination networks are isostructural within the coordination grid (effective dimensions of the diagonals are *ca.* 1.3 × 1.3 nm), the crystal structures of compounds can differ in the manner in which the networks stack with respect to each other. In particular, interlayer separations can lie in the range 0.6–0.8 nm and the quantity of guest molecule can vary. $[M(bipy)_2(NO_3)_2]\cdot$guest (M = Co, Ni)[41–43] exhibits three basic packing modes (Fig. 1). These packing modes are similar in that the square-grid networks are parallel to one another but they differ in the manner in which the square grids pack with respect to one another and the relative proportion of guest molecule that is present. Type A compounds exhibit 2 : 1 guest : host stoichiometry and interplanar separations of *ca.* 0.6 nm, type B compounds generally crystallize with 2.5 guest molecules per metal center and interlayer separations are *ca.* 0.8 nm. Type C compounds have interlayer separations that are similar to those seen for type B compounds and have 3 : 1 stoichiometry.

In all of these compounds the proportion of the crystal that is occupied by guest molecules is *ca.* 50% by volume. In such a situation it becomes reasonable to question whether interactions between the guest molecules determine the cavity shape and crystal packing of the square grid polymers rather than *vice versa.* Careful examination of the crystal packing in $\{[Ni(bipy)_2(NO_3)_2]\cdot 2pyrene\}_n$ reveals that the pyrene molecules

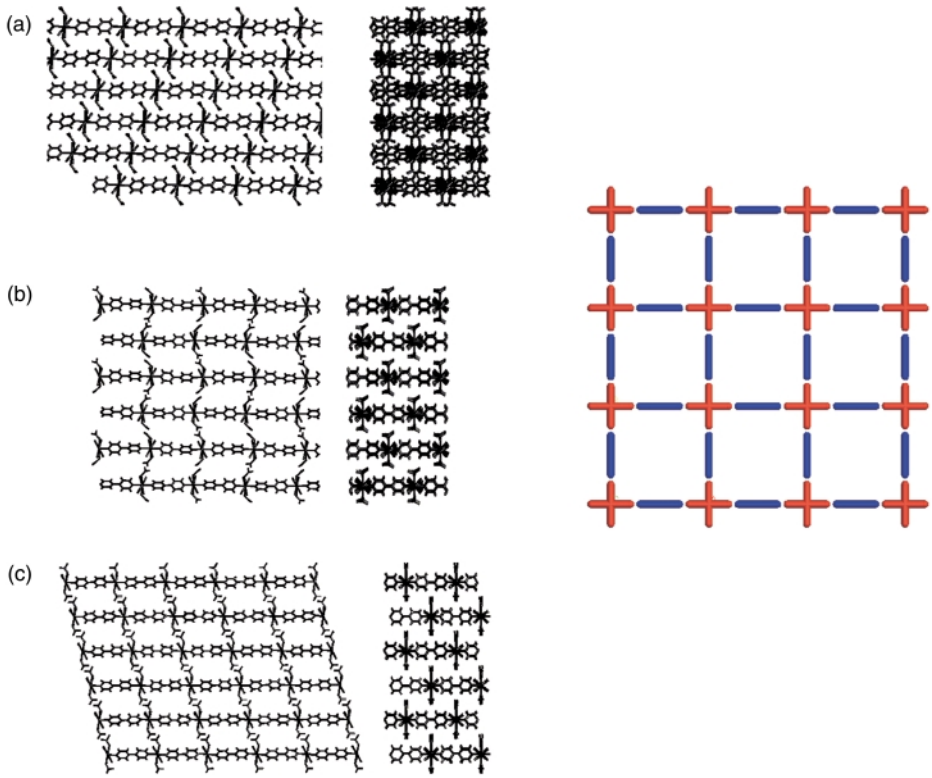

Fig. 1 Perspective views of the stacking of square-grid network architectures of formula $[M(bipy)_2(NO_3)_2]$: (a) A type grids; (b) B type grids; (c) C type grids. The square grid is represented schematically.

form an independent noncovalent network that is complementary from a topological perspective with the square-grid coordination polymer. Indeed, the resulting crystal represents what is to our knowledge the first compound in which it has been revealed that two very different types of 2D net interpenetrate. The square-grid coordination networks [Fig. 2(a)] possess inner cavities of *ca.* 0.8 × 0.8 nm and stack in such a manner that they lie parallel to one another with an interlayer separation of *ca*. 0.79 nm.

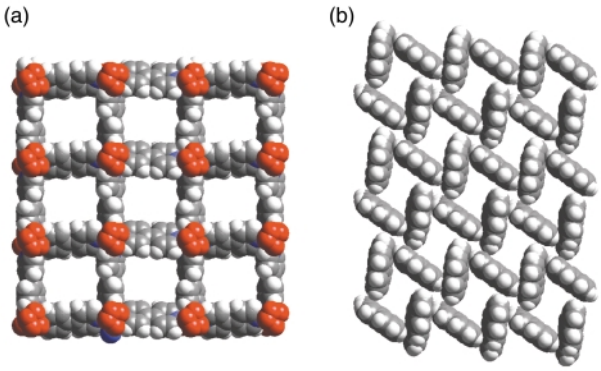

Fig. 2 Space-filling illustrations of the two independent networks in $[M(bipy)_2(NO_3)_2]\cdot 2pyrene$: (a) the metal–organic coordination polymer square-grid, and (b) the noncovalent (4,4) net of pyrene molecules.

The pyrene nets [Fig. 2(b)] are sustained by edge-to-face interactions and contain cavities of dimensions *ca.* 0.65 × 0.35 nm. The planes of the neighboring molecules intersect at an angle of *ca.* 60° and there are no face-to-face stacking interactions between the molecules. The pyrene nets can be regarded as distorted (4,4) nets (if the node is the point in space at which the vectors of the four pyrene planes intersect) or as a distorted brick wall form of a (6,3) net (if the nodes exist at the point of the edge-to-face interactions). It is important to note that, as revealed by Scheme 2, a (6,3) planar net is also complementary from a topological sense with the (4,4) coordination polymer net and that the coordination polymer nets

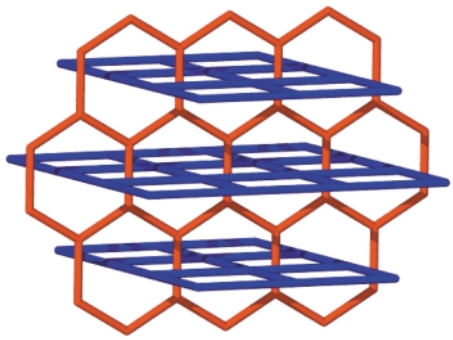

Scheme 2 A schematic diagram that illustrates how honeycomb (6,3) and square (4,4) nets can interpenetrate.

must pack in a staggered manner if they are to fit with the noncovalent net.

That the crystal structure can be viewed as coexistence of interpenetrating covalent and noncovalent nets is potentially important in the context of understanding the structure and stoichiometry of other compounds that are based upon interpenetrated covalent and noncovalent nets. It also illustrates how polarity in crystals can be generated from subtle packing of achiral components, since the pyrene molecules form chiral nets.

This mode of packing is not unique to $\{[Ni(bipy)_2(NO_3)_2]\cdot 2pyrene\}_n$. Indeed, its naphthalene analogue, $\{[Ni(bipy)_2(NO_3)_2]\cdot 3C_{10}H_8\}_n$,[43] can be interpreted as being the result of interpenetration of hexagonal and square nets and a study of a series of related compounds has revealed the presence of noncovalent nets in every compound.[44] The noncovalent hexagonal nets formed by naphthalene and veratrole are illustrated in Fig. 3.

Coordination polymers in which identical (4,4) planar networks interpenetrate have been observed to exhibit two types of interpenetration, both of which are examples of *inclined interpenetration*.[40] The most commonly encountered form might be described as *diagonal/diagonal inclined interpenetration* and was observed in the prototypal $[M(bipy)_2X_2]_n$

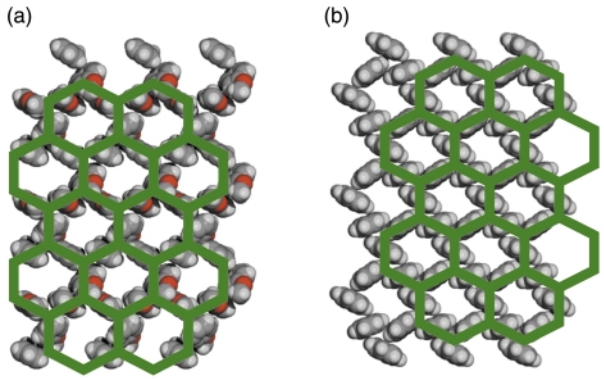

Fig. 3 Space-filling illustrations of the hexagonal (6,3) networks formed by (a) veratrole, and (b) naphthalene in the intepentrated structures [Ni(bipy)$_2$(NO$_3$)$_2$]·3aromatic.

compound [Zn(bipy)$_2$(H$_2$O)$_2$]SiF$_6$.[32] The other mode of interpenetration might be described as *parallel/parallel inclined interpenetration* and to our knowledge has only been reported for two compounds.[45,46] These types of interpenetration are illustrated in Scheme 3(a) and 3(b), respectively, and differ in how the networks orient and cut through each other.

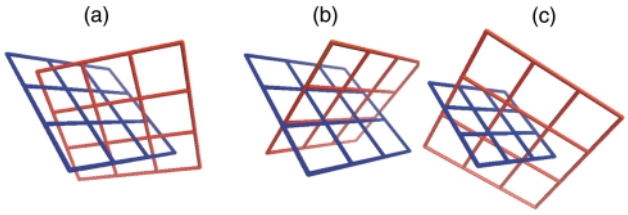

Scheme 3 A schematic that illustrates the three modes of inclined interpenetration that have been observed for square-grid networks: (a) diagonal/diagonal, (b) parallel/parallel, and (c) parallel/diagonal.

Parallel refers to a structure in which a 'spacer' ligand from one network threads through the cavity of the other, *diagonal* refers to a structure in which a 'node' from one network (*e.g.* the metal moiety) is within the cavity of the other. One would anticipate that the structure that is adapted by a particular compound would be influenced by several geometric factors: the relative size of the cavity; the distance between adjacent nodes within a network; the thickness of the layers and how this limits the interlayer separation of adjacent networks; the steric bulk of the node. In this context, it is important to note that, with all other things being equal, the diagonal/diagonal mode of interpenetration facilitates an interlayer separation that is 41.4% greater than that of the parallel/parallel mode. Furthermore, the diagonal/diagonal mode ensures a staggered orientation of parallel layers whereas an eclipsed orientation is necessary if the parallel/parallel structure is present. Therefore, in terms of steric considerations, it would be expected that the diagonal/diagonal mode would be most favored. However, circumstances where the interlayer separation would ideally be shorter, or where the metal atoms in adjacent layers would be eclipsed (*e.g.* to maximize interlayer interactions) could favor the parallel/parallel mode.

The structures we have studied that are based upon complementary covalent and noncovalent networks exhibit a third mode of inclined interpenetration that is a hybrid of the modes described above: *parallel/diagonal inclined interpenetration*. The noncovalent (4,4) arene networks exhibit parallel inclined interpenetration with respect to the (4,4) metal–organic coordination networks, whereas the covalent coordination networks demonstrate diagonal inclined interpenetration with respect to the arene networks [Scheme 3(c)]. This structural feature means that the nitrate groups of adjacent parallel coordination polymer grids are staggered and that the interlayer separation is a consequence of the size of the arene network. It should therefore be unsurprising that Type A grids result when templated by the smallest arenes (benzene and derivatives) as they exhibit smaller interlayer separations than type B and C packing. Grid types B and C occur in the presence of larger or more arenes.

A question that cannot yet be answered with certainty concerns whether or not the noncovalent networks of aromatic molecules can exist in the absence of the coordination polymers. In this context, the existence of a 1 : 1 binary compound between ferrocene and pyrene[45] represents an important prototype since pairs of ferrocene molecules are stacked inside a pyrene 2D network that is sustained by noncovalent C–H···π interactions (Fig. 4). This pyrene network is a slightly distorted version of that observed in {[Ni(bipy)$_2$(NO$_3$)$_2$]·2pyrene}$_n$.

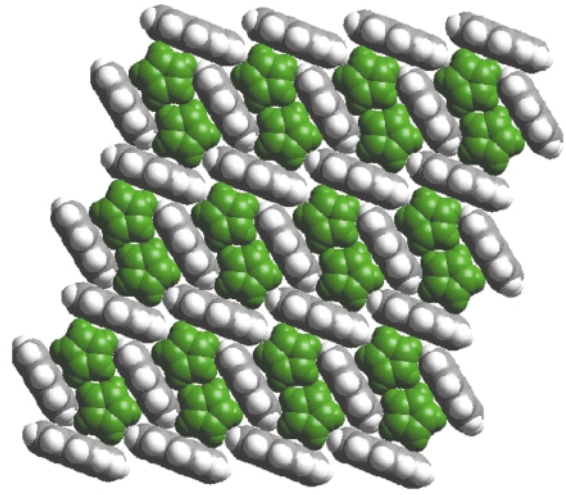

Fig. 4 A space-filling illustration of the crystal structure of the cocrystal formed by ferrocene (green) and pyrene.

From the above it should be clear that even for the relatively narrow class of compounds of formula [M(bipy)$_2$X$_2$]$_n$, there are many permutations of metal, anion and guest. It should be noted that grids in which there are two types of spacer ligand, rectangular grids, have also been reported.[29,30] It therefore seems likely that square and rectangular grids will represent a generic class of synthetic clay mimic.

Other 2D architectures

The existence of supramolecular isomerism is well exemplified by the diverse range of architectures that can be generated by self-assembly of T-shaped nodes. In the context of coordination polymers, this effectively means linking of *mer*-substituted octahedral metal moieties or trisubstituted square-planar metal centers. In such a situation the stoichiometry is based upon a 1 : 1.5 metal : spacer ligand ratio. The T-shape node has thus far produced examples of 1D, 2D and 3D networks. There are three distinct 2D supramolecular isomers: brick wall,[45,48–55] herringbone,[51,56–58] and bilayer.[59–61] Schematic illustrations of these structures are presented in Scheme 4(a)–(c), respectively. It is interesting to note that, if one calculates the possible 2D networks that are possible for T-shaped nodes (Scheme 4), three of the five possibilities have already been realized.

The brick architecture was first observed as the product of the reaction between heptacoordinate Cd(II) and 1,4-bis[(4-pyridyl)methyl]-2,3,5,6-tetrafluorophenylene.[35] The T-shape geometry is the result of two nitrate ligands chelating in a bidentate manner, thereby occupying four of the seven coordination sites. The structure is triply interpenetrated and, as such, does not have channels or cavities. Interestingly, in a similar system using the non-fluorinated pyridyl-based ligand, a 1D ladder structure was observed. In several of the compounds that exhibit the herringbone or 'parquet floor' architecture the coordination sphere is similar to that of the brick architectures: heptacoordinate Cd(II) or Co(II), with two terminal bidentate

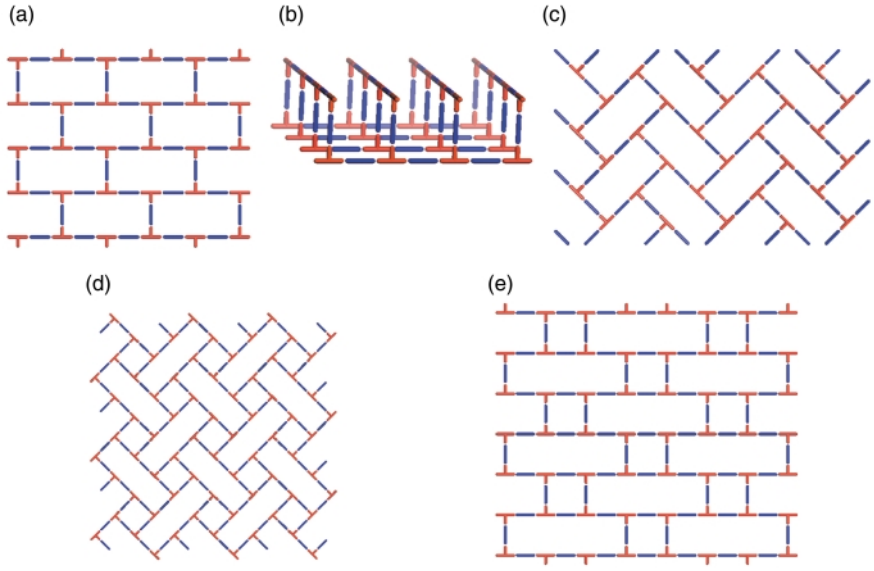

Scheme 4 A schematic illustration of 2D nets that can be generated for T-shape building blocks: that have been characterized or might be expected to occur: (a) brick wall; (b) bilayer; (c) herringbone; (d) long-and-short brick; (e) basket weave; (d) and (e) are yet to be realized.

nitrate ligands and coordination to one end of three 4,4′-azopyridine bridging ligands; an isostructural example has also been reported with 1,2-bis(4-pyridyl)ethyne as the bridging ligand.[60]

The bilayer architecture has been observed in at least three compounds.[59–63] Interestingly, it has been observed as the product from the reaction of $Co(NO_3)_2$ and bipy, which also generates ladder, square-grid and herringbone architectures. The bilayer form of $[Co(bipy)_{1.5}(NO_3)_2]$ is observed if crystallization occurs in the presence of CS_2[59] or H_2O.[61,63] The bilayers pack by partial interdigitation (Scheme 5), which

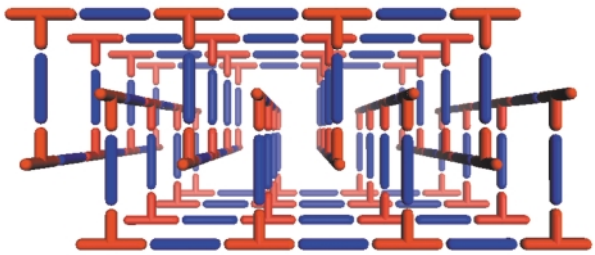

Scheme 5 A schematic that illustrates how porosity can be generated by partial interdigitation of bilayer networks.

allows 1D channels to run through the structure. This structure is somewhat relevant since it represents one of the first reported examples of a synthetic compound that might be regarded as a metal–organic zeolite, *i.e.* the structure is porous and stable to loss of guest.[63] The bilayer architecture has also been reported for systems using 1,2-bis(4-pyridyl)ethane.[64]

The number of supramolecular isomers already observed in the $Co(NO_3)_2$/bipy system indicates the importance of template and crystallization conditions. It seems reasonable to assert that it is only a matter of time and effort before the weave and long-and-short brick motifs, Scheme 4(d) and 4(e), respectively, will also be realized.

In terms of topology, it should be noted that brick and herringbone motifs are both examples of (6,3) nets and can therefore be regarded as being closely related to honeycomb (6,3) nets. Honeycomb networks are quite common in organic structures because of the availability of trigonal nodes (*i.e.* 1,3,5-trisubstituted benzenes such as trimesic acid and species such as the guanadinium cation) but they seldom occur in the context of metal–organic polymers because trigonal and trigonal-bipyramidal coordination geometries are relatively rare. However, $[Cu(pyrazine)_{1.5}]BF_4$[65] is based upon trigonal Cu(I) and it should therefore be unsurprising that it crystallizes as a honeycomb (6,3) net. That there now exist a number of ligands with trigonal geometry means that it is likely that a wider range of honeycomb structures will be generated in the near future.

3D structures *via* 2D structures

Manipulation of 2D structures represents a possible entry into the generation of 3D architectures. In such a context, there are two relatively simple strategies: cross-linking of 2D structures and interpenetration of identical or different 2D networks.

Cross-linking becomes feasible if one selects an appropriate 2D structure that has functionality in the axial direction. Such an approach has been widely used by clay chemists and hence the term ‘pillaring’ might be applied to describe such a process. $[M(bipy)_2(SiF_6)]$ could be used as a prototype in the context of coordination polymers since it can be regarded as having been generated from square-grid coordination polymers that are cross-linked by μ-SiF_6 anions.[20,22]

Interpenetration is a widely encountered phenomenon[40] that can mitigate against the existence of frameworks with very large cavities. However, Scheme 6 reveals that there are

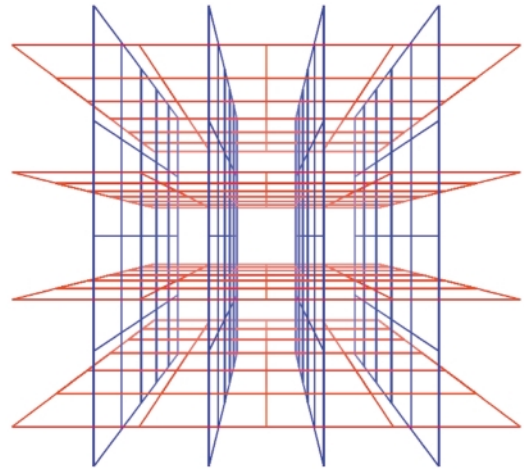

Scheme 6 A schematic diagram that illustrates how square-grids can interpenetrate and generate channels.

situations in which interpenetration can occur, generate porosity and afford 3D structures. Square-grid polymers that are based upon longer spacer ligands such as 1,2-bis(4-pyridyl)ethane

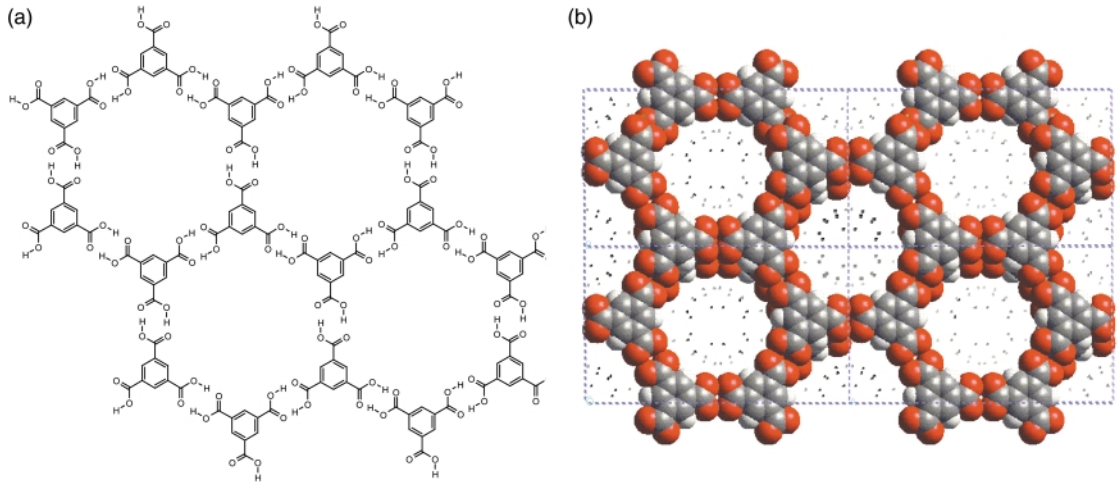

Fig. 5 Schematic (a) and space-filling (b) views of the open-framework phase of trimesic acid.

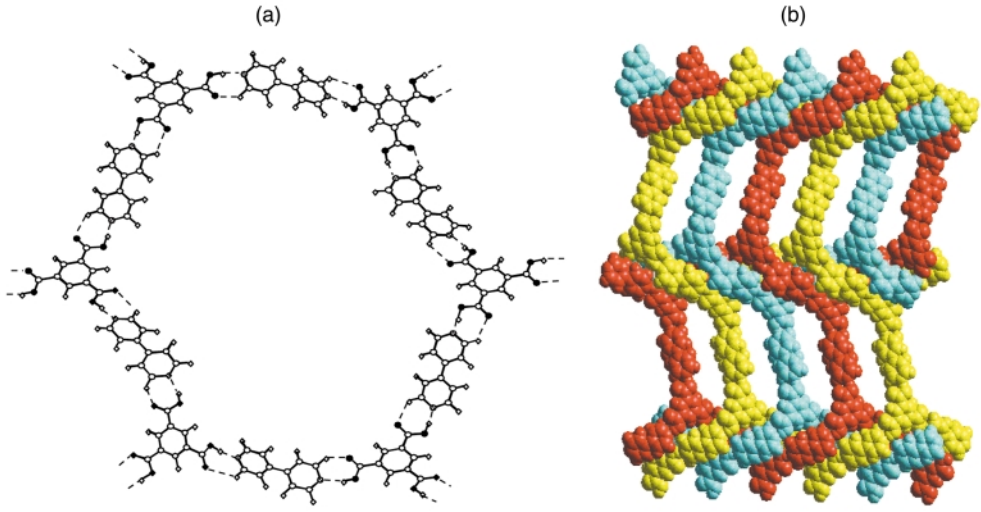

Fig. 6 The cocrystal formed by trimesic acid and 4,4′-bipyridine: (a) a single 'expanded trimesic acid' honeycomb network and (b) a space-filling view of how the puckered honeycomb networks interpenetrate.

(bipy-eta) or 1,2-bis(4-pyridyl)ethylene (bipy-ete) can interpenetrate in such a fashion.[40,41]

Organic networks–molecular and ionic structures involving trimesic acid

It is possible in both principle and practice to draw a number of analogies between organic networks and coordination polymers. In particular, the 'node and spacer' approach can be employed equally well with noncovalent interactions as with coordinate covalent bonds. This is especially true for hydrogen bonds, for which the donor (*i.e.* a protic hydrogen atom) and the acceptor (*i.e.* a region of electron density) can be compared with metal atoms and ligands, respectively. Furthermore, as noted by Etter,[12] in cases where there are multiple hydrogen bonding sites, there is a fair degree of predictability concerning which donors and acceptors will engage. In this context, networks that involve NH···O and/or OH···O hydrogen bonds, including those that exploit the carboxylic dimer or its deprotonated form, represent a wide range of reliable and ubiquitous supramolecular synthons that already have been applied in a broad range of systems.

Molecular networks sustained by trimesic acid

Hydrogen-bonded 2D networks are well exemplified the well known structure of trimesic acid (1,3,5-benzene tricarboxylic acid, H_3TMA), a polyfunctional carboxylic acid that is inexpensive and chemically robust. It possesses trigonal exodentate functionality that facilitates self-assembly into two dimensions. Fig. 5 illustrates how the hydrogen-bonding pattern in 2D networks formed by H_3TMA generates cavities of predictable size (*ca.* 1.4 nm diameter). In pure H_3TMA[66] the honeycomb grid is puckered and the cavities are filled by self-inclusion, or interpenetration, of other networks. However, subsequent reports revealed that there are methods for preparing the non-interpenetrated or open framework form of H_3TMA.[67,68] If crystallized in the presence of alkanes, H_3TMA forms open-framework honeycomb layers that align in such a manner that adjacent sheets are almost eclipsed with respect to each other [Fig. 5(b)]. The resulting architecture observed in the crystal structure is essentially identical to that depicted in Fig. 5(a).

H_3TMA represents an example of a self-assembled motif. However, this limits options in terms of supramolecular synthesis, especially when compared to modular systems. The H_3TMA network can be modified in several ways if modular approaches are employed. For example, $[H_3TMA][bipy]_{1.5}$ would be expected to exist as an expanded form of H_3TMA since the pyridine–carboxylic acid supramolecular synthon appears to be more stable than the carboxylic acid dimer itself.[69] As depicted in Fig. 6, the anticipated expanded honeycomb structure indeed occurs and the cavities are large (*ca.* 2.6 × 3.5 nm). However, the cavities are filled by the interpenetration of three independent networks [Fig. 6(b)], thereby affording a close-packed structure with no cavities. This type of interpenetration, *parallel interpenetration*, resembles weaving, is

facilitated by puckering of the pseudohexagons that form the network. Indeed, the hexagons resemble the chair conformation of cyclohexane.

Rao and coworkers recently reported a related structure that is based upon modular self-assembly:[70] an organic network formed by trithiocyanuric acid (TCA) and bipy. Adjacent layers are aligned parallel to each other and there is no interpenetration.

Networks sustained by anions of trimesic acid

Anionic forms of H_3TMA also represent an appropriate node for generation of 2D superstructures. Ammonium salts of the deprotonated forms of H_3TMA offer a simple entry into such systems.[71–73] Scheme 7 illustrates two motifs that demonstrate how the ammonium moiety might extend anionic forms of H_3TMA into honeycomb networks.

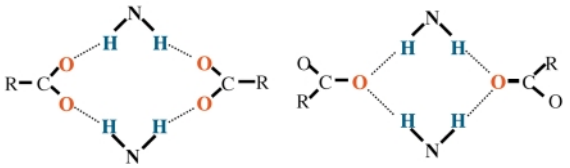

Scheme 7 The two supramolecular isomers that have been seen for self-assembly of carboxylate and ammonium moieties in $[NH_2(c\text{-}C_6H_{11})_2]_3$[TMA].

In the case of TMA^{3-} and the dicyclohexylammonium cation, supramolecular isomers A[74] and B[75] have both been observed to generate laminated structures. The generation of A or B appears to be solvent dependent. It has also been shown that self-assembly of the lamellar structure can occur on surfaces.[74] An important feature of architectures that are sustained by A and B is that some of their components and features can be fine-tuned without destroying the basic architecture. For example, the ammonium cation substituents can be changed without influencing the basic molecular recognition properties in the context of motifs A and B. For secondary amines, organic substituents would extend above and below the network, and in appropriate circumstances would preclude interpenetration.

If alkyl substituents are present on the ammonium cation and the stoichiometry is 1 : 2 then the typical result is a laminated material with poor ability to adsorb molecules because of interdigitation of the alkyl substituents.[72] However, use of dibenzylamine mitigates against interdigitation and promotes reversible incorporation of aromatic guest molecules.[73] The resulting compounds are structurally related to clays, but they are inherently hydrophobic and have generic affinity for a wide range of aromatic guests over alcohols or water. In a series of host–guest compounds, the stoichiometry remains constant, $[NH_2(CH_2Ph)_2]_2$[HTMA], but there is variation in the geometry of the hydrogen bond layer and in the manner in which guest molecules are incorporated. In general, the benzyl groups form a plethora of aromatic C–H$\cdots\pi$ interactions to the surrounding guest molecules. The unit cell lengths are typically multiples of *ca.* 1.2 $\times$ 1.7 $\times$ 2.1 nm (stacking axis, short axis and long axis, respectively). The length of the stacking axis represents the interlayer separation and a doubling of the length of the stacking axis occurs when adjacent layers are not related by translation. Multiples of short and long axes also occur because of differences in the arrangement of guest molecules between benzyl groups. In effect, guest molecules and/or benzyl groups do not necessarily repeat with the asymmetric unit of the H-bonded layer. The crystal structures might be classified based upon the stacking axis as being of one of two types: (a) identical packing of adjacent layers (*i.e.* related by translation); (b) adjacent layers which are different from each other. The hydrogen bonded sheets can be either flat or corrugated. In effect, the host matrix is a flexible, generic host material for aromatic molecules. A representative series of structures is illustrated in Fig. 7 and, as should be clear, there is no interdigitation of benzyl groups.

A series of related structures that is based upon two-dimensional layers resulting from hydrogen bonding of the trigonal guanidinium cation, $C(NH_2)_3^+$, and organic sulfonate ions RSO_3^- has been extensively studied by the Ward group.[76] Interdigitation of the organic substituent of the sulfonate ions on

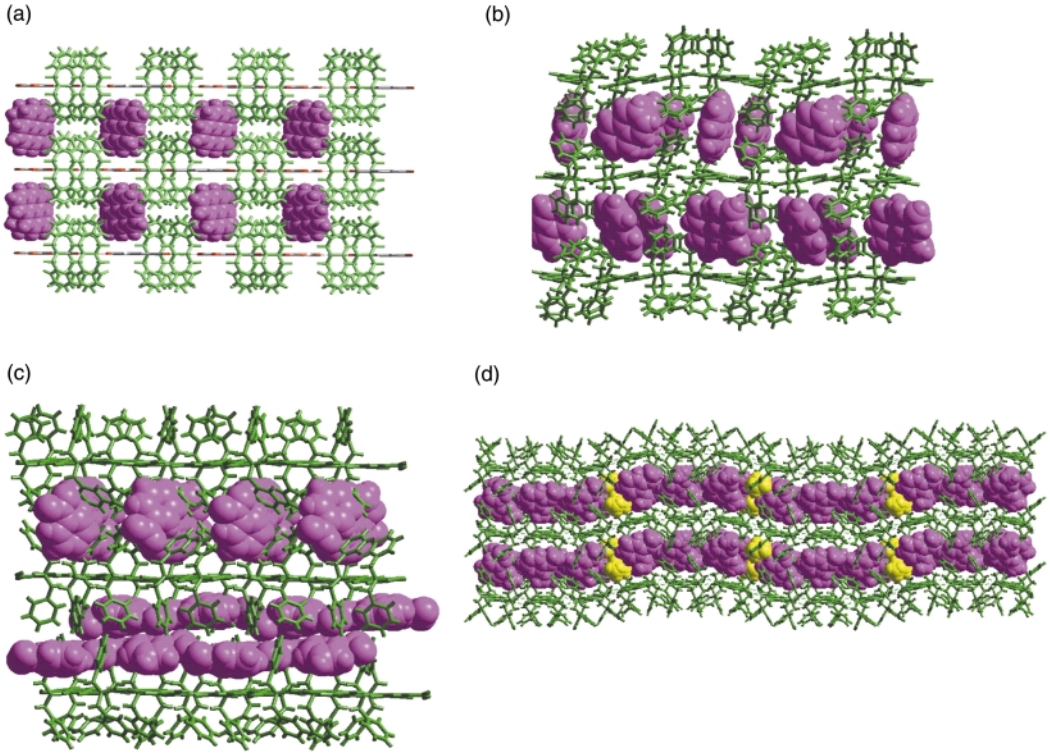

Fig. 7 The crystal structures of four 'organic clays' sustained by [(trimesate){$NH_2(CH_2Ph)_2$}$_2$]. The benzyl moieties preclude interdigitation and facilitate reversible sorption of aromatic molecule: (a) pyrene; (b) naphthalene; (c) nitrobenzene; (d) veratrole.

adjacent layers and ionic hydrogen bonding predictably leads to a series of laminar architectures.

Summary and conclusions

The fundamental precept of crystal engineering is that all information necessary for design of extended 1D, 2D and 3D structures is already present at the molecular level in existing chemical species. However, crystal engineering does not address the important issues of crystal structure prediction, crystal growth and crystal nucleation. In the case of growth and nucleation, the role of kinetic factors and inhibitors in controlling morphology, polymorphs and supramolecular isomers is critical. Crystal engineering does not yet address control of such factors, rather it afford 'recipes'. Based upon this understanding and the results described herein one can make several assertions:

Prediction *vs.* design

It is important to stress the significant conceptual difference between crystal engineering and crystal structure prediction. They are not synonymous. In short, crystal structure prediction is precise (*i.e.* space group and exact details of packing are defined) and deals primarily with known molecules, many of which are not disposed to predictable self-assembly.[77,78] Crystal engineering is far less restrictive from a conceptual perspective since it focuses more broadly upon the design of new and existing network architectures. In effect, the principles of design are based upon a blueprint, in many cases a blueprint that is first recognized *via* a serendipitous discovery, and they allow the designer to select components in a judicious manner. Therefore, a desired network structure or blueprint can be limited to chemical moieties, in many cases commercially available moieties, that are predisposed to a successful outcome. In short, crystal engineering represents a paradigm for supramolecular synthesis of new solid phases and there are no real limits in terms of chemical moieties that can be involved.

What does self-assembly mean in this context of crystal engineering?

That one can exploit self-assembly principles to design new solid phases has important implications. First and foremost, all the information necessary to build networks is already stored in known molecules. In the context of the results reported herein, all structures are air- and water-stable and were generated in one-pot reactions using commercially available reagents. Second, if one uses a modular self-assembly approach then fine-tuning of structures is both facile and can be effected broadly. It should be intuitive that most molecules are not self-complementary, *i.e.* their molecular recognition sites cannot be fully satisfied by self-assembly. It therefore follows that modular structures, *i.e.* those based upon more than one component, are often going to be both more diverse and more controllable than single component phases.

Relevance to 0D structures

The principles of self-assembly have also been applied towards the design and isolation of discrete molecular structures. Such structures are exemplified by molecular squares[79–81] and, more recently, by striking examples of new high molecular weight compounds that can be described as spheroid organic[82,83] or coordination architectures.[15–17,84] The design principles behind the isolation and development of these new classes of compound are based upon applying the concept of self-assembly in the context of geometric considerations found in regular (Platonic) and semi-regular (Archimedean) solids.[82] Interestingly, such structures are also known in zeolites (*e.g.* Linde A, which is based upon an edge-skeleton generated by fused, truncated octahedra[85]) and in biological self-assembled systems such as mammalian picornaoviruses.[86–89]

It is reasonable to expect a great deal of synergy between these two areas of research. In the context of how self-assembly of discrete structures will influence crystal engineering, it is reasonable to assert that a wide range of nanosized molecular species will become available for self-assembly of synthetic clay-like and zeolite-like architectures. Such structures would be unprecedented and offer nanoscale channels and cavities in addition to novel functionality. The hierarchy of such systems, which is inherently a consequence of self-assembly approaches, and the interesting possibilities that exist for use of such 'secondary building units' in materials science have already been highlighted by others.[90,91]

Acknowledgements

I gratefully acknowledge the generous financial support of the NSERC during 1986–99 and Saint Mary's University. I am also indebted for the contributions to this work by a group of talented, hard-working students and coworkers, many of who were undergraduates when they were active in my group. Thanks to them I never need to be reminded that the primary benefit of research is that it is for people and by people. I will only accept a small part of the blame for the contributions that these individuals are now making to science and society.

Notes and references

1 J. Maddox, *Nature*, 1988, **335**, 201.
2 G. M. J. Schmidt, *Pure Appl. Chem.*, 1971, **27**, 647.
3 J. M. Lehn, *Supramolecular Chemistry: Concepts and Perspectives*, VCH, Weinheim, 1995.
4 J. Bernstein, R. J. Davey and J. O. Henck, *Angew. Chem., Int. Ed.*, 1999, **38**, 3441.
5 J. D. Dunitz and J. Bernstein, *Acc. Chem. Res.*, 1995, **28**, 193.
6 K. Tanaka and F. Toda, *Chem. Rev.*, 2000, **100**, 1025.
7 L. R. Macgillivray, J. L. Reid and J. A. Ripmeester, *J. Am. Chem. Soc.*, 2000, **122**, 7817.
8 J. Xiao, M. Yang, J. W. Lauher and F. W. Fowler, *Angew. Chem., Int. Ed.*, 2000, **39**, 2132.
9 J. J. Kane, R. F. Liao, J. W. Lauher and F. W. Fowler, *J. Am. Chem. Soc.*, 1995, **117**, 12 003.
10 G. R. Desiraju, *Angew. Chem., Int. Ed. Engl.*, 1995, **34**, 2311.
11 G. R. Desiraju, *Crystal Engineering: the Design of Organic Solids*, Elsevier, Amsterdam, 1989.
12 M. C. Etter, *Acc. Chem. Res.*, 1990, **23**, 120.
13 A. F. Wells, *Three-Dimensional Nets and Polyhedra*, Wiley, New York, 1977.
14 A. F. Wells, *Structural Inorganic Chemistry*, Oxford University Press, Oxford, 1975.
15 B. Olenyuk, J. A. Whiteford, A. Fechtenkotter and P. J. Stang, *Nature*, 1999, **398**, 796.
16 N. Takeda, K. Umemoto, K. Yamaguchi and M. Fujita, *Nature*, 1999, **398**, 794.
17 A. Muller, E. Krickemeyer, H. Bogge, M. Schmidtmann and F. Peters, *Angew. Chem., Int. Ed.*, 1998, **37**, 3360.
18 B. F. Abrahams, B. F. Hoskins and R. Robson, *J. Am. Chem. Soc.*, 1991, **113**, 3606.
19 M. J. Zaworotko, *Chem. Soc. Rev.*, 1994, **23**, 283.
20 S. Subramanian and M. J. Zaworotko, *Angew. Chem., Int. Ed. Engl.*, 1995, **34**, 2127.
21 H. Li, M. Eddaoudi, M. O'Keeffe and O. M. Yaghi, *Nature*, 1999, **402**, 276.
22 S. Noro, S. Kitagawa, M. Kondo and K. Seki, *Angew. Chem., Int. Ed.*, 2000, **39**, 2081.
23 T. L. Hennigar, D. C. Macquarrie, P. Losier, R. D. Rogers and M. J. Zaworotko, *Angew. Chem., Int. Ed. Engl.*, 1997, **36**, 972.
24 S. Nishikiori and T. Iwamoto, *Inorg. Chem.*, 1986, **25**, 788.
25 S. Nishikiori and T. Iwamoto, *J. Inclusion Phenom.*, 1984, **2**, 341.
26 S. Nishikiori and T. Iwamoto, *Bull. Chem. Soc. Jpn.*, 1983, **56**, 3246.
27 T. Miyoshi, T. Iwamoto and Y. Sasaki, *Inorg. Chim. Acta*, 1972, **6**, 59.
28 S. R. Batten, B. F. Hoskins and R. Robson, *New J. Chem.*, 1998, **22**, 173.

29 B. F. Abrahams, M. J. Hardie, B. F. Hoskins, R. Robson and E. E. Sutherland, *J. Chem. Soc., Chem. Commun.*, 1994, 1049.
30 L. R. Macgillivray, R. H. Groeneman and J. L. Atwood, *J. Am. Chem. Soc.*, 1998, **120**, 2676.
31 M. Aoyagi, K. Biradha and M. Fujita, *Bull. Chem. Soc. Jpn.*, 2000, **73**, 1369.
32 M. Fujita, Y. J. Kwon, S. Washizu and K. Ogura, *J. Am. Chem. Soc.*, 1994, **116**, 1151.
33 R. W. Gable, B. F. Hoskins and R. Robson, *J. Chem. Soc., Chem. Commun.*, 1990, 1677.
34 D. Hagrman, R. P. Hammond, R. Haushalter and J. Zubieta, *Chem. Mater.*, 1998, **10**, 2091.
35 J. Lu, T. Paliwala, S. C. Lim, C. Yu, T. Y. Niu and A. J. Jacobson, *Inorg. Chem.*, 1997, **36**, 923.
36 S. H. Park, K. M. Kim, S. Lee and O. S. Jung, *Bull. Korean Chem. Soc.*, 1998, **19**, 79.
37 M. S. Wang and T. J. Pinnavaia, *Chem. Mater.*, 1994, **6**, 468.
38 A. W. Coleman, S. G. Bott, S. D. Morley, C. M. Means, K. D. Robinson and J. L. Atwood, *Angew. Chem., Int. Ed. Engl.*, 1988, **27**, 1361.
39 J. L. Atwood, G. W. Orr, N. C. Means, F. Hamada, H. Zhang, S. G. Bott and K. D. Robinson, *Inorg. Chem.*, 1992, **31**, 603.
40 S. R. Batten and R. Robson, *Angew. Chem., Int. Ed.*, 1998, **37**, 1461.
41 K. Biradha, D. Dennis, V. A. MacKinnon, C. Seward and M. J. Zaworotko, *Current Challenges on Large Supramolecular Assemblies*, ed. G. Tsoucaris, Kluwer, Dordrecht, 1999, pp. 115–132.
42 K. Biradha, K. V. Domasevitch, B. Moulton, C. Seward and M. J. Zaworotko, *Chem. Commun.*, 1999, 1327.
43 K. Biradha, K. V. Domasevitch, C. Hogg, B. Moulton, K. N. Power and M. J. Zaworotko, *Cryst. Eng.*, 1999, **2**, 37.
44 K. Biradha, A. Mondal, B. Moulton and M. J. Zaworotko, *J. Chem. Soc., Dalton Trans.*, 2000, 3837.
45 L. Carlucci, G. Ciani and D. M. Proserpio, *New J. Chem.*, 1998, **22**, 1319.
46 T. Soma and T. Iwamoto, *Acta Crystallogr., Sect. C*, 1996, **52**, 1200.
47 R. Atencio, K. V. Domasevitch and M. J. Zaworotko, *Cryst. Eng.*, 2000, **3**, 63.
48 L. Carlucci, G. Ciani and D. M. Proserpio, *J. Chem. Soc., Dalton Trans.*, 1999, 1799.
49 M. Kondo, M. Shimamura, S. Noro, S. Minakoshi, A. Asami, K. Seki and S. Kitagawa, *Chem. Mater.*, 2000, **12**, 1288.
50 M. Kondo, A. Asami, K. Fujimoto, S. Noro, S. Kitagawa, T. Ishii and H. Matsuzaka, *Int. J. Inorg. Mater.*, 1999, **1**, 73.
51 M. Fujita, Y. J. Kwon, O. Sasaki, K. Yamaguchi and K. Ogura, *J. Am. Chem. Soc.*, 1995, **117**, 7287.
52 Y. B. Dong, M. D. Smith, R. C. Layland and H. C. Zur Loye, *Chem. Mater.*, 2000, **12**, 1156.
53 Y. B. Dong, M. D. Smith, R. C. Layland and H. C. Zur Loye, *J. Chem. Soc., Dalton Trans.*, 2000, 775.
54 C. V. K. Sharma and R. D. Rogers, *Cryst. Eng.*, 1998, **1**, 19.
55 H. J. Choi and M. P. Suh, *J. Am. Chem. Soc.*, 1998, **120**, 10 622.
56 R. Masse, J. F. Nicoud, M. Bagieu-Beucher and C. Bourgogne, *Chem. Phys.*, 1999, **245**, 365.
57 M. A. Withersby, A. J. Blake, N. R. Champness, P. A. Cooke, P. Hubberstey and M. Schroder, *New J. Chem.*, 1999, **23**, 573.
58 Y. B. Dong, R. C. Layland, N. G. Pschirer, M. D. Smith, U. H. F. Bunz and H. C. Zur Loye, *Chem. Mater.*, 1999, **11**, 1413.
59 K. N. Power, T. L. Hennigar and M. J. Zaworotko, *New J. Chem.*, 1998, **22**, 177.
60 A. Rujiwatra, C. J. Kepert and M. J. Rosseinsky, *Chem. Commun.*, 1999, 2307.
61 S. Kitagawa and M. Kondo, *Bull. Chem. Soc. Jpn.*, 1998, **71**, 1739.
62 C. J. Kepert and M. J. Rosseinsky, *Chem. Commun.*, 1999, 375.
63 M. Kondo, T. Yoshitomi, K. Seki, H. Matsuzaka and S. Kitagawa, *Angew. Chem., Int. Ed. Engl.*, 1997, **36**, 1725.
64 R. Atencio, K. Biradha, T. L. Hennigar, K. M. Poirier, K. N. Power, C. M. Seward, N. S. White and M. J. Zaworotko, *Cryst. Eng.*, 1998, **1**, 203.
65 L. R. Macgillivray, S. Subramanian and M. J. Zaworotko, *Chem. Commun.*, 1994, 1325.
66 D. J. Duchamp and R. E. Marsh, *Acta Crystallogr., Sect. B*, 1969, **25**, 5.
67 F. H. Herbstein, M. Kapon and G. M. Reisner, *J. Inclusion Phenom.*, 1987, **5**, 211.
68 F. H. Herbstein, *Top. Curr. Chem.*, 1987, **140**, 107.
69 C. V. K. Sharma and M. J. Zaworotko, *Chem. Commun.*, 1996, 2655.
70 A. Ranganathan, V. R. Pedireddi, G. Sanjayan, K. N. Ganesh and C. N. R. Rao, *J. Mol. Struct.*, 2000, **522**, 87.
71 K. Biradha, D. Dennis, V. A. Mackinnon, C. V. K. Sharma and M. J. Zaworotko, *J. Am. Chem. Soc.*, 1998, **120**, 11 894.
72 C. V. K. Sharma, C. B. Bauer, R. D. Rogers and M. J. Zaworotko, *Chem. Commun.*, 1997, 1559.
73 R. E. Melendez and M. J. Zaworotko, *Supramol. Chem.*, 1997, **8**, 157.
74 R. E. Melendez, C. V. K. Sharma, M. J. Zaworotko, C. Bauer and R. D. Rogers, *Angew. Chem., Int. Ed. Engl.*, 1996, **35**, 2213.
75 D. J. Plaut, K. M. Lund and M. D. Ward, *Chem. Commun.*, 2000, 769.
76 K. T. Holman and M. D. Ward, *Angew. Chem., Int. Ed.*, 2000, **39**, 1653.
77 P. Ball, *Nature*, 1996, **381**, 648.
78 A. Gavezzotti, *Acc. Chem. Res.*, 1994, **27**, 309.
79 S. Belanger, M. H. Keefe, J. L. Welch and J. T. Hupp, *Coord. Chem. Rev.*, 1999, **192**, 29.
80 P. J. Stang and B. Olenyuk, *Acc. Chem. Res.*, 1997, **30**, 502.
81 M. Fujita and G. Ogura, *J. Am. Chem. Soc.*, 1990, **112**, 5645.
82 L. R. MacGillivray and J. L. Atwood, *Nature*, 1997, **389**, 469.
83 M. M. Conn and J. Rebek, *Chem. Rev.*, 1997, **97**, 1647.
84 D. L. Caulder and K. N. Raymond, *Acc. Chem. Res.*, 1999, **32**, 975.
85 W. M. Meier and D. H. Olson, *Atlas of Zeolite Structure Types*, Butterworth-Heinemann, Boston, MA, 1992.
86 S. Kim, T. J. Smith, M. S. Chapman, M. G. Rossmann, D. C. Pevear, F. J. Dutko, P. J. Felock, G. D. Diana and M. A. Mckinlay, *J. Mol. Biol.*, 1989, **210**, 91.
87 R. Acharya, E. Fry, D. Stuart, G. Fox, D. Rowlands and F. Brown, *Nature*, 1989, **337**, 709.
88 M. Luo, G. Vriend, G. Kamer, I. Minor, E. Arnold, M. G. Rossmann, U. Boege, D. G. Scraba, G. M. Duke and A. C. Palmenberg, *Science*, 1987, **235**, 182.
89 J. M. Hogle, M. Chow and D. J. Filman, *Science*, 1985, **229**, 1358.
90 M. Eddaoudi, H. L. Li and O. M. Yaghi, *J. Am. Chem. Soc.*, 2000, **122**, 1391.
91 G. A. Ozin, *Chem. Commun.*, 2000, 419.

Supramolecular structures based on dimetal units: simultaneous utilization of equatorial and axial connections†

F. Albert Cotton,*[a] Chun Lin[a] and Carlos A. Murillo*[ab]

[a] *Laboratory for Molecular Structure and Bonding and the Department of Chemistry, PO Box 30012, Texas A&M University, College Station, TX 77842-3012, USA. E-mail: cotton@tamu.edu; murillo@tamu.edu*
[b] *Department of Chemistry, University of Costa Rica, Ciudad Universitaria, Costa Rica*

Received (in Columbia, MO, USA) 6th September 2000, Accepted 20th October 2000
First published as an Advance Article on the web 12th December 2000

As determined by X-ray crystallography, tetranuclear metal–metal bound molecular loops $[Rh_2(DAniF)_2]_2(O_2CCH_2CO_2)_2$ (DAniF = *N*,*N*′-di-*p*-anisylformamidinate) react with 2-*N* donor linkers to give a tubular structure $\{[Rh_2(DAniF)_2]_2(O_2CCH_2CO_2)_2(NC_5H_4CHCHC_5H_4N)_2\}_n$ 1, and a sheet-like structure with interstitial dichloromethane molecules for $[Rh_2(DAniF)_2]_2(O_2CCH_2CO_2)_2(NCC_6H_4CN)_2\}_n$ 2; when the assembly unit was changed from $[Rh_2(DAniF)_2(O_2CCH_2CO_2)]_2$ to the square $[Rh_2(DAniF)_2(O_2CCO_2)]_4$ and the linker $NCC_6F_4C_6F_4CN$ was used, the compound $\{[Rh_2(DAniF)_2]_4(O_2CCO_2)_4(NCC_6F_4C_6F_4CN)_4\}_n$ 3, was formed, in which there are infinite tubes of square cross section having entrained CH_2Cl_2 molecules.

Oligomers and polymers in which a key organizing element is a coordinated metal atom, for example, a square-coordinated Pd^{II} or Pt^{II} atom or a tetrahedral zinc atom, are currently the subjects of vigorous study in many laboratories.[1] This work is driven by the search for novel materials, distinguished by special magnetic properties,[2] micro- and meso-porous structures,[3] or catalytic properties.[4]

Several years ago we began to explore the possibilities of employing strongly bonded dimetal units, such as Mo_2^{4+} and Rh_2^{4+}, that can be suitably complexed to control their reactivity and then linked to form linear,[5a,b] square,[5c,d] triangular[5c] and polyhedral[5e] structures. The linking process entails the use of di- and tri-carboxylic acids which attach themselves to adjacent pairs of equatorial sites in the M_2^{4+} entities, as shown

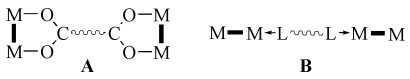

schematically in **A**. The arrays that can be built up in this way have as great a range of sizes as those previously made[2] but differ from most of those in forming initially as neutral species rather than as highly charges ones. However, charge may readily be introduced—in a controlled, stepwise fashion[5b,d]—by oxidation of the Mo_2^{4+} units.

Here we report that by using axial linking, as shown schematically in **B**, it is possible to take simple oligomers and connect them to form one- and two-dimensional polymers. These, again, are initially neutral but can be oxidized. This is the first time such architectures have been created by using dimetal building blocks. We also show how the nature of the polymeric structure can be controlled by choosing axial linkers of the right length, a principle that will be of importance in all future work.

In the examples reported here we have utilized dirhodium, Rh_2^{4+}, building blocks shown as **II** and **III** in Fig. 1. The square, **III**, has been reported before[5c] but the loop, **II**, is a new unit, not reported before, though it is somewhat similar to loops that have been made with Mo_2^{4+} units.[6] Dirhodium units were used here because they have a strong affinity for axial ligands, unlike Mo_2^{4+} units. As axial linkers we have employed **IV**, **V**, and **VI**, (Fig. 1).

With **IV**, $\{[Rh_2(DAniF)_2]_2(O_2CCH_2CO_2)_2(NC_5H_4CHCHC_5H_4N)_2\}_n$ **1** is obtained.‡ It has a tubular structure shown in Fig. 1(a). In Fig. 1(b) there is a schematic representation of this structure§ showing how the rings (**II**) are related alternately by centers of inversion and two-fold axes.

While the formation of such tubes might be considered the 'obvious' outcome of linking units of type **II** by axial bridges, it can only result when the linkers are long enough to keep the bulky *p*-anisyl groups from clashing with each other. With a shorter linker, **V**, major clashes would occur and therefore a different structure arises in $\{[Rh_2(DAniF)_2]_2(O_2CCH_2CO_2)_2(NCC_6H_4CN)_2\}_n$ **2**. This sheet-like structure is shown as 2(a), where dichloromethane molecules are omitted, as 2(b) where the sheets are viewed edge-on and the CH_2Cl_2 molecules are included, and in schematic form as 2(c). The CH_2Cl_2 molecules were well ordered and refined without difficulty. The sheet belongs to the two-dimensional space group C*mm*, the highest symmetry possible in a rectangular sheet structure.

When the assembly unit was changed from **II** to **III** and the linker **VI** was used, the compound $\{[Rh_2(DAniF)_2]_4(O_2CCO_2)_4(NCC_6F_4C_6F_4CN)_4\}_n$, **3** was formed, in which there are infinite tubes of square cross section. A portion of the entire structure is shown as 3(a) while 3(b) shows a portion of one of the units, including one of the entrained CH_2Cl_2 molecules; 3(c) shows a schematic representation of this structure.

Other studies of these compounds and the syntheses of other assemblies of different topologies containing different dimetal units and axial ligands are in progress.

We are grateful to the National Science Foundation for support of this work, and to Johnson Matthey for a generous loan of $RhCl_3$.

Notes and references

‡ The general experimental conditions were described in ref. 1. Elemental analyses were satisfactory for all compounds. The following procedure describes the preparation of $\mathbf{1}\cdot 3CH_2Cl_2\cdot 0.5Et_2O$. A CH_2Cl_2 solution (10 mL) of **II** (82 mg, 0.05 mmol) was carefully layered with a CH_2Cl_2–Et_2O solution (1:1, 20 mL) of *trans*-1,2-bis(4-pyridyl)ethylene (18 mg, 0.10 mmol). Red crystals formed after several days. A similar method was used for $\mathbf{2}\cdot 4CH_2Cl_2$ and $\mathbf{3}\cdot 12.36CH_2Cl_2$. The yields are essentially quantitative.

§ *Crystal data*: for $\mathbf{1}\cdot 3CH_2Cl_2\cdot 0.5Et_2O$: $C_{95}H_{95}Cl_6N_{12}O_{16.5}Rh_4$, M = 2293.17, monoclinic, space group $C2/c$, a = 56.521(4), b = 19.016(2), c = 19.564(2) Å, β = 103.053(2)°, V = 20484(3) Å^3, Z = 8, μ(Mo-Kα) = 0.857 mm^{-1}, T = 213(2) K. The structure, refined on F^2, converged for 13458 unique reflections and 613 parameters to give $R1$ = 0.082 and $wR2$ = 0.182 and a goodness-of-fit = 1.031.

For $\mathbf{2}\cdot 4CH_2Cl_2$: $C_{86}H_{80}Cl_8N_{12}O_{16}Rh_4$, M = 2232.86, triclinic, space group $P\bar{1}$, a = 12.708(2), b = 14.378(2), c = 14.997(3) Å, α = 65.810(3), β = 72.693(3), γ = 74.766(3)°, V = 2355.0(7) Å^3, Z = 1, μ(Mo-Kα) = 0.984 mm^{-1}, T = 213(2) K. The structure, refined on F^2, converged for

† Most of the results reported here were presented in a poster at *Contemporary Inorganic Chemistry, II*, March 12–15, 2000, College Station, TX, USA.

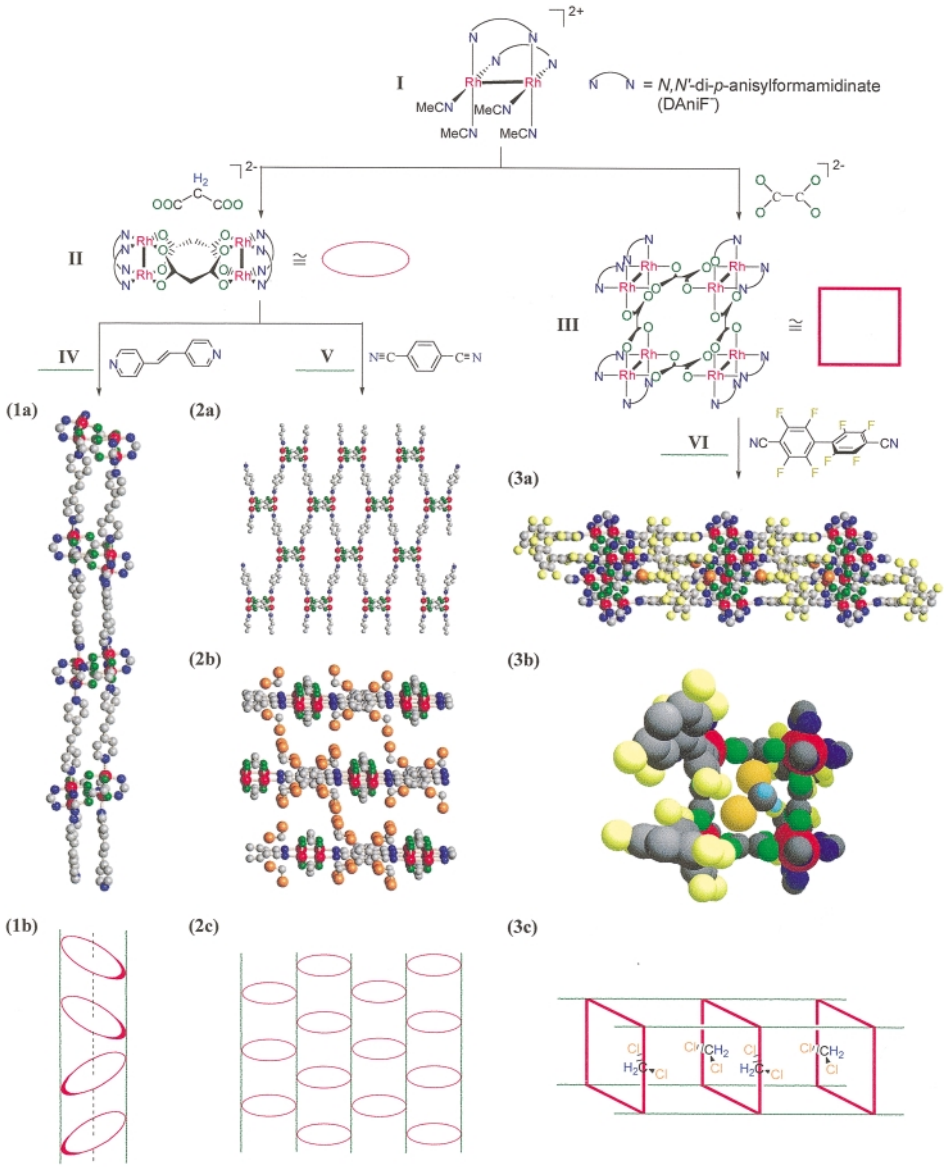

Fig. 1 Synthesis of compounds **1**·3CH_2Cl_2·0.5Et_2O, **2**·4CH_2Cl_2 and **3**·12.36CH_2Cl_2. Views of the extended structures are given in the middle section as follows: (1a) structure of **1**; (2a) structure of **2**; (2b) intercalating architecture in **2**; (3a) structure of **3** and (3b) a space filling drawing of **3** showing CH_2Cl_2 molecules inside the square tube. A schematic view of the corresponding structure is shown in the lower section. In the top section, there are axial CH_3CN molecules (not shown for clarity) at each Rh atom in **I** and **III**. For **II**, there are two CH_3CN molecules distributed on the four Rh atoms. The *p*-anisyl or DAniF groups have also been omitted for clarity. Color labels: Rh, red; N, blue; O, green; C, gray; F, yellow; Cl, orange; H, turquoise.

6163 unique reflections and 578 parameters to give $R1$ = 0.051 and $wR2$ = 0.119 and a goodness-of-fit = 1.010.

For **3**·12.36CH_2Cl_2: $C_{196.36}H_{144.72}Cl_{24.72}F_{32}N_{24}O_{32}Rh_8$, M = 5660.01, triclinic, space group $P\bar{1}$, a = 18.235(6), b = 18.430(6), c = 18.665(6) Å, α = 81.839(7)°, β = 81.775(6), γ = 80.742(7)°, V = 6082(3) Å^3, Z = 1, μ(Mo-Kα) = 0.891 mm^{-1}, T = 223(2) K. The structure, refined on F^2, converged for 15333 unique reflections and 814 parameters to give $R1$ = 0.094 and $wR2$ = 0.211 and a goodness-of-fit = 1.014. CCDC 182/1852. See http://www.rsc.org/suppdata/cc/b0/b007347o/ for crystallographic files in .cif format.

1 See, for example: S. Leininger, B. Olenyuk and P. J. Stang, *Chem. Rev.*, 2000, **100**, 853 and references therein; M. Fujita, *Chem. Soc. Rev.*, 1998, **27**, 417 and references therein; P. Espinet, K. Soulantica, J. P. H. Charmant and A. G. Orpen, *Chem. Commun.*, 2000, 915; J. A. R. Navarro and B. Lippert, *Coord. Chem. Rev.*, 1999, **185**–**186**, 653; D. Whang and K. Kim, *J. Am. Chem. Soc.*, 1997, **119**, 451; S. Mann, G. Huttner, L. Zsolnai and K. Heinze, *Angew. Chem., Int. Ed. Engl.*, 1996, **35**, 2808; M. Scherer, D. L. Caulder, D. W. Johnson and K. N. Raymond, *Angew. Chem., Int. Ed.*, 1999, **38**, 1588; S.-W. Lai, M. C.-W. Chan, S.-M. Peng and C.-M. Che, *Angew. Chem., Int. Ed.*, 1999, **38**, 669; C. J. Jones, *Chem. Soc. Rev.*, 1998, **27**, 289; K. K. Klausmeyer, S. R. Wilson and T. B. Rauchfuss, *J. Am. Chem. Soc.*, 1999, **121**, 2705; H. Li, M. Eddaoudi, M. O'Keeffe and O. M. Yaghi, *Nature*, 1999, **402**, 276.

2 O. Kahn and C. J. Martinez, *Science*, 1998, **279**, 44; Ø. Hatlevik, W. E. Buschmann, J. Zhang, J. L. Manson and J. S. Miller, *Adv. Mater.*, 1999, **11**, 914.

3 T. J. Barton, L. M. Bull, W. G. Klemperer, D. A. Lay, B. McEnaney, M. Misono, P. A. Monson, G. Pez, G. W. Sherer, J. C. Vartuli and O. M. Yaghi, *Chem. Mater.*, 1999, **11**, 2633.

4 M. Fujita, Y. J. Kwon, S. Washizu and K. Ogura, *J. Am. Chem. Soc.*, 1994, **116**, 1151.

5 F. A. Cotton, C. Lin and C. A. Murillo, *J. Chem. Soc., Dalton Trans.*, 1998, 3151; F. A. Cotton, J. P. Donahue, C. Lin and C. A. Murillo, *Inorg. Chem.*, in press; F. A. Cotton, L. M. Daniels, C. Lin and C. A. Murillo, *J. Am. Chem. Soc.*, 1999, **121**, 4538; F. A. Cotton, C. Lin and C. A. Murillo, *Inorg. Chem.*, in press; F. A. Cotton, L. M. Daniels, C. Lin and C. A. Murillo, *Chem. Commun.*, 1999, 841.

6 F. A. Cotton, C. Lin and C. A. Murillo, *Inorg. Chem.*, in press; E. Whelan, M. Deveraux, M. McCann and V. McKee, *Chem. Commun.*, 1997, 427.

Selective anion binding and solid-state host–guest chemistry of an extended cavity calix[6]pyrrole

Boaz Turner,[a] Alexander Shterenberg,[a] Moshe Kapon,[a] Kinga Suwinska[b] and Yoav Eichen*[ac]

[a] *Department of Chemistry, Technion–Israel Institute of Technology, Technion City, 32000 Haifa, Israel. E-mail: chryoav@tx.technion.ac.il*
[b] *Institute of Physical Chemistry, Polish Academy of Sciences, Kasprzaka 44/52, PL-01 224 Warszawa, Poland*
[c] *Solid-State Institute, Technion–Israel Institute of Technology, Technion City, 3200 Haifa, Israel*

Received (in Cambridge, UK) 26th September 2000, Accepted 7th November 2000
First published as an Advance Article on the web

Easily prepared, cone-like, extended cavity calix[6]pyrrole is shown to form strong complexes with iodine and other halide ions as well as with trihaloalkanes and electron deficient aromatic systems.

The host–guest chemistry of calixpyrroles has been the subject of intensive research aimed at gaining both understanding and control on guest recognition and binding.[1] Recently, Sessler and coworkers[2] reported that calix[4]pyrroles **1** are effective and

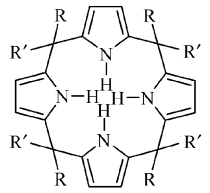

1

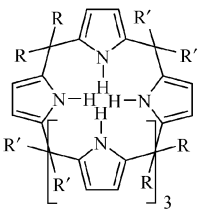

2: R = Ph; R′ = Me

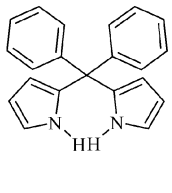

3

selective receptors for anions and neutral guest species. Calixpyrroles that have been tailored to the size, shape and binding modes of target guests were shown to exhibit improved binding ability.[3] Here we report the selective binding of anions, haloalkanes and aromatic guests by recently reported, cone-like, extended-cavity 1,1,3,3,5,5-*meso*-hexaphenyl-2,2,4,4,6,6-*meso*-hexamethylcalix[6]pyrrole.[2,4] Calix[6]pyrroles are a new class of molecules characterized by a six-pyrrolemethane rim. The cross section of the hexapyrrolemethane rim is significantly larger than that of calix[4]pyrroles, *ca.* 110 *cf.* 24 Å^2. Additionally, in the stable conformation of calix[6]pyrroles, such as **2**, three of the *meso* phenyl substituents form a trigonal cavity with a volume of *ca.* 500 Å^3. Such extended-cavity receptors may allow efficient and selective binding of electron defficient aromatic guests as well as large anions such as I^-. These substrates can not be efficiently recognized nor complexed by the smaller calix[4]pyrrole systems.[3b,5]

Calix[6]pyrrole **2** was prepared using a modification of a previously reported method.[4a] Benzophenone (5 g, 27.4 mmol), pyrrole (5 mL, 72.3 mmol) and BF_3·OEt (5 mL, 39.5 mmol) were dissolved in dry ethanol (250 mL) and stirred at room temperature for 5 days under an inert atmosphere. The precipitate was then filtered off and washed with cold ethanol, offering di(phenyl)di(pyrrol-2-yl)methane **3** as a colorless solid (40% yield). An additional crop of **3** could be isolated from the mother-liquor using column chromatography [silica, dichloromethane–hexane (1:10), 50% total yield for **3**]. Calix[6]pyrrole **2** was obtained by stirring a solution of **3** (300 mg, 1 mmol) in 60 mL of dry acetone–ethanol (1:1) containing CF_3CO_2H for 5 days under inert atmosphere. The product was isolated by filtration (43% yield). An additional crop of **2** could be isolated from the mother-liquor using column chromatography [silica, dichloromethane–hexane (3:7), 52% total yield for **2**].

Similarly to earlier studies by Sessler and coworkers on the complexation of calix[4]pyrroles with different guest species, proton NMR spectroscopy was found to be a useful tool for the determination of binding constants between different guests and calix[6]pyrrole, **2**.[6] Quantitative assessments of anion binding constants were made by following the induced shifts in the ^{1}H NMR spectra of the host as a function of the concentration of the guest in an acetonitrile–chloroform (1:9) solution at room temperature (298 K). Table 1 lists the association constants between **2** and the different guests. For comparison, the complexation of octamethylcalix[4]pyrrole with the same guest species was studied under the same conditions (Table 1).

In accordance with previous studies performed by Sessler and coworkers octamethylcalix[4]pyrrole displays a clear preference towards fluoride ions over larger anions, the binding order being $F^- >> Cl^- > Br^- > I^-$. In contrast, probably due to its extended cavity, **2** exhibits a clear preference to iodide over smaller halides. Here the binding order switches to $I^- > F^- >> Cl^- > Br^-$. We interpret this binding order and the high affinity towards iodide in terms of the geometrical fit between the extended cavity of **2** and the iodide ion, allowing full binding of the anion by up to six pyrrole rings. Being the smallest halide, the fluoride ion may fit and bind efficiently to only part of the pyrrolemethane ring. Similar effects have previously been reported for the binding of cations to the cavities of crown ethers.[7]

Calix[6]pyrrole **2** is found to bind also to trihalogenated species such as trichloroethanol, trifluoroethanol, tetrafluoroborate and trifluoroacetate and forms significantly stronger complexes with such guests than with their nonhalogenated ananolgs (Table 1). The reason for this is revealed from the crystal structure† of such a complex between 2,2,2-trichloroethanol and **2** (Fig. 1). Unlike simple calixpyrroles that bind their guests predominantly through X$^-$···H–N bonds,[2,3b] **2** anchors the 2,2,2-trichloroethanol guest through one (disordered) H–O···H–N hydrogen bond with the hydroxy group, *d*(O84b···H–N18) = 2.411 Å; α(O–H–N) = 169.11°; *d*(O84a···H–N70) = 2.412 Å; α(O–H–N) = 175.95°; *d*(O84a···H–N44) = 2.725 Å; α(O–H–N) = 156.97°, and three π_{phenyl}···Cl–C bonds between the Cl atoms of the guest and the three π electron clouds of the three axial *meso*-phenyl groups forming

Table 1 Binding constants of calix[6]pyrrole **2** and 1,2,3,4-*meso*-octamethylcalix[4]pyrrole **1**, with different guest molecules

Guest	Calix[4]pyrrole	Calix[6]pyrrole
F^-	23 800	1080
Cl^-	6800	650
Br^-	270	150
I^-	< 10	6600
SCN^-	< 10	< 10
p-$MeC_6H_4SO_3^-$	< 10	150
BF_4^-	< 10	2350
$MeCO_2^-$	400	< 10
$CF_3CO_2^-$	70	1150
EtOH	< 10	< 10
CF_3CH_2OH	< 10	80
CCl_3CH_2OH	< 10	60

DOI: 10.1039/b007788g

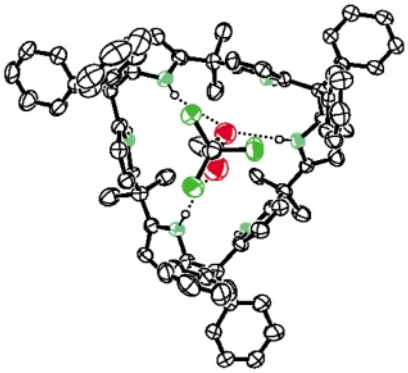

Fig. 1 The molecular structure of the complex between 2,2,2-trichloroethanol and calix[6]pyrrole **2**. Solvent and other molecules not situated in the cavity of the host have been omitted for clarity.

the pseudo-threefolded cavity of **2**: *d*(Cl79–π(C34–C39)) = 3.38 Å; *d*(Cl80–π(C60–C65)) = 3.00 Å; *d*(Cl81–π(C8–C13)) = 3.45 Å.

The stable conformation of **2** brings two electron-rich pyrrole rings, situated in a 1,4 position to one another, into a parallel and cofacial orientation. These two rings are spaced *ca*. 7.1 Å apart. Being an electron rich ring system, the hexapyrrolemethane ring is suitable for hosting electron poor conjugated species in between a pair of cofacial pyrrole rings. The additional four pyrrole rings are capable of forming multiple hydrogen bonds with appropriate guests, making the system an interesting host for different nitro- and carboxy-aromatic compounds. Fig. 2 shows the crystallographic structure† of a complex between *p*-nitrotoluene/nitrobenzene and **2**. Interestingly, though crystallized from a solution containing nitrobenzene and *p*-nitrotoluene in a 10 : 1 ratio, the crystal structure clearly indicates the 1 : 1 inclusion of nitrobenzene and *p*-nitrotoluene within the cavity of **2**. As can be seen in Fig. 2, the nitroaromatic guest is fixed to the cavity of the host through short range π–π interactions between the nitro group of the guest and the two sandwiching pyrrole rings of the host, *d*(nitro(plane)···pyrrole-(plane)) = 3.55 Å. Three of the other four pyrrole rings are involved in hydrogen bonding with the nitro group of the encapsulated guest, *d*(NH1···O80) = 2.23 Å, *d*(N1···O80) = 3.06 Å, *α*(O–H–N) = 172.94°, *d*(NH31···O80) = 2.38 Å, *d*(N31···O80) = 3.18 Å, *α*(O–H–N) = 143.67°, *d*(NH19···O81) = 2.45 Å, *d*(N19···O81) = 3.23 Å, *α*(O–H–N) = 165.11°.

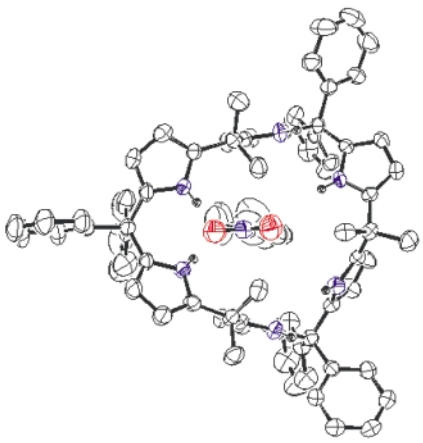

Fig. 2 The molecular structure of the complex between calix[6]pyrrole and nitrotoluene/nitrobenzene. Molecules that are not situated in the cavity of the host have been omitted for clarity.

In conclusion, calix[6]pyrrole **2** shows a wealth of binding modes to different substrates, ranging from simple anions to aromatic derivatives. The axial *meso* phenyl groups form a genuine preorganized cavity and actively participate in binding trihalogenated compounds. The application of calix[6]pyrroles to the separation and identification of such compounds is under investigation.

This work was supported by the Israel Science Foundation, Administrated by the Israel Academy of Sciences and Humanities and by the Fund for the Promotion of Sponsored Research at the Technion.

Notes and referenecs

† *Crystal data*: for **2**·2.5CCl_3CH_2OH·1.5$CHCl_3$·3CH_3CH_2OH·5.5H_2O: grown in the dark from 2,2,2-trichloroethanol–chloroform–ethanol. A single crystal was mounted on the Nonius Kappa CCD diffractometer,[8] and cooled to 170 K under a nitrogen stream. Data were collected with graphite-monochromated Mo-Kα radiation (λ = 0.71070 Å) by applying φ and ω rotations. Data reduction was performed using DENZO-SMN software.[9] The structure was solved using direct methods (SHELXS-97[10]) and refined by SHELXL-97.[11] All non-H atoms of the macrocycle and the trichloroethanol inside the cavity, excluding the disordered hydroxy oxygen, were refined anisotropically. Hydrogen atoms of these moieties were placed at calculated positions and refined as riding on their carbon and nitrogen atoms. Difference Fourier maps based on the macrocycle and the guest inside, revealed another moderately disordered trichloroethanol bound to the macrocycle outside the cavity, and another four sites of severely disordered molecules such as trichloroethanol, chloroform, ethanol and water. All the disordered positions of the solvent molecules were refined isotropically. 38 hydrogen atoms belonging to some of the disordered solvent molecules were not allocated. M_r = 1804.83, monoclinic, space group $P2_1/n$, a = 17.773(10), b = 20.2090(10), c = 26.2590(10) Å, β = 107.730(3)°, V = 8983.6(8) Å^3, T = 170.0(1) K, Z = 4, μ = 0.076 mm^{-1}, 14 385 relections measured, 14 385 unique which were used in all calculations. The final $R(F^2)$ was 0.1168 [$I > 2\sigma(I)$].

For **2**·2.5$C_6H_5NO_2$·0.5$C_7H_9NO_2$: grown in the dark by slow evaporation of a chloroform solution. A single crystal was mounted on the Nonius Kappa CCD diffractometer, at 293 K. Data collection and reduction as above. The structure was also solved and refined as above. All non-H atoms of the macrocycle and the guests were refined anisotropically. Hydrogen atoms were placed at calculated positions and refined as riding on their carbon and nitrogen atoms except for the N–H hydrogen atoms of the pyrrole rings which were localized on a Fourier difference map and refined isotropically. M_r = 1392.66, monoclinic, space group $P2_1/n$, a = 19.455(1), b = 19.762(1), c = 22.027(1) Å. β = 115.405(2)°, V = 7649.8(5) Å^3, T = 293 K, Z = 4, μ = 0.076 mm^{-1}, 16 018 relections measured, 15 694 unique which were used in all calculations. The final $R(F^2)$ was 0.0740 [$I > 2\sigma(I)$].

CCDC 182/1864. See http://www.rsc.org/org/suppdata/cc/b0/b007788g/ for crystallographic files in .cif format.

1 J. M. Lehn, *Supramolecular Chemistry, Concepts and Prespectives*, VCH, Weinheim, 1995.
2 P. A. Gale, J. L. Sessler, V. Kral and V. Lynch, *J. Am. Chem. Soc.*, 1996, **118**, 5140.
3 (*a*) P. Anzenbacher, Jr., K. Jursikova, V. M. Lynch, P. A. Gale and J. L. Sessler, *J. Am. Chem. Soc.*, 1999, **121**, 11 020; (*b*) G. Cafeo, F. H. Kohnke, G. L. La Torre, A. J. P. White and D. J. Williams, *Chem. Commun.*, 2000, 1207; (*c*) S. Camiolo and P. A. Gale, *Chem. Commun.*, 2000, 1129.
4 (*a*) B. Turner, M. Botoshansky and Y. Eichen, *Angew. Chem., Int. Ed.*, 1998, **37**, 2475; B. Turner, M. Botoshansky and Y. Eichen, *Angew. Chem.*, 1998, **110**, 2633; (*b*) for an alternative approach to calix[6]pyrroles see: G. Cafeo, F. H. Kohnke, G. L. La Torre, A. J. P. White and D. J. Williams, *Angew. Chem., Int. Ed.*, 2000, **39**, 1496.
5 P. A. Gale, L. J. Twyman, C. I. Handlin and J. L. Sessler, *Chem. Commun.*, 1999, 1851.
6 W. E. Allen, P. A. Gale, C. T. Brown, V. M. Lynch and J. L. Sessler, *J. Am. Chem. Soc.*, 1996, **118**, 12 471; H. Miyaji, P. Anzenbacher, J. L. Sessler, E. R. Bleasdale and P. A. Gale, *Chem. Commun.*, 1999, 1723; P. A. Gale, J. L. Sessler and V. Kral, *Chem. Commun.*, 1998, 1; P. A. Gale, J. L. Sessler, W. E. Allen, N. A. Tvermoes and V. Lynch, *Chem. Commun.*, 1997, 665.
7 A. Alvanipour, J. L. Atwood, S. G. Bott, P. C. Junk, U. H. Kynast and H. Prinz, *J. Chem. Soc., Dalton Trans.*, 1998, 1223; J. L. Atwood, S. G. Bott, S. Harvey and P. C. Junk, *Organometallics*, 1994, **13**, 4151.
8 Nonius, KappaCCD Server software. Nonius BV, Delft, The Netherlands.
9 Z. Otwinowski and W. Minor, *Methods Enzymol.*, 1997, **276**, 307.
10 G. M. Sheldrick, *Acta Crystaltogr. Sect. A*, 1990, **46**, 467.
11 G. M. Sheldrick, SHELXL97, University of Göttingen, Germany.

ChemComm

Selective formation of rectangular grid coordination polymers with grid dimensions 10 × 15, 10 × 20 and 15 × 20 Å

Kumar Biradha* and Makoto Fujita*

Department of Applied Chemistry, Graduate School of Engineering, Nagoya University and CREST, Japan Science and Technology Corporation (JST), Chikusaku, Nagoya 464-8603, Japan. E-mail: kbiradha@org.mol.nagoya-u.ac.jp; mfujita@apchem.nagoya-u.ac.jp

Received (in Cambridge, UK) 29th August 2000, Accepted 23rd November 2000
First published as an Advance Article on the web 15th December 2000

Using four linear bifunctional ligands of different lengths and $Ni(NO_3)_2$, three coordination polymers containing big rectangular cavities were shown to form selectively, despite the fact that all the four ligands are known to form square grid coordination polymers when they are reacted independently with $M(NO_3)_2$.

The utility of linear bifunctional ligand such as 4,4′-bipyridine **1** has been well explored in the studies of crystal engineering of coordination polymers.[1–4] Although there are a considerable number of reports dealing with designing square grid coordination polymers, their rectangular counterparts are not explored to that extent. The synthesis of rectangular grids at will allows the modulation of size and function of the cavity. Only few rectangular grid polymers have been designed either using two charged ligands or using charged and neutral ligands.[6–9] However using two neutral ligands to date only one rectangular grid coordination polymer has been reported.[10] In this structure the rectangular cavities are too small to enclatharate guest molecules. Recently we have shown that the higher analogues of **1**, 1,4-bis(4-pyridyl)benzene **2** and 4,4′-bis(4-pyridyl)biphenyl **3**, can also be used in designing open square grid polymers with dimensions of 15 × 15 and 20 × 20 Å.[11,12] Herein we show that one can employ these longer ligands to design their rectangular counterparts.

Single crystals of $\{Ni(\mathbf{1})(\mathbf{2})(NO_3)_2\cdot 6C_6H_6\}_n$ **4** in 62% yield were obtained by layering a MeOH solution (2 ml) of $Ni(NO_3)_2$ (6 mg, 0.002 mmol) over a benzene solution (7 ml) of **1** (3.2 mg, 0.002 mmol) and **2** (4.6 mg, 0.002 mmol). Similarly single crystals of $\{Ni(\mathbf{1})(\mathbf{3})(NO_3)_2\cdot 8C_6H_6\}_n$ **5** were prepared in 76% yield by using **3** instead of **2**. The crystal structures of **4** and **5** revealed the selective formation of rectangular grids with the entrapment of benzene molecules.[13]† In both the complexes the Ni atom has octahedral geometry with four pyridyl groups at the equatorial and two nitrates at the apical positions.

Complex **4** forms 2D-network containing rectangular grids of dimension 11.3 × 15.6 Å and encloses six benzene molecules per metal, two of them are embodied in the rectangular cavities while the other four exist between the layers [Fig. 1(a)].[14] Ligands **1** and **2** bridge the metal atoms in the (010) and (001) directions, respectively. The rectangular grid planes sit in (011) plane and pack in the direction of (100). Benzene molecules form a two-dimensional layer [Fig. 1(b)] which is similar to that of naphthalene molecules in the crystal structure of $\{M(4,4'\text{-bipy})_2(NO_3)_2\cdot 3C_{10}H_8\}_n$ (M = Co or Ni).[15] The network of benzene molecules can be described as one of the semi-regular planar networks, which are described by Wells,[16] when benzene molecules are depicted as nodes and aromatic interactions as node connections. The packing of the grids is as follows: the moieties of **1** deposit on each other such that 2,6 and 2′,6′-C–H groups of **1** form C–H···O hydrogen bonds (C···O 3.126, 3.568 Å; C–H···O 151,148°) with the uncoordinated O atoms of the $Ni(NO_3)_2$ moiety. As a result this leads to a C–H···O hydrogen bonded layer that divides the whole structure into an infinite number of two-dimensional compartments with a width of the longer ligand [Fig. 1(c)]. Each of these compartments accommodates two benzene layers which interpenetrates through the moieties of **2** such that each molecule of **2** interacts with 12 benzene molecules *via* edge-to-face aromatic interactions.

Complex **5** also formed 2D-network containing rectangular grids of dimension 19.9 × 11.3 Å and enclosed eight benzene molecules per metal. Similarly to **4**, only two benzene molecules were encapsulated in the cavities while the remaining six exist between the layers (Fig. 2). Ligands **1** and **3** bridge

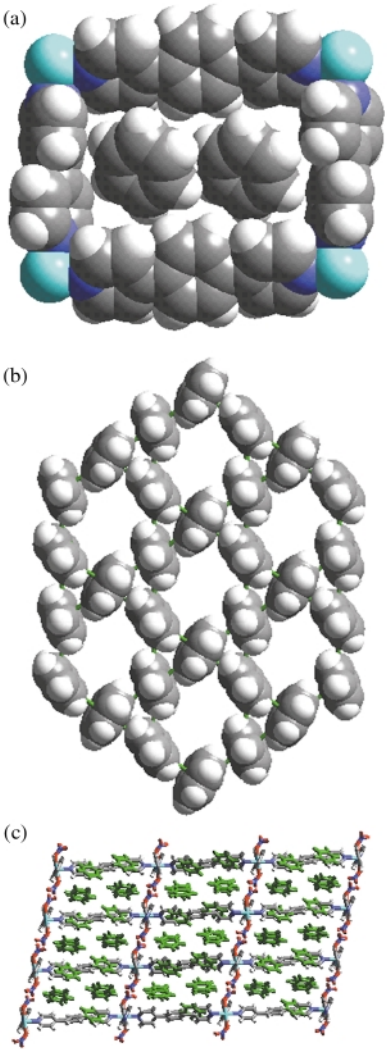

Fig. 1 Space filling representations for (a) rectangular grid unit of **4** containing two benzene molecules; (b) layer of benzene molecules exhibited by complex **4**; (c) side view (101) of the packing of grids and benzene layers in **4**. Note that the C–H···O bonded layers and benzene layers (110) are parallel to each other but perpendicular to grid planes (011).

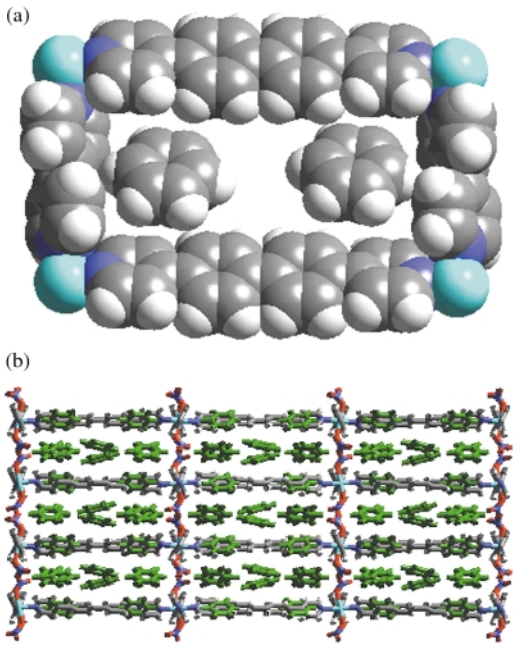

Fig. 2 (a) Space filling representation of rectangular grid unit in **5** containing two benzene molecules. (b) Packing of the grids in **5**. Note that each compartment accommodates three layers of benzene (disorder of the benzene molecules in the middle layer is not shown).

metal atoms in (001) and (100) directions, respectively, and the grid planes pack in the (010) direction. The packing of the grids is similar to that of **4** but now there are three layers of benzene molecules accommodated in each compartment as the width of the compartment is increased from 15.6 to 19.9 Å [Fig. 2(b)]. In this triple layer the outer layers have the same topology as shown in Fig. 1(b) and are linked together by a middle layer, (6,3) net, that is generated by two disordered benzene molecules. In effect each moiety of **3** is surrounded by 18 benzene molecules *via* edge-to-face aromatic interactions.

Our attempts to prepare a 15 × 20 Å grid polymer by using ligands **2** and **3** and $Ni(NO_3)_2/Cu(NO_3)_2/Co(NO_3)_2$ were futile as single crystals suitable for X-ray studies were not obtained. Hence we considered 9,10-bis(4-pyridyl)anthracene **6** as a replacement for **2**. The layering of an MeOH solution of $Ni(NO_3)_2$ over a benzene solution of ligands **3** and **6** resulted in single crystals of the complex $\{Ni(\mathbf{3})(\mathbf{6})(NO_3)(H_2O)\cdot 2C_6H_6\cdot NO_3\}_n$ **7** (yield 55%).† Single crystal analysis reveals

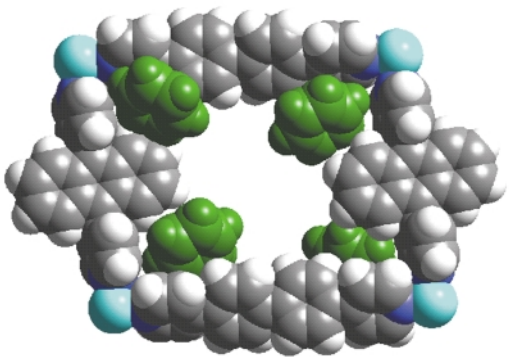

Fig. 3 (a) Space filling representation of a rectangular grid unit in **7**. Note that this contains four benzene molecules.

the formation of a coordination polymer containing rectangular grids of dimension 20 × 15.7 Å (Fig. 3). Each grid accommodates four benzene molecules (two are only partly in the cavity), disordered nitrates and H_2O. Unlike **4** (8 Å) and **5** (7.8 Å), **7** has an interlayer separation of only 4 Å as no guests exist between the layers. The packing of the grids is different from that of the above structures as the layers here deposit on each other in an offset fashion over the two ligands. It is interesting that the rectangular grids formed selectively from two different ligands although ligands **1**–**3** and **6** are known to form square grids when they reacted independently with $M(NO_3)_2$. Given the big size of these rectangular cavities it is also noteworthy that these grid layers are non-interpenetrated.

K. B. thanks the Japan Society for the Promotion of Science (JSPS) for postdoctoral fellowship.

Notes and references

† *Crystal data* for **4**: $C_{62}H_{56}N_6NiO_6$, monoclinic, space group *C*2/*c*, a = 16.123(2), b = 11.341(1), c = 31.106(4) Å, β = 104.190(2)°, U = 5514.0(11) Å^3, T = 193 K, Z = 4, D_c = 1.253 g cm^{-3}, λ = 0.7107 Å, 17 529 reflections measured, 6477 unique (R_{int} = 0.0549) which are used in all calculations. $R1$ = 0.062 and $wR2$ = 0.141.

For **5**: $C_{80}H_{72}N_6NiO_6$, orthorhombic, space group *Pnna*, a = 39.824(3), b = 15.5840(9), c = 11.2915(9) Å, U = 7007.7(8) Å^3, T = 193 K, Z = 4, D_c = 1.206 g cm^{-3}, λ = 0.7107 Å, 42836 reflections measured, 8301 unique (R_{int} = 0.0435) which are used in all calculations. R_1 = 0.069 and wR_2 = 0.173.

For **7**: $C_{58}H_{44}N_6NiO_7$, monoclinic, space group *C*2/*c*, a = 15.774(1), b = 19.975(2), c = 16.207(1) Å, β = 106.398(2)°, U = 4898.8(7) Å^3, T = 193 K, Z = 4, D_c = 1.350 g cm^{-3}, λ = 0.7107 Å, 15 750 reflections measured, 5732 unique (R_{int} = 0.0560) which are used in all calculations. $R1$ = 0.069 and $wR2$ = 0.192. The coordinated H_2O and NO_3 groups were disordered on two sides of the layer with 0.5 occupancy.

CCDC 182/1861. See http//www.rsc.org/suppdata/cc/b0/b007014i/ for crystallographic files in .cif format.

1 R. W. Gable, B. F. Hoskins and R. Robson, *J. Chem. Soc., Chem. Commun.*, 1990, 1677.
2 M. Fujita, Y. J. Kwon, S. Washizu and K. Ogura, *J. Am. Chem. Soc.*, 1994, **116**, 1151.
3 S. Subramanian and M. J. Zaworotko, *Angew. Chem., Int. Ed. Engl.*, 1995, **34**, 2127.
4 S. Kitagawa and M. Kondo, *Bull. Chem. Soc. Jpn.*, 1998, **71**, 1739.
5 M. Fujita, *Acc. Chem. Res.*, 1999, **32**, 53.
6 S. Kawata, S. Kitagawa, M. Konda, I. Furuchi and M. Munakata, *Angew. Chem., Int. Ed. Engl.*, 1994, **33**, 1665.
7 L. R. MacGillivray, R. H. Groeneman and J. L. Atwood, *J. Am. Chem. Soc.*, 1998, **120**, 2677.
8 R. H. Groeneman, L. R. MacGillivray and J. L. Atwood, *Chem. Commun.*, 1998, 2735.
9 L.-M. Zheng, X. Fang, K.-H. Lii, H.-H. Song, X.-Q. Xin, H.-K. Fun, K. Chinnakali and I. A. Razak, *J. Chem. Soc., Dalton Trans.*, 1999, 2311.
10 M.-L. Tong, X.-M. Chen, X.-L. Yu and T. C. W. Mak, *J. Chem. Soc., Dalton Trans.*, 1998, 5.
11 K. Biradha and M. Fujita, *J. Chem. Soc., Dalton Trans.*, 2000, 3805.
12 K. Biradha, Y. Hongo and M. Fujita, *Angew. Chem., Int. Ed.*, 2000, **39**, 3843.
13 The crystals lose the guest molecules at room temperature and become opaque.
14 The distances between the metal atoms of the grid were taken as the dimensions of the grid.
15 K. Biradha, K. V. Domasevitch, B. Moulton, C. Seward and M. J. Zaworotko, *Chem. Commun.*, 1999, 1327; K. Biradha, K. V. Domasevitch, C. Hogg, B. Moulton, K. N. Power and M. J. Zaworotko, *Cryst. Eng.*, 1999, **2**, 37.
16 A. F. Wells, *Structural Inorganic Chemistry*, Clarendon Press, Oxford, 5th edn., p. 82 [see also p. 613 (M_xO_3), p. 1006 (β-quartz), p. 1302 ($CaCu_5$)].

Synthesis of a hybrid fullerene–trimethoxyindole–oligonucleotide conjugate

Massimo Bergamin,[a] Tatiana Da Ros,[a] Giampiero Spalluto,[a] Alexandre Boutorine[b] and Maurizio Prato*[a]

[a] *Dipartimento di Scienze Farmaceutiche, Università di Trieste, Piazzale Europa 1, 34127 Trieste, Italy. E-mail: prato@univ.trieste.it*

[b] *Laboratoire de Biophysique, INSERM U 201 - CNRS UMR 8646, Museum National d'Histoire Naturelle, 43 rue Cuvier, 75231 Paris Cedex 05, France*

Received (in Cambridge, UK) 30th October 2000, Accepted 14th November 2000
First published as an Advance Article on the web 11th December 2000

The synthesis of novel functionalized fullerene derivatives is reported: a DNA minor groove binder such as trimethoxyindole-2-carboxylate (TMI) and an oligonucleotide chain have been covalently linked to C_{60} with the aim of duplicating DNA interactions for increasing sequence selectivity.

Fullerene C_{60} and its organofunctionalized derivatives have recently become a topic of interest in bioorganic and medicinal chemistry. This class of compounds has shown high potential in a wide variety of biological activities, such as DNA photocleavage, HIV protease inhibition, neuroprotection and apoptosis.[1] In particular, the excited state properties of C_{60} may offer viable routes to novel pharmacological tools.[2]

One of the problems of photodynamic therapy is the addressed delivery of a photoactive agent to its target. That is why conjugates of fullerene with molecules possessing biological affinity to certain nucleic acids, proteins, cell types, organelles, *etc.*, might be of particular interest. Additionally, C_{60} itself might facilitate the interactions of certain biologically active molecules with lipophilic membranes of living cells and consequently improve cellular uptake due to its high hydrophobicity.

Recently, some conjugates between C_{60} and nucleic acid-specific agents (acridine,[3] netropsin[4] and complementary oligonucleotides[5,6]) have been reported, with the aim of better understanding the mechanism of action and to increase their cytotoxic properties and specificity. Coupling of fullerene to an intercalator or a minor groove binder already leads to higher affinity and specificity of the derivatives towards target DNA.[4] The next step envisages the improvement of the photocleavage efficiency of the conjugates, possibly by stabilizing their duplexes and triplexes and increasing their sequence selectivity.

In order to achieve these goals, we have designed derivative (**1**) of fulleropyrrolidine linked to trimethoxyindole (TMI) and

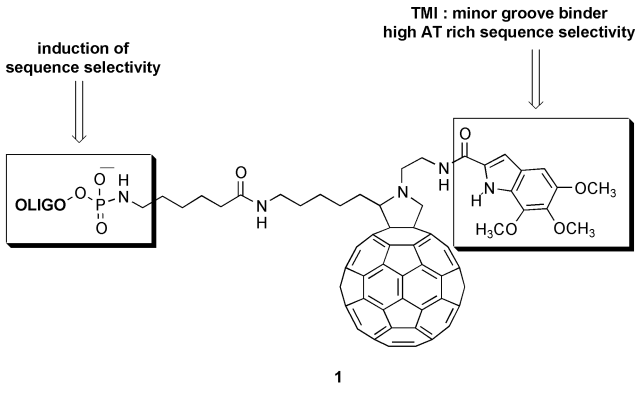

1

OLIGO = 5'-TTT-TC*T-TTT-C*C*C*-C*C*C*-T-3'
C* = Methylated Cytosine

an oligonucleotide chain simultaneously. The rational design of this derivative was based on a synergistic effect of two different linkers such as TMI and oligonucleotide. The TMI unit is characteristic of a class of natural antibiotics named duocarmycins, possessing antitumor activity in the picomolar range, in part due to high affinity and selectivity of the TMI group for the minor groove in AT-rich sequences of DNA.[7] The effect of the oligonucleotide chain could be considered both to induce high sequence-selectivity and to increase water solubility, one of the main problems of C_{60} derivatives for biological application.

The designed compound **1** was prepared following the general synthetic strategy summarized in Schemes 1–2, according to the known procedure for the synthesis of fulleropyrrolidines, based on the 1,3-dipolar cycloaddition of azomethine ylides to C_{60}.[8,9]

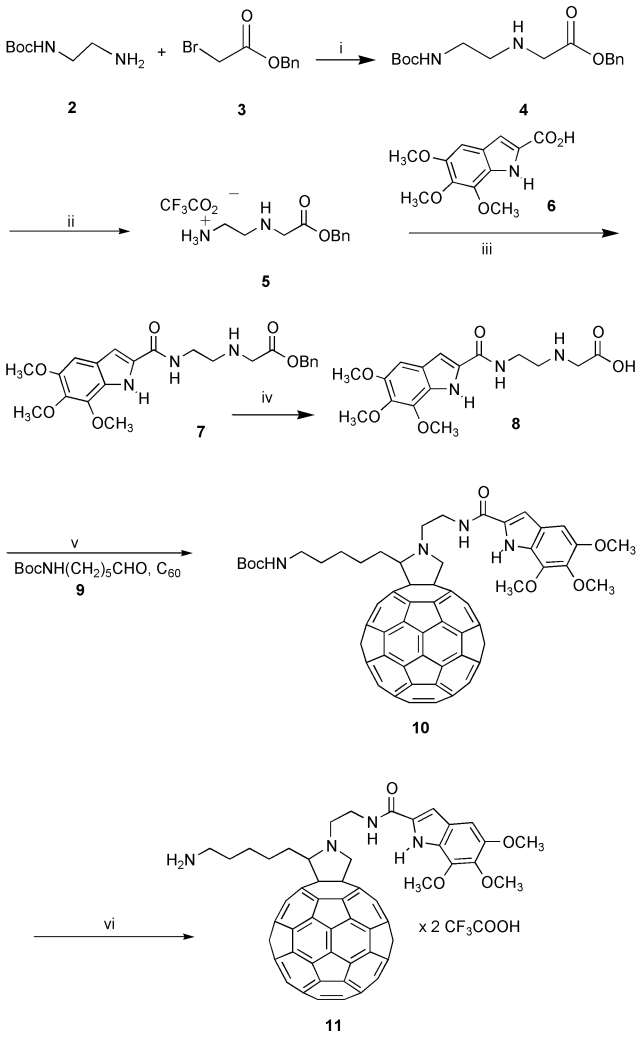

Scheme 1 *Reagents*: i, dioxane, 0 °C, then rt 18 h; ii, TFA, CH_2Cl_2, rt, 20 min; iii, NMM, HOBT, EDC, CH_2Cl_2; iv, Pd/C 10%, H_2, MeOH; v, toluene, reflux, 50 min; vi, TFA, CH_2Cl_2, rt, 1 h.

DOI: 10.1039/b008744k

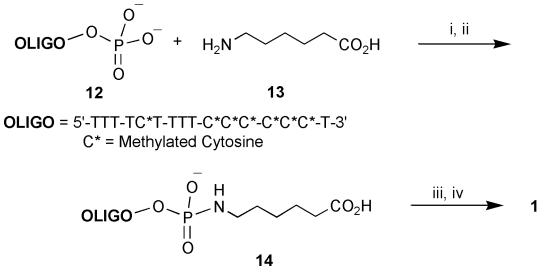

Scheme 2 *Reagents*: i, PPh_3, DMSO, DMAP, Py_2S_2; ii, DMSO; iii, PPh_3, DMSO, Py_2S_2; iv, Et_3N, DMSO, **11**.

The appropriate *O*-benzylaminoacid **4** was prepared by alkylation of the mono protected (Boc) ethylenediamine **2** with benzyl α-bromoacetate **3** (Scheme 1).

Deprotection of the amino functionality by TFA in **8** led to amine **5**, which was coupled to trimethoxyindole-2-carboxylic acid **6**[10] to afford amino ester **7**. The latter was deprotected at the carboxylic function by catalytic hydrogenation and the resulting acid **8** was allowed to react with C_{60} and *N*-Boc-6-aminohexanal **9** to yield the desired multifunctional fulleropyrrolidine **10**.† The latter compound was in turn deprotected to obtain the desired salt **11** by treatment with TFA (Scheme 1).

The designed product **1** was synthesized following a general synthetic strategy for the preparation of oligonucleotide conjugates previously reported[11–13] and summarized in Scheme 2, but the new procedure contained several modifications. Originally the reaction was initiated by activation of the oligonucleotide terminal phosphate by means of Mukaiyama reagents, triphenylphosphine–dipyridyl-2,2′-disulfide in the presence of DMAP.[14] However, it appeared that interaction of the activated phosphate with the amino group of the fullerene derivative did not lead to satisfactory yields of conjugation. Thus, it was necessary to use 6-aminocaproic acid as a spacer between the two moieties.

The phosphorylated oligonucleotide (16-mer) **12** was activated at its terminal phosphate, precipitated by lithium perchlorate in acetone according to the method described by Knorre *et al.*[11] and attached to the ε-amino group of 6-aminocaproic acid **13** in water in the presence of triethylamine to afford the carboxylic acid derivative of oligonucleotide **14** in quantitative yield. Coupling of **14** with fullerene derivative **11** was performed in a similar way, by activation of the carboxylic group with Mukaiyama reagents in organic media to obtain the desired conjugate **1**. Purification of **1** was performed by electrophoresis in 1% agarose–0.1% triton X-100 gel using tris-acetate buffer, followed by excision of the colored band and electroelution, or digestion of agarose with β-agarase.[5,6]

In summary, we have described the synthesis of the bis-functionalized fulleropyrrolidine **1** containing two different linkers capable of modulating and inducing high sequence selectivity. Results on duplex and triplex helicex DNA formation and the synthesis of an enlarged series of compounds for structure–activity relationship studies will be reported in due course.

This work was supported by MURST (cofin. ex 40%, prot. n. mm03198284), by Regione Friuli-Venezia Giulia, fondo Anno 1998, and by the European Community (TMR program BIOFULLERENES, contract No. ERB FMRX-CT98-0192).

Notes and references

† *Analytical and spectroscopic data* of derivative **10**: $C_{86}H_{40}N_4O_6$ (MW 1225.30), yield: 19%. ^{1}H-NMR: δ 9.27 (br s, 1H), 7.30 (br s, 1H), 6.93 (s, 1H), 6.75 (s, 1H), 4.98 (d, J = 10.3 Hz, 1H), 4.52 (m, 1H), 4.37 (t, J = 5.9 Hz, 1H), 4.30 (d, J = 10.5 Hz 1H), 4.08–3.95 (m, 4H), 4.05 (s, 3H), 3.89 (s, 3H), 3.85 (s, 3H), 3.25 (m, 1H), 3.11 (m, 2H), 2.45 (m, 2H), 1.89 (m, 2H), 1.49 (m, 2H), 1.43 (s, 9H). ^{13}C-NMR: δ 166.9, 156.4, 154.4, 153.2, 150.0, 147.1, 146.3, 146.2, 146.1, 146.0, 145.9, 145.5, 145.2, 145.1, 144.6, 144.4, 144.3, 143.0, 142.6, 142.2, 142.1, 142.0, 141.9, 141.7, 140.2, 139.7, 136.7, 135.8, 135.6, 135.4, 130.6, 123.3, 97.1, 71.2, 67.4, 65.4, 61.1, 56.2, 44.1, 41.1, 31.0, 29.9, 28.5. ES-MS (THF–MeOH 1:1): m/z 1225 (MH^+). UV–VIS (cyclohexane) λ_{max}: nm 254, 312, 431, 703. IR (KBr, DRIFT) cm^{-1}: 3330, 2935, 2850, 1690, 1645, 1245, 1169, 526.

1 T. Da Ros and M. Prato, *Chem. Commun.*, 1999, 663.
2 D. Guldi and M. Prato, *Acc. Chem. Res.*, 2000, **33**, 695.
3 Y. N. Yamakoshi, T. Yagami, S. Sueyoshi and N. Miyata, *J. Org. Chem.*, 1996, **61**, 7236.
4 E. Nakamura, H. Tokuyama, S. Yamago, T. Shiraki and Y. Sugiura, *Bull. Chem. Soc. Jpn.*, 1996, **69**, 2143.
5 A. Boutorine, H. Tokuyama, M. Takasugi, H. Isobe, E. Nakamura and C. Hélène, *Angew. Chem., Int. Ed. Engl.*, 1994, **33**, 2462.
6 Y.-Z. An, C.-H. B. Chen, J. L. Anderson, D. S. Sigman, C. S. Foote and Y. Rubin, *Tetrahedron*, 1996, **52**, 5179.
7 D. L. Boger and D. S. Johnson, *Angew. Chem., Int. Ed. Engl.*, 1996, **35**, 1438.
8 M. Maggini, G. Scorrano and M. Prato, *J. Am. Chem. Soc.*, 1993, **115**, 9798.
9 M. Prato and M. Maggini, *Acc. Chem. Res.*, 1998, **31**, 519.
10 D. Boger, T. Ishizaki, H. Zarrinmayeh, P. Kitos and O. Suntornwat, *J. Org. Chem.*, 1990, **55**, 4499.
11 D. G. Knorre, P. V. Alekseyev, Y. V. Gerassimova, V. N. Silnikov, G. A. Maksakova and T. S. Godovikova, *Nucleosides, Nucleotides*, 1998, **17**, 397.
12 T. S. Godovikova, V. F. Zarytova, T. V. Maltseva and L. M. Khalimskaya, *Bioorg. Khim.*, 1989, **15**, 1246.
13 A. S. Boutorine, T. Le Doan, J. P. Battioni, D. Mansuy, D. Dupré and C. Hélène, *Bioconj. Chem.*, 1990, **1**, 350.
14 T. Mukaiyama, R. Matsueda and M. Suzuki, *Tetrahedron Lett.*, 1970, **22**, 1901.

ChemComm

Antibody-catalyzed hydrolysis of oligomeric esters: a model for the degradation of polymeric materials†

Oliver Brümmer, Timothy Z. Hoffman, Da-Wei Chen and Kim D. Janda*

Department of Chemistry, The Scripps Research Institute and The Skaggs Institute for Chemical Biology, 10550 North Torrey Pines Road, La Jolla, CA 92037, USA. E-mail: kdjanda@scripps.edu

Received (in Cambridge, UK) 5th October 2000, Accepted 15th November 2000
First published as an Advance Article on the web 11th December 2000

A catalytic antibody has been discovered that degrades oligomeric ester substrates.

A topic of current interest to both the chemical and global community alike concerns the development of readily degradable polymers and benign agents necessary for polymer breakdown.[1,2] From an environmental perspective, microbial/enzymatic approaches for polymer breakdown are very attractive, and while a number of commercially used polymers are sensitive to biodegradation, a large variety of commonly used materials are essentially resistant.[3–5] Furthermore, our current understanding is not sufficient to fully predict a degradability profile or to specifically target an enzyme/microorganism that could degrade a man-made, synthetic polymer.[6]

Antibodies bind biological macromolecules or haptens with high affinities and specificities.[7] We and others have reported antibodies that bind phosphorus transition-state analogues can catalyze the hydrolysis of carbonate, ester, carbamate and amide substrates.[8] Yet, to date there have been no reports of antibody catalysts that accept oligomeric versions of these simple substrate classes. Herein we report the first example of a catalytic antibody capable of degrading synthetic oligomeric esters.

Several tactics could be envisioned in a hapten design for an antibody-catalyzed hydrolysis of an oligomer. Among the ones we considered include: (1) a transition-state analogue used as a repeating unit, and (2) a pseudo-symmetric transition-state analog. Both approaches have merit, but to date no methodology for antibody-catalyzed oligomer degradation has been disclosed.[8] We recently synthesized the new transition-state analogue phosphorodithioate hapten **1** and used this molecule attached to keyhole limpet hemocyanin (KLH) to obtain antibodies with excellent catalytic activity for the hydrolysis of carbonate **2a** (k_{cat} 2.7 min^{-1}) and good activity to ester **2b** (k_{cat} 0.27 min^{-1}).[9] Based on the carbonate and esterolytic activities seen from antibodies derived from **1** and its pseudo-symmetric structure we reexamined this panel of antibodies for possession of 'deoligomerase' activity. Our objective was thus to see if an antibody could perform either a stepwise degradation from an oligomer's terminus or mediate nonselective endo-cleavage on a starting oligomer and resulting subunit structures.

Before antibody screening could be engaged a set of oligomers that could be recognized based on **1**'s haptenic structure needed to be prepared. While aromatic oligocarbonate structures were deemed to be the most highly congruent substrates for antibody library recognition we found such molecules to be unstable for screening. As a second choice, consideration was given to oligoesters. Polyesters are notoriously insoluble in both aqueous and organic solvents.[2] However, we found that smaller molecular weight oligoesters could be synthesized in a controlled stepwise and highly pure manner.[10] Furthermore, these oligomers displayed good stability and workable solubility parameters for the kinetic analysis of the appearance and disappearance of distinct oligomeric subunits. Based on these considerations (*vide supra*), and the need for maximal antibody substrate recognition, 4-hydroxyphenylacetic acid **3** was chosen as our monomer for oligomeric synthesis.

Twenty-five monoclonal antibodies (mAbs) were screened against tetramer **4**, where the term 'tetramer' refers to the total number of aromatic residues, that contained distinct terminal units (Fig. 1). Though **4** was only soluble up to 250 μM in aqueous buffer (50 mM PIPES, 50 mM NaCl, pH 6.7, 5% DMSO cosolvent), we were still able to conduct the assay at 500 μM of **4** under heterogeneous conditions using an orbital shaker. Three mAbs were found that cleaved the tetramer by cutting at

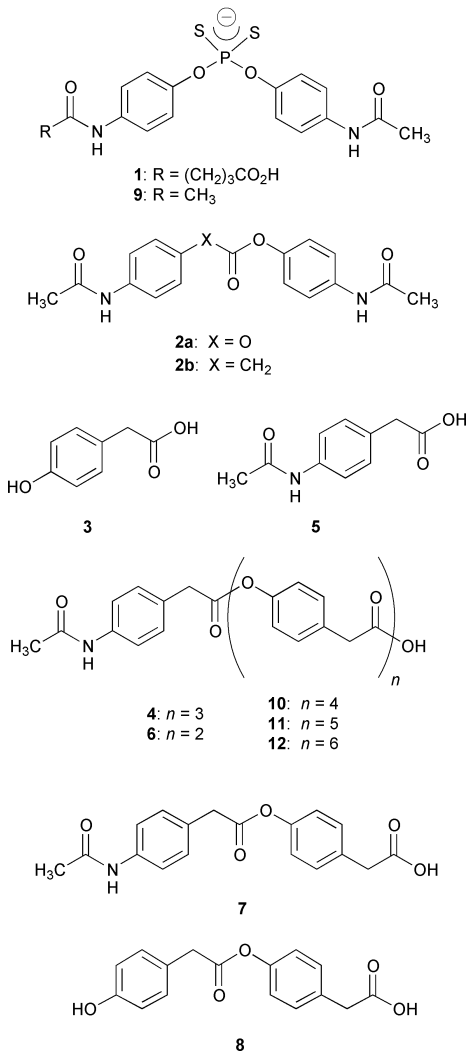

Fig. 1 Structures of hapten **1**, inhibitor **9**, carbonate **2a**, oligoesters **4**, **6**, **10**–**12**, simple esters and products derived from hydrolysis, **2b**, **3**, **5**, **7** and **8**.

† Electronic supplementary information (ESI) available: experimental procedures are provided including kinetic assays, and full characterization (^{1}H and ^{13}C NMR, HRMS, HPLC traces) of the compounds under discussion (**4, 6**–**8**, **10**–**12**). See http://www.rsc.org/suppdata/cc/b0/b008065i/

DOI: 10.1039/b008065i

all three ester linkages. Interestingly, none of these antibodies were noted previously to be catalysts for the hydrolysis of the simple carbonate **2a**, hence they had not been previously examined as catalytic antibodies for monoester hydrolysis.[9] The most impressive mAb, OB2-48F8, was studied in greater detail since it degraded **4** to the products **3**, **5**, **6**, **7** and **8** (Fig. 1) with the best overall rate estimated semi-quantitatively from the sum of product concentrations measured by HPLC. Thereafter, the antibody was freshly prepared and extensively purified by protein G affinity chromatography followed by MonoQ ion exchange chromatography. Notably, the antibody specific activity increased upon purification, as required. Also, the Fab fragment of OB2-48F8 was prepared, purified, and displayed a similar activity compared to the whole IgG. Hence, we ruled out contamination by esterases as a source of the deoligomerization reaction.

Due to the solubility limitations of **4**, the trimer **6** was used as a substrate to quantitatively obtain an assessment of antibody activity. The upper limit of solubility of **6** in the above buffer–cosolvent system was 750 μM and allowed a full kinetic analysis of the formation of **3** and **7** by OB2-48F8 (k_{cat} = 2.2 × 10^{-2} min^{-1}, K_m = 580 μM, k_{cat}/k_{uncat} = 1.5 × 10^3). The phosphorodithioate **9** was a competitive inhibitor (K_i = 6.2 μM) for this route of trimer degradation.[11,12] Concurrently, the antibody also catalyzed the cleavage of **6** to subunits **5** and **8** (k_{cat} = 1.5 × 10^{-3} min^{-1}, K_m = 520 μM, k_{cat}/k_{uncat} = 1.2 × 10^2). The observed activity was interesting in the light of the haptenic structure for which conventional wisdom would predict a preferred hydrolysis to yield **5** and **8**. We also tested the antibody-catalyzed hydrolysis of **2b**,[9] the ester most congruent to **1** and **9**, as well as the cleavage of the two primary ester products **7** and **8**. OB2-48F8 catalyzed the hydrolysis of **2b** (k_{cat} = 1.0 × 10^{-2} min^{-1}, K_m = 289 μM, k_{cat}/k_{uncat} = 3.3 × 10^2) and was competitively inhibited by **9** (K_i = 16.5 μM). The antibody also cleaved **7** (k_{cat} = 1.7 × 10^{-3} min^{-1}, K_m = 695 μM, k_{cat}/k_{uncat} = 1.1 × 10^2) and **8** (k_{cat} = 2.0 × 10^{-3} min^{-1}, K_m = 940 μM, k_{cat}/k_{uncat} = 90). Thus, mAb OB2-48F8 was capable of completely degrading **6** to its component monomeric building blocks. Unexpectedly, the trimer **6** was a better substrate than ester **2b** for reasons that remain unclear. Additional studies employing the novel phosphorodithioate moiety might reveal unusual features with regard to the correlation between hapten and substrate structures.

Finally, to investigate the capabilities of OB2-48F8 for degrading larger oligomers approaching 'real' polymers, we synthesized polyesters **10**–**12** that contained additional repeating units (Fig. 1). The pentamer **10** (MW 729) was sparingly soluble (less than 30 μM) in our aqueous buffer conditions, however using a 500 μM heterogeneous mixture of **10** degradation still occurred into subunit structures (Fig. 2). As detailed in Fig. 2, there was an initial increase in the dimers **7** and **8** followed by a decrease as monomers **3** and **5** increased. This was rationalized based on the above cleavage preferences and consecutive-reaction kinetics. Over a one month period near neutral pH at ambient temperature in the presence of antibody, approximately 200 mM of **3** was formed from degraded **10**. Without antibody, less than 3% occurred. In a similar fashion, OB2-48F8 also broke down polyesters **11** (MW 863) and **12** (MW 997) that were virtually insoluble under our assay conditions, yet cleavage occurred at multiple sites to yield suboligomers as primary products (data not shown). Significantly, the antibody was stable for more than a month under heterogeneous conditions while the progress of these reactions was being monitored.[13] All the observations and data confirmed that the antibody performed oligomer degradations by 'multimer' processing using nonregioselective, kinetically biased endo-cleavage, rather than a stepwise deoligomerization through cleavage of monomers from a terminus.

In conclusion, a catalytic antibody has been discovered that degrades oligomeric esters. Our findings are of fundamental importance as now catalytic antibodies share another trait thought only to be associated with enzymes, the biodegradation of oligo and polymeric materials.[1]

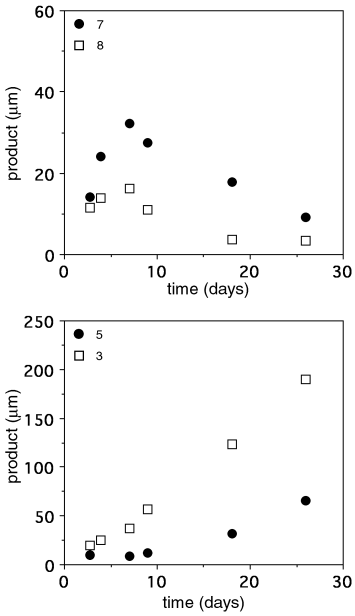

Fig. 2 Reaction profiles showing products from the antibody-catalyzed hydrolysis of oligoester **10**. Reactions were carried out in 50 mM PIPES, 50 mM NaCl, pH 6.7, 5% DMSO at 21 °C in the presence of 500 μM **10** and 20 μM OB2-48F8. The uncatalyzed reactions were carried out under the same conditions in the absence of antibody and the rates subtracted.

We thank Dr Peter Wirsching for reviewing the manuscript. Financial support was provided by The National Institute of Health (GM 43858) and The Skaggs Institute of Chemical Biology.

Notes and references

1 A. C. Albertsson and S. Karlsson, *Acta Polym.*, 1995, **46**, 114.
2 M. P. Stevens, *Polymer Chemistry*, 2nd edition, Carl-Hanser Verlag, Munich, 1990.
3 U. Witt, M. Yamamoto, U. Seeliger, R.-J. Muller and V. Warzelhan, *Angew. Chem., Int. Ed.*, 1999, **38**, 1438; S. Kobayashi, H. Uyama and T. Takamoto, *Biomacromolecules*, 2000, **1**, 3.
4 E. C. King, A. J. Blacker and T. D. H. Bugg, *Biomacromolecules*, 2000, **1**, 75; K. Tabata, H. Abe and Y. Doi, *Biomacromolecules*, 2000, **1**, 157.
5 J. J Jesudason, R. H. Marchessault and T. Saito, *J. Environ. Polym. Degrad.*, 1993, **1**, 89.
6 E. Rantze, I. Kleeberg, U. Witt, R.-J. Mueller and W.-D. Deckwer, *Macromol. Symp.*, 1998, **130**, 319; U. Witt, R.-J. Mueller and W.-D. Deckwer, *Macromol. Chem. Phys.*, 1996, **197**, 1525.
7 H. N. Eisen, *General Immunology*, 3rd ed., J. B. Lippincott Company, Philadelphia, 1990.
8 K. D. Janda, C. G. Shelvin and C.-H. L. Lo, in *Comprehensive Supramolecular Chemistry, Vol. 4: Supramolecular Reactivity and Transport: Bioorganic Systems*, ed. J. L. Atwood, J. E. D. Davies, D. D. MacNicol, F. Vögtle, J.-L. Lehn, Y. Murakami, Elsevier, New York, 1996, p. 43; P. Wentworth and K. D. Janda, *Curr. Opin. Chem. Biol.*, 1998, **2**, 138.
9 O. Brümmer, P. Wentworth, D. P. Weiner and K. D. Janda, *Tetrahedron Lett.*, 1999, **40**, 7307.
10 The synthesis of the compounds under discussion (**4, 6**–**8** and **10**–**12**) can be found in the supplementary information.
11 Phosphorodithioate **9** is a tight-binding inhibitor of OB2-48F8. K_i determinations were therefore not made using the classical Lineweaver–Burk analysis over a range of inhibitor concentrations, since this is known to be subject to error for tight-binding inhibitors. Rather the method of Copeland *et al*. (R. A. Copeland, D. Lombardo, J. Glannaras and C. P. Decicco, *Bioorg. Med. Chem. Lett.*, 1995, **5**, 1947) was employed, which allows for the accurate determination of the K_i values of tight-binding inhibitors.
12 Symmetrical phosphorodithioate **9** was prepared starting from 4-acetamidophenol.[9]
13 Aliquots of sample were removed periodically and checked by ELISA for hapten binding.

ChemComm

Cellulose: a new bio-support for aqueous phase catalysts

Françoise Quignard and Agnès Choplin*

Institut de Recherches sur la Catalyse-CNRS, 2 avenue A. Einstein, 69 626 Villeurbanne Cedex, France. E-mail: choplin@catalyse.univ-lyon1.fr

Received (in Cambridge, UK) 25th September 2000, Accepted 20th November 2000
First published as an Advance Article on the web 11th December 2000

The choice of a hydrophilic bio-polymer, such as cellulose, as the support of the water soluble $Pd(OAc)_2$/5 TPPTS system, leads to a new and efficient heterogeneous catalyst for the Trost Tsuji allylic alkylation reaction.

The heterogeneous catalysts designed for the synthesis of fine chemicals are usually supported either on inorganic oxides (silica, carbon..) or on organic synthetic polymers.[1] If one excludes the case of supported metal particles modified with the appropriate asymmetric inductor (tartaric acid, cinchona alkaloids…),[2–5] most of these catalysts are anchored metal complexes; the anchoring bond links a surface atom either to the metal centre or to an atom of one of the ligands at a position as remote as possible from the active metal centre. The control of the selectivity of the surface anchoring reactions is one of the major difficulties; yet this affects directly the selectivity of the target organic reaction.

About ten years ago, the so-called Supported Aqueous Phase Catalysts were developed for the heterogenization of biphasic water/organic catalysts.[6] This immobilisation procedure takes advantage of the hydrophilicity and of the high specific surface area of an inorganic support. The former character is necessary to maintain the catalyst-containing water film on the solid, the latter is responsible for the substantial activity increase as compared to that achieved in a biphasic medium. Silica is the most used support; mesoporous glass beads of controlled pore size distribution are the favourite, although the precise role of the porosity is so far not unambiguously demonstrated. This methodology is particularly well suited to the reactions non-feasible under conventional biphasic conditions such as, for example, those which involve water non-soluble reactants[7] or water-sensitive reactions.[8] We wish to report here the first example, to our knowledge, of a catalyst supported in an aqueous film on a natural polysaccharide, cellulose.

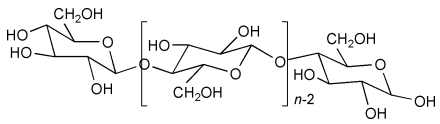

This polymer, which has unlimited availability as a renewable agro-resource and is biodegradable, presents a number of interesting structure related properties[9] which have so far, to our knowledge, never been explored in the field of catalysis. Here, we have used its high hydrophilic character, induced by the presence of numerous hydroxy groups. Thus, we have immobilised on a cellulose powder the water soluble catalytic precursor $Pd(OAc)_2$/5 TPPTS [TPPTS = $P(m\text{-}C_6H_4SO_3Na)_3$] using the SAP methodology and we have tested the catalytic properties of this solid for the allylic substitution of (*E*)-cinnamyl ethyl carbonate by morpholine [eqn. (1)].

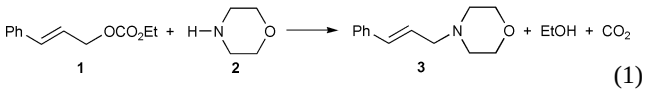

(1)

The cellulose powder (a generous gift from Institut Textile de France, Ecully, France, particles size: 80 μm) is characterised by a degree of crystallinity of 53% (determined by XRD), a specific surface area equal to 1.35 $m^2\ g^{-1}$ (from the isotherm of N_2 adsorption of the solid evacuated at 108 °C) and a wetting volume equal to 4.5 mL g^{-1} (defined as the volume of water which can be added to 1 g of solid before a drop of liquid can be visualised). All the manipulations are performed under inert atmosphere using classical Schlenk tube techniques. The catalyst is synthesised following the so-called incipient wetness method as described in ref. 10. Typically, $Pd(OAc)_2$ (52.5 mg, 0.23 mmol) and TPPTS (732 mg, 1.3 mmol) are dissolved in de-aerated water (12 mL) under magnetic stirring (30 min, 40 °C). This solution is then poured onto cellulose (2.5 g, pre-evacuated at 120 °C (10 h, 10^{-4} Torr)) and the mixture stirred at 40 °C for 30 min. Water is then evacuated at rt (2 h at 10^{-1} Torr, 2 h at 10^{-4} Torr). The dry mustard yellow solid (CELL–SAP-Pd) is characterised by a 0.75% Pd content (determined by ICP) and a 3% wt water content (determined by TGA). The latter parameter is varied by addition of the desired quantity of water directly onto the solid with a syringe under magnetic stirring (rt, 30 min).

The catalytic tests are performed as described in ref. 10 under the following conditions: solvent: PhCN, T = 50 °C, [**1**]–[**2**]–[Pd] = 25:30:1; [**1**] = 30 mmol L^{-1}. The reaction is followed by GPC (HP 5890, HP5 column, T_{inj} = 240 °C, $T_{det.}$ = 280 °C), calibrated against authentic samples. Analysis of the palladium content of the organic solutions at the end of each catalytic test is performed by ICP or ICP-MS when necessary.

The activity of CELL–SAP-Pd is strongly dependent on its water content (Fig. 1), a phenomenon which has already been observed with most silica–SAP catalysts.[10–13] For these latter, one maximum is generally observed which seems to depend on the precise reaction (catalyst, reactants) under investigation. With CELL–SAP-Pd, two maxima of activity are evidenced. The first corresponds to a water content of 26 wt% or 0.5 g H_2O/g CELL; **1** is converted after 100 min to a 60% level with a 100% selectivity for **3**. The second is with 66 wt% H_2O or 6 g H_2O/g CELL; then the solid is much more active and **1** is fully converted to **3** within 100 min.

For the most active solid (66 wt% H_2O), we tested the influence of the method of introduction of water on the solid.

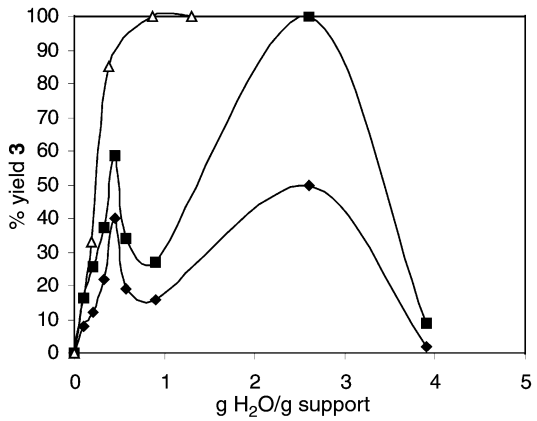

Fig. 1 Influence of the water amount (g H_2O/g CELL) on the catalytic activity of ($Pd(OAc)_2$/5 TPPTS) supported on CELL, ◆: t_R = 50 min; ■: t_R = 100 min and on silica Δ (t_R = 10 min. Exp. cond.: solvent: PhCN, T = 50 °C, [**1**] = 30 mmol L^{-1}, [**1**]–[**2**]–[Pd] = 25:30:1.

DOI: 10.1039/b007776n

For this purpose, we added the desired water amount to the benzonitrile solution of the reactants. This biphasic solution is then poured on the 'dry' CELL–SAP-Pd sample. Instantaneously, the solution becomes monophasic but remains colourless; this confirms the high hydrophilicity of the surface of cellulose and suggests that palladium remains essentially on the solid. The activity of this sample is lower than that obtained with the general method (60 *vs*. 95% yield **3** after 100 min). But, we suspect that the main origin of this discrepancy is the uncontrolled agglomeration of the solid particles under the catalytic conditions; this necessarily induces major problems of diffusion of the reactants to the active centres. Accordingly, we observe also some irreproducibility of the activity of the solid CELL–SAP-Pd as soon as its water content lies above 1 g H_2O/g CELL.

In none of these catalytic tests, is the presence of palladium detected in the organic catalytic solutions once the reactants are fully converted: the leaching of palladium, if any, is below 0.6%. This result is very encouraging because it is the first condition which must be met before one can envisage the possibility of recycling a supported catalyst, one of the advantages which is expected from the heterogenization of any molecular catalyst. It is then worth finding a way to improve the dispersion of the solid particles in the liquid organic medium.

In water, the surface of cellulose is anionic;[9] therefore cationic surfactants should easily interact with the outer surface of the particles, and confer on them a hydrophobic character. This should facilitate their dispersion in an organic medium such as benzonitrile. When a small amount of cetyltrimethylammmonium bromide (CTAB) is added to the solution of the reactants, the dispersion of the solid particles CELL–Pd-SAP (2.6 g H_2O/g CELL) is *de visu* excellent and concomitantly their activity increases sharply (Fig. 2). The increase of the concentration of CTAB (given as the initial concentration in PhCN) is beneficial for the activity, but concomitantly the palladium leaching increases up to an unacceptable level (Table 1). The addition of triethylpropylammonium bromide NEt_3PrBr, which is not a surfactant but a common phase transfer agent in catalysis, improves neither the activity of the same solid, (Fig. 2) nor its dispersion, but simultaneously the palladium leaching is less severe (Table 1). Finally, we observe that CTAB, even at low concentrations, kills the activity of the related silica–SAP-Pd (40 wt% H_2O) (Fig. 2).

The interpretation of all these data clearly needs a more detailed investigation; yet, some important comments can already be made. The increase of the activity of CELL–SAP-Pd

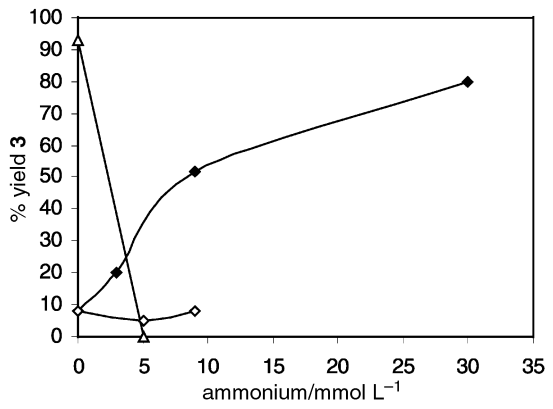

Fig. 2 Influence of NEt_3PrBr (◇) and of CTAB (◆) on the activity of CELL–SAP-Pd (2.6 g H_2O/g CELL and of CTAB on the activity of silica–SAP-Pd (0.87 g H_2O/g silica) (Δ). t_R = 5 min. Exp. cond.: solvent: PhCN, T = 50 °C, [**1**]: 33 mmol L^{-1}, [**1**]–[**2**]–[Pd] = 25:30:1.

Table 1 Palladium leaching from CELL–SAP-Pd (2.6 g H_2O/g CELL) into the organic solvent after the catalytic tests performed under the conditions given below Fig. 1 and 2

Ammonium bromide Nature	Conc/mmol L^{-1}	Pd/ppm	% Pd
CTAB	0	1.2	0.6
	3	9	3
	9	14	8
	30	47	20
NEt_3PrBr	9	9	5

with its water content may be related to a greater mobility of the complex with increasing thickness of the water layer on the surface. But some properties must clearly be correlated to the nature of the support itself: water induces a swelling of the cellulose,[9] a property which increases the surface accessibility. Thus for example, it is known that the specific surface of a cotton powder is very low when determined from the adsorption isotherm of N_2, and raises values two orders of magnitude larger when determined from the adsorption of H_2O.[9] The double maximum may also reflect the structure of cellulose and more specifically the fact that the amorphous part is more accessible to the reactants than the crystalline part. Finally, CTAB clearly has a complex role, but it acts definitely as a surfactant, favouring the dispersion of the cellulose particles in the organic reaction medium and most probably also its swelling.

These data are very encouraging; they show the potential of cellulose as a support for the immobilisation of water soluble catalysts for fine chemical synthesis, these latter reactions are generally compatible with the thermal stability of this natural polymer. We are currently exploring the many other means of immobilisation of complexes which are possible on this type of solid, so as to take advantage of the specific chemical and structural properties of these polysaccharides as compared to the inorganic oxide supports traditionally used in the field of catalysis.

This work was financially supported by CNRS. M. R. Chatelin and P. Gayrine (ITF) are acknowledged for many encouraging and stimulating discussions.

Notes and references

1 For recent reviews, see: A. Choplin and F. Quignard, *Coord. Chem. Rev.*, 1998, **178**–**180**, 1679 and references therein.
2 Y. Orito, S. Imai and S. Niwa, *J. Chem. Soc. Jpn.*, 1979, **8**, 1118.
3 Y. Izumi, M. Iwaida, H. Fukawa and S. Akabori, *Bull. Chem. Soc. Jpn.*, 1963, **36**, 21.
4 H.-U. Blaser, H. P. Jalett, M. Müller and M. Studer, *Catal. Today*, 1997, **37**, 441.
5 T. Osawa, T. Harada and A. Tai, *Catal. Today*, 1997, **37**, 465.
6 J. P. Arhancet, M. E. Davis, J. S. Merola and B. E. Hanson, *Nature*, 1989, **339**, 454.
7 J. P. Arhancet, M. E. Davis and B. E. Hanson, *J. Catal.*, 1991, **129**, 100.
8 S. dos Santos, F. Quignard, D. Sinou and A. Choplin, *Topics in Catalysis*, 2000, **13**, 311.
9 *Comprehensive Cellulose Chemistry, vol. 1 Fundamentals and Analytical Methods*, ed. D. Klemm, B. Philipp, T. Heinze, U. Heinze and W. Wagenknecht, Wiley-VCH, Weinheim, 1998.
10 S. dos Santos, Y. Tong, F. Quignard, A. Choplin, D. Sinou and J. P. Dutasta, *Organometallics*, 1998, **17**, 78.
11 J. P. Arhancet, M. E. Davis, J. S. Merola and B. E. Hanson, *J. Catal.*, 1990, **121**, 327.
12 G. Frémy, E. Monflier, J. F. Carpentier, Y. Castanet and A. Mortreux, *J. Mol. Catal.*, 1996, **162**, 339.
13 B. B. Bunn, B. Barlik, W. R. Bebout, T. E. Glass and B. E. Hanson, *J. Mol. Catal.*, 1994, **94**, 157.

The biosynthesis of bisorbicillinoids: evidence for a biosynthetic route from bisorbicillinol to bisorbibutenolide and bisorbicillinolide

Naoki Abe,* Kazunobu Yamamoto, Tadaharu Arakawa and Akira Hirota

School of Food and Nutritional Sciences, University of Shizuoka, 52-1 Yada, Shizuoka 422-8526, Japan. E-mail: abe@fns1.u-shizuoka-ken.ac.jp; Tel: +81-54-264-5555; Fax: +81-54-264-5099

Received (in Cambridge, UK) 5th September 2000, Accepted 16th November 2000
First published as an Advance Article on the web 11th December 2000

Biosynthetic incorporation of labelled sodium acetates into bisorbicillinol in *Trichoderma* sp. USF-2690 suggests that bisorbicillinol is derived from 12 acetate units. Successful bioconversion of the labelled bisorbicillinols to bisorbibutenolides (bislongiquinolides) and bisorbicillinolides using the washed mycelium of the strain suggests that there are biosynthetic routes from bisorbicillinol to bisorbibutenolide and from bisorbicillinol to bisorbicillinolide.

The 'Bisorbicillinoids', comprised of dimeric sorbicillin-related natural products, have recently been described by Nicolaou *et al*.[1] Several compounds in the group, possessing complex structures, exhibit interesting biological activities, *e.g.*, inhibition of the production of TNF-α by macrophages and monocytes,[2] inhibition of β-1,6-glucan biosynthesis,[3] and scavenging of the 1,1-diphenyl-2-picrylhydrazyl (DPPH) radical.[4–7] The biosynthesis of bisorbicillinoids is of interest to many investigators[5,8–10] and, recently, biomimetic total synthesis has been investigated.[11–13] In particular, the biosynthetic pathway of bisorbibutenolide[5] (bislongiquinolide, **3**)[14] has been proposed to involve several distinct routes.[5,10] We recently reported that *Trichoderma* sp. USF-2690 produced seven bisorbicillinoids, including bisorbicillinol **1**, bisorbibutenolide **2**, and bisorbicillinolide **3**,[4,5] with presumed biogenetic routes from **1** to **2** and from **1** to **3** through a branch point as a common intermediate anion (Scheme 1).[5] The routes were postulated based on the finding that ^{13}C-labeled sodium acetate was incorporated into **1** *via* a polyketide pathway prior to incorporation into **2** and **3**. We wished to establish the biosynthetic relationship between **1**, **2**, and **3**, and report herein the result of a preliminary labelling experiment that provides evidence of the biosynthetic routes from **1** to **2** and from **1** to **3**.

Trichoderma sp. USF-2690 was first cultivated on a reciprocal shaker at 30 °C for 2 d.† The washed mycelium from the fermentation broth was then suspended in five 0.5-liter flasks each holding 150 mL of the medium (pH 7) containing 0.1% sodium [1-^{13}C]acetate or 0.1% sodium [2-^{13}C]acetate and 0.5% polypeptone, and again fermented with reciprocal shaking at 30 °C for 2 d. The filtered broth (1 L) was extracted with ethyl acetate (0.5 L × 2) at pH 3. The organic extract, concentrated *in vacuo*, was applied to a Sephadex LH-20 column and eluted with methanol. The fraction including **1** was rechromatographed using medium-pressure liquid chromatography (MPLC) under the following conditions: support, YMC-ODS-AQ 120-S50; solvent, acetonitrile–H_2O (1 : 1, containing 0.1% trifluoroacetic acid); detection, UV at 370 nm. Two types of labelled bisorbicillinol **1** were obtained. The experiment using sodium [1-^{13}C] acetate gave **1** ([1-^{13}C]-**1**) with 10 ^{13}C-enriched carbons (C-1, C-3, C-5, C-7, C-1′, C-3′, C-5′, C-1″, C-3″, and C-5″) in the ^{13}C-NMR spectrum. The expected incorporations at C-9 and C-11 were not observed. We previously reported that bisorbicillinol **1** had a keto–enol tautomation between C-9 and C-11 in solution, and the ^{13}C signals of C-9 and C-11 did not appear in the ^{13}C-NMR spectrum.[4] Therefore, the lack of peaks at C-9 and C-11 did not necessarily mean that the ^{13}C atoms from sodium [1-^{13}C]acetate were not incorporated at C-9 and

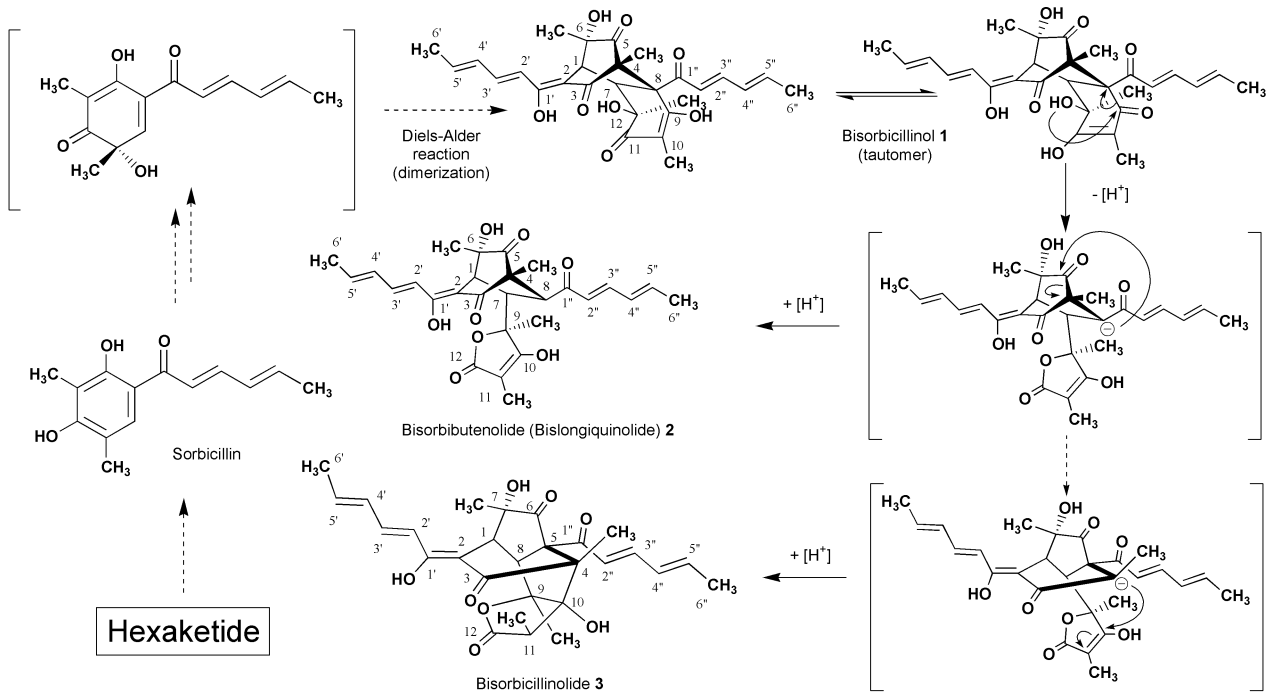

Scheme 1 Biosynthetic pathway from bisorbicillinol **1** to bisorbibutenolide (bislongiquinolide **2**) and bisorbicillinolide **3**.

DOI: 10.1039/b007181l

C-11. On the other hand, the feeding experiment using sodium [2-^{13}C]acetate enhanced the peak strength of 12 carbons (C-2, C-4, C-6, C-8, C-10, C-12, C-2′, C-4′, C-6′, C-2″, C-4″, and C-6″) in the ^{13}C-NMR spectrum of **1** ([2-^{13}C]-**1**). These results suggested that **1** was formed by the dimerization of six acetate units, which combined in the head-to-tail manner typical of fatty acids and polyketides, to give linkages between C-1 and C-7 and between C-4 and C-8 according to the Diels–Alder reaction.

The incorporation study employing each labelled bisorbicillinol **1** as a precursor of bioconversion was accomplished in the following manner. The fungus, inoculated in 0.5 L flasks containing 150 mL of the medium (pH 7) composed of 2.0% glucose and 0.5% polypeptone, was preincubated on a reciprocal shaker at 30 °C for 9 d. Mycelia were washed with sterilized water and then the washed mycelium was inoculated in 0.5 L flasks containing 150 mL of sterilized water with 10 mg of non-labelled and 5 mg of ^{13}C-labelled bisorbicillinol **1**. The cultures for isolation of bisorbibutenolide **2** and bisorbicillinolide **3** were incubated for 72 and 10 h, respectively. The filtrate obtained from each broth was adjusted to pH 3 and extracted with ethyl acetate. LH-20 column chromatography and repetitive MPLC yielded **2** and **3**, respectively.

The ^{13}C-NMR spectrum of bisorbibutenolide **2** obtained from the broth fed with [1-^{13}C]-**1** had 12 ^{13}C-enriched peaks at C-1, C-3, C-5, C-7, C-10, C-12, C-1′, C-3′, C-5′, C-1″, C-3″, and C-5″. This definitive result established the existence of a biological synthetic route from **1** to **2**, as we had proposed previously.[5] In addition, the enrichment of C-10 and C-12 of **2** meant that the two invisible carbons in the ^{13}C-NMR spectrum of **1** were enriched by sodium [1-^{13}C]acetate. Furthermore, the consecutive feeding study of [2-^{13}C]-**1** confirmed the validity of bioconversion from **1** to **2** in the fungal strain. This finding was consistent with the expectation based on a typical polyketide pathway that the ^{13}C–enrichments at C-2, C-4, C-6, C-8, C-9, C-11, C-2′, C-4′, C-6′, C-2″, C-4″, and C-6″ were observed in the ^{13}C-NMR spectrum of **2**.

Proof of biosynthesis of bisorbicillinolide **3** *via* bisorbicillinol **1** as a precursor, was then performed in the same manner. The bisorbicillinolide **3** obtained from the broth fed with [1-^{13}C]-**1** gave the characteristic ^{13}C-NMR spectrum of **3**, which had 12 peaks enhanced at C-1, C-3, C-6, C-8, C-10, C-12, C-1′, C-3′, C-5′, C-1″, C-3″, and C-5″. The continued experiment using [2-^{13}C]-**1** led to the expected **3**, into which excess ^{13}C-atoms were incorporated at C-2, C-4, C-5, C-7, C-9, C-11, C-2′, C-4′, C-6′, C-2″, C-4″, and C-6″. The results of a feeding study using [1-^{13}C]-**1** and [2-^{13}C]-**1** ascertained that bisorbicillinolide **3** was biosynthesized from bisorbicillinol **1** as a precursor.

To examine the possibility that the biosynthesis from bisorbicillinol **1** to bisorbibutenolide **2** occurred *via* bisorbicillinolide **3**, or from **1** to **3** *via* **2**, time course studies on bioconversion of products in the washed mycelium were performed using high performance liquid chromatography analysis. Non-labeled bisorbibutenolide **2** or bisorbicillinolide **3** was added to the washed mycelium prepared above, and the culture broth was incubated at 30 °C for 72 h. No other products were detected in either experiment.

These observations from the ^{13}C-feeding studies indicate that there are biosynthetic routes from **1** to **2** and from **1** to **3** in *Trichoderma* sp. USF-2690. The supporting experiments might rule out the possibility of biosynthesis from **1** to **2** *via* **3** or from **1** to **3** *via* **2** and the reverse biosynthesis from **2** or **3** to **1**. These results suggest the presence of the first anion as a branch point and the second anion following the C–C bond cleavage. Further incorporation studies will clarify the detailed biosynthetic mechanisms through the two precursor anions.

This work is supported in part by a grant-in-aid for Scientific Research (C) (No. 12660100) to A. H. from the Ministry of Education, Science, Sports and Culture of Japan.

Notes and references

† The fermentation broth was pooled from ten 0.5 L flasks each containing 150 mL of the following medium: 2.0% glucose, 0.05% polypeptone, 0.2% yeast extract, 0.1% KH_2PO_4, 0.1% $MgSO_4 \cdot 7H_2O$, and 0.1% trace salt mixture at pH 7. The filtered mycelial cake was washed with 2 L of sterilized water.

1 K. C. Nicolaou, R. Jautelat, G. Vassilikogiannakis, P. S. Baran and K. B. Simonsen, *Chem. Eur. J.*, 1999, **5**, 3651.
2 G. A. Warr, J. A. Veitch, A. W. Walsh, G. A. Hesler, D. M. Pirnik, J. E. Lett, P-F. M. Lin, I. A. Medina, K. D. McBrien, S. Forenza, J. M. Clark and K. S. Lam, *J. Antibiot.*, 1996, **49**, 234.
3 M. Kontani, Y. Sakagami and S. Marumo, *Tetrahedron Lett.*, 1994, **35**, 2577.
4 N. Abe, T. Murata and A. Hirota, *Biosci. Biotechnol. Biochem.*, 1998, **62**, 661.
5 N. Abe, T. Murata and A. Hirota, *Biosci. Biotechnol. Biochem.*, 1998, **62**, 2120.
6 N. Abe, T. Murata, K. Yamamoto and A. Hirota, *Tetrahedron Lett.*, 1999, **40**, 5203.
7 N. Abe, K. Yamamoto and A. Hirota, *Biosci. Biotechnol. Biochem.*, 2000, **64**, 620.
8 L. S. Trifonov, H. Hilpert, P. Floersheim, A. S. Dreiding, D. M. Rast, R. Skrivanova and L. Hoesch, *Tetrahedron*, 1986, **42**, 3157.
9 O. Shirota, V. Pathak, C. F. Hossain, S. Sekita, K. Takataori and M. Satake, *J. Chem. Soc., Perkin Trans. 1*, 1997, 2961.
10 S. Sperry, G. J. Samuels and P. Crews, *J. Org. Chem.*, 1998, **63**, 10 011.
11 D. Barnes-Seeman and E. J. Corey, *Org. Lett.*, 1999, **1**, 1503.
12 K. C. Nicolaou, K. B. Simonsen, G. Vassilikogiannakis, P.S. Baran, V. P. Vidali, E. N. Pitsinos and E. A. Couladouros, *Angew. Chem., Int. Ed.*, 1999, **38**, 3555.
13 K. C. Nicolaou, G. Vassilikogiannakis, K. B. Simonsen, P. S. Baran, Y.-L. Zhong, V. P. Vidali, E. N. Pitsinos and E. A. Couladouros, *J. Am. Chem. Soc.*, 2000, **122**, 3071.
14 R. Andrade, W. A. Ayer and L. S. Trifonov, *Aust. J. Chem.*, 1997, **50**, 255.

ChemComm

Metal extractions using water in carbon dioxide microemulsions

M. Z. Yates,[a] D. L. Apodaca,[a] M. L. Campbell,[a] E. R. Birnbaum[b] and T. M. McCleskey*[a]

[a] *Actinide, Catalysis, and Separations Chemistry, MS J514, Los Alamos National Laboratory, Los Alamos, NM 87545, USA. E-mail: tmark@lanl.gov*

[b] *Analytical Chemistry Sciences, MS E518, Los Alamos National Laboratory, Los Alamos, NM 87545, USA*

Received (in Columbia, MO, USA) 17th July 2000, Accepted 16th October 2000
First published as an Advance Article on the web 11th December 2000

Water in supercritical carbon dioxide microemulsions are examined as a new medium for the extraction of metal ions from contaminated surfaces, and are shown to extract > 99% of the copper from a spiked filter paper with as little as a two-fold excess of surfactant.

Supercritical carbon dioxide ($scCO_2$) has many advantages as a solvent for extractions in environmental remediation including enhanced diffusivity (mass transfer), chemical stability, and pressure-dependent solvation properties that facilitate simple separations. The absence of a liquid–vapor interface above the critical temperature (31 °C) results in zero surface tension, and is particularly advantageous for extraction from solid surfaces since $scCO_2$ may easily penetrate the pores of solid matrices. The challenge for extracting metal ions comes from the fact that supercritical carbon dioxide has no permanent dipole moment and a low dieletric constant (*ca.* 1.5). Hence, hydrophiles and metal salts typically have near zero solubility. Ligands such as β-diketones, dithiocarbamates, and organophosphorus reagents have been used to solubilize metals into $scCO_2$.[1] The solubility of the ligands is quite good in some cases, but solubility of the metal–ligand complexes remains low, limiting practical applications. Solubility of the metal complexes can be enhanced with highly fluorinated ligands,[2] but complexes that have moderate CO_2 solubility often require a large excess of ligand for efficient extraction.[1e,g,i,2e] Yazdi and Beckman have shown that attaching 'CO_2-philic' tails, consisting of either highly fluorinated or polysiloxane groups, to ligands increases the solubility of the metal complexes and results in moderately efficient metal extractions (up to 87%) in liquid CO_2.[3] The approach of designing specific fluorinated ligands has the drawback that efficient extraction depends on the metal being present as a simple metal salt in a specific oxidation state.

Our approach differs significantly from strategies to date in that we solubilize the metal ion with water in CO_2 microemulsions. Johnston *et al.*[4] and Eastoe *et al.*[5] first demonstrated that a perfluoropolyether ammonium carboxylate surfactant was effective in forming water microemulsion droplets (< 10 nm in diameter) in supercritical carbon dioxide. We report here on using these water-based microemulsions as a new medium for metal extraction from contaminated surfaces. The nanodroplets of water suspended in CO_2 take advantage of both the high solubility of metal ions in water and the high difussivity of CO_2 to penetrate pores that are inaccessible to bulk water. The pressure-dependent solvent strength of CO_2 can be used to control formation and disruption of the nanodroplets. This extraction scheme is particularly attractive for remediation of heterogeneous waste in which small amounts of metal contaminants are dispersed throughout a large volume of solid waste. Typically, such extractions require an amount of water or solvent proportional to the volume of solid material. With microemulsions, CO_2 is effectively used as a diluent and the amount of water need only be proportional to the amount of metal to be extracted, making it possible to decontaminate grams of waste with μL of water.

Water in carbon dioxide microemulsions were formed in a stainless steel variable volume view cell.[6] The standard amounts of material added for microemulsion formation were 0.2 g PFPE-NH_4, 10 g CO_2 and 60 μL water. Selected experiments were done with 0.122 g PFPE-NH_4, 10 g CO_2 and 42 μL water (data in Table 1). All extractions were conducted at 207 bar and 45 °C. Filter paper was spiked by two different methods. A 42.5 mm diameter filter paper was submerged in aqueous 1 M copper nitrate for at least 48 h (method 1). After drying, the filter paper was cut into quarter sections and extractions were conducted on one section of the paper. For method 2, 5–6 mg of $Cu(NO_3)_2$ was dissolved in 30 μL of water and the entire solution was added dropwise to a piece of filter paper. Each filter paper was dried for at least 24 h and placed in a small extraction cell (ISCO, 3 mL cell). The microemulsion was recirculated through the extraction cell at a flow rate of 10 mL min^{-1}. The kinetics of extraction from the filter paper were followed with UV–VIS spectroscopy (Hewlett–Packard model 8453). At the completion of the extraction, at least 50 mL of neat CO_2 was passed through the extraction cell (207 bar, 25 °C) to remove residual fluorinated surfactant from the filter paper. The filters were digested and copper concentrations were determined by ICP-AES.

The extinction coefficient for the 733 nm band of $Cu(NO_3)_2$ in the water/CO_2 microemulsion was determined to be 59.3 M^{-1} cm^{-1}.[7] The low energy absorption band is blue shifted compared to copper nitrate in nitric acid (810 nm) at ambient conditions (Fig. 1). We attribute this shift to two factors: copper binding to the surfactant head groups and a decrease in the polarity of water in the micelle core. The maximum solubility of copper in the microemulsion was found to be 3 M.

Extractions of copper from spiked filter paper were conducted to examine the effectiveness of the microemulsion in removing metal contaminates from solid surfaces (Table 1). More than 99% of the copper is extracted in one step from smaller pieces of filter paper. Extraction efficiency decreases when a larger piece of filter paper is used, but following with a second extraction improves the efficiency to 82–99%. The kinetics of extraction from a spiked filter paper (method 1) were followed by UV–VIS spectroscopy (Fig. 1). The absorption from copper reached a maximum after 60 min of exposure to the microemulsion, with no further increase after an additional 90 min. The kinetics of extraction with microemulsions are much

Table 1 Extraction of copper from filter paper at 45 °C and 207 bar for 1 h, using 122 mg surfactant and 42 μL water

Number of extractions	Weight of filter paper/g	Concentration, initial/ppm	% Extracted
1[a]	0.018	81400	99.65
1[a,b]	0.019	81400	99.53
1[c]	0.384	3430	58.5
2[c]	0.386	4090	98.0
2[c]	0.238	6630	82.8
2[c]	0.096	16400	99.7

[a] Extraction from Whatman No. 3 filter paper; % extracted based on measured value from an unextracted piece of spiked filter paper; method 1 spiking procedure (saturated solution). [b] Using 50 μL water. [c] Extraction from Whatman No. 5 filter paper; % extracted based on a calculated value for 5 and 6 mg $Cu(NO_3)_2$; method 2 spiking procedure.

DOI: 10.1039/b007331h

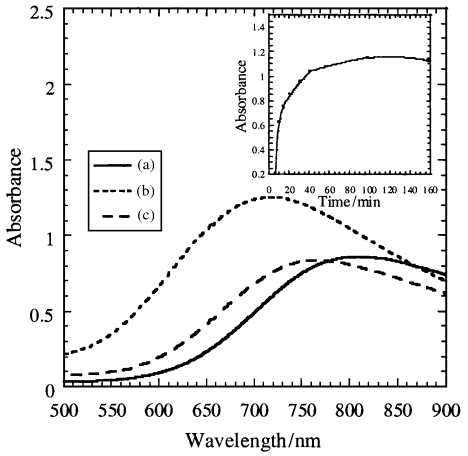

Fig. 1 The absorption spectra of copper(II) from: (a) copper nitrate dissolved in nitric acid at ambient conditions, (b) copper nitrate dissolved in the water/CO_2 microemulsion, and (c) aqueous copper acetate at ambient conditions. The inset shows the intensity at 733 nm *vs.* time for extraction of copper.

faster than those observed recently with CO_2-soluble polymers that required many hours to days for extraction.[8] In addition to improved kinetics, the microemulsions have improved efficiency compared to previous studies with CO_2-soluble chelating agents. In general, past extractions have required a tremendous excess of ligand to achieve reasonable metal extractions (> 1000 fold).[1] By comparison, at the maximum solubility of copper, the molar ratio of surfactant to copper in the microemulsion is approximately 3.

Europium fluorescence lifetimes and emission spectra were examined to probe ion solvation in the water in CO_2 microemulsions. The relative heights of the europium emission bands at 593 and 615 nm provide information on the first solvation sphere around the europium ion.[9,10] In the microemulsion, the 615 nm band gains in intensity, indicating that the center of inversion around europium is removed by displacement of water in the first hydration sphere by another ligand.[11] Two possible ligands are available in the microemulsion core: the carboxylate head group of the surfactant or carbonic acid, formed by CO_2 dissolved in the aqueous phase. As a control, europium chloride was dissolved in D_2O and the headspace over the solution was pressurized to 3000 psi with carbon dioxide to introduce bicarbonate with no surfactant present. The europium emission spectra appeared the same as in water at ambient conditions, suggesting that the carboxylate head group of the surfactant is solely responsible for the changes in the emission spectra of europium ion dissolved in the microemulsion.

Futher evidence for surfactant binding comes from lifetime experiments using H_2O- and D_2O-based microemulsions. The isotope effect provides a way to determine the number of water molecules surrounding the europium ion using the equation: $n = C^*(1/\tau_H - 1/\tau_D)$, where n is the number of water molecules, C is a constant (1.05 for Eu), τ_H is the fluorescenece lifetime in H_2O, and τ_D is the fluorescence lifetime in D_2O (lifetimes in milliseconds).[9] The lifetime of europium(III) ion in the water in supercritical CO_2 microemulsion was found to be 120 μs and increased to 274 μs when the microemulsion was formed with D_2O. Using the above equation with the measured lifetimes gives *ca.* 5 water molecules in the first hydration sphere of the europium ions. As the fully hydrated ion has 8 to 9 water molecules,[12] this result suggests that the surfactant displaces 3 or 4 water molecules from around the europium ion.

Radioactive and heavy metal contaminants are often present as water-insoluble metal oxides in heterogeneous waste. To demonstrate the versatility of the microemulsion in metal extraction, the microemulsion was formed with a 20 wt% nitric acid solution instead of pure water. The increase in acidity was confirmed by dissolving methyl orange indicator in the microemulsion. The indicator appeared bright red when the microemulsion was formed with 20% nitric acid as opposed to orange when distilled water was used. The ability of the acidic microemulsions to extract metal oxides was examined with europium oxide. Based upon visual observation, 10 mg of europium oxide completely dissolved into a microemulsion formed with 20 wt% nitric acid after stirring for 1 h.

Water in supercritical carbon dioxide microemulsions are effective for extraction of metals from solids. At maximum solubility, a 3 M solution of copper can be obtained within the microemulsion core. The nanodroplets offer the advantages of rapid and efficient extractions with a versatile environment. Making the microemulsion with 20 wt% nitric acid rather than pure water allowed europium oxide to be solubilized. Agents that oxidize low valent metal oxides or water-soluble chelating agents could also be introduced into the microemulsions to expand the types of metals that may be extracted and to provide selectivity in mixed metal extractions. Metal is readily recovered by simply dropping the CO_2 pressure below the cloud point, causing the water to coalesce into a single droplet with all of the metal and some surfactant. Initial experimental work has indicated that surfactant recycle should be possible by adding excess water and reducing pressure to destabilize the microemulsion while maintaining surfactant solubility. An additional 270 μL of water was added to a copper-saturated microemulsion at 207 bar, and then pressure was reduced to 101 bar. At 101 bar, phase separation occurred and the aqueous phase settled to the bottom of the cell, while a significant fraction of the surfactant remained in the upper phase. No copper was observable in the upper phase by UV–VIS. The ability of the microemulsion to concentrate the metal into a small volume of water makes it particularly attractive for extractions from contaminated solids that often have small amounts of metal dispersed over a large volume of solid waste.

Notes and references

1 (*a*) J. Darr and M. Poliakoff, *Chem. Rev.*, 1999, **99**, 495; (*b*) Y. Meguro, S. Iso and Z. Yoshida, *Anal. Chem.*, 1998, **70**, 1262; (*c*) Y. Meguro, S. Iso, T. Sasaki and Z. Yoshida, *Anal. Chem.*, 1998, **70**, 774; (*d*) N. G. Smart, T. Carleson, T. Kast, A. A. Clifford, M. D. Burford and C. M. Wai, *Talanta*, 1997, 137; (*e*) Y. Lin, N. G. Smart and C. M. Wai, *Environ. Sci. Technol.*, 1995, **29**, 2706; (*f*) A. F. Lagalante, B. N. Hansen, T. J. Bruno and R. E. Sievers, *Inorg. Chem.*, 1995, **34**, 5781; (*g*) S. Iso, Y. Meguro and Z. Yoshida, *Chem. Lett.*, 1995, 365; (*h*) K. E. Laintz and E. Tachikawa, *Anal. Chem.*, 1994, **66**, 2190; (*i*) J. Wang and W. D. Marshall, *Anal. Chem.*, 1994, **66**, 1658.

2 (*a*) C. M. Wai and S. J. Wang, *Chromatogr. A.*, 1997, **785**, 369; (*b*) M. Z. Özel, M. D. Burford, A. A. Clifford, K. D. Bartle, A. Shadrin, N. G. Smart and N. D. Tinker, *Anal. Chim. Acta*, 1997, **346**, 73; (*c*) J. M. Murphy and C. Erkey, *Ind. Eng. Chem. Res.*, 1997, **36**, 5371; (*d*) J. D. Glennon, S. Hutchinson, A. Walker, S. J. Harris and C. C. McSweeney, *J. Chromatogr. A*, 1997, **770**, 85; (*e*) K. E. Laintz, C. M. Wai, C. R. Yonker and R. D. Smith, *J. Supercrit. Fluids*, 1991, **4**, 194.

3 (*a*) A. V. Yazdi and E. J. Beckman, *J. Mater. Res.*, 1995, **10**, 530; (*b*) A. V. Yazdi and E. J. Beckman, *Ind. Eng. Chem. Res.*, 1996, **35**, 3644; (*c*) A. V. Yazdi and E. J. Beckman, *Ind. Eng. Chem. Res.*, 1997, **36**, 2368.

4 K. P. Johnston, K. L. Harrison, M. J. Clarke, S. M. Howdle, M. P. Heitz, F. V. Bright, C. Carlier and T. W. Randolph, *Science*, 1996, **271**, 624.

5 J. Eastoe, B. M. H. Cazelles, D. C. Steytler, J. D. Holmes, A. R. Pitt, T. J. Wear and R. K. Heenan, *Langmuir*, 1997, **13**, 6980.

6 M. Z. Yates, G. Li, J. J. Shim, S. Maniar, K. P. Johnston, K. T. Lim and S. Webber, *Macromolecules*, 1999, **32**, 1018.

7 The extinction coefficient was determined by dissolving $Cu(NO_3)_2$ in the microemulsion and assuming a homogeneous environment.

8 K. Powell, T. M. McCleskey, W. Tumas and J. DeSimmone, *Macromolecules*, submitted.

9 W. D. Horrocks and D. R. Sudnick, *J. Am. Chem. Soc.*, 1979, **101**, 334.

10 J.-C. G. Bunzli and J. Yersin, *Inorg. Chem.*, 1979, **18**, 605.

11 J.-C. G. Bunzli, in *Lanthanide Probes in Life, Chemical and Earth Sciences*, ed. J.-C. G. Bunzli and G. R. Choppin, Elsevier, Amsterdam, 1989, ch. 7, p. 219.

12 W. Grygiel and M. Starzak, *J. Lumin.*, 1997, **71**, 21.

The effect of solvent on the α-effect: C=O, P=O and SO_2 centers†

Ik-Hwan Um,*[a] Jin-Young Hong[a] and Erwin Buncel*[b]

[a] *Department of Chemistry, Ewha Womans University, Seoul 120-750, Korea*
[b] *Department of Chemistry, Queen's University, Kingston, Ontario K7L 3N6, Canada.*
E-mail: ihum@mm.ewha.ac.kr; Fax: (+1)-(822)-3277-2844; Tel: (+1)-(822)-3277-2349

Received (in Cambridge, UK) 29th August 2000, Accepted 6th November 2000
First published as an Advance Article on the web 11th December 2000

The α-effect for the reaction of a sulfonyl ester exhibits a bell-shaped dependence of the α-effect on solvent composition as do the corresponding reactions with a carbonyl and a phosphinyl ester, and the magnitude of the α-effect is found to be dependent on the magnitude of the β_{nuc} value, suggesting TS stabilization as the cause of the α-effect.

Since the α-effect term was given by Edwards and Pearson in 1962 to the abnormally enhanced reactivity shown by nucleophiles having a pair of unshared electrons adjacent to the nucleophilic center,[1] numerous studies have been performed to account for this phenomenon.[2–11] However, the cause of the α-effect has not been clearly understood.[2–11] One of the intriguing aspects in α-effect studies has been the finding that the magnitude of the α-effect is dependent on the nature of the electrophilic center, generally increasing as $sp^3 < sp^2 < sp$ for carbon centers,[2–4] though some exceptions exist.[5] Equally interesting, as well as controversial, has been the effect of solvent on the α-effect.[6–9]

In order to shed light on the effect of solvent on the α-effect, we initiated systematic studies and in 1986, we investigated the reaction of *p*-nitrophenyl acetate (PNPA) with butane-2,3-dione monoximate (Ox^-) and *p*-chlorophenoxide ($ClPhO^-$), as the α- and corresponding normal-nucleophile, respectively, in DMSO–H_2O mixtures of varying compositions.[6a] We found, unexpectedly, a bell-shaped dependence of the α-effect (k^{Ox^-}/k^{ClPhO^-}) on solvent composition.[6a] A similar bell-shaped trend was observed for the corresponding reaction of *p*-nitrophenyl diphenylphosphinate (PNPDPP).[6b] However, Moss reported that the reaction of PNPA with *o*-iodosylbenzoate (IBO^-) and $ClPhO^-$ in DMSO–H_2O mixtures shows no maximum α-effect but exhibits a decreasing α-effect trend.[7] More surprisingly, a contrasting solvent behaviour was found recently:[8] the reaction of PNPA with Ox^- and $ClPhO^-$ in MeCN–H_2O mixtures exhibits an increasing α-effect trend as the mol% MeCN in the medium is increased.[8a] Similarly, the α-effect for the reaction of PNPA with benzohydroxamates and *m*-chlorophenoxide in MeCN–H_2O mixtures also resulted in an increasing α-effect behaviour as the concentration of MeCN in the reaction medium was increased.[8b]

It appeared to us as potentially highly informative, in investigation of the α-effect, to vary the electrophilic center systematically and to couple that with variation of solvent. We report herein such a study for the reaction of a sulfur centered substrate, *p*-nitrophenyl benzenesulfonate (PNPBS), with Ox^- and $ClPhO^-$ in DMSO–H_2O mixtures as shown in eqn. (1), and compare the results with the data for the corresponding reactions of PNPA and PNPDPP.

$$C_6H_5SO_2\text{-}OC_6H_4NO_2\text{-}p + Nu^- \rightarrow C_6H_5SO_2Nu + {}^-OC_6H_4NO_2\text{-}p \quad (1)$$

$Nu^- = CH_3C(O)C(CH_3)=NO^-$ (Ox^-), an α-nucleophile
$p\text{-}ClC_6H_4O^-$ ($ClPhO^-$), a normal nucleophile

As shown in Fig. 1, the second-order rate constant increases as the mol% of DMSO in the medium increases for both Ox^- and $ClPhO^-$ systems: the rate enhancement upon solvent change from 10 to 90 mol% of DMSO is 2190 and 3330 for Ox^- and $ClPhO^-$, respectively. Interestingly, the plot of log k^{Ox^-} *vs.* mol% of DMSO shows downward curvature, while that of log k^{ClPhO^-} *vs.* mol% DMSO exhibits upward curvature. As a result, the difference in rate constant between Ox^- and $ClPhO^-$ increases up to *ca.* 50 mol% DMSO but decreases beyond this point. Such a differential solvent effect on rates leads to the solvent dependent α-effect profile, shown in Fig. 2; *i.e.* the sulfonyl system exhibits maximum α-effect at *ca.* 50 mol% DMSO, as do the carbonyl and phosphinyl systems. Therefore,

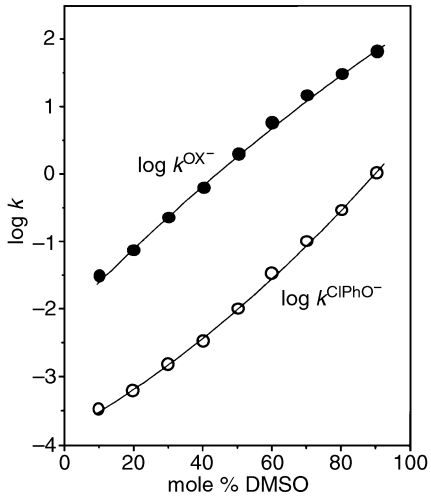

Fig. 1 Plots showing the effect of solvent on second-order rate constants for the reaction of PNPBS with Ox^- and $ClPhO^-$ in DMSO–H_2O mixtures at 25.0 ± 0.1 °C.

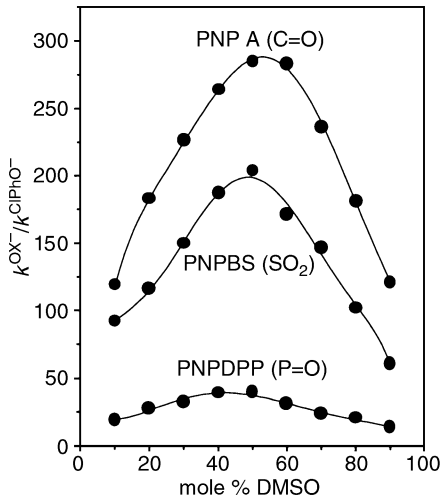

Fig. 2 Plots showing the effect of solvent on the α-effect for the reaction of PNPA, PNPDPP and PNPBS with Ox^- and $ClPhO^-$ in DMSO–H_2O mixtures at 25.0 ± 0.1 °C.

† Electronic supplementary information (ESI) available: Tables of rate constants. See http://www.rsc.org/suppdata/cc/b0/b007000i/

DOI: 10.1039/b007000i

the bell-shaped α-effect behaviour has been found to be general for the reactions of the three different electrophiles with Ox^- and $ClPhO^-$ in DMSO–H_2O mixtures.

Moreover, interestingly, the magnitude of the α-effect is strongly dependent on the electrophilic center; *i.e*. the α-effect in 50 mol% is *ca*. 300, 40 and 200 for the carbonyl, phosphinyl and sulfonyl systems, respectively. The small α-effect for the phosphinyl system compared to the carbonyl and sulfonyl systems is striking. Bruice showed that the magnitude of the α-effect is dependent on the magnitude of the β_{nuc} value for reactions of a variety of substrates with hydrazine and glycylglycine: the α-effect decreases with decreasing β_{nuc} value.[10] Similarly, Bernasconi observed no α-effect for the addition reaction of primary amines including hydrazine and *o*-methylhydroxylamine to Meldrum's acid, a system for which $\beta_{nuc} = 0.22$.[11a]

The β_{nuc} values for the reactions of PNPA with substituted phenoxides in various DMSO–H_2O mixtures are available,[12] but the ones for the reaction of the phosphinyl and sulfonyl systems have not been reported. Therefore, we performed the reaction of PNPDPP and PNPBS with a series of substituted phenoxides in 50 mol% DMSO, in which the maximum α-effect is observed. The plots of log $k^{ZC_6H_4O^-}$ *vs.* pK_a (ZC_6H_4OH) exhibit good Brønsted type correlation: β_{nuc} values are 0.64, 0.21 and 0.54 for the carbonyl, phosphinyl and sulfonyl systems, respectively. Thus, the β_{nuc} value for the phosphinyl systems is much smaller than for the carbonyl and sulfonyl systems, and, moreover, the β_{nuc} value follows the same order as the α-effect in magnitude. Therefore, one can suggest that the small β_{nuc} value is responsible for the small α-effect exhibited by the phosphinyl system. This argument is consistent with our recent report that the reaction for an sp hybridized carbon center exhibited an unexpectedly small α-effect in which the β_{nuc} value was 0.32.[5]

As demonstrated in Fig. 2, the effect of solvent on reactivity is significant. Such a solvent effect on rate can be achieved by destabilizing the ground-state (GS) and/or stabilizing the transition-state (TS). We recently found that the GS of Ox^- and $ClPhO^-$ becomes destabilized upon addition of DMSO to the reaction medium,[6c] however, the GS energy difference between Ox^- and $ClPhO^-$ is constant for the three systems. Therefore, if the GS energy difference between Ox^- and $ClPhO^-$ were mainly responsible for the α-effect, the magnitude of the α-effect should be about the same, regardless of the nature of the electrophilic center. However, our results show that this is not the case. Therefore, the present results clearly suggest that the difference in the GS energy is not solely responsible for the α-effect.

The magnitude of the β_{nuc} value has been understood as a measure of bond formation between the nucleophile and the substrate in the TS of the rate-determining step; hence the TS structures of the carbonyl, phosphinyl and sulfonyl systems would vary according to the different β_{nuc} values. One can expect that the TS stabilizing effect would be smaller for the reaction system in which the degree of bond formation between nucleophile and substrate in the TS is less advanced (reactant-like TS), and *vice versa*. Accordingly, one can suggest that the TS stabilizing effect would be developed to a lesser extent for the phosphinyl system compared with the carbonyl and sulfonyl systems, based on the smaller β_{nuc} value obtained for the former, which would explain the small α-effect observed for the phosphinyl system.

More systematic studies are underway including theoretical investigation for better understanding of solvent effect on the α-effect.

The authors are grateful for the financial support from KOSEF of Korea (1999-2-123-003-5 and 2000-123-02-2) and E. B. also thanks NSERC of Canada for a research grant.

Notes and references

1 J. O. Edwards and R. G. Pearson, *J. Am. Chem. Soc.*, 1962, **84**, 16.
2 Reviews: (*a*) E. Buncel and S. Hoz, *Isr. J. Chem.*, 1985, **26**, 313; (*b*) A. P. Grekov and V. Y. Veselov, *Usp. Khim.*, 1978, **47**, 1200; (*c*) N. J. Fina and J. O. Edwards, *Int. J. Chem. Kinet.*, 1973, **5**, 1.
3 (*a*) G. Moutiers, E. Guevel, L. Villien and F. Terrier, *J. Chem. Soc., Perkin Trans. 2*, 1997, 710; (*b*) F. Terrier, G. Moutiers, L. Xiao, E. Guevel and F. Guir, *J. Org. Chem.*, 1995, **60**, 1748; (*c*) K. R. Fountain, D. B. Tad-y, T. W. Paul and M. V. Golynskiy, *J. Org. Chem.*, 1999, **64**, 6547.
4 (*a*) E. Buncel, C. Chuaqui and H. Wilson, *J. Am. Chem. Soc.*, 1982, **104**, 4896; (*b*) S. Oae and Y. Kadoma, *Phosphorus, Sulfur Silicon Relat. Elem.*, 1997, **123**, 293.
5 I. H. Um, J. S. Lee and S. M. Yuk, *J. Org. Chem.*, 1998, **63**, 9152.
6 (*a*) E. Buncel and I. H. Um, *J. Chem. Soc., Chem. Commun.*, 1986, 595; (*b*) R. M. Tarkka and E. Buncel, *J. Am. Chem. Soc.*, 1995, **117**, 1503; (*c*) I. H. Um and E. Buncel, *J. Org. Chem.*, 2000, **65**, 577.
7 R. A. Moss, S. Swarup and S. Ganguli, *J. Chem. Soc., Chem. Commun.*, 1987, 860.
8 (*a*) I. H. Um and E. Buncel, *J. Chem. Soc., Chem. Commun.*, 2000, 1917; (*b*) I. H. Um, H. W. Yoon, J. S. Lee and H. J. Moon, *J. Org. Chem.*, 1997, **62**, 5939.
9 (*a*) G. Moutiers, E. Guevel, L. Villien and F. Terrier, *J. Chem. Soc., Perkin Trans. 2*, 1997, 7; (*b*) C. A. Bunton, N. D. Gillitt and A. Kumar, *J. Phys. Org. Chem.*, 1997, **10**, 221; (*c*) M. Laloi-Diard, J. F. Verchere, P. Gosselin and F. Terrier, *Tetrahedron Lett.*, 1984, **25**, 1267.
10 H. J. Dixon and T. C. Bruice, *J. Am. Chem. Soc.*, 1972, **94**, 2052.
11 (*a*) C. F. Bernasconi and C. Murray, *J. Am. Chem. Soc.*, 1986, **108**, 5251; (*b*) D. Herschlag and W. P. Jencks, *J. Am. Chem. Soc.*, 1990, **112**, 1951; (*c*) L. E. Fikes, D. T. Winn, R. W. Sweger, M. P. Johnson and A. W. Czarnik, *J. Am. Chem. Soc.*, 1992, **114**, 1493.
12 E. Buncel, I. H. Um and S. Hoz, *J. Am. Chem. Soc.*, 1989, **111**, 971.

ChemComm

Pd-catalysed arylation of propan-1-ol and derivatives: oxidative role of the arylating agent

Laurence Bagnell, Ulf Kreher and Christopher R. Strauss*

CSIRO Molecular Science, Private Bag 10, Clayton South, Victoria 3169, Australia.
E-mail: chris.strauss@molsci.csiro.au

Received (in Cambridge, UK) 3rd July 2000, Accepted 15th November 2000
First published as an Advance Article on the web

With excess PhI under Pd catalysis, 1-PrOH was converted to a mixture of 3,3-diphenylpropenal and *trans*-2,3-diphenylpropenal by a concerted, oxidative sequence that involved two arylative couplings and an olefinic aldehyde that was generated *in situ*.

Recently in our laboratory, Pd on porous glass was developed as a heterogeneous catalyst[1] for promoting Glaser-type and Heck arylative couplings[2] without the need for solubilising or activating ligands. Significantly, with excess allyl alcohol and with PhI in air, Pd on porous glass gave *trans*-cinnamaldehyde (**1**) along with 3-phenylpropanal (**2**; see entry 2, Table 1).[1] Consistent with literature reports,[3,4] in the absence of air, and without the addition of Ag^+ salts, **2** predominated and **1** was not obtained (entry 1, Table 1).

With PhI in excess, the diarylated compounds **3** and **4** appeared as major products from allyl alcohol, along with **1** and **2** (entry 3, Table 1). This diarylation appeared to contrast with a wealth of literature data on the Pd catalysed arylation of that alcohol.[3] Without Ag^+ salts,[4] one might expect that the first arylation of allyl alcohol would be accompanied by rapid migration of the olefinic bond to afford mainly 3-phenylpropanal (**2**), thereby removing the opportunity for a second Heck arylation to occur.

Although air facilitated the dehydrogenation for the reaction in entry 2 of Table 1,[5] the results in entry 3 and co-formation of biphenyl suggested that the arylating agent may have had an additional role. To support this contention, we now report that 1-PrOH with excess PhI can afford a mixture of 3,3-diphenylpropenal (**4**) and *trans*-2,3-diphenylpropenal (**5**), *even under an inert gas atmosphere* (see entry 9). This remarkable transformation has been performed with either $Pd(OAc)_2$ or Pd on porous glass as catalyst[6,7] (which was used for all entries in Table 1) includes microwave heating[8] in a reactor of our design.[9]

A comparable stepwise process would require oxidation of the hydroxy function of 1-PrOH, dehydrogenation of the hydrocarbon chain and two Heck-like arylative couplings of the resultant olefin. However, for the one reaction, successive intermolecular Heck arylative couplings onto the same olefin are rare.[10] Intramolecular examples usually have involved mono-arylations of more than one carbon–carbon double bond.[11]

Mono-arylated products were not observed in the reaction of 1-PrOH, rendering as unlikely, a multi-step sequence involving successive intermolecular Heck arylative couplings with an olefin formed by dehydrogenation *in situ*.[12] The absence of detectable intermediates implies that the process was concerted and may constitute a new reaction.

Formation of biphenyl and benzene as by-products indicates that PhI served as both an oxidant and a reactant. Buchwald and Palucki observed similar behaviour of their arylating agent in the 'Pd' catalysed reaction of cyclohexanol with 4-*tert*-butylbromobenzene to produce the corresponding α-arylated cyclohexanone and *tert*-butylbenzene.[13] They surmised that some of the haloarene was simultaneously reduced during oxidation of the alcohol to cyclohexanone.

Although variations in the order of transformations and alternative routes are possible for the present reaction, the pathway in Scheme 1 appears to account for the products, by-products and their relative proportions.

Preliminary investigations (see Table 1) into the process utilised cinnamaldehyde (**1**),[14] cinnamyl alcohol (**6**), 3-phenylpropanol (**7**) and 3-phenylpropanal (**2**). Cinnamyl alcohol (**6**) afforded diarylenal **4** as a major product (along with **3** and the 2,3-diphenylpropenol isomer **8**), *irrespective of whether or not the atmosphere contained air* (entries 5 and 6). Under argon, 3-phenylpropanal (**2**) gave 2,3-diphenylpropanal (**9**) and products of higher oxidation state, including **1**, **4** and **5** (entry 7). 3-Phenylpropanol (**7**) afforded **4** and **5** as major products, along with traces of **1** and **2** (entry 8). The product distributions obtained from Pd catalysed reactions of excess PhI with **6**, **7** and **2** suggest that several competing processes were operating, including α-arylation,[13] Heck-like arylative coupling of olefinic bonds[2] as well as the new process described herein and illustrated by Scheme 1.

These outcomes may have depended on whether or not coordination of the olefin to Pd occurred in conjunction with the establishment of a strong Pd–O bond, leading to a chelation controlled reaction. Such bonds have been suggested for palladium catalysed oxidation of alcohols.[15] Scheme 1, proposed for the reaction of 1-PrOH commences with Pd–O chelation and proceeds preferably through metallaoxetane intermediates,[16] which account for the observed products and their relative distribution. In the case of allyl alcohol (entry 3), it appears that the double bond and the hydroxy group of the

Table 1 Example reactions and conditions

Entry	Starting material (mmol)	PhI/mmol	Ar or Air	Major products (percentage of total detected)	Turnover Number
1	CH_2=CH–CH_2OH (13)	6	Ar	**2** (59), $CH_3CH(Ph)CHO$ (23)	170
2	CH_2=CH–CH_2OH (13)	6	Air	**1** (60), **2** (40)	120
3	CH_2=CH–CH_2OH (14)	34	Air	**1** (16), **2** (7), **3** (24), **4** (26)	450
4	PhCH=CH–CHO, **1** (13)	34	Ar or Air	**4** (99)	245 (Ar), 170 (Air)
5	PhCH=$CHCH_2OH$, **6** (13)	34	Ar	**3** (36), **4** (18), **8** (15), **9** (10)	700
6	PhCH=$CHCH_2OH$, **6** (13)	34	Air	**3** (6), **4** (62), **8** (13)	560
7	$PhCH_2CH_2CHO$, **2** (6)	34	Ar	**1** (5), **3** (16), **4** (39), **5** (6), **9** (18)	270
8	$PhCH_2CH_2CH_2OH$, **7** (10)	34	Ar	**4** (60), **5** (18)	50
9	$CH_3CH_2CH_2OH$ (20)	34	Ar	**4** (80), **5** (18)	30

DOI: 10.1039/b005323f

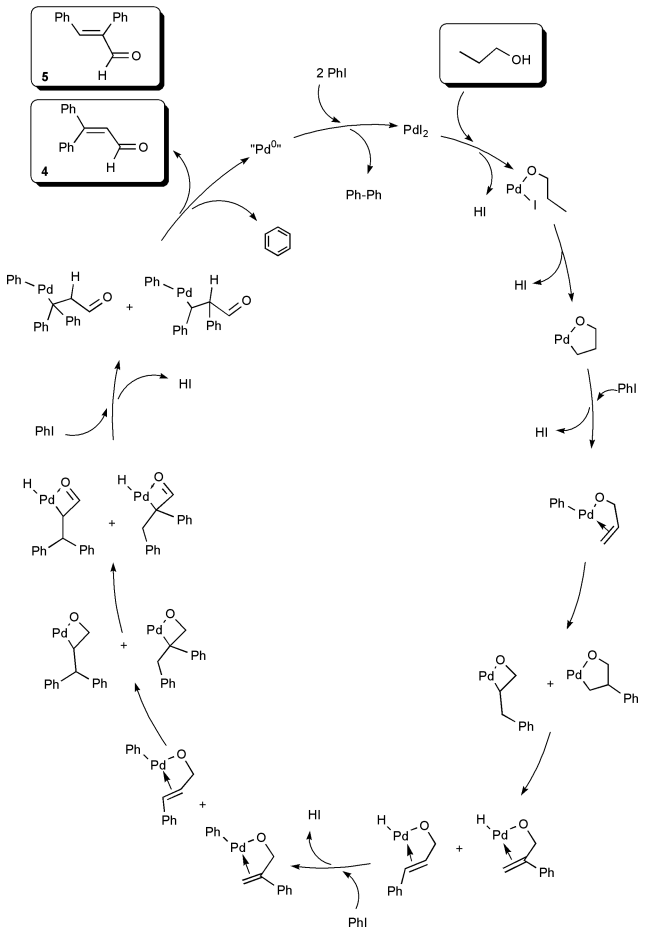

Scheme 1

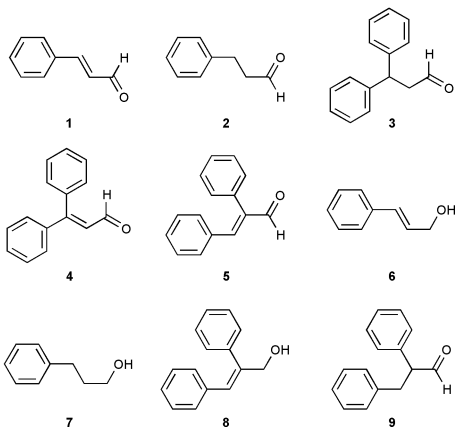

alcohol compete for the Pd and products from both Heck-type arylative coupling (**2** and **3**) as well as the sequence in Scheme 1 (diarylenal **4**) result.

We thank Professor A. Hallberg and Dr M. Larhed of Uppsala University, Sweden, and Dr H. Weigold of CSIRO for reviewing drafts of the manuscript and for helpful discussion. The work was supported by a postdoctoral fellowship (for U.K.) from the German Academic Exchange Service (DAAD).

Notes and references

1 J. Li, A. W.-H. Mau and C. R. Strauss, *Chem. Commun.*, 1997, 1275.
2 A. de Meijere and F. E. Meyer, *Angew. Chem., Int. Ed. Engl.*, 1994, **33**, 2379; R. F. Heck in *Comprehensive Organic Synthesis*, series eds. B. M. Trost, I. Fleming, vol. ed. M. F. Semmelhack, Pergamon, Oxford, 1993, vol. 4, p. 833.
3 J. B. Melpolder and R. F. Heck, *J. Org. Chem.*, 1976, **41**, 265; A. J. Chalk and S. A. Magennis, *J. Org. Chem.*, 1976, **41**, 273; A. J. Chalk and S. A. Magennis, *J. Org. Chem.*, 1976, **41**, 1206; T. Jeffrey, *J. Chem. Soc., Chem. Commun.*, 1984, 1287; R. C. Larock, W.-Y. Leung and S. Stolz-Dunn, *Tetrahedron Lett.*, 1989, **30**, 6629; S.-K. Kang, K.-Y. Jung, C.-H. Park, E.-Y. Namkoong and T.-H. Kim, *Tetrahedron Lett.*, 1995, **36**, 6287; G. Dyker and P. Grundt, *Tetrahedron Lett.*, 1996, **37**, 619.
4 T. Jeffery, *Tetrahedron Lett.*, 1991, **32**, 2121.
5 C. R. Strauss, *Aust. J. Chem.*, 1999, **52**, 83.
6 **A** Into a dry, two-necked flask fitted with a reflux condenser and an inert gas (Ar) bleed line was placed a solution of 1-PrOH (0.784 g; 13.06 mmol) and PhI (12.674 g; 62.12 mmol) in dry, deoxygenated *N*,*N*-dimethyl acetamide (DMA; 50 mL). Anhydrous NaOAc (5.80 g; 70.70 mmol) and $Pd(OAc)_2$ (0.564 g; 2.51 mmol) were added and the mixture was heated at 125 °C for 16 h, then cooled, quenched with 80 mL H_2O and extracted with Et_2O (1 × 80 mL, 2 × 50 mL). The ether extract was washed thrice with water, dried with $MgSO_4$ and the ether removed *in vacuo*. Unconverted PhI was recovered by vacuum distillation at 40 °C and 1×10^{-2} mbar and biphenyl was removed by sublimation (80 °C and 1×10^{-2} mbar). Flash chromatography (silica gel 60, dichloromethane : pentane 1:1) afforded pure product **4** (395 mg). **B** Into a dry, two-necked flask fitted with a reflux condenser and an inert gas (Ar) bleed line was placed a solution of 1-PrOH (749 mg; 12.48 mmol) and PhI (6.971 g; 34 mmol) in dry, deoxygenated *N*,*N*-dimethyl acetamide (DMA; 50 mL). Anhydrous NaOAc (4.127 g; 50 mmol) and Pd on porous glass (containing 19 μmol Pd)[1] were added and the mixture was heated at 125 °C for 16 h, then cooled. Work up as above yielded pure product **4** (73 mg).
7 Although $Pd(OAc)_2$ undergoes thermal decomposition to give finely divided Pd metal and gases including CO_2, methane and ethane (see M. T. Reetz and M. Maase, *Adv. Mat.*, 1999, **11**, 773; M. T. Reetz and G. Lohmer, *Chem. Commun.*, 1996, 1921), no evidence was obtained to associate that redox process with the present reaction.
8 Into a dry PTFE vessel under nitrogen was placed a solution of 1-PrOH (0.803 g; 13.4 mmol) and PhI (6.853 g; 33.6 mmol) in dry, deoxygenated *N*,*N*-dimethyl acetamide (DMA; 50 mL). Anhydrous NaOAc (4.19 g; 51.0 mmol) and $Pd(OAc)_2$ (50.4 mg; 0.22 mmol) were added and the mixture was heated for 10 min at 220 °C in a microwave batch reactor[9] (MBR), then cooled. Work up as in footnote 6 yielded pure product **4** (280 mg). For other examples of Pd catalysed reactions under microwave heating, see M. Larhed and A. Hallberg, *J. Org. Chem.*, 1996, **61**, 9582; U. Bremberg, M. Larhed, C. Moberg and A. Hallberg, *J. Org. Chem.*, 1999, **64**, 1082; M. Larhed, M. Hoshino, S. Hadida, D. P. Curran and A. Hallberg, *J. Org. Chem.*, 1997, **62**, 5583.
9 C. R. Strauss and R. W. Trainor, *Aust. J. Chem.*, 1995, **48**, 1665; K. D. Raner, C. R. Strauss, R. W. Trainor and J. S. Thorn, *J. Org. Chem.*, 1995, **60**, 2456.
10 For examples see, T. Sugihara, M. Takebayashi and C. Kaneko, *Tetrahedron Lett.*, 1995, **36**, 5547; B. M. Choudary, R. M. Sarma and K. K. Rao, *Tetrahedron*, 1992, **48**, 719.
11 L. F. Tietze, *Chem. Rev.*, 1996, **96**, 115; M. Lautens and S. Piguel, *Angew. Chem., Int. Ed.*, 2000, **39**, 1045.
12 In water at high temperature, $Pd(OAc)_2$ catalysed Heck arylations have been reported with olefins generated *in situ*. However, at 400 °C, the reaction between PhI and 1-PrOH gave 1-propylbenzene by a mechanism that was not determined. See E. J. Parsons, *CHEMTECH*, 1996, **26**(7), 30.
13 M. Palucki and S. L. Buchwald, *J. Am. Chem. Soc.*, 1997, **119**, 11 108.
14 A. Amorese, A. Arcadi, E. Bernocchi, S. Cacchi, S. Cerrini, W. Fedeli and G. Ortar, *Tetrahedron*, 1989, **45**, 813.
15 S. Ait-Mohand, F. Henin and J. Muzart, *Tetrahedron Lett.*, 1995, **36**, 2473; V. Bellosta, R. Benhaddou and S. Czernecki, *Synlett*, 1993, 861.
16 E. Bernocchi, S. Cacchi, P. G. Ciattini, E. Morera and G. Ortar, *Tetrahedron Lett.*, 1992, **33**, 3073.

ChemComm

Grignard reagent mediated reaction of Cp_2Zr(II)–ethylene complex with imines†

Tamotsu Takahashi,* Yuanhong Liu, Chanjuan Xi and Shouquan Huo

Catalysis Research Center and Graduate School of Pharmaceutical Sciences, Hokkaido University; and CREST, Science and Technology Corporation (JST), Sapporo 060-0811, Japan. E-mail: tamotsu@cat.hokudai.ac.jp

Received (in Cambridge, UK) 13th September 2000, Accepted 2nd November 2000
First published as an Advance Article on the web 11th December 2000

Imines which do not react with Grignard reagents reacted with EtMgBr in the presence of a catalytic amount of Cp_2ZrCl_2 to give ethylated products in excellent yields; the stoichiometric reaction of the imines and the zirconocene–ethylene complex did not give the ethylated product, whereas addition of MeMgBr or BuMgCl to the mixture afforded the ethylated product after hydrolysis.

We have found that a zircononcene–ethylene complex $Cp_2Zr(CH_2{=}CH_2)$ (**2**)[1] and its ate complex $[Cp_2ZrEt(CH_2{=}CH_2)]MgBr$[2] prepared from Cp_2ZrEt_2 (**1**) and zirconacyclopentanes[1] were involved in the zirconium-catalysed reaction of olefins with EtMgBr[3] which was first reported by Dzhemilev.[4] In order to extend this type of reaction we investigated a catalytic and a stoichiometric reaction of imine with EtMgBr in the presence of zirconocene. In this paper we would like to report a zirconium-catalysed reaction of imine with EtMgBr and the unusual effect of addition of Grignard reagents on the formation of a new C–C bond in the stoichiometric reaction of imines with the zirconocene–ethylene complex.

Imines **3a**–**d**, easily prepared from the corresponding aldehydes and amines, do not react with EtMgBr in THF at even 50 °C to give addition products. When 20 mol% Cp_2ZrCl_2 was added to the mixture of the imines and EtMgBr in THF, the reaction proceeded smoothly at rt to produce substituted amine derivatives **4** in excellent yields after hydrolysis. The results are shown in Table 1. At least 3 eq. of EtMgBr was needed to finish the reaction, and the use of 10 mol% of Cp_2ZrCl_2 decreased the yield of products **4** [eqn. (1)].

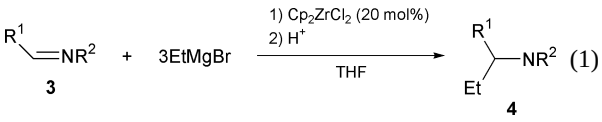

(1)

We investigated the stoichiometric reactions of imines with the zirconocene–ethylene complex. And quite surprisingly, we found that the stoichiometric reaction of **3c** with **2** did not give the coupling product (only 7% of **4c**) after hydrolysis. It puzzled us, however, that when an additional amount of EtMgBr (1 eq.) was added to the reaction mixture, the desired product **4c** was obtained in 64% yield. Moreover, addition of 4 eq. of EtMgBr to the mixture gave an excellent yield of **4c** (93%) [eqn. (2)].

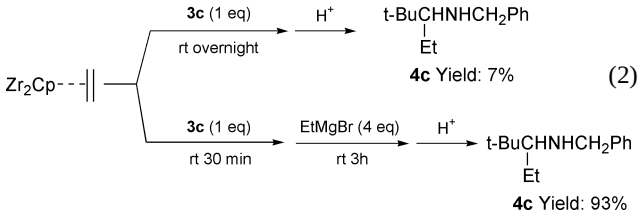

(2)

It is noteworthy that the use of different Grignard reagents also afforded only the same ethylated product **4c**, with improved yields as shown in Table 2.

It is interesting that the reaction of **3a** with **2** gave the ethylated product **4a** in 57% yield after hydrolysis. This indicates that the azazirconacylopentane **5a** was formed in the case of **3a**. A similar effect of addition of a Grignard reagent was also observed. In fact, addition of 1 eq. of MeMgBr to the mixture of **3a** and **2** afforded **4a** in 75% yield after hydrolysis. When 4 eq. of EtMgBr was added to the mixture of **3a** and **2**, the product **4a** was formed in 97% yield after hydrolysis.

These results suggest that there is an equilibrium between azazirconacyclopentane **5** and imine **3** and that the position of the equilibrium lies to the left under the conditions used here. If an irreversible step such as ring-opening and β-hydrogen abstraction is involved in the reaction, in other words, when additional Grignard reagents are added, the reaction goes to the right as expected to give the ethylated products. Deuterolysis instead of hydrolysis of the reaction mixture after addition of 4 eq. of MeMgBr to a mixture of **3c** and **2** afforded deuterated product **4c** DCH_2CH_2(t-Bu)$CHNDCH_2Ph$ (65% D) [eqn. (3)]. This strongly suggests that the complex **6c** is the reaction product of MeMgBr with a mixture of **3c** and **2**. When **6c** was treated with 2 eq. of CuCl for 6 h at rt, ethylated imine tBu(Et)CHN=CHPh (**7**) was obtained in 48% yield after hydrolysis.

We also carried out the reactions of a mixture of Cp_2ZrEt_2 and imine **3a** with various electrophiles[5,6] and the results are summarized in Table 3.

Table 1 Zirconium-catalysed addition of EtMgBr to imines[a]

Imines	R^1	R^2	*T*/°C	*t*/h	Products	Yield (%)[b]
3a	Ph	Bn	20	1	**4a**	96
3b	Ph	Bu	20	12	**4b**	89
3c	t-Bu	Bn	20	1	**4c**	97
3d	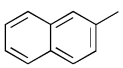	Bn	20	1	**4d**	(87)

[a] 20 mol% Cp_2ZrCl_2 and 3 eq. of EtMgBr were used. [b] GC yields: isolated yield is given in parenthesis.

Table 2 The effect of addition of Grignard reagents under stoichiometric conditions

Grignard reagents	Yield of **4c** (%)[a] 1 eq. of $RMgX$[b]	Yield of **4c** (%)[a] 4 eq. of $RMgX$[b]
MeMgBr	40	70[a]
EtMgBr	64	93
n-BuMgCl	38	64
sec-BuMgCl	22	96
t-BuMgCl	7	15

[a] GC yields of ethylated product **4c**. [b] Amount of addition of RMgX.

† Electronic supplementary information (ESI) available: reaction procedures and NMR data. See http://www.rsc.org/suppdata/cc/b0/b007456j/

Table 3 Reactions of a mixture of Cp_2ZrEt_2 and **3a** with electrophiles[a]

Entry	Additives	Electrophile	*T*/°C	*t*/h	Product[a]		Yield (%)[b]
1	CuCl		r.t.	3	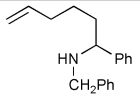	(**8a**)	56 (48)
2	—	C_2H_5COCl	0	1	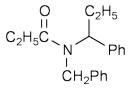	(**8b**)	79 (57)
3[c]	(1) — (ii) CuCl	C_2H_5COCl (2 eq) —	0 50	1 12	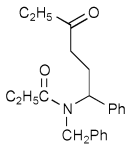	(**8c**)	70 (56)
4[c]	(i) — (ii) CuCl	C_2H_5COCl 	0 r.t.	1 6	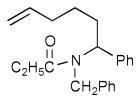	(**8d**)	82 (63)

[a] GC yields; isolated yields are given in parenthesis. [b] Reaction products were isolated after hydrolysis. [c] The mixture was treated with (i) and then (ii).

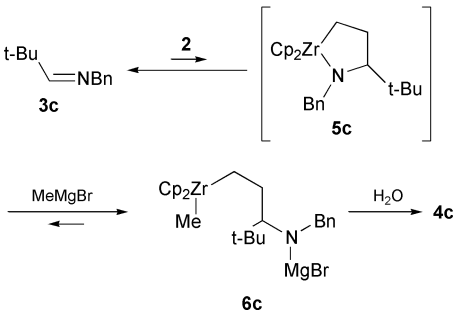

(3)

We have developed several zirconium-catalyzed reactions, in which a zirconocene–olefin complex acts as the key catalytic species. In the light of our previous work, a plausible mechanism for this catalytic addition of EtMgBr to imines is shown in Scheme 1, which involves: (1) generation of zirconocene–ethylene complex **2** from Cp_2ZrCl_2 and two eq. of EtMgBr; (2) coupling with imine **3** to form azazirconacyclopentane **5**; (3) ring-opening reaction by EtMgBr; and (4) β-elimination to regenerate zirconocene–ethylene complex **2** and to release metalated amine **9**.[7] The ring-opening reaction occurred exclusively on the Zr–N bond, because no deuterium incorporation was found in the Et group of products **4** in the catalytic reaction when the reaction mixture was quenched with MeOD. As expected, this catalytic reaction did not proceed with MeMgBr. When higher magnesium alkyls, namely, n-PrMgBr and n-BuMgCl, were used, the formation of addition products was not observed from the reaction with imine **3a**, indicating no coupling reaction between the zirconocene-substituted olefin complex and the imine.

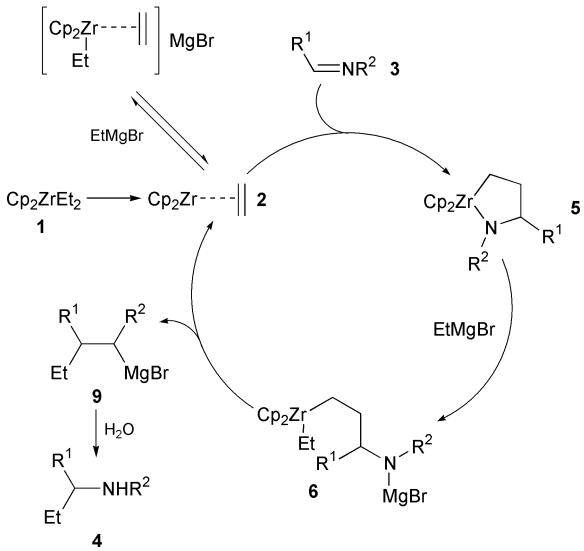

Scheme 1

Notes and references

1 T. Takahashi, T. Seki, Y. Nitto and M. Saburi, *37th Symposium on Organometallic Chemistry, Japan*, Osaka, 1990, 172; T. Takahashi, T. Seki, M. Saburi and E. Negishi, *XIVth International Conference on Organometallic Chemistry*, Detroit, MI, 1990, B17; T. Takahashi, T. Seki, Y. Nitto, M. Saburi, C. J. Rousset and E. Negishi, *J. Am. Chem. Soc.*, 1991, **113**, 6266.

2 T. Takahashi, N. Suzuki, M. Hasegawa, Y. Nitto, M. Kageyama and M. Saburi, *38th Symposium on Organometallic Chemistry, Japan*, Kyoto, 1991, 232. See also T. Takahashi, N. Suzuki, M. Kageyama, Y. Nitto, M. Saburi and E. Negishi, *Chem. Lett.*, 1991, 1579. For the structure of zirconium–olefin ate complex, see H. Lee, T. Hascall, P. J. Desrosiers and G. Parkin, *J. Am. Chem. Soc.*, 1998, **120**, 5830.

3 For related catalytic reactions involving zirconocene, see also K. S. Knight and R. M. Waymouth, *J. Am. Chem. Soc.*, 1991, **113**, 6268; A. H. Hoveyda and Z. Xu, *J. Am. Chem. Soc.*, 1991, **113**, 5079; D. P. Lewis, P. M. Muller and R. J. Whitby, *Tetrahedron Lett.*, 1991, **32**, 6797.

4 U. M. Dzhemilev, O. S. Vostrikova and R. M. Sultanov, *Izv. Akad. Nauk SSSR, Ser. Khim.*, 1983, 218; U. M. Dzhemilev and O. S. Vostrikova, *J. Organomet. Chem.*, 1985, **285**, 43.

5 K. Kasai, M. Kotora, N. Suzuki and T. Takahashi, *J. Chem. Soc., Chem. Commun.*, 1995, 109.

6 T. Takahashi, M. Kotora and Z. Xi, *J. Chem. Soc., Chem. Commun.*, 1995, 1503.

7 Y. Zhang, J. Jiang and Y. Chen, *Tetrahedron Lett.*, 1987, **28**, 3815.

The allylic oxidation of unsaturated steroids by *tert*-butyl hydroperoxide using homogeneous and heterogeneous cobalt acetate†

Jorge A. R. Salvador and James H. Clark

Clean Technology Centre, Chemistry Department, University of York, York, UK YO10 5DD

Received (in Liverpool, UK) 8th September 2000, Accepted 14th November 2000
First published as an Advance Article on the web 11th December 2000

Cobalt acetate is an effective catalyst for the selective allylic oxidation of unsaturated steroids using *tert*-butyl hydroperoxide especially when used in a supported form when it can be easily recovered and reused.

Allylic oxidation is a reaction of fundamental importance in organic chemistry with applications in areas ranging from agricultural products to pharmaceuticals.[1,2]

The allylic oxidation of unsaturated steroids such as Δ^5-steroids has traditionally been carried out with chromium reagents such as CrO_3–pyridine complex,[3] chromium trioxide and 3,5-dimethylpyrazole,[4] pyridinium chlorochromate, (PCC),[5,6] pyridinium dichromate (PDC),[6] sodium chromate,[7] sodium dichromate in acetic acid[8] and pyridinium fluorochromate.[9] However the large excess of reagent used in these procedures along with a difficult work-up and production of environmentally hazardous chromium residues, makes these reactions increasingly unacceptable on a commercial scale. Of greater preparative interest has been the use of hydroperoxides combined with different types of catalysts.[10–17] Despite the good yields reported with CrO_3,[10] hexacarbonylchromium $Cr(CO)_6$,[11,12] pyridinium dichromate[13] and $RuCl_3$[14] to prepare allylic oxidation products from Δ^5-steroids, the toxicity of the chromium compounds and the high cost of the ruthenium catalyst renders the procedures unsuitable for commercialisation and led us to recently report the use of cuprous salts, CuBr, CuCl, CuI, and a cupric salt $CuCl_2$, as well as copper metal as catalysts for this type of reaction.[17]

Allylic oxidation of steroids, particularly at the 7-position, has attracted interest over many years. The Δ^5-steroids can be oxidised to 5-en-7-ones, which are known as inhibitors of sterol biosynthesis and have some use in cancer chemotherapy.[18] This has encouraged us to find new, more environmentally acceptable methods for this reaction. The heterogenisation of inorganic reagents and catalysts useful in organic reactions is a very important area in clean technology.[19] In this communication we report the use of cobalt acetate in homogeneous, ($Co(OAc)_2 \cdot 4H_2O$), and more importantly, heterogeneous forms (catalysts **1**, **2**, and **3** prepared as reported previously[20,21]) for this type of allylic oxidation reaction.

Using Δ^5-steroids **4**–**7** and **12** as substrates (Scheme 1) allylic oxidation products **8**–**11** and **13** were obtained in very high, isolated yields, 70–86% (Table 1). Apart from the reaction with substrate **6** which required benzene as solvent and a temperature of 70 °C all the reactions were performed in acetonitrile using a milder temperature of 50–55 °C. The best results were obtained using the supported catalyst **3** which may be a result of its greater organophilic character. No significant reaction occurs in the absence of catalyst or in the presence of the catalyst support only.

In a typical reaction to a solution of 17-oxoandrost-5-en-3β-yl acetate **4** (660.90 mg 2 mmol) in acetonitrile (12 ml) under nitrogen, catalyst **3** (60 mg, cobalt loading 0.41 mmol g^{-1}) and *tert*-butyl hydroperoxide (*ca.* 2.4 ml 12 mmol) were added. After 24 h under magnetic stirring at 50 °C, the catalyst was removed by filtration and the solution was poured into sodium sulphite solution (10% aq.) and extracted with diethyl ether. The extract was washed with aq. saturated solution of $NaHCO_3$, water, dried and evaporated to dryness to give 7,17-dioxoandrost-5-en-3β-yl acetate. These reactions are very selective compared to those carried out using $Fe(acac)_3$ as catalyst reported by Kimura *et al.*[15,16] $Mo(CO)_6$ has also been described as catalyst for this reaction, but this led to epoxidation of the cholesteryl acetate under similar oxidative conditions.[16]

$Co(OAc)_2/SiO_2$

catalyst **1**

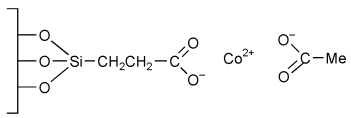

catalyst **2**

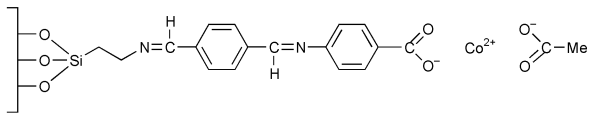

catalyst **3**

While the product yields of the allylic oxidations are very similar under homogeneous and heterogeneous conditions, the easier recovery of the catalyst in the heterogeneous reactions make these more environmentally friendly processes. Furthermore using the heterogeneous catalysts **2** and **3** it was possible to reuse the catalyst with only a small reduction in the product yields, under similar experimental conditions (80% for recycled catalyst **2** and 81% for recycled catalyst **3**, Table 1). Our catalytic method is also effective for other unsaturated steroids. Thus the Δ^4-steroid **14** gives the testosterone acetate **15**, in a yield of 70% (Scheme 2). Furthermore, the method is also effective in the presence of an oxidatively vulnerable secondary alcohol group. The steroid **16** is oxidised to the alcohol product **17** with impressive selectivity (71%) (Scheme 2).

In summary we have discovered a new efficient and relatively environmentally friendly method for the preparation

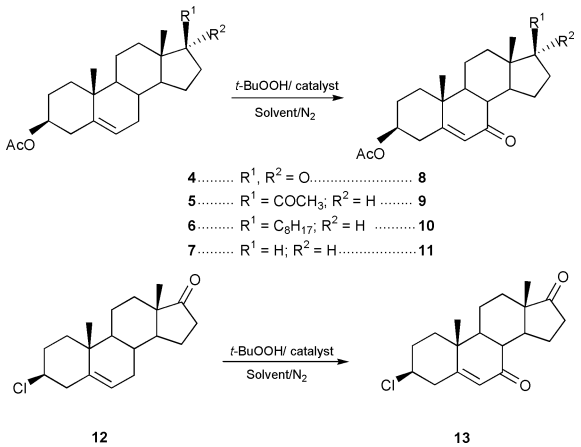

Scheme 1

† UK Patent applied for.

DOI: 10.1039/b007447k

Table 1 Allylic oxidation of unsaturated steroids

Substrate/ mmol	*t*-BuOOH[a]/ml	Catalyst/mmol Co	Solvent	Time/h	Temp./°C	Prod.	Isolated yield (%)
4/1	1.2	$Co(OAc)_2 \cdot 4H_2O$/0.012	CH_3CN	20	50	**8**	84[b]
5/2	2.4	$Co(OAc)_2 \cdot 4H_2O$/0.024	CH_3CN	24	50	**9**	86
4/1	1.2	**1**/0.01	CH_3CN	18	50	**8**	85
4/1	1.2	**2**/0.009	CH_3CN	20	50	**8**	84
4/1	1.2	**2**/(recycled, 0.008)	CH_3CN	20	50	**8**	80
4/1	1.2	**1**/ 0.005	CH_3CN	24	50	**8**	40[c]
6/1	1.2	**2**/0.022	Benzene	48	70	**10**	70[c]
4/1	1.2	**3**/0.016	CH_3CN	20	55	**8**	85
4/1	1.2	**3**/ (recycled, 0.014)	CH_3CN	20	55	**8**	81[b]
4/2	2.4	**3**/0.0025	CH_3CN	24	55	**8**	86
5/2	2.4	**3**/0.0025	CH_3CN	20	50	**9**	82[b]
7/1	1.2	**3**/ 0.007	CH_3CN	24	55	**11**	72[c]
12/0.65	0.8	**3**/0.016	CH_3CN	20	55	**13**	73[c]
14/0.63	0.8	**3**/0.006	CH_3CN	3	55	**15**	70[c]
16/1	1.2	**3**/0.016	CH_3CN	24	55	**17**	71[d]

[a] 5.0-6.0 M solution in decane (Aldrich). [b] Traces of starting material and a by-product are visible by TLC but not detectable in the ^{1}H-NMR spectra (500 MHz) of the crude product. [c] Recovered by flash chromatography (ethyl acetate–petroleum ether 40–60 °C). [d] Calculated on the basis of the ^{1}H-NMR signal (6H) of the crude product.

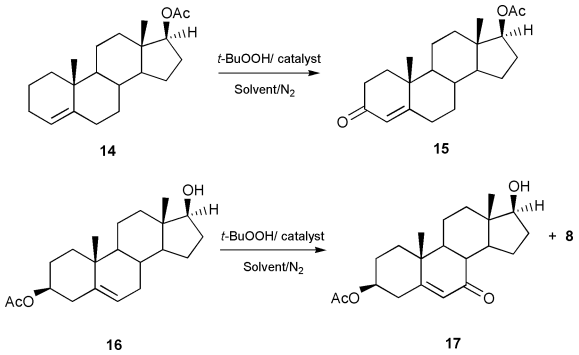

Scheme 2

of Δ^5-7-oxo-steroid and Δ^4-3-oxo-steroid from easily available steroid substrates using *t*-BuOOH as the oxidant and supported Co(II) as an easily recoverable and reusable catalyst. A study of the effects of different oxidants and other types of heterogeneous catalyst on this and related reactions is presently under investigation.

We wish to thank the RAEng-EPSRC for a Clean Technology Fellowship (to J. H. C.) and the Universidade de Coimbra for financial support (to J. A. R. S.).

Notes and references

1 J. Muzart, *Bull. Soc. Chim. Fr.*, 1986, **65**, 2.
2 P. C. Bulman Page and T. J. Mccarthy, in *Comprehensive Organic Synthesis*, ed. B. M. Trost and I. Flemming, 1 Pergamon Press, Oxford, New York, Seoul, Tokyo, 1991, vol. 7, p. 83.
3 G. W. Dauben, M. Lorber and D. S. Fullerton, *J. Org. Chem.*, 1969, **34**, 3587; D. S. Fullerton and C. M. Chen, *Synth. Commun.*, 1976, **6**, 217.
4 W. G. Salmond, M. A. Barta and J. L. Havens, *J. Org. Chem.*, 1978, **43**, 2057.
5 E. J. Parish, S. Chitrakorn and T.-Y. Wei, *Synth. Commun.*, 1986, **16**, 1371.
6 E. J. Parish and T.-Y. Wei, *Synth. Commun.*, 1987, **17**, 1227.
7 C. W. Marshall, R. E. Ray, I. Laos and B. Reigel, *J. Am. Chem. Soc.*, 1957, **79**, 6308.
8 A. Amann, G. Ourisson and B. Luu, *Synthesis*, 1987, 1002.
9 E. J. Parish, H. Sun and S. A. Kizito, *J. Chem. Res.*, 1996, 544.
10 J. Muzart, *Tetrahedron. Lett.*, 1987, **28**, 4665.
11 A. J. Pearson, Y. S. Chen, Y. S. Hsu and T. Ray, *Tetrahedron Lett.*, 1984, **25**, 1235.
12 A. J. Pearson, Y. S. Chen, G. R. Hang, S. Y. Hsu and T. Ray, *J. Chem. Soc., Perkin Trans. 1*, 1985, 267.
13 N. Chidambaram and S. Chandrasekaran, *J. Org. Chem.*, 1987, **52**, 5048.
14 R. A. Miller, W. Li and G. R. Humprey, *Tetrahedron Lett.*, 1996, **37**, 3429.
15 M. Kimura and T. Muto, *Chem. Pharm. Bull.*, 1979, **27**, 109.
16 M. Kimura and T. Muto, *Chem. Phar. Bull.*, 1980, **28**, 1836.
17 J. A. R. Salvador, M. L. Sá e Melo and A. S. Campos Neves, *Tetrahedron Lett.*, 1997, **38**, 119.
18 Y. Sato, Y. Sonoda, M. Morisaki and N. Ikekawa, *Chem. Pharm. Bull.*, 1984, **32**, 3305; K. P. Cheng, H. Nagana, L. Bang and G. Ourisson, *J. Chem. Res. (S)*, 1997, 217; H. Nagana, J. P. Poyser, K. P. Cheng, L. Bang and G. Ourisson, *J. Chem. Res. (S)*, 1997, 218; V. Kumar, A. Alain, G. Ourisson and B. Luu, *Synth. Commun.*, 1987, **17**, 1279.
19 J. H. Clark, *Catalysis of Organic Reactions using Supported Inorganic Reagents*, VCH, New York, 1994; *Chemistry of Waste Minimisation*, ed. J. H. Clark, Chapman and Hall, London, 1995.
20 A. J. Butterworth, J. H. Clark, P. H. Walton and S. J. Barlow, *Chem. Commun.*, 1996, 1859.
21 J. Chisem, I. C. Chisem, J. S. Rafelt, D. J. Macquarrie and J. H. Clark, *Chem. Commun.*, 1997, 2203.

Ellagitannin biosynthesis: oxidation of pentagalloylglucose to tellimagrandin II by an enzyme from *Tellima grandiflora* leaves

Ruth Niemetz,[a] Gerhard Schilling[b] and Georg G. Gross*[a]

[a] *Molekulare Botanik, Universität Ulm, 89069 Ulm, Germany. E-mail: ruth.niemetz@biologie.uni-ulm.de; georg.gross@biologie.uni-ulm.de*

[b] *Universität Heidelberg, Organisch-Chemisches Institut, Im Neuenheimer Feld 270, D-69120 Heidelberg, Germany. E-mail: gerhard.schilling@urz.uni-heidelberg.de*

Received (in Liverpool, UK) 28th July 2000, Accepted 15th November 2000
First published as an Advance Article on the web 11th December 2000

First evidence of the *in vitro* oxidation of 1,2,3,4,6-penta-galloylglucose to the ellagitannins, tellimagrandin II and 1,4,6-tri-*O*-galloyl-2,3-*O*-hexahydroxydiphenoyl-β-D-glucose, has been obtained with a partially purified enzyme from leaves of *Tellima grandiflora* (fringe cups, Saxifragaceae).

It was already recognized in the mid 1950's that ellagitannins, a widespread subclass of hydrolyzable plant tannins, were characterized by 3,4,5,3′,4′,5′-hexahydroxydiphenic (HHDP) acid residues (**5**) that occur in Nature in the form of various glucose esters and which, after hydrolytic release, spontaneously rearranged to the dilactone, ellagic acid (**6**). It was discussed very early on that the biogenesis of such ellagitannins in plants should originate from 1,2,3,4,6-penta-*O*-galloyl-β-D-glucose (**1**) as the principal precursor,[1] a view that was corroborated and refined later by Haslam and coworkers. It was proposed by these authors that the energetically preferred $^4C_1$ conformer of **1** was sequentially oxidized to tellimagrandin II (**2**) and casuarictin (**3**).[2,3] The recently recognized role of ellagitannins as promising chemotherapeutic agents[4,5] has stimulated remarkable success in the challenge of chemically synthesizing such compounds.[6,7] The biosynthesis of ellagitannins, in contrast, still remained completely obscure. The present situation was illustrated in a recent review article[8] with the statement that 'the *in vitro* biaryl coupling of **1** has yet to be achieved by an isolated enzyme.' In several attempts to elucidate the mechanism of such a transition with the enzyme systems laccase/O_2 or peroxidase/H_2O_2[9] only free ellagic acid (**6**) had been detected, while the formation of true ellagitannins, characterized by glucose-bound HHDP residues, has never been achieved.

We concluded that inadequate analytical techniques represented the decisive obstacle in such investigations, which suffered from minimal enzyme reaction rates yielding numerous structurally closely related reaction products and unspecific by-products, and particularly from the inherent risk of contamination with *in vivo* formed ellagitannins that had been transferred into the enzyme assays by complexation with proteins. Such problems are eliminated by using radioactively labeled compounds, a technique that dramatically increases both the sensitivity and specificity of test systems. We therefore produced [*U*-^{14}C]pentagalloylglucose by photoassimilation of $^{14}CO_2$ in leaves of the gallotannin synthesizing plant *Rhus typhina* (staghorn sumac) in >99% purity.[10] This compound was used as standard substrate in an extended screening program for enzymes that formed reaction products liberating [^{14}C]ellagic acid (**6**) upon hydrolysis, thus providing a general probe for the *in vitro* synthesis of ellagitannins of widely differing structures.

By this strategy we were able to discover a novel soluble enzyme in leaves of *Tellima grandiflora* (Pursh) Lindley (fringe cups, Saxifragaceae), a weed that is known as a rich source of ellagitannins. The partially purified protein[11] was found to catalyze the conversion of [*U*-^{14}C]pentagalloylglucose to several radioactively labeled products, while no reaction occurred in the presence of denatured enzyme (Fig. 1). The most prominent peak among these compounds coincided with authentic tellimagrandin II (**2**) in two different HPLC systems with acetonitrile and MeOH gradients, respectively. This fraction was isolated and hydrolyzed (4 M HCl, 100 °C, 4 h) to afford glucose, gallic acid and ellagic acid (**6**) as sole ^{14}C-labeled degradation products as determined by HPLC and liquid-scintillation counting of the eluates, thus indicating the *in vitro* synthesis of a true ellagitannin.

Under the conditions given in Fig. 1, the enzyme reaction proceeded linearly for 30 min and had pH and temperature optima at pH 5 and 45 °C, respectively. Normal Michaelis–

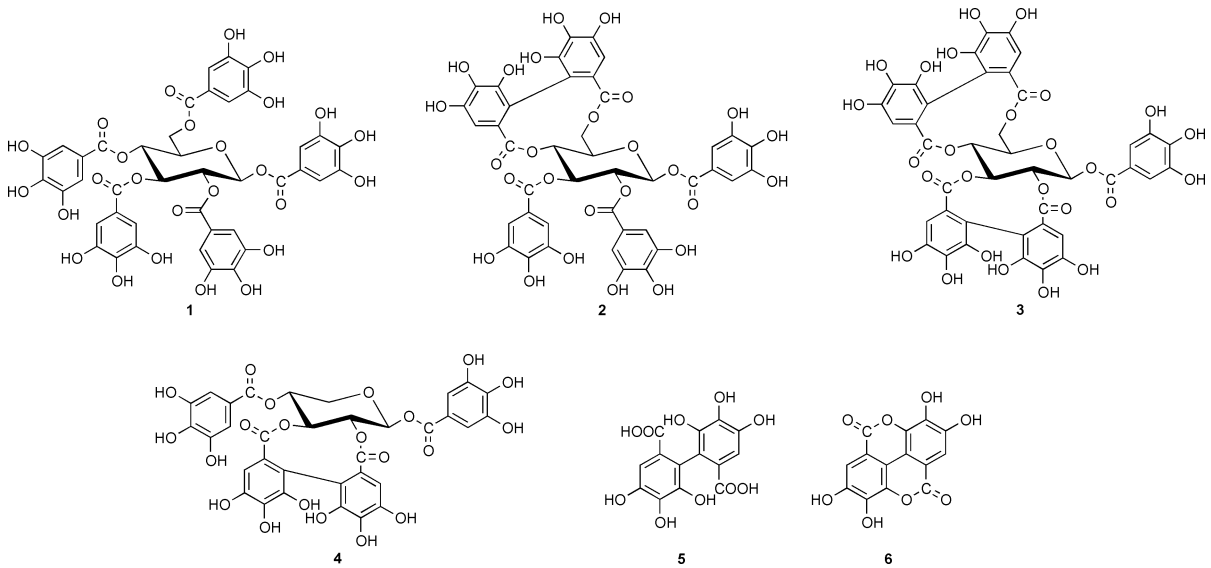

DOI: 10.1039/b006270g

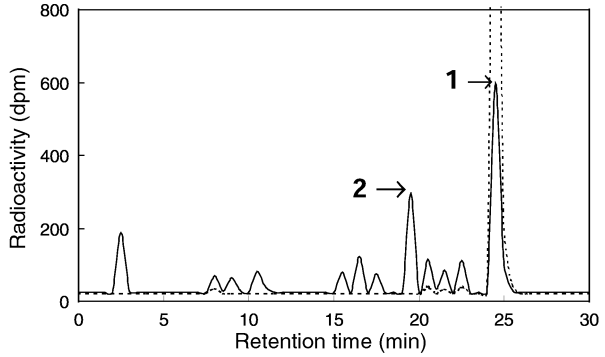

Fig. 1 RP-18 HPLC analysis of *in vitro* formed oxidation products of [^{14}C]pentagalloylglucose with an enzyme from *Tellima grandiflora* leaves. Assay mixtures, containing 12.5 μg (2,500 dpm) **1** and enzyme (4 pkat) in 50 μl HEPES buffer (50 mM, pH 5.0), were incubated at 30 °C for 60 min, stopped by heat-denaturing of enzyme, and analyzed by RP-18 HPLC. (—), Enzyme assay; (···), blank with acid-denatured enzyme. (**1**), Pentagalloylglucose; (**2**) tellimagrandin II. HPLC conditions: Reprosil NE, 5 μm, 250 × 4 mm i.d.; solvent A = 0.05% aq. H_3PO_4, B = 0.05% H_3PO_4, in MeOH; gradient 0–1 min 10% B, 1–3 min 10–30% B, 3–20 min 30–40% B, 20–40 min 40% B; flow rate 0.7 ml min^{-1}. Radioactivity was determined by fractionation of eluates and subsequent liquid-scintillation counting.

Menten kinetics were observed for the substrate, pentagalloylglucose (**1**), up to a maximal concentration of 320 μM, while increasing substrate inhibition occurred above this value. Replots of this data according to Lineweaver-Burk revealed a K_m value of 110 μM (V_{max} = 33 pkat [0.12 μmol h^{-1}]).

For the unequivocal determination of the structure of the reaction product, 100 mg of unlabeled pentagalloylglucose (**1**), chemically synthesized from triacetylgalloylchloride and β-D-glucose[12]) was incubated in a scaled-up enzyme assay, affording 1.7 mg pure reaction product of > 93% purity after semi-preparative HPLC.[13] Negative FAB-MS of this substance revealed prominent peaks for the deprotonated molecular ion $[M - H]^-$ at *m/z* 937 (tellimagrandin II **2**, M_r 938) and *m/z* 635 (trigalloylglucose, M_r 636).[14] Proton NMR spectroscopy (500 MHz) displayed signals that corresponded to those of an authentic sample of tellimagrandin II (**2**). In particular, three characteristic singlets at δ ppm (TMS) 6.91 (2H), 6.94 (2H) and 7.05 (2H) were detected in d_4-MeOH that corresponded to the aryl-2,6 hydrogens at C-1, C-2 and C-3 of **2**, respectively, while the singlets at δ 6.47 (1H) and 6.60 (1H) were due to the 2,2′-hydrogens of diphenic acid (**5**) bound at C-4,6. Also the chemical shifts for the glucose moiety were in full agreement with those of authentic **2**.

The reaction product displayed, however, strong additional singlets at 6.61 (1H) and 6.63 (1H) ppm that apparently were due to a different compound with a C-2,3 linked HHDP unit, as concluded by comparison with ^{1}H NMR data from authentic samples of 2,3-*O*-hexahydroxydiphenoylglucose, casuarictin (**3**) and pedunculagin (structure as **3**, but with a free anomeric OH-group at C-1). Evidently, the enzyme preparation had catalyzed the simultaneous synthesis of both tellimagrandin II (**2**) and isomeric 1,4,6-tri-*O*-galloyl-2,3-*O*-hexahydroxydiphenoyl-β-D-glucose (**4**) that had not been separated by RP-HPLC. This latter, unusual ellagitannin is not known as a natural product; it has been recently obtained, however, by total synthesis in two enantiomerically pure forms, mahtabin A and pterocarinin C, characterized by 2,3-*R*- and *S*-HHDP residues, respectively.[15,16] (An earlier report proposing this structure for a compound named cercidinin A from *Cercidiphyllum japonicum*[17] has been questioned by these authors.) Detection of such a compound raises questions about the specificity of the enzyme(s) catalyzing such transformations that prompt considerations on the eventual cooperation of product-specificity guiding enzymes, analogous to the recently reported 'dirigent' protein involved in lignan biosynthesis.[18]

In summary, first evidence has been provided by our results that the long sought clue to unravel the old enigma of ellagitannin biosynthesis is now available.

We thank Angelika Müller (Ulm) for excellent technical assistence, Dr G. Schmidtberg (Ulm) for MS analyses, and Dr A. Scalbert (Clermont-Ferrand, France) and Professor T. Yoshida (Okayama, Japan) for reference samples of ellagitannins. Financial support from the Deutsche Forschungsgemeinschaft (Bonn), the Fonds der Chemischen Industrie (Frankfurt/M) and from research grants of the University of Ulm is gratefully acknowledged.

Notes and references

1 O. Th. Schmidt and W. Mayer, *Angew. Chem.*, 1956, **68**, 103.
2 R. K. Gupta, S. M. K. Al-Shafi, K. Layden and E. Haslam, *J. Chem. Soc., Perkin Trans. 1*, 1982, 2525.
3 E. A. Haddock, R. K. Gupta, S. M. K Al-Shafi, K. Layden, E. Haslam and D. Magnolato, *Phytochemistry*, 1982, **21**, 1049.
4 K. S. Feldman, K. Sahasrabudhe, R. S. Smith and W. J. Scheuchenzuber, *Bioorg. Med. Chem. Lett.*, 1999, **9**, 985.
5 M. N. Clifford and A. Scalbert, *J. Sci. Food Agric.*, 2000, **80**, 1118.
6 K. S. Feldman, K. Sahasrabudhe, S. Quideau, K. L. Hunter and M. D. Lawlor, in *Plant Polyphenols 2. Chemistry, Biology, Pharmacology, Ecology*, G. G. Gross, R. W. Hemingway and T. Higuchi, eds., Kluwer Academic/Plenum Publishers, New York, 1999, p. 101.
7 K. S. Feldman and K. Sahasrabudhe, *J. Org. Chem.*, 1999, **64**, 209.
8 R. F. Helm, L. Zhentian, T. Ranatunga, J. Jervis and T. Elder, in *Plant Polyphenols 2. Chemistry, Biology, Pharmacology, Ecology*, G. G. Gross, R. W. Hemingway and T. Higuchi, eds., Kluwer Academic/Plenum Publishers, New York, 1999, p. 83.
9 G. G. Gross, in *Comprehensive Natural Products Chemistry. Vol. 3. Carbohydrates and Their Derivatives Including Tannins, Cellulose, and Related Lignins*, B. M. Pinto, ed., Elsevier, Amsterdam, 1999, p. 799.
10 H. Rausch and G. G. Gross, *Z. Naturforsch. C: Biosci.*, 1996, **51**, 473.
11 Fresh leaves (80 g) of *Tellima grandiflora* were homogenized in liquid N_2, extracted with 250 ml Tris-HCl (1.5 M, pH 8.0)–Na borate (0.2 M, pH 7.5) (1:1, by vol.) and centrifuged (30 000 × g, 30 min). The supernatant was depleted of phenolics by stirring with Amberlite XAD (20 min), filtered and fractionated with $(NH_4)_2SO_4$. The 30–80% pellet was resuspended in HEPES buffer (50 mM, pH 6.0), desalted, concentrated by ultrafiltration and chromatographed on a Sephacryl S-300 (Pharmacia Biotech) column (40 × 2.4 cm i.d.) in HEPES buffer.
12 G. G. Gross, *Z. Naturforsch. C: Biosci.*, 1983, **38**, 519
13 The reaction mixture (400 ml vol., pH 5, containing 100 mg **1** and 850 mg protein) was incubated for 60 min at 30 °C. After stopping the reaction by heat-denaturing the enzyme, the mixture was extracted with EtOAc. The contents of the dried organic phase were subjected to semi-preparative RP-18 HPLC on Kromasil (5μ, 250 × 20 mm i.d.; gradient: solvent A = 0.05% aq. H_3PO_4, B = acetonitrile; 0–1 min 5% B, 1–2 min 5–18% B, then isocratic at 18% B; flow rate 22 ml min^{-1}). Relevant fractions were immediately neutralized, depleted of organic solvent *in vacuo*, extracted with EtOAc and rechromatographed twice by RP-18 HPLC on Reprosil NE (5 μm, 250 × 8 mm i.d.; solvents and gradient as in Fig. 1; flow rate 2.4 ml min^{-1}). The purified product was neutralized, depleted of MeOH and applied to a column of Sephadex LH-20 (60 × 12 mm i.d., in water). After rinsing with water to remove H_3PO_4, the product was eluted with MeOH and lyophylized, affording 1.7 mg material of > 93% purity as determined by analytical HPLC under the conditions given in Fig. 1.
14 R. Isobe, T. Tanaka, G. Nonaka and I. Nishioka, *Chem. Pharm. Bull. (Tokyo)*, 1989, **37**, 1748.
15 K. Khanbabaee and K. Lötzerich, *Liebigs Ann.*, 1997, 1571.
16 K. Khanbabaee and K. Lötzerich, *J. Org. Chem.*, 1998, **73**, 8723.
17 G. Nonaka, M. Ishimatsu, M. Ageta and I. Nishioka, *Chem. Pharm. Bull. (Tokyo)*,1989, **37**, 50.
18 L. B. Davin, H. B. Wang, A. L. Crowell, D. L. Bedgar, D. M. Martin, S. Sarkanen and N. G. Lewis, *Science*, 1997, **275**, 362.

Olefin metathesis in non-degassed solvent using a recyclable, polymer supported alkylideneruthenium†

James Dowden* and Jelena Savović

Wolfson Laboratory of Medicinal Chemistry, Department of Pharmacy and Pharmacology, University of Bath, Claverton Down, Bath, UK BA2 7AY. E-mail: J.Dowden@bath.ac.uk

Received (in Liverpool, UK) 6th September 2000, Accepted 16th November 2000
First published as an Advance Article on the web 11th December 2000

Polystyrene-supported ruthenium complex 8 is a robust pro-catalyst for olefin metathesis that can be used in non-degassed solvents and recycled without added stabilisers.

Recent enthusiastic interest in olefin metathesis has been fuelled by the development of well-defined transition metal catalysts.[1] These catalysts have found wide application because they provide facile alkene exchange, often late in a synthetic sequence.[2] Grubb's alkylideneruthenium **1**[3] is particularly

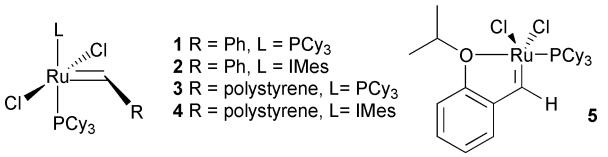

popular because it is easy to handle. Undesirable features of these systems are that they are not amenable to recycling and that they give rise to high levels of ruthenium contamination. Recent work has sought to address these problems.[4–7] Hoveyda and co-workers established **5**[6,7] as a remarkably robust complex that was stable to silica gel chromatography using non-degassed eluent and could therefore be recovered and recycled. Recently, Barrett's group reported a 'boomerang' system **3**[8] for sequestering the catalytic species onto vinyl polystyrene. Indeed **3** could be reused, as long as an alkyl alkene additive was added to intercept the unstable catalytic methylidene carbene ($Cl_2(PCy_3)_2Ru{=}CH_2$).[8] Complex **2** can be transferred to vinyl polystyrene in the same way, with corresponding benefits.[9]

We are interested in developing a robust immobilised catalyst for olefin metathesis that can be readily modified to operate in a range of solvent environments. The ability to utilise non-degassed solvent offers practical simplicity and could widen the scope of this reaction. The reported stability of **5** was attractive and we reasoned that a suitably modified version could be attached to a range of polymer supports. In this communication, we describe initial studies leading to a recyclable, polystyrene-supported analogue of complex **5** that promotes olefin metathesis in non-degassed solvents.

We envisaged that the isopropyl portion of the phenol ether could be extended to accommodate some functional handle that would allow attachment to any chosen support (Scheme 1). Thus, opening of racemic δ-hexanolactone **6** with sodium methoxide,[11] subsequent Mitsunobu reaction with 2-vinylphenol[12] and saponification provided **7**. Treating the pendant acid of **7** with aminomethyl polystyrene under standard conditions afforded the polystyrene supported ligand. Direct formation of the alkylideneruthenium[7] would be expected to be more efficient but we reasoned that reaction of styrene **7** with **1** would generate **8** more simply and in sufficient quantities to permit our initial study. One disadvantage of this approach is that the accumulation of free phosphine effectively inhibits olefin metathesis.[10] This is reflected in the fact that treatment of resin **7** with stoichiometric Grubb's complex afforded loadings of only 0.12 mmol g^{-1} (as determined by phosphorus analysis), while treating the resin with five successive portions of 10 mol% of **1** essentially doubled the loading to 0.20 mmol g^{-1}. Simple filtration and washing of the resin gave **8** as dark brown beads that could be dried, stored in air and used more than a month later with no apparent decrease in activity. In all cases no colour change, or corresponding decomposition was observed during the loading of the catalyst[8] even after extended reaction times.

Polymer-supported complex **8** was then tested for activity using representative diene substrates for ring closing metathesis (Table 1). It is notable that the rates of reaction were somewhat slower than those reported using homogenous Grubb's alkylidene **1**, so that reaction of benchmark substrates such as diethyl diallylmalonate (entry 2) was only 42% complete after 90 min. All of these reactions however, provided good to quantitative yield of product within 5 h. Preparative scale transformation (153 mg, 5 mol%, 4 h) of benzyl *N*,*N*-diallylcarbamate (entry 1) gave isolated product in 91% yield after chromatography.

The easy manipulation of **8** is noteworthy. In each case, general laboratory grade dichloromethane (DCM) was used *without* degassing, in an air atmosphere, so that substrates were simply dissolved and added to the resin in a plastic solid phase organic synthesis tube fitted with a glass frit. The tube was then sealed and subjected to agitation by 360° rotation at rt. Filtration and washing with DCM afforded the product and the remaining resin used for further transformations.

Recycling of **8** was tested by treatment of the same batch of resin with equal, successive portions of benzyl *N*,*N*-diallylcarbamate, without addition of stabilising alkene (Table 2).[8] Indeed **8** proved to be remarkably robust providing good yields over five successive runs at 5 mol% catalyst. In subsequent runs yields declined steadily and the beads turned from dark brown to black.

We have also demonstrated the ability of **8** to perform cross metathesis. Heating a two-fold excess of (*Z*)-1,4-diacetoxybut-2-ene[13] with 4-allylanisole and **8** in DCM under reflux for 9 h furnished the cross-coupled product (33%) along with the anisole homodimer (18%). The recovered resin retained its brown colouration, rather than turning black. Subsequent ring

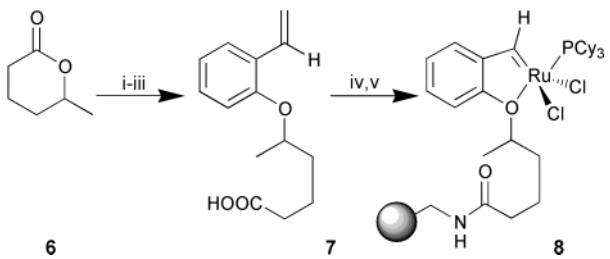

Scheme 1 *Reagents and conditions*: i, sodium methoxide, MeOH, 0 °C to rt, 6 h, 95%; ii, 2-vinylphenol, diisopropyl azodicarboxylate, PPh_3, THF, 0 °C to rt, 14 h, 64%; iii, 1 M NaOH, dioxane, rt, 12 h, 88%; iv, polystyrene-NH_2, DIC, HOBt, CH_2Cl_2–DMF (1 : 1), rt, 12 h; v, $Cl_2(PCy_3)_2Ru{=}CHPh$, DCE, rt, 12 h.

† Electronic supplementary information (ESI) available: experimental details. See http://www.rsc.org/suppdata/cc/b0/b007304k/

DOI: 10.1039/b007304k

closing metathesis of benzyl *N*,*N*-diallylcarbamate using this resin afforded the cyclised product in 85% yield over 90 min, confirming the retention of catalytic activity.

Olefin metathesis using **1** is typically performed in degassed solvent, for example, previous studies of **5** were performed in argon-saturated solvent and atmosphere (only chromatography using non-degassed solvent was reported).[7] We believe that this communication is notable because studies involving non-degassed solvent have not been widely reported. We also found, however, that for reactions corresponding to entries 1 and 5 using non-recyclable complex **1** in non-degassed DCM proceeded in good yield and draw attention to recent discussion relating to the oxidative decomposition of alkylideneruthenium.[14] In the case of Barrett's boomerang system **3** however, it is necessary to add 10 mol% hex-1-ene to prevent decomposition.[8] It is therefore interesting that **8** promotes olefin metathesis for up to five cycles, without added stabiliser.

Table 1 Olefin metathesis using polymer supported complex **8**[a]

Entry	Substrate[b]	Product[cd]
1	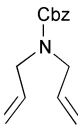	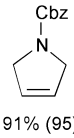 91% (95)
2		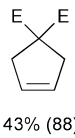 43% (88)[5]
3	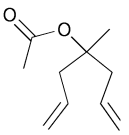	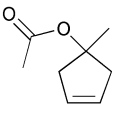 77% (>95)[8]
4	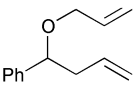	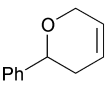 >95% (>95)[16]
5	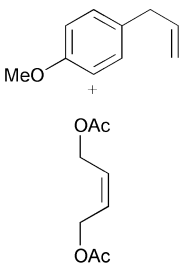	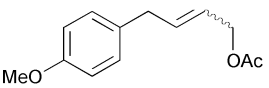 33%[e] 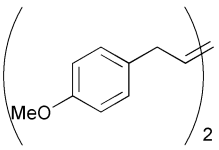 18%
6	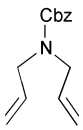	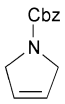 31%[f]

[a] All runs performed with 25 mg substrate and 25 mg of **8** (5 mol%) in non-degassed CH_2Cl_2 for 90 min. [b] E = CO_2Et. [c] Relative integration of ^1H NMR. [d] Conversion after 5 h in parentheses. [e] 9 h at reflux. [f] Methanol, rt, TentaGel-**8** 6 h.

Table 2 Recycling of **8** for the RCM of benzyl *N*,*N*-diallylcarbamate[a]

Conversion[b]						
1	**2**	**3**	**4**	**5**	**6**	**7**
91[c]	81	68	67	63	46	40
81[d]	69	68	33	21	11	—

[a] All runs performed in non-degassed CH_2Cl_2 for 90 min. [b] Relative integration of ^1H NMR. [c] 5 mol% **8**. [d] 1.5 mol% **8**.

The ability to perform olefin metathesis in polar protic solvents is a desirable goal that has so far been addressed by the development of water-soluble phosphine ligands.[14,15] We therefore investigated the effect of a different polymer support on the solubility and catalytic activity of the complex. Thus, amine-functionalised TentaGel (0.3 mmol g^{-1}) was converted into TentaGel-**8** and in preliminary experiments we observed ring-closing metathesis in non-degassed MeOH, although there was significant variation between batches of resin. The best reaction proceeded in 31% yield after 6 h of reaction (entry 6) and the worst gave 18% after overnight reaction with double the quantity of resin (100 mg). The lower yield of this transformation presumably reflects the much lower loading offered by this TentaGel resin but does suggest that modification of the supporting polymer is a viable strategy.

In summary, we have reported a novel polymer supported pro-catalyst for olefin metathesis that is robust and easy to use. That **8** is stable to non-degassed solvents and can be recycled without the use of stabilising additives is notable and interesting. An attractive feature of the precursor **7** is that it can be attached to any solid support.

We are grateful to the University of Bath for a studentship (to J. S.) and to Professor B. V. L. Potter for helpful advice and encouragement.

Note added to proof: two notable papers have been published since the submission of this manuscript: (*a*) S. B. Garber, J. S. Kingsbury, B. L. Gray, A. H. Hoveyda, *J. Am. Chem. Soc.*, 2000, **122**, 8168; (*b*) Q. Yao, *Angew. Chem., Int. Ed.*, 2000, **39**, 3896.

Notes and references

1 For reviews see: (*a*) R. H. Grubbs and S. Chang, *Tetrahedron*, 1998, **54**, 4413; (*b*) S. K. Armstrong, *J. Chem. Soc., Perkin Trans. 1*, 1998, 371.
2 For examples: (*a*) R. Roy and S. K. Das, *Chem. Commun.*, 2000, 519; (*b*) M. J. Bassindale, A. S. Edwards, P. Hamley, H. Adams and J. P. A. Harrity, *Chem. Commun.*, 2000, 1035; (*c*) A. G. M. Barrett, S. D. Baugh, V. C. Gibson, M. R. Giles, E. L. Marshall and P. A. Procopiou, *Chem. Commun.*, 1997, 155; (*d*) S. E. Gibson, V. C. Gibson and S. P. Keen, *Chem. Commun.*, 1997, 1107.
3 P. Schwab, R. H. Grubbs and J. W. Ziller, *J. Am. Chem. Soc.*, 1996, **118**, 100.
4 L. A. Paquette, J. D. Schloss, I. Efremov, F. Fabris, F. Gallou, J. Mendez-Andino and J. Yang, *Org. Lett.*, 2000, **2**, 1259.
5 H. D. Maynard and R. H. Grubbs, *Tetrahedron Lett.*, 1999, **40**, 4137.
6 J. P. A. Harrity, D. S. La, D. R. Cefalo, M. S. Visser and A. H. Hoveyda, *J. Am. Chem. Soc.*, 1998, **120**, 2343.
7 J. S. Kingsbury, J. P. A. Harrity, P. J. Bonitatebus and A. H. Hoveyda, *J. Am. Chem. Soc.*, 1999, **121**, 791.
8 M. Ahmed, A. G. M. Barrett, D. C. Braddock, S. M. Cramp and P. A. Procopiou, *Tetrahedron Lett.*, 1999, **40**, 8657.
9 M. Ahmed, T. Arnauld, A. G. M. Barrett, D. C. Braddock and P. A. Procopiou, *Synlett*, 2000, 1007.
10 E. L. Dias, S. T. Nguyen and R. H. Grubbs, *J. Am. Chem. Soc.*, 1997, **119**, 3887.
11 A. S. Hernandez, A. Thaler, J. Castells and H. Rapoport, *J. Org. Chem.*, 1996, **61**, 314.
12 S. L. Tsaur and R. M. Fitch, *J. Colloid Interface Sci.*, 1987, **115**, 450.
13 D. J. O'Leary, H. E. Blackwell, R. A. Washenfelder and R. H. Grubbs, *Tetrahedron Lett.*, 1998, **39**, 7427.
14 D. M. Lynn, B. Mohr, R. H. Grubbs, L. M. Henling and M. W. Day, *J. Am. Chem. Soc.*, 2000, **122**, 6601.
15 T. A. Kirkland, D. M. Lynn and R. H. Grubbs, *J. Org. Chem.*, 1998, **63**, 9904.
16 Y. S. Shon and T. R. Lee, *Tetrahedron Lett.*, 1997, **38**, 1283.

$AlCl_3$/ICl-Mediated iodo-carbocyclization of α-iodo cycloalkanones: a new entry to spirocyclic ketones

Chin-Kang Sha,* Fong-Cheng Lee and Hsien-Hsun Lin

Department of Chemistry, National Tsing Hua University, Hsinchu 300, Taiwan, ROC.
E-mail: cksha@mx.nthu.edu.tw

Received (in Cambridge, UK) 9th October 2000, Accepted 20th November 2000
First published as an Advance Article on the web 11th December 2000

Treatment of α-iodo cycloalkanones bearing an acetylenic side chain with $AlCl_3$/ICl afforded spirocyclic ketones in good yields.

Spirocyclic systems are core skeletons of several important natural products, such as gloiosiphone A[1] and ginkgolide B.[2] They also constitute the main frameworks of spirocyclic chiral auxiliaries having a C_2 axis of symmetry.[3] During our work on radical cyclization of α-iodo ketones,[4] we became interested in developing a general method for synthesis of spirocyclic ketones from α-iodo ketones. We envisaged that iodo-carbocyclization of α-iodo ketones, as depicted in Scheme 1, could be exploited for annulation of five- and six-membered rings. Generation of enolate from α-iodo ketone **1** with simultaneous transfer of I^+ to the acetylenic moiety might be effected with a Lewis acid, $M(Ln)_x$, to give intermediate **2**. Subsequent cyclization of the intermediate **2** would afford spirocyclic ketone **3**. In the past decade, free-radical atom-transfer cyclization of iodo substrates mediated with hexabutylditin[5] or other reagents[6] has emerged as a routine method. Ionic iodo-carbocyclization of iodo malonates[7] and ionic seleno-carbocyclization of seleno ketones[8] have also been described. In this communication, we report results obtained from our investigation of iodo-carbocyclization of α-iodo ketones.

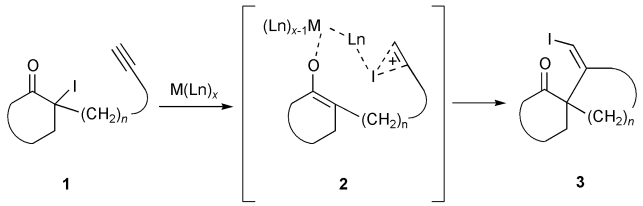

Scheme 1

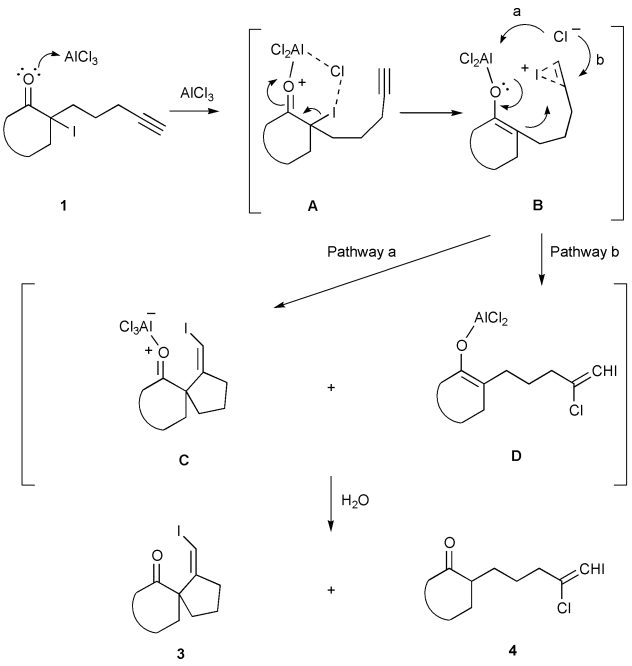

Scheme 2

We first sought appropriate Lewis acids that could effect formation of an enolate from α-iodo ketones. Many Lewis acids including $TiCl_4$, BCl_3, $AlMe_3$, Me_2AlCl, $SnCl_4$, $MgBr_2$ and $AlCl_3$ were examined. We found that $AlCl_3$, Me_2AlCl and $TiCl_4$ effect the desired transformation of **1** to **3** in dichloromethane, although in low yield (10–20%). A plausible mechanism is proposed for the reaction using $AlCl_3$ as catalyst, Scheme 2. $AlCl_3$ reacts with α-iodo ketone to generate an aluminium

Table 1 Ionic iodo-carbocyclization of α-lodo cycloalkanones

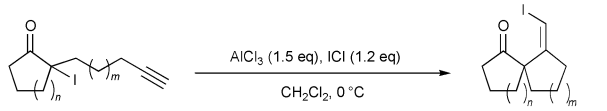

Entry	α-lodo Cycloalkanone	Reaction Time	Product[a]	Yield (%)
1	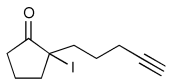 **5**	45 min	 **11**	83
2	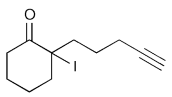 **6**	50 min	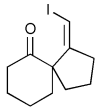 **12**	81
3	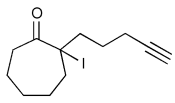 **7**	40 min	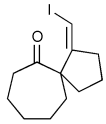 **13**	70
4	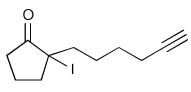 **8**	30 min	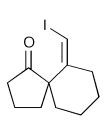	94
5	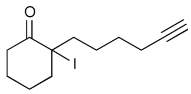 **9**	60 min	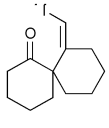 **15**	74
6	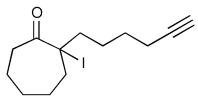 **10**	60 min	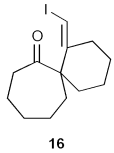 **16**	77

[a] The stereochemistry of the vinyliodide moiety in each product was tentatively assigned as *Z*.

enolate[9] and ICl. The acetylenic moiety on the side chain then complexes with ICl to give intermediate **B**. Cyclization of **B** (pathway a) would afford $AlCl_3$-complex **C**. In principle, $AlCl_3$ is catalytic and gets regenerated at this stage. Because it would complex with the product, one equiv. of $AlCl_3$ is needed. Upon aqueous work-up, complex **C** is hydrolyzed to spiro ketone **3**. According to this mechanism, ICl is generated in the first step and participates in the subsequent cyclization. Therefore, we felt that addition of ICl from an external source might facilitate cyclization. Indeed, we found that treatment of iodo ketones **5**–**10**[10] with a mixture of $AlCl_3$ (1.5 equiv.) and ICl (1.2 equiv.) in dichloromethane at 0 °C afforded spirocyclic products **11**–**16** in good yield.[11] The results are summarized in Table 1. Products **11**–**16** are all obtained as a single geometric isomer and are tentatively assigned to be *Z* isomers.[12] Presumably, the conformation of intermediate **B**, as depicted in Scheme 2, favors the formation of the exclusive *Z* isomers. Annulation of both five-membered rings (entries 1–3) and six-membered rings (entries 4–6) is achieved. In entries 1–3, by-product **4** is formed in trace amount ($< 5\%$) from direct addition of Cl^- to the iodonium moiety, pathway b in Scheme 2.[13] Since addition of an external source of ICl significantly enhances the yield of the carbocyclization process, an alternative mechanism involving enolate formation with simultaneous complexation of ICl to the acetylene unit is also possible.

In conclusion, we have demonstrated that an ionic iodo-carbocyclization of α-iodo cycloalkanones can be effected with Lewis acid, $AlCl_3$. Addition of ICl greatly enhances yields of spirocyclic ketones. In comparison with free-radical atom-transfer cyclization, the present method has two distinct advantages: (i) as tin reagents are not used, tedious separation of products from tin residues is avoided; (ii) whereas free-radical atom-transfer cyclization is only useful for synthesis of the five-membered ring, this method allows annulation of both five- and six-membered rings. Applications of this reaction for total synthesis of natural products are under investigation in our laboratory.

We thank the National Science Council of the Republic of China for financial support.

Notes and references

1 J. L. Chen, M. F. Moghaddam and W. H. Gerwick, *J. Nat. Prod.*, 1993, **56**, 1205.

2 N. Sakabe, S. Takada and K. Okabe, *J. Chem. Soc., Chem. Commun.*, 1967, 259; K. Okabe, K. Yamada, S. Yamamura and S. Takada, *J. Chem. Soc. C*, 1967, 2201; K. Nakanishi, *Pure Appl. Chem.*, 1967, **14**, 89.

3 A. S. C. Chen, C.-C. Lin, J. Sun, W. Hu, Z. Li, W. Pan, A. Mi, Y. Jiang, T.-M. Huang, T.-K. Yang, J.-H. Chen, Y. Wang and G.-H. Lee, *Tetrahedron: Asymmetry*, 1995, **6**, 2953; H. Suemune, K. Maeda, K. Kato and K. Sakai, *J. Chem. Soc., Perkin Trans. 1*, 1994, 3441; R. Brunner and H. Gerlach, *Tetrahedron: Asymmetry*, 1994, **5**, 1613; J. A. Nieman, M. Parvez and B. A. Keay, *Tetrahedron: Asymmetry*, 1993, **4**, 1973.

4 C.-K. Sha, T.-S. Jean and D.-C. Wang, *Tetrahedron Lett.*, 1990, **31**, 3745; C.-K. Sha, R.-T. Chiu, C.-F. Yang, N.-T. Yao, W.-H. Tseng, F.-L. Liao and S.-L. Wang, *J. Am. Chem. Soc.*, 1997, **119**, 4130; C.-K. Sha, K. C. Santhosh and S.-H. Lih, *J. Org. Chem.*, 1998, **63**, 2699; C.-K. Sha and W.-Y. Ho, *J. Chem. Soc., Chem. Commun.*, 1998, 2709; C.-K. Sha, F.-K. Lee and C.-J. Chang, *J. Am. Chem. Soc.*, 1999, **121**, 9875.

5 D. P. Curran and D. Kim, *Tetrahedron Lett.*, 1986, **27**, 5821; D. P. Curran, *Synthesis*, 1988, 417; D. P. Curran and C. Chang, *J. Org. Chem.*, 1989, **54**, 3140; D. P. Curran, M.-H. Chen and D. Kim, *J. Am. Chem. Soc.*, 1989, **111**, 6265; D. P. Curran and J. Tamine, *J. Org. Chem.*, 1991, **56**, 2746.

6 I. Marek and A. Chakraborty, *J. Chem. Soc., Chem. Commun.*, 1999, 2375; I. Marek, *J. Chem. Soc., Perkin Trans. 1*, 1999, 535; K. Oshima, H. Yorimitsu, T. Nakamura and H. Shinokubo, *J. Org. Chem.*, 1998, **63**, 8604; D. P. Curran and C.-T. Chang, *Tetrahedron Lett.*, 1990, **31**, 933.

7 T. Taguchi, O. Kitagawa and T. Inoue, *Tetrahedron Lett.*, 1992, **33**, 2167; T. Taguchi, O. Kitagawa, T. Inoue and K. Hirano, *J. Org. Chem.*, 1993, **58**, 3106; T. Taguchi, O. Kitagawa and T. Inoue, *Tetrahedron Lett.*, 1994, **35**, 1059; T. Taguchi, T. Inoue, O. Kitagawa, S. Kurumizawa and O. Ochiai, *Tetrahedron Lett.*, 1995, **36**, 1479; T. Taguchi, O. Kitagawa, T. Suzuki, T. Inoue and Y. Watanabe, *J. Org. Chem.*, 1998, **63**, 9470; T. Taguchi, O. Kitagawa, T. Suzuki and H. Fujiwara, *Tetrahedron Lett.*, 1999, **40**, 2549; O. Kitagawa, H. Fujiwara, T. Suzuki, T. Taguchi and M. Shiro, *J. Org. Chem.*, 2000, **65**, 6819.

8 T. Toru, S. Kawai and Y. Ueno, *Synlett*, 1996, 539.

9 For the generation of aluminium enolate from α-bromo carbonyl compounds, see: S. Matsubara, N. Tsuboniwa, Y. Morizawa, K. Oshima and H. Zozaki, *Bull. Chem. Soc. Jpn.*, 1984, **57**, 3242.

10 Iodo ketones **5**–**10** were prepared from the corresponding ketones according to our method: C.-K. Sha, J.-J. Young and T.-S. Jean, *J. Org. Chem.*, 1987, **52**, 3919. The required starting ketones were prepared by Yamashita's procedure: T. Mino, S. Masuda, M. Nishio and M. Yamashita, *J. Org. Chem.*, 1997, **62**, 2633.

11 A representative procedure for iodo-carbocyclization: to a solution of compound **5** (200 mg, 0.72 mmol) in CH_2Cl_2 (7.2 mL) was added $AlCl_3$ (150 mg, 1.08 mmol) at 0 °C. The mixture was stirred at 0 °C for 15 min, during which the color turned orange red. A solution of ICl in CH_2Cl_2 (1 M, 0.87 mL, 0.87 mmol) was added dropwise at 0 °C. The color became dark brown. The reaction mixture was stirred at 0 °C for 45 min and then quenched with H_2O (20 mL), saturated $Na_2S_2O_3$ solution (10 mL) and saturated $NaHCO_3$ solution (10 mL). The mixture was extracted with EtOAc (3 × 15 mL). The combined organic layers were washed with brine and dried ($MgSO_4$). Concentration and silica gel column chromatography (hexane–EtOAc, 50 : 1) gave product **11** (160 mg, 83%) as a pale yellow liquid. δ_H(300 MHz; $CDCl_3$) 6.32 (s, 1H), 2.70−2.60 (m, 1H), 2.60−2.34 (m, 1H), 2.34−1.86 (m, 6H), 1.77−1.59 (m, 1H), 1,59−1.15 (m, 3H); δ_C(75 MHz; $CDCl_3$) 211.2, 137.0, 73.4, 55.9, 40.7, 38.0, 34.4, 25.3, 19.5 (two carbons); IR (neat) 3069, 2953, 1732, 1602; MS (EI): *m*/*z* 277 ($M + H^+$), 214 (13), 185 (52), 149 (31), 127 (47), 97 (45), 84 (100), 79 (34), 41 (55); HRMS (EI): Calc. for $C_{10}H_{14}IO$ ($M + H^+$) 277.0090. Found 277.0087.

12 For purposes of comparison, *E* isomers of **11** and **13** were prepared from compounds **5** and **7** according to the photolytic hexabutylditin method (ref. 5). ^{1}H NMR spectra of **11** and **13** were found to be different from those of *E* isomers. Therefore, all products **11**–**16** are tentatively assigned to be *Z* isomers.

13 When the reactions of entries 1 and 2 were performed at −78 °C, products **11** and **12** were both obtained along with some by-product **4**, in ratios of 1 : 0.9 and 1 : 0.8 respectively.

An alternative synthesis method for zeolite Y membranes

Guillaume Clet,*†[a] Leszek Gora,[a] Norikazu Nishiyama,‡[b] Jacobus C. Jansen,[a] Herman van Bekkum[a] and Thomas Maschmeyer[a]

[a] *Laboratory for Applied Organic Chemistry and Catalysis, Delft University of Technology, Julianalaan 136, 2628 BL Delft, The Netherlands. E-mail: guillaume.clet@ismra.fr*

[b] *Laboratory for Industrial Catalysis, Delft University of Technology, Julianalaan 136, 2628 BL Delft, The Netherlands*

Received (in Cambridge, UK) 21st September 2000, Accepted 1st November 2000
First published as an Advance Article on the web 11th December 2000

A new approach for the synthesis of supported zeolite Y membranes is presented, using a synthesis gel containing seeds to avoid any unnecessary *ex situ* pre-treatment of the support.

Zeolitic membranes can be applied in many separations of either liquid or gaseous components. It is important to be able to draw from a large number of different zeolite membranes to enhance the scope of this approach further. Various procedures have been proposed for the synthesis of membranes with different zeolites, *e.g.* for MFI membranes a direct synthesis method has been reported[1–3] as well as a synthesis route involving pre-adsorption of zeolite crystals and subsequent secondary growth.[4,5] However, in some cases membranes become efficient only after many repeated syntheses steps.[2] In another example vapour phase transport was used to synthesise mordenite and ferrierite membranes.[6] Here we report a conceptually new and improved method for membrane preparation.

Owing to its large pore system and its specific counter-ion-dependent adsorption properties, zeolite Y is an interesting material for a membrane and/or a catalytic membrane reactor. Although zeolite Y membranes have been synthesised previously, the methods used involve the deposition of pre-formed crystals employed as seeds on the support[7] or rubbing of the support with zeolite crystals.[8,9] These *ex situ* synthesis methods work well on a laboratory scale, but are unlikely to be applicable for larger scale uses.

We showed recently that a coating of zeolite Y on common stainless steel could be achieved with a new synthesis procedure, using a seeded synthesis mixture.[10] We report here that this method can be successfully employed to synthesise a zeolite Y membrane *in situ*. The behaviour of this material as a membrane was tested in the separation of the light molecules N_2 and CO_2, since membranes able to separate these technologically important gases are not common nor readily available.

Two different synthesis mixtures were prepared. The first mixture, prepared in two steps with sodium silicate as the silica source and sodium aluminate as the alumina source, was seeded according to the procedure described previously,[10] by ageing a mixture highly concentrated in NaOH and incorporating it in a gel of general molar composition 10 SiO_2 : Al_2O_3 : 5.2 Na_2O : 180 H_2O (G1). A second type of gel, unseeded, was prepared in one step using colloidal silica (Ludox HS-40, DuPont) as the silica source with a general molar composition 10 SiO_2 : Al_2O_3 : 4 Na_2O : 180 H_2O (G2). Porous stainless steel disks, coated with a 15 μm thick porous titania layer (Trumem™) were used as supports. They were calcined at 300 °C prior to use to ensure they were free of organic deposits. Synthesis took place at 100 °C under rotational conditions (180 rpm) for 7 h in a Teflon-lined autoclave. During the synthesis, only the titania side was in contact with the synthesis mixture, the stainless steel side being protected by a Teflon disk. After synthesis the coated supports were washed and dried at 120 °C. Permeation measurements using single components of CO_2 and N_2 and binary mixtures of CO_2/N_2 were performed by the Wicke–Kallenbach method at 30 °C. The feed and permeate sides were kept at atmospheric pressure while helium was used as sweep gas with a flow rate of 100 ml min^{-1}. Feed, retentate and permeate streams were analysed with a mass spectrometer. The zeolite layer on the support faced the feed side in the permeation measurements. Characterisation of the materials was performed by XRD and SEM. The Si/Al ratio was measured by ICP-AES of the powder and was equal to 2.

In agreement with previous observations on stainless steel plates,[10] the use of the unseeded synthesis mixture (G2) resulted in a very low coverage of the titania layer even after 24 h of synthesis. Accordingly, no separation of the gas mixture could be observed. By contrast, when using the seeded mixture (G1), a good coverage of the support was obtained, although XRD could not evidence the presence of zeolite Y, probably owing to the thickness of the layer. However, the system did not show any real separation of N_2 or CO_2. When single component experiments were carried out, fluxes of N_2 and CO_2 were 8.58 $\times 10^{-7}$ and 6.05 $\times 10^{-7}$ mol m^{-2} s^{-1} Pa^{-1}, respectively. The ideal selectivity and the selectivity measured for a 1 : 1 mixture were nearly equal, at 0.7 and 0.63, respectively. Besides, large amounts of the sweep gas were found in the retentate. This indicates the presence of pinholes in the membrane. SEM showed that individual crystals were still present. This implies that crystal intergrowth was not achieved.

A second synthesis step can induce the intergrowth of the zeolite crystals supported after the first synthesis, however, when using the same seeded mixture (G1) for the second synthesis, degradation of the first layer occurred and impurities, namely zeolite P, were formed on the surface. This might be caused by the high pH of the synthesis mixture. To avoid the degradation of the zeolite Y layer, the second synthesis was performed, using the *unseeded synthesis* mixture (G2) of lower alkalinity. In this case, XRD evidenced that zeolite Y was present on the surface, and that impurities were not present. SEM images showed that the layer was well intergrown (Fig. 1). This layer was *ca.* 0.7 μm thick and permeation measurements confirmed that a closed layer had been synthesized.

Fig. 2 shows the fluxes of N_2 and CO_2 in the single- and binary-component measurements as a function of CO_2 partial pressure for the latter material. Both curves cannot be explained by the Knudsen diffusion mechanism, since N_2 diffuses faster than CO_2 in the Knudsen diffusion region. The effect of the surface diffusion of CO_2 should be taken into account. When plotting the separation factors of the CO_2/N_2 mixture *vs.* the CO_2 partial pressure, the separation factor is greater than the ideal separation factor calculated with the single component fluxes. This indicates that adsorbed molecules of CO_2 partly blocked the pores and depressed the permeation of N_2. The separation factor CO_2/N_2 increased with increasing partial

† *Present address*: Laboratoire de Catalyse et Spectrochimie, ISMRa, University of Caen, 6, Bd du Maréchal Juin, 14050 Caen (cedex), France
‡ *Present address*: Department of Chemical Engineering, Osaka University, 1-3 Machi-kaneyama, Toyonaka, Osaka 560-8531, Japan.

DOI: 10.1039/b007688k

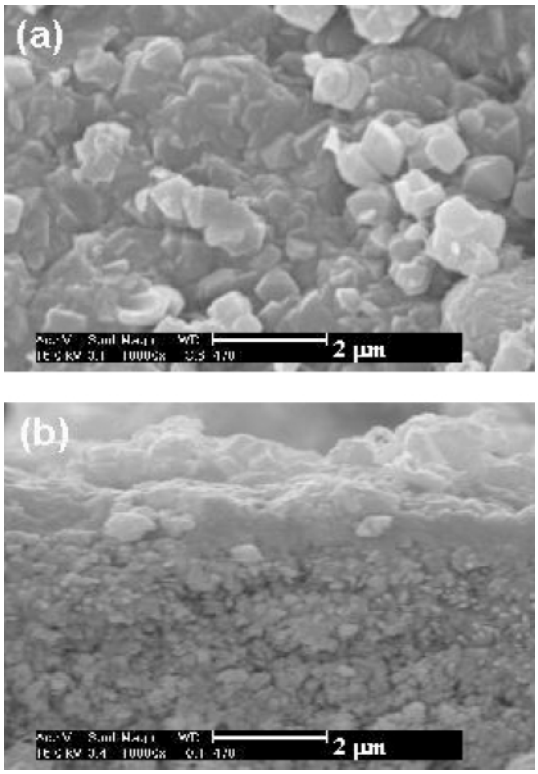

Fig. 1 SEM images of the zeolite Y membrane on a TRUMEM support obtained sequentially after synthesis with G1 and G2 synthesis mixtures: (a) top view, (b) cross-section.

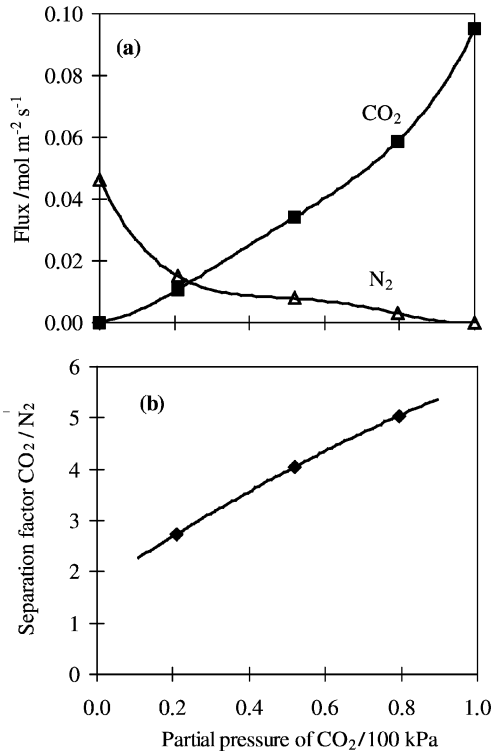

Fig. 2 CO_2/N_2 permeation measurements. (a) fluxes, (b) separation factor (CO_2/N_2).

pressure of CO_2, showing that the effect of pore blocking caused by adsorbed CO_2 is more pronounced when the CO_2 content in the feed stream is higher. This trend is in good agreement with the data obtained for the separation of other gas mixtures such as *n*-butane/methane,[1] *n*-butane/isobutane[11] and ethane/methane[12] over silicalite membranes. Although the separation behaviour was much improved, the fluxes did not decrease significantly (fluxes of N_2 and CO_2 were respectively 4.59×10^{-7} and 9.41×10^{-7} mol m^{-2} s^{-1} Pa^{-1} in single-component experiments). The presence of a dense amorphous phase is thus not likely as this would manifest itself in a lowering of fluxes. Furthermore, this interpretation is consistent with SEM characterisations (Fig. 1).

We have shown that a high quality zeolite Y membrane can be synthesised by combining two synthesis steps. With this method a *seeded gel* layer is first deposited on the support upon dipping it in the synthesis mixture. The seeds initially present in the synthesis mixture are also part of the supported gel layer.[13] Therefore their growth occurs directly on the support and this gives rise to a dense layer when exposing the system to a second synthesis step.

In conclusion, we have shown that seeds on the support are necessary to allow the growth of a supported Y membrane. Unlike previous reports,[8,9] seeds can easily be brought to the support during synthesis. This method simplifies the process of attaching nuclei onto the support and opens up new vistas for supported zeolite membranes.

References

1 E. R. Geus, H. van Bekkum, W. J. W. Bakker and J. A. Moulijn, *Microporous Mater.*, 1993, **1**, 131.
2 J. Coronas, J. L. Falconer and R. D. Noble, *AIChE J.*, 1997, **43**, 1797.
3 L. Gora, J. C. Jansen and Th. Maschmeyer, *Stud. Surf. Sci. Catal.*, 1999, **125**, 173.
4 M. C. Lovallo, A. Gouzinis and M. Tsapatsis, *AIChE. J.*, 1998, **44**, 1903.
5 R. Lai and G.R. Gavalas, *Ind. Eng. Chem. Res.*, 1998, **37**, 4275.
6 N. Nishiyama, K. Ueyama and M. Matsukata, *AIChE J.*, 1996, **7**, 299.
7 H. Kita, T. Inoue, H. Asamura, K. Tanaka and K. Okamoto, *Chem. Commun.*, 1997, 45.
8 K. Kusakabe, T. Kuroda, A. Murata and S. Morooka, *Ind. Eng. Chem. Res.*, 1997, **36**, 649.
9 I. Kumakiri, T. Yamaguchi and S.-I. Nakao, *Ind. Eng. Chem. Res.*, 1999, **38**, 4682.
10 G. Clet, J.C. Jansen and H. van Bekkum, *Chem. Mater.*, 1999, **11**, 1696.
11 L. P. J. van den Broeke, W. J. Bakker, F. Kapteijn and J. A. Moulijn, *AIChE J.*, 1999, **45**, 976.
12 J. M. van de Graaf, E. van der Bijl, A. Stol, F. Kapteijn and J. A. Moulijn, *Ind. Eng. Chem. Res.*, 1998, **37**, 4071.
13 G. Clet, J. A. Peters and H. van Bekkum, *Langmuir*, 2000, **16**, 3993.

Dramatic acceleration of the catalytic process of the amination of allyl acetates in the presence of a tetraphosphine/palladium system

Marie Feuerstein, Dorothée Laurenti, Henri Doucet* and Maurice Santelli*

Laboratoire de Synthèse Organique UMR-CNRS 6009, Faculté des Sciences de Saint Jérôme, Avenue Escadrille Normandie-Niemen, 13397 Marseille Cedex 20, France. E-mail: henri.doucet@lso.u-3mrs.fr; m.santelli@lso.u-3mrs.fr

Received (in Cambridge, UK) 27th September 2000, Accepted 14th November 2000
First published as an Advance Article on the web 15th December 2000

The *cis,cis,cis*-1,2,3,4-tetrakis(diphenylphosphinomethyl)-cyclopentane/$[PdCl(C_3H_5)]_2$ system catalyses allylic amination in good yields with a very high substrate/catalyst ratio; a turnover number of 680 000 and a turnover frequency of 8125 h^{-1} can be obtained for the addition of dipropylamine to allyl acetate in the presence of this catalyst.

Allylamines are fundamental building blocks in organic synthesis and their preparation is an important industrial goal.[1] Allylic amination is an efficient method for the formation of allyl–nitrogen bonds.[2] The classical method to perform this reaction is to employ palladium complexes associated with mono-[3] or di-phosphine[4] ligands. Phosphine-amine[5] ligands have also been used successfully. Even if the catalysts formed by association of these ligands with palladium complexes are efficient in terms of yield of adduct, the efficiency in terms of the ratio of substrate/catalyst is low. In general 1–5% of these catalysts must be used. With one of the most active catalysts based on a polystyrene–phosphine–palladium complex the reaction can be performed with as little as 0.018% catalyst (TON: 3200).[6] Nevertheless, very high values of ratio substrate/catalyst have not been reported for this reaction.

Our aim was to obtain complexes capable of very high turnover numbers in catalysis. The nature of the phosphine ligand on complexes has a tremendous influence on the rate of catalysed reactions. Recently a tetraphosphine based on a cyclobutane ring led to the formation of palladium catalysts for copolymerization that are more efficient than those of dppe by a factor of ten.[7] In order to find more efficient palladium catalysts we decided to study the influence of the new tetrapodal phosphine ligand, *cis,cis,cis*-1,2,3,4-tetrakis(diphenylphosphinomethyl)cyclopentane (Tedicyp **1**)[8,9] in which the four

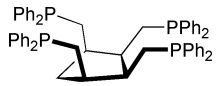

Tedicyp 1

diphenylphosphinoalkyl groups are stereospecifically bound to the same face of the cyclopentane ring, on the rate of allylic amination reaction.

Our first objective was to evaluate the difference of efficiency for allylic amination between a monophosphine ligand such as triphenylphosphine, a diphosphine ligand such as 1,2-bis(diphenylphosphino)ethane (dppe) and our tetraphosphine **1**. We observed that the addition of dioctylamine **8** to allyl acetate **2** in the presence of 0.001% catalyst, led to the addition product **14** in 1 and 3% conversion when PPh_3 and dppe, respectively, were used as ligand and 99% conversion with Tedicyp (Scheme 1, Table 1). A similar tendency was observed for the addition of diallylamine **9** to allyl acetate **2**. In the presence of 0.001% catalyst, only 7% conversion was observed with dppe. With Tedicyp the conversion was 73% in the presence of 0.0001% catalyst.

Next we tried to evaluate the scope and limitations of Tedicyp–palladium complex for this reaction. The addition rate was slightly decreased for the addition of morpholine **11** to **2**. A conversion of 93% is observed in the presence of 0.01%

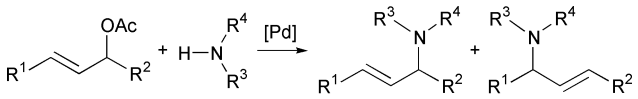

2-5 **6-12** **13-17, 26 18a-25a** **18b-25b**

2: $R^1 = R^2 = H$
3: $R^1 = Ph$, $R^2 = H$
4: $R^1 = Pr^n$, $R^2 = H$
5: $R^1 = R^2 = Ph$

6: $R^3 = Et$, $R^4 = Et$
7: $R^3 = Pr^n$, $R^4 = Pr^n$
8: $R^3 = n\text{-}C_8H_{17}$, $R^4 = n\text{-}C_8H_{17}$
9: $R^3 = CH_2CH{=}CH_2$, $R^4 = CH_2CH{=}CH_2$
10: $R^3\text{-}R^4 = \text{-}(CH_2)_4\text{-}$
11: $R^3\text{-}R^4 = \text{-}(CH_2)_2O(CH_2)_2\text{-}$
12: $R^3 = Pr^i$, $R^4 = Pr^i$

Scheme 1

Table 1 Palladium catalyzed allylic amination[11]

Allyl acetate	Amine	Product (major isomer)	Ratio **a**/**b**[h]	Ratio substrate/ catalyst	Turnover frequency[i]/ h^{-1}	Yield (%)
2	**7**	**13**	—	1 000 000	8125	68[c]
				5 000 000	8333	14[ef]
2	**8**	**14**	—	100 000	2062[j]	99[bf]
				1 000 000	7083	17[af]
2	**9**	**15**	—	100 000	2388	95[e]
				1 000 000	8111[k]	73[df]
2	**11**	**16**	—	10 000	250	93[e]
				100 000	1111	57[e]
2	**12**	**17**	—	1 000	13	81[c]
2	**27**	**29a**	85/15	10 000	250	97[bf]
			90/10	100 000	1229	83[cf]
2	**28**	**30a**	68/32	1 000	49	78[ag]
3	**7**	**18a**	94/6	1 000	45	95[a]
			95/5	10 000	160	36[b]
3	**9**	**19a**	95/5	1 000	30	85[e]
3	**11**	**20a**	86/14	1 000	41	99[a]
			84/16	10 000	183	44[a]
4	**6**	**21a**	100/0	100	2.5	98[e]
			100/0	1 000	6.6	43[e]
4	**7**	**22a**	100/0	1 000	10.3	92[d]
4	**8**	**23a**	100/0	100	3.9	95[a]
			100/0	1 000	13.3	84[b]
4	**10**	**24a**	93/7	100	4.1	98[a]
			94/6	1 000	20.4	49[bf]
4	**11**	**25a**	91/9	100	4.1	100[af]
			92/8	1 000	17.5	51[e]
5	**11**	**26**	—	100	0.5	65[ef]

Conditions: catalyst, see ref 10, THF, 25 °C, [a] 24 h. [b] 48 h. [c] 72 h. [d] 90 h. [e] 130 h. [f] 55 °C. [g] In toluene. [h] For compounds **18**–**25**, **a** corresponds to the linear isomer and **b** to the branched isomer (Scheme 1). For compounds **29** and **30**, **a** corresponds to the monoaddition product and **b** to the diaddition product (Scheme 2). [i] TOF calculated between initial time and 24 h. [j] Calculated after 48 h. [k] Calculated after 90 h.

DOI: 10.1039/b007860n

catalyst. A turnover number (TON) of 57 000 and a TOF of 1111 h^{-1} were obtained in the presence of 0.001% catalyst. On the other hand, a significant steric effect was observed with the bulky diisopropylamine **12**. In the presence of 0.1% catalyst only 81% conversion was obtained after three days.

The complex formed by association of Tedicyp and $[PdCl(C_3H_5)]_2$ seems to be more stable and less sensitive to temperature and poisoning than the complexes formed with diphosphines.

These results prompted us to investigate the allylation of amines with substituted allyl acetates. When we used cinnamyl acetate **3** in the presence of 0.1% catalyst high yields were obtained for the addition of dipropylamine **7** and diallylamine **9**. A TON of 4400 has also been observed with morpholine **11**. We noted a good regioselectivity for the amination of cinnamyl acetate **3** in favour of the linear isomer. Similar selectivities were observed for the addition of diethylamine **6**, dipropylamine **7** and dioctylamine **8** to (*E*)-hex-2-en-1-yl acetate **4**. (*E*)-*N*,*N*-dialkylhex-2-enylamines **21a**–**23a** were obtained regio- and stereo-selectively in good yield. The regioselectivity of the addition of cyclic amines **10** and **11** is slightly lower; 6 and 8% of the branched products **24b** and **25b** are obtained with pyrrolidine **10** and morpholine **11**. Much lower TON and TOF were observed in the course of the amination of hindered 3-acetoxy-1,3-diphenylprop-1-ene **5**.

With primary amines, we obtained mixtures of monoaddition and diaddition products (Scheme 2). Benzylamine **27** led to the monoaddition product **29a** in 83% conversion and 90% selectivity in the presence of 0.001% catalyst with a TOF of 1229 h^{-1}. The addition rate of cyclohexylamine **28** is slower with a TOF of 49 h^{-1} and a lower selectivity in favour of the monoaddition product **30a** is observed.

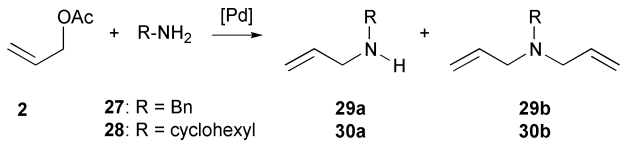

Scheme 2

Finally, we tried to gain some information on the structure of the palladium–Tedicyp complex formed. Addition of 1 equiv. of Tedicyp to 0.5 equiv. of the dimer $[PdCl(C_3H_5)]_2$ gave a clean ^{31}P NMR spectrum which shows two broad signals at δ 19 and 25 (*vs.* H_3PO_4). The characteristic signals of the free phosphine at δ −16.3 and −17.7 were not observed. Addition of 1 equiv. of Tedicyp to 1 equiv. of $[PdCl(C_3H_5)]_2$ gave an identical ^{31}P NMR spectrum. Addition of 2 equiv. of Tedicyp to 0.5 equiv. of $[PdCl(C_3H_5)]_2$ led to a more complicated spectrum; mainly four signals of free phosphines at δ −16.9, −18.2 , −19.3 and −20.9 and some broad peaks between δ 40 and 10 were observed in ^{31}P NMR. In the first case, addition of 1 equiv. of Tedicyp to 0.5 equiv. of the Pd complex, produced broad signals at δ 19 and 25 suggesting that this complex is involved in a succession of equilibria due to a fast coordination–dissociation process of the four phosphines of the ligand. The absence of peaks of free phosphines probably arises from the equilibrium rate which seems to be of the order of the NMR time scale. Similar results have already been described; for example, $Pd(PPh_3)_3$ is largely dissociated and the equilibrium rate is of the order of the NMR time scale even at low temperature.[12] Addition of 10 equiv. of allyl acetate or addition of 10 equiv. of allyl acetate with 10 equiv. of dipropylamine to this Pd–Tedicyp complex (ratio Pd-dimer/Tedicyp = 0.5) has no influence on the ^{31}P NMR spectrum; the two broad signals observed at δ 19 and 25 are unchanged.

We have also examined the importance of the ratio palladium/Tedicyp for the catalysis. We observed that if the reaction is performed with Pd-dimer/Tedicyp ratios of 0.5, 1 and 2, the rate of the reaction decreases. The TONs after 40 min were, respectively, 8100, 4000 and 1300 for the addition of dipropylamine **7** to allylacetate **2** with a ratio substrate/catalyst of 100 000. These results seems to indicate that the active palladium catalyst requires one tetraphosphine for one palladium centre.

In conclusion, the Tedicyp–palladium complex obtained by addition of Tedicyp to $[Pd(C_3H_5)Cl]_2$ provides a convenient catalyst for the allylic amination reaction. This catalyst seems to be more stable and less sensitive to poisoning than the complexes formed with mono- and di-phosphine ligands. This stability probably arises from the presence of the four diphenylphosphinoalkyl groups stereospecifically bound to the same face of the cyclopentane ring. All four phosphines probably cannot bind at the same time to the same palladium centre, but the presence of these four phosphines on the ligand close to the metal centre, along with steric factors, seems to increase the coordination of the ligand to the palladium complex. In the presence of this catalyst the amination reaction can be performed with as little as 0.0001% catalyst. These results represent an inexpensive, efficient, and environmentally friendly synthesis. Further applications of this ligand will be reported in due course.

We thank F. Berthiol for experimental work and the CNRS for providing financial support.

Notes and references

1 For a review on allylic amination: see, M. Johannsen and K. Jorgensen, *Chem. Rev.*, 1998, **98**, 1689.

2 For reviews on palladium catalysed allylic substitution reactions see: T. Hayashi, in *Catalytic Asymmetric Synthesis*, ed. I. Ojima, VCH, New York, 1993, p. 325; J. Tsuji, *Palladium Reagent and Catalysis, Innovation in Organic Synthesis*, Wiley, New York, 1995; R. F. Heck, *Palladium Reagents in Organic Syntheses*, ed A. R. Katritzky, O. Meth-Cohn and C. W. Rees, Academic Press, London, 1985, p. 2; A. Pfaltz and M. Lautens, *Comprehensive Asymmetric Catalysis II*, ed. E. N. Jacobsen, A. Pfaltz and H. Yamamoto, Springer, Berlin, 1999, p. 833; J.-L. Malleron, J.-C. Fiaud and J.-Y. Legros, *Handbook of palladium catalyzed organic reaction*, Academic Press, London, 1997.

3 N. Riegel, C. Darcel, O. Stéphan and S. Jugé, *J. Organomet. Chem.*, 1998, **567**, 219; O. Kuhn and H. Mayr, *Angew. Chem., Int. Ed.*, 1999, **38**, 343; J. P. Genêt, M. Balabane, J. E. Bäckvall and J. E. Nyström, *Tetrahedron Lett.*, 1983, **24**, 2745; C. Thorey, J. Wilken, F. Hénin, J. Martens, T. Mehler and J. Muzart, *Tetrahedron Lett.*, 1995, **36**, 5527; M. Moreno-Manas, L. Morral and R. Pleixats, *J. Org. Chem.*, 1998, **63**, 6160.

4 B. M. Trost, L. T. Calkins, C. Oerlet and J. Zambrano, *Tetrahedron Lett.*, 1998, **39**, 1713; A. Yamazaki and K. Achiwa, *Tetrahedron: Asymmetry*, 1995, **6**, 51; N. Sirisoma and P. Woster, *Tetrahedron Lett.*, 1998, **39**, 1489; Y. Uozumi, A. Tanahashi and T. Hayashi, *J. Org. Chem.*, 1993, **58**, 6826.

5 P. von Matt, O. Loiseleur, G. Koch, A. Pfaltz, C. Lefeber, T. Feucht and G. Helmchen, *Tetrahedron: Asymmetry*, 1994, **5**, 573.

6 B. M. Trost and E. Keinan, *J. Am. Chem. Soc.*, 1978, **100**, 7779.

7 C. Bianchini, H. M. Lee, A. Meli, W. Oberhauser, F. Vizza, P. Brüggeller, R. Haid and C. Langes, *Chem. Commun.*, 2000, 777.

8 D. Laurenti, M. Feuerstein, G. Pèpe, H. Doucet and M. Santelli, unpublished results.

9 *cis,cis,cis*-1,2,3,4-Tetrakis(diphenylphosphinomethyl)cyclopentane Tedicyp **1** was prepared from *cis,cis,cis*-1,2,3,4-tetrakis{[(tolyl-4-sulfonyl)oxy]methyl}cyclopentane **31**[13] by addition of Ph_2PLi. ^{31}P NMR of **1** (162 MHz, THF-d_8) δ −16.3, −17.7.

10 The *cis,cis,cis*-1,2,3,4-tetrakis(diphenylphosphinomethyl)cyclopentane/$[PdCl(C_3H_5)]_2$ complex was prepared by stirring under argon the tetraphosphine **1** (140 mg, 162 μmol) with $[PdCl(C_3H_5)]_2$ (30 mg, 81 μmol) in THF (10 ml) for 10 min at room temperature. This complex is not air stable and must be prepared just before use. δ_P(162 MHz, $CDCl_3$) 25 (w = 80 Hz), 19.4 (w = 110 Hz).

11 In a typical experiment, the reaction of cinnamyl acetate **3** (1.30 g, 7.4 mmol) and dipropylamine **7** (2.07 g, 14.8 mmol) at 50 °C for 90 h in distilled THF (20 mL) in the presence of the Tedicyp–palladium complex (7.4×10^{-3} mmol) under argon affords the corresponding addition product **18** after evaporation and filtration on silica gel (diethyl ether–pentane: 3/7) in 95% (1.52 g) isolated yield.

12 C. Amatore, A. Jutand, F. Khalil, M. M'Barki and L. Mottier, *Organometallics*, 1993, **12**, 3168; C. Amatore, G. Broeker, A. Jutand and F. Khalil, *J. Am. Chem. Soc.*, 1997, **119**, 5176.

13 K. Somekawa, M. Nomura, S. Aoki, S. Noma and T. Shimo, *Org. Prep. Proc. Int.*, 1993, **25**, 449.

Ferromagnetic interactions in the first *dicubane-type* complex involving cyanate ligand: $[Co_4(dpk\text{-}OH)_2(dpk\text{-}OMe)_2(NCO)_4]$

M. Gotzone Barandika,[a] Zurine Serna,[b] Roberto Cortés,*[a] Luis Lezama,[b] M. Karmele Urtiaga,[c] M. Isabel Arriortua[c] and Teófilo Rojo*[b]

[a] *Departamento de Química Inorgánica, Fac. Farmacia, UPV/EHU, Aptdo. 450, Vitoria, E-01080 Spain. E-mail: qipcomor@lg.ehu.es*
[b] *Departamento de Química Inorgánica, Fac. Ciencias, UPV/EHU, Aptdo. 644, E-48080 Bilbao, Spain*
[c] *Departamento de Mineralogía-Petrología, Fac. Ciencias, UPV/EHU, Aptdo. 644, E-48080 Bilbao, Spain*

Received (in Cambridge, UK) 12th October 2000, Accepted 14th November 2000
First published as an Advance Article on the web 15th December 2000

The ligands cyanate and di-2-pyridyl ketone (dpk) are used to construct a tetranuclear cobalt(II) complex involving $\mu_{1,1}$-cyanate bridges: $[Co_4(dpk\text{-}OH)_2(dpk\text{-}OMe)_2(NCO)_4]$, which shows a dicubane-type structure, with two missing vertices, and having ferromagnetic interactions.

A considerable ongoing research has been directed at the preparation of molecule-based magnets over recent years. In this area, great activity has been focused on obtaining nanoscale magnets in which each microcrystal behaves as a single domain. A way to deal with the preparation of nanomagnets concerns single molecules having ground electronic states with a large number of unpaired electrons.[1] In relation to the ligands for the preparation of those clusters, a variety of blocking organic compounds has been used, most of them providing oxo-bridges between metallic centers.[2]

An efficient way for the generation of interactions between metallic centers concerns the use of pseudohalide ligands. Among these, azide has been undoubtedly one of the most interesting magnetic coupling species found so far in molecular magnetism.[3] One of the latest findings found for this ligand is its incorporation into *cubane-type* systems and those exhibiting $\mu_{1,1}$-azido bridges have been observed to be ferromagnetic.[4] The cyanate pseudohalide is a more unusual ligand, its chemistry and bonding properties have been the subject of several studies[5] which focussed upon its ability to coordinate to metals, and its ability and adaptability as a bridging ligand.[6] It shows preference for the end-on bridging mode, through the nitrogen atom. In this kind of bridging, the cyanate ligand has been shown to be able to mediate ferromagnetic interactions.[7]

As mentioned above, in most of the clusters for nanomagnets, the intermetallic connections take place through oxo-bridges. In this way, the coordination behavior of di-2-pyridyl ketone (dpk) as a ligand has also attracted much attention.[8] Its hydrolyzed derivatives, namely, the *gem*-diol[9] and its respective mono- and di-anions, are potential chelating or chelating-bridging ligands. In fact, a number of mononuclear[10] and oligomeric polynuclear[11] complexes derived from these ligands have been isolated and crystallographically characterized. Solvolysis reactions are also observed to occur in contact with other solvents thus widening the possibilities in structural arrangement.

For the indicated reasons above, the simultaneous use of dpk and cyanate ligands could be expected to enhance the formation of intermetallic bridges. Thus, taking into account these considerations, this work reports on a ferromagnetic tetranuclear cobalt(II) system of formula $[Co_2(dpkOH)(dpkOMe)(NCO)_2]_2$, the structural core of which can be described as that of a 'dicubane' having two missing vertices. Very few examples of cobalt(II) dicubanes are known[12] and no cobalt–$\mu_{1,1}$-cyanate polynuclear compound has been characterized structurally and magnetically to date. Furthermore, as far as we are aware, this is the first example of a 'cubane-type' system involving cyanate ligands.

Reaction of dpk, $Co(NO_3)_2{\cdot}4H_2O$ and KNCO yielded,† after evaporation, a brown-red crystalline material, the composition of which was consistent with the formula $[Co_2(C_{23}H_{20}N_4O_4)(NCO)_2]$ **1**. The X-ray crystal structure determination of **1** (Fig. 1)‡ revealed that it consists of centrosymmetric tetranuclear units in which the cobalt(II) ions are connected through the ligands NCO, dpkOH, and dpkOMe (the latter tworesulting from solvolysis of the dpk ligand) to give a face-shared dicubane-like coordination core containing two missing vertices (Fig. 1).

The Co(II) ions exhibit slightly distorted octahedral $[CoN_3O_3]$ and $[CoN_4O_2]$ environments, with the Co–N distances ranging from 2.024(6) (dpk) to 2.146(4) Å (cyanate) and the Co–O distances ranging from 2.025(3) to 2.244(3). The EO cyanate bridges form an angle with the metal of 101.8(2)°, while the Co–O–Co angles range from 97.1(1) to 100.6(2)°. The Co···Co distance through the combined cyanate and oxo bridges is 3.283(2) Å, while those corresponding to the oxo-bridges alone are 3.144(1) and 3.238(2) Å.

The temperature dependence of the magnetic susceptibility χ_m of **1** has been investigated in the range 4–300 K. The product $\chi_m T$ continuously increases upon cooling and its value, per 4 Co atoms, at room temperature is 11.7 $cm^3\ K\ mol^{-1}$, which is larger than the 7.5 $cm^3\ K\ mol^{-1}$ expected for four isolated spin-only $S = 3/2$ ions. This larger value is the result of contributions to the susceptibility from orbital angular momentum at high temperatures, which produces effective moments per cobalt atom in the range 4.7–5.2 μ_B.[13] A maximum of 18.3 $cm^3\ K\ mol^{-1}$ appears at 12 K. After this maximum, $\chi_m T$ decreases [Fig. 2(a)]. This behavior is characteristic of a system exhibiting intramolecular ferromagnetic interactions; while the sudden decrease must be associated to spin–orbit coupling and/or the existence of intermolecular interactions. It is not possible to fit the behavior of an array of four high-spin Co^{II} centers given current theory, even if the centers are orbitally degenerate. Besides, in the present compound the environment of the Co(II) centers which are in distorted octahedra, probably removes the degenereracy. Taking into account that, even for the simplest of the possible Co(II) tetranuclear systems (*i.e.* a square planar cluster with a single *J* value[14]), fitting has not been carried out, the extreme difficulty of modeling a four-*J* system (see Scheme 1) for this cation that should include aspects such as spin–orbit coupling, magnetic anisotropy, orbital degeneracy, *etc*, should be appreciated.

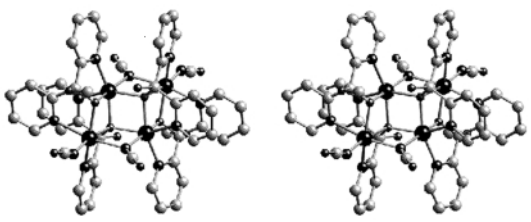

Fig. 1 Stereoview of the tetranuclear structure of compound **1**. Sizes of spheres is in the order Mn > C > N > O. Hydrogen atoms have been omitted for clarity.

DOI: 10.1039/b008256m

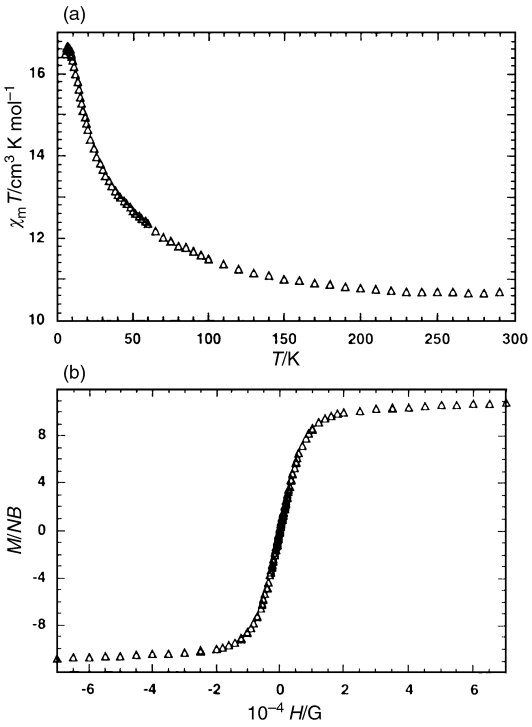

Fig. 2 (a) Thermal variation of $\chi_m T$ for **1**, per tetranuclear unit. (b) Representation of the magnetization *vs.* magnetic field at 5 K.

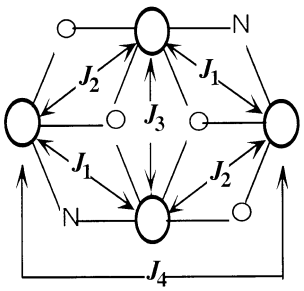

Scheme 1

In order to gain more information on **1**, we investigated the variation of the magnetization *M vs.* the applied magnetic field *H*, in the field range $0 < H/T < 7$ at 5 K and results are shown in Fig. 2(b), where it can be observed that the magnetization reaches the saturation value expected for a tetranuclear ferromagnetic cobalt(II) compound, *i.e.* $N\beta g/2$ ($\approx$ 12). Further studies are being undertaken to thoroughly characterize this system.

The ferromagnetic behavior of this compound can be explained by the existence of *end-on* cyanate bridges, with angles close to 100°, which gives rise to moderately strong ferromagnetic interactions.[7] In addition, the oxo bridges in the compound also promote ferromagnetic interactions, as has been observed in related cubane oxo-bridged compounds.[11b]

In conclusion, the combination of dpk and cyanate ligands has been shown to be a good strategy for obtaining 'cubane-like' systems and related nickel, cobalt and manganese systems are now under investigation. The resulting compound **1** shows a tetranuclear molecular structure of dicubane type which is unprecedented for cyanate ligand. The bridging ligands connecting the cobalt(II) ions provide global ferromagnetic exchange interactions.

Fundings by the Basque Government (grant PI 99/53), the University of the Basque Country (grant UPV 130310-EB201/1998), and the Dirección General de Enseñanza Superior-MEC (Spain) (grant PB97-0637) are gratefully acknowledged. Z. E. S. thanks the University of the Basque Country for a doctoral fellowship.

Notes and references

† *Experimental procedure*: reaction of a methanolic solution (10 cm^3) containing dpk (1 mmol) with a aqueous solution (10 cm^3) containing both $Co(NO_3)_2 \cdot 4H_2O$ (1 mmol) and KNCO (1 mmol) yielded, after two weeks evaporation, a brown crystalline material **1**. Yield 63%. Elemental analysis. Calc. for $C_{25}H_{20}N_6O_6Co_2$: C, 48.56; H, 3.26; N, 13.59; Co, 19.06. Found: C, 48.13; H, 3.15; N, 13.22; Co, 19.06%.

‡ *Crystal data*: $C_{25}H_{20}N_6O_6Co_2$, M = 618.33, monoclinic, space group $P2_1/c$ (no. 14), a = 13.039(1), b = 12.303(1), c = 19.365(1) Å, β = 122.57(1)°, V = 2618.0(4) Å^3, Z = 4, D_c = 1.569 g cm^{-3}, $2\theta_{max}$ = 60°, T = 293 K, ω–2θ scans; Lorentzian, polarization, and extinction corrections were made, μ(Mo-Kα) = 13.2 cm^{-1}, 14672 reflections measured, 6653 unique (R_{int} = 0.1483) all included in the refinement; structure solution by direct methods; 353 parameters refined $R1(F_o)$ = 0.058 [for 6653 reflections with $I > 2\sigma(I)$]; $wR2(F_o^2)$ = 0.098 (all data); quality of fit 0.80. Max./min. residual peaks in the final difference map 0.531/−0.605 e Å^{-3}. Diffraction data were collected on an Enraf-Nonius CAD-4 diffractometer. The structure was solved by direct methods and refined with SHELXL-97.[14] All non-H atoms were refined anisotropically. CCDC 182/1849. See http://www.rsc.org/suppdata/cc/b0/b008256m/ for crystallographic files in .cif format.

1 D. P. Goldberg, A. Caneschi, C. D. Delfs, R. Sesoli and S. J. Lippard, *J. Am. Chem. Soc.*, 1995, **117**, 5789; A. K. Powell, S. L. Heath, D. Gatteschi, L. Pardi, R. Sessoli, G. Spina, F. D. Giallo and F. J. Pieralli, *J. Am. Chem. Soc.*, 1995, **117**, 2491; A. L. Barra, A. Caneschi, D. Gatteschi and R. Sessoli, *J. Am. Chem. Soc.*, 1995, **117**, 8855.

2 S. L. Castro, Z. Sun, C. M. Grant, J. C. Bellinger, D. N. Hendrickson and G. J. Christou, *J. Am. Chem. Soc.*, 1998, **120**, 2365.

3 D. M. Duggan and D. N. Hendrickson, *Inorg. Chem.*, 1973, **12**, 2422; J. Commarmond, P. Plumeré, J. M. Lehn, Y. Agnus, R. Louis, R. Weiss, O. Kahn and I. Morgenstern-Badarau, *J. Am. Chem. Soc.*, 1982, **104**, 6330; P. Chaudhuri, M. Guttmann, D. Ventur, K. Weighardt, B. Nuber and J. Weiss, *J. Chem. Soc., Chem. Commun.*, 1985, 1618; R. Cortés, L. Lezama, F. A. Mautner and T. Rojo, in *Molecule-Based Magnetic Materials*, ed. M. M. Turnbull, T. Sugimoto and L. K. Thomson, ACS Book Series, Washington, 1996, pp. 187–200; J. Ribas, M. Monfort, R. Vicente, A. Escuer, R. Cortés, L. Lezama and T. Rojo, *Coord. Chem. Rev.*, 1999, **193**–**195**, 1027 and references therein.

4 M. A. Halcrow, J. C. Huffman and G. Christou, *Angew. Chem., Int. Ed. Engl.*, 1995, **34**, 889; Z. E. Serna, L. Lezama, M. K. Urtiaga, M. I. Arriortua, M. G. Barandika, R. Cortés and T. Rojo, *Angew. Chem., Int. Ed.*, 2000, **39**, 344.

5 J. L. Bursmeister, *Coord. Chem. Rev.*, 1968, **3**, 225; J. Kohout, M. Havastijova and J. Gazo, *Coord. Chem. Rev.*, 1987, **27**, 141.

6 A. H. Norbury, *Adv. Inorg. Chem. Radiochem.*, 1975, **17**, 232; A. H. Golub, H. Kohler and V. V. Slopenko, *Chemistry of Pseudohalides*, Elsevier, Amsterdam, 1986, p. 239.

7 M. I. Arriortua, R. Cortés, J. L. Mesa, L. Lezama, T. Rojo and G. Villeneuve, *Transition Met. Chem.*, 1988, **13**, 371.

8 J. A. R. Navarro, M. A. Romero, M. J. Salas, M. Quirós and E. R. T. Tiekink, *Inorg. Chem.*, 1997, **36**, 4988; M. C. Feller and R. Robson, *Aust. J. Chem.*, 1968, **21**, 2919; A. Basu, T. G. Kasar and N. Y. Sapre, *Inorg. Chem.*, 1998, **27**, 4539; A. Basu, A. R. Saple and N. Y. Sapre, *J. Chem. Soc., Dalton Trans.*, 1987, 1797.

9 N. Okabe and M. Koizumi, *Acta Crystallogr., Sect. C.*, 1998, **54**, 288; R. Faure, H. Loiseleur and G. Thomas-David, *Acta Crystallogr., Sect. B*, 1973, **29**, 1890.

10 G. Annibale, L. Canovese, L. Cattalini, G. Natile, M. Biagini-Cingi, A. Manotti-Lanfredi and A. Tiripicchio, *J. Chem. Soc., Dalton Trans.*, 1981, 2280; S. Wang, J. W. Richardson, S. J. Briggs, R. A. Jacobson and W. P. Jensen, *Inorg. Chim. Acta*, 1986, **111**, 67; M. L. Tong, G. Yang, X. M. Chen and S. W. Ng, *Acta Crystallogr., Sect. C*, 1998, **54**, 217.

11 (*a*) V. Tangoulis, S. Paschalidou, E. G. Bakalbassis, S. P. Perlepes, C. P. Raptopoulou and A. Terzis, *Chem. Commun.*, 1996, 1297; (*b*) A. Tsohos, S. Dionissopoulou, C. P. Raptopoulou, A. Terzis, E. G. Bakalbassis and S. P. Perlepes, *Angew. Chem., Int. Ed.*, 1999, **34**, 983.

12 J. A. Bertrand, E. Fujita and D. G. VanDeerVeer, *Inorg. Chem.*, 1979, **18**, 230; R. M. Buchanan, B. J. Fitgerald and C. G. Pierpont, *Inorg. Chem.*, 1979, **18**, 3439.

13 R. L. Carlin, *Magnetochemistry*, Springer-Verlag, New York, 1986.

14 O. Waldmann, J. Hassmann, P. Müller, G. S. Hanan, D. Volkmer, U. S. Schubert and J. M. Lehn, *Phys. Rev. Lett.*, 1997, **78**, 3390; O. Waldmann, J. Hassmann, P. Müller, D. Volkmer, U. S. Schubert and J. M. Lehn, *Phys. Rev. B*, 1998, **58**, 3277.

15 G. M. Sheldrick, SHELX-97, Program for structure solution and refinement, University of Göttingen, Germany, 1997.

Unusual products from CO/ethene reactions catalysed by β-ketophosphine and related complexes of rhodium

Ruth A. M. Robertson,[a] Andrew D. Poole,[b] Marc J. Payne[b] and David J. Cole-Hamilton*[a]

[a] *School of Chemistry, University of St. Andrews, St. Andrews, Fife, Scotland, UK KY16 9ST. E-mail: djc@st-and.ac.uk*
[b] *BP, Salt End, Hull, UK HU12 8DS*

Received (in Cambridge, UK) 3rd October 2000, Accepted 20th November 2000
First published as an Advance Article on the web 15th December 2000

Using rhodium complexes of tertiary phosphines with carbonyl groups β to the P atom, ethene and CO react in methanol to give products involving increased chain growth (octane-3,6-dione, methyl 4-oxohexanoate) compared with PEt_3 complexes and unsaturated products (methyl propenoate, penten-3-one and 1-methoxypentan-3-one from addition of methanol to penten-3-one); mechanistic studies suggest that the ligand carbonyl group prevents coordination of the keto group in the growing chain.

Reactions between ethene and CO in methanol generally give perfectly alternating polyketones or methyl propanoate (MP), with the best catalysts being based on palladium complexes of mono- or ditertiary phosphines,[1,2] although we have recently reported that highly electron rich rhodium phosphine complexes can give high selectivities to pentan-3-one (DEK), with the two extra H atoms required being derived from methanol, which forms methyl formate (MF).[3] We presented evidence that the selectivity to pentan-3-one (DEK) arose because of binding of the keto-oxygen atom in the growing chain to the rhodium atom to give an η^2-3-oxopentyl intermediate. Since this complex has 18e, it more readily protonates and reductively eliminates pentan-3-one than undergoing further insertion to give chain growth (Scheme 1).[3]

One of our interests is in the production of CO/C_2H_4 oligomers for use as low-volatility solvents containing relatively high oxygen content, so we were interested in the possibility of encouraging chain growth and hence of preventing the formation of the η^2-3-oxopentyl intermediate. We, therefore, synthesised a range of phosphines which themselves contain carbonyl groups β to the P atom in the hope that these carbonyl groups might compete with coordination of the keto group in the growing chain and encourage chain growth.

The ligands shown in Table 1 were synthesised by the reaction of R_2PH (R = Et, Bu^t, Cy) with the appropriate bromo compound, R′$COCH_2Br$. (R′ = Ph, Et, OEt), followed by removal of HBr with base (Scheme 2). Catalytic reactions were then carried out, synthesising the active catalyst *in situ* from the ligand and $[Rh(acac)(CO)_2]$ (Hacac = pentane-2,4-dione). The results of these reactions are shown in Table 1 and indicate that, apart from the complex derived from $Bu^t_2PCH_2C(O)Ph$, which does not give an active catalyst, catalysts based on these ligands show quite different selectivities compared with those involving PEt_3. In particular, chain growth to octane-3,6-dione (OD) and methyl 4-oxohexanoate (M4OH) has become significant and the unsaturated products, penten-3-one (EVK) and methyl propenoate (MA) are observed. A further product, 1-methoxypentan-3-one (1M3P)† is a major product. We have shown in separate experiments that this is formed by addition of methanol to penten-3-one (EVK) in an uncatalysed reaction under the experimental conditions employed. The selectivity to medium chain products (≥7 chain atoms) can be as high as 57.6%,

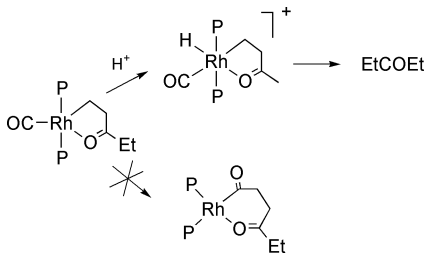

Scheme 1 Proposed role of an η^2-3-oxopentyl intermediate in determining the selectivity of ethene carbonylation to pentan-3-one catalysed by Rh/PEt_3 complexes.[3]

Scheme 2 Sythesis of β-ketophosphine ligands. R″ = H, R = Et, R′ = Ph, OEt, Et; R″ = H, R = Bu^t, R′ = Ph, OEt; R″ = H, R = Cy, R′ = Ph; R″ = Me, R = Et, R′ = Me. *Reagent*: i, NaOH.

Table 1 Products obtained from the carbonylation of ethene catalysed by rhodium complexes of β-ketophosphines and related ligands[a]

Ligand	MA	MP	EVK	DEK	1M3P	M4OH	OD	Total turnover	MCP(%)
$Et_2PCH_2C(O)Ph$	4.4	4.4	2.0	24.0	12.5	2.4	9.0	58.7	40.7
$Et_2PCH_2C(O)Et$	6.7	7.8	3.1	23.4	12.0	2.6	7.1	62.7	34.6
$Et_2PCH_2C(O)OEt$	12.2	6.8	3.7	38.2	14.3	5.8	9.7	90.7	32.9
$Et_2PCH(Me)C(O)Me$	7.2	6.9	1.4	39.7	6.7	2.5	3.1	67.5	18.2
$Cy_2PCH_2C(O)Ph$	—	4.0	—	0.5	1.2	2.0	0.7	8.4	46.4
$Bu^t_2PCH_2C(O)OEt$	—	2.1	1.7	7.7	11.2	—	4.4	27.1	57.6
$Bu^t_2PCH_2C(O)Ph$	—	—	—	—	—	—	—	0	—
$Et_2PC_2H_4OMe$	4.1	15.0	1.5	37.3	17.8	3.0	9.2	87.9	34.1
$Et_2PC_2H_4NEt_2$	—	26.9	trace	41.1	3.3	—	4.4	75.7	10.2
$Me_2PCH_2P(O)Me_2$	—	10.7	0.9	3.5	3.7	—	2.9	21.7	30.4
$Me_2PCH_2P(O)Me_2$[b]	4.4	5.1	3.4	24.9	13.4	2.9	14.3	68.4	44.7

[a] $[Rh(acac)(CO)_2]$ (0.1 mmol), phosphine (0.4 mmol), CO (35 bar), ethene (35 bar), methanol (10 cm^3), 110 °C, 24 h. Amounts expressed as catalyst turnovers. [b] 2 equivalents of ligand used, *i.e.* (0.2 mmol). MA (methyl propenoate, methyl acrylate), MP (methyl propanoate), EVK (penten-3-one, ethyl vinyl ketone), DEK (pentan-3-one, diethyl ketone), 1M3P (1-methoxypentan-3-one), M4OH (methyl 4-oxohexanoate), OD (octane-3,6-dione), MCP (medium chain products, 7+ atoms in backbone).

DOI: 10.1039/b007989h

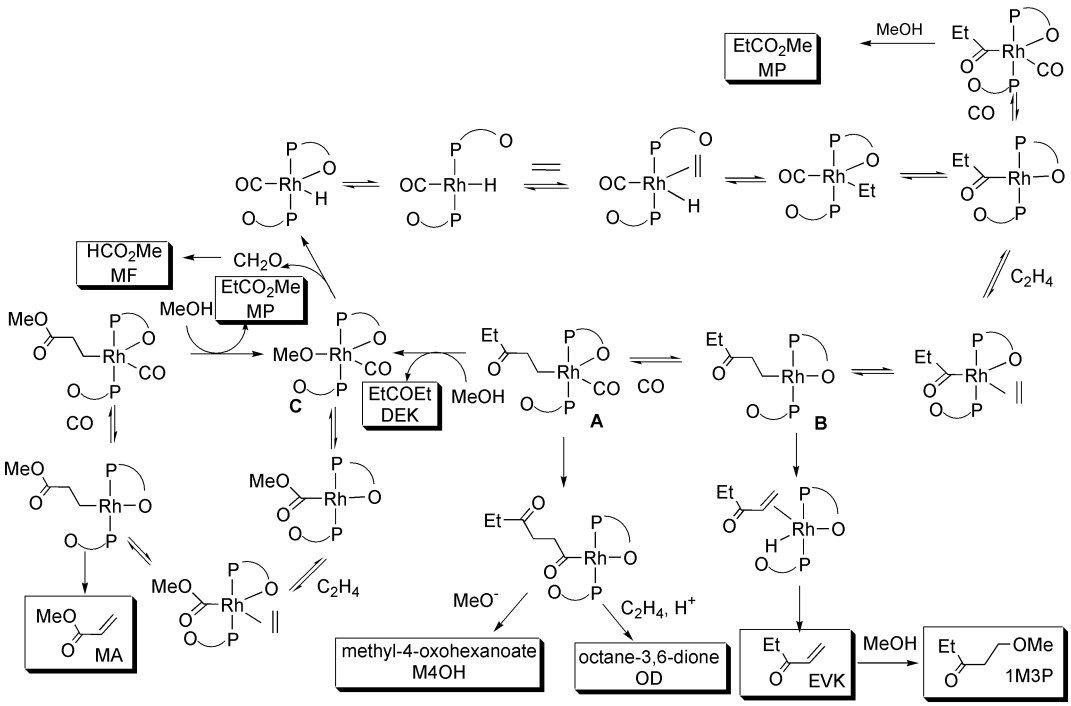

Scheme 3 Proposed mechanism of ethene carbonylation catalysed by Rh/β-ketophosphine (P⁀O) complexes. The products shown in boxes have been observed (Table 1), but the assignments of the metal containing intermediates are tentative.

whereas with PEt_3 the selectivity to pentan-3-one (DEK) can be >80% with only traces of medium chain products being formed. Similar results to those for the β-ketophosphines are obtained (Table 1) using other ligands with O γ to the P atom such as $Me_2PCH_2P(O)Me_2$, or $Et_2PCH_2CH_2OMe$, but not with N in this position; $Et_2PCH_2CH_2NEt_2$ behaves more like PEt_3, although the rate is lower.

We have also carried out the reaction using $PhCOCH_2PEt_2$ in CD_3OD and find that the methyl groups of pentan-3-one (DEK) and of methyl propanoate (MP) contain 0 or 1 D atoms.‡ This contrasts with reactions involving PEt_3,[3] where multiple deuteriation of the methyl groups of pentan-3-one (DEK) is observed.

These results point to the conclusion that, in these systems, the carbonyl group in the growing chain does not coordinate, presumably because the coordination site is blocked by the carbonyl group β to the phosphine (Scheme 3). Intermediate **A** in Scheme 3 is an 18e complex, so may protonate and reductively eliminate pentan-3-one (DEK). Alternatively, CO may insert leading to chain growth. We have shown that multiple D incorporation into the methyl group of pentan-3-one (DEK) in the Rh/PEt_3 catalysed reactions carried out in CD_3OD occurs *via* β-H abstraction in the η^2-3-oxopentyl intermediate to give an enolate. A similar β-H abstraction in the η^1-3-oxopentyl intermediate, **B** in Scheme 3, would lead to penten-3-one (EVK) bound only through the double bond and it appears that this decoordinates to give free penten-3-one (DEK), rather than undergoing reversible C–H bond breakage and multiple D incorporation.

The formation of methyl propenoate (MA) is also of considerable interest, not only because it indicates that acrylates can be products from CO/C_2H_4 reactions under non-oxidative conditions, but also because it indicates that a carbomethoxy mechanism[1] is operating in addition to the hydride mechanism which is responsible for the other products. This suggests that CO insertion into the Rh–OMe bond competes with β-H abstraction and CO can insert in the 18e complex (**C** in Scheme 3). Acrylates can be products of CO/alkene reactions in the presence of oxygen.[5,6]

In conclusion, all of the products obtained from the reaction of CO with ethene in methanol in the presence of rhodium complexes containing phosphine ligands with a carbonyl β to the P atom can be explained as in Scheme 3 if one carbonyl group in the phosphine is coordinated to the rhodium.

We thank BP and the EPSRC for funding (R. A. M. R.) and Dr E. Ditzel and Mr P. Howard for helpful discussions.

Notes and references

† Since this product has seven atoms in the chain and contains two O atoms (bp 62 °C at 24 Torr),[4] it may be a suitable component of a low volatility solvent mixture, so is included when calculating the percentage of medium-chain products produced in the reaction.

‡ The methylene groups contain from 0 to 2 D atoms on account of post-reaction exchange with the solvent.[3]

1 E. Drent, J. A. M. van Broekhoven and P. H. M. Budzelaar, in *Applied Homogeneous Catalysis with Organometallic Compounds*, ed. B. Cornils and W. A. Herrmann, VCH, Weinheim, 1996, vol. 1, p. 333 and references therein.
2 E. Drent and P. H. M. Budzelaar, *J. Organomet. Chem.*, 2000, **593**–**594**, 211.
3 R. A. M. Robertson, A. D. Poole, M. Payne and D. J. Cole-Hamilton, *J. Chem. Soc., Dalton Trans.*, 2000, 1817.
4 I. N. Nazarov and I. V. Torgov, *Chem. Abstr.*, 1948, **42**, 7736a.
5 D. M. Fenton and K. L. Olivier, *US Pat.*, 3 349 119, 1967.
6 W. Gaenzler and K. Kabs, *US Pat.*, 3 907 882, 1975.

ChemComm

Reversible switching of the first hyperpolarisability of an NLO-active donor–acceptor molecule based on redox interconversion of the octamethylferrocene donor unit

Michael Malaun,[a] Zoe R. Reeves,[a] Rowena L. Paul,[a] John C. Jeffery,[a] Jon A. McCleverty,*[a] Michael D. Ward,*[a] Inge Asselberghs,[b] Koen Clays[b] and André Persoons[b]

[a] *School of Chemistry,University of Bristol, Cantock's Close, Bristol, UK BS8 1TS. E-mail: mike.ward@bristol.ac.uk; jon.mccleverty@bristol.ac.uk*

[b] *Laboratory of Chemical and Biological Dynamics, Center for Research on Molecular Electronics and Photonics, University of Leuven, Celestijnenlaan 200D, B-3001 Leuven, Belgium*

Received (in Cambridge, UK) 5th October 2000, Accepted 15th November 2000
First published as an Advance Article on the web 15th December 2000

Compound 1, containing an octamethylferrocene donor linked to a nitrothiophene acceptor *via* an ethenyl linker, shows a static first hyperpolarisability β_0 of 95(±10) × 10^{-30} esu, which is reduced to 10(±2) × 10^{-30} esu on oxidation of the octamethylferrocene unit; this provides for a simple redox-based switching of the NLO characteristics of the compound.

Compounds displaying non-linear optical (NLO) properties are of considerable interest because of their possible applications in the emerging technologies of optoelectronic and photonic devices.[1] Second-order NLO effects, including second-harmonic generation, and especially electro-optic modulation are important in interfacing massive amounts of electronic data to wideband optical communication. At the molecular level, the efficiency for electro-optic modulation is determined by the second-order non-linear polarisability, also called the first hyperpolarisability, β. A large value of β is generally associated with molecules which have a donor/conjugated bridge/acceptor (D-π-A) structure, such that there is a long-range charge-transfer transition from one end to the other and consequently a substantial difference between the ground-state and excited-state dipole moments.

The ability to switch the NLO response of a molecule 'on' and 'off' reversibly by a simple controllable perturbation would add significant value to the utility of NLO molecules, from the point of view of developing molecular photonic devices whose properties can be switched by modifying one of the component parts.[2] Despite the large number of molecules with large first hyperpolarisabilities, there are remarkably few examples in which such reversible switching has been demonstrated. Of these the majority depend on isomerisation or tautomerisation of the molecule, such that the nature of the conjugated bridge linking the donor and acceptor termini undergoes a substantial change.[3] A more appealing method of controlling the second-order NLO response of a molecule would be a reversible redox change, in which either the donor (D) unit is oxidised or the acceptor (A) unit is reduced. The result in either case would be a loss of the charge-transfer capability and a consequent drop in the hyperpolarisability β.[2] To date there is a single example of this in the literature, from the group of Coe, comprising a $\{Ru(NH_3)_5\}^{2+}$ donor linked to a viologen-like acceptor; the value of β decreased by an order of magnitude on one-electron oxidation of the Ru terminus. Subsequent re-reduction of the Ru terminus completely restored the SHG properties of the compound.[4]

We describe here a new molecule for second-order NLO applications (**1**) which contains an octamethylferrocene donor unit and a nitrothiophene acceptor, linked by an ethenyl bridge. The reversible octamethylferrocene–octamethylferrocenium couple, at modest potential, provides an ideal route for redox-based switching of the hyperpolarisability. Compounds which contain ferrocene units as the electron donor, with a single conjugated side-arm linked to an acceptor unit, have been exceptionally popular for studying SHG in the last decade.[5] The redox activity of the ferrocene donor unit however has not until now been exploited for switching purposes; use of the octamethylferrocene unit in **1** will both enhance its electron-donor properties compared to ferrocene, and will reduce the redox potential to make redox-based switching more facile.

Compound **1** was prepared in good yield† by a Wittig reaction between 1′,2,2′,3,3′,4,4′,5-octamethylferrocenylmethyltriphenylphosphonium bromide[6] and 5-nitro-2-thiophenecarbaldehyde in tetrahydrofuran (THF); the crystal structure is in Fig. 1.‡ The cyclopentadienyl ring of the donor, the ethenyl bridge, and the nitrothiophene acceptor are essentially coplanar which will clearly optimise end-to-end charge-transfer *via* the conjugated system. The electronic spectrum in CH_2Cl_2 (Fig. 2)

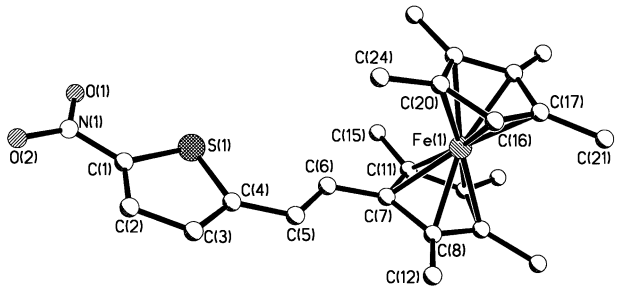

Fig. 1 Crystal structure of **1** together with selected bond distances. The structure of the complex cation of $[\mathbf{1}]^+(PF_6)\cdot CH_2Cl_2$ is essentially identical, and the bond distances for this are given in square parentheses after the corresponding value for **1**. Fe–C (average) 2.05 [2.10], N(1)–O(1) 1.242(4) [1.232(3)], N(1)–O(2) 1.228(4) [1.235(3)], N(1)–C(1) 1.423(4) [1.428(3)], C(1)–C(2) 1.354(5) [1.356(4)], C(2)–C(3) 1.405(4) [1.401(3)], C(3)–C(4) 1.377(4) [1.379(3)], C(1)–S(1) 1.719(3) [1.718(2)], C(4)–S(1) 1.738(3) [1.731(2)], C(4)–C(5) 1.442(4) [1.446(3)], C(5)–C(6) 1.348(4) [1.336(3)], C(6)–C(7) 1.449(4) [1.461(3)] Å.

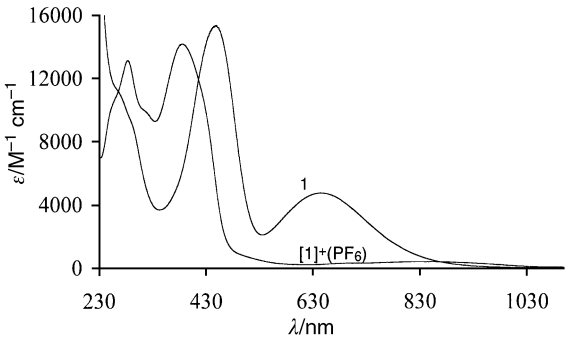

Fig. 2 Electronic spectra of **1** and $[\mathbf{1}]^+(PF_6)$ in CH_2Cl_2.

DOI: 10.1039/b008056j

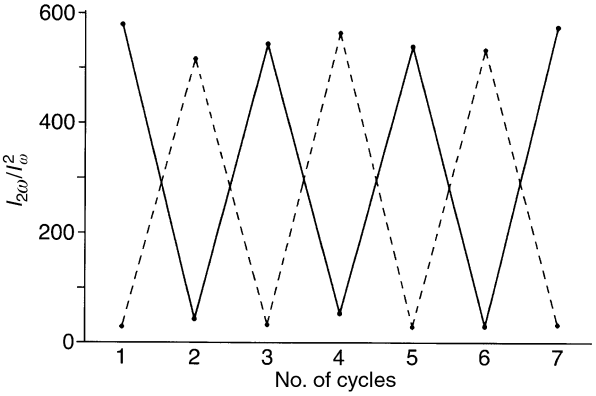

Fig. 3 Redox switching of the hyper-Raleigh scattering response between **1** and $[\mathbf{1}]^+$ in CH_2Cl_2 (concentration of samples, 4×10^{-5} M). The solid line shows the response obtained starting with **1** and then alternately oxidising and re-reducing it; the dotted line shows the response obtained starting with $[\mathbf{1}]^+(PF_6)$ and then alternately reducing and re-oxidising it. The parameter plotted on the *y*-axis ($i_{2\omega}/I^2_{\omega}$) is proportional to β^2.

shows transitions at 644 nm and 447 nm which we ascribe to the two relevant D $\rightarrow$ A charge-transfer transitions;[7] in agreement with this, both transitions are strongly solvatochromic, with the absorption maxima changing from 586 and 409 nm respectively in hexane, to 655 and 453 nm respectively in dimethyl sulfoxide. Compound **1** undergoes a reversible octamethylferrocene–octamethylferrocenium redox interconversion at -0.30 V *vs.* the ferrocene–ferrocenium couple in THF. Accordingly, one-electron oxidation of **1** by treatment with 1 equiv. of ferrocenium hexafluorophosphate in MeCN afforded $[\mathbf{1}]^+(PF_6)$ in high yield.§ This complex has also been structurally characterised,‡ and the structure of the complex cation $[\mathbf{1}]^+$ is essentially identical to that of **1** apart from minor changes in the Fe–C bond distances (see caption to Fig. 1). In the oxidised complex $[\mathbf{1}]^+$ the charge-transfer transitions of **1** are absent, replaced by the characteristic weak LMCT transition of the ferrocenium unit at 851 nm (Fig. 2).

We used the hyper-Raleigh scattering method[8] to measure the first hyperpolarisability β of **1** and $[\mathbf{1}]^+$ in CH_2Cl_2 solution using a 1064 nm laser. The value of β obtained for **1** [316 ($\pm$32) $\times$ 10^{-30} esu] is much greater than that for $[\mathbf{1}]^+$ [25 ($\pm$5) $\times$ 10^{-30} esu], as we would expect based on the above arguments. Part of this change is however ascribable to the fact that the value of **1** is resonantly enhanced due to absorption by the CT transitions in the region of the second harmonic of the excitation laser at 532 nm; this effect is not so significant for $[\mathbf{1}]^+$ whose absorbance at this wavelength is much lower. Consequently the two-level model[9,10]¶ was used to derive the static hyperpolarisability (β_0) in each case, and β_0 values of 95 ($\pm$10) $\times$ 10^{-30} and 10 ($\pm$2) $\times$ 10^{-30} esu were obtained for **1** and $[\mathbf{1}]^+(PF_6)$ respectively. Thus, compound **1** has a SHG efficiency about one order of magnitude greater than does $[\mathbf{1}]^+$.

The redox interconversion of **1** and $[\mathbf{1}]^+$ thus provides a basis for an effective switch of the second-order NLO properties of the complex. The switching effect is illustrated in Fig. 3, which shows (solid line) the alternation in the value of the first hyperpolarisability as a sample of **1** is alternately oxidised (by addition of Bu_4NBr_3) and then reduced (by addition of hydrazine). Exactly similar results were obtained starting with $[\mathbf{1}]^+$ and alternately reducing and oxidising it (dotted line). Given the large number of D–π–A complexes based on ferrocenyl donors which have been prepared for NLO studies,[5] this redox-based switching is clearly of wide applicability for the development of switchable NLO materials.[2]

We thank the Austrian Foundation for Scientific Research (FWF) for an Erwin Schrödinger fellowship and the European Community for a postdoctoral fellowship (EC96-0047) (M. M), the EPSRC for a PhD studentship (Z. R. R.) and the Leverhulme foundation for a post-doctoral fellowship (R. L. P.). We also acknowledge the University of Leuven (GOA 2000/03), the Belgian government (IUAP IV/11) and the Fund for Scientific Research, Flanders (FWO-V G.0407.98 and G.0338.98). M. D. W. is the Royal Society of Chemistry Sir Edward Frankland fellow for 2000/2001.

Notes and references

† To a mixture of 1′,2,2′3,3′,4,4′,5-octamethylferrocenylmethyltriphenylphosphonium bromide (1.75 g, 2.68 mmol) and dry THF (100 cm^3) under N_2 at -78 °C was added potassium *tert*-butoxide (0.33 g, 2.94 mmol). The red suspension was allowed to warm up to 0 °C and was stirred for 30 min at this temperature, after which time 5-nitro-2-thiophenecarbaldehyde (0.50 g, 3.21 mmol) was slowly added. The resulting green solution was stirred at room temperature for 3 h. After quenching with water and removal of solvents *in vacuo*, chromatographic purification (alumina, 1:1 diethyl ether–hexane) afforded pure **1** (0.87 g, 72%). Found: C, 63.8; H, 6.7; N, 3.1%; $C_{24}H_{29}FeNO_2S$ requires C, 63.9; H, 6.4; N, 3.1%. EIMS: *m/z* 451 (M^+, 100%). ^{1}H NMR (300 MHz, $CDCl_3$) δ 1.62, 1.66, 1.82, 1.95 (all 6 H, s, CH_3 groups attached to Cp rings), 3.35 (1 H, s, CH of Cp), 6.73 (1 H, d, J = 16 Hz, C*H*=CH), 6.82 (1 H, d, J = 4 Hz, thienyl CH), 6.99 (1 H, d, J = 16 Hz, CH=C*H*), 7.80 (1 H, d, J = 4 Hz, thienyl CH).

‡ *Crystal data*: for $C_{24}H_{29}FeNO_2S$: M = 451.4, monoclinic, space group $P2_1/n$, a = 14.960(2), b = 9.4435(18), c = 15.639(4) Å, β = 102.200(14)°, U = 2159.4(8) Å^3, Z = 4, D_c = 1.388 Mg m^{-3}, μ(Mo-Kα) = 0.815 mm^{-1}, F(000) = 952, T = 173 K, 4930 independent reflections with 2θ < 55°. Refinement of 270 parameters converged at final $R1$ = 0.0393, $wR2$ = 0.1155. For $C_{24}H_{29}FeF_6NO_2PS{\cdot}CH_2Cl_2$: M = 681.3, triclinic, space group $P\bar{1}$, a = 10.2058(9), b = 12.1655(11), c = 13.0266(11) Å, α = 73.439(2), β = 68.807(2), γ = 77.176(2)°, U = 1432.6(2) Å^3, Z = 2, D_c = 1.579 Mg m^{-3}, μ(Mo-Kα) = 0.906 mm^{-1}, F(000) = 698, T = 173 K, 6498 independent reflections with 2θ < 55°. Refinement of 396 parameters converged at final $R1$ = 0.0390, $wR2$ = 0.0968. X-Ray measurements were made using a Bruker SMART CCD area-detector diffractometer; structure solution and refinement was with the SHELXTL program system version 5.1, 1998. CCDC 182/1853. See http://www.rsc.org/suppdata/cc/b0/b008056j/ for crystallographic files in .cif format.

§ To a solution of **1** (0.15 g, 0.33 mmol) in N_2-purged dry MeCN was added ferrocenium hexafluorophosphate (0.107 g, 0.32 mmol) and the mixture was sonicated in an ultrasound cleaning bath for 15 min. After evaporation of the solvent the residue was washed several times with ether until the filtrate was colourless, and was then dried yielding pure $[\mathbf{1}]^+(PF_6)$ (0.18 g, 91%). Found: C, 47.9; H, 5.1; N, 2.3%; $C_{24}H_{29}FeF_6NO_2PS$ requires C, 48.3; H, 4.9; N, 2.4%. FABMS: *m/z* 451 ($M^+ - PF_6$, 100%).

¶ One of the referees has pointed out that the two-level model (ref. 9) cannot be applied with accuracy to ferrocenyl-based systems such as these in which two charge-transfer processes contribute to β (ref. 7). This is true, however because of its simplicity and the lack of readily applicable alternatives it remains in wide use as long as its limitations are understood (ref. 10).

1 S. R. Marder, B. Kippelen, A. K.-Y. Jen and N. Peyghambarian, *Nature*, 1997, **388**, 845; T. Verbiest, S. Houbrechts, M. Kauranen, K. Clays and A. Persoons, *J. Mater. Chem.*, 1997, **7**, 2175; S. R. Marder, in *Inorganic Materials*, ed. D. W. Bruce and D. O'Hare, Wiley, Chichester, 1992, ch. 3.
2 B. J. Coe, *Chem. Eur. J.*, 1999, **5**, 2464.
3 E. Hendrickx, K. Clays, A. Persoons, C. Dehu and J.-L. Brédas, *J. Am. Chem. Soc.*, 1995, **117**, 3547; R. Loucif-Saïbi, K. Nakatani, J. A. Delaire, M. Dumont and Z. Sekkat, *Chem. Mater.*, 1993, **5**, 229; S. L. Gilat, S. H. Kawai and J.-M. Lehn, *Chem. Eur. J.*, 1995, **1**, 275; S. Houbrechts, K. Clays, A. Persoons, Z. Pikramenou and J.-M. Lehn, *Chem. Phys. Lett.*, 1996, **258**, 485; K. Nakatani and J. A. Delaire, *Chem. Mater.*, 1997, **9**, 2682.
4 B. J. Coe, S. Houbrechts, I. Asselberghs and A. Persoons, *Angew. Chem., Int. Ed.*, 1999, **38**, 366.
5 J. Heck, S. Dabek, T. Meyer-Friedrichsen and H. Wong, *Coord. Chem. Rev.*, 1999, **190**–**192**, 1217; S. Barlow and S. R. Marder, *Chem. Commun.*, 2000, 1555; N. J. Long, *Angew. Chem., Int. Ed. Engl.*, 1995, **34**, 21.
6 A. Hradsky, B. Bildstein, N. Schuler, H. Schottenberg, P. Jaitner, K. H. Ongania, K. Wurst and J.-P. Launay, *Organometallics*, 1997, **16**, 392.
7 S. Barlow, H. E. Bunting, C. Ringham, J. C. Green, G. U. Bublitz, S. G. Boxer, J. W. Perry and S. R. Marder, *J. Am. Chem. Soc.*, 1999, **121**, 3715.
8 K. Clays and A. Persoons, *Phys. Rev. Lett.*, 1991, **66**, 2980; K. Clays and A. Persoons, *Rev. Sci. Instrum.*, 1992, **63**, 3285.
9 J. L. Oudar and D. S. Chemla, *J. Chem. Phys.*, 1977, **66**, 2664; J. L. Oudar, *J. Chem. Phys.*, 1977, **67**, 446; J. Zyss and J. L. Oudar, *Phys. Rev. A*, 1982, **26**, 2016.
10 I. R. Whittall, A. M. McDonagh, M. G. Humphrey and M. Samoc, *Adv. Organomet. Chem.*, 1998, **42**, 291.

ChemComm

$^1J(^{199}Hg^{199}Hg)$ values of up to 284 kHz in complexes of $[Hg–Hg]^{2+}$ with crown ethers: the largest indirect coupling constants

Richard Malleier, Holger Kopacka, Walter Schuh, Klaus Wurst and Paul Peringer*

Institut für Allgemeine, Anorganische und Theoretische Chemie, Universität Innsbruck, Innrain 52a, A-6020 Innsbruck, Austria. E-mail: paul.peringer@uibk.ac.at

Received (in Cambridge, UK) 18th September 2000, Accepted 14th November 2000
First published as an Advance Article on the web

The values of the $^1J(^{199}Hg^{199}Hg)$ coupling constant in solution of the asymmetric dimercury(2+) complexes with the stoichiometries Hg_2^{2+}/18-crown-6 and Hg_2^{2+}/18-crown-6/15-crown-5 are 220 300 and 284 100 Hz, respectively, representing the largest scalar couplings measured.

Very large scalar coupling constants have been observed between heavy metal nuclei and have been attributed to relativistic effects. The largest value known at present is the one-bond $^{199}Hg^{199}Hg$ coupling in the polycation $[Hg–Hg–Hg]^{2+}$ **1** with a magnitude of 139 600 Hz.[1] The largest coupling constant between two different nuclei is a 71 060 Hz $^1J(^{195}Pt^{205}Tl)$ coupling observed for the compound $[(NC)_5Pt–Tl]$.[2]

The use of solid-state ^{199}Hg NMR for the determination of the $^{199}Hg^{199}Hg$ coupling of $[Hg–Hg]^{2+}$ salts involving magnetically inequivalent mercury atoms, has been proposed,[3] but appears not to have been carried out. We report here on the synthesis of asymmetric dimercury(2+)–crown ether complexes which are kinetically stable on the NMR time scale at low temperatures and provide straightforward access to the $^{199}Hg^{199}Hg$ coupling constants.

Treatment of $[Hg–Hg]^{2+}$ with 1 equiv. of 18-crown-6 in CH_2Cl_2 produces the dimercury(2+) complex **2** in which one Hg is complexed to the macrocyclic crown ether.† The mixed ligand complex $[Hg_2(18\text{-crown-6})(15\text{-crown-5})(Me_2SO)](O_3SCF_3)_2$ **3a** containing one 18-crown-6 and one 15-crown-5 co-ordinated to dimercury(2+) was formed upon reaction of **2** with 1 equiv. of 15-crown-5.†

The ^{199}Hg NMR spectra of **2** and **3** consist of a superposition of the patterns of the two isotopomers with one ^{199}Hg nucleus (abundance 14.00% each) and the isotopomer containing two ^{199}Hg nuclei (abundance 2.84%). The latter arises from an AB spin system. The outer transitions of the AB system could not be observed because of very low probabilities (*e.g.* 0.3% of the inner transitions as calculated for **3b**) and because of linewidths of *ca.* 60–80 Hz for **2** and **3**, which are attributed to chemical shift anisotropy (CSA) relaxation. The coupling constant is readily derived from the distances of the inner lines of the AB system and of the shifts ν_a and ν_b which are obtained from the patterns of the isotopomers containing one ^{199}Hg nucleus. The value of the $^1J(^{199}Hg^{199}Hg)$ coupling constant in **2** is 220 300 Hz. An even larger $^{199}Hg^{199}Hg$ coupling constant (263 200 Hz) is observed for the mixed 18-crown-6/15-crown-5 complex **3a** in CH_2Cl_2. The ^{199}Hg NMR spectrum of a solution of **3a** in MeOH at 223 K shows the presence of two asymmetric dimercury(2+) complexes. The parameters of one of these species correspond to those of $[Hg_2(18\text{-crown-6})(15\text{-crown-5})(Me_2SO)](O_3SCF_3)_2$ **3a** in CH_2Cl_2, the other species is assigned to $[Hg_2(18\text{-crown-6})(15\text{-crown-5})(MeOH)](O_3SCF_3)_2$ **3b**, which is thought to be formed according to the equilibrium (1).

$$\underset{\textbf{3a}}{[Hg_2(18\text{-crown-6})(15\text{-crown-5})(Me_2SO)]^{2+}} + MeOH \rightleftharpoons \underset{\textbf{3b}}{[Hg_2(18\text{-crown-6})(15\text{-crown-5})(MeOH)]^{2+}} + Me_2SO \quad (1)$$

The size of the Hg–Hg coupling constant of **3b** is 284100 Hz, and we believe that this represents the largest scalar coupling constant recorded so far. The ^{199}Hg shifts of the mercury atoms complexed to 18-crown-6 macrocycles appear at low frequencies compared with the Hg atoms coordinated by 15-crown-5 or bridging Me_2SO.

The complexes **2** and **3c** (all attempts to isolate **3a** gave **3c**) were characterised by single crystal X-ray diffraction:‡ as can be seen from Fig. 1, **2** exists as a dimer $\{[Hg_2(18\text{-crown-6})(Me_2SO)(\mu\text{-}Me_2SO)](O_3SCF_3)_2\}_2$ in the solid state. Curiously, the crystals of **3c** are built from two different complexes: the asymmetric unit contains one $[Hg_2(18\text{-crown-6})(15\text{-crown-5})(Me_2SO)](O_3SCF_3)_2$ and one $[Hg_2(18\text{-crown-6})(15\text{-crown-5})(H_2O)](O_3SCF_3)_2$ species which is shown in Fig. 2. In **2** and **3c** the coordination geometry of the mercury atoms complexed to a 18-crown-6 is hexagonal-bipyramidal with the other Hg atom and one oxygen of Me_2SO or H_2O in axial position and the crown oxygens in the equatorial sites. The 18-crown-6 ligands are located slightly off-centre with respect to the mercury atoms, presumably as a result of the steric demands of the Me_2SO ligand coordinated to the same Hg atom. The mercury atoms reside slightly off the 18-crown-6 plane which is shifted towards the terminal Me_2SO ligands. The 15-crown-5 macrocycle is coordinated in a 'half-sandwich' manner.

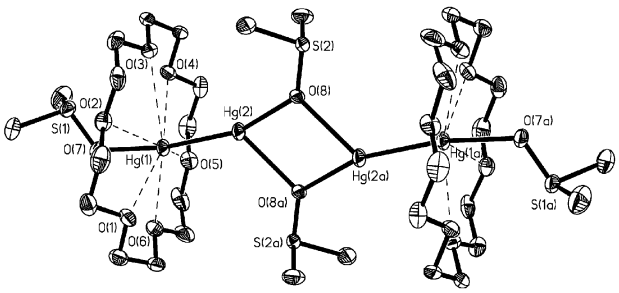

Fig. 1 Structure of $\{[Hg_2(18\text{-crown-6})_2(Me_2SO)(\mu\text{-}Me_2SO)]\}_2^{4+}$ (cation of **2**). Thermal ellipsoids are shown at the 20% probability level.

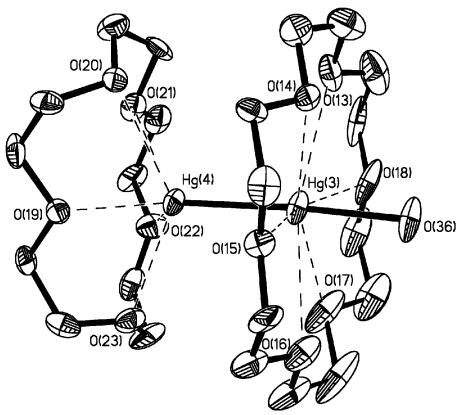

Fig. 2 Structure of $\{[Hg_2(18\text{-crown-6})(15\text{-crown-5})(H_2O)]^{2+}$ (part of **3c**). Thermal ellipsoids are shown at the 20% probability level.

Notes and references

† *Synthesis and data*: for **2**: a mixture of $[Hg(Me_2SO)_6](O_3SCF_3)_2$[4] (0.1 mmol, 0.0968 g) in CH_2Cl_2 (0.5 mL) and elemental mercury (0.1 mL) was stirred vigorously for 2 h and 0.1 mmol (0.0264 g) of 18-crown-6 was then added. Colourless crystals were obtained from a 0.4 M solution in MeOH after 10 days at 277 K (0.060 g, 54%). Anal. Calc. for $C_{36}H_{72}F_{12}Hg_4O_{28}S_8$: C, 19.31; H, 3.24. Found C, 19.34; H, 3.26%. ^{199}Hg NMR (53.63 MHz, shifts relative to 2 mmol HgO in 1 ml 60% $HClO_4$, sweep width 50 kHz, time domain size 64 K, typical number of scans 20000, CH_2Cl_2, 243 K): δ 435 (Hg atom complexed to 18-crown-6), 944; $J(^{199}Hg^{199}Hg)$ 220300 (±790) (corresponding to an uncertainty of the difference of the two inner AB lines of ±4 data points).

For **3a**: a solution of 0.1 mmol (0.1120 g) of **2** in 0.5 mL of MeOH was treated with 0.1 mmol of 15-crown-5 (0.0220 g). All attempts to isolate **3a** gave **3c**: colourless crystals of **3c** were obtained upon standing of a solution of **3a** in MeOH for 3 weeks in contact with the atmosphere (0.070 g, 56%). Anal. Calc. for $C_{50}H_{96}F_{12}Hg_4O_{36}S_5{\cdot}H_2O$: C, 24.20; H, 3.98. Found C, 24.08; H, 3.89%. ^{199}Hg NMR for **3a**, (CH_2Cl_2, 223 K): δ 304 (Hg atom complexed to 18-crown-6), 1023; $J(^{199}Hg^{199}Hg)$ 263200 (±570); i, (MeOH, 223 K): δ 317, 1032, $J(^{199}Hg^{199}Hg)$ 266600 (±590); **3b** (MeOH, 223 K): δ 345, 972, $J(^{199}Hg^{199}Hg)$ 284100 (±860).

‡ *Crystal data*: for **2**: $C_{36}H_{72}F_{12}Hg_4O_{28}S_8$, M = 2239.78, triclinic, space group $P\bar{1}$ (no. 2), a = 9.547(5), b = 11.836(2), c = 15.548(2) Å, α = 78.39(2), β = 77.21(4), γ = 83.79(2)°, V = 1674.5(9) Å^3, T = 213(2) K, Z = 1, Mo-Kα radiation (λ = 0.71073 Å), 5809 reflections collected, 4795 independent reflections (R_{int} 0.0274), 3457 reflections with $I > 2\sigma(I)$, $R1$ [$I > 2\sigma(I)$] = 0.0373, $wR2$ (all data) = 0.0726, goodness-of-fit 1.021. The structure was solved by direct methods (SHELXS-86),[5] and refined by full-matrix least-squares methods on F^2 (SHELXL-93).[6]

For **3c**: $C_{50}H_{96}F_{12}Hg_4O_{36}S_5{\cdot}H_2O$, M = 2481.94, triclinic, space group $P\bar{1}$ (no. 2), a = 12.289(2), b = 15.902(4), c = 21.254(4) Å, α = 92.25(2), β = 93.06(2), γ = 93.35(2)°, V = 4136.7(15) Å^3, T = 213(2) K, Z = 2, Mo-Kα radiation (λ = 0.71073 Å), 8498 reflections collected, 8004 independent reflections (R_{int} = 0.0508), 5405 reflections with $I > 2\sigma(I)$, $R1$ [$I > 2\sigma(I)$] = 0.0566, $wR2$ (all data) = 0.1483, goodness-of-fit 1.032. The structure was solved and refined as for **2**.[5,6] CCDC 182/1851. See http://www.rsc.org/suppdata/cc/b0/b007581g/ for crystallographic files in .cif format.

1 R. J. Gillespie, P. Granger, K. R. Morgan and G. J. Schrobilgen, *Inorg. Chem.*, 1984, **23**, 887.
2 M. Maliarik, K. Berg, J. Glaser, M. Sandström and I. Tóth, *Inorg. Chem.*, 1998, **37**, 2910.
3 R. A. Santos and G. S. Harbison, *J. Am. Chem. Soc.*, 1994, **116**, 3075.
4 P. Peringer, *J. Inorg. Nucl. Chem.*, 1980, **42**, 1501.
5 G. M. Sheldrick, SHELXS-86: program for crystal structure solutions. Universität Göttingen, 1986.
6 G. M. Sheldrick, SHELXL-93: program for refinement of crystal structures. Universität Göttingen, 1993.

Crystal structures of (*R,R*)-{[Ph(Me)CH]$_2$NLi·pmdeta} and {[PhC(=CH$_2$)NH]Na·pmdeta}$_2$: alkali metal amides derived from (*R,R*)-bis(α-methylbenzyl)amine†

Philip C. Andrews,* Peter J. Duggan, Melissa Maguire and Peter J. Nichols

Department of Chemistry, Monash University, Clayton, Melbourne, Victoria 3800, Australia. E-mail: p.andrews@sci.monash.edu.au

Received (in Cambridge, UK) 14th September 2000, Accepted 31st October 2000
First published as an Advance Article on the web

The reaction of Bu^{n}M (M = Li, Na) with [(*R,R*)]-bis(α-methylbenzyl)amine in the presence of pmdeta results in the formation of the chiral lithium amide complex (*R,R*)-{[Ph(Me)CH]$_2$NLi·pmdeta} and, remarkably, the sodium enamide, {[PhC(=CH$_2$)NH]Na·pmdeta}$_2$; both compounds have been authenticated by single crystal X-ray diffraction.

Our knowledge of the structural chemistry of alkali metal amides is now firmly established and indeed, many of the structural features found in these complexes have become largely predictable. As a result of their widespread applicability in synthesis most of our understanding has come from detailed solution and solid state studies on lithium amides, though there has been a steady increase in the study of the heavier metal (Na, K) complexes.[1,2] Limited hydrocarbon solubility, increased reactivity and possible reductions in selectivity are the reasons often quoted for the limited use of Na and K complexes, though implicit within this is also the belief that while structural differences will occur as a result of increasing cation size, the complex formed and the resulting chemistry will be essentially similar to that of the lithium counterpart. While most structural studies have indicated this is probably the case, there is also the possibility that the change in metal can effect dramatic and unexpected structural outcomes, which is important given that many alkali metal reagents are generated and used *in situ*.[3]

We reported recently that in the presence of pmdeta (*N,N,N′,N′,N″*-pentamethylethylenetriamine), α-(methylbenzyl)benzylamido lithium will produce the expected monomer, (*R*)-[(Ph(Me)CH)(PhCH$_2$)NLi·pmdeta], **1**,[4] while the sodium complex will undergo the facile low-temperature transformation to a 2-azaallylic anion system, {[Ph(Me)C⋯N⋯C(H)Ph-]Na·pmdeta} **2**,[6] as has also been described, in detail, for the analogous alkali metal complexes of dibenzylamine.[7] In comparing the Li complexes, the added methyl group increased the stability of the amide complex to azaallyl formation. We also noted the surprising paucity in solid and solution state structural information which is available on enantiomerically pure chiral alkali metal amides,[4] especially in light of their important role in synthesis.[5] With this in mind, we extended our studies to the complexes of [*R*-(*R**,*R**)]-bis(α-methylbenzyl)amine and herein report the solid state structure of (*R,R*)-{[Ph(Me)CH]$_2$NLi·pmdeta}, **3**, and the remarkable transformation of the amide to an enamide with crystallisation of {[PhC(=CH$_2$)NH]Na·pmdeta}$_2$ **4**. Both structures have been determined by single crystal X-ray diffraction.

The preparative methods towards **3** and **4** are shown in Scheme 1. Complex **3** was prepared by the addition of Bu^{n}Li to a hexane solution of (*R,R*)-bis(α-methylbenzyl)amine at −78 °C. Ligand pmdeta (1 equiv.) was added to the bright orange solution on reaching ambient temperature, resulting in a yellow precipitate which was redissolved on addition of toluene. Cooling the pale brown solution to −20 °C resulted in a large crop of pale yellow prismatic crystals, yield 67%.†

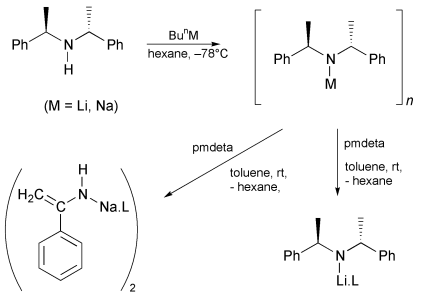

Scheme 1 Synthesis of (*R,R*)-{[Ph(Me)CH]$_2$NLi·pmdeta} **3** and [PhC(=CH$_2$)N(H)Na·pmdeta]$_2$ **4** (L = pmdeta).

Synthesis of **4** was by essentially the same method, the difference being that the amine was added to a hexane suspension of Bu^{n}Na at −78 °C.† Pale yellow crystals of **4** were obtained at room temperature after *ca*. six days, but only after reduction of solvent to a minimum (*ca*. 5 ml for 5 mmol reaction).†

Complex **3** crystallises in the orthorhombic space group $P2_12_12_1$ and is monomeric, as shown in Fig. 1.‡ In general, the structure is similar to that previously described for **1**;[4] the Li centre is four coordinate, bonding with the three available N atoms of pmdeta and N$_{amido}$, is in a distorted tetrahedral environment and with comparable Li–N bonding distances. The most interesting feature of the structure though is the arrangement of the methyl groups, both in terms of their location in relation to the metal centre and their close proximity to the plane defined by C9, N1 and C1. Close H$_3$C⋯Li interactions of 2.74 and 2.78 Å in the dimer (*R,R*)-{[Ph(Me)CH]$_2$NLi·thf}$_2$ are described as being of possible importance in explaining stereochemical outcomes in deprotonation reactions.[8] Given the similarity in the conformations adopted by the amido moieties

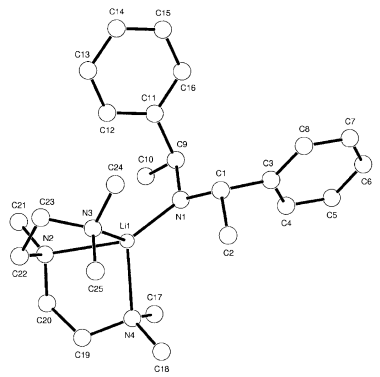

Fig. 1 Molecular structure of (*R,R*)-{[Ph(Me)CH]$_2$NLi·pmdeta}, **3**: all H omitted for clarity. Selected bond distances (Å) and angles (°); Li(1)–N(1) 1.949(6), Li1–N4 2.170(6), Li1–N3 2.222(6), Li1–N2 2.343(6), N1–C1 1.4454, N1–C9 1.446(4); N1–Li1–N4 117.1(3), N1–Li1–N3 119.8(3), N4–Li1–N3 111.2(3), N1–Li1–N2 137.1(3), N4–Li1–N2 81.7(2), N3–Li1–N2 81.9(2), C1–N1–C9 110.4(2), C1–N1–Li1 117.2(3), C9–N1–Li1 125.3(3), N1–C1–C3 115.9(3), N1–C1–C2 109.3(3), C3–C1–C2 106.3(3).

† Electronic supplementary information (ESI) available: analytical data for **3** and **4**. See http://www.rsc.org/suppdata/cc/b0/b007482i/

DOI: 10.1039/b007482i

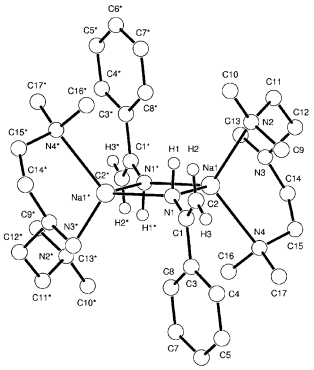

Fig. 2 Molecular structure of $[PhC(=CH_2)N(H)Na{\cdot}pmdeta]_2$ **4**; all H except those on CH_2 and NH omitted for clarity. Selected bond distances (Å) and angles (°); Na1–N1* 2.430(3), Na1–N1 2.406(3), Na1–N2 2.518(4), Na1–N3, 2.577(3), Na1–N4 2.578(4), N1–C1 1.365(4), C1–C2 1.368(5); N1–Na1–N1* 92.9(1), Na1–N1–Na1* 87.1(1), N1–Na1–N2 89.5(1), N1–Na1–N3 160.7(1), N1–Na1–N4 116.7(1), N1–Na1–N2 126.5(1), Na1–N1–C1 128.0(2), Na1–N1–C1 135.4(2), N1–C1–C2 126.5(4), N1–C1–C3 114.3(3).

in the dimeric thf and monomeric pmdeta complexes of $[(Ph(Me)CH)(PhCH_2)NLi]$ it might have been expected that such close interactions and amide conformations would be carried through from (R,R)-$\{[Ph(Me)CH]_2NLi{\cdot}thf\}_2$ into the structure of **3**. As such, in viewing the solid state structure of **3** and the location of the Me groups it would be easy to conclude that the metal centre is dictating the orientation of the Ph(Me)CH moieties. However, while the asymmetry in $Li{\cdots}CH_3$ interactions observed in (R,R)-$\{[Ph(Me)CH]_2NLi{\cdot}thf\}_2$ remains, the analogous distances in **3** are significantly longer at 2.989 Å (C2–Li), and 3.325 Å (C10–Li). The closest distance is therefore only comparable with that observed in **1**, of 3.04 Å. Also, the amido moieties in the thf and pmdeta structures of (R,R)-$[Ph(Me)CH]_2NLi$ do not adopt a similar orientation. In **3** the Me carbons and N_{amido} are almost coplanar, which is evident if we consider a plane defined by N1, C9, C1 above which C10 and C2 lie 4.2 and 15.5°, respectively.

While the monomeric nature of **3** in the solid state was somewhat predictable the crystalline product and subsequent structure obtained from the Na reaction was not. We were probing whether the additional Me groups on the benzylic carbons would effect the formation of an azaallylic anion, as such the formation of the sodium enamide dimer, **4**, was entirely unexpected.

Complex **4** crystallises in the triclinic space group $P\bar{1}$ and is, as evident in Fig. 2, dimeric.‡ What is initially striking about the complex is that it is an amide, with a formal M–N bond, rather than a 1-azaallyl complex in which the Na cation is located above the N∴C∴C fragment as observed in similar systems,[9] and which may have been anticipated on metalation of a primary enamine. The propensity noted for ketimides to undergo a 1, 3 sigmatropic rearrangement to 1-azallyl complexes may hint at a possible mechanism for the formation of **4** involving the formation of [PhC(Me)=NNa] and $PhC(H)=CH_2$ as intermediates. Whether this involves the formation and subsequent cleavage of a C∴N bond from a 2-azaallyl intermediate complex is under investigation. A proton shift from Me onto N as found in $[\{CH_2{\therefore}C(^tBu){\therefore}N(H)Li{\cdot}hmpa\}_2]$[10] with subsequent stabilisation of the enamide over the 1-azallyl structure *via* dimerisation in the solid state would result in **4**. The ^1H and ^{13}C NMR do not give a conclusive answer as to whether the complex in solution adopts a 1-azaallyl arrangement, though the chemical shift of the CH_2 doublet, centred on δ 2.65, is significantly upfield from the region expected for $PhC{=}CH_2$ and is perhaps indicative of a reduction in the double bond character.

The main features of **4** are the central cyclic $(NNa)_2$ ring core about which the amide moieties adopt a *trans* configuration. This is wholly consistent the two other structurally characterised sodium primary amides with which **4** can be compared, $[PhN(H)Na{\cdot}pmdeta]_2$ **5**,[11] and $[2\text{-}PhOC_4H_6N(H)Na{\cdot}pmdeta]_2$,[12] and is a common feature of many sodium secondary amides.[13] In all three cases the Na cation is five coordinate, however the tripodal connectivity of pmdeta in **5** makes it more closely related to **4**. In **5** the anilino moieties tilt at an angle of 65° relative to the $(NNa)_2$ ring plane, whereas in **4** the amide ligands are directly perpendicular, influenced no doubt by the sp^2 nature of C1.

We thank the Australian Research Council and Monash University for financial support.

Notes and references

‡ *Crystallographic data*: for **3**: $C_{25}H_{41}N_4Li$, M = 404.56, T = 123 K, orthorhombic, space group $P2_12_12_1$, a = 9.987(2), b = 13.692(3), c = 18.553(4) Å, V = 2537.0(9) Å^3, D_c = 1.059 g cm^{-3}, Z = 4; $F(000)$ = 888, μ(Mo-Kα) = 0.64 cm^{-1}, $2\theta_{max}$ = 56.9°, final R, R_w = 0.091, 0.126. N_o = 3246 'observed' [$I > 2\sigma(I)$] reflections out of N = 5769 unique. GOF = 1.10.

For **4**: $C_{13}H_{31}N_4Na$, M = 266.4, T = 123 K, triclinic space group $P\bar{1}$, a = 9.8409(2), b = 9.9864(3), c = 10.7169(2) Å, α = 94.128(1), β = 114.261(2), γ = 98.962(1)°, V = 937.59(4) Å^3, D_c = 0.944 g cm^{-3}, Z = 2; $F(000)$ = 296, μ(Mo-Kα) = 0.77 cm^{-1}, $2\theta_{max}$ = 56.6°, final R, R_w = 0.084, 0.083. N_o = 2457 'observed' [$I > 2\sigma(I)$] reflections out of N = 4391 unique. GOF = 2.04.

Crystallographic data collected on a Nonius Kappa CCD with crystals mounted under oil. All H atoms placed in calculated positions.

CCDC 182/1835. See http://www.rsc.org/suppdata/cc/b0/b007482i/ for crystallographic files in .cif format.

1 R. E. Mulvey, *Chem. Soc. Rev.*, 1998, **27**, 339; R. E. Mulvey, 1991, **20**, 167.

2 J. D. Smith, *Adv. Organomet. Chem.*, 1999, **43**, 267; M. A. Beswick and D. S. Wright, *Comprehensive Organometallic Chemistry II*, ed. E. W. Abels, F. G. A. Stone and G. Wilkinson, Pergamon Press, New York, 1995, ch. 1; E. Weiss, *Angew. Chem., Int. Ed. Engl.*, 1993, **32**, 1501; F. S. Mair and R. Snaith, *Dictionary of Organometallic Compounds*, Chapman & Hall, London–New York, 1995, ch. 1; K. Gregory, P. v. R. Schleyer and R. Snaith, *Adv. Inorg. Chem.*, 1991, **37**, 47.

3 C. Lambert and P. v. R. Scheleyer, *Methods in Organic Chemistry*, Thieme, Stuttgart, 1993, vol. 19d; L. Brandsma, *Preparative Polar Organometallic Chemistry*, Springer-Verlag, Berlin–New York, 1987; B. J. Wakefield, *The Chemistry of Organolithium Compounds*, Pergamon Press, Oxford, 1974, p. 204.

4 P. C. Andrews, P. J. Duggan, G. D. Fallon, T. D. McCarthy and A. C. Peatt, *J. Chem. Soc., Dalton Trans.*, 2000, 1937.

5 J. Busch-Peterson and E. J. Corey, *Tetrahedron Lett.*, 2000, **41**, 6941; K. Koga, *Pure Appl. Chem.*, 1994, **66**, 1487; P. J. Cox, A. Persad and N. S. Simpkins, *Synlett*, 1992, **57**, 5438; T. Honda, N. Kimura and M. Tsubuki, *Tetrahedron: Asymmetry*, 1993, **4**, 21; T. Honda, N. Kimura and M. Tsubuki, *Tetrahedron: Asymmetry*, 1993, **4**, 1475; K. Aoki, H. Naguchi, K. Koga and K. Tomioka, *Tetrahedron Let.*, 1993; **34**, 5105; B. J. Bunn and N. S. Simpkins, *J. Org. Chem.*, 1993, **58**, 533; P. J. Cox and N. S. Simpkins, *Tetrahedron: Asymmetry*, 1992, **2**, 1.

6 P. C. Andrews, P. J. Duggan, G. D. Fallon, T. D. McCarthy and A. C. Peatt, *J. Chem. Soc., Dalton Trans.*, 2000, 2505

7 P. C. Andrews, D. R. Armstrong, D. R. Baker, R. E. Mulvey, W. Clegg, L. Horsburgh, P. A. O'Neill and D. Reed, *Organometallics*, 1995, **14**, 427; P. C. Andrews, D. R. Armstrong, R. E. Mulvey and D. R. Reed, *J. Organomet. Chem.*, 1990, **386**, 287.

8 E. J. Edwards, S. Hockey, F. S. Mair, P. R. Raithby, R. Snaith and N. S. Simpkins, *J. Org. Chem.*, 1993, **58**, 6942.

9 M. F. Lappert, *J. Organomet. Chem.*, 2000, **600**, 144; A. Antiñolo, C. Huertas, I. del Hierro, M. F. Lappert, A. Otero, S. Prashar, A. M. Rodriguez and E. Villaseñor, *Organometallics*, 1998, **17**, 5874; B.-J. Deelman, M. F. Lappert, H.-K. Lee, T. C. W. Mak, W.-P. Leung and P.-R. Wei, *Organometallics*, 1997, **16**, 1247; M. F. Lappert and D.-S. Sui, *J. Organomet. Chem.*, 1995, **500**, 203.

10 D. R. Armstrong, W. Clegg, L. Dunbar, S. T. Liddle, M. MacGregor, R. E. Mulvey, D. Reed and S. Quinn, *J. Chem. Soc., Dalton Trans.*, 1998, 3431.

11 D. Barr, W. Clegg, L. Cowton, L. Horsburgh, F. M. MacKenzie and R. E. Mulvey, *J. Chem. Soc., Chem. Commun.*, 1995, 891.

12 I. Cragg-Hine, M. G. Davidson, A. J. Edwards, P. R. Raithby and R. Snaith, *J. Chem. Soc., Dalton Trans.*, 1994, 2901.

13 P. C. Andrews, N. D. R. Barnett, R. E. Mulvey, W. Clegg, P. A. O'Neil, D. Barr, L. Cowton, A. J. Dawson and B. J. Wakefield, *J. Organomet. Chem.*, 1996, **518**, 85.

ChemComm

Responsive nanocapsules

Marc Sauer and Wolfgang Meier*

Department of Physical Chemistry, University of Basel, Klingelbergstrasse 80, CH-4056 Basel, Switzerland. E-mail: wolfgang.meier@unibas.ch

Received (in Cambridge, UK) 1st September 2000, Accepted 16th November 2000
First published as an Advance Article on the web 14th December 2000

Using vesicular polymerization, water-soluble polyelectrolyte nanocapsules have been prepared, that are able to undergo a reversible swelling transition upon changing the pH and/or salt concentration.

In recent years considerable progress has been made in developing synthetic methods that allow preparation of materials with precise control over size and morphology at the nanometer level. One typical example is the formulation of hollow nanoparticles. For such nanocontainers a widespread range of applications such as confined reaction vessels, drug carriers or protective shells for cells or enzymes have been proposed. Similar and very effective nanometer sized containers, *viz.*, micelles and vesicular structures, are already used by nature in biological systems. However, due to the non-covalent interactions responsible for their formation, these objects have only a limited stability and may undergo structural changes. Many applications (*e.g.* in drug delivery) require more stable particles. Mechanically stable polymer nanocapsules can be prepared using a variety of different techniques (see for example refs. 1–9). In view of their high stability and low permeability it is, however, generally rather difficult to load polymeric capsules after formulation or to release substances from their interior in a controlled way at the desired target. Consequently prior to any application of such polymer shells ways have to be found to control their permeability.[10] One possibility to realize this is nicely demonstrated by a naturally occurring polymeric nanocontainer: the protein shells of the cowpea chlorotic mottle virus (CCMV) show a reversible, pH-induced structural transition.[11] Increasing the pH from *ca.* 5 to 7 leads to a swelling of the protein shells by *ca.* 10%. During this swelling gated pores are opened in their shells which allow free molecular exchange between the interior of the virion cages and the bulk medium. Recently this gating transition of the virion particles has been used for host–guest encapsulation.[12] Practical applications of virion cages on a technical scale are not feasible due to the difficulties in handling and producing larger quantities. Here our aim is to find a fairly simple synthetic mimetic of these virion cages able to undergo a similar structural transition.

The conformation of polyelectrolytes is very sensitive towards changes in ionic strength, pH and other external factors. Hence water-soluble polymer hollow spheres formed by a covalently crosslinked polyelectrolyte shell could be a suitable model system. The carboxylate groups of nanocapsules based, for example, on poly(acrylic acid) dissociate increasingly with increasing pH. As a result of the associated electrostatic repulsion between the identically charged carboxylate anions along the polymer backbone the particles should swell considerably. Similar to the virion cages, the permeability of the swollen poly(acrylate) shells should increase and enhance molecular exchange between the interior of the particles and the bulk medium. Here we describe a synthetic route to nanometer-sized poly(acrylic acid) hollow spheres. To demonstrate their potential for host–guest encapsulation and controlled release their swelling behavior in aqueous media of different pH and ionic strength, has been investigated.

Recently we succeeded in preparing hydrophobic polymer hollow spheres with diameters ranging from several nanometers up to hundreds of micrometers by polymerization of hydrophobic monomers in the lipid bilayer of vesicles or liposomes.[5] While the size and shape of the resulting polymer particles are directly determined by the templating vesicles, the polymer scaffold can be modified fairly easily, using conventional chemical reactions.

The preparation of hydrophobic polymer hollow spheres has already been described elsewhere.[5] Therefore we just recall briefly the individual steps. We prepared small unilamellar vesicles from the synthetic surfactant dimethyldioctadecylammonium chloride (DODAC) by ultrasonification of aqueous lipid dispersions (2.1 g DODAC in 97.9 g bidistilled water). This yields unilamellar vesicles with an average diameter of 100 nm, however, with a rather high polydispersity. The lipid bilayers of the vesicles were swollen by incubating them in the presence of hydrophobic monomers (0.52 g, *i.e.*, 25 wt% with respect to the lipid) for 2 h at 60 °C. A crosslinking polymerization of the monomers was initiated by UV-irradiation (2 h) at room temperature. Afterwards the resulting polymer particles were isolated from the vesicles by repeated precipitation in a large excess of methanol–water (3 : 1) until ^{1}H NMR spectroscopy indicated complete removal of the surfactant (yield: 81%). As hydrophobic monomers we used mixtures of *tert*-butyl acrylate (t-BUA) and ethylene glycol dimethacrylate (EGDMA) as the crosslinking agent. For selective saponification of the *tert*-butyl ester groups[13] the crosslinked poly(*tert*-butylacrylate) hollow spheres were dissolved in dioxane and stirred for 8 h at 80 °C in the presence of a catalytic amount of hydrochloric acid. The resulting poly(acrylic acid) particles were precipitated in diethyl ether and finally dried by lyophilization from dioxane (yield 89%). ^{1}H NMR spectroscopy indicates full conversion of the poly(*tert*-butyl acrylate) under these conditions.

The resulting poly(acrylic acid) particles are dispersable in aqueous media. Fig. 1 shows a characteristic cryogenic electron micrograph (cryo-TEM) of a representative sample in an aqueous phosphate buffer at pH = 7. The micrograph shows clearly that the polymer particles are hollow. Although we

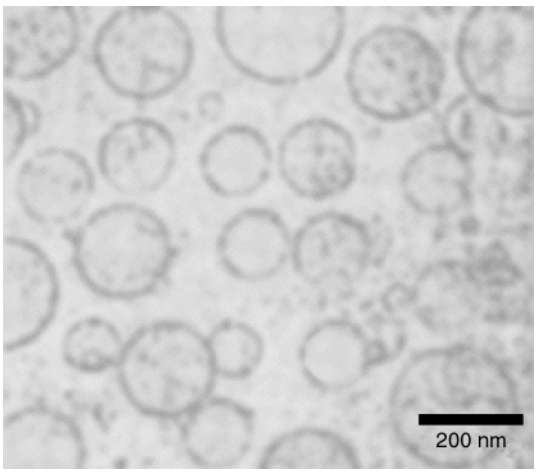

Fig. 1 Cryo-transmission electron micrograph of poly(acrylic acid) hollow spheres in an aqueous phosphate buffer at pH = 7.

DOI: 10.1039/b007118h

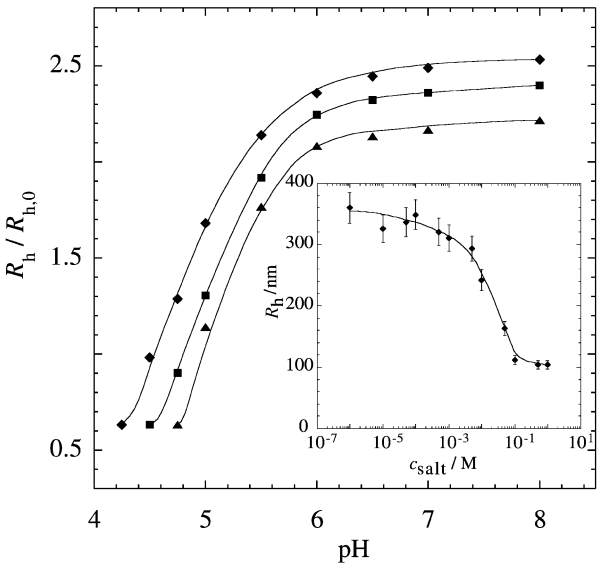

Fig. 2 Reduced hydrodynamic radius $R_h/R_{h,0}$ as a function of pH. The different curves correspond to particles with a different molar fraction of crosslinking comonomers: (◆) 3 mol% EGDMA ($R_{h,0}$ = 49 nm), (■): 5 mol% EGDMA ($R_{h,0}$ = 55 nm), (▲) 10 mol% EGDMA ($R_{h,0}$ = 60 nm). Inset: hydrodynamic radius R_h of poly(acrylic acid) hollow spheres (5 mol% EGDMA) as a function of salt concentration c_{salt} of the buffer.

cannot completely exclude their presence due to the limited resolution of the method, no solid latex particles or fragments of the shells can be detected. The size of the particles is in good agreement with dynamic light scattering experiments (see below) and they are polydisperse as are the parent DODAC vesicles. This reflects that the newly formed poly(acrylic acid) hollow spheres have survived intact the isolation and saponification procedure.

The sensitivity of the particles towards changes of the pH and/or ionic strength of the buffer is the basic requirement for their use as controlled release devices. Therefore we investigated in a first set of experiments the behavior of the poly(acrylic acid) hollow spheres in phosphate buffers of varying pH. It has to be emphasized that the ionic strength of the buffers used for these experiments was carefully kept constant at 0.1 M by addition of sodium chloride. Although electrostatic interactions are shielded considerably this salt concentration is close to physiological conditions (*ca.* 150 mM), the relevant range for most pharmaceutical applications. Additionally the systems are quite insensitive towards small ionic impurities at this concentration.

The pH-induced dimensional changes of the particles were investigated by dynamic light scattering and Fig. 2 shows the results. To take into account small variations in the average radius of different batches of the precursor vesicles we plotted a reduced hydrodynamic radius $R_h/R_{h,0}$ (R_h = hydrodynamic radius of poly(acrylic acid) hollow spheres; $R_{h,0}$ = hydrodynamic radius of the polymer containing vesicular precursors) as a function of pH. As can directly be seen the dimensions of the particles increase considerably with increasing pH. In the range pH 4–8 their radius increases by a factor of about 4 (*i.e.*, their encapsulated volume increases by a factor of 64!). It should be emphasized that this swelling is completely reversible. The different curves in Fig. 2 refer to nanocapsules of different crosslinking density which was controlled by the molar fraction of the crosslinker EGDMA in the particles. With increasing crosslinking density, the maximum swelling decreases and the swelling transition is shifted towards higher pH, which is a result of the increasing fraction of the non-ionic EGDMA comonomers. The same effect has also been observed for other polyelectrolyte gels.[14] It is important to note that the poly(acrylic acid) hollow spheres precipitate at low pH. The first points of the different curves in Fig. 2 represent the lowest pH values for which stable particle dispersions were obtained. Such a pH-induced precipitation could be highly interesting for applications since it represents a convenient way to separate the particles after their loading from the solution.

The effect of varying salt (NaCl) concentration is shown in the inset of Fig. 2. Throughout this series of measurements we kept the pH constant at 6 where the poly(acrylic acid) is highly ionized. As can directly be seen with decreasing salt concentration the swelling of the particles increases and tends towards a saturation value, which is due to decreasing electrostatic shielding effects. Similar observations have been made with macroscopic poly(acrylic acid) based gels.[15] It is interesting that we can conclude from these data an increase of the radius of the poly(acrylic acid) hollow spheres by up to a factor of 10 (*i.e.* the encapsulated volume increase by a factor of 1000!) at low salt concentrations.

In conclusion, we have presented a convenient way to prepare new, pH-sensitive nanocapsules based on crosslinked polyelectrolyte shells. These particles undergo a reversible swelling transition upon changing the pH and/or the salt concentration of the system which reversibly changes their dimensions. We expect that this swelling will have considerable influence on the permeability of the shells of these nanocapsules which makes these systems highly interesting for applications in areas such as drug delivery. Initial preliminary results indicate that this 'gating transition' can successfully be used for controlled encapsulation and release of biopolymers such as enzymes.

Financial support from the Swiss National Science foundation is gratefully acknowledged.

Notes and references

1 J. Murtagh and J. K. Thomas, *Faraday Discuss. Chem. Soc.*, 1986, **81**, 127.
2 J. Kurja, R. J. M. Noelte, I. A. Maxwell and A. L. German, *Polymer*, 1993, **34**, 2045.
3 J. D. Morgan, C. A. Johnson and E. W. Kaler, *Langmuir*, 1997, **13**, 6447.
4 J. Hotz and W. Meier, *Langmuir*, 1998, **14**, 1031.
5 E. Donath, B. Sukhorukov, F. Caruso, S. A. Davis and H. Möhwald, *Angew. Chem., Int. Ed.*, 1998, **37**, 2201.
6 H. Huang, E. E. Remsen, T. Kowalewski and K. L. Wooley, *J. Am. Chem. Soc.*, 1999, **121**, 3805.
7 S. Stewart and G. J. Liu, *Chem. Mater.*, 1999, **11**, 1048.
8 O. Emmerich, N. Hugenberg, M. Schmidt, S. S. Sheiko, F. Baumann, B. Deubzer, J. Weis and J. Ebenhoch, *Adv. Mater.*, 1999, **11**, 1299.
9 C. Nardin, T. Hirt, J. Leukel and W. Meier, *Langmuir*, 2000, **16**, 1035.
10 C. Nardin, S. Thoeni, J. Widmer, M. Winterhalter and W. Meier, *Chem. Commun.*, 2000, 1433.
11 J. A. Speir, S. Munshi, G. Wang, T. S. Baker and J. E. Johnson, *Structure*, 1995, **3**, 63.
12 T. Douglas and M. Young, *Nature*, 1998, **393**, 152.
13 C. Ramireddy, Z. Tuzar, K. Prochazka, S. E. Webber and P. Munk, *Macromolecules*, 1992, **25**, 2541.
14 R. A. Siegel, in *Responsive Gels: Volume Phase Transitions I & II*, in *Advances in Polymer Science*, ed. K. Dusek, Springer, Berlin, 1992/1993, vol. 109/110, p. 234.
15 J. Ricka and T. Tanaka, *Macromolecules*, 1984, **17**, 2916.

Dynamic kinetic resolution of *tert*-butyl 4-methyl-3,5-dioxohexanoate through enzymatic reduction

Aiguo Ji,[ab] Michael Wolberg,[a] Werner Hummel,[c] Christian Wandrey[a] and Michael Müller*[a]

[a] *Institut für Biotechnologie 2, Forschungszentrum Jülich GmbH, 52425 Jülich, Germany. E-mail: mi.mueller@fz-juelich.de*
[b] *Department of Pharmacy, Shandong Medical University, Jinan, Shandong 250012, China*
[c] *Institut für Enzymtechnologie der Heinrich-Heine Universität Düsseldorf im Forschungszentrum Jülich GmbH, 52426 Jülich, Germany*

Received (in Liverpool, UK) 8th September 2000, Accepted 15th November 2000
First published as an Advance Article on the web 14th December 2000

An entirely new method for the dynamic kinetic resolution of a racemic, 2-methyl substituted, unsymmetrical 1,3-diketone *via* enzymatic reduction to give an enantiomerically pure compound is introduced.

The dynamic kinetic resolution of α-substituted β-keto esters by chemical[1] or biocatalytical[2] reduction is particularly useful due to the simultaneous introduction of two stereogenic centres into the molecule in combination with a theoretical maximum yield of 100%. Although this method has proven broad applicability in stereoselective synthesis, the corresponding dynamic kinetic resolution of 2-substituted 1,3-diketones is rarely found in the literature.[3] Our aim is directed toward extending dynamic kinetic resolution to enantio- and regioselective reduction of alkyl-substituted 3,5-dioxoesters, which would enable the introduction of up to four stereogenic centers by two consecutive reduction steps.

The attempted enantioselective ketone reduction of 3,5-dioxohexanoate esters by chemical methods[4] or biotransformation[5] usually results in complex mixtures of several stereo- and regioisomeric products with one or both keto groups reduced. We figured out that this difficult transformation can be accomplished by using isolated enzymes to afford optically pure 5-hydroxy-3-oxohexanoates in high yield.[6] Herein we wish to report in preliminary form on the first enantio- and regioselective enzymatic reduction of 4-alkyl-3,5-dioxohexanoates resulting in formation of one out of a total of 8 monoreduction and 8 bisreduction products.

tert-Butyl 4-methyl-3,5-dioxohexanoate (**1**) was prepared by acylation of the bisenolate of *tert*-butyl 3-oxovalerate with commercially available Weinreb acetamide.[7] For the enzymatic reduction recombinant alcohol dehydrogenase from *Lactobacillus brevis* (recL*B*ADH) was chosen, which has been cloned and overexpressed in *E. coli*.[8] recL*B*ADH exhibits a broad substrate range and considerable stability even towards highly reactive compounds like 6-chloro-3,5-dioxohexanoates.[6,8] Cofactor (NADPH) regeneration succeeds *via* a coupled-substrate process. Propan-2-ol (200 mM) was applied in excess to the reaction mixture as an auxiliary substrate in order to shift the equilibrium of the reaction towards the desired direction (Scheme 1).[9]

NMR data of the major product (4*S*,5*R*)-**2** which was obtained in 66% isolated yield, clearly proved the regioselective monoreduction of the keto group at C-5. Additionally, from GC-MS data of the crude product after derivatisation with $(F_3CCO)_2O$, pyridine, no evidence could be found for the reduction of the keto group at C-3. In order to verify the proposed absolute configuration and to enable precise determination of the enantiomeric excess, (4*S*,5*R*)-**2** was transformed through sodium borohydride reduction into lactone **4** *via* diol (3*RS*,4*S*,5*R*)-**3**. Lactonisation and dehydration gave the unsaturated lactone (5*R*,6*R*)-**4** which is known in racemic form[10] (Scheme 2).

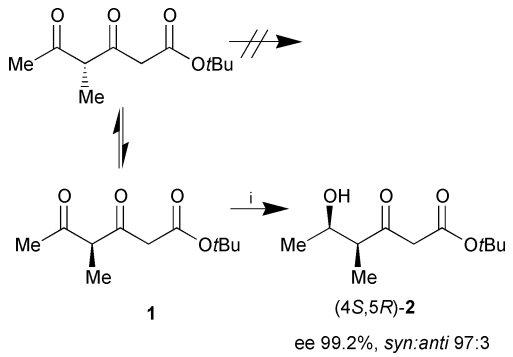

Scheme 1 *Reagents and conditions*: i, **1** (20 mM), propan-2-ol (200 mM), $NADP^+$ (1 mM), pH 6.5, recL*B*ADH (360 U), 23 h, rt (66%).

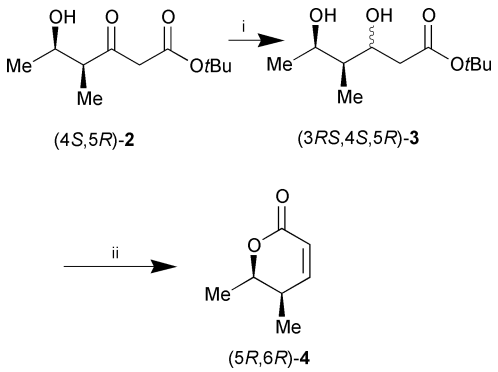

Scheme 2 *Reagents and conditions*: i, $NaBH_4$, EtOH, 0 °C; ii, cat. TsOH, toluene, reflux, 2 h (60% over two steps).

As a standard a racemic 1:1 mixture of *syn*- and *anti*-lactone *rac*-**4** was synthesised from keto ester **5** by sodium borohydride reduction, subsequent chain elongation, and, finally, lactone formation as described above (Scheme 3). The four stereoisomers of *syn/anti-rac*-**4**, which were formed in equal amounts, can be separated by HPLC on chiral stationary phase (Daicel Chiracel OB).

An authentic sample of the enantiomeric *syn*-lactone (5*S*,6*S*)-**4** was synthesised by the same sequence starting from bakers' yeast reduction of **5** *via* the known[11] ethyl (2*R*,3*S*)-2-methyl-3-hydroxybutyrate (2*R*,3*S*)-**6** (Scheme 4).

The spectroscopic data (^{1}H-NMR, ^{13}C-NMR, MS) of (5*S*,6*S*)-**4** and of (5*R*,6*R*)-**4**, produced *via* enzymatic (recL*B*ADH) reduction of **1**, are identical. Comparison of the CSP-HPLC data of both lactones revealed the (4*S*,5*R*)-absolute configuration for the product **2** of the recL*B*ADH reduction. This product is formed in almost enantiomerically pure form (99.2% ee, HPLC data); the diastereomeric ratio of *syn*:*anti* 97:3 is likewise very high (NMR and HPLC data).

DOI: 10.1039/b007448i

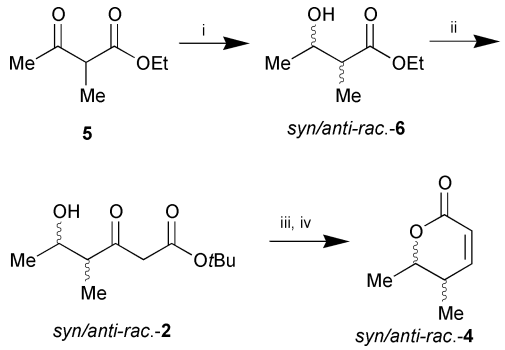

Scheme 3 *Reagents and conditions*: i, $NaBH_4$, EtOH, 0 °C (83%); ii, CH_2=C(OLi)O*t*Bu, THF, −30 °C (53%); iii, $NaBH_4$, EtOH, 0 °C; iv, cat. TsOH, toluene, reflux, 2 h (60% over two steps).

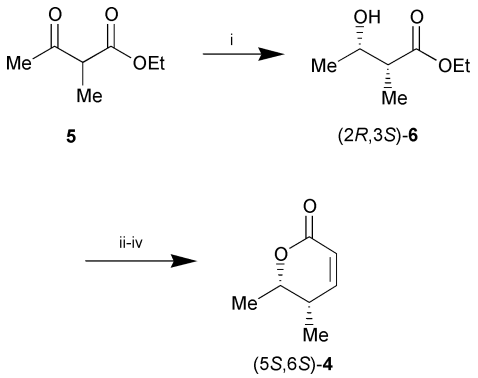

Scheme 4 *Reagents and conditions*: i, bakers' yeast, 10% aq. EtOH, (50%); ii, CH_2=C(OLi)O*t*Bu, THF, −30 °C; iii, $NaBH_4$, EtOH, 0 °C; iv, cat. TsOH, toluene, reflux, 2 h (53% over three steps).

In summary, we have shown the regio- and enantioselective reduction of *tert*-butyl 4-methyl-3,5-dioxohexanoate *via* dynamic kinetic resolution to give an almost enantiomerically and diastereomerically pure compound introducing two stereogenic centers can be done efficiently by enzyme-catalysed reduction. This method represents a novel entry into the chemistry of polypropionates based on a biomimetic approach *via* polyketides. This method should be extendable towards dynamic kinetic resolution of other 2-alkyl-substituted unsymmetrical 1,3-diketones.

A. Ji is the recipient of a Chinese Government Fellowship. The skilful technical assistance of Mrs Silke Bode is gratefully acknowledged. We thank the Deutsche Forschungsgemeinschaft (SFB 380) for financial support.

Notes and references

1 R. Noyori, M. Tokunaga and M. Kitamura, *Bull. Chem. Soc.*, 1995, **68**, 36; and refs. cited therein.
2 H. Stecher and K. Faber, *Synthesis*, 1997, 1; and refs. cited therein.
3 S. Tsuboi, E. Nishiyama, H. Furutani, M. Utaka and A. Takeda, *J. Org. Chem.*, 1987, **52**, 1359; T. Fujisawa, B. I. Mobele and M. Shimizu, *Tetrahedron Lett.*, 1992, **33**, 5567; T. Zelinski, A. Liese, C. Wandrey and M.-R. Kula, *Tetrahedron*: *Asymmetry*, 1999, **10**, 1681; *cf.* R. Hayakawa and M. Shimizu, *Synlett*, 1999, 1298; (α-substituted β-ketoaldehyde).
4 V. Blandin, J.-F. Carpentier and A. Mortreux, *Eur. J. Org. Chem.*, 1999, 3421; L. Shao, H. Kawano, M. Saburi and Y. Uchida, *Tetrahedron*, 1993, **49**, 1997; N. Sayo, T. Saito, H. Kumobayashi, S. Akutagawa, R. Noyori and H. Takaya, (Takasago International Corp.), Eur. Pat. Appl. EP 297,752, 1989 [*Chem. Abstr.*, 1989, **111**, 114745n].
5 R. N. Patel, A. Banerjee, C. G. McNamee, D. Brzozowski, R. L. Hanson and L. J. Szarka, *Enzyme Microb. Technol.*, 1993, **15**, 1014; M. Uko, H. Azuma, T. Sakai, S. Tsuboi (Mitsubishi Kasei Corp.), Jpn. Kokai Tokkyo Koho JP 03-48,641, 1991 [*Chem Abs.* 1991, **115**, 28713b].
6 M. Wolberg, W. Hummel, C. Wandrey and M. Müller, *Angew. Chem.*, in press.
7 S. Nahm and S. M. Weinreb, *Tetrahedron Lett.*, 1981, **22**, 3815; *cf.* J.-F. Lavallée, C. Spino, R. Ruel, K. T. Hogan and P. Deslongchamps, *Can. J. Chem.*, 1992, **70**, 1406; *cf.* K. B. Mullah and J. K. Sutherland, *J. Chem. Soc., Perkin Trans. 1*, 1992, 1237.
8 B. Riebel, *PhD thesis*, University of Düsseldorf, 1996.
9 Enzymatic transformation: A solution of recLBADH was prepared by mechanically disrupting wet cells of recombinant *E. coli* strain recADH-HB101+.[8] One unit (U) enzyme activity is defined as the amount of recLBADH that catalyses the oxidation of 1 μmol NADPH per minute when incubated with acetophenone (10 mM) and NADPH (0.25 mM) at 25 °C and pH 6.5 (100 mM phosphate buffer, 1 mM $MgCl_2$). In a round bottom flask, a solution of diketo ester **1** (0.53 g, 2.5 mmol) in propan-2-ol (1.9 mL, 25 mmol) was added to 120 mL phosphate buffer (100 mM, pH 6.5) containing 1 mM $MgSO_4$, and the mixture was ultrasonicated for 1 minute. The reaction was started by addition of $NADP^+$ (105 mg, 120 μmol; FLUKA Nr. 93210, 90%) and recLBADH (360 U). After slowly stirring for 23 h at ambient temperature, 20 g NaCl were added and the solution was extracted with ethyl acetate three times. The combined organic phases were dried over $MgSO_4$ and evaporated. The crude product was purified by flash chromatography (silica, ethyl acetate isohexane 40/60 (v/v)), yielding 0.35 g (66%) hydroxyketo ester (4*S*,5*R*)-**2** as a colourless oil.
10 M. A. Adams, A. J. Duggan, J. Smolanoff and J. Meinwald, *J. Am. Chem. Soc.*, 1979, **101**, 5364; T. M. Willson, P. Kocienski, K. Jarowicki, K. Isaac, A. Faller, S. F. Campbell and J. Bordner, *Tetrahedron*, 1990, **46**, 1757.
11 H. Akita, A. Furuichi, H. Koshiji, K. Horikoshi and T. Oishi, *Chem. Pharm. Bull.*, 1983, **31**, 4376; G. Fráter, U. Müller and W. Günther, *Tetrahedron*, 1984, **40**, 1269; K. Nakamura, T. Miyai, A. Nagar, S. Oka and A. Ohno, *Bull. Chem. Soc. Jpn.*, 1989, **62**, 1179; W.-R. Shieh and C. J. Sih, *Tetrahedron: Asymmetry*, 1993, **4**, 1259.

Asymmetric cyclopropanation in protic media conducted by chiral bis(hydroxymethyl-dihydrooxazolyl)pyridine–ruthenium catalysts

Seiji Iwasa, Futoshi Takezawa, Yasunori Tuchiya and Hisao Nishiyama*

School of Materials Science, Toyohashi University of Technology, Tempaku-cho, Toyohashi 441-8580, Japan. E-mail: hnishi@tutms.tut.ac.jp

Received (in Liverpool, UK) 23rd October 2000, Accepted 20th November 2000
First published as an Advance Article on the web 14th December 2000

Cyclopropanation of styrene with diazoacetates, performed in aqueous/organic biphasic media or homogeneous alcoholic media in the combination of toluene by using chiral bis(hydroxymethyldihydrooxazolyl)pyridine–ruthenium catalyst, resulted in high enantiomeric excess up to 96–97% and *trans*:*cis* stereoselectivity to 97:3.

Enantioselective reactions of olefins and diazoacetates catalyzed by a variety of metal complexes to provide chiral cyclopropane materials have been well investigated.[1] We have reported ruthenium catalysts of chiral bis(dihydrooxazolyl)pyridine [pybox] for that purpose and their prominent feature of high *trans*-stereoselectivity with higher enantioselectivity.[2,3] Very recently, we reported a characteristic derivative of pybox, *hm*-pybox **1**, having two hydroxymethyl groups as the symmetric chiral stems of the oxazoline rings.[4] We observed that *hm*-pybox exhibits high solubility in water. One of the recent demands for organic synthesis and catalysis, with environmental concerns in mind, has been for the reactions to be carried out in non-halogenated solvents or in aqueous and protic media.[5] We therefore had expectations of developing a new process in aqueous media for asymmetric catalytic cyclopropanation using our water-soluble bis(hydroxymethyldihydrooxazolyl)pyridine–ruthenium catalyst. In addition, however, we demonstrated the tolerance of the catalysis to protic media, such as alcoholic mixtures.

We surveyed previous research related to the catalytic cyclopropanation of olefins and diazoacetates but we could find no systems effective *in aqueous media or protic solvents.*[4] However, we discovered that the existence of a free hydroxy group on chiral ligands does not interfere with the smooth running of cyclopropanation for copper catalyzed reactions, for example, in the case of bis(oxazoline) ligands **2**[6] or **3**[7]. It had also very recently been reported that although a small amount of water in the reaction solvent diminishes enatioselectivity of cyclopropanation with rhodium catalyst, the unfavorable effect of water was reduced by addition of an appropriate phosphite ligand.[8] Accordingly, we were intrigued to examine the catalysis with *hm*-pybox **1** and $[RuCl_2(p\text{-cymene})]_2$ **4**.

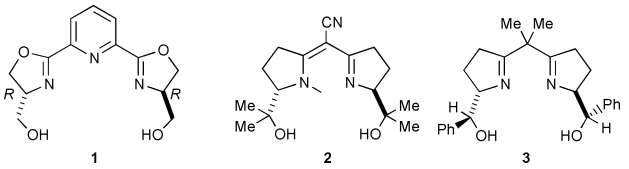

First, we tried an aqueous media for the cyclopropanation of styrene and (+)-menthyl diazoacetate **5a** with *hm*-pybox in the presence of co-solvent THF or toluene (Scheme 1). (+)-Menthyl ester was chosen on the basis of better matching to the (*R*,*R*)-absolute configuration of pybox, which ought to give higher enantioselectivity according to our previous work.[2b] The use of a single organic solvent resulted in lower yields and lower enantioselectivities (run 1 and 2 in Table 1). Surprisingly, addition of water to both media in runs 1 and 2 dramatically improved the enantioselectivities and slightly the yields (runs 4 and 5). This phenomenon can be simply accounted for by the increase of the solubility of the active catalyst Ru(*hm*-pybox)Cl_2(vacant or solvent) derived from *hm*-pybox **1** and pre-catalyst $[RuCl_2(p\text{-cymene})]_2$ **4**. It could easily be seen from the dark-violet coloring of the bottom phase that most of the catalyst was dissolved in the aqueous phase. Into the two-phase system of water and organic solvent (initial ratio = 1:2), a solution of the diazoacetate **5** was slowly added under vigorous stirring to give the desired cyclopropanes **6** in moderate yields with higher enantioselectivity (88% for **6t**, runs 3 and 4). The

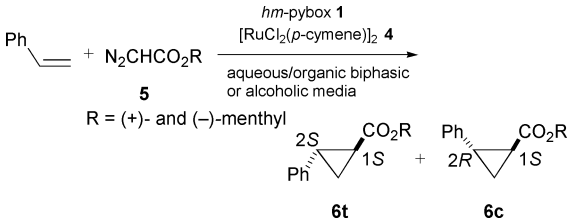

Scheme 1

Table 1 Asymmetric cyclopropanation of styrene and (+)-menthyl diazoacetate **5a** with chiral *hm*-pybox **1** and $[RuCl_2(p\text{-cymene})]_2$[a]

Run	Initial solvent (ml)	Solvent of **5a** (ml)	**6t** + **6c**[b] Yield %	Ratio	%Ee[c] **6t**	**6c**
1	THF (3)	THF (3)	39	83:17	8	30
2	Toluene (3)	Toluene (3)	38	89:11	8	28
3	THF (2) + H_2O (1)	THF (3)	46	95:5	78	45
4	Toluene (2) + H_2O (1)	Toluene (3)	56	96:4	88	51
5_{1st}[d]	Toluene (0.5) + H_2O (0.5)	Toluene (1.5)	57	97:3	94	76
5_{2nd}[e]		Toluene (1.5)	62	97:3	97	90

[a] Styrene (10 mmol), diazoacetate (2.0 mmol), pybox (0.14 mmol), $[RuCl_2(p\text{-cymene})]_2$ (0.05 mmol, 5 mol% of Ru), 40 °C. A solution of diazoacetate in 3.0 ml of the same solvent was slowly added by syringe for 6 h to the mixture of styrene and the catalyst in the initial solvent. [b] Isolated yield, ratios by ^1H NMR. [c] %Ee determined by the reported method, see ref 2. Absolute configuration: **6t** for all runs, (1*S*,2*S*); **6c** for run 1 and 2, (1*R*,2*S*); **6c** for runs 3 and 4, (1*S*,2*R*). [d] Half scale for run 1: diazoacetate (1.0 mmol), styrene (5.0 mmol), catalyst 5 mol%, for 4 h. [e] After ether extraction of the reaction mixture of the first run, styrene (5.0 mmol) and toluene (1.5 ml) were added followed by slow addition of **5a** in toluene.

DOI: 10.1039/b008516m

Table 2 Asymmetric cyclopropanation of styrene and (+)-menthyl diazoacetate **5a** with chiral *hm*-pybox **1** and $[RuCl_2(p\text{-cymene})]_2$ in the presence of alcohols[a]

Run	Initial solvent (ml)	Solvent of **5a** (ml)	**6t** + **6c** Yield %	**6t** + **6c** Ratio	%Ee[b] **6t**	%Ee[b] **6c**
1	Toluene (1) + EtOH (1)	Toluene (3)	67	96:4	35	2
2	Toluene (1) + *t*-BuOH (1)	Toluene (3)	54	91:9	11	15
3	Toluene (1) + *i*-PrOH (1)	Toluene (3)	78	95:5	92	65
4[c]	Toluene (1) + *i*-PrOH (1)	Toluene (3)	52	97:3	96	88
5[d]	Toluene (1) + *i*-PrOH (1)	Toluene (3)	78	95:5	90	88
6	THF (1) + *i*-PrOH (1)	THF (3)	73	96:4	89	58
7	*i*-PrOH (2)	*i*-PrOH (3)	59	95:5	84	30

[a] The reaction scale and procedures were the same as those described in Table 1. [b] Absolute configuration: **6t** for all runs, (1*S*,2*S*); **6c** for run 2 and 6, (1*R*,2*S*); **6c** for runs 1,3,4,5 and 7, (1*S*,2*R*). [c] At 30 °C. The cyclopropanation did not proceed at 20 °C. [d] In place of (+)-menthyl diazoacetate, (−)-menthyl ester **5b** was used.

organic layer was extracted with degassed (or absolute) diethyl ether and concentrated to give the products. As the active species remained in the aqueous phase, the second run was carried out by addition of styrene and diazoacetate to give a similar result (run 5). We are now further investigating the optimization and multi-time reuse of the catalyst.

In this aqueous system, addition of phase-transfer reagents such as $(n\text{-Bu}_4N)(HSO_4)$ (10 mol% of **5a**) into the system of run 4 resulted in no improvement upon the reaction and the selectivities. On the other hand, when alcohols such as ethanol, isopropyl alcohol, and *tert*-butyl alcohol in place of water were adopted to provide a homogeneous protic media, isopropyl alcohol resulted in the best enantioselectivities, up to 96% ee for *trans*-**6t** and 88% ee for *cis*-**6c** at 30 °C (Table 2, run 4). (−)-Menthyl diazoacetate **5b** showed a decrease of ee to 90% for *trans*-product (run 5), because of the unmatched steric pair toward *R*,*R*-absolute configuration of the ligand. Single use of isopropyl alcohol gave moderate ees (run 7). We have thus found that the choice of alcoholic solvents apparently influences the enantioselectivity. However, at present we cannot define the origin of the stereochemical outcomes for protic solvents.

We next intended stereochemical tuning of the hydroxymethyl group of **1** using *hydroxyethyl*-pybox **7** [*he*-pybox] synthesized from (−)-threonine (Scheme 2).† However, in aqueous biphasic media, toluene–H_2O, the enantioselectivities with ruthenium–**7** catalyst were not increased by using (−)-menthyl diazoacetate at 40 °C: 80% ee for *trans* and 50% ee for *cis*, in 96:4 *trans*:*cis* ratio (75% yield). In toluene–*i*-PrOH the enantioselectivities increased to 91% for *trans* and 78% ee for *cis*, in 94:6 *trans*:*cis* ratio (78% yield). In comparison, classic *ip*-pybox **8** with similar bulkiness to **7** was

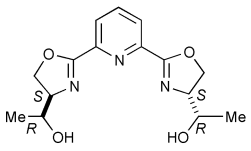

7

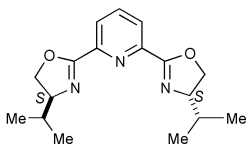

8

found in toluene–*i*-PrOH media to give 93% ee for *trans* and 90% ee for *cis*, in 97:3 *trans*:*cis* ratio (84% yield). *He*-pybox **7** thus proved to be inferior to *iso*-pybox **8**.

In conclusion, the hydroxymethyl derivative of pybox can provide excellent stereoselectivities for cyclopropanation of styrene, compared to the hydroxyethyl or isopropyl derivatives, in moderate yields in aqueous and protic media. We hypothesize that appropriate solvation of water or alcohols around the hydroxy group causes a more favourable stereochemical environment around the active site for the cyclopropanation. Work is now under way to investgate the mechanism of reaction and on applications to other catalytic reactions performed in aqueous media.

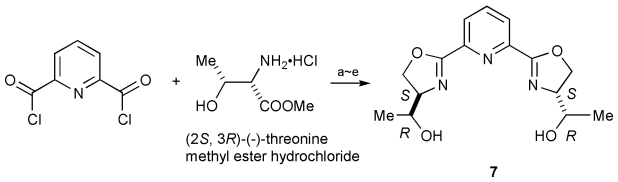

7

Scheme 2 *Reagents and conditions*: (a) Et_3N, $CHCl_3$, rt, 12 h, 92%. (b) TBDMSCl, imidazole, CH_2Cl_2, rt, 3.5 h, 98%. (c) $LiBH_4$, THF, 0 °C ~ rt, 6 h, 75%. (d) PPh_3, imidazole, CCl_4, CH_2Cl_2, rt, 4.5 h, 44%. (e) Bu_4NF (1.0 M in THF), rt, 3 h, 100%.

Footnotes and references

† Synthesis of *he*-pybox: the route is illustrated (Scheme 2) starting from (−)-threonine methyl ester·HCl and 2,6-pyridinecarboxylic acid chloride. **7**; white solid. mp 94–95 °C. δ_H (300 MHz, $CDCl_3$, Me_4Si) 1.30 (d, *J* 6.4, 6 H), 2.70 (br d, 2 H), 3.77 (dq, 2 H), 4.29 (dt, 6 H), 4.59 (dd, 2 H), 7.91 (t, 1 H), 8.15 (d, 2 H). δ_C (75.5 MHz, $CDCl_3$, Me_4Si) 19.5, 70.1, 70.4, 73.2, 126.1, 137.7, 146.5, 163.6.

1 General reviews: *Catalytic Asymmetric Synthesis 2nd*, ed. I. Ojima, Wiley-VCH, New York, 2000; *Comprehensive Asymmetric Catalysis I-III*, ed. E. N. Jacobsen, A. Pfaltz and H. Yamamoto (eds.), Springer-Verlag, Berlin, 1999. For catalytic cyclopropanation: M. P. Doyle, M. A. McKervey and T. Ye, *Modern Catalytic Methods for Organic Synthesis with Diazo Compounds*, John Wiley & Sons, Inc., 1997; M. P. Doyle and M. N. Protopopova, *Tetrahedron*, 1998, **54**, 7919.

2 (*a*) H. Nishiyama, Y. Itoh, H. Matsumoto, S.-B. Park and K. Itoh, *J. Am. Chem. Soc.*, 1994, **116**, 2223; (*b*) H. Nishiyama, Y. Itoh, Y. Sugawara, H. Matsumoto, S.-B. Park and K. Itoh, *Bull. Chem. Soc. Jpn.*, 1995, **68**, 1247; (*c*) H. Nishiyama, N. Soeda, T. Naito and Y. Motoyama, *Tetrahedron: Asymmetry*, 1998, **9**, 2865.

3 Related researches: review for chemistry of oxazoline ligands: K. Ghosh, P. Mathivanan and J. Cappiello, *Tetrahedron: Asymmetry*, 1998, **9**, 1; F. Fache, E. Schulz, M. L. Tommasino and M. Lemaire, *Chem. Rev.*, 2000, **100**, 2159.

4 S. Iwasa, H. Nakamura and H. Nishiyama, *Heterocycles*, 2000, **52**, 939.

5 Reviews: P. A. Grieco, *Organic Synthesis in Water*, Thomson Science, London, 1998; B. Cornils and W. A. Herrmann, *Aqueous-Phase Organometallic Catalysis*, Wiley-VCH, Weinheim, 1998; D. Sinou, *Transition Metals for Organic Synthesis*, Vol. 2, ed. M. Beller and C. Bolm, Wiley-VCH, Weinheim, 1998, 398. Papers for examples: K. Yonehara, T. Hashizume, K. Mori, K. Ohe and S. Uemura, *J. Org. Chem.*, 1999, **64**, 5593; J. Holz, D. Heller, R. Stürmer and A. Börner, *Tetrahedron Lett.*, 1999, **40**, 7059; S. Kobayashi, S. Nagayama and T. Busujima, *Tetrahedron*, 1999, **55**, 8739; W. Xie, J. Fang, J. Li and P. G. Wang, *Tetrahedron*, 1999, **55**, 12 929 and references therein.

6 H. Fritchi, U. Leutenegger and A. Pfaltz, *Helv. Chim. Acta*, 1988, **71**, 1553.

7 O. Hoarau, H. Ait-Haddou, M. Castro and G. G. A. Balavoine, *Tetrahedron: Asymmetry*, 1997, **8**, 3775; O. Hoarau, H. Ait-Haddou, J.-C. Daran, D. Cramailère and G. G. A. Balavoine, *Organometallics*, 1999, **18**, 4718.

8 D. C. Wynne, M. M. Olmstead and P. G. Jessop, *J. Am. Chem. Soc.*, 2000, **122**, 7638 and references for solvent effect in catalytic cyclopropanation cited therein.

A persistent C–H···C(π) T-stacked cation†

Colin D. Abernethy,[a] Charles L. B. Macdonald,[a] Jason A. C. Clyburne[b] and Alan H. Cowley*[a]

[a] *Department of Chemistry and Biochemistry, The University of Texas at Austin, Austin, Texas 78712, USA. E-mail: cowley@mail.utexas.edu*

[b] *Department of Chemistry, Acadia University, Wolfville, Nova Scotia, B0P 1X0 Canada*

Received (in Columbia, MO, USA) 30th June 2000, Accepted 31st October 2000
First published as an Advance Article on the web 15th December 2000

The reaction of 2 equivalents of 1,3-dimesitylimidazolium chloride with Cp_3Yb affords the salt [bis(1,3-dimesitylimidazolium)cyclopentadienide] [bis(cyclopentadienyl)dichloroytterbate]; the T-stacked cation is composed of two imidazolium fragments that are C–H···C(π) hydrogen bonded to the bridging cyclopentadienide anion.

N-Heterocylic carbene transition-metal complexes have been the subject of intense study in recent years.[1] Öfele,[2] and more recently Tilset and coworkers,[3] and our group[4] have demonstrated the utility of imidazolium salts for the preparation of transition-metal (TM) carbene complexes *via* protonolysis of Cp–TM and other suitable ligand-TM bonds. Encouraged by the fact that *N*-heterocyclic carbene complexes of the type Cp'_2M-(carbene) (M = Sm, Yb; Cp′ = $EtMe_4C_5$) have been prepared by traditional methods,[5] we were prompted to seek a new route to such compounds by treatment of lanthanocenes with imidazolium salts. However, the outcome of one of these experiments was unexpected and resulted in the formation of a remarkably persistent T-stacked cation. There is considerable current interest in such X–H···π systems, not only from the structural and theoretical standpoints, but also because of the recognition of this type of interaction in peptide and protein structures[6] and supramolecular architectures.[7] Furthermore, the reactivity patterns of imidazolium salts are of interest because of their use as ionic liquids.[8]

The reaction of 2 equivalents of 1,3-dimesitylimidazolium chloride (ImidCl) with Cp_3Yb in refluxing tetrahydrofuran afforded the golden-orange salt [bis(1,3-dimesitylimidazolium)(μ-cyclopentadienide)][bis(cyclopentadienyl)dichloroytterbate], $[Imid_2Cp][Cp_2YbCl_2]$, upon recrystallisation from toluene.[9] Although the spectroscopic data were consistent with the proposed formulation, unambiguous identification of the structure of the salt required an X-ray crystallographic experiment.‡ The most remarkable structural feature is the unprecedented geometry of the complex cation, $[Imid_2Cp]^+$ (**1**$^+$) which can be regarded as two "interlocked" cationic 1,3-dimesitylimidazolium fragments encapsulating a cyclopentadienide anion (Fig. 1). Interestingly, the "glue" that binds this cation together appears to be two C–H···C(π Cp) hydrogen bonds complemented by interionic attractions. The confined cyclopentadienide anion, which is slightly disordered, has an average C–C bond distance of 1.341(10) Å and an average C–C–C bond angle of 108.0(6)°. Both values are close to those reported for a typical "free" $[C_5H_5]^-$ anion.[10] Likewise, the metrical parameters for the 1,3-dimesitylimidazolium moieties are virtually identical to those reported for 1,3-dimesitylimidazolium chloride.[11] The only significant difference is the slight shortening of the C(1)–H bond in **1**$^+$ [0.819(9) *vs.* 0.944(9) Å for ImidCl] which is an expected consequence of the weaker C–H···Cp hydrogen bond (*vs.* C–H···Cl). The C–X (X is the Cp ring centroid) distance is 3.086(8) Å which is significantly shorter than the 3.85 Å distance in *e.g.* the neutral T-stacked 4-methylpyridine hexamer.[7] Likewise, the H···X distance is 2.295(9) Å and lies at the short end of the range of C–H···Cp contacts reported recently by Harder for ammonium and phosphonium cyclopentadienide salts (2.30–2.63 Å).[12] The C–H–X and H–X–H angles are 162.4(5) and 167.9(5)°, respectively. The average H–C(Cp) distance ($< d >$ = 2.561 Å) and the average C(1)–H–C(Cp) angle ($< \psi >$ = 150.9°) yield a relatively high value of 341 for each of the hydrogen bonds using Harder's C–H···Cp hydrogen bonding scale.[13] Somewhat surprisingly, the two 1,3-dimesitylimidazolium moieties are not mutually orthogonal but are arranged at an angle of 70° with respect to each other. This structural feature is most likely a consequence of crystal packing effects. For example, there is a somewhat close interaction of H(3) with Cl(1) on an adjacent $[Cp_2YbCl_2]^-$ anion (2.662 Å) as shown in Fig. 2. Although the structure of

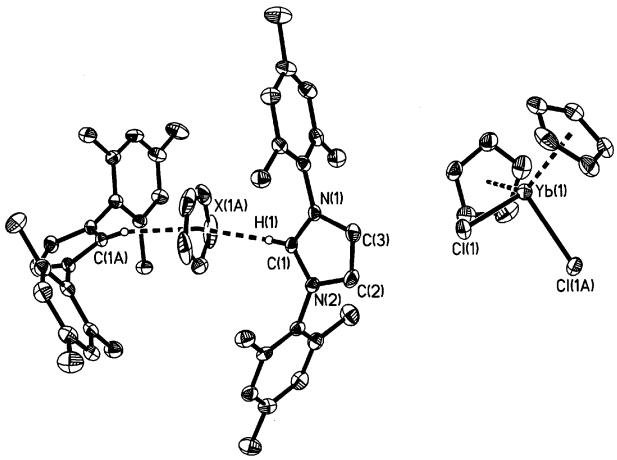

Fig. 1 Thermal ellipsoid plot (30% probability surface) of **1**$[Cp_2YbCl_2]$ (most hydrogen atoms omitted for clarity). Selected metrical parameters including bond lengths (Å) and angles (°); note that X is the Cp ring centroid: C(1)–H(1) 0.819(9), C(1)–N(1) 1.330(4), C(1)–N(2) 1.334(4), N(1)–C(3) 1.381(4), N(2)–C(2) 1.378(4), C(2)–C(3) 1.335(5), N(1)–C(21) 1.451(4), N(2)–C(31) 1.457(4), C(11)–C(12) 1.311(6), C(12)–C(13) 1.352(7), C(13)–C(13A) 1.378(10), H(1)–X(1A) 2.295(9), av H(1)–C(Cp) 2.561(9), Yb(1)–Cl(1) 2.5530(9), Yb(1)–X(1B) 2.329(5), av Yb(1)–C(Cp) 2.614(5); H(1)–X(1A)–H(1A) 167.9(5), X(1A)–H(1)–C(1) 162.4(5), H(1)–C(1)–N(1) 124.1(1), H(1)–C(1)–N(2) 127.9(1), N(1)–C(1)–N(2) 108.0(3), C(1)–N(1)–C(3) 108.8(3), C(1)–N(2)–C(2) 108.7(3), N(1)–C(3)–C(2) 107.2(3), N(2)–C(2)–C(3) 107.4(3), (X1B)–Yb(1)–Cl(1) 107.8(1), (X1B)–Yb(1)–X(1C) 127.3(1), Cl(1)–Yb(1)–Cl(1A) 95.03(4).

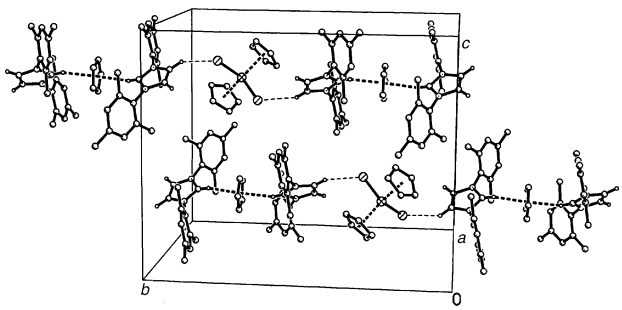

Fig. 2 Partial crystal packing diagram for **1**$[Cp_2YbCl_2]$ showing the cation–anion C–H···Cl interaction (most hydrogen atoms omitted for clarity).

† Electronic supplementary information (ESI) available: DFT calculations. See http://www.rsc.org/suppdata/cc/b0/b005450j/

DOI: 10.1039/b005450j

$[Cp_2YbCl_2]^-$ has not been reported previously, the metrical parameters are unexceptional and are not commented on here.

Interestingly, the complex cation persists in toluene solution. Unfortunately, **1**$[Cp_2YbCl_2]$ is virtually insoluble in aromatic solvents after initial crystallisation and decomposes rapidly in coordinating solvents hence ^{13}C NMR experiments were not informative. However, it was possible to demonstrate the persistence of $\mathbf{1}^+$ by means of an electrospray ionization (ESI) mass spectrum of a saturated toluene solution of **1**$[Cp_2YbCl_2]$ which exhibited an envelope with the anticipated isotopic intensity distribution in the region of *m/z* 674–678. This experiment confirmed the presence of $\mathbf{1}^+$ in solution and revealed that the only other major peak in the positive mode corresponds to the 1,3-dimesitylimidazolium cation. As expected, electron impact (EI) and chemical ionization (CI) mass spectra of solid samples of **1**$[Cp_2YbCl_2]$ did not evidence significant peaks attributable to $\mathbf{1}^+$, presumably because the high energy required to volatilize the solid exceeds the weak binding interactions of the complex cation.

The reaction clearly proceeds differently than had been expected and, although the mechanism remains unclear, some insight into the process can be gleaned from the nature of the products. Instead of protolytic cleavage of a Cp ligand and formation of CpH [eqn. (1)], Cp_3Yb can be regarded as

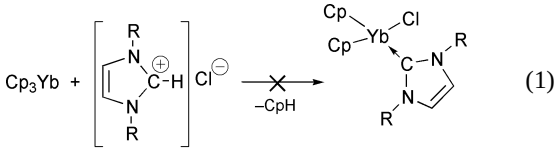

(1)

undergoing nucleophilic attack by two chloride anions to eliminate a Cp^- anion which, in turn, associates with two imidazolium cations to form **1**$[Cp_2YbCl_2]$ [eqn. (2)]. Such

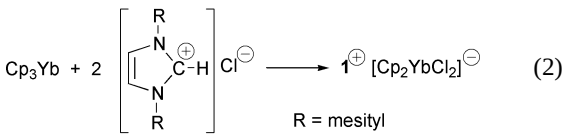

(2)

imidazolium salt reactivity may offer additional insights into the solution structure and catalytic behavior of imidazolium-based ionic liquids.[8]

Interestingly, density functional theory (DFT) calculations (see ESI for details†) indicate that the reaction of Cp^- with a model imidazolium cation (R = Me) is highly exothermic (91.4 kcal mol^{-1}). However, we have not yet calculated the activation energy for such a process; moreover, no account has been taken of solvent effects. Single-point DFT calculations on a model system (R = Ph) predict the bond energy of the imidazolium–Cp interaction to be 31.4 kcal mol^{-1}. As such, this interaction is of a similar magnitude to H···O–R hydrogen bonding and represents the strongest C–H···C(π) bond yet reported.

In conclusion, the formation and persistence of the T-stacked cation $\mathbf{1}^+$ stems both from electrostatic attractions and also from the appreciable acidity of the imidazolium protons which facilitates rather strong C–H···Cp (π) hydrogen bonding. In a sense, $\mathbf{1}^+$ can be regarded as an organic analogue of an "inverse sandwich" complex.

We are grateful to the National Science Foundation, the Robert A. Welch Foundation, the Natural Sciences and Engineering Research Council (Canada) and Acadia University for financial support. We would also like to thank the Atlantic Region Magnetic Resonance Center (Dalhousie University) for the acquisition of some NMR spectra.

Notes and references

‡ *Crystal data* for **1**$[Cp_2YbCl_2]$. Formula (half of each cation and anion in the asymmetric unit): $C_{28.5}H_{32.5}Cl_1N_2Yb_{0.5}$, M_w = 525.04, orange blocks, orthorhombic, space group *Pnma*, a = 16.785(4), b = 19.727(6), c = 15.847(3) Å, V = 5247(2) Å^3, Z = 8, D_c = 1.329 g cm^{-3}, μ(Mo-Kα) = 1.923 mm^{-1}. A single crystal of **1**$[Cp_2YbCl_2]$ was covered with perfluoro(poly)ether and mounted on a Nonius KAPPA CCD diffractometer at 153(2) K. A total of 29 722 reflections were collected in the range of 2.39 < θ < 29.12° using Mo-Kα radiation (λ = 0.71073 Å). Of these, 7037 independent reflections (R_{int} = 0.0859) were used to solve (direct methods, SHELXS) and refine (full matrix, least squares on F^2, SHELXL) the structure of **1**$[Cp_2YbCl_2]$; $wR2$ = 0.0664, R = 0.0403. Note: all hydrogen atoms except those on the encapsulated Cp ring were found in the Fourier difference maps; those on the said Cp ring were placed in calculated positions. CCDC 182/1848. See http://www.rsc.org/suppdata/cc/b0/b005450j/ for crystallographic data in .cif format.

1 See, for example: D. Bourissou, O. Guerret, F. Gabbaï and G. Bertrand, *Chem. Rev.*, 2000, **100**, 39; W. A. Herrmann and C. Köcher, *Angew. Chem., Int. Ed. Engl.*, 1997, **36**, 2162.

2 K. Öfele, *J. Organomet. Chem.*, 1968, **12**, P42.

3 M. H. Voges, C. Rømming and M. Tilset, *Organometallics*, 1999, **18**, 529.

4 C. D. Abernethy, J. A. C. Clyburne, A. H. Cowley and R. A. Jones, *J. Organomet. Chem.*, 2000, **596**, 3.

5 H. Schumann, M. Glanz, J. Winterfeld, H. Hemling, N. Kuhn and T. Kratz, *Chem. Ber.*, 1994, **127**, 2369; H. Schumann, M. Glanz, J. Winterfeld, H. Hemling, N. Kuhn and T. Kratz, *Angew. Chem., Int. Ed. Engl.*, 1994, **33**, 1733.

6 G. R. Desiraju and T. Steiner, *The Weak Hydrogen Bond in Structural Chemistry and Biology*, Oxford University Press, Oxford, 1999; N. Motohiro, M. Hirota and Y. Umezawa, *The CH/π Interaction. Evidence, Nature, and Consequences*, Wiley-VCH, Inc., New York, 1998.

7 See, for example: K. Biradha and M. J. Zaworotko, *J. Am. Chem. Soc.*, 1998, **120**, 6431.

8 T. Welton, *Chem. Rev.*, 1999, **99**, 1071.

9 A mixture of Cp_3Yb (1.0 g, 2.7 mmol) and dimesitylimidazolium chloride[11] (1.8 g, 5.4 mmol) was suspended in 150 mL of tetrahydrofuran then refluxed for 3 h. The volatiles were removed *in vacuo* and the residue was extracted with 150 mL of hot toluene. The resulting orange solution was filtered while hot and the volume was reduced to 100 mL. A crop of golden-orange crystals of **1**$[Cp_2YbCl_2]$ (0.85 g, 30% yield) formed upon storage of the filtrate at 25 °C for 5 days. Mp 158–160 °C (decomp.). Anal. Calc. for $C_{57}H_{65}Cl_2N_4Yb$: C, 65.20; H, 6.24; N, 5.34; Cl, 6.75. Found: C, 64.34; H, 6.32; N, 5.22; Cl, 6.65. Mass spectra: EI, *m/z* 305 (imid$^+$, 100%); CI, *m/z* 305 (imid$^+$, 100%), 675 ($\mathbf{1}^+$, < 1%); ESI, av. *m/z* 305 (imid$^+$, 100%), 675 ($\mathbf{1}^+$, 15%). NMR (note that the salt is virtually insoluble in benzene and toluene after initial precipitation and decomposes rapidly in THF and dichloromethane, thus only the ^1H spectra in the latter solvents, acquired immediately after dissolution, are reported): δ_H(THF-d_8): 1.51 (s, 12 H, *p*-Me), 2.34 (s, 24 H, *o*-Me), 6.35 (s, 5 H, Cp-H), 6.41 (br s, 8H, Mes-H), 6.52 (br s, 4 H, imid C=CH), 8.51 (broad s, 2 H, NCHN). δ_H(CD_2Cl_2): 1.67 (s, 24 H, *o*-Me), 1.97 (s, 12 H, *p*-Me), 6.41 (br s, 8H, Mes-H), 6.49 (br s, 4 H, imid C=CH), 6.55 (s, 5 H, Cp-H), 7.03 (sharp s, 2 H, NCHN). δ_H(toluene-d_8): 2.09 (s, 24 H, *o*-Me), 2.12 (s, 12 H, *p*-Me), 2.68 (br s, 5 H, Cp-H), 6.28 (br s, 4 H, imid C=CH), 6.47 (br s, 8H, Mes-H), 7.08 (sharp s, 2 H, NCHN).

10 See, for example: C. D. Abernethy, J. A. C. Clyburne, A. H. Cowley and R. A. Jones, *J. Am. Chem. Soc.*, 1999, **121**, 2329.

11 A. J. Arduengo, III, S. F. Gamper, M. Tamm, J. C. Calabrese, F. Davidson and H. A. Craig, *J. Am. Chem. Soc.*, 1995, **117**, 572. Refer to CSD #YOFKOT for metrical parameters.

12 S. Harder, *Chem. Eur. J.*, 1999, **5**, 1852.

13 The value is defined as $1000(-\cos\langle\psi\rangle)/\langle d\rangle$. See ref. 12 for details.

Carbon–carbon bond forming reactions of *N*-bound transition metal α-cyanocarbanions: a mechanistic probe for catalytic Michael reactions of nitriles†‡

Takeshi Naota,* Akio Tannna and Shun-Ichi Murahashi*

Department of Chemistry, Graduate School of Engineering Science, Osaka University, Machikaneyama, Toyonaka, Osaka 560-8531, Japan. E-mail: naota@chem.es.osaka-u.ac.jp

Received (in Cambridge, UK) 18th September 2000, Accepted 9th November 2000
First published as an Advance Article on the web 14th December 2000

***N*-Bound α-cyanocarbanion complexes $Ru^+Cp(NCCH^-R^1)(PPh_3)_2$ 1 react with electron deficient olefins to afford the conjugate adduct $Ru^+Cp(NCC^-R^1CHR^2CR^3R^4)(PPh_3)_2$ 2, kinetic studies of which revealed that complex 1-catalyzed Michael reactions of nitriles proceed *via* transformation of 1 to 2 and subsequent ligand exchange with nitriles.**

Transition metal α-cyanocarbanions have attracted much attention as active species for stoichiometric[1] and catalytic[2,3] carbon–carbon bond formations of nitriles, and studies on their structure and reactivity[4,5] are particularly of importance to develop novel transformations of nitriles bearing high selectivities, atom efficiency and sustainability.[6] In 1989 we presented a new methodology for catalytic carbon–carbon bond formation of nitriles initiated by α-C–H activation of nitriles with low-valent transition metal catalysts.[2a] Capture of the α-cyanocarbanion intermediate with electrophiles provides a family of catalytic C–C bond formations at the α-position of nitriles under neutral conditions.[2] *N*-Bound α-cyanocarbanion complexes, *mer*-$Ru^+H(NCCH^-CO_2R)(NCCH_2CO_2R)(PPh_3)_3$, derived by α-C–H activation of alkyl cyanoacetates with $RuH_2(PPh_3)_4$, have proven to be reactive species and active catalysts for the $RuH_2(PPh_3)_4$-catalyzed aldol and Michael reactions of nitriles.[2b,7] Further studies revealed that a variety of *N*-bound transition metal α-cyanocarbanion complexes act as efficient catalysts for the aldol and Michael reactions of nitriles.[8]

One of the most important aspects of this chemistry is to clarify and control the C–C bond forming process on the α-cyanocarbanion intermediates. Direct nucleophilic attack of zwitterionic *N*-bound α-cyanocarbanions to carbon electrophiles has been postulated for the crucial step in these catalytic aldol and Michael reactions.[2b,3b,7,8] Isomerization to *C*-bound α-cyanocarbanions[5] and subsequent carbometallation[1] are alternative possibilities for this process; however, precise mechanistic information on this step still remains to be explored. During the course of our systematic studies on the structure and reactivity of transition metal α-cyanocarbanions[5] we have succeeded in the isolation of intermediate for catalytic Michael reactions of nitriles. We describe here the conjugate addition of *N*-bound α-cyanocarbanions, $Ru^+Cp(NCCH^-R)(PPh_3)_2$ **1** to electron deficient olefins, and mechanism of the catalytic Michael reactions of nitriles.[9]

When a 25.0 mM solution of *N*-bound α-cyanocarbanion $Ru^+Cp(NCCH^-SO_2Ph)(PPh_3)_2$[5] **1a** in benzene was allowed to react with dimethyl ethylidenemalonate (1.0 equiv.) at room temperature under argon atmosphere, conjugate addition and subsequent 1,3-hydrogen shift occurred to give the corresponding *N*-bound α-cyanocarbanion $Ru^+Cp[NCC^-(SO_2Ph)CHMeCH(CO_2Me)_2](PPh_3)_2$ **2a** in 99% isolated yield. Complex **2a** was characterized by ^1H, $^{13}C\{^1H\}$, $^{31}P\{^1H\}$ NMR, IR, mass spectra and elemental analysis.§ Characteristic downfield shifts of the IR absorption (2153 cm^{-1}) and ^{13}C NMR signal (δ 143.7) of the cyano group indicate that the α-cyanocarbanion is *N*-bound,¶ and the zwitterionic structure has been unequivocally established by a ^1H–^{13}C HMBC experiment.‖ Similar treatment of cyanoacetate and ketonitrile analogs **1b** (R^1 = CO_2Et)[8d] and **1c** (R^1 = $COBu^t$) gave the corresponding adducts **2b**, **c** in 98 and 98% isolated yields. Various electron deficient olefins such as dimethyl benzylidenemalonate, benzylidenemalononitrile, pent-3-en-2-one, and acrylonitrile reacted smoothly with **1a** at room temperature to afford **2d**–**g** in 98, 99, 31 and 36% yields, respectively.

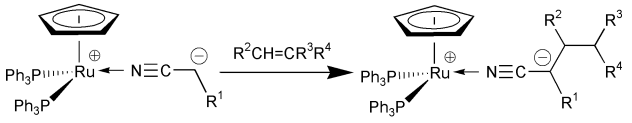

1 **2**

a: R^1 = SO_2Ph, R^2 = Me, R^3 = R^4 = CO_2Me
b: R^1 = CO_2Et, R^2 = Me, R^3 = R^4 = CO_2Me
c: R^1 = $COBu^t$, R^2 = Me, R^3 = R^4 = CO_2Me
d: R^1 = SO_2Ph, R^2 = Ph, R^3 = R^4 = CO_2Me
e: R^1 = SO_2Ph, R^2 = Ph, R^3 = R^4 = CN
f: R^1 = SO_2Ph, R^2 = Me, R^3 = COMe, R^4 = H
g: R^1 = SO_2Ph, R^2 = H, R^3 = CN, R^4 = H

As well as complex **1**,[8d] complex **2** shows comparable catalytic activity for the Michael additions of nitriles. Typically, the reaction of (phenylsulfonyl)acetonitrile **4** (4.00 M) with dimethyl benzylidenemalonate **3** (4.40 M) in the presence of **1a** or **2d** catalyst (0.120 M) in THF at 25 °C for 24 h gave adduct **5** in 86 and 88% isolated yields, respectively. In order to obtain insight into the mechanism of the complex **1**-catalyzed Michael addition of nitriles, kinetic studies on the reaction of **1a** with an excess amount of **3** in THF-d_8 were carried out by means of ^1H NMR (500 MHz) analysis using an internal standard (bibenzyl). The consumption rate of **1a** exhibited clean pseudo-first-order dependence on the concentration of **1a** (k_{obs} = 6.61 ± 0.04 × 10^{-4} s^{-1} at 25.0 °C, $[\mathbf{1a}]_0$ = 2.00 × 10^{-2} M, $[\mathbf{3}]_0$ = 2.00 × 10^{-1} M), and the k_{obs} values showed linear dependence on the initial concentration of **3** ranging from 2.00 to 4.00 × 10^{-1} M, indicating the second-order rate constant k_1 as 2.9 ± 0.1 × 10^{-3} dm^3 mol^{-1} s^{-1} at 25.0 °C. Dependences of k_{obs} *vs.* $[\mathbf{3}]_0$ at 25.0–45.0 °C are shown in Fig. 1. The rate data correlate well (R^2 = 0.990) with the Arrhenius relationship of ln(k_1) *vs.* 1/*T*, where the $\Delta H^‡$ and $\Delta S^‡$ values were determined as 41 ± 3 kJ mol^{-1} and −148 ± 8 J mol^{-1} K^{-1}, respectively. The second-order kinetics and the large negative value of $\Delta S^‡$ clearly indicate that the conjugate addition of **1a** to **3** proceeds *via* a direct ionic pathway without any contact of olefins with the metal center. $Ru^+Cp[NCCH(SO_2Ph)CHMeC^-(CO_2Me)_2](PPh_3)_2$ could not be detected during ^1H NMR experiments, indicating that the process involves a fast 1,3-hydrogen shift after the conjugate addition. When complex **2d** was allowed to react with nitrile **4** at room temperature in THF-d_8,

† Electronic supplementary information (ESI) available. Experimental section. See http://www.rsc.org/suppdata/cc/b0/b007517p/
‡ Dedicated to Professor J. F. Normant on the occasion of his 65th birthday.

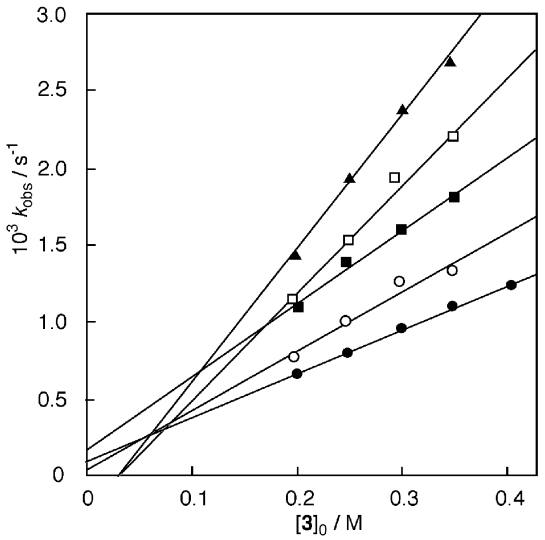

Fig. 1 Dependence of k_{obs} *vs.* $[\mathbf{3}]_0$ for the reactions of **1a** with **3** in THF-d_8 at 25.0 °C (●), 30.0 °C (○) 35.0 °C (■), 40.0 °C (□) and 45.0 °C (▲).

dissociation of Michael adduct **5** and regeneration of complex **1a** can be monitored by ^{1}H NMR spectroscopy. The consumption rate of **2d** was first-order on the concentration of **2d** ($[\mathbf{2d}]_0 = 2.00 \times 10^{-2}$ M, $[\mathbf{4}]_0 = 2.00 \times 10^{-1}$ M) and independent on the concentration of **4** ($[\mathbf{4}]_0 = 2.00$–3.50×10^{-1} M). The first-order rate constant k_2 was determined to be $7.3 \pm 0.3 \times 10^{-6}$ s^{-1} at 25.0 °C. The observed first-order kinetics on the ligand exchange process is ascribed to rate-determining formation of the 16-electron complex $[RuCp(PPh_3)_2]^+$ which would be followed by fast rebound process of the carbanion of **4** from outer sphere of the metal.

The complex **1a**-catalyzed Michael reaction of nitrile **4** with olefin **3** can be rationalized by the mechanism shown in Scheme 1. Direct ionic addition of **1a** to **3** and a subsequent 1,3-hydrogen shift affords complex **2d**, which undergoes a rate determining process of ligand exchange with **4** to form adduct **5** and regenerate catalyst **1a**. In order to verify this mechanism, kinetics on the overall catalytic Michael reaction of **4** with **3** were carried out at 25.0 °C in THF-d_8 using the same NMR technique. The initial rate of the formation of **5** was constant ($d[\mathbf{5}]/dt = k_{obs} = 1.44 \pm 0.03 \times 10^{-7}$ dm^3 mol^{-1} s^{-1}), when the reaction was started at an initial concentration of $[\mathbf{1a}]_0 = 2.00 \times 10^{-2}$ M, $[\mathbf{3}]_0 = 2.00 \times 10^{-1}$ M and $[\mathbf{4}]_0 = 2.00 \times 10^{-1}$ M. Almost the same k_{obs} value of $1.49 \pm 0.03 \times 10^{-7}$ dm^3 mol^{-1} s^{-1} was obtained when complex **2d** was employed as the catalyst ($[\mathbf{2d}]_0 = 2.00 \times 10^{-2}$ M). These rate constants are first-order on the concentration of catalyst **1a** or **2d**, and zero-order on the concentration of both nitrile **4** and olefin **3**. Thus, the rate law for the catalytic reaction can be expressed as $d[\mathbf{5}]/dt = k_3[\mathrm{Ru}]$ ($[\mathrm{Ru}] = [\mathbf{1a}]_0 = [\mathbf{2d}]_0 = [\mathbf{1a}] + [\mathbf{2d}]$), which leads to the relation $k_3 = k_{obs}/[\mathrm{Ru}]$. The calculated k_3 value of $7.7 \pm 0.9 \times 10^{-6}$ s^{-1} (25.0 °C) is well in accord with that of k_2; the rate constant of rate-determining step of the proposed catalytic cycle.

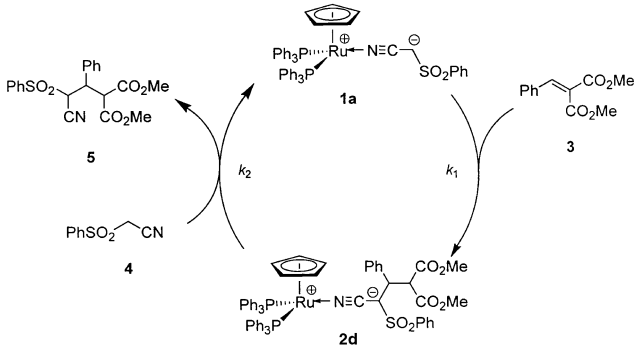

Scheme 1

In summary, we have identified the active species of the catalytic Michael reactions of nitriles, and presented a definitive mechanism for the reactions. This is a rare case because most reported mechanistic investigations for catalytic Michael reactions of nitriles deal mainly with substrate and product analysis while speculating on the crucial step of carbon–carbon bond formation. Efforts are currently underway to investigate more fully the dynamic behavior of transition metal α-cyanocarbanion intermediates in a variety of carbon–carbon bond forming processes of nitriles.

This work was supported by Research for the Future program, the Japan Society for the Promotion of Science, and a Grant-in-Aid for Scientific Research, the Ministry of Education, Science, Sports, and Culture, Japan.

Notes and references

§ *Characterization data* for **2a**: mp 110 °C (decomp.). IR (KBr) 2153 (CN), 1732 (C=O), 1480, 1433, 1281 (C–O, S=O), 1134 (S=O), 1090, 745, 696, 610 cm^{-1}; ^{1}H NMR (500 MHz, C_6D_6) δ 1.26 (d, *J* 7.0 Hz, 3 H, CHC*H*$_3$), 3.27 (s, 3 H, OCH_3), 3.37 (s, OCH_3), 3.63 (dq, *J* 9.6, 7.0 Hz, 1 H, C*H*^{3}CH$_3$), 4.11 [d, *J* 9.6 Hz, 1 H, C*H*^{4}(CO$_2$CH$_3$)$_2$], 4.44 (s, 5 H, C_5H_5), 6.92–7.02 (m, 21 H, ArH), 7.36–7.44 [m, 12 H, PC_6H_5 (*ortho*)], 8.07 [dd, *J* 8.0, 2.5 Hz, 2 H, $SO_2C_6H_5$ (*ortho*)]; ^{13}C{^{1}H} NMR (126 MHz, C_6D_6) δ 169.5 (C=O), 169.4 (C=O), 150.9 [$SO_2C_6H_5$ (*ipso*)], 143.7 (CN), 137.9 [PC_6H_5 (*ipso*)], 134.0 [$SO_2C_6H_5$ (*ortho*)], 133.8 [PC_6H_5 (*ortho*)], 129.3 [$SO_2C_6H_5$ (*para*)], 129.2 [PC_6H_5 (*para*)], 128.5 [PC_6H_5 (*meta*)], 126.4 [$SO_2C_6H_5$ (*meta*)], 83.6 (C_5H_5), 59.9 [*C*H(CO$_2$CH$_3$)$_2$], 58.7 (*C*CN), 52.0 (OCH_3), 51.6 (OCH_3), 34.2 ($CHCH_3$), 20.4 (CH_3); ^{31}P{^{1}H} NMR (202 MHz, C_6D_6) δ 43.2 (s); FAB-MS: *m/z* 1030 ([M]$^+$). Anal. Calc. for $C_{56}H_{51}NO_6P_2RuS$: C, 65.4; H, 5.00; N, 1.36. Found: C, 65.5; H, 4.82; N, 1.36%.

¶ A variety of *N*-bound complexes $RuCp^+(NCCH^-SO_2Ph)(PR_3)_2$ show IR absorption for the CN triple bond in the range *ca.* 2150–2170 cm^{-1}, and ^{13}C chemical shift of a nitrile carbon at δ 140–155, while those of the C-bound isomers have been observed at 2190–2200 cm^{-1} and δ 110–125, respectively.[5]

‖ The ^{1}H NMR signal of **2a** appearing at δ 4.11 strongly correlates with ^{13}C signals of two carbonyl carbons (δ 169.4 and 169.5), which clearly leads to assignment of the ^{1}H signal as the H^4 proton of the zwitterionic α-cyanocarbanion moiety.

1 P. Knochel, N. Jeong, M. J. Rozema and M. C. P. Yeh, *J. Am. Chem. Soc.*, 1989, **111**, 6474; H.-J. Liu and N. H. Al-said, *Tetrahedron Lett.*, 1991, **32**, 5473; T. Kauffmann, H. Kieper and H. Pieper, *Chem. Ber.*, 1992, **125**, 899; M. T. Reetz, H. Haning and S. Stanchev, *Tetrahedron Lett.*, 1992, **33**, 6963.

2 (*a*) T. Naota, H. Taki, M. Mizuno and S.-I. Murahashi, *J. Am. Chem. Soc.*, 1989, **111**, 5954; (*b*) S.-I. Murahashi, T. Naota, H. Taki, M. Mizuno, H. Takaya, S. Komiya, Y. Mizuho, N. Oyasato, M. Hiraoka, M. Hirano and A. Fukuoka, *J. Am. Chem. Soc.*, 1995, **117**, 12 436; (*c*) H. Takaya, T. Naota and S.-I. Murahashi, *J. Am. Chem. Soc.*, 1998, **120**, 4244.

3 (*a*) S. Paganelli, A. Schionato and C. Botteghi, *Tetrahedron Lett.*, 1991, **32**, 2807; (*b*) M. Sawamura, H. Hamashima and Y. Ito, *J. Am. Chem. Soc.*, 1992, **114**, 8295; (*c*) Y. Yamamoto, M. Al-Masum and N. Asao, *J. Am. Chem. Soc.*, 1994, **116**, 6019; (*d*) B. M. Trost, P.-Y. Michellys and V. J. Gerusz, *Angew. Chem., Int. Ed. Engl.*, 1997, **36**, 1750.

4 S. D. Ittel, C. A. Tolman, A. D. English and J. P. Jesson, *J. Am. Chem. Soc.*, 1978, **100**, 7577; J. G. Stack, J. J. Doney, R. G. Bergman and C. H. Heathcock, *Organometallics*, 1990, **9**, 453; G. L. Crocco, K. E. Lee and J. A. Gladysz, *Organometallics*, 1990, **9**, 2819; J. S. Ricci and J. A. Ibers, *J. Am. Chem. Soc.*, 1971, **93**, 2391.

5 T. Naota, A. Tannna and S.-I. Murahashi, *J. Am. Chem. Soc.*, 2000, **122**, 2960, and references therein.

6 S.-I. Murahashi and T. Naota, *Bull. Chem. Soc. Jpn.*, 1996, **69**, 1805.

7 Y. Mizuho, N. Kasuga and S. Komiya, *Chem. Lett.*, 1991, 2127.

8 $Ru^+H(NCCH^-CO_2R)(dppe)_2$: (*a*) M. Hirano, A. Takenaka, Y. Mizuho, M. Hiraoka and S. Komiya, *J. Chem. Soc., Dalton Trans.*, 1999, 3209; $Re^+(NCCH^-CO_2R)(NCCH_2CO_2R)(PMe_2Ph)_4$: (*b*) M. Hirano, Y. Ito, M. Hirai, A. Fukuoka and S. Komiya, *Chem. Lett.*, 1993, 2057; (*c*) M. Hirano, M. Hirai, Y. Ito, T. Tsurumaki, A. Baba, A. Fukuoka and S. Komiya, *J. Organomet. Chem.*, 1998, **569**, 3; $RuCp^+(NCCH^-CO_2R)(PPh_3)_2$: (*d*) S.-I. Murahashi, K. Take, T. Naota and H. Takaya, *Synlett*, 2000, 1016.

9 A preliminary result has been presented: *74th Annual Meeting of the Chemical Society of Japan*, Kyotanabe, March 27–30, 1998, Paper 3A117.

ChemComm

Ruthenium-catalysed oxidation of alkanes with peracetic acid in trifluoroacetic acid: ruthenium as an efficient catalyst for the oxidation of unactivated C–H bonds

Naruyoshi Komiya, Satoru Noji and Shun-Ichi Murahashi*

Department of Chemistry, Graduate School of Engineering Science, Osaka University, 1-3, Machikaneyama, Toyonaka, Osaka 560-8531, Japan. E-mail: mura@chem.es.osaka-u.ac.jp

Received (in Cambridge, UK) 22nd August 2000, Accepted 3rd November 2000
First published as an Advance Article on the web 14th December 2000

The role of ruthenium catalysts for the oxidation of alkanes with peracetic acid in trifluoroacetic acid has been confirmed.

During the course of simulation of the functions of cytochrome P-450 enzyme with transition metal complexes, we have found that transition metal-catalysed oxidations of various substrates can be performed highly efficiently.[1] In 1994 we reported that ruthenium-catalysed oxidation of alkanes with peracetic acid in ethyl acetate gives the corresponding ketones and alcohols.[2] Furthermore, the $RuCl_3$-catalysed oxidation of cyclohexane in TFA proceeds highly efficiently to give cyclohexyl trifluoroacetate and cyclohexanone with high conversion and high selectivity.[2] Recently, Moody and O'Connell reported that the oxidation of cyclohexane using urea hydrogen peroxide (UHP) in TFA without a metal catalyst gives cyclohexyl trifluoroacetate,[3] which was originally reported by Deno *et al.*[4] They obtained the rate constants ($k = 3.3 \times 10^{-5}$ M^{-1} s^{-1}) for the oxidation of cyclohexane with UHP in TFA in the presence or absence of $RuCl_3$ catalyst, indicating that the system is not ruthenium dependent. They claimed our system (peracetic acid–Ru) is not ruthenium dependent. However, our system using peracetic acid is quite different from that of UHP oxidation. Here, we describe our ruthenium-catalysed oxidation of alkanes with peracetic acid, which is very fast and an efficient ruthenium dependent reaction. The kinetics show the rate is 10^5 times faster than previously reported.

As described in our previous paper,[2] the oxidation of cyclohexane with peracetic acid in the presence of ruthenium on charcoal (Ru/C) or $RuCl_3$ (1 mol%) catalyst in ethyl acetate gives cyclohexanone along with a small amount of cyclohexanol [eqn. (1)]. No oxidation takes place without a catalyst.

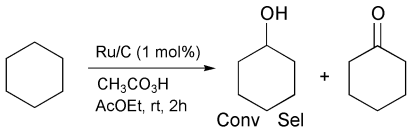

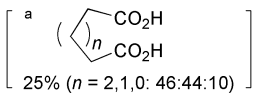

(1)

Treatment of cyclohexane with 0.5 eq. of peracetic acid proceeds in the presence of Ru/C catalyst to give cyclohexanol and cyclohexanone (4:93) with 97% selectivity (conv. 8%). In contrast, treatment of cyclohexane with 3 eq. of peracetic acid afforded cyclohexanol and cyclohexanone (2:68) with 70% selectivity along with dicarboxylic acids (adipic acid–glutaric acid–succinic acid = 46:44:10), which are derived from the oxidation of cyclohexane-1,2- and -1,3-diones under the reaction conditions, with 25% selectivity (conv. 51%). Peracetic acid is quite effective for the ruthenium-catalysed oxidation of alkanes, while hydrogen peroxide does not give any oxidation product because of the decomposition of hydrogen peroxide to give O_2 and H_2O by the contact with $RuCl_3$, indicating that peracetic acid is clearly different from hydrogen peroxide in the present non-TFA system.

In order to generate more active oxo-metal species which may lead to high conversion and high selectivity for the oxidation of alkanes,[5–7] we used TFA. As described in our previous paper,[2] the $RuCl_3$-catalysed oxidation of cyclohexane with peracetic acid in a mixture of TFA and CH_2Cl_2 (5:1) for 4 h gave cyclohexyl trifluoroacetate and cyclohexanone with 90% selectivity (85:15) and 90% conversion [eqn. (2)]. However,

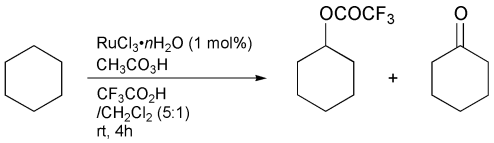

(2)

the same reaction in the absence of $RuCl_3$ for 24 h gave cyclohexyl trifluoroacetate only in $< 3\%$ yield.

The present catalytic oxidation can be applied to a variety of alkanes. The representative results of the ruthenium-catalysed oxidation of alkanes with peracetic acid in a mixture of TFA and CH_2Cl_2 are shown in Table 1. Both linear and cyclic alkanes can be converted into the corresponding esters of trifluoroacetic acid along with ketones. The reaction of adamantane gave adamantan-1-ol, which was formed by hydrolysis of 1-adamantyl trifluoroacetate.

Kinetic experiments on the reaction of cyclohexane with peracetic acid in TFA were carried out. In the presence of a large excess of cyclohexane, the rate was first-order with respect to

Table 1 Ruthenium-catalysed oxidation of alkanes with peracetic acid in TFA[a]

Alkane	Conversion[b] (%)	Product	Yield[c] (%)
Cyclohexane	90	Cyclohexyl trifluoroacetate	77
		Cyclohexanone	13
Cyclooctane	81	Cyclooctyl trifluoroacetate	40
		Cyclooctanone	10
Adamantane[d]	70	Adamantan-1-ol[e]	89
		2-Adamantyl trifluoroacetate	9
Norbornane[f]	90[g]	*exo*-2-Norbornyl trifluoroacetate	61
Hexane	nd	Hexyl trifluoroacetates[h]	24[b]
		Hexanones[i]	6[b]

[a] To a mixture of alkane (2.5 mmol), $RuCl_3$ (0.025 mmol), TFA (5 mL) and CH_2Cl_2 (1 mL) was added dropwise a 30% peracetic acid (5.0 mmol) solution in ethyl acetate over a period of 2 h. After stirring for 2 h, the reaction was quenched by adding 5% aqueous sodium sulfite solution. [b] Determined by GC based on the starting alkane using an internal standard (acetophenone). [c] Determined by GC based on the converted alkane. [d] TFA (5 mL), CH_2Cl_2 (10 mL) and acetic acid (5 mL) were used as a solvent. [e] 1-Adamantyl trifluoroacetate was readily hydrolyzed to give adamantan-1-ol during the work up. [f] The IUPAC name for norbornane is bicyclo-[2.2.1]heptane. [g] Not determined. [h] 2-:3-Hexyl trifluoroacetate = 45:55. [i] 2-:3-One = 34:66.

DOI: 10.1039/b006869l

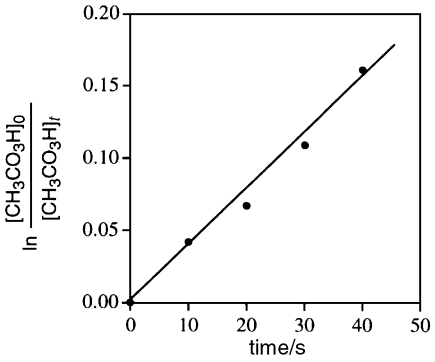

Fig. 1 Pseudo-first-order rate plot of the ruthenium-catalysed oxidation of cyclohexane with peracetic acid in the presence of TFA. Solvent, TFA–CH_2Cl_2–AcOEt = 5:1:1; [$RuCl_3$] = 7.1×10^{-4} M; [CH_3CO_3H] = 1.4×10^{-2} M; [cyclohexane] = 3.6×10^{-1} M; 20 °C; k_{obsd} = 3.9×10^{-3} s^{-1}.

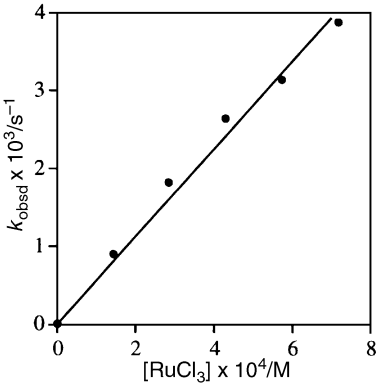

Fig. 2 Dependence of the first-order rate constants k_{obsd} on the concentration of $RuCl_3$. Solvent, TFA–CH_2Cl_2–AcOEt = 5:1:1; [CH_3CO_3H] = 1.4×10^{-2} M; [cyclohexane] = 3.6×10^{-2} M; 20 °C.

the concentration of peracetic acid (Fig. 1). The first-order rate constant increased with an increase in the concentration of $RuCl_3$ (Fig. 2), but the rate constant was independent of the concentration of cyclohexane. The rate law for the ruthenium-catalysed oxidation of cyclohexane with peracetic acid in TFA and CH_2Cl_2 was expressed by the equation $(-d[\text{cyclohexane}]/dt = k[RuCl_3][CH_3CO_3H])$. The second-order rate constant was determined to be $k = 5.4\ M^{-1}\ s^{-1}$. In contrast, the rate constant for the oxidation of cyclohexane without a metal catalyst is very small ($k < 10^{-6}\ s^{-1}$). These results clearly show that the oxidation of cyclohexane is catalysed by $RuCl_3$ catalyst dramatically.

Intermolecular deuterium isotope effect (k_H/k_D) of the ruthenium-catalysed oxidation of cyclohexane–cyclohexane-d_{12} in TFA was determined to be 2.9, which is smaller than the value (6.8) obtained from the same oxidation in ethyl acetate, indicating that a more reactive species is involved in the oxidation in TFA. The oxidation can be rationalized by assuming the mechanism which involves oxo-ruthenium species. The reaction of L_nRu^{III} with peracetic acid would give $L_nRu^{III}OOC(O)CH_3$ which undergoes heterolytic cleavage[8] to give the L_nRu^{V}=O species. Hydrogen abstraction with the oxo-ruthenium species and recombination would give an alcohol. Under the reaction conditions, an alcohol can be converted into either the corresponding trifluoroacetate or ketone. Actually, control experiments show that cyclohexanol is readily converted to a mixture of cyclohexyl trifluoroacetate and cyclohexanone under the reaction conditions.[9] The ruthenium-catalysed oxidation with peracetic acid is quite different from the oxidation with hydrogen peroxide in TFA, where electrophilic reaction of perfluoroacetic acid is involved. It is noteworthy that cyclohexanone has never been obtained from the reaction of H_2O_2–TFA.[3,4]

In summary, the oxidation of alkanes with peracetic acid in TFA proceeds efficiently in the presence of ruthenium catalyst to give the corresponding trifluoroacetic acid ester.

Notes and references

1 (*a*) S.-I. Murahashi, *Angew. Chem., Int. Ed. Engl.*, 1995, **34**, 2443; (*b*) S.-I. Murahashi and N. Komiya, in *Biomimetic Oxidations Catalyzed by Transition Metal Complexes*, ed. B. Meunier, Imperial College Press, London, 2000, pp. 563–611.
2 S.-I. Murahashi, Y. Oda, N. Komiya and T. Naota, *Tetrahedron Lett.*, 1994, **35**, 7953.
3 C. J. Moody and J. L. O'Connell, *Chem. Commun.*, 2000, 1311.
4 N. C. Deno, E. J. Jedziniak, L. A. Messer, M. D. Meyer, S. G. Stroud and E. S. Tomezsko, *Tetrahedron*, 1977, **33**, 2503.
5 T.-C. Lau and C.-K. Mak, *J. Chem. Soc., Chem. Commun.*, 1995, 943.
6 A. Sen, *Acc. Chem. Res.*, 1998, **31**, 550.
7 I. I. Moiseev, in *Transition Metal Catalysed Reactions*, ed. S.-I. Murahashi and S. G. Davies, Blackwell Science, Oxford, 1999, pp. 343–373.
8 W. A. Lee and T. C. Bruice, *J. Am. Chem. Soc.*, 1985, **107**, 513.
9 S.-I. Murahashi, T. Naota, Y. Oda and N. Hirai, *Synlett*, 1995, 733.

ChemComm

A new solid acid catalyst: the first phosphonate and phosphonic acid functionalised microporous polysilsesquioxanes†

Magdalena Jurado-Gonzalez, Duan Li Ou, Bradley Ormsby, Alice C. Sullivan and John R. H. Wilson

Department of Chemistry, Queen Mary and Westfield College, Mile End Road, London, UK E1 4NS. E-mail: a.c.sullivan@qmw.ac.uk

Received (in Cambridge, UK) 10th October 2000, Accepted 17th November 2000
First published as an Advance Article on the web 14th December 2000

A novel microporous solid acid, the phosphonic acid modified polysilsesquioxane $[(HO)SiCH_2CHPO(OH)_2\text{-}CH_2CH_2SiO_2(OH)]_n$ P2, from the new single precursor compound $[(EtO)_3SiCH_2CHPO(OCH_2CH_3)_2CH_2CH_2\text{-}Si(OEt)_3]$ 1, is reported, along with the catalytic activity of P2 for the pinacol–pinacolone rearrangement.

The development of functionalised porous silicas[1a,b] and polysilsesquioxane materials[1c,d] for various applications is proceeding at great pace as evidenced by recent reviews and reports on synthesis and applications in this area. Functional groups or their precursors may be attached to silica *via* compounds $(RO)_3Si(CH_2)_nX$ where X may be further modified if required. Such materials offer a wide spectrum of potential applications for example as acid, base, or oxidation catalysts or asymmetric carbon–carbon coupling catalysts, or as biocompatible surface groups.[1a,b,2] In the context of the present report efforts are also being directed towards the synthesis of functionalised porous polysilsesquioxanes, where the functional group is an integral part of a single framework precursor. Examples include polysilsesquioxanes with built-in NLO and luminescence chromophores,[3a,b] built-in crown-ether[4] or cyclam[5] groups for ion sensing applications or ferrocenyl groups for electrochemical applications.[6]

It occurred to us that phosphonic acid functionalised silicas and polysilsesquioxanes might offer a new class of solid acid materials with wide-ranging potential to act as catalysts, ion exchange and separation materials. There were no examples of such materials previously reported in the literature.

We report here on unique examples of the uniformly modified phosphonate and phosphonic acid polysilsesquioxanes $[(HO)SiCH_2CHPO(OCH_2CH_3)_2CH_2CH_2SiO_2(OH)]_n$ **P1** and $[(HO)SiCH_2CHPO(OH)_2CH_2CH_2SiO_2(OH)]$ **P2** prepared from the new precursor compound $[(EtO)_3SiCH_2CH\text{-}PO(OCH_2CH_3)_2CH_2CH_2Si(OEt)_3]$, **1**, 1,4-bis(triethoxysilyl)-2-(diethylphosphonato)butane. Compound **1** was formed‡ as shown in eqn. (1) by radical addition of $HPO(OEt)_2$ to the *ene* fragment in 1,4-bis(triethoxysilyl)but-2-ene[7] and was fully characterised by solution phase NMR, mass spectrometry and elemental analysis.

$$HPO(OEt)_2 + [(EtO)_3SiCH_2CH{=}CHCH_2Si(OEt)_2] \xrightarrow{Bu^tOOBu^t} [(EtO)_3SiCH_2CHPO(OCH_2CH_3)_2CH_2CH_2Si(OEt)_3] \quad (1)$$

1

P1 was obtained as a transparent monolith after acid-catalysed sol–gel processing of **1** in THF.§ The solid state ^{13}C CP MAS NMR spectrum of **P1** had peaks close to those observed for compound **1**; the ^{29}Si spectrum showed one broad resonance at −63 ppm consistent with predominantly T^2 type silicon sites while the ^{31}P NMR showed a single peak at 35 ppm similar to that of **1**. Treatment of **P1** with concentrated hydrochloric acid gave the corresponding phosphonic acid modified material **P2**.¶ The absence of any Q^n type resonances in the ^{29}Si CP MAS NMR of **P2** indicates that the transformation from ester to acid occurred without any Si–C cleavage. The decrease in C : P ratio and changes in the NMR spectra from **P1** to **P2** (in particular the disappearance of the signals due to the phosphonate ester group $-PO(OCH_2CH_3)_2$ at 63 ppm, see Fig. 1), is consistent with the formation of the phosphonic acid from the ester. Average formulae for these materials derived from C : P ratios and based on predominantly T^2 environments (66% condensation) are $[(HO)SiCH_2CHPO(OEt)_2CH_2CH_2\text{-}SiO_2(OH)]_n$ **P1** and $[(HO)SiCH_2CHPO(OH)_2CH_2CH_2\text{-}SiO_2(OH)]_n$ **P2**.

The material **P2** was found to be microporous by nitrogen sorption porosimetry with very narrow pore size distribution.

It is our intention initially to utilise the phosphonic acid functionality in these and related materials we have prepared for various catalytic transformations. Preliminary experiments based on catalytic pinacol–pinacolone rearrangement and dehydration of cyclohexanol were used to test the reactivity of the phosphonic acid functionality in **P2**. A range of solid acid catalysts have been reported to catalyse pinacol–pinacolone rearrangements; examples include metal substituted aluminophosphates,[8] lanthanide substituted zeolites,[9] heteropolytungstates,[10] various SAPOs (silicoaluminophosphates)[11] and polyphosphoric acid.[12]

A reaction between **P2** (0.2 g) and pinacol (6.0 g) at 140 °C (no solvent) resulted in 80% conversion to pinacolone after 12 h. Control experiments‖ using mesoporous or microporous silicas under the same conditions afforded no rearranged product. Attempted dehydration reactions using **P2** (0.25 g) and cyclohexanol (25 cm^3) ($C_6H_{11}OH : PO(OH)_2$ = 60 : 1) at 120 °C resulted in about 15% conversion to cyclohexene (^1H NMR of the cooled reaction mixture) after 12 h. In control experiments using mesoporous or microporous silica under the same conditions no cyclohexene was produced. Industrial processes for production of cyclohexene require high temperature and pressure whereby cyclohexanol is fed to activated catalysts such as silica, alumina or zinc aluminate at 380–450 °C (see ref. 13 for example). Neat phosphoric acid used in large excess is also active between 160–170 °C. [14]

A detailed systematic study of both reaction types will be carried out to optimise the catalyst performance.

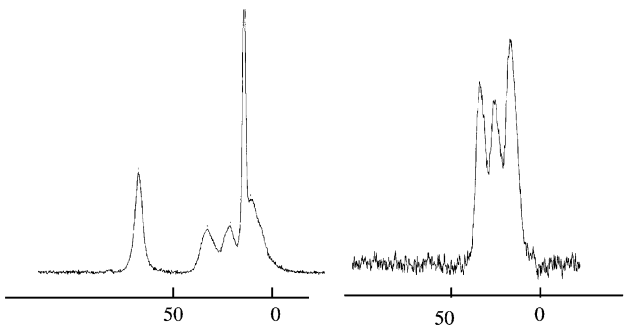

Fig. 1

† Electronic supplementary information (ESI) available: Fig. 2 nitrogen sorption isotherm of **P2** and Fig. 3 BJH pore size distribution of **P2**. See http://www.rsc.org/suppdata/cc/b0/b008192m/

Our material **P2** and related materials we have prepared[15] are also subjects for other studies including rearrangements, condensations, ion exchange and binding of biological molecules.

We thank EPSRC for a quota studentship to Bradley Ormsby, and Grant GR/M78281; Greg Coumbarides (QMW), Peter Haycock and Harold Toms of the ULIRS High Field NMR Service at QMW, Abil Aliev ULIRS solid state NMR service at University College London, for NMR. We also thank the University of London Central Research Fund and the Faculty Research Support Fund of Queen Mary and Westfield College for support.

Notes and references

‡ 1,4-Bis(triethoxysilyl)-2-(diethylphosphonato)butane **1**: 1,4-bis(triethoxysilyl)but-2-ene (30.0 g, 78.8 mmol) and diethyl phosphite (21.8 g, 158 mmol, 20.3 ml) and di-*tert*-butyl peroxide (0.58 g, 3.9 mmol, 0.72 ml) were heated at 140 °C for 18 h under nitrogen. The resultant mixture was distilled under reduced pressure to yield **1** (22.5 g, 55%) bp 147 °C, 0.4 mm Hg; Calcd C 46.3, H 9.1. Found C 46.1, H 9.0; *m/z* 541.5 (M + Na)$^+$ 519.5 (M^+), 473.4 (M − OCH_2CH_3)$^+$; Calcd for $C_{20}H_{48}Si_2P$ 519.2574; Found 519.2569; NMR: [($^6CH_3{}^5CH_2O)_3Si{}^1CH_2{}^2CH\{PO(O^9CH_2{}^{10}CH_3)_2\}$-$^3CH_2{}^4CH_2Si(O^7CH_2{}^8CH_3)_3$] superscripts indicate proton or carbon environments as appropriate ^{1}H($CDCl_3$) δ 0.51–1.03 (complex m, 4H, $^1CH_2$, $^4CH_2$), 1.05 (t, 9 H, $^8CH_3$, $^3J_{HH}$ 8 Hz), 1.06 (t, 9 H, $^6CH_3$, $^3J_{HH}$ 8 Hz), 1.27 (t, 6 H, $^{10}CH_3$, $^3J_{HH}$ 8 Hz), 1.56–1.91 (complex m, 3H, ^2CH, $^3CH_2$), 3.66 (q, $^7CH_2$, $^3J_{HH}$ 8 Hz), 3.69 (q, $^5CH_2$, $^3J_{HH}$ 8 Hz), 3.95 (m, $^9CH_2$, $^3J_{PH}$ 10 Hz); ^{13}C ($CDCl_3$) δ 8.17 (d, $^4CH_2$, $^3J_{PC}$ 4 Hz), 8.92, 9.01 (d, $^1CH_2$, $^2J_{PC}$ 6.5 Hz), 16.30, 16.39 (d, $^{10}CH_3$, $^2J_{PC}$ 6.5 Hz), 18.10 (s, $^6CH_3$,$^8CH_3$), 23.56 (s, $^3CH_2$, $^2J_{PC}$ 4 Hz), 32.16, 34.35 (d, ^2CH, J_{PC} 138 Hz), 58.09 (s, $^5CH_2$), 58.29 (s, $^7CH_2$), 61.16, 61.25 (d, $^9CH_2$, $^2J_{PC}$ 6.5 Hz); ^{29}Si ($CDCl_3$) δ −45.65 (s, ^{4}C-Si), −47.66, −47.94 (d, ^{1}C-Si, $^3J_{PSi}$ 40 Hz); ^{31}P ($CDCl_3$) δ 36.13 (s).

§ **P1**: Compound **1** (4.45 g, 8.58 mmol), THF (37 ml) and 1 M HCl (0.8 ml) were stirred under dynamic nitrogen for 1 h and stored in a polythene bottle. Gelation occurred after 11 d. The transparent monolithic gel obtained was air dried for 1 week and then dried at 60 °C in an oven for 24 h. A transparent monophasic crack-free glass was produced. This was powdered, washed with water, ethanol and ether consecutively, and then dried under vacuum at 120 °C for 24 h; ^{13}C CP MAS δ14.3, 16.9, 23.2, 33.2, 63.1; ^{29}Si CP MAS δ −63.5; ^{31}P CP MAS δ 34.5; Calculated average formula based on T^2 environments $[(HO)SiCH_2CHPO(OEt)_2CH_2CH_2SiO_2(OH)]_n$ C:P = 3.1, Found C/P = 2.8; Calculated for **P1**·$3H_2O$ C, 26.2; H, 6.3, P 8.5. Found C 26.6, H 6.0, P 9.6%.

¶ **P2**: Powdered **P1** (1.00 g) and concentrated HCl (100 ml) were refluxed for 24 h. The mixture was filtered through a fritted funnel and washed with excess H_2O to remove all traces of HCl, followed by ethanol and ether. The residue was dried under vacuum at 120 °C for 24 h; ^{13}C CP MAS δ 16.5, 23.1, 33.6; ^{29}Si CP MAS NMR δ −66.2; ^{31}P CP MAS NMR δ 33.5; Average formula based on T^2 environments $[(HO)SiCH_2CH$-$PO(OH)_2CH_2CH_2SiO_2(OH)]_n$ C:P = 1.55, Found C:P = 1.35; Calculated **P2**·$2H_2O$ C 16.3, H 5.1, P 10.5. Found C 14.2, H 4.3, P 10.5%; BET surface area 354 m^2 g^{-1}; micropore surface area 345 m^2 g^{-1}; micropore volume 0.192 cm^3 g^{-1}; total pore volume 0.219 cm^3 g^{-1}.

‖ Control experiments were carried out with microporous and mesoporous silicas prepared by standard methods from TEOS and with samples of these treated with concentrated HCl and washed in the manner described above for **P2**.

1 (*a*) P. M. Price, J. H. Clark and D. J. Macquarrie, *J. Chem. Soc., Dalton Trans.*, 2000, 101; (*b*) J. H. Clark and D. Macquarrie, *Chem. Commun.*, 1998, 853; (*c*) D. A. Loy and K. J. Shea, *Chem. Rev.*, 1995, **95**, 1431; (*d*) R. J. P. Corriu and D. Leclercq, *Angew. Chem., Int. Ed. Engl.*, 1996, **35**, 1420.

2 I. Rodriguez, S. Iborra, A. Corma, F. Rey and J. L. Jorda, *J. Chem. Soc., Chem. Commun.*, 1999, 593; J. A. Elings, R. Ait-Meddour, J. H. Clark and D. J. Macquarrie, *J. Chem. Soc., Chem. Commun.*, 1998, 2707; R. Ciriminna, J. Blum, D. Anvir and M. Pagliaro, *J. Chem. Soc., Chem. Commun.*, 2000, 1441; Y. Wang, T. Ju Su, R. Green, Y. Tangt, D. Styrkas, T. N. Danks, R. Bolton and J. R. Lu, *J. Chem. Soc., Chem. Commun.*, 2000, 587; S. J. Bae, S.-Wook Kim, T. Hyeon and B. Moon Kim, *J. Chem. Soc., Chem. Commun.*, 2000, 31.

3 H. W. Oviatt, K. J. Shea, S. Kalluri, Y. Shi, W. H. Steier and L. R. Dalton, *Chem. Mater.*, 1995, **7**, 493; A.-C. Franville, D. Zambon and R. Mahiou, *Chem. Mater.*, 2000, **12**, 428.

4 S. Brandes, R. J. P. Corriu, F. Denat, G. Dubois, R. Guilard and C. Reye, *J. Chem. Soc., Chem. Commun.*, 1999, 2283.

5 C. Chuit, R. J. P. Corriu, G. Dubois and C. Reye, *J. Chem. Soc., Chem. Commun.*, 1999, 723.

6 P. Audebert, P. Calas, G. Cerveau, R. J. P. Corriu and N. Costa, *J. Electroanal. Chem.*, 1994, **372**, 275.

7 R. J. P. Corriu, J. J. E. Moreau, P. Thepot and M. Wong Chi Man, *Chem. Mater.*, 1992, **4**, 1217.

8 B. Y. Hsu and S. F. Cheng, *Microporous Mesoporous Mater.*, 1998, **21**, 505.

9 C. P. Bezouhanova and F. A. Jabur, *J. Mol. Catal.*, 1994, **87**, 39.

10 Y. Toyoshi, T. Nakato and T. Okuhara, *Bull. Chem. Soc. Jpn.*, 1998, **71**, 2817; Y. Toyoshi, T. Nakato, R. Tamura, H. Takahashi, H. Tsue, K. Hirao and T. Okuhara, *Chem. Lett.*, 1998, 135.

11 F. A. Jabur, V. J. Penchev and C. P. Bezoukhanova, *J. Chem. Soc., Chem. Commun.*, 1994, 1591.

12 M. A. Kakimoto, T. Seri and Y. Imai, *Bull. Chem., Soc. Jpn.*, 1988, **61**, 2643.

13 T. K. Shioyama and O. K. Bartlesville, Phillips Petroleum Company, US1980000113948 April 7, 1981.

14 W. M. Dehn and K. E. Jackson, *J. Am. Chem., Soc.*, 1933, **55**, 4285.

15 A. Aliev, D. Li Ou, B. Ormsby and A. C. Sullivan, *J. Mat. Chem.*, 2000, **10**, 2758.

A novel Lewis acid-promoted enyne cycloisomerization of triester-substituted alkenes†

Shoko Yamazaki,*[a] Kuriko Yamada,[a] Tetsuya Otsubo,[a] Masayo Haruna,[a] Emiko Kutsuwa[a] and Hatsue Tamura[b]

[a] *Department of Chemistry, Nara University of Education, Takabatake-cho, Nara 630-8528, Japan. E-mail: yamazaks@nara-edu.ac.jp*

[b] *Department of Applied Chemistry, Graduate School of Engineering, Osaka University, 1-16 Machikaneyama, Toyonaka, Osaka 560-0043, Japan*

Received (in Cambridge, UK) 6th October 2000, Accepted 31st October 2000
First published as an Advance Article on the web 15th December 2000

A novel cycloisomerization reaction of enynes 4 in the presence of $ZnBr_2$ and THF (1 eq.) in CH_2Cl_2 at −40 °C gave *exo*-methylenic 1,3-dienes 5 in moderate to good yield.

Lewis acid-promoted reactions are an important part of modern synthetic chemistry.[1] Recently, prototropic cycloisomerization reactions of enynes and dienes have been recognized as atom-economic tools to construct rings, and transition metal-catalyzed cycloisomerizations in particular have received much attention.[2] However, only a few examples of Lewis acid-promoted cycloisomerizations (intramolecular ene reactions) have been reported so far.[3,4a,b]

The design of a Lewis acid-promoted enyne cyclization requires that a highly electrophilic alkene (or alkyne) has coordination sites for a Lewis acid and that the other component (alkyne or alkene) works as a nucleophile. Alkenes with three ester groups are considered to be highly electrophilic and very reactive towards nucleophilic olefins,[5] and they may react intramolecularly with alkynes which are relatively unreactive nucleophiles.[6]‡ We thus examined Lewis acid-promoted intramolecular cyclization of the designed triester-substituted alkene **1**. Reaction of **1** in the presence of $ZnBr_2$ at rt gave cyclized product **2** and H_2O-adduct **3** in 45% and 10% yields, respectively (eqn. (1)).

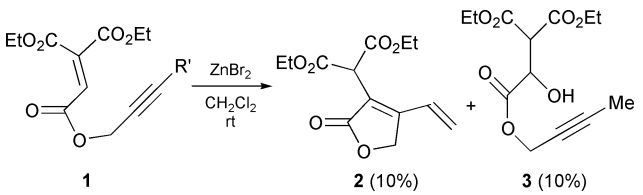

(1)

The formation of **2** can be explained as shown in Scheme 1.§ Nucleophilic attack of the alkyne moiety to the electrophilic olefin complexed with $ZnBr_2$ in **A** gives intermediate **B**.¶ A 1,3-hydride shift then leads to complex **C**, which isomerizes and then forms diene **2** with Et_3N. The formation of hydrated product **3** is presumed to result from attack by trace amounts of water on complex **A**.

If the isomerization step in **C** is prevented, *exo*-methylenic 1,3-dienes should be the primary products in this process. The enyne **4**, which is prevented from undergoing isomerization due to the lack of a proton, was designed and Lewis acid mediated reactions examined. After several conditions were examined (see below), reaction of **4** in the presence of $ZnBr_2$ (1.2 eq.) and THF (1 eq.) in CH_2Cl_2 at −40 °C for 17–19 h gave *exo*-methylenic 1,3-dienes **5** in 29–67% yields (eqn. (2), Table 1).‖ The γ-lactone structure of **5** was suggested by the presence of a characteristic C=O absorption (1771–1779 cm^{-1}). ^1H, ^{13}C, ^1H/^{13}C-HSQC, HMBC and NOESY spectra were in agreement with the lactone structure drawn in eqn. (2). The crystal structure of **5a** was elucidated by X-ray diffraction analysis (Fig. 1).** The diene is slightly twisted from the plane in order to reduce steric repulsion between the ester and HPhC= groups; the torsion angle of the diene moiety (∠C5-C3-C2-C12) is 21.9°. This *cisoid* diene may be effective as an acceptor in the inverse electron demand Diels–Alder reaction (see below).

Scheme 1

Table 1 Cycloisomerization of **4** to **5**

Substrate[a]	R^1	R^2	Ar	Product (yield)
4a	H	Et	Ph	**5a** (67%)
4b	H	Et	*p*-Tol	**5b** (58%)
4c	H	Et	*p*-MeO-C_6H_4	**5c** (41%)
4d	Me	Et	Ph	**5d** (53%)
4e	*n*-Propyl	Et	Ph	**5e** (46%) (**4e** recovered 36%)
4f	H	Me	Ph	**5f** (29%)
4g	H	^{i}Pr	Ph	**5g** (50%)[b]

[a] All reactions were carried out using 0.30–0.58 mmol of **4**, 1.2 eq. of $ZnBr_2$, and 1.0 eq. of THF at 0.41 M for **4** in CH_2Cl_2 at −40 °C for 17–19 h, unless otherwise noted. [b] THF was not added. Addition of THF gave **5g** in 40% yield along with recovered **4g** (24%).

† Electronic supplementary information (ESI) available: experimental procedures and spectral data for described compounds and crystallographic data for **5a**. See http://www.rsc.org/suppdata/cc/b0/b008103p/

DOI: 10.1039/b008103p

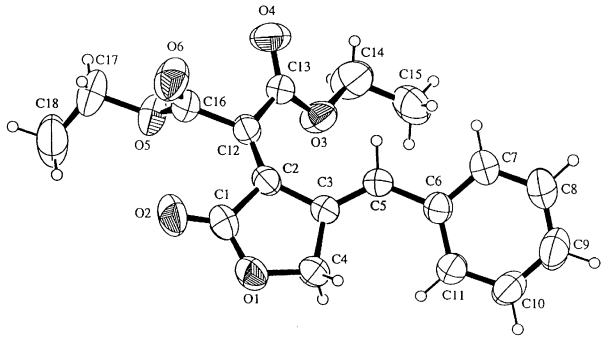

Fig. 1 ORTEP drawing of **5a** (50% probability ellipsoids). Selected bond lengths (Å) and torsion angle (°): C1–C2 = 1.499(3); C2–C3 = 1.460(2); C3–C4 = 1.501(2); C1–O1 = 1.344(2); O1–C4 = 1.444(2); C2–C12 = 1.345(2); C3–C5 = 1.344(2); ∠C5–C3-C2–C12 = 21.9(3). More detailed structure data are given in the supplementary data.

With **4a**,**b**, the yield of **5** decreased when THF was omitted from the reaction (for **5a** to 11–36%, for **5b** to 11–25%).†† The effect of THF is presumed to be that coordination of THF to Zn adjusts the strength of the Lewis acid and prevents side reactions.‡‡ For **4g**, the reaction without THF gave a slightly better yield (see Table 1).

Use of ZnI_2–THF instead of $ZnBr_2$–THF gave **5a** in 62% yield. Use of $SnCl_4$ (−78 °C) or $ZnCl_2$–THF (−40 °C) gave **5a** in lower yield (24–39% including inseparable complex mixtures). The reaction of **4a** with $ZnBr_2$–THF was also performed at a higher temperature (0 °C to rt), however, the yield of **5a** decreased (32%), probably because of the instability of the diene product. The reaction of **4a** using 0.3 eq. of $ZnBr_2$–THF afforded 19% of **5a** along with recovered **4a** (62%), therefore the reaction requires a stoichiometric amount of Lewis acid.§§

Thermal reactions of **4a** and **1** (CH_3CN, 80 °C, 24 h or toluene, 110 °C, 24 h) without Lewis acid only afforded complex mixtures along with recovered starting materials (38–87%). A $RuClH(CO)(PPh_3)_3$-catalyzed reaction (toluene, 110 °C, 7 h) of **4a** was examined but did not proceed.[8]

Only a few examples of synthesis of heterocycles by cycloisomerization using transition metal catalysts have been reported.[9] Therefore, the present method should provide an efficient alternative to transition metal-catalyzed cycloisomerizations. Also, the product cyclic dienes are electron-deficient and suitable for cycloadditions such as inverse electron demand Diels–Alder reaction[10] and transition metal-catalyzed [4 + 3] cycloadditions.[11] The inverse electron demand Diels–Alder reactions of **5a** with the electron rich dienophiles **6** and **8** were thus examined (eqn. (3)). C–C bond formation proceeds readily, however, the observed regio- and stereoselectivity was low.¶¶

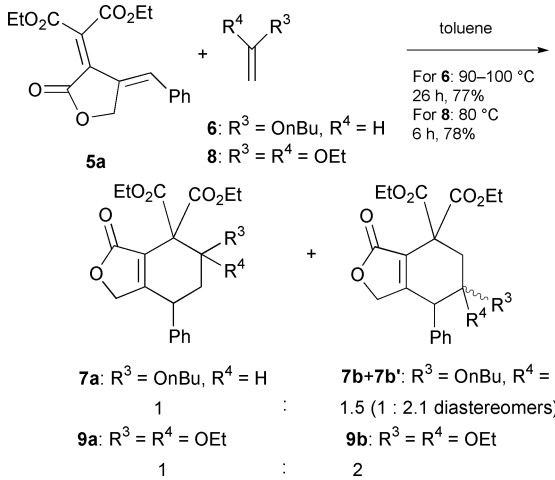

(3)

In summary, a novel Lewis acid-promoted enyne cycloisomerization to give cyclic dienes has been developed. This new reaction provides a highly efficient means to prepare electron-deficient cyclic dienes. The application of this methodology towards the construction of carbocycles and diverse heterocycles is under investigation.

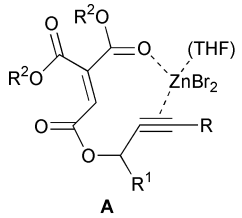

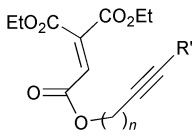

10a: n = 1, R' = H
10b: n = 2, R' = Ph
10c: n = 2, R' = H

We are grateful to Dr K. Yamamoto (Osaka University) for measurement of mass spectra and elemental analysis. We thank Mr Y. Yanase for experimental assistance.

Notes and references

‡ Thermal ene reactions[6a,b] and $FeCl_3$-promoted chlorinated cyclizations[6c] of allylic and propargylic esters of ethylenetricarboxylic acid have been reported.

§ The alternative mechanism is that **1** undergoes an ene reaction initially to give a cyclic allene that rearranges to **2**.

¶ The coordination of a Lewis acid to a C≡C bond was reported recently.[12] The intermediate **A** (Scheme 1) can be drawn as shown above.

‖ Cyclizations were also examined using **10a**–**c** as substrates. Using similar conditions, only starting material was recovered.

** *Crystal data*: $C_{18}H_{18}O_6$, M = 330.34, monoclinic, a = 8.1206(3), b = 10.5914(3), c = 19.7984(7) Å, β = 100.513(1)°, V = 1674.2(1) Å^3, T = 296 K, space group $P2_1/c$ (no. 14), Z = 4, μ(Mo-Kα) = 0.099 mm^{-1}, number of reflections measured = 4062, number of independent reflections = 3845 (R_{int} = 0.025), R, R_w = 0.047, 0.052 for 2473 observed reflections ($I > 2\sigma(I)$). CCDC 182/1839. See http://www.rsc.org/suppdata/cc/b0/b008103p/ for crystallographic files in .cif format.

†† The reaction of **4a** in THF as a solvent did not proceed.

‡‡ Use of propylene oxide instead of THF in the reaction of **4a** gave **5a** in lower yield (28%), along with recovered **4a** (21%). The combination of Lewis acid and Lewis base is used in some Lewis acid-mediated reactions.[7]

§§ Formation of cyclic dienes is in marked contrast with the $FeCl_3$-promoted reaction of dimethyl ester analog of **1** and **4d** giving chlorinated cyclization products.[6c] Investigation of the difference in Lewis acids is underway.

¶¶ The stereochemistries of **7a**, **7b** and **7b′** were tentatively assigned as shown in the supplementary information by the observed NOE's.

1 *Selectivities in Lewis Acid Promoted Reactions*, ed. D. Schinzer, Kluwer Academic Publishers, Dordrecht, 1989; S. Shambayati and S. L. Schreiber, in *Comprehensive Organic Synthesis*, ed. B. M. Trost and I. Fleming, Pergamon Press, Oxford, 1991, Vol. 1, p. 283.
2 B. M. Trost, *Science*, 1991, **254**, 1471.
3 B. B. Snider, *Acc. Chem. Res.*, 1980, **13**, 426; K. Mikami and M. Shimizu, *Chem. Rev.*, 1992, **92**, 1021.
4 (*a*) K. Narasaka, Y. Hayashi and S. Shimada, *Chem. Commn.*, 1988, 1609; (*b*) T. Minami, T. Utsunomiya, S. Nakamura, M. Okubo, N. Kitamura, Y. Okada and J. Ichikawa, *J. Org. Chem.*, 1994, **59**, 6717.
5 W. Srisiri, A. B. Padias and H. K. Hall, Jr., *J. Org. Chem.*, 1994, **59**, 5424.
6 (*a*) T. R. Kelly, *Tetrahedron Lett.*, 1973, 437; (*b*) B. B. Snider, D. M. Roush and T. A. Killinger, *J. Am. Chem. Soc.*, 1979, **101**, 6023; (*c*) B. B. Snider and D. M. Roush, *J. Org. Chem.*, 1979, **44**, 4229.
7 I. Suzuki and Y. Yamamoto, *J. Org. Chem.*, 1993, **58**, 4783.
8 M. Nishida, N. Adachi, K. Onozuka, H. Matsumura and M. Mori, *J. Org. Chem.*, 1998, **63**, 9158.
9 B. M. Trost, E. D. Edstrom and M. B. Carter-Petillo, *J. Org. Chem.*, 1989, **54**, 4489.
10 G. J. Bodwell and Z. Pi, *Tetrahedron Lett.*, 1997, **38**, 309; H. L. Gingrich, D. M. Roush and W. A. Van Saun, *J. Org. Chem.*, 1983, **48**, 4869.
11 B. M. Trost and D. T. Macpherson, *J. Am. Chem. Soc.*, 1987, **109**, 3483.
12 N. Asao, T. Asano, T. Ohishi and Y. Yamamoto, *J. Am. Chem. Soc.*, 2000, **122**, 4817.

Kinetics of formation of the novel peroxide $FC(O)OO(O_2)SF$

María E. Tucceri, María P. Badenes, Adela E. Croce and Carlos J. Cobos*

Instituto de Investigaciones Fisicoquímicas Teóricas y Aplicadas (INIFTA), Departamento de Química, Facultad de Ciencias Exactas, Universidad Nacional de La Plata, CONICET, CICBA, Casilla de Correo 16, Sucursal 4, (1900) La Plata, Argentina. E-mail: cobos@inifta.unlp.edu.ar

Received (in Cambridge, UK) 2nd August 2000, Accepted 14th November 2000
First published as an Advance Article on the web 14th December 2000

The high-pressure rate coefficient for the formation of the new peroxide $FC(O)OO(O_2)SF$ from recombination of $FC(O)O$ and $FS(O_2)O$ radicals has been determined by laser flash photolysis at 296 K; density functional theory calculations indicate peroxide stabilization and allow estimation of an O–O bond dissociation energy of 20.6 ± 3 kcal mol^{-1}.

Early syntheses of fluorinated peroxides involved the coupling of oxy-radicals to form the peroxide bond.[1] In fact, the co-photolysis of the mixtures of peroxides SF_5OOSF_5/CF_3OOCF_3 and $SF_5OOSF_5/FS(O_2)OO(O_2)SF$ have been employed by Cady and coworkers to prepare SF_5OOCF_3 and $SF_5OO(O_2)SF$.[1] The fluorinated peroxides allow study of the role that the electron-withdrawing effect of electronegative groups plays on their reactivity, energetics and conformation. Here we report the determination of the rate coefficient for the recombination of $FC(O)O$ and $FS(O_2)O$ radicals to form the new peroxide $FC(O)OO(O_2)SF$ at 296 K. In addition, the rate coefficient for the reaction of $FS(O_2)O$ with CO has been determined for the first time.

A laser flash photolysis–absorption spectroscopy configuration described in detail elsewhere,[2–7] was employed in the present experiments. Typically, samples of 30–40 mbar of $FS(O_2)OF$ in the presence of 130–300 mbar of CO, 15 mbar of O_2 and up to 900 mbar of SF_6 were irradiated with the emission of an excimer laser operating on the 193 nm ArF transition. No more than 30 single shot experiments from fresh samples were averaged and analysed up to 5 ms for each set of conditions. In the photolysis, electronically excited $FS(O_2)O$ radicals in the B ^2E state are initially formed and afterwards collisionally deactivated to the X $^2A_2$ ground state *via* a manifold of low-lying vibrationally excited states.[4,5] After *ca.* 250 μs the excited radicals are thermalized.[5] On the other hand, photolytically generated F atoms are rapidly consumed by recombination with CO to form FCO radicals, which subsequently recombine with O_2 and yield $FC(O)O_2$ radicals. Finally, these radicals form $FC(O)O$ radicals by self-reaction. The whole reaction mechanism is detailed in refs. 6–9. FCO and $FC(O)O_2$ are almost quantitatively consumed at 200 μs. Thus, the well established mechanisms involved in the $FS(O_2)O$[2–5] and $FC(O)O_x$ (x = 0, 1, 2)[6–9] radical chemistries lead to the conclusion that over 300 μs only $FS(O_2)O$ and $FC(O)O$ survive and the mechanism reduces to eqns. (1)–(5)

$$FC(O)O + FC(O)O \rightarrow FC(O)OO(O)CF \quad (1)$$

$$FS(O_2)O + FS(O_2)O \rightarrow FS(O_2)OO(O_2)SF \quad (2)$$

$$FC(O)O + FS(O_2)O \rightarrow FC(O)OO(O_2)SF \quad (3)$$

$$FS(O_2)O + CO \rightarrow FSO_2 + CO_2 \quad (4)$$

$$FS(O_2)O + FSO_2 \rightarrow FS(O_2)O(O_2)SF \quad (5)$$

Under the present conditions, reactions (1) and (2) are pressure independent with high-pressure rate coefficients of $k_{\infty,1}$ = 5.5 × 10^{-13} [8] and $k_{\infty,2}$ = 4.6 × 10^{-14} cm^3 molecule^{-1} s^{-1}, respectively.[3] Second-order plots of the absorbance monitored at 450 nm after photolysis of $FS(O_2)OO(O_2)SF/CF_4$ and $FS(O)_2OF/CO/O_2/SF_6$ mixtures are depicted in Fig. 1. In the first case, the generated $FS(O)_2O$ radicals [absorption cross-sections $\sigma(FS(O_2)O)$ = 3.64 × 10^{-18} cm^2 molecule^{-1}[3]] react exclusively according to reaction (2). In the latter case, a fast component due to the above mentioned thermalization of excited $FS(O_2)O$ radicals is followed by a second component with a slope much higher than the observed for the first mixture. Absorbance *vs.* time profiles were numerically fitted employing the mechanism described by reactions (1)–(5). The modelling leads to radical concentrations such that the absorbance may be mostly attributed to $FS(O)_2O$ absorption with a small contribution due to $FC(O)O$ radicals [$\sigma(FC(O)O)$ = 6.7 × 10^{-19} cm^2 molecule^{-1} [8]]. Moreover, the calculations show that the higher slope observed in signal (B) of Fig. 1 is predominantly due to $FS(O_2)O$ consumption by reaction (3). At longer times and higher CO pressures these radicals are also consumed in reaction (4). However, the low FSO_2 concentration precludes the determination of k_5, for which reasonable values ranging from 2 × 10^{-12} to 7 × 10^{-11} cm^3 molecule^{-1} s^{-1} do not affect the modelling results. Between *ca.* 175 and 1060 mbar the rate coefficients determined for reaction (3) remain independent on total pressure such that they can be certainly ascribed to the limiting high pressure value. All experimental results are very well reproduced using the $k_{\infty,1}$, $k_{\infty,2}$ and k_5 values given above as well as $k_{\infty,3}$ = (1.2 ± 0.3) × 10^{-12} cm^3 molecule^{-1} s^{-1} and k_4 = (1.8 ± 0.7) × 10^{-17} cm^3 molecule^{-1} s^{-1} for reactions (3) and (4). The errors quoted are 2σ. The value of $k_{\infty,3}$ is normal for this type of reaction[10] while the low value of k_4 is quite consistent with the measured activation energy of 7 kcal mol^{-1}.[11] The experimental study is supplemented by density functional theory thermochemical computations to determine the bond dissociation energies of O–O, C–O and O–S bonds in $FC(O)OO(O_2)SF$. For this, standard enthalpies of formation of the peroxide and the relevant radicals were calculated. The value for $FC(O)OO(O_2)SF$ was estimated using the isodesmic reaction: $FOOF + FC(O)OH + HSO_3F \rightarrow FC(O)OO(O_2)SF + 2FOH$. Energy calculations were carried out on optimized geometries and harmonic frequencies evaluated employing the hybrid B3LYP density functional with the 6-311++G(d,p) basis

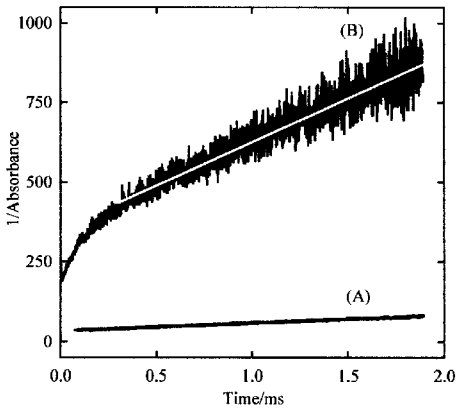

Fig. 1 Plot of the inverse of the absorbance *vs.* time. (A) 8.1 mbar of $FS(O_2)OO(O_2)SF$ and 16.4 mbar of CF_4; (B) 29.3 mbar of $FS(O_2)OF$, 132.4 mbar of CO, 14.3 mbar of O_2 and 890.0 mbar of SF_6. The solid line is the result of the modelling described in the text.

DOI: 10.1039/b006272n

set.[12] Unless otherwise indicated, the experimental enthalpies of formation of the species involved in this and other isodesmic reactions given here are from ref. 10. According to the experimental uncertainties, an error level for all derived thermochemical properties of this work of ±3 kcal mol^{-1} is estimated. From the calculated enthalpy of the isodesmic reaction of ΔH^0_r = 44.7 kcal mol^{-1}, the value $\Delta H^0_{f,298}$(FC(O)OO(O_2)SF) = −229.4 kcal mol^{-1} was derived. The enthalpy of formation for FS(O_2)O was estimated from the experimental bond dissociation energy, D_e(FS(O_2)O–F) = 33.1 kcal mol^{-1},[2] and $\Delta H^0_{f,298}$(FS(O_2)OF) = −136.9 kcal mol^{-1} obtained from the isodesmic reaction FO_2 + HSO_3F → FS(O_2)OF + HO_2 (ΔH^0_r = 40.0 kcal mol^{-1}). In this way, $\Delta H^0_{f,298}$(FS(O_2)O) = −122.8 kcal mol^{-1} results. Using the above enthalpies of formation for FC(O)OO(O_2)SF and FS(O_2)O together with $\Delta H^0_{f,298}$(FC(O)O) = − 86.0 kcal mol^{-1},[13] we obtain the enthalpy change ΔH^0_{298}(FC(O)O–O(O_2)SF) = 20.6 kcal mol^{-1} which is similar to the value measured for the FS(O_2)O–O(O_2)SF bond of 22.1 kcal mol^{-1}.[3]

Finally, using $\Delta H_{f,298}$(FS(O_2)OO) = −110.2 kcal mol^{-1}, estimated using the isodesmic reaction FO_2 + HSO_3F → FS(O_2)OO + FOH (ΔH^0_r = 40.4 kcal mol^{-1}), and $\Delta H^0_{f,298}$(FCO) = 44.6 kcal mol^{-1},[7] $\Delta H^0_{f,298}$(FC(O_2)OO) = −76.1 kcal mol^{-1},[6] and $\Delta H^0_{f,298}$ (FSO_2) = −96.2 kcal mol^{-1},[14] dissociation energies for other bonds in FC(O)OO(O_2)SF were evaluated. The resulting values are: ΔH^0_{298}(FC(O)OO–(O_2)SF) = 57.1 and ΔH^0_{298}(FC(O)–OO(O_2)SF) = 74.6 kcal mol^{-1}. These results indicate that no energetically feasible exit channels for the peroxide decomposition exist. The minimum-energy pathways for the recombination reaction (3) and for FC(O)–OO(O_2)SF and FC(O)OO–(O_2)SF dissociations show a smooth energy profile without a maximum: no transition state was found on the B3LYP/6-311 + G(d) surface. Thus the enthalpy changes can be assimilated to the respective bond dissociation energies. Scarcely probable is the competition between the reaction FC(O)O + FS(O_2)O → CO_2 + FS(O_2)OF and reaction (3). This assumption is supported by the fact that most fluorine abstraction reactions by either FS(O_2)O or other radicals exhibit relatively large activation energy values (*ca.* 10–30 kcal mol^{-1}) and consequently very small room temperature rate coefficients. In particular, for the similar reaction FNO_2 + FS(O_2)O → NO_2 + FS(O_2)OF an activation energy of *ca.* 30 kcal mol^{-1} can be estimated from the measured value of 10 kcal mol^{-1} for the reverse reaction,[15] the enthalpies of formation of FNO_2 and NO_2 molecules[10] and the above values for FS(O_2)O and FS(O_2)OF. The present results indicate that after formation by reaction (3), the new peroxide is mostly collisionally stabilized at room temperature. However, the low O–O bond dissociation energy leads to significant decomposition as temperatures rises, such that a gaseous sample of FC(O)OO(O_2)SF finally degrades to the more stable peroxide FC(O)OO(O)CF.[6–9]

Further experimental and theoretical work on FC(O)OO(O_2)SF is underway.

This work was supported by the Universidad Nacional de La Plata, the CONICET and the CICBA.

Notes and references

1 C. I. Merrill, S. M. Williamson, G. H. Cady and D. F. Eggers, *Inorg. Chem.*, 1962, **1**, 215.
2 A. E. Croce de Cobos, C. J. Cobos and E. Castellano, *J. Phys. Chem.*, 1989, **93**, 274.
3 C. J. Cobos, A. E. Croce de Cobos, H. Hippler and E. Castellano, *J. Phys. Chem.*, 1989, **93**, 3089.
4 C. J. Cobos, A. E. Croce and E. Castellano, *J. Photochem. Photobiol. A: Chem.*, 1991, **59**, 143.
5 A. E. Croce, C. J. Cobos and E. Castellano, *J. Photochem. Photobiol. A: Chem.*, 1990, **55**, 135.
6 M. P. Badenes, E. Castellano, C. J. Cobos, A. E. Croce and M. E. Tucceri, *Chem. Phys. Lett.*, 1999, **303**, 482.
7 M. P. Badenes, E. Castellano, C. J. Cobos, A. E. Croce and M. E. Tucceri, *Chem. Phys.*, 2000, **253**, 205.
8 M. M. Maricq, J. J. Szente, T. S. Dibble and J. S. Francisco, *J. Phys. Chem.*, 1994, **98**, 12 294.
9 T. J. Wallington, T. Ellermann, O. J. Nielsen and J. Sehested, *J. Phys. Chem.*, 1994, **98**, 2346.
10 W. B. DeMore, S. P. Sander, D. M. Golden, R. F. Hampson, M. J. Kurylo, C. J. Howard, A. R. Ravishankara, C. E. Kolb and M. J. Molina, *Chemical Kinetics and Photochemical Data for Use in Stratospheric Modeling. Evaluation Number 12*, JPL Publication 97-4, California Institute of Technology, Pasedena, CA, 1997. http://jpldataeval.jpl.nasa.gov/
11 E. Vasini and H. J. Schumacher, *Z. Phys. Chem. Neue Folge*, 1975, **94**, 39.
12 M. J. Frisch, G. W. Trucks, H. B. Schlegel, G. E. Scuseria, M. A. Robb, J. R. Cheeseman, V. G. Zakrzewski, J. A. Montgomery, Jr., R. E. Stratmann, J. C. Burant, S. Dapprich, J. M. Millam, A. D. Daniels, K. N. Kudin, M. C. Strain, O. Farkas, J. Tomasi, V. Barone, M. Cossi, R. Cammi, B. Mennucci, C. Pomelli, C. Adamo, S. Clifford, J. Ochterski, G. A. Petersson, P. Y. Ayala, Q. Cui, K. Morokuma, D. K. Malick, A. D. Rabuck, K. Raghavachari, J. B. Foresman, J. Cioslowski, J. V. Ortiz, A. G. Baboul, B. B. Stefanov, G. Liu, A. Liashenko, P. Piskorz, I. Komaromi, R. Gomperts, R. L. Martin, D. J. Fox, T. Keith, M. A. Al-Laham, C. Y. Peng, A. Nanayakkara, C. Gonzalez, M. Challacombe, P. M. W. Gill, B. Johnson, W. Chen, M. W. Wong, J. L. Andres, M. Head-Gordon, E. S. Replogle and J. A. Pople, *Gaussian 98, Revision A.7*, Gaussian, Inc., Pittsburgh PA, 1998.
13 T. S. Dibble and J. S. Francisco, *J. Phys. Chem.*, 1994, **98**, 11 694.
14 M. P. Badenes, M. E. Tucceri and C. J. Cobos, *Z. Phys. Chem.*, 2000, **214**, 1193.
15 R. Gatti and H. J. Schumacher, *Z. Phys. Chem. Neue Folge*, 159, **62**, 1968.

Formation of an α-ketocarbene by photolysis of aqueous 2-bromophenol

Florent Bonnichon,[a] Claire Richard*[a] and Gottfried Grabner[b]

[a] *Laboratoire de Photochimie Moléculaire et Macromoléculaire, UMR 6505, Université Blaise Pascal, 63177 Aubière Cedex, France. E-mail: claire.richard@univ-bpclermont.fr; Tel: +33 4 73 40 71 42; Fax: +33 4 73 40 77 00*

[b] *Institut für Theoretische Chemie und Molekulare Strukturbiologie, Universität Wien, Althanstrasse 14, 1090 Wien, Austria*

Received (in Liverpool, UK) 24th July 2000, Accepted 2nd November 2000
First published as an Advance Article on the web 14th December 2000

The α-ketocarbene 2-oxocyclohexa-3,5-dienylidene (λ_{max} = 360, 375 and 388 nm) is detected upon laser flash photolysis of 2-bromophenol in aqueous solution; its formation is confirmed by photoproduct studies.

para-Substituted halogenophenols have been shown to undergo heterolytic photodehalogenation in polar protic solvents.[1–10] The mechanism of this process could be clarified by demonstration of the formation of the carbene 4-oxocyclohexa-2,5-dienylidene (λ_{max} = 370 and 384 nm), which is long-lived enough to be detected by nanosecond laser flash photolysis experiments in aqueous solution.[1]

This intermediate arises from HCl elimination; its characteristic reactivity is governed by its triplet multiplicity: the addition of oxygen yields the *para*-benzoquinone *O*-oxide (λ_{max} = 460 nm) and subsequently *para*-benzoquinone, and the reduction by H-donor molecules such as alcohols gives rise to a phenoxyl radical (λ_{max} = 385 and 400 nm) and subsequently to phenol. Reactions with water and the halogenophenol itself produce hydroquinone and 5-chloro-2,4′-dihydroxybiphenyl respectively, in agreement with earlier studies.[2–5] This mechanism of the photoreactivity of 4-halogenophenols was later confirmed by several studies using transient absorption spectroscopy, EPR, and photoproduct analysis.[6–10]

In the case of aqueous 2-chlorophenol (2-ClP) or 2-bromophenol (2-BrP), UV irradiation leads to photocontraction into cyclopentadienic acids and to photohydrolysis.[11,12]

The ring contraction corresponds to a Wolff rearrangement;[13] it is also observed in the photolysis of α-diazoketones.[14] The similarity of the two reactions led to the proposal of intermediate formation of the α-ketocarbene, 2-oxocyclohexa-3,5-dienylidene, in both cases.[12,14] However, this carbene has not until now been detected, the first intermediate reported in aqueous solution on a nanosecond time scale being the ketene fulvene 6-oxide (λ_{max} = 255 nm), which subsequently adds a water molecule to yield fulvene 6,6-diol (λ_{max} = 295 nm).[15,16]

The photo-Wolff rearrangement is expected to proceed on the excited singlet surface.[13,17] A putative singlet α-ketocarbene arising as an intermediate on the reaction coordinate of ring contraction might have a lifetime in the subnanosecond range, as indicated by time-resolved studies of α-diazocarbonyl compounds.[18,19] On the other hand, α-ketocarbenes may have triplet ground states.[17] Currently available evidence indicates that the photoinduced dehalogenation of 4-halogenophenols proceeds on the excited triplet surface.[1,10] The formation of triplet α-ketocarbenes in the analogous reaction of 2-halogenophenols is therefore conceivable, either preceding ring contraction or in competition to it. A recent photoproduct study of the degradation of 2-ClP in aqueous surfactant solutions indicated that both singlet and triplet pathways may contribute to product formation.[20]

The transient spectrum obtained by laser flash photolysis of aqueous 2-ClP (Nd:YAG laser, Quanta-Ray DCR-1, pulse duration 7 ns, λ_{exc} = 266 nm) is dominated by the strong and broad absorption of the species resulting from ring contraction,[16] which mask a possible contribution from a carbene which, in analogy to that derived from 4-halogenophenols, is expected in the 350–420 nm range. However, careful examination of the transient spectrum in oxygenated solution revealed a very weak band with a maximum around 475 nm ($\varepsilon \times \Phi$ = 11 ± 3 M^{-1} cm^{-1}), reminiscent of the quinone oxide resulting from addition of O_2 to 4-oxocyclohexa-2,5-dienylidene.[1] Upon addition of propan-2-ol (0.085 M), an equally weak new species with a two-band absorption (λ_{max} = 380 and 400 nm, $\varepsilon_{400} \times \Phi$ = 9 ± 3 M^{-1} cm^{-1}) could be detected, indicating the formation of a phenoxyl radical[21] in these conditions.

These results suggested the transient formation of a triplet α-ketocarbene in the photochemistry of aqueous 2-ClP, but a direct proof of its presence was still lacking. Based on the hypothesis that the photoinduced reactions proceed on the triplet surface, it could be argued that 2-BrP, because of its intrinsically faster intersystem crossing, might be better suited as a substrate molecule to detect the carbene.

Laser flash photolysis of aqueous 2-BrP (10^{-3} M) yielded the ring contraction products, ketene and enol, just as with 2-ClP. However, an additional transient absorbing within the wave length range 350–400 nm (λ_{max} = 360, 375 and 388 nm, Fig. 1, spectrum 1) was also observed. This species decayed by first-order kinetics with k_d = 2.5 × 10^5 s^{-1}. In deoxygenated solutions containing propan-2-ol (0.17 M), it was converted into the phenoxyl radical with a formation rate of 1.6 × 10^6 s^{-1} (Fig. 1, spectrum 2). In oxygen-saturated solutions we found again the broad band with maximum around 475 nm (Fig. 1, spectrum 3), which had a formation rate of 9.0 × 10^6 s^{-1}.

As seen in Fig. 2, all these transients derived from monophotonic processes. We deduced from the slopes of the linear relationships of absorbance *vs.* laser pulse energy the following values of $\varepsilon \times \Phi$: 90 ± 20 M^{-1} cm^{-1} for the end-of-pulse transient at 388 nm, 130 ± 25 M^{-1} cm^{-1} for the phenoxyl radical at 400 nm and 175 ± 30 M^{-1} cm^{-1} for the transient observed in oxygenated solution at 475 nm.

Table 1 Quantum yields of photolysis (Φ_d) and of formation of products in neutral aqueous medium

	Conditions	Φ_d	$\Phi_{cyclopentadienic\ Acids}$	$\Phi_{pyrocatechol}$	Other products detected
2-ClP	N_2 or O_2	0.065 ± 0.007	0.042 ± 0.008	0.012 ± 0.001	none
2-BrP	N_2	0.085 ± 0.008	0.035 ± 0.007	0.009 ± 0.001	biphenyls and phenol (ϕ = 0.005)
	O_2	0.065 ± 0.007	0.035 ± 0.007	0.011 ± 0.001	none
	N_2, propan-2-ol (0.17 M)	0.07 ± 0.007	0.025 ± 0.005	0.009 ± 0.001	phenol (ϕ = 0.024)

DOI: 10.1039/b006155g

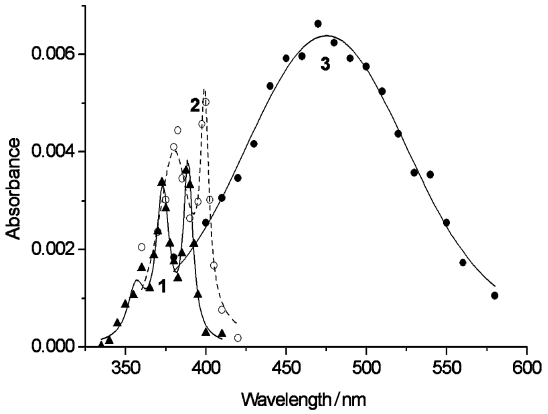

Fig. 1 Transient absorption spectra from neutral 2-BrP (10^{-3} M). Absorbances normalized at P = 1 mJ pulse^{-1} and $A(266)$ = 1.5. **1**: deoxygenated solution, differences between absorbances measured at the pulse end and 16 μs after. **2**: deoxygenated solution containing propan-2-ol (0.17 M), absorbances measured 2 μs after the pulse end. **3**: oxygen-saturated solution, absorbances measured 1 μs after the pulse end.

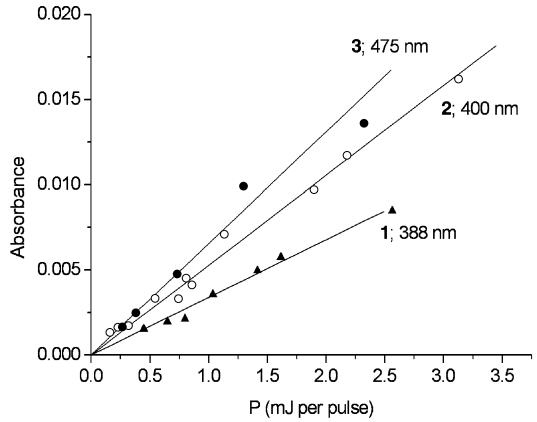

Fig. 2 Dependences of transient absorbances on pulse energy.

The complete analogy of the transients shown in Fig. 1 with those observed in the photochemistry of 4-halogenophenols[1] prompted us to assign the end-of-pulse transient to the α-ketocarbene formed by dehalogenation of 2-BrP. The reactivity with propan-2-ol and O_2 demonstrate the triplet character of this carbene; the 475 nm transient is therefore assigned to the *ortho*-benzoquinone *O*-oxide resulting from addition of O_2. Based on ε = 3000 M^{-1} cm^{-1} for the phenoxyl radical at 400 nm[21] and assuming complete conversion of the α-ketocarbene into the phenoxyl radical, values of Φ = 0.04 ± 0.01 and Φ = 0.003 ± 0.001 are found for the quantum yields of carbene formation from 2-BrP and 2-ClP, respectively. The molar extinction coefficient of the α-ketocarbene at 388 nm is estimated as ε = 2100 ± 500 M^{-1} cm^{-1}.

Product studies were undertaken to confirm the occurrence of an additional reaction pathway in the case of 2-BrP, besides that leading to ring contraction. The substrate (5×10^{-4} M 2-ClP or 2-BrP in neutral aqueous solution) was irradiated at 280 nm with low light intensities and the irradiated solutions were analysed by HPLC (Table 1). Within detection limits, only photocontraction and photohydrolysis are observed in the case of 2-ClP; the reaction is not measurably affected by the presence of O_2 or of propan-2-ol (0.017 M). In the case of 2-BrP, the formation of phenol and of three new products eluted after 2-BrP are observed in deoxygenated solutions. One of them, also obtained by bromination of 2,2′-dihydroxybiphenyl, is likely to be 2-bromo-6-(2′-hydroxyphenyl)phenol. In oxygenated solution biphenyls and phenol are not formed and the quantum yield of 2-BrP photolysis is reduced. The addition of propan-2-ol (0.17 M) clearly favours the formation of phenol, decreases the quantum yield of 2-BrP photolysis and inhibits drastically the formation of biphenyls. These results demonstrate that the photoproduct distribution of 2-BrP is indeed different from that of 2-ClP. The presence of biphenyls and of phenol among the photoproducts is indicative of the characteristic triplet carbene reactions, addition to the substrate and H abstraction, in analogy to the photoproducts from 4-halogenophenols.[1] Quinoid compounds are absent, which is not surprising in view of the instability of *ortho*-benzoquinone.

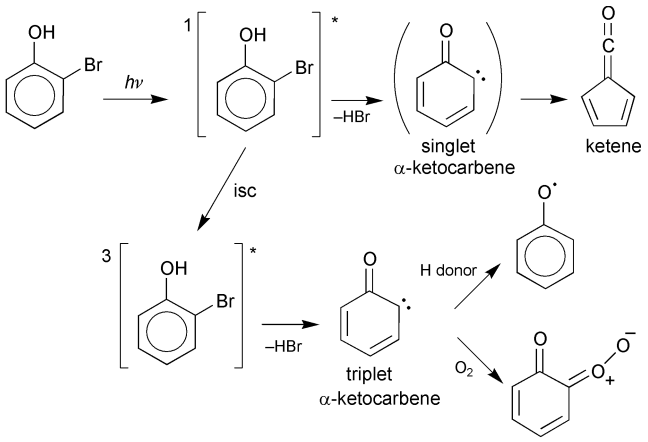

Scheme 1

To summarize, we have been able to characterize a hitherto unknown triplet α-ketocarbene by means of transient absorption spectroscopy and characteristic reactivity. The yield of this carbene is over ten times higher from 2-BrP than from 2-ClP, in agreement with the hypothesis that intersystem crossing at the molecular level precedes its formation. The relatively long triplet α-ketocarbene lifetime, of the order of microseconds, excludes the possibility of it being an intermediate on the way to ring contraction. It is therefore likely that ring contraction and formation of the triplet carbene are competing reactions, as indicated in Scheme 1.

Notes and references

1 G. Grabner, C. Richard and G. Köhler, *J. Am. Chem. Soc.*, 1994, **116**, 11 470.
2 P. Boule, C. Guyon and J. Lemaire, *Toxicol. Environ. Chem.*, 1984, **7**, 97.
3 K. Omura and T. Matsuura, *Tetrahedron*, 1971, **27**, 3101.
4 E. Lipczynska-Kochany and J. R. Bolton, *J. Photochem. Photobiol.*, 1991, **58**, 315.
5 K. Oudjehani and P. Boule, *J. Photochem. Photobiol.*, 1992, **68**, 363.
6 A. Ouardaoui, C. A. Steren, H. van Willigen and C. Yang, *J. Am. Chem. Soc.*, 1995, **117**, 6803.
7 A.-P. Y. Durand, R. G. Brown, D. Worrall and F. Wilkinson, *J. Photochem. Photobiol., A: Chem.*, 1996, **96**, 35.
8 A. Ouardaoui, D. M. Martino, C. A. Steren and H. van Willigen, *Appl. Magn. Reson.*, 1997, **13**, 275.
9 A.-P. Y. Durand, R. G. Brown, D. Worrall and F. Wilkinson, *J. Chem. Soc., Perkin Trans. 2*, 1998, 365.
10 F. Bonnichon, G. Grabner, G. Guyot and C. Richard, *J. Chem. Soc., Perkin Trans. 2*, 1999, 1203.
11 C. Guyon, P. Boule and J. Lemaire, *Tetrahedron Lett.*, 1982, **23**, 1581.
12 C. Guyon, P. Boule and J. Lemaire, *Nouv. J. Chim.*, 1984, **8**, 685.
13 H. Meier and K.-P. Zeller, *Angew. Chem.*, 1975, **87**, 52.
14 M. Yagihara, Y. Kitahara and T. Asao, *Chem. Lett.*, 1974, 1015.
15 B. Urwyler and J. Wirz, *Angew. Chem., Int. Ed. Engl.*, 1990, **29**, 790.
16 P. Boule, K. Othmen, C. Richard, B. Szczepanik and G. Grabner, *Int. J. Photoenergy*, 1999, **1**, 49.
17 R. J. McMahon, O. L. Chapman, R. A. Hayes, T. C. Hess and H.-P. Krimmer, *J. Am. Chem. Soc.*, 1985, **107**, 7597.
18 J. J. M. Vleggaar, A. H. Huizer, P. A. Kraakman, W. P. M. Nijssen, R. J. Visser and C. A. G. O. Varma, *J. Am. Chem. Soc.*, 1994, **116**, 11 754.
19 Y. Chiang, A. J. Kresge and V. V. Popik, *J. Am. Chem. Soc.*, 1999, **121**, 5930.
20 Z. Shi, M. E. Sigman, M. M. Ghosh and R. Dabestani, *Environ. Sci. Technol.*, 1997, **31**, 3581.
21 R. H. Schuler and G. K. Buzzard, *Int. J. Radiat. Phys. Chem.*, 1976, **8**, 563.

A valence isomer of a dialane

John D. Gorden, Charles L. B. Macdonald and Alan H. Cowley*

Department of Chemistry and Biochemistry, The University of Texas at Austin, Austin, Texas 78712, USA. E-mail: cowley@mail.utexas.edu

Received (in Columbia, MO, USA) 14th August 2000, Accepted 13th November 2000
First published as an Advance Article on the web

The compound (η^5-C_5Me_5)Al→Al(C_6F_5)$_3$, which is the first valence isomer of a dialane, has been prepared by treatment of [Al(η^5-C_5Me_5)]$_4$ with Al(C_6F_5)$_3$ and characterized by X-ray crystallography and NMR spectroscopy.

Compounds with aluminium–aluminium bonds are attracting considerable recent attention. The simplest such compounds are the dialanes, R_2AlAlR_2, and a number of these have now been structurally authenticated.[1] It occurred to us that valence isomers of dialanes, *viz.* $RAl{\rightarrow}AlR_3$, might be capable of existence if the appropriate substituents were employed. DFT calculations[2] on the prototypical dialane, H_2AlAlH_2, revealed that the valence isomer $HAl{\rightarrow}AlH_3$, is less stable than H_2AlAlH_2 by 9.17 kcal mol^{-1}. However, replacement of one of the dialane hydride substituents by cyclopentadienide inverted this order and (η^5-C_5H_5)Al→AlH_3 **1** is more stable than the dialane (η^2-C_5H_5)(H)Al→AlH_2 by 10.79 kcal mol^{-1}. In view of the foregoing, [Al(η^5-C_5Me_5)]$_4$ [65 mg, 0.40 mmol of Al(η^5-C_5Me_5) units][3] was treated with Al(C_6F_5)$_3$·$PhCH_3$[4] (250 mg, 0.40 mmol) in 30 mL of toluene at 25 °C. After being stirred for 4 h at 25 °C, the yellow reaction mixture was heated to 50 °C for 30 min. Upon cooling to 25 °C, the reaction mixture was filtered and the solvent and volatiles were removed from the filtrate to afford a dark amber oil from which yellow crystalline (η^5-C_5Me_5)Al→Al(C_6F_5)$_3$ **2** (220 mg, 80% yield, mp 131–133 °C) deposited over a period of 24 h. The mass spectral data† for **2** are consistent with the proposed dialane isomer formulation. The presence of (η^5-C_5Me_5)Al and Al(C_6F_5)$_3$ moieties in **2** is evident from the ^{1}H, ^{13}C, and ^{19}F NMR spectroscopic data,† noting however that the equivalence of the C_5Me_5 ring carbon and Me resonances could be due to the well known fluxional behaviour of cyclopentadienyl–aluminium systems.[5] The ^{27}Al NMR spectrum of **2** comprises singlet resonances at δ −115.7 and 106.9. Given that the ^{27}Al chemical shifts for the model compound **1**, as computed by the GAIO method,[2b,6] are δ −107.9 and 109.0 for the (η^5-C_5Me_5)Al and AlH_3 centres, respectively, analogous assignments have been made for **2**.† Further support for the proposed assignments stems from the experimentally observed ^{27}Al chemical shifts for monomeric (η^5-C_5Me_5)Al (δ −150)[7] and Al(C_6F_5)$_3$·arene [δ 52 (benzene); δ 61 (toluene)].[4] The overall trend of ^{27}Al chemical shifts is consistent with the transfer of electron density from the alanediyl to the Al(C_6F_5)$_3$ fragment upon formation of the Al→Al donor acceptor bond of **2**.

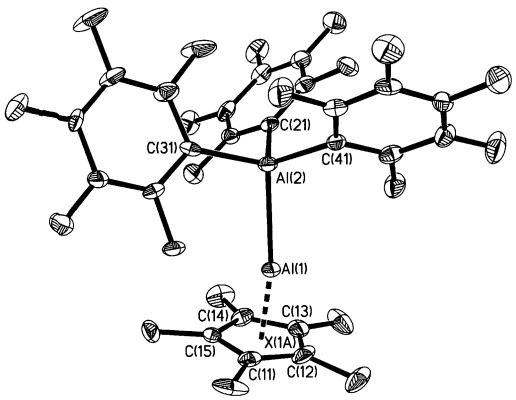

Fig. 1 Thermal ellipsoid plot (30% probability level) for (η^5-C_5Me_5)-Al→Al(C_6F_5)$_3$ **2**. Selected bond lengths (Å) and bond angles (°): Al(2)–Al(1) 2.591(2), Al(1)–X(1A) 2.591(8), Al(1)–C(11) 2.172(7), Al(1)–C(12) 2.162(6), Al(1)–C(13) 2.165(7), Al(1)–C(14) 2.200(7), Al(1)–C(15) 2.189(6), Al(2)–C(21) 1.982(7), Al(2)–C(31) 1.999(7); Al(2)–C(41) 1.997(7); Al(2)–Al(1)–X(1A) 170.1(3), C(21)–Al(2)–C(41) 111.0(3), C(21)–Al(2)–C(31) 108.5(3), C(41)–Al(2)–C(31) 113.5(3), C(21)–Al(2)–Al(1) 104.1(2), C(41)–Al(2)–Al(1) 111.2(2), C(31)–Al(2)–Al(1) 108.0(2).

The foregoing spectroscopic conclusions were confirmed by X-ray crystallography.‡ Compound **2** crystallizes in the *C*2/*c* space group with Z = 8; the solid state consists of individual molecules of the dialane isomer and there are no unusually short intermolecular contacts. The pentamethylcyclopentadienyl substituent is attached in an η^5 fashion and the ring centroid–Al–Al moiety deviates only modestly from linearity [170.1(3)°]. The Al–Al bond length in **2** [2.591(3) Å] is shorter than those in the dialanes {(Me_3Si)$_2$CH}$_4$Al$_2$ [2.660(1) Å],[1a] {2,4,6-Pr^i_3-C_6H_2}$_4$Al$_2$ [2.647(3) Å],[1b] and {Bu^t_3Si}$_4$Al$_2$ [2.751(2) Å][1c] but identical to that in [RIAl–AlClR] {R = [(Me_3Si)$_2$C(Ph)C(Me_3-Si)N]) [2.593(2) Å]}[1d] within experimental error. The average Al(1)–C bond length of 2.178(7) Å [Al–centroid 1.810(8) Å] is considerably shorter than those reported for Al(η^5-C_5Me_5) [2.388(7) Å][8] and [Al(η^5-C_5Me_5)]$_4$ (2.344 Å, av. Al–centroid 2.011 Å).[7] Such a shortening is anticipated as the partially antibonding aluminium 'lone pair' orbital of Al(η^5-C_5Me_5) is transformed into the donor–acceptor bond with the concomitant development of positive and negative charges on the aluminium centres.[9] The same trend is evident for other group 13 (η^5-C_5Me_5)M→acceptor complexes[10] and is true for both main-group and transition element acceptors.

In conclusion, we have prepared (η^5-C_5Me_5)Al→Al(C_6F_5)$_3$, a valence isomer of a dialane. This compound also features the first example of an Al→Al donor acceptor bond.

We are grateful to the National Science Foundation, Robert A. Welch Foundation, and the National Academy of Sciences, through Sigma Xi, The Scientific Research Society for financial support.

Notes and references

† **2**: HRMS (CI, CH_4) calc. for $C_{28}H_{15}Al_2F_{15}$ *m/z* 690.0565; found 690.0572. ^{1}H NMR (499.35 MHz, 295 K, C_6D_6) δ 1.49 (s, 15H, C_5Me_5). ^{13}C{^{1}H} NMR (125.69 MHz, 295 K, C_6D_6) δ 149.99 (d, *o*-C_6F_5, $^1J_{CF}$ 224 Hz), 141.83 (d, *p*-C_6F_5, $^1J_{CF}$ 239 Hz), 137.34 (d, *m*-C_6F_5, $^1J_{CF}$ 226 Hz), 129.28 (s, *ipso*-C_6F_5), 115.94 [s, $C_5(CH_3)_5$], 8.44 [s, $C_5(CH_3)_5$]. ^{19}F NMR (469.81 MHz, 295 K, C_6D_6) δ −122.03 (s, *m*-C_6F_5), −153.19 (s, *p*-C_6F_5), 161.77 (s, *o*-C_6F_5). ^{27}Al NMR (130.25 MHz, 295 K, C_6D_6) δ 106.9 [br, (C_6F_5)$_3$*Al*AlC_5Me_5, $w_{1/2}$ 6122 Hz], −115.7 [s, (C_6F_5)$_3$Al*Al*C_5Me_5].

‡ *Crystal data* for **2**: $C_{28}H_{15}Al_2F_{15}$, monoclinic, space group *C*2/*c*, a = 30.635(6), b = 9.814(2), c = 20.236(4) Å, β = 111.10(3), V = 5676(2) Å^3, Z = 8, D_c = 1.616 g cm^{-3}, μ(Mo-Kα) = 0.220 mm^{-1}. A suitable single crystal of **2** was covered with mineral oil and mounted on a Nonius-Kappa CCD diffractometer at 123 K. A total of 8481 independent reflections were collected in the range 5.96 < 2θ < 50.20° using Mo-Kα radiation (λ = 0.71073 Å). Of these, 3815 were considered observed [$I > 2.0\sigma(I)$] and were used to solve (direct methods) and refine (full matrix, least squares on F^2) the structure of **2**; R = 0.0767, $wR2$ = 0.1944.

CCDC 182/1856. See http://www.rsc.org/suppdata/cc/b0/b007341p/ for crystallographic files in .cif format

1 (*a*) For a review, see: W. Uhl, *Angew Chem., Int. Ed. Engl.*, 1993, **32**, 1386; see also: (*b*) R. J. Wehmschulte, K. Ruhlandt-Senge, M. M.

Olmstead, H. Hope, B. E. Sturgeon and P. P. Power, *Inorg. Chem.*, 1993, **32**, 2983; (*c*) N. Wiberg, K. Amelunxen, T. Blank, H. Nöth and J. Knizek, *Organometallics*, 1998, **17**, 5431; (*d*) K. S. Klimek, C. Cui, H. W. Roesky, M. Noltemeyer and H.-G. Schmidt, *Organometallics*, 2000, **19**, 3085.

2 B3LYP: (*a*) A. D. Becke, *J. Chem. Phys.*, 1993, **98**, 5648; (*b*) A. D. Becke, *Phys. Rev. A*, 1988, **38**, 3098; (*c*) C. Lee, W. Yang and R. G. Parr, *Phys. Rev. B*, 1988, **37**, 785; (*d*) S. H. Vosko, L. Wilk and M. Nusair, *Can. J. Phys.*, 1980, **58**, 1200. All DFT calculations were performed using the Gaussian 94 (revision B2) suite of programs. All-electron basis sets were used for C, H [6-31G(d)] and the group 13 elements [6-31 + G(d]).

3 Prepared according to the method of S. Schulz, H. W. Roesky, H. J. Koch, G. M. Sheldrick, D. Stalke and A. Kuhn, *Angew. Chem., Int. Ed. Engl.*, 1993, **32**, 1729.

4 G. S. Hair, A. H. Cowley, R. A. Jones, B. G. McBurnett and A. Voigt, *J. Am. Chem. Soc.*, 1999, **121**, 4922.

5 P. J. Shapiro, *Coord. Chem. Rev.*, 1999, **189**, 1.

6 R. Ditchfield, *Mol. Phys.*, 1974, **27**, 789; K. Wolinski, J. F. Hinton and P. Pulay, *J. Am. Chem. Soc.*, 1990, **122**, 8251; BP86: J. P. Perdew, *Phys. Rev. B*, 1986, **33**, 8822.

7 C. Dohmeier, D. Loos and H. Schnöckel, *Angew. Chem., Int. Ed. Engl.*, 1996, **35**, 129.

8 A. Haaland, K.-G. Martinsen, S. A. Shlykov, H. V. Volden, C. Dohmeier and H. Schnöckel, *Organometallics*, 1995, **14**, 3116.

9 C. L. B. Macdonald and A. H. Cowley, *J. Am. Chem. Soc.*, 1999, **121**, 12 113.

10 J. D. Gorden, A. Voigt, C. L. B. Macdonald, J. S. Silverman and A. H. Cowley, *J. Am. Chem. Soc.*, 2000, **122**, 950.

ChemComm

Metal ion catalysis in chemisorption and dehydrogenation of alkanes on aluminium hydroxide clusters, revealed by theoretical calculations

Dan Fărcaşiu* and Povilas Lukinskas

Department of Chemical and Petroleum Engineering, University of Pittsburgh, 1249 Benedum Hall, Pittsburgh, PA 15261, USA. E-mail: dfarca@pitt.edu

Received (in Cambridge, UK) 17th August 2000, Accepted 25th October 2000
First published as an Advance Article on the web 14th December 2000

Electron-correlated DFT calculations with a large basis set show that propane adds to coordinatively unsaturated aluminium, as in the clusters $(HO)_3Al(OH_2)_x$ (x = 0, 1), by aluminium insertion into a C–H bond, followed by hydrogen migration to an oxygen atom and predict correctly experimental observations; the alternative pathway involving alkyl–oxygen interaction has a much higher energy barrier and does not predict correctly the experimental results.

Following the progress of superacid chemistry, the reactions of hydrocarbons on aluminosilicates, including zeolites, have been interpreted as involving the activation by hydron transfer to form carbocations as intermediates or transition structures.[1] This type of activation, characteristic of superacids in solutions, *e.g.* $HF–SbF_5$,[2] $HF–TaF_5$,[3] or $H_2O–AlX_3$,[4] is not found for trifluoromethanesulfonic acid (TFMSA), which activates alkanes by an oxidative mechanism.[5] Yet, TFMSA is a much stronger acid than the zeolite catalysts.[6] This paradox, observable to an outsider, has been lost to the researchers in the field.

The computations on the activation of alkane C–H bonds have attempted to describe the accepted mechanism and sought mostly pathways based on hydron transfer.[7] The same held for the hydrogen chemisorption on alumina, responsible for the high-temperature H_2/D_2 exchange,[8] which was thought to involve heterolysis of the H–H bond, with the hydron going to the oxygen (base) and the hydride to aluminium (acid).[9]

Standard *ab initio* (MP2) and DFT (B3LYP) geometry optimizations with large basis sets and search of the reaction coordinate without the imposition of a pathway have shown, however, that hydrogen chemisorption occurs through the interaction of H_2 with the aluminium (metal ion catalysis) until both hydrogen atoms are bonded to Al, after which one hydrogen migrates to oxygen.[10] The reactivity of aluminium centers varied in the order: tri- > tetra- > penta-coordinated and the tetracoordinated aluminium in a silica-alumina cluster chemisorbed hydrogen by the same mechanism.[10*b*]

Alumina catalyzes the H–D exchange of saturated hydrocarbons as well,[11] a reaction also classified as acid–base catalysis.[11] Like the hydrogen chemisorption, the reaction of methane with $Al(OH)_3$ was described as a heterolytic reaction with an acid–base pair on the surface, with a hydron going to the negative oxygen and a methyl anion to the metal.[12] A computational search in which the reaction pathway was not presupposed was, therefore, in order. We studied the reaction of propane with aluminium hydroxide clusters, $(HO)_3Al(OH_2)_x$ (**1**, x = 0; **2**, x = 1).

B3LYP/6-31G** geometry optimizations and frequency analyses (giving also the zero point energy corrections, ZPE),[13] transition structure searching by the STQN (Synchronous Transit-Guided Quasi Newton) method,[14] and reaction pathway identification by intrinsic reaction coordinate (IRC)[15] tracking were conducted with the Gaussian 98 program,[16] as described before.[10] Pathway **b** (defined below) for chemisorption on **1** was also examined by MP2/6-31G**, to check the agreement between the two methods (as done in previous work).[10*a*] To model the alumina surface, the geometry of the tricoordinated aluminium reactant **1** was the optimized geometry of **2**, with the water ligand removed.[10] In the reaction of **1** with propane, the O1–O2–Al–O3 dihedral angle was kept constant. The alternative of freezing the outer atoms of the cluster and allowing the aluminium atom a breathing movement gave a similar potential energy barrier (PEB) for H_2 chemisorption.[10*a*] Our goal was to explore the existence of a reaction pathway, rather than to determine accurately the relative energies of reactants, intermediates, and transition structures.

Weak complexes of propane with **1** (**3**) and **2** (**4**) were located and two types of chemisorption products were identified, with C–Al bond (**5** and **6**, respectively) and with C–O bond (**7** and **8**, respectively), shown in eqns. (1) and (2). The relative reactivities of primary and secondary C–H bonds were also tested [series **a** and **b** in eqns. (1) and (2)]. The O–alkyl complexes were less stable than the Al–alkyl complexes by 5–7 kcal mol^{-1}.

$$\underset{\mathbf{1}(x=0),\ \mathbf{2}(x=1)}{(OH)_3Al(OH_2)_x} + PrH \longrightarrow \underset{\mathbf{5}(x=0),\ \mathbf{6}(x=1)}{(OH)_2Al(OH_2)_{x+1}(R)} \quad (1)$$

$$\mathbf{1}, \mathbf{2} + PrH \longrightarrow \underset{\mathbf{7}(x=0),\ \mathbf{8}(x=1)}{(HO)_2Al(OH_2)_x(H)\text{-}O(R)H} \quad (2)$$

a: R = CH_2Et **b**: R = $CHMe_2$

All chemisorption products react further to form hydrogen and propene, complexed with the aluminium cluster. The energies of intermediates and products, relative to the starting materials, are shown in Table 1.

It is seen that chemisorption and dehydrogenation are catalyzed by both tricoordinated and tetracoordinated aluminium centers. The former are more reactive, just as for the hydrogen chemisorption.[10] For the aluminium–alkyl pathway, eqn. (1), a primary C–H bond (**a**) is more reactive than a secondary C–H bond (**b**). Only option **b** was studied for the O–alkyl pathway [eqn. (2)], because the alkyl group acquired a positive charge. On the aluminium–alkyl pathway, the barrier for alkane chemisorption (TS1) is much smaller than the barrier (TS2) for the dehydrogenation step, whereas in the oxygen–alkyl pathway, TS1 is higher in energy than TS2. The O–alkyl pathway is higher in energy than the aluminium–alkyl pathway. In the second step of the reaction on **2**, the cleavage of an Al–O bond is easier than the elimination of propene. If the cluster was part of a solid, the lattice rigidity would determine the degree of Al–O bond separation. Therefore, the elimination step was followed at two lengths of the labile Al–O bond: the same as in the intermediate (**6** or **8**) and extended by 0.2 Å. Both values are given in Table 1, for each reaction pathway; the latter are smaller.

The transition structure for the chemisorption step on the aluminum–alkyl pathway,[14] shown in Fig. 1 (left)[17] for the reaction **1** → **5a**, was similar to that for hydrogen chemisorption. The imaginary frequency was the bending of the Al–H

Table 1 Relative energies of intermediates, products, and transition structures for the reaction of propane with aluminium hydroxide clusters **1** and **2**[a,b]

Catalyst cluster	Reaction pathway	Physisorbed reactant	TS1	Chemisorbed complex	TS2	Physisorbed product(s)	Isolated products
1	Al–CH_2Et[c]	−4.01	32.19	31.24	57.10	17.63	29.23
1	Al–$CHMe_2$[d]	−4.01[e]	35.14[e]	33.54[e]	62.41	17.63	29.23
1	O–$CHMe_2$[f]	−4.01	72.31	37.34	70.35	34.77[g]	29.23[h]
2	Al–CH_2Et[i]	−1.93	43.95	25.59	74.20,[j] 72.21[k]	26.56	29.23
2	Al–$CHMe_2$[l]	−1.93	—[m]	—	—	—	—
2	O–$CHMe_2$[n]	−1.93	82.22	32.28	75.98,[o] 67.31[p]	43.77	29.23[q]

[a] B3LYP/6-31G**//B3LYP/6-31G**, kcal mol^{-1}, relative to the isolated starting materials (**1** or **2** and Pr^nH). [b] 1 cal = 4.184 J. [c] **1** → **5a**, eqn. (1). [d] **1** → **5b**, eqn. (1). [e] MP2(FC)/6-31G**// MP2(FC)/6-31G** values are −6.33, 33.59 and 31.50 kcal mol^{-1}, respectively. [f] **1** → **7b**, eqn. (2). [g] Propene chemisorbed on the $(H_2O)_2AlH–OH_2$ cluster. [h] 46.65 kcal mol^{-1} if $(H_2O)_2AlH–OH_2$ is a product. [i] **2** → **6a**, eqn. (1). [j] d(Al–OH_2) = 2.11 Å, see text. [k] d(Al–OH_2) = 2.31 Å, see text. [l] **2** → **6b**, eqn. (1). [m] Decomposition to **5b** occurred. [n] **2** → **8b**, eqn. (2). [o] d(Al–OH_2) = 2.00 Å, see text. [p] d(Al–OH_2) = 2.20 Å, see text. [q] 48.14 kcal mol^{-1} if the hydrogenated cluster is a product.

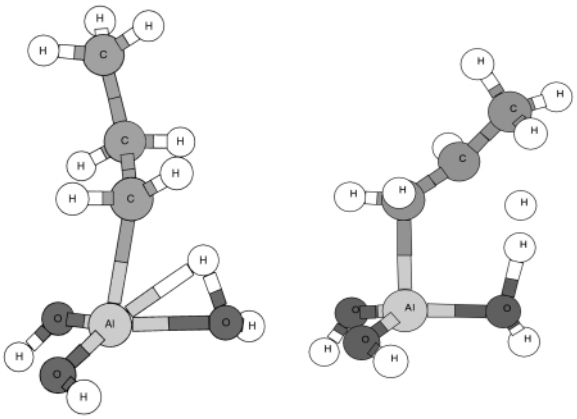

Fig. 1 Left: transition structure (TS1) for the chemisorption of propane (primary C–H) on a tricoordinated aluminium cluster (**1** → **5a**). Right: transition structure (TS2) for the elimination of propane from the chemisorbed complex **5a**.

bond toward O (migration of hydrogen from Al to O).[18] Thus, the reaction mechanism consists of the insertion of aluminium into the C–H bond, followed by hydrogen migration from Al to O, just as for hydrogen chemisorption.[10] In the elimination step, there is less cleavage of the Al–C bond than of the C–H bond at the transition state (Fig. 1, right).[19] For the elimination step of the O–alkyl pathway, the hydrogen is transferred to another oxygen atom.

The reactivity order prim > sec and the prediction that hydrogen exchange [reverse of eqn. (1)] is faster than further reaction of the olefin (*e.g.* on acid sites) agrees with the experiment. (The exchange of H_2 with the clusters has lower barriers than the exchange of the C–H bonds.[10]) The described mechanism is relevant for the hydrogen exchange[11,19] and alkene hydrogenation/alkane dehydrogenation.[20] These reactions have been described as catalyzed by Brønsted acid centers, with carbocations as intermediates or transition structures.[7,9,12,21] The cleavage of H–H and C–H bonds by insertion of metal atoms and ions (metal and metal ion catalysis), known for heavy metals, particularly noble metals, was not considered for aluminium. We show now that Al(O–)$_n$ sites with n = 3 and 4, are active in metal ion catalysis. An increase in reactivity for 'broken lattices' of zeolites or for extraframework aluminium species in steamed zeolites is predicted.

This research was supported by the grant CTS-812704, from NSF, and by a grant of supercomputer time from NCSA, in Urbana, IL.

Notes and references

1 See the discussion in W. K. Hall, E. A. Lombardo and J. Engelhardt, *J. Catal.*, 1989, **115**, 611.
2 D. M. Brouwer and H. Hogeveen, *Prog. Phys. Org. Chem.*, 1972, **9**, 179.
3 D. Fărcaşiu, M. Siskin and R. P. Rhodes, *J. Am. Chem. Soc.*, 1979, **101**, 7671.
4 C. D. Nenitzescu and I. P. Cantuniari, *Ber. Dtsch. Chem. Ges.*, 1933, **66**, 1097; H. S. Bloch, H. Pines and L. Schmerling, *J. Am. Chem. Soc.*, 1946, **68**, 153.
5 D. Fărcaşiu and P. Lukinskas, *J. Chem. Soc., Perkin Trans. 2*, 1999, 2715; D. Fărcaşiu and P. Lukinskas, *J. Chem. Soc., Perkin Trans. 2*, 2000, 2295.
6 T. Xu, E. J. Munson and J. F. Haw, *J. Am. Chem. Soc.*, 1994, **116**, 1962; D. Fărcaşiu, *J. Chem. Soc., Chem. Commun.*, 1994, 1801.
7 S. P. Bates and R. A. van Santen, *Adv. Catal.*, 1998, **42**, 1; P. M. Esteves, M. A. C. Nascimento and C. J. A. Mota, *J. Phys. Chem., B*, 1999, **103**, 10 417.
8 H. S. Taylor and H. Diamond, *J. Am. Chem. Soc.*, 1935, **57**, 1256.
9 I. N. Senchenya and V. B. Kazanskii, *Kinet. Katal.*, 1988, **29**, 1331; F. Ioka, T. Sakka, Y. Ogata and M. Iwasaki, *Can. J. Chem.*, 1993, **71**, 663.
10 (*a*) D. Fărcaşiu and P. Lukinskas, *J. Phys. Chem., A*, 1999, **103**, 8483; (*b*) P. Lukinskas and D. Fărcaşiu, *Appl. Catal. A*, in press.
11 For references, see: S. Yoshida, in *Theoretical Aspects of Heterogeneous Catalysis*, ed. J. B. Moffat, Van Nostrand Reinhold, New York, 1990, p. 506.
12 M. J. Capitán, J. A. Odriozola, A. Márquez and J. F. Sanz, *J. Catal.*, 1995, **156**, 273.
13 W. J. Hehre, L. Radom, P. v. R. Schleyer and J. A. Pople, *Ab initio Molecular Orbital Theory*, Wiley-Interscience, New York, NY, 1986.
14 C. Peng and H. B. Schlegel, *Isr. J. Chem.*, 1993, **33**, 449.
15 C. Gonzales and H. B. Schlegel, *J. Phys. Chem.*, 1989, **90**, 2154.
16 M. J. Frisch, G. W. Trucks, H. B. Schlegel, G. E. Scuseria, M. A. Robb, J. R. Cheeseman, V. G. Zakrzewski, J. A. Montgomery, R. E. Stratmann, J. C. Burant, S. Daprich, J. M. Millam, A. D. Daniels, K. N. Kudin, M. C. Strain, O. Farkas, J. Tomasi, V. Barone, M. Cossi, R. Cammi, B. Mennucci, C. Pomelli, C. Adamo, S. Clifford, J. Ochterski, G. A. Petersson, P. Y. Ayala, Q. Cui, K. Morokuma, D. K. Malick, A. D. Rabuck, K. Raghavachari, J. B. Foresman, J. Cioslowski, J. V. Ortiz, B. B. Stefanov, G. Liu, P. Liashenko, P. Piskorz, I. Komaromi, R. Gomperts, R. L. Martin, D. J. Fox, T. Keith, M. A. Al-Laham, C. Y. Peng, A. Nanayakkara, C. Gonzalez, M. Challacombe, P. M. W. Gill, B. G. Johnson, W. Chen, M. W. Wong, J. L. Andres, M. Head-Gordon, E. S. Replogle and J. A. Pople, *Gaussian 98, Revision A.1*, Gaussian, Inc., Pittsburgh PA, 1998.
17 G. Schaftenaar, *MOLDEN. A Portable Electron Density Program*, available at: ftp ftp.caos.kun.nl Name: anonymous.
18 Projections generated with: *Xmol, version 1.3.1*, Minnesota Supercomputing Center, Inc., Minneapolis, MN, 1993.
19 B. Schoofs, J. Schuermans and R. A. Schoonheydt, *Microporous Mesoporous Mater.*, 2000, **35**–**36**, 99.
20 V. C. F. Holm and R. W. Blue, *Ind. Eng. Chem.*, 1951, **43**, 501.
21 S. Senger and L. Radom, *J. Am. Chem. Soc.*, 2000, **122**, 2613.

Aluminium-containing ring systems and N-heterocycle formation *via* nitrile insertions into Al–N bonds

Vernon C. Gibson,* Carl Redshaw,† Andrew J. P. White and David J. Williams

Department of Chemistry, Imperial College, South Kensington, London, UK SW7 2AY. E-mail: v.gibson@ic.ac.uk

Received (in Cambridge, UK) 7th September 2000, Accepted 6th November 2000
First published as an Advance Article on the web 15th December 2000

Reactions of Me_3Al with 1,2-diaminobenzene [1,2-$(H_2N)_2C_6H_4$] or anthranilic acid, [1,2-$(H_2N)(HO_2$- C)C_6H_4], followed by treatment with acetonitrile, afford tetranuclear and hexanuclear aluminium-containing ring systems; a single crystal X-ray structure on the hexametallic product reveals the construction of quinazoline ligands arising *via* insertion of acetonitrile into Al–N bonds.

It is well over one hundred years since the trimerisation of nitriles to triazines by organometallic reagents was first noted, by Hofmann[1] using sodium, and by Frankland[2] in his studies on Et_2Zn. During the 1960s, Wade[3] and Lappert[4] did much to advance the understanding of nitrile binding and insertion reactions at main group centres; however, the potential of such reactions for synthesising useful heterocycles and interesting metal-containing ring systems has remained largely undeveloped.

Recently, we described the synthesis of large aluminium-containing ring systems *via* treatment of Me_3Al with hydrazines;[5] these included a highly unusual octa-aluminium structural analogue of a tetrapyrrole. The key macrocycle-forming step revolves around the insertion of acetonitrile into the aluminium–nitrogen bonds of intermediate amide species. With a view to probing the generality of this approach for the synthesis of aluminium-containing macrocycles, and also to evaluate the potential of this methodology for constructing nitrogen heterocycles, we have extended the study to other classes of amine substrate. Here, we describe the reactivity of Me_3Al towards 1,2-diaminobenzene [1,2-$(H_2N)_2C_6H_4$] and anthranilic acid [1,2-$(H_2N)(HO_2C)C_6H_4$]. The former gives rise to a tetranuclear complex, the latter to an unprecedented hexanuclear species incorporating N-heterocyclic ligands.

Slow addition of a solution of Me_3Al (2 equivalents) in toluene to 1,2-$(H_2N)_2C_6H_4$, followed by a 12 h reflux, afforded a pale brown solution. After removal of the solvent under reduced pressure, the residue was dissolved in acetonitrile and heated to reflux for 2–3 min. Slow cooling of this solution, followed by standing at room temperature for 2 days, gave colourless needles of **1** in 40% yield (Scheme 1). The ^{1}H NMR spectrum‡ of **1** consists of four equal intensity singlets in the Al–methyl region (δ −0.37 to −0.75) together with a similar intensity singlet at δ 1.29 attributable to carbon-bonded methyl groups. X-Ray analysis§ reveals the product to be the C_i symmetric twelve-membered macrocyclic complex **1** comprising four aluminium atoms (two bridging and two chelating), six nitrogen atoms and two carbon atoms, The structure of this product is closely related to that obtained from the reaction of $MePhNNH_2$ with Me_3Al,[5] and is not described in further detail here.

In the absence of acetonitrile, the 2 : 1 reaction of Me_3Al and 1,2-$(H_2N)_2C_6H_4$ (in toluene) has been shown to afford the asymmetric complex $[(Me_2Al)_2AlMe(C_6H_4(NH)_2)_2]\cdot AlMe_3$ **2**.[6] This, or a closely related derivative, is the likely precursor to **1**. Formation of the 12-membered ring product is brought about by insertion of two acetonitrile molecules into the Al–N bonds, in a related manner to that postulated for the reaction of hydrazines with Me_3Al/MeCN.[5]

Similar treatment of anthranilic acid, [1,2-(NH_2)-$(HO_2C)C_6H_4$] (twice sublimed) with 2 equivalents of a toluene solution of Me_3Al affords, after work-up in acetonitrile, large yellow prisms for which the ^{1}H NMR spectrum possesses nine distinct singlets in the Al–methyl region. The X-ray analysis§ of the product revealed the chiral trimeric hexanuclear complex $[(Me_2AlL)(MeAl)(\mu_3\text{-}O)(\mu\text{-}O)]\}_3$ **3** (L = quinazoline) shown in Fig. 1. The central Al_3O_3 ring has a twisted boat conformation, whereas the three attached Al_2O_2CN rings each have a folded envelope geometry. All six aluminium atoms exhibit marked departures from ideal tetrahedral geometry with angles in the range 100.9(2)–124.4(3)°. Although not possessing strict C_3 symmetry [the methyls on Al(2) and Al(4) are 'up', whilst that on Al(6) is 'down'], the pattern of bonding throughout the structure is essentially three-fold symmetric. It is interesting to note that whilst all of the Al–O bond lengths within the central Al_3O_3 ring and also those to O(2), O(4) and O(6) are all essentially the same [1.770(4)–1.794(4) Å], those to Al(1), Al(3) and Al(5) are all significantly longer [1.811(4)–1.827(4) Å]. As **3** is not the product of a chiral synthesis, the presence in the crystals of molecules of only one chirality is a consequence of spontaneous resolution upon crystallisation.

Whereas the formation of **1** can be rationalised in terms of acetonitrile insertion into the aluminium–nitrogen bonds of **2**, the carboxylic acid group of anthranilic acid contributes oxygen atoms to the Al_3O_3 core around which the quinazoline ligands are clustered. The reaction reproducibly affords **3** in *ca.* 45% yield; its hydrolysis then readily releases the 2-methyl-4(3*H*)-quinazolinone heterocycle **4** (identified by comparison of NMR data with those of an authentic sample) in excellent yield. We

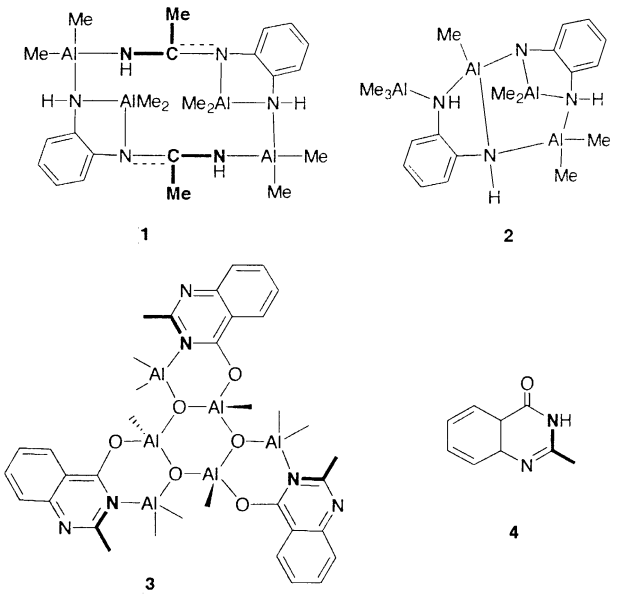

Scheme 1 Compounds **1**–**4** (inserted molecules of acetonitrile are shown in bold).

† Present address: School of Chemical Sciences, University of East Anglia, Norwich, UK NR4 7TJ.

DOI: 10.1039/b007810g

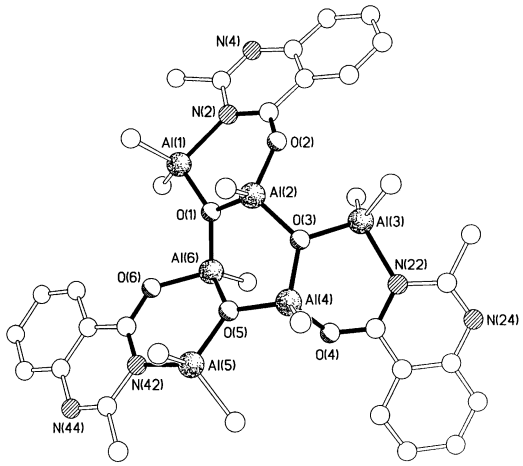

Fig. 1 The molecular structure of **3**. Selected bond lengths (Å); Al(1)–O(1) 1.811(4), Al(1)–N(2) 2.021(5), Al(2)–O(1) 1.785(4), Al(2)–O(3) 1.788(4), Al(2)–O(2) 1.779(4), Al(3)–O(3) 1.827(4), Al(3)–N(22) 2.034(5), Al(4)–O(3) 1.770(4), Al(4)–O(4) 1.783(5), Al(4)–O(5) 1.785(4), Al(5)–O(5) 1.825(4), Al(5)–N(42) 2.015, Al(6)–O(1) 1.784(4), Al(6)–O(5) 1.794(4), Al(6)–O(6) 1.785(5).

note that the formation of N-heterocycles by this methodology is related to the intramolecular Ritter reaction[7–9] in which nitrilium salts, generated in the presence of Friedel–Crafts reagents, react with a second nitrile molecule to give quinazoline ring systems.[9]

Future studies will focus on further exploiting nitrile insertions into aluminium (and gallium) bonds to access unusual inorganic ring systems and nitrogen heterocycle products.

The EPSRC and the Leverhulme Trust (for a Research Fellowship to C. R.) are thanked for financial support. Professor Charles Rees is thanked for helpful discussions.

Notes and References

‡ Satisfactory microanalyses have been obtained.

For **1**: ^{1}H NMR (400 MHz, C_6D_6, 298 K), δ −0.75, −0.48, −0.42, −0.37 (4 × s, 8 × 3H, AlMe), 1.29 (s, 2 × 3H, CMe), 6.36–7.27 (3 × m, 8H, aryl H), NH not seen. ^{13}C NMR (100.6 MHz, C_6D_6, 298 K), δ −12.24, −12.81 (br, AlMe), −8.91 (br, AlMe), −5.99 (br, AlMe). IR: ν(N–H) 3247 cm^{-1}.

For **3**: ^{1}H NMR (400 MHz, $CDCl_3$, 298 K), δ −0.87, −0.82, −0.59, −0.47, −0.46, −0.45, −0.24, −0.23, −0.22 (9 × s, each 3H, AlMe), 2.79 (s, 3H, Me-quin), 2.88 (s, 3H, Me-quin), 2.89 (s, 3H, Me-quin), 7.61 (m, 3H, quinH), 7.82 (m, 3H, quinH), 7.92 (m, 3H, quinH), 8.35 (m, 3H, quinH). ^{13}C NMR (100.6 MHz, $CDCl_3$, 298 K), δ −12.24, −11.56 (2 × m, 3 × AlMe), −7.22, −6.79, −6.45, −5.43, −5.10, −4.57 (6 × s, 3 × $AlMe_2$), 25.53, 25.82, 25.93 (3 × s, Me-quin), 117.15 (m, 3 × aryl C), 125.28–127.61 (overlapping m, 9 × aryl C), 136.33 (m, 3 × aryl C), 150.98 (m, 3 × aryl C), 158.45 (m, 3 × aryl C), 169.31 (m, 3 × aryl C). EI-MS: *m*/*z*: 807 (M^+ − Me). IR: $\nu(\mu_3\text{-O})Al_3$ 800 cm^{-1}.

§ *Crystal data*: For **1**: $C_{24}H_{42}N_6Al_4$, M = 522.6, orthorhombic, space group *Pbca* (no. 61), a = 8.717(1), b = 16.868(1), c = 20.416(2) Å, V = 3002.0(4) Å^3, Z = 4 (the complex has crystallographic C_i symmetry), D_c = 1.156 g cm^{-3}, μ(Cu-Kα) = 16.1 cm^{-1}, F(000) = 1120, T = 183 K; clear prisms, 0.27 × 0.23 × 0.13 mm, Siemens P4/RA diffractometer, ω-scans, 2182 independent reflections. The structure was solved by direct methods and the non-hydrogen atoms were refined anisotropically using full-matrix least squares based on F^2 to give R_1 = 0.069, wR_2 = 0.173 for 1479 independent observed reflections [$|F_o| > 4\sigma(|F_o|)$, $2\theta < 120°$] and 162 parameters.

For **3**: $C_{36}H_{48}N_6O_6Al_6$, M = 822.7, orthorhombic, space group $P2_12_12_1$ (no. 19), a = 12.152(1), b = 16.054(1), c = 22.310(1) Å, V = 4352.3(6) Å^3, Z = 4, D_c = 1.256 g cm^{-3}, μ(Cu-Kα) = 17.9 cm^{-1}, F(000) = 1728, T = 173 K; yellow rhombs, 0.50 × 0.23 × 0.23 mm, Siemens P4/RA diffractometer, ω-scans, 4017 independent reflections. The structure was solved by direct methods and the non-hydrogen atoms were refined anisotropically using full-matrix least squares based on F^2 to give R_1 = 0.055, wR_2 = 0.133 for 3483 independent observed reflections [$|F_o| > 4\sigma(|F_o|)$, $2\theta < 128°$] and 488 parameters. The absolute structure of **3** was determined by use of the Flack parameter which refined to a value of −0.07(7).

CCDC 182/1855. See http://www.rsc.org/suppdata/cc/b0/b007810g/ for crystallographic files in .cif format.

1 A. W. Hofmann, *Chem. Ber.*, 1868, **1**, 194.
2 E. Frankland and J. C. Evans, *J. Chem. Soc.*, 1880, **37**, 563.
3 H. J. Emeléus and K. Wade, *J. Chem. Soc.*, 1960, 2614; J. E. Lloyd and K. Wade, *J. Chem. Soc.*, 1964, 1649; J. E. Lloyd and K. Wade, *J. Chem. Soc.*, 1965, 2662; J. R. Jennings, J. E. Lloyd and K. Wade, *J. Chem. Soc.*, 1965, 5083; I. Pattinson and K. Wade, *J. Chem. Soc.*, 1968, 57; J. R. Jennings and K. Wade, *J. Chem. Soc. A*, 1968, 1946.
4 W. Gerrard, M. F. Lappert and J. W. Wallis, *J. Chem. Soc.*, 1960, 2178; M. F. Lappert and B. Prokai, *Adv. Organomet. Chem.*, 1967, **5**, 225 and references therein.
5 V. C. Gibson, C. Redshaw, A. J. P. White and D. J. Williams, *Angew. Chem., Int. Ed.*, 1999, 961.
6 R. L. Wells, H. Rahbarnoohi, P. B. Glaser, L. M. Liable-Sands and A. L. Rheingold, *Organometallics*, 1996, **15**, 3204.
7 J. J. Ritter and P. P. Minieri, *J. Am. Chem. Soc.*, 1948, **70**, 4045; J. J. Ritter and J. Kalish, *J. Am. Chem. Soc.*, 1948, **70**, 4048.
8 L. I. Krimen and D. J. Cota, *Org. React. (N.Y.)*, 1969, **17**, 213.
9 R. Bishop, in *Comprehensive Organic Synthesis*, ed. B. M. Trost and I. Fleming, Pergamon, Oxford, UK, 1991, vol. 6 and references therein.

ChemComm

Synthesis of hydrolytically stable porphyrin *C*- and *S*-glycoconjugates in high yields†

Paolo Pasetto, Xin Chen, Charles Michael Drain* and Richard W. Franck*

Department of Chemistry and Biochemistry, Hunter College and Graduate Center of The City University of New York, 695 Park Avenue, New York, NY 10021, USA. E-mail: cdrain@shiva.hunter.cuny.edu; rfranck@shiva.hunter.cuny.edu; Phone: (212)650-3791; Fax: (212)772-5332

Received (in Corvallis, OR, USA) 18th October 2000, Accepted 14th November 2000
First published as an Advance Article on the web 14th December 2000

Two *C*-glucosyl porphyrins are prepared using Ramberg–Backlund and Lindsey methods for the key conversions, and thiosugars are shown to react with perfluorophenylporphyrins.

Photofrin®, a mixture of hematoporphyrin oligomers, is currently used clinically for the photodynamic therapy (PDT) of cancers, but suffers from a variety of problems including solubility and dosing.[1] Because of their potential selective binding to various cell types, porphyrins appended with a variety of saccharides have been examined as possible agents for PDT.[1,2] Most recently, sugar-specific binding to rat hepatoma cells by porphyrin glycoconjugates has been described.[2] Their efficacy as antibiotics and anti-viral agents is also under intense investigation.[1] Since metalloporphyrins are well-established catalysts, the attachment of sugars to effect regio- and stereo-selective oxidations has also been examined, albeit with limited success.[3] Additionally, there are several requirements for the successful commercialization of any of these adducts: (a) effective synthesis in high yields, (b) stable products, in this case to hydrolysis, and (c) highly pure compounds.

It is interesting that with few exceptions,[4–6] the glycoconjugate has been oxygen linked *via* a glycosidic bond to a phenolic aryl porphyrin. When the syntheses of these O-linked materials are examined, one finds that disappointingly low yields are reported, considering that the Lindsey porphyrin synthesis yields are typically 45–65%.[7] We believe that one problem may be that the frequently used *O*-glycosyloxybenzaldehyde starting materials, when subjected to the Lindsey porphyrin synthesis using BF_3 catalysis, can undergo a competing and yield-reducing Suzuki *O* to *C*-glycoside rearrangement.[8] Additionally, a perceived problem with the *O*-glycosides is the inherent possibility for glycosyl cleavage by acids, and in biological systems by glycohydrolases. We wish to describe our preliminary results, which provide possible solutions to both the issues of poor yields and hydrolytic instability, namely the preparation of *C*- and *S*-glycosylated aryl porphyrins in high yields. Both yield and stability are crucial factors for the successful incorporation of sugar moieties into porphyrin combinatorial libraries, since the linkage must be stable both during the formation, subsequent reactions, and in the presence of a variety of functional groups.

For the *C*-glycoside series, we chose to exploit earlier work from our laboratory where the Ramberg–Backlund synthesis is used to link sugars to aglycones.[9,10] Thus, after screening several alternative functional equivalents of *p*-bromomethylbenzaldehyde, we settled on α,α′-dibromo-*p*-xylene as an inexpensive starting material. This was condensed with 1-thio-β-D-glucose tetraacetate[11] to afford thioglucoside **1**. Then conversion to the silylated material **2** was accomplished by treatment of **1** with *tert*-butyldimethylsilanol in the presence of silver triflate and 2,6-di-*tert*-butylpyridine.[12] The replacement of the acetyl groups with benzyl ethers to obtain **3** was achieved by deprotection of **2** with sodium methoxide, followed by benzylation. The sulfide **3** was oxidized to the sulfone **4** with monoperoxyphthalic acid (MMPP). The resulting sulfone was employed in the Ramberg–Bäcklund synthesis of the *exo*-glucal **5** under Chan's conditions.[13] The two isomers (*Z*)-**5** and (*E*)-**5** in the ratio 8 : 2 were identified by NOE measurements, which showed an effect between H-1 and H-3 in the case of the *E*-isomer. In some cases the intermediate α-bromosulfone **6** was isolated from the reaction mixture and then converted to the *exo*-glucal **5** by treatment with base. The hydrogenation of **5** with palladium 5% on alumina afforded the β-*C*-glucoside **7**, identified by the coupling constant J = 9.2 Hz, indicating an anti-diaxial configuration of the anomeric H-2 with respect to H-3. The cleavage of the silyl ether **7**, followed by Swern[14] oxidation gave the aldehyde **9**, which was utilized in the synthesis of the porphyrins **10** and **11** in 15 and 53% yields respectively, under Lindsey conditions.[7] The materials obtained showed the expected spectroscopic data. The hydrogenolysis of the benzylic protecting groups yielded the porphyrins **12** and **13**, without reduction of the porphyrin. *S*-Glycosides were chosen as worthy conjugates because they are considered to be good mimics of *O*-glycosides with enhanced stability toward enzymatic hydrolysis.[15]

The second reaction sequence begins with 5,10,15,20-tetra(perfluorophenyl)porphyrin which can be routinely made in gram quantities in high yields by the Lindsey procedure.[7] The reactivity of the *para*-fluoro group toward a large variety of nucleophilic substitution reactions has been well established.[4,16] The tetrakis(thiogalactosyl) and tetrakis(thioglucosyl) derivatives of this fluorinated porphyrin are formed in > 85 and 90% yields, respectively, by modifications of previously described procedures.[16] Specifically, the porphyrin is dissolved in amine-free DMF, five equiv. of the sodium salt of the thiosugar added, and the mixture stirred at rt for 4 h. Purification is accomplished on silica-gel using an ethanol–ethyl acetate gradient as eluent.

DNA photocleavage assays are widely used to evaluate the photoreactivity of porphyrin compounds, though DNA is not the primary site of Photofrin activity.[1,5,6] Thus we used standard plasmid photocleavage assays to evaluate the photoreactivity and compare these results with those for other porphyrins. The conditions used to evaluate the photodamage to plasmid DNA caused by porphyrin compounds varies, but our analysis (see

Table 1

Compound	Partition coeff. octanol–water	DNA photocleavage
5-glu-triPP **12**	68	Fair
Tetra glu PP **13**	30	Poor
Tetra thio glu F4PP	50	Poor
Tetra thio gal F4PP	38	Fair
DiMePy + MeOHP[a]	7	Excellent

[a] Ref. 17.

† Electronic supplementary information (ESI) available: experimental details. See http://www.rsc.org/suppdata/cc/b0/b008489l/

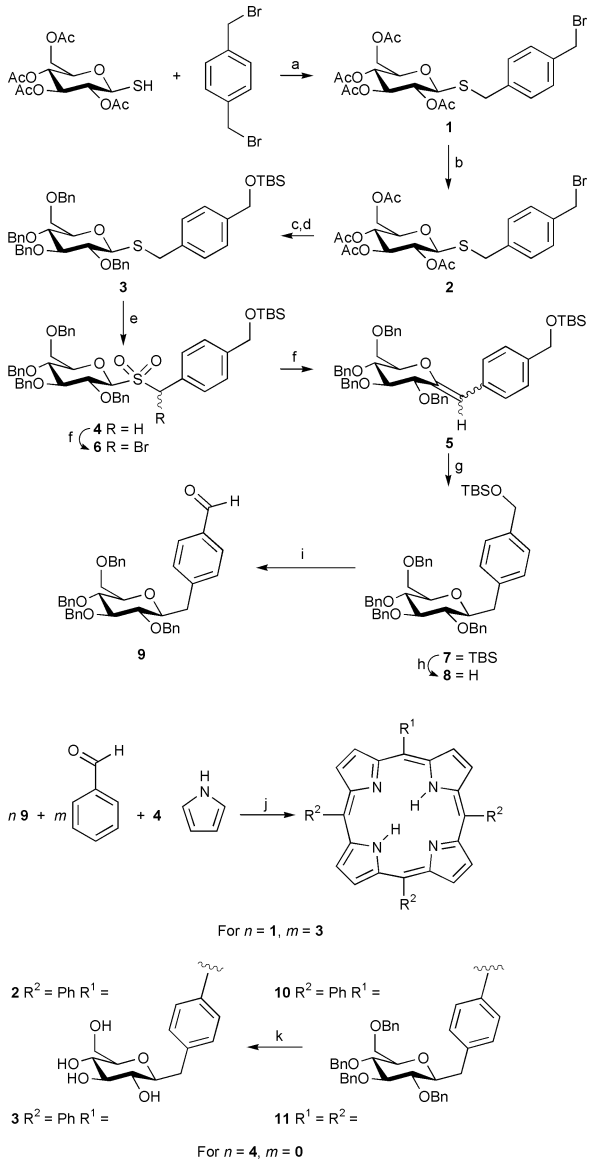

Scheme 1 a, NaH, THF, rt, 2 h, 90%; **b**, TBDMSOH, Ag(OTf), 2,6-di-*tert*-butylpyridine, CH_2Cl_2, rt, 3 h, 60%; **c**, MeONa, MeOH, rt, 3 h; **d**, NaH, BnBr, $Bu_4N^+I^-$, THF–DMF, rt, 8 h, 80% for 2 steps; **e**, MMPP, THF–EtOH–H_2O, 60 ºC, 2 h, 87%; **f**, CBr_2F_2, KOH 25% on alumina, CH_2Cl_2–*t*-BuOH, 0 ºC to rt, 3 h, 88%; **g**, H_2, Pd 5% on alumina, EtOAc, rt, 12 h, 95%; **h**, $Bu_4N^+F^-$, THF, rt, 2 h, 98%; **i**, Oxalyl chloride, DMSO, CH_2Cl_2, −78 °C, then Et_3N, −78 °C to rt, 1.5 h, 85%; **j**, $BF_3{\cdot}OEt_2$, NaCl, rt, 5 h, then DDQ, rt, 30 min, 15% for **10**, 53% for **11**; **k**, H_2, Pd 10% on carbon, EtOAc–MeOH, rt, 16 h, 98%.

Table 1 indicates the compounds reported herein exhibit poor photoreactivity which is consistent with other glycosylated porphyrins.[1,5,6] The amphipathic character of the macrocycle derivative has been shown to correlate to cell toxicity *in vitro*,[1] so the partition coefficients are reported. To date, for this class of compounds, the activity is much poorer than the 5,10-bis(4-methylpyridinium)-15-(4-methylphenyl)-20-(4-hydroxyphenyl)porphyrin (DiMePy$^+$MeOHP) found by combinatorial methods,[17] and for some other tetraphenylporphyrin derivatives.[1]

In conclusion, both the C and S linked glycoporphyrins can be synthesized in high yields exceeding 50% based on starting aldehydes using more efficient synthetic strategies. These compounds are stable to hydrolysis and show some photoactivity. Despite significant efforts by a large number of groups, there are few effective photodynamic therapy (PDT) agents, thus there remains a need to further develop the chemistry and the structure–activity relationships of this class of compounds. In contrast to the present clinical use of Photofrin® for the PDT of cancers, it may be found that different porphyrinic compounds are needed to more effectively treat different cancerous tissues, or for other therapeutic uses.

The authors thank Margareta Sorenson and Dr Clifford Soll, and acknowledge the support of NIGMS SCORE Program 1S06GM60654, NSF CAREER 9732950 to C. M. D.; PSC-CUNY awards to C. M. D. and R. W. F.; NIH GM51216 to R. W. F. Chemistry department infrastructure is partially supported by RCMI grant NIH RR03037. R. W. F. dedicates this article to Professor Steven Weinreb on the occasion of his 60th birthday. ®QLT Phototherapeutics Inc.

Notes and references

1 R. Bonnett, P. Charlesworth, B. D. Djelal, S. Foley, D. J. McGarvey and T. G. Truscott, *J. Chem. Soc.*, 1999, 325; E. D. Sternberg, C. Bruckner and D. Dolphin, *Tetrahedron*, 1998, **54**, 4151; T. J. Dougherty and D. Kessel, *Rev. Contemp. Pharmacother.*, 1999, **10**, 19; B. R. Munson and R. J. Fiel, *Nucleic Acids Res.*, 1992, **20**, 1315.

2 K. Fujimoto, T. Miyata and Y. Aoyama, *J. Am. Chem. Soc.*, 2000, **122**, 3558.

3 P. Maillard, J. L. Guerquin-Kern and M. Momenteau, *Tetrahedron Lett.*, 1991, **32**, 4901.

4 A thioether link between tetra(tetrafluorophenyl)porphyrin and C-6 of glucose embedded in cyclodextrin has been reported: J. Yang and R. Breslow, *Angew. Chem., Int. Ed.*, 2000, **39**, 2692, and references therein.

5 *C*-glycosides: M. Cornia, M. Menozzi, E. Ragg, S. Mazzini, A. Scarafoni, F. Zanardi and G. Casiraghi, *Tetrahedron*, 2000, **56**, 3977, and references therein; M. Momenteau, P. Maillard, M.-A. De Bélinay, D. Carrez and A. Croisy, *J. Biomed. Opt.*, 1999, **4**, 298; N. Ono, M. Baugauchi and K. Maruyama, *Tetrahedron Lett.*, 1992, **33**, 1629.

6 *S*-glycosides linked to alkyl groups: I. Sylvain, R. Benhaddou, V. Carre, S. Cottaz, H. Driguez, R. Granet, M. Guilloton and P. Krausz, *J. Porphyrins Phthalocyanines*, 1999, **3**, 1 and references therein.

7 J. S. Lindsey, I. C. Schreiman, H. C. Hsu, P. C. Kearney and A. M. Marguerettaz, *J. Org. Chem.*, 1987, **52**, 827; F. Li, K. Yang, J. S. Tyhonas, K. A. MacCrum and J. S. Lindsey, *Tetrahedron*, 1997, **53**, 12 339.

8 T. Matsumoto, T. Hosoya and K. Suzuki, *Synlett*, 1991, 709; T. Matsumoto, T. Hosoya and K. Suzuki, *Tetrahedron Lett.*, 1990, **31**, 4629.

9 P. S. Belica and R. W. Franck, *Tetrahedron Lett.*, 1998, **39**, 8225; G. Yang, R. W. Franck, H.-S. Byun, R. Bittman, P. Samadder and G. Arthur, *Org. Lett.*, 1999, **1**, 2149.

10 F. K. Griffin, P. V. Murphy, D. E. Patterson and R. J. K. Taylor, *Tetrahedron Lett.*, 1998, **39**, 8179; M-.L. Alcaraz, F. K. Griffin, D. E. Patterson and R. J. K. Taylor, *Tetrahedron Lett.*, 1998, **39**, 8183; R. J. K. Taylor, F. K. Griffin and D. E. Paterson, *Angew. Chem., Int. Ed.*, 1999, **38**, 2939; A. D. Campbell, D. E. Paterson, T. M. Raynham and R. J. K. Taylor, *Chem. Commun.*, 1999, 1599.

11 D. Horton, in *Methods in Carbohydrate Chemistry*, eds. R. L. Whistler and M. L. Wolfrom, Academic Press Inc., New York, 1963, Vol. II, p. 433–437.

12 R. M. Burk, T. S. Gac and M. B. Roof, *Tetrahedron Lett.*, 1994, **35**, 8111.

13 T. L Chan, S. Fong, Y. Li, T. O. Man and C. D. Poon, *Chem. Commun.*, 1994, 1771.

14 K. Omura and D. Swern, *Tetrahedron*, 1978, **34**, 1651.

15 B. D. Johnston and B. M. Pinto, *J. Org. Chem.*, 2000, **65**, 4607, and references therein; J. C. Wilson, M. J. Kiefel, D. I. Angus and M. von Itzstein, *Org. Lett.*, 1999, **1**, 443; for recent examples of thioglycoside stability toward a glycohydrolase.

16 S. J. Shaw, K. J. Elgie, C. Edwards and R. W. Boyle, *Tetrahedron Lett.*, 1999, 1595.

17 C. M. Drain, X. Gong, V. Ruta, C. E. Soll and P. F. Chicoineau, *J. Comb. Chem.*, 1999, **1**, 286.

ChemComm

Fabrication of a novel polypyrrole/poly(methyl methacrylate) coaxial nanocable using mesoporous silica as a nanoreactor†

Jyongsik Jang,* Byungkwon Lim, Jinwoo Lee and Taeghwan Hyeon*

School of Chemical Engineering, Seoul National University, Seoul 151-742, Korea.
E-mail: jsjang@plaza.snu.ac.kr and thyeon@plaza.snu.ac.kr

Received (in Cambridge, UK) 31st July 2000, Accepted 15th November 2000
First published as an Advance Article on the web 14th December 2000

We report on the fabrication of a polypyrrole/poly(methyl methacrylate) coaxial nanocable through the sequential polymerization of methyl methacrylate and pyrrole monomers inside the channels of mesoporous SBA-15 silica, followed by the removal of the silica template.

There has been tremendous interest in the development of conducting structures with nanometer dimensions. These nanostructured conducting materials could find many attractive applications such as electromagnetic interference shielding, electrochromic devices, supercapacitors, polymeric electrodes and sensors.[1] Recently, many nanotubules and nanowires of polymers, metals and carbons have been produced through template approaches with various membranes,[2] layered inorganic solids,[3] zeolites and mesoporous materials.[4] Generally conducting polymers themselves, however, possess poor mechanical properties, and are very difficult to process. To overcome these drawbacks, much research effort has been focused on the development of processes to combine conducting polymers and polymer matrices with good tractability.[5] Although many different conducting polymer composites have been developed, no nanostructured conducting-polymer/polymer composites have, as yet, been reported. Herein, we report the preparation of polypyrrole/poly(methyl methacrylate) coaxial nanocable using mesoporous silica as a template.‡

In the synthesis, mesoporous SBA-15 silica was utilized as a template. Mesoporous SBA-15 silica with regular hexagonal pores of 7.5 nm was prepared by the reported method.[6] To synthesize tubular PMMA within the pores of SBA-15, methyl methacrylate (MMA) was incorporated into the pores of SBA-15 silica and MMA was subsequently polymerized. The amount of MMA was precisely controlled so that the polymerization could occur selectively on the inner surfaces of mesopores of SBA-15, resulting in a tubular structure of PMMA. Pyrrole monomer was polymerized using $FeCl_3$ as an oxidant inside the tubular holes of the PMMA/SBA-15 composite, resulting in a PPy/PMMA/SBA-15 nanocomposite. The removal of SBA-15 silica template by etching using an aqueous HF solution produced a PPy/PMMA nanocomposite.

The pore size distribution (PSD) curves of SBA-15, PMMA/SBA-15 and PPy/PMMA/SBA-15 were derived from nitrogen adsorption isotherms and are presented in Fig. 1. The pore size of SBA-15 silica (7.5 nm) was decreased to 6.2 nm when the polymerization of MMA was conducted and the TEM image of PMMA incorporated SBA-15 exhibited a nearly hexagonal arrangement of pores, demonstrating the formation of tubular PMMA inside the mesopores of SBA-15 silica. The pore volumes of SBA-15, PMMA/SBA-15, and PMMA/PPy/SBA-15 are 0.63, 0.23, and 0.07 $cm^3\ g^{-1}$, respectively. Thermogravimetric analysis (TGA) showed the weight ratio of SBA-15: PMMA : PPy = 50 : 27 : 23 in the PPy/PMMA/SBA-15 composite. Elemental analysis of the PMMA/PPy nanocomposite revealed a 1 : 1 weight ratio of PMMA and PPy, which matches well with the TGA data. The weight ratio can be also calculated from the change of pore volumes after considering the bulk densities (1.2 g cm^{-3} for PMMA and 1.5 g cm^{-3} for PPy) and the weight increases from the consecutive addition of two polymers. The ratio was calculated to be PMMA : PPy = 1 : 0.8. When the weight ratio was derived simply from the decrease in the pore sizes of the composites, the weight of PMMA is much lower (PMMA : PPy = 0.4 : 1). However, this discrepancy can be explained by the incorporation of PMMA into the complementary pores (micropores) of SBA-15 silica. Recently, Kruk *et al.* revealed that many micropores in the walls of SBA-15 silica interconnect primary mesopores.[7] When polymerization of MMA occurs, PMMA might fill these micropores in addition to partial filling of the mesopores. Therefore, the actual amount of PMMA incorporated into SBA-15 is larger than the calculated amount of PMMA derived solely from the partial filling of mesopores.

Small angle X-ray scattering (SAXS) patterns were obtained at various times during the synthesis. The diffraction pattern of SBA-15 showed typical *hk*0 reflections (100, 110 and 200) from the hexagonal arrangement of pores. The peak intensity in the SAXS of PMMA/SBA-15 and PPy/PMMA/SBA-15 decreased compared with that in SBA-15 silica, but the peak positions of the XRD patterns were nearly identical. These results show that the SBA-15 structure remained intact during the synthesis, demonstrating the usefulness of SBA-15 silica as a nanoreactor.

The PPy/PMMA nanocomposite was obtained by HF etching of the SBA-15 silica template. It has been reported that acid treatment does not decrease the electrical conductivity of PPy.[8] The resulting polymer/polymer nanocomposite was dried at 100 °C under vacuum to obtain the dry powder which was analyzed by FTIR spectroscopy. The IR spectrum of the nanocomposite exhibited characteristic peaks from both PMMA and PPy. One very unusual observation is that there are two carbonyl peaks associated with PMMA. The curve-fitted

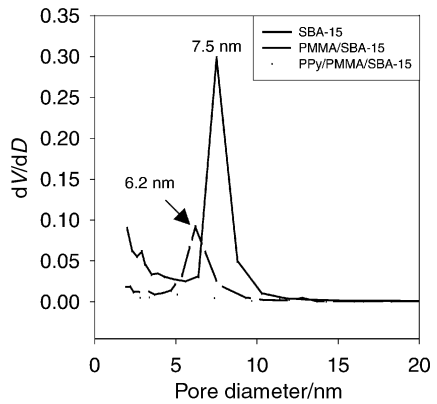

Fig. 1 The pore size distribution curves of SBA-15, PMMA/SBA-15 and PPy/PMMA/SBA-15. The curves were obtained from the adsorption branch of the nitrogen isotherm calculated by the BJH method. The isotherms were collected at 77 K on a Micrometrics ASAP2010 Gas Adsorption Analyzer after degassing at 250 °C at 30 μTorr for 5 h.

† Electronic supplementary information (ESI) available: FTIR spectra, XRD patterns and TEM images. See http://www.rsc.org/suppdata/cc/b0/b006197m/

DOI: 10.1039/b006197m

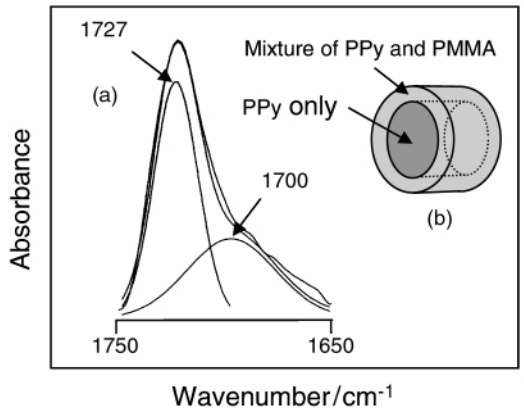

Fig. 2 (a) Curve-fitted IR spectra of the PMMA carbonyl peak for the PPy/PMMA nanocomposite. (b) A schematic illustration of coaxial nanocable of PPy/PMMA.

spectra of the carbonyl region of the PPy/PMMA nanocomposite exhibited one major peak at 1727 cm^{-1} and a shoulder at 1700 cm^{-1} [Fig. 2(a)]. The carbonyl peak at 1700 cm^{-1} indicates hydrogen bonding interactions between PMMA carbonyl groups and PPy N–H groups. On the other hand, the peak at 1727 cm^{-1} arise from the free carbonyl groups of PMMA. Such a strong interaction between PPy and PMMA has not been reported before in the micrometer-sized PPy/PMMA composites. Judging from these data, it seems that the outer PMMA layer is intimately mixed with PPy at the nanometer-scale [Fig. 2(b)].

The PPy/PMMA nanocomposite could be easily molded by compression under 25 kN cm^{-2} at 220 °C for 10 min using a pelletizer. Interestingly, the AFM image of the compression-molded PPy/PMMA composite revealed highly oriented and unidirectional structures (Fig. 3). The well aligned structure was observed nearly all over the sample, which seems to result from template synthesis inside regular hexagonally arranged mesopores of SBA-15. The compression-molded PPy/PMMA nanocomposite exhibited an electrical conductivity of 1.7 S cm^{-1}. Considering that the typical conductivity of chemically synthesized PPy lies in the range 1–10 S cm^{-1}, the conductivity of our PPy/PMMA composite seems to be low. However, when we consider that the PPy wires in the PPy/PMMA nanocomposite are surrounded by insulating PMMA tubules, limiting full exposure of the conducting surface of PPy, the conductivity is relatively high which might result from the good alignment of the PPy chains.

We are grateful to the Brain Korea 21 Program supported by the Korean Ministry of Education for the financial support.

Notes and references

‡ *Experimental details*: SBA-15 was prepared by the reported method. 1 g of methyl methacrylate (MMA) was incorporated into the pores of SBA-15 silica (2 g) by heating for 5 h at 90 °C under reduced pressure. MMA was polymerized with 10 mg of benzoyl peroxide under an argon atmosphere at 70 °C for 2 days and then 120 °C for 2 h, followed by evacuating in a vacuum oven at the same temperature for 18 h. 0.4 g of pyrrole was loaded into the pores of the PMMA/SBA-15 (1.3 g) using the same conditions as in the MMA incorporation, and then polymerized with 20 mL of 0.81 M aqueous $FeCl_3$ solution for 3 h. The resulting solid was retrieved by filtration, followed by drying under vacuum at room temperature for 12 h. To remove the silica template, the PPy/PMMA/SBA-15 composite was dispersed in an aqueous HF solution (48 wt%), and was stirred overnight. The PPy/PMMA nanocomposite was retrieved by vacuum filtration. To fabricate a thin film, the powder form of PPy/PMMA was compression-molded using a pelletizer under 25 kN cm^2 at 220 °C for 10 min.

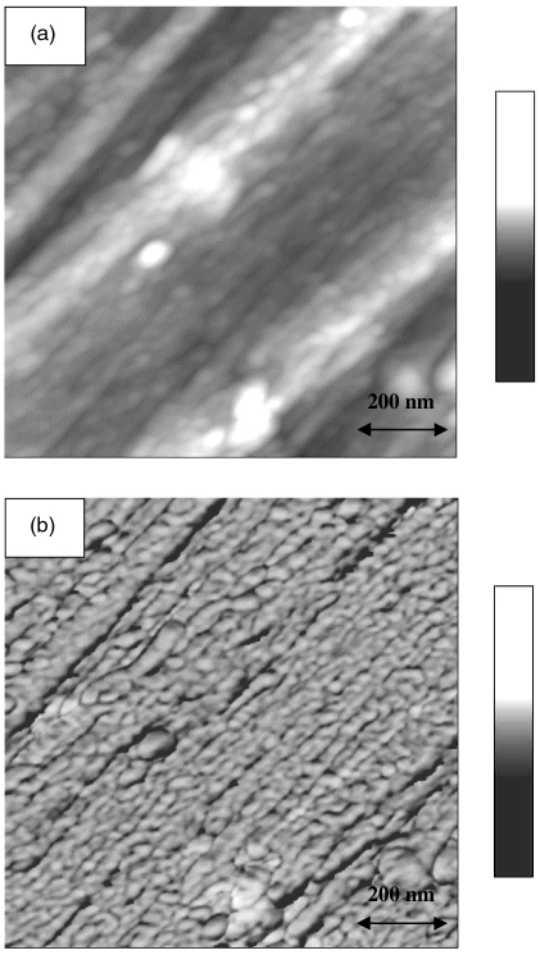

Fig. 3 AFM images of PPy/PMMA nanocomposite: (a) height image and (b) phase image. The film was fabricated by compression-molding of the PPy/PMMA nanocomposite at 220 °C under 25 kN cm^{-2} for 10 min. The images were obtained with Nanoscope IIIa Dimension 3100 SPM (Digital Instruments) in tapping mode.

1 P. Kathirgamanathan, *Adv. Mater.*, 1993, **5**, 281; P. K. Shen, H. T. Huang and A. C. C. Tseung, *J. Electrochem. Soc.*, 1992, **139**, 1840; L. Diederich, E. Barborini, P. Piseri, A. Podesta, P. Milani, A. Schneuwly and R. Gallay, *Appl. Phys. Lett.*, 1999, **75**, 2662; D. K. Moon, A. B. Padias, H. K. Hall, T. Huntoon and P. D. Calvert, *Macromolecules*, 1995, **28**, 6205; J. Kong, N. R. Franklin, C. W. Zhou, M. G. Chapline, S. Peng, K. J. Cho and H. J. Dai, *Science*, 2000, **287**, 622.

2 C. R. Martin, *Science*, 1994, **266**, 1961; C. R. Martin, *Acc. Chem. Res.*, 1995, **28**, 61; G. Che, B. B. Lakshmi, E. R. Fisher and C. R. Martin, *Nature*, 1998, **393**, 346; V. M. Cepak and C. R. Martin, *Chem. Mater.*, 1999, **11**, 1363.

3 M. G. Kanatzidis, L. M. Tonge, T. J. Marks, H. O. Marcy and C. R. Kannewurf, *J. Am. Chem. Soc.*, 1987, **109**, 3797; M. G. Kanatzidis, C. G. Wu, H. O. Marcy and C. R. Kannewurf, *J. Am. Chem. Soc.*, 1989, **111**, 4139.

4 C. G. Wu and T. Bein, *Science*, 1994, **264**, 1757; C. G. Wu and T. Bein, *Science*, 1994, **266**, 1013; S. A. Johnson, E. S. Brigham, P. J. Ollivier and T. E. Mallouk, *Chem. Mater.*, 1997, **9**, 2448; S. A. Johnson, D. Khushalani, N. Coombs, T. E. Mallouk and G. A. Ozin, *J. Mater. Chem.*, 1998, **8**, 13; J. Lee, S. Yoon, S. M. Oh, C.-H. Shin and T. Hyeon, *Adv. Mater.*, 2000, **12**, 359.

5 M. Omastova, J. Pavlinec, J. Pionteck, F. Simon and S. Kosina, *Polymer*, 1998, **39**, 6559; S. F. Lascelles and S. P. Armes, *J. Mater. Chem.*, 1997, **7**, 1339.

6 D. Zhao, J. Feng, Q. Huo, N. Melosh, G. H. Fredrickson, B. F. Chmelka and G. D. Stucky, *Science*, 1998, **279**, 548.

7 M. Kruk, M. Jaroniec, C. Ko and R. Ryoo, *Chem. Mater.*, 2000, **12**, 1961.

8 M. Forsyth and V. T. Truong, *Polymer*, 1995, **36**, 725.

A mannose-6-phosphonate–cholesterylamine conjugate as a specific molecular adhesive linking cancer cells with vesicles

Véronique Barragan,*[a,b] Fredric M. Menger,[a] Kevin L. Caran,[a] Carole Vidil,[b] Alain Morère[b] and Jean-Louis Montero[b]

[a] *Department of Chemistry, 1515 Pierce Drive, Emory University, Atlanta 30322, USA. E-mail: menger@emory.edu*
[b] *Laboratoire de Chimie Biomoléculaire, UMR 5032, Université Montpellier II, Place Eugène Bataillon, 34095 Montpellier cedex 05, France. E-mail: montero@univ-montp2.fr*

Received (in Liverpool, UK) 17th October 2000, Accepted 16th November 2000
First published as an Advance Article on the web 14th December 2000

A hydrolytically stable sugar phosphonate coupled to a steroid *via* a long and semi-rigid spacer (synthesized *via* a 12-step sequence) binds both to the mannose-6-phosphonate receptors of certain cancer cells and to the lipid bilayer of vesicles, thereby serving as a multivalent adhesive between cell and vesicle surfaces.

Mannose-6-phosphate plays a key role in the intracellular retention and secretion of lysosomal hydrolytic enzymes.[1] Thus, this sugar residue inserted on the enzymes directs the transport of the newly synthesized enzymes from the Golgi apparatus to the lysosomes. Membrane-bound mannose-6-phosphate receptors assist in both the secretion and internalization of the lysosomal enzymes. It has been demonstrated that the population of mannose-6-phosphate receptors is increased abnormally in breast cancer cells as compared to those of benign breast disease.[2] The receptors can, therefore, provide a handle with which to attack the cells.[3] For example, drugs and vesicles endowed with mannose-6-phosphate moieties could, in principle, bind selectively to cancer cells owing to the enhanced presence of mannose-6-phosphate receptors. It is this potential vulnerability of the cancer cells which motivates the present paper. A recent paper describing vesicles containing phospholipids bearing a sugar-binding boronic acid that adhere to erythrocytes embodies a similar philosophy.[4]

Actually, the use of mannose-6-phosphate moieties to target bioactive molecules is not as attractive as it might seem. The problem lies in the susceptibility of sugar phosphates to hydrolysis by various phosphatase enzymes. To circumvent this problem, we have recently developed synthetic routes to two phosphonate analogs of mannose-6-phosphate (M6-P); one is isosteric with the phosphate moiety while the other is not.[5] Both, however, are hydrolytically stable. Upon submitting the analogs for biological testing, it was found that the isostere (but not the non-isostere) binds to M6-P receptors as effectively as does M6-P itself.[5]

Encouraged by the results of our biological testing, we proceeded to construct a molecule (**14**) that could bind both to cancer cells and to vesicles and, in this manner, serve as an 'adhesive' between the living and chemical systems. Our interest in attachment to cancer cells arose from the widespread attention given to vesicles (also called 'liposomes') as drug delivery vehicles in cancer therapy.[6]

Vesicles are spherical objects composed of one or more lipid bilayer shells surrounding an aqueous interior. Their diameter ranges from 30 nm ('small') to 10–200 μm ('giant'), and we have had considerable experience with both types.[7] Often in our vesicle research we add cholesterol, owing to its high affinity for lipids bilayers and to its strengthening effect upon the vesicles. It was for these properties that a cholesterylamine unit was selected as the vesicle-adhering unit. All told, about a dozen steps were required to synthesize the cell/vesicle adhesive (Scheme 1). Reactions were generally run at the 50 mg level because scale-up often reduced the yields. Great attention to purification by chromatography was necessary throughout.

4-Nitrophenyl-α-D-pyranoside **1** was used to initiate the synthesis (Scheme 1). Compound **1** was first selectively protected on the primary hydroxy with a 4-methoxytrityl group to give **2**. The secondary hydroxys were then protected with benzoyl groups (**2** to **3**). Attempts to benzylate these hydroxys instead of benzoylating them led to degradation. Compound **3**, fully protected, was selectively deprotected only at C-6 with the

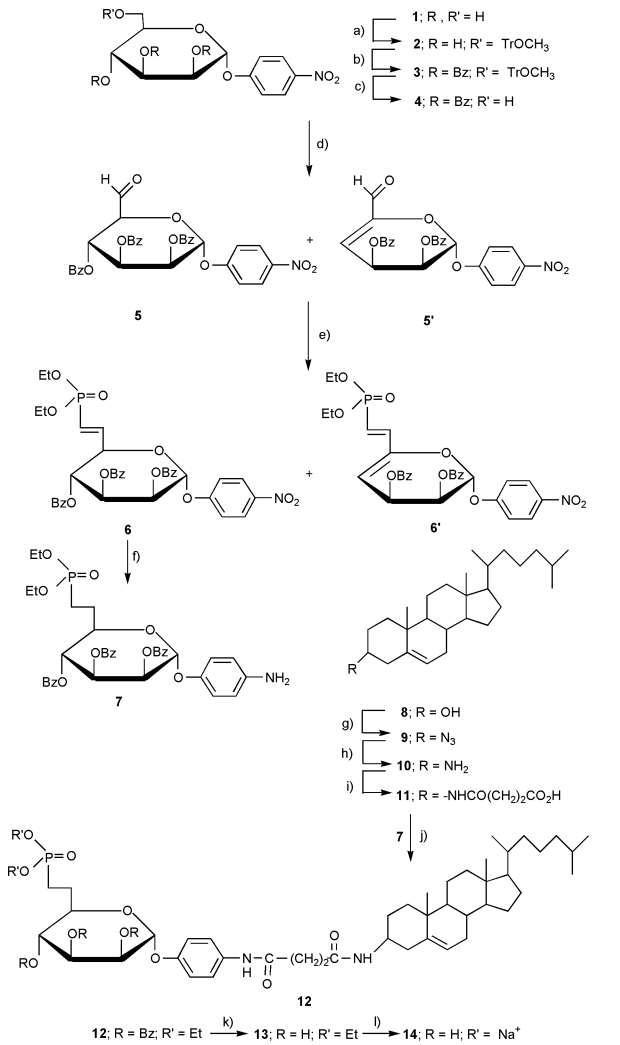

Scheme 1 *Reagents and conditions*: (a) CH_3OTRCl, pyridine, 94%; (b) BzCl, pyridine, 90%; (c) $Ce(NH_4)_2NO_3CN$–H_2O 95:5, 80 °C, 90%; (d) Swern oxidation, $(COCl)_2$, DIEA, DMSO, THF, **5**: 37%, **5′**: 63%; (e) Wittig–Horner, TEMDP, NaH, benzene, **6′**: 40%; (f) H_2 Pd/C, EtOH, 86%; (g) PPH_3, HN_3, DEAD, toluene, 65%; (h) $LiAlH_4$, Et_2O, 95%; (i) succinic anhydride, TEA, Et_2O, 90%; (j) DCC/HOBT, DMAP, *N*-Et-morpholine, CH_2Cl_2, 80%; (k) MeOH–NH_3, 4 °C, 90%; (l) Me_3SiBr, pyridine, CH_2Cl_2 then Na cation exchange resin, 40%.

DOI: 10.1039/b008446h

aid of a redox reaction involving ceric ammonium nitrate. The resulting primary alcohol **4** was then subjected to a Swern oxidation and converted into a product that gave two spots when developed with rhodanine. Both products showed the presence of an aldehyde proton in the NMR (one at 9.70 ppm and the other at 9.28 ppm in a ratio of 37 and 63 respectively). Purification of the mixture by chromatography gave the latter aldehyde whose NMR spectrum indicated the occurrence of a E1cb-type elimination of a benzoate during the Swern oxidation. In the course of the actual synthesis, however, the aldehyde mixture (**5** and **5′**) was used without separation in a Wittig–Horner reaction to produce two phosphonates (**6** and **6′**) in 25% and 40% yields, respectively. At this point, phosphonate **6** was isolated by chromatography and hydrogenated to **7**, a reduction that both removed the unsaturation and converted the nitro group into an amino group. Meanwhile, in this convergent synthesis, chemistry was being performed on the steroidal portion of the molecule starting with cholesterol **8**. Thus, cholesterol was transformed into α-cholesterylamine **10** using a literature procedure with only slight modification.[8] We now had in hand the necessary two amines which were joined together *via* a succinoyl unit by first acetylating **10** with succinic anhydride to give **11**. Carbodiimide coupling of **11** with **7** then gave **12** which needed only to be deprotected to produce the final compound.

Deprotection was accomplished by first debenzoylating **12** with methanolic ammonia. The phosphonate diester **13** was used to obtain the disodium phosphonate salt with the aid of trimethylsilylbromide; purification of **14** was performed by chromatography on silica gel. An overall yield of only 2.6% is indicative, in part, of the difficulties in preparing and purifying this large and bipolar molecule.

Microscopically visible giant vesicles, comprised of 1-palmitoyl-2-oleoyl-*sn*-glycero-3-phosphocholine (POPC), compound **14** or its phosphate counterpart,[9] and 1-palmitoyl-2-oleoyl-3-phosphoglycerol (POPG) were prepared in Hepes solution (1 mM) by the hydration method,[7] using ratios from 87:5:8 to 75:17:8, respectively. An aliquot of the vesicle suspension was added to a petri dish containing MCF-7 breast cancer cells (half-confluent) in Dulbecco's phosphate buffer solution (DPBS, Sigma). The petri dish was gently swirled and placed under a light microscope. Giant vesicles adjacent to cancer cells were grasped with a micropipet under suction and slowly withdrawn from the cells. The majority of the giant vesicles containing **14** or its phosphate counterpart failed to release the cells but continued to stick to them. When such vesicles were pulled away from the cancer cells, either the cell (Fig. 1) or the vesicle (Fig. 2) was substantially distorted. Fig. 1 shows how a withdrawn vesicle retains its contact with the cancer cell *via* an elongated fiber originating from the cancer cell. Fig. 2 shows how a spherical giant vesicle, attached to a cancer cell *via* **14**, deforms into an ellipsoid upon application of a lateral force. Control runs, carried out with identical vesicles except that their bilayers possessed a non-adhesive steroid, the succinate derivative of cholesterylamine, failed to produce a similar effect in the majority of cases. These experiments suggest that **14** does indeed serve as a chemical adhesive.

Submicroscopic vesicles (100 nm in diameter) were prepared by hydration of a film of POPC–14–POPG mixture with a 0.96 mM solution of a water-soluble fluorescent dye (Lucifer Yellow CH, dipotassium salt), followed by 19 extrusions through a 100 nm polycarbonate filter. Elution through a Sephadex G-50 column removed all dye not bound in or on the small vesicles. The fluorescent vesicles were then added to a cancer cell culture in medium and allowed to sit for 40 min. At the end of this period, medium and unbound vesicles were washed away with DPBS, and epifluorescence microscope pictures were taken of the cancer cells (Fig. 3). The cancer cells are seen to display a fluorescence consistent with surface binding of the fluorescent vesicles. As a control experiment, the chemical adhesive **14** was omitted from the vesicles, and the cancer cells failed to display fluorescence. This again suggests the efficacy of the chemical linkage between vesicle and cell. Definite experiments including flow cytometry are being planned. Yet even at this stage of our work the steroidal phosphonate appears to be a promising tool in selective targeting of breast cancer cells.

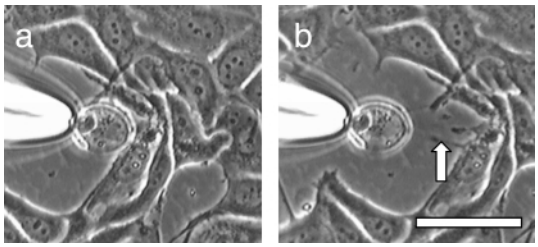

Fig. 1 (a) A giant vesicle containing the phosphate counterpart of **14** has attached itself to a cluster of cancer cells. (b) The vesicle is slowly pulled away from the cells with a micropipet. A fiber (arrow) forms between the vesicle and cells. Bar = 20 μm.

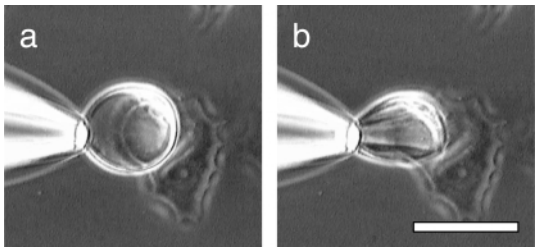

Fig. 2 A giant vesicle containing adhesive **14** and attached to a cancer cell showing a sphere-to-ellipsoid distortion upon application of a lateral force. Bar = 20 μm.

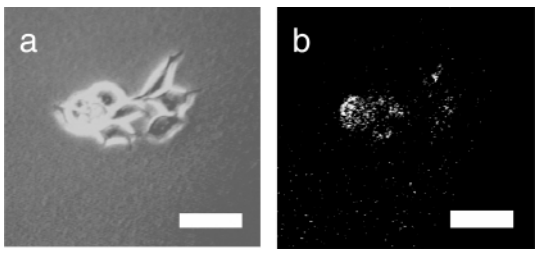

Fig. 3 (a) Phase contrast image of MCF-7 cells that have been incubated with submicroscopic vesicles. The vesicles contain adhesive **14** within their membranes and Lucifer Yellow CH in their aqueous interior. (b) Fluorescence image of the same cluster showing fluorescence-labeled cells. Bar = 25 μm.

This work was supported by grant GM21457 from the National Institutes of Health to F. M. Menger.

Notes and references

1 K. Von Figura and A. Hasilik, *Annu. Rev. Biochem.*, 1986, **55**, 167; S. Kornfeld and I. Mellman, *Annu. Rev. Cell Biol.*, 1989, **5**, 483.
2 S. Meresse, U. Bauer, T. Ludwig, F. Mauxion, A. Schmidt and B. Hoflack, *Med. Sci.*, 1993, **9**, 148; Y. Zhao, C. Escot, T. Maudelonde, C. Puech, P. Rouanet and H. Rochefort, *Cancer Res.*, 1993, **53**, 2901.
3 B. Hamdaoui, G. Dewynter, F. Capony, J.-L. Montero, C. Toiron, M. Hnach and H. Rochefort, *Bull. Soc. Chim. Fr.*, 1994, **131**, 854; N. Yagi, Y. Ogawa, M. Kodaka, T. Okada, T. Tomohiro, T. Konakahara and H. Okuno, *Chem. Commun.*, l999, 1687.
4 Y. R. Vandenburg, Z.-Y. Zhang, D. J. Fishkind and B. D. Smith, *Chem. Commun.*, 2000, 149.
5 C. Vidil, A. Morere, M. Garcia, V. Barragan, B. Hamdaoui, H. Rochefort and J.-L. Montero, *Eur. J. Org. Chem.*, 1999, 447.
6 G. Gregoriadis, *N. Engl. J. Med.*, 1976, **295**, 704; D. D. Lasic, *Liposomes: From Physics to Application*, Elsevier, Amsterdam, 1993, ch. 14.
7 F. M. Menger and D. E. Johnston, *J. Am. Chem. Soc.*, 1991, **113**, 5467; F. M. Menger and K. D. Gabrielson, *Angew. Chem., Int. Ed. Engl.*, 1995, **34**, 2091.
8 C. C. Kan, J. Yan and R. Bittman, *Biochemistry*, 1992, **31**, 1866.
9 V. Barragan, *to be published.*

Sono-emulsion electrosynthesis: electrode-insensitive Kolbe reactions

Jay D. Wadhawan,[a] Frank Marken,†[a] Richard G. Compton,*[a] Steven D. Bull‡[b] and Stephen G. Davies[b]

[a] *Physical and Theoretical Chemistry Laboratory, Oxford University, South Parks Road, Oxford, UK OX1 3QZ. E-mail: compton@ermine.ox.ac.uk*

[b] *Dyson Perrins Laboratory, Oxford University, South Parks Road, Oxford, UK OX1 3QY*

Received (in Cambridge, UK) 30th August 2000, Accepted 16th November 2000
First published as an Advance Article on the web 14th December 2000

The electro-oxidation of water-immiscible liquid aliphatic acids (RCO_2H) leading to decarboxylation to afford a hydrocarbon (R–R) may be achieved using an emulsion formed *via* insonation so that the organic phase continuously extracts the products; in complete contrast to conventional monophasic electrolyses, the type and yield of products obtained from this biphasic Kolbe electrolysis are independent of the electrode material used.

The introduction of power ultrasound into homogeneous solutions has a considerable effect upon mass transport processes due to macroscopic streaming and microscopic interfacial cavitational events;[1] the sonication of biphasic media can result in the formation of an *in situ* emulsion,[2–4] primarily due to cavitational events that occur preferentially at the phase boundary.[3] These mechanical forces act to divide droplets again and again forming microdroplets and effectively 'homogenising' the heterogeneous system.

Electrosynthesis in emulsion media is long established.[5,6] Sono-emulsion systems have considerable potential for application in electrosynthesis because (i) there is no need for emulsion stabilising reagents, (ii) the separation of products is facile, (iii) aqueous solutions may be co-emulsified with a sparingly soluble liquid depolariser, resulting in a medium of high conductivity, (iv) high rates of mass transport can be achieved, and (v) the electrode surface is continually activated.[7]

We report the use of sono-emulsion media to study the electro-oxidation of hexanoic acid (Kolbe reaction). Previous sono-electrosynthetic studies[8–12] have focussed upon the effects of ultrasound on Kolbe electrolysis, exclusively under monophasic conditions, and with seemingly contradictory data. In this work it is shown that under biphasic conditions, although Kolbe electrolysis is conducted at a potential far beyond that required for solvent decomposition, an efficient conversion of hexanoic acid into decane is achieved at both platinum and boron-doped CVD (chemical vapour deposited) diamond film anodes. Surprisingly, the anode material does not affect the type or ratio of products formed.

An electrochemical cell equipped with an ultrasonic probe§ was used as reported earlier.[13] With an ultrasound intensity of 190 W cm^{-2}, this configuration leads to forceful mixing and emulsification of two-phase systems such as water | decane. The biphasic emulsion systems of hexanoic acid (*ca.* 5 mL) in aqueous 1.0 M NaOH (*ca.* 15 ml) had a conductivity of *ca.* 20 mS cm^{-1} and pH of 6.1. These values were kept more or less constant throughout the electrolysis by the reduction of water at the platinum counter electrode, and the gradual dissolution of the organic acid into the aqueous solution phase.

Power ultrasound was used to emulsify *ca.* 15 mmol of hexanoic acid in an aqueous 1.0 M NaOH biphasic system. After the passage of 1 Faraday (per mole of hexanoic acid) of charge (*ca.* 1500 C, sufficient to quantitatively convert hexanoic acid assuming a one-electron oxidation process) the reaction was stopped, excess hydroxide neutralised with acid, and the organic products extracted with ethyl acetate and analysed by GC–MS and NMR spectroscopy. Data summarised in Table 1 describe the conditions used and the yields of the main product, decane—the Kolbe dimer, generated in this electrolysis process. At platinum electrodes, it can be seen that a threshold current density (or applied potential) exists below which the Kolbe process cannot compete against background processes such as oxygen evolution. As in the monophasic case,[14] increasing the temperature at which the reaction takes place causes a decrease in current efficiency; decreasing the aqueous electrolyte concentration also has this effect. The effect of the current density can be rationalised as follows. Initially, increasing the current density causes the current efficiency to improve, and good yields of decane are observed at current densities in the range 0.2–0.3 A cm^{-2}; at values of 0.35 A cm^{-2} and higher, the current efficiency decreases. This can be rationalised in terms of the flux of hexanoate towards the electrode surface. The ultrasound-determined mass transport limiting current (I_{lim}) in homogeneous solution is given by[1] eqn. (1):

$$I_{lim} = \frac{nFADc}{\delta} \quad (1)$$

where n refers to the number of electrons transferred at the electrode, F is the Faraday constant (96485 C mol^{-1}), A is the area of the platinum working electrode (1.1 cm^2), D and c refer to the diffusion coefficient and the concentration of hexanoate in the emulsion respectively, and the Nernstian diffusion layer thickness,[1] δ is *ca.* 5 μm. Using the Wilke–Chang method[15] for estimation of diffusion coefficients, and further assuming the viscosity of the emulsion to be not too different from that of water, a hypothetical mass transport controlled limiting current

Table 1 Results from galvanostatic electrolysis experiments[a]
2 $Me(CH_2)_4CO_2H \rightarrow Me(CH_2)_8Me$

Mass of hexanoic acid/g	Concentration of NaOH/M	Current density/ A cm^{-2}	Tenperature/K	Yield[b] (%) of decane
1.1 cm^2 platinum disc anode				
1.72	1.0	0.08	293	0
1.72	1.0	0.13	293	24 ± 3
1.83	1.0	0.18	293	45 ± 5
1.82	1.0	0.35	293	40 ± 5
1.67	0.1	0.18	293	17 ± 2
1.87	1.0	0.18	313	3 ± 1
0.25 cm^2 free-standing polycrystalline boron-doped CVD diamond anode				
1.80	1.0	0.35	293	40 ± 5
1.80	1.0	0.70	293	14 ± 5

[a] *Reaction conditions*: oxidation of hexanoic acid at a 1.1 cm^2 platinum anode (or at a 0.25 cm^2 free-standing polycrystalline boron-doped CVD diamond electrode) in an aqueous NaOH/hexanoate emulsion system in the presence of power ultrasound (7 mm electrode-to-horn distance, 190 W cm^{-2}). Charge equivalent to 1 Faraday per mol of hexanoic acid was passed before analysis (*ca.* 1500 C). [b] Yields based upon quantitative analysis of ^1H NMR signals.

† Present address: Department of Chemistry, Loughborough University, Loughborough, UK LE11 3TU.
‡ Present address: School of Chemistry, University of Bath, Claverton Down, Bath, UK BA2 7AY.

DOI: 10.1039/b007037h

density of up to *ca.* 1 A cm^{-2} may be inferred. Hence, the oxidation is a mass transport controlled process and not limited by electrode kinetics. Increasing the current density beyond the mass transport limit gives rise to additional oxygen evolution rather than the desired Kolbe process, resulting in loss of efficiency. Decreasing the current density below a critical value of *ca.* 0.1 A cm^{-2} causes the Kolbe process to stop as the anode potential falls below the threshold required for Kolbe electrolysis.

The Kolbe dimer is not produced exclusively: GC–MS and NMR analysis of the electrolytic products permits the identification of the ester, amyl caproate, formed in $< 5\%$ yield. The absence of any pentenes and pentanols is novel and surprising. This is indicative of a trapping of the initial reaction intermediates at the electrode surface; the pentyl carbocation is unlikely to be formed as a free intermediate during electrolysis.

It is widely known that ultrasound damages the surface of platinum electrodes.[1] Recently, boron-doped CVD diamond electrodes have been employed in the presence of ultrasound with negligible damage to the electrode surface.[16] Furthermore, diamond surfaces are chemically inert under hostile conditions and after long-term electrolysis at very positive potentials.[17] The level of boron doping is high, typically *ca.* 10^{20} cm^3, corresponding to a B:C atom ratio of 1:1000, allowing a resistivity of 0.3 mΩ m to be achieved.[18]

Galvanostatic electrosynthesis experiments employing a boron-doped CVD diamond anode were conducted at different current densities, and the products analysed as before. The products observed in conventional Kolbe electrolyses suggest that the electrode material exerts a strong control, with products predominantly derived from carbocation intermediates detected at carbon anodes.[14] Surprisingly, electrosynthesis at a boron-doped CVD diamond anode under sono-emulsion conditions again gives rise to the detection of predominately the Kolbe dimer (see Table 1). Current efficiencies and yields are only slightly lower than those observed at platinum electrodes. Interestingly, the ester, amyl caproate is again the sole by-product, suggesting that a mechanism similar to that at platinum electrodes is operative.

In summary, Kolbe electrolysis has been accomplished under the novel conditions of an emulsion generated *in situ* by power ultrasound. This method of electrosynthesis renders good yields of product and is highly charge efficient. For the first time in 150 years,[19] the electrode material used and conditions employed are observed to have only little effect upon the type of products formed. Although the mechanism of the reaction is unclear, it may involve encapsulation of intermediates within the organic component of the emulsion. This type of electrosynthetic methodology shows promise for wider application.

We thank the Royal Society for financial support through a University Research Fellowship (F. M.), and DeBeers Industrial Diamond Division, UK and the EPSRC (GR/N 12051) for supporting this work.

Notes and references

§ The ultrasound generator employed was a VCX400 model immersion horn (Sonics and Materials, USA) equipped with a 3 mm diameter stepped titanium-alloy tip (electrically insulated) emitting 20 kHz sound with power level set to 190 W cm^{-2} (calorimetrically determined). The horn-to-electrode distance was maintained at 7 mm. Galvanostatic electrosynthesis was undertaken in the thermostatted cell (volume *ca.* 20 cm^3) using a PAR 173 (EG&G) galvanostat fitted with a PAR 178 (EG&G) digital coulometer. The cathode employed was a coil of platinum wire; the anode was either a 12 mm diameter platinum disc (Aldrich) or a 5 $\times$ 5 mm free-standing polycrystalline boron-doped CVD diamond plate (DeBeers Industrial Diamond Division, UK). Chemical reagents and NaOH (Aldrich) were of the highest commercially available purity.

1 For a review see F. Marken, J. C. Eklund and R. G. Compton, *Electroanalysis*, 1997, **7**, 509.
2 F. Marken, R. G. Compton, S. D. Bull and S. G. Davies, *Chem. Commun.*, 1997, 955.
3 F. Marken and R. G. Compton, *Electrochim. Acta*, 1998, **43**, 2157.
4 O. Behrend, K. Ax and H. Schubert, *Ultrason. Sonochem.*, 2000, **7**, 77.
5 H. Fees and H. Wednt, in *Techniques of Electroorganic Chemistry Part III*, ed. N. L. Weinberg, Wiley, New York, 1981, p. 81.
6 J. F. Rusling and D. L. Zhou, *J. Electroanal. Chem.*, 1997, **439**, 89.
7 R. P. Akkermans, S. L. Roberts and R. G. Compton, *Chem. Commun.*, 1999, 1115.
8 H. Fujiwara, M. Atobe, H. Kanetsuna and T. Nonaka, *J. Chin. Chem. Soc.*, 1998, **45**, 175.
9 M. Tashiro, H. Tsuzuki, H. Goto and S. Makata, *Chem. Exp.*, 1991, **4**, 41.
10 D. J. Walton, S. S. Phull, U. Geissler, A. Chyla, A. Durham, S. Ryley, T. J. Mason and J. P. Lorimer, *Electrochem. Commun.*, 2000, **2**, 431.
11 A. Chyla, J. P. Lorimer, T. J. Mason, G. Smith and D. J. Walton, *J. Chem. Soc., Chem. Commun.*, 1989, 603.
12 D. J. Walton, A. Chyla, J. P. Lorimer and T. J. Mason, *Synth. Commun.*, 1990, 1843.
13 A. N. Blythe, R. P. Akkermans and R. G. Compton, *Electroanalysis*, 2000, **12**, 16.
14 C. J. Brockman, *Electroorganic Chemistry*, Wiley, New York, 1926.
15 C. R. Wilke and P. Chang, *AIChE J.*, 1955, **1**, 264.
16 C. H. Goeting, J. S. Foord, F. Marken and R. G. Compton, *Diamond Rel. Mater.*, 1999, **8**, 824.
17 P. A. Michaud, E. Mahe, W. Haenni, A. Perret and C. Comninellius, *Electrochem. Solid State Lett.*, 2000, **3**, 77.
18 R. G. Compton, F. Marken, C. H. Goeting, R. A. J. McKeown, J. S. Foord, G. Scarsbrook, R. S. Sussmann and A. J. Whitehead, *Chem. Commun.*, 1998, 1961.
19 H. Kolbe, *Ann. Chim.*, 1849, **69**, 257.

ChemComm

Solvothermal synthesis of $[Cr_{10}(\mu\text{-}O_2CMe)_{10}(\mu\text{-}OR)_{20}]$ 'chromic wheels' with antiferromagnetic (R = Et) and ferromagnetic (R = Me) Cr(III)··Cr(III) interactions

Eric J. L. McInnes,*†[a] Christopher Anson,‡[a] Annie K. Powell,‡[a] Andrew J. Thomson,[a] Sandrine Poussereau[b] and Roberta Sessoli[b]

[a] *School of Chemical Sciences, University of East Anglia, Norwich, UK NR4 7TJ*
[b] *Universita degli Studi di Firenze, Dipartimento di Chimica, Via Maragliano 75/77, 50144 Firenze, Italy*

Received (in Cambridge, UK) 25th September 2000, Accepted 20th November 2000
First published as an Advance Article on the web

Two decanuclear cyclic Cr(III) complexes have been synthesised in high yield by solvothermal techniques: magnetic susceptibility studies reveal ferromagnetic Cr···Cr exchange in one, and antiferromagnetic Cr···Cr exchange in the other.

The synthesis and magnetic characterisation of molecules with large numbers of unpaired electrons have attracted intense study since the discovery that molecular aggregates stabilising high ground spin states can display the phenomenon of single-molecule magnetism.[1] Cyclic complexes are of particular interest as models of infinite one-dimensional chain compounds and in the study of quantum-size effects,[2,3] and are known for several first row d-transition ions.[4] Among these, Fe(III) rings have received most attention[5] and can generally be made under ambient conditions. By contrast, few cyclic chromium complexes have been reported,[6] and require much harsher synthetic conditions owing to the kinetic inertness of Cr(III).[7]

Solvothermal techniques allow high reaction temperatures in low boiling solvents, whilst maintaining the advantages of solution chemistry (*e.g.* crystallisation of products). However, there are few reports of solvothermal syntheses of molecular clusters.[8] We report here the solvothermal synthesis of $[Cr_{10}(\mu\text{-}O_2CMe)_{10}(\mu\text{-}OR)_{20}]$ (R = Me **1**, Et **2**) in high yield. These are the highest nuclearity *cyclic* clusters yet reported for Cr(III), and **1** displays the rarely observed phenomenon of ferromagnetic Cr(III)··Cr(III) exchange.

Heating trinuclear basic chromium acetate, $[Cr_3(\mu_3\text{-}O)(\mu\text{-}O_2CMe)_6(H_2O)_3]Cl{\cdot}6H_2O$ (100 mg), in MeOH or EtOH (10 ml) in a Teflon-lined autoclave at 200 °C for 1 d followed by slow (0.1 °C min^{-1}) cooling to room temperature over *ca.* 2 d yields large, dark-green crystals of **1** or **2**, respectively (60–70%). Single-crystal X-ray diffraction analyses[9] reveal cyclic decanuclear structures (Fig. 1), similar to the 'molecular ferric wheels' reported by the groups of Lippard[5a] and Winpenny.[5b] The Cr_{10} rings are close to planar, with each pair of neighbouring Cr(III) ions bridged by one μ-acetate and two μ-alkoxide groups. In both compounds the rings are closely aligned perpendicular to the crystal {1 0 −1} plane. In **1**, the Cr_{10} rings in any given layer adopt a staggered configuration relative to those in adjacent layers (Fig. 2), while in **2** they are more closely 'eclipsed'.

The magnetic behaviour of **2** is relatively straightforward: χT *vs.* T decreases slowly from 300 to 120 K and then more quickly to 2 K (Fig. 3). This is indicative of weak, intra-ring antiferromagnetic exchange between Cr(III) ions. The best simulation[10] is obtained with J = +0.9 cm^{-1} (Fig. 3). Introduction of inter-cluster or zero-field splitting (ZFS) effects do not improve the simulation. Corroboration of this number comes from fitting $1/\chi$ *vs.* T (linear to low temperature, data not shown) to the Curie–Weiss law, giving a Curie constant of C = 18.8 $cm^3\ mol^{-1}$ K and a small Weiss constant of Θ = −3.4 K. The Cr··Cr exchange can then be calculated from Θ,[6b] giving J = +0.94 cm^{-1}.

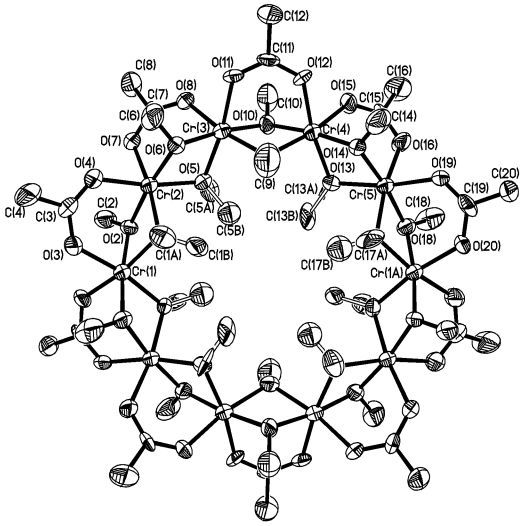

Fig. 1 Molecular structure (50% thermal ellipsoids) of $[Cr_{10}(O_2CMe)_{10}(OMe)_{20}]$ **1**. Bond length ranges: Cr–O(Me) 1.935(7)–1.985(8) Å, Cr–O(acetate) 1.969(8)–2.005(7) Å. Cr··Cr distances: 2.985(3)–2.994(3) Å. Bond angle ranges: Cr–O(Me)–Cr 98.0(3)–100.3(4)°. The analogous ranges for **2** are: Cr–O(Et) 1.951(6)–1.980(6) Å, Cr–O(acetate) 1.981(7)–1.998(7) Å, Cr··Cr 2.992(2)–2.997(2) Å, Cr–O(Et)-Cr 98.5(3)–100.1(3)°.

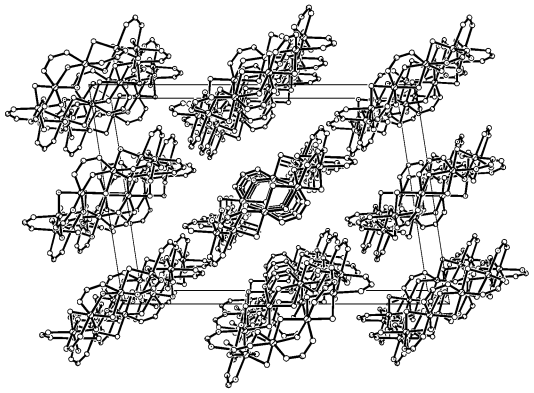

Fig. 2 Packing diagram of **1** viewed down the crystallographic *b* axis. All Me groups have been omitted for clarity.

The magnetic behaviour of **1** is more complicated. χT *vs.* T *increases* from 18.3 to 20.0 $cm^3\ mol^{-1}$ K between 300 and 22 K, indicating the presence of *ferro*magnetic interactions, before decreasing down to 2 K (Fig. 4). The high-temperature data (above 50 K) can be fitted to the Curie–Weiss law with C = 18.2 $cm^3\ mol^{-1}$ K and Θ = +4.1 K. The decrease of χT below

† Present address: Chemistry Department, The University of Manchester, Oxford Road, Manchester, UK M13 9PL. E-mail: eric.mcinnes@man.ac.uk
‡ Present address: Institüt fur Anorganische Chemie, Universitat Karlsruhe, Engesserstrasse Geb 30.45, 76128 Karlsruhe, Germany.

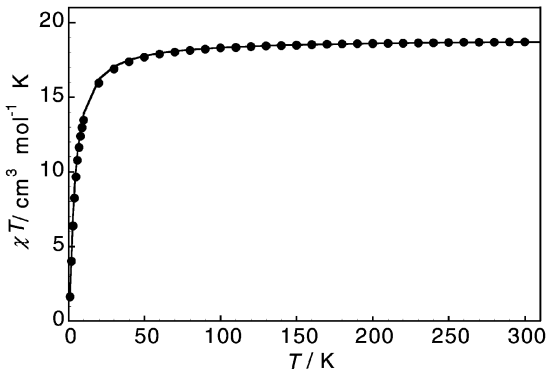

Fig. 3 χT *vs.* T for **2** (●) and best fit with $J = +0.9$ cm^{-1} (——).

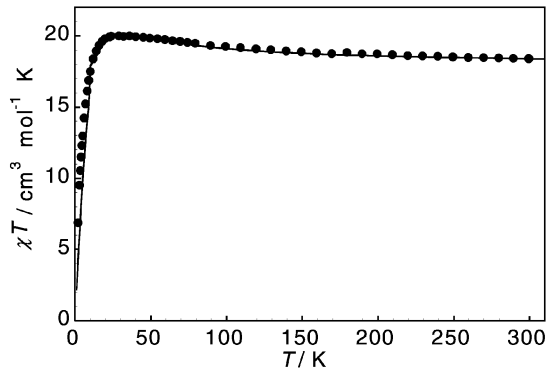

Fig. 4 χT *vs.* T for **1** (●) and best fit with $J = -4.5$ cm^{-1} and $J_{inter} = +0.26$ cm^{-1} (——).

20 K is indicative of an antiferromagnetic contribution to χT. The χT *vs.* T curve can be modelled with a ferromagnetic *intra*-molecular exchange between neighbouring Cr(III) ions of $J = -4.5$ cm^{-1} and a weak antiferromagnetic *inter*-molecular exchange of $J_{inter} = +0.26$ cm^{-1} (see Fig. 4). It is worth noting that it is the ferromagnetic nature of the *intra*-ring coupling in **2** that allows detection of an antiferromagnetic *inter*-ring interaction at temperatures below 20 K: a similar inter-ring coupling in **1** would be barely detectable. The ferromagnetic interaction is predominant as evidenced by the initial increase in χT down to 20 K. The decrease of χT below 20 K could not be modelled by inclusion of ZFS effects, or by having ferromagnetic exchange in one of the two independent molecules of **1** and antiferromagnetic exchange in the other.

The magnetic behaviour of **2** (antiferromagnetic intra-ring exchange, resulting in a non-magnetic $S = 0$ ground state) is common for cyclic complexes. However, $J = +0.9$ cm^{-1} is very weak compared to other cyclic Cr(III) complexes (typically +6 to +10 cm^{-1}).[6] The ferromagnetic interactions observed in **1** are highly unusual: there are very few previous examples of ferromagnetic Cr(III)··Cr(III) exchange in molecular systems[11] and, furthermore, only two previous examples of *ferro*magnetically coupled cyclic complexes of any metal ion.[12]

The so-called GHP model[13] correlates the exchange constant in 'planar' {$Cr_2(\mu\text{-}OR)_2$} dimers with (i) Cr–O(R)–Cr bridging angle (ϕ), (ii) Cr–O(R) bond length (r) and (iii) dihedral angle between the bridging plane and the O–R vector (θ). Our systems are complicated by the non-planarity of the {$Cr_2(\mu\text{-}OR)_2$} bridges imposed by the μ-O_2CMe groups: these bridges are also likely involved in the exchange pathways. However, we note that both **1** and **2** have an average $\phi \approx 99°$ and in the GHP model are in the 'crossover' region between (weak) antiferromagnetic and ferromagnetic coupling regimes. This is consistent with the observed small values of $|J| \approx 0.9$–5 cm^{-1}. Furthermore, the smaller average θ values observed in **2** than in **1** are consistent with the more antiferromagnetic exchange in the former: this effect has been observed previously in ethoxide *vs.* methoxide bridged Cr(III) dimers.[14] Thus, we attribute the differing magnetic behaviour of **1** and **2** to a combination of the above effects.

We thank the EPSRC and Italian MURST for financial support. This work was also supported by 3MD EU network contact no. ERB 4061 PL 97-0197.

Notes and references

1 J. Yoo, E. K. Brechin, A. Yamaguchi, M. Nakano, J. C. Huffman, A. L. Maniero, L. C. Brunel, K. Awaga, H. Ishimoto, G. Christou and D. N. Hendrickson, *Inorg. Chem.*, 2000, **39**, 3615, and references therein.

2 A. Caneschi, D. Gatteschi, C. Sangregorio, R. Sessoli, L. Sorace, A. Cornia, M. A. Novak, C. Paulsen and W. Wernsdorfer, *J. Magn. Magn. Mater.*, 1999, **200**, 182.

3 D. Gatteschi, R. Sessoli and A. Cornia, *Chem. Commun.*, 2000, 725.

4 R. E. P. Winpenny, *Comments Inorg. Chem.*, 1999, **20** A, 233.

5 (*a*) K. L. Taft, C. D. Delfs, G. C. Papaefthymiou, S. Foner, D. Gatteschi and S. J. Lippard, *J. Am. Chem. Soc.*, 1994, **116**, 823; (*b*) C. Benelli, S. Parsons, G. A. Solan and R. E. P. Winpenny, *Angew. Chem., Int. Ed. Engl.*, 1996, **35**, 1825.

6 (*a*) I. M. Atkinson, C. Benelli, M. Murrie, S. Parsons and R. E. P. Winpenny, *Chem. Commun.*, 1999, 285; (*b*) M. Eshel, A. Bino, I. Felner, D. C. Johnston, M. Luban and L. L. Miller, *Inorg. Chem.*, 2000, **39**, 1376; (*c*) N. V. Gerbeleu, Y. T. Struchkov, G. A. Timco, A. S. Batsanov, K. M. Indrichan and G. A. Popovich, *Dokl. Akad. Nauk. SSSR*, 1990, **313**, 1459.

7 F. E. Mabbs, E. J. L. McInnes, M. Murrie, S. Parsons and R. E. P. Winpenny, *Chem. Commun.*, 1999, 643; S. Parsons, A. A. Smith and R. E. P. Winpenny, *Chem. Commun.*, 2000, 579.

8 S. O. H. Gutschke, D. J. Price, A. K. Powell and P. T. Wood, *Angew. Chem., Int. Ed. Engl.*, 1999, **38**, 1088.

9 *Crystal data:* for **1**: $C_{40}H_{90}O_{40}Cr_{10}$, $M = 1731.12$, monoclinic, space group $P2_1/n$, $a = 17.663(5)$, $b = 15.968(4)$, $c = 26.142(4)$ Å, $\beta = 98.89(3)°$, $U = 7285(3)$ Å^3, $T = 293$ K, $Z = 4$ (two half molecules in the asymmetric unit), μ(Mo-Kα) = 1.52 mm^{-1}, 12837 reflections collected, 10960 unique ($R_{int} = 0.0712$), final wR_2 (all data) = 0.1918, R_1 [$I > 2\sigma(I)$] = 0.0887. For **2**: $C_{60}H_{130}O_{40}Cr_{10}$, $M = 2011.64$, monoclinic, space group $P2_1/n$, $a = 9.446(2)$, $b = 16.052(3)$, $c = 28.659(4)$ Å, $\beta = 91.037(14)°$, $U = 4344.8(14)$ Å^3, $T = 293$ K, $Z = 2$, μ(Mo-Kα) = 1.28 mm^{-1}, 9844 reflections collected, 7645 unique ($R_{int} = 0.0552$), wR_2 (all data) = 0.2634, R_1 [$I > 2\sigma(I)$] = 0.0820. Data collected on a Siemens P4 diffractometer to $2\theta = 50°$ and corrected for Lorentz, polarisation and absorption effects. Structures were solved by direct methods and refined by full-matrix least squares on F^2 (all data) (SHELXTL). Eight of the 20 (O)Me groups in **1** showed two-fold disorder, while many of the (O)Et groups in **2** were highly disordered. Non-hydrogen atoms were refined anisotropically, except for carbon atoms of minor disorder components; hydrogen atoms were placed in calculated positions. CCDC 182/1858. See http://www.rsc.org/suppdata/cc/b0/b007773i/ for crystallographic files in .cif format.

10 Magnetic susceptibilities for **1** and **2** were measured on a SQUID magnetometer in the temperature ranges 2–60 and 2–300 K in applied fields of 0.1 and 1 T, respectively, and diamagnetic corrections applied. Corrected χT values for **1** and **2** at 300 K were 18.3 and 18.7 cm^3 mol^{-1} K, respectively. The expected value for 10 Cr(III), $S = 3/2$ ions is 18.4 cm^3 mol^{-1} K. In order to calculate χT for 10 interacting $S = 3/2$ ions we must diagonalise the Heisenberg spin-Hamiltonian matrices ($H = \sum J_{ij} S_i S_j$) for the 116304 spin states of the cluster: the largest matrix (19425 × 19425) is beyond our present computational capabilities. Therefore, we have extrapolated the results from calculations on 6 and 8 interacting $S = 3/2$ ions. An average g-value of 1.98 was assumed for all simulations. Here, a *positive* J value implies an *anti*ferromagnetic interaction.

11 For example, R. P. Scaringe, W. E. Hatfield and D. J. Hodgson, *Inorg. Chem.*, 1977, **16**, 1600; A. Bino, D. C. Johnston, D. P. Goshorn, T. R. Halbert and E. I. Stiefel, *Science*, 1988, **241**, 1479.

12 A. J. Blake, C. M. Grant, S. Parsons, J.M. Rawson and R. E. P. Winpenny, *J. Chem. Soc., Chem. Commun.*, 1994, 2363; E. Rentschler, D. Gatteschi, A. Cornia, A. C. Fabretti, A-L. Barra, O. I. Schegolikhina and A. A. Zhdanov, *Inorg. Chem.*, 1996, **35**, 4427.

13 J. Glerup, D. J. Hodgson and E. Pederson, *Acta. Chem. Scand. Ser. A*, 1983, **37**, 161.

14 H. R. Fischer, D. J. Hodgson and E. Pedersen, *Inorg. Chem.*, 1984, **23**, 4755.

ChemComm

Porphyrins acting as external and internal ligands: preparation of conjugated trimetallic dimeric porphyrins

Sébastien Richeter, Christophe Jeandon, Romain Ruppert* and Henry J. Callot*

Faculté de Chimie, 1 rue Blaise Pascal, 67008 Strasbourg, France. E-mail: callot@chimie.u-strasbg.fr

Received (in Cambridge, UK) 30th October 2000, Accepted 20th November 2000
First published as an Advance Article on the web

A porphyrin bearing a peripheral enaminoketone function allows the preparation of conjugated dimeric porphyrins linked through metal ions.

Multiporphyrin assemblies are involved in several biological processes such as photosynthesis or electron transfer. Mimicking those assemblies and their activity has been a challenge for chemists and numerous examples of multiporphyrin compounds have been described in recent years.[1–22] The connection between porphyrin nuclei may involve C–C bonds, hydrogen bonds, direct metal–metal or μ-X bonds, catenation of porphyrin *ansa*-derivatives, coordination of appropriate peripheral substituents to metal centers, *etc.* More recently, after the molecular wires described earlier by Crossley and Burn,[8] several groups are pursuing efforts to obtain conjugated oligoporphyrinic molecules directly linked through one, two or even three covalent bonds.[10–13] This covalent approach suffers some drawbacks: synthetic and separation problems, iterative reactions to obtain larger molecules, variations of the linking bonds limited to C–C or C–N.

The use of coordination bonds[15–21] has the advantage of offering an additional choice: each metal center may present its own geometry and coordination number depending on the element and its oxidation level, in addition to the variations due to the nature of the internal coordination sites of the porphyrins.

Here we describe a substituted porphyrin acting both as an internal (with the four pyrrole nitrogens) and as an external (with an enaminoketone moiety) ligand. The external coordination site is coplanar and fully conjugated to the porphyrin aromatic system.[22] In contrast to most systems assembled with metal ions, where little or no interaction is observed in the ground state between the porphyrins, the porphyrin–porphyrin conjugation in our dimers linked by metal ions will be illustrated by their electronic spectra and electrochemical behaviour.

meso-Tetraarylporphyrins bearing a keto group located on an additional ring attached to an aryl substituent and a pyrrolic β-carbon have been known since 1980 but their reactivity has been little investigated.[23–26] In the course of a search for extended

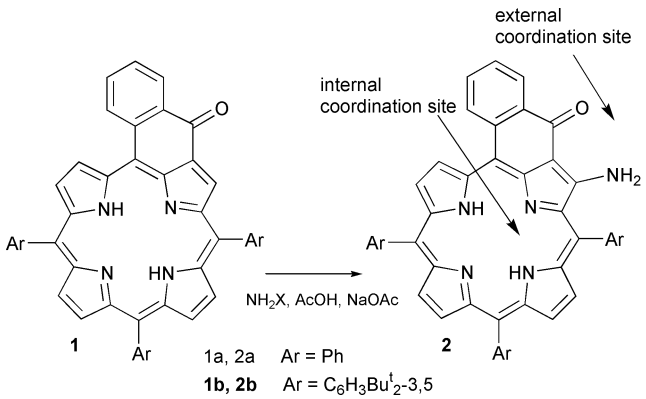

porphyrin chromophores we reacted ketone **1** with nitrogen nucleophiles. Under mild acid catalysis, reagents of the general composition $H_2N–X$ (X = OH, NHTs, OSO_3H) gave in variable yield enaminoketone **2**, the highest yield (90%) being observed with hydroxylamine *O*-sulfonic acid–AcOH–NaOAc in refluxing CH_2Cl_2. Enaminoketone **2a** showed a UV–VIS similar to the starting material (λ_{max} = 451, 568, 614 and 709 nm). The β-N–H NMR signals could be detected at δ 9.0 (N–H involved in a hydrogen bond with the carbonyl group) and δ 5.48 (free N–H, shielded by a vicinal phenyl ring).

Enaminoketone **2** presents remarkable coordinating properties: in addition to the internal 4N tetradentate macrocyclic coordination site, the enaminoketone group is a potential N+O chelating external site (an analog of the acetylacetonate ligand) that might couple porphyrins to form homo- or heteropolymetallic complexes. One would predict that the coordination at the enaminoketone site should be favoured over the introduction of metal ions in the core of the porphyrin, but one also expects the stability of the internal complex to be of orders of magnitude higher for the same metal ion; in particular with first row transition metals the porphyrin–metal–porphyrin connection is expected to be of low stability. Accordingly, heterometallation may be performed along two routes by using as an intermediate either an internal complex or the porphyrin base dimer (Scheme 1).

Metallation of **2a** (R = Ph) with nickel acetylacetonate (one or more equiv.) rapidly gave a highly insoluble product containing one metal and two porphyrins formulated as **3a** (M^1 = Ni; M^2 = M^3 = H_2). Treatment with acetic acid, which is unable to remove nickel from the 4N site of a porphyrin, quantitatively regenerated the starting material. However, on prolonged reaction in refluxing toluene with a 1:1 porphyrin/nickel ratio, metallation of the porphyrin occurred and gave mononuclear **Ni**–**2a**, while excess reagent gave trinuclear **3a** (M^1 = M^2 = M^3 = Ni). The formation of **Ni**–**2a** is best explained by the low stability of the nickel bridge—it did not survive chromatographic conditions—and the slow formation of the most stable metallation product. The same trinuclear compound **3a** (M^1 = M^2 = M^3 = Ni) was formed when **Ni**–**2a** was treated with an excess of nickel acetylacetonate. Similarly, several trimetallic bisporphyrins were prepared (Ni/Cu/Ni; Ni/V=O/Ni; Ni/Pd/Ni).

There remained the question of the relative arrangement of the porphyrins around the metal, since the dimers may have a center or a plane of symmetry. COSY and NOESY experiments

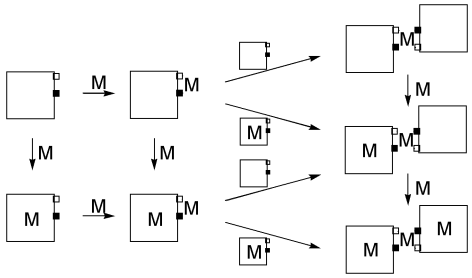

Scheme 1 Metallation of enaminoketone **2** (squares): vertical arrows = metallation of internal site of porphyrin, slow and irreversible under the reaction conditions; horizontal arrows = metallation of external site (fast and possibly reversible reactions).

DOI: 10.1039/b008740h

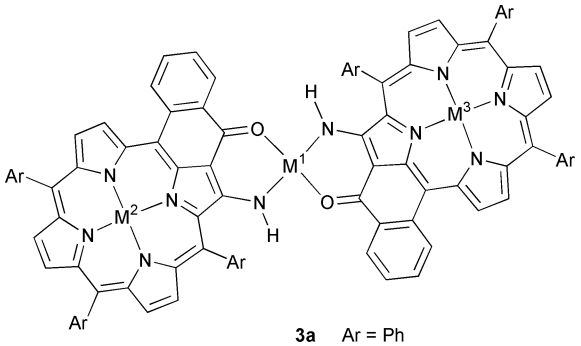

3a Ar = Ph
3b Ar = $C_6H_3Bu^t_2$-3,5

confirmed the structure and the dimeric nature of **3**. Additional information was obtained when we turned to the more soluble *meso*-tri(3,5-di-*tert*-butyl)phenylporphyrin series. Heating equimolecular amounts of palladium(II) acetate and enaminoketone **2b** in refluxing toluene for 3 h led almost exclusively to **3b** (M^1 = Pd; M^2 = M^3 = H_2). Again, NMR experiments (ROESY) confirmed the relative position of the porphyrins: HH ROESY cross signals were observed between two protons of the cyclised phenyl ring and the *para* proton and the *tert*-butyl protons of a *meso*-aryl group belonging to the other porphyrin. This compound survived chromatographic purification and is a good starting material for heterometallic dimer preparation. Indeed, metallation with zinc acetate gave the mono- and bis-metallated **3b** (M^1 = Pd; M^2 = Zn; M^3 = H_2 or Zn).

These new porphyrin dimers all showed similar electronic spectra and an electrochemical behaviour indicative of the conjugation introduced through the connecting metal between the two aromatic rings. For example, the lowest energy band of **3a** ($M^{1–3}$ = Ni) shifts to 700 nm (ε = 33000 dm^3 mol^{-1} cm^{-1}) in comparison to the band observed at 649 nm (ε = 18500 dm^3 mol^{-1} cm^{-1}) for **Ni**–**2a** (Fig. 1). The HOMO–LUMO gap estimated from these data is reduced to 1.77 eV in the dimer **3a** ($M^{1–3}$ = Ni) compared to 1.91 eV for the monomer **Ni**–**2a** (already a very low value compared to the gap reported for nickel porphyrins, $E \approx 2.3$ eV). The corresponding bases such as **3b** (M^1 = Pd; M^2 = M^3 = H_2) display bands at even longer wavelengths (730 nm, ε = 39000 dm^3 mol^{-1} cm^{-1}), which can be compared with that of **2b** (711 nm, ε = 8500 dm^3 mol^{-1} cm^{-1}).

The monomer **Ni**–**2a** showed two one-electron oxidations at 0.46 and 0.83 V *vs.* Fc/Fc$^+$. In trimetallic **3a** ($M^{1–3}$ = Ni), the first oxidation is split into two one-electron oxidation waves (one electron per porphyrin) at 0.32 and 0.50 V, indicative of a strong interaction between the two porphyrins. The removal of the first electron therefore occurs at a potential 0.14 V lower than for the monomer (a value equal to the difference between the gaps taken from the electronic spectra). A two-electron oxidation (or rather twice a one-electron oxidation of each porphyrin ring) is further observed at 0.68 V. It seems that the

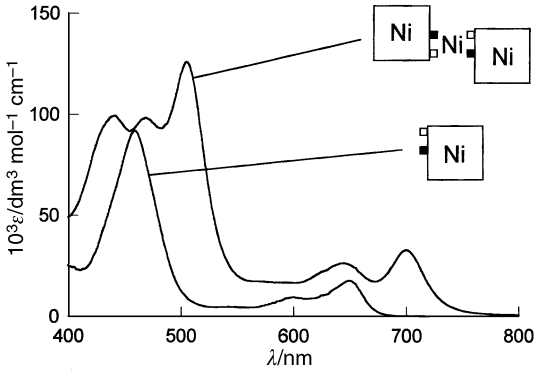

Fig. 1 UV–VIS spectrum of **3a** ($M^{1–3}$ = Ni) and **Ni**–**2a**.

removal of the first two electrons from the dimer has led to a disruption of the conjugation between the two rings. The dimer (already oxidised by two electrons) now behaves like two independant nickel monomers. All waves are quasi-reversible (ΔE_p = 60–90 mV), showing that dimer **3a** ($M^{1–3}$ = Ni) remains intact during this overall four-electron oxidation–reduction process.

In conclusion, we confirmed that efficient porphyrin–porphyrin interaction could be achieved *via* metal coordination. The synthesis of bis-enaminoketoporphyrins where two external coordination sites are located in divergent directions is in progress. These compounds should allow the preparation of more highly conjugated oligomers.

We thank R. Graff for the NMR experiments.

Notes and references

1 J.-C. Chambron, V. Heitz and J.-P. Sauvage, in *The Porphyrin Handbook*, ed. K. M. Kadish, K. M. Smith and R. Guilard, Academic Press, San Diego, 2000, vol. 6, p. 1; J. K. M. Sanders, vol. 3, p. 347; S. Fukuzumi, vol. 8, p. 115; D. Gust and T. A. Moore, vol. 8, p. 153; J.-M. Barbe and R. Guilard, vol. 3, p. 211; J.-H. Chou, M. E. Kosal, H. S. Nalwa, N. A. Rakow and K. S. Suslick, vol. 6, p. 43.
2 A. Osuka, N. Mataga and T. Okada, *Pure Appl. Chem.*, 1997, **69**, 797.
3 F. Li, S. I. Yang, Y. Ciringh, J. Seth, C. H. Martin III, D. L. Singh, D. Kim, R. R. Birge, D. F. Bocian, D. Holten and J. S. Lindsey, *J. Am. Chem. Soc.*, 1998, **120**, 10 001.
4 A. K. Burrell and D. L. Officer, *Synlett*, 1998, 1297.
5 D. P. Arnold, *Synlett*, 1999, 296.
6 M. G. H. Vicente, L. Jaquinod and K. M. Smith, *Chem. Commun.*, 1999, 1771.
7 H. L. Anderson, *Chem. Commun.*, 1999, 2323.
8 M. J. Crossley and P. L. Burn, *J. Chem. Soc., Chem. Commun.*, 1987, 39; M. J. Crossley and P. L. Burn, *J. Chem. Soc., Chem. Commun.*, 1991, 1569.
9 W. J. Belcher, A. K. Burrell, W. M. Campbell, D. L. Officer, D. C. W. Reid and K. Y. Wild, *Tetrahedron*, 1999, **55**, 2401.
10 L. Jaquinod, O. Siri, R. G. Khoury and K. M. Smith, *Chem. Commun.*, 1998, 1261.
11 R. G. Khoury, L. Jaquinod and K. M. Smith, *Chem. Commun.*, 1997, 1057; N. Aratani, A. Osuka, Y. H. Kim, D. H. Jeong and D. Kim, *Angew. Chem., Int. Ed. Engl.*, 2000, **39**, 1458.
12 A. Tsuda, A. Nakano, H. Furuta, H. Yamochi and A. Osuka, *Angew. Chem., Int. Ed. Engl.*, 2000, **39**, 558; K.-i. Sugiura, T. Matsumoto, S. Ohkouchi, Y. Naitoh, T. Kawai, Y. Takai, K. Ushiroda and Y. Sakata, *Chem. Commun.*, 1999, 1957; I. M. Blake, L. H. Rees, T. D. W. Claridge and H. L. Anderson, *Angew. Chem., Int. Ed. Engl.*, 2000, **39**, 1818.
13 A. Tsuda, H. Furuta and A. Osuka, *Angew. Chem., Int. Ed.*, 2000, **39**, 2549.
14 R. Beavington and P. L. Burn, *J. Chem. Soc., Perkin Trans. 1*, 2000, 605.
15 T. Imamura and K. Fukushima, *Coord. Chem. Rev.*, 2000, **198**, 133.
16 J. Wojaczynski and L. Latos-Grazynski, *Coord. Chem. Rev.*, 2000, **204**, 113.
17 A. Harriman, F. Odobel and J.-P. Sauvage, *J. Am. Chem. Soc.*, 1995, **117**, 9461.
18 M. J. Crossley, P. L. Burn, S. J. Langford and J. K. Prashar, *J. Chem. Soc., Chem. Commun.*, 1995, 1921.
19 T. A. Vannelli and T. B. Karpishin, *Inorg. Chem.*, 1999, **38**, 2246.
20 I. M. Dixon, J.-P. Collin, J.-P. Sauvage, F. Barigelletti and L. Flamigni, *Angew. Chem., Int. Ed.*, 2000, **39**, 1292.
21 Y. Diskin-Posner, S. Dahal and I. Goldberg, *Angew. Chem., Int. Ed.*, 2000, **39**, 1288.
22 A porphyrazine allowing the coordination of metal centers in the macrocyclic plane was recently described: N. Bellec, A. G. Montalban, D. B. G. Williams, A. S. Cook, M. E. Anderson, X. Feng, A. G. M. Barrett and B. M. Hoffman, *J. Org. Chem.*, 2000, **65**, 1774.
23 K. Henrick, P. G. Owston, R. Peters, P. A. Tasker and A. Dell, *Inorg. Chim. Acta*, 1980, **45**, 161.
24 H. J. Callot, E. Schaeffer, R. Cromer and F. Metz, *Tetrahedron*, 1990, **46**, 5253.
25 L. Barloy, D. Dolphin, D. Dupré and T. P. Wijesekera, *J. Org. Chem.*, 1994, **59**, 7976.
26 Y. V. Ishkov and Z. I. Zhilina, *Zh. Org. Khim.*, 1995, **31**, 136.

Molecular structure of and exchange coupling in a bis(semiquinone) complex

David A. Shultz,*[a] Scot H. Bodnar[a] and Jeff W. Kampf[b]

[a] *Department of Chemistry, North Carolina State University, Raleigh, North Carolina 27695-8204, USA. E-mail: David_Shultz@ncsu.edu*

[b] *Department of Chemistry, University of Michigan, Ann Arbor, Michigan 48109-1055, USA. E-mail: jkampf@umich.edu*

Received (in Irvine, CA, USA) 29th September 2000, Accepted 30th October 2000
First published as an Advance Article on the web

The first example of a structurally characterized, rationally designed, triplet ground-state bis(semiquinone) complex is presented; the intramolecular exchange coupling is ferromagnetic with $J = +209$ cm^{-1}.

Molecular structures of organic biradical ligands are important to those concerned with construction of molecule-based magnetic materials using the metal-radical approach,[1,2] and to those with an inherent interest in electronic properties of open-shell organic molecules.[3]

Recently, we reported several semiquinone-type ligands to be used as building blocks for high-spin molecules and open-shell materials.[4,5] Among these new ligands is $S = 1/2$ quinonemethide-semiquinone (QMSQ) present in the complex $(LZn)_2$(**1′**-H), the structure of which has been reported as well as its

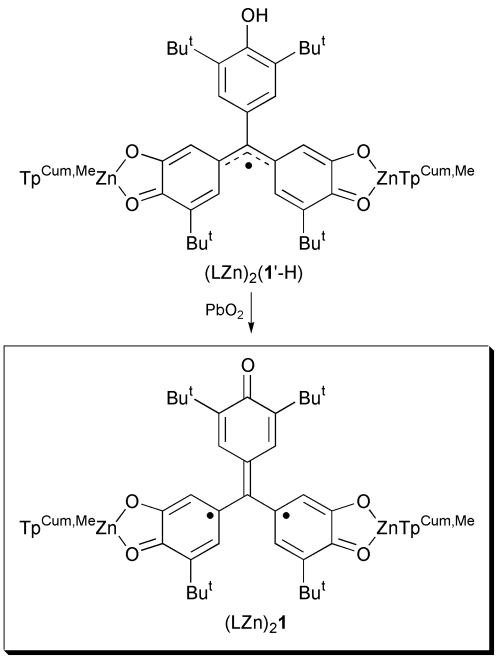

conversion to both a mixed-valent species and to a biradical, $(LZn)_2$**1**, shown below.[5,6] Herein, we report both the molecular structure and magnetic properties of $S = 1$ $(LZn)_2$**1** [Tp^{Cum,Me} = hydrotris(3-cumenyl-5-methylpyrazolyl)borate].

For clarity, we will refer to the mono-oxygenated rings of $(LZn)_2$(**1′**-H) and $(LZn)_2$**1** as A-rings, and the dioxygenated rings as either the dioxolene- or the B-rings. Structural changes that accompany conversion of $(LZn)_2$(**1′**-H) to biradical $(LZn)_2$**1** are consistent with the Lewis structures above.

The crystal structure of biradical $(LZn)_2$**1** shows that the asymmetric unit contains two symmetry-independent molecules that differ primarily in torsion angles of A- and B-rings (and cumenyl ring torsions), and are therefore different conformers that also have an opposite sense of chirality.† An ORTEP of $(LZn)_2$**1** is shown in Fig. 1, where hydrogens and cumenyl groups have been omitted for clarity. Bond lengths, angles, and torsions are summarized in Table 1 and Fig. 2.

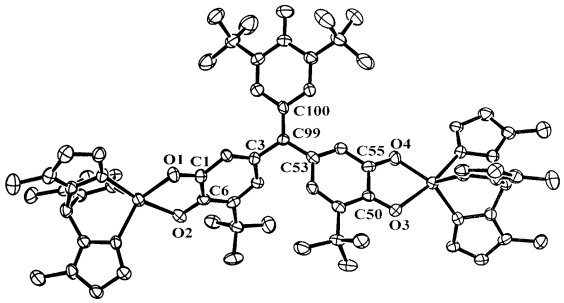

Fig. 1 50% ORTEP of $(LZn)_2$**1**. Hydrogen atoms, cumenyl groups and THF molecules have been omitted for clarity.

Table 1 Average bond lengths and torsion angles for $(LZn)_2$**1**[a,b]

Bond	R_{av}/pm
C1–O1, C55–O4	129.35, 128.35
C6–O2, C50–O3	128.15, 127.15
C1–C6, C50–C55	146.05, 146.55
C3–C99, C53–C99	148.30, 146.95
C99–C100	137.65
Ring	**Average torsion angles**
C1–C6, C50–C55	50.33, 42.68
C100–C105	18.05

[a] Averages for conformers I and II, the two symmetry-independent molecules in the asymmetric unit. [b] Torsion angles are relative to the plane made by atoms C3–C53–C99–C100.

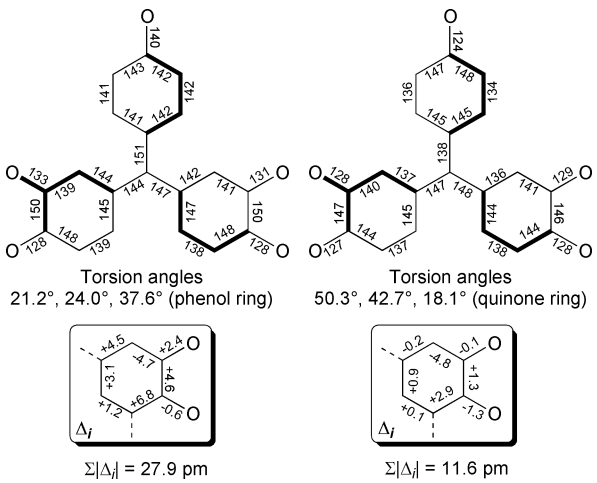

Fig. 2 Comparison of structural features of $(LZn)_2$(**1′**-H) (left) and $(LZn)_2$**1** (right). Averaged bond lengths (in pm) are shown for $(LZn)_2$**1**. See text for details.

DOI: 10.1039/b008037n

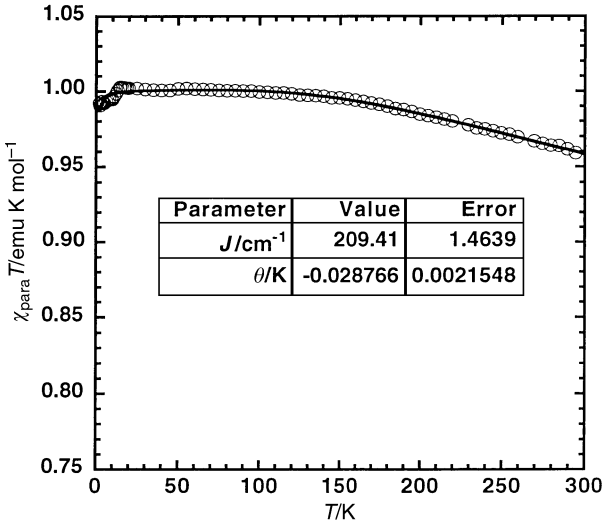

Fig. 3 Temperature dependence of $\chi_{para}T$ for biradical $(LZn)_2$**1**.

The A-ring C–O bond of $(LZn)_2$**1** (*ca.* 124 pm) is substantially shorter than the A-ring C–O single bond of $(LZn)_2$(**1′**-H) (140 pm),[5] consistent with carbonyl character for the former. In fact, as seen in Table 1 and Fig. 2, the pattern of long and short bond lengths for the A-ring in $(LZn)_2$**1** confirms its quinoidal character.

The A-ring of $(LZn)_2$**1** is twisted 18° while the dioxolene rings are twisted *ca.* 46° from the plane made by atoms C3, C53, C99 and C100, allowing conjugation of the dioxolene rings with the A-ring.

Fig. 2 shows bond length deviations ($\Sigma|\Delta_i|$) of the B-rings from a 3,5-di-*tert*-butylorthosemiquinone ring.[7,8] As we pointed out previously, the dioxolene rings of $S = 1/2$ $(LZn)_2$(**1′**-H) are quite different from those of a semiquinone ($\Sigma|\Delta_i| = 27.9$ pm) due to the QMSQ bond formulation.[5] However, $\Sigma|\Delta_i| = 11.6$ pm for the dioxolene rings of $(LZn)_2$**1** indicating a greater similarity to a semiquinone, but also consistent with some delocalization of spin/charge into the A-ring, since we maintain that $\Sigma|\Delta_i| \neq 0$ is an indication of a delocalized electronic structure.

The magnetic susceptibility of microcrystalline $(LZn)_2$**1** was measured from 2 to 300 K using a SQUID magnetometer, and is plotted as $\chi_{para}T$ *vs.* T in Fig. 3. Modeling the temperature-dependent $\chi_{para}T$ product of $S = 1$ molecules can be achieved by fitting to a modified Bleaney–Bowers expression:[9,10]

$$\chi_{para}T = \frac{2Ng^2\beta^2T}{k(T-\vartheta)\left[3+\exp\left(\frac{-2J}{kT}\right)\right]}$$

where, g is the isotropic Landé constant ($g = 2.0023$), β is the Bohr magneton, T is temperature in Kelvin, k is Boltzmann's constant, ϑ is the Weiss constant representing a weak intermolecular interaction, and $2J$ is the singlet–triplet energy gap ($J > 0$ for triplet ground-state and $J < 0$ for singlet ground-state).

The best fit of the data give $J = +209 \pm 1$ cm^{-1} and $\vartheta \approx -0.03$ K. The very small Weiss constant is consistent with negligible intermolecular interactions due to the large, insulating hydrotrispyrazolylborate ligand, while the moderately large, positive exchange parameter, J, indicates that $(LZn)_2$**1** is a triplet ground-state biradical consistent with its π-connectivity. The symmetry of the bis(semiquinone) ligand of $(LZn)_2$**1** precludes degeneracy of the SOMOs, nonetheless, delocalization of spin into the quinone-methide unit (A-ring) gives rise to a substantial exchange integral, stabilizing the triplet state relative to the singlet state. However, the different spin distribution, lower symmetry, and therefore attenuated delocalization into the A-ring results in a slightly smaller J for $(LZn)_2$**1** than for Yang's biradical ($J \geqslant +245$ cm^{-1}).[11,12]

This work is funded by the National Science Foundation. D. A. S. thanks the Camille and Henry Dreyfus Foundation for a Camille Dreyfus Teacher-Scholar Award, and Professor Frank Tsui (Department of Physics, UNC-CH) for the use of his SQUID magnetometer.

Notes and references

† *Crystal data* for $(LZn)_2$**1**: $C_{126}H_{160}B_2N_{12}O_{8.25}Zn_2$ which includes 3.25 molecules of THF solvate per Zn_2 complex, red crystals, $M = 2127.02$, triclinic, space group $P2_1/n$; $a = 38.110(4)$, $b = 18.827(2)$, $c = 38.448(4)$ Å, $\beta = 118.546(2)°$, $V = 24233(4)$ Å^3, $D_c = 1.166$ g cm^{-3}, $Z = 8$, $T = 158(2)$ K, $R = 0.0730$; $wR2 = 0.2174$, GOF = 1.016.

Measurements were carried out on a standard Siemens SMART CCD-based X-ray diffractometer equipped with a normal focus Mo-target X-ray tube ($\lambda = 0.71073$ Å) operated at 2000 W power (50 kV, 40 mA). The structure was solved and refined with the Brüker SHELXTL (version 5.10) software package (G. M. Sheldrick, Bruker AXS, Madison, WI, 1997). All non-hydrogen atoms were refined anisotropically with the hydrogen atoms placed in idealized positions. Modest restraints were placed on the lattice solvates to retain chemically reasonable geometries. Refinement was carried out using blocked least-squares matrices. $F(000) = 9088$; reflections collected, 184229; no. of unique reflections, 34986; no. of parameters, 2655; $R = 0.0730$; $wR2 = 0.2174$; $(\Delta\rho)_{max} = 1.967$ e Å^{-3}.

CCDC 182/1860. See http://www.rsc.org/suppdata/cc/b0/b008037n/ for crystallographic files in .cif format.

1 A. Caneschi, D. Gatteschi, R. Sessoli and P. Rey, *Acc. Chem. Res.*, 1989, **22**, 392.
2 S. Nakatsuji and H. Anzai, *J. Mater. Chem.*, 1997, **7**, 2161.
3 H. Bock, A. John and Z. Havlas, *Angew. Chem., Int. Ed. Engl.*, 1993, **32**, 416.
4 D. A. Shultz, A. K. Boal and N. P. Campbell, *Inorg. Chem.*, 1998, **37**, 1540.
5 D. A. Shultz, S. H. Bodnar, R. K. Kumar and J. W. Kampf, *J. Am. Chem. Soc.*, 1999, **121**, 10 664.
6 D. A. Shultz and S. H. Bodnar, *Inorg. Chem.*, 1999, **38**, 591.
7 C. G. Pierpont and R. M. Buchanan, *Coord. Chem. Rev.*, 1981, **38**, 45.
8 C. G. Pierpont and C. W. Lange, *Prog. Inorg. Chem.*, 1994, **41**, 331.
9 K. Inoue and H. Iwamura, *Angew. Chem., Int. Ed. Engl.*, 1995, **34**, 927.
10 B. Bleaney and K. D. Bowers, *Proc. R. Soc. London, Sect. A*, 1952, **214**, 451.
11 K. Mukai, K. Ishizu and Y. Deguchi, *J. Phys. Soc. Jpn.*, 1969, **27**, 783.
12 P. W. Kopf and R. W. Kreilick, *J. Am. Chem. Soc.*, 1969, **91**, 6569.

Coordination networks derived from antimony(III) halide complexes with thio- and seleno-ether ligation

Andrew J. Barton, Nicholas J. Hill, William Levason, Bhavesh Patel and Gillian Reid*

Department of Chemistry, University of Southampton, Highfield, Southampton, UK SO17 1BJ. E-mail: gr@soton.ac.uk

Received (in Cambridge, UK) 26th September 2000, Accepted 27th November 2000
First published as an Advance Article on the web

Antimony(III) halides form highly unusual infinite one- or two-dimensional networks when coordinated to dithio- or diseleno-ether ligands or macrocyclic selenoethers. The structures adopted are contrasted with those observed for related bismuth(III) species.

We have been interested for some time in the coordination chemistry of group 16 donor ligands. The vast majority of compounds involving thio-, seleno- or telluro-ether coordination incorporate d-block elements.[1] Also, we have shown that σ-donation towards low valent metal centres increases significantly as group 16 is descended.[2] However, there are relatively few examples of complexes involving p-block elements with these ligands. We have therefore extended our work to investigate the interaction of thio-, seleno- and telluro-ether ligands with p-block metalloids. These elements exhibit very different electronic environments compared to d-block elements and π-bonding effects are unimportant. Specifically in this communication we report the synthesis and structural characterisation of three antimony(III) halide complexes involving group 16 donor ligands, including the first examples containing selenoether ligation. Antimony(III) thioether complexes are rare, the only structurally characterised examples being $[SbCl_3$(1,4-dithiacycloheptane)], $[(SbI_3)_2$(1,4-dithiane)], $[SbX_3([9]aneS_3)]$ (X = Cl or I) and $[(SbCl_3)_2([18]aneS_6)]$ ([18]aneS$_6$ = 1,4,7,10,13,16-hexathiacyclooctadecane).[3]

Reaction of $SbBr_3$ with 1 mol equiv. of the dithioether $MeS(CH_2)_3SMe$ in anhydrous MeCN solution yields a pale yellow solid of empirical formula $[SbBr_3\{MeS(CH_2)_3SMe\}]$.† Crystals were obtained by slow evaporation from a solution of the compound in MeCN. The structure shows (Fig. 1)‡ that this species adopts a two-dimensional sheet array derived from distorted octahedral Sb(III) centres coordinated to three mutually *fac* terminal Br ligands and three S-donor atoms from different dithioether ligands, two of which, S(1) and S(1*), may be regarded as μ-bridging since they also form weak interactions to an adjacent Sb centre. While the Sb–Br distances are normal for primary Sb–Br ligation, the Sb–S distances are *ca.* 3.2 Å, suggesting secondary interactions. The second sulfur in each dithioether coordinates to a nearby, symmetry-related Sb centre to generate the infinite array. The *cis* angles at Sb lie in the range 80.3(1)–104.49(7)° and the angle at the bridging thioether, S(1), is 104.4(7)°. The Sb–S distances reported for known Sb(III) thioether species span a considerable range, *e.g.* in $[SbX_3([9]aneS_3)]$, X = Cl (chain structure with seven-coordinate Sb) has *d*(Sb–S) = 3.156(3)–3.409(3), while X = I (discrete monomer with distorted octahedral Sb and *fac* [9]aneS$_3$) gives *d*(Sb–S) = 2.840(2)–2.895(2) Å, while for $[(SbI_3)_2$(1,4-dithiane)] (infinite chain with five-coordinate Sb} *d*(Sb–S) = 3.274 and 2.336 Å.[3] The Sb–S distances in our complex are comparable with those above.

The selenoether analogue $[SbCl_3\{MeSe(CH_2)_3SeMe\}]$ was obtained similarly,† although this species is rather less stable, turning black over a period a few days even when stored in a N_2 purged dry-box. The structure of this complex (Fig. 2)‡ is markedly different from the thioether analogue above, adopting an infinite one-dimensional chain. The Sb centres exhibit a distorted octahedral coordination environment comprising two *cis* terminal Cl, two μ-Cl and two mutually *cis* Se atoms from different diselenoethers. Thus the chains are derived from weakly associated, asymmetric Sb_2Cl_6 units linked by bridging diselenoether ligands, Sb–Cl(2) 2.451(3), Sb–Cl(2*) 3.236(3) Å. Indeed, the Sb–Cl(2) distance is very similar to the terminal Sb–Cl(1) and Sb–Cl(3) distances, with a weak secondary Sb–Cl(2*) interaction. The Sb–Se distances of *ca.* 3.2 Å are very similar to the Sb–S distances in the dithioether species above, again suggesting rather weak, secondary interactions.

The coordination of Sb(III) to the tetraselenoether macrocycle [16]aneSe$_4$ (1,5,9,13-tetraselenacyclohexadecane) was also probed to investigate the effect of the constrained cyclic ligand,

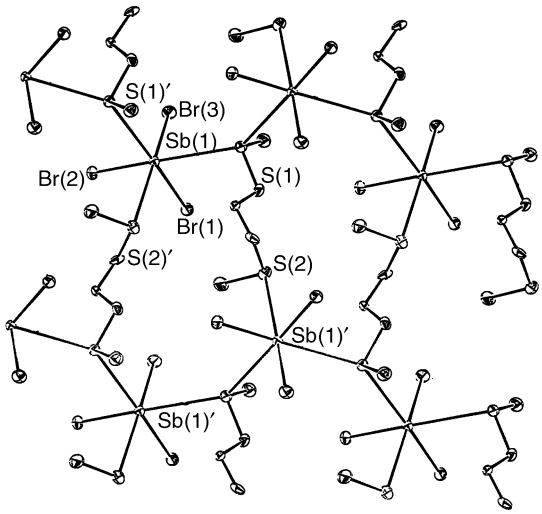

Fig. 1 View of a portion of the two-dimensional structure of $[SbBr_3\{MeS(CH_2)_3SMe\}]$ with the atom numbering scheme. Selected bond lengths (Å): Sb–Br(1) 2.572(2), Sb–Br(2) 2.503(2), Sb–Br(3) 2.575(2), Sb–S(1) 3.253(5), Sb–S(2*) 3.155(5), Sb–S(1*) 3.291(5).

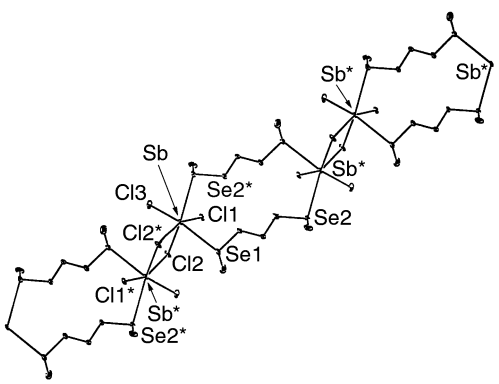

Fig. 2 View of a portion of the one-dimensional structure adopted by $[SbCl_3\{MeSe(CH_2)_3SeMe\}]$ with the atom numbering scheme. Selected bond lengths (Å) and angles (°): Sb–Cl(1) 2.388(3), Sb–Cl(2) 2.451(3), Sb–Cl(3) 2.424(3), Sb–Cl(2*) 3.236(3), Sb–Se(1) 3.204(2), Sb–Se(2) 3.244(2) Å; Cl(2)–Sb–Cl(2*) 76.8(1).

DOI: 10.1039/b007805k

while retaining the trimethylene linkage between the donor atoms. Reaction of $SbBr_3$ with [16]aneSe_4 in MeCN affords a yellow powder of stoichiometry [$(SbBr_3)_2$([16]aneSe_4)].† The crystal structure of this species shows (Fig. 3)‡ a two-dimensional sheet array derived from [16]aneSe_4 molecules coordinated in an exocyclic configuration to four Sb centres each of which bridge to another selenacrown. The geometry at Sb can be described as five-coordinate *via* primary interactions to three *fac* terminal Br and secondary interactions to two *cis* Se atoms from different macrocycles to give a distorted square-pyramidal coordination environment. The Sb–Se distances in [$(SbBr_3)_2$([16]aneSe_4)] are shorter than those in [$SbCl_3${MeSe$(CH_2)_3$SeMe}] above, although this may be due to the lower coordination number at Sb in the former. The weak Sb–Se interactions in these systems are considerably longer than normal Sb–Se bond distances in, for example, [$Sb(SeMe)_3$] which average 2.580 Å.[4]

The main features which these new compounds have in common are the retention of the pyramidal SbX_3 unit observed in the parent antimony trihalide[5] and the occurrence of weak, secondary Sb–S or Sb–Se interactions on the opposite face which leads to the S or Se atoms occupying mutually *cis* coordination sites.

The very low solubilities exhibited by the new compounds, presumably associated with their polymeric nature, has severely hindered attempts to obtain solution NMR spectra, however the IR spectra show features associated with coordinated dithio- or diseleno-ether and ν(Sb–X).

Surprisingly, the structures of the three new antimony species are each quite different from their bismuth(III) analogues. The thioether compound [Bi_4Cl_{12}{MeS$(CH_2)_3$SMe}$_4$]·H_2O forms a three-dimensional open-framework lattice incorporating pseudo-cubane Bi_4Cl_{12} units linked by bridging dithioether ligands, while [$BiBr_3${MeE$(CH_2)_3$EMe}] (E = S or Se) and [$BiCl_3${MeSe$(CH_2)_3$SeMe}] all adopt an infinite two-dimensional sheet array derived from planar Bi_2X_6 units linked by bridging dithio- or diseleno-ether ligands. Finally, [$BiBr_3$([16]aneSe_4)] adopts a one-dimensional ladder structure derived from almost planar Bi_2Br_6 'rungs', which are linked by bridging [16]aneSe_4 'uprights', leaving two mutually *trans* Se atoms within each crown uncoordinated.[6] These differences are unexpected given the subtle change from Bi(III) to Sb(III) and serve to extend further the diverse range of structures identified for thio- and seleno-ether complexes with p-block elements.

We thank the EPSRC for support.

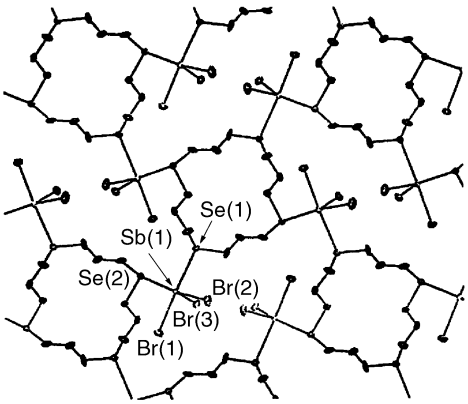

Fig. 3 View of a portion of the two-dimensional sheet adopted by [$(SbBr_3)_2$([16]aneSe_4)] with the atom numbering scheme. Selected bond lengths (Å) and angles (°) Sb–Br(1) 2.687(1), Sb–Br(2) 2.537(1), Sb–Br(3) 2.601(1), Sb–Se(1) 2.989(1), Sb–Se(2*) 3.193(1) Å; Se(1)–Sb–Se(2*) 82.55(3).

Notes and references

† Satisfactory elemental analyses and IR spectroscopic data were obtained for the new compounds.

‡ Colourless {or yellow: [$(SbBr_3)_2$([16]aneSe_4)]} crystals were obtained by slow evaporation from a solution of the appropriate compound in MeCN. X-Ray crystallographic data were collected on a Rigaku AFC7S four-circle diffractometer, T = 150 K. Structure solution and refinement were routine.[7–10]

Crystal data: for [$SbBr_3${MeS$(CH_2)_3$SMe}]: $C_5H_{12}Br_3S_2Sb$, M = 497.73, orthorhombic, space group $Pna2_1$, a = 14.105(2), b = 9.446(1), c = 9.781(1) Å, V = 1303.2(3) Å^3, Z = 4, D_c = 2.537 g cm^{-3}, μ(Mo-Kα) = 116.11 cm^{-1}. 1364 unique reflections of which 1022 with $F > 4\sigma(F)$ were used in all calculations. Final R = 0.041, R_w = 0.049.

For [$SbCl_3${MeSe$(CH_2)_3$SeMe}]: $C_5H_{12}Cl_3SbSe_2$, M = 458.18, monoclinic, space group $P2_1/c$, a = 9.622(5), b = 12.882(3), c = 10.376(4) Å, β = 101.89(4)°, V = 1258.5(8) Å^3, Z = 4, D_c = 2.418 g cm^{-3}, μ(Mo-Kα) = 85.59 cm^{-1}. 2344 unique reflections of which 1934 with $F > 4\sigma(F)$ were used in all calculations. Final R = 0.041, R_w = 0.053.

For [$(SbBr_3)_2$([16]aneSe_4)]: $C_{12}H_{24}Br_6Sb_2Se_4$, M = 1207.08, monoclinic, space group $P2_1/n$, a = 10.276(2), b = 13.340(3), c = 10.755(2) Å, β = 113.71(1)°, V = 1370.1(4) Å^3, Z = 2, D_c = 2.926 g cm^{-3}, μ(Mo-Kα) = 160.58 cm^{-1}. 2536 unique reflections of which 1724 with $F > 4\sigma(F)$ were used in all calculations. Final R = 0.035, R_w = 0.039.

CCDC 182/1865. See http://www.rsc.org/suppdata/cc/b0/b007805k/ for crystallographic files in .cif format..

1 E. G. Hope and W. Levason, *Coord. Chem. Rev.*, 1993, **122**, 109.
2 W. Levason, S. D. Orchard and G. Reid, *Organometallics*, 1999, **18**, 1275.
3 V. M. Schmidt, R. Bender and C. Burschka, *Z. Anorg. Allg. Chem.*, 1979, **454**, 160; T. Bjorvatten, *Acta Chem. Scand.*, 1966, **20**, 1863; G. R. Willey, M. T. Lakin, M. Ravindran and N. W. Alcock., *J. Chem. Soc., Chem. Commun.*, 1991, 271; S. Pohl, D. Haase and M. Peters, *Z. Anorg. Allg. Chem.*, 1993, **619**, 727.
4 H. J. Breunig, S. Gulec, B. Krebbs and M. Dartmann, *Z. Naturforsch., Teil B*, 1989, **44**, 1351.
5 A. Lipka, *Acta Crystallogr., Sect. B*, 1979, **35**, 3020; D. W. Cushen and R. Hulme, *J. Chem. Soc.*, 1962, 2218; *J. Chem. Soc.*, 1964, 4162.
6 A. R. J. Genge, W. Levason and G. Reid, *Chem. Commun.*, 1998, 2159; A. J. Barton, A. R. J. Genge, W. Levason and G. Reid, *J. Chem. Soc., Dalton Trans.*, 2000, 859; A. J. Barton, A. R. J. Genge, W. Levason and G. Reid, *J. Chem. Soc., Dalton Trans.*, 2000, 2163.
7 PATTY, The DIRDIF Program System, P. T. Beurskens, G. Admiraal, G. Beurskens, W. P. Bosman, S. Garcia-Granda, R.O. Gould, J. M. M. Smits and C. Smykalla. Technical Report of the Crystallography Laboratory, University of Nijmegen, The Netherlands, 1992.
8 SHELXS-86, G. M. Sheldrick, *Acta Crystallogr., Sect. A*, 1990, **46**, 467.
9 SHELXL-97, G. M. Sheldrick, University of Göttingen, Germany, 1997.
10 TeXsan: Crystal Structure Analysis Package, Molecular Structure Corporation, The Woodlands, TX, 1995.

ChemComm

Structural studies on dicopper(II) compounds with catechol oxidase activity†

Heidi Börzel, Peter Comba* and Hans Pritzkow

Universität Heidelberg, Anorganisch-Chemisches Institut, INF 270, D-69120 Heidelberg, Germany. E-mail: comba@akcomba.aci.uni-heidelberg.de

Received (in Cambridge, UK) 30th October 2000, Accepted 24th November 2000
First published as an Advance Article on the web 15th December 2000

The X-ray crystal structures of three low molecular weight models of catechol oxidase with three different coordination modes are reported; and the compound with a bridging catecholate is shown to be the catalytically most active form.

A range of biological dicopper sites have similar structures, with three histidine donors for each of the two Cu sites and Cu–Cu distances of *ca.* 3.5 Å. These include the oxygen transport protein hemocyanin, the oxygenation enzyme tyrosinase and the oxidation enzyme catechol oxidase. The active sites of these dicopper proteins are structurally well characterized;[1–6] thorough spectroscopic studies, combined with computational investigations, have defined the electronic structures of the active sites,[7,8] and extensive kinetic studies[9,10] have led to the proposal of mechanisms for oxygen transport and activation, as well as oxygen and electron transfer. The assumption of a bridging catecholate as the active species in catechol oxidase[7] was recently challenged on the basis of crystallographic data, which suggested an active state with a monodentate catecholate.[6]

Low molecular weight model compounds have helped to understand structural, electronic and mechanistic features and are expected to be useful for the development of new catalysts. A number of Cu^{II}-based models with catechol oxidase activity have been reported,[11–16] but only few relevant experimental structures with coordinated catecholate have appeared so far.[11] In particular, there is no example where the various coordination modes of catecholate, including the putative intermediates with bridging or monodentate catecholate, have been analyzed with identical coligands, and for some relevant coordination models there have not been any structural data available so far.

We have successfully used mono- and di-nuclear Cu^{I} and Cu^{II} compounds with bispidine-type ligands to stabilize μ-peroxodicopper(II) compounds.[17,18] We now present preliminary results on the catechol oxidase activity of the corresponding Cu^{II} compounds with 3,5-dtbc in MeOH (3,5-dtbc = 3,5-di-*tert*-butylcatechol; spectrophotometric analysis of the *o*-quinone product).[14,15] The mononuclear Cu^{II} complex of L^1 is inactive, in contrast to the dinuclear compounds with L^2 and L^3.

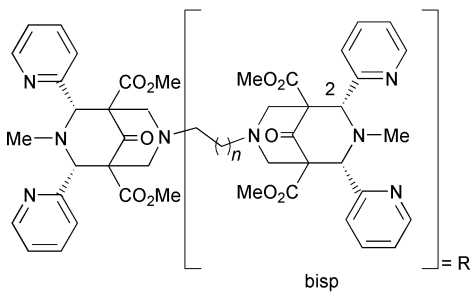

L^1: R = Me, **L^2**: R= bisp, *n* = 1; **L^3**: R = bisp, *n* =2;
L^4: R = bisp, *n* = 2, carbon atoms 2 inverted

One equivalent of $[Cu_2(L^3)(solv)_2]^{4+}$ (solv = solvent) produces in a stoichiometric process 2 equivalents of quinone, while 13 equivalents of quinone are produced per h in a catalytic reaction with $[Cu_2(L^2)(solv)_2]^{4+}$. It emerges that the catalytic activity is a function of the catechol binding mode and stability, and this may differ for all three Cu^{II} compounds.

To examine this, the electronically deactivated substrate $tccH_2$ ($tccH_2$ = tetrachlorocatechol) was added in various concentrations to methanolic solutions of the three Cu^{II} compounds, and substrate binding was monitored spectrophotometrically. For $[Cu(L^1)(solv)]^{2+}$ a strong absorption band appeared at *ca.* 450 nm; for $[Cu_2(L^2)(solv)_2]^{4+}$ and $[Cu_2(L^3)(solv)_2]^{4+}$ equilibria between species with absorptions at *ca.* 450 nm and *ca.* 530 nm were established; with L^2 the species with the lower energy transition was more stable than with L^3, where it disappeared with an excess of catechol (see ESI†). These results are in accord with the assumption that $[Cu_2(L^2)(solv)_2]^{4+}$ and $[Cu_2(L^3)(solv)_2]^{4+}$ lead to catecholate-bridged active compounds, while $[Cu(L^1)(solv)]^{2+}$ leads to a mononuclear catecholate compound. A molecular model[19] (see Fig. 1) indicates that the ethylene-bridged dicopper(II) compound is suitable and highly preorganized for a bridging catecholate.

Single crystals of $[Cu(L^1)(tccH)](ClO_4)$ **1**, $[Cu(L^1)(tcc)]$ **2** and $[Cu_2(L^3)(tcc)](ClO_4)_2$ **3** were obtained by reaction of the Cu^{I} precursors with the fully chlorinated quinone (tcbq) or with $tccH_2$ and O_2, followed by slow evaporation of the solvent (full experimental details, including synthetic procedures, crystal growth, spectroscopic (IR, UV–VIS) and elemental analytical data, are given as ESI†).[20,21] ORTEP plots are shown in Fig. 2. The structure of **1** is of poor quality, but catecholate binds unambiguously as a monodentate, monoprotonated ligand (see analytical data in the ESI†). Also shown in Fig. 2 is an ORTEP plot of $[Cu_2(L^4)(tcc)_2]$ **4**. L^4 has a non-coordinating pyridyl substituent at each copper center and, therefore, leads to copper(II) chromophores with the usual in-plane chelating catecholate coordination mode.

The C–C and C–O bond lengths of tcc^{2-} and $tccH^{-}$ confirm the assignment as coordinated catecholate in all four structures.

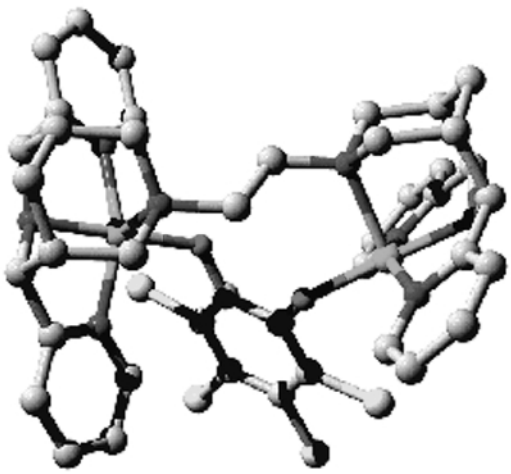

Fig. 1 Molecular model of $[Cu_2(L^2)(tcc)]^{2+}$.

† Electronic supplementary information (ESI) available: S1–S3: titration data; S4: experimental; S5: colour version of Fig. 1. See http://www.rsc.org/suppdata/cc/b0/b008714i/

DOI: 10.1039/b008714i

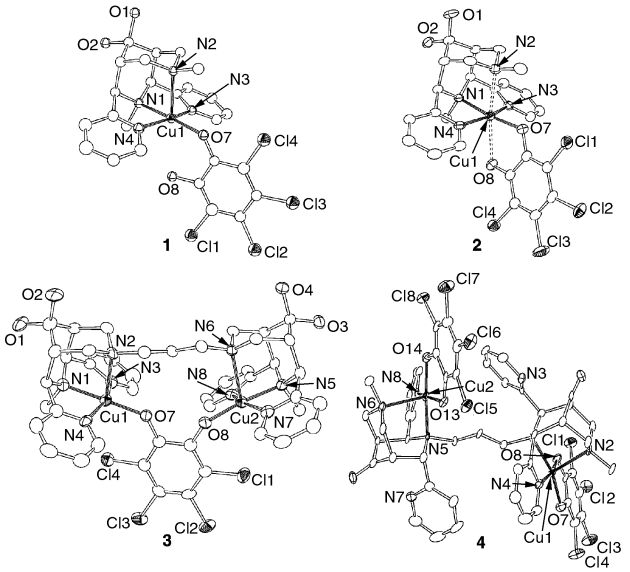

Fig. 2 ORTEP plots of $[Cu(L^1)(tccH)]^+$ **1**, $[Cu(L^1)(tcc)]$ **2**, $[Cu_2(L^3)(tcc)]^{2+}$ **3** and $[Cu_2(L^4)(tcc)_2]$ **4** (50%) probability level). H-atoms, ester groups and counter ions have been omitted for clarity. Selected bond lengths (Å) and angles (°) for **1**; **2**; **3**; **4**; Cu(1)–N(1): 2.020(11); 2.042(2); 2.027(5); 2.094(5). Cu(1)–N(2): 2.320(12); 2.433(2); 2.359(5); 2.293(5). Cu(1)–N(3) 1.987(11); 2.009(2); 2.004(6); —. Cu(1)–N(4) 1.989(11); 2.031(2); 1.985(6); 1.995(5). Cu(1)–O(7) 1.915(9); 1.909(2); 1.898(4); 1.947(4). Cu(1)···O(8) 2.76; 2.46; —; 1.898(4). N(1)–Cu(1)–N(2) 84.06(44); 80.97(8); 83.93(19); 82.24(17). N(1)–Cu(1)–N(3) 81.71(44); 80.56(9); 81.5(2); —. N(1)–Cu(1)–N(4) 81.94(44); 82.15(9); 82.4(2); 80.37(18). N(1)–Cu(1)–O(7) 176.85(47); 172.97(8); 178.1(2); 164.10(18). N(2)–Cu(1)–N(3) 96.66(44); 91.42(8) 95.6(2); —. N(3)–Cu(1)–N(4) 161.28(48); 161.58(9); 161.7(2); —. **4**: O(8)–Cu(1)–O(7) 86.70(17).

The geometry around the Cu^{II} centers can be described as square pyramidal, with N1, the pyridine N-atoms and one of the catecholate O atoms in the square plane and N2 at the axial position; in **2** O8 completes the coordination sphere to an elongated octahedron, and in **4** the second catecholate-O substitutes one of the pyridine-N atoms. **2** is only sparingly soluble in most solvents; the UV–VIS spectrum of a very dilute solution (MeCN) indicates an equilibrium between the mono- and bidentate coordination modes of catecholate, *i.e.* structures **1** and **2** (Fig. 2).

The most prominent structural difference between **3** and the other known structure of a catecholate-bridged dicopper(II) complex is the orientation of the catecholate bridge (angle between the line through the two metal ions and the line through the two catecholate O-atoms: 13.6° in **3**, 32.0° in $[Cu_2(L^2)(TCC)]^{2+}$ (computed), 63.1° in[11]). It is interesting that the increasing puckering of the catecholate bridge correlates with the catalytic activity in the 3,5-dtbc to 3,5-dtbq reaction.

For the model reactions involving bispidine-based ligands it appears that catecholate oxidation occurs at a catecholate-bridged dicopper(II) site by electron transfer from the catechole to the Cu^{II} ions; reoxidation of the Cu centers by molecular oxygen produces water and the active catalyst (the absence of H_2O_2 has been checked by reaction with KI). An interesting question is how thermally stable copper(II) peroxo compounds, generated during the catalytic process, affect the reaction. This and a thorough analysis of the electronic structures of the various structural modes are the subject of further studies in this area.

Generous financial support by the German Science Foundation (DFG), the Fonds of the Chemical Industry (FCI) and the Landesgraduiertenförderungsprogramm of Baden-Württemberg (fellowship to H. B.) is gratefully acknowledged.

Notes and references

1 W. P. J. Gaykema, W. G. J. Hol, J. M. Vereijken, N. M. Soeter, H. J. Bak and J. J. Beintema, *Nature*, 1984, **309**, 23.
2 A. Volbeda and W. G. J. Hol, *J. Mol. Biol.*, 1989, **209**, 249.
3 B. Hazes, K. A. Magnus, C. Bonaventura, J. Bonaventura, Z. Dauter, K. H. Kalk and W. G. J. Hol, *Protein Sci.*, 1993, **2**, 597.
4 K. A. Magnus, B. Hazes, H. Ton-That, C. Bonaventura, J. Bonaventura and W. G. J. Hol, *Proteins*, 1994, **19**, 302.
5 M. E. Cuff, K. I. Miller, K. E. van Holde and W. A. Hendrickson, *J. Mol. Biol.*, 1998, **278**, 855.
6 T. Klabunde, C. Eicken, J. C. Sacchettini and B. Krebs, *Nat. Struct. Biol.*, 1998, **5**, 1084.
7 E. I. Solomon, U. M. Sundaram and T. E. Machonkin, *Chem. Rev.*, 1996, **96**, 2563.
8 H. Decker, R. Dillinger and F. Tuczek, *Angew. Chem.*, 2000, **112**, 1656.
9 B. Salvato, M. Santamaria, M. Beltramini, G. Alzuet and L. Casella, *Biochemistry*, 1998, **37**, 14 065.
10 K. D. Karlin, S. Kaderli and A. D. Zuberbühler, *Acc. Chem. Res.*, 1997, **30**, 139.
11 K. D. Karlin, Y. Gultneh, T. Nicholson and J. Zubieta, *Inorg. Chem.*, 1985, **24**, 3725.
12 M. R. Malachowski, H. B. Huynh, L. J. Tomlinson, R. S. Kelly and J. W. Furbee jun., *J. Chem. Soc., Dalton Trans.*, 1995, 31.
13 J. Manzur, A. M. Garcia, R. Rivas, A. M. Atria, J. Valenzuela and E. Spodine, *Polyhedron*, 1997, **16**, 2299.
14 J. Reim and B. Krebs, *J. Chem. Soc., Dalton Trans.*, 1997, 3793.
15 E. Monzani, L. Quinti, A. Perotti, L. Casella, M. Gullotti, L. Randaccio, S. Geremia, G. Nardin, P. Faleschini and G. Tabbi, *Inorg. Chem.*, 1998, **37**, 553.
16 E. Monzani, G. Battaini, A. Perotti, L. Casella, M. Gullotti, L. Santagostini, G. Nardin, L. Randaccio, S. Geremia, P. Zanello and G. Opromolla, *Inorg. Chem.*, 1999, **38**, 5359.
17 H. Börzel, P. Comba, C. Katsichtis, W. Kiefer, A. Lienke, V. Nagel and H. Pritzkow, *Chem. Eur. J.*, 1999, **5**, 1716.
18 H. Börzel, P. Comba, K. S. Hagen, C. Katsichtis and H. Pritzkow, *Chem. Eur. J.*, 2000, **6**, 914.
19 P. Comba, T. W. Hambley, N. Okon and G. Lauer, 'MOMEC97 a molecular modeling package for inorganic compounds' CVS, Softwareentwicklung, e-mail:cvs@t-online.de, 1997. The force field is that used before for the corresponding peroxo compounds.[17] Structural parameters involving the catecholate bridge were constrained to values derived from the two known structures, see this work and ref. 11.
20 *Crystal structure determination*: data were collected at −100 °C with a Bruker-AXS CCD diffractometer (Mo-Kα radiation, λ = 0.71073 Å, ω-scans). Structures were solved by direct methods and refined against F^2 (SHELXTL V5.10). **2**: $C_{31}H_{31}N_5O_8Cl_4Cu$, M = 806.9, monoclinic $P2_1/c$, a = 16.5741(9), b = 13.5311(7), c = 16.0711(8) Å, β = 110.439(1)°, V = 3377.3(3) Å^3, Z = 4, 8154 independent reflections, θ_{max} = 28.3°, 597 parameters, $R1$ = 0.042, $wR2$ = 0.112. **3**: $C_{55}H_{61}N_9O_{23}Cl_6Cu_2$, M = 1555.9, monoclinic, $P2_1/n$, a = 12.1045(2), b = 33.7116(5), c = 15.8529(2) Å, β = 103.798(1)°, V = 6282.3(2) Å^3, Z = 4, 7686 independent reflections, θ_{max} = 22°, 901 parameters, $R1$ = 0.054, $wR2$ = 0.154. **4**: $C_{75}H_{75}N_{15.50}O_{14}Cl_8Cu_2$, M = 1828.2, triclinic, $P\bar{1}$, a = 19.3832(5), b = 19.5174(5), c = 24.2065(7) Å, α = 71.184(2), β = 80.390(2), γ = 76.041(2)°, V = 8372.5(4)Å^3, Z = 4, 28535 independent reflections, θ_{max} = 24.7°, 2017 parameters, $R1$ = 0.069, $wR2$ = 0.205. CCDC 182/1863. See http://www.rsc.org/suppdata/cc/b0/b008714i/ for crystallographic files in .cif format.
21 We were not able to isolate semiquinone species; when using a Cu^I:Q stoichiometry of 1:1, quantitative formation of Cu^{II}–chloro compounds and a coupling product between catechol (formed by reduction of the quinone by the Cu^I complex) and quinone indicated nucleophilic substitution at the catechol; R. M. Buchanan, B. J. Fitzgerald and C. G. Pierpont, *Inorg. Chem.*, 1979, **18**, 3439.

Development of a light-responsive permeation membrane modified by an azo derivative on a porous glass substrate

Tetsuro Jin,* Aliyar H. Ali and Tetsuo Yazawa

Department of Optical Materials, Osaka National Research Institute, AIST, MITI, 1-8-31 Midorigaoka, Ikeda, Osaka 563-8577, Japan. E-mail: tetsujin@onri.go.jp

Received (in Cambridge, UK) 25th September 2000, Accepted 7th November 2000
First published as an Advance Article on the web 15th December 2000

A photo-responsive gas separation membrane modified by an organic azo derivative in a porous glass tube shows decreased gas permeance upon stimulation with an Xe-lamp, which returns the starting level upon stopping the irradiation.

It is well known that azobenzene derivatives show photo-reversible *cis–trans* isomerization.[1,2] Such conformational change leads to many chemically photoinduced changes so that many applications can be envisaged; among these is the possibility to control the chemical functions by 'on–off switching'. Several investigations considering this concept have been reported.[3–5] In addition, there are many researchers that are attempting to develop membranes with stimuli–response functions. For example, polymeric separation membranes with stimulation–response functions such as pH ultrafiltration membranes[7,8] or liquid membrane separating the intended ions by light[9] are now actively investigated.

On the other hand, porous glass membranes which possess relatively sharp pore size distributions are now actively investigated because of their high gas selectivity, ease of control of the pore size and easier molding.[6] However, the pore size of all such membranes is fixed rigidly so no such membranes can respond to physical and/or chemical stimuli.

In this study, as a new concept, the preparation of a porous glass membrane surface modified by an azo derivative was carried out for use of gas flow control. Furthermore, control of the gas permeability by the photoinduced *cis–trans* switching property of the compound under light irradiation was investigated.

Porous glass tubes were prepared and gas permeance measurements at 300 K were carried out according to the procedure reported elsewhere.[10] The chemicals which were used in this study were purchased either from Wako Pure Chemical Industries Co., Ltd. and Aldrich Inc. or used without any purification. The azo derivative, 11-[4-[(4′-hexylphenyl)-azo]phenoxy]undecanoic acid (6Az10CO_2H) was synthesized using the route reported by Seki *et al.*[11] Initially, a porous glass surface treated with 3-aminopropyldimethylethoxysilane as a coupling agent was placed into a solution of 6Az10CO_2H and THF and refluxed at 373 K for 20 h. Subsequently, the porous glass was refluxed in THF for > 24 h and then washed with THF several times. The azo modification membrane tube (one end was sealed by epoxy resin) was attached to the Pyrex glass tube by epoxy resin and then the support tube with the membrane was placed inside a stainless steel permeation cell equipped with a silica window through a flange connection, after drying at 348 K in vacuum for 1 h. Using the prepared membrane, gas permeances of pure N_2 and He were measured by a mass flow meter. The single feed gas of N_2 and He was passed continuously outside of the membrane under a pressure of *ca.* 3.03×10^5 Pa (3.0 atm) at room temperature (300 K). Light irradiation from a Xe lamp (500 mW cm^{-2}) was directed to the quartz window which could be covered with a thick board to interrupt irradiation. The pore size distribution of the sample after drying at 348 K under vacuum for several hours was measured by a nitrogen adsorption isotherm using a conventional volumetric apparatus (BELSORP 28SA, BEL JAPAN, inc.). Absorption spectra were recorded on a Shimadzu model 2501 instrument controlled by a personal computer.

The pore size distributions of the porous glass membranes before and after modification with the azo derivative were measured by nitrogen adsorption isotherms. As shown in Fig. 1, a main peak at *ca.* 1.7 nm (radius) for the non-modified and azo modified glass tubes was observed. The surface area of the azo modified glass tube (surface area: 108.9 $m^2\ g^{-1}$, pore volume: $9.10 \times 10^{-4}\ m^3\ g^{-1}$) was *ca.* 30% lower than that of the non-treated sample (surface area: 152.0 $m^2\ g^{-1}$, pore volume: $1.36 \times 10^{-3}\ m^3\ g^{-1}$). This suggested that 6Az10CO_2H is mainly located on the surface of the porous glass and not in the pores.

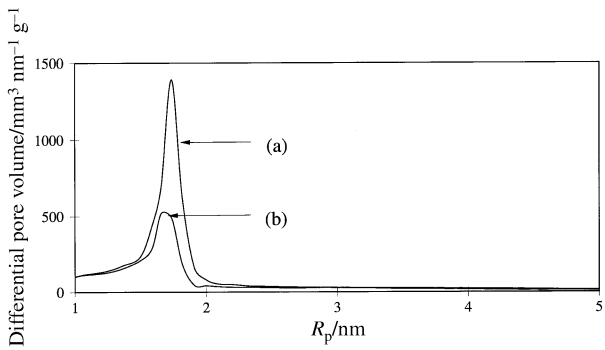

Fig. 1 Pore size distribution for the porous glass tube (a) before and (b) after surface modification with 6Az10CO_2H.

By using the modified membrane, changes of N_2 flow before and after Xe-lamp irradiation were investigated at 300 K. As shown in Fig. 2, the flow of each gas drastically decreased during Xe-lamp irradiation while the flow increased by stopping irradiation. These cycles could be continued > 30 times. Furthermore, there was no light response when similar experiments were performed using non-treated porous glass or porous glass treated with the silane coupling agent only. The increase in temperature close to the modified membrane in the apparatus upon Xe-lamp irradiation was 3–5 K. Thus thermal vibrations around the pores of the glass tube gradually increased the amplitude of N_2 permeance. The length of the folded

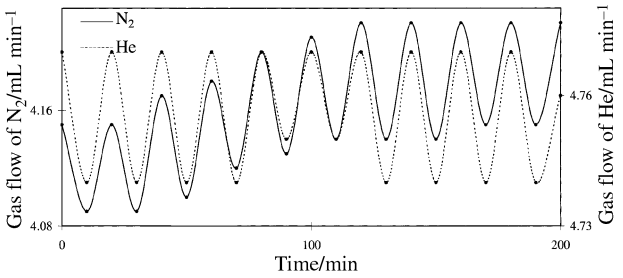

Fig. 2 Gas flow variation of N_2 (——) and He (- - - -) passing through the surface modified glass membrane under Xe-lamp irradiation or non-irradiation.

DOI: 10.1039/b007749f

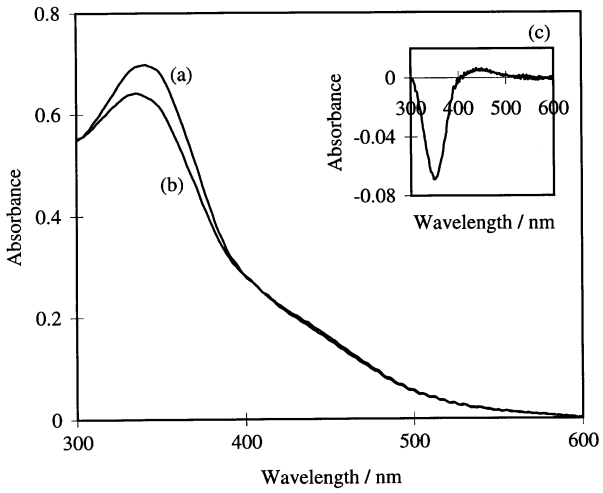

Fig. 3 Absorption spectra of the surface modified glass membrane (a) before irradiation, (b) under Xe-lamp irradiation and (c) differential spectrum (b) − (a).

$=NC_6H_4C_6H_{13}$ moiety of the modifier is 2.377 nm and from these results reorientation of this part of the modifier upon isomerization would reduce the gas permeance by covering the entrance of the pores of the glass substrate.

The absorption spectrum of the azo modified sample under Xe-lamp irradiation is plotted in Fig. 3 which shows a peak at *ca*. 360 nm from the *trans* form and a broad peak at *ca*. 480 nm from the *cis* form with a *trans/cis* ratio of 90/10. On the other hand, this ratio was reduced to 75/25 when UV light (low pressure Hg lamp) was used as a light source and no light response to gas flow was observed. Variation in the permeance relates to rapid *cis* to *trans* isomerization with the *cis* form of the derivative being resistant to permeance (see results of pore size distribution), however, a detailed mechanism could not be established in this study.

Thus, further experiments are now being performed to establish the detailed mechanism of the permeation in an attempt to obtain finer regulation for several gases by considering the interplay between the molecular size of the azo derivative and the pore size of the substrate.

We wish to acknowledge Dr K. Tawa for her assistance in measuring the UV–VIS spectra of the sample. We also thank Mrs H. Kobayashi and Y. Tatematsu for their help on every experiment in this study.

Notes and references

1 D. L. Beveridge and H. H. Jaffe, *J. Am. Chem. Soc.*, 1966, **88**, 1948.
2 S. Llunggren and G. Wettermark, *Acta Chem. Scand.*, 1971, **25**, 1599.
3 S. Shinkai, T. Ogawa, T. Nakaji, Y. Kusano and O. Nanabe, *Tetrahedron Lett.*, 1979, 4569.
4 H. S. Blair and C. B. McArdle, *Polymer*, 1984, **25**, 999.
5 T. Seki, R. Fukuda, M. Yokoi, T. Tamaki and K. Ichikawa, *Bull. Chem. Soc. Jpn.*, 1996, **69**, 2375.
6 T. Yazawa, *Membrane*, 1995, **20**, 183.
7 A. L. Nguyen and J. H. T. Luong, *Biotechnol. Bioeng.*, 1989, **34**, 1186.
8 M. Taniguchi, M. Kobayashi, K. Natsumi and M. Fujii, *J. Ferment. Bioeng.*, 1989, **68**, 32.
9 S. Shinkai, T. Ogawa, T. Nakaji and O. Manabe, *J. Chem. Soc., Chem. Commun.*, 1980, 375.
10 T. Yazawa and H. Tanaka, *Ceram. Trans.*, 1993, **31**, 213.
11 T. Seki, M. Sakuragi, Y. Kawanishi, Y. Suzuki, T. Tamaki, R. Fukuda and K. Ichimura, *Langmuir*, 1993, **9**, 211.

Size and shape controlled ZnTe nanocrystals with quantum confinement effect

Young-wook Jun, Chang-Shik Choi and Jinwoo Cheon*

Department of Chemistry and School of Molecular Science-BK21, Korea Advanced Institute of Science and Technology (KAIST), Taejon 305-701, Korea. E-mail: jcheon@kaist.ac.kr

Received (in Cambridge, UK) 17th October 2000, Accepted 16th November 2000
First published as an Advance Article on the web

A simple one-pot synthesis of size and shape controlled ZnTe nanocrystals using a monomeric molecular precursor, [Zn(TePh)$_2$][TMEDA], has been studied by varying the growth temperature or the templating surfactants.

In recent years, nanomaterials have drawn enormous interest from the scientific community because of their special characteristics that are different from the bulk such as quantum confined electronic band structures,[1,2] novel optical,[3] catalytic,[4] and electronic properties.[5] Since novel properties in nanoscale materials depend on their size and shape, one of the frontier issues of nanochemistry research is morphology controlled synthesis of nanocrystals.

While sulfur and selenium based II/VI nanocrystals such as CdS and CdSe are widely explored,[6–9] there have not been many reports on the preparation of metal telluride nanocrystals. Furthermore, while there are some examples of Cd and Hg based tellurides,[10–14] studies on ZnTe are very limited. ZnTe, an attractive semiconductor with a direct gap of 2.26 eV (*ca.* 548 nm) in the green region of the electromagnetic spectrum, can be a useful material in several applications such as green light-emitting diodes, buffer layers for HgCdTe IR detectors, or as the first unit in a tandem solar cell.[15] Until now, only two reports on the preparation of colloidal ZnTe nanocrystals exist; however the resulting nanocrystals were either large (length 500–1200 nm, width 30–100 nm)[16] or only their optical properties were investigated without isolation or characterization of the nanocrystals.[17] In fact, there have not been any reports on isolated ZnTe nanocrystals < 10 nm. When ZnTe particles are on the order of 10 nm, quantum size effects appear and control of the optical properties is possible by simply changing the particle size. It is then feasible to have tunability of the opto-electronic properties from the green to the UV region.

In this report, we describe a simple one-pot synthesis of morphology controlled ZnTe nanocrystals using a single molecular precursor, [Zn(TePh)$_2$][TMEDA]. Upon thermolysis, this precursor produces ZnTe nanocrystals which are either spherical or of rod-like structure depending on the growth conditions and the choice of stabilizing surfactants. Furthermore, the size of the spherical ZnTe nanocrystals is controlled by the growth temperature and quantum confinement effects are observed. To the best of our knowledge, this paper reports the first isolated and well characterized ZnTe nanocrystals with quantum confined properties.

Even though metal chalcogenolato complexes have been widely studied previously as single-source precursors to group 12 chalcogenide semiconductor materials,[6,12,18] the development of zinc tellurolate molecular chemistry is still limited.[19–21] A pyridine adduct of a mesityltellurolate zinc complex prepared by Bochmann *et al.*[22] and the dimeric compound [Zn{TeSi(SiMe$_3$)$_3$}$_2$]$_2$ prepared by Bonasia and Arnold[23] have been known to generate ZnTe upon pyrolysis. In our study, we synthesized a polymeric phenyltellurolate zinc complex using a dealkylsilation process that was similarly employed to obtain a organotellurolato cadmium compound.[24] The reaction of dimethylzinc with 2 equiv. of PhTeSiMe$_3$ gives the pale yellow product Zn(TePh)$_2$, which was then reacted with TMEDA to give [Zn(TePh)$_2$][TMEDA].[25] X-Ray crystallographic studies of [Zn(TePh)$_2$][TMEDA][26] shows that it is monomeric and that the zinc center adopts a distorted tetrahedral geometry with a large Te–Zn–Te angle of 118.29(6)° and a small N–Zn–N angle of 84.1(4)° (Fig. 1).[27]

A one-pot synthesis of ZnTe nanocrystals was carried out by the thermolysis of [Zn(TePh)$_2$][TMEDA]. According to TGA, it is observed that the thermolysis of [Zn(TePh)$_2$][TMEDA] begins with the dissociation of the TMEDA donor ligand, with ZnTe and Ph$_2$Te produced in the following thermolysis step at higher temperatures.[28] As similarly observed by Yamamoto and Steigerwald in related work on alkyl- or phenyl-chalcogenolate ligand systems,[12,29] the thermolysis of its complexes cleanly produces the desired nanocrystals.

In a typical synthesis of spherical ZnTe nanocrystals, upon injection of the precursor (0.50 g, 0.88 mmol) dissolved in 5 ml of trioctylphosphine into the hot dodecylamine solvent (8.17 g, 44.1 mmol), immediate formation of nanocrystals was observed by the appearance of a pale yellow color. The crystal growth temperature was kept at either 180 or 240 °C for 2 h and the resulting solution was pale yellow in both cases. The solution was treated with butanol and centrifuged to isolate the yellow nanocrystals as a solid product.

Using the same conditions and procedures, the injection of the precursor into the mixed surfactant solvent trioctylamine (20 ml)–dimethylhexylamine (5 ml) and leads to a shape change of the nanocrystals from spherical to rod-like and after 2 h a gray precipitate of ZnTe nanocrystals was obtained from the initially pale yellow solution at 180 °C. It is believed that the combination of the two different surfactants provides rod-like micelles during the one-dimensional crystal growth process.[30]

The obtained spherical ZnTe nanocrystals are moderately monodispersed and their sizes can be controlled by changing the growth temperature. Relative to the position of the 548 nm (2.26 eV) absorption band edge of bulk ZnTe, blue shifts of 0.53 and 1.31 eV are found for the nanocrystals grown at 180 and 240 °C, respectively with larger shifts being seen for samples grown at higher growth temperature (Fig. 2A).[31] Similar blue shifts are also observed in the photoluminescence spectra: band maxima are 451 and 377 nm, respectively, for samples grown at 180 and

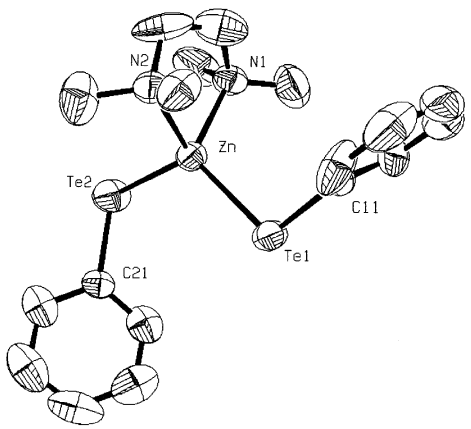

Fig. 1 ORTEP drawing of [Zn(TePh)$_2$][TMEDA]. Selected bond distances (Å) and angles (°): Te(1)–Zn(1) 2.5769(14), Te(2)–Zn(1) 2.5876(15), Zn(1)–N(1) 2.126(9), Zn(1)–N(2) 2.145(9); Te(1)–Zn–Te(2) 118.29(6), N(1)–Zn(1)–N(2) 84.1(4).

DOI: 10.1039/b008376n

240 °C (Fig. 2B). These results suggest that smaller nanocrystals are produced at higher growth temperatures where more nucleation sites exist and relatively less available ZnTe material is present for each nucleus during the growth process.

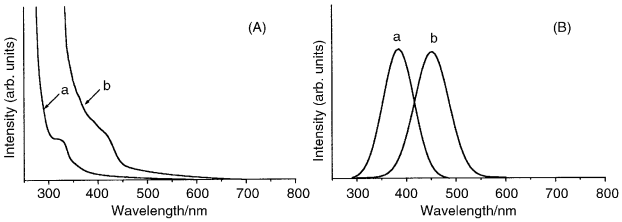

Fig. 2 Optical spectra of ZnTe nanocrystals grown at (a) 240 and (b) 180 °C; (A) UV–VIS absorption spectra, (B) Photoluminescence spectra.

High resolution transmission electron micrographs (HRTEM) show that the spherical ZnTe nanocrystals have average sizes of 4.2 (±1.1) and 5.4 (±0.9) nm for samples grown at 240 and 180 °C, respectively (Fig. 3A). Powder X-ray diffractometry (XRD) and selected area diffractometry (SAED) reveal patterns corresponding to (111), (220) and (311) of the cubic phase of ZnTe nanocrystals (Fig. 3C, D). This result is similar to that of TOPO-capped spherical ZnSe nanocrystals described in a previous report.[31] TEM of the rod-like ZnTe nanocrystals show that the diameters of the rod-like nanocrystals are quite uniform (*ca.* 25 nm) with lengths of several hundred nanometers (200–700 nm) giving an aspect ratio from 8 to 30 (Fig. 3B). The rod-like ZnTe nanocrystals are also cubic phase as confirmed by XRD and SAED analysis.

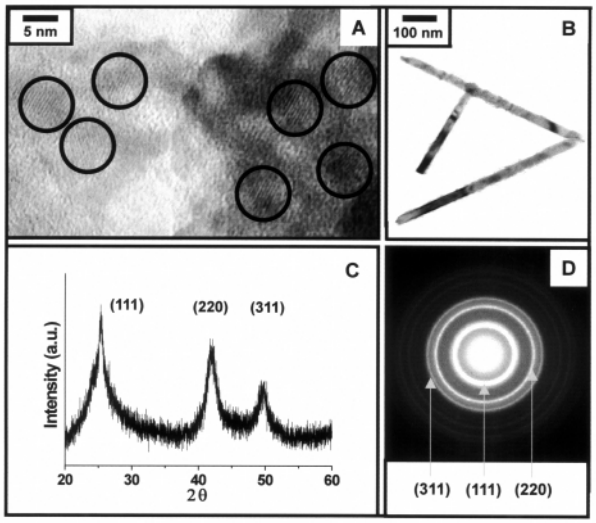

Fig. 3 (A) HRTEM analysis of spherical ZnTe nanocrystals grown at 240 °C, (B) TEM analysis of rod-like ZnTe nanocrystals, (C) powder X-ray diffraction and (D) selected area diffraction patterns of 4.2 nm ZnTe nanocrystals.

In conclusion, the results here constitute a simple and convenient one-pot synthesis of morphology controlled ZnTe nanocrystals using a monomeric molecular precursor, $[Zn(TePh)_2][TMEDA]$. By varying the growth temperature or the choice of the templating surfactants, the size and shape of the nanocrystals are controllable and quantum size effects are observed. We believe that this strategy can be extended to the facile synthesis of nanocrystals of other materials.

This work was supported by the Tera Level Nanodevices National Program of KISTEP. We thank KBSI for the TEM analyses and Professor S. J. Kim and Dr Y.-M. Kim of Ewha Womans' University for X-ray crystallographic analysis of the sample.

Notes and references

1 N. Chestnoy, R. Hull and L. E. Brus, *J. Chem. Phys.*, 1986, **85**, 2237.
2 L. E. Brus, *J. Chem. Phys.*, 1984, **80**, 4403.
3 G. Markovich, C. P. Collier, S. E. Henrichs, F. Remarcle, R. D. Levine and J. R. Heath, *Acc. Chem. Res.*, 1999, **32**, 415.
4 J. P. Wilcoxon, *J. Phys. Chem. B*, 2000, **104**, 7334.
5 S.-H. Kim, G. Markovich, S. Rezvani, S. H. Choi, K. L. Wang and J. R. Heath, *Appl. Phys. Lett.*, 1999, **74**, 317.
6 See reviews: A. P. Alivisatos, *J. Phys. Chem.*, 1996, **100**, 13 226; A. Hagfeldt and M. Gratzel, *Chem. Rev.*, 1995, **95**, 49; H. Weller, *Angew. Chem., Int. Ed. Engl.*, 1993, **32**, 41; J. R. Heath, *Science*, 1995, **270**, 1315.
7 T. Trindade and P. O'Brein, *Chem. Mater.*, 1997, **9**, 523.
8 X. Peng, J. Wickham and A. P. Alivisatos, *J. Am. Chem. Soc.*, 1998, **120**, 5343.
9 C. B. Murray, D. J. Norris and M. G. Bawendi, *J. Am. Chem. Soc.*, 1993, **115**, 8706.
10 M. Mullenborn, R. F. Jarvis, B. G. Yacobi, R. B. Kaner, C. C. Colemann and N. M. Haegel, *Appl. Phys. A*, 1993, **56**, 317.
11 T. Rajh, O. I. Micic and A. J. Nozik, *J. Phys. Chem.*, 1993, **97**, 11 999.
12 J. Brennan, T. Siegrist, P. J. Carroll, S. M. Stuczynski, P. Reynders, L. E. Brus and M. L. Steigerwald, *Chem. Mater.*, 1990, **2**, 403.
13 M. Gao, C. Lesser, S. Kirstein, H. Möhwald, A. L. Rogach and H. Weller, *J. Appl. Phys.*, 2000, **87**, 2297.
14 A. L. Rogach, A. L. Kershaw, M. Burt, M. Harrison, A. Kornowski, A. Eychmüller and H. Weller, *Adv. Mater.*, 1999, **11**, 552.
15 C. Bloomfield, *Compd. Semicond.*, 1995, **1**, 32.
16 Y. Li, Y. Ding and Z. Wang, *Adv. Mater.*, 1999, **11**, 847.
17 U. Resch, H. Weller and A. Henglein, *Langmiur*, 1989, **5**, 1015.
18 M. Bochmann, *Chem. Vap. Deposition*, 1996, **2**, 85; M. B. Hursthouse, M. A. Malik, M. Motevalli and P. O'Brein, *Polyhedron*, 1992, **11**, 45; B. O. Dabbousi, P. J. Bonasia and J. Arnold, *J. Am. Chem. Soc.*, 1991, **113**, 3186; M. Bochmann, A. P. Colemann and A. K. Powell, *Polyhedron*, 1992, **11**, 507.
19 L. Lange and W. W. Du Mont, *J. Organomet. Chem.*, 1985, **286**, C1.
20 P. J. Bonasia and J. Arnold, *J. Chem. Soc., Chem. Commun.*, 1990, 1299.
21 M. Bochmann and K. J. Webb, *J. Chem. Soc., Dalton Tans.*, 1991, 2325.
22 M. Bochmann, G. C. Bwembya, A. K. Powell and X. Song, *Polyhedron*, 1995, **14**, 3495.
23 P. Bonasia and J. Arnold, *Inorg. Chem.*, 1992, **31**, 2508.
24 This compound was prepared according to a modification of the literature procedure: S. M. Stuczynski, J. G. Brennan and M. L. Steigerwald, *Inorg. Chem.*, 1989, **28**, 4431.
25 TMEDA (2.56 g, 22.0 mmol) was slowly added to $Zn(TePh)_2$ (6.97 g, 14.7 mmol) in toluene (100 ml) and the reaction mixture was stirred for 24 h. After pyridine (10 ml) and heptane (50 ml) were added, insolubles were filtered off and the filtrate was concentrated and recrystallized at −24 °C to give colorless needle-shaped crystals. (6.02 g, 72.2%), mp 122–124 °C, Anal. Calc. for $C_{18}H_{26}N_2Te_2Zn$: C, 36.6; H, 4.40; N, 4.74; Te, 43.2; Zn, 11.1. Found: C, 36.6; H, 4.50; N, 4.70; Zn, 11.0%. $\delta_H(CDCl_3$, 25 °C): 7.78 (d, 4H), 7.04 (t, 2H), 6.89 (t, 4H), 2.62 (s, 4H), 2.48 (s, 12H).
26 *Crystal data*: $C_{18}H_{26}N_2Te_2Zn$, M_r = 590.98, monoclinic, space group $P2_1/n$, a = 8.888(1), b = 17.866(3), c = 14.016(2) Å, β = 103.10(1)°, U = 2167.8(5) Å^3, Z = 4, D_c = 1.811 g cm^{-3}, $F(000)$ = 1128, μ(Mo-Kα) = 3.772 mm, R_1 = 0.0616, wR_2 = 0.1659. CCDC 182/1854. See http://www.rsc.org/suppdata/cc/b0/b008376n/ for crystallographic files in .cif form.
27 The Te–Zn–Te angles are slightly smaller than those reported for related compounds with larger ligands such as $[Zn(mesityl)_2(py)_2]$ and $[Zn\{TeSi(SiMe_3)_3\}_2(py)_2]$, (126.9 and 131.9°, respectively). The steric repulsions between these bulkier ligands are responsible for the larger angles as compared to compact phenyl ligands. This trend is clearly shown by the gradual increase of angle from 118.29 to 126.9 to 131.9° as the ligand size increases from phenyl to mesityl to sitel. The Zn–Te and Zn–N bond lengths are 2.5822(65) and 2.136(5) Å which are almost identical to those of $[Zn\{TeSi(SiMe_3)_3\}_2(py)_2]$ and $[Zn(mesityl)_2(py)_2]$ and similar to those seen for other zinc complexes with organochalcogen and amine ligands.[19–21]
28 In TGA, we observed that the dissociation of TMEDA and the generation of Ph_2Te and ZnTe occur at 158 and 178 °C, respectively.
29 K. Osakada and T. Yamamoto, *J. Chem. Soc., Chem. Commun.*, 1987, 1117.
30 M. P. Pileni, T. Gulik-Krzywicki, J. Tanori, A. Filankembo and J. C. Dedieu, *Langmuir*, 1998, **14**, 7359; Y. D. Li, H. W. Liao, Y. Ding, Y. T. Qian, L. Yang and G. E. Zhou, *Chem. Mater.*, 1998, **10**, 2301; C. C. Chen, C. Y. Chao and Z. H. Lang, *Chem. Mater.*, 2000, **12**, 1516.
31 Y. Jun, J. Koo and J. Cheon, *Chem. Commun.*, 2000, 1243.

ChemComm

One-step self-assembly organometallic molecular cages from 11 components†

Shih-Sheng Sun and Alistair J. Lees*

Department of Chemistry, State University of New York at Binghamton, Binghamton, NY 13902-6016, USA. E-mail: alees@binghamton.edu

Received (in Irvine, CA, USA) 18th September 2000, Accepted 15th November 2000
First published as an Advance Article on the web 15th December 2000

Two self-assembly organometallic molecular cages, each comprising 11 components and two different bridging ligands, were prepared from one-step reactions; both of these cages exhibit relatively high affinity and shape-selectivity toward planar aromatic compounds.

Self-assembly has been recognized as a most efficient process that organizes individual molecular components into highly ordered supramolecular species.[1] Relying on strong metal–ligand interactions, the design and study of well arranged metal-containing macrocycles or three-dimensional cage molecules has emerged as a promising research area in modern supramolecular chemistry.[2]

To date, most of the one-step self-assembly transition-metal containing supramolecular species reported in the literature have been synthesized from the same metal components and bridging ligands.[2,3] The incorporation of different metal components or more than two different types of bridging ligands are much rarer.[4] In most cases, such supramolecules were prepared from two or more steps.[5]

Recently, we have prepared a series of self-assembly molecular squares and triangles that incorporate photoactive chromophores. We have demonstrated that the geometry, length and electronic properties of the bridging ligand play an important role in determining the shape of the final self-assembly products and their resultant photophysical, photochemical and electrochemical properties as well as their binding capabilities in molecular sensing applications.[3a,b,6] As an extension of our previous work, we set out to design and synthesize self-assembly cage-type molecules that comprise two different types of ligands, which require more precise bonding directions between the metal components and the bridging ligands in order to avoid the formation of undesired oligomeric species. During the progress of our work, two communications have appeared that describe the two-step preparation of rectangular structures utilizing 2,2′-bipyrimidine (BPM) or bisbenzimidazolate and 4,4′-bipyridine as bridging units.[5a,d]‡ We report, herein, the synthesis of two new cage molecules, each involving two different bridging ligands and assembled from eleven individual components, including a route that involves only one stage and yet leads to high yield. Their photophysical properties and binding behavior toward electron-rich aromatic compounds are also described.

Two synthetic routes to these cage molecules have been investigated (see Schemes 1 and 2). The first involved synthesis of the BPM bridged Re(I) dimer and subsequent replacement of the bromo ligand by triflate (OTf) in acetone to isolate complex **1**.[5d] Subsequent reflux of **1** and the corresponding tridentate ligands, 1,3,5-tris(2′-ethynyl-4″-pyridyl)benzene (TEPB)[7] or 2,4,6-tris(4′-pyridyl)-1,3,5-triazine (TPTA)[8] in THF for 3 days afforded reddish products with general formula {[*fac*-$Re(CO)_3]_2$(μ-BPM)}$_3$(μ-L)$_2$$(OTf)_6$ (**2**, L = TEPB; **3**, L = TPTA).†§

Cages **2** and **3** were characterized by several different analytical techniques including IR, NMR, elemental analysis, and electrospray ionization mass spectrometry (ESI-MS). IR spectra of both cages **2** and **3** indicate typical tricarbonyl patterns with facial arrangements.[9] Elemental analyses confirmed the proposed stoichiometry. ^{1}H NMR spectra of both cages **2** and **3** exhibit very clean and simple chemical shifts, ruling out the possible existence of other oligomeric species. The ESI-MS measurements have provided a straightforward identification of the cage structures of **2** and **3**.† The excellent agreement between the observed and simulated isotopic distributions for the molecular ion unambiguously confirms the proposed molecular structures for **2** and **3**.

After successful isolation of the desired cages **2** and **3**, we wondered if it was possible to prepare them in a simpler one-step process. The synthesis was initiated by refluxing (OTf)-$Re(CO)_5$, BPM and L (TEPB or TPTA) in a 6 : 3 : 2 ratio in THF for one week and, subsequently, cages **2** and **3** were isolated in 47 and 41% yield, respectively. The BPM bridged dimer, $[(CO)_3ReOTf]_2$(μ-BPM), would be expected to form first in the solution considering the extra stabilization through the chelation effect of BPM. Indeed, the formation of one precursor, which is more thermodynamically stable than the other possible intermediates, is important for a self-assembly process that comprises more than one bridging ligand. Subsequently, the thermodynamically driven self-assembly process between $[(CO)_3ReOTf]_2$(μ-BPM) and the corresponding TEPB and TPTA ligands afforded the final cage products.

The absorption spectra of **2** and **3** in MeCN feature intense bands in the near-UV region and a low-energy band at 470 nm, tailing past 600 nm.§ This low energy band is assigned to the

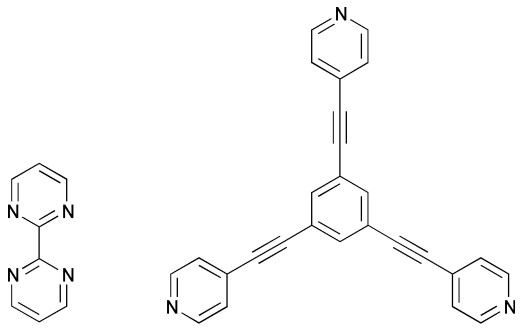

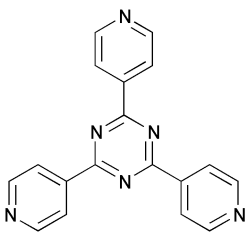

Scheme 1

† Electronic supplementary information (ESI) available: experimental procedures, characterization data for **2** and **3**, a figure showing the ESI mass spectrum of cage **2** and a figure showing the electronic absorption spectra of **2** and **3** in MeCN solution. See http://www.rsc.org/suppdata/cc/b0/b007658i/

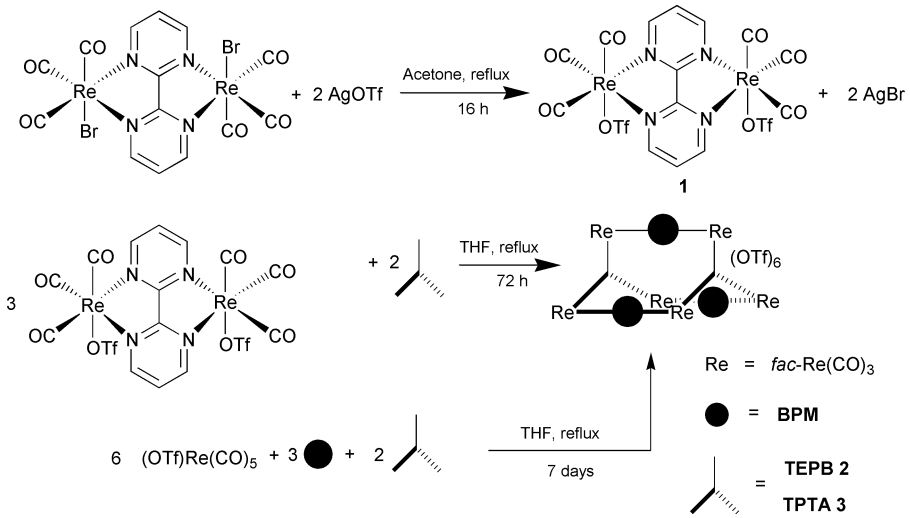

Scheme 2

Table 1 Association constants (K_a/M^{-1}) of **2** and **3** with different guests[a]

Guest	**2**	**3**
o-Dimethoxybenzene	0.81×10^2	0.99×10^2
m-Dimethoxybenzene	5.9×10^2	6.1×10^2
p-Dimethoxybenzene	4.5×10^2	4.2×10^2
1,3,5-Trimethoxybenzene	8.9×10^2	9.1×10^2
2-Naphthalenesulfonic acid, sodium salt	11.2×10^2	11.6×10^2
1,5-Naphthalenedisulfonic acid, disodium salt	26.4×10^2	20.7×10^2
2,6-Naphthalenedisulfonic acid, disodium salt	15.6×10^2	13.8×10^2
Sodium tetraphenylborate	0.75×10^2	0.60×10^2
p-Dimethoxycyclohexane	$< 0.01 \times 10^2$	$< 0.01 \times 10^2$

[a] Binding was monitored by following the phenyl proton of TEPB for cage **2** and β proton of TPTA for cage **3**. The spectra were recorded at 300 MHz in DMSO-d_6 solution at 298 K.

Re(d_π) to BPM (π^*) charge-transfer transition (MLCT). Both **2** and **3** are non-emissive in room-temperature MeCN solution. Several BPM-bridged Re(I) tricarbonyl complexes have been reported that exhibit a lack of emission.[5d,10] These observations have been attributed to the energy gap law effect,[11] resulting in the low-energy ^{3}MLCT excited state undergoing very efficient nonradiative decay. However, it is also possible that an emission band is present but is too red-shifed to detect on our instrumentation.

According to MM2 molecular modeling results, the interplanar distances between the two tridentate ligands in **2** and **3** are 3.5 and 4.2 Å, respectively.[12] These interplanar distances are comparable to the recently reported rectangular structures[5a,d] and the molecules are considered to have very effective π–π stacking that contributes to the highly thermodynamically stable structures.[4a,c] The nearly co-planar arrangement between the two tridentate ligands and the overall six positive charges in **2** and **3** render them promising hosts for electron-rich planar aromatic compounds. Table 1 summarizes the association constants (K_a) of **2** and **3** with different aromatic compounds. Not surprisingly, there is virtually no association between *p*-dimethoxycyclohexane and either **2** or **3** and only a very small association between spherical sodium tetraphenylborate and **2** or **3**. On the other hand, both **2** and **3** showed relatively strong association toward planar aromatic compounds. There are no clear binding differences between **2** and **3**. The shape selectivity, however, deserves more attention and is being further investigated. A significant difference in K_a values was observed for the isomers of dimethoxybenzene, where *m*- and *p*-dimethoxybenzene >> *o*-dimethoxybenzene. A similar trend of shape selectivity has also been observed for Pd and Pt based square complexes.[13]

We are grateful to the U.S. Department of Energy (Grant DE-FG02-89ER14039) for support of this research.

Notes and references

‡ After submission of our manuscript, an article describing the preparation of cages **2** and **3** using a similar two-step procedure appeared.[5e]

§ Two possible geometrical isomers of **1** can exist, namely *syn*- and *anti*-isomers in terms of the mutual arrangement of two triflate ligands. The formation of subsequent cage compounds requires the presence of *syn*-isomers in solution. The high yields (> 50%) of both cage-compounds suggests that either **1** existed mainly as the *syn*-isomer or a mixture of both *syn* and *anti*-isomers where the latter subsequently rearranges to the *syn*-isomer due to more favorable thermodynamic processes.

1 J.-M. Lehn, *Supramolecular Chemistry*, VCH Publishers, New York, 1995.
2 S. Leininger, B. Olenyuk and P. J. Stang, *Chem. Rev.*, 2000, **100**, 853 and references therein.
3 (*a*) S.-S. Sun and A. J. Lees, *J. Am. Chem. Soc.*, 2000, **122**, 8956; (*b*) S.-S. Sun, A. S. Silva, I. M. Brinn and A. J. Lees, *Inorg. Chem.*, 2000, **39**, 1344; (*c*) N. Takeda, K. Umemoto, K. Yamaguchi and M. Fujita, *Nature*, 1999, **398**, 794; (*d*) B. Olenyuk, M. D. Levin, J. A. Whiteford, J. E. Shield and P. J. Stang, *J. Am. Chem. Soc.*, 1999, **121**, 10 434; (*e*) S. M. Woessner, J. B. Helms, J. F. Houlis and B. P. Sullivan, *Inorg. Chem.*, 1999, **38**, 4380.
4 (*a*) M. Fujita, N. Fujita, K. Ogura and K. Yamaguchi, *Nature*, 1999, **400**, 52; (*b*) B. Olenyuk, J. A. Whiteford, A. Fechtenkötter and P. J. Stang, *Nature*, 1999, **398**, 796; (*c*) M. Fujita, M. Aoyagi, F. Ibukuro, K. Ogura and K. Yamaguchi, *J. Am. Chem. Soc.*, 1998, **120**, 611; (*d*) P. N. W. Baxter, J.-M. Lehn, B. O. Kneisel and D. Fenske, *Angew. Chem., Int. Ed. Engl.*, 1997, **36**, 1978; (*e*) P. N. W. Baxter, J.-M. Lehn and A. DeCian, *Angew. Chem., Int. Ed. Engl.*, 1993, **32**, 69.
5 (*a*) K. D. Benkstein, J. T. Hupp and C. L. Stern, *Angew. Chem., Int. Ed.*, 2000, **39**, 2891; (*b*) T. Rajendran, B. Manimaran, F.-Y. Lee, G.-H. Lee, S.-M. Peng, C. M. Wang and K.-L. Lu, *Inorg. Chem.*, 2000, **39**, 2016; (*c*) M. Schweiger, S. R. Seidel, M. Schmitz and P. J. Stang, *Org. Lett.*, 2000, **2**, 1255; (*d*) K. D. Benkstein, J. T. Hupp and C. L. Stern, *J. Am. Chem. Soc.*, 1998, **120**, 12 982; (*e*) K. D. Benkstein and J. T. Hupp, *Mol. Cryst. Liq. Cryst.*, 2000, **342**, 151.
6 S.-S. Sun and A. J. Lees, *Inorg. Chem.*, 1999, **38**, 4181.
7 H. L. Anderson, C. J. Walter, A. Vidal-Ferran, R. A. Hay, P. A. Lowden and J. K. M. Sanders, *J. Chem. Soc., Perkin Trans. 1*, 1995, 2275.
8 H. L. Anderson, S. Anderson and J. K. M. Sanders, *J. Chem. Soc., Perkin Trans. 1*, 1995, 2231.
9 S.-S. Sun, E. Robson, N. Dunwoody, A. S. Silva, I. M. Brinn and A. J. Lees, *Chem. Commun.*, 2000, 201.
10 A. Vogler and J. Kisslinger, *Inorg. Chim. Acta*, 1986, **115**, 193.
11 J. V. Caspar and T. J. Meyer, *J. Phys. Chem.*, 1983, **87**, 952.
12 CAChe Work System 3.8, Oxford Molecular, Oxford, 1995.
13 M. Fujita, J. Yazaki and K. Ogura, *Tetrahedron Lett.*, 1991, **32**, 5589.

ChemComm

The first pillared three-dimensional structure constructed by carboxylate ligands bridging heterometallic trilayers

Long Pan, Bruce S. Finkel, Xiaoying Huang and Jing Li*

Department of Chemistry, Rutgers University, Camden, NJ 08102, USA. E-mail: jingli@crab.rutgers.edu

Received (in Columbia, MO, USA) 30th August 2000, Accepted 14th November 2000
First published as an Advance Article on the web

Reaction of an aqueous solution of Na_2bpdc (H_2bpdc = biphenyldicarboxylic acid) with an organic solution of $Co(NO_3)_2$ *via* a diffusion route leads to a pillared three-dimensional structure in which the heterometallic sodium(I)–cobalt(II) trilayers are connected by carboxylate groups of the pillared ligand $bpdc^{2-}$.

One of the challenges in crystal engineering is to predict the crystal packing from molecular structures. A reasonable approach to build three-dimensional structures based on layered structural motifs is to control the packing of layers by organic pillars of changeable length and/or type. This approach has been demonstrated to be effective towards assembly of both non-covalent and covalent pillared networks.[1] Pillared structures are potentially important for applications in absorption, separation and catalysis.[2] A variety of pillar-layered structures including positively and negatively charged or neutral layers have been synthesized.[3] Organically templated molybdenum oxides MOXI-1, -8, -24, -37 and indium phosphate (InPO) involve nitrogen donor pillars that connect to oxide layers.[4] Metal phosphonates of the type $M^{z+}{}_{4/z}(O_3P–R–PO_3)$ use phosphonate pillars $O_3P–R–PO_3$ where R is an alkyl or aryl group.[5] However, only a few pillared structures are built upon ligands containing carboxylate groups. Limited examples include exo-bicarboxylate in bilayer[6] and isonicotinate (with a carboxylate group and a pyridine nitrogen) in three-dimensional pillared structures.[7] In this contribution, we report a three-dimensional structure consisting of sodium(I)–cobalt(II) heterometallic trilayers and biphenylenecarboxylate pillars, **1**. It is interesting to

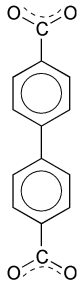

1

note that this structure represents the first example of carboxylate pillared structures containing heterometallic layers.

The title compound was synthesized by mixing organic and aqueous solutions *via* slow diffusion techniques. A DMF solution of $Co(NO_3)_2$ (0.1 M, 1 mL) was carefully layered on an aqueous solution of Na_2bpdc (0.1 M, 1 mL), through a 2 mL mixed (buffer) solution of EtOH–water (2:3). Pink block crystals of $Na_2Co(bpdc)_2(H_2O)$ **2**, suitable for X-ray diffraction analysis,† appeared after several days. Single crystal X-ray analysis revealed that each sodium ion has a distorted triangular bipyramidal (tbp) coordination. The apical positions of the tbp are occupied by two carboxylate oxygen atoms (O1, O2) from two $bpdc^{2-}$, while the equatorial positions are occupied by a η^2-oxygen atom (O5) of a water molecule and two carboxylate oxygen atoms (O3, O4) from another two $bpdc^{2-}$. Each sodium metal is connected with four adjacent sodium atoms located in the same plane through four carboxylate groups *via anti–anti* mode, leading to a two-dimensional grid-like metal network with Na···Na distances of 6.083 Å (along the *b*-axis) and 6.809 Å (along the *c*-axis). Two of these topologically identical Na planes are interconnected by Co. The octahedrally coordinated cobalt ion is located at the inversion center as a node, connected to four adjacent sodium ions through four O atoms at equatorial positions, two of which are *trans* η^2-oxygen atoms (O5, $O5^i$) of water molecules, and the other two, *trans* carboxylate η^2-oxygen (O1, $O1^i$). The remaining two (axial) positions around Co(II) are occupied by terminal water molecules (O6, $O6^i$). This arrangement results in a heterometallic metal slab consisting of a Na(I)–Co(II)–Na(I) trilayer running parallel to the *bc* plane, with the edge-shared sodium(I) and cobalt(II) separated by 3.397(2) Å. A view of the metal slab is illustrated in Fig. 1. This metal trilayer is quite different from that of a pillared zinc biphenylylenebis(phosphonate) $Zn_2(O_3PC_{12}H_8PO_3)\cdot 2H_2O$,[8] in which not only the metal atoms are connected to five neighboring metals by four PO_3 groups, but also they form a monometallic single layer.

The unique heterometallic trilayers in **2** are cross-linked by $bpdc^{2-}$ ligands to form a pillared three-dimensional structure (Fig. 2). Two CO_2^- groups of each bicarboxylate attach the adjacent metal layers as a stud. Each group adopts a different coordination mode. One binds a metal layer through its two oxygen atoms to two sodium ions in a bidentate *anti–anti* mode. The other, at the opposite end of the $bpdc^{2-}$, forms tridentate bonds with the neighboring layer through its two oxygen atoms, coordinating to two sodium ions (in an *anti–anti* mode) and to one cobalt ion (with the η^2-oxygen). The twisting of the $bpdc^{2-}$ ligand is a result of orientation adjustment to achieve a stable coordination geometry for both carboxylate and the metal ions from the layers above and below the pillar, and the *skew–skew* mode of the CO_2^- groups. The width of the heterometallic

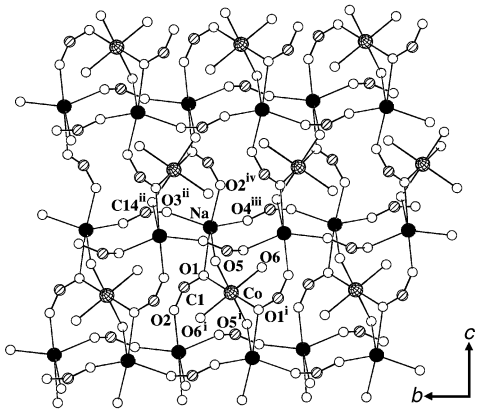

Fig. 1 View of **2** along the crystallographic *a*-axis. Solid and cross-shaded circles are Na and Co, and open and shaded circles are O and C atoms, respectively. Selected bond lengths (Å) and angles (°): Na–Co 3.397(2), Co–O(1) 2.042(3), Co–O(6) 2.044(3), Co–O5 2.210(3), Na–O(1) 2.530(4), Na–O(5) 2.509(3), Na–O(2)^{iv} 2.487(4), Na–O(4)^{iii} 2.271(4), Na–O(3)^{ii} 2.238(5); Na–Co–Na^i 180, Na–O(5)–Co 91.88(11), Na–O(1)–Co 95.36(14). Symmetry codes: i $-x+1/2, -y+1/2, -z-1$; ii $-x, y, -z+1/2$; iii: $-x, y+1, -z+1/2$; iv: $x, -y, z-1/2$.

DOI: 10.1039/b007344j

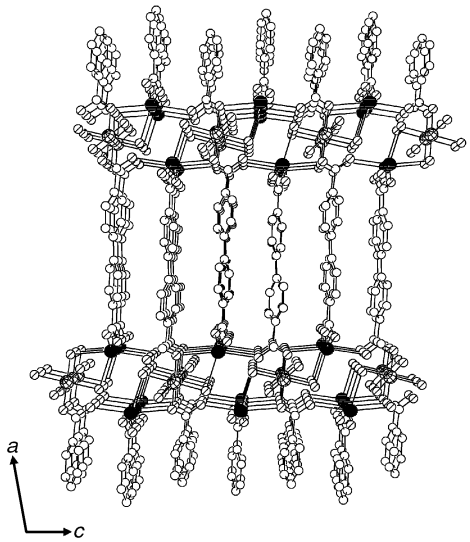

Fig. 2 Perspective view of **2** down the *b*-axis, The same labeling scheme as in Fig. 1 is used. The width of heterometallic trilayer is 3.75 Å and the interlayer distance is 11.5 Å.

trilayer is 3.75 Å. The distance between the two neighboring trilayers is 11.5 Å. The shortest average distance between neighboring benzene rings is 3.75 Å, falling in the range of π–π interactions. This non-covalent interaction may stabilize the pillared structure. However, the closely packed biphenylene groups in the title compound are too close to accommodate guest solvent molecules. The connectivity of $bpdc^{2-}$ (μ_5) in this heterometallic structure cannot be obtained by mixing different ratios of aqueous solutions of Na_2bpdc (0.1 M) and $Co(NO_3)$ (0.1 M), ($V_{Na_2bpdc}/V_{Co(NO_3)_2}$ = 1 : 1, 1 : 5, 1 : 10, 10 : 1, 5 : 1; *V* = volume). The product from these reactions is a one-dimensional structure with a single Co ion center, $^1_\infty[Co(bpdc)(H_2O)_2]$,[9] which was confirmed by powder XRD. The one-dimensional chain in this structure was formed by connecting six-coordinated Co ions through the four μ-H_2O, and two *trans* μ-bpdc.

The present work has shown that heterometallic pillared structures can be effectively synthesized using a bicarboxylate as a pillar molecule. Furthermore, it is likely that other transition metal elements with similar coordination habits and pillars of different length may replace Na/Co and $bpdc^{2-}$, respectively, to form other related pillared structures. Suitable choices of ligands may also lead to porous, 3D pillared networks.

This work is generally supported by the National Science Foundation (Grant DMR-9553066).

Notes and references

† *Crystal data* for **2**: $Na_2CoC_{28}H_{24}O_{12}$, M = 657.38, monoclinic, space group $C2/c$ (no.15), a = 3.746(6), b = 6.083(1), c = 13.363(3) Å, Z = 4, V = 2500.0(8) Å^3, D_c = 1.747 g cm^{-3}, crystal size 0.10 × 0.06 × 0.04 mm, μ(Mo-Kα) = 0.795 mm^{-1}. The intensity data were collected with an Enraf-Nonius CAD4 diffractometer using graphite-monochromated Mo-Kα radiation (λ = 0.71073 Å). 196 unique reflections of which 1097 were measured; $R_1[I > 2\sigma(I)]$ = 0.063, wR_2 (all data) = 0.0668, GOF = 0.951. The structure were solved by direct methods (SHELXS-86) and refined by full-matrix least-squared methods (SHELXL-97). All non-hydrogen atoms were refined anisotropically.

CCDC 182/1862. See http://www.rsc.org/suppdata/cc/b0/b007344j/ for crystallographic files in .cif format.

1 S. C. Zimmerman, *Science*, 1997, **276**, 543; V. A. Russell, C. C. Evans, W. Li and M. D. Ward, *Science*, 1997, **276**, 575; M. Kondo, T. Okubo, A. Asami, S. Noro, T. Yoshitomi, S. Kitagawa, T. Ishii, H. Matsuzaka and K. Seki, *Angew. Chem., Int. Ed.*, 1999, **38**, 140.
2 *Pillared Layered Structures: Current Trends and Applications*, ed. I. V. Mitchell, Elsevier, London, 1990.
3 S. P. Newman and W. Jones, *New J. Chem.*, 1998, **22**, 105; T. J. Pinnavaia, *Science*, 1983, **220**, 365; G. K. H. Shimizu, G. D. Enright, C. I. Ratcliffe and J. A. Ripmeester, *Chem. Commun.*, 1999, 461; G. Alberti, U. Costantino, C. Dionigi, S. Murciamascaros and R. Vivani, *Supramol. Chem.*, 1995, **6**, 29.
4 P. J. Hagrman, D. Hagrman and J. Zubieta, *Angew. Chem., Int. Ed.*, 1999, **38**, 2639; D. E. Hagrman and J. Zubieta, *J. Solid State Chem.*, 2000, **152**, 141; A. M. Chippindale, S. J. Brech and A. R. Cowley, *Chem. Mater.*, 1996, **8**, 2259.
5 A. Clearfield, *Chem. Mater.*, 1998, **10**, 2259; D. Medoukali, P. H. Mutin and A. Vioux, *J. Mater. Chem.*, 1999, **9**, 2553.
6 L. Pan, X. Y. Huang, J. Li, Y. G. Wu and N. W. Zheng, *Angew. Chem., Int. Ed.*, 2000, **39**, 527.
7 O. R. Evans and W. Lin, *Inorg. Chem.*, 2000, 2189.
8 B. Zhang, D. M. Poojary and A. Clearfield, *Inorg. Chem.*, 1998, **37**, 1844.
9 L. Pan, N. Ching, X.-Y. Huang and J. Li, *Inorg. Chem.*, 2000, **39**, 5333.

Synthesis of hyperbranched polymers from commercially available A_2 and BB'_2 type monomers

Chao Gao and Deyue Yan*

College of Chemistry and Chemical Engineering, Shanghai Jiao Tong University, Shanghai 200240, Peoples Republic of China. E-mail: dyyan@mail.sjtu.edu.cn

Received (in Cambridge, UK) 26th July 2000, Accepted 30th October 2000
First published as an Advance Article on the web

This work describes a new strategy for the preparation of hyperbranched polymers from commercially available A_2 and BB'_2 type monomers without any catalysts; the rapid reaction of A groups with B groups results in the formation of dimers that can be regarded as a new sort of AB'_2 type monomer; further polymerization of AB'_2 gives hyperbranched polymers; through this approach a new kind of water-soluble hyperbranched polysulfone-amine was synthesized by polyaddition of *N*-methylpropane-1,3-diamine (BB'_2) to divinyl sulfone (A_2).

Hyperbranched polymers have received attention for about 10 years due to their unique chemical and physical properties.[1–9] It is known that hyperbranched polymers are prepared mainly by polycondensation of AB_x type monomers.[10–14] Most AB_x type monomers are unavailable commercially. A significant approach to hyperbranched polymers, therefore, would be the polymerization of commercially available difunctional and trifunctional monomers. Unfortunately, the polycondensation of A_2 and B_3 type monomers usually leads to the formation of a three-dimensional network.[1] Interestingly, Kakimoto and coworkers[15] reported that hyperbranched aromatic polyamides were synthesized by polycondensation of diamines (A_2) with trimesic acid† (B_3) at low monomer concentration in the presence of special catalysts. The hyperbranched polymers were accessible only when the feed monomer ratio was 1 : 1. Gelation occurred within 10–20 min when the feed ratio of A_2 to B_3 was 3 : 2.[15,16]

This work found that gelation can be avoided at different feed ratios if A_2 monomers and BB'_2 (instead of B_3) monomers are used. Both B and B′ can react with A, and B is more active than B′. The difference in reactivity may be due to the distinction in chemical environment or chemical structure of the two functional groups. If the reaction between B and A is much faster than that between B′ and A, the predominant intermediate formed at the initial stage of the polymerization is the dimer ($AA–BB'_2$), which can be regarded as a new kind of AB'_2 type monomer. Further polymerization of AB'_2 gives a hyperbranched polymer. The approach for synthesis of hyperbranched polymers from two types of reactive monomers is essentially different from that invented by Davis and coworkers in which the new functional group A is formed by reacting a B_3 monomer with a reagent.[17]

To test the aforementioned concept, two kinds of monomers were selected as the raw materials (Scheme 1). Monomer **1** is attractive due to its strong electron-withdrawing group (SO_2) linking double bonds. The sulfone group may guarantee the high reactivity of vinyl groups in the nucleophilic addition, which results in fast reaction without catalyst.[18] The structure of **2** is interesting since it contains an active hydrogen atom in the secondary-amino group and two active hydrogen atoms in the primary-amino group. The former is more active than the latter in the nucleophilic addition due to the effect of the electron-donating group attached to the secondary-amino group.[19,20] At the start of the polymerization, secondary-amino groups of **2** react rapidly with vinyl groups of **1** to afford **3**. Species **3** is now an AB'_2 monomer with one double bond and two active hydrogen atoms. Further polymerization of **3** leads to higher species and finally to a hyperbranched polymer.

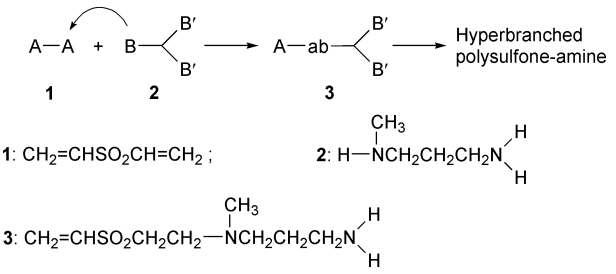

Scheme 1 Polymerization mechanism of A_2 and BB'_2 monomers.

FTIR has been used to investigate the reaction process. For the polyaddition of **1** to **2** with a mole ratio of 1 : 1 (Fig. 1), the area integration of the absorption band from 1625 to 1602 cm^{-1} (assigned to double bonds) decreases to approximately a half of feed **1** during the initial 12 s. However, little change can be observed for the absorption bands from 3240 to 3450 cm^{-1} (assigned to primary-amino groups; the secondary-amino groups can not be observed in the IR spectrum). Then, the peaks of primary-amino groups and double bonds gradually decrease with the reaction. At about 5 h, the peak owing to the double bonds disappears completely, while that of the primary-amino groups is still observed (Fig. 2). These data fully support the polymerization mechanism shown in Scheme 1. Close monitoring of this polymerization by HPLC further demonstrates the reaction is initially very fast. The corresponding peak of monomer **1** vanished after about 10 s. Moreover, in the mass spectrum of the reaction mixture at the initial reaction stage, the molecular ion peak of the AB'_2 monomer (M = 206.3) is observed at m/z = 207.1 (M + 1), and the fragment ion peak (M = 190.3) for AB'_2 losing its primary-amino group is found at m/z = 190.1. These data suggest that dimer **3** is indeed generated by the reaction of the secondary-amino groups with vinyl groups.

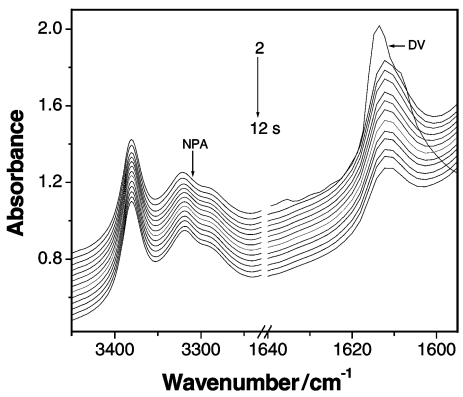

Fig. 1 *In situ* FTIR spectra of the reaction mixture of dinvinyl sulfone (DV) and *N*-methylpropane-1,3-diamine (NPA) with the feed ratio of 1 : 1 in chloroform within initial 12 s.

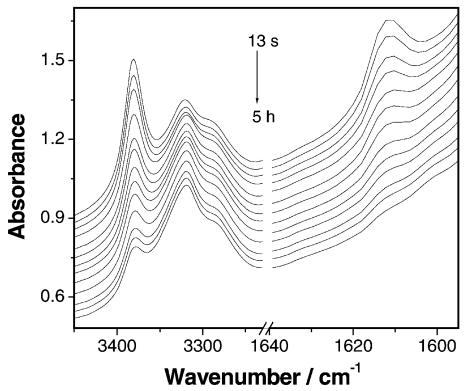

Fig. 2 *In situ* FTIR spectra of the reaction mixture of dinvinyl sulfone and *N*-methylpropane-1,3-diamine with the feed ratio of 1 : 1 in chloroform from 13 s to 5 h.

When the initial mole ratio of A_2 to BB'_2 is equal to 1, the hyperbranched polymer was synthesized through the following procedure (P1 in Table 1): Under vigorous stirring and nitrogen atmosphere, divinyl sulfone (3.5445 g, 30 mmol) was added to a solution of *N*-methylpropane-1,3-diamine (2.6445 g, 30 mmol) in 15 ml of chloroform. The reaction mixture was kept at 40 °C for 96 h. Precipitation of the reaction mixture with 500 ml of MeOH and 8 M aqueous HCl (10 ml) gave the white hyperbranched polymer in 90% yield, which has a molecular weight, M_n, of 18530 (vapour-pressure osmometer) and a glass transition temperature of −22.8 °C (measured on a PE Pyris-1 DSC thermal analyzer under nitrogen at a heating rate of 20 °C min^{-1} from −80 to 200 °C). The resulting polymer shows good solubility in water and polar organic solvents such as DMF, NMP and DMSO, which provides further support for the polymerization mechanism without network formation. A combination of IR, ^1H and ^{13}C NMR spectra confirmed the structure of the hyperbranched polymer. For hyperbranched polymers, the degree of branching (DB)[21] is calculated from the ratio of branched units (N_b) and terminal units (N_t) to the total units (branched units, terminal units and linear units). In this work, the branched unit is the tertiary-amino group, the terminal unit is the primary-amino group, and the linear unit (N_l) is the secondary-amino group. In the ^1H NMR spectrum, the peaks of N_b, N_l and N_t were found at 3.58, 3.31 and 3.19 ppm, respectively. Additionally, a tertiary-amino group is also formed during the reaction of the A group and B group. Since there is a methyl group (CH_3) attached to the tertiary nitrogen, the peaks of the formed tertiary-amino group (N_B) are different from that of the branched tertiary-amino group in the ^1H NMR spectrum. The peak of the methylene group (CH_2) attached to N_B was found at 3.75 ppm, and that of the methyl group at 2.9 ppm. Therefore, N_B has no influence on the calculation of DB. The DB calculated from the integration ratio of corresponding peaks (N_b, N_l and N_t) is summarized in Table 1.

When the feed ratio is equal to 3 : 2, it is more difficult to avoid gelation for the polycondensation systems of A_2 and B_3 monomers.[13,19] In this article, no gelation occurred during the polymerization with the 3 : 2 ratio in organic solvent. The end-capped polymer with benzoyl chloride is soluble in chloroform and other polar solvents such as DMF, NMP, and DMSO. Examination of the FTIR and HPLC showed the expected

Table 1 Direct polymerization of divinyl sulfone with *N*-methylpropane-1,3-diamine

Sample	Ratio[a]	Solvent	Time/h	Yield (%)	DB (%)	η_{inh}[b]	M_n
P1	1 : 1	$CHCl_3$	96	90	58.7	0.17	18530
P2	3 : 2	$CHCl_3$	120	94	71.8	0.15	15385
P3	1 : 1	NMP	96	92	57.4	0.18	19860
P4	3 : 2	NMP	120	95	73.5	0.16	17110

[a] The initial mole ratio of divinyl sulfone to *N*-methylpropane-1,3-diamine. [b] The inherent viscosity (dL g^{-1}) of the resulting polymer measured at a concentration of 0.5 g dL^{-1} in water solution at 25 °C.

reaction mechanism as given in Scheme 1. For the resulting hyperbranched polymer with 3 : 2-feed ratio, the terminal units should contain vinyl groups and primary-amino groups. The peaks of the vinyl groups were observed at 6.4 (CH_2=) and 6.8 (CH=) ppm in the ^1H NMR spectrum.

In conclusion, a novel approach for synthesis of hyperbranched polymers was presented. Water soluble hyperbranched polysulfoneamines were prepared by polyaddition of *N*-methylpropane-1,3-diamine (BB'_2) to divinyl sulfone (A_2). It is likely that the simplicity of this process and the generality of the method will make this new approach attractive for the synthesis of larger scale hyperbranched polymer materials.

This work was supported by the National Natural Science Foundation of China (No. 29974017) and the Gore & Associates Inc. of U. S. A.

Notes and references

† The IUPAC name for trimesic acid is benzene-1,3,5-tricarboxylic acid.

1 P. J. Flory, *J. Am. Chem. Soc.*, 1952, **74**, 2718.
2 Y. H. Kim, *J. Am. Chem. Soc.*, 1992, **114**, 4947.
3 J. M. J. Fréchet, *Science*, 1994, **263**, 1710.
4 B. Voit, *J. Polym. Sci., Polym. Chem.*, 2000, **38**, 2505.
5 J. M. J. Fréchet, C. J. Hawker, I. Gitsov and J. W. Leon, *J. Macromol. Sci.-Pure Appl. Chem.*, 1996, **A33**, 1399.
6 E. Malmström and A. Hult, *J. Macromol. Sci.-Rev. Macromol. Chem. Phys.*, 1997, **C37**, 555.
7 Y. H. Kim, *J. Polym. Sci., Polym. Chem.*, 1998, **36**, 1685.
8 T. Emrick, H. T. Chang and J. M. J. Fréchet, *Macromolecules*, 1999, **32**, 6380.
9 J. M. J. Fréchet, H. Masahiro, I. Gitsov, S. Aoshima, M. R. Leduc and R. B. Grubbs, *Science*, 1995, **269**, 1080.
10 Y. H. Kim and O. W. Webster, *Macromolecules*, 1992, **25**, 5561.
11 V. Percec and M. Kawasumi, *Macromolecules*, 1992, **25**, 3843.
12 T. M. Miller, T. X. Neenan, E. W. Kwock and S. M. Stein, *J. Am. Chem. Soc.*, 1993, **115**, 356.
13 D. H. Bolton and K. L. Wooley, *Macromolecules*, 1997, **30**, 1890.
14 G. Yang, M. Jikei and M. Kakimoto, *Macromolecules*, 1999, **32**, 2215.
15 M. Jikei, S. H. Chon, M. Kakimoto, S. Kawauchi, T. Imase and J. Watanebe, *Macromolecules*, 1999, **32**, 2061.
16 S. M. Aharoni, *Macromolecules*, 1991, **24**, 235.
17 N. J. Davis and S. P. Rannard, PCT Int. Appl. WO 9850453.
18 K. Toda and T. Toda, *Bull. Chem. Soc. Jpn.*, 1968, **41**, 2519.
19 J. R. Mohfig, S. S. Fu, R. W. King, R. Warnet and G. Gustafson, *J. Am. Chem. Soc.*, 1990, **112**, 3665.
20 S. T. McDowell and C. J. M. Stirling, *J. Chem. Soc. (B)*, 1967, 343, 348.
21 C. J. Hawker, R. Lee and J. M. J. Fréchet, *J. Am. Chem. Soc.*, 1991, **113**, 4583.

ChemComm

Supercritical fluid mixing: preparation of thermally sensitive polymer composites containing bioactive materials†

Steven M. Howdle,*[a] Michael S. Watson,[a] Martin J. Whitaker,[b] Vladimir K. Popov,[c] Martyn C. Davies[b] Frederick S. Mandel[d] J. Don Wang[d] and Kevin M. Shakesheff[b]

[a] *School of Chemistry, University of Nottingham, Nottingham, UK NG7 2RD. E-mail: steve.howdle@nottingham.ac.uk*
[b] *School of Pharmaceutical Sciences, University of Nottingham, Nottingham, UK NG7 2RD*
[c] *Institute of Laser and Information Technology, LaserChem Group, Russian Academy of Sciences, 2 Pionerskaya Str., Troitsk, 142092, Russia*
[d] *Ferro Corporation, 7500 E. Pleasant Valley. Rd., Independence, OH 44131, USA*

Received (in Cambridge, UK) 10th October 2000, Accepted 14th November 2000
First published as an Advance Article on the web 15th December 2000

We report the use of supercritical carbon dioxide ($scCO_2$) to create a diverse range of polymeric composites incorporating thermal and solvent labile guest materials such as proteins; no additional co-solvents are required; the entire process can be carried out at near ambient conditions; polymer morphology is controllable; high loadings of guest species can be achieved and the protein function is retained.

Tissue engineering scaffolds and controlled drug delivery devices are polymeric composites designed to release precise amounts of guest species, *e.g.* growth factors and biotechnology drugs, at rates matching the physiological need of the tissue.[1] The challenge is to incorporate such biologically active guest species, without loss or change of activity, into a polymer host. There are well documented problems in maintaining protein conformation and activity under conventional processing methods due to either the presence of an organic/aqueous solvent interface (*e.g.* double emulsion particle formation), elevated temperatures (*e.g.* polymer melt processing), or mechanical agitation of solutions.[2] A further challenge in producing these composites is to control the morphology of the composite, *e.g.* to generate a pore size distribution that promotes cell infiltration or a controlled porosity to influence polymer degradation and controlled release characteristics.

Here, we report a supercritical fluid mixing technology that overcomes both of these limitations in one processing step. The combination of gas-like and liquid-like properties makes $scCO_2$ a unique polymer-processing medium.[3,4] $scCO_2$ has long been proposed as the ideal medium for preparation of polymer based materials containing bioactive species, primarily because no solvent residues would remain in the final product. Progress has been slow because $scCO_2$ is generally a poor solvent for polar guest species[5] and for polymers.[6] and this has resulted in extensive use of $scCO_2$ as an anti solvent.[7,8]

However, $scCO_2$ does interact with a broad range of amorphous polymers leading to depression of the glass transition temperature (T_g).[4] Under these conditions the polymer is plasticised, substantially lowering the viscosity and allowing efficient incorporation of insoluble guest particles into the polymer (see Contents Page illustration). Briefly, powdered samples of polymer and bioactive guest are placed in the autoclave and $scCO_2$ added. Neither the guest, nor the polymer, dissolves in $scCO_2$. The precise conditions of temperature and pressure required to plasticise the polymer are determined by the composition of the polymer. For the biodegradable polymers poly(DL-lactide) (PLA), poly(lactide-*co*-glycolide) (PLGA) and polycaprolactone (PCL), near ambient temperature (35 °C) and modest pressures (200 atm) are sufficient. Efficient agitation of the $scCO_2$ swollen polymer leads to homogeneous distribution of the guest particles throughout the polymer matrix. The vessel is then depressurised to produce either monolithic samples or encapsulated particles. For monoliths, the composite material is formed inside the autoclave. For particles, the entire contents of the vessel are forced out under pressure through a computer controlled orifice. Depressurisation is rapid, and is controlled by the action of a flush valve. The encapsulated particles are retrieved from a cyclone collector and the CO_2 may be repressurised and recycled. The methodology is based on the technique of particle generation from supercritical suspension (PGSS) and was initially developed for the preparation of powder coatings for paint applications, with the aim of decreasing processing temperatures.[9] The whole process can be performed in < 1 h at near ambient temperatures on a gram to multi kg scale in a single processing step. No solvent residues remain after processing and a wide range of loadings (up to 70% by weight), morphologies, and porosities are accessible.

To demonstrate the principle we have prepared porous composites of PLGA (75% DL-lactide : 25% glycolide, M_w = 26 kDa, intrinsic viscosity = 0.6) incorporating a high loading of calcium hydroxyapatite (HA). Such materials are required for bone regeneration applications (Fig. 1A, B). A PLGA composite incorporating the enzyme catalase at 50% w/w loading is also shown (Fig. 1C) The catalase particle morphology is totally unchanged after processing, the protein is intimately mixed with

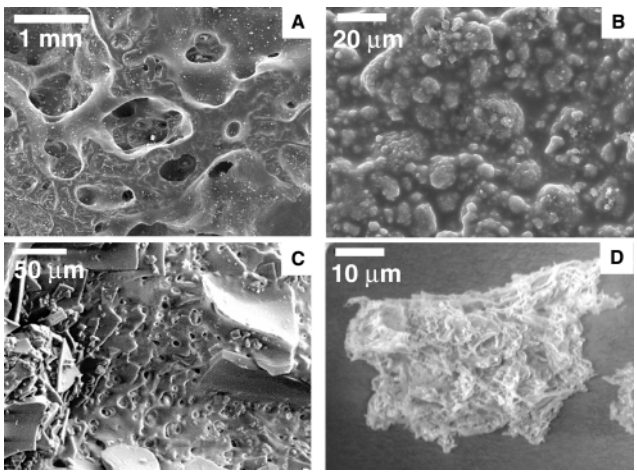

Fig. 1 SEMs of composites. (A and B) Images of internal fracture surface of composite of HA (40 wt%) and PLGA (60 wt%). At low magnification the distribution of HA and the porosity is evident, at higher magnification the intimate mixing of HA and PLGA is observed. (C) Catalase (50 wt%) incorporated into a PLGA matrix (50%). Micron-scale pores in the polymer and the distinctive protein particle morphology are evident. (D) High-surface area microparticle composite [fluorescein (sodium salt) (8 wt%) and PCL (92 wt%)] produced by direct atomisation.

† Electronic supplementary information (ESI) available: methods and measurement of ribonuclease A activity. See http://www.rsc.org/suppdata/cc/b0/b008188o/

DOI: 10.1039/b008188o

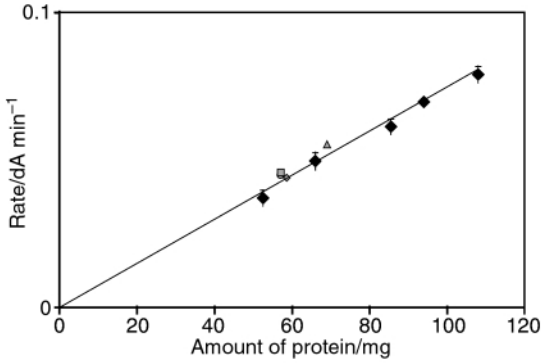

Fig. 2 Evidence of retention of ribonuclease A activity. Measured activities of the released enzyme (four grey-filled symbols) correlate well with calibration data (◆ symbols) and best fit line.

the biodegradable polymer, and porosity in the polymer phase is clearly evident.

The ability to plasticise such polymers at close to 37 °C and the inherently low solubility of proteins in $scCO_2$ provides a key processing advantage; thermal and solvent labile species can be processed easily whilst preserving protein structure and function. We have demonstrated this for three enzymes; ribonuclease A, catalase and β-D-galactosidase. For ribonuclease A, a number of investigators have studied the activity after exposure to a wide range of solvents and environments using a standard assay.[10] Using $scCO_2$ (170 atm; 37 °C for 10 min), we have prepared composites of ribonuclease A (10 wt%) and PLA (M_w 30 kDa). The enzyme was then released to a Tris buffer at 37 °C for 5 min and analysed (see ESI†). The total concentration of protein released was verified by a Coomassie protein assay and the activity of the released protein was measured. The data presented in Fig. 2 demonstrate that the activity of the enzyme is preserved. Thus $scCO_2$ behaves in a similar manner to conventional anhydrous solvents, with the advantage that no solvent residues are introduced. Indeed, $scCO_2$ processing even removes the conventional solvent residues that are almost always found in guest and polymer materials. Clinical use of such composites requires controlled release of the guest from the polymer host. Release of ribonuclease A from the PLA composites over a 70 day period revealed an initial burst release of < 10% of the dose over the first 2 days followed by close to zero-order release kinetics until the delivery device was exhausted.

We have also demonstrated that this $scCO_2$ mixing technology leads to fine control of the morphology of polymer composites. Others have demonstrated that $scCO_2$ can be used to create microcellular foams of amorphous polymers, and that control of the magnitude of pressure drop and the rate of depressurisation influence strongly the porosity and pore size.[11,12] The data in Fig. 3A were recorded following a 'slow' (over a 2 h period), whereas Fig. 3B shows the effect of a 'fast' (2 min) depressurisation. SEM images show that the 'slow' material possesses a small population of large pores (diameter 100–500 μm) whereas the 'fast' material has higher porosity and the pore size distribution, within the resolution of SEM, is more heterogeneous. Mercury porosimetry reveals significant differences in the pore size distribution of small pores that are not visible in the SEM images. 'Slow' depressurisation produced micropores between 50 and 100 nm diameter and no pores in the 500 nm to 5 μm range. Conversely, 'fast' depressurisation produced no micropores in the 50–100 nm range, but many in the 500 nm to 5 μm range. Thus, supercritical mixing offers a mechanism of controlling both macro- and micro-porosity without the addition of porogens[13] and *via* a one-step process. We have also observed such macro- and micro-porosity in protein loaded composites.

For many applications, the polymer/drug composite is required as micron-scale particles particularly for controlled release and lung or subcutaneous delivery systems.[1] Our technique can also produce such micron-scale composite particles. After the mixing step, direct atomisation is achieved

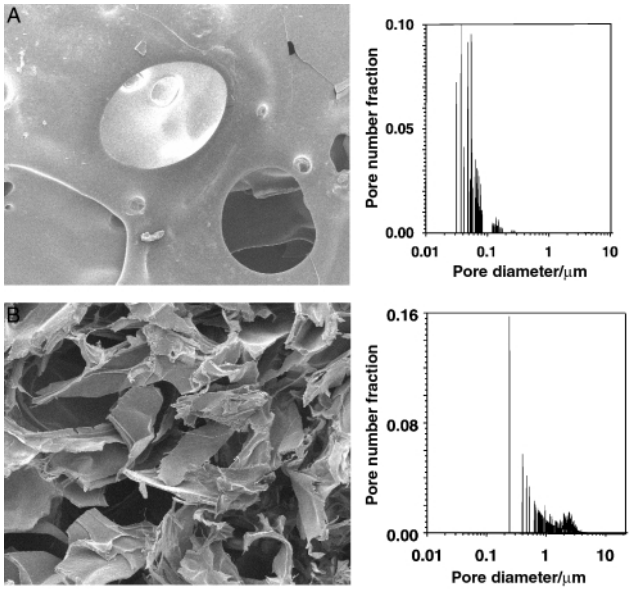

Fig. 3 Controlling PLA pore structure. A, 'slow' depressurisation over a 2 h period. B, 'fast' depressurisation over a 2 min period.

by releasing the pressure of the system across an orifice of known diameter, with particles forming as the CO_2 expands rapidly. The image in Fig. 2D shows an example of the type of particle morphology generated when processing a model system. The composite particles have a high surface area and their size may be fine-tuned by control of the orifice diameter. Typically the mean diameters fall in a range between 24 and 50 μm, a range that has been shown to be suitable for lung delivery of low density particles.[14]

The novel supercritical mixing process described here requires neither the guest nor the polymer to dissolve in $scCO_2$. The process is performed at near ambient temperature and conventional solvents are not required.[15] Hence, it is especially applicable to thermally labile or solvent sensitive guest species and polymers. Most importantly we have demonstrated that protein functioning is retained for a range of enzymes after the processing. The technique is applicable to production of composites for any technology requiring thermally labile materials dispersed throughout a polymer host.

We thank the Royal Society and EPSRC for Fellowships (S. M. H. and K. M. S.) and the RFBR for support.

Notes and references

1 R. Langer, *Nature*, 1998, **392**, 5.
2 K. Fu, A. M. Klibanov and R. Langer, *Nat. Biotechnol.*, 2000, **18**, 24.
3 M. A. McHugh and V. J. Krukonis, *Supercritical Fluid Extraction; Principles and Practice*, Butterworth, London, 1994.
4 A. I. Cooper, *J. Mater. Chem.*, 2000, **10**, 207.
5 A. J. Mesiano, E. J. Beckman and A. J. Russell, *Chem. Rev.*, 1999, **99**, 623.
6 F. Rindfleisch, T. P. DiNoia and M. A. McHugh, *J. Phys. Chem.*, 1996, **100**, 15581.
7 B. Subramaniam, R. A. Rajewski and K. Snavely, *J. Pharm. Sci.*, 1997, **86**, 885.
8 T. J. Young, K. P. Johnston, K. Mishima and H. Tanaka, *J. Pharm. Sci.*, 1999, **88**, 640.
9 F. S. Mandel, *5th Meeting on Supercritical Fluids*, Nice, France, 1998, p. 69.
10 D. B. Volkin, A. Staubli, R. Langer and A. M. Klibanov, *Biotechnol. Bioeng.*, 1991, **37**, 843.
11 S. K. Goel and E. J. Beckman, *Polym. Eng. Sci.*, 1994, **34**, 1137.
12 D. J. Mooney, D. F. Baldwin, N. P. Suh, L. P. Vacanti and R. Langer, *Biomaterials*, 1996, **17**, 1417.
13 M. H. Sheridan, L. D. Shea, M. C. Peters and D. J. Mooney, *J. Controlled Release*, 2000, **64**, 91.
14 D. A. Edwards, J. Hanes, G. Caponetti, J. Hrkach, A. BenJebria, M. L. Eskew, J. Mintzes, D. Deaver, N. Lotan and R. Langer, *Science*, 1997, **276**, 1868.
15 D. D. Hile, M. L. Amirpour, A. Akgerman and M. W. Pishko, *J. Controlled Release*, 2000, **66**, 177.

Metal ion complexation by a new, highly sterically hindered, bowl-shaped carboxylate ligand†

Ferman A. Chavez, Lawrence Que, Jr.* and William B. Tolman*

Department of Chemistry and Center for Metals in Biocatalysis, University of Minnesota, 207 Pleasant St. SE, Minneapolis, Minnesota 55455, USA. E-mail: que@chem.umn.edu; tolman@chem.umn.edu

Received (in Irvine, CA, USA) 7th August 2000, Accepted 14th November 2000
First published as an Advance Article on the web 15th December 2000

A carboxylate encapsulated by arene groups arranged in a bowl-like shape coordinates to Fe(II), Co(II) and Cu(II) to form mononuclear complexes with atypical structures enforced by the extreme steric demands of the ligand.

Carboxylate groups (from Asp or Glu side chains or C termini) play key roles as supporting ligands in a diverse array of metalloprotein active sites.[1] Such carboxylates are notable for the facility with which they adopt different binding modes,[2] in particular during the catalytic cycles of dioxygen-activating mono- and di-iron enzymes.[3] In efforts to synthesize models of these metalloprotein active sites, we[4] and others[5,6] have begun using sterically bulky carboxylate ligands in order to control coordination geometry, mimic the hydrophobic active site environment, and access coordinatively unsaturated species akin to those implicated during enzymatic catalysis. For example, novel biologically relevant structures and reactivity have been discovered for iron complexes of carboxylates **1**[4] and

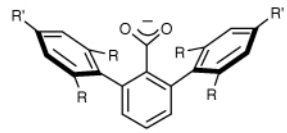

1 (R = R′ = Me)
2 (R = H, R′ = Me)

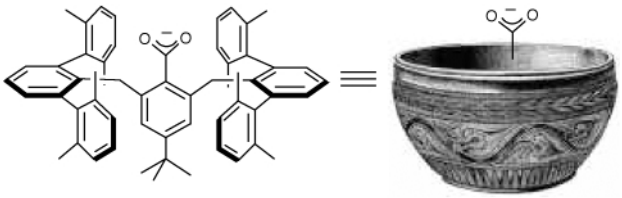

3

2,[5] which contain arene substituents on the benzoate unit that provide a high degree of hydrophobic 'shielding'. In expectation of even greater encapsulation of metal sites in model complexes, we targeted **3**, a carboxylate derivative of the known irregular 'bowl-shaped' 4-*tert*-butyl-2,6-bis[(2,2″,6,6″-tetramethyl-*m*-terphenyl-2′-yl)methyl]phenyl (Bmt) fragment that was used to isolate various species BmtX (X = Br, SH, SO, SI, SO_2H, AlH_3).[7] Herein we report the successful synthesis and X-ray crystallographic characterization of $BmtCO_2H$ (**3**-H) and Fe(II), Co(II) and Cu(II) complexes of **3**, which adopt atypical structures owing to the extreme steric bulk of the new carboxylate ligand.

The synthesis of $BmtCO_2H$ was achieved by lithiation of BmtBr,‡ addition of CO_2(g), acidification, and then column chromatography. The product was identified using spectroscopic (ESI†) and X-ray diffraction§ data. Treatment of $BmtCO_2H$ with Bu^nLi in thf afforded the lithium carboxylate ($BmtCO_2Li$·2thf) that was isolated as an analytically pure solid for use as the starting material for the preparation of metal complexes.

Reaction of $BmtCO_2Li$·2thf (2 equiv.) with MCl_2 in MeOH afforded $[M(BmtCO_2)_2(MeOH)_n]$·*m*MeOH [M = Fe(II), Co(II), $n = m = 4$; M = Cu(II), $n = 2$, $m = 0$]. Use of > 2 equiv. of the carboxylate yielded the same products, indicating that only two of these bulky ligands may be accommodated. The X-ray crystal structures§ of the Fe and Cu complexes are shown in Figs. 1 and 2, respectively. The Co structure is isomorphous with that of Fe, so only data for the Fe case is presented. Common to all of the complexes is a *trans* disposition of two

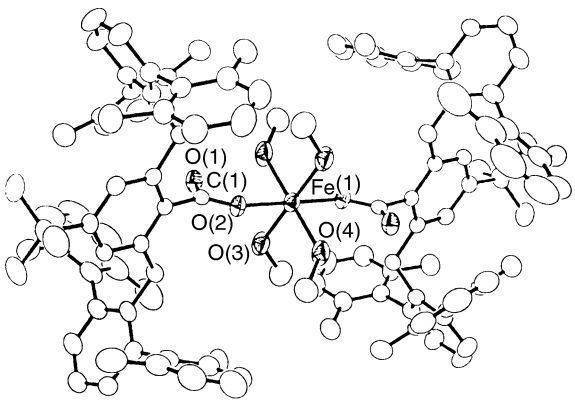

Fig. 1 Representation of the X-ray crystal structure of $[Fe(BmtCO_2)_2(MeOH)_4]$·4MeOH as 50% thermal ellipsoids, with H atoms and the solvent molecules omitted for clarity. Selected bond distances (Å) and angles (°): Fe(1)–O(2) 2.125(18), Fe(1)–O(3) 2.162(2), Fe(1)–O(4) 2.091(2), Fe(1)···O(1) 3.225(2); O(4)–Fe(1)–O(2) 89.69(8), O(4)–Fe(1)–O(3) 90.86(10), O(2)–Fe(1)–O(3) 89.30(8).

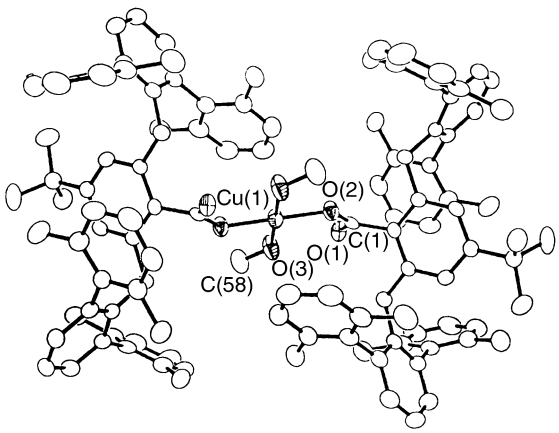

Fig. 2 Representation of the X-ray crystal structure of $[Cu(BmtCO_2)_2(MeOH)_2]$ as 50% thermal ellipsoids, with H atoms omitted for clarity. Selected bond distances (Å) and angles (°): Cu(1)–O(2) 1.893(2), Cu(1)–O(3) 1.950(2), Cu(1)···O(1) 3.245; O(2)–Cu(1)–O(3) 91.70(9), O(2)–Cu(1)–O(3a) 88.30(9).

† Electronic supplementary information (ESI) available: detailed procedures for the syntheses of BmtBr, $BmtCO_2H$ and $BmtCO_2Li$ as well as characterization data for all new compounds. See http://www.rsc.org/suppdata/cc/b0/b006647h/

DOI: 10.1039/b006647h

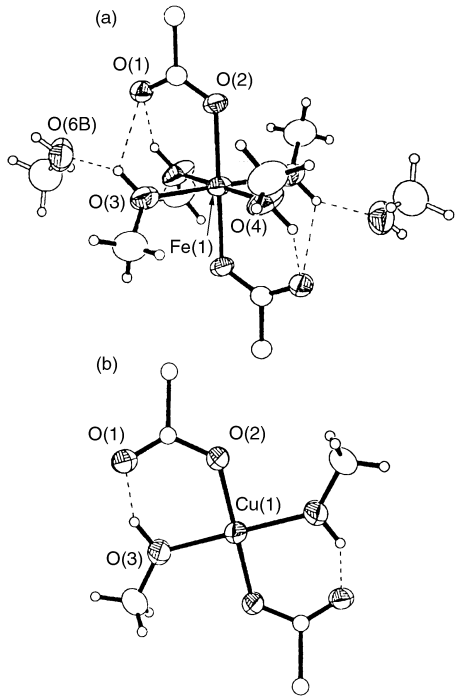

Fig. 3 Coordination spheres of (a) $[Fe(BmtCO_2)_2(MeOH)_4]\cdot 4MeOH$ (showing two of the MeOH solvent molecules; the other two are highly disordered) and (b) $[Cu(BmtCO_2)_2(MeOH)_2]$, with hydrogen bonding interactions indicated by dashed lines. Relevant interatomic distances (Å): (a) O(1)···O(4a) 2.582(3), O(1)···O(3) 3.199(3), O(3)···O(6b) 2.718(7), (b) O(1)···O(3) 2.511(3) Å.

$BmtCO_2^-$ ligands that coordinate in a *syn* monodentate fashion. The noncoordinating carboxylate oxygen atoms participate in hydrogen bonding with the bound MeOH ligands (Fig. 3). Additional hydrogen bonding occurs in the Fe and Co complexes involving included solvent MeOH molecules. Similar intramolecular hydrogen bonding patterns have been seen in other Fe(II)[8] and Cu(II)[9] carboxylate complexes and have been suggested to play a role in stabilizing their structures.

Mononuclear bis(carboxylato) iron(II) complexes possessing *trans* carboxylates are rare,[4a,c,10] and $[Fe(BmtCO_2)_2(MeOH)_4]$ is a unique example with an all-oxygen donor set. The O_{carb}–Fe–O_{carb} angle of 180° presumably results from the tendency of the $BmtCO_2^-$ ligands to position themselves as far apart as possible. This angle in the other two known bis(carboxylato) iron(II) complexes with *trans* monodentate carboxylate groups deviates significantly from linearity [168.5(2) and 154.74(8)°].[4a,c,10] The small space remaining in the equatorial plane of the octahedral $BmtCO_2^-$ complex is ideal for accommodation of small donors such as MeOH.

A Cu(II) complex possessing the same donor set as $[Cu(BmtCO_2)_2(MeOH)_2]$ has been reported,[9a] but in this complex of a functionalized benzoate ('furosemide') there are additional weak axial interactions between the Cu(II) center and the carboxylate oxygen atoms from adjacent molecules [Cu–O 2.720(4) Å]. In the $BmtCO_2^-$ compound, no other potential donor ligand is within bonding distance to the square-planar Cu(II) center due to blocking of the apical site by the carboxylate xylyl groups. The mononuclear structure of the complex contrasts with the familiar dinuclear paddlewheel[11] or other common topologies in which carboxylates bridge between multiple Cu(II) centers.[12] The discrete structure of $[Cu(BmtCO_2)_2(MeOH)_2]$ is also unusual insofar as many Cu(II) carboxylate complexes which exist as monomers in solution form intermolecular hydrogen bonded extended structures in the solid state.[13]

In conclusion, we have developed a synthesis of the carboxylate **3** in which the ligating unit is encapsulated in an irregular 'molecular bowl'. The extreme steric demands of the ligand have been illustrated through characterization of the monomeric Fe(II), Co(II) and Cu(II) complexes comprising two molecules of **3** coordinated *trans* in a *syn* monodentate mode. Further studies will explore the potential for the use of **3** and the complexes described herein for accessing unusual structures pertinent to nonheme, carboxylate rich metalloprotein active sites.

We thank Dr Katherine Aubrecht and Dr Victor G. Young, Jr., for the structural determination of $BmtCO_2H$ (**3**-H), Jamie Schneider for her efforts in improving the synthesis of BmtBr, and the NIH (GM38767 to L. Q.) for financial support.

Notes and references

‡ The precursor BmtBr was synthesized *via* the method described in ref. 7(*e*), but improvements were made that allowed the product to be isolated in higher yield (70% *vs*. 32%). For detailed procedures for the syntheses of BmtBr, $BmtCO_2H$ and $BmtCO_2Li$, see ESI.†

§ *Crystal data* for $BmtCO_2H$ (**3**-H): $C_{171}H_{174}O_6$, M = 2325.10, triclinic, space group $P\bar{1}$, a = 13.2288(7), b = 21.7697(11), c = 26.0770(13) Å, α = 76.040 (1), β = 82.286(1), γ = 84.717(1)°, V = 7208(1) Å^3, T = 173(2) K, Z = 2, μ(Mo-Kα) = 0.062 mm^{-1}, 63 469 reflections measured, 32 161 unique (R_{int} = 0.027) which were used in all calculations. The final $wR(F^2)$ was 0.1298 (all data), $R1$ = 0.0541. For $[Fe(BmtCO_2)_2(MeOH)_4]\cdot 4MeOH$: $C_{122}H_{146}O_{12}Fe$, M = 1860.24, monoclinic, space group $P2_1/n$, a = 21.1152(13), b = 13.3988(9), c = 21.1719(13) Å, β = 115.0900(10)°, V = 5424.7(6) Å^3, T = 173(2) K, Z = 2, μ(Mo-Kα) = 0.198 mm^{-1}, 27 850 reflections measured, 9562 unique (R_{int} = 0.0481) which were used in all calculations. The final $wR(F^2)$ was 0.1772 (all data), $R1$ = 0.0558. For $[Cu(BmtCO_2)_2(MeOH)_2]$: $C_{116}H_{122}O_6Cu$, M = 1675.68, monoclinic, space group $P2_1/n$, a = 15.2154(7), b = 11.1085(5), c = 27.7956(12) Å, β = 97.9700(10)°, V = 4652.6(4) Å^3, T = 173(2), Z = 2, μ(Mo-Kα) = 0.292 mm^{-1}, 23 238 reflections measured, 8203 unique (R_{int}) = 0.0439) which were used in all calculations. The final $wR(F^2)$ was 0.1795 (all data), $R1$ = 0.0598. CCDC 182/1859. See http://www.rsc.org/suppdata/cc/b0/b006647h/ for crystallographic files in .cif format.

1 R. H. Holm, P. Kennepohl and E. I. Solomon, *Chem. Rev.*, 1996, **96**, 2239.
2 R. L. Rardin, W. B. Tolman and S. J. Lippard, *New J. Chem.*, 1991, **15**, 417.
3 A. L. Feig and S. J. Lippard, *Chem. Rev.*, 1994, **94**, 759; L. Que, Jr., in *Bionorganic Catalysis*, ed. J. Reedijk and E. Bouman, Marcel Dekker, Inc., 1999; B. J. Wallar and J. D. Lipscomb, *Chem. Rev.*, 1996, **96**, 2625.
4 J. R. Hagadorn, L. Que, Jr. and W. B. Tolman, *J. Am. Chem. Soc.*, 1998, **120**, 13 531; (*b*) J. R. Hagadorn, L. Que, Jr., W. B. Tolman, I. Prisecaru and E. Münck, *J. Am. Chem. Soc.*, 1999, **121**, 9760; (*c*) J. R. Hagadorn, L. Que, Jr. and W. B. Tolman, *Inorg. Chem.*, 2001, **40**, in press.
5 D. Lee and S. J. Lippard, *J. Am. Chem. Soc.*, 1998, **120**, 12 153; (*b*) D. Lee, J. D. Bois, D. Petasis, M. P. Hendrich, C. Kres, B. H. Huynh and S. J. Lippard, *J. Am. Chem. Soc.*, 1999, **121**, 9893; (*c*) D. Lee, C. Krebs, B. H. Huynh, M. P. Hendrich and S. J. Lippard, *J. Am. Chem. Soc.*, 2000, **122**, 5000.
6 S. C. Payne and K. S. Hagen, *J. Am. Chem. Soc.*, 2000, **122**, 6399.
7 K. Goto, J. Kobayashi and R. Okazaki, *Organometallics*, 1999, **18**, 1357; (*b*) K. Goto, M. Holler and R. Okazaki, *Chem. Commun.*, 1998, 1915; (*c*) K. Goto, M. Holler and R. Okazaki, *J. Am. Chem. Soc.*, 1997, **119**, 1460; (*d*) K. Goto and R. Okazaki, *Liebigs Ann./Recueil*, 1997, 2393; (*e*) K. Goto, M. Holler and R. Okazaki, *Tetrahedron Lett.*, 1996, **37**, 3141.
8 S. Herold and S. J. Lippard, *J. Am. Chem. Soc.*, 1997, **119**, 145; M. M. Morelock, M. L. Good, L. M. Trefonas, R. Majeste and D. G. Karraker, *Inorg. Chem.*, 1982, **21**, 3044.
9 For examples, see: (*a*) P. Bontchev, H. Kadum, G. Gochev, B. Evtimova, J. Macicek and C. Nachev, *Polyhedron*, 1992, **11**, 1973; (*b*) H. Muhonen, *Acta Crystallogr., Sect. C*, 1983, **39**, 536.
10 B. Singh, J. R. Long, G. C. Papaefthymiou and P. Stavropoulos, *J. Am. Chem. Soc.*, 1996, **118**, 5824; B. Singh, J. R. Long, F. F. deBiani, D. Gatteschi and P. Stavropoulos, *J. Am. Chem. Soc.*, 1997, **119**, 7030.
11 R. J. Doedens, *Prog. Inorg. Chem.*, 1975, **19**, 173; M. Melnik, *Coord. Chem. Rev.*, 1982, **42**, 259.
12 G. Psomas, C. P. Raptopoulou, L. Iordanidis, C. Dendrinou-Samara, V. Tangoulis and D. P. Kessissoglou, *Inorg. Chem.*, 2000, **39**, 3042 and references cited therein.
13 For example, see: H. Muhonen, *Acta Crystallogr., Sect. C*, 1983, **39**, 536; C. K. Prout, R. A. Armstrong, J. R. Carruthers, J. G. Forrest, P. Murray-Rust and J. C. Rossotti, *J. Chem. Soc. A*, 1968, 2791; C. K. Prout, M. J. Barrow and F. J. C. Rossotti, *J. Chem. Soc. A*, 1971, 3326.

Stereoselective phenolic coupling in *Blechnum spicant*: formation of 8–2′ linked (−)-*cis*-blechnic, (−)-*trans*-blechnic and (−)-brainic acids†

Chang-Zeng Wang, Laurence B. Davin and Norman G. Lewis*

Institute of Biological Chemistry, Washington State University, Pullman, USA WA 99164-6340.
E-mail: lewisn@wsu.edu; Tel.: 509-335-2682; Fax: 509-335-8206

Received (in Corvallis, OR) 9th October 2000, Accepted 14th November 2000
First published as an Advance Article on the web

***In vivo* administration experiments using stable (^{13}C) and radio (^{14}C) labeled precursors provide further evidence for vascular plant proteins engendering specific but distinct phenolic coupling modes, *i.e.* in this case for stereoselective 8–2′ coupling leading to the optically active lignans, (–)-blechnic and (–)-brainic acids.**

The ferns (*Pteridophytes*) are evolutionary forerunners of the gymnosperms and angiosperms. They contain various phenolic natural products which may represent some of the earliest examples *in planta* of control of stereoselective phenolic coupling. For example, *Blechnum spicant* (deer fern) and *B. orientale*[1] accumulate the unusually linked, optically active, 8–2′ lignans, (−)-blechnic **1** and (−)-brainic **2** acids.

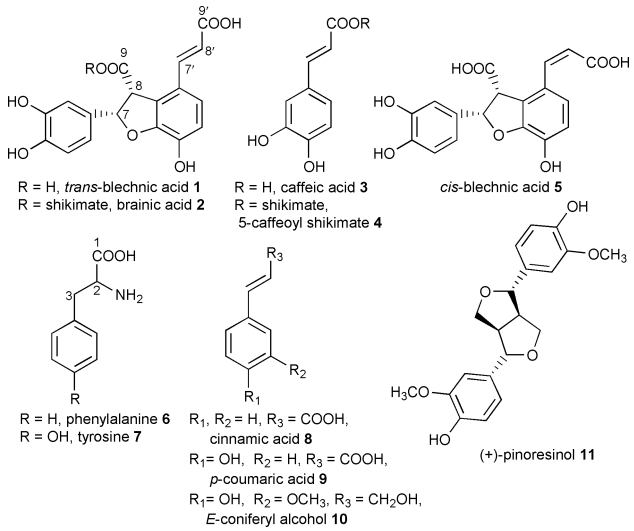

Gymnosperm and angiosperm lignans are frequently derived from stereoselective 8–8′ coupling of two monolignol (hydroxycinnamyl alcohol) radicals,[2] and the recent discovery of dirigent proteins (Latin: *dirigere*, to guide or to align) and their corresponding genes gave a new perspective into how free radical coupling is controlled in plants *in vivo*.[3–5] There have been no reports on the stereoselective control of other coupling modes, and hence establishing the mechanism of 8–2′ linked lignan formation in the Blechnaceae would be instructive.

The MeOH extract of *B. spicant* contains as its principal metabolites, caffeic acid **3**, 5-caffeoyl shikimate **4**, (−)-*trans*-blechnic acid **1** and (−)-brainic acid **2**. An unknown compound **5** was also isolated, which on standing in open solution (in CH_3CN or H_2O) over 72 h, was converted into (−)-*trans*-blechnic acid **1**. Compound **5** ($[\alpha]_D$ −128°, *c* 0.58, MeOH) had a molecular formula of $C_{18}H_{14}O_8$ as evidenced from its HR-MS (381.7373 $[M+Na]^+$); furthermore, comparison of its ^{1}H and ^{13}C NMR spectral data with those of (−)-blechnic acid (−)-**1** revealed that both structures were very similar, except for a *cis*-double bond in **5** [^{1}H NMR: 6.74 (1H, d, J = 12.7 Hz, H-7′), 5.88 (1H, d, J = 12.7 Hz, H-8′); ^{13}C NMR: 139.7 (C-7′) and 120.2 (C-8′)] *vs.* the *trans* double bond in blechnic acid **1** [^{1}H NMR: 7.57 (1H, d, J = 16.1 Hz, H-7′), 6.27 (1H, d, J = 16.1 Hz, H-8′); ^{13}C NMR: 143.3 (H-7′) and 117.8 (H-8′)]. Correlations (or connectivities) for compound **5** were determined by 2D-NMR (^{1}H-^{1}H COSY, HMQC, HMBC) spectroscopic analyses conducted at low temperature (−25°C), and the configuration of the *cis*-double bond was further confirmed by both NOE experiments and a comparison to that of (−)-*trans*-blechnic acid **1**.

The precursor relationships to the optically active 8–2′ linked lignans was examined through deployment of radiolabeled Phe **6**, Tyr **7**, cinnamic **8**, *p*-coumaric **9** and acetic acids as potential precursors over extended durations (Table 1). Thus, caffeic acid **3**, 5-caffeoyl shikimate **4**, (−)-*cis*-blechnic **5**, (−)-*trans*-blechnic **1** and (−)-brainic **2** acids, were individually isolated with the relative total radiochemical incorporation for each estimated by liquid scintillation counting (see Table 1). Significantly, a rapid incorporation into (−)-*cis*-blechnic acid **5** (~3%) was noted within 8 h, relative to that of (−)-*trans*-blechnic **1** and (−)-brainic **2** acids (≤0.1%). This indicated that (−)-*cis*-blechnic acid **5** was the initial coupling product, since it was apparently further metabolized into (−)-*trans*-blechnic **1** and (−)-brainic **2** acids based on the trends of total incorporation noted for **1** and **2** which approached *c.* 1–2 and 3–4% over 48–84 h, respectively. A less likely interpretation is that **5** might be a shunt metabolite and not directly involved in the formation of **1** and **2**. For each time frame examined, the relative incorporation into (−)-brainic acid **2** was higher than that into (−)-blechnic acid **1**, suggesting that *cis*-blechnic acid **5** was more effectively channeled into (−)-brainic acid **2** rather than into (−)-blechnic acid **1**. In a somewhat analogous manner, both [3-^{14}C]cinnamic **8**, and [2-^{14}C]*p*-coumaric **9** acids served as precursors, whereas neither [*U*-^{14}C]tyrosine **7** nor [2-^{14}C]NaOAc were incorporated into any of the various metabolites of *B. spicant* examined, (data not shown).

L-[3-^{13}C], [2-^{13}C] and [1-^{13}C] phenylalanine **6** (1.0 mM) were next individually administered to *B. spicant* fronds for 5 days, with the resulting (−)-brainic **2** and (−)-*trans*-blechnic **1** acids isolated by preparative μBondapak C18 column HPLC and subjected to ^{13}C-NMR spectroscopic analyses (see Fig. 1a–d). Only the data for (−)-brainic acid **2** are presented. Fig. 1a shows the natural abundance NMR spectrum and the corresponding assignments for (−)-brainic **2** acid; these are based on 2-D NMR spectroscopic analyses (HMQC, HMBC and ^{1}H-^{1}H COSY) and previous assignments by Wada *et al.*[1] The (−)-brainic **2** acid obtained following administration of [1-^{13}C]Phe **6** displayed carbon-13 enriched resonances for C-9 and C-9′ at 170.5 and 170.6 ppm, respectively (Fig. 1b). In a

† Electronic supplementary information (ESI) available: ^{13}C-NMR spectra of (a) natural abundance (−)-*trans*-blechnic **1** acid, as well as (−)-*trans*-blechnic acids **1** obtained following administration of (b) [1-^{13}C], (c) [2-^{13}C] and (d) 3-^{13}C]-phenylalanine **6** (1 mM) to *B. spicant* fronds for 5 days; all spectra were recorded under identical conditions.

The relative carbon-13 enrichments noted were higher for (−)-brainic acid **2** than for (−)-*trans*-blechnic **1** due in large part to the much higher endogeneous levels of the latter in *B. spicant*. See http://www.rsc.org/suppdata/cc/b0/b008174o/

Table 1 Incorporation of ^{14}C-labeled potential precursors into various *B. spicant* phenolic metabolites (% incorporation)

	Potential precursor administered (radio-activity)	Metabolic period (h)	Caffeic acid **3** (% incor-poration)	5-Caffeoyl shikimate **4**	(−)-*cis*-Blechnic acid **5**	(−)-*trans*-Blechnic acid **1**	(−)-Brainic acid **2**
A	[*U*-^{14}C] Phenylalanine **6** (200 μL, 148 kBq, 18.5 GBq nmol^{-1})	4	1.2	1.7	1.1	< 0.1	< 0.1
		8	2.3	3.4	3.0	< 0.1	0.1
		12	2.3	2.5	2.6	0.1	0.4
		18	2.0	3.2	3.9	0.5	1.4
		24	2.9	4.1	2.3	0.6	1.6
		30	2.9	5.1	2.7	0.7	1.6
		36	5.0	4.7	2.0	0.7	1.9
		48	4.5	5.3	1.4	1.1	2.9
		84	2.8	3.3	1.3	2.1	4.2
B	[3-^{14}C] Cinnamic acid **8** (200 μL, 185 kBq, 1.89 GBq nmol^{-1})	24	2.9	6.9	3.5	2.0	1.5
		50	3.8	5.6	1.0	1.1	1.4
		84	2.7	5.6	1.2	1.5	1.2
C	[2-^{14}C] *p*-Coumaric acid **9** (200 μL, 148 kBq, 6.07 GBq nmol^{-1})	24	1.0	3.0	1.4	0.5	0.7

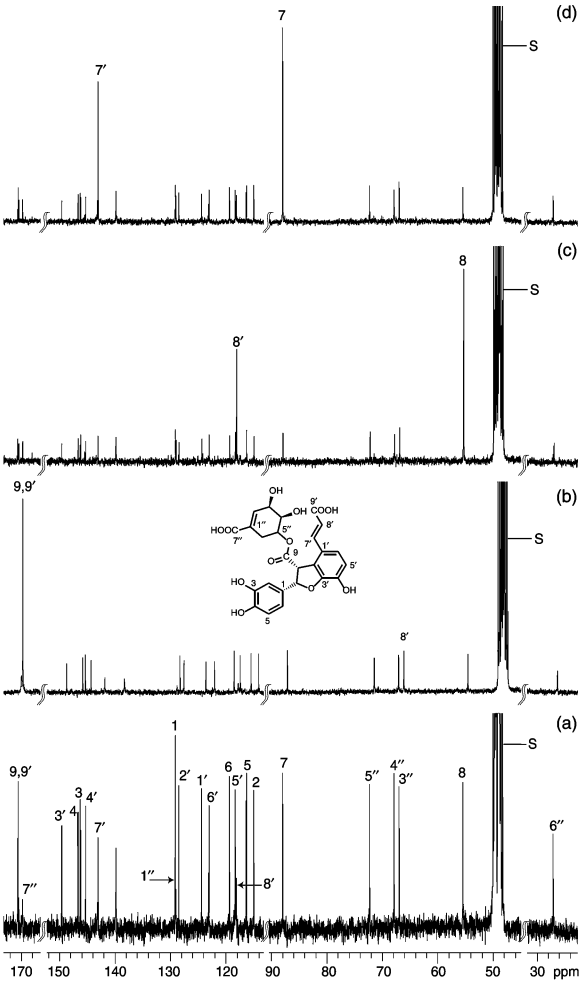

Fig. 1 ^{13}C-NMR spectra of (a) natural abundance (−)-brainic **2** acid, as well as (−)-brainic acids **2** obtained following administration of (b) [1-^{13}C], (c) [2-^{13}C] and (d) [3-^{13}C]phenylalanine **6** (1 mM) to *B. spicant* fronds for 5 days; all spectra were recorded under identical conditions.

similar manner, administration of [2-^{13}C]Phe **6** gave enhanced signals for the C-8 and C8′ resonances of (−)-brainic **2** acid at 55.4 and 118.2 ppm (Fig. 1c), whereas with [3-^{13}C]Phe **6**, the corresponding enhanced signals at C-7 and C7′ were at 88.0 and 142.7 ppm (Fig. 1d). Comparable results were observed for (−)-*trans*-blechnic acid **1** biosynthesis (see ESI†).

We propose that the 8–2′ linked lignans, (−)-blechnic **1** and (−)-brainic **2** acids, result from oxidative coupling of caffeic acid **3** as depicted in Scheme 1. Based on the trends of relative incorporations into **5**, **1** and **2**, this conversion is likely to result *via* stereoselective coupling of two molecules of either *cis*- or

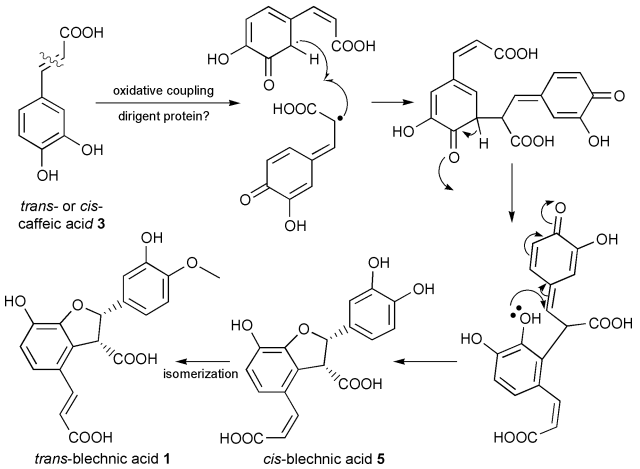

Scheme 1 Proposed stereoselective coupling of caffeic acid **3** leading to (−)-*trans*-blechnic acid **1**.

trans-caffeic acid **3** to first afford (−)-*cis*-blechnic acid **5**. Less likely, stereoselective coupling could involve *p*-coumaric acid **9** with subsequent hydroxylation of the aromatic ring to ultimately afford the corresponding catechols **1** and **2**. In any case, by comparison to the dirigent mediated stereoselective bimolecular coupling of coniferyl alcohol **10** affording (+)-pinoresinol **11**, it is tempting to suggest that the formation of the blechnates **1** and **2** may involve a comparable process.[4,5] This will be established in the future by isolation and characterization of the relevant proteins and enzymes involved in the biosynthesis of (−)-*trans*-blechnic acid **1** and its derivatives in *B. spicant*; nevertheless both 8–8′ and 8–2′ linked phenylpropanoid coupling products are under full proteinaceous control thereby stipulating the outcome of stereoselective coupling.

The authors thank the USDOE (DE-FG03-97ER20259) and the NSF (MCB-9976684), as well as the L. B. and D. Cullman and G. T. Hargrove Center for Land Plant Adaptation.

Notes and references

1 H. Wada, T. Kido, N. Tanaka, T. Murakami, Y. Saiki and C. M. Chen, *Chem. Pharm. Bull.*, 1992, **40**, 2099.
2 N. G. Lewis and L. B. Davin, *Lignans: Biosynthesis and Function*, in *Comprehensive Natural Products Chemistry*, Vol. 1, ed. Sir D. H. R. Barton, K. Nakanishi and O. Meth-Cohn, Elsevier, London, pp 639-712.
3 L. B. Davin and N. G. Lewis, *An. Acad. Bras. Cienc. Suppl. 3*, 1995, **67**, 363.
4 L. B. Davin, H. B. Wang, A. L. Crowell, D. L. Bedgar, D. M. Martin, S. Sarkanen and N. G. Lewis, *Science*, 1997, **275**, 362.
5 D. R. Gang, M. A. Costa, M. Fujita, A. T. Dinkova-Kostova, H. B. Wang, V. Burlat, W. Martin, S. Sarkanen, L. B. Davin and N. G. Lewis, *Chem. Biol.*, 1999, **6**, 143.

Modulation of the water exchange rates in [Gd–DO3A] complex by formation of ternary complexes with carboxylate ligands

Silvio Aime,*[a] Mauro Botta,[b] James I. Bruce,[c] Valentina Mainero,[d] David Parker[c] and Enzo Terreno[a]

[a] *Dipartimento di Chimica IFM, Università di Torino, Via P. Giuria 7, I-10125 Torino, Italy. E-mail: aime@ch.unito.it*
[b] *Dipartimento di Scienze e Tecnologie Avanzate, Università del Piemonte Orientale 'Amedeo Avogadro', C.so Borsalino 54, I-15100 Alessandria, Italy*
[c] *Department of Chemistry, University of Durham, South Road, Durham, UK DH1 3LE*
[d] *Laboratorio Integrato di Metodologie Avanzate, Bioindustry Park Canavese, Via Ribes 5, I-10010, Colleretto Giacosa (TO), Italy*

Received (in Cambridge, UK) 29th September 2000, Accepted 20th November 2000
First published as an Advance Article on the web 15th December 2000

Ternary complexes of formula [Gd–DO3A–L–(H_2O)] (where L is a carboxylate-containing ligand) display exchange lifetimes of the metal-coordinated water that can be modulated as a function of L.

Paramagnetic Gd(III) chelates are currently under intense scrutiny for their use as contrast agents (CAs) for magnetic resonance imaging (MRI).[1] Their efficiency is usually expressed in terms of relaxivity (r_1), which represents the relaxation enhancement of the water protons at mmol concentration of the paramagnetic agent. The relaxivity is the result of a complex interplay of several structural, dynamic and electronic parameters. Recently, it has been shown that the exchange lifetime of the coordinated water, τ_M, may have a key role in determining the relaxivity of a Gd(III) complex.[2] In fact,it has been found that τ_M covers a whole range of values ranging from few ns in the aqua-ion[3] up to several μs in complexes of octadentate neutral macrocyclic ligands.[4] In systems containing one coordinated water only (q = 1) it has been shown that the exchange process occurs through a dissociative mechanism and the relative exchange rate is dependent upon the energy difference between the nona-coordinate ground state and the octa-coordinate transition intermediate.[5] Thus, an increased encumbrance in the ground-state structure results in a smaller energy jump to reach the intermediate state with a consequent increase in the water exchange rate.[6] Moreover, it has been found that in DOTA-like systems, the isomer possessing a twisted antiprismatic structure displays an exchange rate of the bound water that is *ca*. 50 times faster than that observed for the isomer endowed with a more compact square antiprismatic geometry.[7,8] Thus, minor structural variations may have remarkable effect on the exchange lifetime of the coordinated water in lanthanide(III) chelates.

As far as the use as CA for MRI is concerned, optimal values of τ_M for the attainment of high relaxivities [once the Gd(III) is part of a slowly moving macromolecular substrate] fall in the range of few tenths of ns.[9] Thus, it is relevant to gain more insight into the structural factors which are responsible of the exchange rate of the coordinated water. Recently, it has been shown that coordinatively unsaturated Gd(III) chelates with q > 1 are able to readily form ternary complexes with suitable ligands such as carboxylates. The formation of such adducts involves the replacement of one or more Gd-bound water molecules by the ligand.[10,11] Herein, we show that the mixed complexes [Gd–L–L′–(H_2O)], where L is the heptadentate ligand DO3A[12] and L′ is a carboxylate-containing ligand, display exchange lifetimes of the metal coordinated water which can be modulated as a function of the added ligand.

The formation of ternary adducts has been followed by analyzing the changes of relaxivity upon L′ concentration. The [Gd–DO3A] complex has a relatively high r_1 value (6.0 mM^{-1} s^{-1} at 20 MHz and 25 °C[14]) as the largely dominant isomer[13] displays two metal-bound water molecules (average q value = 1.8). Upon adding sodium propionate or L-alanine to a solution of [Gd–DO3A], a progressive decrease of r_1 was observed (Fig. 1). This effect is related to the replacement of one Gd-coordinated water molecule by the entering ligand. The fitting of these data according to the PRE (proton relaxation enhancement) theory[15] allowed us to estimate either the relaxivities of the ternary complexes, which are consistent for Gd(III) chelates of the expected molecular size and q = 1, or the binding constant between the paramagnetic complex and the ligand (Table 1).

As a further check, we evaluated, by luminescence measurements, the metal complex–substrate affinity as well as the hydration state of the resulting mixed complexes. The comparison between the rate constants of the luminescence decay for [Tb–DO3A] adducts in H_2O and D_2O assures about the presence of a residual lanthanide bound water molecule, whereas by looking at the changes in the intensity of the emission spectra at 545 nm [corresponding to the ΔJ = 1 transition of Tb(III) ion] upon the addition of the substrates, K_A values in agreement with those measured by the PRE analysis were obtained (Table 1).

The exchange rate of the metal bound water molecule in this class of paramagnetic complexes may be conveniently deter-

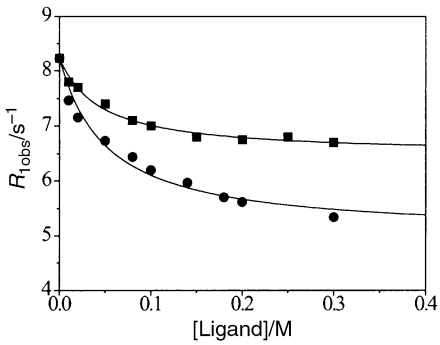

Fig. 1 PRE titration of a 1.15 mM solutions of [Gd–DO3A–(H_2O)$_2$] with L-alanine (■) and sodium propionate (●); 0.235 Tesla, pH 7, 25 °C.

Table 1 Relaxivities, 1:1 association constants and hydration numbers (q) for [Ln–DO3A–L′–(H_2O)] (Ln = Gd or Tb) ternary complexes (20 MHz, 25 °C)

	[Gd–DO3A–L′]		[Tb–DO3A–L′]	
L′	r_1/mM^{-1} s^{-1}	K_A/M^{-1}	K_A/M^{-1}	q
Propionate	3.7	17	25	1.0
L-Alanine	4.7	19	< 50	1.35

DOI: 10.1039/b007901o

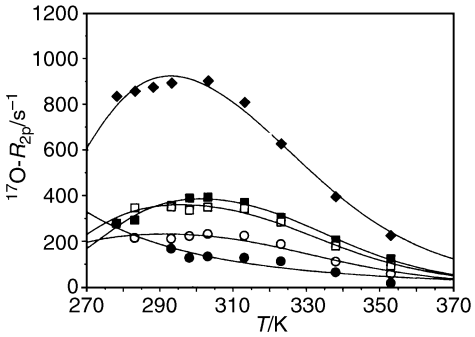

Fig. 2 ^{17}O-R_{2p} *vs.* T of 27.3 mM solutions of [Gd–DO3A–$(H_2O)_2$] (◆), [Gd–DO3A–propionate–(H_2O)]$^-$ (●), [Gd–DO3A–alanine–(H_2O)] (■), [Gd–DO3A–α-aminobutyrate–(H_2O)] (□) and [Gd–DO3A–β-aminobutyrate–(H_2O)] (○); 7.1 Tesla, pH 7.

mined by measuring the temperature dependence of water ^{17}O-R_{2p}.

In fact, the R_{2p} values are basically a function of q, τ_M and the electronic relaxation times of the metal ion T_{ie} (i = 1,2). Two different regimes can be met, one occurring at low temperatures, in which the changes in R_{2p} are mainly determined by τ_M (slow exchange region) and one at higher temperatures, essentially dominated by T_{ie} (fast exchange region). For many systems displaying τ_M in the range of few hundreds of nanoseconds R_{2p} displays a bell-shaped curve (as shown in Fig. 2 for [Gd–DO3A–$(H_2O)_2$] at 7.05 T, τ_M^{298} = 80 ns). The ^{17}O-R_{2p} values for the ternary complexes [Gd–DO3A–propionate–(H_2O)]$^-$ and [Gd–DO3A–alanine–(H_2O)] are significantly smaller than those of the parent chelate owing to the reduction of q in the ternary adduct. Interestingly, the observed behaviour is consistent with the occurrence of a fast exchange of the metal bound water molecule in the case of [Gd–DO3A–propionate–(H_2O)]$^-$ (τ_M^{298} = 8 ns). Thus on going from [Gd–DO3A–$(H_2O)_2$] to [Gd–DO3A–propionate–(H_2O)]$^-$ there is a considerable shortening of the residence lifetime of the inner sphere water molecule. Furthermore, the observed τ_M is much shorter than that of [Gd–DOTA–(H_2O)]$^-$ and, interestingly, it is in the range of optimal values for providing the highest relaxivities for MRI applications.[9]

Surprisingly, the profile for the [Gd–DO3A–alanine–(H_2O)] adduct displays a different shape, indicative of a longer τ_M value (τ_M^{298} = 180 ns). This may reflect the occurrence of a hydrogen-bonding interaction between the metal bound water molecule and the positively charged α-amino group of the amino-acid, which could also be mediated by a solvent water molecule (Scheme 1).

In order to further check this hypothesis ^{17}O-R_{2p} *vs.* T profiles of the adducts between [Gd–DO3A–$(H_2O)_2$] and aminobutyrate anions differing in the position of the protonated amino group were recorded (Fig. 2).

The ^{17}O-R_{2p} values for the adduct with α-aminobutyrate are similar to those of the L-alanine adduct (τ_M^{298} = 120 ns). However, when the $-NH_3^+$ group is shifted to the β-position, the exchange lifetime decreases significantly (τ_M^{298} = 80 ns).

Therefore, these results clearly suggest that the position of the protonated amino group plays a key role for controlling the water exchange rate of the metal bound water molecule.

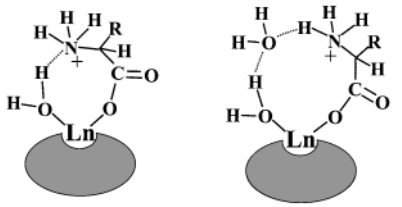

Scheme 1 Proposed representations of the ternary [Ln–DO3A–alanine–(H_2O)] adduct. The elongation of the residence lifetime of the metal bound water molecule may result from the occurrence of the hydrogen bonding network.

In summary, though it is difficult to foresee a MRI application for the Gd(III) based ternary complexes investigated in this work, the results here reported indicate a novel route to the modulation of the exchange rate of the coordinated water in Gd(III) complexes. Moreover, one may seek for the formation of ternary complexes between suitably functionalized Gd(III) chelates and endogenous substrates containing carboxylate functionalities.

Financial support from MURST and CNR (Biotechnology PF and L. 95/95) is gratefully acknowledged. This work was carried out under the framework of the COST-D18 action.

Notes and references

1 J. A. Peters, J. Huskens and D. J. Raber, *Prog. NMR Spectrosc.*, 1996, **28**, 283; P. Caravan, J. J. Ellison, T. J. McMurry and R. B. Lauffer, *Chem. Rev.*, 1999, **99**, 2293.
2 S. Aime, M. Botta, M. Fasano and E. Terreno, *Acc. Chem. Res.*, 1999, **32**, 941.
3 K. Micksei, H. D. Powell, L. Helm, E. Brücher and A. E. Merbach, *Magn. Reson. Chem.*, 1993, **31**, 1011.
4 S. Aime, A. Barge, M. Botta, D. Parker and A. S. De Sousa, *J. Am. Chem. Soc.*, 1997, **119**, 4767.
5 D. H. Powell, O. M. Ni Dhubhghaill, D. Pubanz, L. Helm, Y. S. Lebedev, W. Schlaepfer and A. E. Merbach, *J. Am. Chem. Soc.*, 1996, **118**, 9333.
6 D. Pubanz, G. González, D. H. Powell and A. E. Merbach, *Inorg. Chem.*, 1995, **34**, 4447.
7 S. Aime, A. Barge, M. Botta, A. S. De Sousa and D. Parker, *Angew. Chem.*, 1998, **37**, 2673.
8 F. A. Dunand, S. Aime and A. E. Merbach, *J. Am. Chem. Soc.*, 2000, **122**, 1506.
9 S. Aime, M. Botta, M. Fasano and E. Terreno, *Chem. Soc. Rev.*, 1998, **27**, 19.
10 S. Aime, A. Barge, M. Botta, J. A. K. Howard, R. Kataky, M. P. Lowe, J. M. Moloney, D. Parker and A. De Sousa, *Chem. Commun.*, 1999, 1047.
11 S. Aime, E. Gianolio, E. Terreno, G. B. Giovenzana, R. Pagliarin, M. Sisti, G. Palmisano, M. Botta, M. P. Lowe and D. Parker, *J. Biol. Inorg. Chem.*, 2000, **5**, 488.
12 D. D. Dischino, E. J. Delaney, J. E. Emswiler, G. T. Gaughan, J. S. Prasad, S. K. Srivastava and M. F. Tweedle, *Inorg. Chem.*, 1991, **30**, 1265.
13 E. Tóth, O. M. Ni Dhubhghaill, G. Besson, L. Helm and A. E. Merbach, *Magn. Res. Chem.*, 1999, **37**, 701.
14 S. Aime, M. Botta, S. Geninatti Crich, G. B. Giovenzana, R. Pagliarin, M. Sisti and E. Terreno, *Magn. Reson. Chem.*, 1998, **36**, S200.
15 R. A. Dwek, *Nuclear magnetic resonance in biochemistry, applications to enzyme systems*, Clarendon Press, Oxford, 1973, p. 247.

A molecular photoswitch based on an 'axial-bonding' type phosphorus(v) porphyrin

D. Raghunath Reddy and Bhaskar G. Maiya*

School of Chemistry, University of Hyderabad, Hyderabad 500 046, India. E-mail: bgmsc@uohyd.ernet.in

Received (in Cambridge, UK) 26th September 2000, Accepted 23rd November 2000
First published as an Advance Article on the web 15th December 2000

Reversible isomerization of the two axial azobenzene subunits leads to modulation of the fluorescence due to the basal tetrapyrrolic chromophore in a new hexa-coordinated phosphorus(v) porphyrin 3, illustrating its utility as a molecular photoswitch.

'Emitter–quencher' assemblies based on porphyrin building blocks are attracting increasing attention because of their importance as either model compounds in photosynthetic research or photoswitches in the fabrication of molecular electronic/optical devices.[1,2] While a great variety of covalently or non-covalently bound porphyrin–acceptor motifs are now known to closely mimic the initial, photoinduced electron transfer (PET) events of natural photosynthetic reactions,[1] the utility of such motifs as photoswitches has not been firmly established. In this regard, it is interesting that a key recurring theme of most earlier attempts to construct porphyrin-based photoswitches involves intramolecular PET coupled to isomerization (*E*/*Z*) of the azobenzene group.[3–8] This theme is an appealing one, and especially so, in view of the ready availability of PET-based non-porphyrinic photoswitches that incorporate azobenzene moieties in their architecture.[2] However, barring a recent exception,[4] photoswitching function has not been demonstrated in any of the porphyrin–azobenzene conjugates reported so far. Herein, we describe the luminescence on/off behavior observed in a novel, metalloid porphyrin-based photoswitch **3**, which is constructed by utilizing the 'axial-bonding' capability of a phosphorus(v) porphyrin- (Fig. 1).

The hydroxide salt of photoswitch **3** was synthesized in 70% yield by reacting [5,10,15,20-tetra(tolyl)porphyrinato]phosphorus(v) dichloride **1** and 4-hydroxyazobenzene (excess) **2**, in refluxing pyridine and purifying by column chromatography [silica gel, $CHCl_3$–MeOH 10 : 1, v/v)].[9] The ^{1}H NMR spectrum of this 'axial-bonding' type metalloid-porphyrin shows characteristic, porphyrin ring-current-induced upfield shifts for the protons on the axial aromatic ligands,[10] with the magnitude of shift for a given proton being a function of its separation distance from the porphyrin π-plane (see Fig. 1). On the other hand, effects due to the substitution of axial chlorides by the aryloxo ligands are minimal for the porphyrin pyrrole-β and meso-aryl proton resonances. However, in the ^{31}P NMR spectrum, the signal due to the central phosphorus ion of **3** was seen to be shifted downfield (δ −194.9, 85% H_3PO_4 external reference) compared to that of **1** (δ −229.4) but is within the typical range expected for hexa-coordinated diaryloxo phosphorus(v) porphyrins.[9] Further support for the structural integrity of **3** arises from the appearance of its molecular ion peak at *m/z* = 1093 ([M]$^+$) in the FAB mass spectrum.

The UV/VIS spectrum of **3** is essentially a summation of the spectra of **1** and **2** (1 : 2 molar ratio), with the porphyrin Q- and B-bands [λ_{max}/nm (log ε): 610 (4.03), 566 (4.28), 436 (5.36)] clearly distinguishable from the absorption due to the two *trans* azobenzene moieties in their *E* isomeric form [λ_{max}/nm (log ε): 341 (4.86)] [Fig. 2 (top curve)]. These spectral features suggest that there is no electronic communication between the porphyrin and the azobenzene chromophores and, more importantly, that it is possible to individually address the photochemistry of these two subunits in this bichromophoric system. Accordingly, continuous irradiation of $\mathbf{3}_E$ (5.9×10^{-5} M, MeCN) at 345 ± 5 nm resulted in the time-dependent decrease of its absorption band centered at 341 nm concomitant with a slight increase of absorption in the B-band region, suggesting isomerization of the porphyrin-bound azobenzene subunits to produce $\mathbf{3}_Z$.[11] The reverse thermal reaction was also spectrally monitored and the *E* form could be recovered quantitatively (Fig. 2).

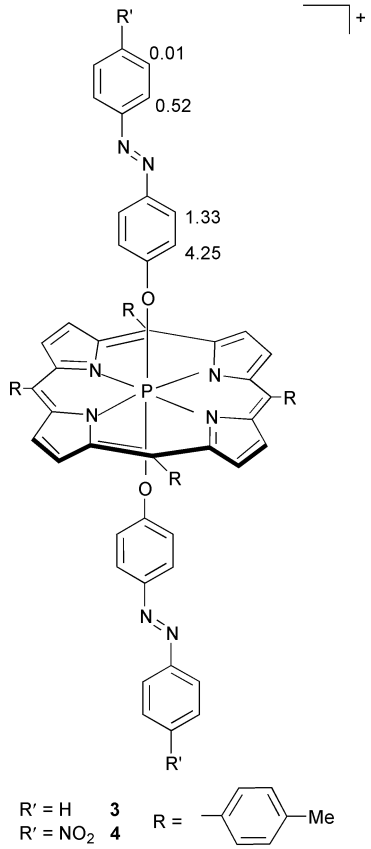

Fig. 1 Molecular structure of photoswitches investigated in the present study. The numbers indicated adjacent to protons on the azobenzene moiety are the corresponding porphyrin ring-current-induced ^{1}H NMR chemical shifts [*i.e.* $\Delta\delta$ (free − bound)] observed for $\mathbf{3}_E$.

Excitation of a MeCN solution of $\mathbf{3}_E$ at 345 nm resulted in no fluorescence emanating from the azo chromophore as is the case with the precursor **2**. On the other hand, the porphyrin component of the complex showed a fluorescence spectrum (λ_{exc} = 465/565 nm) typical of a hexa-coordinated phosphorus(v) porphyrin.[9] The fluorescence quantum yield [Φ_f, estimated using (5,10,15,20-tetraphenylporphyrinato)zinc(II), Zn^{II}TPP, as the standard] of $\mathbf{3}_E$ (0.01) is less than that of [5,10,15,20-tetra(tolyl)porphyrinato]phosphorus(v) dihydroxide {[P^V(TTP)$(OH)_2$]$^+$, Φ_f = 0.045}. Interestingly, the fluorescence intensity due to $\mathbf{3}_Z$ (produced by continuous irradiation at 345 ± 5 nm) is only 60 ± 5% of that due to $\mathbf{3}_E$, and the thermal back reaction regenerates the fluorescence of $\mathbf{3}_E$ as illustrated in Fig. 2 (inset). This *E*/*Z* interconversion was repeated 5–6 times

DOI: 10.1039/b007784o

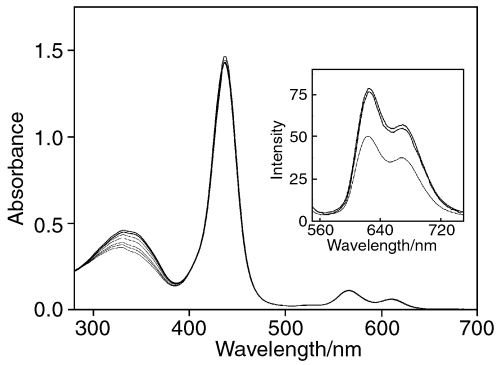

Fig. 2 Time-dependent UV/VIS spectral changes observed upon continuous irradiation of $\mathbf{3}_E$ (solvent: MeCN, [$\mathbf{3}_E$] = 5.9×10^{-5} M). Top curve represents the initial spectrum with the subsequent lower ones resulting from continuous irradiation of the solution at 345 ± 5 nm at 25 °C for 1, 2, 5, 7, 9, 12 and 16 min, respectively (PTI 150 W Xe-arc lamp model A1010, PTI model 1366-MONO monochromator). The dotted curve close to the top curve is the spectrum obtained after keeping the irradiated solution in the dark for several hours. Inset: fluorescence spectra of (——) unirradiated $\mathbf{3}_E$, (– – –) $\mathbf{3}_Z$ obtained upon irradiating $\mathbf{3}_E$ and of (· · · ·) $\mathbf{3}_E$ resulting from the back thermal reaction of $\mathbf{3}_Z$ (solvent: MeCN; λ_{exc} = 465 nm).

with < 5% loss of the material (UV/VIS and fluorescence), thus establishing the ability of **3** to be an effective and stable photoswitch.

What is the origin of weak fluorescence observed for **3** and what is the mechanism of its photoswitching function? Among the various possible mechanisms considered by us,† an intramolecular PET from the axial azobenzene donors to the singlet excited state of the basal phosphorus(v) porphyrin seems to be the most probable pathway for the quenching of fluorescence in $\mathbf{3}_E$. This interpretation is consistent with not only the exoergicity for such a PET reaction (ΔG_{PET} = −0.16 ± 0.03 eV‡), but also a similar interpretation made earlier for the quenching observed in a series of aryloxo phosphorus(v) porphyrins reported by us.[9b] Moreover, Φ_f for complex $\mathbf{4}_E$ (Fig. 1), which is endowed with the electron withdrawing nitro group at the axial azobenzene ligand, was seen (Φ_f = 0.035) to be more than that of $\mathbf{3}_E$.§ Thus, accepting that PET is occurring between the axial ligand and the singlet porphyrin in this donor–acceptor complex, the photoswitching function demonstrated here can be rationalized in terms of the distance dependence of PET. As schematically represented in Fig. 3, the distance between the basal porphyrin and the axial ligand in $\mathbf{3}_Z$ is shorter than that in $\mathbf{3}_E$ explaining the additional fluorescence quenching observed for the former isomer.

Recently, electro-switch and proton-switch properties of an supramolecular ensemble comprising of Zn^{II}TPP and *axially* ligated 4-(phenylazo)pyridine has been reported but, the effect of *E/Z* isomerization on the luminescence properties of this system was not observed.[3] Similarly, studies on the covalently

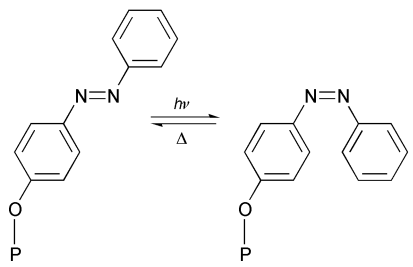

Fig. 3 Reversible *E/Z* isomerization in **3** (P = porphyrin).

connected azobenzene–porphyrin conjugates reported by Hunter and Sarson revealed that photochemistry of the porphyrin components of these novel chromophoric assemblies is essentially unaltered but, the photochemical isomerization of their azobenzene components could not be detected.[5] On the other hand, fluorescence properties of the early azobenzene–porphyrin systems reported by several groups were not investigated in detail.[6–8] While this work was in progress, photoswitching features of an azobenzene-linked diporphyrin complex have been described.[4] However, because of the extensive absorption by the two dissimilar porphyrin chromophores in the UV/VIS region, spectral detection of the *E/Z* isomerization in this system was not as facile as demonstrated here for **3**.

In summary, the new phosphorus(v) porphyrin **3** is an effective and stable photoswitch. Its photoswitching ability is a result of the isomerization-induced modulation of the PET between the axial azobenzene subunits and the basal porphyrin scaffold. Further studies on **3** and other closely related 'axial-bonding' type photoswitches are currently in progress.

We thank the CSIR (New Delhi) for financial support of this work.

Notes and references

† Excitation of **3** at 345 nm resulted in weak fluorescence in the range 550–750 nm but control experiments have suggested this to be entirely due to the residual absorption by the porphyrin chromophore. Moreover, the excitation spectrum of the compound (emission collected at the porphyrin fluorescence band maximum) did not show absorption corresponding to the azobenzene chromophore. In a separate set of experiments, neither the fluorescence of $[P(TTP)(OH)_2]^+$ was found to be quenched by compound **2** nor was any rate enhancement observed for the thermal back reaction of $\mathbf{3}_Z$ in the presence of externally added **2**. Thus, fluorescence quenching observed here for **3** is not due to the energy transfer between the azobenzene and porphyrin subunits or the photochemical disscociation of azobenzene ligands.

‡ Estimation of ΔG_{PET} is based on the electrochemical redox potential data [E_{ox} (axial ligand) = 1.52 V, E_{red} (basal porphyrin) = −0.35 V] and singlet energy of the porphyrin (2.03 eV[9c]).

§ The presence of an electron withdrawing nitro group on the axial ligand is expected to decrease its donor capacity. Indeed, ΔG_{PET} for **4** is close to 0.0 eV, consistent with its high Φ_f value.

1 Reviews: T. Hayashi and H. Ogoshi, *Chem. Soc. Rev.*, 1997, **26**, 355; M. D. Ward, *Chem. Soc. Rev.*, 1997, **26**, 365; M. R. Wasielewski, *Chem. Rev.*, 1992, **92**, 435.
2 See, for example (and references therein): P. Belser, S. Bernhard, C. Blum, A. Beyeler, L. De Cola and V. Balzani, *Coord. Chem. Rev.*, 1999, **190**, 155; A. P. de Silva, H. Q. N. Gunaratne, T. Gunnlaugsson, A. J. M. Huxley, C. P. McCoy, J. T. Rademacher and T. E. Rice, *Chem. Soc. Rev.*, 1997, **26**, 1515.
3 J. Otsuki, K. Harada and K. Araki, *Chem. Lett.*, 1999, 269.
4 S. Tsuchiya, *J. Am. Chem. Soc.*, 1999, **121**, 48.
5 C. A. Hunter and L. D. Sarson, *Tetrahedron Lett.*, 1996, **37**, 699.
6 M. Autret, M. le Plouzennec, C. Moinet and G. Simmonneaux, *J. Chem. Soc., Chem. Commun.*, 1994, 1169
7 H. K. Hombrecher and K. Ludtke, *Tetrahedron*, 1993, **49**, 9489; H. K. Hombrecher, K. Ludtke and D. Koll, *J. Prakt. Chem.*, 1996, **338**, 257.
8 K. H. Neumann and F. Vogtle, *J. Chem. Soc., Chem. Commun.*, 1988, 520.
9 (a) T. A. Rao and B. G. Maiya, *J. Chem. Soc., Chem. Commun.*, 1995, 939; (b) T. A. Rao and B. G. Maiya, *Inorg. Chem.*, 1996, **35**, 4829; (c) L. Giribabu, T. A. Tao and B. G. Maiya, *Inorg. Chem.*, 1999, **38**, 4971.
10 R. J. Abraham, G. R. Bedford, D. McNeille and B. Wright, *Org. Mag. Reson.*, 1980, **14**, 418.
11 S. Shinkai, T. Nakaji, T. Ogawa, K. Shigematsu and O. Manabe, *J. Am. Chem. Soc.*, 1981, **103**, 111.

pH Sensing with mesoporous thin films

Gernot Wirnsberger,*[a] Brian J. Scott[b] and Galen D. Stucky*[b]

[a] *Inorganic Chemistry, Karl-Franzens-University Graz, 8010 Graz, Austria. E-mail: gernot.wirnsberger@kfunigraz.ac.at*

[b] *Department of Chemistry, University of California, Santa Barbara, CA-93106 Santa Barbara, USA. E-mail: stucky@chem.ucsb.edu*

Received (in Columbia, MO, USA) 15th May 2000, Accepted 23rd October 2000
First published as an Advance Article on the web

Optically clear thin mesoporous films with covalently attached fluorescein entities are shown to exhibit very fast response pH sensing.

Dye-doped mesostructured compounds are currently attracting interest with respect to possible optical applications such as materials exhibiting amplified spontaneous emission and lasing.[1–3] The mesoporous forms are also promising for optical applications when doped with dyes. Dyes can be attached covalently to the matrix by introducing hydrolysable units onto the dye molecules.[4] Principally this should allow one to remove the surfactants quantitatively, leaving behind a porous matrix with anchored dye molecules. The porous structure is especially important for optical sensing applications where fast diffusion of the molecules towards the sensing species is of interest.

Previous investigations on optical sensors has focused predominately on sol–gel glasses. The attractive points of sol–gel glasses are their ease of processibility as well as thermal and mechanical robustness. A few examples include oxygen sensing by Ru-complexes,[5] pH sensing,[6] and ion sensing.[7] As far as pH sensing is concerned, the diffusion of the molecules into the dried glass is sometimes a limiting factor, usually leading to rather long response times (up to minutes),[7] a task which could be improved with mesoporous materials. Here, we show that mesosporous thin films[8] prepared by acidic sol–gel chemistry and low-temperature block-copolymer extraction[9] can function very effectively as pH sensors. The pH sensitive dye is covalently anchored to/within the mesoporous SiO_2 wall in order to prevent leaching during optical pH measurements. We also demonstrate that the response of the dye-modified mesoporous silica thin films is very fast, indicating the possibility of using these materials in sensor devices.

Fluorescein isothiocyanate (FITC) was used as the pH sensitive dye and was derivatized with 3-aminopropyltriethoxysilane (APTS). Typically, 7 mg of FITC was dissolved in 20.4 g of EtOH and was allowed to react with 10 mg APTS for 3 h. Afterwards, 2.0 g of the block-copolymer F127 [poly(ethylene oxide)-*block*-poly(propylene oxide)-*block*-poly(ethylene oxide), $(PEO)_{106}(PPO)_{70}(PEO)_{106}$, BASF], 1.6 g H_2O, 0.25 g HCl (2 M) and 8.5 g tetraethylorthosilicate (TEOS) were added. This solution with a molar composition of TEOS–F127–H_2O–HCl–FTIC–APTS–EtOH = $1:4 \times 10^{-3}:2.5:0.012:4.4 \times 10^{-4}:1.1 \times 10^{-3}:10.9$ was refluxed for 1 h. After the solution had cooled to rt, thin films were prepared by dip coating. Films were withdrawn from solutions with 10 cm min^{-1}, resulting in ~900 nm thick films on an area of 2.5×2.5 cm^2. The films show a considerable thickness variation when prepared by dip-coating. Apart from the fact that the ends are swelled thick, the film thickness increases along the dipping direction. When the same solutions are spin-coated (3000 rpm, 30 s), more homogenous thin films (~1500 nm) are produced, with a thickness variation of 5% (apart from the edges which are also swelled thick).

A typical X-ray pattern of an as-synthesized thin film is depicted in Fig. 1(a), showing several peaks in the region between 0.8 and 3.5 $2\theta°$. The peaks can be indexed in the $P6_3/mmc$ space group indicating that the composite thin film consists of a hexagonally packed arrangement of cages (a = 113, c = 181 Å, c/a = 1.60).[8] One further non-indexable peak is observed at a d spacing of 51 Å; this peak may be attributed to the 200 reflection of a cubic $Im3m$ phase which can also be derived under similar conditions with F127 as a block-copolymer.[8] The 110 reflection is hidden by the intense reflection of the hexagonal structure at ~1° 2θ. From the relative intensities we conclude that the hexagonal phase is the major part, whereas the cubic phase is only present in small amounts. However, as both structures are composed of cage-like entities, and porosity itself determines the sensing properties, the presence of minor amounts of a second phase is not of significant importance. We note also that the use of higher concentrations of APTS did not result in ordered mesostructures. This fact is attributed to the pH increase brought about by the basic amine. Hence, we adjusted the concentration of APTS carefully, in order to have an access for complete dye derivatization but still having a pH resulting in thin films with mesostructural order.

A key point is the low temperature removal of the surfactants. Fresh films (~1 d old) show severe cracking when treated in EtOH at 80 °C. The same is true, even when the films are aged for several days at rt. However, we observed that when the films had first been aged at rt for about 10 d and afterwards for 3–5 d at 70 °C, the stability of these films is sufficiently high to allow surfactant removal by extraction without decrease of the optical transparency.

The extraction time itself was optimized in order to completely remove the surfactants. IR spectroscopy was used to

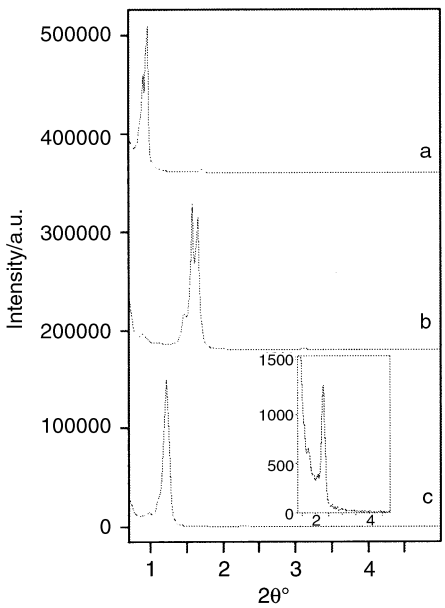

Fig. 1 X-Ray diffraction patterns of fluorescein-doped thin mesostructured/mesoporous films prepared with F127. (a) As-synthesized, (b) after calcination, and (c) after extraction. The inset in (c) shows a magnification of the higher $2\theta°$ range.

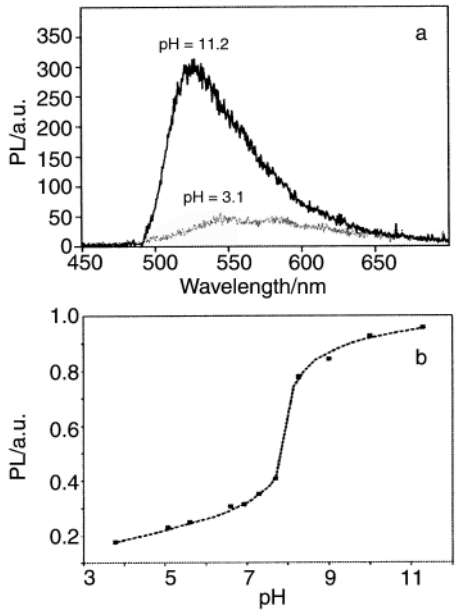

Fig. 2 (a) Photoluminescence of fluorescein doped mesoporous thin films at low and high pH values, (b) typical titration curve.

follow the surfactant removal during extraction by monitoring the C–H vibrations in the range 2700–3000 cm^{-1}. Within the first 4 h of extraction, the intensity of these bands steadily decreased, until finally only weak bands in this wavelength region remained. These bands were still present after 24 h of extraction and may be attributed to vibrations due to the occluded dye and the excess APTS used for the dye derivatization. X-Ray patterns showed that prolonged treatment in EtOH at 80 °C results in a decrease of the unit-cell constants compared to the as-synthesized material (Fig. 1c). The unit-cell parameters (a = 90.1, c = 144.6 Å, c/a = 1.60) are larger than those of a calcined thin film made from the same composition (a = 69.8, c = 111.8 Å, c/a = 1.62), showing a lower contraction of the SiO_2 framework when employing extraction for block-copolymer removal. We note that even after prolonged treatment in EtOH (24 h) not only the optical transparency and the mesostructure are retained but also the X-ray patterns exhibit all reflections seen for the as-synthesized material.

For the demonstration of pH sensing, we chose a simple configuration in which the thin films were excited by the 488 nm line of an Ar^+ ion laser at 45° and the photoluminescence (PL) was detected normal to the film surface. Typical PL spectra are depicted in Fig. 2a at a pH of and 3.1 and 11.2. As expected, the PL intensity of the thin films is dependent on the pH and is stronger under basic conditions. A typical titration curve is depicted in Fig. 2b. Compared to solution, the titration curve is relatively broad. This may be attributed to an inhomogeneous dye environment. Moreover, fluorescein possesses three pK values which can hardly be distinguished in solution (pK_1 = 2.08, pK_2 = 4.31, pK_3 = 6.43) and which might also cause some broadening.[10]

The response time of the mesoporous films upon changing the pH is fast, being in the range of a few seconds. Fig. 3 depicts a typical set of data which was obtained by exchanging the solution from pH 3.8 to 9.4. We attribute the fast response to the fact that the porous structure facilitates the diffusion of H_3O^+ (OH^-). While it is possible the dye is located both at the pore interface and incorporated within the SiO_2 wall, this does not hinder the anchored fluorescein entities to respond rapidly to changes in pH. From time dependent measurements we evaluated the time for the change in the PL signal to 95% of the final value to be in the range of ~7 s. We note that with the exception of small capillaries coated with sol–gel glass,[11] this is faster than in purely sol–gel based optical pH sensors.[7,12]

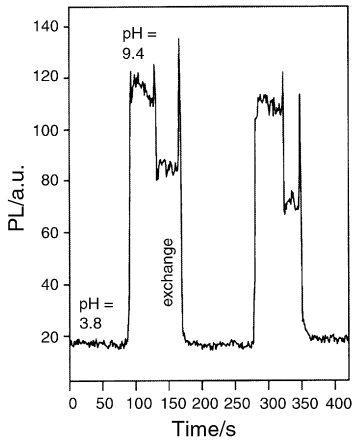

Fig. 3 Time dependent photoluminescence response of a fluorescein doped mesoporous thin film upon change of the pH value.

Here, we have demonstrated that dye-doped mesoporous thin films are suitable candidates for optical solid-state pH sensors. An important point is the careful optimization of the processing conditions which are necessary to obtain thin mesoporous films with high optical quality. As expected, the response time is very fast, due to the mesoporosity of the thin films. On the other hand, the high processibility of the solid state precursor solution should allow one to extend this chemistry to other sensing arrangements, *e.g.* to evanescent wave optical fibers[13] or to pH sensing microtips.[14]

This work was supported by the NSF under grant DMR 95-20971, DMR 9634396, the U.S. Army Research Office under grant DAAH04-96-1-0443 and made use of the Materials Research central facilities supported by the NSF under award DMR-9632716.

During review of this manuscript, Fau *et al.*[15] reported pH sensing in patterned mesoporous materials where the sensing agent was attached by post-synthesis modification.

Notes and references

1 P. Yang, G. Wirnsberger, H. C. Huang, S. R. Cordero, B. Scott, M. D. McGehee, T. Deng, G. M. Whitesides, B. F. Chmelka, S. K. Buratto and G. D. Stucky, *Science*, 2000, **287**, 465.
2 F. Marlow, M. D. McGehee, D. Zhao, B. F. Chmelka and G. D. Stucky, *Adv. Mater.*, 1999, **11**, 632.
3 G. Wirnsberger and G. D. Stucky, *Chem. Mater.*, 2000, **12**, 2525.
4 B. Lebeau, C. F. Fowler, S. R. Hall and S. Mann, *J. Mater. Chem.*, 1999, **9**, 2279.
5 *e.g.* A. K. McEvoy, C. M. McDonagh and B. D. MacCraith, *Analyst*, 1996, **121**, 785.
6 *e.g.* B. Iosefzon-Kuyavskaya, I. Gigozin, M. Ottolenghi, D. Avnir and O. Lev, *J. Non-Cryst. Solids*, 1992, **147–148**, 808.
7 C. Rottman, M. Ottolenghi, R. Zusman, O. Lev, M. Smith, G. Gong, M. L. Kagan and D.Avnir, *Mater. Lett.*, 1992, **13**, 293.
8 D. Zhao, P. Yang, N. Melosh, J. Feng, B. F. Chmelka and G. D. Stucky, *Adv. Mater.*, 1998, **10**, 1380.
9 D. Zhao, J. Feng, Q. Huo, N. Melosh, G. H. Fredrickson, B. F. Chemlka and G. D. Stucky, *Science*, 1998, **279**, 548; D. Zhao, Q. Huo, J. Feng, B. F. Chemlka and G. D. Stucky, *J. Am. Chem. Soc.*, 1998, **120**, 6024.
10 R. Sjöback, J. Nygren and M. Kubista, *Spectrochim. Acta A*, 1995, **51**, L7.
11 J. Samuel, A. Strinkovski, S. Shalom, K. Lieberman, M. Ottolenghi, D. Avnir and A. Lewis, *Mater. Lett.*, 1994, **21**, 431.
12 L. Yang and S. S. Saavedra, *Anal. Chem.*, 1995, **67**, 1307; A. Lobnik, I. Oehme, I. Murkovic and O. S. Wolfbeis, *Anal. Chim. Acta*, 1998, **367**, 159.
13 O. Ben-David, E. Shafir, I. Gilath, Y. Prior and D. Avnir, *Chem. Mater.*, 1997, **9**, 2255.
14 W. Tan, R. Kopleman, S. L. R. Barker and M. T. Miller, *Anal. Chem.*, 1999, **72**, 606A.
15 H. Fau, Y. Lu, A. Stump, S. T. Reed, T. Baer, R. Schunk, V. Perez-Lund, G. P. Lopez and C. J. Brinker, *Nature*, 2000, **405**, 56.

ChemComm

Tungsten–niobium–sulfur composite nanotubes†

Yan Qiu Zhu,[a] Wen Kuang Hsu,[a] Mauricio Terrones,[a] Steven Firth,[b] Nicole Grobert,[a] Robin J. H. Clark,[b] Harold W. Kroto[a] and David R. M. Walton[a]

[a] *Fullerene Science Centre, School of CPES, University of Sussex, Brighton, UK BN1 9QJ. E-mail: d.walton@sussex.ac.uk*

[b] *Christopher Ingold Laboratories, University College London, 20 Gordon St., London, UK WC1H 0AJ*

Received (in Oxford, UK) 31st August 2000, Accepted 6th November 2000
First published as an Advance Article on the web

Novel W–Nb–S composite inorganic nanotubes have been generated by replacing W in the S–W–S sandwich layers of WS_2 by Nb. The tubes are uniform, with the Nb concentration 10 atom%. Raman spectral features of the tubes are described.

Inorganic fullerene (IF) nanotubes, *e.g.* MX_2 (M = W, Mo; X = S, Se), first reported by Tenne *et al.*,[1] have engendered considerable scientific interest because they are good semiconductors and display excellent wear-resistant properties. To date, various approaches to the synthesis of these materials have been developed, such as chemical transport,[2] gas–solid reactions[3] and *in situ* heating,[4] leading to pure MX_2 nanoparticles, short and long tubes, bundles, and even microtubes. The structural features, lubricating properties and electronic behaviour of the IF nanotubes have been widely investigated.[5–8] For example, a single WS_2 nanotube has been used successfully as a microscope probe.[3,9] Recently, Levy and coworkers showed that small amounts of noble metals (Au and Ag) could be intercalated between WS_2 tube walls.[10,11] Akin to their bulk crystals, IF nanotube band gaps are dependent upon tube diameter.[12] It is therefore interesting to prepare doped nanotubes and to assess their electronic and mechanical performance. Here, we describe the generation of a novel $W_xNb_yS_2$ IF nanotube containing *ca.* 10 atom% Nb.

We prepared needle-like WO_x (mainly $W_{18}O_{49}$) nanotubes by the previously described procedure.[13] The needles were then covered with a suspension of Nb_2O_5 (Aldrich, 99.9% pure, particle size < 2 μm) in acetone, and the acetone was allowed to evaporate leaving Nb_2O_5 uniformly distributed over the needles. The sample was then reheated to *ca.* 1100 °C under 200 Torr H_2S. Using a scalpel, the grey needle-like deposit was removed from the quartz surface, subjected to high resolution transmission electron microscopy (HRTEM, JEOL-4000) and to energy dispersive X-ray (EDX, element > B) and Raman spectroscopic (Renishaw system 1000, λ_0 = 514.5 and 632.8 nm) analysis.

Previously, we had refined the oxide–sulfide conversion method[7] and successfully created very long pure WS_2 nanotubes by forming WO_x nanorods prior to oxide–sulfide conversion.[4] We have now found that the constituent atoms of Nb_2O_5-coated WO_x nanorods easily diffuse at high temperature (*ca.* 1100 °C), particularly through materials possessing substantial vacancies. Thus Nb probably occupies some of the W positions within $W_{18}O_{49}$, leading to $W_xNb_yO_z$. This replacement process is reminiscent of the behaviour of the bulk oxides, but in this case the nanorod templates and the suboxide features were retained. The presence of gaseous H_2S in the chamber facilitated oxide-to-sulfide conversion in an identical manner to that found for the synthesis of pure WS_2 or MoS_2 nanotubes,[1,3,4] resulting in homogeneous W–Nb–S composite nanotubes. These tubes are straight, *ca.* 5–10 μm long and *ca.* 20–100 nm in diameter. HRTEM images of the tubes are not different from those of WS_2 nanotubes. The majority have hollow cores, less than 30% of them being fully or partly filled with elongated WO_x crystals. Concentric nanotubes (layer separation *ca.* 0.62 nm) are observed. The outer layers are smooth and appear to be free of lattice defects. All the tubes are closed, *ca.* 20% by flat caps, forming a *ca.* 90-degree connection with the cylinders. Dislocations at the cap–cylinder junctions are apparent [Fig. 1(a), arrowed]. EDX revealed the presence of Nb [Fig. 1(b)] within the nanotubes. Measurements on ten isolated hollow nanotubes revealed a *ca.* 9:1 W to Nb atomic ratio, the metal:sulfur ratio being *ca.* 1:2. The overall stoichiometry of the nanotubes is $W_xNb_yS_2$ (x = 0.9, y = 0.1, 5% uncertainty). The flat tip feature (*ca.* 90-degree angle with the body) of the nanorods is determined by their intrinsic crystalline nature.[13] Hence, the flat nanotube tips probably form as a result of oxide–sulfide template conversion. This conjecture is supported by supplementary experiments, which showed that NbS_2 nanotubes could not be prepared directly from Nb_2O_5 powder alone. These results confirm that the suboxide plays a key role in the IF nanotube formation, and the process can be written in terms of eqns. (1) and (2):

$$WO_{x\,(\text{nanorod})} + Nb_2O_{5\,(\text{particle})} \rightarrow W_{0.9}Nb_{0.1}O_{x\,(\text{nanorod})} \quad (1)$$

$$W_{0.9}Nb_{0.1}O_{x\,(\text{nanorod})} + H_2S_{\,(\text{gas})} \rightarrow W_{0.9}Nb_{0.1}S_{2\,(\text{nanotube})} + H_2O_{\,(\text{gas})} \quad (2)$$

In order to ascertain whether or not Nb was present as an intercalate within the WS_2 tube walls, or as a dopant in the WS_2 structure, we undertook additional EDX analyses. The results showed that the W:Nb:S ratio remained nearly constant, independent of nanotube diameter and position. This behaviour is consistent with the EDX mapping, and implies that the nanotubes are fairly uniform. When intercalated Au and Ag are present, the nanotubes are heterogeneous, irrespective of their diameter and length.[10,11] Heterogeneous intercalation is likely to lead to internal stresses owing to the different atomic diameters of W and Nb, resulting in significant defects. In fact,

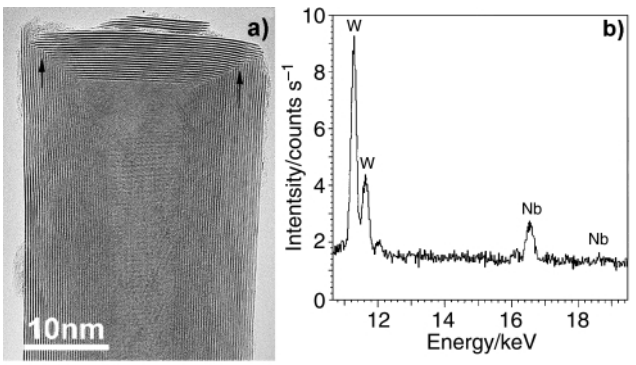

Fig. 1 (a) HRTEM image showing a *ca.* 90-degree flat cap, layer separation = 0.62 nm. Dislocations at the cap-cylinder junctions are apparent (arrowed); (b) EDX of an isolated hollow tube, revealing the presence of W and Nb. S signals are omitted from this profile.

† Electronic supplementary information (ESI) available: HRTEM image of a typical 10-layered $W_{0.9}Nb_{0.1}S_2$ nanotube, layer separation = 0.62 nm and Raman bands of $W_{0.9}Nb_{0.1}S_2$ and WS_2 nanotubes and their assignments. See http://www.rsc.org/suppdata/cc/b0/b007074m/

DOI: 10.1039/b007074m

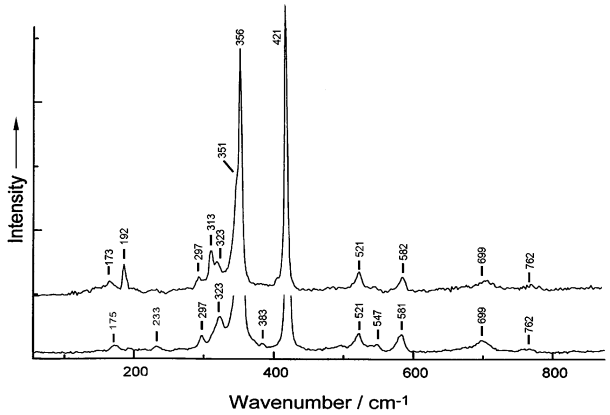

Fig. 2 Raman spectra (λ_0 = 514.5 nm) of $W_{0.9}Nb_{0.1}S_2$ (upper) and WS_2 (lower) nanotubes.

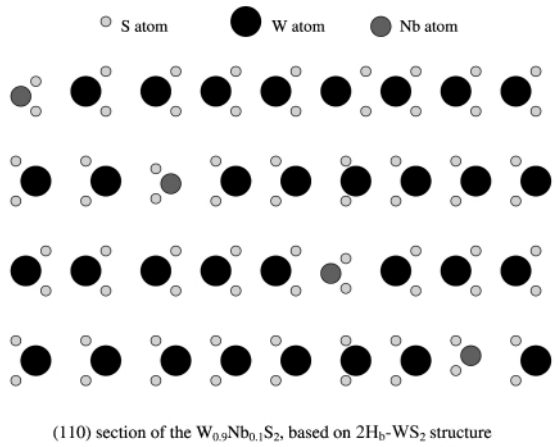

Fig. 3 Proposed model for the layered $W_{0.9}Nb_{0.1}S_2$ structure.

our HRTEM observations show that the distance between layer fringes is *ca*. 0.62 nm [Fig. 1(a)], identical with that in pure WS_2; only a few defects are present. Furthermore, expanded layer separations, *i.e*. > 0.62 nm, would be expected if Nb were to be intercalated between the WS_2 layers. However, very few crystals were found with expanded layer separations. Thus our nanotubes are Nb-doped and not intercalated.

Additional experiments have revealed that the W : Nb ratio can be altered by applying various amounts of Nb_2O_5 coating to the WO_x nanorods, prior to passage of H_2S during heating. The Nb concentration (*ca*. 10% atom%) can be doubled in the nanotubes; however, our results showed that Nb-dominated W–Nb–S tubes are difficult to construct.

The Raman spectrum of $W_{0.9}Nb_{0.1}S_2$ nanotubes taken with 632.8 nm excitation is identical to that of WS_2 nanotubes. The 514.5 nm spectrum of the Nb-doped tubes, however, does show some differences from that of WS_2 (Fig. 2), notably the appearance of a medium intensity band at 313 cm^{-1}, a shoulder on the low wavenumber side of the e_{2g}^1 band at 356 cm^{-1} and an increase in the relative intensity of the 192 cm^{-1} band. The intensity of the 192 cm^{-1} band is *ca*. half that of the disorder-induced zone-edge phonon [LA(M)] band at 173 cm^{-1} for WS_2, whereas its intensity for the Nb-doped tubes is *ca*. 5 times that of the 173 cm^{-1} band. The 192 cm^{-1} band has been observed in the Raman spectra of 2H-bulk and nanotubes of WS_2, but has not been assigned.[14] Its increase in relative intensity on going from pure WS_2 nanotubes to Nb-doped WS_2 nanotubes implies that it is caused by scattering from a disorder-induced zone-edge phonon. The band at 313 cm^{-1} has not previously been seen in the Raman spectra of any form of WS_2, and is also probably due to the increased disorder in the lattice owing to the presence of Nb. The shoulder at 351 cm^{-1} is the first overtone of the LA(M) band, with its apparent intensity enhanced by its proximity to the strong band at 365 cm^{-1}. The Raman bands and their assignments are summarised in Table 1 of ESI.†

The formation of $W_{0.9}Nb_{0.1}S_2$ nanotubes can be accounted for by considering the layered structure of the $W_{0.9}Nb_{0.1}S_2$ crystals. According to our EDX analysis, only *ca*. 10% of the W atoms are replaced by Nb. Therefore, we suggest that the Nb-doped material remains as the $2H_b$-type WS_2 structure, rather than becoming the $2H_a$-type NbS_2 structure. We propose a model for layered $W_{0.9}Nb_{0.1}S_2$ (Fig. 3). In this structure, the doped Nb atoms (medium circles) should not cause severe lattice defects and can easily be stabilised by neighbouring atoms. This suggestion is supported by our Raman spectra; the spectra of the Nb-doped and pure WS_2 tubes are identical using 632.8 nm excitation, whereas new bands attributable to increased lattice disorder are seen using 514.5 nm excitation. The crystal lattice spacing, particularly *c*/2, remains almost unchanged when compared with that of pure WS_2 layers. If a nanotube is to be formed by rolling up such composite layers, one would not expect a significant *c*/2 change. This conjecture is also supported by the facts that the composition of our nanotubes is uniform and that we did not observe severe defects on the tube walls.

We thank the Royal Society, the JFCC, the EPSRC and the ULIRS, for financial support. We are grateful to J. Thorpe and D. Randall (Sussex) for assistance with TEM and SEM facilities. We thank M. Mayne and I. Maurin for helpful discussions.

Notes and references

1 R. Tenne, L. Margulis, M. Genut and G. Hodes, *Nature*, 1992, **360**, 444.
2 M. Remskar, Z. Skraba, M. Regula, C. Ballif, R. Sanjines and F. Levy, *Adv. Mater.*, 1998, **10**, 246.
3 M. Homyonfer, B. Alperson, Y. Rosenberg, L. Sapir, S. R. Cohen, G. Hodes and R. Tenne, *J. Am. Chem. Soc.*, 1997, **119**, 2693.
4 Y. Q. Zhu, W. K. Hsu, N. Grobert, B. H. Chang, M. Terrones, H. Terrones, H. W. Kroto, D. R. M. Walton and B. Q. Wei, *Chem. Mater.*, 2000, **12**, 1190.
5 J. Sloan, J. H. Hutchison, R. Tenne, Y. Felfman, T. Tsirlina and M. Homyonfer, *J. Solid State Chem.*, 1999, **144**, 100.
6 M. Remskar, Z. Skraba, R. Sanjines and F. Levy, *Appl. Phys. Lett.*, 1999, **74**, 3633.
7 L. Rapoport, Y. Bilik, Y. Feldman, M. Homyonfer, S. R. Cohen and R. Tenne, *Nature*, 1999, **387**, 791.
8 G. Seifert, H. Terrones, M. Terrones, G. Jungnickel and T. Frauenheim, *Solid State Commun.*, 2000, **114**, 245.
9 A. Rothschild, S. R. Cohen and R. Tenne, *Appl. Phys. Lett.*, 1999, **75**, 4025.
10 M. Remskar, Z. Skraba, C. Ballif, R. Sanjines and F. Levy, *Surf. Rev. Lett.*, 1999, **6**, 1283.
11 M. Remskar, Z. Skraba, P. Stadelmann and F. Levy, *Adv. Mater.*, 2000, **12**, 814.
12 G. Seifert, H. Terrones, M. Terrones, G. Jungnickel and T. Frauenheim, *Phys. Rev. Lett.*, 2000, **85**, 146.
13 Y. Q. Zhu, W. B. Hu, W. K. Hsu, M. Terrones, N. Grobert, H. Terrones, H. W. Kroto and D. R. M. Walton, *Chem. Phys. Lett.*, 1999, **309**, 327.
14 G. L. Frey, R. Tenne, M. J. Matthews, M.S. Dresselhaus and G. Dresselhaus, *J. Mater. Res.*, 1998, **13**, 2412.

Stable pyrano[2,3-*b*]quinoxalines and pyrano[2,3-*g*]pteridines related to molybdopterin

Ben Bradshaw, David Collison, C. David Garner† and John A. Joule*

Chemistry Department, The University of Manchester, Manchester, UK M13 9PL. E-mail: j.a.joule@man.ac.uk

Received (in Cambridge, UK) 23rd October 2000, Accepted 15th November 2000
First published as an Advance Article on the web

The syntheses of the quinoxaline and pteridine proligands (3 and 4) related to molybdopterin are described and 3 has been characterised complexed *via* its dithiolene group to a CpCo(III) centre (5). Each of 3–5 has the sensitive hemiaminal unit of molybdopterin, unprotected, verifying its stability *in vitro*.

The pioneering studies on representatives of the molybdenum enzymes by Garrett and Rajagopalan[1] showed that each contained a prosthetic group that comprises a pteridine carrying a C_4-side-chain at pteridine C-6, having two sulfur atoms which ligate molybdenum. A series of X-ray crystallographic determinations on molybdenum and tungsten enzymes[2] further clarified the structure of the cofactor and its mode of ligation to Mo and W. Thus, the metals are chelated by an ene-1,2-dithiolate (dithiolene) which is part of a tricyclic system, in which a

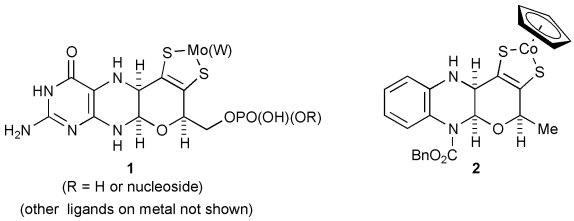

dihydropyran ring is fused to a partially reduced pteridine, **1**. The pterin (2-aminopteridin-4(3*H*)-one) moiety is generally known as molybdopterin.

We have previously described[3] the synthesis of CpCo(III) (where Cp = η^5-cyclopentadienyl) complex **2** which involves ligation of the metal by a dithiolene moiety as part of a dihydropyran fused to a partially reduced pyrazine, as in **1**. However, **2** differs from **1** in several key respects. Firstly, **2** has a benzene ring instead of a pyrimidine ring; secondly the terminal primary hydroxy (phosphate) is absent; and thirdly, and crucially it retains a urethane at the nitrogen of the hemiaminal unit. It was far from certain that, freed from this protection against possible cleavage of the N–C–O system, the cyclic aminal would be stable, especially during the process of ligand release and complexation to a metal centre. Thus, to assess whether there are any special effects operating in the natural system which maintain the hemiaminal linkage, it was essential that structural analogues of **1** without the urethane be prepared. We describe here the synthesis of just such model compounds, the proligands **3** and **4** and the cobalt complex **5** derived from **3**.

We have previously described syntheses of quinoxaline **6**[4] and protected pteridine **10**.[5] Hydrolysis of the acetal in **6** then reaction of **7** with fluoren-9-ylmethyl chloroformate (Fmoc-Cl), under carefully defined conditions gave a high yield of a 2:1 mixture of *cis*[6] (the desired) and *trans* tetracyclic products **8** which could not be separated by chromatography. Reduction of the mixture with sodium cyanoborohydride proceeded stereoselectively producing **9a**[6] and **9b**[6] which could be separated. It

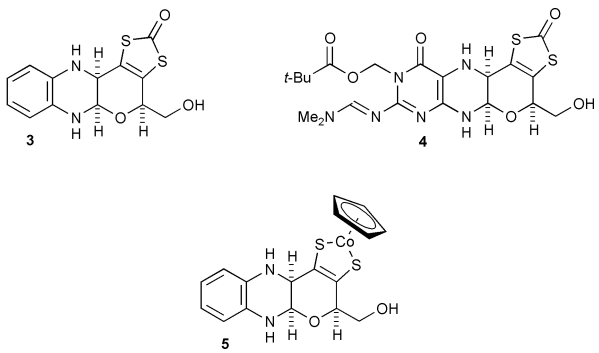

is notable that there were no problems associated with the presence of a second alcohol group—neither cyclisation to give an oxepino[2,3-*b*]quinoxaline nor acylation of the primary hydroxy occurred.

Release of the Fmoc nitrogen protection, most efficiently using diethylamine,[7] gave the unprotected compound **3** *which retained the hemiaminal unit*. It remained to verify that this sensitive functionality would survive conditions to release the enedithiolate and form a metal complex. This indeed proved to be possible for, using caesium hydroxide for hydrolytic ligand release, with subsequent trapping by reaction with $CpCoI_2$, complex **5** was produced (Scheme 1).

A comparable sequence led to the isolation of a pyranopteridine having an unprotected hemiaminal unit. Thus, treatment of pteridine **10** with trifluoroacetic acid allowed selective removal of the acetal protection giving diol **11** then reaction of this with Fmoc-Cl produced a separable mixture of pyran-containing products in which the ratio of *cis*-**12a**[6] (desired) to *trans*-**12b**[6] (2:1) was comparable to that in the quinoxaline series. Conducting the cyclisation reaction at rt produced a more favourable ratio (4:1) of products but the reaction was much slower, not being complete after 1 week. *N*-Deprotection of the 'wrong' isomer **12b** led cleanly back to **11** (incidentally

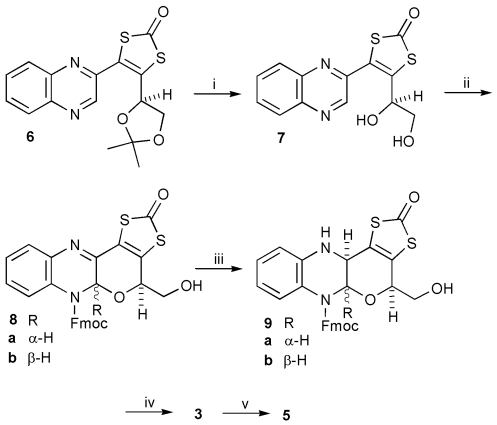

Scheme 1 *Reagents and conditions*: i, $TsOH{\cdot}H_2O$, MeOH, reflux (92%); ii, Fmoc-Cl, 1,4-dioxane, 35 °C, 14 h (92%); iii, $NaB(CN)H_3$, AcOH, CH_2Cl_2, MeOH, rt (92%); iv, **9a**, Et_2NH, THF, rt (80%); v, CsOH, $CHCl_3$, MeOH, rt then $Cp(Co)I_2$ (55%).

† Present address: School of Chemistry, University of Nottingham, University Park, Nottingham, UK NG7 2RD.

DOI: 10.1039/b008544h

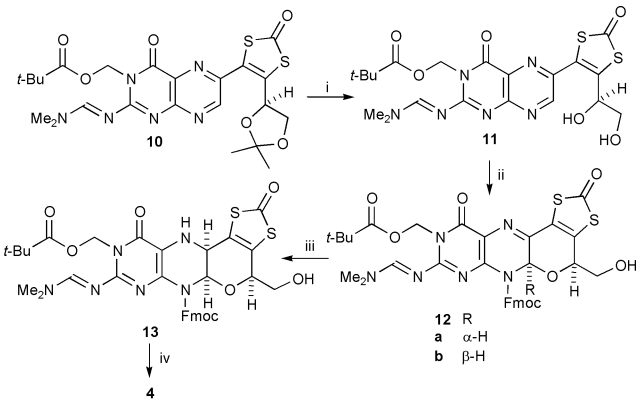

Scheme 2 *Reagents and conditions*: i, TFA, CH_2Cl_2, 0 °C→rt (90%); ii, Fmoc-Cl, 1,4-dioxane, H_2O, 35 °C, 14 h (84%); iii, **11a**, $NaB(CN)H_3$, AcOH, CH_2Cl_2, MeOH, rt (92%); iv, Et_2NH, THF, rt (85%).

confirming the lability of the N–C–O unit) which could thus be recycled. Cyanoborohydride reduction of the *cis* isomer proceeded stereoselectively in high yield and removal of the N-8-protection from **13** gave pro-ligand **4**[6] with the hemiaminal unit intact and having the same relative stereochemistry[8] as the prosthetic groups in the natural cofactors (Scheme 2).

Both **3** and **4** are relatively stable compounds. However, after several weeks at rt, and without protection from moisture or oxygen, each reverted to the corresponding ring opened diol, **7** and **11**. This must involve reversible proton-catalysed cleavage of the N–C–O system revealing dihydro-systems **14** and then irreversible aerial oxidation (Scheme 3). The stabilities of the pyranoquinoxalines and pyranopteridine established in this work make it unlikely that any special properties of the enzyme environment need to be invoked to explain the tricyclic form of molybdopterin found in all the crystal structure determinations,[2] save that it must be protected from oxidation. The proton-catalysed cleavage of the N–C–O system, which we have

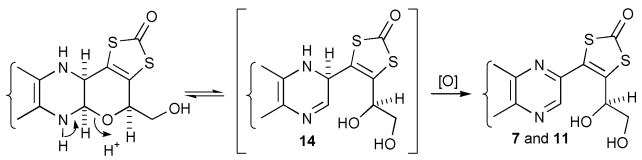

Scheme 3

suggested[9] may be intimately involved with catalysis at the metal centre, can now be studied *in vitro* with the compounds described herein. We shall be reporting on such studies in due course.

We thank the EPSRC for post-graduate (B. B.) and post-doctoral (B. B.) support for this work.

Notes and references

1 For a leading reference see R. M. Garrett and K. V. Rajagopalan, *J. Biol. Chem.*, 1996, **271**, 7387.

2 M. K. Chan, S. Mukund, A. Kletzin, M. W. W. Adams and D. C. Rees, *Science*, 1995, **267**, 1463; M. J. Romão, M. Archer, I. Moura, J. J. G. Moura, J. LeGall, E. Engh, M. Schneider, P. Hof and R. Huber, *Science*, 1995, **270**, 1170; H. Schindelin, C. Kisker, J. Hilton, K. V. Rajagopalan and D. C. Rees, *Science*, 1996, **272**, 1615; F. Schneider, J. Löwe, R. Huber, H. Schindelin, C. Kisker and J. Knäblein, *J. Mol. Biol.*, 1996, **263**, 53; R. Huber, P. Hof, R. O. Duarte, J. J. G. Moura, I. Moura, M.-Y. Liu. J. Legall, R. Hille, M. Archer and M. Romão, *Proc. Natl. Acad. Sci. USA*, 1996, **93**, 8846; J. C. Boyington, V. Sladishev, S. V. Khangulov, T. C. Stadtman and P. D. Sun, *Science*, 1997, **275**, 1305; J. Knäblein, H. Dobbeck, S. Ehlert and F. Schneider, *Biol. Chem.*, 1997, **378**, 293; C. Kisker, H. Schindelin, A. Pacheco, W. A. Wehbi, R. M. Garrett, K. V. Rajagopalan, J. H. Enemark and D. C. Rees, *Cell*, 1997, **91**, 973; M. Czjzek, J.-P. Dos Santos, J. Pommier, G. Giordano, V. Méjean and R. Haser, *J. Mol. Biol.*, 1998, **284**, 435; A. S. McAlpine, A. G. McEwan and S. Bailey, *J. Mol. Biol.*, 1998, **275**, 613; J. M. Dias, M. E. Than, A. Humm, R. Huber, G. P. Bourenkov, H. D. Bartunik, S. Bursakov, J. Calvete, J. Caldeira, C. Carneiro, J. J. G. Moura, I. Moura and M. J. Romão, *Structure*, 1999, **7**, 65; H. Dobbek, L. Gremer, O. Meyer and R. Huber, *Proc. Natl. Acad. Sci. USA*, 1999, **96**, 8884; H.-K. Li, C. Temple, K. V. Rajagopalan and H. Schindelin, *J. Am. Chem. Soc.*, 2000, **122**, 7673.

3 B. Bradshaw, A. Dinsmore, C. D. Garner and J. A. Joule, *Chem. Commun.*, 1998, 417.

4 A. Dinsmore, C. D. Garner and J. A. Joule, *Tetrahedron*, 1998, **54**, 3291

5 A. Dinsmore, C. D. Garner and J. A. Joule, *Tetrahedron*, 1998, **54**, 9559

6 In each case, relative stereochemistry was determined by NOE experiments involving the hydrogen atoms at the pyran/pyrazine ring junction and at the hydroxymethyl-bearing carbon.

7 M. Ueki, N. Nishigaki, H. Aoki, T. Tsurusaki and T. Katoh, *Chem. Lett.*, 1993, 721; K. C. Nicolau, C. W. Hummel, M. Nakada, K. Shibayama, E. N. Pitsinos, H. Saimoto, Y. Mizuno, K. Baldenuius and A. L. Smith, *J. Am. Chem. Soc.*, 1993, **115**, 7625.

8 D. C. Rees, Y. Hu, C. Kisker and H. Schindelin, *J. Chem. Soc., Dalton Trans.*, 1997, 3909.

9 S. P. Greatbanks, I. H. Hillier, C. D. Garner and J. A. Joule, *J. Chem. Soc., Perkin Trans. 2*, 1997, 1529.

ChemComm

Bimetallic μ-cyanoimide complexes prepared by NCN group transfer†

Daniel J. Mindiola, Yi-Chou Tsai, Ryuichiro Hara, Qinghao Chen, Karsten Meyer and Christopher C. Cummins*‡

Department of Chemistry, Room 2-227, Massachusetts Institute of Technology, Cambridge, MA 02139-4307, USA. E-mail: ccummins@mit.edu

Received (in Irvine, CA, USA) 8th August 2000, Accepted 9th October 2000
First published as an Advance Article on the web

A cyanoimide [NCN] transfer reagent has been developed and applied to the synthesis of the μ-NCN systems (μ^2;η^1,η^1-NCN) {M[N(R)Ar]$_3$}$_2$ (Ar = C$_6$H$_3$Me$_2$-3,5; M = V or U, R = Bu^t; M = Mo, R = Pr^i).

Small molecules or ions comprised of combinations of the elements C, N and O hold inherent fascination due to their simplicity and their importance with respect to the global cycles that involve them. Studies in which reactive metal complexes are employed for small molecule activation can shed light on manifolds of processes that permit such substrates to be manipulated. Recent reports involving dinitrogen, nitrous oxide, carbon monoxide, and cyanate ion serve to exemplify this approach. The present work is concerned with cyanoimide ion, $[NCN]^{2-}$, the attributes of which as a ligand in coordination chemistry currently are not well understood. To this end has been developed a new reagent for the synthesis of cyanoimide complexes, a reagent based on the bicyclic amine 2,3 : 5,6-dibenzo-7-azabicyclo[2.2.1]hepta-2,5-diene (Hdbabh). For references relating to this work see ESI.†

As reported by Carpino *et al.*, the synthesis of Hbdabh proceeds *via* an *N*-bromo derivative, Brdbabh or alternatively from the hydrobromide salt BrH$_2$dbabh.[1,2] Treatment of Brdbabh with trimethylsilyl cyanide in DMF has been found to provide the desired *N*-cyano derivative NCdbabh in essentially quantitative yield as colorless leaflets subsequent to recrystallization from diethyl ether.[3] Cyano-dbabh thus prepared constitutes a reagent for transfer of the neutral [NCN] fragment to reducing metal complexes under mild conditions, the reactions being two-electron redox events that occur with concomitant release of anthracene.[4] Methodology based on the ability of the dbabh skeleton to effect group transfer coupled with anthracene formation has been documented previously in the case of $[N]^-$ transfer to form chromium(VI) nitrido complexes.[5]

Several metal complexes have been found to effect smooth [NCN] abstraction from cyano-dbabh. Treatment of a molybdenum metallaziridine–hydride complex known to serve as a source of the relatively unhindered three-coordinate molybdenum(III) fragment Mo[N(Pr^i)Ar]$_3$ **1** (Ar = C$_6$H$_3$Me$_2$-3,5),[6] with 0.5 equiv. of NCdbabh in diethyl ether at 25 °C led to rapid and essentially quantitative formation of the diamagnetic dinuclear μ-cyanamide derivative (μ-NCN)[**1**]$_2$. Anthracene removal was effected by filtration of the reaction mixture through activated charcoal, and orange crystals of (μ-NCN)[**1**]$_2$ were obtained in 63% yield by storing a concentrated Et$_2$O solution at −35 °C (Scheme 1). Prepared analogously using the ^{13}C-labeled reagent N^{13}Cdbabh[3] was the isotopomer (μ-N^{13}CN)[**1**]$_2$, an isotopomer of interest due to its ^{13}C NMR quintet ($^1J_{CN}$ 24 Hz) at 176 ppm and its strong IR ν_{NCN} stretch appearing at 2061 cm^{-1}, this value being red-shifted by 61 cm^{-1} relative to that for its unlabeled counterpart.[3] A low energy band at 475 nm in the visible spectrum of (μ-NCN)[**1**]$_2$ is assigned tentatively to a fully allowed transition from the molecule's e$_u$ HOMO to its e$_g$ LUMO, assuming idealized D_{3d} symmetry for the complex. Calculation of the HOMO–LUMO gap for a model system, using NH$_2$ in place of N(Pr^i)Ar ligands, gave a value (1.38 eV) well in accord with the experimentally observed quantity.[3,7]

Based on the orbital scheme developed for diamagnetic (μ-NCN)[**1**]$_2$, an analogous divanadium complex was expected to exist as a ground-state triplet. Such a complex was obtained upon reaction of V[N(R)Ar]$_3$ **2**[8,9] (R = Bu^t) with 0.5 equiv. of NCdbabh (Scheme 1). The purple–black microcrystalline solid thus obtained analyzed correctly for (μ-NCN)[**2**]$_2$, exhibited the expected strong ν_{NCN} at 2037 cm^{-1} {(μ-N^{13}CN)[**2**]$_2$ had an IR stretch at 1982 cm^{-1}}, and was found to possess a μ_{eff} of 3.01 μ_B in solution at 25 °C.[3] Purification of (μ-NCN)[**2**]$_2$ was accomplished as for the molybdenum derivative, the isolated yield being 91%. The divanadium complex (μ-NCN)[**2**]$_2$ shows an interesting electrochemistry. Two reversible reduction processes can be observed at −1.61 and −2.42 V (*vs.* [FeCp$_2$]$^{0/+}$). An oxidation event at −0.68 V was found to be in a range convenient for chemical oxidation. Oxidation of (μ-NCN)[**2**]$_2$ thus was accomplished using silver triflate, a regimen providing paramagnetic {(μ-NCN)[**2**]$_2$}[O$_3$SCF$_3$] in 56% yield. Oxidized (μ-NCN)[**2**]$_2$ was characterized fully, including its magnetochemistry and X-band EPR spectrum in solution.[3]

That complex (μ-NCN)[**1**]$_2$ contains a linear 5-atom MoNCNMo chain was confirmed by single-crystal X-ray crystallography (Fig. 1(a)),§ the molecular structure in question being found to incorporate a crystallographic center of inversion at the cyanoimide carbon along with a Mo–N–C angle of 176.6(4)° (two crystallographically independent molecules were confined

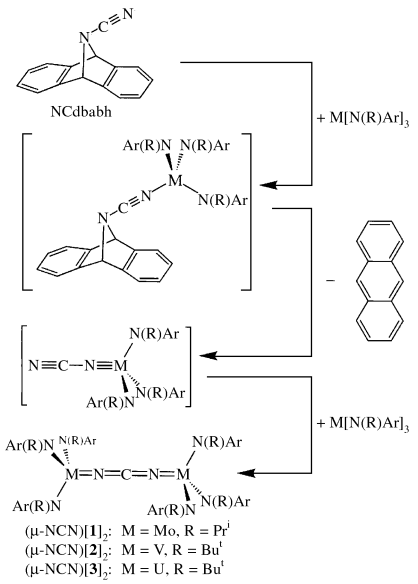

Scheme 1 Reaction scheme for 0.5 equiv. of NCdbabh with the metal complexes M[N(R)Ar]$_3$ to form the μ-cyanoimide complexes of the type (μ-NCN)[M{N(R)Ar}$_3$]$_2$ (M = Mo, R = Pr^i; M = V or U, R = Bu^t). Intermediate complexes have not been observed.

† Electronic supplementary information (ESI) available: introductory section with associated references as well as synthetic, spectroscopic, crystallographic and DFT calculation details for all complexes. See http://www.rsc.org/suppdata/cc/b0/b006517j/

‡ Alfred P. Sloan Fellow, 1997–2000.

DOI: 10.1039/b006517j

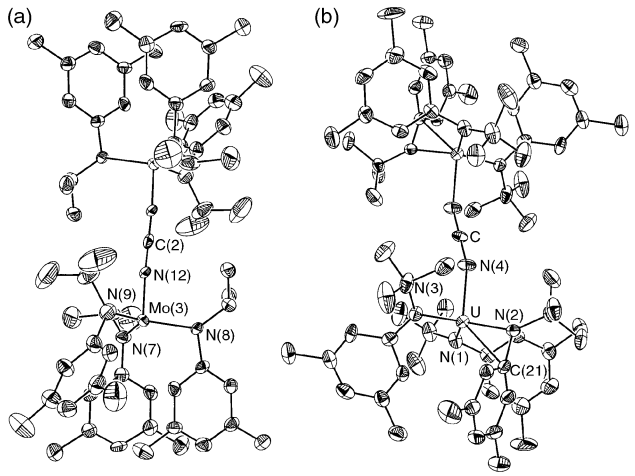

Fig. 1 (a) Structural diagram of (μ-NCN)[**1**]$_2$ with thermal ellipsoids at the 35% probability level. Selected distances (Å) and angles (°): Mo(3)–N(7) 1.947(6), Mo(3)–N(8) 1.994(6), Mo(3)–N(9) 1.960(7), Mo(3)–N(12) 1.852(7), N(12)–C(2) 1.233(7); Mo(3)–N(12)–N(2) 176.6(4). (b) Structural diagram of (μ-NCN)[**3**]$_2$ with thermal ellipsoids at the 35% probability level. Selected distances (Å) and angles (°): U–N(4) 2.226(7), U–N(1) 2.219(6), U–N(2) 2.225(6), U–N(3) 2.291(6), N(4)–C 1.189(8), U–C(21) 2.787(8); C–N(4)–U 162.6(5).

in the asymmetric unit, one of which possessed an inversion center about the cyanoimide carbon). As for the μ-nitrido dimolybdenum complex (μ-N)[**1**]$_2$ studied previously,[6] the six isopropyl substituents are directed to the molecule's interior, the six aryl residues consequently occupying polar positions. Given the properties of vanadium-containing (μ-NCN)[**2**]$_2$, its structure presumably likewise incorporates a linear 5-atom chain with metal termini.[3]

In contrast is the structure of the diuranium derivative (μ-NCN)[**3**]$_2$§ derived from the reaction of (THF)U[N(R)Ar]$_3$ **3**-THF[10,11] with 0.5 equiv. of NCdbabh (Scheme 1). X-Ray crystallography revealed in this case a *bent* geometry at the cyanoimide nitrogens [U–N–C 162.6(5)°], the molecule exhibiting again, however, inversion symmetry at the cyanoimide carbon atom (Fig. 1(b)).[12] The bent geometry adopted by the cyanoimide nitrogens in (μ-NCN)[**3**]$_2$, taken together with the observation of a congruence in the U–N_{amide} and U–$N_{cyanoimide}$ distances, may be indicative of relatively little π bonding in the uranium–cyanoimide interaction. In contrast, the transition-metal derivative (μ-NCN)[**1**]$_2$ exhibits a Mo–$N_{cyanoimide}$ distance shorter by 0.115(6) Å than the Mo–N_{amide} distance in the same complex. Recently it has been suggested that the high nodality of its valence 5 f orbitals renders mid-valent uranium less effective at π bonding than its transition-metal counterparts.[13,14] Using the ^{13}C-labeled reagent N^{13}Cdbabh, it was found that the isotopomer (μ-N^{13}CN)[**3**]$_2$ evinces a broad ^{13}C NMR resonance at 133 ppm.

It is believed that the ultimate step in formation of these μ-cyanoimide systems is the combination of a putative terminal cyanoimide complex with unreacted complex. Formation of the bridged-cyanoimide complexes most likely occurs *via* mononuclear reduction of NCdbabh, a process evidently being slow relative to consumption of unreacted metal complex. This work establishes NCdbabh as an efficient source of the [NCN] moiety, its implementation having led to smooth assembly of dinuclear cyanoimide-bridged complexes of vanadium, molybdenum and uranium. In addition to showing that dbabh represents a versatile platform for group transfer reactions, the present work makes available for study a new class of cyanoimide-bridged dimetal complexes. Mononuclear complexes featuring a *terminal* cyanoimide ligand remain attractive as synthetic targets.[15,16]

For financial support are gratefully acknowledged the National Science Foundation (CAREER Award CHE-9501992), the Alfred P. Sloan Foundation, the National Science Board (1998 Alan T. Waterman award to C. C. C.), and the Packard Foundation. K. M. thanks the DFG for a postdoctoral stipend. We are grateful to Dr Jesper Bendix for helpful comments and providing the EPR simulation program.

Notes and references

§ *Crystallographic data*: for (μ-NCN)[**1**]$_2$: $C_{100.50}H_{144}Mo_3N_{12}$, triclinic, space group $P\bar{1}$, M = 1808.10, a = 15.219(2), b = 18.043(3), c = 20.510(3) Å, α = 63.998(2), β = 81.112(2), γ = 80.611(2)°, U = 4972.1(12) Å^3, Z = 2, T = 183(2) K, μ(Mo-Kα) = 0.422 mm^{-1}, 15823 reflections measured, θ range 2.41–20.75°, 10252 unique reflections, R_1 = 0.0764, wR_2 = 0.1894, GOF = 1.068, residuals based on $I > 2\sigma(I)$. The residual peak and hole electron density was 1.478 and −1.390 e Å^{-3}. Two crystallographically independent molecules were present in the asymmetric unit with one of the chemically equivalent molecules possessing an inversion center about the cyanoimide carbon.

For (μ-NCN)[**3**]$_2$: $C_{73}H_{108}U_2N_8$, monoclinic, space group $P2_1/n$, M = 1573.73, a = 10.9163(8), b = 19.6175(14), c = 17.4079(12) Å, β = 96.8390(10)°, U = 3701.4(5) Å^3, Z = 2, T = 183(2) K, μ(Mo-Kα) = 4.413 mm^{-1}, 12242 reflections measured, θ range 2.10–21.25°, 4091 unique reflections, R (based on F) = 0.0418, wR (based on F^2) = 0.0770, GOF = 1.159, residuals based on $I > 2\sigma(I)$.

Single red-orange crystals of (μ-NCN)[**1**]$_2$ and yellow blocks of (μ-NCN)[**3**]$_2$ were grown from a Et_2O at −35 °C, mounted in inert oil (paratone N oil from Exxon) and transferred to a cold stream of the diffractometer. The structures were solved using direct methods and refined by full-matrix least squares on F^2. CCDC 182/1809.

1 L. A. Carpino, R. E. Padykula, D. E. Barr, F. H. Hall, J. G. Krause, R. F. Dufresne and C. J. Thoman, *J. Org. Chem.*, 1988, **53**, 2565.
2 D. E. Barr, Ph.D. Thesis, University of Amherst, MA, 1965.
3 Experimental details are included as ESI†
4 For an extensive review on arene extrusion reactions, see: H. N. C. Wong, T. K. Hg and T. Y. Wong, *Heterocycles*, 1983, **20**, 1815.
5 D. J. Mindiola and C. C. Cummins, *Angew. Chem., Int. Ed.*, 1998, **37**, 945.
6 Y.-C. Tsai, M. J. A. Johnson, D. J. Mindiola, C. C. Cummins, W. T. Klooster and T. F. Koetzle, *J. Am. Chem. Soc*., 1999, **121**, 10 426.
7 The HOMO and LUMO in question are π-symmetry orbitals extending along the linear 5-atom MoNCNMo chain. The HOMO–LUMO gap was calculated with the aid of DFT to be 1.38 eV, while the experimentally observed value was 1.66 eV at 475 nm. The $E_{excited}$–E_{ground} energy gap was calculated to be 1.42 eV.
8 M. G. Fickes, W. M. Davis and C. C. Cummins, *J. Am. Chem. Soc.*, 1995, **117**, 6384.
9 M. G. Fickes, Ph.D. Thesis, Massachusetts Institute of Technology, MA, 1998.
10 A. L. Odom, P. L. Arnold and C. C. Cummins, *J. Am. Chem. Soc.*, 1998, **120**, 5836.
11 A. L. Odom, Ph.D. Thesis, Massachusetts Institute of Technology, MA, 1997.
12 Experimentals and tables for bond lengths, angles, atomic coordinates and anisotropic displacement parameters are included as ESI†
13 R. B. King, *Inorg. Chem.*, 1992, **31**, 1978.
14 P. L. Diaconescu, P. L. Arnold, T. A. Baker, D. J. Mindiola and C. C. Cummins, *J. Am. Chem. Soc.*, 2000, **122**, in press.
15 A. J. L. Pombeiro, *New. J. Chem.*, 1991, **45**, 444.
16 Attempts to prepare such complexes, *e.g.* by reaction of an equimolar amount of NCdbabh with an appropriate metal complex, gave rise only to the dinculear complexes (μ-NCN)[**1**]$_2$, (μ-NCN)[**2**]$_2$ and (μ-NCN)[**3**]$_2$, along with unreacted NCdbabh.

ChemComm

Structure and polymorphism of the 10.10.10 Simmons and Park cryptand†

Andrei S. Batsanov,[a] Alexander J. Blake,[b] Nicholas M. Hext[b] and Mark Mascal*‡[b]

[a] *Department of Chemistry, University of Durham, South Road, Durham, UK DH1 3LE*
[b] *Department of Chemistry, University of Nottingham, Nottingham, UK NG7 2RD*

Received (in Columbia, MO, USA) 15th September 2000, Accepted 8th November 2000
First published as an Advance Article on the web

The first crystal structure of a 10.10.10 cryptand has been determined, during which an unusual single crystal phase transition was observed; at room temperature, crystals of macrobicycle 1d are monoclinic (α) but undergo a first-order topotactic phase change at 207 K to a triclinic (β) lattice; full structure determinations at 150 and 210 K were carried out and show that both phases adopt the *in–in* cryptand conformation.

The foundations of modern host–guest chemistry were laid in two papers published by independent research groups in 1967 and 1968. The former was the first report of alkali metal complexes of a polyether macrocycle,[1] and the latter the first report of guest inclusion in a diaza macrobicycle.[2] The first result gave birth to the crown ethers, the second to the cryptands, both 'household' words in the field of supramolecular chemistry.[3]

We became interested in the all-hydrocarbon bridged cryptands **1** originally described by Simmons and Park[2] from the point of view of isolating the effects of the two N (or HN^+) sites to produce linear inclusion complexes with various neutral and ionic guests. Although the 'original' crown ether, dibenzo 18-crown-6, has itself been the subject of no less than ninety X-ray crystal structures,[4] only one crystallographic study has been

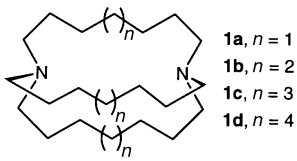

1a, *n* = 1
1b, *n* = 2
1c, *n* = 3
1d, *n* = 4

published on an 'original' cryptand, *i.e.* **1c**.[5] In this work, the bis(hydrochloride) cryptate $[H_2(\mathbf{1c})Cl]^+ Cl^-$ co-crystallizes with the unusual polyaqua cation $H_{13}O_6^+$, the latter species being the main focus of the paper. However, no satisfactory representation of the cage itself was derived from the data, owing to the presence of extensive disorder.

Taking into account the respective melting points in the **1** series indicates that the *n.n.n* cryptands are conformationally mobile where *n* is odd, while those where *n* is even will be conformationally stable.[6] This may explain the difficulties the previous workers experienced with **1c**. We thus prepared the 10.10.10 cryptand **1d**[7] and undertook first to obtain an X-ray crystal structure of the empty, neutral receptor. In the course of the determination, we observed a single-crystal phase transition, and now report on the structure of **1d**, the first of a 10.10.10 cryptand,[8] and this unusual occurrence of polymorphism.

Crystals of **1d** (from light petroleum) were prismatic, but most of them displayed a peculiar form, with a large recess on one of the faces of the prism, often reducing the crystal to a hollow 'box' open on one side. A similar crystal habit has been observed for triethylenetetramine $[H_2N(CH_2)_2NH(CH_2)_2NH(CH_2)_2NH_2]$ and could be attributed to the presence of $N[(CH_2)_2NH_2]_3$, a by-product of the synthesis, which selectively inhibited the development of certain faces.[9]

At ambient temperature crystals of **1d** are monoclinic (α-**1d**), but undergo a sharp phase transition at 207 K. Of several crystals tested, all crumbled to powder or converted to polycrystalline blocks at this temperature, except one which was initially of exceptionally good quality and on which a full structure determination was performed at 210 K in space group *I*2/*a* (a non-standard setting of *C*2/*c*, no. 15). At the moment of transition (monitored by rotational diffractograms taken after every 1 K cooling step) a part of the crystal split off and the remainder appeared to become a non-merohedral twin. Its reflections were indexed on a triclinic lattice (β-**1d**), which was confirmed by a full structure determination at 150 K in space group $P\bar{1}$ (no. 2). No further phase transformations were observed on cooling to 100 K.

The molecular structure of **1d** in the α and β phases is shown in Fig. 1 (ESI†). In the former, monoclinic phase, the molecule lies across a crystallographic twofold axis, which is perpendicular to the N···N′ vector. Two of the decamethylene chains, C(1)– C(10) and C(1′)–C(10′), are related by this axis. In each chain, two atoms [C(7) and C(8) or their equivalents] are disordered over two positions with occupancies of 0.779(8) and 0.221(8). The third decamethylene chain is bisected by the twofold axis, and its four central C atoms are equally disordered over two conformations which are symmetrically related by this axis, but neither of which possesses C_2 symmetry. In the β phase the molecule has no crystallographic symmetry. The average volume per non-hydrogen atom, 24 Å^3 (α-**1d**) or 23 Å^3 (β-**1d**), is considerably higher than the typical value for an organic

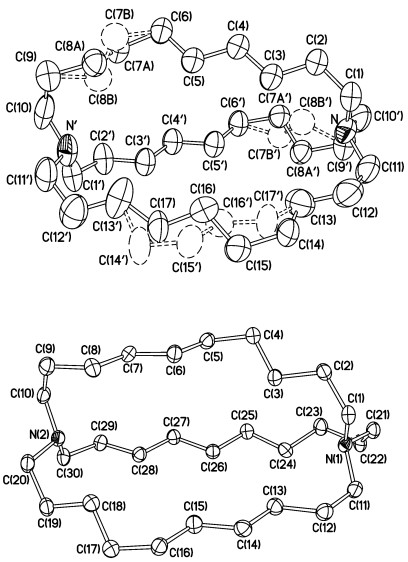

Fig. 1 Molecular structure of **1d** in the monoclinic (α, top) and triclinic (β, bottom) polymorphs, shown in the same crystallographic aspect and scale. Displacement ellipsoids are drawn at the 50% probability level. In α-**1d**, primed atoms are related to their equivalents by the operation of the twofold rotation axis. H atoms are omitted.

† Electronic supplementary information (ESI) available: experimental details of the crystal structure determinations, orientation and phase transformation matrices and diagram of the unit cells of α- and β-**1d**. See http://www.rsc.org/suppdata/cc/b0/b008044f/

‡ Present address: Department of Chemistry and Biochemistry, University of California, Los Angeles, 405 Hilgard Ave., Los Angeles, CA 90095, USA. E-mail: mascal@chem.ucla.edu.

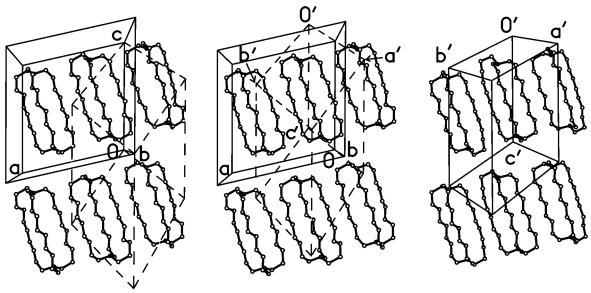

Fig. 2 The phase transformation of **1d**. Left: the structure of α-**1d** and the primitive triclinic cell (dashed lines, origin at 0,0,1); middle: the same with the triclinic cell (primed labels) shifted by $-a'/2$; right: the structure of β-**1d**.

compound of 18 Å^3, but close to the value of 22 Å^3 found in the nearest structurally studied analogue, N[$(CH_2)_4$]$_3$ N.[10,11]

In both structures the lone pairs on the nitrogen atoms point into the cavity, the pro-cryptate '*in-in*' conformation of macrobicyclic hosts.[12] The bond distances are not unusual, while the torsion angles within the chains represent *anti* or *gauche* conformations and their patterns are different in the two structures. The molecule is slightly more elongated in the β than in the α phase, the transannular N···N distances being 9.14 and 9.01 Å, respectively. No significant empty volume was found in either structure or in any disorder component.[13]

As such topotactic phase changes between single crystal phases are relatively rare for molecular crystals, we sought to identify and describe the transformation between the high temperature α form and the low temperature β form, as illustrated in Fig. 2. The β phase is generated from the α form by first transforming the *I*-centered monoclinic lattice onto its primitive trinclinic one by application of the transformation matrix ($-\frac{1}{2}\,\frac{1}{2}\,-\frac{1}{2}\,/\,\frac{1}{2}\,\frac{1}{2}\,-\frac{1}{2}\,/\,0\;0\;-1$), then by an origin shift of *ca.* $a'/2$, and finally a considerable shear of the lattice, roughly along the c' ($=c$) axis, widening all three lattice angles by 7–13°. In both structures the molecules are packed in layers, parallel to the (0 1 0) plane in α-**1d** or the (1 1 0) plane in β-**1d** (Fig. 2 shows the projections on these planes). The intramolecular N···N vector is coplanar with the layer, rigorously in α-**1d**, and within 3° in β-**1d**. The interlayer separations are essentially equal in the α and β forms (8.32 and 8.36 Å, respectively). In either case the adjacent layers are shifted against each other along the *c* axis (which forms the same angle of 15.5° with the N···N vector). In α-**1d** the shift is exactly *c*/2 (*ca.* 7 Å), each molecule fitting the gap in the adjacent layer. In β-**1d** the shift is only 4 Å (*ca.* 0.3*c*) and the molecule adopts an asymmetric conformation to accommodate to a partial overlap.

Although this degree of reorganization could be considered incompatible with a topotactic transition, it is not unprecedented: Gougoutas has identified examples where considerable molecular motions appear to be necessary to effect the observed phase transformations.[14] The difficulties we encountered in retaining singularity suggest that in the present case we were operating at the limits of topotaxy.

The unit cell parameters of **1d** change remarkably between 210 and 293 K (Table 1), while the Laue symmetry and systematic absences remain the same. With increasing temperature, the unit cell actually contracts in the direction of the twofold axis (*b*) by 0.286 Å (1.72%) while expanding in the perpendicular directions, again implying substantial conformational changes. Unfortunately, at room temperature the crystals decay completely in the X-ray beam within a few hours, hence a full structure determination was not possible.

Organic polymorphism is a frequently observed but poorly understood phenomenon which is rarely examined in detail.[15] Despite this, it is of substantial relevance to biomolecular and pharmaceutical sciences.[16] Here we have sought to describe an occurrence of polymorphism in the first structurally characterized 10.10.10 cryptand, requiring a significant degree of molecular reorganization. The historically[2] and practically[7] important Simmons and Park cryptand **1d** has also been shown to reside in the '*in-in*' pro-cryptate macrobicycle conformation in the solid state.

Table 1 Crystal data for **1d**§

T/K	293	210	150	120
Crystal system	Monoclinic	Monoclinic	Triclinic	Triclinic
Space group	$I2/a$	$I2/a$	$P\bar{1}$	$P\bar{1}$
a/Å	14.083(6)	13.515(1)	10.209(1)	10.165(6)
b/Å	16.357(4)	16.643(1)	12.334(5)	12.311(5)
c/Å	14.398(5)	13.934(1)	13.904(1)	13.876(3)
α/°	90	90	63.78(1)	63.95(2)
β/°	106.93(5)	103.12(1)	74.73(1)	74.69(3)
γ/°	90	90	70.54(1)	70.44(4)
U/Å^3	3173(1)	3052.4(4)	1466.9(3)	1456(1)
Z		4	2	
Total reflections		8874	8612	
Unique reflections		2696	4916	
R_{int}		0.045	0.064	
Data with $I > 2\sigma(I)$		1547	3394	
$R[I > 2\sigma(I)]$		0.084	0.065	
$wR(F^2)$, all data		0.254	0.164	

This work was supported in part by the EPSRC, and the authors are grateful to the University of Durham for provision of the X-ray and computational facilities and to Professor J. A. K. Howard for helpful discussions.

Notes and references

§ CCDC 182/1857. See http://www.rsc.org/suppdata/cc/b0/b008044f/ for crystallographic files in .cif format.

1 C. J. Pedersen, *J. Am. Chem. Soc.*, 1967, **89**, 2495.
2 H. E. Simmons and C. H. Park, *J. Am. Chem. Soc.*, 1968, **90**, 2428; C. H. Park and H. E. Simmons, *J. Am. Chem. Soc.*, 1968, **90**, 2429; C. H. Park and H. E. Simmons, *J. Am. Chem. Soc.*, 1968, **90**, 2431.
3 *Comprehensive Supramolecular Chemistry*, ed. G. W. Gokel, Elsevier, Oxford, 1996, vol. 1.
4 Cambridge Structural Database Version 5.17 (197481 structures, April 1999 release): F. H. Allen and O. Kennard, *Chem. Des. Autom. News*, 1993, **8**, 1; F. H. Allen and O. Kennard, *Chem. Des. Autom. News*, 1993, **8**, 31.
5 R. A. Bell, G. G. Christoph, F. R. Fronczek and R. E. Marsh, *Science*, 1975, **190**, 151.
6 *Cf.* melting points, **1a**, 35 °C; **1b**, 120 °C; **1c**, 32 °C; **1d**, 114 °C (from ref. 2). See: J. Dale, *Angew. Chem.*, 1966, **5**, 1000 for a discussion of the effects of chain length on conformational stability in cyclic structures.
7 This cryptand has been used in a number of anion complexation and transport studies, see: B. Dietrich, T. M. Fyles, M. W. Hosseini, J.-M. Lehn and K. C. Kaye, *J. Chem. Soc., Chem. Commun.*, 1988, 691; J.-P. Kintzinger, J.-M. Lehn, E. Kauffmann, J. Dye and A. I. Popov, *J. Am. Chem. Soc.*, 1983, **105**, 7549; E. Graf and J.-M. Lehn, *J. Am. Chem. Soc.*, 1976, **98**, 6403.
8 The crystal structure of a 10.10.10 macrobicycle with tin at the bridgeheads has been published. However, this can not be considered a cryptand due to the tetravalent nature nature of tin and the consequent, forced *out–out* conformation. See: J. H. Horner, P. J. Squatritto, N. McGuire, J. P. Riebenspies and M. Newcomb, *Organometallics*, 1991, **10**, 1741.
9 I. Bernal, personal communication.
10 R. W. Alder, A. G. Orpen and R. B. Sessions, *J. Chem. Soc., Chem. Commun.*, 1983, 999.
11 W. P. Schaefer and R. F. Marsh, *J. Chem. Soc., Chem. Commun.*, 1984, 1555.
12 R. W. Alder and S. P. East, *Chem. Rev.*, 1996, **96**, 2097.
13 A. L. Spek, PLATON, a multi-purpose crystallographic tool. University of Utrecht, The Netherlands.
14 J. Z. Gougoutas, *Pure Appl. Chem.*, 1971, **27**, 305.
15 C. N. R. Rao and K. J. Rao, *Phase Transitions in Solids*, McGraw-Hill, London, 1978; A. Gavezzotti and M. Simonetta, *Chem. Rev.*, 1982, **82**, 1; J. D. Dunitz, *Acta Crystallogr., Sect. B*, 1995, **51**, 619; M. R. Caira, *Top. Curr. Chem.*, 1998, **198**, 163.
16 J. D. Dunitz and J. Bernstein, *Acc. Chem. Res.*, 1995, **28**, 193.

ChemComm

Palladacyclic phosphinite complexes as extremely high activity catalysts in the Suzuki reaction

Robin B. Bedford* and Samantha L. Welch

School of Chemistry, University of Exeter, Exeter, UK EX4 4QD. E-mail: R.Bedford@ex.ac.uk

Received (in Cambridge, UK) 18th October 2000, Accepted 16th November 2000
First published as an Advance Article on the web

Phosphinite based palladacycles show extremely high activity in the Suzuki coupling of both sterically hindered and electronically deactivated aryl bromides, especially in the presence of one equivalent of free ligand.

There has recently been considerable interest in the synthesis of new, high activity palladium-based catalysts that can be used in low concentration in the Suzuki reaction (Scheme 1) since such catalysts have the potential to be used in industrial systems. In particular, palladacyclic catalysts in which a ligand coordinates to the metal centre through both a donor atom and metallated carbon have shown considerable promise. Beller and co-workers demonstrated that palladated phosphine complexes show good activity[1] whilst we have shown that the palladated triaryl phosphite complex **1** and the bis(phosphinite) PCP-

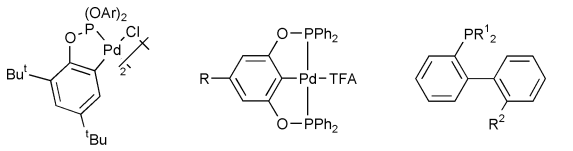

1: Ar = 2,4-^{t}Bu$_2$C$_6$H$_3$ **2**: R = H, Me **5**: R^1 = Cy, ^{t}Bu; R^2 = H, Me, ^{i}Pr, NMe$_2$

pincer complexes **2** show excellent activity.[2,3] High activity is not limited to metallated phosphorus donor systems—Milstein and co-workers have shown that a palladated imine complex shows excellent activity,[4] whilst Zim *et al*. have shown that palladated thioether complexes can also be used.[5]

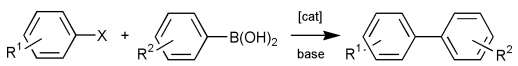

Scheme 1 The Suzuki biaryl coupling reaction.

To the best of our knowledge, the use of *P,C*-bidentate phosphinite palladacycles as catalysts in the Suzuki reaction has not been investigated. We report here the synthesis of such complexes, the remarkable activity they show in the Suzuki reaction and present preliminary evidence that suggests that the active catalysts are likely to be low coordinate palladium(0) species.

The reactions of the ligands **3a** and **b** with palladium chloride in toluene at reflux temperature gives the complexes **4a** and **b** in good yields. Complex **4c** is best prepared by the reaction of [$PdCl_2(NCPh)_2$] with **3c** in THF at reflux temperature. All the complexes **7** are obtained as a mixture of *cis* and *trrans* isomers.[2]

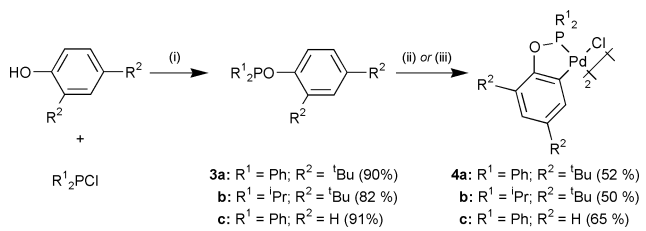

Scheme 2 (i) Et_3N, toluene, reflux temperature, 18–20 h; (ii) For **4a** and **b**: $PdCl_2$, toluene, reflux temperature 18–20 h; (iii) For **4c**: [$PdCl_2(NCPh)_2$], THF, reflux temperature, 20 h.

The application of the complexes **4a**–**c** as catalysts in the Suzuki reaction was studied and the results are summarised in Table 1. The complexes **4a** and **b** prove to be extremely active catalysts for both the 'easy to couple' substrate 4-bromoacetophenone and the more challenging, electronically deactivated substrate 4-bromoanisole. To the best of our knowledge, the activity shown by the catalyst mixture of **4b** and one equivalent of added ligand **3b** (entry 13) is the highest reported for any Suzuki reaction—over five times higher than for the analogous reaction catalysed by palladium complexes of the phosphine ligands **5**.[6] By contrast, the previous highest reported activity with a palladacyclic catalyst in this reaction was with complex **1** which gave a turn-over number (TON) of 1 million.[2] More importantly with the electronically deactivated substrate 4-bromoanisole the catalyst systems reported here show up to 45 times higher activity than the previous best catalysts—the related bis(phosphinite) pincer complexes **2**.[3] Similarly the activities seen with the sterically hindered, electronically deactivated substrates 2-bromotoluene and 2-bromo-*m*-xylene are over an order of magnitude higher than any catalyst systems in the literature.[3]

Complex **4b** generally shows higher activity than **4a**, presumably due to the higher electron density that the phosphinite ligand confers on the palladium centre—this increase in electron density facilitates oxidative addition of the aryl bromide. The observation that **4a** seems to show very little difference in activity in the coupling of phenylboronic acid with either 4-bromoacetophenone or 4-bromoanisole indicates that the oxidative addition of the aryl bromide may not be the rate determining step in the catalytic cycle. Comparing entries 3 and 7 it can be seen that decreasing the steric profile of the metallated ring has a deleterious effect on the rate of reaction, however **4c** still shows substantially higher activity than its previously reported bis(phosphinite) PCP pincer counterpart, **2** (R = H).[3] The importance of the metallation in the pre-catalysts is demonstrated by comparing entries 3, 8 and 9. The addition of a second phosphinite ligand to the metallated complex gives an increase in activity, by contrast the formation of bis(phosphinite) complexes *in situ* leads to substantially *reduced* reactivity. In other words addition of a second phosphinite is only beneficial if there is a metallated ring in the complex, otherwise it is deleterious. This demonstrates that the orthometallation of the pre-catalyst is extremely important; the possible role it plays is addressed below.

By contrast with the extraordinary results obtained with the deactivated aryl bromide 4-bromoanisole, complex **4b** proved to be a very poor catalyst when 4-chloroanisole was used as a substrate, indeed substantial deposition of palladium metal was observed almost immediately upon heating. Interestingly, we found that rapid decomposition of all three complexes **4a**–**c** occurs even if the 4-chloroanisole is left out of the reaction mixture. To gain evidence for the mechanism of decomposition a reaction was performed between **4c**, $PhB(OH)_2$ (4 molar equiv./Pd) and K_2CO_3 (5 molar equiv./Pd) in toluene at reflux temperature. The reaction was performed over 24 h, although decomposition started within seconds of the reaction reaching about 50 °C. After this time the supernatant liquid contained a mixture of compounds which included some unreacted **4c**. A GC-MS spectrum of the mixture revealed the presence of some

DOI: 10.1039/b008470k

Table 1 Suzuki coupling of aryl halides with phenylboronic acid catalysed by palladium phosphinite complexes. Reaction conditions: 10 mmol aryl halide, 15 mmol $PhB(OH)_2$, 20 mmol K_2CO_3, 30 ml toluene, 130 °C, 18 h

Entry	Aryl halide	Catalyst ([Pd]/mol% Pd)	Conversion (%)[a]	TON/10^3 (mol product/ mol Pd)
1	4-Bromoacetophenone	**4a** (10^{-4})	90	900
2	4-Bromoacetophenone	**4a** (10^{-5})	20	2 000
3	4-Bromoanisole	**4a** (10^{-4})	85	850
4	4-Bromoanisole	**4a** (10^{-5})	26	2 600
5	4-Bromoanisole	**4b** (10^{-4})	91	910 000
6	4-Bromoanisole	**4b** (10^{-5})	42	4 200
7	4-Bromoanisole	**4c** (10^{-4})	29	290
8	4-Bromoanisole	**4a** + **3a** (10^{-4})	100	1 000
9	4-Bromoanisole	$Pd(dba)_2$ + 2 **3a** (10^{-4})	36	360
10	4-Bromoanisole	**4a** + **3a** (10^{-5})	87.5	8 750
11	4-Bromoanisole	**4b** + **3b** (10^{-5})	50	5 000
12	4-Bromoacetophenone	**4b** + **3b** (10^{-6})[b]	100	100 000
13	4-Bromoacetophenone	**4b** + **3b** (10^{-7})[b]	47.5	475 000
14	2-Bromotoluene	**4b** + **3b** (10^{-3})	100	100
15	2-Bromo-*m*-xylene	**4b** + **3b** (10^{-3})	48	48
16	4-Chloroanisole	**4b** (1.0)	6	0.006

[a] Determined by GC, based on aryl halide. [b] 24 h reaction time.

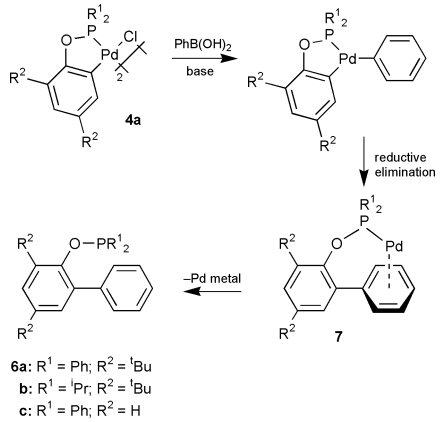

Scheme 3

of the new phosphinite species **6c**, this was confirmed by comparison with the spectrum obtained for a genuine sample of **6c**. In addition, hydrolysis of the reaction mixture led to the formation of 2-phenylphenol, again demonstrated by GC-MS and compared with an authentic sample. A plausible mechanism of decomposition which results in the liberation of **6c** and palladium metal is shown in Scheme 3.

Since the complexes **4** show no reactivity with aryl bromides or chlorides in toluene at reflux temperature it is possible that the transmetallation and reductive elimination steps outlined in Scheme 3 also occur as initiation steps in the catalytic cycles of Suzuki reactions catalysed by these species and that the low coordinate mono-phosphinite species **7** represent the active catalysts in these reactions. Similar low coordinate species have been postulated as being the active catalysts in high activity Suzuki systems which employ palladium complexes of the phosphines **5**.[6] Part of the explanation given for the high activity of these latter complexes is that transient π-coordination of the secondary aryl ring of the ligand to the palladium centre may help to stabilise the low coordinate complex. The introduction of the oxygen atom into the ligands gives a higher degree of flexibility, thus it would be expected that the secondary aryl functions of the ligands **6a**–**c** would participate in π-complexation with the metal centre even more readily than those in the ligands **5**. Furthermore, due to higher π-acidity of the phosphorus donors, the ligands **6** would stabilise the zero-valent palladium complexes better than the ligands **5**.

In summary, the catalysts described here show by far the highest activities yet reported in any Suzuki coupling reactions. These complexes are ideal catalysts for the coupling of deactivated and sterically hindered aryl bromides as they are comparatively inexpensive, very easily synthesised and can be used to give high conversions at extremely low concentrations. In addition preliminary results suggest that the active catalysts in these reactions may be low coordinate Pd(0) species.

We thank the EPSRC for funding and Johnson Matthey Chemicals for funding, the loan of palladium salts and access to their rapid catalyst screening programme.

Notes and references

1 M. Beller, H. Fischer, W. A. Herrmann, K. Öfele and C. Brossmer, *Angew. Chem., Int. Ed. Engl.*, 1995, **34**, 1848.
2 D. A. Albisson, R. B. Bedford, S. E. Lawrence and P. N. Scully, *Chem. Commun.*, 1998, 2095.
3 R. B. Bedford, S. M. Draper, P. N. Scully and S. L. Welch, *New J. Chem.*, 2000, 745.
4 H. Weissman and D. Milstein, *Chem. Commun.*, 1999, 1901.
5 D. Zim, A. S. Gruber, G. Ebeling, J. Dupont and A. L. Monteiro, *Org. Lett.*, 2000, **2**, 2881.
6 J. P. Wolfe, R. A. Singer, B. H. Yang and S. L. Buchwald, *J. Am. Chem. Soc.*, 1999, **121**, 9550.

Variable temperature electrochemistry as a powerful method for conformational investigations on the fluxional organometallic complex Mo(His-N_ε-$C_2H_4CO_2Me$)(η-allyl)$(CO)_2$ (His = N_δ, *N*,*O*-L-histidinate)†

Dave R. van Staveren, Eberhard Bothe, Thomas Weyhermüller and Nils Metzler-Nolte*‡

Max-Planck-Institut für Strahlenchemie, Stiftstraße 34-36, D-45470 Mülheim/Ruhr, Germany

Received (in Cambridge, UK) 26th September 2000, Accepted 25th October 2000
First published as an Advance Article on the web

Square-wave voltammograms of the complex Mo(His-N_ε-$C_2H_4CO_2Me$)(η-allyl)$(CO)_2$ (His = N_δ,*N*,*O*-L-histidinate) 2 recorded at variable temperatures establish the existence of two isomers in solution in both the reduced and the oxidized paramagnetic form of 2; a complete analysis yields thermodynamic parameters such as equilibrium constants, Δ*G* and Δ*H* for all species.

Fluxionality is frequently observed in organometallic complexes in solution.[1,2] In the course of our studies on the labelling of biomolecules with organometallic complexes we have reinvestigated the compound Mo(His)(η-allyl)$(CO)_2$ **1** (His = N_δ,*N*,*O*-L-histidinate). The synthesis of this complex was first reported by Beck and coworkers twenty years ago.[3,4] Since that time, fluxionality in diamagnetic complexes of the general formula M(η-allyl)$(CO)_2L_2X$ (M = Cr, Mo, W) has been studied in some detail by NMR spectroscopy in solution.[5–7] For some derivatives, a good stability of the one-electron oxidized species was demonstrated,[8,9] but related fluxionality was never mentioned. There seems to be no obvious method for investigations of this kind on the paramagnetic species $[M(\eta\text{-allyl})(CO)_2L_2X]^+$.

We were intrigued by the excellent stability of complex **1** and its potential as a covalent marker for biomolecules, in particular by IR or electrochemical detection. In complex **1**, three different orientations of the His ligand with respect to the (allyl)$(CO)_2$ plane are possible. The stereochemical implications of fluxional processes in M(η-allyl)$(CO)_2L_2X$ have been discussed, but all complexes investigated so far were either achiral or racemic mixtures.[7] Here, we report the synthesis of the enantiomerically pure methyl propionate derivative Mo(His-N_ε-$C_2H_4CO_2Me$)(η-allyl)$(CO)_2$ **2** and its complete characterization. The presence of two isomers of **2** is shown by NMR and electrochemical investigations. An unusual case of coalescence in temperature-dependent square-wave voltammograms is reported and we demonstrate how a complete analysis of the electrochemical data gives detailed quantitative information on both isomers of the paramagnetic, one-electron oxidized $\mathbf{2}^+$. This information is difficult to obtain otherwise with such accuracy.

Compound **2** was synthesised in 65% yield by reacting Mo(His)(allyl)$(CO)_2$[3] with 3-bromomethylpropionate in the presence of equimolar amounts of Cs_2CO_3 in DMF, under an atmosphere of Ar. Compound **2** is completely stable under Ar and can be stored in air on the benchtop for several days without decomposition.

X-Ray quality single crystals of **2**·2MeOH were grown by slow pentane diffusion into MeOH at +4 °C. An ORTEP representation of **2**·2MeOH§ is depicted in Fig. 1. The chirality around the metal atom is clearly determined by the known stereochemistry of the amino acid L-His. The Mo(allyl)$(CO)_2$ moiety is in a facial arrangement, with the terminal carbon atoms of the allyl ligand oriented towards the carbonyl ligands. Such a conformation has been shown to be energetically favourable[10] and is observed in all solid-state structures of this type reported thus far.[6,7,11–13] The allyl ligand is located *trans* relative to the histidine-N_δ atom [N(8)] and bound symmetrically to the Mo atom, with Mo–C distances of 2.328(3) Å [Mo(1)–C(17) and Mo(1)–C(19)] and 2.209(2) Å [Mo(1)-C(18)]. The two MeOH molecules form hydrogen bonds with the carboxylato group, with O···O contacts of 2.750(10) Å [O(14)···O(20)] and 2.800(10) Å [O(13)···O(30)].

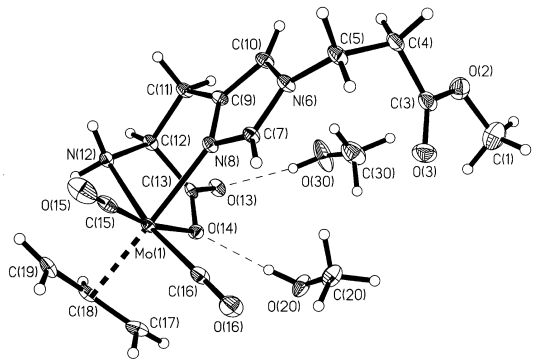

Fig. 1 ORTEP plot for **2**·2MeOH, with thermal ellipsoids at 50% probability level. Selected bond distances (Å): Mo(1)–N(8) 2.216(2), Mo(1)–N(12) 2.256(2), Mo(1)–O(14) 2.214(2), Mo(1)–C(15) 1.945(3), Mo(1)–C(16) 1.944(3), Mo(1)–C(17)=Mo(1)–C(19) 2.328(3), Mo(1)–C(18) 2.209(2).

In solution, the situation is more complex. Two sets of signals are observed in the ^1H NMR as well as in the ^{13}C NMR spectrum of **2**, indicating the presence of two isomers (**2a** and **2b**, see Scheme 1) in solution. The ratio between both isomers is solvent dependent [DMSO 53:47, MeCN (293 K) 57:43, MeOH 77:23]. The presence of two isomers in the special case of Mo(allyl)$(CO)_2L_2X$ with L_2X = cyclopentadienyl (Cp) has been explained by rotation of the allyl group. In the more general case where L_2X comprise heterodonor atoms (N, O, P *etc*.) fluxionality is brought about by a trigonal twist of the L_2X plane with respect to the Mo(allyl)$(CO)_2$ core.[12] Recently, we reported the presence of *two different* allyl orientations in the same crystal structure of a CpMo(allyl)$(CO)_2$ derivative.[14] For **2**, if one of the isomers has the conformation observed in the solid-state structure, the other detectable isomer could either have the NH_2 or the carboxylato group *trans* to the allyl ligand. In accordance with NMR data (*vide infra*), preliminary results from DFT calculations show the latter is the energetically favoured conformer of the two,[15] with the third isomer being too high in energy to be observed by NMR spectroscopy (< 0.1% at

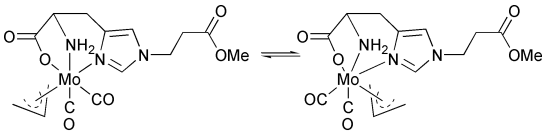

Scheme 1 Molecular structure of the two isomers of **2**.

† Electronic supplementary information (ESI) available: analytical data for **2**. See http://www.rsc.org/suppdata/cc/b0/b007822k

‡ Present address: Institute for Pharmaceutical Chemistry, University of Heidelberg, Im Neuenheimer Feld 364, D-69120 Heidelberg, Germany. E-mail: Nils.Metzler-Nolte@urz.uni-heidelberg.de

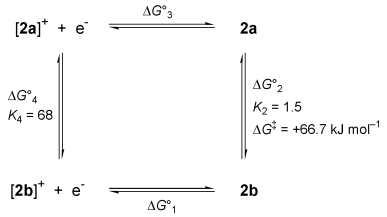

Scheme 2 Square scheme showing the redox reactions and rerrangements of **2**. At −60 °C: ΔG^0_1 = −40.1 kJ mol^{-1}, ΔG^0_2 = −0.72 kJ mol^{-1}, ΔG^0_3 = +48.3 kJ mol^{-1}, ΔG^0_4 = −7.5 kJ mol^{-1}. From electrochemical experiments at variable temperatures: ΔH^0_2 = −2.5 kJ mol^{-1}, ΔH^0_4 = −8.3 kJ mol^{-1}.

500 MHz ^{1}H NMR). The chemical shift of the imidazole proton signals are at δ 8.62 and 7.12 in isomer **2a** and δ 8.02 and 6.92 in isomer **2b**. We assume that the imidazole nitrogen atom is *trans* to the allyl ligand in isomer **2a** and *trans* to a CO in **2b**. The chemical shift difference may then be rationalized by the different *trans* influences of the allyl and CO ligands. Variable temperature measurements in MeCN yielded $\Delta G^{\ddagger}$ = 66.7 ± 0.5 kJ mol^{-1}, consistent with a trigonal twist mechanism of interconversion.[11,12]

The cyclic voltammogram (CV) of **2** in MeCN (scan rate of 0.1 V s^{-1}, 25 °C) shows a wave with reversible appearance at $E_{1/2}$ = +86 mV *vs.* Fc/Fc$^+$. This value is in the range reported for several other analogous pseudo-octahedral Mo complexes.[8,9] Controlled potential coulometry (at +0.5 V *vs.* Fc/Fc$^+$) reveals that the wave arises from a one-electron oxidation of **2**. However, the oxidation of **2** does not proceed *via* an uncomplicated reversible single electron process. At slow scan rates, the peak separation increases with increasing scan rates from 85 mV at 0.025 V s^{-1} to 140 mV at 0.8 V s^{-1}, but at even faster scan rates (up to the highest value measured of 25 V s^{-1}) it remains almost constant (±10 mV). This behaviour can be accommodated in a 'square scheme' shown in Scheme 2, assuming the presence of two isomers in *both* the oxidized and reduced form of **2**.

The presence of two species was readily detected by square-wave voltammetry (SWV). Square-wave voltammograms at four different temperatures are shown in Fig. 2. At −60 °C, the anodic and cathodic scans are fully symmetric [curve (d)]. This shows that the equilibrium composition of the reduced form (the starting material **2**) is maintained after the oxidation for the time period of equilibration at +0.6 V and during the time of the scan, *i.e.* for at least a few seconds. Because the equilibrium constants for the oxidized and reduced forms are quite different (see below), the isomerisation reaction must be correspondingly slow at −60 °C. At −20 °C anodic and cathodic scans are different [curve (b)] and it is observed that oxidized **2**$^+$ exhibits a preference for the state with the lower redox potential. At even higher temperatures two components are no longer discernible by SWV and a situation analogous to coalescence in NMR

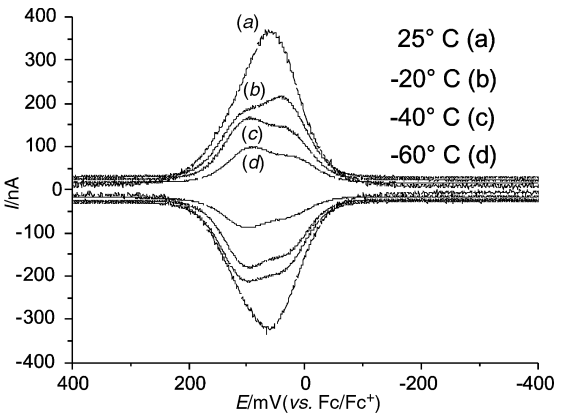

Fig. 2 Square-wave voltammograms of **2** at 25 °C [(a), scan rate 60 Hz], −20 °C [(b), scan rate 20 Hz], −40 °C [(c), 20 Hz] and −60 °C [(d), 20 Hz]. Concentration of **2** 1 mM, 0.1 M NBu_4PF_6 in EtCN, *vs.* Fc/Fc$^+$ as reference.

experiments is reached [curve (a)]. Curve fitting (COOL kinetic software) to the model of reversible oxidation of two independent species with equal diffusion coefficients was performed. At −60 °C the values E_1(1/2) = +15 mV and E_2(1/2) = +100 mV *vs.* Fc/Fc$^+$ were obtained, with relative contributions of 40 and 60% for the species with E_1(1/2) and E_2(1/2), respectively in accordance with ^{1}H NMR data. From the equilibrium data at −60 °C the following ΔG^0 and K values of Scheme 2 are calculated [counter-clockwise direction, starting with the reduction reaction and assuming E°(Fc/Fc$^+$) = 0.400 V *vs.* NHE]: $\Delta G_1{}^0$ = −40.1 kJ mol^{-1}, $\Delta G_2{}^0$ = −0.72 kJ mol^{-1}, $\Delta G_3{}^0$ = +48.3 kJ mol^{-1}, $\Delta G_4{}^0$ = −7.5 kJ mol^{-1}, K_2 = 1.5 and K_4 = 68. It should be noted that in reduced **2** the form with the *higher* redox potential is slightly favoured, whereas the oxidized form exhibits a strong preference for the species with the *lower* redox potential. Analysis in terms of the van't Hoff isochore yields standard reaction enthalpies $\Delta H_2{}^0$ = −2.5 kJ mol^{-1} and $\Delta H_4{}^0$ = −8.3 kJ mol^{-1} for the reduced and the oxidized forms of **2**, respectively. Small values are expected because the same types of bonds and presumably similar geometric parameters are present in all species. The difference of *ca.* 6 kJ mol^{-1} may well be attributed to increased solvation of the oxidized species as a consequence of their positive charge.

Poli and coworkers have investigated stable paramagnetic organometallic Mo compounds in some detail.[16,17] As shown herein, electrochemical measurements provide valuable information about equilibrium constants and thermodynamic parameters for fluxional paramagnetic species. This information cannot easily be derived by other common analytical techniques in organometallic chemistry. Currently, detailed calculations are performed to reveal the structure of all isomers and the mechanism of interconversion along with applications of compound **2** for the labelling of biomolecules.

We are grateful to Professor K. Wieghardt for his support of this work.

Notes and references

§ *Crystal data* for **2**: SMART-CCD diffractometer, Mo-Kα radiation (λ = 0.71073 Å). $C_{17}H_{27}MoN_3O_8$, M = 497.36, monoclinic, space group $P2_1$, a = 12.0928(14), b = 7.5347(8), c = 12.1177(14) Å, β = 101.59(2)° (unit cell parameters determined from 5092 reflections), V = 1081.6(2) Å^3, T = 100(2) K, Z = 2, μ(Mo-Kα) = 0.653 mm^{-1}, 11 346 reflections measured, 4668 unique (R_{int} = 0.0509) which were used in all calculations. $R1$ = 0.0281 (all data) and $wR_2(F^2)$ = 0.0692 (all data). 7 restraints were used. Allyl C–H bond lengths were restrained to be equal within certain errors (0.005 Å). Flack parameter is −0.03(3), in agreement with the absolute configuration (L) of the histidine.

CCDC 182/1846. See http://www.rsc.org/suppdata/cc/b0/b007822k/ for crystallographic files in .cif format.

1 A. Haaland, *Acc. Chem. Res.*, 1979, **12**, 415.
2 N. J. Long, *Metallocenes*, Blackwell Science, Oxford, 1998.
3 W. Beck, W. Petri and J. Meder, *J. Organomet. Chem.*, 1980, **191**, 73.
4 H.-J. Meder and W. Beck, *Z. Naturforsch., Teil B*, 1986, **41**, 1247.
5 J. W. Faller and B. C. Whitmore, *Organometallics*, 1986, **5**, 752.
6 K.-B. Shiu, K.-S. Liou, C. P. Cheng, B.-R. Fang, Y. Wang, G.-H. Lee and W.-J. Vong, *Organometallics*, 1989, **8**, 1219.
7 P. Espinet, R. Hernando, G. Iturbe, F. Villafañe, A. G. Orpen and I. Pascual, *Eur. J. Inorg. Chem.*, 2000, 1031.
8 B. J. Brisdon, K. A. Conner and R. A. Walton, *Organometallics*, 1983, **2**, 1159.
9 B. Brisdon, S. K. Enger, M. J. Weaver and R. A. Walton, *Inorg. Chem.*, 1987, **26**, 3340.
10 M. D. Curtis and O. Eisenstein, *Organometallics*, 1984, **3**, 887.
11 B. J. Brisdon and A. A. Woolf, *J. Chem. Soc., Dalton Trans.*, 1978, 291.
12 J. W. Faller, D. A. Haitko, R. D. Adams and D. F. Chodosh, *J. Am. Chem. Soc.*, 1979, **101**, 865.
13 K.-B. Shiu, C.-J. Chang, S.-L. Wang and F.-L. Liao, *J. Organomet. Chem.*, 1991, **407**, 225.
14 D. R. van Staveren, T. Weyhermüller and N. Metzler-Nolte, *Organometallics*, 2000, **19**, 3730.
15 D. R. van Staveren, E. Bothe, T. Weyhermüller, M. Bühl and N. Metzler-Nolte, 2000, manuscript in preparation.
16 R. Poli and L.-S. Wang, *Coord. Chem. Rev.*, 1998, **180**, 169.
17 L.-S. Wang, J. C. Fettinger and R. Poli, *J. Am. Chem. Soc.*, 1997, **119**, 4453.

Enantioselective hydrolysis of amino acid esters by apomyoglobin: perfect kinetic resolution of a phenylalanine derivative

Katsuhiko Tomisaka, Yasuhiro Ishida, Katsuaki Konishi and Takuzo Aida*

Department of Chemistry and Biotechnology, Graduate School of Engineering, The University of Tokyo, 7-3-1 Hongo, Bunkyo-ku, Tokyo 113-8656, Japan. E-mail: aida@macro.t.u-tokyo.ac.jp; Fax: +81-3-5841-7310

Received (in Cambridge, UK) 18th October 2000, Accepted 20th November 2000
First published as an Advance Article on the web

Apoprotein of horse-heart myoglobin promoted enantioselective hydrolysis of 4-nitrophenyl esters of amino acids, which allowed nearly perfect kinetic resolution of racemic *N*-Boc-phenylalanine ester (Boc-Phe-ONp).

Protein catalysis has a potential for asymmetric synthesis.[1] Apoproteins of cofactor-dependent proteins have attracted attention as the new candidates, since they possess a chiral hydrophobic cavity which can bind asymmetric substrates stereoselectively.[2,3] However, the successful examples are limited. Recently, we have found that the apoprotein of cytochrome b_{562} binds chiral porphyrins enantioselectively[4] and catalyzes template-assisted metalation of porphyrins.[5] Herein we report a novel asymmetric catalysis of apomyoglobin in hydrolysis of amino acid esters,[6] and wish to highlight an extremely high enantioselectivity for *N*-Boc-phenylalanine 4-nitrophenyl ester (Scheme 1).

Apomyoglobin is one of the most extensively studied apoproteins,[7] and has been reported to catalyze hydrolysis of 4-nitrophenyl alkanoates.[8] Horse-heart myoglobin was treated with dilute hydrochloric acid and butanone to give apomyoglobin, which was subjected to extensive dialysis against phosphate buffer (pH = 7.0, 10 mM).[9] Hydrolysis of *N*-Boc-phenylalanine 4-nitrophenyl ester (Boc-Phe-ONp) (Scheme 1) was investigated in a phosphate buffer containing 1% dioxane at 4 °C,[10] where the uncatalyzed hydrolysis ([Boc-Phe-ONp]$_0$ = 6.25 μM) proceeded sluggishly (Fig. 1d; △) to furnish only 11% conversion even after 240 min.[11] On the other hand, addition of apomyoglobin to the system resulted in a considerable acceleration of the reaction, where the L-isomer was preferentially hydrolyzed over the D-isomer. For example, when racemic Boc-Phe-ONp (12.5 μM) was mixed with apomyoglobin (62.5 μM), the hydrolysis proceeded smoothly to reach 60% conversion in only 8 min. Upon mixing of the reaction mixture with ether or ethyl acetate, the products (Boc-Phe-OH and 4-nitrophenol) and unreacted Boc-Phe-ONp were completely extracted into the organic phase. Chiral HPLC analysis of the organic phase with Chiralcel™ OD-H or Sumichiral™ OA-4700 showed that unreacted Boc-Phe-ONp is predominantly the D-isomer with an L : D ratio of 1 : 99 (98% ee), while the hydrolyzed product (Boc-Phe-OH) has an L : D ratio of 18 : 82. Thus, the hydrolysis with apomyoglobin enables nearly perfect kinetic resolution of racemic Boc-Phe-ONp.

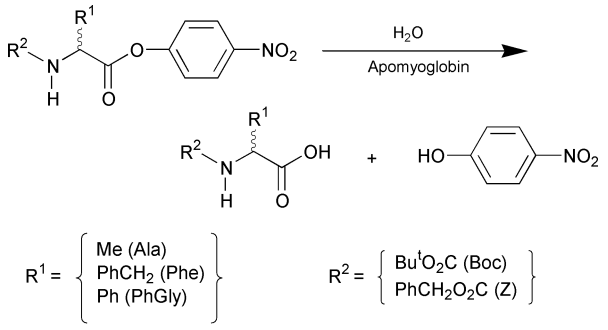

Scheme 1

The hydrolysis of Boc-Phe-ONp (62.5 μM) also proceeded to attain 100% conversion by using an equimolar amount of apomyoglobin. Furthermore, upon addition of a fresh feed of the substrate (0.2 equiv.) to this reaction mixture, the hydrolysis ensued without significant loss of the activity, indicating that the reaction turns over catalytically with respect to apomyoglobin. The hydrolysis most likely occurs *via* acyl transfer to an imidazole group located within the heme pocket. In fact, the reaction was not accelerated by holomyoglobin, whose heme pocket is blocked by the native guest.[8] On the other hand, when imidazole was used as a reference catalyst, Boc-Phe-ONp was hydrolyzed much more slowly than with apomyoglobin. For example, the hydrolysis in the presence of 10 equiv. of imidazole (62.5 μM) with respect to Boc-Phe-ONp proceeded to 4% conversion in 20 min (Fig. 1c; □), where the pseudo first-order rate constant (k_{obs} = 1.4 × 10^{-3} min^{-1}) was only 2.7 times as high as that of the uncatalyzed reaction (k_{uncat} = 5.2 × 10^{-4} min^{-1}) (Fig. 1d; △).[12]

In order to obtain further insight into the enantioselective catalysis of apomyoglobin, the kinetics of the hydrolysis of the L- and D-isomers of Boc-Phe-ONp (12.5 μM) were investigated in the presence of apomyoglobin (62.5 μM). When Boc-L-Phe-ONp was the substrate, the hydrolysis took place smoothly to give Boc-L-Phe-OH and 4-nitrophenol quantitatively within only 10 min (Fig. 1a). The pseudo first-order rate constant (k^L_{obs}) was 4.9 × 10^{-1} min^{-1}, which is 940 times larger than that in the absence of the apoprotein. In contrast, hydrolysis of the D-isomer proceeded very slowly (Fig. 1b) with a rate constant (k^D_{obs}) of only 3.1 × 10^{-2} min^{-1} (k^D_{obs}/k_{uncat} = 59), which is 16 times smaller than that of the L-isomer under the same conditions.

Upon increasing the initial concentration of the apoprotein from 25 to 125 μM, the hydrolysis rates of Boc-L-Phe-ONp and

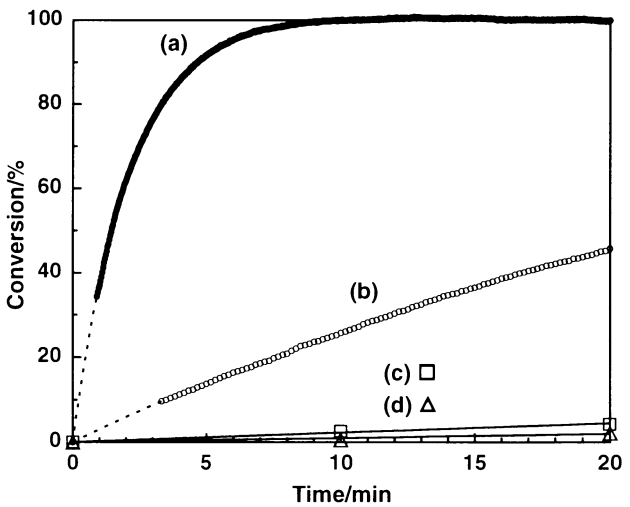

Fig. 1 Time courses of the hydrolysis of Boc-Phe-ONp in phosphate buffer (pH 7.0, 10 mM) containing 1% dioxane at 4 °C: (a) Boc-L-Phe-ONp–apomyoglobin (12.5 : 62.5 μM), (b) Boc-D-Phe-ONp–apomyoglobin (12.5 : 62.5 μM), (c) Boc-Phe-ONp–imidazole (6.25 : 62.5 μM) and (d) Boc-Phe-ONp (6.25 μM) without catalyst.

DOI: 10.1039/b008403o

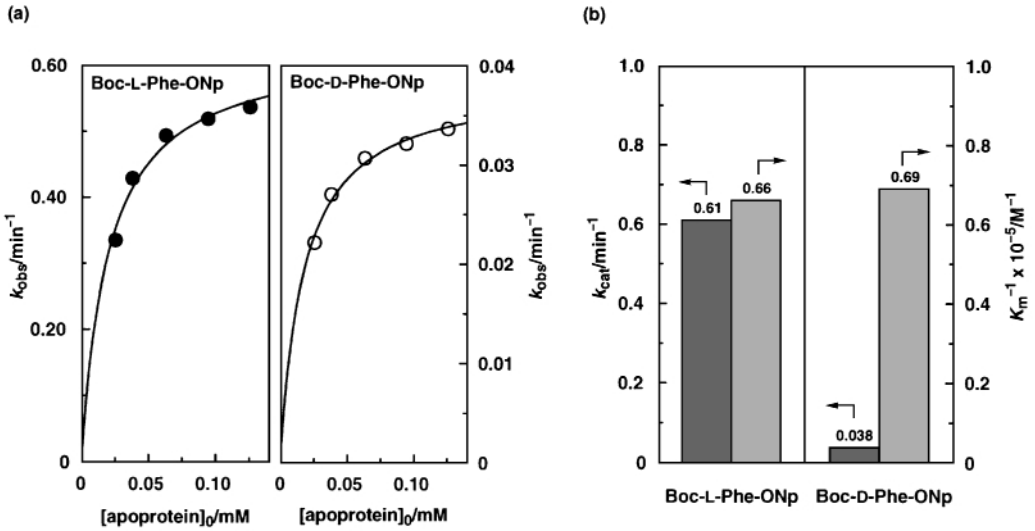

Fig. 2 Hydrolysis of Boc-L-Phe-ONp and Boc-D-Phe-ONp (12.5 μM) in the presence of apomyoglobin (2–10 equiv.) in phosphate buffer (pH 7.0, 10 mM) containing 1% dioxane at 4 °C: (a) plots of hydrolysis rate constant (k_{obs}) *vs.* initial concentration of apomyoglobin, and (b) association constants of the Michaelis complexes (K_m^{-1}) and maximum rate constants (k_{cat}).

Boc-D-Phe-ONp both showed a saturation signature (Fig. 2a), indicating that the apoprotein and Boc-Phe-ONp form a complex which serves as a reactive intermediate. Lineweaver–Burk plots[11,13] gave a maximum rate constant for the L-isomer (k^L_{cat}) of 6.1×10^{-1} min^{-1}, which is approximately 16 times larger than that for the D-isomer ($k^D_{cat} = 3.8 \times 10^{-2}$ min^{-1}) (Fig. 2b).[14] On the other hand, the K_m value for the hydrolysis of Boc-L-Phe-ONp (K^L_m) was evaluated to be 1.5×10^{-5} M, which is comparable to that of the D-isomer ($K^D_m = 1.4 \times 10^{-5}$ M).[12] Thus, the high stereoselectivity of the hydrolysis is not due to the enantioselective binding of the substrate ($K^L_m{}^{-1}/K^D_m{}^{-1} = 0.95$) but is more likely due to the large difference in reactivity between the L- and D-isomers of Boc-Phe-ONp within the heme pocket.

The enantioselectivity of the apomyoglobin-mediated hydrolysis was found to be highly sensitive to the substrate. For example, when the N-protecting Boc group (R^2) of the substrate was replaced with benzyloxycarbonyl (Z-Phe-ONp, 12.5 μM), the rate constant of the hydrolysis of the L-isomer with apomyoglobin (62.5 μM) was considerably decreased ($k^L_{obs} = 5.5 \times 10^{-2}$ min^{-1}, $k^D_{obs} = 3.1 \times 10^{-2}$ min^{-1}) to furnish a $k^L_{obs}:k^D_{obs}$ of only 1.8.[15] Lower enantioselectivities were also observed when Boc-PhGly-ONp (R^1 = Ph, $k^L_{obs}/k^D_{obs} = 1.8$)[16] and Boc-Ala-ONp ($R^1$ = Me, $k^L_{obs}/k^D_{obs} = 1.9$)[16] were the substrates in place of Boc-Phe-ONp, although the L-isomers were again preferentially hydrolyzed.

In conclusion, through the present studies on the utilization of the apoprotein of horse-heart myoglobin as a potential chiral catalyst, we have demonstrated a highly enantioselective hydrolysis of a phenylalanine 4-nitrophenyl ester (Boc-Phe-ONp), whose selectivity is one of the highest reported to date. Exploration with other natural and mutated apoproteins is one of the subjects worthy of further investigation for extending the scope of reactions.

We thank JSPS for financial support. Y. I. thanks the JSPS Young Scientist Fellowship.

Notes and references

1 (*a*) E. T. Kaiser and D. S. Lawrence, *Science*, 1984, **226**, 505; (*b*) G. M. Whitesides and C.-H. Wong, *Angew. Chem., Int. Ed. Engl.*, 1985, **24**, 617; (*c*) P. G. Schultz and R. A. Lerner, *Acc. Chem. Res.*, 1993, **26**, 391; (*d*) R. O. Duthaler, *Tetrahedron*, 1994, **50**, 1539.

2 (*a*) U. G. Wagner, N. Müller, W. Schmitzberger, H. Falk and C. Kratky, *J. Mol. Biol.*, 1995, **247**, 326; (*b*) B. B. Lakshmi and C. R. Martin, *Nature*, 1997, **388**, 758.

3 For utilization of protein hydrophobic domains for catalysis, see: (*a*) M. Nango, Y. Kimura, S. Kanda, Y. Ihara, J. Koga and N. Kuroki, *Chem. Lett.*, 1986, 229; (*b*) F. Hollfelder, A. J. Kirby and D. S. Tawfik, *Nature*, 1996, **383**, 60; (*c*) H. Kuang and M. D. Distefano, *J. Am. Chem. Soc.*, 1998, **120**, 1072.

4 Y. Ishida, K. Konishi, T. Aida and T. Nagamune, *Chem. Eur. J.*, 1998, **4**, 1148.

5 Y. Ishida, K. Konishi, T. Nagamune and T. Aida, *J. Am. Chem. Soc.*, 1999, **121**, 7947.

6 Examples of enantioselective hydrolysis of amino acid esters, see: (*a*) J.-J. Béchet, A. Dupaix and C. Roucous, *Biochemistry*, 1973, **12**, 2566; (*b*) M. Tanihira and Y. Imanishi, *Polym. J.*, 1983, **15**, 499; (*c*) T. Miyazawa, H. Iwanaga, S. Ueji, T. Yamada and S. Kuwata, *J. Chem. Soc., Chem. Commun.*, 1988, 1214; (*d*) R. Ueoka, Y. Matsumoto, K. Harada, H. Akahoshi, Y. Ihara and Y. Kato, *J. Am. Chem. Soc.*, 1992, **114**, 8339; (*e*) ref 3a.

7 (*a*) Y. V. Griko, P. L. Privalov and S. Y. Venyaminov, *J. Mol. Biol.*, 1988, **202**, 127; (*b*) F. M. Hughson, P. E. Wright and R. L. Baldwin, *Science*, 1990, **249**, 1544; (*c*) D. Barrick, F. M. Hughson and R. L. Baldwin, *J. Mol. Biol.*, 1994, **237**, 588.

8 H. Zemel, *J. Am. Chem. Soc.*, 1987, **109**, 1875.

9 F. W. J. Teale, *Biochim. Biophys. Acta*, 1959, **35**, 543.

10 The reaction was followed by a change in absorbance at 400 nm due to 4-nitrophenolate anion (NpO^-). The pseudo first-order rate constants (k_{obs}) were obtained according to the equation $(1\text{-}[NpO^-]/[\text{Boc-Phe-ONp}]_0) = e^{-kt}$.

11 Electronic supplementary information (ESI) available: absorbance spectra and Lineweaver–Burk plots. See http://www.rsc/suppdata/cc/b0/b008403o/

12 The second-order rate constant (k_2) for the hydrolysis of Boc-Phe-ONp with imidazole was 23 M^{-1} min^{-1}, which is much smaller than the catalytic constants (k_{cat}/K_m) for the hydrolysis of Boc-L-Phe-ONp (3.6×10^4 M^{-1} min^{-1}) and Boc-D-Phe-ONp (0.24×10^4 M^{-1} min^{-1}) with apomyoglobin.

13 Examples of Michaelis–Menten kinetics using k_{obs} instead of V_0 in the presence of an excess amount of mediators, see (*a*) V. Jubian, R. P. Dixon and A. D. Hamilton, *J. Am. Chem. Soc.*, 1992, **114**, 1120; (*b*) R. Hetting and H. J. Schneider, *J. Am. Chem. Soc.*, 1997, **119**, 5638.

14 Maximum acceleration factors for the hydrolysis of the L- and D-isomers of Boc-Phe-ONp (k_{cat}/k_{uncat}) were 1200 and 73, respectively.

15 The uncatalyzed reaction was not examined due to a limited solubility of Z-Phe-ONp.

16 Boc-PhGly-ONp: $k^L_{obs} = 1.3 \times 10^{-1}$ min^{-1}, $k^D_{obs} = 7.1 \times 10^{-2}$ min^{-1}, $k_{uncat} = 6.4 \times 10^{-4}$ min^{-1}; Boc-Ala-ONp: $k^L_{obs} = 5.1 \times 10^{-2}$ min^{-1}, $k^D_{obs} = 2.7 \times 10^{-2}$ min^{-1}, $k_{uncat} = 3.1 \times 10^{-4}$ min^{-1}.

Task-specific ionic liquids for the extraction of metal ions from aqueous solutions

Ann E. Visser,[ab] Richard P. Swatloski,[ab] W. Matthew Reichert,[ab] Rebecca Mayton,[c] Sean Sheff,[c] Andrzej Wierzbicki,[c] James H. Davis, Jr.*[ac] and Robin D. Rogers*[ab]

[a] *Center for Green Manufacturing, The University of Alabama, Tuscaloosa, AL 35487, USA. E-mail: RDRogers@bama.ua.edu*
[b] *Department of Chemistry, The University of Alabama, Tuscaloosa, AL 35487, USA*
[c] *Department of Chemistry, University of South Alabama, Mobile, AL 36688, USA. E-mail: JDavis@jaguar1.usouthal.edu*

Received (in Columbia, MO, USA) 19th September 2000, Accepted 14th November 2000
First published as an Advance Article on the web

Imidazolium cations, such as those commonly used in preparing ionic liquids (ILs) can easily be derivatized to include task-specific functionality, such as metal ligating groups that when used as part of the solvent or doped into less expensive ILs, dramatically enhance the partitioning of targeted metal ions into the IL phase from water; the strategy of preparing task-specific ILs is applicable to a wide range of designer solvent needs.

Owing to their unique chemical and physical properties, ionic liquids (ILs) have received recent attention for applications as solvent alternatives,[1–4] where, for example, ILs can be used in place of organic solvents in synthesis, catalysis, electrochemistry and liquid/liquid extractions. The formulations commonly reported for ILs have relied on pyridinium or imidazolium cations bearing simple alkyl appendages as the cation. Changes in IL physical properties have been accomplished by altering the length of the alkyl groups on the rings[4–6] allowing for fine-tuning their viscosity, hydrophobicity and melting points.[6,7] More recently, ionic liquid formulations have been expanded in scope to include other heterocyclic aromatic molecules as well as ions with structurally and functionally complex side chains.[8–10]

It has been demonstrated that organic solutes (*e.g.* aromatic molecules such as simple benzene derivatives)[1,2,4] can be partitioned to specific ILs based on the hydrophobicity of the solute and IL. In contrast, the partitioning of metal ions into an IL extracting phase in liquid/liquid systems is negligible owing to the tendency of the metal cations to remain hydrated and in the aqueous phase, thus necessitating the use of an extractant molecule that forms complexes directly with metal ions to increase their hydrophobicity.[11–15] The drawbacks associated with this approach lie in finding extractant molecules that remain exclusively in the IL under all process conditions and also in understanding the increased complexity of the system upon the addition of solutes. Here, we report the first use of task-specific ILs, *i.e.* those with targeted functionality designed into the IL solvent. In the present example, new compounds which have been designed specifically to both be ionic liquids and to extract heavy metal ions (*e.g.* Hg^{2+} and Cd^{2+}) are reported.

Mercury(II) and cadmium(II) were targeted in this study as part of our ongoing efforts to find alternative separations strategies for removing these toxic, easily transported metal ions from the environment.[16] The bases for the modified ILs were 1-alkyl-3-methylimidazolium, $C_n$mim$^+$ (n = 4, 6, 8) salts of PF_6^- which form two-phase systems when contacted in equal volume with water.[2] ILs that incorporated thiourea, thioether and urea into derivatized imidazolium cations were thus prepared,† that when combined with the PF_6^- anion, functioned as both the hydrophobic solvent and metal ion extractant in liquid/liquid separations. The new ILs (Fig. 1) may either be used directly as the bulk solvent or may be doped‡ as an extractant into less expensive ILs, such as [C_4mim][PF_6].

The distribution ratios§ of Hg^{2+} and Cd^{2+} between our chosen standard for this study, [C_4mim][PF_6], and an aqueous phase at pH = 7 were 0.84 (Hg^{2+}) and 0.03 (Cd^{2+}), indicating a preference for these metal ions to be retained in the aqueous phase. The thioether-appended IL **1**, as either the extracting phase or in 50 : 50 mixtures with [C_4mim][PF_6] at pH = 1 or 7, is effective in partitioning both metal ions to the IL phase (Table 1). The thiourea derivative **2** extracts Hg^{2+} from water comparably to **1**, however distribution ratios are much lower when **2** is diluted with [C_4mim][PF_6]. IL **2** is much less effective at extraction of Cd^{2+} (D values of 20 and 23 at pH of 1 and 7, respectively) and when diluted with [C_4mim][PF_6], IL **2** does not extract Cd^{2+} at all.

IL **3** (another thiourea derivative), and **4**–**6** (urea derivatives) were prepared and their behavior as extractants for Hg^{2+} and Cd^{2+} when mixed in equal mass ratios with [C_4mim][PF_6] measured as a function of aqueous phase pH (Fig. 2). The results are similar, in that each of these ILs {as 1 : 1 (mass) mixtures with [C_4mim][PF_6]} efficiently extract Cd^{2+} and Hg^{2+}, as shown in Fig. 2. In general, the distribution ratios of Cd are

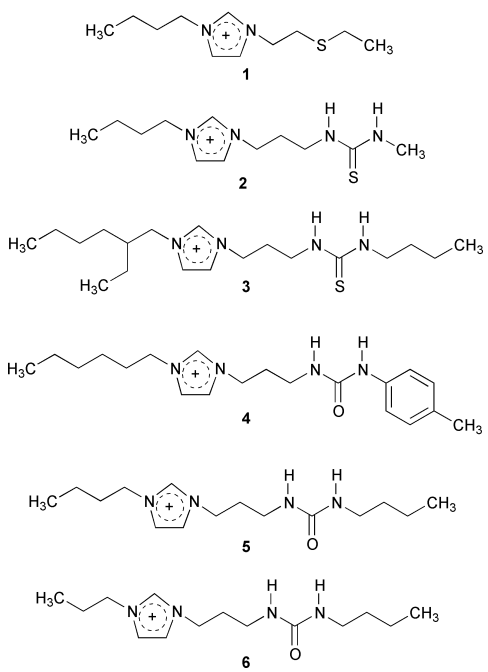

Fig. 1 Structures of the cations combined with PF_6^- to make the ILs utilized in these studies.

DOI: 10.1039/b008041l

Table 1 Distribution ratios for Hg^{2+} and Cd^{2+} in systems incorporating ILs **1** and **2**

IL	M^{2+}	pH (aq)	Distribution ratio	System
1	Hg^{2+}	1	200	**1** only
	Cd^{2+}	1	330	**1** only
1	Hg^{2+}	1	170	**1** + $[C_4mim][PF_6]$ (1 : 1)
	Cd^{2+}	1	310	**1** + $[C_4mim][PF_6]$ (1 : 1)
1	Hg^{2+}	7	210	**1** only
	Cd^{2+}	7	380	**1** only
1	Hg^{2+}	7	210	**1** + $[C_4mim][PF_6]$ (1 : 1)
	Cd^{2+}	7	360	**1** + $[C_4mim][PF_6]$ (1 : 1)
2	Hg^{2+}	1	350	**2** only
	Cd^{2+}	1	20	**2** only
2	Hg^{2+}	1	74	**2** + $[C_4mim][PF_6]$ (1 : 1)
	Cd^{2+}	1	0.0086	**2** + $[C_4mim][PF_6]$ (1 : 1)
2	Hg^{2+}	7	340	**2** only
	Cd^{2+}	7	23	**2** only
2	Hg^{2+}	7	100	**2** + $[C_4mim][PF_6]$ (1 : 1)
	Cd^{2+}	7	0.0074	**2** + $[C_4mim][PF_6]$ (1 : 1)

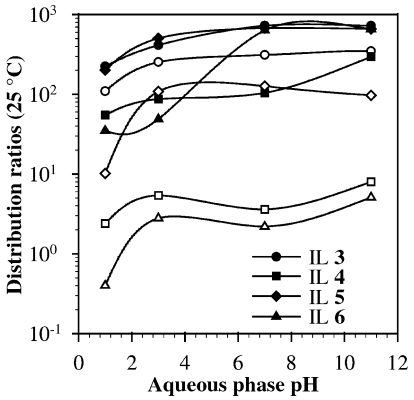

Fig. 2 Distribution ratios for Hg^{2+} (filled symbols) and Cd^{2+} (open symbols) with ILs **3**–**6** utilized in a 1 : 1 weight ratio with $[C_4mim][PF_6]$ and contacted with aqueous phases of variable pH.

lower than observed for Hg, and in the case of ILs **4** and **6**, the differences are over an order of magnitude. ILs **3** and **5** give the highest distribution ratios for each metal ion, and the extraction using IL **6** is the most affected by lowering the pH (although all four ILs exhibit lower distribution rations at the lowest values of pH studied). In comparing these results with those in Table 1, it is to be noted that distribution ratios as high as 710 (Hg^{2+}, IL **3**) were observed in this latter study, even though the ILs were utilized as 1 : 1 mixtures with $[C_4mim][PF_6]$.

Both the appended functional group and the alkyl group appear to affect the extraction. The extended alkyl 'tail' near the thiourea group in **3** results in a significant increase in *D* values for both metals. For the various functional groups, the *D* values for Hg^{2+} are the highest with urea > thiourea with the 'tail' > thioether > thiourea, while those for Cd^{2+} decrease from thiourea with the 'tail' > thioether > urea > thiourea.

We are currently investigating additional series of task-specific ILs with each functional group to elucidate the trends in both structure and function of the IL and to control the physical properties of these new extracting solvents. Additional studies are also required to determine if the metal ions can be effectively stripped from these solvents, although they are currently also being investigated for their ability to retain metallic catalysts in the IL for synthetic applications.

This work was supported by funding from the Division of Chemical Sciences, Office of Basic Energy Sciences, Office of Energy Research, U.S. Department of Energy (R. D. R., Grant No. DE-FG02-96ER14673), the PG Research Foundation (R. D. R), Research Corporation (J. H. D., Grant CC 4758), the Alabama Supercomputer Authority (A. W.), and the Nichols Corporation (A. W.).

Notes and references

† All chemicals were obtained as reagent grade from Aldrich and used without further purification. 1-(3′-aminopropyl)imidazole (20.0 g, 0.160 mol) was mixed with 100 mL of acetonitrile under an atmosphere of dry nitrogen. To the stirred solution was added in a dropwise fashion 15.5 g (0.156 mol) of *n*-butyl isocyanate dissolved in 25 mL of acetonitrile. The combined solution was stirred overnight followed by removing the solvent *in vacuo*. The residue was then dried overnight *in vacuo*. Proton NMR spectroscopy confirmed the structure of the product as being the desired urea-appended imidazole, and the crude material was used in the next step without further purification.

Under a nitrogen atmosphere, the reaction residue was redissolved in acetonitrile (100 mL) and 28.0 g (0.164 mol) of propyl iodide was added. The mixture was then heated gently without refluxing. After stirring with heating overnight, the acetonitrile was removed *in vacuo*, leaving a sticky residue. The residue was washed in water and the aqueous layer washed twice with 100 mL of diethyl ether. To the aqueous solution was added a solution of 36.0 g (0.194 mol) KPF_6 in 100 mL of water. The mixture was stirred overnight at 40 °C, during which time a biphasic system formed comprised of an upper aqueous phase and a lower product phase. (Anion exchange for each of the ureas can also be accomplished using $AgPF_6$ in acetone.) The aqueous phase was decanted and the product was washed four times (2 h contacts) with 100 mL water to remove any remaining KPF_6. After the last water wash, the ionic liquid was dissolved in acetonitrile and toluene was added to aid in the azeotropic removal of water. Any solids were removed by filtration and the solution was then rotary evaporated. The isolated product was dried *in vacuo* for 24 h while being heated to 60 °C. Unoptimized yield: 45.2 g (68%). The general procedure for the preparation of the urea-functionalized ionic liquids **5** and **6** and the thiourea-functionalized ionic liquids **2** and **3** is analogous, each being formed in similar yield.

‡ When preparing the 1 : 1 mixtures of the solid samples with $[C_4mim][PF_6]$, solutions of **5** and **6** were prepared as a 1 : 1 ratio of the cations and added to $[C_4mim][PF_6]$ followed by sonication and gentle heating for 30 min to form the solution. Solutions of **1**–**4** were prepared as 1 : 1 weight ratios in $[C_4mim][PF_6]$ followed by thorough mixing.

§ Metal ion distribution ratios were determined by mixing equal volumes of the IL and aqueous phases followed by vortexing (2 min) and centrifuging (2000 *g*, 2 min) to equilibrate the phases. Addition of either $^{203}HgCl_2$ or $^{109}CdCl_2$ (*ca.* 0.005 μCi, 5 μL) was followed by two intervals of vortexing (2 min) and centrifuging (2000 *g*, 2 min) to ensure that the phases were fully separated. The phases were separated and dispensed into shell vials from which 100 μL of each phase was removed for radiometric analysis. The results are reported as distribution ratios and are calculated as the radioactivity in the lower phase divided by the radioactivity in the upper phase. Each experiment was done in duplicate and the results agreed to within 5%.

1 L. A. Blanchard, D. Hancu, E. J. Beckman and J. F. Brennecke, *Nature*, 1999, **399**, 28.
2 J. G. Huddleston, H. D. Willauer, R. P. Swatloski, A. E. Visser and R. D. Rogers, *Chem. Commun.*, 1998, 1765.
3 M. Freemantle, *Chem. Eng. News*, 1998, **76** (March 30) 32.
4 A. E. Visser, R. P. Swatloski and R. D. Rogers, *Green Chem.*, 2000, **1**, 1.
5 C. M. Gordon, J. D. Holbrey, A. R. Kennedy and K. R. Seddon, *J. Mater. Chem.*, 1998, **8**, 2627.
6 J. D. Holbrey and K. R. Seddon, *J. Chem. Soc., Dalton Trans.*, 1999, 2133.
7 P. Bonhôte, A.-P. Dias, N. Papageorgiou, K. Kalyanasundaram and M. Grätzel, *Inorg. Chem.*, 1996, **35**, 1168.
8 J. H. Davis, Jr., K. J. Forrester and T. J. Merrigan, *Tetrahedron Lett.*, 1998, **39**, 8955.
9 J. H. Davis, Jr. and K. J. Forrester, *Tetrahedron Lett.*, 1999, **40**, 1621.
10 T. K. Merrigan, E. D. Bates, S. C. Dorman and J. H. Davis, Jr., *Chem. Commun.*, 2000, 2051.
11 A. E. Visser, R. P. Swatloski, W. M. Reichert, S. T. Griffin and R. D. Rogers, *Ind. Eng. Chem. Res.*, 2000, **39**, 3596.
12 S. Dai, Y. H. Ju and C. E. Barnes, *J. Chem. Soc., Dalton Trans.*, 1999, 1201.
13 A. E. Visser, R. P. Swatloski, D. H. Hartman, J. G. Huddleston and R. D. Rogers, in *Calixarene Molecules for Separations*, ed. G. J. Lumetta, R. D. Rogers and A. S. Gopalan, American Chemical Society, Washington, DC, ACS Symp. Ser. 757, 2000, p. 223.
14 R. D. Rogers, A. E. Visser, R. P. Swatloski and D. H. Hartman, in *Metal Separation Technologies Beyond 2000: Integrating Novel Chemistry with Processing*, ed. K. C. Liddell and D. J. Chaiko, The Minerals, Metallurgical and Materials Society, Warrendale, PA, 1999, p. 139.
15 A. E. Visser, R. P. Swatloski, S. T. Griffin, D. H. Hartman and R. D. Rogers, *Sep. Sci. Technol.*, 2000, in press.
16 R. D. Rogers and S. T. Griffin, *J. Chromatogr. B*, 1998, **711**, 277.

Synthesis of new types of polysiloxane based surfactants

Josef Bauer, Nicola Hüsing and Guido Kickelbick*

Institut für Anorganische Chemie, Technische Universität Wien, Getreidemarkt 9, A-1060 Wien, Austria. E-mail: kickelgu@mail.zserv.tuwien.ac.at

Received (in Cambridge, UK) 24th October 2000, Accepted 28th November 2000
First published as an Advance Article on the web

New types of amphiphilic polysiloxane diblock copolymers containing a pure polysiloxane backbone were prepared by the functionalization of poly(dimethylsiloxane)-*block*-poly-(methylvinylsiloxane) copolymers, synthesized by 'living' anionic ring opening polymerisation of 1,3,5,7-tetramethyl-1,3,5,7-tetravinylcyclotetrasiloxane (D_4^v) and hexamethyl-cyclotrisiloxane (D_3).

Amphiphilic block copolymers find widespread technological applications especially as non-ionic polymeric surfactants. The coexistence of the dissimilar segments, which show a different solubility in a specific solvent, produces unique properties because of their ability to self-organize at interfaces and in solution and thus modify interfacial properties and enhance compatibility or separation.[1] Typically, purely organic backbones are found in this type of surfactant, nevertheless inorganic polymer segments, especially polysiloxanes show properties that are advantageous, such as biocompatibility, robustness, flexibility *etc*.[2] Although polysiloxanes have superior properties compared to common organic polymers their controlled formation as block copolymers is nearly unexplored.

In recent years the interest in amphiphilic block copolymers has grown especially due to their surface activity and their lyotropic behaviour.[3] Amphiphilic block copolymers with a hydrophobic polysiloxane part are predominantly known in combination with organic hydrophilic blocks such as poly(ethylene oxide) or polymethacrylates.[4] As far as we know there is only one example in literature citing a block copolymer with a pure polysiloxane backbone bearing carboxyl groups pendant to the polysiloxane chain.[5]

In this paper we present the formation and post-functionalization of block copolymers of poly(dimethylsiloxane) (PDMS) and poly(methylvinylsiloxane) by 'living' anionic ring opening polymerisation.

Valuable precursors for a post-functionalization are silane-bonded vinyl groups. For the preparation of a vinyl-functionalized block *via* anionic ring opening polymerisation a cyclic monomer with a sufficient reactivity is needed. The only commercially available monomer that fulfils this demand is 1,3,5,7-tetramethyl-1,3,5,7-tetravinylcyclotetrasiloxane (D_4^v). D_4^v did not show satisfactorily polymerisation initiated by butyllithium with the usual donor solvents (THF, DMF, DMSO, HMPA). Therefore another initiator with a higher basicity, *i.e.* trimethylsilylmethyllithium, $(CH_3)_3SiCH_2Li$, was used to transform the carbanionic acids into the silanolate species.[6] Usually polymerisations of unstrained cyclic siloxanes, such as cyclotetrasiloxanes or larger rings, are more difficult due to the presence of intra- and intermolecular reactions of the active ends leading to an equilibrium reaction between the ring, an oligomeric, and a polymeric species. It was shown that the equilibrium is shifted to the polymeric species if additives able to separate the ion pair between the oxidic end group and the lithium ion are added to the reaction solution. Typical additives are ethylenediamine, diglyme, cryptands and crown ethers like 12-crown-4.[7]

Block copolymers from 'living' ring opening polymerisations are obtained by using a polymer as macroinitiator and extending it with a second monomer. For the PDMS-*block*-poly(methylvinylsiloxane) we observed that the extension of a PDMS chain with poly(methylvinylsiloxane) only leads to the addition of up to five monomeric units until the final equilibrium between polymeric and ring species is reached, while the polymerisation of D_4^v first allows for a much better control of the equilibrium. Therefore, the polymerisation of vinylmethylcyclotetrasiloxane was initiated with trimethylsilylmethyllithium in a first step and the chain was extended by PDMS in a second step[8] (Scheme 1). With this procedure block copolymers with polydispersities around 1.40 and block lengths up to 10.000 with varying poly(methylvinylsiloxane) content were obtained (Table 1).

The resulting block copolymers have purely hydrophobic properties but the vinyl groups can easily be transformed into a variety of other functional groups. The double bonds of the methylvinylsiloxane blocks were modified either by hydrosilation[9] or by epoxidation.[10] In the latter case further modification reactions of the polyepoxide block were carried out[11] (Scheme 2).

The hydrosilation of the double bonds with Karstedt's catalyst at 70 °C worked quantitatively as confirmed by the disappearance of the vinylic protons in ^{1}H NMR. $HSi(OEt)_3$, $HSi(OMe)_3$ and $HSi(CH_3)_2Cl$ were used for this reaction to obtain a functionalized polysiloxane block. While the trialkoxysilane groups can be hydrolysed and used for cross-linking reactions, the chlorosilanes are able to react with a variety of nucleophiles, like alcohols, carboxylic acids, *etc.*

Another possibility of the double bond functionalization is the epoxidation[12] followed by the subsequent ring opening of the oxirane ring. The epoxide was quantitatively formed by a selective oxidation of the double bonds with *m*-chloroperoxybenzoic acid (MCPBA) in methylene chloride or toluene proved by ^{1}H NMR. SEC measurements of the epoxidised samples showed that only a small amount ($< 4\%$) of high molecular weight (cross-linked) polymer was formed. The cross-linking was almost quantitatively suppressed by working in high dilutions.[13] The obtained epoxide was opened with different mono- or difunctional nucleophiles, such as hydroxide ions, diamines, diols, dicarboxylic acids, hydroxy-functionalized ethers and carboxylic acid chlorides (Scheme 3). These reactions resulted in the formation of a hydroxide group at one carbon atom and the coupling product with the nucleophile at

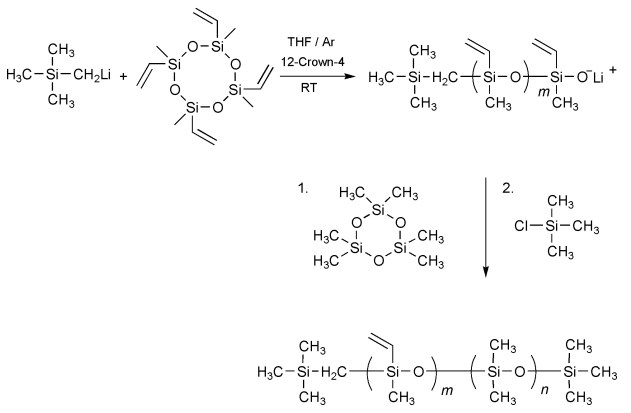

Scheme 1

DOI: 10.1039/b008556l

Table 1 Selected data of typical PD_4^v-*b*-PD_3 block copolymers prepared

Sample	M_n (M_w/M_n) (PD_4^v-block)	*m*	*n*	M_n (M_w/M_n) (PD_4^v-PD_3-diblock)	Ratio by ^{1}H NMR (PD_4^v/PD_3)	Ratio by SEC (PD_4^v/PD_3)
1	2840 (1.36)	33	96	9940 (1.46)	0.38	0.40
2	1900 (1.36)	22	22	3520 (1.38)	0.86	0.85
3	1730 (1.21)	20	82	7840 (1.36)	0.25	0.28
4	1480 (1.14)	17	50	5190 (1.31)	0.35	0.40

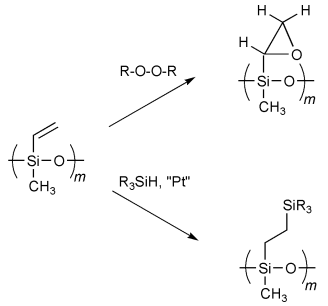

Scheme 2

the other. Modification of the epoxide block by reaction with amines or alcohols was catalysed by $LiClO_4$. Nucleophilic attack of the epoxide by the nucleophile on the more hindered carbon atom ($SiCH{=}CH_2$) was not observed in ^{1}H NMR spectra which indicates an almost quantitative attack on the terminal methylene carbon atom. In the case of modification with oxalic acid the reaction was performed in *N*,*N*′-dimethylformamide to dissolve the reactant and additionally catalysed by pyridine. Hydrolysis of the epoxidised block copolymers leads to the corresponding 1,2-diol side groups and may either be acid- or base-catalysed. Epoxide opening worked quantitatively, which was proved by ^{1}H NMR (disappearance of the signals of the epoxide protons at 2.2, 2.7 and 2.9 ppm). The processing parameters of the ring opening reactions allow for the preparation of different materials. High dilution of the block copolymers in the solvent during the ring opening leads to linear polymers while cross-linked hydrogels are formed in low dilution. To completely suppress cross-linking reactions using multifunctional nucleophiles a large excess of reactants is necessary and harsh purification conditions should be avoided. For a total prevention of cross-linking reactions it is advisable to use monofunctional protected ring opening agents and remove the protecting groups afterwards. Additional advantages of this procedure are simpler purification and analyses. In those cases in which hydroxy groups are formed during the ring opening or other functionalities are present, no elution in the SEC experiments was obtained due to interaction with the column material. This was avoided by protection of the free functional groups.

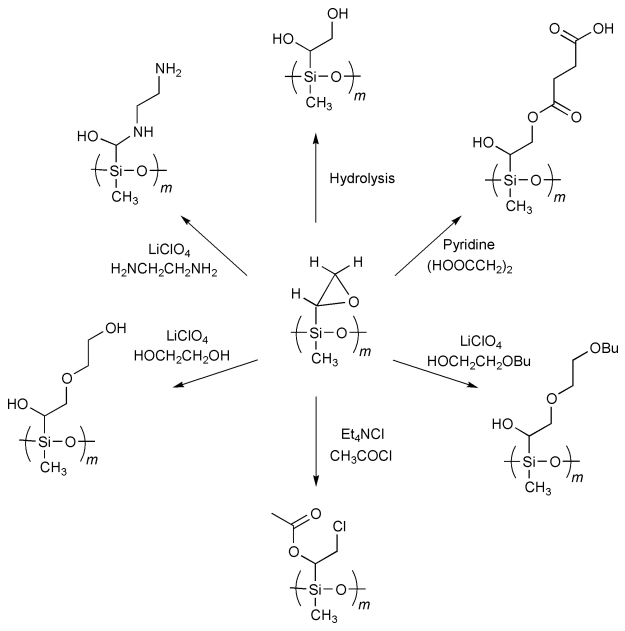

Scheme 3

In summary new methylvinyl-substituted polysiloxane diblock copolymers were prepared by 'living' anionic ring opening polymerisation. The vinyl group was used for a further functionalization to obtain silicon alkoxide substituted or amphiphilic block copolymers with a variety of functional groups.

We gratefully acknowledge the financial support by the Fonds zur Förderung der wissenschaftlichen Forschung Austria and Wacker-Chemie for their kind donation of chemicals.

Notes and references

1 P. Alexandridis, U. Olsson and B. Lindeman, *Langmuir*, 1998, **14**, 2627.
2 P. R. Dvornic and R. W. Lenz, *High temperature siloxane elastomers*, ed. P. Dvornic and R. W. Lenz, Hüthig & Wepf, Verlag, 1990.
3 S. Förster and M. Antonietti, *Adv. Mater.*, 1998, **3**, 195.
4 H.-W. Haesslin, *Makromol. Chem.*, 1985, **186**, 357.
5 M. Scibiorek, N. K. Gladkova and J. Chojnowski, *Polymer Bulletin*, 2000, **44**, 377.
6 R. P. Quirk and D. E. Kester, *J. Organomet. Chem.*, 1977, **127**, 111.
7 J. Chojnowki, K. Ròzga, W. Foruniak and A. Kowalewska, *Makromol. Chem., Makromol. Symp.*, 1993, **67**, 183.
8 Typical procedure: to a solution of D_4^v in THF $(CH_3)_3SiCH_2Li$ was added. The amount of the lithium compound was chosen depending on the target molecular weight of the poly(methylvinylsiloxane) $[I] = \frac{[M]_0}{DP}$ ([*I*] = initiator concentration; $[M]_0$ = monomer concentration; *DP* = degree of polymerisation). After stirring the solution at rt for 1 h 12-crown-4 was added. Propagation progress was determined during the polymerisation by taking samples, quenching the reaction with chlorotrimethylsilane at various reaction times and determining the molecular weights by size exclusion chromatography (SEC) analyses. By adding D_3 to the 'living' polymer the PDMS-blocks were formed. The diblock copolymers were quenched by chlorotrimethylsilane and analysed by SEC and NMR measurements. SEC was performed using a Waters 717 autosampler, 515 HPLC pump, 2410 RI detector and Styragel columns in THF at 40 °C at a rate of 1 ml min^{-1} applying linear polystyrene standards. The DP of each block was calculated by the SEC results of homopolymer and diblock copolymer and compared with the results of the composition determined by ^{1}H NMR. ^{29}Si NMR analyses allowed the determination of the sequence distribution of repeat units, which showed no random copolymerization of D_4^v and D_3.
9 Y. Chang, Y. C. Kwon, S. C. Lee and C. Kim, *Polym. Prepr. (Am. Chem. Soc. Div. Polym. Chem.)*, 1999, **40**, 269.
10 F. Macchia, P. Crotti and M. Chini, *Tetrahedron Lett.*, 1990, **31**, 4661.
11 A. Hassner, in *Small Ring Heterocycles*, ed. A. Weissberger and E. C. Taylor, John Wiley & Sons, New York, 1976.
12 General procedure: MCPBA was dissolved in toluene and dried over Na_2SO_4. Depending on the block length of the poly D_4^v block, a calculated amount of the solution was added to the block copolymer. The resulting mixture was stirred overnight at rt. The organic layer was extracted with an aqueous sodium bicarbonate solution and deionised water several times. The organic layers were collected and dried over Na_2SO_4. Afterwards the solution was filtered and evaporated.
13 K. Udipi, *J. Appl. Polym. Sci.*, 1979, **23**, 3301.

Typeset and printed by Black Bear Press Limited, Cambridge, England

The β-elimination route to stereodefined γ-alkylidenebutenolides†

Reinhard Brückner

Institut für Organische Chemie und Biochemie der Albert-Ludwigs-Universität, Albertstr. 21, D-79104 Freiburg, Germany. E-mail: reinhard.brueckner@organik.chemie.uni-freiburg.de; Fax: Int.+49-761-2036100

Received (in Cambridge, UK) 19th September 2000, Accepted 13th November 2000
First published as an Advance Article on the web 4th January 2001

γ-Alkylidenebutenolides are biologically significant compounds and comprise compounds as structurally and functionally diverse as the inhibitor dihydroxerulin (*Z*-61, Scheme 16) of cholesterol biosynthesis or the carotinoid peridinin (*Z*-18a, Scheme 5) which plays a dominant role in marine photosynthesis. For the stereo-controlled obtention of γ-alkylidenebutenolides *Z*-2 or *E*-2 with or without alkyl substituents at C-α or C-β, a general strategy has been developed (Scheme 1). The key step of this strategy is the stereospecific *anti*-elimination of water from diastereopure γ-(α-hydroxyalkyl)butenolides *lk*-1 or *ul*-1—be they racemic or enantiopure (*lk* = like, *ul* = unlike: γ-(α-hydroxyalkyl)butenolides *lk*-1 give γ-alkylidenebutenolides *Z*-2, while γ-(α-hydroxyalkyl)butenolides *ul*-1 furnish the isomeric γ-alkylidenebutenolides *E*-2. As dehydrating agents we used mixtures of triflic anhydride and pyridine or of diethyl azodicarboxylate and triphenylphosphine. Previous β-eliminations providing γ-alkylidenebutenolides exhibited in general little stereoselectivity and no stereospecifity at all (exception: Scheme 10), irrespective of whether this β-elimination was performed separately or took place *in situ*.

Introduction

Butenolides are γ-butyrolactones with a $C^{\alpha}=C^{\beta}$ bond. They abound in nature, revealing a great variety of substitution patterns.[1] Among many others, one finds γ-alkylidenebutenolides. The most prominent representatives of this class are vitamin C, the pulvinic acids [α-aryl-β-hydroxy-γ-(α-carboxybenzylidene)butenolides], the pulvinones [α-aryl-β-hydroxy-γ-(benzylidene)butenolides], and derivatives thereof. However, there are also γ-alkylidenebutenolides which are totally devoid of heteroatom substituents at C^{α} or C^{β}. Several such γ-alkylidenebutenolides are biologically significant.

Their simplest conceivable representative is γ-methylenebutenolide. This is a natural product ('protoanemonin'[2]) and known to be an antibiotic. The highly unsaturated γ-alkylidenebutenolides dihydroxerulin (*Z*-**61**, Scheme 16) and xerulin (*trans*,*Z*-**66**, Scheme 17) are structurally unique, intensely yellow fungal colorants.[3] Isolated as 90 : 10–65 : 35 mixtures, they were found to inhibit the biosynthesis of cholesterol without being cytotoxic; they prevent the incorporation of ^{14}C-acetate—but not of ^{14}C-mevalonic acid—into cholesterol produced from HeLa S3 cells (ID_{50} = 1 μg g^{-1}).[3] Suppressing a different step of the biosynthesis of cholesterol is what three

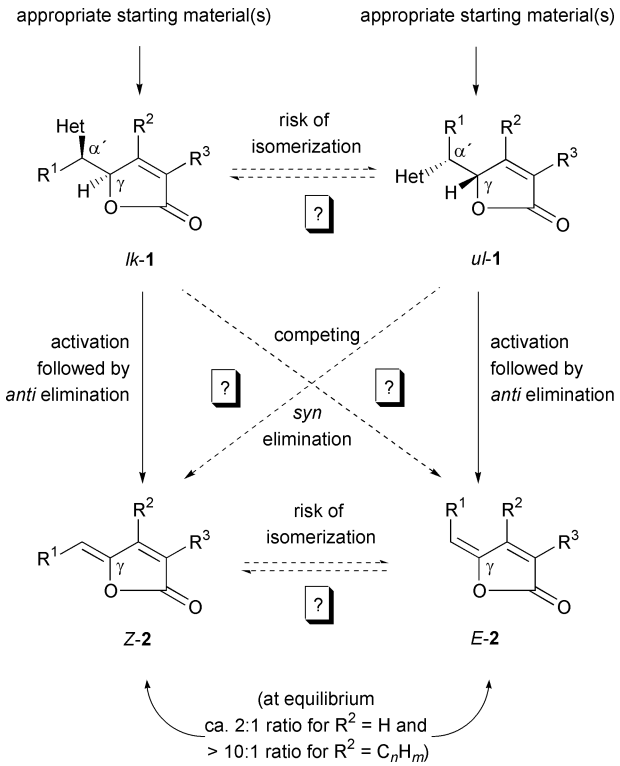

Scheme 1 Strategy for the stereoselective generation of γ-alkylidenebutenolides by *anti*-eliminations from γ-(α-hydroxyalkyl)butenolides.

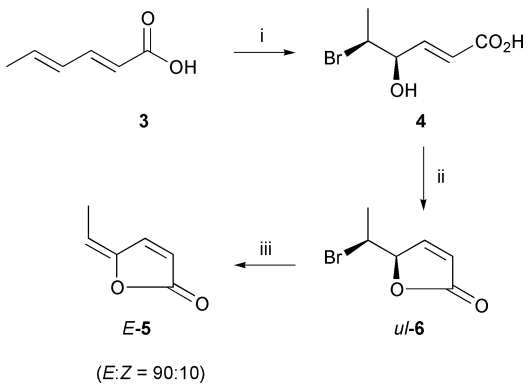

Scheme 2 *Reagents*: i, Br_2, H_2O, 35% **4** + 33% re-isolated **3**; ii, HCl, H_2O, h*ν*, 70%; iii, NEt_3, CH_2Cl_2, 91%.

† Dedicated to Dr Klaus Brückner (retired from Cela-Merck, Ingelheim) on the occasion of his 75th birthday.

Reinhard Brückner prepared his doctoral thesis at the Ludwig-Maximilians-Universität München under the supervision of Professor Rolf Huisgen (1984) and was a postdoctoral fellow with Professor Paul A. Wender at Stanford University. After a habilitation with Professor Reinhard W. Hoffmann at the Philipps-Universität Marburg he became an associate professor at the Julius-Maximilians-Universität Würzburg (1990). He was a full professor at the Georg-August-Universität Göttingen (1992) and moved to the Albert-Ludwigs-Universität Freiburg in 1998. Being a dedicated teacher, he was a visiting professor at the Universities of Wisconsin / Madison and Santiago de Compostela / Spain. His research interests comprise the synthetic chemistry of dienediynes, 1,3,5,7,...-polyols, chiral butyrolactones and butenolides, and the stereochemistry of rearrangements of organolithium compounds.

DOI: 10.1039/b007590f

of the present top ten block busters of the pharmaceutical industry effect—namely Lipitor®, Zocor® and Pravachol®. The structurally most complex γ-alkylidenebutenolides of the substitution pattern under scrutiny are the carotinoids peridinin[4] (*Z*-**18a**, Scheme 5) and pyrrhoxanthin[5] (*Z*-**18b**, Scheme 5). Peridinin plays a key role in marine photosynthesis by dinoflagellates, which make up much of the sea plankton. Light harvesting by *Amphidinium carterae* is effected by a chromoprotein whose 2 active centers contain 2 × four molecules of peridinin, 2 × one molecule of chlorophyll A and 2 × one molecule of a (digalactosyl)diacylglycerol.[6] The conversion of light into chemical energy is a fundamentally important process.[7] Pyrrhoxanthin participates in algal photosynthesis.

Each of the γ-alkylidenebutenolides just mentioned has attracted synthetic attention in recent years[8] (Scheme references: *vide supra*), as have several others, too. The latter comprise the goniobutenolides A (*Z*-**27**) and B (*E*-**27**, Schemes 9, 29), the antibiotic lissoclinolide (*trans*,*Z*,*trans*-**52**, Scheme 14), the isomeric structure *trans*,*E*,*trans*-**52** once assigned to tetrenolin (Scheme 15), constituent *Z*-**72** of the roots of *Chamaemelum nobile* L. (Schemes 19, 22), the alkaloid pandamarilactam-3y (*Z*-**85**, Scheme 23), the cytotoxin nostoclide II (*Z*-**89**, Scheme 24), the wood constituent freelingyne (*Z*-**93**, Scheme 25), melodorinol (*Z*-**99**, Scheme 26), the antibiotic patulin,[9] and an eudesmanolide.[10]

The present article reflects the current interest in the preparation of such compounds.[11] Specifically, it compiles ways of assembling such γ-alkylidenebutenolides by means of

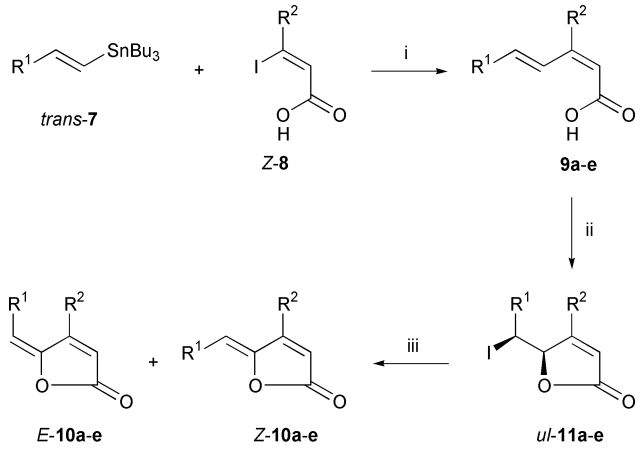

	a	b	c	d	e
R^1	$SiMe_3$	$SiMe_3$	$SiMe_3$	$SiMe_3$	Ph
R^2	H	Me	CH_2OMe	Ph	Me
ii at °C	-78	-78	-78	-78	-30
% Yield **10**	87	85	71	54	70
E : *Z*	99:1[a]	98:2[b]	95:5	46:54	0:100

[a]70:30 at 20 °C; [b] 83:17 at -30 °C.

Scheme 3 *Reagents*: i, Stille coupling; ii, either KI, $Na_2S_2O_8$, H_2O, or ICl, CH_2Cl_2, 48–73%; iii, DBU, CH_2Cl_2.

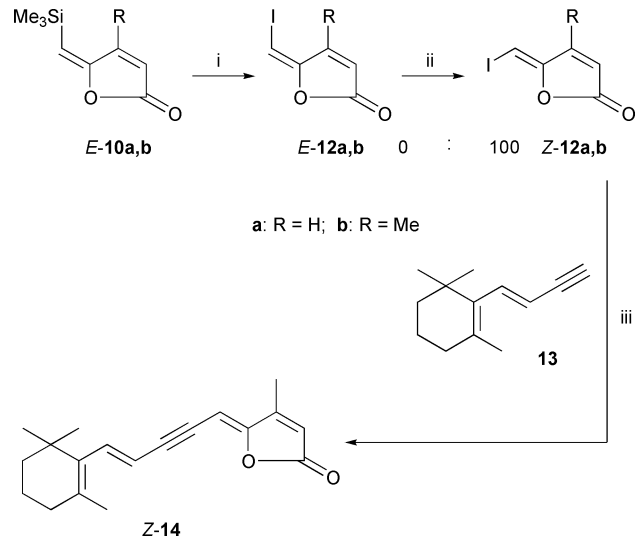

Scheme 4 *Reagents*: i, I_2, AgO_2CCF_3, THF, 'good yield'; ii, Et_2O, 'quantitatively'; iii, for *Z*-**12b**: $Pd(PPh_3)_4$, CuI, $BuNH_2$, benzene, 65%.

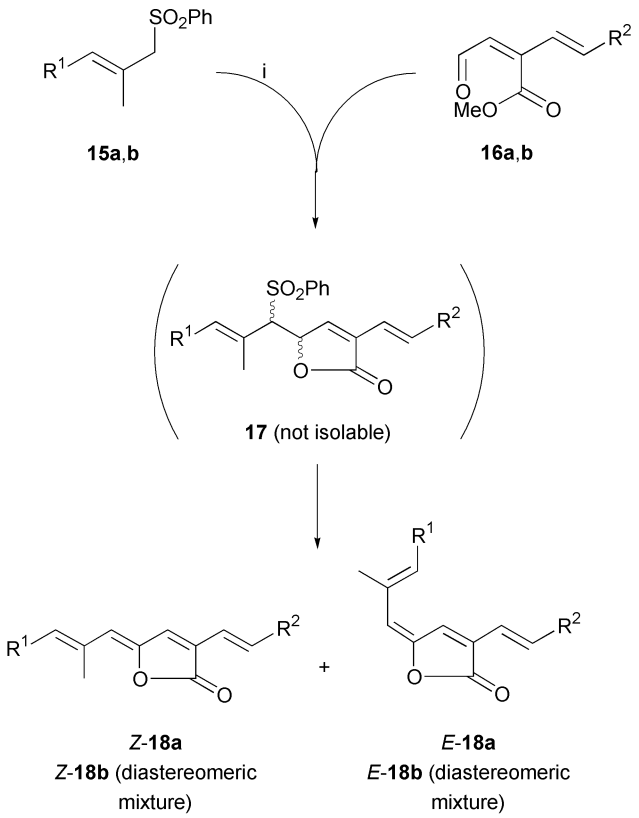

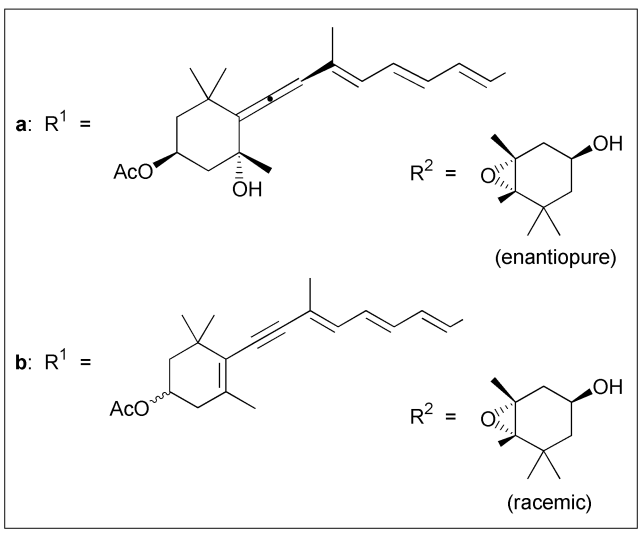

Scheme 5 *Reagents*: i, LDA, THF–hexanes, for **a**: addition of **16a**, *Z*-**18a**:*E*-**18a** mixture: 18% relative to **16a** = 12% relative to **15a**, for **b**: addition of **16b**, *Z*-**18b**:*E*-**18b** mixture after preparative TLC: 13% relative to **16b** = 8.4% relative to **15b**, for **a** and **b**: stereopure products after preparative HPLC, *Z*-**18a**: 2.9% relative to **16a** = 1.9% relative to **15a**, *E*-**18a**: 2.8% relative to **16a** = 1.9% relative to **15a**, *Z*-**18b**: 5.9% relative to **16b** = 3.7% relative to **15b**, *E*-**18b**: 4.9% relative to **16b** = 3.1% relative to **15b**.

the strategy outlined in Scheme 1.[12] Its key step is an *anti*-elimination of a leaving group Het at C$^{\alpha\prime}$ and an adjacent proton at C$^{\gamma}$ from diastereopure γ-(α-heteroalkyl)-substituted butenolides **1**. If the latter possesses stereostructure *lk*-**1**, the *anti*-elimination of α′-Het and γ-H establishes *Z*-configured γ-alkylidenebutenolides *Z*-**2** while the isomeric starting materials *ul*-**1** serve as precursors of the stereocomplementary γ-alkylidenebutenolides *E*-**2**. In order for these eliminations to be stereo*specific*, there must not be competing *syn*-eliminations. Neither may the elimination products *Z*- and *E*-**2** equilibrate under the reaction conditions—*Z*-**2** is slightly or distinctly more stable than *E*-**2**.

To the best of our knowledge, the earliest realization of a (fairly) *anti*-selective elimination of type *ul*-**1** → *E*-**2** is due to Font *et al*. in 1989.[13] As shown in Scheme 2, the dehydrobromination of the γ-(α-bromoethyl)-substituted butenolide *ul*-**6** with NEt_3 gave a 90 : 10-mixture of *E*- and *Z*-**5**.

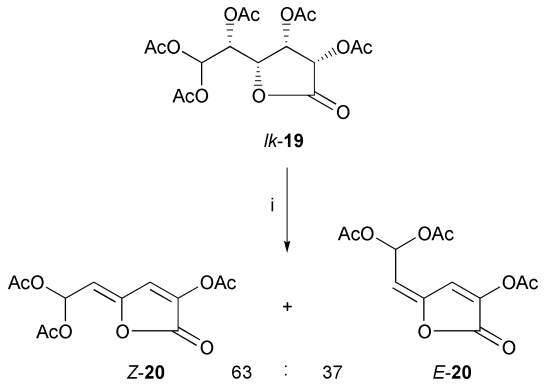

Scheme 6 *Reagents*: i, NEt_3, Ac_2O, 91%.

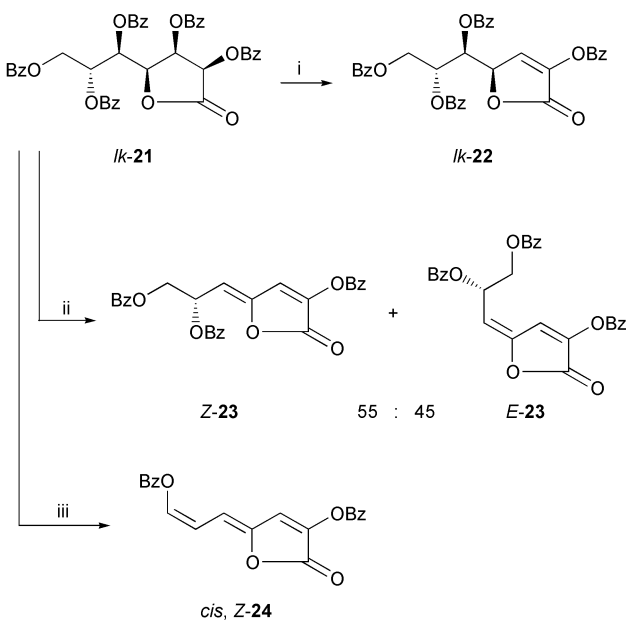

Scheme 7 *Reagents*: i, DBU, CH_2Cl_2, 67%;[18] ii, NEt_3, $CHCl_3$, 85% (experimental part)–90% (according to Scheme);[19] iii, NEt_3–$CHCl_3$, 59%.[20]

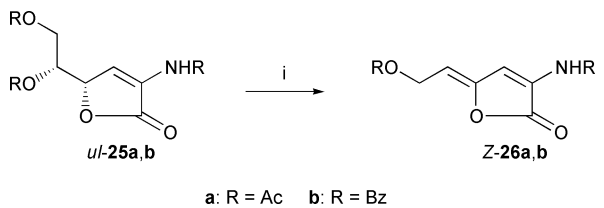

Scheme 8 *Reagents*: i, for **a**: DBU, CH_2Cl_2, 71%, for **b**: DBU, CH_2Cl_2, crystallization, 62%.

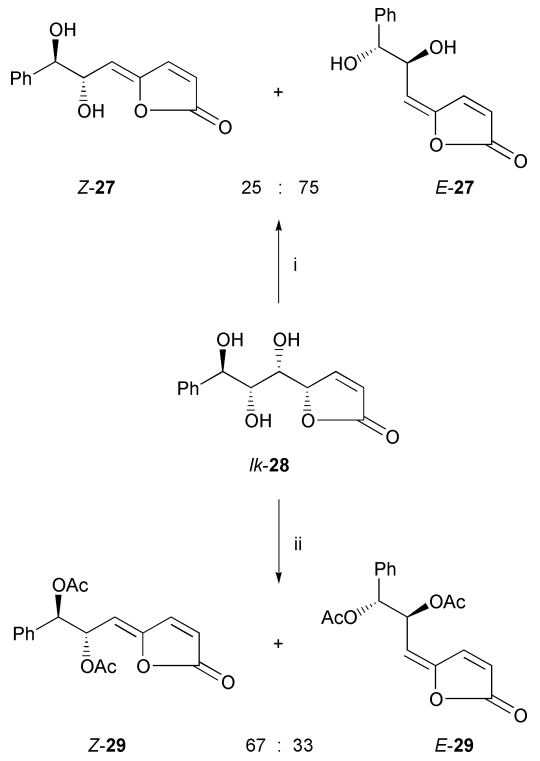

Scheme 9 *Reagents*: i, $(F_3C–CO)_2O$, NEt_3, CH_2Cl_2, then MeOH, 79%; ii, Ac_2O,NEt_3, DMAP, CH_2Cl_2, 99%.

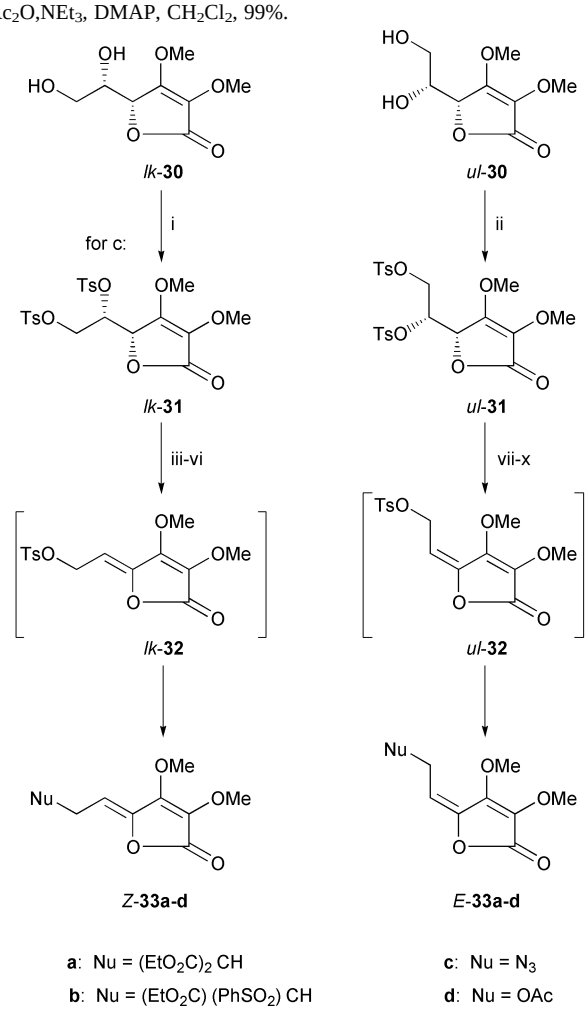

Scheme 10 *Reagents*: i, TsCl, pyridine, 86%; ii, same as (i), 86%; iii, for **a**: $(EtO_2C)_2CH^-Na^+$, THF, 78%; iv, for **b**: $(EtO_2C)(PhSO_2)CH^-Na^+$, THF, 82%; v, for **c**: NaN_3, DMF, 85%; vi, for **d**: NaOAc, DMF, 70%; vii, same as (iii), 70%; viii, same as (iv), 81%; ix, same as (v), 86%; x, same as (vi), 73%.

One must be aware that such an *E*-selectivity can easily be erased by an ensuing (partial or completely) $E \rightarrow Z$ isomerization. This is evidenced, for instance, by the DBU-mediated dehydroiodinations tabulated in Scheme 3.[14] The β-substituents R^2 of elimination products *Z*-**10b**–**e** destabilize the neighboring alkylidene substituents R^1 so much that substrate *ul*-**11e** undergoes a 100% *syn*-selective β-elimination.

Clearly, such a thermodynamically driven $E \rightarrow Z$ isomerization may be exploited for synthesizing *Z*-γ-alkylidenebutenolides selectively. This is underlined by the elaboration of the γ-[(trimethylsilyl)methylene]butenolides *E*-**10a** and **b** shown in Scheme 4.[14] The γ-(iodomethylene)butenolides *E*-**12a** and **b** obtained from these compounds by iodolysis provided the stereopure isomers *Z*-**12a** and **b** within 1 h at room temperature. Compound *Z*-**12b** underwent a Sonogashira–Hagihara coupling with alkyne **13** which proceeded with retention of configuration at the $C^{\alpha'}$=C^{γ} bond and provided the vitamin A lactone analog *Z*-**14** in 65% yield.

The fairly sophisticated β-eliminations of Scheme 5 allowed Ito *et al.* to achieve the first syntheses of the γ-alkylidenebutenolide carotinoids peridinin (*Z*-**18a**) and pyrrhoxanthin (*Z*-**18b**).[15] Benzenesulfonic acid was eliminated from the γ-(α-phenylsulfonyl)-substituted butenolides **17** which were formed *in situ* by the addition of the appropriate lithiated sulfone **15a** or **b** to the respective aldehydoester **16a** or **b**. This addition is expected to lack simple diastereoselectivity—like the first step of the Julia–Lythgoe olefination. Therefore, the corresponding intermediates **17** should arise as *lk*,*ul*-mixtures. The latter circumstance explains, in conjunction with the stereochemical relationships of Scheme 1, why the elimination products **18a** and **b** resulted as *Z*,*E*-*mixtures*.

One concludes that *stereospecific* β-elimination routes to γ-alkylidenebutenolides depend on the availability of diastereopure *lk*- and *ul*-configured γ-(α-heteroalkyl)-substituted butenolides **1**. These compounds have been prepared successfully from sugars, by (Mukaiyama) aldol additions, and by the route of Scheme 30, as specified in the following sections.

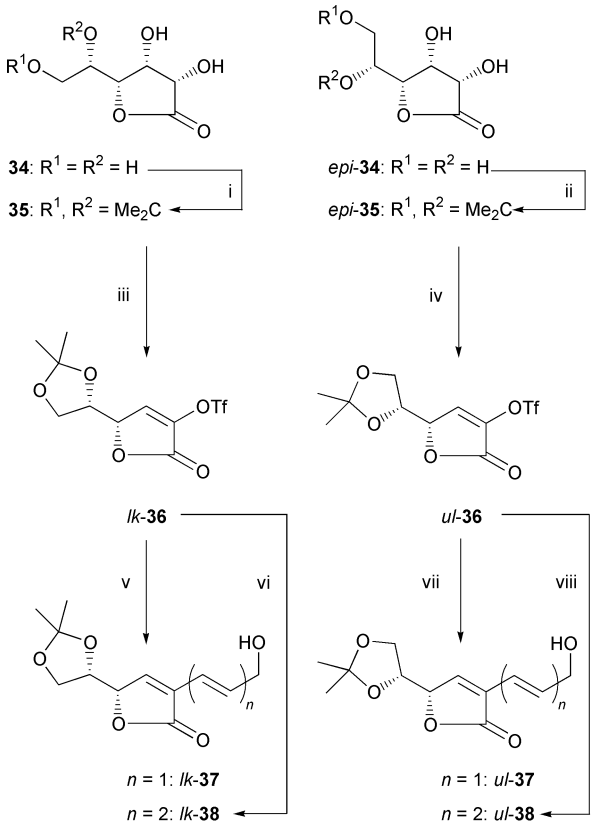

Scheme 11[24] *Reagents*: i, 2,2-Dimethoxypropane Amberlyst-15, DMF, 68% (ref. 25 60%, ref. 26 70%); ii, same as (i), 74% (ref. 25 77%); iii triflic anhydride, pyridine (4.0 equiv.), CH_2Cl_2, 74% (ref. 27 70%); iv, same as (iii), 70% (ref. 27 74%); v, *trans*-3-(tributylstannyl)prop-2-en-1-ol, $Pd_2(dba)_3$·$CHCl_3$, $AsPh_3$, LiCl, THF, 78%; vi, *trans*,*trans*-5-(tributylstannyl)penta-2,4-dien-1-ol, $Pd_2(dba)_3$·$CHCl_3$, $AsPh_3$, LiCl, THF, 57%; vii, same as (v), 68%; viii, same as (vi), 75%.

β-Eliminations from sugar lactones[16]

D-Glucurolactone and acetyl chloride react to give the saturated lactone *lk*-**19** shown in Scheme 6. Treatment with triethylamine in acetic anhydride induced two β-eliminations.[17] First, the C^{α}=C^{β} bond formed, as inferred from the analogous conversion *lk*-**21** → *lk*-**22** in Scheme 7.[18] Then, the $C^{\alpha'}$=C^{γ} bond was established. 57% of the *Z*-configured and 34% of the *E*-configured γ-alkylidenebutenolide **20** resulted,[17] *i.e.* the second elimination was non-stereoselective.

In a similar manner, the perbenzoate *lk*-**21** of D-seduheptulonolactone and triethylamine undergo multiple β-eliminations (Scheme 7).[18–20] As in the case of Scheme 6, the second elimination lacks stereocontrol since the γ-alkylidenebutenolide **23** forms as a 55 : 45 mixture of *anti*-elimination product *Z*-**23** and *syn*-elimination product *E*-**23**.[19] By a 10-fold increase of the reaction time, a third elimination of benzoic acid ensued. It

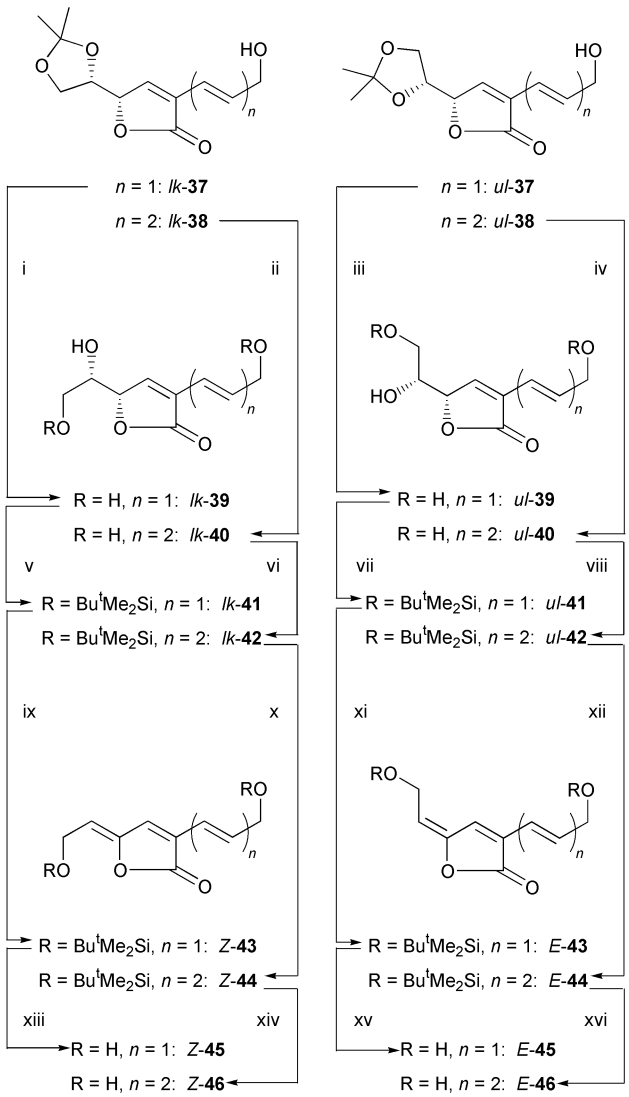

Scheme 12[24] *Reagents*: i, HCl (12 M), CH_2Cl_2, MeOH, 78%; ii, same as (i), 73%; iii, same as (i), 65%; iv, same as (i), 71%; v, Bu^tMe_2SiCl, imidazole, molecular sieves 4 Å, DMF, 73%; vi, same as (v), 48%; vii, same as (v), 70%; viii, same as (v), 51%; ix, triflic anhydride, pyridine, CH_2Cl_2, 81% of a 99 : 1 *Z*-**43** : *E*-**43** mixture; x, same as (ix), 69% of a 97 : 3 *Z*-**44** : *E*-**44** mixture; xi, same as (ix), 63% of a 96 : 4 *E*-**43** : *Z*-**43** mixture; xii, same as (ix), 73% of a 97 : 3 *E*-**44** : *Z*-**44** mixture; xiii, HF·pyridine, THF, 96% of a 94 : 6 *Z*-**45** : *E*-**45** mixture; xiv, same as (xiii), 92% of diastereopure *Z*-**46**; xv, same as (xiii), 86% of a 94 : 6 *E*-**45** : *Z*-**45** mixture; xvi, same as (xiii), 96% of a 95 : 5 *E*-**46** : *Z*-**46** mixture.

created the conjugated γ-alkylidenebutenolide **24** as a pure *cis*,*Z*-isomer.[20] Since the yield of this compound measured 60–80%, the $C^{\alpha'}$=C^{γ} bond of its precursor **23** (55 : 45 *Z* : *E* mixture, 85–90% yield if isolated) must have partly reverted to the *Z*-geometry under the influence of thermodynamic control.

Thermodynamic control must also be responsible for the *syn*(!)-preference of the related, DBU-driven β-eliminations of acetic or benzoic acid from the acylamino-substituted sugar lactones *ul*-**25a** and **b**, respectively (Scheme 8).[21]

Why triethylamine and the tris(trifluoroacetate) derived from the butenolide *lk*-**28** shown in Scheme 9 give a 1 : 3 ratio of *anti*- and *syn*-elimination, while the analogous triacetate does so in a 2 : 1 ratio, is difficult to rationalize.[22] But clearly, the findings of Schemes 6–9 suggest that in γ-(α-heteroalkyl)-substituted butenolides which are to undergo a selective *anti*-elimination and provide sterically homogenous γ-alkylidenebutenolides thereby, the leaving group should *not* be a carboxylic acid. Presumably, a *better* leaving group is called for.

This thought represented *our* start into γ-alkylidenebutenolide syntheses.[12] However, it had already been considered by Khan and Adams in 1995 when they published the study displayed in Scheme 10.[23] The starting materials of these authors were two readily accessible sugar lactones, namely the dimethyl ether *lk*-**30** of L-ascorbic acid and the dimethyl ether *ul*-**30** of D-isoascorbic acid. Treatment of these species with tosyl chloride at room temperature in pyridine provided the diastereomeric ditosylates *lk*-**31** and *ul*-**31**, respectively, both in 86% yield. At 60–80 °C, these compounds became elimination substrates upon treatment with a variety of reagents acting as bases and nucleophiles simultaneously. Behaving as bases, they induced highly stereoselective *anti*-eliminations of toluene-*p*-sulfonic acid which established the homogeneously configured $C^{\alpha'}$=C^{γ} bonds of the presumed intermediates *lk*-**32** and *ul*-**32**, respectively. Then, the same reagents substituted the allylic tosyloxy group nucleophilically: 70–86% of the pure *Z*- and *E*-isomers of the γ-alkylidenebutenolides **33a**–**d** resulted.

Khan's and Adams' results encouraged us to develop *our* β-elimination route[12,24] from sugar lactones to stereodefined γ-alkylidenebutenolides (Schemes 11–17). Clearly, we felt more strongly their message 'this route in principle should work' than we anticipated how profoundly differently our materials behaved in comparison to theirs. We were to deal with 'true' α,β-unsaturated lactones while they had used α,β-unsaturated lactones, which, constituting vinylogous carbonates, are resonance-stabilized. Accordingly, none of our γ-alkylidenebutenolides could be heated overnight at 60–80 °C like theirs (*vide supra*) without suffering decomposition, not to speak of undergoing extensive *E*–*Z*-isomerization much earlier. Indeed, in each step following the installment of the crucial $C^{\alpha'}$=C^{γ} bond skillful experimentation was called for in our work lest the $C^{\alpha'}$=C^{γ} bond geometry be eroded.

Our methodology study (Scheme 11[24]) started from the hydrogenation products **34** ('L-gulonolactone') of L-ascorbic acid and *epi*-**34** ('D-mannonolactone') of D-isoascorbic acid. Acetonide formation, bis(triflate) formation, and *in situ* β-elimination furnished the butenolide-based enol triflates *lk*- and *ul*-**36**, respectively, as described earlier.[27] In the presence of 2 mol% $Pd_2(dba)_3$·$CHCl_3$, $AsPh_3$ and LiCl, these compounds underwent smooth Stille couplings with *trans*-3-(tributyl-

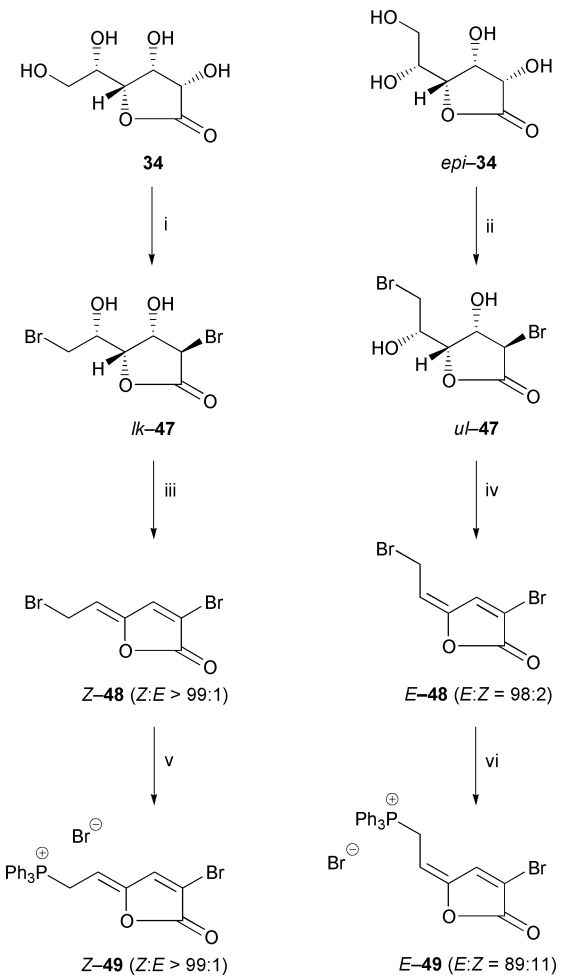

Scheme 13[28] *Reagents*: i, HBr, HOAc, afterwards addition of MeOH, 78% (ref. 29: 90%); ii, same as (i), 71% (ref. 30: 63%); iii, Tf_2O, pyridine, CH_2Cl_2, 95%; iv, same as (iii), 63%; v, Ph_3P, acetonitrile, 96%; vi, same as (v), 80%.

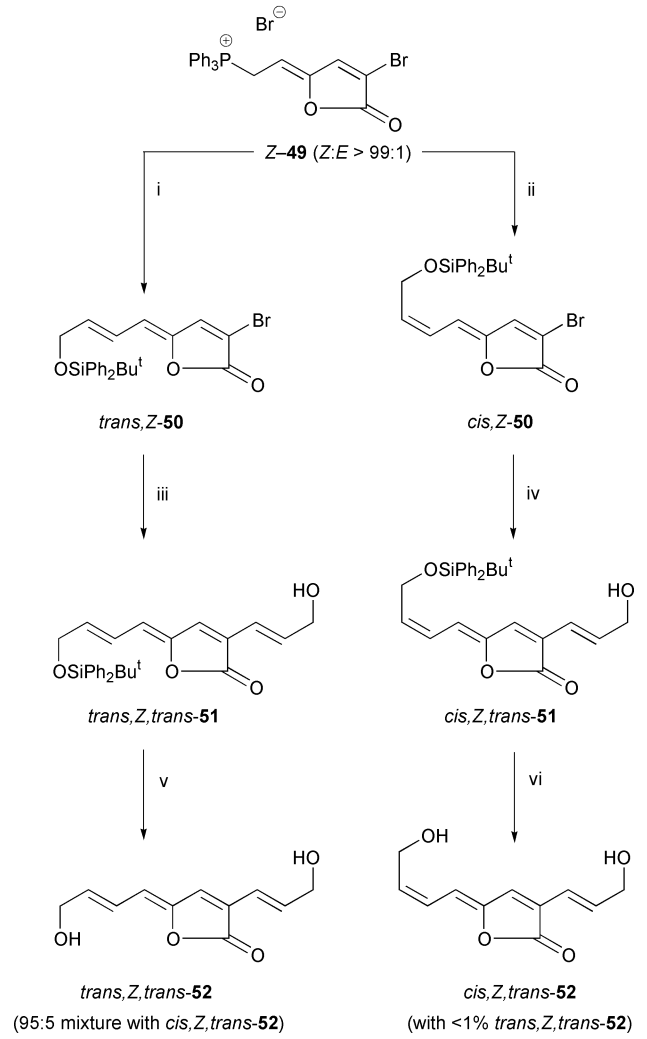

Scheme 14 *Reagents*: i, LDA, THF, $Bu^tPh_2SiOCH_2$–CH=O, −78 °C → 60 °C, 93%; ii, same as (i) but −78 °C → 25 °C, 72%; iii, *trans*-Bu_3Sn–CH=CH–CH_2OH, Pd_2dba_3·$CHCl_3$, $AsPh_3$, THF, 74%; iv, same as (iii), 78%; v, HF·pyridine, THF, 81%; vi, same as (v), 84%.

stannyl)prop-2-en-1-ol and *trans,trans*-5-(tributylstannyl)-penta-2,4-dien-1-ol. The α-alkenylated butenolides **37** and **38** resulted. They were liberated from their acetonide groups, furnishing the triols **39** and **40**, respectively (Scheme 12[24]). After selective *tert*-butyldimethylsilylation of their primary OH groups, the remaining secondary OH group of compounds **41** and **42** was poised to undergo the desired *anti*-elimination after activation with triflic anhydride. Pyridine accomplished this task at −25 °C. The α-alkenyl-γ-alkylidenebutenolides **45** and **46** resulted in 86–96% yield. Their isomeric purities were *Z*:*E* = 94:6 or 6:94 in the former case and *Z*:*E* = 100:0 or 5:95 in the latter. The viability of our strategy had thereby been demonstrated.

In two other sequences, the known[29,30] twofold S_N2-attack of HBr upon the primary and the activated secondary OH group of lactones **34** and *epi*-**34** delivered the dibromodihydroxylactones *lk*- and *ul*-**47** selectively (Scheme 13). Bistriflate formation in the presence of pyridine made possible two β-eliminations. They led to the bromine-containing γ-alkylidenebutenolides *Z*- and *E*-**48** as almost pure diastereomers. Allylic substitution by triphenylphosphine gave the corresponding phosphonium salts **49** with complete retention of the *Z*- and partial loss of the *E*-geometry.

The ylide derived from phosphonium salt *Z*-**49** reacted with $Bu^tPh_2SiOCH_2$–CH=O with complete retention of the $C^{\alpha'}$=Cγ bond geometry (Scheme 14[28]). The newly formed $C^{\beta'}$ = Cγ′ bond of olefination product **50** was either *trans*- or *cis*-configured, depending on whether the Wittig reaction was conducted at 60 or 25 °C. The bromoethylene moiety of the respective product *trans,Z*- or *cis,Z*-**50** could be coupled with *trans*-Bu_3Sn–CH=CH–CH_2OH in the presence of catalytic Pd_2dba_3·$CHCl_3$ and $AsPh_3$. All C=C bonds maintained their configurations under these conditions and did so, too, in the terminating desilylation step. It rendered, in the *trans,Z,trans*-series, the γ-alkylidenebutenolide *trans,Z-trans*-**52**, which had been described as the antibiotic lissoclinolide. This was the third and is the hitherto shortest synthesis of this compound. Two entirely different syntheses of lissoclinolide had been realized shortly before in the laboratories of Rossi[31] and Negishi.[32]

Disappointingly, the ylide derived from phosphonium salt *E*-**49** reacted with $Bu^tPh_2SiOCH_2$–CH=O with complete inversion of the $C^{\alpha'}$=Cγ bond geometry,[28] *i.e.* providing the same *Z*-configured condensation products *trans,Z*-**50** or *cis,Z*-**50** which we had already prepared starting from the isomeric phosphonium salt *Z*-**49** (Scheme 14). This means that the ylide in question underwent a thermodynamically driven *E*→ *Z*-isomerization.

Scheme 15 shows how we managed to get at least small amounts of the Stille coupling product *trans,E,trans*-**51** (which our Wittig approach had failed to give) from the bromoolefin precursor *trans,E*-**50** by a partial isomerization of the previously obtained (*cf.* Scheme 14) coupling product *trans,Z,trans*-**51**. A subsequent desilylation furnished isomer *trans,E,trans*-**52** of lissoclinolide (*trans,Z,trans*-**51**). This isomer was until then suspected to represent 'tetrenolin'.[33] However, having both isomers at hand, we proved by ^{1}H-NMR spectroscopy that "tetrenolin" possesses the structure of lissoclinolide.

Scheme 16 shows the first synthesis of dihydroxerulin (*Z*-**61**).[34] It allowed us to assign a *trans*-configuration to the C=C

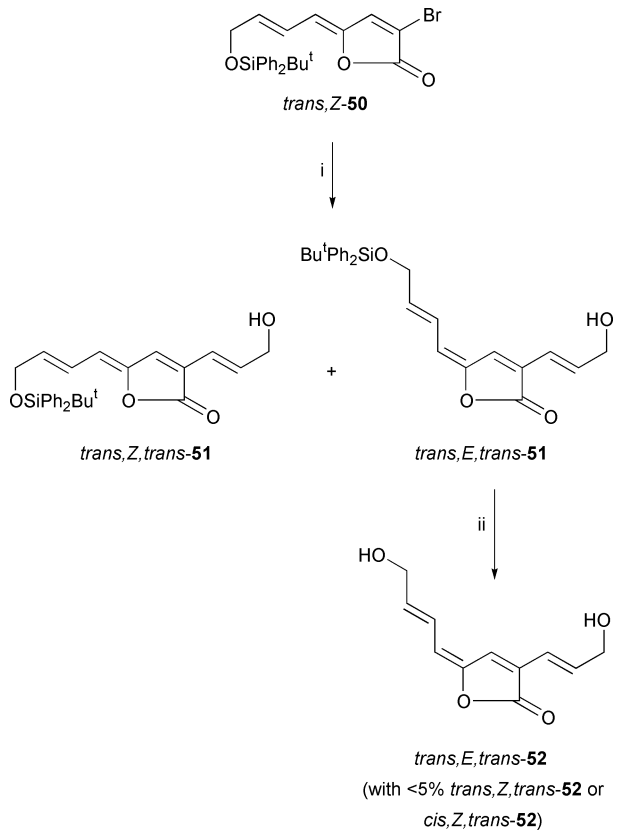

Scheme 15[28] *Reagents*: i, *trans*-Bu_3Sn–CH=CH–CH_2OH, Pd_2dba_3·$CHCl_3$, $AsPh_3$, THF, 71% *trans,Z,trans*-**51** + 20% *trans,E,trans*-**51**; ii, HF·pyridine, THF, 89%.

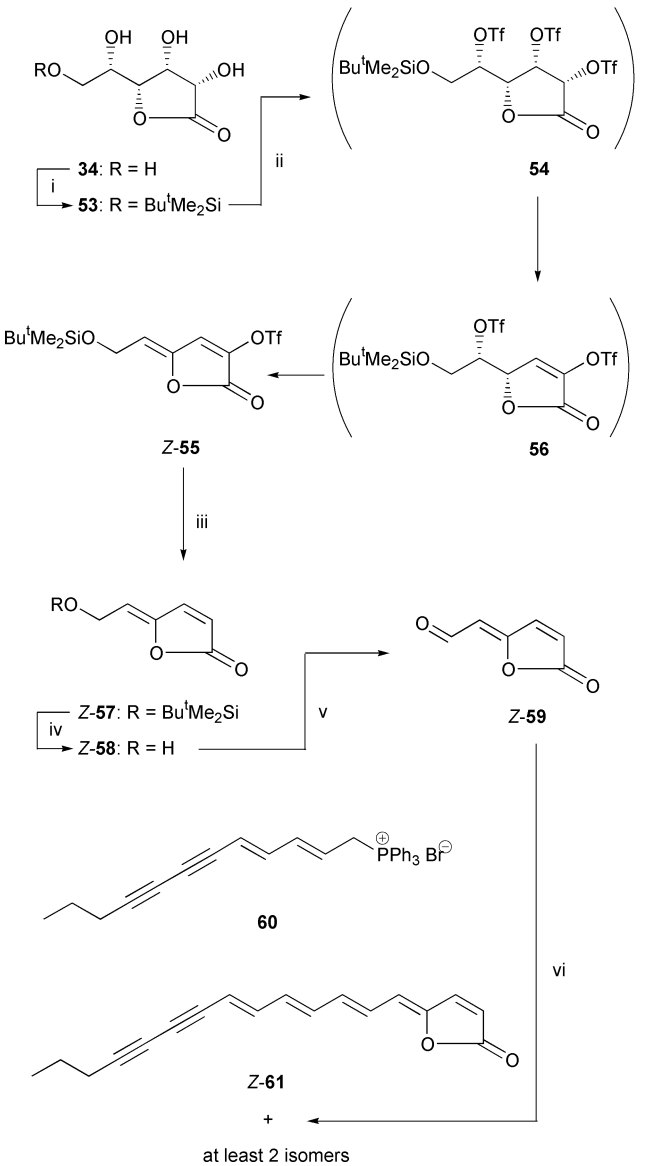

Scheme 16[34] *Reagents*: i, Bu^tMe_2SiCl, imidazole, DMF, 58%; ii, pyridine, triflic anhydride, CH_2Cl_2, 78% (*Z*:*E* > 99:1); iii, LiCl, $NiCl_2(PPh_3)_2$, THF, Bu_3SnH, 83% (*Z*:*E* = 94:6); iv, HF·pyridine, THF, 80% (*Z*:*E* = 96:4); v, Dess-Martin periodinane, CH_2Cl_2, 90% as a 95:5-mixture, recrystallized as a 98:2 *Z*:*E* mixture, 82%; vi, **60**, *n*BuLi, THF, *Z*-**59**, after repeated chromatographies 30% *Z*-**61** and 25% mixture of other isomers.

bond which could not be assigned by the spectroscopic study of the natural specimen[3] because of signal overlap with contaminating xerulin (*trans*,*Z*-**66**, Scheme 17). A conceptionally different synthesis of dihydroxerulin has since been elaborated by Rossi *et al*.[35] Initially, we sulfonylated the three OH groups of the O_{prim}-*tert*-butyldimethylsilyl protected L-gulonolactone **53** with triflic anhydride. The resulting tristriflate **54** underwent two *in situ* β-eliminations of triflic acid, the first elimination rendering butenolide **56**, the second leading to the isomerically pure alkylidenebutenolide *Z*-**55**. The enol triflate moiety of this compound was hydrogenolyzed readily to give lactone *Z*-**57** in the presence of catalytic $NiCl_2(PPh_3)_2$ and stoichiometric Bu_3SnH. A Wittig reaction of the derived aldehyde *Z*-**59** with

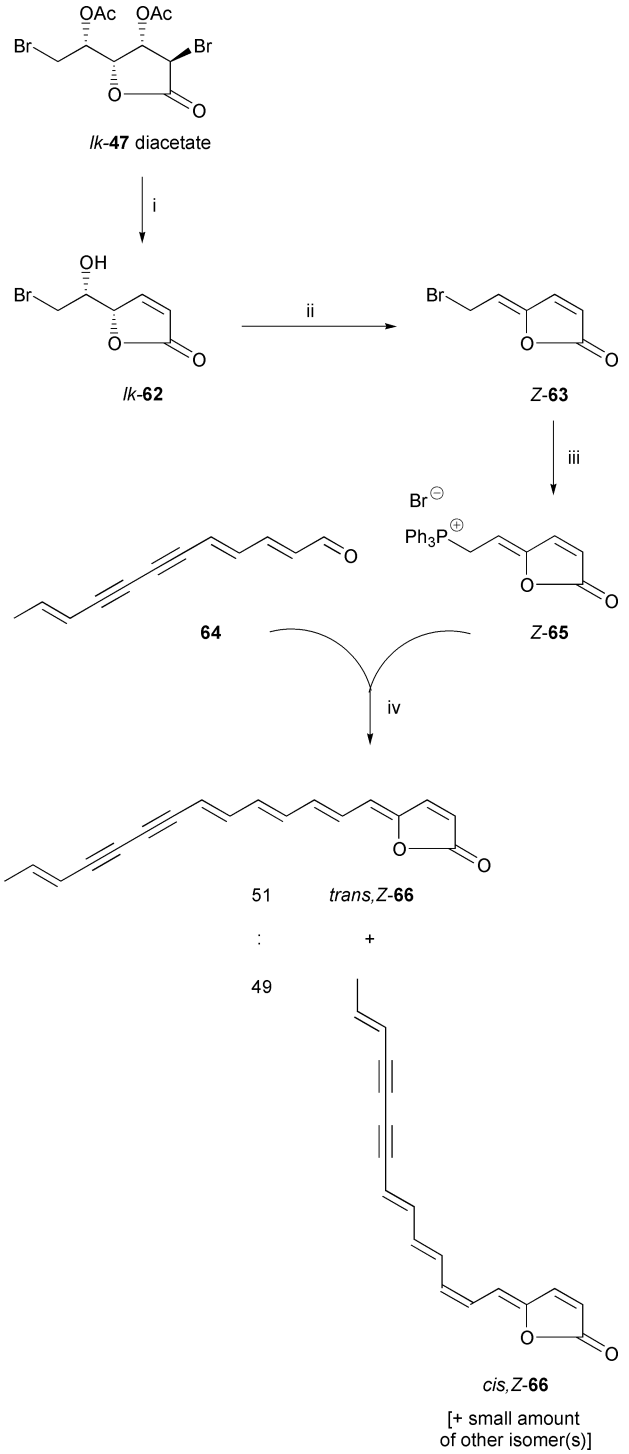

Scheme 17[36] *Reagents*: i, Na_2SO_3, $NaHSO_3$, MeOH, H_2O, crude product treated with MeOH–HCl, 92% overall (ref. 37: 64%); ii, triflic anhydride, pyridine, CH_2Cl_2, 63% (*Z*:*E* 97:3); iii, PPh_3, H_3C–CN, 100%; iv, K_2CO_3, **64**:*Z*-**65** 11:2, CH_2Cl_2, 28% *trans*,*Z*-**66** + 27% [*cis*,*Z*-**66** + small amount of isomer(s)].

the ylide corresponding to the phosphonium salt **60** followed but, unfortunately, exhibited no stereocontrol: it delivered 30% dihydroxerulin *Z*-**61** and 25% of at least two isomers. Yet, this synthesis encompasses only 2 × 5 consecutive steps in the linear sequences and a final converging step.

The first synthesis of xerulin (*trans*,*Z*-**66**) was also effected by our β-elimination strategy (Scheme 17).[36] We started with the diacetate of dibromolactone *lk*-**47** (preparation:[29,30] Scheme 13). A reductive elimination[37] established the $C^{\alpha}=C^{\beta}$ bond of butenolide *lk*-**62** and a subsequent base-promoted elimination the $C^{\alpha'}=C^{\gamma}$ bond of the γ-alkylidenebutenolide **63** (97% *Z*). An S_N2 reaction of this compound with triphenylphosphine provided the corresponding phosphonium salt **65** (96% *Z*). The terminating reaction of Scheme 17 was a Wittig olefination. It showed no more stereocontrol than the Wittig reaction of

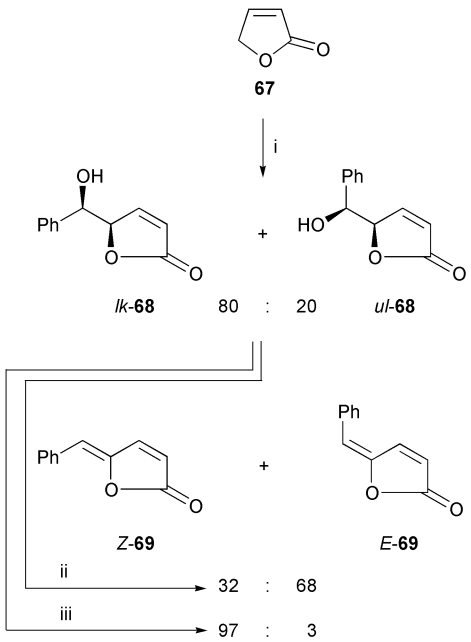

Scheme 18[40] *Reagents*: i, LDA, THF, Ph–CH=O, 76%; ii, MsCl, pyridine, 0 °C → 80–90 °C, 87%; iii, same as (ii) but only rt, 96%.

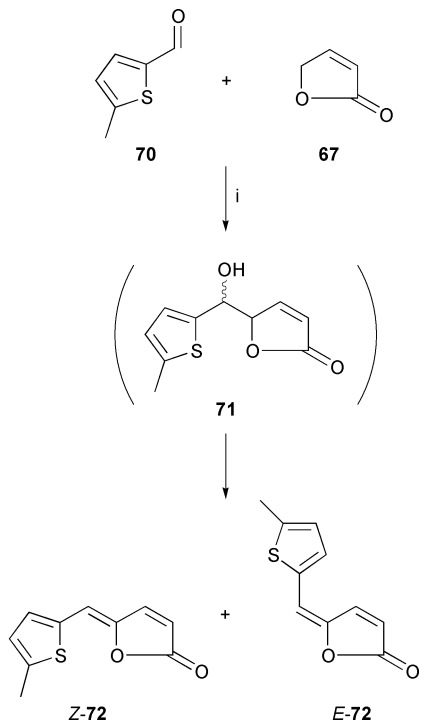

Scheme 19[41] *Reagents*: i, **70**:**67** 1:1, piperidinium acetate, HOAc, 36%.

opposite polarity used for synthesizing dihydroxerulin (*Z*-**61**; Scheme 16). Thus, it furnished equal, but separable, amounts of xerulin (*trans,Z*-**66**; 28% yield) and its isomer *cis,Z*-**66**. The recently published, differently tailored synthesis of xerulin by Negishi *et al*. is free from such a drawback.[38]

β-Eliminations from (Mukaiyama) aldol adducts

Aldol additions of type-**67** butenolides, *via* their quantitatively derived enolate (Schemes 18, 20) or *via* an equilibrium fraction of the same kind of enolate (Scheme 19), as well as the more widely used Mukaiyama aldol additions of the corresponding

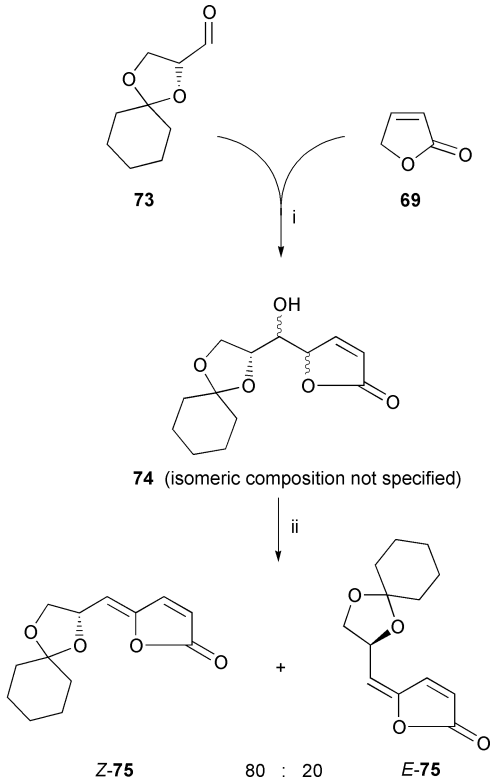

Scheme 20[42] *Reagents*: i, LDA, THF, **73**; ii, crude product from step (i), MsCl, pyridine, 31%.

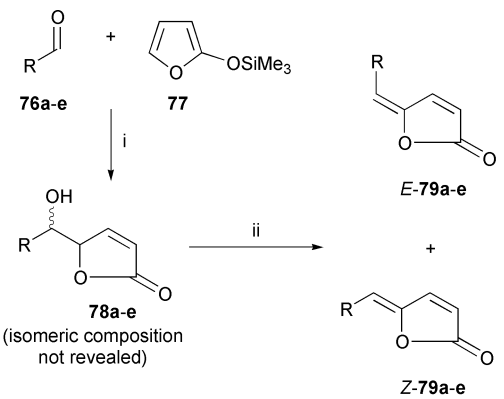

	a	b	c	d	e
R	Pr−C≡C	Ph	Pent	Ph-CH_2-CH_2	
% Yield **78**	70	95	94	90	92
% Yield **79**	90	91	94	96	92
E:*Z*	5:2	1:1	1:1	3:5	1:1

Scheme 21[43] *Reagents*: i, **76a**–**e**:**77** 1:1.2, $SnCl_4$, CH_2Cl_2, aqueous HCl; ii, Ac_2O, NEt_3, 4-pyrrolidinopyridine, CH_2Cl_2.

siloxyfurans (Schemes 21–25, 27–29) constitute versatile preparations of γ-(α-heteroalkyl)-substituted butenolides **1**. The addition of 5-lithio-2-(*tert*-butoxy)furans to an aldehyde followed by hydrolysis of the resulting heterocycle provides an altervative for attaining the same goal (Scheme 26).

In general, a high degree of simple diastereoselectivity in such aldol additions is limited to the use of α-chiral aldehydes (where *lk*-selectivity of Mukaiyama aldol additions occurs[39]) whereas achiral aldehydes usually show little simple diastereoselectivity. Accordingly, the aldol additions shown in Schemes 18–21 provided the aldol addition products **68**, **71** (formed *in situ*, not isolated), **74** and **79** as *lk,ul-mixtures*. Not having separated them, the subsequent *stereoselective* formation of a γ-alkylidenebutenolide was observed in a single case (*lk*-/*ul*-**68** + mesyl chloride–pyridine → *Z*-**69**; Scheme 18) where thermodynamic control was achieved.

A somewhat related *Z*-preference occurred during the deketalization of the γ-alkylidenebutenolides *Z*- and *E*-**75** of Scheme 20: *Z*-**75** underwent this reaction with complete retention of configuration while *E*-**75** exhibited some *E*→*Z*-isomerization.

If the diastereomeric mixtures of (Mukaiyama) aldol addition products initially obtained are separated, the resulting *lk*-isomer, through an *anti*-elimination, gives a *Z*-configured alkylidenebutenolide and the *ul*-isomer, the *E*-alkylidenebutenolide. Thus, treatment of the thiophene-containing Mukaiyama products *lk*- and *ul*-**71** with Tf_2O and pyridine in dichloromethane provided the alkylidenebutenolides *Z*- and *E*-**72** as single isomers in 67 and 70% yield, respectively (Scheme 22). *Z*-**72** is a constituent of the roots of *Chamaemelum nobile* L.

The pyrrolidone-containing Mukaiyama product *lk*-**84** and an excess of both diethyl azodicarboxylate and PPh_3 gave the isomerically pure *Z*-configured alkylidenebutenolide pandamarilactam-3y *Z*-**85** (Scheme 23). It is noteworthy that the BF_3-promoted aldol addition leading to substrate *lk*-**84** was fairly diastereoselective starting from the (trimethylsiloxy)furan **81** (→ *lk*:*ul* = 88:12) and very diastereoselective starting from the (*tert*-butyldimethylsiloxy)furan **82** (→ *lk*:*ul* = 97:3).

The terminating elimination **88**→**89** in the synthesis of the γ-alkylidenebutenolide nostoclide II (*Z*-**89**, Scheme 24) was also

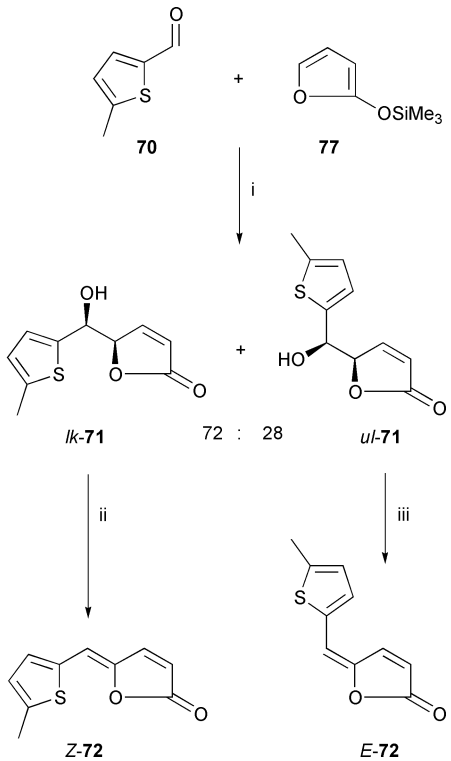

Scheme 22[44] *Reagents*: i, BF_3·OEt_2, aldehyde, CH_2Cl_2, 40%; ii, pyridine, CH_2Cl_2, triflic anhydride, 67%, *Z*-**72**:*E*-**72** 100:0; iii, same as (ii), 70%, *E*-**72**:*Z*-**72** > 99:1.

Z-selective, even when substrate **88** was a mixture (73 : 27) of *lk*- and *ul*-isomers. Probably, *E*-**89** is sterically too hindered to be formed under the reaction conditions (DBU, reflux temperature in chloroform).

Various (trimethylsiloxy)furans and β-iodomethacrolein (**90**) undergo Mukaiyama additions with much more diastereocontrol than simpler α,β-unsaturated aldehydes (*e.g.* crotonaldehyde, cinnamic aldehyde). In the presence of BF_3 etherate, (trimethylsiloxy)furans like compound **81** add to β-iodomethacrolein with > 99% *lk*-selectivity to furnish compounds like *lk*-**91**. Using $ZnBr_2$ as a promoter, the same reactants display an opposite 87 : 13 *ul*-preference. This also makes compound *ul*-**91** accessible as a single isomer (after chromatographic separation). Each of the aldol adducts *lk*- and *ul*-**91** was coupled with 3-ethynylfuran under Pd(0) catalysis (→ *lk*- and *ul*-**92**, respectively).

To our consternation, the *anti*-eliminations *lk*-**92** → *Z*-**93** and *ul*-**92** → *E*-**93** did not yield even trace amounts of product when tried with the elsewhere successful triflic anhydride–pyridine mixture. On the other hand, eliminations with excess diethyl azodicarboxylate–excess PPh_3[48] were high-yielding (94% *Z*-**93**, 87% *E*-**93**) and *anti*-selective. Thus, natural freelingyne (*Z*-**93**) resulted as a 92 : 8 *Z* : *E*- and the unnatural isomer *E*-**93** as a 98 : 2 *E* : *Z*-mixture. Two other stereoselective syntheses of freelingyne are known. They stem from Katsumura *et al.*[49] and Negishi and Liu[50] and are based upon the palladolactonization of a C≡C-containing carboxylic acid followed by a protonolysis of the resulting palladium–carbon bond.

The γ-alkylidenebutenolide syntheses compiled in Schemes 26–29 differ from those collected in Schemes 18–25 since now the $C^{\alpha'}$=C^{γ} bonds are formed through Brønsted (TsOH, HOAc/Δ) or Lewis acid (AgF) mediated β-eliminations. Using the Mukaiyama precursors as diastereomeric mixtures, only the E1-like elimination/fragmentation **96** → *Z*-**97** (Scheme 26) was selective. It furnished, through a subsequent benzoylation, melodorinol (*Z*-**99**).

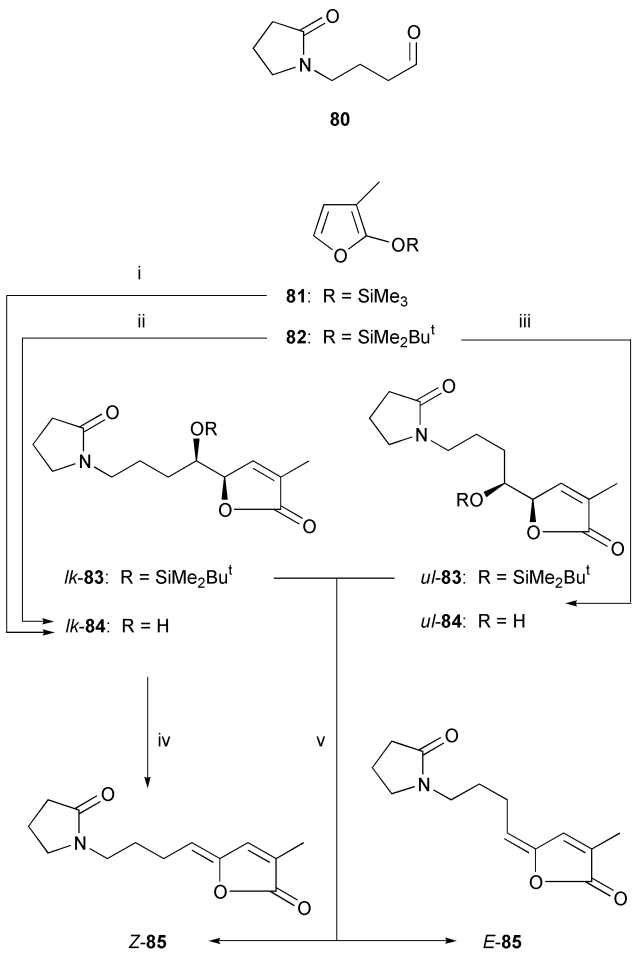

Scheme 23[45] *Reagents*: i, **80**, BF_3·OEt_2, 80% (*lk*-**84** : *ul*-**84** = 88 : 12); ii, **80**, BF_3·OEt_2, 48% **84** (*lk*-**84** : *ul*-**84** = 97 : 3) + 20% recovered **80**; iii, **80**, $Bu_4N^+F^-$ (10 mol%), Bu^tMe_2SiOTf, 37% **83** (*ul*-**83** : *lk*-**83** = 70 : 30) + 11% **84** (*ul*-**84** : *lk*-**84** = 70 : 30); iv, diethyl azodicarboxylate, PPh_3, 82%; v, DBU, 92% (*Z*-**85** : *E*-**85** = 90 : 10).

β-Elimination from a differently prepared γ-(α-hydroxyalkyl)butenolide

Our most recent approach to alkylidenebutenolides is presented in Scheme 30.[54] It is conceptually novel, remarkably stereoselective and, as far as the variablity of the substituents is concerned, potentially versatile. Therefore, it looks promising for an analogously shaped synthesis of peridinin (*Z*-**18a**). The latter is currently being pursued in these laboratories in collaboration with Professor de Lera (Universidade de Vigo, Spain). Peridinin plays a key role in the photosynthesis of marine algae.[6]

The starting point of Scheme 30 is the racemic trihalodiene **109**. So far, its 8-step synthesis[54] from the iodomethacrolein **90** is superior to potential short-cuts. Compound **109** was elaborated with a high degree of regio- and stereocontrol into the target butenolide **116**. First, it underwent a selective Suzuki coupling with the phenyl-substituted vinylboronic acid **110** at the less hindered C=C(–H)–I terminus—for steric and bond-energy reasons. Monocoupling product **111** was isolated in 56% yield. Under the same conditions, but using only 3% $Pd(PPh_3)_4$ rather than 5% as previously, compound **111** underwent a second Suzuki-coupling. Its reaction partner was now the ate-complex formed from the cyclohexyl-substituted vinylboronic acid **112** and aqueous NaOH. According to Roush *et al.*,[55] β-alkyl-*gem*-dibromoolefins undergo Suzuki couplings site-selectively with their *E*–C–Br bond. In agreement with that, we isolated the desired *Z*-configured monobromoolefin **113** in 79% yield. It was converted by Br/Li exchange into an organolithium compound. The latter was quenched by dropwise addition to an excess of neat ethyl chloroformate. This provided ethyl ester **114**. Upon exposure to HCl, the acetonide ring was cleaved and

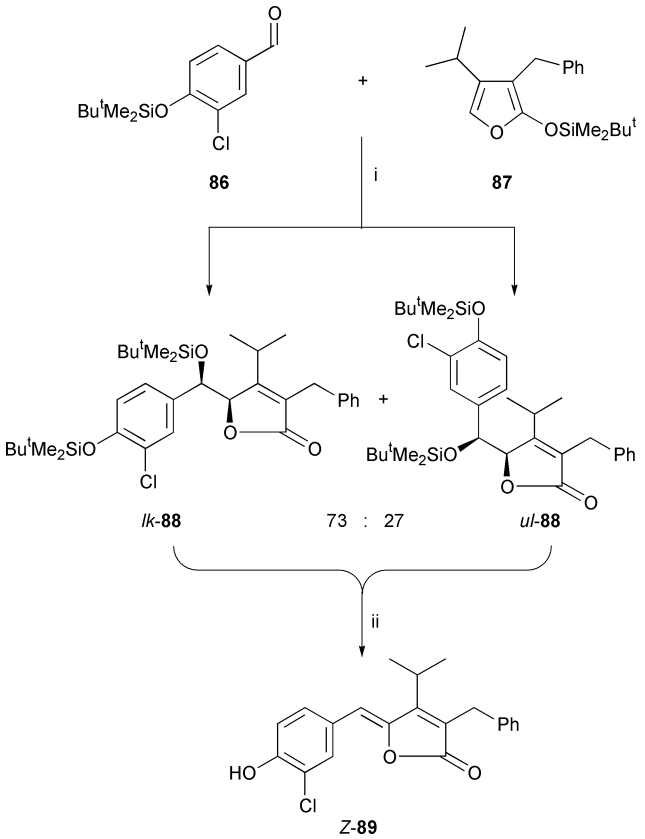

Scheme 24[46] *Reagents*: i, Bu^tMe_2SiOTf (0.5 equiv.), CH_2Cl_2, 93% of the mixture; ii, DBU, $CHCl_3$; HCl, 96%.

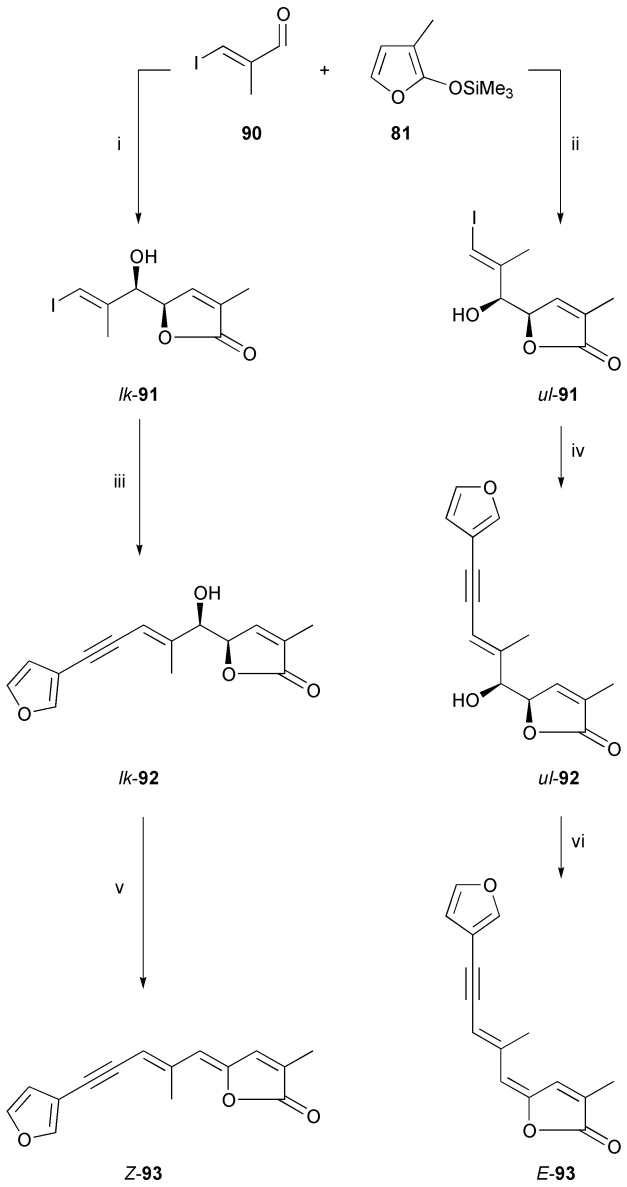

Scheme 25[47] *Reagents*: i, $BF_3{\cdot}OEt_2$–**90**–**81** 1 : 1 : 1, CH_2Cl_2, 56% (*lk*-**91** : *ul*-**91** > 99 : 1); ii, $ZnBr_2$–**90**–**81** 1 : 1 : 1, CH_2Cl_2, 61% (*ul*-**91** : *lk*-**91** = 87 : 13); iii, 3-ethynylfuran, $Pd(PPh_3)_4$, CuI, THF, iPr_2NEt, 70%; iv, same as (iii), 76%; v, diethyl azodicarboxylate, PPh_3, THF, 94% (*Z*-**93** : *E*-**93** = 92 : 8); vi, same as (v), 87% (*E*-**93** : *Z*-**93** = 98 : 2).

a spontaneous lactonization provided the γ-(α-hydroxyalkyl)-butenolide **115**. Its *anti*-selective dehydration was effected by treatment with excess PPh_3 and diethyl azodicarboxylate, *i.e.* by the established protocol of the dehydrations *lk*-**92** → free-lyngine (*Z*-**93**; Scheme 25) and *lk*-**84** → pandamarilactam-3y (*Z*-**85**, Scheme 23). In this way, we obtained butenolide **116** in 94% yield as a 95 : 5 *Z* : *E* mixture or, after recrystallization, in 90% yield as a pure isomer.

Other accesses to γ-alkylidenebutenolides

The best alternative to making *Z*-configured γ-alkylidenebutenolides by the β-elimination route of Scheme 1 is the metallocyclization/protonolysis strategy of Scheme 31. It has been pushed forward in recent years by the combined efforts of the Negishi, Rossi, and other groups.[31,32,35,38,49,50,56]

A reliable route to the less stable alkylidenebutenolides *E*-**119**, except the β-elimination route described, has yet to be developed. It seems conceivable, though, that the strategy of Scheme 32 could work. It represents a tandem metallocyclization/C,C-coupling approach and would start from pentenynoic acids **120** and unsaturated halides or triflates. While itself

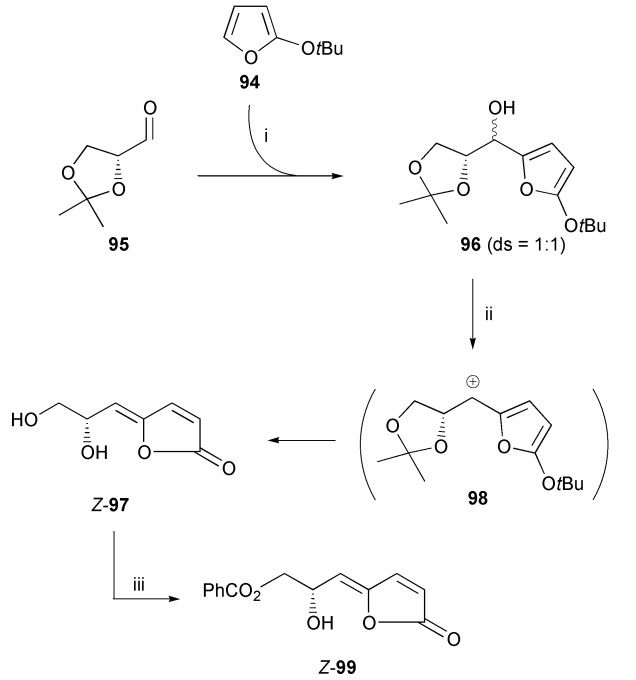

Scheme 26[51] *Reagents*: i, Bu^{t}Li, **94**, THF, addition of **95**, 69%; ii, $TsOH{\cdot}H_2O$, THF, H_2O, 74%; iii, PhC(=O)CN, NEt_3, THF, 54%.

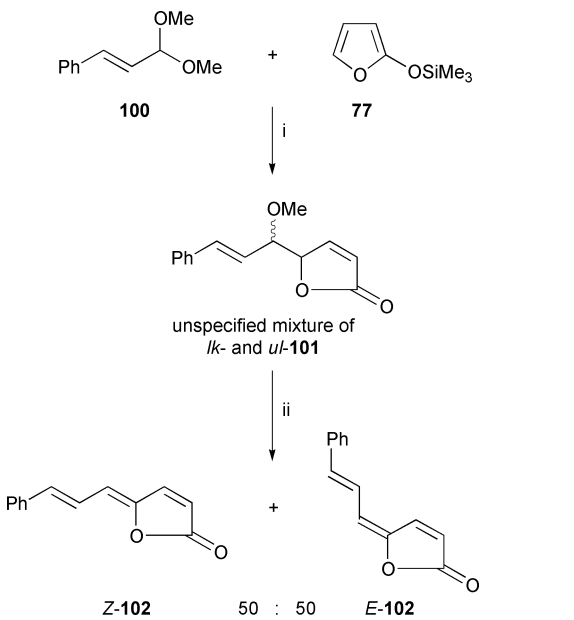

Scheme 27[52] *Reagents*: i, $TiCl_4$; ii, KOAc, HOAc, 80% over the two steps.

apparently unexplored, an analogous formation of *E*-configured γ-alkylidenebutanolides from pentynoic acids and aryl,[57] alkenyl,[58] or alkynyl halides (triflates) has been described.[59]

Notes and references

1 Reviews: Y. S. Rao, *Chem. Rev.*, 1976, **76**, 625; G. Pattenden, *Progr. Chem. Nat. Prod.*, 1978, **35**, 133; D. W. Knight, *Contemp. Org. Synth.*, 1994, **1**, 287; E.-i. Negishi and M. Kotora, *Tetrahedron*, 1997, **53**, 6707.

2 H. Baer, M. Holden and B. C. Seegal, *J. Biol. Chem.*, 1946, **162**, 65.

3 D. Kuhnt, T. Anke, H. Besl, M. Bross, R. Herrmann, U. Mocek, B. Steffan and W. Steglich, *J. Antibiot.*, 1990, **43**, 1413.

4 First isolation: F. Schütt, *Ber. Dtsch. Bot. Ges.*, 1890, **8**, 9. Constitution: H. H. Strain, W. A. Svec, K. Aitzetmüller, M. C. Grandolfo, J. J. Katz, H. Kjøsen, S. Norgård, S. Liaaen-Jensen, F. T. Haxo, P. Wegfahrt and H. Rapoport, *J. Am. Chem. Soc.*, 1971, **93**, 1823; H. H. Strain, W. A. Svec, P. Wegfahrt, H. Rapoport, F. T. Haxo, S. Norgård, H. Kjøsen and

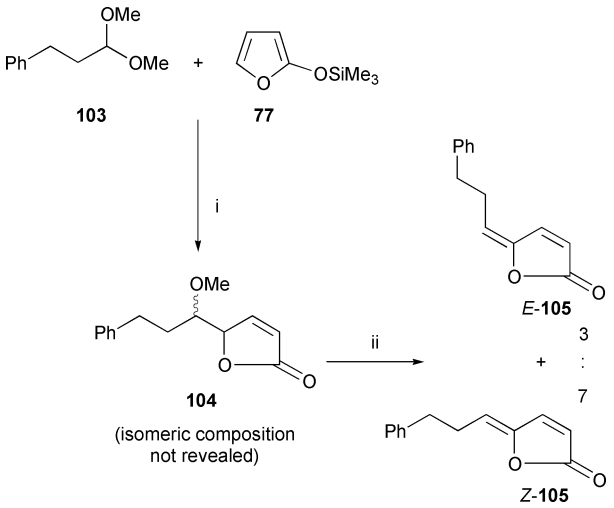

Scheme 28[43] *Reagents*: i, **103**:**77** 1:1.2, $SnCl_4$, CH_2Cl_2; aqueous HCl, 92%; ii, NaOAc, HOAc, 80%.

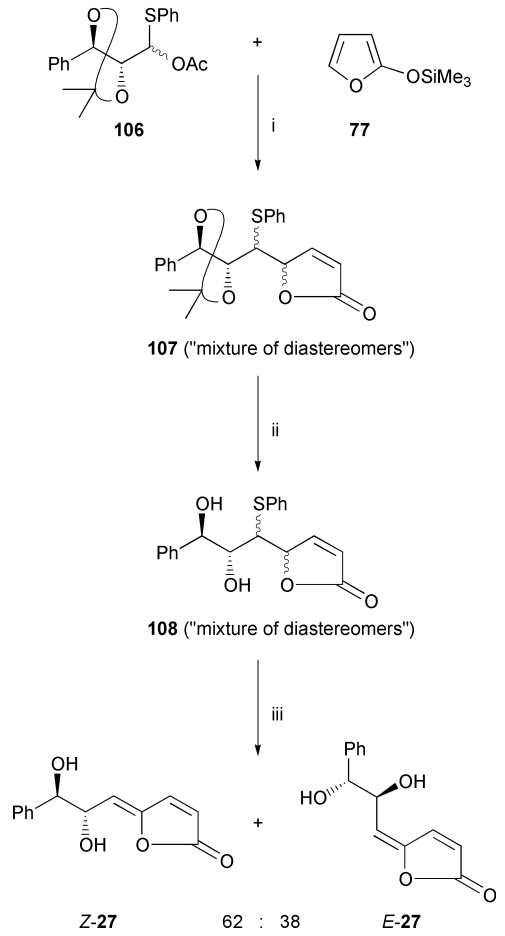

Scheme 29[53] *Reagents*: i, $SnCl_4$, CH_2Cl_2, 39–52% **107** (+ 7–15% **108** + 4% **27** as a *Z*,*E* mixture); ii, $F_3C–CO_2H$, H_2O, 84%; iii, AgF, pyridine, 68%.

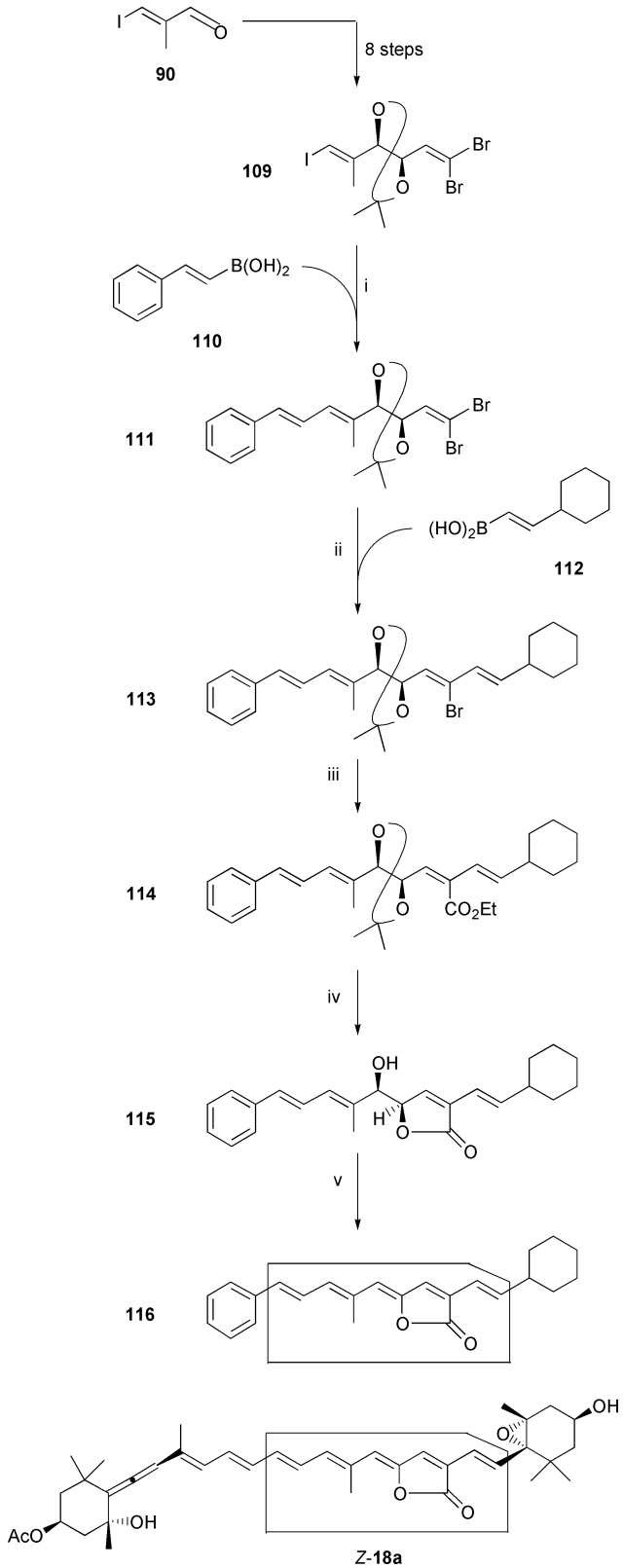

Scheme 30[54] *Reagents and conditions*: i, $Pd(PPh_3)_4$, benzene, **116**; addition of **117**, aqueous NaOH, 56%; ii, $Pd(PPh_3)_4$, toluene, **118**; addition of **119**, aqueous NaOH, 79%; iii, Bu^tLi, Et_2O; addition to pure $ClCO_2Et$, 70%; iv, aqueous HCl, MeOH, 71%; v, PPh_3, THF; addition of diethyl azodicarboxylate, 90% after separation from 4% of the *E*-isomer.

S. Liaaen-Jensen, *Acta Chem. Scand. B*, 1976, **30**, 109. Configuration: J. E. Johansen, G. Borch and S. Liaaen-Jensen, *Phytochemistry*, 1980, **19**, 441.

5 First isolation: A. R. Loeblich and V. E. Smith, *Lipids*, 1968, **3**, 5. Reisolation and constitutional assignment: J. E. Johansen, W. A. Svec, S. Liaaen-Jensen and F. T. Haxo, *Phytochemistry*, 1974, **13**, 2261. Reisolation and configurational assignment: T. Aakermann and S. Liaaen-Jensen, *Phytochemistry*, 1992, **31**, 1779.

6 E. Hofmann, P. M. Wrench, F. P. Sharples, R. G. Hiller, W. Welte and K. Diederichs, *Science*, 1996, **272**, 1788.

7 Leading references: R. G. Hiller, *Adv. Photosynth.*, 1999, **8**, 81; P. Horton, A. V. Ruban and A. J. Young, *Adv. Photosynth.*, 1999, **8**, 271; H. Paulsen, *Adv. Photosynth.*, 1999, **8**, 123; T. Pullerits and V. Sundstroem, *Acc. Chem. Res.*, 1996, **29**, 381; A. Adronov and J. M. J. Fréchet, *Chem. Commun.*, 2000, 1701. Model study with a modified peridinin: A. Osuka and T. Kume, *Tetrahedron Lett.*, 1998, **39**, 655.

8 Syntheses of protoanemonin: S. Tsuboi, H. Wada, S. Mimura and A. Takeda, *Chem. Lett.*, 1987, 937; I. Iovel, Y. Gol'dberg and M. Shimanska, *J. Chem. Soc., Chem. Commun.*, 1990, 1079; R. Alibes, J. Font, A. Mula and R. M. Ortuno, *Synth. Commun.*, 1990, **20**, 2607.

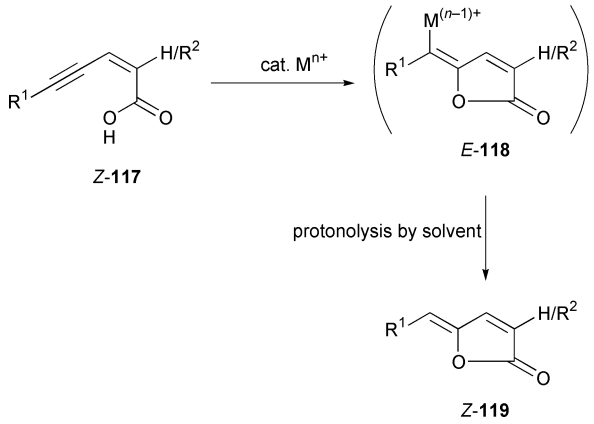

Scheme 31 *Z*-Selective generation of γ-alkylidenebutenolides by the metalolactonization of enynecarboxylic acids followed by protonolysis of the metalolactone.

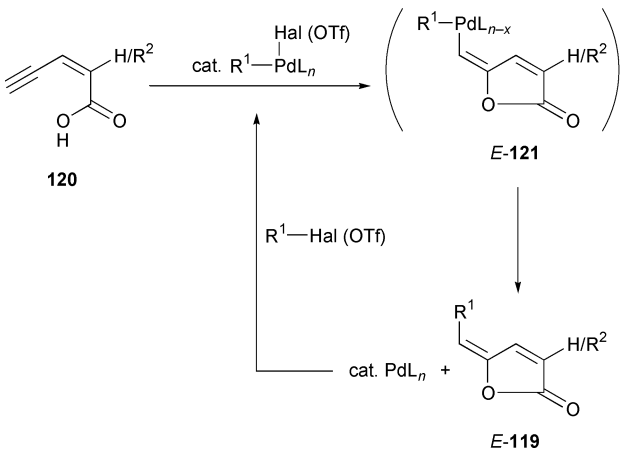

Scheme 32 Suggested *E*-selective generation of γ-alkylidenebutenolides by the metalolactonization of pentenynoic acids followed by reductive elimination.

9 J. Boukouvalas and F. Maltais, *Tetrahedron Lett.*, 1995, **36**, 7175.
10 L. Sun, Y. Tu and W. Xia, *Synth. Commun.*, 1998, **28**, 3751.
11 In addition, α-hydroxy-γ-(alkylidene)butenolides have attracted a great deal of synthetic interest recently due to P. Langer and M. Stoll, *Angew. Chem.*, 1999, **111**, 1919; *Angew. Chem., Int. Ed*, 1999, **38**, 1803; P. Langer, T. Schneider and M. Stoll, *Chem. Eur. J.*, 2000, **6**, 3204; P. Langer and T. Eckardt, *Synlett*, 2000, 844; P. Langer, T. Eckardt and M. Stoll, *Org. Lett.*, 2000, **2**, 2991. Yet, these compounds do not figure in the present account since they contain a heteroatom substituent at C^{α} (which has been exchanged for a methyl or a phenyl substituent *via* the corresponding enol triflate: P. Langer and N. N. R. Saleh, *Org. Lett.*, 2000, **2**, in print). I am grateful to Professor Langer for sending me advance copies of these manuscripts.
12 A. Umland, Diplomarbeit, Universität Göttingen, 1996; K. Siegel, Diplomarbeit, Universität Göttingen, 1997; F. v. d. Ohe, Diplomarbeit, Universität Göttingen, 1997.
13 J. Font, R. M. Ortuño, F. Sánchez-Fernando, C. Segura and N. Terris, *Synth. Commun.*, 1989, **19**, 2977.
14 S. Rousset, J. Thibonnet, M. Abarbri, A. Duchêne and J.-L. Parrain, *Synlett*, 2000, 260.
15 Y. Yamano and M. Ito, *J. Chem. Soc., Perkin Trans. 1*, 1993, 1599.
16 The synthetic chemistry of aldonolactones has been reviewed by R. M. de Lederkremer and O. Varela, *Adv. Carbohydr. Chem. Biochem.*, 1994, **50**, 125.
17 H. Itoh, *Noguchi Kenkyuscho Jiho*, 1984, 15 (cited from *Chem. Abs.* 1986, **104**, 168723c).
18 C. Di Nardo, O. Varela, R. M. Lederkremer, R. F. Baggio, D. R. Vega and M. T. Garland, *Carbohydr. Res.*, 1995, **269**, 99.
19 C. Di Nardo, L. O. Jeroncic, R. M. de Lederkremer and O. Varela, *J. Org. Chem.*, 1996, **61**, 4007.
20 L. O. Jeroncic, O. J. Varela, A. F. Cirelli and R. M. de Lederkremer, *Tetrahedron*, 1984, **40**, 1425.
21 D. Horton, J. K. Thomson, O. Varela, A. Nin and R. M. de Lederkremer, *Carbohydr. Res.*, 1989, **193**, 49.
22 T. K. M. Shing, H.-C. Tsui and Z.-H. Zhou, *J. Org. Chem.*, 1995, **60**, 3121.
23 M. A. Khan and H. Adams, *Synthesis*, 1995, 687.
24 F. C. Görth, A. Umland and R. Brückner, *Eur. J. Org. Chem.*, 1998, 1055.
25 G. J. F. Chittenden, J. A. J. M. Vekemans, J. Boerekamp and E. F. Godefroi, *Recl. Trav. Chim. Pays-Bas*, 1985, 266.
26 C. Hubschwerlen, *Synthesis*, 1986, 962.
27 I. Kalvinsh, K.-H. Metten and R. Brückner, *Heterocycles*, 1995, **40**, 939.
28 F. Görth and R. Brückner, *Synthesis*, 1999, 1520.
29 J. A. J. M. Vekemans, C. W. M. Dapperens, R. Claessen, A. M. J. Koten and E. F. Dodfroi, *J. Org. Chem.*, 1990, **55**, 5336.
30 I. Lundt and C. Pederssen, *Synthesis*, 1992, 669.
31 R. Rossi, F. Bellina, M. Biagetti and L. Mannina, *Tetrahedron Lett.*, 1998, **39**, 7799.
32 C. Xu and E.-i. Negishi, *Tetrahedron Lett.*, 1999, **40**, 431.
33 'Tetrenolin': G. G. Gallo, C. Coronelli, A. Vigevani and G. C. Lancini, *Tetrahedron*, 1969, **25**, 5677; H. Pagani, G. Lancini, G. Tamoni and C. Coronelli, *J. Antibiot.*, 1973, **26**, 1; lissoclinolide: B. S. Davidson and C. M. Ireland, *J. Nat. Prod.*, 1990, **53**, 1036.
34 K. Siegel and R. Brückner, *Chem. Eur. J.*, 1998, **4**, 1116; D. Kuhnt, T. Anke, H. Besl, M. Bross, R. Herrmann, U. Mocek, B. Steffan and W. Steglich, *J. Antibiot.*, 1990, **43**, 1413.
35 R. Rossi, F. Bellina, A. Catanese, L. Mannina and D. Valensin, *Tetrahedron*, 2000, **56**, 479
36 K. Siegel and R. Brückner, *Synlett*, 1999, 1227.
37 J. A. J. M. Vekemans, G. A. M. Franken, C. W. M. Dapperens and E. F. Godefroi, *J. Org. Chem.*, 1988, **53**, 627.
38 E.-i. Negishi, A. Alimardanov and C. Xu, *Org. Lett.*, 2000, **2**, 65.
39 Reviews: (*a*) G. Casiraghi and G. Rassu, *Synthesis*, 1995, 607; (*b*) G. Rassu, F. Zanardi, L. Battistini and G. Casiraghi, *Synlett*, 1999, 1333; (*c*) Cf. also J. Jurczak, E. Kobrzycka and J. Raczko, *Polish J. Chem.*, 1999, **73**, 29.
40 M. Pohmakotr, P. Tuchinda, P. Premkaisorn and V. Reutrakul, *Tetrahedron*, 1998, **54**, 11 297.
41 F. Bohlmann and C. Zdero, *Chem. Ber.*, 1966, **99**, 1226.
42 M. Pohmakotr, P. Tuchinda, P. Premkaisorn, A. Limpongpan and V. Reutrakul, *Heterocycles*, 1999, **51**, 795.
43 M. Asaoka, N. Yanagida, K. Ishibashi and H. Takei, *Tetrahedron Lett.*, 1981, **22**, 4269.
44 F. v. d. Ohe and R. Brückner, *New J. Chem.*, 2000, 659.
45 H. Takayama, T. Kuwajima, M. Kitajima, M. G. Nonato and N. Aimi, *Heterocycles*, 1999, **50**, 75
46 J. Boukouvalas, F. Maltais and N. Lachance, *Tetrahedron Lett.*, 1994, **35**, 7897.
47 F. von der Ohe and R. Brückner, *Tetrahedron Lett.*, 1998, **39**, 1909.
48 Procedure: R. H. Bradbury and K. A. M. Walker, *J. Org. Chem.*, 1983, **48**, 174.
49 H. Mori, H. Kubo, H. Hara and S. Katsumura, *Tetrahedron Lett.*, 1997, **38**, 5311.
50 F. Liu and E.-i. Negishi, *J. Org. Chem.*, 1997, **62**, 8591.
51 C.-C. Shen, S.-C. Chou and C.-J. Chou, *Tetrahedron: Asymmetry*, 1996, **7**, 3141.
52 D. Xu and K. B. Sharpless, *Tetrahedron Lett.*, 1994, **35**, 4685.
53 S. Y. Ko and J. Lerpiniere, *Tetrahedron Lett.*, 1995, **36**, 2101.
54 I. Hanisch and R. Brückner, *Synlett*, 2000, 374.
55 W. R. Roush, B. B. Brown and S. E. Drozda, *Tetrahedron Lett.*, 1988, **29**, 3541; W. R. Roush, K. J. Moriarty and B. B. Brown, *Tetrahedron Lett.*, 1990, **31**, 6509.
56 M. Yamamoto, *J. Chem. Soc., Perkin Trans. 1*, 1981, 582; X. Lu, X. Huang and S. Ma, *Tetrahedron Lett.*, 1993, **34**, 5963; M. Kotora and E.-i. Negishi, *Tetrahedron Lett.*, 1996, **37**, 9041; M. Kotora and E.-i. Negishi, *Synthesis*, 1997, 121.
57 See, for example: L. B. Wolf, K. C. M. Tjen, F. P. J. T. Rutjes, H. Hiemstra and H. E. Schoemaker, *Tetrahedron Lett.*, 1999, **39**, 5081.
58 See, for example: A. Arcadi, A. Burini, S. Cacchi, M. Delmastro, F. Marinelli and B. R. Pietroni, *J. Org. Chem.*, 1992, **57**, 976.
59 See, for example: D. Bouyssi, J. Gore and G. Balme, *Tetrahedron Lett.*, 1992, **33**, 2811.

ChemComm

Palladium-catalysed isomerisation of vinyldisilanes to allyldisilanes

David M. Hodgson,* Sarah F. Barker, Laura H. Mace and Julian R. Moran

Dyson Perrins Laboratory, Department of Chemistry, University of Oxford, South Parks Road, Oxford, UK OX1 3QY. E-mail: david.hodgson@chem.ox.ac.uk

Received (in Liverpool, UK) 19th October 2000, Accepted 27th November 2000
First published as an Advance Article on the web 21st December 2000

The isomerisation of vinyldisilanes 1 to allyldisilanes 2 catalysed by palladium-on-carbon in diethyl ether under hydrogen is described.

Three principle aspects of allylsilane chemistry have contributed to the tremendous utility of allylsilanes in organic synthesis.[1] Firstly, a variety of methods are available for preparing the allylsilane group with high regio- and stereocontrol.[2] Secondly, the allylsilane group is stable to many commonly used reagents, thus allowing the group to be carried through many synthetic sequences unchanged. Thirdly, is the ability of allylsilanes to act as allyl anion equivalents with a range of electrophiles (intramolecular C–C bond formation is particularly useful), generally with high and predictable stereo- and regio-control in the product alkene. Allyldisilanes **2** might be anticipated to possess broadly similar attributes to allylsilanes for use in synthesis. In contrast to allylsilanes however, allyldisilanes **2** are a relatively unexplored class of materials. A deterrent to investigating their chemistry is the lack of concise, general methods available for their preparation, particularly under mild conditions. Lautens and co-workers have developed a six step sequence to allyldisilanes from propargylic alcohols,[3] and Pornet *et al.* have reported a specific synthesis of the simplest allyldisilane [3,3-bis(trimethylsilyl)prop-1-ene] in two steps from 3-(trimethylsilyl)prop-1-yne.[4] The synthetic potential of allyldisilanes is indicated by observations from both Lautens and Pornet that disilylpropenes react with electrophiles (aldehydes and iminium ions) to give *trans*-vinylsilanes.

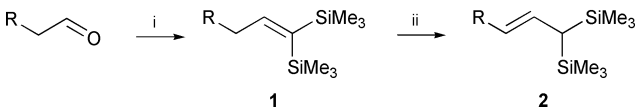

Scheme 1 *Reagents and conditions*: i, $Br_2C(SiMe_3)_2$, $CrCl_2$, DMF, 25 °C, 24 h; ii, see text.

We recently reported a one step highly chemoselective method for the preparation of vinyldisilanes **1** from aldehydes (Scheme 1).[5] During our investigations into the synthetic applications of vinyldisilanes,[5,6] we attempted debenzylation of lactam **3** using Pearlman's catalyst which, however, suprisingly generated the *trans*-allyldisilane **4** in an unoptimised 47% yield (Scheme 2). We communicate here our preliminary results concerning the development of this unusual isomerisation for the synthesis of allyldisilanes **2**.

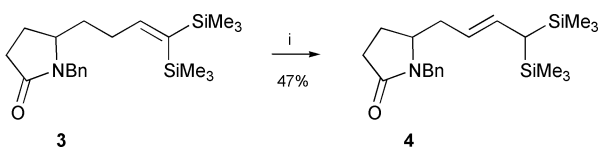

Scheme 2 *Reagents and conditions*: i, 20% Pd)$OH)_2$/C, H_2 (1 atm.), AcOH, 25 °C, 12 h.

Double-bond migrations can occur during homogeneous or heterogeneous hydrogenation to an extent which is profoundly affected by the catalyst used (palladium catalysts being particularly active during heterogeneous hydrogenation),[7] but in many cases the process is not noticeable in the reduced product. Isomerisation of isolated olefins to allylsilanes has been reported under homogeneous catalysis by Matsuda and co-workers using cationic rhodium or iridium catalysts pre-activated with H_2.[8] Also, Mori *et al.* have recently reported the isomerisation of isolated olefins to allyl bis-metalated [$(SnR_3)_2$ and SnR_3/SiR'_3] compounds (formed as 1:1, *cis–trans* mixtures) using $RuClH(CO)(PPh_3)_3$.[9] However, application of Matsuda's conditions {using [Rh(norbornadiene)(dppb)]BF_4} or Mori's conditions to simple vinyldisilanes failed to generate any isomerisation and therefore our attention focused on the heterogeneous process. Initial experiments with Pearlman's catalyst under the original conditions using vinyldisilane **5** established that the presence of H_2 was essential for reaction to proceed, but that incomplete isomerisation was observed and reduction to the disilane **7** was a significant competing reaction (Scheme 3).

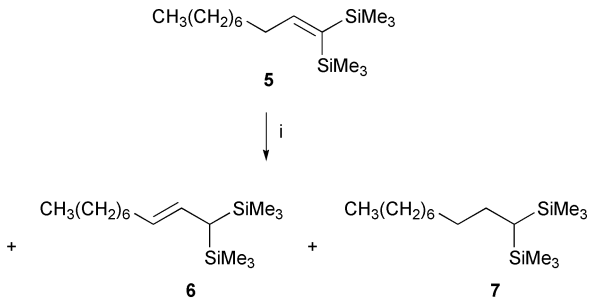

solvent	time	5 : 6 : 7
AcOH	4 h	18 : 61 : 21
hexane	2 h	0 : 24 : 76
CH_2Cl_2	3 h	3 : 88 : 9
Et_2O	2 h	6 : 87 : 7

Scheme 3 *Reagents and conditions*: i, 20% $Pd(OH)_2$/C, H_2 (1 atm.), solvent, 25 °C.

Although a number of different reaction variables with Pearlman's catalyst in acetic acid (and also 10% Pd/C in EtOH) were investigated for the isomerisation of vinyldisilane **5** to allyldisilane **6** (temperature, time, catalyst pre-activation, stirring and not stirring), the most notable variations were obtained by varying the solvent (Scheme 3), which is known to have a large influence on the extent of double bond migration.[7] For Pearlman's catalyst, hexane produced mainly reduction, whereas moving to DCM or ether resulted in a very encouraging ratio of isomerised to reduced material after 2–3 h (the proportion of reduced material increased at longer reaction times). Within the scope of the present study, 10% Pd/C in ether was found to give the best results (Table 1): complete conversion of vinyldisilane **5** to *trans*-allyldisilane **6** and (chromatographically inseparable) disilane **7** (94:6 respectively, 94% yield of allyldisilane **6**). These conditions also successfully isomerised other vinyldisilanes to allyldisilanes: **8** to **9** (88%) and **10** to **11** (91%), for which hydrogenated disilane was also observed at similarly low levels (6 and 7% respectively).

Reaction of vinyldisilane **5** using 10% Pd/C in ether under D_2 instead of H_2 gave allyldisilane **6** for which the ^1H NMR

DOI: 10.1039/b008565k

Table 1 Synthesis of allyldisilanes using 10% Pd/C, H_2 (1 atm.), Et_2O, 25 °C, 1.5 h

Vinyldisilane[5]	Allyldisilane	Yield (%)[a]
$CH_3(CH_2)_6$, $SiMe_3$, $SiMe_3$ **5**	$CH_3(CH_2)_6$, $SiMe_3$, $SiMe_3$ **6**	94
$MeO_2C(CH_2)_3$, $SiMe_3$, $SiMe_3$ **8**	$MeO_2C(CH_2)_3$, $SiMe_3$, $SiMe_3$ **9**	88
$HO(CH_2)_4$, $SiMe_3$, $SiMe_3$ **10**	$HO(CH_2)_4$, $SiMe_3$, $SiMe_3$ **11**	91

[a] Hydrogenated disilane also observed (see text).

spectrum indicated that D had not been incorporated into either of the olefinic positions, but had been incorporated (51% by mass spectrometry) at the carbon atom bearing the two trimethylsilyl groups. One possible mechanistic sequence for the isomerisation consistent with this observation involves initial olefin coordination to palladium, followed by formation of a π-allylpalladium hydride which can undergo partial H/D exchange prior to hydride delivery selectively[3] to the more substituted end of the allylic system.

Density functional theory (DFT) calculations at the B3LYP/6-31+ G* level indicate that the vinyldisilane **1** (R = Et) is less stable than the allyldisilane **2** (R = Et) by 7.2 kJ mol^{-1} (a predicted ratio of 5:95 at 25 °C). The energy minimised structure for the vinyldisilane **1** (R = Et, Fig. 1) shows that the *cis* $SiMe_3$ group orients itself to minimize allylic strain (with the H of the allylic methylene that eclipses the double bond) at the expense of a 1,2-eclipsing interaction [Me–Si(*cis*)–C–Si(*trans*)]. In contrast, the *trans* $SiMe_3$ group has a relatively less demanding 1,3-allylic strain maximised (with the vinylic H) as this leads to the two $SiMe_3$ groups adopting a staggered arrangement of their Si–Me bonds with respect to each other. The 1,2-eclipsing interaction and allylic strain in vinyldisilane **1** (R = Et) could be the origin of its instability compared with the allyldisilane **2** (R = Et).

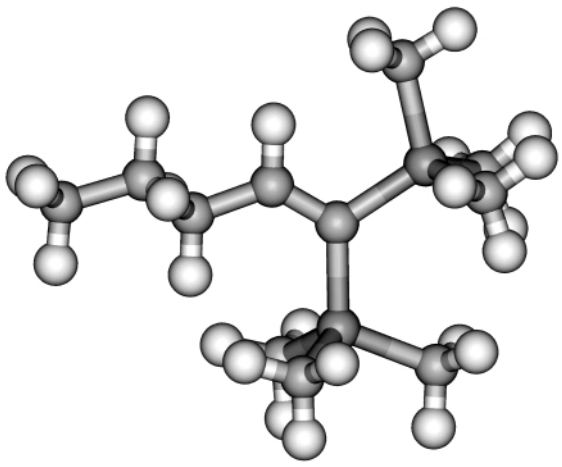

Fig. 1 The B3LYP/6-31+ G* optimised structure of vinyldisilane **1** (R = Et).

The energy minimised structure for the allyldisilane **2** (R = Et, Fig. 2) suggests that the presence of a $SiMe_3$ substitutent both above and below the plane of the double bond might retard (re)association with the catalyst and hence reduction; moreover, since the allylic H substituent [of $CH(SiMe_3)_2$] eclipses the C=C double bond it is now in an unfavourable orientation to reform the π-allylpalladium hydride suggested above.

As discussed earlier, Lautens and Pornet have shown that disilylpropenes undergo reactions with electrophiles. However,

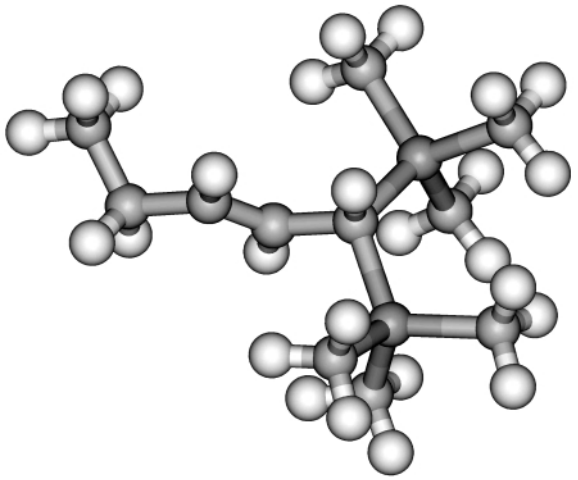

Fig. 2 The B3LYP/6-31+ G* optimised structure of allyldisilane **2** (R = Et).

Lautens and co-workers also observed that higher 1,1-disilylalk-2-enes failed to undergo reaction with aldehydes using a range of Lewis acids.[3] Nevertheless, we have preliminary evidence that such allyldisilanes can undergo synthetically useful reactions. For example, following the conditions of Ito *et al*. for acetalisation–intramolecular allylsilane cyclisation[10] gave, with allyldisilane **11** and benzaldehyde the *trans*-2,3-disubstituted oxepane **12** ($J_{C(2)H\text{-}C(3)H}$ = 10 Hz)[10] possessing a *trans*-vinylsilane moiety ($J_{CH=CHSi}$ = 19 Hz) for further synthetic elaboration (Scheme 4).

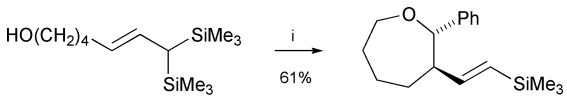

11 **12**

Scheme 4 *Reagents and conditions*: i, PhCHO (1.4 equiv.), TMSOTf (2 equiv.), CH_2Cl_2, −78 °C, 3.5 h.

In summary, we have developed an experimentally straightforward method for the synthesis of allyldisilanes from vinyldisilanes; this allows access to allyldisilanes in two steps from aldehydes and should better allow the potential of allyldisilanes in organic synthesis to be realised.

We thank Dr G. H. Grant (University of Oxford) for performing the DFT calculations, Dr J. M. Goodman (University of Cambridge) for useful discussions and the EPSRC National Mass Spectrometry Service Centre for mass spectra.

Notes and references

1 I. Fleming, A. Barbero and D. Walter, *Chem. Rev.*, 1997, **97**, 2063; Y. Yamamoto and N. Asao, *Chem. Rev.*, 1993, **93**, 2207; I. Fleming, J. Dunoguès and R. Smithers, *Org. React. (N.Y.)*, 1989, **37**, 57.
2 T. K. Sarkar, *Synthesis*, 1990, 969; *idem, ibid*, 1990, 1101.
3 M. Lautens and P. H. M. Delanghe, *Angew. Chem., Int. Ed. Engl.*, 1994, **33**, 2448; M. Lautens, R. N. Ben and P. H. M. Delanghe, *Tetrahedron*, 1996, **52**, 7221.
4 B. Princet, G. Anselme and J. Pornet, *Synth. Commun.*, 1999, **29**, 3329; B. Princet, H. Gardès-Gariglio and J. Pornet, *J. Organomet. Chem.*, 2000, **604**, 186.
5 D. M. Hodgson, P. J. Comina and M. G. B. Drew, *J. Chem. Soc., Perkin Trans. 1*, 1997, 2279.
6 D. M. Hodgson and P. J. Comina, *Chem. Commun.*, 1996, 755.
7 P. N. Rylander, *Hydrogenation Methods*, Academic Press, London, 1985.
8 I. Matsuda, T. Kato, S. Sato and Y. Izumi, *Tetrahedron Lett.*, 1986, **25**, 5747.
9 H. Wakamatsu, M. Nishida, N. Adachi and M. Mori, *J. Org. Chem.*, 2000, **65**, 3966.
10 M. Suginome, T. Iwanami and Y. Ito, *Chem. Commun.*, 1999, 2537.

ChemComm

Electronic effects in the thermal C^2–C^6 biradical cyclisation of enyne-allenes

Michael Schmittel* and Michael Maywald

FB 8 - OC1 (Chemie - Biologie), Universität GH Siegen, Adolf-Reichwein-Str., D-57068 Siegen, Germany. E-mail: schmittel@chemie.uni-siegen.de; Fax: +49-271-740-3270

Received (in Liverpool, UK) 19th September 2000, Accepted 29th November 2000
First published as an Advance Article on the web 4th January 2001

A comprehensive study on the influence of substituents at the alkyne terminus on the thermal biradical cyclisation of enyne-allenes shows a good agreement of the rates with $\sigma^{\cdot}$.

Although the cycloaromatisations of enediynes (Bergman)[1] and enyne-allenes (Myers–Saito)[2] play a fundamental role in the mode of action of the natural enediyne antitumor antibiotics[3] alternative thermal cyclisations with an altered regioselectivity have only been addressed recently. After the discovery of a novel cyclisation of enyne-allenes (C^2–C^6, see Scheme 1) in 1995,[4] this reaction has been studied extensively,[5] and ample evidence for the occurrence of the fulvene biradical **B**[2,6] has been collected through experimental[5f,6] and theoretical investigations.[7]

Moreover, the C^2–C^6 cyclisation has become a valuable synthetic tool for the construction of carbocyclic[8] and heterocyclic[9] ring systems as the intermediate biradical can undergo a second C–C bond formation followed by a formal 1,5-H shift to provide a convenient access to polyaromatic systems.

Engels *et al.*[7a] predicted on the basis of calculations that for **1** (Y,Z = H) the thermal C^2–C^6 cyclisation should be extremely accelerated with X = NH_2 in comparison to X = aryl, or ^{t}alkyl due to a special stabilisation of the biradical intermediate. In order to verify their prediction we decided to study the electronic effect of the substituent X in **1** on the thermal behaviour, which should also give some mechanistic insight in the polarity of the transition state. Herein, we describe the synthesis of the novel enyne-allenes **1a**–**f** and their kinetics.

The key step in the preparation of enyne-allenes **1a**–**f** is based on the rearrangement of the propargyl† alcohols[10] **2a**–**f** with $ClPPh_2$. (Scheme 2) Enyne-allenes **1a**–**f** were purified by low-temperature chromatography as far as possible, but their thermal instability precludes any elemental analysis. Some relevant IR and ^{1}H NMR data are presented in Table 1. Rapid cyclisation of **1f** even at rt prevented both isolation and a reliable kinetic analysis.

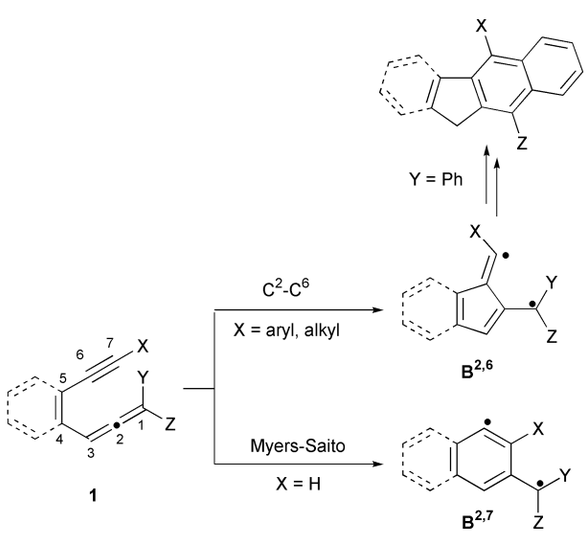

Scheme 1

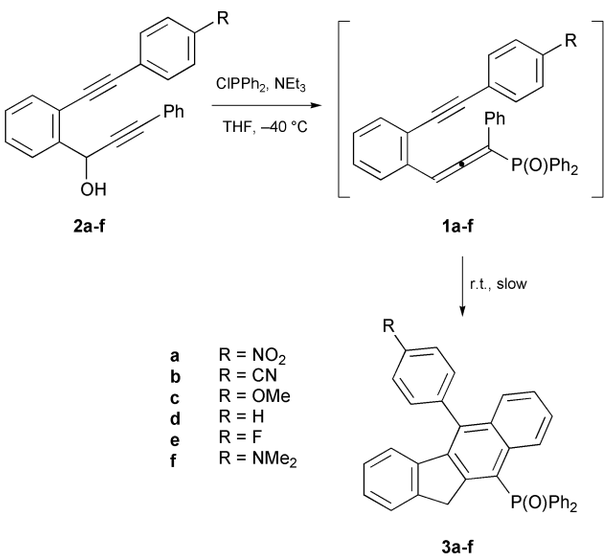

Scheme 2 The reaction of **2a**–**f** with $ClPPh_2$, first at −40 °C and then at rt, leads directly to benzofluorenes **3a**–**f** (**3a**: 42%, **3b**: 47%, **3c**: 62%; **3d**: 68%, **3e**: 31%, **3f**: 45%).

Table 1 The IR (allene, alkyne) and ^{1}H NMR data of the desired enyne-allenes **1a**–**f**

	1a	**1b**	**1c**	**1d**	**1e**
IR (allene)/cm^{-1}	1924	1924	1923	1908	1924
IR (alkyne)/cm^{-1}	2216	2199	2215	2212	2227
^{1}H NMR/ppm[a]	6.75	6.26	6.78	6.80	6.83

[a] Allenic proton showing characteristic doublet with J = 10.1–10.7 Hz.

For the kinetic analysis the enyne-allenes were cooled and subjected to three DSC (differential scanning calorimetry) investigations. This method allows the recording of kinetic data over a range of temperatures in a single experiment.[11] To ensure that we monitor indeed the C^2–C^6 cyclisation, product studies were conducted for both preparative and DSC thermolyses. As rate constants determined at very low and very high temperatures proved to be unreliable, we resigned to make an Eyring analysis. Hence, only the cyclisation onset temperatures, reaction rates in the central temperature range (at 50, 60 and 70 °C) and $\Delta G^{\neq}_{60°C}$ are provided in Table 2. Data for enyne-allene **1g** was added for comparison.[12]

According to the data in Table 2 the lowest cyclisation temperature is found for enyne-allene **1f** with R = NMe_2, which unfortunately could not be isolated. The most stable representative is **1e** with R = F. Quite obviously the cyclisation rate constants do not follow a simple picture with electron-withdrawing substituents on one side, and electron-donating substituents on the other.

For a more detailed discussion we will concentrate on the rate constants at 60 °C that constitute the most reliable data due to the form of the DSC curves. In the above analysis we find a rate acceleration of 2.6 (at 60 °C) when going from R = F to NO_2.

DOI: 10.1039/b007811p

Table 2 Kinetic data of enyne-allenes **1a**–**g** and various σ values[13] for comparison[a]

Enyne-allene R	**1a** NO_2	**1b** CN	**1c** OMe	**1d** H	**1e** F	**1f** NMe_2	**1g** Me
T_{DSC}/°C[b]	43	45	46	51	53	—	50
$k^{50°C}/s^{-1} \times 10^{-3}$	2.06 ± 0.46	1.42 ± 0.43	1.40 ± 0.10	0.86 ± 0.24	0.69 ± 0.05	3.07[c]	0.95[c]
$k^{60°C}/s^{-1} \times 10^{-3}$	5.65 ± 0.98	4.36 ± 1.04	4.23 ± 0.37	2.29 ± 0.49	2.13 ± 0.04	8.20[c]	2.54[c]
$k^{70°C}/s^{-1} \times 10^{-2}$	1.55 ± 0.21	1.22 ± 0.26	1.08 ± 0.08	0.59 ± 0.17	0.56 ± 0.05	2.11[c]	0.66[c]
$\Delta G^{\neq 60°C}$/kJ mol^{-1}	96.27	96.96	97.04	98.74	98.94	95.21[c]	98.46[c]
$\sigma^{\cdot}$	0.57	0.46	0.24	0	−0.08	0.90	0.11
σ_p	0.81	0.70	−0.28	0	0.15	−0.63	−0.14
σ_p^+	0.79	0.66	−0.78	0	−0.07	−1.70	−0.31
σ_p^-	1.27	1.00	−0.26	0	−0.03	−0.12	−0.17

[a] Measured by DSC. [b] Onset temperature in the DSC. [c] Calculated from the correlation of the rate constants with $\sigma^{\cdot}$ (see Fig. 1a).

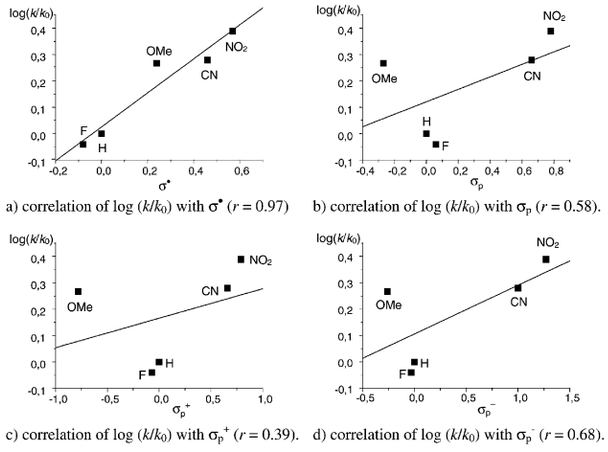

a) correlation of log (k/k_0) with $\sigma^{\bullet}$ (r = 0.97) b) correlation of log (k/k_0) with σ_p (r = 0.58).

c) correlation of log (k/k_0) with σ_p^+ (r = 0.39). d) correlation of log (k/k_0) with σ_p^- (r = 0.68).

Fig. 1 Correlation of the log (k/k_0)-values with the different substituent constants.[13]

Such accelerations are characteristic for radical reactions (2- up to 5-fold acceleration),[13] but much too low for reactions involving polar intermediates where the rates typically change over 2–7 orders of magnitude.

To further evaluate the data we correlated the log (k/k_H) values against the well-known substituent constants, $\sigma^{\cdot}$ (for radical reactions), and σ_p, σ_p^+ and σ_p^- (for polar reactions).[14]

The poor correlation with the polar substituent constants σ_p, σ_p^+ and σ_p^- (Fig. 1) clearly contradicts any polar intermediate in the thermal C^2–C^6 cyclisation, such as a zwitterion. On the contrary, a good correlation is obtained using $\sigma^{\cdot}$ values (reaction constant ρ = 0.643).[15] The latter correlation is strong support, together with earlier mechanistic evidence,[6] that the C^2–C^6 cyclisation is a biradical cyclisation. Moreover, it enables a good insight into the electronic structure of the transition state, as even *bona fide* radical reactions, but with a polar transition state, correlate with polar substituent constants, such as σ_p, σ_p^+ and σ_p^-.[13] Thence, the C^2–C^6 cyclisation of **1** proceeds *via* an extremely unpolar transition state (TS), in contrast to the Myers–Saito cyclisation, where the occurrence of unpolar and polar TS's is discussed.[16]

The reaction constant now allows us to predict the cyclisation rate and the free activation energy of **1f** and **1g** at various temperatures (Table 2). The higher rate constant for **1f** is in agreement with the fact that we have not been able to isolate it. The difference $\Delta\Delta G^{\neq 60°C}$ = −3.5 kJ mol^{-1} when going from R = H to R = NMe_2 is drastically smaller than predicted for **1** (no benzoannelation, Y,Z = H) upon changing from X = H to NH_2 ($\Delta\Delta G^{\neq 25°C}$ = −57 kJ mol^{-1}).[7a] Obviously, the substituent effect in our study is heavily attenuated because of the phenyl spacer between R and the alkynyl group.

In summary, the present study definitely rules out zwitterionic intermediates in the C^2–C^6 cyclisation and supports the biradical hypothesis. For the first time, a thermal biradical cyclisation was demonstrated to follow the radical substituent constant $\sigma^{\cdot}$. This finding is notable as calculations have as yet described the TS to contain no biradical character.[7]

We are indebted to the DFG, the Volkswagenstiftung and the Fonds der Chemischen Industrie for continued support. Additionally, we would like to thank Dr Kiau for providing the temperature onset for **1g**.

Notes and references

† The IUPAC name for propargyl is prop-2-ynyl.

1 R. B. Jones and R. G. Bergman, *J. Am. Chem. Soc.*, 1972, **94**, 660.
2 (*a*) R. Nagata, H. Yamanaka, E. Okazaki and I. Saito, *Tetrahedron Lett.*, 1989, **30**, 4995; (*b*) A. G. Myers, E. Y. Kuo and N. S. Finney, *J. Am. Chem. Soc.*, 1989, **111**, 8057.
3 (*a*) K. Edo, M. Mizugaki, Y. Koide, H. Seto, K. Furihata, N. Otake and N. Ishida, *Tetrahedron Lett.*, 1985, **26**, 331; (*b*) M. D. Lee, T. S. Dunne, M. M. Siegel, C. C. Chang, G. O. Morton and D. B. Borders, *J. Am. Chem. Soc.*, 1987, **109**, 3464; (*c*) K. C. Nicolaou and W.-M. Dai, *Angew. Chem., Int. Ed. Engl.*, 1991, **30**, 1387.
4 M. Schmittel, M. Strittmatter and S. Kiau, *Tetrahedron Lett.*, 1995, **36**, 4975.
5 (*a*) T. Gillmann, T. Hülsen, W. Massa and S. Wocadlo, *Synlett*, 1995, 1257; (*b*) J. G. Garcia, B. Ramos, L. M. Pratt and A. Rodríguez, *Tetrahedron Lett.*, 1995, **36**, 7391; (*c*) M. Schmittel, M. Strittmatter, K. Vollmann and S. Kiau, *Tetrahedron Lett.*, 1996, **37**, 999; (*d*) N. Krause and M. Hohmann, *Synlett*, 1996, 89; (*e*) M. Schmittel, S. Kiau, T. Siebert and M. Strittmatter, *Tetrahedron Lett.*, 1996, **37**, 7691; (*f*) M. Schmittel, J.-P. Steffen, D. Auer and M. Maywald, *Tetrahedron Lett.*, 1997, **38**, 6177.
6 (*a*) M. Schmittel, M. Strittmatter and S. Kiau, *Angew. Chem., Int. Ed. Engl.*, 1996, **35**, 1843; (*b*) M. Schmittel, M. Keller, S. Kiau and M. Strittmatter, *Chem. Eur. J.*, 1997, **3**, 807; (*c*) M. Schmittel, M. Maywald and M. Strittmatter, *Synlett*, 1997, 165.
7 (*a*) B. Engels, C. Lennartz, M. Hanrath, M. Schmittel and M. Strittmatter, *Angew. Chem., Int. Ed.*, 1998, **37**, 1960; (*b*) B. Engels and M. Hanrath, *J. Am. Chem. Soc.*, 1998, **120**, 6356; (*c*) P. R. Schreiner and M. Prall, *J. Am. Chem. Soc.*, 1999, **121**, 8615.
8 Ó. de Frutos and A. M. Echavarren, *Tetrahedron Lett.*, 1997, **38**, 7941; M. Alajarín, P. Molina and A. Vidal, *J. Nat. Prod.*, 1997, **60**, 747; M. Schmittel, J. P. Steffen and I. Bohn, *Heterocyclic Commun.*, 1997, **3**, 443; K. K. Wang, H. R. Zhang and J. L. Petersen, *J. Org. Chem.*, 1999, **64**, 1650.
9 (*a*) M. Schmittel, J.-P. Steffen, M. Á. Wencesla Ángel, B. Engels, C. Lennartz and M. Hanrath, *Angew. Chem., Int. Ed.*, 1998, **37**, 1562; (*b*) M. Schmittel, J.-P. Steffen, B. Engels, C. Lennartz and M. Hanrath, *Angew. Chem., Int. Ed.*, 1998, **37**, 2371; (*c*) C. Shi and K. K. Wang, *J. Org. Chem.*, 1998, **63**, 3517; (*d*) C. Shi, Q. Zhang and K. K. Wang, *J. Org. Chem.*, 1999, **64**, 925; (*e*) M. Schmittel, D. Rodríguez and J.-P. Steffen, *Angew. Chem., Int. Ed.*, 2000, **39**, 2152.
10 The synthesis of the propargyl alcohol is based on the Sonogashira coupling of the substituted phenylacetylene with *o*-bromobenzaldehyde followed by addition of aluminium phenylacetylide.
11 H. J. Borchardt and F. Daniels, *J. Am. Chem. Soc.*, 1957, **79**, 41.
12 S. Kiau, PhD thesis, Würzburg, 1997.
13 C. Hansch and H. Gao, *Chem. Rev.*, 1997, **97**, 2995.
14 (*a*) $\sigma^{\cdot}$: X. Creary, M. E. Mehrsheikh-Mohammadi and S. McDonald, *J. Org. Chem.*, 1987, **52**, 3254; (*b*) σ_p: D. H. McDaniel and H. C. Brown, *J. Org. Chem.*, 1958, **23**, 420; (*c*) σ_p^+: H. C. Brown and Y. Okamoto, *J. Am. Chem. Soc.*, 1958, **80**, 4979; (*d*) σ_p^-: C. Hansch, A. Leo and R. W. Taft, *Chem. Rev.*, 1991, **91**, 165.
15 The exact correlation: log (k/k_0) = 0.643 $\sigma^{\cdot}$ − 0.02484.
16 T. S. Hughes and B. K. Carpenter, *J. Chem. Soc., Perkin Trans. 2*, 1999, 2291.

ChemComm

Highly stereoselective addition to alkoxy or hydroxy ketones using an α-stannyl ester–stannous chloride system in a chelation-controlled manner

Makoto Yasuda, Keishi Okamoto, Toshifumi Sako and Akio Baba*

Department of Applied Chemistry, Faculty of Engineering, Osaka University, 2-1 Yamadaoka, Suita, Osaka 565-0871, Japan. E-mail: baba@ap.chem.eng.osaka-u.ac.jp

Received (in Cambridge, UK) 20th October 2000, Accepted 21st November 2000
First published as an Advance Article on the web 4th January 2001

The reaction of an α-stannyl ester with α-alkoxy or hydroxy ketones in the presence of $SnCl_2$ gave aldol-type products with high selectivity in a chelation-controlled manner.

Stereoselective C–C bond formation is undoubtedly important for organic syntheses. Since the transition state of the reaction concerned demands a rigid structure for a selective reaction, chelation of a substrate bearing coordinative sites to a metal center often has a significant effect on the stereoselectivity. A number of selective reactions under chelation-controlled conditions have been reported for carbonyl addition by carbon nucleophiles.[1] Reetz has developed chelation-controlled aldol-type addition to α-alkoxy aldehydes using enol silane in the presence of Lewis acids.[2] However, chelation-controlled addition of a metal enolate or its equivalent to α-alkoxy ketones is scarcely known in spite of the fascinating structure of the products which would be tertiary alcohols bearing a stereocontrolled *O*-substituent. This is probably because the reaction conditions required to achieve the addition to ketones, which are much less reactive than aldehydes, would be too severe to control the selectivity. In this communication, we report a highly diastereoselective addition of an ester enolate equivalent to α-alkoxy or hydroxy ketones using an α-stannyl ester–stannous chloride system in a chelation-controlled manner.

In the initial trials, we obtained moderate selectivities of diastereomers **2** and **3** in the reactions of α-alkoxy ketone **1** with a lithium enolate[3] or zinc enolate equivalent[4] [eqns. (1) and (2)]. These results prompted us to develop a novel system having high chelation ability.

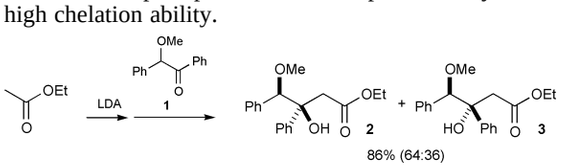

(1)

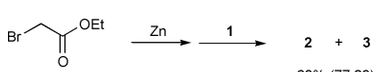

(2)

A stannyl nucleophile is often used for stereoselective organic synthesis.[5] Keck has reported chelation-controlled addition of allylic stannanes in the presence of $TiCl_4$.[6] We examined the reaction of α-stannyl ester **4** in the presence of metal halides, and the results are summarized in Table 1.

Table 1 Reaction of α-stannyl ester **4** with **1**[a]

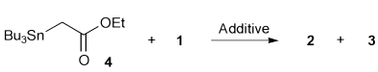

Entry	Additive	Solvent	Conditions	Yield (%)	Ratio of **2**:**3**
1	$TiCl_4$	CH_2Cl_2	−78 °C → rt, 3 h	7	—
2	$BF_3{\cdot}OEt_2$	CH_2Cl_2	−78 °C → rt, 3 h	< 5	—
3	$SnCl_2$	CH_2Cl_2	rt, 3 h	40	> 99 : 1
4	$SnCl_2$	MeCN	rt, 3 h	86	> 99 : 1

[a] All reactions were carried out in solvent (1 mL) using **4** (1.2 mmol), alkoxy ketone **1** (1.0 mmol), and additive (1.2 mmol).

However, the use of $TiCl_4$ as an additive gave a complicated mixture with a small amount of the aldol-type product which was confirmed in a crude reaction mixture by NMR (entry 1). In the presence of $BF_3{\cdot}OEt_2$ almost no reaction took place and the starting ketone was recovered (entry 2). Recently, we have reported a carbonyl addition system using α-stannyl ester or tributylallylic stannane with $SnCl_2$ in which transmetallation occurs to generate an active species.[7] This activation methodology successfully attained the stereoselective reaction of **4** with **1** in the presence of $SnCl_2$ to give the product in 40% yield with excellent selectivity (entry 3). Changing the solvent from CH_2Cl_2 to MeCN improved the yield while retaining high selectivity (86% yield, > 99 : 1, entry 4).†

The relative configuration of the stereochemistry of **2** was unambiguously determined by its X-ray analysis and the ORTEP drawing is shown in Fig. 1.‡ It corresponds to the product which is formed by chelation-controlled alkylation.

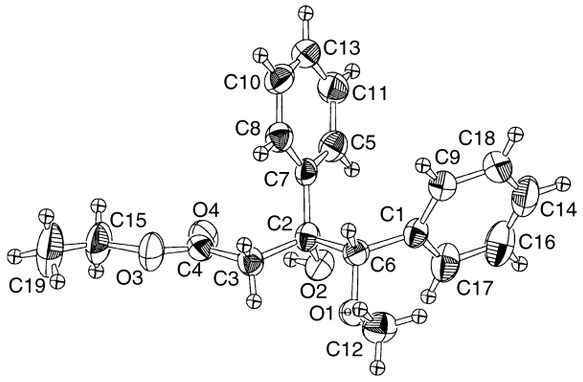

Fig. 1 Molecular structure of **2**.

Although the reaction mechanism is now not clear, we assume that the active species is chlorinated stannous ester **5** which is generated by transmetallation between **4** and $SnCl_2$ (Scheme 1). The metal center has high Lewis acidity and thus high chelation ability to alkoxy ketone. The carbonyl addition proceeds *via* transition states which direct the selective addition by chelation. In fact, a transmetallation was confirmed by the following experiment. A mixture of α-stannyl ester **4** and $SnCl_2$ in MeCN at room temp. gave 71% yield of Bu_3SnCl which was confirmed by ^{119}Sn NMR. A lower yield (16%) of Bu_3SnCl was observed when CH_2Cl_2 was used as a solvent. This significant solvent effect on the transmetallation accounts for the difference in yields in entries 3 and 4 (Table 1). Unfortunately, the signal

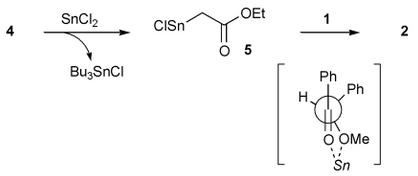

Scheme 1 Plausible path of chelation-controlled addition.

DOI: 10.1039/b008493j

corresponding to the generated nucleophilic tin(II) species was not detected probably because of its broadening in ^{119}Sn NMR.

Various alkoxy ketones were investigated and the results are shown in Table 2. The reaction with the α-ethoxy ketone **6** also gave the aldol product **7** in high selectivity and yield (entry 2). Even isopropoxy ketone **8**, which has a bulky substituent, was also subjected to this reaction system to afford **9** exclusively (entry 3). The reaction with 2-methoxypropiophenone **10** provided the selective aldol-reaction in >95:5 selectivity (entry 4). When the cyclic substrate **12** was used, **13** was selectively formed in a 92:8 ratio (entry 5). The relative configuration of the cyclic product **13** was determined by NOE experiment. The increased intensity at the carbonyl methylene protons was observed by irradiating the axial proton bonded to the methoxy-substituted carbon.

The chelation-controlled reaction using hydroxy carbonyl compounds without protection is a challenging problem because organometals for chelates are readily affected or quenched by the protic sites. Actually, the reaction with α-hydroxy ketone **14** performed under Reformatsky reaction conditions or using a lithium enolate according to the procedures employed in eqns. (1) or (2) did not effectively proceed and a significant amount of the starting ketone was recovered. Surprisingly, the stannyl ester–$SnCl_2$ system can provide high yield and high selectivity of **15** even with the use of hydroxy ketones **14** [eqn. (3)].[8] Other additives, $TiCl_4$ and $BF_3{\cdot}OEt_2$ for the reaction of **4** with **14** gave the recovered ketone **14** and low yields (9 and 26%) of **15**, respectively. The reaction with 2-hydroxypropiophenone **16** also gave the product **17** in high selectivity [eqn. (4)].[9] These results show the strong advantage of our system which tolerates protic conditions.

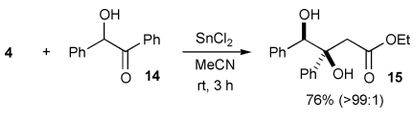

(3)

Table 2 Chelation-controlled reaction of α-stannyl ester **4** with alkoxy ketones in the presence of $SnCl_2$[a]

Entry	Alkoxy ketone	Product	Yield (%)	Dr
1	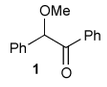	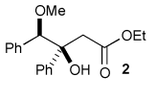	86	>99:1
2	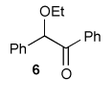	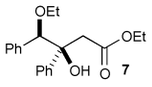	87	>99:1
3	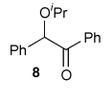	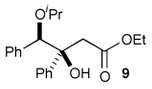	80	>99:1
4	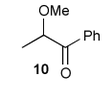	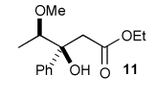	31	>95:5
5	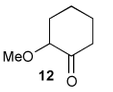	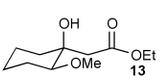	53	92:8

[a] All reactions were carried out in MeCN (1 mL) using **4** (1.2 mmol), alkoxy ketone (1.0 mmol), and $SnCl_2$ (1.2 mmol) at rt for 3 h.

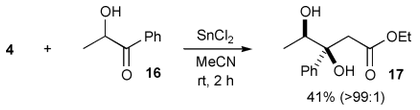

(4)

In conclusion, we have shown a highly diastereoselective addition of an alkoxycarbonylmethyl group to α-alkoxy or hydroxy ketones, controlled by the chelation effect, using an α-stannyl ester–$SnCl_2$ system. The transmetallation between the α-stannyl ester and $SnCl_2$ generates an active species which has high Lewis acidity to form a chelate. Further investigation of the scope and limitations of the methodology, and the reaction mechanism is now under way.

This work was supported by a Grant-in-Aid for Scientific Research from the Ministry of Education, Science, Sports, and Culture, of the Japanese Government.

Notes and references

† *Representative experimental procedure* for the synthesis of **2**: to a mixture of $SnCl_2$ (1.2 mmol) and α-alkoxy ketones **1** (1.0 mmol) in MeCN (1 mL) was added an α-stannyl ester **4** (1.2 mmol) under nitrogen. The solution was stirred for 3 h at ambient temperature. The reaction mixture was poured into the mixed solvent of Et_2O (30 mL) and aq. NH_4F (15%; 15 mL) with vigorous stirring for 10 min. The precipitating Bu_3SnF was filtered off. The filtrate was extracted with Et_2O (30 mL × 2), dried ($MgSO_4$) and evaporated. Recrystallisation (hexane–benzene, 9:1) of the resultant residue gave the pure product **2**.

‡ *Crystal data* for **2**: $C_{19}H_{22}O_4$, M = 314.38, monoclinic, a = 12.14(10), b = 5.9(1), c = 23.99(8) Å, V = 3741.0(9) Å^3, T = 300 K, space group $P2_1/n$ (no. 14), Z = 4, μ(Mo-Kα) = 0.9 cm^{-1}, 4075 reflections measured, 3894 unique (R_{int} = 0.032) which were used in all calculations. The final agreement factors were R = 0.051, R_w = 0.090. CCDC 182/1866.

1 M. T. Reetz, *Acc. Chem. Res.*, 1993, **26**, 462; M. T. Reetz, *Angew. Chem., Int. Ed. Engl.*, 1994, **23**, 556; X. Chen, E. R. Hortelano, E. L. Eliel and S. V. Frye, *J. Am. Chem. Soc.*, 1992, **114**, 1778.

2 M. T. Reetz, K. Kesseler and A. Jung, *Tetrahedron*, 1984, **40**, 4327; M. T. Reetz, B. Raguse, C. F. Marth, H. M. Hugel, T. Bach and D. N. A. Fox, *Tetrahedron*, 1992, **48**, 5731; M. T. Reetz and D. N. A. Fox, *Tetrahedron Lett.*, 1993, **34**, 1119.

3 A flask was charged with $MeCO_2Et$ (1.25 mmol) and dried THF (1 mL) under nitrogen and was cooled to −78 °C. A 2.0 M solution of lithium diisopropylamide (from Aldrich) in THF–heptane–EtPh (0.63 mL) was added and the mixture was stirred for 20 min keeping it at −78 °C. To the mixture was added **1** (1.0 mmol). After 3 h of stirring at −78 °C, the reaction mixture was quenched with 10 mL of aq. NH_4Cl, and extracted with Et_2O.

4 A flask was charged with Zn powder (6.0 mmol) and dried benzene–Et_2O (5:1, 2 mL) under nitrogen. A solution of ethyl 2-bromoacetate (5.5 mmol), **1** (5.0 mmol) in benzene–Et_2O (5:1, 5 mL) was slowly added over a period of 30 min to the mixture at 80 °C. Additional solvent (5 mL) was introduced and the reaction mixture was stirred for 2 h at 80 °C.

5 M. Pereyre, J.-P. Quintard and A. Rahm, *Tin in Organic Synthesis*, Butterworth & Co., London, 1987.

6 G. E. Keck and E. P. Boden, *Tetrahedron Lett.*, 1984, **25**, 265; G. E. Keck and E. P. Boden, *Tetrahedron Lett.*, 1984, **25**, 1879; G. E. Keck and D. E. Abbott, *Tetrahedron Lett.*, 1984, **25**, 1883.

7 M. Yasuda, Y. Sugawa, A. Yamamoto, I. Shibata and A. Baba, *Tetrahedron Lett.*, 1996, **37**, 5951; M. Yasuda, M. Tsuchida and A. Baba, *Chem. Commun.*, 1998, 563; M. Yasuda, Y. Matsukawa, K. Okamoto, T. Sako, N. Kitahara and A. Baba, *Chem. Commun.*, 2000, 2149.

8 The stereochemistry of the product **15** was determined by the following transformation: the methoxy-hydroxy ester **2** was converted by Fujita's method using $AlBr_3$–EtSH–CH_2Cl_2 at rt for 3 h to a dihydroxy ester whose NMR spectrum shows excellent agreement with the product **15** (yield of **15**, 26%, recovery of **2**, 68%). M. Node, K. Nishide, M. Sai, K. Ichikawa, K. Fuji and E. Fujita, *Chem. Lett.*, 1979, 97; M. Node, K. Nishide, M. Sai and E. Fujita, *Tetrahedron Lett.*, 1978, **52**, 5211.

9 The reaction was carried out using **4** (3.6 mmol), **16** (1.0 mmol), and $SnCl_2$ (3.0 mmol).

ChemComm

A molecular ‘hamburger’: bonded benzene in a bun

Douglas N. Butler,* Muhong Shang and Ronald N. Warrener

Centre for Molecular Architecture, Central Queensland University, Rockhampton, Queensland, 4702 Australia. E-mail: d.butler@cqu.edu.au

Received (in Cambridge, UK) 10th October 2000, Accepted 1st December 2000
First published as an Advance Article on the web 8th January 2001

The scaffold bis-succinimide 4 is shown to react twice with 1,2,4,5-tetrakis(bromomethyl)benzene 5 specifically at the *para*-related bromomethyl groups to form a multi-ring alicyclophane system 3 in which the benzene ring is sandwiched between the alicyclic frames to form a molecular ‘hamburger’.

In earlier work on proximity effects and structure–activity, one of us (DNB) demonstrated that the chemistry of an alkene π-bond could be completely negated by screening access to the π-system by suitably positioned benzene rings,[1] as in **1** where the alkene π-bond was situated in the valley between the two benzene rings. In this paper, we report another aspect of reactivity modification by proximity screening in which a benzene ring is positioned in the centre of a pair of extended alicyclic frames in a molecular equivalent of a hamburger, where the benzene ring corresponds to the ‘meat’ and the framework as the protective ‘bun’ (Fig. 1)†.

The synthesis of the molecular ‘hamburger’ **3** represents the second generation of our alicyclophanes[3] and draws on ideas expressed by Vögtle (aliphanes)[4] and the concept of stacked [2.2]cyclophanes (chochins) reported by Misumi[5] and Nakazaki[6]. By building a benzene ring into the alicyclophane and then attaching a second alicyclic spacer component onto the opposite face, it is possible to screen both sides of the benzene ring from reagent approach.‡

Reaction of the bis-succinimide **4**[3] with 1,2,4,5-tetrakis-(bromomethyl)benzene **5** in dimethylformamide containing solid potassium carbonate afforded a bromine free product having *m/z* = 1157.2590 (M + Na^+, calcd. 1157.2607) and thus confirming the 2:1-molecularity of the reaction. Comparisons of the N–N separation in **4** (AM1 6.30 Å) with the different bromomethyl C–C distances in **5** (AM1 C–C distances[8] are annotated on **5** in Scheme 1 and range from 2.91–5.77 Å) support preferential formation of the dual *para*-substituted product **3**§ since less deformation of the molecular frame is required to achieve cyclisation.¶ In order to gain evidence upon which to secure the ‘hamburger’ structure **3**, reactions were conducted between **4** and *o*-, *m*- and *p*-xylylene dibromides **6**–**8** as these subunits are each present in **5**. In all cases, reference to the N–N distances of starting scaffold **4** and product alicyclophanes **3**, **9**, **10** (see Table, Scheme 2) shows that significant frame deformation is required for cyclisation to occur, a feature

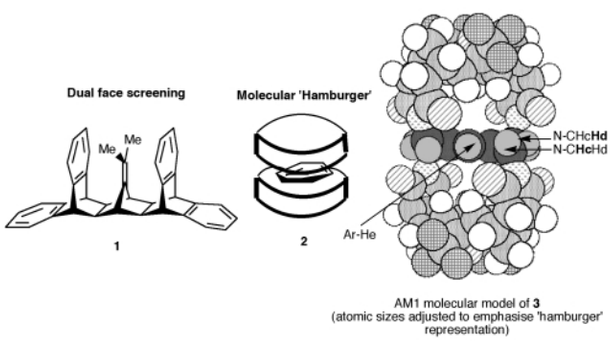

Fig. 1

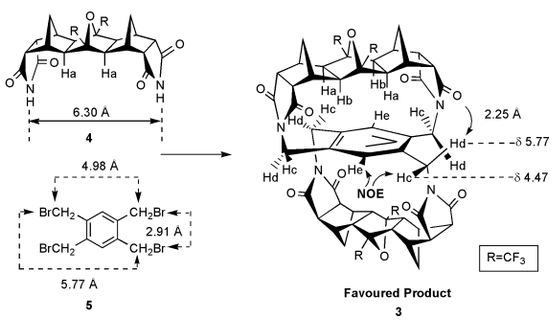

Scheme 1

somewhat surprising considering the expected rigidity in [*n*]polynorbornane frames comprised of fused norbornanes.‖

The product from bis-succinimide **4**** and *p*-xylylene dibromide **6** was assigned the alicyclophane structure **9**** on the basis of mass spectrometry (*m/z* 606.1591, calcd. 606.1589). Product **9**§ displayed ^1H and ^{13}C NMR spectra that reflected its *C*2*v*-symmetry. Similar reaction between *m*-xylylene dibromide **7** and spacer **4** produced an isomeric alicyclophane assigned structure **10**** (*m/z* = 606.1586). The ^1H NMR spectrum of **10** was also indicative of a compound with *C*2*v*-symmetry and was unchanged down to −70 °C supporting a facile ‘flipping’ motion of the *m*-phenylene bridge. By extrapolation, any *meta*,*meta*-linked structure for **3** is considered untenable since the N–CH_2 protons would not be diastereiotropic (as seen in **3**) owing to ring ‘flipping’. The reaction of *o*-xylylene dibromide **8** with **4** takes a different pathway and leads to production of a 2:2 product **11**§ (*m/z* 1212.3197, calcd. 1212.3179) resulting from dual intermolecular alkylation. Significantly, the *endo*-protons in **9** were more shielded than those in **10** and this offers further structural support for the *para*,*para*-structure of molecular ‘hamburger’ **3** in which the *endo*-protons occur at even higher field (δ 1.11, 1.21).

Conclusive chemical support for the structure of **3** was provided by the interrelation between alicyclophane **13**,§ prepared by the reaction of the dichlorodurene†† **12** with

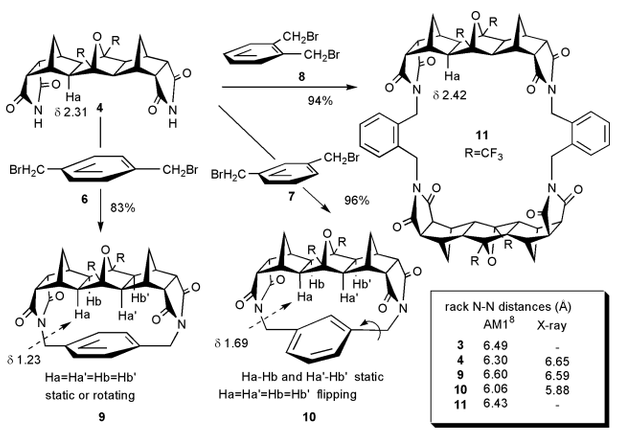

Scheme 2

DOI: 10.1039/b008178g

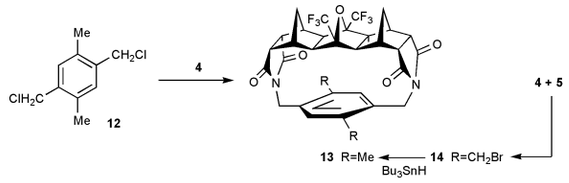

Scheme 3

scaffold **4**, with the alicyclophane **14**§ which has been isolated as an intermediate in the preparation of 'hamburger' **3** (Scheme 3). This was achieved by debromination of **14** by treatment with tributyltin hydride. As the alicyclophane **13** must be *para*-linked (single aryl proton resonance at δ 7.51 is definitive), this shows that **13** has the same motif and the derived 'hamburger' **3** must be *para*,*para*-linked.

In order to assess the steric protection offered by the scaffold structures to reagent approach to the benzene ring in the 'hamburger' **3**, it was treated with hot nitric–sulfuric acid (1:1 v/v). No reaction occurred even at elevated temperatures however blank reactions, conducted on the alicyclophane **9**, produced a mono nitro derivative, while the related alicyclophane **10** produced a mixture of dinitro derivatives similar to that observed for *m*-xylene. This demonstrates that nitration will proceed on the benzene ring when only one face is screened by the scaffold, but that reaction is precluded by incorporation of the second scaffold-containing ring.

In conclusion, we have demonstrated that macrocycles can be produced by reaction of xylylene dibromides with the bis-succinimide **4** and that intramolecular cyclisation occurs to form alicyclophanes with *p*-xylylene dibromide **6** and *m*-xylylene dibromide **7**, whereas intermolecular reaction occurs linking two scaffold units when the shorter *o*-xylylene dibromide is employed. The double cyclisation of the bis-imide **4** with 1,2,4,5-tetrakis(bromomethyl)benzene produced the *para*,*para* substitution 'hamburger' product **3** in which the benzene ring is sandwiched between the alicyclic scaffolds, so much so that it resisted electrophilic substitution even under forcing conditions.

D. N. B. thanks the Centre for Molecular Architecture for a Research Fellowship 1998–2000, and the Central Queensland University merit grants scheme for partial funding. Dr Martin Johnston is thanked for his interest in the project and for conducting the NMR experiments. Dr Alan Lough (Chemistry, University of Toronto) is thanked for the X-ray structures** reported herein.

Notes and references

† Stoddart *et al*. have described[2] a catenated system in which the benzene ring is positioned centrally in a three-dimensional array. Their structure contains other aromatic rings which would make it difficult to conduct reactivity studies of the central aryl ring; further, it does not have the 'hamburger' appearance.

‡ We have recently shown that alicyclophanes containing an isobenzofuran subunit already display increased stability owing to the scaffold frame offering reagent approach control from one face.[7]

§ All new compounds gave appropriate high resolution mass spectra and consistent ^{1}H and ^{13}C NMR spectra.

¶ While there is literature precedent[2,9] for intramolecular cyclisation involving successive nucleophilic reactions at the benzylic bromide positions of 1,2,4,5-tetrakis(bromomethyl)benzene **5** occurring exclusively at the *para*-related sites, literature examples reveal that for more flexible bis-alkylating linkers, such as those forming bis-(crowns ethers), *ortho*- and *meta*-linked products are the preferred mode of cyclisation.[9] Indeed, our finding is one of the few examples in which *para*-linkage occurs and is a direct consequence of the compatibility of the N–N separation of the scaffold (6.30 Å) and the fixed positions of the benzylic carbons (5.77 Å), as mentioned in the text.

‖ The IUPAC name for norbornane is bicyclo[2.2.1]heptane.

** *Crystal data* for **4** $C_{22}H_{18}O_5F_6N_2$, M = 504.38, monoclinic, space group $P2_1/c$ (No. 14), T = 150(1) K, a = 13.7369(6), b = 7.7697(4), c = 20.4778(6) Å, β = 108.483(2)°, U = 2072.9(2) Å^3, Z = 4, D_c = 1.616 g cm^{-3}, μ(Mo Ka) = 0.150 mm^{-1}, 10968 reflections collected, $R(F)$ = 0.0907, $R(wF^2)$ = 0.1209 for all 4696 independent reflections, [$R(F)$ = 0.0518, $R(wF^2)$ = 0.1078 for 3168 data with $F > 4\sigma(F_O)$].

Crystal data for **9** $C_{30}H_{24}O_5F_6N_2$, M = 606.51, orthorhombic, space group $Fdd2$ (No. 43), T = 150(1) K, a = 18.4480(2), b = 28.7380(4), c = 9.6088(8) Å, U = 5094.2(4) Å^3, Z = 8, D_c = 1.582 g cm^{-3}, μ(Mo Ka) = 0.137 mm^{-1}, 7636 reflections collected, $R(F)$ = 0.0459, $R(wF^2)$ = 0.0818 for all 1553 independent reflections, [$R(F)$ = 0.0330, $R(wF^2)$ = 0.0762 for 1326 data with $F > 4\sigma(F_O)$].

Crystal data for **10** $C_{34}H_{32}O_6F_6N_2$, M = 678.62, triclinic, space group $P\bar{1}$ (No. 2), T = 150(1) K, a = 10.1160(7), b = 10.8820(7), c = 14.0090(11) Å, U = 1451.40(4) Å^3, Z = 2, D_c = 1.553 g cm^{-3}, μ(Mo Kα) = 0.131 mm^{-1}, 11411 reflections collected, $R(F)$ = 0.0911, $R(wF^2)$ = 0.1435 for all 5116 independent reflections, [$R(F)$ = 0.0586, $R(wF^2)$ = 0.1292 for 3671 data with $F > 4\sigma(F_O)$].

For all structures the data (collected on a Nonius Kappa-CCD instrument) were integrated and scaled using the DENZO-SMN package (Z. Otwinowski and W. Minor, *Methods in Enzymology*, 1997, **276**, 307). The structures were solved and refined using SHELXTL V5.0 (G. M. Sheldrick, SHELXTL\PC V5.1, Bruker Analytical X-ray Systems, Madison, Wisconsin, U.S.A). CCDC 182/1868. See http://www.rsc.org/suppdata/cc/b0/b008178g/ for crystallographic files in .cif format.

†† The IUPAC name for durene is 1,2,4,5-tetramethylbenzene.

1 D. N. Butler, I. Gupta, W. W. Ng and S. C. Nyburg, *J. Chem. Soc., Chem. Commun.*, 1980, 596.
2 P. R. Ashton, A. S. Reder, N. Spencer and J. F. Stoddart, *J. Am. Chem. Soc.*, 1993, **115**, 5286.
3 D. N. Butler, M. Shang and R. N. Warrener, *Tetrahedron Lett.*, 2000, **41**, 5985.
4 (*a*) J. Dohm, M. Nieger, K. Rissanen and F. Vögtle, *Chem. Ber.*, 1991, **124**, 915; (*b*) F. Vögtle, *Cyclophane Chemistry. Synthesis, Structures and Reactions*, 1993, John Wiley and Sons.
5 T. Otsubo, Y. Aso, F. Ogura, S. Misumi, A. Kawamoto and J. Tanaka, *Bull. Chem. Soc. Jpn.*, 1989, **62**, 164.
6 M. Nakazaki, K. Yamamoto, S. Tanaka and H. Kametani, *J. Org. Chem.*, 1977, **42**, 287.
7 R. N. Warrener, M. Shang and D. N. Butler, unpublished results.
8 Molecular modelling was carried out on a SGI O2 workstation using the SPARTAN version 4 from WaveFunction Inc. 18401 Von Karman Ave., #A370, Irvine, Ca 92715, U.S.A. © 1995 Wavefunction Inc.
9 (*a*) S. J. Loeb and G. K. Shimizu, *Synlett*, 1992, 823; (*b*) W. Y. Lee, W. Sim and O. S. Park, *Synlett*, 1992, 157; (*c*) H. Kurebayashi, T. Haino and Y. Fukazawa, *Tetrahedron Lett.*, 2000, **41**, 477.

ChemComm

Supramolecular organization of fullerenes by quadruple hydrogen bonding†

Minze T. Rispens, Luis Sánchez, Joop Knol and Jan C. Hummelen*

Stratingh Institute and Materials Science Centre, University of Groningen, Nijenborgh 4, 9747 AG Groningen, The Netherlands. E-mail: J.C.Hummelen@chem.rug.nl; Fax: (+31) 50-3634296

Received (in Liverpool, UK) 27th September 2000, Accepted 13th November 2000
First published as an Advance Article on the web 4th January 2001

Quadruple hydrogen bonded fullerene dimer 8 with a very high dimerisation constant ($K_a \geqslant 1.0 \times 10^6$ M^{-1}) was synthesised and fully characterised.‡

Fullerenes have interesting properties that may be utilised in applications such as organic photovoltaic (PV) devices.[1] The bulk-heterojunction version of such cells especially has received much attention recently. In this type of device, a blend of an electron donor (for example a π-conjugated polymer) and an electron acceptor (for example a fullerene derivative) serves as the active PV layer.[2] Very recently, influencing the morphology of the bulk heterojunction layer by simply changing the spincoating solvent resulted in a substantial increase of the PV power conversion efficiency to a record value of 2.5%.[3] A more intimate mixing of the components most likely resulted in both a larger internal donor–acceptor interface area and increased percolation of at least one of the components. Charge carrier transport in the polymer phase was further improved on the nanoscopic scale due to enhanced polymer inter-chain interactions.

Another potential way to obtain desired bulk-heterojunction architectures is through supramolecular assembly of the constituents. Hydrogen bonding is particularly useful in the construction of supramolecular structures.[4] Strong non-covalent binding can be obtained using multiple hydrogen bond arrays, especially with Meijer's self-complementary 2-ureidopyrimidin-4-ones.[5] With this unit, ultra-strong non-covalent coupling can be achieved, reaching association constants of $> 10^8$ M^{-1}.[5c]

Here we report on the preparation of a [60]fullerene derivative bearing one 2-ureidopyrimidin-4-one moiety as the hydrogen bonding unit. This molecule serves as a model compound for supramolecular fullerene arrays based on multiple hydrogen bonding interactions.

The synthesis of target molecule **8** started from easily accessible 1,2-bis(hexyloxy)benzene.[6] Friedel–Crafts acylation yielded keto ester **1**,[7] which was transformed into the corresponding *p*-tosylhydrazone **2**. Subsequently, carboxylic acid **4** was prepared using the following one pot procedure:[8] first, heating the anion of **2** in the presence of [60]fullerene in *o*-dichlorobenzene (ODCB) at 80–90 °C gave fulleroid **3a**, together with methanofullerene **3b**, higher adducts and [60]fullerene. This crude mixture was photoisomerised quantitatively to a mixture of **3b**, higher adducts and [60]fullerene. Hydrolysis of this mixture yielded crude acid **4**, which was purified by column chromatography. The overall yield for the conversion of **2** into **4** was 36%. Carboxylic acid **4** was converted into the corresponding acid chloride **5**, after which reaction with sodium azide yielded the corresponding acyl azide **6**. Heating **6** in the presence of 6-methylisocytosine at 80 °C for 2 h afforded **8** in good yield.

Dimer **8** showed 29 signals for C_{60}-sp^2 carbons in ^{13}C NMR, in accordance with C_{2h} symmetry. The resonances at δ 172.8 (**a**), 156.5 (**b**) and 154.4 (**c**) are characteristic for the 2-ureidopyrimidin-4-one moiety.[5a] The signals at δ 80.6 and 52.4 are diagnostic for the cyclopropyl moiety.[8] The ^{1}H NMR spectrum recorded in $CDCl_3$ showed the typical resonances[5a] for the four dimer bonding hydrogen atoms of **8** at δ 11.81 (H_b) and δ 10.40 (H_c), a signal at δ 12.98 for the intramolecularly bonded H_a, and one at δ 5.75 for the vinylic proton H_d (Scheme 1). When the concentration of compound **8** was lowered to 1.0×10^{-5} mol l^{-1} no dissociation was observed, thus giving a lowest estimate of the dimerisation constant of 1×10^6 M^{-1}, in good agreement with the values obtained for other ureidopyrimidinone derivatives.[5a] To probe a possible influence of the fullerene core on the hydrogen bonding unit, equimolar amounts of dimer **8** and dimer **9** of *N*-butylaminocarbonyl-6-methylisocytosine (**9**)[5] were dissolved in $CDCl_3$. A statistical mixture of the possible dimers was obtained (Fig. 1) as was concluded from the integration of the absorptions of all protons

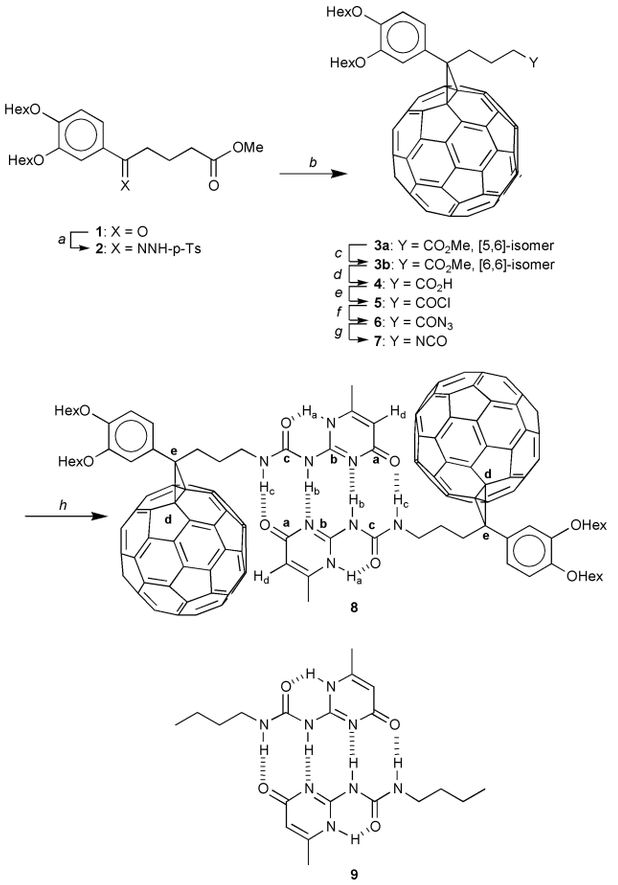

Scheme 1 (*a*) *p*-$TsNHNH_2$, MeOH, 6 h., Δ, 61%; (*b*) 1. NaOMe, py, 30 min., rt, C_{60}, ODCB, 80–90 °C, 16 h; (*c*) ODCB, 500 W flood lamp, 100 min; (*d*) ODCB, HOAc, HCl, H_2O, 16 h, 36% (2⟶4, 3 steps); (*e*) $SOCl_2$, $CHCl_3$, 1 h; (*f*) NaN_3, ODCB, DMAC, rt 75 min; (*g* + *h*) 2-amino-4-hydroxy-6-methylpyrimidine, py, 70–80 °C, 2 h, 71% (4⟶8, 3 steps).

† Electronic supplementary information (ESI) available: details of preparation and spectroscopic characterization of all compounds. See http://www.rsc.org/suppdata/cc/b0/b008006n/

‡ See also the following paper in this issue: J. J. González, S. González, E. M. Priego, C. Luo, D. M. Guldi, J. de Mendoza and N. Martín, *Chem. Commun.*, 2001, DOI: 10.1039/b008005p.

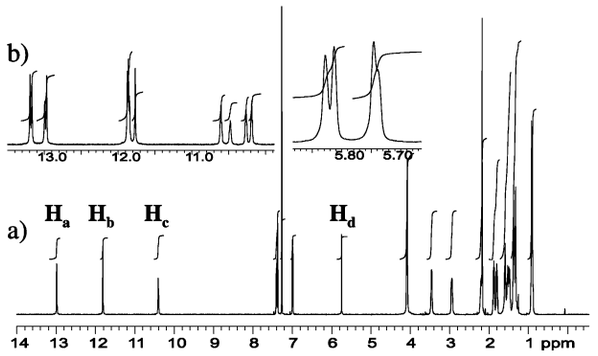

Fig. 1 (a) ^{1}H NMR of **8** in $CDCl_3$. (b) ^{1}H NMR of equimolar solution of **8** and **9** in $CDCl_3$.

Table 1 Redox properties

Com.[a]	E^1_{red}[b]	E^2_{red}[b]	E_{1red}[c]	E^3_{red}[b]	E_{2red}[c]	E^4_{red}[b]
3b	−0.66	−1.04	—	−1.55	—	−2.00
4	−0.72	−1.09	—	−1.60	−1.80	−2.02
8	−0.68	−1.01	−1.15	−1.56	−1.84	−2.02
$\mathbf{C_{60}}$	−0.60	−1.09	—	−1.63	—	−2.07
9	—	—	−1.02	—	−1.60	—

[a] Experimental conditions: V: *vs.* Ag wire, GCE as the working electrode, Bu_4NPF_6 (0.1 M) as the supporting electrolyte, ODCB–MeCN (4 : 1) as the solvent, 100 mV s^{-1} scan rate. [b] Waves corresponding to the reduction processes of the C_{60} cage. [c] Waves corresponding to the reduction processes of the ureidopyrimidinone moiety.

$H_{a–d}$ in ^{1}H NMR. The most pronounced shift is observed for the resonance of H_c.

While **8** shows characteristic absorptions for a methanofullerene in UV-Vis, the FTIR-spectrum showed a peak pattern at 1695, 1658, 1586 and 1513 cm^{-1}, indicative of a pyrimidin-4(1*H*)-one dimer[9] and the typical fullerene absorption at 526 cm^{-1}. The MALDI-TOF spectrum of **8** featured a parent peak at m/z = 1217.8 for the monomer.

The redox behaviour of fullerene derivatives **3b**, **4, 8**, and that of **9**[5a] was determined by cyclic voltammetry (Table 1). The cyclic voltammogram of **3b** showed four reversible waves corresponding to reduction of the fullerene core, with values typical for methanofullerenes.[8] In the case of carboxylic acid **4** an additional wave was observed at −1.80 V, which was attributed to the reduction of the acid moiety. Finally, the cyclic voltammogram of **8** showed the similar four waves corresponding to reduction of the fullerene core as well as a weak wave at −1.84 V and a shoulder at −1.15 V. The latter two waves are related to the 2-ureidopyrimidin-4-one moiety as was confirmed upon comparison with **9**[5a] (−1.02 and −1.60 V).

In an exploratory experiment towards application in a PV device, the processability of dimer **8** was shown as follows: When filtered solutions of MDMO-PPV[10] and **8** [both 1.0 (m/v) % in chloroform] were mixed in a ratio of 1 : 4 and the mixture was subsequently spincoated on a glass substrate, an optical quality film was obtained.

Other supramolecularly interacting fullerene compounds have been reported recently.[11] The synthesis of **8**, however, represents the first example of a hydrogen bonded fullerene dimer. With both fullerene cages connected through the very strong quadruple hydrogen bonding motif, provided by the ureidopyrimidinone moiety, the application in supramolecular electronics is within reach. Non-covalent multifullerene arrays based on bis(ureidopyrimidinone) substituted fullerenes are currently under investigation.

These investigations were financially supported by the Dutch Ministries of EZ, O&W and VROM through the EET program (EETK97115) and by the Netherlands Organization for Energy and the Environment (NOVEM) through the NOZ-PV Program (146.120-008.3).

Notes and references

1 (*a*) N. S. Sariciftci, L. Smilowitz, A. J. Heeger and F. Wudl, *Science*, 1992, **258**, 1474; (*b*) G. Yu, K. Pakbaz and A. J. Heeger, *Appl. Phys. Lett.*, 1994, **64**, 3422.
2 (*a*) G. Yu and A. J. Heeger, *J. Appl. Phys.*, 1995, **78**, 4510; (*b*) G. Yu, J. Gao, J. C. Hummelen, F. Wudl and A. J. Heeger, *Science*, 1995, **270**, 1789; (*c*) J. J. M. Halls, C. A. Walsh, N. C. Greenham, E. A. Marseglia, R. H. Friend, S. C. Moratti and A. B. Holmes, *Nature*, 1995, **376**, 498.
3 S. E. Shaheen, C. J. Brabec, F. Padinger, T. Fromherz, J. C. Hummelen and N. S. Sariciftci, *Appl. Phys. Lett.*, in print.
4 For selected examples, see: (*a*) T. J. Murray, S. C. Zimmerman and S. V. Kolotuchin, *Tetrahedron*, 1995, **51**, 635; (*b*) J. Rebeck Jr., *Chem. Soc. Rev.*, 1996, **25**, 255; (*c*) C. M. Drain, K. C. Russell and J.-M. Lehn, *Chem. Commun.*, 1996, 337; (*d*) J. P. Mathias, E. E. Simanek and G. M. Whitesides, *J. Am. Chem. Soc.*, 1994, **116**, 4326; (*e*) K. A. Jolliffe, P. Timmerman and D. N. Reinhoudt, *Angew. Chem., Int. Ed.*, 1999, **38**, 933.
5 (*a*) F. H. Beijer, R. P. Sijbesma, H. Kooijman, A. L. Spek and E. W. Meijer, *J. Am. Chem. Soc.*, 1998, **120**, 6761; (*b*) B. J. B. Folmer, R. P. Sijbesma, H. Kooijman, A. L. Spek and E. W. Meijer, *J. Am. Chem. Soc.*, 1999, **121**, 9001; (*c*) S. H. M. Söntjes, R.P. Sijbesma, van M. H. P. Genderen and E. W. Meijer, *J. Am. Chem. Soc.*, 2000, **122**, 7487.
6 A. Loupy, J. Sansoulet and F. Vaziri-Zani, *Bull. Soc. Chim. Fr.*, 1987, 1027.
7 G. Kossmehl and H.-C. Frohberg, *Chem. Ber.*, 1986, **119**, 50.
8 J. C. Hummelen, B. W. Knight, F. LePeq, F. Wudl, J. Yao and C. L. Wilkins, *J. Org. Chem.*, 1995, **60**, 532.
9 F. H. Beijer, PhD thesis, University of Eindhoven The Netherlands, 1998.
10 Poly[(2-(3,7-dimethyloctyloxy)-5-methoxy)-1,4-phenylene vinylene].
11 (*a*) F. Diederich, M. Gómez-López, *Chem. Soc. Rev.*, 1999, 263; (*b*) F. Diederich, L. Echegoyen, M. Gómez-López, R. Kessinger and J. F. Stoddart, *J. Chem. Soc., Perkin Trans. 2*, 1999, 1577; (*c*) T. Habicher, J.-F. Nierengarten, V. Gramlich and F. Diederich, *Angew. Chem., Int. Ed.*, 1998, **37**, 1916.

A new approach to supramolecular C_{60}-dimers based in quadruple hydrogen bonding

Juan J. González,[a] Susana González,[b] Eva María Priego,[b] Chuping Luo,[c] Dirk M. Guldi,*[c] Javier de Mendoza*[a] and Nazario Martín*[b]

[a] *Departamento de Química Orgánica, Universidad Autónoma de Madrid Cantoblanco, E-28049, Madrid, Spain*
[b] *Departamento de Química Orgánica, Facultad de Química, Universidad Complutense, E-28040, Madrid, Spain. E-mail: nazmar@eucmax.sim.ucm.es*
[c] *Radiation Laboratory, University of Notre Dame, Notre Dame, IN 46556, USA*

Received (in Liverpool, UK) 27th September 2000, Accepted 27th November 2000
First published as an Advance Article on the web 4th January 2001

A C_{60}-dimer connected through a highly directional fourfold hydrogen bonding motif has been synthesized; photophysical measurements reveal a strong electronic coupling through the hydrogen bond edge.†

The design and synthesis of [60]fullerene dimers is currently attracting considerable attention.[1] Different strategies have been adapted for the construction of C_{60}-dimers: the net result is, however, that the two monomeric units are, in the resulting dimers, attached through diversified, covalent linkages.

Sijbesma, Meijer *et al*. have reported the preparation of remarkably stable dimers ($K_s > 10^6$ M^{-1}) evolving from derivatives of the 2-ureido-4-pyrimidone moiety, *via* a self-complementary array of four hydrogen bonds.[2] The same strategy was afterwards employed for the synthesis of calix-[4]arene dimers.[3]

In this communication, we wish to report on the synthesis of the first, rigid noncovalent C_{60}-dimer system, in which both molecular subunits are linked by a self-complementary DDAA (donor–donor–acceptor–acceptor) array of hydrogen bonding.[4] The selected four-point hydrogen bond motif, based on a 2-ureido-4-pyrimidone moiety, guarantees the molecular recognition in solution and leads to a novel noncovalent constructed model system.

Two different routes, as summarized in Scheme 1, were pursued to synthesize dimers **1a**,**b**. In particular, *N*-substituted 2′,5′-dihydro-1′*H*-pyrrolofullerene **4a** was prepared from *p*-formylbenzoic acid (**2**) and *N*-(3,6,9-trioxadecyl)glycine (**3a**).[5] The polyether chain, located on the pyrrolidine ring, allows the sufficient solubility of compound **4a** in most organic solvents. In **4a**, the carboxy functionality was then transformed into the corresponding isocyanate by a Curtius rearrangement of the intermediate acyl azide generated with diphenylphosphoryl azide (DPPA).[6] Reaction with aminopyrimidone (**5**) afforded dimer **1a** in a 3% overall yield.‡ The poor yield for this three-step, one-pot process can be rationalized in terms of competitive reactions either of the azido group in DPPA or of the amino group in **5** with the C_{60} core of **4a**.

Performing first the C_{60}-based reaction with aldehyde dimer **8**, already containing the ureidopyrimidinone dimerization edge, successfully circumvented these interfering reactions. Accordingly, the reaction of acetal **6** with DPPA, followed by *in situ* reaction of the resulting isocyanate with aminopyrimidone **5**, afforded **7**. Subsequent deprotection of **7** with catalytic $HClO_4$ in 5 : 1 dioxane–$CHCl_3$ led to **8** in a 50% yield from **6**. Reaction of dimer **8** with C_{60} and *N*-substituted glycines **3a**,**b** under the same conditions used for the preparation of pyrrolidinofullerenes, gave the respective dimers (**1a**,**b**) in moderate yields (*ca.* 50%).

From the FTIR spectra characteristic evidence was derived for both subunits, namely, C_{60} and the heterocycle. It is worth mentioning that although a diastereomeric mixture should be formed, the ^{1}H-NMR spectra (500 MHz) show only the presence of a pure compound. Thus, the ^{1}H-NMR spectra of **1a**,**b** disclose the signals of the pyrrolidine protons at *ca*. 5.2 and 4.3 ppm (J = 9.6 Hz; geminal hydrogens) and a singlet at 5.1 ppm (CH), in good agreement with similar monoadducts. Large downfield shifts were found for the urea NH protons in compounds **1a**,**b**, at *ca.* 12.0 ppm, ($CDCl_3$). This observation is consistent with four DDAA hydrogen bonds in the noncovalent

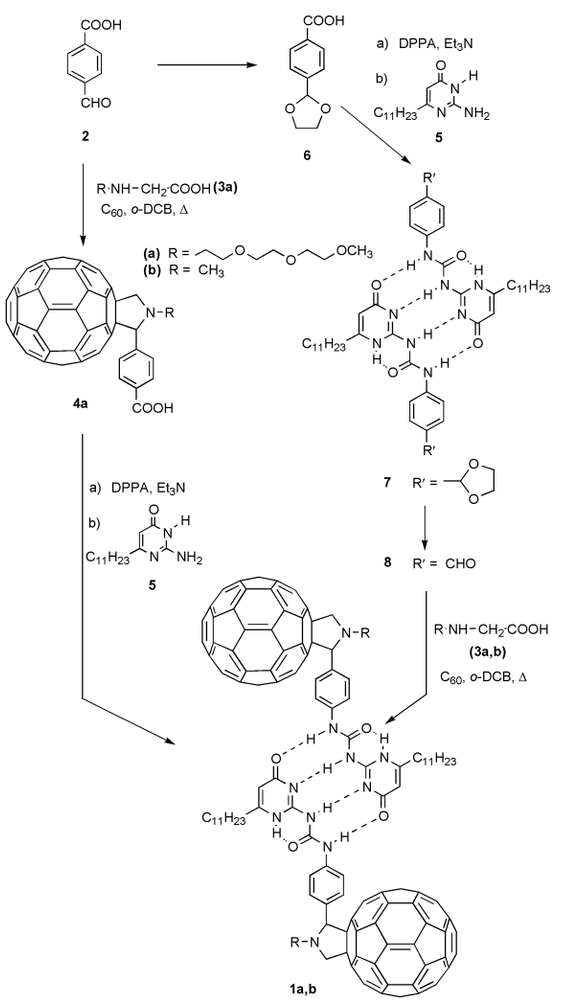

Scheme 1

† See also the preceding paper in this issue: M. T. Rispens, L. Sánchez, J. Knol and J. C. Hummelen, *Chem. Commun.*, 2001, DOI: 10.1039/b008006n.

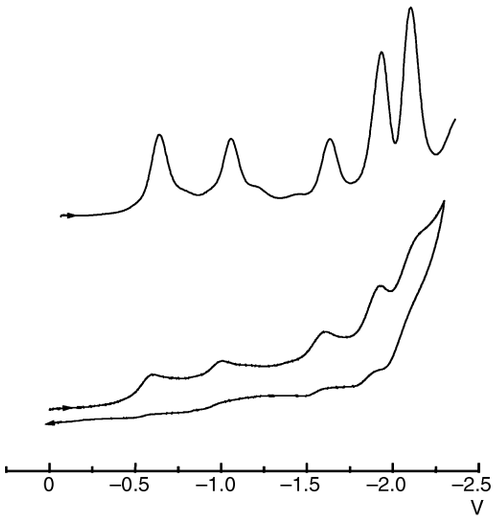

Fig. 1 Cyclic voltammogram and squarewave voltammogran (in V *vs* Ag/Ag^+) of compound **1a** in toluene : MeCN (4 : 1 *v*/*v*) solution containing 0.1 M *n*-Bu_4NClO_4 with glassy carbon; scan rate at 200 mVs^{-1}.

C_{60}-dimer system. In addition, the chelated NH at position 1 was observed at *ca.* 13.0 ppm.

The CV of dimers **1a**,**b** give rise to four reduction waves in deoxygenated CH_2Cl_2, while six reduction waves were found when a toluene–acetonitrile solvent mixture (4 : 1 v/v) was used (Fig. 1). As can be seen from an inspection of the parent C_{60} and related pyrrolidinofullerenes, the waves at −0.62, −1.01, −1.60, −2.08 V (in toluene–MeCN), and −0.69, −1.05, −1.61 V (in CH_2Cl_2) correlate to the one-electron reduction steps of the C_{60} moiety. These values are, nevertheless, cathodically shifted relative to those of C_{60}.[7]

However, it is important to point out that the voltammograms of dimers **1a**,**b** indicate that both fullerene moieties are reduced simultaneously. This observation, in conjunction with the above-listed spectroscopic characterization, supports the critical argument that there is little, if any, electronic interaction between the two C_{60} subunits in the dimers.

The remaining signals at −1.14 and −1.85 V (in toluene–MeCN) and −1.18 V (in CH_2Cl_2), are associated with redox processes of the heterocyclic ureido(oxo)pyrimidinyl addend.

The excited states properties of **1a** were studied by steady-state emission and time-resolved flash photolysis. Emission experiments, carried out with an excitation wavelength of 400 nm, gave rise to a distinctive solvent dependence. For instance, conditions that leave the hydrogen-bonded C_{60}-dimer intact (*i.e.* chlorobutane or CH_2Cl_2), led to an almost 50% quenching of the fullerene fluorescence around 710 nm relative to a 2′,5′-dihydro-1′H-pyrrolofullerene reference (see Table 1). This implies a markedly accelerated deactivation of the fullerene singlet excited state within the C_{60}-dimers and, hereby, resembling a trend established earlier for the most prominent fullerene dimer, namely, C_{120}.

Table 1 Fluorescence quantum yields[a] of **1a** in various solvents, a fulleropyrrolidine reference and C_{120} at room temperature

Compound solvent	Fluorescence quantum yields **1a**
Dichloromethane	3.05×10^{-4}
Chlorobutane/ethanol	3.3×10^{-4}
Chlorobutane/trifluoroethanol	3.65×10^{-4}
Chlorobutane/hexafluoroisopropanol	4.9×10^{-4}
Fulleropyrrolidine dichloromethane	6.0×10^{-4}
C_{120}[b] toluene	3.95×10^{-4}

[a] Measured at 710 nm. [b] See reference 8.

Upon adding protic solvents, such as ethanol, trifluoroethanol and hexafluoroisopropyl alcohol to a CH_2Cl_2 solution of **1a** a progressive enhancement of the fullerene fluorescence was observed. It should be noted that the solvents employed reveal different protic strengths and, therefore, different affinities to interfere in a disruptive manner with the hydrogen bonding along the following order: ethanol < trifluoroethanol < hexafluoroisopropyl alcohol. Importantly, in the most protic solvent (*i.e.* hexafluoroisopropyl alcohol), the emission quantum yield reached almost the value of a reference 2′,5′-dihydro-1′H- pyrrolofullerene. From this we may propose that under the experimental conditions probed the dissociation into monomer subunits is essentially complete. On the other hand, the quantum yield in the weakest protic solvent (*i.e.* ethanol) is close to the values determined in chlorobutane or CH_2Cl_2, suggesting a nearly dimeric appearance of **1a** under such conditions.

In conclusion, we have synthesized the first C_{60}-dimer linked *via* a highly directional fourfold hydrogen bonding motif. Electrochemical results indicate that there is no mutual interaction in the ground state between both C_{60} subunits. In contrast, the photophysical data, disclosing distinguishable differences between the monomer and the dimer, can be taken as first evidence for the strong electronic coupling mediated through the hydrogen bond edge.

Work is currently in progress directed to interface strong electron donor units with the C_{60} core through a self-complementary array of hydrogen bonds.

This work was supported by CICYT (projects PB93-0283 and PB98-0818) and in part by the Office of Basic Energy Sciences of the US Department of Energy. This is contribution NDRL-4280 of the Radiation Laboratory. This paper is dedicated to Professor José Barluenga on the occasion of his 60th birthday.

Notes and references

‡ **1a**: Brown solid; 48% yield; FTIR (KBr): br 3431, 1699 (C=O), 1655 (C=O), 527 (C_{60}) cm^{-1}; ^{1}H-NMR ($CDCl_3$, 500 MHz, 25 °C): δ = 13.02 (s, 2H; NH), 12.26 (s, 4H; NH), 7.78 (br s, 8H; ArH), 5.94 (br s, 2H; pyrim), 5.23 (d, *J*(H,H) = 9.66 Hz, 2H; CH_2N), 5.14 (s, 2H; NCHR), 4.30 (d, *J*(H,H) = 9.66 Hz, 2H; CH_2N), 4.05–3.93 (2m, 4H), 3.80 (br s, 8H), 3.75–3.72 (m, 4H), 3.59–3.50 (m, 4H), 3.38 (m, 8H), 2.80–2.86 (m, 2H), 2.52–2.47 (m, 4H; CH_2), 1.69–1.65 (m, 4H; CH_2), 1.26 (br s, 32H; CH_2), 0.89–0.86 (m, 6H; CH_3); ^{13}C NMR ($CDCl_3$, 125 MHz, 25 °C): δ 173.38, 157.07, 154.99, 154.94, 154.80, 154.10, 154.06, 153.17, 147.68, 147.27, 146.94, 146.81, 146.68, 146.62, 146.59, 146.53, 146.50, 146.46, 146.31, 146.28, 146.16, 145.99, 145.94, 145.91, 145.87, 145.69, 145.63, 145.59, 145.51, 145.11, 145.03, 144.80, 143.52, 143.37, 143.04, 142.92, 142.90, 142.72, 142.70, 142.52, 142.47, 142.41, 142.33, 142.29, 142.05, 141.90, 140.53, 140.49, 140.33, 139.98, 138.91, 137.32, 137.02, 136.21, 136.08, 132.77, 130.52, 128.78, 128.17, 120.68, 106.63, 82.49, 76.80, 72.47, 71.19, 71.11, 71.06, 71.02, 69.69, 68.16, 59.48, 52.44, 33.15, 32.30, 30.09, 29.99, 29.86, 29.72, 29.62, 29.27, 27.38, 23.09, 14.54; UV/Vis (CH_2Cl_2): λ_{max} (ε) = 252 (159148.9), 274 sh (150209.0), 324 sh (69361.6), 430 (8036.3); MS (MALDI-TOF): 1292 (M^+, 100), 1028 (M − $pyrim^+$, 40).

1 For a recent review on [60]fullerene dimers, see: J. L. Segura and N. Martín, *Chem. Soc. Rev.*, 2000, **29**, 13.
2 B. J. B. Folmer, R. P. Sijbesma, H. Kooijman, A. L. Spek and E. W. Meijer, *J. Am. Chem. Soc.*, 1999, **121**, 9001, and references cited therein.
3 J. J. González, P. Prados and J. de Mendoza, *Angew. Chem., Int. Ed. Engl.*, 1999, **38**, 525.
4 A previous supramolecular hydrogen bonding C_{60} dimer in which a C_{60}-dibenzylammonium adduct is threaded through the cavity of the crown ether macrocycle of a C_{60}-dibenzo-24-crown-8 adduct has been recently reported. See: F. Diederich, L. Echegoyen, M. Gómez-López, R. Kessinger and J. F. Stoddart, *J. Chem. Soc., Perkin Trans. 2*, 1999, 1577.
5 T. Da Ros, M. Prato, F. Novello, M. Maggini and E. Banfi, *J. Org. Chem.*, 1996, **61**, 9070.
6 K. Ninomiya, T. Shioiri and S. Yamada, *Tetrahedron*, 1974, **30**, 2151.
7 L. Echegoyen and L. E. Echegoyen, *Acc. Chem. Res.*, 1998, **31**, 593.
8 (*a*) M. Fujitsuka, C. Luo, O. Ito, Y. Murata and K. Komatsu, *J. Phys. Chem. A*, 1999, **103**, 7155; (*b*) B. Ma, J. E. Riggs and Y. P. Sun, *J. Phys. Chem. B*, 1998, **102**, 5999.

ChemComm

A tetraazaporphyrin with an intense, broad near-IR band†

Victor N. Nemykin and Nagao Kobayashi*

Department of Chemistry, Graduate School of Science, Tohoku University, Sendai 980-8578, Japan.
E-mail: nagaok@mail.cc.tohoku.ac.jp

Received (in Cambridge, UK) 19th September 2000, Accepted 5th December 2000
First published as an Advance Article on the web 4th January 2001

A tetraazaporphyrin (TAP) prepared by condensation of 1-ferrocenyl-1,2,2-tricyanoethylene in the presence of magnesium shows an intense, broad near-IR band in the 700–1300 nm region, which may be ascribed to charge-transfer transitions from the ferrocenyl moiety (substituents) to the TAP ligand.

Ferrocene (Fc)-modified porphyrins,[1] porphyrazines,[2] and phthalocyanines (Pcs)[3] have been reported over the past few decades. Although these compounds show characteristics ascribable to the Fc moiety such as the $Fe^{II/III}$ redox couple, their spectroscopic properties are generally similar to normal porphyrins and Pcs, except for a slight change in the shape or positions seen occasionally. In this regard, the TAP compound which we report here, *i.e.* 2,7,12,17-tetracyano-3,8,13,18-tetraferrocenyl-5,10,15,20-tetraazaporphyrinatomagnesium, **1**, is unusual in showing an intense, broad absorption band in the near-IR region (700–1300 nm), beyond the Q band. TAPs are structurally intermediate compounds between porphyrins and Pcs, and some porphyrins[4] and Pcs[5] are known to show near-IR absorption bands having much weaker intensity than the Q band, which can be assigned to either d–d transitions[6] in the central metal or charge-transfer (CT) transitions from the central metal to the ligands. Our compound **1**, on the other hand, has a broad, intense near-IR band, which may be assigned to charge-transfer from the iron in the substituent group to the TAP ligand, as described below.

Compound **1** was synthesized, in the presence of magnesium, by condensation of 1-ferrocenyl-1,2,2-tricyanoethylene, **2**, which was obtained from chloromercurioferrocene and tetracyanoethylene.[7] Fig. 1 shows the electronic absorption and magnetic circular dichroism (MCD) spectra of **1** and **2**. The starting material **2** showed two absorption peaks at 363 and 628 nm, while the TAP **1** had absorption maxima at 382, 623, and 962 nm. From the shape and intensity of the MCD band, the bands at 382 and 623 nm of **1** are assigned as the Soret and Q bands, respectively. The near-IR band can not be a π–π* transition in the TAP ligand, since the Q band corresponds to the HOMO–LUMO transition in the normal porphyrinic compounds. In addition, the possibility of this being a d–d transition is small because of the large absorption coefficient (ε = 13200 $dm^3\ mol^{-1}\ cm^{-1}$), which is a few orders of magnitude larger than normal d–d transitions ($0 < \varepsilon <$ *ca.* $10^2\ dm^3\ mol^{-1}\ cm^{-1}$; the d–d transition is a forbidden transition by the Laporte selection rule). The only feasible possibility appears to be CT transitions between the Fc moiety and the TAP ligand (the magnesium ion in the center of the TAP skeleton does not participate since it does not contain d electrons). However, since this kind of near-IR band has not been detected in Pcs and porphyrins having only a Fc moiety,[1,3] the presence of electron-withdrawing cyano groups in the close proximity may be of crucial importance. In accordance with this conjecture, the peak wavelength of the near-IR band changed from 962 nm in chloroform to 905 nm in ethanol and further to 888 nm in DMSO.

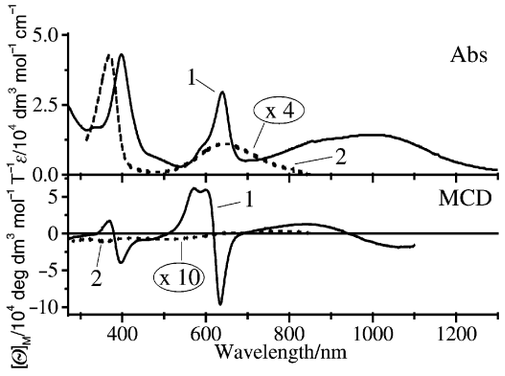

Fig. 1 Electronic absorption and MCD spectra of **1** (solid lines) and **2** (dotted lines) in chloroform.

In order to further gain some insight into the origin of the near-IR band, redox potentials of **1** and **2** were measured in *o*-dichlorobenzene, and the spectra of the electrolysed **1** have been recorded. Compound **2** showed one reversible oxidation peak at 0.38 V *vs.* Fc/Fc^+, which can be assigned to the $Fe^{II/III}$ couple, and one irreversible reduction peak at −1.35 V, which can be tentatively assigned to the formation of the tricyanovinyl-localized anion-radical.[8] The TAP **1** showed two reversible one-electron reduction processes at −0.84 and −1.28 V, and one reversible four-electron oxidation process at 0.06 V and one irreversible quasi one-electron oxidation process at 0.97 V. From the amount of the current and the position, the first oxidation is clearly assigned to the Fc moiety, *i.e.* $Fe^{II/III}$ and other couples are TAP-centered. Of course, an irreversible reduction peak tentatively assigned to the tricyanovinyl moiety in **2** disappeared in **1**, because the two cyano groups of the three cyano groups in **2** were used for the TAP core formation. The potential difference between the 1st oxidation and reduction potential of the TAP ligand (1.81 V) is much smaller than that of general tetraazaporphyrins (*ca.* 2.1–2.2 V)[9] due perhaps to the stabilization of the LUMOs by cyano groups. If the band in the near-IR region of **1** is associated with CT between the Fc moiety and the TAP ligand, the shape of this band should change significantly by electrolysis positive of the first oxidation potential. Accordingly, the solution of **1** was electrolysed at 0.21 V and the concomitant spectroscopic changes were monitored (ESI†). With the progress of electrolysis, the near-IR band faded away, the Soret band lost its intensity by one-third, and the Q band shifted to the red at 663 nm, in accord with the above expectations. From the linear relationship between the absorbance and concentration (Beer's law experiments, ESI†), the possibility of the near IR band being due to the aggregation can also be ruled out.

Furthermore, the molecular orbitals of the starting material **2** were calculated using the time-dependent DFT method, realized in the Gaussian 98W program (B3LYP functional and the SVP basis set).[10] The results of the first 10 lowest transitions are shown in Table 1. Transitions 1–3 and probably 5 correspond to a broad band between *ca.* 500 and 800 nm, and those 7–10 would be related to a strong band at *ca.* 350–400 nm. Taking into account that orbitals 76 (d_{yz}, E = −1.235 eV), 75

† Electronic supplementary information (ESI) available: absorption spectra and Beer's law experiments. See http://www.rsc.org/suppdata/cc/b0/b007515i/

Table 1 Calculated transition energies, oscillator strength (*f*), and configurations for compound **2**

Transition	Energy/ eV (nm)	*f*[a]	Configurations[b]		
1	1.726 (718)	0.0002	72→74 (75%)	72→76(10%)	
2	1.896 (654)	0.0208	73→74(57%)	73→76(15%)	
3	2.297 (540)	0.0012	71→74(24%)	70→74(22%)	72→75(14%)
			71→76(11%)	70→76(10%)	
5	2.629 (472)	0.0073	72→75(28%)	73→74(19%)	72→76(14%)
				73→76(14%)	71→74(12%)
7	3.223 (385)	0.0170	73→76(27%)	70→74(17%)	
8	3.413 (363)	0.0094	69→74(87%)		
9	3.506 (354)	0.2525	71→74(33%)	70→74(29%)	68→74(16%)
10	3.547 (350)	0.0025	72→76(14%)	73→75(11%)	70→75(11%)
				71→75(10%)	

[a] *f* greater than 0.0001 are shown. [b] Configurations greater than 10% are shown.

(LUMO+1, d_{xz}, −1.245), 73 (HOMO, d_{xy}, −6.486), 72 (d_{x2-y2}, −6.563), 71 ($a_1(\pi$, Fc, 47%) and d_{z2}(53%), −7.305), and 70 ($a_1(\pi$, Fc, 51%) and d_{z2}(43%), −7.459) are the iron ion or ferrocene-centered orbitals, while the orbital 74 (LUMO, −3.551) has 76% of its density on the tricyanovinyl fragment, the band to the longest wavelength between *ca.* 500 and 800 nm can be assigned to CT transitions from the filled iron ion orbitals in ferrocene to π* orbitals of the tricyanovinyl group. Unfortunately, similar calculations on **1** could not be performed, because the molecule was too large. However, considering that the Mössbauer parameters of **1** (isomer shift δ = 0.68 mm s^{-1}, quadrupole splitting ΔE_Q = 2.31 mm s^{-1}) and **2** (δ = 0.68, ΔE_Q = 2.06) are similar, and accordingly that the state of the iron ion in the two compounds is similar, the near-IR band of **1** may also be assigned as CT transitions between the Fc moiety and the TAP ligand with electron-withdrawing cyano groups[11] (*i.e.* the above CT transitions in **2** may correspond to the CT transitions from the iron ion in the Fc toward the nitrile groups in the TAP ligand of **1**). Thus, although the CT bands reported so-far on porphyrins and phthalocyanines have always been between the central metal and the ligands,[4,5] compound **1** appears to be the first porphyrin or phthalocyanine which shows a CT band from the metal in the substituent to the parent ligand.

V. N. N. is grateful to JSPS for financial support (grant P98418). This work was partially financed by a Grant-in-Aid for Scientific Research (B) 12020206 from the Ministry of Education, Science, Sports and Culture, Japan to N. K.

Notes and references

1 (*a*) E. S. Schmidt, T. S. Calderwood and T. C. Bruice, *Inorg. Chem.*, 1986, **25**, 3718; (*b*) P. D. Beer and S. S. Kurek, *J. Organomet. Chem.*, 1989, **366**, C6; (*c*) R. W. Wagner, P. A. Brown, T. E. Johnson and J. S. Lindsey, *J. Chem. Soc., Chem. Commun.*, 1991, 1463; (*d*) K. Uosaki, T. Kondo, X. Q. Zhang and M. Yanagida, *J. Am. Chem. Soc.*, 1997, **119**, 8367; (*e*) N. B. Thornton, H. Wojtowicz, T. Netzel and D. W. Dixson, *J. Phys. Chem. B*, 1998, **102**, 2101; (*f*) P. D. Boyed, A. K. Burrell, W. M. Campbell, P. A. Cocks, K. C. Gordon, G. B. Jameson, D. L. Officer and Z. Zhao, *Chem. Commun.*, 1999, 637.

2 T. F. Baumann, J. W. Sibert, M. M. Olmstead, A. G. M. Barrett and B. M. Hoffman, *J. Am. Chem. Soc.*, 1994, **116**, 2639; T. F. Baumann, M. S. Nasir, J. W. Sibert, A. J. P. White, M. M. Olmstead, D. J. Williams, A. G. M. Barrett and B. M. Hoffman, *J. Am. Chem. Soc.*, 1996, **118**, 10 479.

3 (*a*) Z. Jin, K. Nolan, C. R. McArthur, A. B. P. Lever and C. C. Leznoff, *J. Organomet. Chem.*, 1994, **468**, 205; (*b*) M. J. Cook, G. Cooke and A. Jafari-Fini, *J. Chem. Soc., Chem. Commun.*, 1995, 1715; (*c*) S. Dabak and O. Bekaroglu, *New J. Chem.*, 1997, **21**, 267; (*d*) J. Silver, J. L. Sanchez and C. S. Frampton, *Inorg. Chem.*, 1998, **37**, 411; (*e*) A. Gonzalez, P. Vazquez and T. Torres, *Tetrehedron Lett.*, 1999, **40**, 3263; (*f*) K.-W. Poon, Y. Yan, X. Li and D. K. P. Ng, *Organometallics*, 1999, **18**, 3528.

4 M. Gouterman, in *The Porphyrins*, ed. D. Dolphin, Academic Press, New York, 1978, vol. III, p. 1.

5 M. J. Stillman and T. Nyokong, in *Phthalocyanines: Properties and Applications*, ed. C. C. Leznoff and A. B. P. Lever, VCH, New York, 19809, vol. I, p. 133; A. B. P. Lever, S. R. Pickens, P. C. Minor, S. Licoccia, B. S. Ramaswamy and K. Magnell, *J. Am. Chem. Soc.*, 1981, **103**, 6800.

6 W. A. Eaton and E. Charney, *J. Chem. Phys.*, 1969, **51**, 4502.

7 Synthesis of compounds **1** and **2** and their representative data. Compound **2**. Following the method reported in E. G. Prevalova, D. A. Lemonovski, V. P. Alekseev, K. I. Grandberg and A. N. Nesmeyanov, *Izv. Akad. Nauk SSSR, Ser. Khim.*, 1972, **8**, 1867, to a stirred solution of chloromercurferrocene (2.205 g, 0.01 mol) in 150 ml of acetonitrile, tetracyanoethylene (1.28 g, 0.01 mol) was added in one portion. The mixture was refluxed for 3 h and the solvent evaporated to dryness under reduced pressure. The resulting solid was dissolved in chloroform and chromatographed on an alumina column (Act. II) using chloroform–heptane (1:4 v/v) as eluent. The blue band was collected and recrystallized from chloroform–heptane (1:19 v/v), to give 1.15 g (40%) of the dark-blue crystals. Anal. Found: C, 63.02; H, 3.28; N, 14.36%. Calcd for $C_{15}H_9N_3Fe$: C, 62.75; H, 3.16; N, 14.64%. MS (EI, 70V) *m/z*: 287 (M^+, 100%). mp 132–133 °C. ^{1}H NMR δ ($CDCl_3$, TMS): 4.50 (5H, s, β-Cp), 5.17 (2H, t, α-Cp), 5.27 (2H, t, α-Cp). UV-Vis (λ_{max}, nm (log ε), $CHCl_3$): 300sh, 363 (4.04), 628 (3.43). Compound **1**. 3 ml butyl alcohol solution of **2** (70 mg, 4 mmol) and magnesium butoxide from 12 mg magnesium was refluxed for 4 h under a nitrogen atmosphere. After the solution was cooled to rt, the residue was imposed on a silica-gel column using chloroform as eluent. The green band was collected and further chromatographed on an alumina column (Act. I) using toluene–ethanol (4:1 v/v) as eluent. Finally, the green fraction was purified on a gel permeation column (Bio-beads SX-1, Bio-rad) using chloroform as eluent, followed by recrystallization from chloroform–hexane (1:19 v/v), to give *ca.* 11 mg (15%) of dark-green **1** as a mixture of several positional isomers. Anal. Found: C, 61.5; H, 3.1; N, 14.3%. Calcd for $C_{60}H_{36}N_{12}Fe_4Mg$: C, 62.22; H, 3.54; N, 13.84%. MS (MALDI-TOF, dithranol) *m/z*: 1172 (M^+, 100%) mp > 250 °C. ^{1}H NMR δ ($CDCl_3$, TMS): 4.12 (8H, s, α-Cp), 4.23 (20H, s, β-Cp), 5.19 (8H, s, α-Cp). UV-Vis. (λ_{max}, nm (log ε), $CHCl_3$): 320sh, 382 (4.67), 430sh, 590sh, 623 (4.47), 962 (4.12).

8 K. P. Butin, A. A. Moiseeva, I. G. Ilina, E. V. Ivanova and A. N. Ryabtsuev, *J. Gen. Chem. (Engl. Transl.)*, 1993, **63**, 372.

9 N. Kobayashi, in *The Porphyrin Handbook*, ed. K. M. Kadish, K. M. Smith and R. Guilard, Academic Press, New York, 1999, vol. II, p. 301.

10 M. J. Frisch, G. W. Trucks, H. B. Schlegel, P. M. W. Gill, B. G. Johnson, M. A. Robb, J. R. Cheeseman, T. A. Keith, G. A. Petersson, J. A. Montgomery, K. Raghavachari, M. A. Al-Laham, V. G. Zakzewski, J. V. Ortiz, J. B. Foresman, J. Cioslowski, B. B. Stefanov, A. Nanayakkara, M. Challacombe, C. Y. Peng, P. Y. Ayala, W. Chen, M. W. Wong, J. L. Andres, E. S. Replogle, R. Gomperts, R. L. Martin, D. J. Fox, J. S. Binkley, D. J. Defrees, J. Baker, J. P. Stewart, M. Head-Gordon, C. Gonzalez and J. A. Pople, *Gaussian 98W*, (Revision A.7), Gaussian Inc., Pittsburgh PA, 1998.

11 Pcs with directly linked Fc units do not show near-IR bands beyond the Q band.[3a] Accordingly, this suggests that the near-IR band in **1** would not be observed unless cyano groups are not present in the periphery of **1**.

Thermal reactivities of isostructural d^{10} metalloenediynes: metal-dependent Bergman cyclization†

Elbert W. Schmitt, John C. Huffman and Jeffrey M. Zaleski*

Department of Chemistry and Biochemistry, Indiana University, Bloomington, IN 47405, USA.
E-mail: zaleski@indiana.edu

Received (in Irvine, CA, USA) 11th October 2000, Accepted 29th November 2000
First published as an Advance Article on the web 4th January 2001

Isostructural d^{10} metalloenediynes of Cu(I), Pd(0) and Ag(I) exhibit metal-dependent variations in their thermal Bergman cyclization temperatures which correlate with differences in their alkyne termini separations.

The intriguing chemical reactivities and antitumor properties of the enediyne antibiotics[1] have generated considerable interest in controlling thermal Bergman cyclization reactions with simple synthetic motifs. Within this theme, structure/activity relationships for organic enediynes have documented the importance of the alkyne termini separation (*d*) as well as molecular strain in the ground and transition states.[2–5]

Recent work documenting that metal ions can greatly influence the conformation of the enediyne linkage thereby modulating the thermal reactivity of the resulting complex[6–8] broke ground for metal geometry control of Bergman cyclization reactions. It has now been shown that Bergman cyclization temperatures of metalloenediyne complexes of a given metal and enediyne ligand can be reduced by > 80 °C by variations in metal center geometry from tetrahedral to planar or tetragonal.[6,9–11] However, the influence of different metal ions on the Bergman cyclization temperature for a specific enediyne ligand within a well defined metal complex geometry has not been systematically evaluated. To this end, we report the X-ray structures and thermal reactivities of two homoleptic d^{10} metalloenediyne complexes [Cu(I) and Ag(I)] of 1,2-bis(diphenylphosphinoethynyl)benzene (dppeb, **1**). In conjunction with the Pd(dppeb)$_2$ analog **2**,[9] these complexes comprise a unique isoelectronic and isostructural set which exhibit significant differences in alkyne termini separation and consequently Bergman cyclization temperatures.

The Cu(I)‡ and Ag(I)§ metalloenediyne complexes were prepared by reacting 2 equivalents of **1** with the appropriate monovalent metal salt under N_2 to generate the $[M(dppeb)_2]^+$ d^{10} metalloenediyne cation.

Complexes **3** and **4** were isolated and purified by recrystallization from CH_2Cl_2–diethyl ether and MeCN–H_2O, respectively, as well as characterized in solution by NMR (^{1}H, ^{13}C) and mass spectrometry.

The X-ray crystal structures¶ of the cations of **3** (Fig. 1) and **4** (Fig. 2) reveal the isostructural identities of these complexes with respect to **2**.[9] Both d^{10} metal centers have local tetrahedral geometries with nearly idealized P–M–P angles (**3**: 107°, **4**: 108°). The tetrahedral geometries of these species promote a decrease in the alkyne termini separation *d*, relative to the free ligand but force an increase in *d* relative to square planar or tetragonal geometries.[10,11] For **2**–**4**, the average alkyne termini separation increases by 0.19 Å along the series Cu(I) (3.44 Å) < Pd(0) (3.47 Å) < Ag(I) (3.62 Å). For **2** and **3**, the differences in *d* are statistically insignificant. The average M–P bond lengths also increase from Cu(I) (2.33 Å) ≈ Pd(0) (2.33 Å) < Ag(I) (2.52 Å), reflecting contributions from both variations in atomic radii as well as metal–ligand covalency. Both structures exhibit bent alkyne units due to distortion of the enediyne unit induced by metal chelation. For **3**, the P–C≡C and C≡C–C angles are 166 and 170°, respectively, while for **4**, the same angles are 165 and 173°. The dppeb ligands in both complexes are also planar which minimizes out-of-plane structural contributions to the thermal reactivities of the complexes.

Off-resonance (λ = 785 nm) Raman spectra of **1**–**4** as a neat oil (for **1**) or solid states have been obtained in order to assess electronic contributions to the geometric structures which may influence thermal Bergman cyclization reactivities. The spectra (**1**, **3** in Fig. 3) are comprised primarily of alkyne (2150–2170 cm^{-1}), as well as phenyl ring and 1,2-disubstituted benzene group frequencies (500–1600 cm^{-1}).[12] The spectra of the metal complexes **2**–**4** are remarkably similar, indicating that with exception of the alkyne stretch, all of the ligand normal modes are relatively isolated from the effects of metal ion coordination. To this end, $\nu_{C\equiv C}$ for **1** (2160 cm^{-1}) is nearly degenerate with the average alkyne stretch for **3** (2168, 2155 cm^{-1}) and **4** (2165,

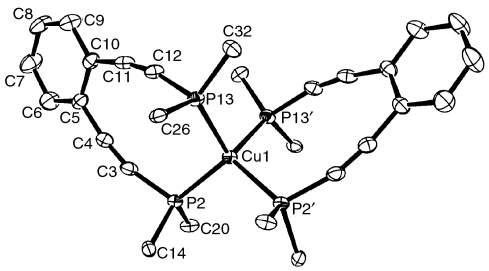

Fig. 1 ORTEP of the X-ray structure of the cation of **3** shown at 50% probability. Only the *ipso* carbon atoms of the phenyl rings are shown for clarity. Selected bond lengths (Å) and angles (°): Cu(1)–P(2) 2.3176(14), Cu(1)–P(13) 2.3406(14); P(2)–Cu(1)–P(2′) 110.14(7), P(2)–Cu(1)–P(13) 111.17(5), P(2)–Cu(1)–P(13′) 110.25(5), P(13)–Cu(1)–P(13′) 103.72(7), P(2)–C(3)–C(4) 166.3(5), P(13)–C(12)–C(11) 167.0(4), C(3)–C(4)–C(5) 171.1(5), C(10)–C(11)–C(12) 169.0(5).

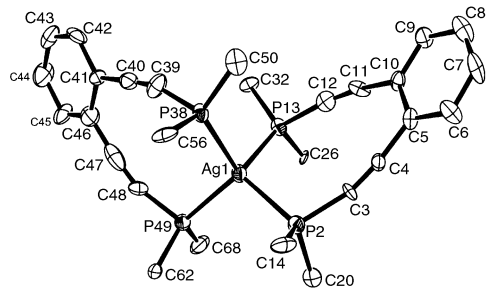

Fig. 2 ORTEP (50% probability) of the X-ray structure of the cation of **4** with phenyl rings removed for clarity. Selected bond lengths (Å) and angles (°): Ag(1)–P(2) 2.477(4), Ag(1)–P(13) 2.524(4), Ag(1)–P(38) 2.527(4), Ag(1)–P(40) 2.508(4); P(2)–Ag(1)–P(13) 110.52(14), P(2)–Ag(1)–P(38) 110.49(12), P(2)–Ag(1)–P(49) 109.97(9), P(13)–Ag(1)–P(38) 105.08(8), P(13)–Ag(1)–P(49) 108.40(12), P(38)–Ag(1)–P(49) 112.26(13), P(2)–C(3)–C(4) 165.1(13), P(13)–C(12)–C(11) 170.0(13), P(38)–C(39)–C(40) 159.9(16), P(49)–C(48)–C(47) 164.6(15), C(3)–C(4)–C(5) 172.6(14), C(10)–C(11)–C(12) 170.7(14), C(39)–C(40)–C(41) 175.9(15), C(46)–C(47)–C(48) 173.4(16).

† Electronic supplementary information (ESI) available: differential scanning calorimetry data for complexes **2**–**4**. See http://www.rsc.org/suppdata/cc/b0/b008337m/

DOI: 10.1039/b008337m

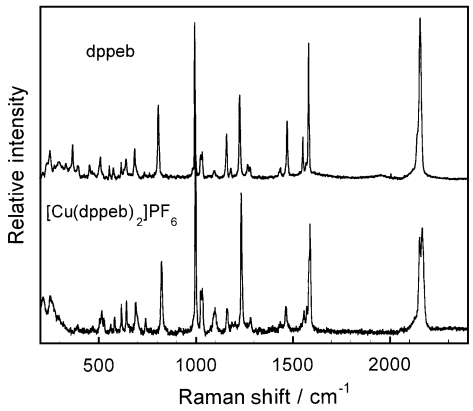

Fig. 3 Off-resonance Raman spectra of neat samples of dppeb **1** and $[Cu(dppeb)_2]PF_6$ **3** obtained with 1 mW at λ = 785 nm.

2153 cm^{-1}) which are comprised of two anisotropic vibrational components within the solid state. For **2** however, these values are shifted to lower energy by an average of 9 cm^{-1} (2155, 2149 cm^{-1}) indicative of only very modest back-donation from Pd(0) to the alkyne π-system through the empty p- and d-orbitals of the phosphine. This electronic contribution is not significant and likely does not strongly influence enediyne reactivity.

The Bergman cyclization temperatures for **2**–**4** have been determined by DSC in the solid state (Table 1) and show the following dependence on metal ion: Cu(I) (227 °C) ≈ Pd(0) (222 °C) < Ag(I) (266 °C). The DSC temperatures correspond to formation of the Bergman cyclized 1,4-phenyl diradical intermediate and rapid reaction to generate intractable black product complexes in the solid state. Unlike thermal cyclization reactions in the presence of H-atom donor in solution, the absence of a large excess of H-atom donor in the solid-state reaction inhibits quenching of the intermediate to specifically trap the disubstituted benzene product. In the absence of H-atom donor, we and others[13] have observed formation of black, insoluble polymeric products for various enediyne thermal cyclization reactions.

Table 1 Bergman cyclization temperatures of d^{10} metalloenediynes

Compound	Cyclization temperature/°C	Alkyne termini separation/Å
2	222[a]	3.47
3	227	3.44
4	266	3.62

[a] This value was originally reported as an onset temperature (209 °C).[9]

The Bergman cyclization temperatures directly correlate with the increased alkyne termini separation between **2** and **3**, and **4**. The 44 °C variation in the cyclization temperatures reflects the intimate relationship between the geometric structure of the metalloenediyne and the Bergman cyclization temperature of the resulting complex. Unlike previous examples of diverse structural variations in either metalloenediyne composition and/or geometry which strongly influence Bergman cyclization temperatures, in this case subtle variations in M–P bonding can introduce significant increases in *d* and consequently the thermal stabilities of the complexes. These results systematically reveal the prominent role that metal ions can play in affecting Bergman cyclization of the enediyne ligands and the intimate contribution that the specific metal ion has in modulating the reactivities of these metalloenediynes.

The generous support of the American Cancer Society (RPG-99-156-01-C), the Donors of the Petroleum Research Fund (PRF#33340-G4), administered by the American Chemical Society, Research Corporation (Research Innovation Award #RI0102 for J. M. Z.), and the NSF-CRIF program (CHE-0077942) are gratefully acknowledged. The authors also wish to thank Dr Diwan Rawat, Nicole Coalter, and Brian Kraft for technical assistance.

Notes and references

‡ *Synthesis* of **3**: dppeb (0.26 g, 0.53 mmol) was stirred with $[Cu(MeCN)_4](PF_6)$ (0.098 g, 0.26 mmol) in dry, degassed MeCN (20 ml) under nitrogen overnight at room temperature. The solvent was then removed *in vacuo* and the residue was dissolved in CH_2Cl_2. The solution was filtered and an off white solid precipitated from solution upon addition of diethyl ether. A white crystalline compound was obtained after recrystallization from CH_2Cl_2–diethyl ether and dried *in vacuo*. Crystals suitable for characterization by X-ray crystallography were grown from a saturated CH_2Cl_2–diethyl ether solution. Yield 150.1 mg (42%). δ_H(400 MHz, CD_2Cl_2), 7.62–7.72 (m, 8H), 7.21–7.24 (m, 24H), 6.96 (t, 16H). $\delta_C(CD_2Cl_2)$, 132.12, 131.05, 130.89, 130.83, 130.67, 129.26, 127.10, 112.03, 88.29. ^{31}P NMR (CD_2Cl_2, −80 °C, rel. to 85% H_3PO_4) −18.20 (br s), −144.33 (sept., PF_6). MS, *m/z* (ESI) 1051.4 ($M^+ - PF_6$).

§ *Synthesis* of **4**: dppeb (0.11 g, 0.22 mmol) was stirred under nitrogen with $AgNO_3$ (0.019 g, 0.11 mmol) in degassed acetone (20 ml) at room temperature for 3 h after which the solvent volume was reduced by half *in vacuo*. A saturated, aqueous solution of NH_4PF_6 was then added producing a white solid that was removed by filtration, recrystallized from acetone–H_2O, and dried *in vacuo*. Crystals suitable for characterization by X-ray crystallography were grown from a saturated MeCN–H_2O solution. Yield 64.9 mg (46%). δ_H(400 MHz, CD_3CN), 7.60–7.70 (m, 8H), 7.30–7.34 (m, 24H), 7.06 (t, 16H). $\delta_C(CD_3CN)$, 132.82, 131.99, 131.79, 131.73, 131.33, 130.17, 126.94, 112.01, 87.60. $\delta_P(CD_3CN$, rel. to 85% H_3PO_4), −17.77 (apparent doublet, unresolved $\Delta J_{Ag(x)-P}$ (x = 107, 109); apparent J_{Ag-P} 223.62 Hz), −143.28 (sept., PF_6). Anal. Calc. for $C_{68}H_{48}AgP_5F_6{\cdot}H_2O$: C, 64.83; H, 4.00. Found: C, 64.76; H, 3.80%.

¶ *Crystallographic data*: for **3**: $C_{70}H_{52}Cl_4CuF_6P_5$, M = 1367.40, orthorhombic, space group *Pbcm*, Z = 4, a = 11.5309(4), b = 20.2376(7), c = 28.5051(11) Å, V = 6651.9(4) Å^3, μ(Mo-Kα) = 0.667 mm^{-1}, T = 135 K, 6846 unique reflections (R_{int} = 0.063) were used in all calculations. A Bruker platform goniometer equipped with a SMART 6000 CCD detector was used for data collection using the ω scan technique. Direct methods (Bruker software: SHELXS) were used in the solution of the structure. Anisotropic thermal parameters were used on the non-hydrogen atoms while isotropic thermal parameters were used on the hydrogen atoms which were included as fixed atom contributors for the final least-squares refinement. Within the unit cell, the cation, anion and solvent molecules lie in special positions. The final agreement factors were R = 0.0495 (observed data), R_w = 0.0610 (all data).

For **4**: $C_{68}H_{54}AgF_6O_3P_5$, M = 1295.9, orthorhombic space group $Pb2_1m$, Z = 4, a = 11.4950(4), b = 20.2486(7), c = 28.7007(9) Å, V = 6680.3(4) Å^3, T = 113 K, μ(Mo-Kα) = 0.4802 mm^{-1}, 8056 unique reflections (R_{int} = 0.063) were used in all calculations. Anisotropic thermal parameters were used on the non-hydrogen atoms and hydrogen atoms were included as fixed atom contributors with isotropic thermal parameters for the final least-squares refinement. The electron density map contained several other partial occupancy peaks that were attributed to water. The structure contains two PF_6 anions, one of which is disordered but well resolved. Both PF_6 anions lie on a crystallographic mirror plane. The final agreement factors were R = 0.0574 (observed data), R_w = 0.0737 (all data). CCDC 182/1867. See http://www.rsc.org/suppdata/cc/b0/b008337m/ for crystallographic files in .cif format.

1 A. L. Smith and K. C. Nicolaou, *J. Med. Chem.*, 1996, **39**, 2103.
2 K. C. Nicolaou, G. Zuccarello, C. Riemer, V. A. Estevez and W.-M. Dai, *J. Am. Chem. Soc.*, 1992, **114**, 7360.
3 P. Magnus, S. Fortt, T. Pitterna and J. P. Snyder, *J. Am. Chem. Soc.*, 1990, **112**, 4986.
4 J. P. Snyder, *J. Am. Chem. Soc.*, 1990, **112**, 5367.
5 J. P. Snyder, *J. Am. Chem. Soc.*, 1989, **111**, 7630.
6 B. P. Warner, S. P. Millar, R. D. Broene and S. L. Buchwald, *Science*, 1995, **269**, 814.
7 B. Konig, W. Pitsch and I. Thondorf, *J. Org. Chem.*, 1996, **61**, 4258.
8 A. Basak and J. Shain, *Tetrahedron Lett.*, 1998, **39**, 1623.
9 N. Coalter, T. E. Concolino, W. E. Strieb, C. G. Hughes, A. L. Rheingold and J. M. Zaleski, *J. Am. Chem. Soc.*, 2000, **122**, 3112.
10 P. B. Benites, D. S. Rawat and J. M. Zaleski, *J. Am. Chem. Soc.*, 2000, **122**, 7208.
11 D. S. Rawat, P. J. Benites and J. M. Zaleski, *J. Am. Chem. Soc.*, 2000, submitted.
12 D. Lin-Vien, *The Handbook of Infrared and Raman Characteristic Frequencies of Organic Molecules*, Academic Press, Boston, MA, 1991.
13 J. A. Jens and J. A. Tour, *J. Am. Chem. Soc.*, 1994, **116**, 5011.

ChemComm

Dimerization of tris(*o*-ureidobenzyl)amines: a novel class of aggregates†

Mateo Alajarín,*[a] Antonia López-Lázaro,[a] Aurelia Pastor,[a] Paul D. Prince,[b] Jonathan W. Steed*[b] and Ryuichi Arakawa[c]

[a] *Departamento de Química Orgánica, Facultad de Química, Campus de Espinardo, Universidad de Murcia, E-30100 Murcia, Spain. E-mail: alajarin@um.es*
[b] *Department of Chemistry, King's College London, Strand, London, UK WC2R2LS. E-mail: jon.steed@kcl.ac.uk*
[c] *Department of Applied Chemistry, Kansai University, Suita, 564-8680 Osaka, Japan. E-mail: arak@ipcku.kansai-u.ac.jp*

Received (in Cambridge, UK) 2nd October 2000, Accepted 11th December 2000
First published as an Advance Article on the web 4th January 2001

Dimeric aggregates are formed by the assembly of two tripodal moieties which are held together, both in solution and in the solid state, by a belt of 6 hydrogen-bonded urea functions.

When two or more identical subunits are geometrically and functionally complementary, they may self-assemble to form a super molecule.[1] Urea or thiourea functionalities are excellent candidates to construct molecules that self-assemble by hydrogen-bonding not only in the solid state but are able to persist in solution.[2] Rebek[3] and Böhmer[4] have independently established that calix[4]arenes containing four urea functions at the upper rim form dimers by interdigitation of the all eight ureas in a head-to-tail directional array of 16 hydrogen bonds. Mendoza and coworkers have described dimeric capsules derived from tris(ureido)calix[6]arenes.[5] Herein we report a novel type of self-assembled dimeric aggregate derived from tris(*o*-ureidobenzyl)amines which resemble the structure of ureidocalixarenes.

The tris(ureas) **1**–**3**[6] shown in Scheme 1, easily available[7] from previously reported tris(*o*-azidobenzyl)amines,[8] showed dramatic differences in their ^{1}H NMR spectra when recorded in $CDCl_3$ or DMSO-d_6. While the spectra of **1**–**3** in DMSO-d_6 displayed the expected patterns consistent with averaged C_{3v} symmetries (Fig. 1a), by changing the solvent to $CDCl_3$ a new set of signals corresponding to a dimer (see below) emerged in each case. The ratio in which both species, monomer and dimer, were present in $CDCl_3$ depended on the substituent R^2 to a great extent. Thus, while for the tris(urea) **1** (R^2 = *p*-tolyl) only the signals attributed to the dimer were apparent, for the tris(ureas) **2** and **3** (R^2 = Bn) their spectra were interpreted as corresponding to equilibrium mixtures of both compounds (Fig. 1b).

The dimeric species featured two well separated doublets assigned to the diastereotopic methylenic protons of the $(ArCH_2)_3N$ fragment (J_{gem} = 14.5–15.7 Hz), instead of the singlet observed for the same nuclei in DMSO-d_6. In the dimers emerging from **2** and **3** the ABX systems formed by the three protons of the –CH_2NH– fragments were clearly evident. The signals assigned to the NH protons of the dimers (near 6.0 and 7.6 ppm, in **2·2** and **3·3**) appeared significantly sharp and shifted to lower field when compared to those attributed to the monomers (near 5.2 and 6.3 ppm). The involvement of the urea carbonyl groups as hydrogen bonding acceptors is supported by the δ value of their carbon atoms in the ^{13}C NMR spectra, which were shifted to downfield in $CDCl_3$ ($\Delta\delta$ = 2.8–3.2 ppm). FT-IR of $CHCl_3$ solutions of **1** (13.7 mM) and **2** (16.4 mM) revealed typical hydrogen-bonded NH-stretching bands[9] at 3317–3327 cm^{-1}.

All those data revealed that the dimers **1·1**, **2·2** and **3·3** should possess a highly ordered, hydrogen-bonded structure. Further indication of the existence of **1·1** and **3·3** in solution came from ESI-MS experiments. This technique was used in virtue of its gentle ionization and has been reported to reflect, at least qualitatively, solution phenomena.[10] The spectra in $CHCl_3$ showed the molecular ions of the protonated dimers **1·1** (1463) and **3·3** (1547).

Thus, monomers and their dimeric aggregates coexist in equilibrium in $CDCl_3$. Preliminary calculations of the dimerization constant of **1** by ^{1}H NMR experiments at three concentrations (in the range 1–10 mM in $CDCl_3$) following known equations[11] showed values (82518, 83832 and 84755 M^{-1}) which are comparable within the experimental error margin.

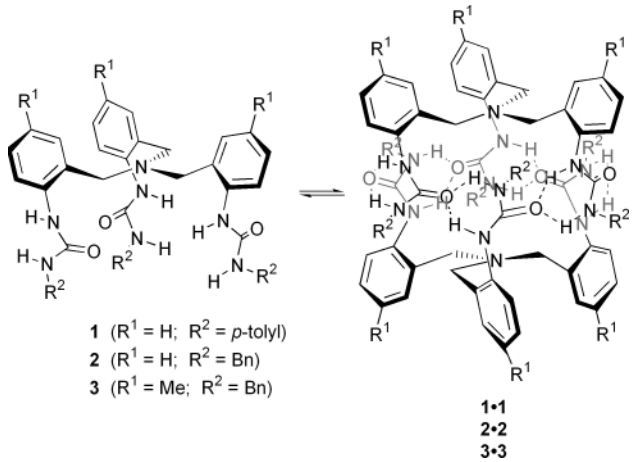

Scheme 1

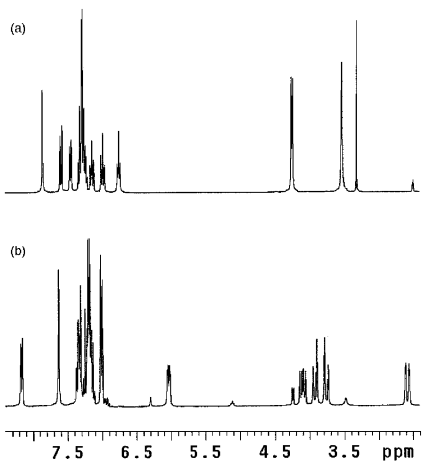

Fig. 1 (a) ^{1}H NMR spectrum (300 MHz) of the tris(urea) **2** in DMSO-d_6 (the singlet at 3.39 ppm is H_2O from the solvent), (b) ^{1}H NMR spectrum measured in $CDCl_3$ showing a mixture of **2** and **2·2**.

† Electronic supplementary information (ESI) available: ^{1}H NMR spectra. See http://www.rsc.org/suppdata/cc/b0/b007955n/

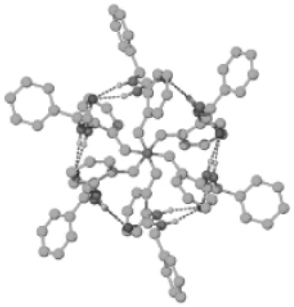

Fig. 2 A perspective view of the molecular structure **2·2**, as projected along the pseudothreefold axis containing the two pivotal nitrogen atoms.

Since DMSO-d_6 is able to disrupt the intermolecular hydrogen bonds, only the monomeric species could be observed in this solvent. The thermodynamic stability of the dimeric aggregate **1·1** proved to be higher than **2·2** and **3·3**. The dimer **1·1** is virtually the only species observed (⩾98%) in a 30 mM $CDCl_3$ solution of **1**. In contrast, the ^{1}H NMR spectra of **2·2** and **3·3** in $CDCl_3$ solutions of the same concentration displayed considerable amounts of their respective monomers (15–20%). These dimerization equilibria were concentration dependent, and could be shifted toward the monomer by decreasing the concentration. These equilibria could be also totally shifted to the monomeric tris(urea) by adding DMSO-d_6 (40%) to the $CDCl_3$ solution. Finally, the composition of a mixture of **2** and **2·2** was found to be temperature dependent; an increase in the temperature shifted the equilibrium toward the monomer. Thus, the 85:15 ratio of **2·2** to **2** measured at 296 K decreased to 72:28 at 323 K (38 mM in $CDCl_3$).

A single crystal X-ray structure[12] of **2·2** confirmed unambiguously the existence of the hydrogen-bonded dimers in the solid state, and provided an exact description of their geometry (Fig. 2). The dimer is composed of two enantiomeric units entangled *via* their urea residues, which form a belt of 12 hydrogen bonds with N···O distances ranging from 2.897(4) to 3.024(4) Å. The dimeric core is of approximate S_6 symmetry, although this is broken by the pendant phenyl substituents. The centre of the capsule is empty and is too small to contain any guest species, however extensive disordered solvent exists in external pockets formed by the aryl groups of the dimer. On the basis of the NMR data ($CDCl_3$) we believe that the conformation shown by the solid state structure of **2·2** is retained in solution.

The formation of heterodimers by the combination of two homodimeric species is a well-known phenomenon in ureidocalixarenes.[3,4] In our case, a mixture of equimolecular amounts of the dimers **1·1** and **2·2** in $CDCl_3$ did not show the formation of heterodimers. However, the ^{1}H NMR spectrum of an equimolecular mixture of **2·2** and **3·3** revealed the appearance of signals attributable to the heterodimer **2·3**, besides those of homodimers **2·2** and **3·3** and monomers **2** and **3**. In this experiment the region of the aryl-NH protons (7.45–7.80 ppm) was especially informative (Fig. 3). Thus, four NH singlets appeared (Fig. 3c), two of them due to the homodimers **2·2** (δ = 7.63 ppm) and **3·3** (δ = 7.61 ppm), and the other two to both aryl-NH protons of the heterodimer **2·3** (δ = 7.51 ppm and δ = 7.73 ppm). The integration revealed a nearly statistical mixture of the three dimers.

In summary, we have shown that tris(*o*-ureidobenzyl)amines **1**–**3** self assemble to form dimeric aggregates in which six urea groups constitute a cyclic array involving a closed network of 12 hydrogen bonds.

This work was supported by DGES (Project PB95-1019) and Fundación Séneca-CARM (Project PB/2/F5/99). J. W. S. thanks the EPSRC and King's College London for the funding of the diffractometer system. A. P. thanks the European Commission for a Marie Curie fellowship (contract HPMF-CT-1999-00126).

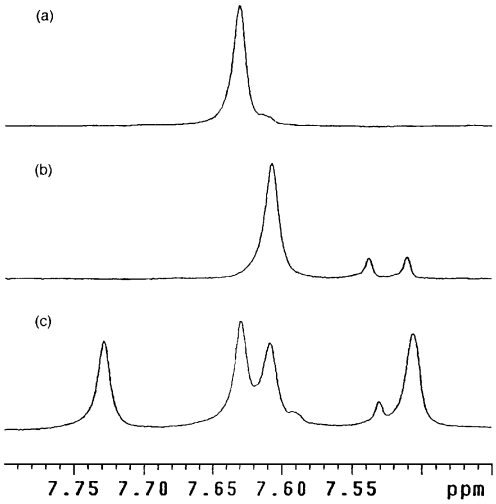

Fig. 3 Partial ^{1}H NMR spectra (300 MHz, $CDCl_3$) showing the N*H*-aryl region: (a) **2·2**; (b) **3·3** (the doublet at 7.53 ppm was assigned to the monomer **3**); (c) mixture of equimolecular quantities of **2·2** and **3·3**.

Notes and references

1 J.-M. Lehn, *Supramolecular Chemistry*, VCH, Weinheim, 1995.
2 M. C. Etter, Z. Urbañczyk-Lipkowska, M. Zia-Ebrahimi and T. W. Panunto, *J. Am. Chem. Soc.*, 1990, **112**, 8415; X. Zhao, Y.-L. Chang, F. W. Fowler and J. W. Lauher, *J. Am. Chem. Soc.*, 1990, **112**, 6627; J. S. Nowick, V. Antonovich, G. Noronha and J. W. Ziller, *J. Org. Chem.*, 1995, **60**, 1888; J. J. Kane, R.-F. Liao, J. W. Lauher and F. W. Fowler, *J. Am. Chem. Soc.*, 1995, **117**, 12 003.
3 B. C. Hamann, K. D. Shimizu and J. Rebek, Jr., *Angew. Chem., Int. Ed. Engl.*, 1996, **35**, 1326; R. K. Castellano, D. M. Rudkevich and J. Rebek, Jr., *J. Am. Chem. Soc.*, 1996, **118**, 10 002; R. K. Castellano, B. H. Kim and J. Rebek, Jr., *J. Am. Chem. Soc.*, 1997, **119**, 12 671; R. K. Castellano and J. Rebek, Jr., *J. Am. Chem. Soc.*, 1998, **120**, 3657; M. S. Brody, C. A. Schalley, D. M. Rudkevich and J. Rebek, Jr., *Angew. Chem., Int. Ed. Engl.*, 1999, **38**, 1640; C. A. Schalley, R. K. Castellano, M. S. Brody, D. M. Rudkevich, G. Siuzdak and J. Rebek, Jr., *J. Am. Chem. Soc.*, 1999, **121**, 4568; R. K. Castellano, C. Nuckolls and J. Rebek, Jr., *J. Am. Chem. Soc.*, 1999, **121**, 11 156.
4 O. Mogck, E. F. Paulus, V. Böhmer, Y. Thondorf and W. Vogt, *Chem. Commun.*, 1996, 2533; O. Mogck, V. Böhmer and W. Vogt, *Tetrahedron*, 1996, **52**, 8489; O. Mogck, M. Pons, V. Böhmer and W. Vogt, *J. Am. Chem. Soc.*, 1997, **119**, 5706; M. O. Vysotsky, I. Thondorf and V. Böhmer, *Angew. Chem., Int. Ed.*, 2000, **39**, 1264.
5 J. J. González, R. Ferdani, E. Albertini, J. M. Blasco, A. Arduini, A. Pochini, P. Prados and J. de Mendoza, *Chem. Eur. J.*, 2000, **6**, 73.
6 All the tris(ureas) **1**–**3** were characterized on the basis of their IR, ^{1}H and ^{13}C NMR spectra and CHN-analyses.
7 Sequential treatment of the corresponding tris(azide) with $LiAlH_4$ (64–68% yield) and *p*-tolyl or benzyl isocyanate, led to the tris(ureas) **1**–**3** in good yields (61–99%).
8 M. Alajarín, P. Molina, A. López-Lázaro and C. Foces-Foces, *Angew. Chem., Int. Ed. Engl.*, 1997, **36**, 67; M. Alajarín, A. López-Lázaro, A. Vidal and J. Berná, *Chem. Eur. J.*, 1998, **4**, 2558.
9 For IR studies of hydrogen bonds, see: I. M. Klotz and J. S. Franzen, *J. Am. Chem. Soc.*, 1962, **84**, 3461; G. P. Dado and S. H. Gellman, *J. Am. Chem. Soc.*, 1994, **116**, 1054.
10 D. E. Clemmer, R. R. Hudgins and M. F. Jarrold, *J. Am. Chem. Soc.*, 1995, **117**, 10 141; M. Scherer, J. L. Sessler, M. Moini, A. Gebauer and V. Lynch, *Chem. Eur. J.*, 1998, **4**, 152.
11 D. J. Cram, H. J. Choi, J. A. Bryant and C. B. Knobler, *J. Am. Chem. Soc.*, 1992, **114**, 7748.
12 Crystallographic data for **2·2**: Formula: $C_{50}H_{51}Cl_2N_7O_3$, triclinic crystal, space group $P\bar{1}$, a = 13.936(3), b = 13.985(3), c = 14.350(3) Å, α = 117.719(3), β = 94.551(3), γ = 108.840(3)°. T = 100(2) K, U = 2253.4(8) Å^3, D_c 1.281 mg m^{-3}, 7864 independent reflections used in refinement, 498 parameters, $R1$ ($I > 2\sigma(I)$) = 0.0805, $wR2$ (all data) = 0.2211. CCDC 182/1878.

ChemComm

The design of second-order nonlinear optical chromophores exhibiting blue-shifted absorption and large nonlinearities: the role of the combined conjugation bridge†

Jingdong Luo,[a] Jianli Hua,[a] Jingui Qin,*[a] Jiqi Cheng,[b] Yaochun Shen,[b] Zuhong Lu,[b] Peng Wang[c] and Cheng Ye[c]

[a] *Department of Chemistry, Wuhan University, Wuhan 430072, P.R. China. E-mail: jgqin@whu.edu.cn; Tel: +86-27-87684117; Fax: +86-27-87647617*
[b] *National Laboratory of Molecular and Biomolecular Electronics, Southeast University, Nanjing 210096, P.R. China*
[c] *Center for Molecular Science, Institute of Chemistry, Chinese Academy of Sciences, Beijing 100080, P.R. China*

Received (in Cambridge, UK) 20th September 2000, Accepted 27th November 2000
First published as an Advance Article on the web 4th January 2001

Two new extended chromophoric systems, in which a 4-aminoazobenzene moiety is linked to a cyclo-bridged hexatriene electron withdrawing group, have been synthesized, and show large optical nonlinearities and unexpected blue-shifted absorption in comparison with shorter chain analogues.

Organic and polymeric second-order nonlinear optical (NLO) materials have been extensively studied for their potential applications involving optical signal processing and telecommunications.[1] One of the major challenges in this area of research is to design and synthesize second-order NLO chromophores simultaneously exhibiting large first molecular hyperpolarizability (β), high chemical and thermal stability, and good optical transparency.[2,3] Most attempts to design molecules with large β since the 1980s have been based upon 'push–pull' compounds,[4] in which a π-conjugated bridge is endcapped with an electron donor group and an electron acceptor group. From the two-level model,[5] the β value of this type of chromophore is a strong function of the absorption maximum (λ_{max}), leading to the so-called nonlinearity–transparency tradeoff.

Among all the attempts to solve this kind of trade-off, it has been proved that the nature of π-conjugated bridge of chromophores is one of the crucial factors in determining the linear and nonlinear optical properties of the chromophores. For example, Alain *et al*. recently reported[6] that chromophore **1** (Fig. 1), in which a biphenyl moiety is present between the diphenylpolyene unit, exhibits a 45 nm (2400 cm^{-1}) blue-shifted absorption and similar optical nonlinearity compared with its all diphenylpolyenic analogue (chromophore **2**, Fig. 1), though the conjugation bridge of **1** is much longer. It seems a worthwhile job to study further the linear and nonlinear optical properties of the chromophores by using a combination of different types of conjugation bridges.

Therefore, we have recently designed two new chromophores (**I** and **II** in Fig. 2)† in which the conjugation bridge of isophorone-protected triene with the terminal acceptors is linked to a donor-substituted azo benzene bridge.

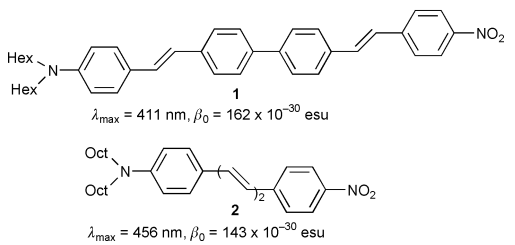

Fig. 1 Chemical structures and properties of chromophores **1** and **2**.

The first molecular hyperpolarizabilities of chromophores **I** and **II** were measured by Hyper-Rayleigh Scattering (HRS) in methanol using the fundamental excitation wavelength of 1064 nm; *p*-nitroaniline (PNA) was used as the external reference. The β values of **I** and **II** were found to be 2890×10^{-30} esu and 3490×10^{-30} esu, respectively, and by using the two-level approximation model, the zero-frequency hyperpolarizabilities β_0 of **I** and **II** were extrapolated to be 337×10^{-30} esu and 198×10^{-30} esu, respectively.

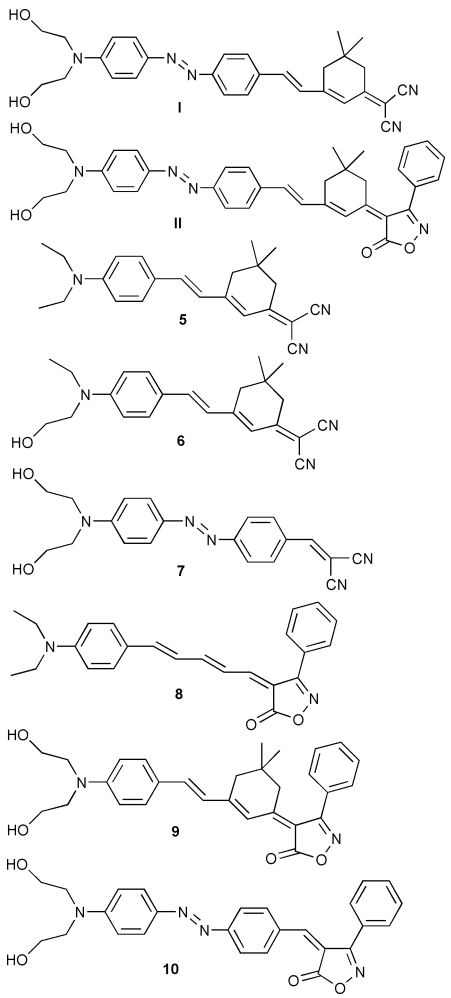

Fig. 2 Chemical structures of chromophores **I**, **II** and their corresponding triene-only and azo-only analogues (chromophores **5**–**10**).

† Electronic supplementary information (ESI) available: synthesis and structural characterization of several new compounds of this work. See http://www.rsc.org/suppdata/cc/b0/b007653h/

DOI: 10.1039/b007653h

Table 1 The linear and nonlinear properties of chromophore **I**, **II** and **5**–**10**

	Solvatochromism data[a] (λ_{max}/nm)				Theoretical investigation[7]		Experimental results	
	$CHCl_3$	AcOEt	DMF	NMP	β_0[b]	f[c]	β^0_{HRS}[d]	f^2
I	490	492	511	519	52.6	2.3302	337	1.0
5	519	504	527	535	46.8	1.5646	—	0.72
6	—	—	—	534	—	—	60[e]	—
7	508	505	525	533	42.5	1.4965	55[e]	0.86
II	510	507	517	533	—	—	198	1.1
8	562	—	—	—	—	—	90[e]	—
9	568	—	—	—	—	—	27[e,13]	—
10	516	524	545	553	—	—	—	0.82

[a] AcOEt: ethyl acetate, DMF: dimethylformamide, NMP: *N*-methylpyrrolidone. [b] AM1/FF results, in units of 10^{-30} esu. [c] ZINDO/S-CI results. [d] Dispersion-corrected β values (in units of 10^{-30} esu) of **I** and **II** were calculated by using an approximate two-level model. [e] β^0_{HRS} values are estimated from the data of β^0_{EFISH} previously reported[8] according to the following equation: $\beta^0_{HRS} = (6/35)^{1/2}\beta^0_{EFISH}$.

Besides the target chromophores **I** and **II**, the other six chromophores (**5**–**10**, see Fig. 2), which are the azo-only or triene-only analogues of **I** and **II**, respectively, will also be discussed below.[8,9]

The linear and the nonlinear properties of these chromophores are summarized in Table 1. It can be seen that **I** and **II**, two chromophores employing the combination of azo benzene and conjugated triene as their conjugation bridge, display unexpectedly blue-shifted absorption compared with the corresponding azo-only or triene-only analogues, although the length of their conjugation bridge is much longer. For instance, the absorption maxima of **I** is about 15 nm (500 cm^{-1}) blue-shifted compared with **5**, **6**, and **7** in different organic solvents. And as shown in Fig. 3, there is no significant broadening of the main absorption band for **I**, if another absorption band around 400 nm in their UV-Vis spectrum is taken into account, and this is also the case for **II**. All these results show that for **I** and **II**, the electron transmission process between donor and acceptor groups is affected, and the intramolecular charge transfer (ICT) efficiency is reduced. This reduction may occur through using different types of bridge with different energy orbitals other than the most efficiently conjugated bridge possible.

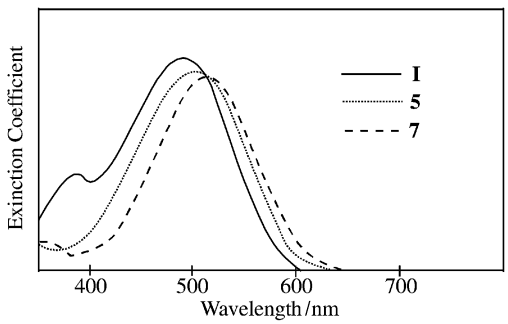

Fig. 3 Comparison of the absorption spectra of chromophores **I**, **5**, and **7** in methanol.

Although the π-electron delocalization efficiency of **I** and **II** is somewhat reduced, it should be noted that the β_0 values of **I** and **II** are quite competitive with those of their corresponding analogues from the theoretical investigation and the experimental results**.** This appears to be at variance with the predictions of the two-level model. However, besides the nonlinearity–transparency trade-off mentioned above, the two-level model also adduces that the β value is a strong function of the oscillator strengths (f) and $\Delta\mu$, the change of dipole moment upon excitation. Thus it can be phenomenologically deduced that the reduction of the ICT efficiency of chromophores **I** and **II** does not accompany a decrease in their f and/or $\Delta\mu$ values, and this has been partially verified by the experimental results. As shown in Table 1, the oscillator strengths (f) of **I** and **II**, respectively determined to be 1.0 and 1.1, are significantly higher than those of the corresponding azo-only or triene-only analogues. It seems that the larger oscillator strengths of **I** and **II** may be one of the major points for counterbalancing the effects of blue shifts. Further study is needed for a full interpretation.

In summary, we have explored two new NLO chromophores with combined conjugation bridges and found that they possess blue-shifted absorption and large molecular nonlinearities. Experimental results indicate that the combined conjugation bridge tunes the linear and nonlinear properties of the chromophores in a different style from those of common homologous chromophores. We expect this methodology to build up new molecular engineering, thereby providing a new opportunity for defeating the 'nonlinearity-transparency trade-off'. Design and synthesis of further chromophores with different types of combined conjugation bridge, and a detailed investigation of the origin of this new effect are currently in progress.

This work was supported by the National Natural Science Foundation of China and by a grant of the Key Fundamental Research Programs of China.

Notes and references

1 S. R. Marder, B. Kippelen, A. K-Y. Jen and N. Peyghambarian, *Nature*, 1997, **388**, 845.
2 C. R. Moylan, R. J. Twieg, V. Y. Lee, S. A. Swanson, K. M. Betterton and R. D. Miller, *J. Am. Chem. Soc.*, 1993, **115**, 12 599.
3 C. Zhang, A. S. Ren, F. Wang, J. Zhu and L. R. Dalton, *Chem. Mater.*, 1999, **11**, 1966.
4 T. Verbiest, S. Houbrechts, M. Kauranen, K. Clays and A. Persoons, *J. Mater. Chem.*, 1997, **7**, 2175.
5 J. L. Oudar, *J. Chem. Phys.*, 1977, **66**, 2664; J. L. Oudar, *J. Chem. Phys.*, 1977, **67**, 446.
6 V. Alain, S. Rédoglia, M. Blandchard-Desce, S. Lebus, K. Lukaszuk, R. Wortmann, U. Gubler, C. Bosshard and P. Günter, *Chem. Phys.*, 1999, **245**, 51.
7 The computational approach has been described in our previous work: P. Zhu, P. Wang and C. Ye, *Chem. Phys. Lett.*, 1999, **311**, 306.
8 C.-F. Shu, W.-J. Tsai and A. K-Y. Jen, *Tetrahedron Lett.*, 1996, **37**, 7055; S. Ermer, S. M. Lovejoy, D. S. Leung, H. Warren, C. R. Moylan and R. J. Twieg, *Mat. Res. Soc. Symp. Proc.*, 1998, **488**, 243; K. D. Singer, J. E. Sohn, L. A. King, H. M. Gordon, H. E. Katz and C. W. Dirk, *J. Opt. Soc. Am. B*, 1989, **6**, 1339; S. R. Marder, L.-T. Cheng, B. G. Tiemann, A. C. Friedli, M. Blandchard-Desce, J. W. Perry and J. Skindh, *Science*, 1994, **263**, 511.
9 Assuming that the dipole moment of chromophore **9** is equal to that of chromophore **8**, the β value of chromophore **9** is estimated from its $\mu\beta$ product reported in the following reference: L. R. Dalton, W. H. Steier, B. H. Robinson, C. Zhang, A. Ren, S. Garner, A. Chen, T. Londergan, L. Irwin, B. Carlson, L. Fifield, G. Phelan, C. Kincaid, J. Amend and A. Jen, *J. Mater. Chem.*, 1999, **9**, 1905.

ChemComm

Formation of nitroethylene during selective catalytic reduction of NO_2 by C_2H_4 over H-ferrierite

Tetsuya Nanba,* Akira Obuchi, Hiroshi Izumi, Yousuke Sugiura, Jiayu Xu, Junko Uchisawa and Satoshi Kushiyama

Atmospheric Environmental Protection Department, National Institute for Resources and Environment, 16-3 Onogawa, Tsukuba, Ibaraki 305-8569, Japan. E-mail: nanba@nire.go.jp

Received (in Cambridge, UK) 23rd October 2000, Accepted 15th November 2000
First published as an Advance Article on the web 4th January 2001

Nitroethylene, formed during the selective catalytic reduction (SCR) of NO_2 by C_2H_4 over H-ferrierite, was determined to be an intermediate in SCR due to its decomposition behavior in forming N_2.

In the selective catalytic reduction (SCR) of NO_x (NO and NO_2) by hydrocarbons, both spectroscopic observation and product analysis support the contention that HNCO and HCN are among the intermediates related to N_2 formation. However, the routes to the formation of these compounds are under discussion. Yokoyama and Misono[1] proposed that nitro compounds are precursors of HNCO and HCN, and Cowan *et al.*[2] speculated that $MeNO_2$ is an intermediate in the SCR of NO_x by CH_4 while Zuzaniuk *et al.* reported that HNCO is produced by nitromethane decomposition over Al_2O_3.[3] Joubert *et al.* also suggested that 2-nitropropane is an intermediate during SCR over a Pt-based catalyst.[4] In this study, we conducted a product analysis of the SCR of NO_2 by C_2H_4 over H-ferrierite, which shows activity for this reaction,[5] and attempted to elucidate the pathway of formation of the nitrogen-containing compounds.

The catalyst sample was obtained by wash-coating *ca.* 30 mg of H-ferrierite (Tosoh; HSZ-720HOA, SiO_2/Al_2O_3 = 17.0) onto a miniature cylindrical cordierite honeycomb (8 mm diameter × 9 mm length, 400 cells in^{-2}).[6] Catalytic activity tests were carried out under conventional flow reactor conditions at ambient pressure. The reactant gas for the SCR of NO_2 was composed of 1000 ppm NO_2, 1000 ppm C_2H_4 and 5% O_2 diluted in He. Products were analyzed with an FTIR spectrometer (Nicolet; Magna 560, resolution set at 0.5 cm^{-1}) equipped with a multi-reflection gas cell (Gemini Specialty Optics; optical path length = 2 m) and GC (Agilent; Micro GC).

Fig. 1(a) shows the gas-phase IR spectrum of the products of SCR at 473 K. To show the unknown band clearly, the absorption bands of coexisting NO_2 and C_2H_4 were subtracted from the original spectrum to an optimum extent. The absorption bands at 1562 and 1546 cm^{-1} were tentatively ascribed to nitro groups. To confirm this assumption, nitroethylene (NE), which was the most probable compound formed, was synthesized according to the literature,[7] and its gas-phase spectrum [Fig. 1(b)] was obtained. Characteristic bands appeared at 1562, 1546, 1384, 1377, 1365, 1355, 963, and 888 cm^{-1}. Comparison with the standard spectrum of 2-nitroethanol [Fig. 1(c)], used as a precursor for the synthesis, shows that this compound was not a contaminant in the synthesized NE. The unknown bands in Fig.1(a) agreed completely with those of NE. To our knowledge, this is the first report of the observation of a gas-phase NE IR spectrum. It is clear that NE is formed during the SCR of NO_2 by C_2H_4. As a comparison, the standard spectrum of nitromethane is shown in Fig. 1(d), which is clearly different from that observed during SCR.

Fig. 2 shows the effect of contact time with a reactant gas on the formation of NE and N_2 at 523 K. The concentration of NE in the product gas decreased drastically at contact times > 0.15 s, becoming negligible at contact times > 0.3 s; on the other hand, the N_2 concentration increased with increasing contact time. This result suggests that NE is an intermediate in the production of N_2. In similar experiments at 623 and 723 K, NE formation was not observed at any contact time, indicating that NE decomposition or a secondary NE reaction is very fast at higher temperatures.

Using the synthesized NE, we further investigated its reactivity over H-ferrierite. In the presence of 5% O_2, decomposition of diluted NE (*ca.* 230 ppm) became prominent above 600 K; CO_2 CO, NH_3 HCN and trace amounts of HNCO and N_2 were observed as the products. The formation of HCN and HNCO is in accord with theoretical calculation results for the thermal decomposition of NE through a four-membered-

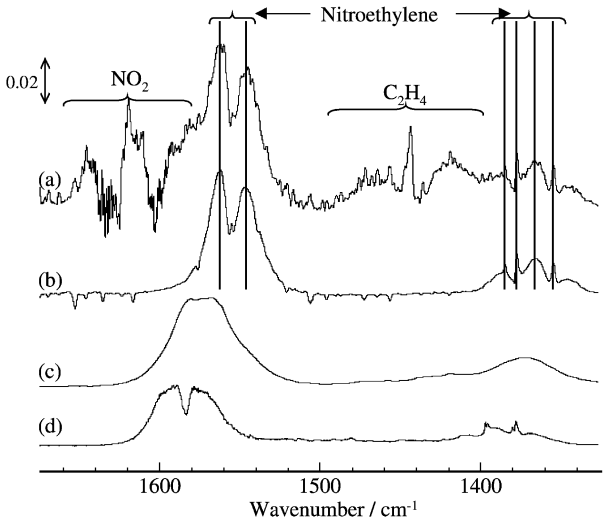

Fig. 1 Gas-phase IR spectra of (a) product gas of SCR of NO_2 by C_2H_4, (b) nitroethylene synthesized in this study, (c) standard 2-nitroethanol and (d) standard nitromethane.

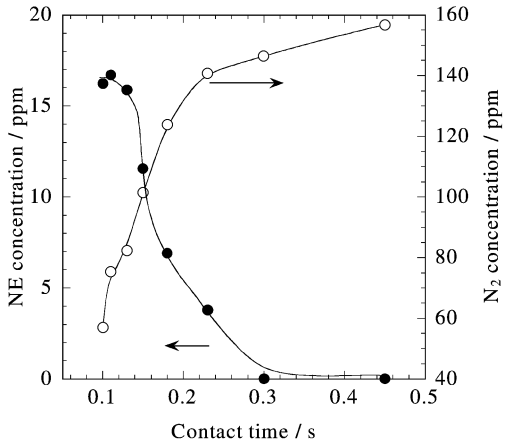

Fig. 2 Effect of contact time on NE and N_2 formation. Symbols indicate the concentration of NE (●) and N_2 (○) in the product gas.

ring structure (4*H*-oxazete *N*-oxide).[8] NH_3 is speculated to be produced by catalytic hydrolysis of HCN[9] and HNCO,[10] which simultaneously form CO and CO_2, respectively.

The formation of NH_3 led us to invoke successive occurrence of the conventional SCR reaction, *i.e.*, selective reaction of NO_x with NH_3 to form N_2 in the presence of excess O_2, over this proton-type zeolite catalyst.[9] Incidentally, under most reaction conditions, the product gas of the SCR of NO_2 with C_2H_4 contains more NO than NO_2; partial reduction of NO_2 to NO by C_2H_4 must have occurred, in addition to the total reduction process. To confirm the above possible role of NH_3 we conducted NE (230 ppm) decomposition over H-ferrierite in the presence of 1000 ppm NO and 5% O_2, as shown in Fig. 3. Conversions in this figure were defined as follows:

NO_x and NE conversion = (Inlet concentration – Outlet concentration)/(Inlet concentration) × 100 (%)

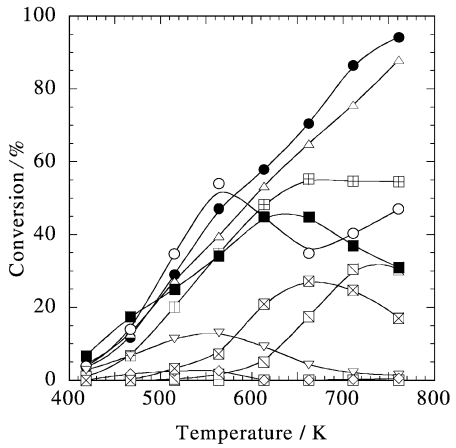

Fig. 3 Behavior of NE decomposition over H-ferrierite. The feed gas was composed of 230 ppm NE, 5% O_2 and 1000 ppm NO. The total flow rate was 160 ml min^{-1}, corresponding to 21 000 h^{-1}. Symbols indicate NE (●) and NO_x conversion (■), and conversion to CO_2 (△), NH_3 (□), N_2 (⊞), CO (○), HNCO (◇), N_2O (▽), HCN (⧅) and HCHO (⊠).

Conversion to products = (Product concentration)/(NE inlet concentration) × 100 (%)

In the presence of NO + O_2, NE decomposition became prominent above 425 K, and the conversion increased with increasing temperature. It is noteworthy that both the NO_x conversion and conversion to N_2 were almost equal to the NE conversion below 623 K. This result strongly suggests that both NE and NO_x molecules supplied, respectively, one nitrogen atom to form one N_2 molecule. The rather high conversion to CO at lower temperatures, amost equal to the NE conversion, might be produced by the decomposition of HCO_2H. We confirmed that HCO_2H is easily produced by the oxidation of HCHO with NO_2 and also decomposed to CO and H_2O over H-ferrierite under conditions similar to that for the present SCR reaction. Formaldehyde should be formed by NE decomposition, simultaneously with HNCO.[8]

To summarize these results, we conclude that the NE we detected is not merely a byproduct in HC-SCR but is very probably an intermediate in the formation of N_2, through conversion to HNCO or HCN followed by formation of NH_3.

Notes and references

1 C. Yokoyama and M. Misono, *Catal. Today*, 1994, **22**, 59.
2 A. D. Cowan, N. W. Cant, B. S. Haynes and P. F. Nelson, *J. Catal.*, 1998, **176**, 329.
3 V. Zuzaniuk, F. C. Meunieer and J. R. H. Ross, *Chem. Commun.*, 1999, 815.
4 E. Joubert, T. Bertin, J. C. Ménézo and J. Barbier, *Appl. Catal. B*, 1999, **23**, 83.
5 K. Yogo, M. Umeno, H. Watanabe and E. Kikuchi, *Catal. Lett.*, 1993, **19**, 131.
6 S. Akaratiwa, T. Nanba, A. Obuchi, J. Okayasu, J. Oi-Uchisawa and S. Kushiyama, *Fifth International Congress on Catalysis and Automotive Pollution Control*, Brussels, 2000, Preprints, vol. 2, p. 127.
7 G. D. Buckley and C. W. Scaife, *J. Chem. Soc.*, 1947, 1471.
8 A. G. Shamov and G. M. Khrapkovskii, *Int. Annu. Conf. ICT*, 1999, pp. 60–1.
9 T. Nanba, A. Obuchi, S. Akaratiwa, S. Liu, J. Uchisawa and S. Kushiyama, *Chem. Lett.*, 2000, 986.
10 R. Dümpelmann, N. W. Cant and D. L. Trimm, *J. Catal.*, 1996, **162**, 96.

Triple-decker main group cations†

Alan H. Cowley,* Charles L. B. Macdonald, Joel S. Silverman, John D. Gorden and Andreas Voigt

Department of Chemistry and Biochemistry, The University of Texas at Austin, Austin, Texas 78712 USA. E-mail: cowley@mail.utexas.edu

Received (in Columbia, MO, USA) 16th June 2000, Accepted 27th November 2000
First published as an Advance Article on the web 8th January 2001

The syntheses of the first main group triple-decker cations are described, namely, [(η⁵-C_5Me_5)Sn(μ-η⁵-C_5Me_5)Sn(η⁵-C_5Me_5)][Ga(C_6F_5)$_4$] and [(η⁶-C_7H_8)In(μ-η⁵-C_5Me_5)In(η⁶-C_7H_8)][(C_6F_5)$_3$BO(H)B(C_6F_5)$_3$], both of which have been characterized by X-ray crystallography; the former was prepared by the reaction of Sn(η⁵-C_5Me_5)$_2$ with Ga(C_6F_5)$_3$, while the latter was prepared by treatment of [In(η⁵-C_5Me_5)]$_6$ with an equimolar mixture of B(C_6F_5)$_3$ and H_2O·B(C_6F_5)$_3$.

An elegant approach to the formation of multidecker, sandwich-type anions of the heavier main group elements consists of the addition of cyclopentadienide anions to neutral metallocenes in the presence of weakly coordinating cations.[1,2] However, to our knowledge, the inverse of this approach has not been reported, *viz.* the synthesis of homonuclear multidecker p-block cations by the addition of positively charged fragments to neutral metallocenes in the presence of appropriate anions. We report two different but complementary reactions that demonstrate the viability of the latter approach.

Since it is known[3] that the reaction of Sn(η⁵-C_5Me_5)$_2$ with a variety of acidic reagents results in salts of [Sn(η⁵-C_5Me_5)]⁺, it was reasoned that, in principle, this cation should be able to add to Sn(η⁵-C_5Me_5)$_2$ to afford the desired triple decker cation [(η⁵-C_5Me_5)Sn(μ-η⁵-C_5Me_5)Sn(η⁵-C_5Me_5)]⁺ **1**⁺. Moreover, it was recognized that the choice of the gegenion would be important, bearing in mind that (a) the anion should be weakly coordinating, and (b) the chance of obtaining a crystalline product would be maximized if the anion and cation were of comparable size. Addition of a toluene solution of Sn(η⁵-C_5Me_5)$_2$[4] (0.38 g, 0.98 mmol) to a solution of Ga(C_6F_5)$_3$[5] (0.60 g, 1.0 mmol) in the same solvent at 0 °C resulted in a yellow precipitate which was recrystallized from hot toluene solution to afford 0.51 g (74.5% yield) of [**1**][Ga(C_6F_5)$_4$]. The positive and negative CI mass spectra for [**1**][Ga(C_6F_5)$_4$] revealed the presence of **1**⁺ and [Ga(C_6F_5)$_4$]⁻ ions, respectively.[6] The ^{1}H, ^{13}C and ^{119}Sn NMR spectra[6] evidenced only one type of C_5Me_5 group and a unique Sn center thus suggesting reversible dissociation of **1**⁺ into Sn(η⁵-C_5Me_5)$_2$ and [Sn(η⁵-C_5Me_5)]⁺. Definitive structural information was provided by a low-temperature X-ray crystal structure.[7] As shown in Fig. 1, the solid state consists of **1**⁺ and [Ga(C_6F_5)$_4$]⁻ ions[8,9] and there are no unusually short interionic contacts. The structure of **1**⁺ is such that a pentahapto C_5Me_5 ring serves as a bridging group for two Sn(η⁵-C_5Me_5) units. Within experimental error, the two Sn atoms are located equidistantly from the ring centroid [X(1C)] of the μ-(η⁵-C_5Me_5) group [2.644(19) Å] and the Sn(1)–X(1C)–Sn(2) angle is close to 180° [174.9(4)°]. The average distance from the Sn atoms to the ring centroids of the two terminal (η⁵-C_5Me_5) rings, X(1A) and X(1B), is shorter than that to the bridging (η⁵-C_5Me_5) moiety [2.246(18) Å] and lies between the values reported for Sn(η⁵-C_5Me_5)$_2$ (2.396 Å)[3c] and [Sn(η⁵-C_5Me_5)]⁺ (2.157 Å).[3c] The X(1A)–Sn–X(1C) and X(1B)–Sn–X(1C) angles of 154.6(7) and 151.8(7)°, respectively are very similar to the values reported for Sn(η⁵-C_5Me_5)$_2$ (av. 154.9°).[3c] An intriguing feature of the overall structure is that **1**⁺ adopts a cis-type geometry while the triple decker anions [(η⁵-C_5H_5)$_3$Tl$_2$]⁻ and [(η⁵-C_5H_5)Cs$_2$]⁻ possess transoid arrangements.[1b,2]

A second method of triple decker cation synthesis recognized the isolobal relationship of *e.g.* [Sn(η⁵-C_5H_5)]⁺ and [In(η⁶-C_6H_6)]⁺ thus suggesting that cations of the latter type should add to In(η⁵-C_5Me_5) units.[10] Since protolytic cleavage of In(η⁵-C_5Me_5) in the presence of an arene solvent represented a potential source of [In(arene)]⁺ cations, we treated In(η⁵-C_5Me_5) (0.1 g, 0.4 mmol) with equimolar quantities (0.195 mmol each) of B(C_6F_5)$_3$[11] and the Brønsted acid H_2O·B(C_6F_5)$_3$[12] in toluene solution at 0 °C. The reaction mixture afforded colorless crystals (0.25 g, 70.4% yield) upon storage at −30 °C for several days. Since the product could not be characterized unambiguously on the basis of spectroscopic data,[6] an X-ray crystallographic study was undertaken.[7] The solid state (Fig. 2) consists of [(η⁶-C_7H_8)In(μ-η⁵-C_5Me_5)In(η⁶-C_7H_8)]⁺ **2**⁺ and [(C_6F_5)$_3$BO(H)B(C_6F_5)$_3$]⁻ ions[8] with 1.5 additional toluene molecules per asymmetric unit. There are no unusually short interionic contacts. The central core of **2**⁺ features an η⁵-bonded In atom on each face of the (μ-C_5Me_5)

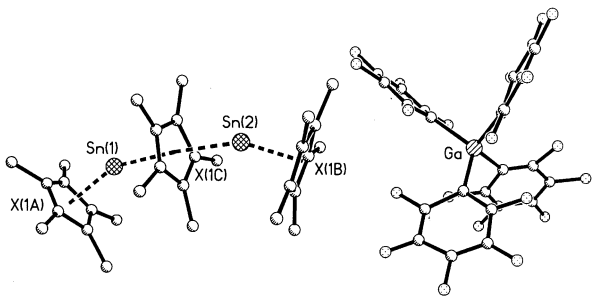

Fig. 1 View of [**1**][Ga(C_6F_5)$_4$] with hydrogen atoms omitted for clarity. Selected bond distances (Å) and angles (°): Sn(1)–C(1*n*) av. 2.556(18), Sn(1)–C(3*n*) av. 2.896(18), Sn(2)–C(2*n*) av. 2.540(14), Sn(2)–C(3*n*) av. 2.92(2), Sn(1)–X(1A) 2.259(18), Sn(1)–X(1C) 2.632(19), Sn(2)–X(1B) 2.232(18), Sn(2)–X(1C) 2.655(19), X(1A)–Sn(1)–X(1C) 154.6(4), Sn(1)–X(1C)–Sn(2) 174.9(4), X(1C)–Sn(2)–X(1B) 151.8(4).

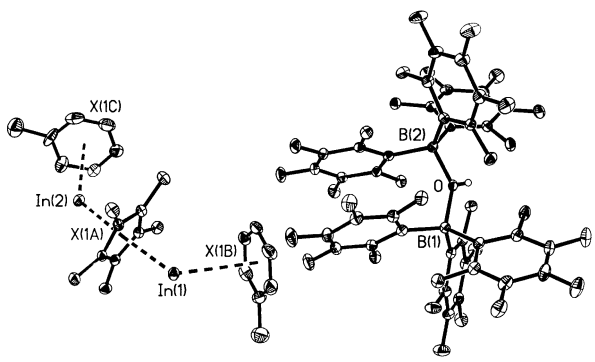

Fig. 2 View of [**2**][(C_6F_5)$_3$BO(H)B(C_6F_5)$_3$]·1.5C_7H_8, with hydrogen atoms and non-coordinated toluene molecules omitted for clarity. Selected bond distances (Å) and angles (°): In(1)–C(1*n*) av. 2.807(3), In(1)–C(2*n*) av. 3.752(3), In(2)–C(1*n*) av. 2.722(3), In(2)–C(3*n*) av. 3.598(3), In(1)–X(1A) 2.528(4), In(1)–X(1B) 3.490(4), In(2)–X(1B) 2.435(4), In(2)–X(1C) 3.325(4), B–C av. 1.646(4), B–O av. 1.559(4); X(1A)–In(1)–X(1B) 124.4(4), In(1)–X(1A)–In(2) 176.0(4), X(1A)–In(2)–X(1C) 130.3(4).

† Electronic supplementary information (ESI) available: summary of theoretical data. See http://www.rsc.org/suppdata/cc/b0/b005425i/

DOI: 10.1039/b005425i

group. The In–ring centroid [X(1A)] distances of 2.528(4) and 2.435(4) Å for In(1) and In(2), respectively are longer than those reported[10] for monomeric [2.288(4) Å] and hexameric [2.302(4) Å] In(η^5-C_5Me_5). As in the case of **1**$^+$, the metal–X–metal angle in **2**$^+$ is close to linear [176.0(4)°]. The triple decker structure of **2**$^+$ is completed by capping η^6-bonded toluene molecules. The In–ring centroid [X(1B) and X(1C)] distances of 3.490(4) and 3.325(4) Å for In(1) and In(2), respectively are considerably longer than those reported for [In(I)·2mesitylene]$^+$ (2.83 and 2.89 Å).[13] Nevertheless, it is interesting to note that, akin to **1**$^+$, the toluene–(μ-C_5Me_5)–toluene moieties are distinctly bent [124.4(4) and 130.3(4)° for X(1A)–In(1)–X(1B) and X(1A)–In(2)–X(1C), respectively] and that the overall cationic geometry is cisoid.

Part of the reason for the long arene distances in **2**$^+$ may relate to the fact that the net +1 charge is delocalized over two In centers. However, the bonding in **2**$^+$ can be interpreted in two different ways, namely (a) as a triple-decker sandwich cation or (b) a base-stabilized inverse sandwich cation. Density functional theory (DFT) optimization[14] of the model system [In(μ-η^5-C_5H_5)In]$^+$ predicts a D_{5h} symmetric structure with a computed In–X distance of 2.515 Å, close to the value observed experimentally for **2**$^+$. Moreover, the η^6-coordination of two benzene molecules to the [In(μ-C_5H_5)In]$^+$ moiety causes only a slight perturbation of the core thus lending credence to model (b). Furthermore, the benzene–In bond dissociation energy (6.6 kcal mol^{-1}) suggests a very weak interaction. In sharp contrast, calculations on [(η^5-C_5H_5)Sn(μ-η^5-C_5H_5)Sn(η^5-C_5H_5)]$^+$ as a model for **1**$^+$ predict a much more tightly bonded triple-decker sandwich environment—the weakest bond (36.6 kcal mol^{-1}) being that between [(η^5-C_5H_5)Sn(η^5-C_5H_5)] and [Sn(η^5-C_5H_5)]$^+$ fragments. Thus the (C_5Me_5) acidolysis methodology may be used to prepare isolobally related compounds with very different properties. We are currently investigating the utility of this technique for the synthesis of larger sandwich, cluster and mixed-metal compounds.

We are grateful to the National Science Foundation and the Robert A. Welch Foundation for financial support.

Notes and references

1 (*a*) M. A. Beswick, H. Gornitzka, J. Kärcher, M. E. G. Mosquera, J. S. Palmer, P. R. Raithby, C. A. Russell, D. Stalke, A. Steiner and D. S. Wright, *Organometallics*, 1999, **18**, 1148, and references therein; (*b*) D. R. Armstrong, A. J. Edwards, D. Moncrieff, M. A. Paver, P. R. Raithby, M.-A. Rennie, C. A. Russell and D. S. Wright, *J. Chem. Soc., Chem. Commun.*, 1995, 927; (*c*) M. A. Beswick, J. S. Palmer and D. S. Wright, *Chem. Soc. Rev.*, 1998, **27**, 225.

2 S. Harder and M. H. Prosenc, *Angew. Chem., Int. Ed. Engl.*, 1996, **35**, 97.

3 (*a*) T. S. Dory and J. J. Zuckerman, *J. Organomet. Chem.*, 1985, **281**, C1; (*b*) F. X. Kohl and P. Jutzi, *Chem. Ber.*, 1981, **114**, 488; (*c*) P. Jutzi, F.Kohl, P. Hofmann, C. Krüger and Y.-H. Tsay, *Chem. Ber.*, 1980, **113**, 757.

4 P. Jutzi and B. Hielscher, *Organometallics*, 1986, **5**, 1201.

5 Ga(C_6F_5)$_3$ was prepared by a similar procedure to that described by K. Ludovici, W. Tyrra and D. Naumann, *J. Organomet. Chem.*, 1992, **441**, 363. We have determined the X-ray crystal structure of Ga(C_6F_5)$_3$·THF; pertinent data have been deposited at the Cambridge Crystallographic Data Centre (file no. CCDC-137250).

6 [**1**][Ga(C_6F_5)$_4$] (74.5% yield, mp >250 °C). HRMS: calc. for $C_{30}H_{45}Sn_2$, *m/z* 641.155; found, 641.155. NMR (CD_2C1_2): ^{1}H, δ 2.07 [s, 45 H, η^5-C_5Me_5, J(^{119}Sn–^{1}H) 27 Hz]. ^{13}C, δ 10.2 [s, η^5-C_5(CH_3)$_5$] 121.0 [s, η^5-C_5(CH_3)$_5$]. ^{19}F, δ −119.8 (s, *o*-C_6F_5), −155.4 (s, *p*-C_6F_5), −160.7 (s, *m*-C_6F_5). ^{119}Sn, δ −2112. Anal. calc. for $C_{54}H_{45}F_{20}GaSn_2$: C, 46.95; H, 3.26. Found: C, 45.61; H, 3.25. [**2**][(C_6F_5)$_3$BO(H)B(C_6F_5)$_3$]·1.5C_7H_8 (70.4% yield, mp 87 °C). HRMS: calc. for $C_{10}H_{15}In$, *m/z* 364.925; found, 364.924. NMR (C_6D_6): ^{1}H: δ 1.494 (s, 15H, η^5-C_5Me_5), 2.091 (s, 6H, Ph*Me*), 2.092 (s, 6H, Ph*Me*), 6.9–7.0 (m, 8H, free *o*- and *m*-Tol), 7.02–7.04 (m, 2H, free *p*-Tol), 7.09–7.12 (m, 8H, bound *o*- and *m*-Tol), 7.12–7.13 (m, 2H, bound *p*-Tol), ^{13}C, δ 9.63 [s, η^5-C_5(CH_3)$_5$], 21.36 (s, Ph*Me*), 116.72 [s, η^5-C_5(CH_3)$_5$], 125.64 (s, *p*-Tol), 128.51 (s, *m*-Tol), 129.28 (s, *o*-Tol), 137.85 (s, *ipso*-Tol). ^{19}F: δ −134.35 (d, $^2J_{FF}$ 17.4 Hz, *p*-C_6F_5), −158.16 ('t', $^2J_{FF}$ 20.9 Hz, *p*-C_6F_5), (m, *m*-C_6F_5). ^{11}B: δ −9.95. Anal. Calc. for $C_{70.5}H_{44}B_2F_{30}In_2O_1$: C, 48.99; H, 2.57. Found: C, 49.66; H, 2.86%.

7 *Crystal data*: for [**1**][Ga(C_6F_5)$_4$]: $C_{54}H_{45}F_{20}GaSn_2$, monoclinic, space group *Cc*, yellow prisms, a = 22.147(4), b = 15.092(3), c = 17.352(4) Å, β = 115.11(3)°, V = 5252(2) Å^3, Z = 4, D_c = 1.747 g cm^{-3}, μ(Mo-Kα) = 1.561 mm^{-1}, R_1 = 0.063, wR_1 = 0.0823, GOF = 1.344. For [**2**][(C_6F_5)$_3$BO(H)B(C_6F_5)$_3$]·1.5C_7H_8: $C_{70.5}H_{44}B_2F_{30}In_2O_1$, monoclinic space group, $P2_1/c$, colorless blocks, a = 16.042(3), b = 20.771(4), c = 21.165(4) Å, β = 107.74(3)°, V = 6717(2) Å^3, Z = 4, D_c = 1.693 g cm^{-3}, μ (Mo-Kα) = 0.814 mm^{-1}, R_1 = 0.0411, wR_1 = 0.1138, GOF = 1.383. Both data sets were collected at 153 K on a Nonius-Kappa CCD diffractometer. CCDC 182/1871. See http://www.rsc.org/suppdata/cc/b0/b005425i/ for crystallographic files in .cif format.

8 The structures of the [Ga(C_6F_5)$_4$]$^-$ and [C_6F_5)$_3$BO(H)B(C_6F_5)$_3$]$^-$ anions are similar to those reported in the literature: K.-F. Tebbe, T. Gilles, F. Conrad and W. Tyrra, *Acta Crystallogr., Sect. C*, 1996, **52**, 1663; A. A. Danopoulos, J. R. Galsworthy, M. L. H. Green, S. Cafferkey, L. H. Doerrer and M. B. Hursthouse, *Chem. Commun.*, 1998, 2529.

9 Presumably, the initially formed anion is [Ga(C_6F_5)$_3$(C_5Me_5)]$^-$. However, since [B(C_6F_5)$_n$R$_{4-n}$]$^-$ anions are known to undergo facile redistribution reactions, a similar process can be postulated to explain the formation of [Ga(C_6F_5)$_4$]$^-$. See: V. K. Dioumaev and J. F. Harrod, *Organometallics*, 1997, **16**, 2798.

10 In(η^5-C_5Me_5) is a weakly-held hexamer in the solid state that undergoes facile dissociation to the monomer in solution and in the vapor phase: O. T. Beachley, Jr., R. Blom, M. R. Churchill, K. Faegri, Jr., J. C. Fettinger, J. C. Pazik and L. Victoriano, *Organometallics,*, 1989, **8**, 346.

11 A. G. Massey, A. J. Park and F. G. A. Stone, *Proc. R. Chem. Soc. London*, 1963, 212; A. G. Massey and A. J. Park, *J. Organomet. Chem.*, 1964, **2**, 245; A. G. Massey and A. J. Park, *J. Organomet. Chem.*, 1966, **5**, 218; W. E. Piers and T. Chivers, *Chem. Soc. Rev.*, 1997, **26**, 345.

12 L. H. Doerrer and M. L. H. Green, *J. Chem. Soc., Dalton Trans.*, 1999, 4325.

13 J. Ebenhöch, G. Müller, J. Riede and H. Schmidbaur, *Angew. Chem. Int. Ed. Engl.*, 1984, **23**, 386; H. Schmidbaur, *Angew. Chem., Int. Ed. Engl.*, 1985, **24**, 893.

14 Details available as ESI†.

Reversible electrochemistry and catalysis with *Mycobacterium tuberculosis* catalase-peroxidase in lipid films

Zhe Zhang,[a] Salem Chouchane,[b] Richard S. Magliozzo[b] and James F. Rusling*[a]

[a] *Department of Chemistry, Box U-60, 55 N. Eagleville Rd., University of Connecticut, Storrs, CT 06269-3060, USA. E-mail: Jrusling@nucleus.chem.uconn.edu*

[b] *Department of Chemistry, Brooklyn College, City Univ. of New York, 2900 Bedford Ave., Brooklyn, New York 11210-2889, USA.*

Received (in Cambridge, UK) 21st November 2000, Accepted 7th December 2000
First published as an Advance Article on the web 4th January 2001

Reversible voltammetry was achieved ($E^{\circ\prime}$ = −0.13 V *vs.* NHE at 25 °C at pH 7.1) for the Fe^{III}/Fe^{II} redox couple of mycobacterial KatG catalase–peroxidase in films of dimyristoyl phosphatidylcholine, which also catalyzed electrochemical reductions of hydrogen peroxide and oxygen.

The mycobacterial KatG catalase–peroxidase[1,2] oxidatively activates the prodrug isoniazid (isonicotinic acid hydrazide) used to treat tuberculosis. *Mycobacterium tuberculosis* catalase-peroxidase is a dimer of 80 kDa subunits, both of which contain an iron heme. Oxidative activation of isoniazid may occur through several possible pathways. The Fe^{III} form of the enzyme can react with peroxides to form an unstable intermediate peroxidase compound I that oxidizes isoniazid.[3] The catalase–peroxidase can oxidize isoniazid in the presence of dioxygen and a reductant, similar to cytochrome P450 catalysis.[4] The Fe^{III} enzyme receives one electron forming Fe^{II} enzyme, to which dioxygen binds to give an Fe^{II}–O_2 intermediate that is the precursor of a high-valent active oxidant.[5,6] Oxidation of isoniazid by the catalase–peroxidase can also be initiated by superoxide.[7] Knowledge of redox chemistry, oxidation kinetics, and reduction of H_2O_2 with the catalase–peroxidase is critical for elucidation of pathways for isoniazid oxidation. Here we report the first example of direct, reversible electron transfer between the Fe^{III}/Fe^{II} redox couple of the catalase–peroxidase from *M. tuberculosis* in thin films of dimyristoyl phosphatidylcholine (DMPC) on electrodes. These enzyme–lipid films catalyzed electrochemical reduction of H_2O_2 and of dioxygen.

Films of stacked lipid bilayers provide a biomimetic environment facilitating direct electrical communication between electrodes and redox sites of incorporated heme enzymes.[8,9] Fig. 1 shows a reversible cyclic voltammogram (CV) for the Fe^{III}/Fe^{II} redox couple of *M. tuberculosis* catalase–peroxidase (enzyme obtained as in ref. 3) in a DMPC film in pH 6.0 buffer. Films were made by spreading 10 μL of an aqueous vesicle dispersion of 1 mM DMPC and 0.05 mM enzyme evenly onto a basal plane PG disc electrode (area = 0.2 cm^2) and drying overnight.[10] The film thickness was *ca.* 0.5 μm.

Catalase–peroxidase/DMPC films in oxygen-free buffers gave symmetric CV peaks with equal reduction and oxidation peak heights that depended linearly on scan rate from 0.01 to 1 V s^{-1}. Peak widths at half-height were *ca.* 200 mV, and reduction–oxidation peak separations were *ca.* 50 mV, exceeding the 90/*n* mV peak width and 0 mV peak separation, respectively, predicted by theory for ideal thin layer voltammetry. Integration of CVs gave enzyme surface concentration of 2.1×10^{-10} mol cm^{-2}. Results are typical for non-ideal thin film protein voltammetry.[9] Formal potentials ($E^{\circ\prime}$) of the catalase–peroxidase obtained as midpoint potentials of reversible CVs are compared with other enzymes in Table 1.

Recently Wengenack *et al.*[11] reported irreversible voltammetry for the KatG catalase–peroxidase on graphite electrodes. Cyclic voltammograms with the enzyme in solution showed a Fe^{III} reduction peak, but no reverse oxidation peak, and reversibility of square-wave voltammograms was unsubstan-

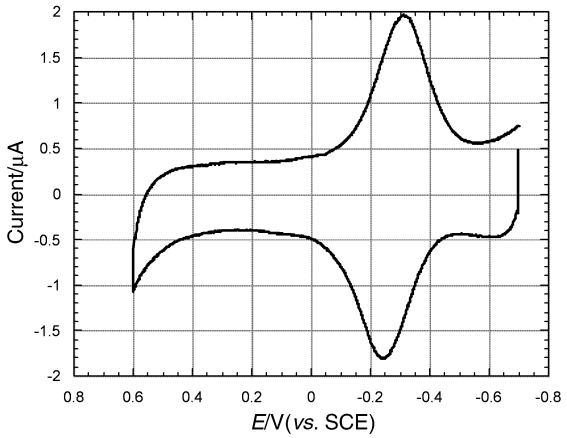

Fig. 1 Background subtracted cyclic voltammogram (CV) at 100 mV s^{-1} and 25 °C of catalase–peroxidase–DMPC film on basal plane PG electrode, in pH 6.0, 20 mM phosphate buffer purged with purified nitrogen for 20 min before CV. Note that *E*/V (*vs.* NHE) = 0.244 + *E*/V (*vs.* SCE).

Table 1 Electrochemical results for enzymes in DMPC films and water[a]

Enzyme	pH	$E^{\circ\prime}$[b]/V (*vs.* NHE)	Γ[c]/ mol cm^{-2}	Slope[d]/nA μM^{-1}	Rel. rates of H_2O_2 redn.[e]
Catalase–peroxidase film	6.0	−0.058	2.1×10^{-10}	1.3	0.06
Catalase–peroxidase film	7.1	−0.128	2.1×10^{-10}		
Catalase–peroxidase in water	7.6	−0.028	(from ref. 11, by titration)		
HRP film	6.0	−0.065	1.8×10^{-11}	1.8	1.0
Catalase film	6.0	−0.18	9.0×10^{-11}	0.11	0.01

[a] Average of at least two electrodes in 20 mM phosphate buffer at pH 6.0, 25 °C. Standard deviations were *ca.* ±5 mV for $E^{\circ\prime}$ and ≤15% for other quantities. [b] Estimated as midpoint potentials of reduction–oxidation peaks in CV. [c] Determined by integration of CV peaks at low scan rates and application of Faraday's law. [d] Calculated by linear regression of amperometric responses to various concentrations of hydrogen peroxide using rotating electrodes at 1800 rpm at 0.24 V *vs.* NHE. [e] From steady state currents as nA $nmol^{-1}$ enzyme at 1800 rpm at 0.24 V *vs.* NHE, proportional to turnover rate, relative to HRP = 1.

DOI: 10.1039/b009348n

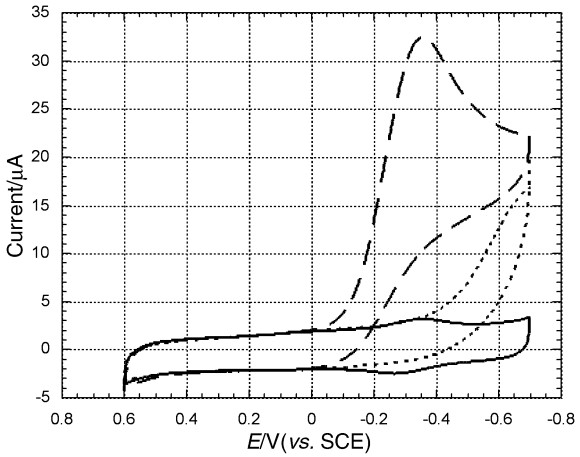

Fig. 2 CVs at 100 mV s^{-1} of KatG–DMPC films in pH 6.0 buffer saturated with air (– —) and without oxygen (—), and enzyme-free DMPC film in pH 6.0 buffer saturated with air (---).

tiated by the data.[11] The potentials of these irreversible redox peaks are controlled by kinetics and do not yield $E°'$ for the Fe^{III}/Fe^{II} couple of the enzyme.

The Soret absorbance band of catalase–peroxidase shifted slightly from 407 nm in pH 7 solution[12] to 409 nm in DMPC films, similar to myoglobin/DMPC films.[13] When the catalase–peroxidase was purposely denatured at pH 3.5, the Soret band disappeared and a new broad band at *ca.* 375 nm appeared. These results suggest that catalase–peroxidase in DMPC films at pH 6–7.5 is similar in secondary structure to the native enzyme.

If the Fe^{II} enzyme generated by reduction reacts with oxygen and product Fe^{II}–O_2 is reduced by the electrode, reduction current will increase due to the catalytic process, and the Fe^{II} oxidation peak will decrease or disappear. Fig. 2 shows such voltammetric behavior of catalase–peroxidase/DMPC in air-saturated buffer. Increased reduction current results from additional electrons injected into Fe^{II}–O_2, and the likely product is hydrogen peroxide as found for other iron heme enzymes.[9] This catalytic reduction is *ca.* 0.4 V more positive than direct reduction of oxygen on DMPC/PG electrodes (Fig. 2).

Catalase–peroxidase/DMPC films also catalyzed the reduction of hydrogen peroxide. Without H_2O_2, enzyme–DMPC films give similar cyclic voltammograms on quiet (*cf.* Fig. 1) and rotating electrodes [Fig 3(b),(d),(f)]. After adding H_2O_2, reduction current was greatly increased to give catalytic steady-state (limiting) currents for the catalase–peroxidase at 0.4 mM H_2O_2 (Fig. 3(a)] and for HRP at 0.05 mM H_2O_2 (Fig. 3(e)]. For catalase (bovine liver), partly reversible Fe^{III}/Fe^{II} redox peaks are still detected even at 1 mM H_2O_2 [Fig. 3(c)], and steady state was not achieved. The onset of catalytic current for reduction of H_2O_2 occurred at *ca.* 0.24 V *vs.* NHE for catalase–peroxidase, 0.14 V for HRP and 0.1 V for catalase. In no case was a direct Fe^{III} *oxidation* peak observed.

Amperometric responses for enzyme–DMPC films at 0.24 V *vs.* NHE to various concentrations of H_2O_2 were measured at rotating electrodes (Table 1). H_2O_2 presumably reacts with the Fe^{III} enzyme to give compound I,[3] which is reduced by the electrode in a catalytic cycle. Relative turnover rates from these steady-state currents[14] in nA $nmol^{-1}$ enzyme were in the order: HRP > catalase–peroxidase > catalase (Table 1).

Results presented above demonstrate direct, reversible electron transfer between electrodes and *M. tuberculosis* catalase–peroxidase in DMPC films. Catalytic reduction of oxygen involving the oxyferrous enzyme proceeded similarly to electrochemical catalytic cycles of cyt P450 enzymes.[8,9] For catalytic electrochemical reduction of H_2O_2, the catalase–peroxidase in DMPC films resembles HRP more than catalase.

Reversible voltammograms allowed estimation of a formal potential of −0.128 V *vs.* NHE in DMPC films at pH 7.1. An observed $E°'$–pH dependence of −53 mV pH^{-1} puts the value

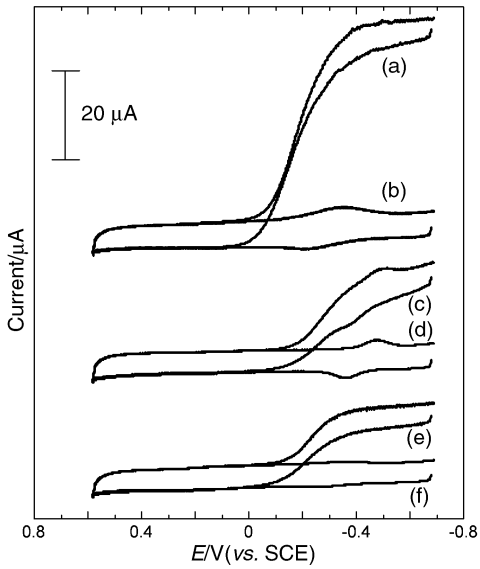

Fig. 3 Rotating disk CVs of enzyme–DMPC films on PG at 1800 rpm and 100 mV s^{-1} in pH 6 buffer illustrating catalytic electrochemical reduction of H_2O_2: KatG enzyme–DMPC films at (a) 0.4 mM H_2O_2, (b) 0 mM H_2O_2; Catalase-DMPC films at (c) 1.0 mM H_2O_2, (d) 0 mM H_2O_2; HRP-DMPC films at (e) 0.05 mM H_2O_2, (f) 0 mM H_2O_2. Buffer solution was purged with purified nitrogen for 20 min before CV; curves for different enzymes were offset for clarity.

at pH 7.6 in DMPC films at −0.155 V. This is significantly more negative than −0.028 V obtained recently in solution at pH 7.6 by spectroelectrochemical titration.[11] Results for other iron heme proteins suggest that $E°'$ values in DMPC films may differ from solution values by 100 mV or more as a result of lipid–enzyme and film–electrode interactions.[9] In comparison, HRP and the catalase–peroxidase have similar formal potentials in DMPC films (Table 1), even though the value for HRP in solution was reported at −0.278 V.[11] Thus, the previous conclusion[11] that the catalase–peroxidase $E°'$ is 200 mV higher than HRP may be modulated by enzyme environment.

We thank the National Institute of Environmental Health Sciences (Grant No. ES03154) and the National Institutes of Allergy and Infectious Diseases (Grant No. AI43582), NIH, for financial support. Contents are solely the responsibility of the authors and do not necessarily represent official views of NIH.

Notes and references

1 Y. Zhang, B. Heym, B. Allen, D. Young and S. Cole, *Nature*, 1992, **358**, 591.
2 K. Johnsson and P. G. Schultz, *J. Am. Chem. Soc.*, 1994, **116**, 7425.
3 S. Chouchane, I. Lippai and R. S. Magliozzo, *Biochemistry*, 2000, **39**, 9975.
4 R. S. Magliozzo and J. A. Marcinkeviciene, *J. Am. Chem. Soc.*, 1996, **118**, 11 303.
5 *Cytochrome P450*, ed. P. R. Ortiz de Montellano, Plenum Press, New York, 1995.
6 *Cytochrome P450*, ed. J. B. Schenkman and H. Greim, Springer-Verlag, Berlin, 1993.
7 N. L. Wengenack, H. M. Hoard and F. Rusnak, *J. Am. Chem. Soc.*, 1999, **121**, 9748.
8 Z. Zhang, A.-E. F. Nassar, Z. Lu, J. B. Schenkman and J. F. Rusling, *J. Chem. Soc., Faraday Trans.*, 1997, **93**, 1769.
9 J. F. Rusling, *Acc. Chem. Res.*, 1998, **31**, 363.
10 A.-E. F. Nassar, Z. Zhang, J. F. Rusling, V. Chynwat, H. A. Frank and K. Suga, *J. Phys. Chem. B*, 1995, **99**, 1103.
11 N. L. Wengenack, H. Lopes, M. J. Kennedy, P. Tavares, A. S. Pereira, I. Moura, J. J. G. Moura and F. Rusnak, *Biochemistry*, 2000, **39**, 11 508.
12 K. Johnsson, W. A. Froland and P. G. Schultz, *J. Biol. Chem.*, 1997, **272**, 2834.
13 Z. Zhang and J. F. Rusling, *Biophys. Chem.*, 1997, **63**, 133.
14 F. A. Armstrong, in *Bioelectrochemistry of Biomacromolecules*, ed. G. Lenaz and G. Milazzo, Birkhauser Verlag, Basel, Switzerland, 1997, pp. 205–255.

Cooperative assistance in a very short O–H··O hydrogen bond. Low-temperature X-ray crystal structures of 2,3,5,6-pyrazinetetracarboxylic and related acids

Peddy Vishweshwar,[a] Ashwini Nangia*[a] and Vincent M. Lynch[b]

[a] *School of Chemistry, University of Hyderabad, Hyderabad 500 046, India. E-mail: ansc@uohyd.ernet.in*
[b] *Department of Chemistry and Biochemistry, University of Texas, Austin, TX 78712, USA*

Received (in Columbia, MO, USA) 30th August 2000, Accepted 7th November 2000
First published as an Advance Article on the web 4th January 2001

In contrast to the well documented role of charge- and resonance-assistance in very short hydrogen bonds, a very short O–H_{acid}···O_{water} hydrogen bond [O···O 2.4791(13) Å] in the title acid is ascribed to the cumulative stabilisation from σ- and π-bond cooperativity.

Very short (very strong) O–H···O hydrogen bonds are formed with unusually activated donors and acceptors, as between an acid and its conjugate base (O–H···O^-) or in the hydrates of strong acids (O^+–H···O). With H···O distances in the range 1.2–1.5 Å (O···O 2.2–2.5 Å), very short H-bonds have a significant covalent component (O–H ≈ H···O) and bond energies in the range 15–40 kcal mol^{-1}. The substantial covalent character of very short H-bonds, a result of three-centre–four-electron contribution, O•–•H···••O ↔ O••···H•–•O, is responsible for their distinctive properties: the near linear geometry (θ = 170–180°), the lengthening of O–H distance (up to 0.2 Å) and the very large IR bathochromic shifts (up to 2000 cm^{-1} in ν_s).[1] Typical examples are the intramolecular hydrogen bonds in monobasic salts of dicarboxylic acids.[2] Very strong hydrogen bonds are relevant in the context of proton transfer phenomena in chemical and biological systems and they have been studied with spectroscopic, crystallographic and computational methods.[1a] The overall picture that emerges from such studies is that very short H-bonds have a quasi-covalent character. This is in contrast to strong hydrogen bonds (H···O 1.5–2.2 Å, O···O 2.5–3.2 Å, energy 4–15 kcal mol^{-1}) that are largely electrostatic in nature.[1b]

In addition to charge-assisted hydrogen bonding (CAHB: O–H···O^-, O^+–H···O) in carboxylic acids, very short hydrogen bonds have been observed in the neutral β-diketone enol fragment, ···O=C–C=C–OH···, wherein resonance-assistance through π-bonds (RAHB) results in unusual bond shortening.[3] We show here that a composite array with σ- and π-bond cooperativity, O–H···O=C–O–H_{acid}···O_{water}–H···O, can shorten an *inter*molecular O–H_{acid}···O_{water} hydrogen bond into the regime of the very short H-bond (O···O < 2.50 Å). This kind of H-bond array has been referred to as 'polarisation enhanced hydrogen bonding' by Jeffrey.[1a] Our example of a very short hydrogen bond is: (i) intermolecular, (ii) not of the charge-assisted type,[4] (iii) not of the acid–conjugate-base type[5] and (iv) does not contain highly activated donor/acceptor groups.[6]

Recrystallisation of 2,3,5,6-pyrazinetetracarboxylic acid **1**† from 20% aqueous HCl afforded diffraction quality crystals of the dihydrate. Low-temperature (123 K) single crystal X-ray analysis of **1**·$2H_2O$ ($P\bar{1}$, Z = 1)‡ showed it to contain a very short O–H_{acid}···O_{water} H-bond [d = 1.50 Å, D = 2.4791(13) Å, θ = 170.3°]§ that is part of cooperative array **I** [Figs. 1 and 2(a)]. In this very short H-bond, both the carboxylic acid O–H donor ability and the water O atom acceptor basicity are simultaneously enhanced through polarisation, as shown in Fig. 2(b). Such a strong polarising effect involving water was noted recently in the complex, Ph_3P=O–1,4-diethynylbenzene–H_2O (4:1:2).[7] The other O–H···O/N bonds in the crystal are in the short to medium range (Table 1).

In order to probe such a polarisation-induced H-bond shortening in related acids, the crystal structures of pyrazine-2,3-dicarboxylic acid **2** and 5,6-dimethylpyrazine-2,3-dicar-

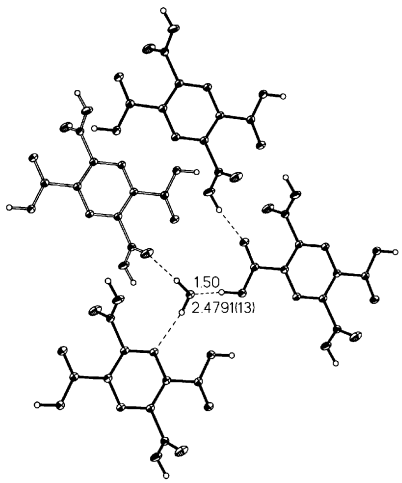

Fig. 1 Crystal structure of tetra-acid **1** showing the cooperative O–H···O synthon **I**. The water molecule acts as a H-bond donor to the CO_2H group of the next layer (shaded differently). Metrics of the very short O–H···O bond are indicated. Displacement ellipsoids are drawn at the 50% probability level for non-H atoms.

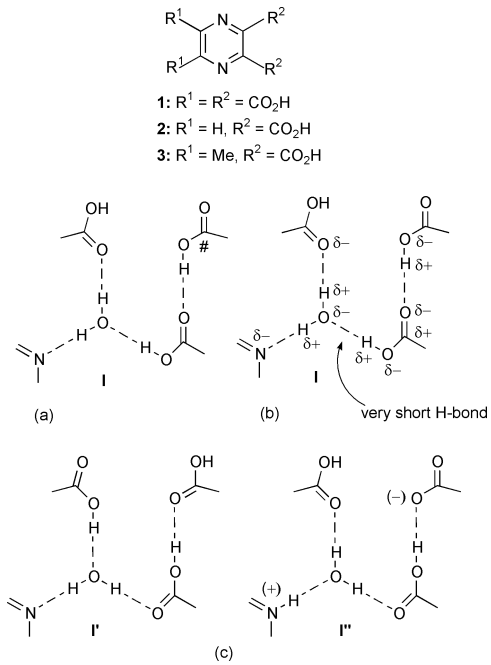

Fig. 2 (a) Cooperative synthon **I** in tetra-acid **1**. The acid group marked # is replaced with H_2O in diacids **2** and **3**. (b) Donor and acceptor groups enhanced by polarisation in **I**. (c) Tautomer synthons **I′** and **I″** (not observed).

DOI: 10.1039/b007346f

Table 1 Geometry of O–H···O/N hydrogen bonds and C–O bond lengths

Acid	Hydrogen bond geometry									
	O–H···O				O–H···N				Bond length	
	O–H/Å	*D*/Å	*d*[a]/Å	*θ*/°	O–H/Å	*D*/Å	*d*[a]/Å	*θ*/°	C–O/Å	C=O/Å
1[b]	0.96(3)	2.4791(13)	1.50	170.3	0.85(3)	2.9393(16)	2.01	156.1	1.3113(17)	1.2022(15)
	0.91(2)	2.7010(12)	1.74	162.6					1.2957(16)	1.2174(14)
	0.89(2)	2.7811(12)	1.80	171.9						
2[c]	1.05	2.562	1.58	170.9	0.73	2.840	1.87	166.4	1.304	1.208
	0.86	2.922	2.04	147.4						
3[b]	0.968(18)	2.5269(12)	1.55	167.2	0.87(2)	2.8963(13)	1.97	155.1	1.3143(13)	1.2122(13)
	0.872(18)	2.8747(12)	1.92	162.4						

[a] *d* Values are neutron-normalised (O–H 0.983 Å). [b] This work. [c] Ref. 8.

boxylic acid **3** were analysed. Diacid **2** is reported as a dihydrate (*C*2/*c*).[8] Diacid **3** was also determined to be a dihydrate by low-temperature X-ray diffraction (*Pbcn*).‡ Both these crystal structures contain synthon **I** with O···O distances in the short (strong) regime [**2**·2H_2O 2.562, **3**·2H_2O 2.5269(12) Å]. The very short O–H···O bond in **1** compared to the short bond in **2** and **3** may be rationalised through differences in their extended arrays: the CO_2H donor in **1** [marked with # in Fig. 2(a)] is replaced by H_2O in **2** and **3**. The relative shortness of the O–H···O bond in **3** compared to **2** could be because the donor O–H_{acid} is more polarised by the stronger O–H_{water}···O = C–O–H bond in **3** [2.922 *vs.* 2.8747(12) Å].

Another reason for the very short O–H_{acid}···O_{water} bond in tetra-acid **1** compared to the short H-bond in diacids **2** and **3** is the presence of twice as many electron-withdrawing groups in the former structure. Thus, molecular (4 CO_2H groups on a *N*-heterocycle) and supramolecular (extended cooperative array **I**) features act in concert, resulting in the very short O–H···O bond in **1**. An analysis of the Cambridge Structural Database (April 2000 update) substantiates our observation. While CO_2H···OH_2 H-bonding is present in many carboxylic acids (*ca.* 150 contacts in the range O···O 2.40–2.80 Å),¶ the very short H-bond region (< 2.50 Å) contains mostly the oxalic acid dihydrates (11/13). In these crystal structures, activation of the donor O–H in the 1,2-dicarboxylic acid moiety results in very short O–H_{acid}···O-$_{water}$ bonds, a point not mentioned in the original publications.[9]

A novel feature of this work is the influence on H-bond shortening of cooperative stabilisation, a phenomenon hitherto not discussed in the extensive literature[1–6] on very short hydrogen bonds. Once again, akin to polarisation by water,[7] precedent for H-bond shortening through cooperative assistance comes from the weak C–H···O category, namely 2-ethynyladamantan-2-ol.[10] The presence of two types of CO_2H groups in the same crystal, one that engages in a very short H-bond and the other with a normal H-bond, permits an assessment of O–H bond lengthening (Table 1). Thus, the very short O–H···O bond in **1** displays the expected characteristics: near linear geometry (θ = 170.3°), O–H lengthening (0.1 Å) and O–H ν_s in agreement with the reported correlation (1398 cm^{-1}).‖

In order that our σ- and π-bond cooperativity argument through synthon **I** is tenable, the presence of tautomers **I′** and **I″** in tetra-acid **1** [Fig. 2(c)] must be rigorously excluded, because such motifs would contribute towards resonance stabilisation (**I** ↔ **I′**↔ **I″**), and in effect negate the present hypothesis. Carboxylic acid groups may be characterised as C=O and C–O or as a delocalised carboxylate by their single and double bond lengths.[11] A difference of > 0.1 Å implies a static CO_2H group while a smaller difference (< 0.02 Å) means a resonating or disordered carboxylate. The > 0.1 Å difference between C–O and C=O bond distances in **1**–**3** (Table 1) confirms that synthon **I** is present in their crystal structures, and not a resonance-stabilised motif.

In summary, we have shown that polarisation through a finite σ- and π-bond cooperative array can shorten an O–H···O bond into the very strong regime. This study adds to our knowledge of the traditional H-bond shortening phenomena, namely through charge- and resonance-assistance.

A. N. thanks the DST for research funding (SP/S1/G29/98). V. M. L. thanks the NSF (CHE-9807702) for support. We thank Professor Gautam R. Desiraju for suggestions.

Notes and references

† *Synthesis*: tetra-acid **1**: oxidation of phenazine with $KMnO_4$ (R. J. Light and C. R. Hauser, *J. Org. Chem.*, 1961, **26**, 1296). Diacid **3**: by the oxidation of 2,3-dimethylquinoxaline under identical conditions.

‡ *Crystal data*: tetra-acid **1**: 2,3,5,6-pyrazinetetracarboxylic acid dihydrate ($C_8H_4N_2O_8·2H_2O$, M = 292.16); triclinic, space group $P\bar{1}$, a = 5.4409(3), b = 6.4041(3), c = 8.6995(3) Å, α = 98.572(3), β = 107.374(3), γ = 105.519(3)°, V = 269.97(2) $Å^3$, Z = 1, D_c = 1.797 Mg m^{-3}, Nonius Kappa CCD area detector, T = 123 K, μ = 0.171 mm^{-1}, λ(Mo-Kα) = 0.71073 Å, ω scan mode, 1219 unique reflections, 1125 with $F_o > 4\sigma(F_o)$, no absorption corrections. Structure solution and refinement with standard methods (SHELX97); H-atoms refined isotropically. Final R = 0.030 (obs.), 0.032 (all); $wR(F^2)$ = 0.080 (obs.), 0.082 (all).

Diacid **3**: 5,6-dimethylpyrazine-2,3-dicarboxylic acid dihydrate ($C_8H_8N_2O_4·2H_2O$, M = 232.19); orthorhombic, space group *Pbcn*; a = 12.6454(3), b = 9.0812(3), c = 8.8800(3) Å, V = 1019.74(5) $Å^3$, Z = 4, D_c = 1.512 Mg m^{-3}, Nonius Kappa CCD area detector, T = 123 K, μ = 0.131 mm^{-1}, λ(Mo-Kα) = 0.71073 Å, ω scan mode, 1161 unique reflections, 1059 with $F_o > 4\sigma(F_o)$, no absorption corrections. Structure solution and refinement with standard methods (SHELX97); H-atoms refined isotropically. Final R = 0.031 (obs.), 0.034 (all); $wR(F^2)$ = 0.084 (obs.), 0.086 (all). CCDC 182/1850. See http://www.rsc.org/suppdata/cc/b0/b007346f/ for crystallographic files in .cif format.

§ *d* Values in this study are neutron-normalised (O-H 0.983 Å).

¶ Screens −28, 35, −55, 57, 85, 88, 153 were applied. Organometallic crystal structures were excluded.

‖ See ref. 1(*a*), p. 222.

1 (*a*) G. A. Jeffrey, *An Introduction to Hydrogen Bonding*, OUP, Oxford, 1997; (*b*) G. R. Desiraju and T. Steiner, *The Weak Hydrogen Bond in Structural Chemistry and Biology*, OUP, Oxford, 1999, ch. 1.
2 M. Currie and J. C. Speakman, *J. Chem. Soc. A*, 1970, 1923.
3 P. Gilli, V. Bertolasi, V. Ferretti and G. Gilli, *J. Am. Chem. Soc.*, 1994, **116**, 909; V. Bertolasi, P. Gilli, V. Ferretti and G. Gilli, *Chem. Eur. J.*, 1996, **2**, 925.
4 D. Braga, L. Maini, F. Grepioni, A. D. Cian, O. Félix, J. Fischer and M. W. Hosseini, *New J. Chem.*, 2000, **24**, 547.
5 T. Steiner, A. M. M. Schreurs, M. Lutz and J. Kroon, *Acta Crystallogr., Sect. C*, 2000, **56**, 577.
6 T. Steiner, C. C. Wilson and I. Majerz, *Chem. Commun.*, 2000, 1231.
7 B. M. Kariuki, K. D. M. Harris, D. Philp and J. M. A. Robinson, *J. Am. Chem. Soc.*, 1997, **119**, 12 679.
8 F. Takusagawa and A. Shimada, *Chem. Lett.*, 1973, 1121.
9 Y. Wang, C. J. Tsai, W. L. Liu and L. D. Calvert, *Acta Crystallogr., Sect. B*, 1985, **41**, 131; D. Zobel, P. Luger, W. Dreissig and T. Koritsanszky, *Acta Crystallogr., Sect. B*, 1992, **48**, 837.
10 F. H. Allen, J. A. K. Howard, V. J. Hoy, G. R. Desiraju, D. S. Reddy and C. C. Wilson, *J. Am. Chem. Soc.*, 1996, **118**, 4081.
11 D. A. Diedrich, I. C. Paul and D. Y. Curtin, *J. Am. Chem. Soc.*, 1974, **96**, 6372.

ChemComm

Chemo- and regioselective cyclotrimerization of monoynes catalyzed by a nickel(0) and zinc(II) phenoxide system†

Naoyoshi Mori, Shin-ichi Ikeda* and Kazunori Odashima

Faculty of Pharmaceutical Sciences, Nagoya City University, Tanabe-dori, Mizuho-ku, Nagoya 467-8603, Japan. E-mail: ikeshin@phar.nagoya-cu.ac.jp

Received (in Cambridge, UK) 6th November 2000, Accepted 6th December 2000
First published as an Advance Article on the web 4th January 2001

A binary metal system of nickel(0) and zinc(II) phenoxide catalyzed the chemo- and regioselective cyclotrimerization of monoynes.

There is considerable interest in organotransition-metal chemistry based on their wide application in organic syntheses. Over the past few years, we have studied the development of new organonickel chemistry.[1,2] In the course of this research, we found that cyclotrimerization (or [2 + 2 + 2] cycloaddition) of enones and alkynes occurred in the presence of both nickel(0) and some other metal species such as aluminum phenoxide or zinc halide.[3,4] Inspired by the synergistic effects of binary metal catalysts, we applied this concept to the cyclotrimerization of two or three different monoynes,[5] in which the control of chemo- and regioselectivity is a crucial problem. We report here the remarkable effects of a zinc(II) phenoxide co-catalyst in the nickel(0)-catalyzed cyclotrimerization of monoynes.[6]

We first investigated the reaction of methyl propargyl‡ ether (**1a**) with methyl propiolate (**2**) (Scheme 1). When a THF solution of **2** (2 eq.) was added dropwise with stirring over 5 min at rt to a THF solution of **1a** (1 eq.), $Ni(acac)_2$ (5 mol%), PPh_3 (10 mol%), Et_2Zn (50 mol%), and PhOH (80 mol%), a mixture of two regioisomeric cycloadducts **3a** and **4a**, which were formed by the chemoselective coupling of one molecule of **1a** and two molecules of **2**, was obtained in 78% yield (Table 1, run 1). The major isomer (95% selectivity) was determined to be **3a** by the spectral analyses. Other benzene derivatives such as **5**, **6**, and **7** were not obtained in this reaction. In contrast, when the reaction was carried out without both Et_2Zn and PhOH, chemoselectivity did not occur (runs 1 and 2 *vs.* run 3). While other metal species such as Et_2Zn itself, $ZnCl_2$, and aluminum phenoxides also assisted the nickel catalyst in the cycloaddition, a noticeable amount of **6** was detected by GC analysis (runs 5–8). The results indicate that the remarkable chemoselectivity is due to the effects of a zinc phenoxide prepared from Et_2Zn and PhOH *in situ.*[7,8]

We explored the scope of the chemo- and regioselective cyclotrimerization of various **1** with **2** in the presence of Ni(0)–PPh_3–Et_2Zn–PhOH (Scheme 2). In each reaction, competing self-trimerizations were suppressed. When **2** was added slowly over 60 min to the reaction medium involving hex-3-yne (**1c**),

Table 1 Catalytic cycloaddition of **1a** and **2**[a]

Run	Catalytic system	Yield[b] (%) (**3a** + **4a**)	**5**	**6**	**7**
1	$Ni(acac)_2$–PPh_3–Et_2Zn–PhOH[c]	81 (78)	0	0	0
2	$Ni(cod)_2$–PPh_3–Et_2Zn–PhOH[d]	(67)	0	0	0
3	$Ni(cod)_2$–PPh_3[e]	10	19	19	11
4	$Ni(acac)_2$–Et_2Zn–PhOH[f]	0	0	0	0
5	$Ni(acac)_2$–PPh_3–Et_2Zn[g]	30	0	8	4
6	$Ni(cod)_2$–PPh_3–Et_2Zn[h]	29	0	13	5
7	$Ni(cod)_2$–PPh_3–$ZnCl_2$[i]	38	0	26	4
8	$Ni(acac)_2$–PPh_3–Me_3Al–PhOH[j]	21	0	56	4

[a] All reactions were carried out as follows: a THF solution of **2** (2 eq.) was added dropwise over 5 min at rt to a THF solution of **1a** (1 eq.) and catalysts. [b] GC yield. Isolated yield is in parentheses. The yield of **7** is estimated on the basis of those of **3**–**6**. [c] $Ni(acac)_2$–PPh_3–Et_2Zn–PhOH = 0.05:0.1:0.5:0.8. [d] $Ni(cod)_2$–PPh_3–Et_2Zn–PHOH = 0.05:0.1:0.4:0.8. [e] $Ni(cod)_2$–PPh_3 = 0.05:0.1. [f] $Ni(acac)_2$–Et_2Zn–PhOH = 0.05:0.5:0.8. [g] $Ni(acac)_2$–PPh_3–Et_2Zn = 0.05:0.1:0.5. [h] $Ni(cod)_2$–PPh_3–Et_2Zn = 0.05:0.1:0.4. [i] $Ni(cod)_2$–PPh_3–$ZnCl_2$ = 0.05:0.1:0.4. [j] $Ni(acac)_2$–PPh_3–Me_3Al–PhOH = 0.05:0.1:0.5:0.8.

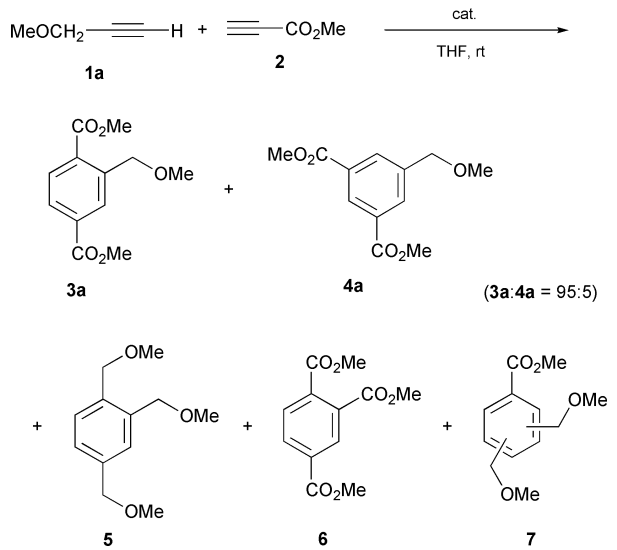

Scheme 1

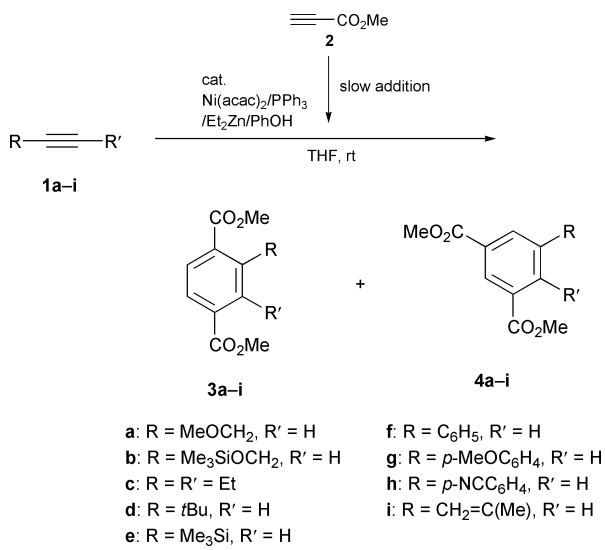

Scheme 2

† Electronic supplementary information (ESI) available: experimental and characterization data. See http://www.rsc.org/suppdata/cc/b0/b008882j/

Table 2 Cylocotrimerization of **1** and **2** in the presence of $Ni(acac)_2$–PPh_3–/Et_2Zn–PhOH[a]

Entry	1	Add. time/min	Product(s)	Yield[b] (%)	Ratio[c] (**3**:**4**)
1	**1a**	5	**3a**, **4a**	78	95:5
2	**1b**	5	**3b**, **4b**	60	95:5
3	**1c**	60	**3c**	41	100:0
4	**1d**	60	**3d**, **4d**	50	92:8
5	**1e**	20	**3e**, **4e**	64	90:10
6	**1f**	10	**3f**, **4f**	53	94:6
7	**1g**	20	**3g**, **4g**	55	93:7
8	**1h**	60	**3h**	49	100:0
9	**1i**	20	**3i**, **4i**	68	93:7

[a] All reactions were carried out as follows: a solution of **2** (2 mmol) in THF (2 mL) was added dropwise with stirring to a mixture of **1** (1 mmol), $Ni(acac)_2$ (0.05 mmol), PPh_3 (0.1 mmol), Et_2Zn (1.0 M in hexane, 0.5 mL), and PhOH (0.8 mmol) in THF (5 mL) at rt. [b] Isolated yield. [c] Determined by integration of the aryl protons of ^1H NMR.

the cross-cyclotrimerization adduct **3c** was obtained as the sole product (Table 2, entry 3). *tert*-Butylacetylene (**1d**) and (trimethylsilyl)acetylene (**1e**) were also applied to the cyclotrimerization (entries 4 and 5). Biaryl compounds **3f**–**h** were synthesized from the reaction with the corresponding arylacetylenes **1f**–**h**, respectively (entries 6–8). The presence of an electron-withdrawing group on arylacetylene tended to increase the regioselectivity. A conjugated enyne **1i** reacted with **2** to give an α-methylstyrene derivative **3i** with an excellent regioselectivity (entry 9).

Interestingly, the cyclotrimerization of three different monoynes was also effectively promoted by the nickel(0) and zinc phenoxide system mentioned above. Thus, when **2** (1 eq.) was added dropwise over 60 min to a mixture of **1c** (1 eq.) and ethylbut-2-ynoate (**8**, 1 eq.) in the presence of the binary metal catalyst (Scheme 3), a mixture of three-component cycloadduct **9** and its regioisomer **10** was preferentially obtained along with small amounts of other benzene derivatives **3c**, **11**, and **12** (Table 3, run 1). On the other hand, in the reactions without zinc phenoxide, the desired **9** and **10** were obtained in lower yields (runs 2–4).

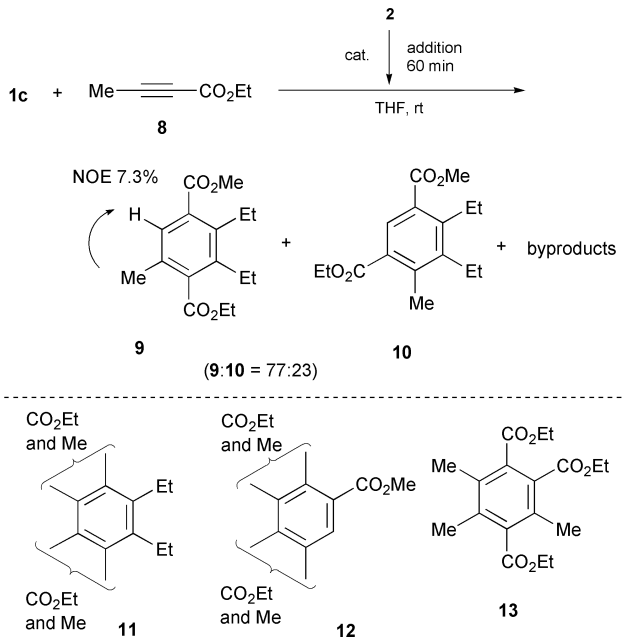

Scheme 3

The transition-metal-catalyzed cyclotrimerization of alkynes has been extensively studied by several research groups.[9] However, in contrast to intramolecular reactions,[10] a fully intermolecular reaction has not yet been established as a useful synthetic method. We have demonstrated that the binary metal system of nickel(0) and zinc(II) phenoxide effectively catalyzes

Table 3 Cyclotrimerization of **1c**, **2**, and **8**[a]

Run	Catalytic system	Yield[b] (%) (**9** + **10**)	Byproducts[c]
1	$Ni(cod)_2$–PPh_3–Et_2Zn–PhOH[d]	45 (48)	**3c** (4) + **11** (1) + **12** (8)
2	$Ni(cod)_2$–PPh_3[e]	(< 3)	**8** (> 90% recovery)
3	$Ni(cod)_2$–PPh_3–Et_2Zn[f]	(13)	**11** + **12** (total 5) + other products
4	$Ni(cod)_2$–PPh_3–Me_3Al–PhOH[g]	24 (27)	**3c** (5) + **6** (3) + **11** (2) + **12** (7) + **13** (13)

[a] All reactions were carried out as follows: a THF solution of **2** (1 eq.) was added dropwise with stirring over 60 min at rt to a THF solution of **1c** (1 eq.), **8** (1 eq.), and catalysts. [b] Isolated yield. GC yield is in parentheses. [c] The yield of **12** (*m/z* = 308) is estimated on the basis of that of **11**. [d] $Ni(cod)_2$–PPh_3–Et_2Zn–PhOH = 0.05:0.1:0.5:0.8. [e] $Ni(cod)_2$–PPh_3 = 0.05:0.1. [f] $Ni(acac)_2$–PPh_3–Et_2Zn = 0.05:0.1:0.5. [g] $Ni(cod)_2$–PPh_3–Me_3Al–PhOH = 0.05:0.1:0.4:0.8.

the chemo- and regioselective cyclotrimerization of two or three different monoynes. While the detail is being investigated further in our laboratory, the present finding should help address a longstanding problem in the cyclotrimerization.

This work was supported by Grants-in-Aid for Scientific Research on Priority Areas (A) (No. 283, 'Innovative Synthetic Reactions') from the Ministry of Education, Science, Sports and Culture, Government of Japan (Monbusho).

Notes and references

‡ The IUPAC name for propargyl is prop-2-ynyl.

1 B. H. Lipshutz and T.-Y. Luh, *Tetrahedron*, 1998, **54**, xiii.
2 S. Ikeda, *Acc. Chem. Res.*, 2000, **33**, 511; for related material, see: J. Montgomery, *Acc. Chem. Res.*, 2000, **33**, 467.
3 S. Ikeda, N. Mori and Y. Sato, *J. Am. Chem. Soc.*, 1997, **119**, 4779; N. Mori, S. Ikeda and Y. Sato, *J. Am. Chem. Soc.*, 1999, **121**, 2722; S. Ikeda, H. Kondo and N. Mori, *Chem. Commun.*, 2000, 815.
4 S. Ikeda, H. Watanabe and Y. Sato, *J. Org. Chem.*, 1998, **63**, 7026; T. Sambaiah, L.-P. Li, D.-J. Huang, C.-H. Lin, D. K. Rayabarapu and C.-H. Cheng, *J. Org. Chem.*, 1999, **64**, 3663.
5 For examples of cyclotrimerization using a stoichiometric amount of metal complex, see: Y. Wakatsuki, T. Kuramitsu and H. Yamazaki, *Tetrahedron Lett.*, 1974, 4549; T. Takahashi, M. Kotora and Z. Xi, *J. Chem. Soc., Chem. Commun.*, 1995, 361; T. Takahashi, Z. Xi, A. Yamazaki, Y. Liu, K. Nakajima and M. Kotora, *J. Am. Chem. Soc.*, 1998, **120**, 1672; T. Takahashi, F.-Y. Tasi, Y. Li, K. Nakajima and M. Kotora, *J. Am. Chem. Soc.*, 1999, **121**, 11093.
6 For recent reports of Ni(0)-catalyzed [2 + 2 + 2] cycloaddition with alkynes, see: Y. Sato, T. Nishimata and M. Mori, *Heterocycles*, 1997, **44**, 443; Y. Sato, K. Ohashi and M. Mori, *Tetrahedron Lett.*, 1999, **40**, 5231.
7 When both **1a** and **2** were successively added to the reaction medium involving the $Ni(acac)_2$–PPh_3–Et_2Zn–PhOH catalytic system, **6** was obtained in 37% yield along with **3a** and **4a** (total 42% yield). On the other hand, prolonging the duration of the addition to 10 min led to the formation of **5** (23% yield, along with **3a** and **4a**: total 57% yield).
8 It has been reported that the reaction of Et_2Zn with PhOH gave not a bis-substituted $Zn(OPh)_2$ but rather a mono-substituted EtZnOPh, which aggregated to form the tetramer as a white solid.[8a] However, this white solid was not efficient in the chemoselective cyclotrimerization of **1a** and **2**. These results suggest that the non-aggregated EtZnOPh species prepared *in situ* acts as the co-catalyst in the reaction; (*a*) G. E. Coates and D. Ridley, *J. Chem. Soc.*, 1965, 1870; J. G. Noltes and J. Boersma, *J. Organomet. Chem.*, 1968, **12**, 425; Also see: G. Allen, J. M. Bruce, D. W. Farren and F. G. Hutchinson, *J. Chem. Soc. B*, 1966, 799.
9 K. P. C. Vollhardt, *Angew. Chem., Int. Ed. Engl.*, 1984, **23**, 539; N. E. Schore, *Chem. Rev.*, 1988, **88**, 1081; M. Lautens, W. Klute and W. Tam, *Chem. Rev.*, 1996, **96**, 49; S. Saito and Y. Yamamoto, *Chem. Rev.*, 2000, **100**, 2901.
10 F. E. McDonald, H. Y. H. Zhu and C. R. Holmquist, *J. Am. Chem. Soc.*, 1995, **117**, 6605; B. Witulski and T. Stengel, *Angew. Chem., Int. Ed.*, 1999, **38**, 2426; Y. Yamamoto, R. Ogawa and K. Itoh, *Chem. Commun.*, 2000, 549.

Reaction of cyclotrisilene with phenylacetylene: an unusual product with a bicyclo[3.2.0]hepta-3,6-diene skeleton†

Masaaki Ichinohe, Tadahiro Matsuno and Akira Sekiguchi*

Department of Chemistry, University of Tsukuba, Tsukuba, Ibaraki, 305-8571, Japan.
E-mail: sekiguch@staff.chem.tsukuba.ac.jp

Received (in Cambridge, UK) 17th October 2000, Accepted 8th December 2000
First published as an Advance Article on the web 8th January 2001

Cyclotrisilene, $(^tBu_2MeSi)_4Si_3$, was reacted with phenylacetylene to produce an unusual 1,2,5-trisilabicyclo[3.2.0]hepta-3,6-diene derivative, whose structure was determined by NMR spectroscopy and X-ray crystallography; a mechanism for its formation is proposed.

The synthesis and characterization of a number of isolable double bond species consisting of the heavier Group 14 elements has been accomplished since the first isolation of tetramesityldisilene by West *et al*. in 1981.[1,2] Cyclotrimetallenes (R_4M_3, M = Si, Ge, Sn), *i.e.* compounds with endocyclic metal–metal double bonds, have been prepared: cyclotrigermenes in 1995,[3] cyclotrisilenes in 1999,[4,5] and cyclotristannene in 1999.[6] Quite recently, we have succeeded in the preparation of the first mixed cyclotrimetallenes consisting of two different Group 14 elements: 1- and 2-disilagermirenes.[7] These compounds exhibit an enhanced reactivity arising from the combination of a highly reactive metal–metal double bond and a highly strained three-membered ring skeleton in one molecule, which gives access to new cyclic and bicyclic compounds by addition and cycloaddition reactions.[8] Recently, we have also succeeded in transforming the cyclotrigermenes and cyclotrisilene into the cyclotrigermenylium ions[9] and cyclotetrasilenylium ion,[10] which are free germyl and silyl cations, respectively. Herein, we report on the reaction of cyclotrisilene **1** with phenylacetylene to produce an unusual product with a bicyclo[3.2.0]hepta-3,6-diene skeleton, and report also on its reaction mechanism.

Cyclotrisilene **1** was allowed to react with excess phenylacetylene in C_6D_6 at rt. The orange colour of **1** disappeared within 15 h to give a 1,2,5-trisilabicyclo[3.2.0]hepta-3,6-diene derivative **2** in a 65% yield (Scheme 1). No reaction occurred with trimethylsilylacetylene, bis(trimethylsilyl)acetylene, or diphenylacetylene, and a complicated reaction mixture was formed with hex-1-yne.

The structure of **2** was determined by mass spectrometry, NMR spectra and X-ray crystallography. The mass spectrum of **2** showed a very weak parent ion at 916, with fragmentation peaks at 859 ($M^+ - {}^tBu$) and at 759 ($M^+ - SiMe^tBu_2$). The ^1H NMR spectrum showed two olefinic protons at 7.42 and 7.98 ppm, as well as peaks indicating the presence of four different $^tBu_2MeSi$ groups, and two phenyl groups. The ^{13}C and ^{29}Si NMR spectra were also consistent with this structure being a 1:2 adduct of **1** and phenylacetylene. As shown in Fig. 1, compound **2** has a bicyclo[3.2.0]hepta-3,6-diene skeleton, the formation of which can be explained by the consecutive addition of one molecule of phenylacetylene to the Si=Si double bond, and by the insertion of a second molecule of phenylacetylene into the Si–Si single bond in the resulting cyclotrisilane ring. The cycloaddition reaction of acetylenes with a Si=Si double bond to give the disilacyclobutene derivative is well known,[11] but the insertion of C–C multiple bonds into a Si–Si single bond at ambient temperature without the use of a catalyst has not been reported.

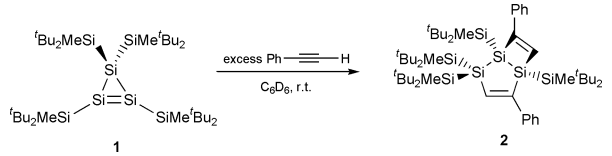

1 2

Scheme 1

The formation of **2** was quite interesting for us, and prompted us to investigate its formation mechanism. Under the same conditions as above, deuterium-labelled cyclotrisilene, **1**–$\mathbf{d}_6$,[12] in which the CH_3 groups in the di-*tert*-butyl(methyl)silyl substituents on the saturated silicon atom were replaced by a CD_3 group, was reacted with phenylacetylene to give **2a**–$\mathbf{d}_6$ and **2b**–$\mathbf{d}_6$ in a 1:1 molar ratio.[13] This result indicates that **2** is not formed *via* a simple [2 + 2] cycloaddition and insertion process. A more likely mechanism is as follows. First, the phenylacetylene undergoes cycloaddition to the Si=Si double bond of **1**–$\mathbf{d}_6$ to form the 1,4,5-trisilabicyclo[2.1.0]pent-2-ene derivative **3**–$\mathbf{d}_6$, which then isomerizes to the 1,2,3-trisilacyclopenta-3,5-diene derivative **4**–$\mathbf{d}_6$, which has a conjugated Si=C–C=Si system in a five-membered ring. Secondly, one $^tBu_2(CD_3)Si$ group on a saturated silicon atom migrates to an unsaturated silicon atom to give the 1,2,3-trisilacyclopenta-2,4-diene derivative **5**–$\mathbf{d}_6$, which has a conjugated Si=Si–C=C system in a five-membered ring.[14] Finally, the silole intermediate **5**–$\mathbf{d}_6$, is trapped by phenylacetylene *via* a [2 + 2] cycloaddition across

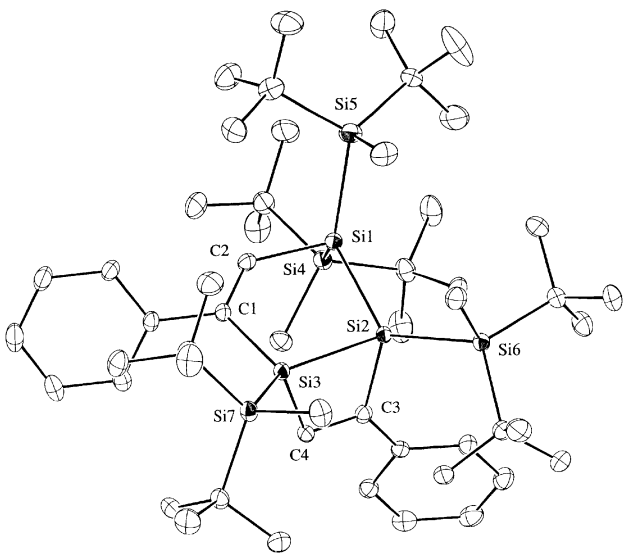

Fig. 1 Structure of **2** (hydrogen atoms are omitted for clarity). Selected bond distances [Å] are: Si1–Si2 2.477(1), Si1–C2 1.893(3), Si2–Si3 2.388(1), Si2–C3 1.943(3), Si3–C 11.909(3), Si3–C4 1.892(3), C1–C2 1.351(4), C3–C4 1.356(4). Selected bond angles [°] are: Si2–Si1–C2 95.8(1), Si1–Si2–Si3 92.6(0), Si3–Si2–C3 73.7(1), Si2–Si3–C1 101.7(1), Si2–Si3–C4 75.0(1), Si3–C1–C2, 119.0(2), Si1–C2–C1 130.5(2), Si2–C3–C4 104.7(2), Si3–C4–C3 106.5(2).

† Electronic supplementary information (ESI) available: experimental procedure, spectral data and X-ray data (CCDC 182/1876) of the products. See http://www.rsc.org/suppdata/cc/b0/b008375p/

DOI: 10.1039/b008375p

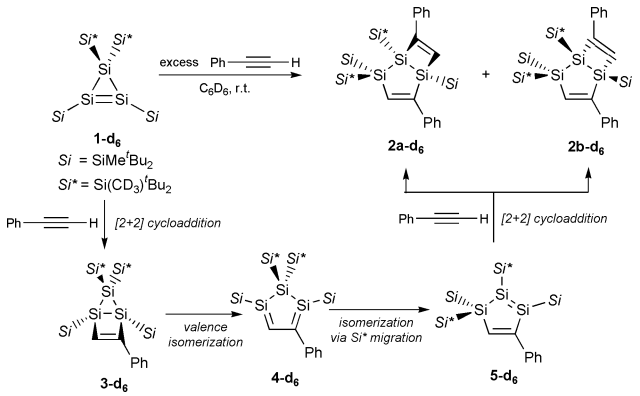

Scheme 2

the Si=Si double bond to afford a mixture of **2a**–$\mathbf{d}_6$ and **2b**–$\mathbf{d}_6$ (Scheme 2). However, the silole intermediates **4** and **5** were not observed in monitoring the reaction of **1** with phenylacetylene using NMR spectroscopy, which is probably due to their high reactivity. Even with equimolar quantity of phenylacetylene, the product **2** was formed together with unreacted **1**.

To have a better understanding of the isomerization of **3** to **5**, *ab initio* calculations on the parent system (**6**–**8**) were carried out at the Beck3LYP/6-31G(d) level, and all isomers **6**–**8** were found as energy minimum structures. The bicyclic structure **6** was the most unfavourable, probably due to the highly strained three- and four-membered bicyclic structure, and the siloles **7** and **8** were more stable by 1.0 and 13.1 kcal mol^{-1} relative to

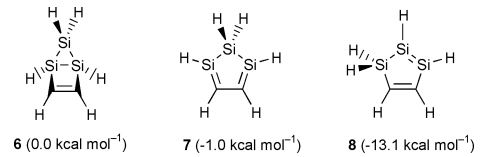

6, respectively. The conrotatory isomerization of **6** to **7** may be unfavourable because of the fixed bicyclic structure of **6**. The last compound consequently isomerizes by the migration of the hydrogen atom to give the thermodynamically most stable silole structure **8**, with a Si=Si–C=C conjugated system.

This work was supported by Grant-in-Aid for Scientific Research (Nos. 10304051, 12020209, 12042213, 12740338) from the Ministry of Education, Science and Culture of Japan, and TARA (Tsukuba Advanced Research Alliance) fund.

Notes and references

1 R. West, M. J. Fink and J. Michl, *Science*, 1981, **214**, 1343.
2 For the recent reviews on $R_2M{=}MR_2$ (M = Si, Ge, Sn), see: M. Weidenbruch, *Eur. J. Inorg. Chem.*, 1999, 373; P. P. Power, *Chem. Rev.*, 1999, **99**, 3463; J. Escudié and H. Ranaivonjatovo, *Adv. Organomet. Chem.*, 1999, **44**, 113.
3 A. Sekiguchi, H. Yamazaki, C. Kabuto, H. Sakurai and S. Nagase, *J. Am. Chem. Soc.*, 1995, **117**, 8025; A. Sekiguchi, N. Fukaya, M. Ichinohe, N. Takagi and S. Nagase, *J. Am. Chem. Soc.*, 1999, **121**, 11 587.
4 T. Iwamoto, C. Kabuto and M. Kira, *J. Am. Chem. Soc.*, 1999, **121**, 886.
5 M. Ichinohe, T. Matsuno and A. Sekiguchi, *Angew. Chem., Int. Ed.*, 1999, **38**, 2194.
6 N. Wiberg, H.-W. Lerner, S.-K. Vasisht, S. Wagner, K. Karaghiosoff, H. Nöth and W. Ponikwar, *Eur. J. Inorg. Chem.*, 1999, 1211.
7 V. Y. Lee, M. Ichinohe, A. Sekiguchi, N. Takagi and S. Nagase, *J. Am. Chem. Soc.*, 2000, **122**, 9034.
8 N. Fukaya, M. Ichinohe and A. Sekiguchi, *Angew. Chem., Int. Ed.*, 2000, **39**, 3881; V. Y. Lee, M. Ichinohe and A. Sekiguchi, *J. Am. Chem. Soc.*, 2000, **122**, 12 604.
9 A. Sekiguchi, M. Tsukamoto and M. Ichinohe, *Science*, 1997, **275**, 60; M. Ichinohe, N. Fukaya and A. Sekiguchi, *Chem. Lett.*, 1998, 1045; A. Sekiguchi, N. Fukaya, M. Ichinohe and Y. Ishida, *Eur. J. Inor. Chem.*, 2000, 1155.
10 A. Sekiguchi, T. Matsuno and M. Ichinohe, *J. Am. Chem. Soc.*, 2000, **122**, 11 250.
11 D. N. Roark and G. J. D. Peddle, *J. Am. Chem. Soc.*, 1971, **94**, 5837; H. Sakurai, T. Kobayashi and Y. Nakadaira, *J. Organomet. Chem.*, 1978, **162**, C43; M. J. Fink, D. J. DeYoung and R. West, *J. Am. Chem. Soc.*, 1983, **105**, 1070.
12 Cyclotrisilene **1**–$\mathbf{d}_6$ was prepared by the reductive condensation of 2,2-dibromo-1,1,3,3-tetra(*tert*-butyl)-1,3-bis-(trideuteriomethyl)trisilane and 2,2,2-tribromo-1,1-di-(*tert*-butyl)-1-methyldisilane with sodium in toluene. See ref. 5.
13 The signal at 0.67 ppm assigned to a methyl group on Si6 completely disappeared, and the relative intensities of two signals at 0.16 and 0.51 ppm, assigned to the methyl groups on Si4 and Si5, were half the magnitude of those of **2**.
14 Thermal rearrangement of tetrakis[di-*tert*-butyl(methyl)silyl]-1-disilagermirene to tetrakis[di-*tert*-butyl(methyl)silyl]-2-disilagermirene by $^tBu_2MeSi$ group migration was reported. See ref. 7.

First report of phase selective gelation of oil from oil/water mixtures. Possible implications toward containing oil spills

Santanu Bhattacharya*† and Yamuna Krishnan-Ghosh

Department of Organic Chemistry, Indian Institute of Science, Bangalore 560 012, India.
E-mail: sb@orgchem.iisc.ernet.in

Received (in Cambridge, UK) 27th September 2000, Accepted 1st December 2000
First published as an Advance Article on the web 8th January 2001

From a two-phase mixture of water and oil (either commercial fuel or pure organic solvent), a simple amino acid derivative, *N*-lauroyl-L-alanine has been shown to be able to gelate the oil phase selectively; SEM and FT-IR provided molecular level insights into the process of gelation.

Much has been achieved in the field of polymeric gels and their applications.[1] Although several excellent non-polymeric *low molecular mass* organogelators have been developed,[2,3] the ability of an organogelator to gelate one solvent in preference to another from a given mixture has still not been evidenced. This becomes an even more daunting task when one of the solvents in such a mixture is water. This is because, in contrast to their macromolecular counterparts, the network structure formed by low molecular weight organogelators are often held together by non-covalent interactions such as hydrogen bonding.[3] Understandably, water competes for the hydrogen bonding sites in the gelator molecule, thereby disrupting the self-association of the gelator and ruining gelation. We discovered that a fatty acid

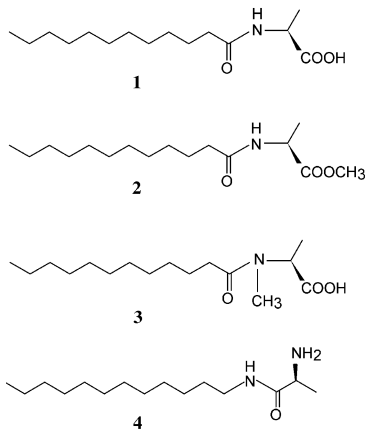

derived amino acid, *N*-lauroyl-L-alanine, **1**, is a simple and effective system for the selective gelation of non-polar organic solvents such as aromatic and aliphatic hydrocarbons. Herein we report for the first time an organogelator, which is capable of achieving solvent-specific gelation from a two-phase mixture. To derive a proper structure–property correlation, related compounds **2**–**4** were also synthesized.‡

First the efficiency of **1** in gelating various aromatic and aliphatic hydrocarbon solvents was examined§ (Table 1). For a series of *n*-alkanes with $6 < n < 12$, the MGC passed through a maximum for $n = 8$, and another minimum was reached for $n = 16$, where n is the number of C-atoms in the aliphatic hydrocarbon. The gels formed in aliphatic hydrocarbons were translucent in nature while those formed in aromatic solvents were found to be transparent. Since the above solvents also form major constituents of petrol, we found that **1** could indeed gelate a wide range of commercial fuels (Table 1).

Representative SEM¶ of the gels of **1** obtained from either *n*-heptane (Fig. 1A) or toluene (Fig. 1B) shows the presence of a network of fibers of varying thicknesses. In the heptane gels, a profusion of thin fibers (0.5–1.5 μm) was seen while in toluene gels individual fibers of regular thickness (3.0 μm) appeared to merge into thicker fibers (6–15 μm). Solvent molecules get entrapped in the fibrous networks due to surface tension resulting in gelation.

We then investigated selective gelation of a discrete volume of such fuels by **1** when it is present in a two-phase system. A mixture of double-distilled water (2 mL) and an oil (2 mL) was taken in a test tube and **1** (10 mg) was added to the two-phase mixture. Compound **1** was solubilized either by heating or by injection of an ethanolic solution of **1** leaving the mixture to equilibrate. Remarkably, as soon as rt was attained, the oily layer was found to be completely gelated leaving the aqueous layer unaffected. Even upon standing for ~1 week, both the phases remained intact with their respective states of gelation and non-gelation. When the experiment was repeated with periodic or continuous violent agitation (a model 'oil-spill situation') the above mixture formed an emulsion which, upon cooling to rt, rapidly solidified into a mass where the phase

Table 1 Gelation properties of **1** (1 mmol) and minimum gelator concentration (MGC) in g L^{-1} (gelator/organic solvent) necessary for gelation of various organic solvents at 25 °C

Organic liquid	MGC	Organic liquid	MGC
n-Hexane	7.0	Benzene	8.0
n-Heptane	2.6	Toluene	3.5
n-Octane	2.4	*o*-Xylene	5.1
n-Decane	2.5	*m*-Xylene	5.5
n-Dodecane	2.7	*p*-Xylene	2.7
n-Hexadecane	2.4	Mesitylene	2.2
Isooctane	3.4	Cyclohexane	4.0
Petrol	11.9	CCl_4	8.8
Kerosene	3.2	1,2-Dichlorobenzene	5.0
Paraffin oil	5.1	Carbon disulfide	5.9

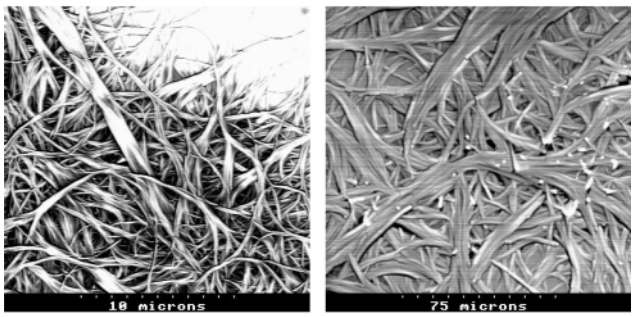

A B

Fig. 1 SEM of gels of (A) *n*-heptane and (B) toluene with **1**.

† Also at the Chemical Biology Unit, JNCASR, Bangalore 560 064, India. This work was supported by the Swarnajayanti fellowship grant of the Department of Science and Technology (Government of India) awarded to S. B.

boundaries were indistinct. Heating of this gelled emulsion to > 50 °C resulted in the 'melting' of the mass which separated into discrete aqueous and organic layers. When this was allowed to cool undisturbed, as before only the organic layer was gelated selectively. Similarly, a given volume of commercially available petrol could be gelated from a two-phase mixture. Importantly the gelation was unaffected even in the presence of (a) NaCl (at various concentrations) or (b) chelation inducing metal salts (*e.g.* $CuSO_4$), or (c) oxidizing agents (*e.g.* $KMnO_4$) or (d) other impurities present in water from natural sources (not shown).

Next, the roles of various functional groups involved in the self-assembly process were investigated by blocking one by one the hydrogen bonding sites in **1** *via* chemical modification. First the carboxylic acid (-CO_2H) in **1** was converted to its methyl ester, **2**. Then the amide moiety (-NH-C(O)) in **1** was subjected to *N*-methylation to give **3**. Interestingly, neither **2** nor **3** induced any gelation. Thus the presence of both the -CO_2H and the secondary amide (-NH-C(=O)) appear to be essential for self-association of the monomer into fibers (Fig. 1) a necessary prerequisite for gelation.

In order to understand the precise roles of the -CO_2H and -NH-C(=O) residues in **1** in the process of gelation, detailed FT-IR studies were carried out.‖ First, FT-IR spectra of (a) the solid (KBr pellet) from a dried benzene gel of **1**, (b) solutions of **1** (c = 60 mg mL^{-1}) in benzene and (c) in a non-gelatable solvent such as $CHCl_3$ were compared (not shown). The amide and the –CO_2H moieties in **1** are as strongly hydrogen bonded in the gel state as they are in the solid state. Benzene does not interfere with the intermolecular association. The *amide I* band in the gel state was almost as strongly hydrogen bonded as in the solid (1646 cm^{-1}). However, in $CHCl_3$ the *amide I* band (1669 cm^{-1}) evidenced a weakly hydrogen bonded species probably between the oxygen of the amide carbonyl and the acidic H of $CHCl_3$. This is confirmed by efficient gelation of CCl_4 by **1**. Thus solvents capable of hydrogen bonding *suppress* gelation in these systems by disallowing the self-assembly process.

The -CO_2H sites of **1** in both solvents form dimers of comparable strength (1732 cm^{-1}). Thus the factor controlling gelation of **1** seems to be hydrogen bonding at the amide sites (-N–H···(O)=C–N–H···(O)=C-), which is significantly affected by the polarity and protic nature of the solvent. However, the strength of the *amide I* band is considerably weaker in $CHCl_3$ (1669 cm^{-1}) than in benzene (1648 cm^{-1}). It is this difference in strength that most probably determines whether the solvent promotes or inhibits perpetuation of the superstructure. In addition to the amide site, the availability of the free -CO_2H is mandatory for the dimer formation leading to gelation. This was confirmed with **4** where the free amine cannot form analogous dimers and despite the presence of amides, the gelation did not occur.

In summary, in order to exhibit gelation, the molecule must have the capacity to self-assemble in three-dimensions to form fibrous networks. Self-assembly of **1** is evident from SEM. IR studies show that this process involves at least two interactions (-CO_2H and (O)=C–N–H) where each residue promotes the formation of a supramolecular array. In water, due to the presence of a lipophilic alkyl chain, **1** exerts a hydrophobic effect[4] and excludes water. Additional stabilization of such aggregates most likely originates from Van der Waals contacts of the polymethylene chains. This promotes the self-organization of **1** and in the process it is able to gelate hydrocarbon-based fuels or solvents even in the presence of water. While the present system is interesting, the necessity to heat and cool the samples in order to achieve phase separation significantly limits its use for the containment of oil-spills. Clearly issues such as requirement of heating to achieve gelation have to be addressed before a real-life application is possible. Nevertheless the present system demonstrates its unique ability to confer phase-selective gelation of toxic solvents from complex mixtures.

Notes and references

‡ All new compounds, **1**–**4**, were synthesized from readily available precursors and were characterized by FT-IR, ^{1}H-NMR, LR-MS and elemental analysis. Selected data: *N*-*n*-dodecanoyl-(*S*)-alanine (**1**) was synthesized by the hydrolysis of **2** in MeOH with 1.0 eq. of 1 M NaOH for 2 h at ~5 °C followed by careful acidification in cold conditions. Isolated as a solid, mp: 84 °C (97% yield). $[\alpha]_D^{25}$ (c = 2 in $CHCl_3$) = +16.6°. IR (cm^{-1}): 3348, 1704, 1646, 1520. ^{1}H-NMR (300 MHz, $CDCl_3$) δ: 0.88 (t, J = 6.5 Hz, 3H), 1.25 (br m, 16H), 1.45 (d, J = 7 Hz, 3H), 1.61 (m, 2H), 2.22 (t, J = 8 Hz, 2H), 4.54 (m, 1H), 6.4 (d, J = 9 Hz, 1H). LR-MS: 271 (M^+, 2%). Anal. calcd. for $C_{15}H_{29}NO_3$: C, 66.38; H, 10.77; N, 5.16. Found: C, 66.62; H, 10.94; N, 4.92%. Methyl *N*-*n*-dodecanoyl-(*S*)-alaninate (**2**) was synthesized by reaction of L-alanine methyl ester hydrochloride (Fluka) with dodecanoyl chloride (1.1 eq.) in dry $CHCl_3$ and Et_3N (2.2 eq.). Isolated as a solid, mp: 65 °C, (97% yield). $[\alpha]_D^{25}$ (c = 2 in $CHCl_3$) = +14.0°. IR (cm^{-1}): 3300, 1732, 1650, 1537. ^{1}H-NMR (300 MHz, $CDCl_3$): δ: 0.88 (t, J = 7 Hz, 3H), 1.26 (br m, 16H), 1.41 (d, J = 6.5 Hz, 3H), 1.62 (m, 2H), 2.18 (t, J = 8 Hz, 3H), 3.73 (s, 3H), 4.56 (m, 1H), 5.93 (d, J = 9 Hz, 1H). LR-MS: 285 (M^+, 2%). Anal calcd. for $C_{16}H_{31}NO_3$: C, 67.33; H, 10.95; N, 4.91. Found: C, 67.52; H, 11.03; N, 5.05%. *N*-*n*-Dodecanoyl-*N*-methyl-(*S*)-alanine (**3**) was synthesized by the reaction of *N*-methyl-L-alanine (Fluka) in dry DMF with dodecanoyl chloride (Fluka) and Et_3N (1.1 eq.). Isolated as a solid, mp: 79 °C, (64% yield). $[\alpha]_D^{25}$ (c = 2 in $CHCl_3$) = +10.1°. IR (KBr) (cm^{-1}): 1701, 1645, 1541. ^{1}H-NMR (300 MHz, $CDCl_3$) δ: 0.87 (t, J = 6.5 Hz, 3H), 1.26 (br m, 16H), 1.44 (d, J = 7 Hz, 3H), 1.62 (m, 2H), 2.21 (t, J = 8 Hz, 3H), 2.91 (s, 3H), 4.53 (m, 1H). LR-MS: 285 (M^+, 2%). Anal. calcd. for $C_{16}H_{31}NO_3$: C, 67.33; H, 10.95; N, 4.91. Found: C, 67.22; H, 10.58; N, 4.74%. *N*-Dodecyl-(*S*)-alaninamide (**4**) was prepared by catalytic hydrogenation (10% Pd/C) in MeOH of *N*-benzyloxycarbonyl-*N*′-hexadecyl-(*S*)-alaninamide, a compound that was prepared by DCC coupling of (*S*)-*N*-Benzyloxycarbonylalanine (Fluka) and *n*-hexadecylamine (Fluka) in dry THF. Isolated as a hygroscopic solid, mp: 54 °C (87% yield). $[\alpha]_D^{25}$ (c = 2 in $CHCl_3$) = +12.8°. IR (KBr) (cm^{-1}): 3320, 1630, 1560. ^{1}H-NMR (300 MHz, $CDCl_3$) δ: 0.86 (t, J = 7 Hz, 3H), 1.2 (br m, 18H), 1.26 (m, 2H), 1.43 (d, J = 7 Hz, 3H), 3.2 (m, 2H), 4.09 (m, 1H), 7.5 (br s, 1H). LR-MS: 256 (M^+, 40%). Anal. calcd. for $C_{15}H_{32}N_2O{\cdot}0.25\ H_2O$: C, 69.04; H, 12.56; N, 10.74. Found: C, 69.36; H, 12.83; N, 10.48%.

§ The ability of **1** to gelate a given solvent was tested by solubilizing **1** (1 mmol) in the desired solvent (7.5 mL) by gentle heating and allowing the solution to spontaneously cool to rt. The gel was allowed to stand for *ca.* 15 min at rt. MGC was calculated as described in the literature.[3a]

¶ Scanning electron micrograph (SEM) was recorded using a Cambridge stereoscan S-360 SEM. A glass plate bearing a droplet of **1** dissolved in benzene or *n*-heptane was attached to the sample stage after completion of gelation and sputtered with gold to 100–150 Å.

‖ **1** was dissolved in the desired concentrations in benzene or $CHCl_3$ and loaded into a solution cell of a JASCO 410 FT–IR spectrometer. Spectra were corrected for solvent absorption.

1 S. Miyazaki, F. Suisha, N. Kawasaki, M. Shirakawa, K. Yamatoya and D. Attwood, *J. Controlled Release*, 1998, **56**, 75; Y. Ito, N. Sugimura, K. Oh and Y. Imanashi, *Nat. Biotechnol.*, 1999, **17**, 73; H. Lee and T. G. Park, *Biotechnol. Prog.*, 1998, **14**, 508; *Using Stimuli-Responsive Polymers in Bioseparation*, ed. I. Yu. Galaev, *Bioseparation Special Issue*, 1999, **7**, 175.

2 See for a recent highlight: J. H. van. Esch and B. L. Feringa, *Angew. Chem., Int. Ed.*, 2000, **39**, 2263.

3 (*a*) K. Hanabusa, M. Yamada, M. Kimura and H. Shirai, *Angew. Chem., Int. Ed.*, 1996, **35**, 1949; (*b*) P. Terech and R. G. Weiss, *Chem. Rev.*, 1997, **97**, 3133; (*c*) K. Yoza, N. Amanokura, Y. Ono, T. Aoka, H. Shinmori, M. Takeuchi, S. Shinkai and D. N. Reinhoudt, *Chem. Eur. J.*, 1999, **5**, 2722; (*d*) A. Aggeli, M. Bell, N. Boden, J. N. Keen, P. F. Knowles, T. C. B. McLeish, M. Pitkeathly and S. E. Radford, *Nature*, 1997, **386**, 259; (*e*) J. Van Esch, F. Schoonbeek, M. de Loos, H. Kooijmann, A. L. Spek, R. M. Kellogg and B. L. Feringa, *Chem. Eur. J.*, 1999, **5**, 937; (*f*) R. Oda, I. Huc and S. J. Candau, *Angew. Chem., Int. Ed.*, 1998, **37**, 2689; (*g*) R. J. H. Hafkamp, M. C. Feiters and R. J. M. Nolte, *J. Org. Chem.*, 1999, **64**, 412; (*h*) S. Bhattacharya and S. N. G. Acharya, *Chem. Mater.*, 1999, **11**, 3121; (*i*) T. Brotin, R. Utermohlen, F. Fages, H. Bouas-Laurent and J.-P. Desvergne, *J. Chem. Soc., Chem. Commun.*, 1994, 1401; (*j*) U. Beginn, S. Keinath and M. Möller, *Macromol. Chem. Phys.*, 1998, **199**, 2379; (*k*) Y. Osada and J.-P. Gong, *Adv. Mater.*, 1998, **10**, 827; (*l*) T. Oya, T. Enoki, A. U. Grosberg, S. Masamune, T. Sakiyama, Y. Takeoka, K. Tanaka, G. Wang, Y. Yilmaz, M. S. Feld, R. Dasari and T. Tanaka, *Science*, 1999, **286**, 1543.

4 C. Tanford, *The Hydrophobic Effect: Formation of Micelles and Biological Membranes*, Wiley, New York, 1980.

ChemComm

Halide redistribution in Pd-catalysed 1,6-diene cycloisomerisation†

Katharine L. Bray, Ian J. S. Fairlamb and Guy C. Lloyd-Jones*

School of Chemistry, Cantock's Close, Bristol, UK BS8 1TS. E-mail: guy.lloyd-jones@bris.ac.uk

Received (in Cambridge, UK) 21st November 2000, Accepted 12th December 2000
First published as an Advance Article on the web 8th January 2001

$[(MeCN)_3PdCl]^+$, generated *in situ*, reversibly disproportionates to give $[(MeCN)_2PdCl_2]$ and $[(MeCN)_4Pd]^{2+}$. The neutral species is a reactive and highly regioselective catalyst for 1,6-diene cycloisomerisation.

Early examples of transition metal-catalysed cycloisomerisation reactions[1] employed hepta-1,6-dienes (*e.g.* **1**) as substrates.[2–4] Since dialkyl diallylmalonates **1** may form cyclopentane **2** and cyclopentenes **3** and **4**, much of the focus in their cycloisomerisation has been the efficient control of regioselectivity (Scheme 1). A pioneer in this area was Grigg,[4] who reported regioselective $[(PPh_3)_3RhCl]$-catalysed isomerization of **1b** to **2b** ($CHCl_3$, reflux 8 h)‡ or **4b** (EtOH, reflux, 12 h).‡ Under palladium catalysis [5 mol% $Pd(OAc)_2$ or $PdCl_2$] isomeric **3b** and **4b** were obtained in good yields (80–88%) and with good regioselectivity (92−94%) for **3b** ($CHCl_3$, reflux 6–8 h).‡ Much more recently, a number of other catalyst systems have been developed for selective isomerisation of **1** to **2** or **4**,[5] although catalysts for selective conversion of **1** to **3** still remain rare.[4,6] Our attention was drawn to the recent report by Heumann and Moukhliss[7] on the use of $[(MeCN)_{(4-m)}Pd(Cl)_m]^{(2-m)+}$ {generated *in situ* from the neutral complex $[(MeCN)_2PdCl_2]$} for cycloisomerisation. By use of 1 or 2 equivalents of $AgBF_4$ (per Pd), **1b** was isomerised to **3b** (79%, 18 h, reflux, 5 mol% Pd, $CHCl_3$) or to **2b** (39%, 8 h, reflux, $CHCl_3$), respectively. This led the authors to conclude that it is the catalyst charge that controls the regioselectivity.[7]

We have recently been studying the mechanism by which $[(MeCN)_2Pd(allyl)]^+$ (5 mol%) in $CHCl_3$ cycloisomerises **1a**.[8] The primary and predominant product is **2a**, however, on co-addition of 1 mol% $[Cl_2Pd_2(allyl)_2]$, which is not itself an active catalyst, both **2a** and **3a** are generated at approximately equal rates. This suggested to us that it could be the presence of chloride, rather than the charge, that determines the regioselectivity in the Heumann system.[7] Consequently, we attempted to isolate $[(MeCN)_3PdCl]^+$ from a freshly prepared solution {AgOTf, MeCN, $CHCl_3$, $[(MeCN)_2PdCl_2]$, filter}. However, chloride redistribution through monomer/μ-halide dimer equilibrium resulted in crystallisation of the neutral dichloride $[(MeCN)_2PdCl_2]$,§ leaving the more soluble complex $[(MeCN)_4Pd][OTf]_2$¶ in solution. Since nearly all Pd-catalysed 1,6-diene cycloisomerisations employ cationic pro-catalysts[5b,c,6,7] there seems to be a general assumption that halide abstraction to generate a mono- or di-cation is a pre-requisite for activity. In fact, pure neutral $[(MeCN)_2PdCl_2]$ turned out to be a far more active catalyst than the analogous mono- or di-cationic complexes. For example, in the presence of 5 mol% $[(MeCN)_2PdCl_2]$, a $CHCl_3$ solution of **1a** was quantitatively cycloisomerised in just a few minutes at 60 °C. The catalyst was also active at lower temperatures, *e.g.* at 40 °C, 100% conversion was achieved in under 2 h with 97% regioselectivity for **3a** and no trace of **2a** evident by GC.‖

Neutrality and the presence of chloride appear to be important features in the activity of $[(MeCN)_2PdCl_2]$: simple salts** $[PdI_2, Pd(OAc)_2, Pd(O_2CCF_3)_2]$ failed to isomerise **1a** at 60 °C in the presence or absence of added MeCN (10 mol%) over a period of many hours. As indicated above, the cations are much less reactive and addition of 5 mol% NBu_4X (X = Cl, Br or I) to $[(MeCN)_2PdCl_2]$, to generate an anionic palladate-type species, completely inhibited catalysis. A stoichiometric reaction between **1a** and $[(MeCN)_2PdCl_2]$ in $CDCl_3$ was followed by ^1H NMR (500 MHz) at 25 °C. There were no observable complexation processes,†† just the slow consumption of **1a** and appearance of **3a**. To gain more information, the kinetics of the catalytic reaction (5 mol% Pd) were measured (HRGC) in $CHCl_3$, CH_2Cl_2 and 1,2-dichloroethane (DCE) at 23, 40 and 60 °C. In nearly all cases, an induction period was followed by a pseudo-zero-order rate profile over three to four half-lives (*ca.* 90% conversion).

The induction period indicates that $[(MeCN)_2PdCl_2]$ must be a pro-catalyst, however, there is no direct reaction between the complex and **1a** observable by NMR, *vide supra*, and although the induction period is followed by pseudo-zero order kinetics (*i.e.* steady-state catalyst concentration) no trace of any co-product from pro-catalyst reaction is evident by GC analysis.‡‡ We also prepared and evaluated $[(PhCN)_2PdCl_2]$, $[(Bu^tCN)_2PdCl_2]$, $[(DMSO)_2PdCl_2]$ and $[(PhCN)_2PdI_2]$ as cata-

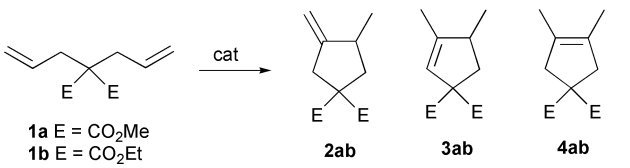

Scheme 1 Transition metal-catalysed cycloisomerisation of 1,6-diene **1**.

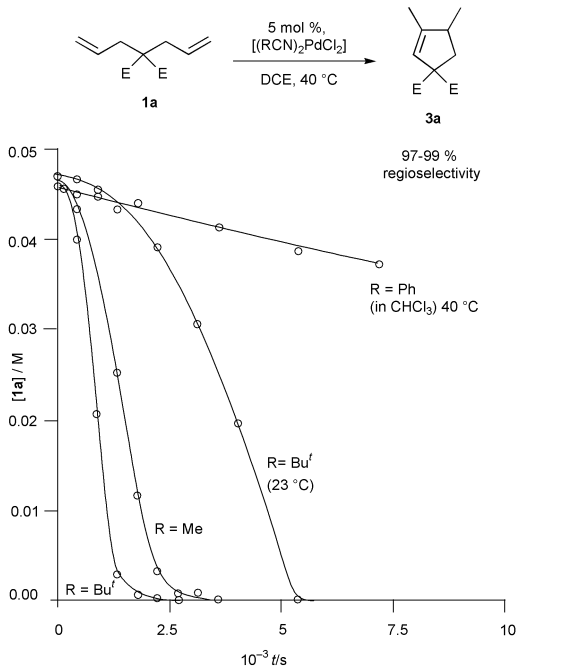

Fig. 1 Plot of variation of the concentration of 1,6-diene **1a** (M, *y*-axis) with time (*s*, *x*-axis) during cycloisomerisation by 5 mol% $[(RCN)_2PdCl_2]$ in 1,2-dichloroethane (DCE) or $CHCl_3$ at 23 or 40 °C. Concentration determined by GC analysis. For full details see ESI†.

† Electronic supplementary information (ESI) available: general experimental procedure, typical GC analyses and table of regioselectivities obtained with the various catalysts. See http://www.rsc.org/suppdata/cc/b0/b009356o/

DOI: 10.1039/b009356o

lysts. Only the chloro-complexes were active for cycloisomerisation of **1a**. The rate of reaction of **1a** using the pro-catalysts of type $[(RCN)PdCl_2]$ were similar, with DCE proving the best solvent. The Bu^{t}CN-bearing complex generally showed the highest activity. With the more coordinating ligand, DMSO, the catalyst was substantially less active (*ca.* 70% conversion in 42 h at 40 °C in DCE). However, it was highly selective, giving a 110 : 1 ratio of **3a** over isomeric **2a** and **4a**. By preparing the μ-halide dimer, $[(DMSO)_2Pd_2(\mu\text{-}Cl_2)Cl_2]$ we obtained a more reactive catalyst (90% conversion, 22 h, 40 °C, DCE) which still displayed excellent regioselectivity for **3a** (99%).

The regioselectivity of the isomerisation of **1a** to **3a** mirrors, but far exceeds, that observed by Grigg using $PdCl_2$, *vide supra*. However, $PdCl_2$, being a relatively insoluble polymeric species, requires use of more vigorous conditions (8 h, reflux in $CHCl_3$).‡ In contrast, monomeric complexes $[L_2PdCl_2]$ (L = RCN or DMSO)[9] allow reaction at lower temperatures, under neutral conditions and extremely high regioselectivity is attained. For example, using $[(Bu^tCN)_2PdCl_2]$ as catalyst, > 99% conversion of **1a** occurred in 90 min at 40 °C in $CHCl_3$ and **3a** was isolated in 96% yield and high purity (97.5%) after chromatography. In summary, compared to the analogous cations $[(RCN)_3PdCl]^+$ and $[(RCN)_4Pd]^{2+}$, complexes of the type $[(RCN)_2PdCl_2]$, are far more active pro-catalysts for 1,6-diene cycloisomerisation.[10] Furthermore, most catalysts[4,6,7] generate isomeric **2** and **4** from **1**, whereas with the neutral catalysts the regioisomer **3** is obtained with very high selectivity. Ironically, $[(MeCN)_2PdCl_2]$ has been used as a precursor for $[(MeCN)_3PdCl]^+$ generation *in situ*, however, due to chloride redistribution, it remains present in the reaction mixture. Nonetheless, preliminary labelling experiments employing $[^2H_2]$-**5**,[11] demonstrate that catalysis by $[(MeCN)_2PdCl_2]$ is not the exclusive process when '$[(MeCN)_3PdCl]^+$' is employed (Scheme 2).

Of note is the finding that, unlike labelling studies of cationic Pd-catalysts that generate the regioisomer **2a**,[5c,8] no scrambling of ^2H is observed with the neutral chloride catalysts (*cf.* $[^2H_2]$-**7**, Scheme 2). This bodes well for elucidation of the complete pathway between **1** and **3** and detailed NMR, kinetic and isotopic labelling studies,[8] to distinguish hydropalladation, cyclometallation and C–H insertion pathways,[1–5] will be reported in full in due course. Additionally, novel chiral ligands allowing the generation of analogous neutral complexes are being tested for asymmetric induction.

We thank the University of Bristol and the EPSRC (GR/N05208) for support. We also thank Professor Ross A. Widenhoefer (Duke University, USA) for sharing results prior to publication.

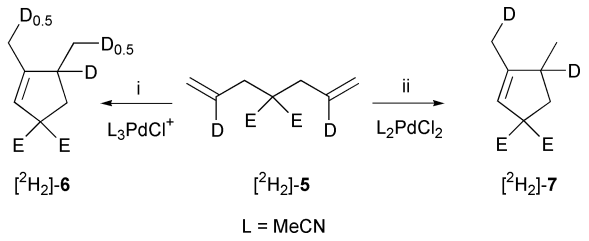

Scheme 2 Conditions: *i*, 5 mol% $[(MeCN)_3PdCl][OTf]$ (prepared from $[(MeCN)_2PdCl_2]$ by halide abstraction in MeCN with 1 equivalent AgOTf, then removal of AgCl by filtration, evaporation and redissolution in $CHCl_3$), 40 °C, $CHCl_3$; *ii*, 5 mol% $[(MeCN)_2PdCl_2]$, 40 °C, $CHCl_3$.

Notes and references

‡ To effect catalyst activation, the solvent was pre-saturated with HCl gas before addition of the substrate and heating to reflux.

§ $[(MeCN)_2PdCl_2]$ was isolated in 66% yield (based on Cl) and its identity confirmed by comparison (FT-IR and mp) with an authentic sample.

¶ Such disproportionation to generate the achiral pro-catalyst $[(MeCN)_2PdCl_2]$ may well explain why cycloisomerisation of **1b** with 5 mol% '$[(MeCN)_3PdCl]^+$/sparteine' in $CHCl_3$, generates **3b** in essentially racemic form, but with '$[(MeCN)_4Pd]^{2+}$/sparteine', **2b** and **3b** are obtained in 60 and 37% ee respectively, see ref. 7.

‖ When pure **2a** was exposed to 5 mol% $[(MeCN)_2PdCl_2]$, no isomerisation could be detected (^1H NMR) over a period of 22 h at 40 °C. However, in some reactions small quantities of the isomer **2a** were generated. Most often, these disappeared in the later stages of reaction and the maximum level of **2a** reached during reaction was < 0.5% of the total mixture of alkenes.

** In contrast to $Pd(OAc)_2$ and $Pd(CF_3CO_2)_2$, it may be noted that PdI_2 is essentially insoluble in $CHCl_3$. However, the soluble complex $[(PhCN)_2PdI_2]$ was also found to be ineffective. Furthermore, the insoluble polymer $PdCl_2$ (or a combination of $Pd(OAc)_2$/HCl) generates a moderately active catalyst, see ref. 4(*c*).

†† However, in the last *ca.* 20% reaction a slight broadening of the signals of **1a** became apparent suggesting reversible and unfavourable complexation at the NMR timescale.

‡‡ This suggests the possibility of substrate-induced establishment of a pre-equilibrium (dissociation of nitrile or chloro-bridged dimers) or solvent–catalyst reaction to generate the active species. Ongoing studies will address this issue through full analysis of the kinetics.

1 Reviews: (*a*) B. M. Trost, *Acc. Chem. Res.*, 1990, **23**, 34; (*b*) B. M. Trost and M. J. Krische, *Synlett*, 1998, 1.
2 A. Bright, J. F. Malone, J. K. Nicholson, J. Powell and B. L. Shaw, *Chem. Commun.*, 1971, 712.
3 E. Schmitz, R. Urban and G. Zimmermann, *J. Prakt. Chem.*, 1976, **318**, 185; E. Schmitz, U. Hench and D. Habisch, *J. Prakt. Chem.*, 1976, **318**, 471.
4 (*a*) R. Grigg, T. R. B. Mitchell and A. Ramasubbu, *J. Chem. Soc., Chem. Commun.*, 1979, 669; (*b*) R. Grigg, T. R. B. Mitchell and A. Ramasubbu, *J. Chem. Soc., Chem. Commun.*, 1980, 27; (*c*) R. Grigg, J. F. Malone, T. R. B. Mitchell, A. Ramasubbu and R. M. Scott, *J. Chem. Soc., Perkin Trans. 1*, 1984, 1745.
5 (*a*) Y. Yamamoto, N. Ohkoshi, M. Kameda and K. Itoh, *J. Org. Chem.*, 1999, **64**, 2178; (*b*) B. Radetich and T. V. RajanBabu, *J. Am. Chem. Soc.*, 1998, **120**, 8007; (*c*) P. Kisanga and R. A. Widenhoefer, *J. Am. Chem. Soc.*, 2000, **122**, 10 017.
6 *N,N*-ligand-bearing cationic Pd–Me complexes '$[(N,N)PdMe]^+$', generated *in situ* from the chloride, have recently been found to be active for selective conversion of **1a** to **3a**; R. A. Widenhoefer, personal communication.
7 A. Heumann and M. Moukhliss, *Synlett*, 1998, 1211.
8 K. L. Bray, I. J. S. Fairlamb, G. C. Lloyd-Jones, P. A. Slatford and J. P. Kaiser, unpublished work.
9 See for example, B. N. Storhoff and H. C. Lewis, *Coord. Chem. Rev.*, 1977, **23**, 1.
10 Although these neutral, stable and homogeneous complexes have previously been overlooked as catalysts for 1,6-diene cycloisomerisation, they are well known to catalyse non-hydride migratory cyclisation reactions such as Cope and related rearrangements and alkyne cyclotrimerisation: for detailed discussion see J. Tsuji, *Palladium Reagents and Catalysts*, John Wiley, Chichester, 1995.
11 K. L. Bray and G. C. Lloyd-Jones, *Eur. J. Org. Chem.*, 2001, in press.

Glycosyldisulfides: a new class of solution and solid phase glycosyl donors†‡

Benjamin G. Davis,* Sarah J. Ward and Phillip M. Rendle

Department of Chemistry, University of Durham, South Road, Durham DH1 3LE, UK.
E-mail: Ben.Davis@durham.ac.uk

Received (in Liverpool, UK) 24th October 2000, Accepted 22nd November 2000
First published as an Advance Article on the web 8th January 2001

Mixed glycosyl disulfides are not only glycomimetics but also glycosyl donors that may be readily constructed in either armed ether-protected or disarmed ester-protected and in soluble or solid-supported forms from corresponding glycosyl methanethiosulfonates and used in the glycosylation of a variety of representative acceptors.

Oligosaccharides and glycopeptides are essential tools for the investigation of the enormous variety of biological functions that require specific carbohydrate-containing structures.[1] Furthermore, their potential as therapeutic agents is clear.[2] As a result, the formation of the glycosidic linkage continues to be a dominant theme in carbohydrate chemistry.[3] Yet despite the development of many elegant strategies, there is still no generally efficient and stereoselective method available. To this end, a number of glycosyl donor systems have been developed in which differences in their anomeric leaving groups have an often critical effect upon reactivity. Of the variety of glycosyl donor systems available, thioglycosides **1** have proved one of

1 **2**

the most popular.[4] Strategies for tuning their reactivity, including armed/disarmed[5] donors, active/latent donors[6] or the use of bulky leaving groups,[7] have culminated in elegant one-pot glycosylation systems.[8]

With the goal of extending the scope of glycosyl donor reagents with sulfur at the anomeric centre, we have examined the utility of glycosyl disulfides **2**. These appeared attractive for several reasons: (i) the mixed disulfide linkage is a flexible one that may be cleaved for ready aglycon adjustment in reactivity tuning methods.[9] (ii) If used as a linker in solid-supported glycosylations, the anomeric mixed disulfide linkage would allow bidirectional (reductive or hydrolytic) cleavage, that would be of great advantage in both the analysis and use of solid supported glycosylation systems. (iii) The coordination of a potential thiophile by both sulfur atoms may offer enhanced reactivity over single sulfur thioglycoside systems.[10]

Remarkably, despite these positive indications and the high utility of thioglycosides **1**, the use of glycosyl disulfides **2** as glycosyl donors in *O*-glycoside bond formation is unexplored.[11] This neglect of glycosyl disulfides may in part be due to the lack of efficiency in existing syntheses.[12] We therefore set ourselves the goals of (a) developing efficient and general methods for the construction of glycosyl disulfides and (b) exploring their utility as glycosyl donors in *O*-glycoside formation.

Methanethiosulfonate (MTS) reagents allow the rapid and efficient formation of mixed disulfides.[13] We have previously demonstrated the utility of glycosyl methanethiosulfonates in the site-selective glycosylation or proteins.[14] In order to test fully the efficiency and scope of their use as reagents we

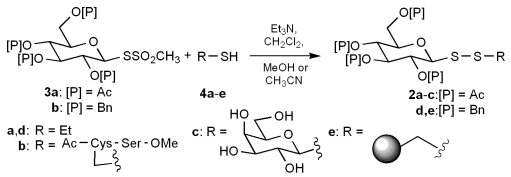

Scheme 1

prepared a representative range of glycosyl disulfides **2a**–**e** (Scheme 1) in which the structure of the coupling thiol **4** was varied. Thus, addition of ethanethiol **4a** to equimolar glucoMTS **3a**[14] gave ethyl glucosyl disulfide **2a**† in an excellent 96% yield. Similarly, more complex dipeptide glucosyl disulfide **2b**[15] (62% yield), as a potential glycopeptide mimic, or galactosyl glucosyl disulfide **2c** (60% yield), as a potential trehalose analogue, were also prepared in fair yield simply by reaction of the appropriate thiol **4b**,**c**, respectively, with **3a**. It should be noted that in all cases the β anomeric stereochemistry of the glucoMTS was preserved in the product disulfides. This also demonstrated the compatibility of this method with partially-, **4b**, or even un-protected, **4c**, thiols. To investigate the effect of protecting groups in the glucoMTS **3**, we prepared perbenzylated glucoMTS **3b**, which also reacted smoothly with ethanethiol to give **2d** (78% yield).[16]

Having demonstrated the efficient synthesis of several different glucosyl disulfides **2a**–**d**, we chose ethyl glycosyl disulfides **2a**,**d** as model systems in which to investigate their utility as glycosyl donors with the representative selection of glycosyl acceptors **5a**–**c** (Scheme 2). As Table 1 shows, glucosyl disulfide **2a** allowed the successful preparation of simple **6a**, disaccharide **6b**[17] and glycopeptide **6c**[18] *O*-glucosides. In all three cases exclusive β-stereoselectivity was observed. However, consistent with the disarmed and peracetylated nature of **2a**, moderate yields and acetyl migration side-products[19] were obtained under a variety of conditions. The disarmed nature of **2a** was further confirmed by the lack of reactivity with I_2 but the efficient conversion of **2a** to acetobromoglucose **7** using IBr.[20] With the aim of improving efficiencies, the activation of armed perbenzylated glucosyl disulfide **2d** was investigated next. We were delighted to find that under the optimal conditions elucidated for the activation of **2a** (NIS, TESOTf, CH_2Cl_2), **2d** rapidly and smoothly[21] gave methyl glucoside **8a** in an excellent 90% yield. Furthermore, reaction of **2d** with more hindered acceptors **5b**,**c** gave good yields of disaccharide **8b**[22] and glycopeptide **8c**[23] *O*-glucosides, respectively.

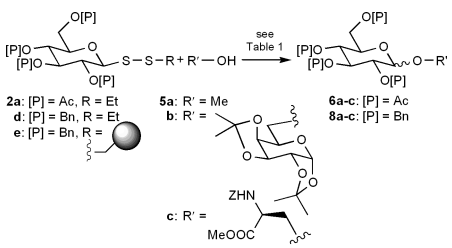

Scheme 2

† Electronic supplementary information (ESI) available: experimental details. See http://www.rsc.org/suppdata/cc/b0/b008734n/

‡ Some of this work was presented at a joint meeting of the RSC Carbohydrate and Bioorganic groups, Warwick, July 6 2000 and at the 20th International Carbohydrate Symposium, Hamburg, August 30, 2000.

DOI: 10.1039/b008734n

Table 1 Results of glycosylation reactions using dithioglycosides **2** as donors

Donor	Conditions[a]	Reaction time/h	Acceptor	Product	Yields (%)[b]
2a	NIS, reflux	24	**5b**	**6b**	32[c] (β only)
2a	NIS, TfOH	22	**5b**	**6b**	26[c] (β only)
2a	NIS, TfOH, CH_3CN	24	**5b**	**6b**	2[c] (β only)
2a	NIS, TMSOTf	4.5	**5b**	**6b**	30[c] (β only)
2a	NIS, TMSOTf, CH_3CN	6	**5b**	**6b**	16[c] (β only)
2a	NIS, TESOTf	2	**5b**	**6b**	36[c] (β only)
2a	I_2	168	**5b**	—	—
2a	IBr	30 min	—	**7**	82 (α only)
2a	NIS, TESOTf	15 min	**5a**	**6a**	24[c] (β only)
2a	NIS, TESOTf	24	**5c**	**6c**	34[c] (β only)
2d	NIS, TESOTf, 0 °C	40 min	**5b**	**8b**	75 (9:11 α:β)
2d	NIS, TESOTf 0 °C	1	**5a**	**8a**	90 (9:15 α:β)
2d	NIS, TESOTf, 0 °C	1.5	**5c**	**8c**	73[d] (1:1 α:β)
2e	NIS, TESOTf	4	**5a**	**8a**	67[e] (1:2 α:β)

[a] All reactions at rt in CH_2Cl_2 unless otherwise stated. [b] All yields are for isolated products. [c] See ref. 19. [d] See ref. 23. [e] Yield over two steps: mercaptomethylpolystyrene **4e** with **3b** then glycosylation.

To test the applicability of glycosyl disulfides to solid-supported glycosylation strategies we used mercaptomethylpolystyrene **4e** as a suitable thiolfunctionalized support (Scheme 3). Such was the reactivity of **3b** that even with solid-supported thiol **4e** reaction proceeded rapidly (1 h) to give solid-supported glycosyl disulfide **2e**.[24] The cleavage of **2e** as a representative disulfide-linked glycoside from the support in a bidirectional manner was then demonstrated. Firstly, a small portion of **2e** was taken and treated with tributylphosphine to yield configurationally stable tetrabenzyl 1-thio-β-D-glucose **9**. The potential ability to retune **9** in a latent/active manner to create a glycosyl donor bearing an alternative aglycon (in this case bearing a methyl) was demonstrated by smooth conversion into **10**[25] using methyl methanethiosulfonate. This also showed the release of solid-supported glycosyl disulfide glycosyl donor **2e** from the resin in the form of a solution phase glycosyl donor **10**, thereby demonstrating the potential of the resin as a platform for the creation of solution-phase donors. Next, the ability of **2e** to act as a solid-supported glycosyl donor was clearly demonstrated by activation with NIS, TESOTf in the presence of glycosyl acceptor **5a** to yield methyl glycoside **8a** in a good overall yield (67% over 2 steps). This is also a traceless cleavage method that installs reducing end functionality.

In summary, we have demonstrated the ready and efficient preparation of a wide range of glycosyl disulfides using differently protected glycosyl methanethiosulfonates. Furthermore, we have shown for the first time that glycosyl disulfides may be used as efficient glycosyl donors in both solution- and solid-phase systems for the preparation of *O*-glycosides including disaccharides and glycopeptides. The disulfide linkage offers enhanced utility in aglycone alteration, use as a linker to solid supports and higher activation rates, the full potential of which is the subject of current investigations.

We thank Dr L. Oates, Mr J. P. Marston for technical assistance, the Mitzutani Foundation for Glycoscience for funding and the EPSRC for a quota studentship (S. J. W.), and access to the Mass Spectrometry Service at Swansea and the Chemical Database Service at Daresbury.

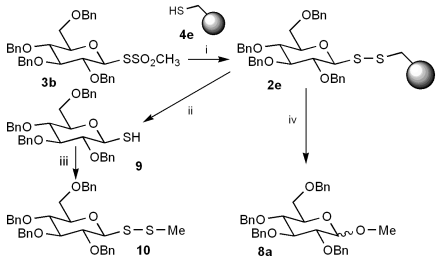

Scheme 3 *Reagents and conditions:* i, Et_3N, CH_2Cl_2; ii, PBu_3, CH_2Cl_2; iii, $MeSSO_2Me$, Et_3N, CH_2Cl_2; iv, MeOH, CH_2Cl_2, NIS, TESOTf.

Notes and references

1 A. Varki, *Glycobiology*, 1993, **3**, 97; R. A. Dwek, *Chem. Rev.*, 1996, **96**, 683; B. G. Davis, *J. Chem. Soc., Perkin Trans. 1*, 1999, 3215.
2 J. C. McAuliffe and O. Hindsgaul, *Chem. Ind.*, 1997, 170; B. G. Davis, *Chem. Ind.*, 2000, 134; K. M. Koeller and C.-H. Wong, *Nature Biotechnol.*, 2000, **18**, 835.
3 H. Paulsen, *Angew. Chem., Int. Ed. Engl.*, 1982, **21**, 155; K. Toshima and K. Tatsuta, *Chem. Rev.*, 1993, **93**, 1503; G. J. Boons, *Contemp. Org. Synth.*, 1996, **3**, 173; G. J. Boons, *Tetrahedron*, 1996, **52**, 1095; B. G. Davis, *J. Chem. Soc., Perkin Trans. 1*, 2000, 2137.
4 P. J. Garegg, *Adv. Carbohydr. Chem. Biochem.*, 1997, **52**, 179.
5 D. R. Mootoo, P. Konradsson, U. Udodong and B. Fraser-Reid, *J. Am. Chem. Soc.*, 1988, **110**, 5583; G. J. Boons, P. Grice, R. Leslie, S. V. Ley and L. L. Yeung, *Tetrahedron Lett.*, 1993, **34**, 8523.
6 R. Roy, F. O. Andersson and M. Letellier, *Tetrahedron Lett.*, 1992, **33**, 6053.
7 G. J. Boons, R. Geurtsen and D. Holmes, *Tetrahedron Lett.*, 1995, **36**, 6325.
8 S. V. Ley and H. W. M. Priepke, *Angew. Chem., Int. Ed. Engl.*, 1994, **33**, 2292; P. Grice, S. V. Ley, J. Pietruszka, H. M. I. Osborn, H. W. M. Priepke and S. L. Warriner, *Chem. Eur. J.*, 1997, **3**, 431; Z. Y. Zhang, I. R. Ollmann, X. S. Ye, R. Wischnat, T. Baasov and C. H. Wong, *J. Am. Chem. Soc.*, 1999, **121**, 734; X. S. Ye and C.-H. Wong, *J. Org. Chem.*, 2000, **65**, 2410.
9 Advantageously, 1-thiohexoses do not mutatrotate in basic or neutral conditions [see W. Schneider and H. Leonhardt, *Ber. Dtsch. Chem. Ges.*, 1929, **62**, 1384] and in glycosyl disulfides the aglycon may be exchanged without loss of anomeric configuration.
10 For enhanced reactivity of disulfides as Lewis bases see H. Böhme and H.-P. Steudel, *Justus Liebigs Ann. Chem.*, 1969, **730**, 121. Since thio(sulfenyl) halides are more stable than corresponding sulfenyl halides (see ref. 11), halonium activation preequilibrium followed by glycosyl cation formation *via* a late transition state of significant product character would lead to enhanced reactivity. Glycosylthio(sulfonium) intermediates are implicated in thioglycoside activation: F. Dasgupta and P. J. Garegg, *Carbohydr. Res.*, 1990, **202**, 225.
11 For one example of *N*-glycoside formation see: M. Hürzeler, B. Bernet and A. Vasella, *Helv. Chim. Acta*, 1992, **75**, 557.
12 Large excess of aglycon thiol under oxidising conditions allows glycosyl disulfide synthesis. Also see G. Hummel and O. Hindsgaul, *Angew. Chem., Int. Engl.*, 1999, **38**, 1782. Unfortunately, these methods are not compatible with the efficient use of sensitive or scarce thiols or with solid supported thiols, respectively.
13 R. Wynn and F. M. Richards, *Methods Enzymol.*, 1995, **201**, 351.
14 B. G. Davis, R. C. Lloyd and J. B. Jones, *J. Org. Chem.*, 1998, **63**, 9614; B. G. Davis and J. Bryan Jones, *Synlett*, 1999, 1495; B. G. Davis, M. A. T. Maughan, M. P. Green, A. Ullman and J. B. Jones, *Tetrahedron: Asymmetry*, 2000, **11**, 245.
15 We are exploring such peptide glycosyl disulfide systems in intramolecular glycosylations: details will be published in due course.
16 A 10:1 mixture of **3b** with its α-anomer also gave exclusively pure β-linked **2d** and recovered MTS enriched in the α-anomer. We are investigating the nature of this apparently stereospecific coupling.
17 K. Freudenberg, A. Noë and E. Knopf, *Chem. Ber.*, 1927, **60**, 238.
18 M. G. Vafina, V. A. Derevitskaya and N. K. Kochetkov, *Bull. Acad. Sci. USSR Div. Chem. Sci. (Engl. Transl.)*, 1965, 1777.
19 Mass balance of 1,3,4,6-tetra-*O*-acetyl-α-D-glucose and acetylated acceptor indicated successful activation of donor but subsequent acetyl migration. See R. U. Lemieux and A. R. Morgan, *Can. J. Chem.*, 1965, **43**, 2190; T. Nukada, A. Berces, M. Z. Zgierski and D. M. Whitfield, *J. Am. Chem. Soc.*, 1998, **120**, 13291.
20 K. P. R. Kartha and R. A. Field, *Tetrahedron Lett.*, 1997, **38**, 8233.
21 **2d** is in fact more rapid than the corresponding ethyl thioglucoside. We are currently investigating other reactivity ratios.
22 R. J. Ferrier, R. W. Hay and N. Vethaviyasar, *Carbohydr. Res.*, 1973, **27**, 55.
23 J. M. Lacombe, A. A. Pavia and J. M. Rocheville, *Can. J. Chem.*, 1981, **59**, 473. *N*-glucosylated succinimide (21%) was also isolated.
24 Ellman's reagent showed lack of thiol: G. L. Ellman, K. D. Courtney, V. Andres and R. M. Featherstone, *Biochem. Pharmacol.*, 1961, **7**, 88.
25 M. Hürzeler, B. Bernet and A. Vasella, *Helv. Chim Acta*, 1993, **76**, 995.

ChemComm

A novel chemiluminescence from the reaction of dioxiranes with alkanes. Proposed mechanism of oxygen-transfer chemiluminescence

Dmitri V. Kazakov,* Anna B. Barzilova and Valeri P. Kazakov

Institute of Organic Chemistry, Ufa Scientific Center of the RAS, 71 Pr. Oktyabrya, 450054 Ufa, Russia. E-mail: chemlum@ufanet.ru

Received (in Cambridge, UK) 16th October 2000, Accepted 7th December 2000
First published as an Advance Article on the web 8th January 2001

Oxidation of adamantane and 2,3-dimethylbutane by methyl(trifluoromethyl)dioxirane is accompanied by chemiluminescence (CL); formation of the emitter of CL, triplet excited trifluoropropanone, is proposed to occur *via* a concerted oxenoid mechanism of oxygen insertion into C–H bond of the hydrocarbons.

Chemiluminescence (CL) is a promising rapidly developing area of chemistry of new class of hyperenergetic molecules—dioxiranes.[1,2,3*a*,*b*,4] In 1981 it was suggested[1] that isomerization of dioxirane into the corresponding ester should lead to the electronic excitation of the latter. Recently it was revealed that decomposition of dioxiranes in the absence of reactive substrates under certain conditions really results in production of the light emission.[2,3*a*,*b*] Apart from the study of CL of isolated dioxiranes, dioxirane intermediate has been also postulated to explain luminescence in biochemical systems.[5]

On the other hand, dioxiranes are known to be highly effective yet selective oxidants in respect to various classes of organic compounds.[3] Some of these oxidation reactions are exothermic enough[6] to generate excited species and consequently to produce CL. The area of oxidative CL of dioxiranes seems to be highly perspective from the viewpoint of fundamental questions of chemistry of excited states since it could provide new valuable information not only on mechanisms of CL, but also on some aspects of generation of light in biochemical reactions as it has been suggested that dioxirane intermediates may be involved in biochemical oxidations.[7*a*] However, in spite of these promising perspectives, so far the literature contained only a single report on generation of CL in the course of oxidative reactions of isolated dioxiranes. In 1994 CL occurring during oxidation of olefin (9-arylmethylene-10-methyl-9,10-dihydroacridine) with isolated dimethyldioxirane (DMD) was reported.[4]

In this communication we report the observation of a novel type of CL of dioxiranes occurring during oxidation of saturated hydrocarbons, such as adamantane (Ad) and 2,3-dimethylbutane (DMB), with isolated methyl(trifluoromethyl)dioxirane (TFD).[7*a*] We also suggest a plausible mechanism of luminescence generation. To the best of our knowledge, CL in the reaction of alkanes with dioxiranes is unprecedented.

We have found that interaction of Ad and TFD is accompanied by light emission in the visible spectrum region (λ_{max} = 430–470 nm). Under air atmosphere, the maximum intensity of CL and the total amount of light (*S*) evolved in the reaction (18 °C, CCl_4, $[Ad]_o$ = 0.063 mol l^{-1}, $[TFD]_o$ = 0.0019 mol l^{-1}) were equal to 2×10^6 photon $s^{-1}ml^{-1}$ and 1.4×10^7 photon ml^{-1} respectively. However, significant increase in CL intensity (I_{CL}) was observed when the reaction was carried out under nitrogen atmosphere. This effect testifies in favour of the triplet nature of the CL emitter since it is known that oxygen quenches triplet excited states.

Reaction of Ad with TFD is known[7*a*,*b*] to obey a second order low (first order on each substrate):

$W = k_2[Ad][TFD]$

or, under pseudo-first order conditions:

$W = k_1[TFD]$, where $k_1 = k_2[Ad]$.

Indeed, under $[TFD]_o << [Ad]_o$, the plots $\ln(I_{CL})$ *vs.* time were found to be linear, yielding reproducible values of k_1. From this k_2 values were estimated at different temperatures (Table 1). The activation parameters for k_2 calculated from the data of Table 1 are equal to $E_a = 8.2 \pm 0.7$ kcal mol^{-1} and $\log A = 6.5 \pm 0.5$.

Under pseudo-first order conditions the rate of the reaction (*W*) is connected with the CL intensity by the following expression:

$$I_{CL} = \varphi_{CL} W = \varphi_{CL} k_2[Ad][TFD] = k_1[TFD] \qquad (1)$$

where φ_{CL} is yield of CL.

The value of φ_{CL} was estimated from eqn. (1) using k_2 values taken from Table 1. Thus, at 18 °C φ_{CL} is equal to 1.2×10^{-11} Einstein mol^{-1}. The yield of CL calculated from the ratio $S/[TFD]_o \approx 1.16 \times 10^{-11}$ Einstein mol^{-1} is in agreement with that obtained from eqn. (1).

CL occurring under interaction of dioxiranes with alkanes appeared to be a more general phenomenon. In fact, we have found that interaction of DMB with TFD is also accompanied by light emission. The yield of CL (estimated as $S/[TFD]_o$ ratio) is equal to 2.6×10^{-12} Einstein mol^{-1} (at 18 °C). It is important to note that the region of CL appeared to be the same as for the reaction of TFD with AD, *i.e.* λ_{max} = 430–470 nm.

What is the mechanism of CL occurring under reaction of TFD with Ad and DMB? Interaction of alkanes with dioxiranes is known[3,7] to result in the formation of the corresponding alcohol and ketone–dioxirane reduction product. In the course of previous studies it was shown[3,7] that oxidation of alkanes (including Ad and DMB) by TFD is a bimolecular reaction implying involvement of high-ordered (so-called butterfly) transition state (Scheme 1 (path (a)).†

Therefore, it seems to be reasonable to attribute the light emission to the mechanism depicted in Scheme 1. According to the proposed mechanism only corresponding alcohol R–OH and trifluoropropanone (TFP) could be regarded as potential CL emitters. However, we can exclude alcohols from the consideration since they emit in the shorter wavelength region of spectrum than that recorded for CL in our system. Indeed, the range of CL observed upon oxidation of DMB and AD by TFD corresponds to the phosphorescence (PS) of TFP, testifying that

Table 1 Dependence of the rate constant of oxidation of Ad by TFD on temperature (solvent-CCl_4, N_2 atmosphere[*d*])

T/K	251	262	272	279.5	283.5	288.5	291.5
[*a*]k_2 ($l\ mol^{-1}\ s^{-1}$)	0.23[*c*] 0.51[*b*]	0.47	0.73	1.42	1.57	1.83	2.25

[*a*] Estimated as $k_2 = (k_1/[Ad]_o)$; k_1 values were obtained from pseudo-first order kinetic plots of CL damping with $[TFD]_o = 1.8–3.8 \times 10^{-3}$ mol L^{-1} and $[Ad]_o = 4–6.3 \times 10^{-2}$ mol L^{-1}; most data are averages (±5%) from duplicate or more runs. [*b*] Value of the rate constant obtained previously[7*a*] (in CH_2Cl_2–TFP mixture) under second-order rate conditions by non-CL method (GLC). [*c*] Extrapolated to 251 K from Arrhenius equation. [*d*] Replacing N_2 with O_2 atmosphere does not affect the rate constant of the reaction.

DOI: 10.1039/b008315l

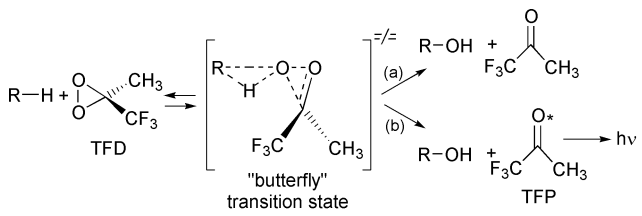

where R-H - adamantane or 2,3-dimethylbutane

Scheme 1

the latter in triplet excited state (TFP^*_T) is indeed an emitter of CL.‡ Recent calculations[5a] also favor the proposed mechanism of CL: oxygen insertion into C–H bonds of saturated hydrocarbons was shown to be about −65–−70 kcal mol^{-1} exothermic[6a] so that the sum of enthalpy and activation energy (according to our data *ca*. 8 kcal mol^{-1} for the reaction of Ad with TFD) should be sufficient for excitation (Scheme 1, path (b)) of, at least, triplet state of TFP. In fact, the energetic level of TFP^*_T is equal[8] to *ca*. 75 kcal mol^{-1}, whereas the singlet excited level of TFP[8] is about 9 kcal mol^{-1} higher and unlikely to be occupied in the reaction.

One may note that the yield of CL arising during oxidation of alkanes with TFD was found to be relatively low.§ This fact is not surprising since numerous oxidation reactions are characterized by rather low yields of CL (ultra-weak CL). In particular, this is characteristic for light emission recorded in certain biological systems.[9]

It is of interest that we failed to record CL upon interaction of Ad with less reactive DMD. This is despite the fact that DMD, similar to TFD, is known to oxidize Ad into the corresponding alcohol.[7e] Probably, the slower rate of Ad oxidation by DMD, compared with that of TFD,[7b] accounts for the impossibility of recording CL due to its low intensity and the quenching of excited acetone (formed by analogy with TFP) by molecules of solvents or other reagents. However, introduction of 9,10-dicyanoanthracene (DCA) in the system results in the appearance of light emission ($[DMD]_o = 3.1 \times 10^{-2}$ mol l^{-1}, $[Ad]_o = 4 \times 10^{-2}$ mol l^{-1}, $[DCA]_o = 6.6 \times 10^{-5}$ mol l^{-1}, CCl_4–acetone = 2:1, 20 °C). DCA was found to be the emitter of the CL observed. One may suppose, that in this case DCA serves as a CL activator and enhances CL intensity as a result of energy transfer from excited acetone, formed by analogy with the mechanism suggested for TFD oxidation of alkanes (Scheme 1, path (b)). However, in contrast to the TFD case, along with triplet ketone, significant contribution of singlet excited states of acetone seems to have taken place since only insignificant quenching (*ca*. 20%) of CL intensity by oxygen is observed in this reaction. Consequently, excitation of DCA is likely to be caused by transfer of energy from both singlet and triplet excited molecules of acetone (Scheme 2).

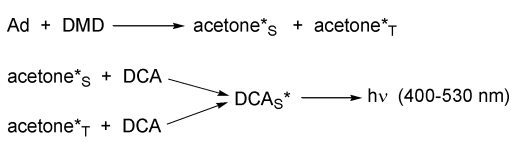

Scheme 2

Likewise, effect of CL enhancement is observed when reaction of TFD and AD is carried out in the presence of DCA, obviously due to transfer of energy from the TFP^*_T on the activator with subsequent radiative deactivation of the latter.

In conclusion, oxidation of alkanes by TFD is accompanied by CL.¶ We have proposed a plausible mechanism of CL (Scheme 1 (path b)) to explain our observations. We suggest to call this novel type of CL *butterfly chemiluminescence* or, in more general sense, *oxygen-transfer chemiluminescence*. To the best of our knowledge, this is a new mode of chemiexcitation not only for dioxiranes but also for other liquid-phase organic reactions with peroxide participation.

We thank Russian Foundation for Basic Research (project No 99-03-32140a) and program of Leading Scientific Schools Support (project No 00-15-97323) for financial support of this work. We are also grateful to Professor Curci (University of Bari, Italy) for supplying us with the first samples of TFD and critical reading of the manuscript.

Notes and references

† Oxidation of DMB by TFD (as 1:1 ratio) leads exclusively to the corresponding alcohol.[7a] Likewise, interaction of Ad and TFD (as 0.9 ratio) results in the formation of 94% of adamantan-1-ol (Ad-OH), 5% of adamantane-1,3-diol and trace amounts of adamantanone (as a result of further oxidation of Ad-OH).[7b] Apart from these compounds and TFP no other products or even intermediates were detected in the course of the reactions of alkanes with TFD.[7] Kinetics evidence and the other experimental data[3,7] also testify in favour of absence of any other routes (including those involving participation of radicals) of the reaction except that depicted in Scheme 1 (path (a)). In particular, very low frequency factor values (logA ~ 6.6–10) noted[7a,c] for oxidation of alkanes by TFD are regarded as support for the existence of a highly ordered transition state preceding the formation of reaction products.

‡ PS spectrum of TFP was recorded on Hitachi MPF-4 fluorimeter at 77K (λ_{exc} = 320 nm): the spectrum has a broad maximum in the region 400–490 nm (spectrum of PS of TFP recorded in gas phase[8] has a shift to longer wavelength region at *ca*. 30 nm).

§ Estimation of the yield of excitation of TFP_T^* was made on the assumption that the quantum yield of its PS is about equal to that of acetone, *i.e.* 10^{-5}. Under this approach, the yield of chemiexcitation of TFP was estimated to be 10^{-4} and 10^{-5}% for the reaction of TFD with AD and DMB respectively.

¶ We have observed CL occurring upon interaction of TFD and DMD with various types of organic compounds including some polyaromatic hydrocarbons, dyes (rhodamine 6G, eosine), europium chelates *etc*. CL intensities recorded in these reactions in many cases are significantly higher then those observed in the reaction of dioxiranes with Ad and DMB (unpublished results). The study of CL arising in reactions of organic compounds with dioxiranes is under progress in our laboratory.

1 W. Adam and R. Curci, *Chim. Ind. (Milan)*, 1981, **63**, 20.
2 (*a*) D. V. Kazakov, A. I. Voloshin, N. N. Kabal'nova, S. L. Khursan, V. V. Shereshovets and V. P. Kazakov, *Russ. Chem. Bull.*, 1997, **46**, 456; (*b*) D. V. Kazakov, A. I. Voloshin, N. N. Kabal'nova, V. V. Shereshovets and V. P. Kazakov, *Mendeleev Commun.*, 1998, 49; (*c*) D. V. Kazakov, N. N. Kabalnova, A. I. Voloshin, V. V. Shereshovets and V. P. Kazakov, *Russ. Chem. Bull.*, 1995, **44**, 2193; (*d*) D. V. Kazakov, A. I. Voloshin, V. V. Shereshovets, V. N. Yakovlev and V. P. Kazakov, *Mendeleev Commun.*, 1998, 169; (*e*) D. V. Kazakov, A. I. Voloshin, V. V. Shereshovets and V. P. Kazakov, in *Bioluminescence and Chemiluminescence: Perspectives for the 21st Century*, ed. A. Roda, M. Pazzagli, L. J. Kricka and P. E. Stanley, John Wiley & Sons, 1999.
3 For reviews on dioxirane chemistry, see: (*a*) V. P. Kazakov, A. I. Voloshin and D. V. Kazakov, *Russ. Chem. Rev.*, 1999, **68**, 253; (*b*) W. Adam, L. P. Hadjiarapoglou, R. Curci and R. Mello, in *Organic Peroxides*, ed. W. Ando, Wiley, New York, 1992, V. 4, p. 195; (*c*) R. W. Murray, *Chem. Rev.*, 1989, **89**, 1187; (*d*) R. Curci, A. Dinoi and M. F. Rubino, *Pure and Appl. Chem.*, 1995, **67**, 811.
4 K. Sakanishi, Y. Kato, E. Mizukoshi and K. Shimizu, *Tetrahedron Lett.*, 1994, **35**, 4789.
5 (*a*) W. A. Francisco, H. M. Abu-Soud, A. J. DelMonte, D. A. Singleton, T. O. Baldwin and F. M. Raushel, *Biochemistry*, 1998, **37**, 2596; (*b*) F. M. Raushel and T. O. Baldwin, *Biochem. Biophys. Res. Commun.*, 1989, **164**, 1137.
6 (*a*) M. N. Glukhovtsev, C. Canepa and R. D. Bach, *J. Am. Chem. Soc.*, 1998, **120**, 10 528; (*b*) A. G. Baboul, H. B. Schlegel, M. N. Glukhovtsev and R. D. Bach, *J. Comput. Chem.*, 1998, **19**, 1353.
7 (*a*) R. Mello, M. Fiorentino, C. Fusco and R. Curci, *J. Am. Chem. Soc.*, 1989, **111**, 6749; (*b*) R. Mello, L. Cassidei, M. Fiorentino, C. Fusco and R. Curci, *Tetrahedron Lett.*, 1990, **31**, 3067; (*c*) W. Adam, G. Asensio, R. Curci, M. E. Gonzalez-Nunez and R. Mello, *J. Org. Chem.*, 1992, **57**, 953; (*d*) W. Adam, R. Curci, L. D'Accolti, A. Dinoi, C. Fusco, F. Gasparrini, R. Kluge, R. Paredes, M. Schulz, A. K. Smerz, L. Angela Veloza, S. Weinkotz and R. Winde, *Chem. Eur. J.*, 1997, **3**, 105; (*e*) R. Curci, A. Dinoi, C. Fusco and M. A. Lillo, *Tetrahedron Lett.*, 1996, **37**, 249.
8 P. A. Hackett and D. Phillips, *J. Phys. Chem.*, 1974, **78**, 665.
9 (*a*) K. Osada, Y. Furukawa, M. Komai and S. Kimura, *J. Clin. Biochem. Nutr.*, 1990, **8**, 185; (*b*) J. S. Sun, Y. H. Tsuang, I. J. Chen, W. C. Huang, Y. S. Hang and F. J. Lu, *Burns*, 1998, **24**, 225; (*c*) I. Kruk, K. Lichszteld, T. Michalska, K. Nizinkiewicz and J. Wronska, *J. Photochem. Photobiol. B-Biology*, 1992, **14**, 329.

ChemComm

Dissolution of small diameter single-wall carbon nanotubes in organic solvents?

Jeffrey L. Bahr, Edward T. Mickelson, Michael J. Bronikowski, Richard E. Smalley* and James M. Tour*

Department of Chemistry and Center for Nanoscale Science and Technology, MS 222, Rice University, 6100 Main Street, Houston, Texas 77005, USA. E-mail: tour@rice.edu

Received (in Columbia, MO, USA) 19th September 2000, Accepted 27th November 2000
First published as an Advance Article on the web 8th January 2001

The solubility of small diameter single-wall carbon nanotubes in several organic solvents is described, and characterization in 1,2-dichlorobenzene is reported.

Owing to their phenomenal electrical and mechanical properties, single-wall carbon nanotubes (SWNTs) have been an area of intense research since their discovery in 1991,[1] and a variety of potential applications have been proposed.[2] Many of these applications will likely require chemical modification to facilitate manipulation of the tubes. Consequently, there have been significant efforts to derivatize SWNTs.[3] These efforts, including our own, have been hampered by minimal or complete lack of solubility in common organic solvents. We report here a screening of organic solvents, many of which have previously been found advantageous towards the dissolution of C_{60} and C_{70} fullerenes.[4] Solubilization of SWNTs is expected to facilitate both their chemical derivatization and investigation of their photophysical properties.

The SWNT samples used for this study were produced by a gas-phase catalytic process developed by Smalley and coworkers.[5] This process is capable of producing SWNTs with diameters of *ca.* 0.7 nm, considerably smaller than SWNTs typically produced by laser oven methods.[5,6] The production material was used directly, with no purification. The material used for this investigation consisted of mostly carbon nanotubes, and contained *ca.* 5 atom% residual iron catalyst, as verified by scanning electron microscopy (Philips XL 30 ESEM) and EDAX (energy dispersive analysis with X-rays). An SEM image of the SWNTs is shown in Fig. 1

UV–VIS absorption spectroscopy was used to determine solubility as follows. Several different concentrations of SWNT solutions in 1,2-dichlorobenzene were prepared by sonication (Cole-Parmer B3-R, 55 kHz). The solutions were then filtered through glass wool until no visible particulate remained, and the absorption spectrum was recorded (Fig. 2). A 100.0 mL aliquot of each sample was placed in a warm water bath, and the solvent was removed with a gentle stream of nitrogen. The samples were dried in an oven at 130 °C for 1 h and then weighed to determine the mass of solubilized SWNT. This concentration (in mg L^{-1}) in conjunction with the absorbance at 500 nm, allowed preparation of the plot shown in the inset of Fig. 2. The slope of the linear-least-squares fit is then analogous to the familiar extinction coefficient of Beer's Law.[7] This value was used to determine the concentration of all subsequent samples, which were prepared in the following manner. Several mg of SWNT material were placed in a scintillation vial containing 10 mL of solvent. The amount of SWNTs used was sufficient to ensure undissolved material. The vial was capped and sonicated for 1 h. The solution was filtered through glass wool until no particulate remained, and the absorption spectrum was recorded. The concentration was determined as described above. The results are shown in Table 1. A single production batch was used to generate the results shown in Table 1. The stability of these solutions varied from *ca.* 4 h to more than 3 days for 1,2-dichlorobenzene. Since the solubility of SWNT samples might vary from batch to batch, two other batches of gas-phase grown material were checked for their solubility properties in 1,2-dichlorobenzene. The results were within *ca.* 10% of the original batch.

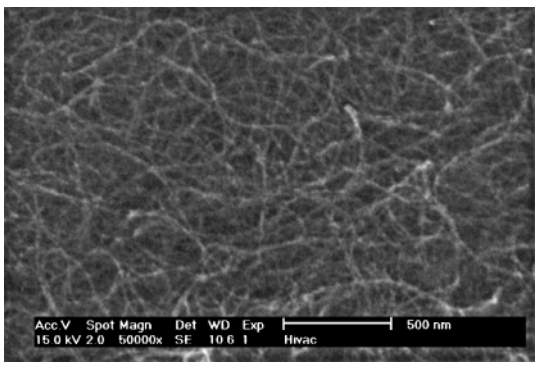

Fig. 1 SEM image of the SWNT material used for this investigation.

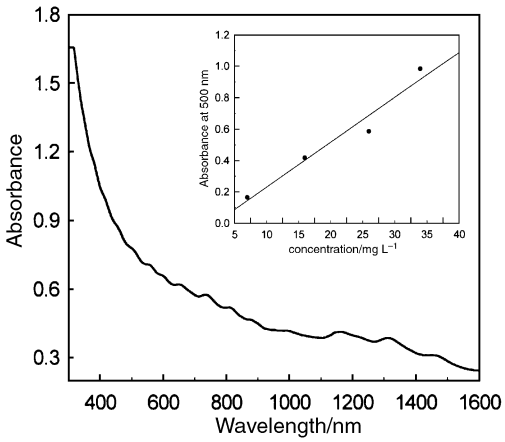

Fig. 2 Absorption spectrum of the SWNT material at a concentration of 27 mg L^{-1} in 1,2-dichlorobenzene. Inset: Optical density at 500 nm of the SWNT material in 1,2-dichlorobenzene at different concentrations. The straight line is a linear-least-squares fit to the data; slope = 0.0286.

Table 1 Room-temperature solubility of the SWNT material[a]

Solvent	mg L^{-1}
1,2-Dichlorobenzene	95
Chloroform	31
1-Methylnaphthalene	25
1-Bromo-2-methylnaphthalene	23
N-Methylpyrrolidinone	10
Dimethylformamide	7.2
Tetrahydrofuran	4.9
1,2-Dimethylbenzene	4.7
Pyridine	4.3
Carbon disulfide	2.6
1,3,5-Trimethylbenzene	2.3
Acetone	—[b]
1,3-Dimethylbenzene	—[b]
1,4-Dimethylbenzene	—[b]
Ethanol	—[b]
Toluene	—[b]

[a] The sonicator bath water temperature rose to *ca.* 35 °C over the course of 1 h. [b] Solubility in these solvents was < 1 mg L^{-1}

DOI: 10.1039/b008042j

1,2-Dichlorobenzene was found to be a reasonable solvent for the SWNTs. A photograph of the SWNT samples dissolved in 1,2-dichlorobenzene at differing concentrations is shown in Fig. 3. The 1,2-dichlorobenzene solutions could be filtered (0.2 μM PTFE, Sartorius), dried for 1 h at 140 °C, and then re-dissolved.

The issue of solution *vs.* suspension for SWNT in organic solvents is unresolved. Although there was no visible particulate in the solutions reported here, the terms 'metastable solution' or indeed even 'suspension' may be equally applicable. The question of whether solvation means exfoliation of nanotube ropes into individual nanotubes is perhaps inherent in this issue. In an attempt to determine whether these solutions/suspensions were comprised of individual tubes, we performed atomic force microscopy (Digital multi-mode SPM)[8] on samples deposited from 1,2-dichlorobenzene solutions. Samples from a *ca.* 5 mg L^{-1} solution showed mostly small bundles which are likely comprised of several nanotubes, based on height analysis of *ca.* 1.5–1.9 nm and lengths of *ca.* 500 nm. Analysis of samples deposited from more concentrated solutions revealed larger bundles or ropes with heights of *ca.* 6 nm and lengths of 1–3 μM. These bundles are a result of the significant van der Waals interaction between the sidewalls of the tubes. It is therefore possible that solubilization in 1,2-dichlorobenzene does not completely exfoliate the SWNT bundles to give individual nanotubes. Alternatively, individual tubes could be present when in solution, but these coalesce when spin-coated on the substrate for imaging.

Solutions in 1,2-dichlorobenzene did not pass through a 1.2 μM PTFE membrane (Sartorius). This does not conclusively mean that all tubes in the solution were longer than 1.2 μM. A few longer tubes may form a mat on the membrane, preventing passage of shorter tubes. In addition, these membranes are 'torturous path' filters, which may require significant solute deformation; a difficult task for these exceedingly rigid tubular structures. We also attempted to pass a *ca.* 30 mg L^{-1} 1,2-dichlorobenzene solution (this solution was sonicated for *ca.* 20 min) through a 3 μM, track-etched polycarbonate membrane (Poretics). The pores in these membranes are nearly 'straight' holes (relative to their diameter) which do not require significant solute deformation for passage. The filtrate contained 13 mg L^{-1} of SWNTs. This solution did not exhibit a Tyndall effect (632 nm) 20 min after filtration. This suggests that most particles in the solution are on the order of 0.6 μM in length or smaller, though this is of course an extremely crude estimate of particle size. In addition, at this concentration, the solution absorbs *ca.* 50% of the incident light at 632 nm. After *ca.* 1 h, the solution did exhibit a Tyndall effect, and particulates became visible shortly thereafter. It is then reasonable to suppose that individual tubes might indeed exist in the solution at low concentrations, but they eventually form ropes, then bundles of larger size. In more concentrated solutions, the tubes are likely to exist only as ropes or bundles. Whenever dealing with such large, rigid molecules however, the question of 'true' solubility persists.

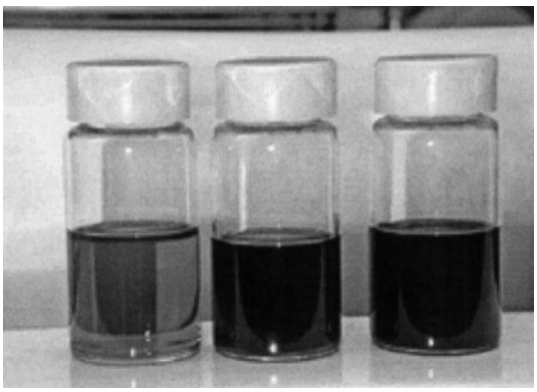

Fig. 3 SWNT solutions in 1,2-dichlorobenzene. From left to right: 10 mg L^{-1}, 25 mg L^{-1}, 95 mg L^{-1}.

A report recently appeared in the literature concerning dissolution of laser-oven produced SWNTs (diameter *ca.* 1.2 nm) in organic solvents.[9] The authors presented extensive spectroscopic characterization of the dispersions, and concluded that highly polar solvents such as dimethylformamide, *N*-methylpyrrolidinone, and hexamethylphorphoramide were the most attractive solvents. We have also investigated the solubility of laser-oven produced tubes (obtained from Tubes@Rice) in 1,2-dichlorobenzene, which was briefly touched upon in the aforementioned report. We found the raw production material to possess a solubility similar to that of the gas-phase catalytically grown tubes in 1,2-dichlorobenzene, at *ca.* 75 mg L^{-1}. However, this material consists of as little as 40% SWNTs, the remainder being comprised of amorphous carbon amd metal catalysts. We found purified material from Tubes@Rice (consisting of *ca.* 90% SWNTs) to be considerably less soluble in 1,2-dichlorobenzene, at 35 mg L^{-1}. It is therefore likely that impurities play a role in dissolution of the laser-oven grown SWNTs. Alternatively, the purification process may affect the integrity of the SWNTs, altering their solubility properties. Concerning the differences observed between the laser-oven produced material and the gas-phase catalytically produced material, it is not clear whether these arise from the nature of the tubes themselves (*i.e.* the diameter or possibly differing helicity mixtures), or merely arise from the different impurities or intermolecular packing characteristics of each production method.

We are currently seeking to take advantage of the dissolution ability of 1,2-dichlorobenzene to facilitate chemical derivatization of the gas-phase catalytically produced SWNTs.

We thank Dr Robert Hauge for helpful discussions. We gratefully acknowledge the financial support of NASA (NASA-JSC-NCC 9-77, OSR#99091801) and the NSF (NSR-DMR-0073046#) for this work.

Notes and references

1 S. Iijima and T. Ichihashi, *Nature*, 1993, **363**, 603.
2 P. M. Ajayan, *Chem. Rev.*, 1999, **99**, 1787 and references therein.
3 E. T. Mickelson, C. B. Huffman, A. G. Rinzler, R. E. Smalley, R. H. Hauge and J. L. Margrave, *Chem. Phys. Lett.*, 1998, **296**, 188; M. A. Harmon, J. Chen, H. Hu, Y. Chen, M. E. Itkis, A. M. Rao, P. C. Eklund and R. C. Haddon, *Adv. Mater.*, 1999, **11**, 834; J. Chen, M. A. Harmon, H. Hu, Y. Chen, A. M. Rao, P. C. Eklund and R. C. Haddon, *Science*, 1998, **282**, 95; S. S. Wong, A. T. Woolley, E. Joselevich, C. L. Cheung and C. M. Lieber, *J. Am. Chem. Soc.*, 1998, **120**, 8557; J. E. Riggs, Z. Guo, D. L. Carroll and Y.-P. Sun, *J. Am. Chem. Soc.*, 2000, **122**, 5879.
4 W. Scrivens and J. M. Tour, *J. Chem. Soc., Chem. Commun.*, 1993, **15**, 1207; R. S. Ruoff, D. S. Tse, R. Malhotra and D. C. Lorents, *J. Phys. Chem.*, 1993, **97**, 3379.
5 P. Nikolaev, M. J. Bronikowski, R. K. Bradley, F. Rohmund, D. T. Colbert, K. A. Smith and R. E. Smalley, *Chem. Phys. Lett.*, 1999, **313**, 91.
6 A. G. Rinzler, J. Liu, H. Dai, P. Nikolaev, C. G. Huffman, K. J. Rodríguez-Macías, P. J. Boul, A. H. Lu, D. Heymann, D. T. Colbert, R. S. Lee, J. E. Fisher, A. M. Rao, P. C. Eklund and R. E. Smalley, *Appl. Phys. A*, 1998, **67**, 29.
7 Beer's Law states that $A = \varepsilon bc$, where A is the optical density, ε is the extinction coefficient, b is the path length, and c is the concentration. The extinction coefficient is somewhat solvent dependent.
8 Samples were spin coated on a mica substrate, rinsed with ethanol, and warmed to evaporate the solvent. Imaging was performed in tapping mode.
9 K. D. Ausman, R. Piner, O. Lourie and R. S. Ruoff, *J. Phys. Chem. B*, 2000, **104**, 8911.

Salt-free C–C coupling reactions of arenes: palladium-catalyzed telomerization of phenols[1]

Andreas Krotz, Frank Vollmüller, Gene Stark and Matthias Beller*

Institut für Organische Katalyseforschung an der Universität Rostock e.V., Buchbinderstr. 5-6, 18055 Rostock, Germany. E-mail: matthias.beller@ifok-uni-rostok.de

Received (in Liverpool, UK) 18th July 2000, Accepted 14th November 2000
First published as an Advance Article on the web 8th January 2001

A salt-free functionalisation of phenols with either butadiene or isoprene in the presence of palladium catalysts has been developed, which gives octadienyl- or decadienylphenols selectively.

Transition metal-catalyzed C–C coupling reactions of arenes with unsaturated organic compounds are of increasing importance for the synthesis of fine chemicals, agrochemicals and intermediates for pharmaceuticals.[2] However, a general problem in most arene transformation reactions is the production of at least stoichiometric amounts of salts due to the necessity of using Lewis acids or suitable activating groups, *e.g.* halides, on the aromatic ring. Despite considerable efforts in the past, only a few examples of direct atom-efficient functionalizations of aromatic compounds are known.[3] Hence, the development of efficient ecologically-favorable protocols for the construction of C–C bonds to aromatic rings is one of the important goals for catalysis.

In 1967 Smutny[4] described the first palladium-catalyzed telomerization reaction[5] of phenol with buta-1,3-diene, which yielded *O*-allylated octa-2,7-dienyl ethers. In the original paper Smutny also reported the observation of *C*-allylated phenols, although neither product yields nor the reaction conditions were given. Later on, telomerizations with phenol were studied by Weigert,[6] Beger[7] and Kaneda *et al.*[8] In all these studies only the corresponding *O*-allylated ethers were obtained.

In this paper we describe the catalytic salt-free reaction of naphthol and electron-rich phenols with buta-1,3-diene and 1,3-isoprene giving selectively *C*-allylated phenols.

While studying the telomerization of buta-1,3-diene with methanol,[1] we became interested in the reaction of 1,3-dienes with substituted phenols and naphthol. Applying our previously optimized conditions (0.1 mol% $Pd(OAc)_2$–1 eq. PPh_3 in THF at 90 °C) the reaction of 100 mmol β-naphthol with 200 mmol buta-1,3-diene yielded both of the expected *O*-allylated products (1-naphthoxyocta-2,7-diene **1**: 30% yield and 3-naphthoxyocta-1,7-diene **2**: 7% yield) as well as significant amount (25%) of the *ortho*-*C*-allylated product 1-(octa-2,7-dienyl)-2-naphthol **3** (Scheme 1).

By variation of the catalyst system, the reaction temperature and the ligand-to-metal ratio we discovered that it is possible to obtain the *C*-allylated products selectively (Table 1). Using optimized conditions (L : Pd = 3 : 1; addition of 1 mol% triethylamine) **3** was obtained in 84% yield (ratio C : O-allylated products = > 50 : 1).† Interestingly, this reaction, which resembles the classic Friedel–Crafts allylation, proceeds with high regioselectivity. Apart from **3**, only a small amount (< 3%) of a second *C*-allylated naphthol was obtained. The efficiency of the simple $Pd(OAc)_2$–PPh_3 catalyst is remarkable: even in the presence of only 0.01 mol% Pd-catalyst, a 76% yield of **3** was obtained (TON = 7600).

In order to understand the formation of the *C*-allylated telomerization product we studied the reaction of **1** in the presence of catalytic amounts (0.5 mol%) of $Pd(OAc)_2$–2 PPh_3 in toluene at 70–90 °C. After 30 min at 70 °C none of the *C*-allylated product **3** was observed. However, after 1.5 h at 90 °C the formation of **3** began, and after 6 h (90 °C) **3** was the main product in the reaction mixture, although other *C*-allylated products (*ca.* 5–10%) were detected. Based on detailed mechanistic studies of the telomerization of butadiene and methanol[9] we propose the following mechanism for the formation of **3** (Scheme 2).

The $Pd(0)$-catalyzed dimerization of buta-1,3-diene affords the L–Pd–(η^1,η^3-octadiendiyl) complex **4**. Subsequent protonation at C6 and attack of the oxygen atom at C1 or C3 yields the corresponding naphthyl allyl ethers **1** and **2**. Due to the improved leaving group ability of naphthol compared to an aliphatic alcohol, **1** and **2** are in equilibrium with **5** under the reaction conditions.[10] Allylation is also possible *ortho* to the hydroxy group, due to the ambident character of napthol. As this reaction step is irreversible, **3** is the main product of this reaction. The large influence of the P : Pd-ratio on the yield of **3**

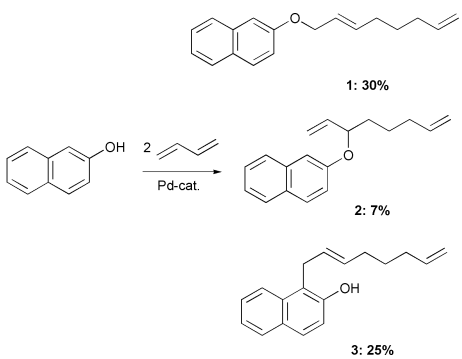

Scheme 1

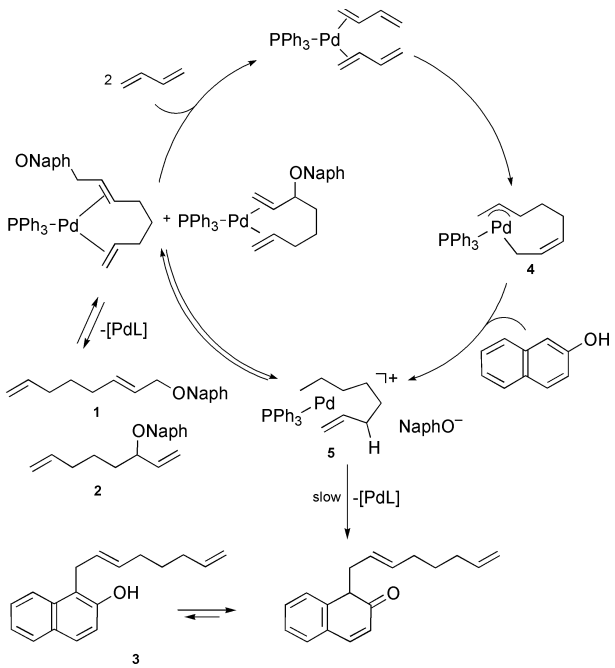

Scheme 2

DOI: 10.1039/b005885h

Table 1 Telomerization of buta-1,3-diene with β-naphthol[a]

Entry	Ligand	L : Pd	Conversion[b] (%)	Yield **3**[c] (%)	Selectivity **3** (%)	Ratio (**3**) : (**1** + **2**)[d]
1	PPh_3	1:1	75	25	33	1
2	**PPh_3**	**3 : 1**	**82**	**76**	**93**	**38**
3	PPh_3	10 : 1	94	75	80	9
4	PPh_3	50 : 1	75[e]	32	42	5
5	PCy_3	3 : 1	73	38	52	2
6	$P(C_6H_2(OMe)_3)_3$[f]	3 : 1	0	—	—	—
7	$P(t\text{Bu})_3$	3 : 1	0	—	—	—
8	$P(OC_6H_3(C_4H_9)_3)_3$[g]	3 : 1	57	16	29	0.3
9[h]	PPh_3	3 : 1	90	8	9	0.1
10[i]	PPh_3	3 : 1	88	69	78	29
11[j]	**PPh_3**	**3 : 1**	**91**	**84**	**92**	**76**

[a] 100 mmol β-naphthol, 200 mmol buta-1,3-diene, 0.1 mol% $Pd(OAc)_2$, 50 ml THF, T = 90 °C, 16 h. [b] Conversion based on β-naphthol. [c] GC-purity > 80%. [d] Ratio of peak areas (GC) (**3**) : (**1** + **2**). [e] *C*-Alkylated products with only one butadiene unit were also formed. [f] Tris(trimethoxyphenyl)phosphine. [g] Tris(2,4-di-*tert*-butylphenyl) phosphite. [h] 60 °C. [i] 120 °C. [j] Addition of 1.0 mol% NEt_3.

Table 2 Telomerization of buta-1,3-dienes with different substrates[a]

Entry	Educt	Ligand	Product	Yield[b] (%)	Ratio C : O-alk[c]
1	α-Naphthol[d]	PCy_3	**6**	47	> 98 : 2
2	β-Naphthol[e]	PPh_3	**3**	84[f]	> 98 : 2
3	Resorcinol monomethyl ether	PCy_3	**7a–c**	63	> 98 : 2
4	Phloroglucinol dimethyl ether[g]	PPh_3	**8**	72	> 98 : 2
5	3-Dimethylaminophenol	PPh_3	**9a–c**	41	> 98 : 2
6	3,4-Methylenedioxyphenol[h]	PCy_3	**10**	46[f]	> 98 : 2
7	β-Naphthol[i]	PCy_3	**11**	55	> 98 : 2

[a] 100 mmol ROH, 200 mmol buta-1,3-diene, 90 °C, 16 h, THF, 0.5 mol% $Pd(OAc)_2$, Pd : PR_3 1 : 3, NEt_3. [b] GC-purity > 98%. [c] Ratio of peak areas (GC). [d] 12 h. [e] 0.1 mol% $Pd(OAc)_2$. [f] GC-purity > 80%. [g] 12 h, toluene, 0.01 mol% $Pd(OAc)_2$. [h] 150 mmol ROH were used. [i] Isoprene was used instead of buta-1,3-diene, 100 °C, toluene, 1 mol% $Pd(OAc)_2$, isoprene–ROH 3 : 1.

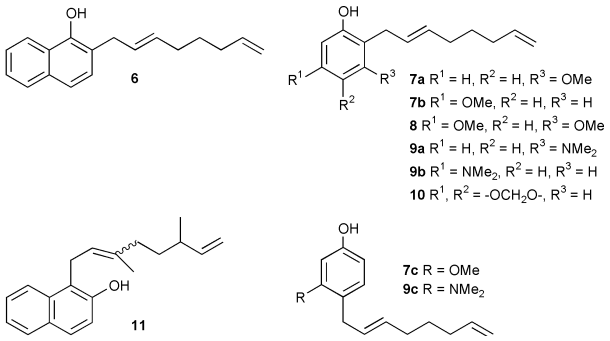

is explained by a deactivation of the Pd catalyst at a low ligand concentration and an inhibition of the catalyst activity in the presence of an excess of phosphine ligand.

In order to demonstrate the generality of the palladium-catalyzed *C*-allylation of phenols we studied the reaction of buta-1,3-diene with electron-rich phenols and the reaction of β-naphthol with isoprene (Table 2). *C*-Allylations similar to β-naphthol are observed with 3-methoxyphenol, 3,5-dimethoxyphenol, α-naphthol, 3-dimethylaminophenol and 3,4-methylenedioxyphenol. In contrast phenol yielded only the corresponding *O*-allylated ethers.

Similar to electrophilic aromatic substitutions, the reaction of butadiene and 3-methoxyphenol, 3,4-methylenedioxyphenol and 3-dimethylaminophenol, gave not only the *ortho*-*C*-allylated products **6**–**10**, but also the *para*-allylated compounds **7c** and **9c**.

The reaction of β-naphthol with isoprene proceeds regioselectively to give the C1-substituted β-naphthol.

In conclusion, we have shown that electron-rich phenols react with 2 molecules of 1,3-dienes in the presence of Pd catalysts to give *C*-allylated phenols. After reduction with hydrogen and Pd/C the corresponding alkylated products are obtained in high yields. The telomerization of phenols with dienes constitutes a salt-free functionalisation of the aromatic nucleus, which proceeds with remarkable catalyst turnover numbers.

We thank Dr W. Baumann (IfOK, Rostock) for performing the NMR studies and Mrs K. Kortus and S. Buchholz for the GC analysis. This work was supported by the Alexander-von-Humboldt-Stiftung (grant for G. S.) and the State Mecklenburg-West Pomerania.

Notes and references

† To a solution of 79 mg (0.3 mmol) triphenylphosphine in 50 ml anhydrous THF in a 100 ml Schlenk tube under an argon atmosphere were added 23 mg (0.1 mmol) palladium acetate and 100 mg (1.0 mmol) triethylamine. The mixture was transferred into a steel autoclave charged with 14.4 g (100 mmol) β-naphthol. After cooling with dry ice 11.0 g (200 mmol) of butadiene were condensed in the autoclave. The reaction was carried out by stirring at 90 °C. After the reaction the resulting residue was purified by flash chromatography (hexane–ethyl acetate) to afford 21.1 g (84%) of **3**.

3: ^{1}H NMR ($CDCl_3$, 400 MHz) δ = 1.29 (m, 2H), 1.88 (pseudo-q, J = 7.5 Hz, 3H), 3.66 (s, 2H), 4.80 (dd, J = 10.0, 2.0 Hz, 1H), 4.84 (dd, J = 17.2, 2.0 Hz, 1H), 5.40 (dt, J = 14.6, 7.1 Hz, 1H), 5.53 (dt, J = 15.1, 6.0 Hz, 1H), 5.60 (ddt, J = 17.1, 10.0, 6.5 Hz, 1H), 5.83 (bs, 1H), 6.96 (d, J = 8.5 Hz, 1H), 7.19 (ddd, J = 8.5, 7.0, 1.0 Hz, 1H), 7.34 (ddd, J = 8.5, 7.0, 1.5 Hz, 1H), 7.50 (d, J = 8.9 Hz, 1H), 7.64 (d, J = 8.5 Hz, 1H), 7.80 (d, J = 8.5 Hz, 1H). ^{13}C NMR ($CDCl_3$, 101 MHz) δ = 28.13, 28.45, 31.75, 33.12, 114.36, 117.66, 117.94, 122.86, 123.04, 126.18, 127.58, 127.91, 128.42, 129.26, 131.55, 133.20, 138.63, 151.28.
MS: m/z: 252 [M^+], 157 [$M^+ - C_7H_{11}$] (100).

1 Part 15 of the series, *Palladium-catalyzed Synthesis of Fine Chemicals*, for part 14 see: F. Vollmüller, S. Klein, J. Krause, W. Mägerlein and M. Beller, *Eur. J. Inorg. Chem.*, 2000, 1825.
2 B. Cornils and W. A. Herrmann, *Applied Homogeneous Catalysis with Organometallic Compounds*, VCH, Weinheim, 1996; M. Beller and C. Bolm, *Transition Metals for Organic Synthesis*, Wiley-VCH, Weinheim, 1998.
3 F. Kakiuchi and S. Murai, in *Activation of Unreactive Bonds and Organic Synthesis*, ed. S. Murai, Springer, 1999, 47; C. Jia, D. Piao, J. Oyamada, W. Lu, T. Kitamura and Y. Fujiwara, *Science*, 2000, **287**, 1992.
4 E. J. Smutny, *J. Am. Chem. Soc.*, 1967, **89**, 6793.
5 For a review on telomerization reactions, see: J. M. Takacs, in *Comprehensive Organometallic Chemistry II*, vol. 12, ed. E. W. Abel, F. G. A. Stone and G. Wilkinson, Pergamon Press, Oxford, 1995, p. 785.
6 F. J. Weigert and W. C. Drinkard, *J. Org. Chem.*, 1973, **38**, 335.
7 J. Beger, C. Duschek, H. Füllbier and W. Gaube, *J. Prakt. Chem.*, 1974, **316**, 26.
8 K. Kaneda, H. Kurosaki, M. Terasawa, T. Imanaka and S. Teranishi, *J. Org. Chem.*, 1981, **46**, 2356.
9 P. W. Jolly, *Angew. Chem.*, 1985, **97**, 279; P. W. Jolly, *Angew. Chem., Int. Ed. Engl.*, 1985, **24**, 283; for an alternative mechanism, see: A. Behr, G. v. Ilsemann, W. Keim, C. Krüger and Y.-H. Tsay, *Organometallics*, 1986, **5**, 514.
10 This equilibrium was also described by Sinou and co-workers in the case of the conversion of β-naphthol with allyl methyl carbonate: C. Goux, M. Massacret, P. Lhoste and D. Sinou, *Organometallics*, 1995, **14**, 4585.

On the calculation of bond energies from atomization energies†

Siân T. Howard,*[a] Michal K. Cyranski[b] and Leszek Z. Stolarczyk[b]

[a] *Department of Chemistry, Cardiff University, Cardiff, UK CF10 3TB. E-mail: howardst@cf.ac.uk*
[b] *Department of Chemistry, University of Warsaw, ul. Pasteura 1, 02-093 Warsaw, Poland*

Received (in Cambridge, UK) 20th September 2000, Accepted 13th December 2000
First published as an Advance Article on the web 8th January 2001

It is possible (and occasionally preferable) to define bond energies of polyatomic molecules by dissociation of the molecule at a given bond into two radical fragments, *e.g.* for a tetra-atomic molecule ABCD.

However it has long been recognized that the quantity derived in this manner will bear little relation to the actual energy content of the bond in the molecular ground-state equilibrium geometry, due to internal reorganization of the radical fragments. Clearly, a rigorous method for determining the distribution of bonding energy at the equilibrium geometry of a polyatomic molecule using its wavefunction or charge density would be highly desirable. In particular, it would provide a powerful analytical tool for quantum chemistry by enabling precise, quantitative statements to be made about the nature of bonds in a given environment, as an alternative to other indirect measures such as bond lengths; bond orders; charges or higher multipoles; or (in some cases) aromaticity indices.[1,2]

$$E\ (\mathrm{B–C}) \equiv E(\mathrm{ABCD}) – E(\mathrm{AB^{\cdot}}) – E(\mathrm{CD^{\cdot}}) \qquad (1)$$

Traditionally, the energies of specific bonds in a molecule have been estimated from its atomization energy ΣD_0 (if vibrationally corrected) or ΣD_e by making assumptions about other bonds in the molecule. For example, the energy of the C–C bond in ethyne, ethene or ethane may be calculated 'precisely' if the C–H bond energy is assumed to be either constant for all three compounds, or the same as the bond energy in methane (trivially $\Sigma D_e/4$). Other approaches to calculating bond energies which should be mentioned here include Grimme's idea of parameterizing the atomization energy in terms of bond critical point (topological) properties;[3] Bader's proposal of relating the bond energy to the integral of the energy density over the interatomic surface;[4] and Krygowski *et al*'s method of parameterizing the C–C bond energies as a single exponential function of experimentally observed bond lengths.[5]

Like Grimme's approach, the method outlined here does not make any assumptions about the constancy of C–C bond energies across any series of compounds, enabling *individual* bond energies to be derived for each such bond in a molecule. Our approach is to parameterize the potential energy surface for each bond in a way which best reproduces the atomization energies across a series of related compounds, assuming only that chemically similar types of atoms interact *via* the same potential.

Molecular geometries and total energies of benzene, naphthalene, five linear polyacenes (anthracene, tetracene, pentacene, hexacene and heptacene), five angular phenacenes (phenanthrene, chrysene, picene, fulminene and [7]phenacene) and four 'composite' benzenoid hydrocarbons (triphenylene, pyrene, perylene, coronene) were obtained at B3LYP/6-311G** level of theory, and used in the subsequent fitting procedure. Comparing the best experimental bond length values for benzene, naphthalene and anthracene, derived from low-temperature crystallographic studies and corrected for librational effects,[6] we find very good agreement with structures optimized at this level of theory, around 0.006 Å mean difference. Vibrationless atomization energies ΣD_e were derived from the molecular total energies by subtracting the energies of the free ground state atoms at the same level of theory, *i.e.* C(^3P) = −37. 85599 and H(^2S) = −0.50216, in Hartree atomic units. The parameterization procedure begins by defining a set of additive bond energies with respect to an estimated vibrationless atomization energy $\Sigma D_e{}^{\mathrm{calc}}$:

$$\Sigma D_e{}^{\mathrm{calc}} = \sum_{n_{\mathrm{CC}}} E(\mathrm{C–C}) + \sum_{n_{\mathrm{CH}}} E(\mathrm{C–H}) \qquad (2)$$

At first glance, the above partitioning of atomization energy seems inappropriate for the systems we have chosen to illustrate the method, namely π-electron molecules with conjugated π-bonds, and aromatic hydrocarbons in particular. An extension of the HMO model due to Longuet-Higgins and Salem[7] predicts the following bond-energy contribution for any pair of neighboring carbon atoms *m* and *n*

$$E_{mn}\ (\mathrm{C–C}) = -\{U(r) + 2p_{mn}\,\beta(r)\} \qquad (3)$$

where *r* is the C–C distance, $U(r)$ and $\beta(r)$ are the σ-bond potential energy and the resonance integral, respectively, and p_{mn} represents the π-electron bond order for atoms *m* and *n*. The latter quantity depends on the LCAO-MO coefficients of all the occupied MOs, and thus is a function of the whole molecular geometry, not just the *m*–*n* distance *r*. On the other hand at the *equilibrium* molecular geometry there is a simple linear relationship between the bond order $p^{\mathrm{e}}{}_{mn}$ and the equilibrium bond distance $r^{\mathrm{e}}{}_{mn}$:

$$p^{\mathrm{e}}{}_{mn} = p(r^{\mathrm{e}}{}_{mn}) = (R_1 - r^{\mathrm{e}}{}_{mn})/(R_1 - R_2) \qquad (4)$$

where R_1 (R_2) is the length of a 'pure' single (double) C–C bond of the sp^2–sp^2 type. It follows from eqs. (3) and (4) that for π-electron hydrocarbons at *equilibrium* there is a *universal* function $E(r)$ which defines bond energies as dependent of equilibrium bond distances $r^{\mathrm{e}}{}_{mn}$,

$$E_{mn}\ (\mathrm{C–C}) = E(r^{\mathrm{e}}{}_{mn}) \qquad (5)$$

The above result is valid providing that all the carbon atoms in the molecule are considered equivalent (a usual assumption in the HMO model). However, in aromatic molecules one finds two kinds of atoms: tertiary (with one hydrogen atom attached) and quaternary (with no hydrogen atom attached). Thus, up to three kinds of C–C bonds may be distinguished in these molecules (see below), with possible different bond-energy functions $E_i(r)$, (i = 1,2,3).

In our approach, the C–C bond energies are represented by one or more Morse functions, slightly modified to give E (C–C) = D_e at $r = r_e$ (rather than zero energy at $r = r_e$).

$$E_i\ (\mathrm{C–C}) = D_e{}^i\,\{1 - [1 - \exp\{-\alpha_i\,(r - r_e{}^i)\}]^2\} \qquad (6)$$

slightly modified to give E (C–C) = D_e at $r = r_e$, rather than zero energy at $r = r_e$ (here r_e and D_e correspond to the minimum of the Morse function, not to some equilibrium bond distance). The subscript/superscript i labels the Morse function to be applied. In fact it would be equally feasible to parameterize E_i(C–C) with a three parameter harmonic model, *i.e.*

† Electronic supplementary information (ESI) available: data for attempted fittings and exact and calculated atomisation energies for the final model. See http://www.rsc.org/suppdata/cc/b0/b007657k/

DOI: 10.1039/b007657k

$$E_i\,(\text{C–C}) = D_e^i\ \{1 - \alpha_i\,(r - r_e^i)^2\} \qquad (7)$$

but since the Morse function allows for anharmonicity without introducing any more parameters, we consider it superior for this application. At first, the bonds to terminal hydrogen atoms were also parameterized with Morse functions, but it was found essentially impossible to extract this data from the atomization energies (the optimized C–H bond lengths vary from just 1.084 to 1.086 Å over the whole data set). Thus the single value of E(C–H) for all such bonds was finally chosen as a parameter in the fitting procedure.

The next step is to define a normalized χ^2 statistic which will be minimized with respect to variations in the model parameters during the fitting procedure.

$$\chi^2 = \sum_{n_{\text{mols}}}\{\Sigma D_e^{\text{calc}} - \Sigma D_e\}^2 \qquad (8)$$

This statistic is minimised in a simple iterative algorithm employing numerical partial first derivatives of eqn. (5) with respect to the model parameters in ΣD_e^{calc}. This has been implemented as a *MATHEMATICA 4*[8] routine which is freely available from the authors, on request.

Topologically we can distinguish three types of C–C bond in polyacenes (see Fig. 1). These are (i) bonds between carbon atoms both bearing hydrogens; (ii) bonds between carbon atoms where only one of the carbons bears a hydrogen; and (iii) bonds between carbon atoms where neither bears a hydrogen. Thus it could be expected that the potential energy surface for these three types of bonds will differ, such that three independent Morse functions for each type of bond will be required to correctly describe all types of polyacene. However, we began the fitting procedure assuming that a single C–C potential energy surface might describe *all* types of C–C bonds, *i.e.* a four-parameter fit of {D_e, α, r_e} plus E(C–H) for all sixteen compounds. The result was quite poor reproduction of the 'exact' B3-LYP/6-311G** atomization energies by the model calculated ones: the average (percentage) accuracy $100(\chi^2/n_{\text{mols}})^{\frac{1}{2}}$ being just 0.5%. Subsequent improvement of the model by distinguishing between chemically distinct types of C–C bond led to a final model with ten parameters (three Morse functions as described above) reproducing the atomization energies with 0.04% average accuracy over all sixteen compounds. The fitted model parameters are as follows (in units of kJ mol^{-1}, Å^{-1} and Å): type (i) C–C bonds {D_e, α, r_e} = {530.83, 5.052, 1.3549}; type (ii) C–C bonds {D_e',α',r_e'} = {498.45, 6.448, 1.3922}; type (iii) C–C bonds {D_e'',α'',r_e''} = {490.49, 4.102, 1.3642}; and E(C–H) = 431.47 kJ mol^{-1}. The data for all of the fits attempted and the exact and calculated atomization energies for the final model are supplied as ESI.†. Here we will just mention that by far the worst agreement between any ΣD_e and ΣD_e^{calc} is found for septacene (ΣD_e = 25212 kJ mol^{-1} and ΣD_e^{calc} = 25232 kJ mol^{-1}, a 0.08% error). It should be noted that an error of 20 kJ mol^{-1} on the atomization energy represents < 1 kJ mol^{-1} error on the average C–C bond energy, since septacene has 30 C–C bonds.

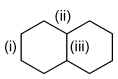

Fig. 1. Definition of C–C bond types.

The bond energies derived from the final model by substituting the optimized C–C bond lengths for r in eqn. (6) vary over a range of 438–531 kJ mol^{-1} in the sixteen compounds, with the C–C bond energy in benzene being at the upper end of this range. The complete distribution of C–C bonding energy is illustrated in Fig. 2 for just a few of the molecules: benzene, perylene and coronene. The values for perylene and coronene nicely demonstrate the Clar classification[9] of so-called 'empty rings' at the centre of composite polyacenes. The energies of innermost C–C bonds are much lower than those of the outermost bonds of the molecules, indicating that π-electron stabilization is concentrated in the peripheral rings (*e.g.* the difference in C–C bond energies between the peripheral rings and the central rings in perylene and coronene is 246 and 107 kJ mol^{-1}, respectively). It should also be mentioned that the bond energies reported here, and those derived by this method in general, will be slightly higher than any experimental estimates because by necessity we use ΣD_e values (*e.g.* the experimental ΣD_0 for benzene is 5464.8 kJ mol^{-1}, compared with our ΣD_e value of 5670 kJ mol^{-1}).

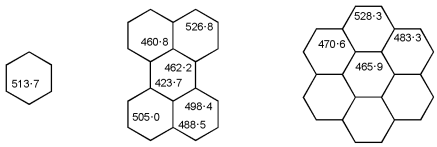

Fig. 2. C–C bond energies (kJ/mol^{-1}) for benzene, perylene and coronene.

To test whether the fitted parameters from our best model are sufficiently general to reproduce atomization energies and hence bond energies for polyacenes not in the fitting set of sixteen compounds, we have optimized four additional molecules at the same level of theory: benz[*a*]anthracene, benzo[*c*]-phenanthrene; benzo[*e*]pyrene and benzo[*g,h,i*]perylene. Indeed, we find that the ten-parameter Morse model reproduces the atomization energies of these compounds to the same accuracy obtained for the compounds present in the fit. So we may conclude that the parameters given here are sufficiently general to predict bond energies for most benzenoid hydrocarbons, with the possible exception of helicenes, where strong steric interactions may need to be explicitly treated in the model.

In addition to providing individual bond energy data, this parameterization procedure leads to a model of the molecules in question whose parameters also lend themselves to chemical interpretation. Consider the harmonic force constant $f = 2\alpha^2 D_e$ computed as the second partial derivative of eqn. (3) with respect to r. The model predicts f for type (i), (ii) and (iii) C–C bonds approximately in the ratio 1.6 : 2.5 : 1.0, information that probably has not been obtained before by any other method, experimental or theoretical.

In conclusion: the method for determining polyatomic molecule bond energies presented here should be applicable to essentially any series of related compounds (not only hydrocarbons); with the proviso that a more detailed treatment of the C–H bond and some types of steric or long-range interactions may be required for some families of compounds.

Financial support by the British Council and Polish Komitet Badan Naukowych for the visit of S. T. H to Warsaw is gratefully acknowledged.

Notes and references

1 P. v. R. Schleyer, C. Maerker, A. Dransfled, H. Jiao and N. J. R. v. E. Hommes, *J. Am. Chem., Soc.*, 1996, **118**, 6317.
2 S. T. Howard and T. M. Krygowski, *Can. J. Chem.*, 1997, **75**, 1174.
3 S. Grimme, *J. Am. Chem. Soc.*, 1996, **118**, 1529.
4 R. F. W. Bader, *Atoms In Molecules: A Quantum Theory*, Oxford University Press, Oxford, 1990.
5 T. M. Krygowski, A. Ciesielski, C. W. Bird and A. Kotschy, *J. Chem. Inf. Comput. Sci.*, 1995, **35**, 203.
6 T. C. W. Mak and G. D. Zhou, *Crystallography In Modern Chemistry*, John Wiley Inc., New York, 1992.
7 H. C. Longuet-Higgins and L. Salem, *Proc. R. Soc. London A*, 1959, **251**, 172.
8 S. Wolfram, *The Mathematica Book*, Wolfram Media/Cambridge University Press, 4th edn., 1999.
9 E. Clar, *The Aromatic Sextet*, J. Wiley and Sons, Chichester, 1972.

ChemComm

Self-assembled dithiocarbamate–copper(II) macrocycles for electrochemical anion recognition†

Paul D. Beer,*[a] Neil Berry,[a] Michael G. B. Drew,[b] O. Danny Fox,[a] Miguel E. Padilla-Tosta[a] and Sarah Patell[a]

[a] *Department of Chemistry, Inorganic Chemistry Laboratory, University of Oxford, South Parks Road, Oxford, UK OX1 3QR. E-mail: paul.beer@chem.ox.ac.uk*

[b] *Department of Chemistry, University of Reading, Whiteknights, Reading, UK RG6 6AD*

Received (in Cambridge, UK) 8th September 2000, Accepted 5th December 2000
First published as an Advance Article on the web

A novel family of redox-active dinuclear copper(II)-based macrocycles self-assembled from dithiocarbamate ligands has been synthesised; a naphthyl-spaced complex exhibits selective electrochemical recognition of perrhenate and dihydrogenphosphate anions.

The use of metal-directed self-assembly techniques provides a facile route to novel host macrocycles capable of binding charged and neutral guest substrates.[1,2] In some instances macrocycle formation can be templated by the guest and therefore the size and stability of the assembly is promoted by the complementarity between host and guest.[3]

We recently demonstrated the utility of the dithiocarbamate (dtc) moiety as a coordinating group[4] in the transition metal-directed construction of nano-sized resorcarene-based assemblies.[5] The incorporation of redox-active metal–ligand units into the macrocycle framework of a host introduces the possibility of using the host as an electrochemical sensor for guest substrates.[6] Herein, we describe the application of dithiocarbamate ligands in the construction of metal-directed self-assembled macrocycles. A range of copper-based, redox-active metallomacrocycles, their structural characterisation and preliminary electrochemical anion sensing results are presented.

The starting diamines were simply prepared by reaction of the appropriate bis(bromomethyl)aromatic compound with neat alkylamine. Dithiocarbamate copper(II) macrocycles were prepared in a one-pot synthesis from the parent secondary amines by reaction with carbon disulfide, potassium hydroxide and copper(II) acetate. The crude powders were recrystallised from dichloromethane–ethanol mixtures to afford the analytically pure metallomacrocycles **1**–**7** in yields of 40–70%.

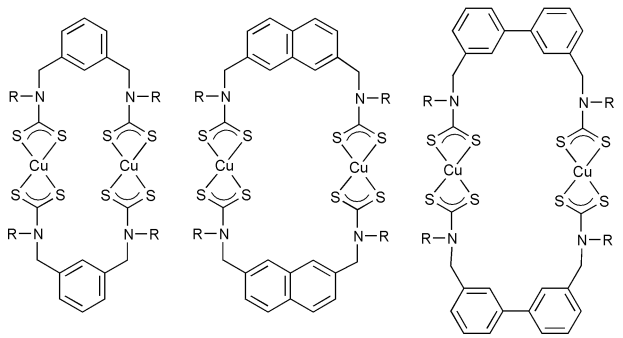

Electrospray mass spectrometry (ESMS) in pure methanol solutions confirmed the presence of all dinuclear macrocyclic structures. Treatment of copper(II) macrocycle **1** with iron(III) chloride gave upon crystallisation the complex $[Cu_2L_2][FeCl_4]_2$ **8**.[7] The structure of **8** was characterised by X-ray crystallography‡ and is shown in Fig. 1. There is only one crystallographically unique copper(III) ion present, a centre of inversion relating the two copper ions. The copper–copper distance in **8** is quite short at 5.5 Å. In profile, the structure of **8** forms a step-like structure, the two aromatic phenyl groups remaining planar and the two dtc–Cu–dtc moieties twisting out of the plane at an angle to the plane of the aromatic rings. There are two tetrachloroferrate(III) anions associated with each macrocycle and each exhibits a single axial interaction *via* a chlorine atom to a copper(III) centre, Cu–Cl 3.00 Å. The nature of this solid-state association led us to consider the possibility of anion interactions with the oxidized macrocycles.

The electrochemical properties of the copper(II) metallomacrocycles **2**, **4** and **7** were investigated in CH_2Cl_2–MeCN (4 : 1) using cyclic and square-wave voltammetry with NBu_4BF_4 as the supporting electrolyte. The xylyl-spaced complex **2** exhibits two quasi-reversible oxidation waves at 0.06 and 0.20 V [Table 1 and Fig. 2(a)]. The observation of two oxidation potentials indicates either electrochemical coupling between the two proximal copper centres or that in solution the two copper centres are in different coordination environments. The naphthyl-spaced complex **4**, with more separated copper centres, exhibits a single, broad, quasi-reversible oxidation wave at 0.19 V suggesting two overlapping waves [Fig. 2(b)]. However interestingly, the biphenyl-spaced copper(II) complex **7** again exhibits two distinct reversible oxidation waves at 0.04 and 0.19 V respectively even though molecular models predict that this complex possesses the longest Cu···Cu distance [Fig. 2(c)].

The copper(II)/(III) redox couples of macrocycles **2**, **4** and **7** in the presence of anions (ReO_4^-, $H_2PO_4^-$, Cl^-, Br^-, NO_3^-) (Table 1) were investigated by square-wave and cyclic voltammetry. Notably, substantial cathodic shifts in oxidation potential are seen for naphthyl-based macrocycle **4** with tetrahedral anions such as dihydrogenphosphate and per-

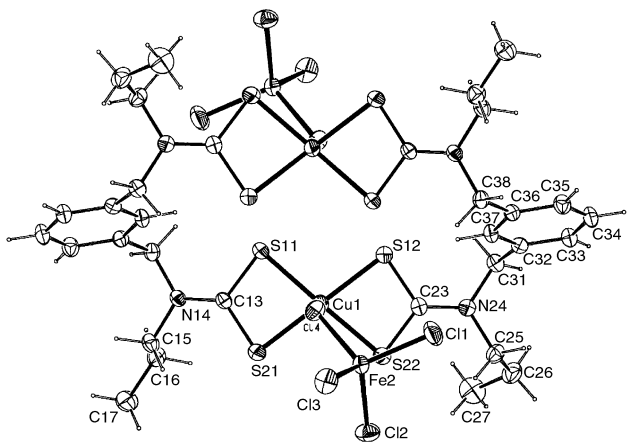

Fig. 1 Structure of the copper(III) complex **8** with associated $FeCl_4^-$ anions; ellipsoids at 20% probability.

† Electronic supplementary information (ESI) available: diamine structures, experimental and characterisation data. See http://www.rsc.org/suppdata/cc/b0/b007296f/

DOI: 10.1039/b007296f

Table 1 Electrochemical data[a]

	Receptor		
	2	**4**	**7**
$E_{1/2}$/V	0.06	0.19[b]	0.04
	0.20		0.19
ΔE (Cl^-)[c]/mV	20	< 10	< 10
ΔE (NO_3^-)[c]/mV	< 10	< 10	< 10
ΔE (Br^-)[c]/mV	< 10	< 10	< 10
ΔE (ReO_4^-)[c]/mV	< 10	85	< 10
ΔE ($H_2PO_4^-$)[c]/mV	< 10	85	< 10

[a] Obtained in CH_2Cl_2–MeCN (4:1) solution containing 0.2 mol dm^{-3} NBu_4BF_4 as supporting electrolyte. Solutions were *ca.* 1×10^{-3} mol dm^{-3} in receptor and potentials were obtained with reference to $Ag–Ag^+$ electrode at 293 K, scan rate = 100 mV s^{-1}. [b] Broad quasi-reversible oxidation wave: E_{pa} = 0.25 V, E_{pc} = 0.11 V, suggesting two overlapping waves. [c] Cathodic shift of $E_{1/2}$ oxidation potential produced by presence of 5 equiv. of anion added as their NBu_4^+ salts.

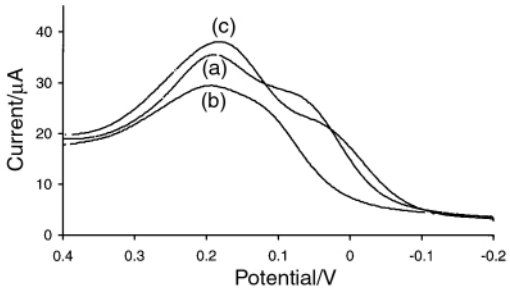

Fig. 2 Square-wave voltammograms of (a) **2**, (b) **4** and (c) **7** in CH_2Cl_2–MeCN (1:1), NBu_4BF_4 supporting electrolyte, Ref: Ag/AgCl.

rhenate.[8] For example with **4** the addition of five equivalents of tetrabutylammoniumperrhenate gave a cathodic shift of 85 mV in the Cu(II)/Cu(III) redox couple (see Fig. 3). The complexed anion effectively stabilises the copper(III) oxidation state. Interestingly no significant perturbations were observed with chloride, bromide or nitrate anions. In contrast the smaller xylyl-spaced macrocycle exhibits a noticeable cathodic perturbation to chloride (20 mV) but little response to nitrate, bromide or the larger anions such as perrhenate or dihydrogenphosphate. For the control bis(diethyldithiocarbamate)copper(II) a single quasi-reversible oxidation wave at 0.07 V is observed which exhibits no significant perturbations in oxidation potential on the addition of anions.

The interaction of **4** with perrhenate was investigated further by UV–VIS spectroscopy. Solutions of **2**, **4** and **7** in CH_2Cl_2–MeCN (0.1 M NBu_4BF_4) were oxidised with $NOBF_4$ to the corresponding dicationic copper(III) complexes.§ On addition of 5 equiv. of NBu_4ReO_4 to freshly prepared $[\mathbf{4}]^{2+}$ (λ_{max} = 421 nm) a bathochromic shift of 10 nm was observed in the maximum absorption. However, no such shifts were observed

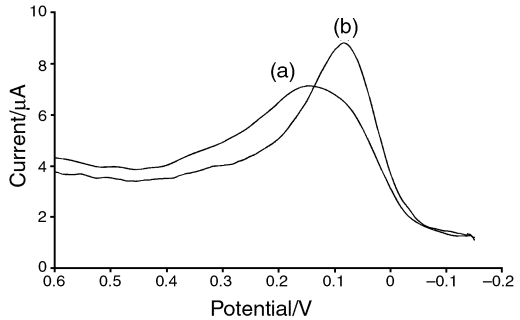

Fig. 3 Square-wave voltammograms of (a) **4** and (b) **4** plus 5 equiv. of NBu_4ReO_4; in CH_2Cl_2–MeCN (1:1), NBu_4BF_4 supporting electrolyte, Ref: Ag/AgCl.

on the addition of NBu_4ReO_4 to $[\mathbf{2}]^{2+}$, $[\mathbf{7}]^{2+}$ or the oxidised monocation of bis(diethyldithiocarbamate)copper(II).¶ Further evidence for the interaction of $[\mathbf{4}]^{2+}$ with ReO_4^- came from ES-MS studies.[9] Oxidation of copper(II) macrocycles in acetonitrile–dichloromethane mixtures with copper(II) triflate, perchlorate or tetrafluoroborate gave in all cases the doubly oxidised species, $[Cu_2L_2]^{2+}$ of the copper(III) macrocycles (L = ligand). Addition of ReO_4^- anions to solutions of macrocycle **4** oxidised with copper(II) triflate or tetrafluoroborate gave the ion corresponding to the doubly oxidised species $[Cu_2L_2][ReO_4]^+$, 1275.2.‖ This species was predominant even in the presence of a large excess of tetrafluoroborate anion. Space filling molecular models indicate anions such as ReO_4^- and $H_2PO_4^-$ may comfortably occupy the cavity and bridge the copper centres in **4**, but are too large for the xylyl-spaced **2** and too small for biphenyl-spaced **7**. This suggests this macrocyclic system may exhibit a measure of anion selectivity based upon the macrocycle ring size.[10]

In summary, copper(II) metallomacrocycles **1**–**7** are novel examples of redox-active macrocyclic hosts whose oxidation states and hence binding affinities can be chemically switched by redox control. In addition we have demonstrated the use of the dtc–copper(II)/(III) redox couple as an electrochemical anion-sensing unit. These preliminary electrochemical sensing results suggest anion selectivity is dictated by the size of dithiocarbamate copper(II) macrocycle.

Financial support for this work was provided by EPSRC, AWE Aldermaston and the Universities of Oxford and Reading.

Notes and references

‡ *Crystal data* for $[Cu_2L_2][FeCl_4]_2$ **8**: $C_{42}H_{56}Cl_8Cu_2Fe_2N_4S_8$, M_r = 1419.78, triclinic, space group $P\bar{1}$, Z = 1, a = 10.751(12), b = 12.229(14), c = 12.598(14) Å, α = 95.657(10), β = 107.331(10), γ = 98.744(10)°, U = 1544 Å^3, D_c = 1.526 g cm^{-3}, μ = 1.76 mm^{-1}, 5535 unique data.

CCDC 182/1869. See http://www.rsc.org/suppdata/cc/b0/b007296f/ for crystallographic files in .cif format.

§ **2**: Cu(II) λ_{max} = 432, Cu(III) λ_{max} = 416; **4**: Cu(II) λ_{max} = 433, Cu(III) λ_{max} = 421; **7**: Cu(II) λ_{max} = 440, Cu(III) λ_{max} = 431; bis(diethyldithiocarbamate)copper(II): Cu(II) λ_{max} = 434, Cu(III) λ_{max} = 425 nm.

¶ UV–VIS spectroscopic anion titrations with the neutral receptors gave no evidence of anion binding. Preliminary UV–VIS titrations of $[\mathbf{4}]^{2+}$ with NBu_4ReO_4 gave a stoichiometry of 1:2 receptor:anion.

‖ Under the same conditions oxidized receptors **2** and **7** gave only very weak peaks for adducts with ReO_4^-.

1 R. W. Saalfrank and I. Bernt, *Curr. Opin. Solid State Mater. Sci.*, 1998, **3**, 407; M. Fujita, *Chem. Soc. Rev.*, 1998, **27**, 417; S. Leininger, B. Olenyuk and P. J. Stang, *Chem. Rev.*, 2000, **100**, 853; C. J. Jones, *Chem. Soc. Rev.*, 1998, **27**, 289.

2 A. W. Maverick, S. C. Buckingham, Q. Yao, J. R. Bradbury and G. S. Stanley, *J. Am. Chem. Soc.*, 1986, **108**, 7430; D. L. Caulder and K. N. Raymond, *J. Chem. Soc., Dalton Trans.*, 1999, 1185.

3 R. W. Saalfrank, I. Bernt, E. Uller and F. Hampel, *Angew. Chem., Int. Ed. Engl.*, 1997, **36**, 2482; M. Fujita, S. Hagao and K. Ogura, *J. Am. Chem. Soc.*, 1995, **117**, 1649; B. Hasenkopf, J. M. Lehn, N. Boumediene, A. Dupont-Gervais, A. V. Dorsselaer, B. Kneisel and D. Fenske, *J. Am. Chem. Soc.*, 1997, **119**, 10 956.

4 D. Coucouvanis, *Prog. Inorg. Chem.*, 1979, **26**, 301.

5 O. D. Fox, M. G. B. Drew and P. D. Beer, *Angew. Chem., Int. Ed.*, 2000, **39**, 135; O. D. Fox, M. G. B. Drew, E. J. S. Wilkinson and P. D. Beer, *Chem. Commun.*, 2000, 391.

6 P. D. Beer, P. A. Gale and G. Z. Chen, *Coord. Chem. Rev.*, 1999, **185**, 3; P. D. Beer and D. K. Smith, *Prog. Inorg. Chem.*, 1997, **46**, 1.

7 R. M. Golding, C. M. Harris, K. J. Jessop and W. C. Tennant, *Aust. J. Chem.*, 1972, **25**, 2567.

8 M. Staffilani, K. S. B. Hancock, J. W. Steed, K. Travis Holman, J. L. Atwood, R. K. Juneja and R. B. Burkhalter, *J. Am. Chem. Soc.*, 1997, **119**, 6324.

9 A. M. Bond, R. Colton, A. D'Agostino, J. Harvey and J. C. Traeger, *Inorg. Chem.*, 1993, **32**, 3952.

10 V. Amendola, E. Bastianello, L. Fabbrizzi C. Mangano, P. Pallavicini, A. Perotti, A. M. Lanfredi and F. Ugozzli, *Angew. Chem., Int. Ed.*, 2000, **39**, 2917.

A Pd complex of a tridentate pincer CNC bis-carbene ligand as a robust homogenous Heck catalyst†

Eduardo Peris,*[a] Jennifer A. Loch,[b] José Mata,[a] and Robert H. Crabtree*[b]

[a] *Dpto. de Química Inorgánica y Orgánica, Universitat Jaume I, 12080 Castellón, Spain. E-mail: eperis@vents.uji.es*
[b] *Department of Chemistry, Yale University, P.O. Box 208107, New Haven, CT 06520-8107, USA. E-mail: robert.crabtree@yale.edu*

Received (in Irvine, CA, USA) 2nd October 2000, Accepted 6th December 2000
First published as an Advance Article on the web

The bis-carbene precursor, 1, gives a thermally very robust Pd(II) catalyst for Heck coupling that maintains activity even in boiling diethylacetamide (bp 184 °C) in air.

One common and significant limitation of some homogeneous catalysts is their relatively rapid deactivation, particularly when high temperatures or harsh conditions are needed; this is often the case for cross-coupling reactions and alkane functionalization.[1] The facility of P–C bond cleavage reactions has been implicated in catalyst deactivation of phosphine complexes.[2] For example, the deactivation of the $[IrH_2(tfa)(P\{C_6H_4F\}_3)_2]$ catalyst in alkane dehydrogenation was shown to correlate with the appearance of C_6H_5F, the product of P–aryl hydrogenolysis.[3]

The recent discovery of imidazole-based carbenes[4] and of their effectiveness as ligands[5] offers an opportunity to develop phosphine-free homogeneous catalysis. These carbenes are not only excellent ligands for late transition metals but are also able to promote a variety of catalytic reactions, including C–C[6] and C–N[7] coupling and olefin metathesis.[8] The thermal stability of carbene complexes is often high and they lack sensitive bonds that might be cleaved in any deactivation process. Since thermal stability of phosphine complexes can be improved by incorporation into a chelating ligand, as in the well known 'pincer' phosphines,[9] the same strategy might be useful in enhancing stability in the carbene case. Several authors have recently reported thermally stable palladium complexes active for the Heck reaction either with carbene or with pincer phosphines of both mono- and multi-dentate types as ligands.[6b,d,e,i,j,10]

We now report that the known carbene precursor,[11] **1**, readily formed by an improved synthesis (95% yield), reacts with $Pd(OAc)_2$ to give a carbene complex, **2**, as shown in Scheme 1 (ESI†). The thermal stability of the product is emphasized by the fact that the final stage of the synthesis of **2** takes place at 160 °C.

Fig. 1 shows the structure and metric parameters of the resulting complex from an X-ray structure determination.‡ The molecule is flat with a ligand bite angle of 79°. Otherwise, the metric parameters are similar to those previously found for related complexes.[6b,d] The Pd–C distance (2.038(6) Å) indicates that the bond is essentially single with very little back donation, as expected for this strongly Fischer-type carbene. This Pd–C distance is somewhat longer than in most prior cases,[6b,d] probably because the two high *trans*-effect carbene ligands are mutually *trans*.

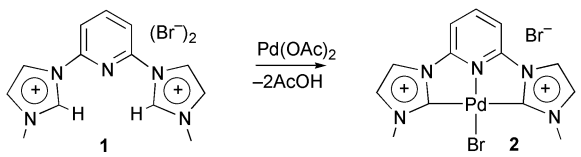

Scheme 1

† Electronic supplementary information (ESI) available: synthesis details and NMR data. See http://www.rsc.org/suppdata/cc/b0/b008038l/

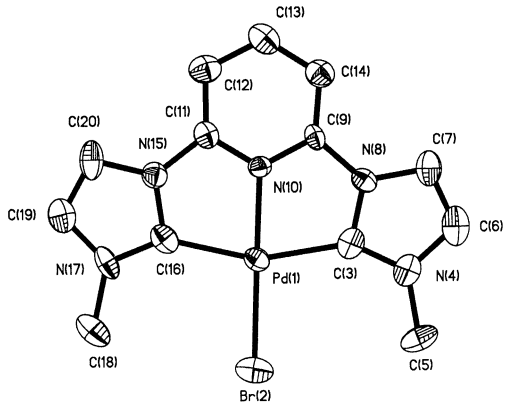

Fig. 1 ORTEP diagram of complex **2** showing the atom numbering scheme. Hydrogen atoms are omitted for clarity. Selected bond distances (Å) and angles (°): Pd(1)–N(10) 1.979(4), Pd(1)–C(3) 2.033(6), Pd(1)–C(16) 2.044(6), Pd(1)–Br(2) 2.4099(7); N(10)–Pd(1)–C(3) 78.9(2), N(10)–Pd(1)–C(16) 79.6(2), C(3)–Pd(1)–C(16) 158.5(2), N(10)–Pd(1)–Br(2) 179.03(13), C(3)–Pd(1)–Br(2) 100.29(16), C(16)–Pd(1)–Br(2) 101.18(16). Thermal ellipsoids are drawn at 50% probability.

The stability that ligand **1** imparts to complex **2** is apparent from comparison with other Heck catalysts containing chelating ligands. Catalysts **3**[6d,e] and **4**[12] are very active for the Heck reaction when used under nitrogen at 140 °C. Complex **3**,

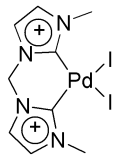

3

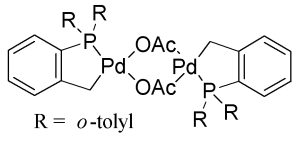

4

however, is reported[6e] to decompose in dimethylacetamide (DMA, bp 165 °C) above 70 °C. Our own work shows that in refluxing DMA in air, complex **3** begins to deposit Pd black after 8 h and complex **4** deposits Pd black after 17 h, while our complex, **2**, is unchanged (> 24 h). Other Pd pincer complexes, of PCP and SCS types, are also known as Heck catalysts.[10]

The new complex **2** shows catalytic activity under argon for a standard Heck reaction between PhI and styrene (Table 1, entry 1) in refluxing diethylacetamide (DEA, bp 184 °C) in the presence of NaOAc as base.§ We find that with 0.2 mol% catalyst, good yields and turnover frequencies are found. Complex **2** shows comparable activity to the Heck catalysts, **3** and **4**, at least for PhI (Table 1, entries 1–3). Bromobenzene and styrene can also be converted to *trans*-stilbene in essentially quantitative yield in the presence of 5 mol% catalyst, NaOAc, and refluxing DMA, within 1 h (Table 2, entry 1). Surprisingly, but not uniquely,[10b,c,e] the catalyst retains activity even under air (Table 2, entry 2). Iodobenzene and styrene can also be converted to *trans*-stilbene in near quantitative yield in the presence of 5 mol% **2**, NaOAc, and refluxing DMA in a reflux

Table 1 Comparison of yields for catalysts **2**–**4** for the reaction of PhI with styrene in refluxing DEA to form *trans*-stilbene (under Ar with 0.2 mol% catalyst and NaOAc)[a]

Entry	Catalyst	0.5 h	1 h	1.5 h	2 h	4 h
1[b]	**2**	48, 494	58, 298	67, 230	73, 188	85, 109
2	**3**	36, 370	48, 247	62, 213	72, 185	84, 108
3	**4**	50, 514	61, 314	67, 230	75, 193	90, 116

[a] Reported as: yield (%), TOF [mol product/(mol Pd × h)]. Yield determined by ^{1}H NMR based on amount of product *vs*. amount of starting material remaining. [b] Average of two runs.

Table 2 Heck reaction between aryl halides and styrene to form *trans*-stilbene. All reactions carried out in refluxing DMA with NaOAc as base

Entry (air/Ar)	Aryl halide	**2** (mol %)	Reaction time/h	Stilbene yield (%)[a]	TOF [mol prod./ (mol Pd)(h)]
1 (Ar)	PhBr	5	1	> 99	20
2 (air)	PhBr	5	1	> 99	20
3 (air)	PhI	5	1	> 99	20
4 (air)	PhI	1	1	89	89
5 (air)	PhI	0.0001	20	33	16.500
6 (Ar)[b]	*p*-(CHO)C$_6$H$_4$Cl	5	20	75	15

[a] Yield determined by ^{1}H NMR based on amount of product *vs*. amount of starting material remaining. [b] In the presence of *n*-Bu$_4$NBr (20 mol% *vs*. Pd).

apparatus open to the air (Table 2, entry 3). A yield of 89% can still be obtained in only 1 h if 1 mol% of **2** is used (Table 2, entry 4). To see if the TOF could be improved at low loading, we find that as little as 10^{-4} mol% of **2** still gives a TOF of 16.500 after 20 h under air (Table 2, entry 5). Aryl chlorides react more slowly (Table 2, entry 6). Other alkenes react satisfactorily—for example, *n*-butyl acrylate and PhI give the Heck product in 99% yield after 1 h in refluxing DMA with 1 mol% catalyst.

In view of recent studies that find evidence that the active species can be metallic palladium,[13] we checked **2**–**4** for heterogeneity by the Hg drop test.[14] Heck catalysis with **2**–**4** was unaffected by the presence of Hg, and no induction period is observed for **2**, so a homogeneous active species is likely.

On the standard model of the Heck reaction, with [Pd(0){PR$_3$}$_2$] as the key intermediate, a pincer carbene might seem to be a poor choice, even if the carbene is an acceptable replacement for the tertiary phosphine of the standard system. On the Amatore–Jutand model,[15] however, [Pd(0)(OAc){PR$_3$}$_2$]$^-$ is the key intermediate. Our work supports this model if the pyridine part of the pincer ligand is considered as replacing the OAc group. It is true that [Pd(0)XL$_2$]$^-$ would normally be expected to adopt a trigonal geometry, but the presumed intermediate Pd(0) form of the metal being d^{10}, there should be no strong penalty to adopt the pincer geometry. Eisenstein and Clot[16] are currently looking at such mechanistic issues in detail.

The results are of interest not so much as an advance in Heck catalysis—other catalysts can be better[6,10]—but as an indication that chelating carbenes can provide ligand systems that give high catalytic activity with excellent stability, even in air. This approach should be widely applicable to the development of non-phosphine late metal homogeneous catalysis.

We thank US DOE (J. A. L.) and NSF (R. H. C.) for funding and Matthew Torres for some preliminary observations.

Notes and references

‡ *Crystal data for* **2**: $C_{11}H_7Br_2N_5Pd{\cdot}H_2O$, monoclinic, space group $P2(1)/n$, a = 8.7782(4), b = 14.3181(6), c = 13.5684(6) Å, α = 90, β = 107.1600(10), γ = 90°, Z = 4, D = 2.011 g cm^{-3}, μ = 6.044 mm^{-1}, 5300 measured reflections, 1467 [R(int) = 0.0310] independent reflections, R = 0.0225 [$F > 2\sigma(F)$]. Crystals were grown by diffusion of CH_2Cl_2 into a DMSO solution. Data collection: Siemens Smart CCD diffractometer (λ = 0.71073 Å). The structure was solved by direct methods and was refined using the SHELXTL 5.1 software package. All non-hydrogen atoms were refined anisotropically. Hydrogen atoms were assigned to ideal positions and refined using a riding model. CCDC 182/1880. See http://www.rsc.org/suppdata/cc/b0/b008038l for crystallographic files in .cif format. The diffraction frames were integrated using the SAINT[17] package and corrected for absorption with SADABS.[18]

§ *General Heck procedure*: NaOAc (360 mg, 4.4 mmol) and the catalyst were placed in a 3-necked flask fitted with a reflux condenser and degassed. Aryl halide (4 mmol), styrene (640 μL, 5.6 mmol), and solvent (DMA or DEA, 5 mL), were added under Ar or air. The reaction vessel was placed into an oil bath preheated to the desired temperature. Aliquots (200 μL) were removed after fixed times and added to 10 mL CH_2Cl_2. The organic layer was extracted five times with 10 mL portions of water and dried with $MgSO_4$. The mixture was then filtered and the CH_2Cl_2 removed *in vacuo*. The residue was dissolved in $CDCl_3$ or CD_2Cl_2 and analyzed by ^{1}H NMR (400 MHz).

1 R. H. Crabtree, *The Organometallic Chemistry of the Transition Metals*, 3rd edn., Wiley, New York, 2001.
2 P. Garrou, *Chem. Rev.*, 1981, **81**, 229.
3 M. J. Burk and R. H. Crabtree, *J. Am. Chem. Soc.*, 1987, **109**, 8025.
4 A. J. Arduengo, III, R. L. Harlow and M. Kline, *J. Am. Chem. Soc.*, 1991, **113**, 361; A. J. Arduengo, III, *Acc. Chem. Res.*, 1999, **32**, 913.
5 K. Öfele, W. A. Herrmann, D. Mihalios, M. Elison, E. Herdtweck, W. Scherer and J. Mink, *J. Organomet. Chem.*, 1993, **459**, 177.
6 (*a*) V. P. W. Böhm, C. W. K. Gstottmayr, T. Weskamp and W. A. Herrmann, *J. Organomet. Chem.*, 2000, **595**, 186; (*b*) J. Schwarz, V. P. W. Böhm, M. G. Gardiner, M. Grosche, W. A. Herrmann, W. Hieringer and G. Raudaschl-Sieber, *Chem. Eur. J.*, 2000, **6**, 1773; (*c*) T. Weskamp, V. P. W. Böhm and W. A. Herrmann, *J. Organomet. Chem.*, 1999, **585**, 348; (*d*) W. A. Herrmann, C.-P. Reisinger and M. Spiegler, *J. Organomet. Chem.*, 1998, **557**, 93; (*e*) W. A. Herrmann, M. Elison, J. Fischer, C. Köcher and G. R. J. Artus, *Angew. Chem., Int. Ed. Engl.*, 1995, **34**, 2371; (*f*) C. Zhang and M. L. Trudell, *Tetrahedron Lett.*, 2000, **41**, 595; (*g*) C. Zhang, J. Huang, M. L. Trudell and S. P. Nolan, *J. Org. Chem.*, 1999, **64**, 3804; (*h*) J. Huang and S. P. Nolan, *J. Am. Chem. Soc.*, 1999, **121**, 9889; (*i*) D. S. McGuiness and K. J. Cavell, *Organometallics*, 2000, **19**, 741; (*j*) D. S. McGuiness, K. J. Cavell, B. W. Skelton and A. H. White, *Organometallics*, 1999, **18**, 1596.
7 S. R. Stauffer, S. Lee, J. P. Stambuli, S. I. Hauck and J. F. Hartwig, *Org. Lett.*, 2000, **2**, 1423; J. Huang, G. Grasa and S. P. Nolan, *Org. Lett.*, 1999, **1**, 1307.
8 C. W. Bielawski and R. H. Grubbs, *Angew. Chem., Int. Ed.*, 2000, **39**, 2903; M. Scholl, S. Ding, C. W. Lee and R. H. Grubbs, *Org. Lett.*, 1999, **1**, 953; T. Weskamp, F. J. Kohl, W. Hieringer, D. Gleigh and W. A. Herrmann, *Angew. Chem., Int. Ed.*, 1999, **38**, 2416; U. Frenzel, T. Weskamp, F. J. Kohl, W. C. Schattenman, O. Nuyken and W. A. Herrmann, *J. Organomet. Chem.*, 1999, **586**, 263; J. Huang, E. D. Stevens, S. P. Nolan and J. L. Petersen, *J. Am. Chem. Soc.*, 1999, **121**, 2674; J. K. Huang, H. J. Schanz, E. D. Stevens and S. P. Nolan, *Organometallics*, 1999, **18**, 5375; S. B. Garber, J. S. Kingsbury, B. L. Gray and A. H. Hoveyda, *J. Am. Chem. Soc.*, 2000, **122**, 8168.
9 C. M. Jensen, *Chem. Commun.*, 1999, 2443; C. J. Moulton and B. L. Shaw, *J. Chem. Soc., Dalton Trans.*, 1976, 1020.
10 (*a*) D. Morales-Morales, R. Redón, C. Yung and C. M. Jensen, *Chem. Commun.*, 2000, 1619; (*b*) D. Morales-Morales, C. Grause, K. Kasaoka, R. Redón, R. E. Cramer and C. M. Jensen, *Inorg. Chim. Acta*, 2000, **300**–**302**, 958; (*c*) M. Ohff, A. Ohff, M. E. van der Boom and D. Milstein, *J. Am. Chem. Soc.*, 1997, **119**, 11687; (*d*) I. P. Beletskaya, A. V. Chuchurjukin, H. P. Dijkstra, G. P. M. van Klink and G. van Koten, *Tetrahedron Lett.*, 2000, **41**, 1075; (*e*) D. E. Bergbreiter, P. L. Osburn and Y. S. Liu, *J. Am. Chem. Soc.*, 1999, **121**, 9531.
11 J. C. C. Chen and I. J. B. Lin, *J. Chem. Soc., Dalton Trans.*, 2000, 839.
12 W. A. Herrmann, C. Brossmer, C.-P. Reisinger, T. H. Riermeier, K. Öfele and M. Beller, *Chem. Eur. J.*, 1997, **3**, 1357.
13 M. Nowotny, U. Hanefeld, H. van Koningsveld and T. Maschmeyer, *Chem Commun.*, 2000, 1877; M. T. Reetz and E. Westermann, *Angew. Chem., Int. Ed.*, 2000, **39**, 165.
14 D. R. Anton and R. H. Crabtree, *Organometallics*, 1983, **2**, 855; P. Foley, R. DiCosimo and G. M. Whitesides, *J. Am. Chem. Soc.*, 1980, **102**, 6713.
15 C. Amatore and A. Jutand, *Acc. Chem. Res.*, 2000, **33**, 314.
16 O. Eisenstein and E. Clot, personal communication, 2000.
17 SAINT, version 5.0, Bruker Analytical X-ray Systems, Madison, WI.
18 G. M. Sheldrick, SADABS empirical absorption program, University of Göttingen, 1996.

ChemComm

Epoxyalcohol route to hydroxyethylene dipeptide isosteres: a new synthesis of the diaminoalcohol core of HIV-protease inhibitor ABT-538 (Ritonavir)

Fabio Benedetti* and Stefano Norbedo

Department of Chemical Sciences, University of Trieste, Via Giorgieri 1, 34127 Trieste, Italy. E-mail: benedett@univ.trieste.it; Fax: +39 040 6763903; Phone: +39 040 6763919

Received (in Liverpool, UK) 13th July 2000, Accepted 8th December 2000
First published as an Advance Article on the web

A stereoselective synthesis of the diaminoalcohol core of Ritonavir illustrates a novel approach to hydroxyethylene dipeptide isosteres, based on the regioselective reduction of amino acid-derived epoxyalcohols.

Ritonavir (**1**), approved in 1996,[1] is a potent and clinically effective peptidomimetic inhibitor of the protease of HIV, with high oral bioavailability.[2] The structure of Ritonavir was designed to target the enzyme's active site and is based on the hydroxyethylene dipeptide isostere **2**.[2a] In the original synthesis of the inhibitor,[3] the diaminoalcohol **2** was obtained from the corresponding diaminodiol **3** by a multi-step deoxygenation

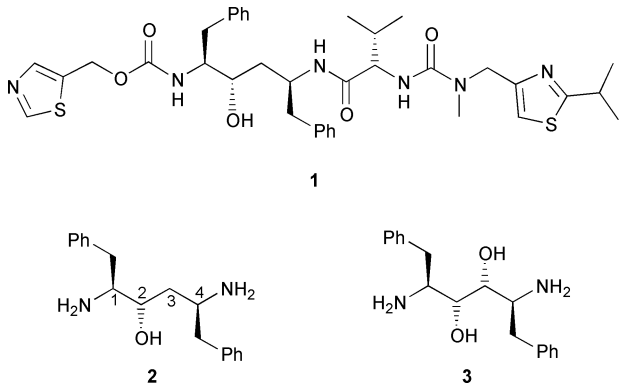

approach.[4] The core **2** was then statistically monoacylated to introduce the first side chain while the second flanking residue was introduced in the final step. This strategy has some drawbacks: loss of **2** through undesired bis-acylation, impossibility of introducing different residues on the isostere's C1 and C4, which originate from the Cα of the same aminoacid *via* the reductive dimerization of the corresponding aminoaldehyde,[4] and a less than optimal stereocontrol in the synthesis of **3**. Several approaches have been proposed to overcome these limitations, based on aminoacids as precursors from the chiral pool[5] or on enantioselective synthetic strategies.[6] In this communication we describe a short and efficient synthesis of the monoprotected Ritonavir core **9** which utilizes the amino-acid derived epoxyalcohol **4** as key intermediate (Scheme 1).

The epoxyalcohol **4** was obtained from phenylalanine, in four steps and 40% overall yield, as described previously.[7] 2,3-Epoxyalcohols are regioselectively converted into the corresponding 1,3-diols by Red-Al;[8] accordingly, when the epoxyalcohol **4** was treated with this reagent (3 equiv.) in THF at 50 °C for 24 h, attack of hydride took place selectively to give the Boc-protected aminodiol **5** {$[\alpha]_D^{25} = -18$ (*c* 0.2, MeOH)} in 60% yield after chromatography. In order to convert this compound into the required diaminoalcohol **9**, it is necessary to: i) selectively activate the hydroxy group on C4 towards displacement by a suitable precursor of the aminogroup and ii) invert the configuration of C2 which is opposite to that of **9**. Differentiation of the two secondary hydroxy groups, selective activation and inversion of the configuration of C2 were obtained in a single step by treating the diol with 3 equiv. of methanesulfonyl chloride and 6 equiv. diisopropylethylamine (DIPEA) in 1,2-dichloroethane, at 80 °C for 6 h. The dimesylate **6** initially obtained spontaneously cyclizes *via* S_N2 attack of the carbonyl oxygen of Boc on the neighbouring sulfonate ester to give the inverted oxazolidinone **7**. Displacement of the second mesylate was obtained by treating crude **7** with 1.5 equiv. NaN_3 in DMSO for 18 h at 50 °C, in the presence of 1 equiv. of 18-crown-6, affording the azide **8** {$[\alpha]_D^{25} = -35$ (*c* 0.2, MeOH)} in which all the stereocenters have the correct configuration (50% for the two steps). The stereochemistry of the oxazolidinone **8** was established from NOE experiments. These show a 3% enhancement between the ring H4 and H5, consistent with a *trans* relationship between these protons, while in the *cis*-oxazolidinone **12** (Scheme 2) a 11% enhancement is detected between the same protons. The Boc-protected amino group was then restored by treatment of **8** with equimolar amounts of Boc_2O and NaH in THF, at 25 °C for 12 h, followed by hydrolysis of the resulting N-Boc heterocycle with Cs_2CO_3 in MeOH–water at 25 °C for 2 h.[9] Finally, hydrogenation of the azide, in MeOH over 10% Pd/C, gave the monoprotected (*S*,*S*,*S*) hydroxyethylene dipeptide isostere **9** {$[\alpha]_D^{25} = -19$ (*c* 0.2, MeOH)} in 20% overall yield from the epoxyalcohol **4**.

The synthetic approach shown here can be expanded to obtain the epimeric Phe-Phe dipeptide isostere **13** with the opposite configuration at the alcoholic carbon (Scheme 2). In this case the diol **5** is treated with sodium hydride in THF at 25 °C for 12 h to give, in 85% yield, the *cis*-oxazolidinone **10** arising from a normal acyl transfer cyclization[10] {$[\alpha]_D^{25} = -42$ (*c* 0.2, MeOH)}. The NOE enhancement between the ring

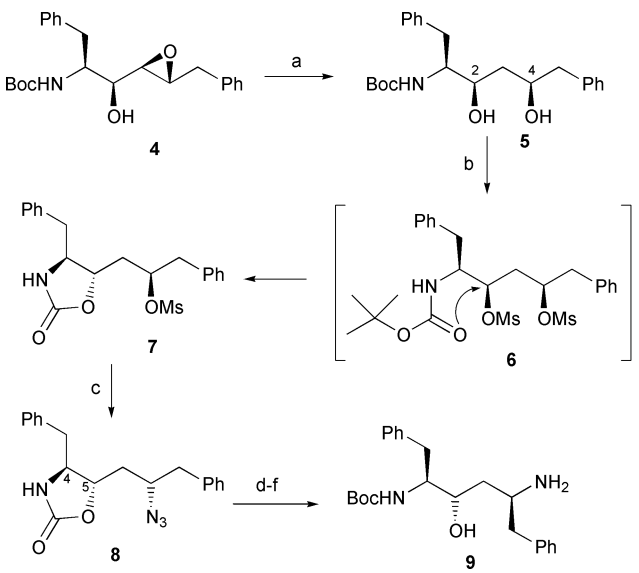

Scheme 1 *Reagents and conditions*: (a) Red-Al, THF, 50 °C, 60%; (b) MsCl, DIPEA, 80 °C; (c) NaN_3, DMSO, 18-crown-6, 50 °C, 50%, 2 steps; (d) NaH, Boc_2O, THF; (e) Cs_2CO_3, MeOH–H_2O, 67%, 2 steps; (f) 1 atm H_2, 10% Pd/C, MeOH, 100%.

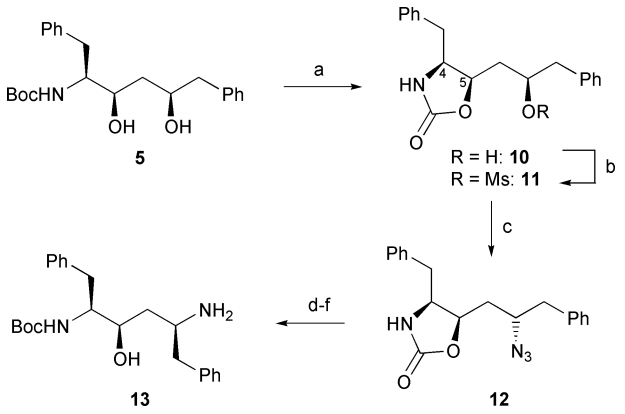

Scheme 2 *Reagents and conditions*: (a) NaH, THF, 25 °C, 85%; (b) MsCl, Et_3N, CH_2Cl_2, 0 °C; (c) NaN_3, DMSO, 18-crown-6, 50 °C, 75%, 2 steps; (d) NaH, Boc_2O, THF; (e) Cs_2CO_3, MeOH–H_2O, 58%, 2 steps; (f) 1 atm H_2, 10% Pd/C, MeOH, 100%.

protons (11%) is consistent with the *cis* stereochemistry of the ring substituents. With the first hydroxy group thus protected, the second OH can be activated as mesylate, in CH_2Cl_2 at 0 °C,[11] and the resulting oxazolidinone **11** is then converted into the selectively protected (*S*,*R*,*S*) isostere **13** {$[\alpha]_D^{25}$ = +1.0 (*c* 2, MeOH)} by the same sequence of reactions seen before for the synthesis of **9** (Scheme 2). The overall yield of **13** is 22%, from the epoxyalcohol **4**.

We have thus described a novel approach to the synthesis of the (*S*,*S*,*S*) dipeptide isostere of Ritonavir **9** and its (*S*,*R*,*S*) epimer **13**, based on the regioselective ring opening of an epoxyalcohol with aluminium hydride. This strategy leads to a mono-protected diaminoalcohol from which peptidomimetic protease inhibitors can be directly obtained by coupling with different peptide, or non-peptide, residues. The approach is not limited to isosteres with identical side chains, and it should thus be possible to extend this methodology to the synthesis of a repertoire of isosteres with different residues, starting from the corresponding, readily available epoxyalcohols.[7] The synthesis of dihydroxyethylene dipeptide isosteres from the same epoxyaminoalcohols **4** has been described previously;[7,12] the present extension to the synthesis of monohydroxyethylene isosteres further demonstrates the synthetic utility of these intermediates.

This work was supported by Istituto Superiore di Sanità, National Research Program on AIDS and the University of Trieste.

Notes and references

1 http://www.niaid.nih.gov/daids/dtpdb/
2 (*a*) D. J. Kempf, H. L. Sham, K. C. Marsh, C. A. Flentge, D. Betebenner, B. E. Green, E. McDonald, S. Vasavanonda, A. Saldivar, N. E. Wideburg, W. M. Kati, L. Ruiz, C. Zhao, L. Fino, J. Patterson, A. Molla, J. J. Plattner and D. W. Norbeck, *J. Med. Chem.*, 1998, **41**, 602; (*b*) D. W. Cameron, M. Heah-Chiozzi, S. Danner, C. Cohen, S. Kravcik, C. Maurath, E. Sun, D. Henry, R. Rode, A. Potthoff and J. Leonard, *Lancet*, 1998, **351**, 543; (*c*) A. P. Lea and D. Faulds, *Drugs*, 1996, **52**, 541; (*d*) D. J. Kempf, K. C. Marsh, J. F. Denissen, E. McDonald, S. Vasavanonda, C. A. Flentge, B. E. Green, L. Fino, C. H. Park, X.-P. Kong, N. E. Wideburg, A. Saldivar, L. Ruiz, W. M. Kati, H. L. Sham, T. Robins, K. D. Stewart, A. Hsu, J. J. Plattner, J. M. Leonard and D. W. Norbeck, *Proc. Natl. Acad. Sci. USA*, 1995, **92**, 2484.
3 D. J. Kempf, K. C. Marsh, L. Codacovi Fino, P. Bryant, A. Craig-Kennard, H. L. Sham, C. Zhao, S. Vasavanonda, W. E. Kohlbrenner, N. E. Wideburg, A. Saldivar, B. E. Green, T. Herrin and D. W. Norbeck, *Bioorg. Med. Chem.*, 1994, **2**, 847.
4 D. J. Kempf, T. J. Sowin, E. M. Doherty, S. M. Hannick, L. M. Codavoci, R. F. Henry, B. E. Green, S. G. Spanton and D. W. Norbeck, *J. Org. Chem.*, 1992, **57**, 5692.
5 T. L. Stuk, A. R. Haight, D. Scarpetti, M. S. Allen, J. A. Menzia, T. A. Robbins, S. I. Parekh, D. C. Langridge, J. J. Tien, R. J. Pariza and F. A. J. Kerdesky, *J. Org. Chem.*, 1994, **59**, 4040.
6 A. K. Ghosh, D. Shin and P. Mathivanan, *Chem. Commun.*, 1999, 1025.
7 F. Benedetti, S. Miertus, S. Norbedo, A. Tossi and P. Zlatoidsky, *J. Org. Chem.*, 1997, **62**, 9348.
8 J. M. Finan and Y. Kishy, *Tetrahedron Lett.*, 1982, **23**, 2719.
9 T. Ishizuka and T. Kunieda, *Tetrahedron Lett.*, 1987, **28**, 4185.
10 D. J. Ager, I. Prakash and D. R. Schaad, *Chem. Rev.*, 1996, **96**, 835.
11 R. K. Crossland and K. L. Servis, *J. Org. Chem.*, 1970, **35**, 3195.
12 A. Tossi, N. Antcheva, F. Benedetti, S. Norbedo, S. Miertus and D. Romeo, *Pept. Prot. Lett.*, 1999, **6**, 145; F. Benedetti, M. Magnan, S. Miertus, S. Norbedo, D. Parat and A. Tossi, *Bioorg. Med. Chem. Lett.*, 1999, **9**, 3027.

A remarkable Cr(III) organometallic compound formed by an unprecedented rearrangement of a formamidinate anion

Rodolphe Clérac,[a] F. Albert Cotton,*[a] Carlos A. Murillo*[ab] and Xiaoping Wang[a]

[a] *The Laboratory for Molecular Structure and Bonding, Department of Chemistry, Texas A&M University, PO Box 30012, College Station, TX 77842-3012, USA. E-mail: cotton@tamu.edu; murillo@tamu.edu*
[b] *Department of Chemistry, University of Costa Rica, Ciudad Universitaria, Costa Rica*

Received (in Irvine, CA, USA) 11th August 2000, Accepted 6th December 2000
First published as an Advance Article on the web

In addition to a quadruply bonded dichromium(II,II) compound of unusual structure, we have obtained a dinuclear, antiferromagnetically coupled, Cr^{III} complex [Cr_2(μ-OMe)$_2$(η^3-*N,C,N′*-H_2DpyF)$_2Cl_2$·MeOH, H_2DpyF = CH(NH-pyridyl)$_2$] containing a transformed formamidinate group in which the central carbon atom has changed from sp^2 to sp^3 hybridization and Cr–C bonds have been formed; details of the crystal structure of the organometallic compound are given here.

The use of formamidinate ligands of the type RNC(H)NR and ArNC(H)NAr to bridge M_2^{n+} dinuclear units (M = various transition metal atoms, n = 4, 5, and 6) has been intensively studied.[1] Typically, paddlewheel structures, **I**, have been obtained. More recently there has been wide interest in creating longer chains of metal atoms.[2] Thus we decided to use amidinate ligands with more than two N atom donors. One such ligand is the anion of *N,N′*-di(2-pyridyl)formamidine, HDpyF, **II**, where the two Ar groups are 2-pyridyl groups. In this way chains of three and four collinear chromium(II) atoms, **III**, were obtained.[3]

After we recently found that dimolybdenum compounds of the DpyF ligand have many coordination isomers in solution,[4] we have carried out the reaction of $CrCl_2$ with LiDpyF in THF in the molar ratio of 1:2. This reaction affords the dinuclear species of Cr_2^{4+} as an unsymmetrical yellow isomer of the type **IV** as the major product.[5] During the work-up process, the

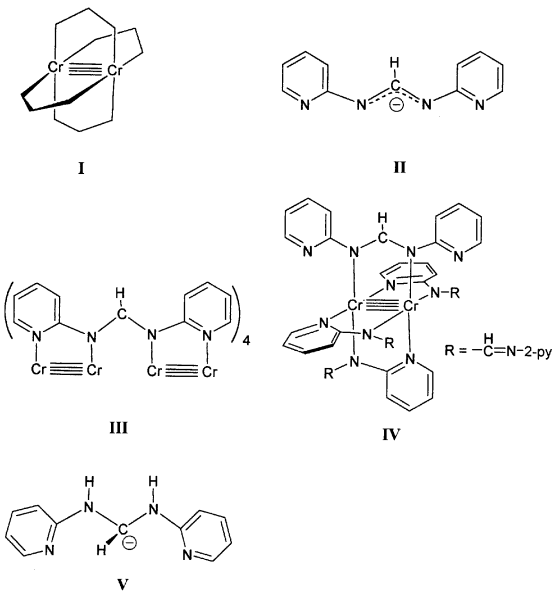

solvent from the reaction mixture was removed under vacuum and the solid residue, which also contained LiCl, was washed with methanol, a solvent in which **IV** is not significantly soluble but LiCl is. We noticed that upon the addition of very dry methanol, a deep red solution was produced above the solid **IV**. After filtration, the red methanol solution was layered with diethyl ether and red crystals of Cr_2(μ-OMe)$_2$(η^3-*N,C,N′*-H_2DpyF)$_2Cl_2$·MeOH were obtained in low yield.†

The structure‡ consists of two very similar but crystallographically independent molecules, one of which is shown in Fig. 1. It comprises an edge-sharing bioctahedral (ESBO) dichromium unit with two methoxy groups defining the shared edge. The Cr_2O_2 unit is planar in accordance with lying on a crystallographic inversion center. A chlorine atom on each chromium atom is *cis* to the methoxy groups. The other three coordination sites comprising a face of each octahedron are occupied by a carbon atom and two nitrogen atoms of a tridentate ligand derived from what was the usual form of the DpyF anion, **II**. The carbon atom is *trans* to the chlorine atom. The DpyF ligand has been transformed to the monoanion, **V**. Binding to the chromium atoms no longer occurs in the usual way, by bonds to the amidinate N atoms, but instead through the two pyridyl N atoms and the central C atom. Thus there are two fused five-membered rings with the N atoms *trans* to the methoxy groups. The methoxy bridges are but slightly asymmetric with Cr–O distances of 1.971(2) and 1.984(2) Å. They are very similar to those found in Cr^{III}–O(H)–Cr^{III} units of hydroxo-bridged amine complexes[6] and in some other compounds with Cr(μ-OMe)$_2$Cr cores[7] where they are in the narrow range of 1.95–1.99 Å. The Cr–N distances of 2.086(2) to 2.101(2) Å are also as expected.[8]

The Cr–C distances of 2.059(3) and 2.068(3) Å in the two nonequivalent molecules are within the normal range of 2.04–2.13 Å. The Cr–Cl distances of 2.4653(8) Å are more

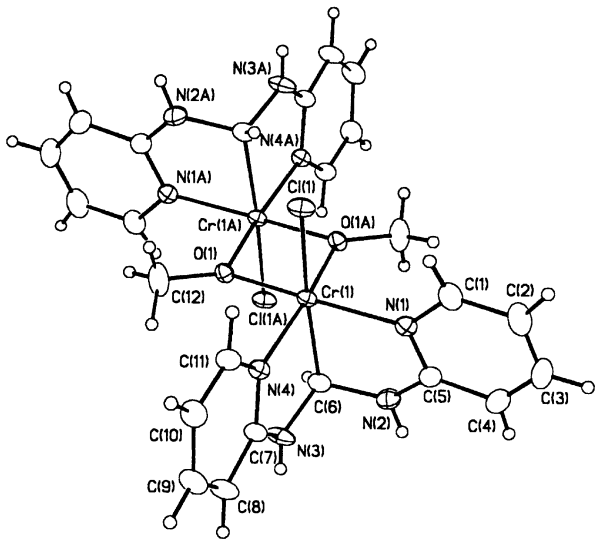

Fig. 1 Plot of one of the independent molecules in Cr_2(μ-OMe)$_2$(η^3-*N,C,N′*-H_2DpyF)$_2Cl_2$·MeOH. Hydrogen atoms refined during the X-ray diffraction study are shown as arbitrarily sized circles. Selected distances (Å) and angles (°) are Cr(1)···Cr(1A) 3.0751(8), Cr(1)–C(6) 2.059(3), C(6)–N(2) 1.444(4), C(6)–N(3) 1.455(4); N(2)–C(6)–N(3) 111.0(2), N(2)–C(6)–Cr(1) 108.8(2), N(3)–C(6)–Cr(1) 108.7(2), N(2)–C(6)–H(6) 105(2), N(3)–C(6)–H(6) 110(2).

DOI: 10.1039/b007813l

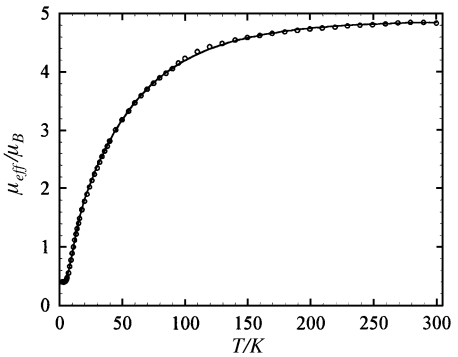

Fig. 2 Temperature dependence of the effective magnetic moment. The solid line is the best fit obtained with a dimer model of $S = 3/2$ magnetic spins (1% of an $S = 3/2$ paramagnetic impurity was taken into account to reflect the residual paramagnetism a low temperature).

difficult to compare with previous results because the presence of halide ions in six-coordinate Cr^{III} organometallic compounds is rare.[9] However, a comparison can be established with *fac*-Cl_3Cr(1,5-diamino-3-azapentane), a coordination compound which has three Cr–N distances varying from 2.08(1) to 2.11(1) Å and three Cr–Cl distances varying from 2.303(7) to 2.332(7) Å.[10] Clearly the Cr–Cl distances in the present case are significantly longer, by more than 0.13 to 0.16 Å. A large *trans* effect for carbon atoms in Cr^{III} organometallic compounds has previously been documented.[11]

All hydrogen atoms were found and refined. In the crystal there is extensive intermolecular hydrogen bonding involving pairs of nonequivalent molecules and also the interstitial methanol molecules. Thus, it is not surprising that the crystalline compound is stable towards exposure to oxygen and moisture.

The most remarkable feature of this compound is the transformation that occurs at the sp^2 methine C atom of the DpyF anion, **II**, whereby the hybridization is changed to sp^3 at the methanide C atom upon hydrogen atom capture by the inner N atoms giving the monoanion **V**. In **II**, the N–C(H)–N unit is typically planar with short C–N distances of 1.31–1.33 Å,[1,12] but in **V** those distances increase to 1.433(4)–1.455(4) Å. These are also *ca*. 0.1 Å longer than those of the corresponding N–$C_{pyridyl}$ bonds. Also consistent with the presence of a methanide group in **V** are the bond angles around the central C atom (including those involving the C–H bond) which are very close to those expected for a tetrahedral atom. Thus the internal consistency of all the structural data supports beyond any doubt the formulation given here.

To our knowledge this is an unprecedented transformation of a formamidinate group (although many other transformations are known[13]) with concomitant formation of a stable Cr(III) organometallic compound. Only one additional report exists of a transformation of an sp^2 C atom in a formamidinate to an sp^3 C atom. This was observed when dimerization of two formamidinate anions was induced by a tantalum compound giving the dianion PhNC(H)N(Ph)*C*(H)$(NPh)_2$,[13] but here the *C* atom has four bonds and is thus unable to bind to metal atoms.

Finally, magnetic measurements (Fig. 2)§ show antiferromagnetic coupling of the two chromium atoms through the methoxy bridges. The fitting of the data using an $S = 3/2$ dimer model[7,14] leads to an exchange interaction, J, of -18 K and a g value of 2.04. This is consistent with the magnetic behavior of other dinuclear Cr^{III}-organometallic compounds.[15]

We gratefully acknowledge the National Science Foundation for financial support and Dr. L. M. Daniels and Professor K. R. Dunbar for help with the crystallographic and magnetic measurements, respectively.

Notes and references

† For $Cr_2(\mu\text{-}OMe)_2(\eta^3\text{-}N,C,N'\text{-}H_2DpyF)_2Cl_2\cdot MeOH$: Anal. Calc. For $Cr_2C_{25}H_{32}N_8O_3Cl_2$: C, 44.98; H, 4.83; N, 16.79. Found: C, 44.52; H, 4.79; N, 16.51%. The process whereby the product is formed is not clear yet but a balanced equation can be written as follows:

$$2CrCl_2 + 4LiDpyF \xrightarrow[\Delta]{THF} \xrightarrow{4MeOH}$$

$$Cr_2(\mu\text{-}OMe)_2(\eta^3\text{-}N,C,N'\text{-}H_2DpyF)_2Cl_2 + 2LiCl + 2LiOMe + 2HDpyF$$

In three runs by two different people yields of 5–10% were obtained.

‡ *Crystal data*: $C_{25}H_{32}Cl_2Cr_2N_8O_3$, $M = 667.49$, monoclinic, space group $P2_1/c$, $a = 15.507(2)$, $b = 9.7562(6)$, $c = 19.920(2)$ Å, $\beta = 98.597(7)°$, $V = 2979.8(5)$ Å^3, $Z = 4$, $T = 213$ K, $\mu = 0.95$ mm^{-1}, 15663 measured/4711 independent reflections, R(int) = 0.056. The final $wR(F^2)$ were 0.093 ($I > 2\sigma$) and 0.098 (all). The positions of all H atoms were clearly indicated in the final difference Fourier maps. CCDC 182/1882. See http://www.rsc.org/suppdata/cc/b0/b007813l/ for crystallographic files in .cif format.

§ Magnetic susceptibility measurements were obtained with the use of a Quantum Design SQUID magnetometer MPMS-XL, from 1.8 to 300 K at 1000 G on a finely divided polycrystalline sample. Data were corrected for the sample holder and for the diamagnetic contributions estimated from Pascal's constants.[16]

1 (*a*) J. Barker and M. Kilner, *Coord. Chem. Rev.*, 1994, **133**, 219; (*b*) F. A. Cotton and R. A. Walton, *Multiple Bonds between Metal Atoms*, 2nd edn., Oxford University Press, 1993; (*c*) J. L. Eglin, C. Lin, T. Ren, L. Smith, R. J. Staples and D. O. Wipf, *Eur. J. Inorg. Chem.*, 1999, 2095 and references therein.

2 See for example: (*a*) R. Clérac, F. A. Cotton, L. M. Daniels, K. R. Dunbar, K. Kirschbaum, C. A. Murillo, A. A. Pinkerton, A. J. Schultz and X. Wang, *J. Am. Chem. Soc.*, 2000, **122**, 6226; (*b*) F. A. Cotton, L. M. Daniels and G. T. Jordan IV, *Chem. Commun.*, 1997, 421; (*c*) F. A. Cotton, L. M. Daniels, G. T. Jordan IV and C. A. Murillo, *J. Am. Chem. Soc.*, 1997, **119**, 10377; (*d*) F. A. Cotton, C. A. Murillo and X. Wang, *J. Chem. Soc., Dalton Trans.*, 1999, 3327; (*e*) F. A. Cotton, C. A. Murillo and X. Wang, *Inorg. Chem.*, 1999, **38**, 6294; (*f*) E.-C. Yang, M.-C. Cheng, M.-S. Tsai and S.-M. Peng, *J. Chem. Soc., Chem. Commun.*, 1994, 2377.

3 F. A. Cotton, L. M. Daniels, C. A. Murillo and X. Wang, *Chem. Commun.*, 1998, 39.

4 R. Clérac, F. A. Cotton, L. M. Daniels, K. R. Dunbar, C. A. Murillo and X. Wang, *Inorg. Chem.*, in print.

5 F. A. Cotton, C. A. Murillo and X. Wang, unpublished results.

6 L. F. Larkworthy, K. B. Nolan and P. O'Brien, in *Comprehensive Coordination Chemistry*, vol. 3, ed. G. Wilkinson, R. D. Guillard and J. A. McCleverty, Pergamon Press, Oxford, 1987, pp. 784–802.

7 See for example: (*a*) E. D. Estes, R. Scaringe, W. E. Hatfield and D. J. Hodgson, *Inorg. Chem.*, 1977, **16**, 1605; (*b*) H. R. Fisher, D. J. Hodgson and E. Pederson, *Inorg. Chem.*, 1984, **23**, 4755.

8 (*a*) M. J. Winter and S. Woodward, in *Comprehensive Organometallic Chemistry II*, vol. 5, ed. E. W. Abel, F. G. A. Stone and G. Wilkinson, Pergamon Press, Oxford, 1995; (*b*) S. W. Kirtley, in *Comprehensive Organometallic Chemistry*, vol. 3, ed. G. Wilkinson, F. G. A. Stone and E. W. Abel, Pergamon Press, Oxford, 1982.

9 M. D. Fryzuk, D. B. Leznoff, S. J. Rettig and V. G. Young, Jr., *J. Chem. Soc., Dalton Trans.*, 1999, 147.

10 A. D. Fowlie, D. A. House, W. T. Robison and S. S. Rumball, *J. Chem. Soc. A*, 1970, 803.

11 J. H. Espenson, *Acc. Chem. Res.*, 1992, **25**, 222.

12 (*a*) F. A. Cotton, C. A. Murillo and I. Pascual, *Inorg. Chem.*, 1999, **38**, 2182; (*b*) K. M. Carlson-Day, J. L. Eglin, R. L. Smith and R. J. Staples, *Inorg. Chem.*, 1999, **38**, 2216; (*c*) K. M. Carlson-Day, J. L. Eglin, C. Lin, L. T. Smith, R. J. Staples and D. O. Wipf, *Polyhedron*, 1999, **18**, 817; (*d*) T. Ren, *Coord. Chem. Rev.*, 1998, **175**, 43; (*e*) C. Lin, T. Ren, E. J. Valente and J. D. Zubkowski, *J. Chem. Soc., Dalton Trans.*, 1998, 571; (*f*) F. A. Cotton, L. M. Daniels, X. J. Feng, D. J. Maloney, J. H. Matonic and C. A. Murillo, *Inorg. Chim. Acta*, 1997, **256**, 291; (*g*) F. A. Cotton, J. H. Matonic and C. A. Murillo, *Inorg. Chim. Acta*, 1997, **264**, 61; (*h*) F. A. Cotton, L. M. Daniels, J. H. Matonic and C. A. Murillo, *Inorg. Chim. Acta*, 1997, **256**, 277; (*i*) A. Singhal and V. K. Jain, *Can. J. Chem.*, 1996, **74**, 2018; (*j*) F. A. Cotton, L. M. Daniels and C. A. Murillo, *Inorg. Chem.*, 1993, **32**, 2881; (*k*) F. A. Cotton and T. Ren, *J. Am. Chem. Soc.*, 1992, **114**, 2495; (*l*) J. L. Bear, C. L. Yao, R. S. Lifsey, J. D. Korp and K. M. Kadish, *Inorg. Chem.*, 1991, **30**, 336.

13 F. A. Cotton, L. M. Daniels, J. H. Matonic, X. Wang and C. A. Murillo, *Polyhedron*, 1997, **16**, 1177.

14 The following spin Hamiltonian was used: $H = -2JS_1S_2$, where J is the exchange parameter and S_1, S_2 are the magnetic spins of the Cr_2 unit ($S = 3/2$).

15 K. H. Theopold, *Acc. Chem. Res.*, 1990, **23**, 263.

16 *Theory and Applications of Molecular Paramagnetism*, ed. E. A. Boudreaux and L. N. Mulay, John Wiley and Sons, New York, 1976.

ChemComm

Preparation and determination of X-ray-crystal and NMR-solution structures of $\gamma^{2,3,4}$-peptides

Dieter Seebach,* Meinrad Brenner, Magnus Rueping, Bernd Schweizer and Bernhard Jaun

Laboratorium für Organische Chemie der Eidgenössischen Technischen Hochschule, ETH-Zentrum, Universitätstrasse 16, CH-8092 Zürich. E-mail: seebach@org.chem.ethz.ch; Fax: +41 1632 1144; Tel: +41 1632 2990

Received (in Cambridge, UK) 17th October 2000, Accepted 27th November 2000
First published as an Advance Article on the web 4th January 2001

(*R*,*R*,*R*)-γ-Amino acids with side chains in the 2-, 3-, and 4-positions, prepared by addition of acyloxazolidinones to a nitroolefin and hydrogenation, have been coupled to γ-tetra-, and γ-hexapeptides which are shown to form (*M*)-2.6_{14} helices in the crystal state and in MeOH solution.

While there is a lot of activity in the field of β-peptides, their homologs, the γ-peptides, have received much less attention, so far.[1–3] It has been discovered that γ-peptides form helical secondary structures in solution, detectable by NMR spectroscopy, with chains as short as four residues, and that homologation of L-α-amino acids to L-β- and L-γ-amino acids leads to peptides, folding to helices of alternating polarity and helicity (α: N ↦ C (*P*), β: N ↤ C (*M*), γ: N ↦ C (*P*)), and of increasing stability. The γ-peptides studied hitherto consisted of γ^4-residues (side chains at C(4))[1,2] or of $\gamma^{2,4}$-residues (two side chains, one at C(2) and one at C(4)),[2,3] rel. configuration *l* or *u*.† Inspection of models leads to the conclusion that $\gamma^{2,3,4}$-peptides of type **1**/**2** (Fig. 1), built of (*R*,*R*,*R*)-amino acid residues, should be able to form a 2.6_{14}-helix without steric interference of the side chains within the helical backbone.

The required γ-amino-acid building blocks were prepared stereoselectively by *Michael* addition of the modified *Evans* acyloxazolidinones **3** to nitrobutene (→ **4**),[4] reductive cleavage (→ **5**), hydrolysis, and *N*-Boc or *C*-OBn protection (→ **6**, **7**) (Scheme 1). Coupling of amino acids **6** and **7** gave dipeptide **8**, which after appropriate deprotection yielded dipeptide building blocks which were coupled to tetra- and hexapeptides **1** and **2**, respectively.

Of the protected γ-tetrapeptide **1** we obtained crystals suitable for X-ray structure analysis.‡ The quality and size of the samples allowed only for isotropic refinement and the determined structure is shown in Fig. 2a. The structure is characterized by two consecutive 14-membered H-bonded rings, one between the NH of residue 3 and the C=O of the Boc-protecting group and the other between the NH of residue 4 and the C=O of residue 1. Thus, both intramolecular H-bonds fit into the typical pattern of the 2.6_{14}-helix (H-bond between NH of residue *i* and C=O of residue (*i* − 3)). The carbamate NH of residue 1 and the amide NH of residue 2 are involved in intermolecular H-bonding to the ester C=O and to the C=O of residue 3 respectively, resulting in a two-dimensional H-bonded network. Residues 1 to 3 show the typical backbone conformation found in the (*M*)-2.6_{14} helix ((−)-*sc* for the C(2)–C(3) and the C(3)–C(4) ethane moieties). The side chains at C(2) and C(4) are in lateral positions, while the C(3)–Me bonds form angles of approximately 35° with the helix axis. The C-terminal residue has an extended backbone conformation ((±)-*ap* for the C(2)–C(3) and the C(3)–C(4) ethane moieties). Since the C-terminal ester group has no NH-group which could form an

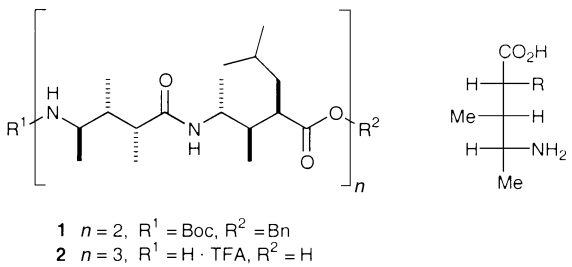

Fig. 1 $\gamma^{2,3,4}$-Tetra- and hexapeptide derivatives **1** and **2** used for the structure determinations and *Fischer* representation of the required amino acid building blocks.

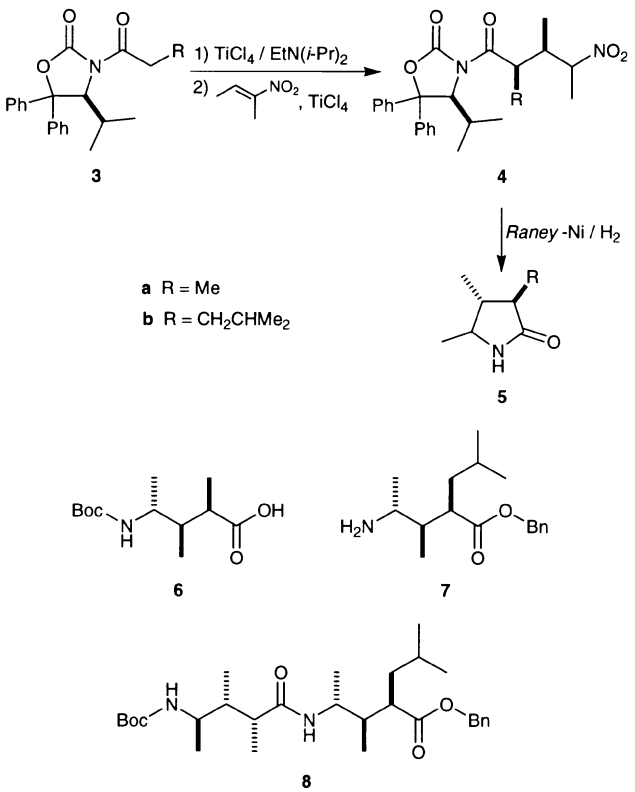

Scheme 1 Synthesis of the building blocks used for the preparation of peptides **1** and **2**. Hydrolysis of lactam **5a** in 6 M HCl and subsequent Boc-protection yielded amino acid **6**. The same procedure was applied with **5b**, followed by benzylation and Boc-deprotection to obtain **7**. Compounds **4** and **5** were used as mixtures of diastereoisomers, and separation was performed at the stage of the corresponding γ-amino acid. Coupling of amino acids **6** and **7** with HATU [*O*-(7-azabenzotriazol-1-yl)-*N*,*N*,*N*′,*N*′-tetramethyluronium hexafluorophosphate] to dipeptide **8** proceeded smoothly. Appropriate deprotected derivatives of **8** were fragment coupled to tetrapeptide **1** and hexapeptide **2** using EDC (1-ethyl-3-[3-(dimethylamino)propyl]carbodiimide·HCl)/DMAP as reagents.

DOI: 10.1039/b008377l

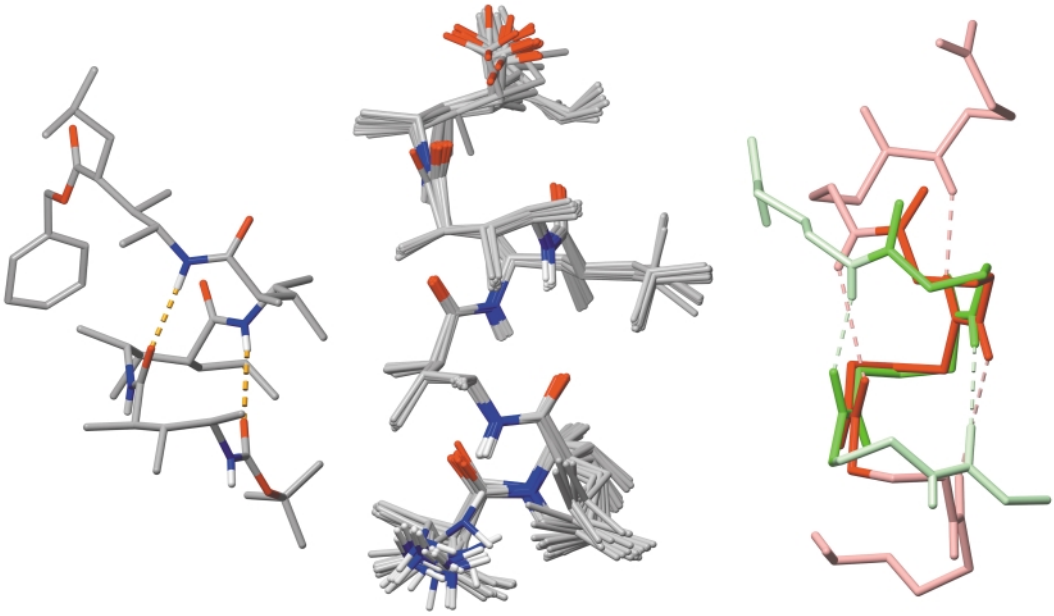

Fig. 2 (*M*)-2.6$_{14}$ Helical structures of γ-peptides **1** and **2**. a, Structure of γ-tetrapeptide **1** in the crystal state determined by X-ray structure analysis. b, Bundle of 20 conformers of hexapeptide **2** in MeOH obtained by simulated annealing calculations using restraints from NMR data. c, Superposition of the peptide backbones from the X-ray diffraction structure (blue) and NMR structure (red).

intramolecular H-bond the conformation of residue 4 may by determined by crystal packing factors.

The observation that γ-peptides with just four residues form a helical structure in the crystal state led us to examining γ-hexapeptide **2** by means of high-resolution NMR techniques. 2D-NMR Studies were carried out on a 500 MHz spectrometer with solutions in CD_3OH. We used DQF-COSY and TOCSY techniques to assign all ^1H resonances in their respective spin systems. HSQC and HMBC experiments led to the assignment of the amino acid sequence. ROESY spectra of **2** at different mixing times were acquired and NOEs were extracted from spectra with a mixing time of 300 ms.

The NOEs were classified according to their relative volume in three distance categories with the following upper bound distance limits: strong < 3.0, medium < 3.5 and weak < 4.5 Å. A total of 83 NOEs were used as distance restraints in simulated annealing, following the XPLOR protocol. This calculation yielded a set of 20 structures with low restraint violation and minimum energy (Fig. 2b). The structures show a well-defined left-handed helix with three 14-membered hydrogen-bonded rings from C=O of residue *i* to NH of residue *i* + 3. The helix has a pitch of *ca*. 5.0 Å and has *ca*. 2.6 residues per turn. An overlay of the backbone of one of the NMR-derived structures of **2** and the backbone from the crystal-structure of tetrapeptide **1** is shown in Fig. 2c. This superposition shows a good agreement between the central residues of the two molecules.

This study shows that γ^{2,3,4}-peptides constructed from (*R*,*R*,*R*)-trisubstituted γ-amino acid residues adopt well defined (*M*)-2.6$_{14}$-helices without steric interferences of the side chains, and allowed for the first time the characterization of this secondary structural motif by X-ray crystal structure analysis.

Notes and references

† Peptides built of γ^{2,4}-amino acids with rel. configuration *l* form 2.6$_{14}$ helical structures, while a tetrapeptide consisting of the corresponding *u* residues was found to form a turn motif.

‡ *Crystal data* for $C_{46}H_{80}N_4O_7$ **1**: M = 801.14, monoclinic, space group $P2_1$, a = 9.462(2), b = 20.472(6), c = 13.866(4) Å, β = 106.14(2)°, V = 2580.1(12) Å^3, Z = 2, D_c = 1.031 g cm^{-3}, μ(Cu-Kα) = 0.543 mm^{-1}, crystal size 0.30 × 0.20 × 0.02 mm. Data were collected on an Enraf Nonius CAD-4 diffractometer using graphite-monochromatized Cu-Kα radiation. A total of 4479 unique reflections (3.32 < 2Θ < 66.23°) were processed of which 1140 were considered significant with $I_{net} > 3\sigma(I_{net})$. Part of the structure was solved by direct method with SIR97,[5] the remaining non-H-atoms were found from a difference Fourier map. The non-H atoms were refined isotropically with SHELXL97.[6] The number of observed reflections did not allow anisotropic refinement. H-atoms were calculated at idealized positions and included in the structure factor calculation with fixed isotropic displacement parameters. Final residuals were R = 0.0898 and R_w = 0.1961 (GOF = 1.525) for 243 parameters. CCDC 182/1874.

The structure was determined by B. Schweizer of our X-ray service.

1 T. Hintermann, K. Gademann, B. Jaun and D. Seebach, *Helv. Chim. Acta*, 1998, **81**, 983.
2 S. Hanessian, X. Luo, R. Schaum and S. Michnick, *J. Am. Chem. Soc.*, 1998, **120**, 8569.
3 S. Hanessian, X. Luo and R. Schaum, *Tetrahedron Lett.*, 1999, **40**, 4925.
4 M. Brenner and D. Seebach, *Helv. Chim. Acta*, 1999, **82**, 2365.
5 A. Altomare, B. Carrozzini, G. L. Cascarano, C. Giacovazzo, A. Guagliardi, A. G. Moliterni and R. Rizzi, SIR97, A Package for Crystal Structure Solution by Direct Methods and Refinement, 1997, Istituto di Ricerca per lo Sviluppo di Metodologie Cristallografiche, CNR, Campus Universitario, Via Orabona 4, 70125 Bari, Italia.
6 G. M. Sheldrick, SHELXL97, Program for the Refinement of Crystal Structures, 1993, University of Göttingen, Germany.

A tandem radical approach to the ABCE-rings of the *Aspidosperma* and *Strychnos* alkaloids

Stephen T. Hilton,[a] Tim C. T. Ho,[b] Goran Pljevaljcic,[b] Marcus Schulte[b] and Keith Jones*[ab]

[a] *School of Chemical and Pharmaceutical Sciences, Kingston University, Penrhyn Road, Kingston-upon-Thames, Surrey, KT1 2EE UK*

[b] *Department of Chemistry, King's College London, Strand, London, WC2R 2LS UK*

Received (in Liverpool, UK) 16th October 2000, Accepted 18th December 2000
First published as an Advance Article on the web

Reaction of indole 19 *via* the derived aryl radical gives the tetracycle 20 in 43% yield. This compound contains the ABCE-rings of both *Aspidosperma* and *Strychnos* alkaloids.

The pentacyclic *Aspidosperma* alkaloids such as aspidospermidine **1** and the heptacyclic *Strychnos* alkaloids such as

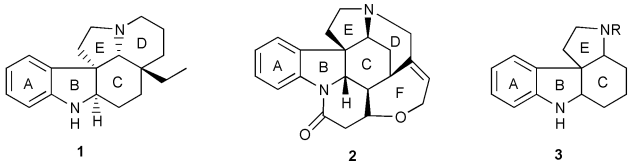

1 **2** **3**

strychnine **2** remain interesting targets for synthetic chemists owing to their chemical architecture and their biological activities.[1] The tetracyclic sub-structure **3**, consisting of the ABCE-rings of both these series of natural products represents the core of these molecules and functionalised examples of this tetracycle have featured in the total synthesis of both *Strychnos* and *Aspidosperma* alkaloids.[2] Efficient approaches to **3** carrying appropriate functionality would allow not only the synthesis of these natural products but also related non-natural products. Some years ago, we commenced a programme of research based on a strategy of radical cyclisation to form oxindoles (indolin-2-ones) followed by carbanion cyclisation to create the B- and C-rings.[3] Murphy has disclosed a tandem radical cyclisation route to this tetracyclic structure in which the B- and E-rings are created by an aryl radical addition to a double bond followed by internal trapping of the resultant radical by an azide.[4] This provides an alternative to the 'radical-polar crossover' chemistry developed by the same group and utilised in a synthesis of (±)-aspidospermidine **1**.[5] Parsons has also reported a conceptually different approach to the *Aspidosperma* skeleton using aryl radicals.[6] We now wish to disclose a new route to the ABCE–tetracycle using a novel tandem radical route to create the C- and E-rings.

The new disconnection sequence is shown in detail in Scheme 1. The key features of this plan involve the addition of radical **6** to the indole 3-position to create the E-ring. The α-amino radical generated in this step can then be captured in a 6-*exo* manner to create the C-ring. In order to generate radical **6**, it was decided to take advantage of the well-known ability of aryl radicals to abstract hydrogen atoms *via* a 6-membered ring transition state.[7] This analysis led back to the tertiary amide **7** as the substrate for a series of radical reaction steps under the usual conditions of tributyltin hydride (TBTH) and a suitable initiator.

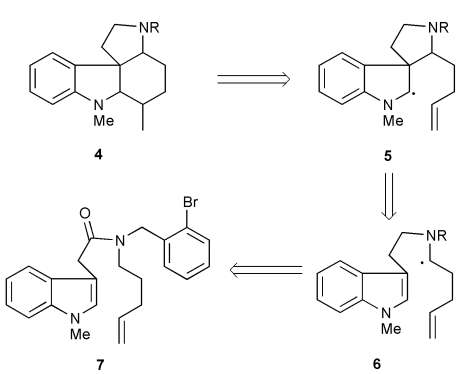

Scheme 1

The synthesis of radical precursor **7** commenced with indole-3-acetic acid **8** (Scheme 2). Treatment with sodium hydride and methyl iodide gave the *N*-methylindole-3-acetic acid **9** in 93% yield. Reaction of **9** with oxalyl chloride in THF at 0 °C gave the acid chloride **10** which was reacted immediately with 2-bromobenzylamine hydrochloride in the presence of excess diisopropylethylamine to give amide **11** in overall 86% yield. Alkylation of **11** with 5-bromopentene using potassium hydride as base in THF and tetrabutylammonium iodide as catalyst proceeded smoothly resulting in tertiary amide **7** in 73% yield. The ^{1}H NMR spectrum of **7** showed clearly the presence of two rotamers caused by restricted rotation about the amide bond. The minor rotamer possessed a singlet resonance at δ 4.72 assigned to the benzyl group in **7a** (Fig. 1) whilst the major rotamer displayed a singlet at δ 4.56 assigned to the benzyl group in **7b**. Integration of these signals revealed a ratio of 6:5 favouring **7b**. It is well known that the timescale for amide bond rotation to occur is considerably longer than the lifetime of radical intermediates which means that cyclisation of the translocated radical derived from major rotamer **7b** is unlikely.[8]

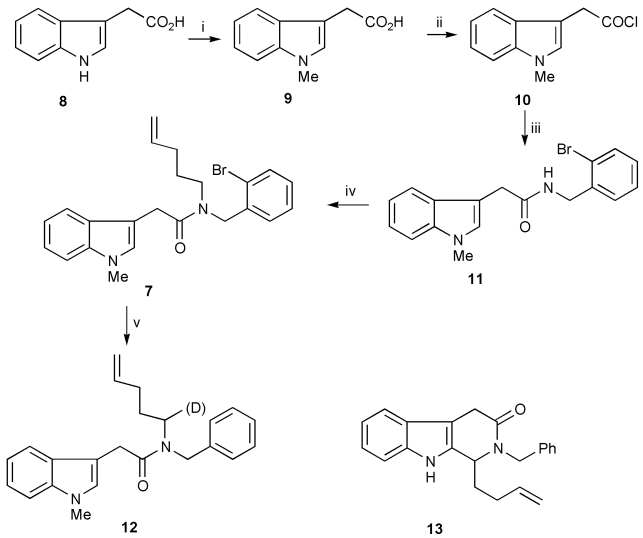

Scheme 2 *Reagents and conditions*: i, NaH, THF, 0 °C, then MeI warm to 20 °C, 12 h, 93%; ii, oxalyl chloride, THF, 0 °C to 20 °C, 20 h; iii, 2-bromobenzylamine hydrochloride, *N*,*N*-diisopropylethylamine, dichloromethane, 0 °C, 2 h, 86%; iv, KH, THF, 0 °C, then 5-bromopentene, tetrabutylammonium iodide, warm to 20 °C for 20 h, 73%, v, TBTH (or TBTD), AIBN, xylene, reflux, 10 h.

DOI: 10.1039/b008465o

With this problem in mind, reaction of **7** with TBTH at reflux in xylene under dilute conditions (0.02 M) was carried out. A complex mixture of products was obtained and to help determine the nature of the products, the reaction was repeated using tributyltin deuteride (TBTD). Extensive spectroscopy on the isolated products allowed assignment of the structure **12** (both rotamers) to the major product (50%) and structure **13** to one of the minor products (18%). Both products contained the intact alkene unit indicating that tetracycle formation had not occurred whilst the product **12** from reaction with TBTD contained deuterium adjacent to the nitrogen indicating successful radical translocation. Addition of the intermediate α-amido radical to the indole C-2 followed by rearomatisation to give **13** is not unreasonable given the results of Moody[9] and related work by Bowman[10] in other heteroaromatic systems. Product **12** could simply be arising from the major rotamer **7b** which cannot cyclise. However, the isolation of **13** indicates that the rather nucleophilic α-amido radical prefers to add to the indole ring at the C-2 position.

Following the precedent in the work of Fang,[11] we decided to introduce an electron-withdrawing group at the 2-position of indole **7** to encourage addition of the nucleophilic α-amido radical to C-3 of the indole. Reaction of 3-methylindole with triphenylphosphine–thiocyanogen has been reported to give 2-cyano-3-methylindole in 85% yield.[12] Treatment of **7** under these conditions led only to starting material. A variety of other studies to introduce a cyano-group at the 2-position were undertaken but eventually it was decided to develop a new route to the desired radical precursor (Scheme 2). The required secondary amine was prepared following the chemistry of Fukuyama and Bowman.[13] Reaction of 2-bromobenzylamine hydrochloride with sulfonyl chloride **14** gave sulfonamide **15** in 86% yield (Scheme 3). Alkylation using 5-bromopentene and caesium carbonate as base gave **16** in 93% yield and removal of the 2-nitrosulfonamide group was achieved in high yield using potassium carbonate and benzenethiol yielding secondary amine **17**. Reaction of **17** with the acid chloride **18** (derived from the acid[14] by reaction with oxalyl chloride in THF at 0 °C) gave the radical precursor **19** in 83% yield. Again the NMR revealed the presence of rotamers in a ratio of 1.1 : 1. Reaction of **19** with TBTH in refluxing 5-*tert*-butyl-*m*-xylene (*ca.* 200 °C) under syringe pump conditions gave some 50% of reduced product (**19** with Br = H) and 43% of **20** which had undergone the desired translocation–cyclisation–cyclisation sequence. Tetracycle **20** was isolated as a mixture of 4 diastereoisomers in a ratio of 8 : 3 : 2 : 1. The relative stereochemistry of the four diastereoisomers obtained cannot be assigned from their NMR spectra owing to the contiguous quaternary centres at the BC- and CE-ring junctions. Calculations show the *trans,trans* stereochemistry at these ring junctions to be of very high energy leaving 6 possible diastereoisomers, four of which possess the natural *cis* CE-ring junction stereochemistry and two of which possess the *trans* CE-ring junction stereochemistry. Although the transition state for the addition of the α-amido radical to the 3-position of the indole would seem to favour creation of a *cis* CE-ring junction, we cannot rule out the formation of isomers containing the *trans*-CE, *cis*-BC stereochemistry.

In summary, we have shown that the sequence of radical reaction steps shown in Scheme 1 is successful if a cyano group is present at the indole C-2. This short sequence to tetracycles such as **20** may provide a rapid entry into indole alkaloid natural products and related compounds and is under active investigation.

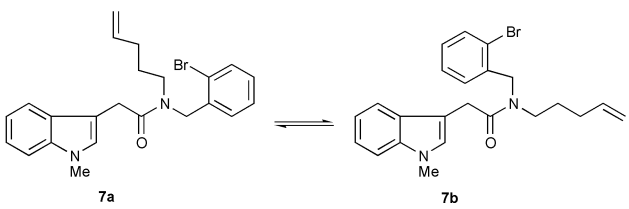

Fig. 1

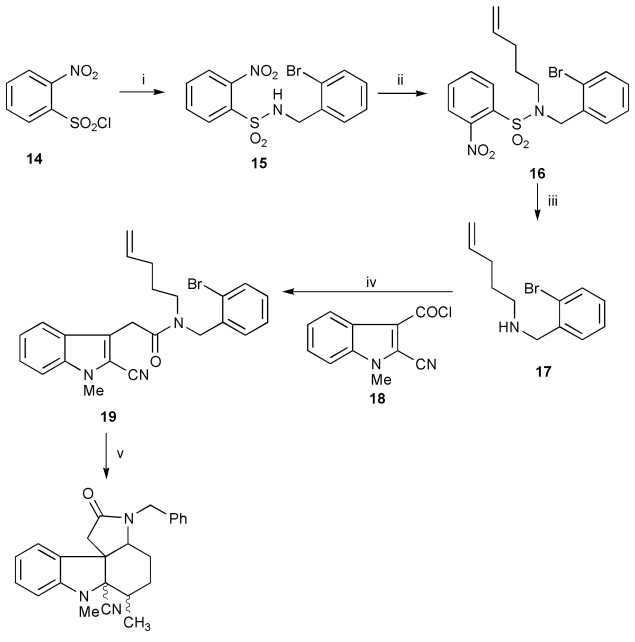

14 15 16 17 18 19 20

Scheme 3 *Reagents and conditions*: i, 2-bromobenzylamine hydrochloride, triethylamine, dichloromethane, 0 °C, 86%; ii, caesium carbonate, DMF, 80 °C, 30 min, then 5-bromopentene, 75 °C, 3 h, 93%; iii, potassium carbonate, PhSH, MeCN, 80 °C, 86%; iv, dichloromethane, diisopropylethylamine, 0 °C, 12 h, 83%; v, TBTH, 5-*tert*-butyl-*m*-xylene, syringe pump, reflux, 6 h, 43%.

We should like to acknowledge financial support from Kingston University (S. T. H.), King's College London (T. C. T. H.) and the EU (G. P. and M. S.).

Notes and references

1 J. E. Saxton, *Nat. Prod. Rep.*, 1996, **14**, 559.
2 J. Bonjoch and D. Sole, *Chem. Rev.*, 2000, **100**, 3455; V. H. Rawal and S. Iwasa, *J. Org. Chem.*, 1994, **59**, 2685; M. E. Kuehne and F. Xu, *J. Org. Chem.*, 1993, **58**, 7490; Y. Ban, T. Ohnuma, M. Nagia, Y. Sendo and T. Oishi, *Tetrahedron Lett.*, 1972, **13**, 5023; P. J. Laronze, J. Laronze-Fontaine, J. Lévy and J. LeMen, *Tetrahedron Lett.*, 1974, **15**, 491; S. J. Veenstra and W. N. Speckamp, *J. Am. Chem. Soc.*, 1981, **103**, 4645.
3 C. McCarthy and K. Jones, *J. Chem. Soc., Chem. Commun.*, 1989, 1717.
4 M. Kizil, B. Patro, O. Callaghan, J. A. Murphy, M. B. Hursthouse and D. Hibbs, *J. Org. Chem.*, 1999, **64**, 7856.
5 O. Callaghan, C. Lampard, A. R. Kennedy and J. A. Murphy, *J. Chem. Soc., Perkin Trans. 1*, 1999, 995.
6 P. J. Parsons, C. S. Penkett, M. C. Cramp, R. I. West, J. Warrington and M. C. Saraiva, *Synlett*, 1995, 507.
7 A. Fiumana and K. Jones, *Tetrahedron Lett.*, 2000, **41**, 4209; D. P. Curran and J. Y. Xu, *J. Am. Chem. Soc.*, 1996, **118**, 3142; A. L. J. Beckwith and J. M. D. Storey, *J. Chem. Soc., Chem. Commun.*, 1995, 977.
8 O. M. Musa, J. H. Horner and M. Newcomb, *J. Org. Chem.*, 1999, **64**, 1022; K. Jones and C. McCarthy, *Tetrahedron Lett.*, 1989, **30**, 2657.
9 C. J. Moody and C. L. Norton, *J. Chem. Soc., Perkin Trans. 1*, 1997, 2639.
10 F. Aldabbagh, W. R. Bowman, E. Mann and A. M. Z. Slawin, *Tetrahedron*, 1999, **55**, 8111.
11 C. C. Yang, H. T. Chang and J. Fang, *J. Org. Chem.*, 1993, **58**, 3100.
12 Y. Tamura, M. Adachi, T. Kawasaki, H. Yasuda and Y. Kita, *J. Chem. Soc., Perkin Trans. 1*, 1980, 1132.
13 T. Fukuyama, C.-K. Jow and M. Cheung, *Tetrahedron Lett.*, 1995, **36**, 6373; W. R. Bowman and D. R. Coghlan, *Tetrahedron*, 1997, **53**, 15 787.
14 S. T. Hilton, T. C. T. Ho, G. Pljevaljcic and K. Jones, *Org. Lett.*, 2000, **2**, 2639.

Heterobimetallic intermediates in alkene insertion reactions into a Pd–acetyl bond†

Pierre Braunstein,[a] Jérôme Durand,[a] Michael Knorr[ab] and Carsten Strohmann[c]

[a] *Laboratoire de Chimie de Coordination (UMR 7513 CNRS), Institut Le Bel, Université Louis Pasteur, 4 rue Blaise Pascal, F-67070 Strasbourg, France. E-mail: braunst@chimie.u-strasbg.fr*
[b] *Laboratoire de Materiaux Moléculaires et Interfaces, Faculté des Sciences et Techniques, Université de Franche-Comté, 16 route de Gray, F-25030 Besançon, France. E-mail: michael.knorr@univ-fcomte.fr*
[c] *Institut für Anorganische Chemie, Universität Würzburg, Am Hubland, D-97074 Würzburg, Germany*

Received (in Cambridge, UK) 5th September 2000, Accepted 12th December 2000
First published as an Advance Article on the web

The reactivity of diphosphine-bridged heterobimetallic Fe–Pd alkyl complexes was evaluated for the insertion of CO, isonitriles, ethylene, methyl acrylate and norbornadienes and the crystal structures of the precursor alkyl complex, the iminoacyl derivative and the five-membered ring complex resulting from ethylene insertion into the palladium–acyl bond are reported.

The insertion of small molecules such as CO, isonitriles, olefins and alkynes into palladium–carbon bonds represents reactions of fundamental importance for stoichiometric organic synthesis and industrial catalysis.[1] An example of the latter is the alternating copolymerisation of CO and olefins, which has triggered considerable research on alkene insertion into the palladium–acyl bond.[1,2] Whereas previous studies have been concerned with the influence of the stereoelectronic properties of the (usually chelating) ligand bonded to the Pd centre on this chemistry, we present here a different approach aimed at evaluating the influence of a metal adjacent to the reactive Pd on its reactivity, with the hope that cooperativity effects may lead to beneficial bimetallic effects.[3]

In the alkyl complexes [$(OC)_4\overline{Fe(\mu\text{-dppx})}PdCl(Me)$] [**1a**, dppx = $Ph_2PNHPPh_2$ (dppa); **1b**, dppx = $Ph_2PCH_2PPh_2$ (dppm)], prepared by reaction of [$Fe(CO)_4$(dppx-*P*)] with [PdCl(Me)(cod)], the methyl ligand is *trans* to the formally dative Fe→Pd bond, both in solution, as deduced from the small $^3J(PH)_{cis}$ coupling constant (< 4 Hz) with the Pd-bound P atom, and in the solid state, as established by X-ray diffraction for **1b** (Scheme 1, Fig. 1).‡§

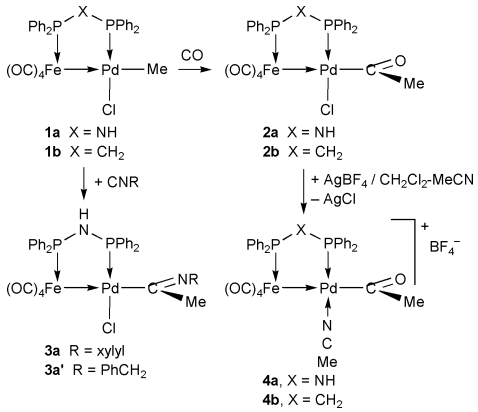

Scheme 1

These complexes react with CO under atmospheric pressure, more rapidly (3 h) in the case of **1b** because of its higher solubility, to form **2a**,**b**. Quantitative carbonylation of **1a** was achieved in CH_2Cl_2 in < 1 h under 20 atm CO. The *trans* arrangement of the acetyl ligand and the metal–metal bond suggested by the spectroscopic data is retained in the solid state, as shown by comparison with the spectroscopic data for the corresponding iminoacyl complexes **3a**,**a′** which were prepared by instantaneous reaction of **1a** with a stoichiometric amount of (xylyl)N≡C or $PhCH_2N{\equiv}C$, respectively, and characterised by X-ray diffraction in the case of **3a** (Fig. 2).‡§ As expected, the iminoacyl ligand is almost orthogonal to the palladium coordination plane.[4]

Since **2a** did not react with ethylene (at 1 atm), we turned our atttention to more electrophilic, cationic systems and prepared complex **4b** by chloride abstraction in CH_2Cl_2 in the presence of MeCN (Scheme 1). Interestingly, this reaction did not lead to CO deinsertion, a reaction often observed with Pd(II) acyl complexes. Complexes **4a**,**b** are more readily prepared by

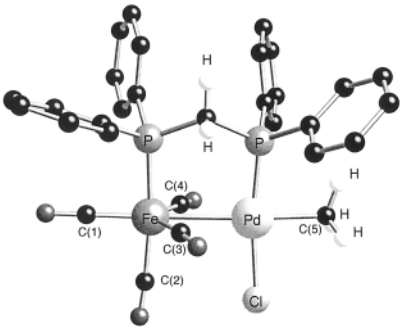

Fig. 1 View of the crystal structure of **1b**. Selected bond lengths (Å) and angles (°): Fe–Pd 2.8408(9), Pd–P(2) 2.2098(14), Pd–C(5) 2.066(6), Pd–Cl 2.361(2), Fe–P(1) 2.256(2), Fe–C(1) 1.761(7), Fe–C(2) 1.897(9), Fe–C(3) 1.799(8), Fe–C(4) 1.869(8); Cl–Pd–Fe 94.10(5), Cl–Pd–C(5) 87.4(2), P(2)–Pd–C(5) 85.2(2), P(2)–Pd–Cl 172.42(6), C(5)–Pd–Fe 174.3(2), Pd–Fe–P(1) 92.35(4), Fe–Pd–P(2) 93.40(4), C(2)–Fe–Pd 93.5(2).

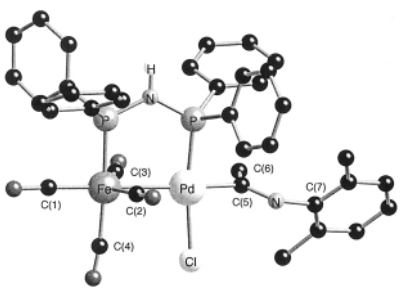

Fig. 2 View of the crystal structure of **3a**. Selected bond lengths (Å) and angles (°): Fe–Pd 2.7356(12), Pd–P(2) 2.274(2), Pd–C(5) 1.978(2), Pd–Cl(1) 2.402(2), Fe–P(1) 2.271(2), Fe–C(1) 1.758(8), Fe–C(2) 1.785(9), Fe–C(3) 1.795(10), Fe–C(4) 1.806(10), C(5)–N(1) 1.319(8); Cl(1)–Pd–C(5) 84.0(2), P(2)–Pd–C(5) 90.8(2), Pd–C(5)–C(6) 116.4(5), Pd–C(5)–N(1) 124.6(5), C(5)–Pd–Fe 164.4(2), C(5)–N(1)–C(7) 127.0(6), Pd–Fe–P(1) 91.86(6), Fe–Pd–P(2) 91.27(5), Cl(1)–Pd–P(2) 171.75(6).

† Electronic supplementary information (ESI) available: Experimental. See http://www.rsc.org/suppdata/cc/b0/b007171o/

DOI: 10.1039/b007171o

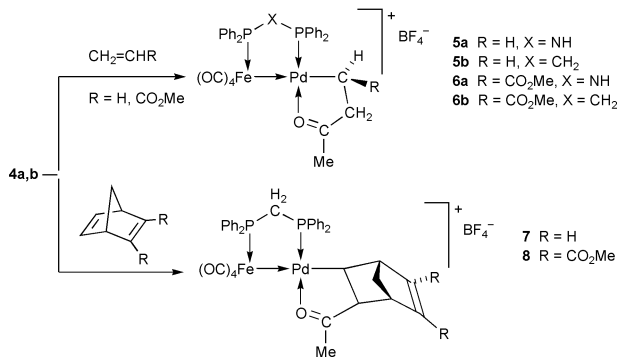

Scheme 2

halide abstraction from **1a**,**b** using $AgBF_4$ in CH_2Cl_2–MeCN, which generates $[(OC)_4Fe(\mu\text{-dppx})Pd(Me)(NCMe)]^+$, followed by instantaneous *in situ* reaction with CO. Complexes **4a**,**b** were indeed more reactive than **2a**,**b** since ethylene insertion into the Pd–acetyl bond occurred under atmospheric pressure to afford after *ca.* 15 h the stable complexes **5a**,**b** in quantitative spectroscopic yields (Scheme 2).‡ The latter represent rare examples of isolable insertion products of an unstrained alkene into a Pd–acyl bond.[5]

IR spectra show an absorption at 1634 cm^{-1} (**5a**) and 1633 cm^{-1} (**5b**) for the acetyl carbonyl coordinated to Pd. The crystal structure of **5a** (Fig. 3)§ established that the σ-bonded carbon atom is *trans* to the metal–metal bond. The BF_4^- counter ion weakly interacts with the N–H proton [d(N···F) = 3.105 Å]. To the best of our knowledge, there are only two precedents for the structural characterisation of a $-CH_2CH_2C(O)Me$ ligand, both in mononuclear Pd complexes.[5]

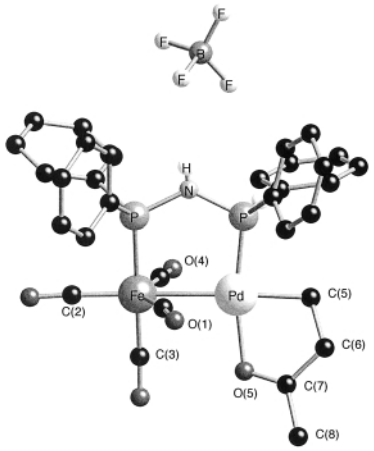

Fig. 3 View of the crystal structure of **5a**. Selected bond lengths (Å) and angles (°): Fe–Pd 2.7208(9), Pd–P(2) 2.1861(14), Pd–C(5) 2.054(6), Pd–O(5) 2.130(4), Fe–P(1) 2.240(2), Fe–C(1) 1.802(6), Fe–C(2) 1.791(7), Fe–C(3) 1.786(6), Fe–C(4) 1.806(6), C(7)–O(5) 1.256(8); O(5)–Pd–Fe 96.13(12), O(5)–Pd–C(5) 81.5(2), P(2)–Pd–C(5) 87.4(2), Pd–C(5)–C(6) 105.7(4), Pd–C(5)–N(1) 124.6(5), C(5)–Pd–Fe 172.5(2), Pd–O(5)–C(7) 112.7(4), Pd–Fe–P(1) 91.12(5), Fe–Pd–P(2) 95.48(5), O(5)–Pd–P(2) 167.93(12), C(6)–C(7)–O(5) 119.0(5), C(3)–Fe–Pd 88.9(2).

The stable methyl acrylate insertion products **6a**,**b** were isolated in *ca.* 90% yield after stirring **4a**,**b** for 18 h in the presence of 10 equiv. of methyl acrylate (Scheme 2). Insertion of norbornadiene or dimethyl norbornadiene-2,3-dicarboxylate into the Pd–C bond of **4b** occurred within *ca.* 30 min with complete regio- and stereo-selectivity to afford yellow **7** or orange **8**, respectively. The ^1H NMR data of **8** unambiguously indicate that insertion across the *exo*-face of the sterically less hindered CH=CH double bond is preferred over that of the more 'activated' $MeO_2C–C=C–CO_2Me$ double bond.

In order to mimic the next step in the alternating CO/olefin insertion chemistry, **5a**,**b** were reacted with CO under atmospheric pressure and the six-membered chelate complexes **9a**,**b** were obtained after *ca.* 4 h [eqn. (1)].

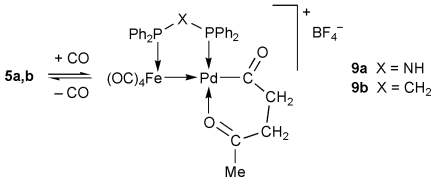

(1)

This reaction is reversible since **5a**,**b** are regenerated under reduced pressure. The lower reactivity of **5a**,**b** compared to $[(OC)_4Fe(\mu\text{-dppa})Pd(Me)(NCMe)]^+$ is most likely due to the presence of a chelating ligand at Pd, suggesting that opening of the dative ketone→Pd bond is necessary for CO insertion into the Pd–CH_2 bond to proceed. The reaction leading to **9a** is indeed much faster in the presence of a few drops of MeCN.

The bimetallic templates around which various C–C coupling reactions have been performed in this work do not appear, at the moment, to be more reactive than mononuclear cationic Pd(II) complexes reported recently.[5b] However, they have allowed the complete characterization of key intermediates, including in the chemistry of functional monomers.

We thank Elf-Atochem and Elf-Aquitaine, the Centre National de la Recherche Scientifique, the Ministère de l' Education Nationale, de la Recherche et de la Technologie and the COST D-12 programme of the European Commission (DG-XII) for financial support.

Notes and references

‡ The dppm complexes are generally more soluble than their dppa analogs and therefore better amenable to NMR studies. Selected spectroscopic data (all ^1H, $^{13}C\{^1H\}$ and $^{31}P\{^1H\}$ NMR spectra were recorded in $CDCl_3$ at 298 K) are provided as ESI.†

§ *Crystal data*: **1b**: $C_{30}H_{25}ClFeO_4P_2Pd$, M_w = 709.14, monoclinic, space group $P2_1/c$, a = 10.931(2), b = 12.0774(15), c = 22.688(3) Å, β = 98.48(3), V = 2962.5(7) Å^3, Z = 4, D_c = 1.590 g cm^{-3}, μ(Mo-Kα) = 1.328 mm^{-1}, 24 209 reflections collected, indep. reflections 5811 (R_{int} = 0.0549), GOF 1.110; final R, R_w indices [$I > 2\sigma(I)$] 0.0599 and 0.1677 for 353 parameters.

3a: $C_{38}H_{33}ClFeN_2O_4P_2Pd{\bullet}0.5CHCl_3$, M_w = 900.99, monoclinic, space group $C2/c$, a = 39.920(8), b = 11.851(2), c = 16.940(3) Å, β = 105.60(3), V = 7719.0(24) Å^3, Z = 8, D_c = 1.551 g cm^{-3}, μ(Mo-Kα) = 1.140 mm^{-1}, 24 525 reflections collected, 6796 indep. reflections (R_{int} = 0.0867), GOF 1.042; final R, R_w indices [$I > 2\sigma(I)$] 0.0574 and 0.1241 for 448 parameters.

5a: $C_{32}H_{28}BF_4FeNO_5P_2Pd{\bullet}CH_2Cl_2$, M_w = 902.52, monoclinic, space group $P2_1/n$, a = 12.468(2), b = 14.540(3), c = 20.969(4) Å, β = 103.40.3, V = 3697.9(12) Å^3, Z = 4, D_c = 1.623 g cm^{-3}, μ(Mo-Kα) = 1.170 mm^{-1}, 29 287 reflections collected, 7202 indep. reflections (R_{int} = 0.0607), GOF 1.001; final R, R_w indices [$I > 2\sigma(I)$] 0.0573 and 0.1404 for 457 parameters.

CCDC 182/1872. See http://www.rsc.org/suppdata/cc/b0/b007171o/ for crystallographic files in .cif format.

1 Recent reviews: E. Drent and P. H. M. Budzelaar, *Chem. Rev.*, 1996, **96**, 663; C. J. Elsevier, *Coord. Chem. Rev.*, 1999, **185–186**, 809; A. Yamamoto, *J. Chem. Soc., Dalton Trans.*, 1999, 1027; G. J. P. Britovsek, V. C. Gibson and D. F. Wass, *Angew. Chem., Int. Ed.*, 1999, **38**, 428; K. Nozaki and T. Hiyama, *J. Organomet. Chem.*, 1999, **576**, 248; B. Milani and G. Mestroni, *Comments Inorg. Chem.*, 1999, **20**, 301; S. D. Ittel, L. K. Johnson and M. Brookhart, *Chem. Rev.*, 2000, **100**, 1169 and references therein.

2 P. Braunstein, M. Knorr and T. Stährfeldt, *J. Chem. Soc., Chem. Commun.*, 1994, 1913; B. A. Markies, D. Kruis, M. H. P. Rietveld, K. A. N. Verkerk, J. Boersma, H. Kooijman, M. T. Lakin, A. L. Spek and G. van Koten, *J. Am. Chem. Soc.*, 1995, **117**, 5263; W. Keim and H. Maas, *J. Organomet. Chem.*, 1996, **514**, 271; M. Sperrle, A. Aeby, G. Consiglio and A. Pfaltz, *Helv. Chim. Acta*, 1996, **79**, 1387; D.-J. Liaw and B.-F. Lay, *Polym. J.*, 1996, **28**, 266; E. Lindner, M. Schmid, P. Wegner, C. Nachtigal, M. Steimann and R. Fawzi, *Inorg. Chim. Acta*, 1999, **296**, 103.

3 P. Braunstein and J. Rosé, in *Metal Clusters in Chemistry*, ed. P. Braunstein, L. A. Oro and P. R. Raithby, Wiley-VCH, Weinheim, 1999, vol. 2, pp. 616–677.

4 K. Onitsuka, M. Segawa and S. Takahashi, *Organometallics*, 1998, **17**, 4335.

5 (*a*) M. J. Green, G. J. P. Britovsek, K. J. Cavell, B. W. Skelton and A. H. White, *Chem. Commun.*, 1996, 1563; (*b*) P. Braunstein, C. Frison and X. Morise, *Angew. Chem., Int. Ed.*, 2000, **39**, 2867.

Reversible α-elimination in the conversion of N–CH_3 to N–CH=Ir by double C–H activation

Dong-Heon Lee,*[a] Junyi Chen,[b] Jack W. Faller*[b] and Robert H. Crabtree*[b]

[a] *Department of Chemistry, Chonbuk National University, Chonju, 561-756, Korea. E-mail: dhl@moak.chonbuk.ac.kr*
[b] *Yale Chemistry Laboratory, 225 Prospect St., New Haven, CT 06520-8107, USA. E-mail: jack.faller@yale.edu; robert.crabtree@yale.edu*

Received (in Irvine, CA, USA) 18th September 2000, Accepted 20th November 2000
First published as an Advance Article on the web

2-Dimethylaminopyridine (pyNMe$_2$; py = 2-pyridyl) reacts with [$H_2Ir(OCMe_2)_2L_2$]$^+$ (L = PPh_3) to give a cyclic carbene complex [H_2Ir(=CHN(Me)py)L_2]$^+$ *via* an oxidative addition, reversible α-elimination sequence.

The conceptual conversion of eqn. (1) is highly endothermic (ΔH = 111 kcal mol^{-1}, triplet; 119 kcal mol^{-1}, singlet). If the carbene is sufficiently stabilized by a metal fragment and by π-donor heteroatom substitution in the α-position (Fischer carbene), however, such a conversion becomes thermodynamically allowed. For example, both alkene to carbene[1–3] and THF to carbene[4,5] rearrangements of this sort are known, but elevated temperatures may be required for satisfactory rates.[4–5]

$$CH_4 \rightarrow :CH_2 + H_2 \quad (1)$$

We now report a room-temperature route for the title reaction [eqn. (2)] *via* the activation of two geminal C–H bonds and liberation of H_2.

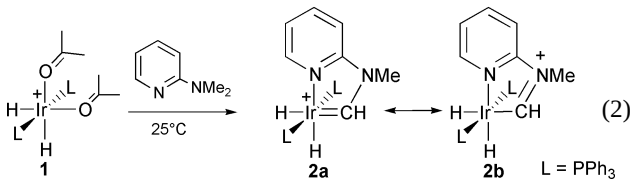

(2)

We find that 2-dimethylaminopyridine (pyNMe$_2$, 1 equiv.) reacts with [$IrH_2(OCMe_2)_2L_2$]BF_4 **1** in CH_2Cl_2 at 25 °C to give the cyclic heteroatom-stabilized carbene complex **2** (25 °C, 15 min, 78%), by a net reaction that resembles eqn. (1).† The identity of the product follows from the ^{1}H NMR spectrum, in particular the appearance of a low-field singlet of intensity 1H at δ 11.71 assigned to the CH=Ir proton. The NMe group of intensity 3H appears as a singlet at δ 3.50. The two inequivalent hydrides (1H each) resonate at δ −9.98 and δ −17.78 as triplets of doublets ($^2J_{PH}$ 16, $^2J_{HH'}$ 4 Hz), indicating each is *cis* to the two phosphines. The ^{13}C NMR shows a low-field resonance at δ 155.9 characteristic of Fischer carbenes.

The reaction is also possible for 2-diethylaminopyridine (pyNEt$_2$, 1 equiv.) to give the analogous product **3** (25 °C, 15 min, 80%), shown in eqn. (3). The spectral data for **3** is similar

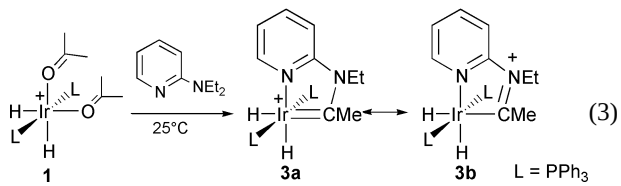

(3)

to that for **2**, in particular, the ^{1}H NMR spectrum shows high-field resonances at δ −10.80 and δ −17.92, characteristic of terminal iridium(III) hydrides. The two hydrides ($^2J_{PH}$ 17 Hz, $^2J_{HH'}$ 4 Hz) are mutually coupled and coupled to the PPh_3 ligands. The formation of **3** was also confirmed by a crystal structure determination (Fig. 1).‡ The Ir–C distance of 2.018 Å is consistent with predominant single bond character while the C–N bond distance of 1.322 Å indicates some multiple bond character as expected from the resonance form **3b** generally preferred by Fischer carbenes. Even with β-hydrogen atoms available, we see only the α-elimination product **3**. Preferred α- *vs.* β-elimination in metal alkyls has been reported.[6,7]

The evidence discussed below suggests formation of **2** proceeds by initial C–H bond activation, perhaps to form an intermediate H_2 complex **5**. Loss of H_2 leads to an alkyl, **6**, which then rearranges to the observed carbene **2,** by α-elimination (Scheme 1).

Formation of an agostic C–H···M bond is typical in complexes related to **1**. For example, the known 2,6-di-

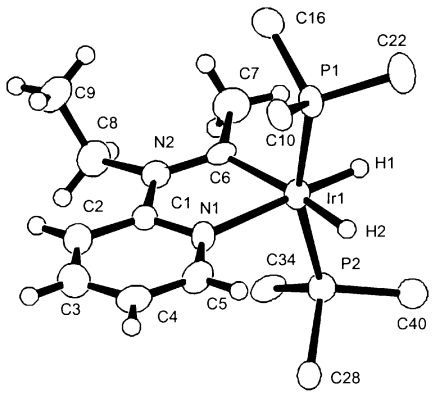

Fig. 1 An ORTEP view of the cation of [$Ir(PPh_3)_2$(pyNEtC-MeH_2]BF_4·CH_2Cl_2 **3**. Selected bond lengths (Å): Ir(1)–C(6) 2.018(5), Ir(1)–N(1) 2.142(4), N(2)–C(1) 1.410(6), N(2)–C(6), 1.332(7). Only the *ipso* carbons of PPh_3 are shown for clarity. The ligand H atoms are in calculated positions. The hydrides were refined with Ir(1)–H(1) 1.43(5) Å and Ir(1)–H(2) 1.47(5) Å, no doubt shortened by systematic error.

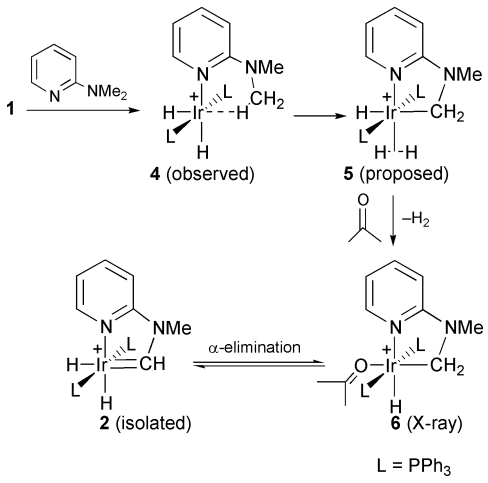

Scheme 1

phenylpyridine species **7**,[8] is fluxional [eqn. (4)] *via* a pathway analogous to that of Scheme 1. To probe the formation of a

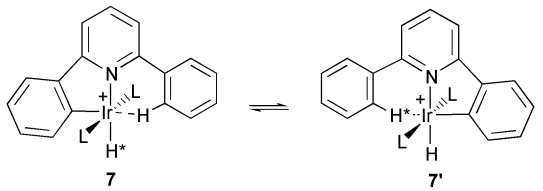

(4)

possible agostic C–H···M intermediate **4** in the present case, we treated **1** in CD_2Cl_2 with $pyNMe_2$ at low temperature and monitored the reaction by ^1H NMR. At −80 °C, a new species, **8**, is seen that is too reactive to isolate [eqn. (5)]. After 40 min

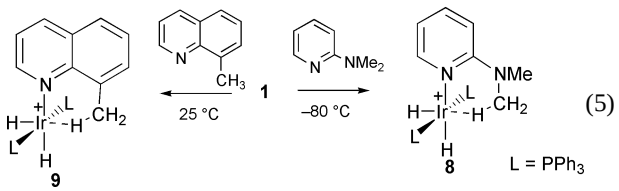

(5)

at 0 °C, it converts to **2**. Comparison of **8** with the fully characterized, stable material **9**, made *via* the route of eqn. (5),[9] shows very close ^1H NMR spectral similarities, suggesting **8** has the agostic structure, **4**, shown in Scheme 1. For example, the inequivalent hydrides resonate as a pair of signals (**8**, δ −20.69, δ −29.84; **9**, δ −19.20, δ −28.60) coupled both to two *cis* phosphines (**8**, $^2J_{PH}$ 17 Hz; **9**, $^2J_{PH}$ 15 Hz) and to each other (**8**, $^2J_{HH'}$ 7 Hz; **9**, $^2J_{HH'}$ 8 Hz).

Net loss of H_2 occurs and free H_2 was detected (δ 4.2) in the ^1H NMR spectrum of the reaction mixture. After loss of H_2 to generate a vacant site *cis* to the newly formed iridium alkyl, an α-elimination gives the final product.

Reversible α-elimination is rare,[6] but remarkably, this process is facile in this system. Dissolving the carbene **2** in acetone rapidly gives **6** by reversal of the α-elimination step. The Ir–H of the product **6** resonates as a triplet at δ −16.14 ($^2J_{PH}$ 14 Hz). This colorless alkyl complex was crystallized from acetone–diethyl ether and characterized by a crystal structure (Fig. 2). The equilibration of **2** and **6** was further probed by ^1H NMR. The colorless alkyl complex **6** dissolved in fresh CD_2Cl_2 at 25 °C with loss of acetone to give the yellow carbene **2** within seconds. In a typical case, **6**:**2** occur as a 1:1 ratio (integration of the hydride peaks). Incremental addition of acetone to the solution then led to displacement of the equilibrium in favor of **6**. For example, when 2 and 3 equivalents of acetone were added, the mole ratio of **6**:**2** became 2:1 and 3.3:1, respectively.

Several factors may make the rearrangement of the agostic species (**8**) to the carbene (**2**) thermodynamically favorable, in contrast with the highly endothermic base case of eqn. (1). The metal complexation stabilizes the carbene but this is not sufficient on its own, as shown by the failure of the agostic 8-methylquinoline species **9** to convert to the corresponding carbene, a species that is as yet unknown. Heteroatom stabilization by the adjacent amino group is clearly an important stabilizing factor. In addition, carbene **2** can be considered as a metallacycle with 10 π-electrons, which could in principle benefit from aromatic stabilization.

In summary, we have a rare double C–H activation route that provides a mild and fast synthetic method to generate chelating Fischer carbene complexes.

We thank the NSF (R. H. C, J. W. F), the DOE (J. C.), and the Korean Research Foundation (D.-H. L., grant KRF-2000-015-DP0305) for funding.

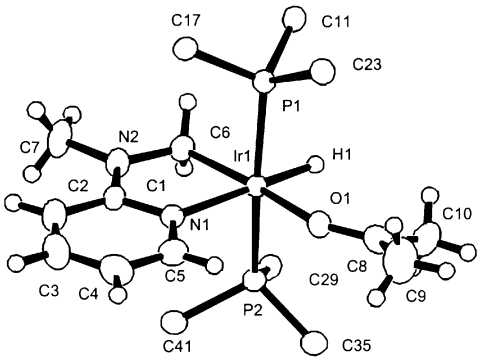

Fig. 2 An ORTEP view of the cation of $[Ir(PPh_3)_2(pyNMeCH_2)(Me_2CO)(H)]BF_4{\cdot}Me_2CO$, **6**. Selected bond lengths (Å) are: Ir(1)–C(6) 2.072(5), Ir(1)–N(1), 2.126(4), N(2)–C(1) 1.338(7), N(2)–C(6) 1.480(7). The ligand H atoms and the hydride are shown in calculated positions.

Notes and references

† *Synthesis*: **2**: the BF_4 salt of **1** (280 mg, 0.3 mmol) was dissolved in degassed CH_2Cl_2 (4 mL) and 2-dimethylaminopyridine (37 mg, 0.3 mmol) was added. The resulting clear yellow solution was stirred for 15 min. Slow addition of diethyl ether (*ca.* 10 mL) gave a light yellow precipitate. The solution was then filtered and the light yellow powder was washed with diethyl ether (15 mL) and dried *in vacuo* to give pure **2**. Yield: 217 mg (78%). Complex **3** can be prepared similarly by treating **1** with 1 equiv. of 2-diethylaminopyridine. Satisfactory analytical and spectroscopic data were obtained for **2** and **3**.

‡ *Crystal data*: **3**: $IrCl_2P_2F_4N_2C_{44}BH_{44}$, pale yellow crystals, M = 1036.74, triclinic; space group $P\bar{1}$ (no. 2), a = 11.8113(4), b = 12.6330(5), c = 16.5025(7) Å, α = 100.210(2), β = 107.894(2), γ = 101.536(2), V = 2219.4(2) Å^3, Z = 2; D_c = 1.551 g cm^{-3}; T = 183 K, λ(Mo-K$_a$) = 0.71069 Å, Nonius KappaCCD; no. reflections [$I > 3.0\sigma(I)$] = 6997; R = 0.043, R_w = 0.042, GOF = 1.34.

6: $IrP_2F_4O_2N_2C_{49}BH_{52}$; colorless crystals, M = 1041.93; monoclinic, space group $P2_1/n$ (no. 14), a = 14.4246(6), b = 14.7760(6), c = 22.8912(7) Å, β = 107.342(2)°, V = 4657.2(3) Å^3, Z = 4; D_c = 1.49 g cm^{-3}; T = 183 K, λ(Mo-K$_a$) = 0.71069 Å, Nonius KappaCCD; no. reflections [$I > 3.0\sigma(I)$] = 5722; R = 0.032, R_w = 0.034; GOF = 0.81.

CCDC 182/1870. See http://www.rsc.org/suppdata/cc/b0/b007679l/ for crystallographic files in .cif format.

1 J. N. Coalter, G. J. Spivak, H. Gerard, E. Clot, E. R. Davidson, O. Eisenstein and K. G. Caulton, *J. Am. Chem. Soc.*, 1998, **120**, 9388.
2 M. W. Holtcamp, J. A. Labinger and J. E. Bercaw, *J. Am. Chem. Soc.*, 1997, **119**, 848.
3 J. N. Coalter, G. Ferrado and K. G. Caulton, *New J. Chem.*, 2000, **24**, 835.
4 H. F. Luecke, B. A. Arndtsen, P. Burger and R. G. Bergman, *J. Am. Chem. Soc.*, 1996, **118**, 2517.
5 C. Slugovc, K. Mereiter, S. Trofimenko and E. Carmona, *Angew. Chem., Int. Ed.*, 2000, **39**, 2158.
6 R. R. Schrock, S. W. Seidel, N. C. Mosch-Zanetti, K. Y. Shih, M. B. O'Donoghue and W. M. Davis, *J. Am. Chem. Soc.*, 1997, **119**, 11 876 and references therein.
7 G. Parkin, E. Bunel, B. J. Burger, M. S. Trimmer, A. Vanasselt and J. E. Bercaw, *J. Mol. Catal.*, 1987, **41**, 21.
8 A. C. Albéniz, G. K. Schulte and R. H. Crabtree, *Organometallics*, 1992, **11**, 242.
9 R. H. Crabtree, E. M. Holt, M. Lavin and S. M. Morehouse, *Inorg. Chem.*, 1985, **24**, 1986.

ChemComm

Reaction of a diarylgermylene with a phosphaalkyne: formation of a germadiphosphacyclobutene with an exocyclic C=Ge double bond

Frank Meiners, Wolfgang Saak and Manfred Weidenbruch*

Fachbereich Chemie, Universität Oldenburg, D-26111 Oldenburg, Germany

Received (in Liverpool, UK) 16th October 2000, Accepted 13th December 2000
First published as an Advance Article on the web

The reaction of bis(2-*tert*-butyl-4,5,6-trimethylphenyl)germylene (Ar_2Ge:) with *tert*-butylphosphaalkyne furnishes a germadiphosphacyclobutene derivative with an exocyclic –C(Bu^t)=GeAr_2 group at one phosphorus atom, which was characterised by an X-ray structure analysis.

The addition of dialkyl-silylenes and -germylenes to the P≡C triple bonds of thermally stable phosphaalkynes represents a simple method for the synthesis of three-membered ring systems containing a P=C double bond that are difficult to prepare by other routes. For example, the silylene R_2Si**:** (R = CMe_3) reacts smoothly with phosphaalkynes to afford the corresponding phosphasilirenes.[1] The dialkylgermylene **1**[2,3] also undergoes a [2 + 1] cycloaddition reaction with *tert*-butylphosphaalkyne from which the germaphosphirene **2** can be isolated (Scheme 1).[4] The diarylsilylene Mes_2Si**:** behaves differently and furnishes a phosphadisilacyclobutene *via* stepwise addition of two silylene molecules to the phosphaalkyne.[5]

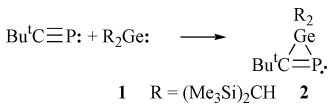

Scheme 1

We have now addressed the question if, similar to the silylenes, the use of a diarylgermylene would furnish a different result. Thus, from the reaction of the germylene **4** (which, in analogy to **1**,[6] exists as the digermene **3** in the solid state)[7] with *tert*-butylphosphaalkyne gave orange-coloured crystals which were isolated in 59% yield. The analytical data for these crystals were indicative of a 1:1 adduct composed of **4** and the phosphaalkyne. However, the ^{31}P NMR spectrum revealed the presence of both two- and three-coordinated phosphorus atoms, thus excluding the formation of a three-membered ring system analogous to **2** and suggesting the presence of a larger ring system (Scheme 2).

In agreement with the analytical and spectral data, an X-ray crystallographic analysis (Fig. 1)‡ revealed that two molecules each of the phosphaalkyne and **4** had reacted to furnish compound **5**† comprised of a germadiphosphacyclobutene with an additional, exocyclic Ge=C double bond. The bond lengths of both the exocyclic Ge=C and the endocyclic P=C double bonds were in accord with those of previously reported, similar

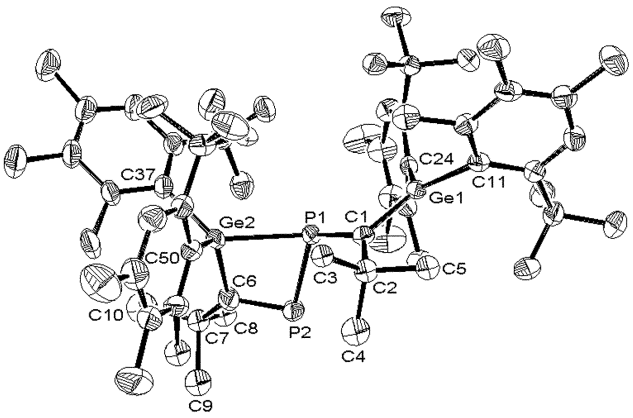

Fig. 1 Molecular structure of **5** (50% probability ellipsoids, hydrogen atoms omitted). Selected bond lengths (Å) and angles (°): P(1)–P(2) 2.1703(14), P(2)–C(6) 1.702(4), C(6)–Ge(2) 1.982(4), P(1)–Ge(2) 2.4351(9), P(1)–C(1) 1.822(3), C(1)–Ge(1) 1.833(4); P(2)–P(1)–Ge(2) 78.73(4), P(1)–Ge(2)–C(6) 79.15(11), Ge(2)–C(6)–P(2) 105.0(2), C(6)–P(2)–P(1) 93.39(15).

bonds. The remaining bond lengths and angles also did not reveal any unusual features.

The unexpected formation of **5** is without precedence in the chemistry of germylenes and phosphaalkynes. It is, at best, comparable with the addition of the germylene **4** to 1,3-diynes, a process proceeding through the C–C bridged bis(germacyclopropenes) **6** as the intermediate on the way to the rearranged, acetylene-linked bis(germaethenes) **7** (Scheme 3).[8] In analogy to the formation of **7**, it may be assumed that here also the reaction sequence is initiated by the addition of **4** to the phosphaalkyne to afford a three-membered ring system of type **8** with subsequent opening of the P–Ge single bond. Cyclodimerisation of this intermediate would then yield compound **5**.

A cyclodimerisation of this type should produce several conformers with varying orientations of the substituents on the exocyclic C atom. In fact, the ^{31}P NMR spectrum of **5** contains two doublets for two-coordinate phosphorus atoms at δ 269.0 and 271.5 as well as two doublets in the high-field region at δ −8.1 and −34.4. These signals remain unchanged even on heating a sample to 80 °C, presumably on account of the steric crowding at the exocyclic carbon atom. The existence of two conformers in solution is further supported by the observation

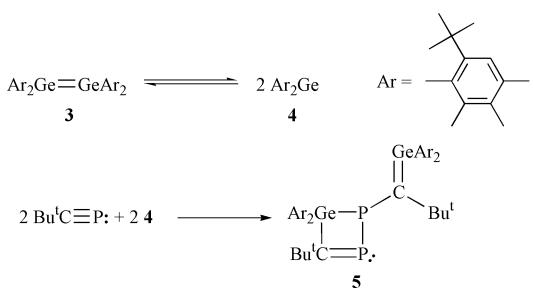

Scheme 2

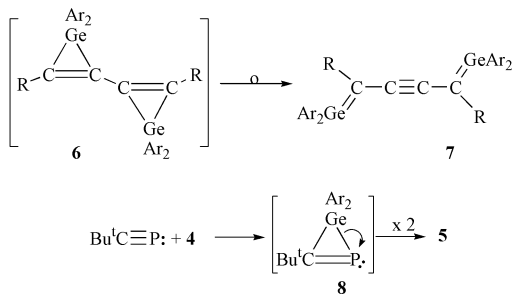

Scheme 3

DOI: 10.1039/b008472g

of numerous, in part overlapping, signals in the ^{1}H and ^{13}C NMR spectra that cannot be assigned unambiguously. The $^{1}J_{PP}$ coupling constants of 16 and 21 Hz for the two conformers are inexplicably small; related ring systems[9] have values of *ca.* 250 Hz.

Financial Support by the Deutsche Forschungsgemeinschaft and the Fonds der Chemischen Industrie is gratefully acknowledged. We thank Professor Marsmann, Paderborn, for the ^{31}P NMR spectra.

Notes and references

† *Preparation* of **5**: to a suspension of **3** (0.35 g, 0.41 mmol) in *n*-hexane (20 mL) was added a solution of *tert*-butylphosphaalkyne (0.30 g, 3.0 mol) in *n*-hexane (20 mL) and the mixture was stirred for 24 h at room temperature. The mixture was then filtered, the filtrate concentrated to a volume of 20 mL, and cooled to −30 °C to furnish 0.255 g (59% yield) of orange crystals of **5**, mp 118–120 °C. $^{31}P\{^{1}H\}$ NMR: δ 271.5, −34.4 ($^{1}J_{PP}$ 16 Hz), 269.0, −8.1 ($^{1}J_{PP}$ 21 Hz). UV–VIS (THF): λ_{max}/nm (ε/dm^3 mol^{-1} cm^{-1}) 366 (29000) nm. Anal. Calc. for $C_{62}H_{94}Ge_2P_2$: C, 71.16; H, 9.05. Found: C, 71.27, H, 9.22%.

‡ *Crystal data* for **5**: $C_{62}H_{94}Ge_2P_2 \cdot n\text{-}C_6H_{14}$, M = 1132.66, crystal dimensions 0.32 × 0.21 × 0.15 mm, triclinic, space group $P\bar{1}$, a = 12.1315(6), b = 15.3937(8), c = 17.6016(7) Å, α = 87.207(5), β = 80.276(5), γ = 87.056(6)°, V = 3232.9(3) Å^3, Z = 2, D_c = 1.164 g cm^{-3}, λ(Mo-Kα) = 0.71073 Å, T = 193(2) K, $2\theta_{max}$ = 52°, 11735 unique reflections, 6979 observed [$I > 2\sigma(I)$] 6979, 624 parameters. The structure was solved by direct methods (SHELXS-97) and refined by the full-matrix least-squares techniques against F^2 (SHELXL-97). The *tert*-butyl groups C2–C5 and C7–C10 are disordered and were refined on two positions with an occupancy factor of 0.5 each. Hydrogen atoms were placed in the calculated positions, and all other atoms were refined anisotropically; $R1$ = 0.0455, $wR2$ (all data) = 0.1064. CCDC 186/1877. See http://www.rsc.org/suppdata/cc/b0/b008472g/ for crystallographic files in .cif format

1 A. Schäfer, M. Weidenbruch, W. Saak and S. Pohl, *Angew. Chem.*, 1987, **99**, 806; *Angew. Chem., Int. Ed. Engl.*, 1987, **26**, 776.
2 D. E. Goldberg, D. H. Harris, M. F. Lappert and K. M. Thomas, *J. Chem. Soc., Chem. Commun.*, 1976, 261.
3 P. J. Davidson, D. H. Harris and M. F. Lappert, *J. Chem. Soc., Dalton Trans.*, 1976, 2268.
4 A. H. Cowley, S. W. Hall, C. M. Nunn and J. M. Power, *J. Chem. Soc., Chem. Commun.*, 1988, 753.
5 M. Weidenbruch, S. Olthoff, K. Peters and H. G. von Schnering, *Chem. Commun.*, 1997, 1433.
6 P. B. Hitchcock, M. F. Lappert, S. J. Miles and A. J. Thorne, *J. Chem. Soc., Chem. Commun.*, 1984, 480.
7 M. Weidenbruch, M. Stürmann, H. Kilian, S. Pohl and W. Saak, *Chem. Ber./Recueil*, 1997, **130**, 735.
8 F. Meiners, W. Saak and M. Weidenbruch, *Organometallics*, 2000, **19**, 2835.
9 F. E. Hahn, L. Wittenberger, D. L. Van, R. Fröhlich and B. Wibbeling, *Angew. Chem.*, 2000, **112**, 2393; F. E. Hahn, L. Wittenberger, D. L. Van, R. Fröhlich and B. Wibbeling, *Angew. Chem., Int. Ed.*, 2000, **39**, 2307.

ChemComm

A microporous framework from a magnetic molecular square: $[Co(HAT)Cl_2]_4$ (HAT = 1,4,5,8,9,11-hexaazatriphenylene)

José R. Galán-Mascarós and Kim R. Dunbar*

Department of Chemistry, Texas A&M University, College Station, TX 77842-3012 USA. E-mail: dunbar@mail.chem.tamu.edu

Received (in Columbia, MO, USA) 9th October 2000, Accepted 12th December 2000
First published as an Advance Article on the web

The neutral, paramagnetic molecular square $[Co(HAT)Cl_2]$ 1,4,5,8,9,11-hexaazatriphenylene (HAT) form stacks with large open, water-filled channels that constitute approximately 37% of the void space in the crystal.

The nitrogen heterocyclic molecule, 1,4,5,8,9,11-hexaazatriphenylene (HAT) and its derivatives have been studied in the context of supramolecular chemistry,[1] photochemistry[2] and organometallic chemistry.[3] The HAT molecule exhibits a symmetrical arrangement of three bidentate binding sites that resemble three fused 1,10-phenanthroline units. The topology of the coordination sites renders HAT an especially interesting ligand for paramagnetic metals due to the fact that the triangular geometries promote spin-frustration if the magnetic interactions between paramagnetic metals are antiferromagnetic. Given that superexchange through similar molecules such as pyrazine, bipyrimidine and pyrazino[2,3-*f*][4,7]phenanthroline (pap)[4] bridges are typically antiferromagnetic, we expect that HAT bridges will also promote antiferromagnetic exchange between paramagnetic metal centers. In terms of HAT coordination chemistry, one can envision the elaboration of a three-dimensional framework, *e.g.* the fascinating chiral compound $[Ag(HAT)ClO_4{\bullet}2MeNO_2]_\infty$,[5] but if fewer than three binding sites are occupied by metal ions, it is conceivable that cyclic oligomers such as molecular squares[6] or one-dimensional polymers will ensue.

In spite of the interest in the HAT molecule, its chemistry has not been widely explored. Presumably, this is due to the fact that it is not commercially available and is insoluble in nearly all common solvents. Two main synthetic approaches to HAT have been reported, one of which employs triaminotrinitrobenzene, a compound that is used as a mild explosive in military applications.[7] We have elected to use an alternative six-step procedure beginning with commercially available precursors that leads to HAT in low overall yields.[8] Colorless, prismatic crystals of HAT were grown from hot water and subjected to a single-crystal X-ray study.† As Fig. 1 clearly shows, HAT forms one-dimensional zigzag chains that run along the *c* axis. Adjacent HAT molecules in the same chain are rotated 180° from each other and engage in π–π interactions at distances of *ca.* 3.25 Å (sum of the van der Waals radii is 3.54 Å).[9] The orientations of HAT molecules between chains are tilted by *ca.* 38° from a parallel arrangement. The packing of the chains is pseudo-tetragonal, with vacancies between the chains being occupied by water molecules that assume close contacts to the nitrogen atoms of the HAT molecules (*ca.* 2.8–3.0 Å).

The title compound was prepared from the addition of aqueous solutions of HAT and $CoCl_2$ in a 1:1 ratio. Slow evaporation of the water led to the formation of orange prismatic crystals of the product in 65% yield.† The solid-state structure of $[Co(HAT)Cl_2]_4{\bullet}27H_2O$ revealed that the compound is a molecular square with four distorted octahedral Co(II) ions coordinated to *cis* HAT molecules (Fig. 2). Each HAT bridge is bound to only two Co atoms and forms an angle of 105° with respect to the plane of the metal atoms. The remaining coordination sites of the Co ions are occupied by two terminal Cl^- ligands. The distortion from a regular octahedron is evident

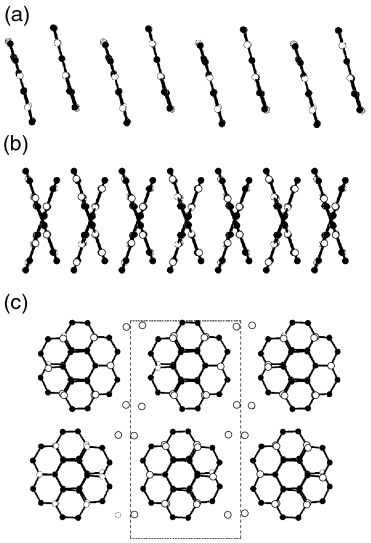

Fig. 1 Structure of $HAT{\bullet}2H_2O$: (a) side view of a dimerized chain, (b) side view of two adjacent chains and (c) projection in the *bc* plane.

from an examination of the Co–N distances [two each at 2.177(10) and 2.145(9) Å] and the Co–Cl distances [2.397(4) Å]. The angles about the Co atoms are *ca.* 90° with the exception of the chelating N–Co–N which is 77.8(3)°. The $CoCl_2(L–L)_2$ corners exhibit alternating chirality (Δ,Λ,Δ,Λ) which allows for the formation of a square rather than the open-chain analog. The individual squares pack in an eclipsed fashion along the *c* axis (Fig. 3) which results in the formation of large, open channels of 6 Å in diameter. The interactions between the stacks are dominated by π–π interactions between HAT ligands at 3.40 Å, a distance that is slightly longer than the interaction observed in $HAT{\bullet}2H_2O$, but shorter than the sum of the van der Waals radii.

It is worth mentioning at this point that the void space in this structure occupied by water molecules represents *ca.* 37%[10] of

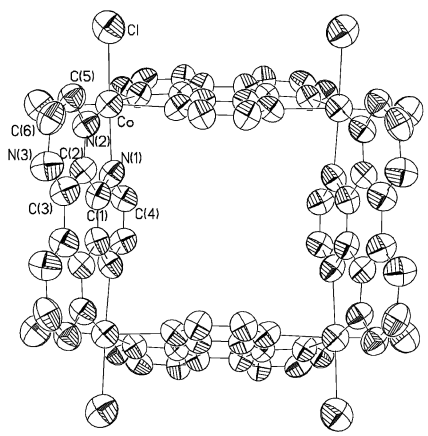

Fig. 2 Molecular structure of the $[Co(HAT)Cl_2]_4$ molecule.

DOI: 10.1039/b008209k

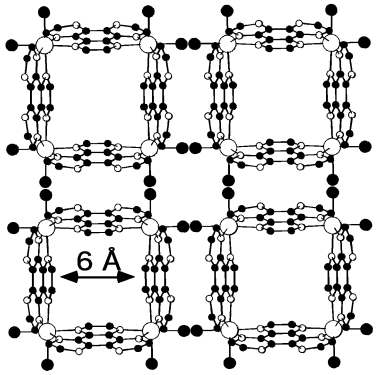

Fig. 3 Projection of the $[Co(HAT)Cl_2]_4 \cdot 27H_2O$ structure on the *ab* plane, showing the channels created by eclipsed stacking of the $[Co(HAT)Cl_2]_4$ squares (solvent molecules are omitted).

the total volume, which places this compound in the category of a microporous material. As many as 27 disordered water molecules were located in the channels created by the stacking of the squares and in the interstices between the stacks. The ability of this material to reversibly absorb and desorb water molecules and other molecules in the solid state is under investigation.

The magnetic properties of $[Co(HAT)Cl_2]_4 \cdot 27H_2O$ were investigated over the temperature range 2–300 K. The behavior of $\chi_m T$ is shown in Fig. 4. The room-temperature value of $\chi_m T$ is 10.41 emu K mol^{-1} which corresponds to four magnetically isolated Co ions ($S = 3/2$; $g = 2.34$). Below 150 K and down to 2 K, $\chi_m T$ steadily decreases which can be attributed to the well known zero-field splitting of high-spin Co(II) ions and also, possibly, to antiferromagnetic exchange between the Co centers. The anisotropy of these Co(II) systems precludes a quantitative analysis of these data, but it is possible to compare these data to the corresponding behavior of the model compound $Co(bpy)_2Cl_2$ with isolated Co ($S = 3/2$) centers. As indicated in Fig. 4, the decrease in χT observed for $Co(bpy)_2Cl_2$ below 150 K is essentially identical to that observed for $[Co(HAT)Cl_2]_4$, thus it must be concluded that the moment decrease is due exclusively to the zero-field splitting of the Co ions. Magnetic exchange through the HAT ligand in this particular case is negligible compared to the ZFS.

In conclusion, a novel magnetic molecular square composed of Co^{II} ions and HAT ligands has been prepared and characterized in the solid state. Several aspects of this molecular structure are particularly noteworthy. It is one of the few neutral molecular squares known to date, and it forms a microporous solid with channels of 6 Å diameter and 37% void space. Efforts to use the HAT ligand to produce new clusters as well as polymeric structures with paramagnetic metal centers are in progress.

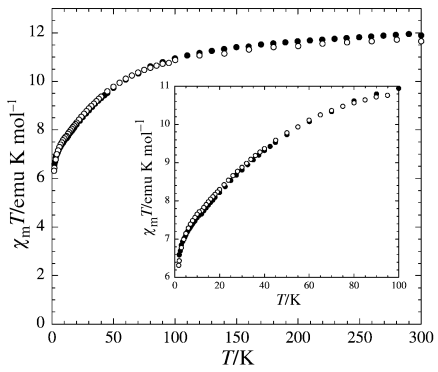

Fig. 4 The $\chi_m T$ *vs.* T plot ($H = 1000$ G) for $[Co(HAT)Cl_2]_4$ (●) compared to 4 × ($\chi_m T$) product for the model compound $Co(bpy)_2Cl_2$ (○).

K. R. D. gratefully acknowledges the National Science Foundation for support of this work (NSF CHE-9906583) and for funding the CCD diffractometer (CHE-9807975) and the SQUID instrumentation (NSF-9974899). J. R. G.-M. thanks the Ministerio de Educacion y Cultura for a postdoctoral fellowship.

Notes and references

† *Crystal data*: for $[C_{12}N_6H_6] \cdot 2H_2O$: $C_{12}H_{10}N_6O_2$, $M_w = 270.26$, monoclinic space group *Pc*, $a = 6.9260(14)$, $b = 9.242(2)$, $c = 18.158(4)$ Å, $\beta = 90.04°$, $V = 1162.3(4)$ Å^3, $T = 110(2)$ K, $Z = 4$, $D_c = 1.544$ Mg m^{-3}, Graphite-monochromated Mo-Kα radiation ($\lambda = 0.71069$ Å), Bruker CCD diffractometer, $F(000) = 560$, $\mu = 0.112$ mm^{-1}, 0.07 × 0.04 × 0.04 mm, 8715 reflections measured, 4374 of which were unique ($R_{int} = 0.0673$). The structure was solved by direct methods (SIR97)[11] followed by Fourier synthesis, and refined on F^2 (SHELX-97. G. M. Sheldrick, University of Göttingen, 1997). The isotropic thermal parameters of equivalent hydrogen atoms were constrained to be identical. All other atoms were refined anisotropically. The final refinement gave $R(F^2) = 0.0522$ and $R^2_w(F^2) = 0.0958$, by using 2601 reflections ($I > 2\sigma$).

For $[Co(HAT)Cl_2]_4 \cdot 27H_2O$: $C_{48}H_{78}Cl_8Co_4N_{24}O_{27}$, $M_w = 1942.64$, tetragonal, space group *P*42/*nnm*, $a = 17.663(3)$, $c = 12.171(3)$ Å, $V = 3797.1(13)$ Å^3, $T = 110(2)$ K, $Z = 2$, $D_c = 1.699$ Mg m^{-3}, graphite-monochromated Mo-Kα radiation ($\lambda = 0.71069$ Å), Bruker CCD diffractometer, $F(000) = 1988$, $\mu = 1.233$ mm^{-1}, 0.05 × 0.04 × 0.02 mm, 32898 reflections measured, 2469 of which were unique ($R_{int} = 0.0925$). The structure was solved by direct methods (SIR97) followed by Fourier synthesis, and refined on F^2 (SHELX-97). The solvent molecules are disordered, and were modeled as 16 crystallographically independent oxygen atoms all of them with occupancy factors less than one. All other non-hydrogen atoms were refined anisotropically. The final refinement gave $R(F^2) = 0.0824$ and $R^2_w(F^2) = 0.2056$, by using 783 reflections ($I > 4\sigma$).

CCDC 182/0000. See http://www.rsc.org/suppdata/cc/b0/b008209k/ for crystallographic files in .cif format

1 P. N. W. Baxter, J.-M. Lehn, G. Baum and D. Fenske, *Chem. Eur. J.*, 1999, **5**, 102; P. N. W. Baxter, J.-M. Lehn, B. O. Kneisel, G. Baum and D. Fenske, *Chem. Eur. J.*, 1999, **5**, 113; C. Moucheron, C. O. Dietrich-Buchecker, J.-P. Sauvage and A. van Dorsselaer, *J. Chem. Soc., Dalton Trans.*, 1994, 885; P. N. W. Baxter, J.-M. Lehn, A. DeCian and J. Fisher, *Angew. Chem., Int. Ed. Engl.*, 1993, **32**, 69.

2 T. J. Rutherford, O. Van Gijte, A. Kirsch-De Mesmaeker and F. R. Keene, *Inorg. Chem.*, 1997, **36**, 4465; T. J. Rutherford and F. R. Keene, *Inorg. Chem.*, 1997, **36**, 3580; C. Moucheron, A. Kirsch-De Mesmaeker and S. Choua, *Inorg. Chem.*, 1997, **36**, 584; I. Ortmans, P. Didier and A. Kirsch-De Mesmaeker, *Inorg. Chem.*, 1995, **34**, 3695; P. Didier, I. Ortmans and A. Kirsch-De Mesmaeker, *Inorg. Chem.*, 1993, **32**, 5239.

3 R. Nasielski-Hinkens, M. Benedek-Vamos, D. Maetens and J. Nasielski, *J. Organomet. Chem.*, 1981, **217**, 179.

4 H. Grove, J. Sletten, M. Julve and F. Lloret, *J. Chem. Soc., Dalton Trans.*, 2000, 515.

5 B. F. Abrahams, P. A. Jackson and R. Robson, *Angew. Chem., Int. Ed.*, 1998, **37**, 2656.

6 S. Leininger, B. Olenyuk and P. J. Stang, *Chem. Rev.*, 2000, **100**, 853; S.-S. Sun, A. S. Silva, I. M. Brinn and A. J. Lees, *Inorg. Chem.*, 2000, **39**, 1344; C. S. Campos-Fernández, R. Clérac and K. R. Dunbar, *Angew. Chem., Int. Ed.*, 1999, **38**, 3477; R. V. Slone, K. D. Benkstein, S. Belanger, J. T. Hupp, A. I. Guzei and A. L. Rheingold, *Coord. Chem. Rev.*, 1998, **171**, 221; M. Fujita, M. Aoyagi, F. Ibukuro, K. Pgura and K. Yamaguchi, *J. Am. Chem. Soc.*, 1998, **120**, 611; P. J. Stang and B. Olenyuk, *Acc. Chem. Res.*, 1997, **30**, 502; B. Olenyuk, J. Whiteford and P. J. Stang, *J. Am. Chem. Soc.*, 1996, **118**, 8221; M. Fujita, O. Sasaki, T. Mitsushashi, T. Fujita, J. Yakazi, K. Yamaguchi and K. Ogura, *Chem. Commun.*, 1996, 1535; M. Fujita, J. Yazaki and K. Ogura, *J. Am. Chem. Soc.*, 1990, **112**, 5645; P. M. Stricklen, E. J. Volcko and J. G. Verkade, *J. Am. Chem. Soc.*, 1983, **105**, 2494.

7 D. Z. Rogers, *J. Org. Chem.*, 1986, **51**, 3904.

8 J. T. Rademacher, K. Kanakarajan and A. W. Czarnik, *Synthesis*, 1994, 378; M. S. P. Sarma and A. W. Czarnik, *Synthesis*, 1988, 72.

9 A. Bondi, *J. Phys. Chem.*, 1964, **68**, 441.

10 PLATON-95 (V-130795); A. L. Spek, *Acta Crystallogr., Sect. A*, **46**, 34.

11 A. Altomare, M. C. Burla, M. Camalli, G. L. Cascarano, C. Giacovazzo, A. Guagliardi, A. G. G. Moliterni, G. Polidori and R. Spagna, *J. Appl. Crystallogr.*, 1999, **32**, 115.

Typeset and printed by Black Bear Press Limited, Cambridge, England

Carbon-rich acetylenic scaffolding: rods, rings and switches†

François Diederich*

Laboratorium für Organische Chemie, ETH-Zentrum, Universitätstrasse 16, CH-8092 Zürich, Switzerland. E-mail: diederich@org.chem.ethz.ch

Received (in Cambridge, UK) 15th November 2000, Accepted 1st December 2000
First published as an Advance Article on the web 16th January 2001

Derivatives of tetraethynylethene (TEE, 3,4-diethynylhex-3-ene-1,5-diyne) and (*E*)-1,2-diethynylethene ((*E*)-DEE, (*E*)-hex-3-ene-1,5-diyne) provide a unique class of π-conjugated building blocks for modular construction of one- and two-dimensional carbon-rich scaffolds such as monodisperse, linearly π-conjugated oligomers extending in length beyond 10 nm or large macrocyclic all-carbon cores. Lateral functionalisation of these novel chromophores with donor–acceptor substituents strongly enhances their advanced materials properties and leads to exceptional third-order optical nonlinearities. New photochromic molecules were prepared which undergo photochemical *cis* → *trans* and *trans* → *cis* isomerisation without competing thermal isomerisation pathways, thereby paving the way for applications as light-driven molecular switches in optoelectronic devices.

Introduction

Acetylenic scaffolding started in 1869 with the discovery of the oxidative alkyne coupling by Glaser.[1,2] Soon after, Baeyer recognized the potential of this reaction for forming infinite all-carbon chains, $[-C\equiv C-]_n$, known today as carbyne.[3] The advent of the Eglinton–Galbraith variant of the Glaser coupling reaction in 1956,[4] which uses cupric salts in donor solvents such as pyridine, paved the way for the pioneering work by Sondheimer and co-workers, who described the first synthesis of [18]annulene in 1959.[5,6] This milestone in physical organic chemistry, which provided experimental support for the Hückel rule defining aromaticity, was followed by the synthesis and investigation of a large number of macrocyclic π-electron perimeters, including many dehydroannulenes containing acetylenic bonds.[7–9] Methodological advances such as the Hay variant for oxidative homo-coupling[10] and the Cadiot–Chodkiewicz protocol for oxidative hetero-coupling[11] expanded the application of acetylenic scaffolding into the fields of polymer and natural product synthesis.[2] Today, progress in acetylene-based molecular construction is greatly fueled by the advent of powerful novel metal-catalyzed acetylenic homo- and cross-coupling protocols.[2,12,13]

In the mid 80s, the observation of fullerene formation by mass spectrometry[14] stimulated our research group to search for other, synthetic carbon allotropes.[15,16] We developed 'precursor' routes to the cyclocarbons (*cyclo*-C_n), *n*-membered monocyclic rings of sp-hybridised C atoms with unique electronic structures resulting from two perpendicular systems of conjugated π-orbitals, one in-plane and one out-of plane.[15–17] In collaborative efforts, we showed that these all-carbon molecules undergo ion-molecule coalescence reactions in the gas phase under clean formation of fullerenes.[18,19] At the same time, we identified two-dimensional all-carbon networks,[20] containing as repeat unit the cross-conjugated framework of tetraethynylethene (**1**, TEE, 3,4-diethynylhex-3-ene-1,5-diyne) (Scheme 1), as potential advanced materials and attractive synthetic targets.[15,16] While our hope of producing such networks with high crystallinity was not substantiated, it initiated the research featured in this article.

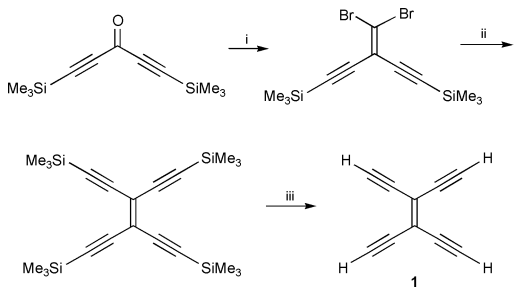

Scheme 1 Synthesis of tetraethynylethene (**1**).[38] i, CBr_4, PPh_3, 50%; ii, $Me_3Si–C\equiv C–H$, $[Pd(PPh_3)_4]$, CuI, $BuNH_2$, PhH, 88%; iii, K_2CO_3, wet MeOH, 87%.

Tremendous synthetic efforts are currently ongoing in the area of acetylenic scaffolding, targeting exceptional molecular architecture and functional advanced materials, and the reader is referred to review articles and monographs for a better appreciation of these developments.[21–32] Here, we describe how derivatives of tetraethynylethene (**1**) and (*E*)-1,2-diethynylethene (**2**, (*E*)-DEE, (*E*)-hex-3-ene-1,5-diyne) have been used to prepare a great diversity of functional carbon-rich compounds such as chromophores with high second- and third-order optical nonlinearities, molecular photochemical switches, large two-dimensional carbon cores, and linearly π-conjugated molecular rods extending in length beyond 10 nm.

† Dedicated to Professor Jean François Normant on the occasion of his 65th birthday.

François Diederich, born in 1952 in the Grand Duchy of Luxembourg, received his PhD degree in 1979 from the University of Heidelberg. Following postdoctoral studies at the University of California at Los Angeles (UCLA) from 1979–1981, he was a research associate at the Max-Planck-Institut für medizinische Forschung in Heidelberg. After his Habilitation in 1985, he joined the faculty of the Department of Chemistry and Biochemistry at UCLA where he became full professor in 1989. Since April 1992, he has been a professor of organic chemistry at ETH Zürich. His research interests encompass the development of covalent fullerene chemistry, the preparation of novel carbon allotropes and acetylenic carbon-rich advanced materials, the exploration of functional dendrimers as models for globular proteins and molecular recognition studies with synthetic and biological receptors.

DOI: 10.1039/b009180o

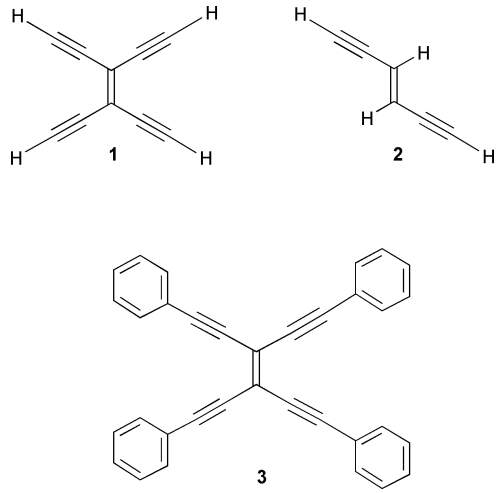

Synthesis and properties of tetraethynylethenes and (*E*)-1,2-diethynylethenes

Tetrakis(phenylethynyl)ethene (**3**) was the first TEE derivative synthesised by Hori *et al.* in 1969,[33,34] and the first peralkylated and persilylated derivatives were reported later in the 70s by Hauptmann.[35] Taking advantage of modern Pd(0)-catalyzed cross-coupling methods,[12] our research group introduced in the early 90s more general synthetic protocols, providing access not only to the parent compound **1**[36] but also to virtually any desired substitution pattern about the central ten-carbon TEE core. These methods have been comprehensively reviewed;[37] they are illustrated in Schemes 1 and 2 for the synthesis of TEE **1**[38] and (*E*)-DEE **4**.[39]

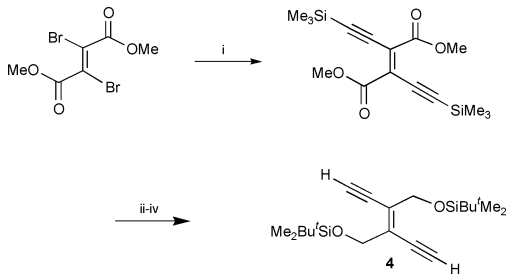

Scheme 2 Synthesis of (*E*)-1,2-diethynylethene **4**.[39] i, Me_3Si–C≡C–H, $[PdCl_2(PPh_3)_2]$, CuI, NEt_3, 20 °C, ≈50%; ii, DIBAL-H, CH_2Cl_2, 0 °C, 85%; iii, Me_2Bu^tSiCl, Et_3N, DMAP, 25 °C, 98%; iv, K_2CO_3, MeOH, 25 °C, 90%. DIBAL-H = diisobutylaluminum hydride, DMAP = 4-(*N*,*N*-dimethylamino)pyridine.

Recently, another general procedure for the synthesis of hex-3-ene-1,5-diynes was described by Jones and co-workers which does not rely on Pd(0)-catalyzed cross-coupling.[40] A large variety of (*E*)- or (*Z*)-DEE and TEE derivatives could be prepared using the carbenoid coupling–elimination strategy shown in Scheme 3.

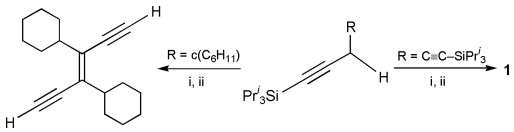

Scheme 3 DEEs and TEEs by a carbenoid coupling–elimination strategy. i, LHMDS, HMPA, THF, −80 °C; ii, Bu_4NF, THF, 70% (DEE), 90% (**1**); yields over 2 steps.[40] LHDMS = lithium hexamethyldisilazane, HMPA = hexamethylphosphorous triamide.

Another synthesis of TEE derivatives results from the acid-catalyzed thermal elimination of an orthoester moiety from 1,1,2,2-tetraethynylethane (3,4-diethynylhexa-1,5-diyne) derivatives (Scheme 4).[41]

The stability of TEE and DEE derivatives largely depends on the number of free ethynyl residues in the molecule. If all

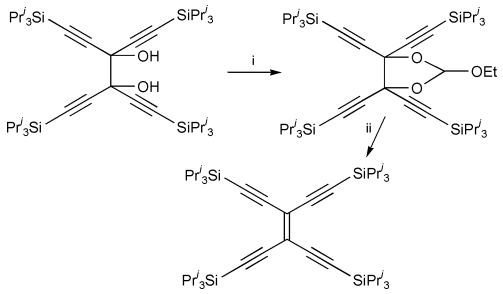

Scheme 4 TEEs by acid-catalysed orthoester thermolysis. i, $(EtO)_3CH$, cat. CSA, CH_2Cl_2, 94%; ii, CSA, 150 °C, 0.1 Torr, 5 min, 25–33%.[41] CSA = camphorsulfonic acid.

acetylene residues are silylated, alkylated or arylated, the compounds are kinetically very stable and display high melting points or decomposition points which in the case of arylated derivatives reach 200 °C and higher. With increasing number of free terminal alkyne groups, the stability rapidly decreases: derivatives with two ethynyl residues already are quite labile in the neat state and the parent TEE **1** rapidly decomposes at 25 °C. Remarkably, we never observed any Bergman cycloaromatisation of TEEs and DEEs;[42,43] at higher temperatures, other decomposition channels presumably become dominant.

Over 30 X-ray crystal structures of TEE and DEE derivatives have been solved.[44] They all revealed fully or nearly planar π-conjugated carbon cores, which in most cases, also include terminal aryl rings. In some solid-state structures, terminal aryl rings are not in plane with the central core, presumably due to crystal packing effects. In these cases, they adopt an orthogonal orientation, thereby maintaining conjugation with the second set of π-orbitals in the adjacent C≡C bond. The length of the central C=C double bond in TEE and DEE cores usually varies between 1.34 and 1.37 Å, whereas the C≡C triple bond lengths vary between 1.17 and 1.22 Å.[45]

One of the striking characteristics of TEE derivatives is the complete chemical inertness of the central olefinic bond. All attempts to add electrophiles, carbenes, 1,3-dienes or 1,3-dipoles to this electron-deficient[46] bond failed.[47] Thus, 1,3-dipolar cycloaddition with diazomethane occurred at one of the C≡C bonds rather than at the central C=C bond. Similarly, oxidations or epoxidations of this bond were unsuccessful and epoxide **5** could only be prepared in an indirect way as shown in Scheme 5.[48]

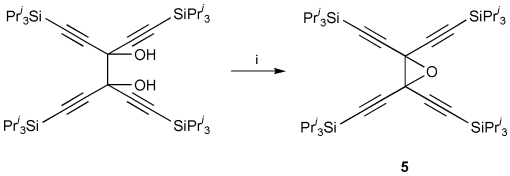

Scheme 5 Synthesis of epoxide **5**. i, $MeSO_2Cl$, NEt_3, CH_2Cl_2, −20 °C → 20 °C, 80%.[48]

Functional advanced materials based on arylated TEEs and DEEs

The physical properties of the TEE and DEE chromophores are further enhanced by arylation, generating a variety of desirable functional derivatives for advanced materials applications. Thus, the fully planar tetraphenyl derivative **3** and the π-acceptors 2,4,7-trinitrofluoren-9-one or (2,4,7-trinitrofluoren-9-ylidene)malononitrile form highly ordered donor–acceptor π-complexes of 1:2 donor–acceptor stoichiometry in the solid state.[49,50] The donor/acceptor orientation in the extended layer structures seen in the crystals is electrostatically controlled and shows a good correlation with the calculated atom-centered point charges on both components.

One of the most interesting properties of arylated TEEs and DEEs is their ability to undergo reversible, photochemical *trans* → *cis* and *cis* → *trans* isomerisation.[51] These isomerisations are not observed in the corresponding derivatives lacking aryl substituents. Since both *cis* and *trans* forms benefit from strain-free planarity—in contrast to azobenzenes[52] and stilbenes[53] which are nonplanar in the *cis* forms—the photochemical processes are not accompanied by undesirable thermal isomerisation, a quality reached only in a very small number of photochromic materials known today.[54] The photoisomerisation is of substantial preparative use and was applied to the synthesis of donor–acceptor substituted TEEs, such as **6** and **7**, for nonlinear optical studies (Scheme 6).[44c] A detailed investigation revealed a strong dependence of the quantum yields for photoisomerisation from the pattern and degree of aryl functionalisation, solvent polarity and excitation wavelength.[51] For a bis(4-nitrophenyl)-substituted DEE, the *trans–cis* isomerisation was also shown to occur electrochemically at the stage of the dianion.[45c]

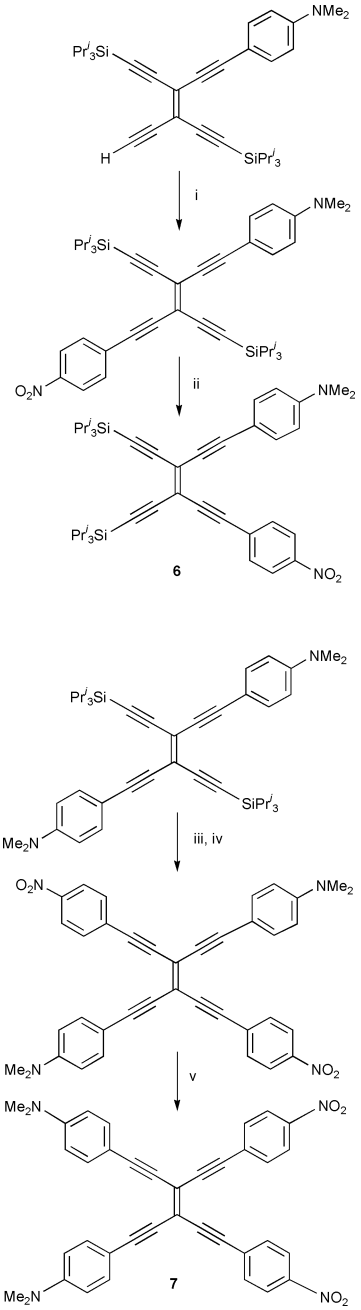

Scheme 6 Synthesis of donor–acceptor substituted TEEs **6** and **7** by photochemical *trans–cis* isomerisation.[44c] i, *p*-O_2N-C_6H_4I, [$PdCl_2(PPh_3)_2$], CuI, NEt_3, 20 °C, 66%; ii, *hv* (366 nm), Et_2O, 37%; iii, Bu_4NF, wet THF; iv, *p*-O_2N-C_6H_4I, [$PdCl_2(PPh_3)_2$], CuI, NEt_3, 20 °C, 56% (2 steps); v, *hv* (366 nm), $CHCl_3$, 20%.

We have taken advantage of the photochemical *trans–cis* isomerisation process to construct light-driven molecular switches.[55] Compounds (*R*,*R*)-**8** and (*R*,*R*)-**9** are hybrid systems consisting of a TEE core with two attached (*R*)-configured 1,1′-binaphthalene moieties (Scheme 7).[56] They can be reversibly

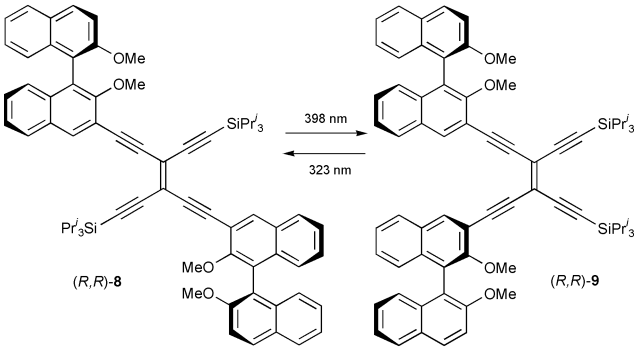

Scheme 7 The couple (*R*,*R*)-**8**/(*R*,*R*)-**9** represents a novel, fully light-driven molecular switch.[56]

interconverted in CH_2Cl_2 solutions with light of λ = 398 or 323 nm. No thermal isomerisation was observed at room temperature, and the system displayed high resistance to photofatigue.

A further enhancement in complexity of molecular functions that can be expressed with TEE derivatives was achieved with the synthesis of the three-way chromophoric molecular switch (*E*)-**10** (Scheme 8).[57] This compound contains three addressable

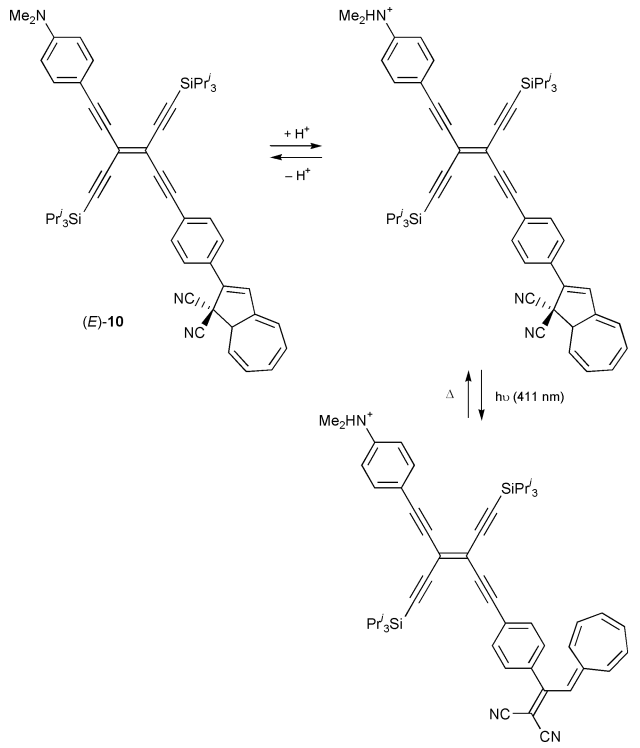

Scheme 8 Two of the three switching functions expressed by the three-way chromophoric molecular switch (*E*)-**10**.[57] The third one (not shown) is the *trans–cis* isomerisation of the TEE core.

subunits which undergo individual reversible switching cycles: (i) a central TEE core which can be reversibly photoisomerised between its *cis* and *trans* forms, (ii) a dihydroazulene unit that can be transformed upon irradiation into a vinylheptafulvene (vinyl-7-methylenecyclohepta-1,3,5-triene) moiety[58] and (iii) a proton-sensitive *N*,*N*-dimethylanilino group. Of the eight resulting possible interconverting states, a total of six could be detected. Individual interconversion processes such as three

'write–erase' processes and one process mimicking the function of an AND logic gate could be separatively addressed. The latter process relies on the interesting observation that the photochemical opening of the dihydroazulene to the vinylheptafulvene moiety occurs only after protonation of the dimethylamino group, as shown in Scheme 8. We are now investigating in interdisciplinary collaboration, whether TEE- and DEE-based molecular switches could find application in photoaddressable memory storage and readout devices or as waveguides.[59]

Donor–acceptor substituted TEEs display some of the highest known third-order optical nonlinearities[60] and in case of acentricity, also very large second-order nonlinear optical effects.[61] Comprehensive investigations by Günter, Bosshard and co-workers under non-resonant conditions helped to establish structure–property relationships which provide useful guidance for the future design of nonlinear optical materials.[60] In particular, these studies clearly demonstrated the important role of two-dimensional conjugation in enhancing third-order nonlinear optical effects.[62] The highest values of the second hyperpolarisability, γ, that describes molecular third-order nonlinear optical effects,[63] were measured for perarylated TEEs such as **7** (Scheme 6), **11**,[44c] **12**[44b] or **13**[44b] in which as many as six conjugation paths are effective (Scheme 9). In addition to

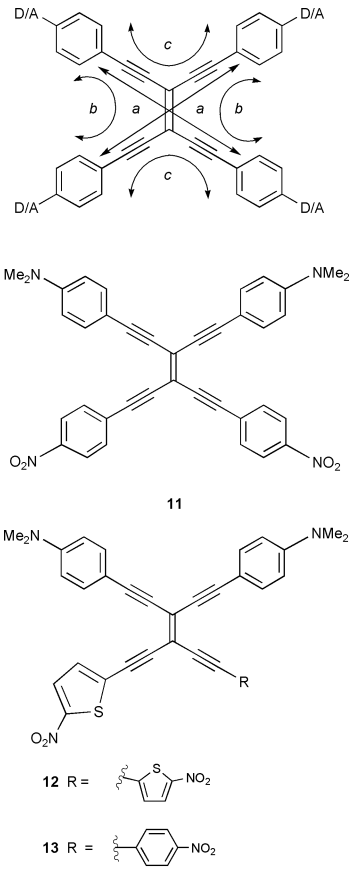

Scheme 9 Top: schematic representation of the possible conjugation pathways in perarylated TEEs. Paths *a* and *b* depict *trans*- and *cis*-linear conjugation, and path *c* depicts geminal cross conjugation. (D donor, A acceptor). Bottom: fully two-dimensionally conjugated chromophores with high second hyperpolarisabilities, γ.[60,64]

full two-dimensional conjugation, low molecular symmetry was also found to be of particular importance for enhancing third-order nonlinear optical effects. Thus, the lower-symmetrical nitrothienyl derivative **13** gave a higher value for γ than obtained for **7**, **11** or **12** possessing higher molecular symmetries. A theoretical model was derived to explain these experimental findings;[64] the reader is referred to the original literature for more details.

Two-dimensional scaffolding: expanded carbon cores

Two families of molecules featuring large all-carbon cores were constructed from suitably functionalised TEE derivatives, perethynylated dehydroannulenes and expanded radialenes. Oxidative Glaser–Hay macrocyclisation of *cis*-bis(trialkylsilyl)-protected TEEs yielded the per(silylethynylated) octadehydro[12]annulenes **14a**,**b** and dodecadehydro[18]annulenes **15a**,**b** with fully planar π-conjugated carbon cores as evidenced by X-ray crystallography (Scheme 10).[65,66] The yellow-colored

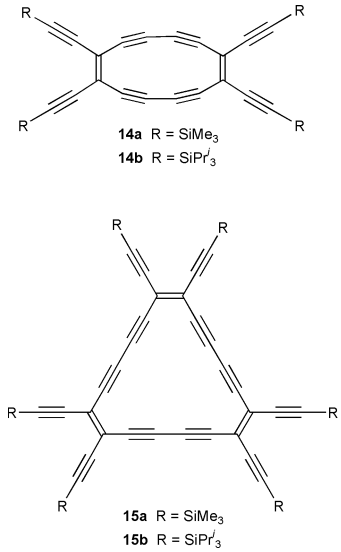

Scheme 10 Planar, perethynylated aromatic (**15a**,**b**) and antiaromatic (**14a**,**b**) dehydroannulenes.[65,66]

[18]annulenes **15a**,**b**, with a large HOMO–LUMO gap (2.57 eV in pentane) are aromatic, whereas the purple-colored [12]annulenes **14a**,**b**, with a smaller HOMO–LUMO gap (1.87 eV), are antiaromatic. Electrochemical studies[46,66] showed that [12]annulene **14b** undergoes stepwise one-electron reductions (E^o = −0.99 and −1.46 eV *vs.* Fc/Fc$^+$ (ferrocene/ferricinium couple) in THF) more readily than [18]annulene **15a** (E^o = −1.12 and −1.52 V). This redox behavior is best explained by the formation of an aromatic [4*n* + 2] π-electron dianion from antiaromatic **14b**, whereas **15a** loses its aromaticity upon reduction. Removal of the six silyl-protecting groups in **15a** yielded the perethynylated derivative with the molecular formula $C_{30}H_6$ which was stable in dilute solutions for a few days at −20 °C in the dark. All attempts, however, to prepare crystalline networks[15,16] by oxidative acetylenic coupling failed.

Formal insertion of ethynediyl[67] or buta-1,3-diynediyl moieties between each pair of vicinal *exo*-methylene units in the cyclic framework of radialenes leads to the carbon-rich expanded radialenes of which the perethynylated derivatives **16a**–**c** are the first representatives (Scheme 11).[66,68] They possess nanometer-sized carbon sheets with diameters, not including the SiPr$^i_3$ groups, of *ca.* 17 (**16a**), 19 (**16b**) and 22 (**16c**) Å. They are amazingly stable and readily soluble compounds with melting points above 220 °C and can be viewed as persilylated C_{40}, C_{50} and C_{60} isomers, respectively. Mass spectrometric analysis revealed that even larger carbon sheets extending to C_{120} cores are formed and, with the recent advances in gel permeation chromatographic (GPC) techniques, we are currently attempting their separation and characterisation. Electrochemical investigations showed that **16a**–**c** are powerful electron acceptors, capable of undergoing multiple reversible one-electron reductions, but are not readily oxidized. Both UV/Vis and electrochemical analyses suggested that cross-conjugation is not very effective in the macrocyclic perimeters and that the extent of π-electron delocalisation in all

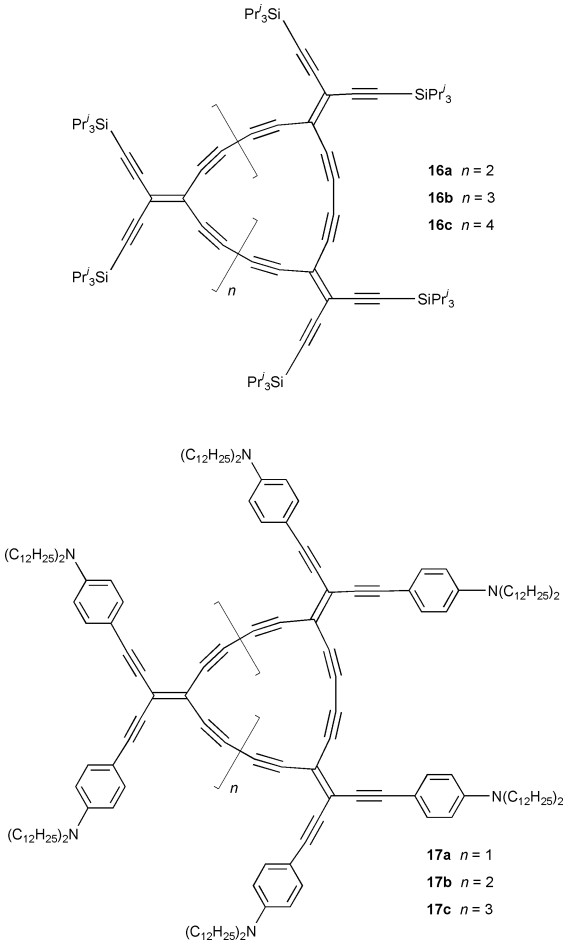

Scheme 11 Expanded radialenes **16a**–**c** and **17a**–**c**.[66,68,69]

three compounds is limited to the longest linearly-conjugated π-electron fragment corresponding to a dodeca-3,9-diene-1,5,7,11-tetrayne-1,12-diyl moiety (–C≡C–CR=CR–C≡C–C≡C–CR=CR–C≡C–).

The materials properties of the expanded radialenes were greatly enhanced upon donor functionalisation, leading to the stable derivatives **17a**–**c** with fully planar π-chromophores.[69] These compounds exhibit large third-order nonlinear optical coefficients, can be reversibly reduced or oxidised, and form Langmuir monolayers at the air–water interface. Particularly intriguing is the UV/Vis spectrum of trimeric **17a**, which features a strong low-energy absorption band in the visible region with an exceptionally large molar extinction coefficient (ε = 171 000 dm^3 cm^{-1} mol^{-1} at λ_{max} = 646 nm). The studies with expanded radialenes executed so far suggest that π-electron delocalisation in these cross-conjugated macrocycles is not well understood, and high-level theoretical calculations of the structural and electronic properties of these large perimeters would be very desirable.

Novel linearly π-conjugated oligomers and polymers with all-carbon backbones

After the introduction of the Pd(0)-catalysed cross-coupling-based syntheses of TEEs and DEEs in 1991,[36] we rapidly became interested in applying these building blocks to the construction of novel oligomers[70] and polymers with linearly π-conjugated all-carbon backbones. In particular, we targeted the first synthesis of poly(triacetylene)s (PTAs),[71] thereby extending the progression of all-carbon polymer backbones which leads from polyacetylene[72] to poly(diacetylene)[73] and, ultimately, to carbyne[74] (Scheme 12).[39]

Starting from suitable TEE or DEE monomers, we prepared by oxidative acetylenic coupling under end-capping conditions

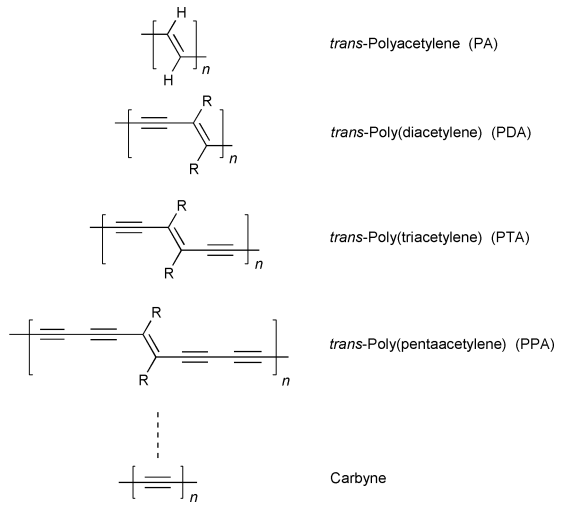

Scheme 12 Progression of linearly π-conjugated all-carbon backbones from *trans*-polyacetylene to carbyne.[39]

several larger-chain PTA polymers such as air-stable **18**–**20** (Scheme 13).[39,69] Deep red–brown **18** was soluble in hot $CHCl_3$

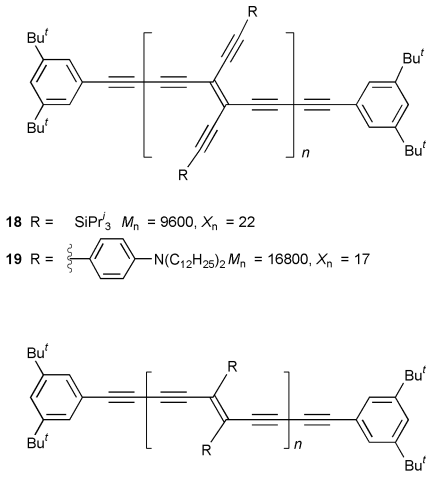

Scheme 13 Poly(triacetylene) polymers prepared by oxidative acetylenic coupling under end-capping conditions.[39,69] M_n = number-averaged molecular weight, X_n = degree of oligomerisation.

and in 1,2-dichlorobenzene above 65 °C and showed an optical gap of E_g = 2.0 eV which is in the range of the values measured for poly(diacetylene)s.[75] It can be reversibly reduced at the remarkably low potential of E = −0.65 V (*vs.* Fc/Fc$^+$).[39] In polymer **19**, with laterally appended donor groups, the optical gap is substantially reduced as compared to **18** and appears at E_g = 1.6 eV.[69] Lacking the laterally appended alkynyl groups, the optical gap in **20** is raised to E_g = 2.4 eV.

A particularly interesting accomplishment in the chemistry of poly(triacetylene)s is their first synthesis by topochemically controlled polymerisation of hexa-1,3,5-triynes in the crystal, which was recently described by Fowler and co-workers.[76] A highly original supramolecular control of spatial alignment and orientation of the hexa-1,3,5-triynes in the crystal lattice was required for this 1,6-polymerisation to occur.

In the largest body of our work on PTA rods, we focused on the preparation and study of monodisperse oligomeric series as models for the corresponding infinite polymers.[77] We first prepared by oxidative coupling under end-capping conditions the two oligomeric series **21a**–**e**[78,79] and **22a**–**f**,[80] extending in length up to 5 nm (Scheme 14). Compounds in series **21a**–**e** undergo facile one-electron reduction, with the number of reversible reduction steps being equal to the number of TEE moieties in each molecular rod. Thus, the first reduction of **21a**

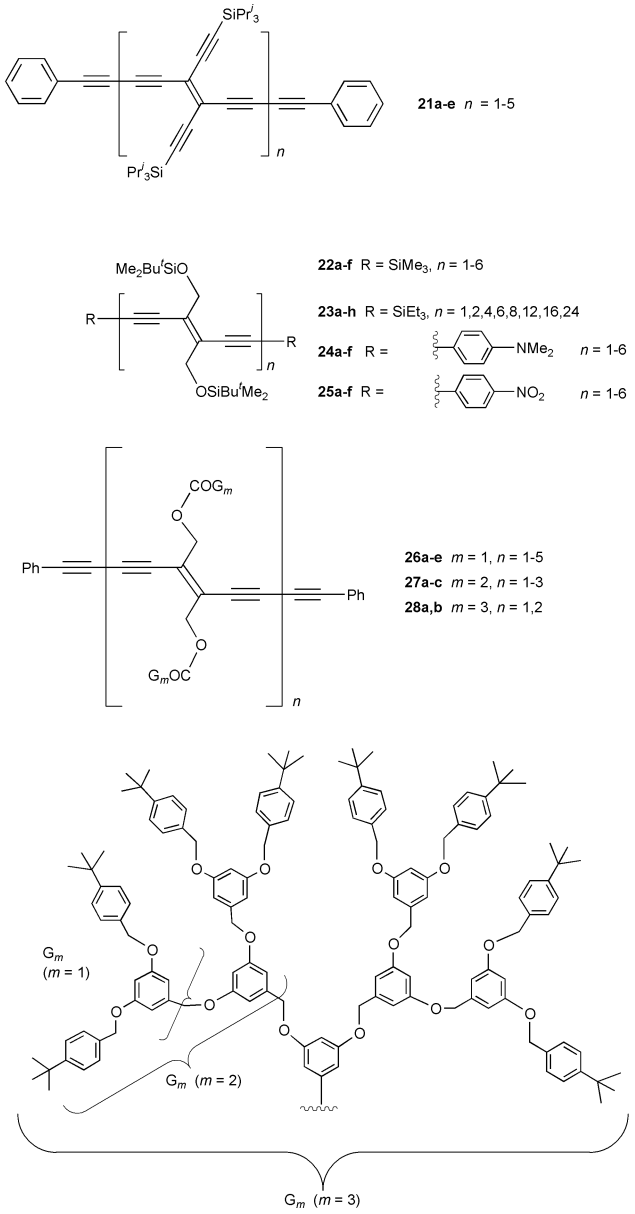

Scheme 14 Poly(triacetylene) oligomers prepared by oxidative acetylenic coupling.[78–80,82,83,85,86]

occurs at $E = -1.57$ V (*vs.* Fc/Fc$^+$ in THF) whereas the first reduction of 49.2 Å long **21e** is much more facile, occurring at -1.07 V. The highly colored oligomers are amazingly stable to air and can be stored on the laboratory bench for months without decomposition. Correspondingly, no oxidation of these rods was observed in THF below 1.0 V (*vs.* Fc/Fc$^+$).

Of particular interest was the determination of the effective conjugation length (ECL)[81] in PTA oligomers and polymers. The effective conjugation length indicates the number of repeat units in a conjugated polymer that is required to furnish size-independent properties. From the chain-length dependence of the linear and third-order nonlinear optical properties of oligomers **22a**–**f** (Scheme 14), the effective conjugation length was extrapolated in the range of 7–10 monomer units, corresponding to 42–60 carbon–carbon bonds. It is noticeable that most linearly π-conjugated polymers show an ECL in this length range.[77a,81]

In more recent work, we prepared the series of stable monodisperse PTA oligomers **23a**–**h** (Scheme 14) which extend up to a 17.8 nm long 24-mer.[82,83] This is the longest known molecular rod featuring a fully conjugated non-aromatic carbon backbone. This series enabled for the first time the investigation of the evolution of the physicochemical properties of PTAs into the higher oligomeric regime where saturation of the properties becomes apparent. In good agreement with the extrapolative studies conducted with the previous oligomeric series **22a**–**f**, evaluation of linear (UV/Vis) and nonlinear (third-harmonic generation (THG) and degenerate four-wave mixing (DFWM)) optical properties, Raman scattering and electrochemical data supported an onset of saturation at about $n = 10$ monomeric units, corresponding to 60 carbon–carbon bonds. Based on the spectroscopic data, we had proposed a preference of the molecular rods for adopting a planar s-*trans* conformation (orientation of two adjacent double bonds with respect to the bridging buta-1,3-diynediyl linker) of the π-conjugated backbone.[82] Such a conformational preference was recently confirmed by an X-ray crystal structure analysis of 4-mer **23c**.[83] The nonlinear optical investigations showed a power law dependence ($\gamma \propto n^a$ with $a \approx 2.5$) of the second hyperpolarisability γ on the number of monomeric repeat units n until a smooth saturation is reached. The experimentally observed power law dependence as well as the measured upper boundary for electron delocalisation in a one-dimensional molecular wire (about 60 carbon–carbon bonds) were nicely reproduced in quantum-mechanical calculations using the Valence Effective Hamiltonian (VEH) method combined to a Sum-Over-States (SOS) formalism.[84]

These investigations were further extended to two families of monodisperse terminally donor–donor and acceptor–acceptor functionalised PTA oligomers **24a**–**f** and **25a**–**f** (Scheme 14).[85] A dramatic influence of the end-groups on the electronic properties of these materials was observed. As an example, saturation of the linear optical properties in the donor–donor series **24a**–**f** occurred already at the stage of 4-mer **24d**, whereas the properties of the acceptor–acceptor series **24a**–**f** resembled much more those of the Me_3Si-end-capped PTA oligomers **22a**–**f**.

In another approach,[86] the PTA oligomers were dendritically encapsulated[87] into shells of Fréchet-type[88] (**26**–**28**, Scheme 14) or carbosilane dendrons.[89] As an important result, UV/Vis studies demonstrated that the insulating dendritic layers do not alter the electronic characteristics of the PTA backbone, even at higher generation level. Electronic conjugation involving the acetylenic fragments in the PTA backbone is presumably best described as being cylindrical rather than resulting from orbital overlap within a distinct plane and is therefore maintained upon rotation about C(sp)–C(sp) and C(sp)–C(sp^2) single bonds. This conclusion, which requires further validation coming from other studies, is of substantial importance for the rich area of acetylenic scaffolding.[90]

Moving further along the progression from polyacetylene to carbyne (Scheme 12), we recently prepared the first series of monodisperse poly(pentaacetylene) (PPA) oligomers **29a**–**c** (Scheme 15).[86b] Compared to the corresponding PTA oligo-

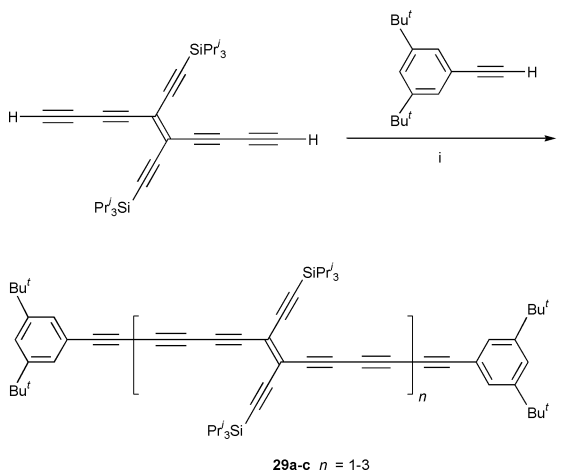

Scheme 15 Synthesis of the first poly(pentaacetylene) oligomers **29a**–**c**.[86b] i, CuCl, TMEDA, air, CH_2Cl_2, 20 °C, 10% (**29a**), 6% (**29b**), 3% (**29c**).

mers **21a**–**e**, we find the PPA derivatives much more delicate in terms of stability and processability. Therefore, it will be interesting to see how much further we will be able to move synthetically along the backbone progression leading to carbyne.

Hybrid systems

TEEs and DEEs are readily combined with other building modules for further enhancement of advanced materials properties. We prepared by Sonogashira cross-coupling a large series of mixed oligomers with a spacer inserted between two DEE moieties (Scheme 16) and found that the resulting hybrid

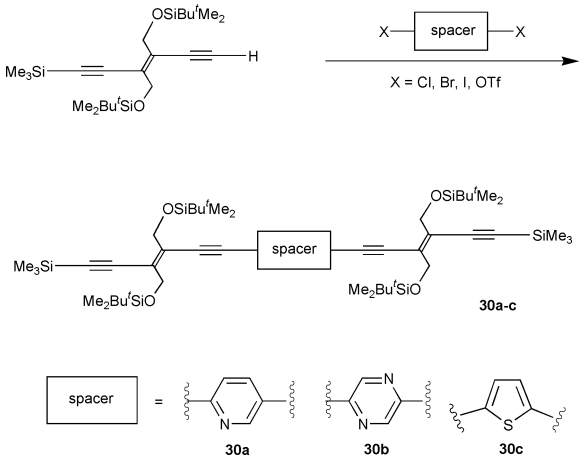

Scheme 16 Incorporation of spacer moieties into DEE oligomers.[91]

systems featured properties not displayed by the individual components.[91] Thus, the heterocyclic derivatives **30a**–**c** containing pyridine, pyrazine or thiophene spacers, respectively, showed a strong fluorescence emission (fluorescence quantum yields in $CHCl_3$ at 20 °C: Φ_F: 0.40 (**30a**), 0.65 (**30b**), 0.21 (**30c**)) which was present to a significant extent neither in DEE oligomers nor in the individual heteroaromatic spacer components. Pyridine derivative **30a** provided an interesting example of a molecular system, in which both the electronic absorption and emission characteristics can be reversibly switched as a function of pH. Upon protonation, the most intense electronic absorption band shifts from 337 to 380 nm and the fluorescence quantum yield decreases strongly from Φ_F = 0.40 to Φ_F = 0.07.

In another study, the porphyrin–DEE hybrid rods **31a**–**c**, extending in length from 2.3 (**31a**) to 3.8 (**31b**) and 5.3 nm (**31c**), were prepared by synthetic routes featuring Sonogashira cross-couplings between *meso*-iodinated porphyrin components and DEE moieties as key steps (Scheme 17).[92] Both UV/Vis and

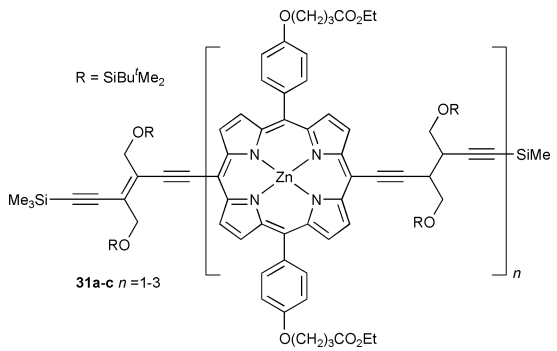

Scheme 17 Porphyrin–DEE hybrid molecular rods.[92]

electrochemical studies confirmed the existence of substantial electronic communication between the two porphyrins rings in **31b** across the *trans*-enediynediyl bridge. On the other hand, the spectra of **31b** and **31c** closely resemble each other, indicating that saturation of the optical properties in the oligomeric series already occurs at the stage of 'dimeric' **31b**. Stationary voltammetric investigations in CH_2Cl_2 showed that the terminal DEE substituents act as strong electron acceptors which induce large anodic shifts (up to ΔE = 190 mV) in the first, porphyrin-based reduction potential.

Finally, novel classes of organometallic macrocycles (such as **32**, Scheme 18)[93] and long molecular rods have become

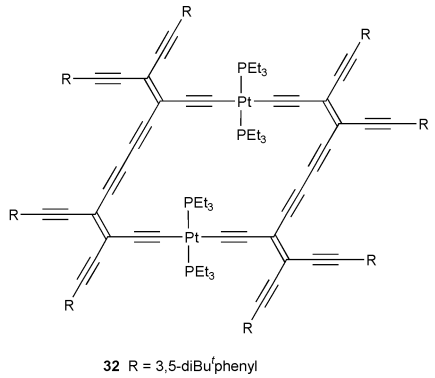

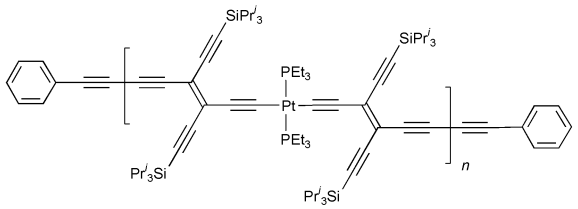

Scheme 18 Novel organometallic macrocycles and molecular rods by Pt–TEE molecular scaffolding.[93,95]

available by Pt–TEE molecular scaffolding.[94,95] The series of stable oligomers **33a**–**f** was prepared by oxidative Glaser–Hay oligomerisation under end-capping conditions. They extend in length from 3.3 (monomeric **33a**) to 12.1 nm (hexameric **33f**). Both linear and nonlinear optical properties of these compounds revealed an almost complete lack of π-electron conjugation along the linear backbones due to the insulating character of the Pt centers and the absence of π-character in the Pt–C(sp) bonds. Purification, separation and characterisation of these remarkable organic–inorganic hybrid materials reached the performance limits of currently available analytical and preparative gel permeation chromatography.

Conclusions

Ten years after we started this research, tetraethynylethene (TEE) and (*E*)-diethynylethene ((*E*)-DEE) building blocks clearly represent one of the most versatile known molecular construction kits for the development of functional molecular architecture. Acetylenic scaffolding, starting from these modules, provided donor–acceptor substituted chromophores with exceptional optical nonlinearities, monodisperse poly(triacetylene) (PTA) oligomers with linearly π-conjugated all-carbon backbones expanding to unprecedented lengths, large carbon sheets with unusual chromophoric properties and a new class of light-driven molecular switches. This research has clearly contributed to expanding the limits in size and complexity of stable, monodisperse functional scaffolds that are accessible by organic synthesis. At the same time, it has advanced the fundamental knowledge of π-electron delocalisation in acetylenic molecular architecture. Only the tip of an immense 'iceberg' of structural diversity accessible through TEE and

DEE scaffolding has been explored today, and this chemistry will undoubtfully provide in the future many new classes of chromophores with multinanometer dimensions which could find use in optoelectronic devices and in the development of molecular-scale electronic circuitry.

I thank the many co-workers and collaborators for their enthusiastic contributions to this research; their names are included in the literature references. Funding for this work was provided by the Swiss National Science Foundation and the ETH research council (TEMA grant and joint grant with Professor P. Günter).

Notes and references

1 C. Glaser, *Ber. Dtsch. Chem. Ges.*, 1869, **2**, 422.
2 P. Siemsen, R. C. Livingston and F. Diederich, *Angew. Chem., Int. Ed.*, 2000, **39**, 2632.
3 A. Baeyer, *Ber. Dtsch. Chem. Ges.*, 1885, **18**, 674.
4 G. Eglinton and A. R. Galbraith, *Chem. Ind. (London)*, 1956, 737.
5 F. Sondheimer and R. Wolovsky, *J. Am. Chem. Soc.*, 1959, **81**, 1771.
6 F. Sondheimer, *Pure Appl. Chem.*, 1963, **7**, 363.
7 F. Sondheimer, *Acc. Chem. Res.*, 1972, **5**, 81.
8 H. A. Staab, J. Ipaktschi and A. Nissen, *Chem. Ber.*, 1971, **104**, 1182.
9 M. Nakagawa, *Angew. Chem., Int. Ed.*, 1979, **18**, 202.
10 A. S. Hay, *J. Org. Chem.*, 1962, **27**, 3320.
11 W. Chodkiewicz and P. Cadiot, *C. R. Hebd. Séances Acad. Sci.*, 1955, **241**, 1055.
12 *Metal-catalyzed Cross-coupling Reactions*, ed. F. Diederich and P. J. Stang, Wiley-VCH, Weinheim, 1998.
13 U. H. F. Bunz and L. Kloppenburg, *Angew. Chem., Int. Ed.*, 1999, **38**, 478.
14 H. W. Kroto, J. R. Heath, S. C. O'Brien, R. F. Curl and R. E. Smalley, *Nature*, 1985, **318**, 162.
15 F. Diederich and Y. Rubin, *Angew. Chem., Int. Ed.*, 1992, **31**, 1101.
16 F. Diederich, *Nature*, 1994, **369**, 199.
17 F. Diederich, Y. Rubin, C. B. Knobler, R. L. Whetten, K. E. Schriver, K. N. Houk and Y. Li, *Science*, 1989, **245**, 1088.
18 S. W. McElvany, M. M. Ross, N. S. Goroff and F. Diederich, *Science*, 1993, **259**, 1594.
19 N. S. Goroff, *Acc. Chem. Res.*, 1996, **29**, 77.
20 A. T. Balaban, *Comput. Math. Applic.*, 1989, **17**, 397.
21 R. Gleiter and R. Merger, in *Modern Acetylene Chemistry*, ed. P. J. Stang and F. Diederich, VCH, Weinheim, 1995, p. 285.
22 L. T. Scott and M. J. Cooney, in ref. 21, p. 321.
23 U. H. F. Bunz, Y. Rubin and Y. Tobe, *Chem. Soc. Rev.*, 1999, **28**, 107.
24 J. S. Moore, *Acc. Chem. Res.*, 1997, **30**, 402.
25 W. J. Youngs, C. A. Tessier and J. D. Bradshaw, *Chem. Rev.*, 1999, **99**, 3153.
26 R. J. Puddephatt, *Chem. Commun.*, 1998, 1055.
27 M. A. Reed and J. M. Tour, *Sci. Am.*, 2000, **282**, (6), 86.
28 H. Hopf, *Classics in Hydrocarbon Chemistry*, Wiley-VCH, Weinheim, 2000.
29 A. de Meijere and S. I. Kozhushkov, *Top. Curr. Chem.*, 1999, **201**, 1.
30 F. Diederich and L. Gobbi, *Top. Curr. Chem.*, 1999, **201**, 43.
31 M. M. Haley, J. J. Park and S. C. Brand, *Top. Curr. Chem.*, 1999, **201**, 81.
32 U. H. F. Bunz, *Top. Curr. Chem.*, 1999, **201**, 131.
33 Y. Hori, K. Noda, S. Kobayashi and H. Taniguchi, *Tetrahedron Lett.*, 1969, 3563.
34 H. Hopf, M. Kreutzer and P. G. Jones, *Chem. Ber.*, 1991, **124**, 1471.
35 (*a*) H. Hauptmann, *Angew. Chem., Int. Ed.*, 1975, **14**, 498; (*b*) H. Hauptmann, *Tetrahedron*, 1976, **32**, 1293.
36 Y. Rubin, C. B. Knobler and F. Diederich, *Angew. Chem., Int. Ed.*, 1991, **30**, 698.
37 R. R. Tykwinski and F. Diederich, *Liebigs Ann./Recueil*, 1997, 649.
38 J. Anthony, A. M. Boldi, Y. Rubin, M. Hobi, V. Gramlich, C. B. Knobler, P. Seiler and F. Diederich, *Helv. Chim. Acta*, 1995, **78**, 13.
39 M. Schreiber, J. Anthony, F. Diederich, M. E. Spahr, R. Nesper, M. Hubrich, F. Bommeli, L. Degiorgi, P. Wachter, P. Kaatz, C. Bosshard, P. Günter, M. Colussi, U. W. Suter, C. Boudon, J.-P. Gisselbrecht and M. Gross, *Adv. Mater.*, 1994, **6**, 786. Although the Stille coupling described in the original work provides better yields, we prefer using the Sonogashira cross-coupling shown in Scheme 2.
40 (*a*) G. Hynd, G. B. Jones, G. W. Plourde, II and J. M. Wright, *Tetrahedron Lett.*, 1999, **40**, 4481; (*b*) G. B. Jones, J. M. Wright, G. W. Plourde, II, G. Hynd, R. S. Huber and J. E. Mathews, *J. Am. Chem. Soc.*, 2000, **122**, 1937.
41 R. R. Tykwinski, F. Diederich, V. Gramlich and P. Seiler, *Helv. Chim. Acta*, 1996, **79**, 634.
42 R. G. Bergman, *Acc. Chem. Res.*, 1973, **6**, 25.
43 K. C. Nicolaou and W.-M. Dai, *Angew. Chem., Int. Ed.*, 1991, **30**, 1387.
44 For X-ray crystal structures, see for example: (*a*) ref. 38; (*b*) R. R. Tykwinski, A. Hilger, F. Diederich, H. P. Lüthi, P. Seiler, V. Gramlich, J.-P. Gisselbrecht, C. Boudon and M. Gross, *Helv. Chim. Acta*, 2000, **83**, 1484; (*c*) R. R. Tykwinski, M. Schreiber, R. P. Carlon and F. Diederich, *Helv. Chim. Acta*, 1996, **79**, 2249; (*d*) J.-F. Nierengarten, M. Schreiber, F. Diederich and V. Gramlich, *New. J. Chem.*, 1996, **20**, 1273; (*e*) R. E. Martin, U. Gubler, C. Boudon, V. Gramlich, C. Bosshard, J.-P. Gisselbrecht, P. Günter, M. Gross and F. Diederich, *Chem. Eur. J.*, 1997, **3**, 1505; (*f*) R. R. Tykwinski, M. Schreiber, V. Gramlich, P. Seiler and F. Diederich, *Adv. Mater.*, 1996, **8**, 226.
45 For theoretical calculations, see: (*a*) B. Ma, Y. Xie and H. F. Schaefer III, *Chem. Phys. Lett.*, 1992, **191**, 521; (*b*) B. Ma, H. M. Sulzbach, Y. Xie and H. F. Schaefer III, *J. Am. Chem. Soc.*, 1994, **116**, 3529; (*c*) A. Hilger, J.-P. Gisselbrecht, R. R. Tykwinski, C. Boudon, M. Schreiber, R. E. Martin, H. P. Lüthi, M. Gross and F. Diederich, *J. Am. Chem. Soc.*, 1997, **119**, 2069.
46 C. Boudon, J.-P. Gisselbrecht, M. Gross, J. Anthony, A. M. Boldi, R. Faust, T. Lange, D. Philp, J.-D. van Loon and F. Diederich, *J. Electroanal. Chem.*, 1995, **394**, 187.
47 For attempted reactions at the central double bond of TEE derivatives, see for example: T. Lange, J.-D. van Loon, R. R. Tykwinski, M. Schreiber and F. Diederich, *Synthesis*, 1996, 537.
48 Epoxide **5** was characterised by X-ray crystallography; T. Lange, ETH Dissertation No. 12036, Zürich 1997.
49 (*a*) F. Diederich, D. Philp and P. Seiler, *J. Chem. Soc., Chem. Commun.*, 1994, 205; (*b*) D. Philp, V. Gramlich, P. Seiler and F. Diederich, *J. Chem. Soc., Perkin Trans. 2*, 1995, 875.
50 H. Taniguchi, K. Hayashi, K. Nishioka, Y. Hori, M. Shiro and T. Kitamura, *Chem. Lett.*, 1994, 1921.
51 R. E. Martin, J. Bartek, F. Diederich, R. R. Tykwinski, E. C. Meister, A. Hilger and H. P. Lüthi, *J. Chem. Soc., Perkin Trans. 2*, 1998, 233.
52 H. Meier, *Angew. Chem., Int. Ed.*, 1992, **31**, 1399.
53 S. Malkin and E. Fischer, *J. Phys. Chem.*, 1962, **66**, 2482.
54 For examples of thermally bistable, fully light-driven switches, see: (*a*) S. Kobatake, M. Yamada, T. Yamada and M. Irie, *J. Am. Chem. Soc.*, 1999, **121**, 8450; (*b*) A. Fernandez-Acebes and J.-M. Lehn, *Chem. Eur. J.*, 1999, **5**, 3285; (*c*) E. M. Geertsema, A. Meetsma and B. L. Feringa, *Angew. Chem., Int. Ed.*, 1999, **38**, 2738; (*d*) Y. Yokoyama, T. Iwai, N. Kera, I. Hitomi and Y. Kurita, *Chem. Lett.*, 1990, 263.
55 V. Balzani, M. Gomez-Lopez and J. F. Stoddart, *Acc. Chem. Res.*, 1998, **31**, 405.
56 L. Gobbi, P. Seiler, F. Diederich and V. Gramlich, *Helv. Chim. Acta*, 2000, **83**, 1711.
57 L. Gobbi, P. Seiler and F. Diederich, *Angew. Chem., Int. Ed.*, 1999, **38**, 674.
58 S. Gierisch and J. Daub, *Chem. Ber.*, 1989, **122**, 69.
59 S. Lecomte, U. Gubler, M. Jäger, C. Bosshard, G. Montemezzani, P. Günter, L. Gobbi and F. Diederich, *Appl. Phys. Lett.*, 2000, **77**, 921.
60 (*a*) C. Bosshard, R. Spreiter, P. Günter, R. R. Tykwinski, M. Schreiber and F. Diederich, *Adv. Mater.*, 1996, **8**, 231; (*b*) R. R. Tykwinski, U. Gubler, R. E. Martin, F. Diederich, C. Bosshard and P. Günter, *J. Phys. Chem. B*, 1998, **102**, 4451.
61 R. Spreiter, C. Bosshard, G. Knöpfle, P. Günter, R. R. Tykwinski, M. Schreiber and F. Diederich, *J. Phys. Chem. B*, 1998, **102**, 29.
62 J. J. Wolff, F. Siegler, R. Matschiner and R. Wortmann, *Angew. Chem., Int. Ed.*, 2000, **39**, 1436.
63 C. Bosshard, K. Sutter, P. Pretre, J. Hulliger, M. Flörsheimer, P. Kaatz and P. Günter, *Organic Nonlinear Optical Materials*, Gordon and Breach, Basel, 1995.
64 U. Gubler, R. Spreiter, C. Bosshard, P. Günter, R. R. Tykwinski and F. Diederich, *Appl. Phys. Lett.*, 1998, **73**, 2396.
65 J. Anthony, C. B.Knobler and F. Diederich, *Angew. Chem., Int. Ed.*, 1993, **32**, 406.
66 J. Anthony, A. M. Boldi, C. Boudon, J.-P. Gisselbrecht, M. Gross, P. Seiler, C. B. Knobler and F. Diederich, *Helv. Chim. Acta*, 1995, **78**, 797.
67 S. Eisler and R. R. Tykwinski, *Angew. Chem., Int. Ed.*, 1999, **38**, 1940.
68 A. M. Boldi and F. Diederich, *Angew. Chem., Int. Ed.*, 1994, **33**, 468.
69 M. Schreiber, R. R. Tykwinski, F. Diederich, R. Spreiter, U. Gubler, C. Bosshard, I. Poberaj, P. Günter, C. Boudon, J.-P. Gisselbrecht, M. Gross, U. Jonas and H. Ringsdorf, *Adv. Mater.*, 1997, **9**, 339.
70 For the first report on a TEE dimer, see: A. M. Boldi, J. Anthony, C. B. Knobler and F. Diederich, *Angew. Chem., Int. Ed.*, 1992, **31**, 1240.
71 J. A. Walker, S. P. Bitler and F. Wudl, *J. Org. Chem.*, 1984, **49**, 4733.

72 (*a*) H. Shirakawa, E. J. Louis, A. G. MacDiarmid, C. K. Chiang and A. J. Heeger, *J. Chem. Soc., Chem. Commun.*, 1977, 578; (*b*) E. J. Ginsburg, C. B. Gorman and R. H. Grubbs in ref. 21, p. 353.
73 (*a*) G. Wegner, *Angew. Chem., Int. Ed.*, 1981, **20**, 361; (*b*) G. W. Coates, A. R. Dunn, L. W. Henling, D. A. Dougherty and R. H. Grubbs, *Angew. Chem., Int. Ed.*, 1997, **36**, 248.
74 R. Eastmond, T. R. Johnson and D. R. M. Walton, *Tetrahedron*, 1972, **28**, 4601.
75 R. H. Baughman, J. L. Brédas, R. R. Chance, R. L. Elsenbaumer and L. W. Shacklette, *Chem. Rev.*, 1982, **82**, 209.
76 J. Xiao, M. Yang, J. W. Lauher and F. W. Fowler, *Angew. Chem., Int. Ed.*, 2000, **39**, 2132.
77 (*a*) R. E. Martin and F. Diederich, *Angew. Chem., Int. Ed.*, 1999, **38**, 1350; (*b*) *Electronic Materials: The Oligomeric Approach*, ed. K. Müllen and G. Wegner, Wiley-VCH, Weinheim, 1998.
78 J. Anthony, C. Boudon, F. Diederich, J.-P. Gisselbrecht, V. Gramlich, M. Gross, M. Hobi and P. Seiler, *Angew. Chem., Int. Ed.*, 1994, **33**, 763.
79 A. M. Boldi, J. Anthony, V. Gramlich, C. B. Knobler, C. Boudon, J.-P. Gisselbrecht, M. Gross and F. Diederich, *Helv. Chim. Acta*, 1995, **78**, 779.
80 R. E. Martin, U. Gubler, C. Boudon, V. Gramlich, C. Bosshard, J.-P. Gisselbrecht, P. Günter, M. Gross and F. Diederich, *Chem. Eur. J.*, 1997, **3**, 1505.
81 H. Meier, U. Stalmach and H. Kolshorn, *Acta Polymer.*, 1997, **48**, 379.
82 (*a*) R. E. Martin, T. Mäder and F. Diederich, *Angew. Chem., Int. Ed.*, 1999, **38**, 817; (*b*) R. E. Martin, U. Gubler, J. Cornil, M. Balakina, C. Boudon, C. Bosshard, J.-P. Gisselbrecht, F. Diederich, P. Günter, M. Gross and J.-L. Brédas, *Chem. Eur. J.*, 2000, **6**, 3622.
83 M. Edelmann, V. Gramlich and F. Diederich, *Helv. Chim. Acta*, in press.
84 U. Gubler, C. Bosshard, P. Günter, M. Y. Balakina, J. Cornil, J. L. Brédas, R. E. Martin and F. Diederich, *Opt. Lett.*, 1999, **24**, 1599.
85 R. E. Martin, U. Gubler, C. Boudon, C. Bosshard, J.-P. Gisselbrecht, P. Günter, M. Gross and F. Diederich, *Chem. Eur. J.*, 2000, **6**, 4400.
86 (*a*) A. P. H. J. Schenning, R. E. Martin, M. Ito, F. Diederich, C. Boudon, J.-P. Gisselbrecht and M. Gross, *Chem. Commun.*, 1998, 1013; (*b*) A. P. H. J. Schenning, J.-D. Arndt, M. Ito, A. Stoddart, M. Schreiber, P. Siemsen, R. E. Martin, C. Boudon, J.-P. Gisselbrecht, M. Gross, V. Gramlich and F. Diederich, *Helv. Chim. Acta*, in press.
87 A. D. Schlüter and J. P. Rabe, *Angew. Chem., Int. Ed.*, 2000, **39**, 864.
88 C. J. Hawker and J. M. J. Fréchet, *J. Chem. Soc., Chem. Commun.*, 1990, 1010.
89 A. W. van der Made and P. W. N. M. van Leeuwen, *J. Chem. Soc., Chem. Commun.*, 1992, 1400.
90 For other series of functional PTA oligomers, see: (*a*) J.-F. Nierengarten, D. Guillon, B. Heinrich and J. F. Nicoud, *Chem. Commun.*, 1997, 1233; (*b*) R. E. Martin, M. Pannier, F. Diederich, V. Gramlich, M. Hubrich and H. W. Spiess, *Angew. Chem., Int. Ed.*, 1998, **37**, 2834; (*c*) E. M. Maya, P. Vazquez, T. Torres, L. Gobbi, F. Diederich, S. Pyo and L. Echegoyen, *J. Org. Chem.*, 2000, **65**, 823.
91 R. E. Martin, J. A. Wytko, F. Diederich, C. Boudon, J.-P. Gisselbrecht and M. Gross, *Helv. Chim. Acta*, 1999, **82**, 1470.
92 J. Wytko, V. Berl, M. McLaughlin, R. R. Tykwinski, M. Schreiber, F. Diederich, C. Boudon, J.-P. Gisselbrecht and M. Gross, *Helv. Chim. Acta*, 1998, **81**, 1964.
93 R. Faust, F. Diederich, V. Gramlich and P. Seiler, *Chem. Eur. J.*, 1995, **1**, 111.
94 F. Diederich, R. Faust, V. Gramlich and P. Seiler, *J. Chem. Soc., Chem. Commun.*, 1994, 2045.
95 P. Siemsen, U. Gubler, C. Bosshard, P. Günter and F. Diederich, *Chem. Eur. J.*, in press.

ChemComm

Post-photoaffinity labeling modification using aldehyde chemistry to produce a fluorescent lectin toward saccharide-biosensors†

Tsuyoshi Nagase, Seiji Shinkai and Itaru Hamachi*‡

Department of Chemistry and Biochemistry, Graduate School of Engineering, Kyushu University, Fukuoka, 812-8581, +PRESTO, JST, Japan. E-mail: itarutcm@mbox.nc.kyushu-u.ac.jp

Received (in Cambridge, UK) 16th October 2000, Accepted 14th December 2000
First published as an Advance Article on the web 11th January 2001

A new method to construct a fluorescent saccharide biosensor based on a lectin protein is successfully proposed using post-photoaffinity labeling modification coupled to aldehyde chemistry.

A biosensor is regarded as one of the ideal systems to monitor ions and molecules of biological importance both *in vivo* and *in vitro*,[1,2] since a protein framework can provide a superior molecular recognition scaffold. To carry out the rational coupling of a signal transduction device with the molecular recognition events on a protein scaffold, most examples rely upon site-directed mutagenesis,[3] GFP (green fluorescent protein) fusion strategy[4] and protein total-[5] or semi-[6]synthesis. In contrast to genetic technologies, however, chemistry-based versatile methods for the manipulation of biomacromolecules have not been satisfactorily developed. In fact, there are still limited numbers of procedures that are capable of the site-directed introduction of unique thiol[3] or ketone[7] groups into native proteins in order to tag unnatural signaling molecules.

We describe herein a new method named as '*post-photoaffinity labeling modification*' to construct a fluorescent saccharide-biosensor based on a naturally occurring saccharide-binding protein, concanavalin A (Con A). Con A, a kind of lectin family, can bind α-D-mannoside and α-D-glucoside derivatives selectively.[8] An active site-directed modification of the lectin was conducted by the photoaffinity-labeling technique using *p*-azidophenyl-α-D-mannopyranoside **1**. The subsequent oxidative degradation of the mannose part to produce aldehyde tags, followed by the chemical modification with a hydrazine derivative yields a fluorescent lectin.

The affinity ligand **1** which has both a α-mannoside unit, the strongest monosaccharide ligand for Con A, and a phenylazide group as a photoaffinity labeling group was synthesized as shown in Scheme 1. Peracetylmannose was glycosylated by *p*-nitrophenol in the presence of $BF_3{\cdot}Et_2O$,[9] followed by deacylation with NaOMe and conversion of the nitro-group to azide in the conventional manner to afford the target **1**.[10]

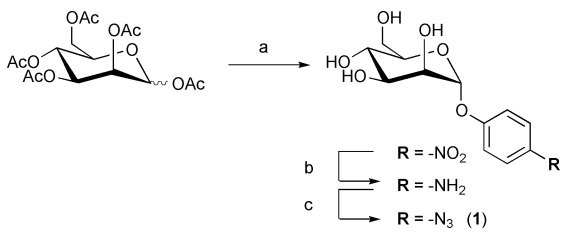

Scheme 1 Synthesis of photoaffinity labeling reagent **1.** *Reagents and conditions*: (a) (i) *p*-nitrophenol, $BF_3{\cdot}Et_2O$ (1 eq.), dry CH_2Cl_2, rt, 3 days; (ii) NaOMe, dry MeOH, rt, 2 h (55% for 2 steps). (b) 10% Pd/C, MeOH, rt, 30 min (95%). (c) (i) $NaNO_2$, 0.4 M HCl, 0 °C, 30 min; (ii) NaN_3, 0 °C, 20 min (61%).

The post-photoaffinity labeling modification for Con A is briefly outlined in Scheme 2. When the ligand **1** was bound to the binding pocket of Con A, photolabeling *via* nitrene generation was carried out by UV light irradiation (λ = 254 nm).[10] The labeled Con A was purified by gel chromatography (Biogel-P-30), followed by affinity chromatography (Sephadex G-100). Two fractions bearing the lessened affinity to the Sephadex column than native Con A were obtained.† The analysis by MALDI-TOF mass spectroscopy shows that the first fraction showing no affinity to Sephadex is a Con A homodimer, the monomer of which is modified with 1 mole of **1** (a mass peak appeared only at 25 850 ± 10 due to Con A plus **1**), and the second one showing moderate affinity is a heterodimer that comprises the modified Con A monomer (1 mole of **1** per 1 mole of Con A**)** and the unmodified monomer [two mass peaks appeared at 25 850 ± 10 and 25 583 (native Con A)]. The total yield of the modified Con A is about 30%. To determine the labeled site, the labeled Con A was digested by lysyl-endopeptidase (at 37 °C, pH 9.0 for 15 h in the presence of 3 M urea).[11] The HPLC (ODS column) and MALDI-TOF mass analyses of the digested peptides showed that only two fragments [the peptide 1 (A1-K30) and the peptide 6 (R60-K101)] among 10 fragments of the digested peptide were labeled with 1 mole of the ligand **1**. The crystal structure of Con A[12] shows that these two peptides are strongly involved in the sugar binding. Especially, Tyr12 in fragment 1 and Tyr100 in fragment 6 form a hydrophobic fence of the binding pocket. These reasonably suggest that the photoaffinity labeling reaction site-selectively proceeds under the present conditions. Subsequently, the mannose unit of **1** introduced by photoaffinity labeling can be converted by oxidation with periodate (IO_4^-) under mild conditions into unique aldehyde groups (CHO-Con A),[13] that can be chemoselectively labeled with hydrazine- or aminooxy-appended fluorophores [DCCH-Con A in the case of DCCH (a coumarin derivative)-hydrazine].[14]

Secondary structure of the modified Con As was monitored by CD spectroscopy. A negative Cotton peak at 218 nm, characteristic of the typical β-sheet, in all of the modified Con As (the labeled, CHO-, and DCCH-Con A), is comparable to that of native Con A,[15] suggesting that the secondary structure is not significantly disturbed by the present modification.

DCCH-Con A showed an absorption at 435 nm[16] (Fig. 1a) and a strong fluorescence at 485 nm (excitation at 435 nm), due to the coumarin unit, an environmentally sensitive fluorophore. Thus, we monitored emission spectral changes of DCCH-Con A by the addition of methyl-α-D-mannoside (Me-α-Man), the strongest mono-saccharide ligand for native Con A (inset of Fig. 1b). With increasing concentration of Me-α-Man, the emission intensity at 485 nm is gradually lessened and the change is saturated at less than 10 mM. The saturation curve (Fig. 1b) obtained by the fluorescent titration can be analyzed by a Benesi–Hildebrandt plot to give a binding constant of 1.9×10^3 M^{-1} for Me-α-Man. Similar saturation curves were observed in the fluorescent titration of other types of saccharides and the association constants are determined as summa-

† Electronic supplementary information (ESI) available: experimental and spectral data for **1**, and a colour version of Scheme 2. See http://www.rsc.org/suppdata/cc/b0/b008323m/

‡ Visiting Professor at the Institute of Molecular Science, Okazaki, 444-8585, Japan.

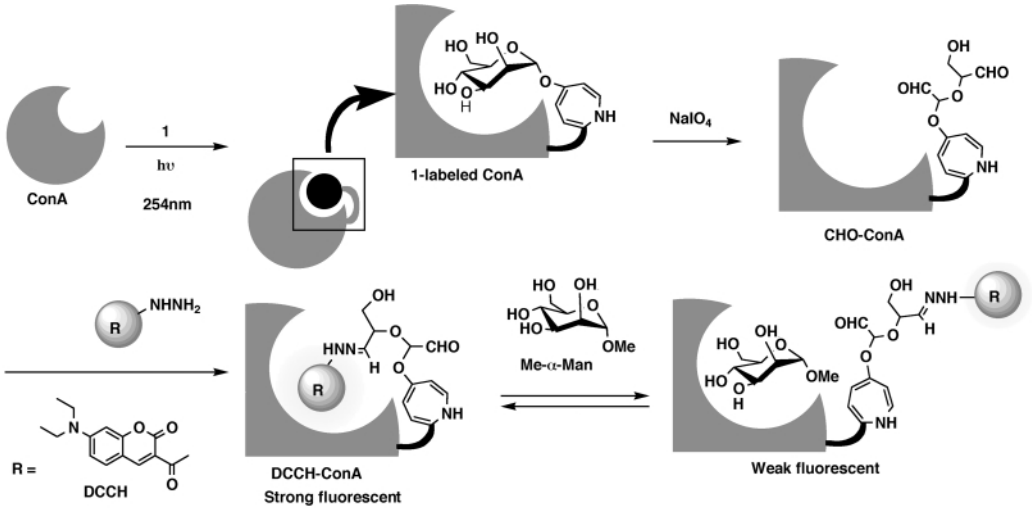

Scheme 2 Schematic illustration for semisynthesis of DCCH-ConA. The typical structures of the oxidative degradation of mannose are shown.

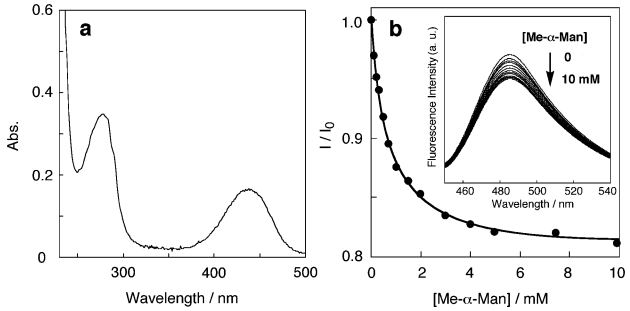

Fig. 1 (a) UV-vis spectrum of DCCH-ConA; (b) fluorescence titration curve of DCCH-ConA with Me-α-Man. [DCCH-ConA] = 3 μM, 50 mM HEPES buffer (pH 7.0), 1 mM $MnCl_2$, 1 mM $CaCl_2$, 0.1 M NaCl at 15 ±1 °C, λ_{ex} = 435 nm; inset: fluorescence spectral change of DCCH-ConA by the addition of Me-α-Man.

Table 1 The binding constants (*K*) of DCCH-ConA for saccharides

	K/M^{-1}	
Saccharide	DCCH-ConA	Native ConA
Me-α-mannoside	1900	11 000[a]
Me-α-glucoside	1450	3 000[a]
Me-β-glucoside	520	—[b]
Me-α-glactoside	570	—[b]

[a] Ref. 16. [b] The binding constants for Me-α-galactoside and Me-β-glucoside have not been reported because of their low affinity.

rized in Table 1. It is clear that the order of the affinity constants for various saccharides is the same as that of native Con A (Me-α-Man > Me-α-Glc > Me-α-Gal, Me-β-Glc), although the affinity constants are lower than the literature values of native Con A[17] determined by ITC (isothermal titration calorimetry) measurement. Significantly these results imply that the molecular recognition event occurring in the binding pocket of DCCH-Con A can be directly transduced by the fluorescence signal. This is the first step toward the rational design of fluorescent saccharide biosensors based on lectins. The reduced selectivity of DCCH-ConA might be due to the partial blocking of the sugar-binding pocket by the appended fluorophore and/or the structural disturbance of the binding site by the unnatural groups. Details are now under investigation in our laboratory.

We believe that this strategy is so general that other fluorescent biosensors may be produced showing different saccharide specificities by the simple replacement of the sugar part of **1** and the usage of the corresponding lectin.

T. N. is a JSPS fellow for Japanese Junior Scientists. This research was partially supported by a specially promoted area (Biotargeting, No. 12019258) and a Grant-in-Aid for COE Research (No. 08CE2005) from the Ministry of Education, Science, Sports and Culture of Japan.

Notes and references

1 For reviews, see; (*a*) D. A. Zachrias, G. S. Baird and R. Y. Tsien, *Curr. Opin. Neurobiol.*, 2000, **10**, 416; (*b*) H. W. Hellinga and J. S. Marvin, *Trends Biotechnol.*, 1998, **16**, 183; (*c*) K. A. Giuliano and D. L. Taylor, *Trends Biotechnol.*, 1998, **16**, 135.

2 Synthetic chemosensors for saccharides have been actively developed in recent years. T. D. James, S. Samankumara and S. Shinkai, *Angew. Chem., Int. Ed. Engl.*, 1996, **35**, 1910.

3 (*a*) J. S. Marvin and H. W. Hellinga, *J. Am. Chem. Soc.*, 1998, **120**, 7; (*b*) G. Gilardi, G. Mei, N. Rosato, A. F. Agro and A. E. G. Cass, *Protein Eng.*, 1997, **5**, 479; (*c*) G. Gilardi, L. Q. Zhou, L. Hibbert and A. E. G. Cass, *Anal. Chem.*, 1994, **66**, 3840.

4 A. Miyawaki, J. Llopis, R. Heim, J. M. McCaffery, J. A. Adams, M. Ikura and R. Y. Tsien, *Nature*, 1997, **388**, 882.

5 (*a*) J. R. Sydor, C. Herrmann, S. B. H. Kent, R. S. Doody and M. Engelhard, *Proc. Nat. Acad. Sci. USA*, 1999, **96**, 7865; (*b*) G. K. Walkup and B. Imperiali, *J. Am. Chem. Soc.*, 1996, **118**, 3053.

6 (*a*) G. J. Cotton and T. W. Muir, *Chem. Biol.*, 2000, **7**, 253; (*b*) I. Hamachi, R. Eboshi, J. Watanabe and S. Shinkai, *J. Am. Chem. Soc.*, 2000, **122**, 4530; (*c*) I. Hamachi, T. Nagase and S. Shinkai, *J. Am. Chem. Soc.*, 2000, **122**, 12 065.

7 V. W. Cornish, K. M. Hahn and P. G. Schultz, *J. Am. Chem. Soc.*, 1996, **118**, 8150.

8 (*a*) H. Bittiger and H. P. Schnebli, *Concanavalin A as a Tool*, John Wiley and Sons, New York, 1976; (*b*) H. Lis and N. Sharon, *Chem. Rev.*, 1998, **98**, 637 and references therein.

9 E. Smits, J. B. F. N. Engberts, R. M. Kellogg and H. A. Doren, *J. Chem. Soc., Perkin Trans. 1*, 1996, 2873.

10 M. Beppu, T. Terao and T. Osawa, *J. Biochem.*, 1975, **78**, 1013. The labeling reagent **1** was identified by FTIR and ^{1}H-NMR.†

11 Y. Shikata, M. Kuwada, Y. Hayashi, A. Hashimoto, A. Koide and N. Asakawa, *Anal. Chim. Acta*, 1998, **365**, 241.

12 J. H. Naismith, C. Emmerich, J. Habash, S. J. Harrop, J. R. Helliwell, W. N. Hunter, J. Raftery, A. J. Kalb and J. Yarib, *Acta Crystallogr., Sect. D*, 1994, **50**, 847.

13 G. A. Lemieux and C. R. Bertozzi, *Trends Biotechnol.*, 1998, **16**, 506.

14 Chemical modification of the aldehyde group produced by the sugar oxidation with $NaIO_4$ is a traditional method to modify glycoproteins (*e.g.* antibody) and RNA with hydrazine derivatives. It has been reported that the mild oxidation does not affect protein function. See the following review articles; (*a*) D. J. O'Shannessy and M. Wilchek, *Anal. Biochem.*, 1990, **191**, 1; (*b*) D. J. O'Shannessy and R. H. Quarles, *J. Immunol. Methods*, 1987, **99**, 153.

15 M. S. Herrmann, L. M. Richardson, L. M. Setzler and W. D. Behnke, *Biopolymers*, 1978, **17**, 2107.

16 UV-vis spectrum of DCCH-ConA showed that 0.5 mol of DCCH was labeled for 1 mol of ConA monomer. This may be due to the incomplete oxidation of the mannose unit. Although the further oxidation for longer than 20 h to complete sugar oxidation was attempted, it was unsuccessful.

17 (*a*) F. P. Schwarz, K. D. Puri, R. G. Bhat and A. Surolia, *J. Biol. Chem.*, 1993, **268**, 7668; (*b*) D. K. Mandal, N. Kishore and C. F. Brewer, *Biochemistry*, 1994, **33**, 1149.

Anion binding by multidentate Lewis acids: a DFT study†

Simon Aldridge,* Ian A. Fallis and Siân T. Howard

Department of Chemistry, Cardiff University, PO Box 912, Cardiff, UK CF10 3TB. E-mail: AldridgeS@cf.ac.uk

Received (in Cambridge, UK) 18th September 2000, Accepted 5th December 2000
First published as an Advance Article on the web 15th January 2001

Density functional studies of model tribora-macrocyclic Lewis acids indicate extremely strong binding of the methyl anion, which in some cases exceeds that of $B(C_6F_5)_3$. In addition anion selectivity for the fluoride ion is implied by binding energies *ca.* 200 kJ mol^{-1} greater than those of other halides.

The formation of donor/acceptor complexes exploiting the well known Lewis acidic nature of organo-boranes and -alanes has been the subject of much recent research interest.[1] In part, this stems from the role of species such as MAO or $B(C_6F_5)_3$ as hydride or alkide abstractors in the generation of highly active cationic olefin polymerisation catalysts.[2] In such cases the activity and stability of catalysts are known to be strongly dependent on the extent of interactions between the cationic transition metal species and the anionic donor/acceptor complex.[3] Attempts have been made to manipulate the nature and strength of ion pairing interactions in solution, for example through the use of sterically more encumbered Lewis acids.[4] An alternative to the manipulation of the steric environment about the Lewis acidic centre is the incorporation of additional acceptor sites within a multidentate framework. By analogy with classical chelating agents such species offer the possibility for even stronger anion binding and the greater delocalisation of negative charge. Recently several groups have investigated this

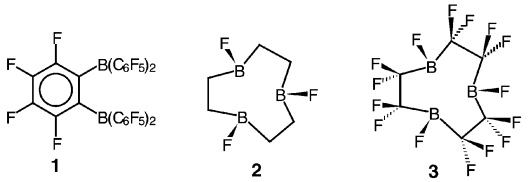

approach using bifunctional Lewis acids such as **1**.[5] A logical extension of this strategy is the development of macrocyclic multidentate Lewis acids. Classical macrocyclic donor ligands are well noted for the formation of exceptionally stable metal complexes and for slow dissociation kinetics.[6] In addition, by the incorporation of acceptor sites into a medium-sized cyclic structure ring strain is released on anion binding *via* the pyramidalization of planar boron centres.

This work explores the nature of two such model compounds, 1,4,7-trifluoro-1,4,7-triboracyclononane **2** and perfluoro-1,4,7-triboracyclononane **3**, and their complexes with a number of anions (H^-, F^-, Cl^-, Br^-, CH_3^-). To facilitate quantitative interpretation of the results, the binding energy of tris(pentafluorophenyl)borane **4** with CH_3^- has also been computed at the same level of theory. Although there are some recent density functional studies of simple mono-functional boranes (BH_3 or BF_3) and their complexes with neutral Lewis bases,[7] studies of anion binding to boranes (either mono- or poly-functional) are limited to a recent high-level study of complexes of BH_3 with PH_2^-, OH^- and Cl^-,[8] and a semi-empirical investigation of anion complexes of macro-bi- and -tri-cyclic boranes.[9]

† Electronic supplementary information (ESI) available: geometry optimization details and results of calibration calculations. See http://www.rsc.org/suppdata/cc/b0/b007544m/

The geometries of **2**, **3** and their various donor–acceptor complexes were optimized at the Hartree-Fock level using 3-21G and 6-31+G* basis sets (Fig. 1 and 2) (see also ESI†). The minimum energy geometries for F^-, Cl^-, and Br^- complexes with both macrocyclic Lewis acids **2** and **3** feature symmetrical binding of the anion to all three boron centres (see Tables 1 and 2). For hydride anion, however, three different BH distances are observed in the minimum energy structure. The H^- anion bridges two boron centres in near symmetrical fashion {*r*(B–H) = 1.429, 1.414 Å for [**2**·H]$^-$; 1.351, 1.364 Å for [**3**·H]$^-$}, but interacts minimally with the third boron atom {*r*(B···H) = 2.668 Å for [**2**·H]$^-$; 2.813 Å for [**3**·H]$^-$}. Such a geometry is unsurprising given the small size of the hydride anion, the μ_2- bonding mode for bridging hydrogen atoms being far more common than the face-capping μ_3-mode in polyhedral boron hydrides, for example. BH distances can be compared to those determined by X-ray diffraction for hydride complexes of bidentate Lewis acids {*e.g.* with 'hydride sponge' [1,8-$(Me_2B)_2C_{10}H_6$·H]$^-$, *r*(B–H) = 1.20(5), 1.49(5) Å and [$(HBC_4H_8)_2$·H]$^-$, *r*(B—H) = 1.28(2), 1.31(2) Å}.[11] In general the closest BH contacts for [**2**·H]$^-$ and [**3**·H]$^-$ are somewhat longer (*ca.* 5–10%) than those determined experimentally. Conceivably this may reflect the anomalous shortening found for E–H bonds determined by X-ray diffraction, as the B···B distances to be spanned by the hydride 'ligand' in both the macrocyclic and bidentate complexes are very similar (2.473 and 2.535 Å for the macrocyclic complexes; 2.480 and 2.544 Å for the bidentate species).

The BCl distances in [**2**·Cl]$^-$ and [**3**·Cl]$^-$ (2.654 and 2.329 Å, respectively) are also somewhat longer than those found in the chloride complex of the bidentate Lewis acid 'chloride sponge', [1,8-$(Cl_2B)_2C_{10}H_6$·Cl]$^-$ [1.86(1)–2.10(1) Å].[12] In this case, however this reflects the significantly longer B···B distance to be spanned by the Cl^- ligand {3.373 and 3.311 Å for the macrocyclic complexes compared to 3.055 Å for [1,8-$(Cl_2B)_2C_{10}H_6$·Cl]$^-$}. Comparison with the structure of the known $B_2F_7^-$ ion shows a similar trend for the fluoride complexes of **2** and **3**.

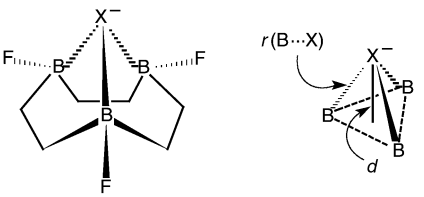

Fig. 1 Definitions of parameters defining the macrocyclic complex geometries.

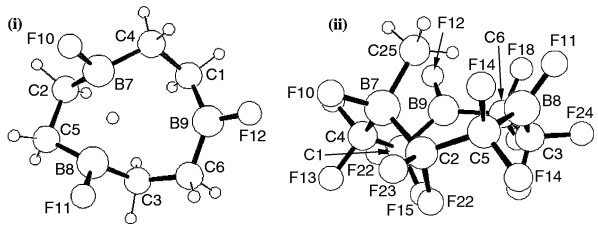

Fig. 2 HF/6-31+G* optimized geometries of (i) [**2**·H]$^-$ and (ii) [**3**·CH_3]$^-$.

DOI: 10.1039/b007544m

Table 1 HF/6-31+G(d) calculated geometrical parameters for complexes of anions with macrocyclic Lewis acids **2** and **3**

	2			**3**		
Lewis base	r(B···X)/Å	d^a/Å	F–B–X/°	r(B···X)/Å	d^a/Å	F–B–X/°
H^-	1.429, 1.414, 2.668	—	—	1.351, 1.364, 2.813	0.413	—
F^-	1.832	0.721	101.9	1.805	0.516	103.8
Cl^-	2.654	1.803	99.7	2.329	1.330	103.4
Br^-	2.857	2.062	98.6	2.445	1.491	104.0
CH_3^-	1.659, 3.276, 3.221	—	—	1.651, 2.984, 3.016	—	—

[a] The perpendicular distance of the anion from the mean plane of the three boron acceptor atoms, as defined in Fig. 1.

Table 2 B3-LYP/6-311+G(d)//HF/6-31+G(d) calculated binding energies (E_b) and anion ↔ macrocycle charge transfers (ΔQ) for complexes of anions with macrocyclic Lewis acids **2** and **3**

	2		**3**	
Lewis base	$E_b{}^a$/kJ mol^{-1}	ΔQ	E_b/kJ mol^{-1}	ΔQ
H^-	359.0	0.90	692.3	0.85
F^-	307.9	0.49	595.7	0.60
Cl^-	107.3	0.52	385.4	0.72
Br^-	73.1	0.58	338.9	0.98
CH_3^-	298.3	0.03	555.3	0.09

[a] These include HF/3-21G harmonic thermal corrections (at 298 K) scaled by 0.893.[10]

The binding energies for F^- and Cl^- complexes of macrocycles **2** (307.9 and 107.3 kJ mol^{-1}, respectively) and **3** (595.7 and 385.4 kJ mol^{-1}, respectively) can be compared to values of 265.7 and 141.8 kJ mol^{-1} calculated by Boutalib and coworkers for the corresponding complexes with BH_3 at the G-2 level of theory.[8] For all the anions examined the binding energy is considerably enhanced by perfluorination of the triboramacrocycle. For the smaller anions H^- and F^- extremely high binding energies are observed for the perfluorinated macrocycle (692.3 and 595.7 kJ mol^{-1}). The weaker binding found for complexes of Cl^- and Br^- reflects a poorer size-match selectivity (anion/macrocycle) and the greater B···X distances (2.329 and 2.445 Å, respectively). Fluoride anion recognition is an area of much current interest,[13] and these data imply that [9]aneB_3 macrocyclic species have much potential in this regard.

The case of methyl anion binding is intriguing; although a strong overall attractive interaction is found for the symmetrically bound (C_3 symmetry) system, [**3**·CH_3]$^-$, reflected by a binding energy (492.9 kJ mol^{-1}) in excess of that calculated for the analogous complex of $B(C_6F_5)_3$ (*vide infra*), the global minimum for both [**2**·CH_3]$^-$ and [**3**·CH_3]$^-$ features less symmetrical anion binding. In each case, binding of the anion within the cavity is essentially monodentate, featuring a single short B···C distance {1.651 Å for [**3**·CH_3]$^-$} and two other B···C distances long enough to preclude any significant interaction {2.984 and 3.016 Å for [**3**·CH_3]$^-$}. For **3** the binding energy for the methyl anion in this asymmetric mode is found to be 555.3 kJ mol^{-1}; for each complex the less symmetrical C_1 binding geometry is found to be energetically more favourable than the C_3 mode of attachment by at least 60 kJ mol^{-1}.

Given the importance of methyl anion abstraction in the initiation of olefin polymerisation processes, we sought to compare the CH_3^- binding capabilities of **2** and **3** with that of the commonly used Lewis acid **4**. At the B3-LYP/6-311+G*//HF/6-31+G* level with a scaled HF/3-21G vibrational correction, we obtained a binding energy of 472.4 kJ mol^{-1} for [$B(C_6F_5)_3$·CH_3]$^-$, a value which is *ca.* 15% lower than the value found for [**3**·CH_3]$^-$. In terms of binding energies for the methyl anion, the value detailed herein for the perfluorinated macrocycle **3** is the highest absolute value yet to be reported in the literature.‡

In summary the calculations presented here reveal that the macrocycle **3** binds CH_3^- at least as strongly as the 'best' recently synthesised Lewis acids. Although binding of CH_3^- by a Lewis acid is only one step in the generation of the active species from metallocene dimethyl derivatives, other factors such ion pairing interactions are known to be important,[3] this result has clear implications in terms of the design of Lewis acids as activators in olefin polymerisation catalysis. With this in mind we are currently investigating anion binding by a range of multidentate and macrocyclic Lewis acids, including species featuring benzyl backbones which may prove to be more synthetically accessible. The results of these studies will be reported in due course.

S. T. H. thanks the EPSRC for access to the Columbus Quantum Chemistry supercomputing facility.

Notes and references

‡ Unpublished work listed in ref. 5 (M. V. Metz, D. J. Schwartz, C. L. Stern, P. N. Nickias and T. J. Marks, *Angew. Chem., Int. Ed.*, 2000, **39**, 1312) indicates that [$(C_6F_4)B(C_6F_5)]_2$ is calculated to have a 10 kcal mol^{-1} stronger affinity for CH_3^- than does $B(C_6F_5)_3$, although no absolute binding energies were given for either species.

1 See, for example, W. E. Piers and T. Chivers, *Chem. Soc. Rev.*, 1997, **26**, 345; J. R. Galsworthy, M. L. H. Green, N. Maxted and M. Müller, *J. Chem. Soc., Dalton Trans.*, 1998, 387.
2 See, for example, P. A. Deck, C. L. Beswick and T. J. Marks, *J. Am. Chem. Soc.*, 1998, **120**, 1772.
3 L. Luo and T. J. Marks, *Top. Catal.*, 1999, **7**, 97.
4 Y.-X. Chen, C. L. Stern, S. Yang and T. J. Marks, *J. Am. Chem. Soc.*, 1996, **118**, 12 451; Y.-X. Chen, C. L. Stern and T. J. Marks, *J. Am. Chem. Soc.*, 1997, **119**, 2582; L. Li and T. J. Marks, *Organometallics*, 1998, **17**, 3996; Y.-X. Chen, M. V. Metz, L. Li, C. L. Stern and T. J. Marks, *J. Am. Chem. Soc.*, 1998, **120**, 6287.
5 V. C. Williams, W. E. Piers, W. Clegg, M. R. J. Elsegood, S. Collins and T. B. Marder, *J. Am. Chem. Soc.*, 1999, **121**, 3244.
6 See, for example, L. F. Lindoy, *The Chemistry of Macrocyclic Ligand Complexes*, Cambridge University Press, Cambridge, 1990.
7 H. Jacobsen, H. Berke, S. Doring, G. Kehr, G. Erker, R. Frohlich and O. Meyer, *Organometallics*, 1999, **18**, 1724; J. H. Ren, D. B. Workman and R. R. Squires, *J. Am. Chem. Soc.*, 1998, **120**, 10 511.
8 H. Anane, A. Boutalib and F. Tomas, *J. Phys. Chem. A.*, 1997, **101**, 7879.
9 S. Jacobson and R. Pizer, *J. Am. Chem. Soc.*, 1993, **115**, 11216.
10 R. F. Hout, B. A. Levi and W. J. Hehre, *J. Comput. Chem.*, 1982, **3**, 234.
11 H. E. Katz, *J. Am. Chem. Soc.*, 1985, **107**, 1421; D. J. Saturnino, M. Yamauchi, W. R. Clayton, R. W. Nelson and S. G. Shore, *J. Am. Chem. Soc.*, 1975, **97**, 6063.
12 H. E. Katz, *J. Am. Chem. Soc.*, 1987, **109**, 1135.
13 S. Camiolo and P. A. Gale, *Chem. Commun.*, 2000, 1129 and references therein.

ChemComm

Fluorodesilylation of alkenyltrimethylsilanes: a new route to fluoroalkenes and difluoromethyl-substituted amides, alcohols or ethers

Benjamin Greedy and Veronique Gouverneur*

University of Oxford, The Dyson Perrins Laboratory, South Parks Road, Oxford, UK OX1 3QY.
E-mail: veronique.gouverneur@chem.ox.ac.uk; Phone and Fax: +44 1865 275 644

Received (in Liverpool, UK) 9th November 2000, Accepted 19th December 2000
First published as an Advance Article on the web 16th January 2001

A range of alkenyltrimethylsilanes are converted to alkenyl fluorides by reaction with one equivalent of Selectfluor™ (1-chloromethyl-4-fluoro-1,4-diazoniabicyclo[2.2.2]octane bis(tetrafluoroborate)), or difluoromethyl-substituted alcohols, ethers or amides using an excess of Selectfluor™ in the presence of various nucleophiles.

In view of the unique features of fluorine-containing compounds, there has been an increasing interest in the development of novel methods for the synthesis of fluorinated molecules.[1] In particular, terminal fluoroalkenes have been used in the design of a number of mechanism-based enzyme inhibitors and other bioactive molecules.[2] Consequently, development of general methodologies for their preparation is an important challenge. Our studies were initiated in order to investigate the hypothesis that electrophilic N–F reagents[3] would react with alkenyltrimethylsilanes to give the corresponding alkenyl fluorides. Fluorodesilylations of aryltrimethylsilanes using xenon difluoride and elemental fluorine have been reported respectively by Lothian and Ramsden[4] and by Stuart *et al*.[5] Surprisingly, in contrast to chloro-, bromo- or iododesilylation,[6] fluorodesilylation has never been applied to alkenylsilanes. In addition, the reactivity of the N–F group of reagents has not been investigated for a fluorodesilylation processes. In this communication, we demonstrate a new and facile approach for the synthesis of alkenyl fluorides as well as difluoromethyl-substituted alcohols, amides and ethers.

The substrate trimethylstyrylsilane **1a** was prepared as a mixture of stereoisomers (*E*:*Z*/8:92).[7] The fluorodesilylation was attempted with several commercially available N–F reagents. The reaction of compound **1a** with 1 eq. of Selectfluor™ in acetonitrile at rt afforded the expected fluoroalkene **2a** with a conversion[8] of 47% after 20 h (Scheme 1, eqn 1 and Table 1, entry 1). Prolonged reaction times did not improve the yield of compound **2a** as the formation of a second product was observed instead. This product was identified as difluoroamide **3a** and is believed to result from further fluorination of **2a** followed by reaction with acetonitrile. When

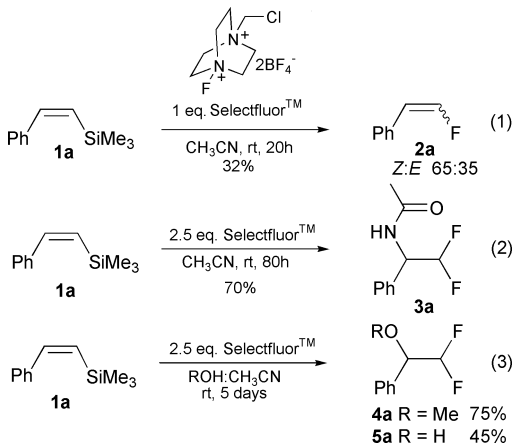

Scheme 1

1-chloromethyl-4-fluoro-1,4-diazoniabicyclo[2.2.2]octane bis-(trifluoromethanesulfonate) was allowed to react with an equimolar amount of compound **1a** in acetonitrile, fluorodesilylation occurred to afford the fluoroalkene **2a** with a conversion of 32%. In contrast, 1-fluoropyridinium pyridine heptafluorodiborate and *N*-fluorobenzenesulfonimide did not react with compound **1a**. These results prompted us to use Selectfluor™ for subsequent fluorodesilylation reactions. A series of alkenyltrimethylsilanes **1b–f** was thus prepared according to known literature procedures[7,9] in order to evaluate the scope and limitation of this reaction. The expected fluoroalkenes **2b**,**c** were obtained as *Z*:*E* mixtures in moderate to good yields (Table 1, entries 2 and 3). In terms of mechanism, the reaction of **1a** to form **2a** might involve an

Table 1 Fluorodesilylation of vinylsilane derivatives **1a–f**

Entry	Substrate	Product	Yield (%)[a] (Conversion (%))[b]
1	Ph, SiMe3 **1a**	Ph, F **2a**	32 (47) *Z*:*E* 65:35
2	*n*C6H13, SiMe3 **1b**	*n*C6H13, F **2b**	(45) *Z*:*E* 80:20
3	Ph, Et, SiMe3 **1c**	Et, Ph, F **2c**	57 (65) *Z*:*E* 58:42
4	Ph, SiMe3 **1a**	MeCONH, F, Ph **3a** F	70 (74)
5	*n*C6H13, SiMe3 **1b**	MeCONH, F, *n*C6H13 **3b** F	0
6	Ph, Et, SiMe3 **1c**	MeCONH, F, Et, Ph **3c** F	86 (88)
7	Et, *n*C6H13, SiMe3 **1d**	MeCONH, F, Et, *n*C6H13 **3d** F	55 (70)
8	Ph, SiMe3 **1a**	MeO, F, Ph **4a** F	75 (82)
9	Ph, SiMe3 **1a**	HO, F, Ph **5a** F	45 (46)
10	Ph, Et, SiMe3 **1c**	MeO, F, Et, Ph **4c** F	79 (87)
11	Ph, Et, SiMe3 **1c**	HO, F, Et, Ph **5c** F	83 (90)
12	HO, *n*, Ph, SiMe3 **1e** *n* = 1 **1f** *n* = 2	F, F, Ph, O, *n*	**6e** *n* = 1 62 **6f** *n* = 2 48

[a] Chemical yield after column chromatography. [b] Evaluated by GCMS.

DOI: 10.1039/b009179k

addition–elimination pathway *via* a carbocationic intermediate. The formation of a mixture of geometrical isomers and the faster reaction with more nucleophilic vinylsilanes are consistent with this mechanism.

Treatment of alkenylsilanes **1a–d** with more than one equivalent of Selectfluor™ produced the corresponding vicinal difluoroamides **3a**, **3c** and **3d** in good yields by a Ritter-type fluoro-functionalisation with acetonitrile (Scheme 1, eqn. 2 and Table 1, entries 4, 6 and 7). The reaction could not be applied to **1b** since the corresponding primary product of the reaction, the fluoroalkene **2b**, failed to react any further (Table 1, entry 5). These results are consistent with the observation made earlier by Stavber *et al.*[10] who reported that monofluoroamides could be prepared from the corresponding alkene by a "fluoro-Ritter" reaction. More recently, Olah *et al.*[11] also reported the formation of difluoroamides by electrophilic fluorination of alkenyl boronic acids and trifluoroborates.

When the reaction was carried out in aqueous acetonitrile or in a mixture of methanol and acetonitrile, the product outcome was different (Scheme 1, eqn. 3). When the alkenyltrimethylsilanes **1a** and **1c** were treated with 2.5 eq. of Selectfluor™ in a 1:1 mixture of MeOH–CH_3CN, the corresponding difluoromethyl ether derivatives **4a** and **4c** were prepared in 75 and 79% yield respectively (Table 1, entries 8 and 10). Similarly, when compounds **1a** and **1c** were treated with 2.5 eq. of Selectfluor™ in a 1:1 mixture of H_2O:CH_3CN, the difluoromethyl alcohols **5a** and **5c** were obtained with chemical yields of 45 and 83% (Table 1, entries 9 and 11). The difluoroamides were always formed as side products but could be easily separated by silica gel chromatography. In addition, the methodology can also be applied to the preparation of the bis-fluorinated tetrahydrofuran **6e** and the tetrahydropyran **6f**† by treating the corresponding alkenyltrimethylsilanes **1e** and **1f** with 2.5 eq. of Selectfluor™ in acetonitrile (Table 1, entry 12).

In summary, substituted alkenylsilanes carrying electron-donating groups undergo smooth mono- or bis-electrophilic fluorination to afford fluoroalkenes or vicinal difluoroamides, alcohols or ethers. The present report opens new possibilities for the direct and effective preparation of alicyclic and cyclic difluorinated derivatives. Mechanistic investigations along with the evaluation of the scope and limitation of this novel methodology are in progress in our laboratory. The generous financial support of Rhodia Organique Fine is acknowledged. We also thank Dr J. M. Paris, Dr J. R. Desmurs, and Dr J. Russell for very helpful suggestions regarding this work.

Notes and references

† *Procedure for the production of* **6f**: A solution of 5-phenyl-6-trimethylsilanyl hex-5-en-1-ol (350 mg, 1.4 mmol) in acetonitrile (35 ml) was treated with Selectfluor™ (1.24 g, 3.5 mmol) and stirred at rt for 48 h. The reaction mixture was poured into saturated aqueous sodium hydrogen carbonate (30 ml) and extracted with diethyl ether (3 × 30 ml). The combined organic phases were dried ($MgSO_4$) and concentrated *in vacuo*. Purification of the residue by silica gel chromatography (1:1 hexane–DCM, R_f = 0.48) gave the product as a colourless oil (142 mg, 48%); ^{1}H NMR (400 MHz, $CDCl_3$): 1.42–1.52 (m, 2H), 1.69–1.79 (m, 2H), 1.96 (td, 1H, J = 13.6, J = 4Hz), 3.53 (td, 1H, J = 12.4Hz, 2.4), 3.80–3.84 (m, 1H), 5.57 (t, 1H, J = 57.2 Hz), 7.35–7.50 (m, 5H); ^{13}C NMR (100.6 MHz, $CDCl_3$): 18.4, 25.3(t, J = 2.3Hz), 25.6, 29.7, 62.5, 117.1 (t, J = 247.8 Hz), 128.1, 128.3, 128.6 and 135.4; ^{19}F NMR (235.3 MHz, $CDCl_3$): −131.1, −131.9 (dxAB, $J_{F–F}$ = 277.6 Hz, $J_{H–F}$ = 56.5 Hz); HRMS calcd. for $C_{12}H_{18}NOF$ $(M + NH_4)^+$ 230.1356, found 230.1349.

1 (*a*) *Organofluorine Compounds in Medicinal Chemistry and Biomedical Applications*, ed. R. Filler, Y. Kobayashi and L. M. Yagupolskii, Elsevier, Amsterdam, 1993; (*b*) *Fluorine-Containing Amino Acids: Synthesis and Properties*, ed. V. P. Kukhar and V. A. Soloshonok, John Wiley & Sons, Chichester, 1995.

2 (*a*) *Biomedical Frontiers of Fluorine Chemistry*, ed. I. Ojima, J. R. McCarthy and J. T. Welch, American Chemical Society, Washington DC, 1996; (*b*) *Synthetic Fluorine Chemistry*, ed. G. A. Olah, R. D. Chambers and G. K. S. Prakash, John Wiley & Sons, New York, 1992; (*c*) *Organofluorine Chemistry: Principles and Commercial Applications*, ed. R. E. Banks, B. E. Smart and J. C. Tatlow, Plenum Press, New York, 1994; (*d*) *Effects of Selective Fluorination on Reactivity*, P. Bey, J. R. McCarthy and I. A. Mcdonald, ACS Symposium Series 456, American Chemical Society, Washington DC, 1991, 105.

3 G. S. Lal, G. P. Pez and R. G. Syvret, *Chem. Rev.*, 1996, **96**, 1737 and references therein.

4 A. P. Lothian and C. A. Ramsden, *Synlett*, 1993, **10**, 753.

5 A. Stuart, P. L. Coe and D. J. Moody, *J. Fluorine Chem.*, 1998, **92**, 179.

6 *The Chemistry of Organic Silicon Compounds Part 2*, ed. S. Patai and Z. Rapoport, John Wiley & Sons, Chichester, 1989.

7 R. B. Miller and G. J. McGarvey, *J. Org. Chem.*, 1978, **23**, 4424.

8 The term 'conversion' is used here to mean the total % of product detected in the reaction mixture by GCMS before isolation.

9 (*a*) N. Chatani, N. Amishiro, T. Morii, T. Yamashita and S. Murai, *J. Org. Chem.*, 1995, **60**, 1834; (*b*) C. Flann, T. C. Malone and L. E. Overman, *J. Am. Chem. Soc.*, 1987, **109**, 6097.

10 S. Stavber, T. S. Pecan, M. Papez and M. Zupan, *Chem. Commun.*, 1996, **19**, 2247.

11 N. A. Petasis, A. K. Yudin, I. A. Zavialov, G. K. S. Prakash and G. A. Olah, *Synlett*, 1997, **5**, 606.

Nitrene-transfer to olefins catalyzed by methyltrioxorhenium: a universal catalyst for the [1+2] cycloaddition of C-, N-, and O-atom fragments to olefins

Hee-Joo Jeon and SonBinh T. Nguyen*

Department of Chemistry, Northwestern University, 2145 Sheridan Road, Evanston, IL 60208, USA

Received (in Corvalis, OR) 28th September 2000, Accepted 5th December 2000
First published as an Advance Article on the web 16th January 2001

Methyltrioxorhenium (MTO) was found to catalyze the transfer of the nitrene unit of [*N*-(*p*-tolylsulfonyl)imino]-iodobenzene to a number of olefins providing aziridines in moderate to good yields, establishing MTO as a universal catalyst for the [1 + 2] cycloaddition of carbene, nitrene, and oxo units to olefins.

The metal-catalyzed [1 + 2] cycloaddition of small functional groups to olefins to yield 3-membered rings comprises a very important class of reactions in organic syntheses.[1,2] Most important among this class of reactions is the addition of isoelectronic second row (ISR) fragments, *e.g.* carbene, nitrene, and oxo species, to olefins to produce cyclopropanes, aziridines, and epoxides, respectively. From a valence-shell electron consideration, it is quite reasonable to propose that these ISR moieties may behave similarly toward olefins in the presence of the *same* metal catalyst. In particular, we were intrigued by the possibility that there may exist a "universal" catalyst which can transfer all three of these ISR species to olefins. The development of a common catalyst for multiple organic reactions is a powerful concept in synthesis. Its significance lies in the possibility that the ligand framework developed for one reaction may be applied to other reactions without further modification of the catalyst system. The advantages are most apparent in the case of enantioselective reactions catalyzed by soluble metal complexes, where the most labor-intensive research is the development of the required chiral ligands. Perhaps the most prominent example of this strategy is the work by Sharpless and coworkers on the osmium-catalyzed asymmetric olefin aminohydroxylation,[3–6] where a chiral alkaloid ligand used in the asymmetric olefin dihydroxylation reaction is applied to the synthesis of chiral β-aminoalcohols. In the area of [1 + 2] cycloadditions, the developers of Cu[2,7–9] and Rh[2,10] catalysts have utilized this strategy to some degree in that both aziridination and cyclopropanation can be carried out by the same metal catalyst.

We report herein the aziridination of olefins catalyzed by methyltrioxorhenium[11] (MTO). Combined with the known olefin epoxidation[12–14] and cyclopropanation[15] catalyzed by the same metal complex, our work establishes *the unique activity of MTO as a 'universal' catalyst for the [1 + 2] cycloaddition of carbene, nitrene, and oxo units to olefins*. To our knowledge, this is the first instance where a single catalyst can be used for three different [1 + 2] cycloaddition reactions.

In the olefin aziridination experiments, we utilized [*N*-(*p*-tolylsulfonyl)imino]iodobenzene (PhINTs) as the nitrene source. General experimental conditions involved the mixing of PhINTs (1 equiv.), olefin (5 equiv.), and MTO (10 mol% relative to PhINTs) in MeCN at the appropriate temperature (Table 1). Although the polymeric PhINTs was initially insoluble, the mixture became homogeneous as the reaction proceeded. The complete consumption of the nitrene source signaled the end of the reaction. In the absence of MTO no reaction occurred, as evidenced both by the lack of dissolution of PhINTs as well as by GC analysis of the reaction solution which shows trace $TsNH_2$ as the only nitrogen-containing product.

As depicted in Table 1, reaction conditions were varied to elucidate their effect on the catalyst activity with respect to the aziridination of styrene. In general, higher substrate concentrations gave better yields in shorter reaction times. A reaction of 40 equiv. of styrene relative to the nitrene source resulted in the highest yield of aziridine (45%, Table 1, entry 5). In refluxing MeCN (*ca.* 82 °C, Table 1, entries 6 and 7), the reaction was essentially instantaneous. There was no noticeable change in yield compared to those at room temperature.

Nitrile solvents (both MeCN and benzonitrile) were the most suitable for this system. In most other solvents, such as Et_2O, CH_2Cl_2 PhMe, THF, and pyridine, aziridine did not form, and all of the nitrene precursor was converted to $TsNH_2$. In the absence of nitrile solvents (neat conditions), the yield of aziridine was 27% based on PhINTs.

In all cases, $TsNH_2$ was the major side product of the aziridination reaction. To determine the hydrogen atom sources for $TsNH_2$ formation, a series of labeling experiments was conducted. A 10:1 mixture of styrene and PhINTs with MTO (10 mol% relative to PhINTs) in deuterated solvent (CD_3CN, rigorously dried and distilled) was allowed to react for 4 h, and the product mixture was analyzed by GC–MS. If the solvent was the major hydrogen source, $TsND_2$ or TsNDH would have been expected to form. However, the product from hydrogen abstraction was mostly $TsNH_2$ with a small amount of TsNDH. When styrene-d_8 in MeCN was used, the byproduct consisted mostly of $TsND_2$ (*m/z* 173) and TsNDH (*m/z* 172). Although both MeCN and styrene can supply hydrogen atoms for the $TsNH_2$ formation, the labeling experiments indicate that the substrate is the major hydrogen source leading to the formation of the $TsNH_2$ side product.

To investigate the scope of the MTO catalyzed aziridination reaction, several substituted olefins were examined using the conditions optimized for the aziridination of styrene (Table 2). In general, electron-withdrawing substituents at the *para* position of styrenes slowed down the overall reaction although yields remained essentially the same (Table 2, entries 1–4). For conjugated aromatic olefins, substitution patterns affected both

Table 1 Substrate concentration effect in the aziridination of styrene catalyzed by MTO

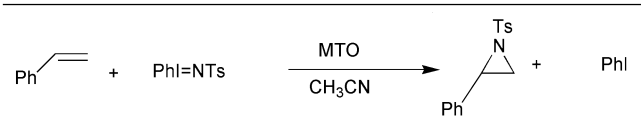

Entry	Substrate[a]	Temperature/°C	Reaction time[b]	Yield (%)[c]
1	5	rt	4–5 h	28
2	10	rt	2–3 h	33
3	20	rt	2–3 h	34
4	30	rt	1–2 h	39
5	40	rt	1–2 h	45
6	10	82	3 min	35
7	20	82	< 2 min	38

[a] Number of equiv. of substrate to PhINTs. [b] Time for complete dissolution of PhINTs. [c] HPLC yield (calibrated with an internal standard) based on the amount of PhINTs. All reactions were performed with PhINTs (0.2 mmol) and MTO (10 mol% relative to PhINTs) in CH_3CN (1 mL) at room temp.

DOI: 10.1039/b007906p

Table 2 Scope of the aziridination reaction catalyzed by methyltrioxorhenium (MTO)

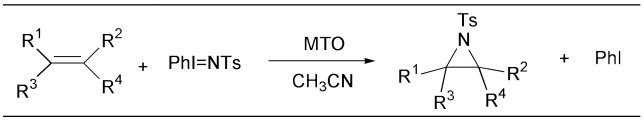

Entry	Substrates	Reaction time[a]/h	Aziridines	Yield (%)[b]
1	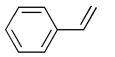	4–5	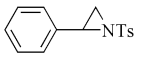	28
2	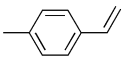	3	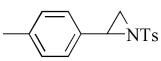	24
3	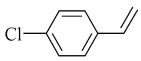	9–10	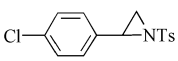	33
4	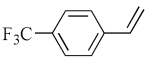	43	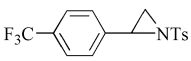	32
5	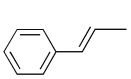	10	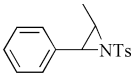	17
6	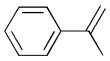	1	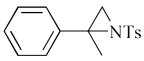	70[c]
7	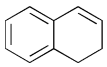	4–5	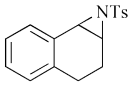	43
8		4–5	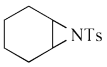	12

[a] Time for complete dissolution of PhINTs. [b] HPLC yield based on the amount of PhINTs. All reactions were performed with PhINTs (0.2 mmol), MTO (10 mol% relative to PhINTs), and substrate (5 equiv. relative to PhINTs) in CH_3CN (1 mL) at room temp. [c] Isolated yield of a mixture of the desired aziridine and the rearranged *N*-Ts-2-phenylpropylidenimine product (*ca.* 4:3).

reaction time and yield. While (*E*)-β-methylstyrene only yielded 17% of the desired *trans*-product after 10 h (Table 2, entry 5), the *cis*-substituted 1,2-dihydronaphthalene showed faster conversion, producing 43% aziridine after 4–5 h (Table 2, entry 7). Aziridination of α-methylstyrene was fastest (1 h reaction time) among the substrates examined, and a mixture of aziridine and *N*-tosyl-2-phenylpropylidenimine was isolated (Table 2, entry 6). Finally, cyclohexene, a substrate known to be very sluggish in atom-transfer reactions, was transformed to the corresponding aziridine in low, but finite, yield (Table 2, entry 8).

Although identification of a complete mechanism accounting for the yields and products obtained from this family of reactions is beyond the scope of this initial communication, we believe that a 3-membered rhenoxaziridine intermediate **A**, formed from the coupling of [NTs] with MTO, is a reasonable common first intermediate (eqn. (1)).[15] This intermediate **A** could then react with olefins to form aziridines or undergo other transformations, such as hydrogen abstraction from the substrate to yield $TsNH_2$.

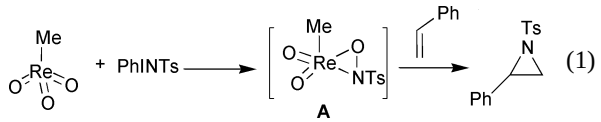

(1)

To summarize, we have demonstrated that MTO can act as a catalyst for the transfer of nitrene to olefins. This reactivity, taken together with the known MTO-catalyzed epoxidation[12–14] and cyclopropanation,[15] represents the first example of three different [1 + 2] cycloadditions of ISR fragments catalyzed by a single metal complex. Further studies, including the isolation and characterization of reaction intermediates, a complete elucidation of the reaction mechanism, the extension of the scope of this reaction to other rhenium(VII) oxo compounds and olefin substrates, as well as the asymmetric version of the MTO-catalyzed olefin aziridination are currently in progress and will be the topic of future reports.

This work was supported by grants from Northwestern University, the Camille and Henry Dreyfus Foundation, the Beckman Foundation, the Packard Foundation, and the Dupont company. We thank Dr Wiechang Jin for helpful discussions.

Notes and references

1 M. Lautens, W. Klute and W. Tam, *Chem. Rev.*, 1996, **96**, 49 and references therein.
2 M. P. Doyle, *Chem. Rev.*, 1986, **86**, 919 and references therein.
3 A. E. Rubin and K. B.Sharpless, *Angew. Chem., Int. Ed. Engl.*, 1997, **36**, 2637.
4 G. G. Li, H. T. Chang and K. B. Sharpless, *Angew. Chem., Int. Ed. Engl.*, 1996, **35**, 451.
5 J. Rudolph, P. C. Sennhenn, C. P. Vlaar and K. B. Sharpless, *Angew. Chem., Int. Ed. Engl.*, 1996, **35**, 2810.
6 G. Li, H. H. Angert and K. B. Sharpless, *Angew. Chem., Int. Ed. Engl.*, 1996, **35**, 2813.
7 D. A. Evans, M. M. Faul and M. T. Bilodeau, *J. Am. Chem. Soc.*, 1994, **116**, 2742.
8 Z. Li, D. R. Conser and E. N. Jacobsen, *J. Am. Chem. Soc.*, 1993, **115**, 5326.
9 P. J. Perez, M. Brookhart and J. L. Templeton, *Organometallics*, 1993, **12**, 261.
10 P. Muller, C. Baud and Y. Jacquier, *Tetrahedron*, 1996, **52**, 1543.
11 W. A. Herrmann, F. E. Kuhn, R. W. R. Fischer, W. Thiel and C. C. Romao, *Inorg. Chem.*, 1992, **31**, 4431.
12 W. W. Herrmann, R. M. Kratzer, H. Ding, W. R. Thiel and H. Gals, *J. Organomet. Chem.*, 1998, **555**, 293.
13 W. A. Herrmann, R. W. Fischer and D. W. Marz, *Angew. Chem., Int. Ed. Engl.*, 1991, **30**, 1638.
14 J. Rudolph, K. L. Reddy, J. P. Chiang and K. B. Sharpless, *J. Am. Chem. Soc.*, 1997, **119**, 6189.
15 Z. Zhu and J. H. Espenson, *J. Am. Chem. Soc.*, 1996, **118**, 9901.

Rhodium-catalyzed allylation of styrenes with allyl tosylate

Naofumi Tsukada,* Tetsuo Sato and Yoshio Inoue

Department of Materials Chemistry, Graduate School of Engineering, Tohoku University, Sendai 980-8579, Japan. E-mail: tsukada@aporg.che.tohoku.ac.jp

Received (in Cambridge, UK) 28th September 2000, Accepted 20th December 2000
First published as an Advance Article on the web 18th January 2001

Rhodium-catalyzed allylation of styrene with allyl tosylate gave 1-phenylpenta-1,4-diene, and various styrene derivatives were also allylated yielding 1,4-dienes or 1,5-dienes.

The palladium-catalyzed arylation of alkenes, the Heck reaction, has proven to be a versatile method for the formation of carbon–carbon bonds.[1] In contrast, the analogous reaction of alkenes with allyl compounds is far more limited in its application, except for intramolecular metallo-ene reactions,[2] and remains a challenge in organic synthesis. Although a few examples of the transition metal-catalyzed allylation of alkenes have been reported,[3–5] to our knowledge, a reaction yielding simple allylation products, *i.e.* 1,4-dienes, is yet to be discovered. For example, strained alkenes such as norbornene† react with allyl compounds in the presence of various transition metal catalysts, however, these reactions do not afford 1,4-dienes because of stereochemical problems.[3] The palladium-catalyzed allylation of activated olefins with allylstannane and allyl chloride gives not mono-allylation products, but double allylation products selectively.[4] Mitsudo *et al.* reported ruthenium-catalyzed reactions of allyl carbonates with *N*,*N*-dimethylacrylamide, in which only 1,3-dienes were obtained in moderate yields.[5] Herein we wish to report the rhodium-catalyzed simple allylation of styrene derivatives with allyl tosylate.[6]

When styrene (**1a**) was treated with two equivalents of allyl tosylate in the presence of a catalytic amount of $[Rh(nbd)(CH_3CN)_2]PF_6$ (nbd = norbornadiene‡) in dioxane at 40 °C, 1-phenylpenta-1,4-diene **2a** was produced in 17% yield (eqn. (1)). Allyl tosylate and styrene were not recovered, and no

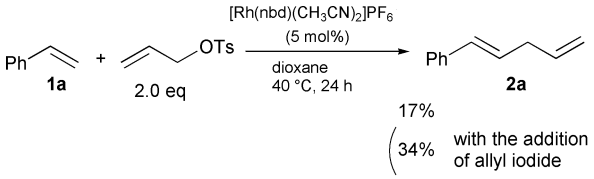

(1)

other product was identified. No allylation product was formed using typical allylating agents such as allyl acetate, allyl carbonate and allyl iodide. Palladium complexes such as $Pd(PPh_3)_4$, $Pd_2(dba)_3{\cdot}CHCl_3$, $[Pd(CH_3CN)_4](BF_4)_2$, or various Lewis acids were ineffective as catalysts for the allylation reaction. The yield of **2a** was improved up to 34% by the addition of allyl iodide (40 mol%). In contrast, the addition of other allylic compounds such as allyl bromide, allyl acetate, or allyl phosphate, decreased the yield slightly. Other organic and inorganic iodides like *n*-propyl iodide, *tert*-butyl iodide and potassium iodide also hindered the reaction to some extent. Furthermore, amounts of allyl iodide less than or exceeding 40 mol% were less effective on the yield of **2a**.

Although satisfactory yield was not obtained in the allylation of *non-substituted* styrene, the reactions of several substituted styrenes gave allylation products in higher yields as illustrated in Table 1. The allylation of 1,1-diphenylethylene **1b** afforded **2b** in 51% yield (run 1). The yield of **2b** increased to 74% with the addition of allyl iodide (run 2). The electron-rich alkene **1c** was so reactive that the product **2c** was obtained in 80% yield

Table 1 Rhodium-catalyzed allylation of styrene derivatives with allyl tosylate[a]

Run	Styrene derivatives **1**	Products, yield (%)[b]
	 **1b-h**	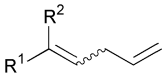 **2b-f**
1	**1b**; R^1, R^2 = Ph	**2b**, 51
2[c]	**1b**	**2b**, 74
3	**1c**; R^1, R^2 = *p*-$CH_3OC_6H_4$	**2c**, 80
4	**1d**; R^1 = Ph, R^2 = *p*-$CH_3OC_6H_4$	**2d**, 73 (53:47)[d]
5	**1e**; R^1 = Ph, R^2 = *o*-$CH_3OC_6H_4$	**2e**, 33 (66:34)[d]
6	**1f**; R^1, R^2 = *p*-ClC_6H_4	**2f**, 26
7	**1g**; R^1 = Ph, R^2 = *n*-C_5H_{11}	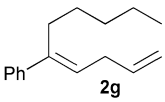 **2g** 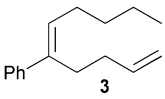 **3** 82 (**2g**:**3** = 43:57)
8	**1h**; R^1 = Ph, R^2 = CH_3	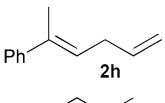 **2h** 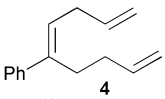 **4** 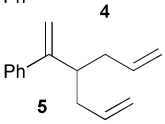 **5** 42 (**2h**:**4**:**5** = 71:29:0)
9[c]	**1h**	63 (**2h**:**4**:**5** = 0:52:48)
10	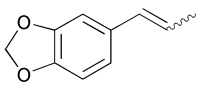 **1i** (*E*:*Z* = 84:16)	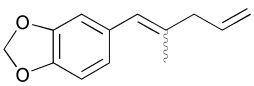 **2i**, 16 (*E*:*Z* = 75:25)
11	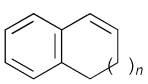 **1j**; *n* = 0	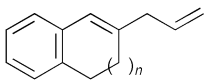 **2j**, 19
12	**1k**; *n* = 1	**2k**, 9
13	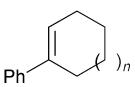 **1l**; *n* = 0	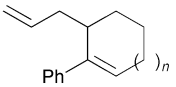 **2l**, 33
14	**1m**; *n* = 1	**2m**, 62
15	**1n**; *n* = 2	**2n**, 68

[a] Reaction conditions: **1** (0.5 mmol), allyl tosylate (1.0 mmol), $[Rh(nbd)(CH_3CN)_2]PF_6$ (0.025 mmol), dioxane, 40 °C, 24 h. [b] Isolated yields. [c] Allyl iodide (0.2 mmol) was added. [d] *E*/*Z* mixture (the stereochemistry cannot be determined).

DOI: 10.1039/b007880h

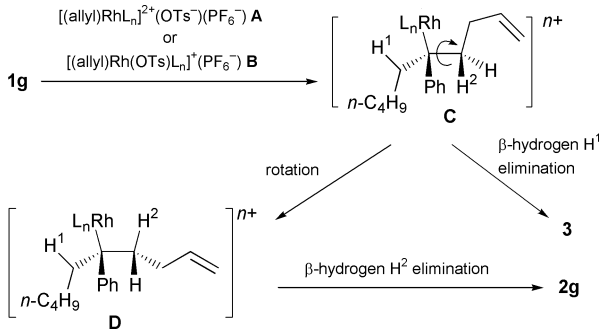

Scheme 1

(run 3). The reaction of 1-(*p*-methoxyphenyl)-1-phenylethylene **1d** also gave **2d** in high yield (run 4), whereas the *ortho*-substituted isomer **1e** was less reactive (run 5). By contrast, the reaction of the electron-poor alkene **1f** afforded **2f** in lower yield (26%, run 6). The α-alkyl-substituted styrenes **1g** and **1h** also reacted with allyl tosylate. In the reaction of **1g** the total yield of the allylated products was high (82%, run 7), although 1,5-diene **3** was yielded in addition to **2g**. The reaction of **1h** gave the monoallylated product **2h** and the diallylated **4**, generated by the allylation of a 1,5-diene product corresponding to **3** (run 8). When allyl iodide was added to the reaction of **1h**, diallylated products **4** and **5** were obtained in 63% yield (run 9). In contrast to the high reactivity of α-substituted styrenes, β-substituted styrenes were less reactive. The reactions of *Z*-stilbene, *E*-stilbene and β-methylstyrene did not give any allylated products. The electron-rich β-substituted styrene derivative **1i** barely reacted with allyl tosylate affording **2i** in only 16% yield (run 10). Indene **1j** was also allylated at the C-2 carbon (runs 11). The allylation reactions of the phenyl-substituted cyclic alkenes **1l**–**n** were also investigated. All the reactions gave only 1,5-dienes **2l**–**n** in satisfactory yields, in which no 1,4-diene was observed (runs 13–15).

Although little mechanistic information has been obtained for the Rh-catalyzed allylation of styrenes, we believe that the reaction proceeds *via* a mechanism similar to that of the palladium-catalyzed Heck arylation reaction. The likely intermediates for the allylation of **1g** are illustrated in Scheme 1. The oxidative addition of allyl tosylate with $[Rh(nbd)(CH_3CN)_2]PF_6$ gives the dicationic complex **A** or the complex **B**, in which tosylate anions weakly coordinate to rhodium, and with the insertion of **1g** to **A** or **B**, the rhodium organometallic intermediate **C** is afforded. In the reaction using allyl acetate or allyl iodide as the allylating agent, the coordination of acetate or iodide ions to rhodium is so strong that the insertion of an alkene does not take place. Subsequent β-hydrogen H^1 elimination in **C** affords 1,5-diene **3**. Since free rotation around the C(H^2)–C(Ph) bond in **C** is possible, alternate *syn*-β-hydrogen H^2 elimination in **D** also occurs, providing 1,4-diene **2g**. The 1,5-dienes were obtained selectively in reactions where free rotation around the C–C bond is not possible in the intermediate corresponding to **C** (runs 13–15). As the formation of **2j** and **2k** is not consistent with the mechanism shown in Scheme 1, the existence of another mechanism, *e.g.* a Friedel–Crafts type reaction, cannot be ruled out, although typical Lewis acids are ineffective in the present allylation reaction. Further investigation of the reaction mechanism and the application to other alkenes are in progress.

Notes and references

† The IUPAC name for norbornene is bicyclo[2.2.1]hept-2-ene.
‡ The IUPAC name for norbornadiene is bicyclo[2.2.1]hepta-2,5-diene.

1 Reviews: (*a*) R. F. Heck, *Palladium Reagents in Organic Synthesis*, Academic Press: London, 1985; (*b*) R. F. Heck, in *Comprehensive Organic Synthesis*, ed. B. M. Trost and I. Fleming, Pergamon Press: Oxford, 1991, Vol. 4, p. 833; (*c*) W. Cabri and I. Candiani, *Acc. Chem. Res.*, 1995, **28**, 2; (*d*) J. Tsuji, in *Palladium Reagents and Catalysts, Innovations in Organic Synthesis*, Wiley: London, 1995, p. 125; (*e*) A. de Meijere and F. Meyer, *Angew. Chem., Int. Ed. Engl.*, 1994, **33**, 2379.

2 Reviews: (*a*) W. Oppolzer, in *Comprehensive Organic Synthesis*, ed. B. M. Trost and I. Fleming, Pergamon Press: Oxford, 1991, Vol. 5, chapter 8.3; (*b*) W. Oppolzer, in *Comprehensive Organometallic Chemistry II*, ed. E. W. Abel, F. G. A. Stone and G. Wilkinson, Pergamon Press, Oxford, 1995, Vol. 12, chapter 1.2.

3 (*a*) M. Catellani, G. P. Chiusoli, E. Dradi and G. Salerno, *J. Organomet. Chem.*, 1979, **177**, C29–31; (*b*) E. Amari, M. Catellani and G. P. Chiusoli, *J. Organomet. Chem.*, 1985, **285**, 383; (*c*) K. Fugami, T. Enokido, K. Kawata, M. Kameyama and M. Kosugi, *Main Group Met. Chem.*, 1999, **22**, 511; (*d*) Y. Morisaki, T. Kondo and T. Mitsudo, *Org. Lett.*, 2000, **2**, 949; (*e*) N. Tsukada, T. Sato and Y. Inoue, *Tetrahedron Lett.*, 2000, **41**, 4181.

4 H. Nakamura, J.-G. Shim and Y. Yamamoto, *J. Am. Chem. Soc.*, 1997, **119**, 8113.

5 T. Mitsudo, S.-W. Zhang, T. Kondo and Y. Watanabe, *Tetrahedron Lett.*, 1992, **33**, 341.

6 N. Tsukada, S. Sugawara and Y. Inoue, *Org. Lett.*, 2000, **2**, 655.

A novel NMR method for screening soluble compound libraries

Philip Hodge,* Pathavuth Monvisade, Gareth A. Morris* and Ian Preece

Department of Chemistry, University of Manchester, Oxford Road, Manchester, UK M13 9PL. E-mail: philip.hodge@man.ac.uk; g.a.morris@man.ac.uk

Received (in Liverpool, UK) 11th November 2000, Accepted 1st December 2000
First published as an Advance Article on the web 16th January 2001

The use of high resolution diffusion-ordered NMR spectroscopy (HR-DOSY) to detect association between a soluble polymer and different components of small libraries of soluble compounds is illustrated for libraries binding respectively to weakly acidic and weakly basic polymers.

In recent years there has been great interest in combinatorial chemistry,[1–3] most commonly involving multi-step polymer-supported syntheses to give *polymer-supported libraries* containing from tens to millions of polymer-supported species. An alternative approach is to synthesise *soluble libraries*[2,4,5] which, to simplify the procedures, may be synthesised with the assistance of polymer-supported reactants or scavengers. Screening of libraries is commonly conducted for biological activity, but may also, for example, be for catalytic activity[6,7] or recognition ability.[8,9]

We report here an NMR method for screening soluble libraries of up to 20–30 components for recognition properties. One possible application would be in refining the design of host molecules for host–guest chemical sensors. The method is based on High Resolution Diffusion-Ordered SpectroscopY (HR-DOSY), a form of multi-dimensional spectroscopy in which signals are dispersed in an extra dimension according to the diffusion coefficient.[10–12]

Diffusion coefficients of organic compounds in common solvents are typically of the order of 10^{-9} m^2 s^{-1}; macromolecules diffuse much more slowly. The basis of the method proposed is to link the species to be recognised (*e.g.* a 'guest') to a suitable soluble polymer. When this polymer is added to a soluble library (of potential 'hosts'), the rates of diffusion of compounds in the library which, on the NMR timescale, bind rapidly and reversibly to the functionalised polymer, will decrease by an amount dependent on the binding constant. The method is related to the DECODES (DOSY-TOCSY) method proposed by Lin *et al*,[13–16] but it differs in the use of a polymer-bound ligand, maximising sensitivity to binding, and in the use of HR-DOSY, which can improve the diffusion resolution and allows the extraction of isolated subspectra for individual components.

As a trial of the method we investigated the interactions between the polymer-supported weak acid **1** and a simulated

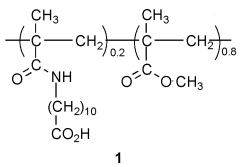

1

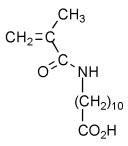

2

library containing 11 commercially available natural products or related compounds (see Table 1). Polymer **1** was prepared by a free radical initiated copolymerisation of monomer **2**[17] and methyl methacrylate (mole ratio, 1:5), to give a copolymer soluble in CD_3OD with no ^{1}H-NMR signals above 4.3 ppm. The polymer had a number average molecular weight M_n of 16500 and a weight average molecular weight M_w of 61500 by gel permeation chromatography (GPC) relative to polystyrene standards. Because the diffusion coefficient of the polymer is small compared with those of the members of the soluble library, such a polydispersity does not affect the estimation of binding constants significantly. A solution in CD_3OD (2.9 mg ml^{-1}) showed a diffusion coefficient by HR-DOSY of 1.0×10^{-10} m^2 s^{-1}. The DOSY spectra of the simulated library alone, and in the presence of the polymer **1**, are shown in Figs. 1 and 2. It is only necessary for there to be one well-resolved characteristic signal for a given component for the diffusion coefficient to be clearly identified. The diffusion coefficients D_f and D_m of the components in the free mixture and with the polymer present are summarised in Table 1.

It is clear from the spectra of Figs. 1 and 2 that the rate of diffusion of hydroquinine **3**, (arrowed signals) is affected strongly by the presence of the polymer, whereas any effect on the other components is much smaller. The small increase in solution viscosity caused by the polymer may be corrected for by calculating estimated diffusion coefficients $D'_m = D_m D_f(\text{ref})/D_m(\text{ref})$, where D_f(ref) and D_m(ref) are the respective diffusion coefficients for a reference compound (in this case residual OH in the solvent) not significantly affected by binding to the polymer. In Table 1, values of D'_m were calculated using the measured MeOH OH diffusion coefficients for the two samples; D'_p, the corrected diffusion coefficient for the dilute free polymer, remained at 1.0×10^{-10} m^2 s^{-1}. Using a simple two-site model, the bound fraction F of a given component is given by $F = (D_f - D'_m)/(D_f - D'_p)$ from which the association constant K between the polymer and that component may be calculated by $K = F/(1 - F)(c_p - Fc)$, where c and c_p are the total concentrations of the component and of the functional polymer repeat unit.

The values of F in Table 1 show clear association between hydroquinine **3** and the polymer; the apparent association constant K is approximately 11 M^{-1}. The spectrum of the

Table 1 Summary of DOSY measurements for library A[a]

Compound	c/mM	$D_f/10^{-10}$ m^2 s^{-1}	$D_m/10^{-10}$ m^2 s^{-1}[b]	$D'_m/10^{-10}$ m^2 s^{-1}[c]	F
Cholest-5-en-3-one	7.8	8.1	7.3	7.8	0.04
(*R*)-(+)-Citronellal	32.4	13.2	12.0	12.7	0.04
(*S*)-(–)-Citronellol[d]	32.0	9.5	8.8	9.3	0.03
Hydroquinine (**3**)	15.6	6.3	3.7	4.0	0.44
Methyl nicotinate	27.7	14.0	12.6	13.3	0.05
N-Methylnicotinamide	24.3	10.3	9.6	10.1	0.01
(1*S*)-(–)-β-Pinene	29.4	13.9	13.1	13.9	0.00
1,6-Dehydopregnenolone acetate	11.8	8.1	7.2	7.7	0.05
Progesterone	15.6	8.3	7.8	8.2	0.01
o-Vanillin	18.1	12.9	12.1	12.9	0.00
Estrone	9.3	7.8	7.0	7.4	0.05
Methanol (solvent)		18.9	17.8	(18.9)	(0.00)

[a] Experiments were carried out in CD_3OD at 20 °C nominal temperature on a Varian Unity 400 spectrometer using the BPPSTE pulse sequence,[12] with gradient levels from 1 to 20 G cm^{-1} and lasting approximately 30 min. Data were analysed as described previously,[11–12] but using explicit correction for field gradient non-uniformity.[19] [b] The concentration c_p of functional repeat units of the polymer was 77.5 mM. [c] Diffusion coefficients were corrected for the difference in viscosity between the solutions of the free library and the library with the polymer present (see text). [d] The signal at 5.1 ppm for which diffusion data are reported contains components from citronellol, citronellal, and higher molecular weight impurities.

DOI: 10.1039/b008412n

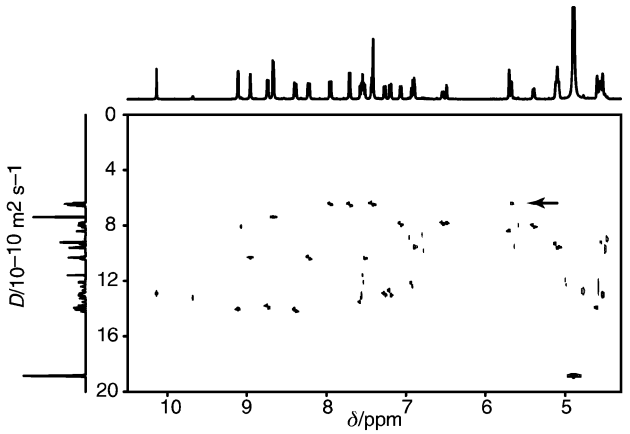

Fig. 1 HR-DOSY spectrum of the library of Table 1 in free CD_3OD solution, with (top) the normal ^1H spectrum and (side) the integral projection onto the diffusion axis.

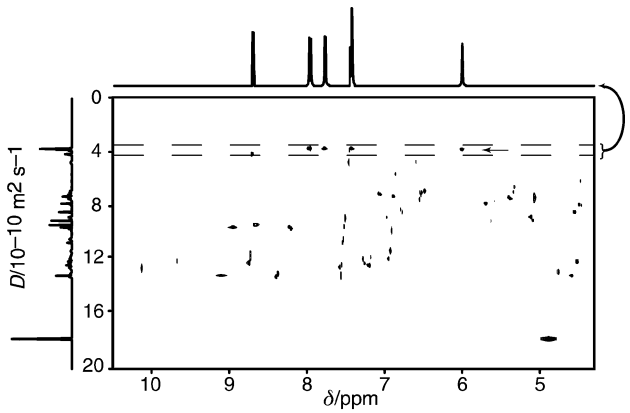

Fig. 2 HR-DOSY spectrum of the library of Table 1 and polymer **1** in CD_3OD, with (top) the integral projection onto the chemical shift axis of the region between the dotted lines, showing the subspectrum of the bound species, and (side) the integral projection onto the diffusion axis.

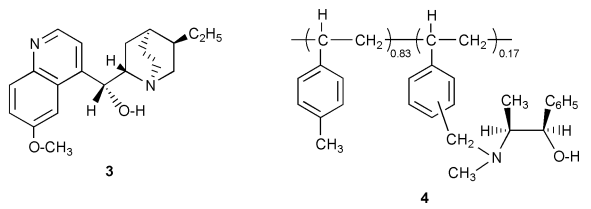

shifted hydroquinine **3** is shown on the top scale in Fig. 2. The changes in chemical shift for **3** between free solution and the polymer mixture show that the quinuclidine moiety in **3** protonates, causing association between the cation and the polyanionic polymer. No detectable change in either diffusion or shift is seen for methyl nicotinate and *N*-methylnicotinamide, both weaker bases than **3**.

In a second trial, the previously-described polymer **4**,[18] with M_n = 4900 and M_w = 9200 by GPC, was used to detect interactions with the β-amino-alcohol unit of (1*R*,2*S*)-*N*-benzylephedrine moieties. Polymer **4** showed a diffusion coefficient of 1.3×10^{-10} m^2 s^{-1} in $CDCl_3$ solution (2.6 mg ml^{-1}). Its interactions with a simulated library of 7 compounds were investigated, with the results summarised in Table 2. Here the only component to show significant binding is α-methoxyphenylacetic acid, which comes close to saturating the polymer binding sites and has an apparent association constant of several thousand M^{-1}. The specific nature of the binding is evidenced by the splitting of the α-proton and methyl signals of the racemic acid on binding to the chiral polymer.

Table 2 Summary of DOSY measurements for library B[a]

Compound	*c*/mM	$D_f/10^{-10}$ m^2 s^{-1}	$D_m/10^{-10}$ m^2 s^{-1}[b]	*F*
Cholest-5-en-3-one	21.3	7.5	7.4	0.02
(*R*)-(+)-Citronellal	21.4	12.2	12.4	−0.02
(*S*)-(–)-Citronellol	19.2	11.3	11.0	0.03
(1*S*)-(–)-β-Pinene	23.5	14.1	14.8	−0.06
1,6-Dehydopregnenolone acetate	21.6	7.8	7.8	0.00
Progesterone	20.0	7.9	8.5	−0.10
(±)-α-Methoxyphenylacetic acid	19.8	9.5	3.1	0.81

[a] Experimental conditions were as for Table 1. [b] The concentration c_p of functional repeat units of the polymer was 17.3 mM. No correction was made for changes in viscosity.

We are currently using the above method to explore interactions of amines, amides and peptides with functional macrocycles.

We thank the Thai Government for a PhD studentship (P. M.), and the EPSRC for grants GR/K44619 and GR/M16863.

Notes and references

1 G. Lowe, *Chem. Soc. Rev.*, 1996, **25**, 309.
2 L. A. Thompson and J. A. Ellman, *Chem. Rev.*, 1996, **96**, 555.
3 N. K. Terrett, M. Gardner, D. W. Gordon, R. J. Kobylecki and J. Steele, *Tetrahedron*, 1995, **51**, 8135.
4 N. K. Terrett, *Combinatorial Chemistry*, Oxford University Press, Oxford, 1998, ch. 4.
5 P. Monvisade, P. Hodge and C. L. Ruddick, *Chem. Commun.*, 1999, 1987.
6 S. R. Gilbertson and X. Wang, *Tetrahedron Lett.*, 1996, **37**, 6475.
7 K. Burgess, H. J. Lim, A. M. Porte and G. A. Sulikowski, *Angew. Chem., Int. Ed. Engl.*, 1996, **35**, 220.
8 K. Lewandowski, P. Murer, F. Svec and J. M. J. Fréchet, *Chem. Commun.*, 1998, 2237.
9 S. J. Rowan, P. S. Lukeman, D. J. Reynolds and J. K. M. Sanders, *New J. Chem.*, 1998, 1015 and references therein.
10 P. Stilbs, *Anal. Chem.*, 1981, **53**, 2135.
11 C. S. Johnson, *Prog. NMR Spectrosc.*, 1999, **34**, 204.
12 M. D. Pelta, H. Barjat, G. A. Morris, A. L. Davis and S. J. Hammond, *Magn. Reson. Chem.*, 1998, **36**, 706.
13 M. Lin and M. J. Shapiro, *J. Org. Chem.*, 1996, **61**, 7617.
14 M. Lin, M. J. Shapiro and J. R. Wareing, *J. Am. Chem. Soc.*, 1997, **119**, 5249.
15 M. Lin, M. J. Shapiro and J. R. Wareing, *J. Org. Chem.*, 1997, **62**, 8930.
16 K. Bleicher, M. Lin, M. J. Shapiro and J. R. Wareing, *J. Org. Chem.*, 1998, **63**, 8486.
17 H. G. Batz and B. Koldehoff, *Makromol. Chem.*, 1976, **177**, 683.
18 D. W. L. Sung, P. Hodge and P. W. Stratford, *J. Chem. Soc., Perkin Trans. 1*, 1999, 1463. The polymer used was labelled (**11d**) in this paper.
19 P. J. Bowyer, A. G. Swanson and G. A. Morris, poster M/T PA061, 41st ENC, Asilomar, CA, 2000.

Mild and efficient methodology for installation of *gem*-diallyl functionality on carbohydrate synthons

Mukund K. Gurjar,* S. V. Ravindranadh and Sukhen Karmakar

National Chemical Laboratory, Pune 411008, India. E-mail: gurjar@dalton.ncl.res.in

Received (in Cambridge, UK) 10th October 2000, Accepted 27th November 2000
First published as an Advance Article on the web 17th January 2001

A versatile approach to construct *gem*-diallyl functionality has been described.

As a part of our ongoing efforts directed toward synthesis of natural products containing a spiro-ring system,[1] we were confronted with a need to synthesize a *geminal* (*gem*) diallyl containing carbohydrate backbone (Fig. 1). The *gem*-diallyl groups can undergo ring closing metathesis to produce the spiro-ring system.[2] Such *gem*-diallyl systems are not reported in carbohydrate chemistry, although they can form valuable synthons for many chemical transformations leading to functionalised products.

Incorporation of *gem*-diallyl groups is usually achieved by base catalyzed dialkylation of active methylene groups with allyl halides.[3] However, we realized that this approach may not be appropriate for carbohydrate molecules because of side reactions resulting from various hydroxy groups. We were particularly interested in the application of Keck's one electron C–C bond-forming reaction[4] to generate a *gem*-diallyl system in a carbohydrate unit by quenching the allylic radical generated *in situ*, with allyltri-*n*-butylstannane.

In accordance with our plan, 5-*O*-*tert*-butyldiphenylsilyl-1,2-*O*-isopropylidene-α-D-xylofuranose (**1**) was oxidized with IBX–DMSO (IBX = *o*-iodoxybenzoic acid) and then the resulting 3-ulose derivative was treated with PPh_3=$CHCO_2Et$ in refluxing benzene to give the α,β-unsaturated product (**2**).[5]

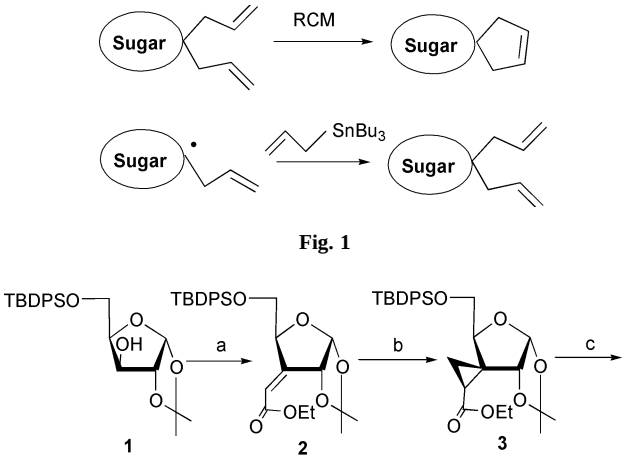

Fig. 1

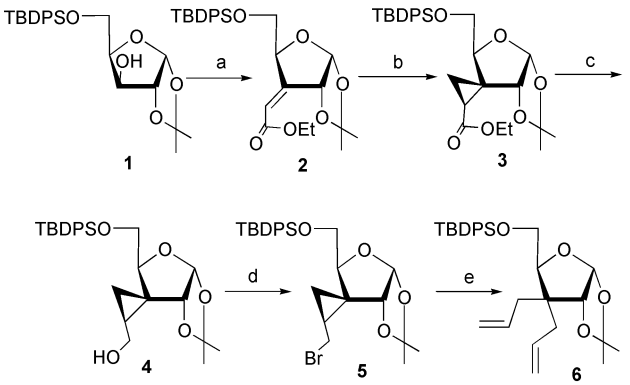

Scheme 1 *Reagents and conditions*: (a) (i) IBX (1.5 eq.), DMSO, rt, 10 h; (ii) PPh_3=CHCOOEt, (1.5 eq.), benzene, 80 °C, 3 h, 70% after two steps; (b) Me_2SOCH_3I (1.1 eq.), NaH (1.1 eq.), DMSO, rt, 3 h, 60%; (c) DIBAL-H (2.5 eq.), −78 °C, 0.5 h, 85%; (d) PPh_3 (2.0 eq.), CBr_4 (2.2 eq.), pyridine (2.5 eq.), 0 °C, 90%; (e) allyltri-*n*-butylstannane (2 eq.), AIBN (5 mol %), benzene, 80 °C,12 h, 80%.

Cyclopropanation of **2** was effected with Me_2SOCH_3I–NaH in dry DMSO to give **3**, as a single diastereomer.[6] Although the stereochemical identification of **3** was of no consequence to the present study, we believe the approach of the ylide occurs from the β-face due to the stereo-controlling effect of the adjacent 1,2-*O*-isopropylidene group. In the ^1H NMR spectrum of **3**, the protons of the cyclopropyl group, as expected, appeared in the high field region. Conversion of the ester function in **3** into the hydroxymethyl group was accomplished by using DIBAL-H at −78 °C to produce **4** in 85% yield. Compound **4** on treatment with CBr_4–PPh_3 in CH_2Cl_2 at rt gave the bromo derivative (**5**) in 90% yield. The ^1H, ^{13}C NMR and MS studies substantiated the assigned structure **4**. Treatment of **5** with allyltri-*n*-butylstannane in the presence of a catalytic amount of AIBN in refluxing benzene under argon atmosphere for 12 h gave the *gem*-diallyl compound **6** in 80% yield.† In the ^1H NMR

Table 1 Compounds **5a**–**e** were prepared essentially by the route shown in Scheme 1 and their structures elucidated by spectral data. Yields are given for isolated products.

Entry	Substrate	Product	Yield (%)
1	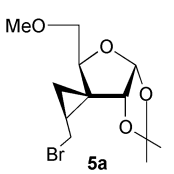 **5a**	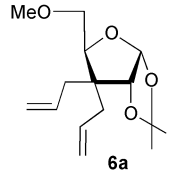 **6a**	72
2	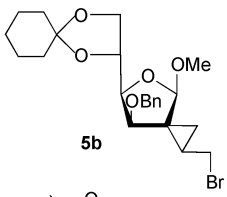 **5b**	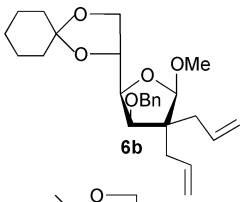 **6b**	63
3	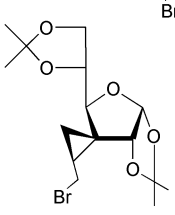 **5c**	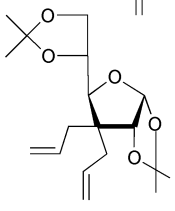 **6c**	76
4	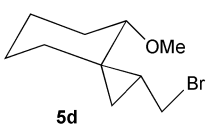 **5d**	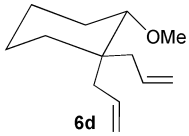 **6d**	75
5	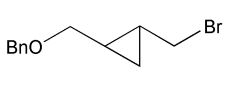 **5e**	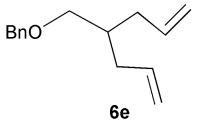 **6e**	70

DOI: 10.1039/b008184l

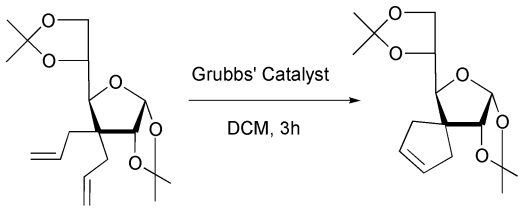

Scheme 2

spectrum of **6**, the characteristic olefinic proton signals of two allylic groups appeared in in the region of 5.0 and 5.7 ppm while the allylic methylene protons were located in the region of 2.2 ppm. In addition, the assigned structure of **6** was further suggested by the ^{13}C NMR, MS and elemental analysis. Table 1 provides other examples in this series which substantiates the versatility of this methodology. Only entry 5 describes an aliphatic example.

The ring closing metathesis reaction of **6c** with Grubbs catalyst in CH_2Cl_2 at rt gave the spiro-ring compound **7** in 80% yield.[7] The structure of **7** was established based on ^{1}H, ^{13}C NMR and MS (Scheme 2).[8]

In summary this communication describes a mild and efficient methodology to construct *gem*-diallylic substituted carbohydrate synthons as precursors for spiro-cyclic systems. The preparation of unsymmetrical *gem*-diallyl substituents at the quaternary carbon will be the next endeavour of this methodology.

Authors (S. V. R. and S. K.) are grateful to CSIR, New Delhi for the award of research fellowships.

Notes and references

† Typical experimental procedure: A solution of the cyclopropylmethyl bromide derivative **5a**–**e** (0.4 mmol), allyltri-*n*-butylstannane (0.8 mmol) and AIBN (5 mol %) in dry benzene (3 mL) was degassed by bubbling argon for 30 min. The reaction mixture was heated under reflux for 12 h and concentrated *in vacuo*. A KF solution (5 mL) and diethyl ether (10 mL) were added, stirred for 1 h, filtered and washed with ether. The ether layer was separated, dried over anhydrous Na_2SO_4 and concentrated. The crude product was purified on silica gel using ethyl acetate–hexane to afford the desired diallyl product.

1 M. Sannigrahi, *Tetrahedron*, 1999, **55**, 9007; A. P. Krapcho, *Synthesis*, 1974, 383; E. J. Corey and A. Guzman-Perez, *Angew. Chem., Int. Ed. Engl.*, 1998, **37**, 389.

2 K. Undheim and J. Efskind, *Tetrahedron*, 2000, **56**, 4857 and reference cited therein.

3 R. K. Singh, *Synthesis*, 1985, 54; S. Kotha and N. Sreenivaschary, *Bioorg. Med. Chem. Lett.*, 1998, **8**, 257; S. Kotha and E. Brahmachary, *Tetrahedron Lett.*, 1997, **3**, 3561.

4 G. E. Keck, E. J. Enholm, J. B. Yates and M. R. Wiley, *Tetrahedron*, 1984, **41**, 4079.

5 J. M. Trouchet and B. Gentile, *Carbohydr. Res.*, 197, **44**, 23.

6 M. K. Gurjar, B. V. N. B. S. Sharma and B. V. Rao, *J. Carbohydr. Chem.*, 1998, **17**, 1107.

7 R. H. Grubbs and S. Chang, *Tetrahedron*, 1998, **54**, 4413; R. H. Grubbs, S. J. Miller and G. C. Fu, *Acc. Chem. Res.*, 1995, **28**, 446.

8 Compound **6**: ^{1}H NMR (200 MHz) data: δ 1.08 (s, 9 H, ^{t}Bu), 1.29, 1.54 (2s, 6 H, 2 × Me, 1.87–2.54 (m, 4H, 2 × CH_2-CH=), 3.82 (m, 2 H, H-5 and H-5′), 4.03 (t, 1 H, J = 6.4 Hz, H-4), 4.25 (d, 1 H, J = 3.4 Hz, H-2), 5.0 (m, 4 H, 2 × CH_2=), 5.70 (d, 1 H, J = 3.4 Hz, H-1), 5.80 (m, 2 H, 2 × CH=), 7.35–7.77 (m, 10 H, 2 × Ph); ^{13}C NMR (50.32 MHz) data: δ 19.3, 26.5, 27.0, 35.6, 36.5, 50.0, 62.9, 84.7, 85.6, 104.2, 111.0, 117.7, 127.8, 129.8, 133.3, 133.5, 134.5, 135.0, 135.7.

Compound **6a**: ^{1}H NMR (200 MHz) data: δ 1.31, 1.53 (2s, 6 H, 2 × Me), 1.91–2.50 (m, 4 H, 2 × CH_2-CH=), 3.35 (s, 3 H, OMe), 3.52 (m, 2 H, H-5 and H-5′), 4.06 (dd, 1H, J = 3.9, 7.3 Hz, H-4), 4.26 (d, 1 H, J = 3.9 Hz, H-2), 5.06 (m, 4 H, 2 × CH_2=), 5.70 (d, 1 H, J = 3.9, H-1), 5.84 (m, 2 H, 2 × CH=); ^{13}C NMR (75.47 MHz) data: δ 26.3, 26.8, 35.3, 35.8, 49.8, 59.2, 71.7, 83.2, 85.3, 104.2, 112.2, 118.0, 134.0, 134.4.

Compound **6b**: ^{1}H NMR (500 MHz) data: δ 1.58 (m, 10 H, 5 × CH_2), 2.05- 2.4 (m, 4 H, 2 × CH_2-CH=), 3.31 (s, 3 H, OMe), 3.9 (d, 1 H, J = 4.4 Hz, H-3), 3.95 (dd, 1 H, J = 5.9, 8.3 Hz, H-4), 4.08 (m, 2 H, H-6 and H-6′), 4.31 (m, 1 H, H-5), 4.49, 4.74 (2d, 2 H, J = 11.0 Hz, CH_2Ph), 4.71 (s, 1 H, H-1), 5.06 (m, 4 H, 2 × CH_2=), 5.77 (m, 2 H, 2 × CH=); ^{13}C NMR (125.75 MHz) data: δ 23.9, 24.1, 25.2, 35.0, 35.3, 36.5, 52.6, 55.9, 67.2, 73.2, 74.2, 80.4, 84.4, 109.2, 109.6, 117.5, 117.7, 127.6, 128.0, 128.3, 135.0, 138.5.

Compound **6c**: ^{1}H NMR (200 MHz) data: δ 1.27, 1.33, 1.45, 1.50 (4s, 12 H, 4 × Me), 2.15–2.45 (m, 4 H, 2 × CH_2-CH=), 3.72 (m, 1 H, H-4), 3.78 (m, 1 H, H-5), 4.09 (m, 2 H, H-6 and H-6′), 4.24 (d, 1 H, J = 3.4 Hz, H-2), 5.03 (m, 4 H, 2 × CH_2=), 5.57 (d, 1 H, J = 3.4 Hz, H-1), 5.9 (m, 2 H, 2 × CH=); ^{13}C NMR (50.32 MHz) data: δ 25.5, 26.4, 26.8, 27.1, 36.1, 37.0, 50.6, 69.0, 73.5, 85.2, 86.0, 104.4, 109.5, 111.3, 117.6, 134.8, 135.5.

Compound **6d**: ^{1}H NMR (200 MHz) data: δ 1.30 (m, 8 H, 4 × CH_2), 1.92–2.30 (m, 4 H, CH_2-CH=), 2.94 (dd, 1 H, J = 3.4, 7.8 Hz, CH), 3.27 (s, 3 H, OMe), 4.94 (m, 4 H, 2 × CH_2=), 5.77 (m, 2 H, 2 × CH=); ^{13}C NMR (50.32 MHz) data: δ 21.0, 22.9, 24.1, 31.4, 36.8, 39.8, 40.9, 56.3, 82.3, 117.0, 117.2, 135.1.

Compound **6e**: ^{1}H NMR (200 MHz) data: δ 1.76 (m, 1 H, methine), 2.10 (m, 4 H, 2 × CH_2-CH=), 3.33 (dd, 2 H, J = 5.9, 11.2 Hz, CH_2O), 4.46 (d, 2 H, J = 11.7 Hz, CH_2Ph), 5.00 (m, 4 H, 2 × CH_2=), 5.73 (m, 2 H, 2 × CH=), 7.26 (m, 5 H, Ph); ^{13}C NMR (50.32 MHz) data: δ 35.4, 38.3, 72.4, 73.1, 116.3, 127.5, 128.3, 136.7.

Modified guanidines as chiral superbases: the first example of asymmetric silylation of secondary alcohols

Toshio Isobe,[ab] Keiko Fukuda,[a] Yukari Araki[b] and Tsutomu Ishikawa*[b]

[a] *Central Research Laboratory, Shiratori Pharmaceutical Co. Ltd., 6-11-24 Tsudanuma, Narashino, Chiba 275-0016, Japan*

[b] *Faculty of Pharmaceutical Sciences, Chiba University, 1-33 Yayoi, Inage, Chiba 263-8522, Japan*

Received (in Cambridge, UK) 15th November 2000, Accepted 13th December 2000
First published as an Advance Article on the web 18th January 2001

Modified guanidines could effectively mediate asymmetric silylation of secondary alcohols as recyclable bases under simple and mild conditions.

Due to their strongly basic character,[1] guanidines can be characterized as superbases[2] and, although chiral guanidines are expected to have potential as asymmetric reagents, their limited use[3] in asymmetric synthesis as chiral auxiliaries is due mainly to the lack of simple preparation methods. We have explored the possibility of modified guanidines as recyclable chiral superbases in organic synthesis under simple and mild conditions and recently reported their application to an asymmetric alkylative esterification of benzoic acid.[4] Kinetic resolution of racemic secondary alcohols is used for the selective preparation of one enantiomer. Enzymes such as esterases have been widely utilized for this purpose,[5] whereas non-enzymatic methods have been succeeded only in acylation.[6] In this communication we present the first example of asymmetric silylation of secondary alcohols mediated by chiral guanidines.

Reactions of indan-1-ol (**1**) with TBDMS (TBDMSCl) or TIPS chlorides (TIPSCl) were chosen as representatives for kinetic silylation of secondary alcohols because of the unsuccessful separation of each enantiomer of the silylated products by chiral HPLC when other acyclic alcohols or silylating agents were used in preliminary experiments.[7] Three different types of monocyclic guanidines [unsubstituted type **I**;[8a] 4-substituted type **II**;[8b,9] (4*S*,5*S*)-4,5-diphenylsubstituted type **III**[8c,9] and bicyclic guanidines **IV**[8b,9] (Fig. 1) were examined for their ability as catalysts in the silylation reaction. Thus, racemic **1** (2 equiv.) was first treated with TBDMSCl (1 equiv.) in DCM at rt in the presence of a chiral guanidine (1 equiv.) for several days to give, as expected, a silylated product **2** with recovery of the starting compound **1** (Table 1).

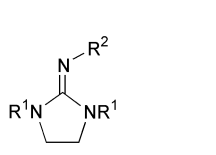

I

a: R^1=Me R^2=(*R*)-CH(Me)Ph
b: R^1=R^2=(*S*)-CH(Me)Ph

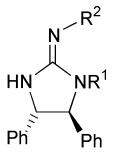

III

a: R^1=H, R^2=Et
b: R^1=H, R^2=CH_2Ph
c: R^1=H, R^2=(*S*)-CH(Me)Ph
d: R^1=H, R^2=(*R*)-CH(Me)Ph
e: R^1=Me, R^2=(*R*)-CH(Me)Ph

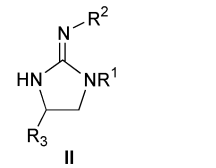

II

a: R^1=R^2=$CHMe_2$ R^3=(*R*)-Ph
b: R^1=R^2=(*S*)-CH(Me)Ph R^3=(*S*)-CH_2Ph
c: R^1=R^2=(*S*)-CH(Me)Ph R^3=(*R*)-CH_2Ph
d: R^1=R^2=(*S*)-CH(Me)Ph R^3=(*R*)-Ph

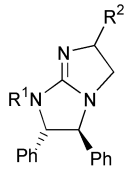

IV

a: R^1=H R^2=(*S*)-CH_2Ph
b: R^1=Me R^2=(*S*)-CH_2Ph
c: R^1=H R^2=(*R*)-Ph
d: R^1=H R^2=(*S*)-Ph

Fig. 1

Simple guanidines **I** were not effective for asymmetric induction (runs 1 and 2). However, moderate ee was observed in the cases of 4-substituted guanidines **II** (runs 3–6), in which the stereogenic center of the silylated product **2** was found to be controlled by the stereochemistry of the imidazolidine ring (C4). Thus, **IIb** with an (*S*)-configuration produced an (*R*)-excess product (run 4), whereas a diastereomeric **IIc** gave an (*S*)-excess product (run 5). Reasonable ee's was obtained when 4,5-diphenylguanidines **III** were used. It was found that the chiral center of the substituent on the external nitrogen atom played an important role in effective asymmetric induction. Thus, (*R*)-phenylethyl-substituted guanidines **IIId** and **IIIe** gave an (*R*)-excess **2** with 37% ee (run 10) and 39% ee (run 11), respectively, whereas a lower ee (6%) was observed in the case of **IIIc** with an (*S*)-phenylethyl-substituent (run 9). The formation of an (*R*)-excess product in each case indicated that the stereochemistry of **2** was controlled by the ring chiral centres of guanidines.

Table 1 Trials for kinetic silylation of **1** with TBDMSCl in the presence of chiral guanidines

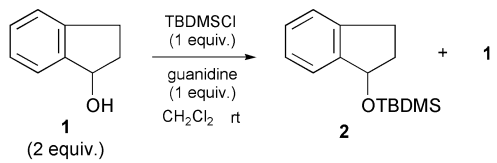

			2[a]		
Run	Guanidine	Time/d	Yield[b] (%)	Ee[c] (%)	Conf.[d]
1	**Ia**	14	82	0	—
2	**Ib**	7	38	0	—
3	**IIa**	3	70	19	*S*
4	**IIb**	6	31	6	*R*
5	**IIc**	9	66	14	*S*
6	**IId**	16	61	13	*S*
7	**IIIa**	8	47	14	*R*
8	**IIIb**	6	67	16	*R*
9	**IIIc**	12	34	6	*R*
10	**IIId**	11	34	37	*R*
11	**IIIe**	9	50	39	*R*
12[e]	**IVa**	10	78	31	*R*
13	**IVb**	9	53	7	*R*
14	**IVc**	7	86	0	—
15	**IVd**	6	32	27	*R*

[a] Authentic (*S*)-**2** was prepared from (*S*)-**1** by a conventional method. [b] The starting **1** was quantitatively recovered. [c] The ee was estimated by chiral HPLC (CHIRALCEL OD, 0.5 ml min^{-1} with hexane). The peak detection was done by UV (254 nm). The retention times of (*R*)- and (*S*)-**2** were 9.67 and 11.61 min, respectively. [d] Absolute configuration of the excess enantiomer. [e] An (*S*)-excess **1** (18% ee) was quantitatively recovered. The guanidine **IVa** was completely recovered in a re-useable form.

DOI: 10.1039/b009173l

Table 2 Asymmetric silylation of **1** or **4** with TlPSCl in the presence of either guanidine **IIId** or **IVd**

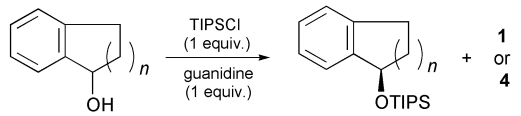

				3 or **5**[a]	
Run	**1** or **4**	Guanidine	Temp.	Yield[b] (%)	Ee (%)
1	**1**	**IIId**	rt	**3**: 36	59[c]
2	**1**	**IIId**	reflux	**3**: 48	59[c]
3	**1**	**IVa**	rt	**3**: 79	58[c]
4	**4**	**IVa**	rt	**5**: 15[d]	70[e]

[a] Authentic (*S*)-**3** and -**5** were prepared from (*S*)-**1** and -**4**, respectively, by conventional methods. [b] The starting **1** was quantitatively recovered. [c] The (*R*)-excess enantiomer was obtained. The ee was estimated by chiral HPLC (CHIRALCEL OD-H, 0.5 ml min^{-1} with hexane). The peak detection was done by UV (254 nm). The retention times of (*R*)- and (*S*)-**3** were 7.75 and 9.29 min, respectively. [d] Side products were detected on TLC during the reaction. [e] The ee was estimated by chiral HPLC (CHIRALCEL OD-H, 0.2 ml min^{-1} hexane). The peak detection was done by UV (254 nm). The retention times of (*R*)- and (*S*)-**5** were 19.82 and 20.68 min, respectively.

With bicyclic guanidines **IV**, equally asymmetric induction was observed when **IVa** was used (run 12). Introduction of a methyl group onto the ring nitrogen did not affect asymmetric induction in the cases of monocyclic guanidines as mentioned above (see runs 10 and 11). However, marked reduction of ee was observed in the reaction using the *N*-methylguanidine **IVb** (run 13). Furthermore, a match–mismatch relationship was observed in reactions using diastereomeric **IVc** and **IVd** similarly to reactions using monocyclic guanidines **IIIc** and **IIId**. Thus, **IVd** with a (2*S*,3*S*,7*S*)-configuration was a more effective base (run 15: 27% ee) than **IVc** (run 14: no ee).

Theoretically, indan-1-ol (**1**) should be obtained as an (*S*)-enantiomer-rich alcohol in these silylation reactions and the guanidine used could be recovered in a re-useable form. Isolation of both **1** and **IVa** in run 12 resulted in their expected and quantitative recovery as an (*S*)-excess alcohol (18% ee) and as a re-useable guanidine, respectively. In addition, we tried the asymmetric silylation in the presence of **IIId** in various solvents such as MeCN, toluene, trifluoromethylbenzene, and THF; however, no improvement of ee was observed in each case.

From the above experiments using TBDMSCl as a silylating agent, **IIId**, **IIIe** or **IVa** among the guanidines examined were suggested to be promising chiral bases for asymmetric silylation. Next, reactions with a more bulky TIPSCl in the presence of either **IIId** or **IVa** were attempted under the same conditions[10] described in Table 1 (Table 2). Reactions of **1** with TIPSCl at rt similarly proceeded to afford an (*R*)-excess **3** in 59% ee with **IIId** (run 1) and 58% ee with **IVa** (run 3), respectively. Interestingly, no loss of ee was observed even in the reaction under heating (run 2), indicating that this silylation would be tolerant to the reaction temperature.[11] Application of the guanidine-mediated silylation using **IVa** to 1,2,3,4-tetrahydro-1-naphthol (**4**) in place of **1** gave a silylated product **5** with high stereoselection (70% ee), albeit the chemical conversion[12] was low (run 4).

In conclusion, we have found that guanidines could effectively mediate asymmetric silylation of secondary alcohols as recyclable bases under simple and mild conditions. Although the ee obtained and reaction rates are not neccessarily perfect, it is noteworthy that these results offer not only the first example of chemical asymmetric silylation of secondary alcohols, but also experimental evidence for a possible ion-pair complex[13] between a silylating agent and a base. Formation of a silylguanidinium salt has been partially suggested by inspection of the ^{1}H NMR spectrum of an equimolar mixture of the guanidine **IIId** and TBDMSCl. Approaches to the mechanistic rationale, kinetics, and optimization of the reaction are at present under study in our laboratory.

Notes and references

1 Y. Yamamoto and S. Kojima, *The Chemistry of Amidines and Imidates*, Vol. 2, ed. S. Patai and Z. Rappoport, John Wiley and Sons Inc., New York, 1991, p. 485.

2 M. Costa, G. P. Chiusoli, D. Taffurelli and G. Dalmonego, *J. Chem. Soc., Perkin Trans. 1*, 1998, 1541.

3 (*a*) For nitroaldol (Henry) reaction, see R. Chinchilla, C. Najera and P. Sanchez-Agullo, *Tetrahedron: Asymmetry*, 1994, **5**, 1393; (*b*) for the Strecker reaction, see M. S. lyer, K. M. Gigstad, N. D. Namdev and M. Lipton, *J. Am. Chem. Soc.*, 1996, **118**, 4910; (*c*) for the Michael reaction, see V. Alcazar, J. R. Moran and J. deMendoza, *Tetrahedron Lett.*, 1995, **36**, 3941. During our research work, application of chiral guanidines to asymmetric synthesis was reported: (*a*) for the Strecker reaction, see E. J. Corey and M. J. Grogan, *Org. Lett.*, 1999, **1**, 157; (*b*) for the Michael reaction, see A. Howard-Jones, P. J. Murphy, D. A. Thomas and P. W. R. Caulkett, *J. Org. Chem.*, 1999, **64**, 1039; M. Dai and K. Cheng, *Tetrahedron: Asymmetry*, 1999, **10**, 713.

4 T. Isobe, K. Fukuda and T. Ishikawa, *Tetrahedron: Asymmetry*, 1998, **9**, 1729.

5 C.-H. Wong, *Science*, 1989, **244**, 1145; J. B. Jones, *Tetrahedron*, 1986, **42**, 3351; C.-S. Chen and C. J. Sih, *Angew. Chem., Int. Ed. Engl.*, 1981, **28**, 695; A. M. Klibanov, *Chem. Rev.*, 1990, **23**, 114.

6 D. A. Evans, J. C. Anderson and M. K. Taylor, *Tetrahedron Lett.*, 1993, **34**, 5563; E. Vedejs and X. Chan, *J. Am. Chem. Soc.*, 1996, **118**, 1809; E. Vedejs, O. Daugulis and S. T. Diver, *J. Org. Chem.*, 1996, **61**, 430; J. C. Ruble, H. A. Latham and G. C. Fu, *J. Am. Chem. Soc.*, 1997, **119**, 1492; T. Kawabata, M. Nagao, K. Takasu and K. Fuji, *J. Am. Chem. Soc.*, 1997, **119**, 3169; S. J. Miller, G. T. Copeland, N. Papajioannou, T. E. Horstmann and E. M. Ruel, *J. Am. Chem. Soc.*, 1998, **120**, 1629.

7 TBDMS, TIPS, and TBDPS derivatives of 1-phenylethyl alcohol and TIPS derivatives of 1-phenylpropyl and 2-phenylcyclohexyl alcohols were examined.

8 (*a*) T. Isobe, K. Fukuda and T. Ishikawa, *J. Org. Chem.*, 2000, **65**, 7770; (*b*) T. Isobe, K. Fukuda, T. Tokunaga, H. Seki, K. Yamaguchi and T. Ishikawa, *J. Org. Chem.*, 2000, **65**, 7774; (*c*) T. Isobe, K. Fukuda, K. Yamaguchi, H. Seki, T. Tokunaga and T. Ishikawa, *J. Org. Chem.*, 2000, **65**, 7779.

9 It is known that substituted guanidines can exist in tautomerization of amino and imino forms depending upon the substitution patterns (see, K. Tanatani, K. Yamaguchi, I. Azumaya, R. Fukotomi, K. Shudo and H. Kagechika, *J. Am. Chem. Soc.*, 1998, **120**, 6433). One tautomer is arbitrarily described as a structure of guanidines with at least one NH function in Fig. 1.

10 We also tried catalytic silylation reactions in the coexistence of Et_3N. The reaction proceeded smoothly (57% conversion after 43 h), but no asymmetric induction was observed.

11 On the other hand, the reaction of **1** with TBDMSCl using **IVa** at −20 °C for 20 days afforded **2** in 16% yield with 33% ee, resulting in no improvement of asymmetric induction.

12 The low yield of **5** probably was caused by considerable production of side-products, whereas only the silylation reaction was observed in the use of **1** as a substrate.

13 E. J. Corey and A. Venkateswariu, *J. Am. Chem. Soc.*, 1972, **94**, 6190; S. K. Chaudhary and O. Hernandez, *Tetrahedron Lett.*, 1979, 99; H. Emde, A. Goetz, K. Hofmann and G. Simehen, *Liebigs Ann. Chem.*, 1981, 1643; S. Kim and H. Cheng, *Synth. Commun.*, 1984, **14**, 899.

Modified guanidines as chiral superbases: application to asymmetric Michael reaction of glycine imine with acrylate or its related compounds

Tsutomu Ishikawa,*[a] Yukari Araki,[a] Takuya Kumamoto,[a] Hiroko Seki,[b] Keiko Fukuda[c] and Toshio Isobe[ac]

[a] *Faculty of Pharmaceutical Sciences, Chiba University, 1-33 Yayoi, Inage, Chiba 263-8522, Japan*
[b] *Chemical Analysis Center, Chiba University, 1-33 Yayoi, Inage, Chiba 263-8522, Japan*
[c] *Central Research Laboratory, Shiratori Pharmaceutical Co. Ltd., 6-11-24 Tsudanuma, Narashino, Chiba 275-0016, Japan*

Received (in Cambridge, UK) 16th November 2000, Accepted 13th December 2000
First published as an Advance Article on the web 18th January 2001

Modified guanidines efficiently catalysed the asymmetric Michael reaction of a prochiral glycine derivative with acrylate or its related compounds either in solution or without a solvent under simple and mild conditions (> 95% ee).

Guanidines can be characterized as superbases[1] in organic synthesis due to their strong basicity.[2] We have explored the possibility of readily available modified guanidines[3] as re-useable chiral superbases in asymmetric synthesis.[4] Glycine imines are used as chiral templates for asymmetric synthesis of α-amino acids, in which enantioselective phase-transfer alkylation with alkyl halides has been established as a general method.[5] Ma and Cheng[6] attempted a conjugate addition of glycine imines with vinyl carbonyl compounds in the presence of C_2-symmetrical linear-type guanidines in place of phase-transfer catalysts;[7] however, the best ee observed by them was up to 30%. Re-examination of the Michael reaction using our modified guanidines under various conditions led to effective asymmetric induction (> 95% ee) when **4** (or **ent-4**, Fig. 1) was used as a catalyst either in solution or without a solvent. In this communication we present the utility of modified guanidines as clean chiral superbases in an asymmetric Michael reaction under simple and mild reaction conditions.

According to the reported conditions[6] we preliminarily examined the Michael reaction of *tert*-butyl diphenyliminoacetate (**1**) (1 equiv.) and ethyl acrylate (**2a**) (3.6 equiv.) in THF (0.26 mmol ml^{-1}) in the presence of 20 mol% of four different types of chiral guanidines **4**,[4] **5**,[3c] **6**,[3c] and **7**[3b] at 20 °C for about one week. Reasonable asymmetric induction (79% ee) was observed only in the case of **4** among the guanidines examined, albeit the chemical conversion was low (15%), in which an (*R*)-excess adduct **3a**[6] was yielded (see Table 1, run 1). In other cases, the reaction did not proceed. However, the guanidines used in these reactions were completely recovered in re-useable forms by chromatographic separation. These results led us to further examine the reaction using **4** under various conditions. Although a stoichiometric reaction in THF slightly increased the yield [34% yield (77% ee)], changing THF to other solvents in the catalytic reaction resulted in no improvement of the reaction rate although high enantioselectivities were maintained [9% yield (84% ee) in chloroform; 4% yield (73% ee) in toluene] except in ethanol [7% yield (42% ee)].

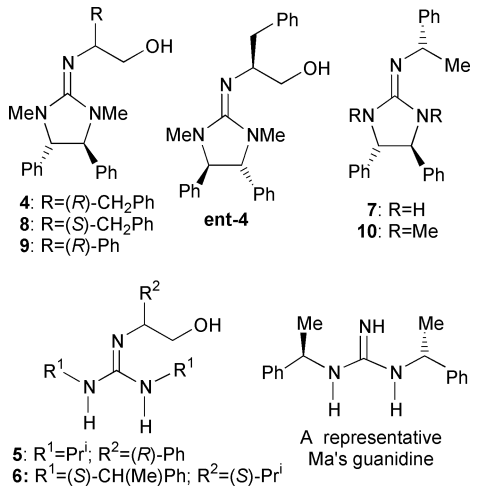

Fig. 1

We next examined the guanidine-catalysed Michael reaction of **1** with methyl vinyl ketone (MVK)[8] (**2b**) and acrylonitrile (**2c**) as a Michael acceptor in place of **2a** under the same conditions. The former reaction smoothly proceeded to afford an adduct **3b** in 90% yield, in which high enantioselectivity (96% ee) was observed (Table 1, run 2), whereas the starting **1** was completely recovered when **2c** was used (Table 1, run 3). These facts suggested that **4** could lead to effective asymmetric induction with the use of reactive Michael acceptors.

Solvent-free reactions,[9] in which rate acceleration is generally observed, have attracted much attention from the ecological point of view. Thus, **1** was treated with **2a** without a

Table 1 Guanidine-catalysed Michael reaction of **1** and **2** using **4** either in THF or without a solvent

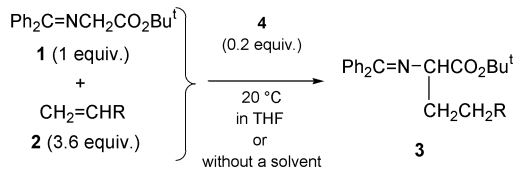

				3		
Run	Solvent	**2** (R)	Time	Yield[a] (%)	Ee (%)	Conf.[b]
1	THF	**a** (CO_2Et)	7 d	15	79[c]	*R*
2		**b** (COMe)	6 d[e]	90	96[f]	(*R*)
3		**c** (CN)	5 d	NR[g]	—	—
4	Without a solvent	**a** (CO_2Et)	3 d	85 (100)	97[c]	*R*
5		**b** (COMe)	15 h	90 (100)	80[f]	(*R*)
6		**c** (CN)	5 d	79 (100)	55[h]	(*R*)
7		**d** (CO_2Me)	3 d	98 (100)	93[i]	(*R*)

[a] Isolated, non-optimized yields. Parentheses show estimation of the product by ^{1}H NMR spectra. [b] Configuration of an excess enantiomer. Parentheses show the expected absolute configuration. [c] The (*R*)- and (*S*)-enantiomers were observed at retention times of 7.2 and 9.3 min, respectively, in HPLC using CHIRALCEL OD (Daicel Co. Ltd.,) under the following conditions; eluent: *n*-hexane–isopropanol = 100 : 1, flow rate: 1.0 ml min^{-1}, detection: 254 nm. [d] Reactions were carried out in 0.26 mmol ml^{-1} concentration of **1** in THF. [e] The adduct **3b** with the same ee was given in 40% yield after 15 h. [f] The (*R*)- and (*S*)-enantiomers were observed at retention times of 11.0 and 15.8 min, respectively, in the same HPLC as **3b**. [g] No reaction. [h] The (*R*)- and (*S*)-enantiomers were observed at retention times of 12.0 and 16.7 min, respectively, the same HPLC as **3b**. [i] The (*R*)- and (*S*)-enantiomers were observed at retention times of 6.5 and 7.3 min, respectively, in the same HPLC as **3b**.

DOI: 10.1039/b009193f

Table 2 Examination of solvent-free asymmetric Michael reaction of **1** with **2a** using various bases

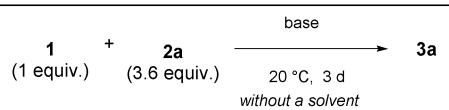

		3a		
Run	Base (mol%)	Yield[a] (%)	Ee (%)[b]	Conf.[c]
1[d]	**4** (20)	85 (100)	97	*R*
2	**4** (5)	40	97	*R*
3	None	NR[e]	—	—
4	(−)-Quinine (20)	NR[e]	—	—
5	**ent-4** (20)	87 (100)	97	*S*
6	**8** (20)	8 (17)	53	*S*
7	**9** (20)	17 (35)	91	*R*
8	**10** (20)	NR[e]	—	—

[a] Isolated, non-optimized yields. Parentheses show estimation of the product by ^{1}H NMR spectra. [b] See footnote *d* in Table 1. [c] Configuration of an excess enantiomer. [d] The data in Table 1, entry 4. [e] No reaction.

solvent (Table 1, run 4). A heterogeneous mixture of the two components containing **4** was simply stirred at 20 °C for 3 d.[10] Interestingly, both product formation and enantioselectivity were dramatically improved to give an (*R*)-excess **3a** with 97% ee in quantitative yield. Similarly, remarkable rate acceleration was observed on two other Michael acceptors **2b** and **2c**. In the former case (Table 1, run 5), reaction was completed after 15 h, in which relatively high enantioselctivity (80% ee) was kept. On the other hand, in the latter case (Table 1, run 6), **1** disappeared after 5 days to afford **3c** with 55% *ee* in spite of no reaction in solution (see Table 1, run 3). In addition, as expected, the use of methyl acrylate (**2d**) as a Michael acceptor led to the same satisfactory results obtained with **2a** (Table 1, run 7).

Thus, as a solvent-free reaction seems to be generally effective in the guanidine-catalysed Michael reaction of **1**, optimization was tried using **2a** as a Michael acceptor (Table 2). The same high *ee* was achieved even on reduction of the catalyst amount, albeit with lower chemical conversion (Table 2, run 2). No reaction was observed in the absence of a guanidine or in the presence of (−)-quinine (Table 2, runs 3 and 4). These facts indicated that **4** effectively catalysed the solvent-free reaction of **1** with **2a** in 20 mol% concentration.

The use of **ent-4**,[11] as expected, afforded an (*S*)-excess **3a** in quantitative yield with the same high enantioselectivity (Table 2, run 5). The (*S*)-excess **3a** was also obtained when **8**,[3a] a diastereomer of **4**, was used as a catalyst, but both chemical yield and asymmetric induction were lowered considerably (Table 2, run 6). Replacement of an (*R*)-phenylalaninol unit in **4** to an (*R*)-phenylglycinol one in **9**[3a] afforded an (*R*)-excess **3a** with relatively high selectivity. However, chemical conversion was not good (Table 2, run 7). On the other hand, the use of a guanidine **10**[4] lacking a hydroxyethyl function resulted in no reaction (Table 2, run 8).

Experimental evidence obtained in the above solvent-free reactions could be summarised as follows: (i) satisfactory chemical conversion with high enantioselectivity in the use of HOC_2H_4-substituted cyclic guanidines with (4*S*,5*S*,1′*R* or 4*R*,5*R*,1′*S*) configuration such as **4** indicates that the relative configurations of these three chiral centers are very important for effective asymmetric induction in addition to rate acceleration; (ii) predominant production of (*R*)-**3a** with **4** and **9** [or (*S*)-**3a** with **ent-4** and **8**] shows that a stereogenic center of the adduct should be strictly reflected by the chirality of a substituent at the external nitrogen; (iii) if the enolate of **1** could be formed by action of **4**, its *re*-face should be attacked by **2a** to yield an (*R*)-excess **3a**, for which the opposite *si*-face is severely blocked by the guanidine unit as shown in Fig. 2; (iv) although the absolute configuration of an excess enantiomer obtained in each reaction of **1** with **2b**, **2c** or **2d** has not been determined, an (*R*)-excess **3b**, **3c** or **3d** should be given in the reaction using **4**

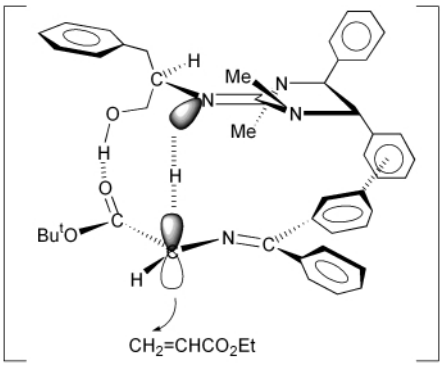

Fig. 2

due to the same face differentiation mentioned above, even in solution.

In summary, it was found that modified guanidines efficiently catalysed the asymmetric Michael reaction of a prochiral glycine derivative with vinyl compounds either in solution or without a solvent under simple and mild conditions. These guanidine-catalysed asymmetric Michael reactions[12] could contribute to development of green chemistry,[13] because modified guanidines are considered to be re-useable (economically favored) and easily functionalizable (widely applicable) artificial organic bases.

Notes and references

1 M. Costa, G. P. Chiusoli, D. Taffurelli and G. Dalmonego, *J. Chem. Soc., Perkin Trans. 1*, 1998, 1541.

2 Y. Yamamoto and S. Kojima, in *The Chemistry of Amidines and Imidates*, Vol. 2, eds, S. Patai and Z. Rappoport, John Wiley and Sons Inc., New York, 1991, pp. 485.

3 (*a*) T. Isobe, K. Fukuda and T. Ishikawa, *J. Org. Chem.*, 2000, **65**, 7770; (*b*) T. Isobe, K. Fukuda, T. Tokunaga, H. Seki, K. Yamaguchi and T. Ishikawa, *J. Org. Chem.*, 2000, **65**, 7774; (*c*) T. Isobe, K. Fukuda, K. Yamaguchi, H. Seki, T. Tokunaga and T. Ishikawa, *J. Org. Chem.*, 2000, **65**, 7779.

4 T. Isobe, K. Fukuda and T. Ishikawa, *Tetrahedron: Asymmetry*, 1998, **9**, 1729.

5 For the early work, see: M. J. O'Donnell, W. D. Bennett and S. Wu, *J. Am. Chem. Soc.*, 1989, **111**, 2353; M. J. O'Donnell, I. A. Esikova, A. Mi, D. F. Shullenberger and S. Wu in *Phase-Transfer Catalysis* (ACS Symposium Series 659), ed. M. E. Halpern, ACS, Washington D. C., 1997, Chapter 10; B. Lygo and P. G. Wainwright, *Tetrahedron Lett.*, 1997, **38**, 8595. For recent work, see: A. Nelson, *Angew. Chem., Int. Ed.*, 1999, **38**, 1583; J. Ezquerra, C. Pedregal, I. Merino, J. Florez, J. Barluenga, S. G.-Granda and M.-A. Llorea, *J. Org. Chem.*, 1999, **64**, 6554; T. Ooi, M. Kameda and K. Maruoka, *J. Am. Chem. Soc.*, 1999, **121**, 6519; T. Abellan, R. Chinchilla, N. Galindo, G. Guillena, C. Najera and J. M. Sansano, *Eur. J. Org. Chem.*, 2000, 2689.

6 D. Ma and K. Cheng, *Tetrahedron: Asymmetry*, 1999, **10**, 713.

7 Corey *et al*. reported the quaternary ammonium salt-catalysed asymmetric Michael reaction: E. J. Corey, M. C. Noe and F. Xu, *Tetrahedron Lett.*, 1998, **39**, 5347; F.-Y. Zhang and E. J. Corey, *Org. Lett.*, 2000, **2**, 1097.

8 Although Ma and Cheng[6] had also tried the Michael reaction of **1** with **2b**, the enantioselectivity was quite low (16.5% ee).

9 For examples, see: K. Tanaka and F. Toda, *Chem. Rev.*, 2000, **100**, 1025; V. K. Aggarwal and A. Mereu, *Chem. Commun.*, 2000, 2310; J. O. Metzger, *Angew. Chem., Int. Ed.*, 1998, **37**, 2975.

10 A heterogeneous mixture turned into a homogeneous one after completion of the reaction.

11 The guanidine was prepared from (*R*,*R*)-1,2-diphenylethylenediamine according to the reported method.[4]

12 Some guanidines have been applied to asymmetric Michael reactions as chiral bases, however low or no enantioselectivity had been observed in the guanidine-catalysed reactions, see: V. Alcazar, J. R. Moran and J. deMendoza, *Tetrahedron Lett.*, 1995, **36**, 3941; A. Howard-Jones, P. J. Murphy, D. A. Thomas and P. W. R. Caulkett, *J. Org. Chem.*, 1999, **64**, 1039. During our research works an effective Strecker reaction catalysed by a C_2-symmetrical bicyclic guanidine was reported in spite of the reaction in solution: E. J. Corey and M. J. Grogan, *Org. Lett.*, 1999, **1**, 157.

13 P. T. Anastas and J. C. Warner in *Green Chemistry: Theory and Practice*, Oxford University Press, Oxford, 1998.

The synthesis of Mo(IV) arene complexes by the hydrogenation of Mo(IV) olefin complexes†

Carlos G. Ortiz,‡ Khalil A. Abboud, Tom M. Cameron and James M. Boncella*

Department of Chemistry and Center for Catalysis, University of Florida, Gainesville, FL 32611-7200, USA. E-mail: boncella@chem.ufl.edu

Received (in Irvine, CA, USA) 11th September 2000, Accepted 7th December 2000
First published as an Advance Article on the web 19th January 2001

The compounds [Mo(NPh)(η²-olefin)(*o*-(Me$_3$SiN)$_2$C$_6$H$_4$)] (olefin = propene (1a), isobutene (1b), and butenes (1c)) react with molecular hydrogen (*ca*. 15 psi) in the presence of excess arene affording Mo(IV) η⁶-arene complexes of the type [Mo(NPh)(η⁶-arene)(*o*-(Me$_3$SiN)$_2$C$_6$H$_4$)] (arene = benzene (2a), toluene (2b), *o*-xylene (2c), *m*-xylene (2d), *p*-xylene (2e), diphenylmethane (2f), and bibenzyl (2g)), while treatment of [Mo(NPh)(η²-styrene)(*o*-(Me$_3$SiN)$_2$C$_6$H$_4$)] (1d) with hydrogen in a pentane solution gives [Mo(NPh)(η⁶-ethylbenzene)(*o*-(Me$_3$SiN)$_2$C$_6$H$_4$)] (2h); the crystal structures of 2d and 2e are reported and reveal highly distorted arene ligands approaching η⁴-coordination modes.

Fisher and Hafner characterized the first transition metal π-arene complex, Cr(η⁶-benzene)$_2$, 45 years ago.[1] Since this discovery the chemistry of π-arene complexes has been extensively explored.[2] It was initially believed that arene complexes were confined to transition metals in low oxidation states and a significant development in this field has involved the synthesis and characterization of high oxidation state Group 4 and 5 transition metal–arene complexes.[3,4] While Group 4 and 5 arene complexes are relatively rare, high valent Group 6 arene complexes are, with one exception,[5] non-existent. Furthermore, the generation of isolable high oxidation state transition metal–arene complexes *via* hydrogenation of η²-olefin complexes remains a rare process.[6] We report herein the synthesis and structure of molybdenum(IV) η⁶-arene complexes obtained upon exposure of various molybdenum η²-olefin complexes,[7] of the form [Mo(NPh)(η²-olefin)(*o*-(Me$_3$SiN)$_2$C$_6$H$_4$)], to molecular hydrogen (*ca*. 15 psi) and excess arene. In addition, these molybdenum(IV) η⁶-arene complexes catalyse the hydrogenation of olefins.

The hydrogenation of **1a**–**c** in the presence of 15 equivalents of arene gave complexes **2a**–**g** as microcrystals after crystallization from pentane (Scheme 1).§ The molecular structures of **2d** and **2e** were determined by single crystal X-ray diffraction studies, and are shown in Fig. 1 and 2, respectively, along with selected crystal data.¶ Complex **2d** adopts a three-legged piano stool geometry in which the arene ligand is strongly distorted toward an η⁴-coordination mode. The structural data suggest that the interaction of the arene ligand with the molybdenum metal center is much like a 1,3-butadiene–metal interaction. A considerable ring distortion of 17.4(3)° was found between the planes formed by C(20)–C(19)–C(24)–C(23) and C(20)–C(21)–C(22)–C(23). Carbons C(19) and C(24) were found to be considerably further from the metal center than the other arene carbons, suggesting that the arene interaction with the metal center is mostly through C(20), C(21), C(22) and C(23). The shorter bond lengths for C(21)–C(22) and C(19)–C(24), in comparison with the remainder of the arene carbon–carbon bonds, are consistent with considerable double bond character between these carbons.

† Electronic supplementary information (ESI) available: ^{1}H NMR spectra for complexes **2b**–**2d** and **2h**, chemical shift data for **2a**–**2h**. See http://www.rsc.org/suppdata/cc/b0/b007812n/

‡ Present address: Dupont Dow Elastomers, L. L. C., Ethylene Elastomers R&D, 2301 N. Brazosport Blvd., B-1470, Freeport, TX 77541, USA.

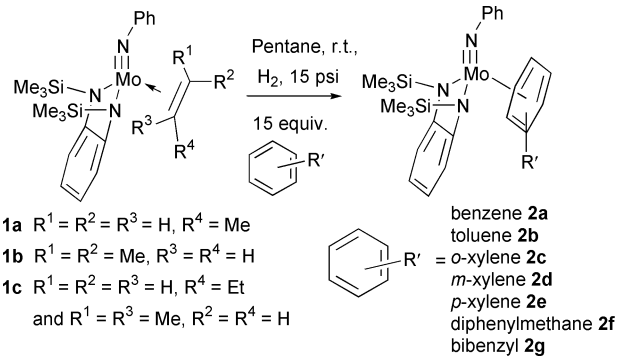

Scheme 1

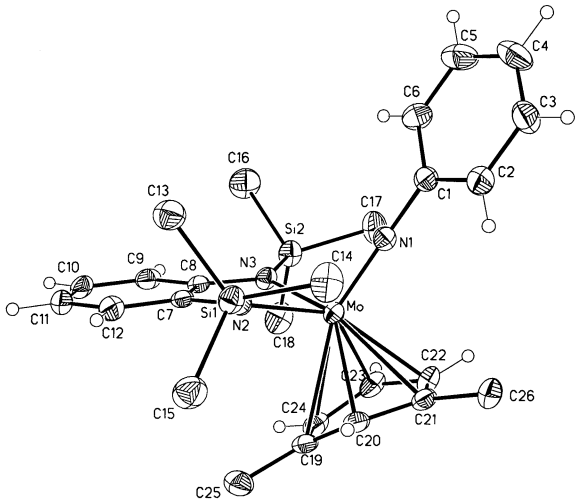

Fig. 1 Thermal ellipsoid plot of **2d** (50% probability thermal ellipsoids). Selected bond lengths (Å) and angles (°): Mo–N(1) 1.761(3), Mo–C(19) 2.519(3), Mo–C(20) 2.313(4), Mo–C(21) 2.425(4), Mo–C(22) 2.371(4), Mo–C(23) 2.286(4), Mo–C(24) 2.506(4), C(19)-C(20) 1.444(5), C(20)–C(21) 1.420(5), C(21)–C(22) 1.387(6), C(22)–C(23) 1.421(5), C(23)–C(24) 1.441(5), C(24)–C(19) 1.381(5); Mo–N(1)–C(1) 178.9(3).

Similar structural parameters were found for **2e** which has a ring distortion of 17.1(1)°. The Mo–N(1) bond lengths in both complexes are virtually identical at 1.761(3) (**2d**) and 1.775(1) Å (**2e**) and are consistent with a Mo–N triple bond interaction.[8] An interesting difference between the two structures arises upon comparison of the Mo–N(1)–C(1) angles which are 178.9(3) (**2d**) and 145.5(1)° (**2e**). It is tempting to suggest that this difference arises from a significant difference in the Mo–N(1) interaction between the two compounds. However, close inspection of the packing diagram of **2d** reveals that there is a π-stacking interaction between the phenyl rings of the phenyl imido groups of neighboring molecules. Given that calculations suggest a very soft bending potential for aryl imido complexes,[9] the differences in the Mo–N(1)–C(1) angles in **2d** and **2e** are most likely due to crystal packing forces.

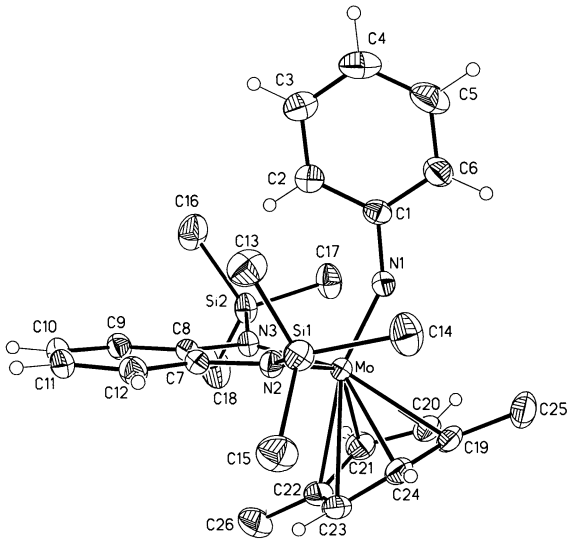

Fig. 2 Thermal ellipsoid plot of **2e** (50% probability thermal ellipsoids). Selected bond lengths (Å) and angles (°): Mo–N(1) 1.7746(14), Mo–C(19) 2.3908(17), Mo–C(20) 2.3900(18), Mo–C(21) 2.3243(19), Mo–C(22) 2.5637(19), Mo–C(23) 2.5410(18), Mo–C(24) 2.2981(18), C(19)–C(20) 1.392(3), C(20)–C(21) 1.4091(3), C(21)–C(22) 1.453(3), C(22)–C(23) 1.359(3), C(23)-C(24) 1.443(3), C(24)-C(19) 1.428(3), Mo-N(1)-C(1) 145.47(12).

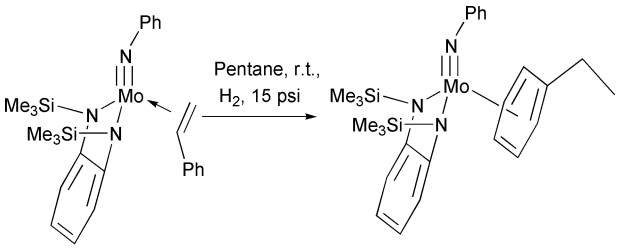

Scheme 2

The chemical shifts associated with the arene protons in the ^{1}H NMR spectra of these complexes are shifted significantly upfield, appearing in the region spanning δ 4.5–5.5 as expected for η^6-bound arene ligands.[10] The arene resonances are well resolved in the ^{1}H NMR spectra at room temperature and only one resonance for the Me_3Si groups is observed, supporting a low barrier to arene ring rotation (ESI†).

When a pentane solution of **1d** was exposed to a slight pressure of dihydrogen (*ca*. 15 psi) for 15 min, **2h** formed and was isolated as a microcrystalline solid by crystallization and filtration at −78 °C (Scheme 2).§ The ^{1}H NMR spectrum of **2h** is similar to those of complexes **2a**–**g** (ESI†).

Compounds **2a**–**h** are catalysts for the hydrogenation of olefins. When C_6D_6 solutions of **2h** (1 mol%) and a substrate olefin (styrene, neohexene, or *trans*-stilbene) were exposed to low pressures of dihydrogen (*ca*. 15 psi) at room temperature, slow conversion to the respective alkanes was observed. Raising the temperature of the reaction to 50 °C increased the rate of hydrogenation of neohexene [1 mol%, (**2b**)] from 17% conversion overnight to 62% over 8 h (TOF *ca.* 7/h).

η^2-Olefin complexes have been widely proposed as intermediates in the catalytic hydrogenation of olefins. As the ethylbenzene ligand of **2h** is readily displaced by styrene giving **1d** at room temperature it is likely that the propagating species in the above hydrogenation reaction is indeed an olefin complex. In general, the arene ligands also undergo exchange reactions with C_6D_6 at room temperature with the rates of reaction depending to some extent upon the identity of the arene ligand that is being displaced.

We thank the National Science foundation (CHE 9523279) for funding of this work. K. A. A. thanks the NSF and the University of Florida for funding X-ray equipment purchases.

Notes and references

§ All reactions and manipulations were carried out using standard Schlenk techniques or in a dry box under a nitrogen atmosphere. Complexes **1a**–**d** were synthesized according to published procedures.[7] Synthesis of **2a**–**g**: to a pentane solution of freshly generated **1a**–**c**, 15 equivalents (relative to the Mo starting material) of the appropriate arene were added followed by freezing of the mixture and evacuation of the headspace. Dry hydrogen was then added to the thawed solution, which was stirred at room temperature for 30 min. The volatiles were then removed *in vacuo* affording **2a**–**g** as blue–green solids that were recrystallized from pentane at −78 °C (80–85% isolated yield). The synthesis of **2h** is analogous to **2a**–**g**; however, no excess arene is employed.

¶ *Crystal data*: for **2d**: $C_{26}H_{37}MoN_3Si_2$, M = 543.71, triclinic, space group $P\bar{1}$, a = 9.2793(6), b = 10.5045(7), c = 15.466(1) Å, α = 87.784(1), β = 76.796(1), γ = 64.068(1)°, V = 1316.7(2) Å^3, Z = 2, μ(Mo-Kα) = 0.608 mm^{-1}, T = 173(2) K, final $R1$ = 0.0453, $wR2$ = 0.0775, Gof (on F^2) = 1.021.

For **2e**: $C_{26}H_{37}MoN_3Si_2$, M = 543.71, monoclinic, space group $P2_1/n$, a = 9.7367(4), b = 14.3272(6), c = 19.5480(8) Å, α = 90, β = 95.080(1), γ = 90°, V = 2716.2(2) Å^3, Z = 4, μ(Mo-Kα) = 0.589 mm^{-1}, T = 173(2) K, final $R1$ = 0.0237, $wR2$ = 0.0590, Gof (on F^2) = 1.021.

CCDC 182/1881. See http://www.rsc.org/suppdata/cc/b0/b007812n/ for crystallographic files in .cif format.

Both structures were solved using the direct methods option of SHELXS. Full matrix least-squares refinements based on F^2 were subsequently performed using SHELXL 97.[11] All non-hydrogen atoms included in calculated positions.

1 E. O. Fisher and W. Hafner, *Z. Naturforsch., Teil B*, 1955, **10**, 665.
2 F. Calderazo and G. Pampaloni, *J. Organomet. Chem.*, 1992, **423**, 307; P. W. Jolly, *Acc. Chem. Res.*, 1996, **29**, 544; G. Marr and B. W. Rockett, in *The Chemistry of the Metal–Carbon Bond*, F. R. Hartley and S. Patai, eds., John Wiley & Sons, New York, 1982.
3 M. G. Thorn, Z. C. Etheridge, P. E. Fanwick and I. P. Rothwell, *Organometallics*, 1998, **17**, 3636; A. D. Horton and J. de With, *Organometallics*, 1997, **16**, 5424; F. Muso, E. Solari, C. Floriani and K. Schenk, *Organometallics*, 1997, **16**, 4889; F. Calderazo, I. Ferri, G. Pampaloni and S. Troyanov, *J. Organomet. Chem.*, 1996, **518**, 187; S. J. Lancaster, G. B. Robinson, M. Bochman, S. J. Coles and M. B. Hursthouse, *Organometallics*, 1995, **14**, 2456; C. Pellechia, A. Grassi and A. Immirzi, *J. Am. Chem. Soc.*, 1993, **115**, 1160.
4 G. M. Diamond, M. L. H. Green, N. M. Walker, J. A. K. Howard and S. A. Mason, *J. Chem. Soc., Dalton Trans.*, 1992, 2641; M. A. Bruck, A. S. Copenhaver and D. E. Wigley, *J. Am. Chem. Soc.*, 1987, **109**, 6525; O. V. Ozerov, B. O. Patrick and F. T. Ladipo, *J. Am. Chem. Soc.*, 2000, **122**, 6423 and references therein.
5 R. C. Mills, K. A. Abboud and J. M. Boncella, *Organometallics*, 2000, **19**, 2953.
6 R. H. Crabtree, M. F. Mellea and J. M. Quirk, *J. Chem. Soc., Chem. Commun.*, 1981, 1217; C. R. Landis and J. Halpern, *Organometallics*, 1983, **2**, 840.
7 T. M. Cameron, C. G. Ortiz, I. Ghiviriga, K. A. Abboud and J. M. Boncella, *Organometallics*, manuscript submitted; we have reported the synthesis of **1b** previously: T. M. Cameron, C. G. Ortiz, K. A. Abboud, J. M. Boncella, R. Tom Baker and B. L. Scott, *Chem. Commun.*, 2000, 573.
8 W. Dyer, V. C. Gibson, J. A. K. Howard, B. Whittle and C. Wilson, *Polyhedron*, 1995, **14**, 103; P. W. Dyer, V. C. Gibson and W. Clegg, *J. Chem. Soc., Dalton Trans.*, 1995, 3313; P. W. Dyer, V. C. Gibson, J. A. K. Howard, B. Whittle and C. Wilson, *J. Chem. Soc., Chem. Commun.*, 1992, 1666; N. Bryson, M. T. Youinou and J. A. Osborn, *Organometallics*, 1991, **10**, 3389.
9 DFT calculations show that changing the Mo–N–Ph angle from 145 to 180° requires only 8.4 kJ mol^{-1}; T. C. Cundari, personal communication.
10 J. P. Collman, L. S. Hegedus, J. R. Norton and R. G. Finke, *Principles and Applications of Organotransition Metal Chemistry*, University Science Books, Mill Valley, 1987.
11 SHELXTL/NT Version 5.10, Bruker Analytical X-Ray Instruments, Inc., Madison, WI, 1997.

ChemComm

Two-dimensional heteronuclear $^{1}H \leftrightarrow {}^{27}Al$-correlated MAS NMR spectra of layered silicates

María D. Alba,* Ana I. Becerro, Miguel A. Castro and Ana C. Perdigón

Departamento de Química Inorgánica, Instituto de Ciencia de Materiales, Universidad de Sevilla, Consejo Superior de Investigaciones Científicas, Avda. Américo Vespucio s/n, 41092-Sevilla, Spain. E-mail: alba@cica.es

Received (in Cambridge, UK) 16th October 2000, Accepted 18th December 2000
First published as an Advance Article on the web 18th January 2001

The structural locations of aluminium in layered silicates, with different chemical environments but similar coordination polyhedra, can be established unequivocally from the correlation between the chemical shifts of protons and ^{27}Al nuclei, *via* their heteronuclear dipole–dipole couplings.

Among the quadrupolar nuclei studied by nuclear magnetic resonance (NMR), the ^{27}Al nucleus has received a great deal of interest for two reasons: on the one hand, aluminium is a main constituent of many interesting basic or applied solid systems; on the other hand, it is a very favourable nucleus for NMR investigations because it is a 100% naturally abundant isotope. However, even when conventional single pulse ^{27}Al MAS NMR spectra are recorded under the best conditions, *i.e.* very high magnetic fields, fast magic angle spinning speeds, and strong radiofrequency pulses with small flip angles,[1] only limited information is obtained. Those ^{27}Al MAS NMR spectra allow the determination of the coordination number of aluminium but they are much less sensitive to the nature of second neighbour species. Thus, very different structural aluminium sites with similar coordination environments can not clearly be differentiated on the basis of those ^{27}Al MAS NMR spectra.

In order to obtain this information, two-dimensional $^{1}H \leftrightarrow {}^{27}Al$ cross-polarisation experiments, which are selective to the existence of dipole–dipole interactions between both nuclei, are very useful in distinguishing similar aluminium coordination environments. The proposed experiments, very recently employed for mesoporous solids,[2] provide spectra with a simple and straightforward interpretation: the identification of the proton species correlated with the aluminium nuclei allows one to obtain precise structural information. However, two difficulties need to be overcome to perform these experiments. First, special care needs to be taken to perform cross-polarisation experiments of quadrupolar nuclei,[3] even though the optimum experimental conditions have already been explored for the case of ^{27}Al nuclei.[4] Second, available and unequivocally assigned high resolution ^{1}H MAS NMR spectra of the studied solid systems are required in order to correlate adequately the 2D signals that appear in the spectra. This second requirement has been recently fulfilled by our group for the solid systems here analysed.[5]

In this report, the advantages of applying this new solid-state NMR method to the family of phyllosilicates are reported for the first time. We describe both the method and the new available information from 2D spectra of aluminosilicates. From these spectra it is demonstrated that the method allows one not only to distinguish between different coordination environments for aluminium, but also to assign to these nuclei a precise structural location. Likewise, useful applications for such measurements are proposed.

The proposed technique is a two-dimensional heteronuclear $^{1}H \leftrightarrow {}^{27}Al$ chemical shift-correlation experiment, HETCOR. It is similar to conventional cross-polarisation, CPMAS NMR, experiments[6] except that the ^{1}H magnetisation is allowed to evolve for a period of time before the magnetisation transfer to the investigated nuclei, *i.e.* the ^{27}Al nuclei.

In order to illustrate the advantages of using this methodology, two well-characterised samples, available from the Source Clay Repository of the Clay Mineral Society, were selected. These samples include the possible structural positions of aluminium in layered silicates. Aluminium ions may occupy

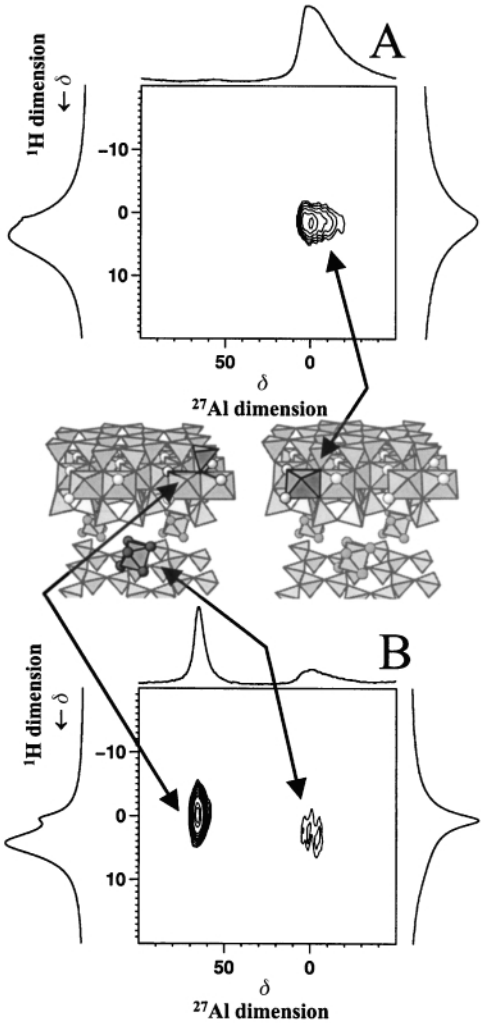

Fig. 1 (A) Contour plot of the 2D $^{1}H \leftrightarrow {}^{27}Al$ correlation experiment on hydrated sodium-saturated SAz-montmorillonite obtained with a ^{1}H $\pi/2$ pulse of 4.8 μs, a 0.3 ms contact time, a 250 ms recycle delay, and a 12.0 kHz spinning rate. A set of 84 FIDs was obtained with a t_1 increment of 5 μs and a dwell time of 5 μs. Separate ^{27}Al and ^{1}H MAS NMR spectra are plotted along their corresponding axes in accordance with the text. A silicate structure drawing is included to emphasize the dipole–dipole coupling found. (B) Contour plot of the 2D $^{1}H \leftrightarrow {}^{27}Al$ correlation experiment on hydrated aluminium-saturated SapCa-saponite. The conditions for this experiment were identical to those presented in (A), with the exception that a set of 96 FIDs was collected. Separate ^{27}Al and ^{1}H MAS NMR spectra and an appropriate silicate structure drawing are also included.

DOI: 10.1039/b008333j

three different positions in these solids. If aluminium is a main constituent of the silicate lattice, *i.e.* the silicate sheet, it can occupy either an octahedral or a tetrahedral location. When aluminium enters in the silicate structure as an exchange cation, *i.e.* in the interlayer space, it exhibits octahedral coordination.[2]

The first location, octahedral aluminium in the silicate sheet, is represented by a sodium-saturated montmorillonite from Arizona, which has been described in detail elsewhere.[7] The 1D ^{27}Al MAS NMR spectrum for this sample, horizontal projection in Fig. 1A, consists of a single peak centred at around 0 ppm that is assigned to these aluminium environments.[8] For the other two locations, tetrahedral aluminium in the silicate sheet and octahedral aluminium in the interlayer space, an aluminium-saturated saponite was selected.[9] In the corresponding 1D ^{27}Al MAS NMR spectrum, horizontal projection in Fig. 1B, two aluminium signals centred at 0 ppm (the octahedral aluminium) and 67 ppm (the tetrahedral aluminium) are observed. A comparison between the 1D NMR peaks obtained for the two different octahedral aluminium environments reveals the difficulties encountered to elucidate the structural location of octahedral aluminium in silicates. Conventional ^{27}Al MAS NMR spectroscopy fails for this purpose.

Fig. 1 also shows the application of the proposed technique to layered silicates for the first time, the 2D spectra for both samples being included. The 2D ^{1}H $\leftrightarrow$ ^{27}Al HETCOR spectra are displayed as contour plots along with the following: ^{27}Al MAS NMR (top) and ^{1}H MAS NMR (left) spectra from the hydrated sample, and ^{1}H MAS NMR (right) spectra from the samples after dehydration at 110 °C which were separately acquired for each. Drawings of the silicate structure are also included in which the coupled aluminium and proton species are outlined in bold to aid in the analysis of the 2D ^{1}H $\leftrightarrow$ ^{27}Al HETCOR spectra obtained.

On the one hand, the 2D spectrum for the sodium-saturated montmorillonite sample (Fig. 1A) consists of a single cross-peak which correlates the unique ^{27}Al signal, corresponding to an indistinguishable octahedral aluminium in the 1D spectrum, with the hydroxyl proton peak from the silicate lattice. Thus, the intensity profile in the contour plot clearly indicates that the aluminium ions are only occupying octahedral positions of the silicate sheet. On the other hand, the 2D spectrum for the aluminium-saturated saponite (Fig. 1B) consists of two cross-peaks, related to the two 1D-aluminium signals. The tetrahedral aluminium, 1D signal at around 67 ppm, is correlated with the hydroxyl proton signal from the silicate lattice in a similar manner as the former case. The octahedral aluminium, 1D signal at around 0 ppm, is correlated with the water proton peak from the interlayer space. This latter correlation reveals the new position of the aluminium species in the silicate mineral, octahedral positions in the interlayer space, in addition to demonstrating the advantages of using this technique. The indistinguishable 1D octahedral aluminium chemical shifts (horizontal projections of each 2D spectrum) are separated from dipole–dipole coupled species into two frequency dimensions, which allow adjacent nuclear species to be readily determined.

In summary, this paper describes a technique that enables, for the first time, the determination of the coordination number of a particular aluminium species from the ^{27}Al chemical shift, in addition to allowing the identification of the location of this polyhedron within the structure, from the dipole–dipole coupling with adjacent protons. Thus, the technique presented here offers a new approach to the improvement of the NMR information extractable from quadrupolar nuclei.

We thank DGICYT for financial support (Project No. PB97-0176)

Notes and references

1 A. Samoson and E. Lippmaa, *Chem. Phys. Lett.*, 1983, **100**, 205.
2 M. T. Janicke, C. C. Landry, S. C. Cristiansen, D. Kumar, G. D. Stucky and B. F. Chmelka, *J. Am. Chem. Soc.*, 1998, **120**, 6940.
3 R. K. Harris and G. J. Nesbitt, *J. Magn. Reson.*, 1988, **78**, 245.
4 (*a*) H. D. Morris and P. D. Ellis, *J. Am. Chem. Soc.*, 1989, **111**, 6045; (*b*) H. D. Morris, S. Bank and P. D. Ellis, *J. Phys. Chem.*, 1990, **94**, 3121; (*c*) J. Rocha and J. Klinowski, *J. Chem. Soc., Chem. Commun.*, 1991, 1121; (*d*) L. Kellberg, M. Linsten and H. J. Jakobsen, *Chem. Phys. Lett.*, 1991, **182**, 120.
5 M. D. Alba, A. I. Becerro, M. A. Castro and A. C. Perdigón, *Chem. Commun.*, 2000, 37.
6 P. Caravatti, G. Bodenhausen and R. R. Ernst, *Chem. Phys. Lett.*, 1982, **89**, 363.
7 R. E. Grim and G. Kulbicki, *Am. Mineral.*, 1961, **46**, 1329.
8 M. D. Alba, R. Alvero, A. I. Becerro, M. A. Castro and J. M. Trillo, *J. Phys. Chem. B*, 1998, **102**, 2207.
9 A. I. Becerro, Ph. D. Thesis, University of Seville, 1997.

ChemComm

The first example of a functional pillared metal sulfonate network

Adrien P. Côté and George K. H. Shimizu*

Department of Chemistry, University of Calgary, 2500 University Drive N.W., Calgary, Alberta, Canada T2N 1N4. E-mail: gshimizu@ucalgary.ca

Received (in Irvine, CA, USA) 17th July 2000, Accepted 20th November 2000
First published as an Advance Article on the web 19th January 2001

Barium 4,5-dihydroxybenzene-1,3-disulfonate, a pillared metal sulfonate network, possesses a microporous interlayer region through the use of a single type of 'bent' sulfonate group, and absorbs H_2S.

The design and synthesis of mixed inorganic–organic solids capable of including small molecules within void spaces in their structures, analogous to natural clays and zeolites,[1] has evolved into a diverse area of research.[2] A widely studied class of metal–organic networks, in this respect, has been the metal phosphonate salts of general formula $M^{n+}(O_3PR)_{n/2}$ where R is an aliphatic or aromatic organic group.[3] These systems often form two-dimensional structures where rigid O–M–O layers assemble, projecting the R groups between the layers. This alternating organic–inorganic layered topology can allow the intercalation of various small molecules between the layers, making these materials useful for chemical separations and/or catalytic applications.[4] However, since, typically, no void space exists between the layers prior to intercalation, an energy cost is associated with the act of separating the layers which can inhibit their usefulness. To overcome this limitation, the layers in these compounds can be 'pillared' to increase the void space between the layers and predispose the structure to guest inclusion. Pillaring is a strategy, first employed with clays and then with other layered materials, where counter ions, organic molecules, or polytopic ligands are used to 'prop' layers apart, resulting in greater porosity in addition to improved structural integrity.[5] Unfortunately, with prototypical metal phosphonate structures, the spacing between simple linear diphosphonate pillars (*e.g.* phenyl or biphenyl) is negligible, rendering the network ineffectual with regard to guest inclusion [Scheme 1(a)].[6] This adverse circumstance can be in part remedied by using mixed phosphonate or phosphate/phosphonate systems where the 'pillar' alternates with a smaller, non-pillaring phosphonate (*e.g.* methylphosphonate) or a phosphate group [Scheme 1(b)], thus generating porosity.[7] However, in addition to complicating the synthesis, this may result in a loss of structural regularity and a greater pore size distribution.[8]

Contrasting the metal phosphonate systems, our research is focused on using weaker metal–sulfonate ($M^{n+}(SO_3R)_n$) interactions to develop new layered and porous compounds.[9] This approach takes advantage of the flexible coordinative behavior of the SO_3^- group to obtain structures not attainable from the rigid O–M–O scaffolding of metal phosphonate networks. Of the relatively few structurally characterized $M_n(SO_3R)_n$ complexes which exist to date, all form layered networks.[9,10] Some of these can be classified as 'pillared' solids but they suffer from the aforementioned problem of virtually no space between adjacent R groups.[11] Even within these layered compounds, there exists substantial diversity with respect to the sulfonate coordination mode.[12] We, therefore, sought to exploit this flexible coordination by generating layered networks which would tolerate the incorporation of a 'bent' pillar. A bent pillar would not pack efficiently in the interlayer and, therefore, generate porosity [Scheme 1(c)] while offering a facile two-component synthesis. Herein, we report the structure, thermal analysis and sorption properties of barium 4,5-dihydroxybenzene-1,3-disulfonate dihydrate, $[Ba(\mathbf{1})(H_2O)]\cdot H_2O$. This compound represents the *first functional pillared metal sulfonate network*.[13] Significantly, interlayer void space is generated and the guests which occupy these sites may be removed while maintaining structural integrity.

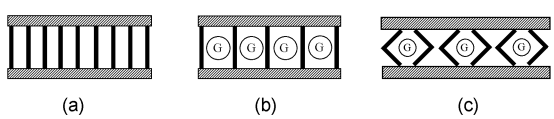

Scheme 1 Pillaring of layered networks showing (a) close packing of linear pillars with no void space; (b) alternating pillars and small R groups to generate porosity; (c) use of 'bent' pillars to create pores with a single type of R group.

$[Ba(\mathbf{1})(H_2O)]\cdot H_2O$ was metathesized from the commercially available $Na_2[\mathbf{1}]\cdot H_2O$ by combining equimolar amounts of $BaCl_2\cdot 2H_2O$ and $Na_2[\mathbf{1}]\cdot H_2O$ in minimal amounts of water. A white precipitate of $[Ba(\mathbf{1})(H_2O)]\cdot H_2O$ formed immediately,

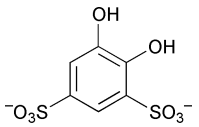

1

which was filtered off in 95% yield. Colorless, X-ray quality crystals were grown by diffusion of acetone vapor into a saturated aqueous solution of the complex.† The structure (Fig. 1) consists of infinite layers of sulfonate-bridged Ba^{2+} centers, in the *xy* plane, with **1** acting as a pillar to bridge adjacent layers through the two sulfonates. One SO_3 group coordinates to a layer in the $+z$ direction and other in the $-z$ direction, to give a *d*-spacing of 9.24(2) Å. The stability of the

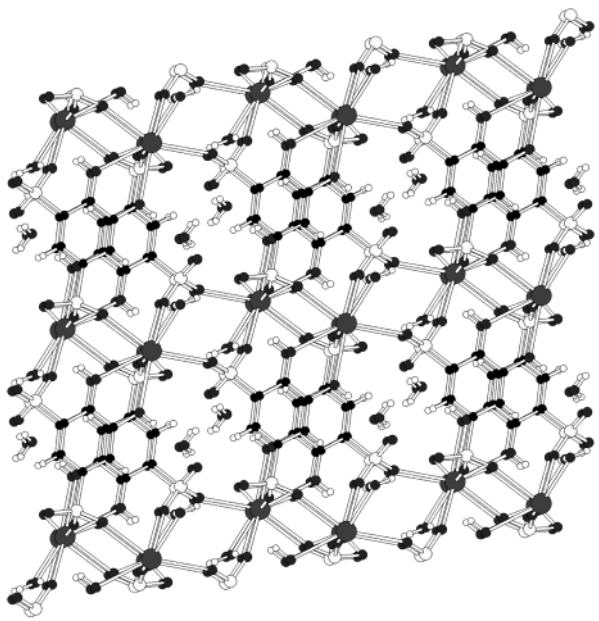

Fig. 1 View of the layered structure of $[Ba(\mathbf{1})(H_2O)]\cdot H_2O$ down the *a*-axis. Ba atoms: large circles, S atoms: medium, light grey circles, O atoms: small, dark grey circles, C atoms: small, black circles. Note the interlayer channels and the water molecules occupying them.

DOI: 10.1039/b005923o

pillars is augmented *via* the chelation of the catechol (4,5-diol) unit of **1** to a single Ba^{2+} center. The bent structure of **1**, with sulfonate groups oriented at 120°, opens up 16-membered rings in the interlayer between the pillars. The rings align along the *a*-axis to form channels which are filled with non-coordinated water molecules. The channels are approximately 4.0 Å in diameter. The construction of the layers is complex, with the one crystallographically unique Ba^{2+} ion being 9-coordinate and each molecule of **1**, in turn, coordinating to six different Ba^{2+} centers. The coordination of **1** is as follows. The catechol moiety of **1** chelates, in a doubly protonated form, to one barium center [Ba–O7 = 2.843(3), Ba–O8 = 2.791(3) Å]. The sulfonate group in the 3-position coordinates to two different Ba^{2+} centers, which are part of the same layer as the catechol-chelated Ba^{2+}, *via* a μ^2,η^2-mode [Ba–O5 = 2.750(3), Ba–O6 = 2.749(3) Å]. Sulfonates in the 1-position adopt a μ^3,η^3-coordination mode where all three Ba^{2+} ions are in the adjacent layer to those coordinating to the sulfonate in the 3-position. One of the Ba^{2+} centers is chelated by two of the sulfonate oxygen atoms resulting in four coordinating interactions in total [Ba–O1 = 2.737(3), 3.002(3), Ba–O2 = 2.875(3), Ba–O3 = 2.765(3) Å]. Each barium ion is 9-coordinate with an irregular geometry. The coordination sphere is comprised of six sulfonate oxygen atoms, from five different sulfonate groups, the two catechol oxygen atoms, and a water molecule [Ba–O9 = 2.751(3) Å] that projects into the interlayer.

The PXRD pattern and the elemental analysis of the bulk precipitate match those of the single crystal sample, indicating that these species have the same structure and composition. Thermal analysis revealed loss of included water at 110 °C and then gradual loss of the coordinated water to 420 °C at which point the sample decomposed.[14] Given that the aversion to employing sulfonates in the generation of extended materials has largely been due to their weaker coordinative tendencies, the stability of this network is quite remarkable. Importantly, the PXRD patterns of the dihydrate and the monohydrate showed that the framework remained intact after loss of the channel water molecules.[15] Removal of only the guest water molecules of $[Ba(\mathbf{1})(H_2O)]\cdot H_2O$ would leave empty channels, possibly with a topology imprinted by the water molecules. Therefore, based upon the structural similarity, the sorbent capabilities of the dehydrated framework with H_2S were examined. It was found that at 50 °C a mass increase of 7.5% was observed, corresponding to the uptake of 0.93 equivalents of H_2S with respect to the equivalent of expelled water.[16] Significantly, analogous experiments with methane and methanol revealed no mass increase, indicating selectivity for H_2S.

In conclusion, $[Ba(\mathbf{1})(H_2O)]\cdot H_2O$ represents the first example of a functional pillared metal sulfonate structure. The flexible coordination of the sulfonate group enables 'bent' pillars to be employed resulting in a microporous network in a system where only a single type of pillar is present. Despite relying on metal–sulfonate interactions in the pillars, the network is highly robust (> 400 °C). With regard to functionality, the guest water molecules can be removed and selectively replaced, almost quantitatively, by hydrogen sulfide.

We would like to thank Dr R. MacDonald at the University of Alberta for the single crystal X-ray data and the reviewers for useful suggestions. This research was supported by the Natural Sciences and Engineering Research Council of Canada.

Notes and references

† *Crystal data* for $[Ba(\mathbf{1})(H_2O)]\cdot H_2O$: $C_6H_8BaS_2O_{10}$, M = 441.58, triclinic, space group $P\bar{1}$, a = 7.3374(6), b = 8.6976(7), c = 9.2006(8) Å, α = 81.923(2), β = 89.368(2), γ = 84.313(2)°, V = 578.47(8) Å^3, Z = 2, D_c = 2.535 g cm^{-3}, μ(18kW RA) = 3.842 mm^{-1}, crystal size 0.25 × 0.08 × 0.03 mm. Data were collected on a Bruker P4 diffractometer with a SMART 1000 CCD area detector using an 18 kW rotating-anode X-ray generator. A total of 2883 reflections ($2.24° < \theta < 26.38°$) were processed of which 2336 were unique and considered significant with $I_{net} > 2\sigma(I_{net})$. Structure solution, refinement and molecular graphics were carried out with the SHELXL software package, release 5.1.[17] Final residuals for $I_{net} > 2\sigma(I_{net})$ were R = 0.0275 and R_w = 0.0665 (GoF = 1.007) for 184 parameters.

CCDC 182/1883. See http://www.rsc.org/suppdata/cc/b0/b005923o/ for crystallographic files in .cif format.

1 D. W. Breck, *Zeolite Molecular Sieves: Structure, Chemistry and Use*, Wiley, New York, 1974; R. M. Barrer, *Zeolites and Clay Minerals as Sorbents and Molecular Sieves*, Academic Press, New York, 1978.

2 C. L. Bowes and G. A. Ozin, *Adv. Mater.*, 1996, **8**, 13; T. J. Barton, L. M. Bull, W. G. Luemperer, D. A. Loy, B. McEnaney, M. Misono, P. A. Monson, G. Pez, G. W. Scherer, J. C. Vartuli and O. M. Yaghi, *Chem. Mater.*, 1999, **11**, 2633; K. Ohtsuka, *Chem Mater.*, 1997, **9**, 2039; O. M. Yaghi, H. Li, C. Davis, D. Richardson and T. L. Groy, *Acc. Chem. Res.*, 1998, **31**, 474.

3 A. Clearfield, *Prog. Inorg. Chem.*, 1998, **47**, 371; G. Alberti, in *Comprehensive Supramolecular Chemistry*, ed. J. L. Atwood, J. E. Davies, D. D. MacNicol and F. Vögtle, Elsevier Science, New York, 1996, vol. 7, p. 151.

4 G. Alberti and U. Costantino, in *Inclusion Compounds*, ed. J. L. Atwood, J. E. Davies and D. D. MacNicol, Oxford University Press, New York, 1991, vol. 5, ch. 5, p. 136; G. Cao, H.-G. Hong and T. E. Mallouk, *Acc. Chem. Res.*, 1992, **25**, 420; M. E. Thompson, *Chem. Mater.*, 1994, **6**, 1168.

5 M. A. Occelli and H. Robson, *Expanded Clays and Other Microporous Solids*, Academic Press, New York, 1992; P. Olivera-Pastor, P. Maireles-Torres, E. Rodríguez-Castellón, A. Jiménex-López, T. Cassagneau, D. L. Jones and J. Rozière, *Chem. Mater.*, 1996, **8**, 1758; A. Clearfield, *Chem. Mater.*, 1998, **8**, 2801.

6 M. B. Dines, P. M. DiGiacomo, P. K. Callahan, P. C. Griffith, R. H. Lane and R. E. Cooksey, in *Chemically Modified Surfaces in Catalysis and Electrocatalysis*, ed. J. S. Miller, *ACS Symp. Ser. 192*, American Chemical Society, Washington, DC, 1982, p. 223; D. M. Poojary, P. C. Bellinghausen, B. Zhang and A. Clearfield, *Inorg. Chem.*, 1996, **35**, 4942; B. Zhang, D. M. Poojary and A. Clearfield, *Inorg. Chem.*, 1998, **37**, 1844.

7 G. Alberti, U. Costantino, F. Marmottini, R. Vivani and P. Zappelli, *Angew. Chem., Int. Ed. Engl.*, 1993, **32**, 1357; G. Alberti, F. Marmottini, S. Murcia-Mascarós and R. Vivani, *Angew. Chem., Int. Ed. Engl.*, 1994, **33**, 1594; N. J. Clayden, *J. Chem. Soc., Dalton Trans.*, 1987, 1877.

8 G. Alberti, U. Costantino, F. Marmottini, R. Vivani and P. Zappelli, *Mater. Res. Soc. Symp. Proc.*, 1991, **233**, 101.

9 G. K. H. Shimizu, G. D. Enright, C. I. Ratcliffe, G. S. Rego, J. L. Reid and J. A. Ripmeester, *Chem. Mater.*, 1998, **10**, 3282; G. K. H. Shimizu, G. D. Enright, C. I. Ratcliffe, K. F. Preston, J. L. Reid and J. A. Ripmeester, *Chem. Commun.*, 1999, 1485.

10 G. Smith, B. A. Cloutt, D. E. Lynch, K. A. Byriel and C. H. L. Kennard, *Inorg. Chem.*, 1998, **37**, 3236; B. J. Gunderman and P. J. Squattrito, *Inorg. Chem.*, 1995, **34**, 2399; B. J. Gunderman and P. J. Squattrito, *Inorg. Chem.*, 1994, **33**, 2924; Y. Garaud, F. Charbonnier and R. Faure, *J. Appl. Crystallogr.*, 1980, **13**, 190; B. J. Gunderman, I. D. Kabell, P. J. Squattrito and S. N. Dubey, *Inorg. Chim. Acta*, 1997, **258**, 237; V. Shakeri and S. Haussuhl, *Z. Kristallogr.*, 1992, **198**, 297.

11 Ag 1,4-butanedisulfonate: F. Charbonnier, R. Faure and H. Loisleur, *Acta Crystallogr., Sect. B*, 1981, **37**, 822; Na anthraquinone-2,6-disulfonate: R. S. K. A. Gamage, B. M. Peake and J. Simpson, *Aust. J. Chem.*, 1993, **46**, 1595; K tetramethylbenzene-1,3-disulfonate: A. Koeberg-Telder, H. Cerfontain, C. H. Stam and G. Kreuning, *Recl. Trav. Chim. Pays-Bas*, 1987, **106**, 142.

12 Even a subtle change such as benzenesulfonate to toluenesulfonate in layered Ag^I complexes shifts an η^6-SO_3 to an η^5-SO_3.[9]

13 Ward *et al*. have employed sulfonates with great success in H-bonded pillared guanidinium sulfonate frameworks. See: V. A. Russell, C. C. Evans, W. Li and M. D. Ward, *Science*, 1997, **276**, 575.

14 TGA/DSC analyses of $[Ba(\mathbf{1})(H_2O)]\cdot H_2O$ were performed on a Netzsch 449C Simultaneous Thermal Analyzer. A mass loss at 110 °C was assigned to loss of the channel water molecules (4.08% calc., 3.62% obs.). Heating beyond 110 °C, a gradual mass loss occurs until decomposition at 420 °C corresponding to the loss of a second molecule of water (4.08% calc. 3.91% obs.).

15 A comparison of the nine most intense peaks in the PXRD patterns of $Ba[\mathbf{1}]\cdot 2H_2O$ and of a sample dehydrated at 150 °C for two hours, to remove channel water molecules, shows a mean deviation of only 1.4%. Full details are given within the crystallographic material.

16 $[Ba(\mathbf{1})(H_2O)]\cdot H_2O$ was placed under a N_2 atmosphere, heated to 150 °C at 10 °C min^{-1}, then held at 150 °C for 10 min to remove the channel water. The sample was cooled to 50 °C and the purge gas changed to H_2S. The sample showed a mass gain of 7.5%. $[Ba(\mathbf{1})(H_2O)]$ has a mass of 423 g mol^{-1}. In terms of molar equivalents, a 7.5% gain is therefore equivalent to 31.68 g mol^{-1} or 31.68/(34.06 g mol^{-1} H_2S) = 0.93 equivalents of H_2S.

17 Bruker AXS Inc., Madison, WI, 1997.

Mainchain pseudopolyrotaxanes *via* post-threading with cucurbituril

Dönüs Tuncel and Joachim H. G. Steinke*

Department of Chemistry, Imperial College of Science, Technology and Medicine, South Kensington, London, UK SW7 2AY. E-mail: j.steinke@ic.ac.uk

Received (in Cambridge, UK) 10th October 2000, Accepted 23rd November 2000
First published as an Advance Article on the web 23rd January 2001

Pseudopolyrotaxanes possessing a controllable number of cucurbituril molecules located along the backbone of poly(iminiohexamethylene chloride) have been prepared *via* an efficient post-threading route.

Although the synthesis of cucurbituril was described almost 100 years ago[1] the exploitation of the supramolecular chemistry of this rigid, nondecacyclic ligand only began recently. Mock and Pierpont reported a molecular switch[2] and both Kim *et al.*[3] and Buschmann *et al.*[4,5] synthesised various inclusion complexes based on cucurbituril. The latter two groups also prepared solid and solution state polyrotaxanes in which cucurbituril features as the macrocyclic component introduced as a pseudorotaxane monomer.[6,7] Steinke *et al.* used the ability of cucurbituril to catalyse 1,3-dipolar cycloadditions, a feature of cucurbituril discovered by Mock *et al.*[8,9] in the synthesis of catalytically self-threading polyrotaxanes.[10]

Formation of polyrotaxanes or pseudopolyrotaxanes *via* post-threading requires an attractive interaction between the macrocycle and the (preformed) polymer backbone. Investigations by Harada *et al.* provided the earliest example of post-threading exploiting the strong hydrophobic interactions between poly(ethylene glycol)s (PEG) and α-cyclodextrins (α-CD) in aqueous media.[11] Since then α-, β- and γ-cyclodextrins, crown ethers and cyclophanes have been post-threaded onto a number of different linear polymer backbones like poly(propylene glycol) (PPG),[12,13] poly(alkylimine)s,[14] PEO-PPO-PEO triblock copolymers,[15] poly(propylene),[16] poly(trimethylene oxide),[13] poly(isobutylene),[16] poly(ε-caprolactone),[16] poly(viologen)s,[16] aromatic poly(ether),[17] poly(ether ester)[17] and poly(urethane)s.[18,19] Recently calorimetric studies by Buschmann *et al.* suggested the formation of a pseudopolyrotaxane between PEG and cucurbituril.[20]

For our contribution to this area we decided to prepare cucurbituril-containing mainchain pseudopolyrotaxanes from poly(iminoalkylene)s. Poly(iminohexamethylene) was deemed to be the most promising linear polyamine because the protonated hexane-1,6-diamine moiety present in its backbone is known to form one of the most stable inclusion complexes with cucurbituril.[21] Poly(iminiohexamethylene chloride) was synthesised according to a procedure by Wenz *et al.*[14] in which Nylon 6,6 was reduced with BH_3·Me_2S (Fig. 1). ^{1}H NMR of the polyamine confirmed that reduction was successful with less than 3% of residual amide groups remaining (M_n = 20000, M_w = 52000, against polystyrene). Cucurbituril was prepared according to the procedure by Behrend *et al.*[1] Samples for the subsequent time-dependent NMR studies were prepared by dissolving poly(iminohexamethylene) in 20% DCl to which the required amount of cucurbituril was added (Fig. 1).

Progress of the threading reaction was monitored at given time intervals by ^{1}H NMR (Fig. 2). Fig. 2 corresponds to a post-threading experiment carried out at 90 °C in DCl–D_2O (20% w/w) with a molar ratio of cucurbituril to the iminiohexamethylene repeat unit of 0.5 : 1.0. Upon threading the original three resonances of the α-, β- and γ-methylene groups of poly(iminiohexamethylene chloride) are split into an additional two sets of resonances (Fig. 2: **A**, **B**, **C** and **a**, **b**, **c**). The integrals of the new resonances are increasing with time to the same extent as the precursor polymer resonances are decreasing. The

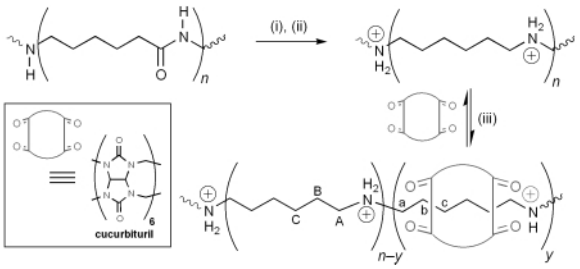

Fig. 1 Synthesis of cucurbituril-threaded mainchain poly(iminiohexamethylene chloride); (i) BH_3·Me_2S, THF, 20 h, rt, 66%; (ii) DCl–D_2O (20% w/w), rt, 100%; (iii) cucurbituril, 0 to 384 h, 90 °C.

set of resonances coded **a**, **b** and **c** can be assigned to threaded hexamethylene segments based on complexation studies with the model compound 1,6-diaminohexane dihydrochloride salt carried out by us which is further supported by earlier work in formic acid carried out by Mock *et al.*[21] Resonances **A**, **B**, and **C** belong to unthreaded hexamethylene segments located next to threaded repeat units along the polymer backbone. This was confirmed by using a five-fold excess of cucurbituril. Under these conditions essentially all precursor resonances disappeared and only the two new sets of resonances remained (not shown). The degree of threading was calculated from the ratio of threaded to non-threaded methylene protons. In this particular example (after 384 h) 43% of all repeat units were threaded by cucurbituril. Threading is also reflected in a small downfield shift in the resonances of cucurbituril (Fig. 2: **QQ** = free macrocycle; **qq** = threaded) which is proportional to the degree of threading over time. Attempts to determine the molecular weight of these pseudopolyrotaxanes by GPC have been hampered by the fact that these polymers are only soluble in water and the necessary analytical equipment has not been available to us.

Data of this very slow threading process are shown in Fig. 3 which suggest that equilibrium has been reached after *ca.* 400 h

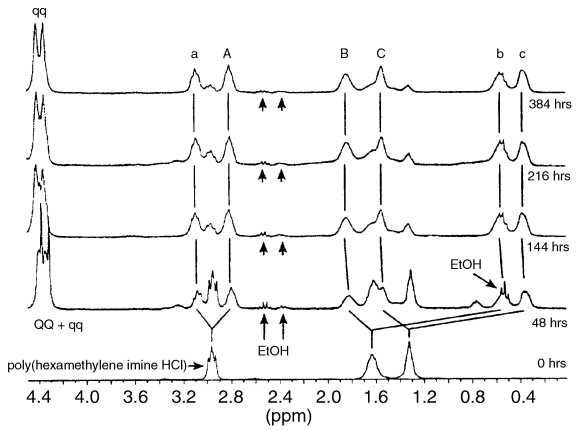

Fig. 2 Progression of post-threading followed by ^{1}H-NMR at 90 °C in DCl–D_2O (20% w/w) with a molar ratio of cucurbituril to iminiohexamethylene repeat unit of 0.5 : 1.0.[27] (Arrows indicate traces of the ethanol inclusion complex with cucurbituril (ethanol was used as co-solvent during recrystallisation). The signal intensity is decreasing with time being replaced by polymer chain repeat units.)

DOI: 10.1039/b008175m

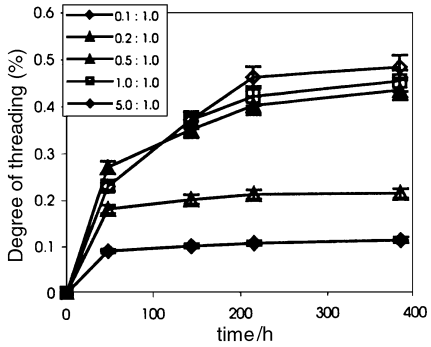

Fig. 3 Time-dependence of the threading of cucurbituril onto poly(iminiohexamethylene chloride) at 90 °C in DCl–D_2O (20% w/w). Molar ratios of cucurbituril to repeat unit: 0.1 : 1.0; 0.2 : 1.0; 0.5 : 1.0; 1.0 : 1.0; 5.0 : 1.0.

at 90 °C for all ratios of cucurbituril to polymer repeat unit. Excess of cucurbituril has very little impact on the maximum degree of threading being close to 50% (experimental error ±2%). From the limiting degree of threading (50%) and the clear splitting of the original ^{1}H NMR signals of the iminiohexamethylene repeat unit into two new sets of peaks of equal intensity, we conclude that a pseudopolyrotaxane has been formed where encapsulated and uncomplexed repeat units alternate. Further evidence comes from encapsulation studies between cucurbituril and bis(6-aminohexyl)amine (a model 'dimer' of the polymer backbone).[22] A two-fold excess of cucurbituril led to 45% threading, a value which is very close to that found for the polymeric case. The inactivity of cucurbituril in the catalytic self-threading of pseudopolyrotaxanes involving hexane-1,6-diamine repeat units[10] can also best be rationalised by assuming that it is energetically unfavourable for two molecules of cucurbituril to complex to the same secondary ammonium ion. We have considered the possibility of other substructures analogous to recent ^{1}H NMR investigations by Hodge *et al.*[17] However, an alternating sequence of complexed and uncomplexed repeat units is the most consistent interpretation of our experimental data.

The slow kinetics of the threading process can be explained through a combination of factors. By far the most important contribution arises from the strong binding constant of cucurbituril to the protonated hexamethylene-spaced repeat unit.[21] A high activation energy is needed for cucurbituril to 'hop' efficiently along the polymer chain during the threading process. This interpretation is supported by recent results from Harada's groups related to slow threading kinetics also affected by strong ionic interactions between macrocycle and polymer chain.[23] Wenz *et al.* have modelled a hopping mechanism for the post-threading of α-CD onto ionene-6,10† which enabled them to explain their observed threading kinetics.[14] Their pseudopolyrotaxane system also required elevated temperatures

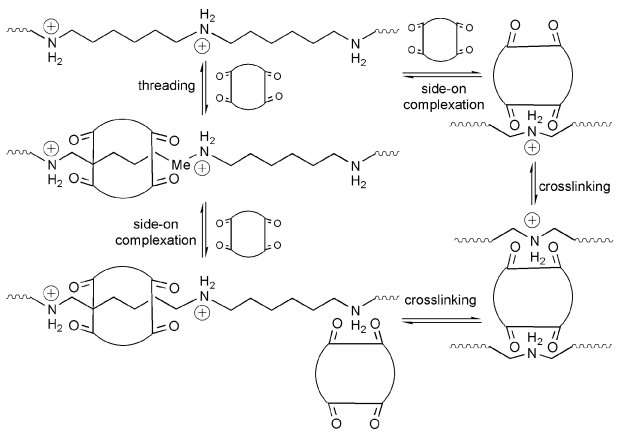

Fig. 4 Modes of complexation of cucurbituril with the corresponding equilibria expected to take part in the threading of cucurbituril onto protonated, linear poly(iminooligoalkylene)s.

and long reaction times (120 h at 80 °C in water) to reach a degree of threading of 0.5. Furthermore we invoke that threading kinetics in our system are retarded further by cucurbituril moieties having to queue. The existence of queuing has been demonstrated by Parsons *et al.*[24,25] during the threading of pseudopolyrotaxanes. The effect of queuing becomes more significant for higher levels of threading as indicated by the corresponding slower threading kinetics (Fig. 3).

The retarded threading kinetics at higher ratios of cucurbituril could also be explained by invoking 'side-on' complexation of cucurbituril to the ammonium groups along the polymer backbone (Fig. 4). Cucurbituril binds to all types of ammonium ions other than quaternary ones.[21,26] Fig. 4 is therefore a more accurate representation of the various competing modes of complexation that have to be considered for our system. However only through further experiments will it be possible to distinguish between queuing and 'side-on' complexation.

Post-threading of cucurbituril onto protonated linear poly(iminohexamethylene) results in a new, synthetically accessible class of pseudopolyrotaxanes, which contain a controllable number of macrocyclic units.

We would like to thank the EPSRC for providing an IPSI project studentship for D. T.

Notes and references

† The IUPAC name for ionene is 1,2,3,4-tetrahydro-1,1,6-trimethylnaphthalene.

1 R. Behrend, E. Meyer and F. Rusche, *Justus Liebigs Ann. Chem.*, 1905, **339**, 1.
2 W. L. Mock and J. Pierpont, *J. Chem. Soc., Chem. Commun.*, 1990, 1509.
3 S. I. Jun, J. W. Lee, S. Sakamoto, K. Yamaguchi and K. Kim, *Tetrahedron Lett.*, 2000, **41**, 471.
4 H. J. Buschmann and T. Wolff, *J. Photochem. Photobiol., A.*, 1999, **121**, 99.
5 H. J. Buschmann, K. Jansen and E. Schollmeyer, *Acta Chim. Slov.*, 1999, **46**, 405.
6 C. Meschke, H. J. Buschmann and E. Schollmeyer, *Polymer*, 1999, **40**, 945.
7 O. S. Jung, Y. J. Kim, Y. A. Lee, J. K. Lee and K. H. Yoo, *Bull. Korean Chem. Soc.*, 2000, **21**, 39.
8 W. L. Mock, T. A. Irra, J. P. Wepsiec and T. L. Manimaran, *J. Org. Chem.*, 1983, **48**, 3619.
9 W. L. Mock, A. Irra, J. P. Websiec and M. Adhya, *J. Org. Chem.*, 1989, **54**, 5302.
10 D. Tuncel and J. H. G. Steinke, *Chem. Commun.*, 1999, 1509.
11 A. Harada, J. Li and M. Kamachi, *Nature*, 1992, **356**, 325.
12 A. Harada, J. Li and M. Kamachi, *Proc. Jpn. Acad. B Phys. Biol. Sci.*, 1993, **69**, 39.
13 S. Kamitori, O. Matsuzaka, S. Kondo, S. Muraoka, K. Okuyama, K. Noguchi, M. Okada and A. Harada, *Macromolecules*, 2000, **33**, 1500.
14 W. Herrmann, B. Keller and G. Wenz, *Macromolecules*, 1997, **30**, 4966.
15 H. Fujita, T. Ooya and N. Yui, *Macromolecules*, 1999, **32**, 2534.
16 A. Harada, M. Okada, Y. Kawaguchi and M. Kamachi, *Polym. Adv. Technol.*, 1999, **10**, 3.
17 P. Hodge, P. Monvisade, G. J. Owen, F. Heatley and Y. Pang, *New J. Chem.*, 2000, **24**, 703.
18 C. G. Gong, Q. Ji, C. Subramaniam and H. W. Gibson, *Macromolecules*, 1998, **31**, 1814.
19 P. E. Mason, W. S. Bryant and H. W. Gibson, *Macromolecules*, 1999, **32**, 1559.
20 H. J. Buschmann, K. Jansen and E. Schollmeyer, *J. Inclusion Phenom. Mol. Recognit. Chem.*, 2000, **37**, 231.
21 W. L. Mock and N. Y. Shih, *J. Org. Chem.*, 1986, **51**, 4440.
22 T. Krasia and J. H. G. Steinke, in preparation.
23 Y. Kawaguchi and A. Harada, *J. Am. Chem. Soc.*, 2000, **122**, 3797.
24 P. E. Mason, I. W. Parsons and M. S. Tolley, *Polymer*, 1998, **39**, 3981.
25 P. E. Mason, I. W. Parsons and M. S. Tolley, *Angew. Chem., Int. Ed. Engl.*, 1996, **35**, 2238.
26 H. J. Buschmann, E. Cleve and E. Schollmeyer, *Inorg. Chim. Acta*, 1992, **193**, 93.
27 We have so far been unable to explain the presence of the resonance at 0.8 ppm in the spectrum recorded after 48 h.

ChemComm

Short and efficient chiral pool and RCM approach towards the synthesis of the macrocyclic core of the salicylihalamides

Gunda I. Georg,* Yu Mi Ahn, Burchelle Blackman, Faryar Farokhi, Patrick T. Flaherty, Craig J. Mossman, Subho Roy and KyoungLang Yang

Department of Medicinal Chemistry, Center for Cancer Experimental Therapeutics, and Drug Discovery Program, Higuchi Biosciences Center, University of Kansas, Lawrence, KS 66045, USA. E-mail: georg@ku.edu

Received (in Corvallis, OR, USA) 1st November 2000, Accepted 20th December 2000
First published as an Advance Article on the web 23rd January 2001

The macrolactone core structure of the salicylihalamides was prepared from diacetone-D-glucose and *via* a ring-closing metathesis reaction.

Salicylihalamides A and B (**1** and **2**) are naturally occurring

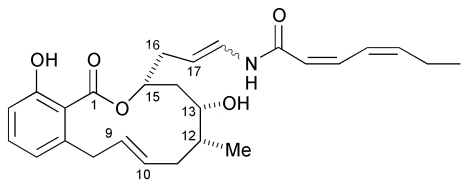

1 Salicylihalamide A (*E*)-enamide
2 Salicylihalamide B (*Z*)-enamide

cytotoxic macrolides isolated from an Australian sponge *Haliclona* sp. in 1997.[1] They were the first examples of a novel class of macrolides that have in common the salicylic acid moiety and an unsaturated enamide side chain.[2–6]

This class of compounds possesses diverse biological activities, including inhibition of tumor cell proliferation.[1–6] Salicylihalamide A displayed a striking pattern of differential cytotoxicity in the NCI's 60-cancer cell line human tumor screen.[1] COMPARE pattern-recognition analyses[7] of the mean-graph profiles of salicylihalamide A suggest that the salicylihalamides may act by a novel mechanism of action. Despite their promise as potential anticancer agents, further studies of this new class of compounds are hampered by limited availability from natural sources. The unique structural features of the salicylihalamides coupled with promising biological activity prompted us to develop a flexible approach toward the synthesis of these molecules and related analogues.

We initially focused on the synthesis of intermediate **3** (Scheme 1), the macrocyclic core structure of the salicylihalamides containing the three chiral centers and the $\Delta^{9,10}$ *E*-alkene. The masked aldehyde functionality in **3** provides an opportunity for side chain attachment at C16 and subsequent completion of the total synthesis.

Our synthetic strategy for the preparation of building block **3** features the use of readily available diacetone-D-glucose as the source for the three chiral centers of the molecule (chiral pool approach). The regioselective formation of the *E*-double bond at C9 was accomplished through a ring-closing metathesis (RCM) reaction employing intermediate **4**. Although the RCM strategy has been used before to form the 12-membered macrolactone ring of unsubstituted or side chain truncated salicylihalamides,[8,9] we herein report the use of the same protocol with a fully-substituted salicylihalamide macrocyclic core. Intermediate **4** can be obtained from lactone **6** *via* Mitsunobu esterification with 6-allylsalicylic acid (**5**). 6-Allylsalicylic acid (**5**) can be prepared from *O*-methylsalicylic acid[10] and diacetone-D-glucose **7** is the precursor for lactone **6**.[11,12]

The macrolide synthesis started with known alcohol **8**, which was prepared in five straightforward steps from diacetone-D-glucose (Scheme 2).[11–13] The secondary hydroxy group in **8**

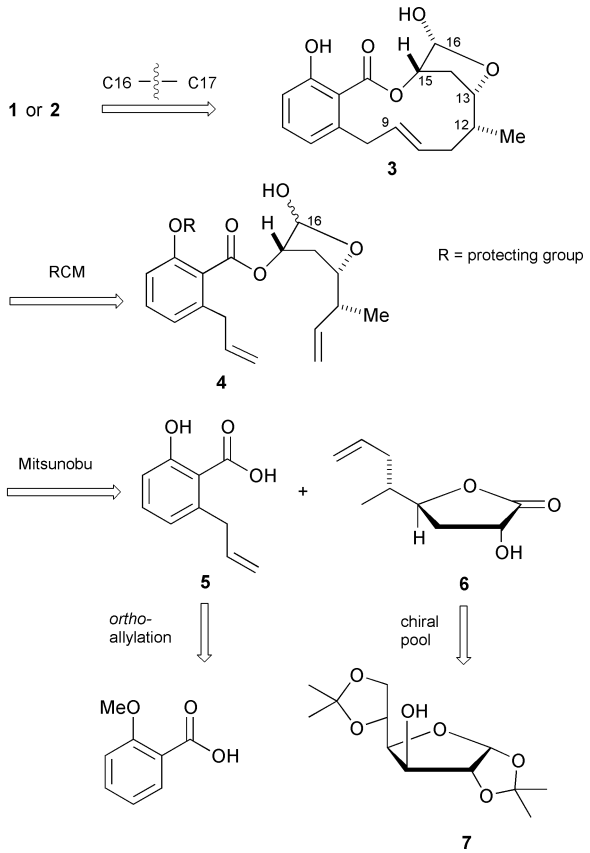

Scheme 1 Retrosynthesis for the salicylihalamide macrolide.

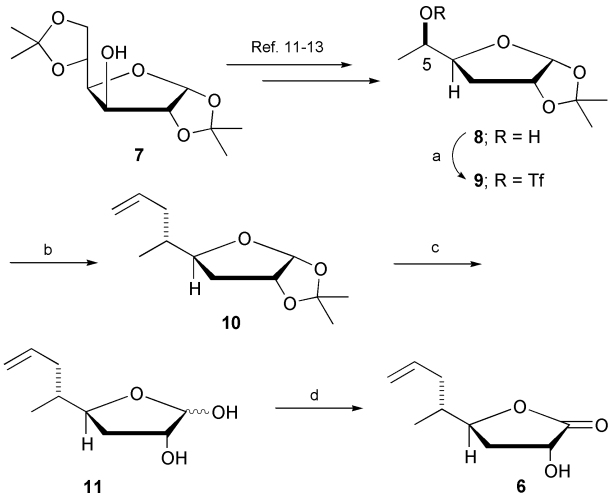

Scheme 2 *Reagents and conditions*: (a) Tf_2O, 2,6-dimethylpyridine, 0 °C, 1.5 h; (b) $(CH_2{=}CHCH_2)_2Cu)CN)Li_2$, THF, −78 °C, 2 h, 78%; (c) 70% aq. acetic acid, 70 °C, 6 h, 98%; (d) Ag_2CO_3–Celite, 80 °C, 1 h, 85%.

DOI: 10.1039/b008842k

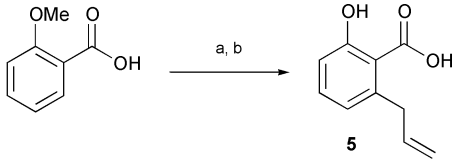

Scheme 3 *Reagents and conditions*: (a) *sec*-BuLi, TMEDA, THF, allyl bromide, −90 °C to rt, 0.5 h, 46% (based on recovered starting material); (b) BCl_3, $(n\text{-Bu})_4NI$, DCM, −78 °C, 2 h, 80%.

was converted to its corresponding triflate **9**, which was reacted immediately and without purification with a higher order allylcyanocuprate to provide **10** with inversion of configuration in 78% yield† (Scheme 2). Deprotection of the acetonide group was carried out with 70% acetic acid to yield alcohol **11**. Selective oxidation of the anomeric hydroxy group with Ag_2CO_3–Celite afforded lactone **6** in excellent yield. The synthesis of **5** was carried out in a two-step sequence as outlined in Scheme 3. Ortho-lithiation of *O*-methylsalicylic acid with *sec*-BuLi–TMEDA and quenching the carbanion with allyl bromide,[10] followed by deprotection of the methyl ether using BCl_3–$(n\text{-Bu})_4NI$,[14] afforded **5** in moderate overall yield.

Esterification of carbohydrate building block **6** with **5** under Mitsunobu conditions (Scheme 4) afforded intermediate **12** in good yield.

After the three stereogenic centers had been installed, the next step was the RCM reaction to form the $\Delta^{9,10}$ alkene. Surprisingly, RCM employing lactone **12** failed to give any of the desired product. Therefore the lactone functionality of **12** was reduced to lactol **14** (88:12, α:β; 80% yield) using DIBAL-H at −78 °C. RCM reaction with this substrate provided the desired reaction product. However, the *Z* isomer

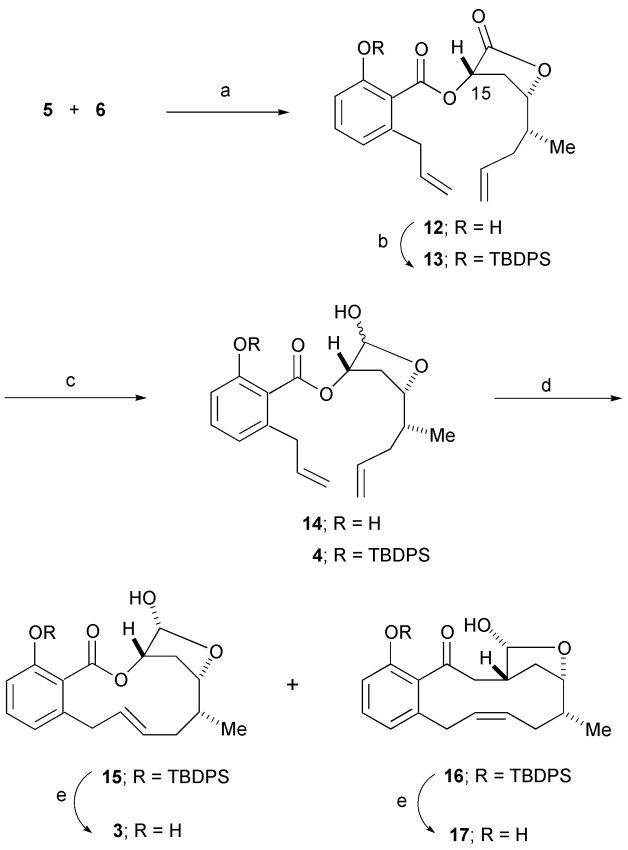

Scheme 4 *Reagents and conditions*: (a) Ph_3P, DEAD, THF, −20 °C to 0 °C, 1 h, 85%; (b) TBDPSCl, imidazole, DMF, rt, 1 h, 85%; (c) DIBAL-H, ether, −78 °C, 2 h, 80%; (d) $RuCl_2$=CHPh)$(PCy_3)_2$, DCM, reflux, 3 h, 60%; (e) TBAF, THF, rt, 1 h, 85%.

was found to be the major reaction product (*E*:*Z* ratio 15:85; 60% yield). When the phenolic hydroxy of **12** was protected as its TBDPS ether **13** (85% yield) and lactone **13** was reduced to lactol **4** (80% yield), RCM of intermediate **4** furnished the two stereoisomeric lactols **15** and **16** in a 70:30 *E*:*Z* ratio and in 60% yield. The introduction of the sterically demanding TBDPS protecting group apparently promotes a conformational change in the transition state of the RCM reaction that favors the formation of the *E*-alkene. After deprotection of the silyl ethers **15** and **16**, the stereoisomers **3** and **17** (85% yield) were separated by column chromatography furnishing the desired *E*-isomer **3** in 60% yield.

Having completed the synthesis of the macrolactone with correct stereo- and regiochemistry,[15] studies directed at introducing the enamide side chain are in progress.

This work was financially supported by the National Cancer Institute (N01-CM-67259 and RO1 CA84173), and the Drug Discovery Program of the Higuchi Biosciences Center at the University of Kansas. B. B. gratefully acknowledges financial support from predoctoral NIH training grant GM-07775 and the American Foundation for Pharmaceutical Education (AFPE) for a predoctoral fellowship. F. F. is grateful for an AAPS-AFPE 'Gateway' Research Scholarship for undergraduate students.

Note added in proof. For a revision of the absolute configuration of salicylihalamide A through total synthesis, see: Y. Wu, L. Esser and J. K. Brabander, *Angew. Chem., Int. Ed.*, 2000, **39**, 4308.

Notes and references

† All new compounds exhibited satisfactory spectral data in accordance with their structures. Yields refer to chromatographically pure compounds.

1 K. L. Erickson, J. A. Beutler, J. H. Cardellina II and M. R. Boyd, *J. Org. Chem.*, 1997, **62**, 8188.
2 K. Suzumura, I. Takahashi, H. Matsumoto, K. Nagai, B. Setiawan, R. M. Rantiatmodjo, K. Suzuki and N. Nagano, *Tetrahedron Lett.*, 1997, **38**, 7573.
3 T. C. McKee, D. L. Galinis, L. K. Pannell, J. H. Cardellina II, J. Laakso, C. M. Ireland, L. Murray, R. J. Capon and M. R. Boyd, *J. Org. Chem.*, 1998, **63**, 7805.
4 K. A. Dekker, R. J. Aiello, H. Hirai, T. Inagaki, T. Sakakibara, Y. Suzuki and J. F. Thompson, *J. Antibiot.*, 1998, **51**, 14.
5 J. W. Kim, K. Shin-ya, K. Furihata, Y. Hayakawa and H. Seto, *J. Org. Chem.*, 1999, **64**, 153.
6 R. Jansen, B. Kunze, H. Reichenbach and G. Höfle, *Eur. J. Org. Chem.*, 2000, 913.
7 K. D. Paull, E. Hamel and L. Malspeis, *Prediction of Biochemical Mechanism of Action from the In Vitro Antitumor Screen of the National Cancer Institute*, in *Cancer Chemotherapeutic Agents*, ed. W. O. Foye, American Chemical Society, Washington, DC, 1995.
8 A. Fürstner, G. Seidel and N. Kindler, *Tetrahedron*, 1999, **55**, 8215.
9 J. T. Feutrill, G. A. Holloway, F. Hilli, H. M. Hugel and M. A. Rizzacasa, *Tetrahedron Lett.*, 2000, **41**, 8569.
10 J. Mortier and J. Moyroud, *J. Org. Chem.*, 1994, **59**, 4042.
11 A. W. M. Lee, W. H. Chan, H. C. Wong and M. S. Wong, *Synth. Commun.*, 1989, **19**, 547.
12 J. J. Patroni and R. V. Stick, *Aust. J. Chem.*, 1978, **31**, 445.
13 S. Iacono, J. R. Rasmussen, P. J. Card and B. E. Smart, *Organic Syntheses*, Wiley & Sons, New York, 1993; Collect. Vol. VII, pp 139.
14 P. R. Brooks, M. C. Wirtz, M. G. Vetelino, D. M. Rescek, G. F. Woodworth, B. P. Morgan and J. W. Coe, *J. Org. Chem.*, 1999, **64**, 9719.
15 The results of this study have been reported: B. Blackman, C. J. Mossman, K. L.Yang, P. T. Flaherty and G. I. Georg, *Progress Towards the Total Synthesis of Salicylihalamide A and B*, Abstracts of papers, 219th National Meeting of the American Chemical Society, San Francisco, CA, American Chemical Society, Washington, D.C., 2000, ORG 808.

Synthesis and antibody binding properties of glycodendrimers bearing the tumor related T-antigen

Myung-Gi Baek,[a] Kate Rittenhouse-Olson,[b] and René Roy*[a]

[a] *Department of Chemistry, University of Ottawa, 10 Marie Curie, Ottawa, Ontario K1N 6N5 Canada*
[b] *Department of Microbiology and Immunology, Roswell Park Division, State University of New York at Buffalo, Buffalo, NY 14214. USA. E-Mail: rroy@science.uottawa.ca; Fax: +1-613-562-5170; Tel: +1-613-562-5800 ext 6055*

Received (in Corvallis, OR, USA) 23rd October 2000, Accepted 8th December 2000
First published as an Advance Article on the web 23rd January 2001

Breast cancer marker T-antigen (Gal(β1-3)αGalNAc) was prepared as an allyl glycoside that was transformed into an active ester and coupled to a series of poly(amidoamine) dendrimers showing strong binding to mouse monoclonal IgG antibodies and serving as useful coating antigens in microtiter plates.

Poly(amidoamine) (PAMAM) dendrimers[1] are actually scrutinized as core structures bearing various pharmacophores for potential applications in biomedical fields such as DNA transfection,[2] inhibition of pathogenic infections,[3] and toxicity, immunogenicity and biodistribution to organs.[4] PAMAM have further broadened their potential usefulness to biological systems by combination with different carbohydrate moieties.[5–7] Chemically well defined monodisperse neoglycoconjugates with several covalently attached carbohydrate residues, can efficiently compensate for the usually weak affinities of individual haptens *via* cooperative binding interactions.[8] However, in spite of these potential biological applications, systematic preparation and biological evaluation of PAMAM-based T-antigen, Gal(β13)αGalNAc, glycodendrimers have not been reported to date.

T-antigen (Thomsen–Friedenrich antigen) has been reported as a cancer-related epitope and as an important antigen for the detection and immunotherapy of carcinomas, particularly relevant in breast cancer.[9] For pharmaceutical applications, T-antigen containing linear glycopolymers have been employed in solid-phase glycosyl transferase assays for high-throughput screening in cancer drug discovery research.[10] Recently, we have reported that mouse monoclonal antibodies raised against the T-antigen recognised breast cancer tissues selectively.[11]

These biological and immunochemical results motivated the synthesis of well defined T-antigen-glycoPAMAMs that can be used as vaccines or as antibody targeting species. Their binding properties against mouse monoclonal IgG antibody has also been evaluated. The synthetic strategy for the construction of T-antigen-containing glycoPAMAMs was based on amide bond formation between amine terminated PAMAM cores **10**–**13** and acid functionalized T-antigen derivative **9**.

α-D-GalNAc derivative **2**† was prepared in 3 steps from *N*-acetylglucosamine (**1**) by a C-4 epimerization strategy using an adaptation of documented procedure (Scheme 1).[12] Compound **2** was debenzoylated under Zemplén conditions (NaOMe, MeOH) and subsequently exposed to either benzaldehyde–zinc chloride or benzaldehyde dimethyl acetal and a catalytic amount of toluene-*p*-sulfonic acid monohydrate to give 4,6-benzylidene protected glycosyl acceptor **3** in 87% yield after deprotection. Compound **3** was coupled with peracylated galactosyl bromide (**4** or **5**) using mercuric(II) cyanide as a promoter at rt to provide disaccharides **6** and **7** in 98 and 78% yields, respectively. Successive de-O-acylation (MeONa–MeOH) and de-acetalation (aq. AcOH, 60 °C) afforded the desired T-antigen **8** in 95% overall yield. Finally, radical initiated 3-mercaptopropionic acid addition to **8** in the presence of UV light (254 nm) under deoxygenated aqueous conditions gave acid functionalized **9** in 83% yield.

PAMAM cores **10**–**13** were conjugated *via* amide bond formation with a slight excess acid **9** (1.1 eq.) using TBTU‡ reagent (Scheme 2). The reaction mixtures were lyophilized to dryness and the residues were purified by either gel permeation chromatography (P-2 or P-4, H_2O) or dialysed against water (2000 molecular weight cut-off). After purification, T-antigen-glycoPAMAMs, **14**–**17** (Fig. 1) with 4, 8, 16, and 32 T-antigen residues were obtained in excellent yields (73, 81, 99, and 79%, respectively).

On the basis of negative ninhydrin tests, mass spectrometry (FAB-MS), and high field ^{1}H NMR spectral data, the extent of conjugations were shown to be complete. The ratios of the NMR signals, fully assigned using COSY and HMQC experiments (D_2O, sensisitivity $\leqslant 2 \sim 3\%$; ± 1 residue/30), clearly confirmed the total incorporation of the T-antigen residues by comparing the relative integration of the two methylene signals of the dendritic cores (δ 2.80 for **14** and **15**, 2.77 for **16** and 3.05 ppm for **17**, respectively) to those of the two anomeric protons of the T-antigen (δ 4.96 for H-1 and 4.56 ppm for H-1′ respectively).

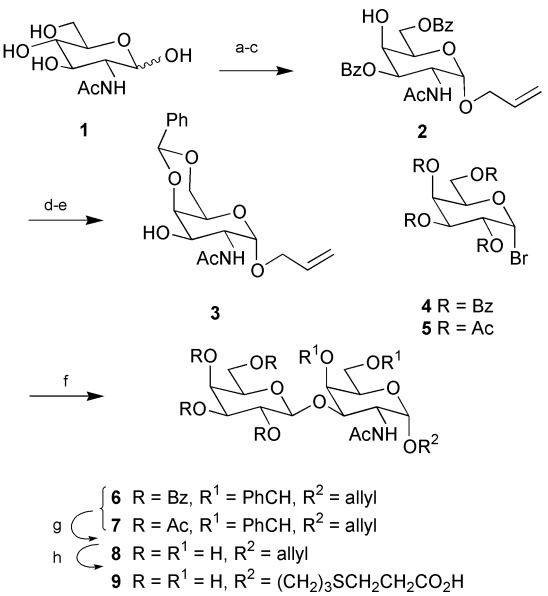

Scheme 1 (a) allyl alcohol, BF_3OEt_2, reflux for 3 h, 65 %; (b) BzCl (2.2 eq.), Py–$CHCl_3$, −60 °C, 92%; (c) (i)Tf_2O (1.5 equiv), Py (3.3 eq.)/CH_2Cl_2, −15 °C, (ii) $NaNO_2$ (10 eq.), DMF, 25 °C, 85% (2 steps); (d) MeONa, MeOH, quantitative; (e) PhCHO, $ZnCl_2$ (2 eq.) or $PhCH(OMe)_2$ (5 eq.), 25 °C, 87%; (f) Gal-Br (**4** (Bz) or **5** (Ac)) (1.5 eq), $Hg(CN)_2$ (1.5 eq) , PhH–$MeNO_2$, 25 °C 78–98 %; (g) i) MeONa, MeOH, (ii) 60% aq. AcOH, 60°C, 93%; (h) $HSCH_2CH_2CO_2H$ (1.1 eq), UV (254 nm), 83%. BzCl = benzoyl chloride, Py = pyridine, Tf_2O = trifluoromethanesulfonic anhydride, AcOH = acetic acid.

DOI: 10.1039/b008664i

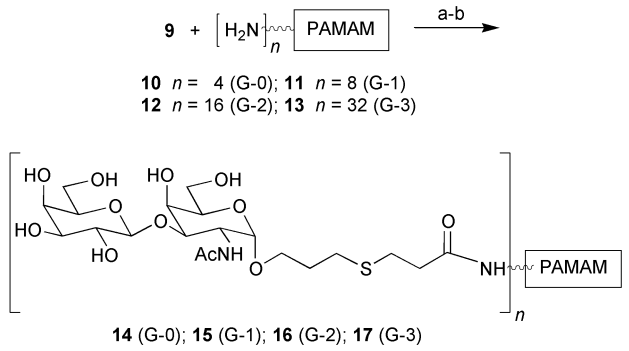

Scheme 2 (a) 1.1 eq **9** per amine, TBTU, DIPEA, DMSO, 25 °C, (b) gel permeation chromatography (P-2, or P-4, water) or dialysis (2000 molecular weight cut-off) 73–99%. DIPEA = diisopropylethylamine, DMSO = dimethylsulfoxide.

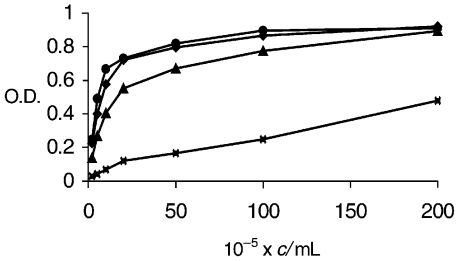

Fig. 1 ELISA of T-antigen-glycoPAMAMs, **14**(●), **15** (×), **16** (◆) and **17** (▲) with mouse monoclonal IgG antibody, goat anti-mouse IgG-horseradish peroxidase conjugate and ABTS-H_2O_2 as enzyme substrate. O.D. (410 nm) = optical density, ABTS = 2,2′-azinobis(3-ethylbenzothiazoline-6-sulfonic acid). *C*: Relative concentration.

The binding properties of glycoPAMAMs to mouse monoclonal IgG antibody (MAb)[11] were initially evaluated by enzyme linked immunosorbent assay (ELISA) (Fig. 1). GlycoPAMAMs were used as coating antigens to determine their ability to capture antibodies on the surface of the microtiter plates. Goat anti-mouse MAb IgG-horseradish peroxidase (HRP) conjugate was used for quantitative detection. The ability of the mouse MAb to recognise all glycodendrimers was clearly demonstrated (Fig. 1). Compound **17**, having 32 T-antigen residues, was shown to be the best ligand. To obtain an optical density value of 0.6, 90 μmol of coating glycodendrimers was needed. This value represents 2- to 4-fold increased binding potentials over those of **15** (16-mer) and **16** (8-mer) (330 and 150 μmol, respectively) which where > 25-fold more potent than tetramer **14** (> 2 mmol).

The efficiency of these glycoPAMAMs for protein-binding interactions were further substantiated by competitive double sandwich inhibition where conjugates **14**–**17** were employed as inhibitors. T-antigen-*co*-polyacrylamide (T-antigen–acrylamide, 1 : 10)[13] was used as a coating antigen. To this end, the T-antigen polymer (1μg well^{-1}, 0.85 nmol of T-antigen in PBS) was deposited in the microtiter plates. In separated plates (Nunclon, Delta), mouse-MAb IgG (50 μL well^{-1}, 0.25 μmol in PBS-tween) and glycoPAMAM inhibitors (50 μL well^{-1} in PBS-tween with varying concentrations from 275 to 1.07 nmol well^{-1}) were preincubated. After blocking the microtiter plates with bovine serum albumin (BSA), the wells were filled with the mixture of antibody–glycoPAMAM inhibitors (100 μL well^{-1}) and the mixtures were then incubated for 1 h at 37 °C. For the quantitative detection of antibodies, goat anti-mouse MAb-HRP was then added, as above. Based on bulk conjugates, the glycoPAMAMs with highest carbohydrate density (**17**) exhibited the strongest inhibitions. Conjugates **14**–**17** showed IC_{50} values of 5.0, 2.4, 1.4 and 0.6 nmol, respectively where monomeric T-antigen **8** needed 2.3 μmol. The inhibitory abilities of these conjugates were thus 460, 960, 1700 and 3800 times higher than that of monomer **8**. Interestingly, when expressed on a per saccharide basis, all dendrimers were equivalent to one another (115 fold better than **8**), thus supporting previous observations that low density glycoPAMAMs are efficient inhibitors.[5]

In conclusion, geometrically well designed starburst T-antigen-glycoPAMAMs were efficiently synthesized with valencies between 4 to 32 using efficient peptide coupling strategy. A series of bioassays with mouse MAb IgG demonstrated that these conjugates strongly bound to the antibody. All conjugates were antigenetically active as previously demonstrated with analogous structures.[5–7] Moreover, some carcinoma cells have been reported to express T-antigen binding sites,[14] it is therefore possible that the compounds described herein may also find applications in specific cancer cell targeting.

Notes and references

† Physical data for representative compounds, NMR assignments are based on COSY and HMQC.

6: mp 109.7–111.0 °C; R_f = 0.59 (benzene–ethyl acetate, 1 : 2); $[\alpha]_D$ = +116.0° (*c* = 1.00, $CHCl_3$); (+) FAB-MS (glycerol) (*m/z*): 928.3 (M + 1); δ_H (500 MHz, $CDCl_3$): 5.16 (m, J_{cis} = 8.0 Hz, 2 H, CH, H1′), 5.10 (d, J_{12} = 3.4 Hz, 1 H, H1); δ_C (500 MHz, $CDCl_3$): 102.0 (C1′), 100.9 (CH), 97.4 (C1); Anal. Calcd. for $C_{52}H_{49}O_{15}N$ (927.49): C, 67.20; H, 5.31; N, 1.53. Found: C, 66.84; H, 5.27; N, 1.48%. **9**: mp 90.0–92.5 °C; $[\alpha]_D$ = +76.0° (*c* = 1, H_2O); R_f = 0.33 ($CHCl_3$–MeOH–H_2O, 10 : 9 : 1); (+) FAB-MS (glycerol): 530.3 (M + 1); δ_H (ppm, D_2O): 4.96 (d, J_{12} = 3.7 Hz, 1 H, H1), 4.54 (d, $J_{1'2'}$ = 7.7 Hz, 1 H, H1′); δ_H (ppm, D_2O): 104.2 (C1′), 96.7 (C1). **17**: δ_H (500 MHz, D_2O): 4.96 (d, J_{12} = 3.7 Hz, 32 H, H1), 4.56 (d, $J_{1'2'}$ = 7.7 Hz, 32 H, H1′); δ_C (D_2O): 104.2 (C1′), 96.8 (C1). Anal. Calcd. for $C_{942}H_{1664}O_{444}N_{154}S_{32}$(23,278.7): C, 48.60; H, 7.20; N, 9.27. Found: C, 48.85; H, 7.21; N, 8.79%.

‡ TBTU = *O*-benzotriazol-1-yl)-*N*,*N*,*N*′,*N*′-tetramethyluronium tetrafluoroborate.

1 M. Fischer and F. Vögtle, *Angew. Chem., Int. Ed.*, 1999, **38**, 884.
2 A. U. Bielinska, C. Chen, J. Johnson and J. R. Baker, Jr., *Bioconjugate Chem.*, 1999, **10**, 843.
3 J. D. Reuter, A. Myc, M. M. Hayes, Z. Gan, R. Roy, D. Qin, R. Yin, L. T. Piehler, R. Esfand, D. A. Tomalia and J. R. Baker, Jr., *Bioconjugate Chem.*, 1999, **10**, 271.
4 (*a*) R. Duncan and N. Malik, *Proc. Int. Symp. Controlled Release Bioact. Mater.*, 1996, **23**, 105; (*b*) J. C. Roberts, M. K. Bhalgat and R. T. Zera, *J. Biomed Mater. Res.*, 1996, **30**, 53.
5 (*a*) R. Roy, *Polymer News*, 1996, **21**, 226; (*b*) R. Roy, *Carbohydr. Eur.*, 1999, **27**, 34.
6 T. Toyokuni and A. K. Singhal, *Chem. Soc. Rev.*, 1995, 231.
7 S. André, P. J. C. Ortega, M. A. Perez, R. Roy and H. J. Gabius, *Glycobiology*, 1999, **9**, 1253.
8 (*a*) R. Roy, *Curr. Opin. Struct. Biol.*, 1996, **6**, 692; (*b*) L. L. Kiessling and N. L. Pohl, *Chem. Biol.*, 1996, **3**, 71; (*c*) M. Mammen, S. K. Choi and G. M. Whitesides, *Angew. Chem., Int. Ed.*, 1998, **37**, 2754.
9 P. O. Livingston, R. Koganty, B. M. Longenecker, K. O. Lloyd and M. Calves, *Vaccine Res.*, 1992, **1**, 99; Y. Chen, R. K. Jain, E. V. Chandrasekaran and K. L. Matta, *Glycoconjuate J.*, 1995, **12**, 55; P. Y. S. Hung, M. Madej, R. R. Koganty and B. M. Longenecker, *Cancer Res.*, 1990, **50**, 4308.
10 R. S. Donovan, A. Datti, M. G. Baek, Q. Q. Wu, I. Sas, B. Korczak, E. G. Berger, R. Roy and J. W. Dennis, *Glycoconjugate J.*, 1999, **16**, 607.
11 K. Rittenhouse-Diakun, Z. Xia, D. Pickhardt, S. Morey, M. G. Baek and R. Roy, *Hybridoma*, 1998, **17**, 165.
12 L.-X. Wang and Y. C. Lee, *J. Chem. Soc., Perkin Trans. 1*, 1996, 581.
13 M.-G. Baek and R. Roy, *Biomacromolecules*, 2000, **1**, 768.
14 H.-J. Gabius, C. Schroter, S. Gabius, U. Brinck and L.-F. Tietze, *J. Histochem. Cytochem.*, 1990, **38**, 1625.

ChemComm

An aurophilicity-determined 3-D bimetallic coordination polymer: using $[Au(CN)_2]^-$ to increase structural dimensionality through gold···gold bonds in (tmeda)Cu$[Au(CN)_2]_2$

Daniel B. Leznoff,*[a] Bao-Yu Xue,[a] Brian O. Patrick,[b] Victor Sanchez[b] and Robert C. Thompson[b]

[a] *Department of Chemistry, Simon Fraser University, 8888 University Drive, Burnaby, B.C., V5A 1S6, Canada. E-mail: dleznoff@sfu.ca*

[b] *Department of Chemistry, University of British Columbia, 2036 Main Mall, Vancouver, B.C., V6T 1Y6, Canada*

Received (in Columbia, MO, USA) 25th August 2000, Accepted 5th December 2000
First published as an Advance Article on the web 23rd January 2001

A coordination polymer with the $[Au(CN)_2]^-$ building block has been prepared and it exhibits weak Au(I)-mediated ferromagnetic interactions; the structure illustrates that aurophilicity is a powerful tool to increase dimensionality, generating a three-dimensional system from a 1-D polymer.

The design of multidimensional coordination polymers is an area of intense current interest.[1] In particular, as many useful properties (magnetism, conductivity, host–guest chemistry, *etc.*) manifest themselves in 2- or 3-D networks, it is important to be able to generate high-dimensionality systems. The incorporation of moieties capable of forming hydrogen bonding interactions into coordination polymers is perhaps the most well-developed method for increasing structural dimensionality.[2] On the other hand, gold(I) centres are known to form weakly bonding interactions with themselves; these 'aurophilic' interactions have the same order-of-magnitude strength as hydrogen bonds.[3] The supramolecular chemistry of gold(I) is replete with systems that are polymeric by virtue of these Au–Au interactions,[4] but aurophilic interactions have not generally been used as a tool to increase structural dimensionality in coordination polymers containing metals other than gold.

Dicyanoaurate, $[Au(CN)_2]^-$, is an ideal building block to explore this concept. The molecule is linear, should readily form coordination polymers as do other anionic metal–cyanide units,[5] is sterically unencumbered and forms aurophilic interactions in the solid state.[6] We present here the first coordination polymer using this building block in which aurophilic interactions increase the dimensionality from one to three dimensions. $M[Au(CN)_2]_2$ (M = Co, Zn) complexes have been reported to form unusual quartz-like nets in which Au···Au bonding plays a secondary role.[7]

The reaction of an aqueous solution of $Cu(ClO_4)_2{\cdot}6H_2O$ containing one equivalent of tmeda (*N*,*N*,*N*′*N*′-tetramethylethylenediamine) with an aqueous solution of $K[Au(CN)_2]$ (2 equiv.) produced an immediate blue precipitate.[8] Elemental analysis indicated a compound of stoichiometry (tmeda)-Cu$[Au(CN)_2]_2$ (**1**). The IR spectrum of **1** is diagnostic due to the presence of multiple absorptions in the CN region. $K[Au(CN)_2]$ has a single absorbance at 2141 cm^{-1}; **1** has three CN absorbances at 2152, 2174 and 2191 cm^{-1}. The high-energy bands likely correspond to bridging CN groups.[5] Single crystals of **1** could be obtained by slow diffusion of the two reagent solutions in an H-shaped tube. Infrared data were identical for both the powder and the crystals.

The X-ray crystal structure of **1** confirms the molecular formula of (tmeda)Cu$[Au(CN)_2]_2$ and reveals a polymeric network.[9] Note that, unlike many other linear building blocks that have been examined (*e.g.* pyrazine, 4,4′-bipyridyl),[10] $[Au(CN)_2]^-$ is anionic, and hence chemically uncharged polymers are generated.[11] The Cu(II) centre in **1** has a five-coordinate, distorted square pyramidal geometry, with one tmeda and three CN nitrogen atoms completing the coordination sphere. The asymmetric unit contains three unique gold centres—Au(2) and Au(3) have CN groups with both ends bound to a Cu(II), while Au(1) has one Cu(II)-bonded CN group and the other CN group is free. As shown in Fig. 1, the Cu(1)–NC–Au(2)–CN–Cu(1*)–NC–Au(3)–CN– fragment infinitely repeats in the *b* direction, giving rise to a coordinately bonded 1-D zig-zag chain. The Cu–N(4) bond length of 2.270(8) Å is significantly longer than the other four Cu–N bond lengths, hence the dangling $[Au(CN)_2]$ unit (Au(1)) is less strongly bound to the Cu centre than those in the polymer backbone. The intrachain Cu(1)–Cu(1*) distance is 10.18(1) Å.

Each gold centre is a site for potential aurophilic interactions to occur. Indeed, the picture of the solid-state structure is incomplete without including them. The Au(2) and Au(3) atoms in the backbone of the 1-D zig-zag chain form *interchain* Au···Au bonds of 3.5378(8) Å in the *a* direction (*i.e.* out of the plane of the paper). This distance is less than the sum of the van der Waals radii of two Au atoms (3.60 Å)[3] and is hence a viable, weak Au···Au interaction. This effectively joins two 1-D chains together to form a 2-D array of alternating 1-D zig-zag chains in the *ab* plane, as shown in Fig. 1. Each Au(2) and Au(3) centre is loosely four-coordinate.[6]

On the dangling $Au(CN)_2$ unit, Au(1) forms moderate Au···Au interactions of 3.345(1) Å with Au(1*) on the adjacent

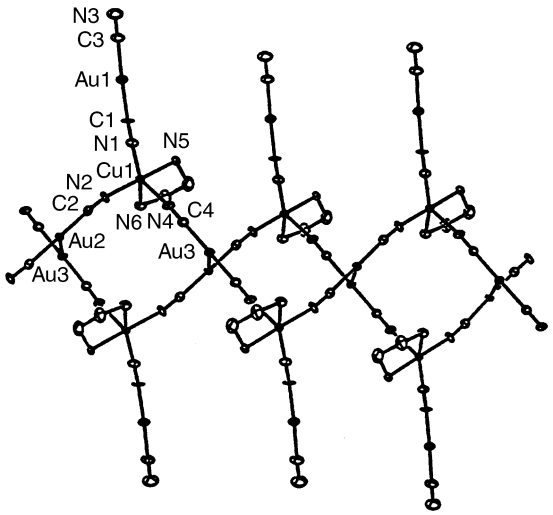

Fig. 1 Extended 2-D structure viewed down the *a* axis of (tmeda)-Cu$[Au(CN)_2]_2$ (**1**), with its numbering scheme, showing a 1-D coordinately bonded zig-zag chain in the *b* direction, connected in the *a* direction by Au···Au bonds to an adjacent, inverse-sense chain (ORTEP, 50% ellipsoids). Tmeda-methyl groups have been removed for clarity. Selected bond lengths (Å) and angles (°): Cu–N(1) 2.006(9), Cu–N(2) 1.992(8), Cu–N(4) 2.270(8), Cu–N(5) 2.048(8), Cu–N(6) 2.080(8), Au(2)–Au(3) 3.5378(8), Cu–Cu* 10.18(1); N(1)–Cu–N(2) 91.6(4), N(1)–Cu–N(4) 103.6(3), N(1)–Cu–N(5) 90.5(3), N(1)–Cu–N(6) 157.2(3), N(2)–Cu–N(4) 89.3(4), N(2)–Cu–N(5) 176.2(4), N(2)–Cu–N(6) 91.2(4), N(4)–Cu–N(5) 93.3(3), N(4)–Cu–N(6) 99.0(3), N(5)–Cu–N(6) 85.7(4), Cu–N(1)–C(1) 165.2(9), Cu–N(2)–C(2) 171.2(9), Cu–N(4)–C(4) 166.9(9).

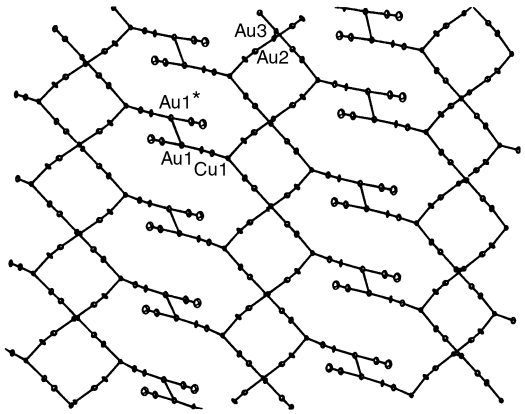

Fig. 2 Complete three–dimensional structure of **1**. Tmeda ligands have been removed for clarity. Au(1)–Au(1*): 3.345(1) Å.

1-D chain in the *b* direction (*i.e.* in the plane of the page), yielding a ladder-rung type motif running parallel to the 1-D chains. This Au···Au bonding in the *bc* plane, connecting the 2-D array of chains illustrated in Fig. 1, transforms the structure into a true three-dimensional system, as shown in Fig. 2. The presence of gold···gold interactions has effectively increased the dimensionality from a 1-D coordination polymer to a 3-D system.

The variable temperature magnetic susceptibility of **1** was measured from 2 to 300 K at a field strength of 1 T.[12] At 300 K, μ_{eff} is equal to 1.94 μ_B, a value typical for a system of isolated Cu(II), d^9, centres. This value steadily increases on decreasing the temperature, behaviour indicative of ferromagnetic interactions, to a maximum value of 2.05 μ_B at 25 K, below which temperature it decreases on further cooling. This latter decrease could arise either from the onset of saturation effects or very weak antiferromagnetic exchange. From a magnetic point of view, **1** could be considered as a 1-D chain, assuming that negligible magnetic interactions are propagated through the Au···Au bonds. We were unable to model the magnetic data over the entire range of temperatures studied. However, the χ_M *vs.* *T* data above 30 K were successfully fitted to theory employing the polynomial expression of Baker *et al*. for a 1-D ferromagnetic chain of $S = 1/2$ spins.[13] The magnetic moment *versus* temperature data are shown in Fig. 3, where the solid line is calculated from theory employing the best fit values of $g = 2.22$ and *J*, the exchange coupling constant, 2.34 cm^{-1}. From this analysis it appears that the diamagnetic $Au(CN)_2^-$ unit may propagate weak ferromagnetic coupling in this compound. Note

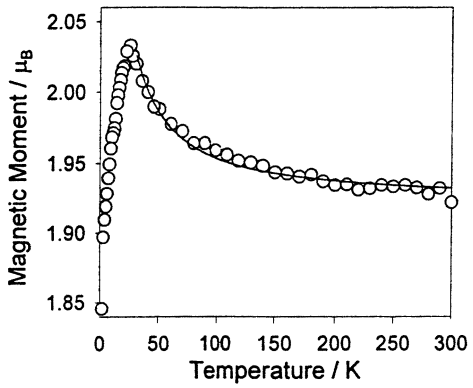

Fig. 3 Magnetic moment *versus* temperature plot for **1**. The solid line is theory (see text).

that in the related $[Ni(en)_2]_3[Fe(CN)_6](PF_6)_2$ system, the diamagnetic Fe(II) cyanide unit also mediates ferromagnetic interactions between the Ni(II) centres.[14]

In summary, a new coordination polymer with the neglected $[Au(CN)_2]^-$ building block has been prepared and crystallized. The structure confirms the concept that aurophilicity is a powerful tool to increase dimensionality in supramolecular coordination polymers.

Financial support from Simon Fraser University (D. B. L.) and NSERC of Canada (R. C. T.) is gratefully acknowledged.

Notes and references

1 O. M. Yaghi, H. L. Li, C. Davis, D. Richardson and T. L. Groy, *Acc. Chem. Res.*, 1998, **31**, 474; D. Braga, F. Grepioni and G. R. Desiraju, *Chem. Rev.*, 1998, **98**, 1375.
2 M. J. Zaworotko, *Chem. Soc. Rev.*, 1994, **23**, 283; S. Subramanian and M. J. Zaworotko, *Coord. Chem. Rev.*, 1994, **137**, 357; P. V. Bernhardt, *Inorg. Chem.*, 1999, **38**, 3481.
3 H. Schmidbaur, *Chem. Soc. Rev.*, 1995, **24**, 391.
4 B.-C. Tzeng, A. Schier and H. Schmidbaur, *Inorg. Chem.*, 1999, **38**, 3978; M. J. Irwin, L. Manojlovic-Muir, K. W. Muir, R. J. Puddephatt and D. S. Yufit, *Chem. Commun.*, 1997, 219; A. Sladek and H. Schmidbaur, *Inorg. Chem.*, 1996, **35**, 3268; P. M. Van Calcar, M. M. Olmstead and A. L. Balch, *J. Chem. Soc., Chem. Commun.*, 1995, 1773.
5 K. R. Dunbar and R. A. Heintz, *Prog. Inorg. Chem.*, 1997, **45**, 283.
6 R. E. Cramer, D. W. Smith and W. Van Doorne, *Inorg. Chem.*, 1998, **37**, 5895; N. Blom, A. Ludi, H.-B. Bürgi and K. Tichy, *Acta Crystallogr., Sect. C*, 1984, **40**, 1767.
7 B. F. Hoskins, R. Robson and N. V. Y. Scarlett, *Angew. Chem., Int. Ed. Engl.*, 1995, **34**, 1203; S. C. Abrahams, L. E. Zyontz and J. L. Bernstein, *J. Chem. Phys.*, 1982, **76**, 5458; S. C. Abrahams, J. L. Bernstein, R. Liminga and E. T. Eisenmann, *J. Chem. Phys.*, 1980, **73**, 4585.
8 *Synthesis of* **1**: a 3 mL aqueous solution of $Cu(ClO_4)_2 \cdot 6H_2O$ (0.055 g, 0.15 mmol) and tmeda (1.5 mL, 0.1 mmol mL^{-1} stock solution, 0.15 mmol) was prepared. To this was added a 5 mL aqueous solution of $KAu(CN)_2$ (0.086 g, 0.3 mmol) dropwise, resulting in an immediate blue-coloured precipitate. This solid was filtered and air-dried to give $(tmeda)Cu[Au(CN)_2]_2$ (**1**) as a blue powder. Yield: 0.068 g (67%). Anal. Calcd. for $C_{10}H_{16}N_6Au_2Cu$: C, 17.72; H, 2.38; N, 12.40. Found: C, 17.65; H, 2.61; N, 12.39%. IR (KBr): ν_{CN} 2152, 2174, 2191 cm^{-1}.
9 *Crystal data*: $C_{10}H_{16}N_6Au_2Cu$; $M = 677.76$, triclinic, space group $P\bar{1}$, $a = 7.076(2)$, $b = 7.669(2)$, $c = 15.909(4)$ Å, $\alpha = 95.924(4)$, $\beta = 94.948(4)$, $\gamma = 113.897(6)°$, $V = 777.2(3)$ $Å^3$, $Z = 2$, $D_c = 2.896$ g cm^{-3}, μ(Mo-Kα) = 202.46 cm^{-1}, $T = 193$ K , 6558 data collected, 2919 unique ($R_{int} = 0.053$), $R_1 = 0.075$ (all data). Data collection, structure solution and refinement of **1** were performed as detailed elsewhere.[15] CCDC 182/1879. See http://www.rsc.org/suppdata/cc/b0/b007342n/ for crystallographic files in .cif format.
10 P. J. Hagrman, D. Hagrman and J. Zubieta, *Angew. Chem., Int. Ed.*, 1999, **38**, 2638; A. J. Blake, N. R. Champness, P. Hubberstey, W. S. Li, M. A. Withersby and M. Schröder, *Coord. Chem. Rev.*, 1999, **183**, 117.
11 A. J. Blake, N. R. Champness, M. Crew, L. R. Hanton, S. Parsons and M. Schröder, *J. Chem. Soc., Dalton Trans.*, 1998, 1533.
12 Magnetic susceptibilities were measured on powdered samples using a Quantum Design (MPMS) SQUID magnetometer. The sample holder and details regarding the use of the equipment have been described elsewhere.[16] Magnetic susceptibilities were corrected for background and for the diamagnetism of all atoms.
13 G. A. Baker Jr., G. S. Rushbrook and H. E. Gilbert, *Phys. Rev. A*, 1964, **135**, 1272; W. E. Estes, W. E. Hatfield, J. A. C. van Ooijen and J. Reedijk, *J. Chem. Soc., Dalton Trans.*, 1980, 2121.
14 N. Fukita, M. Ohba, H. Okawa, K. Matsuda and H. Iwamura, *Inorg. Chem.*, 1998, **37**, 842.
15 D. B. Leznoff, C. Rancurel, J.-P. Sutter, S. J. Rettig, M. Pink and O. Kahn, *Organometallics*, 1999, **18**, 5097.
16 M. K. Ehlert, S. J. Rettig, A. Storr, R. C. Thompson and J. Trotter, *Can. J. Chem.*, 1989, **67**, 1970.

An expedient synthesis of substituted tetraaryltetrabenzoporphyrins†

Olga Finikova,[a] Andrei Cheprakov,*[a] Irina Beletskaya[a] and Sergei Vinogradov*[b]

[a] *Department of Chemistry, Moscow State University, Moscow 119899, Russia. E-mail: avchep@elorg1.chem.msu.ru*
[b] *Department of Biochemistry and Biophysics, School of Medicine, University of Pennsylvania, Philadelphia, PA 19104, USA. E-mail: vinograd@mail.med.upenn.edu; Fax: +01-215-573-3787; Phone: +01-215-898-6382*

Received (in Corvallis, OR, USA) 31st October 2000, Accepted 22nd December 2000
First published as an Advance Article on the web 23rd January 2001

A simple route to tetraaryltetrabenzoporphyrins (Ar_4TBPs) is developed; the procedure allows for the introduction of substituents on both benzo- and phenyl-rings and employs readily available, inexpensive components.

Tetrabenzoporphyrins (TBP's) and their metal complexes have rapidly gained popularity as versatile near infra-red dyes. The spectrum of their applications encompasses PDT (photodynamic therapy),[1a] non-linear optical absorption,[1b] optical limiting[1c] and dioxygen measurements *in vivo* by phosphorescence quenching.[1d] Due to solubility considerations the *meso*-tetraarylsubstituted TBP's (Ar_4TBP) have proven to be the most useful, especially those bearing functional groups in benzo and/or in *meso*-phenyl rings, which permit their further derivatization. However, until very recently all synthetic methods leading to Ar_4TBPs were based on a high temperature condensation between phthalimide and phenylacetic acids,[2a] or similar donors of benzo- and phenyl-groups.[2b] The harsh conditions of this process (fusion at 350–400 °C) allowed for only a few inert substituents, such as alkyl groups or halogens,[3] to be introduced into the TBP macrocycle. In addition, low yields and complex, virtually inseparable mixtures of products[4] made the whole method quite impractical.

Since the obvious precursor of the Ar_4TBP cycle, isoindole, is highly unstable, the recent search for more convenient synthetic protocols centered around isoindole-precursors, *i.e. c*-annelated pyrroles. These are available *via* Barton–Zard isocyanoacetate chemistry and have proven to be useful for the synthesis of other symmetric extended porphyrins.[5] Two methods of TBP synthesis of this kind were reported to date. Both methods are based on the Barton–Zard reaction and involve the initial synthesis of either cycloalkyl[6] or bicycloalkenyl fused porphyrins.[7] These intermediate porphyrins are then aromatized by either base catalyzed elimination of sulfinate[6] or the thermal retro-Diels–Alder extrusion of ethylene.[7] The latter method affords Ar_4TBPs in excellent yields; however, the synthesis of the isoindole precursors themselves, *i.e.* bicycloalkenyl fused pyrroles, involves hazardous compounds such as nitroethyl acetate. Here we report an alternative route to the Ar_4TBP system, which is both simple and general. The procedure allows for the introduction of substituents in both benzo- and *meso*-phenyl rings while employing only inexpensive and readily available components.

In our approach, the common precursor of the synthesis is the inexpensive sulfolene **1**‡ (Scheme 1), which is converted to a tetrahydroisoindole *via* the Diels–Alder reaction with an appropriate dienophile,[8] followed by the introduction of the phenylsulfonyl group and subsequent Barton–Zard-type reaction of the resulting vinyl sulfone.[9] Tetrahydroisoindoles are further introduced into Lindsey condensation, giving tetracyclohexanoporphyrins, which are finally aromatized.

The first successful application of this approach to the synthesis of the substituted Ar_4TBPs is shown in Scheme 1.§

Sulfolene **1** is converted to 3-phenylsulfonyl-3-sulfolene[10] **2** (b1) using earlier published procedures.[11] Alternatively, Diels–Alder adduct **3** with dimethyl maleate (DMM) is obtained in 85% yield (a). Both products, **3** and **2**, are further transformed into sulfone **4**. Compound **3** reacts with PhSCl, which is followed by oxidation and elimination of HCl (b2); **2** participates in the similar Diels–Alder reaction (a) with DMM.[12] Sulfone **4** reacts with *tert*-butyl isocyanoacetate (c)[13] yielding cyclohexanopyrrole **5** in 70–95% yield, which is deprotected and decarboxylated by TFA in CH_2Cl_2 (d) in 35–40% yield. Pyrrole **6** obtained in this way is introduced into the Lindsey condensation (e),[14] which produces porphyrins **7a**–**d** in 25–35% yields. Alternatively, porphyrins **7a**–**d** can be obtained by directly reacting cyclohexanopyrrole **5** with benzaldehydes under Alder–Longo conditions (d+e), in which case deprotection–decarboxylation occurs *in situ* in the presence of TsOH. Such simplification of the synthesis is especially practical when yields of the one-pot procedure (8–12%) are comparable with yields of the stepwise decarboxylation-condensation (8–14%). Noteworthy is that in all cases porphyrins **7a**–**d** were isolated as dications rather than as free-bases (evidenced by UV-VIS

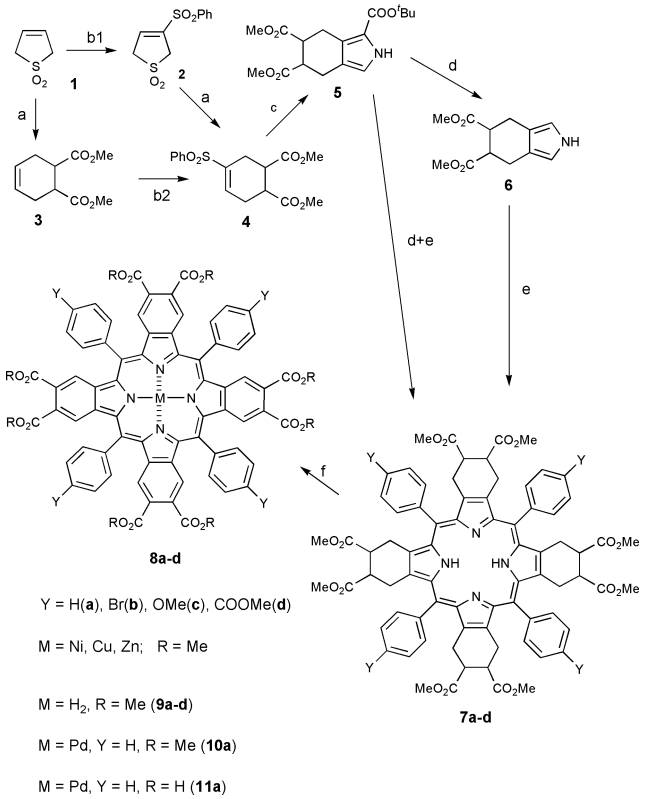

Scheme 1 *Reagents and conditions*: a, DMM, py, 140 °C, pressure tube, 85%; b1, (i) PhSCl. CH_2Cl_2; (ii) Et_3N; (iii) Oxone, MOH, 86% for three steps; b2, (i) PhSCl, CH_2Cl_2; (ii) MCPBA; (iii) DBU, 81% for three steps; c, $CNCH_2CO_2{}^tBu$, ^tBuOK, THF, Ar, 0 °C, 80–95%; d, TFA–CH_2Cl_2, Ar, rt, 35–40%; e, (i) YC_6H_4CHO, $BF_3{\cdot}Et_2O$, CH_2Cl_2; (ii) DDQ, 25–35% for two steps; d + e, YC_6H_4CHO (X = H), AcOH, TosOH, CH_2Cl_2, 8–12%; f, (i) $M(OAc)_2$, MeOH–$CHCl_3$; (ii) DDQ, THF or MeCN, reflux, M = Zn, Cu, Ni, 98% for two steps.

† Electronic supplementary information (ESI) available: experimental data. See http://www.rsc.org/suppdata/cc/b0/b008816l/

DOI: 10.1039/b008816l

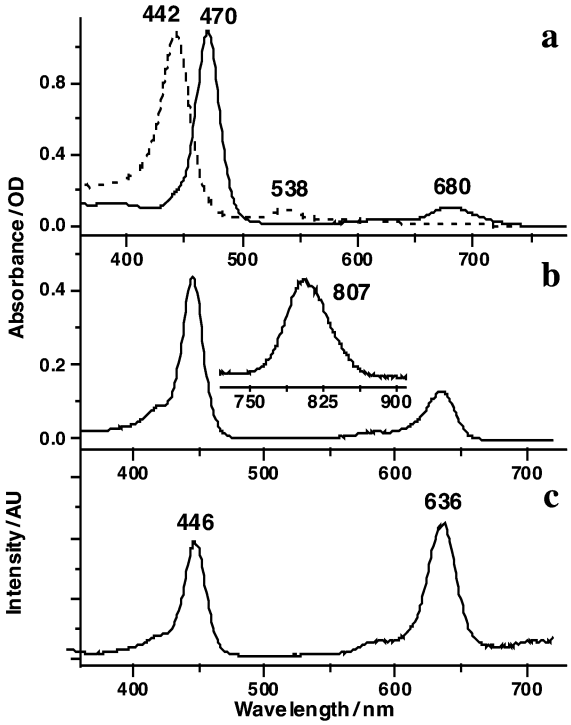

Fig. 1 (a) Absorption spectra of porphyrin **7a** in CH_2Cl_2 (solid line) and in pyridine (dashed line); (b) absorption spectrum of Pd-tetrabenzoporphyrin **11a** in water (pH 8.0). Insert shows uncorrected emission (phosphorescence) spectrum of **11a** in deoxygenated solution; (c) excitation spectrum of **11a** (corrected for the lamp intensity) related to the emission at 807 nm.

spectroscopy Fig. 1a). The dications could be fully deprotonated only in the presence of such bases as Et_3N or pyridine, which suggests that **7a**–**d** exhibit unusually high basicity.[15] The porphyrins **7a**–**d** were converted to their respective metal complexes and aromatized by refluxing with an excess of DDQ (f),[16] giving the MAr_4TBPs (M = Ni, Cu, Zn) **8a**–**d** in nearly quantitative yields. Interestingly, free-base porphyrins could not be aromatized under such conditions, most likely due to the formation of dications, which are apparently not oxidized by DDQ. The net yield of the entire sequence is 3–8%. Given that all starting compounds are readily available, this synthesis can afford gram quantities of substituted Ar_4TBPs in a single preparation.

Zn complexes **8a**–**c** could be quantitatively demetalated by treatment with TFA in CH_2Cl_2, to give free-base tetrabenzoporphyrins **9a**–**c**. The Pd complex of tetraphenyloctamethoxycarbonyltetrabenzoporphyrin **10a** was formed quantitatively upon reacting the free-base porphyrin **9a** with $PdCl_2$ in refluxing benzonitrile. Finally, the methoxycarbonyl groups of **10a** were deesterified ($NaOH–THF–H_2O$), giving tetraphenyloctacarboxytetrabenzoporphyrin **11a**, well soluble in basic aqueous solutions. The absorption and emission spectra of **11a** are shown in Fig 1b. The near infra-red emission with λ_{max} at 807 nm (phosphorescence) is completely quenched in the presence of molecular oxygen. In deoxygenated water solutions this phosphorescence has a lifetime of 107 μsec and a quantum yield of about 10%, which makes metalloporphyrin **11a** well suited for the lifetime oxygen sensing.[1d] Intriguingly the phosphorescence of **11a** has a significantly higher intensity if excited at the weaker Q-band, than at the Soret band. The corrected excitation spectrum of **11a**, recorded at a very high dilution (absorbance at Soret maximum (440 nm) 0.05 OD), is shown in Fig. 1c. Since no emission was observed directly from the S_2-state, such behavior is most likely due to the existence of uncommon non-radiative pathways of S_2 deactivation.

In summary, we have developed a new method of synthesis of Ar_4TBPs, which employs inexpensive, readily available starting materials. The method allows introduction of functional groups in both benzo- and phenyl- rings, thus providing a general route to the modified tetrabenzoporphyrin system. Newly synthesized tetrabenzoporphyrins were found promising basic phosphors for oxygen measurements by phosphorescence quenching.

S. V. acknowledges support of the grant HL-60100 from the National Institutes of Health (NIH) of the USA. O. F. and A. C. acknowledge support of the grant 01-03-33097-A from the Russian Foundation for Basic Research.

Notes and references

‡ The IUPAC name for sulfolene is 2,5-dihydro-1*H*-thiophene-1,1-dioxide.

§ Newly synthesized porphyrins were characterized by ^1H NMR and MALDI-TOF mass spectrometry. The details of the analysis are given in the ESI†. The UV-VIS and phosphorescence spectroscopy was performed as described elsewhere.[1d]

1 (*a*) A. Lavi, F. M. Johnson and B. Ehrenberg, *Chem. Phys. Lett.*, 1994, **231**, 144; R. Bonnet, *Chem. Soc., Rev.*, 1995, **24**, 19 and references therein; (*b*) M. Brunel, F. Chaput, S. A. Vinogradov, B. Campagne, M. Canva and J. P. Boilot, *Chem. Phys.*, 1997, **218**, 301; (*c*) D. V. G. L. N. Rao, F. J. Aranda, D. E. Remy and J. F. Roach, *Int. J. Nonlinear Opt. Prop.*, 1994, **3**, 511; P. L. Chen, I. V. Tomov, A. S. Dvornikov, M. Nakashima, J. F. Roach, D. M. Alabran and P. M. Rentzepis, *J. Phys. Chem.*, 1996, **100**, 17 507; (*d*) S. A. Vinogradov and D. F. Wilson, *J. Chem. Soc., Perkin Trans. 2*, 1994, 103; S. A. Vinogradov, L.-W. Lo, W. T. Jenkins, S. M. Evans, C. Koch and D. F. Wilson, *Biophys. J.*, 1996, **70**, 1609.

2 (*a*) V. N. Kopranenkov, S. N. Dashkevich and E. A. Luk'yanets, *Russ. J. Gen. Chem. (Engl. Transl.)*, 1981, **51**, 2165; (*b*) for review see T. D. Lash, *Synthesis of Novel Porphyrinoid Chromophores* in *Porphyrin Handbook*, ed. K. M. Kadish, K. M. Smith and R. Guilard, Acad. Press, NY, 2000, Vol. 2, Ch. 10, p. 125.

3 V. N. Kopranenkov, E. A. Makarova, S. N. Dashkevich and E. A. Luk'janets, *Russ. Chem. Heterocycl. Comp. (Engl. Transl.)*, 1988, **24**, 630; S. A. Vinogradov and D. F. Wilson, *Tetrahedron Lett.*, 1998, **39**, 8935; R. Bonnet and G. Martinez, *J. Porphyrins Phthalocyanines*, 2000, **4**, 544.

4 K. Ichimura, M. Sakuragi, H. Morii, M. Yasuike, M. Fukui and O. Ohno, *Inorg. Chim. Acta*, 1990, **176**, 31.

5 T. D. Lash and B. H. Novak, *Angew. Chem., Int. Ed. Engl.*, 1995, **34**, 683; J. D. Spence and T. D. Lash, *J. Org. Chem.*, 2000, **65**, 1530.

6 M. G. H. Vicente, A. C. Tome, A. Walter and J. A. S. Cavaleiro, *Tetrahedron Lett.*, 1997, **38**, 3639.

7 S. Ito, T. Murashima, H. Uno and N. Ono, *Chem. Commun.*, 1998, 1661.

8 It could be advantageous to conserve the sulfolene moiety until the last stages of the synthesis. However, the attempts to use sulfolenopyrroles in porphyrin synthesis lead to intractable materials of very low solubility. The only example of fused tetrasulfoleneporphyrin with highly sterically encumbered *meso*-aryl groups has been recently reported by B. Kräutler, C. S. Sheehan and A. Rieder, *Helv. Chim. Acta*, 2000, **83**, 583.

9 G. Haake, D. Struve and F.-P. Montforts, *Tetrahedron Lett.*, 1994, **35**, 9703; Y. Abel, E. Haake, G. Haake, W. Schmidt, D. Struve, A. Walter and F.-P. Montforts, *Helv. Chim. Acta*, 1998, **81**, 1978.

10 In fact, an isomer mixture consisting of **2** and 4-phenylsulfonyl-2-sulfolene was obtained; however, in the subsequent reactions this mixture behaved like pure compound **2**.

11 T.-S. Chou and S.-C. Hung, *J. Org. Chem.*, 1988, **53**, 3020; P. B. Hopkins and P. L. Fuchs, *J. Org. Chem.*, 1978, **43**, 1208.

12 Interestingly, the Diels–Alder reaction between sulfolene **1** and DMM leads almost quantitatively to the *trans*-isomer of **3**, while the reaction of **2** with DMM produces predominantly the *cis*-isomer of **4**. The latter can also be synthesized from the commercially available *cis*-tetrahydrophthalic anhydride. The *trans*-isomer, however, affords higher yields (up to 95%) in the following Barton–Zard condensation with *tert*-butyl isocyanoacetate.

13 B. H. Novak and T. D. Lash, *J. Org. Chem.*, 1998, **63**, 3998.

14 J. S. Lindsey, I. C. Schreiman, H. C. Hsu, P. C. Kearney and A. M. Marguerettaz, *J. Org. Chem.*, 1987, **52**, 827; J. S. Lindsey, K. A. Maccrum, J. S. Tyhonas and Y. Y. Chuang, *J. Org. Chem.*, 1994, **59**, 579.

15 Similar properties were previously observed for other types of non-planar-porphyrins: C. J. Medforth, M. D. Berber, K. M. Smith and J. A. Shelnutt, *Tetrahedron Lett.*, 1990, **31**, 3719.

16 This method was used previously for aromatization of tetrahydrobenzoporphyrins: T. D. Lash, *Energy & Fuels*, 1993, **7**, 166.

Nickel-catalysed acylstannylation of 1,2-dienes: synthesis and reactions of α-(acylmethyl)vinylstannanes

Eiji Shirakawa,*[a] Yoshiaki Nakao[b] and Tamejiro Hiyama*[b]

[a] *Graduate School of Materials Science, Japan Advanced Institute of Science and Technology, Asahidai, Tatsunokuchi, Ishikawa, 923-1292, Japan*

[b] *Department of Material Chemistry, Graduate School of Engineering, Kyoto University, Sakyo-ku, Kyoto, 606-8501, Japan*

Received (in Cambridge, UK) 10th October 2000, Accepted 26th October 2000
First published as an Advance Article on the web 23rd January 2001

Bis(cycloocta-1,5-diene)nickel was found to be an effective catalyst for the acylstannylation of 1,2-dienes to give a wide variety of α-(acylmethyl)vinylstannanes, which were transformed to variously substituted conjugated and unconjugated enones by carbon–carbon bond forming reactions.

Alkenylstannanes are one of the most versatile synthetic reagents, since they can be transformed to various olefinic compounds through the reaction with organic electrophiles, *e.g.* the palladium-catalysed cross-coupling reaction.[1] Although the reaction of other alkenylmetals with stannyl halides provides an easy access to alkenylstannanes, this synthetic method cannot be applied to those having such a reactive substituent as carbonyl. Carbostannylation of alkynes has grown to be a powerful alternative route to alkenylstannanes, especially multi-substituted vinylstannanes (Scheme 1, a).[2] Herein we disclose that acylstannanes add to 1,2-dienes in the presence of a nickel catalyst[3] to give α-(acylmethyl)vinylstannanes[4] as main products (Scheme 1, b) and the resulting alkenylstannanes can be transformed to variously conjugated and/or unconjugated enones. To the best of our knowledge, this is the first demonstration of the transition metal-catalysed addition of a carbon–metal bond of organometallic compounds to 1,2-dienes.[5,6]

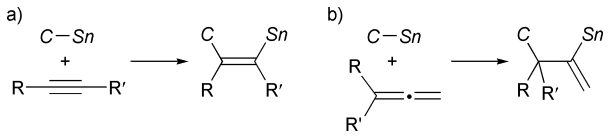

Scheme 1

Acylstannylation of monosubstituted allenes were carried out in the presence of a nickel catalyst (Scheme 2 and Table 1). The following procedure is representative (entry 1). A mixture of trimethyl(benzoyl)tin (**1a**) and 5 mol% of $Ni(cod)_2$ in toluene was heated at 50 °C for 1.5 h under an atmosphere of propa-1,2-diene (**2a**) to give 1-phenyl-3-trimethylstannylbut-3-en-1-one (**3a**) in 64% yield.[7] Analysis of the reaction mixture by ^{119}Sn NMR revealed that the ratio of **3a** and (*E*)-1-phenyl-3-trimethylstannylbut-2-en-1-one, derived probably through the isomerization of **3a**, was 97:3, although trimethyl(phenyl)tin, the decarbonylated product of **1a**, was obtained in a small amount. Addition of **1a** to hepta-1,2-diene (**2b**) took place mainly at the internal C–C double bond to give **3b** in 79% yield (entry 2).[8] Similar regioselectivity was observed in the reaction of 4,4-dimethylpenta-1,2-diene (**2c**) (entry 3). Arylallenes also participated in the acylstannylation with the selectivity of **3** being lowered by an electron-withdrawing substituent on the aromatic ring (entries 4–6). The reaction of 1-methoxypropa-1,2-diene (**2g**) proceeded with the benzoyl group of **1a** adding mainly at the carbon having the methoxy group albeit in a low yield (entry 7). The tributylstannyl derivative (**1b**) of **1a** also gave the acylstannylated product (entry 8). Tributyl(propanoyl)tin (**1c**) also added to various 1,2-dienes (entries 9–12). Noteworthy is that **2g** reacted with **1c** better than with **1a** to afford acylstannylation product **3l** in a higher yield. Aminocarbonylstannane **1d** reacted with allene (**2a**) in a low yield (entry 13).

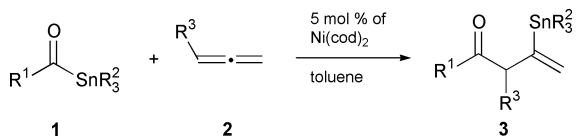

Scheme 2

Disubstituted allenes also participated in the acylstannylation (Scheme 3). Acylstannanes **1a** and **1c** added to 3-methylbuta-1,2-diene (**2h**) with high regioselectivities. In addition, nona-4,5-diene (**2i**) also underwent the reaction, giving a stereoisomeric mixture of **3p** or **3q**.

The catalytic cycle is considered to be initiated by the oxidative addition of an acylstannane to a nickel(0) complex as is the case with the nickel-catalysed acylstannylation of 1,3-dienes, since the decarbonylation of acylstannanes was similarly observed as a side reaction.[3] Although the succeeding pathway remains yet to be clarified, two plausible catalytic cycles leading to the main products are presented in Scheme 4. In any event, the stannyl group invariably attacks the allene central carbon. In Cycle A, coordination of the less hindered double bond of 1,2-diene **2** on the nickel atom of oxidative adduct **4** followed by insertion to the Ni–Sn bond (stannylnickelation) affords the acylstannylation product through π-allylnickel complex **6**. According to Cycle B, the more hindered double bond of **2** coordinates on the nickel and then inserts to

Table 1 Nickel-catalysed acylstannylation of 1,2-dienes[a]

Entry	Acylstannane R1	R2	1,2-Diene R3	Time/h	Yield of **3** (%)[b]	Prod **3**: others[c]	
1[d]	Ph	Me (**1a**)	H (**2a**)	1.5	64	**3a**	97:3
2	Ph	Me (**1a**)	Bu (**2b**)	1.5	79	**3b**	89:11
3	Ph	Me (**1a**)	*t*-Bu (**2c**)	1.5	59	**3c**	86:14
4	Ph	Me (**1a**)	4-$MeOC_6H_4$ (**2d**)	2	50	**3d**	78:22
5	Ph	Me (**1a**)	Ph (**2e**)	2	53	**3e**	77:23
6	Ph	Me (**1a**)	4-$CF_3C_6H_4$ (**2f**)	2	35	**3f**	66:34
7	Ph	Me (**1a**)	MeO (**2g**)	2	26	**3g**	93:7
8[d]	Ph	Bu (**1b**)	H (**2a**)	4	48	**3h**	79:21
9[d]	Et	Bu (**1c**)	H (**2a**)	1.5	67	**3i**	94:6
10[e]	Et	Bu (**1c**)	Bu (**2b**)	2	53	**3j**	89:11
11[e]	Et	Bu (**1c**)	Ph (**2e**)	3.5	43	**3k**	79:21
12[e]	Et	Bu (**1c**)	MeO (**2g**)	2.5	48	**3l**	95:5
13[d,f]	$(CH_2)_5N$	Me (**1d**)	H (**2a**)	2	25	**3m**	—[g]

[a] The reaction was carried out in toluene (0.4 mL) at 50 °C using an acylstannane (0.30 mmol), a 1,2-diene (0.90 mmol) and $Ni(cod)_2$ (15 μmol). [b] Isolated yield based on the organostannane. [c] Determined by ^{119}Sn NMR. [d] The reaction was carried out under an allene atmosphere (1 atm). [e] The reaction was carried out at 80 °C. [f] The reaction was carried out at 100 °C in the presence of 60 μmol of $Ni(cod)_2$. [g] Accompanied by a complex mixture of the products other than **3m**.

DOI: 10.1039/b008190f

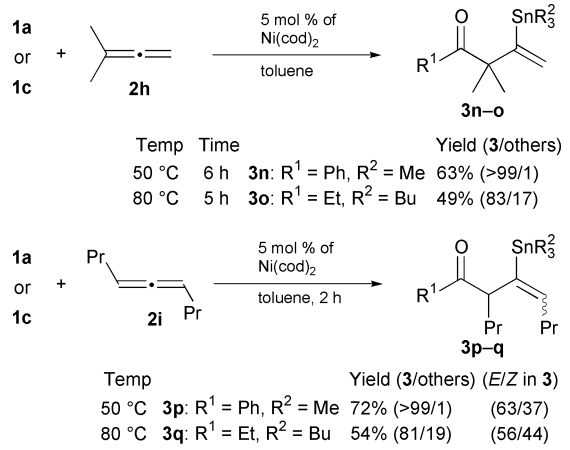

Scheme 3

the C–Ni bond of **4** (acylnickelation), giving the product *via* alkenylnickel **7**.[9] The results that the acylstannylation of nona-4,5-diene (**2i**) gave a mixture of stereoisomers should give us a clue to discriminate the reaction mechanism. In the case that the reaction with **2i** follows Cycle B, only (*E*)-**3p** or **3q** should be provided through *syn*-addition of the C–Ni bond to the C–C double bond and stereo-retained reductive elimination. As this was not the case, Cycle A appears to be more plausible, although it is unclear yet why reductive elimination from **6** takes place mainly at the more hindered carbon of the allyl moiety.

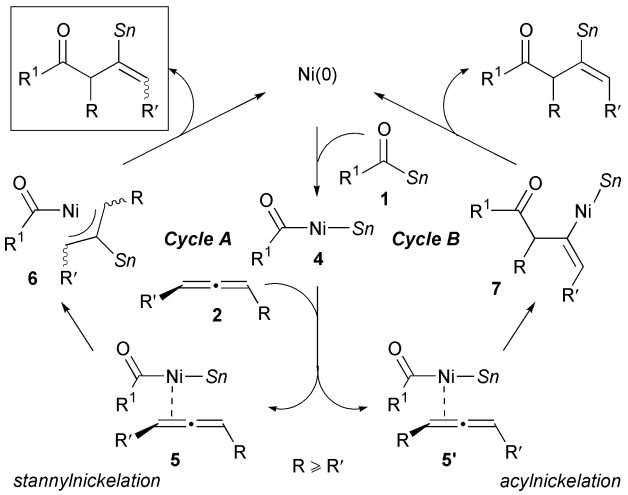

Scheme 4

The applicability of the acylstannylation products was demonstrated by the transformation of **3i** to a wide variety of enones (Scheme 5). The reaction of **3i** with ethyl 4-iodobenzoate (**8**) in the presence of 2.5 mol% of $Pd_2(dba)_3$ gave the corresponding coupling product **9** in 91% yield[10] without cine-substitution.[1b] Conjugated β-arylenone **11** was obtained[11] by cross-coupling reaction with **8** after isomerization of **3i** to **10** by 20 mol% of sodium hydride, whereas the corresponding (*E*)-isomer **12** was obtained by base-catalysed isomerization of **9**. The cross-coupling of **3i** with benzoyl chloride proceeded to give 83% yield of enedione **13**. Stannylenone **3i** reacted with iodomethane in the presence of sodium hydride, giving dimethylation product **14**, which was subjected to the cross-coupling reaction with **8** to afford arylenone **15**. Thus, variously substituted conjugated and unconjugated enones were synthesized from a single acylstannylation product.

In conclusion, we have demonstrated that the acylstannylation of 1,2-dienes readily takes place to give α-(acylmethyl)-vinylstannanes, which were transformed to a wide variety of conjugated and unconjugated enones. Studies on details of the mechanism as well as synthetic applications to various

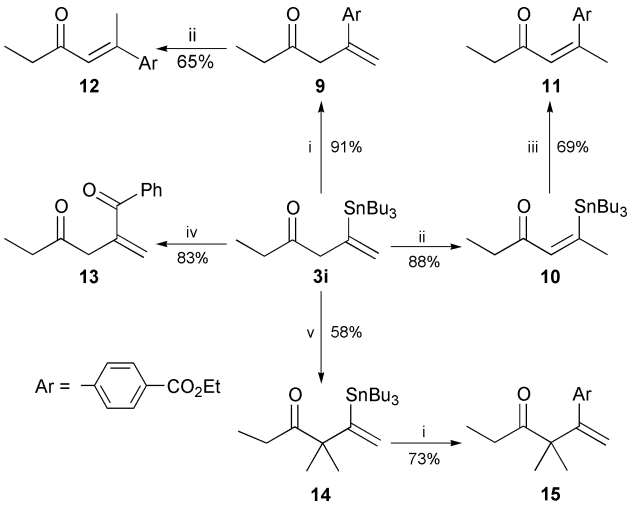

Scheme 5 *Reagents and conditions*: i, 4-EtOCO–C_6H_4–I (**8**, 1.0 equiv), 2.5 mol% of $Pd_2(db\ a)_3$, NMP, 30 °C, 15 h (from **3i** to **9**) or 10 h (from **14** to **15**); ii, NaH (0.2 equiv.), THF, rt, 4 h (from **3i** to **10**) or 3 h (from **9** to **12**); iii, **8** (1.0 equiv.), 5 mol% of $Pd_2(dba)_3$, NMP, 30 °C, 69 h; iv, PhCOCl (1.0 equiv.), 2.5 mol% of $Pd_2(dba)_3$, NMP, 30 °C, 8 h; v, Me–I (3.0 equiv.) THF, rt, 17 h.

unsaturated substrates and organostannanes are in progress in our laboratories.

We thank the Ministry of Education, Science, Sports and Culture, Japan, for the Grant-in-Aids for COE Research on Elements Science, No. 12CE2005 and Scientific Research, No.12750758. E. S. thanks the Asahi Glass Foundation for financial support.

Notes and references

1 (*a*) A. G. Davies, *Organotin Chemistry*, VCH, Weinheim, 1997; (*b*) V. Farina, V. Krishnamurthy and W. J. Scott, *Org. React.*, 1997, **50**, 1.
2 Lewis acid-catalysed reaction: (*a*) N. Asao, Y. Matsukawa and Y. Yamamoto, *Chem. Commun.*, 1996, 1513; (*b*) Y. Matsukawa, N. Asao, H. Kitahara and Y. Yamamoto, *Tetrahedron*, 1999, **55**, 3779; with a radical initiator: (*c*) K. Miura, D. Itoh, T. Hondo, H. Saito, H. Ito and A. Hosomi, *Tetrahedron Lett.*, 1996, **37**, 8539; transition metal-catalysed reaction: (*d*) E. Shirakawa, H. Yoshida, T. Kurahashi, Y. Nakao and T. Hiyama, *J. Am. Chem. Soc.*, 1998, **120**, 2975; (*e*) E. Shirakawa, H. Yoshida, Y. Nakao and T. Hiyama, *J. Am. Chem. Soc.*, 1999, **121**, 4290; (*f*) E. Shirakawa, K. Yamasaki, H. Yoshida and T. Hiyama, *J. Am. Chem. Soc.*, 1999, **121**, 10 221; (*g*) E. Shirakawa, H. Yoshida, Y. Nakao and T. Hiyama, *Org. Lett.*, 2000, **2**, 2209.
3 We reported the nickel-catalysed acylstannylation of 1,3-dienes: E. Shirakawa, Y. Nakao, H. Yoshida and T. Hiyama, *J. Am. Chem. Soc.*, 2000, **122**, 9030.
4 α-Substituted vinylstannanes are available by stannylcupration of alkynes followed by quenching the resulting C–Cu bond with methanol: J. A. Carbezas and A. C. Oehlschlager, *Synthesis*, 1994, 432.
5 There have been many reports on the transition metal-catalysed bismetalation of 1,2-dienes: for example, M. Suginome, Y. Ohmori and Y. Ito, *Synlett*, 1999, 1567 and references cited therein.
6 The palladium-catalysed three component coupling of 1,2-dienes, distannanes and organic iodides is reported to provide allylstannanes: F.-Y. Yang, M.-Y. Wu and C.-H. Cheng, *Tetrahedron Lett.*, 1999, **40**, 6055.
7 The reaction conditions are essentially identical with those used in the nickel-catalysed carbostannylation of alkynes, see ref. 2e.
8 The reaction mixture contains 2-methylene-1-phenyl-3-trimethylstannylheptan-1-one (5% yield) and (*E*)-1-phenyl-3-trimethylstannyloct-3-en-1-one (4% yield). Although we did not characterize the minor isomer(s) in the following entries thoroughly, peak(s) in ^{119}Sn NMR was always observed at −42.2 to 14.2 ppm, being attributed to an alkenyl- or allyl(trialkyl)stannane.
9 Platinum-catalysed diboration of monosubstituted allenes, which is considered to proceed *via* an alkenylplatinum complex similar to **7**, gave the (*Z*)-isomer stereoselectively. T. Ishiyama, T. Kitano and N. Miyaura, *Tetrahedron Lett.*, 1998, **39**, 2357.
10 Conjugated arylenone **12** was also generated in 5% yield.
11 The reaction mixture contains **12** (8% yield).

Silylcupration of styrenes followed by electrophilic trapping reaction

Vilnis Liepins and Jan-E. Bäckvall*

Department of Organic Chemistry, Arrhenius Laboratory, Stockholm University, SE-10691 Stockholm, Sweden. E-mail: jeb@organ.su.se

Received (in Cambridge, UK) 14th November 2000, Accepted 22nd December 2000
First published as an Advance Article on the web 23rd January 2001

Silylcupration reaction of styrene and its analogues with a silylcopper reagent $PhMe_2SiCuCNLi$ followed by an electrophilic trapping has been reported for the first time.

Silylcupration reaction of acetylenes and allenes has been studied by Fleming and co-workers.[1,2] Scarce literature data, however, is available on metallo-metallations of double bonds. Silylmanganation[3] and catalytic silicon–silicon bond addition to double bonds[4] and 1,3-dienes[5] involving silylpalladation have been reported. However, to the best of our knowledge, there are no reports in the literature on silylcupration of double bonds except for allenes.[2,6,7] Most of the silylcupration reactions have been done with the silylcuprate reagent $(PhMe_2Si)_2CuLi{\cdot}LiCN$ or more bulky silylcuprate reagents.[8] Recently, silylcopper reagent $PhMe_2SiCuCNLi$ has been used by Pulido[6] and us[7] in allene silylcupration reactions. The advantage of the silylcopper reagent $PhMe_2SiCuCNLi$ over the disilyl cuprate reagent is that it makes use of all the silyl on copper. With the latter reagent only one of the two groups is transferred and the remaining silylcopper reagent may lead to side products and hence separation problems.

Here we wish to report for the first time a silylcupration reaction of substituted and unsubstituted styrene. The copper intermediate obtained can be easily trapped by different electrophiles, including allylic phosphates, which are reactive and readily accessible allylic substrates for metal-catalysed reactions[7,9] (Scheme 1).

Reaction of styrene with silylcopper reagent $PhMe_2SiCuCNLi$ proceeds smoothly at −30 °C to give an organocopper intermediate, which was trapped by allyl diphenyl phosphate to give compound **1** in 73% yield (Table 1, entry 1).† The corresponding silylcupration of substituted styrenes and subsequent quenching by different allylic phosphates afforded adducts **2**–**8** in yields varying between 44–63% (entries 2–8). When hexenyl phosphate **13** was employed a mixture of α- and γ-regioisomers was obtained in a ratio of 35 : 65 (entry 5). In one case the intermediate silylcupration adduct was trapped by acetyl chloride to give **9** (entry 9).

The silylcupration of styrene was much slower than that of acetylenes[1] and allenes.[2,7] Thus, while the silylcupration of the latter two classes of compounds proceeds within 1 h at −40 °C, the silylcupration of styrenes had to be run at −30 °C for 3 h (for one substrate for 16 h, Table 1, entry 4).

Silylcuprate reagent $(PhMe_2Si)_2CuLi{\cdot}LiCN$[10] was also tried in the silylcupration reaction of styrene. Unfortunately, the desired product could not be isolated upon treatment with an electrophile since the cuprate reagent promoted polymerisation of the starting material, which resulted in a complex reaction mixture.

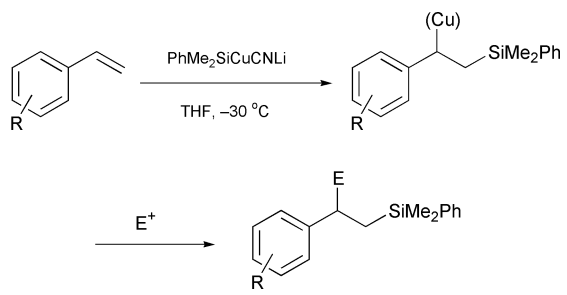

Scheme 1

Several styrenes substituted at the double bond such as α-methylstyrene, (*E*)-β-methylstyrene, indene, and (*E*)-stilbene were tried in this reaction but none of them was reactive enough to give any reaction product. In each case the starting material was recovered after the reaction. We believe that this is due to steric hindrance between the bulky phenyldimethylsilyl group and the substituent on the double bond.

In order to gain some insight into the reaction mechanism we studied the stereochemistry of the addition by the use of a specifically deuterated styrene. Reaction of (*E*)-β-deuteriostyrene[11] **10** with $PhMe_2SiCuCNLi$ followed by allyl diphenyl phosphate gave a 1 : 1 mixture of the two diastereomers **11a** and **11b**, which shows that the addition is non-stereospecific (Scheme 2). (Characteristic NMR data for non-deuterated product **1** (for notations see entry 1, Table 1): δ H_A = 1.26, H_B = 1.16, H_C = 2.73; J_{AB} = 14.8 Hz, J_{AC} = 5.0 Hz, J_{BC} = 10.0 Hz). Trapping of the intermediate copper-species resulting from the silylcupration of deuterated styrene **10** with acetyl chloride as electrophile also resulted in a 1 : 1 mixture of diastereomeric products. This indicates that the addition step of $PhMe_2SiCuCNLi$ to styrene is completely non-stereospecific.

A likely mechanism involves nucleophilic attack by the silylcopper at the terminal carbon of the styrene double bond in analogy with a conjugate addition. This may involve a copper(III)-intermediate[12] and leads to formation of a carbanion in the benzylic position. The latter carbanion would finally form a copper–carbon bond, which now can be formed with either configuration at carbon. A radical intermediate, which would also explain the 1 : 1 diastereomeric ratio of products from **10**, is less likely since in a control experiment in the presence of a radical inhibitor (1 mol% of 4-tBu-catechol) neither the rate nor the stereochemical outcome was changed.

The anionic mechanism is also supported by the fact that styrenes with electron-attracting groups react faster than those with electron-donating groups. This can be seen by the change of colour of the reaction mixture to deep violet, which in the case of 4-fluorostyrene appears almost immediately after the addition of 4-fluorostyrene but for styrene itself it takes longer to form the characteristic colour. Note that for 4-Me-styrene the reaction time had to be extended to 16 h in order to get the desired reaction product (Table 1, entry 4).

In conclusion, the silylcupration of styrenes followed by electrophilic trapping is reported for the first time. The reaction provides an extension to the widely studied silylcupration reaction of other unsaturated compounds. Mechanistic studies suggest that the reaction proceeds through anionic intermediates.

Financial support from the Swedish Natural Science Research Council and The Swedish Foundation for Strategic Research is gratefully acknowledged.

Notes and references

† *A typical procedure is as follows (Table 1, entry 6)*: 0.7 mmol of phenyldimethylsilyllithium[10] (~1 M solution in THF) was added to a

Table 1 Tandem silylcupration–electrophilic trapping reaction

12 =  **13** = 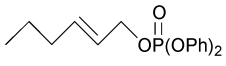

14 = 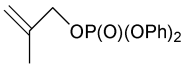 **15** = 

Entry	R on Styrene	Electrophile	Product	Yield, %[a]
1	—	**12**	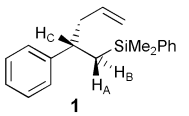 **1**	73%[b]
2	4-F-	**12**	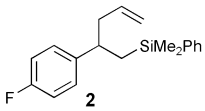 **2**	51%
3	4-Cl-	**12**	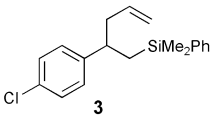 **3**	54%
4	4-Me-	**12**	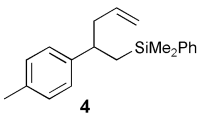 **4**	44%[c]
5	4-F-	**13**	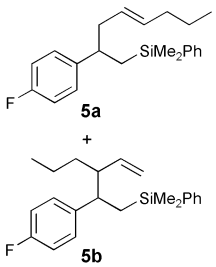 **5a** + **5b**	63% α+γ (35:65)
6	—	**14**	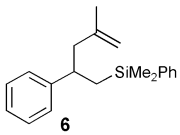 **6**	55%
7	4-F-	**14**	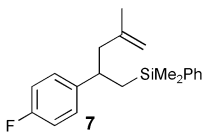 **7**	59%
8	4-Cl-	**14**	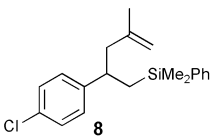 **8**	46%
9	—	**15**	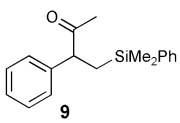 **9**	49%

[a] Isolated yields. [b] 3 equiv. of styrene were used. [c] 16 h reaction time.

stirred suspension of CuCN (1 equiv.) in dry THF (0.5 ml) at 0 °C and stirred at this temperature for 30 min. The mixture was cooled down to −30 °C (cryostat), styrene (2 equiv.) was added dropwise, and the resulting reaction mixture was stirred for 3 h at this temperature. Then allylic phosphate **14** (1.3 equiv.) in 0.7 ml THF was added slowly over 15 min. After the reaction mixture had been stirred for 1 h at −30 °C and for 30 min. at 0 °C, 4 ml of saturated aqueous NH_4Cl was added and the aqueous phase

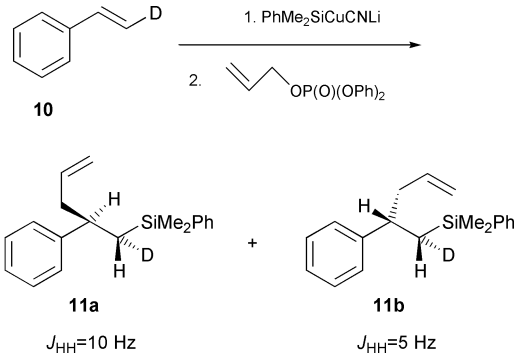

Scheme 2

was extracted with hexane (5 × 3 ml). Column chromatography on silica with pentane as eluent afforded compound **6** as a colourless oil in 55% yield. R_f = 0.29 (hexane). ^{1}H NMR ($CDCl_3$ 300 MHz): δ 7.50–7.14 (m, 10H), 4.72 (m, 1H), 4.61 (m, 1H), 2.89 (dtd, J = 10.3, 7.5, 4.6 Hz, 1H), 2.34 (d, J = 7.5 Hz, 2H), 1.62 (t, J = 1.1 Hz, 3H), 1.31 (dd, J = 14.8, 4.6 Hz, 1H), 1.15 (dd, J = 14.8, 10.3 Hz, 1H), 0.12 (s, 3H), 0.04 (s, 3H). ^{13}C NMR ($CDCl_3$ 75.4 MHz): δ 146.9, 143.9, 139.5, 133.6, 128.8, 128.2, 127.7, 127.6, 126.1, 112.4, 49.7, 40.3, 23.4, 22.4, −1.8, −2.8.

1 (*a*) I. Fleming and F. Roessler, *J. Chem. Soc., Chem. Commun.*, 1980, 276; (*b*) I. Fleming, T. W. Newton and F. Roessler, *J. Chem. Soc., Perkin Trans. 1*, 1981, 2527; (*c*) I. Fleming and E. Martinez de Marigorta, *J. Chem. Soc., Perkin Trans. 1*, 1999, 889.

2 (*a*) I. Fleming and F. J. Pulido, *J. Chem. Soc., Chem. Commun.*, 1986, 1010; (*b*) P. Cuadrado, A. M. Gonzalez, F. J. Pulido and I. Fleming, *Tetrahedron Lett.*, 1988, **29**, 1825; (*c*) P. Cuadrado, A. M. Gonzalez, F. J. Pulido, I. Fleming and M. Rowley, *Tetrahedron*, 1989, **45**, 413; (*d*) A. Barbero, P. Cuadrado, A. M. Gonzalez, F. Pulido and I. Fleming, *J. Chem. Soc., Perkin Trans. 1*, 1991, 2811; (*e*) I. Fleming, Y. Landais and P. R. Raithby, *J. Chem. Soc. Perkin Trans. 1*, 1991, 715.

3 (*a*) K. Fugami, S. Nakatsukasa, K. Oshima, K. Utimoto and H. Nozaki, *Chem. Lett.*, 1986, **6**, 869; (*b*) K. Fugami, K. Oshima, K. Utimoto and H. Nozaki, *Tetrahedron Lett.*, 1986, **27**, 2161; (*c*) K. Fugami, J. Hibino, S. Nakatsukasa, S. Matsubara, K. Oshima, K. Utimoto and H. Nozaki, *Tetrahedron*, 1988, **44**, 4277.

4 T. Hayashi, T. Kobayashi, A. M. Kawamoto, H. Yamashita and M. Tanaka, *Organometallics*, 1990, **9**, 280.

5 (*a*) K. Tamao, S. Okazaki and M. Kumada, *J. Organomet. Chem.*, 1978, **146**, 87; (*b*) H. Matsumoto, K. Shono, A. Wada, I. Matsubara, H. Watanabe and Y. Nagai, *J. Organomet. Chem.*, 1980, **199**, 185; (*c*) H. Sakurai, Y. Eriyama, Y. Kamiyama and Y. Nakadaira, *J. Organomet. Chem.*, 1984, **264**, 229; (*d*) C. W. Carlson and R. West, *Organometallics*, 1983, **2**, 1801.

6 (*a*) F. J. Blanco, P. Cuadrado, A. M. Gonzalez, F. J. Pulido and I. Fleming, *Tetrahedron Lett.*, 1994, **35**, 8881; (*b*) A. Barbero, C. Garcia and F. J. Pulido, *Tetrahedron Lett.*, 1999, **40**, 6649; (*c*) A. Barbero, C. Garcia and F. J. Pulido, *Tetrahedron*, 2000, **56**, 2739.

7 V. Liepins, A. S. E. Karlström and J. E. Bäckvall, *Org. Lett.*, 2000, **2**, 1237.

8 A. Barbero, P. Cuadrado, A. M. Gonzalez, F. J. Pulido and I. Fleming, *J. Chem. Soc., Perkin Trans. 1*, 1991, 2811.

9 Allylic phosphates have previously been used as electrophiles in a copper-catalysed cross coupling reaction with Grignard reagents: (*a*) A. Yanagisawa, Y. Noritake, N. Nomura and H. Yamamoto, *Synlett*, 1991, 251; (*b*) A. Yanagisawa, N. Nomura and H. Yamamoto, *Synlett*, 1993, 689; (*c*) A. Yanagisawa, N. Nomura and H. Yamamoto, *Tetrahedron*, 1994, **50**, 6017.

10 (*a*) I. Fleming, in *Organocopper reagents. A practical approach*, ed. R. J. K. Taylor, Oxford University Press, New York, 1994, 12, 257; (*b*) I. Fleming, R. S. Roberts and S. C. Smith, *J. Chem. Soc., Perkin Trans. 1*, 1998, 1209.

11 (*a*) J. C. Colberg, A. Rane, J. Vaquer and J. A. Soderquist, *J. Am. Chem. Soc.*, 1993, **115**, 6065; (*b*) J. E. Bäckvall, *Tetrahedron Lett.*, 1978, **2**, 163.

12 (*a*) S. Woodward, *Chem. Soc. Rev.*, 2000, **29**, 393; (*b*) C. L. Kingsbury and R. A. J. Smith, *J. Org. Chem.*, 1997, **62**, 4629; (*c*) M. Uerdingen and N. Krause, *Tetrahedron*, 2000, **56**, 2799; (*d*) A. E. Dorigo, J. Wanner and P. von R. Schleyer, *Angew. Chem., Int. Ed. Engl.*, 1995, **34**, 476; (*e*) E. Nakamura and M. Yamanaka, *J. Am. Chem. Soc.*, 1999, **121**, 8941; (*f*) E. Nakamura and S. Mori, *J. Am. Chem. Soc.*, 1998, **120**, 8273; (*g*) E. Nakamura, M. Yamanaka and S. Mori, *J. Am. Chem. Soc.*, 2000, **122**, 1826.

ChemComm

Structural studies of a non-covalently linked porphyrin–fullerene dyad

Francis D'Souza,*[a] Nigam P. Rath,[b] Gollapalli R. Deviprasad[a] and Melvin E. Zandler[a]

[a] *Department of Chemistry, Wichita State University, 1845 Fairmount, Wichita, KS 67260-0051, USA. E-mail: dsouza@wsuhub.uc.twsu.edu*

[b] *Department of Chemistry, University of Missouri, 8001 Natural Bridge Road, St. Louis, MO 63121, USA*

Received (in Corvallis, OR, USA) 27th November 2000, Accepted 18th December 2000
First published as an Advance Article on the web 23rd January 2001

X-ray structural and *ab initio* theoretical investigations of a non-covalently linked *meso*-tetraphenylporphyrinatozinc(II) and *N*-methyl-2-pyrid-4′-yl)-3,4-fullero-pyrrolidine complex is reported

Studies on non-covalently linked donor–acceptor dyads are of current interest because of their potential applications in constructing photovoltaic devices and also, to mimic the primary events of photosynthetic reaction centers.[1] Fullerenes as the electron acceptor in these dyads are particularly appealing because of their unique three-dimensional structure, excellent electron acceptor property, and a small re-organization energy involved in electron transfer reactions.[2] However, studies on non-covalently linked donor–fullerene dyads are limited[3] especially with respect to their crystal structures where no information is yet available even though a number of molecules including calixarenes, cyclodextrins, cyclotriveratrylene and porphyrins are known to form intermolecular complexes with fullerenes.[4] Fullerenes are also well-known to co-crystallize with a variety of molecules which include benzene, ferrocene, Pd_6, Cl_{12}, P_4 and S_8 moieties.[5]

Recently, the formation of stable, non-covalently linked dyads by axial coordination of functionalized C_{60} bearing a pyridine unit to zinc tetrapyrrole macrocycles have been reported.[3] In one such studied dyad, the kinetic analysis of the fullerene π-radical anion transient absorption resulting from irradiation of the ZnTPP-C_{60} dyad yielded a remarkable lifetime of several hundred microseconds with a quantum yield of about 0.14 for the separated radical pair.[3c] This enhanced lifetime of the radical pair was attributed to the diffusional splitting of the initial charge separated radical pair. Since the structural and thermodynamic factors play a crucial role in controlling the charge separation and charge recombination process, we, in the present study have performed X-ray structural analysis and *ab initio* calculations at B3LYP/3-21G(*) level on a non-covalently linked zinc porphyrin–fullerene dyad.

Slow evaporation of a solution mixture of CS_2, CH_2Cl_2 and *n*-heptane containing *meso*-tetraphenylporphyrinatozinc and *N*-methyl-2-(pyrid-4′-yl)-3-4-fulleropyrrolidine of 1 : 1 molar ratio yielded dark purple crystals that subsequently were handled in air. In agreement with the earlier reported solution structure,[3] the X-ray structural analysis of the crystals revealed a 1 : 1 stoichiometry.† Fig. 1 shows the structure of the porphyrin–fullerene complex while the packing diagram is shown in Fig. 2.

In the solid state structure, the zinc to axially coordinated pyridyl nitrogen distance is found to be 2.158(5) Å which compares with a 2.075(5) Å average distance of the porphyrin ring Zn–N bonds and a Zn–N distance of 2.147 Å reported earlier for an intramolecularly linked zinc porphyrin–pyridine adduct.[6] The edge-to-edge distance, that is, the closest distance between the porphyrin π-ring carbon (β-pyrrole) and the C_{60} carbon of the axially linked fulleropyrrolidine, is found to be 3.51 Å while the center-to-center distance between the porphyrin zinc ion and fullerene is ~9.53 Å. The distance between the closely located *meso*-phenyl ring (*meta* carbon) of the porphyrin macrocycle and the C_{60} spheroid is found to be 3.186 Å. In agreement with recent theoretical predictions,[7] the

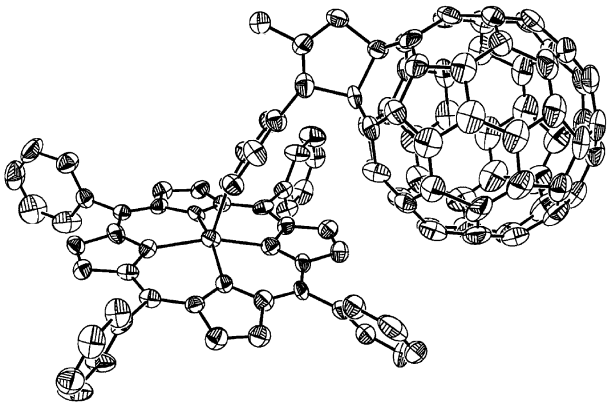

Fig. 1 Projection diagram of the axially coordinated *meso*-tetraphenylporphyrinato-zinc(II) and *N*-methyl-2-(pyrid-4′-yl)-3,4-fulleropyrrolidine complex with 50% thermal ellipsoids. The co-crystallized solvent, *n*-heptane and hydrogen atoms are not shown for clarity.

N-methylpyrrolidine ring on the fullerene spheroid revealed a *syn–trans* conformation. The 6,6 ring carbon atoms of the fullerene to which the pyrrolidine ring is attached is 0.33 Å away from the normal C_{60} spheroid. The porphyrin ring is also slightly ruffled (umbrella mode) with nearly 0.35 Å out-of-plane (defined by the four porphyrin ring nitrogens) displacement of the central zinc because of axial coordination.

Additional inter-complex type interactions between the zinc porphyrin and the C_{60} unit that is not directly coordinated to the zinc but located on the other side of the porphyrin macrocycle have been observed in the crystal packing (Fig. 2). That is, the

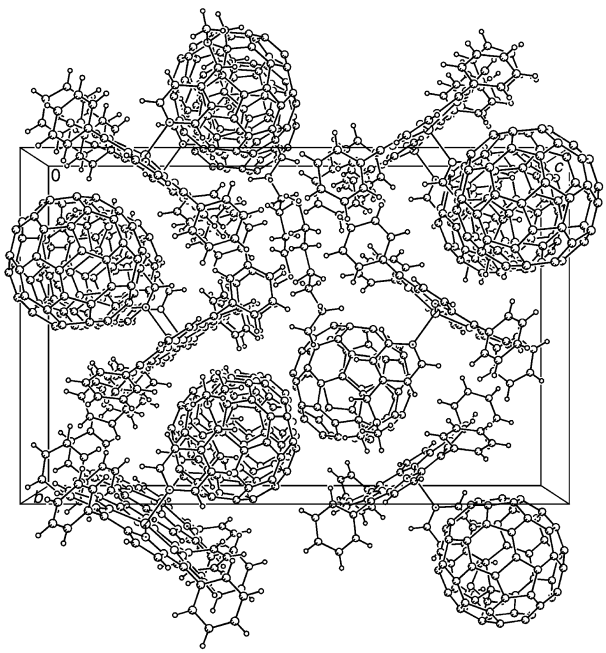

Fig. 2 Packing diagram of the investigated zinc porphyrin–C_{60} complex.

DOI: 10.1039/b009528c

calculated inter-complex distances between the porphyrin ring atoms and C_{60} carbon are close to the calculated van der Waals distances. The central zinc to the closest C_{60} carbon is located at 3.228 Å while this distance between the porphyrin ring nitrogen to C_{60} carbon is 3.114 Å. The nearest porphyrin ring carbon (α-pyrrole) to the C_{60} spheroid carbon is 3.360 Å. These results indicate the existence of significant amounts inter-complex interactions in addition to the strong axial coordinate interactions in the investigated self-assembled supramolecular complex.

In order to further our understanding on the structure of this non-covalently linked dyad, *ab initio* calculations at B3LYP/3-21G(*) level by using Gaussian 98[8] have been performed. For this, first, both the starting compounds, tetraphenylporphyrinatozinc and *N*-methyl-2-(pyrid-4′-yl)-3,4-fulleropyrrolidine were fully optimized to a stationary point on the Born–Openheimer potential energy surface and allowed to interact. The geometric parameters of the dyad were obtained after complete energy minimization. In the calculated structure, the Zn–N distance of the axial coordination bond is found to be ~2.03 Å which is close to the average distance of the four Zn–N bonds (2.10 Å) of the porphyrin and that obtained in the crystal structure (2.074 Å). The center-to-center distance, that is, the distance between the central zinc and the center of the C_{60} spheroid, is found to be ~9.63 Å. The edge-to-edge distance, that is, the distance between the closest *meso*-carbon of the porphyrin ring and the C_{60} carbon, is ~5.17 Å while this distance between the closest β-pyrrole carbon and C_{60} spheroid carbon is ~4.69 Å. Generally, the tilting of the C_{60} unit towards the porphyrin ring is more in the crystal structure than that in the calculated structure, which may be a result of crystal packing. The calculated bond dissociation energy of the axial coordinate bond, that is, the energy difference between the dyad and the sum of the energies of individual zinc porphyrin and fulleropyrrolidine units, is found to be 28.21 kcal mol^{-1} and this compares well with a value of 26.91 kcal mol^{-1} obtained experimentally in 1,2-dichlorobenzene.[3d]

In summary, this paper presents the first X-ray structure of a non-covalently linked porphyrin–fullerene donor–acceptor dyad. The structure agrees well with the theoretically calculated one and the earlier reported spectroscopic studies. Further studies along this line are in progress.

The authors thank Drs David M. Eichhorn and Doug Powell for helpful discussions. The authors are also thankful to the donors of the Petroleum Research Fund, administered by the American Chemical Society (to FD) and to the Dreyfus Foundation (to MEZ), for support of this work.

Notes and references

† *Crystal data for zinc porphyrin–C_{60} complex*: Empirical formula, $C_{119}H_{54}N_6Zn$, M = 1633.05, $P2_12_12_1$, a = 13.2914(5), b = 19.1411(7), c = 29.532(1) Å, V = 7513.2(5) Å^3, Z = 4, μ = 0.393 mm^{-1}, T = 218(2) K. The final residual values were R(F) = 9.2% for 7953 observed reflections [$I > 2\sigma(I)$] and $wR(F^2)$ = 15.4%; s = 0.98 for all data. CCDC 155575. See http://www.rsc.org/suppdata/cc/b0/b009528c/ for crystallographic files in .cif format.

1 *Molecular Electronic Devices*, eds. F. L. Carter, R. E. Siatowski and H. Woltjen, North Holland, Amsterdam, 1999; V. Balzani and F. Scandola, in *Comprehensive Supramolecular Chemistry*, Vol. 10, ed. D. N. Reinhoudt, Pergamon–Elsevier, Oxford, 1996, pp. 687–746; M. D. Ward, *Chem. Soc. Rev.*, 1997, **26**, 365.

2 D. M. Guldi, *Chem. Commun.*, 2000, 321.

3 (*a*) F. D'Souza, G. R. Deviprasad, M. S. Rahman and J.-P. Choi, *Inorg. Chem.*, 1999, **38**, 2157; (*b*) N. Armaroli, F. Diederich, L. Echegoyen, T. Habicher, L. Flamigni, G. Marconi and J.-F. Nierengarten,. *New. J. Chem.*, 1999, 77; (*c*) T. Da Ros, M. Prato, D. Guldi, E. Alessio, M. Ruzzi and L. Pasimeni, *Chem. Commun.*, 1999, 635; (*d*) G. R. Deviprasad, M. E. Zandler and F. D'Souza, in *Fullerenes 2000: Electrochemistry and Photochemistry*, ed. S. Fukuzumi, F. D'Souza and D. M. Guldi, *Proc. Electrochem. Soc.*, 2000, **8**, 182.

4 J. L. Atwood, L J. Barbour, C. L. Raston and I. B. N. Sudria, *Angew. Chem., Int. Ed. Engl.*, 1998, **37**, 981; Z. Yoshida, H. Takekuma, S. Takekuma and Y. Matsubara, *Angew. Chem., Int. Ed. Engl.*, 1994, **33**, 1597; J. W. Steed, P. C. Junk, J. L. Atwood, M. J. Barnes, C. L. Raston and R. S. Burkhalter, *J. Am. Chem. Soc.*, 1994, **116**, 10 346; A. L. Balch, V. J. Catalasono, J. W. Lee and M. M. Olmstead, *J. Am. Chem. Soc.*, 1992, **114**, 5455; P. D. W. Boyd, M. C. Hodgson, C. E. F. Richard, A. G. Oliver, L. Chaker, P. J. Brothers, R. D. Bolskar, F. S. Tham and C. A. Reed, *J. Am. Chem. Soc.*, 1999, **121**, 10 487; M. M. Olmstead, D. A. Costa, K. Maitra, B. C Noll, S. L. Phillips, P. M. Van Calcar and A. L. Balch, *J. Am. Chem. Soc.*, 1999, **121**, 7090; D. Sun, F. S. Tham, C. A. Reed, L. Chaker, M. Burgess and P. D. W. Boyd, *J. Am. Chem. Soc.*, 2000, **122**, 10 704.

5 A. L. Balch, J. W. Lee, B. C. Noll and M. M. Osmstead, *J. Chem. Soc., Chem. Commun.*, 1993, 56; J. D. Cram, P. B. Hitchcock, H. W. Kroto, R. Taylor and D. M. R. Walton, *J. Chem. Soc., Chem. Commun.*, 1992, 1764; M. M. Olmstead, A. S. Ginwalla, B. C. Noll, D.S. Tinti and A. L. Balch, *J. Am. Chem. Soc.*, 1996, **118**, 7737; M. M. Olmstead, *Chem. Rev.*, 1998, **98**, 2123 and references cited therein.

6 M. A. Bobrik and F. A. Walker, *Inorg. Chem.*, 1980, **19**, 3383.

7 F. D'Souza, M. E. Zandler, G. R. Deviprasad and W. Kutner, *J. Phys. Chem. A*, 2000, **104**, 6887.

8 *Gaussian 98* (Revision A.7), M. J. Frisch, G. W. Trucks, H. B. Schlegel, G. E. Scuseria, M. A. Robb, J. R. Cheeseman, V. G. Zakrzewski, J. A. Montgomery, R. E. Stratmann, J. C. Burant, S. Dapprich, J. M. Millam, A. D. Daniels, K. N. Kudin, M. C. Strain, O. Farkas, J. Tomasi, V. Barone, M. Cossi, R. Cammi, B. Mennucci, C. Pomelli, C. Adamo, S. Clifford, J. Ochterski, G. A. Petersson, P. Y. Ayala, Q. Cui, K. Morokuma, D. K. Malick, A. D. Rabuck, K. Raghavachari, J. B. Foresman, J. Cioslowski, J. V. Ortiz, B. B. Stefanov, G. Liu, A. Liashenko, P. Piskorz, I. Komaromi, R. Gomperts, R. L. Martin, D. J. Fox, T. Keith, M. A. Al-Laham, C. Y. Peng, A. Nanayakkara, C. Gonzalez, M. Challacombe, P. M. W. Gill, B. G. Johnson, W. Chen, M. W. Wong, J. L. Andres, M. Head-Gordon, E. S. Replogle and J. A. Pople, *Gaussian, Inc., Pittsburgh PA*, 1998.

Autocatalytic ring opening of *N*-acylaziridines. Complete control over regioselectivity by orientation at interfaces

Peter J. J. A. Buijnsters,[ab] Martinus C. Feiters,[a] Roeland J. M. Nolte,[ac] Nico A. J. M. Sommerdijk*[ac] and Binne Zwanenburg[a]

[a] *Department of Organic Chemistry, NSR Centre, University of Nijmegen, Toernooiveld NL-6525 ED Nijmegen, The Netherlands. E-mail: N.Sommerdijk@tue.nl*
[b] *Department of Medicinal Chemistry, Janssen Research Foundation, Beerse, Belgium*
[c] *Laboratory of Macromolecular and Organic Chemistry, Eindhoven University of Technology, Eindhoven, The Netherlands*

Received (in Cambridge, UK) 20th November 2000, Accepted 20th December 2000
First published as an Advance Article on the web 23rd January 2001

Ring opening of 1-alkanoyl-2-phenoxymethylaziridines by phosphate ions yielding self-assembling phospholipid analogues proceeds in an autocatalytic fashion and with complete regioselectivity at an organic–aqueous interface.

Biological transformations are known to take place with high rates and high degrees of regio- and stereospecificities. This is achieved—amongst others—by positioning the reactants in a well defined manner with respect to each other, *e.g.* in the active site of an enzyme or at the surface of a biomembrane. Many model systems have been developed in order to mimic the supreme action of biomolecules.[1] This has led to important improvements in conversion rates of molecules and in increased regio- and stereospecificities of their reactions. Of special interest in this respect are the autocatalytic[2] and self-replicating[3] biomimetic systems that have been reported in the literature. In the present communication we describe a reaction, *i.e.* the synthesis of chiral amide containing surfactants, which proceeds in an autocatalytic manner and with complete regioselectivity by orienting the reactants at an organic–aqueous interface.

The self-assembly of amide-containing phospholipid analogues (*e.g.* **2** and **3**), has yielded a variety of interesting, and in many cases chiral, aggregate morphologies.[4] Thus far these compounds have been prepared from enantiopure *N*-acylaziridines (**1**) *via* a nucleophilic ring opening with dibenzyl phosphoric acid in organic solvent (Scheme 1). However, in all cases this procedure led to the formation of the two regioisomeric products, *i.e.* compounds **2** and **3**, in molar ratios ranging from 1:1 to 6:1.[5]† We hypothesised that in order to achieve a selective ring opening the *N*-acylaziridine molecules must be preorganised in such a way that only one of the ring carbon atoms is accessible to the nucleophilic species. It was anticipated that compound **1** would orient itself at an aqueous interface such that the C(1) carbon atom of the aziridine ring points towards the aqueous layer while the hydrophobic part of the molecule minimises its contact with water (Fig. 1a).

The ring opening of compound **1** was performed at 40 °C in a two phase system comprising an aqueous phosphate buffer (2.0 mM, pH = 7.0, 4.0 ml) and a top layer in which the starting material (9.0 μmol) is present as an oil. The progress of the reaction was conveniently monitored by determining the concentration of the aziridine in the aqueous phase using reversed phase HPLC.‡ The generated products were analysed by capillary electrophoresis using a borate buffer containing β-cyclodextrin.[6]§

As an example the conversion of **1a** (R = $C_{12}H_{25}$) to **2a** is given. In the first 9 h of the reaction neither compound **1a** nor any reaction products were detected in the aqueous phase, suggesting that at this stage the ring opening was slow since it could only take place at the oil–aqueous buffer interface. After this period vesicles with diameters of 75–350 nm were formed as was demonstrated by electron microscopy (Fig. 1b). Concomitant with the formation of the vesicles the concentration of **1a** in the aqueous phase increased, suggesting that these vesicles facilitated the transfer of the *N*-acylaziridine to the water layer. The concentration of **1a** in the buffer reached a maximum after 24 h (~25% of **1a** in the aqueous phase). Thereafter, it decreased, and the reaction was completed after approximately 80 h. Increasing the buffer concentration to 10.0 mM led to an enhancement of the reaction rate (complete

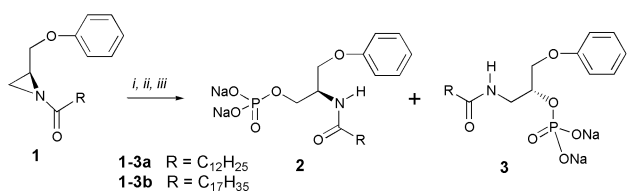

Scheme 1 *i*: $(C_6H_6CH_2O)_2P(O)OH$, CH_2Cl_2, *ii*, H_2, Pd/C, *iii*: Dowex, Na^+-form.

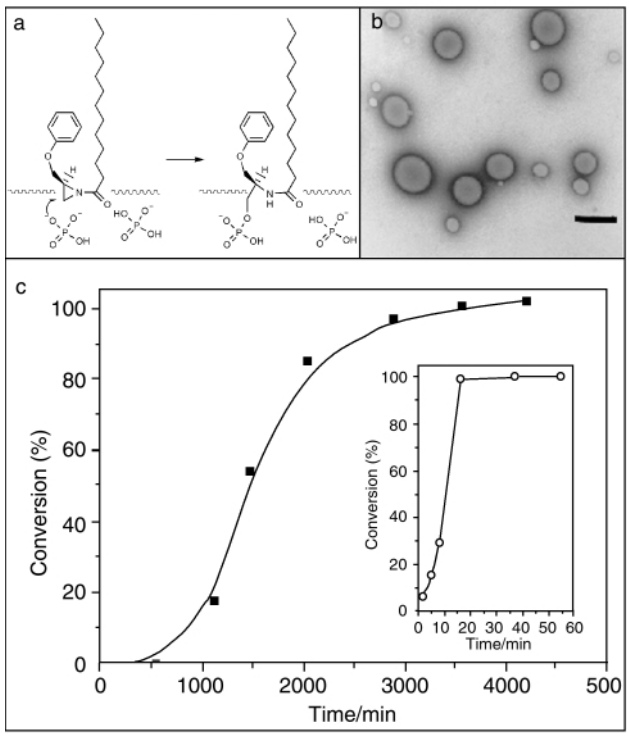

Fig. 1 (a) Proposed mechanism for the regioselective ring opening of **1**; (b) transmission electron micrograph of vesicles produced by ring opening of **1a** (negative staining, bar represents 350 nm); (c) the conversion **1a** in the absence of preformed vesicles of **2a**. Inset: *idem*, in the presence of preformed vesicles of **2a**.

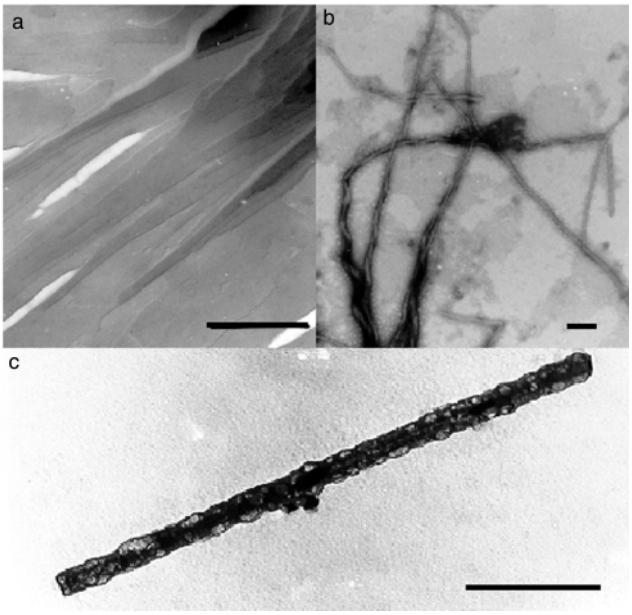

Fig. 2 Transmission electronmicrographs of aggregates of **2b**. (a) Ribbons in 2.0 mM phosphate buffer pH 7.0; (b) tubes in aqueous 9 mM $CaCl_2$ (pH 6.5); (c) rods mineralised in a solution containing 1 mM $FeSO_4$–KNO_2 adjusted to pH 11. Bars represent 250 nm.

conversion after 24 h) indicating that the phosphate anions are the kinetically significant species. Capillary electrophoresis in combination with ^{1}H NMR on authentic samples revealed that in both cases the reaction proceeded with complete regioselectivity (> 99%), leading to the formation of the primary phosphate **2a** exclusively. As outlined above this selectivity can be explained by attack of a phosphate ion on the C(1) ring carbon atom which is exposed to the aqueous phase due to orientation of the *N*-acylaziridine molecules at the interface. Activation of the aziridine ring most probably occurs through reversible protonation of the carbonyl group of **1a** by protonated phosphate groups, either from the buffer or from previously generated molecules of **2a**.

The sigmoidal conversion curve of **1a** (Fig. 1c) suggests that the ring opening reaction is catalysed by the vesicles that are formed. Indeed, when the reaction was carried out in the presence of preformed vesicles prepared from phospholipid **2a** (80 μmol in 4.0 ml 2.0 mM phosphate buffer, pH 7.0), the reaction was complete in 20 min (Fig. 1c). The high concentration of the *N*-acylaziridine detected in the aqueous phase (~95% after 2 min) supports the proposed dissolution of **1a** in the bilayers of the vesicles. When incorporated within these aggregates the hydrophobic alkyl chain will minimise the contact with water by dissolution in the hydrophobic interior of the membrane, leaving the amide carbonyl group of **1a** and consequently also the C(1) ring carbon atom oriented towards the aqueous phase (Fig. 1a).

Similar results are obtained when *N*-acylaziridine **1b** (R = $C_{17}H_{35}$) was used. Interestingly in this case, upon standing for approximately a week, the vesicles formed from compound **2b** slowly converted into flat multilayer ribbons (Fig. 2a). It was found that these ribbons rolled up to form tubuli under conditions that lead to compensation of the head group charge of the lipid, *e.g.* at low pH or in the presence of alkali and transition metal ions (*e.g.* Ca^{2+} and Fe^{2+} ions). Remarkably, the aggregate dimensions did not depend on the conditions used: tubuli of micrometer length and diameters between 20 and 40 nm were generated after lowering the pH to 2.5, after adding calcium ions at pH 5.6 (Fig. 2b) or after exposing the solution to ferric ions at pH 11 (Fig. 2c).[7]

In conclusion, we have shown that the ring opening of the long tail aziridines **1** by phosphate ions at an organic–aqueous interface exclusively leads to the formation of the primary phosphates **2**. The self-assembling properties of these compounds facilitate further conversion of the starting material without compromising the selectivity of the reaction and, ultimately, under the appropriate conditions lead to the formation of well-defined self-assembled objects. A detailed investigation of the autocatalytic nature of the system and possible applications are in progress.

The authors thank B. Martens for performing HPLC and Capillary Electrophoresis experiments.

Notes and references

† For synthetic procedures and for the physical data of **1**–**3b** see reference 5. **(−)-(2*S*)-1-Dodecanoyl(2-phenoxymethyl)aziridine, 1a**: mp 34.6 °C; $[\alpha]_D^{20}$ −45.5 (*c* 1.0, $CHCl_3$); Calc. for **1a** ($C_{21}H_{33}NO_2$) C 76.09, H 10.03, N 4.23. Found: C 75.95, H 9.96, N 4.25%; *m/z* (FAB MS: 495 $[M + Na]^+$, 332 $[C_{21}H_{34}NO_2]^+$; δ_H($CDCl_3$) 0.88 (t, *J* = 6.8 Hz, 3H, C*H*$_3$), 1.25 [m, 16H, CH_3(C*H*$_2$)$_8$], 1.65 [m, 2H, C*H*$_2$CH$_2$C(O)], 2.22 (d, *J* = 3.3 Hz, 1H, NCH*H*), 2.52–2.42 [m, 3H, NC*H*H and C*H*$_2$C(O)], 2.86 (m, 1H, NC*H*), 3.99 (dd, *J* = 6.1, 10.4 Hz, 1H, C*H*HOC$_6$H$_5$), 4.13 (dd, *J* = 10.4, 4.3 Hz, 1H, CH*H*OC$_6$H$_5$) 6.89–7.32 (m, 5H, C$_6$*H*$_5$). **(−)-Disodium (2*R*) -3-phenoxy-2-dodecanoylaminopropan-1-yl phosphate, 2a**: mp 125–128 °C; $[\alpha]_D^{20}$ −33.4 (*c* 1.1, $CHCl_3$); Calc. for **2a** ($C_{21}H_{34}NO_6PN_2$·$2H_2O$) 49.51, H 7.12, N 2.75. Found C 49.72, H 7.15, N 2.80%. **(+)-Disodium (2*R*)-3-phenoxy-1-dodecanoylaminopropan-2-yl phosphate, 3a**: mp 129–131 °C; $[\alpha]_D^{20}$ +15.4 (*c* 1.0, $CHCl_3$); FAB MS [*m/z*]: 495 $[M + Na]^+$, 474 M + 1]$^+$. Calc. for **3a** ($C_{21}H_{34}NO_6PNA_2$·$2.5H_2O$) C 46.85, H 7.58, N 2.70. Found C 46.67, H 7.60, N 2.73%. The enantiomeric purities of the starting aziridines used were > 95% as was determined from NMR analysis of (−)-camphanamide derivatives of both the enantiopure aziridine and the racemate. No loss of enantiomeric integrity during ring opening (either in organic solvents or at organic aqueous interfaces) was observed when comparing enantiomerically pure and racemic compounds.

‡ The concentration of **1** in the aqueous phase was determined using a RP18 reversed phase column, UV detection at 280 nm and a mobile phase of acetonitrile–phosphate buffer [(2 mM, pH = 7.0), 9:1 (v/v)]. Samples (25 μl) of the aqueous phase were diluted with acetonitrile (225 μl) before analysis.

§ The regioselectivity of the reaction was determined by capillary electrophoresis (30 kV, 10 °C, UV detection at 193 nm) using a buffer (Na_2B_4O–NaOH 50 mM, pH = 9.3) containing 26.7 mM β-cyclodextrin to avoid aggregate formation. Samples (25 μl) of the aqueous phase were diluted with sodium borate buffer (150 μl). From authentic samples the retention times of **2** and **3** were determined.

1 M. C. Feiters in *Comprehensive Supramolecular Chemistry*, ed. J. L. Atwood, J. E. D. Davies, D. D. Macnicol, F. Vögtle, series ed., J. M. Lehn, **Vol 10**, *Supramolecular Catalysis*, Pergamon, Elsevier Science Ltd., 1996.

2 (*a*) P. A. Bachmann and P. L. Luisi, *Nature*, 1992, **357**, 57; (*b*) P. Walde, R. Wick, M. Fresta, A. Mangone and P. L. Luisi, *J. Am. Chem. Soc.*, 1994, **116**, 11 649; (*c*) R. Wick, P. Walde and P. L. Luisi, *J. Am. Chem. Soc.*, 1995, **117**, 1435; (*d*) K. Morigaki, S. Dallavlle, P. Walde, S. Colonna and P. L. Luisi, *J. Am. Chem. Soc.*, 1997, **119**, 292.

3 (*a*) D. H. Lee, K. Severin, Y. Yokobayashi and M. R. Ghadiri, *Nature*, 1997, **390**, 591; (*b*) S. Yao, I. Ghosh, R. Zutshi and J. Chmielewski, *Nature*, 1998, **396**, 447; (*c*) A. Luther, R. Brandsch and G. Vonkiedrowski, *Nature*, 1998, **396**, 245; (*d*) S. Yao, I. Ghosh, R. Zutshi and J. Chmielewski, *Angew. Chem., Int. Ed.*, 1998, **37**, 478; (*e*) D. Albagli, R. Vanatta, P. Cheng, B. F. Huan and M. L. Wood, *J. Am. Chem. Soc.*, 1999, **121**, 6954.

4 (*a*) N. A. J. M. Sommerdijk, P. J. J. A. Buynsters, A. M. A. Pistorius, M. Wang, M. C. Feiters, R. J. M. Nolte and B. Zwanenburg, *J. Chem. Soc., Chem. Commun.*, 1994, 1941 and *J. Chem. Soc., Chem. Commun.*, 1994, 2739; (*b*) N. A. J. M. Sommerdijk, P. J. J. A. Buynsters, H. Akdemir, D. G. Geurts, A. M. A. Pistorius, M. C. Feiters, R. J. M. Nolte and B. Zwanenburg, *Chem. Eur. J.*, 1998, **4**, 127.

5 N. A. J. M. Sommerdijk, P. J. J. A. Buijnsters, H. Akdemir, D. G. Geurts, R. J. M. Nolte and B. Zwanenburg, *J. Org. Chem.*, 1997, **62**, 4955.

6 A. D. Dorrego, L. Garcia-Rio, P. Herves, J. R. Leis, J. C. Mejuto and K. Perez-Juste, *Angew. Chem., Int. Ed.*, 2000, **39**, 2945.

7 For the generation of lipid derived tubular aggregates see for example (*a*) J. H. Furhop and W. Helfrich, *Chem. Rev.*, 1993, **93**, 1565; (*b*) J. M. Schnur, *Science*, 1993, **262**, 1669; (*c*) M. Markowitz, S. Baral, S. Brandow and A. Singh, *Thin Solid Films*, 1993, **224**, 242; (*d*) D. D. Archibald and S. Mann, *Nature*, 1993, **364**, 430; (*e*) F. Giulieri, F. Guillod, J. Greiner, M.-P. Krafft and J. G. Riess, *Chem. Eur. J.*, 1996, **2**, 1335; (*f*) M. S. Spector, R. R. Price and J. M. Schnur, *Adv. Mater.*, 1999, **11**, 337.

A hybrid cyclic bisproline designed to adopt a β-fold: crystal structure of cyclo(ProNHCH$_2$CH$_2$NHProCOCH$_2$CH$_2$CO)

Darshan Ranganathan,*[a] M. Gopi Kumar[a] and Isabella L. Karle*[b]

[a] *Discovery Laboratory, Indian Institute of Chemical Technology, Hyderabad 500 007, India. E-mail: ranganathan@iict.ap.nic.in*

[b] *Laboratory for the Structure of Matter, Naval Research Laboratory, Washington, DC 20375-5341, USA*

Received (in Columbia, MO, USA) 6th November 2000, Accepted 5th December 2000
First published as an Advance Article on the web 23rd January 2001

The crystal structure of 14-membered cyclo(ProNHCH$_2$CH$_2$NHProCOCH$_2$CH$_2$CO) reveals the presence of an internal NH···O=C bond dividing the molecule into two halves of 10-membered hydrogen-bonded rings; the molecules self-assemble into cyclic dimers through a symmetrical pair of intermolecular NH···O=C hydrogen bonds; a layered structure is formed, alternating layers of cyclic dimers and layers of chloroform molecules, all of which make strong CH···O hydrogen bonds with the cyclic dimers.

Design of conformationally constrained peptides mimicking receptor-bound conformation is an area of intense current interest in drug design.[1] It is generally believed that a β-folded structure is the most likely conformation present at the active site of many naturally occurring peptides and proteins.[2] Among the natural amino acids, proline is reported to be the most prevalent at the turn locations.[3] In recent years several designs of multiple-stranded β-sheets have been reported[4] using a Pro-Gly motif as the turn inducer. An attractive approach to β-turn folds would be to cyclize proline-containing peptides with a rigid moiety that may force the peptide chain to fold and run in an antiparallel direction. We demonstrate herein the first illustration of this concept and report on the crystal structure of a hybrid cyclic peptide with repeats of L-proline and dimethylene units in a 14-membered ring. The target cyclic peptide **1** was prepared by a two-step procedure (Scheme 1) involving first the formation of a core-modified Z–proline bispeptide which on deprotection and condensation with succinyl chloride under a high-dilution condition yielded the desired cyclic peptide in good yields.[5]

Suitable crystals for **1** were obtained from chloroform solution by slow diffusion of hexane vapour. The colourless shining crystals were found to crumble into an opaque powdery solid when exposed to air. For this reason diffraction measurements were carried out at low temperature on a crystal covered with immersion oil.

The crystal structure[6] of **1** showed the presence of two independent molecules A and B with very similar conformations. The contents of the unit cell also included three chloroform molecules. Molecule A [Fig. 1(a)] and B [Fig. 1(b)] each contain an intramolecular NH···O=C hydrogen bond dividing the macrocycle into two equal halves each enclosing a 10-membered hydrogen-bonded ring. The molecules A and B are further engaged in a dimer formation [Fig. 2(a)] through a similar pair of intermolecular NH···O=C hydrogen bonds. As shown in [Fig. 2(b)] each cyclic dimer is surrounded by three $CHCl_3$ molecules that make strong C–H···O hydrogen bonds with carbonyls O18, O18s and O3s of both macrocycles, and by additional $CHCl_3$ molecules from neighboring cells. Molecule A participates in C–H···O hydrogen bonding only with one of the $CHCl_3$ molecules while molecule B makes C–H···O contacts with two $CHCl_3$ molecules. Table 1 presents the hydrogen bond parameters. The dimers further assemble in infinite columns extending into a layered structure wherein sheets of $CHCl_3$ molecules (three for each dimer) alternate with columns of dimers [Fig. 2(b)]. The chloroform molecules among themselves make only van der Waals contacts. The

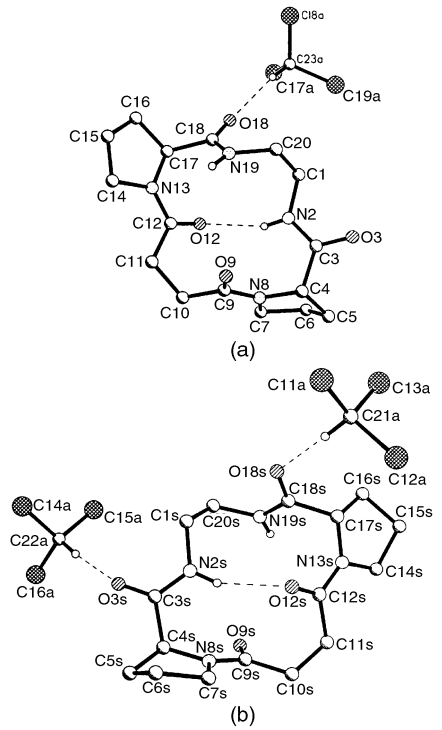

Fig. 1 Molecule A (a) as well as molecule B (b) are each engaged in intramolecular NH···O=C hydrogen bonding dividing the macrocycle into two equal halves of 10-membered hydrogen-bonded rings.

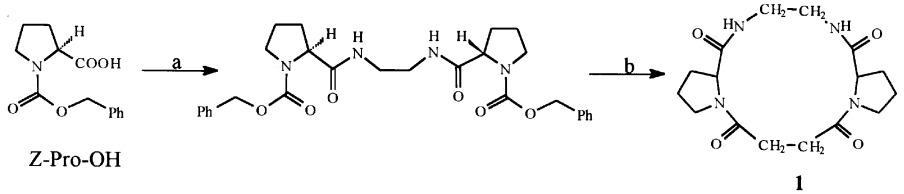

Scheme 1 *Reagents and conditions*: $NH_2CH_2CH_2NH_2$, diphenyl phosphoryl azide (DPPA), DMF–CH_2Cl_2; b, (i) Pd/C 5%, H_2, (ii) $ClCOCH_2CH_2COCl$, NEt_3, CH_2Cl_2.

DOI: 10.1039/b009130h

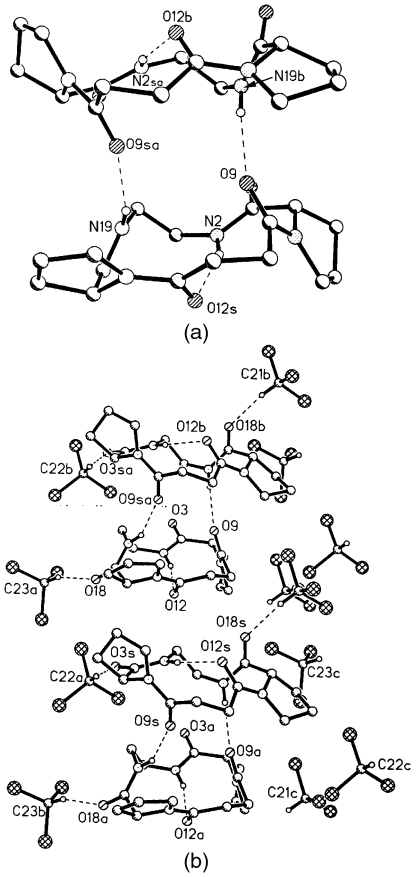

Fig. 2 (a) Hydrogen-bonded cyclic dimer of molecule A and B formed through a similar pair of NH···O=C hydrogen bonds. (b) Packing of dimer columns into a layered structure. Each dimer is surrounded by three $CHCl_3$ molecules that make strong C–H···O contacts with the macrocycles. The remaining $CHCl_3$ molecules in the layers are from neighboring unit cells.

Table 1 Hydrogen bonds

Type	Donor	Acceptor	D–A/Å	H[a]–A/Å	DH···O/°
4 → 1	N2	O12	3.104	2.25	159
4 → 1	N2s	O12s	3.041	2.19	158
Dimer	N19	O9s[b]	2.959	2.12	154
Dimer	N19s	O9[c]	3.071	2.18	172
CH–O	C23	O18	3.085	2.16	160
CH–O	C21	O18s	3.081	2.13	170
CH–O	C22	O3s	3.001	2.04	175

[a] Hydrogen atoms were placed in idealized positions at N–H = 0.90 Å and C–H = 0.96 Å. [b] At symmetry equivalent: *x*, −1 + *y*, *z*. [c] At symmetry equivalent: *x*, 1 + *y*, *z*.

presence of such a large proportion of chloroform molecules in the crystal structure of **1** is rather unusual and may be attributed to the hydrophobic nature of the proline macrocycle.

The β-turns in the proline macrocycle (Fig. 1), mimic true βII′- and βIII-turns in standard peptides, despite a substitution of C1 (methylene) for a N atom in the upper half of the macrocycle and a substituton of C11 for a N atom in the lower half. An inspection of the torsional angles listed in Table 2 shows that the upper half closely resembles a βII′-type turn, whereas the lower half has angles resembling a βIII-type turn.

^{1}H NMR variable-temperature (VT) studies showed a value of −3.75 ppb K^{-1} for the temperature coefficient indicating a moderate amount of intramolecular hydrogen bonding in DMSO solvent. ROESY studies in DMSO-d_6 did not show any significant cross-peaks except weak interaction between NH and methylene spacer units. The presence of dimeric structures was also indicated by electrospray mass spectroscopy.

In conclusion, incorporation of CH_2CH_2 units in an alternating sequence with Pro units in a ring seems to lead to preference

Table 2 Conformation angles (°)

Angle	Molecule A	Molecule B	Std. label[a]	Idealized turns[b] βII′	Idealized turns[b] βIII
C10C11C12C13	167	170	ω_o	180	
C9C10C11C12	61	63	ϕ_1	60	
N8C9C10C11	−138	−138	ψ_1	−120	
C4N8C9C10	−179	−179	ω_1	180	
C3C4N8C9	−79	−80	ϕ_2	−80	
N2C3C4N8	1	3	ψ_2	0	
C1N2C3C4	174	179	ω_2	180	
C11C12N13C17	−178	179	ω'_2		
C12N13C17C18	−60	−49	ϕ_3		−60
N13C17C18N19	−26	−40	ψ_3		−30
C17C18N19C20	171	176	ω_3		180
C18N19C20C1	−66	−62	ϕ_4		−60
N19C20C1C2	−60	−58	ψ_4		−30
C20C1N2C3	−103	−109	X_4		

[a] Conventions for normal peptides in ref. 7. Labeling of torsional angles with the standard ϕ, ψ and ω symbols, and μ or θ for angles about the CH_2–CH_2 is complicated since the order of the backbone atoms in C20 to C11 is in the retro direction as compared to C1 to C10. In the pseudo 4 → 1 turns, atoms C10, C4 and C17, C20 are in the corner positions (C^α atoms) of two standard β-turns. The ϕ, ψ and ω labels were chosen so that torsional angles in the pseudo 4 → 1 turns could be compared directly to standard types of 4 → 1 β-turns. [b] Idealized values in ref. 8.

of a C_{10} hydrogen-bonded turn structure. The presence of all-*trans* amide bonds in the constrained 14-membered ring of **1** and an unusually large amount of chloroform molecules stabilizing the structure through C–H···O hydrogen bonds are additional noteworthy features. The design of related hybrid peptides containing an increasing number of proline units in the ring is in progress.

This work was financially supported by the Department of Science and Technology, New Delhi, National Institute of Health (GM-30902), USA, and the Office of Naval Research. Helpful advice from Professor S. Ranganathan is acknowledged. D. R. is an honorary faculty member of Jawaharlal Nehru Center for Advanced Scientific Research.

Notes and references

1 N. Beeley, *Tib. Tech.*, 1994, **12**, 213; W. M. Kazmierski, *Tib. Tech.*, 1994, **12**, 216; M. Goodman and S. Ro, *Burger's Medicinal Chemistry and Drug Discovery*, ed. M. E. Wollf, Wiley, New York, 1995, vol. 1, pp. 803–861.

2 J. Rizo and L. Gierasch, *Annu. Rev. Biochem.*, 1992, **61**, 387 and references therein.

3 A. Aubry and M. Marraud, *Biopolymers*, 1989, **28**, 109; V. Pavone, A. Lombardi, G. D'Aurtia, M. Saviano, F. Nastri, L. Paolillo, B. DiBlastio and C. Pedone, *Biopolymers*, 1992, **32**, 173; B. Imperiali, S. L. Fischer, R. A. Moats and T. J. Prins, *J. Am. Chem. Soc.*, 1992, **114**, 3182.

4 I. L. Karle, S. K. Awasthi and P. Balaram, *Proc. Natl. Acad. USA*, 1996, **93**, 8189; C. Das, S. Raghotama and P. Balaram, *J. Am. Chem. Soc.*, 1998, **120**, 5812; H. E. Stanger and S. H. Gellman, *J. Am. Chem. Soc.*, 1998, **120**, 4236; H. L. Schenck and S. H. Gellman, *J. Am. Chem. Soc.*, 1998, **120**, 4869; S. C. Shankaramma, S. K. Singh, A. Satyamurthy and P. Balaram, *J. Am. Chem. Soc.*, 1999, **121**, 5360.

5 *Selected data* for **1**: yield 60%; mp 264–269 °C; δ_H(500 MHz, DMSO-d_6) 1.76–1.92 (m, 6H), 2.06–2.16 (m, 2H), 2.25–2.36 (m, 2H), 2.76–2.88 (m, 4H), 3.36 (t, 2H), 3.54 (m, 2H), 3.77 (m, 2H), 4.18 (q, 2H), 6.86 (d, *J* 7.5 Hz, 2H), ES-MS *m/z* (%) 337(5) $(MH)^+$, 359 (100) $(M + Na^+)$, 375(92) $(M + K^+)$, 695(92) $(2M + Na^+)$, 711(20) $(2M + K^+)$.

6 *Crystal data* for **1**: $2[C_{16}H_{24}N_4O_4]\cdot 3CHCl_3$, space group *P*1, *a* = 10.141(1), *b* = 10.892(1), *c* = 12.718(1) Å, α = 67.50(1), *β* = 81.87(1), *γ* = 63.92(1)°, *V* = 1165.1(2) Å^3, D_c = 1.469 g cm^{-3}, Cu-Kα radiation, *λ* = 1.54178 Å, Least-square refinement on F^2, R_1 = 0.083, wR_2 = 0.202. Data collection at −60 °C; crystal covered with microscope oil (severe solvent loss at 20 °C with crystal removed from mother liquor). CCDC 182/1885.

7 IUPAC-IUB Commission on Biochemical Nomenclature, *Biochemistry*, 1970, **9**, 3471.

8 C. M. Venkatachalam, *Biopolymers*, 1968, **6**, 1425.

A unique example of a core-modified bis-proline peptide self-assembling into an infinite hydrogen-bonded β-sheet ribbon: crystal structure of Z-ProNH$(CH_2)_2$NHPro-Z

Darshan Ranganathan,*[a] M. Gopi Kumar,[a] R. S. K. Kishore[a] and Isabella L. Karle*[b]

[a] *Discovery Laboratory, Indian Institute of Chemical Technology, Hyderabad 500 007, India. E-mail: ranganathan@iict.ap.nic.in*

[b] *Laboratory for the Structure of Matter, Naval Research Laboratory, Washington, DC 20375-5341, USA*

Received (in Columbia, MO, USA) 6th November 2000, Accepted 5th December 2000
First published as an Advance Article on the web 23rd January 2001

The crystal structure of Z-ProNH$(CH_2)_2$NHPro-Z exhibits an extended backbone, with occurrence of both a *cis* and a *trans* conformation preceding the two prolyl residues, that self-assembles into an infinite hydrogen-bonded β-sheet ribbon.

Proline, the only amino acid found in proteins with a secondary amino group in a five-membered ring, is known to play an important role in the folding of natural proteins.[1] *N*-Acyl prolines lacking amide NHs display energetically similar *cis*- and *trans*-isomeric forms[2] and both forms are known to occur in proteins, for example, ribonuclease[3] or in bioactive peptides such as bradykinin.[4] Being a cyclic amino acid, proline imposes a certain degree of conformational constraint in the protein or peptide backbone causing bends or breaking helices,[5] and consequently proline-containing peptides are generally not known to display extended structures. We describe herein a unique example of a core-modified bis-proline peptide that is preceded by both a *cis* as well as a *trans* amide bond in its framework and self-assembles to form a hydrogen-bonded infinite β-sheet ribbon in the solid state.

The 1,2-ethylenediamine spacer-linked bis-proline **1** [Fig. 1(a)] was prepared[6] in a single step by coupling Z-proline with 1,2-diaminoethane using a direct azide coupling (diphenyl phosphoryl azide) procedure. The bis-Pro peptide **1** was fully characterized[7,8] by spectral and analytical data.

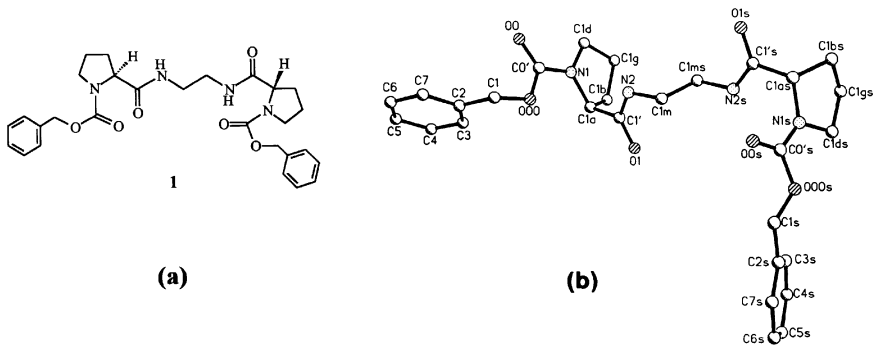

Fig. 1 (a) Molecular formula of **1**. (b) X-Ray structure of **1**. The numbering is the same for each half except that the letter 's' is added for atoms on one side.

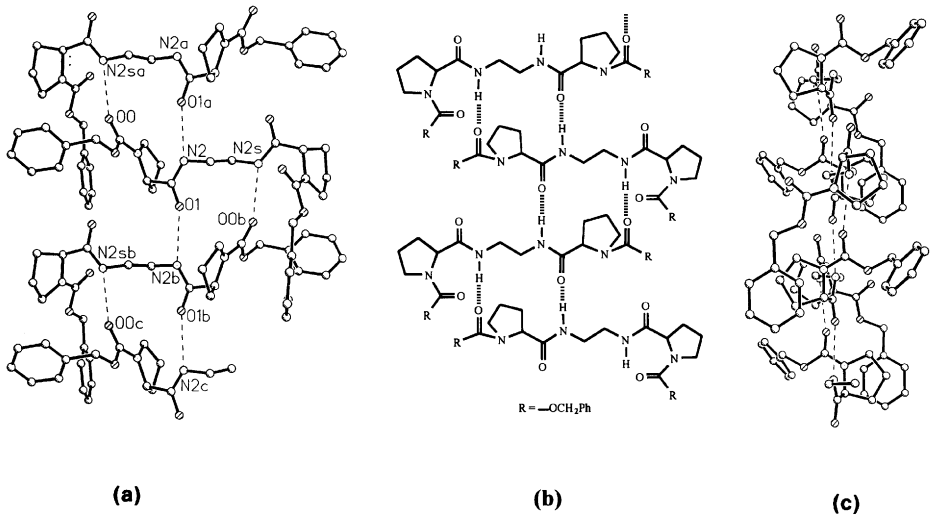

Fig. 2 (a) Flat ribbon formation by connecting the molecules by two types of hydrogen bonds, N(2)H⋯O(1) and N(2s)H⋯O(0). The molecules are repeated by a vertical two-fold screw axis. (b) Schematic representation of the ribbon assembly of **1**. (c) A side view of the ribbon. The dashed lines represent hydrogen bonds. Both surfaces of the ribbon are largely hydrophobic by virtue of the extended placement of the benzyl moieties and prolyl rings.

Suitable crystals for X-ray diffraction were obtained from a mixture of ethyl acetate and hexane. The crystal structure of **1** showed a backbone extended in two sections with a sharp bend at Pro(1s) [Fig. 1(b)]. Interestingly, the two halves of the molecule are not symmetric. On one side of the molecule the Z-L-Pro (1) amide bond C0′–N1 has the *cis* conformation, whereas on the other side the Z-L-Pro (1s) amide bond C0′s–N1s has the *trans* conformation. A similar occurrence of a *cis* amide bond preceding a Pro residue had been noted in 1974 for the Boc-Pro (1) amide bond in Boc-(L-Pro)$_4$-OBzl.[9]

The hydrogen-bonding pattern [Fig.2(a)] in the crystal lattice showed the formation of an infinite ribbon assembly around a two-fold screw axis (space group $P2_1$). There are only two independent hydrogen bonds, N(2)H··O(1) and N(2s)H··O(0) that connect the molecules into ribbons. Fig. 2(b) shows the schematic picture of the ribbon assembly. A side view of the ribbon in Fig. 2(c) shows a relatively flat structure. The protruding phenyl and pyrrolidine rings on either side impart a hydrophobic surface to the ribbon. Table 1 presents the hydrogen bond parameters and torsional angles in **1**. In solution-state conformational studies of **1**, while ^{1}H NMR (variable temperature measurements) has shown agreement with the solid-state structure in exhibiting high dδ/dT values (> 4 ppb K^{-1}) indicating the absence of any intramolecular hydrogen bonding, the FTIR spectrum in chloroform solution at 297 K showed two bands in the NH stretch region. The band at *ca*. 3430 cm^{-1} is assigned to the non hydrogen-bonded NH and the concentration independent, major band at *ca*. 3340 cm^{-1} is attributed to an internally hydrogen-bonded NH, possibly, in a seven-membered ring.

Table 1 Structural characteristics of **1**

(a) Intermolecular hydrogen bonds (Å) and angles (°)					
N2···O1[a]	2.899		N2s···O0[b]	2.877	
H2···O1[a]	2.10		H2s···O0[b]	2.09	
N2···O1=C	153		N2s···O0=C	152	
(b) Selected torsional angles (°)[c]					
C2C1O00C0′		+83	C2sC1sO00sC0′s		+155
C1O00C0′N1	ψ_o	179	C1sO00sC0′sN1s	ψ_{os}	−176
O00C0′N1C1a	ω_o	+12	O00sC0′sN1sC1as	ω_{os}	−171
C0′N1C1aC1′	ϕ_1	−90	C0′sN1sC1asC1′s	ϕ_{1s}	−82
N1C1aC1′N2	ψ_1	−7	N1sC1asC1′sN2s	ψ_{1s}	−12
C1aC1′N2C1m	ω_1	−173	C1asC1′sN2sC1ms	ω_{1s}	177
C1′N2C1mC1ms		+92	C1′sN2sC1msC1m		−99
N2C1mC1msN2s		−175			

[a] Symmetry equivalent $-x$, $-0.5 + y$, $1 - z$. [b] Symmetry equivalent $-x$, $+0.5 + y$, $1 - z$. [c] Conventions for labels in ref. 10.

The present results demonstrate that appropriate core inserts can modify the conformational behavior of proline residues in a peptide.

This work was financially supported by the Department of Science and Technology, New Delhi, National Institute of Health (GM-30902), USA, and the Office of Naval Research. Helpful advice from Professor S. Ranganathan is acknowledged. D. R. is an honorary faculty member of Jawaharlal Nehru Center for Advanced Scientific Research.

Notes and References

1 For reviews on protein folding, see: T. E. Creighton, *Proc. Natl. Acad. Sci. USA*, 1988, **85**, 5082; G. T. Montelione and H. A. Scheraga, *Acc. Chem. Res.*, 1989, **22**, 70; J. King, *Chem. Eng. News*, 1989, **67**, 32; R. L. Baldwin, *Trends Biochem. Sci.*, 1989, **14**, 291; L. M. Gierasch and J. King, *Protein Folding; Deciphering the Second Half of the Genetic Code*, AAAS Pub., Washington D.C., 1990; T. E. Creighton, *Biochem. J.*, 1990, **270**, 1; R. Jaenicke, *Biochemistry*, 1991, **30**, 3147; C. M. Dobson, A. Sali and M. Karplus, *Angew. Chem., Int. Ed.*, 1998, **37**, 868.

2 W. S. Blair and B. L. Semler, *Curr. Opin. Cell. Biol.*, 1991, **3**, 1039 and references therein.

3 P. N. Lewis, F. A. Momany and H. A. Scheraga, *Biochim. Biophys. Acta*, 1973, **303**, 211.

4 R. E. London, J. M. Stewart, R. Williams, J. R. Cann and N. A. Matwiyoff, *J. Am. Chem. Soc.*, 1979, **101**, 2455.

5 J. L. Crawford, W. N. Lipscomb and C. G. Schollman, *Proc. Natl. Acad. Sci., USA*, 1973, **70**, 538; P. Y. Chou and G. D. Fasman, *Biochemistry*, 1974, **13**, 222; C. M. Venkatachalam, *Biopolymers*, 1969, **6**, 1425.

6 The N$^{\alpha}$Z protected proline azide, generated *in situ*, directly from Z-Pro (5 mmol) and diphenylphosphoryl azide (DPPA, 5 mmol) in dry CH_2Cl_2–DMF (5 mL, 3:2) was admixed with 1,2-diaminoethane (2.5 mmol) and the reaction mixture was left stirred for 8 h at 0 °C and 12 h at room temp., the solvents evaporated *in vacuo*, residue mixed with water (*ca*. 50mL), extracted with ethyl acetate (2 × 50 mL), organic extract washed with aq. bicarbonate solution and dried (anhyd. $MgSO_4$). The residue, after solvent removal *in vacuo*, was purified on a short column of silica gel using ethyl acetate–hexane as eluents.

7 *Selected data* for **1**. Yield 80%; mp 158–160 °C; δ_H (200 MHz $CDCl_3$) 1.80–2.31 (m, 8H), 3.05–3.71 (m, 8H), 4.20 (m, 2H), 5.15 (m, 4H), 6.6–7.0 (br, 2H), 7.35 (br s, 10H); FAB-MS (*m*/*z*) 523 (MH)$^+$, 545 (M+Na$^+$).

8 Crystal data for **1**: $C_{28}H_{34}N_4O_6$, space group $P2_1$, a = 9.992(2), b = 10.251(2), c = 13.325(3), β = 90.25(2)°, V = 1364.9(5) Å^3, D_c = 1.272 g cm^{-3}, Cu-Kα radation, λ = 1.54178 Å. Least-squares refinement on F, R = 0.0578 for 1652 data [$F > 3.0\sigma(F)$]. Data collection at 293 °C. CCDC 182/1884.

9 T. Matsuzaki, *Acta Crystallogr., Sect. B*, 1974, **30**, 1029.

10 IUPAC-IUB Commission on Biochemical Nomenclature, *Biochemistry*, 1970, **9**, 3471.

ChemComm

Hierarchical structure of a self-assembled xerogel

Marius Kölbel and Fredric M. Menger*

Department of Chemistry, Emory University, Atlanta, GA 30322, USA. E-mail: menger@emory.edu

Received (in Columbia, MO, USA) 13th September 2000, Accepted 15th December 2000
First published as an Advance Article on the web 23rd January 2001

Removal of the liquid from a glycoluril-based gel produces a macroporous solid (a xerogel) comprised of closely packed fibers that assemble into highly convoluted sheets.

Glycoluril, the bicyclic product of glyoxal reacting with two equivalents of urea, is a molecule with a long history. For three decades, after first being synthesized by Schiff in 1877, glycoluril attracted a fair amount of attention until it faded into the dusty archives of science.[1] Poor solubility of glycoluril and its derivatives in water and organic solvents probably hastened the flagging interest. In the 1980s, however, a renaissance in glycoluril chemistry became apparent. This renewed awareness of glycoluril was driven by its various applications in the design of supramolecular architectures. Among these we find molecular clips and baskets,[2] supramolecular capsules,[3] self-complimentary facial amphiphiles,[4] and complexes of cucurbituril[5] (a macrocyclic condensation product of glycoluril with formaldehyde).

In the course of studying a variety of alkoxyphenyl-substituted glycolurils, we encountered an unexpected ability of the compounds to rigidify organic liquids into so-called organogels. Organogels are a growing class of supramolecular assemblies with potential applications in oil chemistry, nutrition, cosmetics and pharmacology.[6] Diverse molecular structures, among them derivatives of urea,[7] are already known to immobilize organic liquids. Such organogels are categorized as 'physical gels' in that they are formed by low-molecular weight organic molecules that self-assemble into fibrous structures upon cooling of their solutions. The fibers, held together by non-covalent forces, create a network that entrains solvent within the interstices. Removal of the solvent by evaporation or filtration results in a collapsed mat of fibers called a xerogel. The present manuscript focuses on the structure of a xerogel prepared from a glycoluril derivative.

The compound in question, the di(benzyloxyphenyl)-substituted glycoluril **1**, is drawn below. It was obtained by refluxing

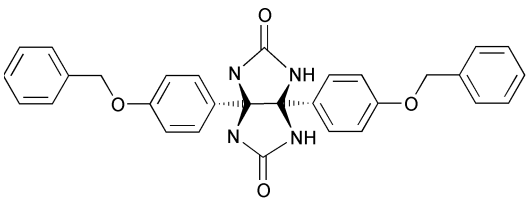

1

a stirred mixture of 1.0 g 4,4′-dibenzyloxybenzil, 4 mL CF_3CO_2H, and 400 mg freshly powdered urea in 150 mL benzene while collecting water in a Dean–Stark trap.[8] After 50 h, the solvent was removed under reduced pressure, leaving a solid that was washed with two 50 mL portions of the following solvents: $CHCl_3$, boiling MeOH, $CHCl_3$ and *n*-pentane to give 51% of the pure compound. Characterization consisted of ^{1}H NMR, ^{13}C NMR, HRMS and elemental analysis.†

The gelation ability of the glycouril derivative was checked by heating suspensions in various organic liquids such as propan-1-ol, decan-1-ol, toluene, DMSO, DMF and benzyl alcohol. Compound **1** proved insoluble in hot propan-1-ol, decan-1-ol, and toluene. On the other hand, clear solutions were obtained in hot DMSO, DMF and benzyl alcohol. Upon cooling these solutions, the compound remained dissolved in DMSO, but rapidly precipitated from DMF. Only with benzyl alcohol, however, did we observe, at a concentration of 20 mg mL^{-1}, the formation of a self-supporting opaque gel that could be turned upside down in a vial without flow or deformation. The gel is thermoreversible and stable for months at room temperature, whereas it is irreversibly destroyed when shaken vigorously.

Light microscopy (400×) on a small portion of the gel (Fig. 1) revealed flexible fibers several hundred μm long and about 2 μm in diameter (often radiating from central points). We assume (partly on the basis of our previous X-ray data on unrelated gel systems[9]) that the fibers in Fig. 1 are a composite of parallel 'elementary' fibers with molecular dimensions (*i.e.* diameters of *ca.* 2.5 nm corresponding to hydrogen-bonded dimers of **1**).

A xerogel was prepared from the **1**/benzyl alcohol gel by filtration. Thus, a portion of gel was placed in a Büchner funnel

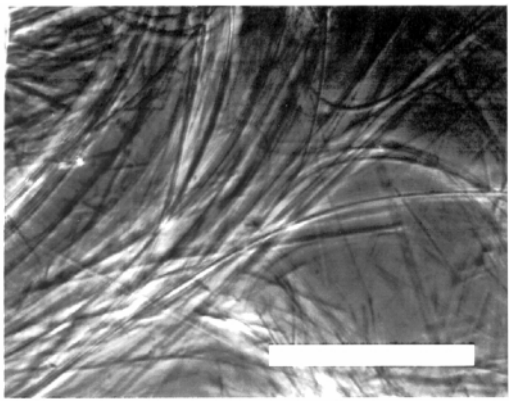

Fig. 1 Optical photomicrograph of the gel **1**/benzyl alcohol (400×, scalebar: 60 μm).

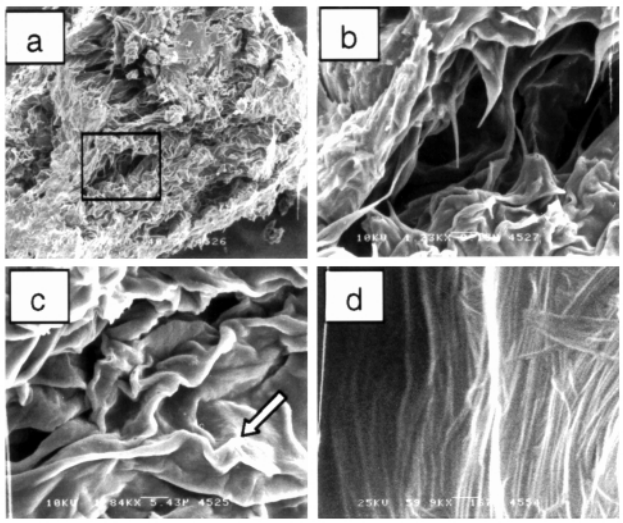

Fig. 2 SEM images of the xerogel obtained from the gel **1**/benzyl alcohol; (a) 246×, scalebar: 40.7 μm; (b) 1230×, scalebar: 8.13 μm; (c) 1840×, scalebar: 5.43 μm; (d) 59 900×, scalebar: 167 nm.

DOI: 10.1039/b008046m

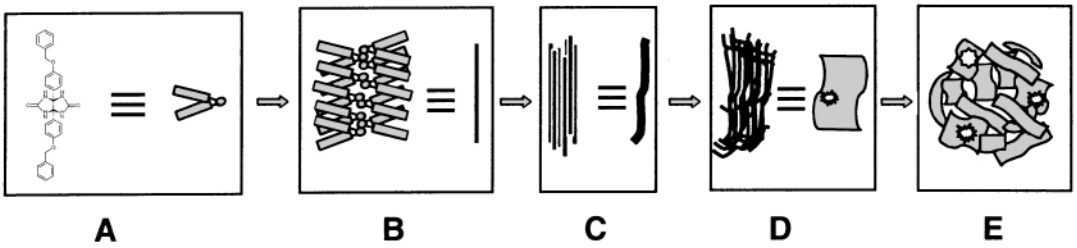

Fig. 3 Schematic representation of the hierarchical levels of the xerogel of **1**.

with a fritted disk, and the solvent was removed under suction for 6 h while a mild N_2 pressure was applied from above. Remaining traces of solvent were then removed under reduced pressure with the aid of a vacuum pump. The resulting xerogel, a brittle material of resin-like appearance, was attached to a metal stub with conductive carbon tape and coated with 3 nm Cr using a Denton DV-602 Cr coater. Representative SEM images were obtained at the lower [Fig. 2(a)–(c)] and upper [Fig. 2(d)] stage of an ISI DS-130 LaB_6 electron microscope.

Macroscopic fibers, as observed by light microscopy, can no longer be found. Instead, we see in Fig. 2(a) (246 × instrumental magnification) a highly convoluted material with pore sizes ranging from *ca.* 5 μm to *ca.* 20 μm. Fig. 2(b) offers a closer look at the concavity framed in Fig. 2(a), using now as 1230 × instrumental magnification. The inside of the orifice is replete with folds, indentations and spikes. Fig. 2(c) at a 1840× instrumental magnification shows how the xerogel is comprised of curved, wrinkled and interconnected sheets. Also seen in Fig. 2(c) is a further underlying fine structure which is particularly noticeable in smoother areas such as that marked with an arrow. At a magnification of 59 900 × [Fig. 2(d)] the fibrous nature of this fine structure becomes apparent. Although the macroscopic fiber bundles observed by light microscopy did not survive the drying process, much smaller fibers, with diameters down to 15 nm and several μm length, remain intact. These microfibers pack themselves into craggy sheet-like structures.

Based on these observations, we can describe this xerogel as a hierarchical structure as depicted schematically in Fig. 3. At the lowest level of structure we postulate single molecules of **1** (**A**) self-assembling into fibers (**B**) *via* hydrogen bonding between the glycoluril head groups. The molecular structure of these elementary fibers is still unknown (a problem that besets most organogel work). The elementary fibers then form bundles (**C**) with diameters of *ca.* 15 nm which are visible by SEM at 60 000 × magnification. These bundles align and pack side-by-side, thereby forming sheets (**D**). Owing to the high disorder and curvature of these sheets, and to their multiple junctions with one another, cavities are formed to give a macroporous solid (**E**). Although individual fibers are curved and seemingly flexible, the bulk material composed of the fibers is hard and brittle. Close packing and interweaving of the fibers into a sponge-like network produces a fairly rigid microstructure.

The gel-to-xerogel transformation upon solvent removal can be understood in terms of our model. As seen in Fig. 4, the organogel is composed of 2 μm fibers (visible by light microscopy) which in turn are composed of 15 nm fibers (visible by SEM). Below our resolution capabilities lie the 2.5 nm elementary fibers. When the gel is dried, the macroscopic fiber bundles disappear, leaving the nanoscopic bundles which self-assemble into the sheets that comprise the xerogel. No comparable transformation has been reported thus far; usually the structure of the original gel is either faithfully preserved or else completely destroyed.

This work has been supported by the National Institutes of Health. We greatly appreciate the assistance of Dr Robert Apkarian and Mr Kevin Caran of the Integrated Microscopy and Microanalytic Facility of Emory University for microscopy services.

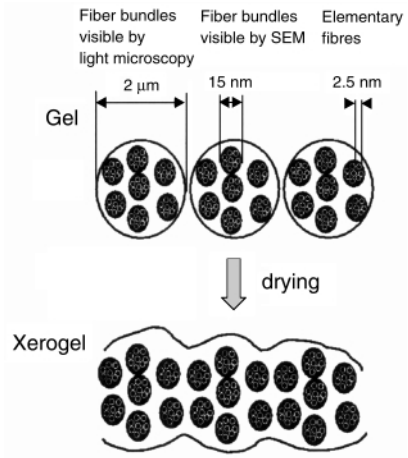

Fig. 4 Schematic representation of cross-sections through fiber bundles in the organogel and through a sheet in the xerogel of **1**.

Notes and references

† δ_H(DMSO-d_6, 400 MHz): 7.65 (s, 4H, –NH), 7.35 (m, 8H, ar. H, benzyl), 7.28 (m, 2H, ar. H, benzyl), 6.97 (d, 4H, J = 8.9 Hz, ar. H), 6.74 (d, 4H, J = 8.9 Hz, ar. H), 4.98 (s, 4H, benzyl, CH_2); δ_C(DMSO-d_6, 100 MHz): 160.6, 157.8, 136.9, 130.7, 128.4, 128.3, 127.7, 127.5, 113.7, 81.6, 69.0; Anal. calc. for $C_{30}H_{26}N_4O_4$: C, 71.13; H, 5.17; N, 11.06; found C, 70.70; H, 5.08; N, 11.08%; HRMS: calc. for $C_{30}H_{26}N_4O_4Li$ $(M + Li)^+$ *m/z* 513.2114, found 513.2120.

1 H. Schiff, *Liebigs Ann. Chem.*, 1877, **189**, 157; R. Behrend, E. Meyer and F. Rusche, *Liebigs Ann. Chem.*, 1905, **339**, 1; H. Biltz, *Chem. Ber.*, 1907, **40**, 4806; H. Biltz, *Chem. Ber.*, 1908, **41**, 167; H. Biltz, *Justus Liebigs Ann. Chem.*, 1909, **368**, 156.
2 A. E. Rowan, J. A. A. W. Elemans and R. J. M. Nolte, *Acc. Chem. Res.*, 1999, **32**, 995.
3 J. Rebek, *Acc. Chem. Res.*, 1999, **32**, 278.
4 L. Isaacs, D. Witt and J. C. Fettinger, *Chem. Commun.*, 1999, 2549.
5 W. A. Freeman, W. L. Mock and N.-Y. Shih, *J. Am. Chem. Soc.*, 1981, **103**, 7367; C. Pintas, *J. Incl. Phenom. Mol. Recognit. Chem.*, 1994, **17**, 205; W. L. Mock, in *Comprehensive Supramolecular Chemistry*, Pergamon/Elsevier Press, New York, 1997, vol. 2, p. 477.
6 P. Terech and R. G. Weiss, *Chem. Rev.*, 1997, **97**, 3133; D. J. Abdallah and R. G. Weiss, *Adv. Mater.*, 2000, **12**, 1237.
7 K. Hanabusa, K. Shimura, K. Hirose, M. Kimura and H. Shirai, *Chem. Lett.*, 1996, 885; J. van Esch, R. M. Kellog and B. L. Feringa, *Tetrahedron Lett.*, 1997, **38**, 281; J. van Esch, S. De Feyter, R. M. Kellog, F. De Schryver and B. L. Feringa, *Chem. Eur. J.*, 1997, **3**, 1238; J. van Esch, F. Schoonbeek, M. de Loos, H. Kooijman, A. L. Spek, R. M. Kellog and B. L. Feringa, *Chem. Eur. J.*, 1999, **5**, 937; F. S. Schoonbeek, J. H. van Esch, R. Hulst, R. M. Kellog and B. L. Feringa, *Chem. Eur. J.*, 2000, **6**, 2633; J. Brinksma, B. L. Feringa, R. M. Kellog, R. Vreeker and J. van Esch, *Langmuir*, 2000, **16**, 9249.
8 C. K. Lee, S. H. Kim and Y. B. Kim, *J. Heterocycl. Chem.*, 1996, **33**, 1019.
9 F. M. Menger, Y. Yamasaki, K. K. Catlin and T. Nishimi, *Angew. Chem., Int. Ed. Engl.*, 1995, **34**, 585.

Photoinduced two-step energy transfer in a Re/Ru dinuclear complex as mediated by an interposed 'reservoir' unit†

Susana Encinas,*[a] Anita M. Barthram,[b] Michael D. Ward,*[b] Francesco Barigelletti*[a] and Sebastiano Campagna[c]

[a] *Istituto FRAE–CNR, Via P. Gobetti 101, 40129 Bologna, Italy. E-mail: franz@frae.bo.cnr.it*
[b] *School of Chemistry, University of Bristol, Cantock's Close, Bristol, UK BS8 1TS. E-mail: mike.ward@bristol.ac.uk*
[c] *Dipartimento di Chimica Inorganica, Chimica Analitica e Chimica Fisica, Università di Messina, Via Sperone 31, I-98166 Messina, Italy*

Received (in Cambridge, UK) 10th October 2000, Accepted 12th December 2000
First published as an Advance Article on the web 23rd January 2001

In a dinuclear complex containing both $[ReCl(CO)_3(bpy)]$ and $[Ru(bpy)_3]^{2+}$ chromophores, the bis(bipyridylethenyl)-benzene bridge acts as an intermediate reservoir of energy for two-step Re→Ru photoinduced energy transfer.

Photoinduced energy transfer between transition metal polypyridine centres is studied because of the widespread interest in processes concerned with light energy collection and conversion.[1,2] The properties of the bridging ligand (L) interposed between the energy donor (D) and acceptor (A) components have accordingly been the object of extensive investigations, because the bridging ligand controls both the important *geometric* properties of the complex (inter-centre distance) and the *electronic* properties (electronic metal–metal coupling). Thus, careful control of the bridging ligand is of great importance in studies of photoinduced energy transfer in D–L–A complexes. However, not many examples are available of cases where L behaves as a photoactive component within the triad D–L–A.[3] This is in contrast to the conceptually similar process of photoinduced electron transfer, a process that can gain in effectiveness if the electron transfer occurs in several discrete steps *via* the bridging ligand.[4]

Here we present spectroscopic results for the dinuclear complex $[ReCl(CO)_3–L–Ru(bpy)_2]^{2+}$ (**Re–L–Ru**), where L is the bis-bipyridyl bridging ligand 1,4-bis[2-(4′-methyl-2,2′-bipyridyl-4-yl)ethenyl]benzene (dstyb), first described by

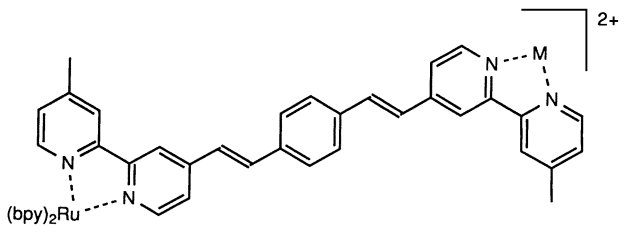

Ru–L (M = nothing); **Re–L–Ru** (M = {*fac*-Re(CO)$_3$Cl})

Schmehl and coworkers[5–7] (ESI †). Data for the reference mononuclear complex $[Ru(bpy)_2(dstyb)]^{2+}$ (**Ru–L**) are also discussed. We show that within **Re–L–Ru**, L behaves as a reservoir of excitation energy collected at the Re-based chromophore and passes some amount of it to the Ru-based emitter, according to a two-step energy transfer scheme [eqn. (1)].

$$\mathbf{Re}*\mathbf{–L–Ru} \rightarrow \mathbf{Re–L}*\mathbf{–Ru} \underset{k_2}{\overset{k_1}{\rightleftarrows}} \mathbf{Re–L–Ru}* \qquad (1)$$

Fig. 1 shows the absorption spectra of **Re–L–Ru** and of the reference mononuclear complex **Ru–L**; the luminescence spectra recorded at room temperature are also shown, as obtained after excitation at 372 nm (an isoabsorbing point for two cases). Luminescence data obtained both at room temperature and at 77 K are collected in Table 1 (ESI †). Comparison of the absorption profiles and intensities for **Re–L–Ru** and **Ru–L** with cases from literature[5–7] allows the following assignments. (i) The bands peaking at 290 nm are of intra-bpy ^{1}IL(bipy) nature; (ii) the bands with maxima in the 360–390 nm region are of intra-dstyb character, ^{1}IL(dstyb); (iii) the bands with maxima at 464 nm are of ^{1}Ru→L MLCT nature; (iv) for Re–L–Ru, the flat region of absorbance in the 380–450 nm region includes the expected ^{1}Re→L CT transition.[6]

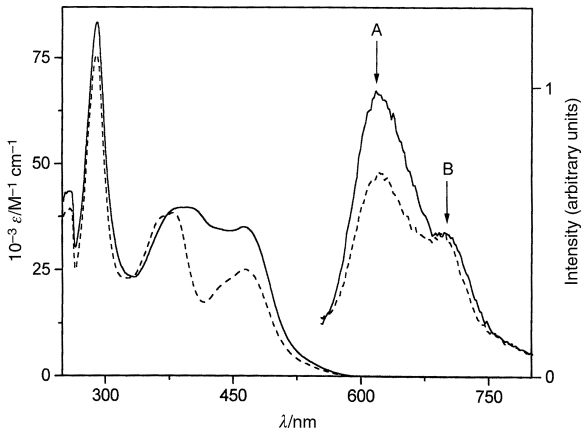

Fig. 1 Room temperature absorption and luminescence spectra of dinuclear **Re–L–Ru** (—) and reference mononuclear **Ru–L** (- - - -) complexes; excitation was at 372 nm, solvent was DMF–CH_2Cl_2. The two luminescence bands are termed A (^{3}Ru→L CT character) and B (^{3}IL[dstyb] character).

The luminescence spectra of both **Re–L–Ru** and **Ru–L** at room temperature (Fig. 1) show two distinct emission features. The band maximum at 621 nm (Table 1, Fig. 1, band A) is ascribed to emission from the ^{3}Ru→L CT excited state; the

Table 1 Luminescence data[a]

	298 K				77 K	
	λ_{max}/nm	τ/ns	ϕ^{Ru}	$10^{-4}k_r$[b]	λ_{max}/nm	τ/μs
Ru–L[c]	621 (A)	183[d]	3.3×10^{-4}[e]	0.18	591 (A)	5.3
	695 (B)	210			693 (B)	11
Re–L–Ru[c]	621 (A)	188	4.5×10^{-4}[e]	0.24	591 (A)	5.3
	695 (B)	216[d]			705 (B)	10
$[Ru(bpy)_3]^{2+}$	608	210	1.5×10^{-2}	7.1	582	5.0

[a] In air-equilibrated DMF–CH_2Cl_2 (9:1, v/v) solvent, unless otherwise noted. [b] $k_r = \phi^{Ru}/\tau$, λ_{exc} = 372 nm. [c] A is the ^{3}MLCT maximum, B is the ^{3}IL band maximum. [d] Major (> 95%) contribution of a dual-exponential decay; the other τ value was 3 ÷ 4 ns. [e] From separation of the overlapping bands constituting the luminescence spectrum.

† Electronic supplementary information (ESI) available: synthetic and spectroscopic details. See http://www.rsc.org/suppdata/cc/b0/b008152n/

DOI: 10.1039/b008152n

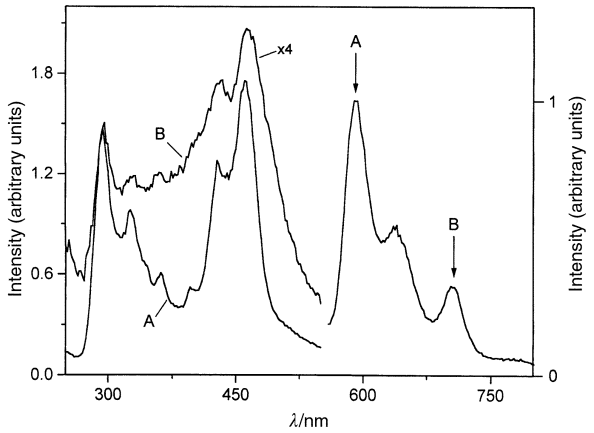

Fig. 2 77 K luminescence spectrum for **Re**–**L**–**Ru** under excitation at 372 nm, and excitation spectra taken at 591 nm (A band, ^{3}Ru→L CT character) and 705 nm (B band, ^{3}IL[dstyb] character); solvent was DMF–CH_2Cl_2.

band maximum peaking at 695 nm (Table 1, Fig. 1, band B), in contrast has previously been established by Schmehl and coworkers as arising from the ^{3}IL(dstyb) excited state.[5–7] In addition, the same authors found that the ^{3}Ru→L and ^{3}IL(dstyb) levels in the homometallic dinuclear complex (**Ru**–**L**–**Ru**, according to our notation above, but where the ancillary ligand was 4,4′-Me_2bpy) are thermally coupled. We are seeing the same effect here for both **Re**–**L**–**Ru** and **Ru**–**L**: *viz* there are two thermally coupled luminescent excited states, of ^{3}Ru→L CT and ^{3}IL(dstyb) character, separated by an energy gap of *ca.* 1750 cm^{-1}. The similar emission lifetime values observed for both A and B bands (for instance, at r.t. for Ru–L, τ = 183 and 210 ns, respectively; see Table 1), are consistent with this coupling. Significantly, we note that for **Re**–**L**–**Ru** no Re-based emission is detected. Any such emission would be expected to be on the blue side of the Ru-based emission maximum. The lack of Re-based emission for **Re**–**L**–**Ru** is ascribed to fast deactivation of the Re-based ^{3}MLCT energy levels, populated after light absorption, in favour of lower lying levels centred on the bridging ligand and/or the Ru fragment (see below).

Fig. 2 shows the 77 K luminescence spectrum for **Re**–**L**–**Ru** (excitation at 372 nm) and the excitation spectra obtained for observation at the emission maxima, 591 nm (band A, ^{3}Ru→L CT nature, τ = 5 μs) and 705 nm [band B, ^{3}IL(dstyb) nature, τ = 10 μs]. At this temperature, the two states are less coupled than at r.t. and comparison of the excitation spectra of **Re**–**L**–**Ru** with the absorption spectra for **Re**–**L**–**Ru** and **Ru**–**L** (Fig. 1) allows identification of the relaxation paths for the excitation energy occurring within the dinuclear complex. For **Re**–**L**–**Ru** the ^{3}IL(dstyb) emission (band B), in addition to intraligand transitions, receives contributions from both ^{1}Ru→L CT (sharp feature at *ca.* 460 nm in the excitation and absorption spectra) and ^{1}Re→L CT transitions (flat region between 380 and 450 nm of the excitation and absorption spectra). Conversely, the ^{3}Ru→L CT emission (band A) is apparently lacking any direct contribution from ^{1}Re→L CT transitions; there is a much weaker intensity in the region characteristic of ^{1}Re→L CT transitions in the excitation spectrum at 77 K and the weak residual intensity in this region of excitation spectrum A may be ascribed to the ^{1}IL(dstyb) transition. We note that at room temperature the excitation spectra taken for the A and B bands of **Re**–**L**–**Ru** are more closely overlapping, as a consequence of the thermal redistribution between the luminescent states.

These results indicate that emission from the ^{3}IL(dstyb) state is directly sensitised by Re-based absorption, whereas the ^{3}Ru→L CT emission is not directly sensitised by Re-based absorption. Thus, some portion of excitation light absorbed by the Re-based chromophore of **Re**–**L**–**Ru** is (i) first transferred to the bridging ligand (giving the ^{3}IL state), and (ii) subsequently redistributed between the luminescent ^{3}IL(dstyb) and ^{3}Ru→L CT levels, a process which is governed by temperature (Scheme 1). According to this description, in **Re**–**L**–**Ru** the overall excitation energy collection process includes an *indirect*, two-

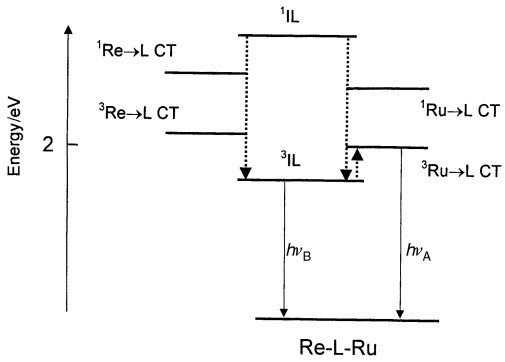

Scheme 1

step Re→Ru energy transfer which is mediated by the spatially interposed dstyb unit such that the ^{3}IL(dstyb) level acts as a 'reservoir' for excitation energy. This reservoir effect has been recognised and documented in a number of recent studies.[8–11]

In order to model the r.t. thermal redistribution between the ^{3}IL(dstyb) and ^{3}Ru→L CT levels [eqn. (1)] of **Re**–**L**–**Ru** and **Ru**–**L**, we have employed τ = 8 μs[6] and 210 ns (Table 1) as intrinsic lifetime values for the separate ^{3}IL(dstyb) and ^{3}CT (Ru-based) luminophores and an energy gap of ΔE = 1750 cm^{-1} between them. We calculate[12] that the thermally equilibrated state contains 86% of the ^{3}Ru→L MLCT level and its decay takes place following a dual exponential law, with τ_1 = 240 ns and τ_2 = 1.4 ns, provided k_1/k_2 = 6 and k_2 = 1 × 10^8 s^{-1} [where k_1 and k_2 are defined in eqn. (1)]. These estimates suggest that the interconversion between the ^{3}IL(dstyb) and ^{3}Ru→L MLCT levels may be affected by different electronic and nuclear factors for the forward (k_1) and backward (k_2) paths, possibly due to the presence of rotamers of dstyb.[13] The fact that the apparent radiative rate constant for the Ru-based luminescence, $k_r \approx 0.2 \times 10^4$ s^{-1} (Table 1), is much lower than that for $[Ru(bpy)_3]^{2+}$, 7.1 × 10^4 s^{-1} (Table 1) has been ascribed to a low efficiency of intersystem processes.[5] However it may well be that the intermixing of ^{3}Ru→L MLCT and ^{3}IL(dstyb) states is in part responsible for this outcome, given that for the latter case k_r is expected 10–10^2 s^{-1}.[7]

We thank the European Community for a post-doctoral fellowship (S. E., contract no. 980226) within the project ERB FMRX-CT98-0226 and for a COST award (COST-D11-0004/98); and the EPSRC (UK) for a Ph.D. studentship (to A. M. B.).

Notes and references

1 V. Balzani, A. Juris, M. Venturi, S. Campagna and S. Serroni, *Chem. Rev.*, 1996, **96**, 759 and references therein; F. Barigelletti and L. Flamigni, *Chem. Soc. Rev.*, 2000, **29**, 1 and references therein.
2 F. Scandola, M. T. Indelli, C. Chiorboli and C. A. Bignozzi, *Top. Curr. Chem.*, 1990, **158**, 75; D. Gust and T. A. Moore, *Top. Curr. Chem.*, 1991, **159**, 103; M. R. Wasielewski, *Chem. Rev.*, 1992, **92**, 365; P. F. H. Schwab, M. D. Levin and J. Michl, *Chem. Rev.*, 1999, **99**, 1863.
3 P. Belser, R. Dux, M. Baak, L. De Cola and V. Balzani, *Angew. Chem., Int. Ed. Engl.*, 1995, **34**, 595.
4 W. B. Davies, W. A. Svec, M. A. Ratner and M. R. Wasielewski, *Nature*, 1998, **396**, 60.
5 J. R. Shaw, R. T. Webb and R. H. Schmehl, *J. Am. Chem. Soc.*, 1990, **112**, 1117.
6 J. R. Shaw and R. H. Schmehl, *J. Am. Chem. Soc.*, 1991, **113**, 389.
7 A. I. Baba, J. R. Shaw, J. A. Simon, R. P. Thummel and R. H. Schmehl, *Coord. Chem. Rev.*, 1998, **171**, 43.
8 W. E. Ford and M. A. J. Rodgers, *J. Phys. Chem.*, 1992, **96**, 2917.
9 G. J. Wilson, W. H. F. Sasse and A. W.-H. Mau, *Chem. Phys. Lett.*, 1996, **250**, 583.
10 D. S. Tyson and F. N. Castellano, *J. Phys. Chem. A*, 1999, **103**, 10 955.
11 M. Hissler, A. Harriman, A. Khatyr and R. Ziessel, *Chem. Eur. J.*, 1999, **5**, 3366; A. Harriman, M. Hissler, A. Khatyr and R. Ziessel, *Chem. Commun.*, 1999, 735.
12 J. N. Demas, *Excited State Lifetime Measurements*, Academic Press, New York, 1983, p. 59.
13 U. Mazzucato and F. Momicchioli, *Chem. Rev.*, 1991, **91**, 1679.

ChemComm

Transcription inhibition by $Rh(phi)_2(phen)^{3+}$

Patty K.-L. Fu and Claudia Turro*

Department of Chemistry, The Ohio State University, Columbus, OH 43210, USA. E-mail: turro.1@osu.edu

Received (in Irvine, CA, USA) 21st September 2000, Accepted 3rd January 2001
First published as an Advance Article on the web 23rd January 2001

$Rh(phi)_2(phen)^{3+}$ (phi = 9,10-phenanthrenequinone diimine, phen = 1,10-phenanthroline) increases the melting temperature (ΔT_m) of a 15-mer duplex DNA by 21 °C and it is able to inhibit transcription *in vitro*; the concentration ratio of $Rh(phi)_2(phen)^{3+}$ relative to DNA bases of the template required to inhibit the RNA transcribed by 50%, R_{inh}^{50}, was found to be 0.13; in contrast, $Rh(phen)_2(phi)^{3+}$, which also possesses the intercalating phi ligand, exhibits only a +7 °C shift in T_m and R_{inh}^{50} = 4.5; $Rh(phen)_3^{3+}$, $RhCl_3$, and ethidium bromide result in negligible or small ΔT_m and exhibit R_{inh}^{50} values that range from 4.8 to 12.5; these results suggest that the intercalation of the phi ligand between the DNA bases and electrostatic binding are not the only means of duplex stabilization by these complexes.

The inhibition of transcription is one of the crucial manners in which the replication of cancerous cells and viruses can be prevented.[1] This mechanism is exploited by antitumor drugs including actinomycin, anthracycline antibiotics and cisplatin, among others.[2] Inhibition of transcription leads to incomplete coding of RNA and proteins, and can ultimately lead to cell death. In the present work we compare duplex stabilization and inhibition of transcription by octahedral $Rh(phi)_n(phen)_{3-n}^{3+}$ (phi = 9,10-phenanthrenequinone diimine, phen = 1,10-phenanthroline; n = 0, 1, 2) complexes, some of which possess the intercalative phi ligand (structures shown in Fig. 1). The interactions and reactivity of phi complexes of Rh(III) with DNA have been extensively investigated.[3]

Two-dimensional ^{1}H NMR spectroscopy was previously utilized to investigate the binding of Rh(III) complexes possessing a single phi ligand to duplex DNA, including $Rh(NH_3)_4(phi)^{3+}$,[4] $Rh(phen)_2(phi)^{3+}$,[5] Δ-α-Rh[(*R*,*R*)-Me_2-trien]phi^{3+} [(*R*,*R*)-Me_2trien = 2*R*,9*R*-diamino-4,7-diazadecane],[6] and $Rh(en)_2(phi)^{3+}$ (en = ethylenediamine).[7] These NMR studies, as well as the crystal structure of Δ-α-Rh[(*R*,*R*)-Me_2trien](phi)$^{3+}$ bound to an eight base-pair oligonucleotide duplex,[8] show that the binding of these complexes to DNA takes place through the intercalation of the phi ligand between the bases of the duplex from the major groove. Although bis-phi complexes of Rh(III), such as $Rh(phi)_2(bpy)^{3+}$ (bpy = 2,2′-bipyridine), are better DNA photocleavage agents than those possessing a single phi ligand,[3] no ^{1}H NMR studies or crystal structures have been reported to date on their DNA binding.

The shifts in the melting temperatures (ΔT_m) of a 15-mer oligonucleotide duplex (see Table 1 for sequence) in the presence of $Rh(phi)_n(phen)_{3-n}^{3+}$ (n = 0, 1, 2), $RhCl_3$, and ethidium bromide are listed in Table 1.[9] The relative concentration of metal complex or ion was fixed at R = 0.067 (R = [complex]/[bases]; two metal complexes per duplex). Inspection of Table 1 reveals that the complex with two phi ligands results in the largest increase in the melting temperature of the duplex. An increase in T_m of 21 °C was measured in the presence of $Rh(phi)_2(phen)^{3+}$ relative to free duplex, and a ΔT_m value of +7 °C was observed for $Rh(phen)_2(phi)^{3+}$. Ethidium bromide, a known DNA intercalator, results in ΔT_m of +5 °C. The Rh^{3+} ion, $RhCl_3$, and the non-intercalative $Rh(phen)_3^{3+}$ complex resulted in negligible changes to T_m.

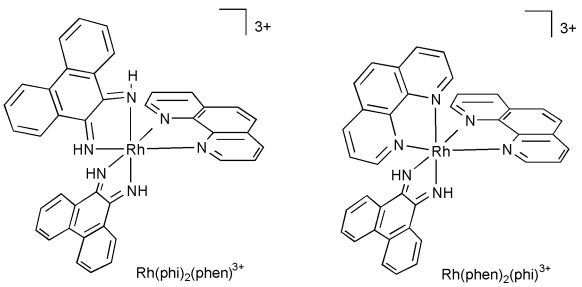

Fig. 1 Structures of $Rh(phi)_2(phen)^{3+}$ and $Rh(phen)_2(phi)^{3+}$.

The ability of $Rh(phi)_2(phen)^{3+}$ to stabilize duplex DNA led us to hypothesize that it may hinder elongation during the transcription process. The imaged agarose gel showing the RNA transcribed *in vitro* in the presence of various concentrations of $Rh(phi)_2(phen)^{3+}$ is shown in Fig. 2.[10] It is clear from Fig. 2 that an increase in the concentration of $Rh(phi)_2(phen)^{3+}$ relative to DNA template, R, results in a decrease in the amount of RNA produced. The ratio at which 50% of the RNA is

Table 1 Changes in melting temperatures (ΔT_m) of a 15-mer duplex in the presence of various metal complexes and R_{inh}^{50} for each complex

Duplex = 5′-AGTGCCAAGCTTGCA-3′ / 3′-TCACGGTTCGAACGT-5′

Complex	ΔT_m[a]/°C	R_{inh}^{50}
$Rh(phi)_2(phen)^{3+}$	21	0.13
$Rh(phen)_2(phi)^{3+}$	7	4.5
$Rh(phen)_3^{3+}$	3	6.2
$RhCl_3$	3	12.5
Ethidium bromide	5	4.8

[a] Error = ±2 °C; for duplex only T_m = 55 °C; measurements performed in 5 mM Tris (pH = 7.5, 50 mM NaCl) with [complex]/[bases] = 0.067 (2 complexes per duplex) and [bases] = 20–30 μM; T_m values determined from the changes in absorbance at 260 nm using the HP Biochemical Analysis software on a diode array spectrometer (HP 8453) in a sample holder equipped with a Peltier temperature controller (1 cm path length).

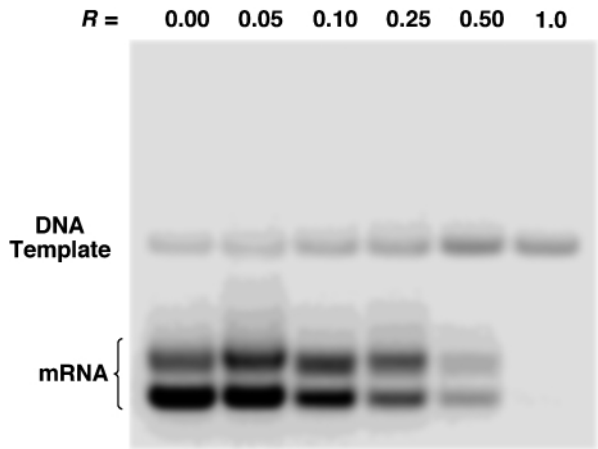

Fig. 2 Ethidium bromide stained agarose gel (1%) of transcribed mRNA in the presence of $Rh(phi)_2(phen)^{3+}$ at various [Rh]/[template DNA base] ratios, R. Both the DNA template (150 μM) and mRNA are imaged on the gel (labeled). See ref. 10 for a detailed description.

transcribed, R_{inh}^{50}, for each complex, $RhCl_3$, and ethidium bromide are listed in Table 1. The values of R_{inh}^{50} presented in Table 1 reveal that $Rh(phi)_2(phen)^{3+}$ inhibits transcription to a much greater extent than $Rh(phen)_2(phi)^{3+}$, although both complexes possess the intercalative phi ligand. In addition, large R_{inh}^{50} values were measured for $Rh(phen)_3^{3+}$, $RhCl_3$ and the intercalator ethidium bromide.

One possible explanation of the observed results is that the complexes that bind more strongly to double stranded DNA might play a greater role in duplex stabilization and transcription inhibition. However, it appears that R_{inh}^{50} is related to ΔT_m rather than K_b. For example, the K_b value for $Rh(phen)_2(phi)^{3+}$ is $\approx 10^6\ M^{-1}$,[11,12] for $Rh(phen)_3^{3+}$ $K_b \approx 10^3\ M^{-1}$,[12] and for ethidium bromide $K_b = 1.7\times10^5\ M^{-1}$,[13] however, the R_{inh}^{50} and ΔT_m values for all three molecules are similar (see Table 1). Although the role of the binding constant cannot be completely discounted at this time, it does not appear that the binding constant of each complex to duplex DNA plays a role in transcription inhibition or duplex stabilization.

Experiments were also performed to ensure that binding of the complexes to T7-RNA polymerase was not the mechanism of transcription inhibition. $Rh(phi)_2(phen)^{2+}$ binds duplex DNA with $K_b \approx 10^7\ M^{-1}$,[11] therefore with 15 μM $Rh(phi)_2(phen)^{2+}$ and 150 μM DNA bases ($R = 0.10$) it would be expected that $\approx 10^{-8}$ M rhodium complex would remain free in solution which could bind to the enzyme ($\approx 10^{-9}$ M). Experiments with an order of magnitude less complex and DNA [1.5 μM $Rh(phi)_2(phen)^{2+}$, 15 μM bases] utilizing the same enzyme concentration ($\approx 10^{-9}$ M) resulted in negligible change to the inhibition of transcription relative to that measured with 15 μM complex and 150 μM DNA bases.[10] In addition, no change in the R_{inh}^{50} was observed with a 10-fold increase in T7-RNA polymerase with 15 μM $Rh(phi)_2(phen)^{2+}$ and 150 μM bases (15 min reaction time).[10] These results are inconsistent with an inhibition mechanism that involves the association of the complex to the enzyme. To exclude displacement of Mg^{2+} ions by the metal complexes, aggregation of oligonucleotides, and non-specific ionic binding of the complexes to the duplex, the transcription reaction was carried out with $Rh(phi)_2(phen)^{3+}$ at $R = 0.10$ and either 6 mM or 12 mM Mg^{2+}. The use of 12 mM instead of 6 mM $MgCl_2$, under the same conditions, did not result in increased transcription.

The largest shifts in the duplex melting temperatures, ΔT_m, and the lowest concentrations of complex required to observe the transcription inhibition, R_{inh}^{50}, were measured for $Rh(phi)_2(phen)^{3+}$, which possesses two quinone diimine phi ligands in the octahedral coordination sphere of the Rh(III) metal center. Since $Rh(phen)_2(phi)^{3+}$ behaves similarly to $Rh(phen)_3^{3+}$ intercalation of the phi ligand or charge on the complex are not the sole reasons for the increased duplex stabilization or transcription inhibition observed for $Rh(phi)_2(phen)^{3+}$. One explanation of our observations is that the four imine protons of the two phi ligands of $Rh(phi)_2(phen)^{3+}$, which are not present in the other complexes, makes hydrogen bonding possible between $Rh(phi)_2(phen)^{3+}$ and the DNA nucleotides and backbone. The recent crystal structure of Δ-α-Rh[(*R*,*R*)-Me_2trien](phi)$^{3+}$ bound to duplex DNA shows that two binding modes are present. In both binding modes the phi ligand is intercalated between the DNA bases. The amino protons of the (*R*,*R*)-Me_2trien ligand located above and below the phi plane are involved in hydrogen bonding with two nearby guanines in one binding mode and with ordered water molecules hydrogen-bonded to the guanines in the other.[8] Furthermore, the two imine protons of the phi ligand are hydrogen bonded to ordered water molecules in the structure.[8]

$Rh(phi)_2(phen)^{3+}$ stabilizes the duplex DNA structure and inhibits the transcription process *in vitro* at 35-fold lower concentration than $Rh(phen)_2(phi)^{3+}$. This finding suggests that intercalation of the phi ligand and the 3+ charge on the complex are not the only factors involved in duplex stabilization. One possible explanation for the observed results is the deformation of the double helix through the binding of the $Rh(phi)_2(phen)^{3+}$ complex at various sites on the DNA template. Another possibility is that hydrogen bonding, either directly to the DNA or through ordered water molecules, may play a role in the binding of $Rh(phi)_2(phen)^{3+}$ to DNA and in the stabilization of the duplex structure, thus resulting in inhibition of transcription.

This work was partially supported by The National Science Foundation (CHE-9733000) and The Arnold and Mabel Beckman Foundation.

Notes and references

1 W. S. Yarnell and J. W. Roberts, *Science*, 1999, **284**, 61; Y. Nibu, H. Zhang and M. Levine, *Science*, 1998, **280**, 101; A. P. Wolffe, *Science*, 1996, **272**, 371; A. P. Wolffe, *Science*, 1994, **264**, 1100; P. C. Hanawalt, *Science*, 1994, **266**, 1957.

2 E. R. Jamieson and S. J. Lippard, *Chem. Rev.*, 1999, **99**, 2467; W. Chu, M. Shinomiya, K. Y. Kamitori, S. Kamitori, R. G. Carlson, R. F. Weaver and F. Takusagawa, *J. Am. Chem. Soc.*, 1994, **116**, 7971; D. J. Taatjes, G. Gaudiano, K. Resing and T. J. Koch, *Med. Chem.*, 1997, **40**, 1276; H. A. Kester, C. Blanchetot, J. Den Hertog, P. T. Van der Saag and B. Van der Burg, *J. Biol. Chem.*, 1999, **274**, 27 439.

3 R. H. Terbrueggen, T. W. Johann and J. K. Barton, *Inorg. Chem.*, 1998, **37**, 6874; C. Turro, D. B. Hall, W. Chen, H. Zuilholf, J. K. Barton and N. J. Turro, *J. Phys. Chem. A*, 1998, **102**, 5708; P. J. Dandliker, R. E. Holmlin and J. K. Barton, *Science*, 1997, **275**, 1465; D. B. Hall, R. E. Holmlin and J. K. Barton, *Nature*, 1996, **382**, 731; N. Y. Sardesai, K. Zimmermann and J. K. Barton, *J. Am. Chem. Soc.*, 1994, **116**, 7502; A. H. Krotz, B. P. Hudson and J. K. Barton, *J. Am. Chem. Soc.*, 1993, **115**, 12 577; A. H. Krotz, L. Y. Kuo, T. P. Shields and J. K. Barton, *J. Am. Chem. Soc.*, 1993, **115**, 3877; A. Sitlani, C. M. Dupureur and J. K. Barton, *J. Am. Chem. Soc.*, 1993, **115**, 12 589.

4 J. G. Collins, T. P. Shields and J. K. Barton, *J. Am. Chem. Soc.*, 1994, **116**, 9840.

5 S. S. David and J. K. Barton, *J. Am. Chem. Soc.*, 1993, **115**, 2984.

6 B. P. Hudson and J. K. Barton, *J. Am. Chem. Soc.*, 1998, **120**, 6877.

7 T. P. Shields and J. K. Barton, *Biochemistry*, 1995, **34**, 15 049.

8 C. L. Kielkopf, K. E. Erkkila, B. P. Hudson, J. K. Barton and D. C. Rees, *Nat. Struct. Biol.*, 2000, **7**, 117.

9 $RhCl_3$ and ethidium bromide were purchased from Aldrich and used without further purification. $Rh(phi)_n(phen)_{3-n}^{3+}$ ($n = 0, 1, 2$) complexes were synthesized following methods previously reported (refs. 3 and 11).

10 The *in vitro* transcription experiments used the pGEM Express Positive Control DNA Template (Promega, 3995 base pairs) and the Ribomax Large Scale RNA Production System with T7 RNA polymerase (Promega). The transcription was allowed to proceed for 1 h at 37 °C (40 mM Tris, 10 mM NaCl, pH = 7.5) in nuclease-free water in the presence of 6 mM $MgCl_2$, 2 mM spermidine and 2.5 mM each ATP, CTP, GTP and UTP. The ethidium bromide stained agarose gels were imaged on a Bio-Rad GelDoc 2000 transilluminator, and quantitative data was determined using Quantiy One software (Bio-Rad).

11 A. Sitlani, E. C. Long, A. M. Pyle and J. K. Barton, *J. Am. Chem. Soc.*, 1992, **114**, 2303.

12 K. Uchida, A. M. Pyle, T. Morii and J. K. Barton, *Nucl. Acids Res.*, 1989, **17**, 10 259.

13 T.-C. Tang and H.-J. Huang, *Electroanalysis (N.Y.)*, 1999, **11**, 1185; C. Paoletti, J. B. Le Pecq and I. R. Lehman, *J. Mol. Biol.*, 1971, **55**, 75.

A novel photoelectrochemical method of metal corrosion prevention using a TiO_2 solar panel

Hyunwoong Park,[a] Kyoo Young Kim[b] and Wonyong Choi*[a]

[a] *School of Environmental Engineering, Pohang University of Science and Technology, Pohang, 790-784, Korea. E-mail: wchoi@postech.ac.kr*

[b] *Department of Materials Science and Metallurgical Engineering, Pohang University of Science and Technology, Pohang, 790-784, Korea*

Received (in Cambridge, UK) 9th October 2000, Accepted 3rd January 2001
First published as an Advance Article on the web 23rd January 2001

By using a simple TiO_2 solar panel connected to a steel electrode, the concept of photoelectrochemical metal corrosion prevention has been demonstrated to be feasible in utilizing solar light for corrosion inhibition.

Ever since Fujishima and Honda[1] reported the water splitting reaction on illuminated TiO_2 electrodes, semiconductor photoelectrochemistry has been applied to a wide variety of issues such as chemical or electrical conversion of solar energy,[2] pollutant degradation,[3] and superhydrophilic materials,[4] all of which are based on photo-induced charge transfer processes at the semiconductor interface. Here we report another novel application of semiconductor photoelectrochemistry: *metal corrosion prevention*.

The common strategy of corrosion prevention is to change the potential of the corroding metal by pumping electrons in, which is widely known as cathodic protection.[5] When using a sacrificial anode that is more active (negative) in corrosion potential than the metal to be protected, the electrons generated from the corroding sacrificial anode are transferred to the metal object to reduce its corrosion rate [Scheme 1(a)]. The basic idea of this investigation is to replace the sacrificial anode with a semiconductor photoanode that generates conduction band (CB) electrons upon band-gap illumination [Scheme 1(b)]. Previous work by Yuan and Tsujikawa,[6] which reported that the potential of a TiO_2-coated copper substrate drastically shifted toward the less noble (negative) direction under illumination, suggests the idea of using a semiconductor photoanode for corrosion prevention is plausible.

Corrosion prevention experiments were carried out with a photoelectrochemical set-up that consists of a flat solar panel containing a semiconductor (TiO_2) photoanode in a hole-scavenging medium and a steel electrode immersed in an aqueous solution. The semiconductor photoanode was prepared by applying a TiO_2 (Degussa P25) suspension (5 wt%) to an indium tin oxide (ITO) glass slide (Delta technology, 14.8 cm^2). The TiO_2 coated slide was dried in air for 1 h and annealed at 450 °C for 30 min. Electrical contact was made by attaching copper wire with silver paste at the uncoated edge of the ITO slide. The TiO_2/ITO electrode was placed in the solid-phase hole-scavenging medium (6.8 g sodium formate per g agar gel) and encased in a transparent Petri dish to form a flat solar cell. The carbon steel electrode was circular (surface area: 1.66 cm^2) and mechanically polished. The backside and edges of the steel electrode were covered with epoxy resin to expose the flat surface to the aqueous solution in the corrosion cell. The TiO_2/ITO electrode and the steel electrode were galvanically coupled through an external circuit and the two cells were connected by a salt bridge (saturated KCl in agar contained in a flexible Tygon tube). When necessary, 0.05 M K_2CO_3 was added as a supporting electrolyte to the cathodic compartment (corrosion cell) in order to eliminate any possible ohmic potential drop. The light source was 10 W blacklight lamps (1, 2 and 3 lamps for 10, 20 and 30 W illumination, respectively) or a 200 W mercury lamp. The intensities of UV light ($300 < \lambda < 400$ nm) (to excite the TiO_2 photoanode) were estimated to be 58, 100, 135 μW cm^{-2} for 10, 20 and 30 W illumination and 1.53 mW cm^{-2} for the 200 W lamp. Natural solar light UV intensity has been measured to be 1.55 mW cm^{-2} around noon. The TiO_2/ITO electrode was illuminated from the ITO side. Potentials (*vs.* SCE) and currents during illumination were measured using a potentiostat (EG&G, model 263A).[7] The corroded steel surface was analyzed by a Raman spectrometer (Renishaw system 3000) in backscatter geometry with an excitation wavelength of 632.8 nm (He–Ne laser).

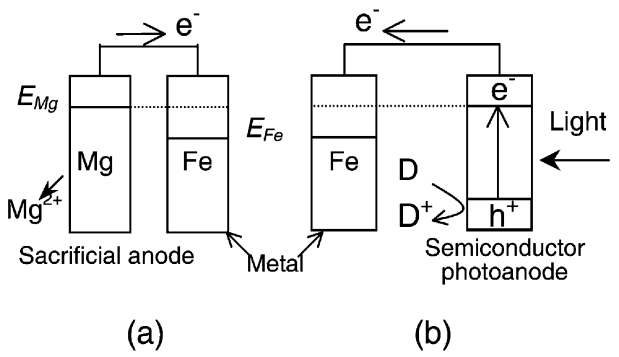

Scheme 1 Schematic representation of metal (Fe) corrosion prevention using (a) a conventional sacrificial anode (*e.g.* Mg) and (b) a semiconductor photoanode investigated in this study; D represents hole scavengers while dashed lines represent the electrochemical potential of the electrons generated in the anode.

Fig. 1(a) shows the changes of potentials and currents in the galvanic couple of the TiO_2 photoanode (solar panel) and the steel electrode in acidic water (pH 4) when the photoanode is illuminated under different sources of light. Under illumination, the coupled photopotential, E_{ph}, immediately shifted to more negative potential with a concurrent increase of photocurrent, I_{ph}. The open circuit potential (E_{oc}) of the TiO_2 anode in the solar panel under 30 W illumination was −0.9 V (*vs.* SCE). Comparing this with E_{oc} of the steel electrode (−0.44 V *vs.* SCE), the illuminated TiO_2 anode can supply CB electrons to the metal electrode to protect the metal cathodically by setting a new mixed potential of the couple, E_{ph}. As monitored in this study the value of E_{ph} remained constant under illumination up to 35 days. Natural solar light was as effective as use of a 200 W lamp in inducing changes in E_{ph} and I_{ph}. In addition, a blank test was performed in the absence of added hole scavengers where E_{ph} and I_{ph} were measured to be *ca.* −0.45 to −0.50 V (*vs.* SCE) and 8 μA under 30 W illumination. Various alcohols and organic acids were tested as hole scavengers of which formate was found to show the best performance.

E_{ph} and I_{ph} were measured as a function of pH in the corrosion cell under constant light intensity [Fig. 1(b)]. The dark corrosion currents (I_{corr}) of the steel electrode increased from 0.1 to 360 μA cm^{-2} on lowering the pH from 11 to 2. As E_{ph} shifted in the positive direction under more corrosive

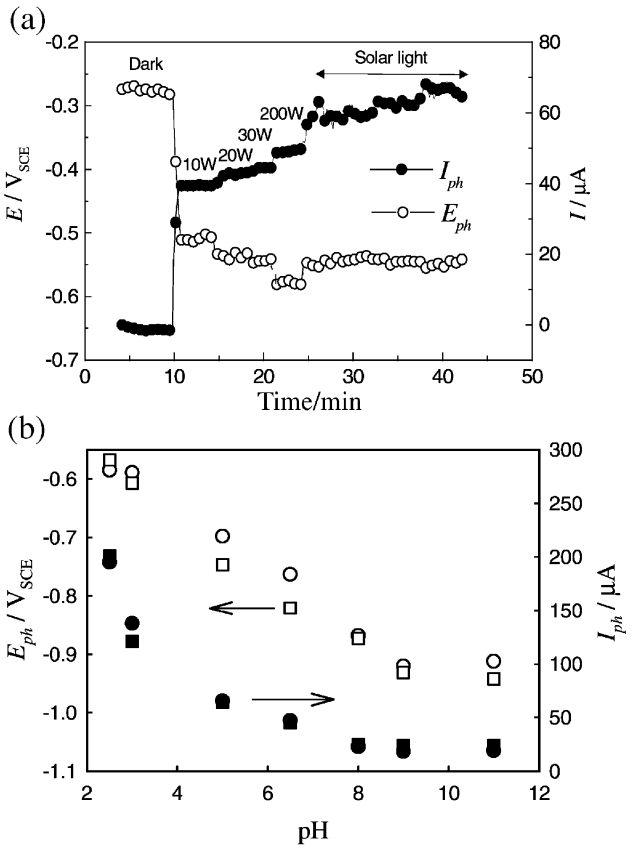

Fig. 1 (a) The change of E_{ph} and I_{ph} in the galvanic couple of a TiO_2 photoanode and the steel electrode when the photoanode was irradiated by 10, 20, 30 or 200 W lamp or solar light. (b) E_{ph} (open symbols) and I_{ph} (filled symbols) as a function of pH under 30 W (circles) or 200 W (squares) illumination.

conditions (lower pH), I_{ph} logarithmically increased even under constant light intensity. There was little dependence on light intensity (30 *vs.* 200 W lamp). Although the present system is essentially identical to a typical photoelectrochemical cell that converts light into electricity where I_{ph} is proportional to the light intensity,[2a] it is clearly distinguished from the latter by the fact that its performance depends little on the light intensity as long as there are enough photons to compensate the dark corrosion current.

Evidence of corrosion prevention of the steel connected to the solar panel was obvious enough to be detected visually. The shiny surface of the steel electrode remained intact in a corrosive electrolyte solution as long as it was connected to the solar panel, while it quickly corroded and was covered by red–brown rust in the absence of light. The progress of corrosion was quantitatively assessed by measuring the Raman spectra of steel surfaces. Fig. 2 compares the Raman spectra of the steel surface corroded in 0.05 M K_2CO_3 solution at pH 6 for 30 h under different illumination conditions. All the peaks generated as a result of corrosion are ascribed to various phases of iron oxides.[8] While the steel surface connected to a continuously illuminated photoanode showed no sign of iron oxide formation, a thick layer of iron oxides covered the steel surface under the dark condition. The steel sample tested under the natural solar light showed an intermediate level of iron oxide formation since more than half of the total corrosion time was during night time or when cloudy.

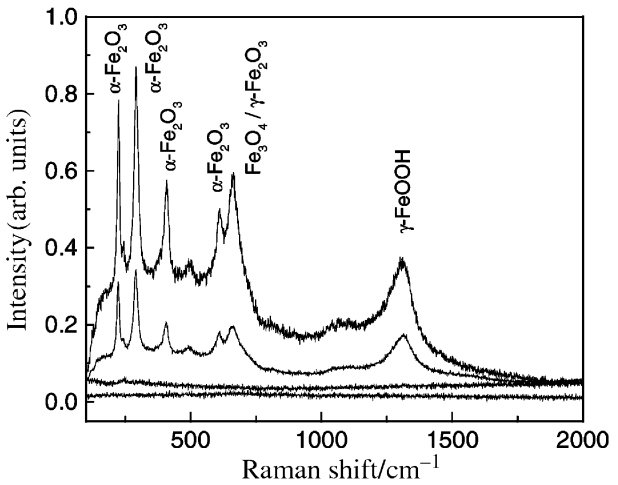

Fig. 2 Raman spectra of the steel surface corroded under different illumination conditions (from the bottom up) of an initial steel surface; a continuously illuminated sample (30 W lamp); sunlight illuminated (16 h day plus 14 h night) sample in the open air; and a control sample not connected to the photoanode.

It has been clearly demonstrated in this work that a simple TiO_2 solar panel can prevent metal corrosion. In view of the fact that the conventional sacrificial anode must be buried or immersed in the medium along with the metal object to be protected and be replaced periodically,[5] use of a photoanode installed on the ground level is easier to maintain. Although the TiO_2 photoanode itself is non-sacrificial, the TiO_2 solar panel is sacrificial since the formate added as a hole scavenger is irreversibly oxidized. However, the hole scavenging medium could be easily refilled to make it regenerative. A similar approach could be possible by using a silicon-based solar cell although it is not economically feasible. Even though the present method suffers from several limitations such as the absence of light at night[9] and the depletion of the hole-scavenging medium, it verifies the possibility of using solar light for corrosion inhibition and could be developed into an alternative or ancillary corrosion prevention method.

Notes and references

1 A. Fujishima and K. Honda, *Nature*, 1972, **238**, 37.
2 (*a*) M. K. Nazeeruddin, A. Kay, I. Rodicio, R. Humphry-Baker, E. Müller, P. Liska, N. Vlachopoulos and M. Grätzel, *J. Am. Chem. Soc.*, 1993, **115**, 6382; (*b*) H. G. Kim, D. W. Hwang, J. Kim, Y. G. Kim and J. S. Lee, *Chem. Commun.*, 1999, 1077; (*c*) K. Hoshino, M. Inui, T. Kitamura and H. Kokado, *Angew. Chem., Int. Ed.*, 2000, **39**, 2509.
3 M. R. Hoffmann, S. T. Martin, W. Choi and D. W. Bahnemann, *Chem. Rev.*, 1995, **95**, 69.
4 R. Wang, K. Hashimoto, A. Fujishima, M. Chikuni, E. Kojima, A. Kitamura, M. Shimohigoshi and T. Watanabe, *Nature*, 1997, **388**, 431.
5 D. A. Jones, *Principles and Prevention of Corrosion*, Prentice Hall, NJ, 2nd edn., 1996.
6 J. Yuan and S. Tsujikawa, *J. Electrochem. Soc.*, 1995, **142**, 3444.
7 The potentiostat that runs a Galvanic corrosion experiment with 'SoftCorr III' software, in effect, functions as a zero-resistance ammeter.
8 L. J. Oblonsky and T. M. Devine, *Corros. Sci.*, 1995, **37**, 17.
9 This could be overcome by charging a battery connected to the solar panel by day and switching the discharging current to the metal object at night. In a preliminary experiment we confirmed that the progress of corrosion was reduced when a rechargeable battery was connected to the steel electrode at night.

ChemComm

A well defined tin(II) initiator for the living polymerisation of lactide

Andrew P. Dove, Vernon C. Gibson,* Edward L. Marshall, Andrew J. P. White and David J. Williams

Department of Chemistry, Imperial College of Science, Technology and Medicine, Exhibition Road, South Kensington, London, UK SW7 2AY. E-mail: v.gibson@ic.ac.uk

Received (in Cambridge, UK) 31st October 2000, Accepted 14th December 2000
First published as an Advance Article on the web

[HC{C(Me)NAr}$_2$]Sn(OPr^i) (Ar = 2,6-Pr$^i_2$C$_6$H$_3$) is shown to be an initiator for the living polymerisation of *rac*-lactide to heterotactic-enriched poly(lactide).

There is increasing interest in the design of polymers for *in vivo* applications such as sutures, artificial tissue networks and drug delivery agents. For these applications it is desirable for the polymer to be non-toxic, biocompatible and resorbable. One of the most promising classes of polymer in this field is the poly(lactide)s[1] which are readily obtained in a controlled manner *via* the living ring-opening polymerisation of lactide, the cyclic diester of lactic acid.[2]

Initiators for lactide polymerisation are typically based on alkoxide or alkanoate complexes of metals such as Al, Mg, Sn, Zn and the rare earths. Tin(II) catalysts such as Sn(ethyl hexanoate)$_2$ are generally preferred in the commercial production of poly(lactide)s[3] for medical or pharmaceutical applications owing to the low toxicity of Sn(II) compared to other metal ions [Sn(ethyl hexanoate)$_2$ is a permitted food additive in many countries]. Although a number of systems based on aluminium,[4] and more recently, magnesium[5] and zinc,[6] have been described that initiate the living ring-opening polymerisation of lactide, there have to date been no reports of well defined tin initiators. Here we describe the first example of a single-site tin catalyst for the living polymerisation of lactide.

The initiator **2** is prepared according to Scheme 1.† Treatment of $SnCl_2$ with [HC{C(Me)NAr}$_2$]Li in diethyl ether followed by crystallisation from pentane affords [HC{C(Me)-NAr}$_2$]SnCl **1** as a yellow crystalline solid. This is converted to **2** by treatment with LiOPr^i followed by recrystallisation from pentane. Crystals of **2** suitable for an X-ray structure determination‡ were grown from pentane; the structure is shown in Fig. 1.

The complex has non-crystallographic C_s symmetry with the three-coordinate tin atom adopting a tripodal geometry with inter-bond angles in the range 83.6(2)–94.1(2)°, the most acute being associated with the bite of the chelating N,N′ ligand. The Sn–N and Sn–O distances are unexceptional, and there is the expected pattern of delocalisation within the β-diketiminate ligand. The six-membered chelate ring has a boat conformation

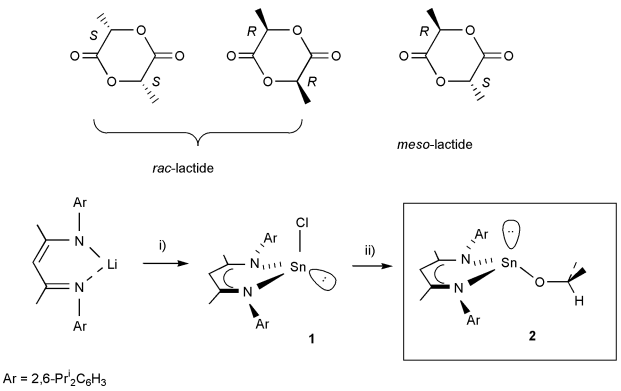

Scheme 1 *Reagents and conditions*: i, $SnCl_2$, Et_2O, 18 h, recrystallisation from pentane, 60% yield (unoptimised); ii, LiOPr^i, Et_2O, 18 h, recrystallisation from pentane, 17% yield (unoptimised).

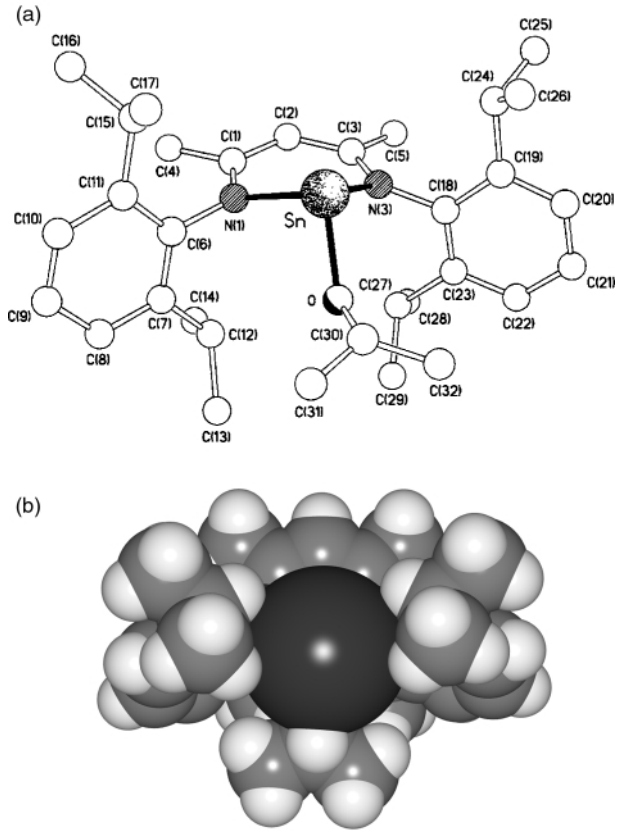

Fig. 1 (a) The molecular structure of **2**. Selected bond lengths (Å) and angles (°); Sn–O 2.000(5), Sn–N(1) 2.206(4), Sn–N(3) 2.208(4), C(1)–N(1) 1.323(6), C(1)–C(2) 1.404(7), C(2)–C(3) 1.387(7), C(3)–N(3) 1.331(6); O–Sn–N(1) 94.1(2), O–Sn–N(3) 92.5(2), N(1)–Sn–N(3) 83.6(2). (b) Space filling representation of the structure of **2** showing the exposed environment of the tin atom.

with C(2) and Sn lying 0.12 and 0.87 Å 'above' the N(1), C(1), C(3), N(3) plane; the isopropoxide oxygen atom lies 0.74 Å 'below' this plane. As a consequence of the folded chelate ring conformation, and retention of near trigonal planar geometries at the two nitrogen centres, the C(12) and C(27) isopropyl groups are drawn together, and those associated with C(15) and C(24) are folded away exposing the non-coordinated 'face' containing the stereochemically active lone pair on the tin atom [Fig. 1(b)]; the shortest intermolecular approach to the tin centre is 3.84 Å from C(13)–H.

The polymerisation of *rac*-lactide (a racemic mixture of L (*S*,*S*) and D (*R*,*R*) lactides) was initially investigated using complex **2** in CH_2Cl_2 at ambient temperature.§ Under these conditions it was found that 100 equivalents of monomer required 96 h for complete conversion (> 99% by ^{1}H NMR). The resultant polymer has a molecular weight close to that calculated from the monomer : initiator ratio (observed M_n = 17 100; calculated M_n = 14 400) and exhibits a narrow polydispersity (M_w/M_n = 1.11), characteristics of a living process. The polymerisation was then repeated at 60 °C in

DOI: 10.1039/b008770j

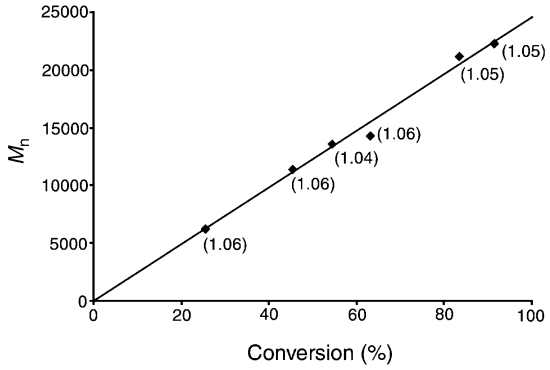

Fig. 2

toluene affording 85% conversion after 4 h, again resulting in a narrow molecular weight distribution product (M_w/M_n = 1.05). The activity of the tin catalyst is lower than that observed for the related zinc system[6] which may be in part due to the lower electrophilicity of the tin centre, and partly a consequence of the stereochemically active lone pair which may disfavour monomer binding. The living characteristics of the polymerisation are supported by the linear increase in M_n with conversion giving in each case a low polydispersity product (Fig. 2).

In order to confirm that the initiator is indeed the isopropoxide complex **2**, a ^{1}H NMR study was carried out in which increasing amounts of lactide were added to **2** in $CDCl_3$. The isopropoxide methine septet resonance at the end of the propagating chain is shifted slightly to higher frequency (0.005 ppm) relative to the unconsumed initiator (δ 4.01). New resonances for the β-diketiminate ligand substituents are also observed for the propagating species. As the number of monomer equivalents is increased, the intensities of the signals attributable to the propagating species increase relative to those of unconsumed **2**. Owing to the overlapping nature of the resonances, accurate integration has not been possible, but the addition of 5 equivalents of monomer leads to an approximately 1 : 1 mixture of initiator : propagating species. This indicates a favourable k_p/k_i ratio (the rate constant of propagation to rate constant of initiation) which is desirable for minimising the polydispersity.

The ^{1}H NMR spectrum of the poly(lactide) derived from **2** (Fig. 3) differs from the spectrum predicted from a Bernouillian analysis of totally random poly(*rac*-lactide), with the *rmr* and *mrm* tetrads much more intense than expected. These observations are consistent with a heterotactic-biased product since the *rmr* microstructure can only arise from two consecutive D–L or L–D interchanges; each *rmr* tetrad is accompanied by two *mrm* tetrads in agreement with the NMR integration. The preference for heterotacticity is not as strong as reported previously for the zinc analogue of **2**, but nonetheless represents the first example of tacticity bias arising from the polymerisation of *rac*-lactide using a tin catalyst.

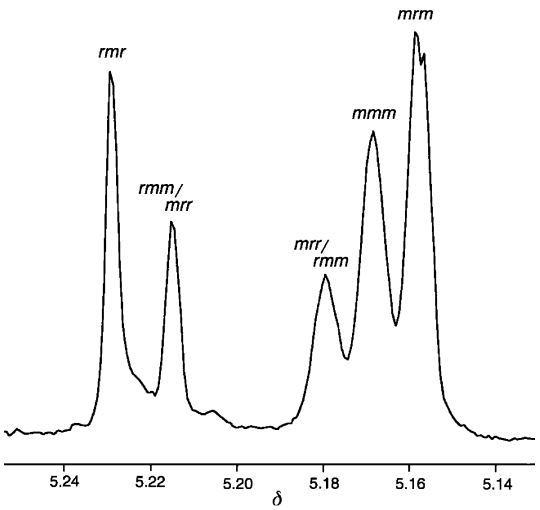

Fig. 3

Further studies are examining the effect of changes to the aryl ligand substituents on the polymerisation behaviour of the tin catalysts and their use in the ring-opening polymerisation of other cyclic ester monomers.

The Engineering and Physical Sciences Research Council is thanked for a studentship (to A. P. D.) and a postdoctoral fellowship (to E. L. M.).

Notes and references

† *Selected spectroscopic data*: for **1**: δ_H(250 MHz, C_6D_6, 25 °C) 1.06 (d, 6H, $^3J_{HH}$ 6.8 Hz, CHMe*Me*), 1.18 (d, 6H, $^3J_{HH}$ 6.9 Hz, CH*Me*Me), 1.22 (d, 6H, $^3J_{HH}$ 6.8 Hz, CHMe′*Me*′), 1.45 (d, 6H, $^3J_{HH}$ 6.6 Hz, CH*Me*′Me′), 1.61 (s, 6H, HC{C(*Me*)NAr}$_2$), 3.12 (sept, 2H, $^3J_{HH}$ 6.8 Hz, C*H*Me$_2$), 3.95 (sept, 2H, $^3J_{HH}$ 6.8 Hz, C*H*Me$_2$), 5.06 (s, 1H, *H*C{C(Me)NAr}$_2$), 7.15 (m, 6H, H_{aryl}). MS: *m/z* 572 $[M]^+$. Anal. Calc. (found) for $C_{29}H_{41}ClN_2Sn$: C, 60.91 (60.77); H, 7.22 (7.32); N, 4.90 (5.07)%. For **2**: δ_H(250 MHz, C_6D_6, 25 °C) δ 0.90 (d, 6H, $^3J_{HH}$ 6.8 Hz, OCH*Me*$_2$), 1.14 (d, 3H, $^3J_{HH}$ 6.8 Hz, CHMe*Me*), 1.24 (d, 3H, $^3J_{HH}$ 6.9 Hz, CH*Me*Me), 1.27 (d, 3H, CHMe′*Me*′), 1.54 (d, 3H, CH*Me*′Me′), 1.59 (s, 6H, HC{C(*Me*)NAr}$_2$), 3.25 (sept, 2H, $^3J_{HH}$ 6.8 Hz, C*H*Me$_2$), 3.86 (sept, 2H, $^3J_{HH}$ 6.8 Hz, C*H*Me$_2$), 4.15 (sept, 1H, $^3J_{HH}$ 6.0 Hz, OC*H*Me$_2$), 4.73 (s, 1H, *H*C{C(Me)NAr}$_2$), 7.16 (m, 6H, H_{aryl}). Anal. Calc. (found) for $C_{32}H_{48}N_2OSn$: C, 64.55 (64.28); H, 8.13 (8.08); N, 4.70 (4.90)%.

‡ *Crystal data* for **2**: $C_{32}H_{48}N_2OSn$, *M* 595.4, monoclinic, space group $P2_1/n$ (no. 14), a = 13.205(2), b = 16.680(2), c = 15.527(2) Å, β = 107.42(1)°, V = 3263.1(6) Å^3, Z = 4, D_c = 1.212 g cm^{-3}, μ(Mo-Kα) = 8.07 cm^{-1}, T = 293 K, yellow blocks; 5742 independent measured reflections, F^2 refinement, R_1 = 0.049, wR_2 = 0.112, 4038 independent observed reflections [$|F_o| > 4\sigma(|F_o|)$, $2\theta \leqslant 50°$], 326 parameters. CCDC 151597. See http://www.rsc.org/suppdata/cc/b0/b008770j/ for crystallographic files in .cif or other electronic format.

§ *Typical polymerisation procedure*: complex **2** (0.005 g, 0.008 mmol) and *rac*-lactide (0.1181 g, 0.819 mmol) were weighed in to a 15 cm^3 glass ampoule fitted with a Teflon stopcock. The mixture was suspended in toluene (6 cm^3) and the ampoule was then sealed and transferred to an oil bath pre-heated to 60 °C. After stirring for the allotted period of time the volatile components were removed *in vacuo*. Conversion was determined by integration of monomer *vs.* polymer methine resonances in the ^{1}H NMR spectrum of the crude product (in $CDCl_3$). The polymer was purified by redissolving in CH_2Cl_2 (5 cm^3) and precipitating from rapidly stirring methanol. GPC chromatograms were recorded on a Knauer differential refractometer connected to a Gynotek HPLC pump (model 300) and two 10 μm columns (PSS) at a flow rate of 1.00 cm^3 min^{-1} using $CHCl_3$ as the eluent. The columns were calibrated against polystyrene standards with molecular weights ranging from 1560 to 128 000. Samples were filtered through a 0.45 μm filter immediately prior to injection. Analysis was performed using Version 3.0 of the Conventional Calibration module of the Viscotek SEC^3 software package.

1 J. C. Middleton and A. J. Tipton, *Biomaterials*, 2000, **21**, 2335.
2 H. R. Kricheldorf and I. Kreiser-Saunders, *Macromol. Symp.*, 1996, **103**, 85; D. K. Gilding and A. M. Reed, *Polymer*, 1979, **20**, 1459.
3 E. E. Schmitt and R. A. Rohistina, *US Pat.*, 3297033, 1967 (*Chem. Abstr.*, 1967, **66**, P38656u); E. E. Schmitt and R. A. Rohistina, *US Pat.*, 3463158, 1969 (*Chem. Abstr.*, **1969**, 71, P92382t); H. R. Kricheldorf, I. Kreiser-Saunders and C. Boettcher, *Polymer*, 1995, **36**, 1253 and references therein.
4 P. Dubois, C. Jacobs, R. Jérome and P. Teyssié, *Macromolecules*, 1991, **24**, 2266; P. A. Cameron, D. Jhurry, V. C. Gibson, A. J. P. White, D. J. Williams and S. Williams, *Macromol. Rapid. Commun.*, 1999, **20**, 616; N. Spassky, M. Wisniewski, C. Pluta and A. LeBorgne, *Macromol. Chem. Phys.*, 1996, **197**, 2627.
5 M. H. Chisholm and N. W. Eilerts, *Chem. Commun.*, 1996, 853.
6 M. Cheng, A. B. Attygalle, E. B. Lobkovsky and G. W. Coates, *J. Am. Chem. Soc.*, 1999, **121**, 11 583.

Synthesis and characterization of new metal-free phthalocyanine substituted with four diazatetrathiamacrobicyclic moieties

Yasar Gök,* Halit Kantekin, Ahmet Bilgin, Durali Mendil and Ismail Degirmencioglu

Department of Chemistry, Karadeniz Technical University, 61080, Trabzon, Turkey. E-mail: ysrgok@yahoo.com

Received (in Cambridge, UK) 20th July 2000, Revised manuscript received 18th December 2000, Accepted 20th December 2000
First published as an Advance Article on the web 23rd January 2001

A novel metal-free phthalocyanine 3 fused in peripheral position with four diazatetrathiabicyclomacrocycles has been prepared by bicyclotetramerization of cryptand 1 and its isoindolinediimine derevative 2; the new compounds were characterized by elemental analyses, IR, ^{1}H and ^{13}C NMR, UV–VIS and MS spectroscopy.

The first synthesis of a soluble copper phthalocyanine with crown ether moieties was reported in 1986[1] and its high tendency towards aggregation by solvents, cations and complexation properties was investigated.[2] Such compounds contain a metal center that is complexed by a phthalocyanine ring and four macrocyclic binding sites.[3] The attachment of polyaza or polyaza-polythia macrocycles to phthalocyanine has received considerable attention because of the transition metal-binding properties of the macrocyclic cavities.[4] Phthalocyanines containing polyaza or mixed-donor macrocycles[5] can form homo- and hetero-pentanuclear transition metal complexes which may allow new functionalized materials to be obtained which are of importance for both biochemistry and materials science.[6]

A range of three-dimensional polycyclic ligand systems (cryptands) have recently been investigated most intensively with respect to their strong selectivity towards individual alkali and alkaline-earth metal ions.[7] The majority of such ligands contain donor sets in which polyether donor functions predominate. However, ligands of general type, incorporating mixed donors such as diaza and/or dithia groups, have also been synthesized.[8] Such ligands show increased affinity for transition metals and many other heavy metals.[9]

This study, describing the synthesis of compound **3**, displaying a suitable combination of diazatetrathiamacrobicycles and phthalocyanine may allow new functionalized materials to be prepared, which are of importance for analytical chemistry as a new type of heavy metal extraction agent. On the other hand, the importance of this new type of phthalocyanine may be regarded as an important step in that it may be a viable sensor material.

The synthesis of macrobicyclic compound **1**, was performed starting from a 14-membered diazadithia macrocycle[10] and 1,2-bis(2-iodoethylmercapto)-4,5-dicyanobenzene[11] in dilute conditions using Cs^+ cation as promotor[12] in acetonitrile. Final purification by recrystallization afforded **1** in 73.2% yield (mp 136 °C).† Compound **1** displays the expected molecular ion peak at *m/z* = 574 $[M]^+$. Conversion of the dicyano compound **1** into the isoiminoindoline derivative **2** was accomplished by bubbling ammonia gas through a solution of **1** in dry methanol in the presence of sodium methoxide for 6 h. Compound **2** was purified by column chromatography on silica gel, using ethanol–chloroform (1 : 1) as eluent and obtained in 63.4% yield (mp 284 °C (decomp.)].† The C, H and N elemental analyses for **2** were satisfactory and a reproductible mass spectrum was obtained using the FAB technique (M^+ at *m/z* 591 corresponding to the molecular ion).

The usual synthetic routes could be applied to synthesize the metal-free phthalocyanine **3**.† Thus, either **1** was cyclotetramerized to **3** in a high boiling solvent such as pentanol at reflux

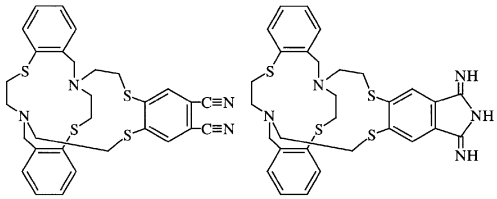

1 **2**

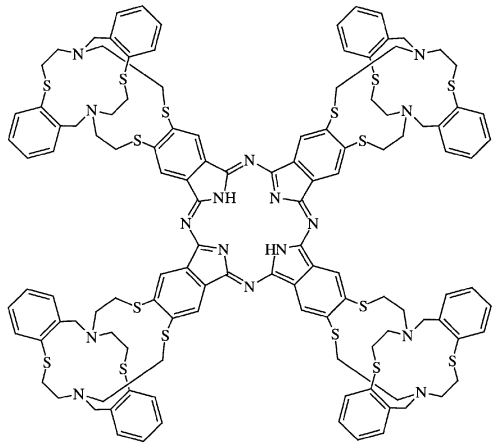

3

temperature in the presence of a strong organic base such as 1,8-diazabicyclo[5.4.0]undec-7-ene(DBU) or alternatively condensation of four isoiminoindoline units **2** into the metal-free

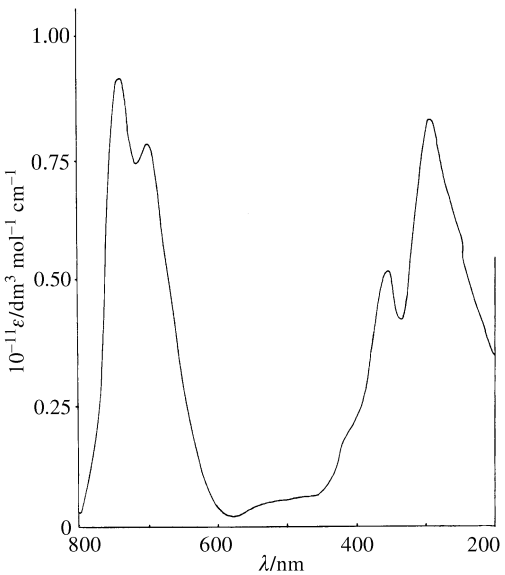

Fig. 1 UV–VIS spectra of **3** in pyridine.

DOI: 10.1039/b010045p

phthalocyanine **3** was carried out in 2-(*N*,*N*-dimethylamino)-ethanol at reflux temperature. In the preparation of the metal-free phthalocyanine, the isoiminoindoline route is more convenient than the phthalonitrile route since the reaction conditions employing isoiminoindolines are mild in comparison to those employing phthalonitriles.[13] The yields (11.3–12.7%) of these reactions were rather low, as encountered for metal-free phthalocyanine with other bulky groups.[5] Elemental analytical results and ^{1}H NMR, IR, MS and UV-VIS spectral data of the new phthalocyanine are consistent with the assigned formulation. A mass spectrometry study by FAB on this compound gave a molecular ion peak the value of which showed good agreement with the calculated value for **3** (*m/z* 2298.3 $[M]^+$).

Fig. 1 shows the electronic absorption spectrum of **3** in pyridine. This spectrum of the phthalocyanine indicates features of both the metal-free phthalocyanine and macro-bicyclic moieties. The cryptand containing phthalocyanine **3** shows intense Q bands at 734 and 704 nm suggesting monomeric species since such species (of D_{2h} symmetry) show two intense absorptions around 700 nm.[13,14] Such split Q band absorptions in pyridine is due to the $\pi \Rightarrow \pi^*$ transition of this fully conjugated 18π electron system.

This study was supported by the Research Fund of Karadeniz Technical University (Trabzon-Turkey).

Notes and references

† Compounds **1** and **2** were characterized by elemental analysis and spectral methods. Compound **1**: anal. Calc. for $C_{30}H_{30}N_4S_4$: C, 62.71; H, 5.22; N, 9.75. Found: C, 62.96; 5.04; N, 9.94%. IR (KBr disc): ν/cm^{-1} 3054, 2916, 2818, 2229, 1588, 1585, 1463, 1429, 1260, 1109, 970, 753. δ_H($CDCl_3$) 7.58(s), 7.55(s), 7.46–7.07(m), 5.89–5.79(m), 3.86(s),3.36(s), 3.28–3.21(m), 2.76–2.70(m). δ_C($CDCl_3$) 142.58, 138.47, 132.36, 131.31, 129.32, 128.31, 127.70, 125.98, 115.14, 112.58, 110.74, 51.52, 45.06, 33.07, 28.01. Compound **2**: anal. Calc. for $C_{30}H_{33}N_5S_4$: C, 60.91; H, 5.58; N, 11.84. Found: C, 61.16; H, 5.40, N, 11.67%. IR (KBr disc): ν/cm^{-1} 3385, 3177, 3048, 2921, 2816, 1636, 1609, 1585, 1541, 1459, 1420, 1376, 1287, 1107, 872, 750. δ_H($CDCl_3$) 7.75 (br), 7.58(s), 7.53(s), 7.33–6.71(m), 5.67–5.58(m), 4.24(m), 3.85(s), 3.34–3.22(m), 2.73–2.67(m). δ_C($CDCl_3$) 138.49, 135.52, 133.49, 132.28, 130.90, 128.82, 128.08, 127.85, 125.46, 121.82, 51.93, 45.25, 33.29, 28.93. Compound **3**: anal. Calc. for $C_{120}H_{122}N_{16}S_{16}$: C, 62.66; H, 5.30; N, 9.74. Found: C, 62.44; H, 5.51; N, 9.59%. Selected spectroscopic data: IR (KBr disc): ν/cm^{-1} 3406, 3055, 2932, 2841,1636, 1617, 1589, 1560, 1508, 1474, 1458, 1423, 1381, 1344, 1296, 1121, 1079, 897, 754; λ_{max}/nm (log ε) (pyridine): 734 (11.44), 704 (10.15), 348 (6.70), 285 (10.74). δ_H(DMSO-d_6) -4.38(s),7.84(m), 7.62–7.50(m), 7.38–6.66(m), 4.28(m), 3.82(s), 3.42–3.29(m), 2.81–2.70(m).

1 A. R. Koray, V. Ahsen and Ö. Bekaroglu, *J. Chem. Soc., Chem. Commun.*, 1986, 932; N. Kobayashi and Y. Nishiyama, *J. Chem. Soc., Chem. Commun.*, 1986, 1462; R. Hendriks, O. E. Sielcken, W. Drenth and R. J. M. Nolte, *J. Chem. Soc., Chem. Commun.*, 1986, 1464.

2 V. Ahsen, E. Yilmazer, M. Erbas and Ö. Bekaroglu, *J. Chem. Soc., Dalton Trans.*, 1988, 401.

3 E. Musluoglu, V. Ahsen, A. Gül and Ö. Bekaroglu, *Chem. Ber.*, 1991, **124**, 2531; A. Gürek, V. Ahsen, A. Gül and Ö. Bekaroglu, *J. Chem. Soc., Dalton Trans.*, 1991, 3367.

4 M. Koçak, A. Cihan, A. I. Okur and Ö. Bekaroglu, *J. Chem. Soc., Chem. Commun.*, 1991, 577; E. Kimura, A. Sakonaka, T. Yatsunami and M. Kodama, *J. Am. Chem. Soc.*, 1981, **103**, 3041.

5 E. Musluoglu, V. Ahsen, A. Gül and Ö. Bekaroglu, *Chem. Ber.*, 1991, **124**, 2531; I. Yilmaz and Ö. Bekaroglu, *Chem. Ber.*, 1996, **129**, 967; G. Gümüs, Z. Z. Öztürk, V. Ahsen, A. Gül and Ö. Bekaroglu, *J. Chem. Soc., Dalton Trans.*, 1992, 2485; S. Z. Yildiz and Y. Gök, *New J. Chem.*, 1998, 1365; S. Z. Yildiz, H. Kantekin and Y. Gök, *J. Porphyrins. Phthalocyanines*, 2000, in press.

6 Ö. Bekaroglu, *Appl. Organomet. Chem.*, 1996, **10**, 605.

7 B. Dietrich, J.-M. Lehn and J. P. Sauvage, *Tetrahedron Lett.*, 1969, **34**, 2885; B. Dietrich, J.-M. Lehn, J. P. Sauvage and J. Balanzat, *Tetrahedron*, 1973, **29**, 1629; A. C. Coxon and J. F. Stoddart, *J. Chem. Soc., Perkin Trans. 1*, 1977, 767; B. Mertz, D. Moras and R. Weiss, *J. Chem. Soc., Perkin Trans. 2*, 1976, 423; D. G. Parsons, *J. Chem. Soc., Perkin Trans. 1*, 1978, 451; J. A. Herbert and M. R. Truter, *J. Chem. Soc., Perkin Trans. 2*, 1980, 1253; G. Anderegg, *Helv. Chim. Acta.*,1981, **64**, 1790; F. Arnaud-Neu, B. Spiess and M. J. Schwing-Weil, *J. Am. Chem. Soc.*, 1982, **104**, 5641; M. C.Almasio, F. Arnaud-Neu and M. J. Schwing-Weil, *Helv. Chim. Acta.*, 1983, **66**, 1296; V. V. Yakshin, A. G. Fedorova and B. N. Laskorin, *Dokl. Akad. Nauk SSSR*, 1984, **276**, 169; V. V. Yakshin, A. G. Fedorova and B. N. Laskorin, *Zh. Anal. Khim.*, 1985, **40**, 45.

8 J.-M. Lehn, *Acc. Chem. Res.*, 1978, **11**, 49; D. G. Blanco, E. F. Alonso and A. Sanz-Medel, *Talanta*, 1985, **32**, 915; A. P. Alonso, D. G. Blanco and A. Sanz-Medel, *J. Mikrochem.*, 1985, **32**, 296.

9 L. F. Lindoy, *The Chemistry of Macrocyclic Ligand Complexes*, Cambridge University Press, Cambridge, 1990, p. 88; B. Dietrich, J.-M. Lehn and J. P. Sauvage, *Chem. Commun.*, 1970, 1055.

10 J. W. L. Martin, G. J. Organ, K. P. Wainwright, K. D. V. Weerasuria, A. C. Willis and S. B. Wild, *Inorg. Chem.*, 1987, **26**, 2963.

11 This compound was characterized elemental analysis, MS, NMR and IR spectroscopy.

12 S. Kulsad and L. A. Malmsten, *Tetrahedron Lett.*, 1980, 643.

13 M. Hanack, H. Heckmann and R. Polley, in *Methods of Organic Chemistry*, Georg Thieme Verlag, Stuttgart, 1998, *Additional Supplementary Volume*, p. 776.

14 A. G. Gürek and Ö. Bekaroglu, *J. Chem. Soc., Dalton Trans.*, 1994, 1419.

ChemComm

Self-assembled multiporphyrin arrays mediated by self-complementary quadruple hydrogen bond motifs†

Charles Michael Drain,* Xinxu Shi, Tatjana Milic and Fotis Nifiatis

Department of Chemistry & Biochemistry, Hunter College & Graduate Center of the City University of New York, 695 Park Avenue, New York, NY 10021, USA. E-mail: Cdrain@shiva.hunter.cuny.edu

Received (in Columbia, MO, USA) 13th September 2000, Accepted 15th December 2000
First published as an Advance Article on the web 23rd January 2001

Discrete squares and tapes of porphyrins are self-assembled by self-complementary hydrogen bonding between diacetamidopyridyl recognition groups rigidly linked to the chromophore.

Porphyrins, and their cousins the phthalocyanines, have attracted considerable attention recently because of their potential use as components of nanometer scale photonic devices and materials.[1] The functionality of many, if not most, photonic devices,[1] including those found in nature,[2] strongly depends on the relative order of the chromophores throughout the entire material and on the mode of assembly. Supramolecular chemistry has been used as a stratagem to achieve the desired geometric order of porphyrin and other entities in both solids and in solution.[3] Crystallization of porphyrins bearing H-bonding groups has yielded fascinating networks,[3,4] and co-crystallization with other compounds has yielded interesting host–guest[3,5] and magnetic[5] materials. Yet consistently predicting long-range three-dimensional order in crystals remains elusive. Several discrete H-bond[6] and metal ion[7] assembled porphyrin systems in solution also have been reported. In order to better understand the role of non-covalent bonds in mediating electron and energy transfer in biological systems,[2] several non-coplanar or non-rigid supramolecular porphyrin–electron acceptor species have been studied.[8,9] One of the primary goals of work reported herein is to understand the process of self-assembly and to reliably predict the structure of self-assembled porphyrin arrays in solution, as opposed to the solid state. We report the self-assembly of several rigid, co-planar multiporphyrin arrays and tapes by self-complementary H-bond motifs that exploit both the directionality of the recognition groups and the square-planar geometry of the porphyrin macrocycle to design predictable arrays in high yields. Though topologically similar to the square porphyrin arrays formed by coordination chemistry,[3,7] the nature of the self-assembly linker has profound effects on the properties of the resultant array, *e.g.* porphyrin fluorescence.

There are several ways in which 5-(3,5-diacetamido-4-pyridyl)-10,15,20-tris(4-*tert*-butylphenyl)porphyrin, **1a**,[10]† may form a dimer by self-complementary hydrogen bonds.[11] The most stable is a linear, quadruple H-bonded system (graphical abstract), albeit this is weak compared to other H-bond systems. A variety of one- and two-dimensional porphyrin structures may be formed *via* this motif. In the present case we demonstrate this by the formation of linear dimers with the 5-substituted compound, linear trimers using a 2:1 stoichiometry of the 5- and the 5,15-substituted compounds **1a**, **2a**, respectively, and a linear tetramer using a 2:2 ratio of **1a** to **2a**.

If there are no dynamic processes occurring on the NMR[12] time scale, both the number of species self-assembling into the final structure, *n*, and the equilibrium constants, *K*, may be determined by ^{1}H NMR experiments that monitor the chemical shift of suitable protons *vs.* the concentration of the self-complementary porphyrin.[6,13] Noting the usual caveats and that these experiments do not yield structural information *per se*, fits of these curves for solutions of **1a**† indicate that the ultimate self-assembled product contains *ca.* 2 units (K = 160 dm^3 mol^{-1}), consistent with the dimeric structure shown in the abstract, where $x = 0$. For the tapes these experiments and their fits show that *ca.* 3.2 units are in the final assembly when a 2:1 mixture of **1a** and **2a** is used to form the trimer (K = 110 dm^6 mol^{-2}), and about 4.1 units are present in the assembly of a 2:2 mixture of **1a** and **2a** (K = 70 dm^9 mol^{-3}). In the case of the linear tapes, there is no *a priori* reason that all of the self-assembled structures in the chloroform solution are the 2:1 trimers, and 2:2 tetramers, thus the NMR results are likely indicative of a mixture of dimers, trimers, tetramers, *etc.* substantially weighted toward the tape resulting from the starting stoichiometries by ΔG.†

The self-assembly of a square tetramer (Scheme 1) from only **3a** is also indicated by similar plots of concentration *vs.* amide NH chemical shifts.† Dramatic differences are observed in the plots for the linear tetramer *vs.* the closed-square tetramer.† For the square array, the rapid increase in the chemical shift at much lower concentrations indicates K (2400 dm^9 mol^{-3}) is much greater compared to the linear tetramer, and thus is a direct measure of the cooperative formation of a closed system with a more favorable ΔG. The fit yields $n \approx 3.9$ units of **3a**.

Because of the different power of the concentration units it is difficult to directly compare the values of K for all but the linear and square tetramers. Additionally, the K values found by this data are about 4-fold weaker then those found by fluorescence

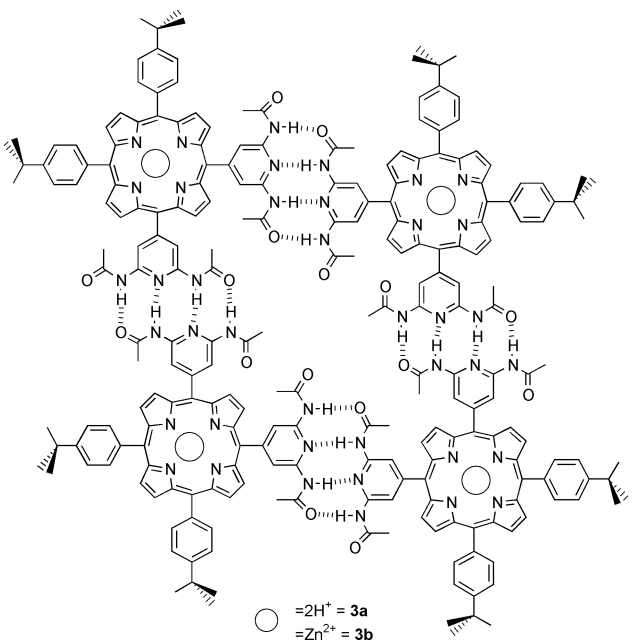

Scheme 1

† Electronic supplementary information (ESI) available: experimental details, NMR data and fits, van't Hoff plots, UV–VIS and fluorescence data, and ESI-MS spectrum for the self-assembled square species. See http://www.rsc.org/suppdata/cc/b0/b008045o/

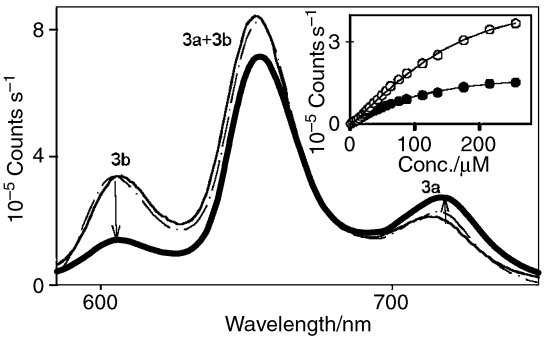

Fig. 1 Fluorescence emission spectra of a solution that is 140 μM in **3a** and 140 μM in **3b** in 2-methylTHF (——) and in ethanol (——) under identical experimental conditions. In ethanol where the H-bonding between the diacetamidopyridyl groups is minimal, the emission spectrum is nearly identical to the sum of the two components (–·–). Whereas in 2-methylTHF where H-bonding is significant, there is a substantial quenching of **3b** and enhanced emission from **3a**. The inset plots the emission intensity of **3b** at 610 nm *vs.* concentration in ethanol (○) and 2-methylTHF (●).

quenching experiments, indicating that dynamic processes are occurring during the NMR acquisition. To contrast the NMR data from all four systems, it may be more informative to compare the $C_{1/2}$ values, where this represents the concentration at the half maximum increase in the chemical shift. The $C_{1/2}$ value from the above NMR data for the closed tetrameric square, 0.8 mM, is a factor of *ca.* 10 less than the comparable open tetrameric tape, consistent with the calculated K values. Note that the linear systems have somewhat similar $C_{1/2}$ values: 8 mM, 5 mM and 9 mM for the dimer, trimer, and tetramer, respectively.†[11] In toluene, where the H-bonds are expected to be stronger, similar results for n are obtained for all systems, but the $C_{1/2}$ values are *ca.* 4-fold lower for the linear assemblies and *ca.* 2-fold lower for the square.

In solvents with low H-bonding potential, the added thermodynamic stability of the closed, square tetramer, as opposed to a open-chain polymer with an average length of four units with enthalpically unfavorable 'unbonded' ends or entropically unfavorable higher order polymers, strongly argues in favor of the square structure when **3a** is the self-assembling species. Estimations of ΔG for these systems from the NMR concentration and temperature data[8] show that the square tetramer ($\Delta G = -19.3$ kJ mol^{-1}) is favored over the tetrameric tapes ($\Delta G = -10.5$ kJ mol^{-1}) by *ca.* 8 kJ mol^{-1}. Van't Hoff plots† of the chemical shift *vs.* temperature are in qualitative agreement with the NMR equilibrium studies above.

As the concentration in chloroform, toluene, 2-methylTHF, and ethanol is increased from 1 μM to *ca.* 250 μM there is little change in the observed UV–VIS spectra, with < 1 nm shifts in the Q bands for both the free bases and the zinc complexes. This indicates very little electronic communication between the macrocycles in the self-assembled tapes and squares in the ground state. However, the relative emission is substantially diminished with increasing concentrations of **1a** or **3a** in chloroform, or 2-methylTHF, compared to ethanol.† This indicates that there is aggregation, which decreases the emission intensity by organization of the chromophores, and quenching of the excited state by energy transfer to neighboring subunits. Significant energy transfer among subunits is well demonstrated by the excitation and emission (Fig. 1) spectra of squares formed from a 1:1 mixture of the free base, **3a** and the zinc complex **3b** in 2-methylTHF. In solvents favoring H-bonding, excitation in the zinc porphyrin Q-band region at 557 nm where **3b** absorbs > 3 times **3a**, the self-complementary square emits predominantly from the free base at 720 nm, with concomitant quenching of **3b** at 610 nm. This direct observation of energy transfer is not observed in dilute solutions (< 10 μM) or in ethanol where the emission is essentially similar to the mathematical addition of the two individual spectra. The emission from **3b** (Fig. 1, inset) is substantially quenched as the concentration of the 1:1 mixture in 2-methylTHF increases, and to a much lesser extent in ethanol. The fluorescence lifetime, determined by phase modulation, of **3a** is 10 ns and that of **3b** is 2 ns at 1 μM concentrations in air in chloroform. At 0.100 mM, **3a** exhibits two time constants 10 ns (80%) and 0.8 ns (20%). A 0.100 mM mixture of 1:1 **3a** and **3b** shows decays of 10 ns (50%), 1 ns (40%) and < 0.2 ns (10%). This is consistent with the notion of energy transfer from the singlet manifold, rather than the triplet manifold for the metallo self-assembled squares.[7]

The characterization of these supramolecular systems will serve as the basis for the characterization of future complex two- and three-dimensional arrays using various combinations of both H-bonding and metal ion coordinating porphyrins.[9] The above data show that the self-complementary H-bonds afforded by the 3,5-diacetamido-4-pyridyl group are surprisingly effective in mediating the self-assembly of these photo- and electroactive species in solution. The solution phase chemistry, in turn, is vitally important for the understanding of how to direct the formation of solid state structures, and will help understanding of the resulting properties of the materials.

This work was supported by NS.F. CHE-9732950, PSC-CUNY-30 grants to C. M. D. We acknowledge the help of Drs M. Blumenstein and C. Soll for NMR and MS experiments.

Notes and references

1 *Molecular Electronics: Science and Technology*, ed. A. Aviram and M. Ratner, *Ann. NY Acad. Sci.*, 1998, p. 852, and references therein; C. M. Drain and D. Mauzerall, *Biophys. J.*, 1992, 1556, and references therein.

2 T. Pullerits and V. Sundstrom, *Acc. Chem. Res.*, 1996, **29**, 381; V. Novoderezhkin, R. Monshouwer and R. van Grondelle, *Biophys. J.*, 1999, **77**, 666.

3 For reviews: A. K. Burrell and M. R. Wasielewski, *J. Porphyrins Phthalocyanines*, 2000 **4**, 401; B. Maiya, *J. Porphyrins Phthalocyanines*, 2000, **4**, 393; K. S. Suslick, N. Rakow, M. E. Kosal and J.-H. Chou, *J. Porphyrins Phthalocyanines*, 2000, **4**, 407; R. Dagani, *Chem. Eng. News*, 1998, **(76)23**, 35.

4 For example: P. Bhyrappa, S. R. Wilson and K. S. Suslick, *J. Am. Chem. Soc.*, 1997, **119**, 8492; S. Dahal and I. Goldberg, *J. Phys. Org. Chem.*, 2000, **13**, 1; Y. Diskin-Posner, S. Dahal and I. Goldberg, *Angew. Chem., Int. Ed.*, 2000, **39**, 1288.

5 For example: T. Hayashi, T. Miyahara, N. Koide, Y. Kato, H. Masuda and H. Ogoshi, *J. Am. Chem. Soc.*, 1997, **119**, 7281; A. J. Epstein, C. M. Wynn, M. A. Girtu, W. B. Brinckerhoff, K.-I. Sugiura and J. S. Miller, *Mol. Cryst. Liq. Cryst.*, 1997, **305**, 321.

6 C. M. Drain, R. Fischer, E. G. Nolen and J.-M. Lehn, *J. Chem. Soc., Chem. Commun.*, 1993, 243; C. M. Drain, K. C. Russel and J.-M. Lehn, *Chem. Commun.*, 1996, 337; C. Ikeda, N. Nagahara, E. Motegi, N. Yoshioka and H. Inoue, *Chem. Commun.*, 1999, 1759.

7 C. M. Drain, F. Nifiatis, A. Vasenko and J. D. Batteas, *Angew. Chem.*, 1998, **37**, 2344; C. M. Drain and J.-M. Lehn, *J. Chem. Soc., Chem. Commun.*, 1994, 2313; J.-C. Chambron, V. Heitz and J.-P. Sauvage in *The Porphyrin Handbook*, ed. K. M. Kadish, K. M. Smith and R. Guilard, Academic Press, San Diego, 2000, pp. 1–41, and references therein; A. Prodi, M. T. Indelli, C. J. Kleverlaan, F. Scandola, E. Alessio, T. Gianferrara and L. G. Marzilli, *Chem. Eur. J.*, 1999, **5**, 2668.

8 J. L. Sessler, B. Wang and A. Harriman, *J. Am. Chem. Soc.*, 1995, **117**, 704; J. L. Sessler, C. T. Brown, D. O'Connor, S. L. Springs, R. Wang, M. Sathiosatham and T. Hirose, *J. Org. Chem.*, 1998, **63**, 7374; T. Arimura, S. Ide, H. Sugihara, S. Murata and J. L. Sessler, *New J. Chem.*, 1999, **23**, 977.

9 P. J. F. de Rege, S. A. Williams and M. J. Therien, *Science*, 1995, **269**, 1409.

10 A distorted porphyrin bearing a single 3,5-diamidopyridyl group has been reported. A. Osuka, R. Yoneshima, H. Shiratori, T. Okada, S. Taniguchi and N. Mataga, *Chem. Commun.*, 1998, 1567.

11 F. H. Beijer, R. P. Sijbesma, J. A. J. M. Vekemans, E. W. Meijer, H. Kooijman and A. L. Spek, *J. Org. Chem.*, 1996, **61**, 6371.

12 Equilibrium constants for weakly H-bonding systems determined by NMR[6,11,13] data are probably internally consistent, but should be treated with caution unless the dynamics are specifically addressed.

13 W. F. DeGrado and J. D. Lear, *J. Am. Chem. Soc.*, 1985, **107**, 7684; D. A. Deranleau, *J. Am. Chem. Soc.*, 1969, **91**, 4044; B. J. Whitlock and H. W. Whitlock, *J. Am. Chem. Soc.*, 1990, **112**, 3910.

14 A. D. Adler, F. R. Longo and W. Shergalis, *J. Am. Chem. Soc.*, 1964, **86**, 3145; C. M. Drain and X. Gong, *Chem. Commun.*, 1997, 2117.

ChemComm

Evolution and atomistic structure of dislocations defects and clusters within CeO_2 supported on ZrO_2

S. Andrada Maicaneanu,[a] Dean C. Sayle*[a] and Graeme W. Watson[b]

[a] *Department of Environmental and Ordnance Systems, Cranfield University, Royal Military College of Science, Shrivenham, Swindon, UK SN6 8LA. E-mail: sayle@rmcs.cranfield.ac.uk*
[b] *Department of Chemistry, Trinity College, Dublin 2, Ireland*

Received (in Cambridge, UK) 8th November 2000, Accepted 20th December 2000
First published as an Advance Article on the web 23rd January 2001

'Simulated amorphisation and recrystallisation' was employed to explore the structural features that evolve within ZrO_2(111) supported CeO_2, including epitaxial relationships, screw and screw-edge dislocations, vacancies and surface clusters.

Ceria and ceria containing materials are used as catalysts and promoters in several heterogeneous catalytic reactions[1] and comprise a major component in three-way catalysts (TWC), which are used for the treatment of automobile exhaust gases. The oxygen storage capacity (OSC), due to the ability of cerium to shift between Ce^{4+} and Ce^{3+}, is one of the key properties of these materials. Accordingly, ceria based catalysts can work in both oxidizing and reducing conditions, converting carbon monoxide, nitrogen oxides and hydrocarbons to non-toxic products. It has been shown experimentally that ceria films, vapour deposited on zirconia and zirconia based substrates such as yttrium-stabilized zirconia (YSZ), are more easily reduced than films supported on α-Al_2O_3.[2]

Here we employ a simulated amorphisation and recrystallisation methodology[3,4] to explore the structural changes that evolve within ZrO_2(111) supported CeO_2. Since elucidation of the atomistic structure, particularly for ultra-thin supported materials is difficult or even intractable experimentally, the simulation provides an invaluable complement.

Simulated amorphisation and recrystallisation[3,4] in this present study involves straining the CeO_2 thin film under considerable pressure and placing it on top of a ZrO_2 support. Dynamical simulation is then applied to the system at high temperature upon which the CeO_2 amorphises. Under prolonged dynamical simulation, the CeO_2 recrystallises revealing a wealth of structural modifications that evolve as the system endeavours to accommodate the lattice misfit, whilst maximising interfacial interactions. Crucially, by ensuring that the CeO_2 thin film recrystallises from an amorphous structure, no influence on the compromise between minimising the lattice misfit whilst maximising the interfacial interactions is introduced artificially into the simulation.

Central to this methodology is that dynamical simulation, as applied to an amorphous structure, allows a more comprehensive exploration of the configurational space due to the high energy amorphous starting point and the conformational freedom this gives rise to. In addition, a single mesoscale simulation has been performed in which a multitude of structural features are present within this simulation cell (in contrast to performing many smaller simulations comprising fewer structural features). Previous simulations on the SrO/MgO(001) system[4] using different simulation cells revealed equivalent thin film energies, epitaxial relationships, dislocation densities and structural configurations suggesting that a single very large simulation cell is sufficiently representative for an initial investigation of the CeO_2/ZrO_2 system. In addition, during experimental fabrication using for example vapour deposition[2] the thin film will endeavour to crystallise into as low an energy structure as possible. Our method is designed to generate low energy structures *via* recrystallisation from an amorphous material and will reflect therefore the structural characteristics present within the experimental system.

The calculations presented in this study are based on the Born model for ionic solids, with potential parameters taken from Lewis and Catlow[5] and Dwivedi and Cormak.[6] These potentials have been employed to model lattice parameters,[7] thermal expansivities,[8] conductivity and diffusion properties[8] for CeO_2 and ZrO_2 solid solutions, in accord with experiment. In addition, a rigid ion model was used to reduce the computational expense. The dynamical simulations, which employ three-dimensional periodicity, were performed using the DL_POLY code,[9] and therefore a void normal to the surface is included to represent the free surface. The simulation cell contains ions distributed in two regions: region I comprises the CeO_2 thin film and the first six repeat units of the ZrO_2(111) support, and ions within this region are allowed to move under the dynamical regime, while region II comprises a fixed region (four repeat ZrO_2 units) of the support and is included to ensure the correct crystalline environment.

In this preliminary study we consider a model system, that of CeO_2 supported on cubic zirconia, as a first step in exploring CeO_2 supported on yttrium stabilised zirconia (YSZ), which will be considered in future studies; it has been shown experimentally that ceria grows epitaxially on YSZ.[10,11]

To generate the CeO_2/ZrO_2(111) interface, two CeO_2(111) repeat units (thick) were placed directly on top of ten repeat units of the ZrO_2(111) support using a 'cube-on-cube' methodology.[3] In particular, a 27 $\times$ 27 (which corresponds to 54 cerium atoms or 27 CeO_2 units for each side of the simulation cell) CeO_2 thin film was placed directly above a 20 $\times$ 20 ZrO_2(111) support, giving an interfacial area of 10 305 Å^2 and 65 496 ions within the simulation cell. The lattice misfit associated with the system is +36%; the CeO_2 is therefore constrained initially under considerable pressure. Dynamical simulation was then applied to the system for 115 ps at 3400 K, 55 ps at 2500 K, 5 ps at 2000, 1500 and 1000 K, 40 ps at 500 K, 10 ps at 100 K and 20 ps at 0 K; the latter acts effectively as an energy minimisation. During the initial dynamical simulation step, the considerable strain within the CeO_2 results in its amorphisation, which, upon prolonged dynamical simulation, recrystallises. That the CeO_2 undergoes an amorphous transition eliminates all 'memory' of the starting configuration enabling the CeO_2 to evolve structurally in response solely to the lattice misfit and underlying ZrO_2.

Inspection of the final structure for the CeO_2/ZrO_2(111) system [Fig. 1(a)] reveals that the CeO_2 thin film has recrystallized into the fluorite structure. The success of the simulated amorphisation and recrystallisation methodology in generating the CeO_2 structure from an amorphous solid suggests that the methodology is applicable to study supported fluorite-structured systems in addition to the supported rocksalt-structured systems considered previously.[3]

The final CeO_2 thin film structure exposes the (111) plane at both the interface and surface and comprises *ca*. five CeO_2 repeat units with an incomplete (*ca*. 25% occupancy) surface layer (layer five), which comprises small clusters ranging from,

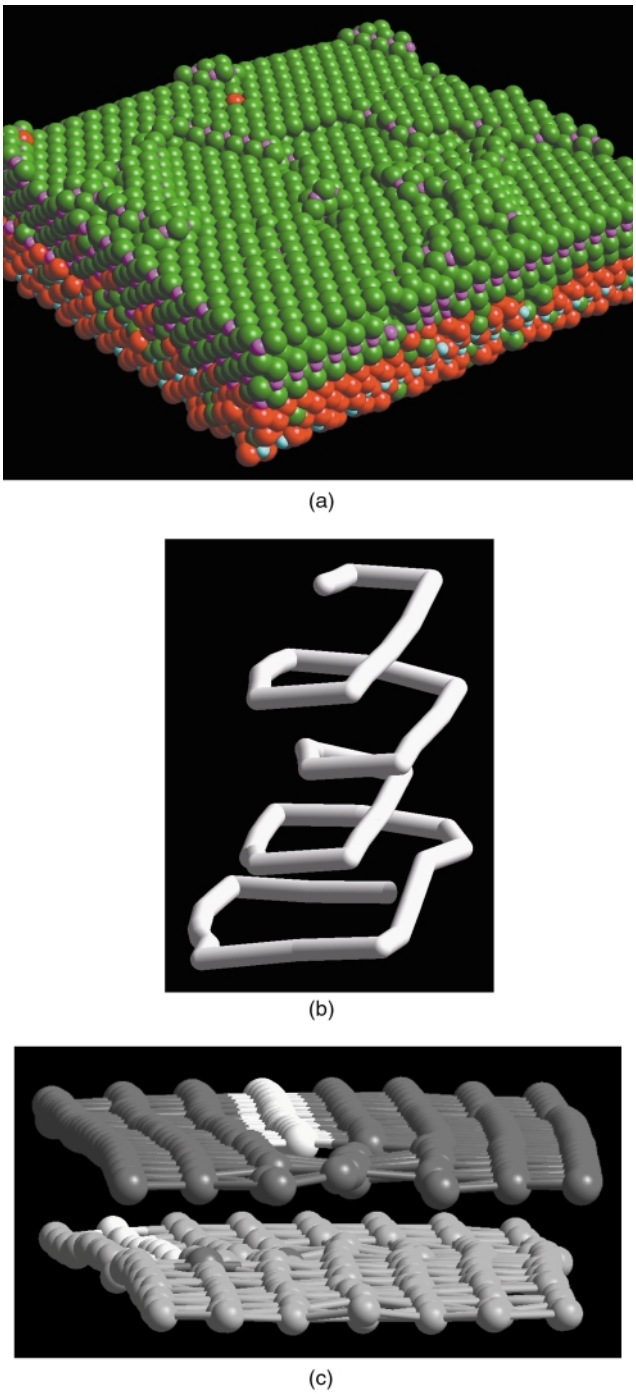

Fig. 1 (a) Representation of the $CeO_2/ZrO_2(111)$ interface. For reasons of clarity, only part of the full simulation cell and three planes of the support are depicted. Zirconium is coloured light blue, cerium is magenta, oxygen (ZrO_2) is red and oxygen (CeO_2) is green; (b) stick representation of the screw-edge dislocation (core structure). Only the cerium sub-lattice is shown to ensure clarity; (c) representation of two edge dislocations (white spheres) within the interfacial ZrO_2 layer (bottom) and second interfacial CeO_2 layer (top). The remaining planes have been omitted to preserve clarity. Zirconium is coloured light grey and cerium dark grey.

for example, Ce_2O_4 and Ce_4O_8, to larger clusters up to 500 Å^2 in size [Fig. 1(a)]. The CeO_2 thin film lies almost coherent with the underlying ZrO_2 support, with the CeO_2 accommodating a 19 × 19 (average) pattern with no rotation of the CeO_2 with respect to the underlying ZrO_2. The lattice misfit associated with such a configuration is therefore reduced from +6.7% based upon 20 CeO_2 units lattice matched with 20 ZrO_2 units (bulk misfit) to *ca*. +1.6% based upon 19 CeO_2 units lattice matched with 20 ZrO_2 units (final structure).† To maintain such a configuration, the CeO_2 lattice must be compressed by 1.6% to accommodate the misfit, which corresponds theoretically to a 'lattice parameter' of 5.34 Å. Experimentally, Dmowski *et al*., who explored the structure and oxygen storage properties of a *ca*. 20 Å CeO_2 thin film supported on zirconia,[10] found the CeO_2 lattice parameter to be reduced from 5.41 to 5.38 Å. In addition, they observed no rotation of the CeO_2 with respect to the underlying support in accord with our findings.

A detailed analysis of the system using molecular graphics techniques revealed that the system comprises cerium (*ca*. 0.8%) and zirconium (*ca*. 0.3%) vacancies charge compensated by associated oxygen vacancies. Moreover, the density of vacancies within the CeO_2 thin film increases within planes further from the interface. In addition, dislocations including pure edge and mixed screw-edge dislocations have evolved within the system. The latter, as depicted in Fig. 1(b), traverses the entire thickness of the CeO_2 thin film and moreover, extends into the first layer of the ZrO_2 support resulting in considerable perturbation of the underlying ZrO_2 support. In response, zirconium and oxygen ions migrate from the support to form a large (*ca*. 30 Å^2) cluster, which emanates from the base of the dislocation core. We also note that pure edge dislocations have evolved in both the CeO_2 thin film *and* within the ZrO_2 support [Fig. 1(c)]. Experimentally, dislocation arrays with periodicity of *ca*. 44 Å were observed to accommodate the lattice misfit for CeO_2 supported on YSZ.[12] We suggest such defects (vacancies and dislocations) help reduce further the +1.6% misfit (19 × 19 CeO_2 supported on 20 × 20 ZrO_2) and hence the associated strain within the system.

In summary, we have shown that computer modelling in conjunction with graphical analysis provides a powerful complementary technique to experiment in characterising the detailed atomistic structure of ZrO_2 supported CeO_2 thin films. In particular, structural features such as dislocations, defects and defect clusters, comprising low coordinatively saturated cerium and oxygen ions, are likely to have a considerable influence on the catalytic behaviour of the system including the mobility of ions through the ceria and zirconia lattices. Accordingly, elucidation of the atomistic structure of such structures as performed here, may help explain the remarkable catalytic properties of supported ceria thin films.

Notes and references

† The bulk and thin-film lattice misfits are given by:

$$F_{\text{bulk}} = \frac{\left|a_{CeO_2} - a_{ZrO_2}\right|}{(a_{CeO_2} + a_{ZrO_2})/2} \times 100 = +6.9\%$$

$$F_{\text{thin\_film}} = \frac{\left|na_{CeO_2} - ma_{ZrO_2}\right|}{(na_{CeO_2} + ma_{ZrO_2})/2} \times 100 = +1.6\%$$

where a_{CeO_2} and a_{ZrO_2} represent the bulk lattice parameters for ceria and zirconia, respectively, and n and m the number of units per side of simulation cell; n = 19CeO_2 units and m = 20ZrO_2 units.

1 A. Trovarelli, *Catal. Rev. Sci. Eng.*, 1996, **38**, 439.
2 E. S. Putna, T. Bunluesin, X. L. Fan, R. J. Gorte, J. M. Vosh, R. E. Lakis and T. Egami, *Catal. Today*, 1999, **50**, 343.
3 D. C. Sayle, C. R. A. Catlow, J. H. Harding, M. J. F. Healy, S. A. Maicaneanu, S. C. Parker, B. Slater and G. W. Watson, *J. Mater. Chem.*, 2000, **10**, 1315.
4 D. C. Sayle and G. W. Watson, *Surf. Sci.*, 2001, **473**, 97.
5 G. V. Lewis and C. R. A. Catlow, *J. Phys. C: Solid State Phys.*, 1985, **18**, 1149.
6 A. Dwivedi and A. N. Cormack, *Philos. Mag. A*, 1990, **61**, 1.
7 G. Balducci, M. S. Islam, J. Kašpar, P. Fornasiero and M. Graziani, *Chem. Mater.*, 2000, **12**, 677.
8 M. S. Khan, M. S. Islam and D. R. Bates, *J. Mater. Chem.*, 1998, **8**, 2299.
9 W. Smith and T. R. Forester, *The DL_POLY Molecular Simulation Package*, URL: http://www.dl.ac.uk/TCSC/Software/DL_POLY.
10 W. Dmowski, E. Mamontov, T. Egami, S. Putna and R. Gorte, *Physica B*, 1998, **248**, 95.
11 R. Aguiar, F. Sánchez, C. Ferrater, M. Aguiló and M. Varela, *Thin Solid Films*, 1998, **317**, 81.
12 A. Wang, J. A. Belot, T. J. Marks, P. R. Markworth, R. P. H. Chang, M. P. Chudzik and C. R. Kannewurf, *Physica C*, 1999, **320**, 154.

Anion selectivity properties of ruthenium(II) tris(5,5′-diamide-2,2′-bipyridine) receptors dictated by solvent and amide substituent†

Lindsay H. Uppadine,[a] Michael G. B. Drew[b] and Paul D. Beer*[a]

[a] *Department of Chemistry, Inorganic Chemistry Laboratory, University of Oxford, South Parks Road, Oxford, UK OX1 3QR. E-mail: paul.beer@chem.ox.ac.uk*

[b] *Department of Chemistry, University of Reading, Reading, UK RG6 6AD*

Received (in Cambridge, UK) 1st November 2000, Accepted 12th December 2000
First published as an Advance Article on the web 23rd January 2001

The ratio of the dichloromethane–methanol solvent mixture medium and nature of the receptor amide substituent critically dictates chloride *vs.* nitrate selectivity properties of new ruthenium(II) tris(5,5′-diamide-2,2′-bipyridine) receptors.

The selective recognition and sensing of anionic guests is a fundamental objective in supramolecular chemistry.[1,2] This is a consequence of the important role played by anions in a range of biological, chemical, medical and environmental processes.[3] Despite the fact that a wide range of solvents and solvent mixtures has been used in anion binding investigations, relatively little attention has been paid as to how the nature of the solvent medium and receptor structure can influence both the strength of anion–receptor complexation and importantly the anion binding selectivity trend the receptor displays. Previous research has shown that bis(heteroleptic) ruthenium(II) bipyridine cations $Ru(bpy)_2(bpy')^{2+}$ can bind and optically sense anions when bpy′ is a 4,4′- or 5,5′-diamide-2,2′-bipyridine ligand.[4,5] These receptors employ a combination of electrostatic and hydrogen bonding interactions to bind anionic guests. We report here the synthesis of new homoleptic receptors based on the ruthenium(II) tris(5,5′-diamide-2,2′-bipyridine) motif and demonstrate the anion binding strength, stoichiometry and chloride *vs.* nitrate anion selectivity critically depend on the nature of the receptor amide substituent and CH_2Cl_2:MeOH solvent mixture ratio.

The condensation of 5,5′-bis(chlorocarbonyl)-2,2′-bipyridine **1** with 2-methoxyethylamine, *n*-butylamine, *n*-dodecylamine 4′-carbonyl-1′,2′-dimethoxyphenyl-1,2-diaminoethane[6] gave the 5,5′-diamide-2,2′-bipyridine ligands **2**–**5** respectively in yields of 61–85% (Scheme 1).[5] The four host molecules **6**–**9** were prepared by reacting ligands **2**–**5** with ruthenium(III) trichloride in EtOH–H_2O (*via* 'ruthenium blue'[7]) or DMF. The receptors were purified by column chromatography on silica gel or Sephadex SP C25 and were isolated as their hexafluorophosphate salts in yields of 17–85%.‡

The Λ- and Δ-enantiomers of host **6** were resolved by cation exchange chromatography (Sephadex SP C25)[8] using sodium (−)-O,O′-dibenzoyl-L-tartrate. Figs. 1 and 2 show the crystal structure of the dichloride salt of Δ-**6**.§ The metal has a six-coordinate distorted octahedral environment being bonded to six nitrogen atoms [2.039(13)–2.095(13) Å] of the three bidentate ligands. The most interesting feature of the structure is that both chloride anions are encapsulated within the cavities formed around two triangular faces in the metal coordination sphere. As shown in Fig. 1, Cl2 forms hydrogen bonds to the three –NH groups at distances of 3.19, 3.29, 3.36 Å for N302, N202 and N602, respectively. However Cl1 forms only two hydrogen bonds to N102 at 3.21 and N502 at 3.27 Å. The third amide N–H group is directed away from the chloride, outwards from the cavity, and forms an intermolecular hydrogen bond N(402)···O(501) (1 − *x*, 0.5 + *y*, 2 − *z*) at 2.99 Å.

† Electronic supplementary information (ESI) available: crystal structure determination of receptor Δ-**6**. See http://www.rsc.org/suppdata/cc/b0/b008822f/

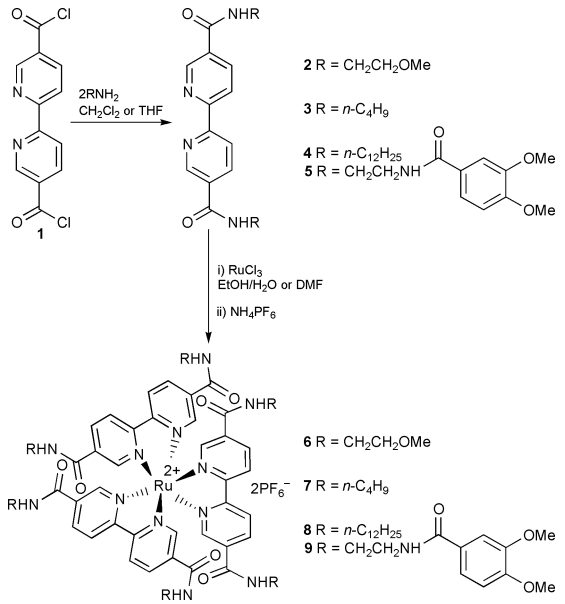

Scheme 1

There is a good geometric complementarity between the chloride anions and the interligand binding clefts, as illustrated in Fig. 2.

UV–VIS spectroscopic anion titrations were performed by adding tetrabutylammonium chloride, acetate and nitrate salts to receptors **6**–**9** in CH_2Cl_2 and CH_2Cl_2–MeOH solutions. Binding was generally signified by decreases in the absorbance and hypsochromic shifts for the MLCT and LC bands at *ca.* 260 and 300 nm, respectively. Values for the stability constants log β_1 and log β_2 were calculated using the Specfit program[9] and the data are summarised in Table 1. The results demonstrate how anion binding strength, stoichiometry and selectivity are

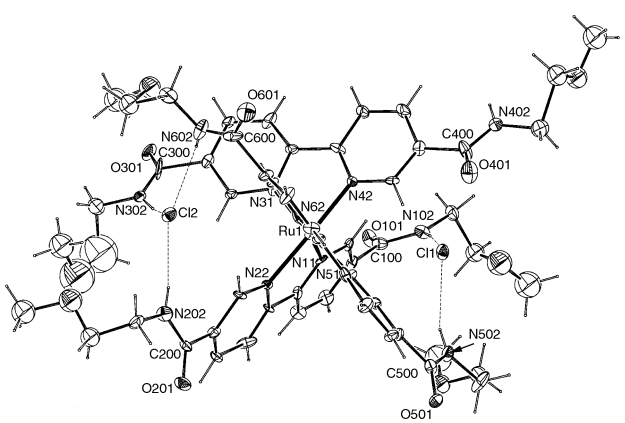

Fig. 1 The structure of Δ-**6** with ellipsoids at 20% probability. Hydrogen bonds to the chloride ions are shown as dotted lines.

DOI: 10.1039/b008822f

strongly dependent on the type of anion, the solvent system and the receptor amide substituent. For example, Table 1 shows the stability constants for all three anions decrease significantly as the methanol content increases from 1:0 to 9:1, 7:3 and then 1:1 CH_2Cl_2:MeOH. This can be rationalised by considering the high polarity of methanol and its ability to hydrogen bond with the receptor and the anionic guest. The complex stoichiometry is dependent on the binding strength and can be either 1:1 or 1:2 (host:guest). In 1:0 and 9:1 CH_2Cl_2:MeOH the host:guest ratio is 1:2. This correlates with the binding stoichiometry exhibited by **Δ-6** in the solid state (Fig. 1). In contrast, the observed host:guest ratio can be 1:2 or 1:1 in 7:3 CH_2Cl_2:MeOH, and is 1:1 in 1:1 CH_2Cl_2:MeOH. Table 1 also reveals how the anion selectivity depends on the solvent system. In 9:1 and 7:3 CH_2Cl_2:MeOH, all receptors display the selectivity sequence $Cl^- > NO_3^- > AcO^-$. The preference for chloride suggests this guest presents a superior match for the shape and/or dimensions of the binding site, while the unfavourable desolvation energy and non-complementary shape of acetate may explain why the weakest complexes are formed with this anion. It is noteworthy that receptors **6** and **7** remain chloride selective in 1:1 CH_2Cl_2:MeOH, while hosts **8** and **9** become selective for the nitrate anion. As the percentage of methanol is raised from 10 to 30 to 50%, the energy required to desolvate the anions prior to complexation increases and this can switch selectivity towards the anion with the lowest desolvation energy.[10] The hydration enthalpies ($-\Delta H_{hyd}$) of NO_3^-, Cl^- and AcO^- are calculated to be 293, 335 and 402 kJ mol^{-1}, respectively,[11] and these provide a good guide to the relative anion solvation energies in 1:1 CH_2Cl_2:MeOH. Hosts **8** and **9** possess large, lipophilic substituents which can partially shield the amide binding site from the surrounding solvent; the anion must therefore undergo significant desolvation prior to binding with these receptors. Consequently, the selectivity trend $NO_3^- > Cl^- > AcO^-$ for hosts **8** and **9** in 1:1 CH_2Cl_2:MeOH reflects the sequence of hydration energies $AcO^- > Cl^- > NO_3^-$ in the Hofmeister series.[12] In contrast, receptors **6** and **7** contain smaller amide substituents than their congeners **8** and **9**, and the anion desolvation energy does not dictate the selectivity sequence. The geometric complementarity between the chloride anion and hosts **6** and **7** is dominant (as exemplified by the crystal structure of **Δ-6** in Fig. 2) and overrides the unfavourable desolvation energy for this guest.

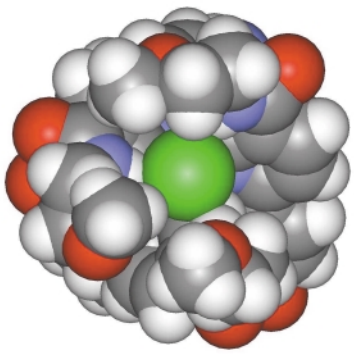

Fig. 2 CPK representation of **Δ-6** based on the crystal structure coordinates, illustrating the geometric complementarity between the chloride guest Cl2 (green) and the interligand binding pocket. (The methoxyethyl chain at the far side of the molecule has been removed to aid clarity.)

Table 1 Stability constants for receptors **6–9** and anions in CH_2Cl_2–MeOH solvent mixtures[a]

		Cl^-		NO_3^-		AcO^-	
Host	Solvent CH_2Cl_2:MeOH (v/v)	log β_1	log β_2	log β_1	log β_2	log β_1	log β_2
8	1:0	[b]		[b]		[b]	
6	9:1	7.47	12.9	6.33	11.3	5.90	10.1
7	9:1	7.69	14.1	6.70	12.3	6.02	10.9
9	9:1	[b]		7.88	13.8	7.06	12.3
6	7:3	5.43		5.27		[c]	
7	7:3	6.44	10.8	5.64		[c]	
8	7:3	6.48	10.5	5.76		[c]	
9	7:3	5.94	10.2	5.42		[c]	
6	1:1	4.31		[c]		[c]	
7	1:1	4.45		[c]		[c]	
8	1:1	4.82		5.39		[c]	
9	1:1	4.51		5.03		[c]	

[a] Errors estimated to be ⩽7%; T = 293 K. [b] Binding too strong for calculation (host:guest complex stoichiometry is 1:2). [c] Binding too weak for calculation.

In summary, the chloride *vs.* nitrate selectivity of new ruthenium(II) tris(5,5′-diamide-2,2′-bipyridine) receptors depends on both solvation factors and the amide substituent on the host. This interrelation between solvation effects and receptor structure is also used to achieve anion binding selectivity in Nature.[11]

We thank Professor F. R. Keene (James Cook University, Townsville, Australia) for supervising the chromatographic resolution of receptor **6**. We also acknowledge the EPSRC for a studentship (L. H. U.) and for use of the mass spectrometry service at the University of Wales, Swansea, and the EPSRC and University of Reading for funds for the Image Plate System.

Notes and references

‡ Receptors **6–9** were fully characterised by ^{1}H and ^{13}C NMR spectroscopy, elemental analysis and mass spectrometry.

§ Receptor **Δ-6** was recrystallised from acetonitrile. *Crystal data*: $[RuL_3]Cl_2 \cdot 0.5\ MeCN \cdot 0.5\ EtOH \cdot 0.5\ H_2O$, $C_{56}H_{70.5}Cl_2N_{12.5}O_{13}Ru$, M = 1298.72, monoclinic, $P2_1$, a = 13.759(14), b = 16.711(17), c = 15.811(16) Å, β = 114.53(10)°, U = 3307 Å^3, Z = 2, D_c = 1.304 g cm^{-3}, 10237 independent reflections were collected with Mo-Kα radiation using the MARresearch Image Plate System at room temperature. The structures were refined on F^2 using SHELXL[13] to $R1$ = 0.1163, $wR2$ = 0.2983 for 5411 data with $I > 2\sigma(I)$ and $R1$ 0.2264, $wR2$ 0.3532 for all data. CCDC 182/1873. See http://www.rsc.org/suppdata/cc/b0/b008822f/ for crystallographic files in .cif format.

1 *Supramolecular Chemistry of Anions*, ed. A. Bianchi, K. Bowman-James and E. García-España, Wiley-VCH, New York, 1997.
2 F. P. Schmidtchen and M. Berger, *Chem. Rev.*, 1997, **97**, 1609.
3 P. D. Beer and D. K. Smith, *Prog. Inorg. Chem.*, 1997, **46**, 1.
4 F. Szemes, D. Hesek, Z. Chen, S. W. Dent, M. G. B. Drew, A. J. Goulden, A. R. Graydon, A. Grieve, R. J. Mortimer, T. Wear, J. S. Weightman and P. D. Beer, *Inorg. Chem.*, 1996, **35**, 5868.
5 P. D. Beer, N. C. Fletcher and T. Wear, *Polyhedron*, 1996, **15**, 1339.
6 J. E. Redman, P. D. Beer, S. W. Dent and M. G. B. Drew, *Chem. Commun.*, 1998, 231.
7 N. Nagao, M. Tsuchida, H. Kumakura, K. Hisamatsu, F. S. Howell and M. Mukaida, *Inorg. Chim. Acta*, 1992, **195**, 221.
8 T. J. Rutherford, P. A. Pellegrini, J. Aldrich-Wright, P. C. Junk and F. R. Keene, *Eur. J. Inorg. Chem.*, 1998, 1677.
9 R. A. Binstead and A. D. Zuberbühler, Specfit Global Analysis, Version 2.90X.
10 P. D. Beer and M. Shade, *Chem. Commun.*, 1997, 2377.
11 J. J. R. Fraústo da Silva and R. J. P. Williams, *Struct. Bonding (Berlin)*, 1976, **29**, 67.
12 F. Hofmeister, *Arch. Exp. Pathol. Pharmacol.*, 1888, **24**, 247.
13 SHELX86, G. M. Sheldrick, 1993, program for crystal structure refinement. University of Göttingen.

Xenon probe for detecting the microporous structure of nanosized HZSM-5 zeolite

Weiping Zhang,*† Xiuwen Han, Xianchun Liu, Hao Lei and Xinhe Bao*

State Key Laboratory of Catalysis, Dalian Institute of Chemical Physics, Chinese Academy of Sciences, Dalian 116023, China. E-mail: w.zhang@tech.chem.ethz.ch

Received (in Cambridge, UK) 8th November 2000, Accepted 3rd January 2001
First published as an Advance Article on the web 23rd January 2001

The secondary pores in the nanosized HZSM-5 zeolite have been observed for the first time *via* ^{129}Xe NMR spectroscopy using xenon as a probe; the location of non-framework Al can also be identified.

As an emerging member of nanometer materials, nanosized zeolites have received considerable attention in the field of catalysis owing to their unique properties. When the crystallite size of HZSM-5 zeolite is reduced to the nanoscale level, it exhibits higher catalytic activity, less coking and longer catalytic life in the conversion of methanol to hydrocarbons,[1] oligomerization of ethylene, *etc.*[2] At present, there is growing interest in the synthesis of nanosized zeolites.[3,4] However, few attempts have been made to characterize the microporous structure of nanosized zeolites. In particular, the effects of crystallite size down to the nanoscale level on the microporous structure of zeolites have not been well established in the literature. ^{129}Xe NMR spectroscopy is a powerful technique for investigating porous materials, especially zeolites.[5–7] The high polarizability of the xenon electron cloud makes it very sensitive to physical interactions with its environment. Here we use xenon as a probe molecule for detecting the variations of microporous structure of dealuminated HZSM-5 zeolites with crystallite sizes of < 100 nm.

The starting HZSM-5 samples (Si/Al = 28) with crystallite sizes of 1000 and 70 nm were prepared according to the procedure published in our previous papers.[8–10] Hydrothermal treatment was performed in a quartz reactor tube with 10 mm maximum bed depth of zeolite. The temperature was increased at a rate of 5 °C min^{-1} to the treatment temperatures of 400 and 700 °C, then 100% water vapor (0.1 MPa) was introduced for 2 h. As established by ^{27}Al MAS and ^{1}H→^{27}Al CP/MAS NMR spectra, there is little non-framework Al in the parent microsized and nanosized HZSM-5 zeolites.[10] However, hydrothermal treatment of the samples leads to dealumination of the zeolite frameworks and to gradual formation of non-framework Al (δ_{Al} at 0 and 30 ppm).[11]

Prior to adsorption, all samples were degassed typically at 723 K and a pressure below 10^{-2} Pa for 10–20 h. ^{129}Xe NMR spectra were collected at room temperature on a Bruker DRX-400 spectrometer operating at 110.6 MHz with a recycle delay of 1 s, 60° pulse width of 8 μs and 1000–4000 scans. Chemical shifts were referenced to a secondary standard of xenon adsorbed in NaY zeolite the resonance of which was previously referenced to xenon gas at zero pressure using Jameson's equation.[12]

XPS measurements were carried out in a modified Leybold LHS-12 MCD system using Mg-Kα excitation and pass energy of 100 eV. The Si/Al ratio on the external surface of the zeolites can be obtained by integrating the calibrated Si 2p (E_b = 102.9 eV) and Al 2p (E_b = 74.3 eV) peaks.

The ^{129}Xe NMR spectra of parent microsized and nanosized HZSM-5 zeolites are shown in Fig. 1. With increase of xenon uptake, the resonance positions shift to low field due to the predominance of Xe–Xe interactions with an increase of xenon concentration. One main signal with a weak high-field shoulder is observed in the spectra of parent microsized HZSM-5 [Fig. 1(a)]. The main peak is associated with xenon adsorbed in the internal channels of microsized HZSM-5. However, for the nanosized HZSM-5, with increase of xenon uptake, a new strong peak appears at higher field [Fig. 1(b)]. The intensity of this new peak increases with xenon pressure up to 400 Torr. Further increase of xenon concentration, however, results in a decrease of the peak intensity where it is observed as a shoulder peak of the low-field signal. It is well known that the average electrostatic field in the internal channels of HZSM-5 zeolite is much stronger than that on the external surface.[6] Thus, xenon is adsorbed preferentially in the internal channels, and its chemical shift is at the low field. When the crystallite size of HZSM-5 zeolite is reduced to the nanoscale level, as demonstrated by a transmission electron microscope (TEM),[8] the particles are present as aggregates of many nanosized crystals with void space between the crystallites, for a high surface energy. Nanosized HZSM-5 zeolite has many secondary pores, which differ from the internal channels. With increasing xenon uptake, more xenon will be distributed in the secondary pores of nanosized HZSM-5, of this, some is adsorbed on the external surface of nanosized HZSM-5 whilst the remainder occupies the void space of the secondary pores. Therefore, as shown in Fig. 1(b), two signals are observed in the ^{129}Xe NMR spectra of nanosized HZSM-5. The low-field peak is assigned to xenon in the internal channels of nanosized zeolite, while the high-field peak is attributed to xenon in the secondary pores. However, under conditions of less aggregation,[8] the xenon signal of the secondary pores appears as a weak shoulder in the spectra of microsized HZSM-5 [Fig. 1(a)]. In addition, it can also be seen from Fig. 1(b) that the line width of the high-field peak is much narrower than that of the low-field peak. This may be due to a higher mobility of xenon atoms in such sites caused by weaker interaction among xenon atoms, which implies that the secondary pore size of the nanosized zeolite might be greater than that of its internal channels.

If we plot the resonance positions of xenon in the internal channels and in the secondary pores of nanosized HZSM-5 at

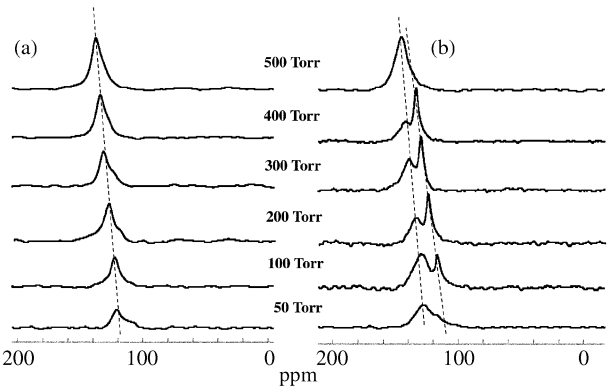

Fig. 1 ^{129}Xe NMR spectra of xenon adsorbed in parent microsized (a) and nanosized (b) HZSM-5 zeolites as a function of xenon pressure.

† Present address: Laboratory of Technical Chemistry, ETH Zurich, CH-8092, Switzerland.

DOI: 10.1039/b009015h

different pressures [Fig. 1(b)], it is found that the slopes of these two lines are different and at higher xenon pressures these two lines will be superposed. This indicates that the chemical shift difference between xenon in the internal channels and in the secondary pores decreases slightly with pressure. Xenon atoms in these two positions also exchange at room temperature and when the xenon pressure is > 500 Torr, this exchange is too fast to be detected by NMR. Thus, one main signal is observed in the ^{129}Xe NMR spectra of nanosized HZSM-5 at higher xenon pressures. To our knowledge, this is the first report that secondary pores in nanosized zeolites are observed by ^{129}Xe NMR spectroscopy.

Fig. 2 and 3 show the ^{129}Xe NMR spectra of microsized and nanosized HZSM-5 zeolites treated by steaming at 400 and 700 °C. There is only a single signal in the ^{129}Xe NMR spectra of microsized HZSM-5 dealuminated by steaming (Fig. 2). This demonstrates that the non-framework Al may migrate to the external surface of the dealuminated microsized HZSM-5, in the presence of steam, leading to a homogeneous distribution of xenon in the channels. However, two signals are evident in the ^{129}Xe NMR spectra of nanosized HZSM-5 treated by steaming at 400 °C [Fig. 3(a)]. The obvious distribution of xenon in the

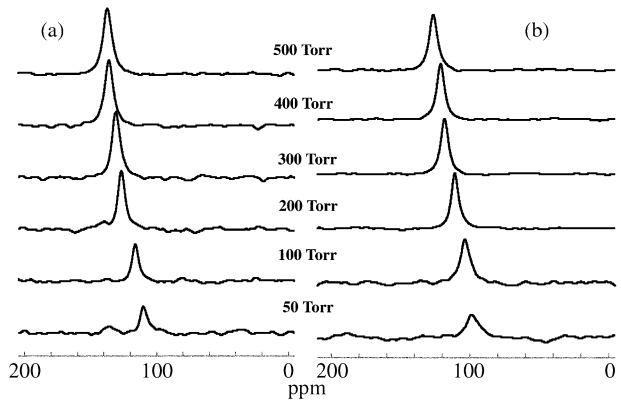

Fig. 2 ^{129}Xe NMR spectra of xenon adsorbed in dealuminated microsized HZSM-5 zeolite steamed at 400 °C (a) and 700 °C (b) as a function of xenon pressure.

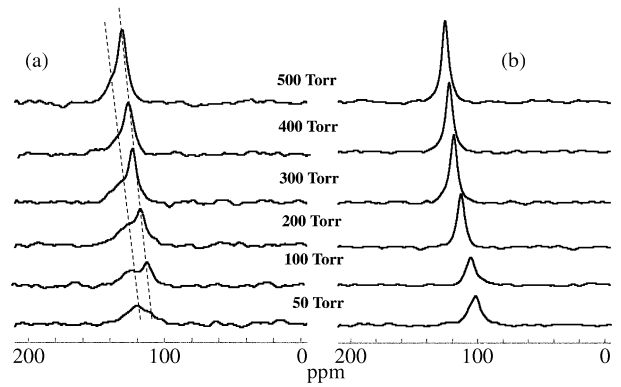

Fig. 3 ^{129}Xe NMR spectra of xenon adsorbed in dealuminated nanosized HZSM-5 zeolite steamed at 400 °C (a) and 700 °C (b) as a function of xenon pressure.

secondary pores of nanosized HZSM-5 indicates that most non-framework Al does not deposit on the external surface of the nanocrystallites. The two lines from the resonance positions of xenon adsorbed in the internal channels and in the secondary pores will not be superposed at high xenon pressures [Fig. 3(a)]. This indicates that the existence of non-framework Al hinders the rapid exchange of the xenon atoms in these two positions. One can speculate that the non-framework Al may deposit near the windows of the nanosized HZSM-5 channels. If hydrothermally treated at higher temperatures, such as at 700 °C, only one signal appears in the ^{129}Xe NMR spectra [Fig. 3(b)]. Thus, the non-framework Al may occupy the secondary pores of nanosized HZSM-5 (*i.e.* on the external surface).

XPS experiments were performed to study the migration of Al atoms in zeolites. It was found that the Si/Al ratio on the external surface of microsized HZSM-5 decreases from 12.5 to 3.5 after steaming at 700 °C, while that of nanosized HZSM-5 decreases from 6.3 to 3.2 under the same conditions. Therefore, hydrothermal treatment of both microsized and nanosized HZSM-5 will lead to Al enrichment on the external surface *i.e.* migration of Al atoms to the external surface. A similar result was obtained by Datka *et al.*[13] in characterizing a dealuminated HZSM-5 zeolite. This also agrees well with the above results from ^{129}Xe NMR.

In conclusion, xenon is a sensitive probe to detect zeolite microporous structure and its variation upon dealumination. Evidence of secondary pores are observed for the first time in the ^{129}Xe NMR spectra of nanosized HZSM-5 zeolite. After hydrothermal treatment, the location of non-framework Al can also be determined.

The support of the National Natural Science Foundation of China and the Ministry of Science and Technology of China through the 973 Project is gratefully acknowledged.

Notes and references

1 M. Sugimoto, H. Katsuno, K. Takatsu and N. Kawata, *Zeolites*, 1987, **7**, 503.
2 M. Yamamura, K. Chaki, T. Wakatsuki and K. Fujimoto, *Zeolites*, 1994, **14**, 643.
3 M. Tsapatsis, M. Lovallo and T. Okubo, *Chem. Mater.*, 1995, **7**, 1743.
4 M. A. Camblor, A. Corma and S.Valencia, *Microporous Mesoporous Mater.*, 1998, **25**, 59.
5 J. A. Ripmeester and C. I. Ratcliffe, *J. Phys. Chem.*, 1990, **94**, 7652.
6 S. M. Alexander, J. M. Coddington and R. F. Howe, *Zeolites*, 1991, **11**, 368.
7 J. L. Bonardet, J. Fraissard, A. Gedeon and M. A. Springud-Huet, *Catal. Rev.-Sci. Eng.*, 1999, **41**, 115.
8 W. Zhang, X. Bao, X. Guo and X. Wang, *Catal. Lett.*, 1999, **60**, 89.
9 W. Zhang, D. Ma, X. Liu, X. Liu and X. Bao, *Chem. Commun.*, 1999, 1091.
10 W. Zhang, D. Ma, X. Han, X. Liu, X. Bao, X. Guo and X. Wang, *J. Catal.*, 1999, **188**, 393.
11 W. Zhang, X. Han, X. Liu, X. Bao, X. Guo and X. Wang, *International Symposium on Zeolites and Microporous Crystals (ZMPC 2000)*, Sendai, Japan, August 2000, organized by Japan Association of Zeolites.
12 A. K. Jameson, C. J. Jameson and H. S. Gutowsky, *J. Chem. Phys.*, 1970, **53**, 2310.
13 J. Datka, S. Marsehmeyer, T. Neubauer, J. Meusinger, H. Papp, F. W. Schutze and I. Szpyt, *J. Phys. Chem.*, 1996, **100**, 1445.

ChemComm

Opportunities for ionic liquids in recovery of biofuels

Andrei G. Fadeev*† and Michael M. Meagher

Biological Process Development Facility, The University of Nebraska, Lincoln, NE, 68583, USA. E-mail: mmeagher@unl.edu; Fax: +1 402-472-1693; Tel: +1 402-472-2342

Received (in Corvallis, OR, USA) 26th July 2000, Accepted 13th December 2000
First published as an Advance Article on the web 23rd January 2001

Room temperature ionic liquids have potential as extractants in recovery of butyl alcohol from fermentation broth; water solubility in ionic liquid and ionic liquid solubility in water are important factors affecting selectivity of butyl alcohol extraction from aqueous solutions.

There has been a renewed interest in processing of biomass into fuels and chemicals *via* fermentation during the last decade. In that respect, ethanol and acetone–butyl alcohol–ethanol (ABE) fermentations are two of the most attractive bioprocesses. Recovery of alcohols from the fermentation broth is the most energy extensive step in fermentative fuel production. The average energy requirement per litre of EtOH produced is 2446 kcal.[1] The amount of energy is about 3 times higher[2] for *n*-BuOH, since ABE fermentation broth contains only about 2 wt% of BuOH *vs.* 6 wt% of EtOH in yeast fermentation broth. EtOH is currently recovered by distillation. Distillative recovery of BuOH from fermentation broth is not economical. Alternative recovery methods have been considered including: solvent extraction, stripping, pervaporation, *etc*. None of the methods has been economically proved yet.

We investigated the potential of ionic liquids for extraction of BuOH from aqueous solutions. Room temperature ionic liquids have extremely low vapor pressure and low solubility in water. These properties make them interesting solvents for extraction of organic compounds from aqueous stream.[3]

Most solvents that have high distribution coefficients for BuOH are flammable, hazardous and toxic to humans and microorganisms.[4] Tri-*n*-butyl phosphate, octan-1-ol and diethyl ether are listed as solvents with high BuOH partition coefficients, 14.6, 7.6, and 4.1, respectively.[5] Tri-*n*-butyl phosphate and octan-1-ol were shown to be toxic to bacteria[6] and diethyl ether is extremely flammable.

Solvent selection criteria for liquid–liquid extractions are numerous, including distribution coefficient, density, viscosity, *etc*. This paper addresses solubility of ionic liquids in water, water coextraction, density and viscosity of extractant. Using the correlation of partitioning data between 1-butyl-3-methyl-1*H*-imidazol-3-ium hexafluorophosphate ([BMIM][PF_6])–water and octan-1-ol–water,[3] it could be found that the BuOH partition coefficient in the [BMIM][PF_6]–water system should be around 0.8–0.85. Professor K. Seddon advised us that 1-octyl-3-methyl-1*H*-imidazol-3-ium hexafluorophosphate ([OMIM][PF_6]) should have lower solubility in water than [BMIM][PF_6].

BMIM[PF_6] was prepared according to the procedure described by Huddleston *et al*.[3] The density of the ionic liquid was 1.34 g cm^{-3}.

1-Octyl-3-methyl-1*H*-imidazol-3-ium chloride was prepared *via* metathesis reaction of equimolar amounts of 1-methylimidazole and 1-chlorooctane. The two components were mixed in a round-bottom flask equipped with stopcock vacuum adapter, and the air was removed from the flask using a vacuum pump. The reaction was carried out at 80 °C for 3–4 d. The product was washed with ethyl acetate and dried in vacuum. OMIM[PF_6] was obtained from 1-octyl-3-methyl-1*H*-imidazol-3-ium chloride by adding an equimolar amount of hexafluorophosphoric acid. The density of [OMIM][PF_6] was 1.21 g cm^{-3}.

To determine distribution coefficients and mutual solubilities, the ionic liquid was mixed with water or BuOH–water solution in an airtight bottle. The mixture was shaken overnight and then left for 1–3 d to achieve phase separation. Mutual solubilities were determined by separating BuOH and water from the IL using a rotary evaporator. The collected BuOH–water solutions were analyzed by GC. BuOH and water distribution coefficients, D, and selectivities, α, were estimated according to eqns. 1 and 2

$$D = c_{IL} \cdot \rho / c_{H_2O} \quad (1)$$

$$\alpha = D_{BuOH} / D_{H_2O} \quad (2)$$

where c_{IL} and c_{H_2O} are the concentrations (g per 1000 g of phase) of BuOH and water in ionic liquid phase and aqueous phase; ρ is the density of ionic liquid, D_{BuOH} and D_{H_2O} are the BuOH and water distribution coefficients.

The BuOH distribution coefficient for [BMIM][PF_6]–water was found to be very close to the predicted value, 0.85 (Table 1). Distribution coefficients of BuOH for both ionic liquids were similar. Increase in the molecular dimensions of the alkylimidazolium cation decreased mutual solubilities of the ionic liquid and water resulting in higher extractive selectivities for [OMIM][PF_6]. Water solubility of [BMIM][PF_6] was 6.5 fold higher than that of [OMIM][PF_6].

The larger size of the $[OMIM]^+$ ion also resulted in higher viscosity of [OMIM][PF_6] (Fig. 1). The viscosity had strong temperature dependence allowing for fast phase separation at elevated temperature. Higher temperature also improved extractive selectivity, Table 1. BuOH solubility for the ionic liquids under investigation was small, 200–400 mol m^{-3}. It is, however, within the range of solubilities in octanol (200 to 2000 mol m^{-3}). Huddleston *et al*.[3] noted that even low partition coefficients could result in an economical recovery process due to the non-volatility of the extractant.

Pervaporation is often mentioned as the most promising technology for recovery of organics from aqueous streams, and polydimethylsiloxane membrane is the most extensively studied for organophilic pervaporation.

Pervaporative BuOH recovery from 1 wt% aqueous solution and [OMIM][PF_6] was investigated using commercial polydimethylsiloxane membrane MEM-100 (MemPro Co., www.MemPro.com). The solution of [OMIM][PF_6]–butanol–water 97.4–1.0–1.6 wt% was prepared to simulate the composition of the ionic liquid phase in equilibrium with 1 wt% BuOH–water solution. The pervaporation set-up is described

† Current address: Santa Fe Science @ Technology, Santa Fe, NM 87505; E-mail: fadeev@sfst.net; Fax: +1 505-474-9489; Phone: +1 505-474-3500.

Table 1 Compositions of phases, distribution coefficients, and extractive selectivity

Initial aqueous phase composition	Aqueous phase, g/1000 g			Ionic liquid phase, g/1000 g					
	BuOH	H_2O	[BMIM][PF_6]	BuOH	H_2O	[BMIM][PF_6]	D_{H_2O}	D_{BuOH}	α
100% H_2O, 23 °C	—	97.703	2.297	—	2.116	97.884	0.029	—	—
2.01 wt% BuOH, 23 °C	1.143	96.463	2.394	0.724	2.400	96.876	0.033	0.849	25.77
4.74 wt% BuOH, 23 °C	2.927	94.664	2.409	1.689	2.576	95.735	0.036	0.773	21.47
4.97 wt% BuOH, 50 °C	1.785	94.639	3.576	2.286	4.791	92.923	0.068	1.716	33.65
Initial aqueous phase composition	BuOH	H_2O	[OMIM][PF_6]	BuOH	H_2O	[OMIM][PF_6]	D_{H_2O}	D_{BuOH}	α
100% H_2O, 23 °C	—	99.65	0.350	—	1.520	98.480	0.018	—	—
2.01 wt% BuOH, 23 °C	1.061	98.458	0.436	0.809	1.321	97.870	0.016	0.923	55.31
4.74 wt% BuOH, 23 °C	2.237	97.225	0.538	1.637	1.922	96.441	0.024	0.885	36.65
4.97 wt% BuOH, 50 °C	1.273	97.257	1.470	1.744	2.970	95.286	0.037	1.658	44.19

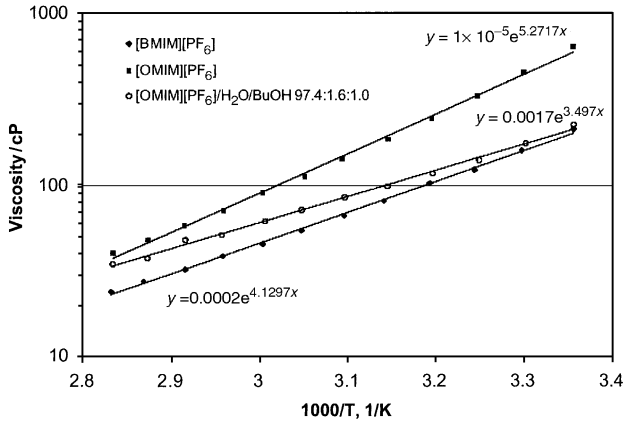

Fig. 1 Viscosity *vs.* 1/*T*.

elsewhere.[7] Pervaporative selectivity was determined according to the equation:

$$\alpha = \left[\frac{C_{BuOH}}{C_{H_2O}}\right]_{permeate} \Big/ \left[\frac{C_{BuOH}}{C_{IL} + C_{H_2O}}\right]_{feed} \quad (3)$$

where C is concentration.

Pervaporation measurements were carried out at 55 °C with permeate pressure 0.01 Torr. Due to the high viscosity of the feed, concentration polarization was anticipated, even though viscosity of [OMIM][PF_6]–water–BuOH solution was noticeably lower than that of pure [OMIM][PF_6] (Fig. 1). The feed flow through the membrane cell was definitely laminar even at a flow rate of 4 L min^{-1}. Flux through the membrane was 67 g m^2 h^{-1} at selectivity 62. As expected, there was no ionic liquid found in the permeate. Pervaporation of 1 wt% BuOH–water solution at the same conditions showed a flux rate of 110 g m^2 h^{-1} at selectivity 42.

Although the viscosity of [OMIM][PF_6]–water–BuOH solution was about 100 fold higher than the viscosity of the BuOH–water mixture, the flux rate through the membrane was only 0.6 fold lower at higher selectivity. BuOH–water ratio in the permeate was close to BuOH–water ratio in ionic liquid feed, suggesting that the membrane did not improve the separation. Distillation is thought to be more economical for BuOH recovery from ionic liquids.

In conclusion, chemical versatility makes ionic liquids interesting solvents for extractive separation in biotechnology. Properties of ionic liquids in that respect remain very much unexplored. We are particularly interested in investigating the mechanism of toxicity of ionic liquids for microorganisms. Preliminary studies of ABE fermentation with [OMIM][PF_6] present at saturation level suggest that the IL suppress biological activity in the system.

The research was supported by the National Corn Growers Association. The authors are grateful to Dr J. Huang for toxicity tests.

Notes and references

1 D. Morris and I. Ahmed, *How Much Energy Does It Take to Make A Gallon of Ethanol*?, Monograph, Institute for Local-Self reliance (ILSR), 1995 (www.ilsr.org)
2 M. Matsumura, H. Kataoka, M. Sueki and K. Araki, *Energy saving effect of pervaporation using oleyl alcohol liquid membrane, Bioprocess Eng.*, 1988, **3**, 93.
3 J. G. Huddleston, H. D. Willauer, R. P. Swatloski, A. E. Visser, R. D. Rogers, *Room temperature ionic liquids as novel media for 'clean' liquid–liquid extraction, Chem. Commun.*, 1998, 1765.
4 K. Schungerl, *Solvent extraction in biotechnology. Recovery of primary and secondary metabolites*, Springer-Verlag, 1994.
5 A. S. Kertes and C. J. King, *Extraction chemistry of low molecular weight aliphatic alcohols, Chem. Rev.*, 1987, **87**, 687.
6 S. R. Roffler, H. W. Blanch and C. R. Wilke, *In situ recovery of fermentation products, Trends Biotechnol.*, 1984, **2**, 129.
7 A. G. Fadeev, M. M. Meagher, S. S. Kelley and V. V. Volkov, *Fouling of poly[1-(trimethylsilyl)prop-1-yne] membranes in pervaporative recovery of butanol from aqueous solutions and ABE fermentation broth, J. Membr. Sci.*, 2000, **173**, 133.

ChemComm

Large chiral discrimination of a molecular probe by bovine serum albumin

Challa V. Kumar,* Apinya Buranaprapuk† and Ho Chou Sze

Department of Chemistry, U-60, University of Connecticut, 55 N. Eagleville Road, Storrs, CT 06269-3060, USA. E-mail: c.v.kumar@uconn.edu

Received (in Columbia, MO, USA) 21st August 2000, Accepted 15th December 2000
First published as an Advance Article on the web 23rd January 2001

A phenylalanine-derived fluorescent probe shows high enantioselectivity for binding to bovine serum albumin; the L-isomer binds nearly one hundred times better than the D-isomer, which suggests the tight fitting of the L-isomer to the binding site.

Although chiral discrimination of substrates by enzymes and other biological macromolecular systems is well known, the design of chiral molecules that can bind to proteins with a high enantioselectivity is challenging.[1] Enantioselective binding of dansyl amino acids, drugs, and metal complexes to bovine serum albumin (BSA), chymotrypsin, and other proteins has been reported, although the selectivity is often low (1.15 to 3).[2] Despite the low selectivity, chiral biochromatography with BSA has been demonstrated to be useful in separating the optical isomers of drugs, amino acids, and small molecules, thereby, indicating the utility of such recognition in a variety of applications.[3] The observed enantiomeric selectivity was explained based on the steric, hydrophobic and hydrogen-bonding interactions between the ligand and the host.[4] The design of ligands that bind tightly to sites that can accommodate only one isomer but not the other, with selectivities > 10, therefore, is challenging.

The design of pyrene labeled peptides that bind to proteins and induce site specific photocleavage of the protein backbone (protein scissors) is of current interest.[5] *N*-[4(1-pyrene)butyroyl]-L-phenylalanine (Py-L-Phe), for example, induces site

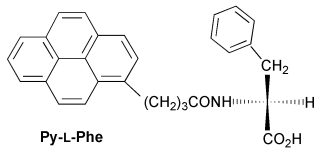

Py-L-Phe

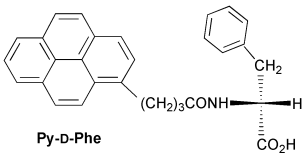

Py-D-Phe

specific photocleavage in BSA between residues Leu 346 and Arg 347, and in lysozyme the cleavage occurs between residues Trp 108 and Val 109.[5c] We now report that Py-L-Phe and its optical isomer, Py-D-Phe, are discriminated by BSA in a 100 : 1 ratio (the ratio of the corresponding binding constants). These observations indicate the importance of the single asymmetric center present in Py-Phe for recognition between ligand and the protein. The chiral discrimination is reflected in the photophysical properties of the protein-bound probes. The protein-bound ligand spectra exhibit contrasting differences between the isomers, indicating the sensitivity of these properties on the chiral nature of the probe microenvironment in the protein.

Py-D-Phe was synthesized by reacting the methyl ester of D-phenylalanine with 4(1-pyrene)butyric acid in tetrahydrofuran using *N*,*N*′-dicyclohexyl carbodiimide (DCC) as the coupling agent in a procedure analogous to the synthesis of the corresponding L-isomer.[5] Mild hydrolysis of the methyl ester (1 M HCl, 12 h, room temp.) followed by column chromatography on silica gel (elution with 20 : 5, chloroform to methanol) resulted in Py-D-Phe in 60% yield. The product was characterized from UV–VIS, fluorescence, circular dichroism, ^{1}H NMR and mass spectral data. ^{1}H NMR (400 MHz, d_6-DMSO) δ 7.8–8.2 (9H), 7.1 (5H), 4.4 (1H), 3.1 (2H), 1.8–2.1 (6H); MS data (FAB): *m/z* 436 (MH^+).

The absorption spectrum of the pyrenyl chromophore in the near UV region (300–360 nm) is sensitive to the binding of the probe to the protein. Addition of BSA (0, 0.5, 1, 1.5, 2, 4, and 8 μM) to Py-D-Phe (10 μM) resulted in dramatic changes in the probe absorption spectrum (Fig. 1). The vibronic band positions are shifted to longer wavelengths as the protein is titrated into the solution, and an isosbestic point (point of constant absorbance) is clearly visible. Such isosbestic behavior is strongly indicative of two distinct chromophores, and we assign these to the bound and free chromophores. A net increase in the absorbance at the 0–0 band (hyperchromism) with protein concentration is also evident in the spectra. In contrast to these results, extensive hypochromism (decrease in absorbance) was observed when Py-L-Phe was titrated with BSA, under similar conditions.

The above absorption titration data were analyzed to construct binding isotherms, using the Scatchard equation,[5] and the corresponding binding constant is 5.3×10^5 dm^3 mol^{-1}. This value is two orders of magnitude less than the corresponding binding constant for the L-isomer (6.7×10^7 dm^3 mol^{-1}).[5] Thus, Py-L-Phe binds nearly 100 times better than Py-D-Phe. The large discrimination between the two chiral isomers is surprising, and it is much greater than the enantioselectivities observed for the binding of gossypol, warfarin, dansyl amino acids and chiral fatty acid analogs to BSA (discussed below). The large differences in the binding constants between the optical antipodes strongly suggest the intimate interaction of the probe with the protein in which only one of the two isomers fits snugly in the binding site. Such intimate interaction with the surrounding protein matrix is expected to result in differences in the spectral properties of the protein-bound chromophores.

The microenvironments of the protein-bound isomers, their access to the aqueous phase, and solvent exposure are expected

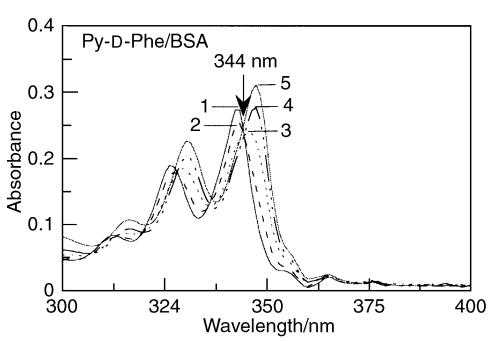

Fig. 1 Absorption spectra of Py-D-Phe (10 μM) (1 cm path length) with increasing concentrations of BSA: (0, 0.5, 2.0, 4.0 and 8.0 μM). The red shift (4 nm) of the peak positions and the isosbestic points at 344, 328, and 315 nm are evident in the spectra.

† Current address: Department of Chemistry, Faculty of Science, Srinakharinwirot University, Sukhumvit 23, Bangkok 10110, Thailand.

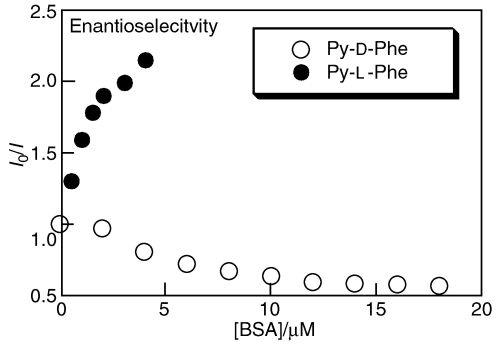

Fig. 2 Plot of the fluorescence intensities (I_0/I) of Py-D-Phe (2 μM, open circles) and Py-L-Phe (2 μM, filled circles) recorded at increasing concentrations of BSA. Note that larger concentrations of BSA are needed to saturate binding of Py-D-Phe. Both samples were excited at 344 nm.

to be different. These details are examined in fluorescence experiments. The protein–probe mixtures are excited at 344 nm (isosbestic point) and the probe emission was monitored at increasing concentrations of the protein. The ratio of initial intensity (I_0) to that in the presence of BSA (I) is plotted as a function of BSA concentration (Fig. 2). The fluorescence intensity of the D-isomer increases initially with protein concentration, and the ratio, I_0/I, reaches a plateau at higher protein concentrations. The fluorescence from the L-isomer, in contrast, is strongly quenched by BSA, and the corresponding plot shows an accidental near-mirror image behavior. These results highlight the differences in the local environment surrounding the fluorophore when the two isomers bind to BSA.

The accessibility of the two isomers to the solvent was probed using the fluorescence quencher, hexamminecobalt(III) chloride. The extent of protection offered by the protein can be readily distinguished in these simple experiments. The emission from the BSA-bound D-isomer was enhanced by the addition of CoHA (Fig. 3) whereas for the L-isomer the emission was quenched, confirming the differences in the binding behavior of the two optical antipodes shown in Figs. 1 and 2.

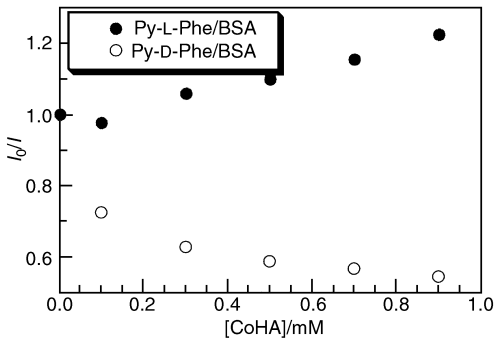

Fig. 3 Chiral selectivity for the quenching of fluorescence emission from the Py-D-Phe (open circles) and Py-L-Phe (filled circles) bound to bovine serum albumin by hexamminecobalt(III) chloride.

The large difference in the affinities of the optical antipodes arising due to a single chiral center is unexpected. For example, the binding of dansyl labeled amino acids to BSA shows only a 3:1 discrimination between the corresponding D- and L-isomers.[2] Treatment of racemic potassium tris(oxalato)cobaltate(III) with BSA resulted in the enrichment of the Δ isomer with an enantiomeric excess of 18%[6] and only minor differences were reported for the binding of the ketoprofen enantiomers to BSA.[7] The first report on the chiral recognition by a *de novo* designed peptide using D-norleucine derivative was reported to be 2:1,[8] and (*R*)-warfarin was retained to a greater extent on an immobilized BSA column than (*S*)-warfarin[9] while no enantioselectivity was observed for the binding of gossypol to BSA.[10] The D-amino acids, on a liquid chromatography column with immobilized BSA as the chiral phase, eluted at different times, but no information on the relative binding affinities of the isomers is reported. Preferential binding of L-phenylalanine to BSA was observed in ultrafiltration experiments,[10b] and in all the above examples, the observed selectivity was only moderate. The larger discrimination observed with Py-Phe, compared to the naphthyl or the dansyl amino acids, can be attributed to the increased hydrophobic surface area of the pyrenyl chromophore. Larger, rigid, hydrophobic surfaces of correct configuration can interact better with the protein, while a wrong isomer will interact poorly, thus widening the gap between the two binding constants.

The chiral center present in Py-Phe is five atoms away from the pyrenyl chromophore and yet it dramatically influences the binding behavior/spectral properties of the pyrenyl chromophore. Both isomers may bind at the same site or may bind at different sites on BSA. These two models can be distinguished in photocleavage experiments in which the pyrenyl probe can be activated with light to cleave the protein backbone at the probe binding site. Such experiments are in progress. Hydrophobic burial of Py-L-Phe at domain II, subdomain C of BSA at residues 346 and 347, was indicated from the photocleavage experiments from this laboratory, and current results are consistent with site specific binding of D and L isomers of Py-Phe to BSA.[5] The marked differences observed in the spectral properties of the bound enantiomers are surprising, and they are primarily due to differences in the residues that line the binding cavity. These results imply that the location of the pyrenyl chromophore, the photoactive moiety used for protein cleavage, is different for the two enantiomers.

Such differences in the binding environment will be exploited in photocleavage experiments to direct the photochemical reagents to different sites on proteins. The large differences in the spectral properties of Py-Phe isomers, in addition, provide a signal transduction mechanism for the translation of the chiral recognition information into an easily measurable spectroscopic quantity for application in chiral biosensors.

Financial support of this work by the National Science Foundation (DMR-9729178), and the sponsors of the Petroleum Research Fund, are gratefully acknowledged.

Notes and references

1 C. J. Suckling, *Enzyme Chemistry: Impact and Applications*, Chapman and Hall, London, 2nd edn., 1990; A. Lehninger, D. L. Nelson and M. M. Cox, *Principles of Biochemistry*, Worth, New York, 1993; F. H. Westheimer, H. Fisher, E. E. Conn and B. Vennesland, *J. Am. Chem. Soc.*, 1951, **73**, 2043.

2 Y. Abe, S. Fukui, Y. Koshiji, M. Kobayashi, T. Shoji, S. Sugata, H. Nishizawa, H. Suzuki and K. Iwata, *Biochim. Biophys. Acta*, 1999, **1433**, 188; A. Haque and J. T. Stewart, *J. Liq. Chromatogr. Relat. Technol.*, 1998, **21**, 2675; C. J. Stefan, M. Ubbink, G. W. Canters and H. P. J. M. Dekkers, *J. Phys. Chem.*, 1996, **100**, 17 957; G. Felix and V. Descorps, *Chromatographia*, 1999, **49**, 595; Y. Yan and M. L. Myrick, *Anal. Chem.*, 1999, **71**, 1958.

3 S. Allenmark and S. Andersson, *Chirality*, 1992, **4**, 24; T. Cserhati and E. Forgacs, *Int. J. Bio-Chromatogr.*, 1999, **4**, 203; L. Lepri, V. Coas and M. Del Bubba, *J. Planar, Chromatogr.-Mod., TLC*, 1999, **12**, 221; T. Kitae, T. Nakayama and K. Kano, *J. Chem. Soc., Perkin Trans. 2*, 1998, 207.

4 K. B. Lipkowitz, *Acc. Chem. Res.*, 2000, **33**, 555.

5 (*a*) A. Buranaprapuk, C. V. Kumar, S. Jockusch and N. J. Turro, *Tetrahedron*, 2000, **56**, 8311; (*b*) C. V. Kumar and A. Buranaprapuk, *J. Am. Chem. Soc.*, 1999, **121**, 4262; (*c*) C. V. Kumar, A. Buranaprapuk, G. J. Opiteck, M. B. Moyer, S. Jockusch and N. J. Turro, *Pro. Natl. Acad. Sci.*, 1998, **95**, 10 361; (*d*) C. V. Kumar and A. Buranaprapuk, *Angew. Chem., Int. Ed. Engl.*, 1997, **36**, 2085.

6 T. Taura, *Inorg. Chim. Acta*, 1996, **252**, 1.

7 M. Levi and M. Zandomeneghi, *Gazz. Chim. Ital.*, 1966, **126**, 599.

8 K. S. Broo, H. Nilsson, J. Nilsson and L. Baltzer, *J. Am. Chem. Soc.*, 1988, **120**, 10 287.

9 G. Massolini, A. F. Aubry, A. McGann and I. W. Wainer, *Biochem. Pharmacol.*, 1993, **46**, 1285.

10 (*a*) D. S. Sampath and P. Balaram, *Biochim. Biophys. Acta*, 1986, **882**, 183; (*b*) A. Higuchi, T. Hashimoto, M. Yonehara, N. Kubota, K. Wanatabe, S. Uemiya, T. Kojima and M. Hara, *J. Membr. Sci.*, 1997, **130**, 31.

Typeset and printed by Black Bear Press Limited, Cambridge, England

Water-accelerated organic transformations

Seth Ribe and Peter Wipf*

Department of Chemistry, University of Pittsburgh, Pittsburgh, PA 15260, USA. E-mail: pwipf+@pitt.edu

Received (in Cambridge, UK) 12th October 2000, Accepted 14th November 2000
First published as an Advance Article on the web 8th January 2001

Rather than quenching all reactive intermediates and arresting the reaction, the addition of catalytic or stoichiometric (1–10 equiv.) quantities of H_2O to organic and organometallic processes can lead to surprisingly beneficial effects on reaction rate, product yield, and regio-, diastereo- and enantioselectivity. A most intriguing aspect of H_2O-promoted transformations is the role that this strong Lewis-base can play in providing a source for more highly Lewis-acidic species. This scenario is most likely operative when H_2O is added to reaction mixtures containing alanes, but organozinc reagents or organocuprates also seem to be transformed accordingly. In addition, the oxide or hydroxide ligand on the metal presents a source for chelation interactions that change aggregation states of organometallics and can provide anchimeric assistance. In many cases, water has been found to be an effective hydrolyzing agent leading to secondary products that serve as catalysts or promoters. In some cases, it has been shown that water provides a quenching agent capable of driving chemical equilibria towards the desired products.

Mr Seth Ribe was born in Bangor, Maine, in 1969. He received his B.S. degree in 1993 from the University of Southern Maine. From 1993–1995, he was at Northern Arizona University where he worked with Professor Michael Eastman studying the chemistry of C_{60} radical anions. He is currently completing the requirements for a PhD degree at the University of Pittsburgh under the direction of Professor Peter Wipf.

Professor Peter Wipf was born in Aarau, Switzerland, in 1959. He received his PhD degree in Organic Chemistry with Professor Heinz Heimgartner in 1987 at the University of Zürich. From 1988–1990, he worked as Swiss National Science Foundation Fellow with Professor Robert E. Ireland at the University of Virginia, where he participated in the total synthesis of FK-506 and studied the ester enolate Claisen rearrangement. In September 1990, he joined the Department of Chemistry at the University of Pittsburgh and was promoted to the rank of full Professor in February 1997. His research interests are centered around the total synthesis of natural products and include heterocyclic, organometallic, combinatorial, computational and medicinal chemistry. Wipf is the Director of the Combinatorial Chemistry Center at Pittsburgh that is involved in many collaborative projects in chemical biology. He has been named an NSF Presidential Faculty, a Japanese Society for the Promotion of Science Fellow and a Lilly Grantee, and he has received a Camille Dreyfus Teacher–Scholar Award, an Alfred P. Sloan Foundation Fellowship, an American Cancer Society Junior Faculty Award, the ETH Ruzicka Award, an American Cyanamid Young Faculty Award, the Merck Young Investigator Award, and the Zeneca Award for Excellence in Chemistry. Most recently, he has received the Chancellor's Distinguished Research Award from the University of Pittsburgh, the Arthur C. Cope Scholar Award from the American Chemical Society, and the Akron Section ACS and Novartis Research Awards. He is a member of the advisory board of the Journal of Organic Chemistry, Molecules, and Chirality, and a co-editor of Organic Reactions, The Chemistry of Heterocyclic Compounds, and eEROS.

Introduction

Reports of stoichiometric or sub-stoichiometric quantities of water resulting in significant increases in the rate and/or the enantioselectivity of organic transformations have sporadically appeared in the literature over the past decade. The means by which water acts as an accelerant in many of these processes is often poorly understood or even counterintuitive. Due to the abundance of primary literature and review articles on subjects concerning organic reactions in aqueous media[1] (*i.e.* Diels–Alder, Aldol, Claisen reactions, *etc.*), this review will focus primarily on transformations in which only stoichiometric or sub-stoichiometric amounts of water are necessary to achieve the desired rate enhancement or reaction improvement. Furthermore, the role that water plays is categorized into three distinct classes of activation: (a) water as a hydrolyzing agent leading to secondary products that serve as catalysts or promoters; (b) water used as an internal quenching agent to drive chemical equilibria, and (c) water as a Lewis acid activator or co-activator. This review is not intended to be comprehensive, and in many cases examples have been selected primarily as illustrations of larger and more comprehensive research efforts.

Water as a hydrolyzing agent leading to secondary products that serve as catalysts or promoters

The controlled *in situ* hydrolysis of TMS-Cl in the presence of NaI led to mild conditions for the preparation of internal alkenyl iodides in good yields and stereoselectivities from both terminal and internal alkynes (Scheme 1).[2] While one could speculate

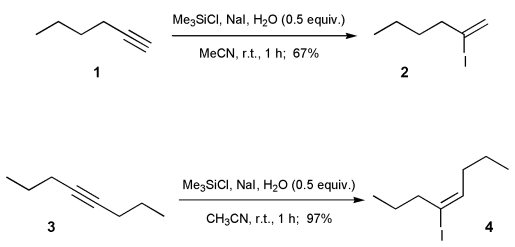

Scheme 1

that a mixture of HCl and HI is formed during the hydrolysis, direct use of an aqueous (57%) HI solution under otherwise identical conditions led mostly to unreacted alkyne.

Acetonitrile was shown to be by far the best solvent for this transformation. The unique selectivity of these mild conditions is highlighted by the clean and stereoselective addition of HI to

prop-2-ynyl alcohol to afford the desired internal alkenyl iodide **6** in 62% yield without any of the undesired prop-2-ynyl iodide (Scheme 2).

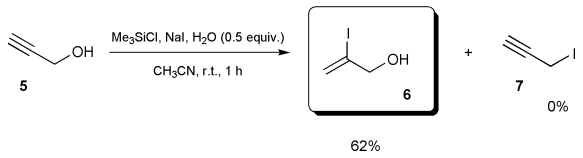

Scheme 2

A related example of this type of H_2O-induced reaction acceleration is represented by the Dess–Martin oxidation. After a serendipitous experimental discovery that only 'aged' (2 years) Dess–Martin periodinane (DMP) reagent was consistently effective in a crucial oxidation step in the total synthesis of rapamycin, a study was undertaken in an attempt to elucidate the general inconsistencies in the preparation of the Dess–Martin periodinane reagent, and to address the 'aging' effect. This study led to the observation that the addition of 1 equiv. of water to DMP accelerated the oxidation reaction dramatically.[3] The inspiration for the use of water as an accelerant came from earlier work in which Dess and Martin observed that the rate of oxidation of ethanol could be increased by the addition of a second equivalent of ethanol.[4] Presumably, an intermediate such as **9** shown in Scheme 3 is formed in the latter process.

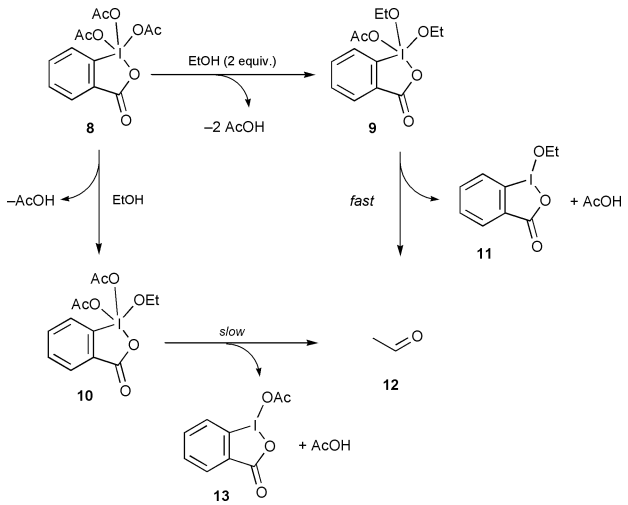

Scheme 3

The increased reactivity of the monoacetate **9** has been ascribed to the difference in basicity of the ethoxy *vs.* the acetoxy substituent. Schreiber and Meyer sought to mimic this effect by replacing an acetoxy group with hydroxide through the addition of one equivalent of H_2O (Scheme 4). Indeed, when

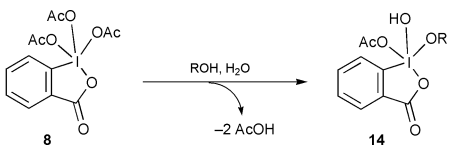

Scheme 4

CH_2Cl_2 containing 1.1 equiv. of water was added dropwise to the alcohol–DMP mixture, a greatly improved rate of oxidation was observed (Scheme 5). Both *trans*-2-phenylcyclohexanol and cholesterol were oxidized in 30 min to 97 and 91% completion, respectively. Under anhydrous conditions, oxidation of these two alcohols was significantly slower, requiring 14 and 8.5 h, respectively. Furthermore, prolonged reaction times under anhydrous conditions resulted in the decomposition of cholesterol, even in the presence of pyridine as a buffer.

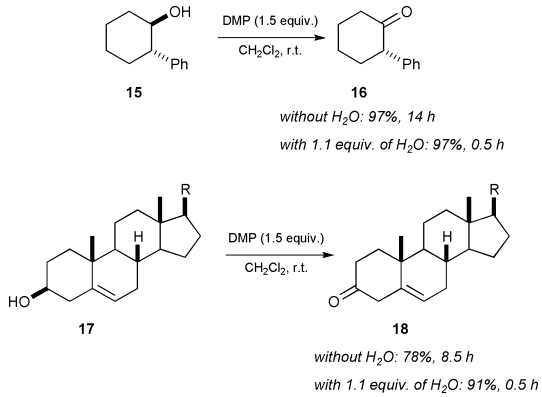

Scheme 5

The preparation of enantiomerically pure homoallylamines by asymmetric allylboration of imines has generated substantial interest.[5] In 1997, Itsuno and co-workers reported that the (apparently) more reactive *N*-trimethylsilylbenzaldimine could be allylated at lower temperatures (−78 °C) to afford the desired homoallylamines in good yields and in good to excellent ee's (depending on the chiral allylboron reagent used).[6] Using Brown's *B*-allylpinan-3-ylborane reagent,[7] the homoallylic benzylamine could be obtained in 70% yield with an ee of 73% (Scheme 6). In efforts to establish comparative rate data for the

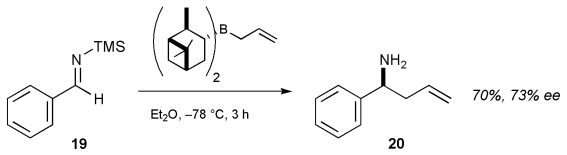

Scheme 6

allylboration of aldimines *vs.* aldehydes, Brown and co-workers subsequently discovered that the reported allylations did not take place under anhydrous conditions, even after a week at room temperature. However, upon aqueous workup of the reaction mixture, a 95% yield of the desired homoallylic amine was obtained.

Surprisingly, this reaction appears to take place quite rapidly upon aqueous workup, but remains dormant in the absence of water. Consequently, cooling the reaction temperature to −100 °C followed by dropwise addition of one equivalent of H_2O afforded an improved yield (87%) and a higher ee (94%, Scheme 7).[8] Presumably, H_2O is necessary to protodesilylate

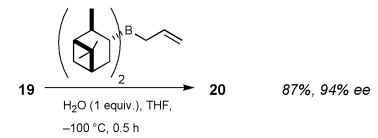

Scheme 7

the aldimine which is rapidly allylated. The improvement in %ee is thought to be due to a controlled, non-exothermic hydrolysis of the imine, allowing the reaction to proceed at much lower temperatures than the previous workup conditions.[9]

Two catalysts for the Mukaiyama aldol condensation, $Cp_2Ti(OTf)_2$ and trityl triflate (Ph_3COTf), both of which have also been used as Lewis acids for Diels–Alder reactions, have recently been shown to be precursors of the active species in this transformation.[10] Rigorous NMR studies have demonstrated that the hydrolysis of these triflates by trace amounts of H_2O leads to the formation of triflic acid, and subsequently, Me_3Si–OTf, which is responsible for catalyzing the reaction. The sequence of events that lead to the formation of Me_3Si–OTf is shown in Scheme 8. This spontaneous hydrolysis is in-

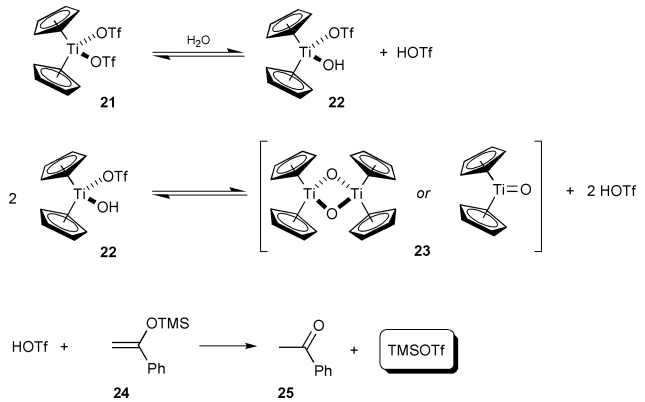

Scheme 8

strumental in explaining why certain chiral $L_2Ti(OTf)_2$ complexes provide racemic products from several substrates and under a broad range of reaction conditions.

An interesting observation was made during attempts to perform a Pt-catalyzed aldol addition of silyl ketene acetals to aldehydes. It was found that both O_2 and H_2O were needed in order to obtain enantiomerically enriched products.[11] Under aerobic and anhydrous conditions, the chiral Pt(II) acyl complex **29** catalyzed the reaction between dimethylketene methyl trimethylsilyl acetal and benzaldehyde at −25 °C. The desired aldol product was obtained after 16 h in a yield of 99% but was formed as a racemic mixture. When the same reaction was conducted in the presence of air, a product with an ee of 35% was obtained. Furthermore, if the reaction mixture was exposed to air and two equivalents of H_2O, the %ee rose to 59% (Scheme 9).

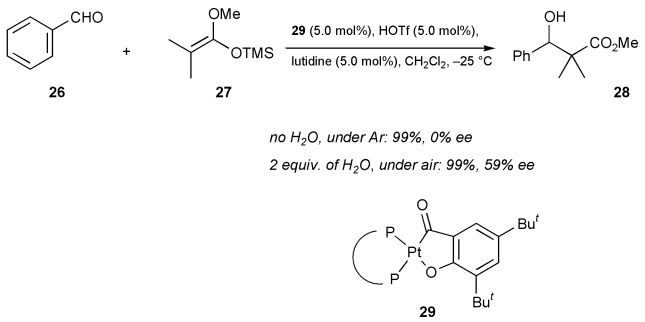

Scheme 9

Based on ^{31}P NMR experiments, the authors of this study speculated that hydrolysis of the salicylaldehyde ligand with two equiv. of H_2O produced the catalytically active dihydroxy platinum complex **32** (Scheme 10).[12] However, further analysis

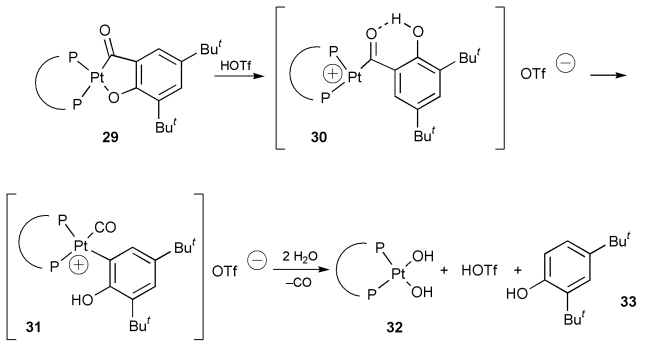

Scheme 10

is needed for verification of the structure of **32** and for the experimental validation of this hypothesis.

In the presence of an excess of the silylketene acetal **27**, the proposed dihydroxy platinum complex **32** was thought to collapse to a C-bound Pt-enolate. A catalytic cycle that is in agreement with this mechanistic hypothesis is shown in Scheme 11.

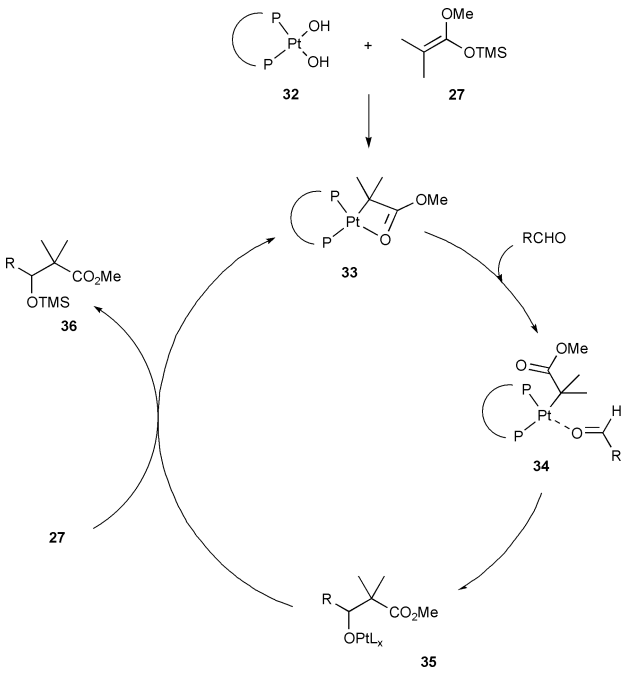

Scheme 11

Water has been postulated to be an essential ingredient in the synthesis of indoles *via* the Pd(0)-catalyzed intramolecular cyclization of alkynes to imines (Scheme 12).[13] The mechanism

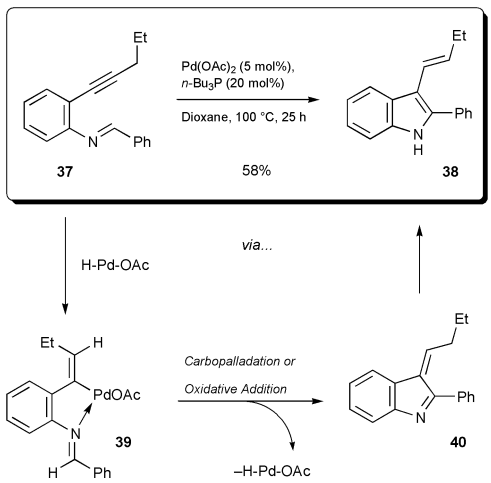

Scheme 12

was thought to involve a regioselective hydropalladation of the alkyne as the first step. The source of Pd-H under these conditions remained unclear.

However, the formation of Pd(0) from the reaction of Bu_3P and $Pd(OAc)_2$ is precedented [eqn. (1)],[14] and, furthermore, the oxidative addition of AcOH to Pd(0) has been reported [eqn. (3)].[15] Although this reaction was performed in dry solvents, it is possible that trace amounts of water were present, thus providing a source for the hydrolysis of Ac_2O [eqn. (2)].

$$Pd(OAc)_2 + Bu_3P \longrightarrow Pd(0) + Bu_3P{=}O + Ac_2O \quad (1)$$

$$Ac_2O + H_2O \rightleftharpoons 2\ AcOH \quad (2)$$

$$Pd(0) + AcOH \rightleftharpoons AcO\text{-}Pd\text{-}H \quad (3)$$

Further evidence for the formation of a Pd-H intermediate *via* this sequence was obtained when 1 equiv. of D_2O was added to

the reaction mixture and the desired indole was obtained in 80% yield (NMR) with 29% deuterium incorporation at C(1) (Scheme 13). Deuterium incorporation at any other position was not observed.

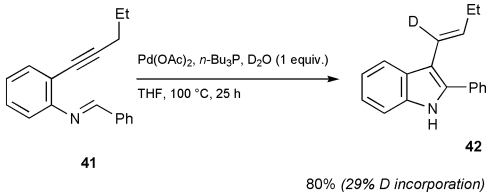

Scheme 13

Water used as an internal quenching agent to drive chemical equilibria

It is well established that silyloxycyclopropanes undergo metal-mediated ring openings to form β-metallo ketones.[16] In 1993, Ryu and co-workers reported their work toward the trapping of the analogous β-Cu(II) keto intermediates with suitable electrophiles such as electron deficient acetylenes. A typical reaction with dimethyl acetylenedicarboxylate (DMAD) is shown in Table 1.[17] Mechanistically, several competing pathways, *i.e.*

Table 1 The effect of additives on the reaction of siloxycyclopropane with $Cu(BF_4)_2$ and DMAD

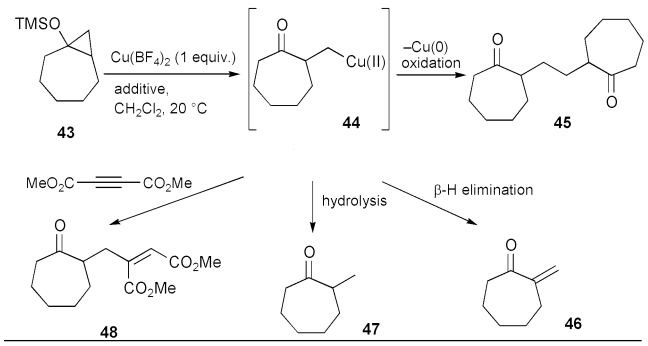

Entry	DMAD/ mmol	Additive (mL)	**45** (%)	**46** (%)	**47** (%)	**48** (%)
1	1	—	0	2	35	45
2	1	BuOTMS (0.2)	0	4	4	65
3	1.1	BuOTMS (0.2) + H_2O (0.02)	0	4	6	73

oxidative homocoupling, β-H elimination and $BF_3{\cdot}OEt_2$-promoted hydrolysis are feasible for this process. Optimal conditions included the use of 0.2 mL of a 10 vol% solution of trimethylsiloxybutane in CH_2Cl_2 containing one equivalent of H_2O (Table 1, entry 3). Trimethylsiloxybutane was used for the suppression of the $BF_3{\cdot}OEt_2$-promoted hydrolysis of the starting silyloxycyclopropane, and the one equivalent of H_2O was apparently needed for the protonation of the resulting vinylcopper intermediate. Internal quenching effectively prevented the reversibility of the addition and therefore decreased the lifetime of the β-Cu(II) ketone species that was prone to side reactions such as β-H elimination or oxidative homocoupling. Interestingly, 1,4-addition of the β-Cu(II) ketone intermediate to reactive electrophiles such as DMAD proceeded faster than protonation of the alkyl–copper bond.

Stannyl- and silylcupration of alkynes was shown to be most effective if H_2O was used as an internal proton source.[18] Stannylcupration of prop-2-ynyl alcohol **49** was conducted in the presence of protic additives with pK_a values of 4–15.5 (Table 2). Surprisingly, the stannylcuprate was stable at pK_a values above 4, but more acidic additives such as 2,4,6-(NO_2)-PhOH (pK_a = 0.3) destroyed the cuprate. When no internal proton source was used (entry 1) the vinylstannane was

Table 2 Effects of proton source on yield and regiochemistry of stannylcupration

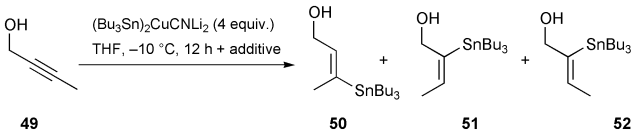

Entry	Additive (equiv.)	Yield (%)	**50** (%)	**51** (%)	**52** (%)
1	—	82	30	0	70
2	MeOH (110)	70	100	0	0
3	PhOH (30)	88	86	14	0
4	AcOH (10)	78	87	13	0
5	2,4-$(NO_2)_2$ PhOH (10)	80	85	15	0
6	H_2O (10)	97	85	15	0

obtained in good yield but as a 30 : 70 mixture favoring the thermodynamically more stable *trans*-addition product **52**. Use of protic additives provided the vinylstannane in similar yields but only the *cis*-addition products were obtained. Although greater control of the ratio of 'distal' *vs.* 'proximal' regioisomers was obtained with MeOH, the best overall yield was obtained when 7–10 equiv. of H_2O were used (Table 2, entry 6).[19]

Stannylcupration of enyne **53** is an example where H_2O proved to be superior to MeOH, providing the (*E*)-dienylstannane **54** in 80% yield as a single isomer (Scheme 14).

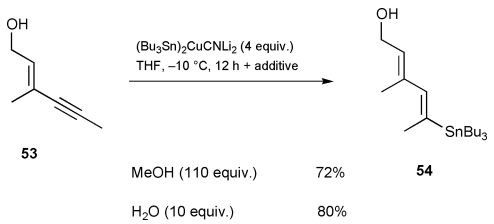

Scheme 14

Similarly, silylcupration of **53** in the absence of any protic quenching agents provided the desired product **55** but with relatively poor regioselectivity (Scheme 15). However, upon

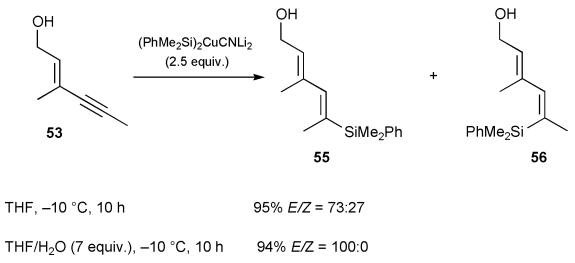

Scheme 15

addition of 7 equiv. of H_2O the desired dienylsilane was obtained in 94% yield as a single regioisomer.

H_2O was also shown to improve the Barbier addition of *in situ* prepared allylzinc to imines derived from (*S*)-valine esters (Table 3).[5d] Under anhydrous conditions (entries 1–3), the diastereoselectivity decreased under prolonged reaction times. Therefore, diastereomerically pure products could only be obtained at the expense of lower chemical yields. The authors suspected that the addition was reversible, which would account for the loss of diastereoselectivity under extended reaction times. In attempts to inhibit possible equilibration, the reaction was conducted in the presence of an internal proton source so that protonation of the zinc salt of **25** would lead to an irreversible process. In the presence of 0.7 equiv. of H_2O, the desired diastereomerically pure product was indeed obtained in 92% isolated yield after 24 h. Although the rate of addition was decreased by the presence of H_2O, the diastereoselectivity improved considerably (Table 3, entries 4 and 5).

Table 3 Effect of H_2O and reaction time on the diastereomeric ratio of **58**

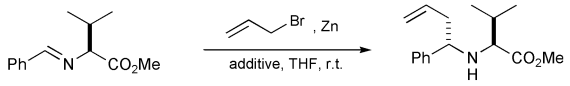

57 **58**

Entry	Additive (equiv.)	Time/h	Product	Yield (%)	dr (%)
1	—	0.5	(*S*,*S*)	80	>99:1
2	—	1.5	(*S*,*S*)	100	94:6
3	—	32	(*S*,*S*)	100	52:48
4	H_2O (0.7)	7	(*S*,*S*)	60	100:0
5	H_2O (0.7)	24	(*S*,*S*)	92	100:0

A study directed towards the development of conditions favorable for nucleophilic additions to imines in the presence of carbonyl groups demonstrated that the combination of water and $BF_3{\cdot}Et_2O$ was a superior catalyst for the selective addition of silyl enolates to imines in the presence of benzaldehyde.[20] $BF_3{\cdot}Et_2O$ alone, if used in catalytic amounts, was sufficient to promote the addition of 1-phenyl-1-trimethylsiloxyethane to benzylideneaniline in the presence of 1 equiv. of benzaldehyde (Table 4, entry 2). However, superior results were obtained

Table 4 Imine-selective addition reactions

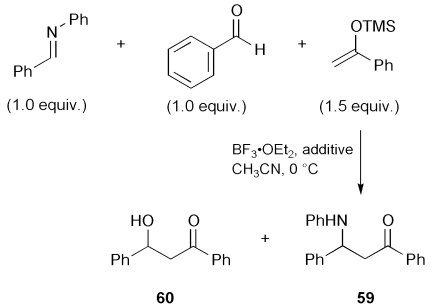

60 **59**

Entry	$BF_3{\cdot}Et_2O$/ equiv.	Additive (equiv.)	Time/h	**59** (%)	**60** (%)
1	1	—	0.5	18	48
2	0.2	—	0.5	60	15
3	0.2	H_2O (0.1)	0.5	92	5
4	0.2	H_2O (1.0)	1	98	1
5	0.2	H_2O (10)	0.5	97	1
6	0.2	H_2O (50)	17	92	0

when 1 equiv. of H_2O was added to the reaction mixture (Table 4, entry 4). The combination of $BF_3{\cdot}Et_2O$ and H_2O might form the hydrate which transfers a proton to give H_3O^+ and BF_3OH^-. Activation of the imine by preferential protonolysis could account for the reversal in selectivity.

Water as a Lewis acid activator or co-activator

Although the Pauson–Khand reaction remains one of the most effective methods for the preparation of cyclopentenones, its scope has been somewhat limited by high temperatures and long reaction times. According to the generally accepted mechanism, the rate-limiting step involves decarbonylation, which generates a free coordination site for the incoming olefin.[21] Many successful attempts at accelerating the reaction by employing various 'hard' Lewis bases as additives have been disclosed. The presence of these 'hard' Lewis bases (*N*-methylmorpholine *N*-oxide,[22a] trimethylamine *N*-oxide,[22a] DMSO,[22b] sulfoxides,[22b] cyclohexylamine and NH_4OH[21c]) is thought to accelerate the decarbonylation step. Water (as a solvent) retarded the reaction.[22c] However, small amounts of H_2O proved to be very effective in accelerating the catalytic variant of the Pauson–Khand reaction.[23] Although H_2O was not the best promoter in this study, it certainly is the cheapest and perhaps most convenient to use (Table 5).

Table 5 The catalytic Pauson–Khand reaction in the presence of various 'hard' Lewis bases

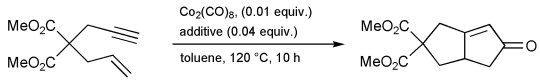

61 **62**

Entry	Additive	CO/atm	**61** (%)	**62** (%)
1	—	7	82	12
2	Cyclohexylamine	7	93	5
3	Diisopropylamine	7	28	64
4	Diisopropylethylamine	7	7	81
5	Benzyl alcohol	7	21	73
6	2-Methoxyethanol	7	71	27
7	Ethylene glycol	7	97	0
8	1,4-Dioxane	7	5	72
9	1,2-Dimethoxyethane	7	0	91
10	1,2-Dimethoxyethane (solvent)	7	78	9
11	1,2-Dimethoxyethane	1	83	5
12	1,2-Dimethoxyethane	3	6	82
13	1,2-Dimethoxyethane	20	0	93
14	H_2O (20 equiv.)	7	33	63
15	H_2O/toluene (1:2)	7	65	21

The cyclization of **63** provides an example where H_2O proved to be a superior additive to DME (Scheme 16).

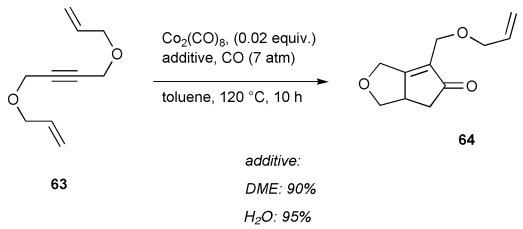

Scheme 16

Buono and co-workers recently described a new chiral copper catalyst for the asymmetric addition of dialkylzinc reagents to cyclic enones.[24] Initially, diethylzinc addition to cyclohexenone proceeded in a yield of 55% with an ee of 45% using a new CuI–QUIPHOS catalyst in toluene at −20 °C (Table 6, entry 1).

Table 6 CuI–QUIPHOS catalyzed addition of Et_2Zn to cyclohexenone

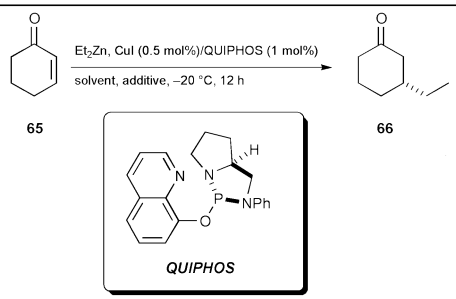

Entry	Solvent	Additive (equiv.)	Yield (%)	Ee (%)
1	Toluene	—	53	45
2	THF	—	53	25
3	CH_2Cl_2	—	55	7
4	1,2-Dichloroethane	—	69	30
5	CCl_4	—	34	7
6	Toluene	H_2O (0.5)	55	6
7	THF	H_2O (0.5)	50	22
8	1,2-Dichloroethane	H_2O (0.5)	55	23
9	Hexane	H_2O (0.5)	0	0
10	CH_2Cl_2	H_2O (0.5)	76	61
11	CH_2Cl_2	$Zn(OH)_2$ (0.1)	64	44
12	CH_2Cl_2	$Zn(OH)_2$ (0.25)	81	53

Attempts to optimize this result by varying the solvent were unsuccessful (entries 1–5). However, a dramatic increase in ee

was observed upon addition of 0.5 equiv. of H_2O. Interestingly, this effect was only observed when CH_2Cl_2 was used as the solvent (Table 6, entries 6–10). The authors proposed that Et_2Zn was hydrolyzed to $Zn(OH)_2$ which supposedly was a stronger, more effective Lewis acid. This hypothesis was tested by adding $Zn(OH)_2$ in place of H_2O (entries 11 and 12). A similar result was obtained when 0.25 equiv. of $Zn(OH)_2$ were used, although further increases in the amount of $Zn(OH)_2$ had deleterious effects.

Apparently, the increased Lewis acidity of the hydrolyzed zinc species activated the carbonyl moiety and, perhaps intramolecularly, provided anchimeric assistance to the approaching Cu species through chelation. This interaction might result in a 'tighter' transition state and higher levels of enantioselectivity (Scheme 17).

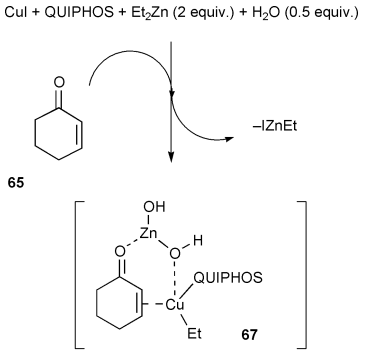

Scheme 17

Although the formation of $Zn(OH)_2$ is plausible, especially since the direct addition of this additive provided results similar to those with H_2O, the formation of alternative agents such as EtZn–O–ZnEt cannot be excluded. The favorable results using $Zn(OH)_2$ could then be explained by the analogous formation of a species such as EtZn–O–Zn–O–ZnEt. We have found that addition of water to a solution of Me_2Zn produces a stronger Lewis acid capable of activating benzaldehyde towards dimethylzinc addition (Scheme 18).[25] This reaction does not proceed to any significant degree in the absence of H_2O.

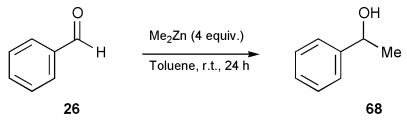

Scheme 18

Corey and co-workers have observed that the addition of 0.3–0.33 equiv. of H_2O to lithium dimethylcuprate at −78 °C generates a substantially more reactive, and selective agent for conjugate addition to the chiral α,β-enone **69** (Table 7).[26]

The authors speculated that the heightened reactivity upon addition of H_2O arose from the formation of a mixed planar cuprate species as shown in Scheme 19. The exocyclic lithium moiety was described as being 'especially suited for chelate formation with the α′-alkoxy-α,β-enone'.

Shibasaki, Sasai and co-workers have seen a significant improvement in their Yb-BINOL catalyzed asymmetric epoxidations of acyclic enones in the presence of H_2O as an additive.[27,28] Both yields and ee's were greatly affected by the amount of added H_2O. The best results were obtained when 5 equiv. of H_2O were used (Scheme 20). Interestingly, and not necessarily easy to reconcile with the effect of water, the use of 4 Å MS was shown to be critical to obtain optimal results.

Addition of H_2O has also been shown to lead to slightly improved enantioselectivities in the addition of 1-naphthol to pyruvate esters.[29] The chiral 1,4:5,8-dimethano-

Table 7 Diastereoselective organocuprate additions

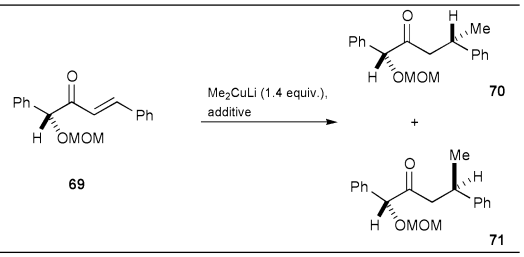

Entry	Solvent	Temperature/°C	Additive (equiv.)	Yield (%)	Ratio **70**:**71**
1	Et_2O	−45	LiI (4)	88	14:1
2	THF	−45	—	80	2.5:1
3	THF	−78	TMS-Cl (5)	>80	2:1
4	Et_2O	−78	H_2O (0.3–0.33)	93–100	16:1
5	Et_2O	−78	H_2O (0.3) + TMS-Cl (5)	>90	33:1

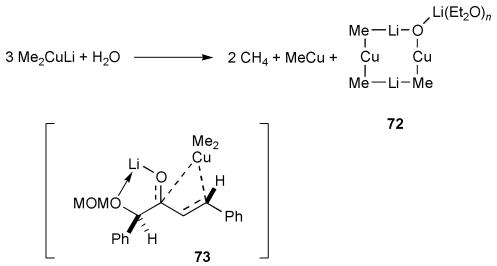

Scheme 19

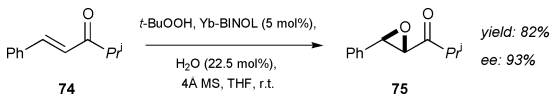

Scheme 20

1,8,10,10,11,11-hexamethyl-1,2,3,4,5,6,7,8-octahydro-4a,4b,8a,9,9a-η-9*H*-fluorenezirconium trichloride **79** (5 mol%), H_2O (27 mol%) and an excess of ethyl pyruvate in CH_2Cl_2 at −10 °C provided the adduct **78** in 70% yield and with an ee of 89% after 5 h (Table 8). Without H_2O and under otherwise

Table 8 Effect of H_2O on yield and ee in the formation of **78**

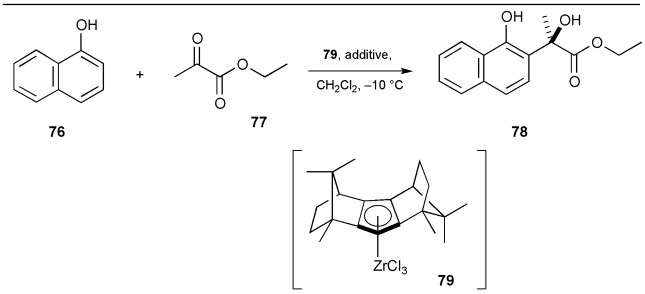

Entry	Additive (equiv.)	Time/h	Conversion (%)	Ee (%)
1	—	2	70	80
2	—	5	85	80
3	—	24	Quant.	72
4	H_2O (0.27)	2	55	89
5	H_2O (0.27)	5	70	89
6	H_2O (0.27)	24	90	84

identical conditions, **78** was obtained in 85% yield with a lower ee of 80%. It is known that $CpZrCl_3$ forms adducts with donor ligands such as THF or DMF to give a stable Zr $d^0/16e^-$ intermediate.[30] Accordingly, it seems possible that two water

molecules coordinate to **79** to provide a related 16e⁻ intermediate. The resulting change in geometry could be responsible for the modest increase in enantiomeric excess. Again, it appears likely that the reversibility of the reaction is partly responsible for the drop in ee under prolonged reaction times. However, unlike the previously discussed reversible addition of allylzinc reagents to imines, the use of water in this case does not appear to inhibit this equilibration as effectively. Alternatively, catalyst decomposition into achiral species can also lead to lower reaction ee's.

Another Zr-catalyzed asymmetric reaction that has been reported to be positively influenced by the presence of water is the Zr-catalyzed enantioselective addition of azide to cyclohexene oxide (Table 9).[31] Both the yield and ee in this process were

Table 9 Enantioselective opening of *meso* epoxides with TMS-azide

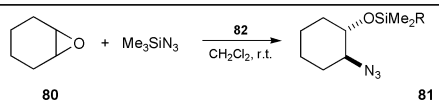

80 81

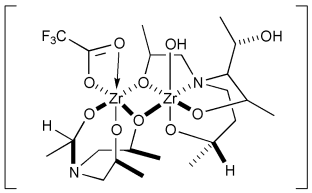

82

Entry	Additive	[Additive]/ [epoxide]	Relative rate	Ee (%)
1	—	—	1.0	84
2	$CyOSiMe_2Pr^i$	2.2	2.1	86
3	CyOH	0.19	2.5	85
4	n-$C_5H_{11}OH$	0.35	2.5	83
5	H_2O	0.63	0	—
6	H_2O	0.32	0.79	79
7	H_2O	0.16	2.2	88
8	H_2O	0.10	2.1	85
9	H_2O	0.073	1.3	85
10	H_2O	0.027	1.3	82
11	4 Å MS	—	0.2	54

increased by addition of silyl ethers, alcohols and H_2O. These additives might be effective in assisting in the catalytic turnover of the Zr-complex.

In 1991, Miyashita and co-workers presented an elegant stereospecific methylation of γ,δ-epoxy acrylates using a trimethylaluminum–H_2O mixture (Scheme 21).[32] Water was

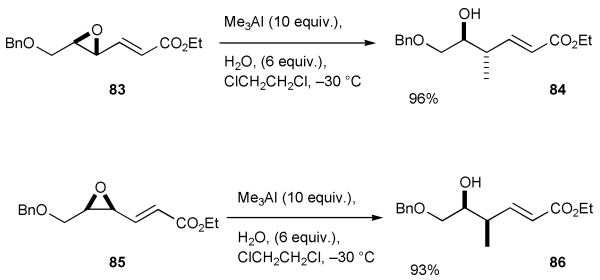

83 84 85 86

Scheme 21

shown to be critical for this transformation; under anhydrous conditions the reaction did not occur. Furthermore, replacing H_2O with MeOH also resulted in recovered starting material. Both *cis*- and *trans*-epoxides were readily methylated with complete regio- and stereocontrol.[33]

This methodology was successfully applied toward a key intermediate in the formal synthesis of *ent*-tirandamycin B (Scheme 22).[34]

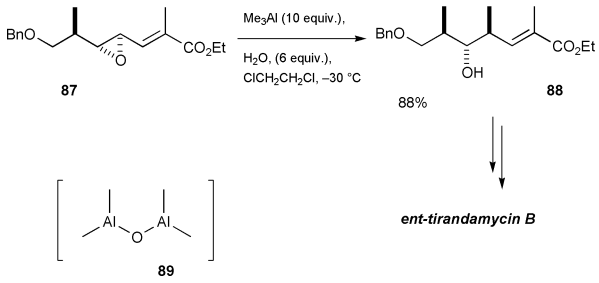

87 88 89

Scheme 22

The bisaluminum-oxo intermediate **89** was proposed to be a reactive intermediate formed by the reaction of H_2O and excess trimethylaluminum in this process. Due to the dual Lewis acid/nucleophilic nature of this species, its exact role remains unclear. It is possible that **89** behaves both as a strong Lewis acid and/or a more reactive methylating agent.

In a related reaction scheme, a water–Me_3Al mixture was found to be useful for accelerating the zirconocene dichloride-catalyzed methylalumination of alkynes. Addition of 1.5 equiv. of H_2O to 3 equiv. of Me_3Al in the presence of 0.2 equiv. of Cp_2ZrCl_2 generated a much more reactive methylating agent.[35] Methylalumination proceeded quite rapidly under these modified conditions, providing the desired methylated product in quantitative yield (as 97 : 3 ratio of regioisomers) after 10 min at −78 °C (Scheme 23). In comparison, under standard conditions oct-1-yne was methylated in a 95 : 5 stereoselectivity after 3 h at room temperature.[36]

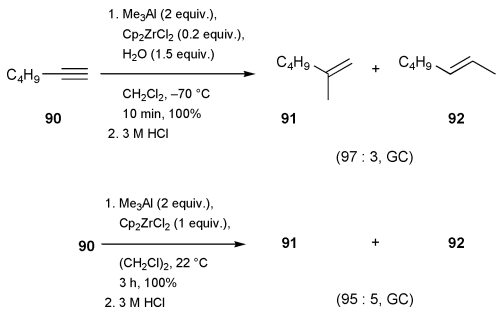

90 91 92

Scheme 23

More recently, this dramatic rate effect of H_2O addition in carbometalation reactions has been extended to the asymmetric methylalumination of terminal alkenes.[37] In 1995, Negishi and Kondakov reported the first asymmetric methylalumination of alkenes using Erker's chiral zirconium catalyst **95**.[38,39] Despite the good to excellent yields and ee's obtained under the original conditions, substrates such as styrene proved quite resistant towards the methylation process, and after 22 days only 30% product was obtained (Scheme 24).[38a] In contrast, a dramatic increase in the reaction rate was achieved by the addition of 1 equiv. of H_2O to 4 equiv. of Me_3Al.[37] The desired product was obtained after 12 h at −5 °C in 73% yield with an ee of 89%. A more quantitative assessment of the rate difference with styrene under the two sets of reaction conditions is shown in Fig. 1. Monitoring the appearance of 2-phenylpropanol at 0 °C by GC revealed that in the presence of 1 equiv. of H_2O the reaction went to > 85% completion after 8 h. Without the benefit of water, no trace of 2-phenylpropanol could be detected. Although more elaborate studies have yet to be conducted in order to shed more light on the mechanism of this water-induced acceleration, it is feasible that a species such as **89** is being formed in this process as well. The degree in which MAO (methylaluminoxane) activates Zr-based catalysts in Ziegler–Natta type polymerizations is relatively well known, and yet also poorly understood in a mechanistic sense.[40] In analogy to the effect of MAO in the Ziegler–Natta process, we believe that a reasonable mechanism involves formation of a cationic

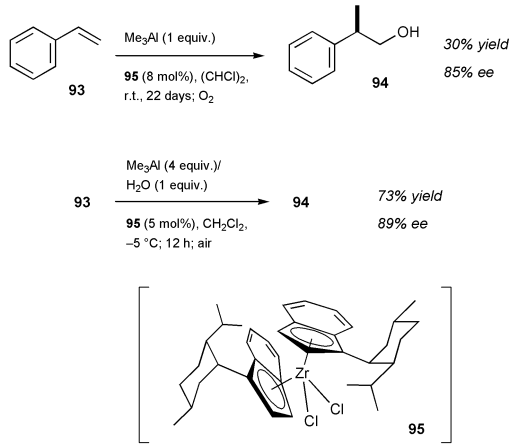

Scheme 24

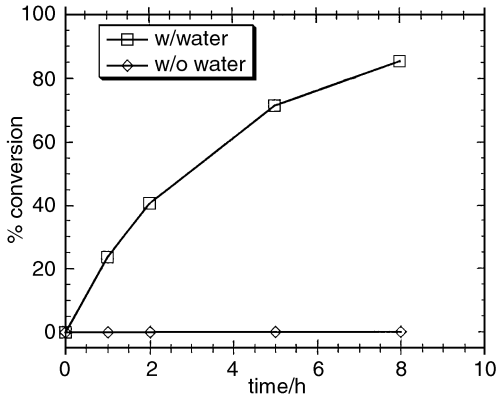

Fig. 1 Rate analysis of the chiral zirconocene-catalyzed methylalumination of styrene at 0 °C using 4 equiv. of trimethylaluminium, 5 mol% of chiral catalyst **95**, and styrene at a 0.17 M concentration in CH_2Cl_2 in the absence and presence of 1 equiv. of H_2O.

zirconocene intermediate formed by ligand (Cl-, or more likely Me-) abstraction from the zirconocene complex by the more Lewis acidic intermediate **89** or a higher molecular weight, more reactive analog thereof that is generated upon addition of H_2O to the reaction mixture.

Conclusions

Maybe one of the most surprising aspects of our survey is the large number of well-documented cases where the addition of catalytic or stoichiometric amounts of H_2O to the reaction mixture of organic and organometallic processes has led to beneficial effects on reaction rate, product yield, and regio-, diastereo- and enantioselectivity. Since, in particular when moisture-sensitive organometallic reagents or Lewis acids are involved, synthetic chemists go to great lengths to avoid traces of water in the reaction mixture, it can only be speculated how many new H_2O-accelerated processes remain to be (re-)discovered, and how many cases of adventitious water effects have played a significant but yet unrecognized role in influencing the course of the reaction. A most intriguing aspect of H_2O-promoted processes is the role that this strong Lewis-base can play in providing the source for transient highly Lewis-acidic species. After a sometimes vigorous exothermic reaction with organometallic derivatives that can only be controlled by careful addition of sub-equimolar quantities of H_2O, the resulting metal oxide or metal hydroxide species is activated at the metal center by the negative inductive effect of the powerful electron-withdrawing oxygen substituent and becomes more Lewis acidic. This scenario is most likely operative when H_2O is added to reaction mixtures containing alanes. In addition, the oxide or hydroxide ligand on the metal presents a source for chelation interactions that change aggregation states of organometallics and can provide anchimeric assistance. Unfortunately, there is a dearth of mechanistic information regarding the interaction and the actual active species obtained upon reaction of H_2O with reactive organometallics or Lewis acids, and beyond empirical experimentation there is little general information that could be used as a guideline when water-effects might prove beneficial. The situation is a bit more transparent in cases when water is used as a hydrolyzing agent leading to secondary products that serve as catalysts or promoters or when water provides a quenching agent intended to drive chemical equilibria. More often than not, the latter working hypotheses can be tested by preforming the active species, monitoring the reaction mixture spectroscopically, or by a thorough analysis of reaction intermediates and products. In all aspects of water-mediated processes, we are anticipating that chemists will continue to discover surprising new effects and beneficial uses of H_2O as a highly versatile reagent in the organic chemistry tool box.

Acknowledgements

We gratefully acknowledge financial support from NSF and NIH as well as from industrial sponsors for our research.

Notes and references

1 (*a*) A. Lubineau and J. Auge, *Top. Curr. Chem.*, 1999, **206**, 1; (*b*) D. Sinou, *Top. Curr. Chem.*, 1999, **206**, 41; (*c*) C.-J. Li and T.-H. Chan, *Tetrahedron*, 1999, **55**, 11 149; (*d*) F. Fringuelli, O. Piermatti and F. Pizzo, *Heterocycles*, 1999, **50**, 611; (*e*) J. B. F. N. Engberts, B. L. Feringa, E. Keller and S. Otto, *Recl. Trav. Chim. Pays-Bas*, 1996, **15**, 457; (*f*) A. Lubineau, J. Auge and Y. Queneau, *Synthesis*, 1994, 741; (*g*) C. J. Li, *Chem. Rev.*, 1993, **93**, 2023.
2 N. Kamiya, Y. Chikami and Y. Ishii, *Synlett*, 1990, 675.
3 S. D. Meyer and S. L. Schreiber, *J. Org. Chem.*, 1994, **59**, 7549.
4 D. B. Dess and J. C. Martin, *J. Org. Chem.*, 1983, **48**, 4155.
5 (*a*) Y. Yamamoto, W. Ito and K. Maruyama, *J. Chem. Soc., Chem. Commun.*, 1985, 1131; (*b*) Y. Yamamoto, T. Koshiaki and K. Maruyama, *J. Org. Chem.*, 1985, **50**, 3115; (*c*) Y. Yamamoto, S. Nishii, K. Maruyama, T. Komatsu and W. Ito, *J. Am. Chem. Soc.*, 1986, **108**, 7778; (*d*) T. Basile, A. Bocoum, D. Savoia and A. Umani-Ronchi, *J. Org. Chem.*, 1994, **59**, 7766; (*e*) D. Enders, J. Schankat and M. Klatt, *Synlett*, 1994, 795; (*f*) Y. Hashimoto, K. Takai, A. Sudo, T. Ogasawara and K. Saigo, *Chem. Lett.*, 1995, 235.
6 S. Itsuno, K. Watanabe, K. Ito, A. A. El-Shehawy and A. A. Sarhan, *Angew. Chem., Int. Ed. Engl.*, 1997, **36**, 109.
7 H. C. Brown and P. K. Jadhav, *J. Am. Chem. Soc.*, 1983, **105**, 2092.
8 G.-M. Chen, P. V. Ramachandran and H. C. Brown, *Angew. Chem., Int. Ed.*, 1999, **38**, 825.
9 In a possibly related scenario, White and co-workers discovered that the presence of 3 equiv. of H_2O was essential for optimal yields in the preparation of homoallylic alcohols by reaction of aldehydes with η^3-allyl- and η^3-crotylmolybdenum complexes. Water as an additive was superior to methanol and trifluoroethanol. The timing of the alkoxide exchange reaction might critically depend on the ability of the additive to bind to the metal: K. P. Gable, M. S. Shanmugham and J. D. White, *Can. J. Chem.*, 2000, **78**, 704.
10 T. K. Hollis and B. Bosnich, *J. Am. Chem. Soc.*, 1995, **117**, 4570.
11 O. Fujimura, *J. Am. Chem. Soc.*, 1998, **120**, 10032.
12 A. Gusso, C. Baccin, F. Pinna and G. Strukul, *Organometallics*, 1994, **13**, 3442.
13 A. Takeda, S. Kamijo and Y. Yamamoto, *J. Am. Chem. Soc.*, 2000, **122**, 5662.
14 T. Mandai, T. Matsumoto, J. Tsuji and S. Saito, *Tetrahedron Lett.*, 1993, **34**, 2513.
15 (*a*) For a review, see: B. M. Trost, *Acc. Chem. Res.*, 1990, **23**, 34; (*b*) B. M. Trost, D. C. Lee and F. Rise, *Tetrahedron Lett.*, 1989, **30**, 651.
16 (*a*) For reviews, see: I. Ryu and N. Sonoda, *J. Syn. Org. Chem. Jpn.*, 1985, **43**, 112; (*b*) E. Nakamura, *J. Syn. Org. Chem. Jpn.*, 1989, **47**, 931; (*c*) I. Kuwajima and E. Nakamura, *Top. Curr. Chem.*, 1990, **133**, 1; (*d*)

I. Kuwajima and E. Nakamura, in *Comprehensive Organic Synthesis*, ed. B. M. Trost and I. Flemming, Pergamon Press, Oxford, 1991, Vol. 2, pp. 441–454.
17 I. Ryu, K. Matsumoto, Y. Kameyama, M. Ando, N. Kusumoto, A. Ogawa, N. Kambe, S. Murai and N. Sonoda, *J. Am. Chem. Soc.*, 1993, **115**, 12 330.
18 J.-F. Betzer and A. Pancrazi, *Synlett*, 1998, 1129.
19 For the first example of using MeOH as an internal proton source, see E. Piers and H. E. Morton, *J. Org. Chem.*, 1980, **45**, 4263.
20 T. Akiyama, J. Takaya and H. Kagoshima, *Chem Lett.*, 1999, 947.
21 N. E. Shore, *Org. React.*, 1991, **40**, 1.
22 (*a*) N. Jeong, Y. K. Chung, B. Y. Lee, S. H. Lee and S.-E. Yoo, *Synlett*, 1991, 204; (*b*) Y. K. Chung, B. Y. Lee, N. Jeong, M. Hudecek and P. L. Pauson, *Organometallics*, 1993, **12**, 220; (*c*) T. Sugihara, M. Yamada, H. Ban, M. Yamaguchi and C. Kaneko, *Angew. Chem. Int. Ed. Engl.*, 1997, **36**, 2801.
23 T. Sugihara and M. Yamaguchi, *Synlett*, 1998, 1384.
24 G. Delapierre, T. Constantieux, J. M. Brunel and G. Buono, *Eur. J. Org. Chem.*, 2000, 2507.
25 P. Wipf and S. Ribe, unpublished results.
26 E. J. Corey, F. J. Hannon and N. W. Boaz, *Tetrahedron*, 1989, **45**, 545.
27 S. Watanabe, Y. Kobayashi, T. Arai, H. Sasai, M. Bougauchi and M. Shibasaki, *Tetrahedron Lett.*, 1998, **39**, 7353.
28 This group also reported an improvement in a catalytic asymmetric aldol reaction if 1 equiv. of H_2O in combination with 1 equiv of BuLi was used. Other additives such as NEt_3, LiCl, and HMPA had little effect on the acceleration: T. Arai, Y. M. A. Yamada, N. Yamamoto, H. Sasai and M. Shibasaki, *Chem. Eur. J.*, 1996, **2**, 1368.
29 G. Erker and A. A. H. van der Zeijden, *Angew. Chem., Int. Ed. Engl.*, 1990, **29**, 512.
30 (*a*) G. Erker, C. Sarter, M. Albrecht, S. Dehnicke, C. Krüger, E. Raabe, R. Schlund, R. Benn, A. Rufinska and R. Mynott, *J. Organomet. Chem.*, 1990, **382**, 89; (*b*) G. Erker, C. Sarter, S. Werner and C. Kruger, *J. Organomet. Chem.*, 1989, **377**, C55.
31 B. W. McCleland, W. A. Nugent and M. G. Finn, *J. Org. Chem.*, 1998, **63**, 6656.
32 M. Miyashita, M. Hoshino and A. Yoshikoshi, *J. Org. Chem.*, 1991, **56**, 6483.
33 For a recent application of this methodology, see: L. Carde, D. H. Davies and S. M. Roberts, *J. Chem. Soc., Perkin Trans. 1*, 2000, 2455.
34 T. Shiratani, K. Kimura, K. Yoshihara, S. Hatakeyama, H. Irie and M. Miyashita, *Chem. Commun.*, 1996, 21.
35 P. Wipf and S. Lim, *Angew. Chem., Int. Ed. Engl.*, 1993, **32**, 1068.
36 D. E. Van Horn and E. Negishi, *J. Am. Chem. Soc.*, 1978, **100**, 2252.
37 P. Wipf and S. Ribe, *Org. Lett.*, 2000, **2**, 1713.
38 (*a*) D. Y. Kondakov and E. Negishi, *J. Am. Chem. Soc.*, 1995, **117**, 10771; (*b*) D. Y. Kondakov and E.-I. Negishi, *J. Am. Chem. Soc.*, 1996, **118**, 1577.
39 G. Erker, M. Aulbach, M. Knickmeier, D. Wingbermühle, C. Krüger, M. Nolte and S. Werner, *J. Am. Chem. Soc.*, 1993, **1215**, 4590.
40 For a useful review of methylaluminoxane (MAO), see: E. Y.-X. Chen and T. J. Marks, *Chem. Rev.*, 2000, **100**, 1391.

Very high titanium content mesoporous silicas

Jamal El Haskouri,[a] Saúl Cabrera,[b] Margarita Gutierrez,[a] Aurelio Beltrán-Porter,[a] Daniel Beltrán-Porter,[a] M. Dolores Marcos*[c] and Pedro Amorós*[a]

[a] *Institut de Ciència dels Materials de la Universitat de València (ICMUV), P.O. Box 2085, 46071-València, Spain. E-mail: pedro.amoros@uv.es*

[b] *Laboratorio de Sólidos y Química Teórica, Instituto de Investigaciones Químicas UMSA, Cota-Cota, Calle nº 27, La Paz, Bolivia*

[c] *Departamento de Química, Universidad Politécnica de Valencia, Camino de Vera s/n, 46071-Valencia, Spain. E-mail: mmarcos@upvnet.upv.es*

Received (in Cambridge, UK) 1st November 2000, Accepted 18th December 2000
First published as an Advance Article on the web 5th February 2001

Titanium content in mesoporous titanosilicate catalysts has been modulated up to a minimum Si/Ti value of 1.9 by using complexing agents able to coordinate both Si and Ti atoms and harmonize the reactivity of the resulting precursors avoiding subsequent phase segregation and leading to chemically very homogeneous materials.

The interest of titanium–silicon mixed oxides in petrochemistry is mainly related to their ability to catalyze olefin epoxidation.[1] Recently, maximum interest was focused, however, on microporous products in which titanium atoms isomorphously replace some of the silicon atoms. Indeed, it was found that zeolites such as TS-1, TS-2 and Ti-β are effective catalysts (although limited to substrates with small molecules) in the oxidation of a variety of organic compounds.[2] Hence, the discovery of the M41S materials opened a new way towards expanding the available pore size. Owing to their large pore-sizes, Ti-substituted MCM-41 materials might be efficient in the oxidation of bulky substrates. In 1994, Corma *et al.*[3] and Tanev *et al.*[4] published the first results on titanium substitution in MCM-41 silicas. Since then a considerable effort has been devoted to this subject.[5]

A major problem concerning the preparation of Si–Ti mixed oxides through sol–gel-derived techniques is to achieve an adequate balance between the hydrolysis and condensation processes affecting the titanium and silicon precursors. Insofar as the catalysts' efficacy substantially depends upon their purity and chemical homogeneity, phase segregation must be avoided.

We report here a new direct and reproducible surfactant-assisted procedure that has allowed us to prepare thermally stable mesoporous titanosilicate molecular sieves in which the Ti content in the framework can be modulated up to a minimum Si/Ti molar ratio value of 1.9. Such a limit value corresponds to a relative Ti content noticeably higher than those previously achieved by using surfactants (Si/Ti = 5.0)[6] or block-copolymers (Si/Ti = 3.9)[7] as supramolecular templates.

The procedure is based on the use of a cationic surfactant (CTAB = cetyltrimethylammonium bromide) as structural directing agent, and a complexing polyalcohol (2,2′,2″-nitrile-triethanol, hereinafter TEAH3) as the hydrolysis retarding agent for Ti species.[8] In a typical synthesis leading to the Si/Ti = 1.9 mesoporous solid, 0.80 g of NaOH (0.02 mol) were dissolved in a TEAH3 (21.55 mL, 0.1624 mol) solution containing 0.0126 mol and 0.051 mol of the titanatrane and the silatrane derivatives of TEAH3 (*e.g.* in the form of $[M(TEA)Cl]_2$ or M(TEA)OR (M = Si, Ti), R being an alkyl chain and TEA meaning the fully deprotonated ligand),[9] respectively, and 0.0116 mol of CTAB. Then, 155 mL of water were slowly added with vigorous stirring. A pale yellow suspension was formed after aging the mixture at 25 °C for 24 h. The resulting mesostructured powder was then collected by filtration, washed with water and ethanol, and air-dried. To obtain the final mesoporous material, the as-synthesized solid was calcined at 500 °C for 5 h under a static air atmosphere. The main synthetic variables and analytical data are summarized in Table 1. All samples were analyzed and characterized by electron probe microanalysis (EPMA, Philips SEM-515), XRD techniques (Seifert 3000TT diffractometer using CuKα radiation), TEM (Philips CM10 electron microscope), UV–Vis diffuse reflectance spectroscopy (Perkin-Elmer Lambda 9), IR spectroscopy (FTIR Perkin-Elmer 1750), and N_2 adsorption–desorption isotherms (Micromeritics ASAP2010).

Our synthesis strategy has been designed to avoid problems due to the great reactivity differences between the usual Ti and Si precursor species (such as alkoxides). Indeed, atrane complexes (*i.e.* complexes which include TEA-like species as ligands) are, in general, unstable but relatively inert towards hydrolysis. In practice, we have observed (Fast Atomic Bombardment coupled with Mass Spectrometry) that, once formed in the absence of water, both titanatrane and silatrane complexes do not react easily with water. In anhydrous solution, the majority species are the complexes $M(TEA)_2H_2$ and $MNa(TEA)_2H_2^+$ (M = Si or Ti). After water addition, both Si and Ti atrane complexes strikingly remain in solution in the majority form of the M(TEA)OH species. In this context, the most outstanding feature concerning the silatranes' and titanatranes' hydrolytic reactivity (when compared to the respective

Table 1 Selected synthetic, physical and catalytic data for some mesoporous titanosilicate samples

Sample	Si/Ti (precusor)	Si/Ti[a]	d_{100}/Å	BJH pore/Å	S_{BET}/m² g^{-1}	IR[b]	C_{ox}(%)[c]	Select.(%)[d]
1	∞	∞	37.5	25.6	1118	2.1	—	—
2	50.0	49.9(3)	40.0	28.0	1110	2.3	97	98
3	32.3	34.9(4)	41.8	28.5	1093	2.5	97	97
4	17.0	19.0(4)	41.2	26.5	959	3.0	—	—
5	10.0	8.3(3)	40.0	25.1	958	3.0	90	83
6	5.0	3.2(3)	38.6	22.0	725	3.0	44	68
7	4.0	1.9(3)	34.5	20.0	595	3.0	—	—

[a] Values averaged from EPMA of *ca.* 50 different particles (statistical esds in parenthesis). [b] Intensity ratio between the 960 and 800 cm^{-1} infrared bands. [c] Oxidant conversion. [d] Selectivity in cyclohexene epoxide.

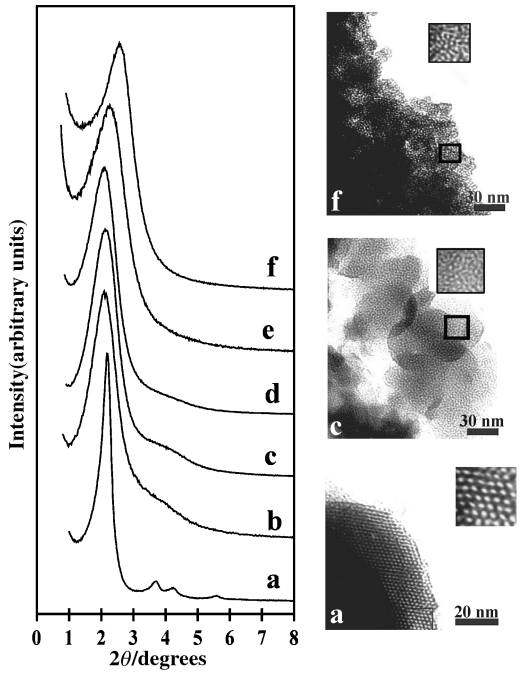

Fig. 1 XRD powder patterns of mesoporous titanosilicates and some selected TEM images: (a) sample 2; (b) sample 3; (c) sample 4; (d) sample 5; (e) sample 6; (f) sample 7.

alkoxides) is that silatranes are more labile than, for example, TEOS, whereas the contrary occurs in the case of titanatranes. Hence, the role of TEAH3, which acts in practice as a hydrolysis retarding agent for Ti species, is the key to achieve an adequate balance between the hydrolysis and subsequent condensation reactions affecting the precursors.

EPMA analysis shows that all the samples are chemically homogeneous (spot area *ca.* 1 μm) with a regular distribution of titanium and silicon atoms. Hence, the solids can be considered as monophasic products, and segregation of TiO_2 can be discarded. This is consistent with the absence of rutile or anatase peaks in the XRD patterns.

Selected low-angle XRD patterns of mesoporous samples are shown in Fig. 1. All solids show diffraction patterns with at least one strong reflection at low 2θ values, which is typical in mesoporous materials. Apart from this intense peak [associated with the (100) reflection if a hexagonal cell is assumed], in the patterns of solids whose titanium content is lower than that defined by the Si/Ti = 49.9 molar ratio, we can observe three other resolved small reflections [(110), (220) and (210)], which are characteristic of highly ordered hexagonal pore systems. Such an evolution indicates that incorporation of Ti in the silica-based hexagonal mesoporous framework (whatever its coordination may be) implies a progressive lowering of order in the pore array. TEM micrographs fully correlate to XRD observations. On the other hand, all materials give typical reversible type IV isotherms with one well defined step in their N_2 adsorption–desorption curves. Incorporation of Ti leads to a slight decrease of the BET surface area. This notwithstanding, high surface area values and unimodal pore distribution are retained even for the highest Ti contents.

Isomorphous substitution of Ti for Si in the framework has been confirmed by UV–Vis and IR spectroscopies. Thus, the UV–Vis spectra (Fig. 2) corresponding to samples with Si/Ti $\geqslant$ 34.9 show an absorption band at *ca.* 220 nm together with a small shoulder in the range 250–275 nm. In contrast, the spectra corresponding to samples with Si/Ti $\leqslant$ 19.0 present an additional band at *ca.* 300 nm whose intensity increases as the titanium content does. These results indicate that nearly all Ti occupies tetrahedral sites in the skeletal net until the Si/Ti = 34.9 molar ratio is reached.[10] Also for samples with Si/Ti $\leqslant$ 19.0, the presence of both tetrahedrally and octahedrally coordinated Ti atoms becomes evident. Nevertheless, even in this last case, the band at 220 nm remains as an intense signal in

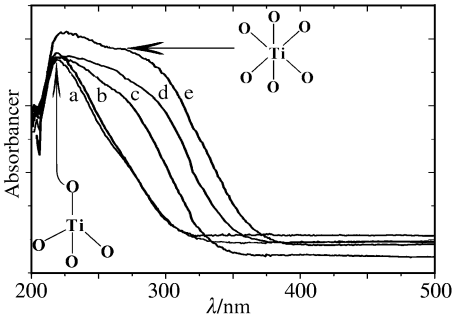

Fig. 2 Diffuse reflectance UV–Visible spectra of mesoporous titanosilicates: (a) sample 2; (b) sample 3; (c) sample 4; (d) sample 5; (e) sample 7.

the UV–Vis spectra. This observation suggests that tetrahedral Ti environments are relevant even for very high titanium contents, although five- and six-coordinated Ti local environments (in the form of small clusters) could be involved in the titanosilicate walls.[11] On the other hand, the IR spectra of all the samples display one band at 960 cm^{-1} that can be assigned to the stretching mode of SiO_4 entities bonded to Ti atoms.[11] Moreover, the intensity ratio (see Table 1) between the bands at 960 and 800 cm^{-1} (SiO_4 symmetric stretching) increases with the titanium content, which is usually taken as proof of isomorphous substitution of Ti for Si.[10]

The catalytic activity of these solids in the epoxidation of cyclohexene with TBHP (*tert*-butyl hydroperoxide) was tested in a stirred glass flask (at 343 K) by mixing 28.15 mmol of cyclohexene with 7.03 mmol of TBPH and 300 mg of catalyst. The results obtained after 3 h of reaction are summarized in Table 1. Such preliminary results seem to represent a significant performance improvement with respect to previous reports based on the use of mesoporous silica,[11] and are comparable to those provided by organo-silica-containing Ti-MCM-41 catalysts.[12] The maximum catalytic activity is maintained in the compositional range 34.9 $\leqslant$ Si/Ti $\leqslant$ 49.9, that is to say the range along which the number of tetrahedral Ti-sites is the highest. The increment in the Ti content implies a slow reduction both in conversion and selectivity related to both the proximity among the active Ti-sites and the growth of small nanodomains of TiO_2-like clusters.

In short, our results demonstrate that by using kinetically inert atrane molecular precursors it is possible to introduce catalytically active Ti-sites into mesoporous silicas. We consider that the atrane route can be extended to the preparation of a diversity of materials of catalytic interest[13]

This research was supported by DGES under grants PB98-1424-C02-01 and MAT2000-1387-C02-01. S. C. and J. E. H. thank the A.E.C.I. for doctoral grants.

Notes and references

1 B. Notari, *Adv. Catal.*, 1996, **41**, 252.
2 P. J. Saxton, W. Chester, J. G. Zajacek, G. L. Crocco and K. S. Wijesekera, *US Pat.*, 5621122, 1997.
3 A. Corma, M. T. Navarro and J. P. Pariente, *J. Chem. Soc., Chem. Commun.*, 1994, 147.
4 P. T. Tanev, M. Chibwe and T. J. Pinnavaia, *Nature*, 1994, **368**, 321.
5 T. Maschmeyer, *Curr. Opin. Solid State Mater. Sci.*, 1998, **3**, 71.
6 M. Alba, A. Becerro and J. Klinowski, *J. Chem. Soc., Faraday Trans.*, 1996, **92**, 849.
7 Z. Luan, E. M. Maes, P. A. W. Van der Heide, D. Zhao, R. S. Czernuszewicz and L. Kevan, *Chem. Mater.*, 1999, **11**, 3680.
8 S. Cabrera, J. El Haskouri, A. Beltrán, D. Beltrán, M. D. Marcos and P. Amorós, *Spanish Pat.*, P200000787, 2000.
9 J. G. Verkade, *Acc. Chem. Res.*, 1993, **26**, 483 and references therein.
10 A. Sayari, *Chem. Mater.*, 1996, **8**, 1840.
11 A. Tuel, *Microporous Mesoporous Mater.*, 1999, **27**, 151.
12 A. Corma, J. L. Jordá, M. T. Navarro and F. Rey, *Chem. Commun.*, 1998, 1899.
13 S. Cabrera, J. El Haskouri, C. Guillem, J. Latorre, A. Beltrán, D. Beltrán, M. D. Marcos and P. Amorós, *Solid State Sci.*, 2000, **2**, 405.

ChemComm

Time-resolved EPR characterisation of radical–triplet pairs formed by host–guest interaction of a photoexcited C_{60}–crown ether with an ammonium aminoxyl in liquid solution

Elena Sartori,[a] Luigi Garlaschelli*[b] and Antonio Toffoletti,[a] Carlo Corvaja,*[a] Michele Maggini*[c] and Gianfranco Scorrano[c]

[a] *Department of Physical Chemistry, University of Padova, via Loredan, 2 35131 Padova, Italy. E-mail: corvaja@chfi.unipd.it*
[b] *Department of Organic Chemistry, University of Pavia, via Taramelli, 10 27100 Pavia, Italy*
[c] *CMRO-CNR, Department of Organic Chemistry, University of Padova, via Marzolo, 1 35131 Padova, Italy*

Received (in Cambridge, UK) 27th November 2000, Accepted 11th January 2001
First published as an Advance Article on the web 30th January 2001

A time resolved EPR (TR-EPR) spectrum of a radical–triplet pair (RTP) in the quartet excited state has been recorded by irradiating with visible laser light a solution of a [60]fullerene–crown ether conjugate and an ammonium aminoxyl radical; this is the first direct observation of a RTP in liquid solution for a stable host–guest complex between a macrocyclic ligand bearing a triplet precursor and an aminoxyl ammonium cation.

Several investigations have shown that triplet excitations are quenched in the presence of free radicals, with a mechanism involving the formation of radical–triplet pairs (RTP).[1] The radical–triplet encounter can form a pair either in a quartet (^{4}[RTP]) or in a doublet state, whose energies are separated by the exchange interaction *J*. These two states are mixed by the electron–electron dipolar interaction.

In a magnetic field, the doublet character of the four quartet components is not the same and they decay with different rates to the ground state, causing a transient deviation of the radical sublevel populations from the thermal equilibrium values. This spin polarisation is revealed as an anomalous EPR line intensity.[2,3] The TR-EPR spectrum of a radical recorded in the presence of a triplet precursor after a laser pulse presents lines in enhanced absorption (A) or in emission (E). Spin polarisation derives also by the radical quenching of the excited singlet state, *i.e.* by enhanced ISC. In this case the polarisation is opposite to that caused by triplet quenching.[4]

The observation of spin polarised EPR spectra of a stable radical, such as aminoxyl radicals, in the presence of a triplet precursor is an indication of the formation of RTPs. However, the direct observation of a RTP in its excited quartet state by EPR spectroscopy is not feasible since collision pairs, in solutions of moderately viscous liquids, have lifetimes too short[5] to be detected *via* their ^{4}[RTP] EPR spectrum. On the other hand, ^{4}[RTP] spectra could be recorded for molecular systems where the radical and triplet precursor were (i) covalently linked,[6] (ii) coordinated[7] or (iii) linked to a molecular template.[8]

In this paper we report the first observation of a RTP that forms upon photoexcitation of a host–guest complex between [60]fullerene–crown ether conjugate **1**[9] and the benzoate ammonium salt of 3-aminomethyl-[2,2,5,5-tetramethylpyrrolidin-1-oxyl] **2**.

Derivative **1** combines in one molecule both the 18-crown-6 ionophore and the [60]fullerene triplet precursor, that has been selected for the long lifetime and high quantum yield of its triplet excited state.[10] The synthetic strategy toward derivative **1** is outlined in Scheme 1 and requires two steps. Esterification between commercially available hydroxymethyl-18-crown-6 and ethylmalonyl chloride in the presence of solid $NaHCO_3$ afforded ester **3** in 33% isolated yield. Cyclopropanation of C_{60}[11] with **3** in the presence of I_2 and 1,8-diazabicyclo[5.4.0]undec-7-ene (DBU) in toluene at rt gave **1** in 42% isolated yield.

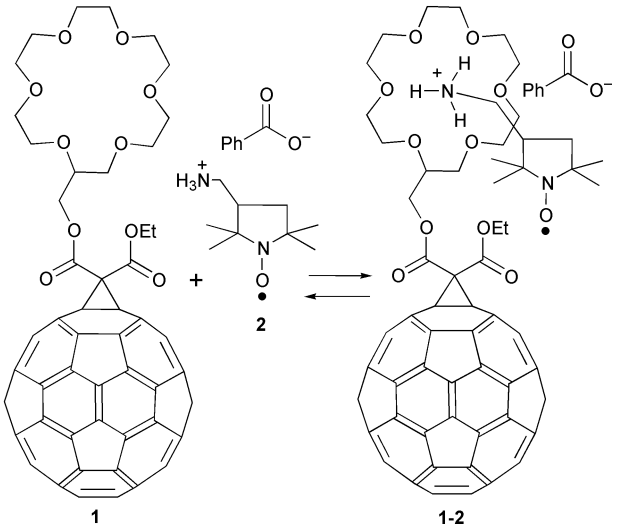

All spectroscopic and analytical data were consistent with the proposed molecular structure.† Ammonium aminoxyl **2** was obtained by mixing equimolar amounts of the corresponding aminomethyl aminoxyl and benzoic acid in diethyl ether. Pink crystals were isolated after crystallization from isopropyl ether.

The TR-EPR spectrum recorded by laser excitation of **1** in $CHCl_3$ solution at 235 K consists of a single broad line (ΔB = 1.66 ± 0.02 mT) centred at g = 2.0016 ± 0.0002 which is attributed to the excited triplet state. The line is broadened because of the incomplete averaging of the electron dipolar interaction. The signal decay is accounted for by two exponential functions with time constants τ_1 = 0.9 μs and τ_2 =

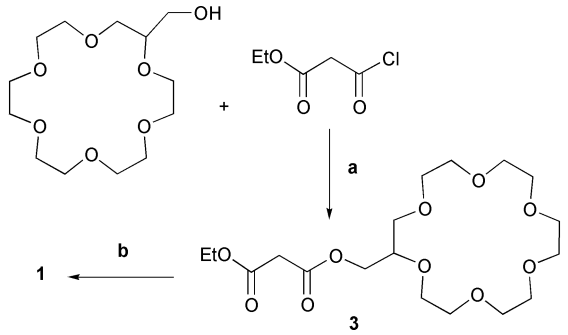

Scheme 1 *Reagents and conditions*: a, solid $NaHCO_3$, toluene, reflux, 8 h, 33%; b, C_{60}, I_2, DBU, toluene, rt, 2 h, 42%.

DOI: 10.1039/b009504o

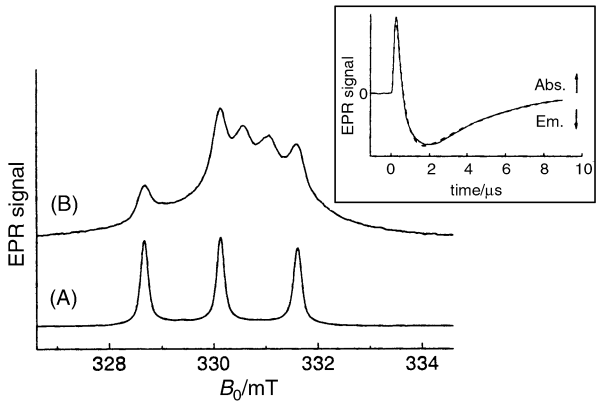

Fig. 1 EPR spectra of a 2 mM $CHCl_3$ solution of **1** and **2** at 235 K. (A) Integrated EPR spectrum. Microwave attenuation 20 dB. (B) TR-EPR spectrum recorded by laser excitation. Time delay from the laser pulse 250 ns. Microwave attenuation 5 dB. In the insert the signal decay of the central quartet line (solid line) and the fitting to a tri-exponential function (dotted line) are shown.

9.2 μs. The first decay time is to be assigned to the spin relaxation process which brings the initially spin polarised sublevel populations to thermal equilibrium values. The larger constant τ_2 is the triplet lifetime.

The EPR spectrum of a 2 mM $CHCl_3$ solution of both **1** and **2** consists of three lines with g_{NO} = 2.0057 ± 0.0002 and hyperfine separation a_N = 1.47 ± 0.02 mT, which are the typical values for an aminoxyl free radical, such as TEMPO, in that solvent (Fig. 1A).

When the solution was illuminated by a laser pulse, a strong spin polarised spectrum was recorded, as shown in Fig. 1B. It consists of three lines at the field positions corresponding to the aminoxyl lines and of three additional lines centred at a lower *g* value (g = 2.0031 ± 0.0002), with a separation of 0.46 ± 0.02 mT. The central line of the aminoxyl spectrum and the low field line of this second multiplet coincide. A broad signal is superimposed to these narrow features.

The three lines with 0.46 mT splitting are assigned to the host–guest complex **1**–**2**.[12] They are typical of the aminoxyl–fullerene triplet pair in the quartet excited state where the three unpaired electron spins interact with a single ^{14}N nuclear spin.[6] Since the electron spins are distributed 2/3 on fullerene and 1/3 on the aminoxyl group, the coupling constant is reduced to 1/3 the typical value for an aminoxyl radical. Also the *g* factor agrees with the value expected for a quartet, obtained from the *g* factor of the triplet state of **1** (g_T = 2.0016) and of the aminoxyl (g_{NO} = 2.0057) according to the formula $g_Q = 2/3g_T + 1/3g_{NO}$.[13] The TR-EPR spectrum of an equimolar amount of **1** and toluene-*p*-sulfonic ester of 3-hydroxymethyl-[2,2,5,5-tetramethylpyrrolidin-1-oxyl][14] in $CHCl_3$ does not show the quartet special features observed for **1**–**2**.

The lifetime of the quartet signal, recorded at 235 K, is about 4 μs (see insert of Fig. 1). This value is much larger than the lifetime of a collisional pair made by the encounter of **1** and **2** in the same solvent at the same temperature, which can be calculated by using[5] the following Einstein–Smoluchowski equation that gives the escape rate of a RTP partner:

$$k_E = 2(D_R + D_T)/(\rho_R + \rho_T)^2$$

where D_R and D_T are the diffusion coefficients of the two partners and ρ_R and ρ_T their van der Waals radii. D_R and D_T are obtained from the Stokes–Einstein relation:

$$D = kT/6\pi\eta\rho.$$

Using η = 1.2 cP[15] and for ρ_R and ρ_T the estimated values 0.35 and 0.70 nm, the RTP lifetime $1/k_E$ = 1.1 ns is obtained.

In the TR-EPR spectra there are signals of three species: excited triplet **1**, **2** and the associated form **1**–**2** in the quartet state. The EPR spectrum of the **1**–**2** host–guest complex in the ground state is not expected to differ significantly from that of free **2**. Unfortunately, the relative concentrations of **2** and **1**–**2** could not be measured directly from the TR-EPR spectra because the signal intensity depends not only on their concentration, but also on the amount of spin polarisation, which is not known. This method for observing host–guest interaction can be extended to other systems, where a partner contains a triplet precursor and the other a free radical.

This work was supported by CNR, through CMRO and CSSRE (legge 95/95), by MURST (Contract Prot. MM03198284) and by European Commission through Joule III, (Contract n. JOR3-CT98-0206).

Notes and references

† *Selected data for* **1**: ^1H NMR (400 MHz, $CDCl_3$) δ (ppm) 1.49 (t, 3H, $COOCH_2CH_3$), 4.07–3.60 (m, 23 H, OCH_2CH_2), 4.57 (q, 2H, $CO_2CH_2CH_3$), 4.67 (d, 2H, CO_2CH_2CH); λ_{max} (CH_2Cl_2)/nm (ε/dm^3 mol^{-1} cm^{-1}) 324 (2700), 257 (8570), 226 (71400); *m/z* (ESI-MS): 1149 (M + Na^+), 1165 (M + K^+).

1 G. Porter and M. R. Wright, *Discuss. Faraday Soc.*, 1959, **27**, 18; G. J. Hoytink, *Mol. Phys.*, 1969, **2**, 114; C. E. Swenberg and N. E. Geacintov, in *Organic Molecular Photophysics*, ed. J. B. Birks, John Wiley, London, 1973, pp. 498–499.
2 C. Blättler, F. Jent and H. Paul, *Chem. Phys. Lett.*, 1990, **166**, 375.
3 A. Kawai, T. Okutsu and K. Obi, *J. Phys. Chem.*, 1991, **95**, 9130.
4 A. Kawai and K. Obi, *J. Phys. Chem.*, 1992, **96**, 52.
5 H. Hayashi, in *Dynamic Spin Chemistry*, eds. S. Nagakura, H. Hayashi and T. Azumi, Kodansha, Tokyo, 1998, p. 40.
6 C. Corvaja, M. Maggini, M. Prato, G. Scorrano and M. Venzin, *J. Am. Chem. Soc.*, 1995, **117**, 8857.
7 K. Ishii, J. Fujisawa, Y. Ohba and S. Yamauchi, *J. Am. Chem. Soc.*, 1996, **118**, 13 079.
8 C. Corvaja, E. Sartori, A. Toffoletti, F. Formaggio, M. Crisma, C. Toniolo, J. Mazaleyrat and M. Wakselman, *Chem. Eur. J.*, 2000, **6**, 2775.
9 [60]Fullerene–crown ether conjugates have been the subject of several investigations in view of possible supramolecular modulation of the electronic properties of fullerenes: F. Diederich, U. Jonas, V. Gramlich, A. Hermann, H. Ringsdorf and C. Thilgen, *Helv. Chim. Acta*, 1993, **76**, 2445; S. Wilson and Y. Wu, *J. Chem. Soc., Chem. Commun.*, 1993, 784; J. Osterod, A. Zett and F. Vögtle, *Tetrahedron*, 1996, **52**, 4949; J. Arias, L. A. Godìnez, S. R. Wilson, A. E. Kaifer and L. Echegoyen, *J. Am. Chem. Soc.*, 1996, **118**, 6068; J.-P. Burgeois, L. Echegoyen, M. Fibbioli, E. Pretsch and F. Diederich, *Angew. Chem., Int. Ed.*, 1998, **37**, 2118; F. Diederich and M. Gómez-López, *Chem. Soc. Rev.*, 1999, **28**, 263.
10 S. L. Murov, I. Carmichael and G. L. Hug, *Handbook of Photochemistry*, Dekker, New York, 1993, p. 22.
11 J.-F. Nierengarten, T. Habicher, R. Kessinger, F. Cardullo, F. Diederich, V. Gramlich, J.-P. Gisselbrecht, C. Boudon and M. Gross, *Helv. Chim. Acta*, 1997, **80**, 2238.
12 The formation of the complex **1**–**2** was evidenced by ES ionisation mass-spectroscopy (ESI-MS). The spectrum recorded from a 1:1 mixture of **1** and **2** in CH_2Cl_2 displayed an intense peak at *m/z* 1298 which corresponds to the supramolecular ion **1**–**2** (1126 + 172).
13 A. Bencini and D. Gatteschi, *EPR of Exchange Coupled Systems*, Springer Verlag, Berlin, 1990, p. 53–55.
14 The 3-aminomethyl aminoxyl, precursor of **2**, was not used for the known reactivity of primary amines with fullerenes.
15 C. L. Yaws, *Handbook of Viscosity*, Gulf Publishing Company, Houston, 1995, vol. 1, p. 16.

ChemComm

Introduction of per(fluoroorganosilyl) peripheries into carbosilane dendrimers and related core-functionalized monodendrons gives rise to anomalous hydrodynamic and viscosimetric behavior

Miguel Angel Casado,[a] Jacques Roovers[b] and Stephen R. Stobart*[a]

[a] *Department of Chemistry, University of Victoria, British Columbia, Canada V8W 2Y2. E-mail: stobartz@uvvm.uvic.ca*

[b] *Institute for Chemical Process and Environmental Technology, National Research Council, Ottawa, Ontario, Canada K1A 0R6*

Received (in Irvine, CA, USA) 3rd November 2000, Accepted 3rd January 2001
First published as an Advance Article on the web 30th January 2001

Platinum-catalyzed hydrosilylation of allyl-terminated carbosilane monodendrons using the silanes $SiHMe_2[(CH_2)_nR_f]$ (1a, n = 2, R_f = n-C_6F_{13}; 1b, n = 3, R_f = $-C_6F_5$) yields fluorous, liquid analogues to [G-3], $BrC_6H_4(CH_2)_3SiMe[(CH_2)_3SiMe[(CH_2)_3SiMe[(CH_2)_3SiMe_2(CH_2)_nR_f]_2]_2]_2$ (7a, n = 2, R_f = n-C_6F_{13}- ; 7b, n = 3, R_f = $-C_6F_5$), intrinsic viscosities [η] for which are unusually low, resulting in calculated hydrodynamic radii/Å (*ca.* 6.3, [G-1]; 8.3, [G-2]; 11.5, [G-3]) that imply unusually compact structures.

The low surface-energy of materials that are required for low-friction coatings and related applications is typically[1] governed by the properties of a fluorine-containing surface layer, a specially effective design for which exposes perfluoroalkyl groups[2] in a microstructural array that[3] minimizes surface disorder. Dendrimer[4] functionalization to prefabricate a suitable hyperbranched subunit, followed by binding of the latter to an appropriate support, is a potentially[5] versatile way of developing such surface coverage; but despite its recent rapid rate of advancement,[4,6] dendrimer chemistry so far offers only a very limited range[7–9] of fluorinated prototypes. Our interest[10,11] in carbosilane[8–12] dendrimers as chemically passive frameworks has led us to explore routes to such species in which a fluorinated organic group is bound to each peripheral silicon atom *directly*, avoiding conjunction through a heteroatom (O or S) as has been reported elsewhere by others.[8,9] We show that by using polyfluoroorgano-substituted silanes in a final convergent step, peripheral modification of allyl-terminated carbosilane dendrimers is possible; and more particularly that, by adaptation of a modular approach[11] to carbosilane monodendrons, members of a family to **[G-3]** of core *p*-bromophenyl-functionalized analogues may be isolated in high yield. These latter products, in which the unique core functionality can be used for further chemistry including polymer or surface attachment, have been fully characterized by size exclusion chromatography (SEC) and viscosimetry as well as by spectroscopic and analytical data. Dendrimers are known[13] to exhibit low intrinsic viscosities [η] that (in sharp contrast to those for other classes of polymer) tend to a limit with increasing molecular weight. Even by such standards, however, the measured [η] values for the fluorinated carbosilane monodendrons are unusual, generating plots *vs.* SEC elution volume that lie below the[10,14] universal calibration curve. We take this to imply (albeit indirectly[15]) that this type of addendum may be useful for surface coverage to promote non-stick behavior.

In preliminary experiments, we set out to introduce fluorous organic groups directly into carbosilane dendrimers by using organometallic reagents to replace Cl in[10] peripheral $-SiMe_xCl_{3-x}$ units. This led, with Grignard reagents of the type $R_fCH_2CH_2MgX$ (R_f = n-C_6F_{13} or $-C_6F_5$; X = I or Br), to extensive formation of unwanted side-products, as well as to mixtures of products that indicated incomplete substitution at the dendrimer periphery. Platinum-catalyzed hydrosilylation of allyl-terminated carbosilane dendrimer precursors proved to be a more satisfactory alternative method for building a modified outer layer: thus regiospecific (anti-Markovnikov, γ-substitution of $Si-CH_2CH{=}CH_2$) addition of the silanes[16] $SiHMe_2[(CH_2)_nR_f]$ (**1a**, n = 2, R_f = n-C_6F_{13}; **1b**, n = 3, R_f = $-C_6F_5$) appeared (through monitoring by NMR) to be essentially quantitative, although limiting the number of fluorous groups to one per silicon atom in the newly-formed periphery. Crude fractions so obtained afforded colorless, viscous liquid products **2a**,**b**–**4a**,**b**, see Scheme 1, although the chromatography required to isolate analytically pure samples resulted in significant losses. These new dendrimers possess a branch hierarchy radiating in the archetypal fashion,[4] from a tetra-substituted core silicon atom to a homofunctional periphery that is not amenable to further adaptation. Construction of analogues that can serve as fluorous mesomolecular building blocks may be accomplished, however, by similarly adding the silanes **1a**,**b** across the peripheral allyl groups of the *p*-bromophenyl-substituted trifurcate monodendrons described elsewhere.[11] This routine has been used to synthesize the new monodendrons **5a**,**b**–**7a**,**b**, (Scheme 1) which proved to be much easier to purify on flash silica gel than their dendrimer counterparts: like the latter, they remain fluid to **[G-3]** (glassy transition temperatures T_g/° C: −66, **5a**; −58, **5b**; −65, **6a**; −53, **6b**; −59, **7a**; −53, **7b**) and have likewise been fully characterized.† Prospective use in[11] modular synthesis led us to investigate the physical behavior of these compounds in more detail, using SEC and viscosity measurements.

Variation of intrinsic viscosity [η] (dL g^{-1}) with nominal molecular weight M for **[G-1]**, **[G-2]** and **[G-3]** homologues (*i.e.* compounds **5a**, **6a**, **7a**; **5b**, **6b**, **7b**), expressed as a double logarithmic relationship, is compared in Fig. 1 with corresponding data for polystyrene standards as well as for unmodified vinyl-terminated, vinyl-derived[10] carbosilane dendrimers (to **[G-4]**). The successive displacement from one plot to the next highlights the lowering in [η] values that accompanies fluorination, with the effect exaggerated for the *n*-perfluorohexyl-terminated species *vs.* their perfluorophenyl-terminated analogues, *i.e.* decreasing with increasing fluorine content and anticipated changes in surface-energy.[2,3] Calculated hydrodynamic radii are as follows (Å, based on nominal M): 6.3, **5a**; 6.3, **5b**; 8.3, **6a**; 8.7, **6b**; 11.5, **7a**; 11.2, **7b**; these are only slightly larger than those for the simple vinyl-terminated prototypes, indicating topology that is unexpectedly compact

$Si[(CH_2)_3SiMe_2(CH_2)_nR_f]_4$ (**[G-1]**: **2a**, **2b**)
$Si[(CH_2)_3Si[(CH_2)_3SiMe_2(CH_2)_nR_f]_3]_4$ (**[G-2]**: **3a**, **3b**)
$Si[(CH_2)_3Si[(CH_2)_3Si[(CH_2)_3SiMe_2(CH_2)_nR_f]_3]_3]_4$ (**[G-3]**: **4a**, **4b**)

$R_cSiMe[(CH_2)_3SiMe_2(CH_2)_nR_f]_2$ (**[G-1]**: **5a**, **5b**)
$R_cSiMe[(CH_2)_3SiMe[(CH_2)_3SiMe_2(CH_2)_nR_f]_2]_2$ (**[G-2]**: **6a**, **6b**)
$R_cSiMe[(CH_2)_3SiMe[(CH_2)_3SiMe[(CH_2)_3SiMe_2(CH_2)_nR_f]_2]_2]_2$ (**[G-3]**: **7a**, **7b**)

Scheme 1 For subset **a**, n = 2, R_f = n-C_6F_{13}–; **b**, n = 3, R_f = $–C_6F_5$; for **5**–**7** core group R_c = $BrC_6H_4(CH_2)_3$–.

DOI: 10.1039/b008992n

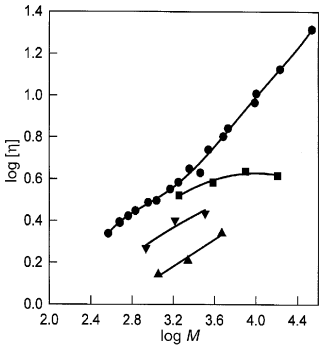

Fig. 1 Plot of log{intrinsic viscosity/dL g^{-1}} *vs.* log{nominal molecular weight}: ● polystyrene standards, ■ vinyl-terminated carbosilane dendrimers (see ref. 10), ▼ pentafluorophenyl-terminated carbosilane monodendrons (**5b**, **6b**, **7b**),▲ polyfluoroalkyl-terminated carbosilane monodendrons (**5a**, **6a**, **7a**).

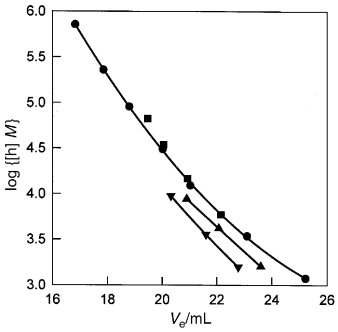

Fig. 2 Plot of log{(intrinsic viscosity/dL g^{-1})(nominal molecular weight)} *vs.* elution volume V_e (mL): for symbol legend, see Fig. 1.

and very much smaller than dimensions that were calculated[8] for extended structures of polyfluoroalkyl ether analogues. Examination of the relationship between log{[η].*M*} and the SEC elution volume (mL) V_e, (Fig. 2) which is the basis[10,14] for the universal calibration curve, shows that while the family of unfluorinated carbosilane dendrimers conform[10] to established expectations, the fluorous monodendrons do not. This is evidence for an anomalous repulsive interaction between the latter and the stationary phase of the SEC column, a phenomenon that may confer resistance to surface penetration on materials that have been treated with reagents like **7a**.

We acknowledge receipt of grant instalments in the form of a N.R.C.-N.S.E.R.C. (Canada) Research Agreement, we are grateful to Organogel Canada Ltd. for generous financial support, and we thank Brad Noren for experimental assistance.

Notes and references

† Measured ^{1}H NMR data were in all cases consistent with the proposed structures. The ^{19}F{^{1}H} NMR spectra which were essentially identical within each family of compounds were useful for diagnostic purposes. Data for compound **5a**: Yield 88%. Anal. Calcd. for $C_{36}H_{45}BrF_{26}Si_3$: C, 38.07; H, 3.99. Found: C, 38.53; H, 4.23. MALDI-TOF (*m/z*) Calcd. (M + Ag^+): 1244. Found: 1244. ^{13}C{^{1}H} NMR ($CDCl_3$, δ): 143.1, 131.3, 130.2 (s, C_6H_4), 121.8 (m, C_6F_{13}), 119.6 (s, C_6H_4), 119.1, 118.0, 115.8, 111.1, 108.2, (m, C_6F_{13}), 39.2 (s, CH_2), 25.9 (t, CH_2CF_2), 25.5, 19.4, 18.4, 18.1, 13.5, 4.4 (s, CH_2), −3.9, −5.2 (s, CH_3). ^{29}Si{^{1}H} NMR ($CDCl_3$, δ): 3.09 (s, 2Si), 1.80 (s, 1Si). **5b**: Yield 92%. Anal. Calcd. for $C_{38}H_{49}BrF_{10}Si_3$: C, 53.07; H, 5.74. Found: C, 53.64; H, 5.97. ^{13}C{^{1}H} NMR ($CDCl_3$, δ): 146.2, 143.4 (m, C_6F_5), 141.6 (s, C_6H_4), 141.5, 139.2, 138.7, 136.1 (m, C_6F_5), 131.2, 130.2, 119.3 (s, C_6H_5), 39.3, 31.5, 25.9, 24.1, 19.9, 18.5, 18.3, 15.2, 13.7 (s, CH_2), −3.5, −5.2 (s, CH_3). ^{29}Si{^{1}H} NMR ($CDCl_3$, δ): 2.21 (s, 2Si), 1.76 (s, 1Si). **6a**: Yield 94%. Anal. Calcd. for $C_{70}H_{95}BrF_{52}Si_7$: C, 38.20; H, 4.35. Found: C, 38.52; H, 4.47. MALDI-TOF (*m/z*) Calcd. (M + Ag^+): 2309. Found: 2309. ^{13}C{^{1}H} NMR ($CDCl_3$, δ): 141.5, 131.2, 130.1 (s, C_6H_4), 121.8 (m, C_6F_{13}), 119.2 (s, C_6H_4), 119.1, 118.0, 115.8, 111.1, 108.2 (m, C_6F_{13}), 39.3 (s, CH_2), 25.8 (t, CH_2CF_2), 25.5, 19.5, 19.0, 18.8, 18.7, 18.6, 18.4, 18.3, 13.7, 4.5 (s, CH_2), −3.9, −5.2, −5.3 (s, CH_3). ^{29}Si{^{1}H} NMR ($CDCl_3$, δ): 3.09 (s, 4Si), 1.70 (s, 1Si), 1.05 (s, 2Si). **6b**: Yield 85%. Anal. Calcd. for $C_{74}H_{103}BrF_{20}Si_7$: C, 53.90; H, 6.30. Found: C, 54.15; H, 6.55. ^{13}C{^{1}H} NMR ($CDCl_3$, δ): 146.2, 143.4 (m, C_6F_5), 141.6 (s, C_6H_4), 141.5, 139.2, 138.7, 136.1 (m, C_6F_5), 131.2, 130.2, 119.3 (s, C_6H_5), 39.4, 26.7, 26.0, 24.0, 19.9, 18.9, 18.7, 18.5, 18.4, 15.3, 15.2, 13.8 (s, CH_2), −3.4, −3.5, −5.1 (s, CH_3). ^{29}Si{^{1}H} NMR ($CDCl_3$, δ): 2.19 (s, 4Si), 1.72 (s, 1Si), 1.18 (s, 2Si). **7a**: Yield 85%. Anal. Calcd. for $C_{138}H_{195}BrF_{104}Si_{15}$: C, 38.27; H, 4.54. Found: C, 38.43; H, 4.67. MALDI-TOF (*m/z*) Calcd. (M + Ag^+): 4439. Found: 4443. ^{13}C{^{1}H} NMR ($CDCl_3$, δ): 141.5, 131.2, 130.1 (s, CH, C_6H_4), 121.8 (m, C_6F_{13}), 119.2 (s, C_6H_4), 119.1, 118.0, 115.8, 111.1, 108.2 (m, C_6F_{13}), 39.3 (s, CH_2), 25.8 (t, CH_2CF_2), 19.5, 18.8, 18.6, 18.5, 18.3, 13.7, 4.5 (s, CH_2), −0.19, −3.9, −5.2 (s, CH_3). ^{29}Si{^{1}H} NMR ($CDCl_3$, δ): 3.06 (s, 8Si), 1.66 (s, 1Si), 1.04 (s, 4Si), 0.95 (s, 2Si). **7b**: Yield 82%. Anal. Calcd. for $C_{146}H_{211}BrF_{40}Si_{15}$: C, 54.33; H, 6.59. Found: C, 54.56; H, 6.84. ^{13}C{^{1}H} NMR ($CDCl_3$, δ): 146.2, 143.4 (m, C_6F_5), 141.6 (s, C_6H_4), 141.5, 139.2, 138.7, 136.1 (m, C_6F_5), 131.2, 130.2, 119.3 (s, C_6H_5), 39.4, 26.7, 26.0, 25.9, 24.1, 24.0, 19.9, 19.8, 18.9, 18.7, 18.5, 18.4, 15.3, 15.2 (s, CH_2), −3.4, −3.5, −5.1, -5.2 (s, CH_3). ^{29}Si{^{1}H} NMR ($CDCl_3$, δ): 2.18 (s, 8Si), 1.69 (s, 1Si), 1.16 (s, 4Si), 0,99 (s, 2Si).

1 R. R. Thomas, D. R. Anton, W. F. Graham, M. J. Darmon and K. M. Stika, *Macromolecules*, 1998, **31**, 4595; I. E. Mayo, E. J. Lochner and A. E. Stiegman, *J. Phys. Chem. B*, 1999, **103**, 9383; I. J. Park, S.-B. Lee and C. K. Choi, *Macromolecules*, 1998, **31**, 7555.
2 D. Schmidt, C. E. Coburn, B. M. DeKoven, G. E. Potter, G. F. Meyers and D. A. Fischer, *Nature*, 1994, **368**, 39; J. Tsibouklis, M. Stone, A. A. Thorpe, P. Graham, T. G. Nevell and R. J. Ewen, *Langmuir*, 1999, **15**, 7076.
3 A. F. Thünemann, U. Schnöller, O. Nuyken and B. Voit, *Macromolecules* 1999, **32**, 7414; S. Perutz, J. Wang, E. J. Kramer and C. K. Ober, *Macromolecules*, 1998, **31**, 4272.
4 E. Buhleier, W. Wehner and F. Vögtle, *Synthesis*, 1978, **155**; D. A. Tomalia, A. M. Naylor and W. A. Goddard III, *Angew. Chem., Int. Ed. Engl.*, 1990, **29**, 138; J. M. J. Fréchet, *Science*, 1994, **263**, 1710; P. R. L. Malenfant, L. Groenendaal and J. M. J. Fréchet, *J. Am. Chem. Soc.*, 1998, **120**, 10 990; G. R. Newkome, A. K. Patri and L. A. Godínez, *Chem. Eur. J.*, 1999, **5**, 1445; M. Fischer and F. Vögtle, *Angew. Chem., Int. Ed.*, 1999, **38**, 884.
5 M. Wells and R. M. Crooks, *J. Am. Chem. Soc.*, 1996, **118**, 3988; V. Chechik and R. M. Crooks, *Langmuir*, 1999, **15**, 7333.
6 F. Zeng and S. C. Zimmerman, *Chem. Rev.*, 1997, **97**, 1681; A. W. Bosman, H. M. Janssen and E. W. Meijer, *Chem. Rev.*, 1999, **99**, 1665; S. L. Gilat, A. Adronov and J. M. J. Fréchet, *Angew. Chem., Int. Ed.*, 1999, **38**, 1422; A. Adronov and J. M. J. Fréchet, *Chem. Commun.*, 2000, 1701.
7 A. I. Cooper, J. D. Londono, G. Wignall, J. B. McClain, E. T. Samulski, J. S. Lin, A. Dobrynin, M. Rubinstein, A. L. C. Burke, J. M. J. Fréchet and J. M. DeSimons, *Nature*, 1997, **389**, 368.
8 B. A. Omotowa, K. D. Keefer, R. L. Kirchmeier and J. M. Shreeve, *J. Am. Chem. Soc.*, 1999, **121**, 11130.
9 K. Lorenz, H. Frey, B. Stühn and R. Mülhaupt, *Macromolecules*, 1997, **30**, 6860.
10 L.-L. Zhou and J. Roovers, *Macromolecules*, 1993, **26**, 963; B. Comanita, B. Noren and J. Roovers, *Macromolecules*, 1999, **32**, 1069.
11 M. A. Casado and S. R. Stobart, *Org. Lett.*, 2000, **2**, 1549.
12 J. Roovers, P. M. Toporowski and L.-L. Zhou, *Poly. Prepr. (Am. Chem. Soc., Div. Polym. Chem.)*, 1992, **33**, 182; A. W. van der Made and P. W. N. van Leeuwen, *J. Chem. Soc., Chem. Commun.*, 1992, 1400; J. Roovers, L.-L. Zhou, P. M. Toporowski, M. van der Zwan, H. Iatrou and N. Hadjichristidis, *Macromolecules*, 1993, **26**, 4324; J. W. J. Knapen, A. W. van der Made, P. W. M. van Leeuwen, J. C. de Wilde, D. Grove and G. van Koten, *Nature*, 1994, **372**, 659; K. Lorenz, R. Mülhaupt, H. Frey, U. Rapp and F. J. Mayer-Posner, *Macromolecules* 1995, **8**, 6657; S. W. Krska and D. J. Seyferth, *J. Am. Chem. Soc.*, 1998, **120**, 3604; P. Wijkens, J. T. B. H. Jastrzebski, P. A. van der Schaaf, R. Kolly, A. Hafner and G. van Koten, *Org. Lett.*, 2000, **2**, 1621.
13 M. C. Moreno-Bondi, G. Orellana, N. J. Turro and D. A. Tomalia, *Macromolecules*, 1990, **23**, 910; T. H. Mourey, S. R. Turner, M. Rubinstein, J. M. J. Fréchet, C. J. Hawker and K. L. Wooley, *Macromolecules*, 1992, **25**, 2401; R. Scherrenberg, B. Coussens, P. van Vliet, G. Edouard, J. Brackman and E. de Brabander, *Macromolecules*, 1998, **31**, 456; C. Cai and Z. Y. Chen, *Macromolecules*, 1998, **31**, 6393.
14 Z. Grubisic, P. Rempp and H. Benoit, *J. Polym. Sci.*, 1967, **B5**, 753.
15 P. G. de Gennes, *Rev. Mod. Phys.*, 1965, **57**, 827.
16 Which are readily accessible from the corresponding, commercially available fluoroalkenes $R_f(CH_2)_xCH{=}CH_2$ (x = 0 or 1). See B. Richter, E. de Wolf, G. van Koten and B.-J. Deelman, *J. Org. Chem.*, 2000, **65**, 3885.

ChemComm

Binding of anthracycline antibiotic nogalamycin to the site of a DNA single strand break engineered between two co-axially stacked hairpins

Michelle L. Colgrave,[ab] Huw E. L. Williams[a] and Mark S. Searle*[a]

[a] *School of Chemistry, University Park, Nottingham, NG7 2RD. E-mail:mark.searle@nottingham.ac.uk; Tel: 0115 951 3567; Fax: 0115 951 3564*

[b] *Department of Chemistry, University of Wollongong, New South Wales 2522, Australia*

Received (in Cambridge, UK) 12th December 2000, Accepted 12th January 2001
First published as an Advance Article on the web 31st January 2001

We show by NMR that the DNA sequence 5′-GCGAAG-CACGAAGT folds to form an intramolecular double hairpin structure containing 5′-GAA loops with co-axial stacking of the two hairpins significantly increasing their stability; the anthracycline antibiotic nogalamycin is able to intercalate between the two hairpins (5′-TG step) despite the break in the phosphodiester backbone.

Hairpins are a common feature of RNA folding and consist of a single-stranded loop region closed by a base paired stem. In contrast, there have been relatively few observations of stable DNA hairpins,[1] however, a number of reports have detailed the extraordinary stability of hairpins containing a 5′-GAA loop.[2–7] High resolution NMR spectroscopy has shown that the structure is folded back between the two As in the loop and is stabilised by a non-Watson–Crick G–A base pair with which there are extensive base stacking interactions.[3]

We have designed a novel intramolecular DNA structure that folds from a single strand of DNA (5′-GCGAAGCACGAAGT) to form a double hairpin structure with 5′-GAA loops (Scheme 1). One half of the structure consists of a hairpin identical to that studied by Hirao *et al.*,[3] 5′-GCGAAGC, whilst the other half consists of a novel hairpin containing an A–T base pair in the stem, 5′-ACGAAGT. Co-axial stacking of the two hairpin structures generates a double-stranded stem region with an effective single strand break in the middle of the duplex region (Scheme 1). We have designed the double hairpin sequence to contain a 5′-TG base step at the strand break site (between the 5′- and 3′-terminal nucleotides; see Scheme 1) and have used this novel structure to investigate (i) the extent to which the two hairpin components are associated through co-axial base stacking and how this affects the stability of the individual hairpin components, and (ii) the role of the phosphate backbone in sequence-specific recognition by the anthracycline antibiotic nogalamycin (Scheme 1) which binds selectively to the 5′-TG step. Nogalamycin is a threading intercalator with sugar moieties interacting in both the major and minor groove of DNA.[8–16]

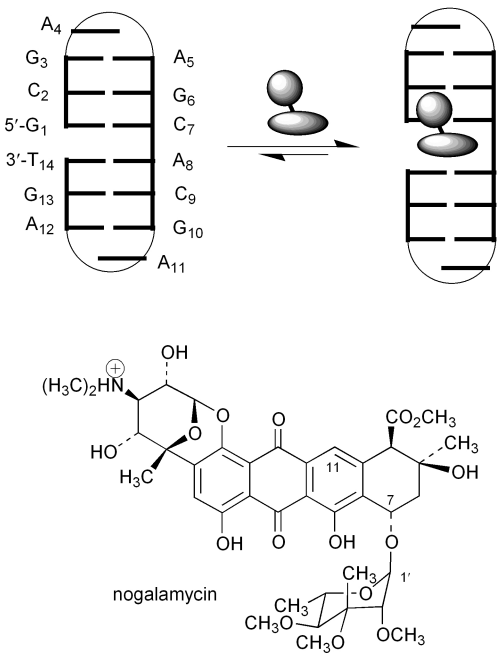

Scheme 1

We first examined the stability of the designed double hairpin sequence by NMR to establish that the sequence was folded into two hairpin conformations and to what extent these hairpins are co-axially stacked (Scheme 1). While the isolated hairpin sequence 5′-GCGAAGC has already been characterised, the hairpin sequence 5′-ACGAAGT has not. We synthesised 5′-ACGAAGT and the full length double hairpin 5′-GCGAAG-CACGAAGT using solid phase methods described previously,[12] and carried out a full NMR assignment.[17] The NMR studies previously reported on the hairpin d(GCGA$_4$AGC) showed that the deoxyribose H4′ of A$_4$ undergoes a large up-field shift as a consequence of stacking interactions in the loop region.[3] We used this shift as one of a number of indicators that the hairpin is folded. Indeed, we see that A$_4$H4′ of 5′-AC$_2$GA$_4$AGT and A$_{11}$H4′ of 5′-GCGAAGCAC$_9$GA$_{11}$AGT are up-field shifted by >2 ppm compared with other H4′ signals. Residues in the stem region also show large shift perturbations as a consequence of stacking of the G–A base pair; C$_2$H2′ in the hairpin and C$_9$H2′ in the double hairpin are located up-field at 1.56 and 1.57 ppm in the two structures. A number of other anomolous chemical shifts, together with the pattern of NOEs close to the loop regions suggest that the loops are well formed. However, the observation of highly exchange broadened imino proton resonances for Watson–Crick hydrogen bonded base pairs suggest that the stem region of 5′-ACGAAG$_6$T is not particularly stable, with the G$_6$NH only visible at low temperature. In contrast, all four imino protons in the stem region of the double hairpin are readily resolved at 25 °C, with that of the terminal thymine (T$_{14}$) showing some evidence of exchange broadening (Fig. 1). We conclude that co-axial stacking of the two hairpins considerably enhances the stability of the less stable 5′-ACGAAGT sequence. Hirao *et al.*,[3] had previously determined the T_m of the isolated hairpin 5′-GCGAAGC as ≈ 76 °C. UV melting studies on 5′-ACGAAGT in isolation under similar salt concentrations (0.30 M NaCl and 30 mM NaH$_2$PO$_4$) gave a broad transition around 48 °C. Thus, substitution of an A–T for a G–C base pair in the stem region significantly reduces the T_m, consistent with the imino proton data. UV melting studies on the intact double hairpin show a broad melting transition with a T_m of 65 °C. The broadness of the transition does not enable us to determine whether this is a biphasic process involving melting of the two individual hairpins in separate transitions, or a single co-operative melting. However, the absence of the low temperature transition seen for the isolated hairpin 5′-ACGAAGT provides further evidence for stabilisation through co-axial stacking between hairpins. Detailed analysis of NMR data for the isolated hairpin 5′-ACGAAGT and the same sequence within the double hairpin

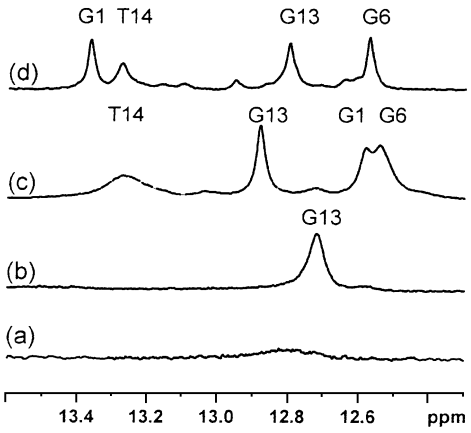

Fig. 1 Portions of the 500 MHz ^{1}H NMR spectra of 5′-ACGAAGT at (a) 15 °C and (b) 5 °C, (c) 5′-GCGAAGCACGAAGT at 15 °C, and (d) 1 : 1 5′-GCGAAGCACGAAGT–nogalamycin complex at 15 °C, all recorded in 90% H_2O solution under identical sample conditions. Imino proton resonances between 12 and 14 ppm are illustrated with assignments (see Scheme 1).

5′-GCGAAGCACGAAGT reveals some differences in chemical shifts of up to 0.2 ppm for nucleotides involved in end-stacking. Further, in NOESY data collected at 15 °C we observe internucleotide NOEs across the break site between G_1 and T_{14} (G_1H8 ↔ T_{14}H1′ and G_1H8 ↔ T_{14}H6), which provide convincing evidence for a significant population of co-axially stacked hairpins.

We subsequently examined the binding of nogalamycin to the 5′-TG site containing the single strand break to examine the role of the phosphate backbone in sequence-specific recognition. Titrating the drug into a solution of the double hairpin sequence, and monitoring the interaction by NMR, showed the emergence of a new set of DNA resonances alongside those of the unbound species. The free and bound DNA signals are in slow exchange at 25 °C, with the change in complexity of the NMR spectrum indicative of the formation of a single bound species. A complete assignment of the 1 : 1 complex has enabled some 30 drug–DNA NOEs to be identified. Fig. 2 shows a number of drug–DNA NOEs that define unambiguously the position and orientation of the bound ligand. In the complex we do not see NOEs across the intercalation site between G_1 and T_{14}, as observed for the free DNA; however, the drug acts as a surrogate base pair with the aromatic proton H11 giving NOEs to both G_1H1′ and T_{14}H1′, consistent with intercalation between the two hairpins. A number of other key NOEs to A_8H1′ at the intercalation site are also highlighted (Fig. 2), while NOEs from drug methyl groups on the nogalose sugar show specific hydrophobic interactions with, for example, G_1H1′ and C_2H1′ on the floor of the minor groove; these are analogous to those observed for nogalamycin binding to the 5′-TG site in duplex DNA.[12] These characteristic NOEs indicate that the drug–base pair stacking geometry is independent of the restraining influence of the phosphodiester backbone. In addition, the chemical shifts of the nucleotide resonances of G_1, C_7, A_8 and T_{14} were most affected by drug binding, consistent with nogalamycin intercalating at the 5′-TG step. UV melting studies on the 1 : 1 complex showed a more co-operative transition than for the free double hairpin, although the T_m of 74 °C is not significantly higher. Examination of the temperature-dependence of imino proton line widths showed that the base pairs forming the intercalation site are highly stabilised at 15 °C (Fig. 1d), indicating that they wrap around the drug to optimise van der Waals interactions, resulting in a highly stable complex templated by stacking and hydrophobic interactions with the bound drug. We can speculate that access of the drug to the intercalation site is greatly facilitated by the single strand break and that the association rate, which is slow for intact duplex DNA due to the requirement for local melting, may be significantly enhanced.

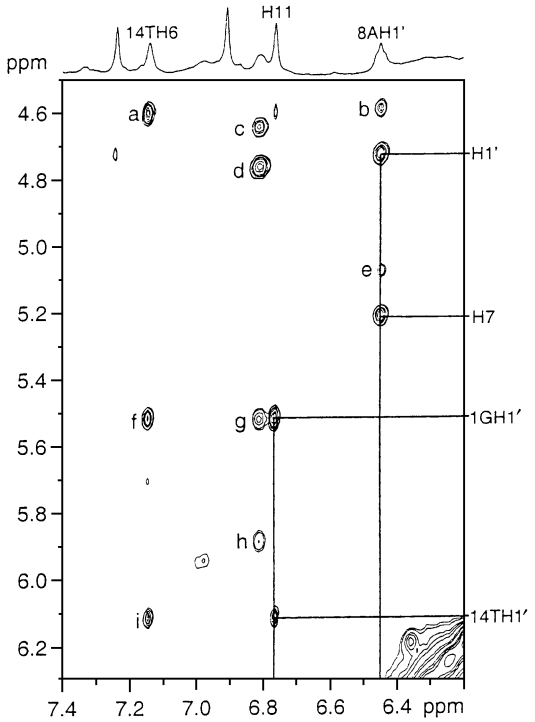

Fig. 2 Portion of the NOESY spectrum (100 ms mixing time) of the 1 : 1 nogalamycin: 5′-GCGAAGCACGAAGT complex recorded in D_2O solution at 15 °C highlighting key drug–DNA NOEs that identify the position and orientation of the bound intercalator at the 5′-TG step (drug H11, H7 and H1′ are marked on the axes), other DNA–DNA cross-peaks are labelled as follows: (a) T_{14}H3′–T_{14}H6, (b) A_8H1′–A_8H4′, (c) C_2H6–C_2H3′, (d) C_2H6–C_2H5, (e) A_8H1′–A_8H3′, (f) G_{13}H1′–T_{14}H6, (g) G_1H1′–C_2H6, (h) C_2H1′–C_2H6, (i) T_{14}H1′–T_{14}H6.

We thank the EPSRC (studentship to H. E. W. L.) for funding this work. M. L. C. thanks the Australian Research Council, Boehringer Ingelheim Fonds and Professor Margaret Sheil for the opportunity to travel to the UK. We are grateful to John Keyte in the School of Biomedical Sciences (Nottingham) for oligonucleotide synthesis.

Notes and references

1 S. Yoshizawa, G. Kawai, K. Watanabe, K. Miura and I. Hirao, *Biochemistry*, 1997, **36**, 4761.
2 I. Hirao, Y. Nishimura, T. Naraoka, K. Watanabe, Y. Arata and K. Miura, *Nucleic Acids Res.*, 1989, **17**, 2223.
3 I. Hirao, G. Kawai, S. Yoshizawa, Y. Nishimura, Y. Ishido, K. Watanabe and K. Miura, *Nucleic Acids Res.*, 1994, **22**, 576.
4 I. Hirao, Y. Nishimura, Y. Tagawa, K. Watanabe, Y. Arata and K. Miura, *Nucleic Acids Res.*, 1992, **20**, 3891.
5 G. Varani, *Annu. Rev. Biophys. Biomol. Struct.*, 1995, **24**, 379.
6 S. Yoshizawa, T. Ueda, Y. Ishido, K. Miura, K. Watanabe and I. Hirao, *Nucleic Acids Res.*, 1994, **22**, 2217.
7 Z. Chraibi, M. Refregiers, B. Jolles and A. Laigle, *J. Raman Spectrosc.*, 2000, **31**, 481.
8 J. F. Fisher and P. A. Aristoff, *Prog. Drug Res.*, 1998, **32**, 411.
9 S. K. Arora, *J. Am. Chem. Soc.*, 1983, **105**, 1328.
10 M. S. Searle and W. Bicknell, *Eur. J. Biochem.*, 1992, **205**, 45.
11 C. K. Smith, J. A. Brannigan and M. H. Moore, *J. Mol. Biol.*, 1996, **263**, 237.
12 H. E. Williams and M. S. Searle, *J. Mol. Biol.*, 1999, **290**, 699.
13 X. L. Zhang and D. J. Patel, *Biochemistry*, 1990, **29**, 9451.
14 Y. G. Gao, Y. C. Liaw, H. Robinson and A. H. J. Wang, *Biochemistry*, 1990, **29**, 10 307; Y. C. Liaw, Y. G. Gao, H. Robinson, G. A. van der Marel, J. H. van Boom and A. H. J. Wang, *Biochemistry*, 1989, **28**, 9913.
15 K. R. Fox and M. J. Waring, *Biochim. Biophys. Acta*, 1984, **802**, 162; K. R. Fox and M. J. Waring, *Biochemistry*, 1986, **25**, 4349.
16 K. R. Fox and Z. Alam, *Eur. J. Biochem.*, 1992, **209**, 31.
17 W. J. Chazin, K. Wuthrich, S. Hyberts, M. Rance, W. A. Denny and W. Leupin, *J. Mol. Biol.*, 1986, **190**, 439.

Synthesis of carbon films with diamond-like structure by electrochemical oxidation of lithium acetylide

Elena Shevchenko,*[a] Eugeny Matiushenkov,[b] Dmitry Kochubey,[d] Dmitry Sviridov,[b] Alexander Kokorin[c] and Anatoly Kulak[a]

[a] *Institute of General & Inorganic Chemistry, National Academy of Sciences, 220072, Belarus*
[b] *Department of Chemistry, Belarussian State University, 220050 Minsk, Belarus*
[c] *Institute of Catalysis, Russian Academy of Sciences, 630090 Novosibirsk, Russia*
[d] *Institute of Chemical Physics, Russian Academy of Sciences, 117977 Moscow, Russia*

Received (in Cambridge, UK) 7th November 2000, Accepted 20th December 2000
First published as an Advance Article on the web 31st January 2001

Electrochemical oxidation of lithium acetylide in aprotic media affords carbon films containing a high fraction of sp^3-type C bonds; the growth conditions and the photoelectrochemical behaviour of these films were investigated.

Much recent attention has been focused on the diamond-like carbon (DLC) films which are considered as promising materials for electronic, optical, and wear protection applications[1–3] because of similarities of their properties to those of diamond. These similarities, which are caused fundamentally by the fact that a greater part of DLC consists of a local sp^3 bonding configuration, ensure superior features such as chemical inertness, hardness, low friction and high thermal conductivity. The use of conductive DLC films as electrodes has also been of great interest due to very low capacitive background currents and a wide potential window in aqueous solutions[4] – these open up fresh opportunities for various electroanalytical applications.[5]

DLC films can be deposited using various chemical and physical vapour deposition techniques such as filament-assisted chemical vapour deposition,[6] filtered cathodic vacuum arc,[7] microwave plasma-assisted deposition,[8] mass-selected ion beam deposition[9] and pulse laser deposition.[10] On the other hand, there are few known reports describing attempts at utilising electrolysis of organic liquids for DLC film deposition despite the fact that the liquid deposition techniques, from the viewpoint of practical use, have many advantages such as an availability for large area deposition and a low deposition temperature. Recently, the possibility of deposition of DLC films by means of electrolysis of methanol has been demonstrated;[11] this deposition process, which occurs at high voltages (2–3 kV) and at high current densities (15 A cm^{-2}), is to be considered rather as an electrochemical plasma-assisted anodic carbonization of organics. It has also been reported that the anodic oxidation of acetylene in liquid ammonia yields transparent fragile carbon films exhibiting an electron diffraction pattern similar to that of diamond; however, the deposition rate showed by this process does not exceed 2×10^{-3} μm h^{-1}.[12]

In this work we demonstrate the possibility of utilizing anodic oxidation of lithium acetylide in dimethyl sulfoxide for electrochemical growing of carbon films containing a high fraction of sp^3 hybridized sites.

To prepare the C_2HLi/DMSO solution, acetylene was passed through lithiated DMSO obtained by dissolving lithium hydride in DMSO at 70 °C. The electrochemical deposition of carbon films has been carried out from a 0.1 M C_2HLi + 0.01 M Bu_4NClO_4/DMSO electrolyte under potentiostatic or galvanostatic conditions. As the electrodes, cathode-sputtered 100 nm platinum films at <111> silicon single-crystal wafers were used. The potentials were measured against an aqueous Ag/AgCl,Cl^-(sat.) reference electrode connected to the electrolysis cell through a salt bridge.

It is seen from Fig. 1 that an effective oxidation of lithium acetylide occurs at potentials more positive than about −0.5 V. The prolonged electrolysis of C_2HLi/DMSO solution is accompanied with the formation of the hard transparent film. As evidenced by Auger electron spectroscopy (AES) the film consists entirely of carbon (carbon content *ca.* 96%). The discharge of lithium acetylide at the carbon-modified surface occurs at higher overvoltages than at the bare platinum and the completion of carbon monolayer formation manifests itself as a pronounced anodic peak on the potentiodynamic polarization curve (Fig. 1). According to the AES depth profiling measurements, the electrolysis of C_2HLi/DMSO solution for 30 min under galvanostatic conditions at $i = 400$ μA cm^{-2} leads to the formation of a *ca.* 50 nm thick carbon film, only a mere increase in the film thickness being observed during the further anodization. During the course of electrolysis, the electrode potential exhibits a gradual shift in the anodic direction (Fig. 1) that can be attributed to the increase of overvoltage for C_2HLi

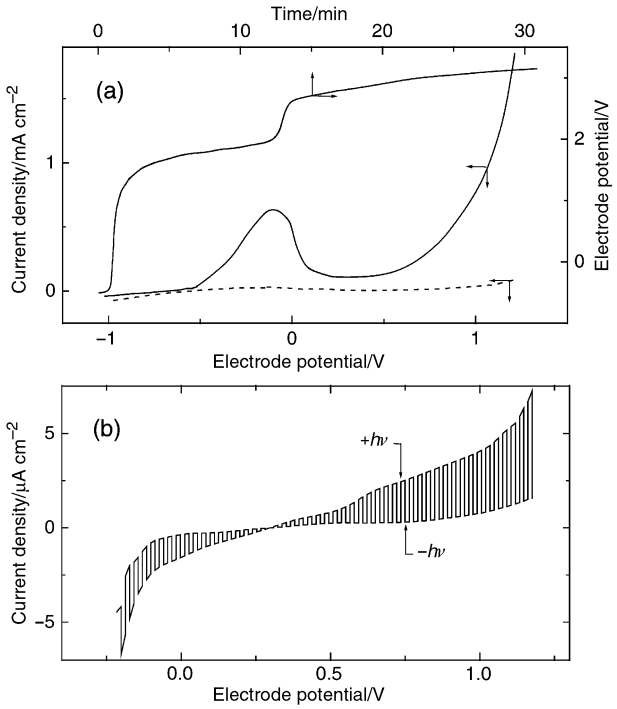

Fig. 1 (a) Current *vs.* time (galvanostatic conditions, $i = 400$ μA cm^{-2}) and current *vs.* potential (potentiostatic conditions, scan rate $dE/dt = 2$ mV s^{-1}) dependencies for anodic oxidation of lithium acetylide (0.1 M) in Bu_4NClO_4/DMSO at Pt electrode. Dashed curve corresponds to the sweep in a supporting electrolyte. (b) Potential dependence of photocurrent in aqueous buffered (pH 4.4) solution for carbon film grown under galvanostatic conditions. Full spectrum of 120 W medium-pressure Hg lamp; chopped illumination; $dE/dt = 5$ mV s^{-1}.

DOI: 10.1039/b008968k

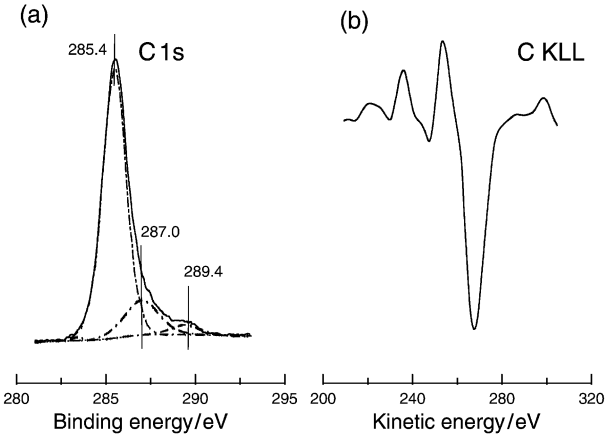

Fig. 2 (a) Spectrum of C 1s photoelectrons and (b) the first-derivative spectrum of X-ray excited C KLL Auger electrons for a carbon film grown under galvanostatic conditions. The Au 4f line of freshly evaporated gold was used as reference.

oxidation, while a step at the chronoammetric curve corresponds to the moment when the anodic decomposition of DMSO becomes dominant and the film growth terminates. The transparent carbon films similar to those obtained at platinum were also successfully grown on F-doped SnO_2 and nickel electrodes.

The photoelectrochemical experiments (potentiostatic conditions, potential given *vs.* Ag/AgCl) carried out in aqueous solution (acetate buffer, pH 4.6, 20 °C) have shown that under illumination with the whole spectrum of a 120 W medium-pressure mercury lamp the electrochemically-grown carbon film generates an anodic current of approximately 20 μA cm^{-2} at a potential of 1.2 V (Fig. 1). The anodic photocurrent was about two times larger in the acetate-containing solution (0.1 M CH_3CO_2H + 0.1 M CH_3CO_2Na + 0.25 M Na_2SO_4) as compared with the solution containing only Na_2SO_4. This fact can be explained by the effective acceptance of photogenerated holes by the acetate, a well known hole scavenger. This process significantly facilitates the transport of the photogenerated carriers through the carbon–solution interface. At a potential of *ca.* 0.3 V, an anodic photocurrent changes its direction and a cathodic photocurrent is evident under cathodic bias (Fig. 1). Photocurrent magnitude was not found to exhibit a pronounced influence on film thickness.

It seen from Fig. 2(a) that the C 1s photoelectron spectrum of electrochemically-deposited carbon film exhibits a main peak at 285.4 eV, *i.e.* at higher binding energies than those typical of amorphous carbon and hydrogenated carbon containing a high concentration of sp^2 sites.[13] A narrow C 1s peak (FWHM = 1.6 eV) points to the presence of a single C–C bonding phase, while a shoulder to the higher-binding-energy side of the C 1s spectrum can be assigned to carbon atoms bonded to oxygen. On the other hand, a large O 1s photoelectron peak composed of double signals with maxima at 532.9 and 534.2 eV indicates the presence of the other oxygen species (*e.g.* adsorbed DMSO). The AES and X-ray photoelectron measurements show very little evidence for the presence of sulfur (*ca.* 3 at.%) and nitrogen (< 1 at.%) at the surface of the carbon film grown under galvanostatic conditions. The S 2p photoelectron spectrum is composed of at least two signals peaking at 164 and 168.9 eV. This points to the fact that the observed contamination of the carbon surface is due to the adsorption not only of the electrolyte components but also of some other sulfur-containing species produced during electrolysis.

Further information on the carbon state in the electrochemically-grown carbon film was obtained from the X-ray excited Auger electron spectra (XAES). The XAES measurements, which are known to be much less destructive as compared to the conventional AES experiments,[14] have shown their suitability for the elucidation the form of carbon at a surface.[13] The main energy feature of the XAES spectrum is a peak at 262 eV, which coincides very closely with the energy of the major transition in the XAES spectrum of DLC.[13] Fig. 2(b) shows C KLL, the first-derivative Auger spectrum obtained from the XPS line. The maximum in the derivative spectrum is located at *ca.* 253 eV which is typical of amorphous carbon and hydrogenated carbon films.[13,15] A secondary feature at *ca* 241 eV, which is generally identified as an energy loss peak,[15] is also observed in the spectrum, while the high-energy shoulder at *ca*. 247 eV is attributable to the contamination of the carbon surface by oxygen.

A narrow C KLL line at *ca*. 265 eV, possessing no secondary features on the high-energy side, implies complete absence of KVV transitions involving pπ electrons which are typical of sp^2 coordination. As a result, the energy distance between the maximum of the positive-going excursion and the excursion and the minimum of the negative-going excursion, which was unambiguously indicated as a fingerprint of the different arrangement of carbon atoms,[13,14] does not exceecd 14 eV. This value is very close to the peak-to-peak width of the main transition of diamond (13 eV),[14] whereas the graphite spectrum is characterized by a far larger width (*ca.* 23 eV) between the negative and the positive maximum peak. The observed peculiarities of the X-ray excited Auger electron spectrum point to the fact that the electrolysis of lithium acetylide solution leads to the formation of the diamond-like carbon films almost free from sp^2-bonded carbon.

Notes and references

1 A. M. Zaitsev, A. V. Denisenko, G. Kosaca, R. Job, W. R. Fahrner, A. A. Melnikov, V. S. Varichenko, B. Buchard, J. von Borany and M. Werner, *J. Wide Bandgap Mater*., 1999, **7**, 4.
2 J. Van der Weide and R. J. Nemanich, *Phys. Rev. Sect. B.*, 1994, **49**, 13 629.
3 A. Grill, *Diamond Relat. Mater*., 1999, **8**, 428.
4 Yu. V. Pleskov, A. Yu. Sakharova, M. D. Krotova, L. L. Bouilov and B. V. Spitsyn, *J. Electroanal. Chem.*, 1987, **228**, 19.
5 E. Popa, H. Notsu, T. Miwa, D. A. Tryk and A. Fujishima, *Electrochem. Solid-State Lett.*, 1999, **2**, 49.
6 K. Ocano, H. Naruki, Y. Akiba, T. Kurosu, M. Ikeda, Y. Hirose and T. Nakamura, *Jpn J. Appl. Phys.*, 1989, **28**, 1066.
7 W. Kautek, S. Pentzien, A. Conradi, J. Krüer and K.-W. Brzezinka, *Appl. Surf. Sci.*, 1996, **106**, 158.
8 B. S. Satyanarayana, A. Hart, W. I. Milne and J. Robertson, *Appl. Phys. Lett.*, 1997, **71**, 1430.
9 Z. Has and S. Miruta, *Thin Solid Films*, 1985, **128**, 353.
10 J. H. Freaman and W. Temple and G. A. Gard, *Vacuum*, 1984, **34**, 305.
11 H. Wang, M. R. Shen, Z. Y. Ning, C. Ye, C. B. Cao, H. Y. Dang and H. S. Zhu, *Appl. Phys. Lett.*, 1996, **69**, 1074.
12 V. P.Novikov and V. P. Dymont, *Appl. Phys. Lett.*, 1997, **70**, 200.
13 J. C. Lascovich, R. Giorgi and S. Scaglione, *Appl. Surf. Sci.*, 1991, **47**, 17.
14 Y. Mizokawa, T. Miyasato, S. Nakamura, K. M. Geib and C. W. Wilmsem, *Surf. Sci.*, 1987, **182**, 431.
15 K. Ohmura, M. Kijima and H. Shirakawa, *Synth. Met.*, 1997, **84**, 417.

ChemComm

Supramolecular dendritic two-component gel

Kevin S. Partridge,[a] David K. Smith,*[a] Graham M. Dykes[a] and P. Terry McGrail[b]

[a] *Department of Chemistry, University of York, Heslington, York, UK YO10 5DD. E-mail: dks3@york.ac.uk*
[b] *ICI Technology, PO Box 90, Wilton Centre, Middlesbrough, Cleveland, UK TS90 8JE*

Received (in Cambridge, UK) 4th December 2000, Accepted 16th January 2001
First published as an Advance Article on the web 31st January 2001

Dendritic peptides with a carboxylic acid at the focal point of the branched structure form a two-component supramolecular organogel with a linear aliphatic diamine in non-hydrogen-bonding solvents.

There has been intense interest in the development of efficient and tunable small molecule gelators for organic solvents,[1] partly because gels possess many varied industrial applications as a consequence of the diversity of gel structures on both a microscopic and mesoscopic scale. Multiple supramolecular interactions[2] between the individual building blocks are critical in the gel forming process—for example hydrogen bonding, metal coordination, hydrophobicity *etc.* The ability of dendritic structures to act as gelators has, as a consequence of their multiplicity of functional groups, been of some interest. Newkome and co-workers reported dendrimers with a hydrophilic periphery and a hydrophobic core which stacked in aqueous solution, forming a gel.[3] Aida and co-workers reported a dendritic branch functionalised with a dipeptide at the focal point, which gelated organic solvents primarily through hydrogen bonding interactions.[4] In addition, Beginn and co-workers described branched amphiphiles functionalised with long aliphatic chains which gelate organic solvents.[5]

Recently, there has been increasing interest in the development of two-component gelling systems in which the presence of two complementary building blocks in solution is essential in order for gel formation to occur.[6–8] In these cases, supramolecular interactions between the complementary units allow a complex to form which is then capable of assembling further *via* inter-complex interactions to form the fully gelated network. Reports of two-component systems are still limited, and in this communication we report for the first time a controllable two-component dendritic system which gelates organic solvents as a consequence of specific supramolecular interactions.[9]

We recently reported the use of dendritic branches **1**, **2** and **3** constructed from L-lysine building blocks using a solution phase approach[10] to solubilise a hydrophilic dye into apolar solvents.[11] It was proposed that these dendritic branches containing a free carboxylic acid unit at the focal point (Fig. 1) interact with molecules containing basic amine sites through the formation of a hydrogen bonded (acid–base) complex with potential proton transfer (and salt bridge formation).[12] We therefore became interested in the ability of this type of dendritic branch to interact with amines possessing different structural motifs, such as long chain aliphatic diamines. We quickly discovered that the combination of dendritic branch **2** and diaminododecane (**4**) was capable of gelating organic solvents (Fig. 2), and we set about discovering the *key criteria required for effective gel formation*.[13]

Neither dendritic branch nor diamine alone are capable of gelating the solvent—branch **2** forms homogeneous solutions up to a concentration of at least 350 mg ml^{-1} (0.44 M), whilst diaminododecane (**4**) is largely insoluble. On mixing a solution of **2** in CH_2Cl_2 and solid **4**, followed by sonication and standing, dissolution of **4** combined with strong gel formation was observed. This indicates that an interaction between **2** and **4** takes place, solubilising **4** into CH_2Cl_2,[11] and that the complex subsequently induces gel formation.

The *concentrations* of dendritic branch **2** and diamine **4** were optimised for the effective gelation of DCM. At low concentrations of dendritic branch **2** (< 20 mg ml^{-1}, < 25 mM), gel formation is largely ineffective, however, above this concentration (> 2.0 wt vol%$^{-1}$) strong gels were observed. In particular, very strong gels were formed at a branch concentration of 25 mg ml^{-1} (31 mM). The strongest gel was observed using 10 mg of solid diaminododecane (**4**). Below a given mass of diamine **4**, however (2.5 mg, 12.5 mM), the diamine was completely solubilised by the dendritic branch, but gel formation would not

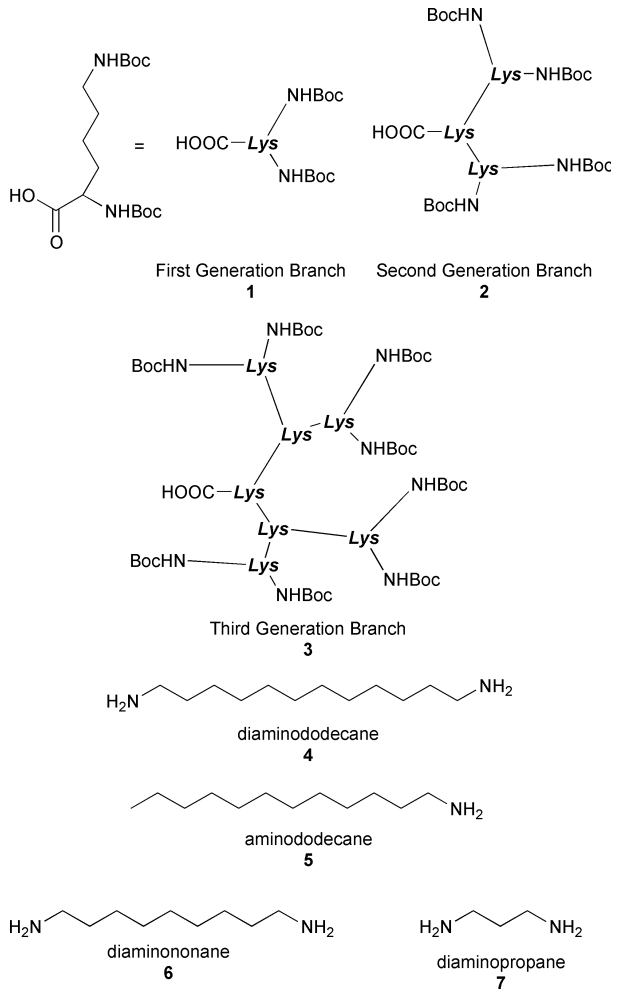

Fig. 1 Dendritic branches (**1**–**3**) and linear aliphatic amines (**4**–**7**) investigated. Combination of certain branches with complementary diamines leads to effective organogel formation.

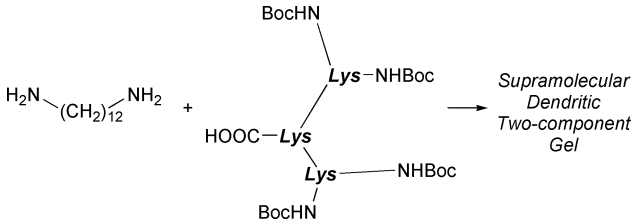

Fig. 2 Dendritic branch **2** solubilises diamine **4** into organic solvents (*e.g.* toluene, CH_2Cl_2 and CH_3CN) and the complex then induces gelation.

DOI: 10.1039/b009672p

Table 1 Effect of solvent on gel formation by compounds **2** (25 mg ml^{-1}, 31 mM) and **4** (10 mg). The Kamlet-Taft α and β parameters (relating to the ability of the solvent to donate and accept hydrogen bonds respectively) are also shown

Solvent	α (H-bond donor ability)	β (H-bond acceptor ability)	Gel formation using branch **2** and diamine **4** (25 mg ml^{-1} and 10 mg, respectively)
Toluene	0.00	0.11	Yes—rapid
Acetone	0.08	0.48	Solvent reacts with amine
CH_3CN	0.19	0.31	Yes—rapid, very strong gels
CH_2Cl_2	0.30	0.00	Yes—slow
$CHCl_3$	0.44	0.00	No
MeOH	0.93	0.62	No

readily occur. It is interesting to note that gelation becomes difficult when the molar ratio of diamine–branch falls below 1:2 and this result indicates that controlling the relative amounts of the two components is important. This would be expected if both components are complementary and essential for gel formation.

The *structure of the dendritic branch* was subsequently varied. First generation dendritic branch **1** did not induce gel formation with diaminododecane (**4**) at any concentration investigated (10–50 mg ml^{-1}, (29–145 mM) [**1**], 1–20 mg, (5–100 mM) [**4**]). This indicates that the dendritic branching of compound **2** plays a key role in enabling gelation to occur. Third generation dendritic branch **3** showed similar behaviour to second generation branch **2**, forming strong gels at 25 mg ml^{-1} (14.5 mM) with diaminododecane (4.5 mg). Interestingly, although the mass of **3** required to gelate the solution was the same as the mass of **2**, this is a lower absolute concentration (14.5 mM—as compared to 31 mM required for compound **2**) as a consequence of the higher molecular mass of the third generation branch. In a control experiment, branch **2** was protected at the focal point as a methyl ester. In this case, no solubilisation of diaminododecane occurred and furthermore, there was no gel formation. This indicates the importance of complementary interactions between carboxylic acid and amine as previously reported for dye solubilisation.[11]

The *structure of the aliphatic diamine* is also important in controlling gel formation. If a monoamine (aminododecane, **5**) was used, no gelation occurred in CH_2Cl_2, even at almost double the concentration of dendritic branch (40 mg ml^{-1}, 50 mM). If a shorter aliphatic diamine (diaminononane, **6**) was used, gelation with branch **2** was less successful, whilst using diaminopropane (**7**) led to no gel formation at all. This indicates the importance of having a sufficiently long aliphatic chain for gelation to occur. Interestingly, however, first generation branch **1** did form a weak gel with diaminononane (**6**) in CH_2Cl_2, although not with any other diamine. This could indicate that it is important to tune the length of the aliphatic diamine to match the generation of the dendritic branching for optimal gel formation. These results clearly illustrate the importance of microscopic structural features in controlling the macroscopic properties of the supramolecular dendritic gel.[14]

The *effect of solvent* on the gelation of **2** and **4** was then investigated (Table 1). The best solvent for gel formation appeared to be CH_3CN in which gelation occurred very rapidly, even at dendritic branch concentrations as low as 15 mg ml^{-1} (18.5 mM). Interestingly, gel formation occurred most readily in solvents which possess a low Kamlet-Taft α parameter.[15] This parameter reflects the ability of the solvent to donate hydrogen bonds (*i.e.* to the amine groups). This clearly indicates the importance of hydrogen bonds—competitive interactions from the solvent prevent gelation. Hydrogen bonds (either with or without associated proton transfer) are responsible for the interaction between the carboxylic acid of **2** and the amines of **4**, and may also play important roles in further mediating the gelation (*e.g.* hydrogen bond interactions between peptide groups in the dendritic branching).

In conclusion, we have demonstrated for the first time that suitably functionalised dendritic branches can undergo supramolecular two-component gelation of an organic solvent in the presence of a suitable complementary guest—a process mediated by hydrogen bond interactions. It is hoped in the future to expand the tunability of these gels by varying the structure of the individual components, and hence generate organogels with desirable physical properties. Furthermore the application of these gels to sensing and catalysis will be investigated.

D. K. S. acknowledges the support of the University of York, EPSRC (G. M. D) and ICI Technology (G. M. D.).

Notes and references

1 For excellent overviews of this area see: (*a*) P. Terech and R. G. Weiss, *Chem. Rev.*, 1997, **97**, 3133; (*b*) J. H. van Esch and B. L. Feringa, *Angew. Chem., Int. Ed.*, 2000, **39**, 2263 and references therein.

2 For reviews of supramolecular chemistry, see (*a*) P. D. Beer, P. A. Gale, D. K. Smith, *Supramolecular Chemistry*, Oxford University Press, Oxford, 1999; (*b*) J.-M. Lehn, *Supramolecular Chemistry: Concepts and Perspectives*, VCH, Weinheim, 1995; (*c*) F. Diederich, *Cyclophanes*, The Royal Society of Chemistry, Cambridge, 1991.

3 (*a*) G. R. Newkome, G. R. Baker, M. J. Saunders, P. S. Russo, V. K. Gupta, Z.-q. Yao, J. E. Miller and K. Bouillon, *J. Chem. Soc., Chem. Commun.*, 1986, 752; (*b*) G. R. Newkome, G. R. Baker, S. Arai, M. J. Saunders, P. S. Russo, K. J. Theriot, C. N. Moorefield, L. E. Rogers, J. E. Miller, T. R. Lieux, M. E. Murray, B. Phillips and L. Pascal, *J. Am. Chem. Soc.*, 1990, **112**, 8458; (*c*) G. R. Newkome, C. N. Moorefield, G. R. Baker, R. K. Behera, G. H. Escamilla and M. J. Saunders, *Angew. Chem., Int. Ed. Engl.*, 1992, **31**, 917; (*d*) G. R. Newkome, X. Lin, C. Yaxiong and G. H. Escamilla, *J. Org. Chem.*, 1993, **58**, 3123.

4 W.-D. Jang, D.-L. Jiang and T. Aida, *J. Am. Chem. Soc.*, 2000, **122**, 3232.

5 (*a*) U. Beginn, *Adv. Mater.*, 1998, **10**, 1391; (*b*) U. Beginn, S. Sheiko and M. Möller, *Macromol. Chem. Phys.*, 2000, **201**, 1008; (*c*) U. Beginn, G. Zipp and M. Möller, *Chem. Eur. J.*, 2000, **6**, 2016.

6 Aminopyridine–isocyanuric acid (hydrogen-bonding interactions): (*a*) K. Hanabusa, T. Miki, Y. Taguchi, T. Koyama and H. Shirai, *J. Chem. Soc., Chem Commun.*, 1993, 1382; (*b*) S. W. Jeong, K. Murata and S. Shinkai, *Supramol. Sci.*, 1996, **3**, 83; (*c*) K. Inoue, Y. Ono, Y. Kanekiyo, T. Ishi-i, K. Yoshihara and S. Shinkai, *J. Org. Chem.*, 1999, **64**, 2933.

7 Phenol–AOT (hydrogen-bond interaction): X. Xu, M. Ayyagari, M. Tata, V. T. John and G. L. McPherson, *J. Phys. Chem.*, 1993, **97**, 11 350 (AOT = sodium bis(2-ethylhexyl)sulfosuccinate).

8 Bile acid-Pyrene–trinitrofluorenone (aromatic donor–acceptor interactions): U. Maitra, P. V. Kumar, N. Chandra, L. J. D'Sousa, M. D. Prasanna and A. R. Raju, *Chem. Commun.*, 1999, 595.

9 For reviews of the growing field of supramolecular dendrimer chemistry see: (*a*) F. W. Zeng and S. C. Zimmerman, *Chem. Rev.*, 1997, **97**, 1681; (*b*) V. V. Narayanan and G. R. Newkome, *Top. Curr. Chem.*, 1998, **197**, 20; (*c*) D. K. Smith and F. Diederich, *Top. Curr. Chem.*, 2000, **210**, 183.

10 (*a*) R. G. Denkewalter, J. Kolc and W. J. Lukasavage, US Patent No. 4 289 872, 1981; assigned to Allied Corp; (*b*) J. P. Tam, *Proc. Natl. Acad. Sci. USA*, 1988, **85**, 5409.

11 D. K. Smith, *Chem. Commun.*, 1999, 1685.

12 For other reports of acid–amine interactions using dendrimers see: (*a*) V. Chechik, M. Zhao and R. M. Crooks, *J. Am. Chem. Soc.*, 1999, **121**, 4910; (*b*) L. J. Twyman, A. E. Beezer, R. Esfand, M. J. Hardy and J. C. Mitchell, *Tetrahedron Lett.*, 1999, **40**, 1743.

13 In a typical gel forming experiment, a sample of the dendritic branch (**1**, **2** or **3**) was dissolved in the organic solvent (1 ml) and to this was added a quantity of solid diaminododecane. The mixture was then sonicated at ambient temperature for 1 hour and allowed to stand. The strength of the gel formed was estimated by a visual investigation of its rheological properties. This involved inversion of the tube containing the gel and checking that neither the gel nor excess solvent ran down the side of the tube, and also lightly shaking the sample to ensure structural integrity was maintained for strong gels.

14 For a paper in which the microscopic structure of the gelator controls its potency see: K. Yoza, N. Amanokura, Y. Ono, T. Akao, H. Shinmori, M. Takeuchi, S. Shinkai and D. N. Reinhoudt, *Chem. Eur. J.*, 1999, **5**, 2722.

15 M. J. Kamlet, J.-L. M. Abboud, M. H. Abraham and R. W. Taft, *J. Org. Chem.*, 1983, **48**, 2877.

ChemComm

An active and selective alkane isomerization catalyst: iron- and platinum-promoted tungstated zirconia

Stefan Kuba,[ab] Bruce C. Gates,*[b] Robert K. Grasselli*[a] and Helmut Knözinger*[a]

[a] *Department Chemie, Physikalische Chemie, Ludwig-Maximilians-Universität München, Butenandtstr. 5-13, Haus E, D-81337 München, Germany. E-mail: helmut.knoezinger@cup.uni-muenchen.de; robert.grasselli@cup.uni-muenchen.de*

[b] *Department of Chemical Engineering and Materials Science, University of California, Davis, CA 95616-5294, USA. E-mail: bcgates@ucdavis.edu*

Received (in Cambridge, UK) 12th December 2000, Accepted 16th January 2001
First published as an Advance Article on the web 31st January 2001

Addition of iron sulfate to Pt-promoted tungstated zirconia increases the activity and selectivity of the catalyst for isomerization of *n*-pentane in the presence of H_2; selectivities > 98% have been observed.

Environmental concerns are motivating the use of motor fuels with increased amounts of high-octane-number branched alkanes. These are made by alkylation and by isomerization of straight-chain alkanes, the latter typically carried out with bifunctional catalysts incorporating hydrogenation/dehydrogenation functions and acidic functions or by very strong acids, such as aluminium chloride supported on alumina, which has the disadvantages of being corrosive and expensive to dispose of without environmental detriment. There is a need for alkane isomerization catalysts with improved activities and selectivities. Recently investigated candidates include tungstated zirconia (WZ), which has a high activity,[1,2] especially when promoted with Pt and when H_2 is contained in the feed.[3–5] The use of group 8 metals as promotors of WZ has been claimed in recent patents.[6–8] Fe has also been incorporated in WZ catalysts,[9] but promotion was not observed in the absence of Pt in the catalyst and H_2 in the feed. We now report WZ catalysts improved by promotion with both Pt and Fe and compare their performance with that of WZ promoted by Pt only.

Catalysts were prepared by slurry impregnation of amorphous $Zr(OH)_4$ (MEL Chemicals, XZO880/01) with aqueous ammonium metatungstate, $(NH_4)_6H_2W_{12}O_{40}{\cdot}nH_2O$ (Aldrich). In the synthesis of Fe-promoted catalysts, the appropriate amount of either $FeSO_4$ or $Fe(NO_3)_3$ was added to the slurry. The resultant suspensions were refluxed overnight at 393 K, dried in an oven at 353 K, and then calcined at 923 K in static air for 3 h. Separate batches of these calcined materials were impregnated by the incipient wetness method with 0.6 M aqueous $Pt(NH_4)(NO_3)_2$ and calcined at 723 K in air.

Each catalyst contained W in an amount corresponding to 17 wt% as WO_3, which is close to the theoretical monolayer capacity (19 wt%).[2] The Pt content was 1 wt%. The catalysts contained either no Fe (denoted as Pt/17WZ) or Fe in amounts corresponding to 1.0 wt% as Fe_2O_3; the latter are denoted as Fe/Pt/17WZ(N) and Fe/Pt/17WZ(S), prepared from iron nitrate or sulfate, respectively. The BET surface areas of Pt/17WZ, Fe/Pt/17WZ(N) and Fe/Pt/17WZ(S) were 126, 110 and 80 $m^2\ g^{-1}$, respectively.

Catalytic conversion of *n*-pentane was carried out in a once-through packed-bed flow reactor under the following conditions: temperature, 523 K; pressure, 101 kPa; *n*-pentane partial pressure, 0.84 kPa; H_2 partial pressure, 16.8 kPa; catalyst mass, 200 mg; feed flow rate (at NTP), 10 ml min^{-1} of 1% *n*-pentane in N_2 mixed with 2 ml min^{-1} of H_2. Under these conditions, the predominant catalytic reaction product was isopentane, formed with small amounts of methane, ethane, propane, butane, isobutane and neopentane. Catalysis was also carried out in the absence of H_2 under the same conditions, except that the feed *n*-pentane partial pressure was 0.84 kPa and the total flow rate was 10 ml min^{-1}. As the Pt precursor in the catalyst was observed to be reduced in H_2 to give zero-valent Pt even at room temperature, we infer that it was also reduced in the presence of the H_2-containing reactant mixture at 523 K during the initial stages.

The dependence of *n*-pentane conversion on time-on-stream (TOS) in the flow reactor is shown for the three catalysts in Fig. 1. Fe/Pt/17WZ(S) almost immediately attained a nearly stable activity corresponding to a conversion of *ca.* 64%. In contrast, induction periods of *ca.* 15 and 60 min were observed for Pt/17WZ and Fe/Pt/17WZ(N), respectively, before a nearly stable conversion of *ca.* 48% was attained. These activities are in the reverse order of the BET surface areas of the catalysts and show that the differences are associated with the catalyst compositions and not just physical properties.

The selectivities of the catalysts for isopentane formation measured during these experiments are shown in Fig. 2. The selectivity of Pt/17WZ dropped from *ca.* 97% to a stable value of *ca.* 95% after 1 h, whereas that of Fe/Pt/17WZ(N) reached a stable selectivity of *ca.* 99.7% after 30 min and that of Fe/Pt17WZ(S) approached 99% after 2.5 h. This small difference in selectivies may be caused by the higher conversion on the sulfate-containing catalyst. Thus, the data show that promotion by Fe enhances the catalytic activity of WZ for *n*-pentane conversion, with the iron sulfate providing a higher activity than iron nitrate but a somewhat lower selectivity.

The importance of H_2 in the reactant feed is emphasized. It was shown[9] that Fe had no promoting effect on WZ when H_2 was absent from the feed. Only 1% conversion of *n*-pentane and 30% selectivity for isopentane were measured under our conditions for the Fe- and Pt-promoted catalyst in the absence of

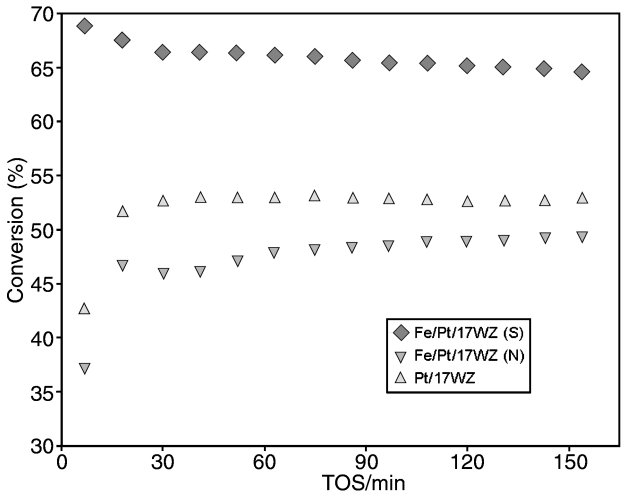

Fig. 1 Conversion of *n*-pentane catalyzed by Fe-promoted and Fe-free Pt/WZ catalysts in a flow reactor (conditions stated in text).

DOI: 10.1039/b009900g

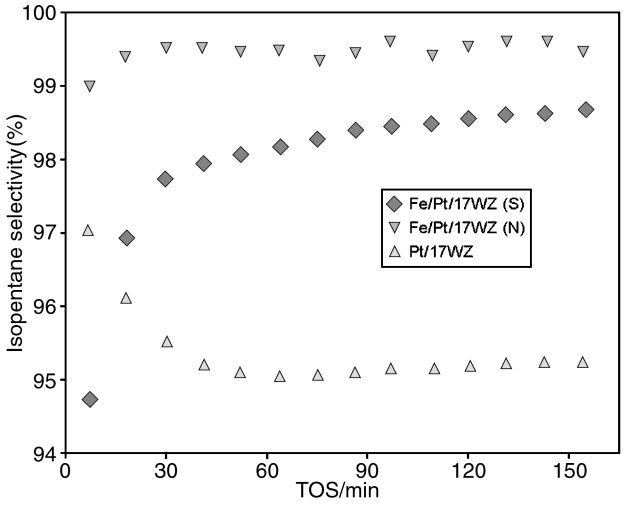

Fig. 2 Selectivity for isopentane formation of Fe-promoted and Fe-free Pt/WZ catalysts in a flow reactor (conditions as for Fig. 1).

H_2. It is therefore inferred that H_2 is essential for the optimal performance of this class of catalysts.

Sulfate is known to be strongly bonded to the zirconia surface,[10] and sulfated zirconia is itself a highly active catalyst for *n*-alkane conversions. The performance of sulfated zirconia is significantly improved by the addition of Fe and/or Pt promoters.[11] We therefore speculate that Fe/Pt17WZ(S) may incorporate surface sulfate and that Fe and sulfate may provide a cooperative promotion effect. Although the function of the Fe is at this juncture not entirely known, it is mechanistically deemed to prevent deep reduction of the tungsten by nascent hydrogen which is produced by Pt from the co-fed H_2. In this manner a redox equilibrium (steady state) is maintained on the catalyst surface which is responsible for the unusually good catalytic efficiency and stability of the Fe/Pt-WZ system.

In summary, we have shown that WZ catalysts promoted by both Fe and Pt exhibit high activity and selectivity for the conversion of *n*-pentane to isopentane. The observed performance indicates a significant improvement over known catalysts for *n*-pentane isomerization, and we suggest that the advantage may extend to other alkanes as well and be of practical value.

We thank F. Lai and A. Argo for their help. The international cooperation was made possible by financial support from the Alexander von Humboldt-Stiftung, the Max Planck-Gesellschaft and the BMBF (Max Planck-Research Award to H. K.). The work done in Munich was supported by the Deutsche Forschungsgemeinschaft (SFB338).

Notes and references

1 M. Hino and K. Arata, *J. Chem. Soc., Chem. Commun.*, 1988, 1259.
2 M. Scheithauer, R. K. Grasselli and H. Knözinger, *Langmuir*, 1998, **14**, 3019.
3 M. Scheithauer, T.-K. Cheung, R. E. Jentoft, R. K. Grasselli, B. C. Gates and H. Knözinger, *J. Catal.*, 1998, **180**, 1.
4 E. Iglesia, D. G. Barton, S. L. Soled, S. Miseo, J. E. Baumgartner, W. E. Gates, G. A. Fuentes and G. D. Meitzner, *Stud. Surf. Sci. Catal.*, 1996, **101**, 533.
5 D. G. Barton, S. L. Soled, G. D. Meitzner, G. A. Fuentes and E. Iglesia, *J. Catal.*, 1999, **181**, 57.
6 S. L. Soled, W. E. Gates and E. Iglesia, *US Pat.*, 5422327, 1993.
7 S. L. Soled, W. E. Gates and E. Iglesia, *US Pat.*, 5648589, 1995.
8 C. D. Chang, C. T. Kresge, J. G. Santiesteban and J. C. Vartuli, *US Pat.*, 5510309, 1996.
9 M. Scheithauer, R. E. Jentoft, B. C. Gates and H. Knözinger, *J. Catal.*, 2000, **190**, 271.
10 C. Morterra and G. Cerrato, *Catal. Lett.*, 1996, **41**, 101.
11 S. Rezgui, R. E. Jentoft and B. C. Gates, *Catal. Lett.*, 1998, **51**, 229.

Synthesis and structure of the $[Mn^{IV}(biguanide)_3]^{4+}$ ion: the simplest source for water-stable manganese(IV)

Gopal Das,[a] Parimal K. Bharadwaj,[a] Debjani Ghosh,[b] Beauty Chaudhuri[b] and Rupendranath Banerjee*[b]

[a] *Department of Chemistry, Indian Institute of Technology, Kanpur 208016, India*
[b] *Department of Chemistry, Jadavpur University, Calcutta 700 032, India. E-mail: dsthcr28@cal2.vsnl.net.in*

Received (in Cambridge, UK) 29th August 2000, Accepted 4th January 2001
First published as an Advance Article on the web 1st February 2001

Aqueous oxidation of alkaline biguanide sulfate with $KMnO_4$ followed by crystallisation from 2 M HNO_3 yields the mononuclear $[Mn(bigH)_3]^{4+}$ ion, which has been characterised crystallographically and provides an easy route to mononuclear, water-stable manganese(IV).

In aqueous solution, some oxo-bridged multinuclear manganese(IV) complexes are known to be stable enough for successful study of their solution chemistry.[1] In contrast, none of the limited number of well characterised mononuclear complexes of manganese(IV) have been synthesised from aqueous media or have been reported to be stable in aqueous solution. This situation has considerably limited our knowledge of the aqueous chemistry of manganese(IV), a key species in photosystem II. We report here the synthesis and structural characterisation of a mononuclear complex of manganese(IV) with the ligand biguanide, $NH_2C(=NH)NHC(=NH)NH_2$, (bigH). The crystals grow from 2 M nitric acid and are stable in aqueous solution over a wide range of acidity (10^{-6} to 2 M).

X-Ray structural studies[2] indicate that the complex ion $[Mn(bigH)_3]^{4+}$ contains Mn^{IV} bound to three biguanide ligands (Fig. 1). Structurally the complex comprises of an axially distorted octahedral MnN_6 coordination sphere with axial Mn–N(av.) 1.98 Å and equatorial Mn–N(av.) 1.917 Å. Such Mn–N distances (usual range 1.955–2.052 Å for other Mn^{IV}–N bonds[3]) effectively establish the Mn^{IV} state. The lattice consists of two types of metrically similar but crystallographically distinct $[Mn(bigH)_3]^{4+}$ units with sulfate and nitrate counter anions along with three molecules of water of crystallization. The two monomeric units are held together by hydrogen bonds *via* the sulfato anion, the latter acting as a bridge between the two. The non-bonded N···N interactions are responsible for packing in the structure (Fig. 2) with an average N···N distance of 2.414 Å. There are no significant covalent bonding contacts between the two molecules. An ORTEP[4] drawing of the complex cation with atom numbering scheme is shown in Fig. 1. The average *cis* and *trans* angles at the metal center are 89.548 and 175.085°, respectively. The four nitrogen atoms N(7), N(8), N(15) and N(21) form the equatorial plane and N(1) and N(14) are in axial positions. The Mn atom lies 0.045 Å towards the N(1) atom from the least-squares plane consisting of N(7), N(8), N(15) and N(21) atoms.

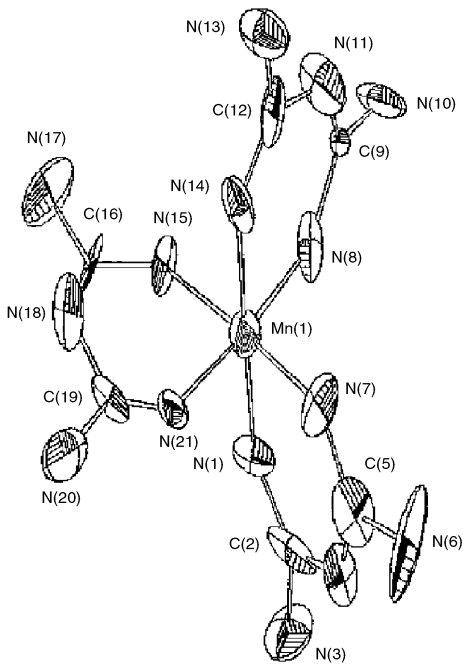

Fig. 1 ORTEP plot and labeling for $[Mn(bigH)_3]^{4+}$. For clarity the hydrogen atoms are not shown. Selected bond lengths (Å) and bond angles (°): Mn(1)–N(1) 1.97(2), Mn(1)–N(7) 1.91(1), Mn(1)–N(8) 1.93(1), Mn(1)–N(14) 1.99(2), Mn(1)–N(15) 1.92(1), Mn(1)–N(21) 1.91(1); N(1)–Mn(1)–N(7) 92.57(6), N(8)–Mn(1)–N(14), 86.22(4), N(15)–Mn(1)–N(21), 84.83(7).

The complex was prepared by a very simple procedure. A solution of $KMnO_4$ (0.158 g, 1.0 mmol in 5 ml water) was added dropwise with stirring to 30 ml of a stirred, ice-cold aqueous solution of $bigH{\cdot}H_2SO_4$ (1.0 g, 5.0 mmol) in NaOH (0.6 g, 15.0 mmol). The resulting deep orange–red solution was nearly neutralised by slow addition of 2–3 mL, 2 M HNO_3 and filtered. The filtrate was acidified to *ca.* 2 M by adding *ca.* 7.5 mL, 12 M HNO_3 and stored overnight at 4 °C. Red crystals suitable for diffraction measurements were collected by filtration. Yield, 0.18 g, (60% based on MnO_4^-). Anal.: calc. (found) for $[Mn(bigH)_3]_2SO_4(NO_3)_6{\cdot}3H_2O$: C, 11.63 (11.3); H 3.88 (3.9); N, 40.71 (39.9)%. UV–VIS (H_2O, pH 2), λ/nm (ε/dm^3 mol^{-1} cm^{-1}) 352 (8942), 430 (8035). Prominant molecular ion peaks (Kratos PC-Kompact MALDI 4 V1.0.3) found at 694.8 $\{[Mn(bigH)_3]SO_4(NO_3)_3{\cdot}3H_2O\}^-$, 585.9 $\{[Mn(bigH)_3]SO_4(NO_3){\cdot}4H_2O\}^+$, 101.7 $\{bigH_2\}^+$, 60 $\{NO_3^-\}$.

The mononuclear structure of the complex appeared somewhat surprising because of the demonstrated tendency of higher-valent manganese complexes for aquation, decomposition and polynucleation in aqueous acids.[2a] It is probably the exceptionally strong basicity of biguanide[5] which discourages the formation of multinuclear oxo-bridged manganese complexes. Hart *et al.*[3] isolated the complex $[Mn^{IV}(big)_3]$-

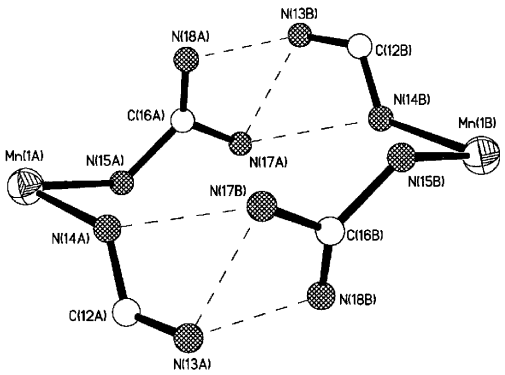

Fig. 2 Non–bonded N···N interactions responsible for packing in the structure.

DOI: 10.1039/b007013k

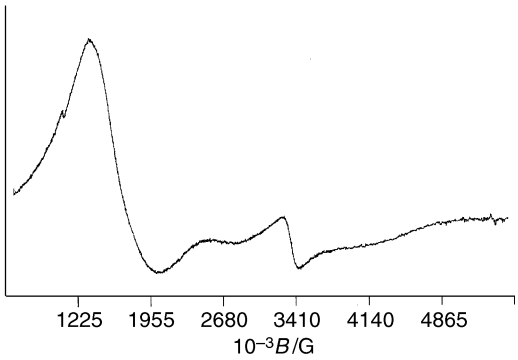

Fig. 3 X-Band EPR spectrum of polycrystalline $[Mn(bigH)_3]^{4+}$ at room temperature.

$(OAc)\cdot 2H_2O$ by the non-aqueous oxidation of Mn^{II} acetate with $NBu^n{}_4MnO_4$ in the presence of bigH in ethanol. They reported no aqueous chemistry for this complex but we found that in water it forms a turbid solution the turbidity of which increased rapidly and a brown precipitate deposited slowly. This is consistent with our earlier kinetic observation[6a] that $[Ag^{III}(bigH)_2]^{3+}$ but not its conjugate base, $[Ag^{III}(big)(bigH)]^{2+}$ survives for an extended period in aqueous solution. An analogous situation was found with $[Ag^{III}\{C_2H_4(bigH)_2\}]$,[6b] $\{[C_2H_4(bigH)_2]$ is tetradentate ethylenebis(biguanide)$\}$. The electron-rich, deprotonated ligands big^- and $[C_2H_4(big)(bigH)]^-$ significantly lower the kinetic barrier to intramolecular redox decomposition forming Ag^+ and oxidation products of the biguanide. Expectedly, a similar redox decomposition is favoured for $[Mn(big)_3]^+$ but not $[Mn(bigH)_3]^{4+}$ in solution in spite of the greater ligand field strength of big^-, as indicated by the fact that both the UV–VIS spectral bands of $[Mn(big)_3]^+$ appear at lower wavelengths than those of $[Mn(bigH)_3]^{4+}$.

The synthetic procedure used for $[Mn(bigH)_3]^{4+}$ failed to produce a stable $[C_2H_4(bigH)_2]$ analogue. The isolated red crystals in this case changed to a nearly colourless solid within hours. The strong-field tetradentate ligand, ethylenebis(biguanide), prefers square-planar coordination and may not be compatible with a d^3 Mn^{IV} system which prefers octahedral geometry. Notably, a square-planar Mn^{III} complex of $[C_2H_4(bigH)_2]$ has been structurally characterised.[7]

In the polycrystalline form **1** exhibits a corrected room-temperature (19 °C) magnetic moment of 3.73 μ_B consistent with a d^3 octahedral complex. Its polycrystalline X-band EPR spetrum (Fig. 3) displays broad resonances at g values (DPPH, g = 2.0037) of *ca.* 2 and 4. The signal at lower field is much more intense and slightly asymmetric with turnover and crossover points at 1550 G (g = 4.3) and 1860 G (g = 3.58). The EPR spectrum fully corresponds to a Mn^{IV} (d^3) ion in octahedral field with axial distortion[8] consistent with the crystal structure. The MnN_6 core in $[Mn(big)_3]^+$ by contrast, is almost undistorted.[3]

The synthesis described here opens an easy route to aqueous stable Mn^{IV} which may be useful for better understanding of the aqueous chemistry of Mn in its +4 state. Presently, the kinetics of $[Mn^{IV}(bigH)_3]^{4+}$ with simple reducing agents in acidic solution are under investigation.

R. B. is grateful to the Department of Science and Technology, New Delhi for sponsoring the research.

Notes and references

1 (*a*) C. Philouze, G. Blondin, J. J. Girerd, J. Guilhem, C. Pascand and D. Lexa, *J. Am. Chem. Soc.*, 1994, **116**, 8557; J. E. Sarneski, H. Didiuk, H. H. Thorp, R. H. Crabtree, G. W. Brudvig, J. W. Faller and G. K. Schulte, *Inorg. Chem.*, 1991, **30**, 2883; (*b*) U. Roychaudhuri, S. Banerjee and R. Banerjee, *J. Chem. Soc., Dalton Trans.*, 2000, 589; (*c*) B. Mondal and R. Banerjee, *Polyhedron*, 2000, **19**, 1213.

2 *Crystal data* for $[Mn(bigH)_3]_2SO_4(NO_3)_6\cdot 3H_2O$; M = 1238.0, monoclinic, space group *Ia*, a = 17.2338(17), b = 15.8698(16), c = 18.3355(18) Å, β = 103.07(1)°, U = 4884.772(46) Å^3, T = 298(1) K, Z = 4, μ(Mo-Kα) = 0.66 mm^{-1}. D_c = 1.6359 Mg m^{-3}. Data were collected (for a crystal of dimensions 0.18 × 0.21 × 0.19 mm) on an Enraf-Nonius CAD4-mach 2 diffractometer and were corrected for Lorentz polarization and decay. The structure was solved by direct methods and refined on F using the full-matrix least squares technique using the XTAL 3.2 program package. The final R, R_w indices were 0.098 and 0.108 and goodness of fit on F^2 was 6.294. Attempts were made to solve the structure in the space group *C*2/*c* but a few atoms including the nitrogen and oxygen of the nitrate anion and water molecules could not be properly located. In addition, a few nitrogen atoms of the chelate ring were also unreliable owing to their high anisotropic thermal parameters leading to high residual electron density which could not be accounted for. CCDC 182/1886. See http://www.rsc.org/suppdata/cc/b0/b007013k/ for crystallographic files in .cif format.

3 R. O. C. Hart, S. G. Bott, J. L. Atwood and S. R. Cooper, *J. Chem. Soc., Chem. Commun.*, 1992, 894.

4 C. K. Johnson, *ORTEPII*, Report ORNL-5138; Oak Ridge National Laboratory: Oak Ridge, TN, 1976.

5 L. Fabbriezi, M. Micheloni, P. Paoletti and G. Schwarzenbach, *J. Am Chem. Soc.*, 1977, **99**, 5574; L. Fabbriezi, M. Micheloni and P. Paoletti, *Inorg. Chem.*, 1978, **17**, 495.

6 (*a*) R. Banerjee, S. Dasgupta and A. Das, *Transition Met. Chem.*, 1989, **14**, 19; (*b*) R. Banerjee and D. Banerjea, *Indian J. Chem. Sect. A*, 1979, **17**, 246.

7 A. De, *Acta Crystallorgr. Sect. C*, 1990, **46**, 1004.

8 S. K. Chandra, P. Basu, D. Ray, S. Pal and A. Chakravorty, *Inorg. Chem.*, 1990, **29**, 2423 and references therein.

ChemComm

Palladium–tetraphosphine catalysed cross coupling of aryl bromides with arylboronic acids: remarkable influence of the nature of the ligand

Marie Feuerstein, Dorothée Laurenti, Céline Bougeant, Henri Doucet* and Maurice Santelli*

Laboratoire de Synthèse Organique associé au CNRS, Faculté des Sciences de Saint Jérôme, Avenue Escardrille Normandie-Niemen, 13397 Marseille Cedex 20, France. E-mail: henri.doucet@lso.u-3mrs.fr, m.santelli@lso.u-3mrs.fr; Fax: 04 91 98 38 65

Received (in Cambridge, UK) 27th November 2000, Accepted 12th January 2001
First published as an Advance Article on the web 31st January 2001

The *cis,cis,cis*-1,2,3,4-Tetrakis(diphenylphosphinomethyl)-cyclopentane–[PdCl(C_3H_5)]$_2$ system catalyses the cross coupling of aryl bromides with arylboronic acids with very high substrate–catalyst ratios in good yields; a turnover number of 28 000 000 can be obtained for the addition of 4-bromobenzophenone to benzeneboronic acid in the presence of this catalyst.

Biaryl compounds are fundamental building blocks in organic synthesis and their preparation is an important industrial goal.[1] The cross coupling reaction is an efficient method for the synthesis of these compounds.[2] The classical method of performing this reaction is to employ aryl halides and organometals containing zinc, magnesium or boron in the presence of palladium catalysts. These palladium complexes are generally associated with the triphenylphosphine ligand.[2] Even if the catalyst formed by association of this ligand with palladium complexes is efficient in terms of yield of adduct, the efficiency in terms of substrate–catalyst ratio is usually low. In general 1–10% of the catalyst must be used. Recently a few bulky monodentate ligands have been successfully used for this reaction.[3] One of the most efficient catalytic systems uses a palladium–phosphite complex. The nature of the phosphite ligand has an important effect on the yield of the reaction, and only hindered phosphites such as P(O-2,4-*t*Bu$_2$C$_6$H$_3$)$_3$ or P(O-*i*Pr)$_3$ are useful ligands.[4] A carbene ligand also leads to the formation of palladium catalysts that are more efficient than those of triphenylphosphine for this reaction. With this complex the reaction can be performed with as little as 0.0004% catalyst.[5] Finally, a very efficient catalyst for this reaction has been prepared with the bulky ligand (*o*-biphenyl)P(*t*-Bu)$_2$.[6] If bulky monodentate ligands have been successfully used for this reaction, to our knowledge, the efficiency of bulky polydentate ligands has not yet been demonstrated.

The nature of the phosphine ligand on complexes has a tremendous influence on the rate of catalysed reactons.[7] In order to find more efficient palladium catalysts we have prepared a new tetrapodal phosphine ligand, *cis,cis,cis*-1,2,3,4-tetrakis(diphenylphosphinomethyl)cyclopentane or Tedicyp **1**[8] (Fig. 1) in which the four diphenylphosphino groups are stereospecifically bound to the same face of the cyclopentane ring. The presence of four phosphines close to the metal centre should increase the coordination of the ligand to the metal centre and therefore increase the stability of the catalyst. We have reported recently the first results obtained in allylic substitution using **1** as ligand.[8] For example, a TON of 680 000 for the addition of dipropylamine to allyl acetate had been observed. In this paper, we wish to report on the superiority of Tedicyp **1** over other diarylphosphines in the cross coupling of arylboronic acid with aryl bromides.

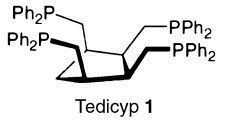

Tedicyp **1**

Fig. 1

First, we tried to evaluate the importance of the presence of phosphine ligands on the complex. So we performed the reaction with [PdCl(C_3H_5)]$_2$ as catalyst in the absence of ligand. We observed that the coupling of 2,4-dimethoxybromobenzene **2** or 3-bromothiophene **3** with benzeneboronic acid **12** in the presence of 4% catalyst led to the biaryl adducts in low yield (Scheme 1 and 2) (Table 1, entries 1 and 2). Next, we tried to evaluate the difference of efficiency between mono, di and polydentate ligands bearing diphenylphosphino groups for this reaction. For this we compared the rate of the reaction in the presence of a monophosphine PPh_3, a diphosphine dppe, and with our tetraphosphine.[9] Addition of 3-bromothiophene **3** to benzeneboronic acid **12** in the presence of 0.0002% catalyst, led to the addition product in 2% conversion when PPh_3 was used as ligand and 61% conversion with dppe (Table 1, entries 3 and 5). With Tedicyp the yield was 91% in the presence of 0.00002% catalyst (substrate–catalyst ratio of 5 000 000) (Table 1 entry 7) and 16% in the presence of 0.0000002% catalyst (Table 1, entry 9). A similar tendency was observed for the addition of 2,4-dimethoxybromobenzene **2** to benzeneboronic acid **12**. In the presence of 0.0002% catalyst, only 2% conversion was observed with PPh_3 (Table 1, entry 4). With Tedicyp, in the presence of 0.00002% catalyst, the conversion was 28% (Table 1, entry 6).

The electronic properties of the ligand are certainly of importance for this reaction, as most triarylphosphines are not sufficiently electron-rich to promote a fast oxidative addition of aryl bromides.[2] However, previous studies have shown that electron-rich trialkylphosphines such as PCy_3 are also rather inefficient ligands for this reaction.[10] In contrast *t*-Bu$_2$P(biphenyl) is an effective ligand for the Suzuki coupling.[6] Although electron-rich ligands such as P(Cy)$_3$ facilitate oxidative addition, they also decrease the rate of the reductive elimination process. These observations indicate that the combination of both steric bulk and electronics is important. The complex formed by association of Tedicyp and [PdCl(C_3H_5)]$_2$ seems to possess a fine balance of steric and electronic properties, which allow a fast catalytic process.

Next we tried to evaluate the scope and limitations of the Tedicyp–palladium complex for this reaction. A survey of

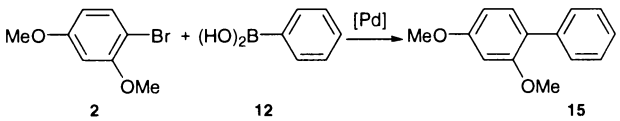

2 **12** **15**

Scheme 1

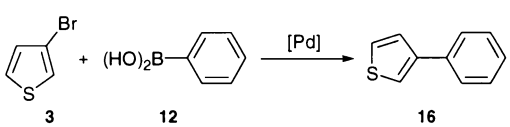

3 **12** **16**

Scheme 2

DOI: 10.1039/b009520f

Table 1 Palladium-catalysed cross-coupling with **12**: influence of the ligand

Entry	Substrate	Ligand	*T*/h	Substrate–catalyst ratio	Yield (%)
1	3-Bromothiophene	No ligand	24	25	33
2	2,4-Dimethoxybromobenzene	No ligand	48	25	16
3	3-Bromothiophene	PPh_3	96	500 000	2
4	2,4-Dimethoxybromobenzene	PPh_3	24	500 000	2
5	3-Bromothiophene	dppe	24	500 000	61
6	2,4-Dimethoxybromobenzene	**1**	20	5 000 000	28
7	3-Bromothiophene	**1**	24	5 000 000	91
8	3-Bromothiophene	**1**	20	100 000 000	34
9	3-Bromothiophene	**1**	24	500 000 000	16

Conditions: catalyst $[Pd(C_3H_5)Cl]_2$/ligand 1/1; 3-bromothiophene 1 eq.; benzeneboronic acid **12** 1.5 eq.; K_2CO_3 2 eq.; 130 °C; xylene.

catalytic cross coupling of aryl bromides with arylboronic acids is provided in Table 2. A wide variety of functional groups are tolerated. Coupling of 4-bromoanisole **4**, 4-bromophenol **5**, 4-bromobenzaldehyde **6**, 4-bromoacetophenone **7** and 4-bromobenzophenone **8** with benzeneboronic acid **12** in the presence of 0.00001% of Tedicyp–palladium complex led to the coupling products in 25, 74, 15, 96 and 98% yields, respectively. A turnover number of 28 000 000 has been obtained for the addition of 4-bromobenzophenone **8** to benzeneboronic acid **12**. Lower TON were observed in the course of the coupling of 1-bromo-4-nitrobenzene **9** and 4-bromo-*N*,*N*-dimethylaniline **10** with **12**. Coupling of 4-bromoacetophenone **7** with the substituted 4-fluorobenzeneboronic acid **13** and 4-methoxybenzeneboronic acid **14**, in the presence of 0.0001% catalyst, led to the coupling products **25** and **26** in 97% and 80% yield (Scheme 3). When we used 3-bromopyridine **11** in the presence of 0.0001% catalyst a complete conversion was observed for the coupling with benzeneboronic acid **12**. Turnover numbers of 75 000 and 96 000 have also been obtained for the coupling of 3-bromopyridine **11** with 4-methoxybenzeneboronic acid **14** and 4-fluorobenzeneboronic acid **13** respectively (Scheme 4). These results seem to indicate that in general electron-poor aryl bromides can be reacted at higher TON than electron-rich aryl bromides. In contrast, substituents on the arylboronic acid seem to have a minor effect. In all cases, only traces (< 1%) of homocoupling products were observed with this catalyst. The best results were usually obtained with K_2CO_3 as base in toluene or xylene as solvents. Use of biphasic solvent systems generally gave inferior results compared to reactions run without added water.

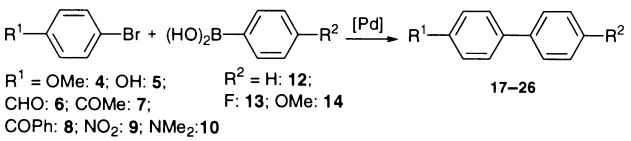

Scheme 3

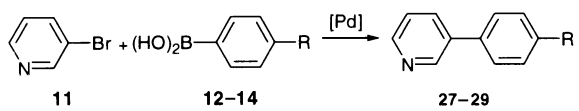

Scheme 4

In conclusion, the use of the tetradentate ligand Tedicyp associated with a palladium complex provides a convenient catalyst for the cross coupling of aryl bromides with arylboronic acids. This catalyst is much more efficient than the complex formed with the triphenylphosphine ligand. This efficiency probably comes from the presence of the four diphenylphosphinoalkyl groups stereospecifically bound to the same face of the cyclopentane ring which probably increases the coordination of the ligand to the metal and presents precipitation of the catalyst. The complex seems also to possess a fine balance of steric and electronic properties which allow a fast catalytic process. The reaction can be performed with as little as 0.000005% catalyst without further optimisation of the reaction conditions. These results represent an inexpensive, efficient, and environmentally friendly synthesis.

Table 2 Tedicyp–Pd catalysed cross-coupling[11]

Aryl bromide	Boronic acid	Product	Substrate–catalyst ratio	Yield (%)
4	**12**	**17**	100 000	93[a]
			10 000 000	25[f]
5	**12**	**18**	1 000 000	98[b]
			10 000 000	74[a]
6	**12**	**19**	10 000 000	15[d]
7	**12**	**20**	10 000 000	96[f]
8	**12**	**21**	10 000 000	98[c]
			100 000 000	28[a]
9	**12**	**22**	100 000	26[b]
10	**12**	**23**	100 000	92[a]
5	**13**	**24**	20 000 000	95[a]
7	**13**	**25**	1 000 000	97[e]
7	**14**	**26**	1 000 000	80[a]
11	**12**	**27**	1 000 000	98[e]
11	**13**	**28**	100 000	96[d]
11	**14**	**29**	100 000	75[d]

Conditions: catalyst see ref. 9; ArX 1 eq; $ArB(OH)_2$ 1.5 eq.; K_2CO_3 2 eq.; xylene; 130 °C.
[a] 24 h, [b] 48 h, [c] 72 h, [d] 90 h, [e] 115 h, [f] 135 h.

We thank the CNRS for providing financial support.

Notes and references

1 For a review on biaryl synthesis: S. Stanforth, *Tetrahedron*, 1998, **54**, 263.
2 For reviews on the cross coupling of aryl bromides with arylboronic acids: (*a*) A. Suzuki, *Metal-catalysed cross-coupling reaction*, ed. F. Diederich and P. J. Stang, Wiley, New York, 1998; (*b*) J.-L. Malleron, J.-C. Fiaud and J.-Y. Legros, *Handbook of palladium catalysed organic reactions*, Academic Press, San Diego, 1997; (*c*) N. Miyaura and A. Suzuki, *Chem. Rev.*, 1995, **95**, 2457.
3 (*a*) M. Beller, H. Fischer, A. Herrmann, K. Ôfele and C. Brossmer, *Angew. Chem., Int. Ed. Engl.*, 1995, **34**, 1848; (*b*) D. A. Albisson, R. B. Bedford, S. E. Lawrence and P. N. Scully, *Chem. Commun.*, 1998, 2095.
4 A. Zapf and M. Beller, *Chem. Eur. J.*, 2000, **6**, 1830.
5 D. McGuiness and K. Cavell, *Organometallics*, 2000, **19**, 741.
6 (*a*) J. Wolfe, R. Singer, B. Yang and S. Buchwald, *J. Am. Chem. Soc.*, 1999, **121**, 9550; (*b*) J. Wolfe and S. Buchwald, *Angew. Chem., Int. Ed.*, 1999, **38**, 2413.
7 C. Bianchini, H. M. Lee, A. Meli, W. Oberhauser, F. Vizza, P. Brüggeller, R. Haid and C. Langes, *Chem. Commun.*, 2000, 777.
8 M. Feuerstein, D. Laurenti, H. Doucet and M. Santelli, *Chem. Commun.*, 2001, 43.
9 For the preparation of the catalyst see D. Laurenti, M. Feurstein, G. Pèpe, H. Doucet and M. Santelli, *J. Org. Chem.*, in press.
10 W. Shen, *Tetrahedron Lett.*, 1997, **38**, 5575.
11 As a typical experiment, the reaction of 4-bromoacetophenone **7** (1.03 g, 5.2 mmol), benzeneboronic acid **12** (0.92 g, 7.6 mmol) and K_2CO_3 (1.38 g, 10 mmol) at 130 °C for 24 h in dry xylene (10 mL) in the presence of *cis*,*cis*,*cis*-1,2,3,4-tetrakis(diphenylphosphinomethyl)cyclopentane–$[PdCl(C_3H_5)]_2$ complex ($5.2\ 10^{-7}$ mmol) under argon affords the corresponding biaryl adduct **20** after evaporation and filtration on silica gel in 96% (0.98 g) isolated yield.

Synthesis and structure of [{$Sn_4(NBu^t)_3P$}{$Sn_4(NBu^t)_3(OSiMe_3)$}]; a low-oxidation state p-block metal complex containing a P^{3-} anion

Marta E. G. Mosquera,*[a] Alexander D. Hopkins,[b] Paul R. Raithby,[b] Alexander Steiner,[c] Alexander Rothenberger,[b] Anthony D. Woods[b] and Dominic S. Wright*[b]

[a] *Departmento de Química Orgánica e Inorgánica, Universidad de Oviedo, 33071 Oviedo, Spain. E-mail: megm@sauron.quimica.uniovi.es*
[b] *Chemistry Department, University of Cambridge, Cambridge, UK CB2 1EW. E-mail: dsw1000@cus.cam.ac.uk*
[c] *Chemistry Department, University of Liverpool, Liverpool, UK L69 3BX*

Received (in Cambridge, UK) 9th October 2000, Accepted 14th December 2000
First published as an Advance Article on the web 1st February 2001

The complex [{$Sn_4(NBu^t)_3P$}{$Sn_4(NBu^t)_3(OSiMe_3)$}] 1 is the first example of a low-oxdation state p-block metal complex containing a P^{3-} anion.

In contrast to transition metal complexes containing bare P^{3-} ions,[1] the analogous complexes of the heaviest (most metallic) p-block elements have been almost unexplored.[2] Among the very few complexes of this type so far structurally characterised are $[(Cp^*Al)_6P_4]$,[2e] $[\{(Me_3Si)_3CGa\}_3P_4]$[2f] and $[\{Me_2Sn\}_nP_2]$ (n = 5[2b] or 6[2c]), all of which contain the Group 13 and 14 elements in their highest oxidation states (*i.e.* corresponding to the formal loss of the valence s and p electrons). Two of the main synthetic strategies used to generate these species are the reactions of high-oxidation state organometallic dihydrides with P_4[2b,c] or oxidative addition of low-oxidation state organometallics with P_4.[2e,f] Norman and coworkers recently showed that the binary Group 15 phosphides EP (E = Sb, Bi) can be generated by the reactions of $E(NMe_2)_3$ with $P(SiMe_3)_3$,[3] a process which is driven thermodynamically by the formation of Si–N bonds. However, although the related reactions of transition metal halides with trimethylsilyl phosphines have been used to generate molecular transition metal phosphides,[1i,j] neither this reaction nor reactions involving amides or imides have previously been used in the generation of molecular main group metal species containing the P^{3-} anion.[4] Our interest in the synthesis and coordination chemistry of Sn^{II} oxo cubanes such as $[Sn_4(NBu^t)_3O]$[5,6] led us to investigate new approaches to the isoelectronic Group 15 anions $[Sn_4(NR)_3E]^-$ (E = N, P). Herein we report the synthesis and structure of [{$Sn_4(NBu^t)_3P$}{$Sn_4(NBu^t)_3(OSiMe_3)$}], a Sn^{II} phosphide which formally contains a $[Sn_4(NBu^t)_3P]^-$ anion.

The reaction of $[SnNBu^t]_4$ (1 equiv.) with an excess of $P(SiMe_3)_3$ in THF–$PhCH_3$ was undertaken initially in order to obtain the substituted cubane $[Sn_4(NBu^t)_3(PSiMe_3)]$ [*via* elimination of $Bu^tN(SiMe_3)_2$]. However, unexpectedly the title complex [{$Sn_4(NBu^t)_3P$}{$Sn_4(NBu^t)_3(OSiMe_3)$}] **1** was obtained as the only isolable crystalline product (in low yield). The incorporation of the O centre within the $OSiMe_3$ group of **1** was confirmed by the subsequent structural characterisation of the complex, and is supported by the observation of a Si–O stretching band in the IR spectrum at 1175 cm^{-1}.[7] The low solubility of the complex once isolated precluded more extensive investigations of its solution structure. However, the observation of only two Bu^t resonances in the ^1H NMR spectrum of **1** (δ 1.15 and 1.11) suggests that the behaviour of the complex in solution is far from simple. The likely pathway to **1** involves the addition reaction of $[Sn_4(NBu^t)_3(PSiMe_3)]$ and the oxo cubane $[Sn_4(NBu^t)_3O]$ (as depicted in Scheme 1). It was assumed that the latter species arose from trace hydrolysis of the imido Sn^{II} cubane $[SnNBu^t]_4$ during storage of the reaction mixture; a previously established route to the oxo cubane.[6] This view is supported by the isolation of **1** from the reaction of $[SnNBu^t]_4$ (1 equiv.) and an excess of $P(SiMe_3)_3$, followed by addition of $[Sn_4(NBu^t)_3O]$ (1 equiv.).† Significantly, attempts

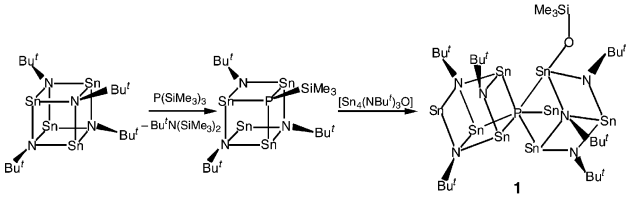

Scheme 1

to prepare the complex by reaction of $[Sn_4(NBu^t)_3O]$ (2 equiv.) with $P(SiMe_3)_3$ (1 equiv.) failed to produce **1**, indicating that the imido cubane $[SnNBu^t]_4$ is involved in the initial step.

The X-Ray crystallographic study of **1** shows that molecules of the complex consist of a pseudo 'double-cubane' $Sn_8(NBu^t)_6P$ core (Fig. 1),‡ in which the two $Sn_4(NBu^t)_3$ cubane subunits are linked together by a P^{3-} ion. Although other Group 13 and 14 metal complexes containing the P^{3-} ion have been structurally characterised,[2] **1** is the first example in

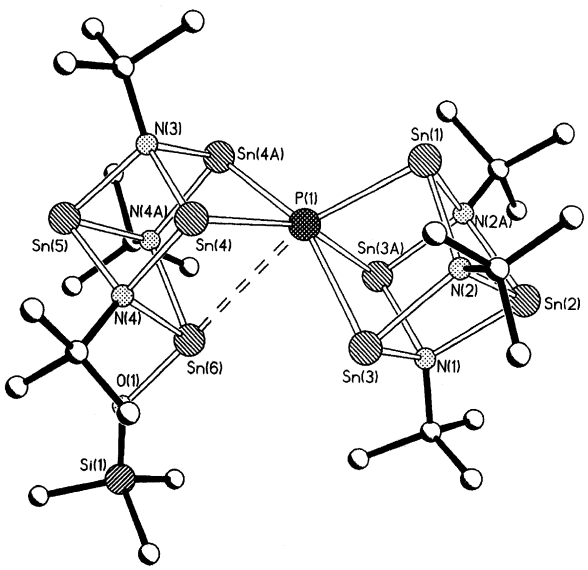

Fig. 1 The cage structure of **1**. H-atoms have been omitted for clarity. Key bond lengths (Å) and angles (°): Sn(1)–P(1) 2.580(4), Sn(1)–N(2) 2.219(7), Sn(1)–N(2) 2.219(8), Sn(2)–N(1) 2.20(1), Sn(2)–N(2,2A) 2.219(8), Sn(3)–P(1) 2.725(3), Sn(3)–N(1) 2.207(6), Sn(3)–N(2) 2.235(7), Sn(4)–P(1) 2.630(3), Sn(4)–N(3) 2.198(7), Sn(4)–N(4) 2.177(7), Sn(5)–N(3) 2.22(1), Sn(5)–N(4,4A) 2.187(7), Sn(6)···P(1) 3.298(4), Sn(6)–N(4) 2.265(8), Sn(6)–N(4A) 2.265(7), Sn(6)–O(1) 1.981(9), Si(1)–O(1) 1.64(1); Sn–N–Sn range 96.9(3)–107.0(3), N–Sn–N range 78.1(3)–81.4(3), N–Sn–P range 82.2(2)–98.3(2), Sn(1)–P(1)–Sn(3) 84.8(1), Sn(1)–P(1)–Sn(4) 118.0(1), Sn(2)–P(1)–Sn(3) 98.8(3), Sn(3)–P(1)–Sn(3A) 101.3(4), Sn(3)–P(1)–Sn(4) 94.70(5), Sn(3)–P(1)–Sn(4A) 155.4(2), Sn(4)–P(1)–Sn(4A) 82.7(1), N(4)–Sn(6)–O(1) 99.8(3), Sn(6)–O(1)–Si(1) 140.5(7).

DOI: 10.1039/b008108f

which the p-block metal is in a low-oxidation state (*i.e.* in which the metal lone-pair of electrons is retained).

Although they occur over fairly broad ranges, the Sn–N bond lengths [2.177(7)–2.265(8) Å] and Sn–N–Sn [96.9(3)–107.0(3)°] and N–Sn–N [78.1(3)–81.4(3)°] angles in **1** are similar to those found in structurally characterised imido Sn(II) cubanes of the type $[SnNR]_4$ [*cf.* Sn–N range 2.15(1)–2.34(2) Å, Sn–N–Sn mean 98.4°, N–Sn–N mean 81.9°].[5,8] An unusual feature of **1** is the distorted six-coordinate geometry of the P^{3-} centre. The five Sn–P bonds involved with Sn(1) [2.580(4) Å], Sn(3,3A) [2.725(3) Å] and Sn(4,4A) [2.630(3) Å] fall within the range previously reported for bonds between anionic (R_2P^- and RP^{2-}) P centres and Sn^{II} (2.60–2.80 Å).[9,10] However, the remaining contact with the chemically distinct tin centre Sn(6) [3.298(3) Å] {which is bonded to the O centre of an Me_3SiO group [Sn–O 1.981(9) Å][11]} is clearly much weaker, and is around the value which could be estimated for that between a neutral phosphine (R_3P) and Sn^{II}.[10] The weakness of this contact is consistent with the absence of a vacant p orbital on Sn(6) and the apparent orientation of the metal lone pair towards the core of **1**. The coordination number of the Sn(II) centre and range of Sn–P distances in **1** are similar to that found in the NaCl-type lattice structure of tetragonal SnP [with Sn–P bond lengths of 2.55(6), 2.74(1) and 3.41(1) Å].[12] However, the bonding pattern in **1** is markedly different to that found in all previously reported molecular p-block metal compounds containing P^{3-} anions, which have three-coordinate P atoms and electron-precise metal–P bonding.[2] Two bonding schemes may be used to rationalise the Sn_6P unit in **1**. Although the description of the structure of **1** as a donor complex of the $[Sn_4(NBu^t)_3P]^-$ anion and a $[Sn_4(NBu^t)_3(OSiMe_3)]^+$ fragment is an attractive one [*i.e.* containing a 2e–3c bond between P(1) and Sn(4) and (4A)], a model involving a 2e–3c bond with Sn(3) and Sn(3A) appears to be most consistent with the variation of the Sn–P bond lengths in the complex.

In conclusion, the first low-oxidation state p-block metal complex containing a P^{3-} anion has been prepared. The synthetic route used in its preparation ('silyl/imido elimination') exemplifies a new, potentially broad-ranging approach to a variety of molecular main group as well as transition metal species containing 'bare' P centres.

We gratefully acknowledge the EPSRC (P. R. R., A. S., A. R., A. D. W., D. S. W.), the E.U. (M. E. G. M.), The DGES and The British Council (M. E. G. M., D. S. W.), Gottlieb Daimler-und Karl Benz-Stiftung (A. R.) and Churchill College (Fellowship for A. D. H.) for financial support.

Notes and references

† *Synthesis of* **1**: $[SnNBu^t]_4$ (0.42 mmol) was prepared *in situ* by reaction of Bu^tNH_2 (0.18 mL, 1.70 mmol) with $Sn(NMe_2)_2$ (0.35 g, 1.70 mmol) in $PhCH_3$ (15 mL). The reaction mixture was brought to reflux briefly and stirred (2 h), to give a bright yellow solution. To this solution was added $P(SiMe_3)_3$ (0.42 mL, 1.45 mmol, excess) at room temperature. Immediately, a solution of $[Sn_4(NBu^t)_3O]$ (0.44 mmol) in THF (10 mL) was added. Stirring at room temperature (20 min) produced a deep red solution. Filtration followed by reduction of the solvent under vacuum (to *ca.* 3 mL) and storage (18 °C, 3 d) gave deep red cubic crystals of **1**. These were washed with Et_2O (2 × 5 mL) prior to analysis. Yield 0.090g (14%). Decomp. 153 °C to black solid. IR (Nujol mull), ν_{max}/cm^{-1} 1355m, 1250m, 1237w, 1175s (Si–O str.), 1092s, 1021s, 937m, 916m, 899w, 871w, 822s(sh), 801vs (air exposure led to a gradual loss of the bands at 1175, 937, 916, 899 and 822 cm^{-1} and to a change in color from red to yellow). ^{1}H NMR (+25 °C, 400.132 MHz, [D$_8$]-THF): δ = 1.15 (s, 18H, Bu^tN), 1.11 (s, 36H, Bu^tN), 0.11 (s, 9H, Me_3Si). ^{31}P NMR (+25 °C, 161.976 MHz, [D$_8$]-THF): δ = ×245.0 (s, poorly resolved shoulders). Anal. Found: C, 21.7; H, 4.2; N 5.4. Calc.: C 21.7; H, 4.2; N, 5.6%.

‡ *Crystal data* for **1**; $C_{27}H_{63}N_6OPSiSn_8$, M = 1496.42, monoclinic, space group *Cm*, Z = 2, a = 13.453(3), b = 15.280(3), c = 12.736(3)Å, β = 116.00(3)°, V = 2353.1(8) Å^3, D_c = 2.109 Mg m^{-3}, μ(Mo–Kα) = 4.257 mm^{-1}, T = 220(2) K. Data were collected on a Nonius Kappa CCD diffractometer. Of a total of 10543 refections collected, 5244 reflections were independent (R_{int} = 0.021). The structure was solved by direct methods and refined by full-matrix least squares on F^2. Final $R1$ = 0.043 [for 4605 reflections $I > 2\sigma(I)$] and $wR2$ = 0.193 (all data).[13] CCDC 182/1887. See http://www.rsc.org/suppdata/cc/b0/b008108f/ for crystallographic files in. cif format.

1 (*a*) J. L. Vidal, W. E. Weller, R. L. Prütt and R. C. Schöning, *Inorg. Chem.*, 1979, **18**, 129; (*b*) S. A. MacLaughlin, N. J. Taylor and A. J. Carty, *Inorg. Chem.*, 1983, **22**, 1409; (*c*) S. B. Colbran, C. M. Hay, B. F. G. Johnson, F. Lahoz, J. Lewis and P. R. Raithby, *J. Chem. Soc., Chem. Commun.*, 1986, 1766; (*d*) L. M. Bullock, J. S. Field, R. J. Haines, E. Minshall, D. N. Smit and G. M. Sheldrick, *J. Organomet. Chem.*, 1986, **310**, C47; (*e*) H. Lang, G. Huttner, L. Zsolnai, G. Mohr, B. Sigwarth, U. Weber, O. Orama and I. Jibrile, *J. Organomet. Chem.*, 1986, **304**, 157; (*f*) S. B. Colbran, F. J. Lahoz, P. R. Raithby, J. Lewis, B. F. G. Johnson and C. J. Cardin, *J. Chem. Soc. Dalton Trans.*, 1988, 173; (*g*) H. Beruda, E. Zeller and H. Schmidbaur, *Chem. Ber.*, 1993, **126**, 2037; (*h*) P. L. Sunick, P. S. White and C. K. Schauer, *Inorg. Chem.*, 1993, **32**, 5665; (*i*) A. Eichofer, D. Fenske and W. Holstein, *Angew. Chem.*, 1993, **105**, 257; *Angew. Chem., Int. Ed. Engl.*, 1993, **32**, 242; (*j*) D. Fenske and F. Simon, *Angew. Chem.*, 1997, **109**, 240; D. Fenske and F. Simon, *Angew. Chem., Int. Ed. Engl.*, 1997, **36**, 230; (*k*) R. E. Bachman and H. Schmidbaur, *Inorg. Chem.*, 1996, **35**, 1399.

2 (*a*) A. R. Dahl, A. D. Norman, H. Shenav and R. Schaeffer, *J. Am. Chem. Soc.*, 1975, **97**, 6364; (*b*) B. Mathiasch and M. Dräger, *Angew. Chem.*, 1978, **90**, 814; B. Mathiasch and M. Dräger, *Angew. Chem., Int. Ed. Engl.*, 1978, **17**, 767; (*c*) M. Dräger and B. Mathiasch, *Angew. Chem.*, 1981, **93**, 1079; M. Dräger and B. Mathiasch, *Angew. Chem., Int. Ed. Engl.*, 1981, **20**, 1029; (*d*) M. Veith, M. Grosser and V. Huch, *Z. Anorg. Allg. Chem.*, 1984, **513**, 89; (*e*) C. Dohmeier, H. Schnöckel, C. Robl, U. Schneider and R. Ahlrichs, *Angew. Chem.*, 1994, **106**, 225; *Angew. Chem., Int. Ed. Engl.*, 1994, **33**, 199; (*f*) W. Uhl and M. Benter, *Chem. Commun.*, 1999, 771.

3 C. J. Carmalt, A. H. Cowley, A. L. Hector, N. C. Norman and I. P. Parkin, *J. Chem. Soc., Chem. Commun.*, 1994, 1987; G. C. Allen, C. J. Carmalt, A. H. Cowley, A. L. Hector, S. Kamepalli, Y. G. Lawson, N. C. Norman, I. P. Parkin and L. K. Pickard, *Chem. Mater.*, 1997, **9**, 1385.

4 Reactions of Group 12 (Zn, Cd) silylamides with $P(SiPh_3)_3$ have been used in the synthesis of metal–$P(SiPh_3)_2$ complexes, see M. A. Matchett, M. Y. Cheing and W. E. Buhro, *Inorg. Chem.*, 1994, **33**, 1109.

5 M. Veith and G. Schlemmer, *Chem. Ber.*, 1982, **115**, 2141.

6 (*a*) G. Galan, J. S. Palmer, M. E. G. Mosquera, P. R. Raithby and D. S. Wright, *J. Chem. Soc., Dalton Trans.*, 1999, 1043; (*b*) C. Brown, M. E. G. Mosquera, J. S. Palmer, P. R. Raithby, A. Steiner and D. S. Wright, *J. Chem. Soc., Dalton Trans.*, 2000, 479.

7 Si–O stretching bands are normally found in the range 800–1100 cm^{-1}.

8 M. Veith and M. Grosser, *Z. Naturforsch., Teil B*, 1982, **37**, 1375; M. Veith and O. Recktenwald, *Z. Naturforsch., Teil B*, 1983, **38**, 1054; W. J. Grigsby, T. Hascall, J. J. Ellison, M. M. Olmstead and P. P. Power, *Inorg. Chem.*, 1996, **35**, 3254; H. Chen, R. A. Barlett, H. V. R. Dias, M. M. Olmstead and P. P. Power, *Inorg. Chem.*, 1991, **30**, 3390; M. A. Beswick, R. E. Allan, M. A. Paver, P. R. Raithby, M.-A. Rennie and D. S. Wright, *J. Chem. Soc., Dalton Trans.*, 1995, 1991.

9 For example, see A. M. Arif, A. H. Cowley, R. A. Jones and J. M. Power, *J. Chem. Soc., Chem. Commun.*, 1986, 1446; R. E. Allan, M. A. Beswick, N. L. Cromhoult, M. A. Paver, P. R. Raithby, A. Steiner, M. Trevithick and D. S. Wright, *Chem. Commun.*, 1996, 1501; M. Westerhausen, M. Krofta, N. Wiberg, H. Nöth and A. Pfitzner, *Z. Naturforsch., Teil B*, 1998, **53**, 1489; M. Driess, S. Martin, K. M. Grützmacher, V. Pintchouk, H. Pritzkow, H. Grutzmacher and M. Kaupp, *Angew. Chem.*, 1997, **109**, 1982; M. Driess, S. Martin, K. M. Grützmacher, V. Pintchouk, H. Pritzkow, H. Grutzmacher and M. Kaupp, *Angew. Chem., Int. Ed. Engl.*, 1997, **36**, 1894.

10 Search of the Cambridge Crystallographic Data Base: Sn–P mean 2.627 Å, Sn(IV)–P(anionic) 2.50–2.60 Å, Sn(II)–P(anionic) 2.60–2.80 Å (like the examples in ref. 9), Sn(V)–P(neutral) 2.90–3.10 Å.

11 Si–O bond lengths of *ca.* 1.90–2.00 Å are typical of terminal Si–O–Sn(II,IV) units, *e.g.* see M. Veith, C. Mathur and V. Huch, *J. Chem. Soc., Dalton Trans.*, 1997, 995.

12 P. C. Donohue, *Inorg. Chem.*, 1970, **9**, 335.

13 SHELXL 97, Programme for structural refinement, G. M. Sheldrick, University of Göttingen, Germany, 1997.

$B(C_6F_5)_3$ as a C_6F_5 transfer reagent in zirconium chemistry: facile formation of the borole-bridged triple-decker complex $[Zr_2Cp''_2(C_6F_5)_2\{\mu\text{-}\eta^5:\eta^5\text{-}C_4H_4BCH_2\text{-}\eta^3,\kappa F\text{-}CHCHCHB(C_6F_5)_3\}]$

Timothy J. Woodman,[a] Mark Thornton-Pett[b] and Manfred Bochmann*[a]

[a] *School of Chemical Sciences, University of East Anglia, Norwich, UK NR4 7TJ. E-mail: m.bochmann@uea.ac.uk*
[b] *School of Chemistry, University of Leeds, Leeds, UK LS2 9JT*

Received (in Cambridge, UK) 8th November 2000, Accepted 5th January 2001
First published as an Advance Article on the web 1st February 2001

Warming mixtures of $(Cp^R)Zr(\eta^3\text{-}C_4H_7)(\eta^4\text{-}C_4H_6)$ and $B(C_6F_5)_3$ leads to complete transfer of all three C_6F_5 substituents of a $B(C_6F_5)_3$ molecule to give borole-bridged triple-decker complexes with a Zr_2C_4B core, a zwitterionic structure and an unusually strong Zr–F donor interaction.

Early transition complexes of the borole dianion $[C_4H_4BR]^{2-}$ have attracted attention as potential alkene polymerisation catalysts.[1] Two general synthetic strategies have been employed: the dehydrogenation of 2,5-dihydo-1*H*-boroles with various transition metal compounds,[2] or the reaction of metal halides with a pre-formed borole dianion.[3] We found recently that zirconium 1,3-diene complexes $(Cp^R)Zr(\eta^3\text{-allyl})(\eta^4\text{-diene})$ **1** react with $B(C_6F_5)_3$ *via* C–H activation and C_6F_5 transfer steps to give boryldiene compounds **2**;[4,5] for Cp^R = 1,3-$C_5H_3(SiMe_3)_2$ **2a**, this decomposes further under carefully controlled conditions (prolonged storage at 5 °C) *via* another C–H activation step to give the pentafluorophenylborole complex **3** (Scheme 1).[6] We now report a similar reaction sequence leading to the unexpected formation of zirconium triple-decker complexes **4** containing a novel *ansa*borole-allyl ligand.

Warming an equimolar mixture of $B(C_6F_5)_3$ and $Zr(\eta^3\text{-}C_4H_7)(\eta^4\text{-}1,3\text{-butadiene})Cp''$ [Cp″ = 1,3-$C_5H_3(SiMe_3)_2$] to 50 °C for 2 h gave a red solution which did not contain the expected **3** but a new product **4a** in high yield. Removal of the volatiles and recrystallisation from diethyl ether provided a red crystalline solid, identified as the triple-decker zirconium complex $Zr_2Cp''_2(C_6F_5)_2\{\mu\text{-}\eta^5:\eta^5\text{-}C_4H_4BCH_2\text{-}\eta^3,\kappa F\text{-}CHCHCHB(C_6F_5)_3\}\cdot 2Et_2O$ (**4a**·2Et$_2$O).† Formation of this product involves complete transfer of all three C_6F_5 substituents of one $B(C_6F_5)_3$ molecule, with C–H activation and loss of one C_6F_5 group as pentafluorobenzene. The role of the boryldiene complex **2a** as a reaction intermediate is supported by the formation of the same product from isolated **2a**.

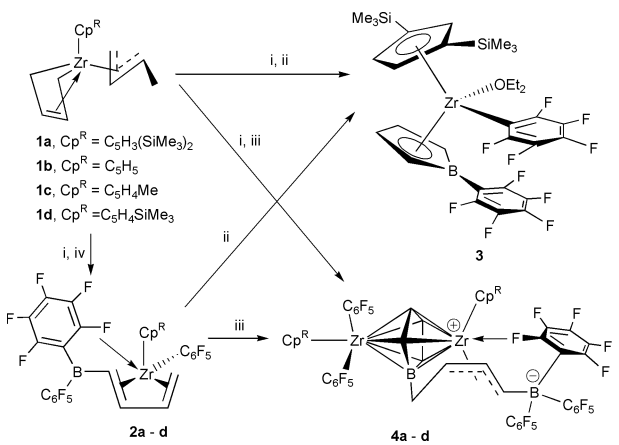

Scheme 1 *Reagents and conditions*: i, $B(C_6F_5)_3$; ii, $-C_6F_5H$, toluene, 5 °C, 4 weeks, followed by addition of Et_2O; iii, $-C_6F_5H$, toluene, 50 °C, 2 h; iv, toluene, room temperature, reduced pressure, 2 h, $-C_4H_8$.

The ambient temperature ^{19}F NMR spectrum features a signal at δ −217.2 indicative of coordination of one of the *o*-F atoms of the formally anionic butenyl–$B(C_6F_5)_3$ moiety to the metal centre. Signal broadening due to *o*-F exchange is observed on heating to 70 °C. Similar evidence of *o*-F coordination is seen in the zwitterionic complex $Cp_2Zr(\eta^3\text{-}CH_2CHCHCH_2B(C_6F_5)_3]$[7] ($\delta$ −213.2), although in this case cooling to −86 °C was required to reach the slow exchange limit. Evidently the Zr···F interaction in **4a** is significantly stronger. The ^{11}B NMR spectrum shows two signals, one extremely broad peak at δ *ca*. 3 (borole-B) and a sharp peak at δ −12.8 for the butenyl–$B(C_6F_5)_3$ moiety. The borole is low-field shifted by *ca*. 20–30 ppm compared with other alkyl–borole systems,[8] probably due to the bridging nature of the ligand.

The structure of **4a** was confirmed by single crystal X-ray diffraction (Fig. 1).‡ The most striking feature of the structure is the bridging borole ligand, the boron atom of which is derived from $B(C_6F_5)_3$ that has lost all three C_6F_5 substituents. The boron is instead bonded to the butenylborate unit which in turn is η^3-bonded to Zr(1). This Zr atom is further coordinated to an *o*-F atom of the butenylborate ligand. The coordination sphere of the second metal centre Zr(2) is completed by a Cp″ and two C_6F_5 ligands.

There is little difference in the bonding distances of the two zirconium atoms with regard to the borole ring, with an average Zr–C length of 2.522(5) Å for Zr(1) and 2.521(5) Å for Zr(2). The Zr–B distances do differ however, with Zr(1)–B(1) of 2.534(6) Å and Zr(2)–B(1) of 2.609(6) Å; this is most probably due to the distortion imposed by the coordination of the allylic fragment to Zr(1). For the related borole complex $Cp''Zr(C_6F_5)\text{-}(\eta^5\text{-}C_4H_4BC_6F_5)\cdot OEt_2$[6] the Zr–C distances are shorter (average Zr–C of 2.455 Å). The Zr–F distance of 2.355(3) Å is significantly shorter than Zr···F interactions in comparable complexes, for example $[NEt_4]_2[\{C_5H_4B(C_6F_5)_3\}Zr(\mu\text{-}Cl)Cl_2]_2$ [2.430(2) Å],[9] $Cp''Zr(C_6F_5)\{\eta^4\text{-}C_4H_5B(C_6F_5)_2\}$ [2.441(7) Å],[4d] and $Cp_2Zr\{\eta^3\text{-}C_4H_6B(C_6F_5)_3\}$ [2.423(3) Å].[7] This is a reflection of the strength of this interaction, in agreement with the ^{19}F NMR evidence.

The reaction leading to **4a** is remarkable in several respects. Although triple-decker complexes involving a central borole ligand have been reported,[10–13] **4a** is the first example containing a group 4 metal. $B(C_6F_5)_3$, widely used as an activator for metallocene polymerisation catalysts because of its chemical stability,[14] acts here as a boron source after loss of all three of its C_6F_5 groups. The decomposition pathways of the boryldiene system **2a** are evidently strongly temperature dependent and are diverted from the formation of **3** at 5 °C to the binuclear complex **4a** by the simple expedient of raising the temperature. However, while **3** is formed only in the case of Cp″, the selective formation of complexes of type **4** is quite general and has led to isolation in high yields of **4b** (Cp^R = C_5H_5, 73%), **4c** (C_5H_4Me, 72.7%) and **4d**, ($C_5H_4SiMe_3$, 66%).

This work was supported by the Engineering and Physical Sciences Research Council.

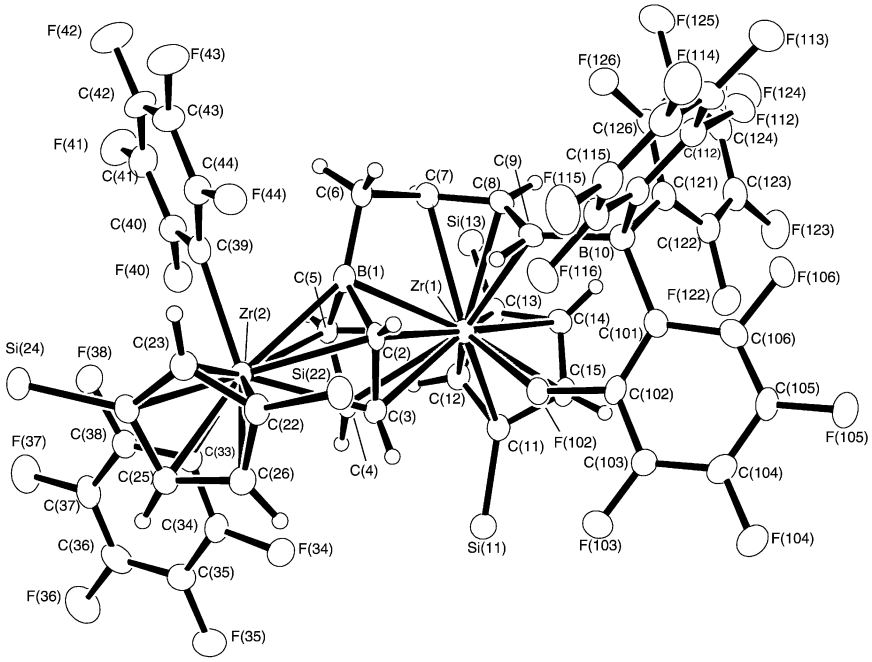

Fig. 1 Molecular structure of **4a**·2Et$_2$O. Selected bond lengths (Å) and angles (°): Zr(1)–F(102) 2.355(3), Zr(1)–B(1) 2.534(6), Zr(2)–B(1) 2.609(6); Zr(1)–B(1)–Zr(2) 117.1(2), B(1)–C(6)–C(7) 100.7(4), C(6)–C(7)–C(8) 126.1(5), C(7)–C(8)–C(9) 125.8(5), C(102)–F(102)–Zr(1) 136.2(3), B(10)–C(9)–C(8) 124.8(5), C(6)–B(1)–Zr(1) 100.4(3), C(6)–B(1)–Zr(2) 142.3(4), C(39)–Zr(2)–C(33) 116.37(19).

Notes and references

† *Synthesis* of **4a**: a solution of Zr(C$_4$H$_7$)(C$_4$H$_6$)Cp″ (1.63 g, 3.98 mmol) in toluene (30 cm^3) at −78 °C was treated with a solution of B(C$_6$F$_5$)$_3$ (1.98 g, 3.87 mmol). The reaction was maintained at this temperature for 30 min and then allowed to reach room temperature. The volatiles were removed *in vacuo*, toluene (40 cm^3) was introduced and the reaction was stirred at 50 °C for 2 h. Removal of the solvent *in vacuo* provided a brown foam which was extracted with diethyl ether (50 cm^3). Concentration of this red solution to *ca*. 10 cm^3 and cooling to −20 °C gave **4a** as red crystals, yield 2.56 g, (82.3%). Anal. Found: C, 45.4; H, 3.3. $B_2C_{60}H_{51}F_{25}Si_4Zr_2$ requires C, 46.1; H, 3.3%. ^{1}H NMR (300 MHz, C$_6$D$_6$, 20 °C): δ −0.38, −0.01, 0.08, 0.20 (s, 9H each, SiMe$_3$), 1.51 (d, 2H, *J* 8.04 Hz, C*H*$_2$CHCHCHB(C$_6$F$_5$)$_3$), 3.36 (q, 1H, *J* 8.27 Hz, CH$_2$C*H*CHCHB(C$_6$F$_5$)$_3$), 4.81 (d, 1H, *J* 19.44 Hz, CH$_2$CHCHC*H*B(C$_6$F$_5$)$_3$), 5.81 (d, 1H, *J* 6.46 Hz, CH$_2$CHC*H*CHB(C$_6$F$_5$)$_3$), 3.91, 7.87 (m, 2H, *m*-C$_4$H$_4$B), 4.98, 6.81 (m, 2H, *o*-C$_4$H$_4$B), 5.51, 6.03, 6.66, 7.08 (m, 4H, 4,5-C$_5$H$_3$), 5.89, 6.74 (m, 2H, 2-C$_5$H$_3$) ^{11}B{^{1}H} NMR (96.2 MHz, C$_6$D$_6$, 20 °C): δ 3.0 (vbr, C$_4$H$_4$B), −12.8 [B(C$_6$F$_5$)$_3$]. ^{13}C NMR (75.6 MHz, C$_6$D$_6$, 20 °C): δ −1.20, −0.84, −0.69, −0.21 (SiMe$_3$), 14.95 [*C*H$_2$CHCHCHB(C$_6$F$_5$)$_3$], 81.40 [CH$_2$*C*HCHCHB(C$_6$F$_5$)$_3$], 98.71, 126.64 (*m*-C$_4$H$_4$B), 105.72, 111.34 (*o*-C$_4$H$_4$B), 119.73, 124.01, 124.78, 129.95 (4,5-C$_5$H$_3$), 121.54 [*C*HB(C$_6$F$_5$)$_3$], 123.87 [*C*HCHB(C$_6$F$_5$)$_3$], 127.69, 129.50 (2-*C*$_5$H$_3$). ^{19}F NMR (75.6 MHz, C$_6$D$_6$, 20 °C): δ −108.2 (s, br, 1F), −112.8 (s, vbr, 1F), −119.9 (s, vbr, 1F), −120.2 (s, br, 1F), −126.2 (s, 1F), −130.0 (s, vbr, 2F), −132.9 (s, br, 2F), −217.2 (m, 1F) (all *o*-C$_6$F$_5$), −152.1 (t, $^3J_{FF}$ 19.8 Hz, 1F), −152.5 (t, $^3J_{FF}$ 19.8 Hz, 1F), −157.1 (t, $^3J_{FF}$ 19.8 Hz, 1F), −157.6 (t, $^3J_{FF}$ 19.8 Hz, 1F), −159.0 (t, $^3J_{FF}$ 19.8 Hz, 1F) (all *p*-C$_6$F$_5$), −160.2 (t, $^3J_{FF}$ 19.8 Hz, 1F), −160.5 (m, 3F), −161.5 (s, br, 1F), −162.6 (m, 1F), −164.2 (m, 2F), −164.4 (m, 2F) (all *m*-C$_6$F$_5$).

‡ *Crystal data* for **4a**·2Et$_2$O: crystals were grown from diethyl ether at −20 °C; $C_{60}H_{51}B_2F_{25}Si_4Zr_2{\cdot}2C_4H_{10}O$, *M* = 1711.67, triclinic, space group $P\bar{1}$, *a* = 13.2618(3), *b* = 13.6828(3), *c* = 22.1150(6) Å, α = 96.858(2), β = 106.311(2), γ = 102.906(2)°, *U* = 3682.30(15) Å^3, *F*(000) = 1732, D_c = 1.544 g cm^{-3}, *Z* = 2, μ(Mo-Kα, λ = 0.71073 Å) = 0.455 mm^{-1}. Final *R* indices [$I > 2\sigma(I)$] R_1 = 0.0599, wR_2 = 0.1232 for 8712 absorption-corrected reflections. CCDC 152834. See http://www.rsc.org/suppdata/cc/b0/b009016f/ for crystallographic data in .cif or other electronic format.

1 R. W. Quan, G. C. Bazan, A. F. Kiely, W. P. Schaefer and J. E. Bercaw, *J. Am. Chem. Soc.*, 1994, **116**, 4489; A. Pastor, A. F. Kiely, L. M. Henling, M. W. Day and J. E. Bercaw, *J. Organomet. Chem.*, 1997, **528**, 65; G. C. Bazan, S. J. Donnelly and G. J. Rodriguez, *J. Am. Chem. Soc.*, 1995, **117**, 2671; G. C. Bazan and G. J. Rodriguez, *Polyhedron*, 1995, **14**, 93; C. K. Sperry, W. D. Cotter, R. A. Lee, R. J. Lachiotte and G. C. Bazan, *J. Am. Chem. Soc.*, 1998, **120**, 7791.

2 G. E. Herberich, B. Hessner, W. Boveleth, H. Lüthe, R. Saive and L. Zelenka, *Angew. Chem., Int. Ed. Engl.*, 1983, **22**, 1024; G. E. Herberich, M. Negele and H. Ohst, *Chem. Ber.*, 1991, **124**, 25; G. E. Herberich, T. Carstensen, N. Klaff and M. Neuschütz, *Chem. Ber.*, 1992, **125**, 1801; M. Enders, H. Pritzkow and W. Siebert, *Chem. Ber.*, 1992, **125**, 1981; G. E. Herberich, T. Carstensen and U. Englert, *Chem. Ber.*, 1992, **125**, 2351; P. Braunstein, U. Englert, G. E. Herberich and M. Neuschütz, *Angew. Chem., Int. Ed. Engl.*, 1995, **34**, 1010; G. E. Herberich, T. Carstensen, D. P. J. Koffer, N. Klaff, R. Boese, I. Hylakryspin, R. Gleiter, M. Stephan, H. Meth and U. Zenneck, *Organometallics*, 1994, **13**, 619; G. E. Herberich, H. J. Eckenrath and U. Englert, *Organometallics*, 1997, **16**, 4292.

3 G. E. Herberich, M. Hostalek, R. Laven and R. Boese, *Angew. Chem., Int. Ed. Engl.*, 1990, **29**, 317; G. E. Herberich, U. Englert, M. Hostalek and R. Laven, *Chem. Ber.*, 1991, **124**, 17; G. E. Herberich, U. Eigendorf and U. Englert, *Chem. Ber.*, 1993, **126**, 1397; G. E. Herberich, H. W. Marx and T. Wagner, *Chem. Ber.*, 1994, **127**, 2135; G. E. Herberich, T. Wagner and H. J. Marx, *J. Organomet. Chem.*, 1995, **502**, 67.

4 (*a*) M. Bochmann, *Top. Catal.*, 1999, **7**, 9; (*b*) G. Jiménez Pindado, M. Thornton-Pett, M. Bowkamp, A. Meetsma, B. Hessen and M. Bochmann, *Angew. Chem., Int. Ed. Engl.*, 1997, **36**, 2358; (*c*) G. Jiménez Pindado, M. Thornton-Pett and M. Bochmann, *J. Chem. Soc., Dalton Trans.*, 1997, 3115; (*d*) G. Jiménez Pindado, M. Thornton-Pett, M. B. Hursthouse, S. J. Coles and M. Bochmann, *J. Chem. Soc., Dalton Trans.*, 1999, 1663.

5 M. Corradi, G. Jiménez Pindado, M. J. Sarsfield, M. Thornton-Pett and M. Bochmann, *Organometallics*, 2000, **19**, 1150; M. Bochmann, S. J. Lancaster, G. Jiménez Pindado, D. A. Walker, S. Al-Benna and M. Thornton-Pett, *Contemporary Boron Chemistry*, ed. M. Davidson, A. K. Hughes, T. B. Marder and K. Wade, Royal Society of Chemistry, Cambridge, 2000, p. 9.

6 G. Jiménez Pindado, S. J. Lancaster, M. Thornton-Pett and M. Bochmann, *J. Am Chem. Soc.*, 1998, **120**, 6816.

7 B. Temme, G. Erker, J. Karl, R. Luftmann, R. Fröhlich and S. Kotila, *Angew. Chem., Int. Ed. Engl.*, 1995, **34**, 1755; J. Karl, G. Erker and R. Frölich, *J. Am Chem. Soc.*, 1997, **119**, 11 165.

8 G. E. Herberich, H. J. Eckenrath and U. Englert, *Organometallics*, 1997, **16**, 4800.

9 S. J. Lancaster, M. Thornton-Pett, D. M. Dawson and M. Bochmann, *Organometallics*, 1998, **17**, 3829.

10 G. E. Herberich, B. Hessner and R. Saive, *J. Organomet. Chem.*, 1987, **319**, 9.

11 G. E. Herberich, J. Hengesbach, G. Huttner, A. Frank and U. Schubert, *J. Organomet. Chem.*, 1983, **246**, 141.

12 G. E. Herberich, B. Hessner, J.A.K. Howard, D. P. J. Koffer and R. Saive, *Angew. Chem., Int. Ed. Engl.*, 1986, **25**, 165.

13 G. E. Herberich, J. Hengesbach, U. Kolle, G. Huttner and A. Frank, *Angew. Chem., Int. Ed. Engl.*, 1976, **15**, 433.

14 Reviews: E. Y. X. Chen and T.J. Marks, *Chem. Rev.*, 2000, **100**, 1391; M. Bochmann, *J. Chem. Soc., Dalton Trans.*, 1996, 255; H. H. Brintzinger, D. Fischer, R. Mülhaupt, B. Rieger and R. Waymouth, *Angew. Chem., Int. Ed. Engl.*, 1995, **34**, 1143.

A short synthesis of biologically active lignan analogues

Stefan Kamlage,[a] Michael Sefkow,[a] Beatrice L. Pool-Zobel[b] and Martin G. Peter*[a]

[a] *Institut für Organische Chemie und Strukturanalytik, Universität Potsdam, Karl-Liebknecht-Str. 24-25, D-14476 Golm, Germany. E-mail: peter@serv.chem.uni-potsdam.de*

[b] *Institut für Ernährungswissenschaften, Friedrich-Schiller-Universität Jena, Dornburger Str. 25, D-07743 Jena, Germany*

Received (in Cambridge, UK) 20th October 2000, Accepted 12th January 2001
First published as an Advance Article on the web 31st January 2001

β-Benzyl-γ-butyrolactones were synthesized in four transition metal catalysed reactions from butynediol, and alkylated to afford new, biologically active lignan analogues.

Lignans, dimers of phenylpropenes, are ubiquitous secondary plant metabolites.[1] They exhibit notable biological activities, in particular antiviral,[2] cytotoxic[3] and canceroprotective[4] properties. Many lignan syntheses have been reported in the past.[1,5] Two different strategies were most frequently followed for the synthesis of butyrolactone lignans **1**: 1. oxidative dimerization of *p*-hydroxycinnamic acids[6] and 2. alkylation of β-benzyl-γ-butyrolactones **2**.[7] Following these routes, between 6 and 13 steps were necessary to obtain this class of lignans. We reported recently the Stille coupling[8] of unsymmetrically protected 2-tributylstannylbuten-1,4-diols **3** with a variety of benzyl bromides.[9] This coupling reaction was the key step for the preparation of lactones **2** from butynediol **4** (Scheme 1, Route A) but several protecting group manipulations were necessary and the overall yields were low (6–15%). Thus, a regioselective oxidation of 2-tributylstannylbut-2-en-1,4-diol (**5**) to lactone **6** was desirable for a short synthesis of lactone **2** (Scheme 1, Route B). Herein we report the synthesis of lactone **2** using only four transition metal catalysed reactions. Key step was the hitherto unknown, regioselective oxidation of diol **5** to lactone **6**.[10]

The palladium catalysed *cis*-selective addition of tributylstannane to butynediol **4** is well documented.[11] The quality of diol **4** was crucial in this step. Purification of this compound prior to its use was necessary to obtain diol **5** in 92% yield (Scheme 2).

The hydroxy group at C(4) of diol **5** can be regioselectively protected using bulky silyl groups like the TBDMS group.[12] We assumed that selective oxidation of this hydroxy group may occur if a sterically demanding oxidation reagent like TPAP[13] in conjunction with NMO was employed. The selective oxidation of a primary hydroxy group in the presence of a secondary using this oxidation system was reported by Bloch and Brillet[14] but a regioselective oxidation of one of two primary hydroxy groups has not been published yet.

Treatment of diol **4** with 2.5 equivalents of NMO and 5 mol% TPAP at rt for 17 h afforded the lactones **6** and **7** in 15% yield and in a 4:1 ratio (Table 1, entry 1). The major compound isolated was furane **10** (30%) formed by elimination of water after initial oxidation to lactol **11** (Scheme 3).

Improved yields and selectivities were achieved when the initial temperature was below 0 °C and the reaction mixture gradually warmed to rt over a period of 17 h (entries 2 and 3). Increasing the amount of TPAP and longer reaction times produced the lactones **6** and **7** in *ca.* 50% yield but the

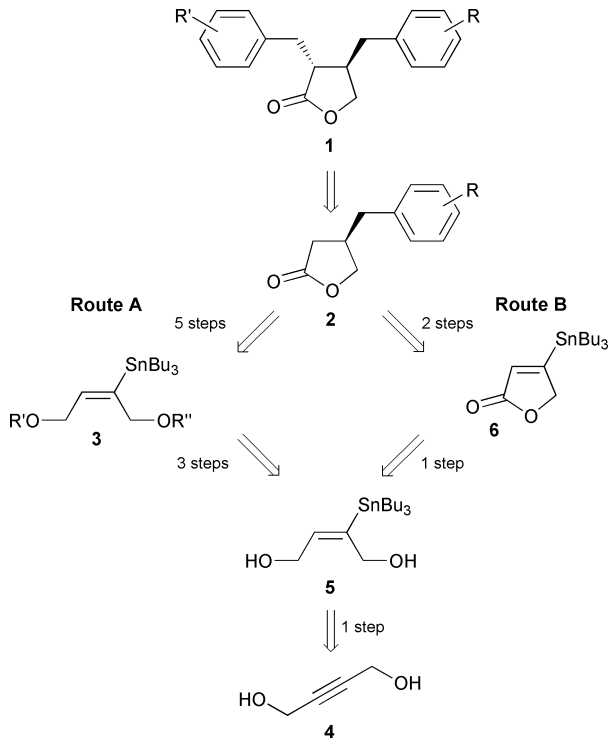

Scheme 1

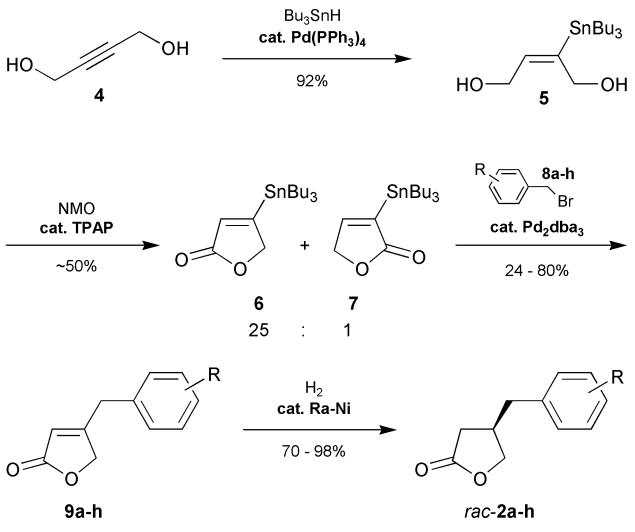

Scheme 2

Table 1 Reaction conditions for the TPAP-catalysed oxidation of diol **5** to lactones **6** and **7**

Entry	TPAP/mol%	*T*/°C	*t*/h	Yield (%)	Ratio **6**:**7**[a]
1	5	23	17	15	3,7:1
2	5	−30 → 23	17	21	22:1
3	5	−78 → 23	17	32	22:1
4	7,5	−78 → 23	62	47	**25**:**1**
5	10	−78 → 23	62	49	20:1
6	7,5 + 2,5 +2,5	−78 → 23	62	**50**	5,4:1

[a] Estimated by ^{1}H NMR spectra of crude reaction products.

DOI: 10.1039/b008499i

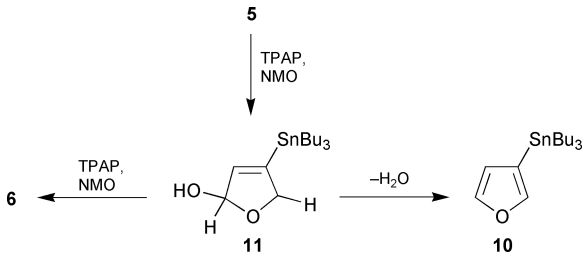

Scheme 3

selectivity decreased with higher contents of the oxidation reagent (entries 4–6).

Lactones **6** and **7** were inseparable by flash chromatography and were therefore used as a mixture for the Stille coupling. This reaction was performed with benzyl bromides **8a**–**h** as described previously.[9] The α,β-unsaturated lactones **9a**–**h** were isolated as isomerically pure compounds (Scheme 2). Sweeney *et al.* described recently, that the reaction rates for the Stille coupling of lactones **6** and **7** with aryl halides are different.[15] In analogy, only lactone **6** reacted with benzyl bromides **8a**–**h** to the coupling products **9a**–**h** (Table 2).

Table 2 Benzyl bromides **8a**–**h** employed for the Stille coupling and yields of the reaction products **9a**–**h**

Entry	Residue (R)	Bromide	Lactone	Yield (%)
1	4-Mesyl-3-methoxy	**8a**	**9a**	80
2	3,4,5-Trimethoxy	**8b**	**9b**	56
3	4-Methyl	**8c**	**9c**	76
4	H	**8d**	**9d**	70
5	4-Nitro	**8e**	**9e**	24
6	2,4,6-Trimethyl	**8f**	**9f**	77
7	3-Methoxy	**8g**	**9g**	59
8	3,4-Methylendioxy	**8h**	**9h**	45

Hydrogenation of lactones **9a**–**h** to lactones **2a**–**h** were achieved by means of 10% Pd on charcoal or Ra-Ni T4 (Table 3). The former catalyst, however, gave irreproducible results or no conversion. Additionally, high pressure (100 bar) and long reaction times (> 24 h) were required. With Ra-Ni T4 as catalyst, complete conversion was found in all cases within 2 h at 0.1 bar positive pressure.

Table 3 Hydrogenation of the unsaturated lactones **9a**–**h** using different catalysts

Entry	Unsat. lactone	Product	Catalyst	*p*/bar	*t*/h	Yield (%)
1	**9a**	**2a**	Pd/C	0.1	14	93
2	**9a**	**2a**	Ra-Ni T4	0.1	2	98
3	**9b**	**2b**	Pd/C	0.1	14	0
4	**9b**	**2b**	Ra-Ni T4	0.1	2	70
5	**9c**	**2c**	Pd/C	0.1	24	98
6	**9d**	**2d**	Pd/C	50	48	97
7	**9e**	**2e**	Pd/C	0.1	14	0
8	**9f**	**2f**	Pd/C	0.1	14	0
9	**9f**	**2f**	Pd/C	100	72	88
10	**9f**	**2f**	Ra-Ni T4	0.1	2	98
11	**9g**	**2g**	Pd/C	100	14	92
12	**9h**	**2h**	$Pd(OH)_2$	100	16	0
13	**9h**	**2h**	Ra-Ni T4	0.1	2	70

Alkylation of lactones **2** with benzyl halides using LDA as base and HMPA as cosolvent provides lactone lignans **1**.[1,7,16] We found that alkylation using LHMDS as base and DMPU[17] as non-carcinogenic substitute for HMPA afforded lactones **1** in moderate yields (Scheme 4 and Table 4).

Bioassay of the synthetic lignan analogues using colon-tumor lines HT29 revealed that compound **1f** possesses high cytotoxic activity (IC_{50} = 40 mM).[18]

We have shown that β-benzyl-γ-butyrolactones **2** were effectively synthesised from butynediol **4** in four transition

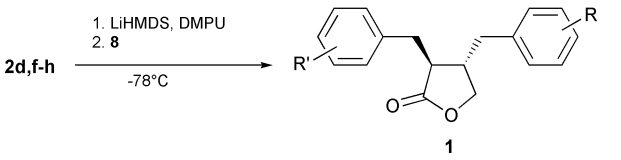

Scheme 4

Table 4 Alkylation of lactones **2d**,**f**–**h** to the symmetrically and unsymmetrically substituted lignan analogues **1**

Entry	Lactone	Bromide	Residue (R′)	Lignan	Yield (%)[a]
1	**2d**	**8d**	H	**1d**	30
2	**2f**	**8f**	2,4,6-Trimethyl	**1f**	43
3	**2f**	**8h**	3,4-Methylendioxy	**1fb**	25
4	**2g**	**8g**	3-Methoxy	**1g**	18
5	**2h**	**8h**	3,4-Methylendioxy	**1h**	35

[a] Reaction conditions not optimized.

metal catalysed reactions. Alkylation of these compounds produced lignan analogues **1** with cytotoxic activities. An enantioselective route to this class of lignans is in progress.

This research was supported by the Deutsche Forschungsgemeinschaft (DFG) (INK A26/1-1 and B26/1-1). MS acknowledges a habilitation grant from the DFG (Se875/1-1).

Notes and references

1 D. C. Ayres and J. D. Loike, *Lignans: Chemical, Biological and Clinical Properties*, Cambridge University Press, Cambridge, 1990; R. S. Ward, *Nat. Prod. Rep.*, 1999, **16**, 75.
2 Recent reviews: J. L. Charlton, *J. Nat. Prod.*, 1998, **61**, 1447; E. Eich, *ACS Symp. Ser.*, 1998, **691**, 83; A. J. Vlietinck, T. De Bruyne, S. Apers and L. A. Pieters, *Planta Med.*, 1998, **64**, 97.
3 Recent reviews: S. E. Rickard and L. U. Thompson, *ACS Symp. Ser.*, 1997, **662**, 273; D. M. Tham, C. D. Gardner and W. L. Haskell, *J. Clin. Endocrinol. Metab.*, 1998, **83**, 2223; C. D. N. Humfrey, *Nat. Toxins*, 1998, **6**, 51; J. M. Cline and C. L. Hughes, Jr., *Cancer Treat. Res.*, 1998, **94**, 107; W. Mazur and H. Adlercreutz, *Pure Appl. Chem.*, 1998, **70**, 1759; S. Bingham, *Pure Appl. Chem.*, 1998, **70**, 1777.
4 S. R. Stitch, J. K. Toumba, M. B. Groen, C. W. Funke, J. Leemhuis, J. Vink and G. F. Woods, *Nature*, 1980, **287**, 738; K. D. R. Setchell, A. M. Lawson, F. L. Mitchell, H. Adlercreutz, D. N. Kirk and M. Axelson, *Nature*, 1980, **287**, 740; M. Axelson, J. Sjövall, B. E. Gustafsson and K. D. R. Setchell, *Nature*, 1982, **298**, 659; L. U. Thompson, P. Robb, M. Serraino and F. Cheung, *Nutr. Cancer*, 1991, **16**, 43.
5 R. S. Ward, *Chem. Soc. Rev.*, 1982, **11**, 75; R. S. Ward, *Tetrahedron*, 1990, **46**, 5029.
6 N. J. Cartwright and R. D. Haworth, *J. Chem. Soc.*, 1944, 535; K. Weinges and R. Spänig, in *Oxidative Coupling of Phenols*, ed. W. I. Taylor and A. R. Battersby, Marcel Dekker, New York, 1967; D. E. Bogucki and J. L. Charlton, 1997, **75**, 1793.
7 J. M. de L. Vanderlei, F. Coelho and W. P. Almeida, *Synth. Commun.*, 1998, **28**, 3047.
8 J. K. Stille, *Angew. Chem.*, 1986, **98**, 504; V. Farina, V. Krishnamurthy and W. J. Scott, *Org. React.*, 1997, **50**, 512.
9 S. Kamlage, M. Sefkow and M. G. Peter, *J. Org. Chem.*, 1999, **64**, 2938.
10 H. X. Zhang, F. Guibe and G. Balavoine, *J. Org. Chem.*, 1990, **55**, 1857.
11 A. G. M. Barrett, T. E. Barta and J. A. Flygare, *J. Org. Chem.*, 1989, **54**, 4246.
12 G. J. Hollingworth, G. Perkins and J. Sweeney, *J. Chem. Soc., Perkin Trans. 1*, 1996, 1913.
13 S. V. Ley, J. Norman, W. P. Griffith and S. P. Marsden, *Synthesis*, 1994, 639–666.
14 R. Bloch and C. Brillet, *Synlett*, 1991, 829.
15 R. Mabon, A. M. E. Richecœur and J. B. Sweeney, *J. Org. Chem.*, 1999, **64**, 328.
16 R. Chênevert, G. Mohammadi-Zirani, D. Caron and M. Dasser, *Can. J. Chem.*, 1999, **77**, 223.
17 T. Mukhopadhyay and D. Seebach, *Helv. Chim. Acta*, 1982, **65**, 385.
18 T. W. Becker, M. G. Peter and B. L. Pool-Zobel, in *Proceedings of the Food and Cancer Prevention III Meeting, Norwich, UK*, 1999, ed. I. T. Johnson and G. R. Fenwick, Special Publication No 255, Royal Society of Chemistry, Cambridge, UK, p. 151.

Structure and magnetic properties of a high-spin $Mn_6^{II}Cr^{III}$ cluster containing cyano bridges and Mn centres capped by pentadentate ligands

Richard J. Parker,[a] Leone Spiccia,*[a] Kevin J. Berry,[b] Gary D. Fallon,[a] Boujemaa Moubaraki[a] and Keith S. Murray[a]

[a] *School of Chemistry, PO Box 23, Monash University, Victoria, 3800, Australia. E-mail: leone.spiccia@sci.monash.edu.au*
[b] *Westernport Secondary College, Hastings, Victoria 3915, Australia*

Received (in Cambridge, UK) 1st September 2000, Accepted 11th January 2001
First published as an Advance Article on the web 1st February 2001

The formation of an elaborate H-bonding network between heptanuclear cations, consisting of a hexacyanochromate capped by six $[Mn(dmptacn)]^{2+}$ moieties, and hexacyanochromate counterions results in the assembly of novel 1-D chains with short-range ferrimagnetic behaviour occurring between the $S = 27/2$ clusters and $S = 3/2$ ions.

A major challenge in the field of molecular magnetism is to design discrete polynuclear entities with high-spin ground states and tunable magnetic properties.[1–3] Such materials allow the study of the transition from molecular to bulk-like magnetic behaviour exhibited by, for example, bulk ferromagnets. An important area is that of 'single-molecule' magnets based on high-spin clusters, *e.g.* $Mn_{12}O_{12}(O_2CR)_{16}(OH_2)_4$, for which magnetic anisotropy and negative zero-field splitting are prerequisites.[1,2] One approach to isolating discrete molecules with high-spin states, albeit of a symmetrical type, has focussed on the use of hexacyanometallates as building blocks in the construction of heterometallic assemblies.[4–7] We have reported the structure of $[Fe\{(CN)Cu(tpa)\}_6](ClO_4)_8{\cdot}3H_2O$, [tpa = tris(2-pyridylmethyl)amine]. While this was the first heptanuclear complex of this type to be structurally characterized, new techniques, such as X-ray MCD, have since been applied to probe the magnetisation in $Mn_6^{II}Cr^{III}$ and $Ni_6^{II}Cr^{III}$ complexes, for which X-ray structures were not obtained.[6] Two other structurally characterised cyano-bridged clusters with large high-spin ground states were reported recently.[8,9] Based on octacyanometallates, they consist of $Mn^{II}_9M^{V}_6$ fully-capped cubane structures but, surprisingly, that with M = W[8] has an $S = 39/2$ ground state (*i.e.* $S = 9S_{Mn} - 6S_W$) while that with M = Mo[9] is reported to have an $S = 51/2$ ground state (*i.e.* $S = 9S_{Mn} + 6S_{Mo}$). Inter-cluster coupling, *via* H-bonded pathways, led to long-range order being observed in the Mo case[9] while some features of single molecule magnetism were noted in the W case.[8] We report here the structure and magnetism of $[\{Mn(dmptacn)(CN)\}_6Cr][Cr(CN)_6](ClO_4)_6{\cdot}6H_2O$ **1** [dmptacn = 1,4-bis(2-methylpyridyl)-1,4,7-triazacyclononane], a complex featuring intimate H-bonding between heptanuclear $[\{Mn^{II}(dmptacn)(CN)\}_6Cr^{III}]^{9+}$ cations and $[Cr(CN)_6]^{3-}$ counter anions.

Complex **1** initially formed in an aqueous solution containing a 1:6 mixture of $[Cr(CN)_6]^{3-}$ and $[Mn(dmptacn)(OH_2)]^{2+}$, a reactant ratio expected to yield a heptanuclear complex. However, microanalysis and crystallography confirmed a Mn:Cr ratio of 3:1, and the IR spectrum exhibited CN stretches attributable to both bridging and terminal CN groups. Reactant ratios corresponding to the product stoichiometry afforded better yields of **1**.† The encapsulation of $[Cr(CN)_6]^{3-}$ by six $[Mn(dmptacn)]^{2+}$ moieties has generated a heptanuclear cation [Fig. 1(a)] whose 9+ charge is balanced by one $[Cr(CN)_6]^{3-}$ and six perchlorates even in the presence of excess ClO_4^-. This gives rise to a novel crystallographic feature described below.‡

The geometry of the Cr centres in **1** is little distorted from octahedral, *viz.*, C–Cr–C(*cis*) and C–Cr–C(*trans*) angles are close to 90 and 180°, respectively, and the Cr–C–N angles in both the 'capped $Cr(CN)_6$' core and $[Cr(CN)_6]^{3-}$ anions are almost linear. These features are common to clusters incorporating $[Cr(CN)_6]^{3}$,[11] except for $(VO)_3[Cr(CN)_6]_2{\cdot}10H_2O$.[10,11] The Mn–N–C(CN) angles in **1** [158.4(5)°] deviate from linearity [Fig. 1(b)]. Such deviations have been found in extended lattices formed by cyanometallates and manganese chelates[12] but not in discrete molecules like **1**. For each Mn^{II} centre, the CN ligand is *cis* to the secondary amine of dmptacn,[13] and the Mn^{II} cations adopt a geometry intermediate between trigonal prismatic and octahedral. A trigonal twist angle of 29.2° is calculated from the orientation of the three tacn N atoms relative to the two pyridyl and cyano N atoms. The slightly bent *trans*-C≡N–Mn–N angles [164.9(2)°] cause the three sets of *trans*-Cr–C≡N–Mn units to adopt *anti*-configurations.

Intimate H-bonding interactions exist between the terminal CN nitrogens in the $[Cr(CN)_6]^{3-}$ counter ion and the hydrogen on the sec. amine of dmptacn [Fig. 1(c)]. The C≡N···H–N distance is 2.53 Å while the C≡N···N distance is 3.075(7) Å.

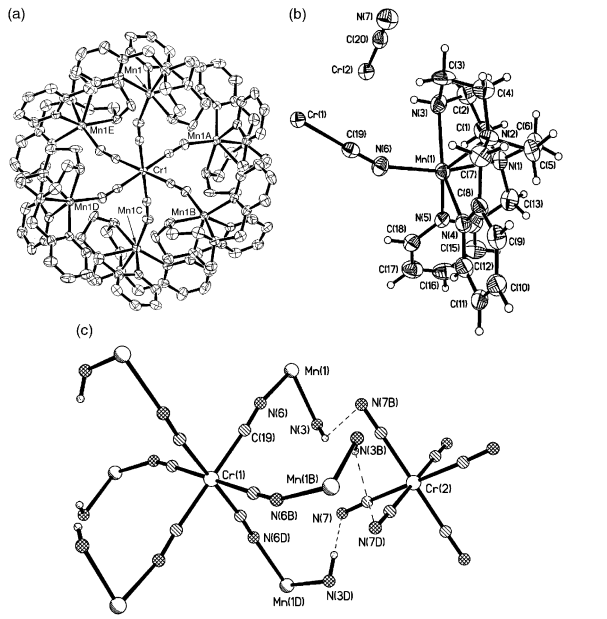

Fig. 1 (a) View of the heptanuclear cation in **1**; (b) atomic labeling scheme (50% probability ellipsoids); (c) 1-D chains formed by H-bonding between the cyano groups on the $[Cr(CN)_6]^{3-}$ counter ion and the secondary amine proton on each dmptacn. Selected bond lengths (Å) and angles (°): Cr1–C19 2.074(6), Cr2–C20 2.050(6), Mn1–N1 2.316(4), Mn1–N2 2.306(4), Mn1–N3 2.236(5), Mn1–N4 2.308(4), Mn1–N5 2.197(4), Mn1–N6 2.196(5), C19–N6 1.150(6), C20–N7 1.173(7), Cr1···Mn1 5.318, Cr2···Mn1 5.849, Cr1···Cr2 6.882, N3···N7b 3.075(7); Cr1–C19–N6 175.0(5), Cr2–C20–N7 177.5(5), Mn1–N6–C19 158.4(5), N1–Mn1–N2 75.4(1), N1–Mn1–N3 76.7(2), N1–Mn1–N5 75.4(2), N1–Mn1–N6 164.9(2), N2–Mn1–N5 140.0(2), N3–Mn1–N4 146.6(2), N3–Mn1–N5 122.3(2), N3–Mn1–N6 88.7(2), N5–Mn1–N6 110.1(2).

DOI: 10.1039/b007113g

This interaction results in a pseudo 1-D chain of alternating $[\{Mn(dmptacn)(CN)\}_6Cr]^{9+}$ cations and $[Cr(CN)_6]^{3-}$ anions running along the *c*-axis. Each complex anion is sandwiched between two heptanuclear cations, forming three H-bonds to one of the two sets of three sec. amine N atoms on each cation. Of importance to the supramolecular assembly of the cations and anions into H-bonded 1-D chains is the geometric arrangement of each set of three sec. amine N atoms, and their hydrogens, at the corners of an equilateral triangle (thus, the cation has a C_{3v} axis of symmetry). The excellent match in the symmetry and size of the extended octahedral faces of $[Cr(CN)_6]^{3-}$ and these triangular arrays of sec. N atoms facilitate the establishment of H-bonded contacts between the exposed N atoms on the anion and the heptanuclear cations.

Fig. 2 shows the temperature dependence of the $\chi_M T$, per Mn_6Cr_2, measured in a field of 1 T. The room-temperature $\chi_M T$ value of 27.1 cm^3 K mol^{-1} is slightly lower than the spin-only value of 30.0 expected for an uncoupled spin system [6(S_{Mn} = 5/2), 2(S_{Cr} = 3/2)] with g = 2.0. As the temperature is lowered, $\chi_M T$ decreases slightly to a broad minimum of 26.3 at 203 K and then slowly increases to 30.1 at 100 K. As the temperature is decreased further, $\chi_M T$ increases rapidly to a maximum of 71.0 at 12 K. This is below the value expected for a fully antiferromagnetically coupled heptanuclear spin system plus $[Cr(CN)_6]^{3-}$ [*viz.*, 99.9 cm^3 K mol^{-1} for {6(S_{Mn} = 5/2) − (S_{Cr} = 3/2)} + (S_{Cr} = 3/2)]. The drop in $\chi_M T$ observed below 12 K can be attributed to a competing intermolecular antiferromagnetic interaction and/or thermal population of low lying Zeeman levels, as noted in other clusters.[14] The χ_M values obey the Curie–Weiss law above *ca*. 140 K with a Weiss constant θ = − 4.2 K. This is consistent with intracluster antiferromagnetic coupling. A ground-state spin value of 27/2 for the cluster corresponds to the spins on the Mn^{II} atoms being antiparallel to those on the central Cr^{III}, *i.e.* $6S_{Mn} - S_{Cr}$. This was also the case for the related $Mn^{II}{}_6Cr^{III}$ cluster[5,6] and the $Mn^{II}{}_9W^{V}{}_6$ cluster.[8] Indeed, a good fit to the $\chi_M T$ *vs.* T data in a field of 1 T was obtained using the spin Hamiltonian of Scuiller *et. al.*,[5] allowing for an additional S_{Cr} = 3/2 Curie contribution in **1**. The best-fit, shown in Fig. 2, corresponds to the parameters of g = 1.96 and J_{Cr-Mn} = −5 cm^{-1} (J_{Mn-Mn} 0) which are similar to those for $[Mn(L)(NC)_6Cr]^{9+}$ {g = 1.97; J_{Cr-Mn} = −8.0 cm^{-1}, L = *N*,*N*,*N*′-[tris(2-pyridylmethyl)-*N*′-methylethane)-1,2-diamine}.[5,6] The ability to simulate the maximum in $\chi_M T$ at 12 K, using the thermodynamic form of the susceptibility,[14] shows that field-dependent Zeeman level depopulation effects are responsible for this maximum.

The broad minimum in $\chi_M T$ noted at 203 K most likely reflects short-range 1D-ferrimagnetic behaviour occurring through weak antiferromagnetic coupling between the S = 27/2 cation and the S = 3/2 $[Cr(CN)_6]^{3-}$ *via* the H-bonding pathways that connect them. Tests for long-range order in **1** proved negative. Thus, the field-cooled and zero-field magnetization data at very low temperatures, in H = 5Oe, showed no bifurcation. At low-fields and 2 K, the magnetization, M, increases rapidly with increasing fields then saturates above H = ≈ 2 T to a M_{sat} value of 24 μ_B, a value consistent with the 1D-ferrimagnet proposal. There is no hysteresis in magnetization at 2 K. Further, the rapid increase in M observed at low fields, such as 100 and 50 Oe, lead to values of $\chi_M T$, as a function of temperature (50–2 K) which do not show the maximum of Fig. 2. Anomalously high values are observed, that continue increasing as T is decreased, reaching $\chi_M T$ of 358 cm^3 K mol^{-1} at 2 K. Such behaviour gives further confirmation of **1** being a 1D-ferrimagnet. However, further work, including ac susceptibility measurements, is needed to fully understand this unusual behaviour at low temperatures and variable fields. Finally, we note that Hashimoto and coworkers,[15] have obtained a 3-D network in their octacyanotungstate(V)–Mn(II) species which is a ferrimagnet displaying long-range order (T_c = 54 K) and with W–CN–Mn chains linking the clusters.

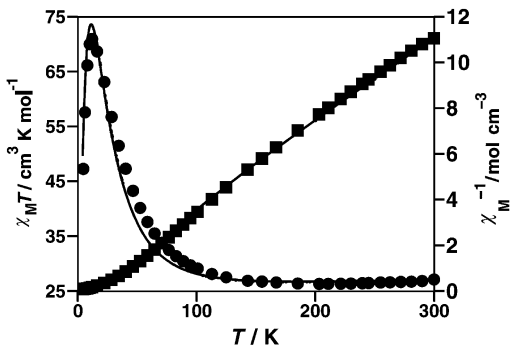

Fig. 2 Plots of $\chi_M T$ (■) and χ_M^{-1} (●) per $Mn_6{}^{II}Cr_2{}^{III}$, for **1** *vs.* T measured in a field of 1 T . The solid line was calculated using the heptanuclear model (see text).

Financial support from the Australian Research Council is gratefully acknowledged.

Notes and references

† *Experimental details*: **Caution!** Perchlorates are potentially explosive and should be handled in small quantities. An aqueous solution of $K_3[Cr(CN)_6]$ (0.05 g, 0.15 mmol) was added to a stirring solution of $[Mn(dmptacn)(OH_2)](ClO_4)_2$[13] (0.26 g, 0.44 mmol) in water (45 ml), resulting in a change from colourless to pale yellow. Evaporation of this solution gave yellow needles of $[Cr\{(CN)Mn(dmptacn)\}_6][Cr(CN)_6](ClO_4)_6{\cdot}6H_2O$ suitable for crystallography (yield: 0.16 g, 37%). Anal Calc. for $C_{120}H_{162}N_{42}Cl_6O_{30}Mn_6Cr_2$: C, 43.4; H, 4.9; N, 17.7. Found: C, 43.3; H, 5.0; N, 17.5%. IR (KBr, cm^{-1}): 3632, 3543 (H_2O); 3330 (N–H); 2142, 2118 (C≡N); 1608vs, 1572m (py); 1097vs, 624 (ClO_4).

‡ *Crystal data* for **1**: $C_{120}H_{162}N_{42}Cl_6O_{30}Mn_6Cr_2$, M = 3319.2, trigonal, space group $R\bar{3}$ (no. 148), a = 30.1382(9), c = 13.7641(9) Å, V = 10827.1(7) $Å^3$, Z = 3, D_c = 1.386 g cm^{-3}, μ = 8.31 cm^{-1}, $F(000)$ = 4686, T = 173 K, Nonius Kappa CCD, Mo-Kα radiation (λ = 0.71069 Å), $2\theta_{max}$ = 56.5°, ϕ-scans, 5378 unique data, final R = 0.062, wR = 0.056 for 2908 observed reflections [$I > 3.00\sigma(I)$] and 311 variables. The structure was solved by and expanded using Fourier techniques and non-hydrogen atoms refined anisotropically. CCDC 182/1889. See http://www.rsc.org/suppdata/cc/b0/b007113g/ for crystallographic files in .cif format.

1 R. Sessoli, D. Gatteschi, A. Caneschi and M. A. Novak, *Nature*, 1993, **365**, 141.
2 Z. Sun, D. Ruiz, E. Rumberger, C. D. Incarnito, K. Folting, A. L. Rheingold, G. Christou and D. N. Hendrickson, *Inorg. Chem.*, 1998, **37**, 4758 and references therein.
3 D. Gatteschi, A. Müller, F. Peters and M. Pope, *Chem. Rev.*, 1998, **98**, 239; D. Gatteschi, G. L. Abbati, A. Cornia, A. C. Fabretti and A. Caneschi, *Inorg. Chem.*, 1998, **37**, 3759.
4 T. Mallah, C. Auberger, M. Verdaguer and P. Veillet, *Chem. Commun.*, 1995, 61.
5 A. Scuiller, T. Mallah, M. Verdaguer, A. Nivorozkhin, J. Tholence and P. Veillet, *New J. Chem.*, 1996, **20**, 1.
6 M.-A. Arrio, A. Scuiller, Ph. Saintctavit, Ch. Cartier de Moulin, T. Mallah and M. Verdaguer, *J. Am. Chem. Soc.*, 1999, **121**, 6414.
7 R. J. Parker, D. C. R. Hockless, B. Moubaraki, K. S. Murray and L. Spiccia, *Chem. Commun.*, 1996, 2789.
8 Z. J. Zhong, H. Seino, Y. Mizobe, M. Hidai, A. Fujishima, S.-I. Ohkoshi and K. Hashimoto, *J. Am. Chem. Soc.*, 2000, **122**, 2952.
9 J. Larianova, M. Gross, M. Pilkington, H. Audres, H. Stoeckli-Evans, H. U. Güdel and S. Decurtins, *Angew. Chem., Int. Ed.*, 2000, **39**, 1605.
10 D. G. Fu, J. Chen, X. Shi Tan, L. J. Jiang, S. W. Zhang, P. J. Zheng and W. X. Tang, *Inorg. Chem.*, 1997, **36**, 220; T. Mallah, S. Ferlay, J. Vaissermann, F. Bartolome, P. Veillet and M. Verdaguer, *Chem. Commun.*, 1996, 2481; M. Ohba and H. Okawa, *Coord. Chem. Rev.*, 2000, **198**, 313.
11 S. Ferlay, T. Mallah, R. Ouahes, P. Veillet and M. Verdaguer, *Inorg. Chem.*, 1999, **38**, 229.
12 H. Miyasaka, H. Ieda, N. Matsumoto, N. Re, R. Crescenzi and C. Floriani, *Inorg. Chem.*, 1998, **37**, 255 and references therein.
13 S. J. Brudenell, L. Spiccia, A. M. Bond, G. D. Fallon, D. C. R. Hockless, G. Lazarev, P. J. Mahon and E. R. T. Tiekink, *Inorg. Chem.*, 2000, **39**, 881.
14 K. Van Langenberg, S. R. Batten, K. J. Berry, D. C. R. Hockless, B. Moubaraki and K. S. Murray, *Inorg. Chem.*, 1997, **36**, 5006.
15 Z. J. Zhong, H. Seino, Y. Mizobe, M. Hidai, M. Verdaguer, S.-I. Ohkoshi and K. Hashimoto, *Inorg. Chem.*, 2000, **39**, 5095.

Novel starch–polyalkane composite materials

Jeffrey J. E. Hardy, James H. Clark,* Christopher N. Rhodes and Karen Wilson

Clean Technology Centre, Chemistry Department, University of York, York, UK YO10 5DD. E-mail: jhc1@york.ac.uk

Received (in Cambridge, UK) 8th November 2000, Accepted 5th January 2001
First published as an Advance Article on the web 31st January 2001

The polymerisation of dibromoalkanes adsorbed in potato starch leads to a novel class of hydrophobic starch–polyalkane composite materials with very high capacity for surface derivitisation.

Starch is the second largest biomass on earth and depleting fossil hydrocarbon resources will require an increasing range of novel applications for starch-based materials.[1] More than 6 MT y^{-1} of starch materials are currently produced in industry with chemically modified starches (through fundamental processes such as hydrolysis, esterification and oxidation) as well as native starches finding diverse uses.[2] Composite materials incorporating starch are less well known although physical mixtures of starch with polyethylene for example, have value as films, coatings and biodegradable plastics.[3] The high degree of functionality of starch along with its low cost, widespread availability and biodegradability makes it a potentially attractive surface-active material but this is hindered by the apparent low site availability and its hydrophobicity and instability in many environments.

The helical structure of native starch leads to hydrophobic channels in which polarisable organic molecules such as haloalkanes can be adsorbed.[2] We have attempted to polymerise intercalated α,ω-dihaloalkanes so as to create a thermally and chemically stable hydrocarbon polymeric core which could open up the starch structure creating a more surface-active material and making it more accessible to derivatisation. Our strategy for accomplishing these goals is illustrated by the following example. Native potato starch was stirred together with 1,10-dibromodecane in cyclohexane. The slurry was then reacted with sodium metal at 80 °C for 24 h. The mixture develops a distinct blue colour over this period and filtration under nitrogen gives an intensely colored blue solid. The FTIR spectrum of the solid shows a number of remarkable features notably a highly resolved hydroxyl stretching region and further sharp bands at 1615, 600 and 450 cm^{-1} (Fig. 1). These bands can at least in part be attributed to a composite matrix stabilised sodium colloid that is also likely to be the origin of the colour.[4] The blue colour of the solid slowly disappears on exposure to the atmosphere and can rapidly be destroyed by washing with water to give a highly particulate white solid. The well resolved FTIR bands noted above are absent in the white solid that has a spectrum essentially consistent with a combination of starch and a polyalkane (Fig. 1). The following discussions refer to the water-washed white solid.

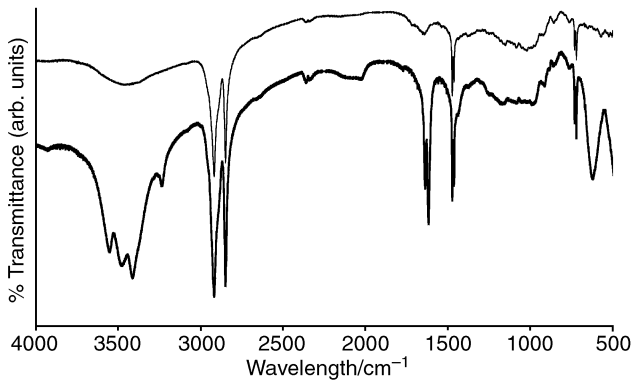

Fig. 1 Diffuse reflectance FTIR spectra of a starch–polyalkane material (STPAM) before (—) and after (—) removal of sodium colloid by water washing.

We have carried out materials preparations as described above at various starch–dibromodecane ratios and thermal analysis can be used to determine the relative amount of the starch and polyalkane (an example of which is shown in Fig. 2). Thermal analysis shows weight losses typical for starch (*ca.* 200 °C) and a polyalkane (*ca.* 400 °C) although it also shows a small but reproducible weight loss between these temperatures which suggests that the two components are not entirely distinct. The bulk of the starch can be removed from the composite materials by treatment with aqueous acid and GPC analysis of the residual polymer shows that it has a rather low molecular weight comparable to that of a polydecane prepared in the absence of starch (Table 1). Bromine analysis reveals the presence of small amounts of organobromine (residual NaBr can be removed by thorough washing) which can be accounted for as polymer terminating CH_2Br groups (based on a 'true' M_w for the polyalkane of 4000).

Other analytical techniques show more obvious evidence of the materials being more than an intimate mixture of starch and polyalkane. Molecular probes can be used to give information about the polarity of surfaces. Reichardt's dye for example, a well known indicator of polarity in the liquid phase can also be used on solids.[5] Remarkably, the spectroscopic shift of the dye adsorbed on the starch–polyalkane composites is considerably greater than that observed for ordinary starch or a polyalkane.

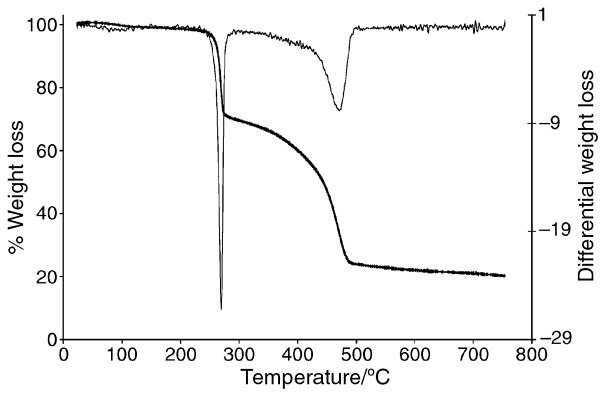

Fig. 2 Thermogravimetric (TG) trace for a typical starch–polyalkane (STPAM) material (10 °C min^{-1}; 20 mg in a ceramic pan; flowing N_2 atmosphere).

Table 1 Representative GPC data for polydecane synthesised with (starch-polydecane material, STPDM) and without (polydecane, PD) the presence of potato starch

Sample	PD : starch ratio	$\bar{M}_w$	$\bar{M}_n$	Polydispersity
PD 1[a]	N/A	1980	890	2.2
PD 2[b]	N/A	3440	1010	3.4
STPDM 4[a]	2.84 : 1	1530	620	2.5
STPDM 5[b]	0.81 : 1	3120	870	3.6

[a] Sodium metal to 1,10-dibromodecane ratio 2 : 1. [b] Sodium metal to 1,10-dibromodecane ratio 1 : 1.

DOI: 10.1039/b009100f

Table 2 Comparative surface polarities of starch, a typical polyalkane and a typical starch–polyalkane material

Sample	Polyalkane : starch ratio	$\lambda_{max/nm}$	Sample polarity
Potato starch	N/A	592	0.543
Polyalkane	N/A	630	0.453
Starch–polyalkane material	1.33 : 1	538	0.693

This indicates a surface polarity for the composites that is greater than either of its component parts (Table 2). Scanning electron microscopy may help to explain the origin of this effect (Fig. 3). Potato starch exists as pebble-like granules which vary between 10 and 100 μm in size. The composite materials however, are apparently made up of smaller particles (< 5 μm) bound to larger (polyalkane) particles (up to 200 μm). The higher effective surface area of the starch may also result in a higher available concentration of surface hydroxyl groups leading to greater surface polarity. Despite the relatively high surface polarity as measured by Reichardt's dye, the materials are hydrophobic and float on water unchanged for periods of several weeks before water eventually permeates the structure sufficiently for them to sink.

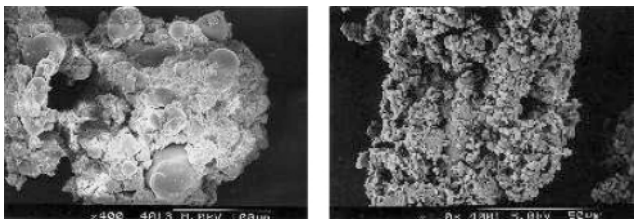

Fig. 3 Scanning electron microscopy (SEM) images of a typical starch–polyalkane material (STPAM) before (left) and after (right) removal of sodium colloid by water washing.

Perhaps the most dramatic effect of the enhanced surface activity of the new materials is their capacity for chemical modification with silanes. Stirring the materials with 3-(trimethoxy)aminopropylsilane in refluxing toluene for 24 h before filtration followed by through washing with toluene and then refluxing aqueous ethanol gives solid materials which were dried at 110 °C for 24 h. The measured loadings of aminoalkyl groups of up to 0.6 mmol g^{-1} (1.4 mmol g^{-1} based on the starch present) are over 10× greater than the maximum loading that can be obtained with potato starch (0.05 mmol g^{-1}). It is interesting to calculate that the level of derivatisation of potato starch corresponds to < 1% of the total number of hydroxyl groups that are present—an indication of the poor availability of these groups. By increasing the availability of the groups in the new materials the degree of functionalisation has increased to *ca.* 10%.

The derivatisation values that can be achieved with the new materials are comparable to those that can be obtained on a high surface area porous silica gel.[6] This comparison is further reinforced by measuring the activity of the aminoalkyl-derivitised starch–polyalkane materials in a typically base-catalysed reaction. The reaction chosen was the Knoevenagel reaction, a useful carbon–carbon bond forming reaction that relies on the base-activation of a carbon acid. The rates of the Knoevenagel reaction between ethyl cyanoacetate and cyclohexanone in cyclohexane catalysed by a typical aminopropyl-starch–polyalkane composite material, an aminopropyl-functionalised mechanical mixture of starch and a polyalkane, and aminopropyl-potato starch are compared in Fig. 4. The

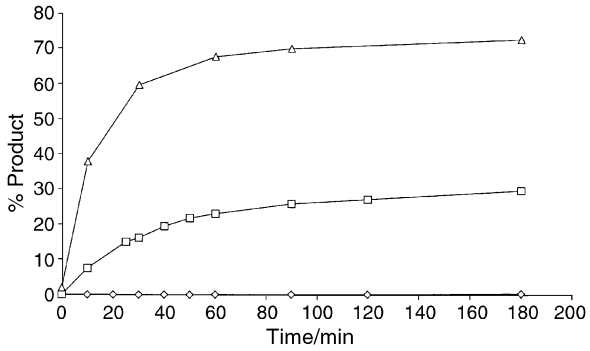

Fig. 4 Reaction profiles for the Knoevenagel condensation reaction of ethyl cyanoacetate and cyclohexanone catalysed by aminopropylsilane on starch (◇), aminopropylsilane on a typical starch–polyalkane material (△) and aminopropylsilane on a mechanical mixture of starch and a typical polyalkane (□).

differences are dramatic. While the ordinary starch based material has almost no activity in the reaction and that based on the starch–polyalkane mechanical mixture is low, the derivitised new material is very active and comparable to their porous silica analogues.[6] Starch that has been treated with sodium metal or sodium hydroxide solution but in the absence of the halocarbon gives a material that has an unchanged FTIR spectrum, thermal analysis and interaction with Reichard's dye compared to ordinary starch. It does however show a higher capacity for reaction with the aminopropylsilane although the resulting material is only as active in the model reaction as the starch–polyalkane mechanical mixture.

We have extended the synthetic methodology to other α,ω-dibromoalkanes. 1,6-Dibromohexane and 1,2-dibromoethane can be used in place of 1,10-dibromodecane with apparently very similar reactions occurring. All of the materials are resistant to water over periods of several weeks, all can be derivatised to high levels with aminoalkylsilanes (0.3–0.6 mmol g^{-1}) and all of the resulting derivatised solids are active solid base catalysts in the test reaction. The ability to increase substantially the availability of the starch hydroxyl groups enabling high degrees of derivatisation while rendering the materials water-resistant would seem to be an attractive combination of properties. The method of polymerising starch-intercalated monomers to achieve this may well open the door to a family of new and useful materials based on an inexpensive renewable resource.

We gratefully acknowledge the support of the Royal Academy of Engineering and the Engineering and Physical Sciences Research Council (EPSRC) for a Clean Technology Fellowship to J. H. C. and ICI/EPSRC for a studentship to J. E. H.

Notes and references

1 J. Jane, *Pure Appl. Chem.*, 1995, **A32**, 751.
2 *Carbohydrates as Organic Raw Materials*, ed. H. Van Bekkum, Carbohydrate Research Foundation, VCH, New York, 1994; J. A. Radley, *Industrial uses of Starch and its Derivatives*, Applied Science, London, 1976.
3 R. B. Seymour and C. E. Carraher, *Polymer Chemistry, an Introduction*, Marcel Dekker, 2nd edn.,1998; G. J. L. Griffin, *Proc. Symp. Degradable Plastics*, Soc. Plastic. Indust., Washington, 1987.
4 R. E. Benifield, R. H. Cragg, R. G. Jones, S. A. McIntosh, A. C. Swain and A. J. Wiseman, *Z. Phys. D*, 1993, **26(S)**, 18.
5 S. J. Tavener, J. H. Clark, G. W. Grey, P. A. Heath and D. J. Macquarrie, *Chem. Commun.*, 1997, **12**, 1147.
6 D. J. Macquarrie, J. H. Clark, J. E. G. Mdoe and A. Priest, *React. Functional Polym.*, 1997, **35**, 153.

ChemComm

Site-selective coordination behaviour of the Py_2P^--anion: the N–C–P-allylic system as σ- and π-donor in $[(PMDETA)Cs\{(\mu\text{-}PPy)Py\}]_2$ and as a μ_2-σ-phosphorus-donor in $[\{Cp(CO)_2Fe\}_2\{(\mu\text{-}P)Py_2\}][BMe_4]$†

Matthias Pfeiffer,[a] Thomas Stey,[a] Heinrich Jehle,[a] Bernd Klüpfel,[a] Wolfgang Malisch,[a] Vadapalli Chandrasekhar[b] and Dietmar Stalke*[a]

[a] *Institut für Anorganische Chemie der Universität Würzburg, Am Hubland, D-97074 Würzburg, Germany. E-mail: dstalke@chemie.uni-wuerzburg.de*

[b] *Indian Institute of Technology, Kanpur, Department of Chemistry, Kanpur-208 016, India*

Received (in Cambridge, UK) 26th October 2000, Accepted 11th January 2001
First published as an Advance Article on the web 1st February 2001

The coordination flexibility of the ambidentate Py_2P^--anion (Py = 2-pyridyl) spans the wide range from σ-all-nitrogen chelation to hard organometallic moieties, σ-phosphorus μ_2-bridging in dinuclear iron complexes to π-N,C,P heteroallyl coordination to the soft caesium.

Primary and secondary alkali metal phosphides MPR_2 and MPHR are key transfer reagents in organophosphorus synthesis and in the introduction of phosphide ligands to catalytically active transition metal fragments.[1] The structural topology of these species has been reviewed recently[2] and is mainly determined by the donor base, *e.g.* in the [(donor)$LiPPh_2$] complexes,[3] by the radius and polariseability of the alkali metal[4] and the size of the substituents.[5] In general, bulky groups (*e.g.* 2,4,6-$(F_3C)_3C_6H_2$[5a] or terphenyl[5b–d]) and heavier alkali metals prompt M–aryl π interactions in addition to M–P σ bonds.[2b] Rather than varying the bulk of the aryl substituent we incorporate donor centres in group 14 and 15 element bonded rings such as di(2-pyridyl)-amides, -phosphides and -arsenides Py_2E^- (Py = 2-pyridyl, E = N, P, As) to modulate the coordinaton behaviour.[6] In the Py_2P^- anion both ring nitrogen atoms chelate the metal to leave the phosphorus divalent.[7] The alkali metal coordination in the substituent periphery opens up the door to unique reactivity in these complexes, *e.g.* the reduction of the iminophosphorane $Py_3P{=}NSiMe_3$ to chiral phosphane amines $RPyPN(H)SiMe_3$ *via* lithium organics involving the cleavage of two P–C Py bonds in a single step.[8] The adaptability of these pyridyl substituted ligands is exemplified by the flexible coordination behaviour towards various metal centres. Thus, the pyridyl nitrogen atoms may be involved in coordination exclusively (Scheme 1, **A**)[6,7] or in conjunction with the bridging heteroatom (Scheme 1, **B**).[9]

Although it is anticipated that in species **A**, the central atom E can further function either as a 2e or 4e donor to form heterometallic derivatives, recent theoretical calculations, supported by experiments, have shown that while in the amides (E = N) the amido nitrogen does function as a typical Lewis base,[9] the situation in the corresponding phosphides (E = P) is different.[10] In the latter, nearly all the charge density couples into the pyridyl rings, leaving the central phosphorus atom only attractive for soft metals in the form of a π-acid type of coordinating centre. In order to test the coordination abilities further, we reacted the pyridyl phosphides with two contrasting type of metals *viz.*, Cs(I) and Fe(II). Towards the soft caesium metal in the complex $[(PMDETA)Cs\{(\mu\text{-}PPy)Py\}]_2$ **2** [PMDETA = $(Me_2NCH_2CH_2)_2NMe$] an unprecedented coordination behaviour of the di(2-pyridyl)phosphide ligand is observed. In this complex the ligand is involved *simultaneously* in a σ (through P and N) as well as a π (through the P–C–N segment) interaction with the caesium ions. This hetero aza allylic coodination represents an entirely new facet of coordination capability of the pyridyl phosphide ligands. In the iron complex $[\{Cp(CO)_2Fe\}_2\{(\mu\text{-}P)Py_2\}][BMe_4]$ **5** the phosphorus atom of the ligand bridges two Fe(II) centres without any further Fe–N contacts. The reaction of di(2-pyridyl)phosphane, Py_2PH[7] **1** with caesium metal in the presence of PMDETA afforded the dimeric complex **2** [eqn. (1)].‡ In an attempt to prepare

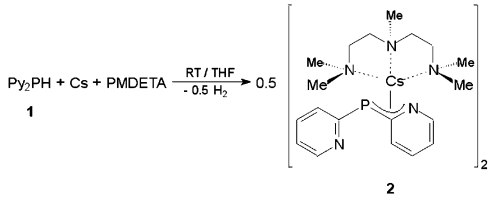

(1)

heterobimetallic compounds we have reacted the aluminium derivative $[Me_2Al(Py_2P)]$ **3**[7] with $[CpFe(CO)_3][BF_4]$ **4**[11] where in general a carbonyl group can easily be replaced by a phosphane.[12] We aimed to utilise the vacant phosphorus site for coordination with Fe(II) while retaining the Al–N bonds. However, the Al–N bonds in the complex are cleaved presumably by the formation of the thermodynamically favourable AlF_3 accompanied by the alkylation of the tetrafluoroborate anion. This leads to the formation of $[\{Cp(CO)_2Fe\}_2\{(\mu\text{-}P)Py_2\}][BMe_4]$ **5** [eqn. (2)].‡

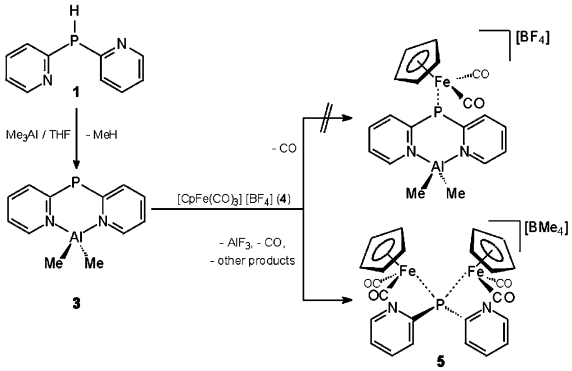

(2)

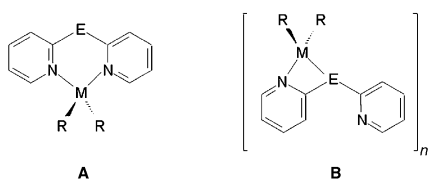

Scheme 1

† Dedicated to Professor Siegfried Hünig on the occasion of his 80th birthday.

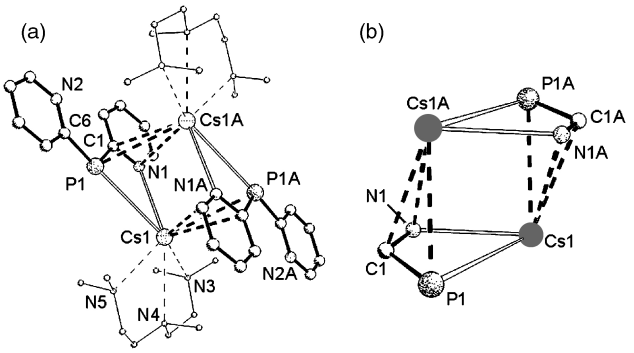

Fig. 1 Solid-state structure of **2**. Selected bond distances (pm) and angles (°): P1–C1 179.4(4), P1–C6 179.8(4), P1–Cs1 365.2(2), P1–Cs1A 369.3(2), N1–Cs1 321.2(4), N1–Cs1a 337.3(4), C1–Cs1a 334.6(4); C1–P1–C6 108.67(18), P1–C1–N1 111.3(3), P1–C6–N2 126.2(3).

Both $[(PMDETA)Cs\{(\mu\text{-}PPy)Py\}]_2$ **2** and $[\{Cp(CO)_2Fe\}_2\{(\mu\text{-}P)Py_2\}][BMe_4]$ **5**, were structurally investigated,§ allowing the ambidentate coordination flexibility of the Py_2P^- anion toward soft metals to be probed. The dimeric structure of **2** comprises of two distinct modes of bonding of the Py_2P^- ligand [Fig. 1(a)].

The atoms P1 and N1 are involved in a σ-type of interaction with Cs1. At the same time the hetero aza allylic P1–C1–N1 moiety is η^3-coordinated through a π-type of interaction with the second caesium ion Cs1A of the dimeric complex [Fig. 1(b)]. One pyridyl nitrogen on each of the Py_2P^- ligands remains non-coordinated. The P–C bond lengths in the anion are not affected by the metal coordination and are identical within esds [179.4(4), π-coordinated and 179.8(4) pm, non-coordinated] and as long as in other metal di(2-pyridyl)phosphides.[7] Even the P–Cs distances are only marginally different [365.2(2), σ-coordinated and 369.3(2) pm, π-coordinated] and are similar to other caesium phosphides.[5] It is only in the N–Cs distances where the different bonding mode is mirrored in different lengths [321.2(4), σ-coordinated and 337.3(4) pm, π-coordinated]. The different coordination of the ring nitrogen atoms gives rise to two different signals in the ^{15}N MAS NMR spectrum (δ −68.2 and −71.7) although these environments equilibrate in solution. The Cs1–C1 bond of 334.6(4) pm is as short as found in Cs–η^6-carbon coordination[1b] and considerably shorter than to terphenyl substituted phosphides.[5] Hence the P,C,N–Cs π bonding has to be considered a hetero aza allyl coordination with the negative charge not only delocalized to the coordinated ring but also to the other. This clearly proves the anticipated ability of the phosphorus centre in the Py_2P^- anion to coordinate soft metals. This is further substantiated in the structure of $[\{Cp(CO)_2Fe\}_2\{(\mu\text{-}P)Py_2\}][BMe_4]$ **5**. Two soft Lewis acidic metal fragments $[CpFe(CO)_2]^+$ are bridged by the phosphorus atom of a single di(2-pyridyl)phosphide ligand to give the $[\{Cp(CO)_2Fe\}_2\{(\mu\text{-}P)Py_2\}]^+$ cation (Fig. 2).

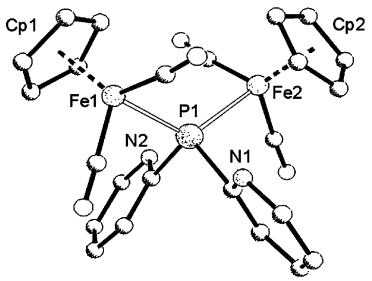

Fig. 2 Solid state structure of the $[\{Cp(CO)_2Fe\}_2\{(\mu\text{-}P)Py_2\}]^+$ cation in **5**. Selected bond distances (pm) and angles (°): P1–C1 184.9(5), P1–C6 184.4(5), P1–Fe1 226.4(2), P1–Fe2 226.5(2), Fe1···Cp1(centre) 172.7, Fe2···Cp2(centre) 171.5, Fe–CO 176.1(7)–176.9(7), C–O 113.7(7)–115.1(7); C1–P1–C6 101.7(3), Fe1–P1–Fe2 120.49(7).

In conclusion the di(2-pyridyl)phosphide ligand shows a metal-dependant coordination response and is involved in a highly unusual σ/π interaction with caesium ion. The latter is clearly reminiscent of the coordination of an allylic type of ligand. On the other hand the phosphorus atom in the Py_2P^- anion is Lewis basic enough to bridge two soft iron metal centres. Yet again the structure determining influence of different metals is obvious.[4]

We gratefully acknowledge the continued financial support of the DFG (SFB 347; D. S., M. P., W. M.) Fonds der Chemischen Industrie (D. S.) and the Alexander von Humboldt foundation (D. S., V. C.).

Notes and references

‡ *Preparation* of **2**: to a suspension of caesium (1.00 g; 7.52 mmol) in 10 ml thf a solution of Py_2PH (1.62 g; 8.77 mmol) in 10 ml thf was added. The deep red reaction mixture was stirred for 12 h at room temperature. It was gently warmed and filtered through Celite. The clear filtrate was treated with PMDETA (1.34 ml; 6.39 mmol) and stirred for 24 h at room temperature. The reaction mixture was kept at −38 °C. Red crystals of compound **2** were isolated. Yield (3.11 g; 72%). Mp: 49 °C. Satisfactory elemental analysis.

§ *Crystal data* for **2**: $C_{19}H_{31}CsN_5P$, M = 493.37, triclinic, space group $P\bar{1}$, a = 935.6(3), b = 1076.6(3), c = 1277.5(4) pm, α = 71.29(3), β = 72.89(3), γ = 83.82(2)°, U = 1.165(1) nm^3, T = 173(2) K, Z = 2, D_c = 1.273 g cm^{-3}, μ(Mo-Kα, λ = 71.073 pm) = 1.670 mm^{-1}. $R1[F > 4\sigma(F)]$ = 0.027 and $wR2$ = 0.066 (all data). For **5**: $C_{28}H_{30}BFe_2N_2O_4P$, M = 493.37, monoclinic, space group $P2_1/c$, a = 1310.7(6), b = 840.3(2), c = 2600.5(10) pm, β = 96.37(2)°, U = 2.846(2) nm^3, T = 193(2) K, Z = 4, D_c = 1.428 g cm^{-3}, μ(Mo-Kα, λ = 71.073 pm) = 1.111 mm^{-1}. $R1[F > 4\sigma(F)]$ = 0.051 and $wR2$ = 0.113 (all data); (G. M. Sheldrick, *Acta Crystallogr. Sect. A*, 1990, **46**, 467; G. M. Sheldrick, SHELXL-96, program for crystal structure refinement, 1996, Göttingen). CCDC 152867 and 152868. See http://www.rsc.org/suppdata/cc/b0/b008662m/ for crystallographic data in .cif or other electronic format.

1 Alkali metal–P: F. Pauer, P. P. Power, in *Lithium Chemistry: A Theoretical and Experimental Overview*, ed. A.-M. Sapse and P. v. R. Schleyer, John Wiley & Sons, New York, 1994, ch. 9; heavier alkali metal–C: J. D. Smith, *Adv. Organomet. Chem.*, 1999, **43**, 267.
2 (*a*) G. Becker, B. Eschbach, D. Käshammer and O. Mundt, *Z. Anorg. Allg. Chem.*, 1994, **620**, 29; (*b*) J. D. Smith, *Angew. Chem., Int. Ed.*, 1998, **37**, 2071.
3 H. Hope, M. M. Olmstead, P. P. Power and X. Xu, *J. Am. Chem. Soc.*, 1984, **106**, 819; R. A. Bartlett, M. M. Olmstead and P. P. Power, *Inorg. Chem.*, 1986, **25**, 1243; R. E. Mulvey, K. Wade, D. R. Armstrong, G. T. Walker, R. Snaith, W. Clegg and D. Reed, *Polyhedron*, 1987, **6**, 987.
4 C. Lambert and P. v. R. Schleyer, *Angew. Chem., Int. Ed.*, 1994, **33**, 1129.
5 (*a*) M. Driess, H. Pritzkow, M. Skipinski and U. Winkler, *Organometallics*, 1997, **16**, 5108; (*b*) G. W. Rabe, S. Kheradmandan, L. M. Liable-Sands, I. A. Guzei and A. L. Rheingold, *Angew. Chem., Int. Ed.*, 1998, **37**, 1404; (*c*) G. W. Rabe, H. Heise, G. P. A. Yap, L. M. Liable-Sands, I. A. Guzei and A. L. Rheingold, *Inorg. Chem.*, 1998, **37**, 4342; (*d*) G. W. Rabe, L. M. Liable-Sands, C. D. Incarvito, K.-C. Lam and A. L. Rheingold, *Inorg. Chem.*, 1999, **38**, 4324; (*e*) M. Drieß, G. Huttner, N. Knopf, H. Pritzkow and L. Zsolnai, *Angew. Chem., Int. Ed.*, 1995, **34**, 316; (*f*) U. Englich, K. Hassler, K. Ruhlandt-Senge and F. Uhlig, *Inorg. Chem.*, 1998, **37**, 3532.
6 For review see: T. Kottke and D. Stalke, *Chem. Ber./Recl.*, 1997, **130**, 1365.
7 A. Steiner and D. Stalke, *J. Chem. Soc., Chem. Commun.*, 1993, 444; A. Steiner and D. Stalke, *Organometallics*, 1995, **14**, 2423.
8 A. Steiner and D. Stalke, *Angew. Chem., Int. Ed. Engl.*, 1995, **34**, 1752; S. Wingerter, M. Pfeiffer, F. Baier, T. Stey and D. Stalke, *Z. Anorg. Allg. Chem.*, 2000, **626**, 1121.
9 H. Gornitzka and D. Stalke, *Eur. J. Inorg. Chem.*, 1998, 311.
10 M. Pfeiffer, F. Baier, T. Stey, D. Leusser, D. Stalke, B. Engels, D. Moigno and W. Kiefer, *J. Mol. Model.*, 2000, **6**, 299.
11 M. E. Grees and R. A. Jacobson, *Inorg. Chem.*, 1973, **12**, 1746.
12 W. Malisch, H. Blau, K. Blank, C. Krüger and L. K. Liu, *J. Organomet. Chem.*, 1985, **C32**, 296; W. Ries, T. Albright, J. Silvestre, I. Bernal, W. Malisch and C. Burschka, *Inorg. Chim. Acta*, 1986, **11**, 119; J. D. Goodrich, P. N. Nichias and J. P. Selegue, *Inorg. Chem.*, 1987, **26**, 3424; W. Malisch, J. Zöller, M. Schwarz, V. Jäger and A. M. Arif, *Chem. Ber.*, 1994, **127**, 1243; W. Malisch, K. Thirase and J. Reising, *Z. Naturforsch., Teil B*, 1998, **53**, 1084.

Snapshots of a Stille reaction

Arturo L. Casado, Pablo Espinet,* Ana M. Gallego and Jesús M. Martínez-Ilarduya

Departamento de Química Inorgánica, Facultad de Ciencias, Universidad de Valladolid, E-47005 Valladolid, Spain. E-mail: espinet@qi.uva.es

Received (in Liverpool, UK) 1st November 2000, Accepted 12th January 2001
First published as an Advance Article on the web 31st January 2001

The main sequential intermediates involved in a real catalytic cycle of the Stille reaction (the coupling of ROTf with CH_2=$CHSnBu_3$ catalyzed by [PdR(OTf)(dppe)]; R = aryl) are observed and characterized unequivocally before the coupling product is released.

Only in rare occasions can real intermediates in a catalytic cycle be observed and unambiguously identified. The Stille reaction (palladium-catalyzed coupling of organotin reagents with carbon electrophiles) is nowadays one of the most powerful synthetic methods for the formation of carbon–carbon bonds.[1] Its catalytic cycle involves a number of intermediates, but evidence for these only comes from model reactions outside a real cycle. Echavarren and coworkers have synthesized oxa- and aza-palladacycles using the oxidative addition of haloarylstannanes to Pd(0) complexes, followed by an intramolecular transmetalation, thus the products can be considered intermediates of a frustrated Stille cycle, which do not undergo coupling because of the high energy of the coupling product.[2] We have shown that the coupling of halides R^1I with SnR^2Bu_3 (R^2 = vinyl or phenyl) follows a S_E2 mechanism involving an associative L-for-R^2 substitution on *trans*-[PdR^1IL_2]. This Pd(II) complex, which can be prepared separately, was actually observed as involved in the catalytic cycle.[3] More recently we have observed the formation and fading out of *trans*-[$PdR^1R^2L_2$] in the coupling of triflates R^1OTf with Sn(vinyl)Bu_3.[4] Here we present a catalytic Stille coupling in which all the main intermediates involved are observed, as they are formed and disappear, using ^1H, ^{19}F and ^{31}P NMR spectroscopy.

[$Pd(C_6F_5)$(OTf)(dppe)] **1a** [dppe = 1,2-bis(diphenylphosphino)ethane] is a poor catalyst for the coupling, in THF at 50 °C (Pd : Sn = 1 : 20), of C_6F_5OTf and CH_2=$CHSnBu_3$ **2** to give CH_2=CHC_6F_5. When the reaction was carried out in THF-d^8 at low temperature, starting with [$Pd(C_6F_5)$(OTf)(dppe)] and CH_2=$CHSnBu_3$ in 1 : 1 molar ratio, several intermediate species could be detected and identified until the coupling product was formed. For an easier monitoring of the cycle the studies were repeated on [$Pd(C_6Cl_2F_3)$(OTf)(dppe)] **1b** ($C_6Cl_2F_3$ = 3,5-dichlorotrifluorophenyl), which behaves identically to **1a** and shows the same intermediates, but has more simple ^{19}F NMR spectra, facilitating a more accurate integration of the signals.[5] Scheme 1 shows, step by step, the mechanism of the catalytic cycle and the ^1H NMR spectra of the intermediates identified in the stoichiometric cycle for **1b** while Fig. 1 shows the evolution of the reaction, as monitored by ^{19}F NMR.

The first intermediate in the cycle is **1a** (or **1b**). Under catalytic conditions **1a** is formed very slowly by oxidative addition of C_6F_5OTf to [Pd(0)], but stoichiometrically these compounds are better prepared from [PdRCl(dppe)] (R = C_6F_5, $C_6Cl_2F_3$) and AgOTf. Complexes **1a** and **1b** are stable in the solid state and have been isolated and fully characterized.[6] In solution in dry THF they give the ionic species [PdR(dppe)(THF)](OTf) (specific molar conductivity, Λ_m = 4.66 S cm^{-1} mol^{-1} for **1a**),[7] on which the transmetallation occurs.[4]

The next step is the transmetalation on **1b** leading to a σ-vinyl complex [$Pd(C_6Cl_2F_3)(CH{=}CH_2)$(dppe)] **3**, characterized by NMR. Its ^{19}F NMR spectrum shows the characteristic resonances expected for a $C_6Cl_2F_3$ group linked to Pd(II), with the

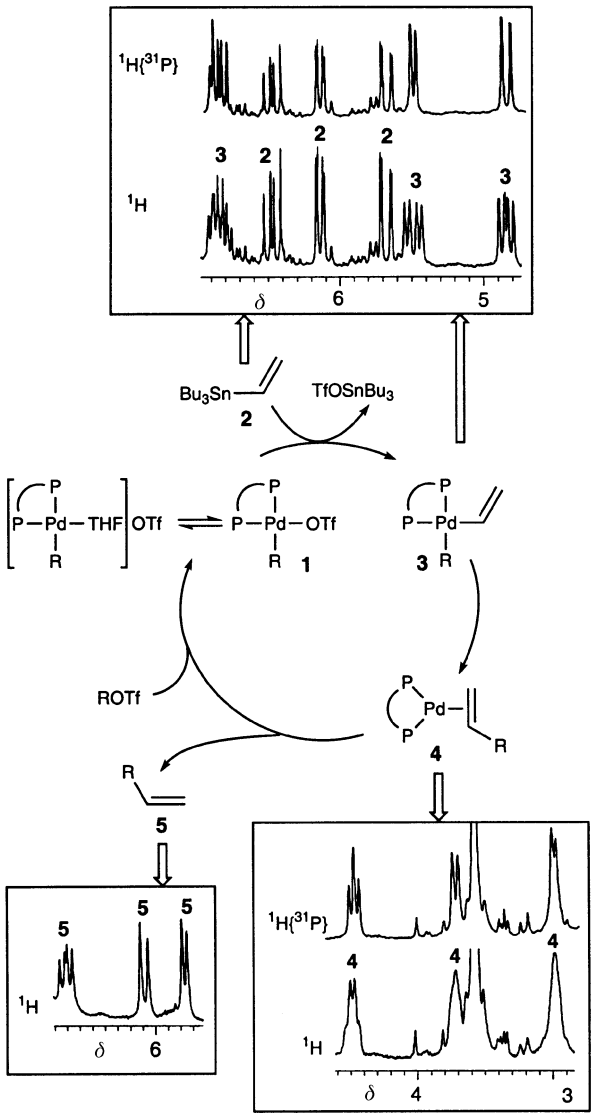

Scheme 1 Catalytic cycle showing the ^1H NMR spectra of the products detected in the range of vinylic protons.

F_{ortho} coupled to the *trans* phosphorus atom (coupling to the *cis* phosphorus is not observed). In the $^{31}P\{^1H\}$ NMR spectrum two signals are observed: one for the P *trans* to $C_6Cl_2F_3$, which appears as an overlapped doublet of triplets, and one for the *cis* phosphorus which appears as a doublet. The ^1H NMR spectrum (Scheme 1) shows three resonances for the three vinylic protons, coupled to phosphorus (see changes upon ^{31}P irradiation in the corresponding $^1H\{^{31}P\}$ NMR spectrum).

Complex **3** is unstable and can be observed only at low temperature.[8] In spite of the *cis* configuration of this complex, the reductive elimination step takes place less easily than with PPh_3 because of the small bite angle chelating ligand,[9] and this stabilizes the compound sufficiently for it to be observed.[10] The

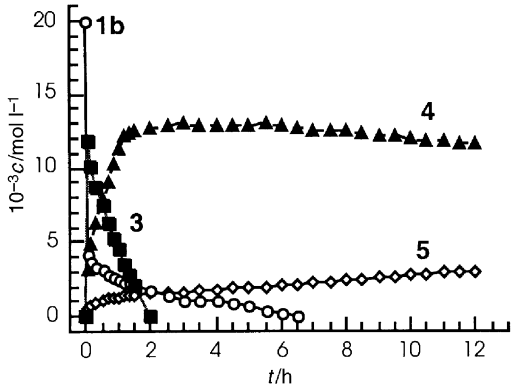

Fig. 1 Profiles of the reaction between [Pd($C_6Cl_2F_3$)(OTf)(dppe)] **1b** and CH_2=CHSnBu_3 **2** in THF at 243 K. Concentrations were obtained by integration in the ^{19}F NMR spectra. Starting concentration: 0.02 mol L^{-1} in **1b**.

coupling product remains coordinated stabilizing a Pd^0 complex [Pd(dppe)(η^2-CH_2=$CHC_6Cl_2F_3$)] **4**. Its ^{1}H NMR spectrum (Scheme 1) shows three broadened signals, at higher field than in the σ-vinyl complex **3** due to the bigger shielding produced by the metallic center. They are coupled to each other (as seen by ^{1}H COSY) and also coupled with the phosphorus nuclei of the dppe ligand. In the ^{1}H{^{31}P} NMR spectrum (Scheme 1) only the coupling between protons is observed. The ^{31}P NMR spectrum of **4** shows an AB system. This chemical inequivalence of the two P atoms is consistent with a trigonal-planar coordination of the palladium, with the double bond of the asymmetric olefin lying in the plane containing the palladium atom and two phosphorus atoms. Similar complexes have been reported in the literature.[11] This compound is again rather stable and can be observed even at room temperature in the stoichiometric reaction. Upon decomposition (or when it undergoes oxidative addition) the olefin CH_2=$CHC_6Cl_2F_3$ **5** is released.

In catalytic conditions the cycle should close upon oxidative addition to **4** or to a low coordinated [Pd(0)] complex formed by decoordination of **5**. This oxidative addition is extremely slow and decomposition pathways compete, causing the low efficiency of the catalyst.[11*a*] However, four to five turnovers are observed showing that the cycle is actually catalytic. Alternatively, the oxidative addition step can be accelerated very efficiently by adding LiCl once **4** has been formed [the accelerating effect of LiCl on some Stille catalytic cycles is well documented in ref. 1(*a*), and is discussed in ref. 11(*a*)]. This leads to the easy formation of [PdRCl(dppe)] on which, however, transmetalation is extremely slow. A thorough discussion of these observations will be made in a forthcoming full paper.

This article is dedicated to Professor Rafael Usón on occasion of his 75th birthday. The work was supported by the Dirección General de Investigación Científica y Técnica (Project No. PB96−0363) and the Junta de Castilla y León (Project No. VA80-99). A. M. G. is grateful for a grant from the Dirección General de Enseñanza Superior (Spain).

Notes and references

1 (*a*) V. Farina, V. Krishnamurthy and V. J. Scott, *The Stille Reaction*, in *Organic Reactions*, 1997, vol. 50, p. 1; (*b*) V. Farina, V. Krishnamurthy and V. J. Scott, *The Stille Reaction*, Wiley, New York, 1999; (*c*) S. P. Stanforth, *Tetrahedron*, 1998, **54**, 263; (*d*) V. Farina and G. P. Roth, *Adv. Met-Org. Chem.*, 1996, **5**, 1; (*e*) T. N. Mitchell, *Synthesis*, 1992, 803; (*f*) J. K. Stille, *Angew. Chem., Int. Ed. Engl.*, 1986, **25**, 508.

2 D. J. Cárdenas, C. Mateo and A. M. Echavarren, *Angew. Chem., Int. Ed. Engl.*, 1994, **33**, 2445; C. Mateo, D. J. Cárdenas, C. Fernández-Rivas and A. M. Echavarren, *Chem. Eur. J.*, 1996, **2**, 1596.

3 A. L. Casado and P. Espinet, *J. Am. Chem. Soc.*, 1998, **120**, 8978.

4 A. L. Casado, P. Espinet and A. M. Gallego, *J. Am. Chem. Soc.*, 2000, **122**, 11 771.

5 M. A. Alonso, J. A. Casares, P. Espinet, J. M. Martínez-Ilarduya and C. Pérez-Briso, *Eur. J. Inorg. Chem.*, 1998, 1745.

6 **1a** and **1b** were prepared from their corresponding precursors,[12] by treatment of [PdRCl(dppe)] with AgOTf, removal of the AgCl led to crystallisation. **1a**: yield: 89%; calc. for $C_{33}H_{24}F_8O_3P_2PdS$: C, 48.28; H, 2.95; found: C, 48.62, H 3.17%; ^{19}F NMR (ref. $CFCl_3$, $CDCl_3$–THF), δ −78.22/−74.71 (s, CF_3), −118.52/−113.70 (m, *o*-CF), −158.88/−157.76 (t, $^3J_{FF}$ 19.5 Hz, *p*-CF), −162.50/−160.43 (m, *m*-CF); ^{31}P{^{1}H} NMR (ref. 85% H_3PO_4, $CDCl_3$–THF), δ 61.9/67.9 (m, P_{cis}), 46.3/52.6 (m, P_{trans}); ^{1}H NMR (300 MHz, ref. TMS, $CDCl_3$), δ 7.85–7.40 (m, arom-CH), 2.57 (m, CH_2), 2.19 (m, CH_2). **1b**: yield: 87%; calc. for $C_{33}H_{24}Cl_2F_6O_3P_2PdS$: C, 46.42, H, 2.83%; found: C 46.28, H, 2.83%; ^{19}F NMR ($CDCl_3$–THF), δ −78.19/−74.72 (s, CF_3), −92.46/−87.43 (dd, $^4J_{FP(trans)}$ 13.5, $^4J_{FP(cis)}$ 7.5 Hz, *o*-CF), −117.26/−115.14 (s, *p*-CF); ^{31}P{^{1}H} NMR ($CDCl_3$–THF), δ 61.6/67.5 (dt, $^2J_{PP}$ 15.5, $^4J_{FP}$ 7.5 Hz, P_{cis}), 46.0/51.7 (dt, $^2J_{PP}$ 15.5, $^4J_{FP}$ 13.5 Hz, P_{trans}); ^{1}H NMR ($CDCl_3$), δ 7.85–7.43 (m, arom-CH), 2.55 (m, CH_2), 2.18 (m, CH_2).

7 The formation of very similar ionic complexes, with either THF or H_2O displacing the triflate, has been reported, and similar molar conductivity values have been found: J. M. Brown and K. K. Hii, *Angew. Chem., Int. Ed. Engl.*, 1996, **35**, 657–659.

8 *NMR characterization* of the intermediates: **3**: ^{19}F NMR (THF, 243 K), δ −85.41 (d, $^4J_{FP}$ 10.8 Hz, *o*-CF), −119.11 (s, *p*-CF); ^{31}P{^{1}H} NMR (THF, 243 K), δ 47.2 (dt, $^2J_{PP}$ 21.3, $^4J_{FP}$ 10.8 Hz, P_{trans}), 44.0 (d, $^2J_{PP}$ 21.3 Hz, P_{cis}); ^{1}H NMR ([D_8]THF, 243 K), δ 8.00–6.88 (m, arom-CH), 6.83 (m, $^{trans}J_{HH}$ 18.3, $^{cis}J_{HH}$ 10.9, $^3J_{HP(trans)}$ 10.9, $^3J_{HP(cis)}$ 8.3 Hz, CH), 5.49 (dddd, $^{cis}J_{HH}$ 10.9, $^{gem}J_{HH}$ 2.2, $^{4,trans}J_{HP(trans)}$ 25.1, $^4J_{HP(cis)}$ 2 Hz, CH), 4.84 (ddd, $^{trans}J_{HH}$ 18.3, $^{gem}J_{HH}$ 2.2, $^{4,cis}J_{HP(trans)}$ 11.7 Hz, CH), 3.00 (br, CH_2), 2.40 (br, CH_2). **4**: ^{19}F NMR (THF, 243 K), δ −114.64 (s, *o*-CF), −123.24 (s, *p*-CF); ^{31}P{^{1}H} NMR (THF, 243 K), δ 42.5 (d, $^2J_{PP}$ 48.4 Hz, P), 38.7 (d, $^2J_{PP}$ 48.4 Hz, P); ^{1}H NMR ([D_8]THF, 243 K), δ 7.85–6.80 (m, arom-CH), 4.49 (br. m, $^{trans}J_{HH}$ 12.5, $^{cis}J_{HH}$ 9.6, $^3J_{HP(trans)}$ 9.5 Hz, CH), 3.72 (br, $^{trans}J_{HH}$ 12.5 Hz, CH), 2.98 (br, $^{cis}J_{HH}$ 9.6 Hz, CH), 2.50 (br, CH_2), 2.10 (br, CH_2).

9 G. Mann, D. Baranano, J. F. Hartwig, A. L. Rheingold and I. A. Guzei, *J. Am. Chem. Soc.*, 1998, **120**, 9205, and references therein.

10 A similar complex [Pd(CH_2Ph)(CH=CHC_6H_4OMe-*p*)(dppf)] [dppf = 1,1′-bis(diphenylphosphino)ferrocene], obtained treating [PdBr(CH=CHC_6H_4OMe-*p*)(dppf)] with $ClMgCH_2$Ph at −70 °C, has been detected previously: N. A. Cooley and J. M. Brown, *Organometallics*, 1990, **9**, 353. In that case its observation is likely facilitated by the slower elimination when sp^3 carbons are involved: M. J. Calhorda, J. M. Brown and N. A. Cooley, *Organometallics*, 1991, **10**, 353.

11 (*a*) A. Jutand, K. K. Hii, M. Thornton-Pett and J. M. Brown, *Organometallics*, 1999, **18**, 5367; (*b*) J. Krause, W. Bonrath and K. R. Pörschke, *Organometallics*, 1992, **11**, 1158; (*c*) F. Ozawa, T. Ito, Y. Nakamura and A. Yamamoto, *J. Organomet. Chem.*, 1979, **168**, 375.

12 [PdRCl(dppe)] (R = C_6F_5, $C_6Cl_2F_3$) were prepared by a general method reported previously: P. Espinet, J. M. Martínez-Ilarduya, C. Pérez-Briso, A. L. Casado and M. A. Alonso, *J. Organomet. Chem.*, 1998, **551**, 9.

ChemComm

Size effects of ultrafine Pt–Ru particles on the electrocatalytic oxidation of methanol

Yoshio Takasu,* Hiroyuki Itaya, Tomoya Iwazaki, Ryo Miyoshi, Takefumi Ohnuma, Wataru Sugimoto and Yasushi Murakami

Department of Fine Materials Engineering, Faculty of Textile Science and Technology, Shinshu University, 3-15-1 Tokida, Ueda 386-8567, Japan. E-mail: ytakasu@giptc.shinshu-u.ac.jp

Received (in Cambridge, UK) 1st November 2000, Accepted 12th January 2001
First published as an Advance Article on the web 31st January 2001

The specific activity, i_{sp}/A m^{-2} (current density per real surface area), of Cl-free well-homogenized Pt–Ru particles at 25 and 60 °C in aqueous acidic solutions has been found to decrease with a decrease in the size of the Pt–Ru alloy particles, and the mass activity, i_{mass}/A g^{-1} (current density per mass of catalyst metal loaded), showed the same dependency when the size of the alloy particles was < *ca.* 3 nm in diameter.

For the development of methanol fuel cells,[1] many investigations have been made on the catalytic activity of Pt–Ru alloy electrocatalysts which perform as active anodes for methanol and carbon monoxide-containing hydrogen.[2] Among the various factors possibly affecting the catalytic activity of the Pt–Ru alloy catalysts for methanol oxidation, the dependence of the Pt–Ru particle size on the catalytic oxidation of methanol, *e.g.* the 'size effect', is an important factor for recognizing the fundamental catalytic properties of ultrafine alloy particles. The size effect of platinum particles of Pt/C catalysts for the oxidation of methanol has been examined by some research groups;[3] however, that for well-homogenized Pt–Ru alloy particles has not yet been reported. Ultrafine catalyst metal particles are often more active compared to larger ones probably due to their higher concentration of low-coordinated surface metal atoms.

The present investigation has been carried out to clarify the 'size effect' for the electrocatalytic oxidation of methanol on well-homogenized ultrafine Pt–Ru particles supported on a carbon. The alloy composition used was Pt_{50}–Ru_{50}, (Pt : Ru = 1 : 1 mol/mol), since this composition was the most active in the binary alloy catalyst system.[4] The Pt_{50}–Ru_{50}/C catalyst powders were prepared by an impregnation method with carbon black powder (Vulcan XC72R; 254 m^2 g^{-1}) and ethanolic solutions of $Pt(NO_2)_2(NH_3)_2$ and $RuNO(NO_3)_x$. The combination of these metal complexes can give well-homogenized alloy particles.[4] The decomposition of the metal complexes supported on the carbon black powder was made in a stream of $H_2 + N_2$ at 450 °C to attain almost complete alloying, while the catalytic activity for the oxidation of methanol decreased with the preparation temperature from 200 to 450 °C.[4]

Fig. 1 shows high-resolution scanning electron micrographs of Pt_{50}–Ru_{50}/C catalysts with different loading amounts of the alloy. The mean size of Pt_{50}–Ru_{50}, *d*, determined from these electron micrographs increases with the amount of catalyst loading. As shown in Fig. 2, the X-ray diffraction patterns of these Pt_{50}–Ru_{50}/C catalysts show that the lattice constant of the fcc Pt_{50}–Ru_{50} alloys is almost the same value as measured by Gasteiger *et al.* using a bulk Pt_{48}–Ru_{52} alloy, 0.38624 nm.[5]

Fig. 3 shows the relationships between the catalytic activities,[6] specific activity (i_{sp}) and the mass activity (i_{mass}), for the oxidation of methanol in 0.5 mol dm^{-3} H_2SO_4 at 60 °C and the loading amount of the alloys. Some of the mean particle sizes of the Pt_{50}–Ru_{50} particles are marked on the figure. It should be noted that i_{sp} decreases with a decrease in the particle size of Pt_{50}–Ru_{50} at all potentials studied, while i_{mass} gives a maximum value at 40 mass% of alloy loading at all polarization potentials,

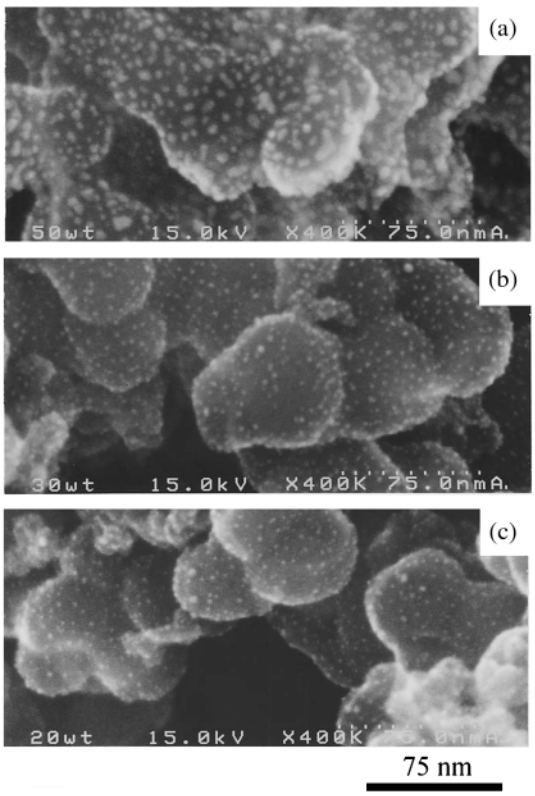

Fig. 1 High-resolution scanning electron micrographs (Hitachi, S-5000) of Pt_{50}–Ru_{50}/C catalysts with different loadings. Loading amount: (a) 20 mass%, (b) 30 mass%, (c) 50 mass%.

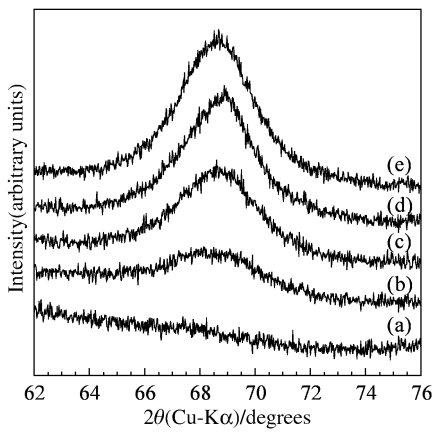

Fig. 2 XRD patterns of Pt_{50}–Ru_{50}/C catalysts with different loadings. Loading amount of Pt–Ru and the mean particle size, *d*, determined from the high-resolution SEM: (a) 10 mass% (*d* = 1.9 Å ± 0.7 nm), (b) 20 mass% (*d* = 2.1 Å ± 0.7 nm), (c) 30 mass% (*d* = 2.7 Å ± 0.6 nm), (d) 40 mass% (*d* = 3.0 Å ± 0.8 nm), (e) 50 mass% (*d* = 3.5 Å ± 1.0 nm).

DOI: 10.1039/b008821h

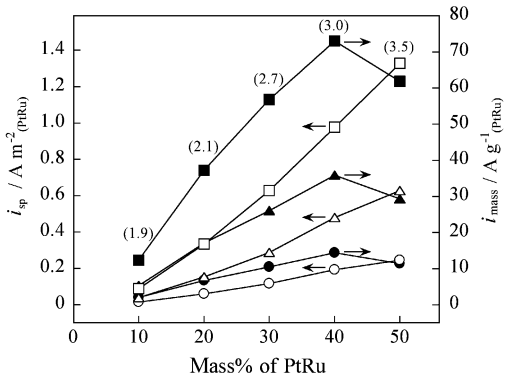

Fig. 3 Dependence of the specific activity (i_{sp}) and mass activity (i_{mass}) for the oxidation of methanol on the size of alloy particles of Pt_{50}–Ru_{50}/C electrodes in 0.5 mol dm^{-3} H_2SO_4 containing 1 mol dm^{-3} MeOH at 60 °C. The values of i_{sp} and i_{mass} correspond to mean quasi-steady state current densities at 30 min after polarization at each electrode potentials per real surface area of alloy particles and per mass of alloy particles, respectively. Open symbols (○, △, □): i_{sp}, Solid symbols (●, ▲, ■): i_{mass}. Polarization potential of the test electrode (*vs.* RHE): ○ and ●, 400 mV; △ and ▲, 450 mV; □ and ■, 500 mV.

where *d* is *ca*. 3 nm. The fact that the specific activities of the larger Pt_{50}–Ru_{50} particles are higher than the smaller ones suggests a larger surface area of alloy particles is more effective for the oxidation. A similar size effect was observed in the experiments at 25 °C. The possible effect of adsorption of the anion, SO_4^{2-}, on the oxidation of methanol can be neglected because similar size effects were also observed in the reaction in 0.020 mol dm^{-3} $HClO_4$. Since no obvious difference in the average distance between Pt_{50}–Ru_{50} particles in Fig.1 (a)–(c) is found, the 'size effect' observed in the catalytic activity is not caused by the diffusion interference between the spherical diffusion areas around the alloy particles.[3] The findings of this investigation suggest, at least, that low-coordinated surface atoms should not be the limiting factor for the electrocatalytic oxidation of methanol.

In order to clarify the origin of the 'size effect' found in this investigation, the electronic structure and surface alloy composition[6] of the Pt–Ru particles as well as the surface species[7] of OH_{ad}, CO_{ad} and CHO_{ad} should be characterized. Such information; however, concerns the overall properties of the alloy catalysts. Furthermore, characterization of the exposed crystal planes[8] and the precise shapes of the alloy particles and elucidation of the optimum ensemble of the surface Pt and Ru atoms[9] for the oxidation of methanol are needed as a function of particle size.

The present work was partly supported by a Grant-in-Aid for Scientific Research on Priority Area of *Electrochemistry of Ordered Interface* from the Ministry of Education, Science and Culture, Japan (grant no. 10131230). We are also grateful to Ishifuku Metal Industry Company Ltd. for supplying us with the platinum complex.

Notes and references

1 A. J. Appleby, *J. Power Sources*, 1992, **37**, 223; A. Hamnett, *Catal. Today*, 1997, **38**, 445; S. Wasmus and A. Kuver, *J. Electroanal. Chem.*, 1999, **461**, 14; B. D. McNicol, D. A. J. Rand and K. R. Williams, *J. Power Sources*, 1999, **83**, 15; X. Ren, T. E. Springer and S. Gottesfeld, *J. Electrochem. Soc.*, 2000, **147**, 92.

2 J. O'M. Bockris and H. Wroblowa, *J. Electroanal. Chem.*, 1964, **7**, 428; M. Watanabe and M. Motoo, *J. Electroanal. Chem.*, 1975, **60**, 267; B. D. McNicol and R. T. Short, *J. Electroanal. Chem.*, 1977, **81**, 249; D. Chu and S. Gilman, *J. Electrochem. Soc.*, 1996, **143**, 1685; J. W. Long, R. M. Stroud, K. E. Swider-Lyons and D. R. Rolison, *J. Phys. Chem. B*, 2000, **104**, 9772.

3 B. D. McNicol, P. A. Attwood and R. T. Short, *J. Chem. Soc., Faraday Trans. 1*, 1981, **77**, 2017; M. Watanabe, S. Saegusa and P. Stonehart, *J. Electroanal. Chem.*, 1989, **271**, 213; A. Kabbabi, F. Gloaguen, F. Andolfatto and R. Durand, *J. Electroanal. Chem.*, 1994, **373**, 251; T. Frelink, W. Visscher and J. A. R. Veen, *J. Electroanal. Chem.*, 1995, **382**, 65; Y. Takasu, T. Iwazaki, W. Sugimoto and Y. Murakami, *Electrochem. Commun.*, 2000, **2**, 671.

4 Y. Takasu, T. Fujiwara, Y. Murakami, K. Sasaki, M. Oguri, T. Asaki and W. Sugimoto, *J. Electrochem. Soc.*, 2000, **147**, 4421.

5 H. A. Gasteiger, P. N. Jr. Ross and E. J. Cairns, *Surf. Sci.*, 1993, **293**, 67.

6 The catalyst electrodes for the examination of the electrocatalytic activity were prepared with a glassy carbon rod (5 mm diameter) on which *ca*. 0.10 μg of the catalyst powder Pt_{50}–Ru_{50}/C was fixed with a dispersion of Nafion 117. The surface area of Pt–Ru particles was determined by cyclic voltammetry for the oxidation of monolayer-adsorbed carbon monoxide, where the Coulombic charge necessary for the oxidation is 420 μC cm^{-2}. The catalytic activity of the electrodes was determined by chronoamperometry.[4] A typical quasi-steady state current density at 30 min after setting of a test electrode at a polarization potential used for the evaluation of the activity gave a *ca*. 15% lower value than that at 15 min.

7 J.-M. Leger and C. Lamy, *Ber. Bunsenges. Phys. Chem.*, 1990, **94**, 1021; R. Ianniello, V. M. Schmidt, U. Stimming, J. Stumper and A. Wallau, *Electrochim. Acta*, 1994, **39**, 1863; J. McBreen and S. Mukerjee, *J. Electrochem. Soc.*, 1995, **142**, 3399.

8 K. Yahikozawa, Y. Fujii, Y. Matsuda, N. Nishimura and Y. Takasu, *Electrochim. Acta*, 1991, **36**, 973.

9 H. A. Gasteiger, N. Markovic, P. N. Ross and E. Cairns, *J. Phys. Chem.*, 1993, **97**, 12 020; H. A. Radmilovic, H. A. Gasteiger and D. N. Jr. Ross, *J. Catal*, 1995, **154**, 98; M. S. Nashner, A. I. Frenkel, D. L. Adler, J. R. Shapley and R. G. Nuzzo, *J. Am. Chem. Soc.*, 1997, **119**, 7760; W. Chrzanowski, H. Kim and A. Wieckowski, *Catal. Lett.*, 1998, **50**, 69; C. W. Hills, M. S. Nashner, A. I. Frenkel, J. R. Shapley and G. R. G. Nuzzo, *Langmuir*, 1999, **15**, 690.

ChemComm

Control of hydrogen bond network dimensionality in tetrachloroplatinate salts†

Alessandro Angeloni and A. Guy Orpen*

School of Chemistry, University of Bristol, Bristol, UK BS8 1TS. E-mail: guy.orpen@bristol.ac.uk

Received (in Cambridge, UK) 27th November 2000, Accepted 16th January 2001
First published as an Advance Article on the web 5th February 2001

Tetrachloroplatinate salts of 4,4-bipiperidinium, piperazinium and *N*-protonated isonicotinic acid or isonicotinamide show two-dimensional NH···Cl hydrogen bond networks related in a rational way to the one-dimensional ribbon polymer network of [4,4′-H_2bipy][$PtCl_4$].

In the synthesis of crystal structures by design, the assembly of molecular units in predefined arrangements is a key goal.[1] Directional intermolecular interactions are the primary tools in achieving this goal and hydrogen bonding is currently the best among them.[2] We have shown[3] that the chelate hydrogen bond moiety **A** (Scheme 1) is a useful supramolecular synthon[1a,c] for the construction of crystal structure of perhalometallate salts of the 4,4′-bipyridinium dication. In these salts the motif **B** is observed, most clearly in [4,4′-H_2bipy][$PtCl_4$] **1** but also in cases where the MCl_4 species forms a chain polymer [4,4′-H_2bipy][MCl_4] (M = Mn, Cd, Pb).[3c] In **1** the NH···Cl hydrogen bond network is one-dimensional (although there are longer CH···Cl contacts[3c]) and the crystal structure can be viewed as arising from close packing of the **B**-type ribbons.[3] To control the crystal structure more completely it is critical to be able to raise the dimensionality of the hydrogen bond networks in such structures in a rational and planned manner. In so doing we will probe the range of cations able to form **B**-type ribbons.

In the first instance we employed cations with two rather than one NH unit per charge starting with the saturated analogue of [4,4′-H_2bipy]$^{2+}$, 4,4-bipiperidinium ([4,4′-H_2bipip]$^{2+}$, **C**). On treatment of an aqueous solution of $K_2[PtCl_4]$ with 4,4′-bipiperidine hydrochloride a crystalline salt [4,4′-H_2bipip][$PtCl_4$] **2** is formed.‡ The crystal structure of **2** has an

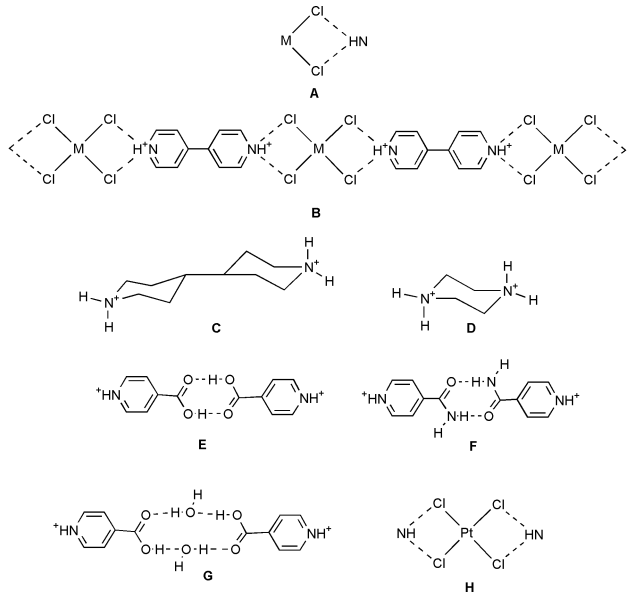

Scheme 1

† Electronic supplementary information (ESI) available: syntheses of **2**–**5**. See http://www.rsc.org/suppdata/cc/b0/b009515j/

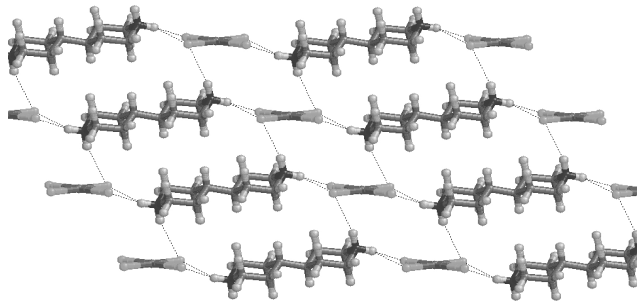

Fig. 1 Structure of the NH···Cl hydrogen bonded layer in crystalline [4,4′-H_2bipip][$PtCl_4$] **2**. The NH···Cl hydrogen bonds are indicated. Hydrogen bond lengths and angles include: in-ribbon NH···Cl 2.79 Å, N–H···Cl 132°, Pt–Cl···HN 89°; NH···Cl 2.45 Å, N–H···Cl 147°, Pt–Cl···HN 98°. Between ribbons: NH···Cl 2.55 Å, N–H···Cl 158°, Pt–Cl···HN 74°.

hydrogen bonded ribbon motif analogous to that of **1** (see Fig. 1). In addition to the chelate hydrogen bond of type **A** in the **B**-like ribbon, which is formed by the equatorial hydrogen at the nitrogens of the [4,4′-H_2bipip]$^{2+}$ cation, a second NH···Cl interaction links parallel ribbons by NH···Cl bonds. The **B**-like ribbons are not flat as they are in **1** because of the chair form of the saturated bipip rings and the inter-ribbon distance is rather larger than in **1** (4.0 Å in **2** compared with 3.5 Å in **1**) as a consequence of the thicker cation in **2**. The chelate hydrogen bond is rather asymmetric in **2**, presumably because one of the chloride ligands involved is also forming a hydrogen bond to the axial NH hydrogen. It is this chloride which forms the longer NH···Cl contact in the **A**-type interaction. The net result is that the NH···Cl hydrogen bond network is two-dimensional. Although, as in **1**, each ribbon is surrounded by six near neighbours the ribbons in **2** are tilted with respect to the hydrogen bonded layers they form so that all ribbons within a layer are parallel but ribbons in adjacent layers are not parallel.

To probe the generality of the NH_2 hydrogen bond donor approach, we also prepared the piperazinium (**D** in Scheme 1) salt, [$C_4H_{12}N_2$][$PtCl_4$] **3** by a similar route.‡ In the crystal structure§ of **3** (Fig. 2) a two-dimensional NH···Cl hydrogen bond network results in which the **B**-like ribbons are more distorted from planarity than in **2**. Thus the type **A** chelate interaction is not planar (see Fig. 3) and is formed by the *axial* NH groups of the piperazinium (*cf.* **2** in which the equatorial NH groups are used). The NH···Cl bonds between **B**-type ribbons are only slightly longer than those within the rows (2.61 *cf.* 2.56 Å) and are also of the chelate type.

Clearly the replacement of the bipyridinium moieties of **1** by bipiperidinium or piperazinium does not prevent the formation of a **B**-type motif. We therefore sought to test other aspects of this motif for robustness by replacing part of the covalent framework of the bipyridinium cation with supramolecular units. Thus protonated isonicotinic acid and isonicotinamide were used in preparation of salts of $[PtCl_4]^{2-}$ from acidic (HCl) aqueous solution in the expectation that supramolecular dications **E** and **F** would replace bipyridinium. In the case of **F**, additional NH hydrogen bond donor capability is available parallel to the plane of the supramolecular dication. In this way

DOI: 10.1039/b009515j

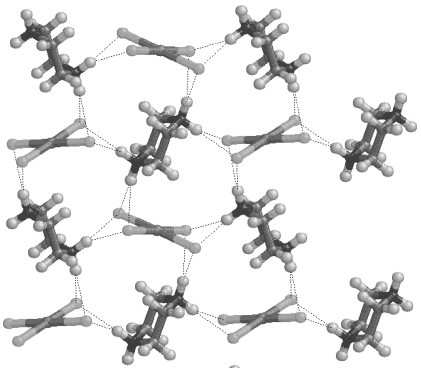

Fig. 2 The NH···Cl hydrogen bonded layer in crystalline [piperazinium][$PtCl_4$] **3**. The NH···Cl hydrogen bonds are indicated. Hydrogen bond lengths and angles include: in-ribbon (across page): NH···Cl 2.56 Å, N–H···Cl 141°, Pt–Cl···HN 87°. Between ribbons: NH···Cl 2.61 Å, N–H···Cl 141°, Pt–Cl···HN 69°.

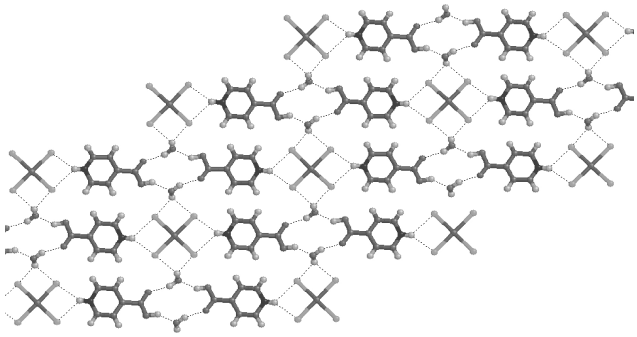

Fig. 3 The hydrogen bonded layer in crystalline [$HNC_5H_4CO_2H$-4]$_2$[$PtCl_4$]·$2H_2O$ **4**. The NH···Cl, OH···Cl and OH···O hydrogen bonds are indicated. Hydrogen bond lengths and angles include: in-ribbon NH···Cl 2.45 Å, N–H···Cl 145°, Pt–Cl···HN 97°; NH···Cl 2.63 Å, N–H···Cl 134°, Pt–Cl···HN 92°; HOH···O(1) 1.90 Å, O-H···O 163°, H···O-C 133°; OH···OH_2 1.74 Å, O-H···OH_2 147°. Between ribbons: OH···Cl 2.63 Å, O–H···Cl 141°, Pt–Cl···HO 85°; OH···Cl 2.77 Å, O–H···Cl 145°, Pt–Cl···HO 82°.

the salts [$HNC_5H_4CO_2H$-4]$_2$[$PtCl_4$]·$2H_2O$ **4** and [$HNC_5H_4CONH_2$-4]$_2$[$PtCl_4$] **5** were prepared‡ and characterised by single crystal X-ray diffraction analyses.§

Both **4** and **5** contain **B**-type ribbons (see Fig. 3 and 4) with supramolecular dications in the chain as anticipated. However the incorporation of water in **4** was unexpected and instead of the R2,2(8) cyclic dimer (**E**), the dihydrate variant (**G**) of this structure, is formed. Thus an R4,4(12) supramolecular motif is incorporated in the **B**-type ribbon of **4** (see Fig. 3). As a result of water incorporation there is a pair of extra hydrogen bond donors present in the supramolecular dication **G** compared with **E**. In contrast **5** has the expected motif containing the classic amide dimer R2,2(8) unit (see Fig. 4). As in **4** there are

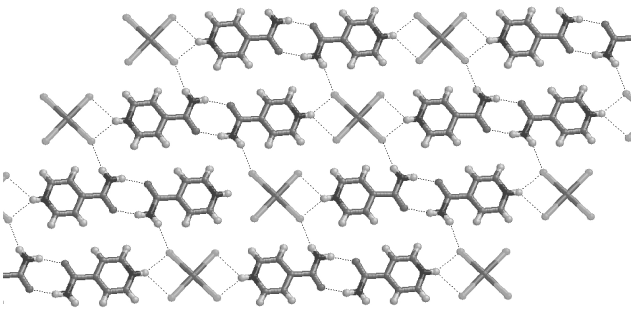

Fig. 4 The hydrogen bonded layer in crystalline [$HNC_5H_4CONH_2$-4]$_2$[$PtCl_4$] **5**. The NH···Cl and NH···O hydrogen bonds are indicated. Hydrogen bond lengths and angles include: in-ribbon NH···Cl 2.47 Å, N–H···Cl 146°, Pt–Cl···HN 97°; NH···Cl 2.60 Å, N–H···Cl 133°, Pt–Cl···HN 80°; NH···O 2.03 Å, N–H···O 161°, NH···O-C 124°. Between ribbons: NH···Cl 2.58 Å, N–H···Cl 156°, Pt–Cl···HN 144°.

additional acidic hydrogens (OH in **4** and NH in **5**) available to cross-link the ribbons. In **4** the spare OH is inclined at 59° to the plane of the ribbon, while in **4** the spare NH bond is near coplanar with the ribbon. As a consequence the resultant cross-linked ribbons are of pleated and planar form in **4** and **5**, respectively.

These results establish:

(1) The robustness of motif **A** in its doubled form **H**; both saturated and aromatic cationic NH donors are compatible with this supramolecular synthon.
(2) The robustness of the periodic structural motif **B** with respect to the nature of the framework to which the NH group(s) are attached, whether saturated or aromatic, molecular or supramolecular. Furthermore the metric of this motif is very flexible, the repeat distance along the **B**-like ribbon in **1** is 15.76 Å while in **2**–**5** it is 15.87, 10.15, 23.38 and 21.32 Å, respectively.
(3) That the presence of additional hydrogen bond donors, beyond those required to form interaction **H** or to form the supramolecular dications of **4** and **5**, may be exploited to add dimensionality to the NH···Cl hydrogen bond network in a rational manner.

Financial support of the EPSRC and the Royal Society and the Leverhulme Trust (a Royal Society Leverhulme Trust Senior Research Fellowship for A. G. O.) is gratefully acknowledged.

Notes and references

‡ *Syntheses* of **2**–**5**. Details are given in ESI†. In general, stoichiometric amount of the nitrogen base (or its hydrochloride) dissolved in aqueous HCl was added to an aqueous solution of K_2PtCl_4 and crystalline samples grown from solution. For **5** this yielded a mixture of products, presumably as a result of hydrolysis of the isonicotinamide. A sample of crystalline **5** was obtained by hand selection of crystals.

§ *Crystal structure analyses of* **2**–**5**: *Crystal data*: [4,4′-H_2bipip][$PtCl_4$] **2**, $C_{10}H_{22}Cl_4N_2Pt$, M = 507.19, monoclinic, space group $P2_1/n$ (no. 14), a = 5.9922(11), b = 10.766(3), c = 11.601(2) Å, β = 95.545(12)°, U = 744.9(3) Å^3, Z = 2, μ = 10.117 mm^{-1}, T = 173 K, 1700 unique data, $R1$ = 0.018. [piperazinium][$PtCl_4$] **3**, $C_4H_{12}Cl_4N_2Pt$, M = 425.05, orthorhombic, space group $Cmca$ (no. 64), a = 12.0729(24), b = 8.6976(28), c = 10.1510(25) Å, U = 1065.9(4) Å^3, Z = 4, μ = 14.112 mm^{-1}, T = 173 K, 646 unique data, $R1$ = 0.016. [$HNC_5H_4CO_2H$-4]$_2$[$PtCl_4$]·$2H_2O$ **4**, $C_{12}H_{16}Cl_4N_2O_6Pt$, M = 507.19, triclinic, space group $P\bar{1}$ (no. 2), a = 6.9551(13), b = 8.5188(12), c = 8.9795(10) Å, α = 86.462(13), β = 73.017(9), γ = 66.472(10)°, U = 465.61(11) Å^3, Z = 1, μ = 8.139 mm^{-1}, T = 173 K, 2114 unique data, $R1$ = 0.019. [$HNC_5H_4CONH_2$-4]$_2$[$PtCl_4$] **5**, $C_{12}H_{14}Cl_4N_2O_2Pt$, M = 583.16, triclinic, space group $P\bar{1}$ (no. 2), a = 6.8888(13), b = 7.7068(18), c = 8.2032(15) Å, α = 88.779(15), β = 72.911(19), γ = 89.466(19)°, U = 416.19(15) Å^3, Z = 1, μ = 9.083 mm^{-1}, T = 173 K, 1900 unique data, $R1$ = 0.018. In **2**, **4** and **5** the metal atoms lie at sites of C_i symmetry as does the dication in **2**. In **3** both cations and anions lie at sites of C_{2h} symmetry. All hydrogen atoms were located in difference maps and included in idealised positions except for OH group hydrogens in **4** which were refined without constraints. CCDC 154209–54212. See http://www.rsc.org/suppdata/cc/b0/b009515j/ for crystallographic data in .cif or other electronic format.

1 (*a*) G. R. Desiraju, *Angew Chem., Int. Ed. Engl.*, 1995, **34**, 2311; (*b*) J. C. MacDonald and G. M. Whitesides, *Chem. Rev.*, 1995, **95**, 37; (*c*) G. R. Desiraju, *Chem. Commun.*, 1997 1475; (*d*) D. Braga, F. Grepioni and G. R. Desiraju, *Chem. Rev.*, 1998, **98**, 1375.
2 (*a*) M. C. Etter, *Acc. Chem. Res.*, 1990, **23**, 120; (*b*) C. B. Aakeröy and K. R. Seddon, *Chem. Soc. Rev.*, 1993, 397; (*c*) A. D. Burrows, C.-W. Chan, M. M. Chowdry, J. E. McGrady and D. M. P. Mingos, *Chem. Soc. Rev.*, 1995, 329; (*d*) S. Subramanian and M. J. Zaworotko, *Coord. Chem. Rev.*, 1994, **137**, 357; (*e*) M. J. Zaworotko, *Nature*, 1997, **386**, 220; (*f*) F. H. Allen, W. D. S. Motherwell, P. R. Raithby, G. P. Shields and R. Taylor, *New J. Chem.*, 1999, **23**, 25; (*g*) G. R. Desiraju, *J. Chem. Soc., Dalton Trans.*, 2000, 3745; (*h*) D. Braga and F. Gresioni, *Acc. Chem. Res.*, 2000, **601**, 33.
3 (*a*) G. R. Lewis and A. G. Orpen, *Chem. Commun.*, 1998, 1873; (*b*) A. L. Gillon, A. G. Orpen, J. Starbuck, X.-M. Wang, Y. Rodríguez-Martín and C. Ruiz-Pérez, *Chem. Commun.*, 1999, 2287; (*c*) A. L. Gillon, G. R. Lewis, A. G. Orpen, S. Rotter, J. Starbuck, X.-M. Wang, Y. Rodríguez-Martín and C. Ruiz-Pérez, *J. Chem. Soc., Dalton Trans.*, 2000, 3897.

The first syntheses of diformamides by carbonylation of aliphatic diamines with Au(I) complex catalysts

Feng Shi, Youquan Deng,* Hongzhou Yang and Tianlong SiMa

State Key Laboratory for Oxo Synthesis and Selective Oxidation and Laboratory of Environmental and Applied Catalysis, Lanzhou Institute of Chemical Physics, Chinese Academy of Sciences, Lanzhou, 730000, China. E-mail: ydeng@ns.lzb.ac.cn; Fax: +86-931-8417088

Received (in Cambridge, UK) 17th November 2000, Accepted 12th January 2001
First published as an Advance Article on the web 7th February 2001

Organic Au(I) complexes could be highly effective catalysts for the synthesis of diformamides by carbonylation of aliphatic diamines, with selectivity significantly enhanced in the presence of the appropriate amount of oxygen.

Gold as a catalytic material has recently been receiving growing attention. Many reactions catalysed over Au catalyst such as CO oxidation,[1,2] selective oxidation,[3,4] removal of NO_X,[5] selective hydrogenation,[6] methane combustion,[7,8] carbonylation of olefins,[9] dehydrogenation dimerization of trialkylstannane,[10] asymmetric aldol reactions[11] and C–C bond making reactions,[12–14] have been reported to have excellent performances. These results indicate that the potential of gold as a catalyst may be tremendous and is worthy of further investigation, since gold has been little explored in comparison with precious metals such as Pd, Pt, Rh *etc*.

In this communication, we show that organic Au(I) complexes can be highly effective catalysts for the synthesis of diformamides, which are useful as intermediate compounds to pharmaceutical substances,[15] by carbonylation of aliphatic diamines in the presence of appropriate amounts of oxygen [eqn. (1)].

$$H_2N(CH_2)_mNH_2 + CO \xrightarrow[O_2]{[Au(PPh_3)_a]_bX} OHCHN(CH_2)_mNHCHO \quad (1)$$

m = 6 or 8; a = 1 or 2; b = 1 or 2; X = Cl, NO_3, or S

$Au(PPh_3)Cl$, $Au(PPh_3)_2Cl$, $Au(PPh_3)NO_3$ and $[Au(PPh_3)]_2S$, synthesized according to the literature,[16–18] were used as the catalysts. $HAuCl_4$ and $Pd(PPh_3)_2Cl_2$ were also employed for the purpose of comparison. All reactions were performed in a 90 cm^3 stainless steel autoclave equipped with a magnetic stirrer. Typically, for each reaction we employed catalyst 0.75–1.6 mol% (relative to the substrate), solvent 20 ml, substrate 0.5 ml or 0.5 g (3–6.5 mmol). These were successively charged into the reactor, and then CO 4–5 MPa and O_2 0–1 MPa were successively introduced with an initial pressure 5.0 MPa at room temperature. The reaction was allowed to proceed with stirring at 150–200 °C for 3 h. The resulting liquid mixture was analyzed with a Hewlett-Packard 6890/5793 GC/MS equipped with a HP 5MS column. The concentrations of reactant and product were given directly by the GC/MS chemstation from the area of each chromatograph peak.

The results of carbonylation of aliphatic amines are shown in Table 1. Although the oxygen was not involved directly in the carbonylation reaction according to eqn. (1), it was found that oxygen had a remarkable impact on the selectivity. For example, when 1,6-hexanediamine was used as the substrate in the presence of $Au(PPh_3)Cl$ as catalyst, entry 1, only 47.2% of the selectivity for desired diformamide could be obtained in the absences of oxygen although the conversion was almost 100%. The main by-product was monoformamide (52.5%), and a very small amount of *N*,*N*,*N*′,*N*′-tetramethyl 1,6-hexanediamine was also detected, which probably resulted from the reaction of 1,6-hexanediamine with methanol. The selectivity, however, was significantly enhanced when a small amount of O_2 was introduced, and it can also be seen that high selectivities could not be achieved if the addition of O_2 was deficient or excessive (entries 2–4), *i.e*. there existed an optimum $P(CO):P(O_2)$ ratio for high selectivities of *ca*. 4.5:0.5, under which only monoformamide (8%) was detected. Hexanolactam (1%), an over oxidized by-product, could be found if the ratio of $P(CO):P(O_2)$ reached 4.0:1.0. Since O_2 was not directly incorporated into the products it was conjectured that O_2 plays a role in maintaining the Au species in an appropriately active state during the reaction.

Although 150 °C was high enough for almost complete conversion of the substrate (entry 5), the highest selectivity for

Table 1 The results of catalytic carbonylation of aliphatic amines with different Au(I) complexes

Ent.	Sub.	Cat.	Sol.	$P(CO):P(O_2)$	T/°C	Con. (%)	Sel. (%)	TOF[a]	TOFP[b]
1	HDA[c]	$Au(PPh_3)Cl$	MeOH	5.0/0	175	100	47.2	30	14.2
2	HDA	$Au(PPh_3)Cl$	MeOH	4.8/0.2	175	100	59.5	30	17.9
3	HDA	$Au(PPh_3)Cl$	MeOH	4.5/0.5	175	100	92	30	27.6
4	HDA	$Au(PPh_3)Cl$	MeOH	4.0/1.0	175	100	87	30	26.1
5	HDA	$Au(PPh_3)Cl$	MeOH	4.5/0.5	150	100	63	30	18.9
6	HDA	$Au(PPh_3)Cl$	MeOH	4.5/0.5	200	100	99	30	29.7
7	HDA	$Au(PPh_3)Cl$	CH_3CN	4.5/0.5	175	100	90	30	27
8	HDA	$Au(PPh_3)Cl$	C_6H_6	4.5/0.5	175	100	95	30	28.5
9	HDA	$Au(PPh_3)_2Cl$	C_6H_6	4.5/0.5	175	100	94	30	28.2
10	HDA	$Au(PPh_3)NO_3$	C_6H_6	4.5/0.5	175	100	93	30	27.9
11	HDA	$[Au(PPh_3)]_2S$	C_6H_6	4.5/0.5	175	100	96	30	28.8
12	HDA	$HAuCl_4$	C_6H_6	4.5/0.5	175	100	10	30	3.0
13	DDA[d]	$Au(PPh_3)Cl$	MeOH	4.5/0.5	200	100	98	20	19.6
14	n-HA[e]	$Au(PPh_3)Cl$	MeOH	4.5/0.5	200	95	51.8	26	13.5
15	c-HA[f]	$Au(PPh_3)Cl$	MeOH	4.5/0.5	200	68	70	38	26.6
16	HDA	$Pd(PPh_3)_2Cl_2$	MeOH	4.5/0.5	150	100	39.5	30	11.9
17	HDA	$Pd(PPh_3)_2Cl_2$	MeOH	4.5/0.5	175	100	79.7	30	23.9

[a] Mole substrate per mole Au per h. [b] Turnover frequency for product. [c] 1,6-Hexanediamine. [d] Decanediamine. [e] n-Hexylamine. [f] Cyclohexylamine.

DOI: 10.1039/b009257f

the desired product was achieved at *ca.* 175 °C, and by-products, such as hexanolactam (0.1%) were detected if the temperature was further increased to 200 °C (entry 6). From entries 3, 7 and 8 it can be seen that the best results were obtained when benzene was employed as solvent, with 95% selectivity achieved; 92% and 90% selectivities were obtained if methanol or acetonitrile were used as solvents, respectively.

$Au(PPh_3)_2Cl$, $Au(PPh_3)NO_3$ and $[Au(PPh_3)]_2S$ were also tested for catalytic activity (entries 9–11). The best catalytic performance was achieved with $[Au(PPh_3)]_2S$ although the differences in selectivities for the desired product were not large with these Au complexes, while the selectivity, when using $HAuCl_4$ as catalyst, was significantly inferior to that with the Au(I) complexes, indicating that the chemical state of Au and the organic ligands played an important role in the selectivity.

The carbonylation of other substrates using $Au(PPh_3)Cl$ as catalyst was further examined under the same reaction conditions (entries 13–15). For decanediamine, almost 100% of conversion and 98% of selectivity were achieved. But $Au(PPh_3)Cl$ as catalyst was less effective when n-hexylamine and cyclohexylamine were used as substrates. The selectivities for the desired products were only 51.8% and 70% respectively, and the main by-products were the corresponding dialkylureas. These results suggested that the organic Au(I) complex catalysts used here were especially effective for the carbonylation of aliphatic diamines to form the corresponding alkyldiformamide.

$Pd(PPh_3)_2Cl_2$ as catalyst was also employed for this reaction, and only 79.7% selectivity was obtained at 175 °C (entry 16) although the conversion could be almost 100%. The main by-products were hexanolactam (5.7%) and monoformamide (14.6%). The catalytic performance of $Pd(PPh_3)_2Cl_2$ was even poorer at 150 °C. This indicates that Au(I) complexes as catalysts for such specific carbonylation are better than the corresponding Pd(II) complexes, although it was well known that Pd complexes are the most effective catalysts for many other carbonylation processes.

It is worth noting that the TOFs listed in Table 1 do not distinguish clearly the differences in performance among these catalysts. For example, the TOFs for entries 1–4 are the same. So, in this work, TOFP (turnover frequency for product), *i.e.* mole product per mole catalyst per hour has been used to characterize the performance of a catalyst. The differences in the catalytic performances are clearly shown with TOFP, for example, at 175 °C the best catalyst is $[Au(PPh_3)]_2S$.

In summary, the organic Au(I) complexes mentioned above can effectively catalyse the carbonylation of aliphatic diamines to produce the corresponding diformamides in the presence of an appropriate amount of oxygen. To our knowledge, this is the first reported study of organic Au(I) complexes as homogeneous catalysts for the synthesis of diformamides by carbonylation of aliphatic diamines. Further optimization towards the gold catalyst system for the carbonylation reaction is now ongoing.

Notes and references

1 A. Sanchez, S. Abbet, U. Heiz, W.-D. Schneider, H. Hakkinen, R. N. Barnett and Uzi Landman, *J. Phys. Chem. A.*, 1999, **103**, 9573.
2 J. Jansson, *J. Catal.*, 2000, **194**, 55.
3 L. Prati and M. Rossi, *J.Catal.*, 1998, **176**, 552.
4 T. Hayashi, K. Tanaka and M. Haruta, *J.Catal.*, 1998, **178**, 566.
5 T. M. Salama, R. Ohnishi and M. Ichikawa, *Chem. Commun.*, 1997, 105.
6 J. E. Bailie and G. J. Hutching, *Chem. Commun.*, 1999, 2151.
7 R. J. H. Grisel, P. J. Kooyman and B. E. Nieuwenhuys, *J. Catal.*, 2000, **191**, 430.
8 R. D. Waters, J. J. Weimer and J. E. Smith, *Catal. Lett.*, 1995, **30**, 181.
9 Q. Xu, Y. Imamura, M. Fujiwara and Y. Souma, *J. Org. Chem.*, 1997, **62**, 1594.
10 H. Ito, T. Yajima, J.-i Tateiwa and A. Hosomi, *Tetrahedron Lett.*, 1999, **40**, 7807.
11 V. A. Soloshonok and A. D. Kacharov, *Tetrahedron.*, 1996, **52**, 245H.
12 A. S. K. Hashmi, L. Schwarz, J.-H. Choi and T. M. Frost, *Angew. Chem., Int. Ed*, 2000, **39**, 2285.
13 T. Hayashi, M. Sawamura and Y. Ito, *Tetrahedron.*, 1992, **48**, 1999.
14 Y. Ito, M. Sawamura and T. Hayashi, *J. Am. Chem. Soc.*, 1986, **108**, 6405.
15 J. W. Mitchell and T. A. Johnson, US Patent 5919979.
16 *Inorganic Syntheses*, ed. R. N. Grimes, Wiley, New York, 1992, **29**, 280.
17 C. A. McAuliffe, R. V. Parish and P. D. Randall, *J. Chem. Soc., Dalton. Trans.*, 1979, **1**, 1730.
18 F. Canales, C. Gimeno, A. Laguna and M. D. Villacampa, *Inorg. Chim. Acta*, 1996, **244**, 95.

Catalytic enantioselective alkylation of heteroaromatic compounds using alkylidene malonates

Wei Zhuang, Tore Hansen and Karl Anker Jørgensen*

Center for Metal Catalysed Reactions, Department of Chemistry, Aarhus University, DK-8000 Aarhus C, Denmark. E-mail: kaj@kemi.aau.dk

Received (in Cambridge, UK) 8th November 2000, Accepted 15th January 2001
First published as an Advance Article on the web 7th February 2001

A catalytic enantioselective alkylation of heteroaromatic compounds using alkylidene malonates has been developed; the reaction proceeds for different heteroaromatic compounds with alkylidene malonates in high yield and enantiomeric excess.

The addition of aromatic C–H bonds to alkenes, the Friedel–Crafts alkylation, is a highly important reaction in synthetic chemistry for the formation of new C–C bonds.[1] A challenge for the Friedel–Crafts alkylation is to perform the reaction in a catalytic enantioselective fashion as this would be a simple and attractive method for the synthesis of optically active aromatic compounds using easily available starting materials. The first examples of catalytic enantioselective addition reactions of aromatic compounds to conjugated compounds such as carbonyls and imines have recently appeared.[2] In the following we will present the first catalytic enantioselective alkylation of heteroaromatic compounds using alkylidene malonates catalyzed by chiral Lewis acids.

The reaction of indole **1a** with alkylidene malonate **2a**[3] in the presence of the chiral bisoxazoline–metal(II) complexes, (*S*)-**4a**-Cu(II), (*S*)-**4b**-Zn(II), as the catalysts[4] proceeds well giving the Friedel–Crafts alkylation adduct **3a** in good yield and high ee [eqn. (1)]. Table 1 gives some representative results for the screening of catalysts and reaction conditions.

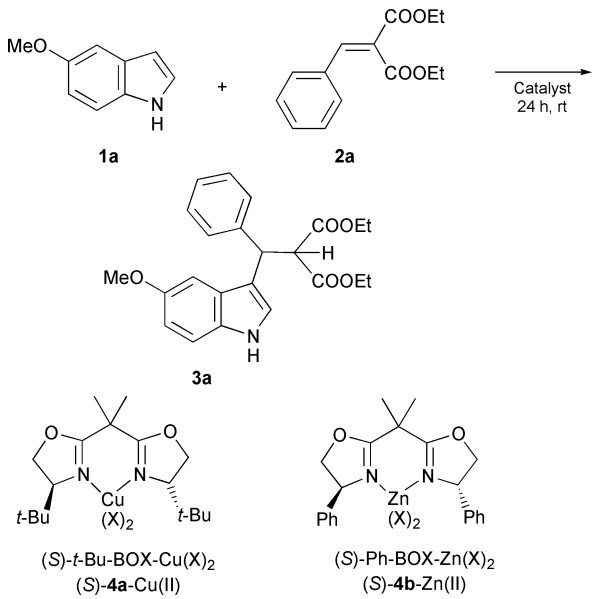

(1)

The reactions were performed with 2 eq. of hexafluoro-*i*-PrOH (HFIP) and 10% catalyst loading.[5] No reaction took place with (*S*)-**4a**-Cu(OTf)$_2$ in MeCN or $MeNO_2$ as solvents, while in Et_2O high conversion to **3a** and good ee was achieved (entries 1–3). The catalyst (*S*)-**4b**-Zn(OTf)$_2$ also gave high conversion, however, the enantioselectivity was low (entry 4). The catalytic activity of (*S*)-**4a**-Cu(OTf)$_2$ in THF was very good and **3a** was obtained in 91% yield and 60% ee (entry 5). The activity increased further by changing counterion from OTf to SbF_6 in CH_2Cl_2 giving high conversion at 0 °C, however, the ee of **3a** dropped from 57 to 35% ee (entry 6 and 7). The effect of addition of HFIP to the reaction was found to be negligible; the reaction rate decreased only slightly and the ee was essentially unchanged in the absence of HFIP (entry 3 *vs.* 8).[5] The effect of other parameters such as lower catalyst loading, concentration and temperature all gave lower conversion to **3a** with very little increase in ee.

Table 1 Screening of chiral Lewis acids and reaction conditions for the reaction of indole **1a** with alkylidene malonate **2a**

Entry	Catalyst	Solvent	X	Conv.[a] (%)	Ee[bc] (%)
1	(*S*)-**4a**-CuX$_2$	MeCN	OTf	—	—
2	(*S*)-**4a**-CuX$_2$	$MeNO_2$	OTf	—	—
3	(*S*)-**4a**-CuX$_2$	Et_2O	OTf	95	60
4	(*S*)-**4b**-ZnX$_2$	Et_2O	OTf	89	8[d]
5	(*S*)-**4a**-CuX$_2$	THF	OTf	91	60 (93)
6	(*S*)-**4a**-CuX$_2$	CH_2Cl_2	OTF	71	57
7[e]	(*S*)-**4a**-CuX$_2$	CH_2Cl_2	SbF_6	92	35
8[f]	(*S*)-**4a**-CuX$_2$	Et_2O	OTf	93	57

[a] Determined by ^{1}H-NMR spectroscopy. [b] Determined by chiral HPLC. [c] Number in parentheses is ee after recrystallization. [d] Opposite enantiomer. [e] Reaction performed at 0 °C. [f] No HFIP used.

A selection of β-substituted alkylidene malonates **2a**–**e** were examined in this reaction with indole **1b** catalyzed by (*S*)-**4a**-Cu(OTf)$_2$ (Table 2). Indole **1b** reacted with **2a** to give the Friedel–Crafts alkylation product **3b** in 73% yield and 60% ee (entry 1).† The dimethyl benzylidene malonate **2b** was significantly more reactive compared to the diethyl derivative (**2a**) giving the addition product in 95% isolated yield, however, the ee was lower for **3b** (entry 1 *vs.* 2). The reactivity of dimethyl *p*-nitrobenzylidene malonate **2c** was comparable to **2b**, and product **3d** was formed in high yield and with 56% ee

Table 2 Reaction of indole **1b** with various β-substituted alkylidene malonates **2a**–**e** catalyzed by (*S*)-**4a**-Cu(OTf)$_2$

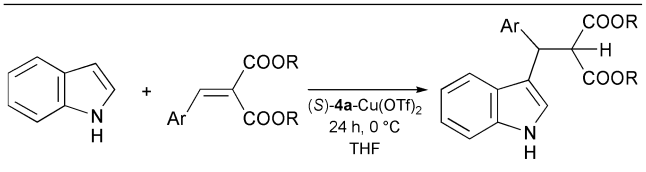

1b **2a-e** **3b-f**

Entry	R, Ar	Yield[a] (%)	Ee[bc] (%)
1	Et, Ph–**2a**	**3b**–73	60 (92)
2	Me, Ph–**2b**	**3c**–95	50
3	Me, 4-NO_2-Ph–**2c**	**3d**–92	56
4	Et, 4-Br-Ph–**2d**	**3e**–45	50
5[d]	Et, 2-Cl-Ph–**2e**	**3f**–87	69

[a] Isolated yield after column chromatography. [b] Determined by chiral HPLC. [c] Number in parentheses is ee after recrystallization. [d] Reaction performed at 30 °C.

DOI: 10.1039/b009008p

(entry 3). The diethyl 2-chlorobenzylidene malonate derivative **2e** was considerably less reactive compared to the other malonates and required a 30 °C reaction temperature for the reaction to go to completion. The enantioselectivity of **3f** was 69% ee, the highest enantioselectivity obtained in this selection.

Dimethyl *p*-nitrobenzylidene malonate **2c** was then used as a standard substrate to probe the reactivity of different aromatic compounds **1a**, **c**–**f** in this Friedel–Crafts alkylation reaction [eqn. (2)] (Table 3).

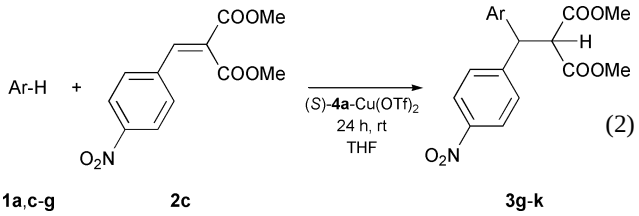

(2)

1a,**c**-**g** **2c** **3g**-**k**

Table 3 Friedel–Crafts alkylation reaction of different heteroaromatic compounds **1a**, **c**–**g** with dimethyl *p*-nitrobenzylidene malonate **2c** catalyzed by (*S*)-**4a**-Cu(OTf)$_2$

Entry	Ar	Yield[a] (%)	Ee[bc] (%)
1[d]	5-MeO-indole–**1a**	**3g**–99	58
2[e]	4-Cl-indole–**1c**	**3h**–62	46
3	*N*-Me-indole–**1d**	**3i**–99	48
4	*N*-Me-pyrrole–**1e**	**3j**–99	36
5	Pyrrole–**1f**	**3k**–99	28
6	2-Me-furan–**1g**	**3l**–99	12

[a] Isolated yield after column chromatography. [b] Determined by chiral HPLC. [c] Determined by chiral HPLC. [d] Reaction performed at 0 °C. [e] Reaction performed at 30 °C.

The reaction with 5-methoxyindole **1a** gave the Friedel–Crafts alkylation product **3g** in excellent yield and with 58% ee (entry 1). 4-Chloroindole **1c** reacted to give the desired product **3h**, although in a lower yield and ee compared to the more electron-rich indole (entry 2). *N*-Methylindole **1d** and *N*-methylpyrrole **1e** both yielded the alkylation products **3i** and **3j**, respectively, with great efficiency and with a small drop in ee (entries 3, 4). Both pyrrole **1f** and 2-methylfuran **1g** reacted in a Friedel–Crafts fashion in excellent yields, but the enantioselectivity of the products was low compared to the other substrates (entries 5, 6).

A further advantage of this Friedel–Crafts alkylation reaction is that the products all are solid and the optical purity can be greatly enhanced to > 90% ee by crystallization as shown for several of the entries in Table 1, 2.

The Friedel–Crafts adducts such as **3b** can undergo decarboxylation[6] to give the mono ester **5** in high yield [eqn. (3)], showing that the present reaction formally can be considered as a Friedel–Crafts alkylation of cinnamates.

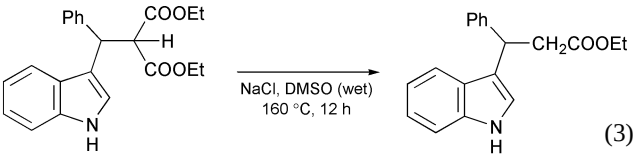

(3)

3b **5**
74% isolated yield

In summary, a new catalytic enantioselective alkylation of heteroaromatic compounds using alkylidene malonates catalyzed by chiral bisoxazoline–copper(II) complexes has been presented. The reactions proceed in high yields and with moderate ee for different aromatic compounds and alkylidene malonates. The optical purity of the products can be enhanced by recrystallization and it is demonstrated that the reaction can be considered as a formal Friedel–Crafts alkylation of cinnamates.

We are indebted to The Danish National Research Foundation for financial support.

Notes and references

† *Representative experimental procedure*: A powdered mixture of Cu(OTf)$_2$ (18 mg, 0.05 mmol) and (*S*)-**4a**-Cu(OTf)$_2$ (16 mg, 0.054 mmol) was dried under vacuum for 1 h. THF (1 mL) was added under N_2 and the solution stirred for 1 h. Compound **2a** (113 μL, 0.5 mmol) was added and stirred for 15 min, followed by addition of **1b** (65 mg, 0.55 mmol). After 24 h the reaction mixture was filtered through a plug of silica gel, washed with Et_2O, and the solvent removed. The product **3b** was obtained as a white solid in 73% yield after purification by chromatography (CH_2Cl_2 as eluent). The ee was determined by HPLC analysis to be 60% (Chiralpack AS, 1.0 mL min^{-1}, 95:5 hexane–*i*-PrOH, R_t = 23 (major) and 26 (minor) min). $\delta_H(C_3D_6O$, 400 Hz) 10.1 (s, 1H), 7.56 (m, 1H), 7.47 (m, 3H), 7.33 (m, 1H), 7.21 (m, 2H), 7.13 (m, 1H), 7.05 (m, 1H), 6.95 (m, 1H), 5.03 (d, J = 11.6 Hz, 1H), 4.40 (d, J = 11.6 Hz, 1H), 3.96 (q, J = 7.2 Hz, 2H), 3.92 (q, J = 7.2 Hz, 2H), 0.98 (t, J = 7.2 Hz, 3H), 0.97 (t, J = 7.2 Hz, 3H); $\delta_C(C_3D_6O$, 100 Hz) 167.7, 167.6, 142.5, 136.9, 128.6, 128.3, 127.1, 126.6, 121.7, 121.6, 119.0, 118.9, 116.7, 111.4, 60.9, 58.9, 43.0, 13.5; HRMS (ES) calcd for $C_{22}H_{23}NO_4$ 365.1627, found (M + Na)$^+$ 388.1525; mp 164–167 °C; $[\alpha]^{20}_D$ = +37.1° (69 mg mL^{-1} $CHCl_3$).

1 For reviews of Friedel–Crafts alkylation reactions see *e.g.*: (*a*) G. A. Olah, R. Krishnamurit and G. K. S. Prakash, *Friedel–Crafts Alkylation* in *Comprehensive Organic Synthesics*, ed. B. M. Trost and I. Flemming, Pergamon Press, Oxford, (1st Edn.) 1991, Vol III, p. 293; (*b*) R. M. Roberts and A. A. Khalaf, *Friedel–Crafts Alkylation Chemistry A Century of Discovery*, Dekker, New York, 1984; (*c*) G. A. Olah, *Friedel–Crafts and Related Reactions*, Wiley-Interscience, New York, 1964, Vol. II, part 1.

2 Activated carbonyl compounds: (*a*) F. Bigi, G. Casiraghi, G. Casnati, G. Sartori, G. Fava and M. F. Belicchi, *J. Org. Chem.*, 1985, **50**, 5018; (*b*) A. Ishii, V. A. Soloshonok and K. Mikami, *J. Org. Chem.*, 2000, **65**, 1597; (*c*) A. Ishii and K. Mikami, *J. Fluorine Chem.*, 1999, **97**, 51; α-dicarbonyl compounds: (*d*) G. Erker and A. A. H. Zeijden, *Angew. Chem., Int. Ed. Engl.*, 1990, **29**, 512; (*e*) N. Gathergood, W. Zhuang and K. A. Jørgensen, *J. Am. Chem. Soc.*, 2000, **122**, 12 517; (*f*) W. Zhuang, N. Gathergood, R. G. Hazell and K. A. Jørgensen, *J. Org. Chem.*, in press; imines: (*g*) M. Johannsen, *Chem. Commun.*, 1999, 2233; (*h*) S. Saaby, X. Fang, N. Gathergood and K. A. Jørgensen, *Angew. Chem., Int. Ed.*, 2000, **39**, 4114.

3 For enantioselective Lewis acid catalyzed Michael reactions of alkylidene malonates see: D. A. Evans, T. Rovis, M. C. Kozlowski, C. W. Downey and J. S. Tedrow, *J. Am. Chem. Soc.*, 2000, **122**, 9134.

4 For recent reviews see (*a*) J. S. Johnson and D. A. Evans, *Acc. Chem. Res.*, 2000, **33**, 325; (*b*) K. A. Jørgensen, M. Johannsen, S. Yao, H. Audrain and J. Thorhauge, *Acc. Chem. Res.*, 1999, **32**, 605; (*c*) A. K. Ghosh, P. Mathivanan and L. Cappiello, *Tetrahedron: Asymmetry*, 1998, **9**, 1.

5 Addition of HFIP was crucial for catalytic activity in the Micheal addition of silylketene acetals to alkylidene malonate see ref 4.

6 A. P. Krapcho, *Synthesis*, 1982, 805.

ChemComm

Modification of SBA-15 pore connectivity by high-temperature calcination investigated by carbon inverse replication

Hyun June Shin,[a] Ryong Ryoo,[a] Michal Kruk[b] and Mietek Jaroniec*[b]

[a] *Department of Chemistry (School of Molecular Science-BK21) Korea Advanced Institute of Science and Technology, Taejon 305-701, Korea. E-mail: rryoo@sorak.kaist.ac.kr*

[b] *Department of Chemistry, Kent State University, Kent, OH 44242, USA. E-mail: jaroniec@columbo.kent.edu*

Received (in Irvine, CA, USA) 5th December 2000, Accepted 17th January 2001
First published as an Advance Article on the web 7th February 2001

Two-dimensional hexagonally ordered CMK-3 carbons were synthesized using SBA-15 templates calcined at a temperature of 1153 K, whereas a disordered carbon was obtained using SBA-15 calcined at 1243 K, demonstrating that the pores connecting ordered mesopores in SBA-15 silica persist up to *ca.* 1153 K, but are eliminated at temperatures close to 1243 K.

During the last several years, SBA-15 silica[1] with a two-dimensional (2-D) hexagonal arrangement of uniform mesopores has attracted much attention and is being evaluated for numerous applications in the fields of catalysis, separations, water purification, and advanced optics devices (see for instance refs. 2 and 3 for references). This remarkable interest stems from the many desirable features of SBA-15, including tailored pore size, high degree of structural ordering, ease of synthesis, availability of economically facile synthesis pathways, high hydrothermal/thermal stability and so forth. Despite all this interest in the synthesis, modification and application of SBA-15, the very structural identification of this material was largely uncertain until recently. Initially,[1] SBA-15 was considered to be an extra-large-pore MCM-41[4] analog with a honeycomb structure of disconnected channel-like pores. Later, much evidence for microporosity in numerous SBA-15 samples was reported,[2,3,5–8] although some SBA-15 samples were claimed to be non-microporous in contrast to others,[7,8] and the very evidence of microporosity was questioned[9] by the authors who first suggested the presence of micropores in SBA-15.[5] As we first pointed out,[2,3] the development of microporosity in SBA-15 and its evolution during the synthesis are consequences of the fact that poly(ethylene oxide) blocks of the poly(ethylene oxide)–poly(propylene oxide)–poly(ethylene oxide) template penetrate the silicate walls of as-synthesized SBA-15, which was convincingly shown by others.[10,11] To end the controversy about the SBA-15 structure and to fully reveal its nature, we carried out an extensive study involving platinum[3] and carbon[12] replication, as well as characterization *via* selective pore blocking *via* chemical modification.[3] The latter method in addition to nitrogen and argon adsorption confirmed the presence of micropores and small mesopores (later referred to as complementary pores) of the size below 3.4 nm.[3] In addition, the replication studies revealed for the first time the interconnected nature of SBA-15 porosity, since bundles of ordered platinum nanowires,[3] and high-surface-area carbon (denoted as CMK-3) with uniform pores between 2-D hexagonal arrangement of uniform rods[12] were obtained through SBA-15 templating. It is otherwise known that similar structures cannot be obtained using MCM-41 as a template under analogous conditions.[13–15] It is also noteworthy that replication is widely considered as a convincing and reliable tool of structure characterization,[16] and carbon replication[17] in particular has already been employed[13] to confirm the worm-like interconnected nature of porosity in HMS silica.[18] The SBA-15 samples studied by platinum and carbon replication were synthesized by employing aging at 373 K which is a standard procedure for SBA-15 synthesis[1] (referred to by some authors as hydrothermal treatment).[8] Therefore, our findings about the interconnected nature of SBA-15 porosity are relevant to the overwhelming majority of SBA-15 preparations reported to date, including some of the materials, which were claimed non-microporous in contrast to other SBA-15 samples.[7,8]

In the current study, we employed carbon replication to confirm that not only typical SBA-15 silica has interconnected porous structure, but also the connecting pores are exceptionally persistent and are not eliminated even after calcination at 1153 K, although there is evidence that they are largely eliminated at somewhat higher temperatures. The remarkably high thermal stability of connecting pores and the possibility of their elimination only at temperatures as high as *ca.* 1273 K were suggested in our earlier study based solely on nitrogen adsorption data.[3]

SBA-15 samples were prepared using the triblock copolymer, $EO_{20}PO_{70}EO_{20}$ (Pluronic P123, BASF) and tetraethoxysilane (TEOS, 98%, Acros). The details of the synthesis procedure are described elsewhere.[12] The synthesis procedure was similar to that originally developed by Stucky and coworkers,[1] except for the particle growth under static conditions and the starting composition of 10 g P123 : 0.10 mol TEOS : 0.60 mol HCl : 20 mol H_2O. The SBA-15 products were filtered off, dried without washing, and calcined in dry air flow at various temperatures. The carbon replication was performed with sucrose as described in detail elsewhere.[12] Briefly, the SBA-15 sample was infiltrated twice with sucrose in the presence of sulfuric acid and subsequently, the carbonization was completed by heating at 1173 K under vacuum. These calcined SBA-15 silicas are referred to as SBA-15-*x*, where *x* denotes the calcination temperature, whereas the SBA-15-*x* templated carbons are referred to as CMK-3-*x* or C-*x*, in the case of ordered and disordered carbons, respectively.

As can be seen in Fig. 1(a), SBA-15 retains a highly ordered hexagonal structure even after calcination at 1243 K, despite the large decrease (*ca.* 25%) in the unit-cell size. The structural shrinkage was accompanied by a major loss of the BET specific surface area and total pore volume (from 850 to 390 and 220 m^2 g^{-1}, and from 1.03 to 0.49 and 0.23 cm^3 g^{-1}, after heating at 1153 and 1243 K, respectively) and significant pore size decrease, but the narrow pore size distribution persisted [Fig. 1(b)]. It should be noted that the specific surface areas, total pore volumes, and pore size distributions reported herein were evaluated as described in our previous work.[2,3] When the resulting SBA-15 silica templates were employed in the carbon synthesis, only samples calcined at 823 and 1153 K afforded 2-D hexagonally ordered carbons, whereas SBA-15 template calcined at 1243 K rendered carbon with no long-range ordering [Fig. 1(a)]. All the carbon replicas exhibited high BET specific surface areas and total pore volumes (1160, 1160 and 750 m^2 g^{-1}, as well as 1.24, 1.08 and 0.53 cm^3 g^{-1}, for CMK-3-823, -1153 and C-1243 samples, respectively). However, only CMK-3-823 and -1153 samples exhibited capillary condensation steps on nitrogen adsorption isotherms, and consequently, narrow mesopore size distributions [Fig. 1(c)], whereas C-1243 carbon was primarily microporous with a relatively small amount of

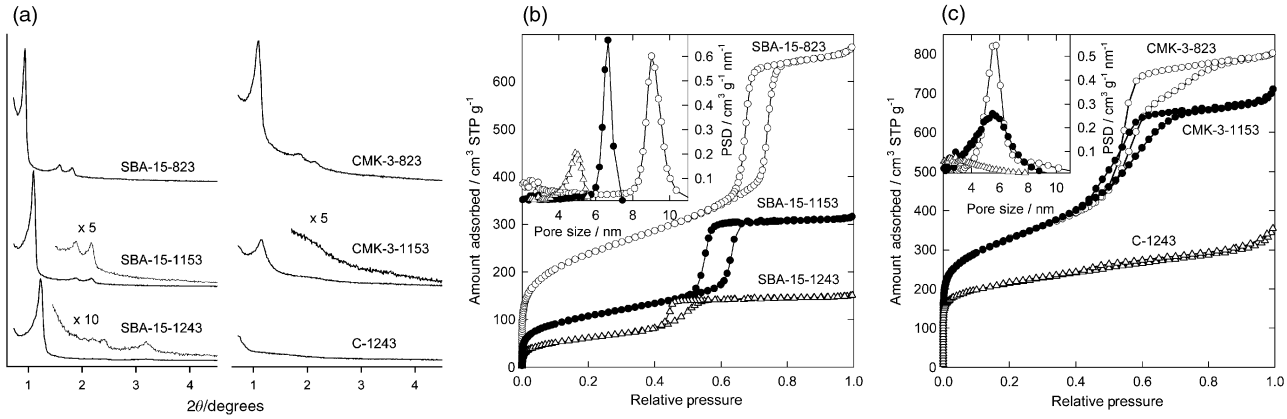

Fig. 1 (a) Powder X-ray diffraction spectra for the SBA-15 and carbon samples. (b) Nitrogen adsorption isotherms and pore size distributions for the SBA-15 silicas. (c) Nitrogen adsorption isotherms and pore size distributions for the carbons synthesized using the SBA-15 silica templates.

disordered mesopores, thus being similar to the high-surface-area carbon synthesized using MCM-41 as a template.[14] It should be noted that the carbon framework of CMK-3 is microporous to some extent,[12] similarly to other ordered mesoporous carbons synthesized using the same carbon precursor.[14,17] Therefore, the overall porosity of CMK-3 is a combination of uniform pores between ordered carbon rods, and micropores within these rods.

The successful synthesis of ordered mesoporous carbons using SBA-15 templates calcined at 823 and 1153 K showed that the structure of SBA-15 prepared under standard conditions is clearly interconnected, otherwise periodic carbon structures would not form. Indeed, as inferred from the structures of C-1243 carbon and carbons templated using MCM-41 silicas,[13,14] disconnected uniform carbon rods do not exhibit a tendency to agglomerate in ordered structures. The carbon templated using SBA-15-1153 exhibited mesoporous structure similar to that of the material prepared from the SBA-15-823 template, thus suggesting that the large structural shrinkage during the high-temperature calcination did not result in the complete elimination of the complementary pores. However, it needs to be kept in mind that the complementary pores are likely to be largely depleted after such a treatment. One can infer this from the examination of the relation between the primary mesopore diameter (w), primary pore volume (V) and primary pore surface area (S) for the SBA-15 templates. Primary pores are defined here as primary (ordered) mesopores and complementary (connecting) pores. The factor wS/V is theoretically expected to be 4 for cylindrical and 4.2 for hexagonal pores. For highly ordered MCM-41 silicas, we found wS/V values of 4.5–5.0 and therefore we can consider this range of values as that characteristic of disconnected cylindrical (or hexagonal) mesopores of size of several nanometers. The difference between the theoretical and experimental values can be largely attributed to the overestimation of surface area using the BET method that was discussed elsewhere.[19] For SBA-15 calcined at 823 K, the wS/V factor was equal to 7.6 (consistent with earlier studies),[3] whereas for the samples calcined at 1153 and 1243 K, it was 5.3 and 4.9, respectively. So, on the basis of data for MCM-41, it is not unexpected that SBA-15 samples with wS/V = 7.6 and 5.3 were suitable as templates for ordered porous carbons, and SBA-15 with wS/V = 4.9 was not. However, it is surprising that as small a difference in wS/V factor as 0.4, and corresponding expected small difference in the pore structure may lead to completely different templating effects. This suggests that either even a small content of connecting pores in SBA-15 is capable of imparting stable CMK-3 frameworks, or connecting pores in SBA-15 are abundant and even their significant depletion leaves an appreciable population, or both of the above. Anyway, further studies of structures of SBA-15 and CMK-3 carbons are highly desirable. In addition, a search for criteria useful for reliable prediction of pore connectivity of templates, and in particular, further work on refinement of the wS/V criterion, appear to be worthwhile. To this end, we should emphasize that w, S and V values need to be evaluated using reliable methodology, for instance the same as or equivalent to that employed herein.[2,3] Where calculation procedures providing different results are used, the threshold value of the wS/V factor for connected pore structures would have to be re-evaluated. Moreover, the value of the wS/V factor should not be treated as fully conclusive as to pore connectivity. The final conclusions about the presence or absence of connecting pores should be based preferably on replication procedures, among which carbon replication appears to be the most convenient.

The Donors of the Petroleum Research Fund administrated by the American Chemical Society are gratefully acknowledged for support of this research.

Notes and references

1 D. Zhao, J. Feng, Q. Huo, N. Melosh, G. H. Fredrickson, B. F. Chmelka and G. D. Stucky, *Science*, 1998, **279**, 548.
2 M. Kruk, M. Jaroniec, C. H. Ko and R. Ryoo, *Chem. Mater.*, 2000, **12**, 1961.
3 R. Ryoo, C. H. Ko, M. Kruk, V. Antochshuk and M. Jaroniec, *J. Phys. Chem. B*, 2000, **104**, 11 465.
4 C. T. Kresge, M. E. Leonowicz, W. J. Roth, J. C. Vartuli and J. S. Beck, *Nature*, 1992, **359**, 710.
5 W. W. Lukens, Jr., P. Schmidt-Winkel, D. Zhao, J. Feng and G. D. Stucky, *Langmuir*, 1999, **15**, 5403.
6 Y.-H. Yue, A. Gedeon, J.-L. Bonardet, J. B. d'Espinose, N. Melosh and J. Fraissard, *Stud. Surf. Sci. Catal.*, 2000, **129**, 209.
7 K. Miyazawa and S. Inagaki, *Chem. Commun.*, 2000, 2121.
8 M. Imperor-Clerc, P. Davidson and A. Davidson, *J. Am. Chem. Soc.*, 2000, **122**, 11 925.
9 M. S. Morey, S. O'Brien, S. Schwarz and G. D. Stucky, *Chem. Mater.*, 2000, **12**, 898.
10 N. A. Melosh, P. Lipic, F. S. Bates, F. Wudl, G. D. Stucky, G. H. Fredrickson and B. F. Chmelka, *Macromolecules*, 1999, **32**, 4332.
11 N. Melosh, P. Davidson and B. F. Chmelka, *J. Am. Chem. Soc.*, 2000, **122**, 823.
12 S. Jun, S. H. Joo, R. Ryoo, M. Kruk, M. Jaroniec, Z. Liu, T. Ohsuna and O. Terasaki, *J. Am. Chem. Soc.*, 2000, **122**, 10 712.
13 J. Lee, S. Yoon, S. M. Oh, C.-H. Shin and T. Hyeon, *Adv. Mater.*, 2000, **12**, 359.
14 M. Kruk, M. Jaroniec, R. Ryoo and S. H. Joo, *J. Phys. Chem. B*, 2000, **104**, 7960.
15 Z. Liu, Y. Sakamoto, T. Ohsuna, K. Hiraga, O. Terasaki, C. H. Ko, H. J. Shin and R. Ryoo, *Angew. Chem., Int. Ed.*, 2000, **39**, 3107.
16 S. A. Johnson, D. Khushalani, N. Coombs, T. E. Mallouk and G. A. Ozin, *J. Mater. Chem.*, 1998, **8**, 13.
17 R. Ryoo, S. H. Joo and S. Jun, *J. Phys. Chem. B*, 1999, **103**, 7743.
18 P. T. Tanev and T. J. Pinnavaia, *Science*, 1995, **267**, 865.
19 M. Kruk, V. Antochshuk, M. Jaroniec and A. Sayari, *J. Phys. Chem. B*, 1999, **103**, 10 670.

ChemComm

The controlled glycosylation of a protein with a bivalent glycan: towards a new class of glycoconjugates, glycodendriproteins†‡

Benjamin G. Davis

Department of Chemistry, University of Durham, Science Laboratories, South Road, Durham, UK DH1 3LE. E-mail: ben.davis@durham.ac.uk

Received (in Liverpool, UK) 10th November 2000, Accepted 12th January 2001
First published as an Advance Article on the web 7th February 2001

The use of a novel bivalent carbohydrate modification reagent, based on a flexible, branched divalent core in a combined site-directed mutagenesis and chemical modification strategy has allowed the first controlled synthesis of a pure protein bearing a branched glycan or a first generation glycodendriprotein.

The glycosylation of proteins plays a key role in determining their expression, folding,[1] thermal and proteolytic stability[2] and in the case of enzymes, catalytic activity.[3] Furthermore, the role of glycoproteins as cell surface markers in communication events such as microbial invasion,[4] inflammation,[5] immune responses and tissue development[6] depends crucially on the correct glycosylation pattern.[7] There is evidence that even very slight alterations in the sugars that decorate the exterior of a protein can cause remarkable changes in these properties. For example, we have recently shown that correct and controlled glycosylation of a model enzyme system with a single saccharide unit allows fine tuning of activity to levels that are up to 8.4-fold greater than the native unglycosylated enzyme.[8] Models for glycoprotein interactions, including activity and binding to corresponding receptor proteins, have been suggested[9,10] and the elucidation of the mechanism of this binding and its consequences is a dominant primary goal in glycoscience and continues to drive the synthesis of glycoconjugates.[11] Access to well-defined scaffolds to probe the nature of these models is essential.[12]

Despite their very shallow binding sites, sugar-binding proteins, lectins, show a remarkable specificity in their binding of multivalent complex carbohydrate structures.[13] The monosaccharide–lectin interaction stands out as an unusually weak and relatively undiscriminating one ($K_d \sim 10^{-3}$ M).[14] However, when more than one saccharide of the right type and in the right orientation are clustered together there is a rapid increase in both affinity and specificity by the corresponding lectin.[15] This increase appears in some cases to be greater than would be expected due to the increase in local concentration (statistical effect) alone and has been termed the 'cluster' or 'multivalent effect', although its origin is yet to be rigorously determined.[10]

† Some of this work was presented at a joint meeting of the RSC Carbohydrate and Bioorganic groups, Warwick, July 6, 2000 and at the 20th International Carbohydrate Symposium, Hamburg, August 30, 2000.
‡ Electronic supplementary information (ESI) available: selected NMR data. See http://www.rsc.org/suppdata/cc/b0/b009184g/

Exploitation of lectin binding does not necessarily rely on mimicking natural multiantennary structures as long as an energetically efficient method for their presentation to binding sites may be found.[15] We have recently demonstrated that glycoproteins bearing a single monosaccharide ligand bind to lectins with a low affinity that is dependent both on the nature of the carbohydrate and the site of glycosylation.[16] We have set ourselves the goal of constructing glycoproteins bearing branched multivalent glycans at predetermined sites to probe the nature of this binding interaction further. Furthermore, by choosing an enzyme as our protein model we aim to investigate the effect of multivalent site-selective glycosylation, by displaying multiple copies of a glycan that previously allowed dramatic enhancement of enzyme actvities.[8] This communication describes the successful construction of the first generation of this new class of glycoconjugates: glycodendriproteins.

To achieve our goals we employed a combined site-directed mutagenesis (SDM) and chemical modification approach (Scheme 1).[17] This strategy involves the introduction of cysteine as a chemoselective tag at preselected positions within a given protein and then reaction of its thiol residue with (polyglyco)methanethiosulfonate reagents, such as **1**. Methanethiosulfonate (MTS) reagents react specifically and quantitatively with thiols[18] and allow the controlled formation of neutral disulfide linkages. We chose as our model protein the serine protease enzyme, subtilisin *Bacillus lentus* (SBL, EC 3.4.21.14).[19] SBL is an ideal model since wildtype (WT)-SBL contains no natural cysteines and methanethiosulfonate reagents therefore react only with the cysteine residue that has been introduced by SDM. In addition, SBL has been well characterized,[20] has been over-expressed and purified,[21] and its crystal structure is known.[22]

Two representative bivalent branched glycan MTS reagents **1a**,**b** based on a trivalent tris(2-aminoethyl)amine (TREN) core were chosen as targets (Scheme 2). **1a** bears at the end of its two glycan branches the same untethered peracetylglucose unit that had previously allowed dramatic enhancement of enzyme activity.[8] **1b** would bear ethyl-tethered mannose moieties that had been used in the construction of previous glycoproteins that had shown low levels of lectin binding.[16] These two reagents would therefore allow the introduction of multivalent, tethered or untethered, glycans with α or β anomeric stereochemistry from different parent carbohydrates systems.

After differentiation of one of the amine termini of TREN **2** through selective protection as its mono-Boc derivative,[23] the two remaining free amine termini were reacted with chloro-

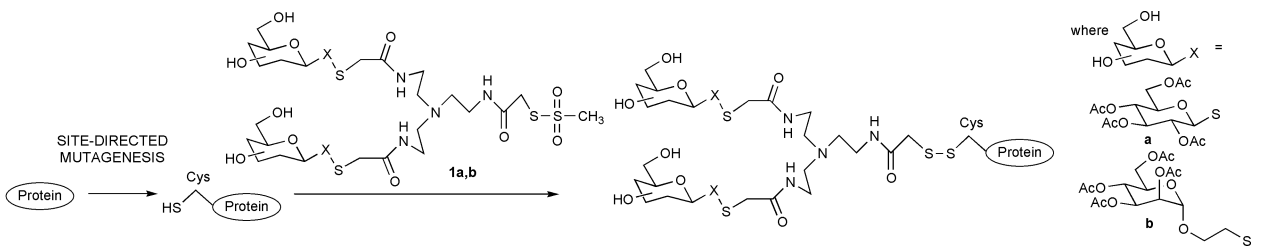

Scheme 1

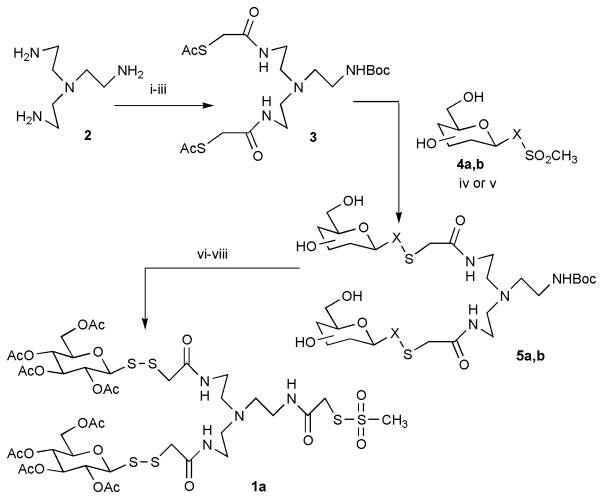

Scheme 2 *Reagents and conditions*: i, 1 equiv. Boc_2O, CH_2Cl_2, −78 °C, 68%; ii, $(ClCH_2CO)_2O$, pyridine, CH_2Cl_2, 97%; iii, KSAc, DMF, 50 °C, 88%; iv, NaOH (aq.) then **4a**, 73%; v, NaOH (aq,) then **4b**, 62%; vi, CF_3COOH, CH_2Cl_2, 88%; vii, $(ClCH_2CO)_2O$, pyridine, CH_2Cl_2, 87%; viii, $NaSSO_2CH_3$, DMF, 50 °C, 68%.

acetic anhydride to give the corresponding bis-α-chloroamide. Treatment of this branched dichloride with the potassium salt of thioacetic acid gave the bis-thioester **3** in a good overall yield (58% over 3 steps from **2**). One-pot selective deprotection and glycosylations of **3** were achieved by treatment with dilute aqueous NaOH solution to hydrolyse the labile thioacetates and then modification of the free thiol groups produced with the appropriate untethered β-gluco **4a** or tethered α-manno **4b** methanethiosulfonate reagents to yield the corresponding bivalent branched glycans **5a**,**b** in 73 and 62% yield, respectively. It should be noted that the use of a basic TREN-core as a scaffold allowed the scavenging of **5a**,**b** from reaction mixtures using acidic ion exchange resin and therefore greatly simplified their purification. With the ability to introduce two distinct glycan endgroups **a** or **b** thus suitably demonstrated, **5a** was selected and the remaining Boc-protected amine terminus elaborated to introduce a methanethiosulfonate group and to create **1a** as the first representative reagent that would allow protein modification. Thus, **5a** was deprotected through treatment with CF_3COOH and the free amine produced converted to the corresponding α-chloroamide. Displacement of α-chloro group through treatment with $NaSSO_2CH_3$ in DMF at 50 °C proceeded smoothly and yielded the target bis-glycan MTS **1a** in good yield (52% over 3 steps from **5a**).

We used **1a** as the first example of a bivalent protein glycosylating reagent to treat mutant protein SBL-S156C in aqueous buffer (Scheme 1). S156C was obtained through site-directed mutagenesis of SBL[8] and bears an outwardly directed reactive thiol on its surface close to its substrate-binding region. Gratifyingly, the reaction was rapid and quantitative, as judged by monitoring changes in specific activity and by titration of residual free thiols with Ellman's reagent.[24] The first generation glycodendriprotein S156C-(S-**a**)$_2$ formed was purified by size-exclusion chromatography and dialysis, and its structures confirmed by rigorous ES-MS analysis (Found 27811, Expected 27805 Da, Fig. 1b). The protein also appeared as a single band on non-denaturing gradient PAGE (Fig. 1(a)), thereby establishing its formation as a single glycoform. This is the first example of a homogeneous protein bearing branched multivalent glycans, or first-generation glycodendriprotein, in which both the site of glycosylation and the structure of the glycan introduced has been predetermined.

Work towards the synthesis of higher generations based on this novel-type of disulfide constructed dendrimeric system is now in progress and the details of kinetics and binding analysis of glycodendriprotein S156C-(S-**a**)$_2$ will be published in due course.

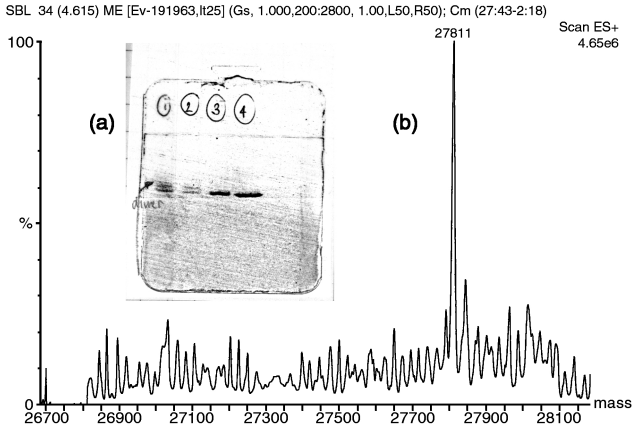

Fig. 1(a) PAGE analysis: Lanes 1,2 crude S156C, Lane 3 pure S156C, Lane 4 pure glycodendriprotein S156C-(S-**a**)$_2$ (b) MaxEnt™ deconvoluted ES^+-MS spectrum of S156C-(S-**a**)$_2$ indicating found mass 27811, expected 27805.

We gratefully acknowledge the generous financial support of Genencor International Inc. and the University of Durham. We also thank Dr R. R. Bott and Professor J. B. Jones for helpful discussions and J.P Marston and Dr M. Jones for technical assistance.

Notes and references

1 A. Helenius, *Mol. Biol. Cell*, 1994, **5**, 253.
2 G. Opdenakker, P. M. Rudd, C. P. Ponting and R. A. Dwek, *FASEB J.*, 1993, **7**, 1330.
3 P. M. Rudd, H. C. Joao, E. Coghill, P. Fiten, M. R. Saunders, G. Opdenakker and R. A. Dwek, *Biochemistry*, 1994, **33**, 17.
4 N. Sharon and H. Lis, *Essays Biochem.*, 1995, **30**, 59.
5 L. A. Lasky, *Annu. Rev. Biochem.*, 1995, **64**, 113; W. I. Weis and K. Drickamer, *Annu. Rev. Biochem.*, 1996, **65**, 441.
6 K. Brueckner, L. Perez, H. Clausen and S. Cohen, *Nature*, 2000, **406**, 411.
7 A. Varki, *Glycobiol.*, 1993, **3**, 97; R. A. Dwek, *Chem. Rev.*, 1996, **96**, 683.
8 R. C. Lloyd, B. G. Davis and J. B. Jones, *Bioorg. Med. Chem.*, 2000, **8**, 1537.
9 R. B. Parekh and C. J. Edge, *TIBTECH*, 1994, 339.
10 S. M. Dimick, S. C. Powell, S. A. McMahon, D. N. Moothoo, J. H. Naismith and E. J. Toone, *J. Am. Chem. Soc.*, 1999, **121**, 10286; J. B. Corbell, J. J Lundquist and E. J. Toone, *Tetrahedron: Asymmetry*, 2000, **11**, 95.
11 B. G. Davis, *J. Chem. Soc., Perkin Trans. 1*, 1999, 3215.
12 B. G. Davis, *Chem. Ind.*, 2000, 134.
13 N. Sharon and H. Lis, *Essays Biochem.*, 1995, **30**, 59.
14 Y. C. Lee and R. T. Lee, *Acc. Chem. Res.*, 1995, **26**, 323.
15 Y. C. Lee, R. R. Towsend, M. R. Hardy, J. Lönngren, J. Arnarp, M. Haraldsson and H. Lönn, *J. Biol. Chem.*, 1983, **258**, 199.
16 B. G. Davis, D. Hodgson, A. Ullman, K. Khumtaveeporn, R. Sala, R. R. Bott and J. B. Jones, unpublished work. Lectin binding led to enhanced selectivity in the degradation of a mannose specific lectin by SBL glycosylated with a single mannose residue.
17 B. G. Davis, R. C. Lloyd and J. B. Jones, *J. Org. Chem.*, 1998, **63**, 9614; B. G. Davis and J. Bryan Jones, *Synlett*, 1999, 1495; B. G. Davis, M. A. T. Maughan, M. P. Green, A. Ullman and J. B. Jones, *Tetrahedron: Asymmetry*, 2000, **11**, 245.
18 R. Wynn and F. M. Richards, *Methods Enzymol.*, 1995, **201**, 351.
19 C. Betzel, S. Klupsch, G. Papendorf, S. Hastrup, S. Branner and K. S. Wilson, *J. Mol. Biol.*, 1992, **223**, 427.
20 H. Gron, M. Meldal and K. Breddam, *Biochemistry*, 1992, **31**, 6011.
21 M. R. Stabile, W. G. Lai, G. DeSantis, M. Gold, J. B. Jones, C. Mitchinson, R. R. Bott, T. P. Graycar and C.-C. Liu, *Bioorg. Med. Chem. Lett.*, 1996, **6**, 2501.
22 P. Kuhn, M. Knapp, S. M. Soltis, G. Ganshaw, M. Thoene and R. Bott, *Biochemistry*, 1998, **37**, 13446.
23 P. Tecilla, U. Tonellato, A. Veronese, F. Felluga and P. Scrimin, *J. Org. Chem.*, 1997, **62**, 7261.
24 G. L. Ellman, K. D. Courtney, V. Andres and R. M. Featherstone, *Biochem. Pharmacol.*, 1961, **7**, 88.

A bridging ethyl complex of aluminium

Zhengkun Yu, Mary Jane Heeg and Charles H. Winter*

Department of Chemistry, Wayne State University, Detroit, Michigan 48202, USA. E-mail: chw@chem.wayne.edu

Received (in Columbia, MO, USA) 13th September 2000, Accepted 20th December 2000
First published as an Advance Article on the web 7th February 2001

Treatment of triethylaluminium (2 equiv.) with diphenylpyrazole (1 equiv) affords a pyrazolate-bridged dialuminium complex that contains a bridging ethyl group between the two aluminium centers; this complex has been structurally characterized and its reactivity and properties are described.

The bridging of saturated hydrocarbon groups between two aluminium ions is widely recognized.[1,2] Despite widespread interest in this phenomenon, there are actually very few such compounds that have been structurally characterized and nearly all contain methyl bridges.[2] Hexakis(cyclopropyl)dialuminium has been structurally characterized and contains two bridging cyclopropyl groups per dimeric unit.[3] In addition to homobimetallic complexes, there is a small family of structurally characterized complexes in which methyl[4] or ethyl[5] groups act as bridges between aluminium and a different metal center [mostly lanthanide(III) ions]. The degree of association of several saturated higher alkyl derivatives of aluminium has been investigated in solution and in the gas phase by several different techniques.[6–9] Triethylaluminium and tri-*n*-propylaluminium were found to be dimeric by freezing point depression measurements in benzene, while triisopropylaluminium and triisobutylaluminium are predominantly monomeric in this medium apparently due to steric hindrance to dimerization.[7] Triethylaluminium was reported to be predominantly dimeric in the gas phase, as determined by vapor density measurements.[8] The low-temperature ^{1}H NMR spectrum of triethylaluminium has been interpreted in terms of a dimeric structure similar to that of trimethylaluminium dimer.[9] However, despite extensive investigation of aluminium alkyls over many years, there have been no reports of structurally characterized complexes in which an *n*-alkyl group other than methyl serves as the bridging group. In this context, we report the synthesis, structure, properties and reactivity of an aluminium pyrazolate complex that contains an ethyl group bridging between two aluminium atoms.

Treatment of diphenylpyrazole with triethylaluminium (2 equiv.) in hexane at ambient temperature led to slow ethane evolution over 18 h. The bridging ethyl complex **1** was isolated as colorless needles after crystallization of the crude residue from hexane (Scheme 1).† The formulation of **1** as the ethyl-bridged structure was suggested initially by the ^{1}H and ^{13}C{^{1}H} NMR spectra. At –40 °C in toluene-d_8, resonances due to terminal ethyl groups were observed in the ^{1}H NMR spectrum at δ 1.27 (t) and −0.30 (q) while another set of ethyl resonances appeared at δ 1.00 (t) and 0.93 (q). The ratio of these two sets of peaks (δ 1.27, −0.30 and 1.00, 0.93) was 4:1, suggesting that the presence of a bridging ethyl ligand. In the ^{13}C{^{1}H} NMR spectrum at −40 °C, the terminal ethyl carbons resonated at δ 9.79 and 1.79, while sharp bridging ethyl ligand resonances were observed at δ 7.35 and 4.08. At or below −40 °C in toluene-d_8, static NMR spectra with sharp resonances were obtained for **1**. Upon warming from −40 to 20 °C in toluene-d_8, the methyl and methylene resonances of the bridging ethyl resonance gradually broadened and shifted downfield slightly. Above 20 °C, only one type of ethyl group was observed, suggesting rapid exchange of terminal and bridging ethyl sites. The bridged ethyl structure of **1** was established in the solid state by X-ray crystallography, as described below.

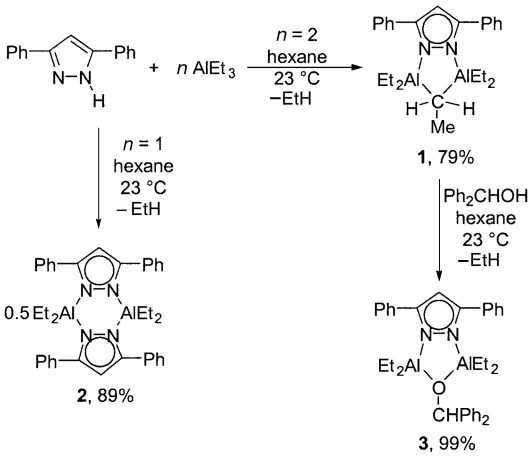

Scheme 1

Other reactions relating to **1** are outlined in Scheme 1. Treatment of diphenylpyrazole with triethylaluminium (1 equiv.) afforded the dimeric pyrazolato complex **2** (89%) as colorless crystals after crystallization from hexane. Protonolysis of **1** with diphenylmethanol in hexane at 23 °C was complete within 0.25 h to afford the diphenylmethoxo complex **3** (99%) as colorless crystals. The structures of **2** and **3** were established by a combination of spectral and analytical techniques.

The X-ray crystal structure of **1** was determined.‡ Fig. 1 shows a perspective view of **1** along with selected bond lengths and angles. Consistent with the NMR analysis, the molecule consists of a diphenylpyrazolato ligand with a diethylalumino group bonded to each nitrogen atom. An ethyl group acts as a bridge between the two aluminium atoms. The two nitrogen atoms and two aluminium atoms occupy an approximate plane, but the methylene carbon of the bridging ethyl group is situated 0.95 Å above this plane. The aluminium–nitrogen bond lengths are 1.928(2) and 1.936(2) Å. The aluminium–carbon bond lengths lie in the range 1.942(4)–1.967(3) Å for the terminal ethyl groups and are 2.144(4) and 2.150(4) Å for the bridging ethyl group. These aluminium–carbon bond lengths are very similar to the related values in structurally characterized aluminium complexes with bridging methyl groups.[2] The carbon–carbon bond length of the bridging ethyl group [1.535(4) Å] is within the normal range for such bonds and does not differ significantly from the values for the terminal ethyl groups. The geometry about the aluminium centers is distorted tetrahedral.

The crystal structure of **1** provides the first structural documentation of a saturated *n*-alkyl group other than methyl bridging between two aluminium centers. The bridging ethyl ligand in **1** appears to be far more stable than the analogous group in triethylaluminium. In the ^{1}H NMR spectrum of triethylaluminium the bridging methylene resonance is only resolved below −60 °C, suggesting that bridge–terminal ethyl group exchange is fast on the NMR timescale above this temperature.[9] In **1**, the bridging ethyl resonance is resolved at temperatures as high as 20 °C. We have recently reported the synthesis, structure and molecular orbital calculations of pyrazolate-bridged dialuminium complexes that contain bridg-

DOI: 10.1039/b008047k

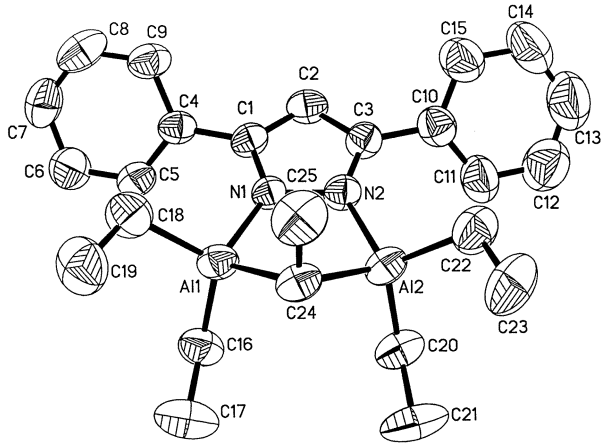

Fig. 1 Perspective view of **1**. Selected bond lengths (Å) and angles (°): Al(1)–N(1) 1.928(2), Al(2)–N(2) 1.936(2), Al(1)–C(16) 1.942(4), Al(1)–C(18) 1.967(3), Al(2)–C(20) 1.947(3), Al(2)–C(22) 1.942(4), Al(1)–C(24) 2.144(4), Al(2)–C(24) 2.150(4), C(16)–C(17) 1.496(5), C(18)–C(19) 1.533(5), C(20)–C(21) 1.508(5), C(22)–C(23) 1.544(5), C(24)–C(25) 1.535(4), N(1)–N(2) 1.378(2), N(1)–Al(1)–C(16) 111.93(14), N(1)–Al(1)–C(18) 109.79(13), N(1)–Al(1)–C(24) 100.54(13), C(16)–Al(1)–C(18) 117.67(19), C(16)–Al(1)–C(24) 110.75(17), C(18)–Al(1)–C(24) 104.56(16), N(2)–Al(2)–C(20) 110.38(13), N(2)–Al(2)–C(22) 112.18(14), N(2)–Al(2)–C(24) 100.92(12), C(20)–Al(2)–C(22) 116.23(19), C(20)–Al(2)–C(24) 112.12(17), C(22)–Al(2)–C(24) 103.79(18), Al(1)–C(24)–C(25) 112.6(2), Al(2)–C(24)–C(25) 112.0(2), Al(1)–C(24)–Al(2) 90.44(12).

ing methyl groups.[10] The bridging aluminium–carbon bond strengths in these complexes are 6–7 kcal mol^{-1} stronger than the analogous bonds in trimethylaluminium dimer, and calculations indicate that this increased bond strength is due to extended bonding interactions involving pyrazolate π-orbitals. Similar extended bonding interactions in **1** could account for the slower bridge–terminal exchange of the ethyl groups, compared to triethylaluminium. The preparation of **1** suggests that other main group metal complexes with bridging *n*-alkyl ligands may be accessible synthetically by inclusion of pyrazolate or other unsaturated groups in the cyclic array incorporating the bridging alkyl.

Financial support for this work from the National Science Foundation (Grant No. CHE-9807269) and the Defense Advanced Research Projects Agency is gratefully acknowledged.

Notes and references

† *Spectroscopic data*: for **1**: mp 66–67 °C; ^{1}H NMR (300 MHz, C_6D_6, 298 K): δ 7.42 (m, 4 H, CH of phenyl rings), 7.09 (m, 6 H, CH of phenyl rings), 6.24 (s, 1 H, pz ring CH), 1.13 (t, *J* 7.8 Hz, 15 H, CH_2CH_3), 1.04 (br s, 2 H, bridging CH_2CH_3), 0.21 (q, *J* 7.5 Hz, 8 H, terminal CH_2CH_3); ^{13}C{^{1}H} NMR (75 MHz, C_6D_6, 298 K): δ 155.38 (s, pz ring C-Ph), 131.35 (s, *ipso*-C of phenyl rings), 129.43 (s, *para*-CH of phenyl rings), 128.74 (s, *ortho*-CH of phenyl rings), 128.54 (s, *meta*-CH of phenyl rings), 107.13 (s, pz ring CH), 9.40 (s, terminal CH_2CH_3), 7.4 (br s, bridging CH_2CH_3), 3.9 (br s, bridging CH_2CH_3), 1.80 (s, terminal CH_2CH_3); MS (EI, 70 eV) *m/z* 304 ([M − $AlEt_3$]$^+$, 16%), 220 ([Ph_2pz]$^+$, 100%). Anal. Calc. for $C_{25}H_{36}Al_2N_2$: C, 71.74; H, 8.67; N, 6.69. Found: C, 71.48; H, 8.60; N, 6.52%. For **2**: mp. 117–118 °C; ^{1}H NMR (300 MHz, C_6D_6, 298 K): δ 7.49 (m, 8 H, CH of phenyl rings), 7.05 (m, 12 H, CH of phenyl rings), 6.26 (s, 2 H, pz ring CH), 0.86 (t, *J* 7.8 Hz, 12 H, CH_2CH_3), −0.16 (q, *J* 7.8 Hz, 8 H, CH_2CH_3); ^{13}C{^{1}H} NMR (75 MHz, C_6D_6, 298 K): δ 158.71 (s, pz ring C-Ph), 131.91 (s, *ipso*-C of phenyl rings), 129.53 (s, *ortho*-CH of phenyl rings), 129.41 (s, *para*-CH of phenyl rings), 128.40 (s, *meta*-CH of phenyl rings), 109.56 (s, pz ring CH), 8.74 (s, CH_2CH_3), 2.91 (s, CH_2CH_3); MS (EI, 70 eV) *m/z* 220 ([Ph_2pzH]$^+$, 100%). Anal. Calc. for $C_{38}H_{42}Al_2N_4$: C, 74.98; H, 6.95; N, 9.20. Found: C, 74.67; H, 7.02; N, 9.29%. For **3**: decomp. pt. 122 °C; ^{1}H NMR (300 MHz, C_6D_6, 298 K): δ 7.56 (m, 4 H, CH of pz phenyl rings), 7.37 (m, 8 H, $CHPh_2$), 7.12 (m, 12 H, $CHPh_2$), 7.01 (m, 6 H, CH of pz phenyl rings), 6.40 (s, 1 H, OCH), 6.37 (s, 1 H, pz ring CH), 0.98 (t, *J* 7.8 Hz, 12 H, CH_2CH_3), 0.00 (m, 8 H, CH_2CH_3); ^{13}C{^{1}H} NMR (75 MHz, C_6D_6, 298 K): δ 155.59 (s, pz ring C-Ph), 140.18 (s, *ipso*-C of $CHPh_2$), 131.81 (s, *ipso*-C of pz phenyl rings), 129.30 (s, CH of phenyl rings), 128.94 (s, CH of phenyl rings), 128.81 (s, CH of phenyl rings), 128.74 (s, CH of phenyl rings), 128.59 (s, 2 CH of phenyl rings), 107.33 (s, pz ring CH), 79.91 (s, $OCHPh_2$), 9.16 (s, CH_2CH_3), 2.03 (s, CH_2CH_3); MS (EI, 70 eV) *m/z* 347 ([M − Ph_2CH − 2Et]$^+$, 6%), 105 (100%). Anal. Calc. for $C_{36}H_{42}Al_2N_2O$: C, 75.50; H, 7.39; N, 4.89. Found: C, 75.27; H, 7.42; N, 4.87%.

‡ Single crystals suitable for X-ray diffraction analysis were grown from hexane at –20 °C. Data were collected on a Siemens/Bruker P4-CCD diffractometer. *Crystal data* for **1**: $C_{25}H_{36}Al_2N_2$, M_r = 418.52, monoclinic, space group $P\bar{1}$, *a* = 12.0348(14), *b* = 11.7684(12), *c* = 18.159(2) Å, β = 101.661(2)°, *V* = 2518.8(5) Å^3, *T* = 296 K, *Z* = 2, μ(Mo-Kα) = 0.126 mm^{-1}, 5850 independent reflections harvested from 1650 frames of data containing 9276 integrated intensities, R_{int} = 0.050. All data were included in the refinement. For $I \geq 2\sigma(I)$, R_1 = 0.0392, wR_2 = 0.0615. Including weak data R_1 = 0.2215, *wR*2 = 0.0808. CCDC 182/1888. See http://www.rsc.org/suppdata/cc/b0/b008047k/ for crystallographic files in .cif format.

1 For leading references, see: F. A. Cotton, G. Wilkinson, C. A. Murillo and M. Bochmann, *Advanced Inorganic Chemistry*, Wiley, New York, 5th edn., pp. 194–195; N. N. Greenwood and E. A. Earnshaw, *Chemistry of the Elements*, Butterworth-Heinemann, Oxford, 1997, 2nd edn., pp. 257–262; J. J. Eisch, in *Comprehensive Organometallic Chemistry*, ed. G. Wilkinson, F. G. A. Stone and E. W. Abel, Pergamon, Oxford, 1982, vol. 1, pp 555–682; T. Mole and E. A. Jeffery, *Organoaluminium Compounds*, Elsevier, Amsterdam, 1972.

2 P. E. Lewis and R. E. Rundle, *J. Am. Chem. Soc.*, 1953, **63**, 986; J. C. Huffman and W. E. Streib, *J. Chem. Soc. D*, 1971, 911; S. K. Byram, J. K. Fawcett, S. C. Nyburg and R. J. O'Brien, *J. Chem. Soc. D*, 1970, 16; R. G. Vranka and E. L. Amma, *J. Am. Chem. Soc.*, 1967, **89**, 3121; V. R. Magnuson and G. D. Stucky, *J. Am. Chem. Soc.*, 1969, **91**, 2544; V. R. Magnuson and G. D. Stucky, *J. Am. Chem. Soc.*, 1968, **90**, 3269; S. D. Waezsada, F.-Q. Liu, E. F. Murphy, H. W. Roesky, M. Teichert, I. Uson, H.-G. Schmidt, T. Albers, E. Parisini and M. Noltemeyer, *Organometallics*, 1997, **16**, 1260; E. Ihara, V. G. Young Jr. and R. F. Jordan, *J. Am. Chem. Soc.*, 1998, **120**, 8277.

3 D. A. Sanders and J. P. Oliver, *J. Am. Chem. Soc.*, 1968, **90**, 5910; J. W. Moore, D. A. Sanders, P. A. Scherr, M. D. Glick and J. P. Oliver, *J. Am. Chem. Soc.*, 1971, **93**, 1035; D. A. Sanders, P. A. Scherr and J. P. Oliver, *J. Am. Chem. Soc.*, 1976, **15**, 861; W. H. Ilsey, M. D. Glick, J. P. Oliver and J. W. Moore, *Inorg. Chem.*, 1980, **19**, 3572.

4 D. G. H. Ballard and R. Pearce, *J. Chem. Soc., Chem. Commun.*, 1975, 621; J. Holton, M. F. Lappert, G. R. Scollary, D. G. H. Ballard, R. Pearce, J. L. Atwood and W. E. Hunter, *J. Chem. Soc., Chem. Commun.*, 1976, 425. J. Holton, M. F. Lappert, D. G. H. Ballard, R. Pearce, J. L. Atwood and W. E. Hunter, *J. Chem. Soc., Dalton Trans.*, 1979, 45; J. Holton, M. F. Lappert, D. G. H. Ballard, R. Pearce, J. L. Atwood and W. E. Hunter, *J. Chem. Soc., Dalton Trans.*, 1979, 54; C. J. Burns and R. A. Andersen, *J. Am. Chem. Soc.*, 1987, **109**, 5853; W. J. Evans, R. Anwander and J. W. Ziller, *Organometallics*, 1995, **14**, 1107; W. T. Klooster, R. S. Lu, R. Anwander, W. J. Evans, T. F. Koetzle and R. Bau, *Angew. Chem. Int. Ed.*, 1998, **37**, 1268.

5 W. J. Evans, L. R. Chamberlain and J. W. Ziller, *J. Am. Chem. Soc.*, 1987, **109**, 7209; H. Yamamoto, H. Yasuda, K. Yokota, A. Nakamura, Y. Kai and N. Kasai, *Chem. Lett.*, 1988, 1963; see also: M. L. Montero, H. Wessel, H. W. Roesky, M. Teichert and I. Usón, *Angew. Chem., Int. Ed. Engl.*, 1997, **36**, 629.

6 For overviews, see: G. E. Coates and K. Wade, in *Organometallic Compounds*, ed. G. E. Coates, M. L. H. Green and K. Wade, Butter & Tanner, London, 3rd edn., 1967, vol. 1, pp. 295–343; J. P. Oliver, *Adv. Organmet. Chem.*, 1970, **8**, 167.

7 K. S. Pitzer and H. S. Gutowsky, *J. Am. Chem. Soc.*, 1946, **68**, 2204; E. G. Hoffman, *Liebigs Ann. Chem.*, 1960, **629**, 104; M. B. Smith, *J. Organomet. Chem.*, 1970, **22**, 273; J. N. Hay, P. G. Hooper and J. C. Robb, *J. Organomet. Chem.*, 1971, **28**, 193; M. B. Smith, *J. Organomet. Chem.*, 1972, **46**, 31; B. Champagne, D. H. Mosley, J. G. Fripiat, J.-M. André, A. Bernard, S. Bettonville, P. François and A. Momatz, *J. Mol. Struct. (THEOCHEM)*, 1998, **454**, 149.

8 A. W. Laubengayer and W. F. Gillam, *J. Am. Chem. Soc.*, 1941, **63**, 477.

9 O. Yamamoto, *Bull. Chem. Soc. Jpn.*, 1964, **37**, 1125; O. Yamamoto, K. Hayamizu and M. Yanagisawa, *J. Organomet. Chem.*, 1974, **73**, 17; Z. Cerný, S. Hermánek, J. Fusek, O. Kri and B. Césenský, *J. Organomet. Chem.*, 1988, **345**, 1; see also: E. G. Hoffman, *Proc. Faraday Soc.*, 1962, **58**, 642; O. Yamamoto, *Bull. Chem. Soc. Jpn.*, 1963, **36**, 1463; K. C. Ramey, J. F. O'Brien, I. Hasegawa and A. E. Borchert, *J. Phys. Chem.*, 1965, **69**, 3418; O. Yamamoto and K. Hayamizu, *J. Phys. Chem.*, 1968, **72**, 822.

10 Z. K. Yu, J. M. Wittbrodt, M. J. Heeg, H. B. Schlegel and C. H. Winter, *J. Am. Chem. Soc.*, 2000, **122**, 9338.

ChemComm

Unprecedented C–H bond oxidative addition of the imidazolium cation to Pt^0: a combined density functional analysis and experimental study

David S. McGuinness,[a] Kingsley J. Cavell*[b] and Brian F. Yates*[a]

[a] *School of Chemistry, University of Tasmania, GPO Box 252-75 Hobart, Tasmania 7001, Australia*
[b] *Department of Chemistry, Cardiff University, PO Box 912, Cardiff, UK CF1 3TB. E-mail: cavellkj@cf.ac.uk*

Received (in Cambridge, UK) 4th December 2000, Accepted 17th January 2001
First published as an Advance Article on the web 7th February 2001

Density functional studies predict that oxidative addition of an imidazolium salt to a Pt^0 complex is an exothermic process, and consistent with this proposal, the reaction of the 1,3-dimethylimidazolium cation with $Pt(PPh_3)_4$ yields a hydrido–Pt^{II} carbene complex.

Heterocyclic carbene complexes of transition metals have been reported to act as precatalysts for a variety of reactions,[1] in particular complexes of the group 10 metals have been found to catalyse a number of C–C couplings.[2–5] In recent reports we have shown that heterocyclic carbene complexes of Pd^{II} and Ni^{II} which contain alkyl, aryl or acyl groups may decompose *via* elimination of 2-organyl imidazolium salts,[4,6,7] and that this reaction occurs *via* concerted reductive elimination of the hydrocarbyl and carbene moieties.[8] Inasmuch as hydrocarbyl–metal species are considered to be intermediates in many catalytic reactions, this reaction represents a significant pathway for catalyst deactivation. As a method of catalyst stabilisation, it seems possible that the energetics of this reaction may be shifted such that the oxidative addition of imidazolium to M^0 is favoured over reductive elimination. Related to this, the use of group 10 metals for catalysis in imidazolium based ionic liquids (ILs) is common, and in several cases heterocyclic carbene complexes have been implicated as the active species.[9,10] A recent report on the use of Pd^0 complexes in imidazolium based ionic liquids[11] prompted us to report our results of a density functional theoretical study, which shows oxidative addition of imidazolium to Pt^0 to be energetically feasible, and experimental results which confirm this.

As oxidative addition to Pt^0 is expected to be more favourable than to Pd^0,[12] the oxidative addition of the 1,2,3-trimethylimidazolium cation to $Pt(PH_3)_2$ was modelled† [eqn. (1)]. The

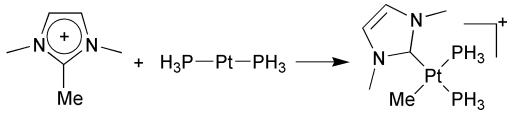

(1)

2-methylimidazolium cation was studied instead of 2*H*-imidazolium to allow comparison with the same reaction with Pd.[8] Furthermore, this reaction is the reverse of the ubiquitous reductive elimination reaction we have observed for hydrocarbyl–Pd carbene complexes.[4,6–8] Optimised geometries of the reactants **1**, precursor complex **2**, transition structure **3** and product **4** are shown in Scheme 1 while a potential energy profile for the reaction is shown in Fig. 1. The first step in the reaction yields the precursor complex **2** with a stabilisation energy of 5.3 kcal mol^{-1}. The initially linear PH_3 groups are slightly distorted such that the angle between them is 167.5°, however the imidazolium cation remains unchanged indicating a weak interaction with Pt. The transition structure **3** lies 33.1 kcal mol^{-1} above **2**, giving an apparent activation enthalpy ($\Delta H^{\ddagger}$) of 27.8 kcal mol^{-1} relative to the separated reactants. The Me–$C_{carbenoid}$ distance increases to 1.78 Å in the transition structure and the Pt–$C_{carbenoid}$ distance is short at 2.06 Å. Importantly, the product of oxidative addition lies 13.5 kcal mol^{-1} *below* the reactants, showing that oxidative addition is

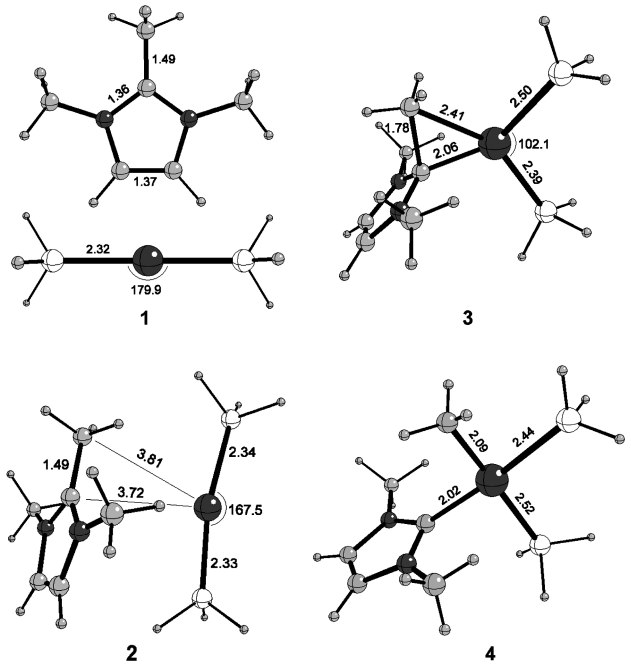

Scheme 1 Optimised geometries (Å and °) of the reactants **1**, precursor complex **2**, transition structure **3** and product **4**.

predicted to be exothermic. In contrast, oxidative addition to the analogous Pd system is found to be slightly endothermic.[8] The Gibbs free energy change of the gas phase reaction (ΔG_{react}) is predicted to be 0.1 kcal mol^{-1}, indicating that oxidative addition should proceed to some extent.

To date we have not been able to observe oxidative addition of the 1,2,3-trimethylimidazolium cation to Pt^0 (or Pd^0). However, oxidative addition of a C–H bond is known to proceed with a lower barrier than oxidative addition of a C–C bond. Furthermore, imidazolium salts used as ILs are usually unsubstituted and have a proton in the 2-position. We therefore studied the reaction of 1,3-dimethylimidazolium tetrafluoroborate with $Pt(PPh_3)_4$. Heating equimolar quantities of the imidazolium salt and $Pt(PPh_3)_4$ in refluxing THF resulted in the formation of *ca.* 15% (by NMR) of the oxidative addition

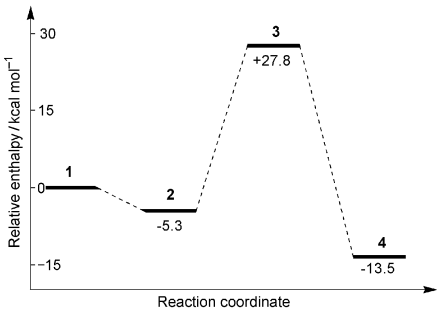

Fig. 1 Potential energy profile for oxidative addition.

DOI: 10.1039/b009674l

product *cis*-[PtH(1,3-dimethylimidazolin-2-ylidene)$(PPh_3)_2$]-BF_4 **5** relative to unreacted imidazolium and $Pt(PPh_3)_4$ [eqn. (2)]. Complex **5** was identified by ^1H, ^{31}P NMR

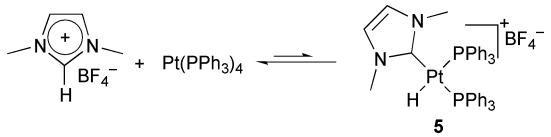

(2)

5

and HRMS. The ^1H NMR spectrum of **5** features a doublet of doublets centred at δ −5.23 (J_{PH} 19, 176 Hz) with Pt satellites (J_{PtH} 511 Hz) corresponding to PtH. The ^{31}P NMR spectrum of **5** gives rise to two doublets (J_{PP} 18 Hz) at δ 24.0 and 20.1 with Pt satellites (J_{PtP} 654, 663 Hz). To the best of our knowledge, this is the first example of oxidative addition of a C–H bond to a Pt^0 complex that does not contain a chelating ligand,[13] which was thought to be requisite for this reaction.[12]

Attempts to drive the reaction to completion by heating the reactants to 150 °C in DMSO resulted in approximately the same amount of oxidative addition product relative to the reactants, however, in this case the *trans* isomer of **5** was formed. This result suggests that the oxidative addition product is in equilibrium with the reactants, and the low amount of **5** results not from a high barrier to oxidative addition but rather the equilibrium concentration of the reactants and product. The ΔG_{react} value is therefore close to zero, which is consistent with the value predicted by the calculations on the theoretical system. The formation of *trans*-**5** can be explained by a *cis–trans* isomerisation of *cis*-**5**, which is probably the kinetically favoured product obtained from oxidative addition. Thermally induced or polar solvent induced isomerisations of Pt carbene complexes are well known,[14] it is therefore not surprising that hot DMSO can promote the isomerisation. The PtH resonance for *trans*-**5** appears as a triplet (J_{PH} 13 Hz) with Pt satellites (J_{PtH} 336 Hz) at δ −6.03 in the ^1H NMR spectrum. The related complex [PtH(1,3-dimethylimidazolidin-2-ylidene)$(PEt_3)_2$]-BF_4 has a very similar hydride resonance.[14]

The oxidative addition of 2-iodo-1,3,4,5-tetramethylimidazolium tetrafluoroborate has also been successfully carried out to give *trans*-[PtI(1,3,4,5-tetramethylimidazolin-2-ylidene)-$(PPh_3)_2$]BF_4 **6** [eqn. (3)]. The complex has been isolated as

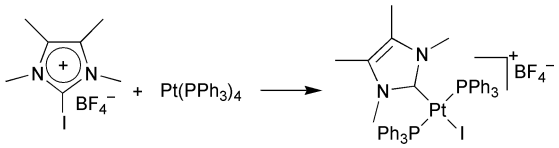

(3)

6

colourless crystals and an X-ray structure analysis carried out. Details will be reported in a full paper on this topic.

The above results indicate a potentially important method of limiting decomposition of M–carbene catalysts, by operating in a large excess of the imidazolium ion, any M^0 that forms as a consequence of alkyl–carbene reductive elimination may re-form the M^{II}–carbene complex through oxidative addition of the imidazolium ion. For this reason, catalysts based on heterocyclic carbene complexes should be particularly suited to reactions in imidazolium based ILs. Furthermore, these results show unambiguously for the first time that the imidazolium cation, which is usually considered an unreactive solvent when used as an ionic liquid, can react with low valent metals to give a carbene complex. While interaction of the imidazolium cation with $Pd(OAc)_2$ has been shown to yield carbene complexes,[10] this work shows that a basic metal salt is not necessarily required to deprotonate the imidazolium. Thus, when group 10 metal complexes, particularly M^0 complexes, are used in imidazolium based ILs the possibility of carbene complexes as the active species must be considered. The large excess of imidazolium present under these conditions can be expected to drive the oxidative addition reaction. It is important to note that not only does oxidative addition of an imidazolium ion produce a carbene complex, but it also generates a metal hydride that could effectively initiate numerous catalytic processes.

In summary, density functional studies show that oxidative addition of an imidazolium cation to Pt^0 is possible both in terms of the activation barrier and relative energies of the reactants and product. We have experimentally demonstrated this by the reaction between $Pt(PPh_3)_4$ and the 1,3-dimethylimidazolium cation, which yields the hydrido–Pt carbene complex **5**. Further theoretical and experimental studies are in progress dealing with the effect of different metals, ligands and imidazolium salts on this remarkable oxidative addition reaction. A full account of these results will be reported shortly.

This work was supported by the Australian Research Council (financial support, postgraduate award to D. S. M), and the staff of the Central Science Laboratory (University of Tasmania) are gratefully acknowledged for their assistance.

Notes and references

† Full geometry optimisations were carried out with the use of the B3LYP[15,16] density functional level of theory combined with the LANL2DZ basis set which incorporates the Hay and Wadt[17] small-core relativistic effective core potential and double-zeta valence basis set on Pt and P together with the Dunning/Huzinaga[18] double-zeta basis set on other atoms. Sets of five d-functions were used in the basis sets throughout these calculations. For the optimised geometries, harmonic vibrational frequencies were calculated at the B3LYP level and zero-point vibrational energy corrections obtained using unscaled frequencies. The vibrational frequencies were also used to obtain thermodynamic corrections and entropies. All transition structures possessed one and only one imaginary frequency, and they were further characterised by following the corresponding normal mode towards each product and reactant. All structures were treated as singlets and electronic wavefunction stability optimisations reveal no singlet–triplet instability. Finally, single-point energies on B3LYP/LANL2DZ optimised geometries were calculated at the B3LYP level with the LANL2augmented:6-311 + G(2d,p) basis set, which incorporates the LANL2TZ + (3f) basis set on platinum[19] and 6-311 + G(2d,p) on all other atoms.[20–22] The energy values in the text refer to this final level of theory. All calculations were carried out with the Gaussian 98 program.[23]

1 W. A. Herrmann and C. Köcher, *Angew. Chem., Int. Ed. Engl.*, 1997, **36**, 2162.
2 W. A. Herrmann, M. Elison, J. Fischer, C. Köcher and G. R. J. Artus, *Angew. Chem., Int. Ed. Engl.*, 1995, **34**, 2371.
3 W. A. Herrmann, C.-P. Reisinger and M. Spiegler, *J. Organomet. Chem.*, 1998, **557**, 93.
4 D. S. McGuinness, M. J. Green, K. J. Cavell, B. W. Skelton and A. H. White, *J. Organomet. Chem.*, 1998, **565**, 165.
5 D. S. McGuinness and K. J. Cavell, *Organometallics*, 2000, **19**, 741.
6 D. S. McGuinness, K. J. Cavell, B. W. Skelton and A. H. White, *Organometallics*, 1999, **18**, 1596.
7 D. S. McGuinness and K. J. Cavell, *Organometallics*, 2000, **19**, 4918.
8 D. S. McGuinness, N. Saendig, B. F. Yates and K. J. Cavell, submitted for publication.
9 A. J. Carmichael, M. J. Earle, J. D. Holbrey, P. B. McCormac and K. R. Seddon, *Org. Lett.*, 1999, **1**, 997.
10 L. Xu, W. Chen and J. Xiao, *Organometallics*, 2000, **19**, 1123.
11 C. J. Mathews, P. J. Smith and T. Welton, *Chem. Commun.*, 2000, 1249.
12 A. Dedieu, *Chem. Rev.*, 2000, **100**, 543.
13 M. Hackett and G. M. Whitesides, *J. Am. Chem. Soc.*, 1988, **110**, 1449.
14 B. Çetinkaya, E. Çetinkaya and M. F. Lappert, *J. Chem. Soc., Dalton Trans.*, 1973, 906.
15 A. D. Becke, *J. Chem. Phys.*, 1993, **98**, 5648.
16 P. J. Stephens, J. F. Devlin, C. F. Chabalowski and M. J. Frisch, *J. Phys. Chem.*, 1994, **98**, 11623.
17 P. J. Hay and W. R. Wadt, *J. Chem. Phys.*, 1985, **82**, 299.
18 T. H. Dunning and P. J. Hay, in *Modern Theoretical Chemistry*, ed. H. F. Schaefer, Plenum, New York, 1976, vol. 3, p. 1.
19 B. F. Yates, *J. Mol. Struct. (THEOCHEM)*, 2000, **506**, 223.
20 R. Krishnan, J. S. Binkley, R. Seeger and J. A. Pople, *J. Chem. Phys.*, 1980, **72**, 650.
21 A. D. McLean and G. S. Chandler, *J. Chem. Phys.*, 1980, **72**, 5639.
22 M. J. Frisch, J. A. Pople and J. S. Binkley, *J. Chem. Phys.*, 1984, **80**, 3265.
23 *Gaussian 98 A.1.*, Gaussian, Inc., Pittsburgh, PA, 1998.

ChemComm

Allyl- and propargylchromium reagents generated by a chromium(III) ate-type reagent as a reductant and their reactions with electrophiles†

Makoto Hojo, Rie Sakuragi, Satoru Okabe and Akira Hosomi*

Department of Chemistry, Graduate School of Pure and Applied Sciences, University of Tsukuba, Tsukuba, Ibaraki 305-8571, Japan. E-mail: hosomi@chem.tsukuba.ac.jp

Received (in Cambridge, UK) 21st November 2000, Accepted 16th January 2001
First published as an Advance Article on the web 8th February 2001

A chromium ate-type reagent 'Bu_5CrLi_2' reacts with allylic and propargylic phosphates to generate the corresponding allyl- and propargylchromium (propargyl = prop-2-ynyl) reagents which further react with a variety of electrophiles such as aldehydes, ketones, imines, and isocyanates to afford the corresponding adducts in high yields.

Organochromium(III) reagents are well-known to be nucleophilic, and have been used for the selective transformation of organic molecules. These reagents are usually generated from organic halides or their equivalents by reduction with chromium(II) as a 'one-electron' reductant.[1] We found that a chromium ate-type reagent, 'Bu_5CrLi_2'‡ easily prepared from chromium(III) chloride and butyllithium reacted with an equimolar amount of allylic phosphates to produce a nucleophilic allylation agent[2] where the butylchromium ate reagent served not as an alkylation agent, but formally as a 'two-electron' reductant [eqn. (1)].

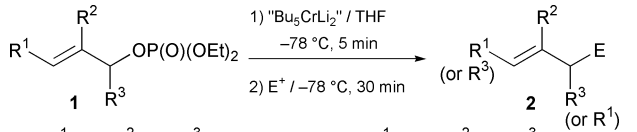

1a: R^1 = H, R^2 = H, R^3 = $Ph(CH_2)_2$ **1d**: R^1 = Me, R^2 = H, R^3 = H
1b: R^1 = $Ph(CH_2)_2$, R^2 = H, R^3 = H **1e**: R^1 = H, R^2 = Me, R^3 = H
1c: R^1 = H, R^2 = H, R^3 = H **1 f** : R^1 = H, R^2 = H, R^3 = Me

(1)

At the outset, we had found that 'Bu_4CrLi' reacted with an allylic phosphate, which can be easily prepared from the corresponding allyl alcohol, to produce reduction products, after aqueous workup. Therefore, we examined the reactivity of some butylchromium(III) reagents to 5-phenylpent-1-en-3-yl diethyl phosphate (**1a**) in a simple reduction to yield a mixture of terminal and internal alkenes. As can be seen in Table 1, 'Bu_5CrLi_2' was the most reactive toward the allyl phosphate **1a**. With 'Bu_4CrLi' it took 3 h to consume the starting material, and in a reaction of 'Bu_3Cr', 31% of **1a** was recovered even after 24 h.§ Next, we tested reactions of allyl bromide,[3] phosphate,[4] and acetate with 'Bu_5CrLi_2'. Allyl phosphate, diethyl 5-phenylpent-2-enyl phosphate (**1b**) was the best choice as precursor of the postulated allylchromium reagent, compared to 5-phenylpent-2-enyl bromide and acetate (Table 2). With an allylic bromide, butylation and dimerization competed with the desired reduction, and the acetate gave the starting allyl alcohol, suggesting a nucleophilic reaction of the 'Bu_5CrLi_2' reagent to the carbonyl of an acetoxy moiety.

By virtue of the reducing ability of the chromium ate-type reagent 'Bu_5CrLi_2', an allylchromium reagent was prepared from allyl phosphate **1c** under mild conditions, and the thus-generated reagent reacted with many types of electrophiles (Table 3).¶ Throughout this conversion, an allylic moiety of phosphate **1c** changes from electrophilic to nucleophilic.[5] Besides aliphatic (entries 1–3) and aromatic aldehydes (entry 4), ketones also reacted with the present allylchromium reagent (entries 5 and 6). To cyclohex-2-enone, 1,2-addition took place to give the corresponding homoallyl alcohol **2g** (entry 7). Imine and isocyanate gave homoallylamine **2h** and but-3-enoyl amide **2i**, respectively, in high yields (entries 8 and 9). The generation and reactions of other substituted allylchromium reagents were also successful. A β-methallyl-type reagent reacted efficiently with an aldehyde [(eqn. (2)]. Unsymmetrical reagents were also

Table 1 Reaction with allyl phosphate **1a**[a]

Entry	Chromium reagent	Conditions	Alkene (%)[b]
1	'Bu_5CrLi_2'	−78 °C, 5 min	96 (83 : 17)
2	'Bu_4CrLi'	−78 °C, 1 h	77 (82 : 18)[c]
3	'Bu_4CrLi'	−78 °C, 3 h	91 (83 : 17)
4	'Bu_3Cr'	−78 °C, 24 h	61 (80 : 20)[d]

[a] The reduction was conducted at −78 °C for 5 min using 1.2 equiv. of 'Bu_5CrLi_2'. Reactions were quenched with saturated NH_4Cl solution. [b] Isolated yield and isomeric ratio are shown in parentheses. [c] 20% of starting material **1a** was recovered. [d] 31% of starting material **1a** was recovered.

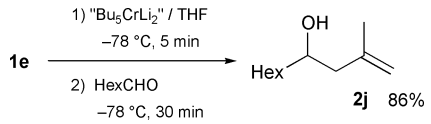

(2)

generated from **1d** and **1f** under the same conditions, −78 °C, 5 min, and these isomeric reagents both reacted with heptanal to give the same mixture of α- and γ-allylation products, suggesting that these reactions proceeded through a common intermediate [eqn. (3)].‖ Interestingly, the same reagent derived

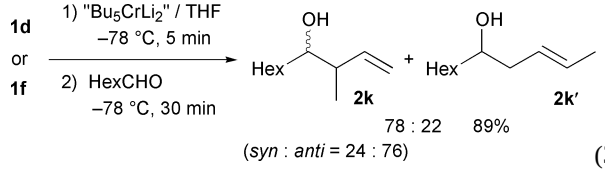

(3)

from **1d** afforded only γ-allylation product **2l**, when reacted with pivalaldehyde [eqn. (4)]. These results imply that the

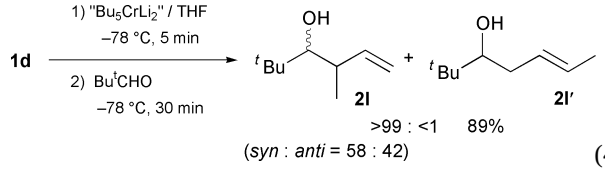

(4)

common intermediate would possibly be labile or not responsible for the regiochemical outcome, and the regioselectivity would be affected by the steric requirements of both a bulky allylchromium reagent and an aldehyde in the transition state for the allylation. The reagent was chemoselective for ketones in the presence of esters. The chemoselective allylation with the present allylchromium reagent is exemplified by eqn. (5).

† Electronic supplementary information (ESI) available: experimental details. See http://www.rsc.org/suppdata/cc/b0/b009351n/

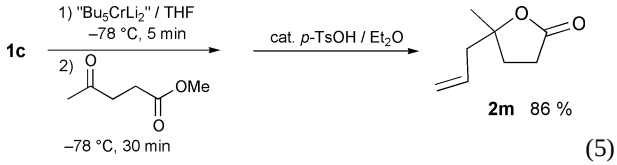

(5)

The present protocol can be applied even to the generation of a propargylic reagent[6] from the corresponding phosphate **3** [eqn. (6)]. With aromatic aldehydes, only homopropargyl

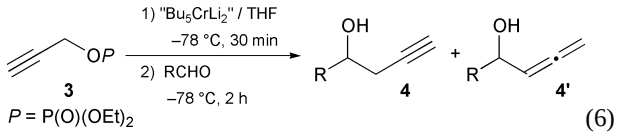

(6)

alcohols **4** were obtained, while with an aliphatic aldehyde, allenylmethyl alcohol **4′** was also co-produced as well as homopropargyl alcohol **4** (Table 4).

Table 2 Reactions of allylic bromide, phosphate and acetate with 'Bu_5CrLi_2'[a]

Entry	Substrate	Conditions	Alkene (%)[b]
1	Ph, Br	–78 °C, 5 min	73 (70 : 30)[c]
2	Ph, OP(O)(OEt)$_2$ (**1b**)	–78 °C, 5 min	96 (83 : 17)
3	Ph, OAc	–78 °C, 3 h	18 (69 : 31)[d]

[a]The reduction was conducted at –78 °C for 5 min using 1.2 equiv. of "Bu_5CrLi_2". Reactions were quenched with saturated NH_4Cl solution. [b]Isolated yield and isomeric ratio are shown in parentheses. [c]15% of butylated product and 4% of dimer were detected. [d]35% of allylic alcohol and 40% of the starting material were recovered.

Table 3 Reaction of allyl phosphate **1c** with electrophile[a]

Entry	Electrophile	Product **2**		Yield (%)
1	Hex, H	Hex, OH	**2a**	93
2	Cy, H	Cy, OH	**2b**	85
3	Bu^t, H	Bu^t, OH	**2c**	79
4	Ph, H	Ph, OH	**2d**	91
5	=O	OH	**2e**	96
6	Ph, Me	Ph, OH, Me	**2f**	91
7	=O	OH	**2g**	83
8	N-Ts, Ph	NHTs, Ph	**2h**	84
9	PhNCO	Ph, N, H, O	**2i**	75

[a]The reduction was conducted at –78 °C for 5 min using 1.2 equiv. of "Bu_5CrLi_2". To the allylchromium reagent, 4 equiv. of an electrophile were added, and the mixture was stirred at –78 °C for 30 min. Reactions were quenched with saturated NH_4Cl solution. [b]Isolated yield.

Table 4 Reaction of propargylchromium reagent[a]

Entry	R′CHO	Product ratio (%) **4**	**4′**	Yield (%)[b] (**4** + **4**)
1	Ph	99 **4a**	<1	75
2	O	99 **4b**	<1	73
3	Hex	88 **4c**	12 **4c′**	70

[a]The reduction was conducted at –78 °C for 30 min using 1.2 equiv. of "Bu_5CrLi_2". An aldehyde (4 equiv.) was added at –78 °C and the mixture was stirred at the same temperature for 2 h. Reactions were quenched with saturated NH_4Cl solution. [b]Isolated yield.

In conclusion, a chromium ate-type reagent 'Bu_5CrLi_2' reduces allyl and propargyl phosphates to generate allyl- and propargylchromium reagents, respectively, where no alkylation takes place, while these thus-generated reagents act as nucleophilic reagents toward a variety of electrophiles. From a synthetic point of view, many types of allyl- and propargylchromium reagents can be generated by the present protocol, starting from allyl and propargyl alcohols. Further study on the generation and reaction of these reagents is now in progress.

The present work was partly supported by Grants-in-Aid for Scientific Research, Grants-in-Aid for Scientific Research on Priority Areas (No. 706: Dynamic Control of Stereochemistry) from the Ministry of Education, Science, Sports and Culture, Japan.

Notes and references

‡ Formulae 'Bu_nCrLi_{n-3}' are tentatively used, since the precise structures of the species are not clear at present.

§ These 'Bu_nCrLi_{n-3}' species are possibly in equilibrium through disproportionation.

¶ A solution of 'Bu_5CrLi_2' in THF was prepared from BuLi in hexane (1.62 mL, 2.6 mmol) and a suspension of chromium(III) chloride in THF (0.52 mmol in 5 mL) with stirring at −78 °C for 30 min. Allyl phosphate (0.43 mmol) was added at −78 °C, and the mixture was stirred for 5 min. To the flask, an electrophile (1.72 mmol) was added and the resulting mixture was further stirred for 30 min. After quenching with saturated NH_4Cl and conventional workup, the crude mixture was subjected to chromatography to give a pure product.

‖ The stereoselectivity in the reactions of a crotyl-type reagent to aldehydes was not so high compared to that of the reported crotylchromium reagent generated by the reduction with a chromium(II) reagent. At the moment, reaction conditions for the selectivity were not optimized, and more likely, this lower selectivity may possibly be due to the crowded chromium-metal center to which remaining butyls would coordinate.

1 (*a*) A. Fürstner, *Chem. Rev.*, 1999, **99**, 991; (*b*) P. Cintas, *Synthesis*, 1992, 248.
2 Y. Yamamoto and N. Asao, *Chem. Rev.*, 1993, **93**, 2207.
3 Y. Okude, S. Hirano, T. Hiyama and H. Nozaki, *J. Am. Chem. Soc.*, 1977, **99**, 3179.
4 (*a*) K. Takai and K. Utimoto, *J. Synth. Org. Chem. Jpn.*, 1988, **46**, 66; (*b*) C. Jubert, S. Nowotny, D. Kornemann, I. Antes, C. E. Tucker and P. Knochel, *J. Org. Chem.*, 1992, **57**, 6384.
5 (*a*) Y. Tamaru, A. Tanaka, K. Yasui, S. Goto and S. Tanaka, *Angew. Chem., Int. Ed. Engl.*, 1995, **34**, 787; (*b*) T. Tabuchi, J. Inanaga and M. Yamaguchi, *Tetrahedron Lett.*, 1987, **28**, 215; (*c*) Y. Masuyama, Y. Nimura and Y. Kurusu, *Tetrahedron Lett.*, 1991, **32**, 225; (*d*) S. Torii, H. Tanaka, T. Katoh and K. Morisaki, *Tetrahedron Lett.*, 1984, **25**, 3207; (*e*) K. Takai, M. Tagashira, T. Kuroda, K. Oshima, K. Utimoto and H. Nozaki, *J. Am. Chem. Soc.*, 1986, **108**, 6048.
6 (*a*) P. Place, F. Delbecq and J. Gore, *Tetrahedron Lett.*, 1978, 3801; (*b*) P. Place, C. Vernière and J. Gore, *Tetrahedron*, 1981, **37**, 1359; (*c*) K. Belyk, M. J. Rozema and P. Knochel, *J. Org. Chem.*, 1992, **57**, 4070.

Preparation of polycyclodextrin hollow spheres by templating gold nanoparticles

Li Sun,[a] Richard M. Crooks[a] and Victor Chechik*[b]

[a] *Department of Chemistry, Texas A&M University, College Station, TX 77843, USA*
[b] *Department of Chemistry, The University of York, Heslington, York, UK YO10 5DD. E-mail: vc4@york.ac.uk*

Received (in Cambridge, UK) 27th November 2000, Accepted 16th January 2001
First published as an Advance Article on the web 8th February 2001

Oxidation of gold nanoparticles protected by thiolated β-cyclodextrin molecules, leads to formation of water-soluble polycyclodextrin nanocapsules held together by S–S bonds.

Recent advances in supramolecular chemistry have given chemists unprecedented control over the composition and shape of nanoscopic objects. An example of such development is the synthesis of nanometer-sized organic hollow spheres, which can find numerous applications in drug delivery/targeting, extraction and as nanoreactors.[1] Here, we describe a new method for preparation of nanometer-sized hollow, monolayer-thick spheres using thiolated β-cyclodextrins templated around gold nanoparticles.

Reduction of Au(III) compounds in the presence of thiols results in the formation of Au nanoparticles coated with organic shells [[eqn. (1)].[2] Re-oxidation of such nanoparticles with

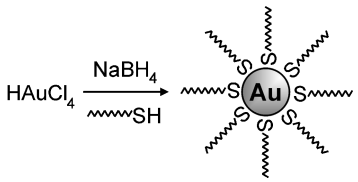

(1)

iodine is known to dissolve gold as a mixture of Au(I) and Au(III) complexes[3] and liberate organic substrates as disulfides [eqns. (2) and (3)].[4,5]

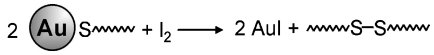

(2)

$$AuI + I_3^- \rightleftarrows AuI_4^- \quad (3)$$

Our strategy relies on these disulfide bridges to form hollow spheres. Indeed, if organic substrate molecules (R–SH) possess several thiol groups, then formation of multiple S–S bonds in reaction (2) would cross-link the whole structure. Such disulfide bridges are often used to stabilize supramolecular assemblies.[6] A minimum of three thiol groups per substrate molecule is required for efficient cross-linking.

To test this hypothesis, we synthesized 2.3 nm Au nanoparticles coated with a monolayer of thiolated β-cyclodextrin molecules (Scheme 1, β-CD-S/Au), according to a recently published procedure.[7] Every molecule of thiolated β-cyclodextrin (β-CD-SH) contains seven thiol groups, and formation of disulfide bonds will therefore lead to multiple cross-linking of the organic shell (Scheme 1).

Aqueous β-CD-S/Au nanoparticles were added to a dilute solution of excess I_2 in aqueous KI to effect oxidation (Scheme 1). Reaction could be monitored by the disappearance of the brown colour of the Au nanoparticles. Excess iodine is required to prevent decomposition of unstable gold iodide [eqn. (4)].[3]

$$AuI_2^- \rightleftarrows Au^0 + I_2 \quad (4)$$

After reaction was complete, gold complexes and excess iodine were extracted into ethyl acetate, and the aqueous phase was exhaustively dialysed to remove KI and filtered to eliminate a small amount of water-insoluble material.

The resulting nanocapsules were characterized by ^{1}H NMR and FTIR spectroscopy. Importantly, NMR spectra of the nanoparticles before (β-CD-S/Au) and after removal of gold (β-CD-S/capsules) were almost identical, an observation consistent with formation of well defined structures containing β-CD-S units (Fig. 1). FTIR spectra of the nanocapsules were found to be identical with the spectrum of a polymer $(\beta\text{-CD-S})_n$ obtained by oxidation of β-CD-SH with I_2 in DMSO [eqn. (5)]. This further confirmed the proposed macrocomposition of the nanocapsules.

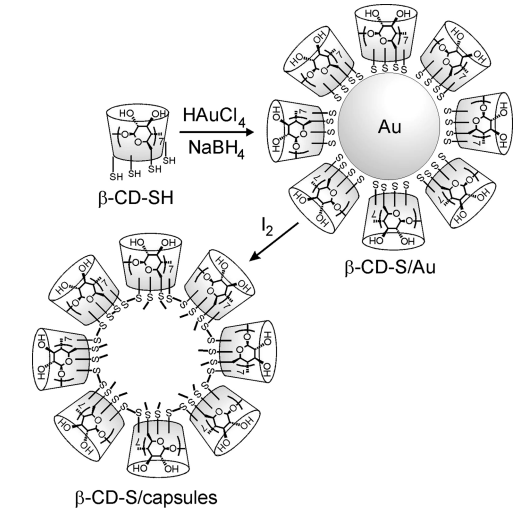

Scheme 1 Preparation of polycyclodextrin hollow spheres.

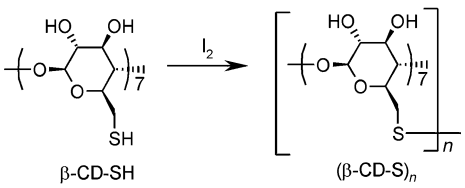

(5)

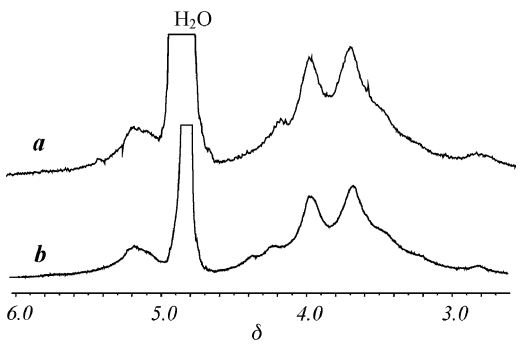

Fig. 1 ^{1}H NMR spectra (D_2O) of thiolated β-cyclodextrin/Au nanocomposites before (β-CD-S/Au, a) and after removal of Au template (β-CD-S/capsules, b).

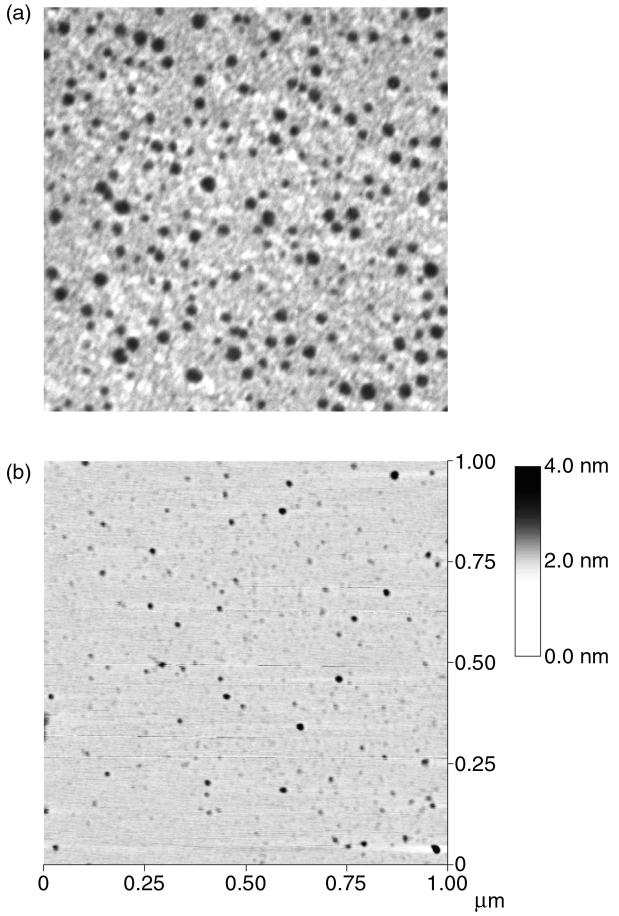

Fig. 2 (a) TEM image (100 nm × 100 nm) of Au nanoparticles protected with thiolated β-cyclodextrin (β-CD-S/Au). (b) AFM image of poly-cyclodextrin hollow spheres (β-CD-S/capsules) deposited on mica.

It proved more difficult to confirm the nanostructure of the materials obtained, *i.e.*, that they are indeed hollow spheres. Strong evidence came from solubility experiments. β-CD-SH is completely insoluble in water due to the hydrophobic nature of the SH group. At the same time, β-CD-S/Au nanoparticles are very soluble in water, as all hydrophobic groups are now hidden inside the nanoparticles, their surface being dominated by the hydrophilic OH groups (Scheme 1). Importantly, β-CD-S/capsules are also very soluble in water, which is consistent with the retention of the shell structure. In contrast, most (> 90%) of the polymer $(\beta\text{-CD-S})_n$ [eqn. (5)] is insoluble in water.

This very different water solubility of polymers $(\beta\text{-CD-S})_n$ and β-CD-S/capsules (materials which have the same molecular composition) confirms the hydrophilic nature of the proposed hollow shell structure.

Prolonged storage (over several weeks) of hollow shells in aqueous solution at room temperature leads to precipitation of insoluble disulfide polymer $(\beta\text{-CD-S})_n$ as a result of a disproportionation reaction (6) which is known to be fast for hydrophilic disulfides in water.[8]

$$2R^1\text{–SS–}R^2 \longrightarrow R^1\text{–SS–}R^1 + R^2\text{–SS–}R^2 \qquad (6)$$

This further supports a non-equilibrium structure for the nanocapsules obtained and is consistent with the hollow sphere model. A better understanding of the kinetics of reaction (6) might lead to a means for controlled release of small molecules within the capsules.

The ultimate proof of the hollow shell structure should come from microscopy. Unfortunately, we have been unable to obtain electron microscopy (TEM) images of hollow spheres due to their small size and low contrast. However, AFM analysis of hollow spheres deposited on mica from a dilute aqueous solution, showed nearly monodisperse round features.[9] The diameter of these features (*ca.* 30 nm) substantially exceeds the diameter of the Au particles [*ca.* 2.3 nm, Fig. 2(a)] due to the tip convolution,[10] which is a familiar scanning probe microscopy phenomenon. The height of the features [*ca.* 1.6 nm, Fig. 2(b)] corresponds approximately to the double height of the β-CD-SH molecule (*ca.* 0.78 nm). This might suggest that the nanocapsules collapse on the mica surface upon drying in air, but one must be cautious in interpreting height data as not much is known about the tip–surface interactions.[11] We believe that our observation of monodisperse round features strongly supports formation of hollow spheres.

The inner surface of the hollow spheres is dominated by the disulfide bonds and is therefore hydrophobic. To probe if the voids inside nanocapsules can accommodate external guests, we studied solubilisation of ferrocene, a hydrophobic molecule, in aqueous β-cyclodextrin (β-CD) and β-CD-S/capsules. Ferrocene is known to form inclusion complexes with β-CD, leading to its partial solubilisation in β-CD solutions.[12] We have found that β-CD-S/capsules can solubilise *ca.* 50 times more ferrocene than β-CD in aqueous solution.[13] This result can be explained either by accumulation of ferrocene in the inner voids of the hollow spheres, or by an increase in the value of the ferrocene-β-CD binding constant. More experiments are needed to distinguish unambiguously between these possibilities.

In conclusion, we have demonstrated a new strategy for synthesizing nanometer-scale organic hollow spheres using Au colloids as templates. The whole structure is held together by S–S bonds. We are currently working on broadening the described strategy to other substrates/templates and probing the encapsulation properties of the hollow spheres.

V. C. thanks the University of York and Astra-Zeneca for financial support.

Notes and references

1 S. M. Marinakos, J. P. Novak, L. C. Brousseau, A. B. House, E. M. Edeki, J. C. Feldhaus and D. L. Feldheim, *J. Am. Chem. Soc.*, 1999, **121**, 8518; M. Wu, S. A. O'Neill, L. C. Brousseau, W. P. McConnell, D. A. Shultz, R. J. Linderman and D. L. Feldheim, *Chem. Commun.*, 2000, 775.
2 M. Brust, M. Walker, D. Bethell, D. J. Schiffrin and R. Whyman, *Chem. Commun.*, 1994, 801.
3 R. J. Puddephatt, *The Chemistry of Gold*, Elsevier, Amsterdam, 1978.
4 A. C. Templeton, M. J. Hostetler, C. T. Kraft and R. W. Murray, *J. Am. Chem. Soc.*, 1998, **120**, 1906; J.-B. Kim, M. L. Bruening and G. L. Baker, *J. Am. Chem. Soc.*, 2000, **122**, 7616.
5 Reaction (2) is likely to proceed *via* oxidative addition of I_2 to Au(I) thiolate followed by fast elimination of disulfide from the resulting Au(II) complex, see T. Jiang, G. Wei, C. Turmel, A. E. Bruce and M. R. M. Bruce, *Met. Based Drugs*, 1994, **1**, 419.
6 S. Otto, R. L. E. Furlan and J. K. M. Sanders, *J. Am. Chem. Soc.*, 2000, **122**, 12063; Y. Kakizawa, A. Harada and K. Kataoka, *J. Am. Chem. Soc.*, 1999, **121**, 11247.
7 J. Liu, W. Ong, E. Román, M. J. Lynn and A. E. Kaifer, *Langmuir*, 2000, **16**, 3000.
8 L. Field, in *Organic Chemistry of Sulfur*, ed. S. Oae, Plenum Press, New York, 1977, pp. 304–382.
9 AFM samples were prepared by spin-coating of a 10 ng mL^{-1} aqueous solution of nanocapsules onto a freshly-cleaved mica surface at 2000 rpm. The samples were then oven-dried briefly at 80 °C for 1 min. Images were obtained using a tapping-mode NanoScope III scanner (Digital Instruments, Santa Barbara, CA).
10 M. J. Waner, M. Gilchrist, M. Schindler and M. Dantus, *J. Phys. Chem. B*, 1998, **102**, 1649 and references therein.
11 J. Yang, L. K. Tamm, A. P. Somlyo and Z. Shao, *J. Microscopy (Oxford)*, 1993, **171**, 183.
12 R. Castro, I. Cuadrado, B. Alonso, C. M. Casado, M. Morán and A. E. Kaifer, *J. Am. Chem. Soc.*, 1997, **119**, 5760 and references therein.
13 Powdered ferrocene was vigorously stirred overnight with aqueous solutions of β-CD or β-CD-S/capsules. The resultant mixture was then filtered through a 0.45 μm filter and analysed by UV spectroscopy.

Increased selectivity in hydroformylation reactions using dendrimer based catalysts; a positive dendrimer effect

Loïc Ropartz,[a] Russell E. Morris,[a] Douglas F. Foster[b] and David J. Cole-Hamilton*[a]

[a] *School of Chemistry, University of St. Andrews, St. Andrews, Fife, Scotland, UK KY16 9ST. E-mail: djc@st.andrews.ac.uk*

[b] *Catalyst Evaluation and Optimistaion Service (CATS), School of Chemistry, University of St. Andrews, St. Andrews, Fife, Scotland, UK KY16 9ST*

Received (in Cambridge, UK) 29th November 2000, Accepted 11th January 2001
First published as an Advance Article on the web 8th February 2001

Dendrimers based on polyhedral oligomeric silsesquioxanes (POSS) cores with 16 PPh_2 arms give much higher linear selectivities (14 : 1) than their small molecule analogues (3–4 : 1) in the hydroformylation of oct-1-ene.

Dendrimers are globular molecules in which the groups on the periphery are all the same. They have been used for a variety of applications, but interesting opportunities are offered if the dendrimer is used as a ligand in homogeneous catalysis. Most research in this area is aimed at using the dendrimer to overcome the main problem of homogeneous catalysts, that the reaction products can be hard to separate from the catalyst and the solvent. Because of their persistent shape and size (1–10 nm), there is interest in attempting to remove the catalyst by nanofiltration through a suitable membrane. Filtration of this kind has been demonstrated.[1–3] Another possible advantage of dendrimers is that crowding in the periphery might lead to constrained geometries in the metal binding, which might affect the activity or selectivity of the catalyst. In many cases, reaction rates are slowed in the presence of a dendrimer, but there are also examples of reactions being totally or partially inhibited because the dendrimer is present. In one case it is believed that an unpaired electron is passed from metal to metal on the dendrimer, thus inhibiting its use in the Kharasch reaction.[4]

Examples of enhanced reactivity in C–C coupling reactions have been reported[3,5] and very recently it has been shown that epoxidation reactions can be accelerated if the catalyst is bound to the dendrimer and this is thought to be because the oxidising peroxide binds to one metal, whilst the substrate is activated by another. Having the two metals held in close proximity increases the reaction rate.[6] To our knowledge, examples of positive dendrimer effects on the *selectivity* of catalytic reactions have not been reported, but we now report such an effect in the hydroformylation of oct-1-ene. Hydroformylation using metals bound to dendrimers with phosphines on the periphery have been reported,[7,8] but generally the selectivity to the desired linear product is similar to that using model small molecule ligands, although we noted a slightly enhanced linear selectivity using dendrimer-bound trialkylphosphines.[8]

Dendrimers based on polyhedral oligomeric silsesquioxane (POSS) cores were prepared as shown in Scheme 1 such that they had up to 16 PPh_2 groups on the periphery (**1**). Attempts to prepare the dendrimer with 24 PPh_2 arms leads to incomplete conversion to phosphines, presumably because of excessive steric crowding.[8] Analysis of **1** by NMR and by MALDI-TOF mass spectrometry shows that they have 14, 15 or 16 PPh_2 groups per dendrimer, with the average number being *ca* 15. Within one arm of the dendrimer, the P atoms are separated by five atoms. Simple diphosphines separated by five or six atoms are only expected to favour bidentate binding when constrained, as in the case of Xantphos[9] and bis(diphenylphosphinomethyl)biphenyl (BISBI)[10] ligands. For such constrained ligands, the linear : branched ratios can be very high. Indeed, using the unconstrained small molecules, **2** and **3**, l : b ratios are only of the order of 3-4 (Table 1 and Fig. 1). In contrast, under

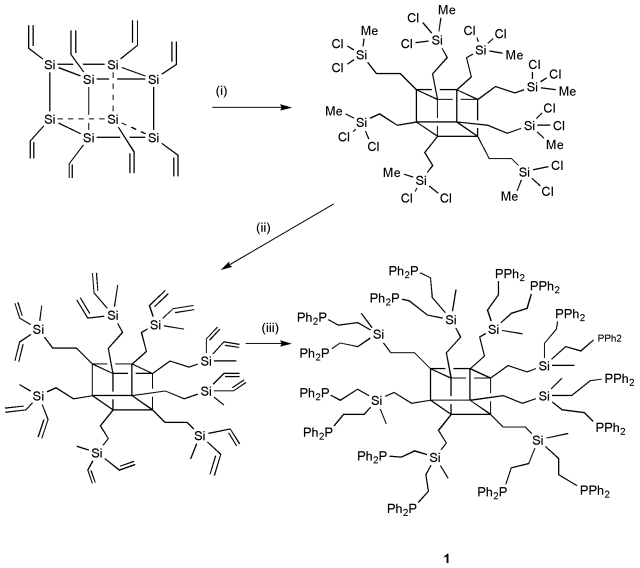

1

Scheme 1 Synthesis of 16-arm dendrimer phosphine **1**. *Reagents and conditions*: i, $MeSiHCl_2$, H_2PtCl_6 (catalyst); ii, (vinyl)MgBr; iii, Ph_2PH, azodi(isobutyryl)nitrile. **1** has an average of 15 PPh_2P groups, **5** has an average of 12 PPh_2 groups. In the POSS core, each edge of the cube represents Si–O–Si.

exactly the same conditions, catalysts prepared *in situ* from **1** and [Rh(acac)$(CO)_2$] (acacH = pentane-2,4-dione) give l : b ratios of up to 14. A ratio this high would be very unusual for an unconstrained ligand of this size and certainly shows that a positive dendrimer effect is operating. The reaction rate and l : b ratio increase with increasing temperature or decreasing gas pressure (Table 1) but are only slightly affected by the Rh : P ratio (3.6–10.8) at a given Rh concentration. The generally high l : b ratios suggest that strong bidentate coordination occurs or that the high local concentration of P atoms on the surface of the dendrimer increases the concentration of complexes containing three P donors. Further confirmation that the metal is strongly bound to the dendrimer comes from ^{31}P NMR studies of solutions prepared from [Rh(acac)$(CO)_2$] and **1** (1 : 3) under CO and H_2. Two resonances are observed at room temperature, one (δ 37) for P bound to Rh and the other (δ − 9.5) from the free P atoms (**1** resonates at δ − 9.5). Both resonances are very broad (width at half maximum = 470 and 88 Hz respectively), possibly because of different binding environments for the rhodium since the spectrum is the same in different solvents (CH_2Cl_2, tetrahydrofuran) and the linewidth at half maximum of the signal from the unbound P atoms only changes slightly

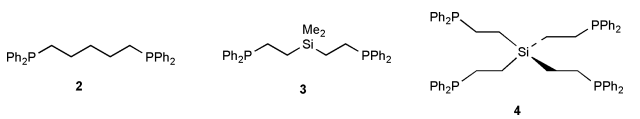

2 **3** **4**

DOI: 10.1039/b009574p

Table 1 Results of hydroformylation reactions using various ligands[a]

Ligand	*T*/°C	*p*/bar	$k^b/10^{-3}$ s^{-1}	Conversion (%)	l:b	Nonanal (%)
1	120	10	1.2	> 99.9	13.9	86
5[c]	120	10	1.1	> 99.9	12.0	86
5[c,d]	100	10	0.42	> 99.9	10.8	86
5[c,e]	80	10	0.08	> 99.9	8.8	84
5[c,f]	100	20	0.33	> 99.9	7.5	85
5[g]	120	10	1.5	> 99.9	12.2	85
5[h]	120	10	0.95	> 99.9	11.9	84
2	120	10	3.6	> 99.9	3.4	70
3	120	10	3.0	> 99.9	3.8	73
4	120	10	2.1	> 99.9	5.2	77

[a] [Rh(acac)(CO)$_2$] (2.0×10^{-5} mol); P:Rh = 6:1, toluene (4 cm^3), heated under CO/H$_2$ (6 bar) for 1 h. Oct-1-ene (8.3×10^{-3} mol) injected and pressure increased. Pressure kept constant through mass flow controller and fed from a ballast vessel. Pressure drop in ballast vessel monitored every 5 s. Total reaction time, 2 h. [b] First-order rate constant measured from gas uptake plots at constant pressure. [c] P:Rh = 5.4:1. [d] t = 4 h. [e] t = 19 h. [f] t = 6 h. [g] P:Rh = 10.8. [h] P:Rh = 3.6.

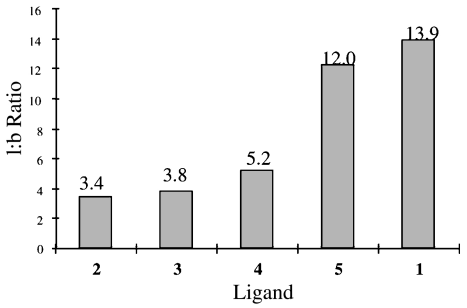

Fig. 1 l:b Ratio of product C$_9$ aldehydes at 120 °C and 10 bar. P:Rh = 6:1, except for **5** (P:Rh = 5.4:1).

between −40 (63 Hz) and +60 °C (150 Hz). This shows that the rhodium is not migrating rapidly around the surface of the dendrimer, nor dissociating on the NMR timescale. The resonance from the Rh-bound phosphines appears as two broad overlapping doublets (δ 37 and 36) at −40 °C, but as a single broad doublet (δ 37 $J_{P-H} \approx$ 130 Hz) at +60 °C, suggesting fluxionality within the bound complex. A broad hydride signal is observed at δ −10.5 (width at half maximum = 80 Hz) in the ^{1}H NMR spectrum at room temperature.

In order to try to understand the higher l:b ratios observed with the dendrimer bound catalysts, we have carried out some molecular modelling of the dendrimer using the Discovery programme contained in the Insight(II) Molecular Modelling Suite of Molecular Simulations Inc.[11] This shows that within an arm, the P atoms are separated by 4–7 Å, whilst between arms there are always some distances in the 5–10 Å region. Rh–P distances are of the order of 2.5 Å, so very little disruption of the ground state structure of the dendrimer is required to facilitate bidentate binding. Presumably the orientation of the PPh_2 groups relative to one another is determined by steric repulsions on the surface of the dendrimer whilst models of the small molecules show that the lowest energy structures have the phosphine groups far away from one another. If this is the case, one might expect that the compound prepared from addition of Ph_2PH across the double bonds of tetravinylsilane **4**, for which the X-ray crystal structure shows that the P atoms are 6.94 and 8.33 Å apart,[12] might show intermediate behaviour between **1** and **3**. Indeed this is the case, with the l:b ratio being 6 (Table 1 and Fig. 1). Reducing the PPh_2 loading on the dendrimer to an average value of 12 PPh_2 groups (**5**)† gives a slightly lower l:b ratio (12.0, Table 1, Fig. 1) than the more completely substituted dendrimer, again suggesting that steric crowding on the dendrimer periphery is important.

It seems that the chain length between the two P atoms is also important since extensive studies on a compound derived from tetravinylsilane containing 16 Ph_2P arms, but with only one CH_2 spacer between Si and P, *i.e.* with a potential ring size of six atoms for bidentate bonding, shows no special enhancement over the small molecule analogue.[7]

We conclude that the dendrimers synthesised here have sufficient steric crowding to make eight-membered ring bidentate coordination favourable and that these rings enhance the linear selectivity in hydroformylation reactions. Whether the binding in five-coordinate intermediates is equatorial–equatorial, which has been shown to give enhanced selectivity,[9,10] whether the P atoms are mutually *trans* throughout the reaction, which may also give enhanced selectivity, or whether the reason for the enhanced selectivity is the locally high Ph_2P concentration is not clear at present, although the low-temperature ^{31}P NMR spectrum of the rhodium complex under CO/H$_2$ suggests that the P atoms bound to rhodium are not all equivalent.

We thank the University of St. Andrews for a studentship (L. R.), the Royal Society for a University Research Fellowship (R. E. M.) and Professor Dieter Vogt and Dr Joost Reek for helpful discussions.

Notes and references

† This dendrimer was prepared for **1**, but the reaction was not taken to completion. It was shown to have an average of 12 PPh_2 groups by MALDI-TOF mass spectrometry.

1 D. de Groot, E. B. Eggeling, J. C. de Wilde, H. Kooijman, R. J. van Haaren, A. W. van der Made, A. L. Spek, D. Vogt, J. N. H. Reek, P. C. J. Kamer and P. W. N. M. van Leeuwen, *Chem. Commun.*, 1999, 1623.
2 N. J. Hovestad, E. B. Eggeling, H. J. Heidbüchel, J. T. B. H. Jastrzebski, U. Kragl, W. Keim, D. Vogt and G. van Koten, *Angew. Chem., Int. Ed.*, 1999, **38**, 1655.
3 N. Brinkmann, D. Giebel, G. Lohmer, M. T. Reetz and U. Kragl, *J. Catal.*, 1999, **83**, 163.
4 A. W. Kleij, R. A. Gossage, J. T. B. H. Jastrzebski, J. Boersma and G. van Koten, *Angew. Chem., Int. Ed.*, 2000, **39**, 176.
5 V. Maraval, R. Laurent, A.-M. Caminade and J.-P. Majoral, *Organometallics*, 2000, **19**, 4025.
6 R. Breinbauer and E. N. Jacobsen, *Angew. Chem., Int. Ed.*, 2000, **39**, 3604.
7 D. de Groot, P. G. Emmerink, C. Coucke, J. N. H. Reek, P. C. J. Kamer and P. W. N. M. van Leeuwen, *Inorg. Chem. Commun.*, 2000, **3**, 711.
8 L. Ropartz, R. E. Morris, G. P. Schwarz, D. F. Foster and D. J. Cole-Hamilton, *Inorg. Chem. Commun.*, 2000, **3**, 714
9 M. Kranenburg, Y. E. M. van der Burgt, P. C. J. Kamer and P. W. N. M. van Leeuwen, *J. Am. Chem. Soc.*, 1995, **14**, 3081
10 C. P. Casey, E. L. Paulsen, E. W. Bettenmueller, B. R. Proft, L. M. Petrovich, B. A. Matter and D. A. Powell, *J. Am. Chem. Soc.*, 1997, **119**, 11 817.
11 *Discover*, MSI. Inc., San Diego, 1996.
12 L. Ropartz, A. M. Z. Slawin, R. E. Morris and D. J. Cole-Hamilton, to be published.

ChemComm

Single-crystalline photochromism of a linear coordination polymer composed of 1,2-bis[2-methyl-5-(4-pyridyl)-3-thienyl]perfluorocyclopentene and bis(hexafluoroacetylacetonato)zinc(II)

Kenji Matsuda,* Kohsuke Takayama and Masahiro Irie*

Department of Chemistry and Biochemistry, Graduate School of Engineering, Kyushu University, and CREST, Japan Science and Technology Corporation, 6-10-1 Hakozaki, Higashi-ku, Fukuoka 812-8581, Japan.
E-mail: irie@cstf.kyushu-u.ac.jp

Received (in Cambridge, UK) 21st November 2000, Accepted 17th January 2001
First published as an Advance Article on the web 8th February 2001

A linear coordination polymer composed of diarylethene and bis(hexafluoroacetylacetonato)zinc(II) has been synthesized and its photochromism in the single-crystalline phase studied by polarized absorption spectroscopy.

Photochromic compounds have attracted much attention because of their potential ability for photonic switching devices.[1] Among them diarylethenes with heterocyclic aryl groups are the most promising compounds for such applications. Diarylethenes undergo fatigue resistant and thermally irreversible photochromic reactions.[2] In addition, it has recently been found that some diarylperfluorocyclopentenes undergo photochromic reactions in the single crystalline phase.[3]

When metal ions are located at both ends of the aryl groups of the diarylethenes, the interaction between metal ions can be switched by photoirradiation, because the π-conjugated bond structures between the two aryl groups are different in the two isomers.[4] Therefore, the use of a diarylethene as a photoswitching bridging ligand is of interest. The synthesis and photochromism of metal complexes of diarylethenes was first reported in 1996 by Munakata *et al.*[5] They prepared a linear polymer, bridged by cyano groups, of *cis*-1,2-dicyano-1,2-bis[2,4,5-trimethyl-3-thienyl)ethene and copper(I) ions. In the present work we report on the synthesis of a linear chain polymer complex of 1,2-bis[2-methyl-5-(4-pyridyl)-3-thienyl]-perfluorocyclopentene **1a**[6] with $Zn(hfac)_2$ (hfac = 1,1,1,5,5,5-hexafluoroacetylacetonate) and its photochromic reaction in the single-crystalline phase (Scheme 1).

Rhombus-shaped single crystals of **1a** were obtained by recrystallization from hexane. An X-ray crystallographic study showed that two independent molecules were present in the asymmetric unit.[7] The distances between the reactive carbons of **1a** were 3.570 and 3.546 Å, short enough to react in the crystalline phase. Single crystals of **1a** turned blue upon irradiation with 366 nm light whilst retaining their shape. The blue color is considered to arise from the closed-ring form isomer **1b**.[3,6] The blue color disappeared upon irradiation with 578 nm light. The color of a crystal was observed under polarized light. Fig. 1(a) and (b) show the polarized absorption spectra and the polar plot. The polarized absorption spectrum at a selected angle showed its maximum at 610 nm. The absorption maximum in the crystal showed a bathochromic shift as much as 20 nm in comparison with the maximum in ethyl acetate solution (λ_{max} = 589 nm). The absorption intensity was strongly dependent on rotation, which indicates that the colored form isomers were regularly oriented in the crystal lattice. The order parameter $[(A_{\parallel} - A_{\perp})/(A_{\parallel} + 2A_{\perp})]$ was as high as 0.72.

$Zn(hfac)_2 \cdot 2H_2O$ was chosen as the metal source for complexation because of its high affinity for pyridyl ligands.[8] A solution of **1a** (200 mg) in dichloromethane (2 mL) was mixed with a solution of $Zn(hfac)_2 \cdot 2H_2O$ (197 mg) in methanol–dichloromethane (1 : 1, 2 mL) to afford a pale green powder. Recrystallization from methanol–dichloromethane (1 : 1) gave

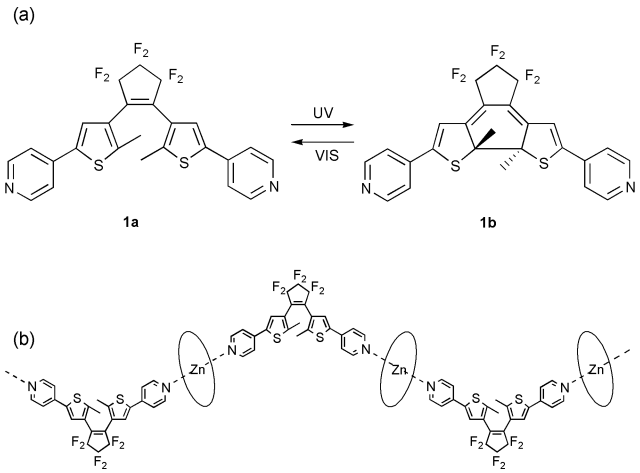

Scheme 1 (a) Photochromism of ligand **1a**. (b) Schematic drawing of the linear chain polymer composed of **1a** and $Zn(hfac)_2$.

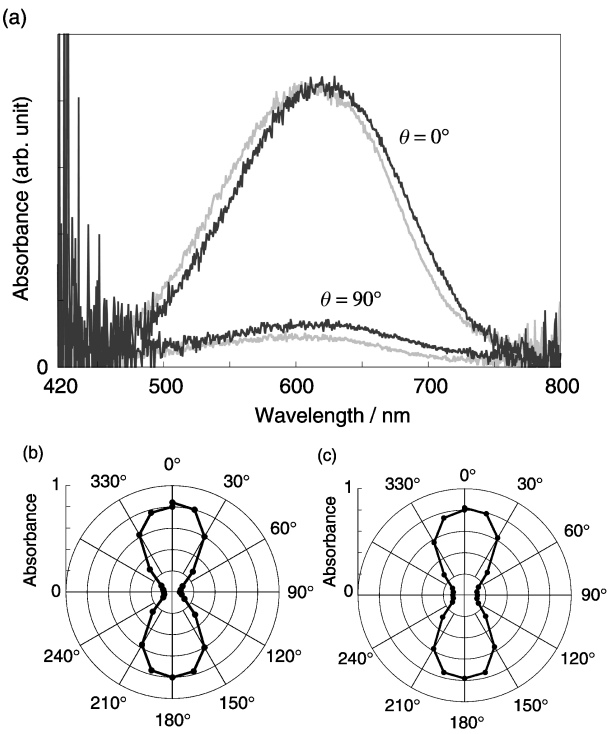

Fig. 1 (a) Polarized absorption spectra of single crystals of **1a** (grey line) and **1a**·$Zn(hfac)_2$ (black line) after irradiation with 366 nm light. (b) Polar plot at the absorption maximum of **1a**. (c) Polar plot at the absorption maximum of **1a**·$Zn(hfac)_2$. The angle of maximum intensity of the absorption is defined as θ = 0° for **1a** and the direction of the linear chain was defined as θ = 0° for **1a**·$Zn(hfac)_2$.

DOI: 10.1039/b009352l

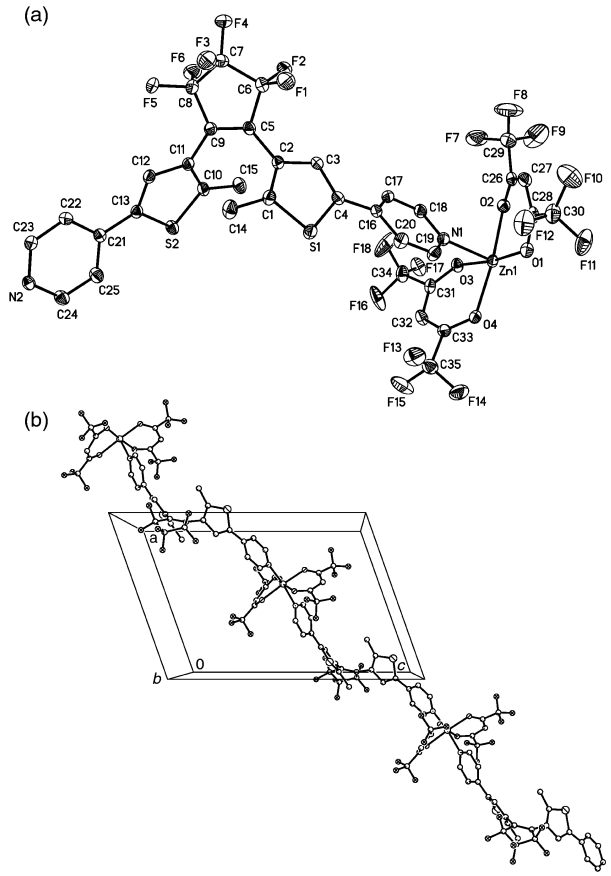

Fig. 2 (a) ORTEP drawing of the molecular structure of **1a**·Zn(hfac)$_2$ for one unit (50% probability) with hydrogen atoms omitted for clarity. (b) Ball-and-stick model of the linear polymer chain of **1a**·Zn(hfac)$_2$ viewed normal to the (010) face.

pale yellow block crystals.[9] The IR spectrum of the crystal was a superposition of **1a** and Zn(hfac)$_2$·2H$_2$O, indicating formation of the complex. X-Ray crystallography revealed the formation of a linear chain polymer complex composed of **1a** and Zn(hfac)$_2$ (Fig. 2).[10] The two pyridyl nitrogens of two different molecules of **1a** are coordinated with Zn(hfac)$_2$ in a *trans* configuration to produce a linear chain structure parallel to the [2 0 −1] direction. The molecular structure of **1a** in the complex is almost identical to that of **1a** itself. The distance between reactive carbons was 3.557 Å, again short enough to react.

An ethyl acetate solution of **1a**·Zn(hfac)$_2$ underwent a photochromic reaction by alternate irradiation with 313 and 578 nm light. The absorption maximum of the colored form isomer **1b**·Zn(hfac)$_2$ was at 590 nm, the same as the maximum of **1b** itself in ethyl acetate solution.

Crystals of **1a**·Zn(hfac)$_2$ also showed photochromic reactivity in the single-crystalline phase. Upon irradiation with 366 nm light single crystals of **1a**·Zn(hfac)$_2$ turned blue with formation of the closed-ring isomer **1b**·Zn(hfac)$_2$ considered to be the origin of the blue color.[3] Upon irradiation with 578 nm light the blue color disappeared. The polarized absorption spectra and the polar plot measured normal to the (010) plane of the face-indexed crystal are shown in Fig. 1(a) and (c). Here, the [2 0 −1] direction, the direction of the linear polymer chain, is defined as θ = 0°. The absorption intensity was strongly dependent on rotation, indicating a regular orientation of the closed-ring form isomer **1b**·Zn(hfac)$_2$. The transition moment was almost identical to the direction of the linear chain. The absorption maximum of **1b**·Zn(hfac)$_2$ in the crystal was 620 nm, 10 nm longer than that observed for crystals of **1b**.

Table 1 summarizes the absorption maxima of the colored closed-ring isomer **1b** and **1b**·Zn(hfac)$_2$, which are generated by irradiation with UV light in solution and in the single crystalline phase. In solution there was no difference between the free ligand and the complex, but in the single-crystalline phase the absorption maximum of the polymer complex showed a bathochromic shift upon complexation. The absorption shift upon complexation in the single crystal can be attributed to an increase in the strain upon complexation.

Table 1 Absorption maxima (nm) of the closed-ring form isomers generated by irradiation with UV light

	1b	**1b**·Zn(hfac)$_2$
In solution	589	590
In single crystal	610	620

In conclusion we have synthesized a linear chain polymer complex composed of 1,2-bis[2-methyl-5-(4-pyridyl)-3-thienyl]perfluorocyclopentene **1a** and Zn(hfac)$_2$. The complex undergoes a photochromic reaction in the single-crystalline state. While there was no shift in solution, the absorption maximum in the single crystal showed a 10 nm bathochromic shift upon complexation.

This work was partly supported by CREST (Japan Science and Technology Corporation) and by a Grant-in-Aid for Scientific Research on Priority Area 'Creation of Delocalized Electronic Systems' (No. 12020244) from the Ministry of Education, Science, Culture, and Sports, Japan.

Notes and references

1 G. H. Brown, *Photochromism*, Wiley-Interscience, New York, 1971; H. Dürr and H. Bouas-Laurent, *Photochromism: Molecules and Systems*, Elsevier, Amsterdam, 1990; *Chem. Rev.*, 2000, **100**, issue 5, thematic issue on *Photochromism: Memories and Switches*, ed. M. Irie.

2 M. Irie and K. Uchida, *Bull. Chem. Soc. Jpn.*, 1998, **71**, 985; M. Irie, *Chem. Rev.*, 2000, **100**, 1685.

3 M. Irie, K. Uchida, T. Eriguchi and H. Tsuzuki, *Chem. Lett.*, 1995, 899; S. Kobatake, T. Yamada, K. Uchida, N. Kato and M. Irie, *J. Am. Chem. Soc.*, 1999, **121**, 2380; S. Kobatake, M. Yamada, T. Yamada and M. Irie, *J. Am. Chem. Soc.*, 1999, **121**, 8450; T. Yamada, S. Kobatake and M. Irie, *J. Am. Chem. Soc.*, 2000, **122**, 1589; M. Irie, T. Lifka, S. Kobatake and N. Kato, *J. Am. Chem. Soc.*, 2000, **122**, 4871; T. Kodani, K. Matsuda, T. Yamada, S. Kobatake and M. Irie, *J. Am. Chem. Soc.*, 2000, **122**, 9631; T. Yamada, S. Kobatake and M. Irie, *Bull. Chem. Soc. Jpn.*, 2000, **73**, 2179.

4 K. Matsuda and M. Irie, *Chem. Lett.*, 2000, 16; K. Matsuda and M. Irie, *J. Am. Chem. Soc.*, 2000, **122**, 7195; K. Matsuda and M. Irie, *J. Am. Chem. Soc.*, 2000, **12**, 8309.

5 M. Munakata, L. P. Wu, T. Kuroda-Sowa, M. Maekawa, Y. Suenaga and K. Furuichi, *J. Am. Chem. Soc.*, 1996, **118**, 3305; A. Fernández-Acebes and J.-M. Lehn, *Chem. Eur. J.*, 1999, **5**, 3285; G. E. Collins, L.-S. Choi, K. J. Ewing, V. Michelet, C. M. Bowen and J. D. Winkler, *J. Chem. Soc. Chem. Commun.*, 1999, 321.

6 S. L. Gilat, S. H. Kawai and J.-M. Lehn, *J. Chem. Soc., Chem. Commun.*, 1993, 1439; S. L. Gilat, S. H. Kawai and J.-M. Lehn, *Chem. Eur. J.*, 1995, **1**, 275.

7 *Crystal data*: for **1a**: $C_{25}H_{16}F_6N_2S_2$, M = 522.53, triclinic, $P\bar{1}$, a = 11.6091(18), b = 12.899(2), c = 15.818(3) Å, α = 76.850(2), β = 85.771(2), γ = 77.020(2)°, V = 2247.0(6) Å^3, Z = 4, μ(Mo-Kα) = 0.304 mm^{-1}, R [$I > 2\sigma(I)$] = 0.0554, $wR2$ (all data) = 0.1535, 8955 data, 635 parameters. For **1a**·Zn(hfac)$_2$: $C_{35}H_{18}F_{18}N_2O_4S_2Zn$, M = 1002.01, monoclinic, $P2_1/c$, a = 12.3592(9), b = 18.3531(14), c = 17.9411(13) Å, β = 109.4780(10)°, V = 3836.7(5) Å^3, Z = 4, μ(Mo-Kα) = 0.879 mm^{-1}, R [$I > 2\sigma(I)$] = 0.0309, $wR2$ (all data) = 0.0777, 8418 data, 561 parameters. CCDC 154005 and 154006. See http://www.rsc.org/suppdata/cc/b0/b009352l/ for crystallographic data in .cif or other electronic format.

8 M. L. Morris, R. W. Moshier and R. E. Sievers, *Inorg. Chem.*, 1963, **2**, 411; Y. Sano, M. Tanaka, N. Koga, K. Matsuda, H. Iwamura, P. Rabu and M. Drillon, *J. Am. Chem. Soc.*, 1997, **119**, 8246; Y.-B. Dong, M. D. Smith, R. C. Layland and H.-C. zur Loye, *Inorg. Chem.*, 1999, **38**, 5027; M. J. Plater, M. R. St. J. Foreman and A. M. Z. Slawin, *Inorg. Chim. Acta*, 2000, **303**, 132.

9 *Analytical data* for **1a**·Zn(hfac)$_2$: mp 274 °C (decomp.); ^{1}H NMR (400 MHz, DMSO-d_6) δ 2.01 (s, 6H), 5.55 (s, 2H), 7.65 (d, J 4 Hz, 4H), 7.83 (s, 2H), 8.59 (br s, 4H); IR (KBr) ν 1130, 1230, 1500, 1600 cm^{-1}; UV–VIS (AcOEt) λ_{max}/nm (ε/dm^3 mol^{-1} cm^{-1}) 300 (6.0 × 10^4). Anal. calc. for $C_{35}H_{18}F_{18}N_2O_4S_2Zn$: C, 41.95; H, 1.81; N, 2.80. Found: C, 42.13; H, 1.82; N, 2.95%. Corresponding closed-ring form isomer **1b**·Zn(hfac)$_2$: ^{1}H NMR (400 MHz, DMSO-d_6) δ 2.14 (s, 6H), 5.55 (s, 2H), 7.30 (s, 2H), 7.72 (d, J 6 Hz, 4H), 8.70 (br s, 4H).

A unique synthesis of a well-defined block copolymer having alternating segments constituted by maleic anhydride and styrene and the self-assembly aggregating behavior thereof

Ming-Qiang Zhu,[a] Liu-He Wei,[a] Mei Li,[b] Lei Jiang,[b] Fu-Sheng Du,[a] Zi-Chen Li[a] and Fu-Mian Li*[a]

[a] *Department of Polymer Science and Engineering, College of Chemistry, Peking University, Beijing 100871, China. E-mail: fmli@chemms.chem.pku.edu.cn; Fax: +86-10-6275-2054; Tel: +86-10-6275-7155*
[b] *Institute of Chemistry, Chinese Academy of Science, Beijing, 100080, China*

Received (in Cambridge, UK) 7th December 2000, Accepted 16th January 2001
First published as an Advance Article on the web 8th February 2001

A unique synthesis of a well-defined block copolymer having alternating maleic anhydride(MAn)/styrene(St) segments and PSt segments was achieved *via* radical addition–fragmentation chain transfer (RAFT) copolymerization and the self-assembly aggregating behavior of its hydrolyzed amphiphilic product in water was demonstrated.

One of the extensively studied CTC (charge transfer complex) forming monomer pairs is the combination of maleic anhydride (MAn) and styrene (St),[1] which can be alternately copolymerized under ordinary free radical initiating techniques to give a functional copolymer by further modification. However, the molecular weight and molecular weight distribution (M_w/M_n) of the copolymer thus obtained are not well-defined.

Recently developed 'living' free radical polymerization has received rapidly increasing interest, since it not only furnishes control over the resulting polymers with narrow M_w/M_n but also can be performed under ordinary radical polymerization procedures avoiding the stringent conditions needed for living ionic polymerization. The preparative technique for well-defined polymers of vinyl monomers *via* precision free radical polymerization has witnessed explosive growth in nitroxide-mediated polymerization,[2] atom transfer radical polymerization (ATRP),[3] and consequently developed radical reversible addition–fragmentation chain transfer (RAFT) polymerization.[4] They are marked with their respective features and limitations. A RAFT polymerization can be achieved by using thiocarbonylthio compounds as a reversible capping agent to produce 'living' polymer chains *via* a free radical mechanism.[4] The 'living' controlled radical copolymerization of electron-deficient and electron-rich monomer pairs is an elusive target, but the works are scarce.[5,6] The challenge associated with ATRP is to obtain an alternating copolymer of MAn, which destroys the ATRP catalytic system. Recently, Hawker *et al.* reported a one-step controlled copolymerization of MAn with St by nitroxide-mediated polymerization, giving a P(St-*co*-MAn)-*b*-PSt block copolymer,[2] and the same polymerization system was also reported for the copolymerization of St with MAn.[7] However, there is no alternating structure observed in the MAn-St copolymer. More recently, there was a report on a copolymerization of MAn and St *via* the RAFT process in which a dithiobenzoate residue was linked to a polyolefine chain end affording a block copolymer.[8] Here we describe a copolymerization of MAn with an excess amount of St in molar feed *via* the RAFT technique affording a well-defined block copolymer, P(MAn-*alt*-St)-*b*-PSt and the self-assembly aggregating behavior of its hydrolyzed amphiphilic product in water.

A typical RAFT initiating system used is the combination of (*S*)-benzyl dithiobenzoate (BTBA) with AIBN. The copolymerization of MAn with St takes place readily at 80 °C and the results are listed in Table 1. During the polymerization, both monomer conversion and number average molecular weight (M_n) increase with polymerization time. The copolymers obtained possess narrow M_w/M_n(~ 1.2), and the composition of P(MAn-*co*-St) is approximately 1:1 in molar ratio. The M_n determined by GPC method increases linearly with the monomer conversion, and matches well with the theoretical value. A thermal copolymerization of MAn with St at 80 °C in the absence of BTBA was demonstrated as a comparison. It can be seen that the copolymer obtained by using AIBN as an initiator possesses a higher M_n up to 6.3×10^4, with a broader M_w/M_n of 2.96. This firmly supports the conclusion that the RAFT copolymerization of MAn and St is of a controlled polymerization nature.

To further reveal the alternating nature of the MAn-St copolymer, a RAFT copolymerization of MAn and St with a molar feed of 1:9 was demonstrated at 60 °C. The conversions of both MAn and St were determined by GC. As can be seen from Fig. 1, the conversion of MAn apparently increases faster than that of St, but the absolute consumption of MAn and St are approximately the same until 80% of MAn was consumed. This indicates that the copolymer obtained possesses a predominantly alternating character at any monomer conversion before MAn has been exhausted. After MAn was completely consumed, the alternating copolymer chain subsequently continued to propagate forming a block copolymer with St sequence. Thus, the copolymerization basically involves: the simultaneous incorporating of MAn and St resulting in an alternating copolymer (Stage I), and the consumption of essentially pure St to continue chain propagation affording a block copolymer with a PSt segment (Stage II). At both stages, Mn increases linearly

Table 1 Molecular weight, molecular weight distribution and composition of MAn-St copolymers obtained *via* RAFT polymerization[a]

Copolymer	Time/h	Conversion (%)[b]	M_n[f] (theory)	M_n[c] (found)	M_w/M_n[c]	St in copolymer (mol%)[e]
MAn-St-1	0.1	17.4	1 580	2 450	1.19	45.9
MAn-St-2	0.3	64.1	5 820	6 180	1.24	48.6
MAn-St-3	1.0	93.3	8 480	7 250	1.22	47.9
MAn-St-4[d]	0.5	96.5	—	63 000	2.96	50.2

[a] $[MAn]_0:[St]_0:[BTBA]_0:[AIBN]_0 = 90:90:2:1$ in molar ratio, $[MAn]_0 = 2.0$ mol L^{-1}, dioxane, 80 °C. [b] Determined by gas chromatography (GC) method. [c] Determined by GPC, THF as an eluent, 35 °C. [d] Thermal polymerization, the monomer feed was 1:1 in molar ratio, 80 °C; [e] Calculated by ^{1}H-NMR analysis (200 MHz); [f] Mn (theory) = [MW (MAn) + MW (St)] × $[MAn]_0$ × conversion /$[BTBA]_0$.

DOI: 10.1039/b009815i

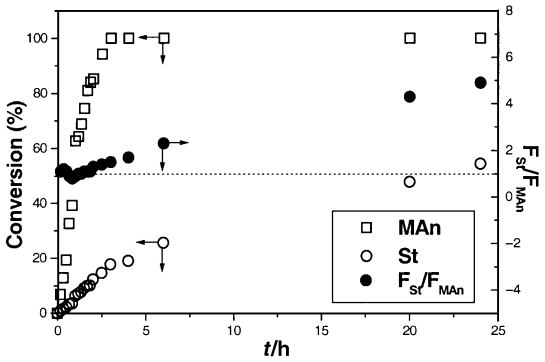

Fig. 1 Evolution of monomer conversions for St and MAn and their consumed molar ratio (F_{St}/F_{MAn}) with the polymerization time *via* RAFT polymerization. $[MAn]_0:[St]_0:[BTBA]:[AIBN] = 100:900:2:1$ in molar ratio, [MAn] = 0.2 mol L^{-1}, 60 °C.

with the conversion and M_w/M_n lies in the range of 1.2–1.4. It is thus concluded that, under RAFT polymerization conditions, the consuming rate of MAn is approximately equal to that of St during Stage I regardless of the large excess of St presented in the monomer feed. A well-defined block copolymer, P(MAn-*alt*-St)-*b*-PSt, composed of P(MAn-*alt*-St) and PSt sequences can thus be obtained by RAFT polymerization. Similar results were also manifested by the RAFT copolymerization of *N*-phenylmaleimide with St conducted at 60 °C.

It should be pointed out that the composition and sequence of the copolymer in the present work were different from the nitroxide-mediated ones reported by Hawker *et al*.[2] and Yoon *et al*.[7] There was no alternating character in the copolymer of MAn-St observed during the early stage of nitroxide-mediated polymerization performed at above 120 °C. In this work, the RAFT polymerization was carried out at 60 °C, where the CTC formation of MAn and St plays an important role in the copolymerization. On the contrary, the nitroxide-mediated copolymerization is always conducted at 120 °C or higher, which would destroy the CTC formed by MAn and St, hence the copolymerization of St or MAn favorably takes place in a 'free' monomer manner. In this regard, Seymour and Garner[1] reported that there is a change of the copolymer sequential distributions from alternating to random structure when the polymerization temperature increased from 80 to 130 °C for the MAn/St comonomer pair. Obviously, the polymerization temperature of 120 °C or higher and the large excess of St would lead to the tendency of homopolymerization of St.

DSC profile can provide valuable information about the block copolymer. The final copolymer possessed two distinct glass transition temperatures (T_g) at 104 and 167 °C, while the copolymer from Stage I showed only one T_g at 164 °C. This also strongly supports the conclusion that the final product is a block copolymer.

The P(MAn-*alt*-St) segment in the block copolymer can easily be hydrolyzed resulting in an amphiphilic block copolymer which can form uniform nanoscale particles by self-assembly. Fig. 2 shows the AFM (atomic force microscopy) image of the amphiphilic block copolymer in water obtained by hydrolyzing P(MAn-*alt*-St)$_{50}$-*b*-PSt$_{80}$ as illustrated in Scheme 1. The particles possess a uniform size with an average diameter of 63 nm and height of 30 nm. In addition, P(MAn-*alt*-St)-*b*-PSt can also form similar micelles in polar solvents such as propan-2-ol. These architectural particles in nanoscale size constructed

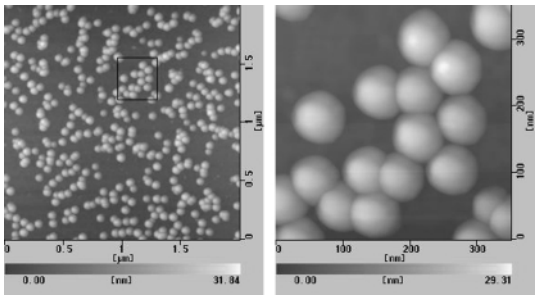

Fig. 2 AFM images of the hydrolyzed product of P(MAn-*alt*-St)$_{50}$-*b*-PSt$_{80}$ (M_n = 18,000, M_w/M_n = 1.34) by spin-coating 5.0×10^{-4} wt% aqueous solution (pH = 9.7) on mica. (a) 2 × 2 μm region; (b) 350 × 350 nm area from (a).

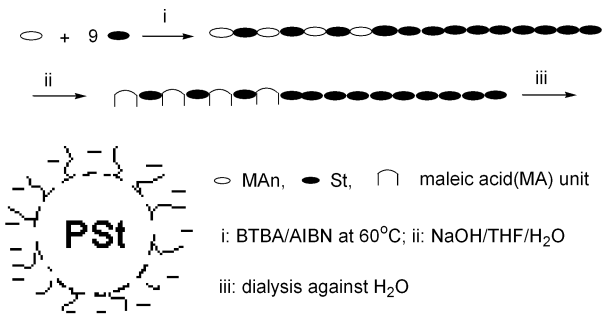

Scheme 1

by PSt segment as a core, and P(MAn-*alt*-St) or P(MA-*alt*-St) segment as a corona, which provides reactive anhydride or carboxylic groups on the surface of particles, are of interest in further chemical or biological modification. The surface modification of the copolymer micelle and the morphology of their derivatives in selective solvents are underway.

This research was supported by the National Natural Science Foundation of China (No. 59773018).

Notes and references

1 R. B. Seymour and D. P. Garner, *Polymer*, 1976, **17**, 21.
2 D. Benoit, C. J. Hawker, E. E. Huang, Z. Lin and T. P. Russell, *Macromolecules*, 2000, **33**, 1505, and references therein.
3 J. S. Wang and K. Matyjaszewski, *J. Am. Chem. Soc.*, 1995, **117**, 5614.
4 R. T. A. Mayadunne, E. Rizzardo, J. Chiefari, J. Krstine, G. Moad, A. Postma and S. H. Thang, *Macromolecules*, 2000, **33**, 243, and references therein.
5 S. G. Gaynor and K. Matyjaszewski, in *Controlled Radical Polymerization*, ACS Symp. Series 685; American Chemical Society, Washington D.C., 1998, p. 258, p. 396.
6 (*a*) G.-Q. Chen, Z.-Q. Wu, J.-R. Wu, Z.-C. Li and F. M. Li, *Macromolecules*, 2000, **33**, 232; (*b*) F.-M. Li, G.-Q. Chen, M.-Q. Zhu, P. Zhou, F.-S. Du and Z.-C. Li, in *Controlled Radical Polymerization*, ACS Symposium Series 768, American Chemical Society, Washington D.C., 2000, Chpt. 27, p. 384.
7 E.-S. Park, M. N. Kim, I.-M. Lee, H. S. Lee and Y. S. Yoon, *J. Polym. Sci.: Part A: Polym. Chem.*, 2000, **38**, 2239.
8 H. D. Brouwer, M. A. J. Schellekens, B. Klumperman, M. J. Monteiro and A. L. German, *J. Polym. Sci.: Part A: Polym. Chem.*, 2000, **38**, 3596.

ChemComm

A highly efficient synthetic procedure for deuteriating imidazoles and imidazolium salts

Christopher Hardacre,*[ab] John D. Holbrey[b] and S. E. Jane McMath[a]

[a] *School of Chemistry, The Queen's University of Belfast, Belfast BT9 5AG, Northern Ireland*
[b] *The QUILL centre, The Queen's University of Belfast, Belfast BT9 5AG, Northern Ireland.*
E-mail: c.hardacre@qub.ac.uk; Fax: +44 28 9038 2117; Tel: +44 28 9027 4592

Received (in Cambridge, UK) 13th November 2000, Accepted 17th January 2001
First published as an Advance Article on the web 8th February 2001

Both substituted imidazoles and 1,3-dialkylimidazolium salts can be fully deuteriated on the heterocyclic ring using D_2O over heterogeneous Pd catalysts: deuteriated 1-alkyl-3-methylimidazolium chloride and hexafluorophosphate ionic liquids can also be prepared in good yields utilising readily available and relatively low cost sources of deuterium.

Imidazole and imidazolium salts are key systems in nature (in, for example, histidine and vitamin B_{12}, and as components in DNA base-pair structure, biotin, *etc*).[1] As such they have a tremendous range of applications in pharmaceutical, veterinary and agrochemical products. Other important applications include formulation of high temperature polymers and corrosion inhibitors,[2] for the formation of carbenes (as replacements for phosphine ligands in transition metal catalysis),[3] and as the basis for ionic liquids - clean solvents for catalysis, extraction technology and electrochemical applications.[4]

For our ongoing investigations of the liquid structure of ionic liquids by neutron diffraction, access to deuteriated materials in order to provide neutron-scattering contrast was required. For these studies, it was necessary to prepare significant quantities (3–5 g) of both fully deuteriated and selectively deuteriated (exchange on the ring positions only) samples of 1,3-dimethylimidazolium chloride or hexafluorophosphate and 1-ethyl-3-methylimidazolium chloride or hexafluorophosphate. Only one of these materials, 1-ethyl-3-methylimidazolium-d_{11} chloride, is currently commercially available and is supplied in small quantities and at prohibitively high cost for this experiment. This paper describes a versatile low cost methodology to prepare these deuteriated materials. Although ionic liquids research provided the driving force behind this investigation, these molecules are also of significant interest as mechanistic probes, particularly in biochemical studies, especially where ^{1}H and ^{2}D NMR spectroscopies are utilised.[5]

Ring deuteriation of imidazolium cations has been performed using D_2O by Dieter *et al*.[6] In this study, shaking with D_2O was sufficient to exchange the most acidic ring-hydrogen, H(2); however, exchange of the ring-hydrogens, H(4/5), was found to require more forcing conditions, *i.e.* heating in D_2O–K_2CO_3. Using this method, the ring-deuteriated salt, 1-ethyl-3-methylimidazolium-d_3 chloride could be prepared. In contrast, imidazoles are much less susceptible to H/D exchange (10^6–10^8 times slower) than the corresponding imidazolium salts.[7,8] Full ring deuteriation of imidazole is also possible under forcing acidic conditions. Lui *et al.* incorporated 90% deuterium using D_2O–D_2SO_4 at 200 °C for 4 h after two passes.[5] Here we show that by using D_2O and a heterogeneous catalyst, both imidazolium salts and substituted imidazoles can be ring deuteriated easily under mild, neutral conditions.

The deuteriation of 1-methylimidazole and 1,3-dimethylimidazolium chloride was screened using palladium and platinum catalysts on a variety of supports† (Table 1). The deuteriations were performed following a pre-reduction of the catalyst in flowing dihydrogen at rt. The substrate dissolved in D_2O was added to the catalyst and underwent a number of freeze-pump thaw cycles, after which the temperature was raised to 100 °C and left for 1 h. This technique has been used extensively for the deuteriation of other heterocycles, commonly pyridines and related molecules.[9] Using this method, 1,3-dimethylimidazolium chloride was deuteriated at the ring H(2) (99%) and H(4/5) (90%) positions using a 10% Pd/C catalyst. The general applicability of this system was demonstrated by deuteriation of imidazole, 1-methylimidazole and 1,3-dimethyl-, 1-ethyl-3-methyl- and 1,3-dibutylimidazolium chlorides with 90–96% deuterium incorporation at the ring H(4/5) positions after one cycle. Exhaustive deuteriation of alkylimidazolium salts was tested at elevated temperatures, and showed that, although exchange of the alkyl group hydrogens is possible, it is inefficient. For example, the maximum deuterium incorporation in methyl side chains on 1,3-dimethylimidazolium chloride at 250 °C over any catalyst was 43% after 12 h.

Table 1 Percentage deuterium incorporation at the ring H(4/5) positions in (i) 1,3-dimethylimidazolium chloride and (ii) 1-methylimidazole using various catalysts

	% Of ring H(4/5) deuteriated	
Catalyst[a]	(i)	(ii)
10% Pd/C	90	91
—	99[b]	—
10% Pd/Al_2O_3	95	87
5% Pt/C	33	0
5% Pt/Al_2O_3	45	5

[a] Little difference was found varying the catalyst loading between 5 and 10%. [b] Second deuteriation cycle.

In general, palladium catalysts are much more active for the exchange reaction than platinum catalysts in both imidazole and imidazolium-based systems. The lack of H/D exchange at the H(4/5) positions using platinum is not well understood at present. Explanations include a change in molecular adsorption geometry between the two metals or site blocking by strongly adsorbed molecules (originating *via* a surface reaction of the imidazole).[10,11] Experiments are currently underway to understand this process more fully.

Using the methodology described above to deuteriate the ring positions, a general procedure was devised in which the synthesis and deuteriation of the 1,3-dialkylimidazolium salts is divided into three discrete steps which can be manipulated in a modular fashion (Scheme 1). This involved a sequence in which imidazole is alkylated to 1-alkylimidazole, then ring-deuter-

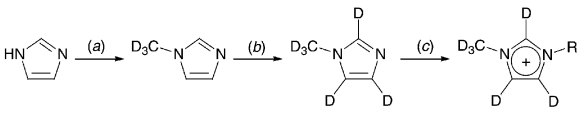

Scheme 1 (*a*) CD_3OD, $RuCl_3$/(*n*-BuO)$_3$P; (*b*) D_2O, 10% Pd/C; (*c*) RX (CD_3Cl, C_2D_5I).

DOI: 10.1039/b009097m

iated with subsequent quaternisation with a second alkylating agent to yield the desired deuteriated 1,3-dialkylimidazolium salt. The order of the sequence depends on the relative efficiency of each step and the nature of the anions in the final 1,3-dialkylimidazolium salt. It is also important to consider whether deuteriation of the ring should be performed before or after the quaternisation. This is dependant on the relative stability of the H/D exchanged hydrogens with respect to scrambling in the subsequent reactions, *e.g.* quaternisation.

Here, the initial alkylation of the imidazole could not be performed cleanly using conventional procedures,[12] since a number of by-products were also formed. For example, methylation of imidazole with iodomethane under neutral conditions led to the formation of a mixture of 1H-imidazolium iodide, 1-methylimidazole and 1,3-dimethylimidazolium iodide. Under these reaction conditions, the imidazole acts as a base for the alkylation. However, since 1-methylimidazole is more reactive towards methyl iodide than imidazole itself, this leads to a final product mixture, which cannot easily be separated. Due to this problem, this method can only be applied to symmetrically substituted 1,3-dialkylimidazolium salts. In the field of room temperature ionic liquids, cation asymmetry is an important feature in order to provide the variation in properties such as melting point, viscosity and density, which allows their use as tuneable solvents.[13]

Alkylimidazoles may be synthesised *via* a number of other routes. Arduengo *et al.*[14] prepared 1,4,5-trimethyl-d_9-imidazole as a precursor to perdeuteriated carbenes *via* a cyclisation route using perdeuteriated methylamine, prepared by deuteriation of deuteriated nitromethane. Alkylation of imidazole has also been performed catalytically with methanol over a homogeneous ruthenium–tributylphosphite catalyst; Tanaka *et al.*[15] claimed 99.5% conversion and greater than 98% selectivity for the production of methylimidazole. This presents a potentially more effective route than that of Arduengo *et al.*[14] for the formation of 1-methyl-d_3-imidazole using deuteriated methanol as a low-cost methylating agent and also gives the opportunity to utilise longer-chain alcohols (for instance, deuteriated ethanol).

Here, 1,3-dimethylimidazolium-d_9 chloride was prepared from imidazole in three steps, introducing deuteriatated functionality at one nitrogen (*via* an alkyl group), to the ring and finally in a quaternisation step adding a deuteriated methyl group to the second nitrogen.‡ In the first step, imidazole was *N*-methylated with deuteriated methanol to 1-methyl-d_3-imidazole over a homogeneous ruthenium–tributylphosphite catalyst in 1,4-dioxane at 200 °C/40 bar pressure[15] with overall 75% yield (based on recovered imidazole) and was isolated by vacuum distillation. The resulting 1-methyl-d_3-imidazole was then deuteriated on the ring with D_2O over a Pd/C catalyst to give the fully perdeuteriated 1-methylimidazole. This was then alkylated with chloromethane-d_3 to give the 1,3-dimethylimidazolium-d_9 chloride, and with iodoethane-d_5 to 1-ethyl-3-methylimidazolium-d_{11} iodide in good overall yields. This approach allows the greatest flexibility in the chemistry and permits the selective introduction of deuterium to any of the functional areas of the imidazolium cation using relatively inexpensive and readily available deuteriated starting materials. The hexafluorophosphate salts were obtained by metathesis from the halide salt with $Na[PF_6]$ in D_2O. 1-Ethyl-3-methylimidazolium-d_{11} chloride was then isolated from the corresponding hexafluorophosphate salt by metathesis with LiCl in acetone-d_6. All the salts were collected as colourless crystals. ^1H and ^{13}C NMR spectra were obtained to assess the levels of deuteriation in the salts and in all cases the deuterium incorporation was greater than 97%. It should be noted that, for the ring deuteriations, this required two cycles in order to increase the deuterium level from 90 to >97%.

This procedure (Scheme 1) enables the preparation of ionic liquids and other 1,3-dialkylimidazolium salts (*i.e.* as precursors to carbene ligands) in which deuteriation of the cation can be selectively applied to any position; one or two *N*-alkyl substituents and ring. Moreover, combined with the lability of the ring H(2) in aqueous solution, it is also possible to selectively control the H/D substitution of the ring H(2) and H(4/5) by H/D exchange.

Financial support from the Department of Education in Northern Ireland (S. E. J. M.) and the Queen's University Ionic Liquids Laboratory (S. E. J. M., J. D. H) is gratefully acknowledged. Johnson Matthey and Degussa are thanked for the generous donation of the carbon catalysts and aluminium oxide respectively.

Notes and references

† Oxide supported catalysts were synthesised by wet impregnation from $PdCl_2$ and H_2PtCl_6 precursors on Degussa Alumina grade C, the catalysts were then calcined and reduced under hydrogen. ICP analysis of metal content was used to confirm catalyst loading. Pd/C and Pt/C catalysts were supplied by Johnson Matthey.

‡ Methanol-d_4 (99.8%) from Apollo Scientific Ltd. All other reagents were obtained from Aldrich and used as supplied.

1-Methyl-d_3-imidazole. Ruthenium chloride hydrate (0.63 g, 2.41 mmol), tri(*n*-butyl)phosphite (2.30 g, 9.19 mmol) and imidazole (10.78 g, 0.158 mol) were sequentially dissolved in 1,4-dioxane (300 cm^3) in a stirred 1 L autoclave. After addition of methanol-d_4 (20 g, 0.554 mol), the mixture was heated at 200 °C under 40 bar pressure of nitrogen for 18 h. Following reaction, the liquid was decanted from the spent catalyst and solvent/excess methanol were removed. The resulting pale yellow oil was vacuum distilled at 100 °C to give 1-methyl-d_3-imidazole as a colourless oil (6.5 g, 49%) and analysed by GC-MS. *m/z* (EI) 85, accurate mass 85.072 (Calc for $C_4H_3N_2D_3$, 85.072), NMR δ_H/ppm ($CDCl_3$) 7.49 (1H, s), 7.01 (1H, s), 7.86 (1H, s); δ_C/ppm ($CDCl_3$) 135.26 (C2), 126.93 (C4), 118.05 (C5), 30.59 ($-CD_3$); δ_D/ppm ($CDCl_3$) 29.64 ($-CD_3$). Unreacted imidazole (34%) was recovered from the distillation flask. Overall yield, based on imidazole was 75%, unreacted deuteriated methanol was recovered from the solvents by distillation and could be reused.

1-Methylimidazole-d_6. Palladium on activated carbon (2 g, 10% Pd) was reduced under dihydrogen (1 atm), for 1 h at rt. 1-Methylimidazole (10 g, 0.117 mol) was dissolved in pure D_2O (50 g, 0.28 mol), and added to the reduced catalyst. The reaction mixture was degassed by three freeze pump thaw cycles, then heated with stirring at 100 °C for 1 h. The reaction mixture was filtered to remove the catalyst, and the aqueous solvent was removed under reduced pressure, and then *in vacuo* to give the ring-deuteriated 1-methylimidazole (9.4 g, 91%). Extent of deuteriation was analysed by loss in ^1H and changes in ^{13}C NMR.

1,3-Dimethylimidazolium-d_9 chloride. Chloromethane-d_3 (1.0 g, 18.7 mmol) was condensed onto 1-methylimidazole-d_6 (1.0 g, 11.4 mmol) in a carius tube cooled to −180 °C with liquid nitrogen. The tube was then sealed and brought to rt, then heated at 80 °C for 15 h to give the 1,3-dimethylimidazolium-d_9 chloride as a colourless crystalline solid (1.6 g, 99%).

1 R. J. Sundberg and R. B. Martin, *Chem. Rev.*, 1974, **74**, 471.
2 F. Eng and H. Ishida, *J. Mater. Sci.*, 1986, **21**, 1561.
3 W. A. Herrmann, L. J. Goossen, C. Kocher and G. R. J. Artus, *Angew. Chem., Int. Ed. Engl.*, 1996, **35**, 2805.
4 T. Welton, *Chem. Rev.*, 1999, **99**, 2071.
5 K. Lui, J. Williams, H. R. Lee, M. M. Fitzgerald, G. M. Jensen, D. B. Goodin and A. E. McDermott, *J. Am Chem. Soc.*, 1998, **120**, 10 199.
6 K. M. Dieter Jr., C. J. Dymek, N. E. Heimer, J. W. Rovang and J. S. Wilkes, *J. Am. Chem. Soc.*, 1988, **110**, 2722.
7 O. Clement, A. W. Roszak and E. Buncel, *J. Am. Chem. Soc.*, 1996, **118**, 612; E. Buncel, O. Clement and I. Onyido, *J. Am. Chem. Soc.*, 1994, **116**, 2679; J. R. Jones and S. E. Taylor, *Chem. Soc. Rev.*, 1981, **10**, 329.
8 J. L. Wong and J. Keck Jr., *J. Org. Chem.*, 1974, **39**, 2398.
9 For example, J. A. Elvidge, J. R. Jones, R. B. Mane and J. M. A. Al-Rawi, *J. Chem. Soc., Perkin Transactions 2*, 1979, 386; G. E. Calf, J. L. Garnett and V. A. Pickles, *Aust. J. Chem.*, 1968, **21**, 961.
10 K. Pekmez and A. Yildiz, *Z. Phys. Chem.*, 1996, **96**, 109.
11 R. T. Carlin, T. H. Cho and J. Fuller, *Proceedings of the 12th International Symposium on Molten Salts*, ed. P. C. Truelove, H. C. De Long, G. Stafford and S. Deki, PV99-41, p. 90, The Electrochemical Proceedings Series, Pennington NJ, 1999; K Anderson, P. Goodrich, C. Hardacre, S. E. J. McMath, in preparation.
12 M. R. Grimmett, *Imidazole and benzimidazole synthesis*, 1997, Academic Press, London.
13 A. S. Larsen, J. D. Holbrey, F. S. Tham and C. A. Reed, *J. Am. Chem. Soc.*, 2000, **122**, 7264.
14 A. J. Arduengo III, H. V. R. Dias, D. A. Dixon, R. L. Harlow, W. T. Klooster and T. F. Koetzle, *J. Am. Chem. Soc.*, 1994, **116**, 6812.
15 N. Tanaka, M. Hatanaka and Y. Watanabe, *Chem. Lett.*, 1992, 575.

A novel route towards formylated 1,3-dithiole-2-thiones *via* an unprecedented allylic 1,4-diol rearrangement†

Tahir Khan,[a] Peter J. Skabara*[a] Simon J. Coles[b] and Michael B. Hursthouse[b]

[a] *Department of Chemistry, University of Manchester, Oxford Road, Manchester, UK M13 9PL. E-mail: peter.skabara@man.ac.uk*

[b] *Department of Chemistry, University of Southampton, Highfield, Southampton, UK SO17 1BJ*

Received (in Cambridge, UK) 28th November 2000, Accepted 16th January 2001
First published as an Advance Article on the web 8th February 2001

In the presence of perchloric acid, an unusual 1,4-aryl shift is observed for two electron-rich 4,5-bis[hydroxy(aryl)methyl]-1,3-dithiole-2-thiones; the X-ray crystal structure of compound 8 confirms the structural identity of the rearrangement product.

The chemistry of the 1,3-dithiole-2-thione heterocycle and its derivatives has been studied extensively,[1] mainly because these compounds are efficient precursors to tetrathiafulvalenes (TTFs), which are famous components in conducting materials.[2] Innovative steps towards the functionalisation of 1,3-dithiole-2-thiones and TTFs continue to attract attention and the formyl group has been one of the most commonly used functional groups for the preparation of TTFs with simple or complex architecture.[3]

Some of our recent work has involved the synthesis of triaryl systems annelated to the 1,3-dithiole-2-thione heterocycle.[4] During these investigations, we discovered that one of our key intermediates, 4,5-bis[hydroxy(thien-2-yl)methyl]-1,3-dithiole-2-thione **1**, rearranges under acidic conditions to give a variety of products (*e.g* **2**), depending on the choice of solvent

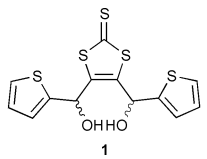

1

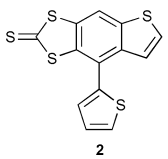

2

and acid.[5] *En route* to a series of dihydrofuran derivatives, we have discovered that electron-rich benzyl analogues undergo a different type of rearrangement to **1**, involving an unexpected 1,4-aryl shift and the concomitant formation of an aldehyde functionality. Herein, we discuss the likely mechanism involved in the reaction sequence and comment on substituent effects.

Using a four-step procedure,[4a] 1,3-dithiole-2-thione **3** can be lithiated by LDA and reacted with aryl carbaldehydes to afford bisalcohol products. Thus, compounds **4** (Ar = phenyl, 2-methoxyphenyl, 4-methoxyphenyl, 2,4-dimethoxyphenyl and 3,5-dimethoxyphenyl) were prepared in 75–90% yield, according to Scheme 1.‡ The diols slowly decomposed under ambient conditions; treatment of 3-6 drops of perchloric acid to solutions of **4** in DCM increased the rate of decomposition of the starting material and in all cases the diol was consumed within 24 h. Dihydrofurans **5** and **6** (87 and 23%, respectively)[6] were isolated from the corresponding diols as mixtures of stereoisomers, whereas the 4-methoxyphenyl and 2,4-dimethoxyphenyl diols gave the rearrangement products **7** and **8** in 44 and 83% yields, respectively. The rearrangement products from **4** were all obtained as the major product (by TLC), however, the diol obtained from the reaction of 3,5-dimethoxybenzaldehyde gave an intractable series of reaction products on addition with $HClO_4$.

† Electronic supplementary information (ESI) available: molecular structure of compound **6**. See http://www.rsc.org/suppdata/cc/b0/b009550h/

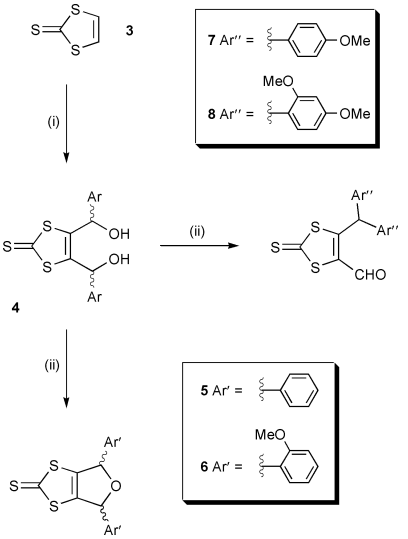

Scheme 1 *Reagents and conditions*: (i) LDA (1 eq.), ArCHO (1 eq.), then repeat, −78 °C, THF; (ii) $HClO_4$, CH_2Cl_2, rt.

Crystals of compounds **6**† and **8**§ were grown from DCM–petroleum ether.

The X-ray crystal structure of compound **8**§ (Fig. 1) provides irrevocable proof for the structure of the rearrangement product. There are considerably less weak interactions in **8** when compared to **6**, allowing more flexible conformations of the dimethoxyphenyl substituents and forming a supramolecular assembly of one-dimensional chains (C(13)···2O(5) = 3.394 Å).

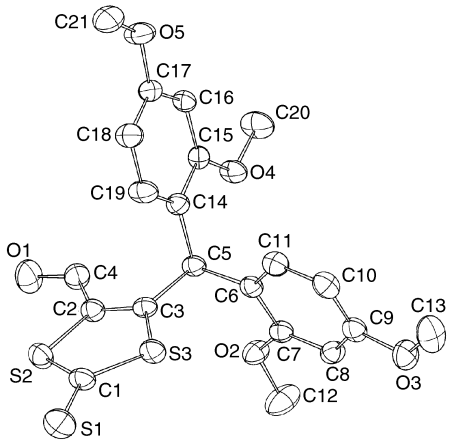

Fig. 1 Molecular structure of compound **8**.

The Pinacol rearrangement of 1,2-diols, affording aldehydes or ketones, is one of the classic transformations in organic chemistry. The reaction involves the acid-mediated 1,2-shift of an alkyl or aryl group as part of a concerted mechanism. Despite the similarity in structure of the reaction products **7** and **8**, one

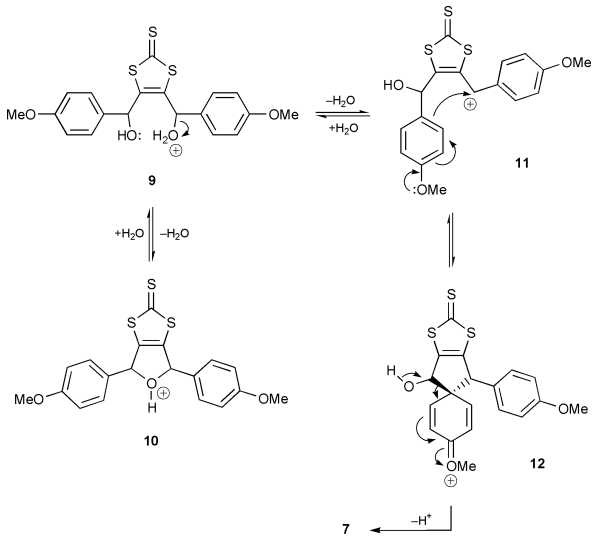

Scheme 2

cannot assume that the mechanism is Pinacol-type. The proposed mechanism for the decomposition of **4** in the presence of perchloric acid is depicted in Scheme 2, using **7** as the example. Protonation of the diol **4** (Ar = 4-methoxyphenyl) gives intermediate **9** which, upon loss of water, generates the dihydrofuran derivative **10** or the free cation **11**. In the case of compounds **5** and **6**, the dihydrofuran species predominates and there is no further transformation. However, for compounds **7** and **8**, the *p*-methoxy group assists in the formation and stabilisation of a phenonium intermediate **12**. The loss of a proton from this species results in **7** *via* an overall step-wise migration of the aryl unit and the formation of a formyl group.

The involvement of a phenonium intermediate in aryl shifts has been seen previously.[7] Theoretical studies have shown that there is significant stabilisation of the phenonium ion through back-bonding from the ethylene unit of spirocyclopropylbenzenium species.[8] However, we propose a spirocyclopentylbenzenium intermediate **12** in Scheme 2, which can only be stabilised by the methoxy unit. The position of the electron releasing groups is important and it is obvious that complications arise in the case of the 3,5-dimethoxy species, since neither the dihydrofuran or 1,4-shift products are observed. In this case, the formation of a spirocyclic intermediate is not possible. It is also unusual that the sole product from the 2-methoxyphenyl species is the dihydrofuran derivative **6**, particularly since the electron donating substituent effect should be identical to that of the 4-methoxy derivative, which gives the rearrangement product **7**. One possible explanation for this can be derived from the X-ray crystal structure of compound **6**.† The intramolecular close contacts between O(2)··S(2) and O(3)··S(3) arise from a π–d orbital interaction, which decreases the electron releasing ability of the methoxy groups towards the benzene ring, thereby conferring a weaker stabilising effect upon the phenonium ion.

Finally, it is worth noting that we have carried out a similar study on analogous benzene derivatives (**13**). In each case, the

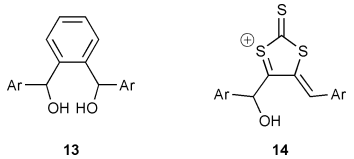

addition of perchloric acid resulted in a complex mixture of products, which could not be easily separated. None of the isolated fractions proved to be the dihydrofuran or rearrangement products such as compounds **5**–**8** (by MS and ^{1}H NMR). The function of the 1,3-dithiole heterocycle in stabilising the allylic cation (shown in structure **14**) is, therefore, an important process in the formation of compounds **5**–**8**. To check the generality of this stabilisation effect in diols such as **4**, we also substituted the 1,3-dithiole-2-thione ring with thiophene, *via* the lithiation (*n*-BuLi) of 2,3-dibromothiophene and subsequent reaction with 2,4-dimethoxybenzaldehyde. The resulting diol decomposed to the corresponding dihydrofuran (by MS and ^{1}H NMR) on standing, whilst the addition of perchloric acid did not yield the 1,4-rearrangement product. Clearly, there is further scope to investigate the versatility of structure **14** by replacing the 1,3-dithiole-2-thione unit with alternative electron-rich moieties and this will be the focus of future work.

In conclusion, we have reported the first example of a 1,4-aryl shift in an allylic 1,4-diol system. This reaction is important for understanding the stabilising effects of substituents upon the allylic cation and, independently, the phenonium intermediate, as well as providing an alternative strategy towards the functionalisation of benzylated 1,3-dithiole-2-thione and TTF derivatives.

We thank the EPSRC for research grant GM/M36342 (T. K.).

Notes and references

‡ Satisfactory spectroscopic data was obtained for all new compounds.

§ *Crystal Data for* **8**: $C_{21}H_{20}O_5S_3$, M_r = 448.55, Monoclinic space group $P2_1/n$, a = 12.732(3), b = 13.131(3), c = 13.040(3) Å, β = 96.88(3), U = 2164.3(7) Å^3, Z = 4, D_c = 1.377 g cm^{-3}, μ = 0.372 mm^{-1}, $F(000)$ = 936, crystal size 0.3 × 0.25 × 0.1 mm, 4938 unique data produced from 16442 measured reflections (R_{int} = 0.0533). 266 parameters refined to R_1 = 0.0493 and wR_2 = 0.1220 [$I > 2\sigma(I)$] (R_1 = 0.1006 and wR_2 = 0.1432 for all data), with residual electron densities of 0.226 and −0.337eÅ^{-3}.

All data were collected at 150 K, on a Nonius KappaCCD area detector diffractometer,[9] equipped with a Nonius FR591 rotating anode (λ Mo-Kα = 0.71073 Å). A correction was applied to account for absorption effects by means of comparing equivalent reflections, using the program SORTAV.[10] A solution was obtained *via* direct methods and refined[11] by full-matrix least-squares on F^2, with hydrogens included in idealised positions.

CCDC 154927 and 154928. See http://www.rsc.org/suppdata/cc/b0/b009550h/ for crystallographic files in .cif format.

1 N. Svenstrup and J. Becher, *Synthesis*, 1995, 215.

2 M. R. Bryce, *Chem. Soc. Rev.*, 1991, **20**, 355; J. M. Williams, J. R. Ferraro, R. J. Thorn, K. D. Carlson, U. Geiser, H. H. Wang, A. M. Kini, M.-H. Whangbo, *Organic Superconductors (including Fullerenes)*, Prentice Hall, New Jersey, 1992; M. R. Bryce, *J. Mater. Chem.*, 1995, **5**, 1481.

3 See for example: M. R. Bryce, W. Devonport and A. J. Moore, *Angew. Chem., Int. Ed. Engl.*, 1994, **33**, 1761; R. Andreu, J. Garin, J. Orduna, M. Saviron, J. Cousseau, A. Gorgues, V. Morrison, T. Nozdryn, J. Becher, R. P. Clausen, M. R. Bryce, P. J. Skabara and W. Dehaen, *Tetrahedron Lett.*, 1994, **35**, 9243; Y. Ishikawa, T. Miyamoto, A. Yoshida, Y. Kawada, J. Nakazaki, A. Izuoka and T. Sugawara, *Tetrahedron Lett.*, 1999, **40**, 8819.

4 (*a*) P. J. Skabara, I. M. Serebryakov, D. M. Roberts, I. F. Perepichka, S. J. Coles and M. B. Hursthouse, *J. Org. Chem.*, 1999, **64**, 6418; (*b*) P. J. Skabara, I. M. Serebryakov and I. F. Perepichka, *Synth. Met.*, 1999, **102**, 1336; (*c*) P. J. Skabara, D. M. Roberts, I. M. Serebryakov and C. Pozo-Gonzalo, *Chem. Commun.*, 2000, 1005.

5 I. M. Serebryakov, P. J. Skabara and I. F. Perepichka, *J. Chem. Soc., Perkin Trans. 2*, 1999, 1405.

6 Related compounds containing dihydrofurans fused to the 1,3-dithiole heterocycle have been reported previously: S. Y. Hsu and L. Y. Chiang, *Synth. Met.*, 1988, **27**, B651.

7 For example see: W. Kirmse and B.-R. Günther, *J. Am. Chem. Soc.*, 1978, **100**, 3619.

8 E. del Rio, M. I. Menéndez, R. López and T. L. Sordo, *J. Phys. Chem. A*, 2000, **104**, 5568.

9 DENZO: Z. Otwinowski and W. Minor, *Methods in Enzymology*, Volume 276, *Macromolecular Crystallography*, ed. C.W. Carter, Jr. and R. M. Sweet, Part A, p. 307–326, 1997, Academic Press. COLLECT: Data collection software, R. Hooft, Nonius B.V., 1998.

10 R. H. Blessing, *Acta Cryst.*, 1995, **A51**, 33; R. H. Blessing, *J. Appl. Cryst.*, 1997, **30**, 421.

11 G. M. Sheldrick, SHELXL-97, Program for the refinement of crystal structures, University of Göttingen, 1997.

ChemComm

A new approach for the formation of alloy nanoparticles: laser synthesis of gold–silver alloy from gold–silver colloidal mixtures†

Yu-Hung Chen and Chen-Sheng Yeh*

Department of Chemistry, National Cheng Kung University, Tainan, Taiwan 701, R.O.C.
E-mail: csyeh@mail.ncku.edu.tw

Received (in Cambridge, UK) 8th December 2000, Accepted 16th January 2001
First published as an Advance Article on the web 8th February 2001

A new methodology has been developed to synthesize gold–silver alloy nanoparticles by laser irradiation of mixtures consisting of gold and silver nanoparticles.

Nanoscale materials have attracted a great deal of interest in scientific research and industrial applications, owing to their unique large surface-to-volume ratio and quantum size effect properties.[1] In principle, the preparations of metal nanometer-sized particles could be classified into two categories: physical and chemical techniques. Evaporation[2] or laser ablation[3] from metal bulk samples is utilized to generate nanoparticles in the physical methods whilst reduction of metal ions to neutral atoms, followed by metal growth is the common strategy in chemical syntheses, including conventional chemical (one- or two-phase systems),[4] photochemical,[5] sonochemical,[6] electrochemical[7] and radiolytic reductions.[8] In this report, a novel methodology is developed to fabricate gold–silver alloy nanoparticles, using laser irradiation of gold and silver colloidal solutions.

Nanocomposites, *i.e.* alloy and core–shell particles, are an attractive subject because of their composition-dependent optical and catalytic properties. To date, Papavassiliou has successfully prepared Au/Ag alloy particles *via*. evaporation of Au/Ag alloys.[2a] Kim and coworkers[4c] and El-Sayed and coworkers[4d] employed simultaneous reduction of gold and silver salts to form Au/Ag alloy nanoparticles of 4 nm and ≈ 18 nm diameter, respectively. Although Lis-Marzán *et al.* used a similar chemical method to synthesize gold–silver bimetallic colloids, the detailed structures of these remained ambiguous.[4b] It should be noted that the formation of alloy particles by co-reduction of different metal salts strongly relies on the reduction rates of the metal ions. A core–shell structure could be readily prepared through a heteronucleation process: the metal with the faster reduction forms the core and the other is the surrounding shell.

Recently, pulsed laser irradiation to nanorods or spherical particles was studied to unravel the photophysical properties of these particulates. The groups of El-Sayed and Koda suggested that the interaction between laser light and metal particles may lead to conformational changes *via* a melting process.[9] We have attempted to take advantage of this melting state, if present, to alloy a mixture containing two different kinds of metal particles under laser light irradiation. A gold–silver system was selected since both metals are miscible in the bulk phase, owing to very similar lattice constants.[10] Moreover, the UV–VIS absorption spectra of the Au/Ag bimetallic particles show a substantial difference between the alloy and a core–shell structure, which has been studied explicitly by experimental and theoretical measurements.[4b–d,11]

In this study, Au and Ag nanoparticles were prepared in aqueous solution following the methods employed by Natan and coworkers[12] and Lee and Meisel,[13] respectively. The mean diameters of the prepared colloids were 13.7 ± 0.8 nm for Au and 16.8 ± 6.6 nm for Ag. Assuming that metal salts ($HAuCl_4$ and $AgNO_3$) are completely reduced into neutral metals completely, gold and silver colloids were mixed in molar ratios (Au : Ag) of 1 : 2, 1 : 1 and 2 : 1 (see ESI†).

Fig. 1 shows the UV–VIS absorption development of the 1 : 1 molar ratio (Au : Ag) colloidal suspensions before and after laser irradiation. Two distinct absorbance maxima at 396 and 519 nm, corresponding to Ag and Au plasmon bands, respectively, indicate segregated Ag and Au particles in the mixed suspension before exposure to laser light [Fig. 1(a)]. For solutions exposed to the laser [Fig. 1(b) and (c)] the absorption spectra changed as the irradiation time was increased. The Au surface plasmon band increases in magnitude and shifts to lower wavelength while the Ag plasmon band moves in the opposite direction with reduced intensity and absorption maximum. This variation in UV–VIS spectra clearly imply changes in the colloidal properties. Further irradiation [Fig. 1(d)], leads to a single absorption peak at 459 nm, located at an intermediate position between the Au and Ag plasmon bands. This surface plasmon band is likely due to the formation of the gold–silver alloy.[4c,d,11] Two plasmon bands (Au and Ag) would be expected if the colloids consisted of individual Au and Ag particles or of bimetallic composites with a core–shell structure.[11] A similar evolution in absorption spectra appeared in mixtures with Au : Ag molar ratios of 1 : 2 and 2 : 1 (see ESI†). A linear relationship was obtained from the plot of the plasmon band position *vs.* the gold mole fraction, as shown in Fig. 2. Previous studies on Au/Ag alloy nanoparticles showed a linear red-shift in the position of the plasmon absorption with an increase in gold composition.[2a,4c,d,11] The final temperatures of the solutions rose by *ca.* 20 °C from room temperature (24 °C) after

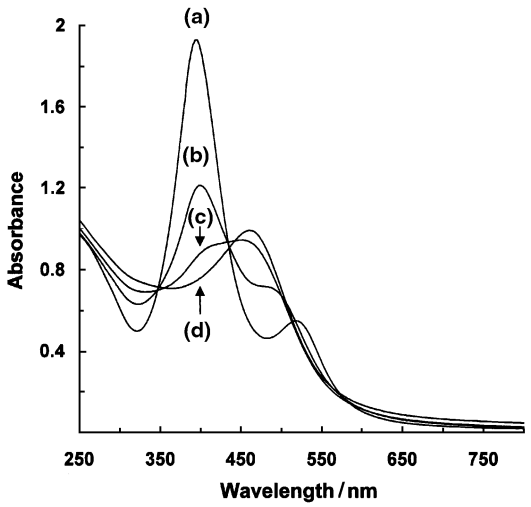

Fig. 1 Development of the UV-VIS absorption spectra of the 1 : 1 molar ratio (Au : Ag) colloidal suspension during irradiation using a pulsed laser, as a function of the exposure time: (a) 0 min, (b) 5 min, (c) 10 min, (d) 25 min. A 532 nm wavelength was utilized as light source and the laser intensity was maintained at 2.45×10^2 mJ pulse^{-1}.

† Electronic supplementary information (ESI) available: experimental details, UV–VIS spectra, TEM images and EDX analysis for molar ratios (Au : Ag) of 1 : 2 and 2 : 1. See http://www.rsc.org/suppdata/cc/b0/b009854j/

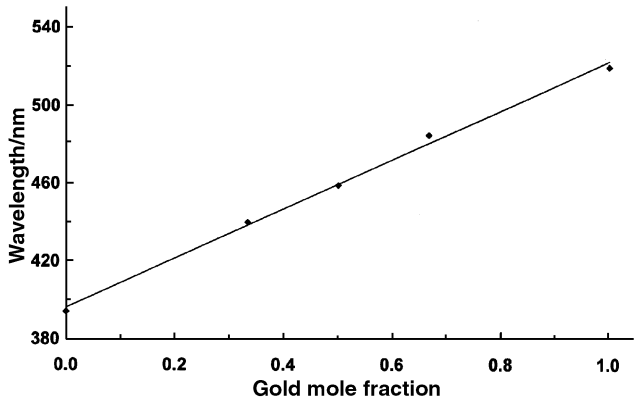

Fig. 2 Absorption position of the surface plasmon maximum as a function of the gold mole fraction.

irradiation. We also found that a lower laser fluence required a longer irradiation time to form gold–silver alloys.

Fig. 3 displays the TEM images of the 1:1 molar ratio (Au:Ag) colloid suspension. The most striking feature is the formation of an interconnected network, as shown in Fig. 3(a). The network appearance can be readily observed at various stages, where two Au and Ag plasmon peaks appeared in the absorption spectra, in the course of colloidal mixture irradiation. On closer inspection of Fig. 3(a), the particles (indicated by arrows) seem to develop as ramification structures in a radial fashion and are interconnected with each other, leading to a network morphology. However, the shape changes back to spherical after the alloying process is complete [Fig. 3(b)]. According to the TEM images, the morphology changes in the alloy nanoparticle formation can be described as follows: spherical (initially prepared Au and Ag particles) → network structure → spherical (alloy particles). Fig. 3(b) indicates highly dispersed tiny gold–silver alloy nanoparticles. The average particle sizes are 4.9 ± 1.8 nm (molar ratio Au:Ag = 1:2), 4.9 ± 1.9 nm (molar ratio Au:Ag = 1:1), and 5.1 ± 2.1 nm (molar ratio Au:Ag = 2:1). The minor variation in size is in contrast to the results of an increase in particle size when increasing the shell element amount in core–shell composites.[4b–d,11] The resulting alloy sizes are significantly less than those of the initially prepared Au and Ag colloids. In addition, the composition of the discrete bimetallic particles was analyzed using EDX. EDX measurements of selected particles, chosen at random, for molar ratio of 1:1 (Au:Ag) suspension, yielded the atomic ratios (Au:Ag): 49.1:50.9, 52.1:47.9, 47.2:52.8, 44.5:55.5 and 44.7:55.3. The compositions of the 1:2 and 2:1 molar ratios (Au:Ag) were also investigated using EDX analysis (see ESI†). Finally, from the viewpoint of their stability, the resulting alloy nanoparticles are preserved for at least one month with no sign of decay under aerobic conditions.

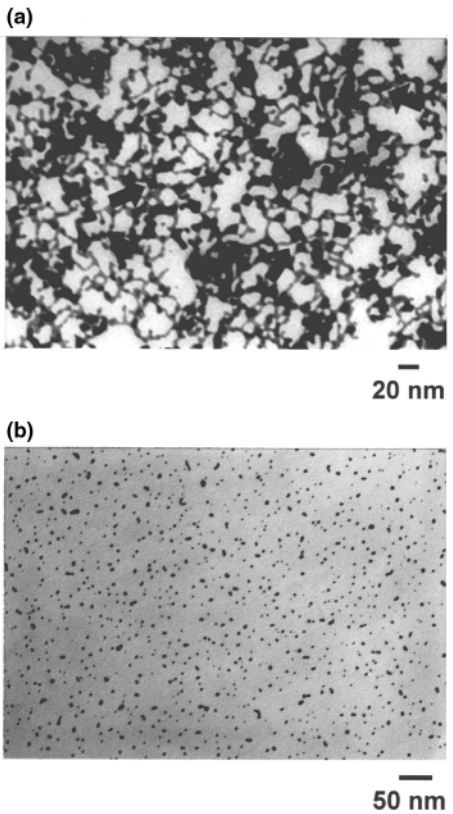

Fig. 3 TEM images of the 1:1 molar ratio (Au:Ag) colloidal suspensions after exposure to laser light for (a) 5 min and (b) 25 min.

In summary, we have demonstrated that Au/Ag bimetallic particles, forming a mixture at the atomic level, can be synthesized *via* the methodology introduced here. It is expected that this strategy could be applied to prepare other binary systems. Although the original idea of this experiment is based on the melting state, leading to alloy particles, the detailed formation mechanism remains to be resolved. However, the intermediate morphology, as seen in Fig. 3(a), reveals that the particles (indicated by arrows) appear to show that the metals are at the melting stage. Studies of the compositions and structures of the irradiated colloidal mixtures as a function of irradiation time are in progress.

We thank the National Science Council of the Republic of China for financial support of this work. We also acknowledge Ms. S. Y. Hsu and Mr. S. Y. Yao for the TEM and EDX measurements at Tainan Regional Instrument Center, National Cheng Kung University, R. O. C.

Notes and references

1 A. Henglein, *Chem. Rev.*, 1989, **89**, 1861; M. G. Bawendi, M. L. Steigerwald and L. E. Brus, *Annu. Rev. Phys. Chem.*, 1990, **41**, 477.
2 See for example: (*a*) G. C. Papavassiliou, *J. Phys. F: Met. Phys.*, 1976, **6**, L103; K. J. Klabunde, Y.-X. Li and B.-J. Tan, *Chem. Mater.*, 1991, **3**, 30; (*c*) N. Sato, H. Hasegawa, K. Tsujii and K. Kimura, *J. Phys. Chem.*, 1994, **98**, 2143; (*d*) Y. Takeuchi, T. Ida and K. Kimura, *J. Phys. Chem. B*, 1997, **101**, 1322.
3 See for example: A. Fojtik and A. Henglein, *Ber. Bunsen-Ges. Phys. Chem.*, 1993, **97**, 252; M. S. Sibbald, G. Chumanov and T. M. Cotton, *J. Phys. Chem.*, 1996, **100**, 4672; A. M. Morales and C. M. Lieber, *Science*, 1998, **279**, 208; M. S. Yeh, Y. S. Yang, Y. P. Lee, H. F. Lee, Y. H. Yeh and C. S. Yeh, *J. Phys. Chem. B*, 1999, **103**, 6851.
4 See for example: (*a*) M. Brust, M. Walker, D. Bethell, D. J. Schiffrin and R. Whyman, *J. Chem. Soc., Chem. Commun.*, 1994, 801; (*b*) L. M. Liz-Marzán and A. P. Philipse, *J. Phys. Chem.*, 1995, **99**, 15 120; (*c*) S. W. Han, Y. Kim and K. Kim, *J. Colloid Interface Sci.*, 1998, **208**, 272; (*d*) S. Link, Z. L. Wang and M. A. El-Sayed, *J. Phys. Chem. B*, 1999, **103**, 3529.
5 See for example: Y. Yonezawa, T. Sato, S. Kuroda and K. I. Kuge, *J. Chem. Soc., Faraday Trans.*, 1991, **87**, 1905; H. H. Huang, X. P. Ni, G. L. Loy, C. H. Chew, K. L.Tan, F. C. Loh, J. F. Deng and G. Q. Xu, *Langmuir*, 1996, **12**, 909.
6 See for example: M. M. Mdleleni, T. Hyeon and K. S. Suslick, *J. Am. Chem. Soc.*, 1998, **120**, 6189; B. Li, Y. Xie, J. Huang, Y. Liu and Y. Qian, *Chem. Mater.*, 2000, **12**, 2614.
7 See for example: M. T. Reetz and W. Helbig, *J. Am. Chem. Soc.*, 1994, **116**, 740; Y. Y. Yu, S. S. Chang, C. L. Lee and C. R. C. Wang, *J. Phys. Chem. B*, 1997, **101**, 6661.
8 See for example: J. L. Marignier, J. Belloni, M. O. Delcourt and J. P. Chevalier, *Nature*, 1985, **317**, 344; A. Henglein, *J. Phys. Chem. B*, 2000, **104**, 2201.
9 A. Takami, H. Kurita and S. Koda, *J. Phys. Chem. B*, 1999, **103**, 1226; S. Link, C. Burda, M. B. Mohamed, B. Nikoobakht and M. A. El-Sayed, *J. Phys. Chem. A*, 1999, **103**, 1165; S. Link, C. Burda, B. Nikoobakht and M. A. El-Sayed, *J. Phys. Chem. B*, 2000, **104**, 6152.
10 M. Hansen and K. Anderko, *Constitution of Binary Alloys*, McGraw-Hill Inc., New York, 2nd edn, 1989.
11 P. Mulvaney, *Langmuir*, 1996, **12**, 788.
12 K. C. Grabar, R. G. Freeman, M. B. Hommer and M. J. Natan, *Anal. Chem.*, 1995, **67**, 735.
13 P. C. Lee and D. Meisel, *J. Phys. Chem.*, 1982, **86**, 3391.

ChemComm

New paramagnetic ruthenium complexes *via* one-electron reduction of metallacumulenes†

Stéphane Rigaut,* Olivier Maury, Daniel Touchard* and Pierre H. Dixneuf

Institut de Chimie de Rennes, UMR 6509 CNRS-Université de Rennes: Organométalliques et Catalyse, Campus de Beaulieu 35042 Rennes, France. E-mail: daniel.touchard@univ-rennes1.fr

Received (in Cambridge, UK) 6th November 2000, Accepted 11th January 2001
First published as an Advance Article on the web 8th February 2001

One-electron reductions of $[Cl(dppe)_2Ru{=}C{=}C{=}CR_2]PF_6$ (R = Ph, Me) and $[Cl(dppe)_2Ru{=}C{=}C{=}C{=}CPh_2]PF_6$ with $Co(C_5H_5)_2$ provide radical species with the unpaired electron localized on the trisubstituted carbon atom of the cumulene moiety as shown by hydrogen atom capture and EPR spectroscopy.

Transition metal complexes are useful to stabilize the otherwise highly reactive **:**(C=)$_n$CR$_2$ species which behave as strong electron withdrawing ligands. Following the development of vinylidene derivatives[1] [M]=C=CR$_2$, the Selegue methodology[2] has allowed the synthesis and reactivity study of a large variety of metal allenylidene [M]=C=C=CR$_2$.[3,4] This chemistry has been extensively developed towards material science[5] and alkene metathesis catalyst precursors.[6] Stimulated by the fact that radical species have been recently proposed as intermediates in metathesis[7] and by the design of new magnetic materials with carbon-rich chains, monoelectronic reduction of metal allenylidene and higher metallacumulenes now appears as an important field to explore. Apart from a recent specific reduction of a 3-alkylthioallenylidene complex[8] which leads to a heteroatom-bonded carbon-stabilized radical, no information has yet been obtained on the nature of the reduction site, *e.g.* on the metal or on the cumulene ligand. We now wish to report here the preliminary results of a general study on reduction of all carbon metallacumulenes including allenylidene[9] L$_n$Ru=C=C=CR$_2$ and pentatetraenylidene[10] L$_n$Ru=C=C=C=C=CPh$_2$ complexes. We show on the basis of electrochemical, spin trapping and EPR spectroscopic evidences that: (i) monoelectronic reduction leads to a radical stabilized on the most remote carbon of the cumulene chain as a general trend; (ii) a striking difference of reactivity of L$_n$Ru=C=C=C=C=CPh$_2$ with respect to reduction *vs.* nucleophilic addition.

Complexes $[Cl(dppe)_2Ru{=}C{=}C{=}CR_2]PF_6$ [R = Ph (**1**$^+$), Me (**2**$^+$)[9a] and $[Cl(dppe)_2Ru{=}C{=}C{=}C{=}C{=}CPh_2]PF_6$ (**3**$^+$)[10] [dppe = 1,2-bis(diphenylphosphino)ethane], were studied using cyclic voltammetry (Fig. 1). Allenylidene **1**$^+$ undergoes two, well defined, one-electron reduction waves: the first one is reversible ($E°$ = −1.03 V *vs.* ferrocene, ΔE_p = 60 mV, $I_{pa}/I_{pc} \cong 1$), whereas the second one is irreversible (E_{pc} = −2.11 V). By contrast, complex **2**$^+$ undergoes only one irreversible reduction (E_{pc} = −1.31 V) which is consistent with the first reduced species undergoing following chemical reaction. The pentatetraenylidene complex **3**$^+$ shows a similar behavior to **1**$^+$, *i.e.* a reversible reduction ($E°$ = −0.63 V, ΔE_p = 65 mV, $I_{pa}/I_{pc} \cong 1$) followed by an irreversible one (E_{pc} = −1.67 V).

It is worth noting that by replacing the phenyl groups in **1**$^+$ with methyl groups in **2**$^+$ induces a significant cathodic shift of first the reduction wave by more than 250 mV. Lengthening the carbon chain from Ru–(C)$_3$ **1**$^+$ to Ru–(C)$_5$ **3**$^+$ surprisingly lowers the reduction potential by 400 mV and shows that the Ru–(C)$_5$ **3**$^+$ species is dramatically easier to reduce. The strong impact of these modifications of the metallacumulene on the reduction processes is a clear indication of the key role played by the cumulene chain. It is then obvious that increasing the length of the delocalized path on the cumulene ligand has a crucial stabilizing influence on the LUMO.[11]

We attempted to generate *in-situ* the first reduced species allowing further spin trapping experiments or EPR spectroscopy investigations. The most appropriate reducing agent is the cobaltocene, Cp$_2$Co, since (i) the reduction potential[12] ($E°$ = −1.33 V *vs.* ferrocene) will selectively induce the first reduction process in **1**$^+$ and **3**$^+$, and (ii) it is EPR-silent down to temperatures considerably below that of liquid nitrogen.[12b] Indeed, reduction of the deep colored cationic compounds **1**$^+$ (red), **2**$^+$ (green) and **3**$^+$ (blue), carried out with one equivalent of cobaltocene in THF, quickly lead to colorless solutions. Simultaneous addition of Ph$_3$SnH, which is known as a specific radical quencher by H· transfer,[13] leads to the complete disappearance of **1**$^+$, **2**$^+$ or **3**$^+$, on the basis of NMR data, and to the formation of the pale yellow, neutral acetylide compounds [Cl(dppe)$_2$Ru–C≡C–CHPh$_2$] **4**, [Cl(dppe)$_2$Ru–C≡C–CHMe$_2$] **5** and [Cl(dppe)$_2$Ru–C≡C–C≡C–CHPh$_2$] **6** (Scheme 1). These complexes have been characterized by ^{1}H, ^{13}C, ^{31}P NMR and high resolution mass spectrometry.† In addition, characteristic IR vibration stretches are obtained: $\nu_{C\equiv C}$ = 2085 (**4**), 2086 (**5**), 2179 and 2023 (**6**) cm^{-1}. All of these observations show that radical trapping only occurs at the end of the carbon skeleton.

Furthermore, achieving the reduction *in situ* of complexes **1**$^+$, **2**$^+$ and **3**$^+$ by dropping a crystal of cobaltocene in a THF solution into a capped EPR tube allows the direct observation of the radical species **1**, **2** and **3**. Reduced complexes **1** and **3** generated an intense and persistent signal. By contrast, the EPR spectrum generated from **2** disappears within few seconds, indicating fast evolution of the reduced species as observed on the electrochemistry scale.[14a,b] All the reduced forms **1**, **2** and **3** exhibit signals at 293 K in a characteristic region for organic radicals with g = 2.0042, 2.0097 and 2.0089 respectively. The signals

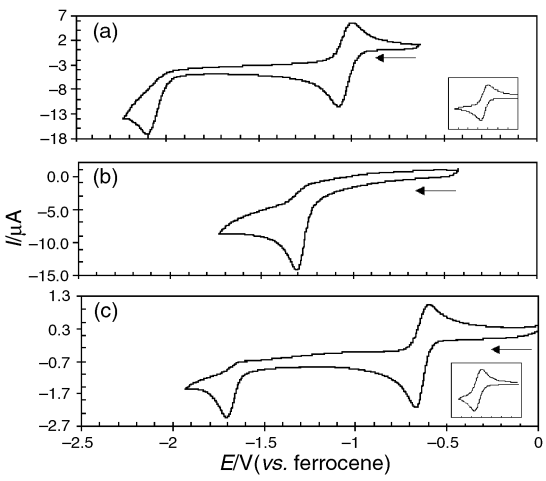

Fig. 1 Cyclic voltammetry responses (CH_2Cl_2, Bu_4NPF_6 0.1 M, scan rate 100 mV s^{-1}) *vs.* internal ferrocene for (a) **1**$^+$, (b) **2**$^+$ and (c) **3**$^+$. Insets show first reduction waves.

† Electronic supplementary information (ESI) available: selected spectroscopic data. See http://www.rsc.org/suppdata/cc/b0/b008893p/

DOI: 10.1039/b008893p

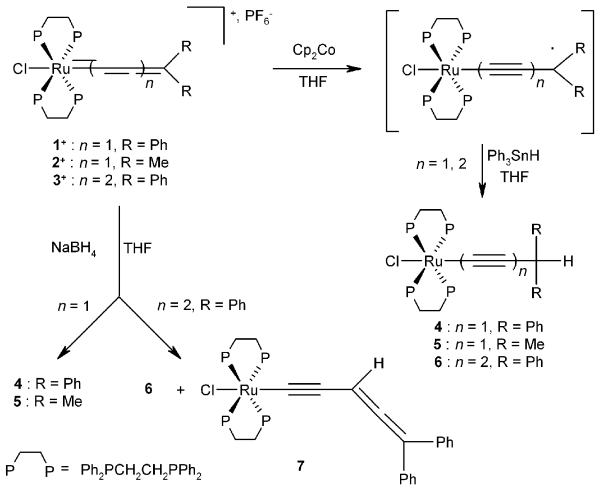

Scheme 1

are resolved only in the case of **1** and **2**. The EPR spectrum of **2** gave a poorly resolved quintet [Fig. 2(b)] showing the hyperfine coupling with the four phosphorus nuclei with a_P = 3.0 G. For compound **1**, the EPR spectrum is complex [Fig. 2(a)]. This could be best rationalized by the coupling of the unpaired electron with the four phosphorus nuclei on one hand and further coupling with the *ortho*, *meta* and *para* hydrogens of the phenyl group of the carbon-rich bridge. These results suggest that the radical is centered on the organic bridges in **1**, **2**, **3** and is stabilized by delocalization along the two neighbouring phenyl rings in **1**. In the case of **2**, identification of such a radical neighbouring methyl groups is quite unexpected. These EPR data added to the trapping experiments indicate the organic nature of radicals **1**, **2** and **3** and show that the radical stabilization on the cumulene chain takes place at the trisubstituted carbon atom and thus is not controlled by the presence of a heteroatom bonded to the unsaturated chain.[8]

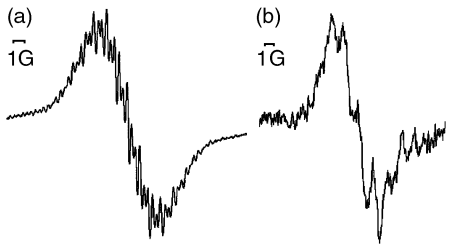

Fig. 2 EPR spectra resulting from reduction of (a) $\mathbf{1}^+$, g = 2.0042; (b) $\mathbf{2}^+$, g = 2.0097.

The synthesis of complexes **4**–**6** were achieved on successive addition to the cumulene chain of one electron and one hydrogen atom. This led us to study the reactivity difference with the simultaneous addition, *i.e.* the nucleophilic addition, of H^-. Nucleophiles are susceptible to attack either the C_α or the C_γ atom of an allenylidene ligand,[3,11*a*] but using the bulky phosphines additions only occur on C_γ.[9*b*] Reductions were performed using $NaBH_4$ in THF (Scheme 1). As expected for $\mathbf{1}^+$ and $\mathbf{2}^+$, additions of H^- take place at the C_γ carbons yielding the acetylide compounds $[Cl(dppe)_2Ru–C{\equiv}C–CHPh_2]$ **4** and $[Cl(dppe)_2Ru–C{\equiv}C–CHMe_2]$ **5**. When complex $\mathbf{3}^+$ was reduced, a mixture of two compounds was obtained. The presence of $[Cl(dppe)_2Ru–C{\equiv}C–CH{=}C{=}CPh_2]$ **7** (42% estimated by ^1H NMR), which displays a ^{13}C NMR signal at δ 216.7 characteristic for the cumulenic carbon (C=*C*=C),† is consistent with the electrophilicity of carbon C_γ in $\mathbf{3}^+$.[10] The main product $[Cl(dppe)_2Ru–C{\equiv}C–C{\equiv}C–CHPh_2]$ **6** (58%) shows the unknown electrophilic character of the C_ε atom. The fact that **7** is not observed in the free radical trapping experiment with H· is very promising, suggesting the location of the radical on the C_ε atom in **3** and the higher selectivity of radical addition *vs.* nucleophilic attack.

This last observation associated with cyclic voltammetry, trapping experiments and EPR spectroscopy re-enforces the conclusion that the reduction of Ru(II) allenylidene or pentatetraenylidene generate radical species located on the termini of the cumulene chain that can be written as shown in Scheme 1. More detailed investigations are in progress, including the study of the striking difference in selectivity between reduction/radical trapping and nucleophilic attack on the pentatetraenylidene complex and the potential of cumulenylidene in radical chemistry.

We thank the CNRS and the Université de Rennes for support, P. Guénot from the Centre de Mesures Physiques de l'Ouest and F. Monnier for assistance.

Notes and references

1 M. I. Bruce, *Chem. Rev.*, 1991, **91**, 197.
2 J. P. Selegue, *Organometallics*, 1982, **1**, 217.
3 H. Werner, *Chem. Commun.*, 1997, 903; M. I. Bruce, *Chem. Rev.*, 1998, **98**, 2797.
4 D. Touchard and P. H. Dixneuf, *Coord. Chem. Rev.*, 1998, **178**–**180**, 409.
5 M. Tamm, T. Jentzsh and W. Werncke, *Organometallics*, 1997, **16**, 1418; G. Roth, H. Fischer, T. Meyer-Friedrichsen, J. Heck, S. Houbrechts and A. Persoons, *Organometallics*, 1998, **17**, 1511.
6 A. Furstner, M. Picquet, C. Bruneau and P. H. Dixneuf, *Chem. Commun.*, 1998, 1315; M. Picquet, C. Bruneau and P. H. Dixneuf, *Chem. Commun.*, 1998, 2249; A. Furstner, A. F. Hill, M. Liebl and J. D. E. T. Wilton-Ely, *Chem. Commun.*, 1999, 615; M. Picquet, D. Touchard, C. Bruneau and P. H. Dixneuf, *New J. Chem.*, 2000, **24**, 141; D. Sémeril, J. Le Nôtre, C. Bruneau, P. H. Dixneuf, A. F. Kolomiets and S. N. Osipov, *New J. Chem.*, 2000, **25**, 16
7 V. Amir-Ebrahimi, J. G. Hamilton, J. Nelson, J. J. Rooney, J. M. Thompson, A. J. Beaumon, A. D. Rooney and C. J. Harding, *Chem. Commun.*, 1999, 1621.
8 R. F. Winter, *Eur. J. Inorg. Chem.*, 1999, 2121.
9 (*a*) D. Touchard, P. Haquette, A. Daridor, A. Romero and P. H. Dixneuf, *Organometallics*, 1998, **17**, 3844; (*b*) D. Touchard, N. Pirio and P. H. Dixneuf, *Organometallics*, 1995, **14**, 4920.
10 D. Touchard, P. Haquette, A. Daridor, L. Toupet and P. H. Dixneuf, *J. Am. Chem. Soc.*, 1994, **116**, 11 157.
11 These results are in agreement with previous theoretical studies on analogous allenylidene $[(C_5H_5)(CO)(PPh_3)Ru{=}C{=}C{=}CH_2]^+$ and $[(C_9H_7)(PPh_3)_2Ru{=}C{=}C{=}CH_2]^+$ suggesting that the LUMO is strongly located on the cumulenic ligand. See: (*a*) M. A. Esteruelas, A. V. Gomez, A. Lopez, J. Modrego and E. Oñate, *Organometallics*, 1997, **16**, 5826; (*b*) V. Cadierno, M. P. Gamasa, J. Gimeno, M. González-Cueva, E. Lastra, J. Borge, S. García-Granda and E. Pérez-Carreño, *Organometallics*, 1996, **15**, 2137.
12 (*a*) N. G. Connelly and W. E. Geiger, *Chem. Rev.*, 1996, **96**, 877; (*b*) J. H. Ameter and J. D. Swallen, *J. Phys. Chem.*, 1972, **57**, 678.
13 (*a*) D. D. Tanner, G. E. Diaz and A. Potter, *J. Org. Chem.*, 1985, **50**, 2149; (*b*) K. J. Covert, P. T. Wolczanski, S. A. Hill and P. J. Krusic, *Inorg. Chem.*, 1992, **31**, 66.
14 (*a*) The irreversibility of the reduction wave of $\mathbf{2}^+$ was also observed in THF at room temperature and at low temperature (−30 °C). (*b*) Many organometallic species are known to undergo reductive coupling reactions *via* radical intermediates. For examples see: ref. 13(*b*); Z. Hou, A. Fujita, H. Yamazaki and Y. Wakatsuki, *J. Am. Chem. Soc.*, 1996, **118**, 7843; E. J. Roskamp and S. F. Pedersen, *J. Am. Chem. Soc.*, 1987, **109**, 3152. However, in the present reaction we have observed that evolution of **2** led to a mixture of products. The two main compounds have been identified as **5** and $[Cl(dppe)_2Ru–C{\equiv}C–C(=CH_2)CH_3]$, certainly result from an intermolecular hydrogen abstraction [such an intermolecular abstraction reaction has already been reported for ketyl radicals, see ref. 13(*b*).

ChemComm

Hydrolysis of phosphodiester with hydroxo- or carboxylate-bridged dinuclear Ni(II) and Cu(II) complexes

Kazuya Yamaguchi,*[a] Fumio Akagi,[a] Shuhei Fujinami,[b] Masatatsu Suzuki,[b] Mitsuhiko Shionoya,[c] and Shinnichiro Suzuki[a]

[a] *Department of Chemistry, Graduate School of Science, Osaka University, 1-16 Machikaneyama, Toyonaka, Osaka 560-0043, Japan. E-mail: kazu@ch.wani.osaka-u.ac.jp*
[b] *Department of Chemistry, Faculty of Science, Kanazawa University, Kakuma-machi, Kanazawa 920-1192, Japan*
[c] *Department of Chemistry, Graduate School of Science, The University of Tokyo, 7-3-1 Hongo, Bunkyo-ku, Tokyo 113-0033, Japan*

Received (in Cambridge, UK) 8th November 2000, Accepted 15th January 2001
First published as an Advance Article on the web 8th February 2001

A hydroxo- or carboxylate-bridged dinuclear Ni(II) complexes with *N,N,N′*,N′-tetrakis{(6-methyl-2-pyridyl)methyl}-1,3-diaminopropan-2-ol has been synthesized as models for Ni(II)-substituted phosphotriesterase, which are more active catalysts for hydrolysis of phosphodiester than the corresponding dinuclear Cu(II) and Zn(II) complexes.

It has recently been shown that a number of phosphate esterases are activated by two metal ions.[1] For example, phosphotriesterases which hydrolyze organophosphate triesters, known to be potent insecticides and neurotoxins, require several metal ions [Zn(II), Cd(II), Ni(II), Co(II) and Mn(II)] for their activities.[2] *Pseudomonas diminuta* phosphotriesterase has two Zn(II) atoms per subunit. The binuclear metal site was confirmed by the 2.1 Å resolution X-ray crystal structure of the enzyme.[3] The structure of the active site is very similar to urease, a Ni(II) enzyme catalyzing the hydrolysis of urea, characterized by a bridging carbamylated Lys, two His ligands for each metal ion, and a bridging solvent ligand.[4] Interestingly, Ni(II)-substituted phosphotriesterase has a higher specific activity than the native Zn(II) enzyme, while the Cu(II)-substituted enzyme has a similar activity to the native one.[2] Although there have been numerous reports of esterase model systems using well defined metal complexes [Zn(II), Cu(II), Co(III) and Ln(III)],[5] only a few Ni(II) model complexes have been studied in relation to the structure and reactivity in the hydrolysis of phosphodiesters.[6] In order to understand the mechanistic roles of the metal ions in phosphate ester hydrolysis, we have examined hydrolysis catalyzed by hydroxo- or carboxylate-bridged dinuclear Ni(II) and Cu(II) complexes. We have found that the hydrolysis activities of the dinuclear Ni(II) complexes are significantly greater than those of the Cu(II) and Zn(II) complexes.

$[Ni_2(Me_4\text{-tpdp})(MeCO_2)(H_2O)_2](ClO_4)_2$ **1** was prepared by the reaction of $[Ni_2(Me_4\text{-tpdp})(OH)](ClO_4)_2$ **2** with equimolar $MeCO_2H$ in acetone at room temp. and was recrystallized from MeCN–H_2O as light green crystals.[7] The X-ray crystal structure[8] of **1** reveals that the two hexacoordinate Ni(II) ions bridged by alkoxide and acetate anions are 3.62 Å apart. The geometries of both the Ni(II) sites are octahedral, with oxygen atoms of water molecules at the sixth coordination site. $[Cu_2(Me_4\text{-tpdp})(CH_3CO_2)](ClO_4)_2$ **3** was prepared by the reaction of $[Cu_2(Me_4\text{-tpdp})(OH)(H_2O)](ClO_4)$ **4** with equimolar $MeCO_2H$ in acetone at room temperature and was recrystallized from methanol–diethyl ether as dark green crystals. The X-ray crystal structure[8] of **3** reveals that the two pentacoordinate Cu(II) ions bridged by alkoxide and acetate anions are 3.54 Å apart. The geometries of both the Cu(II) centers are distorted square pyramidal.

As a model reaction of phosphotriesterase, we examined the hydrolysis of bis(4-nitrophenyl)phosphate (BNP) with the dinuclear metal complexes **1**–**4**. The hydrolysis rates (v) catalyzed by the complexes (2.0 mM) were measured by the initial slope method following an increase in the 395 nm absorption band of released 4-nitrophenolate in 20% MeCN aqueous solution at 35.0 ± 0.1 °C. Buffer solutions (20 mM HEPES, pH 6.5–8.0; TAPS, pH 8.5–9.0; CAPS, pH 9.5–10.7)[9] were used, and the ionic strength adjusted to 0.10 with $NaNO_3$. The observed first-order rate constant, k_{obs}/s^{-1} for the hydrolysis reaction was calculated from the dependency of v on the initial concentration (2.0–8.0 mM) of BNP. The second-order rate constants, $k_{BNP}/M^{-1}\ s^{-1}$ for BNP hydrolysis are given by fitting of the kinetic eqn (1).

$$v = k_{obs}[BNP] = k_{BNP}[complex][BNP] \quad (1)$$

The k_{BNP} values for the Ni(II) and Cu(II) complexes (**1**, **2**, **3**, and **4**) were determined to be $(3.4 \pm 0.2) \times 10^{-2}$, $(3.5 \pm 0.1) \times 10^{-2}$, $(1.8 \pm 0.1) \times 10^{-4}$ and $(1.8 \pm 0.1) \times 10^{-4}\ M^{-1}\ s^{-1}$ at pH 10.1 and 35.0 °C, respectively. The results demonstrate that the nucleophilic reactions catalyzed by the Ni(II) complexes are *ca.* 200 times faster than those by the Cu(II) complexes. Koike and Kimura reported that mononuclear Zn(II) complexes [Zn([12]aneN$_3$)(OH) and Zn([12]aneN$_4$)(OH)][10] catalyze the hydrolysis of BNP, with k_{BNP} of 2×10^{-5} and $13 \times 10^{-5}\ M^{-1}\ s^{-1}$, respectively, at 35.0 °C.[5d] The second-order rate constant for BNP hydrolysis with the $Zn_2(Me_4\text{-tpdp})$ complex is $6.7 \times 10^{-4}\ M^{-1}s^{-1}$ under almost the same conditions.[11] It is interesting that the Ni(II) complexes are more effective than the Cu(II) and Zn(II) complexes for phosphate ester hydrolysis. It should be noted that the hydrolysis activity of a mononuclear Ni(II) complex $(Ni(Me_2\text{-bpa})(H_2O)(ClO_4)_2$, **5**)[12] is lower than those of dinuclear **1** and **2**; k_{BNP} for the mononuclear Ni(II) complex ($6.4 \times 10^{-3}\ M^{-1}s^{-1}$ at pH 10.1) is 5–6 times smaller than those for the dinuclear Ni(II) complexes **1** and **2**. The result suggests that the dinuclear Ni(II) complexes are the cooperative hybrid catalysts.[5d]

The DPP-bridged dinickel complexes,[13] $[Ni_2(Me_4\text{-tpdp})(DPP)](ClO_4)_2$ **5**, and the BNP-bridged dicopper complex, $[Cu_2(Me_4\text{-tpdp})(BNP)](ClO_4)_2$ **6**, were obtained by the reaction of **2** with equimolar DPP, and **4** with equimolar BNP in acetone solution, respectively. For X-ray crystal structure analysis, **5** was recrystallized from dry methanol while **6** was recrystallized from dry acetonitrile–diethyl ether. As shown in Fig. 1, the X-ray crystal structures of **5** and **6** reveal that the metal ions are bridged by alkoxide and phosphate diester.[8] The geometries of both the Cu sites in **6** are distorted square pyramidal, while the geometries of both the Ni sites in **5** are octahedral, with oxygen atoms of methanol at the sixth coordination site. The crystal structures of **1**, **3**, **5**, **6** and $[Zn_2(M_4\text{-tpdp})(BNP)]^{2+}$ indicate that the Ni(II) centers are hexacoordinate, whereas the Cu(II) and Zn(II)[11] centers are pentacoordinate; the hexacoordinate Ni(II) sites would be more favorable for the formation of an active intermediate complex bound BNP than the pentacoordinate Cu(II) and Zn(II) sites. The substrate could coordinate to Ni(II) ions under conditions that the nucleophile remains bound, and might react with the nucleophile, whereas the substrate

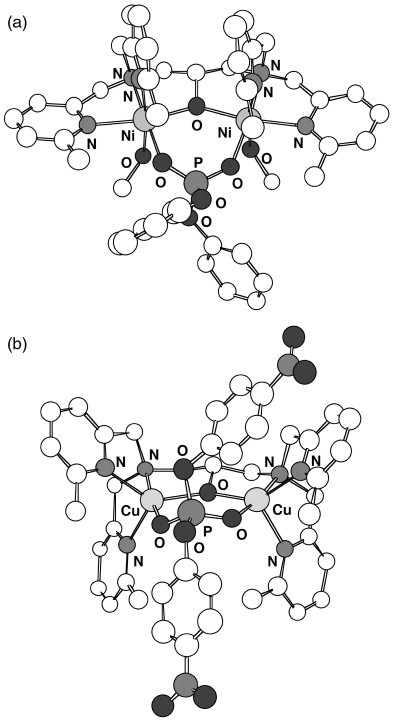

Fig. 1 Perspective views of $[Ni_2(Me_4\text{-tpdp})(DPP)(MeOH)_2]^{2+}$ (a) and $[Cu_2(Me_4\text{-tpdp})(BNP)]^{2+}$ (b). Hydrogen atoms are omitted for clarity.

coordinated to Cu(II) or Zn(II) ions could react only with exogenous nucleophile.

k_{BNP} Values for **1** and **2** are plotted against pH in Fig. 2. The inflection point at pH 8.0 for **2** almost coincides with the pK_a value of 7.9 for the coordinated water of **2**. Therefore, the OH^- ligand in **2** must be a good nucleophile for phosphodiester. On the other hand, the inflection point for **1** is shifted to a higher pH. These findings might be caused by ligand exchange of acetate with the substrate. The pH dependence of the UV–VIS spectrum of **1** was measured at 25.0 ± 0.1 °C. The UV–VIS spectrum of **1** was similar to that of **2** at high pH, with isosbestic points being observed (data not shown). The equilibrium constant for acetate binding was calculated as 25 ± 2 from the absorbance change at 488 nm in the pH range 7.5–11.0 and suggests that the acetate ligand in **1** readily dissociates and exchanges with hydroxide at high pH. This is consistent with the fact that the reactivity of **1** is similar to that of **2** at high pH while acetate ion in **1** would be a competitive inhibitor of the hydrolysis of BNP at low pH. Complex **2** behaves as a catalyst as revealed by the yield of product (>200% relative to complex) when the reaction of 8.0 mM BNP with 2.0 mM complex was carried out for 12 h at pH 10.1 and 35.0 °C. However, BNP hydrolysis with **2** inhibited (by 30%) upon the addition of an equimolar amount of 4-nitrophenyl phosphate (NPP), the hydrolysis product of BNP, at pH 10.1 and 35.0 °C NPP is also a competitive inhibitor with the substrate.

In conclusion, the mechanism of BNP hydrolysis with the dinuclear Ni(II) and Cu(II) complexes can be summarized by

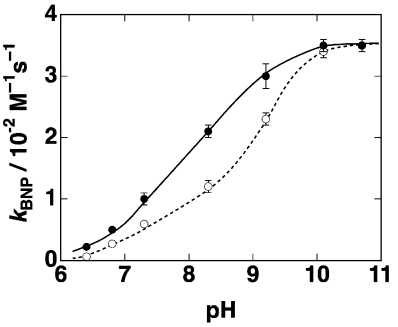

Fig. 2 Dependence of k_{BNP} on pH for the hydrolysis with complex **1** (○) and complex **2** (●) in 20% MeCN aqueous solution at 35.0 °C.

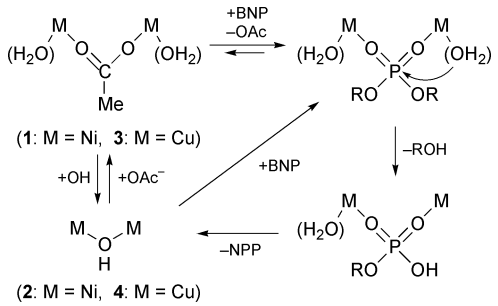

Scheme 1 Suggested mechanism of BNP hydrolysis with hydroxo- or carboxylate-bridged dinuclear complexes (M = Ni or Cu; R = $C_6H_4NO_2$).

Scheme 1. The hexacoordinate dinuclear Ni(II) complexes are more active catalysts for phosphate diester hydrolysis than the corresponding pentacoordinate dinuclear Cu(II) and Zn(II) complexes. The coordination number of the metal ions in an intermediate complex would be important for phosphodiester hydrolysis.

This work was supported by Grant-in-Aids for Scientific Research on Priority Area No.12640538 from the Ministry of Education, Science, Sports and Culture of Japan, to whom we express our thanks.

Notes and references

1 D. E. Wilcox, *Chem. Rev.*, 1992, **96**, 2435.
2 G. A. Omburo, J. M. Kuo, L. S. Mullins and F. M. Raushel, *J. Biol. Chem.*, 1992, **267**, 13278.
3 J. L. Vanhooke, M. M. Benning, F. M. Raushel and H. M. Holden, *Biochemistry*, 1996, **35**, 6020.
4 E. Jabri, M. B. Carr, R. P. Hausinger and P. A. Karplus, *Science*, 1995, **268**, 998.
5 For example: (*a*) E. L. Hegg and J. N. Burstyn, *Coord. Chem. Rev.*, 1998, **173**, 133; (*b*) J. R. Morrow and W. C. Trogler, *Inorg. Chem.*, 1988, **27**, 3387; (*c*) N. H. Williams, B. Takasaki, M. Wall and J. Chin, *Acc. Chem. Res.*, 1999, **32**, 485; (*d*) T. Koike and E. Kimura, *J. Am. Chem. Soc.*, 1991, **113**, 8935; (*e*) D. H. Vance and A. W. Czarnik, *J. Am. Chem. Soc.*, 1993, **115**, 12 165.
6 M. A. De Rosch and W. C. Trogler, *Inorg. Chem.*, 1990, **29**, 2409; J. R. Morrow, L. A. Buttrey and K. Berback, *Inorg. Chem.*, 1992, **31**, 16.
7 Me_4-tpdp: *N,N,N′,N′*-tetrakis{(6-methyl-2-pyridyl)methyl}-1,3-diaminopropan-2-ol (Y. Hayashi, T. Kayatani, H. Sugimoto, M. Suzuki, K. Inomata, A. Uehara, Y. Mizutani, T. Kitagawa and Y. Maeda, *J. Am. Chem. Soc.*, 1995, **117**, 11 220).
8 *Crystal data*: for **1**: $C_{33}H_{46}O_{14}N_6Cl_2Ni_2$, M = 936.06, monoclinic, $P2_1/n$ (no. 14), a = 17.336(1), b = 13.045(1), c = 18.060(1) Å, β = 100.938(5)°, V = 4010.0(5) Å^3, Z = 4, μ(Mo-Kα) = 11.45 cm^{-1}, 6698 reflections measured, 5724 unique reflections collected [$I > 3\sigma(I)$], T = 153 K, R_{int} = 0.0264, R = 0.060, R_w = 0.096. For **3**: $C_{37}H_{50}O_{12}N_6Cl_2Cu_2$, M = 968.83, monoclinic, $P2_1/c$ (no.14), a = 17.577(3), b = 17.387(2), c = 14.257(2) Å, β = 100.63(1)°, V = 4282(1) Å^3, Z = 4, μ(Mo-Kα) = 11.84 cm^{-1}, 7300 reflections measured, 6088 unique reflections collected [$I > 3\sigma(I)$], T = 153 K, R_{int} = 0.0305, R = 0.053, R_w = 0.079. For **5**: $C_{46}H_{59}Cl_2N_6O_{16}Ni_2P$, M = 1171.28, monoclinic, $P2_1/n$, a = 13.5091(4), b = 20.927(1), c = 18.0299(9) Å, β = 96.4758(5)°, V = 5064.6(4) Å^3, Z = 4, μ(Mo-Kα) = 0.956 cm^{-1}, 11459 reflections measured, 8547 unique reflections collected [$I > 3\sigma(I)$], T = 138.2 K, R_{int} = 0.02299, R = 0.052, and R_w = 0.078. For **6**: $C_{48}H_{59.5}Cl_2Cu_2N_{8.5}O_{19.5}P$, M = 1296.52, orthorhombic, *Pnma*, a = 22.941(4), b = 36.360(4), c = 14.160(2) Å, V = 11812(2) Å^3, Z = 8, μ(Mo-Kα) = 9.15 cm^{-1}, 7732 reflections measured, 5142 unique reflections collected [$I > 2.60\sigma(I)$], T = 288.2 K, R = 0.081, R_w = 0.114. CCDC 153180–153183. See http://www.rsc.org/suppdata/cc/b0/b008994j/ for crystallographic data in .cif or other electronic format.
9 HEPES: *N*-2-hydroxyethylpiperazine-*N′*-2-ethanesulfonic acid; TAPS: *N*-tris(hydroxymethyl)methyl-3-aminopropanesulfonic acid; CAPS: cyclohexylaminopropanesulfonic acid.
10 [12]aneN$_3$: 1,5,9-triazacyclododecane; [12]aneN$_4$: 1,4,7,10-tetraazacyclododecane.
11 M. Suzuki *et al.*, unpublished data.
12 Me_2-bpa: bis{(6-methyl-2-pyridyl)methyl}amine.
13 DPP: diphenylphosphate.

1,1′-Bis(trimethylsilylseleno)ferrocene in cluster synthesis: a redox active surface on a copper–selenide core†‡

Andrew I. Wallbank and John F. Corrigan*

Department of Chemistry, The University of Western Ontario, London, Ontario, N6A 5B7, Canada. E-mail: jfcorrig@julian.uwo.ca

Received (in Cambridge, UK) 15th December 2000, Accepted 17th January 2001
First published as an Advance Article on the web 8th February 2001

1,1′-Bis(trimethylsilylseleno)ferrocene 1 has been prepared from the reaction of [1,1′-Fe(η^5-$C_5H_4SeLi)_2$(TMEDA)] and $ClSiMe_3$ in good yield. The reactive silyl groups on 1 are used as a driving force for the synthesis of [Cu_8{Fe(η^5-$C_5H_4Se)_2$}$_4$($PPh_2Et)_4$] 2, a cluster possessing four peripheral ferrocenyl moieties.

Owing to the inherent redox active metal centre, the functionalisation of the cyclopentadienyl rings in ferrocene and subsequent ligation to metal centres are currently of great research interest in cluster, materials and inorganic synthesis.[1] Many of these ferrocene-containing molecules display interesting charge transport, non-linear optical and magnetic properties related to the metal–metal interactions between the ferrocene units and other metal centres in the structure.[2] It has been demonstrated that nanoparticle (Au) surfaces can be functionalised with ferrocenyl units, although these redox centres are spatially removed from the metallic core due to the micellar type of stabilisation provided by the thiolate ligands.[3] Bidentate 1,1′-bis(diphenylphosphino)ferrocene[4] (dppf) has been shown to be an excellent ligand in carbonyl cluster chemistry due to the flexibility of the ferrocene unit, through a combination of ring twisting and tilting. 1,1′-Ferrocenyldichalcogenolates have many similar characteristics and have been shown to bridge metal centres[5] and bind in a chelating fashion to one metal.[6] These dichalcogenolates are synthesized either *via* insertion of chalcogens into the C–Li bond of dilithioferrocene[7] or *via* deprotonation of the corresponding dichalcogenols.[8]

The use of silylated selenium reagents offers a powerful entry into the formation of metal–selenium bonds in both coordination and polynuclear chemistry.[9] Their utility in the latter exploits the bridging capacity of the selenium centre in alkyl– and aryl–selenolate ligands and has been used to effectively stabilise metal–selenide cores. Herein we describe the unprecedented complexation of 1,1′-diselenolatoferrocene units onto a polymetallic core.

We reasoned that the synthesis of the bis-silylated reagent [Fe(η^5-$C_5H_4SeSiMe_3)_2$] **1** and its use in the synthesis of metal–chalcogen clusters would permit facile introduction of redox active iron centres onto metal–chalcogen cluster surfaces, which may be intimately coupled (*via* the C_5–Se rings) to the cluster core. Owing to the large variety of bonding modes for selenium and the success of the use of silylselenoethers in cluster synthesis,[9] [Fe(η^5-$C_5H_4SeSiMe_3)_2$] **1** was targeted and prepared from the corresponding dilithiodiselenolate.§ When chlorotrimethylsilane is added to a suspension of [Fe(η^5-$C_5H_4SeLi)_2$(TMEDA)][10] in pentane at 0 °C, **1** is isolated as a golden yellow powder in 65% yield. Compound **1** is susceptible to rapid air decomposition both in solution and the solid state. Even under an inert atmosphere, **1** must be stored cold and in the absence of light in order to avoid decomposition. The molecular structure of **1** (Fig. 1) shows that the selenolate groups are held in a *trans* configuration in the solid state with the two Cp rings adopting a staggered conformation. The iron atom sits on a crystallographic inversion centre with the planes of the cyclopentadienyl rings parallel and the selenium atoms lie slightly above (0.02 Å) the C_5 rings.¶

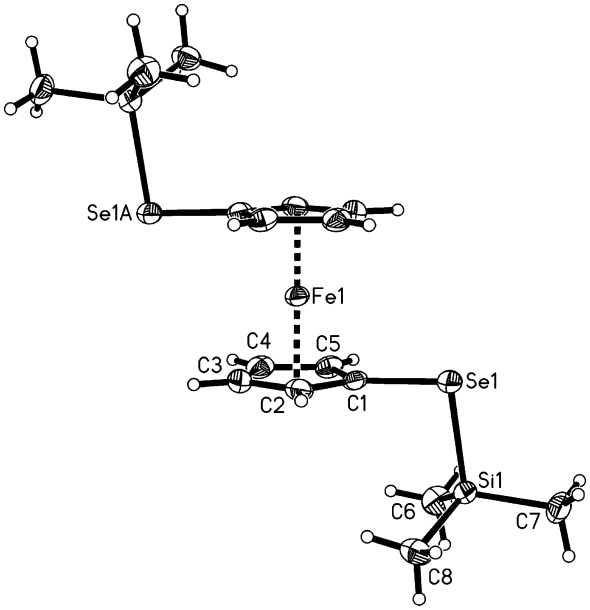

Fig. 1 Molecular structure of Fe(η^5-$C_5H_4SeSiMe_3)_2$ **1**. Selected bond lengths (Å) and angles (°): Fe1–C 2.041(3)–2.048(3), C1–Se1 1.916(3), Sel–Si1 2.2930(8); C1–Se1–Si1 95.32(8).

The reaction of **1** with 2 equivalents of CuOAc : $3PPh_2Et$ in THF affords [Cu_8{Fe(η^5-$C_5H_4Se)_2$}$_4$($PPh_2Et)_4$]·(OC_4H_8) **2**·THF in good yield, the reaction driven by the formation and elimination of Me_3SiOAc.‖ The molecular structure of **2** is shown in Fig. 2. There are two crystallographically independent and chemically equivalent molecules in the unit cell, both of which reside on a two-fold rotation axis.** Bond lengths and angles discussed in the text for **2** refer to molecule 1.

Cluster **2** contains a copper–selenium core shielded by four ferrocenyl and four phosphine ligands. All of the copper centres exhibit a trigonal planar geometry either through a combination of two selenium and one phosphorus bonds (Cu1, Cu3, Cu1A, Cu3A) or three Cu–Se interactions (Cu2, Cu2A, Cu4, Cu4A). The Cu–Se [2.356(1)–2.463(1) Å] and Cu–P distances [2.214(2)-2.226(2) Å] are similar to those found in other copper–selenium clusters.[11] Both of the crystallographically independent ferrocenyl moieties display moderate deviations from co-planarity of the two C_5 rings (2.0 and 5.3° for Fe2 and Fe1, respectively). Whilst the two Cp rings about Fe1 deviate 15.7° from being eclipsed, the two about Fe2 are better described as adopting a staggered (29.5°) conformation. The selenium atoms in **2** are slightly displaced (0.07–0.28 Å) from the planes defined by their respective C_5 rings. Overall, the eight Se centres define a non-bonded [3.352(1)–4.411(1) Å] dodecahedral framework bridging either two (Se1, Se1A, Se3,

† Electronic supplementary information (ESI) available: cyclic voltammograms for **1** and **2**, ^{1}H NMR spectrum for **1**. See http://www.rsc.org/suppdata/cc/b0/b010023o/

‡ Dedicated to Dr Arthur J. Carty on the occasion of his 60th birthday.

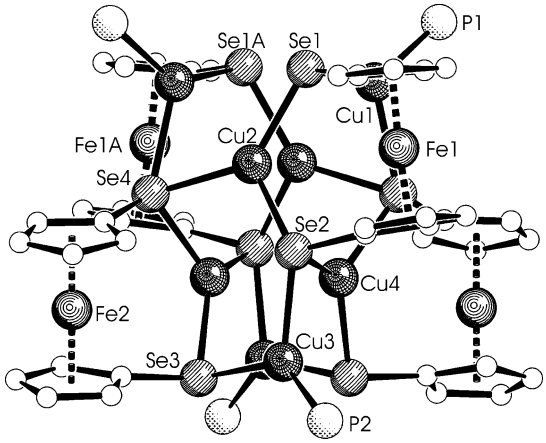

Fig. 2 Molecular structure of $[Cu_8\{Fe(\eta^5\text{-}C_5H_4Se)_2\}_4(PPh_2Et)_4]$ **2** (molecule 1; phosphine carbon atoms omitted). Selected bond lengths (Å): Se(1)–Cu(2) 2.355(1), Se(1)–Cu(1) 2.411(1), Se(2)–Cu(2) 2.362(1), Se(2)–Cu(4) 2.397(1), Se(2)–Cu(3) 2.434(1), Se(3)–Cu(4A) 2.354(1), Se(3)–Cu(3) 2.399(1), Se(4)–Cu(4A) 2.380(1), Se(4)–Cu(2) 2.431(1), Se(4)–Cu(1A)–Cu(1A) 2.463(1).

Se3A) or three (Se2, Se2A, Se4, Se4A) metals. It is interesting to note that the observed Cu_8Se_8 core geometry in **2** has been predicted to be unstable for related $[(FeCl)_{4-x}Cu_{4+x}(SePr^i)_8]$ complexes.[11b]

The cyclic voltammogram of **1** (ESI†) displays one irreversible wave at +1.33 V (*versus* $CoCp_2/CoCp_2^+$), complicated by the deposition of the material onto the electrode surface. In **2**, two irreversible oxidation waves of equal current are observed at +1.11 and +1.35 V,†† although the first wave may be due to oxidation of Cu(I) centres. Unlike surface modified Au particles with ferrocenylalkanethiolate ligands where the Fe centres are spatially 'removed' from the cluster,[3] in **2** the Fe centres are intimately associated with the polymetallic core. Oxidation of **2** to higher potential results in cluster decomposition only. Any electronic communication between the iron and copper centres in the molecular complex **2** suggests similar effects in related *nanoscale* $[Cu_{2m}\{Fe(\eta^5\text{-}C_5H_4Se)_2\}_{m-n}Se_n(PR_3)_x]$ complexes and we are actively pursuing their synthesis.

This work was supported by the Natural Sciences and Engineering Research Council Canada. J. F. C. thanks the Canada Foundation for Innovation and the Ontario Research and Development Challenge Fund for equipment funding. The authors thank Professor Mark S. Workentin for the use of his electrochemical equipment and Mr Robert L. Donkers for his assistance with these experiments.

Notes and references

§ *Synthesis of* **1**: $ClSiMe_3$ (0.13 mL, 3.26 mmol) was added dropwise to a suspension of $[Fe(\eta^5\text{-}C_5H_4SeLi)_2(TMEDA)]$ (0.16 mmol) in pentane (40 mL) at 0 °C. The orange suspension gradually became yellow in colour and after two hours the suspension was filtered to remove LiCl and the filtrate was concentrated slowly to afford X-ray quality golden orange crystals of **1**. Yield 65%. ^{1}H NMR (C_6D_6): δ 4.30 vt (CH, J_{HH} 1.8 Hz, 4), 4.05 vt (CH, J_{HH} 1.8 Hz, 4), 0.225 (Si–CH_3, s, 18). ^{13}C{^{1}H} NMR: δ 77.3 (CH, s), 71.5 (CH, s), 69.3 (C–Se, s), 1.6 (CH_3, s). ^{77}Se: δ 9.7 (s); ^{29}Si: δ 13.7 (s) ppm. Exact mass: Calcd. 489.925276. Found 489.924389.

¶ *Crystal data* for **1**: $C_{16}H_{26}FeSe_2Si_2$, M = 488.3, triclinic, space group $P\bar{1}$, a = 6.1366(2), b = 9.1532(5), c = 10.1063(6) Å, α = 65.321(2), β = 81.568(3), γ = 79.697(3)°, V = 505.85(4) Å^3, T = 200 K, Z = 1, μ = 4.454 mm^{-1}, $2\theta_{max}$ = 54.9, 7283 measured, 2282 independent reflections (R_{int} = 0.069) on an Enraf-Nonius Kappa-CCD diffractometer. All non-hydrogen atoms were refined anisotropically to yield R = 0.0432, wR_2 = 0.1020, GoF = 1.043.

‖ *Synthesis of* **2**: CuOAc (0.07 g, 0.57 mmol) was dissolved with PPh_2Et (0.35 mL, 1.72 mmol) in THF (5 mL). After stirring for 30 min, a solution of **1** (0.14 g, 0.28 mmol) in THF (0.5 mL) was added dropwise. After stirring for a further hour, the orange solution was layered with pentane (20 mL). Pale orange crystals of **2**·THF formed within a few days. Yield 60% (based on Cu). ^{1}H NMR (C_6D_6): δ 7.74 (br s, H_{phenyl}, 8 H), 7.64 (br s, H_{phenyl}, 8 H); 7.07–7.02 (mult., H_{phenyl}, 24H), 5.25 (br s, H_{Cp}, 4H, $\Delta\nu_{\frac{1}{2}}$ 11.1 Hz), 4.60 (br s, H_{Cp}, 4H, $\Delta\nu_{\frac{1}{2}}$ 11.1 Hz), 4.30 (br s, H_{Cp}, 4H, $\Delta\nu_{\frac{1}{2}}$ 11.1 Hz), 4.03 (s, H_{Cp}, 4H, $\Delta\nu_{\frac{1}{2}}$ 11.1 Hz), 3.90 (s, H_{Cp}, 8H, $\Delta\nu_{\frac{1}{2}}$ 12.8 Hz), 3.87 (s, H_{Cp}, 4H, $\Delta\nu_{\frac{1}{2}}$ 12.8 Hz), 3.81 (s, H_{Cp}, 4H); 2.13 (mult., –CH_2–, 8H), 1.28 (mult., –CH_3, 12H). ^{31}P{^{1}H} NMR: δ −4.1 ($\Delta\nu_{\frac{1}{2}}$ 19.2 Hz, due to J_{PCu}[12]) ppm. Anal. Calcd. for $C_{96}H_{92}Cu_8P_4Se_8Fe_4$·$(OC_4H_8)$: C, 42.8; H, 3.59%. Found: C, 42.6; H, 3.46%.

** *Crystal data* for **2**: $C_{96}H_{92}Fe_4Cu_8Se_8P_4$·THF, M = 2805.1, monoclinic, space group $P2/n$, a = 24.051(1), b = 15.5641(8), c = 28.042(6) Å, β = 108.202(1)°, V = 9971.8(9) Å^3, T = 223 K, Z = 4, μ = 5.261 mm^{-1}, $2\theta_{max}$ = 56.6, 59974 measured, 23541 independent reflections (R_{int} = 0.072) on a Siemens SMART CCD diffractometer. All non-hydrogen atoms (with the exception of solvent atoms) were refined anisotropically to yield R = 0.0553, wR_2 = 0.1154, GoF = 0.973.

CCDC reference number 182/1890. See http://www.rsc.org/suppdata/cc/b0/b010023o/ for crystallographic files in .cif format.

†† Electrochemical experiments were performed under an argon atmosphere in glass distilled THF with a platinum working, platinum flag counter and silver wire in THF/electrolyte reference electrode using a Princeton Applied Research (PAR) 263 potentiostat. Potentials are referenced to cobaltocene as an internal reference, added at the end of the experiments.

1 *Ferrocenes: Homogeneous Catalysis, Organic Synthesis, Materials Science*, ed. A. Togni and T. Hayashi, VCH, Weinheim, 1994.
2 I. Manners, *Adv. Organomet. Chem.*, 1995, **37**, 131; I. Manners, *Chem. Commun.*, 1999, 857; Y. Zhu, O. Clot, M. O. Wolf and G. P. A. Yap, *J. Am. Chem. Soc.*, 1998, **120**, 1812.
3 A. C. Templeton, W. P. Wuelfing and R. W. Murray, *Acc. Chem. Res.*, 2000, **33**, 27; R. S. Ingram, M. J. Hostetler and R. W. Murray, *J. Am. Chem. Soc.*, 1997, **119**, 9175.
4 S.-W. A. Fong and T. S. A. Hor, *J. Cluster Sci.*, 1998, **9**, 351.
5 R. Broussier, Y. Gobet, R. Amardeil, A. Da Rold, M. M. Kubicki and B. Gautheron, *J. Organomet. Chem.*, 1993, **445**, C4.
6 S. Takemoto, S. Kuwata, Y. Nishibayashi and M. Hidai, *Inorg. Chem.*, 1998, **37**, 6428.
7 M. Herberhold, M. Hübner and B. Wrackmeyer, *Z. Naturforsch, Teil B*, 1993, **48**, 940.
8 A. G. Osborne, R. E. Hollands, R. F. Bryan and S. Lockhart, *J. Organomet. Chem.*, 1982, **224**, 129.
9 D. Fenske and J. F. Corrigan, in *Metal Clusters in Chemistry*, ed. P. Braunstein, L. A. Oro and P. R. Raithby, Wiley-VCH, Weinheim, 1999, vol. 3, p. 1302.
10 R. Broussier, A. Abdulla and B. Gautheron, *J. Organomet. Chem.*, 1987, **332**, 165.
11 (*a*) N. Y. Zhu and D. Fenske, *J. Chem. Soc., Dalton Trans.*, 1999, 1076; (*b*) J. Lackmann, R. Hauptmann, S. Weißgräber and G. Henkel, *Chem. Commun.*, 1999, 1995.
12 R. K. Harris, *Nuclear Magentic Resonance Spectroscopy*, Longman Scientific & Technical, Essex, 1986, p. 139.

$[Bu^tNHP(\mu\text{-}NBu^t)_2PNH_2]$, a novel building block for neutral and anionic polycyclic main group arrangements†

Michael A. Beswick,* Benjamin R. Elvidge, Neil Feeder, Sara J. Kidd and Dominic S. Wright*

University of Cambridge, Lensfield Road, Cambridge, UK CB2 1EW. E-mail: dsw1000@cus.cam.ac.uk

Received (in Cambridge, UK) 8th November 2000, Accepted 17th January 2001
First published as an Advance Article on the web 8th February 2001

The novel precursor $[Bu^tNHP(\mu\text{-}NBu^t)_2PNH_2]$ (1) provides easy access to polycyclic main group systems; reaction with $Sb(NMe_2)_3$ gives the tricyclic species $\{[Bu^tNHP(\mu\text{-}NBu^t)_2\text{-}P]_2\{Me_2NSb(\mu\text{-}N)\}_2]$ (2), whereas reaction with an excess of Bu^nLi results in elimination of $LiNH_2$ and the formation of the co-complex $[\{Bu^tNP(\mu\text{-}NBu^t)_2P\}_2N]Li_3\ (Bu^nLi)_2$, (3), containing the unprecedented $[\{Bu^tNP(\mu\text{-}NBu^t)_2P\}_2N]^{3-}$ trianion.

In recent years the synthesis and coordination chemistry of a range of new anionic ligands based on p-block element frameworks has become a rich area of study. This work has been dominated by a number of related Group 15 and 16 element/nitrogen arrangements, such as the tripodal systems $[E(NR)_3]^{2-}$ (E = S–Te)[1] and $[E(NR)_3]^{3-}$ (E = As, Sb),[2] which provide the means to an extensive range of cage complexes, containing well-defined mixed-element compositions.[2] Such cages have potentially far-ranging applications as single-source materials to a number of technologically important mixed-element phases.[3] The normally easy access to these multifunctional p-block element ligand arrangements contrasts with the generally far more involved synthetic procedures required to prepare related systems based on carbon. However, a key issue is whether systematic routes can be devised to more elaborate polyfunctional p-block element species (beyond the simple systems previously investigated). To this end, we present here a simple design approach to a family of polycyclic Group 15 imido frameworks, providing a new direction in this area.

The principal starting material for these investigations, $[Bu^tNHP(\mu\text{-}NBu^t)_2PNH_2]$ (**1**), is prepared in good yield (59%) by the reaction of $[Bu^tNHP(\mu\text{-}NBu^t)_2PCl]$[4] with NH_3(g) in THF solution.† Previous studies of imido phosphorus anions have dealt almost exclusively with species of the type $[R'NP(\mu\text{-}NR)]_2^{2-}$, prepared by deprotonation of $[R'NHP(\mu\text{-}NR)]_2$.[5] Although **1** has a similar P_2N_2 core arrangement to the latter, it presents the unique opportunity for deprotonation at up to three positions (*i.e.* the Bu^tNH and NH_2 groups). The reaction of **1** with $Sb(NMe_2)_3$ (1:1 equiv.) in toluene gives $[\{Bu^tNHP(\mu\text{-}NBu^t)_2P\}_2\{Me_2NSb(\mu\text{-}N)\}_2]$ (**2**) (Scheme 1). This result is similar to that observed between simple primary amines (RNH_2) and $Sb(NMe_2)_3$,[6] which gives dimers of the type $[Me_2NSb(\mu\text{-}NR)]_2$. However, in the case of **2** a tricyclic arrangement is established in a single step. The low reactivity of the Bu^tNH protons in **2** (which could potentially react further with the Sb-bonded NMe_2 groups) contrasts with the deprotonation of **1** with Bu^nLi (1:3 equiv., respectively). The product is the unusual co-complex $[\{Bu^tNP(\mu\text{-}NBu^t)_2P\}_2N]Li_3{\cdot}(Bu^nLi)_2$ (**3**), the framework of which results from a combination of deprotonation and coupling of the dimer units of **1** (with elimination of $LiNH_2$) (see ESI†).

The low-temperature X-ray structures of **1**, **2** and **3** were obtained.‡ Although simple, **1** is the first non-symmetrically substituted cyclophosphazane containing the NH_2 functionality (Fig. 1). Related species containing the NH_2 functionality are

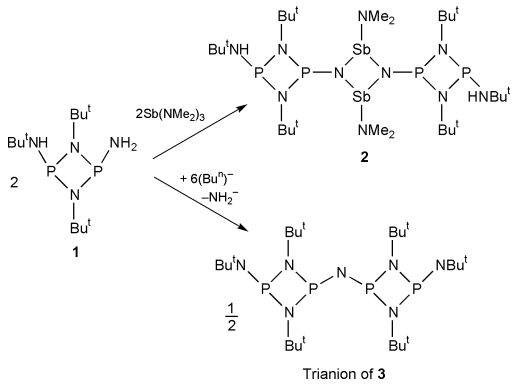

Scheme 1

rare[7] and the only structurally characterised dimers previously reported are chlorides of the type $[R_2NP(\mu\text{-}NR')(\mu\text{-}NR'')PCl]$[8] and $[Bu^tNHP(\mu\text{-}NBu^t)_2PCl]$[4] (the immediate precursor to **1**). The *cisoid* disposition of the Bu^tNH and NH_2 groups found in molecules of **1** is similar to that observed for the previous chlorides. However, the similarity of the ^1H and ^{31}P NMR behaviour of **1** in toluene solution with that of $[PhNHP(\mu\text{-}NPh)]_2$ suggests that two closely related *cisoid* isomers are present (in *ca.* 2:1 ratio, corresponding to rotation of the Bu^tNH group *exo* or *endo* to the P_2N_2 ring).[9]

Complex **2** (Fig. 2) has a tricyclic arrangement composed of a central Sb_2N_2 ring symmetrically substituted with bridging $[Bu^tNHP(\mu\text{-}NBu^t)_2P]$ groups. The orientation of these ring units approximately *trans* to the Sb_2N_2 ring plane gives molecules an overall S-shape, in which the *cisoid* conformation found in the precursor **1** is retained in the $[Bu^tNHP(\mu\text{-}NBu^t)_2PN]$ ring units of **2**. The bias for the *cisoid* conformation of these substituents is apparently reinforced by H-bonding of the terminal Bu^tNH protons to the *trans* Me_2N groups of the Sb_2N_2 core [N(2)···N(5) 3.178(9) Å (H(2)···N(5) 2.34 Å), N(2)H(2A)···N(5A) 165.3°]. Although (unlike **1**) the

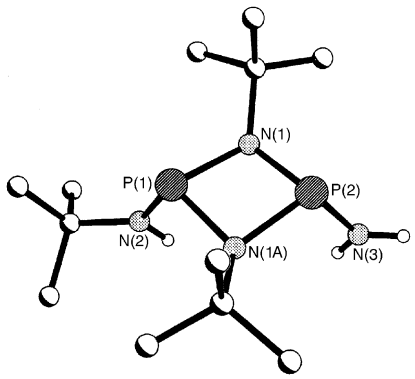

Fig. 1 *Cisoid* conformation of molecules of **1**. Key bond lengths (Å) and angles (°): P(1)–N(1) 1.728(1), P(2)–N(2) 1.663(2), P(2)–N(1) 1.729(1), P(2)–N(3) 1.663(2); N(1)–P(1)–N(2) 105.54(7), N(1)–P(1)–N(1A) 80.79(9), N(1)–P(2)–N(3) 105.81(8), N(1)–P(2)–N(1A) 80.78(9), P(1)–N(1)–P(2) 97.48(7).

† Electronic supplementary information (ESI) available: synthetic and crystallographic details for **1**–**3**, See http://www.rsc.org/suppdata/cc/b0/b009000j/

DOI: 10.1039/b009000j

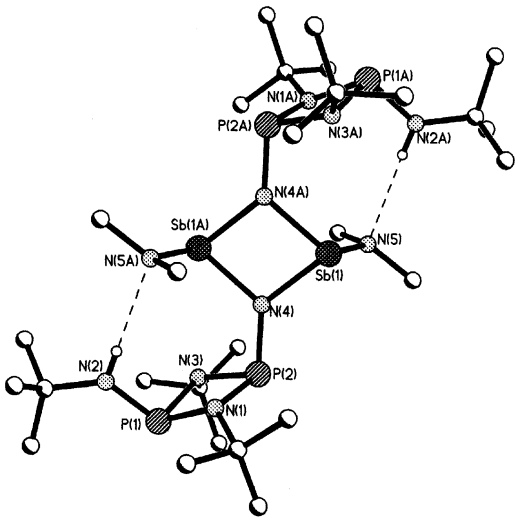

Fig. 2 Tricyclic molecules of **2**. Key bond lengths (Å) and angles (°): Sb(1)–N(4) 2.071(9), Sn(1)–N(4A) 2.048(9), Sb(1)–N(5) 2.06(1), P(2)–N(4) 1.680(9), P(2)–N(1) 1.726(9), P(2)–N(3) 1.729(9), P(1)–N(1) 1.739(9), P(1)–N(3) 1.778(9), P(1)–N(2) 1.66(1), N(2)···N(5) 3.178(9) [H(2)···N(5) 2.34, N(2)H(2A)···N(5A) 165.3]; N(4)–Sb(1)–N(4A) 77.3(4), Sb(1)–N(4)–Sb(1A) 102.7(4), N(4,4A)–Sb(1)–N(5) mean 100.2, Sb(1)–N(4)–P(2) 130.5(5), Sb(1A)–N(4)–P(2) 126.8(5), N(4)–P(2)–N(1) 108.3(5), N(4)–P(2)–N(3) 101.0(4), N(1)–P(2)–N(3) 82.5(4), P(2)–N(1,3)–P(1) mean 97.6, N(1)–P(1)–N(3) 80.8(4), N(2)–P(1)–N(1,3) mean 105.0.

[$Bu^tNHP(\mu\text{-}NBu^t)_2PN$] units of **2** are no longer symmetric, deprotonation of the NH_2 group of the precursor has comparatively little effect on the overall bond lengths and angles found in these units.

The surprising result of attempted deprotonation of **1** with Bu^nLi is the formation of the elaborate cage complex **3**, consisting of a $[\{Bu^tNP(\mu\text{-}NBu^t)_2P\}_2N]^{3-}$ trianion coordinated to three Li^+ cations and further associated with two monomer units of Bu^nLi (Fig. 3). Although uncommon, a number of co-complexes with Bu^nLi of this kind have been structurally characterised in recent years.[10] The composition of **3** resembles that of $[Al_2(NHBu^t)_3(NBu^t)_3Li_3{\cdot}2Bu^nLi]$, which contains an $[Al_2(NHBu^t)_3(NBu^t)_3]^{3-}$ trianion unit and two Bu^nLi monomers.[11c] Nonetheless, the bicyclic $[\{Bu^tNP(\mu\text{-}NBu^t)P\}_2N]_2^{3-}$ trianion is an unprecedented Group 15 imido ligand arrangement. The closest comparison that can be made with the trianion framework of **3** is with the neutral cyclophosphazane

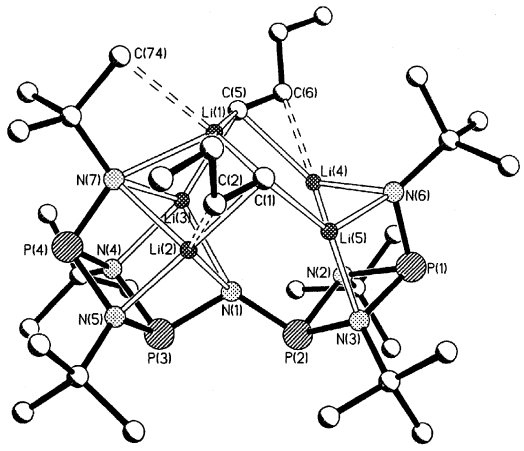

Fig. 3 Cage structure of the co-complex **3**. Key bond lengths (Å) and angles (°): within the $[\{Bu^tNP(\mu\text{-}NBu^t)P\}_2N]_2^{3-}$ trianion: P(1)–N(6) 1.655(3), P(1)–N(2) 1.792(3), P(1)–N(3) 1.784(3), P(2)–N(2) 1.774(3), P(2)–N(3) 1.762(3), P(2)–N(1) 1.676(3), P(3)–N(1) 1.689(3), P(3)–N(4) 1.768(2), P(3)–N(5) 1.768(2), P(4)–N(4) 1.779(2), P(4)–N(5) 1.785(2), P(4)–N(7) 1.668(3); N(2,4)–P(1,4)–N(3,5) mean 82.3, N(2,4)–P(2,3)–N(3,5) mean 83.3, P(2)–N(1)–P(3) 113.1(1); within Li–N/C framework: terminal Bu^tN–Li(2,3,4,5) range 1.987(6)–2.208(6), μ-Bu^tN–Li(2,3,4,5) range 2.014(6)–2.102(6), N(1)–Li(2) 2.313(6), N(1)–Li(3) 2.193(7), N(7)–Li(1) 2.147(7), C(1,5)–Li(2,3,4,5) range 2.124(7)–2.218(6), C(1,5)–Li(1) mean 2.26, C(2)···Li(2) 2.461(6), C(6)···Li(4) 2.341(6), C(74)···Li(4) 2.783(6).

[$\{PhNHP(\mu\text{-}NPh)_2P\}_2NPh$] (a product of condensation of $PhNH_2$ with PCl_3), consisting of a similar arrangement of two P_2N_2 rings linked by an NPh bridge.[11] All five of the Li^+ cations of **3** have distinct coordination geometries. The positioning of Li(2) and Li(3), and Li(4) and Li(5) within the 'hemisphere' of the coordinating $[\{Bu^tNP(\mu\text{-}NBu^t)P\}_2N]_2^{3-}$ trianion of **3** is broadly similar. Each of these cations is coordinated by one of the μ-NBu^t groups and by the terminal Bu^tN group of the [$Bu^tNP(\mu\text{-}NBu^t)P$] halves of the trianion unit. However, presumably owing to the geometric constraints involved, the μ-N centre linking the [$Bu^tNP(\mu\text{-}NBu^t)P$] units [N(1)] only bonds to Li(2) and Li(3) [*cf.* > 2.84 Å for Li(4,5)···N(2)], giving a pseudo-cubane fragment on this side of the molecule which is reminiscent of the structure of $[\{Bu^tNP(\mu\text{-}NBu^t)\}_2Li_2{\cdot}2THF]$.[5b] The two Bu^n groups bridge Li^+ cations associated with each [$Bu^tNP(\mu\text{-}NBu^t)P$] half of the trianion. The involvement of the α-C and β-C centres of each of the Bu^{n-} anions with Li(2) and Li(4) is similar to that found in the hexameric structure of $[Bu^nLi]_6$ in the solid state [*β*-C(–H)···Li *ca.* 2.28 Å;[12] *cf.* C(2)···Li(2) 2.461(6) and C(6)···Li(4) 2.341 (6) Å in **3**]. The remaining Li cation [Li(1)] is located above the pseudo-cubane half of the cage, being bonded to the α-C atoms of both of the $(Bu^n)^-$ anions and to a terminal Bu^tN group. Further agostic interaction with the Me group of this Bu^tN ligand [C(74)···Li(1) 2.783(6) Å[15] results in a pseudo-tetrahedral geometry for Li(1).

We gratefully acknowledge the EPSRC (N. F., S. J. K.) and the Leverhulme Trust (M. A. B.) for financial support. We also thank Dr J. E. Davies for collecting X-ray data for the compounds reported.

Notes and references

‡ CCDC reference number 150926-150928. See http://www.rsc.org/suppdata/cc/b0/b009000j/ for crystallographic data in .cif or other electronic format.

1 For examples see: R. Fleischer, S. Freitag, F. Pauer and D. Stalke, *Angew. Chem.*, 1996, **108**, 208; *Angew. Chem., Int. Ed. Engl.*, 1996, **35**, 204; T. Chivers, X. Gao, M. Parvez and G. Schatte, *Inorg. Chem.*, 1996, **35**, 4094.
2 M. A. Beswick and D. S. Wright, *Coord. Chem. Rev.*, 1998, **176**, 373.
3 M. A. Beswick, C. N. Harmer, A. D. Hopkins, M. McPartlin and D. S. Wright, *Science*, 1998, **281**, 1500.
4 A. Bashall, M. A. Beswick, B. R. Elvidge, S. J. Kidd, M. McPartlin and D. S. Wright, *Chem. Commun.*, 2000, 1439.
5 (*a*) G. Linti, H. Nöth, E. Schneider and W. Storch, *Chem. Ber.*, 1993, **126**, 619; (*b*) I. Schranz, L. Stahl and R. J. Staples, *Inorg. Chem.*, 1998, **37**, 1493; (*c*) D. F. Moser, I. Schranz, M. C. Gerrety, L. Stahl and R. J. Staples, *J. Chem. Soc., Dalton Trans.*, 1999, 751; (*d*) L. Grocholl, V. Huch, L. Stahl, R. Staples, P. Steinhart and A. Johnson, *Inorg. Chem.*, 1997, **36**, 4451; (*e*) L. Grocholl, I. Schranz, L. Stahl and R. J. Staples, *Inorg. Chem.*, 1998, **37**, 2496; (*f*) J. K. Brask, T. Chivers, M. L. Krahn and M. Parvez, *Inorg. Chem.*, 1999, **38**, 290; (*g*) N. Burford and D. J. LeBlanc, *Inorg. Chem.*, 1999, **38**, 2248.
6 For example see: A. J. Edwards, M. A. Paver, M.-A. Rennie, C. A. Russell, P. R. Raithby and D. S. Wright, *J. Chem. Soc., Dalton Trans.*, 1994, 2963.
7 For example $[NP(NH_2)_3]_3$, H. Jacobs and R. Kirchgassner, *Z. Anorg. Allg. Chem.*, 1990, **581**, 125.
8 G. David, E. Nieke, M. Nieger, V. von der Gönna and W. W. Schoeller, *Chem. Ber.*, 1993, **126**, 1513.
9 A. Tarassoli, M. L. Thomson, R. C. Haltiwanger, T. G. Hill and A. D. Norman, *Inorg. Chem.*, 1988, **27**, 3382 and references therein.
10 For recent examples see: (*a*) P. G. Williard and C. Sun, *J. Am. Chem. Soc.*, 1997, **119**, 11693; (*b*) J. G. Donkervoort, J. L. Vicario, E. Rijnberg, J. T. B. H. Jastrzebski, H. Kooijman, A. L. Spek and G. van Koten, *J. Organomet. Chem.*, 1998, **550**, 463; (*c*) J. K. Brask, T. Chivers and G. A. P. Yap, *Chem. Commun.*, 1998, 2543.
11 M. L. Thomson, R. C. Haltiwanger and A. D. Norman, *J. Chem. Soc., Chem. Commun.*, 1979, 647; M. L. Thomson, A. Tarassoli, R. C. Haltiwanger and A. D. Norman, *Inorg. Chem.*, 1987, **26**, 684.
12 T. Kottke and D. Stalke, *Angew. Chem.*, 1993, **105**, 619; *Angew. Chem., Int. Ed. Engl.*, 1993, **32**, 580.
13 These agostic interactions are similar to those occurring in $[\{Sb(NBu^t)_3\}_2Li_6]$: M. A. Beswick, N. Choi, C. N. Harmer, A. D. Hopkins, M. A. Paver, M. McPartlin, P. R. Raithby, A. Steiner, M. Tombul and D. S. Wright, *Inorg. Chem.*, 1998, **37**, 2177.

ChemComm

Practical entry into the HIJKLM ring segment of ciguatoxin CTX3C

Tohru Oishi,† Hisatoshi Uehara, Yoko Nagumo, Mitsuru Shoji, Jean-Yves Le Brazidec, Masashi Kosaka and Masahiro Hirama*

Department of Chemistry, Graduate School of Science, Tohoku University, and CREST, Japan Science and Technology Corporation (JST), Sendai 980-8578, Japan. E-mail: hirama@ykbsc.chem.tohoku.ac.jp

Received (in Cambridge, UK) 27th November 2000, Accepted 18th January 2001
First published as an Advance Article on the web 8th February 2001

The HIJKLM ring segment (27) of the right half portion of ciguatoxin CTX3C (1) has been synthesized using a ring-closing reaction mediated by a low-valent titanium reagent.

During the course of our synthetic studies directed toward ciguatoxins,[1,2] we have recently reported the convergent synthesis of the ABCDE[3] and IJKLM[4] ring fragment of **1**, based

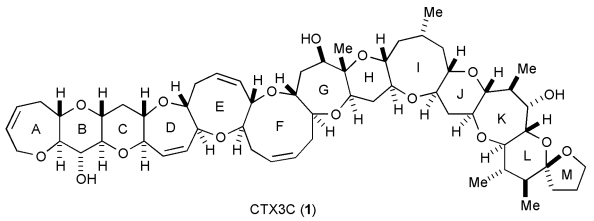

upon an alkylation-ring closing metathesis (RCM) strategy[5,6] and a Tebbe reagent (**3**)[7] mediated ester olefination-ring closing metathesis sequence,[8] respectively. Occasionally, however, the key transformation of **2** into **4** in the latter sequence turned out to be non-reproducible. The yield of **4** fluctuated between trace amount to 63% and concomitant formation of an inseparable mixture of enol ethers, **5**, **6**, and **7** tended to occur (Scheme 1). Unfortunately, irrespective of extensive investigation, secure conditions to yield **4** uniformly could not be found. At low conversions **5** sometimes predominated, while **6** and then **7** gradually increased as the reaction time was extended. Since the intermediacy of the diene **5** in the formation of **4** was conceivable,[8] mixtures which contained **5** as the major product were treated with **3** or the Schrock catalyst, 2,6-(^{i}Pr)$_2$C$_6$H$_3$-N=Mo[OC(CF$_3$)$_2$Me]$_2$=CHCMe$_2$Ph.[9–11] However, in remarkable contrast to literature precedent, **4** was not produced in appreciable amounts; instead **6** and **7** increased.[8] Steric hindrance around the diene system of **5** is likely to account for this unexpected failure of converting **5** into **4**. Mechanistically, there should exist an alternative pathway (**2** ⇌ **8** ⇌ **9** ⇌ **10** ⇌ **4**) to provide **4**, in which the ester carbonyl group reacts with an

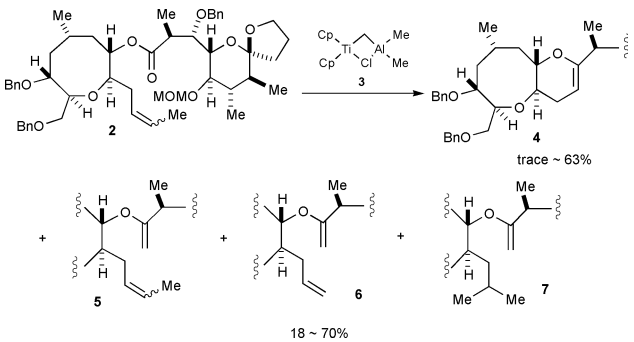

Scheme 1

internal carbenoid species such as **9** (Scheme 2). Thus, we reasoned that exclusive formation of **9** would improve the yield of **4** and that **9** could be prepared from the phenylthioacetal **11** using the low-valent titanium complex Cp$_2$Ti[P(OEt)$_3$]$_2$ recently developed by Takeda.[12]

The dithioacetal **11** was synthesized as shown in Scheme 3. Although we had synthesized the I-ring moiety of **1** based on a ring-expansion strategy,[13] we developed an alternative route applicable to large-scale synthesis. Aldol reaction of glycolate **12**[14] with acrolein gave diene **13** as an epimeric mixture of alcohols (47%), which was separated from other diastereomers by flash column chromatography (40% combined yield). RCM reaction of **13** using Grubbs catalyst, (PCy$_3$)$_2$Cl$_2$Ru=CHPh,[15] proceeded smoothly to give the eight-membered cyclic ether **14** (60%). Reduction of the ester **14** followed by selective protection of the resulting primary alcohol as TBDPS ether, and Swern oxidation of the secondary alcohol gave the enone **15** (3 steps, 68%). Stereoselective introduction of the secondary methyl group was successfully achieved by conjugate addition with Me$_2$Cu(CN)Li$_2$ to afford **16** in 74% yield. Removal of the TBDPS group of **16** using TBAF in the presence of AcOH, and reduction of the resulting hydroxy ketone with NaBH(OAc)$_3$ gave the diol **17** as a single isomer (92%).[16] Bis-benzylation, acetal hydrolysis followed by a two step cyanation sequence yielded the nitrile **18** (46% overall yield). Protection, DIBAL-H reduction and thioacetalization gave the dithioacetal **19** (3 steps, 73%), which was condensed with the carboxylic acid **20**[4] to afford **11** (58%). Ring-closing reaction of **11** was then examined. A THF solution of **11** was added to excess Takeda reagent (Cp$_2$Ti[P(OEt)$_3$]$_2$)[12] at rt and then refluxed under an argon atmosphere for 1 h. Using this protocol, the cyclic enol ether was formed reproducibly in 52–67% yield even on a one or two gram scale, while reduction and elimination products of the phenylthio group, **21** and **22**, respectively, were only produced in minor amount, *ca.* 10% combined yield.

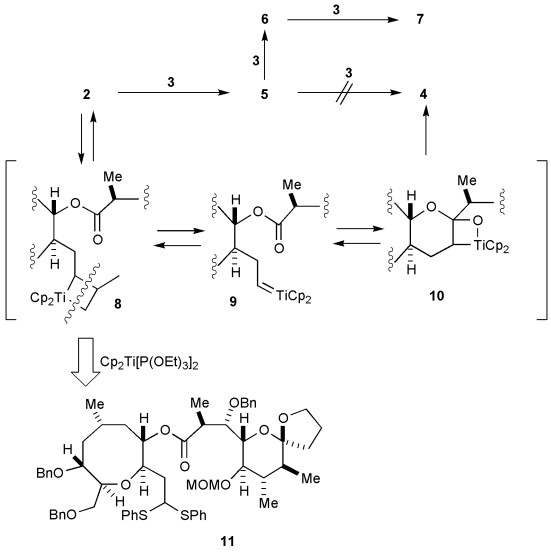

Scheme 2

† Present address: Department of Chemistry, Graduate School of Science, Osaka University, Osaka 560-0043, Japan.

DOI: 10.1039/b009506k

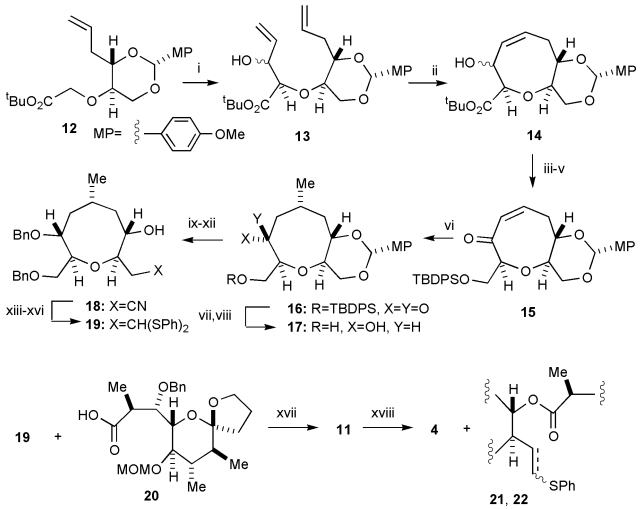

Scheme 3 *Reagents and conditions*: i, LDA, acrolein, THF, −78 °C, 10 min, separation, 47%; ii, $(PCy_3)_2Cl_2Ru$=CHPh (10 mol%), CH_2Cl_2 (0.01 M), reflux, 24 h, 60%; iii, LAlH, THF, 0 °C to rt, 5 h, 98%; iv, TBDPSCl, Et_3N, DMAP, CH_2Cl_2, rt, 16 h, 88%; v, $(COCl)_2$, DMSO, Et_3N, CH_2Cl_2, −60 °C, 30 min, 79%; vi, $Me_2Cu(CN)Li_2$, Et_2O, −78 °C, 30 min, 74%; vii, TBAF, AcOH, THF, rt, 5 h, 95%; viii, $NaBH(OAc)_3$, AcOH, CH_3CN, −20 °C, 2 h, 97%; ix, BnBr, NaH, THF, DMF, 0 °C to rt, 20 h; x, $TsOH·H_2O$, MeOH, H_2O, rt, 1 d, 68%; xi, I_2, PPh_3, imidazole, THF, 0 °C to rt, 1 d, 87%; xii, NaCN, DMSO, 40 °C, 2 d, 78%; xiii, TESOTf, 2,6-lutidine, CH_2Cl_2, −30 to −20 °C, 15 min, quant.; xiv, DIBAL-H, CH_2Cl_2, −70 to −60 °C, 1 h; xv, PhSSPh, Bu_3P, benzene, rt, 12 h, 73% (2 steps); xvi, TBAF, THF, rt, 3 h, 95%; xvii, EDC·HCl, DMAP, CH_2Cl_2, rt, 12 h, 58%; xviii, $Cp_2Ti[P(OEt)_3]_2$ (3 or 4 eq.), THF, reflux, 1 h, **4**: 52–67%, **21**, **22**: ~10%.

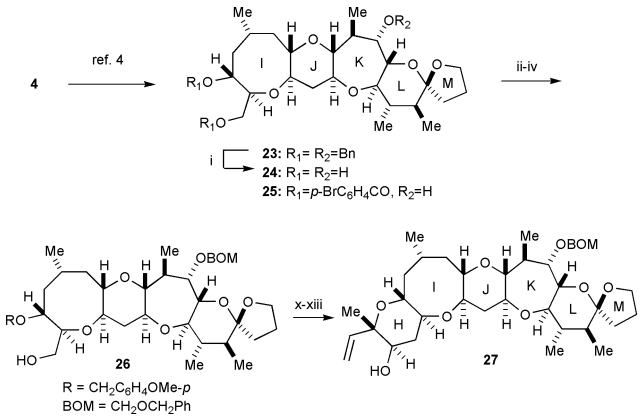

Scheme 4 *Reagents and conditions*: i, H_2, $Pd(OH)_2$/C, EtOAc, MeOH, rt, 1 d; ii, *p*-$MeOC_6H_4CH(OMe)_2$, CSA, CH_2Cl_2, rt, 30 min, 89% (2 steps); iii, BOMCl, $^iPr_2NEt$, $(CH_2Cl)_2$, 40 °C, 12 h, 88%; iv, DIBAL-H, CH_2Cl_2, −80 to −30 °C, 2 h, 85%; v, MsCl, Et_3N, $(CH_2Cl)_2$, 0 °C, 40 min; vi, NaCN, 18-crown-6, DMF, 50 °C, 3 d, 98% (2 steps); vii, DIBAL-H, CH_2Cl_2, −80 to −70 °C, 30 min; viii, Ph_3P=C(Me)CO_2Et, toluene, rt, 3 h, 84% (2 steps); ix, DIBAL-H, CH_2Cl_2, −70 °C, 20 min, 94%; x, D-(−)-DET, $Ti(O^iPr)_4$, Bu^tOOH, MS4A, CH_2Cl_2, −50 to −30 °C, 2 h, 80%; xi, SO_3·Py, Et_3N, CH_2Cl_2, 0 °C to rt, 2 h; xii, $Ph_3P^+CH_3Br^-$, NaHMDS, THF, 0 °C, 20 min, 96% (2 steps); xiii, DDQ, H_2O, CH_2Cl_2, rt, 2 h, 82%.

The enol ether **4** was converted to the IJKLM-ring fragment **23** according to our previously reported procedure (Scheme 4).[4] The stereochemistry of **23** was unambiguously determined by X-ray crystallography of the corresponding bis-*p*-bromobenzoate **25** (Fig. 1).[17] Furthermore, the H-ring moiety was successfully constructed in **23** in a similar manner to our previously established route[18] in 32% overall yield utilizing acid catalyzed vinylepoxide–alcohol cyclization methodology.[19]

In short, a practical synthetic route to the HIJKLM ring fragment **27** has been established. Further studies directed towards the total synthesis of ciguatoxin CTX3C (**1**) are currently in progress in our laboratory.

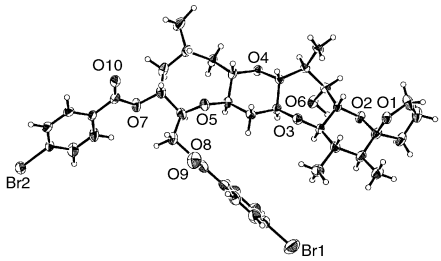

Fig. 1 ORTEP drawing of bis-*p*-bromobenzoate **25**.

Notes and references

1 For structures of ciguatoxins, see: M. Murata, A. M. Legrand, Y. Ishibashi, M. Fukui and T. Yasumoto, *J. Am. Chem. Soc.*, 1990, **112**, 4380; M. Satake, M. Murata and T. Yasumoto, *Tetrahedron Lett.*, 1993, **34**, 1975; M. Satake, A. Morohashi, H. Oguri, T. Oishi, M. Hirama, N. Harada and T. Yasumoto, *J. Am. Chem. Soc.*, 1997, **119**, 11 325; M. Satake, M. Fukui, A. M. Legrand, P. Cruchet and T. Yasumoto, *Tetrahedron Lett.*, 1998, **39**, 1197.

2 T. Suzuki, O. Sato, M. Hirama, Y. Yamamoto, M. Murata, T. Yasumoto and N. Harada, *Tetrahedron Lett.*, 1991, **32**, 4505; H. Oguri, S. Hishiyama, T. Oishi and M.Hirama, *Synlett*, 1995, 1252; H. Oguri, S. Hishiyama, O. Sato, T. Oishi, M. Hirama, M. Murata, T. Yasumoto and N. Harada, *Tetrahedron*, 1997, **53**, 3057; T. Oishi, M. Shoji, N. Kumahara and M. Hirama, *Chem. Lett.*, 1997, 845; T. Oishi, Y. Nagumo and M. Hirama, *Synlett*, 1997, 980; H. Oguri, S. Sasaki, T. Oishi and M. Hirama, *Tetrahedron Lett.*, 1999, **40**, 5405; H. Oguri, S. Tanaka, S. Hishiyama, T. Oishi, M. Hirama, T. Tumuraya, Y. Tomioka and M. Mizugaki, *Synthesis*, 1999, 1431; H. Oguri, S. Tanaka, T. Oishi and M. Hirama, *Tetrahedron Lett.*, 2000, **41**, 975; K. Maeda, T. Oishi, H. Oguri and M. Hirama, *Chem. Commun.*, 1999, 1063. For recent synthetic studies of other groups, see: M. Sasaki, H. Fuwa, M. Ishikawa and K. Tachibana, *Org. Lett.*, 1999, **1**, 1075; M. Inoue, M. Sasaki and K. Tachibana, *J. Org. Chem.*, 1999, **64**, 9416; K. Fujiwara, H. Tanaka and A. Murai, *Chem. Lett.*, 2000, 610; T.-Z. Liu and M. Isobe, *Tetrahedron*, 2000, **56**, 5391.

3 M. Maruyama, K. Maeda, T. Oishi, H. Oguri and M. Hirama, *Heterocycles*, 2001, **54**, 93.

4 T. Oishi, Y. Nagumo, M. Shoji, J.-Y. Le Brazidec, H. Uehara and M. Hirama, *Chem. Commun.*, 1999, 2035.

5 T. Oishi, Y. Nagumo and M. Hirama, *Chem. Commun.*, 1998, 1041.

6 Recent reviews on ring-closing metathesis reactions, see: S. K. Armstrong, *J. Chem. Soc., Perkin Trans. 1*, 1998, 371; R. H. Grubbs and S. Chang, *Tetrahedron*, 1998, **54**, 4413.

7 S. H. Pine, R. Zahler, D. A. Evans and R. H. Grubbs, *J. Am. Chem. Soc.*, 1980, **102**, 3270.

8 K. C. Nicolaou, M. H. D. Postema and C. F. Claiborne, *J. Am. Chem. Soc.*, 1996, **118**, 1565.

9 R. R. Schrock, J. S. Murdzek, G. C. Bazan, J. Robbins, M. DiMare and M. O'Regan, *J. Am. Chem. Soc.*, 1990, **112**, 3875.

10 J. S. Clark and J. G. Kettle, *Tetrahedron Lett.*, 1997, **38**, 123; J. S. Clark and J. G. Kettle, *Tetrahedron Lett.*, 1997, **38**, 127; J. S. Clark and J. G. Kettle, *Tetrahedron*, 1999, **55**, 8231.

11 J. D. Rainier and S. P. Allwein, *J. Org. Chem.*, 1998, **63**, 5310; J. D. Rainier, S. P. Allwein and J. M. Cox, *Org. Lett.*, 2000, **2**, 231.

12 Y. Horikawa, M. Watanabe, T. Fujiwara and T. Takeda, *J. Am. Chem. Soc.*, 1997, **119**, 1127; M. A. Rahim, T. Fujiwara and T. Takeda, *Tetrahedron*, 2000, **56**, 763.

13 T. Oishi, M. Shoji, K. Maeda, N. Kumahara and M. Hirama, *Synlett*, 1996, 1165; T. Oishi, M. Maruyama, M. Shoji, K. Maeda, N. Kumahara, S. Tanaka and M. Hirama, *Tetrahedron*, 1999, **55**, 7471.

14 The glycolate **12** was prepared from D-2-deoxyribose in 3 steps by standard procedures.

15 G. C. Fu, S. T. Nguyen and R. H. Grubbs, *J. Am. Chem. Soc.*, 1993, **115**, 9856; P. Schwab, R. H. Grubbs and J. W. Ziller, *J. Am. Chem. Soc.*, 1996, **118**, 100.

16 D. A. Evans, K. T. Chapman and E. M. Carreira, *J. Am. Chem. Soc.*, 1988, **110**, 3560.

17 *Crystal data*: $C_{39}H_{48}O_{10}Br_2$, M = 836.61, orthorhombic, space group $P2_12_12_1$, Dc = 1.440 g cm^{-3}, Z = 4, a = 5.5284(3), b = 25.006(2), c = 27.913(2) Å, V = 3858.7(4) Å^3, F(000) = 1728, μ(Mo-Kα) = 21,63 cm^{-1}, R = 0.053, Rw = 0.152. CCDC 154471. See http://www.rsc.org/suppdata/cc/b0/b009506k/ for crystallographic files in .cif format.

18 T. Oishi, K. Maeda and M. Hirama, *Chem. Commun.*, 1997, 1289.

19 K. C. Nicolaou, C. V. C. Prasad, P. K. Somers and C.-K. Hwang, *J. Am. Chem. Soc.*, 1989, **111**, 5330.

First anti-oestrogen in the cyclopentadienyl rhenium tricarbonyl series. Synthesis and study of antiproliferative effects

Gérard Jaouen,*[a] Siden Top,[a] Anne Vessières,[a] Pascal Pigeon,[a] Guy Leclercq[b] and Ionna Laios[b]

[a] *Laboratoire de Chimie Organométallique, Ecole Nationale Supérieure de Chimie de Paris, UMR 7576, 11 rue Pierre et Marie Curie, 75231 Paris Cedex 05, France. E-mail: jaouen@ext.jussieu.fr*

[b] *Laboratoire de Cancérologie Mammaire, Institut Jules Bordet, Rue Héger Bordet, 1 Brussels 1000, Belgium. E-mail: lcanmamm@ulb.ac.be*

Received (in Cambridge, UK) 28th November 2000, Accepted 18th January 2001
First published as an Advance Article on the web 8th February 2001

A route to the organometallic complex 8 is described, along with a study of its antiproliferative effects on breast cancer cell lines; in the examples studied, 8 behaves in a very similar manner to tamoxifen, suggesting new possibilities for applications in organometallic chemistry.

Tamoxifen **1** and its active metabolite, 4-hydroxytamoxifen **2** (Scheme 1) have been the subject of numerous studies owing to their efficacy in breast cancer treatment.[1,2] Currently however, substitutes are being sought in order to obviate the effects of resistance build up, as well as to improve the therapeutic effectiveness of the current treatments.[3,4] Our study is an attempt to potentiate the effects of these medications by introducing an organometallic-type modification to the base skeleton. Some organometallic complexes have in fact proven to be of interest either as antitumour agents, as in the case of the metallocenes of Fe and Ti,[5,6] or as radiopharmaceuticals, for example certain isotopes of Tc and Re.[7,8] If the organometallic moiety could be incorporated into this molecule while still preserving its character as an anti-oestrogen vector, this would provide a route to new products of added interest in a variety of applications. The question of preservation of antagonist activity is not an idle concern; we have shown that merely substituting the phenyl in the β position in **2** with a ferrocenyl group in **3** resulted in a significant drop in anti-oestrogenic effects *in vitro* on breast cancer cell lines, as well as *in vivo*, in nude mice.[9,10] Here we show that by attaching to the diphenylethylene skeleton a moiety of Re(I), in the form of cyclopentadienyl $Re(CO)_3$, small in size and difficult to oxidize, we obtain an anti-oestrogenic organometallic complex comparable to hydroxytamoxifen **2** but with the added advantage, owing to the presence of the metal Re, of allowing access to a new type of radiopharmaceutical compounds of ^{99m}Tc, ^{186}Re or ^{188}Re.

Compound **8** is prepared as shown in Scheme 2 starting from dihydroxybenzophenone **4** and the $(\eta^5\text{-}C_5H_4COEt)Re(CO)_3$ complex **6**, itself prepared by a Friedel–Crafts reaction between cyclopentadienyl rhenium tricarbonyl and propionyl chloride. The aromatic ketone **4** is first reacted with KH, to give the potassium salt, which reacts with dibromobutane. The monobrominated compound **5** is obtained in 35% yield. A McMurry cross-coupling reaction[11,12] between **5** and the organometallic compound **6** in the presence of $TiCl_4$ and Zn in THF under reflux gives **7** in 62% yield, and the latter when heated with dimethylamine in an autoclave produces **8** (***Z*** + ***E*****)** in a yield of 64%.† Separation of the isomers **8*Z*** and **8*E*** was done by reverse phase preparative HPLC. Identification of the isomers was ascertained by NOE NMR on the *E* isomer (effect between the protons $CH_3\text{-}CH_2$ and $C_6H_4\text{-}O(CH_2)_4N(CH_3)_2$, as well as between $\eta^5\text{-}C_5H_4\text{–}Re(CO)_3$ and $C_6H_4\text{-}OH$). In contrast to what is observed in the ferrocene series, no rapid interconversion was noticed between **8*Z*** and **8*E***, then showing a similarity of the rhenium derivatives with tamoxifen.

The relative binding affinity values (RBA) of **8** were measured for the mixture (*Z* + *E*) and for the individual isomers *Z* and *E* on the two oestrogen receptor subtypes ERα and ERβ using a competitive radiometric binding assay, with tritium-labeled oestradiol as tracer and protamine sulfate precipitation

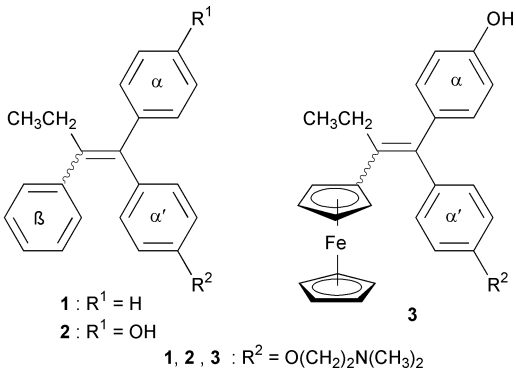

Scheme 1

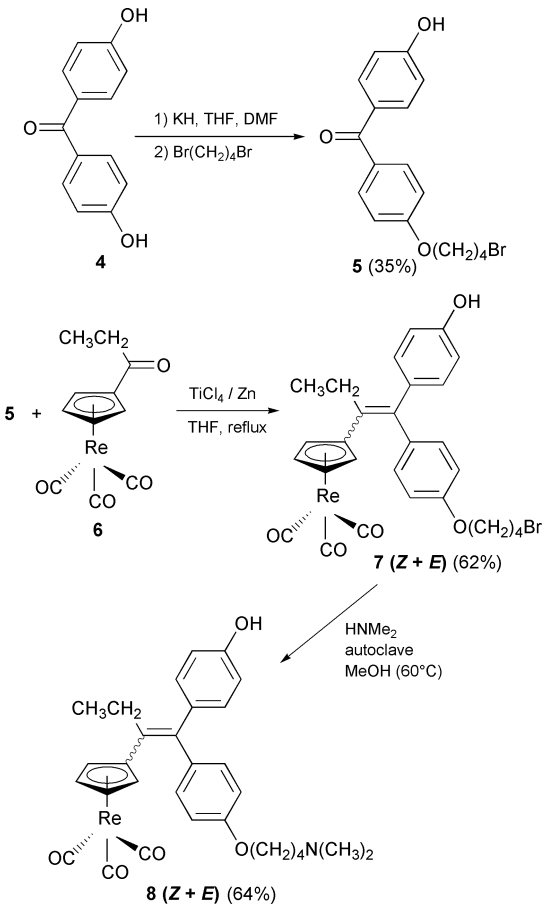

Scheme 2

DOI: 10.1039/b009553m

Table 1 Antiproliferative activity of compounds **8**, **2** and E_2 on different cell lines

Compound	Molarity (M)	Cell	
		MVLN[a]	MDA-MB231[b]
8	1×10^{-6}	55.5 [97][c]	n d
	1×10^{-7}	51.5 [101][c]	91
2	1×10^{-7}	51.5	88
E_2	1×10^{-10}	258	91

[a] Cells with a high level of ERα. Results are expressed as percentage of the luciferase induction after 24 h of culture.[14] [b] Cells with no ERα, but presumably with ERβ.[15] Results are expressed as the percentage of DNA/control after 120 h of culture.[16] [c] Value obtained after simultaneous addition in the medium of 10 nM of E_2.

of the bound fraction of the tracer.[13] ERα was prepared from sheep uterus and ERβ, expressed in baculovirus, was obtained commercially from PanVera. The RBA values (mean of 2 or 3 experiments) found at 0 °C for **8** on ERα are 8% for the mixture **8** (***Z*** + ***E***), 7.4% for **8*Z*** and 5.2% for **8*E***, thus showing only a slight difference between the two isomers. In contrast, the RBA value obtained for ERβ is higher with **8*Z*** (17.8%) than for the mixture **8** (***Z*** + ***E***) (6%) or the *E* isomer **8*E*** (5.6%). However it is important to notice that ERβ is a purified receptor devoid of the effectors naturally present in the receptor alpha preparation obtained from sheep. Nevertheless the affinity for both ERα and ERβ are still satisfactory even if these RBA values are lower than the values found for **2** (***Z*** + ***E***) on ERα (38.5%) and ERβ (20%). This decrease probably reflects the greater steric crowding of $(\eta^5\text{-}C_5H_4)Re(CO)_3$ in **8** relative to the phenyl group in **2**.

We studied the agonist–antagonist effect of compound **8 (*Z*** + ***E***) on cell lines derived from breast cancer tumours (MVLN, MDA-MB231) (Table 1). In the MVLN line recently developed by Pons[14] it has been shown that the expression of the luciferase gene is proportional to the oestrogenic effect of the product tested. It contains a high level of ERα while the MDA-MB231 line does not contain any. In these tests, the control value is set by definition at 100%. For any given product, a value above 100% indicates an oestrogenic effect, and a value below 100% an anti-oestrogenic effect. As usual oestradiol is used as the reference for oestrogens and hydroxytamoxifen **2** (***Z*** + ***E***) for anti-oestrogens. The results obtained with MVLN cells show that the Re complex **8** behaves as an anti-oestrogen with almost identical efficacy as **2**. The observed effect with **8** is certainly hormonally based, since it is abolished by addition of oestradiol into the medium (values in square brackets in the Table). On MDA-MB231 cells which do not possess ERα but may possess ERβ,[15] **8** and **2** have no effect. It thus appears that the observed antiproliferative effect is dependent on the oestradiol receptor α, as is also the case with tamoxifen.

It appears that **8** may have a higher potential as an organometallic radiopharmaceutical, despite the fact that up to now the chelate route has been the one explored with tamoxifen;[17] in the latter case the ER binding rate was found to be too small to measure, which was not the case with **8**. It is therefore important to find a rapid route by which to attach useful isotopes of Tc and Re to **8**. To this end, we plan to use a selective photochemical decomplexation reaction that we have recently discovered, followed by rapid recomplexation in water with a new reagent reported by Alberto,[18,19] $(H_2O)_3M^+(CO)_3$ with M = ^{99m}Tc, ^{188}Re.

Notes and references

† Procedure for the preparation of **7** and **8**. Titanium tetrachloride (2 ml, 18 mmol) was added dropwise to a suspension of zinc powder (2.34 g, 36 mmol) in 60 ml of THF at 0 °C. The mixture obtained was heated at reflux for 2 h and then cooled to rt. A second solution was prepared by dissolving 4-(4-bromobutoxy)-4′-hydroxybenzophenone (4.25 g, 6 mmol) and cyclopentadienyltricarbonylrhenium ethyl ketone (2.35 g, 6 mmol) in 30 ml of THF. This latter solution was added dropwise to the first one and then the resulting mixture was heated for 2 h. After cooling to rt, the mixture was stirred with water and CH_2Cl_2. After treatment the pure oily *Z* + *E* mixture of **7** was obtained with a yield of 62%; MS (IE, 70 eV) *m*/*z*: 708 ($M^{+\cdot}$), 624 ($M - 3CO)^+$. Halide **7** (3 mmol) and a solution of dimethylamine in MeOH (2 M, 15 ml, 30 mmol) were heated with stirring in an autoclave at 60 °C for 1 day. After cooling, the solution was concentrated under reduced pressure. After treatment the pure amines **8** (***Z*** + ***E***) were isolated as oil containing a mixture of *Z* and *E* isomers with a yield of 64%; MS (IE, 70 eV) *m*/*z*: 673 ($M^{+\cdot}$). The *Z* and *E* isomers were separated on reverse phase preparative Kromasil C18 column, solvent MeOH phosphate buffer (KH_2PO_4, 25 mM, pH 7) 80/20, flow rate 6 mL min^{-1}. The retention times obtained on an analytical column of the same type (Kromasil C18, 10 μM, 250 mm) are repectively of 19.4 min for **8*Z*** and 26.4 min for **8*E*** in the proportion 48.5/51.5. Selected data for the two isomers: **8*E***: mp 153 °C, ^{1}H NMR δ 7.04 (d, *J* = 8.4 Hz, 2H, H_{arom}), 6.93 (d, *J* = 8.4 Hz, 2H, H_{arom}), 6.78 (d, *J* = 8.4 Hz, 2H, H_{arom}), 6.70 (d, *J* = 8.4 Hz, 2H, H_{arom}), ^{13}C NMR δ (all aromatic carbons) 135.5 (C), 134.6 (C), 130.6 (2 CH), 130.1 (2 CH), 129.9 (C), 115.6 (2 CH), 114.1 (2 CH). **8*Z***: mp 134°C, ^{1}H NMR δ 7.00 (d, *J* = 8.4 Hz, 2H, H_{arom}), 6.99 (d, *J* = 8.4 Hz, 2H, H_{arom}), 6.75 (d, *J* = 8.4 Hz, 2H, H_{arom}), 6.74 (d, *J* = 8.4 Hz, 2H, H_{arom}), ^{13}C NMR (all aromatic carbons) δ 135.9 (C), 134.8 (C), 130.5 (2 CH), 129.9 (2 CH + C), 115.3 (2 CH), 114.3 (2 CH).

1 K. Dhingra, *Invest. New Drugs*, 1999, **17**, 285.
2 J. I. MacCregor and V. C. Jordan, *Pharmacol. Rev.*, 1998, **50**, 151.
3 M. Cognlan and M. Kort, *Expert Opin. Ther. Patents*, 1999, **9**, 1524.
4 V. C. Jordan, *J. Nat. Cancer Inst.*, 1998, **90**, 967.
5 A. Houlton, R. Roberts and J. Silver, *J. Organomet. Chem.*, 1991, **418**, 107.
6 P. Köpf-Maier, *Eur. J. Clin. Pharmacol.*, 1994, **47**, 1.
7 J. R. Dilworth and S. J. Parrott, *Chem. Soc. Rev.*, 1998, **27**, 43.
8 G. Jaouen, A. Vessières, S. Top and R. Alberto, *J. Organomet. Chem.*, 2000, **600**, 23.
9 G. Jaouen, S. Top, A. Vessières, G. Leclercq, J. Quivy, L. Jin and A. Croisy, *C. R. Acad. Sci. Paris*, 2000, **Série IIc**, 89.
10 S. Top, J. Tang, A. Vessières, D. Carrez, C. Provot and G. Jaouen, *Chem. Commun.*, 1996, 955.
11 S. Gauthier, J. Mailhot and F. Labrie, *J. Org. Chem.*, 1996, **61**, 3890.
12 S. Top, B. Dauer, J. Vaisserman and G. Jaouen, *J. Organomet. Chem.*, 1997, **541**, 355.
13 A. Vessières, S. Top, A. A. Ismail, I. S. Butler, M. Louer and G. Jaouen, *Biochemistry*, 1988, **27**, 6659.
14 M. Pons, D. Gagne, J. C. Nicolas and M. Mehtali, *Bio Techniques*, 1990, **9**, 450.
15 G. G. J. M. Kuiper, E. Enmark, M. Pelto-Huikko, S. Nilsson and J.-A. Gustafsson, *Proc. Natl. Acad. Sci. USA*, 1996, **93**, 5925.
16 G. Leclercq, N. Devleeschouwer and J. C. Heuson, *J. Steroid Biochem.*, 1983, 75.
17 D. H. Hunter and L. G. Luyt, *Bioconjugate Chem.*, 2000, **11**, 175.
18 R. Alberto, R. Schibli, A. Egli, A. P. Schubiger, U. Abram and T. A. Kaden, *J. Am. Chem. Soc.*, 1998, **120**, 7987.
19 S. Top, E. B. Kaloun and G. Jaouen, *J. Am. Chem. Soc.*, 2000, **122**, 736.

ChemComm

Efficient catalytic oxidation of primary and secondary alcohols using a non-heme dinuclear iron complex

Alette G. J. Ligtenbarg,[a] Peter Oosting,[a] Gerard Roelfes,[a] René M. La Crois,[a] Martin Lutz,[b] Anthony L. Spek,[b] Ronald Hage*[a] and Ben L. Feringa*[a]

[a] *Department of Organic and Molecular Inorganic Chemistry, University of Groningen, Nijenborgh 4, 9747 AG Groningen, The Netherlands. E-mail: b.l.feringa@chem.rug.nl*

[b] *Department of Crystal and Structural Chemistry, Utrecht University, Padualaan 8, 3584 CH, Utrecht, The Netherlands*

Received (in Cambridge, UK) 22nd November 2000, Accepted 18th January 2001
First published as an Advance Article on the web 8th February 2001

A novel μ-oxo diiron(III) complex is capable of fast and selective oxidation of primary and secondary alcohols in the presence of H_2O_2 and a remarkable increase in reaction rate is achieved by addition of 1 eq. of CF_3SO_3H.

In nature, a variety of non-heme metalloenzymes are present which are capable of oxidation of substrates with high turnover frequencies and excellent selectivity.[1] An example is the mononuclear copper enzyme galactose oxidase (GOase) which catalyses the aerobic oxidation of benzylic and allylic alcohols to their corresponding aldehydes with concomitant formation of H_2O_2. The study of model complexes not only provides invaluable information about metalloenzymes, but also can result in the development of new generations of oxidation catalysts.[2] Beautiful examples are the GOase models developed by the groups of Wieghardt and Stack, which are capable of oxidation of alcohols to the corresponding aldehydes with high yield and selectivity.[3] An iron(II) complex of a pentadentate ligand N4Py† was developed as a model system for Fe-BLM.[4,5]† This system is capable of oxidising alkanes using H_2O_2 *via* a radical type mechanism. To explore the effect of ligand variations on the oxidation behaviour of the complex, we prepared a ligand HL^1† in which one of the pyridyl groups is replaced by a phenolate moiety. The corresponding μ-oxo dinuclear iron complex of HL^1 proved to be a selective and efficient catalyst for the oxidation of alcohols to aldehydes and ketones using H_2O_2 as the oxidant. Yields up to 65% based on H_2O_2 can be reached.

The synthesis of HL^1 is shown in Scheme 1. Complexation of the ligand with $Fe(II)(ClO_4)_2 \cdot x\,H_2O$ in MeOH, in the presence of 1 eq. of Et_3N followed by slow diffusion of ethyl acetate into the methanolic solution yielded purple crystals of complex **1** (λ_{max} = 540 nm, ε_M = 5.6 10^3 M^{-1} cm^{-1}) in 50% yield.‡ The complex was characterised as an antiferromagnetically coupled diiron(III) species based on its EPR silent nature and its ^{1}H-NMR spectrum, which exhibits paramagnetically shifted signals in the 0–40 ppm range. The ESI/MS spectrum shows a peak at *m/z* 445 ($[(L^1)Fe(\mu\text{-}O)Fe(L^1)]^{2+}$), which is consistent with the formulation of **1** as $\{[(L^1)Fe(\mu\text{-}O)Fe(L^1)](ClO_4)_2\}$. Further proof for this assignment was obtained from the crystal structure of the corresponding μ-oxo diiron(III) complex $[(L^1)Fe(\mu\text{-}O)Fe(L^1)](PF_6)_2$ (**2**), depicted in Scheme 1, which was synthesised by adding $Fe(NO_3)_3 \cdot 9H_2O$ to a solution of the ligand in methanol, followed by the addition of 1 eq. of Et_3N and 2 eq. of NH_4PF_6. Dark purple–blue crystals were obtained by slow diffusion of ether into the solution of **2**. Each iron(III) ion adopts a distorted octahedral coordination geometry involving a tertiary amine, three pyridine nitrogens, a phenolate oxygen atom and the bridging oxygen atom, with the Fe–O–Fe angle being 151.22(10)°.§ The crystal structure of **2** gave no indications that a proton is present at the phenolate moiety, which is consistent with the ESI/MS results of **1** (*vide supra*).

Complex **1** was examined as a catalyst (0.1 mol%) in the oxidation of various substrates using H_2O_2 as the oxidant.¶ Primary and secondary alcohols are oxidised rapidly (Table 1).‖

The oxidation of benzyl alcohol was monitored in time by GC. In Fig. 1 the turnovers per iron centre are plotted against time. Surprisingly, already 4 eq. of benzaldehyde have been formed in a reproducible manner, 30 s after the reaction was started by adding H_2O_2. The origin of this initial burst of activity is unclear. After the initial oxidation, a lag phase was observed. A significant increase in catalytic activity occurred after approximately 40 min and after 75 min the catalytic activity ceased because all the H_2O_2 was consumed. A total of 50 turnovers towards benzaldehyde was reached. Although a trace of benzoic acid was obtained, no other side products were produced according to GC. When another aliquot of H_2O_2 is added after 90 min, the catalyst is immediately active and no lag phase is observed. A value of 96 turnovers per iron centre can be obtained after 180 min. This can be repeated at least 3 times without significant loss of activity, showing a good stability of the system during catalytic turnover.

The UV/Vis absorption of **1** at 540 nm was monitored concomitantly with the oxidation of benzyl alcohol to benzaldehyde. During the lag phase the solution remains purple but after 45 min the colour changes to yellow. This colour change coincides with the end of the lag phase, suggesting that the yellow species is responsible for the oxidation activity.

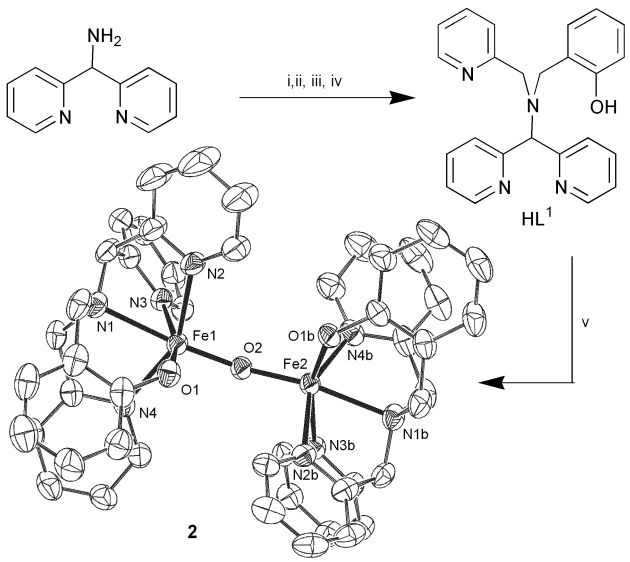

Scheme 1 Synthesis of HL^1 and **2** and crystal structure of the cation of **2** (displacement ellipsoid plot with 50% probability level in which hydrogen atoms are omitted for clarity). *Reagents and conditions*: i, 2-pyridine carbaldehyde, 2 h, 97%; ii, $NaBH_4$, MeOH, 2 h, 90%; iii, 2-(bromomethyl)phenyl acetate, $^iPr_2EtN$, EtOAc, 3 d, 66%; iv, K_2CO_3, MeOH, 1 h, 89%; v, $Fe(NO_3)_3$, Et_3N, NH_4PF_6, 29%; Selected interatomic distances (Å): Fe–O: 1.93, Fe(1)–O(2) 1.79, Fe(1)–N(1) 2.26, Fe(1)–N(2) 2.17Å, Fe(1)–N(3) 2.22, Fe(1)–N(4) 2.13.

DOI: 10.1039/b009368h

Table 1 Turnover numbers (t.o.n.) of the catalytic oxidation experiments with **1** using H_2O_2

Entry	Substrate	Product	Time/min	t.o.n.[a]
1[b]	Benzyl alcohol	Benzaldehyde	75	50
2[c]	Benzyl alcohol	Benzaldehyde	15	50
3[d]	Benzyl alcohol	Benzaldehyde	90	15
4[e]	Benzyl alcohol	Benzaldehyde	180	96
5	Cyclohexanol	Cyclohexanone	60	28
6	Cyclohexanol	Cyclohexanone	60	65
7	Cyclooctanol	Cyclooxtanone	180	11
8	Octan-1-ol	Octanal[f]	180	11
9	*sec*-Phenylethyl Alcohol	Acetophenone	60	50

[a] t.o.n. = mol product/mol catalyst. [b] In the absence of catalyst a negligible amount of 0.004 mmol of benzaldehyde was formed under the standard reaction conditions after 90 min, whereas in the presence of Fe(II)$(ClO_4)_2$ only 8 turnovers were reached. [c] In the presence of 1 eq. CF_3SO_3H. [d] With 100 eq. of substrate instead of 1000 eq. [e] Addition of another aliquot of H_2O_2 after 90 min. [f] Octanoic acid was formed as side product.

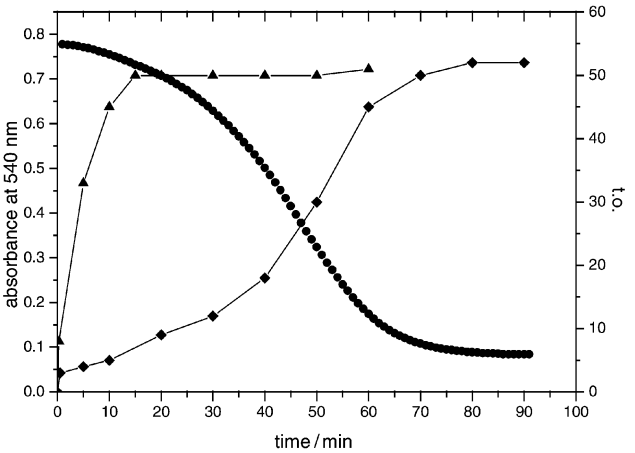

Fig. 1 Catalytic oxidation of benzyl alcohol to benzaldehyde using **1**: (■) time course of the turnovers, (●) time dependent decay of the UV band at λ = 540 nm and (▲) oxidation in the presence of 1 eq. CF_3SO_3H.

Several observations suggest that the active oxidising complex is a mononuclear species. First, complex **1** is EPR silent whereas upon addition of benzyl alcohol and H_2O_2, when the solution becomes yellow, a strong EPR signal can be observed at g = 4.3 which is characteristic for a mononuclear high-spin iron(III) complex.[6] Secondly, it was found that alcohols, which are known to be capable of breaking up the oxo-bridge of some dinuclear iron μ-oxo complexes to form monomeric structures by coordination to the metal centre,[6] are oxidised rapidly. In contrast, the active yellow species is formed very slowly in the absence of substrate or with a non-coordinating substrate like cyclohexene. Finally, we envisaged that protonation of the oxo-bridge in **1** would facilitate the formation of the mononuclear species and hence would speed up the reaction. Upon addition of triflic acid (CF_3SO_3H) to **1** in acetone a blue colour appears. The ^{1}H-NMR spectrum of this solution shows broad signals in the −10 to 120 ppm range consistent with the presence of mononuclear high-spin Fe(III) species. The ESI/MS spectrum shows prominent peaks at m/z 581 and 472, which corresponds to $[L^1Fe^{III}\text{-}OTf]^+$ and $[(HL^1)Fe^{III}(OH)_2]^+$, respectively. Indeed when CF_3SO_3H (1 eq.) was used, the reaction rate increased dramatically (Fig. 1). The yellow species was formed immediately upon addition of H_2O_2 and after 15 min already 50 turnovers are reached in the oxidation of benzyl alcohol.

Although the exact reaction mechanism is not known yet, some tentative conclusions can be drawn. The fact that benzene, which can act as a hydroxyl radical trap,[5] is not oxidised by this system, combined with the large kinetic deuterium isotope effect (KIE, k_H/k_D = 4.0) that was observed in a competition experiment between benzyl alcohol and benzyl alcohol-d_7, it can be concluded that oxidising species more selective than hydroxyl radicals are present. When the KIE was determined 30 s after starting the reaction by addition of H_2O_2, *i.e.* after the initial burst of activity, a value of 1.8 was obtained indicating the presence of a highly reactive oxidising species in the initial stage of the reaction. Finally, since the purple colour of **1** is indicative of a LMCT transition between the phenolic part of the ligand and the iron(III) center,[7,8] it is most likely that the phenolic moiety is no longer coordinated to the iron centre in this yellow species, which is thought to be responsible for oxidation activity.

In conclusion, a new Fe(III) containing catalyst has been developed for selective oxidation of primary and secondary alcohols using H_2O_2. A dramatic enhancement in the reaction rate upon addition of acid has been observed, which is attributed to accelerated formation of the active mononuclear catalyst.

Mrs C. M. Jeronimus-Stratingh is gratefully acknowledged for performing the ESI-MS measurements. This work was supported in part (A. L. S., M. L.) by the Council for Chemical Sciences of the Netherlands Organization for Scientific Research (CW-NWO).

Notes and references

† Abbreviations used: N4Py = *N*,*N*-bis(2-pyridylmethyl)-*N*-bis(2-pyridyl)methylamine; HL^1 = 2-({[di(2-pyridyl)methyl](2-pyridylmethyl)-amino}methyl)phenol; Fe-BLM = iron bleomycin.

‡ Anal. calcd. for $C_{48}H_{42}N_8O_{11}Fe_2Cl_2{\cdot}H_2O$: C 52.07, H 4.01, N 10.13%; found: C 52.17, H 3.80, N 10.03%.

§ *Crystal data*: $[C_{48}H_{42}Fe_2N_8O_3](PF_6)_2$, *F*w = 1180.54, dark blue needle, 0.45 × 0.24 × 0.15 mm^3, monoclinic, *C*2/*c* (No. 15), a = 31.0660(6), b = 11.1832(2), c = 33.8507(7) Å, β = 100.6240(7)°, V = 11558.7(4) Å^3, Z = 8, ρ = 1.357 g cm^{-3}. 83260 reflections were measured on a Nonius KappaCCD diffractometer with rotating anode (λ = 0.71073 Å) at a temperature of 150(2) K. 10198 reflections were unique (R_{int} = 0.043). *R*-values [$I > 2\sigma(I)$]: *R*1 = 0.0416, *wR*2 = 0.1173. Molecular illustration, structure checking and calculations were performed with the PLATON package. CCDC 154063. See http://www.rsc.org/suppdata/cc/b0/b009368h/ for crystallographic files in .cif format.

¶ Oxidation reactions were performed in acetone, under an argon atmosphere in a water bath thermostatted at 25 °C. In a typical reaction, 3.5 mmol of substrate (1000 eq.) was added to 4 ml of a stock solution of 1.75 μmol of the catalyst (*i.e.* 3.5 μmol of iron) and a known amount of the internal standard bromobenzene. The reaction was initiated by addition of 35 μl of H_2O_2 (30% solution in water, 100 eq.) and monitored by GC.

‖ Alkenes and alkanes were also investigated, but these reactions are slow (6–18 h), less selective and turnover numbers are lower (typically 10–20).

1 For reviews on iron based enzymes, see: E. I. Solomon, T. C. Brunold, M. I. Davis, J. N. Kemsley, S.-K. Lee, N. Lehnert, F. Neese, A. J. Skulan, Y.-S. Yang and J. Zhou, *Chem. Rev.*, 2000, **100**, 235; L. Que, Jr. and R. Y. N. Ho, *Chem. Rev.*, 1996, **96**, 2607.

2 H. J. Krüger, *Angew. Chem., Int. Ed.*, 1999, **38**, 627.

3 Y. Wang, J. L. DuBois, B. Hedman, K. O. Hodgson and T. D. P. Stack, *Science*, 1998, **279**, 537; P. Chaudhuri, M. Hess, U. Flörke and K. Wieghardt, *Angew. Chem., Int. Ed.*, 1998, **37**, 2217.

4 M. Lubben, A. Meetsma, E. C. Wilkinson, B. Feringa and L. Que, Jr., *Angew. Chem., Int. Ed. Engl.*, 1995, **34**, 1512; G. Roelfes, M. Lubben, K. Chen, R. Y. N. Ho, A. Meetsma, S. Genseberger, R. M. Hermant, R. Hage, S. K. Mandal, V. G. Young, Jr., Y. Zang, H. Kooijman, A. L. Spek, L. Que, Jr. and B. L. Feringa, *Inorg. Chem.*, 1999, **38**, 1929; R. Y. N. Ho, G. Roelfes, B. L. Feringa and L. Que, Jr., *J. Am. Chem. Soc.*, 1999, **121**, 264.

5 G. Roelfes, M. Lubben, R. Hage, L. Que, Jr. and B. L. Feringa, *Chem. Eur. J.*, 2000, **6**, 2152.

6 J. Kim, E. Larka, E. C. Wilkinson and L. Que, Jr., *Angew. Chem., Int. Ed. Engl.*, 1995, **34**, 2048.

7 S. Ito, M. Suzuki, T. Kobayashi, H. Itoh, A. Harada, S. Ohba and Y. Nishida, *J. Chem. Soc., Dalton Trans.*, 1996, 2579.

8 S. Yan, L. Que, Jr., L. F. Taylor and O. P. Anderson, *J. Am. Chem. Soc.*, 1988, **110**, 5222.

A new cascade for the one-pot synthesis of linear homoallylic alcohols with an allylic diindium reagent

Tsunehisa Hirashita, Hatsuo Yamamura, Masao Kawai and Shuki Araki*

Department of Applied Chemistry, Nagoya Institute of Technology, Gokiso-cho, Showa-ku, Nagoya 466-8555, Japan. E-mail: araki@ach.nitech.ac.jp

Received (in Cambridge, UK) 19th December 2000, Accepted 17th January 2001
First published as an Advance Article on the web 8th February 2001

A new cascade based on a novel allylic diindium reagent has been developed; the indium reagent prepared from 3-bromo-1-iodopropene successively coupled with carbonyl compounds and then with aryl, alkenyl or allyl halides in the presence of a Pd(0) catalyst to afford a convenient one-pot synthesis of linear homoallylic alcohols.

Organodimetallic compounds, which possess two metal–carbon bonds in one molecule, are synthetically attractive reagents; because, when they couple successively with two electrophiles, a three-component coupling can be achieved in one pot.[1] Although a number of organodimetallic reagents have hitherto been prepared and utilized, allylic dimetal compounds of type **1** are rare and only a few examples such as M = Li[2], Zn[3] and Sn[4] are known. Recently we described the preparation of the diindium reagent **1** (M = In) by oxidative addition of indium to 3-bromo-1-iodopropene (**2**).[5] This reagent couples readily with carbonyl compounds leading to the corresponding homoallylic alcohols **4** *via* the vinylic indium compound **3** (Scheme 1). However, the reagent **3** could not be utilized for further transformations owing to the poor nucleophilicity of the vinylic indium–carbon bond. Now we have established a new cascade based on **1** (M = In) involving allylation of carbonyls followed by Pd(0)-catalyzed coupling of the resulting vinylindium with aryl, alkenyl or allyl halide, which provides a convenient one-pot synthesis of linear homoallylic alcohols.

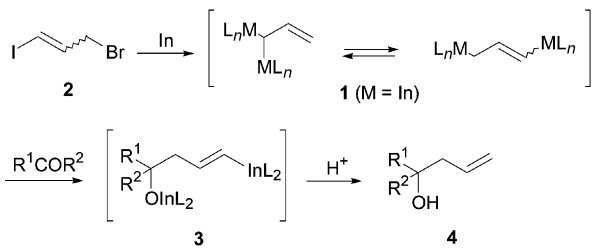

Scheme 1

Table 1[a] Tandem couplings of **1** (M = In) with benzaldehyde and iodobenzene

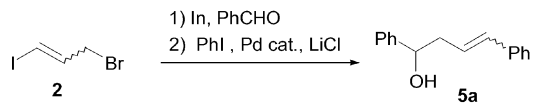

Entry	Solvent	$Pd(PPh_3)_4$/mmol	*T*/°C	Yield of **5a** (%)
1[b]	DMA	0.03	rt	0 [72][c]
2[b]	DMA	0.05	110	18 (*E*:*Z* = 46:54)
3	DMA	0.03	rt	0 [68][c]
4	DMA	0.03	110	56 (*E* only)
5	NMP	0.05	100	57 (*E* only)
6[d]	NMP	0.03	100	34 (*E* only)
7	NMP	0.04[e]	100	47 (*E* only)
8[f]	NMP	0.10	100	67 (*E*:*Z* = 85:15)

[a] Unless otherwise noted, reactions were carried out with **2** (1.0 mmol), PhCHO (0.50 mmol), PhI (1.0 mmol) and LiCl (3.0 mmol) in a solvent (6 mL) for 24 h. [b] Without LiCl. [c] Yield of 1-phenylbut-3-en-1-ol. [d] NaOEt was added in place of LiCl. [e] $Pd_2(dba)_3$ (0.02 mmol) and tris(2-furyl)phosphine (0.13 mmol) were used in place of $Pd(PPh_3)_4$. [f] With PhCHO (0.39 mmol).

Iodobenzene and a catalytic amount of $Pd(PPh_3)_4$ were added to the vinylindium reagent **3** prepared by the indium-mediated coupling of **2** with benzaldehyde at rt for 1 h. Although the addition of the second electrophile did not occur at rt (Table 1, Entry 1), the expected three-component coupling product **5a** was obtained in 18% yield at 110 °C with an *E*:*Z* ratio of 46:54 (Entry 2). The addition of LiCl resulted in the dramatic improvement both in the yield and *E*:*Z* selectivity: (*E*)-**5a** was obtained stereoselectively in 56% yield (Entry 4). The solvent NMP gave almost coincident results (Entry 5). The addition of NaOEt or the use of $Pd_2(dba)_3$–tris(2-furyl)phosphine in place of $Pd(PPh_3)_4$ also resulted in the selective formation of (*E*)-**5a** (Entries 6 and 7). The yield increased with increasing amounts of $Pd(PPh_3)_4$, though the *E*/*Z* selectivity was diminished (Entry 8).

The scope of this cascade was examined by changing the carbonyl compounds and the second electrophiles (Table 2).

Table 2[a] Scope of the cascade reaction with **1** (M = In)

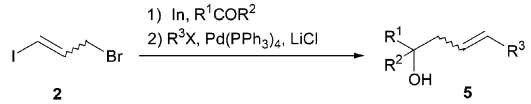

Entry	R^1COR^2	R^3X	Yield (%) (*E*:*Z*)
1	$CH_3(CH_2)_6CHO$	PhI	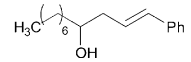 **5b:** 43 (100:0)
2	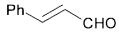	"	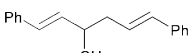 **5c:** 47 (100:0)
3	$CH_3(CH_2)_5COCH_3$	"	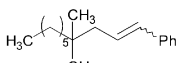 **5d:** 67 (70:30)
4	$PhCOCH_3$	"	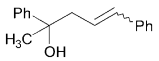 **5e:** 81 (59:41)
5	"	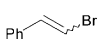 (*E*:*Z*=86:14)	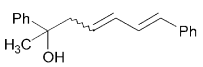 **5f:** 50 (68:32)
6	"	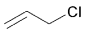	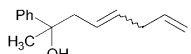 **5g:** 49 (76:24)[b]

[a] Reactions were carried out in NMP by mixing **2** (1.0 mmol), indium (1.0 mmol) and a carbonyl compound (0.50 mmol) at rt for 1 h, and then the second electrophile (1.0 mmol) was reacted in the presence of $Pd(PPh_3)_4$ (0.10 mmol) and LiCl (3 mmol) at 100–110 °C for 24 h. [b] This *E*/*Z* assignment is tentative.

DOI: 10.1039/b010176l

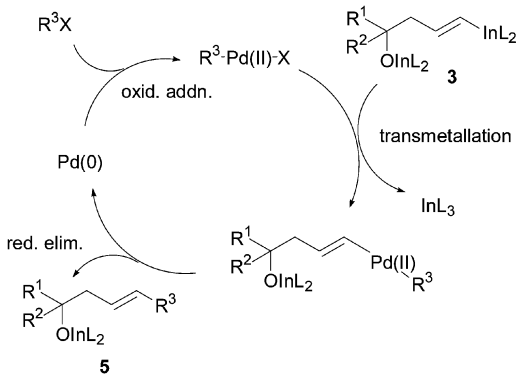

Scheme 2

Aliphatic and α,β-unsaturated aldehydes gave the corresponding three-component coupling products (Entries 1 and 2). The coupling with the aldehydes underwent with complete *E*-selectivity, though the yields were somewhat lower. Ketones also gave the linear homoallylic alcohols (Entries 3 and 4). As the second electrophiles, β-bromostyrene and allyl chloride were successfully used to give 1,3- and 1,4-dienes, respectively (Entries 5 and 6). The most plausible mechanism is depicted in Scheme 2. The vinylindium **3** undergoes transmetallation to a vinylpalladium(II) intermediate, which gives the three-component coupling products **5** by reductive elimination.

In contrast to the highly reactive nature of allylic indium reagents,[6] the preparation and synthetic applications of vinylic indium compounds are strictly limited.[7] The allylic diindium reagent **1** (M = In) possessing the two indium–carbon bonds of distinct reactivity can be prepared readily and can now be utilized for the tandem couplings with two electrophiles. The success of the present cascade not only provides a new synthetic route for linear homoallylic alcohols, but also expands the scope of organoindium chemistry in organic synthesis by means of a combination with palladium catalysts.[8]

This work was supported by a Grant-in-Aid for Scientific Research (No. 12640515) from the Ministry of Education, Science, Sports and Culture, Japan.

Notes and references

1 (*a*) I. Marek and L.-F. Normant, *Chem. Rev.*, 1996, **96**, 3241; (*b*) I. Marek, *Chem. Rev.*, 2000, **100**, 2887.
2 (*a*) J. Vollhardt, H. J. Gais and K. L. Lukas, *Angew Chem., Int. Ed. Engl.*, 1985, **24**, 610; (*b*) H. J. Gais and J. Vollhardt, *Tetrahedron Lett.*, 1988, **29**, 1529.
3 (*a*) J. F. Normant, J. C. Quirion, A. Alexakis and Y. Masuda, *Tetrahedron Lett.*, 1989, **30**, 3955; (*b*) L. Labaudinière, J. Hanaïzi and J. F. Normant, *J. Org. Chem.*, 1992, **57**, 6903; (*c*) J. F. Normant, *New J. Chem.*, 1990, **14**, 461; (*d*) L. Labaudinière and J. F. Normant, *Tetrahedron Lett.*, 1992, **33**, 6139.
4 (*a*) D. Madec and J.-P. Férézou, *Tetrahedron Lett.*, 1997, **38**, 6657; (*b*) D. Madec and J.-P. Férézou, *Tetradron Lett.*, 1997, **38**, 6661.
5 T. Hirashita, T. Kamei, T. Horie, H. Yamamura, M. Kawai and S. Araki, *J. Org. Chem.*, 1999, **64**, 172.
6 (*a*) P. Cintas, *Synlett*, 1995, 1087; (*b*) J. A. Marshall, *Chemtracts-Organic Chemistry*, 1997, **10**, 481; (*c*) C.-J. Li and T.-H. Chan, *Tetrahedron*, 1999, **55**, 11 149; (*d*) B. C. Ranu, *Eur. J. Org. Chem.*, 2000, 2347.
7 (*a*) I. Pérez, J. P. Sestelo and L. A. Sarandeses, *Org. Lett.*, 1999, **1**, 1267. Vinylindium compounds prepared from allylindation of alkynes were reported to couple with iodobenzene in the presence of Pd(0) catalyst. (*b*) N. Fujiwara and Y. Yamamoto, *J. Org. Chem.*, 1999, **64**, 4095.
8 Recently, palladium–indium mediated Barbier-type allylations of carbonyls were reported. (*a*) J. A. Marshall and C. M. Grany, *J. Org. Chem.*, 1999, **64**, 8214; (*b*) U. Anwar, R. Grigg, M. Rasparini, V. Savic and V. Sridharan, *Chem. Commun.*, 2000, 645; (*c*) U. Anwar, R. Grigg and V. Sridharan, *Chem. Commun.*, 2000, 933; (*d*) S. Araki, T. Kamei, T. Hirashita, H. Yamamura and M. Kawai, *Org. Lett.*, 2000, **2**, 847.

Typeset and printed by Black Bear Press Limited, Cambridge, England

The application of micro reactors to synthetic chemistry

Stephen J. Haswell,*[a] Robert J. Middleton,[a] Brian O'Sullivan,[a] Victoria Skelton,[a] Paul Watts[a] and Peter Styring[b]

[a] *Department of Chemistry, University of Hull, Cottingham Road, Hull, UK HU6 7RX. E-mail: s.j.haswell@chem.hull.ac.uk*
[b] *Department of Chemical and Process Engineering, University of Sheffield, Mappin Street, Sheffield, UK S1 3JD*

Received (in Cambridge, UK) 20th October 2000, Accepted 19th December 2000
First published as an Advance Article on the web 5th February 2001

A feature article describing the fundamental characteristics and emerging applications of micro technology in the field of synthetic chemistry.

Introduction

It is interesting to observe that despite the many advances made in synthetic chemistry over recent decades the basic practical methodology used remains unchanged. This situation arises primarily because reactions tend to be carried out on a bulk scale using a batch approach which chemists feel comfortable manipulating. At the molecular level however, it makes little difference fundamentally whether a reaction takes place in a 10 ml or 10 pl container. By applying technology developed for the electronics industry, it is now possible to produce reactors in which one can manipulate and analyse materials on a micron to nanometer scale. It is our belief that so called micro reactor technology can do for synthetic chemistry what the solid-state transistor has done for computing, vastly increasing the versatility and the amount of chemical information that a single person can generate. In short it represents a paradigm shift, changing the way we think about the way we work.

Stephen Haswell is Professor of Analytical Chemistry at the University of Hull. His current research activities are in the areas of micro reactors including analytical developments, microwave enhanced reaction chemistry, trace elemental speciation and process analysis. He is author of over 100 research papers, a number of books and patents and is widely known nationally and internationally for his enthusiastic lectures. For a number of years one of the underlying principles of Professor Haswell's research has been to break down the sectorial walls which exist in science, in particular, the integration of analytical science with main line chemistry, physics, engineering and biology. Many of these ideals are encompassed in his research into micro-chemical reactors the subject of this feature article.

Robert Middleton obtained a B.Sc. (Hons) from the University of Nottingham and carried out postgraduate studies in synthetic organic chemistry with Professor David Knight at Cardiff University focusing on the synthesis of highly substituted tetrahydrofurans via *electrophilic cyclisation. Now working at the University of Hull as part of the 'Lab on a Chip' Consortium, developing enzymatic and other catalytic reactions in micro reactors.*

Brian O'Sullivan obtained a Ph.D. in physical organic chemistry from the University of Exeter, and has spent some time at the University of Reading researching heterogeneous catalysis and organic synthesis in supercritical fluids. He is currently working at the University of Hull as part of the 'Lab on a Chip' Consortium, studying metal-catalysed carbon–carbon bond forming reactions in micro reactors and using electro-osmotic flow to control reagent mobilisation. Brian is also interested in modelling currents within micro reactors, in order to achieve a greater understanding of the fundamental processes underlying this technology.

Victoria Skelton graduated from the University of Hull in 1997 with a B.Sc. Hons. degree in Chemistry with Analytical Chemistry and toxicology. This included a year of industrial pharmaceutical experience in the analytical research and development department within Pfizer Central Research, Kent. Vikki obtained her Ph.D. at Hull University in 2000, investigating the role of micro reactors for organic synthesis and combinatorial applications and has continued a collaboration with GlaxoSmithKline. She is currently developing a number of chemical reactions and detection systems in micro reactors in order to establish the physical and chemical requirements of such devices.

Paul Watts graduated from the University of Bristol in 1995 with a B.Sc. in chemistry. He continued his studies at Bristol, obtaining a Ph.D. in bio-organic chemistry in 1999 under the supervision of Professor Tom Simpson and Professor Chris Willis. His Ph.D. focussed on the synthesis of isotopically labelled compounds for use in the determination of biosynthetic pathways to polyketide-derived natural products of biological interest. Paul is currently researching methods of peptide synthesis using micro reactor technology at the University of Hull. The project is funded by Novartis Pharmaceuticals, Basel, Switzerland.

Peter Styring is Senior Lecturer in the Process Fluidics Group at the University of Sheffield, Department of Chemical and Process Engineering. Previously he was the Thorn-EMI—BNR and DERA Lecturer in Chemistry at the University of Hull between 1990–2000. Peter gained his B.Sc. and Ph.D. from the University of Sheffield, Department of Chemistry. He has a background in Liquid Crystal Chemistry but moved into the field of Chemical Micro Reactors in 1997 where he addresses aspects of high throughput organic chemistry and catalysis within miniaturised devices.

DOI: 10.1039/b008496o

Basic concepts of micro reactors

A micro reactor is generally defined as a series of interconnecting channels (10 to 300 microns in diameter) formed in a planar surface in which small quantities of reagents are manipulated. The reagents can be brought together in a specified sequence, mixed and allowed to react for a specified period of time in a controlled region. The product may then be analytically monitored and if necessary separated for further steps in a reaction, or collected for analysis or testing.

In what is basically a diffusion limited environment, where laminar flow characteristics dominate, the micro reactor confers many advantages over conventional scale chemistry. The decrease in linear dimensions allows heat transfer coefficients to exceed those of conventional heat exchangers by an order of magnitude.[1] Micromixers can reduce mixing times to milli- or nano-seconds.[2] The increased surface to volume ratio in micro reactors (10 000 to 50 000 $m^2\ m^{-3}$, compared to 1000 $m^2\ m^{-3}$ in conventional laboratory vessels) has implications for surface-catalysed reactions.[3] Other properties include localised control of concentration gradients, separation of reaction products and the possibility of eliminating unwanted side reactions. For example, when Ehrfeld *et al.*[4] prepared hydrogen cyanide in a micro reactor *via* the Andrussow route, the rapid cooling of the products by a micro heat exchanger prevented hydrolysis of the HCN to ammonia. Jensen and coworkers[5] demonstrated that the synthesis of organic peroxides from acid chlorides and hydrogen peroxide may even be carried out beyond the 'explosion limit', as the transfer of heat energy from the area of reaction is rapid enough to prevent explosion.

In addition the small scales used reduce exposure to toxic or hazardous materials, and the enclosed nature of the micro reactors means greater ease of containment in the event of a runaway reaction. The greatest contribution to safety is the fact that hazardous materials can be synthesised as required at the point of use, in precisely defined quantities, thus eliminating the problems associated with transportation and storage.

Although the small size of the micro reactors would seem to preclude industrial scale synthesis, it has been shown[6] that only 1000 micro reactors operating continuously could produce 1 kg of material in a day. This so called 'scaling out' concept has clear implications in process development where the costly and time-consuming process of going from lab to pilot plant to full-scale production is by-passed simply by optimising the reaction on a single chip and replicating it 1000 or 1 000 000 times. The main attraction of this approach is not only the elimination of the problems associated with the scaling up procedure but also the ability to maintain the high level of control and selectivity made possible through using micro reactor technology.

The micro total analysis systems (μ-TAS)

In recent years, research in the area of miniaturised analytical systems has become well established with a large rapidly growing number of publications reflecting this trend.[7–14] The first fully miniaturised system fabricated was a gas chromatographic device reported by Terry *et al.*[15] at Stanford University in 1979. This micro device was constructed using a silicon wafer, which included a sample inlet port, a 1.5 m long column, an injector and thermal conductivity detector allowing the separation of a mixture of hydrocarbons within 10 s. However, it took a further 10 years before Manz and colleagues[16] at Ciba-Geigy laboratories in Switzerland fabricated a micro capillary electrophoresis device. The μ-TAS was fabricated from glass and allowed the rapid separation of two fluorescent dyes. During the past decade, the main research thrust in academia and industry has centred on the separation and characterisation of DNA.[17–22] This has now led to commercially available micro analytical devices such as the DNA analyser from Agilent, formerly Hewlett–Packard. More recently, a number of research groups worldwide have shifted the focus of research from μ-TAS to developing micro reactor technology building on the already existing μ-TAS concept. Some of the unique features of such devices will be described in the remainder of this paper but it is worth stressing that integration between μ-TAS and micro reactors is essential if chemical and biochemical reactions, at the micro scale or less, are to be effectively monitored and controlled.

Fabrication techniques

Many of the existing fabrication methods described for the μ-TAS systems have been successfully transferred to the field of chemical micro reactors.[23] A number of materials such as silicon, glass, quartz, metals and some polymers can be used to construct micro reactors. Glass and certain polymers have been particularly useful because of their physical properties and chemical inertness. These substrates also allow the mobilisation of organic reagent and aqueous solutions using a number of pumping mechanisms such as hydrodynamic pumping and electro-osmotic flow (EOF).[24–26] A range of fabrication methods such as photolithography, hot embossing, powder blasting, injection moulding, laser micro forming and LIGA, from the German *Lithographie*, *Galvanioformung* (electroforming) and *Abformung* (moulding), are available and can be both versatile and relatively low cost processes.

Fig. 1 shows the steps that are involved in the popular technique of photolithography and wet etching to produce

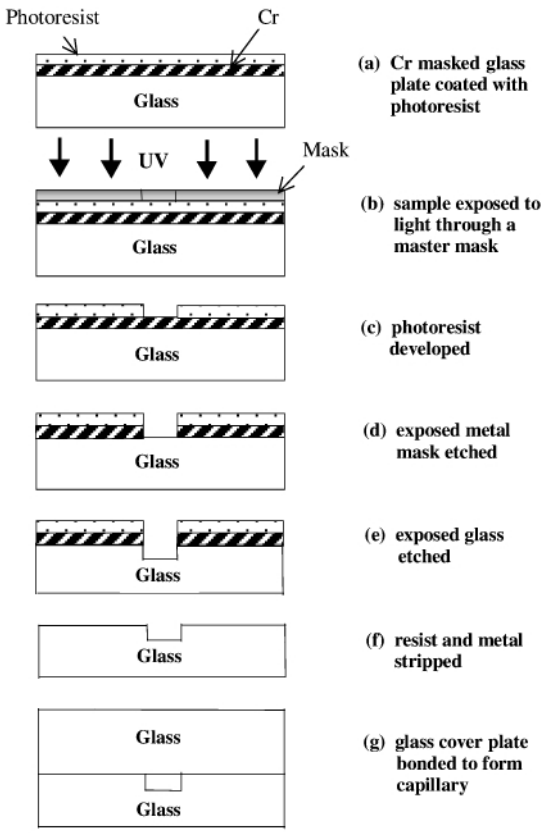

Fig. 1 Sequence of processes in photolithographic fabrication.

channels in a glass micro reactor. A thin layer of metal, such as chromium, is deposited on the surface of a glass plate to control the degree of undercutting during the etching process. A layer of positive photoresist is then spin coated on top of the chromium to a depth of 0.5 to 2.0 μm. The pattern of the required network of interconnecting channels is transferred to the photoresist layer using photolithography. After exposure, the photoresist is developed and removed together with the chromium layer to

reveal the areas of glass to be etched. The plate is then heated to allow volatiles to evaporate, before performing the chemical etch. The channels are then etched using, for example, a mixture of 1% HF and 5% NH_4F in water at 65 °C, resulting in an etch rate of 0.3 to 0.5 μm min^{-1}. A glass top block, with pre-drilled holes to act as reservoirs and if necessary electrode supports, is aligned with the channel geometry and thermally bonded to the glass base plate, producing an all glass device. An example of such a micro reactor, produced by the photolithographic, wet etch and thermal bonding method outlined above is shown in Fig. 2. It should be noted that a range of alternative fabrication

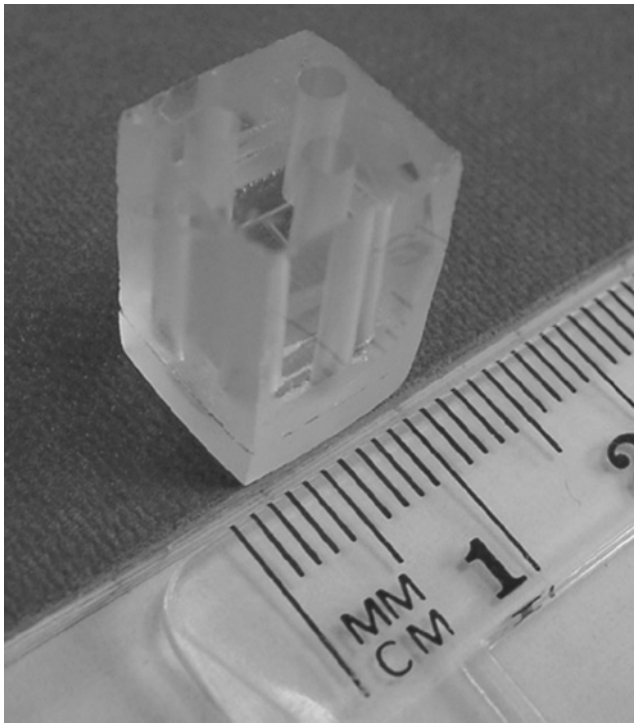

Fig. 2 A simple all-glass micro reactor.

techniques have been reported describing a number of different masking layers, etchant solutions, low temperature bonding, anodic bonding, and polymer based substrates. A recent review of these may be found in ref. 3.

Chemical control in micro reactors

Flow mechanics of liquids in micro channels

One of the main areas that liquid based micro reactor research has focused on to date has been the accuracy with which fluids in capillaries can be manipulated. Owing to the microlitre flow rates that are generally required, some groups have used methods such as syringe pumps, HPLC pumps and peristaltic pumps with high reproducibility being achieved through computer control. Syringe pumps can also be used to infuse and withdraw fluids through channels in both directions. These techniques provide a relatively quick and simple method for pumping reagents through a micro reactor in a controlled manner. However, these systems can build up high back-pressure due to capillary effects, which may lead to pulsing in the flow: this could be a particular problem when using peristaltic pumps.[24] Another problem is the cost associated with HPLC and syringe pumps. These pumps can also be intolerant of mixed-phase liquid systems, or systems that contain particulate matter.

Several companies have developed pumps specifically for micro reactor applications. These pumps are typically based on a piezoelectric driven one way valve to mobilise liquids.[27] For example, the Institut für Mikrotechnik, Mainz has developed a membrane pump that operates with microlitre volumes, but can also pump at up to 0.4 ml min^{-1}. These pumps, which are very small, can deliver the microlitre volumes that are required for managing the movement of liquids in typical devices. However, as they have been constructed from a polymer, practical difficulties may arise when using organic solvents, and depending upon the micro channel geometry, excessive back pressures may be generated.

As one of the attractive features of using micro reactors is their capacity to perform high throughput parallel processing, the use of hydrodynamic pumping may become impractical due to the large number of different solutions that will be required within the reactor. To overcome the need therefore for a large number of pumps and to simplify the construction of micro fluidic systems, electro-osmotic flow (EOF) which has no moving parts, has proved to be a widely preferred method for reagent and solvent pumping.

EOF can be used to move reagents and solvents around a system of channels as a function of applied voltages, with a very high degree of control and allowing the processes to be readily automated. In addition, due to the high electric field (*e.g.* 200 V per centimetre of channel) associated with the EOF, variations in the electrophoretic mobility of individual species enables separation to be achieved. The combination of EOF and electrophoretic mobility can be used to both model and practically control the spatial and temporal position of components in a micro reactor system.[28]

To illustrate the principles of EOF, one can consider a microchannel fabricated from a material (*e.g.* glass), having naturally negatively charged functional groups on its surface. If a liquid, displaying some degree of dissociation, is brought into contact with the material, positive counter ions will form a double layer such that the positively charged ions are attracted to the negatively charged surface. If an electric field is now applied through the liquid phase, the positive mobile ions will migrate to the negative electrode inducing a drag on the bulk liquid. In an aqueous buffered system (pH 3–9) the solution flows towards the cathode with volumetric flow rates in the order of nl min^{-1} to μl min^{-1} depending on the channel dimensions and applied field. The flow velocity achieved with EOF is given by eqn. (1)

$$\upsilon_{EOF} = \frac{V}{L}\mu$$

where V is the applied field, L is the length of the channel and μ is electro-osmotic mobility (dependent on factors such as zeta potential, ionic strength and pH).

Since V and L are controlled by the user, a very high level of control is achievable. Furthermore, this control can be automated and a relatively simple LabVIEW™ program, such as that developed at Hull which allows one to control the output from a power supply to a number of channels in a micro reactor (Fig. 3) has been developed. By varying the potentials across each channel section, it is possible to rapidly optimise the relative flows of different reagents, or to inject plugs of one reagent into a stream of another, or to introduce a number of reagents in a specified sequence for multi-step reactions.

Unlike conventional (hydrodynamic) flow systems, solutions that are moved by EOF have a flat velocity profile across the channel. This, together with an absence of back pressure effects and an inherent low Reynolds number, affords minimal band broadening and efficient electrophoretic separation of reactants and products.

Although EOF has mainly been used in applications with aqueous solutions, it is not restricted to these systems and EOF may be applied to reagents in polar solvents such as methanol, tetrahydrofuran, acetonitrile and dimethylformamide. For example, Harrison and coworkers[29] used EOF to achieve valveless

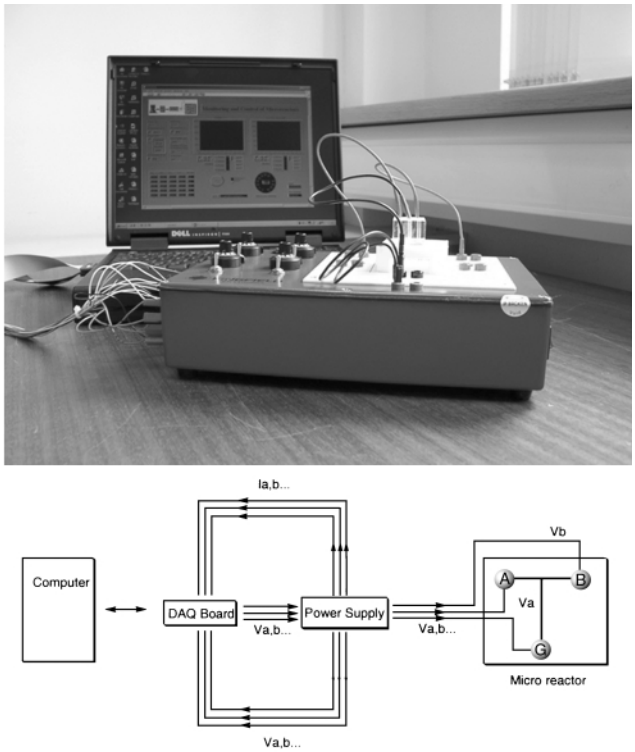

Fig. 3 An automated computer controlled chemical reaction, showing the hardware and a schematic of the system. Using the configuration shown, the duration and magnitude of voltage applied to each reservoir can be selected and the resulting current monitored.

pumping of acetonitrile reagent solutions during the synthesis of an azo dye in a glass micro reactor. This degree of solvent choice greatly extends the types of EOF-controlled chemistry that can be carried out in micro reactors. Obviously the solvent systems used must exhibit some level of polarity, and strictly non-polar solvents cannot be pumped by EOF unless a polar modifier is added.

Applications of micro reactors in synthesis

The inherent benefits of micro reactors, namely rapid generation of small but detectable quantities of reaction products, efficient heat transfer and fluidic control, are now being applied successfully to synthetic chemistry. In theory, these factors might give a research worker using a micro reactor the ability to greatly increase the rate at which new compounds are produced. The work highlighted in this section demonstrates how some of the initial findings obtained by research groups developing micro reactor systems could be applied to high throughput synthesis. There are also some operating characteristics of the micro reactor environment that result in fundamental differences in chemistry. Of more immediate and perhaps significant impact to the research community is the opportunity micro reactors offer in terms of performing a large number (many hundreds) of reactions to explore and optimise a single reaction or a series of chemical reactions. For example, the capability to generate information about reaction conditions, kinetics and product selectivity is now readily accessible using micro reactors, an option not easily available using conventional methodology.

Micro reactor systems have so far been successfully deployed in gas and liquid phase chemistry, including catalyst testing. A recent example of the application of micro reactors to gas phase chemistry was reported at the IMRET 4 conference. Hönicke and coworkers reported the gas phase partial hydrogenation of cyclododeca-1,5,9-triene (CDT), cycloocta-1,5-diene (COD) and benzene over palladium and ruthenium/zinc catalysts (see Scheme 1).[30] The micro reactor system consisted of alumina wafers with mechanically etched channels, which were then

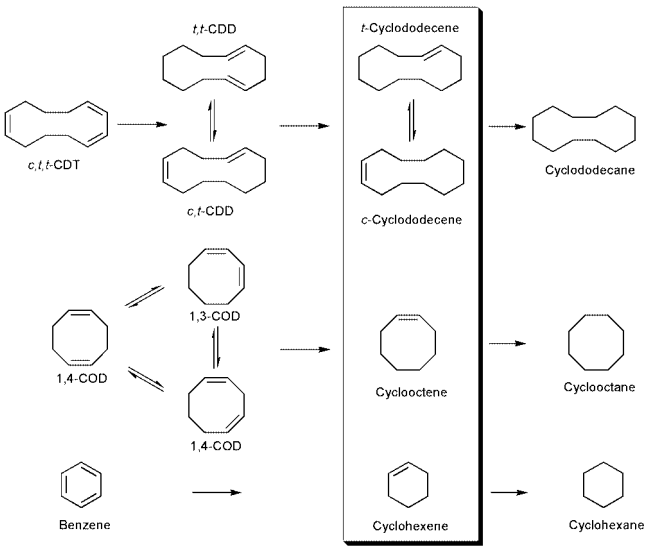

Scheme 1 The mild reaction conditions and the unique mass transfer properties of micro reactors allow hydrogenation of cyclic trienes and dienes to industrially important monoalkenes (ref. 26).

activated by anodic oxidation and impregnation with an organic solution of palladium(II) acetylacetonate. This gave an 18 μm thick activated layer with 0.18 wt% palladium. Twenty four of these wafers were then stacked to give 672 micro channels with internal geometries of 200 μm × 200 μm × 30 mm. A similar process was used for the construction of the Ru/Zn reactor, which contained 0.2 wt% each of ruthenium and zinc. The organic solvent was then removed *via* oxidation in air at 417 °C followed by hydrogen reduction at 150 °C to give the activated catalyst. Although palladium showed no conversion of benzene to cyclohexene, CDT was converted with high yield and selectivity to cyclododecene at 150 °C, with the catalyst bed giving > 80% conversion to cyclododecene for over 20 h. The COD conversion went from 75 to 100% at 150 °C by increasing the residence time in the reactor from 40 to 115 ms. This system proved to be robust, in that throughput could be increased ten-fold from 50 to 500 mg h^{-1} whilst conversion to cyclooctene remained above 80%. Partial hydrogenation of benzene by Ru/Zn was less successful with conversion falling rapidly, and only low yields of cyclohexene were obtained, with the major product being cyclohexane. This work shows that high conversions may be achieved given only a short residence time. By controlling the rate of flow, conversion rate and product yields may be selected or rapidly optimised. This micro reactor system also allows easy re-activation of the catalyst, and it would be readily possible to allow the mixture and velocity of gases to be adjusted automatically in real-time *via* feedback control from analysis of exhaust gases.

Micro reactors using heterogenous catalysts have been applied in liquid-phase organic synthesis. An early, though still comparatively recent development was reported from the Micro Reactor Group in Hull by Greenway *et al.*.[31] The micro reactor utilised EOF to mobilise the reagents and allowed the catalytic synthesis of 4-cyanobiphenyl using a modified Suzuki coupling reaction (Scheme 2). The incorporation of micro porous silica frits[32] within the reactor manifold enhanced EOF and allowed the immobilisation of the heterogeneous catalyst (1.8% palladium on silica). The catalyst immobilisation method produced a leaching rate in the region of ppb (1.2 to 1.6 ppb) removing the need for subsequent purification from metal residues. The micro reactor device was optimised using flow injection analysis principles producing a 67 ± 7% (n = 6) yield of the 4-cyanobiphenyl product at room temperature within 25 min.

The flow injection method adopted allowed the periodic injection of the aryl halide (5 s injection length with a 25 s injection interval) into a continuous flow of phenylboronic acid. Flow was maintained using an external applied voltage of 200 V. The yield obtained using the device was comparable with Suzuki reactions performed on a large (batch) scale using homogeneous catalysts. One of the interesting observations of this reaction was that, unlike conventional Suzuki couplings performed in a flask, base was not required. Although the reason for this is as yet unclear, it is thought that the applied electric field may be sufficient to cause localised ionisation of solvent water to H^+ and OH^- at the metal surface. It may be this so-formed hydroxide that performs the function of a conventional inorganic or amine base. However, the micro reactor demonstrated the potential application of such devices to perform chemical reactions, allowing high throughput screening, rapid method development or reaction optimisation.

The Hull group have also demonstrated that a superacid catalyst (sulfated zirconia) could be immobilised onto the surface of a polydimethylsiloxane (PDMS) micro reactor top plate. This was achieved by dusting the pre-cured PDMS surface with activated catalyst and baking the plate at 100 °C for 1 h. The PDMS top plate (containing the catalyst) was clamped to a glass base plate (with etched micro channels) and syringe pumps were used to mobilise the hexan-1-ol, which underwent dehydration to hex-1-ene. The micro reactor featured an *in situ* resistive heater wire cast into the PDMS top plate, which was operated at 155 to 160 °C.[33]

An attractive feature of micro reactors is their ability to carry out chemical processes that may be hazardous. For example Burns and Ramshaw[34] at the University of Newcastle have described the nitration of toluene and benzene in stainless steel or PTFE micro reactors, demonstrating the approach is suited to a hazardous processes involving organic solvents and concentrated acids. In addition, they are also investigating the challenge of manipulating bi-phasic liquid–liquid systems and the control of product distribution to avoid hazardous trinitrated aromatic products. Their studies have yielded some elegant ways to control immiscible liquid layers in capillary systems that include (i) segmented flow, in which plugs of alternate phases travel down a capillary and (ii) parallel laminar flow, where similar amounts of two phases run together through the capillary producing an interfacial contact zone.

Burns and Ramshaw's studies on benzene nitration also demonstrated that conversion, while showing a near linear relationship with temperature, can be increased substantially by the use of smaller capillaries that enhance diffusion effects by reducing the size of the slugs of material in the channel. Halving the capillary diameter from 250 to 130 μm more than doubled the rate of nitration. Flow rates were also found to be important, with faster flow rates giving rise to higher conversion as they promoted internal circulation of the liquid plugs travelling down the capillary.

In comparison with conventional nitration techniques, the results showed that rate constants for the micro reactor process (1–8 min^{-1}) in 178 μm capillaries were similar to those in the published literature (1–5 min^{-1}). It is expected that further optimisation of the micro reactor device and its operation, particularly by increasing the sophistication of the technology to decrease droplet size, will result in substantial improvement to the efficiency of the devices.

To demonstrate the advantages that micro reactors offer when dealing with potentially hazardous reagents, Chambers and Spink[35] recently reported the development of a micro reactor fabricated from a block of nickel, which was used for the elemental fluorination of organic substrates. Conversions compare well with results from conventional reactors. The small amount of fluorine involved, together with the heat and mass transfer properties of the micro reactor, overcame many of the safety issues associated with this type of reaction.

Optimisation of catalytic processes

To demonstrate the testing and optimisation of catalytic processes, the Hull group has developed a simple procedure for the immobilisation and introduction of supported reagents in micro reactors (Fig. 4). Such configurations enable solutions to

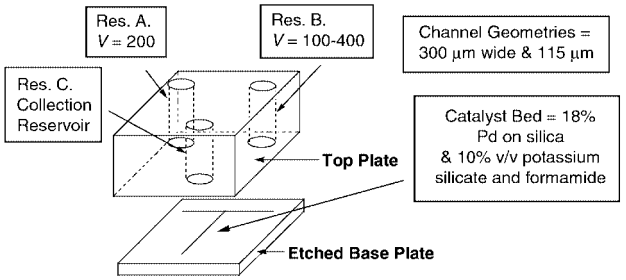

Fig. 4 A Hull micro reactor, configured for the Suzuki reaction. Reservoir A contains 100 μl of 4-bromobenzonitrile (0.1 M) and reservoir B 100 μl of phenylboronic acid (0.1 M), both in 75% $THF_{(aq)}$. Products from the reaction are taken from reservoir C and analysed by GCMS.

be passed over catalysts in either a continuous or plug mode with a high degree of fluidic control. Catalyst types under investigation include immobilised enzymes (such as lipases and esterase), metals, sulfated zirconia and zeolite-based materials. For example, in the case of an enzyme system based on porcine liver esterase, symmetrical diesters are passed over this catalyst bed to effect desymmetrisation to a chiral mono-ester, creating a high-throughput reactor for biocatalysis.

A second approach is to pulse several different reagents one by one over the catalyst bed. Given the computer-based flow-control possible with micro reactors, it is now relatively easy to achieve accurate and reproducible reaction sequencing. In the Suzuki reaction performed at Hull, the aryl halide and boronic acid were alternately pulsed over a catalyst bed of palladium on silica. This had the effect of increasing yields from < 5% to 68% by simulating the catalytic cycle (Scheme 2).[31] The catalyst was

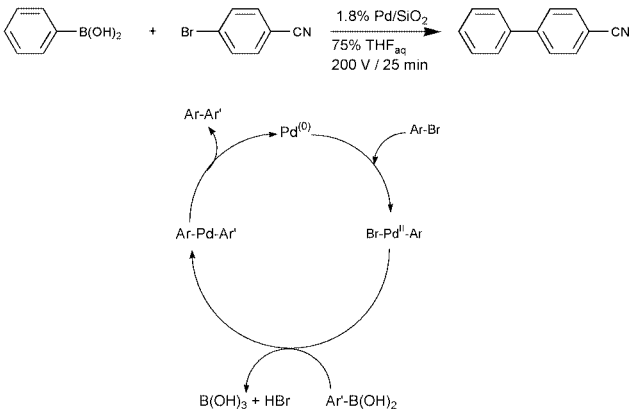

Scheme 2 The catalytic cycle of the Suzuki reaction.

flushed with the aryl bromide to drive the oxidative addition to the metal, and then flushed with boronic acid to effect conversion to the biphenyls.

Using a system of five continuous flow micro reactors, the Suzuki reaction has been carried out on an industrial scale by Merck in Germany, where researchers found improvements over conventional batch reactors.[30] For example, in the reaction of 3-bromobenzaldehyde with 4-fluorophenylboronic acid, 90% yields were reported for the micro reactors, compared with 50% in stirred flasks.

One of the chief limitations of the studies in Hull has been the high temperatures (680 °C) required to anneal the top glass plate

to the etched glass base plate as any organic material would be destroyed in these processes, hence metals on silica have been favoured as catalysts.

These early studies into catalytic processes demonstrate the potential of using micro reactor technology for a continuous production line approach to single compound production. However, the design of such devices could be easily modified to evaluate the performance of a catalyst across a broad range of substrates. Another opportunity would be in using multi-channel systems that would allow the evaluation of a number of different catalysts for a single reaction. These studies allow rapid evaluation of reaction conditions to allow the best catalyst for a given reaction to be studied, or the efficacy of a catalyst over a range of substrates to be evaluated.

Multi-step and analog based reactions

At the recent IMRET 4 conference, the Hull group reported a micro reactor device that allowed the synthesis of a number of nitrostilbene esters using a borosilicate micro reactor.[36] The micro reactor allowed the development of the Wittig reaction investigating a number of reaction features such as stoichiometry, stereochemistry and reaction diversity (Scheme 3).

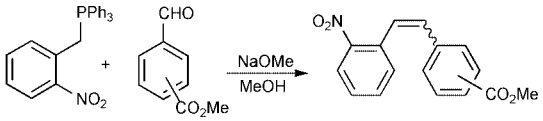

Scheme 3 The Wittig reaction.

Initial investigations centred on using the device for synthetic method development and optimisation, allowing rapid reaction design in conjunction with EOF as the mobilisation method. With a 2 : 1 reaction stoichiometry (aldehyde in excess) a yield of 70% was achieved using the micro reactor in a continuous flow mode with an optimum voltage of 400 V. The micro reactor demonstrated an increase in reaction efficiency of 10% over the conventional batch method. The reaction stoichiometry was then reduced to 1 : 1 but the yield was poor (39%) so a flow injection technique was adopted. This resulted in the injection of the phosphonium salt into the continuous flow of the aldehyde compound at 400 V. A 59% yield was obtained, but more importantly it allowed a series of aldehydes to be reacted in sequential injections using the optimum conditions established at 1 : 1 stoichiometry. This demonstrated the micro reactors diversity and high through-put capability.

The above research has been extended to investigate the stereoselective control of the chemical reaction by applying electrical fields which generate controlled concentration gradients of the reagent streams.[37] The stereoselective synthesis of the *cis* (*Z*) and *trans* (*E*) isomers was controlled by varying the applied voltages to the reagent reservoirs within the device. The variation in the external applied voltage subsequently altered the relative reagent concentrations within the device producing *Z/E* ratios in the region of 0.57 to 5.21. In comparison, a traditional batch reaction was performed based on the same reaction length, concentration, solvent and stoichiometry resulting in a *Z/E* ratio of 3.0. The unique flow control created in the micro reactor system has allowed the localised concentration gradients, produced by a diffusion limited non-turbulent mixing regime, to generate the observed stereoselectivity. The control of these localised diffusion-limited concentration gradients is an important feature of micro reactors and one that can be effectively exploited for yield and product selectivity.

Multi-step reactions

So far, micro reactors appear to be limited to carrying out a single synthetic step. One of the thrusts of the research in Hull is to develop methodology that will give the chemist the ability to look as multi-step reactions, culminating in target or diversity based synthesis.

To extend the capability of performing multi step reactions in micro reactors, processes such as peptide synthesis represent a good model system. Peptides have been traditionally prepared combinatorially *via* solid supported techniques[38,39] but this approach has the disadvantage that a fairly expensive polymer support is required and that the product requires post-synthetic cleavage. In addition, extra steps are added to the synthesis as a result of having to initially link the amino acid to the polymer support. The preparation of peptides in micro reactors, using solution phase chemistry, offers the possibility of overcoming such problems.

Using solution phase chemistry there are several methods that may be used to form peptide bonds such as diethyl azodicarboxylate[40] (DEAD) or carbodiimide reagents such as dicyclohexylcarbodiimide (DCC)[41] or 1-(3-dimethylaminopropyl)-3-ethylcarbodiimide hydrochloride (EDCI).[42] In addition acyl halides, anhydrides and azides may be utilised in the formation of peptide bonds.[43] Once the methodology for the formation of peptide bonds has been fully established, selective deprotection of either of the protecting groups will allow longer peptide chains to be assembled. This multi-step synthesis will clearly allow the rapid generation of libraries of peptides, which could then be used in determining their biological properties.

In situ detection methods in micro reactors

As indicated earlier, research focused on μ-TAS has developed a number of suitable detection methods for micron scale systems, with the most common method adopted being fluorescence. Other detection systems developed have included UV–VIS[44–48] and electrochemical[49–52] detection offering sensitivity and simple detection with environmental micro systems. The information provided is however generally insufficient for structural characterisation of unknown chemical species. For the micro reactor system to become truly versatile, the development of hyphenated techniques and specialised equipment such as NMR and Raman spectrometry would allow direct, real time characterisation and spatial determination of concentration and pH information. Currently a range of analytical techniques are being investigated by a number of research groups. These include mass spectrometry (MS)[53] and near infrared (NIR).[54–57]

One area of analysis which has been readily reported in the literature is the hyphenation of micro reactor to mass spectrometers.[58–61] Lazar *et al.*[58] from Oakridge National Laboratories have coupled a micro fluidic device with a nanospray tip for electrospray ionisation, allowing dilute peptide and protein solutions to be characterised using a time of flight mass spectrometer. The hyphenated system allowed the capture of spectra within milliseconds (10 to 20 ms) resulting in 50 to 100 spectra per second. The second study by Mitchell *et al.*, presented at the recent Micro Total Analytical Systems conference,[59] described the detection of a multicomponent reaction using an electrospray ionisation (EIS)-MS. The multicomponent synthesis investigated was the Ugi reaction (Scheme 4) in which a solution of formaldehyde and pure

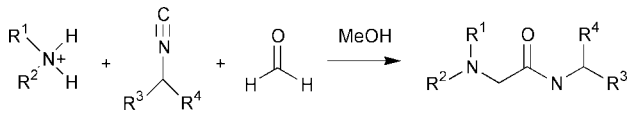

Scheme 4 The Ugi reaction.

solvent was infused through one of the inlets whilst a multicomponent mixture (isocyanide, amine salt) was also added. The hyphenated micro reactor-MS system allowed the real time detection of the synthetic Ugi coupling reaction.

Other detection systems reported have been NIR and Raman spectrometry. A miniaturised NIR spectroscopic system fabri-

cated in borosilicate glass has been developed by Ache.[56] The micro device contains a circular wave guide covered by a sensing membrane. In addition, the micro NIR system contained an incandescent light source, a NIR micro spectrometer with a self-focusing reflection grating and NIR diode. At the University of Michigan, Reshni and co-workers[62] demonstrated one early example of Raman spectrometry on a micro device. The system was fabricated using a Raman microprobe stage coupled to a capillary electrophoresis chip. Traditionally, Raman spectroscopy has a limit of detection in the millimolar region, however Reshni's micro device achieved a limit of detection in the micromolar region and below. This was due to the addition of a preconcentration stage using isotachophoresis. This system has allowed the successful fingerprinting and quantification of reactions on-chip.

Commercialisation of micro reactor technology

A commercially available chemical synthesiser using micro reaction technology already exists, and is produced by IMM-Mainz. It consists of a pumping module, a micro-reactor that results in very efficient mixing of reagents, followed by a capillary to allow time for the reaction to go to completion. The outflow is then collected for further manipulation by the user. This could be just the first step along a road which will see the integration of automated reagent manipulation, reaction monitoring and product purification into a single instrument containing several interconnected micro reactors, or possibly a single micro reactor device. In common with microelectronic chips, once the facilities to fabricate micro reactors are in place, they become progressively cheaper to produce in quantity. This should make the production of chemicals in massive parallel arrays of reactors an economic possibility. It is likely that some of the peripheral equipment required will still represent a considerable cost, but this should be set against the potential increase in productivity per research worker. In addition, the effective production of molecules in terms of energy, safety and environmental impact will emerge as important factors in the future exploitation of micro reactor technology. One of the underlying features of any future commercially available automated synthesis system must be versatility. Research is now moving towards a 'plug and play' approach in which the reaction and detection configurations can be customised. The next couple of years will undoubtedly see significant development in this area of the technology. We should now prepare ourselves, including university courses for undergraduates, for the impact the micro reactor is going to have on the whole area of chemical research and production.

Acknowledgements

We wish to thank the EPSRC Lab-on-a-chip Consortium (B. O'S., R. J. M.), Novartis Pharmaceuticals (P. W.) and GlaxoSmithKline (V. S.) for financial support.

Further information

See the following websites:
http://analyticalsciencehull.org/
Further information about conferences relating to this topic may be found at the following websites:
IMRET 5 (Strasbourg, France, 27–30 May 2001):
http://www.aiche.org/conferences/cosponsored/#2001
μ-TAS 2001 (Monterey, CA, USA, 21–25 Oct 2001):
http://www.casss.org/tas2001

Notes and references

1 K. Schubert, W. Bier, J. Brandner, M. Fichtner, C. Franz and G. Linder, *Process Miniaturisation: 2nd International Conference on Microreaction Technology*, AIChE, New Orleans, 1998, p. 89.
2 J. B. Knight, A. Vishwanath, J. P. Brody and R. H. Austin, *Phys. Rev. Lett.*, 1998, **80**, 386.
3 W. Ehrfeld, V. Hessel and H. Löwe, *Microreactors*, Wiley-VCH, Weinheim, 2000, ch. 1.
4 W. Ehrfeld, V. Hessel, S. Kiesewalter, H. Löwe, T. Richter and J. Schiewe, *Proceedings of the Third International Conference on Microreaction Technology*, Frankfurt, Germany, 1999, p. 14.
5 T. M. Floyd, M. W. Losey, S. L. Firebaugh, K. F. Jensen and M. A. Schmidt, *Proceedings of the Third International Conference on Microreaction Technology*, Frankfurt, Germany, 1999, p. 171.
6 P. D. I. Fletcher and S. J. Haswell, *Chem. Br.*, 1999, **35**, 38.
7 S. J. Haswell, *Analyst*, 1997, **112**, 1R.
8 A. Manz, D. J. Harrison, E. Verpoorte, J. C. Fettinger, H. Ludi and H. M. Widmer, *Chimia*, 1991, **45**, 103.
9 A. Manz, D. J. Harrison, E. Verpoorte and H. M. Widmer, *Adv. Chromatogr.*, 1993, **33**, 1.
10 A. Manz, C. S. Effebhauser, N. Burggraf, E. Verpoorte, D. E. Raymond and H. M. Widmer, *Anal. Mag.*, 1994, **22**, M25.
11 *Proceedings of the Micro Total Analytical Systems 98' Workshop*, ed. D. J. Harrison and A. van den Berg, Kluwer Academic Press, Dordrecht, 1998.
12 A. van den Berg and T. S. J. Lammerink, *Top. Curr. Chem.*, 1998, **194**, 21.
13 D. J. Harrison, K. Fluri, K. Seiler, Z. H. Fan, C. S. Effenhauser and A. Manz, *Science*, 1993, **261**, 895.
14 S. C. Jacobson, R. Hergenroder, L. B. Koutny and J. M. Ramsey, *Anal. Chem.*, 1994, **66**, 1114.
15 S. C. Terry, J. H. Jerman and J. B. Angel, *IEEE Trans. Electron Devices*, 1979, **ED26**, 1880.
16 A. Manz, N. Graber and H. M. Widmer, *Sens. Actuators B*, 1990, **1**, 24.
17 A. T. Woolley, D. Hadley, P. Ladre, A. J. deMello, R. A. Mathies and M. A. Northrup, *Anal. Chem.*, 1996, **68**, 4081.
18 A. T. Woolley and R. A. Mathies, *Anal. Chem.*, 1996, **67**, 3676.
19 A. T. Woolley, G. F. Sensabaugh and R. A. Mathies, *Anal. Chem.*, 1997, **69**, 2181.
20 S. C. Jacobson and J. M. Ramsey, *Anal. Chem.*, 1996, **68**, 720.
21 C. S. Effenhauser, A. Paulus, A. Manz and H. M. Widmer, *Anal. Chem.*, 1994, **66**, 2949.
22 D. Schmalzing, A. Adourian, L. Koutny, L. Ziagura, P. Matsudaria and D. Ehrlich, *Anal. Chem.*, 1998, **70**, 2303.
23 T. McCreedy, *TrAC*, 2000, **19**, 396.
24 D. M. Spence and S. R. Crouch, *Anal. Chem.*, 1998, **358**, 95.
25 B. H. Schoot, S. Jeanneret and A. Berg, *Anal. Methods Instrum.*, 1993, **1**, 38.
26 P. K. Das Gupta and S. Lui, *Anal. Chem.*, 1994, **66**, 1792.
27 H. T. G. van Lintel, F. C. M. van de Pol and S. Bouwstra, *Sens. Actuators*, 1988, **15**, 153.
28 S. J. Haswell, P. D. I. Fletcher and V. N. Paunov, *Analyst*, 1999, **124**, 1273.
29 H. Salimi-Moosavi, T. Tang and D. J. Harrison, *J. Am. Chem. Soc.*, 1997, **119**, 8716.
30 E. Dietzsch, D. Hönicke, M. Fichtner, K. Schubert and G. Weißmeier, *IMRET 4: 4th International Conference of Micro Reaction Technology Topical Conference Proceedings, AIChE Spring National Meeting, March 5–9 2000*, Atlanta GA, USA, p. 89.
31 G. M. Greenway, S. J. Haswell, D. O. Morgan, V. Skelton and P. Styring, *Sens. Actuators B*, 2000, **63**, 153.
32 P. D. Christensen, S. W. P. Johnson, T. McCreedy, V. Skelton and N. G. Wilson, *Anal. Commun.*, 1998, **35**, 341.
33 N. G. Wilson and T. McCreedy, *Chem. Commun.*, 2000, 733.
34 J. R. Burns and C. Ramshaw, *IMRET 4: 4th International Conference of Micro Reaction Technology Topical Conference Proceedings, AIChE Spring National Meeting, March 5–9 2000*, Atlanta GA, USA, p. 133.
35 R. D. Chambers and R. C. H. Spink, *Chem. Commun.*, 1999, 883.
36 V. Skelton, G. M. Greenway, S. J. Haswell, P. Styring, D. O. Morgan, B. H. Warrington and S. Y. F. Wong, *Analyst*, 2000, **126**, 7.
37 V. Skelton, G. M. Greenway, S. J. Haswell, P. Styring, D. O. Morgan, B. H. Warrington and S. Y. F. Wong, *Analyst*, 2000, **126**, 11.
38 R. B. Merrifield, *J. Am. Chem. Soc.*, 1963, **85**, 2149.
39 D. B. Whitney, J. P. Tam and R. B. Merrifield, *Tetrahedron*, 1984, **40**, 4237.
40 O. Mitsunobu, *Synthesis*, 1981, 1.
41 A. Hassner and V. Alexanian, *Tetrahedron Lett.*, 1978, 4475.
42 P. D. Bailey and K. D. Morgan, *Organonitrogen Chemistry*, Oxford University Press, 1996.
43 D. S. Perlow, J. M. Erb, N. P. Gould, R. D. Tung, R. M. Freidinger, P. D. Williams and D. F. Veber, *J. Org. Chem.*, 1992, **57**, 4394.
44 G. M. Greenway, S. J. Haswell and P. Petsul, *Anal. Chim. Acta*, 1999, **387**, 1.
45 G. N. Doku and S. J. Haswell, *Anal. Chim. Acta*, 1999, **382**, 1.

46 E. Verpoorte, A. Manz, H. Lüdi, A. E. Bruno, F. Maystre, B. Krattiger, H. M. Widmer, B. H. van der Schoot and N. F. de Rooij, *Sens. Actuators*, 1992, **6**, 66.
47 Z. Liang, N. Chiem, G. Ocvirk, T. Tang, K. Fluri and D.J. Harrison, *Anal. Chem.*, 1996, **68**, 1040.
48 H. Salimi-Moosavi, Y. Jiang, L. Lester, G. McKinnon and D. J. Harrison, *Electrophoresis*, 2000, **21**, 1291.
49 J.-J. Gau, E. H. Lan, B. Dunn and C.-H. Ho, *Micro Total Analysis Systems 2000*, ed. A. van den Berg, W. Olthius and P. Bergveld, Kluwer Academic Publishers, Dordrecht, 2000, p. 509.
50 A. T. Woolley, K. Q. Lao, A. N. Glazer and R. A. Mathies, *Anal. Chem.*, 1998, **70**, 684.
51 J. S. Rossier, M. A. Roberts, R. Ferrigno and H. H. Girault, *Anal. Chem.*, 1999, **71**, 4294.
52 R. S. Martin, A. J. Gawron, S. M. Lunte and C. S. Henry, *Anal. Chem.*, 2000, **72**, 3196.
53 A. Feustel, J. Muller and V. Reilling, *Micro Total Analysis Systems '95*, ed. A. van den Berg and P. Bergveld, Kluwer Academic Press, Dorchecht, 1995, p. 299.
54 J. P. Cozen, *Appl. Spectrosc.*, 1993, **37**, 753.
55 H. J. Ache, *Chem. Ind.*, 1993, **1**, 40.
56 H. J. Ache, *Micro Total Analysis Systems '95*, ed. A. van den Berg and P. Bergveld, Kluwer Academic Press, Dorchecht, 1995, p. 47.
57 R. J. Jackman, T. M. Floyd, M. A. Schmidt and K. Jensen, *Micro Total Analysis Systems 2000*, ed. A. van den Berg, W. Olthius and P. Bergveld, Kluwer Academic Publishers, Dordrecht, 2000, p. 155.
58 I. M. Lazar, R. S. Ramsey, S. Sundberg and J. M. Ramsey, *Anal. Chem.*, 1999, **71**, 3627.
59 M. C. Mitchell, V. Spikmans, F. Bessoth, A. Manz and A. de Mello, *Micro Total Analysis Systems 2000*, ed. A. van den Berg, W. Olthius and P. Bergveld, Kluwer Academic Press, Dordrecht, 2000, p. 463.
60 I. Ugi, R. Meyr, C. Fetzer and C. Steinbrückner, *Angew. Chem.*, 1959, **71**, 386.
61 J. Li, C. Wang, J. F. Kelly, D. J. Harrison and P. Thibault, *Electrophoresis*, 2000, **21**, 198.
62 K. A. Reshni, M. D. Morris, B. N. Johnson and M. A. Burns, *Micro Total Analysis Systems '98*, ed. A. van den Berg, W. Olthius and P. Bergveld, Kluwer Academic Press, Dordrecht, 1998, p. 109.

Strong intramolecular electronic interactions in an anthraquinone bridged bis-ethenylphthalocyaninatozinc(II) triad

Andreas Gouloumis,[a] Sheng-Gao Liu,[bc] Purificación Vázquez,[a] Luis Echegoyen*[b] and Tomás Torres*[a]

[a] *Departamento de Química Orgánica (C-I), Facultad de Ciencias, Universidad Autónoma de Madrid, Cantoblanco 28049 Madrid, Spain. E-mail: tomas.torres@uam.es*
[b] *Department of Chemistry, University of Miami, Coral Gables, Florida 33124, USA. E-mail: echegoyen@miami.edu*
[c] *National Renewable Energy Laboratory, 1617 Cole Blvd., Golden, Colorado 80401, USA*

Received (in Cambridge, UK) 12th December 2000, Accepted 18th January 2001
First published as an Advance Article on the web 9th February 2001

Two metallophthalocyanines bridged by ethenyl spacers to an anthraquinone moiety have been synthesized; both spectroscopic and electrochemical experiments have demonstrated strong intramolecular electronic interactions between the phthalocyanine donors and the anthraquinone acceptor unit.

There has been a great deal of recent research on the properties of phthalocyanine (Pc)-based molecular assemblies for the construction of new molecular materials.[1] However, few systems possess sufficient structural constraints to influence the factors that control electron transfer processes between the donor and acceptor moieties. [2–4] We describe here the synthesis and electrochemical behaviour of an anthraquinone (AQ) covalently linked by ethenyl spacers with two tri-*tert*-butylphthalocyaninatozinc(II) moieties **1**† (Scheme 1), for the study of intramolecular electronic interactions between the Pc donor and AQ acceptor.

The synthesis was carried out by palladium-catalysed Heck-type coupling between tri-*tert*-butylvinylphthalocyaninatozinc(II) (**2**)[5a] and 2,6-diiodo-9,10-anthraquinone, which was in turn prepared by a double Sandmeyer reaction from commercially available 2,6-diamino-9,10-anthraquinone. The model compound, 2,6-divinyl-9,10-anthraquinone, **4**, has been prepared for comparison by a Stille coupling reaction.[6]

The UV–Vis spectrum of triad **1** in THF shows a split Q-band at 696 and 675 nm, and a Soret band at 352 nm (Fig. 1). Splitting of the Q-band in this case could be attributed to an effect of 'local asymmetry' in the molecule.[5b] Importantly, comparing the spectra with those of the model compound **2** (675, 351 nm) and tetra-*tert*-butylphthalocyaninatozinc(II) **3** (672, 348 nm)

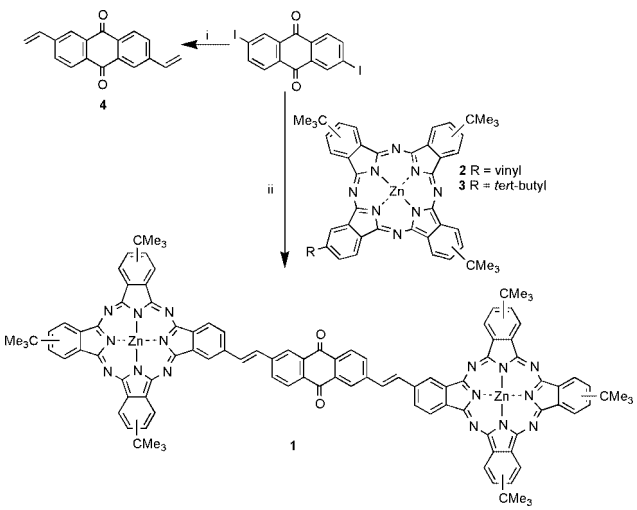

Scheme 1 Synthesis of bis(tri-*tert*-butylphthalocyanine)–anthraquinone triad **1**, and 2,6-divinylanthraquinone **4**. *Reagents and conditions*: i, tributyl(vinyl)tin, $Pd(PPh_3)_4$, toluene, 100 °C; ii, $(MeCN)_2PdCl_2$, Bu_4NBr, Et_3N, toluene, 100 °C.

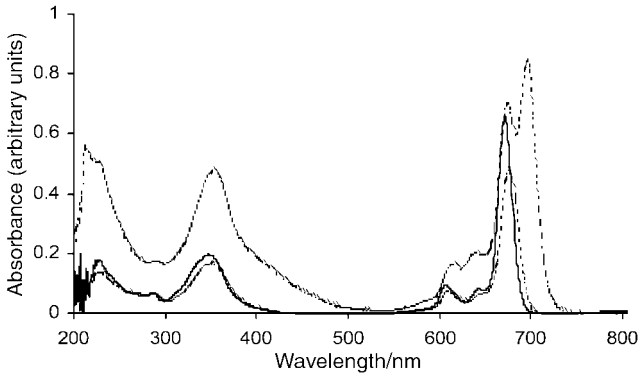

Fig. 1 Electronic spectra of **1** (dashed line), **2** (dotted line) and **3** (solid line) in THF. [C] *ca.* 1×10^{-5} mol L^{-1}.

reveals a very significant red shift of about 21 and 24 nm for the Q-bands with respect to **2** and **3**, respectively. This indicates a substantial extension of the π system in triad **1**. If this is correct, there may also be strong intramolecular electronic interactions between the electron-donating Pc moiety and the acceptor AQ unit. This is perfectly supported by the electrochemical analysis discussed below.

Solution electrochemistry of triad **1** and model compounds **2**, **3**, **4** and AQ in THF was studied by cyclic voltammetry (CV) and Osteryoung square voltammetry (OSWV). The voltammetric results are summarised in Fig. 2 and Table 1. As shown in Fig. 2, the CV of triad **1** shows that it is electrochemically active in both anodic and cathodic sweep directions between +1.2 and −3.0 V. In the anodic scan, all the redox processes are Pc-based because no oxidations can be observed for either AQ or its derivative **4** in this potential region. In the cathodic scan, triad **1** exhibits five reduction waves. Fig. 2 shows that the first wave is a chemically irreversible process when swept to −0.84

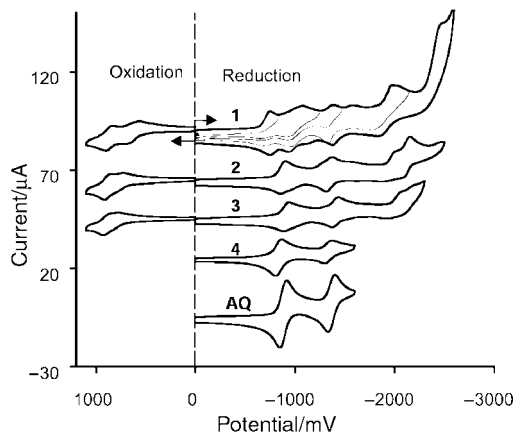

Fig. 2 CVs (0.1 V s^{-1}) for compounds **1**, **2**, **3**, **4** and AQ in THF–$TBAPF_6$ system at room temperature.

DOI: 10.1039/b009917c

Table 1 Electrochemical data (mV *vs.* Ag/AgCl) for the redox processes of compounds **1**, **2**, **3**, **4**, AQ and **2** + AQ (1 : 1) detected by OSWV in THF solution (0.1 mol dm^{-3} $TBAPF_6$) at room temperature under identical experimental conditions[a]

	E^1_{ox}[b]	E^2_{ox}[b]	E^1_{red}[b]	E^2_{red}[c]	E^3_{red}[b]	E^4_{red}[c]	E^5_{red}[b]	E^6_{red}[b]	E^7_{red}[d]
1	652	868	−764	−1076[e]	−1076[e]	−1376	−2024		−2472
2	790	876	−876		−1336		−2008		−2154
3	912[f]		−912		−1404		−2064	−2620	
4				−840		−1348			−2620
AQ				−884		−1384			
2 + AQ	612	808	−864[g]	−864[g]	−1288	−1428	−1984[h]		−1984[h]

[a] OSWVs were obtained using a sweep width of 25 mV, a frequency of 15 Hz, a step potential of 4 mV, and a quiet time of 2 s on a Windows-driven BAS 100w electrochemical analyzer (Bioanalytical Systems, West Lafayette, IN). [b] Pc-based. [c] AQ-based. [d] Pc- and vinyl-based. [e] First AQ and second Pc potentials overlapped. [f] Two-electron process. [g] First Pc and AQ potentials overlapped. [h] Third Pc and Pc-vinyl potentials overlapped.

V at 100 mV s^{-1}, and the process can be assigned to a Pc-based reduction when compared to the results observed for the models **2**, **3**, **4** and AQ. Thus, on the whole, this is a chemically irreversible Pc-based two-electron process (1e per Pc moiety). When the sweep (100 mV s^{-1}) is extended cathodically to −1.5 V, a second reduction process is observed which is chemically reversible but electrochemically irreversible (ΔE_p = 146 mV), and it can be assigned to an overlap of the first AQ-based and the second Pc-based reductions based on direct comparison, for a total of three electrons. Similarly, the next two cathodic processes are assigned to the second AQ-based one-electron process (ΔE_p = 82 mV) and to the third Pc-based electrochemically irreversible reduction, respectively. The fifth reduction process, which is chemically irreversible, can either be assigned to the Pc moiety or to the vinyl groups, but a definitive assignment based solely on comparisons with the model compounds is not possible.

Interestingly and most importantly, all of the measurements discussed above show that the redox behaviour of both the Pc and AQ moieties in triad **1** significantly changed when compared to those of the model compounds, indicating strong electronic interactions (inter- and/or intra-molecular) between the donating Pc and the acceptor AQ at ambient conditions. In the case of intermolecular interactions, a control experiment with an equimolar solution of model compounds **2** and AQ was performed. The results indicate, to some degree, the presence of intermolecular electronic interactions between the electron acceptor AQ and the electron Pc donor **2** since there are some changes in both AQ- and Pc-based redox processes (Table 1). This is not surprising because Pcs are known to self-aggregate as well as with other molecules in solution and in the solid state. Recent results published by us for the [60]fullerene–Pc dyads also showed similar intermolecular electronic interactions.[5a] Although some intermolecular effects are visible, pronounced differences between triad **1** and the mixture **2** + AQ are observed, Table 1, especially for the reduction processes. However, the differences for the reductions between the mixture and models **2** or **3** are much smaller. This means that strong intramolecular electronic interactions are present in triad **1** (compare data in Table 1).

In conclusion, the redox potentials of both Pc and AQ moieties in **1** were significantly changed when compared to the related models, showing some degree of intermolecular electronic interactions, but mainly strong intramolecular electronic interactions between the covalently bonded electron-donating Pc and the accepting AQ moieties at ambient conditions in the ground state. This results in a pronounced negative potential shift for the AQ-based reductions and significant positive potential shift for the Pc-based reductions in triad **1**. Owing to the significant extension of the conjugation as evidenced by the large red shift for the Q-bands, the Pc-based oxidations are negatively shifted.

This work was supported by CICYT, Comunidad de Madrid (Spain) and European Commission through grants MAT-99-0180, 07N/0020/98 and HPRN-CT-2000-00020, respectively. A Graduated Research Fellowship of the Ministerio de Educación y Cultura to A. G. is gratefully acknowledged. L. E. and S. G. L. would like to acknowledge support from the National Science Foundation (grant CHE-9816503) for generous financial support. S.G.L. also acknowledges Dr Brian A. Gregg at the National Renewable Energy Laboratory for partial support during the writing stages of this work.

Notes and references

† *Selected data* for **1**: ν_{max} (KBr)/cm^{-1}: 2953, 1672 (C=O), 1613, 1585, 1486, 1392, 1304, 1255, 1146, 1088, 1047, 920, 831, 747. δ_H(THF, 300 MHz): 9.6–7.6 (m, 34H, arom and vinyl), 2.1–1.8 (m, 54H, Bu^t). MALDI-TOF: *m*/*z* 1744–1753 [M^+]. Elem. Anal. for $C_{106}H_{88}N_{16}O_2Zn_2$: Calc. C, 72.81; H, 5.07; N, 12.82: Found: C, 72.27; H, 4.98; N, 12.33%. UV–Vis (THF): λ_{max}/nm (log ε) = 696 (5.18), 675 (5.10), 352 (4.94).

1 *Phthalocyanines: Properties and Applications, Vol. 1*, C. C. Leznoff and A. B. Lever, ed., VCH, Weinheim, 1989; *Phthalocyanines: Properties and Applications, Vol. 2*, C. C. Leznoff and A. B. Lever, ed., VCH, Weinheim, 1993; *Phthalocyanines: Properties and Applications, Vol. 4*, C. C. Leznoff and A. B. Lever, ed., VCH, Weinheim, 1996; M. Hanack, H. Heckman and R. Pollay, in *Methods in Organic Chemistry* (Houben-Weyl), *Vol. E 94*, E. Schauman, ed., Thieme, Stuttgart, 1998, p. 717; G. de la Torre, M. Nicolau and T. Torres, in *Phthalocyanines: Syntheses, Supramolecular Organization and Physical Properties* (*Supramolecular Photo-sensitive and Electro-active Materials*), H. S. Nalwa, ed., Wiley, Chichester, in press.

2 N. Kobayashi, T. Ohya, M. Sato and S. Nakajima, *Inorg. Chem.*, 1993, **32**, 1803; L. Li, S. Shen, Q. Yu, Q. Zhou and H. Xu, *J. Chem. Soc., Chem. Commun.*, 1991, 619.

3 H. Ali and J. E. van Lier, *Chem. Rev.*, 1999, **99**, 2379.

4 M. R. Wasielewski, *Chem. Rev.*, 1992, **92**, 435; A. Harriman, *Photochemistry*, 1999, **30**, 13.

5 (*a*) A. Gouloumis, S.-G. Liu, Á. Sastre, P. Vázquez, L. Echegoyen and T. Torres, *Chem. Eur. J.*, 2000, **6**, 3600; (*b*) E. M. Maya, P. Vázquez and T. Torres, *Chem. Eur. J.*, 1999, **5**, 2004.

6 J. K. Stille, *Angew. Chem.*, 1986, **98**, 504; J. K. Stille, *Angew. Chem., Int. Ed. Engl.*, 1986, **25**, 508.

ChemComm

Application of KIE and thia approaches in the mechanistic study of a plant stearoyl-ACP Δ^9 desaturase

Behnaz Behrouzian,[a] Peter H. Buist*[b] and John Shanklin*[a]

[a] *Brookhaven National Laboratory, Department of Biology, Upton, NY, USA, 11973*
[b] *Ottawa-Carleton Chemistry Institute, Department of Chemistry, Carleton University, 1125 Colonel By Drive, Ottawa, Ontario, Canada, K1S 5B6. E-mail: shanklin@bnl.gov*

Received (in Corvallis, OR, USA) 3rd November 2000, Accepted 8th January 2001
First published as an Advance Article on the web 9th February 2001

The mechanism of the castor stearoyl-ACP Δ^9 desaturase has been investigated; it has been shown that C–H cleavage at carbons 9 and 10 is not sensitive to deuterium substitution and oxo-trapping experiments using thia analogues revealed that sulfoxidation occurs when the substrate bears sulfur at the 9 and 10 positions.

Fatty acid desaturases[1] constitute an important family of O_2-dependent non-heme diiron-containing enzymes which catalyze the regio- and stereoselective *syn*-dehydrogenation of adjacent unactivated methylene groups. Two structurally unrelated classes[2] of these remarkable catalysts have been identified: a) a large set of membrane-bound proteins which have a probable multi-histidine diiron coordination site[3] and act on CoA- or phospholipid-linked substrates; b) soluble plant desaturases which contain a well-characterized, carboxylate-bridged, diiron cluster[4] similar to that found in methane monooxygenase and which convert the acyl carrier protein (ACP) derivative of substrates to the corresponding product (**1**, **2**, Scheme 1). A generic mechanism for desaturation involves oxidative attack† to give a very short-lived radical intermediate or its iron-bound equivalent which then collapses to give the olefinic product (Scheme 1).‡[5] Recently, a number of substrate-based mechanistic probes[6] have been developed by Buist *et al.*, using a convenient, *in vivo*, yeast Δ^9 desaturase system and some preliminary information has been obtained for the family of membrane-bound desaturases which is consistent with the model presented in Scheme 1.[6] However, very little is known regarding the mechanism of desaturation by the soluble plant desaturases[7] and the issue of whether or not the two classes of desaturases share the same mechanistic features, has yet to be addressed. The availability of homogenous preparations of a soluble plant Δ^9 desaturase from castor seed has prompted us to turn our attention to the bioorganic chemistry of this enzyme system. Here, we describe the application of our kinetic isotope effect (KIE) and 'thia' approaches[6a–c] in the mechanistic study of the soluble castor stearoyl-ACP Δ^9 desaturase.

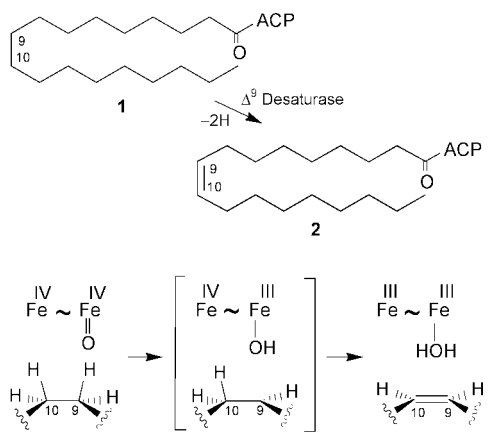

Scheme 1

Our first experiments involved an attempt to decipher the cryptoregiochemistry (site of initial oxidation) of desaturation by determining the individual primary deuterium isotope effects for each individual C–H cleavage: according to Scheme 1, the first, energetically difficult, hydrogen abstraction should be much more sensitive to isotopic substitution than the second C–H bond cleavage. The required regiospecifically deuterium labelled substrates **3b**,**c** along with the non-labelled parent **3a** were available from previous studies.§[6b] 1 : 1 Mixtures of **3b** : **3a** and **3c** : **3a** as their ACP thioesters (14 nmol) were incubated separately with freshly prepared desaturase (0.02 nmol) and required cofactors[7,8] (total volume of 250 μL) under conditions adjusted to allow *ca*. 15% conversion of substrate.[9] The reactions were quenched *via* addition of THF and after reductive workup ($NaBH_4$), extraction with hexane and derivatization with trimethylchlorosilane (TMCS), the product mixtures **6b** : **6a** and **6c** : **6a** were analyzed by GC-MS (60 m SP-23 capillary column, MS scan rate: 2.14 scans s^{-1}). The competitive primary deuterium KIE was computed by comparing the isotopic content of substrates and products[6b,c] and found to be $k_H/k_D = 1.03 \pm 0.02$ at C-9 and $k_H/k_D = 0.95 \pm 0.02$ at C-10

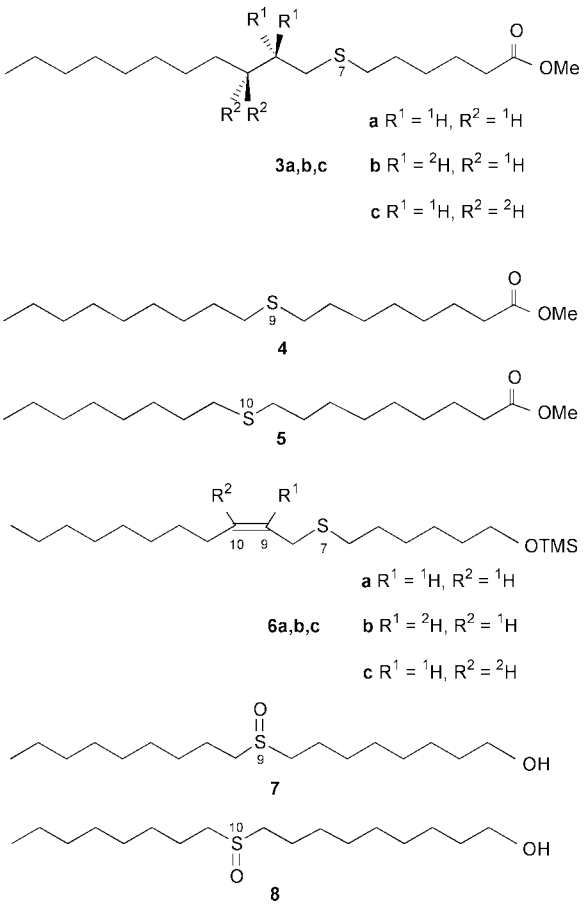

DOI: 10.1039/b008972i

(average of two incubations). Similar results were obtained when the incubations of **3a**–**c** were run[7,8] in the noncompetitive mode: k_H/k_D = 1.10 ± 0.10 at C-9 and k_H/k_D = 1.13 ± 0.18 at C-10 (average of two incubations). These findings are in marked contrast with those reported for all membrane-bound desaturases studied to date.[6b,c,10] These include bacterial Δ^5, protozoan Δ^6, yeast, algal and bacterial Δ^9, insect Δ^9 and Δ^{11}, plant and algal Δ^{12} and animal and plant ω-3. All of these systems show a similar pattern of isotope effects (one large (k_H/k_D = 4–7), one negligible (k_H/k_D ~ 1)), clearly indicating the stepwise nature of the reaction for this class of desaturase and the kinetic importance of the initial C–H activation step. The absence of a measurable KIE for both C–H cleavages in the case of the soluble stearoyl-ACP Δ^9 desaturase is almost certainly due to the fact that these steps are masked by other enzymatic events such as electron transfer, substrate binding, product release, *etc*.[11] Thus it is clear that the substantial differences in protein structure, enzyme location, and substrate head group for the two classes of desaturases result in very different overall kinetic mechanisms.

We then turned to our 'thia' approach which probes the relative distance between the putative iron oxidant and substrate methylene groups by comparing the efficiency of oxo transfer to 9- and 10-thia analogues. In a preliminary set of experiments, the required pair of thiastearates **4** and **5** along with **3a** as control were incubated separately as their ACP thioesters with soluble stearoyl-ACP Δ^9 desaturase under conditions similar to those used for KIE experiments but adjusted for higher conversion (0.04 nmole enzyme, 10 min incubation). Products of these incubations were isolated and analyzed by GC-MS as the TMS derivatives. Under these conditions, the thia substrate bearing sulfur at the 7-position **3a** was cleanly converted to the corresponding *cis*-olefinic product **6a**; only traces of unreacted starting material were observed for incubations using **4**- and **5**-ACP.

To probe for products of oxo transfer, a second set of incubations was carried out using the ACP-derivative of each thiastearate (**3a**, **4**, **5**, 60 nmol) along with enzyme (4 nmol) and required cofactors[7,8] (in a total volume of 1.5 ml for 30 min). The CH_2Cl_2 extracts of reduced ($NaBH_4$) reaction mixtures were examined by silica gel TLC (90% EtOAc–hexane, H_2O spray detection, detection limit = 1–2 nmole). A search for the anticipated sulfoxide product alcohols was conducted with the use of authentic standards.¶ Significantly, only in the case of 9- and 10-thia substrates (**4**-, **5**-ACP), were the corresponding sulfoxides (**7**, **8**) detected (R_f = 0.20 and 0.16, respectively). Sulfoxidation of **4**- and **5**-ACP was not observed in the absence of enzyme or enzyme lacking a supply of NADPH. No sulfones were detectable. The structural assignments of the sulfoxide products were confirmed by electrospray MS analysis of material isolated from the TLC by CH_2Cl_2 extraction.‖ This constitutes the first report of an *in vitro* desaturase-mediated sulfoxidation and substantiates earlier reports of similar results for an *in vivo* yeast Δ^9 desaturase system.[12] However, it is interesting to note that in the latter case, sulfoxidation of a series of 9-thia-analogues was always more efficient (2–3-fold) than the production of the corresponding 10-sulfoxides,[6a,13] which led to the conclusion that the site of initial oxidation was at C-9 in good agreement with the observance of a large KIE effect at C-9 but not at C-10 (see above).[6b] In contrast, it appears that for the soluble Δ^9 desaturase, the trend is the reverse: we consistently see a greater amount of sulfoxide (7–12-fold)†† from the 10-thia substrate (**5**-ACP) than from the corresponding 9-isomer under conditions of partial and complete substrate consumption. This clearly implies that the 9-thia substrate is being converted to additional products possibly arising from oxidative attack α to the sulfur; experiments designed to address this issue are currently in progress. In addition, the determination of the absolute configuration of the sulfoxide products presents an impressive challenge to the methodology we have developed previously.[6a]

In summary, we have demonstrated fundamental differences in the behaviour of the two major classes of desaturase enzymes and have taken our first steps towards defining the crypto-regiochemistry of a structurally well-defined plant stearoyl-ACP Δ^9 desaturase. It is hoped that these efforts will complement ongoing active-site X-ray crystallographic work[4a] and other mechanistic studies[7] on this fascinating catalytic system.

This work was supported by an NSERC PDF (B. B.), an NSERC operating grant (P. H. B.) and the Office of Basic Energy Research of the U.S. Department of Energy (J. S.). The technical assistance of Dr. Clem Kazakoff (University of Ottawa), and Dr. Simin Maleknia (Albert Einstein College of Medicine) in obtaining the electrospray MS is gratefully appreciated.

Notes and references

† We have chosen to use a generic iron oxo representation of the active oxidant although other structures are possible. For an in depth analysis of the inorganic chemistry involved in diiron-mediated oxidations, see Ref. 4*c*.

‡ The intermediate could collapse rapidly to give alkene *via* a one electron oxidation–deprotonation sequence, simple disproportionation or Lewis acid (Fe^{3+})-catalyzed dehydration of a hydroxy intermediate. Newcomb *et al.*, have recently raised the possibility that these sorts of C–H activations may proceed, in part, *via* cationic intermediates produced by insertion of OH^+ into the unactivated C–H bond as the first step, followed by rapid loss of water from a protonated alcohol intermediate.[5a,b]

§ A trial incubation using **3a**-ACP revealed that this material was an excellent substrate and the structure of the 7-thia alkene **6a** was confirmed by comparison with an authentic standard on the basis of MS and GC retention time. The presence of the thia-substituent does not affect the regiochemistry of desaturation.[6b,c,10] The standard was prepared by LAH reduction of the carbomethoxy group of the methyl 7-thiaoleate available from previous experiments[12] followed by derivatization *via* TMCS.

¶ Authentic standards were prepared from available synthetic methyl thiastearates[12] by LAH reduction of the terminal methyl ester group followed by sulfoxidation using *m*-chloroperbenzoic acid.

‖ **7**: *m*/*z* 305 ($M + H^+$), 287 [$(M - H_2O) + H^+$], 269 [$(M - 2H_2O) + H^+$], 177 [$(M - HOCH_2(CH_2)_5CH{=}CH_2) + H^+$], 161 [$((M - H_2O) - CH_3(CH_2)_6CH{=}CH_2) + H^+$], 111 ($C_8H_{14} + H^+$); **8**: *m*/*z* 305 ($M + H^+$), 287 [$(M - H_2O) + H^+$], 269 [$(M - 2H_2O) + H^+$], 175 [$((M - H_2O) - CH_3(CH_2)_5CH{=}CH_2) + H^+$], 163 [$(M - HOCH_2(CH_2)_6CH{=}CH_2) + H^+$], 125 ($C_9H_{16} + H^+$).

†† The amount of sulfoxide products was estimated using known amounts of authentic standards on the same TLC plate.

1 H. Cook, in *Biochemistry of Lipids and Membranes*, D. E. Vance and J. E. Vance, eds, The Benjamin Cumming Publishing Co. Ltd., Menlo Park, CA, 1985, p. 191.
2 (*a*) J. Shanklin and E. B. Cahoon, *Annu. Rev. Plant. Physiol. Plant. Mol. Biol.*, 1998, **49**, 611; (*b*) J. Shanklin and C. Somerville, *Proc. Natl. Acad. Sci. U.S.A.*, 1991, **88**, 2510.
3 J. Shanklin, E. Whittle and B. G. Fox, *Biochemistry*, 1994, **33**, 12787.
4 (*a*) Y. Lindqvist, W. Huang, G. Schneider and J. Shanklin, *EMBO J.*, 1996, **15**, 4081 and unpublished data; (*b*) B. G. Fox, J. Shanklin, C. Somerville and E. Münck, *Proc. Natl. Acad. Sci. U.S.A.*, 1993, **90**, 2486; (*c*) J. A. Broadwater, B. G. Fox and J. A. Haas, *Fett/Lipid*, 1998, **100**, 103.
5 (*a*) M. Newcomb and P. H. Toy, *Acc. Chem. Res.*, 2000, **33**, 449; (*b*) S. Choi, P. E. Eaton, D. A. Kopp, S. J. Lippard, M. Newcomb and R. Shen, *J. Am. Chem. Soc.*, 1999, **121**, 12198.
6 (*a*) P. H. Buist and D. M. Marecak, *J. Am. Chem. Soc.*, 1992, **114**, 5073; (*b*) P. H. Buist and B. Behrouzian, *J. Am. Chem. Soc.*, 1996, **118**, 6295; (*c*) P. H. Buist and B. Behrouzian, *J. Am. Chem. Soc.*, 1998, **120**, 871; (*d*) P. H. Buist, B. Behrouzian, K. Alexopoulos, B. Dawson and B. Black, *Chem. Commun.*, 1996, 2671.
7 J. A. Broadwater, B. J. Laundre and B. G. Fox, *J. Inorg. Biochem.*, 2000, **78**, 7.
8 J. A. Haas and B. G. Fox, *Biochemistry*, 1999, **38**, 12833.
9 L. Melander and W. H. Saunders, in *Reaction Rates of Isotopic Molecules*, R. E. Krieger Publishing, Florida, 1987, p. 91.
10 (*a*) G. J. Schroepfer and K. Bloch, *J. Biol. Chem.*, 1965, **240**, 54; (*b*) A. Pinilla, F. Camps and G. Fabrias, *Biochemistry*, 1999, **38**, 15272; (*c*) J. E. Baenziger, I. C. P. Smith and R. J. Hill, *Chem. Phys. Lipids*, 1990, **54**, 17; (*d*) D. Meesapyodsuk, D. W. Reed, C. Savile, P. H. Buist and P. Covello, *Biochemistry*, in press; (*e*) L. Fauconnot and P. H. Buist, unpublished data.
11 D. Northrup, *Biochemistry*, 1975, **14**, 2644.
12 P. H. Buist, H. G. Dallmann, R. R. Rymerson, P. M. Seigel and P. Skala, *Tetrahedron Lett.*, 1987, **28**, 857.
13 P. H. Buist and D. M. Marecak, *Can. J. Chem.*, 1994, **72**, 176.

A novel oxime to pentathiepin cascade reaction

Sonia Macho,[a] Charles W. Rees,*[b] Teresa Rodríguez[a] and Tomás Torroba[a]

[a] *Departamento de Química, Facultad de Ciencias, Universidad de Burgos, 09001 Burgos, Spain*
[b] *Department of Chemistry, Imperial College of Science, Technology and Medicine, London, UK SW7 2AY. E-mail: c.rees@ic.ac.uk*

Received (in Liverpool, UK) 9th January 2001, Accepted 16th January 2001
First published as an Advance Article on the web 9th February 2001

An extensive domino sequence, including a vinylogous sulfur-assisted Beckmann fragmentation, is involved in the one-pot conversion of a dioxime 3 by S_2Cl_2 into a cyanoethyl-1,2,3-dithiazole 5 and a novel tricyclic pentathiepin 6; the yield of 6 is increased by added lithium sulfide, and both 5 and 6 are formed in higher yield from 2-(cyanoethyl)cyclopentanone oxime 7; reaction mechanisms are proposed for these cascade reactions.

Benzopentathiepins have attracted much attention recently because of their remarkable stability, the very high barrier (up to *ca*. 30 kcal mol^{-1}) for inversion of the chair-like heterocyclic ring[1] and their potent biological activity. The first naturally occurring examples varacin **1a**[1] and lissoclinotoxin A **1b**,[1,2] and

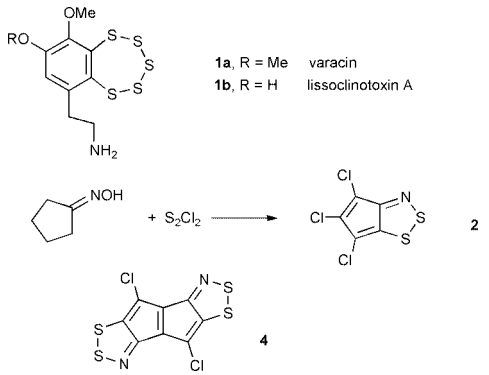

related dopamine-like structures, have strong antimicrobial and antifungal activity, selectively inhibit protein kinase C,[3] and varacin is highly toxic towards human colon cancer HCT 116.[1] Furthermore 7-methylbenzopentathiepin, lacking the aminoethyl group, is a potent thiol-dependent DNA cleaving agent.[4] The pentasulfur ring appears to be essential for biological activity. However, with the notable exceptions of Chenard's isothiazolo and pyrazolo pentathiepins[5] and Sato's trithiolobenzopentathiepins,[6] very little is known about heterocyclic fused pentathiepins. We now describe an unusual and unexpected one-pot synthesis of a new polyheteroatom pentathiepin **6**.

The reaction of simple saturated ketoximes with disulfur dichloride, S_2Cl_2, in the presence of tertiary amines provides an effective one-pot route to 1,2,3-dithiazoles; the initial cyclocondensation is followed by extensive dehydrogenation and chlorination to yield fully unsaturated heteroaromatic products.[7] A typical example is the conversion of cyclopentanone oxime into the deep violet 10 π pseudoazulene **2**.[8]

In an extension of this work we treated the dioxime **3** of tricyclo[3.3.0]octan-2,6-dione[9] (Scheme 1) with S_2Cl_2 and Et_3N hoping to produce the tetracyclic 18 π bis-dithiazole **4**, but instead we isolated two mono-dithiazoles **5** and **6**.

Better yields of products were obtained from silylated oximes, so we first treated dioxime **3** with TMSCl and Et_3N in boiling THF for 1 h. Then the mixture was cooled (−20 °C) and Et_3N (20 equiv.) and S_2Cl_2 (20 equiv.) were added and the mixture stirred for 3 d at 4 °C. Chromatography gave a purple product **5**, $C_8H_4Cl_2N_2S_2$ (19%) and, in some reactions, a very minor mauve product **6**, $C_8H_4N_2S_7$ (1–3%). The purple product was similar to cyclopentadithiazole **2** but had a nitrile and two methylene groups in addition to the five sp^2 carbons. Based on this, and mechanistic considerations, structure **5** was assigned to this compound. One cyclopenta-1,2,3-dithiazole has been formed but the second carbocyclic ring has been opened, together with dehydrogenation and chlorination, as before.[7]

The mauve product with five extra sulfur atoms in place of the two chlorines in **5** also showed a cyanoethyl group, but now one of the methylenes gave a complex signal in the ^{1}H NMR compounded of two quintets; each quintet was the sum of two overlapping triplets, suggesting the presence of conformational isomers. This information supported the (chiral[10]) structure **6** with a slowly inverting chair-like pentathiepin ring fused to a cyclopentadithiazole, a new ring system.

The pentathiepin ring in **6** is presumably formed by substitution of the chlorines in **5** by some nucleophilic sulfur species. The 7-membered ring could then be completed by S_2Cl_2 in a reaction related to the known formation of benzopentathiepins,[2,5,11] the thermodynamically favoured products. To test this possibility we ran the reaction of dioxime **3** with S_2Cl_2 as before but after 3 days we added Li_2S (20 equiv.), stirred the mixture for 6 h at 4 °C, then added more S_2Cl_2 (20 equiv.) at −20 °C and stirred for 20 min. Chromatography gave a higher yield (17%) of **6** as the only isolable product.

We then synthesized the dithiazoles **5** and **6** in a more rational way from preformed 2-(2-cyanoethyl)cyclopentanone oxime **7**[12] to confirm their structures and improve their yields. Firstly, oxime **7** was treated with S_2Cl_2 (10 equiv.) and Hünig's base (10 equiv.) in THF for 3 d at 4 °C to give **5** (47%) and **6** (3%). Secondly, oxime **7** was treated with S_2Cl_2 (10 equiv.) and Hünig's base (10 equiv.) in THF for 3 d at 4 °C, then with Li_2S (20 equiv.) in THF for 8 h at 4 °C and then with S_2Cl_2 (10 equiv. for 18 h at 4 °C and then another 10 equiv. at RT) all in one pot to give the pentathiepin **6** (30%) as the only product. The same product was obtained in similar yield (28%) when the final aliquot of S_2Cl_2 (20 equiv.) was added in one portion and stirred for 12 min at RT.

Surprisingly, exposure of the reaction mixture to the final portion of S_2Cl_2 (20 equiv.) for longer periods resulted in the

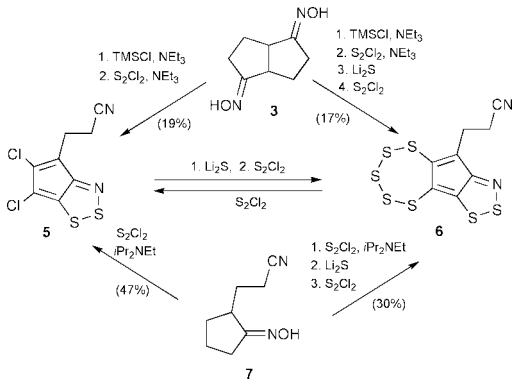

Scheme 1

DOI: 10.1039/b100366f

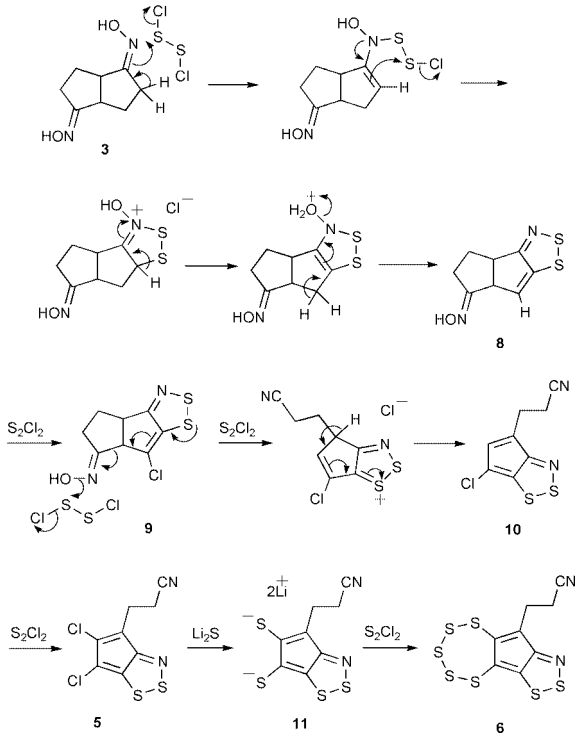

Scheme 2

formation of **5** as well as **6** and, after 1 d at 4 °C, **5** (25%) was the only product isolated. Separate experiments showed that **5** is converted into **6** by excess of sulfide anion followed by S_2Cl_2, and that **6** reverts to **5** when treated with excess of S_2Cl_2 for longer periods. These results, summarised in Scheme 1, support the structures of **5** and **6** and a pathway for the formation of **6** from **3** and from **7**.

A plausible mechanism, starting for simplicity from the free oximes, is shown in Scheme 2. Electrophilic attack by S_2Cl_2 at one oxime (or silylated oxime) group in **3** is followed by cyclisation and dehydration to give the 1,2,3-dithiazole **8**. Both sulfur atoms of **8** would activate it to chorination to give **9** in which the chlorine atom disfavours the *Z* configuration of the oxime necessary for formation of the second dithiazole ring, and the steric repulsion would be greater for the TMS derivative. Thus Beckmann fragmentation (arrows in **9**),[13] catalysed by S_2Cl_2 or by liberated acid, can supervene to give the cyanoethyl intermediate **10**. This ring fission, which is activated by both dithiazole sulfur atoms, is a vinylogous version of the long-known sulfur assisted fragmentation of oximes of β-keto-sulfides.[14] Further chlorination of **10** gives the cyclopenta-1,2,3-dithiazole **5** isolated. Nucleophilic sulfur species produced in, or added to, the reaction mixture could afford the dithiolate **11** and hence, with two equiv. of S_2Cl_2, the pentathiepin **6**, by a mechanism similar to that proposed by Toste and Still.[11]

These one-pot syntheses of the fused pentathiepin **6** from the mono-oxime **7** or the dioxime **3** provide a new and easy route to compounds related to the naturally occurring pentathiepins that are of considerable pharmaceutical and agrochemical potential.

We gratefully acknowledge financial support from the *Dirección General de Enseñanza Superior* of Spain (DGDES Project ref. PB96-0101), *Junta de Castilla y León, Consejería de Educación y Cultura* (Project ref. BU07/00B), MDL Information Systems (UK) Ltd and the Wolfson Foundation for establishing the Wolfson Centre for Organic Chemistry in Medical Science at Imperial College.

Notes and references

1 P. A. Searle and T. F. Molinski, *J. Org. Chem.*, 1994, **59**, 6600 and references therein.
2 B. S. Davidson, T. F. Molinski, L. R. Barrows and C. M. Ireland, *J. Am. Chem. Soc.*, 1991, **113**, 4709; P. W. Ford, M. R. Narbut, J. Belli and B. S. Davidson, *J. Org. Chem.*, 1994, **59**, 5955.
3 R. S. Compagnone, D. J. Faulkner, B. K. Carté, G. Chan, A. Freyer, M. E. Hemling, G. A. Hofmann and M. R. Mattern, *Tetrahedron*, 1994, **50**, 12 785.
4 T. Chatterji and K. S. Gates, *Biorg. Med. Chem. Lett.*, 1998, **8**, 535.
5 B. L. Chenard and T. J. Miller, *J. Org. Chem.*, 1984, **49**, 1221; B. L. Chenard, R. L. Harlow, A. L. Johnson and S. A. Vladuchick, *J. Am. Chem. Soc.*, 1985, **107**, 3871; B. L. Chenard, D. A. Dixon, R. L. Harlow, D. C. Roe and T. Fukunaga, *J. Org. Chem.*, 1987, **52**, 2411.
6 R. Sato, T. Kimura, T. Goto and M. Saito, *Tetrahedron Lett.*, 1988, **29**, 6291; R. Sato, T. Kimura, T. Goto, M. Saito and C. Kabuto, *Tetrahedron Lett.*, 1989, **30**, 3453; T. Kimura, M. Hanzawa, E. Horn, Y. Kawai, S. Ogawa and R. Sato, *Tetrahedron Lett.*, 1997, **38**, 1607 and references therein.
7 M. J. Plater, C. W. Rees, D. G. Roe and T. Torroba, *Chem. Commun.*, 1996, 427; O. A. Rakitin, C. W. Rees, D. J. Williams and T. Torroba, *J. Org. Chem.*, 1996, **61**, 9178.
8 M. J. Plater, C. W. Rees, D. G. Roe and T. Torroba, *J. Chem. Soc., Perkin Trans. 1*, 1993, 769.
9 A. A. Hagedorn and D. G. Farnum, *J. Org. Chem.*, 1977, **42**, 3763; J. Pérard-Viret and A. Rassat, *Tetrahedron Asymmetry*, 1994, **5**, 1.
10 For the first isolation of both invertomers of an unsymmetrical benzopentathiepin, see K. Kimura, Y. Kawai, S. Ogawa and R. Sato, *Chem. Lett.*, 1999, 1305.
11 V. Behar and S. J. Danishefsky, *J. Am. Chem. Soc.*, 1993, **115**, 7017; F. D. Toste and I. W. J. Still, *J. Am. Chem. Soc.*, 1995, **117**, 7261.
12 R. J. Vijn, H. J. Arts, P. J. Maas and A. M. Castelijns, *J. Org. Chem.*, 1993, **58**, 887.
13 C. A. Grob, H. P. Fischer, W. Raudenbusch and J. Zergenyi, *Helv. Chim. Acta*, 1964, **47**, 1003.
14 R. L.Autrey and P. W. Scullard, *J. Am. Chem. Soc.*, 1968, **90**, 4924; R. K. Hill and D. A. Cullison, *J. Am. Chem. Soc.*, 1973, **95**, 2923; P. A. Grieco and K. Hiroi, *Tetrahedron Lett.*, 1973, 1831; K. Hiroi, M. Otsuka and S. Sato, *Chem. Lett.*, 1985, 1907.

Palladium(II)-promoted aziridination of olefins with bromamine T as the nitrogen transfer reagent

Alexandra M. M. Antunes, Susana J. L. Marto, Paula S. Branco,* Sundaresan Prabhakar* and Ana M. Lobo

Departamento de Química, Faculdade de Ciências e Tecnologia, Universidade Nova de Lisboa, Centro de Química Fina e Biotecnologia, 2825-114 Monte de Caparica, Portugal

Received (in Liverpool, UK) 23rd October 2000, Accepted 17th January 2001
First published as an Advance Article on the web 9th February 2001

The palladium(II)-promoted reaction of a variety of olefins and bromamine T, as the nitrogen atom transfer reagent, provided *N*-tosyl-2-substituted aziridines under mild conditions.

Aziridines have been shown to be valuable starting materials, for the synthesis of useful nitrogen containing compounds, due to the highly regio- and stereoselective ring opening reactions that they undergo.[1,2]

Recently two copper-catalysed aziridination methods for olefins have been reported. Whilst the first,[3] which involved the use of PhI=NTs, is of wide applicability, the second method that utilised chloramine T[4] or bromamine T,[5] as the nitrogen transfer agent, is limited to non-deactivated olefins. The aziridination procedure of Bäckvall[6] [olefins, Pd(II) and primary aliphatic amines] also suffers from a similar disadvantage.

We report herein our preliminary results, collected in Table 1, of a novel $PdCl_2$-assisted aziridination[7]† of olefins **1**, both simple and electron-deficient, by bromamine T.

An examination of the Table shows that all olefins examined participate with varying degrees of efficiency. The electron deficient olefins in general react to give better yields of aziridines than the simple alkenes. Amongst the former class of compounds, *N*,*N*-dimethylacrylamide (**1b**) (entry 2) afforded the highest yield (81%) and phenylvinylsulfoxide (**1g**) (entry 7) the lowest (20%). Whilst methyl acrylate (**1a**) (entry 1) afforded the synthetically useful aziridine **2a**[8] in acceptable yield (60%), as the only isolable product, acrylonitrile (entry 4) however provided a mixture of bromosulfonamide **3d** and the aziridine **2d**[9] in almost equal amounts‡ (*ca.* 20%). A methyl substituent in the β-position **1c** (entry 3) completely inhibited the reaction possibly due to steric reasons. In contrast to styrene (**1i**) (entry 9) and cyclohexene (**1h**) (entry 8), which provided negligible yields of the corresponding heterocycles, allyl alcohol (**1j**) (entry 10), containing an additional metal coordinating centre (OH), afforded the expected product[10] in modest yield (40%). Although the exact nature of the palladium reagent involved in the reaction is not known, a possible mechanism is outlined in Scheme 1 for the substrate *N*,*N*-dimethylacrylamide. Thus, the initially formed π-complex **4** leads, on nucleophilic attack by TsNBrNa,[11] to the σ-alkylpalladium species **5**. Subsequent intramolecular oxidative addition would furnish the 4-member palladocycle Pd(IV) **6**, which collapses to the aziridine **2b**,[12] regenerating the Pd(II) salt. Organopalladium(IV) complexes are known[13] and have been occasionally invoked as intermediates in reactions of Pd(II) species with electrophiles.[14]

Table 1 Aziridination of olefins with bromamine T promoted by Pd(II) compounds

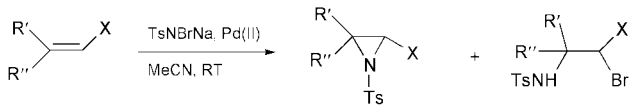

Entry	R″	R′	X	1	Reaction conditions[a]	Yield[b] of **2** (%)	Yield[b] of **3** (%)
1	H	H	COOMe	**a**	*A*	60	—
2	H	H	$CONMe_2$	**b**	*B*	81	12
3	Me	H	$CONMe_2$	**c**	*B*	—	—
4	H	H	CN	**d**	*A*	22	19
5	H	H	COMe	**e**	*C*	44	7
6	H	$CO(CH_2)_3$		**f**	*D*	33	—
7	H	H	SOPh	**g**	*D*	20	7
8	H	$(CH_2)_4$		**h**	*B*	2.5	—
9	H	H	Ph	**i**	*B*	—	—
10	H	H	CH_2OH	**j**	*B*	40	—

[a] *Method A*—Olefin (3 eq., 0.55 mmol), TsNBrNa (1.2 eq., 0.22 mmol), $Pd(MeCN)_2Cl_2$ (0.5 eq., 0.09 mmol); *Method B*—Olefin (1.2 eq., 0.22 mmol), TsNBrNa (1.5 eq., 0.27 mmol), $PdCl_2$ (0.2 eq., 0.04 mmol); *Method C*—Olefin (3 eq., 0.55 mmol), TsNBrNa (1.2 eq., 0.22 mmol), $PdCl_2$ (0.5 eq., 0.09 mmol); *Method D*—Olefin (3 eq., 0.55 mmol), TsNBrNa (1 eq., 0.18 mmol), $Pd(MeCN)_2Cl_2$ (0.5 eq., 0.09 mmol). [b]Isolated yield.

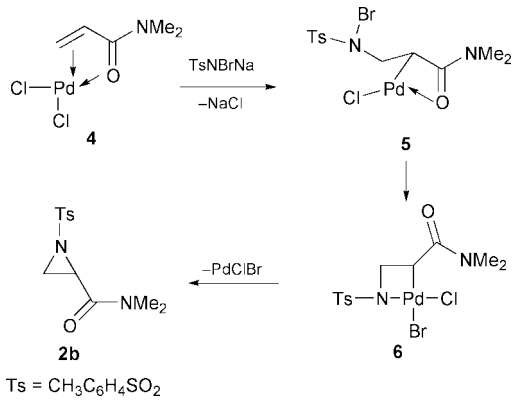

Scheme 1

In conclusion a mild one-pot procedure for the preparation of *N*-tosyl-2-substituted aziridines§ is reported. Further experiments to define the palladium species involved in the process and the stereochemical aspects of the reaction are in progress.

We thank Fundação para a Ciência e a Tecnologia (Lisbon, Portugal), PRAXIS program, for partial financial support and Dr S. N. Swami (Pfizer, UK) for the interest shown. Two of us (A. M. M. Antunes and S. J. L. Marto) also thank PRAXIS program for the award of research fellowships.

Notes and references

† No significant aziridination occurred in the absence of $PdCl_2$.

‡ It is likely that the bromosulfonamides are formed from the initially produced aziridines undergoing nucleophilic ring opening with bromide ion. A blank experiment performed with pure **2d** and NaBr in CH_3CN did indeed afford **3d** in excellent yield. Compound **3d** in CH_3CN on treatment with NaH furnished **2d** in 64% yield.

§ All spectral data were in accord with the structures assigned. *Selected data for* **2f**: δ_H (400 MHz, $CDCl_3$) 7.81 (2H, d, *J* 8.2, ArH_{2+6}), 7.35 (2H, d, *J* 8.2, ArH_{3+5}), 3.46 (1H, d, *J* 6.5, H_2), 3.15 (1H, d, *J* 6.5, H_3), 2.45 (3H, s, ArCH_3), 2.20–2.16 (1H, m), 2.07–1.99 (1H, m), 1.94–1.84 (2H, m), 1.70–1.54 (2H, m); δ_C (100 MHz, $CDCl_3$) 200.8 (CO), 144.9 (ArC_4), 135.2 (ArC_1), 129.9 (ArC_{3+5}), 128.0 (ArC_{2+6}), 44.12 (C_2), 41.23 (C_3), 37.0 (C_6), 22.0 (C_4), 21.5 ($ArCH_3$), 17.61 (C_5); HR-EIMS calcd for $C_{13}H_{15}NO_3S$ (M^+) 265.076715,

found 265.07666. *Selected data for* **2g**: δ_H (400 MHz, $CDCl_3$) 7.75 (2H, d, *J* 8.0 Hz, ArH_{2+6}), 7.60–7.47 (5H, m, Ar*H*), 7.31 (2H, d, *J* 8.0 Hz, ArH_{3+5}), 3.82 (1H, dd, *J* 6.0, 3.7 Hz, H_2), 2.91 (1H, d, *J* 3.8 Hz, H_3), 2.79 (1H, d, *J* 6.4 Hz, H_3), 2.46 (3H, s, ArCH_3); δ_C (100 MHz, $CDCl_3$) 145.1 (ArC_4), 140.0 (ArC_1), 131.6 (ArC), 129.7 (ArC_{3+5}), 129.3 (ArC), 128.1 (ArC_{2+6}), 124.4 (ArC), 55.3 (C_2), 28.4 (C_3), 21.3 ($ArCH_3$); HR-EIMS calcd for $C_{14}H_{15}NS_2O_3$ (MH^+) 322.056610, found 322.05693.

1 D. Tanner, *Angew. Chem., Int. Ed. Engl.*, 1994, **33**, 599.
2 T. Ibuka, *Chem. Soc. Rev.*, 1998, **27**, 145.
3 D. A. Evans, M. M. Faul and M. T. Bilodeau, *J. Am. Chem. Soc.*, 1994, **116**, 2742.
4 T. Ando, S. Minakata, I. Ryu and M. Komatsu, *Tetrahedron Lett.*, 1998, **39**, 309. For the aziridination of simple olefins with chloramine T in the presence of Br_2 or I_2, see J. U. Jeong, B. Tao, I. Sagasser, H. Henniges and K. B. Sharpless, *J. Am. Chem. Soc.*, 1998, **120**, 6844 and T. Ando, D. Kano, S. Minakata, I. Ryu and M. Komatsu, *Tetrahedron*, 1998, **54**, 13 485, respectively.
5 R. Vyas, B. M. Chanda and A. V. Bedekar, *Tetrahedron Lett.*, 1998, **39**, 4715.
6 J. E. Bäckvall, *Chem. Commun.*, 1977, 413.
7 The reaction was performed by adding the indicated quantity of TsNBrNa in portions, over a period of time, to a solution of $PdCl_2$ and olefin in dry acetonitrile (3 ml) at rt. Each addition was performed only after a negative test (starch–iodide paper) for bromamine T was observed. Following the evaporation of the solvent, the residue obtained was dissolved in methylene chloride, washed with aqueous sodium metabisulfite solution (15%) and then water. The products were isolated by preparative TLC.
8 J. E. Baldwin, A. C. Spivey, C. J. Schofield and J. B. Sweeney, *Tetrahedron*, 1993, **49**, 6309.
9 C. S. Pak, T. H. Kim and S. J. Ha, *J. Org. Chem.*, 1998, **63**, 10 006.
10 N. Fujii, K. Nakai, H. Habashita, Y. Hotta, H. Tamamura, A. Otaka and T. Ibuka, *Chem. Pharm. Bull.*, 1994, **42**, 2241.
11 The nucleophilicity of TsNBrNa is reported to be comparable to that of azide ion: F. E. Hardy, *J. Chem. Soc. B*, 1971, 1899.
12 G. A. Molander and P. J. Stengel, *Tetrahedron*, 1997, **53**, 8887.
13 R. Uson, J. Fornies and R. Navarro, *J. Organomet. Chem.*, 1975, **96**, 307.
14 W. D. Graaf, J. Boersma and G. V. Koten, *Organometallics*, 1990, **9**, 1479; J. E. Bäckvall, *Tetrahedron Lett.*, 1975, 2225; J. E. Bäckvall, *Tetrahedron Lett.*, 1978, 163.

ChemComm

Reductive electrolysis of [60]fullerene mono-methanoadducts in THF leads to the formation of bis-adducts in high yields

Marcel W. J. Beulen,[a] José A. Rivera,[b] M. Ángeles Herranz,[c] Ángel Martín-Domenech[c] Nazario Martín*[c] and Luis Echegoyen*[a]

[a] *Department of Chemistry and Center for Supramolecular Science, University of Miami, Coral Gables, Florida 33124, USA. E-mail: echegoyen@miami.edu*
[b] *Department of Chemistry, Pontifical Catholic University of Puerto Rico, Ponce, Puerto Rico 00731, USA*
[c] *Departamento de Química Orgánica, Facultad de Ciencias Químicas, Universidad Complutense, E-28040-Madrid, Spain*

Received (in Columbia, MO, USA) 30th October 2000, Accepted 19th January 2001
First published as an Advance Article on the web 9th February 2001

A new reaction, electrolytically induced adduct transfer between [60]fullerene mono-adducts, leads to bis-adducts with a unique regioisomer distribution.

Cyclopropanation of fullerenes by the addition of malonate derivatives (the Bingel reaction) has been widely used for the preparation of fullerene adducts.[1] The groups of Diederich and Echegoyen reported the reverse of this reaction, the retro-Bingel reaction, an electrolytic reduction reaction performed in dichloromethane, which efficiently removes di[alkoxycarbonyl]methano (Bingel) adducts to yield the parent fullerene (see Scheme 1).[2] The 'Bingel–retro-Bingel' strategy as a protection–deprotection scheme has already found several uses in fullerene chemistry, such as the isolation of enantiomerically pure C_{76}[2a] and of a new C_{2v}-C_{78} bis-adduct,[2b] and in the separation of constitutional isomers of C_{84}.[2c] The groups of Diederich and Echegoyen also described a chemical retro-Bingel reaction (using Mg/Hg, THF, heat) which also efficiently removes the Bingel addends.[3]

Very recently we reported that the range of fullerene adducts that can be removed *via* electrolytic reduction is not limited to di[alkoxycarbonyl]methano adducts (see fullerene **3**), but includes those present in structures **1** and **2** (Scheme 1). Controlled potential electrolysis (CPE) in dichloromethane after the first (**2**) and third (**1**) electrochemical reduction wave induces the efficient removal of the adducts, to form the parent C_{60}.[4]

While electrolytic reduction can lead to the efficient removal of the adducts mentioned, it has been shown that methano-adduct formation can also result from the reaction between electrolytically prepared fullerene anions and dihalo-compounds, even with dichloromethane.[5] Dichloromethane reacts efficiently with the [60]fullerene trianion to form methano-fullerenes of the type $C_{60}>(CH_2)_n$,[5b] and forms similar adducts with C_{84} [$C_{84}>(CH_2)_n$] during the reductive retro-Bingel reaction of di[alkoxycarbonyl]methano-adducts of C_{84}.[2c] In order to avoid these reactions and to further explore the potential and mechanism of the electrolytic methods of fullerene adduct removal, we decided to investigate the electrolysis of compounds **1**–**3** in THF. In the process we found an electrochemically induced intermolecular reaction that leads to the formation of multiple fullerene adducts.[6]

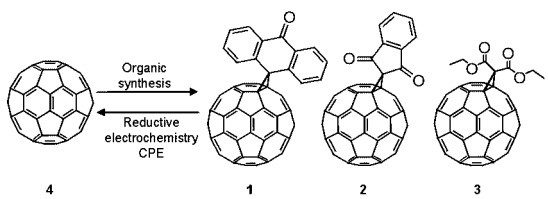

Scheme 1 Protective group system for fullerenes: synthesis of methano-fullerenes **1**–**3** and subsequent adduct removal by reductive electrochemistry.

The cyclic voltammograms of the methanofullerenes **1** and **2** in THF are shown in Fig. 1.[7] These compounds exhibit irreversible electrochemistry in THF, similar to that observed in dichloromethane. Compound **1** exhibits, in addition to several reversible electrochemical processes, an irreversible reduction process between the first and third reduction potentials whilst **2** undergoes an initial two-electron reduction, followed by a one-electron reduction. The irreversible behavior presumably results from the cleavage of one of the cyclopropane bonds connecting the addend to C_{60} after reduction.[8]

Compounds **1** and **2** were subjected to CPE in 0.1 M NBu_4PF_6–THF and the products were separated and analyzed. CPE of **1** was performed at *ca.*100–150 mV more cathodic than the third, reversible, reduction wave (Fig. 1, arrow a); 2.7 electrons per molecule were discharged and clear changes in the CV and OSWV were observed, indicating that a chemical reaction had taken place. Subsequent re-oxidation at 0 V and purification of the product mixture by column chromatography (eluent: toluene) yielded fullerene products in *ca.* 91% yield. Analysis of this mixture by HPLC, UV–VIS spectroscopy, and MALDI-TOF spectrometry clearly showed the formation of C_{60} as the main product (41%). Thus reductive electrochemistry removes the addend in THF (as also observed in CH_2Cl_2), leading to the formation of C_{60}. A second fraction (39%) containing the starting material **1** was also recovered. Interestingly and unexpectedly, a third fraction (11%) with a higher polarity was also isolated. Analysis showed this fraction to be composed of the bis-adducts: fullerenes with two spiro-anthraquinone groups attached (MALDI-TOF: *m*/*z* 1104).

CPE of **2** in THF was performed after the first two-electron reduction wave (Fig. 1, arrow b), and 1.8 electrons per molecule were discharged. Re-oxidation and purification yielded 81% of fullerene products, consisting of 40% C_{60}, 27% recovered **2**, and 14% of bis-adducts. Adduct removal is also the main

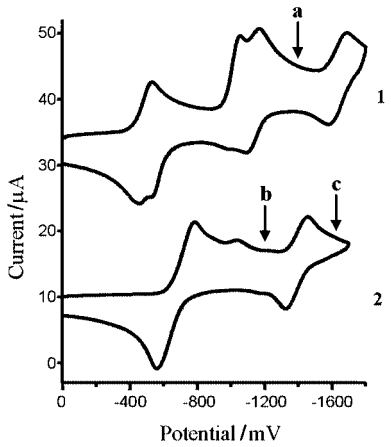

Fig. 1 Cyclic voltammograms of **1** and **2** in THF.

DOI: 10.1039/b008769f

reaction pathway but again a significant amount of regioisomeric bis-adducts was isolated (MALDI-TOF: *m*/*z* 1010). A separate CPE experiment conducted after the second reduction wave (Fig. 1, arrow c) discharged 3.0 electrons and led to similar results (C_{60} : **2** : bis-adducts **7** = 35 : 30 : 19%).

As stated in the introduction, Bingel-adduct removal from fullerenes like **3** by electrochemical (CH_2Cl_2) or chemical reduction (THF) yields C_{60} and starting material (Scheme 1).[2] However, no bis-adduct formation was observed using either of these reductive methods. In view of the results already described for **1** and **2** in THF, we decided to electrolyze **3** in the same solvent. CPE after the second reduction wave of **3** discharged 2.6 electrons, considerably less than the typical value obtained in CH_2Cl_2 (4.0 electrons). Re-oxidation and purification gave fullerene products in a quantitative yield, with 62% C_{60} and 38% **3**. Interestingly, no bis-adducts were detected. Thus profound mechanistic differences exist between the behavior of **1** and **2** and that of **3** under electrolytic conditions.

Our electrochemical experiments show that in THF (but not in CH_2Cl_2) there is a second reaction pathway, besides simple addend removal, that leads to bis-adduct formation. The regioisomer distribution of these bis-adducts is of great interest, as this could provide information on the mechanism of this intermolecular adduct crossover reaction. The unambiguous assignment of regioisomers of several fullerene bis-adducts has been described in detail by Hirsch *et al.*[9] The quantities of bis-adducts that are isolated from the electrolysis experiments in THF are small (typically *ca.* 0.5 mg), thus for characterization purposes we prepared a large amount of the bis-adduct regioisomer mixture (defined as **7**) using the same synthetic procedures used to prepare the original compound, **2**.[10] We separated the regioisomeric bis-adducts **7** on a preparative HPLC column (eluent: toluene). The structures of the different fractions were assigned by ^{1}H NMR spectroscopy and UV–VIS spectroscopy: *trans*-2 14%, *trans*-3 16%, *e* 41%, *cis*-3 5%, *cis*-2 19%. The regioisomers of the bis-adducts obtained by electrolysis were then assigned using HPLC. The two CPE-experiments performed with **2** at different reductive potentials yield similar regioisomer distributions, which are clearly different from that obtained by the regular synthetic route (CPE-b: *trans*-2 3%, *trans*-3 7%, *e* 37%, *cis*-3 49%; CPE-c: *trans*-2 6%, *trans*-3 11%, *e* 43%, *cis*-3 37%).[11] The electrochemical formation of the *cis*-3 bis-adduct as one of the predominant regioisomers is particularly remarkable. Such a relatively large percentage of the *cis*-3 bis-adduct regioisomer had never been seen before during the preparation of bis-Bingel-adducts[9] or bis-methanofullerenes **7**, nor during bis-adduct formation obtained *via* 'shuffle-isomerization' of bis-Bingel adducts[12] or by retro-Bingel of tris-adducts.[13] This offers a possible clue about the mechanism of the reaction in THF.

A possible mechanism to explain these observations is shown in Scheme 2 for **2**. Reductive electrochemistry heterolytically opens the cyclopropane ring, leading to charge formation in the addend as well as in the fullerene core.[8] Two pathways are then possible: (1) the addend can be removed from the fullerene, leading to C_{60} formation, or (2) the anionic addend can add to another fullerene *via* the depicted intermediate **6**, leading to the corresponding bis-adducts.[14] One possible explanation for the favored formation of the *cis*-3 and *e* isomers is the existence of an intermediate like **5**, where both addends interact with the two fullerene cores. Molecular mechanics modeling[15] shows that **5** is highly unfavored for the *trans* isomers while the resulting *cis*-1 and *cis*-2 bis-adducts products have higher energy than the *cis*-3 and *e*.

In conclusion, we have shown an electrolytically induced adduct transfer between fullerenes. The unique bis-adduct regioisomer distribution found deviates significantly from that obtained by the direct synthetic route. These observations are potentially useful for the preparation of specific regioisomer bis-adducts. Mechanistic studies are underway to understand these reaction pathways.

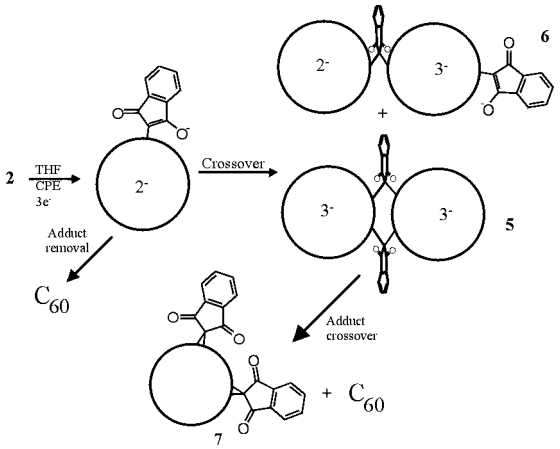

Scheme 2 Possible mechanism for the formation of bis-adducts from electroreduced **2**.

Financial support for this work from the National Science Foundation through grant CHE-9816503, the Netherlands Organization for Scientific Research (NWO, talent stipendium, M. W. J. B.) and the DGICYT of Spain (PB98-0818) is greatly apreciated. We also thank to the Fulbright Foundation (Project 99125) for financial support.

Notes and references

1 C. Bingel, *Chem. Ber.*, 1993, **126**, 1957.
2 (*a*) R. Kessinger, J. Crassous, A. Herrmann, M. Rüttimann, L. Echegoyen and F. Diederich, *Angew. Chem., Int. Ed.*, 1998, **37**, 1919; (*b*) C. Boudon, J.-P. Gisselbrecht, M. Gross, A. Herrmann, M. Rüttimann, J. Crassous, F. Cardullo, L. Echegoyen and F. Diederich, *J. Am. Chem. Soc.*, 1998, **120**, 7860; (*c*) J. Crassous, J. Rivera, N. S. Fender, L. Shu, L. Echegoyen, C. Thilgen, A. Herrmann and F. Diederich, *Angew. Chem., Int. Ed.*, 1999, **38**, 1613.
3 N. N. P. Moonen, C. Thilgen, L. Echegoyen and F. Diederich, *Chem. Commun.*, 2000, 335.
4 M. W. J. Beulen, L. Echegoyen, J. A. Rivera, M. Ángeles Herranz, Á. Martín-Domenech and N. Martín, *Chem. Commun.*, 2000, 917.
5 (*a*) P. L. Boulas, Y. Zuo and L. Echegoyen, *Chem. Commun.*, 1996, 1547; (*b*) M. W. J. Beulen and L. Echegoyen, *Chem. Commun.*, 2000, 1065.
6 A precedent for a similar reaction involving a C_{70} mono-adduct was described previously, but only traces of bis-adducts were detected by HPLC: R. Kessinger, N. S. Fender, L. E. Echegoyen, C. Thilgen, L. Echegoyen and F. Diederich, *Chem. Eur. J.*, 2000, **6**, 2184.
7 For full details of our electrochemical setup and general characterization methods see ref. 5(*b*).
8 B. Knight, N. Martín, T. Ohno, E. Ortí, C. Rovira, J. Veciana, J. Vidal-Gancedo, P. Viruela, R. Viruela and F. Wudl, *J. Am. Chem. Soc.*, 1997, **109**, 9871; N. Martín, L. Sánchez, B. Illescas and I. Pérez, *Chem. Rev.*, 1998, **98**, 2527.
9 A. Hirsch, I. Lamparth and H. R. Karfunkel, *Angew. Chem., Int. Ed. Engl.*, 1994, **33**, 437; A. Hirsch, I. Lamparth and H. R. Karfunkel, in *Fullerenes: Recent advances in the chemistry and physics of fullerenes and related materials; The regiochemistry of nucleophilic addition reactions to C_{60}*, ed. K. M. Kadish and R. S. Ruoff, The Electrochemical Society, Inc., Pennington, NJ, 1994, p. 734.
10 Full details of the organic synthesis and characterization of the bis-adducts **7** will be published elsewhere.
11 The regioisomers of the bis-adduct of **1** could not be assigned due to the small quantity. However, HPLC measurements indicated a similar regioisomer pattern with three predominant isomers.
12 R. Kessinger, M. Gómez-López, C. Boudon, J.-P. Gisselbrech, M. Gross, L. Echegoyen and F. Diederich, *J. Am. Chem. Soc.*, 1998, **120**, 8545.
13 L. E. Echegoyen, F. D. Djojo, A. Hirsch and L. Echegoyen, *J. Org. Chem.*, 2000, **65**, 4994.
14 The formation of bis-adducts *via* reaction of addends in solution (completely removed from the fullerene instead of attached to a fullerene) is unlikely, as the removed addend is not stable in the electrolyte solution. For example, we were not able to isolate any trace of addend after an electrolysis experiment, performed either in THF or dichloromethane.
15 Software used for molecular mechanics: PC Spartan Pro.

Kinetic *versus* thermodynamic control of the self-assembly of isomeric double-stranded dinuclear titanium(IV) complexes from a phenylalanine-bridged dicatechol ligand

Markus Albrecht,*[a] Matthias Napp,[a] Matthias Schneider,[a] Patrick Weis[b] and Roland Fröhlich[c]

[a] *Institut für Organische Chemie der Universität, Richard-Willstätter-Allee, D-76131 Karlsruhe, Germany. E-mail: albrecht@ochhades.chemie.uni-karlsruhe.de*
[b] *Institut für Physikalische Chemie der Universität, Fritz-Haber-Weg, D-76128 Karlsruhe, Germany*
[c] *Organisch-Chemisches Institut der Universität, Corrensstraße 40, D-48149 Münster, Germany*

Received (in Cambridge, UK) 1st December 2000, Accepted 25th January 2001
First published as an Advance Article on the web 9th February 2001

The phenylalanine-bridged dicatechol ligand L-H_4 forms under kinetic reaction conditions a double-stranded dinuclear titanium(IV) complex $[(\mathbf{L})_2Ti_2(OCH_3)_2]^{2-}$, as a mixture of seven regio- and stereo-isomers, which in solution transforms into the thermodynamically favored major product and two minor side products.

Peptides are biopolymers which are built up from amino acid monomers. Hereby hydrogen bonding, electrostatic and steric interactions of the amino acid residues lead to the formation of α-helical, β-sheet, turn or random coil structures.[1] Recently we introduced amino acids as spacers into dicatechol ligands to use the unique features of this moiety for the formation of helicates.[2,3]

When we perform a complexation study of the phenylalanine-bridged dicatechol ligand **L**-H_4 with $[TiO(acac)_2]$ and alkali metal carbonate in methanol (15 h, r.t.), we obtain red solids (Scheme 1). Negative ESI MS in methanol (Fig. 1 shows the spectrum of the sodium salt as a representative example) reveals that only traces of a triple-stranded helicate-type complex $M_4[(\mathbf{L})_3Ti_2]$ {*m/z* = 698, charge 2−, $Na_2[(\mathbf{L})_3Ti_2]^{2-}$} are present while the major component $M_2[(\mathbf{L})_2Ti_2(OCH_3)_2]$ is composed of two ligands **L**, two titanium(IV) ions and two coligands CH_3O^- {for M = Na: *m/z* = 1017, charge 1−, $Na[(\mathbf{L})_2Ti_2(OCH_3)_2]^-$; and *m/z* = 497, charge 2−, $Na_2[(\mathbf{L})_3Ti_2]^{2-}$}. The isotopic patterns are in accordance with the proposed formulae.

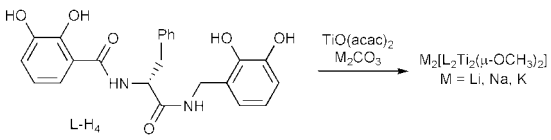

Scheme 1

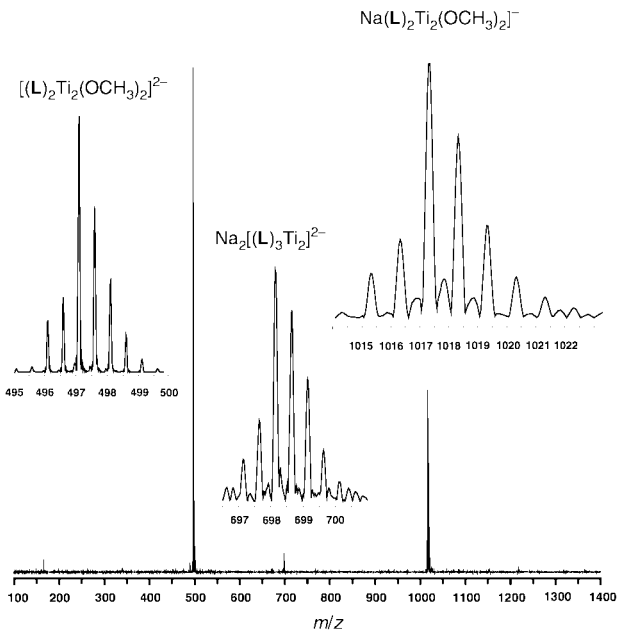

Fig. 1 Negative ESI mass spectrum (methanol) of $Na_2[(\mathbf{L})_2Ti_2(OCH_3)_2]$.

Stack and coworkers already reported a similar dinuclear iron(III) complex. They were able to control the formation of double- *versus* triple-stranded complexes by the stoichiometry of the components.[4] With our system we could not shift the reaction towards the triple-stranded complexes $M_4[(\mathbf{L})_3Ti_2]$.

The NMR spectra of the complexes $M_2[(\mathbf{L})_2Ti_2(OCH_3)_2]$ are very complicated because of the directionality[5] of the ligand **L** and of the stereochemistry at the complex units.[6] Fig. 2 shows a schematic representation of the different stereo- and regioisomers which can be formed. The two directional ligands (N-*versus* C-terminus) can be orientated parallel or antiparallel to each other and the two complex units can be homo- or heterochiral. The isomers **I**, **II** and **IV**–**VII** possess a C_2 axis and lead to only one set of NMR signals for the ligands, whereas **III** possesses C_1 symmetry and thus would result in two sets of signals. If a ^1H NMR spectrum of freshly synthesized (r.t., 15 h, methanol) $[(\mathbf{L})_2Ti_2(OCH_3)_2]^{2-}$ in methanol-d_4 is recorded, up to eight sets of signals—all seven isomers—are observed [Fig. 3 (top), only the signals of one of the diastereotopic benzylic CH_2N protons are shown, the other signals are partly overlapping and cannot be interpreted unambigously].

After two weeks at room temperature the spectrum gets much simpler and one major (a) and two minor species (b, c) are observed [Fig. 3 (bottom)]. From the NMR spectrum it is seen that the complexes which are present in significant amounts belong to the C_2-symmetric isomers **I**, **II** and/or **IV**–**VII**.

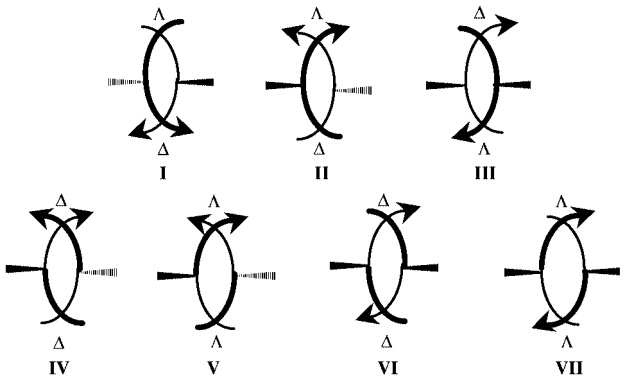

Fig. 2 Schematic representation of the possible isomers of the double-stranded complex $[(\mathbf{L})_2Ti_2(OCH_3)_2]^{2-}$. Only the two directional ligand strands **L** are shown as arrows. Additionally, the configuration at the complex units (Λ or Δ) and at the ligand are indicated. Bold lines are at front, thin lines are at the back.

DOI: 10.1039/b009657l

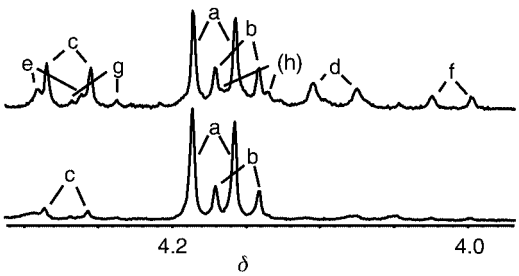

Fig. 3 Part of the ^{1}H NMR spectrum (methanol-d_4) of $Li_2[(\mathbf{L})_2Ti_2(OCH_3)_2]$ (only the signal of one of the diastereotopic protons in benzylic $[NCH_2]$-position is shown). (Top) spectrum of a freshly prepared (r.t., 15 h, methanol) sample of $Li_2[(\mathbf{L})_2Ti_2(OCH_3)_2]$ showing up to eight doublets (a)–(h) (→ seven isomers) ('kinetic control'). (Bottom) spectrum after two weeks at room temperature in methanol-d_4 with the dominating species (a) and the minor components (b) and (c) ('thermodynamic control').

Following the optical rotation of $[(\mathbf{L})_2Ti_2(OCH_3)_2]^{2-}$ (c = 0.1, methanol, 20 °C) we observed a drop of $[\alpha]_D$ from +70° to about 0° within 18 days. Those results indicate that under kinetic control a mixture of complexes is formed which slowly transforms in solution into the thermodynamically most stable coordination compounds as the major product.[7] The decrease of the optical rotation gives some evidence that, initially, the helical isomers **IV**–**VII**, which should lead to high $[\alpha]_D$ values,[8] are formed in significant amounts but are only minor species in the thermodynamically favored mixture. Model considerations indicate, that for the helical structures **IV**–**VII** the stabilizing intramolecular hydrogen bonding is disturbed.

The X-ray structure of $Li_2[(\mathbf{L})_2Ti_2(OCH_3)_2]$ (Fig. 4) shows a central four-membered $[Ti(\mu\text{-}OCH_3)]_2$ unit which is bridged by two ligands **L**.† The two ligands **L** are orientated in opposite directions and are bound in a 'side-by-side' fashion to the metal centers leading to a 'meso'-relation between the two complex units . This unsymmetrical isomer **III**, which should lead to two sets of signals by NMR, cannot be detected in significant amounts in solution. Investigation of a second crystal showed the presence of the same isomer **III**.

A conformational analysis following Ramachandran's method[1] shows that one of the ligands adopts a conformation as found in left-handed α-helical peptides (Φ = 80.53°, Ψ = 30.69°) whereas the other one has a conformation somewhere in-between a right-handed helix and a sheet structure (Φ = −115.11°, Ψ = 5.80°).[1]

Herein we presented the coordination chemistry of the phenylalanine-bridged dicatechol ligand **L** with titanium(IV) ions. ESI MS shows that the ligand **L** preferably forms double-stranded coordination compounds $[(\mathbf{L})_2Ti_2(OR)_2]^{2-}$ and not triple-stranded helicate-type complexes $[(\mathbf{L})_3Ti_2]^{4-}$. Hereby a complex mixture of isomers which is obtained under kinetic control transforms in solution within several days into the more simple 'thermodynamic' product mixture.

This work was supported by the Deutsche Forschungsgemeinschaft and the Fonds der Chemischen Industrie. We thank Professor Dr M. Kappes and the Nanotechnology Institute, Forschungszentrum Karlsruhe for facilitating the ESI-MS measurements.

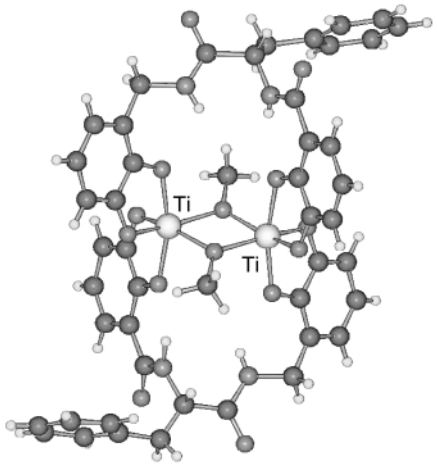

Fig. 4 SCHAKAL representation of the molecular structure of the dianion $[(\mathbf{L})_2Ti_2(OCH_3)_2]^{2-}$ in the crystal. Selected distances (Å) and angle (°) for the central four-membered ring: Ti(1)···Ti(2) 3.188(1); Ti(1)–μ-O(1/2) 1.996(6), 2.018(6); μ-O(1)–Ti(1)–μ-O(2) 73.1(2). Distances (Å) of the intramolecular hydrogen bonds: N–H/H···O 0.854/2.508, 0.866/2.055, 0.780/2.229 and 1.101/1.786.

Notes and references

† *Crystal data* for $C_{60}H_{74}N_8O_{20}Li_2Ti_2$, M = 1336.95, monoclinic, space group $P2_1$ (no. 4), a = 9.404(1), b = 22.726(1), c = 15.382(1) Å, β = 95.04(1), V = 3274.7(4) Å^3, μ = 3.22 cm^{-1}, Z = 2, T = 198 K, 17559 reflections collected ($\pm h$, $\pm k$, $\pm l$), 10574 independent (R_{int} = 0.062) and 6559 observed reflections [$I \geqslant 2\sigma(I)$], R = 0.068, wR^2 = 0.121, Flack parameter 0.01(6).

CCDC 149452. See http://www.rsc.org/suppdata/cc/b0/b009657l/ for crystallographic data in .cif or other electronic format.

1 A. Fersht, *Structure and Mechanism in Protein Science*, W. H. Freeman, New York, 1998.
2 M. Albrecht, M. Napp and M. Schneider, *Synthesis*, in press.
3 For amino acid-bridged ligands see: C. J. Carrano and K. N. Raymond, *J. Am. Chem. Soc.*, 1978, **100**, 5371; A.-K. Duhme, Z. Dauter, R. C. Hider and S. Pohl, *Inorg. Chem.*, 1996, **35**, 3059.
4 E. J. Enemark and T. D. P. Stack, *Inorg. Chem.*, 1996, **35**, 2719.
5 For double-stranded dinuclear complexes of directional ligands, see: E. C. Constable, F. Heirtzler, M. Neuburger and M. Zehnder, *J. Am. Chem. Soc.*, 1997, **119**, 5606; M. J. Hannon, S. Bunce, A. I. Clarke and N. W. Alcock, *Angew. Chem.*, 1999, **111**, 1353; *Angew. Chem., Int. Ed.*, 1999, **38**, 1277.
6 M. Albrecht, *Chem. Eur. J.*, 2000, **6**, 3485.
7 B. Hasenknopf, J.-M. Lehn, N. Boumedijene, E. Leize and A. Van Dorsselaer, *Angew. Chem.*, 1998, **110**, 3458; *Angew. Chem., Int. Ed.*, 1998, **37**, 3265.
8 E. J. Corey, C. L. Cywin and M. C. Noe, *Tetrahedron Lett.*, 1994, **35**, 69; M. Albrecht, *Synlett*, 1996, 565.

Poly-carbon chemistry: reactions of the multi-site coordinated diyndiyl ligand in $\{Fe_2(CO)_6(\mu\text{-}PPh_2)\}_2(\mu\text{-}\eta^1,\eta^2:\mu\text{-}\eta^1,\eta^2\text{-}C{\equiv}C{-}C{\equiv}C)$ with the nucleophiles $P(OMe)_3$ and $NHEt_2$†

Paul J. Low,*[ab] Arthur J. Carty,*[ac] Konstantin A. Udachin[a] and Gary D. Enright[a]

[a] *Steacie Institute for Molecular Sciences, National Research Council of Canada, 100 Sussex Drive, Ottawa, Ontario, Canada, K1A 0R6*

[b] *Department of Chemistry, University of Durham, South Road, Durham, UK DH1 3LE. E-mail: p.j.low@durham.ac.uk*

[c] *Ottawa-Carleton Research Institute, Department of Chemistry, University of Ottawa, 1125 Colonel By Drive, Ottawa, Ontario, Canada, K1A 5B6*

Received (in Cambridge, UK) 6th December 2000, Accepted 22nd January 2001
First published as an Advance Article on the web 9th February 2001

The diyndiyl complex $\{Fe_2(CO)_6(\mu\text{-}PPh_2)\}_2(\mu\text{-}C{\equiv}C{-}C{\equiv}C)$ reacts with $P(OMe)_3$ or $NHEt_2$ to give products derived from addition to C_α and facile P–C, N–C and/or C–C bond formation.

Transition metal diyndiyl (M–C≡C–C≡C–M) complexes are members of a rapidly expanding class of organometallic molecules bearing poly-unsaturated, all-carbon molecules as ligands. While the synthesis of compounds featuring polyynyl and polyyndiyl ligands has advanced rapidly,[1] the reactivity of these carbon-rich materials is relatively unexplored.[2] Herein we describe some remarkable reactions of the diyndiyl complex $\{Fe_2(CO)_6(\mu\text{-}PPh_2)\}_2(\mu\text{-}C_\alpha{\equiv}C_\beta{-}C_\gamma{\equiv}C_\delta)$ (**1**) with the nucleophiles $NHEt_2$ and $P(OMe)_3$.

The tetra-iron diyndiyl complex $\{Fe_2(CO)_6(\mu\text{-}PPh_2)\}_2(\mu\text{-}C_\alpha{\equiv}C_\beta{-}C_\gamma{\equiv}C_\delta$ (**1**), previously obtained in only very low yields from a two-step reaction,[3] may be conveniently obtained (35%) directly from the reaction of $Fe_3(CO)_{12}$ with $Ph_2PC{\equiv}CC{\equiv}CPPh_2$ in THF *via* a facile P–C (alkynyl) bond cleavage reaction. Treatment of **1** with an excess of $P(OMe)_3$ in benzene resulted in the formation of the dark red adduct **2** (Scheme 1, Fig. 1),[4,5]† together with the simple phosphite-substituted complexes $\{Fe_2(\mu\text{-}PPh_2)(CO)_5[P(OMe)_3]\}(\mu\text{-}C{\equiv}CC{\equiv}C)\{Fe_2(\mu\text{-}PPh_2)(CO)_5(L)\}$ [L = CO, $P(OMe)_3$]. Compound **2** is derived from addition of the phosphite reagent to only one ynyl functionality of the original butadiyndiyl ligand at C_α, followed by migration of the associated diphenylphosphido group to C_β and P–C bond formation to give a simple 2e-phosphine. This contrasts with the reactions of the analogous mono-acetylide complex $Fe_2(\mu\text{-}C{\equiv}CPh)(CO)_6(\mu\text{-}PPh_2)$ with $P(OR)_3$ (R = Me, Et, Bu^n) which gave $Fe_2(CO)_6\{C[P(OR)_3]CPh\}(\mu\text{-}PPh_2)$ quantitatively.[6] An examination of the molecular structure of the Et product suggests that C_β is sterically protected by both $P(OEt)_3$ and Ph groups, which probably hinders the migration of the PPh_2 moiety.[6]

While **1** failed to react with the bulky reagents dicyclohexylamine and diphenylamine (benzene, 80 °C), treatment of **1** with an excess of $NHEt_2$ (r.t., 2 d) resulted in the formation of purple **3** (Fig. 2) and red **4** (Fig. 3) in 19 and 33% yield respectively (Scheme 1).[4,5] Complex **3** contains two $Fe_2(CO)_6$ moieties bridged by an unusual 1-diethylamino-3-diphenylphosphinobuteneylidene ligand, obtained from 1,2-addition of the amine N–H bond across one acetylide moiety in **1**, with migration of a PPh_2 phosphino group to C_γ. The major product **4** is also derived from 1,2-addition of the amine to the carbon ligand, although in this case it is a carbonyl ligand rather than the PPh_2 group that has migrated from iron to C_γ yielding the five-membered metallacyclic ligand. The addition of the

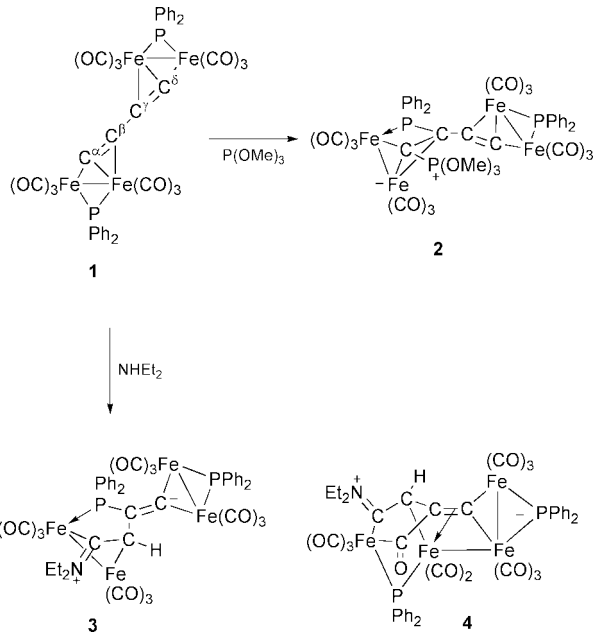

Scheme 1 Reaction of **1** with $P(OMe)_3$ and $NHEt_2$.

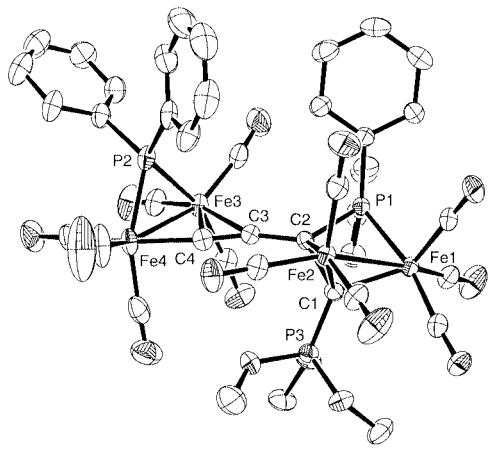

Fig. 1 ORTEP drawing of **2**. Selected bond lengths (Å) and angles (°): Fe(1)–Fe(2) 2.6033(4), Fe(3)–Fe(4) 2.5754(4), C(1)–C(2) 1.498(3), C(2)–C(3) 1.443(2), C(3)–C(4) 1.229(3), Fe(1)–C(1) 2.025(2), Fe(2)–C(1) 1.9457(2), Fe(2)–C(2) 2.072(2), Fe(1)–P(1) 2.2316(6), P(1)–C(2) 1.782(2), Fe(3)–C(3) 2.469(2), Fe(3)–C(4) 2.105(2), Fe(4)–C(4) 1.906(2), P(3)–C(1) 1.708(2); C(1)–C(2)–C(3) 126.5(1), C(2)–C(3)–C(4) 162.2(2), C(3)–C(4)–Fe(4) 171.5(2), Fe(1)–P(1)–C(2) 86.10(7).

† Electronic supplementary information (ESI) available: reaction details and spectroscopic data. See http://www.rsc.org/suppdata/cc/b0/b009797g/

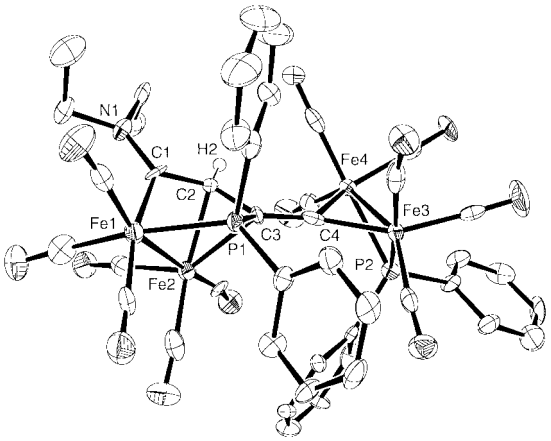

Fig. 2 Molecular structure of one molecule of **3**. Selected bond lengths (Å) and angles (°): Fe(1)–Fe(2) 2.665(2), Fe(3)–Fe(4) 2.540(2), Fe(1)–C(1) 2.020(9), Fe(1)–P(1) 2.233(3), N(1)–C(1) 1.33(1), P(1)–C(3) 1.813(9), Fe(2)–C(1) 2.458(9), Fe(2)–C(2) 2.033(9), Fe(2)–C(3) 2.212(9), Fe(3)–C(4) 1.95(1), Fe(4)–C(4) 1.933(9), C(1)–C(2) 1.43(1), C(2)–C(3) 1.46(1), C(3)–C(4) 1.40(1); Fe(1)–P(1)–C(3) 98.9(3), Fe(1)–C(1)–N(1) 127.4(7), N(1)–C(1)–C(2) 118.2(8), C(2)–C(3)–C(4) 121.4(8).

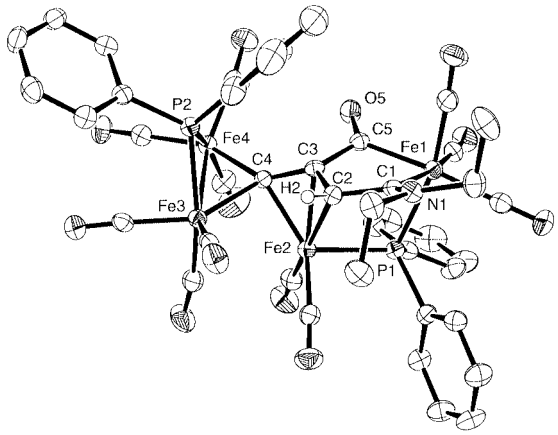

Fig. 3 Molecular structure of **4**. Selected bond lengths (Å) and angles (°): Fe(2)–Fe(3) 2.831(1), Fe(3)–Fe(4) 2.582(1), Fe(1)–P(1) 2.315(1), Fe(1)–C(1) 2.008(3), Fe(1)–C(5) 2.032(3), N(1)–C(1) 1.324(4), C(1)–C(2) 1.457(5), C(2)–C(3) 1.434(4), C(3)–C(4) 1.390(5), C(3)–C(5) 1.518(5), Fe(2)–C(2) 2.110(3), Fe(2)–C(3) 2.015(3), Fe(2)–C(4) 2.034(3), Fe(3)–C(4) 2.036(3), Fe(4)–C(4) 1.928(3); Fe(1)–P(1)–Fe(2) 106.14(4), Fe(1)–C(1)–N(1) 130.3(3), N(1)–C(1)–C(2) 117.8(3), C(1)–C(2)–C(3) 114.6(3), C(2)–C(3)–C(4) 119.9(3), C(2)–C(3)–C(5) 114.1(3), Fe(4)–C(4)–C(3) 140.6(2).

nucleophile is accompanied by significant rearrangement of the metal framework. The regiospecific 1,2-addition of $NHEt_2$ to C_α/C_β in the diyndiyl complex **1** is unusual in that the corresponding mono-ynyl iron complexes give β-addition products exclusively,[7] while the related ruthenium diynyl compounds give products derived from 1,4-addition of an N–H bond.[8]

Further studies of these remarkable rearrangements, which proceed with total atom conservation and demonstrate facile N–C, P–C and C–C bond formation involving the diyndiyl ligand, are in progress.

We are grateful to the National Research Council of Canada and the Natural Sciences and Engineering Research Council of Canada for financial support of this work. We thank Dr H. Puschmann for crystallographic assistance. P. J. L. held an NRC/NSERC Canadian Government Laboratories Visiting Fellowship.

Notes andreferences

1 R. Dembinski, T. Bartik, B. Bartik, M. Jaeger and J. A. Gladysz, *J. Am. Chem. Soc.*, 2000, **122**, 810; F. Paul and C. Lapinte, *Coord. Chem. Rev.*, 1998, **178–180**, 431; M. I. Bruce, M. Ke, P. J. Low, B. W. Skelton and A. H. White, *Organometallics*, 1998, **17**, 3539; M. Akita, M.-C. Chung, A. Sakurai, S. Sugimoto, M. Terada, M. Tanaka and Y. Moro-oka, *Organometallics*, 1997, **16**, 4882; P. Blenkiron, J. F. Corrigan, D. Pilette, N. J. Taylor and A. J. Carty, *Can. J. Chem.*, 1996, **74**, 2349 and references therein.

2 M. I. Bruce, B. C. Hall, B. D. Kelly, P. J. Low, B. W. Skelton and A. H. White, *J. Chem. Soc., Dalton Trans.*, 1999, 3719; M. I. Bruce, P. J. Low, N. N. Zaitseva, S. Kahal, J.-F. Halet, B. W. Skelton and A. H. White, *J. Chem. Soc., Dalton Trans.*, 2000, 2939; M. Akita, A. Sakurai and Y. Moro-oka, *Chem. Commun.*, 1999, 101. R. Dembinski, T. Lis, S. Szafert, C. L. Mayne, T. Bartik and J. A. Gladysz, *J. Organomet. Chem.*, 1999, **578**, 229; M. Akita, M.-C. Chung, M. Terada, M. Miyauti, M. Tanaka and Y. Moro-oka, *J. Organomet. Chem.*, 1998, **565**, 49; F. Leroux, R. Stumpf and H. Fischer, *Eur. J. Inorg. Chem.*, 1998, 1225; P. Blenkiron, G. D. Enright, N. J. Taylor and A. J. Carty, *Organometallics*, 1996, **15**, 2855.

3 C. J. Adams, M. I. Bruce, B. W. Skelton and A. H. White, *J. Organomet. Chem.*, 1993, **450**, C9.

4 *Selected spectroscopic data* for **2**: IR (cyclohexane, ν/cm^{-1}): 2061m, 2044vs, 2020s, 2003s, 1997s, 1985s, 1980s, 1958m, 1944w. FAB-MS: *m*/*z* 1102 $[M]^+$, 1046–794, $[M - nCO]^+$ (n = 1–11). For **3**: IR (cyclohexane, ν/cm^{-1}): 2058m, 2040vs, 2017s, 2008s, 1988sh, 1984s, 1968s, 1959m, 1943m. FAB-MS: *m*/*z* 1023–715 $[M - nCO]^+$ (n = 1–12). For **4**: IR (CH_2Cl_2, ν/cm^{-1}) 2069m, 2047vs, 2011vs, 1998m, 1987sh, 1965m, 1954sh, 1936sh. FAB-MS: *m*/*z* 968 $[M - 3CO + H]^+$, 912 $[M - 5CO + H]^+$, 854 $[M - 7CO]^+$. Satisfactory microanalytical data were obtained for all complexes reported.

5 X-Ray data were collected on a Siemens SMART CCD diffractometer [graphite monochromatised Mo-Kα radiation, λ = 0.71070 Å, T = 173(2) K] and ω-scan frames and structures solved using the SHELXTL suite of programs. Refinement on F^2 by full-matrix least squares techniques. *Crystal data* for **2**: $Fe_4P_3O_{15}C_{43}H_{29}{\cdot}0.7CH_2Cl_2$, M = 1101.97, triclinic, space group $P\bar{1}$, a = 10.9884(5), b = 11.1706(5), c = 22.0560(10) Å, α = 81.65(1), β = 75.71(1), γ = 61.36(1)°, V = 2301.4(2) Å^3, Z = 2, μ = 1.407 mm^{-1}. 20767 reflections measured, 8085 unique (R_{int} = 0.0773) which were used in all calculations. $wR2$ = 0.1243 (all data). For **3**: $Fe_4NO_{12}P_2C_{44}H_{31}$, M = 1051.04, monoclinic, space group $P2_1/c$, a = 39.793(4), b = 11.639(1), c = 19.552(2) Å, β = 102.08(1)°, V = 8855(1) Å^3, Z = 4, μ = 1.577 mm^{-1}. 33404 reflections measured, 10058 unique (R_{int} = 0.1178), $wR2$ = 0.1549 (all data). For **4**: $Fe_4NO_{12}P_2C_{44}H_{31}$, M = 1051.04, monoclinic, space group $P2_1/n$, a = 14.404(1), b = 21.879(1), c = 14.448(1) Å, β = 105.52(5)°, V = 4387.2(5) Å^3, Z = 4, μ = 1.433 mm^{-1}. 37566 reflections measured, 10107 unique (R_{int} = 0.0722), $wR2$ = 0.1030 (all data). CCDC reference numbers 155050–155052. See http://www.rsc.org/suppdata/cc/b0/b009797g/ for crystallographic data in .cif or other electronic format.

6 Y. S. Wong, H. N. Paik, P. C. Chieh and A. J. Carty, *J. Chem. Soc., Chem. Commun.*, 1975, 309.

7 A. A. Cherkas, L. H. Randall, N. J. Taylor, G. N. Mott, J. E. Yule, J. L. Guinmant and A. J. Carty, *Organometallics*, 1990, **9**, 1677.

8 P. Blenkiron, D. Pilette, J. F. Corrigan, N. J. Taylor and A. J. Carty, *J. Chem. Soc., Chem. Commun.*, 1995, 2165.

How polar are room-temperature ionic liquids?

Sudhir N. V. K. Aki,[a] Joan F. Brennecke*[a] and Anunay Samanta*†[b]

[a] *Department of Chemical Engineering, University of Notre Dame, Notre Dame, IN 46556 USA. E-mail: jfb@nd.edu*
[b] *Radiation Laboratory, University of Notre Dame, Notre Dame, IN 46556, USA*

Received (in Columbia, MO, USA) 25th September 2000, Accepted 18th January 2001
First published as an Advance Article on the web 9th February 2001

The solvent strength and polarity of four imidazolium and pyridinium based ionic liquids, as measured using two different fluorescent probes, indicate that these liquids are more polar than acetonitrile but less polar than methanol.

The realization that pollution prevention is frequently more cost effective than remediation has catalyzed tremendous effort in the development of environmentally benign solvents and processes. Room-temperature ionic liquids (ILs) are one such class of solvents. They are organic molten salts that in their pure state are liquids at temperatures around ambient. The typical IL is based on a bulky *N*-alkylpyridinium or *N*,*N*′-dialkylimidazolium cation, with a variety of substituents paired with a variety of anions. These, along with alkylammonium and alkylphosphonium compounds, are most popular.[1] Interestingly, even though ILs are organic solvents, they exhibit vanishingly small vapor pressures.[2,3]

Since the synthesis of air- and water-stable ionic liquids in 1992,[4] they have been widely explored as solvents and/or catalysts in synthetic chemistry. Welton[1] has reviewed many of these reaction studies in a recent paper. For example, catalytic hydrogenation of cyclohexene[5] using rhodium based homogeneous catalysts and hydrogenation of olefins[6] using ruthenium and cobalt based homogeneous catalysts in several ionic liquids showed enhancement in reaction rates and selectivity, compared to normal liquid solvents. In addition, very recent efforts have explored the separation of organic solutes from ILs with water[7] and with carbon dioxide,[8] as well as their use in the extraction of metal compounds such as strontium nitrate.[9]

A significant barrier to the use of ILs is the absence of understanding of how the structure of the IL affects its physical properties and solvent strength. Perhaps more importantly, there is a lack of understanding of how solvent strength and solvent polarity of various ILs affect reaction rates. Since polarity and polarizability are the simplest indicators of solvent strength, organic solvents are frequently classified on their ability to dissolve and stabilize dipolar or charged species. Fluorescent probes are commonly used to determine the solvent strength of organic solvents and recent studies indicate that these probes can be used to determine the solvent strength of ILs. For example, the solvent strength of alkylammonium thiocyanate organic salts was determined to be similar to cyclohexanone using fluorescent probes such as pyrene.[10] Bonhote *et al.* found that the solvent strength of 1-ethyl-3-methylimidazolium bis-(triflyl)amide, using pyrene and pyrenecarbaldehyde, was similar to ethanol and hexane respectively, depending on the choice of the fluorescent probe.[11] In the present paper we report on the polarity of several ILs, (**I**–**IV**, Fig. 1) as measured by two fluorescent probes (**V** and **VI**).‡

While betaine dye (Reichardt's dye) is a common probe used to measure the polarity of homogeneous media,[12] neutral fluorescence probe molecules may be preferred when the large size and charge on the betaine dye is problematic. However, it is still quite common to express microscopic polarities in terms of the absorption energy of the betaine dye, $E_T(30)$. Another advantage with the fluorescent probes is that multiple solvent sensitive parameters, *e.g.* the location of the fluorescence maximum, the fluorescence quantum yield and the fluorescence lifetime, can be monitored. Taking this into consideration, we have chosen AP (**V**) and DAP (**VI**), fairly small, neutral molecules whose fluorescence properties are known to be highly sensitive to the polarity of the media[13–15] to explore the solvent strength of [bmim][PF_6], [C_8mim][PF_6], [bmim]NO_3] and [*N*-bupy][BF_4] (**I**–**IV**). The fluorescence properties of these probe molecules are shown in Table 1 in several protic and aprotic organic solvents. All three properties are very sensitive to the nature of the medium. The effect of the nature of the solvent on the fluorescence properties of these probes has been discussed in detail elsewhere.[12–14]

The frequency maxima, lifetimes and quantum yields of AP and DAP correlate reasonably well with the microscopic solvent polarity parameter, $E_T(30)$. For instance, the λ_{max} of AP can be related to the $E_T(30)$ by $E_T(30)$ (kcal mol^{-1}) = 0.225 λ_{max}(nm) − 62.677 with a correlation coefficient of 0.94. We use these probes as general measures of the solvent strength of the various ILs shown in Fig. 1. As a result, we also report the equivalent $E_T(30)$ values determined from these correlations.[13,14]

The fluorescence properties of DAP were measured in four different ILs **I**–**IV**. The results are shown in Table 2, along with the equivalent $E_T(30)$ values estimated from the correlations that are obtained using the data given in Table 1. It is interesting to note that the solvent strength [as indicated by the equivalent $E_T(30)$ values] of the ILs, does not depend very strongly on which fluorophore is used, as demonstrated by the measurements in **I**. Moreover, the values do not depend strongly on what particular fluorescence parameter (λ_{max}, fluorescence lifetime or quantum yield) is used. These data provide more convincing estimates of the solvent strength than a single $E_T(30)$ measurement. Nonetheless, we did measure the $E_T(30)$ value of **I** using Reichardt's dye. A value of 55 kcal mol^{-1} was obtained and this value compares reasonably well with the estimated values reported in Table 2.

All of the ILs exhibit solvent strengths as great or greater than the most polar aprotic solvent (acetonitrile) shown in Table 1. Clearly, these ILs are more polar than hexane, as has been suggested previously for some other ILs.[11] In fact, the equivalent $E_T(30)$ values for the ILs fall in the range of the various alcohols. The data presented in Table 2 suggest that both **I** and **III** provide more polar environments than those offered by

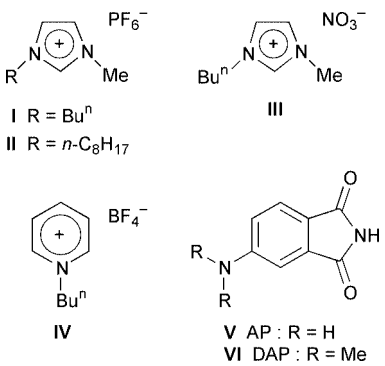

Fig. 1 Structures of fluorescent probes and ionic liquids.

† Present address: School of Chemistry, University of Hyderabad, Hyderabad 500046, India. E-mail: assc@uohyd.ernet.in

DOI: 10.1039/b008039j

Table 1 Fluorescence properties of the probe molecules in selected organic solvents at room temperature[13,14]

Solvent	Relative permittivity	$E_T(30)$[12]/ kcal mol^{-1}	AP[13,14]			DAP[13,14]		
			λ_{fluo}^{max}/nm	ϕ_{fluo}	τ_{fluo}/ns	λ_{fluo}^{max}/nm	ϕ_{fluo}	τ_{fluo}/ns
Hexane	1.887	31	416[a]			437[a]		
Diethyl ether	4.2	34.5	425			440		
1,4-Dioxane	2.21	36	435	0.73	15.0	457	0.62	14.9
Tetrahydrofuran	7.58	37.4	445	0.7	12.4	459	0.52	13.8
Acetone	20.56	43.1	457	0.68		483	0.17	
Acetonitrile	35.94	45.3	458	0.63	14.0	490	0.12	3.9
tert-Butyl alcohol	12.42	43.5	501			516		
Propan-2-ol	19.92	48.5	505			523		
Ethanol	25.3	51.9	509[a]			523[a]		
Methanol	32.66	55	518	0.1		534		
Water	78.3	63.1	540	0.01		562		

[a] These values were estimated using the $E_T(30)$ values and the correlations developed.

Table 2 Fluorescence properties of DAP in ILs at room temperature and the estimated $E_T(30)$ values (kcal mol^{-1}) in parentheses for the ILs[a]

Solvent	DAP		
	λ_{fluo}^{max}/nm	ϕ_{fluo}	τ_{fluo}/ns
[bmim][PF_6]	526 (52.39)	0.028 (51.69)	2.9 (46.16)
[C_8mim][PF_6]	503 (46.84)	0.18 (47.16)	8.5 (41.51)
[bmim][NO_3]	525 (52.14)	0.045 (51.18)	
[*N*-bupy][BF_4]	495 (44.91)		2.51 (46.48)
[bmim][PF_6] (dried)	512 (49.01)	0.036 (51.44)	

[a] The steady state emission spectra were obtained in a 1 × 1 cmSuprasil quartz cell using a SLM-AMINCO 8100 spectrofluorometer. The fluorescence lifetime measurements were obtained with a PTI laserstrobe fluorescence spectrometer with excitation at 337 nm.

II and **IV**. In addition, we can conclude that replacing the counter ion, PF_6^-, by NO_3^- does not change the apparent polarity of the medium. This may be caused by the fluorophore preferentially positioning itself near the imidazolium ring, thus not being significantly influenced by the anion. The fact that **I** is determined to be more polar than **II** is understandable, as an octyl group is expected to provide a more hydrophobic (hence non-polar) environment than the butyl substituent.

These ILs are expected to be at least partially miscible with water. In fact, measurements in our laboratory indicate that the equilibrium solubility of water in **I** at room temperature is *ca.* 1.735 M. In addition, the ILs are hygroscopic. In general, we would expect the probes used in the current work to be sensitive to the presence of water. To reduce the amount of water in the samples, they were dried *in vacuo* for at least 48 h at room temperature. Subsequent analysis by Karl–Fisher titration suggests that the water content is reduced to *ca.* 0.43 wt% (0.324 M) with this treatment. To further explore the effect of water on the measured $E_T(30)$ values, **I** was dried under even more stringent conditions, (*in vacuo* at 75 °C for 24 h), and Karl–Fisher analysis indicates that the water content should be down to 0.015 M. The fluorescence properties of DAP in this dried salt were measured and are shown at the bottom of Table 2. As expected, the fluorescence properties of the DAP in the dried sample did change somewhat, but the estimated $E_T(30)$ values indicate that the overall solvent strength of the sample is only reduced slightly from the previous measurements. Thus, we are confident that the solvent strengths of the ILs shown in Table 2 are faithful indications of their relative polarities.

In conclusion, the solvent strengths of **I**–**IV**, as represented by their equivalent $E_T(30)$ values, have been estimated using two fluorescent dyes. The results indicate that **I** is more polar than acetonitrile and less polar than methanol. The replacement of the counter ion, PF_6^-, by NO_3^- did not change the apparent polarity of the medium. Also, both **I** and **III** provide more polar environments than those offered by **II** and **IV**. The presence of small amounts of water was found to have only a small effect on the estimated $E_T(30)$ values.

We appreciate the supply of samples of **II**, **III** and **IV** from the group of Professor Kenneth R. Seddon at the Queen's University of Belfast. In addition, financial support from the Environmental Protection Agency (R826734-01-0) and the National Science Foundation (EEC97-00537-CRCD) is gratefully acknowledged. The Notre Dame Radiation Laboratory is supported by the Division of Chemical Sciences of the U.S. Department of Energy. This is contribution No. NDRL 4254 from the Notre Dame Radiation Laboratory.

Notes and references

‡ **I** was obtained from Sachem. The remaining ILs used in this work were prepared by the group of Professor Kenneth R. Seddon at the University of Belfast. All samples were dried *in vacuo* at room temperature for 24 h unless indicated otherwise in the text. The fluorescent probes were synthesized, as described elsewhere.[13,14]

1 T. Welton, *Chem. Rev.*, 1999, **99**, 2071.
2 C. L. Hussey, *Pure Appl. Chem.*, 1988, **60**, 1763.
3 K. R. Seddon, *Kinet. Catal.*, 1996, **37**, 693.
4 J. S. Wilkes and M. J. Zaworotko, *Chem. Commun.*, 1992, **13**, 965.
5 P. A. Z. Suarez , J. E. L. Dullis, S. Einloft, R. F. de Souza and J. Dupont, *Polyhedron*, 1996, **15**, 1217.
6 P. A. Z. Suarez, J. E. L. Dullis, S. Einloft, R. F. de Souza and J. Dupont, *Inorg. Chim. Acta*, 1997, **255**, 207.
7 J. G. Huddleston, H. D. Willauer, R. P. Swatloski, A. E. Visser and R. D. Rogers, *Chem. Commun.*, 1998, **16**, 1765.
8 L. A. Blanchard, D. Hancu, E. J. Beckman and J. F. Brennecke, *Nature*, 1999, **399**, 28.
9 S. Dai, Y. H. Ju and C. E. Barnes, *J. Chem. Soc., Dalton Trans.*, 1999, **8**, 1201.
10 K. W. Street Jr., W. E. Acree Jr., J. C. Fetzer, P. H. Shetty and C. F. Poole, *Appl. Spectrosc.*, 1989, **43**, 1149.
11 P. Bonhote. A. Dias, N. Papageorgiou, K. Kalyanasundaram and M. Gratzel, *Inorg. Chem.*, 1996, **35**, 1168.
12 T. Soujanya, R. W. Fessenden and A. Samanta, *J. Phys. Chem.*, 1996, **100**, 3507.
13 T. Soujanya, S. R. Krishna and A. Samanta, *J. Phys. Chem.*, 1992, **96**, 8544.
14 B. Saroja, B. Ramachandram, S. Saha and A. Samanta, *J. Phys. Chem. B*, 1999, **103**, 2906.
15 C. Reichardt, *Solvent and Solvent Effects in Organic Chemistry*, VCH Verlagsfesellschaft mbH, D-6940, Weinheim, Germany, 2nd edn., 1988.

Low temperature reforming of methane to synthesis gas with direct current pulse discharge method

Shigeru Kado,* Kouhei Urasaki, Yasushi Sekine and Kaoru Fujimoto

Department of Applied Chemistry, School of Engineering, The University of Tokyo, 7-3-1 Hongo, Bunkyo-ku, Tokyo 113-8656, Japan. E-mail: tt97208@mail.ecc.u-tokyo.ac.jp

Received (in Cambridge, UK) 7th November 2000, Accepted 24th January 2001
First published as an Advance Article on the web 13th February 2001

Synthesis gas was produced by pulsed irradiation of electrons on a mixture of CH_4 and CO_2 (or H_2O) at low temperature and atmospheric pressure without catalysts; especially in the CO_2 reforming reaction, the H_2:CO ratio could be controlled and depended on the concentration of CO_2 in the feed gas.

Authors have shown that when dc pulse discharge (DCPD) was applied to non-catalytic activation of methane, dehydrogenation of methane proceeded by electron collision and acetylene was produced with 95% selectivity under the conditions of ambient temperature and atmospheric pressure. Coexisting oxygen was found to be very effective in suppressing carbon deposition.[1] In this paper, carbon dioxide or steam was added, a possibility to produce synthesis gas was examined. Because carbon dioxide and steam reforming of methane are highly endothermic reactions, these reactions require temperatures > 800 K in the presence of catalysts. It has been reported that carbon dioxide reforming of methane with plasma techniques, such as di-electric-barrier discharge[2,3] and radio-frequency discharge,[4] give syngas at ambient temperature.

A flow-type tubular discharge reactor (4.0 mm i.d.) used in the present study is the same as that reported previously.[1] In the steam reforming reaction, water was fed as liquid with the micro feeder and vaporized in the preheater upstream of the reactor at 453 K. Before sampling, water was trapped in an ice trap. The temperature of the whole reactor and line to the ice trap was maintained at 453 K to prevent condensation. Carbon dioxide reforming was conducted at ambient temperature. Stainless steel rods of 1.0 mm diameter were used as the electrodes and were located 1.5 mm or 10.0 mm apart. The total flow rate was fixed at 10 cm^3 min^{-1}. All experiments were conducted at atmospheric pressure and all the products were analyzed by gas chromatography. Product selectivity was defined as based on the carbon.

In the presence of CO_2 or steam, the state of discharge was stable and carbon deposition on the electrodes and the wall of the reactor was not observed. Table 1 shows the effect of supplied energy on CO_2 and steam reforming of methane. Since trace amounts of C_3 and C_4 hydrocarbons were produced, the sum of the selectivity did not reach 100%. In the reforming reaction, CO was formed as well as C_2 hydrocarbons in both reaction systems. Also, in the presence of steam, CO_2 was produced by the water gas shift reaction. Although the formation of CO_2 is one of the serious problems in the conventional steam reforming process for making syngas, its selectivity was as low as 4% in the DCPD method in spite of the low reaction temperature of 453 K. The main component of C_2 compounds was acetylene, so the H_2:CO ratio was larger than the stoichiometric ratio. With an increase of supplied energy, the conversion increased and CO selectivity increased slightly while C_2 selectivity decreased slightly. It was clarified that the DCPD method had a possibility to proceed the reforming reaction at low temperature.

Fig. 1 shows the effect of CO_2 content in the feed gas on the conversion, the selectivity and H_2:CO ratio. With increasing CO_2 content, CH_4 conversion rose and reached 76% at CH_4:CO_2 = 1:4 while CO_2 conversion remained almost stable at *ca.* 40%. The selectivity strongly depends on the feed gas composition. With the increase of CO_2 content, C_2 selectivity decreased sharply while CO selectivity increased dramatically. Under the conditions of high CH_4 concentration, the formation

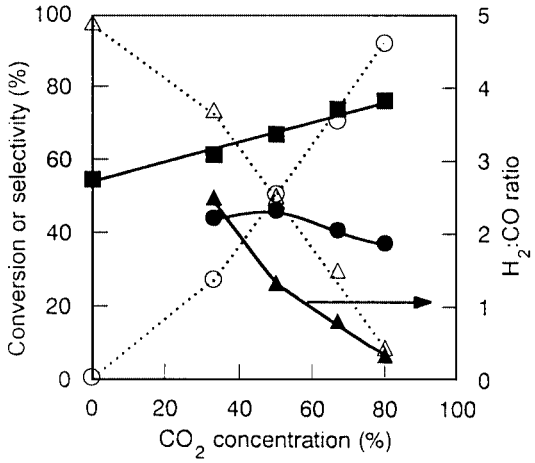

Fig. 1 Effect of carbon dioxide concentration on CO_2 reforming. Reaction conditions: 10 cm^3 min^{-1} total flow rate, ambient temperature, 0.1 MPa, 1.5 mm electrode distance, 52 W supplied energy; (■) CH_4 conv., (●) CO_2 conv., (△) C_2 sel., (○) CO sel., (▲) H_2:CO ratio.

Table 1 Effect of supplied energy on reforming of methane[a]

Added gas	Supplied energy/W	Conversion(%)		Selectivity(%)			
		CH_4	CO_2 or H_2O	C_2	CO	CO_2	H_2:CO ratio
CO_2	3.2	16.3	8.1	64.2	35.6	—	1.74
	10.4	30.4	17.0	62.5	37.3	—	1.56
	21.0	41.2	24.3	54.9	44.7	—	1.48
H_2O	4.4	20.2	9.4	57.0	38.0	3.2	5.44
	11.8	29.9	15.7	52.1	41.3	4.4	5.25
	24.0	39.8	22.2	48.6	45.8	3.7	4.87

[a] Reaction conditions: 10 cm^3 min^{-1} total flow rate, CH_4:CO_2 or H_2O = 1, 1.5 mm distance of electrodes, 0.1 MPa, ambient temperature in CO_2 reforming and 453 K steam reforming.

DOI: 10.1039/b008922m

Table 2 Effect of H_2O concentration and distance of electrodes on steam reforming of methane[a]

CH_4:H_2O	Electrode distance/mm	Conversion(%)		Selectivity(%)			H_2:CO ratio
		CH_4	H_2O	C_2	CO	CO_2	
5:5	1.5	39.8	22.2	48.6	45.8	3.7	4.87
2:8	1.5	49.2	11.7	19.7	64.3	15.3	4.37
2:8	10.0	82.4	19.5	11.0	83.1	5.7	3.46

[a] Reaction conditions: 10 cm^3 min^{-1} total flow rate, 453 K, 0.1 MPa, 3.0 mA.

of C_2H_2 was predominant by the coupling of CH that was produced from CH_4, whereas under conditions of high CO_2 concentration, CO became the main product because of the higher collision probability between CH and activated CO_2 species. The selectivity of C_2 and CO was equal for CH_4:CO_2 = 1:1. The feed gas composition also had a great influence on H_2:CO molar ratio. That ratio was inversely proportional to CO_2 content and could be approximated over the whole range by the formula $R = 1.258 \times r$, where R is the H_2:CO ratio and r is the mixing ratio of CH_4:CO_2. Synthesis gas with a H_2:CO ratio of 2 was obtained at 40% CO_2 content, which is suitable for methanol synthesis *via* a catalytic process.

As shown in Table 2, increasing the steam content caused a decrease in C_2 selectivity together with an increase in CO selectivity during steam reforming. However, CO_2 selectivity increased to *ca.* 15% at CH_4:H_2O = 1:4. Lengthening the distance apart of the electrodes increased CH_4 conversion and CO selectivity dramatically and decreased the C_2 and CO_2 selectivity. The results at a 10 mm distance gave 83% CO selectivity with 82% CH_4 conversion under the conditions of CH_4:H_2O = 1:4.

In CO_2 reforming also, an increased distance apart of electrodes caused the same promotional effect on the conversion and selectivity (Table 3) as was observed in steam reforming. Under the conditions of CH_4:CO_2 = 1:1 and 10.0 mm gap, the discharge region was filled with $Ni_{0.03}Mg_{0.97}O$ prepared by the same method as Tomishige *et al.*[5] NiMgO had a great effect on the selectivity: C_2 selectivity decreased drastically to 1% and CO selectivity increased to 99%. Other hydrocarbons such as C_3 and C_4 compounds were not detected. Also, CO_2 conversion became higher than that of CH_4 probably because of the promotion of the reverse water gas shift reaction. From these results, the catalyst was found to demonstrate some effect on the DCPD reaction at low temperature. The precursor of C_2 hydrocarbons might be adsorbed onto Ni and be subjected to reforming by CO_2. As a consequence, by the combined NiMgO–DCPD system, synthesis gas was produced from methane with 70% CH_4 conversion and little C_2 hydrocarbon formation at ambient temperature.

Table 3 Effect of distance of electrodes and catalyst on CO_2 reforming of methane[a]

Catalyst	Electrode distance/mm	Conversion(%)		Selectivity(%)		H_2:CO ratio
		CH_4	CO_2	C_2	CO	
None	1.5	41.2	24.3	54.9	44.7	1.48
None	10.0	80.9	72.7	33.6	65.4	1.00
NiMgO	10.0	69.5	79.5	1.0	99.0	0.86

[a] Reaction conditions: 10 cm^3 min^{-1} total flow rate, CH_4:CO_2 = 1, ambient temperature, 0.1 MPa, 3.0 mA, $Ni_{0.03}Mg_{0.97}O$ = 0.13 g.

In conclusion, the DCPD method could be applied for CO_2 and steam reforming of methane at low temperature with or without the use of catalysts. The selectivity strongly depended on the composition of the feed gas, and a desired H_2:CO ratio could be obtained. NiMgO had the great effect of increasing CO selectivity to 99%. If the energy efficiency is improved in the future, the catalyst–DCPD combined system has the possibility of being developed as a brand-new reaction process.

Notes and references

1 S. Kado, Y. Sekine and K. Fujimoto, *Chem. Commun.*, 1999, 2485.
2 L. M. Zhou, B. Xue, U. Kogelschatz and B. Eliasson, *Energy Fuels*, 1998, **12**, 1191.
3 B. Eliasson, C. J. Liu and U. Kogelschatz, *Ind. Eng. Chem. Res.*, 2000, **39**, 1221.
4 S. Y. Savinov, H. Lee, H. K. Song and B. K. Na, *Ind. Eng. Chem. Res.*, 1999, **38**, 2540.
5 K. Tomishige, Y. Himeno, Y. Matsuo, Y. Yoshinaga and K. Fujimoto, *Ind. Eng. Chem. Res.*, 2000, **39**, 1891.

Extraction of lanthanides and actinides by a magnetically assisted chemical separation technique based on CMPO-calix[4]arenes†

Susan E. Matthews,*‡[a] Pavel Parzuchowski,§[a] Alejandro Garcia-Carrera,[b] Cordula Grüttner,[c] Jean-François Dozol[b] and Volker Böhmer[a]

[a] *Fachbereich Chemie und Pharmazie, Abteilung Lehramt Chemie, Johannes-Gutenberg-Universität, Duesbergweg 10-14, Mainz, D-55099, Germany*
[b] *CEA Cadarache, DCC/DESD/SEP/LPTE, St. Paul lez Durance, F-13108, France*
[c] *micromod Partikeltechnologie GmbH, Friedrich-Barnewitz-Str. 4, D-18119 Rostock, Germany, www.micromod.de*

Received (in Cambridge, UK) 4th December 2000, Accepted 23rd January 2001
First published as an Advance Article on the web 14th February 2001

A novel particulate system carrying CMPO ligands pre-organised on a calixarene scaffold has been synthesised and demonstrated to extract Eu^{3+}, Am^{3+} and Ce^{3+} at high efficiency from simulated nuclear waste streams.

The recovery of lanthanides and actinides from high level nuclear waste is an area of world-wide concern. Current approaches are based on the TRUEX process which utilises the highly efficient, neutral, organophosphorus ligand; octyl(phenyl)(*N*,*N*-diisobutylcarbamoylmethyl)phosphine oxide (CMPO).[1] Previously, we have reported calix[4]arene-based extractants which incorporate CMPO moieties at either the wide[2,3] or narrow rim.[4] Such pre-organisation of the chelating ligands leads to a 100-fold (or greater) increase[2] in extraction efficiency combined with an enhanced selectivity for actinides and lighter lanthanides.[5]

Recently, interest has been focused on magnetic fluidised bed separation technology and the development of magnetically assisted chemical separation (MACS) systems for nuclear waste remediation.[6] These combine the selectivity of a ligand developed for liquid/liquid extraction with improved separation due to the magnetic field, resulting in an effective system suitable for use at low concentrations. Adsorption of CMPO to magnetic polyacrylamide particles enhances extraction of americium and plutonium through a putative synergistic relationship between the extractant and magnetic particle.[7–9]

Here we report the first extraction results, for lanthanides and actinides, obtained with magnetic and non-magnetic silica particles[10] which allow evaluation of the role of pre-organisation of chelating groups through direct comparison of CMPO-substituted calixarenes and derivatives with single CMPO groups. Unlike previously reported systems, in which the extractant is adsorbed onto magnetic particles, our system uses covalent attachment of ligands to the particle surface, allowing controlled ligand loading with defined orientation.

Ligands carrying amines were developed for straightforward attachment to silica particles modified with carboxylic acids. The simple ligand **1** was easily synthesised by monoacylation of 1,5-diaminopentane with 4-nitrophenyl(diphenylphosphoryl)-acetate.[2] In contrast, the calix[4]arene-based system[11] **8** was designed to allow chelation at the wide rim and attachment *via* a two-point interaction at the narrow rim. The multi-step synthesis is outlined in Scheme 1.¶ Selective 1,3 alkylation at the narrow rim with *N*-(3-bromopropyl)phthalimide enabled incorporation of masked amines, whilst subsequent treatment of the remaining 2,4-positions with bromopropane fixed the calix[4]arene in the desired *cone* conformation. *ipso*-Nitration[12]

† Electronic supplementary information (ESI) available: full synthetic procedures and extraction studies. See http://www.rsc.org/suppdata/cc/b0/b009679m/

‡ Present address: Inorganic Chemistry Laboratory, University of Oxford, South Parks Road, Oxford, UK OX1 3QR. E-mail: susan.matthews@chem.ox.ac.uk

§ Present address: Faculty of Chemistry, Warsaw University of Technology, Warsaw PL-00664, Poland

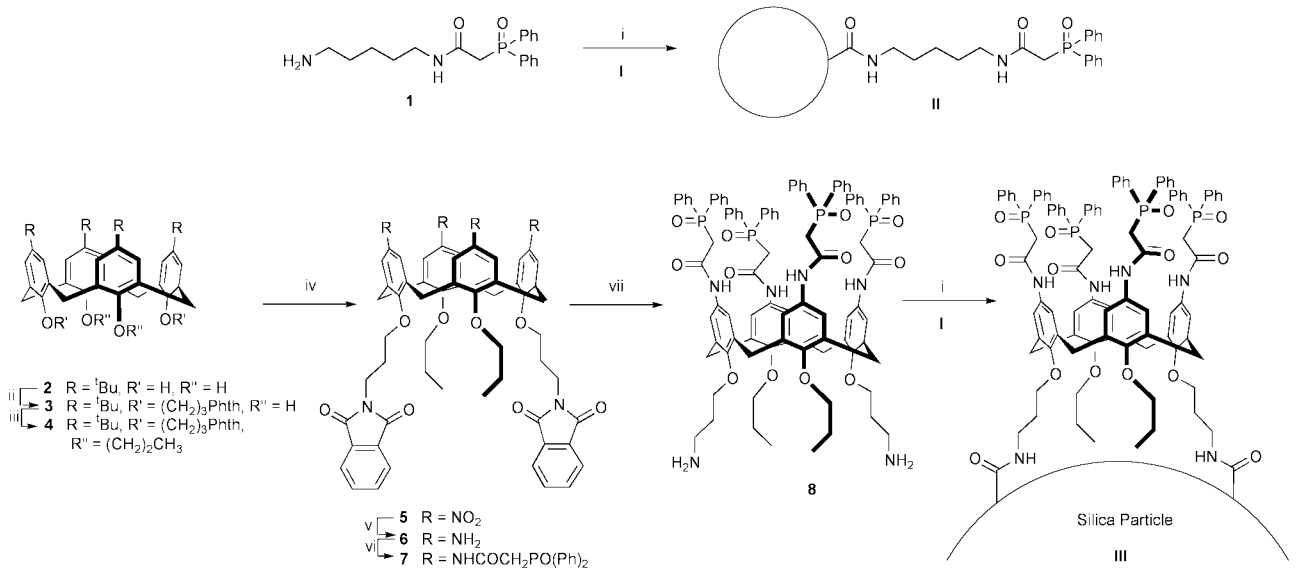

Scheme 1 Synthesis of CMPO particles. *Reagents and conditions*: i, preactivated polymeric beads (I), quant.; ii, $Br(CH_2)_3Phth$, K_2CO_3, MeCN, reflux, 48 h, 68%: iii, $Br(CH_2)_2Me$, NaH, DMF, 2 d, 82%; iv, TFA, HNO_3 (fuming), CH_2Cl_2, 30 min, 65%; v, $Sn(II)Cl_2$, EtOH, reflux, 18 h, 89%; vi, *p*-nitrophenyl(diphenylphosphoryl)acetate, toluene, 50 °C, 68%; vii, hydrazine hydrate, EtOH, reflux, 1 h, 96%.

followed by reduction [Sn(II)Cl_2] yielded the tetraamine derivative **6** which could be effectively acylated to give the pre-organised ligand **7**. Removal of the phthalimide protecting groups gave the required amino ligand **8**.

The amino CMPO derivatives **1** and **8** were covalently bound to the surface of carboxylic acid modified magnetic (**I_m**) and (for comparison) non-magnetic (**I_n**) silica particles *via* carbodiimide activation. The optimal binding capacity of *ca*. 50 μmol CO_2H functions per g particles was determined by preliminary electrokinetic studies. An equivalent loading of CMPO units on the particle surface was achieved through stoichiometric treatment of the particles with either 50 μmol g^{-1} of compound **1** containing a single CMPO unit or with 12.5 μmol g^{-1} of calixarene **8** containing four pre-organised CMPO units.

Solid–liquid extraction experiments were performed under conditions that simulate European nuclear waste streams (4 M $NaNO_3$, 1 M HNO_3). Separation of europium, cerium or americium, as representatives of the early lanthanides and actinides, was evaluated. γ-Ray spectroscopic measurements of the initial nuclide activity in the aqueous phase and the activity after shaking with the particles were used to calculate the percentage extraction (%E = $100(A_0 - A)/A_0$ where A_0 and A symbolise the initial and final activity of the aqueous phase) (Table 1).‖

Table 1 Percentage extraction of lanthanides and actinides by CMPO and CMPO–calix[4]arene silica particles

	^{152}Eu	^{241}Am	^{139}Ce
Non-magnetic silica particles			
I_n	0	0	—
II_n	3	12	—
III_n	62	88	—
Magnetic silica particles			
I_m	4	0	9
II_m	2	1	9
III_m	78	82	92

Attachment of simple CMPO ligands directly onto the particle surface (**II**) enables extraction of the trivalent cations, albeit at a very low level which is only slightly higher than for the untreated silica particles (**I**). However, the calix[4]arene-based particles (**III**), with a comparable concentration of ligating functions, show a significantly higher level of extraction of all cations studied. This demonstrates the importance of pre-organisation of the chelating ligands on a suitable macrocyclic scaffold, prior to their attachment at the particle surface.

Partition coefficients for europium extraction are comparable to those seen for the particulate systems with adsorbed ligands.[13] However, in contrast, larger K_D values per mass of particles are found for americium. Taking into account the lower density of ligands on the particle (50 μmol g^{-1} *vs*. 4.8 mmol g^{-1}), the apparent K_D ($\approx$425 ml g^{-1} *vs.* 3500 ml g^{-1}) represents a *ca*. 12-fold advantage in extraction. This reinforces the importance of initial pre-organisation in imparting selectivity. CMPO extractants, such as octyl(phenyl)(*N*,*N*-diisobutylcarbamoylmethyl)phosphine oxide are unable to discriminate greatly between actinides and lanthanides showing only a slight preference for the heavier lanthanides. In contrast, it has previously been shown, with non-particulate systems,[2,3] that incorporation onto a calix[4]arene allows differentiation between the actinides and lanthanides based on their cationic radii, the actinides and lighter lanthanides with larger radii being extracted more efficiently.

Interestingly, preliminary results on the extraction of ^{139}Ce for the magnetic particles are in marked contrast to those found previously for flexible wide-rim CMPO-calix[4]arenes.[3] The minimal extraction of cerium by CMPO-calix[4]arenes, has been rationalised by the oxidation of Ce^{3+} to the smaller radius Ce^{4+} in the extremely acidic extraction conditions. However, with the solid–liquid extraction conditions reported here, 90% extraction of cerium is achieved within 19 h of shaking, providing an opportunity for effective and selective separation of this cation.

Both non-magnetic and magnetic particles proved effective in the extraction of lanthanides and actinides. However, the ease of separation of magnetic particles from the waste stream using magnetic fluidised bed techniques makes this system more attractive for future industrial development.

These preliminary results are the starting point for a novel MACS process based on particles bearing pre-organised CMPO-calix[4]arenes as ligands. Efficient extraction of americium and europium from simulated nuclear waste conditions has been achieved together with surprisingly high levels of cerium sequestration. Currently, we are developing a range of particulate systems based on suitably functionalised conformationally mobile and narrow-rim CMPO-calix[4]arenes and extending the system to industrial applications.

These studies were supported by the Commission of the European Communities (contract F12W-CT96-0022).

Notes and references

¶ Full synthetic procedures are given in the supplementary material (ESI†).

‖ Methods for extraction studies are reported in the supplementary material (ESI†). Distribution coefficients are defined as $K_D = (A_0 - A)V/Am$ with V = volume of the aqueous phase and m = mass of the particles.

1 E. P. Horwitz, D. G. Kalina, H. Diamond, D. G. Vandegrift and W. W. Schultz, *Solv. Extr. Ion Exch.*, 1985, **3**, 75.
2 F. Arnaud-Neu, V. Böhmer, J.-F. Dozol, C. Grüttner, R. A. Jakobi, D. Kraft, O. Mauprivez, H. Rouquette, M.-J. Schwing-Weill, N. Simon and W. Vogt, *J. Chem. Soc., Perkin Trans. 2*, 1996, 1175.
3 S. E. Matthews, M. Saadioui, V. Böhmer, S. Barboso, F. Arnaud-Neu, M-J. Schwing-Weill, A. Garcia-Carrera and J.-F. Dozol, *J. Prakt. Chem.*, 1999, **341**, 264.
4 S. Barboso, A. Garcia-Carrera, S. E. Matthews, F. Arnaud-Neu, V. Böhmer, J.-F. Dozol, H. Rouquette and M.-J. Schwing-Weill, *J. Chem. Soc., Perkin Trans. 2*, 1999, 719.
5 L. H. Delmau, N. Simon, M.-J. Schwing-Weill, F. Arnaud-Neu, J.-F. Dozol, S. Eymard, B. Tournois, V. Böhmer, C. Grüttner, C. Musigmann and A. Tunayar, *Chem. Commun.*, 1998, 1627.
6 L. Nuñez and M. D. Kaminski, *CHEMTECH*, 1998, 41.
7 L. Nuñez, B. A. Buchholz and G. F. Vandegrift, *Sep. Sci. Technol.*, 1995, **30**, 1455.
8 L. Nuñez, B. A. Buchholz, M. Kaminski, S. B. Aase, N. R. Brown and G. F. Vandegrift, *Sep. Sci. Technol.*, 1996, **31**, 1393.
9 M. D. Kaminski, L. Nuñez and A. E. Visser, *Sep. Sci. Technol.*, 1999, **34**, 1103.
10 For a general survey, see: *Scientific and Clinical Applications of Magnetic Carriers*, ed. U. Häfeli, W. Schütt, J. Teller and M. Zborowski, Plenum Press, New York, 1997. Nonmagnetic (sicastar®) and magnetic (sicastar®-M) silica particles used in these studies are available from micromod Partikeltechnologie GmbH (www.micromod.de).
11 For general reviews on calixarenes see: V. Böhmer, *Angew. Chem.*, 1995, **107**, 785; C. D. Gutsche, *Calixarenes Revisited*, Royal Society of Chemistry, Cambridge, 1998.
12 P. J. A. Kenis, O. F. J. Noordman, N. F. van Hulst, J. F. J. Engbersen, D. N. Reinhoudt, B. H. M. Hams and C. P. J. M. van der Vorst, *Chem. Mater.*, 1997, **9**, 596.
13 M. Kaminski, S. Landsberger, L. Nuñez and G. F. Vandegrift, *Sep. Sci. Technol.*, 1997, **32**, 115.

ChemComm

Electrostatic and covalent immobilisation of enzymes on ITQ-6 delaminated zeolitic materials

A. Corma,*[a] V. Fornés,[a] J. L. Jordá,[a] F. Rey,[a] R. Fernandez-Lafuente,[b] J. M. Guisan[b] and C. Mateo[b]

[a] *Instituto de Tecnología Química (UPV-CSIC), Universidad Politécnica de Valencia, Avda. de los Naranjos s/n, 46022 Valencia, Spain. E-mail: acorma@itq.upv.es*

[b] *Instituto de Catálisis y Petroleoquímica (CSIC), Departamento de Biocatálisis, Campus de la UAM, Cantoblanco, 28049 Madrid, Spain*

Received (in Cambridge, UK) 16th November 2000, Accepted 4th January 2001
First published as an Advance Article on the web 13th February 2001

ITQ-6, a delaminated material derived from the lamellar precursor of the Ferrierite zeolite, is an excellent support for immobilisation of enzymes; this has been proved by supporting two different enzymes, β-galactosidase from *Aspergillus Oryzae* and penicillin G acylase from *Escherichia Coli*, by electrostatic and covalent interactions, respectively; the adequacy and versatility of the ITQ-6 support and the high stability and catalytic activity of the resultant supported enzymes are shown, with ITQ-6 clearly superior to other already well optimised laboratory and industrial supports for enzymes.

It is well known that enzymes are the most active and selective catalysts for many reactions of commercial interest. However, their low thermal and/or solvent stability and difficult recycling are the major drawbacks for a broader industrial application. In order to improve the stability and performance of enzymes as catalysts, they have been supported in a variety of solids which include organic gels, resins, silicas[1–5] or more recently mesoporous molecular sieves such as MCM-41 or SBA-15.[6–8] Inorganic supports have the advantage of allowing the regeneration of the carrier when the enzyme has been deactivated. Moreover, in the case of ordered mesoporous materials a good selectivity to some enzymes can be obtained by varying the pore diameter and functional groups of the support.[8] Unfortunately, owing to the limited stability in aqueous media of some of these materials and the large steric volume of many enzymes which can result in the blocking of the channels, their possibilities as useful catalysts will be limited. Recently, a series of delaminated zeolites have been obtained as crystalline materials with a well defined external surface area of >600 m^2 g^{-1}, easily accessible to very large molecules, and containing regularly distributed silanol groups.[9,10] By taking advantage of these remarkable properties, it appears that this type of material can offer new opportunities as supports for enzymes.

Generally speaking, with conventional supports, enzyme immobilisation *via* covalent bonding has the advantage of forming strong and stable linkages that result in very robust enzyme supported catalysts. However, the irreversible covalent binding has the drawback that enzyme and support are disposed as waste after deactivation.[1–5,11–13] However, as shown here, when a delaminated zeolite, ITQ-6[10] is used as support, this can be easily recovered and recycled simply by calcination.

There are other cases in where the reversible electrostatic immobilisation of enzymes on pre-existing supports could be of industrial interest. If the enzyme becomes deactivated and can not be further used in the industrial reactor, it can be desorbed and the support can be recovered free of protein, and so available for a new immobilisation of a fresh solution of soluble enzyme.[14] Again, the surface of a delayered zeolite, such as ITQ-6,[10] appears to be highly suitable for activation and use as a reversible enzyme support.

ITQ-6, a delaminated material derived from the lamellar precursor of the Ferrierite zeolite,[10] is an excellent support for immobilisation of enzymes. This has been proved by supporting two different enzymes, β-galactosidase from *Aspergillus Oryzae* and penicillin G acylase from *Escherichia Coli*, by electrostatic and covalent interactions, respectively. The suitability and versatility of the ITQ-6 support and the high stability and catalytic activity of the resultant supported enzymes represent an alternative to other well optimised laboratory and industrial supports for enzymes.

Pure silica ITQ-6, with a specific surface area of 600 m^2 g^{-1} and 0.75 cm^3 g^{-1} pore volume was prepared by a procedure reported previously.[10]

ITQ-6 was functionalised by reacting a solution of 3-aminopropyltriethoxysilane (APS) in toluene with dehydrated ITQ-6 samples resulting in aminopropyl functionalised ITQ-6, denoted N-ITQ-6. When this material (1.0 g) was contacted with a solution of β-galactosidase enzyme (60 mg) from *Aspergillus Oryzae* (MW = 105 kD, pI < 6) to achieve its electrostatic immobilisation on the N-ITQ-6 carrier, it was found that the adsorption of the enzyme was > 99% within 1 h. The amount of adsorbed enzyme was determined from the activity of the resulting solution, after removal of the solid, for the hydrolysis of *o*-nitrophenyl-β-D-galactopiranoside (ONPG) using a 100 mM acetate buffer at pH = 4.5 and 298 K. Hydrolysis of ONPG was monitored by the appearance of a characteristic band of the hydrolysis product at 405 nm. In order to check that the negligible activity of the liquid phase is due to the adsorption of the enzyme onto the solid and not to the deactivation of the enzyme, the solid was recovered and used to catalyse the hydrolysis of ONPG. It is remarkable that the activity of the electrostatically supported enzyme was the same as the activity of the free enzyme before adsorption (the absorbances at 405 nm of the reaction mixtures after 7 min of reaction were 0.43 and 0.41 for the supported and free enzymes, respectively), indicating that all the enzyme has been immobilised, and more importantly, it remains active and accessible to the reactants upon immobilisation. No activity was found when the support, prior of adsorption of the enzyme, was used as catalyst. Also, no leaching of the supported enzyme was detected as can be concluded from the zero activity observed in the reaction media after filtering off the enzyme containing solid.

The immobilised enzyme is highly stable even in contact with solutions of relatively high ionic strength. Specifically, 98% of the immobilised enzyme is still retained on the N-ITQ-6 support in 0.30 M NaCl medium, as determined from the enzyme activity of the resulting solution after removal of the supported enzyme. This level of enzyme retention is much higher than observed for most traditional supports, and it is at least as high as that found for the best performance highly optimised supports (Fig. 1). When desired, the enzymes can be desorbed from N-ITQ-6 by increasing the NaCl concentration of the eluent solution to 1 M. This allows the regeneration of the carrier after the enzyme deactivation in the same reactor or in a fixed bed. At this point the support is ready to be recharged again with enzyme simply by contacting again the regenerated N-ITQ-6 carrier with a fresh solution of the enzyme in the appropriate conditions.

DOI: 10.1039/b009232k

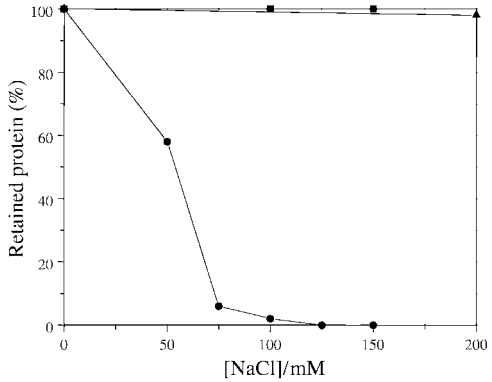

Fig. 1 Desorption of β-galactosidase from *A. Oryzae* adsorbed on diverse supports by increasing ionic strength. (▲) N-ITQ-6; (■) PEI–glyoxil–agarose composite (from ref. 14); (●) DEAE–agarose (from ref. 14).

Up to now, enzymes have been supported into mesoporous molecular sieves *via* electrostatic bonding.[6–8] However, for ITQ-6, the enzymes can also be easily supported by covalent bonding resulting in extremely stable catalysts. To do this, a portion of N-ITQ-6 was reacted with a solution of glutaraldehyde at pH = 7 yielding to a material denoted G-ITQ-6. This solid contains imine and aldehyde functional groups and now is ready for covalently immobilising the enzymes by reacting the amino groups of the enzyme with the anchored aldehyde groups at pH = 8, forming imine bonds which are further reduced with sodium borohydride to secondary amines (Scheme 1).

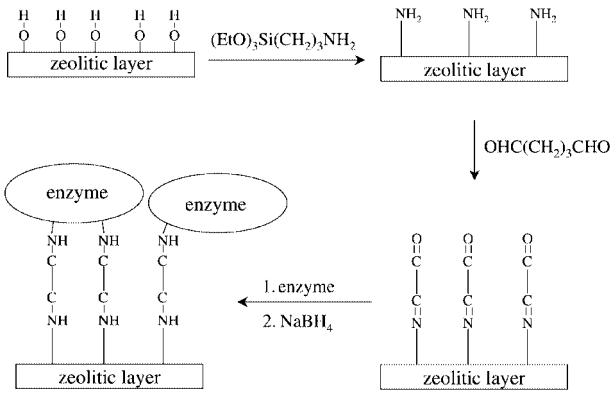

Scheme 1 Covalent immobilisation of enzymes on delaminated mesoporous materials.

Following the above procedure, 2050 IU of a highly voluminous enzyme, penicillin G acylase (PGA, MW = 86000) was immobilised. The catalytic activity and accessibility under reaction conditions of the covalently bonded enzyme were studied by performing the hydrolysis of penicillin G at pH = 8 and 298 K. The progress of the reaction was followed by continuous titration of the released protons with a 25 mM NaOH solution using an automatic burette. In this way, the activity of the supported enzyme was found to be 2440 IU g^{-1} of G-ITQ-6 indicating that the supported enzyme is very active and accessible to the penicillin G reactant.

Moreover, we have proved that the enzyme covalently bonded to the G-ITQ-6 support displays higher stability by comparing its deactivation rate with that of the free enzyme and also with PGA chemically bonded to amorphous silica, which has been widely used as an inorganic carrier of enzymes[15] and particularly for PGA.[16] In order to perform this experiment, aliquots of the covalently supported enzymes on both ITQ-6 and amorphous silica supports (200 IU g^{-1} support) or equivalent amounts of free enzyme were incubated in a 100 mM phosphate buffer at pH = 8 and 319 K for different times. Then, the activity for hydrolysis of penicillin G was measured and compared to that obtained for the non-incubated enzyme. The

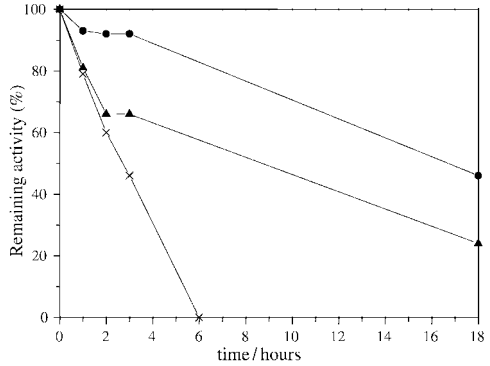

Fig. 2 Deactivation of penicillin G acylase at 319 K and pH = 8 in 100 mM phosphate buffer. (×) Free enzyme remaining activity; (▲) glutaraldehyde-modified silica immobilised enzyme remaining activity; (●) G-ITQ-6 immobilised enzyme remaining activity. Penicillin G hydrolysis reaction was carried out at 298 K and pH = 8, using 25 mM NaOH solution as a titrant.

results shown in Fig. 2 indicate that the stability of the enzyme is substantially improved when it is covalently bonded to the surface of the G-ITQ-6, in such a way that, while the activity of the unsupported enzyme was zero after 6 h of incubation, the remaining activity of the supported enzyme was close to 90%. This value was also clearly higher than that found for the enzyme supported on amorphous silica (60%), The increase in the enzyme stability suggests a multipoint attachment between the enzyme and the supports, perhaps involving the most reactive groups of the protein surface. Moreover, it is reasonable to suppose that a well structured surface, such as that found on ITQ-6, may facilitate the interactions with the enzyme and the dispersion forces might have a positive effect on the enzyme stability.

In conclusion, ITQ-6, owing to its well structured high external surface area and by regularly distributed silanol groups, opens new possibilities for supporting and stabilising many enzymes and using them for reaction with large substrates. It has been proved that the enzymes can be adequately supported by either ionic or covalent bonding whilst retaining full activity.

We thank the Spanish CICYT for financial support (Project MAT97-1016-C02-01 and MAT97-1207-C03-01). J. L. J. thanks the M. E. C. for a doctoral fellowship).

Notes and references

1 I. Chibata, T. Tosa and T. Sato, *J. Mol. Catal.*, 1986, **37**, 1.
2 A. Rosevear, *J. Chem. Technol. Biotechnol. B*, 1984, **34**, 127.
3 G. P. Royer, *Catal. Rev.*, 1980, **22**, 29.
4 A. M. Klibanov, *Science*, 1983, **219**, 722.
5 J. F. Kennedy, E. H. M. Melo and K. Jumel, *Chem. Eng. Prog.*, 1990, **45**, 81.
6 J. F. Diaz and K. J. Balkus, *J. Mol. Catal. B, Enzymatic*, 1996, **2**, 115.
7 M. E. Gimonkinsel, V. L. Jimenez, L. Washmon and K. J. Balkus, *Stud. Surf. Sci. Catal.*, 1998, **117**, 373.
8 Y. J. Han, G. D. Stucky and A. Butler, *J. Am. Chem. Soc.*, 1999, **121**, 9897.
9 A. Corma, V. Fornés, S. B. Pergher, T. L. M. Maesen and J. G. Buglass, *Nature*, 1998, **396**, 353.
10 A. Corma, U. Diaz, M. E. Domine and V. Fornés, *J. Am. Chem. Soc.*, 2000, **122**, 2804.
11 M. N. Gupta, *Biotechnol. Appl. Biochem.*, 1991, **14**, 1.
12 W. Hartmeier, *Trends Biotechnol.*, 1985, **3**, 149.
13 E. Katchalski-Katzir, *Trends Biotechnol.*, 1993, **11**, 471.
14 C. Mateo, O. Abian, R. Fernandez-Lafuente and J. M. Guisan, *Biotechnol. Bioeng.*, 2000, **68**, 98.
15 J. V. Sinisterra, *Immobilization of enzymes and cells (Methods in Biotechnology 1)*, ed. E. Gordon and F. Bickerstaff, Humana Press, Totowa, NJ, 1997, p. 331.
16 G. H. A. Pereira, J. M. Guisan and R. L. C. Giordanoi, *Braz. J. Chem. Eng.*, 1997, **14**, 327.

ChemComm

A rapid screening, 'combinatorial-type' survey of the metalloligand chemistry of $Pt_2(PPh_3)_4(\mu\text{-}S)_2$ using electrospray mass spectrometry

S.-W. Audi Fong,[a] Jagadese J. Vittal,[a] William Henderson,*[b] T. S. Andy Hor*[a] Allen G. Oliver[c] and Clifton E. F. Rickard[c]

[a] *Department of Chemistry, Faculty of Science, National University of Singapore, 3 Science Drive 3, Singapore 117543*

[b] *Department of Chemistry, University of Waikato, Private Bag 3105, Hamilton, New Zealand. E-mail: b.henderson@waikato.ac.nz*

[c] *Department of Chemistry, University of Auckland, Private Bag 92019, Auckland, New Zealand*

Received (in Cambridge, UK) 30th November 2000, Accepted 25th January 2001
First published as an Advance Article on the web 14th February 2001

Electrospray mass spectrometry is a rapid and powerful technique for a combinatorial-like survey of the chemistry of the metalloligand $Pt_2(PPh_3)_4(\mu\text{-}S)_2$, leading to the successful isolation and crystallographic characterisation of the novel protonated species $Pt_2(PPh_3)_4(\mu\text{-}S)(\mu\text{-}SH)$ together with a range of metallated derivatives.

The sulfido complex $Pt_2(PPh_3)_4(\mu\text{-}S)_2$ **1** has attracted much interest in recent years, particularly for its ability to act as a metalloligand in the assembly of a diverse range of sulfido-bridged higher nuclearity aggregates.[1,2] In this communication, we describe how electrospray mass spectrometry (ESMS) can be used as a rapid, powerful combinatorial-type tool for surveying the metalloligand chemistry of **1** with a range of metal substrates. The utility of ESMS as a general technique for the characterisation of coordination and organometallic complexes is well known,[3] but as far as we are aware there are no previous extensive studies which have used ESMS as the primary screening tool for surveying the reactivity of coordination complexes, the results of which are then used to target subsequent synthetic efforts. Advantages of this approach include the need for only minute amounts of material, rapid screening of potential substrates for further study, and the accepted general agreement between mass spectrometric data and solution speciation.[3] In parallel studies, we are investigating the reactivity of the selenide analogue $Pt_2(PPh_3)_4(\mu\text{-}Se)_2$.[4]

The positive-ion ES spectrum of **1** in methanol gives ions due to protonated **1**, $[\mathbf{1} + 2H]^{2+}$ (*m/z* 752) and $[\mathbf{1} + H]^+$ (*m/z* 1504), together with ions $[(\mathbf{1})_2 + Ag + H]^{2+}$ (*m/z* 1557) and $[(\mathbf{1})_2 + 2Ag]^{2+}$ (*m/z* 1611) formed by adventitious Ag^+ ions in the spectrometer. Addition of a small quantity of formic acid increased the intensity of the *m/z* 752 ion. The novel mono-protonated complex $[Pt_2(PPh_3)_4(\mu\text{-}S)(\mu\text{-}SH)]PF_6$ **2** was subsequently obtained by titration of **1** with HCl, followed by metathesis with NH_4PF_6. This complex, which is related to the monomethyl complex $[Pt_2(PPh_3)_4(\mu\text{-}S)(\mu\text{-}SMe)]^+$,[5] has not been isolated previously. Complex **2** gives two distinct ^{31}P NMR signals [δ 20.2, ^1J(PtP) 2705 and 23.0, ^1J(PtP) 3582, ^2J(PP) 15] together with a resonance for the SH proton at δ 3.48 in the ^1H NMR spectrum. Confirmation of its identity was obtained from an X-ray diffraction study, Fig. 1.† The dihedral angle of the four-membered Pt_2S_2 ring is 135°, which is similar to the methylated analogue $[Pt_2(PPh_3)_4(\mu\text{-}S)(\mu\text{-}SMe)]^+$ (138°).[5] There have only been two previous structural determinations on underivatised Pt(μ-sulfide)$_2$Pt systems, with [(dppe)Pt(μ-S)$_2$Pt(dppe)] being folded (140.2°)[6] and [(dppy)$_2$Pt(μ-S)$_2$Pt(dppy)$_2$] (dppy = 2-diphenylphosphinopyridine)[7] being planar. Structural features of such $\{M_2S_2\}$ systems has attracted recent interest.[1,8] The structure of **2** is the first containing the Pt–SH–Pt moiety, although μ-SH complexes of other metals such as palladium[9] and nickel[10] have been structurally characterised.

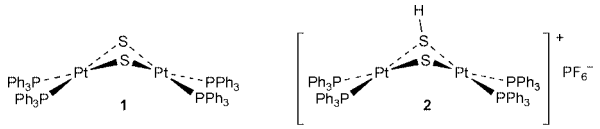

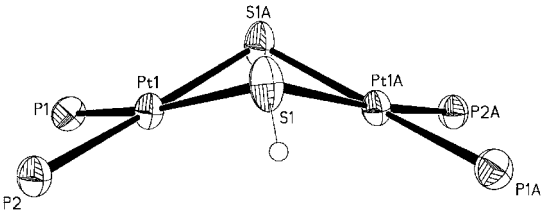

Fig. 1 Molecular structure of $[Pt_2(PPh_3)_4(\mu\text{-}S)(\mu\text{-}SH)]PF_6$ **2**. The phenyl rings of the PPh_3 ligands have been omitted for clarity. Selected bond distances (Å) and angles (°): Pt(1)–S(1) 2.3289(8), Pt(1)–S(1A) 2.3536(8), Pt(1)–P(1) 2.2965(8), Pt(1)–P(2) 2.2712(8), Pt(1)–S(1)–Pt(1A) 91.01(3), Pt(1)–S(1A)–Pt(1A) 91.01(3), S(1)–Pt(1)–S(1A) 78.91(4), S(1)–Pt(1A)–S(1A) 78.91(4), P(1)–Pt(1)–P(2) 98.97(3), P(1)–Pt(1)–P(2) 98.97(3), P(1)–Pt(1)–S(1) 167.60(3), P(2)–Pt(1)–S(1) 92.88(3), P(1)–Pt(1)–S(1A) 89.06(3), P(2)–Pt(1)–S(1A) 171.27(3).

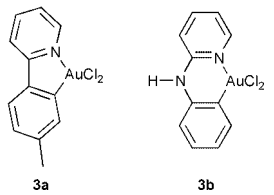

The reactivity of complex **1** towards a range of halide-containing main group (*e.g.* Sn and Hg) and transition metal (*e.g.* Au) complexes can conveniently be monitored by ESMS, and allows the identification of novel, sulfide-bridged aggregates. As an illustrative example, the reaction of **1** with the organogold(III) complexes $AuCl_2$(tolpy) **3a**[11] and $AuCl_2$(pap) **3b**[12] monitored by positive-ion ESMS shows a single major peak in each case, due to the aggregate cations $[Pt_2(PPh_3)_4(\mu_3\text{-}S)_2Au(tolpy)]^{2+}$ and $[Pt_2(PPh_3)_4(\mu_3\text{-}S)_2Au(pap)]^{2+}$, as illustrated for the pap system in Fig. 2, with excellent agreement between observed and calculated isotope patterns. On a synthetic scale, metathesis of the $AuCl_2$(tolpy) reaction solution with NH_4BF_4 gave yellow $[Pt_2(PPh_3)_4(\mu_3\text{-}S)_2Au(tolpy)][BF_4]_2$ **4**, Fig. 3.‡ While there have been several studies on aggregates with $\{M_3S_2\}$ cores containing Pt and Pd,[1,13] this is the first time that the isoelectronic gold(III) centre has been incorporated, though gold(I) and silver(I) derivatives of the $\{Pt_2S_2\}$ core have been known for some time.[1,14] The isolation of silver(I) halide aggregates containing the isoelectronic $\{Au^{III}_2S_2\}$ core has been reported.[15] The successful formation of **4** is facilitated by the increased stability towards reduction (by sulfur-based ligands) of gold(III) complexes bearing *N,C*-cyclometallated ligands.[16] The structure confirms the formulation of **4** as the

DOI: 10.1039/b009616b

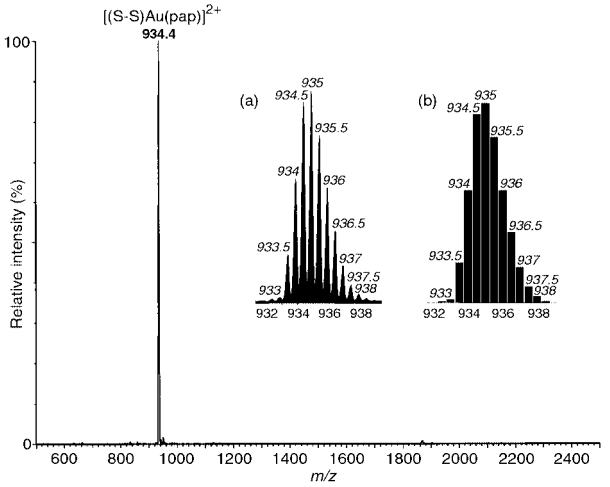

Fig. 2 Positive ion ES spectrum of a 1:1 mixture of **1** and $AuCl_2$(pap) **3b** in MeOH at a cone voltage of 20 V, demonstrating the facile and exclusive formation of $[Pt_2(PPh_3)_4(\mu_3\text{-}S)_2Au(pap)]^{2+}$. The inset shows (a) observed and (b) calculated isotope patterns for the dication.

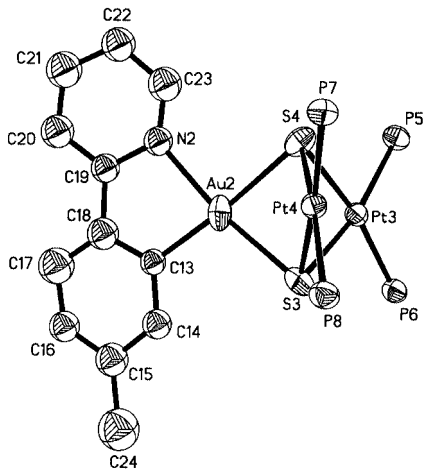

Fig. 3 Molecular structure of one of the cations of $[Pt_2(PPh_3)_4(\mu_3\text{-}S)_2Au(tolpy)][BF_4]_2$ **4** with thermal ellipsoids at the 50% probability level. The phenyl rings of PPh_3 have been omitted for clarity. Selected bond distances (Å) and angles (°): Pt(3)–S(3) 2.371(3), Pt(3)–S(4) 2.362(3), Pt(4)–S(3) 2.377(3), Pt(4)–S(4) 2.360(3), Au(2)–S(3) 2.357(4), Au(2)–S(4) 2.371(4), Pt(3)–P(5) 2.302(3), Pt(3)–P(6) 2.274(3), Pt(4)–P(7) 2.269(3), Pt(4)–P(8) 2.296(3), Au(2)–C(13) 1.94(3), Au(2)–N(2) 2.18(2), Pt(3)–S(3)–Pt(4) 87.66(11), Pt(3)–S(4)–Pt(4) 88.25(11), Pt(3)–S(3)–Au(2) 82.81(11), Pt(3)–S(4)–Au(2) 82.68(11), Pt(4)–S(3)–Au(2) 82.42(11), Pt(4)–S(4)–Au(2) 82.46(11), S(3)–Pt(3)–S(4) 78.20(12), S(3)–Pt(4)–S(4) 78.12(12), P(5)–Pt(3)–P(6) 99.92(12), P(7)–Pt(4)–P(8) 98.92(12), P(5)–Pt(3)–S(3) 167.06(12), S(3)–Au(2)–S(4) 78.31(11), C(13)–Au(2)–N(2) 81.0(9).

first heterometallic aggregate of the $\{Pt_2S_2\}$ core containing gold(III), and the presence of the methyl group allows for unambiguous assignment of N(1) and C(1) on the square-planar gold atom. The $\{Pt_2S_2\}$ ring is, as expected, puckered (126.8°) with average Au–S bond distances 2.358(2) Å.

The successful isolation and characterisation of the novel species, initially identified by mass spectrometry experiments, clearly demonstrates the power of this methodology. It helps researchers to identify possible products before they are synthesized on a macroscopic scale. This pre-synthesis scanning helps to cut down wastage and increases the chance of achieving successful syntheses. Extension to organotin(IV) halides leads to the successful isolation of a range of adducts of complex **1** with $SnMeCl_2^+$, $SnMe_2Cl^+$, and $SnPhCl_2^+$ moieties (derived from $SnMeCl_3$, $SnMe_2Cl_2$ and $SnPhCl_3$, respectively), their formulation being confirmed by single crystal X-ray diffraction studies. Full details will be reported in due course. Although **1** is a good model for this methodology, it is neither unique nor exclusive. One can anticipate similar success in other systems.

We thank the National University of Singapore and the University of Waikato for financial support of this work, including a visiting scholarship (to S.-W. A. F.), and G. K. Tan for assistance with the X-ray crystallography.

Notes and references

† Crystal data for **2**·CH_2Cl_2: $C_{73}H_{62.5}Cl_2F_6P_5Pt_2S_2$, M = 1733.78, monoclinic, space group $C2/c$, a = 21.3742(6), b = 18.7308(6), c = 17.1833(5) Å, β = 90.025(1)°, V = 6879.4(4) Å^3, T = 223(2) K, Z = 4, ρ_{calc} = 1.674 g cm^{-3}, λ(Mo-Kα) = 0.71073 Å, μ(Mo-Kα) = 4.376 mm^{-1}, 17188 reflections measured, 6043 unique (R_{int} = 0.0217) which were used in all calculations. The data were collected on a Bruker AXS SMART diffractometer and solved by direct methods in conjunction with standard difference Fourier techniques. Non-hydrogen atoms were refined anisotropically and hydrogen atoms were included at calculated positions. Refinement converged to R_F = 0.0218, $wR(F^2)$ = 0.0518 (all data).

‡ *Crystal data* for **4**: $C_{168}H_{130}Au_2B_2F_8N_2P_8Pt_4S_4$, M = 3900.65, triclinic, space group = $P\bar{1}$, a = 18.0900(2), b = 21.3643(2), c = 23.0658(2) Å, α = 98.643(1), β = 95.966(1), γ = 93.923(1)°, V = 8733.4(2) Å^3, T = 220(2) K, Z = 2, ρ_{calc} = 1.483 g cm^{-3}, λ(Mo-Kα) = 0.71073 Å, μ(Mo-Kα) = 5.040 mm^{-1}, 83105 reflections measured, 30322 unique (R_{int} = 0.0562) which were used in all calculations. There are two independent cations present, one of which exhibits little disorder. In the other cation, the tolpy ligand is disordered (occupancies 50:50). Isotropic thermal parameters of all the non-hydrogen atoms of the disordered ligands were refined. The two BF_4^- anions show high thermal activities; one BF_4^- was disordered (occupancies 70:30), and the anion with 70% occupancy was found to be further disordered along one B–F axis (40:30). Refinement converged normally with R_F = 0.0735, $wR(F^2)$ = 0.1208 (all data). CCDC 154466–154467. See http://www.rsc.org/suppdata/cc/b0/b009616b/ for crystallographic data in .cif or other electronic format.

1 S.-W. A. Fong and T. S. A. Hor, *J. Chem. Soc., Dalton Trans.*, 1999, 639.
2 Selected recent references: Z. Li, X. Xu, S. B. Khoo, K. F. Mok and T. S. A. Hor, *J. Chem. Soc., Dalton Trans.*, 2000, 2901; H. Liu, C. Jiang, J. S. L. Yeo, K. F. Mok, L. K. Liu, T. S. A. Hor and Y. K. Yan, *J. Organomet. Chem.*, 2000, **595**, 276.
3 W. Henderson, B. K. Nicholson and L. J. McCaffrey, *Polyhedron*, 1998, **17**, 4291; R. Colton, A. D'Agostino and J. C. Traeger, *Mass Spectrom. Rev.*, 1995, **14**, 79; I. I. Stewart, *Spectrochim. Acta, Part B*, 1999, **54**, 1649.
4 J. S. L. Yeo, J. J. Vittal, W. Henderson and T. S. A. Hor, *J. Chem. Soc., Dalton Trans*, 2001, 315.
5 C. E. Briant, C. J. Gardner, T. S. A. Hor, N. D. Howells and D. M. P. Mingos, *J. Chem. Soc., Dalton Trans.*, 1984, 2645.
6 M. Capdevila, Y. Carrasco, W. Clegg, R. A. Coxall, P. Gonzáles-Duarte, A. Lledós, J. Sola and G. Ujaque, *Chem. Commun.*, 1998, 597.
7 V. W.-W. Yam, P. K.-Y. Yeung and K.-K. Cheung, *J. Chem. Soc., Chem. Commun.*, 1995, 267.
8 M. Capdevila, W. Clegg, P. González-Duarte, A. Jarid and A. Lledós, *Inorg. Chem.*, 1996, **35**, 490.
9 S. Wirth and D. Fenske, *Z. Anorg. Allg. Chem.*, 1999, **625**, 2064.
10 R. J. Pleus, H. Waden, W. Saak, D. Haase and S. Pohl, *J. Chem. Soc., Dalton Trans.*, 1999, 2601.
11 S. J. Faville and W. Henderson, unpublished results.
12 Y. Fuchita, H. Ieda, A. Kayama, J. Kinoshita-Nagaoka, H. Kawano, S. Kameda and M. Mikuriya, *J. Chem. Soc., Dalton Trans.*, 1998, 4095.
13 Z. Li, H. Liu, K. F. Mok, A. S. Batsanov, J. A. K. Howard and T. S. A. Hor, *J. Organomet. Chem.*, 1999, **575**, 223; M. Capdevila, Y. Carrasco, W. Clegg, R. A. Coxall, P. González-Duarte, A. Lledós and J. A. Ramírez, *J. Chem. Soc., Dalton Trans.*, 1999, 3103.
14 H. Liu, A. L. Tan, C. R. Cheng, K. F. Mok and T. S. A. Hor, *Inorg. Chem.*, 1997, **36**, 2916; C. E. Briant, T. S. A. Hor, N. D. Howells and D. M. P. Mingos, *J. Organomet. Chem.*, 1983, **256**, C15; W. Bos, J. J. Bour, P. P. J. Schlebos, P. Hageman, W. P. Bosman, J. M. M. Smits, J. A. C. van Wietmarschen and P. T. Beurskens, *Inorg. Chim. Acta*, 1986, **119**, 141; V. W.-W. Yam, P. K.-Y. Yeung and K.-K. Cheung, *Angew. Chem., Int. Ed. Engl.*, 1996, **35**, 739.
15 M. B. Dinger, W. Henderson, B. K. Nicholson and W. T. Robinson, *J. Organomet. Chem.*, 1998, **560**, 169.
16 Selected references: U. Abram, K. Ortner, R. Gust and K. Sommer, *J. Chem. Soc., Dalton Trans.*, 2000, 735; R. V. Parish, B. P. Howe, J. P. Wright, J. Mack, R. G. Pritchard, R. G. Buckley, A. M. Elsome and S. P. Fricker, *Inorg. Chem.*, 1996, **35**, 1659; M. A. Cinellu, G. Minghetti, M. V. Pinna, S. Stoccoro, A. Zucca and M. Manassero, *J. Chem. Soc., Dalton Trans.*, 1999, 2823.

Synthesis and properties of a stable, cationic, rhodium Lewis-acid catalyst for hydrosilation, Mukaiyama aldol and cyclopropanation reactions†

Eric L. Dias, Maurice Brookhart* and Peter S. White

Department of Chemistry, University of North Carolina at Chapel Hill, Chapel Hill, NC 27599-3290, USA. E-mail: mbrookhart@unc.edu

Received (in Irvine, CA, USA) 22nd September 2000, Accepted 9th January 2001
First published as an Advance Article on the web 14th February 2001

The remarkably stable cationic, three-coordinate, 14-electron rhodium complex 1 has been synthesized, isolated and used as a catalyst for hydrosilation, Mukaiyama aldol and cyclopropanation reactions.

Of the several different catalyst types available for organic reactions, the most diverse are probably the Lewis acids. Ranging from a simple proton to boranes or main group and transition metal complexes, Lewis-acid catalysts now allow for a variety of transformations to be accomplished efficiently and, in many cases, selectively.[1] The requirements for a Lewis-acid catalyst are straightforward: (1) the complex should be electrophilic, and (2) there should be a vacant coordination site. Here, we report the synthesis of the surprisingly stable, cationic, three-coordinate, 14-electron rhodium compound **1**.[2] Complexes of **1** with aldehydes and ketones are also described, in addition to preliminary studies employing **1** in catalytic reactions.

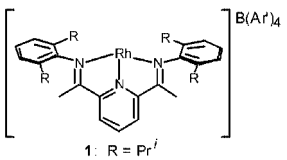

Addition of $NaB(Ar')_4$ [Ar′ = 3,5-bis(trifluoromethyl)phenyl] to a solution of the rhodium(I) chloride compound **2** in dichloromethane results in quantitative formation of the cationic complex **1** after 1–2 h at room temp., as evidenced by the change in solution color from dark green to orange [eqn. (1)].

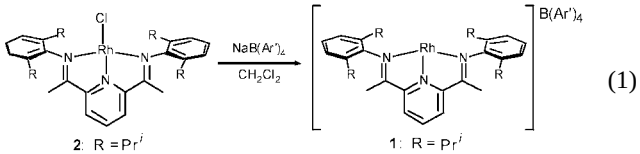

(1)

After removing the NaCl by cannula filtration, evaporation of the solvent yields **1** as a stable, dark orange solid which usually contains *ca*. 0.25 equiv. of CH_2Cl_2, as determined by ^1H NMR spectroscopy in d_8-THF. Although **1** can be stored under an inert atmosphere for an indefinite period of time, it is extremely susceptible to hydration, such that it is often more convenient to generate **1** *in situ* immediately prior to use in any subsequent experiments.

The stability of **1** towards the oxidative addition of dichloromethane, a reaction common to rhodium(I) complexes of this type,[3] is of particular significance.[4] Complex **1** was found to be stable in dichloromethane solution indefinitely at room temperature, and even at 40 °C. In addition, **1** can be heated to 70 °C in chlorobenzene without any decomposition. On the other hand, addition of 1 equiv. of methyl iodide to a dichloromethane solution of **1**, generated *in situ* from **2** and $NaB(Ar')_4$, results in quantitative formation of the rhodium(III) methyl iodide complex **3** after 15–20 min [eqn. (2)]. While we had previously

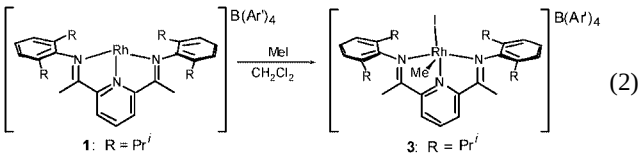

(2)

synthesized **3** from the ethylene-bound adduct of **1**,[5] this has proven to be a much more simple and convenient route.

The use of chlorinated solvents, whch are very weakly coordinating at best, allows the Lewis-acid characteristics of **1** to be fully exploited. For example, addition of 1 equiv. of either *p*-tolualdehyde or acetophenone to a dichloromethane solution of **1** produces the corresponding adducts **4a** and **4b** [eqn. (3)], which were isolated as stable solids. From the crystal

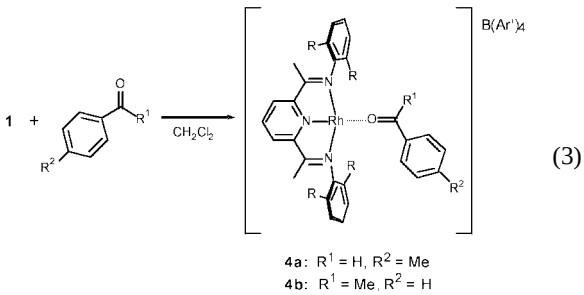

(3)

structure of the aldehyde complex **4a** (Fig. 1),[6] it can be seen that the aldehyde coordinates in an η^1 fashion. It is also apparent that the imine moieties of the ligand are pulled close to the metal center, such that the attached aryl groups create a 'wedge' in which the aldehyde binds. In fact, when hydrogens are included in the structure, the intramolecular distance of 2.70 Å between the aldehydic hydrogen and the centroid of one of the aryl rings

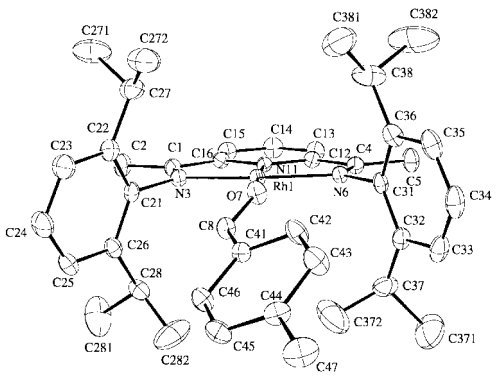

Fig. 1 X-Ray crystal structure of **4a**. Thermal ellipsoids are drawn at the 50% probability level. Selected bond lengths (Å) and angles (°): Rh(1)–O(7) 2.0728(18), Rh(1)–N(3) 2.0124(23), Rh(1)–N(11) 1.8854(20), O(7)–C(8) 1.227(3); Rh(1)–O(7)–C(8) 129.44(19), O(7)–Rh(1)–N(11) 174.81(9), N(6)–C(4)–C(12) 113.80(25), C(1)–N(3)–C(22) −104.8(6), N(3)–Rh(1)–O(7)–C(8) 41.5(3).

† Electronic supplementary information (ESI) available: experimental information, van't Hoff plot, temperature and equilibrium data, ^1H NMR spectrum of **1** and crystallographic data. See http://www.rsc.org/suppdata/cc/b0/b007815h/

suggests a van der Waals interaction with the aromatic π-cloud. Likewise, the distance of 3.06 Å between the *ortho*-protons on the *p*-tolualdehyde and the other ring indicates a potentially similar interaction. This geometry is verified by the ^{1}H NMR spectrum of **4a**. Resonances for the aldehydic and *ortho* protons appear at 7.45 and 6.68 ppm, respectively, shifted upfield due to the shielding provided by the aryl groups.

When the acetophenone complex **4b** is redissolved in dichloromethane, an equilibrium between the bound and free acetophenone is established. ^{1}H NMR spectroscopy reveals that at room temp., *ca*. 25% of the ketone is not bound to the rhodium center, unlike the aldehyde complex **4a** in which *all* of the aldehyde remains complexed. At lower temperatures, the equilibrium lies further towards complexed acetophenone as expected, and a van't Hoff plot (see ESI†) provides an estimated value of $\Delta H^0 = -16 \pm 2$ kJ mol^{-1} for acetophenone binding.

The availability of complexes **4a** and **4b** led us to screen transformations involving aldehydes and ketones, utilizing **1** as a Lewis acid catalyst. Using 2.5 mol% **1**, the hydrosilation of benzaldehyde and acetophenone with triethylsilane could be effected [eqn. (4)].[1a,7] While the reaction of triethylsilane with

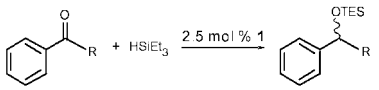

(4)

5a: R = H
5b: R = Me

benzaldehyde proceeds to 95% conversion to **5a** after 2 h at 70 °C in chlorobenzene, the reaction with acetophenone to produce **5b** required *ca*. 17 h to reach 90% conversion under similar conditions. Given the lack of reactivity of triethylsilane with **1** and the steric environment imposed by the ligand, it is believed that this reaction in fact proceeds by a Lewis acid-catalyzed mechanism.

The Mukaiyama aldol condensation of a trimethylsilyl enol ether with benzaldehyde can also be catalyzed by **1** [eqn. (5)].[8]

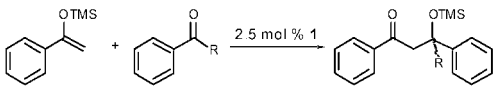

(5)

6a: R = H
6b: R = Me

The reaction of benzaldehyde with 1-trimethylsilyloxy-1-phenyl ethylene in chlorobenzene proceeds to 88% conversion to **6a** after heating at 65 °C for 24 h; however, when dichloromethane is used as the solvent, the reaction only proceeds to *ca*. 50% conversion after 24 h at room temperature.

Finally, since carbenes are also two-electron donors, complex **1** seemed to be ideally suited to catalyze cyclopropanation reactions.[9] The reaction of ethyl diazoacetate with α-olefins such as hex-1-ene and oct-1-ene proceeds smoothly; however, carbene insertion into the vinylic C–H bonds was also observed to some extent [eqn. (6)]. Upon monitoring the reaction of

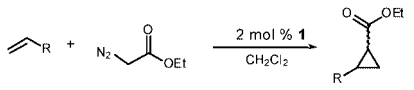

7a: R = *n*-C_4H_9
7b: R = *n*-C_6H_{13}
+

(6)

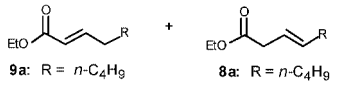

9a: R = *n*-C_4H_9
9b: R = *n*-C_6H_{13}
8a: R = *n*-C_4H_9
8b: R = *n*-C_6H_{13}

hex-1-ene and ethyl diazoacetate by ^{1}H NMR spectroscopy, it was determined that in addition to forming the cyclopropane **7a**, the C–H insertion product **8a** appears initially as well, and slowly isomerizes to the α,β-unsaturated ester **9a** in what is likely a rhodium-catalyzed process. For oct-1-ene, the combined products **7b**, **8b** and **9b** were isolated in 95% yield, and the product distrubution was determined by ^{1}H NMR to be 85 : 9 : 6 respectively.[10]

Surprisingly, these cyclopropanations do *not* proceed using trimethylsilyldiazomethane as a carbene source. Because of the steric limitations imposed by the ligand, incorporation of the TMS group appears to make the diazoalkyl fragment too bulky to coordinate to the rhodium center through the α-carbon, and thus ultimately produce a reactive carbene. In fact, the N-bound adduct of TMS–diazomethane is actually stable enough to be isolated, and we are currently exploring the unique reactivity that results.[11]

In summary, we have demonstrated that **1** is an easily synthesized, isolable compound which shows remarkable stability for a three-coordinate, 14-electron complex. As expected, **1** is a fairly potent Lewis acid, and the steric environment imposed by the ligand creates a binding pocket that must accommodate potential substrates.[12] It is this steric environment, however, which is responsible for the stability of **1** towards oxidative addition reactions common to Rh(I) complexes—in particular, reaction with chlorinated solvents is suppressed, allowing them to be used as the preferred solvents for synthetic and catalytic applications. In future papers, we will describe the integral role that steric effects play in stabilizing complexes of this type, and report on further studies utilizing **1** as a Lewis acid catalyst.

Acknowledgment is made to the National Institutes of Health (GM-29838) for support of this work.

Notes and references

1 (*a*) *Lewis Acid Reagents: A Practical Approach*, ed. H. Yamamoto, Oxford University Press, New York, 1999; (*b*) *Lewis Acids and Selectivity in Organic Synthesis* ed. M. Santelli and J.-M. Pons, CRC Press, Boca Raton, FL, 1996.

2 A complex employing a similar PNP ligand has been implicated (C. Hahn, M. Spiegler, E. Herdtweck and R. Tabue, *Eur. J. Inorg. Chem.*, 1999, 435), although it was not observed directly and its stability is not evident.

3 H. F. Haarman, J. M. Ernsting, M. Kranenburg, H. Kooijman, N. Veldman, A. L. Spek, P. W. N. M. vanLeeuwen and K. Vrieze, *Organometallics*, 1997, **16**, 887; K. J. Bradd, B. T. Heaton, C. Jacob, J. T. Sampanthar and A. Steiner, *J. Chem. Soc., Dalton Trans.*, 1999, 1109; H. Nishiyama, M. Horihata, T. Hirai, S. Wakamatsu and K. Itoh, *Organometallics*, 1991, **10**, 2706.

4 In a separate study, we have determined that *steric* effects are responsible for the stability of **2** towards the oxidative addition of dichloromethane, and this stability extends to **1** as well. In the series of complexes analogous to **2** where only the *ortho* substituents are varied, we have found that the oxidative addition of dichloromethane occurs when R = H or Me.

5 E. L. Dias, M. Brookhart and P. S. White, *Organometallics*, 2000, **19**, 4995.

6 *Crystal data*. $BC_{73}F_{24}H_{63}N_3ORh$, M = 1567.98, triclinic, space group $P\bar{1}$, a = 13.3839(6), b = 16.3962(7), c = 16.8506(7) Å, α = 80.160(1), β = 79.835(1), γ = 86.890(1)°, U = 3585.1(3) Å^3, Z = 2, μ(Mo-Kα) = 0.35 mm^{-1}, 45 784 reflections measured, 17 165 unique (R_{int} = 0.018) which were used in all calculations. The final $wR(F^2)$ was 0.056 (all data). CCDC 182/1892. See http://www.rsc.org/suppdata/cc/b0/b007815h/ for crystallographic files in .cif format.

7 For examples of Lewis-acid catalyzed hydrosilation, see; D. J. Parks, J. M. Blackwell and W. M. Piers, *J. Org. Chem.*, 2000, **65**, 3090; D. J. Parks and W. E. Piers, *J. Am. Chem. Soc.*, 1996, **118**, 9440; Y. S. Song, B. R. Yoo, G. H. Lee and I. N. Jung, *Organometallics*, 1999, **18**, 3109.

8 See: T. Mukaiyama, *Org. React.*, 1982, **28**, 203 and references therein.

9 For reviews of transition metal-catalyzed cyclopropanations, see: M. P. Doyle and D. C. Forbes, *Chem. Rev.*, 1998, **98**, 911; M. P. Doyle, *Acc.Chem. Res.*, 1986, **19**, 348; G. Maas, *Top. Curr. Chem.*, 1987, **137**, 75.

10 It was observed in NMR experiments that the product distribution does not change over the course of these reactions, indicating that the products **8** and **9** are not formed by acid-assisted opening of the cyclopropanes **7**.

11 E. L. Dias, M. Brookhart and P. S. White, *J. Am. Chem. Soc.*, in press.

12 For a recent review of Lewis-acid catalysts with designed binding pockets, see: H. Yamamoto and S. Saito, *Pure Appl. Chem.*, 199, **71**, 239 and references therein.

Enzyme catalysis in ionic liquids: lipase catalysed kinetic resolution of 1-phenylethanol with improved enantioselectivity

Sonja H. Schöfer,[a] Nicole Kaftzik,[a] Peter Wasserscheid[b] and Udo Kragl*[a]

[a] *Rostock University, Dept. of Chemistry, 18051 Rostock, Germany. E-mail: udo.kragl@chemie.uni-rostock.de*
[b] *RWTH Aachen, Institut für Technische Chemie und Makromolekulare Chemie, 52066 Aachen, Germany*

Received (in Liverpool, UK) 16th November 2000, Accepted 26th January 2001
First published as an Advance Article on the web 13th February 2001

Lipases show good activity and, in some cases, improved enantioselectivity when employed in pure ionic liquids for dynamic kinetic resolution of 1-phenylethanol by transesterification.

Today, more than 100 one-step biotransformations making use of whole cells or isolated enzymes are employed on an industrial scale, including a very recent process established by BASF for the kinetic resolution of chiral amines using lipases.[1,2] On a lab scale more than 13000 enzyme-catalysed reactions have been described.[3,4] Nevertheless, there are still problems with substrate solubility, yield or (enantio-)selectivity. Some progress has been made by addition of organic solvents,[5] addition of high salt concentrations[6] or use of microemulsions[7] or supercritical fluids.[8] Recently, ionic liquids (IL) have gained increasing attention for performing all types of reactions with sometimes remarkable results.[9–11] By modification of the cation and anion their properties can be tuned in many ways. For all catalytic processes, there are basically three modes of operation: use of the IL as a co-solvent, as pure solvent or in a biphasic system. After the first trials using ethylammonium nitrate in salt water mixtures more than 15 years ago,[12] recently the first results of the use of pure ILs as a reaction medium for enzymatic reactions have been published.[13,14] A biphasic system containing an IL for *in situ* product extraction for a whole cell process has been described as well.[15]

In this paper we report our results about the application of lipases for an enantioselective reaction in pure ILs based on 1-butyl-3-methylimidazolium (BMIM) ions such as [BMIM]PF_6 **1**, [BMIM]CF_3SO_3 **2** and [BMIM]$(CF_3SO_2)_2N$ **3** or on *N*-butylpyridinium ions such as [4-MBP]BF_4 **4**. As a model system the kinetic resolution of *rac*-1-phenylethanol **6** by transesterification with vinyl acetate **7** was investigated (Scheme 1). Our results on the β-galactosidase catalysed synthesis of *N*-acetyllactosamine are reported elsewhere.[16] In that case, addition of 25% v/v of [MMIM]$MeSO_4$ **5** as a water-miscible co-solvent suppresses the secondary hydrolysis of the formed product resulting in doubling the yield to almost 60%! The reaction investigated here yields two products: the remaining alcohol **(*S*)-6** or the formed acetate **(*R*)-8**. Unless stated otherwise the enantioselectivity is always given for the (*R*)-acetate. When the enzyme shows low enantioselectivity it is not possible to reach high ee-values for the (*R*)-acetate whereas for the (*S*)-alcohol high ee is possible at the expense of the yield.

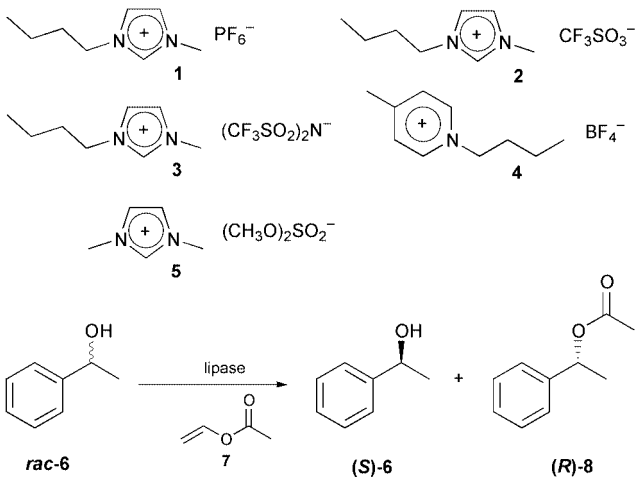

Scheme 1

A set of nine lipases and two esterases (Roche Diagnostics Chirazyme Screening Set 2) was screened for activity in ten different ionic liquids.[17] The results were compared with the reaction performed in methyl *tert*-butyl ether (MTBE) as solvent. MTBE is widely used as solvent for transesterification in industry and academia. Therefore it was used for this study despite the fact that some other solvents might be favourable as well.

The data are summarised in Table 1. Under the conditions employed the two pig liver esterases showed no activity. Best results were obtained with *Candida antarctica* lipase B (L-2) and *Pseudomonas* sp. lipase (L-6) in several ionic liquids. There is no 'best ionic liquid' in general, but [BMIM]$(CF_3SO_2)_2N$ seems to have some advantages. Surprisingly, with the lipases from *Pseudomonas* sp. and *Alcaligenes* sp. (L-10) the enantioselectivity for the formation of the acetate **(*R*)-8** is improved to a large extent compared to the reaction in MTBE. For the *Candida antarctica* lipase A (L-5) the opposite is observed. The increase of enantioselectivity is reproducible under different conditions. It is likely that the ILs will interact with charged residues found in or near the active centre of the enzyme. For two of the enzymes, L-2 and L-6 concentrations and enantioselectivity were followed as a function of time in MTBE, [BMIM]CF_3SO_3 and [BMIM]$(CF_3SO_2)_2N$. The reaction velocity is equal in both media, MTBE or IL.

One of the major advantages of ILs is that they are not volatile. Therefore it is possible to remove the products by distillation and repeat the catalytic cycle after addition of fresh substrate. This was investigated for L-2 in [BMIM]-$(CF_3SO_2)_2N$. The lipase shows good thermal stability up to 100 °C in MTBE as well as in the IL. Unfortunately, the substrate chosen and the product have boiling points around 200 °C at atmospheric pressure. Therefore, even at a pressure of 0.06 mbar a temperature of 85 °C was necessary to remove the reactants. But the enzyme suspended in the IL could be reused three times with less than 10% loss of activity per cycle. The enantioselectivity was not influenced. Certainly the recycling of the ionic liquid–enzyme system would be easier for other substrates as well as on a larger scale. These aspects as well as the improved enantioselectivity are subject to further studies. Additionally, other factors such as the water content, the viscosity or the question of which of the ions is responsible for the effects will be investigated as well.

The results presented here clearly demonstrate the potential of ionic liquids for enzymatic biotransformations. The variations possible for tailor-made solvents may have a similar impact as the pioneering work of the use of enzymes in pure organic solvents.[18]

DOI: 10.1039/b009389k

Table 1 Results of the screening of lipases in various ionic liquids. Conversion (%) of **rac-6** and ee's (%) of **(*R*)-8** (in brackets) are given. Conversion and ee were estimated by HPLC. Purified L-3 is also part of the Roche Chirazyme screening set

	Enzymes								
Solvent	L-2[h]	L-3[i]	L-3 purified	L-5[j]	L-6[k]	L-7[l]	L-8[m]	L-9[n]	L-10[o]
MTBE	43 (> 98)	13 (47)	< 5	11 (22)	53 (84)	45 (> 98)	10 (> 98)	29 (> 98)	> 98 (0)
[BMIM]PF_6[a]	< 5	< 5	0	10 (37)	0	< 5	< 5	< 5	44 (77)
[NMIM]PF_6[b]	10 (> 98)	7 (70)	0	41 (71)	17 (> 98)	< 5	11 (> 98)	33 (> 98)	68 (14)
[BMIM]BF_4[a]	< 5	41 (> 98)	< 5	< 5	7 (53)	0	< 5	< 5	60 (81)
[HMIM]BF_4[c]	10 (> 98)	0	0	27 (34)	0	0	0	0	26 (> 98)
[OMIM]BF_4[d]	41 (> 98)	< 5	< 5	59 (13)	< 5	< 5	< 5	< 5	50 (> 98)
[4-MBP]BF_4[e]	46 (> 98)	< 5	< 5	> 98 (3)	9 (> 98)	< 5	< 5	< 5	15 (> 98)
[BMIM]CF_3SO_3[a]	50 (> 98)	< 5	< 5	44 (45)	50 (> 98)	< 5	9 (> 98)	< 5	70 (82)
[BMIM]$(CF_3SO_2)_2N$[a]	50 (> 98)	10 (69)	< 5	> 98 (0)	47 (> 98)	8 (> 98)	12 (> 98)	40 (> 98)	89 (15)
[MMIM]$MeSO_4$[f]	Dark brown solution, analysis not possible								
[EMIM]benzoate[g]	Dark brown solution, analysis not possible								

[a] BMIM: 1-butyl-3-methylimidazolium. [b] NMIM: 1-methyl-3-nonylimidazolium. [c] HMIM: 1-hexyl-3-methylimidazolium. [d] OMIM: 1-methyl-3-octylimidazolium. [e] 4-MBP: *N*-butyl-4-methylpyridinium. [f] MMIM: 1,3-dimethylimidazolium. [g] EMIM: 1-ethyl-3-methylimidazolium. [h] L-2 *Candida antarctica* lipase B. [i] L-3 *Candida rugosa* lipase. [j] L-5 *Candida antarctica* lipase A. [k] L-6 *Pseudomonas* sp. lipase. [l] L-7 Pig pancreas lipase. [m] L-8 *Thermomyces lanuginosa* lipase. [n] L-9 *Mucor miehei* lipase. [o] L-10 *Alcaligenes sp.* lipase.

In a typical experiment 1 mg of lipase is added to 400 μl substrate solution containing 54 μl ***rac*-6** and 122 μl **7** in 4.4 ml ionic liquid or MTBE. The suspension is incubated for 3 d at 24 °C in a thermomixer. For analysis 100 μl of the reaction mixture are extracted with 1 ml *n*-hexane–propan-2-ol (97.5 : 2.5). The extract is analysed by HPLC using a chiral stationary Phase Chiracel OJ (Daicel). The eluent consists of 96.5% (v/v) *n*-hexane, 3% (v/v) propan-2-ol and 0.5% (v/v) ethanol with a flow rate of 1 ml min^{-1}; temperature 38 °C, UV-detection at 205 nm.

For the distillative workup 600 mg lipase L-2 (10 U mg^{-1}) is mixed with 4 ml [BMIM]$(CF_3SO_2)_2N$, 0.7 ml **6** and 1.2 ml **7**, mixed thoroughly and incubated at 40 °C for 40 min. Non-converted starting material and **(*R*)-8** are removed by vacuum distillation at 85 °C and 0.06 mbar. After cooling down the same amount of substrates is added again and the cycle is repeated.

We thank Roche Diagnostics GmbH, Mannheim, for providing the Chirazyme Screening set and additional amount of CAL, and the *Fonds der Chemischen Industrie* for financial support.

Notes and references

1 A. Liese, K. Seelbach and C. Wandrey, *Industrial Biotransformations*, Wiley-VCH, Weinheim, 2000.
2 G. Carrea and S. Riva, *Angew. Chem., Int. Ed.*, 2000, **112**, 2312.
3 K. Faber, *Biotransformations in Organic Chemistry*, Springer, Berlin, 2000.
4 U. T. Bornscheuer and R. J. Kazlauskas, *Hydrolases in Organic Synthesis*, Wiley-VCH, Weinheim, 1999.
5 J. M. S. Cabral, M. R. Aires-Barros, H. Pinheiro and D. M. F. Prazeres, *J. Biotechnol.*, 1997, **59**, 133.
6 A. M. Blinkorsky, Y. L. Khmelnitzky and J. S. Dordick, *J. Am. Chem. Soc.*, 1999, **116**, 2697
7 B. Orlich and R. Schomäcker, *Biotechnol. Bioeng.*, 1999, **65**, 357.
8 T. Hartmann, E. Schwabe and T. Scheper, in *Stereoselective Biocatalysis*, ed. R. Pathel, Marcel Dekker, 2000, 799.
9 P. Wasserscheid and W. Keim, *Angew. Chem., Int. Ed.*, 2000, **112**, 3926.
10 K. R. Seddon, *J. Chem. Tech. Biotechnol.*, 1997, **68**, 351.
11 T. Welton, *Chem. Rev.*, 1999, **99**, 2071.
12 D. K. Magnuson, J. W. Bodley and D. F. Evans, *J. Solution Chem.*, 1984, **13**, 583.
13 M. Erbeldinger, A. J. Mesiano and A. J. Russel, *Biotechnol. Prog.*, 2000, **16**, 1129.
14 R. Madeira Lau, F. van Rantwijk, K. R. Seddon and R. A. Sheldon, *Org. Lett.*, 2000, **2**, 4189.
15 S. G. Cull, J. D. Holbrey, V. Vargas-Mora, K. R. Seddon and G. J. Lye, *Biotechnol. Bioeng.*, 2000, **69**, 227.
16 N. Kaftzik, P. Wasserscheid and U. Kragl, *Angew. Chem., Int. Ed.*, submitted.
17 Ionic liquids are commercially available from Solvent Innovation GmbH, Cologne (http://www.solvent-innovation.de).
18 A. M. Klibanov, *CHEMTECH*, 1986, **16**, 354.

ChemComm

Synthesis and properties of the first series of mixed thioether/telluroether macrocycles

William Levason, Simon D. Orchard and Gillian Reid

Department of Chemistry, University of Southampton, Highfield, Southampton, UK SO17 1BJ. E-mail: gr@soton.ac.uk

Received (in Cambridge, UK) 17th October 2000, Accepted 22nd January 2001
First published as an Advance Article on the web 13th February 2001

The preparations of the first examples of mixed thioether/telluroether macrocycles, [9]aneS_2Te (1,4-dithia-7-telluracyclononane), [11]aneS_2Te (1,4-dithia-8-telluracycloundecane), [12]aneS_2Te (1,5-dithia-9-telluracyclododecane) and [14]aneS_3Te (1,4,7-trithia-11-telluracyclotetradecane) *via* a 'disguised dilution' method are described, together with the crystal structure of [Ag([11]aneS_2Te)]BF_4 which serves to authenticate the macrocyclic ligand.

In recent years thioether macrocycles have attracted considerable interest in the chemical community. A variety of ring sizes and denticities have been prepared and their metal ion chemistry studied, yielding a diverse range of structures and unexpected electronic and redox responses.[1] The tridentate [9]aneS_3 probably displays the most interesting chemistry, facilitating the stabilisation of a range of unusual oxidation states, including mononuclear Pd(III), Rh(II) and Au(II).[1] We have been conducting comparative studies of the ligating characteristics of acyclic bi- and tri-dentate thio-, seleno- and telluro-ethers to a variety of d- and p-block metal centres and have shown that to low-valent metal centres E→M donation increases in the order S < Se << Te.[2] Incorporation of telluroether functions in a macrocyclic environment is expected to significantly enhance their bonding to metal centres and should lead to rich new chemistry. However, while several macrocyclic selenoethers are now known, telluroether crowns are extremely rare[3] and indeed only a handful of multidentate telluroethers have been synthesised.[4] This really reflects the synthetic difficulties which need to be overcome. Thus, since Te–H and Te–C bonds are considerably weaker than those in their lighter Group 16 analogues, the methods used to prepare thioether and selenoether macrocycles are not usually suited to telluroether derivatives. We have therefore begun to develop new synthetic routes to macrocyclic telluroethers and report here the preparations of four new mixed S/Te-donor macrocycles involving different ring sizes and denticities, including [9]aneS_2Te, the direct analogue of [9]aneS_3. The successful incorporation of dimethylene linkages between the S and Te centres is significant since the ditelluroethers RTe$(CH_2)_2$TeR cannot be isolated, instead undergoing facile elimination of ethene and forming ditellurides.[4] The combination of both S and Te functions within a macrocyclic configuration will permit a direct comparison of their ligating properties to transition metal guests. Silver(I) complexes of the new ligands are also described, together with the crystal structure of [Ag([11]aneS_2Te)]BF_4 which serves to authenticate the macrocyclic ligand.

The synthetic method used for the macrocycles is depicted in Scheme 1.† In a typical preparation a freshly prepared sample of Na_2Te in liquid NH_3 was taken to −78 °C and a THF solution of the appropriate α,ω-dichlorothioalkane species was added dropwise over *ca.* 30 min. Evaporation of the NH_3 followed by subsequent hydrolysis and extraction with CH_2Cl_2 yielded a red oil. The macrocyclic ligands are obtained as light yellow, poorly soluble solids in moderate yields (20–30%) following purification by flash chromatography on silica using ethyl acetate : hexane 1 : 3 or, in the case of [9]aneS_2Te, by recrystallisation from

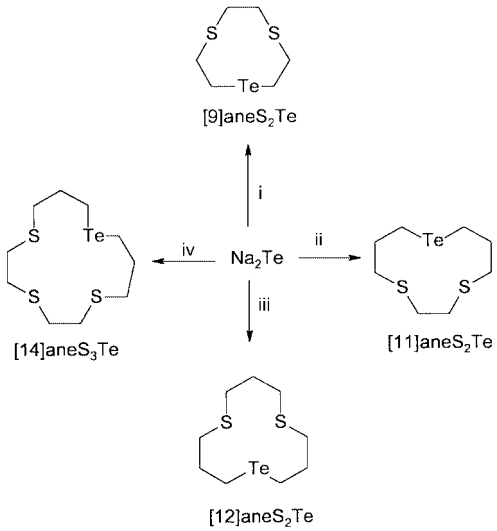

Scheme 1 *Reagents and conditions*: i, $Cl(CH_2)_2S(CH_2)_2S(CH_2)_2Cl$, THF/$NH_3$(liq); ii, $Cl(CH_2)_3S(CH_2)_2S(CH_2)_3Cl$, THF/$NH_3$(liq); iii, $Cl(CH_2)_3S(CH_2)_3S(CH_2)_3Cl$, THF/$NH_3$(liq); iv, $Cl(CH_2)_3S(CH_2)_2S(CH_2)_2S(CH_2)_3Cl$, THF/$NH_3$(liq); T = −78 °C, reagents added dropwise over 30 min.

CH_2Cl_2–MeOH. NMR spectroscopic studies and microanalyses are entirely consistent with the formulations, while mass spectrometry confirms the products as [1+1] cyclisation species, showing envelopes of peaks with the correct isotopic distributions associated with the parent ion, together with peaks at lower *m*/*z* consistent with fragments arising from Te–C and S–C bond cleavage. There is no evidence from FAB mass spectrometry for higher macrocycles even in the crude reaction products.

The macrocycles (L) react readily with one mol. equiv. of Ag$[CF_3SO_3]$ in CH_2Cl_2 at r.t. for one hour to yield light yellow, very poorly soluble, powdered species of formula [AgL]$[CF_3SO_3]$. Electrospray mass spectrometry (MeCN) shows major peaks associated with $[AgL]^+$ for all four complexes (as well as $[AgL_2]^+$ for L = [9]aneS_2Te, [11]aneS_2Te and [12]aneS_2Te). Crystals of the analogous tetrafluoroborate salt, [Ag([11]aneS_2Te)]BF_4, were obtained from $MeNO_2$–MeOH–Et_2O solution and a crystal structure‡ of this species established unequivocally the macrocyclic configuration. The cation assumes a one-dimensional polymeric structure [Fig. 1(a) and 1(b)] in which Ag centres are bridged by [11]aneS_2Te ligands, with a silver(I) ion coordinated to each macrocyclic donor atom. The Ag(I) ions adopt a distorted trigonal planar coordination environment. The Ag–Te bond distance [2.674(1) Å] is slightly shorter than those observed in [Ag{MeTe$(CH_2)_3$TeMe}$_2$]BF_4 [*d*(Ag–Te) = 2.785(2)–2.837(2) Å],[5] while the Ag–S distances [2.521(3), 2.634(3) Å] are comparable to those observed for [Ag{PhS$(CH_2)_3$SPh}$_2$]-BF_4 [*d*(Ag–S) = 2.573(3)–2.623(3) Å][6] (both of which also adopt infinite structures).

DOI: 10.1039/b008370o

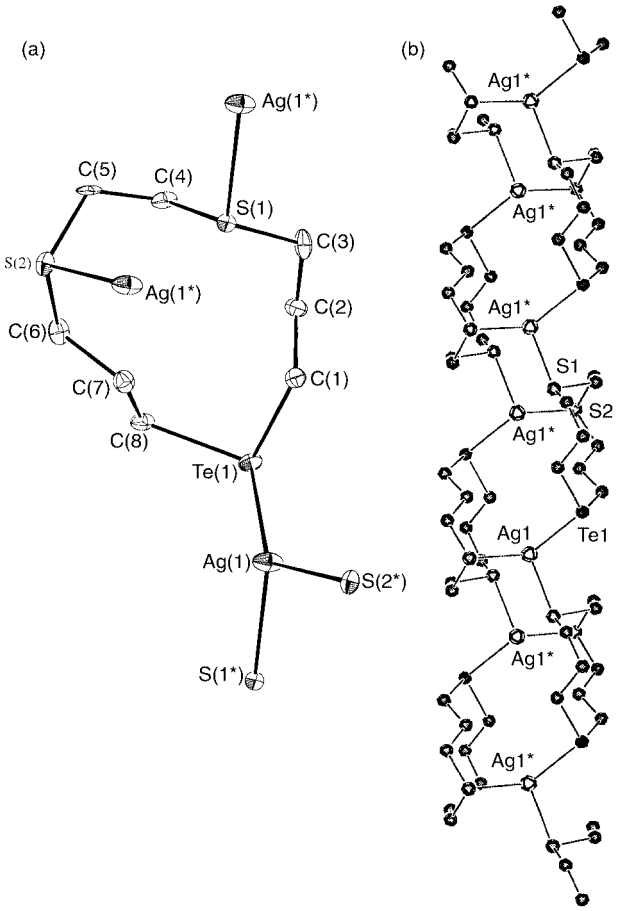

Fig. 1 (*a*) View of the asymmetric unit of $[Ag([11]aneS_2Te)]^+$, together with nearest symmetry-related atoms. H atoms are omitted for clarity and ellipsoids are shown at the 40% probability level. Selected bond lengths (Å) and angles (°): Ag(1)–S(1*) 2.634(3), Ag(1)–S(2*) 2.521(3), Ag(1)–Te(1) 2.674(1); S(1*)–Ag(1)–S(2*) 106.7(1), S(1*)–Ag(1)–Te(1) 107.46(7), S(2*)–Ag(1)–Te(1) 135.67(9). (b) View of a portion of the one-dimensional lattice adopted by $[Ag([11]aneS_2Te)]BF_4$.

Studies on the coordination chemistry and associated reaction chemistry of these and other related macrocycles are in progress.

We thank the EPSRC for support.

Notes and references

† Satisfactory analytical data were obtained for all new compounds. *Selected spectroscopic data*: for **[9]aneS$_2$Te**: ^{1}H NMR: δ 2.84 (s, 4H, SCH_2CH_2S), 2.93 (t, 4H, SCH_2CH_2Te), 3.06 (t, 4H, $TeCH_2$). $^{13}C\{^1H\}$ NMR: δ 38.9 (CH_2S), 32.9 (CH_2S), 2.9 (CH_2Te). $^{125}Te\{^1H\}$ NMR: δ 345. FAB-MS: *m*/*z* 278, 204; calc. for $[C_6H_{12}S_2{}^{130}Te]^+$ 278, $[C_3H_6S^{130}Te]^+$ 204. For **[11]aneS$_2$Te**: ^{1}H NMR: δ 2.74 (s, 4H, SCH_2CH_2S), 2.73 (t, 4H, $SCH_2CH_2CH_2Te$), 2.67 (t, 4H, $TeCH_2$), 2.05 (*q*, 4H, $CH_2CH_2CH_2$). $^{13}C\{^1H\}$ NMR: δ 34.7 ($CH_2CH_2CH_2$), 32.9 (CH_2S), 32.6 (CH_2S), 2.2 (CH_2Te). $^{125}Te\{^1H\}$ NMR: δ 234. FAB-MS: *m*/*z* 306, 204; calc. for $[C_8H_{16}S_2{}^{130}Te]^+$ 306, $[C_3H_6S^{130}Te]^+$ 204. For **[12]aneS$_2$Te**: ^{1}H NMR: δ 2.78 (t, 4H, SCH_2), 2.73 (t, 4H, SCH_2), 2.66 (t, 4H, $TeCH_2$), 2.06 (q, 4H, $SCH_2CH_2CH_2Te$), 1.86 (q, 2H, $SCH_2CH_2CH_2S$). $^{13}C\{^1H\}$ NMR: δ 33.5 ($SCH_2CH_2CH_2Te$), 30.1 (CH_2S), 29.0 (CH_2S), 27.7 ($SCH_2CH_2CH_2S$), 1.0 (CH_2Te). $^{125}Te\{^1H\}$ NMR: δ 217. FAB-MS: *m*/*z* 320, 246, 204; calc. for $[C_9H_{18}S_2{}^{130}Te]^+$ 320, $[C_6H_{12}S^{130}Te]^+$ 246, $[C_3H_6S^{130}Te]^+$ 204. For **[14]aneS$_3$Te**: ^{1}H NMR: δ 2.78 (m, 8H, SCH_2), 2.73 (t, 4H, SCH_2), 2.62 (t, 4H, $TeCH_2$), 2.09 (q, 4H, $CH_2CH_2CH_2$). $^{13}C\{^1H\}$ NMR: δ 36.1 ($CH_2CH_2CH_2$), 34.5, 34.9, 35.7 (CH_2S), 4.7 (CH_2Te). $^{125}Te\{^1H\}$ NMR: δ 254. FAB-MS: *m*/*z* = 366, 264; calc. for $[C_{10}H_{20}S_3{}^{130}Te]^+$ 366, $[C_5H_{10}S_2{}^{130}Te]^+$ 264.

‡ *Crystal data* for $[Ag([11]aneS_2Te)]BF_4$: M = 498.61, monoclinic, space group $P2_1/n$, a = 8.885(2), b = 17.329(3), c = 9.018(2) Å, β = 93.48(2)°, V = 1386.0(4) Å^3, Z = 4, D_c = 2.389 g cm^{-3}, μ(Mo-Kα) = 38.34 cm^{-1}. Rigaku AFC7S four-circle diffractometer, T = 150 K, Mo-Kα X-radiation (λ = 0.71073 Å), 2548 unique reflections, 2022 reflections with $I > 2\sigma(I)$. Structure solution and refinement were routine.[7,8] R = 0.038, R_w = 0.071.

CCDC 151895. See http://www.rsc.org/suppdata/cc/b0/b008370o/ for crystallographic data in .cif or other electronic format.

1 A. J. Blake and M. Schröder, *Adv. Inorg. Chem.*, 1990, **35**, 1; S. R. Cooper and S. C. Rawle, *Struct. Bonding (Berlin)*, 1990, **72**, 1 and references therein.
2 W. Levason, S. D. Orchard and G. Reid, *Organometallics*, 1999, **18**, 1275; A. J. Barton, W. Levason and G. Reid, *J. Organomet. Chem.*, 1999, **579**, 235; W. Levason, S. D. Orchard, G. Reid and J. M. Street, *J. Chem. Soc., Dalton Trans.*, 2000, 2537.
3 Y. Takaguchi, E. Horn and N. Furukawa, *Organometallics*, 1996, **15**, 512; S. C. Menon, A. Panda, H. R. Singh and R. J. Butcher, *Chem. Commun.*, 2000, 143.
4 E. G. Hope, T. Kemmit and W. Levason, *Organometallics*, 1987, **6**, 206; E. G. Hope, T. Kemmit and W. Levason, *Organometallics*, 1988, **7**, 78; T. Kemmit and W. Levason, *Organometallics*, 1989, **8**, 1303; J. Connolly A. R. J. Genge, W. Levason, S. D. Orchard, S. J. A. Pope and G. Reid, *J. Chem. Soc., Dalton Trans.*, 1999, 2343.
5 W.-F. Liaw, C.-H. Lai, S.-J. Chiou, Y.-C. Horng, C.-C. Chou, M.-C. Liaw, G.-S. Lee and S.-M. Peng, *Inorg. Chem.*, 1995, **34**, 3755.
6 J. R. Black, N. R. Champness, W. Levason and G. Reid, *J. Chem. Soc., Dalton Trans.*, 1995, 3439.
7 PATTY, The DIRDIF Program System, P. T. Beurskens, G. Admiraal, G. Beurskens, W. P. Bosman, S. Garcia-Granda, R. O. Gould, J. M. M. Smits and C. Smykalla, Technical Report of the Crystallography Laboratory, University of Nijmegen, The Netherlands, 1992.
8 TeXsan: Crystal Structure Analysis Package, Molecular Structure Corporation, Texas, 1995.

Thermally induced conformational-transition of polydeoxyadenosine in the complex with schizophyllan and the base-length dependence of its stability†‡

Masami Mizu,[a] Taro Kimura,[a] Kazuya Koumoto,[a] Kazuo Sakurai*[b] and Seiji Shinkai*[a]

[a] *Chemotransfiguration Project Japan Science and Technology Corporation (JST), Kurume Research Center Bldg, 2432 Aikawa, Kurume, Fukuoka 839-0861, Japan*

[b] *PRESTO "Function and Organization", Japan Science and Technology Corporation (JST), Kurume Research Center Bldg, 2432 Aikawa, Kurume, Fukuoka 839-0861, Japan. E-mail: seijitcm@mbox.nc.kyushu-u.ac.jp*

Received (in Cambridge, UK) 13th December 2000, Accepted 22nd January 2001
First published as an Advance Article on the web 13th February 2001

A single chain of schizophyllan, one of the β-1,3-glucan family, can form a stoichiometric complex with poly(dA) and the poly(dA)'s conformation and the complex stability strongly depends on the base length.

Conformational changes in polynucleotides play an important role in biological systems.[1] Powell and Gray[2] have explored the conformational change induced by a single-stranded polynucleotide binding protein (SSB), using poly(dA) as a model single-stranded DNA (ssDNA). Their CD data clearly demonstrated that SSB induces the same conformational change in ssDNA as that of heating poly(dA) or of protonating the polymer at low pH. More recently, Sakurai and Shinkai[3] found that a single chain of schizophyllan (s-SPG) can form a complex with single-stranded RNAs, such as poly(A) and poly(C), and RNA's conformation is altered by complexation.[3] Their finding led us to examine if s-SPG can interact with ssDNA. This report presents our preliminary results for an interaction observed between poly(dA) and s-SPG.

SPG (produced by *Schizophyllum commune* of the Basidiomycota) belongs to the β-1,3-glucan family.[4] SPG exists in a triple helix in water and a single chain in DMSO.[5] When s-SPG in DMSO solution is diluted with water (renature), SPG can gain the triple helical conformation again.[6] We found that when RNA such as poly(C) or poly(A) coexists in the renaturing process, a new triple helix consisting of one polynucleotide chain and two s-SPG chains is formed instead of the original triple helix reforming from three s-SPG chains.[7]

Fig. 1 demonstrates the base lengths (X_b) dependence of the CD spectra ([θ] is the molar ellipticity) for poly(dA) itself (left) and for the mixture of poly(dA) and s-SPG (poly(dA)+s-SPG) (right). The spectra for poly(dA) themselves are overlaid for X_b = 18–60 and that for X_b = 250 shows slight deviation from the others in the 260–280 nm region. Since the overall feature of the spectra seems identical, we can assume that both the helix content and conformation of poly(dA) do not depend on X_b.

On the other hand, the mixtures show that the conformation of poly(dA) strongly depends on X_b. In the case of X_b = 18, there is no difference between poly(dA) itself and the mixture, indicating that no significant interaction exists. From X_b = 30 to 45, the difference between the poly(dA) themselves and the mixtures becomes evident (*i.e.* increase at 260 nm and decrease at 250 nm). Thus complexation occurs at this base length, and becomes more favourable with increasing X_b. In the case of X_b = 60 and 250, the spectra are different from those of $X_b \leqslant 60$ (*i.e.* two new positive bands at 257 and 285 nm and one negative band at 267 nm), indicating that the longer poly(dA) exhibits a different conformation from the shorter poly(dA). As shown in the ESI†[8] this novel interaction is only observed for s-SPG and other polysaccharides (including triple-helix of s-SPG[7]) show no interaction at all.

Fig. 2 presents the temperature dependence of the CD spectra for both poly(dA) and the mixture at X_b = 250. For convenience, the spectra for the shorter wavelength (180–240 nm) and the longer (240–300 nm) are presented on different [θ] scales. For poly(dA) (the solid line), the CD spectrum at shorter wavelength does not change much upon heating. On the other hand, heating induces a dramatic change in that for poly(dA) of the complex. At T = 5 °C, there are two positive bands at 257 and 285 nm and one negative band at 267 nm in the complex. At T = 60 °C, however, there is a strong negative band at 250 nm, a strong positive band at 260 nm, and the 285 nm band disappears. At T = 40 °C, it seems that the spectrum is a hybrid of those at 5 and 60 °C. At T = 90 °C, there is no spectral difference between poly(dA) and the complex. This feature indicates that heating induces a conformational transition of poly(dA) in the complex between 40 and 60 °C, and that the complex is dissociated above 90 °C. Interestingly, the transition

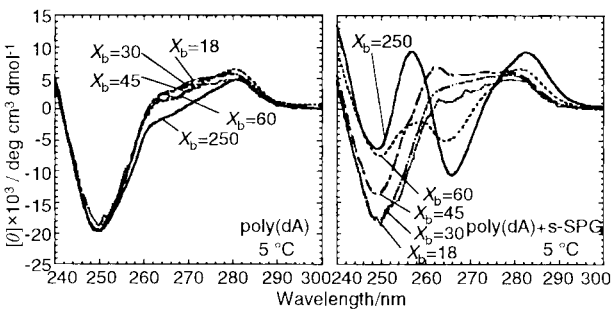

Fig. 1 The base length (X_b) dependence of the CD spectra for poly(dA) (left) and for the mixture made from poly(dA) and s-SPG (right) measured at 5 °C.

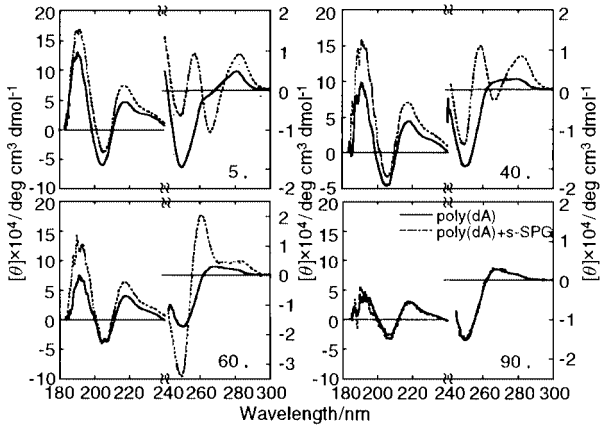

Fig. 2 Spectral change upon heating (from 5 °C, 40 °C, to 90 °C) for both poly(dA) (solid line) and its complex (broken line) for X_b = 250. The spectra at longer wavelengths and at shorter ones are plotted on separate vertical scales to make comparison easy.

† Electronic supplementary information (ESI) available: structure of s-SPG, experimental method, gel electrophoresis of poly(dA) plus dextran (Fig. S1) and s-SPG (Fig. S2). See http://www.rsc.org/suppdata/cc/b0/b009943k/

from 'positive 257 nm + negative 267 nm bands at 5 °C' to 'negative 250 nm + positive 260 nm bands at 60 °C' is correlated with a reverse of the Cotton effect. This feature resembles the feature observed for the B- to Z-form transition in DNA duplexes.[9]

One method to classify polynucleotide conformations is to examine the CD bands related to the phosphoric ester around 170–200 nm. Three typical conformations in DNA duplexes can be characterized as follows: a small negative band at 210 nm and a very large positive band at 190 nm in the A-form, a large positive band (smaller than the A-form) at 190 nm and a fairly small band at 210 nm in the B-form and a relatively large negative band at 185–195 nm and a large positive band at 180 nm in the Z-form. Namely, inversion of the Cotton effect is usually observed between the Z- and B- (or A-) forms. This criterion has been used to study the influence of the ionic strength on the conformational transition from the B- to Z-form[10] and the medium polarity on the conformational transition from the B- to A-form[11]

We apply the above criteria to the present system.[12] By comparing the left hand spectra in each panel in Fig. 2, we can conclude that the poly(dA)'s helicity does not undergo any transition. From the similarity between the spectra of poly(dA) and the complex at 5 °C and the fact that poly(dA) itself takes the B-form (C_2'-*endo* of the ribose and *anti* of the adenosine) in aqueous solution,[1,13] it can be considered that poly(dA) in the complex at 5 °C also takes the B-form. Even for the same type of conformation, the spectra in 240–300 nm are different between poly(dA) and the complex. This difference can be attributed to the difference in the conformation or the electronic state in adenosine, because the complexation can alter both. At 60 °C, the 190 nm band of the complex is larger than that of poly(dA), while the intensities of the 210 nm band are same. This feature can be interpreted in two ways. One possible rationale is that poly(dA) in the complex takes the A-form. This speculation is based on the fact that the CD spectrum in 240–300 nm resembles that of poly(A)[14] which is already known to take the A-form.[1,15] Another rationale is that poly(dA) in complex retains the B-form and the spectral change in 240–300 nm is due to a conformational transition of the adenosine such as *anti* to *syn*. However, the final assignment of the spectral change needs more extensive work using NMR spectroscopy.

Fig. 3 shows the temperature dependence of $[\theta]_{250}$ ($[\theta]$ at 250 nm) in the left panel and of the extinction coefficient at 257 nm (ε_{257}) in the right one, comparing poly(dA) and the mixture. Table 1 summarizes schematically the temperature dependence of the poly(dA) conformation for each X_b. Poly(dA) for all X_b values shows a monotonous increment in both $[\theta]_{250}$ and ε_{257}. We consider that this change is due to decrease in the helix content in the original B-form. On the other hand, for X_b = 250 in the complex, $[\theta]_{250}$ drastically decreases in the range T = 20–60 °C, then increases in the range T = 60–80 °C, and finally merges into the data of poly(dA) itself. The data for the ε_{257} change are clearly correlated with those of CD. This temperature dependence confirms that the poly(dA) in the complex

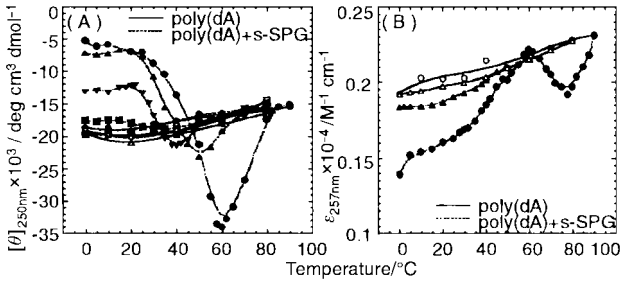

Fig. 3 The temperature dependence of $[\theta]$ at 250 nm (A) and ε at 257 nm (B) for poly(dA) (solid line and unfilled marks) and their mixtures with s-SPG (broken line and filled marks). X_b = 250 (○ and ●), X_b = 60 (△ and ▲), (x_b = 45 (▽ and ▼), x_b = 30 (■ and □) and X_b = 18 (◇ and ◆), respectively.

Table 1 The conformational transition for poly(dA) and poly(dA) in the complex

Poly(dA)	Conformation of poly(dA)			
Poly(dA)	B	→		
Complex				
X_b = 18	B	→		
X_b = 30	LL	→ 22 °C		
X_b = 45	LL	→ 23 °C	H	→ 45 °C
X_b = 60	HL	→ 30 °C	H	→ 65 °C
X_b = 250	HL	→ 30 °C	H	→ 80 °C

B = B-form. LL = conformation of a low molecular weight (Mw) and low temperature (T). HL = conformation of a high Mw and low T. H = conformation of high T.

undergoes a conformational transition (*i.e* a high molecular weight (*Mw*) and low *T* conformation (HL) to a high *T* conformation (H) as denoted in Table 1) before the complex dissociation. With decreasing X_b, H becomes less obvious. At X_b = 45, HL disappears and a low *Mw* and low *T* conformation (LL) is cooperatively dissociated at 35 °C and a small amount of H appears. These features indicate that the presence of this conformation is characteristic of long poly(dA) chains. As discussed above, HL is considered to be the B-form and H can be the A-form or a conformational transition of adenosine. At this moment, however, the origin of LL is not clear yet. In conclusion, we have substantiated that s-SPG forms a novel macromolecular complex with poly(dA). This novel interaction between s-SPG and poly(dA)[16] should provide new insight into the polysaccharide–DNA interactions, frequently important in biological systems.

Notes and references

‡ Polysaccharide–polynucleotide complexes (V).

1 W. Saenger, in *Principles of Nucleic Acid Structure*, Springer-Verlag, New York, 1984.
2 M. D. Powell and D. M. Gray, *Biochemistry*, 1995, **34**, 5635.
3 K. Sakurai and S. Shinkai, *J. Am. Chem. Soc.*, 2000, **122**, 4520.
4 K. Tabata, W. Ito, T. Kojima, S. Kawabata and A. Misaki, *Carbohydr. Res.*, 1981, **89**, 121.
5 T. Norisuye, K. Yanaki and H. Fujita, *J. Polym. Sci.*, 1980, **18**, 547; K. Yanaki, T. Norisuye and H. Fujita, *Macromolecules*, 1980, **13**, 1462.
6 T. M. McIntire, and D. A. Brant, *J. Am. Chem. Soc.*, 1998, **120**, 6909.
7 K. Sakurai, M. Mizu and S. Shinkai, submitted to *Biomacromolecules*.
8 As shown in Fig. S1 (ESI),† we examined whether dextran can bind with poly(dA), using gel electrophoresis. We found that dextran can not interact with poly(dA) and confirmed that there is no interaction such as we clearly observed in the s-SPG system.
9 J. H. Riazance, W. A. Baase, W.C. Johnson, Jr., K. Hall, P. Cruz and I. Tinoco, Jr., *Nucl. Acids Res.*, 1985, **13**, 4983.
10 J. H. Riazance-Lawrence and W. C. Johnson, Jr., *Biopolymers*, 1992, **32**, 271.
11 C. A. Sprecher, W. A. Baase and W. C. Johnson, Jr., *Biopolymers*, 1979, **18**, 1009.
12 N. Berova, K. Nakanishi and R. W. Woody, *Circular dichroism: Principles and applications*, 2nd edn., Wiley-VCH, Canada, 2000, Chapter 24.
13 C. S. M. Olsthoorn, L. J. Bostelaar, J. F. M. de Rooij, J. H. van Boom and C. Altona, *Eur. J. Biochem.*, 1981, **115**, 309; C. S. M. Olsthoorn, L. J. Bostelaar, J. H. van Boom and C. Altona, *Eur. J. Biochem.*, 1980, **112**, 95.
14 G. C. Causley and W. C. Johnson, Jr., *Biopolymers*, 1982, **21**, 1763.
15 W. Saenger, J. Riecke and D. Suck, *J. Mol. Biol.*, 1975, **93**, 529; F. E. Evans and R. H. Sarma, *Nature*, 1976, **263**, 567.
16 As shown in Fig. S2 (ESI),† we determined the stoichiometric ratio of the complex, using gel electrophoresis. The ratio we found for this system is that two s-SPG repeating units interact with three bases, which is the same result as that for the poly(C) and the poly(A) systems.

Ruthenium complexes bearing π-conjugated pendant moieties for a redox-switching system

Toshikazu Hirao* and Koichiro Iida

Department of Applied Chemistry, Faculty of Engineering, Osaka University, Yamada-oka, Suita, Osaka 565-0871, Japan. E-mail: hirao@ap.chem.eng.osaka-u.ac.jp

Received (in Cambridge, UK) 15th December 2000, Accepted 4th January 2001
First published as an Advance Article on the web 14th February 2001

A ruthenium(II) complex bearing *N*,*N*′-bis(4-aminophenyl)-1,4-phenylenediamine moieties, which can be chemically oxidized to the corresponding *N*,*N*′-bis(4-aminophenyl)-1,4-benzoquinonediimine moieties, was synthesized, characterized electrochemically and photochemically, and found to afford a redox-switching system.

The construction of efficient systems for electron transfer is a key factor in the development of versatile catalysts and functionalized materials. Photoinduced electron-transfer systems have been investigated with a variety of ruthenium bipyridyl complexes. A ruthenium complex bearing a redox-active moiety provides an electro-photoswitching device, as exemplified by complexes bearing a benzoquinone[1] or viologen function.[2] Ruthenium(II) complex systems have also been recognized as receptors for anion recognition[3] and photosynthetic models.[4] In a previous paper, quinonediimine derivatives were revealed to afford redox-active catalysts and d,π-conjugated complexes.[5] Furthermore, four π-conjugated pendant groups have been incorporated into a porphyrin scaffold to give atropisomeric three-dimensionally oriented redox-active systems.[6] We herein report redox-switchable ruthenium(II) complexes bearing π-conjugated pendant moieties.

A bipyridyl ligand **1** bearing aniline trimer pendant groups was prepared by amidation of the acid chloride derivative of 2,2′-bipyridine-4,4′-dicarboxylic acid with 2 mol equiv. of *N*-(4-acetylaminophenyl)-*N*′-(4-aminophenyl)-1,4-phenylenediamine.† The ruthenium(II) complex **2** was synthesized by complexation with *cis*-$Ru(bpy)_2Cl_2$ and subsequent treatment with NH_4PF_6. Chemical oxidation of complex **2** was achieved with 2 mol equiv. of Ag_2O to give the corresponding oxidized complex **3** (Scheme 1). Furthermore, **3** could be reduced to **2** on treatment with $N_2H_4{\cdot}H_2O$ at room temperature for 3 h under argon. These complexes were identified by spectral data and cyclic voltammetry.‡ For example, **3** exhibited a CT band at *ca.* 400–600 nm together with an MLCT band, in contrast to the observation of only the MLCT band for **2**.

The redox properties were studied by cyclic voltammetry. The redox waves were assigned by comparison with those of the corresponding complexes **4** and **5** bearing anilino and anilino-anilino groups, respectively (Table 1). The electrochemical behavior of complex **2** in acetonitrile is explained by the redox processes $D^0 \rightarrow D^+ \rightarrow D^{2+} \rightarrow D^{4+}$ of the quinonediimine moieties as shown in Scheme 2. The redox behavior of the ruthenium bipyridyl moiety was similar to that for complexes **4** or **5**. A multiredox system has thus been achieved with complex **2**. It should be noted that the redox processes were found to depend on the solvent. The redox waves in DMF were different from those observed in acetonitrile, suggesting the redox processes $D^0 \rightarrow D^{2+} \rightarrow D^{3+} \rightarrow D^{4+}$ in the former. Two quinonediimine moieties exhibited the same redox potential at each step in both solvents.

The radical cationic species **6** could be generated by treatment of **2** with **3** in the presence of a proton source ($HClO_4$) with the appearance of a broad absorption (600–1100 nm) in the UV–VIS–NIR spectrum.§ EPR spectroscopy also supported the formation of **6** (g = 2.004, A_N = 6.7 G, $A_{H(CH)}$ = 1.6 G, $A_{H(NH)}$ = 3.4 G). These findings are consistent with the reported redox behavior of *N*,*N*′-diphenyl-1,4-benzoquinonediimine and *N*,*N*′-diphenyl-1,4-phenylenediamine.[7] The above-mentioned solvent effect might be due to the difference in equilibrium between the diprotonated quionediimine and corresponding reduced species, and the radical cationic species.

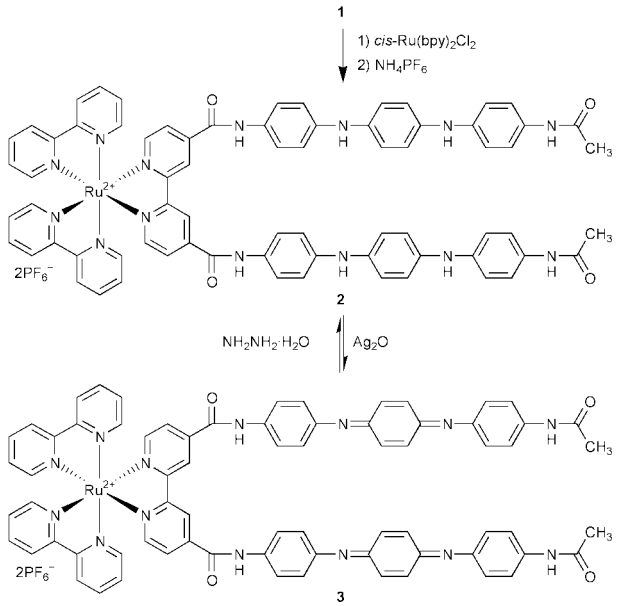

Scheme 1

In the emission spectrum of complex **2** excited at 477 nm, almost complete quenching was observed in acetonitrile (Fig.

Table 1 Electrochemical data for **2**, **4** and **5**[a]

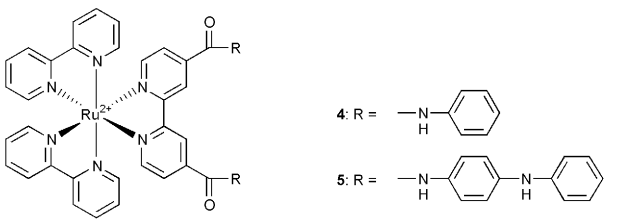

	$E_{1/2}$/V (*vs.* Fc/Fc$^+$)					
Complex	bpy$^{-/0}$	D$^{0/+}$	D$^{+/2+}$	D$^{2+/3+}$	D$^{3+/4+}$	Ru$^{2+/3+}$
2	−1.50	−0.01	+0.38	+0.93[c]	+0.93[c]	+0.93[c]
2[b]	−1.50	−0.10[c]	−0.10[c]	+0.63	+0.93[c]	+0.93[c]
4	−1.48					+0.94
5	−1.49	+0.48	+0.88			+0.94

[a] [Complex] = 0.25 mM; solv, MeCN. Recorded with NBu_4PF_6 as electrolyte (0.1 M). Potentials were obtained by cyclic voltammetry with a scan rate of 100 mV s^{-1}. D: π-conjugated pendant group. [b] Solv, DMF. [c] Observed simultaneously.

DOI: 10.1039/b010039k

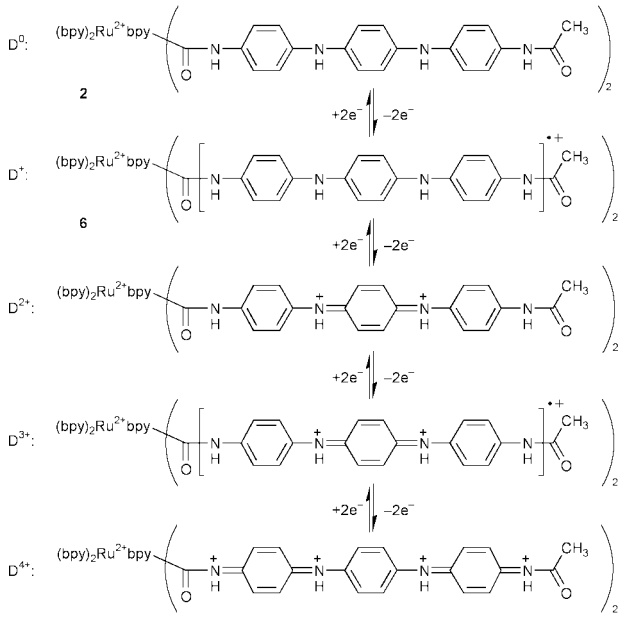

Scheme 2

1). Such quenching was not observed with **4**, indicating that the π-conjugated chain of **2** contributes to the quenching. An efficient photoinduced electron transfer is likely to operate in complex **2**, where the reduced form of the π-conjugated pendant groups serves as an electron donor. Use of the oxidized form **3** also resulted in a quenched spectrum upon excitation at 477 nm. Taking the reported electron-transfer mechanism of complexes bearing viologen or benzoquinone moiety into account,[1,2] this result might be explained by electron transfer in a direction opposite to that of **2**. A much less effective quenching of ruthenium(II) complex **4** with *N*,*N*′-bis(4-acetylaminophenyl)-1,4-phenylenediamine or *N*,*N*′-bis(4-acetylaminophenyl)-1,4-benzoquinonediimine was observed intermolecularly, indicating that the quenching process for both **2** and **3** occurs intramolecularly. Such intramolecular quenching processes are considered to be thermodynamically feasible.

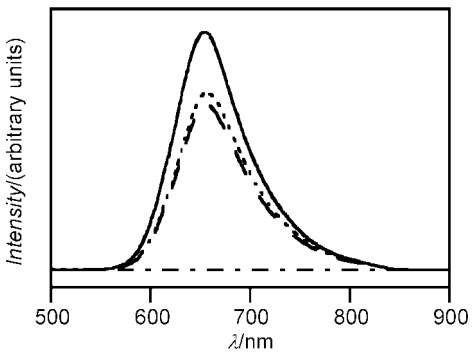

Fig. 1 Emission spectra of **2** or **3** (·-·-), **4** (—), **4** with 2.0 mol equiv. of *N*,*N*′-bis(4-acetylaminophenyl)-1,4-phenylenediamine (····), and **4** with 2.0 mol equiv. of *N*,*N*′-bis(4-acetylaminophenyl)-1,4-benzoquinonediimine (- -). [Complex] = 2.0×10^{-5} M; solv, MeCN, λ_{exc} = 477 nm.

In conclusion, we have described a versatile and efficient redox-switching system with variable oxidation state of the π-conjugated pendant moieties. Further investigation on the electron-transfer mechanism and molecular recognition is now in progress.

Thanks are due to the Analytical Center, Faculty of Engineering, Osaka University, for the use of their facilities. Partial financial support by a Grant-in-Aid for Scientific Research from the Ministry of Education, Culture, Sports, Science and Technology, Japan is also acknowledged.

Notes and references

† The acid chloride derivative prepared by treatment of 2,2′-bipyridine-4,4′-dicarboxylic acid (122 mg, 0.50 mmol) with $SOCl_2$ (238 mg, 2.0 mmol) was dissolved in DMF (40 mL) and added dropwise over 2 h to a solution of *N*-(4-acetylaminophenyl)-*N*′-(4-aminophenyl)-1,4-phenylenediamine[5] (332 mg 1.0 mmol), 4-dimethylaminopyridine (12 mg, 0.10 mmol) and Et_3N (0.50 mL) in DMF (20 mL) at 0 °C. After stirring at room temp. for 24 h, work-up gave the pure bipyridyl ligand **1** (342 mg, 0.39 mmol, 78%). **1**: IR (KBr) 3408, 3305, 3265, 1652 cm^{-1}; δ_H(300 MHz, DMSO-d_6) 10.51 (s, 2H), 9.69 (s, 2H), 8.94 (d, 2H, *J* 5.2 Hz), 8.91 (d, 2H, *J* 1.6 Hz), 7.97 (dd, 2H, *J* 5.2, 1.6 Hz), 7.87 (s, 2H), 7.76 (s, 2H), 7.62 (d, 4H, *J* 9.0 Hz), 7.39 (d, 4H, *J* 8.8 Hz), 7.04–6.90 (m, 16H), 1.99 (s, 6H); MS (FAB) *m*/*z* 872 M^+.

‡ **2**: IR (KBr) 3405, 3291, 1654 cm^{-1}; δ_H(600 MHz, DMSO-d_6) 10.55 (s, 2H), 9.67 (s, 2H), 9.34 (s, 2H), 8.88–8.87 (m, 4H), 8.23–8.20 (m, 4H), 7.96–7.95 (m, 4H), 7.89 (s, 2H), 7.81–7.75 (m, 4H), 7.76 (s, 2H), 7.59–7.54 (m, 4H), 7.54 (d, 4H, *J* 8.9 Hz), 7.38 (d, 4H, *J* 8.9 Hz), 7.01–6.96 (m, 12H), 6.91 (d, 4H, *J* 8.9 Hz), 1.99 (s, 6H); MS (FAB) *m*/*z* 1431 $(M - PF_6)^+$; UV–VIS (MeCN) λ_{abs}/nm (log ε) 289 (5.08) 304 (5.04) 477 (4.42). **3**: IR (KBr) 3404, 1669, 1529 cm^{-1}; UV–VIS (MeCN) λ_{abs}/nm (log ε) 288 (5.00) 482 (4.64).

§ UV–VIS–NIR (MeCN) λ_{abs}/nm (log ε) 288 (4.96) 405 (4.72) 847 (4.44).

1 V. Goulle, A. Harriman and J.-M. Lehn, *J. Chem. Soc., Chem. Commun.*, 1993, 1034.
2 E. H. Yonemoto, R. L. Riley, Y. I. Kim, S. J. Atherton, R. H. Schmehl and T. E. Mallouk, *J. Am. Chem. Soc.*, 1992, **114**, 8081.
3 P. D. Beer, *Acc. Chem. Res.*, 1998, **31**, 71 and references therein; S. Watanabe, O. Onogawa, Y. Komatsu and Y. Katsuhira, *J. Am. Chem. Soc.*, 1998, **120**, 229; M. J. Deetz and B. D. Smith, *Tetrahedron Lett.*, 1998, **39**, 6841; S.Watanabe, N. Higashi, M. Kobayashi, K. Hamanaka, T. Tanaka and Y. Katsuhira, *Tetrahedron Lett.*, 2000, **41**, 4583.
4 M. Seiler, H. Dürr, I. Willner, E. Joselevich, A. Doron and J. F. Stoddart, *J. Am. Chem. Soc.*, 1994, **116**, 3399; S. Yamada, Y. Koide and T. Matsuo, *J. Electroanal. Chem.*, 1997, **426**, 23; A. Magnuson, H. Berglund, P. Korall, L. Hammarström, B. Åkermark, S. Styring and L. Sun, *J. Am. Chem. Soc.*, 1997, **119**, 10 720; S. H. Bossmann, M. F. Ottaviani, D. Loyen, H. Dürr and C. Turro, *Chem. Commun.*, 1999, 2487; K. A. Maxwell, M. Sykora, J. M. DeSimone and T. J. Meyer, *Inorg. Chem.*,2000, **39**, 71; D. Burdiniski, E. Bothe and K. Wieghardt, *Inorg. Chem.*, 2000, **39**, 105; Y.-Z. Hu, S. Tsukiji, S. Shinkai, S. Oishi, H. Dürr and I. Hamachi, *Chem. Lett.*, 2000, 442.
5 T. Hirao and S. Fukuhara, *J. Org. Chem.*, 1998, **63**, 7534; T. Moriuchi, S. Bandoh, M. Miyaishi and T. Hirao, *Eur. J. Inorg. Chem.*, 2001, 651.
6 T. Hirao and K. Saito, *Tetrahedron Lett.*, 2000, **41**, 1413.
7 J. F. Wolf, C. E. Forbes, S. Gould and L. W. Shacklette, *J. Electrochem. Soc.*, 1989, 2887.

Phase-separable catalysis using room temperature ionic liquids and supercritical carbon dioxide

Fuchen Liu, Michael B. Abrams, R. Tom Baker* and William Tumas*

Los Alamos Catalysis Initiative, Chemistry Division, MS J514, Los Alamos National Laboratory, Los Alamos, New Mexico 87545, USA. E-mail: weg@lanl.gov; tumas@lanl.gov

Received (in Cambridge, UK) 4th December 2000, Accepted 29th January 2001
First published as an Advance Article on the web 14th February 2001

A new phase-separable catalysis concept is demonstrated using supercritical carbon dioxide and the room temperature ionic liquid 1-butyl-3-methylimidazolium hexafluorophosphate for hydrogenation of alkenes and carbon dioxide.

There is a continuing interest in developing new concepts for biphasic or phase-separable catalysis where a homogeneous catalyst is immobilized in one liquid phase and the reactants and/or products reside largely in another liquid phase.[1] Brennecke and Beckman[2] have recently reported that the room temperature ionic liquid (IL) 1-butyl-3-methylimidazolium hexafluorophosphate, **1**, ([BMIM][PF_6]), exhibits very interesting phase behavior with supercritical carbon dioxide ($scCO_2$), where CO_2 can dissolve significantly (up to 0.6 mole fraction) into the lower IL phase, but no polar IL dissolves in the upper $scCO_2$ phase. They further illustrated that organics such as naphthalene could be extracted from the IL phase using $scCO_2$. Kazarian *et al.*[3] recently provided corroborating spectroscopic evidence that CO_2 dissolves in **1**. This intriguing discovery of phase behavior suggested that a reaction system comprised of $scCO_2$ and an ionic liquid might offer particular advantages as a new biphasic catalysis system. Herein, such a $scCO_2$/IL biphasic system is demonstrated, where a homogeneous transition metal catalyst is immobilized in an IL phase and products can be isolated from a distinct $scCO_2$ phase.[4]

Room temperature ionic liquids[5] and supercritical carbon dioxide[6] have both been extensively studied as alternative solvents for a wide range of homogeneously catalyzed reactions including hydrogenation, hydroformylation, selective oxidation and carbon–carbon bond formation. We chose to examine the $scCO_2$/IL system through investigations of the hydrogenation of dec-1-ene and cyclohexene using Wilkinson's catalyst $RhCl(PPh_3)_3$, **2**, which is insoluble in $scCO_2$ but soluble in water-stable [BMIM][PF_6], **1**.

All reactions were run in custom-designed, high pressure stainless steel view cells with a sapphire window using magnetic stirring at 50 °C, as described previously.[7]† The hydrogenation of dec-1-ene proceeded in 98% conversion to *n*-decane in 1 h at 48 bar H_2 and a total pressure of 207 bar, which implies a time-averaged reaction turnover frequency (TOF) of 410 h^{-1}. The reaction mixture was biphasic throughout the reaction with a colorless carbon dioxide phase above a yellow ionic liquid phase. Hydrogenation of cyclohexene proceeded more slowly under identical conditions with 82% conversion being observed after 2 h reaction at 50 °C (time-averaged TOF = 220 h^{-1}) and 96% conversion measured after 3 h. Product recovery and catalyst recycling were demonstrated for dec-1-ene using a variable volume reaction vessel to transfer the upper $scCO_2$ phase to a separate receiver under high pressure after reaction.[8] The reaction vessel was then recharged with dec-1-ene, hydrogen and carbon dioxide and allowed to react for 1 h. This process was repeated up to four times and the reaction proceeded to *ca.* 98% conversion each time, thereby demonstrating efficient catalyst recycling through immobilization of the rhodium catalyst in the ionic liquid.

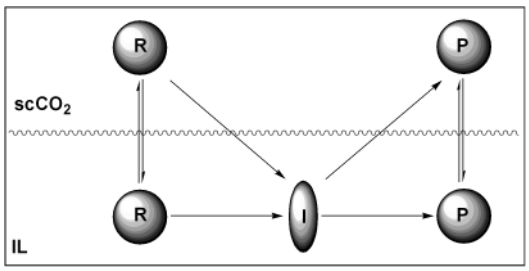

Scheme 1 Pictorial illustration of a $scCO_2$/IL biphasic system **R** = reactant, **P** = product, **I** = polar intermediate (*e.g.* carbamate **4**).

Since many organic compounds are not miscible with imidazolium-based ionic liquids, many of the reported catalytic reactions in ILs can be considered to be organic/IL biphasic systems. Product separation has been demonstrated in a number of cases.[9] In order to benchmark the reactivity of the $scCO_2$/IL system with organic/IL systems, we also examined the above hydrogenation reactions using *n*-hexane in place of carbon dioxide, under otherwise identical conditions.‡ The reaction of dec-1-ene to form *n*-decane proceeded to 99% conversion after 1 h at 50 °C in *n*-hexane/[BMIM][PF_6]. Conversions of cyclohexene to cyclohexane were similar to those measured in the $scCO_2$/[BMIM][PF_6] experiments: 88% after 2 h, 98% after 3 h at 50 °C. These results suggest that there is no reactivity advantage for CO_2 over *n*-hexane for simple hydrogenation reactions.

In order to capitalize on advantages arising from the polar nature of the ionic liquid phase, we sought to examine reactions that proceed through polar intermediates which would be soluble in the IL phase and not in $scCO_2$ (Scheme 1). We studied the hydrogenation of carbon dioxide in the presence of dialkylamines to produce *N*,*N*-dialkylformamides. Noyori *et al.*[10] and Baiker *et al.*[11] have reported elegant studies on the catalytic hydrogenation of CO_2 to formamides in $scCO_2$ using $scCO_2$-soluble $RuCl_2(PMe_3)_4$ and $scCO_2$-insoluble $RuCl_2(dppe)_2$ (dppe = $Ph_2PCH_2CH_2PPh_2$), **3**, respectively. These reactions involve ionic carbamate intermediates, since dialkylamines react with CO_2 reversibly to form dialkylammonium dialkylcarbamates, **4** [eqns (3), (4)].[12]

$$CO_2 + H_2 \overset{[cat]}{\rightleftharpoons} HCO_2H \quad (1)$$

$$HCO_2H + R_3N \rightleftharpoons [HNR_3]^+[HCO_2]^- \quad (2)$$

$$HNR_2 + CO_2 \rightleftharpoons R_2NCO_2H \quad (3)$$

$$R_2NCO_2H + NHR_2 \rightleftharpoons \underset{\mathbf{4}}{[NH_2R_2]^+[O_2CNR_2]^-} \quad (4)$$

$$[NH_2R_2]^+[O_2CNR_2]^- + 2HCO_2H \rightarrow 2HCON(R)_2 + 2H_2O + CO_2 \quad (5)$$

Noyori *et al.* reported that salt **4a** (R = CH_3) separated from the $scCO_2$ phase right from the start of the reaction starting with dimethylamine and rates using **4a** were similar to those using dimethylamine. Very high rates for selective *N*,*N*-dimethylformamide (DMF) formation were reported using either liquid **4a**,[10] or dimethylamine.[10,11] Significantly Noyori *et al.* found that activity and selectivity (*i.e.* formic acid *vs.*

Table 1 Production of formamides from amines and CO_2 in different solvent systems

Amine	Solvent	Catalyst	*T*/°C	*t*/h	Con (%)	Sel (%)	TON[a]	TOF (h^{-1})[b]
$NH(C_2H_5)_2$[c]	$scCO_2$	$RuCl_2(PMe_3)_4$	100	13	38	46[d]	820	63
$NH_2(n\text{-}C_3H_7)$[c]	$scCO_2$	$RuCl_2(PMe_3)_4$	100	5	18	30[d]	260	52
$NH(n\text{-}C_3H_7)_2$	$scCO_2$/IL	$RuCl_2(dppe)_2$	80	5	100	> 99	110	> 22

[a] TON = mol product/mol ruthenium. [b] Time-averaged TOF. [c] Ref. 10. [d] Other product is formic acid.

formamide production) decreased rapidly with longer chain amines (R ≠ CH_3) which lead to solid, $scCO_2$-insoluble carbamate intermediates.[10]

In the $scCO_2$/IL system, catalyst **3** and carbamate **4** are both soluble in the IL phase. Carbamate **4a** could be completely converted to DMF after 4 h at 80 °C using 55 bar hydrogen under a total pressure of 276 bar.§ While this unoptimized reactivity is significantly less than that reported by Baiker for the liquid carbamate,[11]‡ we found that the reactivity and more importantly the selectivity is higher for amines other than dimethylamine in the $scCO_2$/IL biphasic system. Under similar reaction conditions, di-*n*-propylamine¶ led to complete amine conversion and exclusive production of the corresponding *N*,*N*-di-*n*-propylformamide after only 5 h at 80 °C. The activity and selectivity are higher than those reported[10] for less bulky diethylamine and *n*-propylamine in neat $scCO_2$ (Table 1). The increased selectivity in the $scCO_2$/IL biphasic system likely arises from the increased solubility of the solid dialkylcarbamate intermediates in the IL phase or through rate enhancement of amidation of formic acid derived from CO_2 hydrogenation [eqn (5)].

The highly polar formamide products appear to be very soluble in the ionic liquid phase, **1**. Preliminary experiments reveal that they do not partition strongly into the $scCO_2$ phase after only one reaction cycle. Quantitative data on the partitioning of organic compounds between ionic liquids and either organic solvents or $scCO_2$ are just starting to appear in the literature.[13,14] We have demonstrated extraction of DMF from IL **1** in a separate experiment. After stirring 30 mL $scCO_2$ (P_{tot} = 276 bar) over a solution of 1.0 mL ionic liquid **1** and 1.0 mL DMF for 1 h at 80 °C, the upper CO_2 phase was transferred under high pressure to another vessel. Subsequent pressure let-down led to 151 mg of isolated DMF (16% recovery). We have been able to demonstrate effective product recovery for *N*,*N*-di-*n*-propylformamide after several reaction/recovery cycles. The recovery yield in the first cycle was poor (less than 5%), however, the yield in the second cycle improved significantly to 61%. *N*,*N*-di-*n*-propylformamide can be almost quantitatively recovered in the third and fourth cycle, suggesting the IL phase becomes saturated with the product in the first two cycles.[15]

In conclusion, we demonstrate one of the first examples[4] of catalysis in a biphasic system incorporating supercritical carbon dioxide and ionic liquids and more importantly the first example involving CO_2 reaction chemistry. High selectivity, catalyst recycling and product recovery were observed for hydrogenation of CO_2 in the presence of dialkylamines, demonstrating the potential advantages arising from dissolving polar reaction intermediates in the IL phase. We are in the process of investigating other reactions, particular those involving polar intermediates, as well as quantifying the partitioning of reactants (including gases), products and catalyst between the two phases.

We gratefully acknowledge support of this research by the U.S. Department of Energy through a Laboratory Directed Research and Development (LDRD) grant at Los Alamos National Laboratory.

Notes and references

† *Typical experimental procedure for olefin hydrogenation*: 20 mg (21 μmol) of **2** were added to 10.5 mmol of olefin (500 equiv. relative to catalyst **2**) and 1 mL of ionic liquid **1** in the reaction cell which was then pressurized with hydrogen (48 bar) and CO_2 to a total pressure of 207 bar. All the experiments were conducted at 50 °C using *n*-nonane as an internal standard.

‡ While magnetic stirring may not be optimal for these reactions, our preliminary experimental conditions allow for a semi-quantitative comparison.

§ *Typical experimental procedure for CO_2 hydrogenation*: 0.5 mL (4.3 mmol) of **4a** was charged into a 33 mL stainless steel reaction cell with a solution of 10 mg (10 μmol) of **3** in 1 mL of **1**. The cell was heated to 80 °C after being filled with 55 bar H_2, then it was pressurized to a total pressure of 276 bar with CO_2. The start of the reaction was defined as the time of CO_2 gas introduction. The yield and identification of formamide were performed by GC, GC-MS and ^{1}H NMR.[10]

¶ 0.15 mL (1.1 mmol) of di-*n*-propylamine and 1 mL of **1** were used. Higher concentration of amine (*e.g.* 7.3 mmol di-*n*-propylamine in 1 mL of **1**) led to precipitation of a white solid (carbamate).

1 B. Cornils and W. A. Herrmann, in *Applied Homogeneous Catalysis with Organometallic Compounds*, ed. B. Cornils and W. A. Herrmann, Weinheim: New York, 1996, Chapter 4.1, pp. 1167–1197; An entire issue of *Catalysis Today* (1998, **42** (2)) was devoted to biphasic homogeneous catalysis.
2 L. A. Blanchard, D. Hancu, E. J. Beckman and J. F. Brennecke, *Nature*, 1999, **399**, 28.
3 S. G. Kazarian, B. J. Briscoe and T. Welton, *Chem. Commun.*, 2000, 2047.
4 While this manuscript was in preparation we learned that other groups have been working on asymmetric hydrogenation reactions in a $scCO_2$/IL biphasic system: P. G. Jessop, private communication; R. A. Brown, P. Pollett, E. McKoon, C. A. Eckert, C. L. Liotta and P. G. Jessop, *J. Am. Chem. Soc.*, 2001, **123**, 1254.
5 T. Welton, *Chem. Rev.*, 1999, **99**, 2071; P. Wasserscheid and W. Keim, *Angew. Chem., Int. Ed.*, 2000, **39**, 3772.
6 P. G. Jessop and W. Leitner, in *Chemical Synthesis Using Supercritical Fluids*, ed. P. G. Jessop and W. Leitner, Weinheim, Wiley-VCH, 1999; P. G. Jessop, T. Ikariya and R. Noyori, *Chem. Rev.*, 1999, **99**, 475.
7 D. K. Morita, D. R. Pesiri, S. A. David, W. H. Glaze and W. Tumas, *Chem. Commun.*, 1998, 1397.
8 G. B. Jacobson, C. T. Lee, K. P. Johnston and W. Tumas, *J. Am. Chem. Soc.*, 1999, **121**, 11 902.
9 Y. Chauvin, L. Mussmann and H. Olivier, *Angew. Chem., Int. Ed.*, 1995, **34**, 2698; B. Ellis, W. Keim and P. Wasserscheid, *Chem. Commun.*, 1999, 337; C. J. Mathews, P. J. Smith and T. Welton, *Chem. Commun.*, 2000, 1249.
10 P. G. Jessop, Y. Hsiao, T. Ikariya and R. Noyori, *J. Am. Chem. Soc.*, 1994, **116**, 8851; P. G. Jessop, Y. Hsiao, T. Ikariya and R. Noyori, *J. Am. Chem. Soc.*, 1996, **118**, 344.
11 O. Kröcher, R. A. Köppel and A. Baiker, *Chem. Commun.*, 1997, 453.
12 H. B. Wright and M. B. Moore, *J. Am. Chem. Soc.*, 1948, **70**, 3865; K. Takeshita and A. Kitamoto, *J. Chem. Eng. Jpn.*, 1988, **221**, 411.
13 L. A. Blanchard and J. F. Brennecke, *Ind. Eng. Chem. Res.*, 2001, **40**, 287.
14 L. A. Blanchard, Z. Gu and J. F. Brennecke, *J. Phys. Chem.*, submitted.
15 D. E. Bergbreiter, Y. S. Liu and P. L. Osburn, *J. Am. Chem. Soc.*, 1998, **120**, 4250.

Photocatalytic reactions on chromium containing mesoporous silica molecular sieves (Cr-HMS) under visible light irradiation: decomposition of NO and partial oxidation of propane

Hiromi Yamashita,*[a] Katsuhiro Yoshizawa,[a] Masao Ariyuki,[a] Shinya Higashimoto,[a] Michel Che[b] and Masakazu Anpo*[a]

[a] *Department of Applied Chemistry, Graduate School of Engineering, Osaka Prefecture University, Gakuencho 1-1, Sakai, Osaka 599-8531, Japan. E-mail: yamashita@chem.osakafu-u.ac.jp*

[b] *Laboratoire de Réactivité de Surface, Université P. et M. Curie, UA 1106-CNRS, 4 Place Jussieu Tour 54, 75252 Paris Cedex 05, France*

Received (in Cambridge, UK) 23rd October 2000, Accepted 29th January 2001
First published as an Advance Article on the web 13th February 2001

Cr-containing mesoporous silica molecular sieves (Cr-HMS) containing tetrahedrally coordinated isolated chromium oxide (chromate) moieties can operate as an efficient photocatalyst for the decomposition of NO and the partial oxidation of propane with molecular oxygen under visible light irradiation.

Highly dispersed transition metal oxides incorporated within the framework of zeolites and mesoporous molecular sieves show unique reactivities not only for catalytic reactions[1] but also for photocatalytic reactions.[2] In particular, highly dispersed transition metal oxides such as titanium,[3] vanadium[4] and molybdenum[5] exhibit high photocatalytic reactivities for various reactions. However, these metal oxides can operate as efficient photocatalysts only under UV light irradiation and exhibit no photocatalytic reactivity under visible light irradiation. To establish the clean photocatalysis system using the most environmentally ideal energy source—solar light—it is vital to develop a photocatalyst that can operate efficiently under visible light irradiation.

In the present study, chromium-containing mesoporous silica molecular sieves (Cr-HMS) have been prepared and characterized by various spectroscopic methods (XRD, EXAFS, EPR, UV–VIS, photoluminescence) and their photocatalytic reactivities under UV and visible light irradiations have been investigated. It has been found that chromium oxide (Cr-oxide) highly dispersed on the mesoporous silica can adsorb and utilize visible light in photocatalytic reactions such as the decomposition of NO into N_2 and O_2 and the partial oxidation of propane with O_2.

Cr-HMS mesoporous molecular sieves (0.02, 0.2, 1.0, 2.0 wt% as Cr) were synthesized using tetraethyl orthosilicate and $Cr(NO_3)_3{\cdot}9H_2O$ as the starting materials and dodecylamine as a template.[6,7] Calcination of the sample was carried out in a flow of dry air at 773 K for 5 h. Prior to spectroscopic measurements and photocatalytic reactions, the catalysts were degassed at 723 K for 2 h, heated in O_2 at the same temperature for 2 h and then finally evacuated at 473 K for 2 h to 10^{-6} Torr. The photocatalytic reactions were carried out with the catalysts (100 mg) in a flat-bottomed quartz cell (80 ml) connected to a conventional vacuum system (10^{-6} Torr range). Photocatalytic reactions were carried out under UV ($\lambda > 270$ nm) or visible light ($\lambda > 450$ nm) irradiation at 273 K using a high pressure mercury lamp (310–400 nm, 29 W m^{-2}; 360–480 nm, 44 W m^{-2}) through water and colored filters. The photocatalytic decomposition of NO was carried out on a starting amount of 135 μmol and the products in the gas phase were analyzed by GC. For the photocatalytic oxidation of propane with O_2, reactions were carried out on mixtures containing 240 μmol propane and 180 μmol O_2, and products in the gas phase and the products desorbed from the catalysts by heating to 573 K were also analyzed by GC.

The results of the XRD analysis indicated that the Cr-HMS have a mesopore structure[7] and that the Cr-oxide moieties are highly dispersed in the framework of HMS, while no other phases are formed. Cr-HMS exhibited a sharp and intense pre-edge peak in the XANES region which is characteristic of Cr-oxide moieties in a tetrahedral coordination.[8] In the Fourier transforms of EXAFS spectra, only a single peak due to the neighboring oxygen atoms (Cr–O) were observed, showing that Cr ions are highly dispersed in the Cr-HMS. Analysis of EXAFS spectra of Cr-HMS indicated that tetrahedrally coordinated Cr-oxide (chromate) moieties having two terminal C=O bonds existed as in an isolated state [two oxygen atoms (Cr=O) at 1.57 Å and two oxygen atoms (Cr–O) at 1.82 Å]. The EPR technique was also applied to investigate the coordination state of the Cr-oxide species by monitoring the Cr^{5+} ions formed under UV irradiation of the catalyst in the presence of H_2 at 77 K. After photoreduction with H_2 at 77 K, Cr-HMS exhibited a sharp, axially symmetric signal at around $g = 1.9$ ($g_{\|} = 1.880$, $g_{\perp}$ 1.945), attributed to the isolated mononuclear Cr^{5+} ions in tetrahedral coordination.[9]

As shown in Fig. 1, the UV–VIS spectra of the Cr-HMS catalysts exhibit three distinct absorption bands at around 250, 360 and 480 nm which can be assigned to charge transfer from O^{2-} to Cr^{6+} of the tetrahedrally coordinated Cr-oxide moieties.[10] Without Cr ion, HMS exhibit no absorption band above 220 nm. The absorption bands assigned to the absorption of dichromate or Cr_2O_3 cluster cannot be observed above 550 nm, indicating that tetrahedrally coordinated Cr-oxide species exist in an isolated state. Cr-HMS exhibited photoluminescence spectra at *ca*. 550–750 nm upon excitation of the absorption (excitation) bands at *ca*. 250, 360 and 480 nm. These absorption and photoluminescence spectra are similar to those obtained with well defined, highly dispersed Cr-oxides anchored on to Vycor glass or silica[11] and can be attributed to the charge transfer processes on tetrahedrally coordinated Cr-oxide moieties involving an electron transfer from O^{2-} to Cr^{6+} and a reverse radiative decay, respectively.

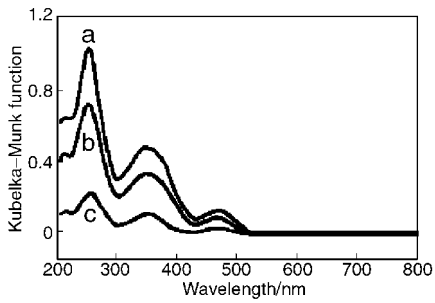

Fig. 1 The UV–VIS spectra of Cr-HMS catalysts (a) 2.0 wt%, (b) 1.0wt%, (c) 0.2 wt%, as Cr.

DOI: 10.1039/b008527h

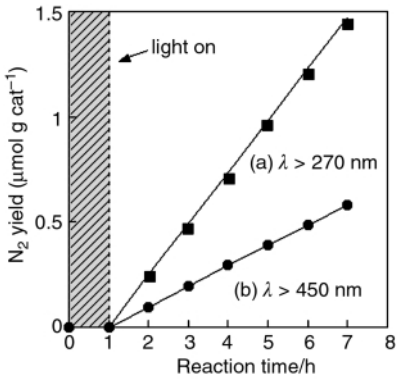

Fig. 2 The reaction time profile of N_2 formation in the photocatalytic decomposition of NO on the Cr-HMS catalyst at 273 K (2.0 wt% as Cr) under UV light irradiation (a) $\lambda > 270$ nm and visible light irradiation (b) at $\lambda > 450$ nm.

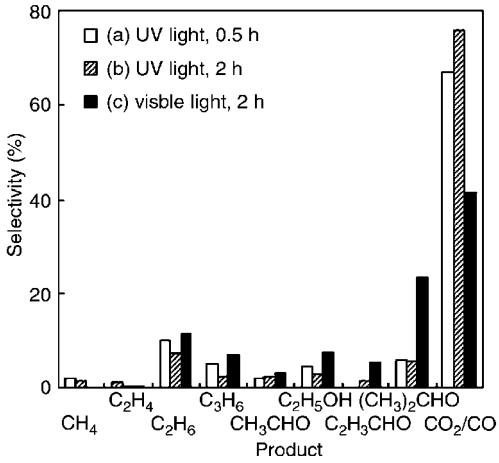

Fig. 3 The distribution of the photo-formed products in the photocatalytic oxidation of propane with O_2 on the Cr-HMS catalyst at 273 K (2.0 wt% as Cr) under UV light irradiation ($\lambda > 270$ nm) for (a) 0.5 h and (b) 2 h, and visible light irradiation ($\lambda > 450$ nm) for (c) 2 h.

UV light irradiation ($\lambda > 270$ nm) of the Cr-HMS in the presence of NO in the gas phase at 275 K led to the photocatalytic decomposition of NO and the evolution of N_2, N_2O and O_2. The Cr-HMS also showed photocatalytic reactivity even under visible light irradiation ($\lambda > 450$ nm). As shown in Fig. 2, the N_2 yields increase linearly with the irradiation time. The reaction stopped immediately when irradiation was ceased. Formation of these reaction products was not detected under dark conditions, or from irradiation of the HMS itself without Cr-oxide. After prolonged irradiation, the amount of decomposed NO to form N_2 per total number of Cr ions included within the catalyst exceeded unity [after 96 h on the Cr-HMS (0.02 wt% as Cr)]. These results clearly indicate that the presence of both Cr-oxide species (included within the HMS) as well as light irradiation are indispensable for the photocatalytic reaction to take place and that the direct decomposition of NO to produce N_2, O_2 and N_2O occurs photocatalytically on the Cr-HMS. Although the reaction rate under visible light irradiation is less than under UV light irradiation, the selectivity for N_2 formation (97%) under visible light irradiation is higher than that of UV light irradiation (45%). These results indicate that Cr-HMS can absorb visible light and act as an efficient photocatalyst under not only UV light but also visible light irradiation, and especially, Cr-HMS can be useful to form N_2 under visible light irradiation.

The addition of NO to the Cr-HMS led to an efficient quenching of the photoluminescence spectrum of the catalyst, its extent depending upon the amount of NO added. These results indicate that the charge transfer excited state of the tetrahedrally coordinated isolated Cr-oxide moieties, $(Cr^{5+}–O^{-})^*$, easily interact with NO, and this photo-excited species plays an important role in the photocatalytic reaction under UV and visible light irradiation.

On the other hand, light irradiation of the Cr-HMS in the presence of propane and O_2 led to the photocatalytic oxidation of propane. As shown in Fig. 3, partial oxidation of propane with a high selectivity for the production of oxygen-containing hydrocarbons such as acetone and acrolein proceeds under visible light irradiation, while further oxidation proceeds mainly under UV light irradiation to produce CO_2 and CO. The selectivity of partial oxidation production under visible light irradiation observed at 12% propane conversion is higher than that observed under UV light irradiation at 26% conversion and even under UV light irradiation for the shorter reaction time with 11% conversion. These results indicate that the tetrahedrally coordinated, isolated Cr-oxide moieties in HMS can exhibit an efficient photocatalytic reactivity for the oxidation of propane under visible light irradiation with a high selectivity for the partial oxidation of propane.

The present results have clearly demonstrated that the Cr-HMS can absorb visible light and act as an efficient and selective photocatalyst under visible light irradiation. This photocatalytic system with tetrahedrally coordinated Cr-oxide moieties dispersed on mesoporous silica seems to be a good candidate for the conversion of abundant visible or solar light energy into useful chemical energy.

Notes and references

1 L. Marchese, E. Gianotti, V. Dellarocca, T. Maschmeyer, F. Rey, S. Coluccia and J. M. Thomas, *Phys. Chem. Chem. Phys.*, 1999, **1**, 585; J. Dédécék and B. Wichterlova, *Phys. Chem. Chem. Phys.*, 1999, **1**, 629; A. Corma, *Chem. Rev.*, 1997, **97**, 2373; B. Notari, *Adv. Catal.*, 1996, **41**, 253.

2 M. Anpo and M. Che, *Adv. Catal.*, 1999, **44**, 119; H. Yamashita, J. Zhang, M. Matsuoka and M. Anpo, in *Photofunctional Zeolites*, ed. M. Anpo, Nova Sci. Pub. Inc., New York, 2000, p. 129.

3 H. Yamashita, Y. Ichihashi, M. Anpo, M. Hashimoto, C. Louis and M. Che, *J. Phys. Chem.*, 1996, **100**, 16 041; M. Anpo, H. Yamashita, Y. Ichihashi, Y. Fujii and M. Honda, *J. Phys. Chem. B*, 1997, **101**, 2632.

4 M. Anpo, S. G. Zhang, S. Higashimoto, M. Matsuoka, H. Yamashita, Y. Ichihashi, Y. Matsumura and Y. Souma, *J. Phys. Chem. B*, 1999, **103**, 9295.

5 S. Higashimoto, R. Tsumura, S. G. Zhang, M. Matsuoka, H. Yamashita, C. Louis, M. Che and M. Anpo, *Chem. Lett.*, 2000, 408.

6 H. Yamashita, M. Ariyuki, S. Higashimoto, S. G. Zhang, J. S. Chang, S. E. Park, J. M. Lee, Y. Matsumura and M. Anpo, *J. Synchrotron Radiat.*, 1999, **6**, 453.

7 W. Zhang, P. T. Tanev and T. J. Pinnavaia, *Chem. Commun.*, 1996, 979.

8 D. Wei, N. Yao and G. L. Haller, *Stud. Surf. Sci. Catal.*, 1999, **121**, 239.

9 B. M. Weckhuysen, R. A. Schoonheydt, J. M. Jehng, I. E. Wachs, S. J. Cho, R. Ryoo and E. Poels, *J. Chem. Soc., Faraday Trans.*, 1995, **91**, 3245; Z. D. Zhu, Z. X. Chang and L. Kevan, *J. Phys. Chem. B*, 1999, **103**, 2680.

10 B. M. Weckhuysen, A. A. Verberckmoes, A. L. Buttiens and R. A. Schoonheydt, *J. Phys. Chem. B*, 1994, **98**, 579.

11 M. Anpo, I. Takahashi and Y. Kubokawa, *J. Phys. Chem.*, 1982, **86**, 1; M. F. Hazenkamp and G. Blasse, *J. Phys. Chem.*, 1992, **96**, 3442.

Synthesis of novel non-cross-linking pyrrolobenzodiazepines with remarkable DNA binding affinity and potent antitumour activity

Ahmed Kamal,*[a] N. Laxman,[a] G. Ramesh,[a] K. Neelima[b] and Anand K. Kondapi[b]

[a] *Division of Organic Chemistry, Indian Institute of Chemical Technology, Hyderabad 500 007, India. E-mail: ahmedkamal@iict.ap.nic.in*

[b] *Department of Biochemistry, School of Life Sciences, University of Hyderabad, Hyderabad 500 046, India*

Received (in Cambridge, UK) 16th November 2000, Accepted 23rd January 2001
First published as an Advance Article on the web 13th February 2001

Mixed imine–amide pyrrolobenzodiazepine dimers have been prepared which exhibit potent antitumour activity and have significant DNA binding affinity; one of them, 1c, has been shown to cause a remarkable rise in the melting temperature of calf thymus DNA.

There has been increasing interest in discovering and developing small molecules that are capable of interacting with nucleic acids in a sequence-selective manner.[1–3] Such compounds have potential in the therapy of genetic-based diseases (some cancers),[4] diagnostics, and validation of DNA sequences. The pyrrolo[2,1-*c*][1,4]benzodiazepines (PBD's) are a well known class of antitumour antibiotics with sequence-selective DNA binding ability that are derived from various *Streptomyces* species. Their interaction with DNA has been extensively studied and is considered unique since they bind within the minor groove of DNA, forming a covalent aminal bond between the C11 position of PBD B-ring and the N2-amino group of a guanine base.[5] Further, the requirement of (*S*)-stereochemistry at C11a for these compounds enables a snug fit in the minor groove of DNA.[6] It has also been shown that PBD's inhibit both endonuclease activity and *in vitro* transcription in a sequence-selective manner.[7]

The naturally occurring PBD's (*e.g.* anthramycin and tomaymycin) span approximately 3 base pairs with a preference for purine–guanine–purine sequences. Thurston and co-workers[8] have synthesized C8 diyldioxy ether-linked PBD dimers (DSB-120), that span approximately six base pairs of DNA and in which the sequence selectivity is also increased (*e.g.* purine–GATC–pyrimidine for DSB-120). Moreover, the cytotoxic potency and large change in calf thymus (CT) DNA melting temperature has been attributed to its ability to irreversibly cross-link DNA *via* guanine residues on opposite strands because of the presence of two active sites (*i.e.* two imine functionalities). Recently, another new cross-linking PBD dimer (SJG-136) having C2/C2′-*exo* unsaturation has been prepared by the same group and exhibits extraordinary DNA binding affinity.[9] It has been established that the imine functionality or its equivalent methanolamine form is a primary requirement for the covalent binding, whereas the non-covalent interactions of PBD's with DNA bases help in rationalising the sequence selectivity and drug orientations.[10] Therefore, it has been considered of interest to design and synthesize C8 linked PBD-dimers, wherein one ring of PBD has the imino function while the other has an amide group. It has been envisaged that such a mixed dimer could offer more insight into not only the covalent binding but also the role played by non-covalent interactions with DNA bases.

In recent years a number of hybrid molecules containing the PBD ring system have been synthesized to improve upon the DNA binding ability and sequence selectivity.[11] We have been interested in the structural modifications of the PBD ring system and the development of new synthetic strategies.[12–16] In continuation of these efforts, we report a new synthesis of novel mixed dimers of PBD containing the imino function in one of the PBD rings and an amido group in the other, linked at the C8 position by a suitable alkane spacer. Interestingly, the larger sized spacer (n = 5) increases the melting temperature of CT DNA by a significant 17 °C after 18 h incubation at a (PBD) : (DNA) ratio of 1 : 5 for **1c**.

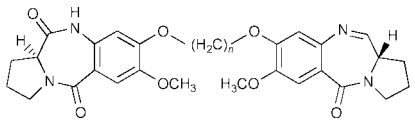

1a n = 3
1b n = 4
1c n = 5

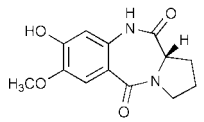

2

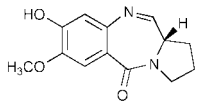

3 (DC-81)

Synthesis of the imine–amide mixed dimers of PBD has been carried out employing the commercially available vanillin. Oxidation of vanillin followed by benzylation and nitration by literature methods[17] provides the starting material **4**. L-Proline methyl ester has been coupled to **4** followed by debenzylation with BF_3·OEt_2–EtSH to give the nitro ester **6** (Scheme 1). Another precursor has been prepared from vanillic acid methyl ester **7** by its etherification with dibromoalkanes to afford **8**. The mono alkylation of **7** has been achieved by using 3 molar equivalents of the dibromo alkanes. Nitration of **8** followed by ester hydrolysis and coupling (2*S*)-pyrrolidinecarbaldehyde diethyl thioacetal gives **11**. The key intermediate has been prepared by linking **6** and **11**. Reduction of both nitro groups provides **13** which has a dilactam moiety at one end and the amino functionality on the other. Deprotection of the thioacetal group by using the method of Thurston and coworkers[8] affords the target molecules **1a**–**c** (Scheme 2).

Interestingly, the data presented in Table 1 show that as the size of the linker spacer increases from n = 3 to 5 the DNA stabilization is also enhanced. In this assay for a 1 : 5 molar ratio of (PBD) : (DNA), one of these mixed imine–amide PBD dimers (**1c**) elevates the helix melting temperature of CT DNA by a remarkable to 17.0 °C after incubation for 18 h at 37 °C. Under similar conditions, the dimer having two imino functionalities *i.e.* DSB-120 provides a ΔT_m of 15.4 °C. On the other hand, the naturally occurring DC-81 having only one imino group

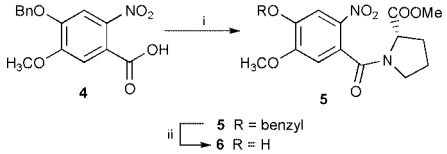

5 R = benzyl
6 R = H

Scheme 1 *Reagents and conditions*: i, $SOCl_2$ L-proline methyl ester hydrochloride, Et_3N, H_2O, 0 °C, 30 min, 85%; ii, BF_3·OEt_2–EtSH, CH_2Cl_2, rt, 8 h, 88%.

DOI: 10.1039/b009195m

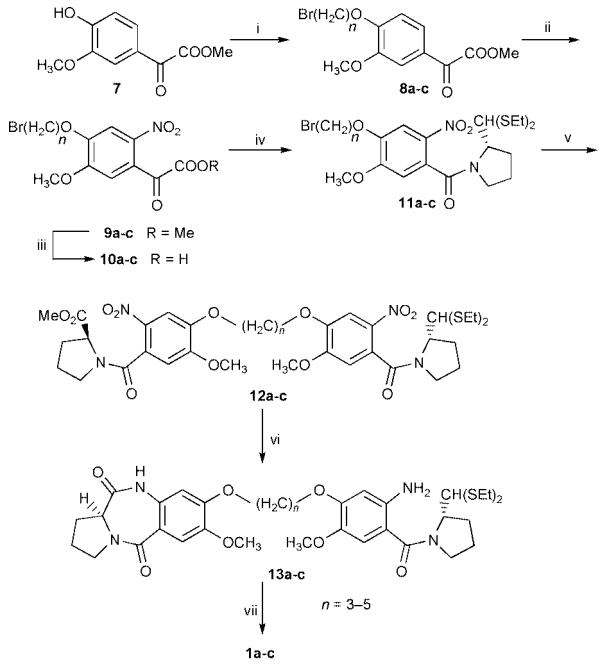

Scheme 2 *Reagents and conditions*: i, $Br(CH_2)_nBr$, K_2CO_3, CH_3COCH_3, reflux, 48 h, 82–86%; ii, $SnCl_4$–HNO_3, CH_2Cl_2, −25 °C, 5 min, 88–91%; iii, 1 M LiOH, THF, MeOH, H_2O (3 : 1 : 1), rt, 12 h, 89–93%; iv, $SOCl_2$ then DMF, THF, H_2O, 2(*S*)-pyrrolidinecarbaldehyde diethyl thioacetal, Et_3N, 3 h, 89–92%; v, **6**, K_2CO_3, CH_3COCH_3, reflux, 48 h, 85–90%; vi, $SnCl_2{\cdot}2H_2O$, MeOH, reflux, 40 min, 80–85%; vii, $HgCl_2$, $CaCO_3$, CH_3CN–H_2O (4 : 1), 3–8 h, 55–61%.

Table 1 Thermal denaturation with calf thymus DNA,[a] at a [PBD] : [DNA] molar ratio of 1 : 5[b] and *in vitro* one dose primary anticancer assay[c] in the NCI-H460, MCF 7 and SF-268 for **1a–c**

Induced ΔT_m/°C[ab] after incubation at 37 °C for			Growth percentages		
Compound	0 h	18 h	(Lung) NCI-H460	(Breast) MCF7	(CNS) SF-268
1a	6.5	7.0	4	10	11
1b	5.0	8.5	−16	−41	−81
1c	14.0	17.0	−39	7	−21
DC-81(**3**)	0.3	0.7	—	—	—
DSB-120	10.2	15.4	—	—	—

[a] For CT-DNA at pH 7.00 ± 0.01, ΔT_m = 66.5 °C ± 0.01 (mean value from 60 separate determinations), all ΔT_m values ± 0.1–0.2 °C. [b] For a 1 : 5 molar ratio of [ligand] : [DNA], where CT-DNA concentration = 100 μM in aqueous buffer [10 mM sodium phosphate + 1 M EDTA, pH 7.00 ± 0.01]. [c] One dose of **1a–c** at 10^{-4} molar concentration.

exhibits a ΔT_m of 0.7 °C. This demonstrates that compound **1c** containing a single imino functionality has a very significant DNA binding affinity. To the best of our knowledge, this is the first synthetic non-cross-linking molecule to exhibit a remarkable DNA binding effect similar to the naturally occurring sibiromycin (ΔT_m = 16.3 °C at 18 h).[11] These data indicates that non-covalent interactions play an important role for the enhancement of DNA binding affinity. The preliminary anticancer assays carried out on three human cell lines; lung (NCI-H460), breast (MCF7) and CNS (SF-268), exhibit significant anticancer activity for these compounds as illustrated in Table 1.

In summary, the synthesis of **1a–c**† reported here describes the importance of non-covalent interactions for increasing the DNA binding affinity and potent antitumour activity of the non-cross-linking mixed imine–amide PBD dimers. These findings may allow researchers to design newer analogues with improved therapeutic potential, particularly for antitumour activity. The sequence selectivity, endonuclease activity and detailed anticancer activity of these non-cross-linking PBD compounds will be reported elsewhere.

We thank the National Cancer Institute, Maryland for the primary anticancer assay in human cell lines. We are also thankful to CSIR, New Delhi for the award of research fellowship to two of us (N. L. and G. R.).

Notes and references

† *Selected data for compound* **1a**: δ_H(200 MHz, DMSO-d_6 + $CDCl_3$) 1.89–2.5 (m, 10H), 3.4–4.05 (m, 13H), 4.1–4.4 (m, 3H), 6.6 (s, 1H), 6.82 (s, 1H), 7.4 (s, 1H), 7.5 (s, 1H), 7.65 (d, 1H), 9.9 (s, 1H, NH exchangeable); ν_{max} (KBr)/cm^{-1} 3450–3460 (br), 2993, 2345, 1686, 1654, 1606, 1518, 1491, 1437, 1384, 1265, 1228, 1119, 1021, 839, 784; $[\alpha]_D^{30}$ +202.6 (*c* 0.5, $CHCl_3$); *m/z* (FAB): 549 $(M + H)^+$ (calc. for $C_{29}H_{31}N_4O_7$).

1 P. B. Dervan, *Science*, 1986, **232**, 464.
2 D. E. Thurston and A. S. Thompson, *Chem. Br.*, 1990, **26**, 767.
3 S. White, J. W. Szewczyk, J. M. Turner, E. E. Baird and P. B. Dervan, *Nature*, 1998, **391**, 468.
4 S. Neidle and D. E. Thurston, *New Targets for Cancer Chemotherapy*, ed. D. J. Kerr and P. Workman, CRC Press, London, 1994, p. 159.
5 D. E. Thurston, in *Molecular Aspects of Anticancer Drug–DNA Interactions*, ed. S. Neidle and M. J. Waring, Macmillan, London, 1993, p. 54.
6 R. L. Petrusek, G. L. Anderson, T. F. Garner, Q. L. Fannin, D. J. Kaplan, S. G. Zimmer and L. H. Hurley, *Biochemistry*, 1981, **20**, 111.
7 M. S. Puvvada, S. A. Forrow, J. A. Hartley, P. Stephenson, I. Gibson, T. C. Jenkins and D. E. Thurston, *Biochemistry*, 1997, **36**, 2478.
8 D. E. Thurston, D. S. Bose, A. S. Thompson, P. W. Howard, A. Leoni, S. J. Croker, T. C. Jenkins, S. Neidle, J. A. Hartley and L. H. Hurley, *J. Org. Chem.*, 1996, **61**, 8141.
9 S. J. Gregson, P. W. Howard, T. C. Jenkins, L. R. Kelland and D. E. Thurston, *J. Chem. Soc., Chem. Commun.*, 1999, 797.
10 G. B. Jones, C. L. Davey, T. C. Jenkins, A. Kamal, G. G. Kneale, S. Neidle, G. D. Webster and D. E. Thurston, *Anticancer Drug Design*, 1990, **5**, 249.
11 P. G. Baraldi, G. Balboni, B. Cacciari, A. Guiotto, S. Manfridini, R. Romagnoli, G. Spalluto, D. E. Thurston, P. W. Howard, N. Bianchi, C. Rutigliano, C. Mischiati and R. Gambari, *J. Med. Chem.*, 1999, **42**, 5131.
12 Y. Damayanthi, B. S. P. Reddy and J. W. Lown, *J. Org. Chem.*, 1999, **64**, 290.
13 A. Kamal, P. W. Howard, B. S. N. Reddy, B. S. P. Reddy and D. E. Thurston, *Tetrahedron*, 1997, **53**, 3223.
14 A. Kamal, Y. Damayanthi, B. S. N. Reddy, B. Lakshminarayana and B. S. P. Reddy, *Chem. Commun.*, 1997, 1015.
15 A. Kamal, M. V. Rao and B. S. N. Reddy, *Khim. Geterosilil. Soedin. Chem. (Chem. Heterocycl. Compd. Engl. Transl.)*, 1998, **12**, 1588.
16 A. Kamal, E. Laxman, N. Laxman and N. V. Rao, *Bioorg. Med. Chem. Lett.*, 2000, **10**, 2311.
17 D. E. Thurston, V. S. Murty, D. R. Langley and G. B. Jones, *Synthesis*, 1990, 81.

Enantiocontrol in the intermolecular cyclopropanation reaction catalyzed by dirhodium(II) complexes with *ortho*-metalated aryl phosphine ligands

Mario Barberis,[a] Pascual Lahuerta,*[b] Julia Pérez-Prieto*[a] and Mercedes Sanaú[b]

[a] *Departamento de Química Orgánica/Instituto de Ciencia Molecular, Facultad de Farmacia Universidad de Valencia, Vicént Andrés Estellés s/n, Burjassot, Valencia, 46100 Spain. E-mail: julia.perez@uv.es; Fax: (34)963864939*

[b] *Departamento de Química Inorgánica, Facultad de Químicas, Universidad de Valencia, Dr. Moliner 50, 46100 Burjassot,Valencia, Spain. E-mail: pascual.lahuerta@uv.es; Fax: (34)963864322*

Received (in Liverpool, UK) 8th December 2000, Accepted 25th January 2001
First published as an Advance Article on the web 14th February 2001

(*P*) and (*M*) dirhodium(II) complexes with *ortho*-metalated aryl phosphines are assessed as chiral catalysts in the enantioselective cyclopropanation of styrenes by ethyl diazoacetate; enantioselectivities up to 91% and up to 87%, respectively, for *cis*- and *trans*-2-arylcyclopropanecarboxylates are observed.

A great deal of effort is presently being devoted to the development of new chiral catalysts to induce enantiocontrol in carbene transfer reactions.[1–3] The catalytic reaction of ethyl diazoacetate with styrene is a model reaction with which stereo- and enantioselectivity for intermolecular cyclopropanation is measured and catalytic effectiveness is determined. Chiral copper catalysts,[4–8] especially those with bis-oxazoline ligands and ruthenium catalysts,[9] have been found to induce the highest levels of enantiocontrol. Thus, enantioselectivities up to 99% for ethyl 2-phenylcyclopropanecarboxylates have been obtained in the cyclopropanation of styrene with ethyl diazoacetate catalyzed by Cu catalysts. In general, chiral dirhodium(II) catalysts do not provide high enantioselectivities; there is a remarkable exception in chiral azetidine-4-carboxylate-ligated dirhodium(II) catalysts.[10] They produce enantioselectivities up to 76 and 52% ee, respectively, for **2a** and **3a** (Scheme 1).†

Dirhodium(II) catalysts of general formula $Rh_2(O_2CR)_2(PC)_2$, containing two *ortho*-metalated aryl phosphines (PC) in a head to tail arrangement,[11] (Fig. 1), have backbone chirality and they can be isolated as pure enantiomers by conventional resolution methods.[12] Until now, all approaches to the design of enantiomerically pure Rh(II) catalysts have depended on the attachment of enantiomerically pure ligands to the dirhodium core.

The racemic $Rh_2(O_2CR)_2(PC)_2$ compounds have been used in intramolecular processes.[13,14] Those with high electron-withdrawing carboxylate groups (CF_3CO_2) have shown the best selectivity values.

We now report, from results obtained with a series of Rh(II) catalysts, $Rh_2(O_2CCF_3)_2(PC)_2$, that they induce low diastereoselectivity in the intramolecular cyclopropanation of styrenes **1a**–**1d** (Scheme 1), but both cyclopropane diastereoisomers are obtained with high optical purity.

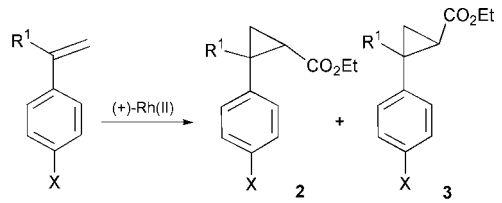

1a X = H, R^1 = H
1b X = Cl, R^1 = H
1c X = OMe, R^1 = H
1d X = H, R^1 = Me

Scheme 1 Catalyzed cyclopropanation of styrenes.

Use of catalysts **4**–**8** for cyclopropanation of styrene with ethyl diazoacetate gave the results reported in Table 1 (Fig. 1). Catalysts **4**–**7** showed low diastereoselectivity in the obtention of both diastereoisomers, **2a** and **3a**. However, all of them induced high asymmetry in the cyclopropanation of styrene; those catalysts with a more basic phosphine (catalysts **4**–**6** compared to **7**) led to the best ee values. The influence of the olefin on enantioselectivity was studied using styrenes of varying nucleophilicity (Table 2). Product yields were higher with the more nucleophilic olefins **1c** and **1d**. However, no remarkable differences on diastero- and enantioselectivity were found for catalysts **4**–**7**. These results confirm that degradation to an achiral rhodium catalyst is not a major competing pathway.

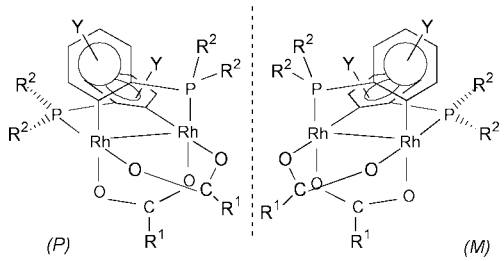

Rh	Phosphine Ar_3P (Ar)	R^1	R^2	Y
4	C_6H_5	CF_3	C_6H_5	H
5	*p*-MeC_6H_4	CF_3	*p*-MeC_6H_4	CH_3
6	*m*-MeC_6H_4	CF_3	*m*-MeC_6H_4	CH_3
7	*p*-FC_6H_4	CF_3	*p*-FC_6H_4	F
8	C_6H_5	$C(C_6H_5)_3$	C_6H_5	H

Fig. 1 List of Rh(II) catalysts with *ortho*-metalated aryl phosphine ligands.

Table 1 Asymmetric cyclopropanation of styrene catalyzed by the (*M*)-enantiomer

		% ee			Configuration	
Rh	Yield %[a]	**2a**/**3a**[b]	**2a**[c]	**3a**[c]	**2a**[d]	**3a**[d]
4	55	48:52	91	87	1*S*, 2*R*	1*S*, 2*S*
5	40	61:39	87	75	1*S*, 2*R*	1*S*, 2*S*
6	36	51:49	88	81	1*S*, 2*R*	1*S*, 2*S*
7	71	47:53	74	74	1*S*, 2*R*	1*S*, 2*S*
8	94	43:57	39	6	1*R*, 2*S*	1*R*, 2*R*

[a] Cyclopropanation yield based on ethyl diazoacetate. [b] Determined by GC analysis. [c] Ee values were based on GC analysis with a 2,3-di-*O*-acetyl-6-*O*-*tert*-butyldimethylsilyl-beta-CDX column. [d] Configuration was determined by correlation of the sign of the rotation of polarized light with that of the known enantiomer (ref. 15).

DOI: 10.1039/b010145c

Table 2 Influence of the olefin on enantioselectivity in the cyclization catalyzed by (***M***)-**4**

Olefin	Yield %	% ee		
		2/3	**2**	**3**
1a	55	48:52	91	87
1b	62	49:51	86	—[a]
1c	88	51:49	—[a]	85
1d	90	51:49	84	—[a]

[a] Not determined.

We suggest that the olefin approaches to the carbenoid through its less substituted carbon and also that the carbene transfer to olefin occurs through an early transition state. The interaction between the carbenoid ester group (CO_2Et) and the olefinic substituents (R, Ar) would be weak in such a case. These two mechanistic details, altogether, could explain the low influence of the olefin on diastereoselectivity observed in our experiments.

A tentative rationale for the observed high ee values for both stereoisomers, and for the sense of asymmetric induction in the cyclopropanation of styrenes with Rh(II) catalysts **4**–**7** is based on the model depicted in Fig. 2 for the *M*-catalyst. The non-metalated aryl substituents of the phosphorus atom protrude into the region where carbene transfer takes place, thereby limiting the possible orientations of the coordinated carbene and favoring those orientations placing the ester group at the less sterically demanding quadrants (orientation $\mathbf{A_1}$ and $\mathbf{B_1}$ in Fig. 2). The cyclopropanation step, $\mathbf{A_1} \rightarrow \mathbf{A_2}$ appears to be more favored than $\mathbf{B_1} \rightarrow \mathbf{B_2}$, since in the latter, a repulsive interaction builds up between the ester group and the metalated aryl group at some level of the proccess.

Additional evidence supporting such a model was obtained from the crystal structure determination of the enantiomerically pure catalyst ***(M)*-8** having bulky carboxylate ligands

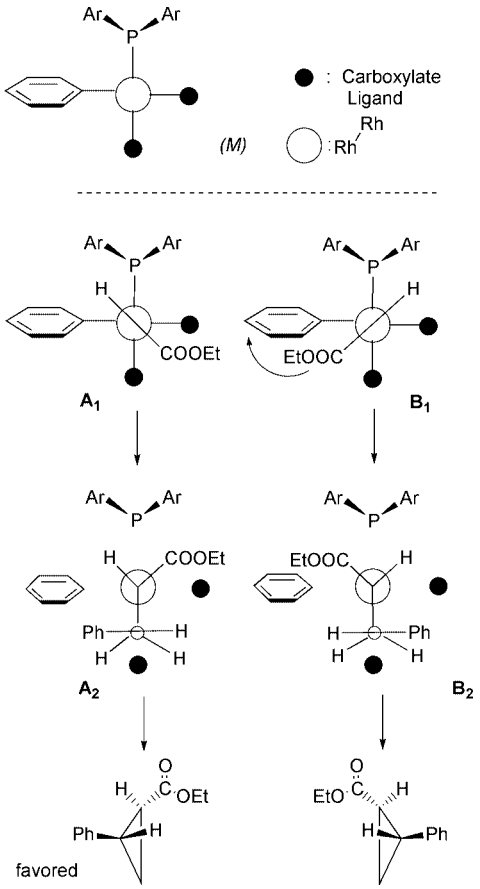

Fig. 2 Model transition state for the reaction of styrene catalyzed by the (*M*)-enantiomer.

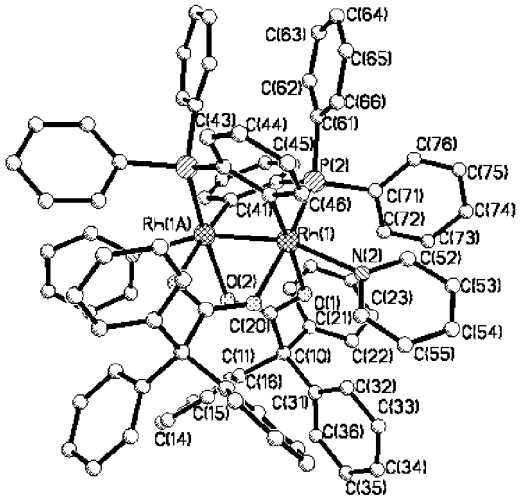

Fig. 3 Molecular view of the complex $Rh_2[(C_6H_5)_3CCO_2]_2[(C_6H_5)_2(C_6H_4)P]_2$ [***(M)*-8**]. Selected distances (Å) are Rh(1)–Rh(1A) = 2.5587(7), Rh(1)–O(2) = 2.151(3), Rh(1)–O(1) = 2.164(3), Rh(1)–P(2) = 2.280(13), Rh(1)–N(2) = 2.302(4). Selected angles (°) are C(41)–Rh(1)–O(2) = 88.08(15), O(2)–Rh(1)–O(1) = 85.65(12), O(2)–Rh(1)–P(2) = 171.46(9), N(2)–Rh(1)–Rh(1A) = 162.02.

$[(C_6H_5)_3CCO_2]$ (Fig. 3). In this case two relevant observations are made: the enantioselectivity was much lower (almost zero for one of the diastereoisomers) and there was a reversal of induction. These two facts may be attributed to increased steric interactions in the area of the carboxylate ligands, due to the higher steric requirements of the $[(C_6H_5)_3CCO_2]$ in **8** compared to (CF_3CO_2) in **4**–**7**, that make a carbenoid intermediate $\mathbf{A_1}$ less favored than $\mathbf{B_1}$ (Fig. 2). Additional studies oriented to confirm the reliability of the model depicted in Fig. 2 are in progress.

In summary, results indicate a high chiral recognition in the intermolecular cyclopropanation of styrenes showed by these dirhodium(II) compounds. The ee values clearly exceed those previously observed with other Rh(II) catalysts for this particular intermolecular reaction.

We thank the Dirección General de Investigación Científica y Técnica (DGICYT) (Project PB98-1437) and the EC (Project TMR Network ERBFMRXCT 60091).

Notes and references

† CCDC 155434. See http://www.rsc.org/suppdata/cc/b0/b010145c/ for crystallographic files in .cif format.

1 M. P. Doyle and M. N. Protopopova, *Tetrahedron*, 1998, **54**, 7919.
2 M. P. Doyle and D. C. Forbes, *Chem. Rev.*, 1998, **98**, 911.
3 G. A. Sulikowski, K. L. Cha and M. M. Sulikowski, *Tetrahedron: Asymmetry*, 1998, **9**, 3145.
4 T. Aratani, Y. Yoneyoshi and T. Nagase, *Tetrahedron Lett.*, 1982, **23**, 685.
5 Z. Li, Z. Zheng and H. Chen, *Tetrahedron: Asymmetry*, 2000, **11**, 1157.
6 D. A. Evans, K. A. Woerpel, M. M. Hinman and M. M. Faul, *J. Am. Chem. Soc.*, 1991, **113**, 726.
7 R. E. Lowenthal, A. Abiko and S. Masamune, *Tetrahedron Lett.*, 1990, **31**, 6005.
8 H. Fritschi, U. Leutenegger and A. Pfaltz, *Helv. Chim. Acta*, 1988, **71**, 1553.
9 H. Nishiyama, N. Soeda, T. Naito and Y. Motoyama, *Tetrahedron: Asymmetry*, 1998, **9**, 2865.
10 M. P. Doyle, S. B. Davies and W. Hu, *Chem. Comm.*, 2000, 867.
11 A. R. Chakravarty, F. A. Cotton, D. A. Tocher and J. H. Tocher, *Organometallics*, 1985, **4**, 8.
12 D. F. Taber, S. C. Malcolm, S. K. Bieger, P. Lahuerta, S.-E. Stiriba, J. Pérez-Prieto, M. Sanaú and M. A. Monge, *J. Am. Chem. Soc.*, 1999, **121**, 860.
13 F. Estevan, P. Lahuerta, J. Pérez-Prieto, M. Sanaú, S. E. Stiriba and M. A. Ubeda, *Organometallics*, 1997, **16**, 880.
14 F. Estevan, P. Lahuerta, J. Pérez-Prieto, I. Pereira, S. E. Stiriba and M. A. Ubeda, *Organometallics*, 1998, **17**, 3442.
15 T. Aratani, Y. Nakanisi and H. Nozaki, *Tetrahedron*, 1970, **26**, 1675.

Novel CuX_2-mediated cyclization of acid–base salts of (L)-cinchonidine or (D)-/(L)-α-methylbenzylamine and 2,3-allenoic acids in an aqueous medium. An efficient entry to optically active β-halobutenolides

Shengming Ma* and Shulin Wu

Laboratory of Organometallic Chemistry, Shanghai Institute of Organic Chemistry, Chinese Academy of Sciences, 354 Fenglin Lu, Shanghai 200032 People's Republic of China. E-mail: masm@pub.sioc.ac.cn

Received (in Cambridge, UK) 1st November 2000, Accepted 16th January 2001
First published as an Advance Article on the web 15th February 2001

The treatment of 1:1 salts of 2,3-allenoic acid–chiral base with CuX_2 (4 equiv.) in an aqueous medium, *i.e.* acetone–H_2O (2:1), at 60–65 °C afforded β-halobutenolides with high enantiopurities in good to excellent yields.

Polysubstituted butenolides are a class of compounds of current interest due to their potential broad range of biological activities[1] and abundant occurrence in natural products.[2] However, the methods for the highly stereoselective synthesis of optically active butenolides are limited.[3,4] In this paper, we wish to report a highly efficient CuX_2-mediated cyclization of the salts formed between chiral bases and 2,3-allenoic acids. The method provides a novel route to β-halobutenolides with high enantiopurity, important building blocks for polysubstituted butenolides.[5]

Recently, we have developed several methodologies for the synthesis of β-halobutenolides from 2,3-allenoic acids.[5,6] The interesting point of these reactions is that the starting 2,3-allenoic acids are a class of compounds with chirality when properly substituted. Thus, it would be possible to use a cheap optically active base to resolve 2,3-allenoic acids and transfer the axial chirality in allenes into central chirality in butenolides in a highly stereoselective manner. One major issue here is the use of the salt of an optically active base with 2,3-allenoic acids *directly* as the starting point, the release of 2,3-allenoic acids from the salts would not be necessary, which makes this strategy more attractive.

The resolution of racemate 2-methyl-4-phenylbuta-2,3-dienoic acid **1a** with 0.5 equiv. of (L)-cinchonidine, a readily available and relatively cheap base, afforded a salt which could be readily recrystallized in *ethyl acetate* to afford the optically active salt (+)-**2a** in 43% yield with $[\alpha]_D^{20}$ = +85.4°.[7] Release of the acid from the corresponding salt (+)-**2a** by the treatment with dilute H_2SO_4 afforded *S*-(+)-**1a**, indicating the (*S*)-configuration of the allene moiety according to the Lowe–Brewster rule (Scheme 1).[8]

Luckily, when (+)-**2a** was treated with $CuBr_2$ in an aqueous medium (acetone–H_2O (2:1)), at 60–65 °C for 3 h, a methodology recently developed by ourselves for the halolactonization of 2,3-allenoic acids,[6] the reaction afforded (+)-**3a** in 95% yield with 98% ee, [9] the corresponding β-chlorobutenolide (+)-**3b** was also obtained in 90% yield with 99% ee by using $CuCl_2$ instead of $CuBr_2$ (Scheme 2).

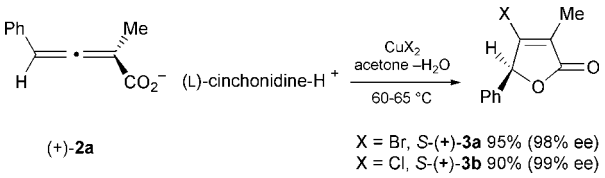

With the standard aqueous reaction conditions in hand, a series of β-bromobutenolides with high optical purity were prepared and the results are summarized in Table 1. It is obvious: (1) the yields are from good to excellent; and (2) the efficiency of the chirality transfer process is almost 100% since the %ee of the products from the resolved salts are similar to those from the released free 2,3-allenoic acids (Scheme 3),indicating that the chirality of (L)-cinchonidine has almost no impact on the chirality transfer of the allene moiety. Similar results were obtained for all substrates using $CuCl_2$ in place of $CuBr_2$ to afford β-chlorobutenolides. The absolute configuration of the chiral centers in the products **3c** and **3d** were determined by X-ray diffraction using the bromine atoms as the reference.[10] The absolute configuration of other products are based on these X-ray studies and further confirmed by the study of their CD spectra.[11]

Furthermore, it is interesting to observe when we used (*S*)-(+)-α-methylbenzylamine as the resoluting agent, the salt (−)-**4a** was obtained and its treatment with $CuBr_2$ afforded the opposite enantiomers (*R*)-(−)-**3a** (98% ee) and (*R*)-(−)-**3b** (98% ee) in 90% and 93% yields, respectively (Scheme 4).

By using (*R*)-(−)-α-methylbenzylamine instead of its *S*-enantiomer, the corresponding salt (+)-**4a** afforded the same enantiomer as with (L)-cinchonidine, *i.e.* (*S*)-(+)-**3a** and (*S*)-(+)-**3b** in 92 (98% ee) and 90% yield (97% ee), respectively (Scheme 4).

In conclusion, we have developed an efficient aqueous synthesis of highly optically active β-halobutenolides. The current methodology will show its utility in organic synthesis due to the ready availability of starting materials with different substitution patterns,[7,12] direct cyclization from the salts, and availability of both enantiomers.

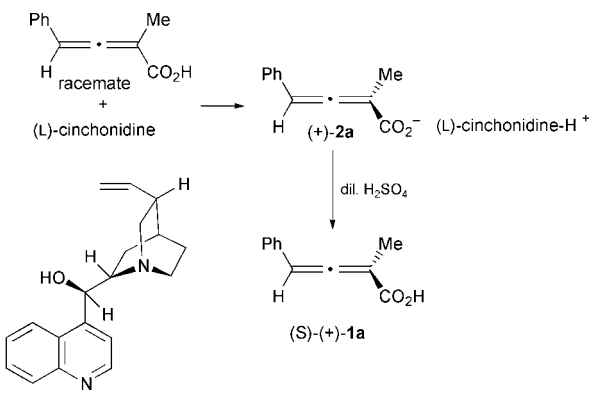

Scheme 1

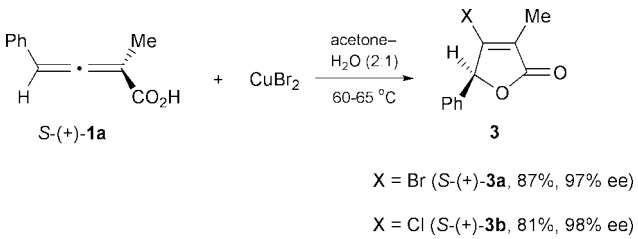

Scheme 3

DOI: 10.1039/b008818h

Table 1 Highly stereoselective cyclization of (L)-cinchonidine salts of 2,3-dienoic acids[a]

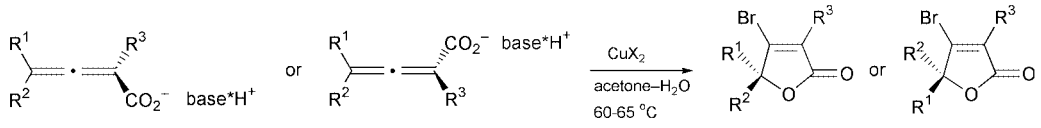

Entry	Acid R1	R2	R3	Optical rotation of the salt[b]	CuX_2 X =	Reaction time/h	Yield (%) (product, ee%[g])
1	C_6H_{13}	H	Me (**1b**)	−9.10	Cl	6	90 (*S*-(−)-**3c**, 94)
2	C_6H_{13}	H	Me (**1b**)	−9.10	Br	3	95 (*S*-(−)-**3d**,[c] 95)
3	$C_{10}H_7$[d]	H	Me (**1c**)	+58.3	Cl	10	88 (*S*-(+)-**3e**, 98)
4	$C_{10}H_7$[d]	H	Me (**1c**)	+58.3	Br	3	86 (*S*-(+)-**3f**,[c] 98)
5	Ph	H	C_3H_7 (**1d**)	+37.8	Cl	8	92 (*S*-(+)-**3g**, 96)
6	Ph	H	C_3H_7 (**1d**)	+37.8	Br	3	96 (*S*-(+)-**3h**, 96)

reaction was carried out using the salt and CuX_2 (4 equiv.) in acetone–H_2O (2:1) at 60–65 °C. [b] The specific optical rotation $[\alpha]_D^{20}$ (c = 1, . [c] The absolute configuration was determined by X-ray diffraction studies. [d] $C_{10}H_7$ = α-naphthyl.

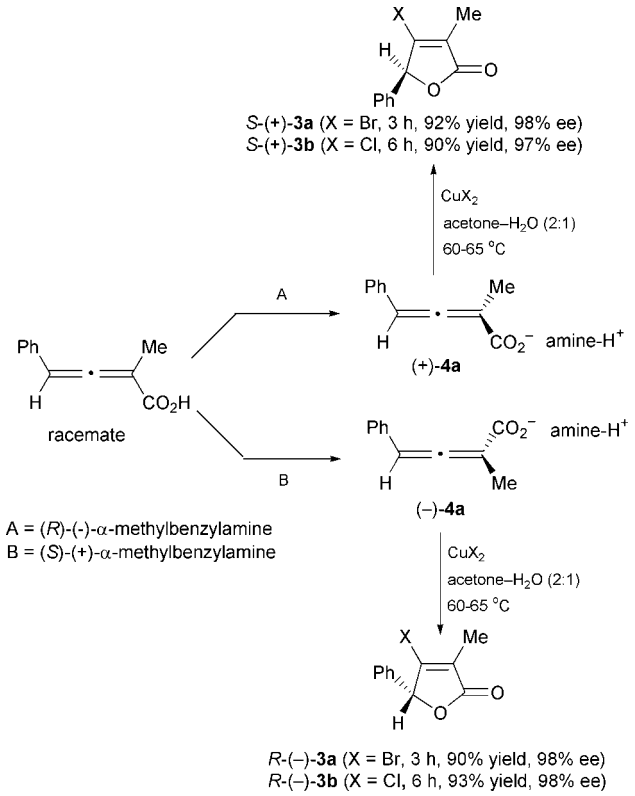

Scheme 4

Financial support from National NSF of China (No. 29932020) and the Major State Basic Research Development Program (Grant No. G2000077500) are greatly appreciated. Shengming Ma is the recipient of 1999 Qiu Shi Award for Young Scientific Workers issued by Hong Kong Qiu Shi Foundation of Science and Technology (1999–2002) and the Special Starting Grant for Outstanding Young Chemists issued by National Natural Science Foundation of China (29525202).

Notes and references

1 (*a*) T. S. Brima, US 4,968,817, 1990 [*Chem. Abstr.*, 1991, **114**, 185246y]; (*b*) A. Tanabe, *Jpn. Kokai. Tokyo. Koho JP*. 63,211,276 [88,211,276], 1988 [*Chem. Abstr.* 1989, **110**, 94978q]; (*c*) G. C. M. Lee, Eur. Pat. EP. 372,940, 1990 [*Chem. Abstr.*, 1990, **113**, 191137j]; (*d*) Y. Ducharme, J. Y. Gauthier, P. Prasit, Y. Leblanc, Z. Wang, S. Leger and M. Thrien, PCT Int. Appl. WO 95, 00,501, 1995 [*Chem. Abstr.*, 1996, **124**, 55954y]; (*e*) C. M. Lee Gary and M. E. Gast, PCT Int. Appl. WO. 91 16,055, 1991 [*Chem. Abstr.*, 1992, **116**, 59197m].

2 For recent examples, see: (*a*) Y. Chia, F. Chang and Y. Wu, *Tetrahedron Lett.*, 1999, **40**, 7513; (*b*) S. Takahashi, K. Maeda, S. Hirota and T. Nakata, *Org. Lett.*, 1999, **1**, 2025; (*c*) D. A. G. Cortez, J. B. Fermandes, P. C. Vieria, M. F. Das, G. F. Da Silva, A. G. Ferreira, Q. B. Cass and J. R. Pirani, *Phytochemistry*, 1998, **49**, 2493; (*d*) H. Ostuka, K. Kotani, M. Bando, M. Kido and Y. Takeda, *Chem. Pharm. Bull.*, 1998, **46**, 1180; (*e*) T. Ishikawa, K. Nishigaya, H. Uchikoshi and I. Chen, *J. Nat. Prod.*, 1998, **64**, 534; (*f*) S. Driol, F. Felluga, C. Forzeto, P. Nitti, G. Pitacco and E. Valentin, *J. Org. Chem.*, 1998, **63**, 2385.

3 For a summary of methodologies for the synthesis of racemic butenolides, see: (*a*) D. W. Knight, *Contemp. Org. Synth.*, 1994, 287; (*b*) S. Ma and Z. Shi, *J. Org. Chem.*, 1998, **63**, 6387, and the references cited therein. For some of the most recent examples, see: (*c*) N. Chatani, T. Morimoto, Y. Fukumoto and S. Murai, *J. Am. Chem. Soc.*, 1998, **120**, 5335; (*d*) M. J. Bassindalem, P. Hamley, A. Leitner and J. P. A. Harrity, *Tetrahedron Lett.*, 1999, **40**, 3247.

4 For some of the representative examples of the stereoselective synthesis of optically active butenolides, see: (*a*) A. G. Schultz, M. Dai, S. Khim, L. Pettus and K. Thakkar, *Tetrahedron Lett.*, 1998, **39**, 4203; (*b*) S. M. Dankwardt, J. W. Dankwardt and R. H. Schlessinger, *Tetrahedron Lett.*, 1998, **39**, 4971, 4975 and 4979; (*c*) A. van Oeveren and B. L. Feringa, *J. Org. Chem.*, 1996, **61**, 2920; (*d*) M. Renard and L. Ghosez, *Tetrahedron Lett.*, 1999, **40**, 6237; (*e*) T. Mukaiyama and K. Suzuki, *Chem. Lett.*, 1980, 255; (*f*) S. Tsuboi, J. Sakamoto, H. Yamashita, T. Sakai and M. Utaka, *J. Org. Chem.*, 1998, **63**, 1102; (*g*) Q. Yu, Y. Wu, L.-J. Xia, M.-H. Tang and Y.-L. Wu, *Chem. Commun.*, 1999, 129; (*h*) T. Berkenbusch and R. Bruckner, *Tetrahedron*, 1998, **54**, 11 471.

5 (*a*) S. Ma, Z. Shi and Z. Yu, *Tetrahedron Lett.*, 1999, **40**, 2393; (*b*) S. Ma, Z. Shi and Z. Yu, *Tetrahedron*, 1999, **55**, 12 137.

6 S. Ma and S. Wu, *J. Org. Chem.*, 1999, **64**, 9314.

7 The known resolving process in acetone lacks efficiency and affords the salts in 27.5% yield with $[\alpha]_D^{25}$ = +60°, see: W. Runge and G. Kresze, *Liebigs Ann. Chem.*, 1975, 1361.

8 S. R. Landor, *The Chemistry of the Allenes*, Academic Press, New York, 1982, vol. 3, pp. 587–590.

9 The ee values were determined by HPLC on a Chiralpack AS column using *n*-hexane–isopropyl alcohol (65:35) as the eluent. The racemic butenolides were prepared by starting from the racemic 2,3-allenoic acids using the method reported in ref. 6.

10 The absolute configuration was determined using Texsan software. The Bijvoet reflections were collected and refined with Bijvoets not flagged as redundant. CCDC 152077 and 152078. See http://www.rsc.org/suppdata/cc/b0/b008818h/ for crystallographic data in .cif format.

11 (*a*) J. K. Gawronski, A. van Oeveran, H. van der Deen, C. W. Leung and B. L. Feringa, *J. Org. Chem.*, 1996, **61**, 1513; (*b*) J. K. Gawronski, Q. Chen, Z. Geng, B. Huang, M. R. Martin, A. I. Mateo, M. Brzostowska, U. Rychlewska and B. Feringa, *Chirality*, 1997, **9**, 537.

12 (*a*) H.-J. Bestmann and H. Hartung, *Chem. Ber.*, 1966, **99**, 1198; (*b*) H. D. Venkruijsse and L. Brandsma, *Synthesis of Acetylenes, Allenes and Cumulenes. A Laboratory Manual*, Elsevier: Amsterdam, The Netherlands, 1981, p. 33.

First gold(I) complex-catalyzed oxidative carbonylation of amines for the syntheses of carbamates

Feng Shi and Youquan Deng*

State Key Laboratory for Oxo Synthesis and Selective Oxidation, and Laboratory of Environmental and Applied Catalysis, Lanzhou Institute of Chemical Physics, Chinese Academy of Sciences, Lanzhou, 730000, China. E-mail: ydeng@ns.lzb.ac.cn; Fax: +86-931-8277088

Received (in Cambridge, UK) 29th November 2000, Accepted 25th January 2001
First published as an Advance Article on the web 14th February 2001

At 200 °C and 5 MPa of initial total pressure, the oxidative carbonylation of amines for the synthesis of the corresponding carbamates by Au(I) complexes as catalysts was conducted with excellent conversion and selectivity.

Gold catalysts have been receiving growing attention and many reactions catalyzed over Au catalysts,[1] such as CO oxidation,[2] selective oxidation,[3] water-gas shift reactions,[4] asymmetric aldol reactions,[5] carbonylation of olefins[6] and dehydrogenative dimerization of trialkylstannane,[7] have been reported to be high performance. These reactions indicate that using gold complexes as catalysts for those synthetic reactions traditionally catalyzed with Pd, Rh *etc.* complexes should be not only possible but also practical and even highly efficient.

Produced either by oxidative carbonylation of amines or by reductive carbonylation of nitro compounds in the presence of an alcohol, carbamates as intermediates for the synthesis of isocyanates by non-phosgene routes have been extensively studied over the past two decades.[8] Pd, Ru and Rh complexes and other transition metals were employed as the catalysts,[9] and complexes of Pd coordinated with N-containing compounds were among the most effective of these catalyst systems.[10] Although reductive carbonylation of nitro compounds should be the more attractive route for indirect production of isocyanates, the occurrence of catalyst deactivation due to the reduction of noble metal ions, *e.g.* Pd^{2+} to Pd^0, under the strong reductive conditions may be difficult to be overcome,[11] and the catalyst systems were generally more complicated than those for oxidative carbonylation. Furthermore, no studies concerning the oxidative carbonylation of amines or reductive carbonylation of nitro compounds for carbamate formation by Au complexes have been reported yet.

Herein, the first example of the oxidative carbonylation of amines for the synthesis of the corresponding carbamates by Au complexes, *i.e.* $HAuCl_4$ **1**, $Au(PPh_3)Cl$ **2**, $Au(PPh_3)_2Cl$ **3**, $Au(PPh_3)NO_3$ **4** and $[Au(PPh_3)]_2S$ **5** as the catalysts with excellent performance, is reported:

$$R(NH_2)_n + CO + O_2 + R'OH \xrightarrow[PPh_3]{[Au(PPh_3)_x]_yZ} R(NHCO_2R')_n + H_2O$$

R = Ph, Alkyl; R′ = CH_3, CH_3CH_2; $n = 1$ or 2;

$x, y = 1$ or 2; Z = Cl, NO_3, S.

The oxidative carbonylation of a series of aromatic and aliphatic amines over the above mentioned Au(I) complexes was examined (Table 1). When aniline as substrate was subjected to carbonylation, different catalytic performances were observed over catalysts **1**–**5**. The highest selectivity was 70% over **2**, and the highest conversion 62.2% over **3**. The catalyst **5** was even less effective than catalyst **1**. The main by-product resulting from catalyst **1** was azobenzene, while *N*-methylaniline and quinazoline were detected over the catalysts **2**–**5**. Other by-products such as azoxybenzene over catalyst **1** and quinazoline over catalyst **2** were also identified. When catalyst **1** was employed, decomposition of the catalyst, *i.e.* reduction of Au^{3+} to Au^0, occurred. A very thin film, light-yellow in color, was observed to have been deposited on the wall of the glass tube inside the reactor after the reaction; no such phenomenon was observed with catalysts **2**–**4**.

The conversion and selectivity for the desired products were greatly enhanced if extra PPh_3, (0.1 g) was further added into the reaction, entries 6–9. It is noteworthy that 97.2% conversion and 89% selectivity were achieved over catalyst **2** + PPh_3. The TOF reached 36, which is comparable to the result of $Pd(PPh_3)_2Cl_2$ (**6**) + PPh_3 used as the catalyst, where 98.5% conversion and 86% selectivity was obtained, entry 8. Such enhancement in catalytic activity may partially be attributed to the stabilization of organic Au(I) complexes by the additional PPh_3 which may replace the oxidized ligand, since it is possible that small amounts of PPh_3 could be oxidized under oxidative conditions during the reaction. The same main by-product, quinazoline, was found over catalysts **2** + PPh_3 and **6** + PPh_3, indicating that a similar reaction mechanism occurred over catalysts **2** and **6**.

Using alcohol as one of the reaction substrates and solvent had a strong impact on the reaction. Much higher selectivity could be achieved when methanol was used, entry 6, although slightly higher conversion was obtained with ethanol under the same reaction conditions, entry 7. This may be due to the easier formation of quinoline in the simultaneous presence of aniline and ethanol. Treatment of 2,4-diaminotoluene and 4,4′-diaminodiphenylmethane with carbon monoxide and methanol in the presence of catalyst **2** + PPh_3 afforded excellent conversion and selectivity, entries 11 and 12. The main by-product from 2,4-diaminotoluene was the mono-carbonylated product, while the main by-product from 4,4′-diaminodiphenylmethane was 4,4′-diaminobenzophenone.

An attempt was also made to test the oxidative carbonylation of aliphatic amines using catalyst **2** + PPh_3, the best catalyst system found for the carbonylation of aromatic amines. Although the conversion of the corresponding amines was almost complete for n-hexylamine (entry 13) and cyclohexylamine (entry 14), poor selectivities for the desired product were obtained, but relatively high selectivities for the corresponding alkylureas were achieved. For 1,6-hexanediamine (entry 15) almost no desired product could be observed, but it is noteworthy that 63% selectivity for *N*,*N*′-hexylmethylene diformamide could be achieved. This may imply that the Au(I) complexes could be a promising catalyst for the synthesis of other N-containing compounds from aliphatic amines under suitable reaction conditions.

In summary, the experimental results suggest that organic Au(I) complexes show an excellent performance towards the oxidative carbonylation of aromatic amines to form corresponding carbamates, and also exhibit a promising catalytic performance towards the carbonylation of aliphatic amines to produce either alkylureas or formamides. To the best of our knowledge this is the first reported study of Au(I) complexes for this kind of reaction.

DOI: 10.1039/b009575n

Table 1 The catalytic performances of Au(I) complexes towards oxidative carbonylation of amines

Entry	Sub.	Cat.	Con. (%)	Sel. (%)	TOF[a]	Products	By-products		Others[b]
1	aniline	$HAuCl_4$	33.7	37	11	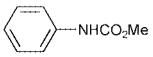	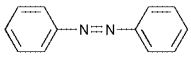	9	34(20)
2	aniline	$Au(PPh_3)Cl$	38.8	70	14	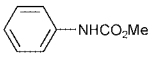	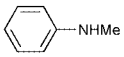	10	18(2)
3	aniline	$Au(PPh_3)_2Cl$	62.2	60	23	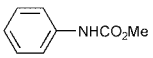	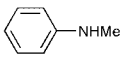	15	23(2)
4	aniline	$Au(PPh_3)NO_3$	42.1	43	16	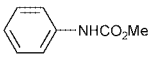	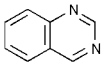	13	41(3)
5	aniline	$[Au(PPh_3)_3]_2S$	32.2	30	11	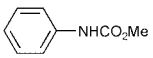	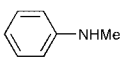	30	39(1)
6	aniline	$Au(PPh_3)Cl$ $+PPh_3$	97.2	89	36	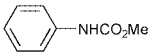	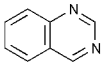	7	3(1)
7[c]	aniline	$Au(PPh_3)Cl$ $+PPh_3$	98.8	60	36.5	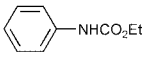	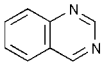	21	19
8	aniline	$Pd(PPh_3)_2Cl_2$ $+PPh_3$	98.5	86	36	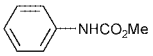	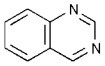	11	2(1)
9	aniline	$Au(PPh_3)NO_3$ $+PPh_3$	96	83	36	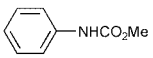	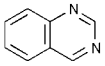	13	41(3)
10	aniline	$[Au(PPh_3)_3]_2S$ $+PPh_3$	48	69	17	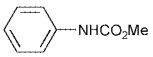	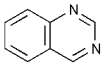	5	23(3)
11	TDA[d]	$Au(PPh_3)Cl$ $+PPh_3$	98	93	28	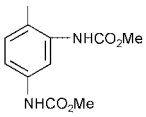	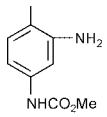	5	(2)
12	MDA[e]	$Au(PPh_3)Cl$ $+PPh_3$	89	88	17	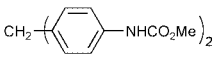	DBP[f]	2	(10)
13	n-hexyl-amine	$Au(PPh_3)Cl$ $+PPh_3$	99	35	30	$C_6H_{15}NHCO_2Me$	$(CH_3C_5H_{10}NH)_2CO$	40	24(1)
14	cyclohexyl-amine	$Au(PPh_3)Cl$ $+PPh_3$	100	58	30	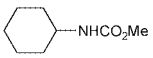	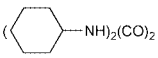	22	18(2)
15	1,6-hexane-diamine	$Au(PPh_3)Cl$ $+PPh_3$	99	–	30	$(CH_2)_6(NHCO_2CH_3)_2$	$(OHCHN)_2(CH_2)_6$	63	37

[a]Mol substrate converted per mol Au per hour. [b]Unidentified in brackets. [c]Ethanol as solvent. [d]2,4-Diaminotoluene. [e]4,4′-Diaminodiphenylmethane. [f]4,4′-Diaminobenzophenone.

The following experimental procedure was used: the syntheses of the Au(I) complexes were as reported in previous papers.[12] $Pd(PPh_3)_2Cl_2$ (**6**) was also employed for the purpose of comparison. The reactions were performed in glass tubes with magnetic stirring within an autoclave. For each reaction, 0.05mmol Au(I) complex or the mixture of 0.05 mmol Au(I) complex and 0.1 g PPh_3 was added to the solution of amine (0.5 g or 0.5 ml) and alcohol (20 ml, MeOH or EtOH) at rt. Then O_2 (99.99% purity 1 MPa) and CO (99.99% purity, 4 MPa) were respectively introduced into the reactor to 5 MPa total pressure. The reaction was allowed to proceed at 200 °C for 3 h and the resulting liquid mixture was then directly analyzed with a HP 6890/5973 GC-MS.

Notes and references

1 C. B. Geoffrey and T. T. David, *Cat. Rev.*, 1999, 319.
2 J. D. Grünwaldt and A. Baiker, *J. Phys. Chem. B.*, 1999, **103**, 115; Y. z. Yuan, A. P. Kozalova, K. Asakura, K. Tsai and Y. Iwasawa, *J. Catal.*, 1997, **170**, 191; M. Valden, X. Lai and D. W. Goodman, *Science*, 1998, **281**, 1647.
3 D. Andreeva, T. Tabakova and A. Andreev, *J. Catal.*, 1996, **158**, 354.
4 L. Prati and M. Rossi, *J. Catal.*, 1998, **176**, 552; J. Zou, Z. Guo, J. A. Parkinson, Y. Chen and P. J. Sadler, *Chem. Commun.*, 1999, 1359.
5 V. A. Soloshonok and A. D. Kacharov, *Tetrahedron*, 1996, **52**, 245.
6 Q. Xu, Y. Imamura, M. Fujiwara and Y. Souma, *J. Org. Chem.*, 1997, **62**, 1594.
7 H. Ito, T. Yajima, J.-i. Tateiwa and A. Hosomi, *Tetrahedron Lett.*, 1999, **40**, 7807.
8 S. Cenini and F. Ragaini, *Catalytic Reductive Carbonylation of Organic Nitro Compounds*, Kluwer Academic Publishers, The Netherlands, 1997; A. M. Tafesh and J. Weiguny, *Chem. Rev.*, 1996, **96**, 2035.
9 V. L. K. Valli and H. Alper, *J. Am. Chem. Soc.*, 1993, **115**, 3778; D. K. Mukherjee, B. K. Palit and C. R. Saha, *J. Mol. Cat.*, 1994, **91**, 19; P. Wehman, P. C. J. Kamer and P. W. N. M. Leeuwen, *J. Chem. Soc., Chem. Commun.*, 1996, 217.
10 S. M. Islam, D. Mal, B. K. Palit and C. R. Saha, *J. Mol. Catal.*, 1999, **142**, 169; P. Giannoccaro, C. F. Nobile, P. Mastrorilli and J. N. Ravasio, *J. Organomet. Chem.*, 1991, **419**, 251; V. L. K. Valli and H. Alper, *Organometallics*, 1995, **14**, 80.
11 E. Alessio and G. Mestroni, *J. Mol. Catal.*, 1984, **26**, 337; R. Ugo, R. Psaro, M. Pizzotti, P. Nardi, C. Dossi, A.Andreetta and G. Capparella, *J. Organomet. Chem.*, 1991, **417**, 211.
12 N. G. Russell, *Inorganic Syntheses*, Wiley, New York, 1992, **29**, 280; C. A. McAuliffe, R. V. (Dick) Parish and P. D. Randall, *J. Chem. Soc., Dalton Trans.*, 1979, 1730; F. Canales, C. Gimeno, A. Laguna and M. D. Villacampa, *Inorg. Chim. Acta*, 1996, **244**, 95.

ChemComm

In situ, time resolved, and simultaneous multi-edge determination of local order change during reduction of supported bimetallic (Pt–Ge) catalyst precursors using energy dispersive EXAFS†

Steven G. Fiddy,[a] Mark A. Newton,[a] Tom Campbell,[a] Judith M. Corker,[a] Andrew J. Dent,[b] Ian Harvey,[b] Guiseppe Salvini,[b] Sandra Turin[a] and John Evans[a]

[a] *Department of Chemistry, University of Southampton, Southampton, UK SO17 1BJ. E-mail: je@soton.ac.uk*
[b] *CLRC Daresbury, Warrington, UK WA4 4AD*

Received (in Cambridge, UK) 1st November 2000, Accepted 24th January 2001
First published as an Advance Article on the web 14th February 2001

***In situ*, time resolved, simultaneous multi-edge energy dispersive EXAFS (EDE) reveals Ge precursor induced perturbations of the reduction of supported $Pt(acac)_2$ to form Pt particles, and details the subsequent thermally induced formation of PtGe species.**

Many heterogeneously catalysed processes may be enhanced through the formation of alloyed, rather than elemental, metal particles (*e.g.* hydrocarbon reforming, PtSn,[1] PtRe[1] and PtGe[2,3] rather than Pt) or *via* addition of other oxides (*e.g.* ZnO to Cu/Al_2O_3 in methanol synthesis[4]). It is therefore of considerable interest to delineate the details of how these interactions evolve during synthesis, and are affected by the synthetic approach applied.

Time resolved measurements have the potential for gaining an understanding of the processes resulting in a given catalyst; indeed the combination of Quick EXAFS (QuEXAFS)[5] [or energy dispersive EXAFS (EDE)[6]] and XRD has been reported, but only for the interrogation of a one-elemental edge in EXAFS (Cu K in both cases). EDE has the potential for extremely rapid data acquisition, and therefore considerable potential for quantitative structural and kinetic determinations: we have previously demonstrated this for heterogeneous systems on a timescale of 1–8 s for supported metal systems.[7,8] EDE also potentially allows truly simultaneous multiple edge sampling and analysis. This situation cannot be achieved by QuEXAFS,[5,9] as this still requires movement of a monochromator through a given energy window. Here we show the application of EDE to follow the changes that lead to the formation of Pt/Ge alloy particles from mono-metallic precursors supported upon H_ISiO_2 mesoporous silicas *via in situ* sampling of the Pt L_{III} and Ge K edges simultaneously. PtGe catalysts have been shown to exhibit enhanced properties in hydrocarbon reforming reactions[2,3,10,11] particularly, increased selectivity toward aromatics[10] and tolerance towards sulfur,[11] the latter property being associated with the formation of PtGe alloy particles, which requires reduction at 773 K in H_2 for typical H_2PtCl_2/$GeCl_4$/Al_2O_3 derived catalysts.[11]

The preparation of the mesoporous silica has been described previously.[12] In the current case Pt was incorporated in these supports through impregnation [$Pt(acac)_2$] in dry toluene. The toluene was subsequently removed by rotary evaporation and drying. $GeBu_4$ was incorporated by injection under vacuum to the pre-prepared $Pt(acac)_2/H_ISiO_2$ sample. The final catalyst precursors contained 5 wt% Pt and 1.9 wt% Ge yielding a Pt : Ge ratio of 1 : 1. EDE experiments were performed using a flow microreactor described previously,[7,8] based around thin walled quartz tubes, into which the sieved (*ca.* 100 μm) particles of catalyst precursors were packed into a bed (10 mm long). The experimental conditions used for reduction of these samples under 10% H_2–N_2 (8 ml min^{-1}) were identical to those described previously for the reduction of the analogous elemental [$Pt(acac)_2/H_ISiO_2$] system.[7] The EDE measurements were made on station 9.3 at the SRS using a four-point bending mechanism[13] to manipulate a Si[111] monochromator. Spectra were recorded in 8 s (8 ms × 1000 scans). Data reduction was carried out using PAXAS[14] with multiple scattering spherical wave analysis performed using EXCURVS98.[15] Errors in coordination number are quoted at a fixed ±10%.

Fig. 1 shows EDE spectra derived simultaneously from both Pt L_{III} and Ge K edges whilst the $Pt(acac)_2/GeBu_4/H_ISiO_2$ sample was heated to 673 K under a flow of H_2–N_2. At least two regions of change can be observed as the sample is reduced. The first, occurring in the range 450–473 K, is observed only in the Pt edge spectra with the Ge EXAFS remaining essentially constant. It is only at higher temperature (> 543 K) that changes in the Ge EXAFS, together with further changes in the Pt spectra, are evident. Fig. 2 shows representative k^3 weighted EXAFS from both Pt and Ge edges at 543 K during *in situ* reduction of the sample; Table 1 summarises both the local order and statistical data resulting from spherical wave analysis. The EDEXAFS (8 s of acquisition time) from the Pt edge may be reasonably analysed in the range 2–11 $Å^{-1}$; for the Ge edge this data length is reduced to *ca.* 9 $Å^{-1}$. At temperatures as low as 543 K, Pt–Ge interactions and alloy formation are indicated. At this temperature it also reveals the persistence of Ge–C interactions.

Fig. 3 shows the results of a comprehensive analysis of the spectra shown in Fig. 1 and gives a detailed insight into the formation of the PtGe particles. The temperature dependence of the Pt–Pt, Pt–Ge, Ge–Pt coordination numbers are shown in the temperature range 300–673 K; no Ge–Ge interactions were observed. This clearly shows that the reduction of the precursor

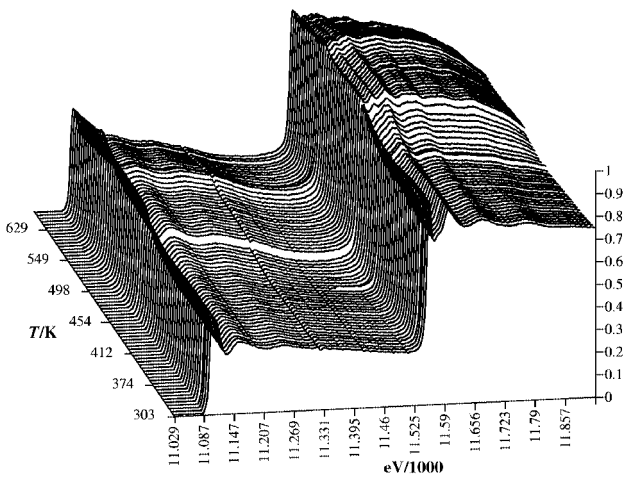

Fig. 1 EDEXAFS spectra for the Pt L_{III} and Ge K edges in the temperature range 298–670 K. Each spectra represents a total acquisition time of 8 s (1000 acquisitions @ 8 ms each).

† Electronic supplementary information (ESI) available: background to EDE measurements. See http://www.rsc.org/suppdata/cc/b0/b008809i/

DOI: 10.1039/b008809i

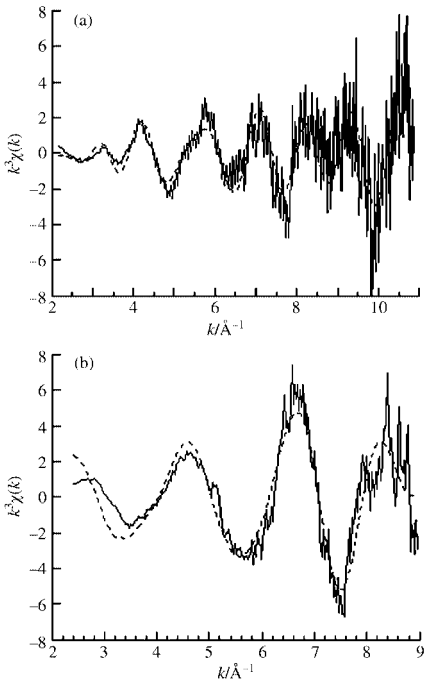

Fig. 2 Representative k^3 EXAFS for (a) Pt L_{III} and (b) Ge K edges derived from data shown in Fig. 1 for T = 543 K; experiment (—); fit derived from explicit analyis in EXCURV98 (- - -).

Table 1 Structural and statistical parameters derived from the dual edge analysis shown in Fig. 2[a]; method as in ref. 7

Edge	Shell	CN	r/Å	1.5% error in r	$2\sigma^2$/Å^2	R factor (%)
Ge K	C	1.9(0.2)	1.98(2)	0.0297	0.004(3)	46.3
	Pt	2.0(0.3)	2.52(2)	0.0378	0.011(3)	
Pt L_{III}	Ge	0.5(1)	2.42(1)	0.0363	0.006(3)	62.3
	Pt	7.3(3)	2.74(1)	0.0411	0.020(2)	

[a] Δk(Pt L_{III} = 2–12 Å^{-1}).

system to form Pt–Ge alloy particles occurs in at least three stages and allows determination of the effect of Ge on the reductive process.

The initial reduction stage appears to involve only the formation of Pt clusters with no concomitant formation of Pt–Ge bonds. The formation of the Pt particles however is very different to that observed for the analogous Pt only system.[7] The initial reduction is similar in terms of light-off temperature, however, whereas the elemental system develops a Pt–Pt coordination of 10 (±1) over a *ca.* 20 K temperature range, the Pt–Ge sample displays a much slower evolution of Pt–Pt coordination: over a *ca.* 40 K temperature window only a metastable coordination of 4 (±0.4) is reached. At temperatures >440 K the observed Pt–Pt coordination slowly rises to a maximal Pt–Pt coordination of 9 (±1.8) attained at *ca.* 475 K. Low Z (C/O) coordination (from the Pt L_{III} edge) is also retained over a considerably extended temperature range relative to that observed in the elemental system.

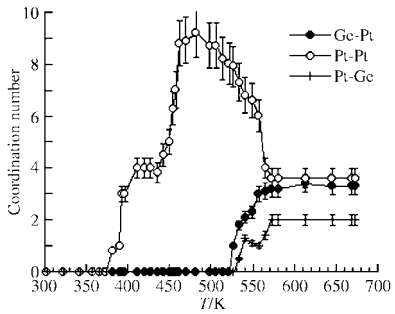

Fig. 3 Temperature dependence of Pt–Pt, Pt–Ge, Ge–Pt coordination during reduction of the $Pt(acac)_2/GeBu_4/H_1SiO_2$ sample from analysis of individual spectra shown in Fig. 1. Error bars are shown at a fixed ±10%.

At temperatures above *ca.* 460 K the Pt–Pt coordination starts to decline indicating either the onset of alloy formation and/or a morphological change in the particulate Pt. Concomitant changes in the Ge environment start to be observable with a gradual loss of low Z (C/O) coordination. Above >500 K a signal fitting Pt–Ge components is apparent. These interactions continue to evolve until a stable phase emerges above 570 K, characterised from the Ge edge by an average coordination of 3.4 Pt coordination, and from the Pt edge by 3.4 Pt and 2 Ge. It is not however until 650 K that the fitting of low Z components at the Ge K edge is not observed to produce a significant reduction in obtained R factor.

Reduction of the mixed organometallic system results in significant alloy formation at temperatures *ca.* 250 K lower than seen in more conventional systems supported upon Al_2O_3,[11] though carbon retention from cracking of the ligands initially present persists to *ca.* 650 K. The EDEXAFS results also indicate the production of alloy particles that are smaller than the elemental particles produced from the Pt-only system;[7] this differential is deemed to be a direct result of the Ge induced modification of the initial stage of the reductive process.

This work shows that considerable structure/phase information may be derived from explicit analysis of the EXAFS from two edges interrogated simultaneously. This methodology could be used for the simultaneous interrogation of a number of systems containing elements showing K or Li_{III} edges in the correct energetic proximity (see ESI†), for example Pt–Au, Cu–Ni and the aforementioned, Cu–Zn system.

This work was carried out under the 'Catalysis and Chemical Processes' initiative of the EPSRC, who are also thanked for access to CLRC Daresbury, postdoctoral funding to M. A. N. and doctoral funding for S. G. F. and T. C. (with CASE support from BNFL Plc). The University of Southampton and BP Chemicals Plc are thanked for provision of a studentship to S. T. We would also like to acknowledge the technical assistance of Mike Caplin, Melanie Hill, Bruce Hancock, and John James.

Notes and references

1 For instance: N. Macleod, J. R. Fryer, D. Stirling and B. Webb, *Catal. Today*, 1998, **46**, 37.
2 J. Goldwasser, B. Arenas, C. Bolivar, G. Castro, A. Rodriguez, A. Fleitas and J. Giron, *J. Catal.*, 1986, **100**, 75.
3 A. Borgna, T. F. Garetto, C. R. Apesteguia and B. Moraweck, *Appl. Catal. A*, 1999, **182**, 189.
4 For instance, G. C. Chinchen, P. J. Denny, D. G. Parker, M. S. Spencer and D. A. Whan, *Appl. Catal.*, 1987, **30**, 333.
5 See, for instance: B. S. Clausen, L. Grabaek, G. Steffensen, P. L. Hansen and H. Topsøe, *Catal. Lett.*, 1993, **20**, 23.
6 For instance, J. W. Couves, J. M. Thomas, D. Waller, T. H. Jones, A. J. Dent, G. E. Deryshire and G. N. Greaves, *Nature*, 1991, **354**, 465.
7 S. G. Fiddy, M. A. Newton, A. J. Dent, G. Salvini, J. M. Corker, S. Turin, T. Campbell and J. Evans, *Chem. Commun.*, 1999, 851.
8 M. A. Newton, D. G. Burnaby, A. J. Dent, S. Diaz-Moreno, J. Evans, S. G. Fiddy, T. Neisius, S. Pascarelli and S. Turin, *J. Phys. Chem. B*, submitted.
9 For instance: R. Frahm, *Nucl. Instrum. Methods A*, 1988, **270**, 578.
10 S. R. DeMiguel, J. A. M. Correa, G. T. Baronetti, A. A. Castro and O. A. Scolza, *Appl. Catal. A*, 1990, **60**, 47.
11 For instance, A. Borgna, T. F. Garetto, C. R. Apesteguia and B. Moraweck, *Appl. Catal. A*, 1999, **182**, 189; T. F. Garretto, A. Borgna and A. Monzon, *Catalyst Deactivation*, ed. B. Delmont and G. F. Froment, Elsevier, Amsterdam, 1994.
12 G. Attard, J. C. Clyde and C. G. Göltner, *Nature*, 1995, **378**, 366.
13 M. Hagelstein, C. Ferraro, U. Hatje, T. Ressler and W. Metz, *J. Synchrotron Radiat.*, 1995, **2**, 174.
14 N. Binsted, PAXAS, Programme for the analysis of X-ray adsorption spectra, University of Southampton, 1988.
15 S. J. Gurman, N. Binsted and I. Ross, *J. Phys. C.*, 1984, **17**, 143; S. J. Gurman, N. Binsted and I. Ross, *J. Phys. C*, 1986, **19**, 1845; N. Binsted, EXCURVE98, CCLRC Computer Programme, 1998.

ChemComm

Synthesis and assembly of $BaWO_4$ nanorods

Serena Kwan, Franklin Kim, Jennifer Akana and Peidong Yang*

Department of Chemistry, University of California, Berkeley, CA 94720, USA. E-mail: pyang@cchem.berkeley.edu

Received (in Cambridge, UK) 2nd January 2001, Accepted 31st January 2001
First published as an Advance Article on the web

Uniform, large aspect-ratio, monocrystalline $BaWO_4$ nanorods were synthesized using a reversed micelle templating method; novel nanorod superstructures were observed in both as-made materials and Langmuir–Blodgett monolayer assemblies.

There has been a recent heightened interest in one-dimensional nanoscale building blocks, such as nanotubes, nanowires, and nanorods.[1–10] These 1-D systems offer fundamental scientific opportunities for investigating the influence of size and dimensionality with respect to their collective optical, magnetic and electronic properties. Recent efforts have been focused on the development of new synthetic methodologies for making nanorods with uniform sizes and aspect ratios, including, for example, $BaCrO_4$,[4] CdSe,[1,8] Fe,[5] Ag[3] and Au nanorods.[2,7,9] Simple chemical reactions in a micellar or reversed micellar solution have been shown to be powerful in the synthesis of colloidal particles of different sizes and shapes. In these reactions, the size and shape control of the resulting particles was usually achieved by adjusting the water : oil : surfactant ratio. Nanorods of different compositions reported so far generally have small aspect ratios (length : diameter) of 2–10.

With its interesting excitonic luminescence, thermoluminescence and stimulated Raman scattering (SRS) properties, $BaWO_4$ is a potential material for designing all-solid-state lasers that can emit radiation in a specific spectral region and will have applications for medical treatment, up-conversion lasers and spectroscopy.[11,12] Herein, we report a simple reversed micelle templating method for the synthesis of uniform $BaWO_4$ nanorods. These nanorods are highly uniform with diameter of 9.5 nm and length of 1500 ± 200 nm. Owing to the high uniformity of these nanorods, they spontaneously form superstructures resembling crossed haystacks. Furthermore, upon removal of excess surfactant in the system, these uniform nanorods can be used as anisotropic building blocks for Langmuir–Blodgett studies.

A simple reversed micelle templating method was used to synthesize uniform $BaWO_4$ nanorods. Briefly, barium bis(2-ethylhexyl)sulfosuccinate [$Ba(AOT)_2$] reverse micelles[4] were added to NaAOT microemulsion droplets containing sodium tungstate (Na_2WO_4), to give final molar ratios of $[Ba^{2+}]:[WO_4^{2-}]$ = 1 and water content $[H_2O]:[NaAOT]$ = 10. This produced a white precipitate *ca.* 2 h after addition of the reactants under ambient conditions. Transmission electron microscopy (TEM) images of the samples taken from the liquid phase of the microemulsion show nanorod arrays resembling crossed haystacks (Fig. 1a,b). The nanorods are uniform in length (*ca.* 1500 nm) and diameter (*ca.* 9.5 nm), and generally arrange in a side-by-side geometry. Energy dispersive X-ray analysis and X-ray diffraction indicate that the nanorods are single crystalline $BaWO_4$ with a tetragonal Scheelite unit cell (a = 0.561 nm, c = 1.272 nm). Eight slightly broadened diffraction peaks with d spacings of 0.511, 0.336, 0.317, 0.280, 0.245, 0.210, 0.198, 0.187 nm can be readily indexed as (101), (112), (004), (200), (114), (204), (220), (116), respectively, of the Scheelite structures. No impurity peaks were detected in the experimental range.

High resolution TEM studies were carried out to examine the crystallinity of individual nanorods. It was found that each nanorod was separated from the neighboring ones by 1–2 nm (Fig. 1c), consistent with the presence of the surfactant molecules. Although the surface of these nanorods is slightly zigzag shaped, high-resolution TEM images (Fig. 1d) show that these nanorods are monocrystalline. The lattice fringe in Fig. 1d has a spacing of 0.317 nm, indicating that these nanorods grow preferentially along their c axes.

These as-made nanorods were washed with isooctane to remove excess surfactant AOT so that they could be redispersed in isooctane to make a stable nanorod colloidal suspension. This colloidal suspension was spread dropwise (typically 1–2 ml of 3 mg ml^{-1} concentration) on the water surface of a Langmuir–Blodgett (LB) trough (Nima Technology, M611). The nanorod monolayer was then compressed slowly while the surface pressure was monitored. During the compression process, the nanorod assemblies at the water–air interface were transferred carefully onto transmission electron microscope (TEM) grids covered with continuous carbon thin film using the Langmuir–Schäffer horizontal liftoff procedure. Initially, these nanorods were fairly dispersed; the directors of nanorod are isotropically distributed, and no superstructures were observed (Fig. 2a). After compression, these nanorods tend to align in roughly the same direction and form a nematic layer (Fig. 2b). With strong compression, these nanorods form bundles that have almost perfect side-by-side alignment between the nanorods (Fig. 2c).

It should be mentioned that the organization of the $BaWO_4$ nanorods here differs significantly from the assembly of the short $BaCrO_4$ and CdSe nanorods where ribbon-like and vertical rectangular/hexagonal superstructures are favored.[1,4] We believe this is due to the higher aspect ratio (*ca.* 150) of our

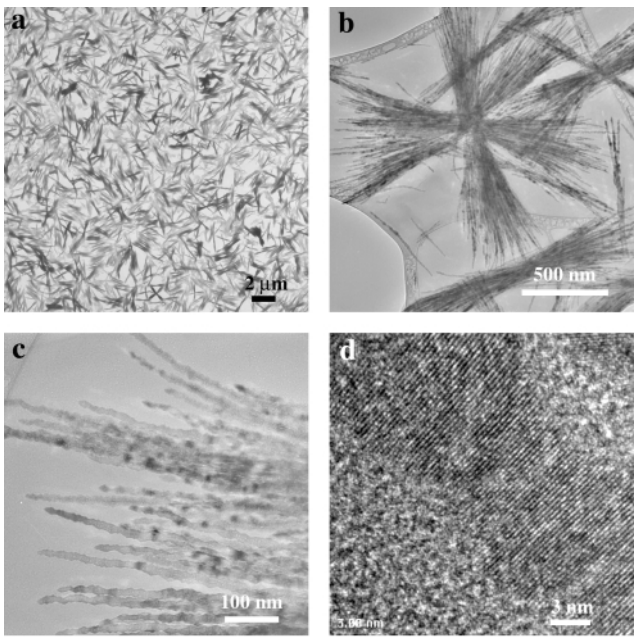

Fig. 1 TEM images of the as-made $BaWO_4$ nanorod assemblies. (a) Large area overview of the sample; (b) individual crossed haystack nanorod superstructure; (c) high magnification image of the assembly; (d) high resolution image of individual monocrystalline nanorods showing the lattice fringe.

DOI: 10.1039/b100005p

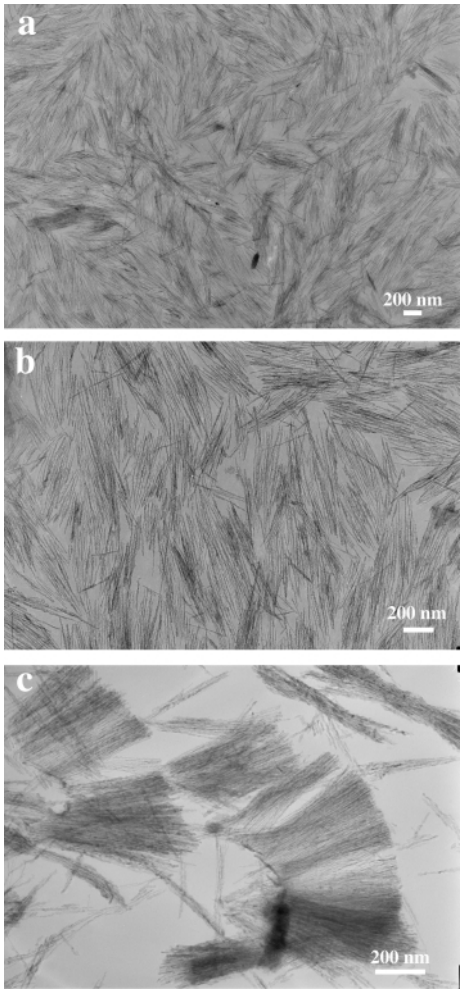

Fig. 2 TEM images of the $BaWO_4$ nanorod assemblies at the air–water interface after compression: (a) and (b) at low surface pressure; (c) at high surface pressure.

nanorods as compared with those (2–10) of $BaCrO_4$–CdSe systems. With a larger aspect ratio, it is less favorable for the nanorods aligning vertically on top of substrates (TEM support) to form a vertical superlattice, instead they prefer to lie parallel to the substrate. The reasons for these rods to align in parallel are two-fold: first, within hard-rod approximation,[13–15] this side-by-side ordering occurs in order to maximize the entropy of the self-assembled structure by minimizing the excluded volume per particle in the array as first proved by Onsager.[15] Secondly, the higher lateral capillary forces along the length of a nanorod, as compared with its width, could be another important driving force for the side-by-side alignment of nanorods rather than end-to-end. We expect that the super-structural formation of these large aspect ratio nanorods should be generally applicable to many other metal or semiconductor systems.

This work was supported in part by a New Faculty Award from the Dreyfus Foundation and start-up funds from the University of California, Berkeley. P. Y. thanks the 3M company for an untenured faculty award. We thank the National Center for Electron Microscopy for the use of their facilities.

Notes and references

1 X. Peng, L. Manna, W. Yang, J. Wickham, E. Scher, A. Kadavanich and A. P. Alivisatos, *Nature*, 2000, **404**, 59.
2 S. Chang, C. Shih, C. Chen, W. Lai and C. R. C. Wang, *Langmuir*, 1999, **15**, 701.
3 B. A. Korgel and D. Fitzmaurice, *Adv. Mater.*, 1998, **10**, 661.
4 M. Li, H. Schnablegger and S. Mann, *Nature*, 1999, **402**, 393.
5 S. J. Park, S. Kim, S. Lee, Z. G. Khim, K. Char and T. Hyeon, *J. Am. Chem. Soc.*, 2000, **35**, 8581.
6 J. Tanori and M. P. Pileni, *Langmuir*, 1997, **13**, 639.
7 B. R. Martin, D. J. Dermody, B. D. Reiss, M. Fang, A. Lyon, M. J. Natan and T. E. Mallouk, *Adv. Mater.*, 1999, **11**, 1021.
8 C. Chen, C. Chao and Z. Lang, *Chem. Mater.*, 2000, **12**, 1516.
9 B. Nikoobakht, Z. L. Wang and M. A. El-Sayed, *J. Phys. Chem. B*, 2000, **104**, 8635.
10 H. Liao, Y. Wang, X. Liu, Y. Li and Y. Qian, *Chem. Mater.*, 2000, **12**, 2819.
11 M. Nikl, P. Bohacek, E. Mihokova, M. Kobayashi, M. Ishii, Y. Usuki, V. Babin, A. Stolovich, S. Zazubovich and M. Bacci, *J. Lumin.*, 2000, **87**, 1136.
12 P. Cerny, P. G. Zverev, H. Jelinkova and T. T. Basiev, *Opt. Commun.*, 2000, **177**, 397.
13 J. A. C. Veerman and D. Frenkel, *Phys. Rev. A*, 1991, **43**, 4334.
14 M. Adams, Z. Dogic, S. Keller and S. Fraden, *Nature*, 1998, **393**, 349.
15 G. J. Vroege and H. N. W. Lekkerkerker, *Rep. Prog. Phys.*, 1992, **55**, 1241.

ChemComm

Synthesis of an amylose–polymer inclusion complex by enzymatic polymerization of glucose 1-phosphate catalyzed by phosphorylase enzyme in the presence of polyTHF: a new method for synthesis of polymer–polymer inclusion complexes

Jun-ichi Kadokawa,* Yoshiro Kaneko, Hideyuki Tagaya and Koji Chiba

Department of Chemistry & Chemical Engineering, Faculty of Engineering, Yamagata University, Yonezawa, Yamagata 992-8510, Japan. E-mail: kadokawa@chem.yz.yamagata-u.ac.jp

Received (in Cambridge, UK) 10th October 2000, Accepted 23rd January 2001
First published as an Advance Article on the web 14th February 2001

The enzymatic polymerization of α-D-glucose 1-phosphate (Glc-1-P) with phosphorylase in the presence of polytetrahydrofuran (polyTHF) leads to an amylose–polyTHF (polymer–polymer) inclusion complex; the present reaction system provides a new method for the preparation of polymer–polymer inclusion complexes.

Recent studies on molecular recognition and self-assembly in the field of supramolecular chemistry have received considerable attention because of possible applications in numerous scientific fields, such as materials science and chemical sensing.[1] As it concerns those research fields, host–guest chemistry, which is often compared to the relation between an enzyme and a substrate, has been of importance for chemists, from the viewpoint not only of pure chemistry but also in connection with biological work.[2] Representative host molecules have cyclic structures like crown ethers[3] and cyclodextrins.[4] Amylose, a natural linear polysaccharide linked through (1→4)-α-glycosidic linkages, is also a well-known host molecule forming helical inclusion complexes with monomeric organic compounds by hydrophobic interaction between guest molecules and the cavity of amylose.[5] Although amylose has been reported to form inclusion complexes with a few polymeric guest molecules, *i.e.* polymer–polymer inclusion complexes,[6] the scope and limitation for formation of polymer–polymer inclusion complexes using not only amylose but also the other host molecules has not been well surveyed. The polymeric hosts may not have sufficient ability to include the long chains of the polymeric guests directly into those cavities.

Amylose has been prepared by an *in vitro* approach from α-D-glucose 1-phosphate (Glc-1-P) monomer catalyzed by phosphorylase enzyme.[7] The enzymatic polymerization initiated from a primer of maltoheptaose (Glc_7) proceeds through the following reversible reaction, where a glucose unit is transferred from Glc-1-P to the non-reducing 4-OH terminus of a (1→4)-α-glucan chain, resulting in inorganic phosphate (P).

$$((\alpha, 1 \rightarrow 4)\text{-Glc})_n + \text{Glc-1-P} \rightleftharpoons ((\alpha, 1 \rightarrow 4)\text{-Glc})_{n+1} + \text{P}$$

This polymerization forming amylose has inspired us to develop a new method for preparation of polymer–polymer inclusion complexes, because we have assumed that the polymerization proceeds with the formation of an inclusion complex when the enzymatic polymerization is carried out in the presence of a hydrophobic synthetic guest polymer. Here, we report this new method for preparation of the amylose–polymer inclusion complex by enzymatic polymerization of Glc-1-P monomer catalyzed by phosphorylase enzyme in the presence of polyTHF as a hydrophobic polymer (Scheme 1).†

When the enzymatic polymerization of Glc-1-P from Glc_7 as a primer catalyzed by the phosphorylase (E.C.2.4.1.1)[8] in citrate buffer was carried out in the presence of polyTHF (M_n = 4000), the inclusion complex was obtained (Scheme 1), and its structure was characterized by X-ray powder diffraction and ^{1}H NMR measurements.

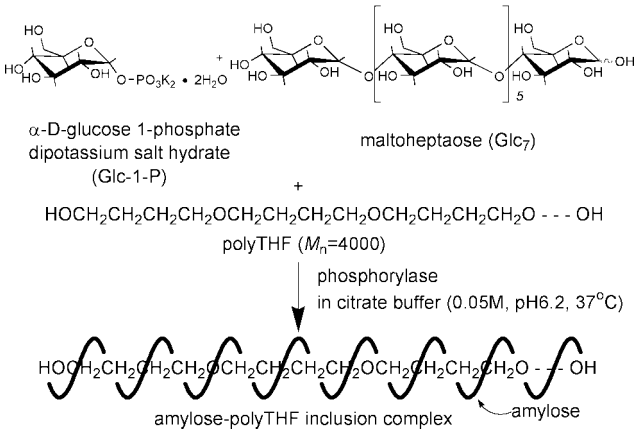

Scheme 1

The X-ray powder diffraction scan of the product indicates two strong diffraction maxima at 2θ = 12.4 and 19.8°, corresponding to d = 7.1 and 4.5 Å, respectively. The X-ray pattern of the product is completely different from that of amylose and polyTHF, and is similar to that of the inclusion complexes of amylose with monomeric compounds as shown in previous studies.[9] These data indicate that the product has a conformation similar to that of the helical inclusion complexes obtained from amylose and monomeric guests.

The ^{1}H NMR spectrum in DMSO-d_6 of the product in Fig. 1 shows the signals due not only to the amylose but also the polyTHF, in spite of the washing with MeOH, which is a good solvent of polyTHF. Furthermore, the methylene peak $\mathbf{H_a}$ of polyTHF is broadened and shifts to upfield (δ 1.48) compared to that of the original polyTHF (δ 1.50). This is because each methylene group of polyTHF is basically immobile and interacts with the protons inside the cavity of the amylose. When polyTHF was added to the NMR sample of the product in DMSO-d_6, two different signals due to methylene protons $\mathbf{H_a}$ of polyTHF were observed. This result suggests that the polyTHF of the product exists in a different environment. These NMR data can be taken to support the structure of the helical inclusion complex, which was also confirmed based on the spin-lattice relaxation time (T_1) measurements in the ^{1}H NMR analysis.‡ The T_1 value of the methylene peak $\mathbf{H_a}$ of polyTHF in the product was 0.24 s, whereas that of the original polyTHF was 0.74 s. The shorter T_1 in the product confirms the restriction of the methylene movement due to included conditions.

When the NMR sample was kept at rt, the intensity of the methylene peak $\mathbf{H_a}$ of polyTHF gradually decreased and the solution became turbid. These observations indicate that polyTHF was coming out of the amylose cavity and precipitating owing to the relative lower solubility of the polyTHF in DMSO-d_6. The degree of polymerization (DP) value of the precipitated polyTHF was calculated from ^{1}H NMR analyses to be *ca.* 39 (M_n = 2800), indicating that amylose preferred to

DOI: 10.1039/b008180i

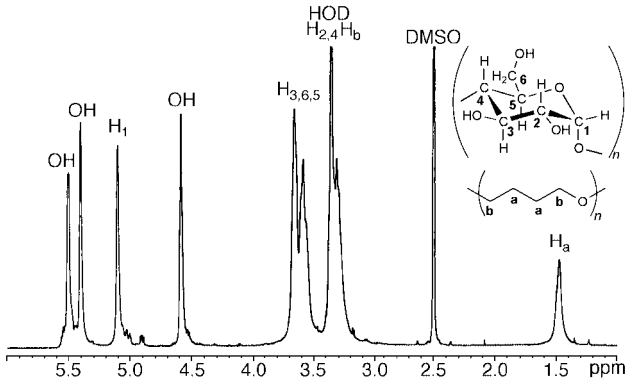

Fig. 1 ^{1}H NMR spectrum of the product in DMSO-d_6. Chemical shifts were referenced to DMSO (δ 2.50 ppm).

include the relative lower molecular weight polyTHF present in the original polyTHF, with an average molecular weight of 4000 (by ^{1}H NMR); the molecular weight was also estimated by gel permeation chromatographic (GPC) measurement as 3200.

Generally, one helical turn of amylose is composed of *ca*. 6 repeating glucose units when linear molecules of small cross reactional area, *e.g*. fatty acids, are included.[10] The repeat distance of the helix of amylose has been reported as 7.95 Å,[10] whereas the length of one unit of polyTHF is presently calculated as *ca*. 6.0 Å,§ as shown in Fig. 2. Therefore, 4.5 repeating glucose units in amylose correspond to the length of one polyTHF unit (Fig. 2). From the above calculations, the integrated ratio of the signal due to **H_1** of amylose to the signal due to **H_a** of polyTHF (H_a/H_1) in the ^{1}H NMR spectrum is assessed to be 0.89. Actually, the integrated ratio of these two signals in the ^{1}H NMR spectrum of the product was *ca*. 1, relatively close to the calculated value. This also supports the structure of the inclusion complex as shown in Scheme 1.

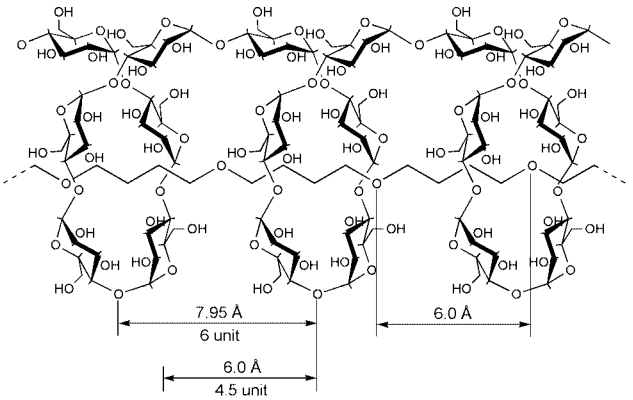

Fig. 2 Illustration of repeat distance of amylose helix and length of one polyTHF unit.

The molecular weight of the amylose in the inclusion complex was evaluated by means of GPC measurement after the acetylation of the inclusion complex and the precipitation of the products into i-PrOH.[11] The GPC value of the precipitated triacetyl amylose was 22800 (M_w/M_n = 1.29), which corresponds to M_n = 12800 of the original amylose. This value is in good agreement with the molecular weight values determined by ^{1}H NMR spectra (M_n = 12200–14600, DP = 75–90).¶ These values correspond to 99–119 Å of molecular lengths in helical form,‖ whereas the chain length of the included polyTHF (M_n = 2800) is calculated as *ca*. 230 Å.§ Therefore, one polyTHF molecule is probably included by two amylose molecules.

The inclusion complex was not formed by mixing amylose (DP = 75–90, M_n = 12200–14600) and polyTHF (M_n = 4000) in the same solvent as described above (sodium citrate buffer, 0.05 mol L^{-1}, pH = 6.20) at 37 °C. This observation suggests that the inclusion complex forms during the enzymatic polymerization. Such a formation behavior for the inclusion complex was further supported by the following experiments. When polyTHF was added to the reaction solution immediately after the general enzymatic polymerization of Glc-1-P had started, an identical inclusion complex to that mentioned above was obtained, judging by the H_a/H_1 value in the NMR spectrum, which was *ca*. 1. However, the H_a/H_1 values decreased as the time delay between adding polyTHF into the solution and the start of the enzymatic polymerization was increased (after 1 h; H_a/H_1 = 0.96, after 3 h; H_a/H_1 = 0.78, after 5 h; H_a/H_1 = 0.33). These observations reveal that the inclusion complex was not formed after the polymerization produced amyloses with relative higher molecular weights. These results indicate that polymerization proceeds with the formation of the inclusion complex.

In conclusion, we have synthesized an amylose–polyTHF (polymer–polymer) inclusion complex by the enzymatic polymerization of Glc-1-P with phosphorylase in the presence of polyTHF. The present reaction system provides a new method for the preparation of polymer–polymer inclusion complexes. Detailed studies on how the complex forms during the polymerization process are now in progress.

We acknowledge the gift of the polyTHF sample from Hodogaya Chemical Co., Ltd., Kanagawa. We are also indebted to Ms M. Karasu and Messrs K. Fujita and S. Nagase of our research group for performing X-ray measurement and technical assistance.

Notes and references

† Synthesis of the amylose–polyTHF inclusion complex: typically, polyTHF (M_n = 4000, 50.0 mg) was suspended in 5 mL of sodium citrate buffer (0.05 mol L^{-1}, pH = 6.20) with ultrasonication and heated to 37 °C. After addition of 2.31 mg (2 μmol) of maltoheptaose (Glc_7) primer, 186 mg (500 μmol) of α-D-glucose 1-phosphate dipotassium salt hydrate (Glc-1-P), and 6.40 mg (~160 units) of phosphorylase, the solution was stirred vigorously for 10 h at 37 °C. The precipitated product was collected by centrifugation, washed with MeOH and water, and then lyophilized, to yield *ca*. 20 mg of the inclusion complex (yields *ca*. 21% based on Glc-1-P and Glc_7, and *ca*. 4% based on polyTHF).

‡ The measurements of T_1 values of inclusion complexes have often been used for the identification of their structures. The T_1 values of the inclusion complexes are shorter than those of the corresponding individual molecules.[3]

§ The calculation of this value was performed with MM2 in the CS Chem 3D program package.

¶ The DP values were calculated by the integrated ratio of the peak of **H_1** of amylose chain (δ 5.1) to the peaks of **H_1** (α and β) of the reducing terminus (δ 4.9 (α) and 4.3 (β)) by the ^{1}H NMR spectra in DMSO-d_6–D_2O. The DPs were changeable depending on reaction conditions, especially the activity of enzyme.

‖ The reported DP 75 and 90 corresponds to 75/6 = 12.5 and 90/6 = 15 helical turns, and hence 12.5 × 7.95 Å = 99 Å and 15 × 7.95 Å = 119 Å represent the length of helical amylose and not that of the extended molecule.

1 J. M. Lehn, *Supramolecular Chemistry: Concepts and Perspectives*, VCH, Weinheim, 1995.
2 J. M. Lehn, *Angew. Chem., Int. Ed. Engl.*, 1990, **29**, 1304.
3 C. Gong and H. W. Gibson, *Angew. Chem., Int. Ed. Engl.*, 1997, **36**, 2331; C. Gong, T. E. Glass and H. W. Gibson, *Macromolecules*, 1998, **31**, 308.
4 M. L. Bender and M. Komiyama, *Cyclodextrin Chemistry*, Springer, Verlag, 1978.
5 S. Kubik, O. Höller, A. Steinert, M. Tolksdorf and G. Wulff, *Macromol. Symp.*, 1995, **99**, 93.
6 R. L. Shogren, R. V. Greene and Y. V. Wu, *J. Appl. Polym. Sci.*, 1991, **42**, 1701; R. L. Shogren, *Carbohydr. Polym.*, 1993, **22**, 93.
7 G. T. Cori and C. F. Cori, *J. Biol. Chem.*, 1940, **135**, 733.
8 A. Kamogawa, T. Fukui and Z. Nikuni, *J. Biochem.*, 1968, **63**, 361.
9 H. D. Seneviratne and C. G. Biliaderis, *J. Cereal Sci.*, 1991, **13**, 129; N. Jeannette, S. Bettina, C. P. Béatrice and E. Felix, *Food Hydrocolloids*, 1997, **11**, 27.
10 Y. Yamashita, *J. Polym. Sci. Part A.*, 1965, **3**, 3251; H. F. Zobel, A. D. French and M. E. Hinkle, *Biopolymers*, 1967, **5**, 837; H. F. Zobel, *Starch*, 1988, **40**, 1.
11 J. Einfeldt, A. Kwasniewski, D. Klemn, R. Dicke and L. Einfeldt, *Polymer*, 2000, **41**, 9273.

ChemComm

Cationic phosphine ligands with phenylguanidinium modified xanthene moieties—a successful concept for highly regioselective, biphasic hydroformylation of oct-1-ene in hexafluorophosphate ionic liquids

Peter Wasserscheid,*[a] Horst Waffenschmidt,[a] Peter Machnitzki,[a] Konstantin W. Kottsieper[b] and Othmar Stelzer[b]

[a] *Institut für Technische Chemie und Makromolekulare Chemie, RWTH Aachen, Worringer Weg 1, D-52074 Aachen, Germany. E-mail: Wasserscheidp@itc.rwth-aachen.de*

[b] *Anorganische Chemie, Bergische Universität—GH Wuppertal, Gaußstr. 20, D-42097 Wuppertal, Germany. E-mail: Stelzer@uni.wuppertal.de*

Received (in Liverpool, UK) 6th December 2000, Accepted 29th January 2001
First published as an Advance Article on the web 14th February 2001

New guanidinium-modified diphosphine ligands with a xanthene backbone show high overall activity and high regioselectivity in the biphasic hydroformylation of oct-1-ene using hexafluorophosphate ionic liquids.

Biphasic catalysis is a well-established method for effective catalyst separation and recycling. In the case of Rh-catalysed hydroformylation reactions this principle is technically realised in the Ruhrchemie–Rhône-Poulenc process where an aqueous catalyst phase is used.[1,2] Unfortunately, this process is limited to C_2–C_5 olefins due to the low water solubility of higher olefins. As an alternative polar medium for biphasic hydroformylation, Chauvin *et al.* suggested novel solvents known as ionic liquids (for general reviews see refs. 3–5). These authors described in detail the biphasic hydroformylation of pent-1-ene with $[Rh(CO)_2acac]$/triarylphosphine in *e.g.* 1-butyl-3-methylimidazolium hexafluorophosphate ($[BMIM]PF_6$).[6,7] However, none of the tested ligands (PPh_3, sulfonated triaryl phosphines) allowed a combination of high activity, complete retention of the catalyst in the ionic liquid and high selectivity for the desired linear hydroformylation product. Recently, some of us described the successful application of cobaltocenium ligands in the Rh-catalysed hydroformylation of oct-1-ene in hexafluorophosphate ionic liquids, demonstrating that the reaction benefits from the use of ligand systems that are specifically designed for this application.[8]

Cationic phosphine ligands containing phenylguanidinium moieties were originally developed to make use of their pronounced solubility in water.[9,10] They have been shown to form active catalyst systems in Pd-mediated C–C coupling reactions between aryl iodides and alkynes[9,11] (Castro–Stephens–Sonogashira reaction) and Rh-catalysed hydroformylation of *n*-hexene in aqueous two-phase systems.[12]

In the present article, we report a new and very general approach to immobilise homogeneous Rh-catalysts in hexafluorophosphate ionic liquids. We found that the modification of neutral phophine ligands with cationic phenylguanidinium groups represents a very powerful tool to immobilise Rh complexes in these ionic liquids. In detail, we describe the synthesis of the new ligand **1a** and its catalytic performance in the biphasic, Rh-catalysed hydroformylation of oct-1-ene using the ionic liquid $[BMIM]PF_6$ as catalyst solvent. This ionic liquid has been prepared from [BMIM]Cl[13] according to a method described by Fuller and Carlin[14] or has been purchased from Solvent Innovation GmbH, Cologne.[15] First experiments aimed to prove the general concept by comparing the ligand PPh_3 with the related guanidinium-substituted ligand **2a** (Table 1, entries 1–5). **2a** was prepared from **2b** by anion exchange with NH_4PF_6 in aqueous solution. **2b** was prepared as previously described by Stelzer *et al.*[10]

In the reaction with PPh_3, good catalytic activity is observed but obviously a significant part of the hydroformylation reaction takes place in the organic layer. After the first catalytic run, 53% of the used Rh is found in the organic layer (according to ICP analysis) (Table 1, entry 1). In contrast, with ligand **2a** the hydroformylation reaction takes place uniquely in the ionic liquid layer (Table 1, entries 3, 4). In the first catalytic run the hydroformylation activity was found to be lower than in the case of PPh_3 (probably due to some mass transfer limitation of oct-1-ene into the ionic liquid). However, due to the excellent immobilisation of the Rh-catalyst with **2a** (leaching is < 0.07% per run according to ICP analysis (detection limit)), the catalytic activity of the ionic catalyst solution is even slightly higher in the third recycling run compared to the first run (probably due to some preformation time of the active catalyst). Since NaTPPTS is the most widely used ligand for immobilisation of Rh-catalysts in aqueous catalyst phases, this ligand was tested as well (Table 1, entries 5, 6). The results reveal good immobilisation of the Rh-complex in the ionic liquid but much lower activity of the resulting catalyst in the hydroformylation of oct-1-ene in comparison with **2a**.

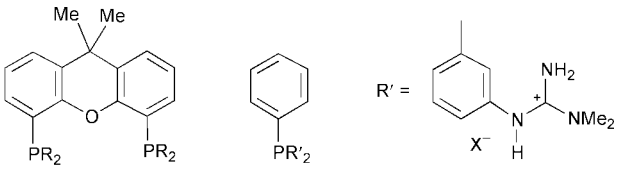

1a: R = R', X = I
1b: R = phenyl
1c: R = H

2a: X = PF_6
2b: X = I

Encouraged by the good results with the guanidinium-substituted ligand, we decided to adopt this new immobilisation

Table 1 Hydroformylation results with different ligands in $[BMIM]PF_6$

No.	Ligand (cycle)	Conversion (%)	TOF[a] h^{-1}	Octane + i-octenes (%)	n : iso[b]
1	PPh_3 (1)	69.1	680	0.4	2.8
2	PPh_3 (3)	10.2	100	0.1	2.7
3	**2a** (1)	32.1	276	2.5	2.0
4	**2a** (3)	35.3	330	3.5	1.7
5	NaTPPTS	7.8	80	4.9	2.6
6	NaTPPTS	7.7	78	4.9	2.6
7	**1a** (1)	10.6	15	1.5	19.1
8	**1a** (3)	21.9	30	2.4	20.9
9	**1a** (5)	38.3	52	3.4	21.3
10	**1a** (7)	44.3	58	3.9	18.0

[a] Turnover frequency (TOF) in mol of octene converted per mol of Rh per h. [b] Ratio of linear to branched aldehyde products; general conditions: $CO:H_2$ = 1; $p(CO/H_2)$ = 30 bar; T = 100 °C; L : Rh = 2; Rh-precursor: $Rh(CO)_2acac$, preformation time 30 min; t = 1 h (runs 1–6), 8 h (runs 7–10).

DOI: 10.1039/b009919h

concept to a ligand structure that promises better regioselectivity in the hydroformylation reaction. It is well-known that diphosphine ligands with large natural P–metal–P bite angles form catalysts for highly regioselective hydroformylation reactions.[16] Here, xanthene-type ligands (P–metal–P ~110°) developed from van Leeuwen's group proved to be especially suitable showing, *e.g.* an overall selectivity of 98% towards the desired linear aldeyde in oct-1-ene hydroformylataion.[17–19] Recently, some work has been published where xanthene-based ligands have been immobilised on silica support.[20]

We describe here the first use of xanthene-based ligands in biphasic catalysis using ionic liquids as catalyst solvent. Since xanthene ligands such as, *e.g.* **1b** show highly preferential solubility in the organic phase in a biphasic oct-1-ene/[BMIM]PF_6 mixture, even at rt we developed the guanidinium-modified xanthene ligand **1a** for this purpose. The cationic ligand **1a** was synthesised in four steps according to Scheme 1.†

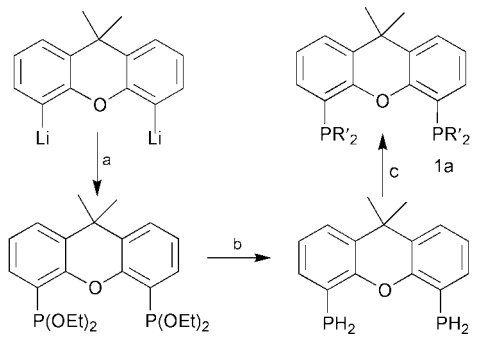

Scheme 1 Synthesis of ligand **1a**. a) diethylchlorophosphite; b) $LiAlH_4$–chlorotrimethylsilane; c) 4 eq. 3-iodophenylguanidine, 2 mol% Pd_2dba_3 * $CHCl_3$, 80 °C, 24 h in DMF.

The structure of **1a** was established by its mass spectrum and its $^{31}P\{^1H\}$NMR chemical shift ($\delta P = -15.9$) comparable to that of **1b** ($\delta P = -17.9$)[21] and of the *meta* guanidinium phosphines **2a** ($\delta P = -4.7$).[10] The signal at $\delta C = 157.1$ in the $^{13}C\{^1H\}$NMR spectrum of **1a** may be assigned to the carbonium carbon atoms of the guanidinium moieties, the δC value of which compares well with that in **2a**[10] ($\delta C = 155.8$). Some of the $^{13}C\{^1H\}$NMR resonances appear as higher order line pattern (X-parts of AA′X spin systems, A, A′ = ^{31}P, X = ^{13}C) in agreement with the diphosphine structure proposed for **1a**.

After each hydroformylation run, in which **1a** was used as crude product, the organic layer was decanted off (under normal atmosphere) and the remaining ionic catalyst layer remained in the autoclave for the next run. It is noteworthy that the catalytic activity increases during the first runs to obtain a stable level only after the forth recycling run (Table 1, entries 7–10). This behaviour is attributed to a certain catalyst preforming time as well as to impurities of 3-iodophenylguanidine in the used ligand sample (about 5 mass%). The latter are slowly washed out from the catalyst layer over the first catalytic runs. After ten consecutive runs an overall turnover number of 3500 mol oct-1-ene per mol Rh-catalyst could be obtained. In good agreement with the recycling experiments, the Rh-leaching into the organic layer was found to be very low. With AAS and ICP analysis no rhodium could be detected in the organic layer indicating a leaching of less than 0.07%. In all experiments with **1a** very good selectivities for the linear aldehyde were obtained thus proving that the attachment of the guanidinium moiety to the xanthene backbone does not influence its known positive effect on the regioselectivity of the reaction. This is in line with previous IR and NMR studies in our laboratories showing that the steric and electronic properties of arylphosphines is not significantly changed by introduction of polar groups like SO_3^-, PO_3^{2-} and guanidinium in *meta*- or *para*-position to phosphorus.[10]

In conclusion, we could show that the modification of known phosphine ligands with guanidinium groups represents a simple and very efficient method to fully immobilise transition metal complexes in hexafluorophosphate ionic liquids. Hereby, the electronic properties of the phosphine is not changed significantly. Our approach may therefore be of interest not only for hydroformylations but also for many other catalytic reactions in ionic liquids. Further work to develop methods for the immobilisation of neutral catalyst complexes in ionic liquids is in progress.

We wish to thank the Fonds der Chemischen Industrie and the Deutsche Forschungsgemeinschaft for financial support. P. W. and H. W. thank Professor W. Keim for his continuous interest in this research and the European Community for founding under the BRITE 96-3745 project.

Notes and references

† *Preparation of* **1a**: to a solution of 0.75 g (2.74 mmol) of the diprimary phosphine **1c** (prepared according to van Leeuwen *et al.*[22]) and 3.17 g (10.96 mmol) of 3-iodophenylguanidine 227 mg (2 mol%) of tris(benzylidene acetone)dipalladium(0) were added and the reaction mixture was heated to 80–100 °C for 24 h. $^{31}P\{^1H\}$ NMR spectroscopic control of the reaction mixture indicated that all of the diprimary phosphine had been consumed. On evaporation of the solvent *in vacuo* (80 °C, 0.01 mbar) 4.14 g of a yellow–brownish coloured powder were obtained. It contains small amounts of 3-iodophenylguanidine as indicated by the $^{13}C\{^1H\}$-NMR spectrum.

Mass spectrum [SIMS(DTE/DTT/Sul)]: cation: *m/z* = 919; $^{31}P\{^1H\}$-NMR data (161.98 MHz, 298 K, d_4-methanol, referenced to H_3PO_4) for **1a**: $\delta P = -15.9$. $^{13}C\{^1H\}$-NMR *data* (100.63 MHz, 298 K, d_4-methanol, referenced to TMS_{int}, values in parentheses $N = J_{PC} + J_{P'C}$) for **1a**: 157.1, 153.3 (*C*–O, 19.3 Hz), 141.0, 139.9 (13.2 Hz), 139.1 (6.0 Hz), 133.1 (12.0 Hz), 132.9, 131.5, 131.1 (6.0 Hz), 130.6 (19.3 Hz), 128.6, 126.2, 125.2, 39.5 (N*Me*$_2$), 35.5 (*C*Me$_2$), 32.3 (C*Me*$_2$).

1 E. G. Kuntz, *Fr. Pat. 2314910*, (to Rhone-Poulenc); E. G. Kuntz, *CHEMTECH*, 1987, 570.
2 W. A. Herrmann and C. W. Kohlpaintner, *Angew. Chem., Int. Ed. Engl.*, 1993, **32**, 1524.
3 P. Wasserscheid and W. Keim, *Angew. Chem., Int. Ed.*, 2000, **39**, 3772.
4 T. Welton, *Chem. Rev.*, 1999, **99**, 2071.
5 J. D Holbrey and K. R. Seddon, *Clean Products and Processes*, 1999, **1**, 223.
6 Y. Chauvin, H. Olivier and L. Mußmann, *EP*, 0776 880 A1 (to IFP).
7 Y. Chauvin, L. Mußmann and H. Olivier, *Angew. Chem.*, 1995, **107**, 2941.
8 C. C. Brasse, U. Englert, A. Salzer, H. Waffenschmidt and P. Wasserscheid, *Organometallics*, 2000, **19**, 3818.
9 A. Heßler, O. Stelzer, H. Dibowski, K. Worm and F. P. Schmidtchen, *J. Org. Chem.*, 1997, **62**, 2362.
10 P. Machnitzki, M. Tepper, K. Wenz, O. Stelzer and E. Herdtweck, *J. Organomet. Chem.*, 2000, **602**, 158.
11 H. Dibowski and F. P. Schmidtchen, *Angew. Chem., Int. Ed. Engl.*, 1998, **37**, 476.
12 A. Heßler, M. Tepper, O. Stelzer, F. P. Schmidtchen, H. Dibowski, H. Bahrmann and M. Riedel, *DE*, 197 01 245, (23.7.1998), (Hoechst AG).
13 J. S. Wilkes, J. A. Levisky, R. A. Wilson and C. L. Hussey, *Inorg. Chem.*, 1982, **21**, 1263.
14 R. T. Fuller, H. C. Carlin, H. C. de Long and D. Haworth, *J. Chem. Soc., Chem. Commun.*, 1994, 299.
15 http://www.solvent-innovation.com
16 C. P. Casey, G. T. Whiteker, M. G. Melville, L. M. Petrovich, J. A. Gavey and D. R. Powell, *J. Am. Chem., Soc.*, 1992, **114**, 5535.
17 M. Kranenburg, Y. E. M. van der Burgt, P. C. J. Kamer, P. W. N. M. van Leeuwen, K. Goubitz and J. Fraanje, *Organometallics*, 1995, **14**, 3081.
18 L. A. van der Veen, M. D. K. Boele, F. R. Bregman, P. C. J. Kamer, P. W. N. M. van Leeuwen, K. Goubitz, J. Fraanje, H. Schenk and C. Bo, *J. Am. Chem. Soc.*, 1998, **120**, 11 616.
19 P. W. N. M. van Leeuwen, P. C. J. Kamer, J. N. H. Reek and P. Dierkes, *Chem. Rev.*, 2000, 100.
20 A. J. Sandee, L. A. van der Veen, J. N. H. Reek, P. C. J. Kamer, M. Lutz, A. L. Spek and P. W. N. M. van Leeuwen, *Angew. Chem., Int. Ed.*, 1999, **38**, 3231.
21 S. Hillebrand, J. Bruckmann, C. Krüger and M. W. Haenel, *Tetrahedron Lett.*, 1995, **36**, 75.
22 P. Dierkes, S. Ramdeehul, A. De Cian, J. Fischer, P. C. J. Kamer and W. N. M. van Leeuwen, *Angew. Chem., Int. Ed.*, 1998, **37**, 3299.

Oligo-ligandosides: a DNA mimetic approach to helicate formation

Haim Weizman and Yitzhak Tor*

Department of Chemistry and Biochemistry, University of California, San Diego, La Jolla, CA 92093-0358, USA. E-mail: ytor@ucsd.edu

Received (in Corvallis, OR, USA) 5th December 2000, Accepted 8th January 2001
First published as an Advance Article on the web 14th February 2001

A novel 'ligandoside' dimer, where 2,2′-bipyridine chelators are attached to the anomeric carbons of a D-ribose–phosphate backbone, forms double stranded multinuclear complexes.

The distinct geometry of coordination complexes has been extensively employed for the programmed assembly of exquisite structures.[1] Among these assemblies, double stranded multinuclear complexes known as helicates, have attracted special attention due to their structural resemblance to the DNA double helix and intriguing stereochemistry.[2] While some control over the stereochemical elements involved in helicate formation (*e.g.* the helix chirality and the relative orientation of non-symmetrical strands) has been achieved, controlling this multicomponent assembly remains a challenging problem.[3]

Although assembling helical complexes was inspired by the structure of the DNA double helix, none of the structural elements inherent to DNA has been exploited in helicate design. This is especially intriguing as both the chirality of the DNA helix and its anti-parallel orientation are encoded in the sugar–phosphate backbone.[4] We have sought to explore if incorporation of native DNA structural elements into synthetic binders can be employed to dictate the formation of defined complexes. In these novel structures, ligands are attached to the anomeric carbon of the D-ribose–phosphate backbone replacing the DNA nucleobases (Fig. 1). Unlike helicates where the ligands are integrated into the helical backbone, here the ligands project away from the backbone. Importantly, the backbone phosphodiester groups may be considered as 'built-in' counter ions that can balance the charges associated with metal complex formation. In this contribution we present the design and synthesis of first generation polynuclear complexes based on this approach.

The building block for synthesizing these polytopic ligands is a nucleoside mimic, coined ligandoside, where the heterocyclic base is replaced by a metal-binding ligand.[5,6] Our first model is based on 2,2′-bipyridine (bpy) as a chelator (Scheme 1). A methylene bridge is introduced between the bpy and the sugar to allow for a more relaxed structure and dimensions similar to the DNA double helix. The synthesis of the binding strand utilizes the standard DNA phosphoramidite chemistry.[7] The 5′-protected ligandoside **1** is converted to the phosphoramidite **2** or to the 3′-protected acetate **3**. The two components are then coupled in the presence of 1*H*-tetrazole. Oxidation of the trivalent phosphorus with iodine–water–pyridine mixture gives the phosphate triester derivative **4**. Removal of the protecting groups provides the ditopic ligand **5** (Scheme 1). The structure of **5** was confirmed by NMR and MS.† The development of this phosphoramidite chemistry is particularly attractive for future solid phase synthesis of longer oligomeric strands.

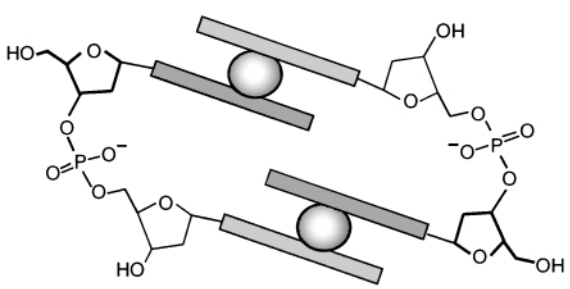

Fig. 1 Schematic representation of a DNA mimetic metal binding dimer.

The absorption spectrum of ligand **5** shows the characteristic π–π* absorption bands of the aromatic bpy at 242 and 287 nm. Upon titration with Cu^+ under an inert atmosphere, new bands at 266 and 300 nm appear with three isosbestic points (Fig. 2). An additional metal to ligand charge transfer (MLCT) band at 440 nm, characteristic of copper–bpy complex formation, also emerges. The titration establishes a 1 : 1 ratio between the metal and the ligand. This stoichiometry can be attributed either to the formation of a mononuclear (**5**Cu) or a dinuclear ($\mathbf{5}_2Cu_2$) complex. ESI mass spectrometry reveals the formation of a mononuclear complex only (*m*/*z* 696 calcd. for **5**CuNa). The pattern and isotopic distribution exclude the possibility that this peak represents the doubly charged complex $\mathbf{5}_2Cu_2$.

Titration of ligand **5** with Pd^{2+} results in the appearance of new absorption bands at 248 and 314 nm with two isosbestic points (Fig. 2). The mass spectrum indicates the formation of the mononuclear complex **5**Pd (*m*/*z* 739 calcd. for **5**Pd) together with a dinuclear species (*m*/*z* 1479 calcd. for $\mathbf{5}_2Pd_2$–H, 1500 calcd. for $\mathbf{5}_2Pd_2Na$–H). It is difficult to establish the actual equilibrium ratio between the various species in the mass spectrum due to their different ionization abilities.‡

Upon titration of ligand **5** with Ag^+ in MeOH, complex formation is manifested as a shift in absorption bands to 250 and 296 nm associated with the appearance of three isosbestic points (Fig. 2). This titration verifies the formation of a 1 : 1 complex between the metal ion and the ditopic ligand (Fig. 2). The ESI mass spectrum indicates the formation of the dinuclear complex $\mathbf{5}_2Ag_2$ (*m*/*z* 1483 calcd. for $\mathbf{5}_2Ag_2H$, 1505 calcd. for $\mathbf{5}_2Ag_2Na$).

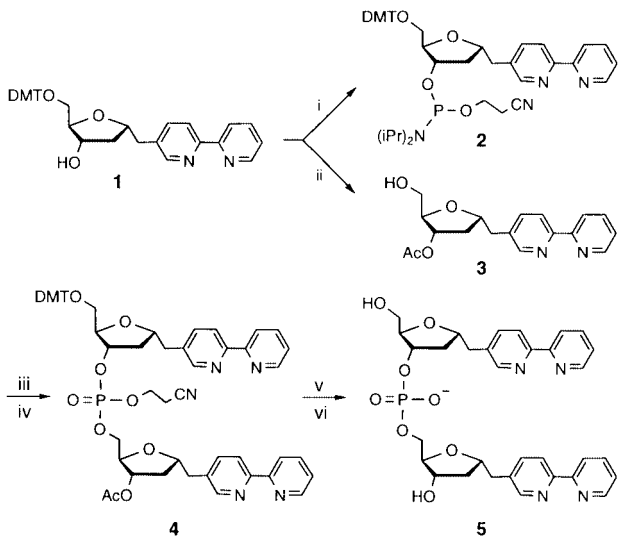

Scheme 1 *Reagents and conditions*: i, 2-cyanoethyl-*N*,*N*,*N*′,*N*′-tetraisopropylphophordiamidite, 1*H*-tetrazole, CH_3CN, 1.5 h; ii, a. Ac_2O, Py, 12 h, b. 8 : 2 AcOH–H_2O, 1.5 h; iii, 1*H*-tetrazole, CH_3CN, 3 h; iv, I_2–THF–H_2O–Py; v, 8 : 2 AcOH–H_2O, 1 h; vi, NH_4OH, CH_3CN–MeOH, 12 h.

DOI: 10.1039/b009855h

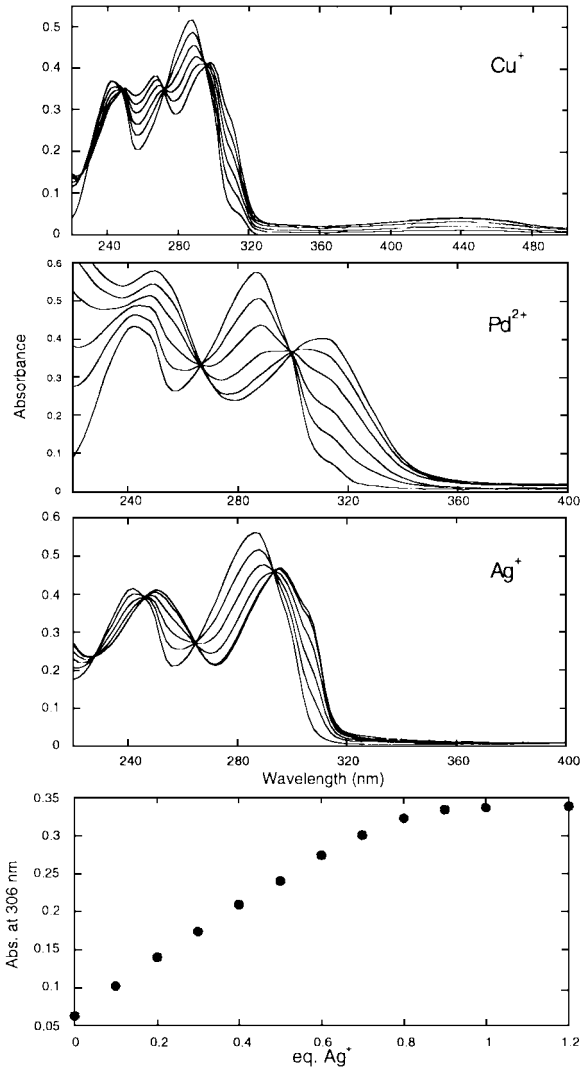

Fig. 2 Uv-vis titrations of di-ligandoside monophosphate **5** in MeOH with a. $Cu(CH_3CN)_4BF_4$ in CH_3CN, b. $Pd(CH_3CN)_4(BF_4)_2$ in CH_3CN, c. $AgCF_3SO_3$ in MeOH. Bottom: a representative curve illustrating the formation of a 1 : 1 complex.

The theoretically predicted pattern and isotopic distribution perfectly matches the experimentally observed one (Fig. 3).

These results demonstrate that threading ligands on a sugar–phosphate backbone can lead to the formation of double stranded structures. In the prototypical ligandoside system described here, the formation of double stranded structures is in competition with the formation of single stranded complexes. This can be attributed to the flexibility of both the sugar–phosphate backbone and the bpy–CH_2 ligand. It is anticipated that further refinement of the ligand structure (*i.e.* changes to the bridging unit between the sugar and the ligand, changes to the connection position of the bpy ring) will further increase the tendency to form double stranded structures.

We thank the National Institutes of Health (Grant Number GM 58447) for generous support.

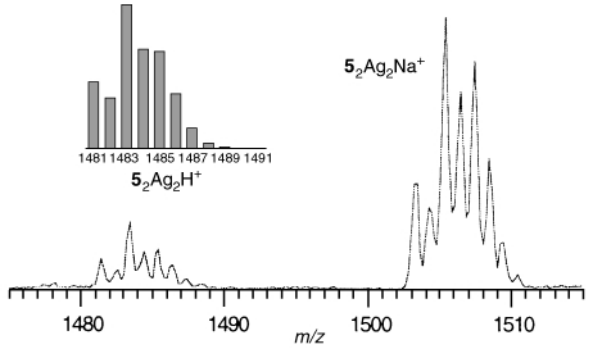

Fig. 3 ESI mass spectrum of the dinuclear complex $\mathbf{5}_2Ag_2$ and its sodium adduct. The insert shows the corresponding theoretical isotopic pattern.

Notes and references

† Full synthetic procedures will be published elsewhere. The DMT-protected **1** is chromatographically resolved into the α and β anomers. Structural assignment is based on NOE experiments, where the β anomers shows a key NOE signal between the H-1′ and H-4′. Selected data for **5**: ^{1}H NMR (400 MHz, CD_3OD) δ 8.61 (br s, 2H, bpy), 8.51 (br d, J = 10.0 Hz, 2H, bpy), 8.24 (br d, J = 7.6 Hz, 2H, bpy), 8.18 (br d, J = 7.6 Hz, 2H, bpy), 7.90 (m, 2H, bpy), 7.82 (m, 2H, bpy), 7.39 (m, 2H, bpy), 4.62 (m, 1H, H3′$_a$), 4.37 (m, 2H, H3′$_b$ and H1′$_b$), 4.26 (m, 1H, H1′$_a$), 4.06 (m, 1H, H4′$_a$), 3.95 (m, 1H, H4′$_b$), 3.89 (m, 2H, H5′$_b$), 3.57 (m, 2H, H5′$_a$), 3.04–2.84 (m, 4H, C*H*$_2$bpy), 2.37 (m, 1H, H2′$_b$), 2.28 (m, 1H, H2′$_a$), 1.91 (m, 1H, H2′$_a$), 1.71 (m, 1H, H2′$_b$). FAB-MS calcd for $C_{32}H_{35}N_4O_8P$ 635 found *m*/*z* 635.

‡ The mononuclear complex is singly charged and may appear as the major component since it can be detected with no further dissociation.

1 For recent reviews see: M. Fujita, *Acc. Chem. Res.*, 1999, **32**, 53; D. L. Caulder and K. N. Raymond, *J. Chem. Soc., Dalton Trans.*, 1999, 1185; G. F. Swiegers and T. J. Malefetse, *Chem. Rev.*, 2000, **100**, 3483; S. Leininger, B. Olenyuk and P. J. Stang, *Chem. Rev.*, 2000, **100**, 853.

2 J.-M. Lehn, A. Rigault, J. S. Siegel, J. Harrowfield, B. Chevrier and D. Moras, *Proc. Natl. Acad. Sci. U.S.A.*, 1987, **84**, 2565; C. Piguet, G. Bernardinelli and G. Hopfgartner, *Chem. Rev.*, 1997, **97**, 2005; A. F. Williams, *Chimia*, 2000, **54**, 585.

3 W. Zargas, J. Hall, J.-M. Lehn and C. Bolm, *Helv. Chim. Acta*, 1991, **74**, 1843; C. Piguet, G. Hopfgartner, B. Bocquet, O. Schaad and A. F. Williams, *J. Am. Chem. Soc.*, 1994, **116**, 9092; C. R. Woods, M. Benaglia, F. Cozzi and J. S. Siegel, *Angew. Chem., Int. Ed. Engl.*, 1996, **35**, 1830; M. Albrecht and R. Frohlich, *J. Am. Chem. Soc.*, 1997, **119**, 1656; G. Baum, E. C. Constable, D. Fenske and T. Kulke, *Chem. Cummun.*, 1997, 2043; E. C. Constable, T. Kulke, G. Baum and D. Fenske, *Inorg. Chem. Commun.*, 1998, **1**, 80; H. Weizman, J. Libman and A. Shanzer, *J. Am. Chem. Soc.*, 1998, **120**, 2188; C. Piguet, *J. Inclusion Phenom. Macrocycl. Chem.*, 1999, **34**, 361; C. Provent, E. Rivara-Minten, S. Hewage, G. Brunner and A. F. Williams, *Chem. Eur. J.*, 1999, **5**, 3487; G. Baum, E. C. Constable, D. Fenske, C. E. Housecroft, T. Kulke, M. Neuburger and M. Zehnder, *J. Chem. Soc., Dalton Trans.*, 2000, 945; M. Albrecht, *Chem. Eur. J.*, 2000, **6**, 3485.

4 K. Groebke, J. Hunziker, W. Fraser, L. Peng, U. Diederichsen, K. Zimmermann, A. Holzner, C. Leumann and A. Eschenmoser, *Helv. Chim. Acta*, 1998, **81**, 375; R. Micura, R. Kudick, S. Pitsch and A. Eschenmoser, *Angew. Chem., Int. Ed.*, 1999, **38**, 680; A. Eschenmoser, *Science*, 1999, **284**, 2118.

5 For the incorporation of a copper-containing 'base-pair' into DNA see: E. Meggers, P. L. Holland, W. B. Tolman, F. E. Romesberg and P. G. Schultz, *J. Am. Chem. Soc.*, 2000, **122**, 10 714.

6 For the modification of DNA oligonucleotides with ligandoside building blocks, see: H. Weizman and Y. Tor, submitted for publication.

7 M. J. Gait, *Oligonucleotide Synthesis, A Practical Approach*, IRL Press, 1984.

Amphipathic hydrogen bonding of CO in protonic zeolites

Carlos Otero Areán,*[a] Alexey A. Tsyganenko,[b] Olga V. Manoilova,[b] Gemma Turnes Palomino,[a] Margarita Peñarroya Mentruit[a] and Edoardo Garrone[c]

[a] *Departamento de Química, Universidad de las Islas Baleares, 07071 Palma de Mallorca, Spain. E-mail: dqueep@clust.uib.es*
[b] *Institute of Physics, St. Petersburg University, 198904 St. Petersburg, Russia*
[c] *Dipartimento di Scienza dei Materiali ed Ingegneria Chimica, Politecnico di Torino, 10126 Torino, Italy*

Received (in Cambridge, UK) 5th December 2000, Accepted 17th January 2001
First published as an Advance Article on the web 14th February 2001

CO interacts with Brønsted acid sites of protonic zeolites to form both ZH···CO and ZH···OC hydrogen bonds (Z = zeolite framework); by means of variable-temperature FTIR spectroscopy, these hydrogen-bonded species were found to be in a temperature-dependent equilibrium which, for the faujasite-type H-Y zeolite, involves an enthalpy change of 4.3 kJ mol^{-1}.

Studies on hydrogen bonding are relevant to a number of biological and chemical fields, including theoretical chemistry,[1] molecular recognition,[2] crystal engineering[3] and catalysis. Regarding the field of heterogeneous catalysis, interaction of CO with acidic hydroxy groups (Brønsted acid sites) of metal oxides and zeolites is well known[4,5] to give rise to OH··CO adducts which can easily be observed by low-temperature IR spectroscopy. In fact, the corresponding shift of the O–H stretching frequency is often used to quantify zeolite Brønsted acidity.[6,7] There is some evidence[8] that CO can also form OH··OC hydrogen bonds when adsorbed on acid (protonic) zeolites, but detailed experimental studies on this interaction mode are not available.

The aim of this work was to analyse variable-temperature FTIR spectra of CO adsorbed on the faujasite-type zeolite H-Y, which show not only that both OH··CO and OH··OC hydrogen-bonded species are formed upon interaction of CO with the zeolite Brønsted acid sites, but also that these hydrogen-bonded adducts are in a temperature-dependent equilibrium; the C-bonded adduct showing the higher interaction energy. These findings extend recent work on cation-exchanged zeolites, where a similar behaviour of adsorbed CO was found.[9] They are also in consonance with the known ability of CO to form hydrogen bonded OC··HF and CO··HF adducts with hydrogen fluoride.[10]

The H-Y zeolite used was prepared following standard methods. For IR studies, a thin self-supported wafer was outgassed (activated) for 2 h at 700 K inside an infrared cell, described elsewhere,[11] which allowed *in situ* high-temperature activation, gas dosage, and variable-temperature spectroscopy to be carried out. After running the blank spectrum of the zeolite, *ca.* 0.3 Torr of helium (to secure good thermal equilibrium)† and 3 Torr of CO (at room temperature) were dosed. The cell was then closed and a series of spectra were taken at *ca.* 10 K intervals from 77 K to room temperature.

As shown in Fig. 1, the blank spectrum of H-Y displays characteristic bands at 3545 and 3648 cm^{-1} arising, respectively, from bridged Si(OH)Al hydroxy groups inside the sodalite cages and in the supercage.[4] A minor silanol band at 3748 cm^{-1} is also observed. After dosing with CO (at 77 K) the band at 3648 cm^{-1} is reduced, and there is a simultaneous growth of a new band at 3353 cm^{-1} which proves hydrogen bonding between CO and the acidic OH groups at the supercage. The band at 3545 cm^{-1} is not affected, which is consistent with the known fact that the sodalite cages are not accessible to CO.

Fig. 2 shows selected variable-temperature spectra in the C–O stretching region. The major band seen at 2173 cm^{-1} (HF band) corresponds to the fundamental C–O stretching mode of OH··CO adducts,[4] while the minor band at 2124 cm^{-1} (LF band), downward shifted with respect to the 2143 cm^{-1} value

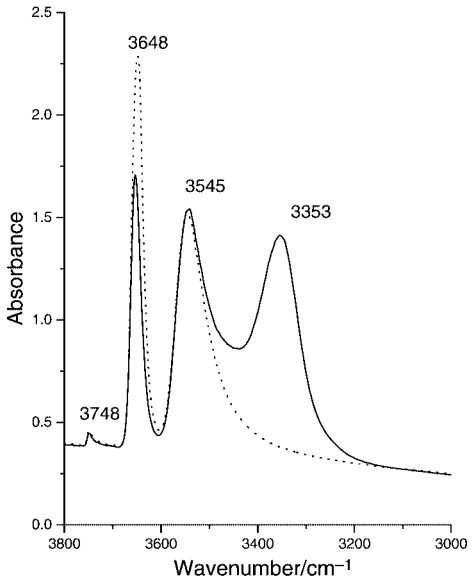

Fig. 1 IR spectra in the O–H stretching region of CO adsorbed, at 77 K, on H-Y. The dotted line is the zeolite blank spectrum while the continuous line is the spectrum obtained after dosing with CO.

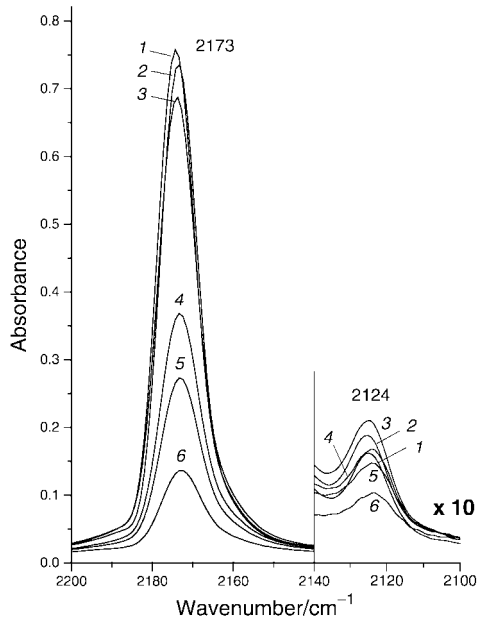

Fig. 2 Selected FTIR spectra of CO (*ca.* 3 Torr) adsorbed on H-Y at variable temperatures: 1, 119; 2, 138; 3, 153; 4, 173; 5, 179; 6, 191 K.

for free CO, is due to OH··OC adducts[9,10,12] in which the CO molecule interacts with a positively charged centre through the oxygen atom. A distinctive feature of the spectra in Fig. 2 is the temperature dependence of the intensity of the HF and LF bands. When temperature is raised from 119 to 153 K, the intensity of the HF band (A_{HF}) decreases, whereas that of the LF band (A_{LF}) increases. At higher temperatures both bands decrease, since the net amount of adsorbed CO decreases, but the ratio of integrated intensities, A_{LF}/A_{HF}, was found to increase over the whole temperature range. It should be noted that the ^{13}CO counterpart of the HF band occurs in the same frequency region as the LF band. For this reason, integrated A_{LF} values were corrected by subtracting 1% of the corresponding A_{HF} values (1% is approximately the natural abundance of the ^{13}CO isotope). A variable contribution from C-bonded ^{13}CO explains the slight variations observed in the peak position of the LF band.

The temperature dependence of the intensity of the HF and LF bands can be explained in terms of a temperature-dependent equilibrium between C- and O-bonded species: [eqn. (1)] (Z = zeolite framework):‡

$$ZH\cdot\cdot CO \rightleftarrows ZH\cdot\cdot OC \quad (1)$$

The equilibrium constant, K, for this process should be equal to the ratio of fractional coverages of O- and C-bonded species. If ε_{LF} and ε_{HF} are the corresponding molar absorption coefficients, the well known van't Hoff relationship [eqn. (2)] leads to eqn. (3):

$$\ln K = -(\Delta H°/RT) + (\Delta S°/R) \quad (2)$$

$$\ln(A_{LF}/A_{HF}) = -(\Delta H°/RT) + (\Delta S°/R) + \ln(\varepsilon_{LF}/\varepsilon_{HF}) \quad (3)$$

Fig. 3 shows that the above equation is obeyed for the whole temperature range studied, therefore proving that hydrogen-bonded OH··CO and OH··OC species are in a temperature-dependent equilibrium. The enthalpy change was found to be $\Delta H° = 4.3$ kJ mol^{-1}, as derived from the linear plot in Fig. 3.§ Knowledge of this enthalpy value is relevant to theoretical studies on weak hydrogen bonding. On the other hand, the amphipathic behaviour shown by carbon monoxide could also be manifested by other heteroatomic molecules adsorbed on zeolites, and this would have important consequences for zeolite mediated catalytic processes. This is a field deserving further studies.

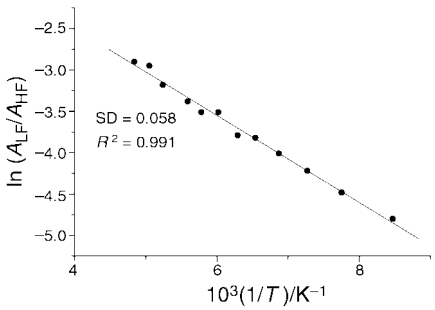

Fig. 3 van't Hoff plot of the natural logarithm of the intensity ratio of the LF and HF bands *vs.* reciprocal temperature.

Finally, it can be stated that preliminary results on the CO/H-ZSM-5 system have shown a similar equilibrium between hydrogen-bonded species as that found for CO/H-Y. It is also relevant to add, that for the CO/Na-Y system,[13] the corresponding enthalpy change for the isomerization equilibrium between C- and O-bonded adducts of CO with Na^+ ions was found to be $\Delta H° = 2.4$ kJ mol^{-1}. It is clear that the value of $\Delta H°$ depends upon the nature of the active centre interacting with adsorbed CO, and on the nature of such an interaction. However, more experimental work is needed before general trends can be established.

Notes and references

† Liquid nitrogen was used for refrigeration, and its gradual removal allowed variable-temperature spectra to be taken. The actual temperature was measured with a platinum resistance thermometer inserted close to the sample wafer.

‡ A similar equilibrium was recently documented[9] for CO adsorbed on Na-ZSM-5, but data for hydrogen-bonded species are reported here for the first time.

§ Correct application of the van't Hoff relationship for equilibrium data obtained over a large temperature range implies constant values of $\Delta H°$ and $\Delta S°$. Theoretical calculations[8,14] have shown that the difference in specific heat, $\Delta C_p°$, between C- and O-bonded adducts of CO with alkali-metal cations is negligible. It seems safe to assume that the same applies to hydrogen-bonded species.

1 M. J. Calhorda, *Chem. Commun.*, 2000, 801.
2 J. M. Lehn, *Supramoleular chemistry: Concepts and Perspectives*, VCH, Weinheim, 1995.
3 D. Braga and F. Grepioni, *J. Chem. Soc., Dalton Trans.*, 1999, 1.
4 A. Zecchina and C. Otero Areán, *Chem. Soc. Rev.*, 1996, **25**, 187.
5 J. C. Lavalley, *Catal. Today*, 1996, **27**, 377.
6 E. A. Paukshtis and E. N. Yurchenko, *React. Kinet. Catal. Lett.*, 1981, **16**, 131.
7 M. A. Makarova, K. M. Al-Ghefaili and J. Dwyer, *J. Chem. Soc., Faraday Trans.*, 1994, **90**, 383.
8 P. Ugliengo, E. Garrone, A. M. Ferrari, A. Zecchina and C. Otero Areán, *J. Phys. Chem. B*, 1999, **103**, 4839.
9 C. Otero Areán, A. A. Tsyganenko, E. Escalona Platero, E. Garrone and A. Zecchina, *Angew. Chem., Int. Ed.*, 1998, **37**, 3161.
10 G. Schatte, H. Willner, D. Hoge, E. Knözinger and O. Schrems, *J. Phys. Chem.*, 1989, **93**, 6025.
11 M. A. Babaeva, D. S. Bystrov, A. Yu. Kovalin and A. A. Tsyganenko, *J. Catal.*, 1990, **123**, 396.
12 A. J. Lupinetti, S. Fau, G. Frenking and S. H. Strauss, *J. Phys. Chem. A*, 1997, **101**, 9551.
13 A. A. Tsyganenko, E. Escalona Platero, C. Otero Areán, E. Garrone and A. Zecchina, *Catal. Lett.*, 1999, **61**, 187.
14 A. M. Ferrari, P. Ugliengo and E. Garrone, *J. Chem. Phys.*, 1996, **105**, 4129.

The synthesis of bimetallic manganese tricarbonyl-capped metallocenes

Eric J. Watson,[a] Kurtis L. Virkaitis,[a] Huazhi Li,[a] Anne J. Nowak,[a] Jason S. D'Acchioli,[a] Kunquan Yu,[a] Gene B. Carpenter,[a] Young K. Chung[b] and Dwight A. Sweigart*[a]

[a] *Department of Chemistry, Brown University, Providence, Rhode Island 02912, USA. E-mail: Dwight_Sweigart@Brown.edu*

[b] *Department of Chemistry, Seoul National University, Seoul 151-742, Korea*

Received (in Irvine, CA, USA) 8th November 2000, Accepted 23rd January 2001
First published as an Advance Article on the web 15th February 2001

Stable bimetallic 'capped' metallocenes are formed by the reaction of Cp^*_2M (M = Fe, Ru, Os) with the manganese tricarbonyl transfer reagent $[(\eta^6\text{-naphthalene})Mn(CO)_3]^+$.

Multimetallic complexes have generated great interest for many years due to their potentially useful electronic, redox and catalytic properties in comparison to monometallic analogues. Bimetallic 'triple-decker' complexes **1** containing cyclopentadienyl, arene, and/or related heterocyclic π-ligands have been widely studied.[1] Bimetallics having the general structure **2**, in which a coordinated π-ring system is 'capped' with a $M(CO)_n$ carbonyl moiety, are much less common. Furthermore, in each complex of type **2** reported, the ring bridging the two metals is heterocyclic, most commonly being a borole based system.[2] Here we report the synthesis and characterization of bimetallic $[Mn(CO)_3]^+$ capped metallocenes **3**-Fe,Ru,Os, in which the bridging ligand is strictly carbocyclic.

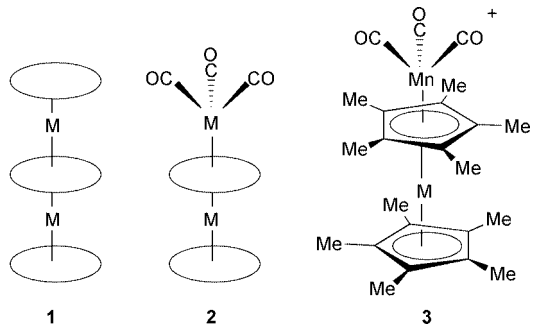

1 **2** **3**

It was recently shown by Chung and coworkers,[3] that ferrocene undergoes ring exchange with $[(\eta^6\text{-naphthalene})Mn(CO)_3]^+$ according to eqn. (1). Since it is known[4] that

$$[(\eta^6\text{-}C_{10}H_8)Mn(CO)_3]^+ + [Cp_2Fe] \rightarrow [(\eta^6\text{-}C_{10}H_8)FeCp]^+ + [CpMn(CO)_3] \quad (1)$$

$[(\eta^6\text{-polyarene})Mn(CO)_3]^+$ complexes readily transfer the $[Mn(CO)_3]^+$ moiety to suitable donor sites, it seemed possible that the bimetallic species $[Cp–Fe–Cp–Mn(CO)_3]^+$, in which one of the Cp rings is coordinated to both metals, occurs as an intermediate in this reaction. No such intermediate was actually observed with ferrocene, but we now report that changing the potential 'donor' from Cp_2Fe to the more electron-rich Cp^*_2M (M = Fe, Ru, Os) results in the formation of stable isolable bimetallic capped metallocenes **3**-Fe, **3**-Ru and **3**-Os.

Refluxing equimolar amounts of Cp^*_2M and the manganese tricarbonyl transfer reagent[4] $[(\eta^6\text{-polyarene})Mn(CO)_3]BF_4$ (polyarene = 1-methylnaphthalene or acenaphthene) in CH_2Cl_2, followed by standard work-up procedures, led to moderate yields of the air-stable capped metallocenes $[\mathbf{3}]BF_4$ (M = Fe, Ru, Os).[5] The iron complex is green while the ruthenium and osmium complexes are orange. The capped structure indicated for **3** is supported by IR, elemental analysis, MS, ^{1}H NMR, and ^{13}C NMR data (Table 1). Attempts to grow crystals of $[\mathbf{3}]BF_4$ suitable for X-ray diffraction were not successful. However, acceptable crystals of $[\mathbf{3}\text{-Ru}]PF_6$ were obtained by diethyl ether vapor diffusion into a CH_2Cl_2 solution of $[\mathbf{3}\text{-Ru}]BF_4$ containing a large excess of NH_4PF_6.

Table 1 Characterization data for the capped metallocenes $[Cp^*MCp^*Mn(CO)_3]BF_4$

	Fe	Ru	Os
ν_{CO}/cm^{-1} (CH_2Cl_2)	2050, 1975	2048, 1974	2051, 1976
EA (%):			
C(calc., found)	50.04, 49.85	46.25, 46.15	40.24, 40.34
H(calc., found)	5.48, 5.43	5.06, 5.00	4.40, 4.14
$\delta_H(CD_2Cl_2)$	2.61(s), 1.66(s)	2.44(s), 1.59(s)	2.57(s), 1.62(s)
$\delta_C(CD_2Cl_2)$	81.86, 81.33, 12.60, 8.31	87.56, 82.07, 12.96, 9.13	85.66, 72.66, 13.15, 9.63
$E_{1/2}$/V (CH_2Cl_2)[a]	−1.44	−1.46	−1.42

[a] At 25 °C, 0.10 M NBu_4PF_6, 500 mV s^{-1}, relative to Fc^+/Fc = 0.00 V.

The X-ray structure of the cation in $[\mathbf{3}\text{-Ru}]PF_6$ is shown in Fig. 1.[6] Both Cp* rings are highly planar (rms deviations 0.030, 0.019 Å) and adopt a staggered conformation. In contrast, the rings in Cp^*_2Ru are eclipsed in the solid state.[7] The singly coordinated Cp* ring in $[\mathbf{3}\text{-Ru}]PF_6$ has an average Ru–C bond length of 2.16 Å and an average ring C–C bond length of 1.42 Å. The corresponding distances in Cp^*_2Ru are 2.18 and 1.42 Å.[7]

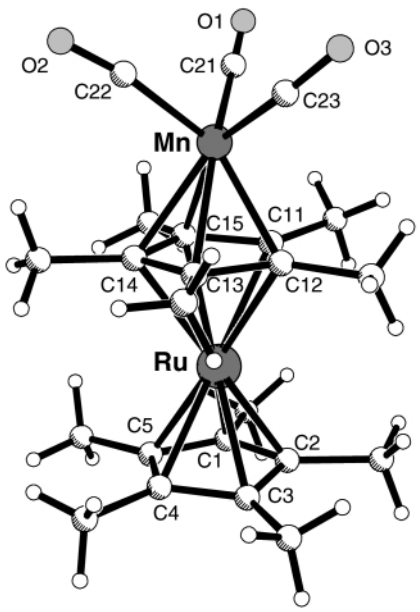

Fig. 1 Crystal structure of the cation in $[\mathbf{3}\text{-Ru}]PF_6$. Selected bond lengths (Å) and angles (°): Mn–C(11) 2.180(7), Mn–C(12) 2.136(9), Mn–C(13) 2.186(5), Mn–C(14) 2.222(10), Mn–C(15) 2.163(13), Ru–C(11) 2.181(7), Ru–C(12) 2.225(7), Ru–C(13) 2.223(5), Ru–C(14) 2.215(11), Ru–C(15) 2.238(12), Ru–C(1) 2.144(5), Ru–C(2) 2.114(13), Ru–C(3) 2.203(12), Ru–C(4) 2.160(9), Ru–C(5) 2.182(9); Mn–C(21)–O(1) 176.1(10), Mn–C(22)–O(2) 169.6(9), Mn–C(23)–O(3) 167.6(10).

The reduced electron density in the doubly coordinated Cp* ring is reflected in longer average Ru–C and C–C bonds, 2.22 and 1.46 Å, respectively. The average Mn–C bond distance to the Cp* ring is 2.18 Å, which is *ca*. 0.04 Å longer than that typically found in neutral [(cyclopentadienyl)$Mn(CO)_3$] complexes.[8]

The ^{1}H NMR data in Table 1 for the Cp* methyls show a resonance at δ *ca*.1.6, which is near that found for free Cp^*_2M. The Cp* ring in **3**-Fe,Ru,Os that is bonded to both metals, however, has methyls shifted *ca*. 1 ppm downfield. This demonstrates the deshielding effect of the cationic $[Mn(CO)_3]^+$ fragment. Table 1 shows that the ν_{CO} bands for **3**-Fe,Ru,Os are at *ca*. 2050 and 1975 cm^{-1}. By comparison, the ν_{CO} bands occur at 2005 and 1914 cm^{-1} for $[Cp^*Mn(CO)_3]$ and at 2062 and 2002 cm^{-1} for $[(\eta^6\text{-}C_6Me_6)Mn(CO)_3]^+$. From this one concludes that electron donation to the $[Mn(CO)_3]^+$ moiety is in the order $C_5Me_5^-$ >> Cp*MCp* > C_6Me_6 and that much of the positive charge (LUMO) in **3** resides on the $[Mn(CO)_3]$ fragment. This assertion is supported by electrochemical data, which show that the 30-electron bimetallic **3** is reduced in a one-electron chemically *reversible* manner at *ca*. −1.4 V relative to ferrocene. This is about the potential at which $[(\eta^6$-mono-arene$)Mn(CO)_3]^+$ complexes undergo reduction, although these species do so in a chemically *irreversible* manner.[9] In any case, the 31-electron neutral radical produced from **3** must have substantial stability for all three metals, and this aspect of the chemistry will be explored in future work.

Complexes **3**-Fe,Ru,Os are remarkably stable in CH_2Cl_2 and did not undergo a detectable reaction with $P(OEt)_3$ over 30 min. Similarly, a CH_2Cl_2 solution of **3**-Ru in the presence of naphthalene was unchanged after refluxing overnight. In MeCN solvent at room temperature, **3**-Ru was found to react with a half-life of *ca*. 1 h to afford predominantly the ring transfer product, $[Cp^*Mn(CO)_3]$, along with $[Cp^*Ru(MeCN)_3]^+$. In contrast, the major products obtained from **3**-Fe in MeCN were $[(MeCN)_3Mn(CO)_3]^+$ and Cp^*_2Fe, with a half-life of *ca*. 5 h. This difference in reaction pathway may be due to easier nucleophilic attack by MeCN at the larger ruthenium center, with concomitant Cp* ring displacement. The isolation and stability of **3**-Fe,Ru,Os strongly suggests a capped bimetallic as an intermediate in eqn. (1). An attempt was made to detect this species in the reaction of $[(naphthalene)Mn(CO)_3]^+$ with the bridged metallocene [3]ferrocenophane, the idea being that the $-(CH_2)_3-$ strap would slow or prevent the Fe–Cp cleavage for entropy reasons. Unfortunately, the reaction was found to proceed analogously to eqn. (1).

In conclusion, we have shown that stable metal carbonyl capped metallocenes can be prepared from Cp^*_2M.

This work was supported by grant CHE-9705121 from the National Science Foundation. We wish to thank Professor Thomas Bitterwolf for providing a sample of [3]ferrocenophane and for valuable discussions.

Notes and references

1 J. L. Priego, L. H. Doerrer, L. H. Rees and M. L. H. Green, *Chem. Commun.*, 2000, 779; A. R. Kudinov, M. I. Rybinskaya, Y. T. Struchkov, A. I. Yanovskii and P. V. Petrovskii, *J. Organomet. Chem.*, 1987, **336**, 187; E. Herberich, U. Englert and F. Marken, *Organometallics*, 1993, **12**, 4039; G. E. Herberich and B. Ganter, *Organometallics*, 1997, **16**, 522; M. Munakata, L. P. Wu and G. L. Ning, *Coord. Chem. Rev.*, 2000, **198**, 171.

2 G. E. Herberich, I. Hausmann and N. Klaff, *Angew. Chem., Int. Ed. Engl.*, 1989, **28**, 319; G. E. Herberich, B. J. Dunne and B. Hesser, *Angew. Chem., Int. Ed. Engl.*, 1989, **28**, 737; W. Siebert, C. Bohle, C. Kruger and Y.-H. Tsay, *Angew. Chem., Int. Ed. Engl.*, 1978, **17**, 527; W. Siebert and K. Kinberger, *Angew. Chem., Int. Ed. Engl.*, 1976, **15**, 434; R. Gleiter, I. Hyla-Kryspin and G. E. Herberich, *J. Organomet. Chem.*, 1994, **478**, 95; M. A. Benvenuto, M. Sabat and R. N. Grimes, *Inorg. Chem.*, 1992, **31**, 3904; M. Stephan, P. Müller, U. Zenneck, H. Pritzkow, W. Siebert and R. N. Grimes, *Inorg. Chem.*, 1995, **34**, 2058.

3 J. E. Kim, S. U. Son, S. S. Lee and Y. K. Chung, *Inorg. Chim. Acta*, 1998, **281**, 229.

4 S. Sun, L. K. Yeung, D. A. Sweigart, T.-Y. Lee, S. S. Lee, Y. K. Chung, S. R. Switzer and R. D. Pike, *Organometallics*, 1995, **14**, 2613.

5 Syntheses: [**3**-Fe]BF_4: [(1-methylnaphthalene)$Mn(CO)_3$]BF_4 (100 mg, 0.275 mmol) and Cp^*_2Fe (99 mg, 0.302 mmol) were added to CH_2Cl_2 (15 mL) under N_2 at room temperature. The solution was refluxed for 40 min, during which the color quickly changed from orange to green. The solution was cooled, the volume reduced to a few mL, and diethyl ether added to precipitate the product as a green powder. The product was redissolved in a minimal amount of CH_2Cl_2 and placed on a silica gel column wetted with CH_2Cl_2. Neutral species were eluted with CH_2Cl_2 and the green product was eluted with 1 : 10 (v/v) acetone–CH_2Cl_2, while unreacted [(1-methylnaphthalene)$Mn(CO)_3$]BF_4 remained on the column. The solvent was stripped and the product taken up in CH_2Cl_2 and reprecipitated with Et_2O. Yield 61% (93 mg); HRMS. calc. for $C_{23}H_{30}FeMnO_3$: *m*/*z* 465.0947; obs.: 465.0925. See Table 1 for other characterization data. [**3**-Ru]BF_4: A procedure essentially identical to that described for [**3**-Fe]BF_4 was followed, with Cp^*_2Ru (112 mg, 0.30 mmol) replacing the Cp^*_2Fe. Yield 32% (53 mg); HRMS: calc. for $C_{23}H_{30}RuMnO_3$: *m*/*z* 511.0626; obs.: 511.0619. See Table 1 for other characterization data. [**3**-Ru]BF_4 was also synthesized in a similar yield by reacting $Mn(CO)_5Br$ with $AgBF_4$ in CH_2Cl_2 solution, followed by the addition of Cp^*_2Ru. [**3**-Os]BF_4: A procedure essentially identical to that described for [**3**-Fe]BF_4 was followed, with Cp^*_2Os (92 mg, 0.20 mmol) replacing the Cp^*_2Fe and [(acenaphthene)$Mn(CO)_3$]BF_4 (83 mg, 0.22 mmol) replacing the [(1-methylnaphthalene)$Mn(CO)_3$]BF_4. Yield 30% (41 mg); HRMS: calc. for $C_{23}H_{30}OsMnO_3$: *m*/*z* 601.1190; obs.: 601.1186. See Table 1 for other characterization data. The yield in this reaction was artificially low because a significant amount of reactant [(acenaphthalene)$Mn(CO)_3$]BF_4 was found to remain when the reaction was stopped.

6 The crystal structure of [**3**]PF_6 was determined by standard procedures. The crystal showed (chiral) $P2_1$ symmetry, but proved to be a racemic twin. The structure was readily solved. Each hydrogen was introduced in an ideal position, riding on the atom to which it is bonded; each was refined with an isotropic temperature factor 20% greater than that of the ridden atom. Both Cp* groups showed some librational disorder, and the atomic parameters were gently restrained to physically possible values. The three carbonyl groups and the PF_6^- anion also showed evidence of disorder. In spite of the somewhat poorly defined parameters of the lighter atoms, the connectivity is clear. *Crystal data* for [**3**]PF_6: $C_{23}H_{30}F_6MnO_3PRu$, M = 655.45, data collected at 25 °C, monoclinic, space group $P2_1$, a = 8.8909(11), b = 8.9536(12), c = 16.406(2) Å, β = 94.905(2)°, V = 1301.2(3) Å^3, Z = 2, μ = 1.193 mm^{-1}, 327 variables refined with 5673 independent reflections (R_{int} = 0.0341) to R = 0.0530, *wR*2 = 0.1113, GOF = 1.319. CCDC 148380. See http://www.rsc.org/suppdata/cc/b0/b009054i/ for crystallographic data in .cif or other electronic format.

7 D. C. Liles, A. Shaver, E. Singleton and M. B. Wiege, *J. Organomet. Chem.*, 1985, **288**, 33.

8 Y. Huang, G. B. Carpenter, D. A. Sweigart, Y. K. Chung and B. Y. Lee, *Organometallics*, 1995, **14**, 1423.

9 C. C. Neto, C. D. Baer, Y. K. Chung and D. A. Sweigart, *J. Chem. Soc., Chem. Commun.*, 1993, 816.

A novel approach to the construction of medium-ring carbocycles utilising the rearrangement of oxonium ylides generated from metal carbenoids

J. Stephen Clark,*[a] Andrea L. Bate[a] and Trevor Grinter[b]

[a] *School of Chemistry, University of Nottingham, University Park, Nottingham, UK NG7 2RD. E-mail: j.s.clark@nottingham.ac.uk*

[b] *SmithKline Beecham Pharmaceuticals, Old Powder Mills, Leigh, Tonbridge, Kent, UK TN11 9AN*

Received (in Cambridge, UK) 8th January 2001, Accepted 25th January 2001
First published as an Advance Article on the web

Medium-ring carbocycles have been prepared by intramolecular reactions of metal carbenoids with tethered α-vinyl methyl ethers and subsequent [2,3] rearrangement of the presumed cyclic oxonium ylide intermediates.

Natural products containing medium-ring carbocycles continue to be important targets because of the synthetic challenges that they present and the potent biological activity they frequently possess.[1] As a consequence, the discovery of new reactions which permit the implementation of novel strategies for medium-ring construction continues to be an important endeavour in organic synthesis.[2]

Recently, several research groups, including our own, have shown that cyclic ethers can be prepared by rearrangement of the putative oxonium ylides generated by *intramolecular* reaction of ethers with metal carbenoids derived from diazocarbonyl compounds.[3–11] When allylic ethers are employed as substrates, an apparent [2,3] rearrangement occurs to give the corresponding cyclic ether.[4–6,8,9] In the case of acetals and non-allylic ethers, ylide generation is usually followed by a [1,2] rearrangement,[6,7,8c,10] which is generally efficient when the migrating group is benzylic.[6,7]

The substrates used in our previous studies possess an allylic ether group pendant to the main carbon chain (Scheme 1).[4] In these cases, oxonium ylide formation results in ring closure and subsequent rearrangement delivers the cyclic ether with preservation of ring size.

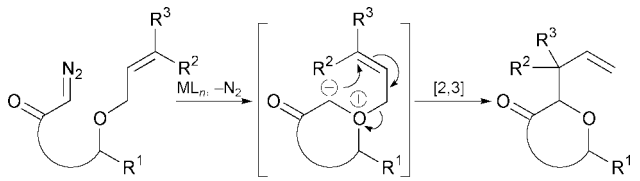

Scheme 1

It occurred to us that it might be possible to broaden the scope of the tandem ylide generation and rearrangement reaction to the preparation of carbocycles, by employing substrates in which the unsaturated group is incorporated into the main chain (Scheme 2). For example, the carbenoid derived from the diazoketone **1** should undergo intramolecular cyclisation to give the cyclic ylide **2** and subsequent [2,3] rearrangement would then deliver the carbocycle **3**. During the rearrangement process, the ring size would be increased by one and the ether substituent would be positioned outside the ring.

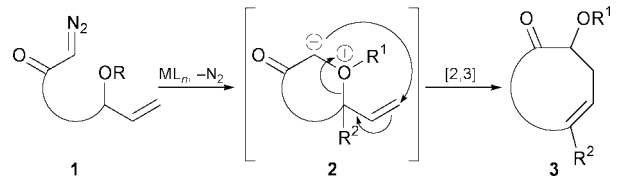

Scheme 2

There are few literature precedents for catalytic oxonium ylide generation and rearrangement using systems of the type shown in Scheme 2. In fact, the only example comes from Johnson's original studies on the generation of oxonium ylides by intramolecular reaction of metal carbenoids with ethers (Scheme 3).[6] In this case however, treatment of the diazoketone **4** with rhodium(II) acetate afforded mainly the cyclobutanone **5**, resulting from [1,2] rearrangement with ring contraction, and only a small amount of the [2,3] rearrangement product **6** was isolated (Scheme 3).[6]

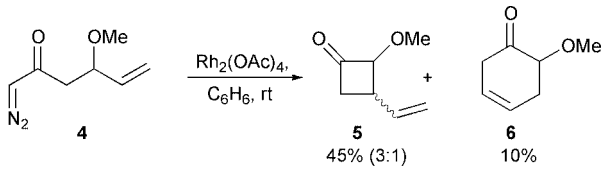

Scheme 3

Although the literature precedent above did not bode well for the development of a general reaction of the type outlined in Scheme 2, we explored the construction of cycloheptenones and cyclooctenones by an analogous ylide formation and rearrangement process (Scheme 4, Table 1). The cyclisation reaction of the diazoketone **7a** was investigated first, and treatment of this precursor with rhodium(II) acetate delivered the required cycloheptenone **9a** in 39% yield. The copper(II) hexafluoroacetylacetonate mediated reaction was also performed with the expectation that it would deliver a higher yield of the required product. However, the yield of cycloheptenone **9a** was

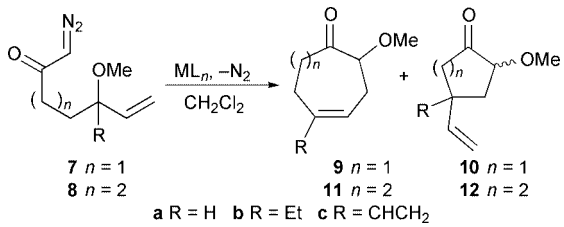

Scheme 4

Table 1 Metal-mediated ylide formation and rearrangement

Precursor	Catalyst ML_n	Temp. (°C)[a]	Product and yield (%)
7a	$Rh_2(OAc)_4$	Rt	**9a** 39[b]
7a	$Cu(hfacac)_2$	Reflux	**9a** 11[b]
7b	$Rh_2(OAc)_4$	Rt	**9b** 49 **10b** 16 (~1:1)
7b	$Cu(hfacac)_2$	Reflux	**9b** 15[b]
7c	$Rh_2(OAc)_4$	Rt	**9c** 63 **10c** 11
7c	$Cu(hfacac)_2$	Reflux	**9c** 46[b]
8b	$Rh_2(OAc)_4$	Rt	**11b** 8 **12b** 22 (~2:1)
8c	$Rh_2(OAc)_4$	Rt	**11c** 26 **12c** 9

[a] Reactions performed in DCM at rt or reflux. [b] Traces of the corresponding [1,2] rearrangement products were formed.

DOI: 10.1039/b100292i

substantially lower than that obtained from the corresponding rhodium carbenoid.† This result was surprising because we have found that copper-catalysed oxonium ylide generation and rearrangement is more efficient than the corresponding rhodium-catalysed process in most cases.[4,7]

It seemed likely that the modest yield of the ketone **9a** was due to the relatively low rate of [2,3] rearrangement as a consequence of vinyl group adopting an equatorial position in the lowest energy conformation of the cyclic oxonium ylide. We reasoned that introduction of another substituent adjacent to the ether should help populate the conformer in which the vinyl group is disposed to participate in the rearrangement reaction. In order to explore this possibility, the substrates **7b** and **7c** were prepared. Higher product yields were obtained from the rhodium- and copper-catalysed cyclisation reactions of the ethyl-substituted diazoketone **7b** (Table 1). The yields were increased further when an additional vinyl substituent was present; treatment of the substrate **7c** with rhodium(II) acetate afforded the expected product **9c** in a yield of 63% and the corresponding copper-catalysed reaction delivered the same product in 46% yield.

The construction of cyclooctenones by oxonium ylide formation and rearrangement was also explored. As expected, treatment of the substrates **8b** and **8c** with rhodium(II) acetate afforded the desired products **11b** and **11c** in much lower yields (8 and 26% respectively) than had been obtained from reactions of the homologues **7b** and **7c** (Table 1). In the case of the diazoketone **8b**, the major product **12b** was that arising from [1,2] rearrangement of the intermediate ylide. The divinyl substrate **8c** underwent cyclisation and [2,3] rearrangement in a higher yield (26%) than the diazoketone **8b**, and a small amount of the corresponding [1,2] rearrangement product **12c** (8%) was also isolated.

The divinyl susbtrates **7c** and **8c** underwent the most efficient cyclisations in each series and the products from these reactions are synthetically useful because they are amenable to further elaboration as Diels–Alder substrates. The Diels–Alder reactions of the dienes **9c** and **11c** were investigated (Scheme 5). Treatment of the diene **9c** with DMAD in toluene at reflux afforded the 1,4-diene **13a**‡ in 20% yield along with the aromatised product **13c** in 14% yield. When the reaction was performed in 1,2-dichloroethane at reflux, the isomers **13a**‡ and **13b**‡ were obtained in yields of 47 and 33% respectively, without formation of the aromatised product **13c**.

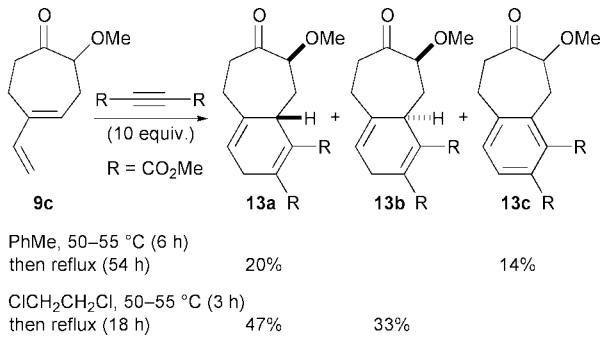

Scheme 5

The Diels–Alder reactions of **9c** and **11c** with the reactive dipolarophile maleic anhydride were also explored (Scheme 6). Cycloaddition of the diene **9c** with maleic anhydride afforded two cycloadducts. The major adduct was the tricyclic compound **14a**‡ produced by *endo* addition of the dipolarophile. The available data suggests that the minor isomer is the product **14b** resulting from *endo* addition of the other face of diene by analogy with the reaction of the same diene with DMAD (Scheme 5). In the case of the diene **11c**, Diels–Alder reaction with maleic anhydride delivered **15a** as a single isolable product in 47% yield.‡

Finally, the oxonium ylide formation and rearrangement reaction and Diels–Alder reaction were performed in a one-pot fashion. Thus, addition of the diazoketone **7c** to a solution of

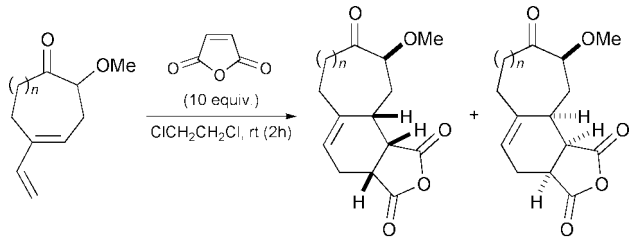

Scheme 6

rhodium(II) acetate (1 mol%) and DMAD (10 equiv.) in 1,2-dichloroethane at reflux provided the isomers **13a** and **13b** in a combined and unoptimised yield of 34%.

In summary, we have shown that it is possible to construct medium-ring carbocycles by rearrangement of oxonium ylides generated by intramolecular reaction of metal carbenoids with allylic ethers (Scheme 2). We have also shown that the diene products resulting from this reaction undergo Diels–Alder addition, and that the two reactions can be coupled to give a one-pot reaction.

We thank the EPSRC for the award of an Industrial Studentship to A. Bate, and we thank Dr A. J. Blake and Dr C. Wilson for performing X-ray crystallography.

Notes and references

† Carbenoids were also generated using $Rh_2(O_2CCF_3)$, $Rh_2(NHCOCF_3)$, and $Rh_2(O_2CC_3F_7)$, but they generally gave inferior yields of the cycloheptenone **9a**.

‡ The structure and relative stereochemistry were confirmed by X-ray crystallography.

1 For examples of bioactive medium-ring carbocycles see: (*a*) P. B. Schiff, J. Fant and S. B. Horwitz, *Nature*, 1979, **277**, 665; (*b*) *Naturally Occurring Phorbol Esters*, ed. F. J. Evans, CRC Press, Boca Raton, Florida, 1986.

2 (*a*) N. A. Petasis and M. A. Patane, *Tetrahedron*, 1992, **48**, 5757; (*b*) *The Total Synthesis of Natural Products*, Vol. 5, ed. J. ApSimon, J. Wiley & Sons, 1983.

3 A. Padwa and S. F. Hornbuckle, *Chem. Rev.*, 1991, **91**, 263.

4 (*a*) J. S. Clark, A. G. Dossetter, A. J. Blake, W.-S. Li and W. G. Whittingham, *Chem. Commun.*, 1999, 749; (*b*) J. S. Clark, M. Fretwell, G. A. Whitlock, C. J. Burns and D. N. A. Fox, *Tetrahedron Lett.*, 1998, **39**, 97; (*c*) J. S. Clark, A. G. Dossetter and W. G. Whittingham, *Tetrahedron Lett.*, 1996, **37**, 5605; (*d*) J. S. Clark and G. A. Whitlock, *Tetrahedron Lett.*, 1994, **35**, 6381; (*e*) J. S. Clark, S. A. Krowiak and L. J. Street, *Tetrahedron Lett.*, 1993, **34**, 4385; (*f*) J. S. Clark, *Tetrahedron Lett.*, 1992, **33**, 6193.

5 (*a*) M. C. Pirrung, W. L. Brown, S. Rege and P. Laughton, *J. Am. Chem. Soc.*, 1991, **113**, 8561; (*b*) M. C. Pirrung and J. A. Werner, *J. Am. Chem. Soc.*, 1986, **108**, 6060.

6 E. J. Roskamp and C. R. Johnson, *J. Am. Chem. Soc.*, 1986, **108**, 6062.

7 (*a*) R. W. Tester and F. G. West, *Tetrahedron Lett.*, 1998, **39**, 4631; (*b*) F. G. West, B. N. Naidu and R. W. Tester, *J. Org. Chem.*, 1994, **59**, 6892; (*c*) F. G. West, T. H. Eberlein and R. W. Tester, *J. Chem. Soc., Perkin Trans. 1*, 1993, 2857; (*d*) T. H. Eberlein, F. G. West and R. W. Tester, *J. Org. Chem.*, 1992, **57**, 3479.

8 (*a*) M. P. Doyle and W. H. Hu, *Tetrahedron Lett.*, 2000, **41**, 6265; (*b*) M. P. Doyle and C. S. Peterson, *Tetrahedron Lett.*, 1997, **38**, 5265; (*c*) M. P. Doyle, D. G. Ene, D. C. Forbes and J. S. Tedrow, *Tetrahedron Lett.*, 1997, **38**, 4367.

9 (*a*) N. Pierson, C. Fernandez-Garcia and M. A. McKervey, *Tetrahedron Lett.*, 1997, **38**, 4705; (*b*) T. Ye, C. Fernandez-Garcia and M. A. McKervey, *J. Chem. Soc., Perkin Trans. 1*, 1995, 1373.

10 (*a*) J. B. Brogan and C. K. Zercher, *Tetrahedron Lett.*, 1998, **39**, 1691; (*b*) J. B. Brogan, C. K. Zercher, C. B. Bauer and R. D. Rogers, *J. Org. Chem.*, 1997, **62**, 3902; (*c*) J. B. Brogan, C. B. Bauer, R. D. Rogers and C. K. Zercher, *Tetrahedron Lett.*, 1996, **37**, 5053.

11 (*a*) A. Oku and M. Numata, *J. Org. Chem.*, 2000, **65**, 1899; (*b*) A. Oku and T. Mori, *Chem. Commun.*, 1999, 1339; (*c*) A. Oku, N. Murai and J. Baird, *J. Org. Chem.*, 1997, **62**, 2123.

ChemComm

Catalysis of a hydroxyapatite-bound Ru complex: efficient heterogeneous oxidation of primary amines to nitriles in the presence of molecular oxygen

Kohsuke Mori, Kazuya Yamaguchi, Tomoo Mizugaki, Kohki Ebitani and Kiyotomi Kaneda*

Department of Chemical Science and Engineering, Graduate School of Engineering Science, Osaka University, 1-3 Machikaneyama, Toyonaka, Osaka 560-8531, Japan. E-mail: kaneda@cheng.es.osaka-u.ac.jp; Tel: +81-6-6850-6260 and Fax: +81-6-6850-6260

Received (in Cambridge, UK) 12th December 2000, Accepted 30th January 2001
First published as an Advance Article on the web 14th February 2001

A hydroxyapatite-bound Ru complex could efficiently catalyze the aerobic oxidation of various *primary* amines to nitriles which were further hydrated to amides in the presence of water.

Nitriles are versatile synthetic intermediates which are generally prepared by nucleophilic displacement of halides with cyanide ions, ammoxidation, and the Sandmeyer reaction. These conventional methods often require hazardous reagents and severe reaction conditions. Direct synthesis of nitriles from *primary* amines by the oxidative dehydrogenation is one powerful candidate for a clean synthesis. Many stoichiometric reagents in the above dehydrogenation have, however, been used,[1] which often result in the production of a vast amount of environmental waste.[2] Catalytic methods using molecular oxygen as an oxidant[3] are more desirable from the consideration of 'green and sustainable chemistry'.[2]

We have recently succeeded in creating a monomeric Ru^{3+} species on the surface of hydroxyapatite (RuHAP), which acts as a highly efficient heterogeneous catalyst for the aerobic oxidation of various alcohols.[4] During the course of these studies, we have also found and herein wish to report that the aerobic oxidation of amines to the corresponding nitriles smoothly occurred in the presence of this RuHAP catalyst. Compared with other catalysts for this amine oxidation, *the RuHAP system has many advantages as follows: (i) high catalytic activity for the oxidation of both aromatic and aliphatic amines under mild reaction conditions, (ii) a reusable heterogeneous catalyst, (iii) use of molecular oxygen as an ultimate oxidant, and (iv) applicability to the hydration of nitriles to amides.*

A calcium hydroxyapatite, $Ca_{10}(PO_4)_6(OH)_2$, was synthesized according to the literature procedure.[5] 1.0 g of the calcium hydroxyapatite was stirred at 25 °C for 24 h in 75 mL of a 2.67×10^{-2} M aqueous $RuCl_3$ solution. The obtained slurry was filtered, washed with deionized water and dried overnight at 110 °C, yielding the RuHAP as a dark brown powder (Ru^{3+} content: 1.69 mmol g^{-1}). The surface structure of the present RuHAP was determined by X-ray absorption fine structure.[4] A typical RuHAP-catalyzed amine oxidation is as follows. Into a reaction vessel with a reflux condenser were successively placed the RuHAP (0.2 g, Ru^{3+}: 6.5 mol%), *p*-xylene (15 mL), and *n*-dodecylamine (0.96 g, 5.2 mmol). The reaction mixture was stirred at 125 °C under atmospheric pressure of O_2. After 24 h, the RuHAP was separated by filtration and the organic layer was distilled to afford pure *n*-dodecanenitrile (0.88 g, 94% yield).

Oxidation of various *primary* amines is summarized in Table 1. Many benzylic amines were converted into the benzonitriles in high yields (entries 1–8).† Notably, our RuHAP could oxidize aliphatic amines to the corresponding nitriles in high yields (entries 9–12). It is said that aliphatic amines give low yields of the nitriles in homogeneous Ru-catalyzed systems such as *trans*-$[Ru^{VI}(tmp)(O_2)]$[3a] (H_2tmp = 5,10,15,20-tetramesitylporphyrin) and $RuCl_2(PPh_3)_3$[3c] using molecular oxygen. When an equimolar mixture of *n*-octylamine and octan-1-ol was used as substrate, the oxidation of *n*-octylamine occurred exclusively to afford *n*-octanenitrile in 91% yield for 12 h without any oxidation products derived from octan-1-ol.‡ Also, an intramolecular competitive oxidation of 4-(aminomethyl)-benzyl alcohol afforded chemoselectively 4-cyanobenzyl alcohol in a quantitative yield [eqn. (1)] because the amino function

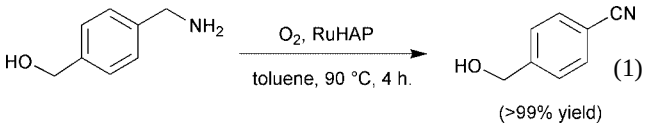

(1)

(>99% yield)

coordinates more strongly to a Ru center than the hydroxy one. 2-(1-Cyclohexenyl)ethylamine and geranylamine gave the allylic and vinylic nitriles in high yields without geometrical isomerization of double bonds, respectively (entries 13 and 14). In a *secondary* amine of dibenzylamine, *N*-benzylidenebenzylamine could be obtained in 91% yield (entry 16). Other *secondary* amines such as *N*-methylbenzylamine and *N*-ethylbenzylamine afforded the corresponding imines accompanied with benzaldehyde through the imine hydrolysis. Oxidation of *tertiary* amines did not proceed under the present conditions. The spent RuHAP catalyst was easily separated from the reaction mixture and the ICP analysis of the filtrate showed that no leaching of the Ru species was observed during the above oxidation. This catalyst could be reused with retention of its high catalytic activity and selectivity for the oxidation (entry 3).

Interestingly, when water was used as a solvent instead of toluene under N_2 atmosphere, the RuHAP could also catalyze the hydration reaction of many nitriles, *i.e. n*-hexanenitrile, *n*-octanenitrile, benzonitrile, 4-methoxybenzonitrile, and 3-cyanopyridine to afford excellent yields of the corresponding amides without any formation of carboxylic acids, respectively, as shown in Table 2. This hydration system using RuHAP has advantages over other reported methods because of its simple and clean operation under neutral conditions and its high reactivity for both aliphatic and aromatic nitriles.[6] Finally, the RuHAP catalyst could be applied to the one-pot synthesis of nicotinamide, a highly versatile intermediate of nicotinamide nucleotides, directly from 3-aminomethylpyridine, giving an excellent yield of a pure amide (Scheme 1).

We here propose a possible mechanism for this amine oxidation. Initially, a ligand exchange between an amine and a surface Cl moiety of the RuHAP[4] gives a Ru–$NHCH_2R$ species, followed by elimination to produce a Ru–H species and an

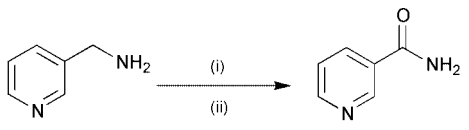

(91% isolated yield)

Scheme 1 Reaction conditions: (i) RuHAP (0.1 g), amine (10 mmol), 1,2-diethoxyethane (25 mL), O_2 atmosphere, 120 °C, 16 h, (ii) followed by adding water (5 mL), N_2 atmosphere, 150 °C, 48 h.

DOI: 10.1039/b009944i

Table 1 Oxidation of various amines using RuHAP in the presence of O_2[a]

Entry	Substrate	Conversion[b](%)	Yield of nitrile[b] (%)
1	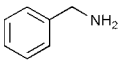	100	90[c]
2	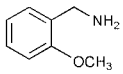	100	96
3[d]		100	97
4	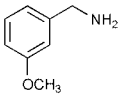	92	90
5	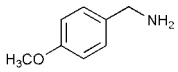	100	97
6	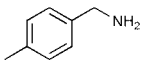	100	96
7	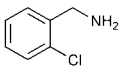	100	>99
8	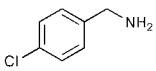	95	95
9	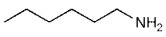	100	91
10[e]	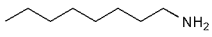	100	>99
11[e]	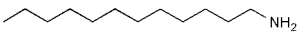	100	98
12[e]	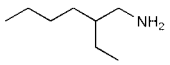	100	>99
13[e]	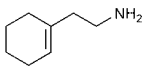	100	>99
14	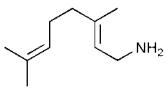	100	81
15[e]	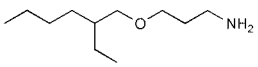	100	94
16[e,f]	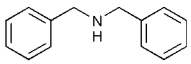	98	91[g]

[a] Amine (1 mmol), RuHAP (0.1 g), toluene (10 mL), O_2 atmosphere, 110 °C, 12 h. [b] Determined by GC using biphenyl as an internal standard. [c] *N*-Benzylidenebenzylamine was also formed (10% yield). [d] Recycling experiment. Same conditions except that the recovered RuHAP catalyst was used. [e] 24 h. [f] *p*-Xylene (10 mL) was used as a solvent instead of toluene, 130 °C. [g] Yield of *N*-benzylidenebenzylamine.

intermediate imine. Attack of molecular oxygen on the hydride species affords a Ru–OOH species, which reacts with the imine to produce a Ru–N=CHR species. The second dehydrogenation of the imine to nitrile proceeds *via* a similar path to that described above. In the nitrile hydration, the reaction of the surface Cl moiety with water yields a Ru–OH species, which attacks nucleophilically to a nitrile. A formed iminol intermediate, Ru–N=C(OH)R,[6b] subsequently undergoes a ligand exchange with water to give the amide accompanied by the Ru–OH species.

Table 2 Hydration of various nitriles using RuHAP in the presence of H_2O[a]

Entry	Substrate	Conversion[b](%)	Yield of amide[b] (%)
1		100	>99
2	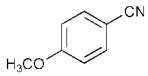	100	96
3		100	97
4	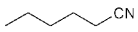	100	98
5	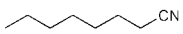	100	97

[a] Nitrile (1 mmol), RuHAP (0.1 g), water (3 mL) , N_2 atmosphere, 150 °C, 24 h. [b] Determined by GC using biphenyl as an internal standard.

In conclusion, the RuHAP efficiently catalyzed the oxidation of many *primary* amines using molecular oxygen, and could be further extended for the nitrile hydration. No leaching of the Ru species in the reaction solution was observed, which allows the hydroxyapatite catalyst to be recycled with retention of its high catalytic activity and selectivity. We have continuously designed hydroxyapatite catalysts containing various other transition metal complexes for developing many functional transformations in organic synthesis.

This work is supported by the Grant-in-Aid for Scientific Research from Ministry of Education, Culture, Sports, Science and Technology of Japan (11450307). We are also grateful to the Department of Chemical Science and Engineering, Osaka University, for scientific support by 'Gas-Hydrate Analyzing System (GHAS)'.

Notes and references

† In the oxidation of *para*-substituted benzylamines, the Hammett plot showed a negative ρ value, −0.137, which is close to that with a monomeric $RuCl_2(PPh_3)_3$, $\rho = -0.118$.

‡ Octan-1-ol alone was smoothly oxidized to afford 1-octanoic acid in 82% yield within 6 h under the same reaction conditions as in Table 1: See ref. 4.

1 (*a*) P. Capdevielle, A. Lavigne and M. Maumy, *Synthesis*, 1989, 453; (*b*) M. V. George and K. S. Balachandran, *Chem. Rev.*, 1975, **75**, 491; (*c*) J. B. Lee, C. Parkin, M. J. Shaw, N. A. Hampson and K. I. MacDonald, *Tetrahedron*, 1973, **29**, 751.

2 (*a*) R. A. Sheldon, *Green Chem.*, 2000, **2**, G1; (*b*) P. T. Anastas, L. B. Bartlett, M. M. Kirchhoff and T. C. Williamson, *Catal. Today*, 2000, **55**, 11.

3 Examples on the catalytic amine oxidation are as follows: (*a*) A. J. Bailey and B. R. James, *Chem. Commun.*, 1996, 2343; (*b*) S. Yamazaki and Y. Yamazaki, *Bull. Chem. Soc. Jpn.*, 1990, **63**, 301; (*c*) F. Porta, C. Crotti and S. Cenini, *J. Mol. Catal.*, 1989, **50**, 333; (*d*) S. Cenini, F. Porta and M. Pizzottio, *J. Mol. Catal.*, 1982, **15**, 297.

4 K. Yamaguchi, K. Mori, T. Mizugaki, K. Ebitani and K. Kaneda, *J. Am. Chem. Soc.*, 2000, **122**, 7144.

5 J. C. Elliott, *Structure and Chemistry of the Apatites and Other Calcium Orthophosphates*, Elsevier: Amsterdam, 1994.

6 For examples of catalytic nitrile hydration: (*a*) C. J. Cobley, M. van den Heuvel, A. Abbadi and J. G. de Vries, *Tetrahedron Lett.*, 2000, **41**, 2467; (*b*) N. V. Kaminskaia and N. M. Kostic, *J. Chem. Soc., Dalton Trans.*, 1996, 3677; (*c*) T. Ghaffar and A. W. Parkins, *Tetrahedron Lett.*, 1995, **36**, 8657; (*d*) S.-I. Murahashi, S. Sasao, E. Saito and T. Naota, *J. Org. Chem.*, 1992, **57**, 2521.

Synthesis and thermolysis of novel spiroselenuranes bearing two oxaselenetane rings: double oxirane formation reactions from 1,5-dioxa-4λ⁴-selenaspiro[3.3]heptanes†

Fumihiko Ohno, Takayuki Kawashima* and Renji Okazaki*‡

Department of Chemistry, Graduate School of Science, The University of Tokyo, 7-3-1 Hongo, Bunkyo-ku, Tokyo 113-0033, Japan. E-mail: takayuki@chem.s.u-tokyo.ac.jp

Received (in Cambridge, UK) 6th December 2000, Accepted 29th January 2001
First published as an Advance Article on the web 14th February 2001

The first stable spiroselenuranes bearing two oxaselenetane rings have been synthesized, chracterized by X-ray crystallographic analysis, and shown to be thermally reactive giving two molar equivalents of the corresponding oxirane with elimination of elemental selenium, in sharp contrast to the behavior of the phosphorus and silicon analogues.

In the course of our study on oxetanes containing high-coordinate main group elements at the position adjacent to the oxygen atom,[1] we have reported the syntheses and isolation of intermediates of Wittig- and Peterson-type olefin formation reactions.[2,3] For the purpose of elucidating the influence of ring size of the spiro-ring system on the reactivity of the heteracyclobutanes, we have investigated the synthesis and reactivity

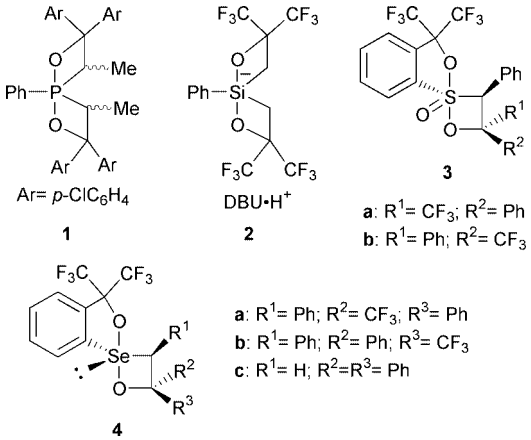

of compounds **1** and **2**, which have two oxaphosphetane and oxasiletane rings, respectively, and found that **1** undergoes double olefin extrusion,[4] while **2** undergoes homo-Brook rearrangement to give the corresponding alcohol.[5] On the other hand, we have recently found that the oxirane formation reactions from pentacoordinate 1,2λ⁶-oxathietanes **3a**,**b** or tetracoordinate 1,2λ⁴-oxaselenetanes **4a**,**b** proceed with retention of configuration,[6] which is the first example for the oxirane formation without backside attack of oxide anion on the carbon attached to the chalcogen atom, in sharp contrast to the Corey–Chaykovsky reaction.[7] These results prompted us to study tetracoordinate 1,5-dioxa-4λ⁴-selenaspiro[3.3]heptanes, a novel type of a spiroselenurane bearing two oxaselenetane rings. We now report, for the first time, their synthesis and unique thermal behavior.

Sequential treatment of $(PhSCH_2)_2Se$ **5** with 1.1 equiv. of lithium diisopropylamide (LDA), with 2.0 equiv. of freshly generated hexafluoroacetone (HFA), and then with aqueous NH_4Cl gave mono(β-hydroxyalkyl) selenide **6** (28%) (Scheme 1). A diastereomer mixture of bis(β-hydroxyalkyl) selenides **7** was obtained from **6** by repetition of the same procedure as the addition of HFA to **5** (2.0 equiv. of LDA and 3.0 equiv. of HFA). Separation by flash column chromatography (SiO_2) gave *dl*-**7** (7%) and *meso*-**7** (61%). Oxidative cyclization of *dl*-**7** and *meso*-**7** with Br_2 in the presence of Et_3N afforded the corresponding tetracoordinate 1,5-dioxa-4λ⁴-selenaspiro[3.3]heptanes *trans-trans*-**8** (30%) and *trans-cis*-**8** (49%), respectively. Recrystallization of *trans-trans*-**8** and *trans-cis*-**8** from hexane–diethyl ether gave colorless plates which melted at 93.5–108.4 and 105.0–106.2 °C with decomposition, respectively.§

In the ^1H, ^{13}C and ^{19}F NMR spectra of *trans-trans*-**8**, the two oxetane rings were observed equivalently, whereas those of *trans-cis*-**8** were non-equivalent. Downfield shifts from *dl*-**7** (δ_H 4.98, δ_C 52.31) to *trans-trans*-**8** (δ_H 6.35, δ_C 88.07) were observed for the proton and carbon of the methine adjacent to the central selenium, which is a common spectral feature for tetracoordinate 1,2-oxachalcogenetanes.[1,6] In the ^{77}Se NMR spectra of *trans-trans*-**8** (δ_{Se} 835.3) and *trans-cis*-**8** (δ_{Se} 882.0) were observed multiplets due to the long-range coupling with ^{19}F nuclei. The large downfield shifts in δ_{Se} from **7** [δ_{Se} 521.1 (*dl*), 521.7 (*meso*)] to **8** and their similar chemical shifts to compounds **4** (**4a**: δ_{Se} 781; **4b**: δ_{Se} 793; **4c**: δ_{Se} 840.8) strongly support the selenurane structure for **8**. We have also synthesized *trans-trans*-**9** with two phenyl groups instead of two phenylthio groups of *trans-trans*-**8**.¶

X-Ray crystallographic analysis indicated that the asymmetric unit of a crystal of *trans-trans*-**9** contains one and a half molecules, A and B, the latter of which is disordered in two different orientations on the crystallographic inversion center.‖ Both molecules have a distorted pseudo-trigonal bipyramidal (TBP) structure with two oxygen atoms at apical positions and two carbon atoms and a lone pair at equatorial positions. The

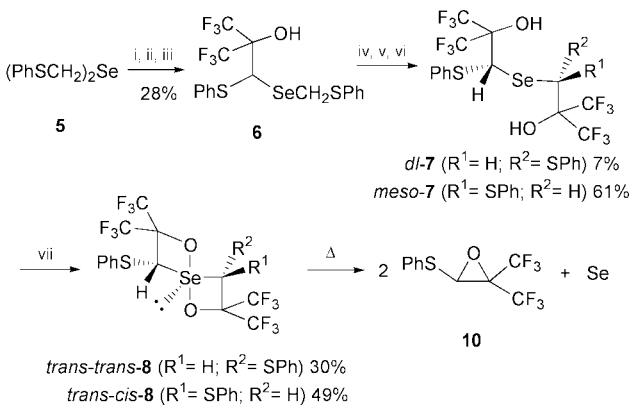

Scheme 1 *Reagents and conditions*: i, 1.1 equiv. of LDA, THF, −78 °C, 10 min; ii, 2.0 equiv. of $(CF_3)_2C{=}O$, –78 °C, 30 min; iii, aqueous NH_4Cl; iv, 2.0 equiv. of LDA, THF, –78 °C, 10 min; v, 3.0 equiv. of $(CF_3)_2C{=}O$, –78 °C, 30 min; vi, 1.1 eq Br_2, 8.3 equiv. of Et_3N, CCl_4, 0 °C, 30 min.

† Electronic supplementary information (ESI) available: full experimental details and spectroscopic data. See http://www.rsc.org/suppdata/cc/b0/b009789f

‡ Present address: Department of Chemical and Biological Sciences, Faculty of Science, Japan Women's University, 2-8-1 Mejirodai, Bunkyo-ku, Tokyo 112-8681, Japan.

DOI: 10.1039/b009789f

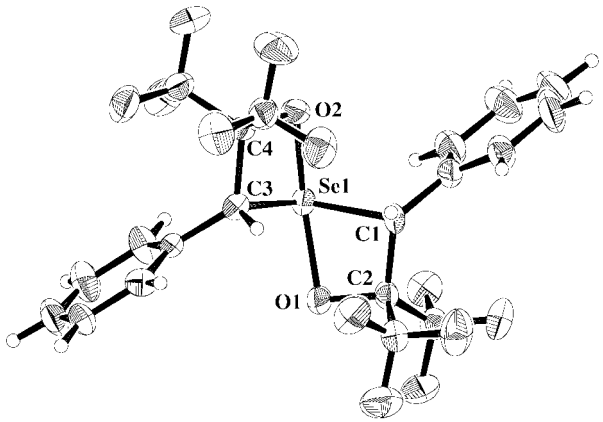

Fig. 1 ORTEP drawing of *trans-trans*-**9** with thermal ellipsoid plot (30% probability for all non-hydrogen atoms). Selected bond lengths (Å), bond angles (°) and torsion angles (°): Se1–O1 1.971(4), Se1–O2 1.955(4), Se1–C1 1.979(6), Se1–C3 1.978(6), C1–C2 1.532(8), C2–O1 1.388(6), C3–C4 1.531(8), O2–C4 1.392(7); O1–Se1–O2 155.26(18), C1–Se1–O1 71.1(2), Se1–C1–C2 90.0(4), C1–C2–O1 103.7(5), Se1–O1–C2 94.7(3), C1–Se1–C3 109.2(3), O2–Se1–C3 71.9(2), O2–C4–C3 104.3(5), Se1–C3–C4 89.1(4); Se1–C1–C2–O1 −5.9(5), Se1–C3–C4–O2 −6.1(5).

ORTEP drawing of molecule A (Fig. 1) shows that both the phenyl groups at the 3- and 3′-positions are *cis* to the lone pair of selenium and *trans* to the Se–C bond of another four-membered ring. The apical Se–O bonds are bent away from the lone pair leading to the deviation of the O–Se–O angle by 22.74(18)° from linearity, which is a common structural feature of the hypervalent species containing a four-membered ring.[1,4,6*a*] The apical Se–O bond lengths [1.971(4) and 1.955(4) Å)] are between those [1.977(4) and 1.902(4) Å] of selenurane **4c**.[1*b*] The two oxaselenetane rings of *trans-trans*-**9** are almost planar [Se–C–C–O; −6.2195(10)° and −6.5439(10)°] similar to **4c** [Se–C–C–O 4.7(4)°].[1*b*]

Thermolyses of *trans-trans*-**8** (C_6D_6, 120 °C, 11 h) and *trans-cis*-**8** (C_6D_6, 60 °C, 19 h) in a degassed sealed tube gave oxirane **10** in 72 and 83% yields,** respectively, with black precipitates and minor unidentified products, indicating that both compounds underwent double oxirane extrusion reaction. The formation of elemental selenium (black precipitates) was confirmed by observation of the signal due to tris(dimethylamino)phosphine selenide (δ_P 84.9) after treatment of the reaction mixture with tris(dimethylamino)phosphine (δ_P 121.5). On the other hand, the thermolysis of *trans-trans*-**9** ($CD_3C_6D_5$, 200 °C, 12 d) gave a somewhat complicated mixture containing oxirane **11** (31%) and deuterated alcohol **12** (19%). (Scheme 2)** The formation of **12** indicates that radical species were generated by homolytic bond cleavage, probably because drastic conditions were necessary for the thermolysis.

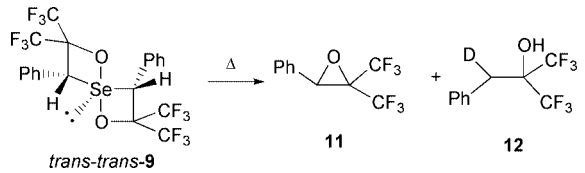

Scheme 2

Although oxetanes containing a pentacoordinate group 14 or 15 element give rise to olefins,[1*a*] spiro oxachalcogenetanes yielded oxiranes, regardless of the ring size (five- or four-membered ring). This indicates that the thermal reactivity mainly depends on the bond energy of the oxygen and the central atom. Investigation of the stereochemistry of the oxirane formation is now in progress.

This work was partially supported by Grants-in-Aid for Scientific Research on Priority Areas No. 09239101 and General Scientific Research (B) No. 10440212 (T. K.) from the Ministry of Education, Science, Sports and Culture, Japan. We are grateful to Professor N. Tokitoh of Kyoto University for the determination of the X-ray structure of *trans-trans*-**9**. We also thank Central Glass, Shin-etsu Chemical, and Toso Akzo Co. Ltd. for the gifts of organofluorine compounds, trialkylsilanes and alkyllithiums, respectively.

Notes and references

§ *Selected data*: for *trans-trans*-**8**: colorless plates (hexane–Et_2O); mp 93.5–108.4 °C (decomp.); ^{1}H NMR (C_6D_6, 500 MHz) δ 6.35 (s, 2H, SeCH), 6.86–6.95 (m, 6H), 7.43–7.46 (m, 4H); ^{19}F NMR (C_6D_6, 254 MHz) δ –74.0 (q, $^4J_{FF}$ = 8.3 Hz, 6F), −78.7 (q, $^4J_{FF}$ 8.3 Hz, 6F); ^{77}Se NMR ($CDCl_3$, 51.5 MHz) δ 835.3 (m). HRMS (70 eV): *m*/*z* calc. for $C_{20}H_{12}F_{12}O_2S_2{}^{80}Se$ 655.9252, found 655.9263. For *trans-trans*-**9**: colorless plates (hexane–Et_2O); mp 178.2–179.8 °C (decomp.); ^{1}H NMR ($CDCl_3$, 500 MHz) δ 6.86 (s, 2H, SeCH), 7.40 (d, ^3J 7.2 Hz, 4H), 7.45–7.53 (m, 6H); ^{19}F NMR ($CDCl_3$, 254 MHz) δ −73.4 (q, $^4J_{FF}$ 9.0 Hz, 6F), –78.2 (q, $^4J_{FF}$ 9.0 Hz, 6F); ^{77}Se NMR ($CDCl_3$, 51.5 MHz) δ 723.1 (s). HRMS (70 eV): *m*/*z* calc. for $C_{20}H_{12}F_{12}O_2{}^{80}Se$ 591.9811, found 591.9816. Satisfactory ^{13}C NMR spectra were obtained for both *trans-trans*-**8** and *trans-trans*-**9**.

¶ Synthesis of *trans-trans*-**9** is described in the supporting information (ESI†).

‖ Crystal data for *trans-trans*-**9**: $C_{20}H_{12}F_{12}O_2Se$, M = 591.25, monoclinic, space group $P2_1/n$, a = 9.621(2), b = 22.144(3), c = 16.221(2) Å, β = 106.209(4)°, U = 3318.3(9) Å^3, T = 298 K, Z = 6, μ(Mo-Kα) = 18.14 cm^{-1}, 8261 refelections measured, 7812 (R_{int} = 0.075) which were used in all calculations. The final w$R(F^2)$ was 0.221 (all data). CCDC 154648. See http://www.rsc.org/suppdata/cc/b0/b009789f/ for crystallographic data in .cif or other electronic format.

** The yields were calculated assuming that 1 mol of **8** or **9** gives 2 mol of products.

1 (*a*) T. Kawashima and R. Okazaki, *Synlett*, 1996, 600; T. Kawashima and R. Okazaki, in *Advances in Strained and Interesting Organic Molecules*, ed. B. Halton, JAI Press Inc., Stamford, 1999, vol. 7, pp. 1–41; (*b*) T. Kawashima, F. Ohno and R. Okazaki, *J. Am. Chem. Soc.*, 1993, **115**, 10 434.

2 For the Wittig reactions, see: D. J. H. Smith, in *Comprehensive Organic Chemistry*, ed. D. H. R. Barton and W. D. Ollis, Pergamon, Oxford, 1979, vol. 2, pp. 1316–1329; B. E. Maryanoff and A. B. Reitz, *Chem. Rev.*, 1989, **89**, 863; E. Vedejs and M. J. Peterson, *Top. Stereochem.*, 1994, **21**, 1.

3 For the Peterson reactions, see: W. P. Weber, *Silicon Reagents for Organic Synthesis*, Springer-Verlag, New York, 1983, pp. 58–73; D. J. Ager, *Org. React. (New York)*, 1990, **38**, 1.

4 T. Kawashima, R. Okazaki and R. Okazaki, *Angew. Chem., Int. Ed. Engl.*, 1997, **36**, 2500.

5 T. Kawashima, K. Naganuma and R. Okazaki, *Organometallics*, 1998, **17**, 367.

6 (*a*) T. Kawashima, F. Ohno, R. Okazaki, H. Ikeda and S. Inagaki, *J. Am. Chem. Soc.*, 1996, **118**, 12455; (*b*) F. Ohno, T. Kawashima and R. Okazaki, *Chem. Commun.*, 1997, 1671.

7 For the Corey–Chaykovsky reactions, see: J. Aubé, in *Comprehensive Organic Synthesis: Selectivity, Strategy, and Efficiency in Modern Synthetic Chemistry*, ed. B. M. Trost and I. Fleming, Pergamon, Oxford, 1991, vol. 1, pp. 822–825.

ChemComm

Adsorption and activity of cytochrome c on mesoporous silicates†

J. Deere, E. Magner,* J. G. Wall and B. K. Hodnett

Materials and Surface Science Institute and Department of Chemical and Environmental Sciences, University of Limerick, Limerick, Ireland. E-mail: edmond.magner@ul.ie

Received (in Cambridge, UK) 27th November 2000, Accepted 29th January 2001
First published as an Advance Article on the web 14th February 2001

Cytochrome c (horse heart) has been adsorbed onto a range of mesoporous silicate materials with the extent of adsorption dependent on the silicate pore size; adsorption and activity profiles of the adsorbed protein are reported.

Mesoporous silicate materials (MPS) such as those which are formed by mediated pathways involving surfactants as structure directing reagents[1,2] are very suitable as hosts for large organic molecules[3] and proteins.[4–6] MPS exhibit highly ordered pore structures and very tight pore size distributions, as exemplified by the first type of these materials reported, MCM-41.[1] As a direct consequence of their mesopore structures, MPS possess large surface areas of the order of 1000 $m^2\ g^{-1}$. Owing to their silicate inorganic framework, they are chemically and mechanically stable[2] and are resistant to microbial attack. In addition, it is possible to chemically modify MPS with various functional groups, enabling electrostatic attraction or repulsion between MPS and the protein(s) of interest to be maximised.[7] Materials such as sol–gels display similar stability as MCS and have been used to encapsulate proteins for use as biosensors. However, sol–gels suffer from the disadvantage of possessing a highly variable pore size distribution.[8] More importantly, their preparation can involve the use of harsh conditions or reagents which are detrimental to proteins, resulting in denaturation of the protein.[8] With MPS, protein encapsulation occurs after synthesis of the support, avoiding this difficulty. MPS therefore hold great promise for use as supports to immobilise enzymes,[6,7,9] and may find applications in biosensors,[5] biocatalytic[9] and biomolecule separation[7] systems. For example, Stucky and coworkers[7] have used MPS to sequester and release proteins of similar size but varying charge, while Díaz and Balkus[9] have used MPS to immobilise cytochrome c. To date, there have been no reports on the adsorption isotherms obtained with MPS–protein systems, nor on the catalytic activity of a stable, adsorbed, protein–silicate system. In this report, we describe adsorption isotherms for cytochrome c onto four MPS materials covering a range of pore sizes, and peroxidative activity profiles of the adsorbed protein.

Cytochrome c is a small (12 384 Da) redox protein, with an approximate spherical diameter of 40 Å.[10] The cytochrome c (horse heart) (Sigma-Aldrich) used in this study was *ca.* 95% pure and was further purified using standard methods.[11] The MPS materials used consisted of a commercially available silicate (COS) (Fluka, Reidel-de Haën), a cyano-modified silicate (CNS), an MCM-41 material and an MPS material (MPS-F127) synthesised using a non-ionic triblock surfactant Pluronic-F127 as the structure directing agent. The physicochemical properties of the MPS materials are presented in Table 1 and the pore size distributions in Fig. 1.

Cytochrome c has been previously adsorbed onto MPS materials such as MCM-41,[9] SBA-15[14] (MPS of pore diameter 90–110 Å), Nb-TMS4[4] (MPS modified with Nb^{5+}). However, neither the adsorption isotherms nor the peroxidative activity of the protein were reported. The latter, in particular, is important if MPS are to be of use in biosensors and biocatalytic systems.

† Electronic supplementary information (ESI) available: experimental details. See http://www.rsc.org/suppdata/cc/b0/b009478l/

Table 1 Physicochemical properties of mesoporous silicates used in adsorption studies

MPS	BET surface area/$m^2\ g^{-1}\ SiO_2$	Average pore size/Å	Mesopore volume /$cm^3\ g^{-1}\ SiO_2$	Cytochrome c maximum load/μmol $g^{-1}\ SiO_2$	Volume cytochrome c adsorbed[a]/ $cm^3\ g^{-1}\ SiO_2$
COS	470	55	0.46	3.8	0.3
CNS	379	130	0.61	10.2	0.7
MCM-41	1000	28	0.31	1.7	0.1
MPS-F127	537	50	0.38	6.8	0.5

[a] The volume of cytochrome c was calculated from the crystal structure to be 121 nm^3.[14]

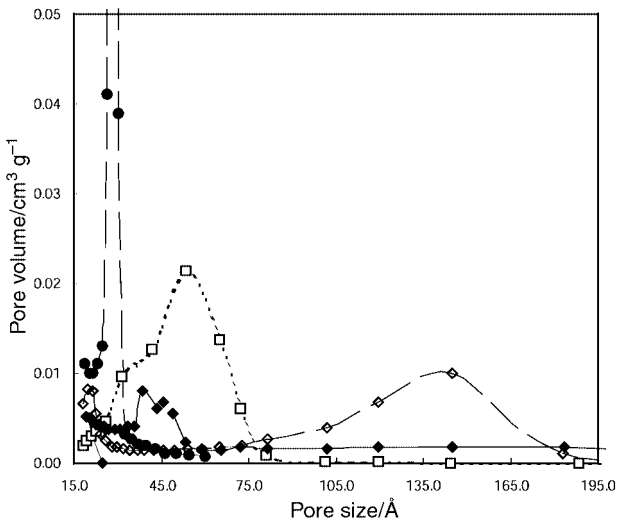

Fig. 1 Pore size distributions of COS (□), MCM-41 (●), CNS (◇) and MPS-F127 (◆).

Fig. 2 shows protein adsorption isotherms for the cytochrome c–MPS systems. It can be clearly seen from Table 1 and Fig. 1 that CNS has the largest average pore size (130 Å) with MCM-41 exhibiting a pore size of 28 Å. The isotherms in Fig. 2 demonstrate that CNS has a much larger affinity for cytochrome c compared with MCM-41. The latter has a very tight pore size distribution at 28 Å (Fig. 1), a pore diameter too small for cytochrome c to penetrate, yielding a maximum adsorption of only 1.7 μmol g^{-1} MCM-41. The CNS material on the other hand, with a much larger pore diameter (130 Å), allows for a maximum adsorption of 10.2 μmol g^{-1} silicate. Clearly, the pore size of the material is a major factor in the adsorption process.[9] The pores in the COS material with an average diameter of 55 Å (Fig. 1) are also large enough to allow penetration of the protein molecule into the pores. With MCM-41, the amount of cytochrome c adsorbed does not change significantly over the range of concentrations studied from the initial 1.7 μmol g^{-1} SiO_2 level), indicating that adsorption is largely confined to the outside surface of the silicate.[9] The MPS-F127 allows for more protein to be adsorbed than in the

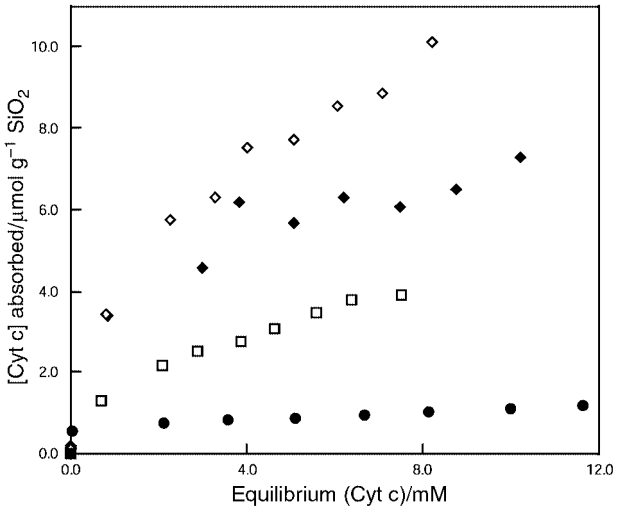

Fig. 2 Adsorption isotherms for pure cytochrome c on to COS (□), MCM-41 (●), CNS (◇) and MPS-F127 (◆).

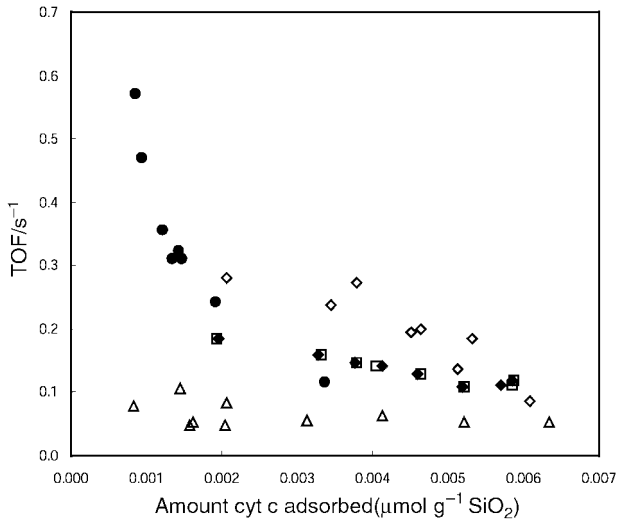

Fig. 3 Peroxidative activity (ABTS assay) profiles for cytochrome c adsorbed on to COS (□), MCM-41 (●), CNS (◇) and MPS-F127 (◆) and of aqueous cytochrome c (Δ). The standard deviations for the assays were 18, 24, 11 18 and 12%, respectively.

case of COS, despite having a similar pore size distribution; this is likely due to the presence of a small subgroup of mesopores with diameters in the range 60–200 Å in the former material (Fig. 1). In contrast to the adsorption of trypsin onto MCM-41,[9] where the enzyme leached out of the silicate, adsorbed cytochrome c was found to be stable to repeated washing in buffer (minimum of four washings). As with the adsorption of conalbumin onto MPS,[7] the ionic strength was found to strongly influence the amount of protein adsorbed, with little absorption occurring at high ionic strengths.[13]

Peroxidative activity profiles‡ over the range of adsorbed cytochrome c are shown in Fig. 3. Aqueous cytochrome c activity was constant over this range (TOF§ ≈ 0.075 s^{-1}). The similarity of the activity profiles of adsorbed protein on COS and MPS-F127 silicates may be a reflection of the similarity in the pore size distributions of these two materials. The general trend of higher TOF at lower amounts of adsorbed protein indicates that access of the ABTS substrate to cytochrome c molecules may be limited at higher protein loadings. This is seen clearly in the MCM-41 profile, where the TOF decreases to that of aqueous solution. From the data in Fig. 1, adsorption of cytochrome c onto MCM-41 appears to occur largely on the outside of the silicate, implying that diffusion of the substrate into the pores cannot be rate limiting. The high TOF values at the lower levels of protein adsorbed may be a result of assaying externally adsorbed protein, where increased substrate access would be expected. The CNS silicate activity profile is similar to the COS and MPS-F127 silicates, but with marginally higher TOF. This is possibly due to the larger pores of the CNS material allowing for faster substrate access. The TOF values obtained for the adsorbed protein are marginally higher for the aqueous protein. This is in marked contrast to the results obtained with trypsin where the activity of the entrapped enzyme was only 13% of that of the protein in solution.[9]

We have shown that a protein–mesoporous silicate system can be readily generated and that cytochrome c is readily adsorbed by such mesoporous materials, provided that the pore sizes of the mesoporous silicate are large enough to accommodate the protein structure and therefore allow access to the large internal surface areas of these materials. The activity of the adsorbed protein at the interface has also been clearly defined and is comparable with the activity of the protein in solution over the same concentration range.

This research was funded by the Higher Education Authority through the Programme for Research in Third Level Institutions (1999–2000).

Notes and references

‡ The activity profiles for each of the silicates were adjusted to reflect only the activity of the adsorbed cytochrome c.
§ TOF is the turnover frequency defined as μmol of reduced ABTS s^{-1}/μmol cytochrome c on silicate.

1 J. S. Beck, J. C. Vartuli, W. J. Roth, M. E. Leonowicz, C. T. Kresge, K. D. Schmitt, C. T.-W. Chu, D. H. Olson, E. W. Sheppard, S. B. McCullen, J. B. Higgins and J. L. Schlenker, *J. Am. Chem. Soc.*, 1992, **114**, 10 834.
2 D. Zhao, Q. Huo, J. Feng, B. F. Chmelka and G. D. Stucky, *J. Am. Chem. Soc.*, 1998, **120**, 6024.
3 B. F. G. Johnson, S. A. Raynor, D. S. Shephard, T. Mashmeyer, J. M. Thomas, G. Sankar, S. Bromsley, R. Oldmoyd, L. Gladden and M. D. Mantle, *Chem. Commun.*, 1999, 1167.
4 K. J. Balkus, M. E. Gimon-Kinsel, V. L. Jimenez and L. Washmon, *Stud. Surf. Sci. Catal.*, 1998, **117**, 373.
5 L. Washmon-Kriel, V. L. Jimenez and K. J. Balkus, *J. Mol. Catal. B: Enzymatic*, 2000, **10**, 453.
6 J. He, X. Li, D. G. Evans, X. Duan and C. Li, *J. Mol. Catal. B: Enzymatic*, 2000, **11**, 45.
7 Y.-J. Han, G. D. Stucky and A. Butler, *J. Am. Chem. Soc.*, 1999, **121**, 9897.
8 I. Gills and A. Ballesteros, *J. Am. Chem. Soc.*, 1998, **120**, 8587.
9 J. F. Díaz and K. J. Balkus, *J. Mol. Catal. B: Enzymatic*, 1996, **2**, 115.
10 *Cytochrome c, A multidisciplinary approach*, ed. R. A. Scott and A. G. Mauk, University Science Books, Sausalito, CA, 1996.
11 E. Margoliash and J. Lustgarten, *J. Biol. Chem.*, 1962, **237**, 3397.
12 D. Zhou, J. Feng, Q. Huo, N. Melosh, G. H. Fredrickson, B. F. Chmelka and G. D. Stucky, *Science*, 1998, **279**, 548.
13 J. Deere, E. Magner, J. G. Wall and B. K. Hodnett, to be submitted.
14 G. W. Bushnell, G. V. Louie and G. D. Brayer, *J. Mol. Biol.*, 1990, **214**, 585.

A new class of single-molecule magnets: mixed-valent $[Mn_{12}O_8Cl_4(O_2CPh)_8(hmp)_6]$

Colette Boskovic,[a] Euan K. Brechin,[a] William E. Streib,[a] Kirsten Folting,[a] David N. Hendrickson*[b] and George Christou*[a]

[a] *Department of Chemistry and the Molecular Structure Center, Indiana University, Bloomington, IN 47405-7102, USA. E-mail: christou@indiana.edu*

[b] *Department of Chemistry-0358, University of California at San Diego, La Jolla, CA 92093-0358, USA. E-mail: dhendrickson@ucsd.edu*

Received (in Cambridge, UK) 15th December 2000, Accepted 12th January 2001
First published as an Advance Article on the web 19th February 2001

The reaction of $(NBu^n_4)[Mn_8O_6Cl_6(O_2CPh)_7(H_2O)_2]$ with 2-(hydroxymethyl)pyridine (hmpH) or 2-(hydroxyethyl)pyridine (hepH) gives the $Mn^{II}_2Mn^{III}_{10}$ complexes $[Mn_{12}O_8Cl_4(O_2CPh)_8(hxp)_6]$ [hxp$^-$ = hmp$^-$ (1) or hep$^-$ (2)]; these compounds are core isomers with markedly different magnetic properties, compound 1 having an $S = 7$ ground state and displaying strong out-of-phase ac susceptibility signals that establish it as a new class of single-molecule magnet, whereas compound 2 is a low-spin molecule with an $S = 0$ ground state.

In recent years, the search for the ultimate high-density memory devices has afforded so-called single-molecule magnets (SMMs). Each independent molecule in these materials possesses the ability to function as a magnetizable magnet below a critical temperature, owing to intrinsic intramolecular properties rather than intermolecular interactions and long-range ordering. Known SMMs include $[Mn_{12}O_{12}(O_2CR)_{16}(H_2O)_x]^{n-}$ (n = 0–2),[1–4] complexes with the $[Mn^{IV}Mn^{III}_4O_3X]^{6+}$ core,[5] $[Mn_4(O_2CMe)_2(Hpdm)_6]^{2+}$ salts (pdm = anion of pyridine-2,6-dimethanol),[6] $[Fe_8O_2(OH)_{12}(tacn)_6]^{8+}$ salts (tacn = 1,4,7-triazacyclononane),[7] $[Fe_4(OMe)_6(dpm)_6]$ (dpmH = dipivaloylmethane)[8] and $[V_4O_2(O_2CR)_7(L–L)]^z$ (L–L = 2,2′-bipyridine, pyridine-2-carboxylate anion).[9] A convenient way to detect the slow magnetic relaxation of SMMs is by the appearance of an out-of-phase signal (χ_M'') in ac susceptibility studies, which indicates that the rate of relaxation is insufficient to keep up with the oscillating applied field. We herein report a new class of dodecanuclear Mn-based SMMs with an $S = 7$ ground state and a strong χ'' signal, which occurs at temperatures higher than those observed for all previously reported SMMs, except the $[Mn_{12}O_{12}(O_2CR)_{16}(H_2O)_x]^{n-}$ family. We also report a structurally related species, whose structural differences result in a low-spin ground state.

Treatment of $(NBu^n_4)[Mn_8O_6Cl_6(O_2CPh)_7(H_2O)_2]$[10] with 4 equivalents of 2-(hydroxymethyl)pyridine (hmpH) or 2-(hydroxyethyl)pyridine (hepH) in MeCN leads to a precipitate after several days. Extraction of the soluble component into CH_2Cl_2 and diffusion of Et_2O into the resulting solution results in crystalline $[Mn_{12}O_8Cl_4(O_2CPh)_8(hxp)_6]$, where hxp$^-$ = hmp$^-$ (**1**) or hep$^-$ (**2**), in yields of ⩽15%.

The centrosymmetric structures of **1** and **2**†‡ (Figs. 1 and 2) each consist of an $[Mn^{III}_{10}Mn^{II}_2(\mu_4\text{-}O)_4(\mu_3\text{-}O)_4(\mu_2\text{-}O)_8(\mu_3\text{-}Cl)_2]$ core, with peripheral ligation provided by six hmp$^-$ (**1**) or hep$^-$ (**2**) ligands, eight O_2CPh^- ligands and two terminal Cl$^-$ ligands. The cores are isomers and can be described as three pairs of face-sharing cuboidal units, (*i.e.* incomplete face-sharing double cubanes). The difference between the cores arises from the manner in which these three units are linked together; the orientation of the 'middle' unit of one compound is related to that of the other by a 120° rotation. Bond valence sums indicate that the two Mn^{II} atoms of each cluster are Mn(6) and Mn(6′). As expected, the ten Mn^{III} atoms in each cluster display a Jahn–Teller elongation. For each cluster, the hxp$^-$ ligands chelate and bridge the Mn atoms of the 'end' units, while the O_2CPh^- groups bridge Mn atoms in the 'middle' unit with those in the 'end' units. However, the arrangement of the peripheral ligands differs between **1** and **2**.

Solid-state dc magnetization measurements were performed on **1** in the range 1.8–300 K in a field of 10.0 kG. The $\chi_M T$ value of 36.6 cm^3 mol^{-1} K at 300 K remains approximately constant as the temperature is decreased until *ca.* 100 K when it begins to increase to a maximum value of 38.3 cm^3 mol^{-1} K at 50 K before rapidly decreasing to 5.3 cm^3 mol^{-1} K at 1.8 K. The spin-only ($g = 2$) value for a unit composed of non-interacting $Mn^{II}_2Mn^{III}_{10}$ ions is 38.8 cm^3 mol^{-1} K. Hence, the molecule appears to have a high spin ground state, with the low temperature decrease assigned to zero field splitting and other effects. In order to determine the ground state spin, magnetization data were collected in the ranges 1.8–4.0 K and 1–70 kG. The data were fit using a full-matrix diagonalization approach; the best fits were with $S = 6$, $g = 2.09$, $D \approx -0.8$ cm^{-1} and $S = 7$, $g = 1.79$, $D \approx -0.6$ cm^{-1}, which were of comparable quality but poorer than those normally obtained. This is a common problem in higher nuclearity Mn_x systems[11,12] and is assignable to relatively low-lying excited states, particularly when Mn^{II} ions are present since these typically give weak exchange interactions. We conclude that the molecule has $S = 6$ or 7, although we favour the latter given that $g < 2$.

Ac magnetization measurements were performed on **1** in the 1.8–10 K range in a 3.5 G ac field oscillating at 50–1500 Hz.

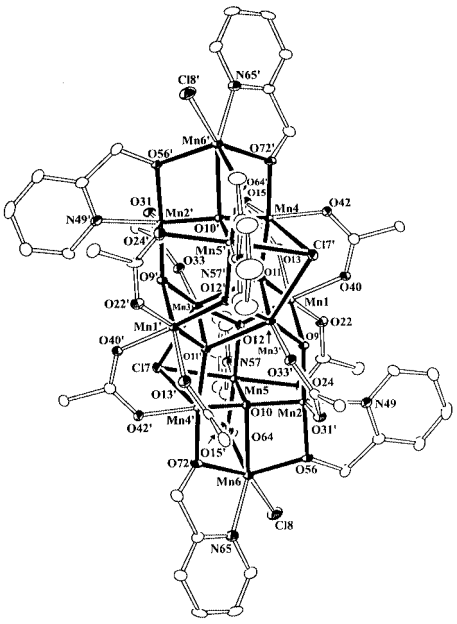

Fig. 1 ORTEP representation of complex **1** at the 50% probability level. For clarity, only the *ipso* carbon atom of each phenyl ring is included.

DOI: 10.1039/b010038m

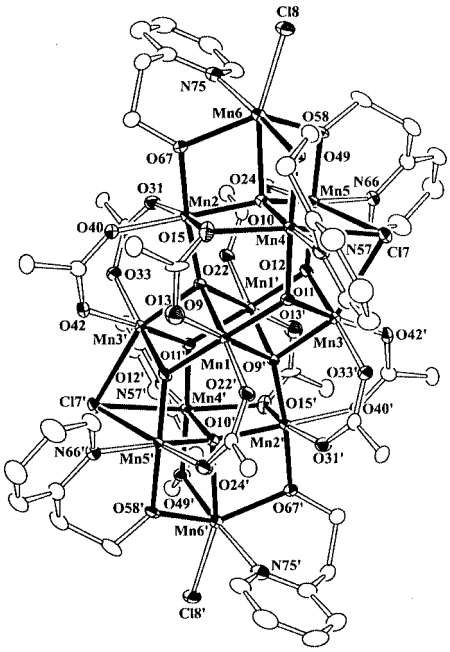

Fig. 2 ORTEP representation of complex **2** at the 50% probability level. For clarity, only the *ipso* carbon atom of each phenyl ring is included.

The in-phase $\chi_M'T$ signal (Fig. 3) shows a frequency dependent decrease at $T < 4$ K, indicative of the onset of slow relaxation on the ms timescale diagnostic of a SMM. This was confirmed by the concomitant appearance of an out-of-phase (χ_M'') signal due to the inability of **1** to relax sufficiently rapidly at these temperatures to keep up with the oscillating field. The χ_M'' signal has a peak at *ca.* 2.75 K at a 997 Hz ac frequency, where the position of the peak corresponds to the temperature at which the relaxation rate is equal to the ac oscillation frequency. Data obtained by varying the frequency of oscillation of the ac field was fit to the Arrhenius equation to obtain the energy barrier (U_{eff}) for the relaxation of the magnetization. The slope of the Arrhenius plot (Fig. 4) gave a U_{eff} of 30.3 K (21.1 cm^{-1}). For an integer spin system, the barrier to thermally activated magnetic relaxation is $S^2|D|$. Thus the experimentally determined kinetic energy barrier of 30.3 K (21.1 cm^{-1}) implies a minimum value of D of −0.62 K (−0.43 cm^{-1}), assuming that $S = 7$. High-field EPR studies will be performed to obtain a more precise value of D.

Solid-state dc magnetization measurements were performed on **2** in the range 1.8–300 K in a 10.0 kG field. The $\chi_M T$ value increases slightly from 37.9 $cm^3\ mol^{-1}$ K at 300 K to 38.5 $cm^3\ mol^{-1}$ K at 200 K before steadily decreasing to 1.5 $cm^3\ mol^{-1}$ K at 1.8 K, indicating a low ground state spin value. Ac susceptibility measurements were performed with a 3.5 G ac field oscillating at 997 Hz. The ac and dc data are essentially superimposable (not shown) except at the lowest temperatures and appear to be heading for $\chi_M T = 0$ $cm^3\ mol^{-1}$ K at 0 K,

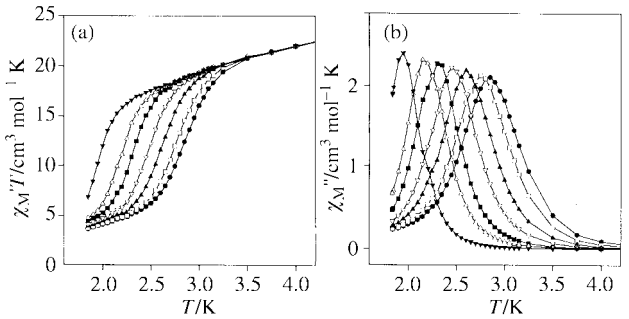

Fig. 3 Plots of (a) the in-phase (χ_M') signal as $\chi_M'T$ and (b) out-of-phase (χ_M'') signal in ac susceptibility studies *vs.* temperature of complex **1** in a 3.5 G field oscillating at 1488 (●), 997 (□), 499 (▲), 250 (▽), 100 (■), 50 (△) and 10 Hz (▼).

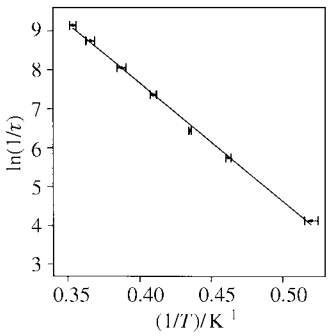

Fig. 4 Arrhenius plot with error bars for complex **1**. The solid line is a fit of the data (see text).

suggesting an $S = 0$ ground state. Its very different S value compared with **1** must clearly be due to the core isomerism, which will affect many of the Mn_2 pairwise exchange interactions in the core. No χ_M'' signal is observed for **2** and thus it is not a SMM. In contrast, the structurally related complex **1** displays strong out-of-phase signals in ac susceptibity studies that firmly establish it as a new class of SMM. These signals for **1** occur at relatively high temperatures reflecting the relatively large value of U_{eff}. Indeed, only $[Mn_{12}O_{12}(O_2CR)_{16}(H_2O)_4]^{n-}$ complexes have exhibited greater U_{eff} values (Mn_{12} 70 K, $[Mn_{12}]^-$ 55 K, $[Mn_{12}]^{2-}$ 40 K). Thus, the new Mn_{12} complex **1** represents an important new member of the SMM family, and studies of magnetization hysteresis and quantum tunneling of magnetization in this molecule are in progress.

This work was supported by the National Science Foundation.

Notes and references

† The complexes analyzed satisfactorily (C, H, N) as solvent-free. Crystals were kept in contact with the mother liquor to avoid solvent loss and were crystallographically identified as **1**·2Et_2O·4CH_2Cl_2 and **2**·7CH_2Cl_2.

‡ *Crystal data:* **1**: $C_{104}H_{104}N_6O_{32}Cl_{12}Mn_{12}$ (including solvate molecules), M_r = 3034.68, triclinic, space group $P\bar{1}$, a = 14.2602(12), b = 14.8241(12), c = 15.7931(14) Å, α = 15.7931(14), β = 94.5578(22), γ = 94.5578(22)°, U = 3005.87 Å^3, Z = 1, T = −160 °C. Residuals R and R_w were 0.0623 and 0.0698, respectively, from refinement on F using 9578 unique data with $F > 2\sigma(F)$. **2**: $C_{105}H_{102}N_6O_{30}Cl_{18}Mn_{12}$ (including solvate molecules), M_r = 3225.39, monoclinic, space group $C2/c$, a = 36.774(3), b = 14.930(1), c = 27.037(3) Å, β = 121.884(3) °, U = 312604 Å^3, Z = 4, T = −168 °C. Residuals R and R_w were 0.0353 and 0.0379, respectively, from refinement on F using 7908 unique data with $F > 2\sigma(F)$.

CCDC 154915 and 154916. See http://www.rsc.org/suppdata/cc/b0/b010038m/ for crystallographic data in .cif or other electronic format.

1 R. Sessoli, H.-L. Tsai, A. R. Schake, S. Wang, J. B. Vincent, K. Folting, D. Gatteschi, G. Christou and D. N. Hendrickson, *J. Am. Chem. Soc.*, 1993, **115**, 1804.

2 R. Sessoli, D. Gatteschi, A. Caneschi and M. A. Novak, *Nature*, 1993, **365**, 141.

3 H. J. Eppley, H.-L Tsai, N. de Vries, K. Folting, G. Christou and D. N. Hendrickson, *J. Am. Chem. Soc.*, 1995, **117**, 301.

4 M. Soler, S. K. Chandra, D. Ruiz, J. C. Huffman, D. N. Hendrickson and G. Christou, *Chem. Commun.*, 2000, 2417.

5 S. M. J. Aubin, M. W. Wemple, D. M. Adams, H.-L Tsai, G. Christou and D. N. Hendrickson, *J. Am. Chem. Soc.*, 1996, **118**, 7746.

6 J. Yoo, E. K. Brechin, A. Yamaguchi, M. Nakano, J. C. Huffman, A. L. Maniero, L.-C Brunel, K. Awaga, H. Ishimoto, G. Christou and D. N. Hendrickson, *Inorg. Chem.*, 2000, **39**, 3615.

7 C. Sangregorio, T. Ohm, C. Paulsen, R. Sessoli and D. Gatteschi, *Phys. Rev. Lett.*, 1997, **78**, 4645.

8 A.-L. Barra, A. Caneschi, A. Cornia, F. Fabrizi de Biani, D. Gatteschi, C. Sangregorio, R. Sessoli and L. Sorace, *J. Am. Chem. Soc.*, 1999, **121**, 5302.

9 S. L. Castro, Z. Sun, C. M. Grant, J. C. Bollinger, D. N. Hendrickson and G. Christou, *J. Am. Chem. Soc.*, 1998, **120**, 2997.

10 H.-L Tsai, S. Wang, K. Folting, W. E. Streib, D. N. Hendrickson and G. Christou, *J. Am. Chem. Soc.*, 1995. **117**, 2503.

11 M. Soler, E. Rumberger, K. Folting, D. N. Hendrickson and G. Christou, *Polyhedron*, in press.

12 E. K. Brechin, J. Yoo, D. N. Hendrickson and G. Christou, in preparation.

Microtubes and balls of amorphous phosphorus nitride imide (HPN_2) prepared by a benzene-thermal method

Zhaoyu Meng,*[a] Yiya Peng[b] and Yitai Qian[ab]

[a] *Department of Chemistry, University of Science and Technology of China, Hefei, Anhui 230026, P. R. China. E-mail: meng_zhaoyu@sina.com*

[b] *Structure Research Laboratory, University of Science and Technology of China, Hefei, Anhui 230026, P. R. China.*

Received (in Cambridge, UK) 14th December 2000, Accepted 15th January 2001
First published as an Advance Article on the web 19th February 2001

Microtubes, hollow balls, solid balls and square frameworks of amorphous phosphorus nitride imide (HPN_2) were obtained through the reaction of PCl_5 and NaN_3 using benzene as solvent and hydrogen source under mild conditions; as an inorganic polymer, amorphous HPN_2 with these interesting morphologies may be of potential uses in industries.

The discoveries of fullerene and carbon nanotubes as new forms of matter in the nanoscale range have opened a challenging new field in solid state physics, chemistry, and materials science with many possible applications.[1,2] Since then, much attention has been paid to the development of new methods for the preparation of nanotubes and fullerene-like structures of other materials.[3,4] Besides crystalline nanotubes and fullerene-like structures, amorphous microtubes of molybdenum polysulfide have recently been reported, which undoubtedly indicate that amorphous materials can also aggregate into tube- and ball-like morphologies.[5]

As an inorganic polymer, phosphorus nitride imide (HPN_2) is one of the tenary phosphorus nitrides. It has been researched for many years,[6] and has a network structure consisting of PN_4 tetrahedra linked through all four vertices by corner sharing; it has isometric analogues in the silicate family.[7,8] Recently, amorphous phosphorus nitride (P_3N_5) was synthesized in our laboratory by a solvent-free reaction between PCl_5 and NaN_3 in an autoclave.[9] However, when the reaction was carried out in benzene, amorphous HPN_2 was formed instead of P_3N_5. It was also found that microtubes, balls (hollow and solid) and square frameworks of the amorphous HPN_2 could be formed under different reaction conditions. The results are presented here.

The preparation technique was as follows. Manipulations were carried out in a dry glovebox with N_2 gas flowing. Analytically pure PCl_5 (0.005 mol) and NaN_3 (0.025 mol) were put into four stainless steel autoclaves of 25 ml capacity. These were filled with benzene to within 90% of the total volume. Two autoclaves were maintained at 190 °C for 3 d and 10 d, the other two were kept at 250 °C for 12 h and 3 d, respectively. When the heating was over, the autoclaves were allowed to cool to room temperature naturally. The precipitates were collected, washed with carbon disulfide, benzene, absolute ethanol and distilled water several times and dried under vacuum at 80 °C for 4 h.

Elemental† and chemical analyses show that the H : N : P : C ratio in the samples is *ca.* 1 : 2.02 : 0.99 : 0.02. XPS‡ showed that the binding energies of P 2p and N 1s were 133.3 and 398.7 eV, which are close to the values of P_3N_5.[10–12] The quantification of peaks confirmed that the atomic ratio of P : N was nearly 1 : 2.01. No other element except a trace amount of chlorine was detected in the samples. Fig. 1 shows the infrared spectrum§ of the sample, which is in good agreement with the reported spectrum of HPN_2.[7] Taking the above results into consideration, it is believed that the products are phosphorus nitride imide, HPN_2.

TEM¶ images of the samples prepared under different conditions are shown in Fig. 2. Microtubes [Fig. 2(a), (b)] were found to exist in the samples prepared at 250 °C for 12 h and 190 °C for 3 d. The proportion of microtubes in the samples was 20–25%. It is evident that the boundary of the wall of the tubes is quite well defined. The external diameter of the tubes is 350–450 nm and the thickness of the walls is *ca.* 100 nm. However, the samples prepared at 250 °C for 3 d and 190 °C for 10 d consisted of hollow balls (15–20%), solid balls (60–70%) and square frameworks (1–2%) [Fig. 2(c), (d) and (e)], respectively. The balls are perispherical with a diameter of 200–300 nm. The thickness of the shell of the hollow balls is *ca.* 50 nm. The frameworks are a uniform square and the length is about 500 nm. Electron diffraction did not reveal any crystal ordering in the tubes, balls and frameworks, and they may be considered as completely amorphous. The result was consistent with the XRD patterns of the samples.

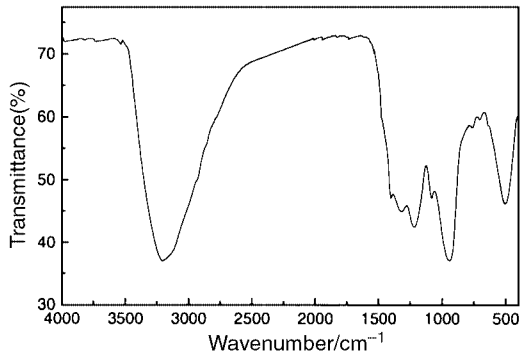

Fig. 1 IR spectrum of the amorphous HPN_2.

It is believed that the hydrogen element in HPN_2 originated from benzene because P_3N_5 instead of HPN_2 was produced when the reaction was carried out in a solvent-free environ-

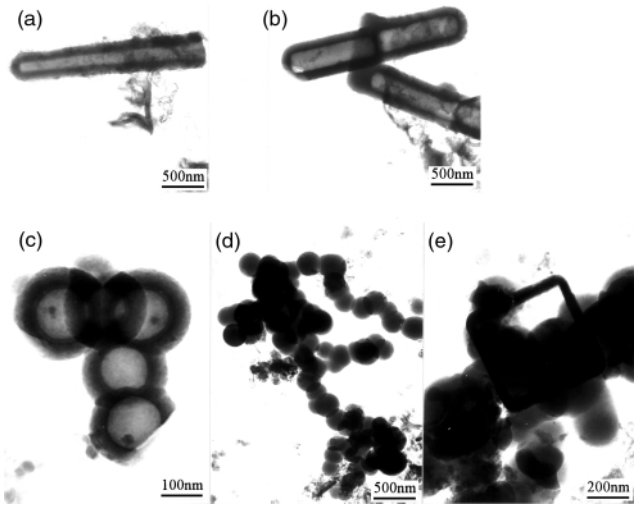

Fig. 2 TEM images of the amorphous HPN_2 prepared (a) at 250 °C for 12 h, (b) at 190 °C for 3 d, and (c–e) at 250 °C for 3 d or 190 °C for 10 d.

DOI: 10.1039/b009994p

ment.[9] Benzene plays an important role in the reaction: it acts not only as a solvent but also as a hydrogen element source, and may be the key to the formation of the interesting morphologies. This process is a complicated reaction and the exact mechanism needs further research. It was found that sodium chloride was the by-product, which was determined by the XRD patterns of the samples not washed with water.

The influence of temperature and time on the synthesis of amorphous HPN_2 was also studied. If the reaction temperature is lower than 190 °C the reaction is very incomplete and only a small amount of HPN_2 can be obtained. But when the reaction temperature is above 300 °C, P–H adsorption at 2080 cm^{-1} is detected through IR spectra, indicating that PN_4 tetrahedra are destroyed.[10] For the sample prepared at 190 °C for 12 h, no special morphology was found. The samples prepared at 190 °C for 3 d and 10 d have the same morphologies as those prepared at 250 °C for 12 h and 3 d, respectively, which indicates that a long reaction time and low temperature have the same effect as a short reaction time and high temperature, in the appropriate temperature range. Considering the facts that balls are formed instead of tubes with lengthened reaction time, and that some tubes are found truncated at the middle part [Fig. 2(b)], it is proposed that the hollow balls are transformed from the tubes. Solid balls might be formed through the aggregation of amorphous fragments, which is consistent with the fact that the ball was the most stable state in liquid.

In the reaction temperature range, nothing dangerous took place in our experiments, which indicated that this process was safe even though PCl_5 and NaN_3 were used. As an inorganic polymer, phosphorus nitride imide, HPN_2, with the above interesting morphologies may have some potential uses in industry.

Notes and references

† Elemental analyses were taken on a 240C elemental analysis instrument.

‡ XPS were recorded on an ESCALAB MKII instrument with Mg Kα radiation as the exciting source.

§ IR spectra were obtained on a Magna IR-750FT spectrometer.

¶ TEM measurements were made on a Hitachi H-800 transmission electron microscope with an accelerating voltage of 200 kV.

1 H. W. Kroto, J. R. Heath, S. C. O'Brien, R. F. Curl and R. E. Smalley, *Nature*, 1985, **318**, 162.
2 S. Iijima, *Nature*, 1991, **354**, 56.
3 M. Terrones, W. K. Hsu, H. W. Kroto and D. R. M. Walton, *Top. Curr. Chem.*, 1999, **199**, 189.
4 R. Tenne, M. Homyonfer and Y. Feldman, *Chem. Mater.*, 1998, **10**, 3225.
5 P. Afanasiev, C. Geantet, C. Thomazeau and B. Jouget, *Chem. Commun.*, 2000, 1001.
6 *Gmelins Handbook of Inorganic Chemistry*, Verlag Chemie, Weinheim, 1964, 8th edn., vol. P.
7 W. Schnick and J. Lucke, *Z. Anorg. Allg. Chem.*, 1992, **610**, 121.
8 H. Dai, E. W. Wong, Y. Z. Lu, S. Fan and C. M. Liber, *Nature*, 1995, **375**, 769.
9 Z. Meng, Y. Peng, Z. Yang and Y. Qian, *Chem. Lett.*, 2000, 1252.
10 S. Vepřek, Z. Iqbal, J. Brunner and M. Scharli, *Philos. Mag. B*, 1981, **43**, 527.
11 C. M. Zelenski and P. K. Dorhout, *J. Am. Chem. Soc.*, 1998, **120**, 734.
12 L. S. Dake, D. R. Baer and D. M. Friedrich, *J. Vac. Sci. Technol., A*, 1989, **7**, 1634.

Alloy nanowires: Invar inside carbon nanotubes

N. Grobert,[a] M. Mayne,†[a] M. Terrones,[bc] J. Sloan,[de] R. E. Dunin-Borkowski,[e] R. Kamalakaran,[b] T. Seeger,[b] H. Terrones,[c] M. Rühle,[b] D. R. M. Walton,*[a] H. W. Kroto[a] and J. L. Hutchison[e]

[a] *School of Chemistry, Physics and Environmental Science, University of Sussex, Brighton, UK BN1 9QJ. E-mail: D.Walton@sussex.ac.uk*
[b] *Max-Planck-Institut für Metallforschung, Seestraße 92, 70174 Stuttgart, Germany*
[c] *Instituto de Física, Laboratorio Juriquilla, UNAM, A.P. 1-1010, 76000, Querétaro, México*
[d] *Wolfson Catalysis Centre (Carbon Nanotechnology Group), Inorganic Chemistry Laboratory, University of Oxford, South Parks Road, Oxford, UK OX1 3QR*
[e] *Department of Materials, University of Oxford, Parks Road, Oxford, UK OX1 3PH*

Received (in Cambridge, UK) 4th January 2001, Accepted 29th January 2001
First published as an Advance Article on the web 19th February 2001

Invar ($Fe_{65}Ni_{35}$), a 'zero' thermal expansion alloy consisting of Fe and Ni, has been successfully introduced into carbon nanotubes by pyrolysing, at 800 °C, aerosols of $NiCp_2/FeCp_2$ mixtures dissolved in C_6H_6; scanning electron microscopy (SEM) and high-resolution transmission electron microscopy (HRTEM) studies reveal the presence of flake-like structures (*ca.* 1–2 mm²) consisting of filled/aligned carbon nanotubes (⩽200 μm in length and ⩽80 nm in diameter) in a carpet pile-like configuration; analysis of the filling material (⩽500 nm in length and ⩽40 nm in diameter) by X-ray powder diffraction and high-resolution electron energy loss spectroscopy (HREELS) line scans, confirmed that Invar was formed; this appears, to the best of our knowledge, to be the first report of mixed metal alloy nanowires forming inside carbon nanotubes.

Invar ($Fe_{65}Ni_{35}$) alloy, discovered by Guillaume in 1897,[1] exhibits an extremely low thermal expansion coefficient, *ca.* one tenth of that of steel.[2] Furthermore, Fe/Ni alloys are interesting not only for their low thermal expansion, but also for their remarkable magnetic properties. These alloys have various uses in, for instance, the fabrication of electronic devices, aircraft controls, laser systems, bimetallic thermostats, *etc.*[2–4]

To date, various techniques for encapsulating metals, metal oxides and chlorides in multi-walled (MWNT) or single-walled carbon nanotubes (SWNT) have been developed.[5,6] However, the encapsulation of alloys has so far been unsuccessful although the formation of segregated phases of Sn and Pb has been observed in carbon-coated nanowires.[7] High temperature routes involving the arc-discharge of graphite and metal mixtures, such as Fe:Co, Fe:Ni or Ni:Y, results in the formation of SWNTs rather than alloy-filled MWNTs. Here we report, for the first time, the encapsulation of Invar in MWNTs by pyrolysing aerosols consisting of $NiCp_2/FeCp_2/C_6H_6$ mixtures in an Ar atmosphere at 800 °C.

A benzene solution containing $FeCp_2$ (Aldrich, 99%) and $NiCp_2$ (Aldrich, 98%) mixtures (atomic ratios 65:35 Fe:Ni; 5% by weight), was prepared ultrasonically during 3–5 min. The solution was transferred to the reservoir of an aerosol generator (sprayer), then nebulized by a high Ar flow rate (*ca.* 2000 sccm), and dispersed through the sprayer (nozzle diameter *ca.* 0.45 mm). The aerosol was passed through a quartz tube (2 cm i.d. and 50 cm in length) placed in a furnace (30 cm in length) fitted with a temperature-controller. The sprayer was operated for 5 min while the furnace was maintained at 800 °C. Subsequently, spraying was discontinued and the Ar flow rate reduced to 300–500 sccm in order to avoid oxidation of the products upon cooling. The product, a black powder, was scraped from the inner walls of the hot zone of the quartz tube. A detailed description of the aerosol generator is given elsewhere.[8]

SEM studies (JEOL-JSM 6300F operating at 2–5 kV) revealed the presence of flake-like material (*ca.* 1–2 mm²) consisting of arrays of aligned nanotubes (⩽200 μm in length, ⩽80 nm in diameter) similar to those reported previously (Fig. 1).[9] The material resembles a carpet of exceptionally uniform length (or height), and the purity of the material is strikingly high when compared to experiments carried out with $FeCp_2$ only. In this context, only small amounts of particles and other by-products were observed. HRTEM (JEM3000F FEG-TEM operating at 300 kV and JEOL-JEM4000 EX operating at 400 kV) images showed the presence of partly filled nanotubes, the walls of which are relatively disordered in places where there was no metal filling. The nanowires exhibit lengths ⩽500 nm and widths ⩽40 nm and were mainly found within highly crystalline carbon walls (Fig. 2). This result is in agreement with that reported by Itoh and Sinclair, who described the graphitisation of amorphous carbon layers in the presence of Ni.[10] It has also been observed that metal-filled carbon nanotubes, generated by pyrolysis, generally tend to exhibit a higher degree of graphitisation than unfilled nanotubes.[9–12]

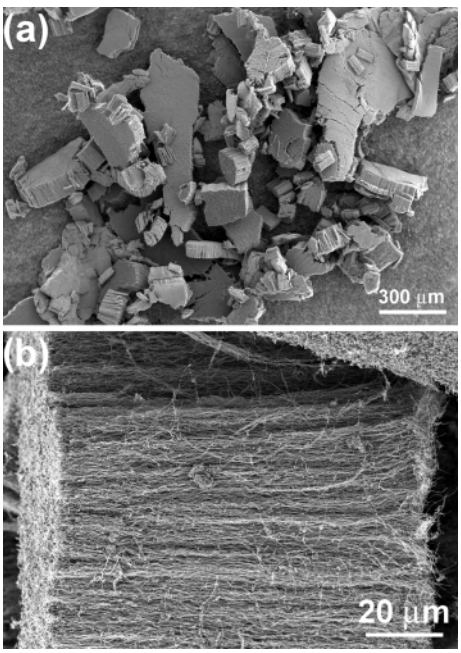

Fig. 1 (a) SEM images of aligned nanotube films (flakes) grown on the walls of the pyrolysis tube; other carbonaceous material is notably absent. (b) Higher magnification of an individual 'flake' showing the degree of alignment and that the nanotubes possess uniform diameters (< 80 nm) and lengths (< 200 μm).

† Permanent address: CEA Saclay, DRECAM-SPAM Bat. 522, 91191 Gif sur Yvette, France.

DOI: 10.1039/b100190f

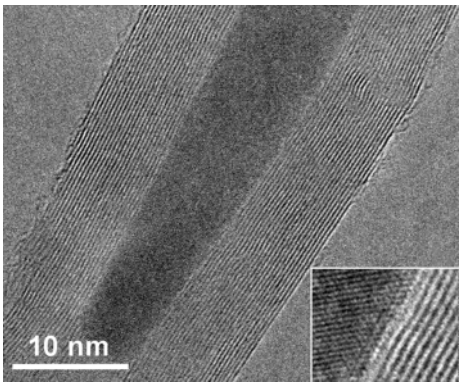

Fig. 2 HRTEM image of an Invar-filled nanotube with an inset showing the crystallinity of the filling (carbon interlayer spacing 0.34 nm).

X-Ray powder diffraction measurements (XRD, Siemens Diffraktometer D5000; Cu-Kα radiation) were carried out on the samples as well as on a commercially available Invar foil (Fe65 : Ni35, Goodfellow) for comparison. The diffraction patterns of the sample exhibit graphite peaks with a small shift of the (00l) reflections due to curvature of the concentric graphene sheets constituting the carbon nanotubes (*d*-spacing 0.34 nm). Distinct peaks for 2θ are observed at *ca.* 43.5, 50.7, 74.7 and 90.7, in agreement with those resulting from the Invar foil. They correspond to the (111), (200), (220) and (311) reflections of γ-FeNi alloys (fcc structure containing 30 atom% Ni and above) respectively. It is noteworthy that individual peaks for Fe or Ni were not observed, confirming the absence of segregated Fe or Ni domains [Fig. 3(a)]. The variation of Ni content in the fcc structure of γ-FeNi alloys induces a linear change in the lattice parameter (Vegard's Law).[13,14] Determinations of this parameter for the fcc structure of the γ-FeNi alloy present in the samples indicate an overall Ni content of *ca.* 45 ± 2 at%.

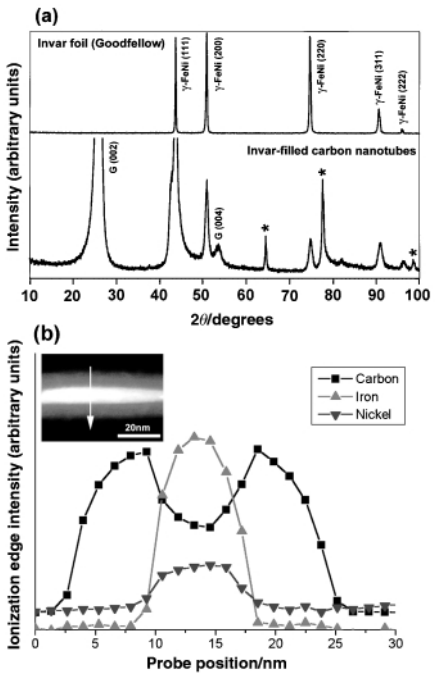

Fig. 3 (a) X-Ray powder diffraction pattern showing distinct peaks for 2θ at *ca.* 43.5, 50.7, 74.7 and 90.7, in agreement with peaks resulting from the Invar foil and corresponding to the (111), (200), (220) and (311) reflections of γ-FeNi alloys (fcc structure containing $\geqslant$30 at% Ni) respectively. (* signals belong to the XRD holder). (b) High-spatial-resolution EELS spectra profile of an Invar-filled nanotube axis (*ca.* 23 nm across) showing the relative concentrations of C, Fe and Ni. Ni and Fe are homogeneously distributed within the inner core of the carbon tube. The inset shows the high angular dark field (HADF) image of the nanowire contained within the carbon nanotube as well as the line-scan recorded during the measurement. The EELS spectra reveal that the wires contain Ni and Fe with a *ca.* 0.55±0.03 Ni/Fe ratio including the Invar composition ($Fe_{65}Ni_{35}$, Ni/Fe = 0.54).

Elemental mapping (Zeiss EM 912 Omega, operated at 120 kV) using EELS revealed that Ni and Fe are uniformly distributed within the wires. HREELS line scans along and across the fillings (carried out using a dedicated STEM VG- HB 501UX equipped with a Gatan Digi-PEELS 766) also confirmed that Ni and Fe concentrations correlate, which is consistent with alloy formation. The C and Ni–Fe concentration profiles anti-correlate, indicating that the metal is located in the nanotube core [Fig. 3(b)]. The presence of sharp features corresponding to the π^* and σ^* excitations on the energy loss near-edge structure (ELNES) of the carbon K edge at 284.5 eV indicates that the material is highly 'graphitic'. The edges at 708 and 854 eV are characteristic of Fe-L and Ni-L respectively. Quantification of representative EEL spectra reveal that the wires consist of Ni and Fe with a *ca.* 0.55 ± 0.03 Ni/Fe ratio, commensurate with the Invar composition ($Fe_{65}Ni_{35}$, Ni/Fe = 0.54).

We have demonstrated that pyrolysis of aerosols obtained from $C_6H_6/NiCp_2/FeCp_2$ mixtures generates aligned Invar-filled carbon nanotubes of high purity. It is important to note that the pyrolysis of $NiCp_2/FeCp_2$ powder mixtures or of hydrocarbons over metal powder mixtures at higher temperatures does not result in the formation of alloy nanowires because the metals tend to segregate. The generation of Invar nanowires opens up new avenues for further exploration at the nanoscale level. The magnetic and mechanical properties of these novel structures may find applications in the fabrication of magnetic storage devices and nanoscale thermostats.

We thank the EPSRC, the Royal Society (N. G. and H. W. K.), the Wolfson Foundation, the European Community Marie-Curie-Fellowship Cat. 30 (M. M.), the Alexander von Humboldt Stiftung (M. T.), CONACYT-México grants J31192U (M. T. and H. T.) and 25237-E (H. T.) and DGAPA-UNAM IN 108199 (H. T.) for financial support. We are grateful to S. Kühnemann, K. Hahn and S. Nufer for stimulating discussions and technical support.

Notes and references

1 C. E. Guillaume, *CR Acad. Sci.*, 1897, **125**, 235.
2 D. Wenschof, *Alloy Phase Diagrams*, ed. H. Baker *et al.*, American Society for Metals, Materials Park: The Society, vol. 3, 1992.
3 S. Eroglu, S. C. Zhang and G. L. Messing, *J. Mater. Res.*, 1996, **11**, 1231.
4 M. van Schilfgaarde, I. A. Abrikosov and B. Johansson, *Nature*, 1999, **400**, 46 and references therein.
5 M. Terrones, N. Grobert, W. K. Hsu, Y. Q. Zhu, W. B. Hu, H. Terrones, J. P. Hare, H. W. Kroto and D. R. M. Walton, *MRS Bull.*, 1999, **24**, 43 and references therein.
6 J. Sloan, D. M. Wright, H. G. Woo, S. Brown, A. P. E. York, K. S. Coleman, J. L. Hutchison and M. L. H. Green, *Chem. Commun.*, 1999, 699.
7 W. K. Hsu, S. Trasobares, H. Terrones, M. Terrones, N. Grobert, Y. Q. Zhu, W. Z. Li, R. Escudero, J. P. Hare, H. W. Kroto and D. R. M. Walton, *Chem. Mater.*, 1999, **11**, 1747.
8 M. Mayne, N. Grobert, M. Terrones, R. Kamalakaren, M. Rühle, H. W. Kroto and D. R. M. Walton, *Chem. Phys. Lett.*, submitted.
9 N. Grobert, W. K. Hsu, Y. Q. Zhu, J. P. Hare, H. W. Kroto, D. R. M Walton, M. Terrones, H. Terrones, P. Redlich, M. Rühle, R. Escudero and F. Morales, *Appl. Phys. Lett.*, 1999, **75**, 3363.
10 T. Itoh and R. Sinclair, *Mater. Res. Soc. Symp. Proc.*, 1994, **349**, 31.
11 N. Grobert, M. Terrones, A. J. Osborne, H. Terrones, W. K. Hsu, S. Trasobares, Y. Q. Zhu, J. P. Hare, H. W. Kroto and D. R. M. Walton, *Appl. Phys. A*, 1998, **67**, 595.
12 M. Terrones, N. Grobert, J. P. Zhang, H. Terrones, J. Olivares, W. K. Hsu, J. P. Hare, A. K. Cheetham, H. W. Kroto and D. R. M. Walton, *Chem. Phys. Lett.*, 1998, **285**, 299.
13 E. R. Jette and F. Foote, *AIME Tech. Publ.*, 1936, **670**.
14 A. J. Bradley and W. H. Taylor, *Phil. Mag.*, 1937, **23**, 545.

Gold–platinum alloy nanoparticle assembly as catalyst for methanol electrooxidation

Yongbing Lou, Mathew M. Maye, Li Han, Jin Luo and Chuan-Jian Zhong*

Department of Chemistry, State University of New York at Binghamton, Binghamton, New York 13902, USA. E-mail: cjzhong@binghamton.edu

Received (in Columbia, MO, USA) 24th October 2000, Accepted 18th January 2001
First published as an Advance Article on the web 19th February 2001

This paper describes preliminary findings of a thiolate-capped gold–platinum alloy nanoparticle assembly (metallic core and organic shell) as a novel catalyst for electrooxidation of methanol.

The study of catalytic oxidation of methanol and carbon monoxide has broad technological applications, including fuel-cell technology, purification of air in gas products and in long duration space travel, and conversion in automobile exhaust systems.[1–3] The search for highly effective catalysts and detailed mechanistic understanding[4–7] has spanned to the exploration of nanometer-size catalysts.[1–3] Two critical issues facing the exploration of nanosized catalysts for methanol oxidation are however the propensity of poisoning at traditional platinum group catalysts by adsorbed CO-like species and the tendency of nanoparticle aggregation. To address these issues, we have recently reported a proof-of-concept demonstration of electrocatalytic oxidation of CO at core–shell nanostructured alkyl thiolate-capped gold nanoparticles,[8] a new expansion of recent interest in exploring nanosized bare gold catalysts.[4,5] We report herein preliminary findings of an investigation of thiolate-encapsulated gold–platinum (Au–Pt) alloy nanoparticles as catalysts for methanol electrooxidation (Scheme 1). In addition to aggregation-resistant and poison-resistant properties arising from shell encapsulation and networking, an important attribute is the bimetallic core composition with different catalytic functions: methanol oxidation at Pt-sites and CO oxidation at Au-sites. Whether such encapsulated alloyed nanosites are catalytically active under the encapsulation is a critical question. The basic understanding will also be useful to much of the recent interest in Pt–Ru based bimetallic catalysts[1] and other related systems such as polypyrrole-supported[9,10] and dendrimer-encapsulated[11] Pt nanoparticles.

The catalyst preparation involved Schiffrin's two-phase synthesis of thiolate-capped gold and alloy nanoparticles.[12,13] Fig. 1 shows a transmission electron microscopic (TEM) image of decanethiolate (DT) encapsulated Au–Pt nanoparticles which were synthesized from a 5 : 1 feed ratio (Au : Pt) of $HAuCl_4$ and K_2PtCl_6. The average core size determined was *ca.* 2.5 ± 0.4 nm. The UV–VIS spectrum of the nanoparticles showed a subtle difference of surface plasmon resonance band intensity from Au nanoparticles (*ca.* 2 nm) synthesized under similar conditions, consistent with the presence of Pt in the Au nanoparticles.[13] On the basis of previous XPS data that showed a 1 : 0.3 ratio of Au : Pt in the nanoparticles synthesized from a 1 : 1 feed ratio,[13] the Pt content estimated for our alloy nanoparticles was *ca.* 5%. Using 1,9-nonanedithiol (NDT) as the crosslinking agent, the nanoparticles were assembled on a glassy carbon (GC) electrode surface as a shell-linked particle ensemble *via* an exchange–crosslinking–precipitation route.[14] Briefly, a GC electrode was immersed into a hexane solution of DT-capped nanoparticles (30 mM) and NDT (50 mM) for *ca.* 24 h. The NDT–DT exchange reaction was followed by crosslinking, leading to nucleation and growth of a nanoparticle thin film on GC, *i.e.* NDT–$(Au–Pt)_{2.5\text{-nm}}$. The thickness of the film was controlled by immersion time. A typical film had *ca.* 8 equivalent number of particle layers, estimated from quartz-crystal microbalance measurements.[14] Electrochemical measurements were performed in a conventional three-electrode cell with Ag/AgCl (saturated KCl) as reference electrode. The electrolyte solution was purged with argon before measurements.

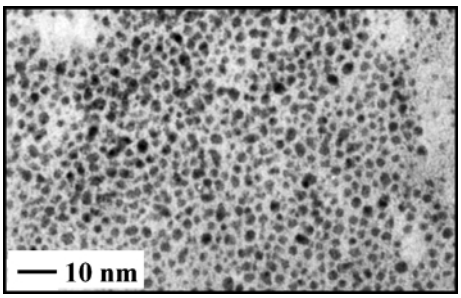

Fig. 1 TEM micrograph of DT-capped Au–Pt (5 : 1) nanoparticles.

As recently demonstrated for the case of CO oxidation,[8] the NDT–$(Au–Pt)_{2\text{-nm}}$/GC electrode was initially activated in the presence of methanol by potential polarization to *ca.* 0.8 V. Fig. 2 shows a typical set of cyclic voltammetric curves [(b)–(e)] at such an activated electrode in an alkaline solution of methanol (99.99%) purged with argon. Curve (a) is the result obtained after transferring the electrode to methanol-free electrolyte. In the absence of methanol (a), the voltammetric curve displays a small and broad oxidation wave at +300 mV extending to the positive potential limit, and a sharp reduction wave at +120 mV. These two waves are attributed to the formation and reduction of surface Au oxide (AuO_x)[8] on the nanocrystals. Contribution from Pt oxide should be minimal because its redox potential is more positive than that of Au oxide and the alloyed Pt is a very small fraction (*ca.* 5%). The shell encapsulation may become partially open as a result of either surface oxide formation or a change in shell packing due to possible thiolate desorption or reorganization. In the presence of methanol of different concentrations [(b)–(e)], two voltammetric features are remarkable. First, a large anodic wave is evident at +300 mV. The anodic peak current (i_{pa}) increases with increasing methanol concentration, exhibiting a linear relationship (Fig. 2, insert). The peak potential closely matches the potential for Au oxide formation, suggesting the participation of Au oxide in the overall catalytic oxidation mechanism. An integration of the

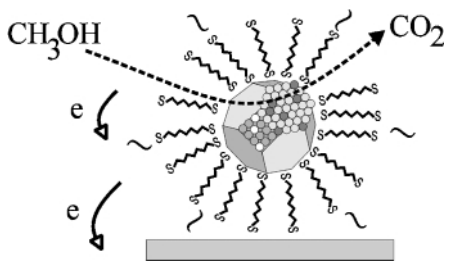

Scheme 1 A schematic illustration of catalytic oxidation of methanol at a thiolate-capped core–shell nanoparticle catalyst.

DOI: 10.1039/b008669j

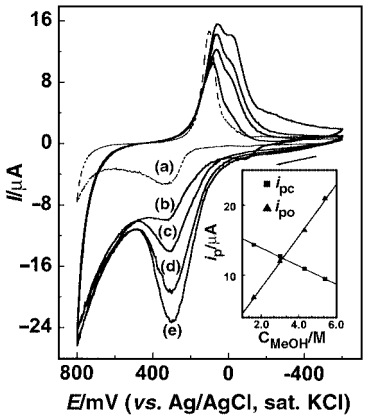

Fig. 2 Cyclic voltammetric curves for an activated NDT–(Au–Pt)$_{2.5\text{-nm}}$/GC electrode in an electrolyte solution of 0.5 M KOH with methanol concentration of 0 (a), 1.6 M (b), 3.0 M (c), 4.3 M (d) and 5.4 M (e). Geometric electrode area: 0.07 cm^2. Scan rate: 50 mV s^{-1}.

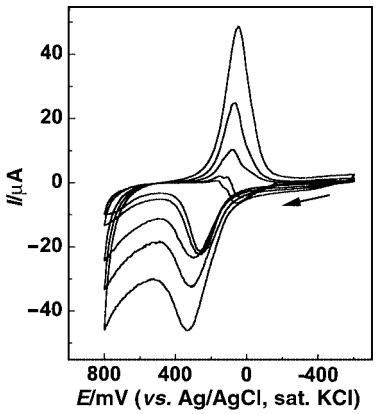

Fig. 3 Scan rate dependence of cyclic voltammetric curves for an activated NDT–(Au–Pt)$_{2.5\text{-nm}}$/GC electrode in a solution of 0.5 M KOH + 5.4 M methanol. Geometric electrode area: 0.07 cm^2. Scan rate: 10, 20, 50, 100 and 200 mV s^{-1}. Both anodic peak and cathodic currents increase with increasing scan rate.

charge from the cathodic wave translates to *ca.* 9×10^{-9} mol cm^{-2} of the amount of reactive Au. Second, in contrast to the trend for the anodic wave, the peak current for the cathodic wave (i_{pc}) decreases with increasing methanol concentration, which also exhibits a linear relationship (Fig. 2 insert). These two features are the first set of evidence demonstrating that methanol is oxidized at the nanostructured catalyst. The opposite trend between the oxidation and reduction peak currents as a function of methanol concentration is suggestive of a catalytic mediation mechanism likely by surface Au oxide species.[6–8]

There is another distinctive feature for the data in comparison with voltammetric characteristics reported for bulk Pt. No oxidation wave is detected in the negative-going sweep of the above data, which is usually observed for Pt-based catalysts due to methanol oxidation at partially reduced surface oxide. Although such an oxidation wave becomes evident at *ca.* −100 mV for a slower scan rate for NDT–(Au–Pt)$_{2.5\text{-nm}}$ (Fig. 3), the relative magnitude of the wave is much smaller. We also note that the overall potential of methanol oxidation is *ca.* 200 mV more positive for the NDT–(Au–Pt)$_{2.5\text{-nm}}$ than Pt. This difference is presumably due to a conductivity effect of the film.[14]

Fig. 3 shows the voltammetric dependence on scan rate (v) as a further piece of evidence for the electrocatalytic mediation of the catalyst. Both i_{pa} and i_{pc} increase with increasing v. A close examination reveals that the i_{pa} *vs.* $v^{1/2}$ relationship is approximately linear for $v > 20$ mV s^{-1}, indicative of an diffusion-controlled process for methanol oxidation. Remarkably, the ratio of i_{pa}:i_{pc} decreases with increasing v, which is characteristic of an surface redox-mediated catalytic oxidation process. At $v < 20$ mV s^{-1}, the reduction wave basically disappears whereas a small anodic wave is evident on the negative-going sweep. This feature resembles those observed for electrooxidation of methanol at a Pt-based surface[3] and of CO at core–shell Au nanoparticle assembies.[8] Overall, the data further support an electrocatalytic mechanism by which the oxidation of methanol is mediated by surface oxide redox species.[6]

Other preliminary data are also supportive of the above assessment. An insignificant change of C–H stretching bands of alkyl thiolates in IR reflection spectroscopic data before and after the catalytic activation supports the presence of shell encapsulation. Voltammetric data with a similar catalytic activity but different characteristics have also been noticed using thiolate-capped Au nanoparticles, which is under further investigation. Moreover, the catalytic activity is remarkably stable against repetitive cycling (at least 2 h at 10–200 mV s^{-1}) in the indicated potential region. We believe that the catalytic oxidation proceeds predominantly at surface Au oxide sites within the core–shell nanoparticle assembly. As reviewed recently by Burke and Nugent[6] for gold-based catalysis, oxygen transfer reactions have been considered using an incipient hydrous oxide/adatom mediator model. In a few recent examples, metal oxides are used as supports for bare Au nanoparticle catalysts.[5]

The result is, to our knowledge, the first example of electrocatalytic oxidation of methanol at core–shell nanostructured Au–Pt nanoparticles upon catalytic activation. A systematic manipulation of the bimetallic core composition is under way, including further investigations using nanoparticle size and shape processing methods,[15] IR reflection spectroscopy and atomic force microscopy to gain insights into effects of nanostructured voids, nanocrystal corners or edges, surface activation and segregation.

The ACS Petroleum Research Fund is acknowledged for support of this research.

Notes and references

1 S. Wasmus and A. Kuever, *J. Electroanal. Chem.*, 1999, **461**, 14.
2 *Electrocatalysis, Frontiers in Electrochemistry*, ed. J. Lipkowski and P. N. Jr. Ross, VCH, New York, 1997, vol. 5.
3 T. D. Jarvi, S. Sriramulu and E. M. Stuve, *J. Phys. Chem. B.*, 1998, **101**, 3649.
4 M. Valden, X. Lai and D. W. Goodman, *Science*, 1998, **281**, 1647.
5 M. Haruta, *Catal. Today*, 1997, **36**, 153.
6 L. D. Burke and P. F. Nugent, *Gold Bull.*, 1998, **31**, 39.
7 G. C. Bond, *Catal. Rev.*, 1999, **41**, 319.
8 M. M. Maye, Y. Lou and C. J. Zhong, *Langmuir*, 2000, **16**, 7520.
9 M. Hepel, *J. Electrochem. Soc.*, 1998, **145**, 124.
10 P. J. Kulesza, M. Matczak, A. Wolkiewicz, B. Crzybowska, M. Galkowski, M. A. Malik and A. Wieckowski, *Electrochim. Acta*, 1999, **44**, 2131.
11 M. Q. Zhao and R. M. Crooks, *Adv. Mater.*, 1999, **11**, 217.
12 M. Brust, M. Walker, D. Bethell, D. J. Schiffrin and R. Whyman, *J. Chem. Soc., Chem. Commun.*, 1994, 801.
13 M. J. Hostetler, C. J. Zhong, B. K. H. Yen, J. Anderegg, S. M. Gross, N. D. Evans, M. D. Porter and R. W. Murray, *J. Am. Chem. Soc.*, 1998, **120**, 9396.
14 F. L. Leibowitz, W. X. Zheng, M. M. Maye and C. J. Zhong, *Anal. Chem.*, 1999, **71**, 5076.
15 M. M. Maye, W. X. Zheng, F. L. Leibowitz, N. K. Ly and C. J. Zhong, *Langmuir*, 2000, **16**, 490.

Synthesis of 7-methoxybenzolactam-V8 using a diastereoselective Strecker synthesis

Sukumar Sakamuri and Alan P. Kozikowski*

Drug Discovery Program, Georgetown University Medical Center, 3900 Reservoir Road, NW, Washington, DC 20007-2197, USA. E-mail: kozikowa@giccs.georgetown.edu; Fax: +1-202-687-5065, Tel: +1-202-687-0686

Received (in Corvallis, OR, USA) 3rd November 2000, Accepted 19th January 2001
First published as an Advance Article on the web 19th February 2001

7-Methoxybenzolactam-V8 (4) was synthesized using a diastereoselective Strecker reaction as the key step employing an *ortho*-substituted phenylacetaldehyde and (*R*)-phenylglycinol as the chiral auxiliary.

Protein kinase C (PKC) consists of a growing family of closely related isozymes that mediate a wide range of cellular signal transduction processes.[1] Compounds that are able to selectively modulate the individual PKC isozymes can serve as valuable research tools in the elucidation of their physiological roles. Additionally, such compounds hold promise in the development of novel therapeutics for the treatment of human diseases, such as cancer and Alzheimer's dementia. However, very few isozyme-selective activators have been reported to date. The teleocidins (*e.g.* indolactam V, **1**) are potent PKC activators,

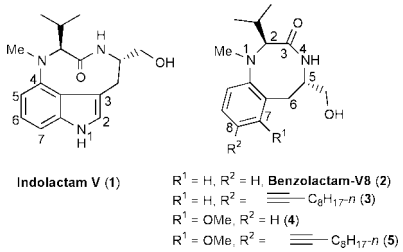

however, they show little selectivity.[2] Endo's group and ours have reported[3] that the benzolactam-V8 derivative **3**, a mimic of the twist-like conformation of indolactam V, is a potent activator of PKC. Recently, our group has shown that introduction of a methoxy substituent at the C7-position of benzolactam-V8 leads to a compound (**5**) that retains potency at PKCα, PKCδ and PKCε.[4] The total synthesis of benzolactam-V8 analogs depends mainly on the effective construction of the 8-membered lactam ring, which in turn depends on an efficient synthesis of a suitably substituted phenylalanine moiety. An improved synthesis of 7-methoxybenzolactam-V8 (**4**) would permit access to further analogs by making use of the heteroatom at the 7-position. We have recently developed the first synthesis of 7-methoxybenzolactam-V8,[4] which makes use of a catalytic asymmetric alkylation. The poor selectivity in this step induced us to explore an alternative approach. In the present communication, we describe a diastereoselective Strecker reaction for the synthesis of the required substituted phenylalanine which after a series of further reactions leads to the title compound **4**.

Our synthetic sequence began with the introduction of an allyl group in the ortho position to the hydroxy group using the Claisen rearrangement. Thus, 3-hydroxyacetanilide (**6**) was transformed into its allyl ether **7** using allyl bromide and potassium carbonate in refluxing acetone in 88% yield (Scheme 1). Compound **7** was subjected to the Claisen rearrangement in refluxing dimethylaniline for 6 h to give a mixture of products **8** and **9** in a 1 : 1 ratio.[5] The required regioisomer **8** was isolated by fractional crystallization and protected as its methyl ether in 82% yield. The *N*-acetyl group in compound **10** was unstable to the conditions of a subsequent nitrile methanolysis step, resulting in the formation of an undesired six-membered lactam.[6] We therefore masked the amine as a 2,5-dimethylpyrrole which can be easily cleaved under mild conditions but is stable to the conditions of acidic nitrile methanolysis. Accordingly, compound **10** was deprotected to give aniline **11**, which on treatment with acetonylacetone in toluene utilizing a Dean–Stark trap for azeotropic water removal gave compound **12** in 72% yield.[7] Compound **12** was converted to the aldehyde in a two step sequence. First, compound **12** on treatment with osmium tetroxide in acetone in the presence of NMO at rt gave diol **13** in 74% yield. Compound **13** was oxidized to the aldehyde **14** using sodium metaperiodate in a 1 : 1 mixture of ^{t}BuOH and H_2O at rt in 69% yield. Compound **14** was now subjected to the Strecker synthesis using (*R*)-phenylglycinol.[8] It is important to note that previously Chakraborty *et al.*[8] reported

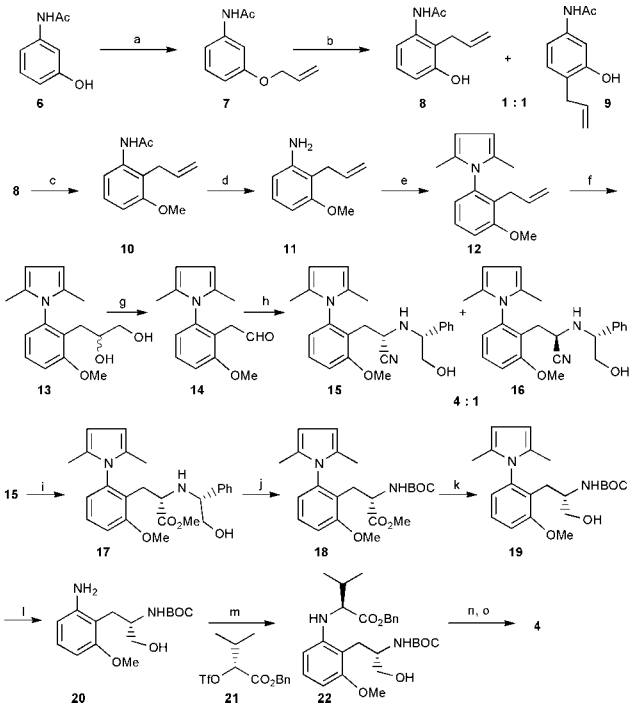

Scheme 1 *Reagents and conditions*: (a) K_2CO_3, allyl bromide, acetone, reflux, 88%; (b) $PhNMe_2$, reflux, 6 h, 84%; (c) K_2CO_3, MeI, acetone, reflux, 82%; (d) 7% HCl, reflux, 2 h, 81%; (e) acetonylacetone, toluene, reflux, 24 h, 72%; (f) OsO_4, NMO, rt, acetone, 74%; (g) $NaIO_4$, t-BuOH–H_2O, rt, 69%; (h) i, (*R*)-phenylglycinol, $CHCl_3$, ii, Me_3SiCN, 0 °C–rt, 10 h, iii, TBAF, 66% for three steps; (i) HCl in ether, MeOH, 0 °C–rt, 48 h, 81% (j) i, $Pb(OAc)_4$, CH_2Cl_2–MeOH (2 : 1), 15 min; ii, 20% $Pd(OH)_2$/C, EtOH, 50 psi of H_2, overnight; iii, BOC_2O, Et_3N, THF, rt, 44% for three steps; (k) $LiBH_4$, THF, 0 °C–rt, 8 h, 96%; (l) NH_2OH·HCl, Et_3N, *i*-PrOH–H_2O, reflux, 24 h, 81%; (m) 2,6-lutidine, 1,2-dichloroethane, 87%; (n) H_2, Pd/C, EtOH, quantitative; (o) i, *N*-hydroxysuccinimide–DCC, CH_2Cl_2, ii, trifluoroacetic acid, then $NaHCO_3$, EtOAc, 82%; iii, HCHO, $NaCNBH_3$, AcOH, CH_3CN, reflux, 87%.

DOI: 10.1039/b008970m

that the Strecker reaction of phenylacetaldehyde with (*R*)-phenylglycinol gave a 1 : 1 ratio of isomers. The poor selectivity was attributed to steric factors. Compound **14** on reaction with (*R*)-phenylglycinol in chloroform at rt overnight gave the imine which on reaction with Me_3SiCN at rt for 10 h followed by treatment with tetrabutylammonium fluoride gave the amino nitriles **15** and **16** in a 4 : 1 ratio in 66% yield over the three steps. The amino nitriles **15** and **16** were easily separated by column chromatography. The structure of the isomer **15** was confirmed by X-ray crystallography. This compound was subjected to acidic hydrolysis to afford the ester **17** in 81% yield based on recovered starting material. No cyclization product was formed in the hydrolysis reaction, thus supporting our choice of protecting group. Oxidative removal of the phenylglycinol moiety was carried out with lead tetraacetate in CH_2Cl_2–MeOH to give a Schiff's base, which on catalytic hydrogenation over $Pd(OH)_2$/C gave the free amine. The amine was isolated as the BOC-protected intermediate **18**, and the overall yield for the three steps was 44%.

With the substituted phenylalanine fragment in hand, we now needed to add the valine fragment. Compound **18** was reduced to alcohol **19** using $LiBH_4$ in THF in near quantitative yield. The aromatic amino group was unmasked in good yield by refluxing in a solvent mixture of ^iPrOH–H_2O with hydroxylamine hydrochloride and triethylamine. The aniline **20** was reacted with the D-valine derived triflate **21**[9] to give compound **22** in 87% yield. Compound **22** on hydrogenation gave the carboxylic acid in quantitative yield, which was converted to the eight-membered lactam using the active ester method as reported previously.[3b] *N*-Methylation using HCHO–$NaCNBH_3$–HOAc gave 7-methoxybenzolactam **4** in 87% yield.[10]

In conclusion, we report an improved synthesis of 7-methoxybenzolactam-V8 making use of a diastereoselective Strecker synthesis. This compound may serve as an intermediate in the preparation of a variety of C7-substituted benzolactam analogs, which may exhibit better isozyme selectivity.

We are indebted to the National Institutes of Health for support of this work (CA 79601).

Notes and references

1 (*a*) Y. Nishizuka, *Science*, 1992, **258**, 607; (*b*) Y. Nishizuka, *Nature*, 1988, **334**, 661; (*c*) S. Bhagavan, D. Ibarreta, D. Ma, A. P. Kozikowski and R. Etcheberrigaray, *Neurobiol. Disease*, 1998, **5**, 177.

2 (*a*) Y. Endo, K. Shudo and T. Okamoto, *Chem. Pharm. Bull.*, 1982, **30**, 3457; (*b*) Y. Endo, K. Shudo, K. Furuhata, H. Ogura, S. Sakai, N. Aimi, Y. Hitotsuyanagi and Y. Koyama, *Chem. Pharm. Bull.*, 1984, **32**, 358; (*c*) K. Irie, T. Isaka, Y. Iwata, Y. Yanai, Y. Nakamura, F. Koizumi, H. Ohigashi, P. A. Wender, Y. Satomi and H. Nishino, *J. Am. Chem. Soc.*, 1996, **118**, 10733.

3 (*a*) Y. Endo, M. Ohno, M. Hirano, A. Itai and K. Shudo, *J. Am. Chem. Soc.*, 1996, **118**, 1841; (*b*) A. P. Kozikowski, S. Wang, D. Ma, J. Yao, S. Ahmad, R. I. Glazer, K. Bogi, P. Acs, S. Modarres, N. E. Lewin and P. M. Blumberg, *J. Med. Chem.*, 1997, **40**, 1316.

4 D. Ma, T. Zhang, G. Wang, A. P. Kozikowski, N. E. Lewin and P. M. Blumberg, *Bioorg. Med. Chem. Lett.*, 2001, **11**, 99.

5 (*a*) *Chem. Abstr.*, 1955, **49**, 3880; (*b*) Z. Budesinsky and E. Rockova, *Chem. Listy*, 1954, **48**, 427.

6 Compound **10** after a sequence of reactions as reported in Scheme 1 gave compound **A**, which on acid hydrolysis gave lactam **B**.

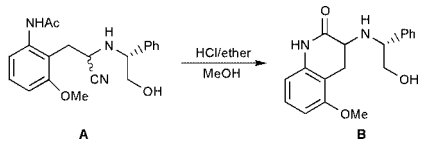

A B

7 J. E. Macor, B. L. Chenard and R. J. Post, *J. Org. Chem.*, 1994, **59**, 7496.

8 T. K. Chakraborty, A. Hussain and G. V. Reddy, *Tetrahedron*, 1995, **51**, 9179.

9 T. P. Kogan, T. C. Somers and M. C. Venuti, *Tetrahedron*, 1990, **46**, 6623.

10 Selected data for compound **4**: $[\alpha]_D^{22}$ − 262° (*c* 0.6, $CHCl_3$), lit[4]: $[\alpha]_D^{22}$ − 275° (*c* 0.82, $CHCl_3$); ^1H NMR (300 MHz, $CDCl_3$) δ 7.12 (1H, t, *J* = 8.3 Hz), 6.65 (1H, d, *J* = 8.0 Hz), 6.61 (1H, br s), 6.49 (1H, d, *J* = 8.0 Hz), 4.36 (1H, s), 3.80 (3H, s), 3.71 (1H, dd, *J* = 10.9, 4.2 Hz), 3.57 (1H, d, *J* = 8.5 Hz), 3.50 (1H, d, *J* = 9.3 Hz), 3.24 (1H, d, *J* = 17.5 Hz), 2.80 (3H, s), 2.76–2.64 (2H, m), 2.45–2.38 (1H, m), 1.04 (3H, d, *J* = 6.3 Hz), 0.83 (3H, d, *J* = 6.9 Hz); ^{13}C NMR ($CDCl_3$) δ 19.7, 20.7, 27.8, 28.2, 34.9, 54.2, 55.6, 66.4, 69.7, 103.4, 112.3, 118.7, 127.3, 157.9, 173.9.

Solvothermal synthesis of $[Ni(C_4H_{13}N_3)_2]_2Sb_4S_8$: the first compound with a cyclic $[Sb_4S_8]^{4-}$ anion

Wolfgang Bensch,* Christian Näther and Ralph Stähler

Institut für Anorganische Chemie, Universität Kiel, Olshausenstr. 40, D-24098-Kiel, Germany. E-mail: wbensch@ac.uni-kiel.de

Received (in Cambridge, UK) 29th November 2000, Accepted 30th January 2001
First published as an Advance Article on the web 19th February 2001

Under mild hydrothermal conditions the novel thioantimonate(III) $[Ni(C_4H_{13}N_3)_2]_2Sb_4S_8$ was synthesised using elemental nickel, antimony and sulfur; the structure is composed of cyclic isolated $[Sb_4S_8]^{4-}$ anions and $[Ni(C_4H_{13}N_3)_2]^{2+}$ cations.

Open framework structures based on interconnected chalcogenometallates are of great interest as possible 'zeolite' similar phases, for which highly interesting properties could be expected. Condensation of maingroup-thioanions in the presence of large organic cations[1–3] acting as structure directing agents was achieved under solvothermal conditions. The incorporation of transition metals (tm) into the thiometallate network should lead to new connections and to changed physical properties. Our main goals are the investigation of the synthetic conditions necessary to connect tmS_x fragments with main group thiometallates and to study the influence of the 'template' on the dimensionality of the products. Thioantimonates(III) exhibit a variable coordination behaviour caused by the stereochemically active lone pair.[4–6] However, until now large isolated Sb_xS_y anions were observed in only very few compounds. Recently, we and other groups reported the first examples of transition metal containing thioantimonates(III).[7,8] During our continuing work in this field the new thioantimonate(III), $[Ni(DETA)_2]_2Sb_4S_8$† [DETA = diethylenetriamine], containing the new and unusual isolated ring anion $[Sb_4S_8]^{4-}$ was obtained. The present contribution reports the synthesis and crystal structure of this new compound.

In the crystal structure of $[Ni(DETA)_2]_2Sb_4S_8$‡ two crystallographically independent $[Sb_4S_8]^{4-}$ ring anions [Fig. 1(a) and (b)] and two crystallographically independent $[Ni(DETA)_2]^{2+}$ cations are found. Four pyramidal SbS_3 units sharing common corners build a Sb_4S_4 hetero ring. Each Sb atom is bounded to a terminal S atom thus forming the final $[Sb_4S_8]^{4-}$ anion. The cyclo-octathiotetraantimonate anion belongs to the class of the medium-sized rings that preferably adopt the bent flexible chair conformation. Charge balancing is achieved by the two isolated $[Ni(DETA)_2]^{2+}$ cations.

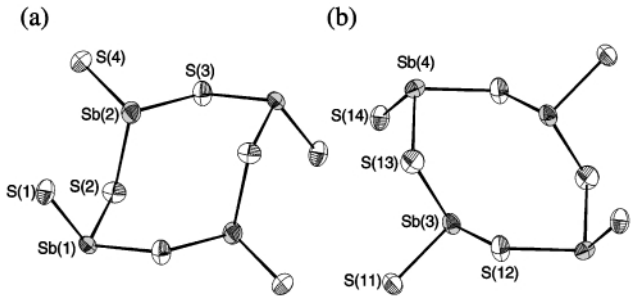

Fig. 1 (a) and (b): The two $[Sb_4S_8]^{4-}$ anions in $[Ni(DETA)_2]_2Sb_4S_8$ with labelling and displacement ellipsoids drawn at the 50% level. Selected bond lengths (Å) and angles (°): Sb(1)–S(1) 2.337(2), Sb(1)–S(2) 2.429(2), Sb(1)–S(3) 2.453(2), Sb(2)–S(4) 2.315(3), Sb(2)–S(3) 2.471(2), Sb(3)–S(11) 2.328(2), Sb(3)–S(13) 2.492(2), Sb(3)–S(12) 2.497(2), Sb(4)–S(14) 2.326(2), Sb(4)–S(13) 2.426(2); S(1)–Sb(1)–S(2) 104.32(7), S(2)–Sb(1)–S(3) 101.62(7), Sb(1)–S(3)–Sb(2) 110.88(7), S(11)–Sb(2)–S(12) 101.48(7), S(14)–Sb(4)–S(13) 100.38(8), Sb(4)–S(13)–Sb(3) 102.60(8).

The Sb–S distances within the Sb_4S_4 rings are between 2.426(2) and 2.497(2) Å and the S–Sb–S angles vary from 87.92(7) to 107.53(8)°, both being in good agreement with data found in the literature.[9] As expected, the terminal Sb-S distances [Sb(1)–S(1), Sb(2)–S(4), Sb(3)–S(11) and Sb(4)–S(14)] are shorter ranging from 2.315(3) to 2.337(2) Å. They are significantly shorter than the Sb–μ_2-S links [Sb(1)–S(2), Sb(2)–S(2), Sb(2)–S(3), Sb(3)–S(12), Sb(3)–S(13), Sb(4)–S(13)], which are often observed in literature.[10] The pertinent angles vary between 93.90(9) and 104.32(7)°. If the lone pair of Sb(III) is considered, the coordination of the SbS_3 pyramids can be viewed as distorted ψ-SbS_3 tetrahedra.[11] The two independent $[Sb_4S_8]^{4-}$ anions have a similar geometry. The Sb_4S_8 rings are stacked onto each other forming rods parallel to the *a*-axis (Fig. 2). We note that the shortest intramolecular Sb–S contacts are above 3.9 Å and no intermolecular Sb–S separations shorter than 4 Å are observed.

The Ni^{2+} cations are in a distorted octahedral environment of six nitrogen atoms of two DETA ligands. The Ni–N distances vary between 2.080(8) and 2.193(6) Å and are in the normal range.[12] The angles range from 78.0(3) to 174.8(3)°. In one cation the DETA ligands take up an u-facial (Ni1) and in the second a *mer* geometry.[20]

The three-dimensional arrangement of cations and anions (Fig. 2) is achieved by N–H···S close contacts. Every anion shows seven such contacts with distances between 2.513 and 2.837 Å and angles N–H···S ranging from 144.15 to 175.53°. The H atoms of $[Ni(1)(DETA)_2]^{2+}$ are involved in eight and those of the second complex in six S···H contacts. It is well known that S···H hydrogen bond interactions are weak and a definite decision as to whether genuine hydrogen bonding occurs cannot be drawn alone on the basis of crystal structure determination. Nevertheless, the distinct differences of intermolecular cation–anion interactions may be responsible for the above mentioned differences in the conformations of the anions and cations. Raman spectra of pure DETA and of the title

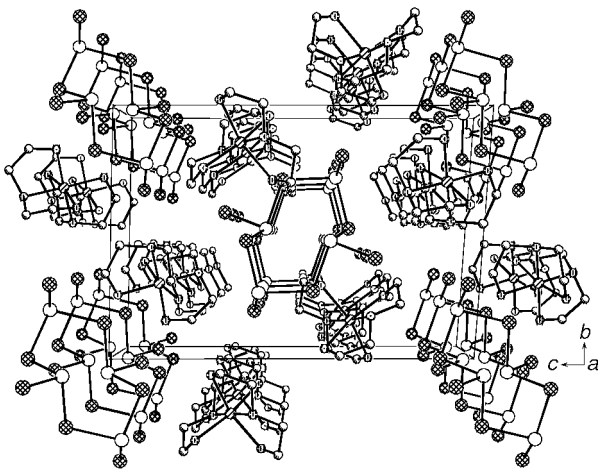

Fig. 2 Crystal structure of $[Ni(DETA)_2]_2Sb_4S_8$ with view along the *a*-axis (hydrogen atoms omitted for clarity).

DOI: 10.1039/b009583o

compound were recorded to monitor the differences in the νNH_2 and δNH_2 regions. For the free ligand the νNH_2 resonances are between about 3100 and 3400 cm^{-1} with a pronounced peak at 3297 cm^{-1}. The δNH_2 line is located at 1601 cm^{-1}. In the title compound the whole region of νNH_2 modes is broader extending from *ca*. 3030 to 3410 cm^{-1} with a peak at 3232 cm^{-1}. The δNH_2 line is slightly shifted to 1594 cm^{-1}. We note that all modes of the $[Ni(DETA)_2]^{2+}$ complexes are in good agreement with data published in the literature.[20–25] The shift to lower wavenumbers as well as the broadening may be caused by both the N–Ni bonding interactions and possible S···H–N hydrogen bonds.

As can be seen in Fig. 3 the material decomposes in two steps with individual weight changes of 31.1 and 2.7% giving a total weight loss of 33.8% which roughly corresponds to the emission of the four DETA ligands (Δm_{theo} = 32.4%).§ Decomposition starts at T_{onset} = 222 °C and is accompanied by two endothermic peaks at T_p = 260 and 319 °C. The first endothermic signal exhibits a complex shape with two shoulders located at T_p = 251 and 273 °C. In further experiments decomposition of the educt was stopped at 300 and 350 °C. The residues were characterised by CHN analysis, X-ray powder diffraction (XPD), energy dispersive X-ray analysis (EDX) and IR spectroscopy. In the XPD pattern of the grey residue [C, 1.8; H, 0.25; N, 1.15; EDX (atom%): S, 48(1); Sb, 32.2(1.4); Ni, 19.7(2.7)] obtained after the 300 °C treatment, NiS, Sb_2S_3, NiSbS and a small amount of an unknown fourth phase were identified. In the IR spectrum no C–H, C–N, C–C or N–H vibrations could be detected. From the elemental analyses it can be assumed that not only DETA is emitted but also S, and a small amount of C, H, and N remain in the residue. In the XPD pattern of the dark grey sample obtained after heating to 350 °C (C, 1.6%; H, 0%; N, 0.72%; EDX(atom%): S, 47.8(8); Sb, 31.7(1.0); Ni, 20.5(1.9)%] the reflections of the unknown phase disappeared and only NiS, Sb_2S_3 and NiSbS could be identified. The small weight loss between 300 and 350 °C of *ca*. 2.7% may be attributed to the decomposition of the unknown phase accompanied by the emission of C, H and N as well as of sulfur.

The endothermic event at T_p = 556 °C agrees well with the melting point of Sb_2S_3 (literature value: T_m = 550 °C). In the grey reaction product the two phases Sb_2S_3 and NiS could be identified.

In conclusion, we note that the stabilisation of the high negatively charged $[Sb_4S_8]^{4-}$ anion may be achieved by an extended hydrogen bond network as well as by the shape and size of the counterion. There is no simple relationship between cation size and shape and the dimensionality of the anionic thioantimonate network. In addition, hydrothermal crystallisations are multicomponent heterogeneous reactions that are not well understood and we are far from being able to predict structures or physical properties of the products. The successful synthesis and characterisation of new thioantimonates(III) may provide the information that is necessary to lead to more rational syntheses of such compounds.

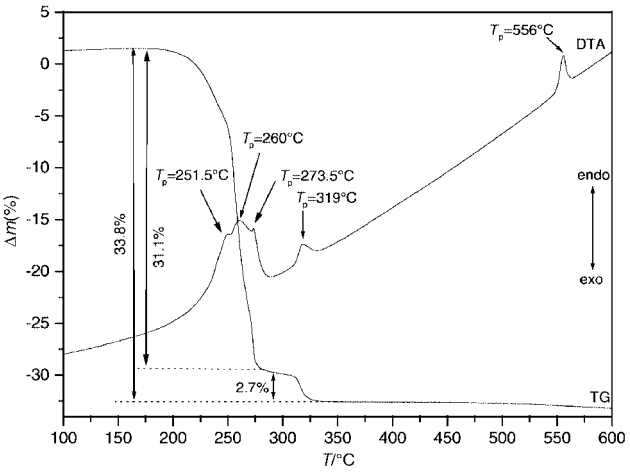

Fig. 3 DTA and TG curves for $[Ni(DETA)_2]_2Sb_4S_8$.

Notes and references

† *Synthesis:* dark yellow platy crystals of $[Ni(DETA)_2]_2Sb_4S_8$ were synthesised from elemental Ni (58.69 mg, 1 mmol), Sb (121.76 mg, 1 mmol) and S (96.19 mg, 3 mmol) in a solution of 100% diethylenetriamine (3 mL, 27 mmol). The mixture was heated to 145 °C for 11 days in a Teflon-lined steel autoclave (*ca*. 20 mL) under autogenous pressure. The crystalline product was filtered off and washed with acetone and stored under vacuum. The yield based on Ni is *ca*. 40%. C, H, N analysis: found: N, 12.0; C, 14.95; H, 4.1; calc.: N, 13.2; C, 15.09; H, 4.12%. EDX analysis (%): found: Ni, 12.7(3); Sb, 29.3(1.4); S, 58(1); calc. Ni, 14.3; Sb, 28.6; S, 57.

‡ *Crystal structure determination*: $[Ni(DETA)_2]_2Sb_4S_8$, M = 1273.6, triclinic, space group $P\bar{1}$ (no. 2), a = 9.0249(6), b = 12.7607(2), c = 18.037(2) Å, α = 92.299(9), β = 91.058(8), γ = 105.735(9)°, U = 1996.6(3) $Å^3$, T = 293 K, Z = 2, Imaging Plate Diffraction System (IPDS) (Mo-Kα; λ = 71.073 pm), μ(Mo-Kα) = 4.04 mm^{-1}, 7843 reflections collected in the range $3 \leqslant 2\theta \leqslant 51.87°$, 3873 unique reflections. Face-indexed absorption correction; structure solution with SHELXS-97: structure refinement against F^2 using SHELXL-97. 380 parameters, $R1$ for 3182 reflections [$F_o > 4\sigma(F_o)$] = 0.0313, $wR2$ for all 3873 data = 0.0814, GOF 1.049. Residual electron density: 0.73/−0.51 e $Å^{-3}$. The non-hydrogen atoms were refined anisotropically. The hydrogen atoms were positioned with idealised geometry and refined with individual isotropic displacement parameters using the riding model. CCDC 154455. See http://www.rsc.org/suppdata/cc/b0/b009583o/ for crystallographic data in .cif or other electronic format.

§ The thermal stability of the compound was investigated using DTA/TG measurements. The sample was heated under argon atmosphere in a Al_2O_3 crucible (heating rate: 3 °C min^{-1}, temperature range: 25–600 °C, mass: 48.6 mg. EDX analysis: EDAX unit attached to an XL 30 ESEM, Philips.

1 B. Krebs, *Angew. Chem.*, 1983, **95**, 113.
2 R. L. Bedard, S. T. Wilson, L. D. Vail, J. M. Bennett and E. M. Flanigan, in *Zeolites: Facts, Figures, Future*, ed. P. A. Jacobs and R. A. van Santen, Elsevier, Amsterdam, 1989, p. 375.
3 C. L. Bowes and G. A. Ozin, *Adv. Mater.*, 1996, **8**, 13.
4 X. Wang and F. Liebau, *Acta Crystallogr., Sect. B*, 1996, **52**, 7.
5 M. Schur and W. Bensch, *Z. Anorg. Allg. Chem.*, 1998, **624**, 310.
6 H. Rijnberk, C. Näther, M. Schur, I. Jeß and W. Bensch, *Acta Crystallogr., Sect. C*, 1998, **54**, 920.
7 H.-O. Stephan and M. G. Kanatzidis, *J. Am. Chem. Soc.*, 1996, **118**, 12 226.
8 W. Bensch and M. Schur, *Eur. J. Solid State Inorg. Chem.*, 1996, **33**, 1149.
9 X. Wang and F. Liebau, *J. Solid State Chem.*, 1994, **111**, 385.
10 W. Bensch and M. Schur, *Z. Naturforsch., Teil B*, 1997, **52**, 405.
11 M. Schur, H. Rijnberk, C. Näther and W. Bensch, *Polyhedron*, 1998, **18**, 107.
12 J. Ellermeier, C. Näther and W. Bensch, *Acta Crystallogr., Sect. C*, 1999, **55**, 501.
13 G. H. Searle, S. F. Lincoln, F. R. Keene, S. G. Teague and D. G. Rowe, *Aust. J. Chem.*, 1977, **30**, 1221; F. G. Mann, *J. Chem. Soc.*, 1934, 466.
14 F. R. Keene and G. H. Searle, *Inorg. Chem.*, 1972, **11**, 148.
15 Y. Yoshikawa and K. Yamasaki, *Bull. Chem. Soc. Jpn.*, 1972, **45**, 179.
16 G. H. Searle and D. A. House, *Aust. J. Chem.*, 1987, **40**, 361.
17 A. K. Mukherjee, S. Korner, A. Ghosh, N. R. Chaudhuri, M. Mukherjee and A. J. Welch, *J. Chem. Soc. Dalton Trans.*, 1994, 2367.
18 F. S. Stephens, *J. Chem. Soc. A*, 1969, 883; F. S. Stephens, *J. Chem. Soc. A*, 1969, 2233.
19 K. Harada, *Bull. Chem. Soc. Jpn.*, 1993, **66**, 2889.
20 A. Mondal, I. R. Laskar and N. R. Chaudhuri, *Transition Met. Chem.*, 1999, **24**, 282.
21 H. H. Schmidtke and D. Garthoff, *Inorg. Chim. Acta*, 1968, **2**, 357.
22 V. Rodriguez, J. M. Gutierrez-Zorrilla, P. Vitoria, A. Luque, P. Roman and M. Martinez-Ripoll, *Inorg. Chim. Acta*, 1999, **290**, 57.
23 S. Koner, A. Ghosh and N. R. Chaudhuri, *Transition Met. Chem.*, 1988, **13**, 291.
24 S. Koner, A. Ghosh and N. R. Chaudhuri, *Transition Met. Chem.*, 1990, **15**, 394.
25 A. R. Gainsford and D. A. House, *Inorg. Chim. Acta*, 1969, **3**, 367.
26 G. L. Schimek and J. W. Kolis, *Chem. Mater.*, 1997, **9**, 2776.

ChemComm

Synthesis of the first polymer-supported tripodal triphosphine ligand and its application in the heterogeneous hydrogenolysis of benzo[*b*]thiophene by rhodium catalysis

Claudio Bianchini,* Marco Frediani and Francesco Vizza

ISSECC-CNR, Via J. Nardi 39, Firenze 50132, Italy. E-mail: bianchin@fi.cnr.it

Received (in Cambridge, UK) 19th December 2000, Accepted 2nd January 2001
First published as an Advance Article on the web 19th February 2001

A *p*-styrenyl substituent attached to the ligand framework allows the tripodal triphosphine moiety –C(CH$_2$PPh$_2$)$_3$ to be introduced as a pendant group in polystyrene matrices *via* free-radical copolymerisation; in conjunction with rhodium(I), the polytriphos material forms an effective heterogeneous catalyst for the hydrogenolysis of benzo[*b*]thiophene to 2-ethylthiophenol and ethylbenzene.

The immobilisation of metal complexes on solid supports to obtain single-site heterogeneous catalysts is a research topic of much current interest. Several heterogenisation techniques are available which span from hydrogen-bonding to covalent grafting, to physical and ionic immobilisation.[1,2] Similarly, many different types of materials (metal oxides, dendrimers, polyolefins, heteropoly acids, gels, *etc*.) may be employed as the support, which may be either inert or chemically interacting with metal, substrate and/or product. Irrespective of the grafting mode and of the type of support, a major drawback of any heterogenised catalyst is represented by metal leaching into the mobile phase. In order to reduce, and ultimately inhibit, undesired loss of metal during the catalysis, the structure of the tethered complex must be thermally and chemically robust. In general, tertiary phosphines meet these requisites and beyond, as they behave as strong ligands towards most transition metals and can also be finely tuned so as to determine the steric and electronic properties of the metal centre. Polydentate phosphines show superior control properties over monophosphines and those having tripodal structure, such as MeC(CH$_2$PPh$_2$)$_3$ (triphos), are almost insuperable with regard to the stability of the metal complexes.[3]

Here, we describe the synthesis of the first tripodal triphosphine anchored to a cross-linked styrene/divinylbenzene polymer and of its complex with the 'Rh(cod)$^+$' moiety (cod = cycloocta-1,5-diene). It is also shown here that the supported rhodium complex is a powerful catalyst for the hydrogenolysis of benzo[*b*]thiophene to 2-ethylthiophenol and ethylbenzene, which represents the first evidence of a successful single-site catalyst in the heterogeneous hydrodesulfurisation (HDS) of a thiophenic substrate.[4,5]

The synthetic route to the triphosphine-containing styrene monomer is illustrated in Scheme 1. The strategy is to prepare a triphos ligand bearing a single reactive hydroxy functionality for attachment of the styrene group. Nucleophilic attack by diphenylphosphide at the heterocycle of 3,3-bis(diphenylphosphinomethyl)oxacyclobutane,[6] followed by reaction with 4-vinylbenzyl chloride is an excellent method to accomplish the high-yield synthesis of the desired *p*-styrenyl-functionalised triphos ligand 2,2,2-tris(diphenylphosphinomethyl)ethyl 4-vinylbenzyl ether (TVBE).† Copolymerisation of TVBE with divinylbenzene alone (DVB) or with styrene–DVB in THF/MeOH using AIBN as the radical initiator generates cross-linked triphosphine polymers (polytriphos) as off-white solids insoluble in organic solvents. Besides elemental analysis (C, H, P), the presence of triphosphine units is shown by CP MAS ^{31}P NMR spectroscopy.‡ The spectrum of a polytriphos sample obtained by copolymerisation of TVBE with DVB (1:1) is given in Fig. 1a. Note that the chemical shift (δ −25.6) is similar to that of monomeric TVBE as well as silica-supported triphos.[2] A soluble polystyrene-bound diphosphine ligand with the 1,3-bis(diphenylphosphino)propane moiety has been described previously.[7]

Advantages of the present technique over heterogenisation procedures involving the reaction of functionalised phosphines with functionalised cross-linked styrene–DVB resins[8] are: (1) the ease of synthesis since only the phosphine needs to be chemically modified; (2) the effective control on the phosphine loading (and hence of the metal loading) by simply varying the phosphine : DVB : styrene ratio; (3) the absence of residual functional groups on the resins.

Supported complexes of the general formula [Rh(cod)(polytriphos)]PF$_6$ have been prepared by stirring CH$_2$Cl$_2$ solutions of [RhCl(cod)]$_2$ and NBu$_4$PF$_6$ in the presence of polytriphos at room temperature for 24 h. The filtered yellow solids are washed with CH$_2$Cl$_2$ at reflux temperature using a Soxhlet

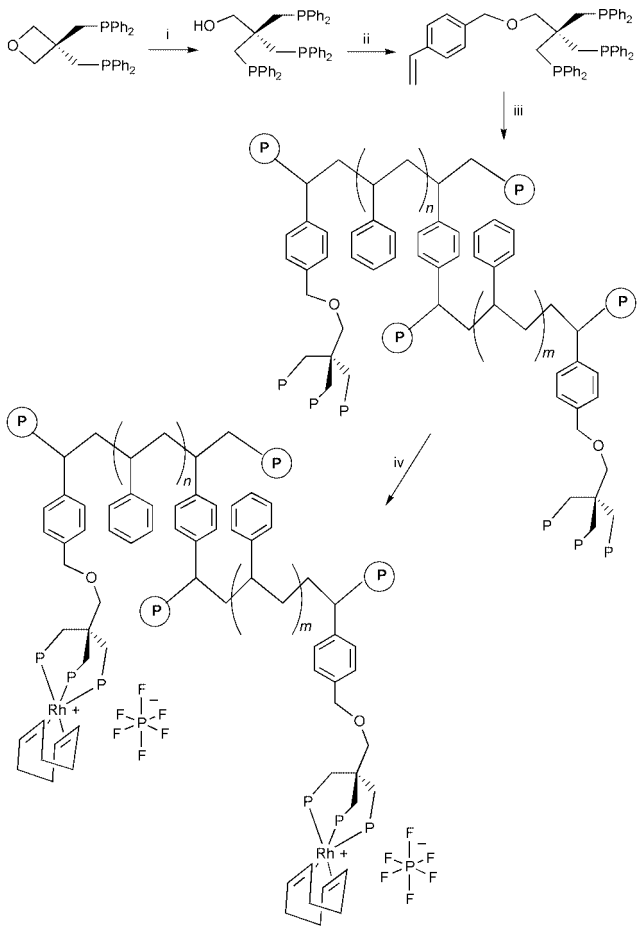

Scheme 1 *Reagents and conditions*: i, HPPh$_2$, BuLi, THF (65%); ii, NaH, 4-vinylbenzyl chloride, DMF (90%); iii, styrene–divinylbenzene, AIBN, THF/MeOH (1:2, v/v), 85 °C; iv, [RhCl(cod)]$_2$, NBu$_4$PF$_6$, CH$_2$Cl$_2$ (98%).

DOI: 10.1039/b010128l

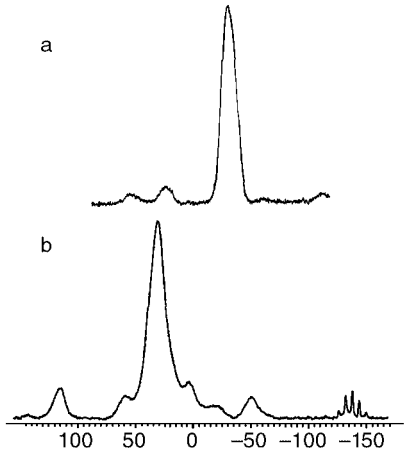

Fig. 1 CP MAS ^{31}P NMR (121.50 MHz) spectra of polytriphos (a) and [Rh(cod)(polytriphos)]PF_6 (b).

apparatus and then dried. The rhodium content in the heterogeneous catalysts depends on the polytriphos sample; in particular, a loading of 7.24 wt% has been found for a polymer obtained by copolymerising TVBE and DVB in a 1:1 ratio, while a loading of 0.94 wt% has been found for a polymer obtained by copolymerising TVBE, DVB and styrene in a 0.6:1:36 ratio. The coordination of rhodium(I) to the tethered phosphine is demonstrated by the low-field shift to δ 28.4 of the phosphorus resonance as well as the presence of the PF_6^- sextuplet at δ −143.5 (Fig. 1b).

As an example of the great potential of polytriphos metal complexes in heterogeneous catalysis, [Rh(cod)(polytriphos)]PF_6 (0.94 wt%) has been employed to hydrogenate benzo[*b*]thiophene (BT) in tetrahydrofuran (THF) under basic conditions (Scheme 2).[4,5]

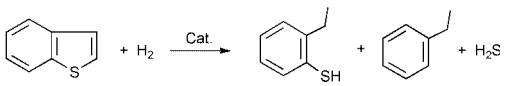

Scheme 2 Hydrogenolysis of BT to 2-ethylthiophenol and ethylbenzene.

Under rather harsh experimental conditions (160 °C, 30 bar H_2), the thiophenic substrate is mainly converted to 2-ethylthiophenol (ET) but appreciable formation of the desulfurised product ethylbenzene (EB) also occurs. Interestingly, no trace of 2,3-dihydrobenzo[*b*]thiophene was detected by GC. Table 1 reports catalytic data obtained for runs at 2, 5 and 10 h. In all cases, no rhodium leaching was observed by ICP-AES (< 1 ppm), while an effective catalyst recycling with no loss of catalytic activity was accomplished by removing the liquid phase *via* the liquid sampling valve and recharging the autoclave with a solution containing substrate and base (entries 4 and 5).

Under comparable experimental conditions, both the aqueous-biphase catalyst [Rh(cod)(sulphos)] in MeOH/*n*-heptane [sulphos = $^-O_3S(C_6H_4)CH_2C(CH_2PPh_2)_3$][5] and the homogeneous catalyst [Rh(DMAD)(triphos)]PF_6 in THF (DMAD = dimethyl acetylenedicarboxylate)[9] are slightly less efficient than [Rh(cod)(polytriphos)]PF_6 for the hydrogenolysis of BT to ET (TON *ca*. 90 *vs*. 124) and cannot be recycled after catalysis.

The data reported in Table 1 are of great relevance in the field of model studies of heterogeneous HDS as they show that a single metal site belonging to the class of the HDS promoters[10] can open and hydrogenate a thiophenic substrate without the need of any cooperative effect.[4,5] Besides this important result, we have succeeded for the first time in producing a polymer-supported tripodal triphosphine ligand with which we intend to prepare a large variety of metal catalysts and study their performance in heterogeneous processes.

Table 1 Hydrogenation of BT with [Rh(cod)(polytriphos)]PF_6 (0.94 wt%)[a]

Entry	*t*/h	ET (%)	EB (%)	TON (ET)	Conv. (%)
1	2	48.5	2.5	97	51.0
2	5	62.2	4.0	124	66.2
3	10	74.3	5.5	349	79.8
4[b]	2	47.6	3.1	95	50.7
5[b]	2	48.0	3.5	96	51.5

[a] Experimental conditions: 30 mL THF, Rh 3.5×10^{-2} mmol, BT 7 mmol, Bu^{t}OK 7 mmol, 160 °C, 30 bar H_2, 1500 rpm; product composition determined by GC–MS after acidification of the catalytic mixture with aqueous HCl. [b] Recycling in the same conditions of entry 1.

We are grateful to Claudia Forte (ICQEM-CNR of Italy) for assistance in recording the CP MAS ^{31}P NMR spectra and to MURST (Italy) for financial support (legge 95/95).

Notes and references

† *Selected NMR data* for 2,2,2-tris(diphenylphosphinomethyl)ethyl 4-vinylbenzyl ether (TVBE): ^{1}H NMR ($CDCl_3$) δ_H 2.57 (d, 6H, CH_2P, ^3J 2.91 Hz), 3.16 (s, 2H, OCH_2C$(CH_3)_3$), 3.71 (s, 2H, OCH_2Ph), 5.24 (dd, H_{cis}, CH_2=CH, J_{cis} 10.90 Hz, J_{gem} 0.97 Hz), 5.74 (dd, H_{trans}, CH_2=CH, J_{trans} 17.53 Hz, J_{gem} = 0.97 Hz), 6.71 (dd, 1H C*H*=CH_2), 6.91–7.31 (m, 34H, Ph). ^{13}C{^{1}H} NMR ($CDCl_3$) δ_C 38.87 (m, CH_2P), 43.58 (q, $CH_2C(CH_2PPh_2)$, J(CP) 12.4 Hz), 72.50 (s, O*C*H_2Ph), 77.19 (m, O*C*$H_2C(CH_3)_3$), 114.03 (s, *C*H_2=CH), 123.48-137.42 (m, Ph), 133.92 (s, *C*H=CH_2). ^{31}P{^{1}H} NMR ($CDCl_3$) δ_P −26.1 (s). Satisfactory elemental analyses were obtained for all compounds.

‡ Solid-state ^{31}P NMR spectra were recorded at room temperature on a Bruker AMX 300 WB spectrometer equipped with a 4 mm BB-CP MAS probe at a working frequency of 121.50 MHz. The spectra were acquired using the cross-polarisation pulse sequence under magic angle spinning at a spinning rate of 10 kHz. The 90° pulse was 3.3 μs, and the contact pulse was 1 ms. The spectra of the supported triphosphine were collected after 400 scans with a recycle delay of 1 s and a line broadening of 30 Hz, whereas the spectra of the supported rhodium complex were acquired with 700 scans, a recycle delay of 1 s and a line broadening of 50 Hz. H_3PO_4 (85%) was used as the external standard.

1 *Applied Homogeneous Catalysis*, ed. B. Cornils and W. A. Herrmann, VCH, Weinheim, Germany, 1996, ch. 3; E. Lindner, T. Schneller, F. Auer and H. A. Mayer, *Angew. Chem., Int. Ed.*, 1999, **38**, 2154; E. M. Carnahan and G. B. Jacobsen, *CATTECH*, 2000, **4**, 74.
2 C. Bianchini, D. G. Burnaby, J. Evans, P. Frediani, A. Meli, W. Oberhauser, R. Psaro, L. Sordelli and F. Vizza, *J. Am. Chem. Soc.*, 1999, **121**, 5961; C. Bianchini, V. Dal Santo, A. Meli, W. Oberhauser, R. Psaro and F. Vizza, *Organometallics*, 2000, **19**, 2433; C. Bianchini, P. Barbaro, V. Dal Santo, R. Gobetto, A. Meli, W. Oberhauser, R. Psaro and F. Vizza, *Adv. Synth. Catal.*, 2001, **343**, XX.
3 C. Bianchini, A. Meli, M. Peruzzini, F. Vizza and F. Zanobini, *Coord. Chem. Rev.*, 1992, **120**, 193; H. A. Mayer and W. C. Kaska, *Chem. Rev.*, 1994, **94**, 1239.
4 C. Bianchini and A. Meli, *J. Chem. Soc., Dalton Trans.*, 1996, 801; C. Bianchini, A. Meli, S. Moneti, W. Oberhauser, F. Vizza, V. Herrera, A. Fuentes and R. A. Sánchez-Delgado, *J. Am. Chem. Soc.*, 1999, **121**, 7071; T. Kabe, A. Ishihara and W. Qian, *Hydrodesulfurization and Hydrodenitrogenation*, Kodansha, Tokyo, Japan and Wiley-VCH, Weinheim, Germany, 1999.
5 C. Bianchini, A. Meli, V. Patinec, V. Sernau and F. Vizza, *J. Am. Chem. Soc.*, 1997, **119**, 4945.
6 Th. Seitz, A. Muth, G. Huttner, Th. Klein, O. Walter, M. Fritz and L. Zsolnai, *J. Organomet. Chem.*, 1994, **469**, 155.
7 F. Benvenuti, C. Carlini, A. M. Raspolli Galletti, G. Sbrana, M. Marchionna and R. Patrini, *J. Mol. Catal. A: Chem.*, 1999, **137**, 49.
8 C. U. Pittman, Jr., L. R. Smith and R. M. Hanes, *J. Am. Chem. Soc.*, 1975, **97**, 1742; F. Benvenuti, C. Carlini, M. Marchionna, R. Patrini, A. M. Raspolli Galletti and G. Sbrana, *J. Inorg. Organomet. Polym.*, 1997, **7**, 183.
9 C. Bianchini, J. A. Casares, A. Meli, V. Sernau, F. Vizza and R. A. Sánchez-Delgado, *Polyhedron*, 1997, **16**, 3099.
10 H. Topsøe, B. S. Clausen and F. E. Massoth, *Hydrotreating Catalysis*, Springer-Verlag, Berlin, Germany, 1996.

Photocycloaddition reactions of 2-acylcyclohex-2-enones

Leticia Oliveira Ferrer and Paul Margaretha*

Institute of Organic Chemistry, University of Hamburg, D-20146 Hamburg, Germany. E-mail: margpaul@chemie.uni-hamburg.de

Received (in Liverpool, UK) 28th November 2000, Accepted 6th February 2001
First published as an Advance Article on the web 19th February 2001

The newly synthesized 2-acylcyclohex-2-enones 1 photocycloadd selectively to the C–C triple bond of 2-methylbut-1-en-3-yne giving diacylcyclobutene derivatives 4 and 5, and they react with 2,3-dimethylbut-2-ene in an overall [4+2]-photocycloaddition to afford benzopyranones 7.

We have recently published results[1,2] on the photocycloaddition of cyclohex-2-enones to 2-methylbut-1-en-3-yne, showing that the substitution pattern on C(2) of the enone has a pronounced influence on the outcome of the reaction. While the (parent) cyclohex-2-enone affords mainly bicyclo[4.2.0]octan-2-ones resulting from [2 + 2]-cycloaddition to the C–C double bond of the enyne, 2-alkylcyclohex-2-enones give naphthalen-1(2*H*)-ones *via* 1,6-cyclization of the triplet biradical intermediate. Finally, 2-cyanocyclohex-2-enone yields a mixture of these two types of compounds and, in addition, one product resulting from cycloaddition to the C–C triple bond of the enyne. Here we report on the synthesis of the hitherto unknown 2-acylcyclohex-2-enones **1a** and **1b** and on their unprecedented behaviour on irradiation in the presence of this same enyne or of 2,3-dimethylbut-2-ene, respectively. *C*-Acylation of 2,2-dimethylcyclohexanone (**2**)[3] with either LDA–acetyl cyanide or NaOMe–ethyl trifluoroacetate affords 2-(1-hydroxyethylidene)-6,6-dimethylcyclohexanones **3a** and **3b** in 60 and 62% yield, respectively.[4] Dehydrogenation to **1a** and **1b** is then achieved by treatment[5] of **3** with PhSeCl and then H_2O_2 in 96 and 90% yield, respectively (Scheme 1).[6–8]

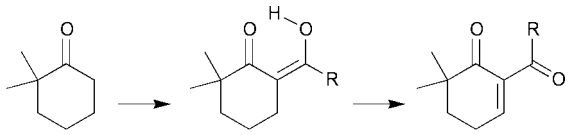

Scheme 1

Monitoring the irradiation (λ > 340 nm) of an argon-degassed solution of **1a** (0.1 M) and 2-methylbut-1-en-3-yne (1 M) in benzene by GC indicates the formation of two new products, **4a** and **5a**, in a 1:1 ratio. At degrees of conversion of **1a** higher than 40–45% the photoproducts start to undergo secondary reactions. Under the same conditions **1b** gives a 2:3 mixture of **4b** and **5b**. In preparative runs[9] the photoproducts were separated, isolated and identified as being regioisomeric 1-acylbicylo[4.2.0]oct-7-en-2-ones (Scheme 2).[10]

Similarly, monitoring the irradiation of **1** in the presence of a tenfold molar excess of 2,3-dimethylbut-2-ene in benzene

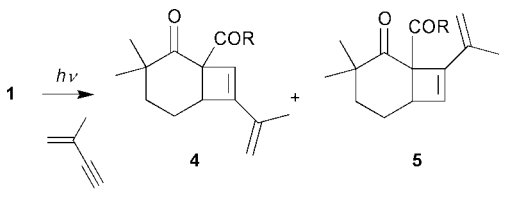

Scheme 2

indicates the formation of two new products **6** and **7**, in a 3:1 ratio from **1a** and in a 2:1 ratio from **1b**, the major products **6** again undergoing consecutive photoreactions. After isolation as above[9] the major products **6** turned out to be (the expected) 1-acylbicyclo[4.2.0]octan-2-ones—which then undergo α-cleavage to afford aldehydes—while the minor products **7** were identified as being 3,4,4a,5,6,7-hexahydro-8*H*-isochromen-8-ones (Scheme 3).[11]

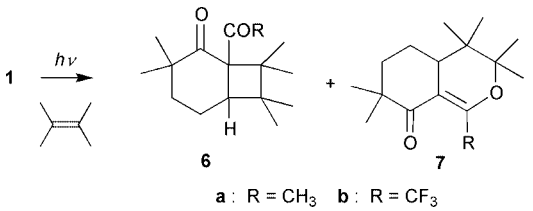

Scheme 3

The behaviour of **1a** and **1b** contrasts that of 6,6-dimethyl-2-pivaloylcyclohex-2-enone[12] which on the one hand is thermally more stable, *i.e.* it does not enolize, but on the other hand does not photocycloadd to alkenes or enynes, most probably because of the (steric) bulk of the *tert*-butyl substituent. Despite their pronounced lack of (thermal) stability, which can nevertheless be controlled by careful handling,[5,13] 2-acylcyclohex-2-enones **1a** and **1b** turn out to be remarkable substrates for intermolecular photocycloaddition reactions *a*) due to the fact that on reaction with the enyne excited cyclohexenones **1** give (novel) cyclobutene adducts selectively, thus corroborating the assumption[2] that the amount of this type of cycloadduct will increase with decreasing reduction potential of the (excited) enone, and *b)* because photochemical [4 + 2]-cycloadditions of s-*cis* enones to alkenes to give dihydropyrans have not been reported so far in the literature. Further studies aiming at the improvement in the product ratio pyran *vs*. cyclobutane are in progress.

We thank the Deutsche Forschungsgemeinschaft and the Fonds der Chemischen Industrie for support.

Notes and references

1 B. Witte and P. Margaretha, *Org. Lett.*, 1999, **1**, 173.
2 B. Witte, L. Meyer and P. Margaretha, *Helv. Chim. Acta*, 2000, **83**, 554.
3 R. Z. Andriamialisoa, N. Langlois and Y. Langlois, *Tetrahedron Lett.*, 1985, **26**, 3563.
4 **3a**: δ_H(500 MHz, $CDCl_3$) 16.27 (O**H**), δ_C(125 MHz, $CDCl_3$) 199.4, 188.1, 105.4 (sp^2 C-atoms); **3b**: δ_H(500 MHz, $CDCl_3$) 15.53 (O**H**), δ_C(125 MHz, $CDCl_3$) 195.8, 179.5 (q, J_{CF} = 33.9 Hz), 103.4 (sp^2 C-atoms). Both **3a** and **3b** gave satisfactory elemental analyses.
5 H. Reich, J. M. Renga and I. L. Reich, *J. Am. Chem. Soc.*, 1975, **97**, 5434.
6 Both compounds **1** are sensitive to acids and bases in undergoing irreversible (*cf.* ref. 5) enolization to 2-(1-hydroxyethylidene)-6,6-dimethylcylohex-3-en-1-ones.
7 In the normal (ref. 5) work-up trifluoroacetylcyclohexenone **1b** is obtained in a mixture with its hydrate, *i.e.* 2-(1,1-dihydroxy-2,2,2-trifluoroethyl)-6,6-dimethylcyclohex-2-enone; pure **1b** is obtained by azeotropic removal of water by distillation of added benzene.

8 **1a**: light yellow liquid, δ_H(500 MHz, C_6D_6) 7.13 (t, J = 4 Hz), 2.41 (s, 3H), 1.65 (dt, J = 4 and 6 Hz, 2H), 1.18 (t, J = 6 Hz, 2H), 0.88 (s, 6H), δ_C(125 MHz, C_6D_6) 201.4, 197.6, 153.6 (**C**H), 138.0, 42.1, 35.7 (**C**H_2), 30.7 (**C**H_3), 24.1 (**C**H_3), 23.4 (**C**H_2); **1b**: light yellow liquid, δ_H(500 MHz, C_6D_6) 7.31 (t, J = 4 Hz), 1.81 (dt, J = 4 and 6 Hz, 2H), 1.29 (t, J = 6 Hz, 2H), 0.96 (s, 6H), δ_C(125 MHz, C_6D_6) 199.5, 184.8 (q, J_{CF} = 37.5 Hz), 156.3 (**C**H), 135.2, 126.6 (q, J_{CF} = 290 Hz), 42.2, 35.5 (**C**H_2), 23.7 (**C**H_3), 23.6 (**C**H_2).

9 *Preparative Details*: an argon degassed solution of **1** (1 mmol) and enyne/alkene (0.01 mol) in benzene (10 ml) is irradiated with a 250 W mercury lamp using a liquid filter with cutoff < 340 nm for 24 h up to a degree of conversion of **1** of 40–45%. After evaporation of the solvent the residue is chromatographed (SiO_2, pentane–ether 9 : 1). The orders of elution are **4a** < **5a**, **5b** < **4b**, **6a** < **7a** and **6b** < **7b**, the enones **1** always having much lower R_f values. The new compounds **4**, **5**, **6** and **7**—all colourless liquids—have been fully characterized and have spectroscopic properties compatible with the structures assigned.

10 **4a**: δ_H(500 MHz, C_6D_6) 5.90 (s), 4.92 (s), 4.89 (s) (olefinic H-atoms), δ_C(125 MHz, C_6D_6) 211.4, 204.3, 153.7, 137.5, 128.1 (**C**H), 115.7 (**C**H_2) (sp^2 C-atoms); **5a**: δ_H(500 MHz, C_6D_6) 5.81 (s), 5.71 (s), 5.08 (s) (olefinic H-atoms), δ_C(125 MHz, C_6D_6) 212.0, 203.7, 148.0, 135.6, 134.2 (**C**H), 117.7 (**C**H_2) (sp^2 C-atoms); **4b**: δ_H(500 MHz, C_6D_6) 5.80 (s), 4.90 (s), 4.81 (s) (olefinic H-atoms), δ_C(125 MHz, C_6D_6) 211.1, 189.7 (q, J_{CF} = 35 Hz), 154.2, 137.0, 123.7 (**C**H), 117.1 (**C**H_2) (sp^2 C-atoms); **5b**: δ_H(500 MHz, C_6D_6) 5.60 (s), 5.40 (s), 4.93 (s) (olefinic H-atoms), δ_C(125 MHz, C_6D_6) 212.4, 190.2 (q, J_{CF} = 34 Hz), 144.3, 135.6, 133.6 (**C**H), 117.9 (**C**H_2) (sp^2 C-atoms).

11 **7a**: δ_C(125 MHz, C_6D_6) 204.3, 161.0, 109.2, 81.4, 43.4 (**C**H), 43.0, 38.4 (**C**H_2), 36.1, 20.2 (**C**H_2) and seven signals for **C**H_3; **7b**: δ_C(125 MHz, C_6D_6) 203.6, 142.5 (q, J_{CF} = 26.3 Hz), 123.0 (q, J_{CF} = 275 Hz), 119.1, 83.1, 45.4 (**C**H), 45.0, 38.9 (**C**H_2), 36.3, 20.6 (**C**H_2) and six signals for **C**H_3.

12 L. O. Ferrer and P. Margaretha, *J. Chem. Res. (S)*, 1999, 204.

13 B. B. Snider, *Tetrahedron Lett.*, 1980, **21**, 1133.

ChemComm

First structural characterization of a covalently bonded porphyrin–carborane system

M. Graça H. Vicente,*[a,b] Daniel J. Nurco,[a] Shankar J. Shetty,[a,b] Craig J. Medforth[a] and Kevin M. Smith[a]

[a] *Department of Chemistry, University of California, Davis, CA 95616, USA*
[b] *Department of Neurological Surgery, School of Medicine, University of California, Davis, CA 95817, USA. E-mail: mgvicente@ucdavis.edu*

Received (in Corvallis, OR, USA) 20th December 2000, Accepted 22nd January 2001
First published as an Advance Article on the web 19th February 2001

The first definitive crystal structure of a covalently bonded carborane–porphyrin system is reported; unusual inter- and intra-molecular carborane–porphyrin interactions are observed in the molecular structure and in variable temperature ^{1}H NMR experiments.

In the past few decades, porphyrins have assumed broad importance in applications as diverse as medicine,[1,2] catalysis,[3] and molecular electronics.[4,5] Many of these novel applications have employed 5,10,15,20-tetraarylporphyrins as the substrate because this type of porphyrin platform can be readily synthesized.[6] Recently, carboranyl-substituted tetraarylporphyrins have been identified as useful agents in boron neutron capture therapy (BNCT) of cancer because of their ability to localize in tumors, and their high boron content.[7,8] However, to date, carboranyl-substituted tetraarylporphyrins have not been well-characterized and it is not known if the large carborane substituent confers any novel structural or spectroscopic properties on these porphyrins. Herein, we present the first crystal structure of a carboranylporphyrin [**1** (M = Zn)] and detailed proton NMR studies of several carboranyl-substituted tetraphenylporphyrins (**2**–**5**) which demonstrate unusual interactions between the carborane group and the porphyrin macrocycle.

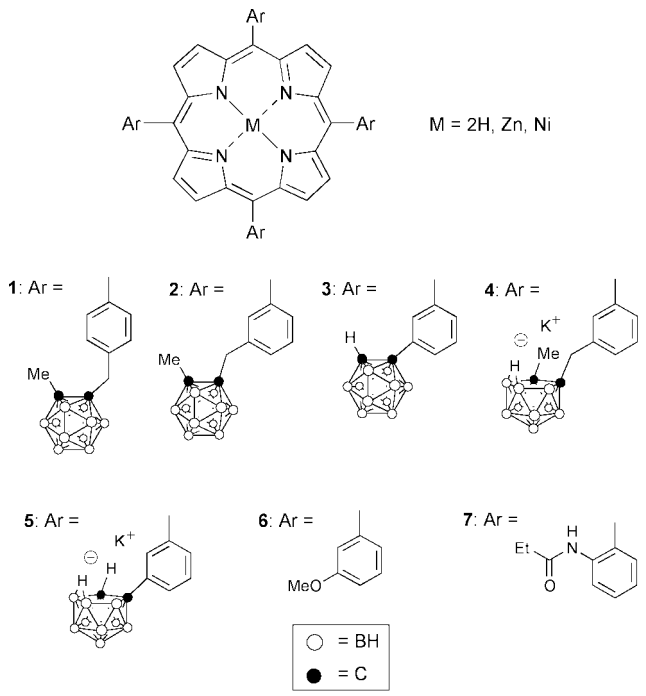

Several *m*- and *p*-carboranylarylporphyrins were synthesized in order to investigate structure–activity relationships in BNCT.[9] Insertion of zinc and nickel using normal procedures ($ZnCl_2$ in THF–CH_2Cl_2 1:10 or Ni(II) acetylacetonate in toluene) produced the corresponding metallo-carboranylporphyrins. Repeated attempts to grow X-ray quality crystals of these compounds were unsuccessful until the *para*-substituted porphyrin **1** (M = Zn) was crystallized and the structure determined.† The molecular structure of **1** (M = Zn), the first definitive crystallographic investigation for a covalently bonded porphyrin–carborane molecule, is shown in Figs. 1 and 2.‡[10]

The porphyrin macrocycle exhibits a non-planar waved conformation[11] (Fig. 2) with a mean deviation of the 24 macrocycle atoms from their least-squares plane of 0.062 Å. The Zn–N bond lengths of 2.062(2) Å are within the range typically seen for zinc porphyrins.[12] An unusual feature of the structure is the close intermolecular contacts between the BH hydrogens of one porphyrin and the zinc atom of another; this produces a *pseudo-hexacoordinate* zinc complex (Fig. 2). Zinc

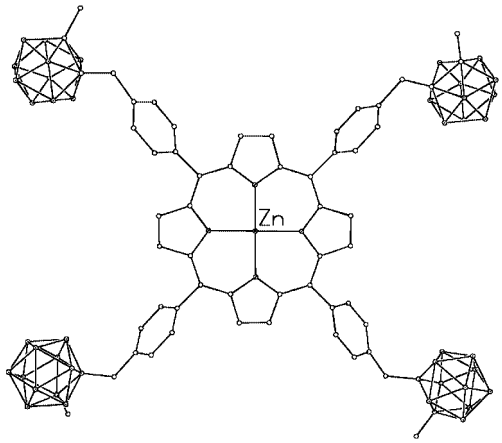

Fig. 1 The molecular structure of **1** (M = Zn). Hydrogen atoms have been omitted for clarity.

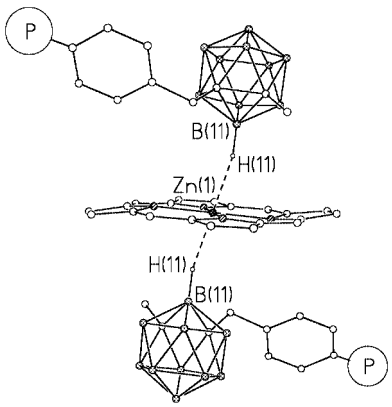

Fig. 2 View of the crystal structure of **1** (M = Zn) showing the waved porphyrin macrocycle and *pseudo-hexacoordinate* zinc(II) ion. Hydrogen atoms, except for the two involved in the B(11)–H(11)···Zn1···H(11)–B(11) bridge, and methylcarboranylphenyl substituents attached to the illustrated porphyrin macrocycle have been omitted (P = porphyrinyl).

Table 1 Activation energies ($\Delta G^{\ddagger}$; kJ mol^{-1}) for aryl–porphyrin rotation in porphyrins **2**–**7**[a]

Porphyrin	M = 2H	M = Zn	M = Ni
2	72 (313 K)[b]	80 (368 K)	
3	72 (323 K)	79 (348 K)	55 (243 K)
4	73 (323 K)	79 (353 K)	
5	71 (323 K)	76 (338 K)	54 (258 K)
6	45[16]		
7	122[15]	131[15]	108[15]
Δ (**7**–**3**)[c]	50	52	53

[a] Proton NMR spectra were measured at 400 MHz using $CDCl_3$ [**2** (M = 2H) and **3** (M = 2H, Ni)], $C_6D_5CD_3$ [**2** and **3** (M = Zn)], CD_3COCD_3 [**4** (M = 2H) and **5** (M = 2H, Ni)] or CD_3SOCD_3 [**4** and **5** (M = Zn)] as solvent. [b] Activation energies for aryl–porphyrin rotation in porphyrins **2**–**5** were calculated at the coalescence temperatures which are given in parentheses. [c] Difference in activation energies for aryl–porphyrin rotation in porphyrins **7** and **3**.

porphyrin structures are generally either four-coordinate or contain one or two axial ligands bound *via* a lone pair from nitrogen or oxygen.[12] The hydrogen atom positions were treated with a riding model which afforded Zn(1)···H(11)–B(11) distances of 2.09 and 1.12 Å [when H(11) was freely refined the bond distances 2.16 and 1.06 Å were obtained]. An examination of the more than 250 zinc porphyrin crystal structures in the Cambridge Structural Database did not reveal any examples of axial ligands coordinating *via* a hydrogen atom, so this appears to be the first example of this type of bonding. There were however, two reported crystal structures that are similar enough to be mentioned; firstly, the structure of [Fe(III)TPP]·[$(CB_{11}H_{12})^-$][13] shows the $(CB_{11}H_{12})^-$ anion coordinated to the Fe(III) ion *via* one of its hydrogen atoms, with Fe···H–B distances of 1.82 and 1.25 Å. Secondly, the structure of $[(C_6H_5)_3P]_3Rh(CB_{10}H_{10}C–C_6H_5)$[14] exhibits a Rh···H–B bridge with a Rh–H distance of 2.06 Å. We believe that the unusual interaction between the carborane and the zinc ion in **1** (M = Zn) is probably a result of the electronic properties of the carborane cages combined with an efficient cell packing of this structural motif.

The ^{1}H NMR spectrum of the *para*-substituted carboranylporphyrin **1** (M = 2H) showed a singlet (8.85 ppm) for the pyrrole protons and two doublets (7.59 and 8.20 ppm, J = 8.0 Hz) for the *ortho* and *meta* phenyl protons, consistent with the fourfold symmetry expected for this molecule. In contrast, the ^{1}H NMR spectra of the *meta*-substituted carboranylporphyrins **2** and **3** (M = 2H) and the open cage species **4** and **5** (M = 2H) showed multiple signals for the pyrrole protons consistent with the presence of atropisomers (due to restricted rotation about the aryl–porphyrin bond).[15] *meta*-Substituted tetraarylporphyrins [*e.g.* **6** (M = 2H)][16] normally show fast exchange between atropisomers at rt. The presence of multiple β-pyrrolic signals for porphyrins **2**–**5** (M = 2H) at rt thus suggests that the barriers for aryl rotation in these compounds are markedly increased by the carborane substituents. This suggestion was confirmed by variable temperature ^{1}H NMR studies, which showed that the activation energies for aryl rotation in porphyrins **2**–**5** (M = 2H) were intermediate between those of porphyrins with *meta*-substituents [*e.g.* **6** (M = 2H)] and porphyrins with *ortho*-substituents [*e.g.* **7** (M = 2H)] (Table 1).

Proof that aryl–porphyrin rotation was the dynamic process being observed was obtained by varying the core substituent M, which is known to modulate the rotational barriers in *ortho*-substituted porphyrins such as **7**.[15] The activation energies determined for the dynamic processes in porphyrins **2**–**5** showed a similar response to the incorporation of zinc or nickel into the porphyrin core (Table 1). Interestingly, no significant difference in the aryl–porphyrin rotational barriers was seen for the *o*-carboranes (**2** and **3**) *vs.* the anionic *nido*-carboranes (**4** and **5**) nor for the porphyrins with methylene bridges between the carborane and aryl groups (**2** and **4**) and those without bridges (**3** and **5**). No attempt was made to physically separate the atropisomers given the short lifetimes calculated from the activation energies in Table 1.

In summary, the present work provides evidence of novel carborane–porphyrin inter- and intra-molecular interactions that can be related to the unusual size and electronic properties of the carborane group.

This research was supported by grants from the Department of Energy (98ER62633) and the National Institutes of Health (HL 22252).

Notes and references

† Crystals were grown by slow diffusion of MeOH into a chlorobenzene solution of **1** (M = Zn) [$C_{60}H_{84.8}B_{40}N_4Zn_{0.6}\cdot(C_6H_5Cl)$, FW = 1447.21]. The crystals were found to consist of **1** (M = Zn) and **1** (M = 2H) due to acid catalyzed demetalation. The selected crystal (0.30 × 0.10 × 0.10 mm) had a monoclinic unit cell, space group $P2(1)/c$, with cell dimensions a = 13.3139(5), b = 18.6428(8), c = 15.7642(6) Å, β = 93.9630(10)°, V = 3903.5(3) Å^3, and Z = 2. Data were collected on a Bruker SMART 1000 diffractometer with a sealed tube source [λ(Mo-Kα) = 0.71073 Å] at 90(2) K. A 2θ cutoff of 55° was applied to the data to afford 33815 total reflections of which 8971 were unique and of those 5897 were observed ($I > 2\sigma$) [R_{int} = 0.071, T_{min} = 0.92, T_{max} = 0.97, ρ_{calc} = 1.226 g cm^{-3}, μ = 0.274 mm^{-1}]. The structure was solved by direct methods and refined (based on F^2 using all data) by full matrix least-squares methods with 515 parameters (Bruker SHELXS-97, SHELXL-97). All hydrogen atom positions were refined with a riding model. The occupancy of the zinc atom was determined to be 60% from free variable refinement with fixed isotropic parameter of 0.020 Å. Final R factors were $R1$ = 0.069 (observed data) and w$R2$ = 0.191 (all data). Atomic coordinates, bond lengths and angles, and thermal parameters for **1** (M = Zn) have been deposited at the Cambridge Crystallographic Data Center (CCDC). Any request to the CCDC for this material should quote the full literature citation and reference number 155418. See http://www.rsc.org/suppdata/cc/b1/b100231g/ for crystallographic files in .cif format.

‡ A search of the Cambridge Structural Database did not reveal any structures of carborane-substituted porphyrins. However, a semiquantitative structure (R = 0.25) has been reported.[10]

1 R. K. Pandey and G. Zheng, in *The Porphyrin Handbook*, ed. K. M. Kadish, K. M. Smith and R. Guilard, Academic Press, Boston, 1999, Vol. 6, p. 157.
2 H. Ali and J. E. van Lier, *Chem. Rev.*, 1999, **99**, 2379.
3 J. P. Collman, P. S. Wagenknecht and J. E. Hutchinson, *Angew. Chem., Int. Ed. Engl.*, 1994, **33**, 1537.
4 M. R. Wasielewski, *Chem. Rev.*, 1992, **92**, 435.
5 J.-H. Chou, H. S. Nalwa, M. E. Kosal, N. A. Rakow and K. S. Suslick, in *The Porphyrin Handbook*, ed. K. M. Kadish, K. M. Smith and R. Guilard, Academic Press, Boston, 1999, Vol. 6, p. 43.
6 J. S. Lindsey, in *The Porphyrin Handbook*, ed. K. M. Kadish, K. M. Smith and R. Guilard, Academic Press, Boston, 1999, Vol. 1, p. 45.
7 A. H. Soloway, W. Tjarks, B. A. Barnum, F.-G. Rong, R. F. Barth, I. M. Codogni and J. G. Wilson, *Chem. Rev.*, 1998, **98**, 1515.
8 M. G. H. Vicente, A. Wickramasighe, S. J. Shetty and K. M. Smith, *Abstracts 9th Int. Symp. Neutron Capture Therapy for Cancer*, Osaka (Japan), 2000, 121; B. Edwards, K. Matthews, Y. Hou, M. G. H. Vicente, S. Autry-Conwell and J. Boggan, *Abstracts 9th Int. Symp. Neutron Capture Therapy for Cancer*, Osaka (Japan), 2000, 61.
9 M. G. H. Vicente, S. J. Shetty, A. Wickramasighe and K. M. Smith, *Tetrahedron Lett.*, 2000, **41**, 7623.
10 R. C. Haushalter, W. M. Butler and R. W. Rudolph, *J. Am. Chem. Soc.*, 1981, **103**, 2620.
11 W. Jentzen, X.-Z. Song and J. A. Shelnutt, *J. Phys. Chem. B*, 1997, **101**, 1684.
12 M. P. Byrn, C. J. Curtis, Y. Hsiou, S. I. Khan, P. A. Sawin, S. K. Tendick, A. Terzis and C. E. Strouse, *J. Am. Chem. Soc.*, 1993, **115**, 9480.
13 K. Shelly, C. A. Reed, Y.-J. Lee and W. R. Scheidt, *J. Am. Chem. Soc.*, 1986, **108**, 3117; G. P. Gupta, G. Lang, Y.-J. Lee, W. R. Scheidt, K. Shelly and C. A. Reed, *Inorg. Chem.*, 1987, **26**, 3022.
14 G. Allegra, R. Calligaris, R. Furlanetto, G. Nardin and L. Randaccio, *Cryst. Struct. Commun.*, 1974, **3**, 69.
15 R. A. Freitag and D. G. Whitten, *J. Phys. Chem.*, 1983, **87**, 3918.
16 M. J. Crossley, L. D. Field, A. J. Forster, M. M. Harding and S. Sternhell, *J. Am. Chem. Soc.*, 1987, **109**, 341.

Evidence for α-lactone intermediates in addition of aqueous bromine to disodium dimethyl-maleate and -fumarate

James J. Robinson,[ab] J. Grant Buchanan,*[a] Michael H. Charlton,[b] Richard G. Kinsman,[a] Mary F. Mahon[a] and Ian H. Williams*[a]

[a] *Department of Chemistry, University of Bath, Bath UK BA2 7AY. E-mail: i.h.williams@bath.ac.uk*
[b] *Oxford Asymmetry International, 151 Milton Park, Abingdon, UK OX14 4SD*

Received (in Cambridge, UK) 8th January 2001, Accepted 5th February 2001
First published as an Advance Article on the web 20th February 2001

Crystallographic analysis of the bromo-β-lactones obtained by addition of bromine to aqueous solutions of disodium 2,3-dimethylmaleate and 2,3-dimethylfumarate reveals stereochemistries opposite to those originally assigned and suggests that the first-formed intermediate in each case is an α-lactone.

It is widely accepted that the addition of halogens to an alkene occurs in two stages and in an *anti* manner.[1] In 1937, Tarbell and Bartlett[2] found that the disodium salts of 2,3-dimethylmaleic acid and 2,3-dimethylfumaric acid (**1** and **2**) reacted stereospecifically with aqueous bromine, each yielding a single crystalline bromo-β-lactone; similar results were obtained with chlorine. The stereospecific nature of the reaction implied that the addition of the two components to the alkene was concerted. The authors proposed that the addition of bromine to give a carbocation was followed 'in the quickest possible succession' by attack of the carboxylate group leading directly to a β-lactone. The structures of the lactones (**3** and **4**, respectively) were assigned on this basis, corresponding to *anti* addition at the double bond. This work shortly predated the important paper by Roberts and Kimball[3] proposing cyclic halonium ion intermediates for halogen addition to alkenes. In Scheme 1 we have illustrated the two possible interpretations given at that time.[2,4]

We suspected that the reaction might be more complex than had been supposed, and have therefore prepared the two bromolactones from **1** and **2** by the published method[2] and established their structures by X-ray crystallography. The structures found (**4** from **1**,† and **3** from **2**,‡ Fig. 1) correspond to overall *syn* addition to the alkene. This unequivocal result is in contrast to the *anti* addition supposed by the Tarbell and Bartlett mechanism or arising from direct attack by carboxylate anion on a cyclic bromonium ion intermediate.[4,5] We believe that the most satisfactory explanation of our results (Scheme 2) involves formation of an α-lactone intermediate[6] (**5** and **6**) as the first step in the decomposition of the bromonium ion. Subsequently the other carboxylate group attacks the α-lactone, with a second inversion of configuration, to give the β-lactone. This scheme accounts simply and satisfactorily for the overall

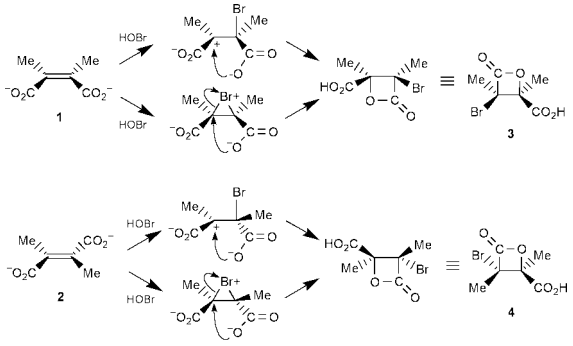

Scheme 1

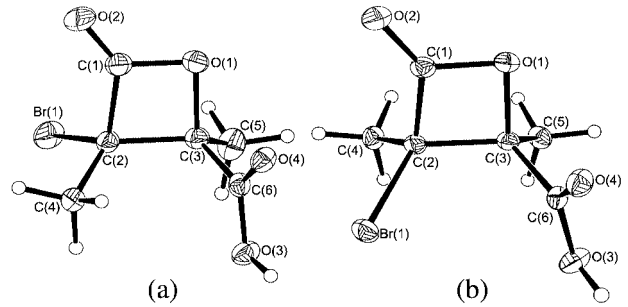

Fig. 1 X-Ray crystallographic structures for bromo-β-lactones: (a) compound **4** from disodium 2,3-dimethylmaleate; (b) compound **3** from disodium 2,3-dimethylfumarate.

stereochemical outcome. Furthermore, both of the individual steps, the formation of the α-lactone from the bromonium ion followed by formation of the β-lactone, are favoured *exo* processses in the Baldwin sense.[7–10] It is known that β-lactones are formed as kinetically controlled products in halolactonisation of salts of β,γ-unsaturated acids,[11,12] involving ring opening of the halonium intermediate in an *exo* manner.[13] Scission of the bromonium ion derived from a salt of an α,β-unsaturated monocarboxylic acid to give a β-lactone directly has been recognised as a relatively unfavourable pathway,[7,12–14] and can only be achieved under certain conditions.[13–16]

In support of our proposed mechanism, it is known that halogenation of certain allylic alcohols leads to epoxides by rearrangement of the halonium ion.[17–22] More pertinent is the behaviour of maleic acid and fumaric acid towards halogens; bromine in ether converts the free acids into the dibromides expected from *anti* addition.[23] On the other hand, treatment of disodium maleate with aqueous chlorine affords the *erythro* chlorohydrin[24] or, in the presence of an excess of chloride ions, the *erythro* (*meso*) dichloro compound,[25] the products of overall *syn* addition; disodium fumarate reacts *via* both *anti* and *syn* addition (80 : 20).[24,26] During the course of this work we became aware of the suggestion by Badea,[27] without experimental evidence, that an α-lactone intermediate might account for the *syn* addition.

α-Lactones are known to undergo intramolecular nucleophilic attack under aqueous conditions. Reaction of 2-amino-2-deoxy-D-gluconic acid with nitrous acid affords 2,5-anhydro-D-gluconic acid by double inversion *via* an α-lactone intermediate.[28] Similar reactions of L-glutamic acid and L-

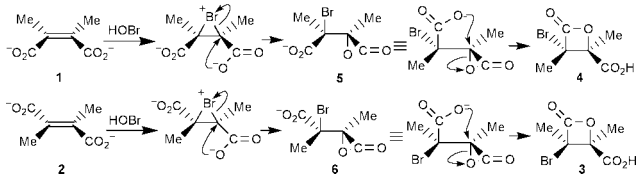

Scheme 2

DOI: 10.1039/b100335f

glutamine result in the γ-lactone of L-α-hydroxyglutaric acid.[29,30] It appears that in the system we have studied ring closures are facilitated by alkyl substitution (the 'Thorpe–Ingold' effect);[31] there is no evidence for β-lactone formation during the chlorination of disodium maleate,[24–26] nor in the deamination of L-asparagine.[30]

Despite their high instability,[32] α-lactones may be more prevalent as reaction intermediates than has generally been imagined. Computational studies are in progress to evaluate structural and energetic aspects of the alternative mechanisms in Schemes 1 and 2 in order to elucidate the factors determining the preferred course of reactivity *via* the α-lactone intermediate.

Notes and references

† **4**, [3*S*(3*R*),4*S*(4*R*)]-3-Bromo-4-carboxy-3,4-dimethyloxetan-2-one, mp 92–94 °C (lit.,[2] 95–96 °C); δ_H [400 MHz, $(CD_3)_2SO$] 1.81 (s, 3H, Me), 1.93 (s, 3H, Me); δ_C [100 MHz, $(CD_3)_2SO$] 22.9 (Me), 23.1 (Me), 64.4 (C-3), 83.6 (C-4), 166.5 (C=O), 168.2 (C=O). *Crystal data*: $C_6H_7BrO_4$, M = 223.03, monoclinic, a = 10.4057(9), b = 6.4044(4), c = 12.0468(11) Å, β = 92.812(4)°, U = 801.86(11) Å^3, T = 170(2) K, space group $P2_1/c$, Z = 4, μ(Mo-Kα) = 5.090 mm^{-1}, 8001 reflections (R_{int} = 0.0514), R_1 = 0.0364 and wR_2 = 0.1021 based on 1328 F^2 data with $F_o > 4\sigma(F_o)$. Software used SHELXS,[33] SHELXL[34] and ORTEX.[35] CCDC 149760. See http://www.rsc.org/suppdata/cc/b1/b100335f/ for crystallographic data in .cif or other electronic format.

‡ **3**, [3*R*(3*S*),4*S*(4*R*)]-3-Bromo-4-carboxy-3,4-dimethyloxetan-2-one, mp 148 °C (lit.,[2] 148–150 °C); δ_H [400 MHz, $(CD_3)_2SO$] 1.77 (s, 3H, Me), 1.99 (s, 3H, Me); δ_C [100 MHz, $(CD_3)_2SO$] 18.3 (Me), 21.0 (Me), 61.4 (C-3), 85.0 (C-4), 166.7 (C=O), 168.9 (C=O). *Crystal data*: $C_6H_7BrO_4$, M = 223.03, triclinic, a = 6.0820(4), b = 6.3270(4), c = 11.6600(8) Å, α = 81.416(4), β = 88.333(5), γ = 62.060(4)°, U = 391.52(4) Å^3, T = 170(2) K, space group $P\bar{1}$ (No. 2), Z = 2, μ(Mo-Kα) = 5.212 mm^{-1}, 4102 reflections (R_{int} = 0.0675) $R1$ = 0.0330 and $wR2$ = 0.0918 based on 1469 F^2 data with $F_o > 4\sigma(F_o)$. Software used SHELXS,[33] SHELXL[34] and ORTEX.[35] CCDC 149759. See http://www.rsc.org/suppdata/cc/b1/b100335f/ for crystallographic data in .cif or other electronic format.

1 P. B. D. de la Mare and R. Bolton, *Electrophilic Additions to Unsaturated Systems*, 2nd edn., Elsevier, New York, 1982.
2 D. S. Tarbell and P. D. Bartlett, *J. Am. Chem. Soc.*, 1937, **59**, 407.
3 I. Roberts and G. E. Kimball, *J. Am. Chem. Soc.*, 1937, **59**, 947.
4 S. Winstein and H. J. Lucas, *J. Am. Chem. Soc.*, 1939, **61**, 1576.
5 E. S. Gould, *Mechanism and Structure in Organic Chemistry*, Holt, Rinehart and Winston, New York, 1959, pp. 522 and 611.
6 C. F. Rodriquez and I. H. Williams, *J. Chem. Soc., Perkin Trans. 2*, 1997, 959 and references therein.
7 J. E. Baldwin, *J. Chem. Soc., Chem. Commun.*, 1976, 734 (p.736).
8 J. G. Buchanan and A. R. Edgar, *Carbohydr. Res.*, 1969, **10**, 295; J. A. Mills, *Adv. Carbohydr. Chem.*, 1955, **10**, 1 (p. 8).
9 J. G. Buchanan and H. Z. Sable, in *Selective Organic Transformations*, ed. B. S. Thyagarajan, Wiley, New York, 1972, vol. 2, p. 53.
10 G. Stork and J. F. Cohen, *J. Am. Chem. Soc.*, 1974, **96**, 5270.
11 W. E. Barnett and W. H. Sohn, *J. Chem. Soc., Chem. Commun.*, 1972, 472, and references therein.
12 K. E. Harding and T. H. Tiner, in *Comprehensive Organic Synthesis*, ed. B. M. Trost, Pergamon, Oxford, **1991**, vol. 4, p. 363, and references therein.
13 F. Homsi and G. Rousseau, *J. Org. Chem.*, 1999, **64**, 81.
14 C. A. Kingsbury and G. Max, *J. Org. Chem.*, 1978, **43**, 3131.
15 C. C. Price and H. W. Blunt, *J. Org. Chem.*, 1969, **34**, 2484.
16 D. Solas and J. Wolinsky, *Synth. Commun.*, 1981, **11**, 609.
17 S. Winstein and L. Goodman, *J. Am. Chem. Soc.*, 1954, **76**, 4373.
18 B. Ganem, *J. Am. Chem. Soc.*, 1976, **98**, 858.
19 R. D. Evans, J. W. Magee and J. H. Schauble, *Synthesis*, 1988, 862.
20 B. O. Lindgren and C. M. Svahn, *Acta. Chem. Scand.*, 1970, **24**, 2699.
21 M. Santelli and J. Viala, *Tetrahedron Lett.*, 1977, 4397.
22 M. M. Midland and R. L. Halterman, *J. Org. Chem.*, 1981, **46**, 1229.
23 A. McKenzie, *J. Chem. Soc.*, 1912, **101**, 1196.
24 R. Kuhn and F. Ebel, *Ber.*, 1925, **58**, 919;
25 E. M. Terry and L. Eichelberger, *J. Am. Chem. Soc.*, 1925, **47**, 1067.
26 R. Kuhn and T. Wagner-Jauregg, *Ber.*, 1928, **61**, 504.
27 F. Badea, *Reaction Mechanisms in Organic Chemistry*, Abacus Press, Tunbridge Wells, Kent, 1977, p. 496.
28 A. B. Foster, *Chem. Ind. (London)*, 1955, 627.
29 H. Sachs and E. Brand, *J. Am. Chem. Soc.*, 1954, **76**, 3601.
30 A. T. Austin and J. Howard, *J. Chem. Soc.*, 1961, 3278; A. T. Austin and J. Howard, *J. Chem. Soc.*, 1961, 3284; A. T. Austin and J. Howard, *J. Chem. Soc.*, 1961, 3593.
31 A. J. Kirby, *Adv. Phys.Org.Chem.*, 1980, **17**, 183.
32 C. F. Rodriquez and I. H. Williams, *J. Chem. Soc., Perkin Trans. 2*, 1997, 953.
33 G. M. Sheldrick, *Acta Cryst.*, 1990, **A46**, 467.
34 G. M. Sheldrick, *SHELXL–97*, a computer program for crystal structure refinement, University of Göttingen, 1997.
35 P. McArdle, *J. Appl. Cryst.*, 1995, **28**, 65.

A new non-metal heterogeneous catalyst for the activation of hydrogen peroxide: a perfluorinated ketone attached to silica for oxidation of aromatic amines and alkenes

Karine Neimann and Ronny Neumann*

Department of Organic Chemistry, The Weizmann Institute of Science, Rehovot, Israel 76100. E-mail: ronny.neumann@weizmann.ac.il

Received (in Cambridge, UK) 10th January 2001, Accepted 31st January 2001
First published as an Advance Article on the web 20th February 2001

A silane functionalized by octafluoroacetophenone was polymerized by the sol–gel method to form an insoluble silicate with perfluoroketone pendants; the silicate was used as a heterogeneous catalyst for the activation of aqueous hydrogen peroxide and the oxidation of aromatic amines and alkenes.

The preparation of heterogeneous catalysts for the activation of hydrogen peroxide and their use for oxidation of organic substrates has been the subject of rather intense research efforts over the last 10–15 years. Almost exclusively this effort has been concentrated on the incorporation of metal-based catalysts onto or into inert matrices. This has been achieved either by substitution of active metals (titanium, vanadium *etc*.) into molecular sieves[1] or amorphous silica,[2] or by encapsulation or attachment of organometallic catalysts onto supports.[3] There are only a few organic compounds capable of activating hydrogen peroxide. Thus, under basic conditions hydrogen peroxide can be used for the epoxidation of electron deficient alkenes[4] and this has led to guanidine functionalized silica for such reactions.[5] A perfluorinated ketone, hexafluoroacetone, also is a known compound capable of reacting with hydrogen peroxide to yield an α-hydroperoxyperfluoro alcohol intermediate capable of reacting with nucleophilic substrates to give oxygenated products,[6] Scheme 1. The high toxicity and volatility of hexafluoroacetone has prevented the wide use of this catalytic system. Recently, a high molecular weight perfluoroketone with less volatility has been suggested as a suitable improvement for hexafluoroacetone in similar oxidation reactions.[7]

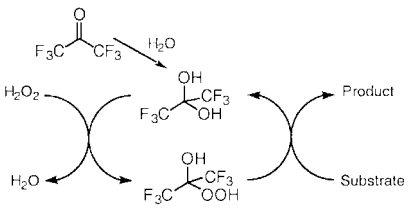

Scheme 1

Now we present a silica immobilized perfluoroketone as an effective heterogeneous recyclable catalyst for the oxidation of aromatic amines such as pyridine and its derivatives and aniline and its derivatives in addition to alkenes, using aqueous hydrogen peroxide as oxygen donor. The strategy for the preparation of the perfluoroketone non-metal silicate catalyst is presented in Scheme 2. First, the ketone moiety of octafluoroacetophenone was protected by formation of an imine with *n*-butylamine. The protected perfluoroketone was then attached to an aminosilane by nucleophilic substitution and the insoluble silicate was prepared by co-polymerization with tetraethoxysilane by the sol–gel method. The final heterogeneous catalyst was then obtained by removal of the *n*-butylamine protecting group.†

The perfluoroketone–silicate catalyst was tested for activity with several substrate types.‡ First, the oxidation of pyridine and derivatives to the corresponding *N*-oxides, showed that the catalyst was quite effective for this reaction, Table 1. The yields were generally high for some representative substrates such as pyridine, 2- and 4-methylpyridine, quinoline, and 4-methylquinoline; *N*-oxides were the only products. Interestingly, 8-hydroxyquinoline was less reactive, presumably because of steric considerations, and the electron-poor 2,6-dichloropyridine was unreactive as expected. The oxidation of aniline and its derivatives catalysed by the perfluoroketone–silicate gave somewhat more surprising results, Table 2. Aniline, alkyl-

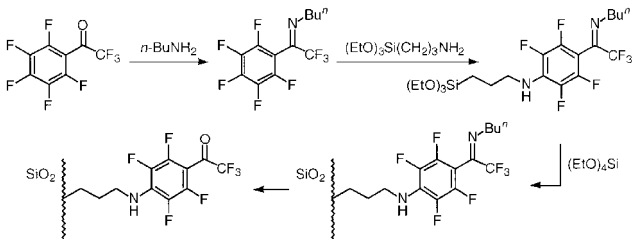

Scheme 2

Table 1 Oxidation of pyridine derivatives with 60% H_2O_2 catalysed by the perfluoroketone–silicate

Substrate	Product	Yield (mol%)
Pyridine	Pyridine 1-oxide	99
2-Methylpyridine	2-Methylpyridine 1-oxide	84
4-Methylpyridine	4-Methylpyridine 1-oxide	93
Quinoline	Quinoline 1-oxide	87
4-Methylquinoline	4-Methylquinoline 1-oxide	83
8-Hydroxyquinoline	8-Hydroxyquinoline 1-oxide	20
2,6-Dichloropyridine	2,6-Dichloropyridine 1-oxide	0

Reaction conditions: 0.8 mmol substrate, 20 mg (0.05 mmmol ketone) perfluoro–silicate, 1 mL acetonitrile, 3 mmol 60% H_2O_2, 24 h, 80 °C. Yields were computed by GC analysis.

Table 2 Oxidation of aniline derivatives with 60% H_2O_2 catalysed by the perfluoroketone–silicate

Substrate	Product	Yield (mol%)
Aniline	Diphenyldiazene 1-oxide	100
3-Methylaniline	Bis(3-methylphenyl)diazene 1-oxide	100
2-Ethylaniline	Bis(2-ethylphenyl)diazene 1-oxide	100
3-Trifluoromethylaniline	Bis(3-trifluorophenyl)diazene 1-oxide	100
3-Fluoroaniline	Bis(3-Fluorophenyl)diazene 1-oxide	100
3-Nitroaniline	1,3-Dinitrobenzene	100
2-Methyl-4-hydroxyaniline	4-Nitro-5-methylphenol	100
4-Hydroxyaniline	4-Nitrophenol	100
2-Nitroaniline	None	—
4-methoxy-2-nitroaniline	None	—

Reaction conditions: 0.8 mmol substrate, 20 mg (0.05 mmmol ketone) perfluoro–silicate, 1 mL acetonitrile, 3 mmol 60% H_2O_2, 12 h, 80 °C. Yields were computed by GC analysis.

DOI: 10.1039/b100421m

substituted aniline and halogen-substituted aniline derivatives all yielded the dimeric azoxy compounds as *sole* products in quantitative yields. On the other hand aniline with electron donating hydroxy substitution or electron withdrawing nitro substitution yielded the corresponding nitro derivatives, provided the nitro was not *ortho* to the amino substituent. In this latter case there was no reaction, possibly related to intramolecular hydrogen bonding between the amino and nitro substituents. For the other cases, we have as yet no satisfactory explanation for partial oxidation and the *selective* formation of azoxy compounds on the one hand for aniline, alkylated anilines and halogenated anilines and full oxidation to nitro derivatives in the case of 3-nitroaniline and 4-hydroxyaniline.

The catalytic activity of the perfluoroketone–silicate was also tested for oxidation of alkenes, Table 3. For less nucleophilic substrates such as oct-1-ene and oct-2-ene, activity was low although the initial epoxide product formed was stable under the reaction conditions and epoxides were obtained selectively. More nucleophilic substrates such cyclohexene, 1-methylcyclohexene and 2,3-dimethylbut-2-ene were much more reactive and high conversions were obtained. However, selectivity to the epoxide was very low due presumably to acid catalysed formation of diols or pinacol rearrangement. Interestingly, primary allylic alcohols reacted to yield mostly aldehyde as the product using 30% H_2O_2; no epoxidation was observed. Thus, 0.8 mmol (Z)-hex-2-en-1-ol was reacted with 2 mmol 30% H_2O_2 in 1 mL EtOAc at 80 °C for 24 h to yield 94% hex-2-enal.

Finally, the stability and activity of the catalyst was tested in a multi-recycle experiment. Thus, 4 mmol aniline, 100 mg (0.25 mmmol ketone) perfluoro–silicate and 15 mmol 60% H_2O_2 were mixed in 5 mL acetonitrile at 80 °C for 18 h. More than 98% of the aniline reacted to diphenyldiazene 1-oxide. The mixture was filtered and the catalyst washed twice with dichloromethane, dried and reused in an additional reaction. Over a period of five reaction cycles, as described above, no significant loss of activity was observed and yields of diphenyldiazene 1-oxide remained > 95%.

Table 3 Oxidation of alkenes with 60% H_2O_2 catalysed by the perfluoroketone–silicate

Substrate	Products (Yield (mol%))	Conversion (mol%)
Cyclooctene	Cyclooctene oxide (100)	78
Oct-2-ene	Oct-2-ene oxide (100)	16
Oct-1-ene	Oct-1-ene oxide (100)	6
Cyclohexene	Cyclohexane-1,2-diol (80) Cyclohex-2-en-1-ol (15) Other (5)	61
1-Methylcyclohexene	1-Methylcyclohexane-1,2-diol (86) 2-Methylcyclohexanone (10) Other (4)	100
2,3-Dimethylbut-2-ene	2,3-Dimethylbut-2-ene oxide (16) 2,3-Dimethylbutane-2,3-diol (21) 2,3-Dimethylbutan-2-one (63)	100

Reaction conditions: 0.8 mmol substrate, 20 mg (0.05 mmmol ketone) perfluoro–silicate, 1 mL acetonitrile, 3 mmol 60% H_2O_2, 24 h, 80 °C. Yields were computed by GC analysis.

Notes and references

† Octafluoroacetophenone (6 mmol, 1 g) was reacted with *n*-butylamine (6 mmol, 0.57 mL) in 50 mL dry toluene for 5 h at 60 °C in a 250 mL flask. After this time 3-aminopropyl(trimethoxy)silane (6 mmol, 1.43 mL) was added and the solution was heated and stirred under reflux while the reaction was monitored by ^{19}F NMR ($CDCl_3$). The starting compound (Shiff base) has peaks at −75.7 ppm (s, β position, 3F), −161.6 ppm (d, *ortho* position, 2F), −138.2 ppm (m, *meta* position, 2F) and −153.2 ppm (d, *para* position, 1F), whereas the product has peaks at −75.7 ppm (s, β position, 3F), −160.3 ppm (d, *ortho* position, 2F) and −141.5 ppm (m, *meta* position, 2F). After one week the reaction was complete and tetraethoxysilane (9 mmol, 2 mL), water (3 mL), dibutyltin dilaurate (0.09 mL, 0.15 mmol) in 100 mL of ethanol were added; the solution was then heated at 60 °C for 12 h. After this time, the reaction mixture was transferred into a beaker and the solvent(s) was allowed to evaporate at rt until a yellow–brown solid was obtained. After grinding the silicate to a course powder, the solid was treated by Soxlet extraction with diethyl ether followed by dichloromethane. The silicate was then treated with 100 mL 30% H_2O_2 under reflux for 16 h to remove the protecting group (verified by IR spectroscopy—carbonyl peak at 1640 cm^{-1}). The white powder that was obtained was filtered and washed consecutively by water, acetonitrile and finally with dichloromethane. After drying under vacuum at 60 °C overnight, the silicate was used in the catalytic studies.

‡ The reaction ingredients as noted in the tables were placed in 5 mL vials; the vials were closed and placed in an oil bath at 80 ± 2 °C and the contents stirred magnetically for the noted time period. After the reaction was completed the organic phase was extracted with dichloromethane (5 mL) and analyzed by GC and GC-MS using a 30 m 5% phenylmethylsilicone capillary column (0.32 mm id, 0.25 μm coating).

1 I. W. C. E. Arends, R. A. Sheldon, M. Wallau and U. Schuchardt, *Angew. Chem., Int. Ed. Engl.*, 1997, **36**, 1143.
2 R. Hutter, T. Mallat, D. Dutoit and A. Baiker, *Topics Catal.*, 1996, **3**, 421; R. Hutter, T. Mallat and A. Baiker, *J. Catal.*, 1995, **153**, 165; R. Hutter, T. Mallat and A. Baiker, *J. Catal.*, 1995, **153**, 177; R. Neumann and M. Levin-Elad, *Appl. Catal. A*, 1995, **122**, 85; R. Neumann and M. Levin-Elad, *J. Catal.*, 1997, **166**, 206.
3 R. A. Sheldon and I. W. C. E. Arends, *Catal. Today*, 1998, **41**, 387.
4 R. D. Temple, *J. Org. Chem.*, 1970, **35**, 1275.
5 Y. V. Subba-Rao, D. E. de Vos and P. A. Jacobs, *Angew. Chem., Int. Ed. Engl.*, 1997, **36**, 2661.
6 R. P. Heggs and B. Ganem, *J. Am. Chem. Soc.*, 1979, **101**, 2346; A. J. Biloski, R. P. Heggs and B. Ganem, *Synthesis*, 1980, 810; P. A. Ganespure and W. Adam, *Synthesis*, 1996, 179
7 M. C. A. van Vliet, I. W. C. E. Arends and R. A. Sheldon, *Chem. Commun.*, 1999, 263.

ChemComm

Fabrication of heterogeneous macroporous materials based on a sequential electrostatic deposition process

Dayang Wang and Frank Caruso*

Max Planck Institute of Colloids and Interfaces, D-14424 Potsdam, Germany.
E-mail: frank.caruso@mpikg-golm.mpg.de

Received (in Cambridge, UK) 11th December 2000, Accepted 6th February 2001
First published as an Advance Article on the web 20th February 2001

Heterogeneous macroporous materials are prepared by the sequential electrostatic deposition of fluorescein isothiocyanate-labeled poly(allylamine hydrochloride) and cadmium telluride nanocrystals onto macroporous titania structures.

Ordered macroporous materials with pore diameters in the nanometer to micrometer range have attracted significant interest because of their unique properties, *e.g.* high specific surface area, high damping capacity, low thermal conductivity and low dielectric permittivity. They have a wide range of applications (both structural and functional), including their use as light-weight structural materials,[1] catalytic supports and surfaces,[2] thermal and acoustic insulators,[3] optical devices[4] and as candidates for high speed computer device packaging.[5]

Recently, considerable effort has been devoted to the use of colloidal assemblies as templates for the fabrication of interconnected three-dimensional (3D) macroporous materials.[6] Monodisperse colloidal spheres, either polystyrene, silica or poly(methyl methacrylate),[6] or emulsion droplets,[7] can self-assemble into ordered 3D arrays. These ordered structures offer a 3D scaffold for a variety of precursor materials, which can be infiltrated in the voids between the colloidal spheres. After subsequent solidification of the precursors and removal of the templated colloids, 3D macroporous materials are obtained. The pore dimensions of the structures depend on the diameters of the colloidal spheres employed. This method provides a simple and effective route to the fabrication of macroporous materials with controlled pore sizes and well-defined periodic structures. In the last few years, a variety of organic, inorganic, and metal precursor materials have been used to prepare a wide range of 3D ordered macroporous structures.[6]

The development of heterogeneous (*i.e.* multicomponent) 3D ordered macroporous structures is expected to yield promising materials for use in the areas of catalysis and optical devices based on photonic crystals. However, to date there have been few studies on the fabrication of such materials. For example, Yin and Wang have recently doped macroporous titania with cobalt by the precipitation of mixed precursors,[8] while Stein and co-workers have prepared 3D ordered macroporous organic/inorganic hybrids[9] and alloys[10] using a similar procedure. Here we report a method for creating 3D heterogeneous structures by using a sequential electrostatic deposition process that involves the post-modification of macroporous titania. This technique is based on the electrostatic attraction between sequentially deposited species, and represents a general approach for the fabrication of multicomponent films on planar supports[11] and colloid particles.[12]

Based on electrostatic attractions, poly(allylamine hydrochloride) (M_w 8000–11 000) labeled with fluorescein isothiocyanate (FITC-PAH) and cadmium telluride (CdTe) nanocrystals (3–4 nm in diameter)[14] were consecutively deposited on macroporous titania (TiO_2), which was produced by templating colloidal crystals of polystyrene (PS) spheres with titanium isopropoxide (TIP). The advantages of our approach are that it allows tailoring of the composition (and consequently function) of the heterogeneous macroporous structures through the electrostatic deposition of charged components that coat the inner surface of the materials.

Colloidal crystals of monodisperse PS spheres of diameter 640 nm were used as the template and TIP as the precursor for the formation of macroporous TiO_2 structures, as described earlier.[13] The resulting TiO_2 material was treated with basic solution (1 M sodium hydroxide aqueous solution), after which the macroporous TiO_2 was placed into 2 mL of a 0.5 mg mL^{-1} FITC-PAH solution containing 0.5 M NaCl, and 12 h was allowed for FITC-PAH adsorption. After removal of the FITC-PAH solution, the TiO_2 material was washed five times with 2 mL of water to ensure removal of FITC-PAH not electrostatically bound to the TiO_2. The adsorption of FITC-PAH changes the surface charge of the macroporous TiO_2 to positive due to charge overcompensation.[11] Subsequently, negatively charged CdTe nanocrystals were adsorbed from aqueous solution onto the surface and within the pores of the macroporous TiO_2 modified with FITC-PAH (the electrostatic interactions occur between the NH_3^+ groups of the FITC-PAH and the negatively charged hydroxy and thiol moieties on the surface of the nanocrystals[14]). This resulted in the sample turning red, suggesting a relatively high loading of the CdTe nanoparticles.[15]

The macroporous materials prepared were examined by scanning electron microscopy (SEM). Fig. 1 shows a SEM micrograph of a cross-section of the macroporous TiO_2 produced when using PS colloidal crystals as templates. The center-to-center average distance between the pores is 432 ± 10 nm, reflecting a linear shrinkage of 33% (compared to the diameter of the PS spheres, 640 nm). The round channels in the pore walls are clearly visible, and confirm that the pores in the structure are interconnected with each other. There are small openings in the middle of each of the triangular intersections of the macroporous TiO_2 (indicated by the arrow). These openings are likely caused by incomplete filling of the voids between the spheres.[16]

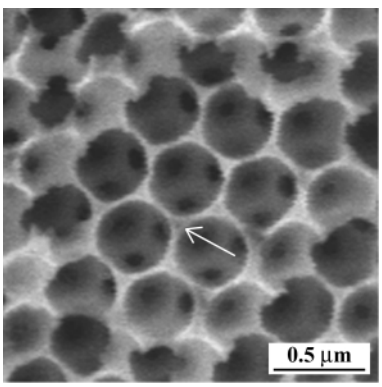

Fig. 1 SEM micrograph of the macroporous TiO_2 structure fabricated by templating pure PS colloidal spheres of diameter 640 nm. The arrow points to the small openings that are present in the middle of each of the triangular intersections of the macroporous TiO_2 material.

DOI: 10.1039/b009897n

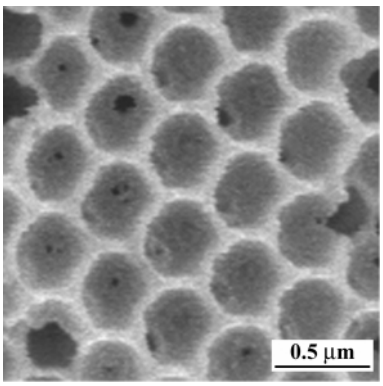

Fig. 2 SEM micrograph of the heterogeneous (TiO_2–FITC-PAH/CdTe) macroporous structure fabricated by the sequential electrostatic adsorption of FITC-PAH and CdTe nanocrystals onto macroporous TiO_2.

Fig. 2 displays a SEM micrograph of a cross-section of the macroporous TiO_2 structure modified with FITC-PAH and CdTe nanocrystals. The resulting heterogeneous (TiO_2–FITC-PAH/CdTe) macroporous material has the same structure as that of the original macroporous TiO_2 (Fig. 1). The center-to-center distance of 427 ± 10 nm is also the same (within experimental error) to that obtained for the unmodified TiO_2 structure. It is clearly observed that the pores are still interconnected with each other (round channels are seen). However, the small openings in the middle of each of the triangular intersections of the pure macroporous TiO_2 material (Fig. 1) are not observed. This suggests that the TiO_2 structure has been coated with the FITC-PAH/CdTe hybrid layer. Energy disperse X-ray (EDX) analysis of the heterogeneous macroporous material indicates the presence of Ti, O, Cd and Te [Fig. 3(a)], demonstrating that the CdTe nanocrystals were adsorbed on the TiO_2. Fig. 3(b) shows the luminescence spectrum of the heterogeneous macroporous material. The shoulder observed around 530 nm corresponds to the emission of the FITC molecules of the labeled PAH, confirming that FITC-PAH was also deposited. The maximum at 570 nm is attributed to the 'excitonic' emission of the 3–4 nm CdTe nanocrystals. It is important to note that the SEM, EDX and fluorescence experiments were conducted on cross-sections of the heterogeneous macroporous structures. The above results verify that the PAH-FITC and CdTe nanocrystals infiltrated the macroporous TiO_2 structure and coated the inside surface. In addition, all of the cross-sectioned samples showed a red color. Preliminary experiments revealed an intensified color for cross-sections of the heterogeneous material when additional FITC-PAH/CdTe nanocrystal multilayers were deposited. Characterization of the growth of FITC-PAH/CdTe nanocrystal multilayers on macroporous TiO_2 structures is currently in progress.

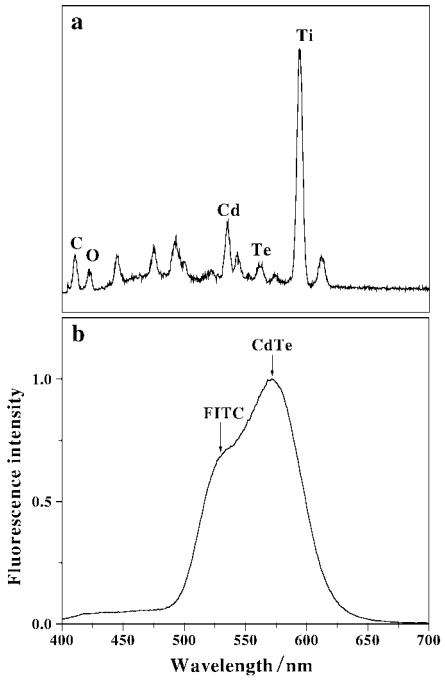

Fig. 3 (a) EDX and (b) luminescence spectra of the heterogeneous macroporous material shown in Fig. 2.

In this study, we have used FITC-PAH, CdTe nanocrystals and macroporous TiO_2 to demonstrate the feasibility of fabricating heterogeneous macroporous materials by using the sequential electrostatic deposition approach. This strategy provides a simple and versatile means to prepare novel macroporous materials, allowing control over their composition and functional properties. Given the general nature of the method, it is expected that complex and tailored structures can be produced with defined multilayers of polyelectrolytes, small organic molecules, inorganic nanoparticles, clays and proteins. Such studies are being undertaken. The creation of such structures should open up new and interesting possibilities for the applications of heterogeneous macroporous materials.

We thank Dangsheng Su and Gisela Weinberg (Fritz Haber Institute, Berlin) for assistance with SEM, and Andrey L. Rogach (Hamburg University) for the CdTe nanocrystals. This work was supported by the BMBF and the Volkswagen Foundation.

Notes and references

1 M. Wu, T. Fuji and G. L. Messing, *J. Non-Cryst. Solids*, 1990, **121**, 407.
2 M. P. Harold, C. Lee, A. J. Burggraaf, K. Kaizer, V. T. Zaspalis and R. S. A. de Lange, *MRS Bull.*, 1994, **19**, 34.
3 E. Litovsky, M. Shapiro and A. Shavit, *J. Am. Ceram. Soc.*, 1996, **79**, 1366.
4 Y. Xia, B. Gates, Y. Yin and Y. Liu, *Adv. Mater.*, 2000, **12**, 693.
5 R. D. Miller, *Science*, 1999, **286**, 421.
6 O. D. Velev and A. M. Lenhoff, *Curr. Opin. Colloid Interface Sci.*, 2000, **56**, 5.
7 A. Imhof and D. J. Pine, *Nature*, 1997, **389**, 943.
8 J. S. Yin and Z. L. Wang, *Adv. Mater.*, 1999, **11**, 469.
9 B. T. Holland, C. F. Blanford, T. Do and A. Stein, *Chem. Mater.*, 1999, **11**, 795.
10 H. Yan, C. F. Blanford, W. H. Smyrl and A. Stein, *Chem. Commun.*, 2000, 1477.
11 G. Decher, *Science*, 1997, **277**, 1232.
12 F. Caruso, R. A. Caruso and H. Möhwald, *Science*, 1999, **282**, 1111; F. Caruso, *Chem. Eur. J.*, 2000, **6**, 413.
13 D. Wang, R. A. Caruso and F. Caruso, *Chem. Mater.*, 2001, in press.
14 A. Rogach, A. Susha, F. Caruso, G. Sukhorukov, A. Kornowski, S. Kershaw, H. Möhwald, A. Eychmüller and H. Weller, *Adv. Mater.*, 2000, **12**, 333.
15 The loading of CdTe nanocrystals was higher (as assessed by visual observation of the color change) when the macroporous TiO_2 material was first immersed in the 1 M NaOH solution for 6 h prior to FITC-PAH/CdTe nanocrystal adsorption steps. The absence of the FITC-PAH layer resulted in only a very low coverage of CdTe nanocrystals on the TiO_2 structure.
16 J. E. G. J. Wijnhoven and W. L. Vos, *Science*, 1998, **281**, 802.

Concerted and stepwise Grignard additions, probed with a chiral Grignard reagent

Reinhard W. Hoffmann* and Bettina Hölzer

Fachbereich Chemie, Philipps-Universität Marburg, Hans-Meerwein-Strasse, D-35032 Marburg, Germany. E-mail: rwho@chemie.uni-marburg.de; Fax: +49 6421 2828917; Tel: +49 6421 2825571

Received (in Cambridge, UK) 4th December 2000, Accepted 30th January 2001
First published as an Advance Article on the web 20th February 2001

The Grignard reagent 6, in which the magnesium-bearing carbon atom is the sole stereogenic centre has been added to CO_2, PhNCO, PhNCS and certain aldehydes with full retention of configuration. Reaction with benzophenone, electron-deficient aldehydes and several allyl halides proceeded with partial or complete racemization. The findings are discussed with respect to a dichotomy between concerted polar and stepwise SET reaction pathways.

Grignard reagents are among the oldest organometallic reagents known.[1] Their chemistry has evolved as the prototype of polar organometallic compounds. Yet, despite the enormous body of polar addition reactions recorded,[2] the mechanism of these additions cannot be considered as settled.[3] Most textbooks describe the addition of Grignard reagents to aldehydes—being representative of carbonyl compounds—as a simple addition, *cf.* **1**. Evidence has however been provided[4] that it is a Grignard dimer (halogen-bridged or alkyl-bridged) that enters into the reaction with the carbonyl group, *cf.* **2**.

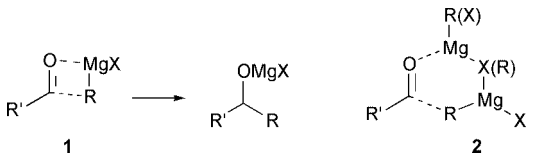

1 **2**

But still, this says little about the nature of the C–C bond forming step. At least in some cases it has been shown that electron transfer precedes the C–C bond formation, especially in addition reactions to carbonyl compounds with a low reduction potential, such as benzophenone.[5,6] While it is tempting to formulate[5,7,8] all polar additions as being initiated by an electron-transfer step, there is at the moment no meaningful way to address the question to what extent electron motion precedes nuclear motion in the formation of the new C–C bond. Rather we have to be content with the heuristic approach that a two-step process can be considered as established, if it is possible to prove the existence of an intermediate (likely the radical R· or radical pair **3**).[9]

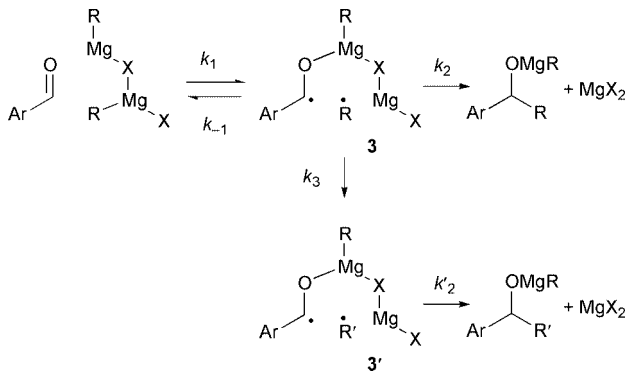

3 **3′**

This is usually done by diverting the radical R· to give another radical R′·, a process that becomes manifest if the rate of conversion (k_3) of R· into R′· is similar to or larger than the rate of collapse (k_2) of the postulated radical pair **3**. Radical rearrangements of known k_3 (radical clocks) have been studied in this context.[5] It is clear, that an ultrafast radical reorganization reaction would enlarge the scope of this approach.[10] This would hold *e.g.* for the conversion of a chiral carbon radical R· to its enantiomer R′·. The barrier to the inversion of the *tert*-butyl radical has been experimentally bracketed to be < 0.5 kcal mol^{-1}.[11] For most practical purposes alkyl radicals can be considered as being planar, that is prochiral. Therefore, the stereochemical probes such as **4**[12,13] and **5**[14] have been used to probe the mechanism of Grignard additions.[15,16]

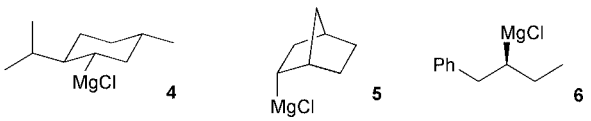

4 **5** **6**

Yet in the case of **4** and **5** it is a moot point, to what extent the stereochemical outcome is influenced by the presence of the additional stereogenic centres (only one case of epimerisation[13] has been so far observed). The ideal probe would be a Grignard reagent such as **6**, in which the magnesium-bearing carbon atom is the sole stereogenic centre. We have recently described an access to such a species of *ca.* 90% ee by asymmetric synthesis.[17] We report here on the use of this reagent as a mechanistic probe in Grignard additions to carbonyl compounds and in Grignard-substitution reactions.

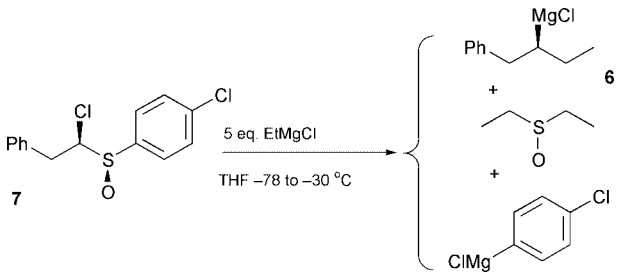

7

The reagent **6** is generated in *ca.* 90% ee from the enantiomerically and diastereomerically pure sulfoxide **7**.[17] Due to the mode of generation, the solution of **6** contains *ca.* 2 equiv. of EtMgCl, one equiv. of *p*-Cl-C_6H_4-MgCl and one equiv. of diethyl sulfoxide. The reagent **6** is configurationally stable in this cocktail in THF solution up to −30 °C; racemization proceeds with $t_{1/2}$ = 5 h at −10 °C.

Therefore those polar additions can be investigated that proceed readily at −30 °C or below. This holds *e.g.* for the addition of **6** to CO_2, PhNCO, or PhNCS which provides the adducts **8**, **9**, and **10**. The same level of enantiomeric purity of these adducts suggests that the value of 90 ± 2% ee represents the enantiomeric purity of **6** and that the addition proceeds without racemization (Table 1).

The absolute configuration of compounds **8**[18] and **10**[17] is known, that of **9** has been established by chemical correlation

DOI: 10.1039/b009678o

Table 1 Trapping of the Grignard reagent **6** (*ca.* 90% ee) with various electrophiles

Electrophile	Product(s)	Configuration[a]	Yield (%)	ee (%)
CO_2	HOOC-CH(Et)Bn **8**	*S*	80	92
PhNCO	PhNHCO-CH(Et)Bn **9**	*S*	60	89
PhNCS	PhNHCS-CH(Et)Bn **10**	*S*	56	91
ArCHO[b]	ArCHOH-CH(Et)Bn	n.d.	41	D1: 89 D2: 84
PhCHO	PhCHOH-CH(Et)Bn	*S*	42	D1: 88 D2: 84
C_6F_5CHO **11**	C_6F_5CHOH-CH(Et)Bn	n.d.	45	D1: 43 D2: 47
Ph_2CO **12**	Ph_2COH-CH(Et)Bn	—	85	12

[a] At the former Grignard C-atom. [b] Ar = *p*-MeO-C_6H_4—. n.d.: not determined.

with compound **8**. This establishes that the addition reactions proceeded with retention of configuration. This is in line with the finding for the carboxylation of **5**.[14] As the addition of formaldehyde to **5** proceeded as well without epimerisation,[15] we looked at the addition of **6** to aromatic aldehydes, where the intervention of electron transfer steps is more likely. Addition of **6** to aldehydes generates two diastereomeric adducts (D1; D2), which were derivatized with Mosher's reagent and analysed by ^{1}H-NMR spectroscopy. Both for addition to benzaldehyde and *p*-methoxybenzaldehyde the formation of the major diastereomer proceeded without loss in enantiomeric purity. There is a slight decrease in enantiomeric purity of the minor diastereomer, a fact of uncertain significance. Addition to the more electron deficient pentafluorobenzaldehyde clearly led to partially racemized adducts. On addition to benzophenone, which has a reduction potential that is by +0.20 V more positive than that of benzaldehyde,[19] racemization is extensive but not complete.

The partial racemization observed in the addition to **11** and **12** can be interpreted in terms of a competition between a concerted polar addition and a SET initiated process. This would imply that even benzophenone undergoes a polar addition to the extent of 12%. One could also argue that all of these reactions proceed by SET[5,8] and that rotation of R· within the radical pair **3** is only in few instances faster than the collapse of the radical pair.

We then turned our attention to the reaction of Grignard reagent **6** with allylic halides, which proceeds in high yield even at −90 °C and therefore intuitively suggests an SET process.

While allylation with allyl iodide led indeed to racemic product **13** (R = H) we were surprised to find sizeable enantiomeric enrichment when allyl bromide or allyl chloride were allowed to react with **6**. We tend to interprete this as being caused by a competition between a polar S_N2-reaction and an SET process. This is in line with the ordering of the reduction potentials recorded for allyl chloride, bromide and iodide (−1.91; −1.29; −0.23 V *vs.* Hg).[20] The SET process should be faster with ethyl α-bromomethylacrylate and indeed, this gave rise to 79% of racemic product, **13** (R = COOEt).

Thus, with the chiral Grignard reagent **6** it was possible to probe the mechanism of Grignard addition to carbonyl compounds and Grignard substitution reactions with respect to the competition between polar concerted and stepwise SET pathways.

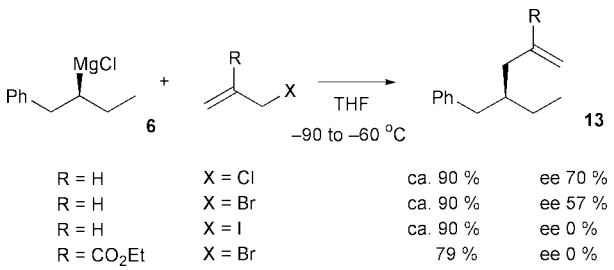

We are grateful to the Deutsche Forschungsgemeinschaft (SFB 260 and Graduiertenkolleg Metallorganische Chemie) as well as the Fonds der Chemischen Industrie for support of this study. We thank Dr O. Knopff for preliminary experiments in the racemic series.

Notes and references

1 J. Cologne, *Bull. Chem. Soc. Fr.*, 1950, **17**, 910.
2 (*a*) M. S. Kharash and O. Reinmuth, *Grignard Reactions of Nonmetallic Substances*, Prentice Hall, New York, 1954; (*b*) B. J. Wakefield, *Organomagnesium Methods in Organic Synthesis*, Academic Press, 1995.
3 T. Holm and I. Crossland, in *Grignard Reagents: New Developments*, ed. H. G. Richey, Jr., J. Wiley & Sons Ltd., New York, 2000, pp. 1–26.
4 (*a*) C. G. Swain and H. B. Boyles, *J. Am. Chem. Soc.*, 1951, **73**, 870; (*b*) E. C. Ashby, R. B. Duke and H. M. Neumann, *J. Am. Chem. Soc.*, 1967, **89**, 1964.
5 E. C. Ashby, *Pure Appl. Chem.*, 1980, **52**, 545.
6 E. C. Ashby, J. Laemmle and H. M. Neumann, *Acc. Chem. Res.*, 1974, **7**, 272.
7 C. Walling, *J. Am. Chem. Soc.*, 1988, **110**, 6846.
8 H. Yamataka, T. Matsuyama and T. Hanafusa, *J. Am. Chem. Soc.*, 1989, **111**, 4912.
9 Other approaches have used *e.g.* isotope effects or linear free energy relationships to demonstrate that the addition of certain alkyl Grignard reagents to benzophenone is not a one-step process: (*a*) T. Holm and I. Crossland, *Acta Chem. Scand.*, 1971, **25**, 59; (*b*) T. Holm, *Acta Chem. Scand.*, 1973, **27**, 1552; (*c*) J. J. Gajewski, W. Bocian, N. J. Harris, L. P. Olson and J. P. Gajewski, *J. Am. Chem. Soc.*, 1999, **121**, 326; and ref. 8.
10 J. M. Tanko and L. E. Brammer, Jr., *J. Chem. Soc., Chem. Commun.*, 1994, 1165.
11 D. Griller, K. U. Ingold, P. J. Krusic and H. Fischer, *J. Am. Chem. Soc.*, 1978, **100**, 6750.
12 (*a*) M. Tanaka and I. Ogata, *Bull. Chem. Soc. Jpn.*, 1975, **48**, 1094; (*b*) H. Schumann, B. C. Wassermann and F. E. Hahn, *Organometallics*, 1992, **11**, 2803.
13 D. Dakternieks, K. Dunn, D. J. Henry, C. H. Schiesser and E. R. Tiekink, *Organometallics*, 1999, **18**, 3342.
14 F. R. Jensen and K. L. Nakamaye, *J. Am. Chem. Soc.*, 1966, **88**, 3437.
15 J. S. Filippo and J. W. Nicoletti, *J. Org. Chem.*, 1977, **42**, 1940.
16 D. E. Bergbreiter and O. M. Reichert, *J. Organomet. Chem.*, 1977, **125**, 119.
17 R. W. Hoffmann, B. Hölzer, O. Knopff and K. Harms, *Angew. Chem.*, 2000, **112**, 3206; *Angew. Chem., Int. Ed.*, 2000, **39**, 3072.
18 W. Kirmse, P. Feyen, W. Gruber and W. Kapmeyer, *Chem. Ber.*, 1975, **108**, 1839.
19 H.-W. Buckel and F. Wasgestian, *Ber. Bunsen-Ges. Phys. Chem.*, 1983, **87**, 154.
20 M. v. Stackelberg and W. Stracke, *Z. Elektrochem. Angew. Phys. Chem.*, 1949, **53**, 118.

Synthesis of fluorescent stilbene and tolan rotaxanes by Suzuki coupling

Carol A. Stanier,[a] Michael J. O'Connell,[a] William Clegg[b] and Harry L. Anderson*[a]

[a] *Department of Chemistry, University of Oxford, Dyson Perrins Laboratory, South Parks Road, Oxford, UK OX1 3QY. E-mail: harry.anderson@chem.ox.ac.uk*

[b] *Department of Chemistry, University of Newcastle, Newcastle-upon-Tyne, UK NE1 7RU and CCLRC Daresbury Laboratory, Warrington, UK WA4 4AD*

Received (in Cambridge, UK) 15th December 2000, Accepted 24th January 2001
First published as an Advance Article on the web 15th February 2001

Highly fluorescent stilbene and tolan cyclodextrin [2]rotaxanes have been synthesised in good yield using aqueous Suzuki coupling, and the crystal structure of one of these rotaxanes has been determined.

A rotaxane is a supramolecular assembly of a dumbbell locked through the cavity of a macrocycle.[1] The formation of rotaxanes provides a means of stabilising dumbbell-shaped chromophores, by shielding them from the external environment. This type of encapsulation can also enhance the fluorescence efficiency.[2] Hydrophobic binding is a convenient way of directing rotaxane formation, provided the dumbbell can be synthesised in water. Recently we reported the synthesis of poly-*p*-phenylene rotaxanes and polyrotaxanes using aqueous Suzuki coupling, although in this case the [2]rotaxane (**1a** in Table 1) was only obtained in low yield (4%).[3] While exploring the scope of this route to rotaxanes, we discovered that the right combinations of aryl iodide stopper, diboronic acid core and macrocycle components give highly fluorescent cyclodextrin encapsulated stilbenes and tolans, such as **1g**, in high yield. Previous stilbene rotaxanes have been prepared by aromatic nucleophilic substitution[4] and by slipping macrocycles over pre-formed dumbbells.[5]

Six new rotaxanes **1b**–**g** have been prepared by reacting bulky water-soluble aryl iodides **2a** and **2b** with diboronic acids **3a**–**c**[6] in the presence of cyclodextrins (α-CD and β-CD; *ca*. 5 eq.), in aq. sodium carbonate containing palladium(II) acetate, as summarised in Scheme 1 and Table 1.† As expected, the 5-iodoisophthalic acid stopper **2b** is too narrow to form rotaxanes with β-CD, and the biphenyl diboronic acid core **3a** is too bulky to form rotaxanes with α-CD. Apart from these exceptions, all combinations of aryl iodides, diboronic acids and macrocycles yield rotaxanes. The lower yields obtained with the 1-iodonaphthalene-3,6-disulfonate stopper **2a** can be attributed to an unfavourable interaction between the bound CD and the inwardly pointing H8 of the naphthalene. The tetracarboxylate

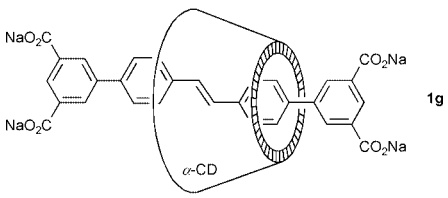

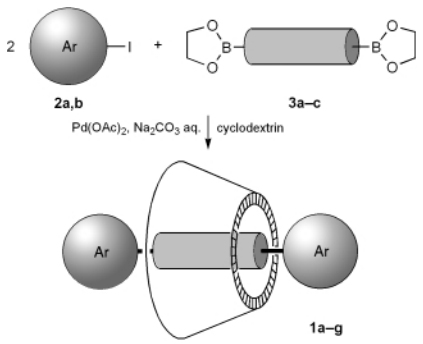

Scheme 1

Table 1 Yields for rotaxane synthesis, and fluorescence behaviour of rotaxanes and dumbbells[a]

Stopper	Diboronic acid core	Macrocycle	Rotaxane	Yield (%) Rotaxane	Φ_F Rotaxane	Φ_F Dumbbell	λ_{max}(em)/nm Rotaxane	λ_{max}(em)/nm Dumbbell
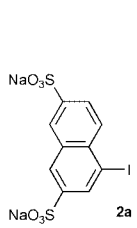	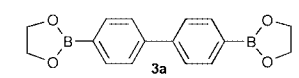	β-CD	**1a**	4	1.04	0.67	394	418
	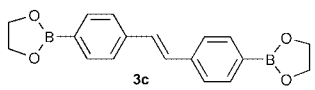	α-CD	**1b**	31	1.08	0.81	387	409
		β-CD	**1c**	16	0.98		390	
	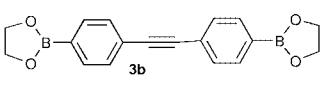	α-CD	**1d**	25	1.03	0.30	416	445
		β-CD	**1e**	14	0.72		425	
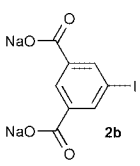	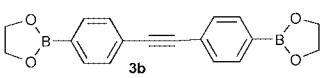	α-CD	**1f**	50	0.99	0.89	360, 378	359, 378
	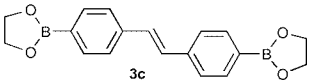	α-CD	**1g**	73	0.94	0.67	387, 406	385, 405

[a]Yields are for isolated rotaxanes; reaction conditions were similar to those detailed for **1g**. Fluorescence spectra were measured in water; quantum yields (Φ_F) are relative to quinine bisulfate in 0.5 M H_2SO_4 (Φ_F = 0.546) and are reproducible to within ± 10%.

DOI: 10.1039/b010015n

rotaxanes **1f** and **1g** are easier to isolate than the sulfonates **1a**–**e**, because they precipitate from aqueous solution at low pH. The smaller isophthalic acid stopper is still large enough to prevent unthreading of α-CD. For example **1g** shows no sign of unthreading after 10 d in D_2O at 80 °C; even after 10 d at 120 °C in d_6-DMSO no unthreading was detected.

One objective of this investigation was to explore how encapsulation affects the fluorescence efficiencies of tolan and stilbene chromophores. Comparison of the fluorescence quantum yields of all seven rotaxanes **1a**–**g** with those of their free dumbbells (Table 1) demonstrates that encapsulation always enhances the fluorescence yield. In both cases where α- and β-CD rotaxanes can be compared (**1b**/**c** and **1d**/**e**) the α-CD is found to give greater fluorescence enhancement. The cyclodextrin probably reduces the rate of non-radiative decay by restricting the flexibility of the excited state, and by hindering the approach of quenchers. A similar effect has recently been reported for stilbenes bound to antibodies.[7] Epoxidation of rotaxane **1g** and its dumbbell analogue with dimethyldioxirane was explored, in order to test the shielding of the chromophore. Dimethyldioxirane (Me_2CO_2) was selected for this experiment because it is small and highly reactive. The dumbbell reacted with dimethyldioxirane in aqueous acetone over a few hours to form the epoxide, whereas no reaction was detected with the rotaxane under the same conditions, even after 24 h, demonstrating that the C=C double bond of the rotaxane is hidden from this reagent.

In order to understand in more detail how the cyclodextrin interacts with the chromophore in these rotaxanes, we have determined the crystal structure of **1g** (as the tetracarboxylic acid).‡ To the best of our knowledge, this is the first crystal structure determination of any cyclodextrin-based rotaxane, although many such rotaxanes have been synthesised[1b] and crystal structures have been reported for cyclodextrin-based pseudorotaxanes and pseudopolyrotaxanes.[9] The α-CD sits round the centre of the chromophore (as shown in Fig. 1a). The stilbene unit is essentially planar (deviation from mean plane < 0.2 Å), with slight twists about both biphenyl links (torsional angles: 29° near the 6-rim; 24° near the 2,3-rim). The CD is distorted into an elliptical conformation, to accommodate the flat π-system, and this distortion is most pronounced around the narrower 6-rim of the macrocycle (Fig. 1b). For example the cavity width defined by the van der Waals surfaces of the H5 hydrogens is 5.3 Å for the transannular H5–H5 distance in the plane of the stilbene, but 4.0 and 4.3 Å for the other two transannular H5–H5 distances. NMR spectra show that the rotaxane is dynamic in solution at 298 K. Only one set of ^{1}H and ^{13}C glucose resonances is observed, showing that the CD rotates rapidly relative to the dumbbell. The H5 protons of the α-CD show NOEs to all six stilbene resonances, indicating that there is significant lateral motion of the macrocycle.

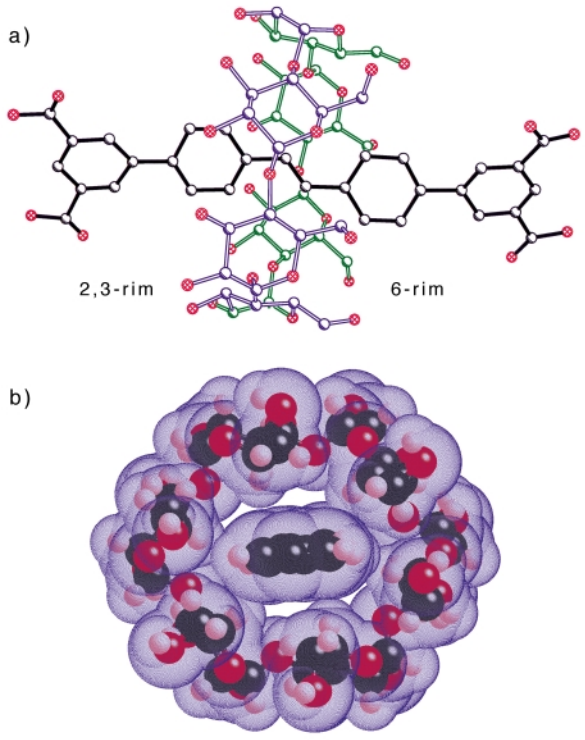

Fig. 1 Structure of rotaxane **1g** in the solid state: (a) view of whole molecule and (b) view of van der Waals surface, from the 6-rim end, with isophthalic acid units deleted for clarity.

In summary, we have shown that Suzuki coupling can be used to prepare cyclodextrin-based rotaxanes in good yield, and that this chemistry can be used to prepare stilbene and tolan rotaxanes with very high fluorescence quantum yields. The crystal structure of one of these compounds shows that the α-cyclodextrin clasps tightly round the centre of the stilbene chromophore.

This work was generously supported by the EPSRC and Avecia Ltd. We are grateful to Dr P. N. Taylor for valuable discussion, and to Dr M. G. Hutchings of DyStar UK Ltd. (Cheadle Hulme) for providing sodium 1-aminonaphthalene-3,6-disulfonate, for preparation of **2a**.

Notes and references

† Procedure for synthesis of **1g**: Water (8 cm^3), **2b** (151 mg, 0.63 mmol), **3c** (100 mg, 0.31 mmol), α-CD (1.6 g, 1.64 mmol), Na_2CO_3 (0.41 g, 3.9 mmol) and $Pd(OAc)_2$ (1.6 mg, 4 mol %) was stirred at 45 °C overnight. The mixture was diluted with Na_2CO_3 aq. (100 cm^3, 0.2 M), filtered, then acidified to pH 1 with HCl, to give a white suspension. The precipitate was separated by centrifugation, redissolved in Na_2CO_3 aq. (100 cm^3, 0.2 M), reprecipitated with acid, washed with water, dissolved in NH_3 aq. and evaporated to yield the ammonium salt of rotaxane **1g** (312 mg, 73%).

‡ Crystals of **1g** were grown over 2 weeks from aqueous solution in a 5 mm NMR tube by warming the lower region to 40 °C while the upper region was cooled to 20 °C. The structure was solved using synchrotron X-rays at Daresbury Station 9.8. *Crystal data* for **1g**: $C_{66}H_{80}O_{38}$, M = 1481.3, monoclinic, space group $I2$ (alternative setting of $C2$), a = 20.767(5), b = 13.960(3), c = 28.085(7) Å, β = 107.479(3)°; U = 7766(3) Å^3, Z = 4, λ = 0.6942 Å, μ = 0.11 mm^{-1}, T = 160 K, $R1$ = 0.164 for 9681 'observed reflections' [$F^2 > 2\sigma(F^2)$] and $wR2$ = 0.394 for all 10443 unique reflections ($\theta < 45°$). Methods and programs were as described elsewhere (ref. 8). Refinement included application of the SQUEEZE procedure (A. L. Spek, PLATON program, University of Utrecht, The Netherlands, 2000) to model diffuse electron density in two substantial voids per unit cell, presumably occupied by highly disordered solvent molecules. No H atoms were included, as they did not appear clearly in difference syntheses and those attached to oxygen atoms cannot be unambiguously placed from purely geometrical considerations. These limitations of the structural model and the weak diffraction due to disorder and crystal size and quality are reflected in the relatively high crystallographic residual factors, as is often found for cyclodextrin-containing materials. CCDC 156256. See http://www.rsc.org/suppdata/cc/b0/b010015n/ for crystallographic files in .cif format.

1 (*a*) *Molecular Catenanes, Rotaxanes and Knots*, ed. J.-P. Sauvage and C. Dietrich-Buchecker, Wiley-VCH, Weinheim, 1999; (*b*) S. A. Nepogodiev and J. F. Stoddart, *Chem. Rev.*, 1998, **98**, 1959; (*c*) H. Ogino, *J. Am. Chem. Soc.*, 1981, **103**, 1303.
2 J. E. H. Buston, J. R. Young and H. L. Anderson, *Chem. Commun.*, 2000, 905.
3 P. N. Taylor, M. J. O'Connell, L. A. McNeill, M. J. Hall, R. T. Aplin and H. L. Anderson, *Angew. Chem., Int. Ed.*, 2000, **39**, 3456.
4 M. Kunitake, K. Kotoo, O. Manabe, T. Muramatsu and N. Nakashima, *Chem. Lett.*, 1993, 1033; C. J. Easton, S. F. Lincoln, A. G. Meyer and H. Onagi, *J. Chem. Soc., Perkin Trans. 1*, 1999, 2501.
5 C. Heim, A. Affeld, M. Neiger and F. Vögtle, *Helv. Chim. Acta*, 1999, **82**, 746.
6 M. Baumgarten and T. Yüksel, *Phys. Chem. Chem. Phys.*, 1999, **1**, 1699.
7 A. Simeonov, M. Matsushita, E. A. Juban, E. H. Z. Thompson, T. Z. Hoffman, A. E. Beuscher, M. J. Taylor, P. Wirsching, W. Rettig, J. K. McCusker, R. C. Stevens, D. P. Millar, P. G. Schultz, R. A. Lerner and K. D. Janda, *Science*, 2000, **290**, 307.
8 W. Clegg, M. R. J. Elsegood, S. J. Teat, C. Redshaw and V. C. Gibson, *J. Chem. Soc., Dalton Trans.*, 1998, 3037.
9 S. Kamitori, O. Matsuzaka, S. Kondo, S. Muraoka, K. Okuyama, K. Noguchi, M. Okada and A. Harada, *Macromolecules*, 2000, **33**, 1500.

ChemComm

Crystal engineering of a 3-D coordination polymer from 2-D building blocks†

Timothy J. Prior and Matthew J. Rosseinsky*

Department of Chemistry, University of Liverpool, Liverpool, UK L69 7ZD. E-mail: m.j.rosseinsky@liv.ac.uk

Received (in Cambridge, UK) 27th November 2000, Accepted 31st January 2001
First published as an Advance Article on the web 19th February 2001

Linking of 'all chair' two-dimensional honeycomb networks, structurally analogous to CF_x, with the 4-aminopyridine ligand leads to a three-dimensional molecular framework.

The construction of porous hosts[1] through crystal engineering[2] is currently attracting a great deal of interest in pursuit of novel materials which may act as catalysts or selective sorbents. Approaches include construction of hydrogen bonded architectures,[3] pillared clay mimics,[4] zeolite analogues[5] such as the AlPOs and GaPOs, and coordination polymer chemistry.[6] A considerable challenge in the field is to achieve predictable combination of structural features, which we have effected by linking the two-dimensional honeycomb motif in three dimensions with a bidentate amine ligand, identified by simple chemical reasoning.

1,3,5-Benzenetricarboxylic acid, H_3btc, has received considerable interest as a tridentate ligand capable of forming coordination polymers.[7] The structures are controlled by the extent of deprotonation of the H_3btc and the nature of the auxiliary ligands coordinated to the metal centre. The graphene-like (6,3) net[8] is well matched to the molecular geometry of btc, and thus two-dimensional honeycomb sheets,[9] some with pyridine projecting perpendicular to the sheets,[10] are a common feature of this chemistry. This opens up the opportunity of linking together these honeycomb layers, thereby predictably generating a three-dimensional architecture, using a suitable bidentate auxiliary ligand.

A wide variety of potential linking ligands to combine these infinite two-dimensional building blocks may be envisaged. We reasoned that a bidentate linker chemically resembling pyridine but without the marked framework forming tendency of, for example, 4,4′-bipyridine, was required. These considerations led to the choice of 4-aminopyridine (4AP). The Cambridge Crystallographic Database‡ currently contains twelve examples where 4AP binds to metal cations through the pyridine function, but there are no examples in the current literature where it, or its *N*-methylated derivatives, act as bidentate ligands. Reaction of tridentate layer-forming and bidentate layer-linking components yields a phase with the desired structural features.

Controlled diffusion§ of 4AP into a butan-1-ol solution of nickel nitrate and H_3btc yields pure UOL-1, $Ni_3(btc)_2(\mu\text{-}4AP)_2(4AP)_4{\cdot}6C_4H_9OH{\cdot}2H_2O$. Analysis of single-crystal X-ray diffraction data collected using synchrotron radiation§ reveals that the structure consists of concertina sheets, shown in Fig. 1, composed of hexagonal 48-membered rings, linked by 4AP. Each ring is made up of six btc units joining six Ni^{II} cations and each sheet may be described topographically as a (6,3) net. In the present case the (6,3) net is not the ubiquitous flat graphene sheet but a topologically equivalent (6,3) net of chair conformation six-rings, which form a coordination polymer analogue of the puckered layers in graphite monofluoride, CF_x.[11]

Every btc is fully deprotonated and binds to three nickel cations: one carboxylate arm of the btc is monodentate to nickel, while the other two arms are bidentate with bite angles of 62.6(1) and 62.3(1)°. Two nickel cations (Ni2) act as linear connectors in the side of the concertina layer and these display

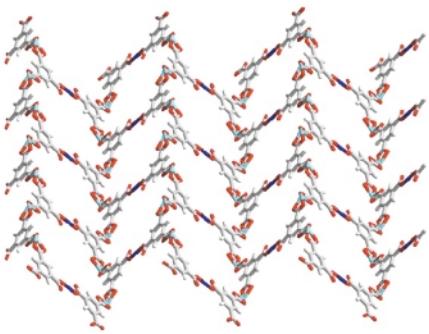

Fig. 1 A single concertina sheet composed of Ni^{2+} and 1,3,5-benzenetricarboxylate. The 'all chair' conformation of the six-membered rings generates a corrugated sheet which is structurally analogous to the layers in CF_x. 4-Aminopyridine ligands and encapsulated solvent have been omitted (colour scheme: Ni1, light blue; Ni2, dark blue; C, grey; O, red; H, light grey).

slightly distorted octahedral coordination. The other four Ni cations (Ni1) are each six-coordinate with an environment that may be described as an extremely distorted octahedron. Two btc units are linked together at Ni1 and the angle subtended between their mean planes is 81.7(9)°. This is reflected in the extreme puckering of the layers: adjacent corrugations subtend an angle of 76.4° to each other (Fig. 2). The coordination about the two crystallographically different nickel atoms is completed entirely by the btc described above and 4AP. Both monodentate (through the pyridine function) and bidentate 4AP are observed. Nickel cations (Ni1) at the peaks and troughs of each corrugated layer are linked by two bidentate 4AP molecules to nickel (Ni2) at the midpoints of the hexagons in adjacent layers, as shown in Fig. 2. To our knowledge this is the first crystallographic report of bidentate 4-aminopyridine.

While it might be possible to link plane (6,3) graphene nets using a bridging ligand with *linear* coordination geometry (such as pyrazine), this is not the case for 4AP. Unlike the pyridine function, which can bind a metal in the plane of the aromatic

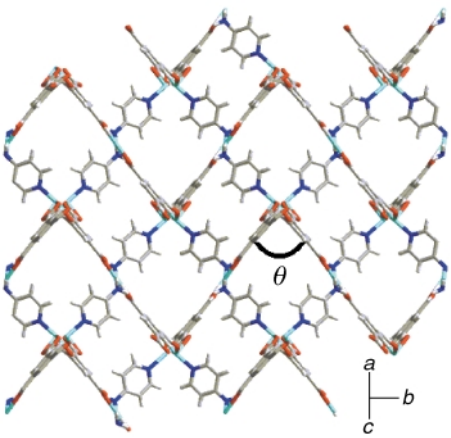

Fig. 2 Linking of ABAB stacked concertina sheets by bidentate 4-aminopyridine (4AP). The angle denoted θ is 76.4°. Monodentate 4AP and solvent are omitted (colour scheme: Ni, light blue; N, dark blue; C, grey; O, red; H, light grey).

† Electronic supplementary information (ESI) available: single-crystal and powder diffraction data and an ORTEP plot of UOL-1. See http://www.rsc.org/suppdata/cc/b0/b009455m/

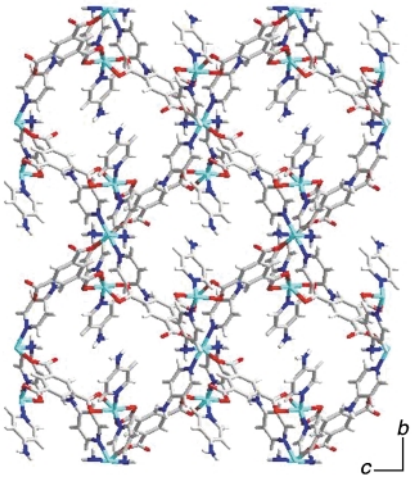

Fig. 3 View down ***a*** showing protrusion of monodentate 4AP into rectangular pores 15.4 × 7.7 Å in size. Pore solvent is omitted (colour scheme: Ni, light blue; N, dark blue; C, grey; O, red; H, light grey).

ring, the amino function can only bind a cation lying out of the plane of the ring because of the directionality of its coordination. Adoption of the graphite monofluoride layer allows the pyridine function of 4AP to bind in a linear mode, while the amino function can bind forming a C–N–Ni angle of 119.0(1)°. Thus the different geometric requirements of the two ends of the linker enforce the CF_x geometry on to the sheets: puckering must occur if the 4AP is to link the octahedral cations in adjacent layers.

The concertina sheets are stacked in an ABAB manner producing a three-dimensional architecture with pores running parallel to ***a*** (15.4 × 7.7 Å shortest van der Waals contacts) and ***c*** (15.1 × 6.0 Å). Monodentate 4AP protrudes into these pores forming necks where the pore is narrowed to *ca*. 3.4 Å, while providing an extremely hydrophilic lining to the cavities (Fig. 3). The program PLATON[12] reveals that the total solvent accessible volume within the crystal, summing voxels more than 1.2 Å away from the framework, is 42.2%. In the pristine material this pore volume is filled with butan-1-ol and water molecules, all engaged in hydrogen bonding with the framework. The hydroxyl groups of two of the three independent butan-1-ol molecules act as donors to btc carboxylates in the framework (O···O distances are 2.68(1) and 2.83(1) Å). The remaining butan-1-ol forms a hydrogen bond to water [2.70(1) Å] which in turn binds to a framework carboxylate [2.73(1) Å]. Removal of this solvent from within the pores may be effected thermally and leads to framework collapse.

The bidentate 4-aminopyridine ligand therefore allows the construction of molecular frameworks in which the infinite two-dimensional honeycomb building blocks characteristic of btc are linked to form a three-dimensional pore network. The (6,3) net unusually adopts the corrugated conformation of CF_x to allow connection of the layers, driven by the geometry of the connecting 4AP ligand. This systematic construction of a framework using linking units to join identifiable structural features may have wider application in coordination polymer chemistry.

We thank Dr S. J. Teat of the SRS, Daresbury Laboratories for help with data processing and the EPSRC for a studentship to T. J. P. and support from GR/N 08537.

Notes and references

‡ Cambridge Structural Database, Version 5.20 (October 2000) with 224 400 entries. www.ccdc.cam.ac.uk

§ 4-Aminopyridine (80 mg, 0.85 mmol) was allowed to mix with $Ni(NO_3)\cdot 6H_2O$ (17.4 mg, 60 μmol) and H_3btc (8.4 mg, 40 μmol) by diffusion through butan-1-ol in an H-cell (height 60 mm, crossbar 90 mm, circular cross-section diameter 15 mm). Extremely small single crystals were obtained after *ca*. 4 weeks. Single-crystal X-ray diffraction was carried out on a Bruker AXS SMART CCD area detector diffractometer at Station 9.8 of the CLRC Daresbury Laboratory Synchrotron Radiation Source, UK. A light green rod-shaped crystal of dimensions 15 × 15 × 40 μm was removed from the mother liquor and covered with a thin film of perfluoropolyether oil and mounted on the tip of a two-stage glass fibre. The crystal was cooled to 123 K in an Oxford Instruments nitrogen gas cryostream. Synchrotron radiation of wavelength 0.6923 Å was employed (determined by measurement of a known crystal). A sphere of data was collected in three series of ω-rotation exposure frames each with different crystal orientation φ angles: each 3 s exposure employs a 0.15° rotation in ω. Data were integrated using Bruker software[13] and semi-empirical corrections[14] were applied to account for beam decay and absorption. The structure was solved using direct methods within SHELXS-86.[15] Full-matrix least-squares refinement on F^2 was carried out with SHELXL-93.[16] Hydrogen atoms were located from the difference Fourier and fitted with a riding model.

UOL-1 crystallises in the centrosymmetric monoclinic space group $P2_1/n$ (no. 14): a = 13.1698(9), b = 19.1965(12), c = 16.6969(11) Å, β = 108.9670(11)°, V = 3992 Å^3. Using a single detector position, 14 214 intensities were recorded, producing 9505 unique data (θ_{max} 30.24 °), R_{int} = 0.0749, conventional R [$I > 2\sigma(I)$, all data] 0.0866 (0.1069), $wR2$ 0.2068 (0.2222). GOF on F^2 1.083 (1.083). CCDC 154064. See http://www.rsc.org/suppdata/cc/b0/b009455m/ for crystallographic data in .cif or other electronic format.

The diffusion synthesis affords phase-pure UOL-1 as demonstrated by the fully indexed powder diffraction patterns given as ESI.†

1 T. J. Barton, L. M. Bull, W. G. Klemperer, D. A. Loy, B. McEnaney, M. Misono, P. A. Monson, G. Pez, G. W. Scherer, J. C. Vartuli and O. M. Yaghi, *Chem. Mater.*, 1999, **11**, 2633.
2 C. B. Aakeröy and A. S. Borovik, *Coord. Chem. Rev.*, 1999, **183**, 1; A. J. Blake, N. R. Champness, P. Hubberstey, W. S. Li, M. A. Withersby and M. Schröder, *Coord. Chem. Rev.*, 1999, **183**, 117; D. Braga and F. Grepioni, *Coord. Chem. Rev.*, 1999, **183**, 19; M. O'Keeffe, M. Eddaoudi, H. L. Li, T. Reineke and O. M. Yaghi, *J. Solid State Chem.*, 2000, **152**, 3.
3 F. H. Herbstein, *Top. Curr. Chem.*, 1987, **140**, 107; R. E. Melendez and M. J. Zaworotko, *Supramol. Chem.*, 1997, **8**, 157; R. E. Melendez and A. D. Hamilton, *Top. Curr. Chem.*, 1998, **198**, 97.
4 M. L. Kantam, P. L. Santhi, K. V. R. Prasad and F. Figueras, *J. Mol. Catal. A: Chem.*, 2000, **156**, 289; A. Rujiwatra, C. J. Kepert and M. J. Rosseinsky, *Chem. Commun.*, 1999, 2307; K. Biradha, D. Dennis, V. A. MacKinnon, C. V. K. Sharma and M. J. Zaworotko, *J. Am. Chem. Soc.*, 1998, **120**, 11 894; K. Bahranowski, R. Grabowski, B. Grzybowska, A. Kielski, E. M. Serwicka, K. Wcislo, E. Wisla-Walsh and K. Wodnicka, *Top. Catal.*, 2000, **11**, 255.
5 A. K. Cheetham, G. Ferey and T. Loiseau, *Angew. Chem., Int. Ed.*, 1999, **38**, 3269; P. A. Wright, M. J. Maple, A. M. Z. Slawin, V. Patinec, R. A. Aitken, S. Welsh and P. A. Cox, *J. Chem. Soc., Dalton Trans.*, 2000, **8**, 1243.
6 B. F. Abrahams, S. R. Batten, M. J. Grannas, H. Hamit, B. F. Hoskins and R. Robson, *Angew. Chem., Int. Ed.*, 1999, **38**, 1475; K. Biradha, C. Seward and M. J. Zaworotko, *Angew. Chem., Int. Ed.*, 1999, **38**, 492; M. Eddaoudi, H. L. Li and O. M. Yaghi, *J. Am. Chem. Soc.*, 2000, **122**, 1391; H. Gudbjartson, K. Biradha, K. M. Poirier and M. J. Zaworotko, *J. Am. Chem. Soc.*, 1999, **121**, 2599; T. M. Reineke, M. Eddaoudi, D. Moler, M. O'Keeffe and O. M. Yaghi, *J. Am. Chem. Soc.*, 2000, **122**, 4843; P. Lightfoot and A. Snedden, *J. Chem. Soc., Dalton Trans.*, 1999, 3549.
7 M. J. Plater, M. R. S. Foreman, E. Coronado, C. J. Gomez-Garcia and A. M. Z. Slawin, *J. Chem. Soc., Dalton Trans.*, 1999, 4209; O. M. Yaghi, G. M. Li and H. L. Li, *Nature*, 1995, **378**, 703; C. J. Kepert, T. J. Prior and M. J. Rosseinsky, *J. Am. Chem. Soc.*, 2000, **122**, 5158; S. S. Y. Chui, S. M. F. Lo, J. P. H. Charmant, A. G. Orpen and I. D. Williams, *Science*, 1999, **283**, 1148.
8 A. F. Wells, *Three Dimensional Nets and Polyhedra*, Wiley Interscience, New York, 1977.
9 H. J. Choi and M. P. Suh, *J. Am. Chem. Soc.*, 1998, **120**, 10 622; H. J. Choi, T. S. Lee and M. P. Suh, *Angew. Chem., Int. Ed. Engl.*, 1999, **38**, 1405.
10 C. J. Kepert, T. J. Prior and M. J. Rosseinsky, *J. Solid State Chem.*, 2000, **152**, 261.
11 N. N. Greenwood and A. Earnshaw, *Chemistry of the Elements*, Butterworth-Heinemann, London, 2nd edn., 1997, p. 290.
12 A. L. Spek, *Acta Crystallogr., Sect. A*, 1990, **46**, C34.
13 Bruker AXS Inc., Madison, WI, SMART (control) and SAINT (integration) software, version 4, 1994.
14 G. M. Sheldrick, SADABS, Universität Göttingen, 1997.
15 G. M. Sheldrick, SHELXS-86, Universität Göttingen, 1986.
16 G. M. Sheldrick, SHELXL-93: Program for the refinement of crystal structures, Universität Göttingen, 1993.

Molecular paneling *via* coordination

Makoto Fujita,* Kazuhiko Umemoto, Michito Yoshizawa, Norifumi Fujita, Takahiro Kusukawa and Kumar Biradha

Department of Applied Chemistry, Graduate School of Engineering, Nagoya University and CREST, Japan Science and Technology Corporation (JST), Chikusaku, Nagoya 464-8603, Japan. E-mail: mfujita@apchem.nagoya-u.ac.jp

Received (in Cambridge, UK) 27th October 2000, Accepted 8th January 2001
First published as an Advance Article on the web 7th February 2001

This article deals with a coordination approach to three-dimensional assemblies *via* '*molecular paneling*'. Families of planar exo-multidentate organic ligands (molecular panels) are found to assemble into large three-dimensional assemblies through metal-coordination. In particular, *cis*-protected square planar metals, (en)Pd^{2+} or (en)Pt^{2+} (en = ethylenediamine), are shown to be very useful to panel the molecules. Metal-assembled cages, bowls, tubes, capsules, and polyhedra are efficiently constructed by this approach.

Introduction

The last decade has witnessed the syntheses of several complex 3D-molecules that are assembled by linking molecules *via* non-covalent bonds such as coordination and/or hydrogen bonds and has led to the development of a new paradigm denoted *non-covalent synthesis*.[1] This non-covalent synthesis has become a reliable approach to prepare 3D-complex molecules and has been considered as an alternative approach to organic synthesis. Earlier the important examples of metal-directed assembly of 3D structures, for example Saalfrank's M_4L_6 cages and Lehn's cylindrical cages, have been well documented.[2,3] Remarkable progress in the construction of 3D structures *via* metal coordination has been made by the groups of Raymond, Stang, Steels, Robson, Shinkai and others.[4–8] The focus of this article will be on our efforts in the construction of three-dimensional (3D) structures by linking two-dimensional (2D) planar organic components *via* metal-coordination. Before going into the main topic, we would like to brief the basic concept of the present study that prompted us to develop a concept of *molecular paneling* which points to a highly efficient approach for constructing large 3D molecules.

Makoto Fujita is a Professor of the Department of Applied Chemistry, Graduate School of Engineering, Nagoya University, Japan. He received his Ph.D. degree from Tokyo Institute of Technology in 1987. Then he joined Department of Applied Chemistry at Chiba University as an Assistant Professor in 1988 and was promoted to a Lecturer in 1991 and to Associate Professor in 1994. In 1997, he moved to Institute for Molecular Science (IMS) at Okazaki as an Associate Professor. Since 1999, he has been in the current position. He is currently a leader of the CREST (Core Research for Evolutional Science and Technology) project of Japan Science and Technology Corporation (JST). His current research interests include metal-assembled complexes, molecular recognition, and nanometer-sized molecules.

Takahiro Kusukawa is an Assistant Professor of the Department of Applied Chemistry, Graduate School of Engineering, Nagoya University. He received his Ph.D. degree from Tsukuba University in 1995. After working in Tsukuba for two years, he joined Fujita's group in 1997 as a Research Associate and moved to Nagoya in 1999 where he got the current position. His interests focus upon the synthesis, assembly, and structural analysis of giant molecules.

Kumar Biradha is also an Assistant Professor of the Department of Applied Chemistry, Graduate School of Engineering, Nagoya University. He received his Ph.D. degree from the University of Hyderabad, India in 1997. He was a postdoctoral fellow in Canada from 1997–1998. In 1998, he joined Fujita's group as a JSPS postdocotral fellow and got the current position in 2000. His interests focus upon the crystal engineering and supramolecular chemistry.

Norifumi Fujita and Kazuhiko Umemoto are doctoral students of the Graduate University for Advanced Studies and will soon receive Ph.D. degrees in March of 2001. Michito Yoshizawa is a doctoral student of Nagoya University.

A basic concept

It was more than a decade ago when we first had the idea to incorporate 90° coordination angles of transition metals into metal–organic frameworks.[9] We paid special attention to the geometry of square-planar metals since non-distorted 90° bond angles can not be afforded by the hybridization of organic elements. To exploit this angle, we designed a *cis*-protected square-planar metal as illustrated in Fig. 1. Accordingly, an

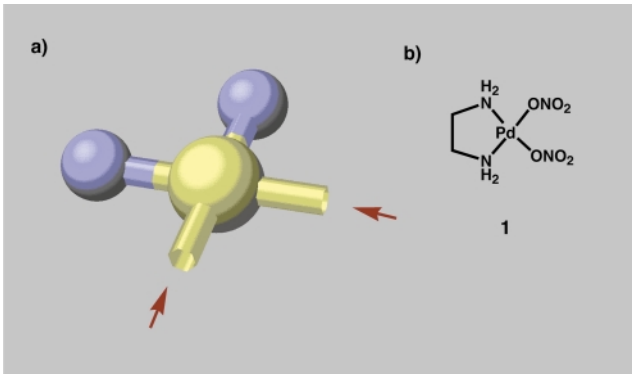

Fig. 1 (a) Cartoon representation of the *cis*-protected Pd(II) building block **1** and (b) structural drawing of **1**.

ethylenediamine-protected Pd(II) complex was prepared and successfully incorporated into a tetranuclear square framework by complexation with one of the simplest bridging ligands: 4,4′-bipyridine (Fig. 2). The design of the *cis*-protected Pd(II) as well as the formation of the square complex **1** cultivated the basic concept of our study which has been carried out over the last decade and can be dictated as follows:

Upon *cis*-protection, the coordination nature of the metal ion changes from divergent to convergent. Owing to the convergent nature, the discrete framework **1** was efficiently generated without formation of any oligomeric products, in striking contrast to the previous coordination chemistry of 4,4′-

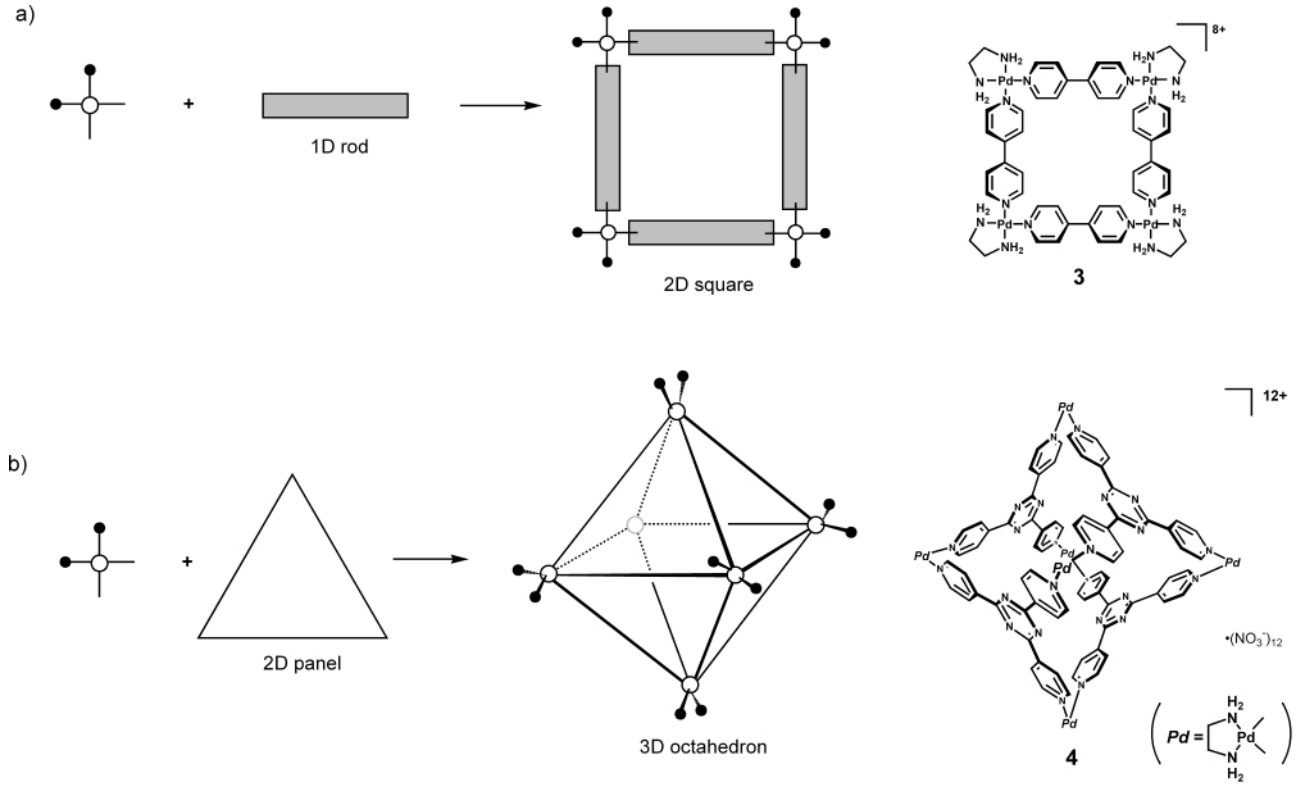

Fig. 2 (a) Schematic representation of molecular paneling: (a) from 1D-rods to 2D-molecules and (b) from 2D-panels to 3D-molecules.

bipyridine where infinite complexes were afforded in most cases.[10] The Pd(II)–pyridine coordination bond is labile and hence the product is formed under thermodynamic control. Thus, under a set of appropriate conditions, the square molecule is spontaneously generated in quantitative yield.

A square molecule in which the transition metal provides a 90° angle at each corner of the square has been recently termed as a 'molecular square' by Stang.[11] The extensive studies by Stang and others stirred considerable current interest in such square molecules. Prior to our study, there have been some important studies on the synthesis of metal-linked macrocycles. One of the excellent examples is the Cu(II)-linked dinuclear complex **2** synthesised by Maverick *et al.*[12]

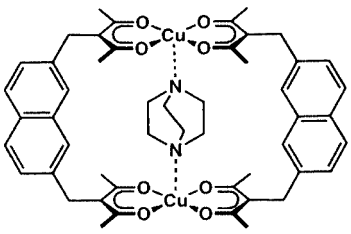

2

From 2D to 3D structures

A 1D molecular rod, 4,4′-bipyridine, upon linking with 90° coordination block **1** was assembled into a 2D square as discussed above. This molecular design was extended to the construction of 3D structures by considering 2D molecular components. Namely, instead of 1D rod, a 2D triangular panel was used as an organic component (Fig. 2). In 1995 this idea was first realized by the synthesis of an octahedral 3D structure **4** (Fig. 2b).[13] This example illustrates that the molecular paneling of a 2D organic component is undoubtedly an efficient method for the construction of large 3D entities. In the following sections, we will show a family of molecular panels that are successfully paneled into various 3D molecules *via* metal coordination. In addition to the coordination approach, 3D molecules are also accessible by hydrogen-bond directed self-assembly. The groups of Rebek[14] and Atwood[15] have demonstrated the efficient self-assembly of capsules through hydrogen bonding. The cavity volumes of these capsules range from 0.3 to 1.7 nm^3.[14,15]

Molecular panels

3D-molecular structures can be well designed by deducing the molecular components from polyhedra. For example, the basic components (polygons) to construct Platonic solids are equilateral triangles, squares and pentagons.[16] The common feature in these solids is that they are made up of regular polygons which are arranged in space such that the edges, vertices and three coordinate directions of each solid are equivalent. Here we have designed several molecular panels with the basic shapes of triangle, square and rectangle (Fig. 3). The assembling of these panels with the 90° *cis*-protected coordination block **1** can be considered as a new concept that we term as '*molecular paneling*'.

Paneling triangles

An important aspect of regular polygons is that they enclose space. In particular, four triangles enclose space, without the use of curved surface, and this is the lowest number of polygons which will do so.[16] Thus we first deal with a triangle which is a very basic building block of several polyhedra. For example out of five Platonic solids, three (tetrahedron, octahedron and icosahedron) are originated from equilateral triangles indicating the importance of triangular panels in the construction of polyhedra (Fig. 4). Accordingly we designed triangular molecular panels **5**–**9** to assemble them into several 3D-structures (polyhedra). The differences between these triangular panels is the number (varying from three to six) and position of the binding sites. Molecular panels **5** and **6** contain three binding

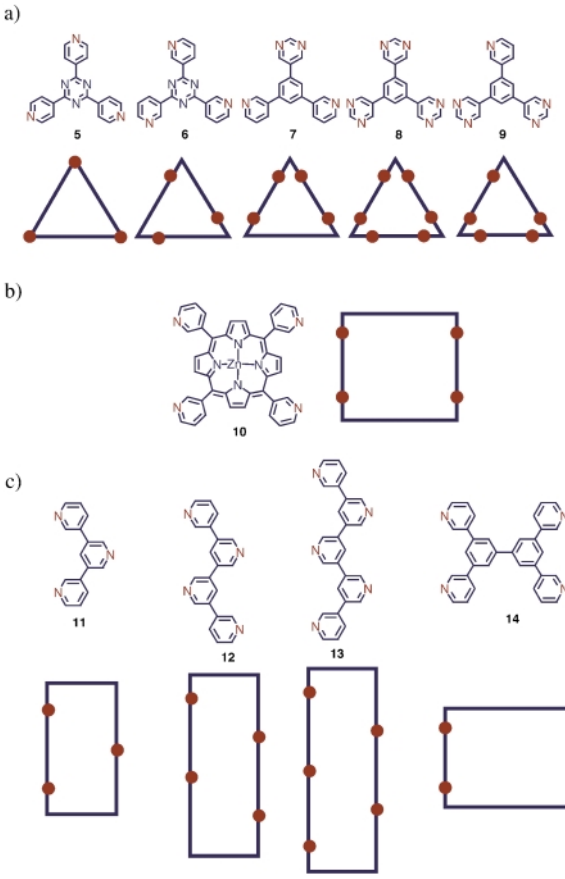

Fig. 3 Structural and cartoon representation of molecular panels: (a) triangular, (b) square and (c) rectangular. The filled circles represent the binding sites.

sites each but the position of the sites differs, whereas molecular panels **7**, **8** and **9** contain four, six and five binding sites each, respectively. The assembled architectures from these molecular panels include octahedra, square pyramids, tetrahedra and hexahedra.

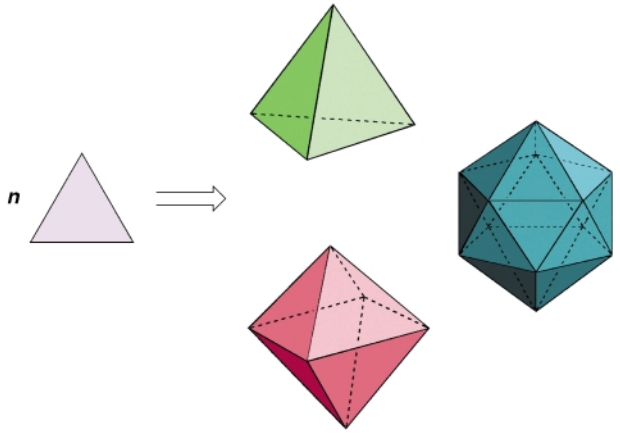

Fig. 4 Schematic representation of assembling of three types of Platonic solids from a triangular unit.

M_6L_4 octahedral cage

As discussed above, the first example of using the molecular panel approach to obtain a 3D discrete structure is an M_6L_4 octahedral assembly **4**, reported in 1995.[13] By treating **1** with **5** in 3:2 ratio, the octahedral complex **4** is assembled in quantitative yield (Fig. 5). In this complex, the four triangular panels are linked together at the corners of the triangles such that every alternate face of the octahedron contains either molecular panel or portal. Complex **4** is a thermodynamically stable product because the formation of the product is not affected by the presence of an excess of **1**. The synthetic procedure is so simple that a 10–50 g scale synthesis can be carried out in a laboratory.

It has been shown that the cage complex **4** effectively binds various organic guest molecules in its cavity. The structure of the clathrate complex of **4** with the adamantane carboxylate ion has been determined by X-ray crystallography (Fig. 5c), which showed that four guest molecules are tightly encapsulated inside the nano-sized cavity of **4**. The inclusion geometry of the guest in the cavity is interesting as the hydrophobic and hydrophilic groups (CO_2^-) are located inside and outside of the cavity, respectively. A space filling presentation of **4** shows that the

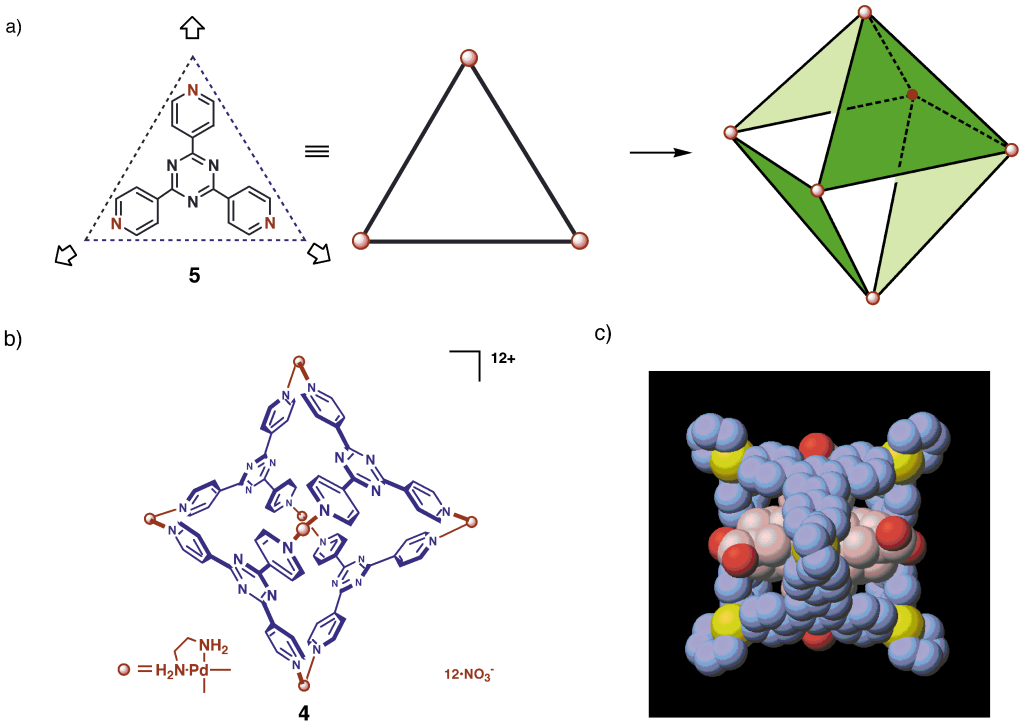

Fig. 5 (a) Schematic representation of molecular paneling of **5** to form **4**, (b) structural drawing of **4** and (c) X-ray structure of **4** with adamantane carboxylates in the cavity.

dimension of the portal of the cage is comparable to that of adamantane, whereas the interior space can hold as many as four guest molecules. The ^{1}H NMR study showed that the same host–guest aggregation was retained even in aqueous media.

A kinetically stable octahedral M_6L_4 cage

The Pd(II) self-assembly described above is a result of thermodynamical equilibration and the product is not stable under extreme conditions (*e.g.* acidic, basic or nucleophilic). In order to prepare a kinetically stable M_6L_4 complex, a Pt(II) analogue of **4**, **15** was used instead of **1**. In contrast to the Pd cage, the formation of Pt cage was quite slow to form in a reasonable yield. However, heating the solution and adding a guest molecule, adamantanecarboxylate, dramatically improved the reaction rate as well as the yield. The host–guest ratio and the guest inclusion geometry were found to be similar to those of Pd structure **4**. Usually, a receptor framework organized by guest induced fit will be lost when the guest is removed. In contrast, the assembled Pt cage did not lose its cage structure even after removal of the guest because of the locking, irreversible nature of Pt(II)–pyridine bond. As anticipated, the Pt(II) complex was very stable and did not decompose even in the presence of an acid (HNO_3), a base (K_2CO_3) or a nucleophile (NEt_3) owing to the inertness of a Pt(II)–pyridine coordinate bond.[17]

M_6L_4 square-pyramidal cone

The triangular molecular panel **6** was used to assemble a bowl-like M_6L_4 square-pyramidal cone. Although **6** has a similar structure as **5**, due to the different placement of N-atoms in the ligand this component formed a square-pyramidal cone **16** upon treatment with **1** (Fig. 6).[18a] The structure of **16** was characterized in solution by ^{1}H NMR spectroscopy and in the solid state by X-ray crystallography. The framework is held together by 10 molecular components (six metal ions and four ligands) having nanometer dimensions (*ca.* 3 × 2 × 2 nm) in spite of the small size of the molecular components.

In aqueous media the square-pyramidal cone **16** is expected to assemble into a dimeric capsule that contains a large hydrophobic pocket inside the framework because of its amphiphilic properties: hydrophobic inside and hydrophilic outside. In fact, such a dimeric structure does assemble in the solid state. That is, X-ray structures have been obtained for host–guest complexes with large guest molecules, all of which showed the dimeric capsule structure of the host accommodating as many as six neutral organic molecules.[18b] The solid structure of the complex with *o*-terphenyl (Fig. 7a) is recognized as a dimer of 1:2 host–guest complexes because the whole structure can be divided into two identical 1:2 complexes. On the other hand, the solid structure of the complex with *m*-terphenyl (Fig. 7b) can not be divided into two halves and thus the whole structure is regarded as a 2:4 complex rather than a dimer of 1:2 complex. With *cis*-stilbene, 1:6 complexation has been confirmed by X-ray analysis.

Dynamic assembly of an M_8L_4 cone and tetrahedron

Whilst molecular panels **5** and **6** contain C_3-symmetry, molecular panel **7** has C_2-symmetry, and therefore is expected to link in two different ways upon treatment with **1**: parallel and antiparallel fashions. Linking in parallel fashion is expected to generate the square-pyramidal cone **17** whereas linking in antiparallel fashion is expected to generate a closed tetrahedron **18** (Fig. 8). Interestingly, these two routes are found to be controlled effectively by the guest molecules.[19] Larger guest molecules such as dibenzoyl templated formation of the square-pyramidal cone **17** while small tetrahedral guests like CBr_4 templated formation of the closed tetrahedron **18**. Ligand **7** and dibenzoyl were suspended in aqueous solution of **1** and stirred for 24 h. The ^{1}H NMR spectra and ESI-MS of this solution revealed the formation of **17** which accommodated one molecule of dibenzoyl. In the ESI-MS, major peaks corresponding to $\{[\mathbf{17}(\text{dibenzoyl})_m\cdot(NO_3)_{16-n}]^{n+}$ (m = 0–2, n = 3, 4)$\}$ were observed suggesting the formation of a cone structure. In ^{1}H NMR spectra eight signals appeared corresponding to the C_2-symmetric environment of **7**. The signals of dibenzoyl were substantially upfield shifted suggesting its inclusion in the cone-shaped cavity. Other bulky guest molecules such as 1,2-dibenzoyl, ethane-1,2-diol and 1,1′-ferrocenedicarboxylic acid were also found to template the same square pyramidal cone **17**.

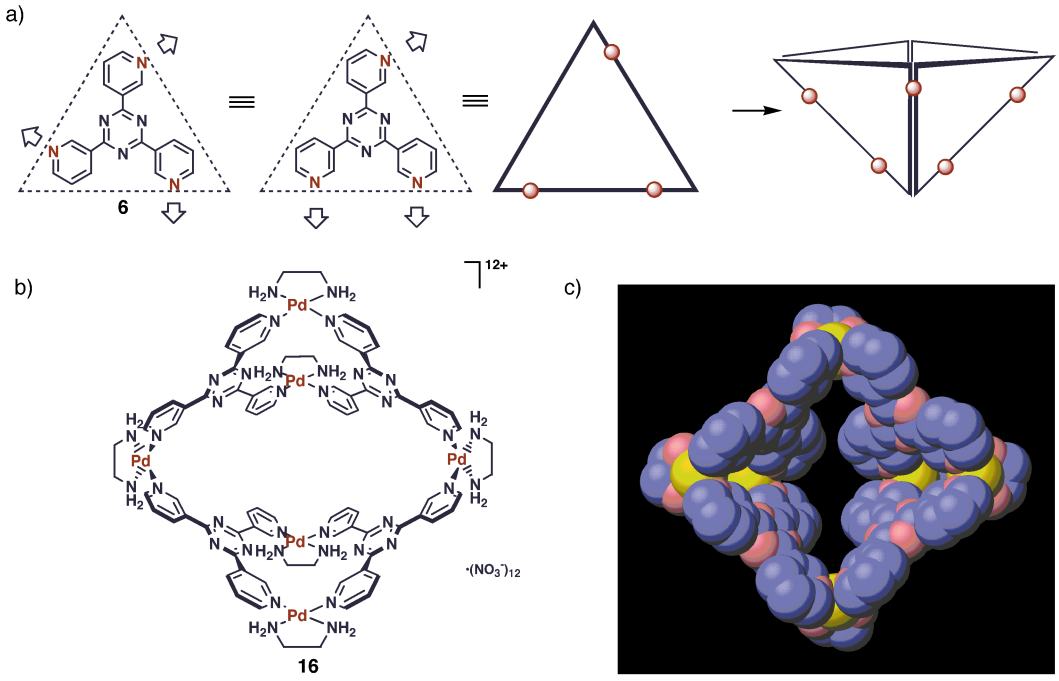

Fig. 6 (a) Schematic representation of molecular paneling of **6** to form **16**, (b) structural drawing of **16** and (c) space-filling representation of **16** exhibited in its crystal structure.

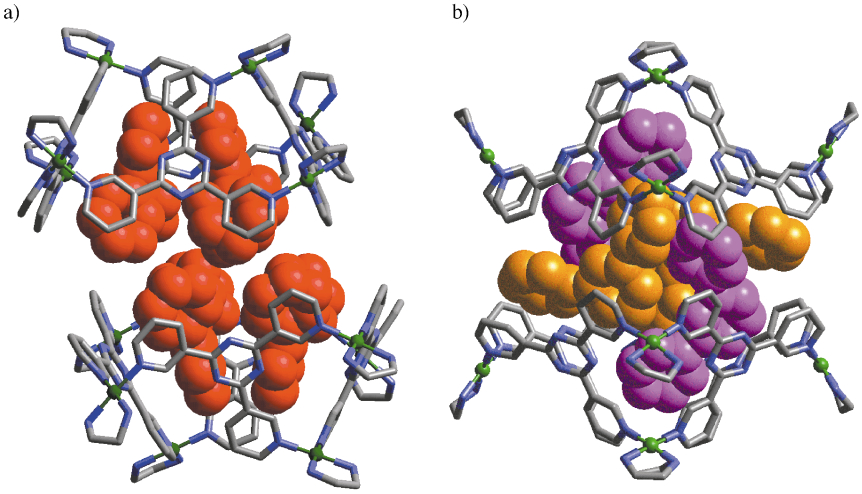

Fig. 7 Dimeric capsules of **16** accommodating (a) *o*-terphenyl and (b) *m*-terphenyl exhibited in their crystal structures.

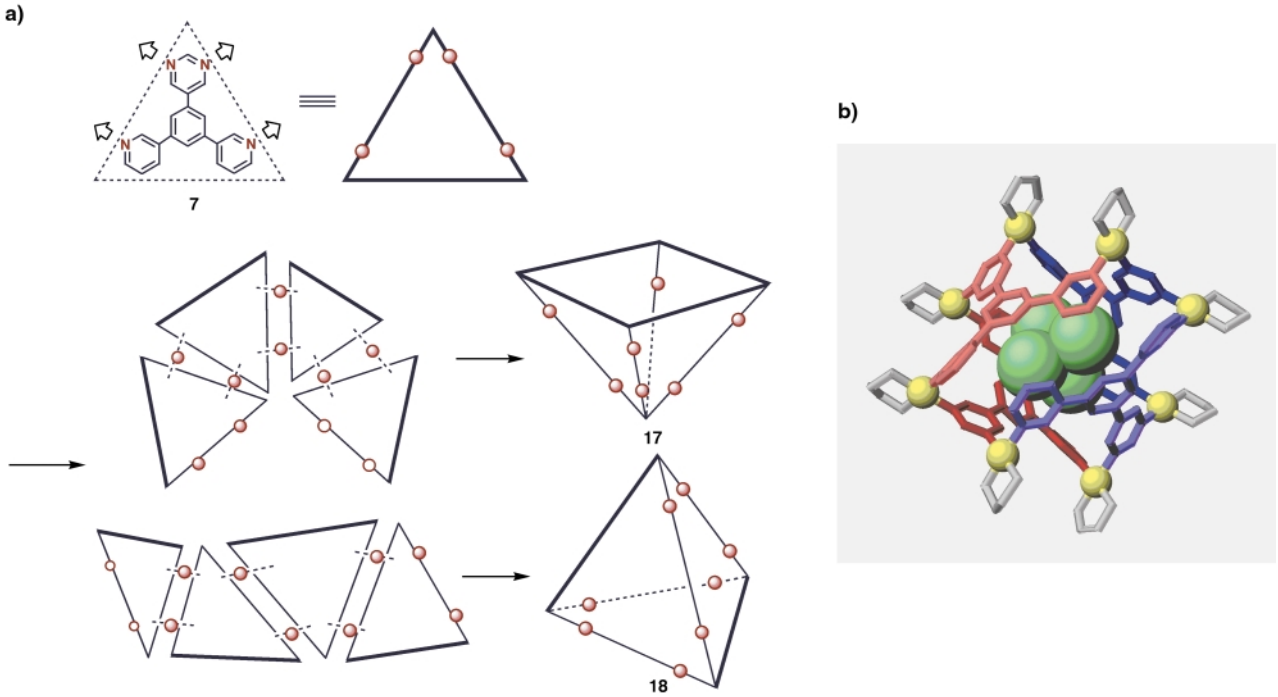

Fig. 8 (a) Schematic representation of molecular paneling of **7** to form **17** and **18** and (b) X-ray structure of the tetrahedron **18** (cylinder mode) with CBr_4 (space filling) in its cavity.

The closed tetrahedron structure **18** resulted when **1** and **7** were allowed to react in the presence of CBr_4 in D_2O. The antiparallel linking of the ligands was strongly supported by the observation of NOE between adjacent ligands. The complex was precipitated in 93% yield after adding an excess of EtOH and an elemental analysis supported a 1:1 host–guest ratio. Similarly $CHCl_3$ and $CBrCl_3$ were also found to template a similar type of structure. Further the assigned structure was supported by the single-crystal X-ray structure which showed the complete entrapment of CBr_4 in its closed tetrahedral cavity (Fig. 8b).

In the absence of guest molecules at 25 mM concentration, **1** and **7** were found to assemble into a 3:2 mixture of two products. According to ^{1}H NMR spectroscopy the minor product was identified as square-pyramidal cone **17** whereas an increase in the percentage of the major product was observed when the reaction was conducted at lower concentrations. This fact indicates that the major component could be a trimeric open-cone structure assembled from a lower number of molecular components than the tetrameric cone. These assembled trimeric and tetrameric cones and tetrahedron were found to reorganize from one structure to the other by the guest addition/exchange.

$M_{18}L_6$ hexahedron

Following the exotridentate ligands **5** and **6**, an exohexadentate ligand, 1,3,5-tris(3,5-pyrimidyl)benzene **8** was also designed as a triangular unit. As already discussed, the triangle is a basic unit for the self-assembly of polyhedra. Ligand **8** is an almost coplanar triangle and is expected to give an edge-sharing polyhedron when it is self-assembled with **1**. When ligand **8** is treated with **1** in D_2O, the predominant formation of a single component was observed, the ^{1}H NMR spectrum of which showed seven singlet-like signals in an integral ratio of 2:2:2:2:2:1:1. Of several possibilities, the assembly of the molecular hexahedron **19** was strongly suggested by ^{1}H NMR spectroscopy (Fig. 9).[20] This observation confirms that, after complexation, ligand **8** is placed in a less-symmetrical environment with one symmetry axis passing through a 3,5-pyramidyl (pym) ring and a core benzene ring. This symmetry is in good agreement with the trigonal-bipyramidyl structure of the

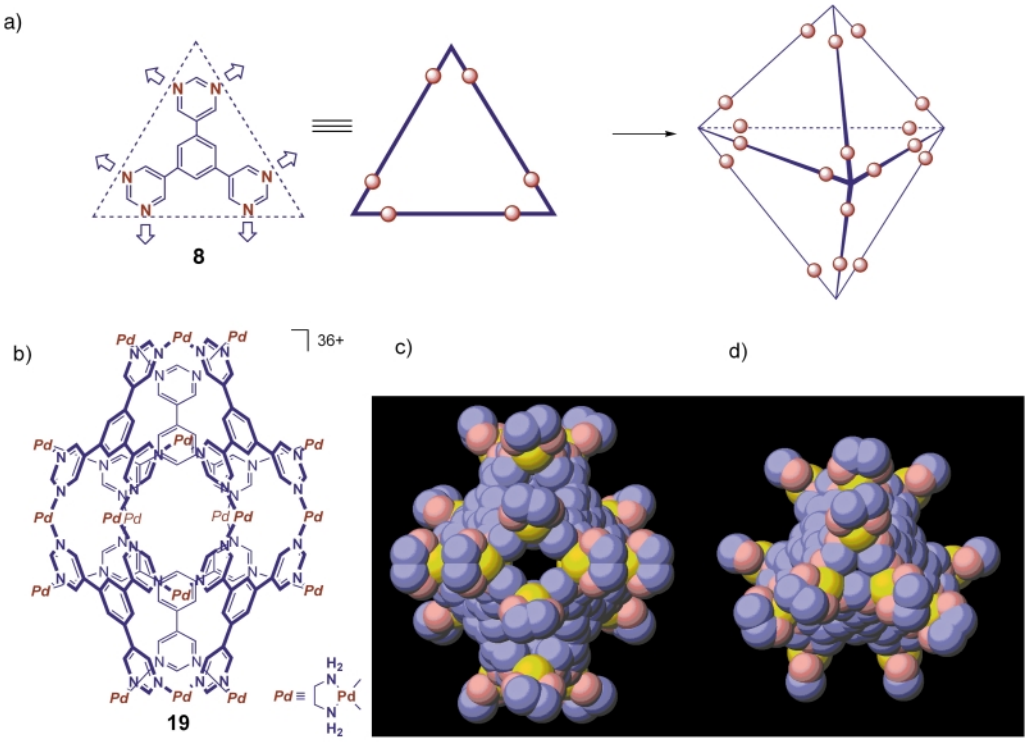

Fig. 9 Schematic representation of molecular paneling of **8** to form hexahedron **19**, (b) structural drawing of **19** and space filling representation of the X-ray structure of **19**: (c) equatorial and (d) apical views.

molecular hexahedron **19** in which the pym groups at the apical corners are not equivalent to those at equatorial corners. The metal-linked dimer and trimer of **8**, which are the possible intermediates for assembly process of **19**, were observed when ligand **8** was treated with **1** in D_2O in 1:1 and 3:4 ratios, respectively.

Reliable evidence for the hexahedron structure of **19** was provided by X-ray crystallography (Fig. 9c and d). The crystal structure clearly demonstrates that the assembly is a trigonal-bipyramidal capsule with a chemical formula of $C_{144}H_{216}N_{108}Pd_{18}$, a molecular mass of 7103 Da, and dimensions of 3 × 2.5 × 2.5 nm. Each equatorial corner of the hexahedron is the assembly of four triangle units, where [Pd(II)–pym]$_4$ leads to a small pinhole (2 × 2 Å). Only small molecules such as water and molecular oxygen may pass through these holes, whereas, ordinary organic molecules cannot enter or escape. The free volume inside the capsule, into which guests can be accommodated, is *ca.* 900 Å^3.

$M_{15}L_6$ hexahedron: reversible guest inclusion

As described above hexahedron **19** is a very closed and rigid structure making it difficult to encapsulate/exchange guest molecules. To prepare a hexahedron that has more flexibility to encapsulate/exchange guest molecules we designed another molecular panel **9**, which is similar to **8**, but has one binding site less than **8**. We found that the treatment of **9** with **1** in D_2O affords hexahedron **20** (Fig. 10). Interestingly as anticipated molecules of **20** can exchange the encapsulated encapsulates and small guest molecules.[21]

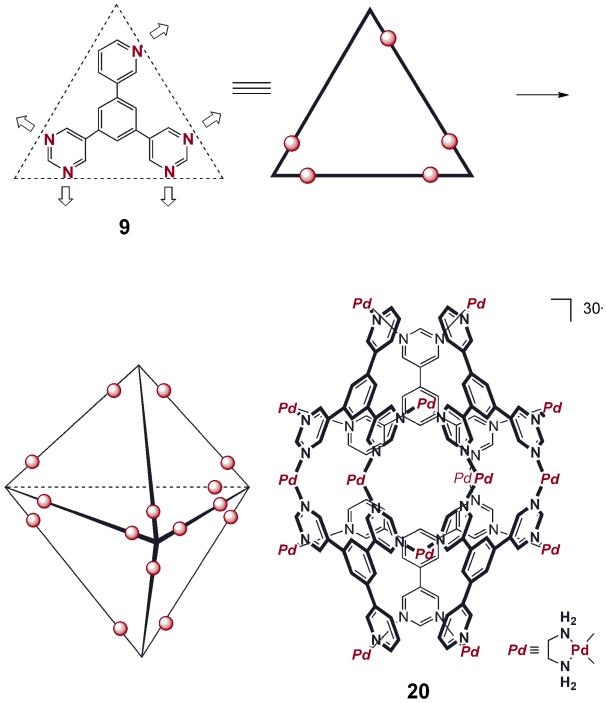

Fig. 10 Molecular paneling of **9** to form **20**.

Some functions of M_6L_4 octahedral cages

Cage compounds prepared by conventional covalent synthesis usually contain small cavities and can encapsulate only one or two small molecules. The *molecular paneling* approach gives us an opportunity to construct larger frameworks containing relatively large cavities. For example, the octahedral cage compound **4** has a very large cavity with a diameter of 1 nm and exhibited a remarkable ability to encapsulate large and neutral molecules. In the following sections we describe its abilities in molecular recognition, catalysis and condensation of trialkoxysilanes.

Molecular recognition

It has been already described that M_6L_4 can bind four molecules of aqueous guest such as adamantanecarboxylate. Further, it efficiently encapsulates neutral and spherical guest molecules such as adamantane, 1- and 2-adamantanol, *o*-carborane, and aromatic compounds such as 1,3,5-trimethoxybenzene, anisole and toluene in the cavity.[22] Interestingly, adamantane was found to transfer into the aqueous phase even in a solid–liquid

two-phase system. The very efficient guest binding by **4** can be ascribed to the amphiphilic nature of the cage: *i.e.* the inside of **4** is surrounded by 16 aromatic rings and thus hydrophobic, whereas the outside surface of the cage is hydrophilic due to the exposure of six charged Pd(II) centers.

Notably, complexation is faster with smaller guest molecules and slower with larger guest molecules. For example 1,3,5-tri-*tert*-butylbenzene which is slightly larger than the portal of **4**, was encapsulated very slowly. Tetrabenzylsilane required a few hours to be completely encapsulated by **4′** which is the 2,2′-bipyridine protected analogue of **4**. Crystallographic analysis showed a good fit for the tetrahedral symmetry of the guest in the octahedral cage (Fig. 11).[23]

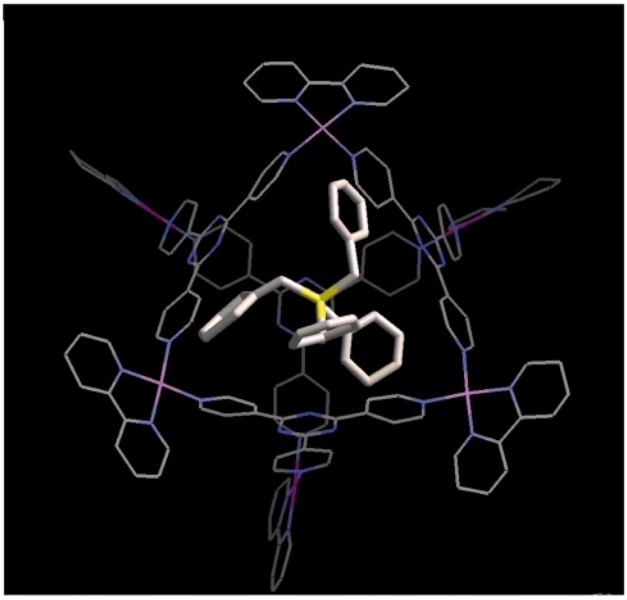

Fig. 11 X-Ray crystallographic structure of **4′** (stick mode) enclathrating tetrabenzylsilane (cylinder mode).

Compound **4** also exhibited a remarkable ability to encapsulate C-shaped molecules such as *cis*-azobenzene **21** and *cis*-stilbene **22**, derivatives.[24] These guest molecules are enclathrated in the cavity *via* the formation of a hydrophobic dimer with a topology reminiscent of a hydrogen-bonded tennis ball (Fig. 12a).[24] The formation of a hydrophobic dimer was

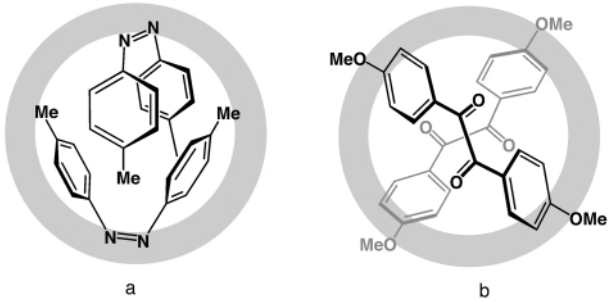

Fig. 12 Schematic drawing of formation of a hydrophobic dimer of (a) *cis*-stilbene and (b) 4,4′-dimethoxydibenzoyl within the cavity of **4** (shown as circle).

suggested by NOE and also by molecular dynamic simulation. Further the selective enclathration of only the *cis* isomer was observed when *cis–trans* mixtures of either **21** or **22** in hexane were stirred in a D_2O solution of **4**. The NMR spectra confirm the encapsulation of dimers of *cis*-isomers in the cavity. Notably, the *cis* isomer of **21** was significantly stabilized in the cavity and not isomerised to the *trans* isomer even after allowing the solution to stand for a few weeks under visible light at room temperature. Molecular modeling calculations suggest that the hydrophobic dimers are a perfect fit for cavity of **4**. Dimerization of the guests prior to enclathration is unlikely because the dimension of the spherical dimer (*ca.* 11 Å in diameter) is larger than that of the portals of **4** (*ca.* 7 Å diameter). Therefore, two guest molecules can subsequently, but not simultaneously, be enclathrated in the cavity leading *in situ* into the stable hydrophobic dimer.

A similar dimer formation was observed when 1,2-diketone **23** was employed as a guest (Fig. 12b). In the 1:2 complex, dissymmetrization of the host structure was observed by NMR spectroscopy: that is, before addition of guest the four ligands in host are equivalent, but after addition of guest, 12 protons on each ligand were observed independently. This observation was clearly revealed by X-ray crystallographic analysis. As shown in Fig. 13, two guest molecules are assembled in a similar way

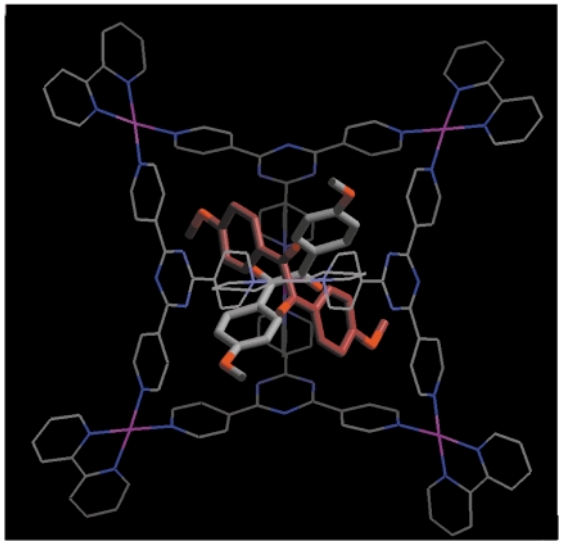

Fig. 13 X-Ray crystallographic structure of **4′** (stick mode) enclathrating the hydrophobic dimer of 4,4′-dimethoxydibenzoyl (cylinder mode).

to that of **21** and **22**. However, each guest adapts a twisted conformation: one is *P*-form and another is *M*-form. As a consequence, the formed dimer has a *meso* configuration with no centrosymmetry making all protons on each ligand inequivalent.[22]

Catalysis in the cavity of M_6L_4 cage

Reactivity and catalysis represent one of the most important features of the functional properties of self-assembled molecular systems.[25] The existence of a large cavity in **4** motivated us to test its ability to catalyze the oxidation of styrene and isomerization of allylbenzene.[26] When **1** and **5** were mixed in D_2O in 2:1 ratio, formation of only **4** was observed and excess of **1** remained in the solution. Our strategy was to use the remaining amount of **1** as a mediator between organic and aqueous phases: that is to use **1** to transfer the substrate, cyclically and continuously, into a aqueous phase that contains **4** and then the formed product into the organic phase (Scheme 1). It was observed that **4** can accommodate nearly three molecules of styrene in its cavity. The oxidation of styrene at 80 °C in an aqueous solution of either **1** or **4** gave acetophenone only in 4% yield. Importantly, the presence of both **1** and **4** in an aqueous solution increased the yield of the reaction up to 86%. Similarly, the isomerization of allylbenzenes catalyzed by the presence of **1** and **4** in aqueous solution gave β-methylstyrene in 50% yield, whereas the reaction did not occur in the absence of either **1** or **4** (Scheme 2). The presence of trimethoxybenzene in the reaction media inhibited these reactions because the cavity of **4** was strongly occupied by this molecule. The yields of these reactions reveal that as the size and electron deficiency of the substrate increases the yield of the reaction decreases. These are

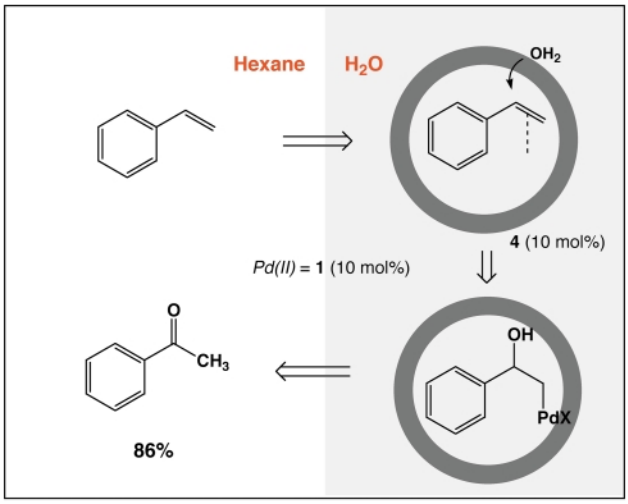

Scheme 1 Schematic representation of reversed phase-transfer catalysis of **4**. Wacker oxidation is promoted by a slight excess of **1**.

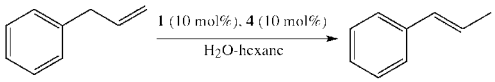

Scheme 2 Olefin isomerization in an aqueous phase with the aid of **1** (10 mol%) and **4** (10 mol%).

good examples of organic reactions in solutions but in the absence of organic solvents.

Condensation of trialkoxysilanes

Isolated cavities in molecular capsules are well known to stabilize labile molecules formed *in situ* by the reaction of smaller molecular components.[27] These components, being smaller in size, can enter into the cavity through the portals and react with each other to form a larger molecule that can not leave the cavity since it is larger than the portal. By using the same principles here we studied the condensation reaction of trialkoxysilanes in the cavity of an M_6L_4 cage.[28] Cyclic oligomers of silanols **23** and **24** are considered to be ephemeral

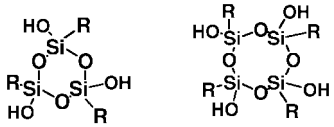

23 **24**

intermediates in the poly-condensation of trialkoxysilanes.[29] Cyclic tetramer **24** has been isolated in moderate yields whereas cyclic trimer **23** has never been isolated in a pure and stable form. Interestingly, when we conducted the condensation of trialkoxysilanes in the M_6L_4 cavity we observed the exclusive formation of cyclic trimer **23** as a stable form. In a typical reaction, phenyltrimethoxysilane **25** was suspended in D_2O solution of **4** at 100 °C. The ^{1}H NMR of the solution after 5 min showed the formation of complexes **4**·(**25**)$_3$ and **4**·(**25**)$_4$. After 1 h, the ^{1}H NMR spectrum showed the presence of only one complex **4**·**A**. The formation **4**·**A** was also evidenced by ESI-MS and single crystal X-ray crystallography (Scheme 3). We note the following important features of this reaction. First, the cyclic trimers are formed in a *ship-in-a-bottle* fashion. Secondly, the formed cyclic trimers, which are protected by the cavity, are very stable even in acidic aqueous solutions and isolable as pure clatharate compounds. Lastly, the stereochemistry of the condensation is highly controlled within the cage giving only all-*cis* isomers.

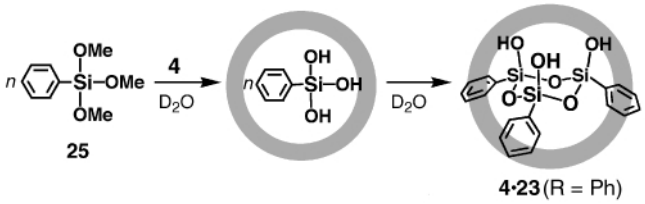

Scheme 3 Schematic representation of trimer formation in the cavity of **4** (shown as circle).

Paneling squares

The square is a basic unit for the construction of cubes and prisms (trigonal, square, pentagonal, hexagonal, *etc.*) Tetrakis(pyridyl)porphyrins are the most common and easily available square panels. Indeed tetrakis(4-pyridyl)porphyrin is already known to form coordination polymers and also some 2D-molecular squares with transition metal atoms.[30] However, 3D-discrete molecules using porphyrin molecular panels have not yet reported. We found the formation of a triangular prism **26** by the self-assembly of tetrakis(3-pyridyl)porphyrin **10** (Fig. 14).[31] The formation of the prism structure was confirmed by ^{1}H NMR ESI-MS and X-ray analyses.

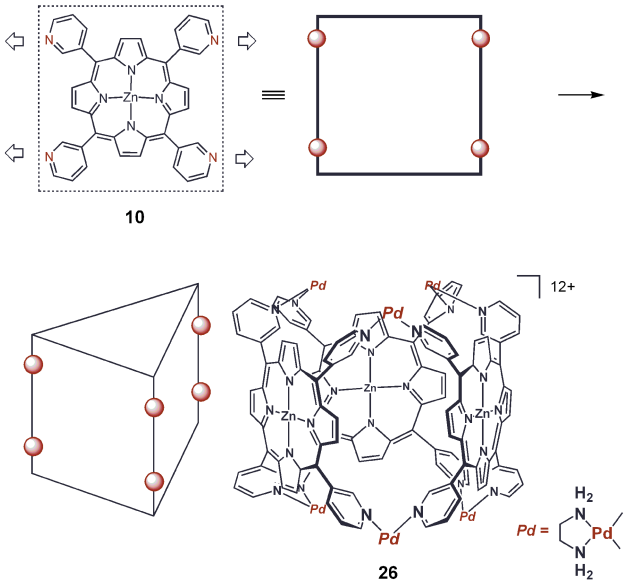

Fig. 14 Schematic representation of molecular paneling of **10** to form **26**.

Paneling rectangles

Similar to square panels, rectangular panels can also be used to construct prismatic structures of (triangles, squares, pentagonal, hexagonal *etc.*) However, depending on the length and width of the rectangular panel the assembled structures can be denoted as either tubes or boxes. Further a number of important topological surfaces such as torus, Möbius strip, Klein bottle and projective plane can also be constructed from rectangular panels. Here, we describe the self-assembly of a family of rectangular panels **11**–**13** to form molecular tubes, and that of **14** to form a molecular nano-box.

Coordination nanotubes

Molecular-based tubular structures have attracted considerable current interest because of their potential abilities for selective inclusion and transportation of ions and molecules and catalysis of specific chemical transformations.[32] Rectangular panels **11**–**13** were designed in anticipation of such tubular structures upon treatment with **1**.[33] For **13**, a coordination nanotube **27** is

expected from four molecules of **13** and 10 molecules of **1** (Fig. 15). However, the formation of coordination nanotubes were observed only in the presence of a rod-like template molecule

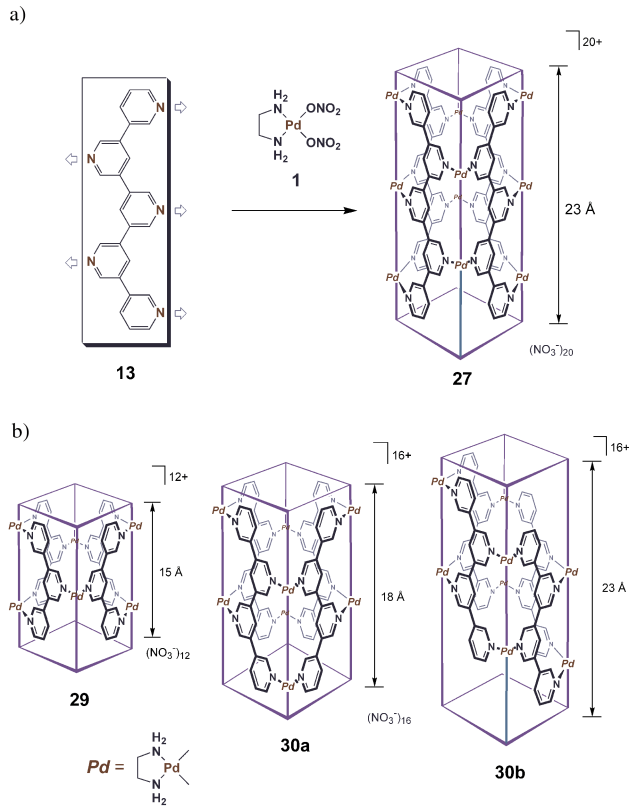

Fig. 15 (a) Schematic representation of molecular paneling of **13** and (b) structural drawings of **29**, **30a** and **30b**.

such as sodium 4,4′-biphenylenedicarboxylate **28**. Similarly, coordination nanotubes **29** and **30** were also obtained and characterized using NMR and ESI-MS. According to NMR spectroscopy, the protons of **28** were up-field shifted by up to 2.6 ppm indicating its encapsulation in the nanotube. A similar template effect was observed with two other rod-like molecules biphenyl and *p*-terphenyl. Spherical and large molecules such as adamantane carboxylate failed to template the nanotubes. Interestingly, it is found that the formation of these tubes is a completely reversible process. That is, the tube dissociates into its components by the removal of the guest molecule and again associates by the addition of guest molecule.

Shuttle movements of guest molecules were observed: at low temperatures the guest stays at a fixed position of the tube, shuttles on the NMR time scale at 60 °C, and rapidly moves or partially goes out at above 60 °C. NMR studies of nanotube **30** revealed that it is a 1 : 1 mixture of structural isomers **30a** and **30b**. In isomer **30a**, each ligand is placed on a C_2-symmetry site and only seven protons corresponding to half of **30a** were observed. On the other hand, in isomer **30b**, all 14 protons were observed as the C_2-symmetry of the ligands was removed. Tubes **29** and **30b** were characterized by X-ray crystallography. The crystal structures display tubular structures of **29** and **30b** efficiently assembled around template **28** *via* strong π–π and CH–π interactions (Fig. 16). The shape of the tube, which ideally should be square, is significantly distorted in order to maximize strong aromatic interactions. That is, the two faces which are interacting with **28** *via* π–π interactions, are squeezed towards the inside, while the remaining two faces, which interact with **28** *via* CH–π interactions, are pushed outwards. Another interesting feature of this crystal structure is the presence of a second molecule of **28** which is enclathrated between the nanotubes.

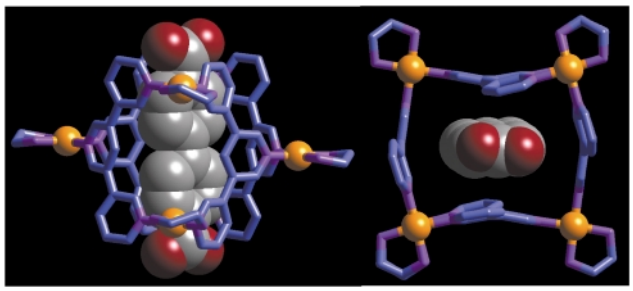

Fig. 16 The X-ray structure of **29**, side view (left) and top view (right).

Coordination box with dynamic property

A 1D rod-like ligand, such as biphenyl, upon treatment with **1** is known to be in equilibrium with two types of two-dimensional structures, namely square **3** and a triangle.[9] In order to extend this property into 3D structures we designed a rectangular molecular panel **14** which has four exodentate coordination sites. As anticipated the molecular panel **14** upon treatment with **1** was found to be in rapid equilibrium with several products which constitute a dynamic library of box structures. From the library we were able to isolate two box structures: namely trimeric box **31** and tetrameric box **32** which are minor products under normal conditions (Fig. 17).[34]

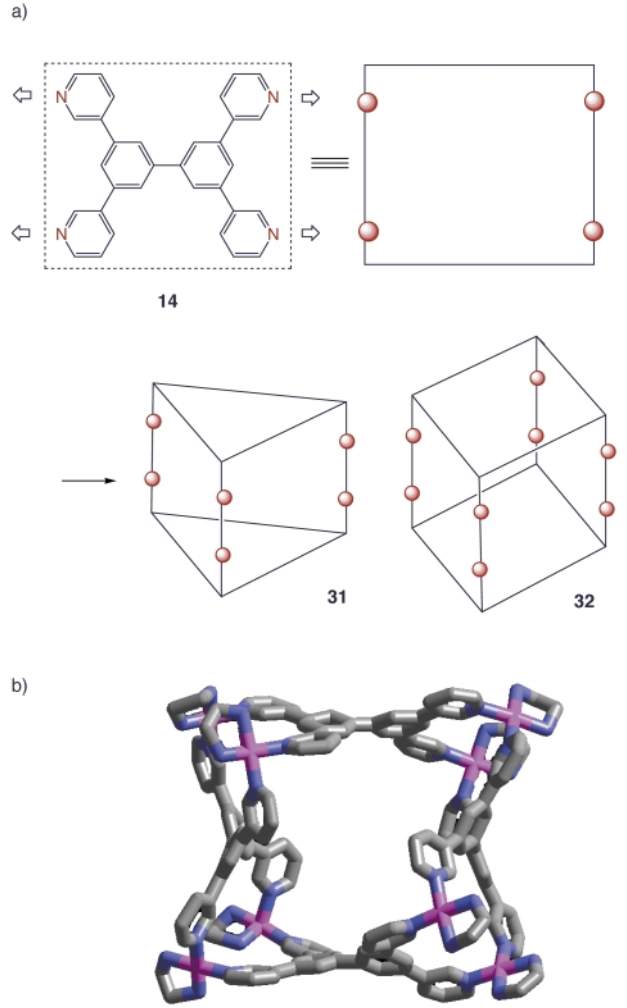

Fig. 17 Schematic representation of molecular paneling of **14** to form **31** and **32** and (b) X-ray crystal structure of an isomer of **32**.

The trimeric molecular box **31** was isolated quantitatively when a template such as biphenyl was suspended in a D_2O solution of **1** and **14** at 80 °C. The ^{1}H NMR of the solution showed two sets of signals: one set corresponds to triangular box **31** (δ 7–10) while the other set corresponds to biphenyl (δ

4.8–6.5). The biphenyl protons were significantly up-field shifted due to the inclusion in the box and the integration of the signals suggests that there are two biphenyl molecules per box. Moreover the proposed formula is in agreement with ESI-MS which shows five peaks at *m/z* 1502.9{[**31**·10NO_3]$^{2+}$}, 982.1{[**31**·9NO_3]$^{3+}$},720.8{[**31**·8NO_3]$^{4+}$},564.3{[**31**·7NO_3]$^{5+}$} and 460.3 {[**31**·6NO_3]$^{6+}$}.

Tetrameric box **32** was isolated as the major product when ligand **14** was treated with **1** at 50 °C for four days in D_2O–CD_3OD. In its ^{1}H NMR spectrum a set of six signals were observed in accord with D_{4h} symmetry of **32**, while CSI-MS of its PF_6 salt also supported the tetrameric box structure (*m/z* 1688.8 [**32**·13PF_6]$^{3+}$ and 1230.8 [**32**·12PF_6]$^{4+}$). Slow diffusion of THF vapor into an H_2O–CH_3CN solution of **1** and **14** for a few weeks resulted in single crystals suitable for X-ray analysis. The crystal structure revealed the formation of an unexpected structure that has the same composition as **32** but is composed of two structural isomers of **14**. The differences between solution and solid-state structures could be due to the presence of THF vapor that possibly shifted the equilibrium during the crystallization. However, the formation of a similar box structure in solution was not observed as it is rapidly isomerizes into box structure **32**.

The dynamic behavior of these box structures in solution was studied by ^{1}H NMR and CSI-MS. When the PF_6 salt of trimeric box **31**·2(biphenyl) was dissolved in CD_3CN the guest was liberated immediately leaving empty **31**. Interestingly monitoring of this solution by ^{1}H NMR and CSI-MS showed the reorganization of trimeric box **31** into tetrameric box **32** in 24 h and also revealed the presence of a pentameric box as a kinetic intermediate during the reorganization process.

Conclusions

Here we have described a highly successful strategy, which we term as *molecular paneling*, to construct various 3D-molecules that resembles several existing polyhedra. We note the following as advantages of using the concept of *molecular paneling* to construct 3D-architectures.

The syntheses are very facile: most of the compounds described here can be synthesized on a several gram scale in the laboratory simply by mixing the components in water, and the yield is quantitative in most cases.

This method provides the opportunity for the construction of larger cage-like molecules with larger cavities. Such larger cavities allow for the existence of isolated spaces which can be used for chemical transformations as described for octahedral cage **4**.

The involvement of transition metals in the molecular frameworks may lead to new properties (photo, redox, magnetic and/or thermal).

Notes and references

1 *Templating, Self-Assembly and Self-Organization*, Exec. ed. J.-P. Sauvage and M. W. Hosseini, *Comprehensive Supramolecular Chemistry*, ed. J.-M. Lehn, Chair ed. Pergamon Press, Oxford, 1995, vol. 9. This volume includes excellent reviews of metal-associated self-assembly. In particular, see the following: J.-P. Sauvage, C. Dietrich-Buchecker and J.-C. Chambron, ch. 3; J. K. M. Sanders, ch. 4; P. N. W. Baxter, ch. 5; E. C. Constable, ch. 6; M. Fujita, ch. 7; K. Biradha and M. Fujita, in *Advances in Supramolecular Chemistry*, ed. G. W. Gokel, Connecticut, vol. 6, p. 1–40.

2 R. W. Saalfrank, E. Uller, B. Demleitner and I. Bernt, *Struct. Bonding (Berlin)*, 2000, **96**, 149; R. W. Saalfrank and I. Bernt, *Curr. Opin. Solid State Mater. Sci.*, 1998, **3**, 407 and references therein.

3 P. Baxter, J.-M. Lehn and A. DeCian, *Angew. Chem., Int. Ed. Engl.*, 1993, **32**, 69; P. N. W. Baxter, J.-M. Lehn, G. Baum and D. Fenske, *Chem. Eur. J.*, 1999, **5**, 102; P. N. W. Baxter, J.-M. Lehn, B. O. Kneisel, G. Baum and D. Fenske, *Chem. Eur. J.*, 1999, **5**, 113.

4 D. L. Caulder and K. N. Raymond, *Acc. Chem. Res.*, 1999, **32**, 975.

5 S. Leininger, B. Olenyuk and P. J. Stang, *Chem. Rev.*, 2000, **100**, 853; P. J. Stang and B. Olenyuk, *Acc. Chem Res.*, 1997, **30**, 502.

6 C. M. Hartshorn and P. J. Steel, *Inorg. Chem.*, 1996, **35**, 6902; C. M. Hartshorn and P. J. Steel, *Chem. Commun.*, 1997, 541.

7 S. R. Batten and R. Robson, *Angew. Chem., Int. Ed.*, 1998, **37**, 1461.

8 A. Ikeda, M. Yoshimura, H. Udzu, C. Fukuhara and S. Shinkai, *J. Am. Chem. Soc.*, 1999, **121**, 4296.

9 M. Fujita, J. Yazaki and K. Ogura, *J. Am. Chem. Soc.*, 1990, **112**, 5645; M. Fujita, J. Yazaki and K. Ogura, *Tetrahedron Lett.*, 1991, **32**, 5589; M. Fujita, J. Yazaki and K. Ogura, *Chem. Lett.*, 1991, 1031; M. Fujita, O. Sasaki, T. Mitsuhashi, T. Fujita, J. Yazaki, K. Yamaguchi and K. Ogura, *Chem. Commun.*, 1996, 1535.

10 R. W. Gable, B. F. Hoskins and R. Robson, *J. Chem. Soc., Chem. Commun.*, 1990, 1677; M. Fujita, Y. J. Kwon, S. Washizu and K. Ogura, *J. Am. Chem. Soc.*, 1994, **116**, 1151.

11 P. J. Stang and D. H. Cao, *J. Am. Chem. Soc.*, 1994, **116**, 4981; P. J. Stang and B. Olenyuk, *Acc Chem Res.*, 1997, **30**, 502.

12 A. W. Maverick and F. E. Klavetter, *Inorg. Chem.*, 1984, **23**, 4129; A. W. Maverick, S. C. Buckingham, Q. Yao, J. R. Bradbury and G. G. Stanley, *J. Am. Chem. Soc.*, 1988, **108**, 7430.

13 M. Fujita, D. Oguro, M. Miyazawa, H. Oka, K. Yamaguchi and K. Ogura, *Nature*, 1995, **378**, 469.

14 R. Wyler, J. de Mendoza and J. Jr. Rebek, *Angew. Chem., Int. Ed. Engl.*, 1993, **32**, 1699; J. Jr. Rebek, *Chem. Soc. Rev.*, 1996, 255.

15 L. R. MacGillivray and J. L. Atwood, *Nature*, 1997, **389**, 469; G. W. Orr, L. J. Barbour and J. L. Atwood, *Science*, 1999 **285**, 1049.

16 L. R. MacGillivray and J. L. Atwood, *Angew. Chem., Int. Ed.*, 1999, **38**, 1019; M. J. Wenninger, *Polyhedron Models*, Cambridge University Press, New York, 1971.

17 F. Ibukuro, T. Kusukawa and M. Fujita, *J. Am. Chem. Soc.*, 1998, **120**, 8561.

18 (*a*) M. Fujita, S.-Y. Yu, T. Kusukawa, H. Funaki, K. Ogura and K. Yamaguchi, *Angew. Chem., Int. Ed.*, 1998, **37**, 2082; (*b*) S.-Y. Yu, T. Kusukawa, K. Biradha and M. Fujita, *J. Am. Chem. Soc.*, 2000, **122**, 2665.

19 K. Umemoto, K. Yamaguchi and M. Fujita, *J. Am. Chem. Soc.*, 2000, **122**, 7150.

20 N. Takeda, K. Umemoto, K. Yamaguchi and M. Fujita, *Nature*, 1999 **398**, 794.

21 K. Umemoto, K. Biradha and M. Fujita, manuscript in preparatipon.

22 T. Kusukawa and M. Fujita, *Angew. Chem., Int. Ed.*, 1998, **37**, 3142.

23 T. Kusukawa, M. Yoshizawa and M. Fujita, submitted.

24 T. Kusukawa and M. Fujita, *J. Am. Chem. Soc.*, 1999, **121**, 1397.

25 J.-M. Lehn, *Pure Appl. Chem.*, 1978, **50**, 871.

26 H. Ito, T. Kusukawa and M. Fujita, *Chem. Lett.*, 2000, 598.

27 D. J. Cram and J. M. Cram, *Container Molecules and Their Guests*, Royal Society of Chemistry, Cambridge, UK, 1995; D. J. Cram, *Nature*, 1992, **356**, 29; R. Warmuth and M. A. Marvel, *Angew. Chem., Int. Ed.*, 2000, **39**, 1117.

28 M. Yoshizawa, T. Kususkawa, M. Fujita and K. Yamaguchi, *J. Am. Chem. Soc.*, 2000, **122**, 6311.

29 R. H. Baney, M. Itoh, A. Sakakibara and T. Suzuki, *Chem. Rev.*, 1995, **95**, 1409.

30 B. F. Abrahams, B. F. Hoskins and R. Robson, *J. Am. Chem. Soc.*, 1991, **113**, 3606; B. F. Abrahams, B. F. Hoskins, D. M. Michail and R. Robson, *Nature*, 1994, **369**, 727; C. V. K. Sharma, G. A. Broker, J. G. Huddleston, J. W. Baldwin, R. M. Metzer and R. D. Rogers, *J. Am. Chem. Soc.*, 1999, **121**, 1137; C. M. Drain, R. Fisher, E. Nolen and J.-M. Lehn, *J. Chem. Soc., Chem. Commun.*, 1993, 243; P. J. Stang, J. Fan and B. Olenyuk, *Chem. Commun.*, 1997, 1453.

31 N. Fujita, K. Biradha, K. Yamaguchi and M. Fujita, submitted.

32 S. Iijima, *Nature*, 1991, **354**, 56; A. Harada, in *Modular Chemistry*, ed. J. Michl, Kluwer Academic Publishers, Dordrecht, The Netherlands, 1997, p. 361; J. D. Hartgerink, T. D. Clark and M. R. Ghadiri, *Chem. Eur. J.*, 1998, **3**, 1367.

33 M. Aoyagi, K. Biradha and M. Fujita, *J. Am. Chem. Soc.*, 1999, **121**, 7457.

34 Y. Yamanoi, Y. Sakamoto, T. Kusukawa, M. Fujita, S. Sakamoto and K. Yamaguchi, *J. Am. Chem. Soc.*, 2001, **123**, in press.

Phase-transfer synthesis of novel water-soluble gold clusters with tripodal thioether based ligands

W. Matthias Pankau,[a] Karen Verbist†[b] and Günter von Kiedrowski*[a]

[a] *Lehrstuhl für Bioorganische Chemie, Ruhr-Universität-Bochum, 44780 Bochum, Germany. E-mail: kiedro@ernie.orch.ruhr-uni-bochum.de*
[b] *EMAT, University of Antwerp, Groenerborgerlaan 171, B-2020 Antwerp, Belgium*

Received (in Cambridge, UK) 7th November 2000, Accepted 24th January 2001
First published as an Advance Article on the web 28th February 2001

Tripodal, water-soluble thioethers based on 1,3,5-trismethylbenzene scaffolds are suitable ligands for the Au_{55} cluster.

The so called 'Schmid-cluster',[1] $Au_{55}(PPh_3)_{12}Cl_6$, has stimulated many different areas of chemistry ranging from catalysis research[2] to the concept of nanocrystals[3,4] and quantum electronics.[5] Monofunctionalized water-soluble derivatives of the cluster are commercially available and have found numerous applications as TEM markers for biomolecules.[6] We have recently reported on trisoligonucleotidyls,[7] a novel class of branched oligonucleotides that can be used for an informational self assembly of defined nanometer sized objects. TEM imaging of such objects proved to be successful in those cases where heating steps involving oligonucleotide gold conjugates could be avoided. The exploration of general strategies for the non-covalent synthesis of nanoobjects, however, requires sufficient thermal stability of the TEM markers, especially if one conceives a chemical replication of such nanoobjects.

We report here on the synthesis[8] and preliminary characterisation of water-soluble gold clusters bearing tripodal thioether based ligands **1**–**6** (Fig. 1). The rationale behind these ligands, shown in Fig. 2, relates to the general ideas of symmetry-based host design as outlined by MacGillivray and Atwood.[9] The Au_{55} cluster core may be described as a cuboctahedron whose surface

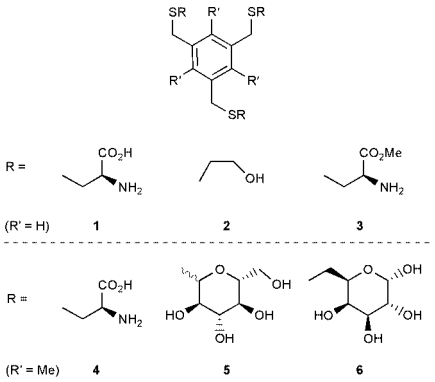

Fig. 1 Structures of examined thioethers.

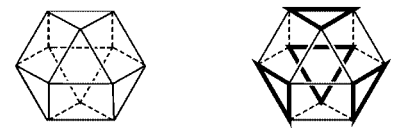

Fig. 2 Proposed cuboctahedron geometry of the Au_{55} cluster and some possibilities of coverage with multidentate ligands.

† Present address Soft Imaging System GmbH, Hammerstr. 89, 48153 Münster, Germany.

is composed of eight edge-connected triangles (111) and six squares (110). As such, Au_{55} is expected to bind four tripodal ligands if the binding mode of the ligands is comparable to the Schmid cluster where the 12 triphenylphosphanes most likely occupy the edges of the cuboctahedron. The affinity of C_3-symmetrical thioethers towards the (111) gold surface has already been reported in the context of self assembled monolayers.[10] Molecular modelling studies suggested that tris-thioethers derived from 1,3,5-trismethylbenzene scaffolds are suitable candidates for tripodal binding as they seem to match the geometric requirements for covering the (111) triangles of Au_{55}. A model of the Au_{55} core surrounded by ligand **1** is shown in Fig. 3.

Ligands **1**–**6** were tested for their ability to extract gold into the aqueous phase from a solution of the triphenylphosphane cluster in methylene chloride, a method used previously by Schmid *et al.*[11] to exchange the ligand into monosulfonated triphenylphosphane. The degree of phase transfer was monitored from the partition of the brown color after stirring the two-phase system for varying periods of time. Complete phase transfer resulting in an decolorization of the organic phase was achieved with ligand **6** after 16 h and with ligands **1** and **4** after 7 days (in buffered[12] solution or when using the sodium salt respectively). Extraction using the other ligands (**2**, **3** and **5**) did not show any phase transfer. The absence of remaining triphenylphosphane ligands was shown by NMR investigation of the precipitated and redissolved clusters with ligands **1**, **4** and **6** (in D_2O). In all cases neither signals of the phosphane aromatics (in ^1H NMR) nor P resonance signals could be detected. The clusters were precipitated from the aqueous phase by addition of propan-2-ol and purified by cycles of dissolution in water and reprecipitation with the alcohol. The solvent was

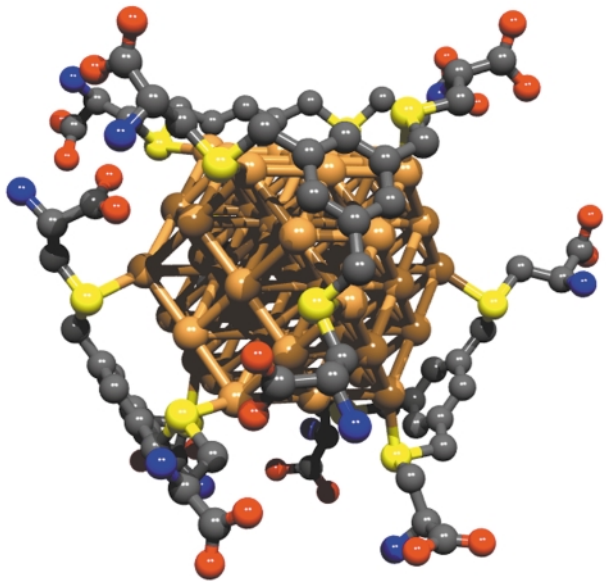

Fig. 3 Computational model structure of the ligand **1** cluster complex.

DOI: 10.1039/b008967m

evaporated *in vacuo* at room temperature, yielding a brownish powder. Elemental analyses were carried out with the cluster bearing ligand **1** as its sodium salt[13a] or with trishydroxymethylaminomethane (TRIS) as counter ion.[13b] The results suggest a ratio of four ligand molecules (with counter ions) per $Au_{55}Cl_6$ core.

Dynamic light scattering/photon correlation spectroscopy (PCS) proved to be a quick and comfortable method for studying the size distribution of the clusters. The mean diameters (and half value widths) were 2.6 ± 0.34 nm for clusters with ligands **1** and **4** and 2.8 ± 0.20 nm for ligand **6**, respectively. These data are not incompatible with the assumption of an Au_{55} core if one considers the hydrodynamic radius estimated from PCS is affected by the nature and solvation properties of the ligands. For ligand **1** the distribution of cluster core sizes was further monitored using high resolution TEM (400 kV). A fairly uniform size distribution with a mean diameter of 1.4 nm was found. The cluster preparations were stable in aqueous solution for weeks at ambient temperature, before slow aggregation to larger colloids and precipitation occurs, hinting at their high kinetic stability. A sample that was stored in aqueous solution at room temperature for 70 days still showed a very narrow size distribution (diameter *ca.* 1.4 nm) according to TEM (Fig. 4).

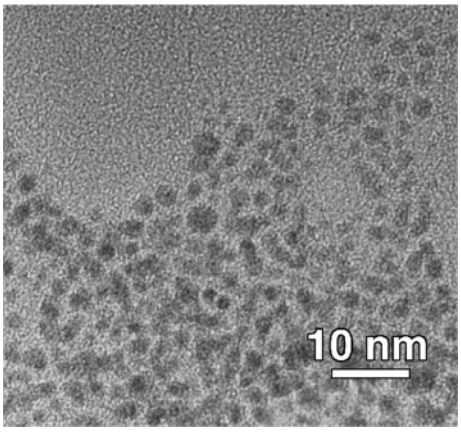

Fig. 4 HRTEM image of the Au_{55} cluster with ligand **1** after storing the sample solution for 70 days.

Gel electrophoresis using 1% agarose gel proved applicable to investigate the charge, uniformity and kinetic stability of the different clusters. The agarose gel of clusters with ligands **1** and **4** reveals a discrete brownish band moving to the anode. Its appearance in terms of broadness is comparable to bromophenyl blue hinting at its uniformity and proving the expected anionic character of the cluster. Under the same conditions, the clusters formed from ligand **6** did not show any mobility, as expected for neutral ligands, if the six chloride ions are tightly bound to the cluster core, with only diffusive broadening at the flanks of the gel pocket being observed. Furthermore, clusters from ligands **1** and **4** show only little smearing of the electrophoresis band so revealing their kinetic stability. All attempts to establish the molecular weight of the clusters by MALDI-TOF mass spectroscopy have failed so far.

To the best of our knowledge, this work represents the first examples of the utilisation of tripodal ligands and on the use of thioether ligands for the preparation of gold clusters. Future approaches towards the synthesis of stable, water soluble, biocompatible and monofunctionalizable gold clusters may now employ peptide chemistry for further sealing and packaging of Au_{55} cores.

We thank Deutsche Forschungsgemeinschaft (SFB 452) for support, Degussa-Hüls AG for the generous gift of tetrachloroauric acid, and G. Schmid for a sample of $Au_{55}(PPh_3)_{12}Cl_6$.

Notes and references

1 G. Schmid, R. Boese, R. Pfeil, F. Bandermann, S. Meyer, G. H. M. Calis and J. W. A- van der Velden, *Chem. Ber.*, 1981, **114**, 3634.
2 M. Haruta, S. Tsubota, T. Kobayashi, H. Kageyama, M. J. Denet and D. Delmon, *J. Catal.*, 1993, **144**, 175.
3 C. A. Mirkin, *Nature*, 1996, **382**, 607.
4 C. J. Loweth, W. B. Caldwell, X. Peng, A. P. Alivisatos and P. G. Schultz, *Angew. Chem., Int. Ed.*, 1999, **38**, 1808.
5 G. Schmid and N. Beyer, *Eur. J. Inorg. Chem.*, 2000, 835.
6 'Nanogold' available from Nanoprobes Inc., Yaphank, NY, USA. As an example of utilisation see: P. A. Alivisatos, K. P. Johnsson, X. Peng, T. E. Wilson, C. J. Loweth, M. P. Bruchez and P. G. Schultz, *Nature*, 1996, **382**, 609.
7 M. Scheffler, A. Dorenbeck, S. Jordan, M. Wüstefeld and G. von Kiedrowski, *Angew. Chem., Int. Ed.*, 1999, **38**, 3311.
8 The synthesis of the ligands was straightforward: *S*-alkylation of sodium cysteinate and potassium 2-hydroxyethylthiolate using 1,3,5-tris(bromomethyl)mesitylene[8a] in H_2O–methanol (1 : 1) yielded ligands **1** and **2** in 90 and 77% yields, respectively. Ligand **1** was converted into its trimethylester **3** in 91% yield using $SOCl_2$ in methanol. Treatment of 1,3,5-tris(bromomethyl)benzene[8b] with sodium cysteinate in H_2O–methanol gave ligand **4** in 94% yield while the analogous conversion of 1-deoxy-1-thioglucose sodium salt[8c] into ligand **5** proceeded with 45% yield under the same conditions. The sugar-based thioether ligand **6** was obtained in an overall yield of 54% from 6-deoxy-6-tosyldiacetonegalactose,[8d] which was converted into the 6-bromo derivative, condensed with 1,3,5-tris(mercaptomethyl)benzene sodium salt[8e] in DMF and deprotected with methanolic HCl. (*a*) J. Závada, M. Pánková, P. Holý and M. Tichý, *Synthesis*, 1994, 1132; (*b*) W. Offermann and F. Vögtle, *Synthesis*, 1977, 273; (*c*) commercialy available from ALDRICH Chemicals; (*d*) B. Iselin and T. Reichstein, *Helv. Chim. Acta*, 1946, 508; (*e*) A. Ricci, R. Danieli and S. Rossini, *J. Chem. Soc., Perkin Trans. 1*, 1976, 1691.
9 L. R. MacGillivray and J. L. Atwood, *Angew. Chem., Int. Ed.*, 1999, **38**, 1018.
10 H. Schoenherr, F. J. B. Kremer, S. Kumar, J. A. Rego, H. Wolf, H. Ringsdorf, M. Jaschke, H.-J. Butt and E. J. Bamberg, *J. Am. Chem. Soc.*, 1996, **118**, 13051.
11 G. Schmid, N. Klein and L. Korste, *Polyhedron*, 1988, **7**, 605.
12 1 mM TRIS/HCl, pH = 7.90
13 (*a*) Found: C, 5.92; H, 0.81; N, 0.94; S, 3.09; Au, 81.98%(av.) Calc: C, 6.54; H, 0.73; N, 1.27; S, 2.91, Au, 81.26%. (*b*) Found: C, 10.64; H, 1.40; N, 1.87; S, 4.14; Au, 77.89%(av.). Calc: C, 10.00; H, 1.68; N, 2.33; S, 2.67, Au, 75.18% (calculated for a 1 : 4 ratio of metal core (with 6 chloride atoms) to ligands).

ChemComm

Highly selective induction of metal-centered chirality in the ligand exchange reaction of planar-chiral cyclopentadienyl–ruthenium complex bearing an anchor phosphine ligand†

Kiyotaka Onitsuka, Noriko Dodo, Yuji Matsushima and Shigetoshi Takahashi*

The Institute of Scientific and Industrial Research, Osaka University, 8-1 Mihogaoka, Ibaraki, Osaka 567-0047, Japan. E-mail: takahashi@sanken.osaka-u.ac.jp

Received (in Cambridge, UK) 23rd November 2000, Accepted 6th February 2001
First published as an Advance Article on the web 26th February 2001

Treatment of planar-chiral cyclopentadienyl–phosphine ruthenium complexes with phosphine and phosphite induces metal-centered chirality with a high stereoselectivity (≥99 % de).

Planar-chiral cyclopentadienyl (Cp) complexes generated by coordination of unsymmetrically substituted Cp ligands to metal atoms have attracted much attention as novel asymmetric catalysts.[1] Although planar-chiral Cp complexes of early transition metals have been applied to asymmetric reactions with high selectivities, limited numbers of studies on such types of complex involving late transition metals are found in the literature. We have been investigating the synthesis, optical resolution and properties of planar-chiral organometallic complexes of Group 8 metals with trisubstituted Cp ligands.[2] Recently we prepared planar-chiral Cp–phosphine ruthenium complexes **1**,[3] which may serve as a good asymmetric environment around the ruthenium atom to prevent the rotation of the trisubstituted Cp ring by an anchor phosphine.[4] Now we examined the efficiency of the planar-chiral Cp–phosphine ligand on the induction of metal-centered chirality since the control of stereochemistry at a metal center is very important to develop highly enantioselective reaction using three-legged piano-stool complexes.[5]

Significant numbers of attempts to induce metal-centered chirality in three-legged piano-stool complexes have been found in the literature.[6] However, successive examples of the control of metal-centered chirality with a high selectivity are still limited. Very recently, with planar-chiral Cp and indenyl Rh and Ir complexes having anchor phosphine ligands it has been shown that the metal-centered chirality is induced by oxidative addition to the metal with high stereoselectivities.[7] Herein we report the thermodynamically or kinetically controlled induction of metal-centered chirality in the ligand exchange reactions of planar-chiral Cp–phosphine Ru complexes with various phosphines and phosphites.

Treatment of complex **1a** with 1.1 equiv. of PPh_3 in acetone at room temperature resulted in the replacement of one of the two MeCN ligands to give complex **2a** in quantitative yield. Resulting complex **2a** contained two diastereomers, each of which consists of a pair of enantiomers when racemic **1a** was used as the starting material (Scheme 1). Thus, the stereoselectivity at a chiral metal center was appraised by the ratio of the major diastereomer (**2a-1**) to the minor one (**2a-2**). ^1H and ^{31}P NMR spectra of **2a** clearly showed that the diastereoselectivity was 52% de. Fortunately, single crystals of **2a-1** were able to be grown in a CH_2Cl_2–ether solution of a mixture of the two diastereomers. The stereochemistry of **2a-1** was unequivocally identified by X-ray crystallography to be $S_{1C}S_{Ru}$/$R_{1C}R_{Ru}$ as shown in Fig. 1.‡

The stereoselectivity was then examined for the reactions of **1a**–**1c** with phosphines and phosphites (Table 1), and it was found that the selectivity depends upon the steric bulkiness of incoming phosphines and phosphites, and of the substituents on the Cp group. In the reactions with bulky phosphines, such as PPh_3 and PBu_3, the selectivities were higher than those with smaller ones such as PMe_3. The reaction of complex **1c** having a *t*-butyl group on the Cp ring gave products with a high selectivity relative to those for complexes **1a** and **1b**. Thus, the reactions of **1c** with bulky phosphines and phosphites (entries 11, 12 and 14) produced single diastereomers exclusively (> 99% de). The X-ray analyses of major products **2d-1**, **2f-1**, **2h-1**, **2m-1**, **2n-1** and **2o-1** revealed that all of them have the same stereochemistry as that of **2a-1**.†‡§ Similar reactions of planar-chiral Ru complexes **3** involving a $P(OMe)_3$ ligand instead of an anchor phosphine one were performed (Scheme 2, Table 2). Although the yields of products **4** were high, the

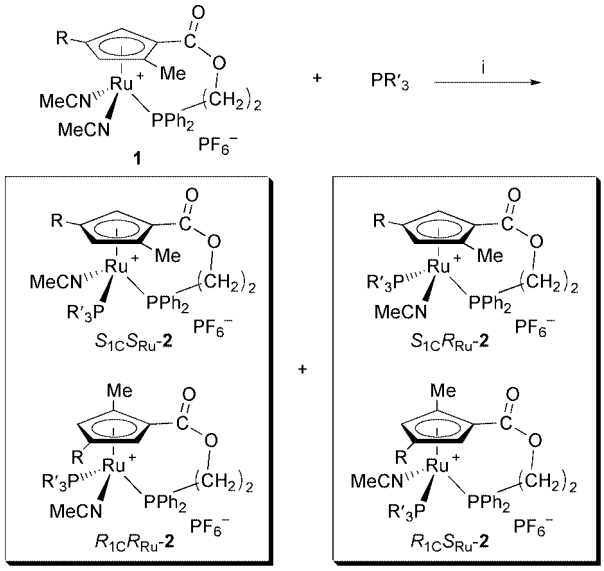

Scheme 1 *Reagents and conditions*: i, acetone, room temp., 3 h.

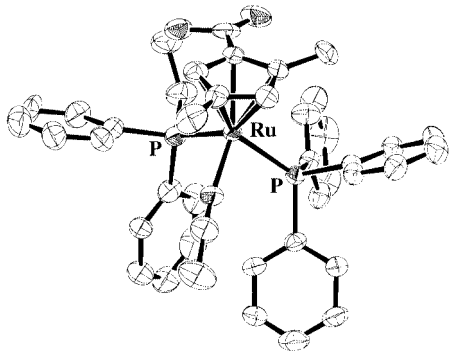

Fig. 1 Molecular structure of complex **2a-1**·$2CH_2Cl_2$. Hydrogen atoms, a counter anion and a solvent molecule are omitted for clarity.

† Electronic supplementary information (ESI) available: crystal data and ORTEP diagrams for complexes **1a**, **2d-1**, **2f-1**, **2h-1**, **2m-1**, **2n-1** and **2o-1**. See http://www.rsc.org/suppdata/cc/b0/b009412i/

Table 1 Reactions of complexes **1a**–**1c** with phosphines and phosphites

Entry	Complex	PR'_3	Product	Yield (%)[a]	% de[a]
1	**1a** (R = Me)	PPh_3	**2a**	100	52[b]
2	**1a**	PBu_3	**2b**	100	92
3	**1a**	PMe_3	**2c**	100	64
4	**1a**	$P(OPh)_3$	**2d**	100	38[b]
5	**1a**	$P(OMe)_3$	**2e**	100	40
6	**1b** (R = Ph)	PPh_3	**2f**	100	80[b]
7	**1b**	PBu_3	**2g**	96	86
8	**1b**	PMe_3	**2h**	100	46[b]
9	**1b**	$P(OPh)_3$	**2i**	100	42
10	**1b**	$P(OMe)_3$	**2j**	100	44
11	**1c** (R = Bu^t)	PPh_3	**2k**	91	> 99
12	**1c**	PBu_3	**2l**	100	> 99
13	**1c**	PMe_3	**2m**	100	70[b]
14	**1c**	$P(OPh)_3$	**2n**	100	> 99[b]
15	**1c**	$P(OMe)_3$	**2o**	96	82[b]

[a] Determined by ^{1}H and ^{31}P NMR spectroscopy. [b] The structures of major products were determined by X-ray crystallography.

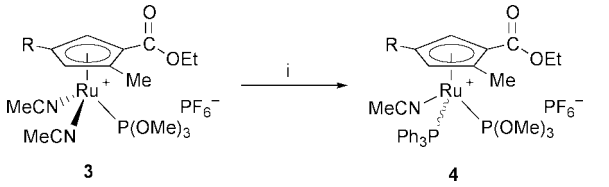

Scheme 2 *Reagents and conditions*: i, 1.1 PPh_3, acetone, room temp., 3 h.

Table 2 Reactions of complexes **3a**–**3c** with phosphines

Entry	Complex	Product	Yield (%)[a]	% de[a]
1	**3a** (R = Me)	**4a**	92	28
2	**3b** (R = Ph)	**4b**	100	2
3	**3c** (R = Bu^t)	**4c**	100	34

[a] Determined by ^{1}H and ^{31}P NMR spectroscopy.

diastereoselectivities were very low (< 34% de) relative to those of **2**, suggesting that the anchor phosphine ligand has an important role in control of the stereochemistry at the metal center.

It should be noted that complexes **2a-1** and **2f-1** slowly isomerized into minor isomers **2a-2** and **2f-2**, respectively, in acetone at room temperature. For example, diastereomerically pure complex **2a-1** was converted into a mixture of complexes **2a-1** and **2a-2** in a 74:26 ratio (48% de), which is almost the same diastereoexcess as that observed for the reaction of **1a** with PPh_3. Since easy replacement of the MeCN ligands in **2a-1** and **2f-1** with CD_3CN was confirmed by means of ^{1}H NMR, the selectivities in these cases must be determined by the thermodynamic stability of the products. On the other hand, no epimerization at a metal center as well as no exchange of MeCN with CD_3CN were observed in other major products **2-1** in solution. These results strongly suggest that the selectivities of products **2**, except for **2a** and **2f**, were controlled kinetically. The kinetic preference of $S_{1C}S_{Ru}/R_{1C}R_{Ru}$ isomers to $S_{1C}R_{Ru}/R_{1C}S_{Ru}$ ones can be reasonably explained considering the stereochemistry of intermediate **5** as shown in Scheme 3. Ligand exchange reactions would proceed *via* unsaturated species **5**, which is generated by dissociation of MeCN from **1**. Coordination of incoming phosphines or phosphites from side (a) gives ($S_{1C}S_{Ru}/R_{1C}R_{Ru}$)-**2**, while coordination from side (b) produces ($S_{1C}R_{Ru}/R_{1C}S_{Ru}$)-**2**. The structures of planar-chiral ruthenium complexes with Cp–phosphine ligands including starting complex **1a**‡ clearly show that the attack of phosphines to the ruthenium center receives steric hindrance caused by the equatorial phenyl group and the substituent (R) on the Cp group. Thus, the attack from side (a) must be faster than that from side

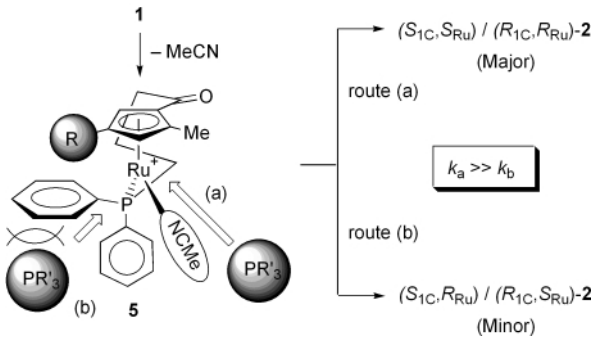

Scheme 3

(b), resulting in the selective formation of ($S_{1C}S_{Ru}/R_{1C}R_{Ru}$)-**2**. This explanation is in good agreement with the steric influence of incoming phosphines and the substituents on the Cp group upon the selectivity of the reactions (*vide supra*).

In summary, we have disclosed here the first example of the kinetic control of metal-centered chirality by planar-chirality of the Cp group in the three-legged piano-stool complexes. Since the resulting complexes are conformationally stable, they may be applicable to novel asymmetric catalysts.

Notes and references

‡ *Crystal data* for complex **2a-1**·$2CH_2Cl_2$: $C_{44}H_{44}Cl_4F_6NO_2P_3Ru$, M = 1068.63, triclinic, $P\bar{1}$ (no. 2), a = 11.480(3), b = 19.232(5), c = 11.334(3) Å, α = 98.40(2), β = 107.45(2), γ = 80.66(2)°, V = 2342(1) Å^3, Z = 2, D_c = 1.515 cm^{-3}, μ(Mo-Kα) = 7.26 cm^{-1}, $2\theta_{max}$ = 55°, −50 °C, R (R_w) = 0.075 (0.137) for 550 parameters against 9502 reflections with I > 3.0σ(I) out of 11 004 unique reflections (R_{int} = 0.019), GOF = 1.53.

CCDC 147977–84. See http://www.rsc.org/suppdata/cc/b0/b009412i/ for crystallographic files in .cif or other electronic format.

§ In the reaction with PBu_3 and PMe_3, the assignments of configuration at a metal center (R_{Ru} or S_{Ru}) in resulting complexes **2b**, **2c**, **2g**, **2h**, **21** and **2m** are reversed relative to those of other complexes with the same conformation due to the change of the priorities of the anchor phosphine ligand and the incoming P ligands. Thus, the stereochemistries of **2b-1**, **2c-1**, **2g-1**, **2h-1**, **2l-1** and **2m-1** are $S_{1C}R_{Ru}/R_{1C}S_{Ru}$ whereas those of other major products are $S_{1C}S_{Ru}/R_{1C}R_{Ru}$.

1 R. L. Halterman, *Chem. Rev.*, 1992, **92**, 965.
2 T. Katayama, Y. Morimoto, M. Yuge, M. Uno and S. Takahashi, *Organometallics*, 1999, **18**, 3087 and references therein.
3 N. Dodo, Y. Matsushima, M. Uno, K. Onitsuka and S. Takahashi, *J. Chem. Soc., Dalton Trans.*, 2000, 35.
4 Y. Matsushima, K. Onitsuka and S. Takahashi, *Chem. Lett.*, 2000, 760.
5 H. Brunner, K. Fisch, P. G. Jones and J. Salbeck, *Angew. Chem., Int. Ed. Engl.*, 1989, **28**, 1521; S. G. Davies, *Aldrichchim. Acta*, 1990, **23**, 31; M. Brookhart, Y. Liu, E. W. Goldmman, D. A. Timmers and G. D. Williams, *J. Am. Chem. Soc.*, 1991, **113**, 927; J. W. Faller, M. R. Mazzieri, J. T. Nguyen, J. Parr and M. Tokunaga, *Pure Appl. Chem.*, 1994, **66**, 1463; J. A. Gladysz and B. J. Boone, *Angew. Chem., Int. Ed. Engl.*, 1997, **36**, 550.
6 F. Morandini, G. Consiglio, B. Straub, G. Ciani and A. Sironi, *J. Chem. Soc., Dalton Trans.*, 1983, 2293; E. Cesarotti, A. Chiesa, G. F. Ciani, A. Sironi, R. Vefghi and C. White, *J. Chem. Soc., Dalton Trans.*, 1984, 653; Y. Nishibayashi, I. Takei and M. Hidai, *Organometallics*, 1997, **16**, 3091; W. A. Schenk, J. Kümmel, I. Reuther, N. Burzlaff, A. Wuzik, O. Schupp and G. Bringmann, *Eur. J. Inorg. Chem.*, 1999, 1745; A. J. Davenport, D. L. Davis, J. Fawcett, S. A. Garratt and D. R. Russell, *Chem. Commun.*, 1999, 2331; B. M. Trost, B. Vidal and M. Thommen, *Chem. Eur. J.*, 1999, **5**, 1055; D. Carmona, F. J. Lahoz, R. Atencio, L. A. Oro, M. P. Lamata, F. Viguri, E. San José, C. Vega, J. Reyes, F. Joó and Á. Kathó, *Chem. Eur. J.*, 1999, **5**, 1544; M. R. Meneghetti, M. Grellier, M. Pfeffer, J. Dupont and J. Fischer, *Organometallics*, 1999, **18**, 560; J. W. Faller, B. P. Patel, M. A. Albrizzio and M. Curtis, *Organometallics*, 1999, **18**, 3096; C. Slugovc, W. Simanko, K. Mereiter, R. Schmid, K. Kirchner, L. Xiao and W. Weissensteiner, *Organometallics*, 1999, **18**, 3865; H. Brunner and T. Zwack, *Organometallics*, 2000, **19**, 2423.
7 T. A. Mobley and R. G. Bergman, *J. Am. Chem. Soc.*, 1998, **120**, 3253; Y. Kataoka, A. Shibahara, Y. Saito, T. Yamagata and K. Tani, *Organometallics*, 1998, **17**, 4338; Y. Kataoka, Y. Iwato, T. Yamagata and K. Tani, *Organometallics*, 1999, **18**, 5423.

A bromine-catalysed free-radical oxidation of acetamides from primary and secondary alkylamines by H_2O_2

Hans-René Bjørsvik,[a] Francesca Fontana,[b] Lucia Liguori[c] and Francesco Minisci*[c]

[a] *Department of Chemistry, University of Bergen, Allégaten 41, N-5007 Bergen, Norway*
[b] *Department of Engineering, University of Bergamo, viale Marconi 5, I-24044 Dalmine (BG), Italy*
[c] *Department of Chemistry, Politecnico di Milano, via Mancinelli 7, I-20131 Milano, Italy. E-mail: Francesco.Minisci@polimi.it*

Received (in Liverpool, UK) 7th November 2000, Accepted 8th February 2001
First published as an Advance Article on the web 26th February 2001

New procedures based on the oxidation by bromine-catalysed hydrogen peroxide in a two-phase system provide simple and cheap transformations of alkylamines to carbonyl derivatives (aldehydes, ketones, carboxylic acid, imides, lactams) through the corresponding acetamides.

Classical rearrangement reactions, such as the Hofmann[1,2] and Curtius[1,3] rearrangements, allow the transformation of carboxylic acids to amines through the corresponding amides or acyl azides [eqn. (1)], while the Beckmann[4,5] rearrangement involves the formation of amides from ketones through the oximes [eqn. (2)].

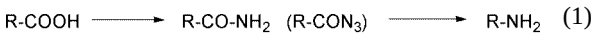

(1)

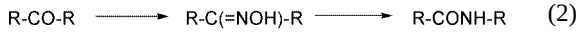

(2)

In this Communication we report a new simple oxidation procedure, which allows the reverse transformation of alkylamines to carboxylic acids, aldehydes, ketones and imides through the intermediates acetamides [eqn. (3)].

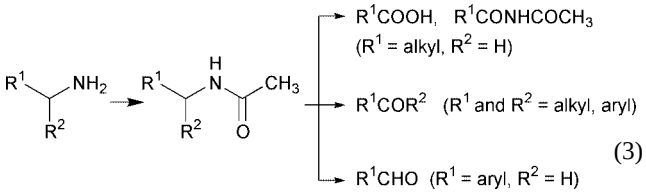

(3)

Recently we have reported[6,7] simple and highly selective methods for the oxidation of primary alcohols to either aldehydes or esters, depending on the benzylic or aliphatic nature of the alcohol, by bromine-catalysed H_2O_2 [eqns. (4) and (5)].

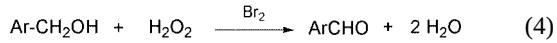

(4)

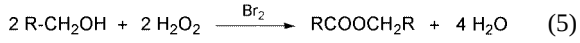

(5)

The selectivity of these reactions is determined by the relative rates of hydrogen abstraction by bromine atom from the alcohol (k_4) and from the corresponding aldehyde (k_5). For benzylic alcohols $k_4 > k_5$ and the reaction gives high selectivity in aldehyde with complete conversion, whereas for non-benzylic alcohols $k_4 << k_5$ and the oxidation gives high selectivity in esters even at very low conversion, without formation of a significant amount of aldehydes.

Aliphatic amines, in principle, should be more reactive, both for enthalpic and polar reasons, than the corresponding alcohols towards hydrogen abstraction by Br•. The acidic medium, however, deactivates the amines by protonation, which reverses the polar effect and increases the strength of the C–H bonds in the α-position. To avoid this limitation we have investigated the bromine-catalysed H_2O_2 oxidation of the corresponding acetamides.

With primary alkyl groups, the carboxylic acid was easily obtained, but when the primary alkyl group was benzylic the corresponding aldehyde was formed instead, with good selectivity at complete conversion. A free-radical chain is involved according to Scheme 1.

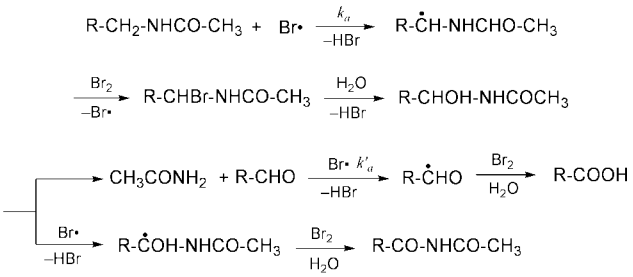

Scheme 1

Also in this case, as for alcohol oxidation, the selectivity was determined by the relative rates of hydrogen abstraction by Br• from the amide (k_a) or from the aldehyde (k'_a). Since $k_a > k'_a$ for R = aryl, while $k_a << k'_a$ for R = alkyl, an opposite behaviour is observed in the two cases. Polar and enthalpic effects, due to the different electronic configurations of the alkyl (π-type) and acyl (σ-type) radicals,[8] determine this different reactivity, as previously[6,7] discussed for the oxidation of alcohols.

With secondary alkyl groups the corresponding ketones were obtained, but under the reaction conditions a partial bromination of the ketones occurs; conversion and selectivity are low with cyclohexyl derivatives, due to the particular ease of bromination of cyclohexanone, compared to acyclic ketones.[9]

By-products of the oxidation according to Scheme 1 are the imides, formed by further oxidation of α-hydroxyamides before cleavage. In any case, imides can be easily hydrolysed, so that high overall yields of carboxylic acids can be obtained by refluxing the acidic reaction mixture; under the reaction conditions (room temperature) the imides are not substantially hydrolysed, supporting the mechanism of Scheme 1 for the formation of carboxylic acids.

With cyclic amines, such as **1** and **2**, the higher stability of α-hydroxyamides leads to the corresponding imides **3** and **4** with high yields and to the corresponding lactams **5** and **6** by hydrolysis [eqns. (6) and (7)].

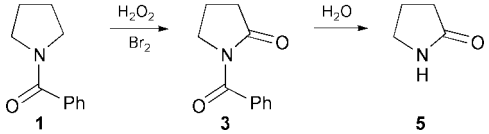

(6)

DOI: 10.1039/b008965f

Table 1 Oxidation of R^1R^2NCOMe (1 mmol) by H_2O_2 and Br_2 in a two-phase system (H_2O–DCE[a])

#	R^1	R^2	Br^2/mmol	H_2O_2/ mmol	Solvent ml H_2O–DCE	Conv. %	Reaction products (%)
1[b]	*n*-C_4H_9	H	0.4	1.8	1/4	> 99	Carboxylic acid (68) Imide (26)
2[b]	*n*-C_6H_{13}	H	0.4	1.8	1/4	97	Carboxylic acid (72) Imide (24)
3[b]	Me_2CH-CH_2	H	0.4	1.8	1/4	95	Carboxylic acid (63) Imide (25)
4[b]	*n*-$C_{12}H_{23}$	H	0.4	1.8	1/4	98	Carboxylic acid (72) Imide (23)
5[b]	*n*-C_4H_9	*n*-C_4H_9	0.8	3.6	1/4	98	Carboxylic acid (66) Imide (28)
6[b]	*n*-C_6H_{13}	*n*-C_6H_{13}	0.8	3.6	1/4	92	Carboxylic acid (61) Imide (23)
7[c]	*n*-C_4H_9	H	2.2	—	4/8	> 99	Carboxylic acid (48) Imide (45)
8[c]	*n*-C_6H_{13}	H	2.2	—	4/8	> 99	Carboxylic acid (47) Imide (48)
9[c]	*n*-$C_{12}H_{23}$	H	2.2	—	4/8	96	Carboxylic acid (44) Imide (43)
10[d]	*n*-C_4H_9	H	HBr 4.4	H_2O_2 2.2	4/8	93	Carboxylic acid (46) Imide (44)
11[c]	Me_2CH-*n*-C_5H_{11}	H	1.3	—	4/8	95	Ketone (70) α-Br-ketone (12)
12[c]	(*n*-Bu)$_2$CH	H	1.3	—	4/8	93	Ketone (69) α-Br-ketone (13)
13[c]	Ph-CH-Me	H	1.3	—	4/8	> 99	Ketone (73) α-Br-ketone (13)
14[c]	Cyclohexyl	H	1.3	—	4/8	26	Cyclohexanone (49) α-Br-cyclohexanone (51)
15[c]	Cyclohexyl	H	2.2	—	4/8	35	Cyclohexanone (46) α-Br-cyclohexanone (53)
16[b]	(*n*-Bu)$_2$CH	H	0.3	1	1/4	41	Ketone (56) α-Br-ketone (41)
17[d]	(*n*-Bu)$_2$CH	H	HBr 2.6	1.3	4/8	89	Ketone (71) α-Br-ketone (12)
18[c]	**1**	**1**	2.2	—	4/8	98	**3** (96)
19[c]	**2**	**2**	2.2	—	4/8	100	**4** (95)
20[b]	**2**	**2**	1.2	0.8	1/1	100	**4** (98)
21[c]	$PhCH_2$	H	0.5	—	2/2	49	Aldehyde (95) Imide (5)
22[c]	*p*-Me-C_6H_4-CH_2	H	1.0	—	4/4	83	Aldehyde (81) Imide (12)
23[b]	*p*-Me-C_6H_4-CH_2	H	0.3	1.2	1/6	96	Aldehyde (73) Imide (4)
24[d]	*p*-Me-C_6H_4-CH_2	H	HBr 2.4	1.2	4/4	85	Aldehyde (82) Imide (6)
25[b]	*p*-Cl-C_6H_4-CH_2	H	0.4	0.8	0.6/3	100	Aldehyde (89) Imide (4)

[a] DCE = 1,2-dichloroethane. [b] Procedure: the aqueous solution of H_2O_2 was added dropwise to the mixture of the other reagents and solvents reported in the Table, at rt and under effective stirring for 3 h. [c] Procedure: the mixture of the reagents and solvents reported in the Table 1 was effectively stirred for 3 h at rt. [d] Procedure: as in *c* but 2 mol of HBr and 1 mol H_2O_2 were used instead of 1 mol Br_2. All the reaction products were known and characterised by comparison with authentic samples (GLC-MS and NMR); quantitative yields were determined by GLC using as internal standards *n*-$C_7H_{15}COOH$ for carboxylic acids, *p*-MeO-C_6H_4-CHO for aromatic aldehydes, *n*-Pr-CO-Pr-*n* for ketones and *n*-$C_6H_{13}CONHCOMe$ for imides.

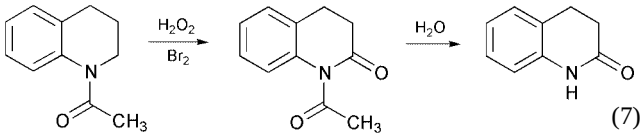

(7)

2 **4** **6**

The reactions, carried out in a two-phase system (H_2O–$ClCH_2CH_2Cl$), are initiated by ambient light and the active oxidant is Br_2, which acts in the organic phase; the formed HBr is extracted by the aqueous phase and oxidised to Br_2 by H_2O_2 making the process catalytic in Br_2. Two procedures were utilised as reported in Table 1. In both cases the overall process is catalytic in Br_2, but a higher concentration of Br_2 makes the overall process faster; an aqueous solution of HBr and H_2O_2 can be utilised instead of Br_2 in a two-phase system. Procedure a) gives better results for the synthesis of carboxylic acids because a higher concentration of Br_2 accelerates the oxidation of a-hydroxyamides to imides, while procedure b) is more suitable for the synthesis of ketones, which consumes the catalytic amount of Br_2 by electrophilic bromination and inhibits the free-radical oxidation.

Notes and references

1 J. R. Molpass, *Comprehensive Organic Chemistry*, vol. 2, ed. I. O. Sutherland, 1979, p. 17.
2 D. V. Banthorpe, *The chemistry of the amino group*, ed. S. Patai, 1968, p. 630.
3 D. V. Banthorpe, *The chemistry of the amino group*, ed. S. Patai, 1968, p. 623.
4 B. C. Chollis and J. A. Chollis, *Comprehensive Organic Chemistry*, vol. 2, ed. I. O. Sutherland, 1979, p. 966.
5 D. V. Banthorpe, *The chemistry of the amino group*, ed. S. Patai, 1968, p. 623.
6 A. Amati, G. Dosualdo, F. Fontana, F. Minisci and H.-R. Bjørsvik, *Org. Process Res. Dev.*, 1998, **2**, 261 and references therein.
7 F. Minisci and F. Fontana, *Chim. Ind. (Milan)*, 1998, **80**, 1309 and references therein.
8 F. Minisci, *Top. Curr. Chem.*, 1976, **62**, 1.
9 A. J. Waring, Ref. 1, pp. 1027, 1036, **vol. 1**.

ChemComm

Phosphide coupling in the reaction of $Sn(NMe_2)_2$ with MesPHLi; synthesis and structure of the Sn(II) phosphide dianion $[\{Sn(\mu\text{-}PMes)\}_2(MesP)_2]^{2-}$ (Mes = 2,4,6-$Me_3C_6H_2$)

Andrew D. Bond, Alexander Rothenberger, Anthony D. Woods and Dominic S. Wright*

University of Cambridge, Lensfield Road, Cambridge, UK CB2 1EW. E-mail: dsw1000@cus.cam.ac.uk

Received (in Cambridge, UK) 20th December 2000, Accepted 2nd February 2001
First published as an Advance Article on the web 26th February 2001

In contrast to the reactions of other primary phosphides with $Sn(NMe_2)_2$, the reaction of MesPHLi with $Sn(NMe_2)_2$ results in partial coupling of MesP groups in the product (which contains the novel Sn(II) dianion $[\{(Sn(\mu\text{-}PMes)\}_2(MesP)_2]^{2-}$).

We recently showed that the heterometallic Sb(III) cage $[\{Sb(PCy)_3\}_3Li_6]$ (Cy = C_6H_{11}) decomposes at relatively low temperature (30–40 °C) into Zintl compounds containing the Sb_7^{3-} anion.[1] The isolation of $[CyP]_4$ from this 'cage-to-alloy' reaction suggests that the formation of P–P bonds (the strongest homonuclear Group 15 bond) provides the thermodynamic driving force.[1] In related studies it was shown that probable intermediates in the formation of E_7^{3-} Zintl ions (E = As, Sb) are cyclic anions of the type $[(RP)_nE]^-$.[2,3] A key observation was that the ease of formation of the Zintl compounds is dependent (among other factors) on the nature of the R substituent of the RP^{2-} groups.[3] Thus, reaction of MesPHLi with $As(NMe_2)_3$ at room temperature in the presence of TMEDA [= $(Me_2NCH_2)_2$] leads to rapid (1 h) formation of $As_7Li_3\cdot3$TMEDA, whereas prolonged reaction (12 h) of a range of aliphatic primary phosphides with $As(NMe_2)_3$ under similar conditions gives complexes containing $[(RP)_nAs]^-$ anions (n = 3 or 4), it being necessary to reflux these reactions in order to effect formation of Zintl compounds.[3] The synthesis and structure of $[\{(Sn(\mu\text{-}PMes)\}_2(MesP)_2]Li_2\cdot2$TMEDA **2** reported here provides the first evidence that the reactivity pattern established for Group 15 phosphides has broader implications to other p block elements.

In earlier studies we had observed that the reaction of $[SnNBu^t]_4$ with CyPHLi (1:6 equiv.) in thf gives the heterometallic complex $[\{Sn(\mu\text{-}PCy)_2\}_2(\mu\text{-}PCy)]_2Li_4\cdot4$thf **1**, containing the metallacylic tetraanion $[\{Sn(\mu\text{-}PCy)_2\}_2(\mu\text{-}PCy)]_2^{2-}$.[4] The impetus for further studies came with the surprising finding that the same complex is also produced by the reaction of $Sn(NMe_2)_2$ with CyPHLi in thf using a range of stoichiometries (from 1:1.5 to 1:3 equiv., respectively) (Scheme 1).[5] In fact other aliphatic primary phosphides react similarly with $Sn(NMe_2)_2$ in thf. For example, reaction of Bu^tPHLi with $Sn(NMe_2)_2$ gives $[\{Sn(\mu\text{-}PBu^t)_2\}_2(\mu\text{-}PBu^t)]_2Li_4\cdot4$thf **2** (in *ca.* 60% yield), whose structure is essentially identical to **1**.[5] However, the analogous reaction of MesPHLi (Mes = 2,4,6-$Me_3C_6H_2$) with $Sn(NMe_2)_2$ gives a radically different result. The product isolated in the presence of the bidentate donor TMEDA (addition of which was necessary to facilitate crystallisation) is $[\{(Sn(\mu\text{-}PMes)\}_2(PMes)_2]Li_2\cdot2$TMEDA **3** (in 96% yield).† Some indication of the different outcome of the reaction with MesPHLi is provided by room-temperature NMR studies. In contrast to **1** and **2** where the two ^{31}P NMR environments are markedly different (*e.g.* δ −180 and −249 in **1**), the P environments of **3** occur at very similar chemical shifts (δ −156.7 and −157.5). In addition, the electronic environment of the Sn centres in **3** (δ −154.6) is clearly vastly different from that found in **1** and **2** (*ca.* δ +690).[4] However, the Sn–P coupling was poorly resolved in the spectra of **3** so that no information concerning the connectivities of either nucleus within the core of the complex could be gleaned.

The low-temperature X-ray structure of **3**‡ shows that the complex is an ion-paired species, arising from the association of a $[\{(Sn(\mu\text{-}PMes)\}_2(PMes)_2]^{2-}$ dianion with two TMEDA solvated Li^+ cations (Fig. 1). In addition, there are two molecules of toluene in the lattice for each molecule of **3**. Although only a few Sn(II) and Pb(II) complexes containing RP^{2-} ligands have been structurally characterised,[4,6] (like **3**) the majority of these are ion-paired molecular species contain-

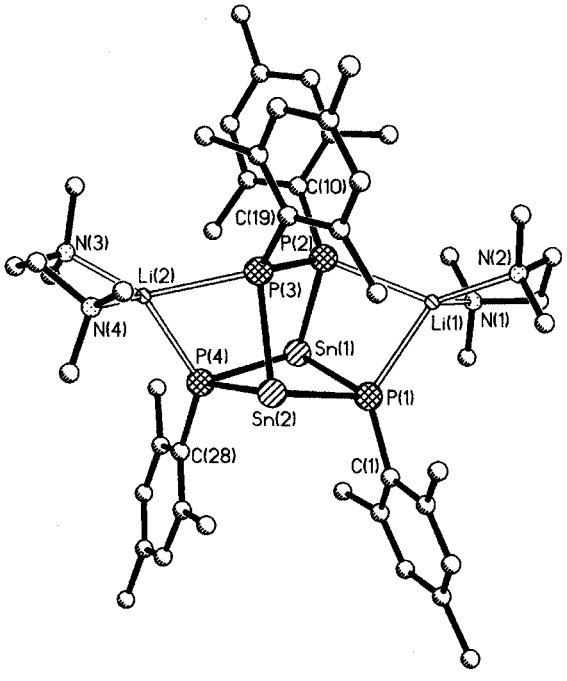

Fig. 1 The heterometallic cage structure of **3**. H atoms, lattice-bound toluene molecules and the disorder about the $-CH_2CH_2-$ groups of the TMEDA ligands have been omitted for clarity. Key bond lengths (Å) and angles (°); Sn(1)–P(1) 2.635(1), Sn(1)–P(2) 2.636(1), Sn(1)–P(4) 2.627(1), Sn(2)–P(1) 2.615(1), Sn(2)–P(3) 2.648(1), Sn(2)–P(4) 2.646(1), Li(1)–P(1) 2.518(8), Li(1)–P(2) 2.596(7), Li(2)–P(3) 2.609(7), Li(2)–P(4) 2.533(7), P(2)–P(3) 2.186(2), Li(1,2)–N(1,2,3,4) range 2.090(8)–2.118(8); Sn(1)–P(1,2)–Sn(2) mean 86.8, P(1)–Sn(1,2)–P(4) mean 90.6, P(1)–Sn(1)–P(2)/P(3)–Sn(2)–P(4) mean 75.8, P(4)–Sn(1)–P(2)/P(4)–Sn(2)–P(3) mean 93.7, Sn–{P(2)–P(3)} mean 99.8.

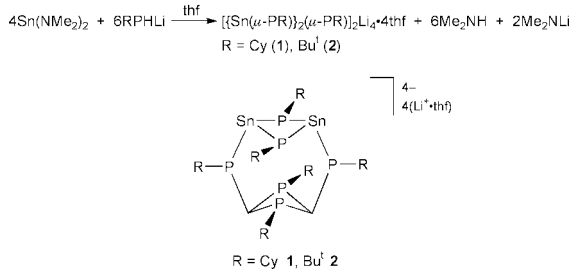

Scheme 1

ing Sn(II) phosphide anions coordinated to alkali or alkaline earth metal cations. However, in none of these previous examples has the formation of a P–P bond (*via* coupling of RP^{2-} anions) been observed. Of particular note in comparison with **3**, is the formation of $[(Me_3Si)PSn(\mu\text{-}PSiMe_3)]_2(Ca{\cdot}2thf)_2$ in the reaction of $[Ca\{PSiMe_3\}_2]$ with $SnCl_2$.[6b] The latter complex contains a $[(Me_3Si)PSn(\mu\text{-}PSiMe_3)]_2^{4-}$ tetraanion whose framework can be regarded as related to the $[\{(Sn(\mu\text{-}PMes)\}_2(PMes)_2]^{2-}$ dianion of **3** by 2e reduction and cleavage of the P–P bond.

Examination of the bond lengths and angles found in the bicyclic Sn_2P_4 core of **3** indicates that there is a considerable amount of strain in this arrangement. Thus, although the Sn–P bond lengths are similar to those found in the few structurally characterised Sn(II) complexes containing RP^{2-} ligands,[6] these bonds fall over a wide range of values [2.615(1)–2.648(1) Å]. In addition, the Sn(II) centres adopt highly irregular pyramidal geometries, with the P–Sn–P angles involved being in the range 75.75(3)–94.71(3)°. Clearly, the distortions found in the Sn_2P_4 core can be partly attributed to the geometric constraints involved in the coordination of the MesPPMes ligand to the two Sn centres of the $Sn_2(PMes)_2$ dimer unit. Some evidence for this view is seen in the compression of the P–P bond of the MesPPMes ligand [P(2)–P(3) 2.186(2) Å]; a value which is significantly shorter than that observed for the Bu^tPPBu^t groups in the Sn(IV) complex $[ClSn\{Bu^tPPBu^t\}_3SnCl]$[7] (2.237 Å). However, the highly distorted geometry of the Sn(II) centres in **3** is primarily the result of the chelation of each of the pseudo-tetrahedral Li^+ cations by a P centre of the MesPPMes group [Li(1,2)–P(2,3) mean 2.60 Å[7]] and by a MesP ligand [Li(1,2)–P(1,4) mean 2.53 Å[7]] of the $[\{(Sn(\mu\text{-}PMes)\}_2(MesP)_2]^{2-}$ dianion. This coordination to the Li^+ ions results in the compression of the associated P–Sn–P angles [P(1)–Sn(1)–P(2) and P(3)–Sn(2)–P(4) mean 75.8°; *cf*. 90.59(3)–94.71(3)° for the remaining P–Sn–P angles].

In summary, the reactions of $Sn(NMe_2)_2$ with RPHLi (R = Cy, Bu^t) and MesPHLi parallel those with Group 15 reagents $E(NMe_2)_3$ (E = As, Sb, Bi) and a range of lithium primary phosphides (RPHLi). In this context, the $[\{(Sn(\mu\text{-}PMes)\}_2(PMes)_2]^{2-}$ dianion core of **3** can be regarded as the Group 14 counterpart of the previously studied Group 15 $[(RP)_nE]^-$ anions. The $[\{(Sn(\mu\text{-}PMes)\}_2(MesP)_2]^{2-}$ anion of **3** has the potential to act as a multi-electron donor to a range of main group and transition metal complexes, yielding a variety of mixed-metal complexes. Furthermore, the thermolysis of **3** and similar complexes may lead to further P–P bond formation, providing a route to Sn Zintl phases.

We gratefully acknowledge the EPSRC (A. D. B., A. D. W.) and the Gottlieb Daimler- and Karl Benz-Stiftung (A. R.) for financial support.

Notes and references

† *Synthesis of* **3**: to a solution of $MesPH_2$ (0.94 ml, 6.0 mmol) in toluene (20 ml) at −78 °C was added Bu^nLi (4.0 ml, 6.0 mmol, 1.6 mol dm^{-3} in hexanes). Stirring at room temperature (1 h) produced a yellow precipitate of the monolithiate. To this suspension at −78 °C was added a solution of $Sn(NMe_2)_2$ (0.42 g, 2.0 mmol) in toluene (10 ml). Warming to room temperature led to the formation of a red–orange precipitate which was dissolved by the addition of TMEDA (1 ml, excess). Storage at 5 °C for 24 h gave orange crystalline blocks of **3**. Spectroscopic and analytical studies of **3** show that the toluene solvation found in the lattice is removed by placing crystalline samples under vacuum (*ca*. 15 min, 10^{-1} atm) during isolation. Yield 1.04 g (96%). ^{1}H NMR (400.16 MHz, d_8-toluene, +25 °C), δ 6.92 (S, 8H, aryl C–H), 2.90 (s, 12H, 4-Me of Mes), 2.65 (s, 24H, 2,6-Me of Mes), 1.97 (s, 24H, Me_2N of TMEDA), 1.83 (br s, 8H, $–CH_2CH_2–$ of TMEDA). ^{31}P NMR (161.98 MHz, d_8-toluene, +25 °C, rel. 80% H_3PO_4–D_2O), δ −156.7 (s), –157.5 (s). ^{7}Li NMR (155.55 MHz, d_8-toluene, +25 °C), δ 0.20 (s). ^{119}Sn NMR (141.21 MHz, d_8-toluene, +25 °C, rel. sat. $SnCl_2$–D_2O), δ −154.6 (br s). Satisfactory (C,H,N) analysis was obtained for **3**(−2toluene).

‡ *Crystal data* for **3**: $C_{62}H_{92}Li_2N_4P_4Sn_2$, M = 1268.54, monoclinic, space group $P2_1/c$, Z = 4, a = 21.4284(3), b = 13.5986(2), c = 22.9153(2) Å, β = 94.644(9)°, V = 6655.51(15) Å^3, μ(Mo-Kα) = 0.884 mm^{-1}, T = 180(2) K. Data were collected on a Nonius KappaCCD diffractometer. Of a total of 60891 reflections collected, 15148 were independent (R_{int} = 0.059). The structure was solved by direct methods and refined by full-matrix least squares on F^2. Final $R1$ = 0.053 [$I > 2\sigma(I)$] and $wR2$ = 0.174 (all data).[8] The $–CH_2CH_2–$ groups of one of the TMEDA ligands are disordered over two sites. This was modelled with 50% occupancy in each. CCDC 156336. See http://www.rsc.org.suppdata/cc/b0/b010201f/ for crystallographic data in .cif or other electronic format.

1 See: M. A. Beswick, J. M. Goodman, C. N. Harmer, A. D. Hopkins, M. A. Paver, P. R. Raithby, A. E. H. Wheatley and D. S. Wright, *Chem. Commun.*, 1997, 1897; M. A. Beswick, C. N. Harmer, A. D. Hopkins, M. McPartlin and D. S. Wright, *Science*, 1998, **281**, 1500.

2 M. A. Beswick, N. Choi, A. D. Hopkins, M. E. G. Mosquera, M. McPartlin, P. R. Raithby, A. Rothenberger, D. Stalke, A. E. H. Wheatley and D. S. Wright, *Chem. Commun.*, 1998, 2485.

3 A. Bashall, M. A. Beswick, N. Choi, A. D. Hopkins, S. J. Kidd, Y. G. Lawson, M. E. G. Mosquera, M. McPartlin, P. R. Raithby, A. E. H. Wheatley, J. A. Wood and D. S. Wright, *J. Chem. Soc., Dalton Trans.*, 2000, 479.

4 R. E. Allen, M. A. Beswick, N. L. Cromhout, M. A. Paver, P. R. Raithby, M. Trevithick and D. S. Wright, *Chem. Commun.*, 1996, 1501.

5 The reactions of $Sn(NMe_2)_2$ with CyPHLi and Bu^tPHLi occur most smoothly using an apparent excess of the primary phosphide, in a 1:3 ratio. Details of the new synthesis of **1** and **2** and of the structure of **2** will be published as part of a full paper.

6 (*a*) M. Westerhausen, R. Low and W. Schwarz, *J. Organomet. Chem.*, 1996, **513**, 213; (*b*) M. Westerhausen and W. Schwarz, *Z. Anorg. Allg. Chem.*, 1996, **622**, 903; (*c*) M. Driess, S. Martin, K. Merz, U. Pintchouk, H. Pritzkow, H. Grützmacher and M. Kaupp, *Angew. Chem., Int. Ed. Engl.*, 1997, **36**, 1894; (*e*) M. Westerhausen, M. Krofta, N. Wiberg, H. Nöth and A. Pfitzer, *Z. Naturforsch., Teil B*, 1998, **53**, 1489.

7 P–Li bond lengths are typically in the range 2.47–2.70 Å (depending on the coordination number of the Li^+ cations involved). For examples, see: R. A. Jones, A. L. Stuart and T. C. Wright, *J. Am. Chem. Soc.*, 1983, **105**, 7459; L. M. Engelhardt, G. E. Jacobsen, C. L. Raston and A. H. White, *J. Chem. Soc., Chem. Commun.*, 1984, 220; P. B. Hitchcock, M. F. Lappert, P. P. Power and S. J. Smith, *J. Chem. Soc., Chem. Commun.*, 1984, 1669; A. M. Arif, A. H. Cowley, R. A. Jones and J. M. Power, *J. Chem. Soc., Chem. Commun.*, 1986, 1446; R. E. Mulvey, K. Wade, D. R. Armstrong, G. T. Walker, R. Snaith, W. Clegg and D. Reed, *Polyhedron*, 1987, **6**, 987.

8 SHELXTL PC version 5.03, Siemens Analytical Instruments, Madison, WI, 1994.

ChemComm

Zoned MFI films by seeding

Qinghua Li, Jonas Hedlund,* Derek Creaser and Johan Sterte

Division of Chemical Technology, Luleå University of Technology, S-971 87, Luleå, Sweden. E-mail: johe@km.luth.se

Received (in Cambridge, UK) 23rd November 2000, Accepted 6th February 2001
First published as an Advance Article on the web 26th February 2001

The synthesis and characterization of zoned MFI films consisting of intergrown TPA-silicalite-1 and ZSM-5 crystals are described.

ZSM-5 is a zeolite which is used for shape selective acid catalysis. However, it is only the internal sites that are shape selective, the external sites are not. Various strategies have been used to improve the ratio of shape selective sites to non-selective sites. Large crystals have a higher ratio, but the increased diffusional length reduces activity, and deactivation can be more severe for larger crystals.[1] Chemical vapour deposition (CVD) of silica has been used to coat the external surface in order to eliminate the external sites.[2–5] However, the pore opening size and the activity may be reduced if this method is employed. A more elegant way to eliminate the external acid sites would be to prepare a compositionally zoned zeolite catalyst, *i.e*. to synthesize an inactive outer shell of aluminium free silicalite-1 on aluminium-containing ZSM-5 crystals. The pore openings would be unaffected if the channels propagate continuously from the interior of the ZSM-5 catalysts and through the external silicalite-1 shell. Materials that are claimed to be zoned have been evaluated previously by adsorption and catalytic testing.[5–7] It has been shown that at least some of the external acid sites of the materials were eliminated and shape selectivity increased. However, extensive characterization by means other than catalytic evaluation have not been carried out to determine whether such materials truly consist of a continuously propagating channel system through the compositionally zoned regions. The present communication describes the preparation and characterization of relatively thick zoned zeolite films consisting of TPA-silicalite-1 and ZSM-5 layers on quartz substrates. Such samples are well suited for characterization by techniques such as SEM, EDS and the preferred orientation of the crystals can be evaluated by XRD in order to elucidate the channel structure of the material. Additionally, these materials themselves possess a potential for various applications.[7]

A method employing seeding[8] was used for preparation of the zeolite films. TPA-silicalite-1 crystals with an average size of 60 nm were adsorbed on charge-reversed quartz substrates. The seeded substrates were further used to synthesize three different types of zeolite films (samples A, B, C). TPA-silicalite-1 films (A) were prepared by hydrothermal treatment of the seeded quartz substrate in a synthesis solution with a molar composition of 3 TPAOH : 25 SiO_2 : 1500 H_2O : 100 EtOH at 100 °C for 3 days.[8] After the first synthesis step, the samples were rinsed with a 0.1 M ammonia solution and a fresh synthesis solution with the same composition was used for further hydrothermal treatment. This sequence was repeated four times in total to reach a crystallization time of 12 days. ZSM-5 films (B) were prepared by hydrothermal treatment of the seeded quartz substrate in a synthesis gel free from organic templates at 180 °C for 18 h.[9] The molar composition of the gel was 30 Na_2O : 1 Al_2O_3 : 103 SiO_2 : 4000 H_2O. Zoned TPA-silicalite-1/ZSM-5 films (C) were prepared by a two-step crystallization procedure. In the first step, a TPA-silicalite-1 film was synthesized in the same way as for sample A. In the second step, the rinsed TPA-silicalite-1 film obtained from the first step was hydrothermally treated in the same way as for sample B. After completion of the two-step procedure the samples were rinsed with a 0.1 M ammonia solution to remove sediments and unreacted gel adsorbed on the film as described for sample B.

Fig. 1 shows SEM micrographs of the three samples. Fig. 1(a) and (b) show the top- and side-view images of sample A. The film thickness is *ca.* 2.8 μm and the texture is columnar. The surface of the film is relatively smooth. Fig. 1(c) and (d) show the top- and side-view images of sample B. The film consists of well intergrown crystals of ZSM-5 with very well developed crystal faces. The thickness of this film is *ca*. 3.4 μm. Fig. 1(e) and (f) show the top- and side-view images of sample C. After the second step, the morphology of the film has changed completely. The surface of the film is no longer smooth as for sample A, but well defined crystal faces constitute the surface, as in sample B. The thickness of film is *ca*. 6.3 μm, which agrees well with the sum of the film thickness of samples A and B. No border can be seen between the two different layers of silicalite-1 and ZSM-5 and the texture is still columnar.

The marker in Fig. 1(f) indicates the position of the EDS line scan shown in Fig. 2 which shows the Al Kα and Si Kα signals. The start of the EDS line scan at 0 μm in Fig. 2 corresponds to the dot in Fig. 1(a) on the quartz substrate. The Si signal is approximately constant over the quartz support and the zeolite, indicating an equal amount of Si in the zeolite and quartz. The Al signal from the support and the silicalite-1 film, (×5) is not

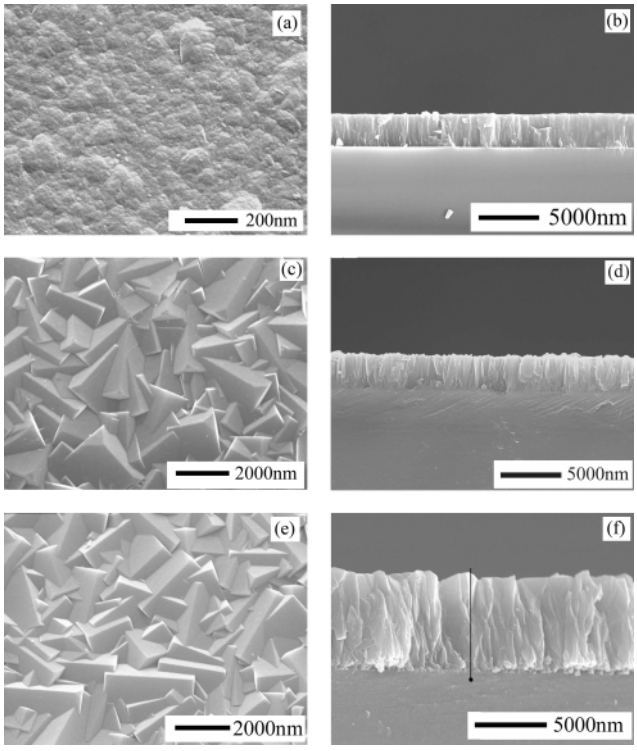

Fig. 1 SEM micrographs of the films. Top-view image of sample A (a), side-view image of sample A (b), top-view image of sample B (c), side-view image of sample B (d), top-view image of sample C (e) and side-view image of sample C (f).

DOI: 10.1039/b009414p

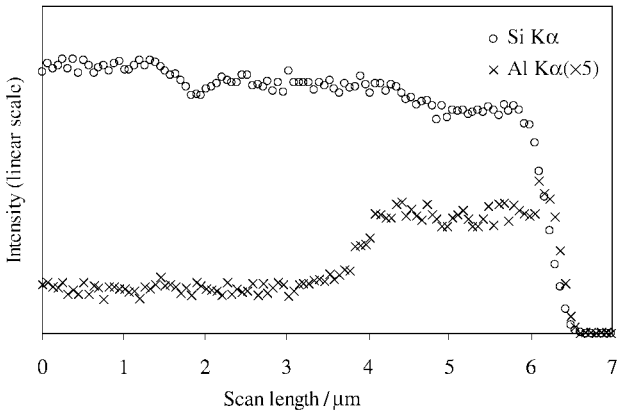

Fig. 2 Si Kα and Al Kα signals of the EDS line scan indicated by the line in Fig. 1(f), the scan starts at the position of the dot. The Al Kα signal was multiplied by 5.

zero owing to the continuous background signal (no Al atoms could be detected by EDS in sample A). The Al signal increases abruptly after *ca*. 3 μm which agrees well with the silicalite-1 film thickness of sample A of *ca*. 2.8 μm. From the EDS analysis the Si/Al ratio for the ZSM-5 layer was estimated to be *ca*. 10, which is a quite low value for ZSM-5 and identical to one reported previously.[9]

Fig. 3 shows X-ray diffraction patterns of samples A–C and a purified bulk product powder sample from TPA-silicalite-1 film synthesis. The powder sample [Fig. 3(d)] was used as a reference and considered to have a random orientation. It was reported previously that the (501) peak dominates in the pattern for TPA-silicalite-1 films with thickness of *ca*. 1.0 μm on silicon wafers.[8,10] However, in the pattern for sample A [Fig. 3(a)], the (303) peak dominates. This suggests that with increasing crystallization time not only the film thickness increases, but also the preferred orientation of the crystals changes so that the (303) peak dominates in films with a thickness of 2.8 μm. In the pattern for sample B [Fig. 3(b)], the (133) peak is dominant, which is in agreement with previous findings.[8] In the pattern for sample C [Fig. 3(c)], two (303) peaks, one from ZSM-5 and one from TPA-silicalite-1 dominate. Since the unit cell of ZSM-5 is larger than that of TPA-silicalite-1, the ZSM-5 peak occurs at lower 2θ.[11] The exact location of the (303) peaks was also determined by mixing silicon powder with TPA-silicalite-1 powder and ZSM-5 powder prepared from the synthesis mixtures used for film growth. The position of the (303) peak for ZSM-5 and for TPA-silicalite-1 was 23.86 and 23.98°, respectively. The fact that the (303) peak and not the (133) peak dominate in the zoned film indicates that the orientation of the crystals in the ZSM-5 part of the zoned films is controlled by the orientation of the TPA-silicalite-1 crystals in the first film. In other words, according to the XRD data, the TPA-silicalite-1 crystals in the first film continue to grow to form the ZSM-5 film, resulting in a zoned MFI film with a continuous channel system. Because the ZSM-5 layer covers the TPA-silicalite-1, based on the thickness, diffraction angle and absorption coefficient of the ZSM-5 film, about 20% of the signal from the silicalite-1 film should be absorbed by the ZSM-5 film. Also, the crystal size in the ZSM-5 film should be larger due to the continued growth of the crystals in the silicalite-1 layer. Therefore, the (303) peak from the ZSM-5 part should be more intense than from the TPA-silicalite-1 part since the films have similar thickness. However, Fig. 3(c) shows the opposite, *i.e*. the (303) peak from the ZSM-5 part is weaker than from the TPA-silicalite-1 part. This could be due to somewhat lower crystallinity of the ZSM-5 layer in the zoned film, which was also indicated by XRD data from powders of ZSM-5 and TPA-silicalite-1 with similar crystal size.

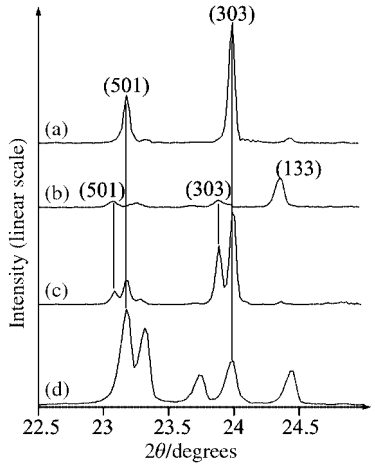

Fig. 3 XRD patterns of sample A (a), sample B (b), sample C (c) and TPA-silicalite-1 powder (d).

In summary, this communication presents a method for preparation of zoned MFI type films containing TPA-silicalite-1 and ZSM-5 layers. The most significant finding is that such films are not only compositionally zoned but also appear to consist of a continuously propagating channel system through the zoned regions, according to SEM/EDS and XRD data. In order to further verify that the channel system propagates continuously, TEM studies of the interface of zoned films on carbon fibres will be carried out and the results presented elsewhere. The same general method can be used for the preparation of zoned films with the reversed positioning of the layers, *i.e*. silicalite-1 covering ZSM-5, which is of more practical interest for preparation of catalysts free of external sites as discussed in the introduction. Also, the preparation method has been modified to synthesize zoned films with a non-continuous channel system. Characterization results for these zoned films will be presented in a subsequent publication.

The authors acknowledge the Swedish Research Council for Engineering Sciences (TFR) for the financial support of this work.

Notes and references

1 H. Guo, X. Wang and G. Wang, in *Proceedings of the 12th International Zeolite Conference*, ed. M. M. J. Treacy, B. K. Marcus, M. E. Bisher and J. B. Higgins, Baltimore, Maryland, U.S.A., p. 141.
2 M. Niwa, M. Kato, T. Hattori and Y. Murakami, *J. Phys. Chem.*, 1986, **90**, 6233.
3 G. P. Handreck and T. D. Smith, *Zeolites*, 1990, **10**, 746.
4 R. W. Weber, J. C. Q. Fletcher, K. P. Möller and C. T. O'Connor, *Microporous Mater.*, 1996, **7**, 15.
5 C. S. Lee, T. J. Park and W. Y. Lee, *Appl. Catal. A*, 1993, **96**, 151.
6 L. D. Rollmann, *US Pat.* 4088605, 1976.
7 J. C. Jansen, J. M. V. d. Graff, N. V. D. Puil, S. B. G. Seijger and S. P. J. Simth, in *Proceedings of the 12th International Zeolite Conference*, ed. M. M. J. Treacy, B. K. Marcus, M. E. Bisher and J. B. Higgins Baltimore, Maryland, USA, p. 603.
8 J. Hedlund, S. Mintova and J. Sterte, *Microporous Mesoporous Mater.*, 1999, **28**, 185.
9 J. Hedlund, M. Noack, P. Kölsch, D. Creaser, J. Sterte and J. Caro, *J. Membr. Sci.*, 1999, **159**, 263.
10 J. Hedlund, *J. Porous Mater.*, 2000, **7**, 455.
11 M. Tielen, M. Geelen and P. A. Jacobs, *Acta Phys. Chem.*, 1985, **31**, 1.

Synthesis of novel cage molecules bicapped with tris(2-thienyl)methanes

Hiroyuki Kurata, Hiromichi Nakaminami, Kouzou Matsumoto, Takeshi Kawase and Masaji Oda*

Department of Chemistry, Graduate School of Science, Osaka University, Toyonaka, Osaka 560-0043, Japan. E-mail: moda@chem.sci.osaka-u.ac.jp

Received (in Cambridge, UK) 7th December 2000, Accepted 8th February 2001
First published as an Advance Article on the web 27th February 2001

The McMurry coupling of tris(5-formyl-2-thienyl)methanes affords novel cage molecules which are bicapped with tris(2-thienyl)methanes and where all the sulfur atoms of thienyl groups direct inward.

Cage molecules have been attracting increasing attention from the viewpoint of host–guest or supramolecular chemistry.[1] There are a number of types in the basic skeleton of cage molecules and one of such families is that of cage molecules bicapped with triphenylmethanes (triphenylmethanophanes).[2] Here we report on the first synthesis of cage molecules bicapped with tris(2-thienyl)methanes **1a** and **1b** (trithienylmethanophanes) where the thiophenes are bridged with etheno groups and the sulfur atoms are direct inward forming a three dimensional cavity. Related three or two dimensional sulfur-rich and unsaturated cyclophanes, macrobicyclic tetrathiafulvalene-bridged cage molecules or sulfur bridged annulenes have been reported.[3,4] Differing from triphenylmethanophanes, the thienyl groups in trithienylmethanophanes act as either π-electron donors, as aryl groups or electron-pair donors due to the sulfur atoms.

For the synthesis of **1a** and **1b** we chose tris(2-thienyl) methane **2** as the starting material because it has a number of favorable features such as easy lithiation–alkylation at the central methyl carbon (Cα-alkylation)[5] and possible metalation and functionalization at C5 of the thienyl groups in the Cα-alkylation products. It has been reported that treatment of **2** with BuLi–TMEDA in THF followed by addition of alkyl halides selectively yielded Cα-alkylation products.[5] In our case, however, C5-alkylation appreciably competed against Cα-alkylation under similar conditions and the separation of both the products was difficult. We have found that treatment of **2** with BuLi (1.2 equiv.) in THF in the presence of an excess amount (1.5 equiv.) of diisopropylamine (−70 °C then rt) followed by addition of alkyl halides provides a simpler procedure as well as excellent selectivity for Cα-alkylation with primary alkyl halides (Scheme 1).†[6]

Treatment of 1,1,1-tris(2-thienyl)ethane **3a**, thus obtained by methylation with methyl iodide, with five equivalents of BuLi in THF and subsequent addition of excess DMF afforded, after chromatographic purification on silica gel, trialdehyde **4a**‡ in 64% yield from **2**. Similarly hexyl compound **4b**‡ was obtained in 83% yield from **2** *via* **3b**. The McMurry coupling[7,8] of **4a** with low valent titanium in DME gave the trithienylmethanophane **1a**‡ in 5–8% yield as a sole, readily isolable, yellow crystalline substance. Trialdehyde **4b** also gave **1b**‡ in 7% yield. Although **1a** and **1b** are stable at solid state and in neutral solution, they slowly decomposed in $CHCl_3$–CF_3COOH (9 : 1 v/v) at rt when the effect of acid or encapsulation of proton in the cavity was examined by means of NMR spectroscopy.

^1H and ^{13}C NMR spectra show a high symmetry of **1a** and **1b** exhibiting only three proton-signals and six carbon-signals besides the signals of the alkyl groups. The vicinal coupling constants obtained from the ^{13}C satellite signals of the olefin protons of **1a** (δ 6.45, $J^{13}_{C\text{-}H}$ = 161.6 Hz, $J_{H\text{-}H}$ = 11.7 Hz) and **1b** (δ 6.50, $J^{13}_{C\text{-}H}$ = 161.4 Hz, $J_{H\text{-}H}$ = 11.9 Hz) indicate the *cis* configuration of the three etheno bridges. The UV-vis absorptions (325, 270 nm) are at slightly longer wavelengths than those of *cis*-1,2-bis(2-thienyl)ethene (322, 250 nm).[9] Inter-

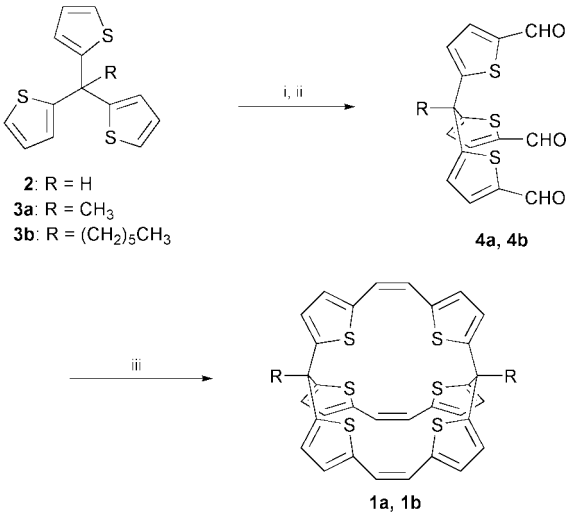

Scheme 1 i, 5.0 eq. BuLi–THF, 0 °C, 2 h; ii, excess DMF (**4a**: 64%; **4b**: 83%); iii, $TiCl_4$, Zn, CuI–DME, rt, overnight → reflux, 24 h (**1a**: 8%; **1b**: 7%).

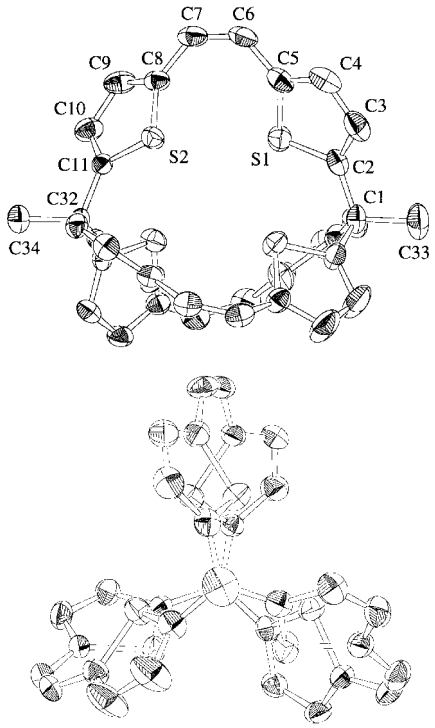

Fig. 1 ORTEP drawing (30% thermal ellipsoids) of the cage molecule **1a** (upper: side view; lower: viewed along the C_3 axis). Selected bond lengths (Å) and angles (°): C1–C2 1.523(5), C2–C3 1.369(5), C3–C4 1.403(5), C4–C5 1.369(5), C5–C6 1.444 (5), C6–C7 1.330(5), S1–C2 1.712(4), S1–C5 1.715(4), C2–C1–C33 110.2(3), C5–C6–C7 130.5(3), C6–C7–C8 130.3(3), C11–C32–C34 109.7(3).

DOI: 10.1039/b009811f

estingly, the mass spectra of the trithienylmethanophanes, in particular the EI spectrum of **1b**, suggest fair stability of dealkylated monocation and dication showing strong peaks at *m/z* 679 ([*M* − hexyl]$^+$, 100%) and 297 ([*M* − 2 × hexyl]$^{2+}$, 38%). Upon cyclic votammetry, **1b** shows an irreversible oxidation peak at +1.12 V (*vs*. Ag/Ag$^+$, in 0.1 M $Bu_4N^+ClO_4^-$/CH_3CN, ferrocene/ferrocene$^+$ = 0.33 V).

Recrystallization of **1a** from benzene–hexane afforded a single crystal suitable for X-ray structure analysis.§ The X-ray results establish the cage structure (Fig. 1) and reveal several structural features of **1a**. First, all the three etheno bridges have *cis* configuration, as ^{1}H NMR spectrum suggests, with considerably widened bond angles (av. 131.0°). Second, all the sulfur atoms of the six thienyl groups direct inward. Third, the molecule thus has a three dimensional cavity, though rather small, surrounded with six sulfur atoms, the cavity-size being about 0.7 Å in diameter. The cavity might encapsulate a Cu(II) ion. In a preliminary experiment, treatment of **1a** with $Cu(ClO_4)_2$·*n*AcOH in toluene–nitromethane precipitated dark green powder which was sparingly soluble in organic solvents.

In conclusion, the McMurry coupling of tris(5-formyl-2-thienyl)methanes affords novel cage molecules bicapped with tris(2-thienyl)methanes. The host–guest chemistry of **1a** and **1b**, further synthetic utility of trialdehyde **4**, and the synthesis of the cage cations suggested by the mass spectra are in progress. In addition, reductive desulfurization of trithienylmethanophanes **1** would form novel three dimensional hydrocarbons having a bicyclo[10.10.10]dotriacontane skeleton, and such attempts are also ongoing.

This work was supported by a Grant-in-Aids for Scientific Research of Priority Area (No. 10146102) from the Ministry of Education, Science, Sports and Culture, Japan.

Notes and references

† Diisopropylamine mediates rapid equilibrium between Cα-lithio-species (thermodynamically more stable and hence less reactive) and C5-lithio-species (less stable and much more reactive) in nearly exclusive favor for the former which gives Cα-alkylation products with non-bulky, reactive alkyl halides. It is also important to add alkyl halides above 0 °C so as to keep the reactivity of the Cα anion high enough. The crude product from this procedure was used for the next step.

‡ *Selected physical and spectroscopic data* for **4a**: yellow powder; mp 134.5–136.0 °C; MS (EI) *m/z* (rel intensity) 360 ([*M*]$^+$, 42), 345 ([*M* − CH_3]$^+$, 100), 331 ([*M* − CHO]$^+$, 47); δ_H(270 MHz, $CDCl_3$): 9.88 (s, 3H), 7.65 (d, *J* = 3.8 Hz, 3H), 6.99 (d, *J* = 3.8 Hz, 3H), 2.39 (s, 3H); δ_C(67.8 MHz, $CDCl_3$): 182.80, 160.52, 143.27, 135.76, 127.60, 47.96, 32.83; **4b**: yellow oil; δ_H(270 MHz, $CDCl_3$) 9.87 (s, 3H), 7.65 (d, *J* = 3.8 Hz, 3H), 7.10 (d, *J* = 3.8 Hz, 3H), 2.62 (m, 2H), 1.24–1.42 (m, 8H), 0.87 (m, 3H); **1a**: yellow plates; mp > 270 °C (decomp.); MS (FAB) *m/z* = 624 (*M*$^+$), 609 ([*M* − CH_3]$^+$); δ_H(270 MHz, $CDCl_3$) 6.86 (d, *J* = 3.6 Hz, 6H), 6.80 (d, *J* = 3.6 Hz, 6H), 6.45 (s, 6H), 2.25 (s, 6H); δ_C(67.8 MHz, $CDCl_3$) 153.96, 136.98, 128.99, 123.87, 122.55, 45.77, 29.35; UV-vis (CH_2Cl_2) λ_{max} nm 325 (log ε = 4.23), 288 sh, 270 (4.62); **1b**: yellow powder; mp 209.5–211.5; MS (EI) *m/z* (rel intensity) 764 ([*M*]$^+$, 36%), 679 ([*M* − C_6H_{13}]$^+$, 100), 594 ([*M* −2 C_6H_{13}]$^+$, 42), 297 ([*M* – 2 C_6H_{13}]$^{2+}$, 38); NMR; ^{1}H δ_H(270 MHz, $CDCl_3$) 6.88 (d, *J* = 3.7 Hz, 6H), 6.78 (d, *J* = 3.7 Hz, 6H), 6.50 (s, 6H), 2.49 (m, 4H), 1.25–1.49 (m, 16H), 0.87 (m, 6H); δ_C(67.8 MHz, $CDCl_3$) 153.35, 137.14, 127.92, 124.52, 123.47, 50.63, 41.06, 31.85, 29.88, 25.22, 22.80, 14.25; UV-vis (CH_2Cl_2) λ_{max} nm 315 sh, 290 sh, 268 (log ε = 4.58).

§ *Crystal data* for **1a**: $C_{34}H_{24}S_6$, *M* = 624.94, triclinic, space group $P\bar{1}$ (no. 2), *a* = 10.596(3), *b* = 15.960(2), *c* = 9.860(1) Å, α = 92.75(1), β = 106.40(2), γ = 88.74(2)°, *U* = 1597.8(5) Å^3, *Z* = 2, D_c = 1.374 M gm^{-3}, μ = 0.455 mm^{-1}, *F*(000) = 684. 8871 reflections measured, 8867 unique (R_{int} = 0.037) used in refinement. *R1* = 0.040 (3859 data, $I > 2\sigma(I)$), *wR* = 0.113 (all data).

CCDC 156652. See http://www.rsc.org/suppdata/cc/b0/b009981f/ for crystallographic files in .cif format.

1 *Comprehensive Supramolecular Chemistry*, Vol. 2, ed. F. Vögtle, Pergamon, 1996.

2 J. Franke and F. Vögtle, *Angew. Chem., Int. Ed. Engl.*, 1985, **24**, 219; D. O'krongly, S. R. Denmeade, M. Y. Chang and R. Breslow, *J. Am. Chem. Soc.*, 1985, **107**, 5544; H. Schrage, M. Franke, F. Vögtle and E. Steckhan, *Angew. Chem., Int. Ed. Engl.*, 1986, **25**, 336; F. Vögtle, R. Bersheid and W. Schnick, *J. Chem. Soc., Chem. Commun.*, 1991, 414; F. Vögtle, M. Nieger and R. Bersheid, *J. Chem. Soc., Chem. Commun.*, 1991, 1364; R. Bersheid and F. Vögtle, *Synthesis*, 1992, 58; R. Bersheid, W. Schnick and F. Vögtle, *Chem. Ber.*, 1992, **125**, 1687; M. Bauer and F. Vögtle, *Chem. Ber.*, 1992, **125**, 1675.

3 P. Blanchard, N. Svenstrup, J. Rault-Berthelot, A. Riou and J. Becher, *Eur. J. Org. Chem.*, 1998, 1743.

4 E. Vogel, P. Röhrig, M. Sicken, B. Knipp, A. Herrmann, M. Pohl, H. Schmickler and J. Lex, *Angew. Chem., Int. Ed. Engl.*, 1989, **28**, 1651; Z. Hu and M. P. Cava, *Tetrahedron Lett.*, 1994, **35**, 3493; Z. Hu, J. L. Atwood and M. P. Cava, *J. Org. Chem.*, 1994, **59**, 8071; E. Vogel, M. Pohl, A. Herrmann, T. Wiss, C. König, J. Lex, M. Gloss and J. P. Gisselbrecht, *Angew. Chem., Int. Ed. Engl.*, 1996, **35**, 1520.

5 J. Nakayama, M. Sugino and M. Hoshino, *Chem. Lett.*, 1992, 703.

6 M. Oda, T. Kawase and C. Wei, *Pure & Appl. Chem.*, 1996, **68**, 267.

7 J. E. McMurry and M. P. Fleming, *J. Am. Chem. Soc.*, 1974, **96**, 4708; J. E. McMurry, M. P. Fleming, K. L. Kees and L. R. Krepski, *J. Org. Chem.*, 1978, **43**, 3225; J. E. McMurry, T. Lectka and J. G. Rico, *J. Org. Chem.*, 1989, **54**, 3748.

8 T. Kawase, N. Ueda, H. R. Darabi and M. Oda, *Angew. Chem., Int. Ed. Engl.*, 1996, **35**, 1556; T. Kawase, H. R. Darabi and M. Oda, *Angew. Chem., Int. Ed. Engl.*, 1996, **35**, 2664; T. Kawase, N. Ueda and M. Oda, *Tetrahedron Lett.*, 1997, **38**, 6681. See also ref. 4.

9 A. A. Zimmerman, C. M. Orlando and M. H. Gianni, *J. Org. Chem.*, 1969, **34**, 73.

ChemComm

Understanding Si/Al distributions in Al-rich zeolites: the role of water in determining the structure of Goosecreekite†

Neyvis Almora-Barrios,[ab] Ariel Gómez,*[b]‡ A. Rabdel Ruiz-Salvador,[a]‡ Manisha Mistry[c] and Dewi W. Lewis[c]

[a] *Zeolites Engineering Laboratory, IMRE–Faculty of Physics, University of Havana, Havana 10400, Cuba*
[b] *Structural Analysis Laboratory, IMRE–Faculty of Physics, University of Havana, Havana 10400, Cuba. E-mail: ariel@lae.ff.oc.uh.cu*
[c] *Centre for Theoretical and Computational Chemistry, Department of Chemistry, University College London, 20 Gordon Street, London, UK WC1H 0AJ*

Received (in Cambridge, UK) 30th November 2000, Accepted 8th February 2001
First published as an Advance Article on the web 26th February 2001

Inclusion of hydration in atomistic simulations of the zeolite Goosecreekite allowed the determination of the most stable structure, including the distribution of Al in the framework and the position of extra-framework cations and water, and highlight how hydration appears to control the framework distribution.

The increasing use of zeolites in many branches of the chemical industry and, in particular, for environmental pollution control, demands a better understanding of the structure if we are to optimise their application. For catalysis and ion exchange, the number and location of aliovalent atoms in the framework and the charge balancing species govern the performance of a particular material. Thus, being able to determine and understand the location of such species will allow us to produce optimised compositions for specific applications. Whilst diffraction methods can identify extra-framework cation (efc) sites they often do not provide any accurate information on the spatial distribution of framework atoms. Similarly, NMR provides only short-range co-ordination of the framework Al and Si. Thus, whist there are established 'rules' of Al distribution in zeolites—Lowenstein's and Dempsey's rules—there is little further detail available from experiment.[1]

Computational methods, based on interatomic potentials, are well established in modelling the structure of zeolites:[2] for example, demonstrating an energetic basis for Lowenstein's rule.[3] Recently, we have developed a methodology to study the distribution of Al in the frameworks of low and medium Si/Al zeolites.[4–6] Whilst the results obtained are generally in excellent agreement with experimental data on the siting of Al atoms, we find that certain efcs shift away from experimental sites towards the framework – a consequence of the omission of water from our models. We now wish to determine the role of water in controlling both the distribution of Si and Al within the framework and the location of efcs. The limited number of theoretical studies of hydrated zeolites have considered only the location and dynamics[7–10] of water in fixed, ordered or 'random' distributions of Al.

Therefore, as a first step in modelling hydrated zeolites, we consider here the mineral Goosecreekite (IZA code GOO).[11] Experimentally, the material is found to have an ordered Al distribution with a Si/Al of 3, providing a rigorous test of our methodology[4–6] for identifying stable Al distributions. Goosecreekite has a three-dimensional channel structure with a maximum pore opening of 4.7 × 2.9 Å.

We employ lattice energy minimisation techniques[2] as implemented in the program GULP.[12] For the zeolite and efc interactions we used the potential parameters described by Jackson and Catlow,[13] while the water related interactions were taken from the work of de Leeuw *et al.*[14,15] These water potentials were originally derived for modelling of solvation at ionic mineral surfaces (*e.g.* $CaCO_3$). They are, therefore, more suitable for simulations of hydrated zeolites (where the most accurate models are also formally charged) than other water potentials such as those derived for the modelling of proteins and other biomolecules. They include a description of polarisation, which will be significant.

The Goosecreekite unit cell ($Ca_2Al_4Si_{12}O_{32}$) comprises eight unique tetrahedral sites,[11] each with a multiplicity of two. Six of the sites are found to be occupied by Si (labelled Si1, Si2,…Si6), the remaining two sites by Al (Al1 and Al2). We therefore considered a total of 1820 different framework configurations at the outset, with four Al distributed over the 16 sites. On the basis of our previous work[4–6] we applied Lowenstein's rule and eliminated those related by symmetry elements of the experimental[11] space group $P2_1$, reducing the number of structures considered to 89.

For the resulting minimised structures we calculated a Boltzmann distribution probability (Table 1) at 600 K, which is typical for volcanic mineral formation. We find that the most stable calculated configuration (C1§) possesses an ordered Al distribution, but that the Al is at the sites labelled Si3 and Si4. The second most stable configuration, C2, (Fig. 1) does have the experimental Al distribution, but is significantly less stable. We also find significant differences in the location of the efc sites.

Table 1 The calculated most stable configurations for Goosecreekite without water. Those configurations (of the 89 considered) with a Boltzmann population (*P*) greater than 5% at 600 K are shown

Configuration	E_{latt} per u.c./eV	*P* (%)	Al location
C1	−1936.389	53.2	2 at Si3, 2 at Si4
C2	−1936.345	22.5	2 at Al1, 2 at Al2
C3	−1936.308	11.0	Si1, Si3, Si4, Al1
C4	−1936.285	7.1	Si3, Si6, Al1, Al2

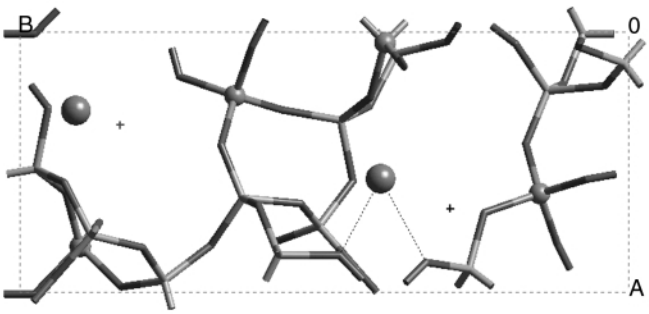

Fig. 1 The second most stable calculated structure (C2) of Goosecreekite without water. The Al (spheres in framework) is located at the experimentally found sites. The Ca^{2+} are two-fold co-ordinated to the framework and are significantly displaced from the experimental sites (black crosses).

† Electronic supplementary information (ESI) available: structure of C1 with and without water and further illustration of the experimental structure. See http://www.rsc.org/suppdata/cc/b0/b009623g/

‡ Also at the Computational and Theoretical Materials Science Group, Faculty of Physics, University of Havana, Havana 10400, Cuba.

Table 2 The unit cell parameters for the two most stable calculated structures, with and without water, are given and compared with experiment. For each structure the cell angle α and γ are calculated to be 90.00°. Experimentally, $\alpha = \gamma = 90°$

	E_{latt} per u.c./eV	a/Å	b/Å	c/Å	β/°	V/Å^3
Expt.[11]		7.401	17.439	7.293	105.44	907.3
C1 (dehyd.)	−1936.389	7.358	16.124	7.092	110.31	853.5
C2 (dehyd.)	−1936.345	7.409	17.036	7.155	109.10	789.1
C1 (hyd.)	−2036.357	7.385	16.855	7.211	108.17	852.9
C2 (hyd.)	−2036.598	7.398	17.017	7.236	106.38	874.0

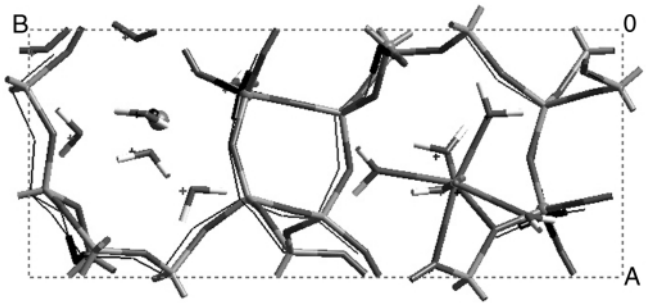

Fig. 2 The most stable calculated structure of Goosecreekite with water (C2) and the experimental unit cell (thin black lines with Al highlighted as tubes). Highlighted in the right channel is the co-ordination sphere of the Ca^{2+}. Also shown in the left channel are the experimental water oxygen (black crosses) and Ca^{2+} (black sphere) positions for comparison to the calculated sites (tubular water and larger spheres).

In the most stable calculated configuration, C1, we find that the Ca^{2+} are located along *a*, which are not observed experimentally, and coordinate strongly to four framework oxygens. Conversely, in C2 the Ca^{2+} are located close to the experimental sites in the channel along [001]. However, these cations can coordinate to only two framework oxygen atoms. We also note the reduced lattice parameters (Table 2) compared with experiment.

Although our methodology has successfully identified stable configurations that are indeed very similar to experiment, notable differences remain. In particular, the experimental framework structure is not sufficiently stabilised by the dehydrated cations (in the calculation) and as a consequence is not the most stable configuration calculated. It is also clear that there is considerable interplay between the location of Al and the siting of the efc sites. Thus, we now need to consider whether the omission of water from these calculations is significant and responsible for the observed discrepancies.

We placed 10 water molecules[11] in the unit cells of C1 and C2 and re-optimised the structures. On energy minimisation, we now find that C2 is more stable than C1 by 0.32 eV per unit cell (Table 2). Furthermore, the calculated structure is now in even better agreement with experiment (Fig. 2, Table 2), with a discrepancy of only 3.6% in the cell volume.

The cations in the calculated, hydrated C2 structure are now located very close to the experimental sites, being 7-fold co-ordinated to five H_2O and two framework oxygens (Fig. 2), as in experiment.[11] Whilst the position and co-ordination of Ca^{2+} in C1 are also in good agreement with experiment, the efcs are more distant from the AlO_4 tetrahedra, which destabilises this particular Al distribution. Thus, the role of water in influencing the Si/Al distribution in this zeolite can be considered as a combination of both electrostatic—screening the electrostatic interaction between the efc and the framework—and steric factors—preventing the efcs from occupying the smaller channels. These effects are reflected in the changes in cell volume (Table 2). A dramatic increase is seen in the cell volume of C2 upon hydration, where water screens the electrostatics and also occupies the same channels as the efcs. For C1, in contrast, the efcs are in the small channels in the dehydrated structure, whilst they move into the larger channels on hydration, resulting in only a small overall change in cell volume.

Our results show how, once solvation is considered, our methodologies and models are able to identify stable Si/Al distributions as well as reproducing the extra-framework structure of both cations and water. Agreement with the experimental structure is excellent. The work clearly demonstrates how water is critical, not only in stabilising the structure but also in actually determining the position of efc sites and framework Al distributions. The successful reproduction of the extra-framework structure also shows that the water potentials of de Leeuw *et al.*[14,15] are suitable for simulations of hydrated zeolites. Further evaluation of the water potential is underway, as are studies of cation exchange.

Dr N. de Leeuw is thanked for providing us with the water potentials prior to publication. Dr J. D. Gale is also thanked for the provision of GULP. A. R. R. S. acknowledges the Royal Society for a Postdoctoral Fellowship and the RSC for a Grant for International Authors. We also thank the University of Havana for an Alma Mater Research Grant.

Notes and references

§ The structure of C1 with and without water and a further illustration of the experimental structure are provided as ESI†.

1 T. Takaishi, M. Kato and K. Itabashi, *Zeolites*, 1995, **15**, 21.
2 *Modelling of Structure and Reactivity in Zeolites*, ed. C. R. A. Catlow, Academic Press, London, 1992.
3 R. G. Bell, R. A. Jackson and C. R. A. Catlow, *Zeolites*, 1992, **12**, 870.
4 A. R. Ruiz-Salvador, D. W. Lewis, J. Rubayo-Soneira, G. Rodríguez-Fuentes, L. R. Sierra and C. R. A. Catlow, *J. Phys. Chem. B*, 1998, **102**, 8417.
5 A. R. Ruiz-Salvador, A. Gómez, D. W. Lewis, G. Rodríguez-Fuentes and L. Montero, *Phys. Chem. Chem. Phys.*, 1999, **1**, 1679.
6 A. R. Ruiz-Salvador, A. Gómez, D. W. Lewis, C. R. A. Catlow, L. M. Rodríguez-Albelo, L. Montero and G. Rodríguez-Fuentes, *Phys. Chem. Chem. Phys.*, 2000, **8**, 1803.
7 D. O'Connor, P. Barnes, D. R. Bates and D. F. Lander, *Chem. Commun.*, 1998, 2527.
8 Y. M. Channon, C. R. A. Catlow, A. M. Gorman and R. A. Jackson, *Microporous. Mesoporous Mater.*, 1998, **102**, 4045.
9 D. A. Faux, *J. Phys. Chem. B*, 1999, **103**, 7803.
10 J. R. Hill, A. R. Minihan, E. Wimmer and C. J. Adams, *Phys. Chem. Chem. Phys.*, 2000, **2**, 4255.
11 R. C. Rouse and D. R. Peacor, *Am. Mineral.*, 1986, **71**, 1494.
12 J. D. Gale, *J. Chem. Soc., Faraday Trans.*, 1997, **93**, 629.
13 R. A. Jackson and C. R. A. Catlow, *Mol. Sim.*, 1988, **1**, 207.
14 N. H. de Leeuw and S. C. Parker, *J. Am. Ceram. Soc.*, 1999, **82**, 3209.
15 N. H. de Leeuw, personal communication.

Access to optically active linear ketones by one-pot catalytic deprotection, decarboxylation, asymmetric tautomerization from racemic benzyl β-ketoesters

Olivier Roy, Mira Diekmann, Abdelkhalek Riahi, Françoise Hénin* and Jacques Muzart

Unité Mixte de Recherche «Réactions Sélectives et Applications», CNRS – Université de Reims Champagne-Ardenne, BP 1039, 51687 Reims Cedex 2, France. E-mail: francoise.henin@univ-reims.fr

Received (in Liverpool, UK) 1st December 2000, Accepted 25th January 2001
First published as an Advance Article on the web 26th February 2001

Benzyl 2-benzoyl-2-phenylpropanoate 1b subjected to heterogeneous hydrogenolysis conditions in the presence of catalytic amounts of commercially available cinchonia alkaloids as chiral protic source, led to (*R*)-1,2-diphenylpropanone with up to 71% ee, through a cascade reaction involving deprotection, decarboxylation and asymmetric tautomerization of enolic species.

Numerous diastereoselective methods exist in enol chemistry to prepare linear ketones bearing an α-stereogenic centre: they use various protecting groups as chiral auxiliaries[1,2] or an alkylating reagent having a chiral leaving group.[3,4] Another efficient way involves the asymmetric protonation of metal enolates generated from ketones[5] or ketenes[6] by stoichiometric quantities of a chiral protic source. In some cases, these latter methods become catalytic in chiral inducing entity,[7,8] but meticulous adjustments of the experimental conditions are then required. The development of catalytic methods in asymmetric protonation of open chain ketone enolates can be complicated by two main factors: i) in contrast to ester or amide derivatives, these simple enolates have no additional chelation sites able to enhance the rigidity of a transition state in coordinating the chiral protic source[9] and ii) *Z*- and *E*-enolates can provide similar[10] or opposite[4] enantiomers. Currently no rule can predict the olefin configuration effect; thus, the preparation of a single enol geometrical isomer is required and is difficult to achieve.

We have shown that 2-carboxy-2-methyltetralone provided optically active 2-methyltetralone in a two step reaction consisting of a decarboxylation and an asymmetric protonation of the resulting enolic species assisted by catalytic amounts of enantiopure aminoalcohols.[11] In acyclic series, a similar methodology has been studied by Brunner's group and was also effective starting from malonic substrates[12] [eqn. (1)]; furthermore, this has been applied to the preparation of optically active naproxen derivatives, the selectivity being higher, starting from 2-cyano-2-arylpropionic acid[13] than from 2-ethoxycarbonyl-2-arylpropionic acid.[14]

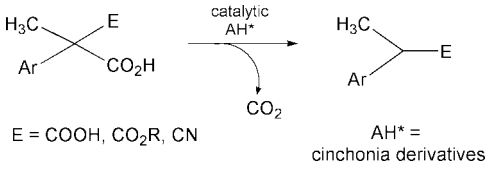

(1)

Using this methodology, we envisaged to prepare aliphatic non racemic ketones. Since we have observed that solutions of 2-carboxy-2-methyltetralone where the acidic group is tertiary were not stable at rt,[11] we decided to start from protected β-ketoacids. The acidic group was protected as benzylic ester as the reductive cleavage of the benzyl group would allow a gradual generation of the acid and of the enolic species. The *in situ* generation of the intermediates under palladium–aminoalcohol catalysis[15] could improve both chemical and optical yields. We present here our results [eqn. (2)].

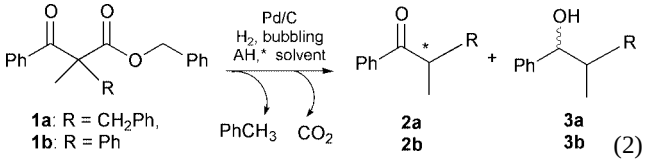

(2)

In the first experiments, we applied the conditions previously defined from cyclic substrates:[15] to an acetonitrile solution of substrate **1a**† and chiral aminoalcohol (0.3 eq.) was added palladium on charcoal (0.025 eq., Ref. 5011 from Engelhard Company), then, H_2 was continuously bubbled into the mixture for the time indicated in Table 1. From the results assembled in Table 1, it appears that ketone **2a** was obtained with good chemical yields but usually accompanied by alcohol **3a**,[16] which corresponds to an over-reduction of **2a**, the amount of **3a** increasing slowly with the reaction time (runs 1 and 2). As aminoalcohols, we used (−)-ephedrine (**4**) and aminoborneol (**5**) which gave satisfying results from cyclic substrates,[15] and also cinchonia alkaloids **6** or **7** which afforded good enantioselectivities from malonic substrates.[12–14] However these chiral inducing entities led to poor enantioselectivities even in varying the reaction temperature (Table 1); the results were not improved by modifying the nature of the supported palladium catalyst or the solvent (toluene and THF instead of acetonitrile).

Table 1 Enantioselective hydrogenolysis–decarboxylation–tautomerization from **1a**

				2a		**3a**
Run	AH* 0.3 eq.	T °C	Time[a]/h	Yield[b](%)	ee (config.)[c]	Yiled[b] (%)
1	**4**	22	0.25	79	2 (*S*)	17
2	**4**	22	1	71	4 (*S*)	22
3	**4**	50	0.25	58	6 (*S*)	11
4	**5**	22	0.5	74	5 (*S*)	n.d.[d]
5	**5**	50	0.25	60	10 (*S*)	n.d.[d]
6	**5**	80	0.17	62	10 (*S*)	n.d.[d]
7	**6**	0	7[e]	19	16 (*S*)	n.d.[d]
8	**6**	22	1	89	10 (*S*)	n.d.[d]
9	**6**	50	0.37	81	9 (*S*)	n.d.[d]
10	**7**	22	1.1	82	5 (*R*)	n.d.[d]

[a] Reaction time to reach full conversion of the substrate, as indicated by TLC. [b] Isolated yields of purified products. [c] Enantiomeric excess determined by HPLC (column Daicel, Chiralcel OD; n-hexane–*i*-PrOH = 99 : 1, 0.6 mL min^{-1}, t_r (*R*) = 14.1 min, t_r (*S*) = 15.5 min, α = 1.2); configuration determined by optical rotation comparison:[2,17] $[\alpha]_D^{20}$ = +5 (*c* 1 $CHCl_3$, ee_{HPLC} = 10%). [d] Not determined. [e] Conversion: 35%.

Then we examined substrate **1b**† where the benzyl group in the 2-position was replaced by a phenyl substituent capable of stabilizing the enolic species (Table 2). From this substrate compared to **1a**, the chemical yield of ketone **2b** increased since alcohol **3b** was not produced. Again the use of **4** and **5** led to no or low enantioselectivity (runs 11 and 12). In contrast, the enantiomeric excess of **2b** increased dramatically with cincho-

DOI: 10.1039/b009828k

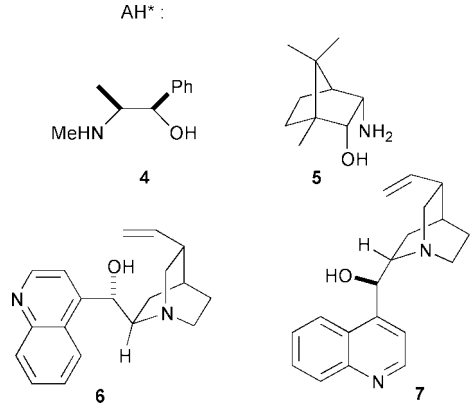

Table 2 Enantioselective cleavage–decarboxylation–tautomerization from **1b** at room temperature

Run	Solvent	AH* (eq.)	Time[a]/h	**2b** Yield[a] (%)	ee (config.)[b]
11	MeCN	**4** (0.3)	1	97	0
12	”	**5** (0.3)	0.5	85	16 (*S*)
13	”	**6** (0.3)	0.5	70	49 (*S*)
14	”	**7** (0.3)	1	94	56 (*R*)
15	”	**7** (0.5)	1	100	56 (*R*)
16	”	**7** (0.1)	1	100	61 (*R*)
17	”	Adsorbed[c]			
		7 (0.3)	7	95	64 (*R*)
18	THF	**7** (0.3)	17	85	52 (*R*)
19	AcOEt	**7** (0.3)	1	100	71 (*R*)
20	”	**7** (0.05)	2	100	68 (*R*)
21	”	Adsorbed[c]			
		7 (0.3)	8	49[d]	70 (*R*)

[a] See Table 1. [b] Enantiomeric excess determined by HPLC (column Daicel, Chiralcel OD; n-hexane–*i*-PrOH = 99:1, 0.6 mL min^{-1}, t_r (*R*) = 11.8 min, t_r (*S*) = 13.9 min, α = 1.46); configuration determined by optical rotation comparison:[2,18] $[\alpha]_D^{20}$ = +167 (*c* 1.2 $CHCl_3$, ee_{HPLC} = 71%). [c] The suspension is prepared as following: the palladium on charcoal is added to a solution of **7** in chloroform; then the solvent is evaporated under reduced pressure and replaced by the solution of the substrate in MeCN or AcOEt. [d] Only 49% of conversion.

nia aminoalcohols; indeed we observed 49 and 56% ee with cinchonidine (**6**) (run 13) and cinchonine (**7**) (run 14) respectively. As these latter chirality inductors were insoluble in acetonitrile, we studied the effects of the amount of **7** and of its distribution in the medium. As expected, increasing the amount of **7** from 0.3 (run 14) to 0.5 eq. (run 15) did not change the selectivity. Dropping to 0.1 eq. the amount of **7** was not detrimental to both chemical yield and ee (run 16). Adsorbing **7** on the supported catalyst by its dissolution in chloroform followed by a solvent exchange allowed a slight increase of the enantioselectivity, but a concomitant decrease of the reaction rate (run 17). Switching from acetonitrile to THF led to a slower reaction and a decreased ee (run 18). The best solvent for both yield and ee was ethyl acetate, since ee could reach 71% for a quantitative chemical yield (runs 19); even in the presence of only 0.05 eq. of **7**, ee remained high (68%, run 20). In this solvent however, the adsorption of **7** on palladium on charcoal was detrimental to the conversion without change of the ee.

Thus we have shown that, in spite of their non-fixed geometry, enolic species corresponding to open chain ketones could be asymmetrically protonated in using a catalytic amount of commercial cinchonine, the one pot procedure starting from **1** being easily carried out.

We thank Eva Berssen for a few experiments and Socrates Institution for financial support to M. D. and E. B. who were on leave from Oldenburg University, Germany. Part of this work has been carried out in the framework of the COST D12/0028/99 program. We are grateful to the “Ministère de la Recherche et de la Technologie” for a PhD studentship to O. R. and to Engelhard Company for a loan of Pd catalysts.

References and notes

† *Selected data for* **1**: **1a**: δ_H (250 MHz, $CDCl_3$) 7.7–7.8 (m, 2H), 6.9–7.4 (m, 13H), 5.09 (br s, 2H, OC*H*$_2$Ph), 3.44 (d, 1H, C*H*HPh, *J* = 13.7 Hz), 3.35 (d, 1H, CH*H*Ph, *J* = 13.7 Hz), 1.50 (s, 3H, C*H*$_3$). **1b**: δ_H (250 MHz, $CDCl_3$) 7.62–7.66 (m, 2H), 7.06–7.50 (m, 13H), 5.16 (d, 1H, OC*H*HPh, *J* = 12.6 Hz), 5.08 (d, 1H, OCH*H*Ph, *J* = 12.6 Hz), 1.94 (s, 3H, C*H*$_3$).

1 Reviews: J. S. McCallum and L. S. Liebeskind, in *Stereoselective Synthesis* (Houben-Weyl), ed. G. Helmchen, R. W. Hoffmann, J. Mulzer and E. Schaumann, Thieme Verlag: New York, 1996, p. 916. P. Fey and W. Hartwig, *ibid*, p. 969. P. Fey, *ibid*, p. 1030.
2 W. Oppolzer, C. Darcel, P. Rochet, S. Rosset and J. De Brabander, *Helv. Chim. Acta*, 1997, **80**, 1319.
3 P. Duhamel, in *Stereoselective Synthesis* (Houben-Weyl), ed. G. Helmchen, R. W. Hoffmann, J. Mulzer and E. Schaumann, Thieme Verlag: New York, 1996, p. 1101.
4 C. Fehr and J. Galindo, *J. Am. Chem. Soc.*, 1988, **110**, 6909.
5 K. Ishibara, H. Nakamura and H. Yamamoto, *J. Am. Chem. Soc.*, 1999, **121**, 7720.
6 For examples: Ref. 4; J. Pracejus and H. Mätje, *J. Prakt. Chem.*, 1964, **24**, 195; Y. Nakamura, S. Takeuchi, Y. Ohgo, M. Yamaoka, A. Yoshida and K. Mikami, *Tetrahedron*, 1999, **55**, 4595.
7 C. Fehr and J. Galindo, *Angew. Chem., Int. Ed. Engl.*, 1994, **33**, 1888.
8 Y. Nakamura, S. Takeuchi, A. Ohira and Y. Ohgo, *Tetrahedron Lett.*, 1996, **37**, 2805; S. Takeuchi, Y. Nakamura, Y. Ohgo and D. P. Curran, *Tetrahedron Lett.*, 1998, **39**, 8691; B. L. Hodous, J. C. Ruble and G. C. Fu, *J. Am. Chem. Soc.*, 1999, **121**, 2637.
9 C. Fehr, *Angew. Chem., Int. Ed. Engl.*, 1996, **35**, 2566.
10 F. Hénin, S. Létinois and J. Muzart, *Tetrahedron: Asymmetry*, 2000, **11**, 2037 and references cited therein.
11 F. Hénin, J. Muzart, M. Nedjma and H. Rau, *Monatsh. Chem.*, 1997, **128**, 1181.
12 H. Brunner, J. Müller and J. Spitzer, *Monatsh. Chem.*, 1996, **127**, 845.
13 H. Brunner and P. Schmidt, *Eur. J. Org. Chem.*, 2000, 2119.
14 H. Brunner and P. Schmidt, *Z. Naturforsch.*, 2000, **55b**, 369.
15 J. Muzart, F. Hénin and S. Jamal Aboulhoda, *Tetrahedron: Asymmetry*, 1997, **8**, 381; S. Jamal Aboulhoda, I. Reiners, J. Wilken, F. Hénin, J. Martens and J. Muzart, *Tetrahedron: Asymmetry*, 1998, **9**, 1847.
16 A *syn* relative configuration has been determined for the diastereomer in slight excess (around 55±3%) which could be compared with analogous values observed for **3a** resulting of the hydride reduction of **2a**: C. Alvarez Ibarra, F. Fernandez Gonzalez, M. L. Quiroga Feijoo and J. Santoro, *An. Quim.*, 1978, **74**, 449; C. Alvarez Ibarra, R. Pérez-Ossorio, M. L. Quiroga, M. S. Arias Pérez and M J. Fernandez Dominguez, *J. Chem. Soc., Perkin Trans. 2*, 1988, 101.
17 T. Izawa, Y. Terao and K. Suzuki, *Tetrahedron: Asymmetry*, 1997, **8**, 2645.
18 A. I. Meyers, D. R. Williams, S. White and G. W. Erickson, *J. Am. Chem. Soc.*, 1981, **103**, 3088.

Immobilisation of heteropoly anions in Si-MCM-41 channels by means of chemical bonding to aminosilane groups

Waldemar Kaleta and Krystyna Nowińska*

Faculty of Chemistry, A. Mickiewicz University, Poznań, Poland. E-mail: krysnow@main.amu.edu.pl

Received (in Cambridge, UK) 27th August 2000, Accepted 30th January 2001
First published as an Advance Article on the web 26th February 2001

Heteropoly acids (HPA) have been immobilised inside the channels of Si-MCM-41 mesoporous molecular sieve by means of chemical bonding with amine groups introduced into the system during a previous aminosilylation procedure, which resulted in the strong anchoring of heteropoly anions and prevented the HPA leaching when applied as a catalyst in polar solvent media.

The encapsulation of heteropoly compounds of Keggin structure into the pores of a molecular sieve may provide an active, stable catalyst. However, the anchoring of HPA into MCM-41 walls occurs by means of the interaction of the HPA acidic protons with the silanol groups and results in the formation of only very weak bonds between HPA and MCM-41. As a consequence, leaching of heteropoly acid was always observed when the HPA/MCM-41 system was applied in polar solvent media.[1–3] Our earlier reports[3] and those of others[4] have shown that the generation of insoluble non-stoichiometric caesium or ammonium salts of HPA inside the channels of the support prevents leaching of active phase.

In the following study we utilised modification of the silica gel surface with aminoalkoxysilanes, as reported by Vansant and coworkers,[5–7] in order to incorporate functional groups inside the channels of the mesoporous molecular sieve which would be able to react with heteropoly acid and form strong bonds. According to the mechanism proposed by Vansant and Van der Voort,[6,7] aminosilane molecules, initially connected to the silica surface *via* the amine groups, turn to display an amine-upward position as a result of the so-called flip mechanism.[6,7] It seems probable that the exposed basic amine groups might react with heteropoly acids to form the salt $\equiv Si(CH_2)_3NH_3 \cdot HPA$, which will be linked strongly to the modified surface.

Two samples of MCM-41 molecular sieves of different pore size were synthesised using $C_{14}H_{29}(CH_3)_3NBr$ [merystyltrimethylammonium bromide (MTMABr)] and $C_{16}H_{31}(CH_3)_3NBr$ [cetyltrimethylammonium bromide (CTMABr)] as surfactants according to ref. 8. These samples are denoted MCM-41-A and MCM-41-B, respectively.

After template removal the calcined materials were treated with the aqueous solution of ammonium nitrate to remove the sodium cations remaining after the synthesis. The samples were calcined again at 400 °C under nitrogen. The aminosilylation procedure was performed with γ-aminopropyltriethoxysilane (APTS) according to the procedure given in ref. 5 with some minor modification. MCM–41 dehydrated at 400 °C was contacted with a refluxing toluene solution containing 1% APTS for 5 h. The resulting materials were filtered off, washed with toluene and the remaining solvent removed under vacuum, firstly at RT and then at 140 °C for 20 h. MCM-41 modified by aminosilylation is denoted as ASIL/MCM-41 (A or B). The modified samples (1 g) were treated with 60 mL of a refluxing methanol solution containing 5% $H_6PMo_9V_3O_{40}$ for 3 h. After this time the samples were allowed to cool and the solids subsequently filtered off and washed four times with methanol. Finally, the filtered samples were heated *in vacuo* at 100 °C to remove the remaining methanol. The two resulting samples, HPMoV/ASIL/MCM-41-A and HPMoV/ASIL/MCM-41-B contained 10 and 30 wt% of HPMoV, respectively, the amount of heteropoly acid immobilised in the MCM-41 channels being estimated from analysis of the remaining methanol solution. The presence of heteropoly anions in the modified systems was also monitored by FTIR spectra.

We also introduced heteropoly acid (HPMoV) into MCM-41-B (unmodified with aminotriethoxysilane) using exactly the same procedure as for the modified sample. MCM-41-B after impregnation with HPMoV from methanol solution (denoted HPMoV/MCM-41-B) showed distinctive yellow colour indicating the introduction of heteropoly acid into the molecular sieve. Washing the sample with methanol (four times) resulted, however, in decoloration of the sample indicating removal of the HPMoV. By contrast, the aminosilane modified matrix releases very few Keggin units even after extraction with boiling methanol. Only 0.8 wt% of HPA anchored in APTS modified MCM-41 was removed after 2 h extraction with boiling methanol, while 95 wt% of HPA was removed from the unmodified support when treated with methanol at RT.

XRD patterns of MCM-41-A and MCM-41-B indicated that mesoporous materials were obtained (Fig. 1, curve 1). The APTS modified sample (ASIL/MCM-41-B) showed an XRD pattern which was almost unchanged relative to the parent MCM–41 matrix (Fig. 1, curve 2), while the XRD pattern of ASIL/MCM-41-B modified with 30 wt% heteropoly acid showed almost no reflectance in the low angle region (Fig. 1, curve 3). The disappearance of XRD patterns characteristic of the MCM structure has already been observed as a result of introduction of a relatively high number of HPA anions into MCM-48 channels.[9,10] The removal of heteropoly compound from unmodified MCM-41-B upon rinsing with methanol restored the XRD patterns characteristic of the MCM-41 structure (Fig. 1, curve 4). Considering that the heteropoly anions introduced into APTS modified samples are firmly connected to the MCM-41 by chemical bonds, destruction of the amine group by relatively high temperature treatment (320 °C) and subsequent removal of the HPA by washing with polar solvents (methanol and water) was performed. Removal of heteropoly anions from the MCM-41-B matrix restored the XRD pattern which were very similar to that of the parent MCM-41 sample (Fig. 1, curve 5).

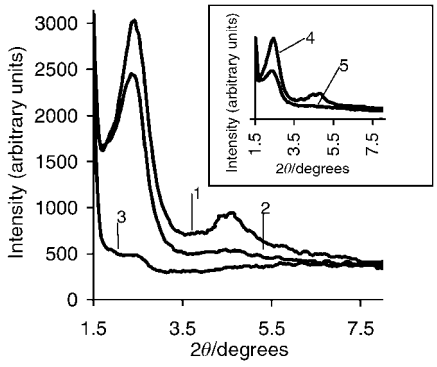

Fig. 1 XRD patterns of the MCM–41 samples before and after modification. 1, parent MCM–41; 2, ASIL/MCM-41 (aminosilylated MCM–41); 3, HPMoV/ASIL/MCM–41 (ASIL/MCM–41 modified with HPMoV); 4, HPMoV/MCM–41 (unmodified MCM–41 impregnated with HPMoV and subsequently rinsed with methanol); 5, HPMoV/ASIL/MVM–41 (after HPMoV removal).

DOI: 10.1039/b007111k

Table 1 Catalytic activity of MCM-41 modified with heteropoly acid for cyclohexane oxidation

Catalyst	Catalyst loading/mg	HPMoV content		Cyclohexane conversion (mol%)	TON
		mg	mmol of KU		
HPMoV(30)/ASIL/MCM-41-B (first run)	50	15	0.009	14.6	24.6
HPMoV(30)/ASIL/MCM-41-B (second run)	50	15	0.009	13.5	23
HPMoV(30)/ASIL/MCM-41-B (after previous treatment with oxidative mixture)	50	14.8	0.0087	13.5	24
HPMoV(10)/ASIL/MCM-41-A (first run)	50	5	0.003	13.0	68
Free HPMoV dissolved in the reaction mixture	5	5	0.003	15.0	78

BET surface areas and pore distributions were calculated using N_2 adsorption at 77 K (ASAP equipment, Micromeritics). Aminosilylation and introduction of heteropoly anions affect the surface area and pore distribution of the modified samples significantly [Fig. 2(a) and (b)]. The parent MCM-41 samples (A and B) show a maximum of pore diameter at 22 and 25 Å and surface areas of 1330 and 1000 $m^2\ g^{-1}$, respectively. Aminosilylation of the molecular sieves results in a shift of the pore maximum to lower diameters and a decrease of the pore volume and surface area (*ca.* 720 $m^2\ g^{-1}$). Introduction of heteropoly anions leads to a further decrease in surface area and in pore volume. Taking into consideration the pore diameter of the MCM-41 modified with APTS (Fig. 2), and the diameter of the Keggin unit (12 Å), monolayer coverage can be expected at an HPMoV loading of *ca.* of 30 wt% (only one Keggin unit may be located along the ASIL/MCM-41 channels). It is unlikely that an ideal distribution of the Keggin units inside the channels, will be obtained, so encapsulation of *ca.* 30 wt% of HPMoV into the ASIL/MCM-41 matrix may result in partial blocking of the pores and makes some of the Keggin units inaccessible to reagents which should also affect the catalytic activity of the modified samples. The catalytic activity of heteropoly anions (HPMoV) anchored in the ASIL/MCM-41 channels (10 and 30 wt%) as well as of free HPMoV heteropoly acid was examined for cyclohexane oxidation reaction in the liquid phase (Table 1). 12–Molybdophosphoric acid modified with vanadium has been reported to be an active catalyst for liquid-phase oxidation of different organic and inorganic substrates with H_2O_2 or organic peroxides as oxidants.[11] The oxidation reaction was carried out in the liquid phase (sealed vials, 90 °C, 20 h, no stirring, 50 mg of ASIL/MCM-41 modified with HPMoV or 5 mg of free HPMoV) using *tert*-butyl hydroperoxide (TBHP) and acetonitrile as oxidant and solvent, respectively. A negligible cyclohexane conversion was observed in the presence of unmodified ASIL/MCM-41. Comparing the activity of samples containing different amounts of HPMoV, the TON (mol of reacted cyclohexane per KU) was calculated (Table 1). The results presented in Table 1 indicate that the heteropoly anions occupying the pores in ASIL/MCM-41-A (50 mg of sample, 10 wt% of HPMoV) show almost the same activity (TON) as 5 mg of free heteropoly acid dissolved in the reaction medium. This suggests that the distribution of the Keggin units in the HPMoV(10)/ASIL/MCM-41 is very close to monomolecular coverage and almost every heteropoly anion is accessible to the reagents. When the concentration of the Keggin units in the mesoporous material was increased to 30 wt%, the activity for cyclohexane oxidation (expressed as TON), decreased, which shows that a proportion of the heteropoly anions introduced may not be accessible to the reagents because of the pores being blocked.

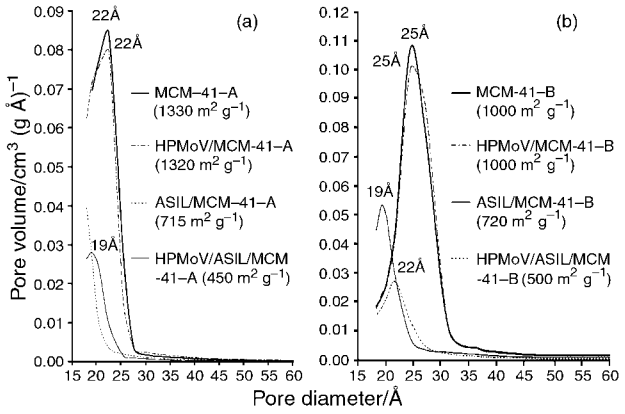

Fig. 2 Pore size distribution of the MCM–41 samples synthesised with MTMABr (a) and CTMABr (b) as surfactants before and after modification.

To investigate the stability of HPMoV/ASIL/MCM-41 system towards a powerful oxidant such as TBHP, two additional experiments have been carried out. The spent catalyst containing 30 wt% HPMoV (after cyclohexane oxidation process) was carefully separated from the products and reused for cyclohexane oxidation (second run, Table 1). The decrease in oxidative activity was insignificant. To check the effect of possible removal of HPMoV from the catalytic system as a result of potential oxidative degradation of aminopropyl groups, a fresh HPMoV(30)/ASIL/MCM-41 sample was treated with a mixture of TBHP and acetonitrile under exactly the same conditions as the oxidation process (90 °C, 20 h). The liquid phase was carefully separated and analysed for the presence of molybdenum. The remaining solid was treated again with the mixture of acetonitrile and TBHP under the same conditions with subsequent analysis for molybdenum. It was assumed that if partial decomposition of aminopropyl groups took place as a result of possible oxidation with TBHP it should result in some release of HPMoV. The first treatment resulted in the removal of 1.5 wt% HPMoV (anchored to ASIL/MCM-41) while the second treatment released an additional 0.8 wt% (ICP–AEC). These results indicate that 98 wt% of anchored HPMoV still remains in the HPA/ASIL/MCM-41 system and the leaching of HPA from this system is negligible even under drastic conditions. The HPA(30)/ASIL/MCM-41 sample was also used after the first treatment with a mixture of acetonitrile and TBHP as catalyst for cyclohexane oxidation. The decrease of oxidative activity was negligible.

Notes and references

1 M. J. Verhoef, P. J. Kooyman, J. A. Peters and H. van Bekkum, *Microporous Mesoporous Mater.*, 1999, **27**, 365.
2 B. L. C. Passoni, F. J. Luna, M. Wallau, R. Buffon and U. Schuchardt, *J. Mol. Catal.*, 1998, **134**, 229.
3 K. Nowińska and W. Kaleta, *Appl. Catal. A: Gen.*, 2000, **203**, 91.
4 Á. Molnár, T. Beregszászi, Á. Fudala, B. Török, M. Rózsa-Tarjáni and I. Kiricsi, *Proceedings of The Royal Society of Chemistry, Third International Symposium on Supported Reagents and Catalysts in Chemistry*, Limerick, RSC, Cambridge, 1998, p. 25.
5 K. C. Vrancken, P. Van Der Voort, K. Possemier and E. F. Vansant, *J. Colloid Interface Sci.*, 1995, **174**, 86.
6 P. Van Der Voort and E. F. Vansant, *J. Liq. Chromatogr. Rel. Technol.*, 1996, **19**, 2723.
7 P. Van Der Voort and E. F. Vansant, *Pol. J. Chem.*, 1997, **71**, 550.
8 W. A. Carvalho, P. B. Varaldo, M. Wallan and U. Schurchardt, *Zeolites*, 1997, **18**, 408.
9 I. V. Kozhevnikov, A. Sinnema, R. J. J. Jansen, K. Pamin and H. van Bekkum, *Catal. Lett.*, 1995, **30**, 241.
10 A. Ghanbari-Siahkali, A. Philippou, J. Dwyer and M. W. Andreas, *Appl. Catal.*, 2000, **192**, 57.
11 R. Neumann and M. Cohen, *Angew. Chem., Int. Ed. Engl.*, 1997, **36**, 1738.

The role of the 'glow phenomenon' in the preparation of sulfated zirconia catalysts†

Alexander Hahn, Thorsten Ressler, Rolf E. Jentoft and Friederike C. Jentoft *

Fritz-Haber-Institut der Max-Planck-Gesellschaft, Department of Inorganic Chemistry, Faradayweg 4–6, 14195 Berlin, Germany. E-mail: jentoft@fhi-berlin.mpg.de

Received (in Cambridge, UK) 9th January 2001, Accepted 9th February 2001
First published as an Advance Article on the web 26th February 2001

During the calcination procedure that is necessary to obtain sulfated zirconia catalysts from hydroxide precursors an exothermic reaction occurs in the heat-up period which can lead to a rapid overheating ('glow') of the sample bed; the batch size is identified as a critical parameter that influences heat transfer and thus the extent of the temperature overshoot and the catalytic activity of the product.

Sulfated zirconia has attracted interest as a solid acid catalyst[1,2] because it is capable of isomerizing alkanes at temperatures below 373 K where the more valuable branched alkanes are thermodynamically favored. The activity of sulfated zirconia for *n*-butane isomerization increases 1–2 orders of magnitude upon addition of transition metal cations (Fe, Mn, typically *ca.* 2 wt%) as promoters,[3,4] whose function has not yet been clarified. For preparation of these materials, X-ray amorphous zirconium hydroxide is treated with sulfate solutions (*e.g.* ammonium sulfate, sulfuric acid) and, optionally, with solutions containing the respective cations (*e.g.* metal nitrates). The final step of the preparation is a thermal treatment at 773–973 K, typically conducted in air (calcination). Important catalyst properties such as sulfur content, surface area, phase composition and activity are seemingly correlated to the calcination temperature.[2,5–7] A number of reactions occur during calcination–typically already in the heat-up period–among them water loss, decomposition of species (*e.g.* ammonium, nitrate) and changes of morphology and structure (crystallization). Using thermal analysis, the heat of these reactions has been monitored, and for pure zirconium hydroxide typically a broad endothermic signal is found between 273–373 K, followed by a sharp exothermic signal around 725 K.[2,8] Not only is the origin of the exothermic signal–crystallization or a surface area reduction–still under debate,[6,8–11] the extent of the temperature increase has also never been accurately determined for catalyst precursor samples not of analytical (*ca.* 10 mg) but of preparative scale (*ca.*10 g). We measured the temperature in the sample bed when calcining gram amounts of zirconium hydroxide-based catalyst precursors and tested the activity of the obtained catalysts.

Zirconium hydroxide (ZH) and sulfated zirconium hydroxide with 5–6% SO_3 (SZH) (from MEL Chemicals) were used as starting materials. SZH was promoted by adding aqueous solutions of $Mn(NO_3)_2{\cdot}4H_2O$ or $Fe(NO_3)_3{\cdot}9H_2O$ (both Merck p.a.) under vigorous stirring, followed by room temperature drying (incipient wetness method[4]) to give *x*FSZH and *x*MSZH (*x* = nominal promoter content after calcination in wt% metal). For calcination, the powders were loaded into differently sized quartz boats (2.2, 8.4, 17.1 ml) providing different surface-to-volume ratios. Single boats were placed in a 29 mm i.d. quartz tube in a tubular furnace (Heraeus RO 4/25) with PID control. In order to monitor the bed temperature during calcination, an additional thermocouple was placed in the center of the bed. Sheath thermocouples with 0.5 mm o.d. were used for fast response and to minimize heat-sink effects. The quartz tube was continuously purged with 200 ml min^{-1} synthetic air and the oven was heated to 923 K at 3 K min^{-1}, held for 3 h at 923 K–a temperature recommended for best activity of promoted sulfated zirconia[7]–and then cooled to room temperature. Isomerization of *n*-butane to isobutane was conducted at atmospheric pressure in a once-through plug-flow fixed bed reactor employing 500 mg of catalyst. After a 30 min activation at 723 K in dry nitrogen, the isomerization was run at 338 K, feeding 80 ml min^{-1} of 1% *n*-butane in nitrogen mixture. Analysis was performed with on-line gas chromatography.

Fig. 1 shows the bed temperature *vs.* oven temperature during the calcination of ZH, SZH, 2FSZH, and 2MSZH in the largest boat. During the heat-up period, at oven temperatures of 650–850 K, a rapid temperature rise inside the bed was observed for all samples with maximum rates of 60 K s^{-1} (ZH). The bed temperature rose by up to 300 K (ZH) and exceeded the desired maximum temperature of 923 K in all cases. Increasing promoter content shifted the start of the temperature rise to higher oven temperatures, with Mn exerting a stronger effect than Fe. The position of the temperature rise was reproducible within 5 K, and the extent of the temperature rise was reproducible within 15 K.

Fig. 2(a) shows the bed *vs.* oven temperature for three differently sized batches (ESI†) taken from a single preparation of 2MSZH. The temperature rise in the large batch started first during the ramp, followed by the medium and the small batch. The largest batch produced the highest temperature rise and only this sample reached more than 923 K. These three batches underwent the entire calcination program as described above, the only difference being the batch size, and were then tested for *n*-butane isomerization. The sample taken from the large batch exhibited a significantly higher maximum conversion than the samples taken from the smaller batches [Fig. 2(b)]. For a number of samples with different promoter contents (Mn and/or Fe in the range 0.5–3.5%) calcination in a large batch led to higher activity *vs.* calcination in smaller batches. The BET surface area of Fe- or Mn-promoted samples increased with

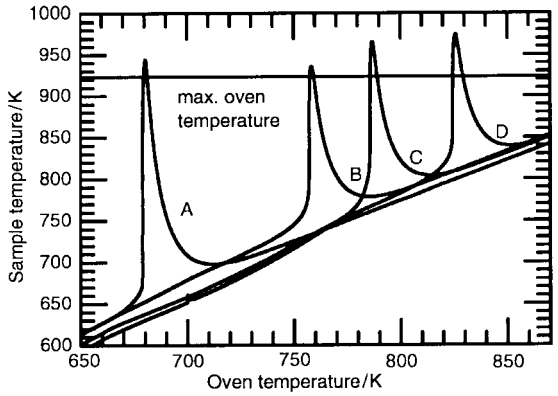

Fig. 1 Bed temperature *vs.* oven temperature during calcination of zirconium hydroxide (A), sulfated zirconium hydroxide (B), sulfated zirconium hydroxide promoted with 2 wt% Fe (C), and sulfated zirconium hydroxide promoted with 2 wt% Mn (D). Conditions: 17.1 ml boat (20–25 g sample), flowing air, nominal heating rate 3 K min^{-1}.

† Electronic supplementary information (ESI) available: boats used for calcination. See http://www.rsc.org/suppdata/cc/b0/b100364j/

DOI: 10.1039/b100364j

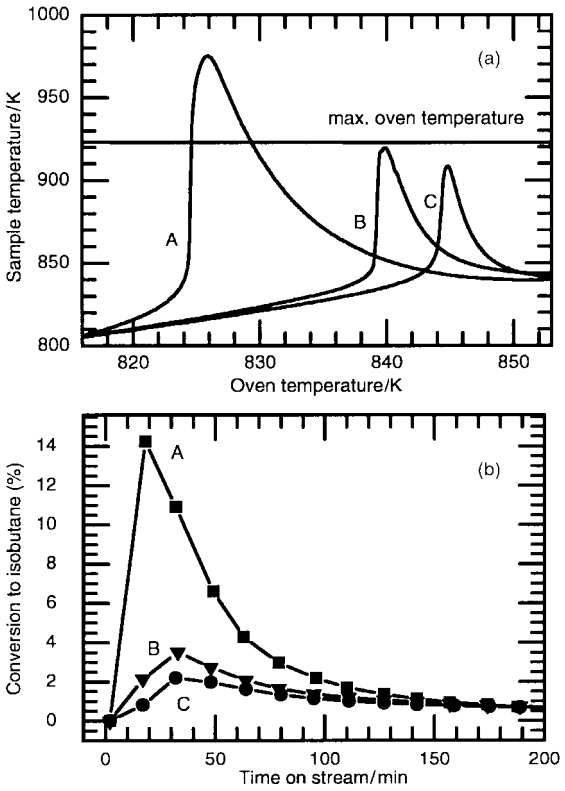

Fig. 2 (a) Bed temperature *vs.* oven temperature with the sample amount as parameter. Sample: sulfated zirconium hydroxide promoted with 2 wt% Mn. Conditions: flowing air, nominal heating rate: 3 K min^{-1}, holding time 3 h at 923 K. Large boat 25 g (A), medium boat 12 g (B), and small boat 3 g (C). (b) Butane isomerization reaction performance of the samples from Fig. 2(a). Reaction conditions: 500 mg sample, 1% *n*-butane in nitrogen, 80 ml min^{-1} total flow, $p = 1$ atm, $T = 338$ K.

increasing calcination batch size, covering a range of 85–115 $m^2\ g^{-1}$. Fe- or Mn-promoted samples consisted predominantly of tetragonal zirconia, and the size of the crystalline domains decreased with increasing calcination batch size, covering a range of 8–13 nm.

The spontaneous temperature rise in the sample bed during the heat-up phase corresponds to the reported thermal analysis data[2,6] in that an exothermic reaction occurs. Older literature gives some indication that the temperature rise may be considerable, depending on the amount and packing, *e.g.* Wöhler[11] heated as much as 0.25 g zirconium hydroxide and measured a *ca.* 60 K temperature rise. The effect has been observed for a number of different hydroxides and is also referred to as a 'glow phenomenon'[9,11,12] because it can lead to a visible light emission. In the presence of sulfate[6] or other hydroxides,[8,9] the 'glow'[9] or the thermal signals[6,8] were found to be subdued and/or shifted to higher temperature.[6,8,9] Our results are consistent with previous findings but additionally demonstrate how an extensive and typically not reported quantity, *i.e.* the mass to be calcined, influences heat transfer and thus the temperatures reached, and the catalytic properties of the final product. In sufficiently large and compact batches, the peak temperature may exceed the desired maximum calcination temperature; if this is the case, then for equally sized batches of differently promoted zirconium hydroxides, the nature and amount of additive (sulfate, Fe, Mn) may determine the true maximum temperature. Thus, the promoters have a systemic influence in that they alter the calcination chemistry. The start temperature correlates with the batch size, as does the catalytic activity. The series of events–rapid temperature increase, high peak temperature, rapid temperature decrease–allows for a chemistry that is reflected in the final product although the sample is subsequently treated for 3 h at 923 K.

Similar effects are potentially possible in the processing of other hydroxides that exhibit the 'glow', namely hydroxides of iron, chromium and titanium.[9,11] Certainly for the preparation and characterization of zirconia catalysts all details of the thermal treatment must be reported, *i.e.* the heating rate and any parameter influencing heat transfer such as sample size and shape. This applies particularly to experiments involving very small or large amounts (thermal analysis, scale-up) and *in situ* calcinations with the sample pressed into a pellet or wafer. Our results suggest that any two experiments involving thermal treatment of a zirconium hydroxide under non-identical conditions may not yield the same material and may not deliver related analytical data.

The authors thank Gisela Lorenz for preparing the catalysts and Robert Schlögl for continuous support. T. R. thanks the Deutsche Forschungsgemeinschaft, DFG, for financial support.

Notes and references

1 M. Hino, S. Kobayashi and K. Arata, *J. Am. Chem. Soc.*, 1979, **101**, 6439.
2 X. Song and Y. Sayari, *Catal. Rev.–Sci. Eng.*, 1996, **38**, 329.
3 C.-Y. Hsu, C. R. Heimbuch, C. T. Armes and B. C. Gates, *J. Chem. Soc., Chem. Commun.*, 1992, 1645.
4 F. C. Lange, T.-K. Cheung and B. C. Gates, *Catal. Lett.*, 1996, **41**, 95.
5 F. R. Chen, G. Coudurier, J.-F. Joly and J. C. Védrine, *J. Catal.*, 1993, **143**, 616.
6 S. Chokkaram, R. Srinivasan, D. R. Milburn and B. H. Davis, *J. Colloid Interface Sci.*, 1994, **165**, 160.
7 S. X. Song and R. A. Kydd, *Catal. Lett.*, 1998, **51**, 95.
8 A. Keshavaraja, N. E. Jacob and A. V. Ramaswamy, *Thermochim. Acta*, 1995, **254**, 267.
9 M. Sorrentino, L. Steinbrecher and F. Hazel, *J. Colloid Interface Sci.*, 1969, **31**, 307.
10 R. Srinivasan and B. H. Davis, *J. Colloid Interface Sci.*, 1993, **156**, 400.
11 L. Wöhler, *Kolloid-Z.*, 1926, **38**, 97.
12 R. Ruer, *Z. Anorg. Allg. Chem.*, 1905, **43**, 282.

Easy formation of indium–silicon bonds: reaction of decamethylsilicocene with trimethylindium

Thorsten Kühler, Peter Jutzi,* Anja Stammler and Hans-Georg Stammler

Universität Bielefeld, Fakultät für Chemie, Universitätsstraße 25, 33615 Bielefeld, Germany. E-mail: peter.jutzi@uni-bielefeld.de

Received (in Cambridge, UK) 7th December 2000, Accepted 9th February 2001
First published as an Advance Article on the web 26th February 2001

The reaction of decamethylsilicocene 1 with trimethylindium yields the disilyl indium compound [Cp*$_2$Si(Me)]$_2$InMe (2) in nearly quantitative yield; 2 is characterised by ^{1}H, ^{13}C and ^{29}Si NMR and microanalytical data and by X-ray crystallography.

For the majority of main group elements a variety of silyl derivatives have been previously described in the literature. It is therefore somewhat surprising that silyl indium compounds are rarely known. Although $(Me_3Si)_3In$[1] has previously been synthesised by Bürger and Götze in 1969 it took nearly 20 years before a second representative of this class of compound, namely $[(Me_3Si)_3Si]_2InCl_2Li\cdot 2THF$, was reported by Cowley *et al.* in 1986.[2] It was not until the late 1990's that further silyl indium compounds were reported in the literature. Besides the silyl indium halides $(Bu^t_3Si)_nInHal_{3-n}$ (n = 1 and 2) prepared by Wiberg,[3] these were mainly examples of low valent indium compounds like the sterically crowded diindanes $\{[(Me_3Si)_3Si]_2In\}_2$ described by Weidlein *et al.*[4] and $[(Bu^t_3Si)_2In]_2$ synthesized by Wiberg.[5] The most recent examples are the indium cluster compounds $(Bu^t_3Si)_6In_8$[6] and $(Bu^t_3Si)_8In_{12}$[7] which were again prepared by Wiberg *et al.* Of the aforementioned compounds only the diindanes, the cluster compounds and the lithium indanate have been structurally characterised. It is of great interest to find new preparations for silyl–indium compounds and to structurally identify them.

In the course of our investigations on the reactivity of decamethylsilicocene[8] **1** we have already reported on the reactions of **1** with halides and organo halides of group 13 compounds.[9] Here we present the result of the reaction of **1** with trimethylindium (Scheme 1) where the disilyl indium compound **2** is formed by insertion of **1** into two of the three indium–carbon bonds.

When an excess of trimethylindium was added to **1** in pentane at low temperature a colourless solution was formed which turned yellow on warming to room temperature. Evaporation of all volatiles *in vacuo* gave **2** as a bright yellow, air and moisture sensitive solid in nearly quantitative yield.† Recrystallisation from pentane gave single crystals of **2** that were suitable for X-ray structure analysis. Fig. 1 shows the molecular structure of **2** in the solid state.‡

The indium atom is surrounded by the methyl group and the two silyl substituents in a trigonal planar fashion. The sum of the bond angles at the indium centre is 360°. The indium–silicon distances are 2.642(2) Å for In(1)–Si(1) and 2.640(3) Å for In(1)–S(2) and thus slightly longer than the sum of the covalent radii of 2.61 Å. However, they are decidedly shorter than the mean Si–In distances of 2.78 Å in the sterically crowded diindane $(Bu^t_3Si)_4In_2$[5] and of 2.68 Å in the somewhat less demandingly substituted conjuncto cluster $(Bu^t_3Si)_8In_{12}$.[7] Only in the indanate anion $[(Me_3Si)_3Si]_2InCl_2^-$ are shorter Si–In distances of 2.605(7) and 2.591(7) Å observed.[2] The widening of the C_{Cp}–Si–C_{Cp} angle (116° as compared to 109.5° for a perfect tetrahedral coordination) is due to the steric bulk of the Cp* groups. The Cp* moieties are in van der Waals contact with those on the other silicon centre as well as with the methyl groups on the silicon and indium atoms (for details see Fig. 1). This provides a tight organic wrapping of the inorganic core of the molecule.

This rigid structure of **2** is not retained in solution as is shown by the NMR spectra where conformational changes and sigmatropic rearrangements of the Cp* substituents are observed. In the room temperature ^{1}H NMR spectrum (500 MHz) of **2** in C_6D_6 the resonances for the methyl groups at indium and silicon are detected as singlets at δ 0.45 and 0.82, respectively. For the 60 methyl protons of the Cp* moieties the spectrum shows one broad signal of low intensity at δ 1.17 and a higher intensity broad signal at δ 1.82; only one broad signal at δ 1.66 is detected for the Cp* methyl protons in toluene-d_8 at 100 °C. The room-temperature ^{13}C NMR spectrum shows five signals for the ring carbon atoms of the Cp* groups and four broad signals for the Cp* methyl carbon atoms.[10] Owing to the prochiral character of the silicon centers five signals each would be expected. The observations described above are in accordance with the assumption that the Cp* groups perform rather slow sigmatropic shifts due to the steric interference of the Cp* groups as deduced from the molecular structure. In the ^{29}Si NMR spectrum one resonance at δ 20.6 can be detected for the two equivalent silicon centres. The mass spectrum (CI) of **2** shows no M^+ peak; however the $[M - Cp^*_2SiMe]^+$ ion is observed in low intensity at m/z = 443.

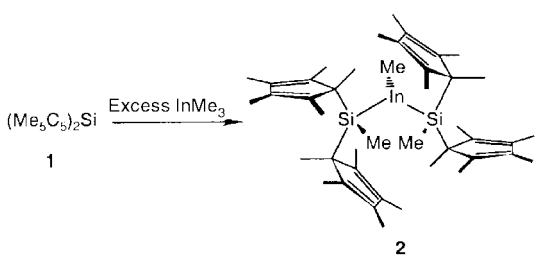

Scheme 1 Reaction of **1** with trimethylindium. *Reagents and conditions*: −90 °C → RT, pentane.

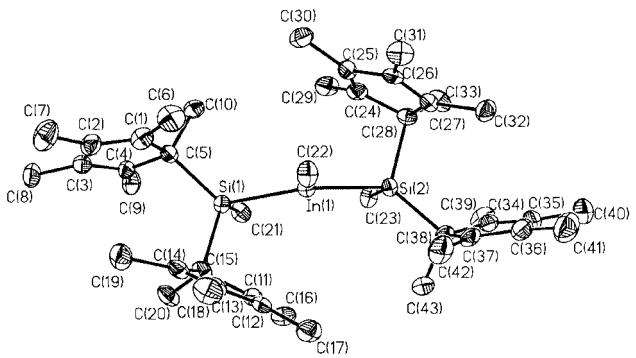

Fig. 1 Molecular structure of **2**. Selected interatomic distances (Å) and angles (°): In(1)–Si(1) 2.642(2), In(1)–Si(2) 2.640(3), In(1)–C(22) 2.172(6), C(10)–C(29) 3.7428(115), C(17)–C(42) 3.8451(119), C(22)–C(30) 3.9836(115), C(16)–C(21) 3.43, C(22)–In–(1)–Si(2) 120.40(18), C(22)–In(1)–Si(1) 120.87(18), Si(2)–In(1)–Si(1) 118.73(7), C(15)–Si(1)–C(5) 116.7(3), C(38)–Si(2)–C(28) 116.4(3).

DOI: 10.1039/b009839f

The thermal stability of **2** in solution and in the gas phase is limited. Thermal decomposition is observed to result in the formation of Cp*In. Evidence for this process can be found in the ^{1}H NMR spectrum of **2** at 100 °C which in addition to the aforementioned resonances shows a signal at δ 2.01 for the methyl groups of Cp*In[11] which grows on prolonged heating. No further defined decomposition products can be identified. As far as the stability of **2** in the gas phase is concerned the CI mass spectrum of **2** is very instructive. Here a very strong signal (rel. int. 94%) for the $[Cp^*In]^+$ ion is observed. This can also be explained as the result of thermal decomposition of **2** in the spectrometer. The thermolability of silyl indium compounds has been previously described.[4]

Concerning the mechanistic aspects of the formation of **2** we assume that the reaction is started by a nucleophilic attack of **1** on the Lewis acidic indium centre *via* the silicon lone pair. This attack is followed by a migration of one methyl group from indium to silicon accompanied by a rearrangement of the Cp* moieties from $\eta^{2/3}$ to η^1 thus forming an intermediate monosilyl substituted indium compound. This intermediate is again attacked by a silylene molecule in the way described above leading to the final product. The formation of **2** is one of the very few examples for the insertion of a silylene into a metal–carbon bond.[12]

Notes and references

† To a solution of **1** (298 mg, 1.0 mmol) in pentane (20 ml) was added a solution of $InMe_3$ in pentane (2.2 molar, 1.5 ml) at −100 °C. On warming to room temperature the solution changed to a light yellow. After 2 h all volatiles were removed *in vaco* to yield **2** (388 mg) as a yellow solid that can be recrystallized from pentane. Yield (after recrystallization): 302 mg (0.4 mmol, 80%). ^{1}H NMR (C_6D_6): 0.45 (s, 3 H, InMe), 0.82 (s, 6 H, SiMe), 1.17, 1.82 (br, 60 H, C_5Me_5). ^{1}H NMR (toluene-d_8, 100 °C): 0.38 (s, 3 H, InMe), 0.69 (s, 6 H, SiMe), 1.66 (brs, 60 H, C_5Me_5), 2.01 (s, Cp*In). ^{13}C NMR (C_6D_6): 10.32 (SiMe), 10.46 (InMe), 11.71, 12.97, 13.20, 18.63 (br, $C_5\mathit{Me}_5$), 57.66 (br, allyl-C_5Me_5), 134.15, 134.71, 140.68, 141.90 (br, vinyl-C_5Me_5). ^{29}Si NMR (C_6D_6): 20.6. MS (CI, NH_3: 137 (100%) $Me_5C_5H_2^+$, 251 (94) $Me_5C_5In^+$, 443 (2) $(Me_5C_5)_2SiInMe_2^+$. $C_{43}H_{69}InSi_2$, M_r = 757.00 g mol^{-1}; calc.: C 68.23, H 9.19; found: C 68.10, H 9.18%.

‡ *Crystal data for* **2**: $C_{43}H_{69}InSi_2$; M = 756.98; T = 173(2) K; λ(Mo-Kα) = 0.71073 Å; triclinic, $P\bar{1}$; a = 10.808(7), b = 12.425(9), c = 16.592(11) Å, α = 71.99(5)°, β = 77.40(6)°, γ = 81.18(6)°; V = 2059(2) Å^3; Z = 2; D_c = 1.221 Mg m^{-3}; μ = 0.659 mm^{-1}; reflections collected/unique: 7680/7249 [R(int) = 0.1046]; final R indices [$I > 2\sigma(I)$]: R_1 = 0.0614, wR_2 = 0.1462 [5534]; R indices (all data): R_1 = 0.0903, wR_2 = 0.1628. Data collected on a Siemens P2(1) diffractometer. CCDC 154849. See http://www.rsc.org/suppdata/cc/b0/b009839f/ for crystallographic data in .cif or other electronic format.

1 H. Bürger and U. Götze, *Angew. Chem., Int. Ed. Engl.*, 1969, **8**, 140.
2 A. M. Arif, A. H. Cowley, T. M. Elkins and R. A. Jones, *J. Chem. Soc., Chem. Commun.*, 1986, 1776.
3 N. Wiberg, K. Amelunxen, H. W. Lerner, H. Nöth, J. Knizek and I. Krossing, *Z. Naturforsch. B: Chem. Sci.*, 1998, **53**, 333.
4 R. Wochele, W. Schwarz, K. W. Klinkhammer, K. Locke and J. Weidlein, *Z. Anorg. Allg. Chem.*, 2000, **626**, 1963.
5 N. Wiberg, K. Amelunxen, H. Nöth, M. Schmidt and H. Schwenk, *Angew. Chem., Int. Ed. Engl.*, 1996, **35**, 65.
6 N. Wiberg, T. Blank, A. Purath, G. Stösser and H. Schnöckel, *Angew. Chem., Int. Ed. Engl.*, 1999, **38**, 2563.
7 N. Wiberg, T. Blank, H. Nöth and W. Ponikwar, *Angew. Chem.*, 1999, **111**, 887.
8 P. Jutzi, D. Kanne and C. Krüger, *Angew. Chem.*, 1986, **98**, 163.
9 U. Holtmann, P. Jutzi, T. Kühler, B. Neumann and H.-G. Stammler, *Organometallics*, 1999, **18**, 5531.
10 The static character of the Cp* ring in the ^{13}C NMR spectrum in contrast to the dynamic character in the ^{1}H NMR spectrum is caused by the different chemical shift range.
11 O. T. Beachley Jr., R. Blom, M. R. Churchill, K. Faegri Jr., J. C. Fettinger, J. C. Pazik and L. Victoriano, *Organometallics*, 1989, **8**, 346.
12 (*a*) N. Metzler and M. Denk, *Chem. Commun.*, 1996, 2657; (*b*) C. Drost, B. Gehrhus, P. B. Hitchcock and M. F. Lappert, *Chem. Commun.*, 1997, 1845; (*c*) J. Belzner, V. Ronneberger, D. Schär, C. Brönnecke, R. Herbst-Irmer and M. Noltemeyer, *J. Organomet. Chem.*, 1999, **577**, 330.

ChemComm

Sol–gel synthesis of an array of C_{70} single crystal nanowires in a porous alumina template

Huaqiang Cao,[a] Zheng Xu,*[a] Xianwen Wei,[a] Xiang Ma[b] and Ziling Xue[c]

[a] *Coordination Chemistry Institute, State Key Laboratory of Coordination Chemistry, Center of Nanometer Science and Technology, Nanjing University, 210093, China. E-mail: profzxu@jlonline.com*
[b] *Center for Materials Analysis, Nanjing University, 210093, China*
[c] *Department of Chemistry, University of Tennessee, Knoxville, TN 37996-1600, USA*

Received (in Cambridge, UK) 24th January 2001, Accepted 12th February 2001
First published as an Advance Article on the web 1st March 2001

An ordered array of C_{70} single crystal nanowires was prepared by a sol–gel template method which is composed of three steps: generation of the C_{70} sol; deposition of C_{70} sol particles in the pores of the alumina membrane; and annealing of the resulting C_{70} composite in an argon atmosphere.

Fullerene-C_{70} chemistry[1] has been established since first detection of these species by Kroto *et al.*[2] and the subsequent macroscopic preparation by Krätschmer *et al.*[3] Photophysical properties,[4–7] conductivity,[8] photoconductivity[9] and optical limiting performance[10,11] of C_{70} have been reported frequently in the literature. Recently, C_{70} self-organization into short- and long-range order[12,13] has aroused great interest among scientists, but there has been little work on C_{70} nanostructures such as nanowires and nanotubules. As we all know, one-dimensional (1D) structures with nanometer diameters, such as nanotubes and nanowires, have a great potential for the testing and understanding of fundamental concepts about the roles of dimensionality and size in, for example, optical, electrical and mechanical properties and for applications ranging from probe microscopy tips to interconnections in nanoelectronics.[14] But developing the techniques for synthesizing and characterizing nanostructures is one of the grand challenges to chemists.

Here, we report the first generation of an ordered array of C_{70} single crystal nanowires obtained by a sol–gel template method. This is a key step for the construction of molecular devices.

A simple method to generate an aqueous colloidal solution has recently been developed by our group:[11] 8.0 mg C_{70} powder (99% purity), 100 mg Al–Ni alloy (excess) and 400 mg solid NaOH pellets were put in a bottle, which was evacuated and filled with argon; then 10 ml THF (distilled from sodium–benzophenone in a Schlenk system) were added with stirring. With the exception of C_{70}, which is slightly soluble in THF, the other starting materials do not dissolve. NaOH solid pellets dissolve with accompanying effervescence after the addition of 3 ml of deoxygenated water. The colour of the THF layer turned from slightly yellow to red–orange. After 1 h the red–orange THF solution was separated from the colourless aqueous caustic NaOH solution. Then, the solution of C_{70}^- in THF was added dropwise to 50 ml of undegassed distilled water. The THF was removed under reduced pressure to give an aqueous colloidal solution of containing 0.45 mg l^{-1} C_{70} (0.54 mM).[11]

An alumina template (Anodise®) made by Whatman Inc. (SEM images revealed a pore diameter ranges of 100–300 nm) was immersed in the C_{70} sol for 4–5 h under *ca.* 1.3 atm at ambient temperature. The template was then taken out from the C_{70} sol and dried at *ca.* 75 °C for 30 min. The deposits on both faces of the alumina membrane were removed by polishing with alumina powder, and annealed under argon atmosphere with the temperature ramping up to 500 °C for 5 h, before ramping back down to room temperature.

Fig. 1 shows scanning electron microscope (SEM)† images of the sample which was treated with a 6 M NaOH solution for *ca.* 3 min in order to dissolve the top layer of alumina. Without tetrabutylammonium hydroxide (TBAH) as catalyst, C_{70} cannot form C_{70} fullerol; also, without a reducing agent, C_{70} cannot form C_{70} anions in aqueous caustic solution. It can be seen that the C_{70} nanowires are well ordered and are perpendicular to the alumina template.

Fig. 2(a) is a transmission electron microscopy (TEM)† image of selected C_{70} nanowires. The diameter varies from 100 to 300 nm, which corresponds to the pore diameter of the alumina template. Bright field TEM images revealed that the

Fig. 1 Scanning electron micrograph of an array of C_{70} nanowires embeded in the alumina template matrix: (a) general cross-section view; (b) and (c) part view, magnifying power ×4000 and ×12 000, respectively.

DOI: 10.1039/b100863n

(a)

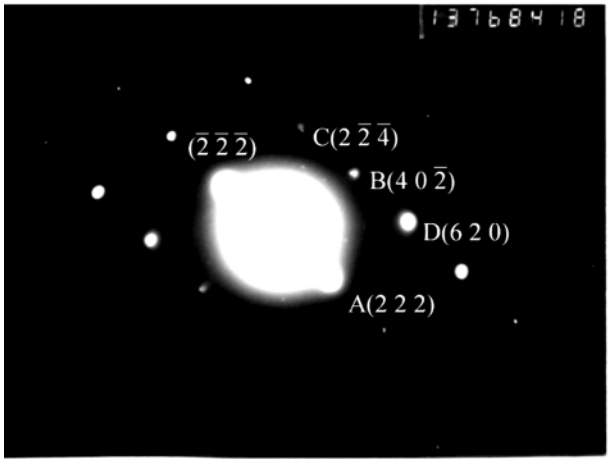

(b)

Fig. 2 (a) Transmission electron micrograph (TEM) images of a piece of *ca.* 150 nm diameter C_{70} nanowire after removing the alumina matrix, scale bar is 100 nm; (b) fcc [1$\bar{3}$2] zone axis electron diffraction pattern of corresponding C_{70} nanowires.

C_{70} nanowires were stable under the 200 keV electron beam. Fig. 2(b) is an electron diffraction pattern of the selected C_{70} nanowires. The ratio of $R_A^2:R_B^2:R_C^2:R_D^2 \approx 12:20:24:40$, R corresponding to the distance between the reflection spot and the reflection pattern center. These results suggest that the C_{70} crystal is of cubic structure, whose reflection spots may be indexed as A(222), B(40$\bar{2}$), C(2$\bar{2}\bar{4}$) and D(620), and the zone axis is [1$\bar{3}$2]. The sharp [1$\bar{3}$2] zone axis pattern contains D(620) reflections at *ca*. 44°, B(40$\bar{2}$) reflections at *ca*. 78°, and C(2$\bar{2}\bar{4}$) reflections at *ca*. 120° from A(222). Hence, the C_{70} single crystal samples prepared by this method, similar to the samples prepared by sublimation, are face-centered cubic, and thermal annealing is in favor of the fcc phase forming. This result is in accordance with the observation by Heiney and coworkers,[15] *i.e.* that the fcc phase is the equilibrium state of pure C_{70} above 300 K.

In conclusion, the sol–gel template method is a convenient and powerful method for generation the array of single-crystal C_{70} nanowires. The morphology and structure of the C_{70} nanowires array were studied by SEM and TEM. The C_{70} nanowires are single crystals with fcc structure and the zone axis is along the [1$\bar{3}$2] direction. The morphology of the array of C_{70} nanowires is brush-like and well ordered and is stable under a 200 keV electron beam.

We gratefully acknowledge the National Natural Science Foundation of China for the key project (No. 29823001), the Natural Science Foundation of Jiangsu Province for the key project (No. BK99207) and U.S. National Science Foundation for a Camille Dreyfus Teacher–Scholar Award.

Notes and references

† SEM images were obtained using a Hitachi, X650/EDAX, PV9100 scanning electron microanalysis instrument. TEM images were obtained using a Transmission Electron Microscope JEM-200CX, JEOL. The accelerating voltage of the electron beam was 200 keV.

1 C. Thilgen, A. Herrmann and F. Diederich, *Angew. Chem., Int. Ed. Engl.*, 1997, **36**, 2269 and references therein.
2 H. W. Kroto, J. R. Health, S. C. O'Brien, R. F. Curl and R. E. Smalley, *Nature*, 1985, **318**, 162.
3 W. Krätschmer, L. D. Lamb, K. Fostiropoulos and D. R. Huffman, *Nature*,1990, **347**, 354.
4 J. W. Arbogast and C. S. Foote, *J. Am. Chem. Soc.*, 1991, **113**, 8886.
5 J. Catalán and J. Elguero, *J. Am. Chem. Soc.*, 1993, **115**, 9249.
6 M. Lee, O.-K. Song, J.-C. Seo, Y. D. Suh, S. M. Jin and S. K. Kim, *Chem. Phys. Lett.*, 1992, **196**, 325.
7 S. P. Sibley, S. M. Argentine and A. H. Francis, *Chem. Phys. Lett.*, 1992, **188**, 187.
8 R. C. Haddon, A. F. Hebard, M. J. Rosseinsky, D. W. Murphy, S. J. Duclos, K. B. Lyons, B. Miller, J. M. Rosamilia, R. M. Fleming, A. R. Kortan, S. H. Glarum, A. V. Makhija, A. J. Muller, R. H. Eick, S. M. Zahurak, R. Tycko, G. Dabbagh and F. A. Thiel, *Nature*, 1991, **350**, 320.
9 Y. Wang, *Nature*, 1992, **356**, 585.
10 L. W. Tuff and A. Kost, *Nature*, 1992, **356**, 225.
11 X. W. Wei, Z. Y. Suo, K.-Y. Zhou, Z. Xu, W. J. Zhang, P. Wang, H. Y. Shen and X. Li, *J. Chem. Soc., Perkin Trans. 2*, 1999, 121.
12 D. Arčon, R. Blinc, P. Cevc, G. Chouteau and A.-L. Barra, *Phys. Rev. B*, 1997, **56**, 10786.
13 M. M. Olmstead, L. Hao and A. L. Balch, *J. Organomet. Chem.*, 1999, **578**, 85.
14 A. P. Alivisatos, *Science*, 1996, **271**, 933; B. I. Yakobson and R. E. Smalley, *Am. Sci.*, 1997, **85**, 324.
15 G. B. M. Vaughan, P. A. Heiney, J. E. Fischer, D. E. Luzzi, D. A. Ricketts-Foot, A. R. McGhie, Y.-W. Hui, A. L. Smith, D. E. Cox, W. J. Romanow, B. H. Allen, N. Coustel, J. P. McCauley, Jr. and A. B. Smith III, *Science*, 1991, **254**, 1350.

Solid-state photolysis of sterically congested *cis*-1,2-dibenzoylalkenes: isolation and characterization of vinylketenes

Mithu Chanda, Dwijendralal Maji and Saswati Lahiri*

Department of Organic Chemistry, Indian Association for the Cultivation of Science, Calcutta 700032, India. E-mail: ocsl@mahendra.iacs.res.in

Received (in Cambridge, UK) 8th November 2000, Accepted 12th February 2001
First published as an Advance Article on the web 28th February 2001

Hitherto non-isolable vinylketenes from the solid state photolysis of *cis*-1,2-dibenzoylalkene compounds have been isolated and characterized and their stabilities were found to be enhanced with the extent of steric congestion in the molecules.

Formation of vinylketenes from the photoreactions of *cis*-1,2-dibenzoylethylenes was first speculated in 1962[1] (Scheme 1). Its intermediacy was confirmed later from a strong peak for $\nu_{C=C=O}$ at 2103 cm^{-1} in the IR spectrum of the photolyzed reaction mixture.[2] Such photoinduced intramolecular phenyl migration from carbon to the proximate oxygen is a general reaction route for *cis*-1,2-dibenzoylalkene chromophore and has been observed in tetrabenzoylethylene[3] as well as in other *cis*-1,2-dibenzoylalkene derivatives.[4,5] In unsymmetrical derivatives, such migrations have been found to take place from the benzoyl group attached to the more crowded olefinic carbon atom.[1,4a,b,5] However, in our work with 5,6-dibenzoyl-4-methoxybicyclo[2.2.2]oct-5-en-2-one (**1**) such migration was observed to occur from both the benzoyl groups in solution, whereas in solid state, only the expected vinylketene (**1K**) was identified.[6] In all of these cases the intermediate vinylketenes have so far been neither isolated nor characterized fully because of their instability. The vinylketene **1K** was found to be fairly stable in cyclohexane solution at 20 °C. It took almost 48 h for the total disappearance of the ketene band at 2100 cm^{-1}. Such an observation encouraged us to take up the present project to enhance the steric congestion in such molecules and try to isolate the intermediate vinylketenes and characterize them.

In this attempt, the residue from the solid-state photoreaction of **1** was carefully chromatographed on a silica gel column.[7] Ketene **1K** as a pale-yellow solid (25%) and the starting compound **1** (70%) were separated from this reaction mixture. The spectral data of **1K** agreed well with the proposed structure. Since all attempts for recrystallization led to its decomposition, elemental analysis for **1K** could not be performed. However, its structure was finally confirmed by trapping it with MeOH which gave 4-methoxy-6-(phenoxyphenylmethylene)-5-*exo*-carbomethoxybicyclo[2.2.2]octan-2-one (**1E**).

To increase the persistency of such vinylketenes, we decided to enhance steric congestion in the molecule and hence prepared compound **2** with a methyl group at the bridgehead. Solid-state photolysis of **2** and chromatography of the photolyzed residue gave white crystals of the corresponding vinylketene **2K** (27%) whose analytical and spectral data were in agreement with the proposed structure. Further elution gave back unreacted starting material **2** (68%). The ketene **2K** was stable at rt and could be trapped with MeOH only at elevated temperature (~40 °C) to give 4-methyl-6-(phenoxyphenylmethylene)-5-*exo*-carbomethoxybicyclo[2.2.2]octan-2-one (**2E**) as the major product along with its 5-*endo* epimer (**2E′**) in minor yield.

The preference of photo-phenyl migration in *cis*-1,2-dibenzoylalkene chromophore from the more crowded olefinic carbon atom in the solid state, was further confirmed from the solid state photoreaction of compound **3**. Chromatography of the reaction mixture yielded the vinylketene **3K** (35%), unreacted starting material **3** (37%) and an unidentified gummy material (25%). The ketene **3K** was found to be less stable than its isomer **2K** and on stirring with MeOH at rt it yielded 1-methyl-5-(phenoxyphenylmethylene)-6-*exo*-carbomethoxybicyclo[2.2.2]octan-2-one (**3E**).

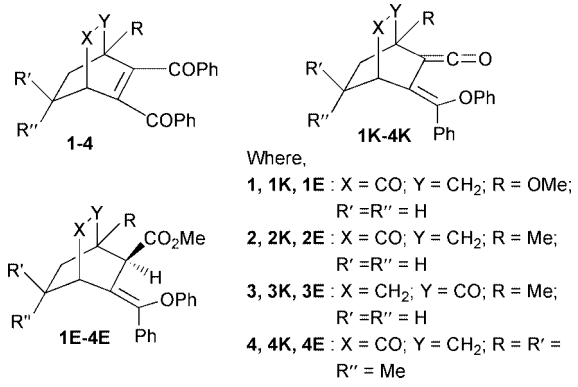

Addition of nucleophiles to ketenes is thought to occur in the plane of the ketene and the approach occurs from the least sterically hindered site of the ketene.[8,9] Increasing the steric congestion in a molecule thus could remarkably enhance persistency of vinylketenes and retard the nucleophilic addition to it. This was further confirmed from the solid state photolysis of 5,6-dibenzoyl-4,7,7-trimethylbicyclo[2.2.2]oct-5-en-2-one (**4**), which gave white crystals of the vinylketene **4K** (28%) along with the unreacted starting material (65%). Even under atmospheric conditions, solid **4K** could be stored without decomposition for a long time and its cyclohexane solution was stable at rt for more than 5 days. Addition of MeOH to **4K** took place only under refluxing conditions to yield 4,7,7-trimethyl-6-(phenoxyphenylmethylene)-5-*exo*-carbomethoxybicyclo-[2.2.2]octan-2-one (**4E**).

The ketene bands of **1K**–**4K** appeared near 2100 cm^{-1} in the IR spectrum. The ^{1}H-NMR spectra of these compounds were very similar to their parent molecules but their ^{13}C-NMR data were found to be much more useful (Table 1). In ^{1}H-NMR, the *endo*-protons around δ 3 ppm appeared as doublets for **1E, 2E** and **4E** and as a singlet for **3E** (Table 1).

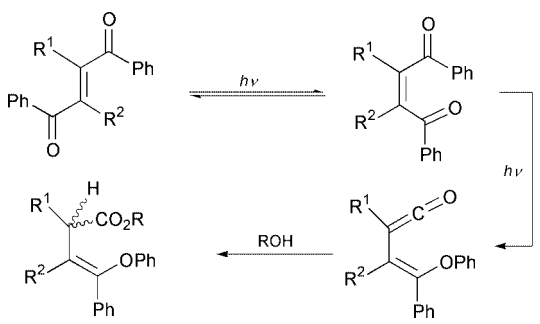

Scheme 1

DOI: 10.1039/b009013l

Table 1 Characteristic data for **1K**–**4K** and **1E**–**4E**

Starting compound[a]	Products[b] (mp/°C)	Yield (%)	IR/cm^{-1} $\nu_{C=C=O}$	^{1}H-NMR/ppm $\delta_{Bridgehead}$	$\delta_{Bridgehead}$	^{13}C-NMR/ppm δ_{C+O}	δ_{+C+O}	δ_{C+C+O}	$\delta_{+C\text{-}OPh}$
1	**1K**[c] (157)	85[d]	2103	3.6 (m)		207.0	199.4	34.9	155.7
2	**2K** (187)	84[d]	2100	3.65 (t, *J* 3 Hz)		210.5	202.3	34.2	155.7
3	**3K** (122)	55[d]	2092	3.38 (t, *J* 2.4Hz)		210.0	200.2	40.8	155.8
4	**4K** (125)	82[d]	2100	3.21 (s)		210.3	208.9	34.4	155.7
1K	**1E** (41)	93[e]		3.45 (m)	3.95 (d, *J* 2 Hz)				
2K	**2E** (125)	59[e]		3.46 (t, *J* 3 Hz)	3.46 (t, *J* 1.5 Hz)				
	2E′(132)	28[e]		3.44 (t, *J* 3 Hz)	3.52 (d, *J* 1.5 Hz)				
3K	**3E** (158)	89[e]		3.3 (m)	3.6 (s)				
4K	**4E** (156)	90[e]		3.06 (s)	3.26 (d, *J* 1.5 Hz)				

[a] Compounds **1**–**4**, for the first time were prepared following reported procedures.[5,10] [b] Elemental analyses have been performed for all compounds excepting **1K**. [c] Unstable to prepare analytical sample. [d] Based on recovered starting materials. [e] Isolated yields.

In summary, we report here the first isolation and characterization of the intermediate vinylketene formed by photo-phenyl migration in *cis*-dibenzoylalkenes. In the solid state, the migration always occurred from the more crowded center to the less crowded one. By controlling the degree of steric congestion in the molecule, the stability of these vinylketenes can remarkably be enhanced.

Financial support from DST, India is gratefully acknowledged.

Notes and references

1 (*a*) G. W. Griffin and E. J. O'Connell, *J. Am. Chem. Soc.*, 1962, **84**, 4148; (*b*) H. E. Zimmerman, H. G. C. Dürr, R. G. Lewis and S. Bram, *J. Am. Chem. Soc.*, 1962, **84**, 4149.

2 A. Padwa, D. Crumrine and R. A. Shubber, *J. Am. Chem. Soc.*, 1966, **88**, 3064.

3 M. B. Rubin and W. W. Sander, *Tetrahedron Lett.*, 1987, **28**, 5137.

4 (*a*) S. Lahiri, V. Dabral, S. M. S. Chauhan, E. Chakachery, C. V. Kumar, J. C. Scaiano and M. V. George, *J. Org. Chem.*, 1980, **45**, 3782; (*b*) B. A. R. C. Murty, C. V. Kumar, V. Dabral, P. K. Das and M. V. George, *J. Org. Chem.*, 1984, **49**, 4165; (*c*) B. B. Lohray, C. V. Kumar, P. K. Das and M. V. George, *J. Org. Chem.*, 1984, **49**, 4647; (*d*) R. Barik, K. Bhattacharya, P. K. Das and M. V. George, *J. Org. Chem.*, 1986, **51**, 3420.

5 R. Singh, A. Sinha and S. Lahiri, *J. Chem. Res. (S)*, 1992, 372.

6 D. Maji, R. Singh, G. Mostafa, S. Roy and S. Lahiri, *J. Org. Chem.*, 1996, **61**, 5165.

7 In a typical solid state photoreaction, a suspension of the compound (0.5–1 g) in distilled water (150 ml) was irradiated with stirring using a Hanovia medium pressure 450 W lamp and a pyrex filter for ~35 h. The suspension was then extracted with CH_2Cl_2 and the residue obtained after removal of solvent was chromatographed on a silica gel column (60–120 mesh). The ketene was eluted with a mixture of ethyl acetate (5–10%) in petroleum ether (bp 60–80 °C).

8 T. T. Tidwell, *Acc. Chem. Res.*, 1990, **23**, 273.

9 C. O. Kappe, R. A. Evans, C. H. L. Kennard and C. Wentrup, *J. Am. Chem. Soc.*, 1991, **113**, 4234.

10 S. Lahiri and R. Singh, *Indian J. Chem.*, 1980, **28B**, 860.

ChemComm

Syntheses and luminescence behaviour of dinuclear copper(I) selenolate and tellurolate complexes. X-Ray crystal structures of $[Cu_2(\mu\text{-dppm})_2(\mu\text{-SePh})]BF_4$ and $[Cu_2(\mu\text{-dppm})_2(\mu\text{-TePh})]BF_4$

Vivian Wing-Wah Yam,* Chi-Ho Lam and Kung-Kai Cheung

Department of Chemistry, The University of Hong Kong, Pokfulam Road, Hong Kong, P.R. China
E-mail: wwyam@hku.hk

Received (in Cambridge, UK) 4th December 2000, Accepted 8th February 2001
First published as an Advance Article on the web 1st March 2001

A series of novel dinuclear copper(I) μ-chalcogenolate complexes is synthesized and their photophysics studied; the X-ray crystal structures of $[Cu_2(\mu\text{-dppm})_2(\mu\text{-SePh})]BF_4$ and $[Cu_2(\mu\text{-dppm})_2(\mu\text{-TePh})]BF_4$ are reported.

Increasing interest in the investigation of copper(I) complexes with chalcogenide ligands has emerged.[1,2] The closely related class of ligands, the chalcogenolates, has also attracted enormous attention owing to their importance in biological systems and their propensity to form metal complexes and clusters of various bonding modes and structural motifs.[3] In view of this and the ready functionalization of the chalcogenolate ligands *via* a change in the substituent on the heteroatom to effect steric and electronic control of the ligating ability, it would be of interest to synthesize and study the related copper(I) chalcogenolate complexes. Compared with copper(I) thiolates, reports on selenolate and tellurolate complexes are relatively rare.[4] Moreover, the luminescence properties of copper(I) chalcogenolate complexes are almost unexplored[5] and represent a challenging area of research. Here we report the syntheses and photophysics of a new class of dinuclear copper(I) chalcogenolates and the X-ray crystal structures of $[Cu_2(\mu\text{-dppm})_2(\mu\text{-SePh})]BF_4$ and $[Cu_2(\mu\text{-dppm})_2(\mu\text{-TePh})]BF_4$.

Reaction of $[Cu_2(\mu\text{-dppm})_2(MeCN)_2](BF_4)_2$ with the corresponding sodium chalcogenolate (prepared *in situ* from the diaryldiselenide or diarylditelluride and $NaBH_4$) in a molar ratio of 1:1 in THF and under anaerobic and anhydrous conditions afforded dinuclear copper(I) μ-chalcogenolate complexes, $[Cu_2(\mu\text{-dppm})_2(\mu\text{-EAr})]BF_4$ (EAr = SePh **1**, SeC_6H_4Cl-*p* **2**, TePh **3**, TeC_6H_4Me-*p* **4**) in *ca*. 19–62% yield. Single crystals of **1** and **3** suitable for diffraction studies were grown by layering of diethyl ether on concentrated solutions of the complexes in acetone. All of the newly synthesized dinuclear copper(I) complexes gave satisfactory elemental analyses, and have been characterized by ^1H and ^{31}P NMR spectroscopy, and positive FAB mass spectrometry.† The X-ray crystal structures of complexes **1** and **3** have also been determined.‡

Fig. 1 shows the perspective drawing of the complex cation of **3**. The two copper atoms of the dinuclear complexes are held in close proximity by three bridging ligands, two dppm ligands acting through the P atoms and one chalcogenolate ligand acting through the Se/Te atom. The Se/Te atom asymmetrically bridges the two copper atoms, with the Cu(2)–Se/Te distances [**1**, Cu(2)–Se(1) 2.485 Å; **3**, Cu(2)–Te(1) 2.608 Å] longer than those of Cu(1)–Se/Te [**1**, Cu(1)–Se(1) 2.371 Å; **3**, Cu(2)–Te(1) 2.532 Å]. In addition, a short non-bonded contact of *ca*. 2.4 Å is observed between the Cu(2) atom of the complex cation and an oxygen atom of the acetone solvent molecule, with a tendency to afford a distorted trigonal bipyramidal arrangement about Cu(2) [**1**, Cu(1)···Cu(2)···O(1) 150.5(3)° with Cu(2) deviated 0.43 Å towards O(1); **2**, Cu(1)···Cu(2)···O(1) 153.7(3)° with Cu(2) deviated 0.39 Å towards O(1)], while Cu(1) assumes a distorted tetrahedral arrangement. It is noted that the phenyl ring of the chalcogenolate is bent towards one side of the Cu_2E triangle (E = Se, Te) due to the sp^3 hybridization of the Se/Te atom. The Cu···Cu distances in **1** and **3** are in the range 2.723–2.739 Å. They are shorter than the sum of van der Waals radii for copper (2.8 Å)[6] and this may indicate weak metal–metal interactions in the complexes.

The electronic absorption spectra for complexes **1**–**4** in dichloromethane are characterized by absorption shoulders at *ca*. 250 and 260–295 nm (Table 1). Since the electronic absorption spectra were rather featureless, no further attempts were made to unambiguously assign the absorption bands. The emission spectra of the dinuclear complexes **1**–**4** in degassed acetone showed a low energy emission at *ca*. 600–630 nm, with emission energies in the order **4** ≥ **3** > **2** ≥ **1** (Table 1). Complexes **3** and **4** with tellurolate ligands show slightly higher emission energies than those with selenolate ligands **1** and **2**. Such an energy trend appears to depend upon the π-accepting ability of the chalcogenolate ligand, in which the areneselenolate is a better π-acceptor ligand than the arenetellurolate. This suggests that the low energy emission involves an excited state

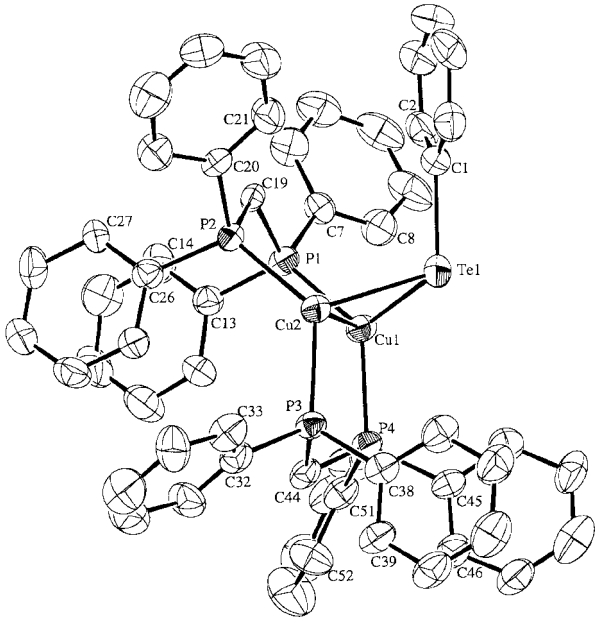

Fig. 1 Perspective drawing of the complex cation of **3** with the atomic numbering scheme. Hydrogen atoms have been omitted for clarity. Thermal ellipsoids are shown at the 40% probability level. Selected bond distances (Å) and bond angles (°) for complex **3**: Cu(1)···Cu(2) 2.723(1), Cu(1)–Te(1) 2.532(1), Cu(2)–Te(1) 2.608(1), Cu(1)–P(1) 2.243(3), Cu(2)–P(2) 2.283(3), Cu(2)–O(1) 2.36(1); Te(1)–Cu(1)–P(1) 116.80(8), Te(1)–Cu(2)–P(2) 112.40(8), Te(1)–Cu(1)–P(4) 112.44(9), Te(1)–Cu(2)–P(3) 111.01(8), P(1)–Cu(1)–P(4) 129.3(1), P(2)–Cu(2)–P(3) 128.46(10), Cu(1)–Te(1)–C(1) 110.7(3), Cu(2)–Te(1)–C(1) 107.1(3). Selected bond distances (Å) and bond angles (°) for complex **1**: Cu(1)···Cu(2) 2.739(2), Cu(1)–Se(1) 2.371(2), Cu(2)–Se(1) 2.485(2), Cu(1)–P(1) 2.241(4), Cu(2)–P(2) 2.296(3), Cu(2)–O(1) 2.39(1); Se(1)–Cu(1)–P(1) 118.3(1), Se(1)–Cu(2)–P(2) 112.91(10), Se(1)–Cu(1)–P(4) 111.1(1), Se(1)–Cu(2)–P(3) 108.9(1), P(1)–Cu(1)–P(4) 129.0(1), P(2)–Cu(2)–P(3) 128.0(1), Cu(1)–Se(1)–C(1) 113.5(3), Cu(2)–Se(1)–C(1) 106.4(3).

DOI: 10.1039/b009676h

Table 1 Photophysical and electrochemical data of complexes **1**–**4**

Complex	Absorption,[a] λ/nm (ε_{max}/ dm^3 mol^{-1} cm^{-1})	Emission[b] Medium (T/K)	Emission[b] λ_{em}/nm (τ_o/μs)	Oxidation,[d,e] $E_{1/2}$ (V *vs.* SCE)
1	286sh (21 850)	Acetone (298)	630 (6.0)[c]	+0.68
		Solid (298)	431, 452 (< 0.1)	
2	266sh (34 290), 296sh (31480)	Acetone (298)	626 (< 0.1)[c]	+0.70
		Solid (298)	440, 468sh (< 0.1)	
3	256sh (42 380)	Acetone (298)	607 (< 0.1)[c]	+0.79
		Solid (298)	439, 464sh (< 0.1)	
4	256sh (40 530)	Acetone (298)	601 (< 0.1)[c]	+0.80
		Solid (298)	438, 463sh (< 0.1)	

[a] In CH_2Cl_2. [b] Excitation wavelength at 350 nm. [c] Excitation wavelength at 370 nm. [d] In MeCN (0.1 M $^nBu_4NPF_6$), glassy carbon electrode, scan rate 100 mV s^{-1}, 298 K. [e] $E_{1/2}$ is taken to be the average of E_{pa} and E_{pc}, where E_{pa} and E_{pc} are the anodic and cathodic peak potentials of the quasi-reversible couple, respectively.

of metal-to-ligand charge transfer (MLCT) [$Cu_2 \rightarrow ER^-$] origin. A related dinuclear copper(I) complex, [Cu_2(μ-dppm)$_2$(μ-O_2CMe)]$^+$,[7] in which the lowest lying excited state was suggested to be MLCT [copper → phosphine/acetate] in character, as supported by molecular orbital calculations, shows a relatively high energy emission at *ca*. 470 nm. However, low energy emissions at *ca*. 600–630 nm are observed for complexes **1**–**4** and the emission energy difference between the dinuclear copper(I) selenolate and tellurolate complexes is relatively small. This, together with the fairly short Cu···Cu contacts (*ca*. 2.7 Å) found in these dinuclear complexes, may be more suggestive of an assignment of the emission as having a metal-centered ds/dp origin. Thus, the low energy emission in the dinuclear copper(I) chalcogenolate complexes is tentatively assigned as derived from an excited state that is predominantly metal-centered ds/dp in origin, mixed with some MLCT [copper → chalcogenolate/phosphine] character.

The cyclic voltammograms of complexes **1**–**4** show quasi-reversible oxidation couples in the range 0.68 to 0.80 V *vs*. SCE (Table 1). A relatively small shift in the potential of the oxidation couples is observed. The oxidation couple is tentatively assigned as a copper(I/II) metal-centered oxidation. No reduction wave was observed even when the potential was scanned to −2.4 V *vs*. SCE. Further oxidation and reduction of the complexes resulted in decomposition, as suggested by the irreversibility of the couples at higher anodic and cathodic potentials.

V. W. W. Y. acknowledges financial support from the Research Grants Council and The University of Hong Kong. The receipt of a Croucher Senior Research Fellowship by V. W. W. Y. from the Croucher Foundation is gratefully acknowledged. C. H. L. acknowledges the receipt of a postgraduate studentship, administered by The University of Hong Kong.

Notes and references

† *Selected spectroscopic data* for **1**. ^{1}H NMR (300 MHz, acetone-d_6, 298 K): δ 3.6 (m, 4H, CH_2), 6.6–7.6 (m, 45H, Ph); ^{31}P{^{1}H} NMR (202 MHz, acetone-d_6, 298 K): δ −6.3. Positive FAB-MS: *m/z* 1052 [M − BF_4]$^+$. Calc. for $Cu_2C_{56}H_{49}P_4SeBF_4$: C, 59.21; H, 4.63; Found: C, 59.13; H, 4.75%. For **2**. ^{1}H NMR (300 MHz, acetone-d_6, 298 K): δ 3.6 (m, 4H, CH_2), 6.7–7.6 (m, 44H, Ph); ^{31}P{^{1}H} NMR (202 MHz, acetone-d_6, 298 K): δ −5.9. Positive FAB-MS: *m/z* 1088 [M − BF_4]$^+$. Calc. for $Cu_2C_{56}H_{48}P_4SeClBF_4{\cdot}CH_2Cl_2$: C, 54.42; H, 4.01; Found: C, 54.67; H, 3.96%. For **3**: ^{1}H NMR (300 MHz, CD_2Cl_2, 298 K): δ 3.5 (m, 4H, CH_2), 6.5–7.7 (m, 45H, Ph); ^{31}P{^{1}H} NMR (202 MHz, acetone-d_6, 298 K): δ −6.9. Positive FAB-MS: *m/z* 1102 [M − BF_4]$^+$. Calc. for $Cu_2C_{56}H_{49}P_4TeBF_4{\cdot}CH_2Cl_2$: C, 53.81; H, 4.04; Found: C, 53.81; H, 3.97%. For **4**. ^{1}H NMR (300 MHz, acetone-d_6, 298 K): δ 2.1 (s, 3H, CH_3), 3.5 (m, 4H, CH_2), 6.5–7.7 (m, 44H, Ph); ^{31}P{^{1}H} NMR (202 MHz, acetone-d_6, 298 K): δ −6.8. Positive FAB-MS: *m/z* 1116 [M − BF_4]$^+$. Calc. for $Cu_2C_{57}H_{51}P_4TeBF_4{\cdot}CH_2Cl_2$: C, 54.16; H, 4.15. Found: C, 54.36; H, 4.05%.

‡ *Crystal data* for [Cu_2(μ-dppm)$_2$(μ-SePh)]BF_4 **1**: [$(C_{56}H_{49}P_4SeCu_2)^+$ $BF_4^-{\cdot}(CH_3)_2CO{\cdot}(C_2H_5)_2O$], M_r = 1270.96, orthorhombic, space group $P2_12_12_1$ (no. 19), a = 13.539(3), b = 21.137(4), c = 21.223(4) Å, V = 6073(2) Å^3, Z = 4, D_c = 1.390 g cm^{-3}, μ(Mo-Kα) = 14.59 cm^{-1}, F(000) = 2608, T = 301 K, using Mo-Kα radiation (λ = 0.71073 Å). 5305 unique reflections were measured, of which 3923 reflections with $I > 3\sigma(I)$ were used in the structural analysis. Convergence for 430 variable parameters by least-squares refinement on F with $w = 4F_o^2/\sigma^2(F_o^2)$, where $\sigma^2(F_o^2) = [\sigma^2(I) + (0.024F_o^2)^2]$ for 3923 reflections with $I > 3\sigma(I)$ was reached at R = 0.054 and wR = 0.071 with a goodness-of-fit of 2.98. For [Cu_2(μ-dppm)$_2$(μ-TePh)]BF_4 **3**: [$(C_{56}H_{49}P_4TeCu_2)^+BF_4^-{\cdot}(CH_3)_2CO{\cdot}(CH_3CH_2)_2O$], M = 1319.60, orthorhombic, space group $P2_12_12_1$ (no. 19), a = 13.546(2), b = 21.094(3), c = 21.274(3) Å, V = 6078(1) Å^3, Z = 4, D_c = 1.442 g cm^{-3}, μ(Mo-Kα) = 13.29 cm^{-1}, F(000) = 2680, T = 301 K, using Mo-Kα radiation (λ = 0.71073 Å). 6114 unique reflections were obtained from a total of 32593 measured reflections (R_{int} = 0.056). 4642 reflections with $I > 3\sigma(I)$ were used in the structural analysis. Convergence for 624 variable parameters by least-squares refinement on F with $w = 4F_o^2/\sigma^2(F_o^2)$, where $\sigma^2(F_o^2) = [\sigma^2(I) + (0.034F_o^2)^2]$ for 4742 reflections with $I > 3\sigma(I)$ was reached at R = 0.055 and wR = 0.072 with a goodness-of-fit of 2.09. CCDC 155745 and 155746. See http://www.rsc.org/suppdata/cc/b0/b009676h/ for crystallographic files in .cif or other electronic format.

1 D. Fenske, T. Langetepe, M. M. Kappes, O. Hampe and P. Weis, *Angew. Chem., Int. Ed.*, 2000, **39**, 1857; D. Fenske and N. Y. Zhu, *J. Cluster Sci.*, 2000, **11**, 135; V. Saltas, C. A. Papageorgopoulos, D. C. Papageorgopoulos, D. Tonti, C. Pettenkofer and W. Jaegermann, *Surf. Rev. Lett.*, 2000, **7**, 235; M. F. Beck, A. Swartzlander, R. Matson, J. Keane and R. Noufi, *Sol. Energy Mater. Sol. Cells*, 2000, **64**, 135; M. Kemell, H. Saloniemi, M. Ritala and M. Leskela, *Electrochim. Acta*, 2000, **45**, 3737; V. M. Glazov, A. S. Pashinkin and V. A. Fedorov, *Inorg. Mater.*, 2000, **36**, 641; Z. H. Han, Y. P. Li, H. Q. Zhao, S. H. Yu, X. L. Yin and Y. T. Qian, *Mater. Lett.*, 2000, **44**, 366; J. F. Corrigan and D. Fenske, *Angew. Chem., Int. Ed.*, 2000, **36**, 1981.

2 V. W. W. Yam, K. K. W. Lo and K. K. Cheung, *Inorg. Chem.*, 1996, **35**, 3459; V. W. W. Yam, K. K. W. Lo and C. R. Wang, *Inorg. Chem.*, 1996, **35**, 5116; V. W. W. Yam, K. K. W. Lo, C. R. Wang and K. K. Cheung, *J. Phys. Chem. A*, 1997, **101**, 4666; C. R. Wang, K. K. W. Lo and V. W. W. Yam, *J. Chem. Soc., Dalton Trans.*, 1997, 227; C. R. Wang, K. K. W. Lo and V. W. W. Yam, *Chem. Phys. Lett.*, 1996, **262**, 91; V. W. W. Yam and K. K. W. Lo, *Comments Inorg. Chem.*, 1997, **19**, 209; V. W. W. Yam, *J. Photochem. Photobiol.*, 1997, **106**, 75; V. W. W. Yam, K. K. W. Lo, W. K. M. Fung and C. R. Wang, *Coord. Chem. Rev.*, 1998, **171**, 17; V. W. W. Yam, K. K. W. Lo, W. K. M. Fung and C. R. Wang, *Chem. Phys. Lett.*, 1998, **296**, 505.

3 W. F. Liaw, N. H. Lee, C. H. Chen, C. M. Lee, G. H. Lee and S. M. Peng, *J. Am. Chem. Soc.*, 2000, **122**, 488; C. W. Liu, R. J. Staples and J. P. Fackler Jr., *Coord. Chem. Rev.*, 1998, **174**, 147; J. J. Ellison, A. Nienstedt, S. C. Shoner, D. Barnhart, J. A. Cowen and J. A. Kovacs, *J. Am. Chem. Soc.*, 1998, **120**, 5691; I. G. Dance and K. Fisher, *Prog. Inorg. Chem.*, 1994, **41**, 637; N. Ueyama, H. Oku and A. Nakamura, *J. Am. Chem. Soc.*, 1992, **114**, 7310; P. K. Gowik and T. M. Klaoietke, *Inorg. Chim. Acta*, 1990, **169**, 1; I. J. Hollander, Y. Q. Shen, J. Heim, A. L. Demin and S. Wolf, *Science*, 1984, **224**, 610.

4 I. Davies, W. R. McWhinnie, N. S. Dance and C. H. Jones, *Inorg. Chim. Acta*, 1978, **29**, L217; W. Hirpo, S. Dhingra, A. C. Sutorik and M. G. Kanatzidis, *J. Am. Chem. Soc.*, 1993, **115**, 1597; P. J. Bonasia, G. P. Mitchell, F. J. Hollander and J. Arnold, *Inorg. Chem.*, 1994, **33**, 1797; J. F. Corrigan, D. Fenske and W. P. Power, *Angew. Chem., Int. Ed. Engl.*, 1997, **36**, 1176.

5 F. Sabin, C. K. Ryu, P. C. Ford and A. Vogler, *Inorg. Chem.*, 1992, **31**, 1941; D. M. Knotter, G. van Koten, H. L. van Maanen, D. M. Grove and A. L. Spek, *Angew. Chem., Int. Ed. Engl.*, 1989, **28**, 341; D. M. Knotter, H. L. van Mannen, D. M. Grove, A. L. Spek and G. van Koten, *Inorg. Chem.*, 1991, **30**, 3309; D. M. Knotter, A. L. Spek and G. van Koten, *J. Chem. Soc., Chem. Commun.*, 1989, 1738; D. M. Knotter, A. L. Spek, D. M. Grove and G. van Koten, *Organometallics*, 1992, **11**, 4083.

6 J. C. Slater, *J. Chem. Phys.*, 1964, **41**, 3199.

7 P. D. Harvey, M. Drouin and T. Zhang, *Inorg. Chem.*, 1997, **36**, 4998.

The selective oxidation of benzyl alcohols in a membrane reactor

G. Grigoropoulou,[a] J. H. Clark,*[a] D. W. Hall[b] and K. Scott[b]

[a] *Centre for Clean Technology, Chemistry Department, University of York, UK YO10 5DD. E-mail: jhc1@york.ac.uk*
[b] *Department of Chemical and Process Engineering, University of Newcastle, Metz Court, Newcastle upon Tyne, UK NE1 7RU*

Received (in Liverpool, UK) 14th November 2000, Accepted 29th January 2001
First published as an Advance Article on the web 28th February 2001

The selective oxidation of benzyl alcohols by hypochlorite and a phase transfer catalyst has been successfully carried out in a membrane reactor.

Selective oxidation is one of the most important synthetic transformations in organic chemistry based on hydrocarbon resources. It is essential that these transformations are based on the principles of green chemistry and avoid heavy metal reagents, toxic solvents and the generation of large volumes of hazardous waste. The major source of waste in many organic reactions is commonly aqueous or salt effluent produced at the work-up stage when the organic and inorganic components are separated, often *via* an aqueous quench.[1]

Phase transfer catalysis (PTC) has been widely used to transfer inorganic anions into organic media by using catalytic amounts of lipophilic quaternary ammonium or phosphonium salts.[2] Sodium hypochlorite is a non-toxic oxidant, which has been reported to be transferred into the organic phase in the presence of quaternary ammonium salt[3–6] and is capable of oxidising alcohols including benzyl alcohol although it can be difficult to control selectivity.[7–9]

Most PTC reactions are carried out on an industrial scale in stirred tank reactors, which require the separation of products afterwards. Key criteria required in a PTC reactor are high interfacial area with little emulsification to enable easy phase separation. The use of a membrane reactor for a PTC reaction could fulfil these criteria as well as offering the advantages of easy product recovery. Furthermore, the organic-free reduced aqueous phase can be electrochemically regenerated while the organic phase remains uncontaminated with aqueous species thus facilitating continuous reactions. The use of a membrane reactor in a phase transfer catalysed reaction has been theoretically modelled before[10] and tested in a simple anion displacement reaction. It has been shown that the reactor performance depends on the flow rate ratio and conversions are slower than predicted due to mass transfer resistance. The membrane acts as a stable interface and no emulsification problems are involved.

Here we report the selective oxidation of benzyl alcohols using a porous PTFE membrane to separate the aqueous and organic phases. A flat sheet diaphragm reactor shown in Fig. 1, was used to carry out the reaction. In a typical reaction, a 13% aqueous solution of hypochlorite (25 ml), was adjusted to pH 9 and then added in the aqueous side of the reactor. Benzyl alcohol (3 mmol), and tetrabutylammonium hydrogen sulfate (0.3 mmol), were dissolved in DCM on the organic side. A hydrophobic microporous PTFE (0.2 μm) membrane was used and a slight pressure was applied to the aqueous side to avoid any transport of the organic phase into the aqueous phase. The hydrophobic PTFE membrane kept the aqueous phase from entering into the organic phase. The reaction could be run static or continuous with counter flowing aqueous and organic phases.

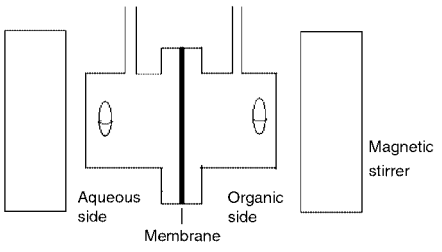

Fig. 1 Schematic diagram of flat sheet diaphragm cell.

The influence of several parameters has been investigated so as to optimise the performance of the system and in particular to avoid further oxidation of the benzaldehyde to benzoic acid [eqn. (1)].

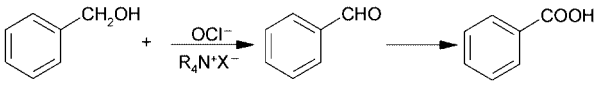

(1)

The effect of benzyl alcohol concentration on the reaction profiles was first investigated (Fig. 2). As the concentration of benzyl alcohol increases the rate of conversion increases slightly. For each reaction a small induction period is observed, due to slow mass transfer of hypochlorite although this is not observed if the system is allowed to equilibrate before the alcohol substrate is added. The rate of the reaction does not depend as much on the concentration of benzyl alcohol as expected, however the concentration of PTC increases the rate due to easier mass transfer. Selectivity to the aldehyde is also reduced at low concentrations of the PTC. Changing the counter anion in the PTC (HSO_4^-, Cl^-, Br^-) has little effect on reaction rate or selectivity but little reaction occurs in the absence of a PTC. While the hypochlorite concentration has only a small effect on the rate of conversion of benzyl alcohol, it strongly influences the selectivity of the reaction. The amount of hypochlorite transferred into the organic phase is dependant on both the concentration of quaternary ammonium in the organic phase and that of the hypochlorite in the aqueous phase. The optimum concentration of hypochlorite at which we obtain a good rate of conversion and very high selectivity to the aldehyde is 13%.

Toluene can be used as a solvent for the reaction, although it decreases the rate of conversion due to slower mass transfer and benzyl chloride was produced from its oxidation under the standard reaction conditions.

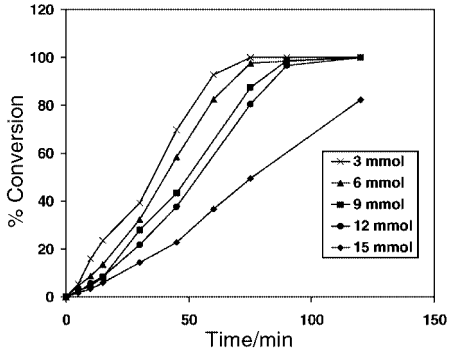

Fig. 2 Influence of the concentration of benzyl alcohol on the conversion of the reaction.

DOI: 10.1039/b009178m

Table 1 Oxidation of substituted benzyl alcohols to aldehydes under optimum conditions[a]

Substrate (benzyl alcohol)	Time/min	Product	Yield (%)[b]	Selectivity (%)
2-Methylbenzyl alcohol	60	2-Methylbenzaldehyde	97	98
4-Methylbenzyl alcohol	60	4-Methylbenzaldehyde	93	97
4-*tert*-Butylbenzyl alcohol	45	4-*tert*-Butylbenzaldehyde	90	95
4-Methoxybenzyl alcohol	120	4-Methoxybenzaldehyde	78	87
4-Chlorobenzyl alcohol	75	4-Chlorobenzaldehyde	75	84

[a] Reaction conditions: substrate (3 mmol), aqueous solution of NaOCl 13% (25 ml) at pH 9, $TBAHSO_4$ (0.9 mmol) and DCM (25 ml) at rt. [b] By quantitative NMR.

The optimised system was successfully used for the selective oxidation of a series of substituted benzyl alcohols (Table 1). It appears that moving the substituent away from the reaction centre did not affect the yield of the reaction. Insertion of an electron-withdrawing substituent on the benzene ring increases the reaction time and reduces the yield of the produced substituted benzaldehyde products.

In summary, we have shown that it is possible to develop a membrane reactor system for the static or continuous production of benzaldehyde as well as substituted benzaldehydes.

We thank the EPSRC for funding this work and we are grateful for valuable discussions with other members of the York–Newcastle Chemistry–Chemical Engineering collaboration. J. H. C. also thanks the RAEng-EPSRC for a Clean Technology Fellowship.

Notes and references

1 J. H. Clark, *Green Chem.*, 1999, **1**, 1.
2 C. M. Starks, C. L. Liotta and M. Halpern, *Phase-transfer catalysis: fundamentals, applications, and industrial perspectives*, Chapman & Hall, New York, London, 1994.
3 G. A. Lee and H. H. Freedman, *Tetrahedron Lett.*, 1976, **20**, 1641.
4 G. Lee and H. Freedman, *Isr. J. Chem.*, 1985, **26**, 229.
5 H. E. Fonouni, S. Krishnan, D. G. Kuhn and G. A. Hamilton, *J. Am. Chem. Soc.*, 1983, **105**, 7672.
6 S. Abramovici, R. Neumann and Y. Sasson, *J. Mol. Catal.*, 1985, **29**, 291.
7 S. Abramovici, R. Neumann and Y. Sasson, *J. Mol. Catal.*, 1985, **29**, 299.
8 J. S. Do and T. C. Chou, *Ind. Eng. Chem. Res.*, 1990, **29**, 1095.
9 S. Asai, H. Nakamura and T. Sumita, *AIChE J.*, 1994, **40**, 2028.
10 T. J. Stanley and J. A. Quin, *Chem. Eng. Sci.*, 1987, **42**, 2313.

Metal-containing DNA hairpins as hybridization probes†

Hima S. Joshi and Yitzhak Tor*

Department of Chemistry and Biochemistry, University of California, San Diego, La Jolla, CA 92093-0358, USA. E-mail: ytor@ucsd.edu

Received (in Corvallis, OR, USA) 21st December 2000, Accepted 25th January 2001
First published as an Advance Article on the web 28th February 2001

A Ru^{II}–based emission, while almost entirely quenched in a Ru^{II}/Os^{II} heterodimetallated DNA hairpin, is dramatically restored upon hybridization to a complementary oligonucleotide, while hybridization to an oligonucleotide that contains a single mismatch results in significantly lower emission intensity.

Luminescent polypyridine transition metal complexes have been gaining interest as molecular probes for bioanalytical applications.[1] Several important features distinguish emissive coordination compounds from their organic counterparts: (a) they are typically chemically inert and photostable, (b) their photophysical characteristics can be tuned while maintaining very similar structural features, (c) their photophysical properties are commonly insensitive to environmental changes (*e.g.* pH, ionic strength), although functional groups can be appended to affect sensing capabilities, (d) they exhibit rather large Stokes' shifts, and (e) their excited states are relatively long-lived, a feature that facilitates their utilization in polarization assays with relatively high molecular weight assemblies. Most of these traits can be attributed to their unique excited-state manifold, where the emission results from a metal-to-ligand-charge-transfer (MLCT) state.[2]

Oligonucleotides containing emissive transition metal complexes have become an important tool for the study of energy- and electron-transfer processes in nucleic acids.[3,4] In an early contribution, we have reported the synthesis of Ru^{II}- and Os^{II}-containing nucleosides **1** and **2** and their corresponding phosphoramidites (Fig. 1).[5] The Ru^{II} nucleoside exhibits a long-lived excited state in phosphate buffer pH 7.0 (τ = 1.08 μs) associated with a relatively high emission quantum efficiency (ϕ = 0.051). In contrast, the Os^{II}-containing nucleoside is quite non-emissive in an aqueous environment (τ = 0.027 μs, ϕ = 1×10^{-4}) and serves as a quencher of the Ru^{II} excited state.[6,7] Since this donor/acceptor interaction is distance-dependent,[5] we have envisioned its application for the detection of DNA hybridization events. In this contribution we demonstrate the utilization of novel metal-containing oligonucleotides as hybridization probes following the molecular beacons principle (Fig. 2).[8]

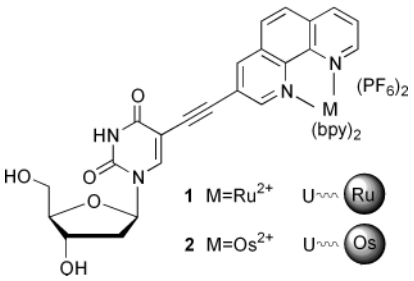

Fig. 1 Metal-containing nucleosides **1** and **2** serve as a donor and an acceptor, respectively.

† Electronic supplementary information (ESI) available: synthesis, enzymatic degradation, composition analysis and thermal denaturation studies of oligonucleotides. See http://www.rsc.org/suppdata/cc/b1/b100036p/

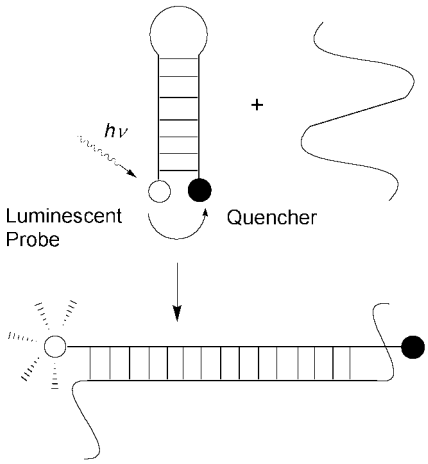

Fig. 2 General principle of molecular beacons technology: the quenched emission of a donor is restored upon hybridization to a target oligonucleotide.

The oligonucleotides used for this study are shown in Fig. 3.‡ The heterodimetallated hairpin **3**, which holds the donor and acceptor in close proximity, possesses a single mismatch in its 8-mer stem and a stable T_4 loop. Upon hybridization to its perfect complementary oligonucleotide **4a**, a 20-mer duplex **3·4a** with an additional six base pairs is formed, while placing the quencher away from the Ru^{II} donor (Fig. 3).§ Thermal denaturation studies confirm the enhanced stability of duplex **3·4a** when compared to the hairpin **3** (Table 1 and Fig. 4).

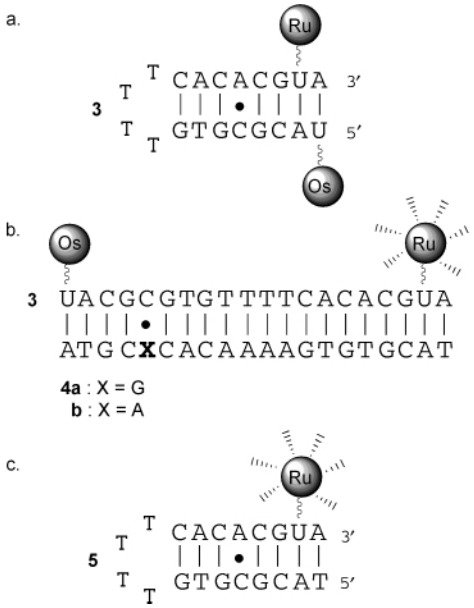

Fig. 3 Oligonucleotides used in this study: (a) Ru^{II}/Os^{II} heterodimetallated hairpin **3**, (b) duplexes **3•4a** and **3·4b** formed upon hybridization of **3** to the perfect (**4a**) and single-mismatch (**4b**) complement, respectively, and (c) a control Ru^{II}-containing hairpin **5**.

Table 1 Thermal denaturation and photophysical data

Sample	T_m/°C[ac]	I_{em} (arbitrary units)[bc]
3	69	5
3·4a	70	89
3·4b	70	38
5	69	100
5·4a	65	99
5·4b	69	98

[a] Melting temperature, ±1 °C. [b] Percent luminescence intensity (with respect to **5**), ±3%, 25 °C. [c] In 10 mM phosphate buffer pH 7.0 with 100 mM NaCl.

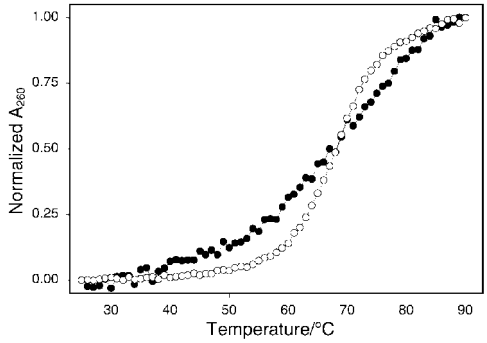

Fig. 4 Thermal denaturation curves of **3** (●) and **3·4a** (○).

Hybridization of hairpin **3** to oligonucleotide **4b** yields a less stable duplex **3·4b** that contains a single AC mismatch (Table 1 and ESI).

Steady-state emission spectra of iso-absorptive oligonucleotide solutions are shown in Fig. 5.§ The Ru-based emission intensity of the dimetallated hairpin **3** increases 17-fold when it hybridizes to its complementary strand to give duplex **3·4a**. The presence of a non-complementary strand **4b**, whose sequence differs from the perfect complement by merely one base, does not fully restore the Ru-based emission of the probe. The emission intensity of duplex **3·4b** is only 43% of the luminescence intensity of the perfect duplex **3·4a**. Hence, the hairpin hybridization probe **3** is able to distinguish between the target strand and a strand that contains a single mutation. We attribute this difference to the less favorable association between the unmatched oligonucleotides that is likely to lead to an equilibrium mixture of the quenched hairpin **3** and emissive

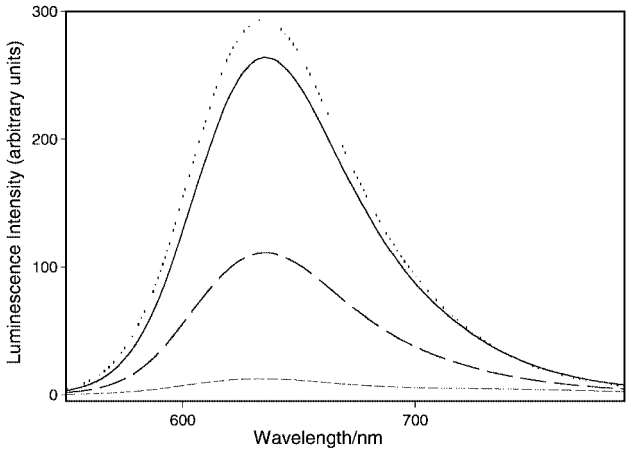

Fig. 5 Steady-state emission spectra of **3** (- - -), **3·4a** (—), **3·4b** (– – –) and **5** (···).

duplex **3·4b**.¶ Importantly, the luminescence of oligonucleotide **5**, the Ru^{II}-only control, does not significantly change in the presence of the complementary strand **4a** or the non-complementary strand **4b** (Table 1).‖

To the best of our knowledge, this is the first example of metallated hairpin oligonucleotides that serve as 'metallo-beacons'. The unique photophysical features of coordination compounds and their chemical compatibility with functional groups found on biomolecules hold great promise for future studies. In particular, advanced designs that include modulated emission and tailored quenchers that can undergo electron-transfer processes can further enhance the sensitivity and dynamic range of metal-based hybridization probes.

We thank the National Institutes of Health (Grant Number GM 58447) for generous support.

Notes and references

‡ Oligonucleotides were synthesized using the standard solid-phase phosphoramidite chemistry as previously described.[5] Purification was accomplished by preparative polyacrylamide gel electrophoresis and reversed-phase HPLC. The composition of each oligonucleotide was confirmed by enzymatic digestion followed by quantitative HPLC analysis of the resulting nucleosides. See ESI for experimental details.

§ Solutions of the oligonucleotides in 10 mM phosphate buffer, pH 7.0 containing 100 mM NaCl were heated to 90 °C for 5 min and slowly cooled to rt prior to measurements. Emission spectra of degassed solutions were measured upon excitation at 456 nm. The spectra were converted to an energy scale (cm^{-1}) and typically integrated between 520 and 850 nm.

¶ Supporting evidence can be found in the thermal denaturation curves of the corresponding oligonucleotides. See ESI.

‖ It is of interest to mention that the Ru-based emission in the Ru^{II}/Os^{II} perfect duplex **3·4a**, where the metal complexes are separated by 17 base pairs, is quenched by 10% in comparison to the Ru^{II}-only perfect duplex **5·4a**. This is consistent with the anticipated distance-dependent interaction between these coordination compounds.[5]

1 J. R. Lackowicz, *Principles of Fluorescence Spectroscopy*, Kluwer Academic/Plenum Publishers, New York, 1999, pp. 573–594.

2 A. Juris, V. Balzani, F. Barigelletti, S. Campagna, P. Belser and A. Von Zelewsky, *Coord. Chem. Rev.*, 1988, **84**, 85; J.-P. Sauvage, J.-P. Collin, J.-C. Chambron, S. Guillerez, C. Coudret, V. Balzani, F. Barigelletti, L. De Cola and L. Flamigni, *Chem. Rev.*, 1994, **94**, 993; V. Balzani, A. Juris, M. Venturi, S. Campagna and S. Serroni, *Chem. Rev.*, 1996, **96**, 659; F. Barigelletti, L. Flamigni, J.-P. Collin and J.-P. Sauvage, *Chem. Commun.*, 1997, 333.

3 For selected examples, see: C. J. Murphy, M. R. Arkin, Y. Jenkins, N. D. Ghatlia, S. H. Bossmann, N. J. Turro and J. K. Barton, *Science*, 1993, **262**, 1025; T. J. Meade and J. F. Kayyem, *Angew. Chem., Int. Ed. Engl.*, 1995, **34**, 352; P. J. Dandliker, R. E. Holmlin and J. K. Barton, *Science*, 1997, **275**, 1465; I. Ortmans, S. Content, N. Boutonnet, A. Kirsch-De Mesmaeker, W. Bannwarth, J.-F. Constant, E. Defrancq and J. L'homme, *Chem. Eur. J.*, 1999, **5**, 2712; T. T. Williams, D. T. Odom and J. K. Barton, *J. Am. Chem. Soc.*, 2000, **122**, 9048.

4 For overview articles, see: R. E. Holmlin, P. J. Dandliker and J. K. Barton, *Angew. Chem., Int. Ed. Engl.*, 1997, **36**, 2714; K. E. Erkkila, D. T. Odom and J. K. Barton, *Chem. Rev.*, 1999, **99**, 2777; M. W. Grinstaff, *Angew. Chem., Int. Ed.*, 1999, **38**, 3629.

5 D. J. Hurley and Y. Tor, *J. Am. Chem. Soc.*, 1998, **120**, 2194.

6 D. J. Hurley and Y. Tor, submitted.

7 Polypyridine Ru^{II} and Os^{II} complexes are a well-established couple for the study of energy and electron transfer processes. The transfer of electronic excitation from Ru^{II} to Os^{II} centers is energetically allowed and has been demonstrated in multinuclear systems. See ref. 2 and F. Barigelletti and L. Flamigni, *Chem. Soc. Rev.*, 2000, **29**, 1.

8 S. Tyagi and F. R. Kramer, *Nature Biotech.*, 1996, **14**, 303; S. Tyagi, D. P. Bratu and F. R. Kramer, *Nature Biotech.*, 1998, **16**, 49; L. G. Kostrikis, S. Tyagi, M. M. Mhlanga, D. D. Ho and F. R. Kramer, *Science*, 1998, **279**, 1228; S. A. E. Marras, F. R. Kramer and S. Tyagi, *Genet. Anal-Biomol. Eng.*, 1999, **14**, 151; L. J. Brown, J. Cummins, A. Hamilton and T. Brown, *Chem. Commun.*, 2000, 621.

Easy synthesis of polyphenolic 4-thiaflavans with a 'double-faced' antioxidant activity

Giuseppe Capozzi,*[a] Pierandrea Lo Nostro,[b] Stefano Menichetti,*[c] Cristina Nativi[a] and Paolo Sarri[a]

[a] *Centro C.N.R. 'Chimica dei Composti Eterociclici', Dipartimento di Chimica Organica, Università di Firenze, Via G. Capponi 9, I-50121, Firenze, Italy*
[b] *Dipartimento di Chimica e CSGI, Università di Firenze, Via G. Capponi 9, I-50121, Firenze, Italy*
[c] *Dipartimento di Chimica Organica e Biologica, Università di Messina, Salita Sperone 31, I-98166, Messina, Italy. E-mail: menichet@isengard.unime.it*

Received (in Cambridge, UK) 9th January 2001, Accepted 12th February 2001
First published as an Advance Article on the web 28th February 2001

Inverse electron demanding Diels–Alder reactions of *o*-thioquinones with styrenes, followed by simple manipulations of the obtained cycloadducts, allowed the synthesis of polyphenolic 4-thiaflavans which showed antioxidant activity miming either flavonoid or tocopherol behaviour.

Flavonoids, natural products containing the 2-phenylchromane skeleton, are almost ubiquitous in higher plants and have been related to a huge number of biological effects[1] including anti-inflammatory, anti-viral and anti-cancer activity. Flavonoids bearing OH groups on A, B and C rings (Fig. 1) represent one of the most important families of natural antioxidants, able to prevent oxidation by oxyl radicals.[2] A high polyphenolic flavonoid content in the diet has been indicated as the reason why certain populations show statistically low levels of cardiovascular disease (the so-called *French paradox*) and most types of cancer.[3]

We have reported that *o*-hydroxy-*N*-thiophthalimides, prepared by *N*-phthalimidesulfenylation of activated phenols, are suitable precursors of *ortho*-thioquinones, a synthetically useful class of electron-poor heterodienes, which react with styrenes giving rise to the formation of aryl-substituted benzoxathiin cycloadducts with complete regioselectivity.[4]

This hetero Diels–Alder approach, can be involved in the preparation of 4-thiaflavan derivatives as shown in Fig. 1. Thus we decided to exploit this procedure for access to polyphenolic 4-thiaflavans with the aim of verifying their potential performance as antioxidants.

We focused our attention on the 5,7,3′,4′ and 5,7,4′ substitution patterns, two of the more common structural characteristics in natural flavonoids.[1]

The sulfenylation of 3,5-dimethoxyphenol and 3,5-(dimethyl-*tert*-butylsilyloxy)phenol with phthalimidesulfenyl chloride gave, as expected, the sulfenamide derivatives **1** and **2** as suitable precursors of the corresponding *o*-thioquinones.†

The reaction of compounds **1** or **2** with styrenes **3**–**5** in $CHCl_3$ at 60 °C, in the presence of TEA,[4] allowed the isolation of the required cycloadducts which were transformed into the hydroxy derivatives **6**–**12** by direct fluoro desilylation using wet TBAF in THF at 0 °C.‡ For sulfoxides **7**, **11** and **12** the oxidation with *m*CPBA of the corresponding sulfides was performed before the deprotection of the silyl ethers (Scheme 1).§

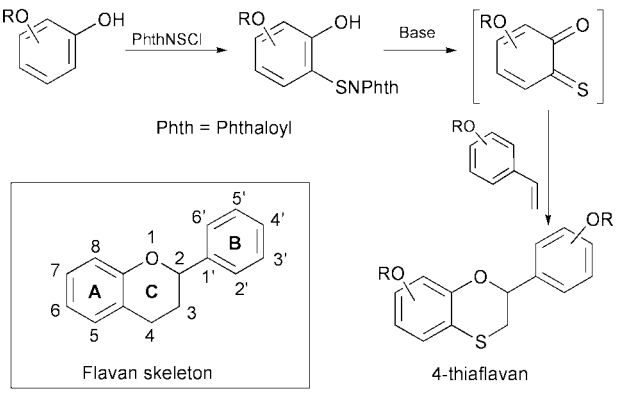

Fig. 1 Flavan skeleton and access to 4-thiaflavan structure.

The antioxidant activity of compounds **6**–**12** was evaluated,[5] as fading of the purple colour of commercially available DPPH radical measured at 517 nm. Thus the value of the absorbance of a 10^{-4} M solution of DDPH in absolute ethanol (A_0) and the absorbance after 20 min from its mixing with an equimolar solution of the thiaflavans (A_1), were used for calculating the reducing activity ***RA*** as: $\boldsymbol{RA} = [(A_0 - A_1)/A_0] \times 100$. The obtained ***RA*** for derivatives **6**–**12** and the one measured for commercially available (+)-catechin hydrate are reported in Scheme 1.

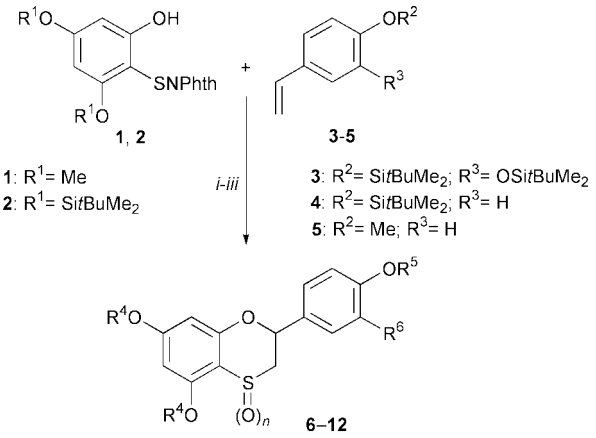

Product	R^4	R^5	R^6	*n*	Yield (%)	***RA***
6	H	H	OH	0	36	***83***
7	H	H	OH	1	26	***83***
8	H	H	H	0	34	***85***
9	Me	H	H	0	38	—
10	H	Me	H	0	42	***83***
11	H	H	H	1	28	***23***
12	H	Me	H	1	30	***6***
(+)-catechin						***83***

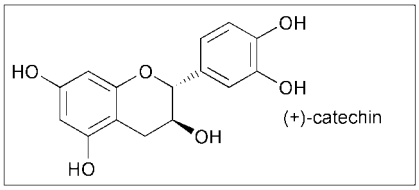

Scheme 1 *Reagent and conditions. i*: TEA (1 equiv.), $CHCl_3$, 60 °C, 20–120 h; *ii* (only for **7**, **11** and **12**): *m*CPBA (1 equiv.) CH_2Cl_2, 0 °C, 0.5–2h; *iii*: TBAF (1–4 equiv.), THF, 0 °C, 1–2 h.

DOI: 10.1039/b100359n

Satisfactorily, derivatives **6** and **7** showed the same activity as catechin. The high efficiency as antioxidants of natural flavonoids showing a catechol-like ring B, has been explained on the basis of the formation of a stable *o*-quinone species arising from two consecutive hydrogen abstractions by the radical reagent.[2] Clearly thiaflavans **6** and **7** could show a similar behaviour demonstrating that the above mentioned catechol-like mechanism is maintained with the introduction of a sulfide or a sulfoxide sulfur into the C ring.

Surprisingly compound **8**, bearing only one hydroxy group on C4′ of ring B, was even more efficient than previously considered 4-thiaflavans and catechin. This is in sharp contrast with the literature data on antioxidant activity of flavonoids[2] and prompted us to envisage a different oxidation mechanism probably involving the A and C rings. This hypothesis was corroborated by the substitution of hydroxy by methoxy groups on the A ring which caused a complete loss of consumption of DPPH colour for derivative **9**, while compound **10**, bearing a methoxy group on the B ring but hydroxy groups on the A ring, exhibited the same activity as **8**. Moreover the transformation of sulfides **8** and **10** into the corresponding sulfoxides **11** and **12** gave rise to an almost complete loss of activity. Thus the observed antioxidant activity of compounds **8** and **10** requires both hydroxy groups on the A ring and a sulfide sulfur in the C ring (Scheme 1).

A simple rationalization of these results can be obtained by considering that a 5,7-dihydroxy-4-thiaflavan moiety, like in **8** or **10**, could behave as an antioxidant with the same mechanism operative in tocopherols and related compounds, which, with flavonoids, represent the most important families of natural antioxidants (Fig. 2).

Literature data regarding the activity of modified tocopherols[6] are in perfect agreement with the observed high efficiency of 4-thiaflavans **8** and **10**. Actually it is known that the introduction of electron donating groups in the aromatic ring (*i.e*. OH on C5) facilitates hydrogen abstraction by the oxyl radical, while the substitution of the oxygen by the sulfur atom, on the saturated condensed ring, increases the stability of the intermediate radical[7] (Fig. 2).

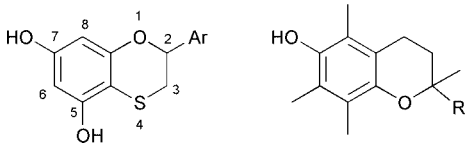

Fig. 2 4-Thiaflavan and tocopherol skeletons.

The oxidation of the sulfide sulfur causes the decrease of activity exhibited by sulfoxides **11** and **12** since it introduces an electron withdrawing group which, at the same time, is known to possess less ability in stabilizing radicals.[8]

These results seem to indicate that both the flavonoid-like and the tocopherol-like mechanisms are operative in compound **6**. Recent observations indicate that '*in vivo*' these two classes of natural polyphenols have to operate synergistically for a fast and safe protection against LDL (low density lipoprotein) damaging radicals.[9] Thus the possibility of joining in a single compound the very fast reaction of flavonoids with oxyl radicals and the high chain breaking ability of tocopherols, makes these thiaflavans very stimulating and promising new 'double-faced' antioxidant derivatives.

Moreover, since several 4-thiaflavans, including derivatives **8**–**10**, appeared active against *Staphylococcus aureus*, *Pseudomonas aeruginosa* and *Candida albicans* growth,[10] more detailed studies on the activity of 4-thiaflavans as antioxidants and antimicrobials are in progress in these laboratories.

This work was carried out under the auspices of the National Project: 'Stereoselezione in Sintesi Organica. Metodologie ed Applicazioni' supported by the Ministero dell'Università e della Ricerca Scientifica e Tecnologica, Rome, and by the University of Florence.

Notes and references

† 3,5-(Dimethyl-*tert*-butylsilyloxy)phenol was prepared by direct silylation of 1,3,5-trihydroxybenzene hydrate (fluorglucinol hydrate) with *t*-Bu-Me_2SiCl and imidazole in DMF.

‡ Representative experimental procedure: to a solution of **2** (150 mg, 0.28 mmol) and *p*-methoxystyrene (**5**) (38 mg, 0.28 mmol) in dry $CHCl_3$ (3 mL), TEA (28 mg, 0.28 mmol) was added and the mixture heated at 60 °C for 22 h. Evaporation of the solvent and flash chromatography afforded the required cycloadduct (145 mg, 60%), which was directly desilylated by reaction with TBAF hydrate (146 mg, 0.56 mmol) in THF (5 mL) for 35 min at 0 °C. Evaporation of the solvent and flash chromatography gave derivative **10** (57 mg, 70%) as a white solid; mp 169 °C.

§ Sulfoxides **7**, **11** and **12** were obtained, and tested, as 82 : 18, 86 : 14 and 93 : 7 mixtures of *trans* and *cis* isomers, respectively. For the synthesis and geometry of related sulfoxides see: G. Capozzi, P. Fratini, S. Menichetti and C. Nativi, *Tetrahedron*, 1996, **52**, 12 233. Using 1 equiv. of *m*CPBA the formation of sulfones is not observed, the latter can be easily prepared carrying out the oxidation with 2 equiv. of *m*CPBA at rt for 2–12 h.

1 J. B. Harborne, *The Flavonoids Advances in Research Since 1986*, Chapman & Hall, London, 1994; N. C. Cook and S. Samman, *Nutritional Biochemistry*, 1996, **7**, 66; B. A. Bohm, *Introduction to Flavonoids*, Harwood Academic Publishers, Amsterdam, 1998; L. Bravo, *Nutr. Rev.*, 1998, **56**, 317 and references cited therein.

2 S. V. Jovanovic, S. Steenken, M. Tosic, B. Marjanovic and M. G. Simic, *J. Am. Chem. Soc.*, 1994, **116**, 4846; O. Dangles, G. Fargei and C. Dufour, *J. Chem. Soc., Perkin Trans. 2*, 1999, 1387 and references cited therein.

3 O. Dangles, G. Fargeix and C. Dufour, *J. Chem. Soc., Perkin Trans. 2*, 2000, 1653 and references cited therein.

4 G. Capozzi, C. Falciani, S. Menichetti and C. Nativi, *J. Org. Chem.*, 1997, **62**, 2611.

5 P. Lo Nostro, G. Capuzzi, N. Mulinacci and A. Romani, *Langmuir*, 2000, **16**, 1744.

6 G. W. Burton, T. Doba, E. J. Gabe, L. Hughes, F. L. Lee, L. Praasad and K. U. Ingold, *J. Am. Chem. Soc.*, 1985, **107**, 7053.

7 H. A. Zahalka, B. Robillard, L. Hughes, J. Lusztyk, G. W. Burton, E. G. Janzen, Y. Kotake and K. U. Ingold, *J. Org. Chem.*, 1988, **53**, 3739; L. Engman, M. J. Laws, J. Malmstrom, C. H. Schiesser and L. M. Zugaro, *J. Org. Chem.*, 1999, **64**, 6764.

8 I. Biddles, A. Hudson and J. T. Wiffen, *Tetrahedron*, 1972, **28**, 867; D. D. M. Wayner and D. R. Arnold, *Can. J. Chem.*, 1984, **62**, 1164; D. Griller, D. C. Nonhebel and J. C. Walton, *J. Chem. Soc., Perkin Trans. 2*, 1984, 1817; A. E. Luedtke and J. W. Timberlake, *J. Org. Chem.*, 1985, **50**, 268.

9 O. Dangles, G. Fargeix and C. Dufour, *J. Chem. Soc., Perkin Trans. 2*, 2000, 1215.

10 G. Capozzi, A. Lo Nostro, S. Menichetti, C. Nativi and P. Sarri, unpublished results.

Alkali metal-templated assembly of the tetrahedral cyanometallate cages $[M\subset Mo_4(\mu\text{-}CN)_6(CO)_{12}]^{5-}$ (M = Li, Na)

Stephen M. Contakes and Thomas B. Rauchfuss*

Department of Chemistry, University of Illinois at Urbana Champaign, Urbana, IL 61801,USA. E-mail: rauchfuz@uiuc.edu

Received (in Irvine, CA, USA) 11th December 2000, Accepted 16th January 2001
First published as an Advance Article on the web 28th February 2001

Acetonitrile solutions of (mesitylene)$Mo(CO)_3$, 1.5 equiv. Et_4NCN, and 0.25 equiv M^+ afford the inorganic tetrahedranes $(Et_4N)_5[M\subset Mo_4(\mu\text{-}CN)_6(CO)_{12}]$ (M = Na, Li), the strained nature of which is indicated by their ready reaction with CsO_3SCF_3 to give trigonal prismatic $(Et_4N)_8[Cs\subset Mo_6(\mu\text{-}CN)_9(CO)_{18}]$.

We have reported that the cyanometallate box $[Cp^*Rh]_4[Mo(CO)_3]_4(\mu\text{-}CN)_{12}^{4-}$ selectively binds Cs^+ (*vs.* K^+).[1] This mirrors behavior exhibited by solid state cyanometallates, which have been of interest for radiowaste separations.[2,3] We have recently discovered that in cyanometallate cages with labile M–CN bonds, Cs^+ and K^+ promote the formation of trigonal prismatic, not cubic, cages, *e.g.* $[Cs\subset Mo_6(\mu\text{-}CN)_9(CO)_{18}]$.[4] We now report that use of the smaller Na^+ (r_{ionic} = 116 pm[5]) and Li^+ (r_{ionic} = 90 pm) ions in place of Cs^+ (r_{ionic} = 181 pm) and K^+ (r_{ionic} = 152 pm) in the Mo–CO/CN^- system affords tetrahedral cages, a third member of the series $\{M\subset[Mo(\mu\text{-}CN)_{1.5}L_x]_n\}^{(1.5n-1)-}$. This result establishes that the alkali metal not only templates cage formation, but that *the size of the alkali metal ion determines the cage structure*. Of further interest, tetrahedral $M_4(\mu\text{-}CN)_6$ cages are unprecedented within the area of cyanometallates.[2]

Treatment of acetonitrile solutions of (mesitylene)$Mo(CO)_3$ with 1.5 equiv. Et_4NCN in the presence of 0.25 equiv. $NaSbF_6$ gives a yellow solution from which golden crystals, analyzed as $(Et_4N)_5[Na\subset Mo_4(\mu\text{-}CN)_6(CO)_{12}]$ ($Na\subset T^{5-}$), can be precipitated in 77% yield.†‡ 159 MHz ^{23}Na NMR spectroscopy indicates that this reaction is complete within 1 h. The IR spectrum shows that the anion is rather electron rich (ν_{CO} = 1997, 1876, 1745 cm^{-1}). X-Ray diffraction analysis revealed an anionic tetrahedrane with four $Mo(CO)_3$ vertices and six μ-CN edges (Fig. 1). Not unlike $[K\subset Mo_6(\mu\text{-}CN)_9(CO)_{18}]^{8-}$ ($K\subset TP^{8-}$),[4] each Mo atom is octahedral with acute CN–Mo–CN angles (82.1°) and 90° C–Mo–CO angles. The Na^+–C/N distance of *ca.* 2.56 Å is comparable to that in Na-alkyls.[6–10] The Mo–CN linkages are bent with Mo–C/N–N/C bond angles of 165.9°. In the molecular triangle $Re_3(\mu\text{-}CN)_3(CO)_{12}$, the M–C–N angles are *ca.* 180° with most of the bending occurring at the *ca.* 135° M–N–C angles.[11] A similar situation may apply to $Na\subset T^{5-}$ but the presence of four structurally similar linkage isomers, each of which can adopt four different orientations in the crystal structure, made this difficult to establish unambiguously. Evidence for the four different possible linkage isomers comes from ^{13}C NMR spectroscopy (Fig. 2), which shows the predicted 16 signals in the μ-CN region. The Li^+-containing tetrahedrane, $(Et_4N)_5[Li\subset Mo_4(\mu\text{-}CN)_6(CO)_{12}]$ ($Li\subset T^{5-}$), was prepared from (mesitylene)$Mo(CO)_3$, 1.5 equiv. Et_4NCN, and 0.25 equiv. LiO_3SCF_3.

The availability of two classes of cages of formula $M\subset[Mo(\mu\text{-}CN)_{1.5}(CO)_3]_n^{(1.5n-1)-}$ (M = Cs, K, *n* = 6 *vs.* M = Na, Li, *n* = 4) prompted a study of their interconversion. Cage interconversion is also relevant to cage assembly mechanisms, a topic that has only recently come under scrutiny.[12] The 233 MHz ^7Li NMR spectrum of $Li\subset T^{5-}$ in MeCN consists of a single signal at δ −0.28 (apparently the Na chemical shift is insensitive to the CN linkage isomerism). On addition of one equiv. of LiO_3SCF_3 to a MeCN solution of square $(Et_4N)_4[Cs\subset Mo_6(\mu\text{-}CN)_9(CO)_{18}]$ (**1**),[4] a broad signal at δ −1.8 as well as small amounts of $Li\subset T^{5-}$ (Fig. 3) were observed. Upon adjusting the CN^- : $Mo(CO)_3$ ratio to 1.5, the signal for $Li\subset T^{5-}$ becomes dominant. Further Et_4NCN, however, degrades the $Li\subset T^{5-}$ giving only $Mo(CO)_3(CN)_3^{3-}$ and free Li^+.[4] Similar observations were obtained by ^{23}Na NMR spectroscopy for the formation of $Na\subset T^{5-}$ from $NaSbF_6$ and **1**. These results confirm the ready formation of the tetrahedrane when $Mo(CO)_3$, CN^-, and the alkali metal are present in the appropriate ratio.

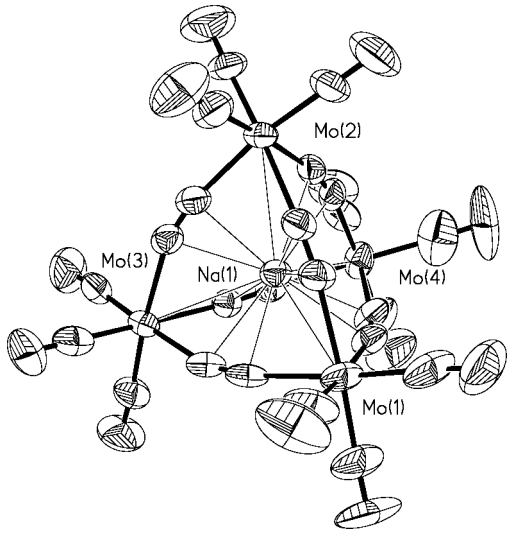

Fig. 1 Structure of the anion in $(Et_4N)_5[Na\subset Mo(\mu\text{-}CN)_6(CO)_{12}]\cdot 4MeCN$ with thermal ellipsoids set at the 50% probability level. Selected average distances (Å) and angles (°): Mo–C/N 2.25, Mo–CO 1.93, Na–C/N 2.56, C/N–Mo–C/N 82.1, OC–Mo–CO 90.0; Mo–C/N–Mo 165.9.

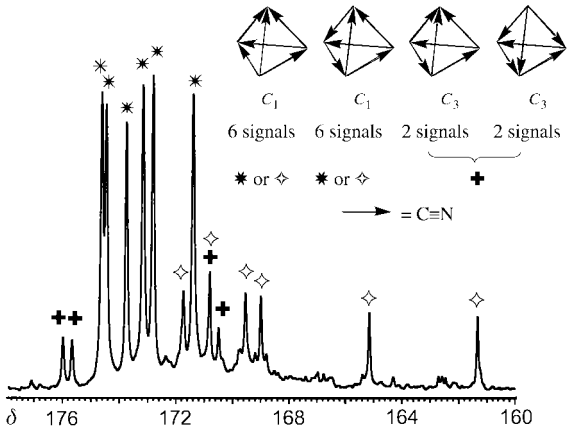

Fig. 2 187.5 MHz ^{13}C NMR spectrum of $(Et_4N)_5[Na\subset Mo(\mu\text{-}CN)_6(CO)_{12}]$ showing the 14 signals observed in the μ-CN region and breakdown of signals into groups attributable to the four linkage isomers.

DOI: 10.1039/b010192n

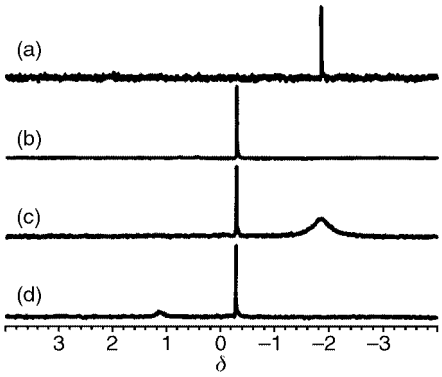

Fig. 3 233.2 MHz ^{7}Li NMR spectra illustrating the effect of Mo:CN ratio on cage synthesis (MeCN solutions): (a) 0.18 M LiO_3SCF_3; (b) 0.018 M $(Et_4N)_5[Li{\subset}Mo(\mu\text{-}CN)_6(CO)_{12}]$; (c) 0.019 M $(Et_4N)_4\{[Mo(CO)_3(NCMe)]_4(CN)_4\}$ and 0.019 M LiO_3SCF_3; and (d) 0.019 M $(Et_4N)_4\{[Mo(CO)_3(NCMe)]_4(CN)_4\}$, 0.019 M LiO_3SCF_3 and 0.038 M Et_4NCN.

We also examined the effect of alkali metal stoichiometry. Addition of one equiv. $NaSbF_6$ to a solution of $Na{\subset}T^{5-}$ gave a broad ^{23}Na NMR signal for Na^+ centered at δ −4.5 along with undiminished signal for $Na{\subset}T^{5-}$, indicating that excess alkali metal does not degrade the cage. Using substoichiometric amounts of $NaSbF_6$ shows only formation of $Na{\subset}T^{5-}$. Thus, alkali metal is required for cage formation, only the tetrahedral cage forms at low stoichiometry, and excess alkali metal does not affect cage formation.

Experiments involving mixed alkali metals clarified the relative thermodynamic and kinetic stabilities of the new families of CN-based cages. LiO_3SCF_3 has no effect on the ^{23}Na spectrum of $Na{\subset}T^{5-}$ whereas one equiv of $NaSbF_6$ converts $Li{\subset}T^{5-}$ into $Na{\subset}T^{5-}$. This reaction is likely due to the better fit of the sodium ion within the cavity and may also be partially driven by the entropic advantage for encapsulation of $[Na(MeCN)_6]^+$ *vs.* $[Li(MeCN)_4]^+$.[13,14] ^{7}Li NMR measurements showed that one equiv. of CsO_3SCF_3 causes release of free Li^+ from $Li{\subset}T^{5-}$. Complementarily, 79 MHz ^{133}Cs NMR measurements showed that Cs^+ converts both $Na{\subset}T^{5-}$ and $Li{\subset}T^{5-}$ predominantly into $Cs{\subset}TP^{8-}$ (Scheme 1). Consistent with the greater stability of the larger cages, the ^{133}Cs NMR spectrum of $Cs{\subset}TP^{8-}$ is unaffected by the presence of Li^+, Na^+, and K^+. The higher reactivity of the tetrahedral cages is attributed to the weakened M-NC bonding associated with strained Mo–C–N–Mo angles (*vide supra*).

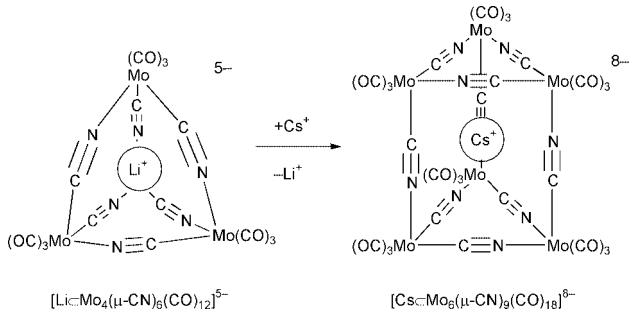

Scheme 1

The literature on tetrahedral cages is rapidly growing,[15–18] although the previously reported cages are guided by the directionality and denticity of organic ligands, whereas in the present case only CN^- is the linker and guidance is provided by the size of the encapsulated ion.

This research was supported by the Department of Energy. We thank Dr Paul Molitor for assistance with the NMR measurements.

Notes and references

† *Synthesis* of $(Et_4N)_5[Na{\subset}Mo_4(\mu\text{-}CN)_6(CO)_{12}]$ (**1**). A solution of 156 mg (1.00 mmol) Et_4NCN in 15 mL MeCN was added dropwise to a stirred solution of 200 mg (0.666 mmol) (mesitylene)$Mo(CO)_3$ and 43 mg (0.167 mmol) $NaSbF_6$ in 10 mL MeCN. The resulting solution was allowed to stand for 18 h and then 100 mL Et_2O was added to precipitate the product as a yellow powder. The product was collected by filtration, washed twice with 10 mL portions of Et_2O, and dried under vacuum for 12 h. Yield 210 mg (77%). IR ($\nu_{C\equiv X}$, KBr/cm^{-1}): 2089 (w), 1997 (vw), 1934 (m), 1876 (vs), 1745 (vs). Anal. Calc. (found) for $C_{58}H_{100}Mo_4NaN_{11}O_{12}$: C, 44.94 (45.02); H, 6.50 (6.62); Mo, 24.75 (24.53); Na, 1.48 (1.42); N, 9.94 (10.10)%. The Li derivative was prepared identically using LiOTf in place of $NaSbF_6$. Single crystals of **1** were grown from MeCN solutions by vapor diffusion using ether.

‡ *Crystal data* for **1**: M = 1550.3, monoclinic, space group $P2_1/c$, a = 19.1292(16), b = 19.3643(16), c = 24.966(2) Å, β = 96.764°, Z = 4, D_c = 1.290 Mg m^{-3}, λ = 0.71073 Å, μ = 0.601 mm^{-1}, $R1$ = 0.0735, $wR2$ = 0.1894, GoF = 1.0098.

CCDC 13795. See http://www.rsc.org/suppdata/cc/b0/b010192n/ for crystallographic data in .cif or other electronic format.

1 K. K. Klausmeyer, S. R. Wilson and T. B. Rauchfuss, *J. Am. Chem. Soc.*, 1999, **121**, 2705.
2 K. R. Dunbar and R. A. Heintz, *Prog. Inorg. Chem.*, 1997, **45**, 283.
3 J. T. Davis, S. K. Tirumala and A. L. Marlow, *J. Am. Chem. Soc.*, 1997, **119**, 5271.
4 S. M. Contakes and T. B. Rauchfuss, *Angew. Chem., Int. Ed.*, 2000, **39**, 1984.
5 J. A. Huheey, E. A. Keiter and R. L. Keiter, *Inorganic Chemistry: Principles of Structure and Reactivity*, Harper Collins, New York, 1993.
6 S. S. Al-Juaid, C. Eaborn, P. B. Hitchcock, K. Izod, M. Mallien and J. D. Smith, *Angew. Chem., Int. Ed. Engl.*, 1994, **33**, 1268.
7 C. Eaborn, W. Clegg, P. B. Hitchcock, M. Hoppman, K. Izod, P. N. O'Shaugnessy and J. D. Smith, *Organometallics*, 1997, **16**, 4728.
8 P. B. Kitchcock, M. F. Lappert, W.-P. Leung, L. Diansheng and T. Shun, *J. Chem. Soc., Chem. Commun.*, 1993, 1386.
9 C. Schade, P. v. R. Schleyer, M. Geissler and E. Weiss, *Angew. Chem., Intl. Ed. Engl.*, 1986, **25**, 1986.
10 H. Viebrock, U. Behrend and E. Weiss, *Chem. Ber.*, 1994, **127**, 1399.
11 F. Calderazzo, U. Mazzi, G. Pampaloni, R. Poli, F. Tisato and P. F. Zanazzi, *Gazz. Chim. Ital.*, 1989, **119**, 241.
12 M. D. Levin and P. J. Stang, *J. Am. Chem. Soc.*, 2000, **122**, 7428.
13 Y. Yokota, J. Young, V. G. Verkade and J. G. Verkade, *Acta Crystallogr., Sect. C*, 1999, **55**, 196.
14 C. L. Raston, C. R. Whitaker and A. H. White, *Aust. J. Chem.*, 1989, **42**, 201.
15 R. L. Paul, S. M. Couchman, J. C. Jeffrey, J. A. McCleverty, Z. R. Reeves and M. D. Ward, *J. Chem. Soc., Dalton Trans.*, 2000, 845.
16 D. L. Caulder and K. N. Raymond, *Acc. Chem. Res.*, 1999, **32**, 975.
17 S. Leininger, B. Olenyuk and P. J. Stang, *Chem. Rev.*, 2000, **100**, 853.
18 K. Umenoto, K. Yamaguchi and M. Fujita, *J. Am. Chem. Soc.*, 2000, **122**, 7150.

ChemComm

Novel ferrocene receptors for barbiturates and ureas

Simon R. Collinson,[a]† T. Gelbrich,[b] Michael B. Hursthouse[b] and James H. R. Tucker*[a]

[a] *School of Chemistry, University of Exeter, Stocker Road, Exeter, UK EX4 4QD*
[b] *Department of Chemistry, University of Southampton, Southampton, UK SO17 1BJ.*
E-mail: j.h.r.tucker@exeter.ac.uk

Received (in Cambridge, UK) 7th December 2000, Accepted 6th February 2001
First published as an Advance Article on the web 5th March 2001

The complexation *via* complementary hydrogen bonds, of three novel ferrocene receptors with barbital, ethylene urea and trimethylene urea is described with the binding mode and stoichiometry clearly shown by NMR spectroscopy and X-ray crystallography.

As part of the continued interest in the development of novel molecular switches and sensors, redox-active receptors for inorganic cations and anions have been studied in much detail,[1] although reports of similar receptors for organic molecules, be they charged or neutral, are less common.[2] Interest in the development of functional receptors for organic molecules such as barbiturates arises due to their importance as sedatives and anticonvulsants,[3] whilst the detection of ureas is important with regard to possible applications in dialysis. Previous studies concerning the binding of barbiturates and ureas have largely focused on organic receptors that bind the neutral guest through hydrogen bonds.[4] In particular, Hamilton and coworkers have reported the complexation of barbiturates by both macrocyclic and acyclic receptors (*e.g.* **1** and **2**) containing two 2,6-diaminopyridine units linked *via* an isophthaloyl group.[4a,b] Here we report that a similar binding motif can be constructed through the incorporation of the redox-active ferrocene unit into the receptor framework.

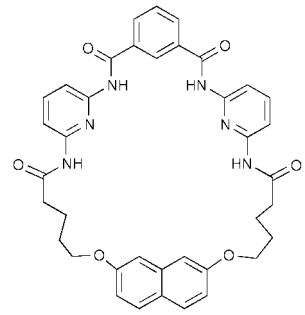

1

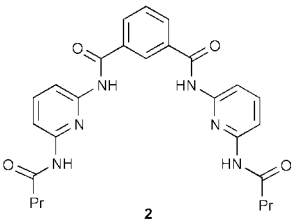

2

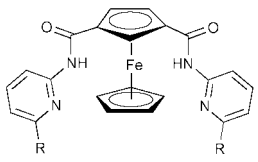

3 R = CH_3
4 R = NH_2
5 R = HNCOEt

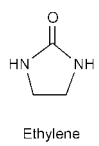

Ethylene urea

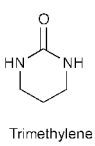

Trimethylene urea

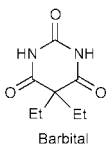

Barbital

The synthetic strategy involved the synthesis of ferrocene-1,3-dicarbonylchloride,[5] which was then reacted, in the presence of triethylamine, with either two equivalents of 2-amino-6-methylpyridine or with an excess of 2,6-diaminopyridine, to yield compounds **3** and **4** respectively. Further reaction of **4** with propionyl chloride, again in the presence of triethylamine, yielded compound **5**. These reactions thus produced a series of ferrocene receptors containing either two hydrogen bond donor groups (D) with two hydrogen bond acceptor groups (A) (receptor **3**) or four hydrogen bond donor groups with two hydrogen bond acceptor groups (receptors **4** and **5**).

The interaction of each ferrocene receptor with a range of neutral guests was monitored by ^{1}H NMR spectroscopy in dry $CDCl_3$. Downfield shifts in the resonances corresponding to the amide protons and also the proton in the 2-position of the disubstituted ferrocene Cp ring were observed. For example, this Cp-H resonance in receptor **5** underwent a downfield shift of +0.25 ppm upon the addition of one molar equivalent of barbital. The stoichiometry of each of the complexes was confirmed as 1:1 *via* Job plots derived from the NMR data, which displayed a maximum at 0.5 mole fraction of the receptor. The values of the binding constants for each complexation experiment were then determined using the EQNMR program (Table 1).[6]

From Table 1 it is clear that there is a correlation between the number of the hydrogen bonds and the value of the binding constant. Receptor **3** forms the most stable complex *via* four hydrogen bonds with trimethylene urea, suggesting that ethylene urea is too small for the cavity formed by these receptors. Interestingly, **3** only forms a weak complex with barbital which is a similar size to trimethylene urea. This reflects the fact that there are two carbonyl groups on the barbital guest, which are not involved directly in hydrogen bonding but nevertheless are adjacent to a hydrogen bond, leading to unfavourable diagonal secondary electrostatic interactions.[7] In a related manner, trimethylene urea forms weaker complexes with receptors **4** and **5** compared to receptor **3**. The additional hydrogen bond donor groups on **4** and **5** are not directly involved in hydrogen bond formation but still contribute to unfavourable diagonal secondary electrostatic interactions with the adjacent hydrogen bonds. As expected, the highest binding constants, *via* the formation of six hydrogen bonds, are observed between barbital and receptors **4** and **5**. In fact, **4** binds more strongly than **5**, where the difference beween these two receptors arises at the hydrogen bond donor groups in position R, being amines or amides respectively. A related effect has previously been reported with ferrocene receptors used in anion recognition studies.[8]

Single crystals suitable for study by X-ray crystallography were obtained *via* the diffusion of diethyl ether into a chloroform solution of barbital and **5**.‡ The structures in Fig. 1 show that, as expected, barbital is complexed in a 1:1 stoichiometry through complementary hydrogen bonds. The hydrogen bond lengths in Table 2 show that the closest contacts are between barbital and the amide groups at the position R (*i.e.* N3 and N3′). The two bonds to the apical O3 atoms of the guest in fact are, in fact, very long for a hydrogen bond. However, it

Table 1 Binding constants (M^{-1}) for complexes **3**–**5**, as determined from ^{1}H NMR titration experiments ($CDCl_3$, 298 K)

Receptor	Ethylene urea	Trimethylene urea	Barbital
3	250 ± 5	600 ± 20	195 ± 6
4	—[a]	110 ± 2	3200 ± 242
5	—[a]	25 ± 2	2150 ± 127

[a] Weak binding with several complexes formed in solution.

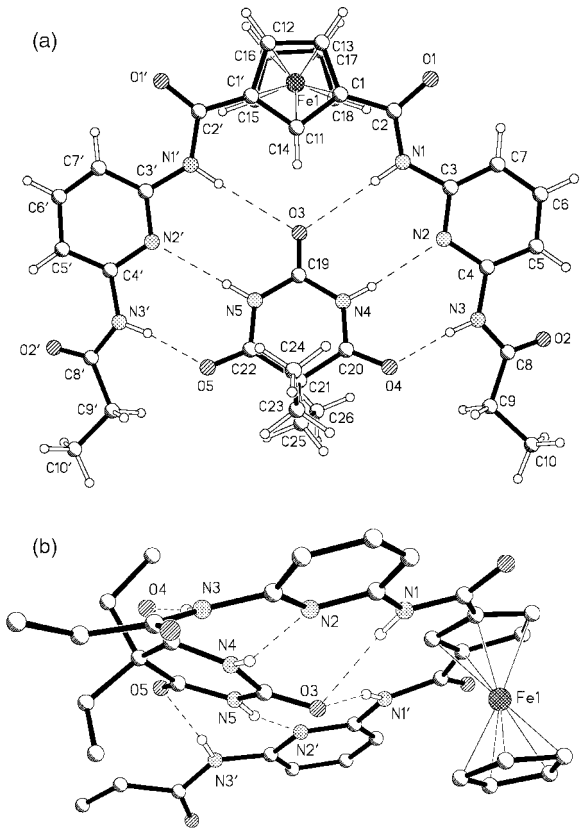

Fig. 1 (a) Top and (b) side views of the X-ray structure of [**5**:barbital].

Table 2 Hydrogen bond lengths and anglesin the X-ray structure of [**5**:barbital]

	Separation (D···A/Å	Angle (DHA)/°
N1–O3	3.434(7)	174.2
N1′–O3	3.494(7)	164.7
N4–N2	3.105(8)	156.6
N5–N2′	3.116(8)	165.3
N3–O4	2.865(7)	174.4
N3′–O5	2.892(8)	171.5

is clear that in solution, these two hydrogen bonds are formed since both resonances for the amide protons of the receptor undergo large downfield shifts upon addition of barbital. In fact, unambiguous assignment of the two resonances corresponding to these two pairs of amide protons was achieved through NOE experiments, allowing the observation that in the presence of 1.5 equiv. of barbital, the resonance for the amide protons adjacent to the Cp-ferrocene ring shifted by +0.9 ppm compared to a larger shift of +1.19 ppm for the resonance for the amide protons at position R. These findings are therefore in agreement with the solid state results in that the strongest amide hydrogen bonds are those that are the furthest away from the ferrocene unit. It is interesting to note that a similar trend in bond lengths was found in the crystal structure of the same guest with the macrocyclic host **1**.[4b] Furthermore, in both structures, the guest is oriented at an angle with respect to the plane formed by the 1,3-arms of the host (**1**:barbital = 27°,[4b] **5**:barbital = 38°).

The nature of the spacer group affects the binding constant with barbital. For Hamilton's analagous acyclic receptor **2**, where the spacer is a 1,3-isophthalic acid group,[4a] the binding constant with barbital in $CDCl_3$ is approximately one order of magnitude higher than that between **5** and barbital (K = 2.08 × 10^4 and 2.15 × 10^3 M^{-1} respectively). A likely explanation for this difference is that the angle between the 1,3-arms in the ferrocene host is larger (the angle geometry is 144 and 120° respectively for five and six-membered rings) which results in the guest having to position itself even closer to the spacer group, with its protuding Cp–H proton, to form hydrogen bonds of any reasonable length. However, additional electronic effects can not be completely ruled out since the Cp unit should lower the acidity of the proximate amide hydrogens, as it is more electron donating than benzene. To examine this effect further, electrochemical measurements were undertaken to assess the effect of oxidising the ferrocene unit on the binding strength. Receptor **5** undergoes a reversible oxidation in dry CH_2Cl_2 at 298 K [E = 0.41 V *vs.* ferrocene internal reference, where E = (E_{pa} + E_{pc})/2], corresponding to the Fe^{II}/Fe^{III} redox couple. Upon addition of excess barbital, a modest cathodic shift of −20 (±5) mV in this redox couple was observed, reflecting a slightly stronger binding of the guest upon oxidation of the ferrocene unit,§ as found previously with related hydrogen bonding ferrocene receptors.[2a] Therefore, the introduction of a positive charge and the resulting electron withdrawing effect from the spacer group would appear to increase the hydrogen bonding strength, although this effect is not as pronounced as when the guest is bridged between the two Cp rings.[2a,b] In conclusion, we have shown that a series of ferrocene compounds can form discrete complexes with a range of biologically relevant molecules through hydrogen bonding interactions. Further binding studies with these and other related receptors are currently underway.

We thank the EPSRC for the award of a PDRA grant (S. R. C.).

Notes and references

† Present address: School of Chemistry, University of Nottingham, University Park, Nottingham, UK NG7 2RD.

‡ *Crystal data* for the 1:0.5 solvate of receptor **5**-barbital with $CDCl_3$; orange blocks from $CDCl_3$–Et_2O, T = 150 K, $C_{36.56}H_{40.50}Cl_{1.50}FeN_8O_7$, M = 812.29, monoclinic, a = 11.281(2), b = 26.560(5), c = 13.995(3) Å, β = 107.39(3)°, U = 4001.5(14) Å^3, space group $P2_1/n$, Z = 4, D_c = 1.348 Mg m^{-3}, μ(MoKα) = 0.789 mm^{-1}, crystal size = 0.10 × 0.07 × 0.07 mm^3, Final R [on 6173 $F > 2\sigma(F^2)$] = 0.0841 and wR (on F^2) = 0.1740. CCDC 154652. See http://www.rsc.org/suppdata/cc/b0/b009820p/ for crystallographic data in .cif or other electronic format.

§ Reference electrode Ag/AgCl; scan rate 100 mV s^{-1}; for other conditions used, see reference 2*b*. Although a clear negative shift in the redox couple was observed upon complexation, the small magnitude of this shift along with the slight increase in peak separation (E_{pa} − E_{pc} (±5 mV); **5**, 75 mV; **5**: barbital, 85 mV; ferrocene internal reference, 70 mV) made the binding enhancement difficult to quantify without a computer simulation.

1 (*a*) P. D. Beer, P. A. Gale and G. Z. Chen, *J. Chem. Soc., Dalton Trans.*, 1999, 1897 and references therein; (*b*) P. D. Beer, *Acc. Chem. Res.*, 1998, **31**, 71 references therein; (*c*) H. Plenio and C. Aberle, *Angew. Chem., Int. Ed.*, 1998, **37**, 1397; (*d*) K. S. Bang, M. B. Neilsen, R. Zubarev and J. Becher, *Chem. Commun.*, 2000, 215.

2 (*a*) J. D. Carr, S. J. Coles, M. B. Hursthouse, M. E. Light, J. H. R. Tucker and J. Westwood, *Angew. Chem., Int. Ed.*, 2000, **39**, 3296 and references therein; (*b*) J. D. Carr, L. Lambert, D. E. Hibbs, M. B. Hursthouse, K. M. A. Malik and J. H. R. Tucker, *Chem. Commun.*, 1997, 1649 and references therein; (*c*) T. H. Galow, F. Ilham, G. Cooke and V. M. Rotello, *J. Am. Chem. Soc.*, 2000, **122**, 3595; (*d*) Y. Ge and D. K. Smith, *Anal. Chem.*, 2000, **72**, 1860.

2 T. DuQuesne and J. Reeves, *A Handbook of Psychoactive Medicine*, Quartet Books Ltd, 1982.

4 (*a*) S. K. Chang and A. D. Hamilton, *J. Am. Chem. Soc.*, 1988, **110**, 1318; (*b*) S. K. Chang, D. Van Engen, E. Fan and A. D. Hamilton, *J. Am. Chem. Soc.*, 1991, **113**, 7640; (*c*) I. Aoki, Y. Kawaharay, T. Sakaki, T. Hanada and S. Shinkai, *Bull. Chem. Soc. Jpn.*, 1993, **66**, 927.

5 R. Deschenaux, I. Kosztics and B. Nicolet, *J. Mater. Chem.*, 1995, **5**, 2291 and references therein.

6 M. J. Hynes, *J. Chem. Soc., Dalton Trans.*, 1993, 311.

7 (*a*) W. L. Jorgensen and J. Prahata, *J. Am. Chem. Soc.*, 1990, **112**, 2008; (*b*) S. C. Zimmerman and T. J. Murray, *Tetrahedron Lett.*, 1994, **35**, 4077; (*c*) J. E. McGrady and D. M. P. Mingos, *J. Chem. Soc., Perkin Trans. 2*, 1995, 2287.

8 P. D. Beer, A. R. Graydon, A. O. M. Johnson and D. K. Smith, *Inorg. Chem.*, 1997, **36**, 2112.

Facile synthesis of cofacial porphyrin dimer and trimer using a diarylurea linkage†

Shigeyuki Yagi,* Isamu Yonekura, Minori Awakura, Masayuki Ezoe and Toru Takagishi*

Department of Applied Materials Science, Graduate School of Engineering, Osaka Prefecture University, Gakuen-cho, Sakai, Osaka 599-8531 Japan. E-mail: yagi@ams.osakafu-u.ac.jp; Tel: +81-722-54-9324; Fax: +81-722-54-9913

Received (in Cambridge, UK) 29th November 2000, Accepted 8th February 2001
First published as an Advance Article on the web 5th March 2001

Diarylurea-linked zinc porphyrin dimer and trimer were newly prepared: taking advantage of the structural characteristics of the diarylurea skeleton led to a convenient arrangement of the porphyrin chromophores in a cofacial manner.

Multi-porphyrin arrays and their photochemical properties have been attracting much attention from the viewpoint of the construction of suitable models for photosynthetic functions such as light gathering, excitation energy relay and long-range charge separation as well as their potential applications as molecular photonic devices such as solar cells, photon-gated molecular wires, and so on.[1] In multi-porphyrin arrays, photochemical processes, especially photo-induced energy and electron transfer are significantly affected by the inter-chromophore distance. Much effort has been devoted to regulating orientation among porphyrin chromophores by means of both covalent and non-covalent approaches,[2,3] but more convenient methods are still required to arrange the chromophores in various well-defined manners. In the present communication, we report the facile synthesis and conformational control of porphyrin dimer and trimer by using a diarylurea linkage, where the porphyrin chromophores are arranged in a cofacial manner.

As shown in Fig. 1a, *N*,*N*′-diarylurea predominantly adopts a *trans*,*trans*-conformation.[4] If porphyrin skeletons are introduced into the 5 and 5′ positions and the rotation of the N–C bonds (arrows a and a′ in Fig. 1a) is fixed by steric repulsion between the substituents introduced into the 2 and 2′ positions (*e.g.* methyls) and the carbonyl oxygen, the chromophores should be forced into a cofacial arrangement (Fig. 1b). In addition, diarylurea is easily obtained by the reaction of the corresponding amine and isocyanate in good yield. Thus, a diarylurea skeleton is a good candidate for the linkage in the construction of a cofacial porphyrin array. In Scheme 1 is shown the synthesis of diarylurea-linked zinc porphyrin dimer **1**, which is carried out in a similar manner to the preparation of urea-functionalized porphyrins reported by Collman.[5] Aminoporphyrin **3** was converted to the corresponding isocyanate **4** by treating with triphosgene in dry dichloroethane containing a small amount of dry pyridine. The reaction of **4** with another molecule of **3** followed by insertion of zinc(II) ions afforded zinc porphyrin dimers **1a** and **1b** in 73 and 49% yields from **3a** and **3b**, respectively. In the similar way, the reaction of 2 equiv. of **4a** with 1 equiv. of diaminoporphyrin **5** afforded trimer **2** in 44% yield from **3a**. The reference monomer **6** was also prepared from **3a** and aniline in 90% yield. Each compound was identified by ^{1}H NMR, ^{1}H–^{1}H COSY, electronic absorption, IR and FAB mass spectra and elemental analysis.†

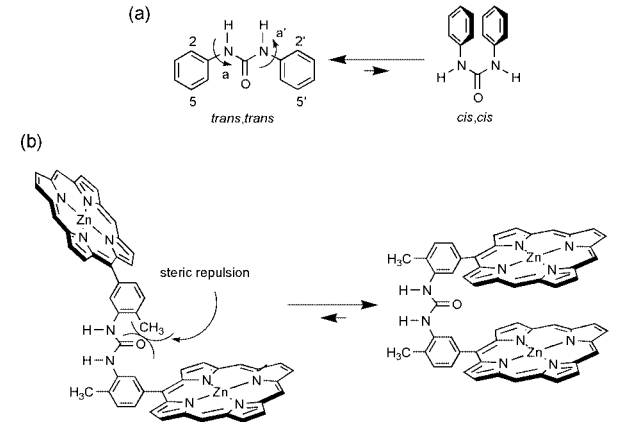

Fig. 1 (a) Conformational equiliblium in diarylurea. (b) An illustration of the conformational control of diarylurea-linked porphyrin dimer.

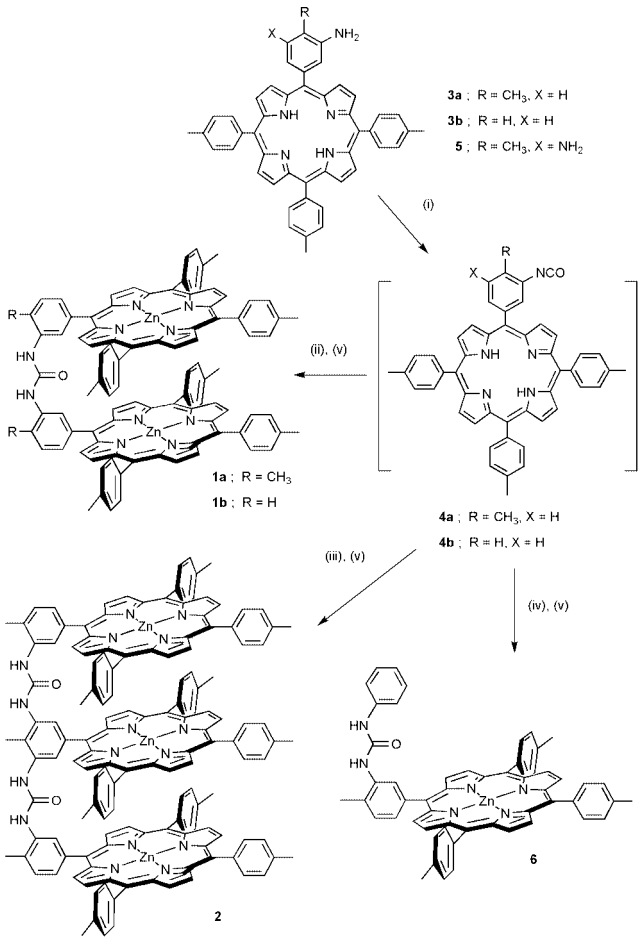

Scheme 1 *Reagents and conditions*: (i) triphosgene, dry pyridine, dry CH_2ClCH_2Cl, rt; (ii) **3** (1 eq.), reflux; (iii) **4a** (2 eq.) and **5** (1 eq.), reflux; (iv) aniline, reflux; (v) $Zn(OAc)_2$, CH_2Cl_2–EtOH, reflux.

† Electronic supplementary information (ESI) available: ^{1}H NMR, electronic absorption, IR and FAB mass spectra and elemental analysis data for **1a**, **1b**, **2** and **6**. See http://www.rsc.org/suppdata/cc/b0/b009578h/

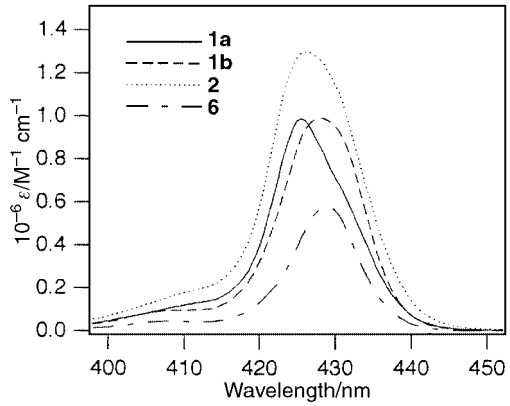

Fig. 2 Electronic absorption spectra of **1a**, **1b**, **2** and **6** in the Soret region in $CHCl_3$–DMSO (20/1, v/v) at 293 K.

Firstly, electronic absorption spectra gave us some information about the orientation between the chromophores in the zinc porphyrin oligomers **1** and **2**. The absorption spectra in the Soret region for **1**, **2** and **6** are shown in Fig. 2. The dimer **1b**, which possesses no substituents in the diarylurea skeleton except for the porphyrins, exhibited a similar absorption spectrum to **6**, whereas the absorption maximum of **1a** exhibited a slight blue shift of 4 nm compared to that of **6**, indicating an exitonic coupling between the transitions in the two porphyrin moieties adopting the cofacial arrangement.[6,7] The trimer **2** also exhibited the similar blue shift (λ_{max} = 426 nm), indicating a well-defined cofacial array of three porphyrin units, although the half band width is a little bit larger than that of **1a** (half band widths; 12 and 14 nm for **1a** and **2**, respectively).

The cofacial orientation between the porphyrin units in **1a** was also confirmed by formation of a complex with 1,4-diazabicyclo[2.2.2]octane (DABCO). The porphyrin face-to-face distance in **1a** estimated by a molecular modeling study was 7.0 Å,[8] suitable distance for binding of DABCO through two Zn–N coordination interactions. Addition of an equimolar amount of **1a** to a solution of DABCO in $CDCl_3$–DMSO-d_6 (20 : 1, v/v, 0.34 mM) induced a significantly large upfield shift of the $-CH_2CH_2-$ signal of DABCO from 2.80 to −4.75 ppm, which apparently originated from ring current anisotropy of the two porphyrin rings.[9] In Fig. 3 are shown absorption spectra of **1a** and **1b** in $CHCl_3$–DMSO (20 : 1, v/v) upon addition of varying concentrations of DABCO, and the titration data are summarized in Table 1. An isosbestic point observed in each spectral change (426 and 427 nm for **1a** and **1b**, respectively) indicates 1 : 1 complex formation in the present condition, which was supported by the Job plot. The spectra of **1a** and **1b** both exhibited blue shifts upon complexation with DABCO to

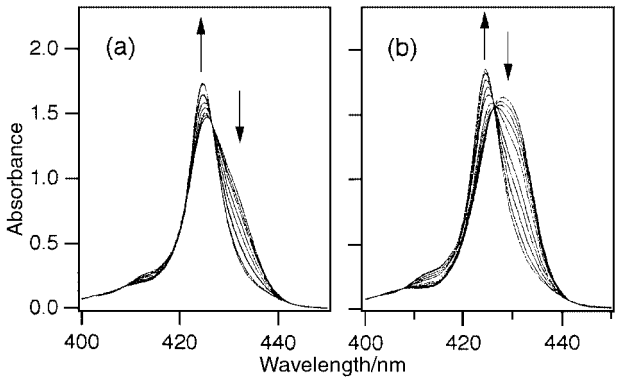

Fig. 3 Electronic absorption spectra of **1a** and **1b** in the presence of varying concentrations of DABCO in $CHCl_3$–DMSO (20/1, v/v) at 293 K. (a) [**1a**], 1.50 μM; [DABCO], 0, 1.22, 2.44, 4.83, 7.75, 11.7, 23.3, 34.8 μM. (b) [**1b**], 1.64 μM; [DABCO], 0, 0.0260, 0.0515, 0.0827, 0.125, 0.249, 0.372, 0.614, 2.50, 3.67 mM.

Table 1 Electronic absorption titration data for **1a**, **1b** and **6** with DABCO in $CDCl_3$–DMSO (20/1, v/v) at 293 K

Compound	λ_{free}[a]/nm	$\lambda_{complex}$[a]/nm	$\Delta\lambda$[b]/nm	K[c]/M^{-1} (s.d., %)
1a	425 (12)	424 (8)	−1	1.48×10^5 (11)
1b	428 (12)	424 (8)	−4	3.59×10^3 (7)
6	429 (10)	431 (9)	2	1.02×10^3 (5)

[a] Absorption maximum in the Soret region. λ_{free}; in the absence of DABCO, $\lambda_{complex}$; upon complexation with DABCO. Half band width in parenthesis. [b] $\lambda_{complex} - \lambda_{free}$. [c] Determined by computer-assisted least-squares analysis of the absorbance changes.

afford an identical narrow Soret absorption (λ_{max} = 424 nm; half band width, 8 nm), although monomer **6** exhibited a red shift upon complexation, induced by the coordination of DABCO's nitrogen to the central zinc of the porphyrin moiety.[10] This suggests that the blue shifts observed in **1a** and **1b** are due to the exitonic interaction between the porphyrin chromophores tightly fixed in a cofacial manner. It is emphasized that the binding constant K for **1a** was 41 times larger than that for **1b**, indicating that the introduction of methyl groups at the 2 and 2′ positions in the diarylurea skeleton of **1a** effectively forces the porphyrin moieties to adopt a cofacial orientation.

In summary, we have demonstrated here a facile method for construction of cofacial porphyrin oligomers by linking porphyrin units by a diarylurea linkage as well as the introduction of appropriate intramolecular steric interactions. As can be seen, alternative copolymerization of **5** with the corresponding porphyrin diisocyanate should afford a linear cofacial porphyrin array. This research is on going.

Notes and references

1 R. W. Wagner and J. S. Lindsey, *J. Am. Chem. Soc.*, 1994, **116**, 9759; J. Seth, V. Palaniappan, T. E. Johnson, S. Prathapan, J. S. Lindsey and D. F. Bocian, *J. Am. Chem. Soc.*, 1994, **116**, 10 578 and references therein; H. L. Anderson, *Chem. Commun.*, 1999, 2323.

2 Covalently linked porphyrin arrays: K. Sugiura, H. Tanaka, T. Matsumoto, T. Kawai and Y. Sakata, *Chem. Lett.*, 1999, 1193; E. K. L. Yeow, K. P. Ghiggino, J. N. H. Reek, M. J. Crossley, A. W. Bosman, A. P. H. J. Schenning and E. W. Meijer, *J. Phys. Chem. B*, 2000, **104**, 2596; F. Takei, K. Onitsuka, N. Kobayashi and S. Takahashi, *Chem. Lett.*, 2000, 914; A. Nakano, T. Yamazaki, Y. Nishimura, I. Yamazaki and A. Osuka, *Chem. Eur. J.*, 2000, **6**, 3254.

3 Supramolecular systems of porphyrin assemblies: C. A. Hunter and R. K. Hyde, *Angew. Chem., Int. Ed. Engl.*, 1996, **35**, 1936; A. P. H. J. Schenning, F. B. G. Benneker, H. P. M. Geurts, X. Y. Liu and R. J. M. Nolte, *J. Am. Chem. Soc.*, 1996, **118**, 8549; S. Knapp, B. Huang, T. J. Emge, S. Sheng, K. Krogh-Jespersen, J. A. Potenza and H. J. Schugar, *J. Am. Chem. Soc.*, 1999, **121**, 7977; N. Nagata, S. Kugimiya and Y. Kobuke, *Chem. Commun.*, 2000, 1389; Y. Kuroda, K. Sugou and K. Sasaki, *J. Am. Chem. Soc.*, 2000, **122**, 7833.

4 M. C. Etter, Z. Urbanczyk-Lipkowska, M. Zia-Ebrahimi and T. W. Panunto, *J. Am. Chem. Soc.*, 1990, **112**, 8415; A. Tanatani, I. Azumaya and H. Kagechika, *J. Syn. Org. Chem., Jpn.*, 2000, **58**, 556.

5 J. P. Collman, Z. Wang and A. Straumanis, *J. Org. Chem.*, 1998, **63**, 2424.

6 M. Kasha, H. R. Rawls and M. A. El-Bayoumi, in *Molecular Spectroscopy VIII*, Butterworths, London, 1965, p. 371.

7 The electronic absorption spectrum of **1a** did not exhibit any significant changes between temperatures 283–323 K. This suggests that **1a** predominantly adopts a cofacial conformation, and does not exist in equilibrium with other conformers.

8 The molecular modeling was performed at MOPAC PM3 level by using the PC Spartan *Pro* program package (Wavefunction Inc., Irvine, California, 1999).

9 In the presence of an excess of DABCO, no porphyrin ligands other than **1a** and **1a**·DABCO complex were observed in the ^1H NMR spectrum, indicating following complexation of DABCO to **1a**·DABCO scarcely occurs.

10 Although the possibility exists of the monomer **6** forming a 1 : 2 complex with two equivalents of DABCO, 1 : 1 complex formation is predominant under dilute conditions: P. N. Taylor and H. L. Anderson, *J. Am. Chem. Soc.*, 1999, **121**, 11 538.

Synthesis of highly ordered nanoporous carbon molecular sieves from silylated MCM-48 using divinylbenzene as precursor

Suk Bon Yoon, Jeong Yeon Kim and Jong-Sung Yu*

Department of Chemistry, Hannam University, Taejon, 306-791, Korea. E-mail: jsyu@mail.hannam.ac.kr

Received (in Cambridge, UK) 4th December 2000, Accepted 13th February 2001
First published as an Advance Article on the web 5th March 2001

Calcined pure silica MCM-48 is modified by silylating its mesopores with trimethylsilyl chloride; such pore modification along with polymerization and carbonization of divinylbenzene as a carbon precursor is found to be a very efficient way of fabricating highly ordered carbon molecular sieves with three-dimensionally interconnected uniform pore arrays, greatly improving structural integrity and thermal stability.

Porous carbons have been greatly studied as adsorbents and electrode materials.[1,2] Since zeolites and other molecular sieves including mesoporous materials possess several attractive characteristics such as high surface area and periodic arrays of uniform pores, they can be used as synthesis templates for carbon with regular pore structures.[3,4] Polymerization and pyrolysis of acrylonitrile were demonstrated in zeolite Y and mordenite channels.[5] The formation of porous carbon by carbonization of poly(acrylonitrile) and poly(furfuryl alcohol) was reported in Y zeolite template.[6] The phenol–formaldehyde polymers and their carbons were also studied in Y, β and L zeolites.[7] However, the pore ordering was not well maintained in the porous carbon structure due to the non-rigidity of the carbon frameworks formed in the narrow pores of zeolites. Most recently, carbon frameworks with ordered pores were reported using mesoporous templates. Ordered porous carbon replicas of the MCM-48 template were reported by converting sucrose in the channels into carbon using an acid catalyst.[8] Mesoporous carbon was also synthesized by acid-catalyzed polymerization of phenol and formaldehyde in Al-implanted MCM-48 followed by carbonization.[9] Here we report the novel synthesis of highly ordered mesoporous carbon materials using a pure silica MCM-48 template with surface-modified pores and divinylbenzene as a carbon precursor. Particularly, this method provides the first example of mesoporous carbon with much improved structural integrity and thermal stability.

High quality silica MCM-48 was prepared using $C_{16}H_{33}N(CH_3)_3Br$ and Brij 30 as surfactants and colloidal silica Luodx HS40 as the silica source based on the modification of reported methods.[10] Calcined silica MCM-48 was first modified by a simple silylation using trimethylsilyl (TMS) chloride according to methods described in literature.[11] After such a silylation, more than 90% of the silanol groups in the pores were replaced with TMS groups [eqn. (1)].

$$(\text{silica})\equiv\text{SiOH} + (CH_3)_3\text{SiCl} \rightarrow (\text{silica})\equiv\text{SiOSi}(CH_3)_3 + \text{HCl} \quad (1)$$

This was confirmed by the decrease of a signal at 960 cm^{-1} corresponding to Si–O stretching in the Si–OH groups before silylation and by the concomitant development of two new signals at 845 and 2960 cm^{-1} ascribed to attached $OSi(CH_3)_3$ groups in the infrared spectra as reported in previous work.[11–13] We denote TMS-modified MCM-48 as TMS-MCM-48 in order to distinguish it from pure silica MCM-48. Such TMS-MCM-48 showed higher hydrophobicity and nonpolarity[11,13] which were confirmed by a marked decrease of a broad signal centered at 3450 cm^{-1} due to physically attached water in the mesopore. The modified pores in the templates were filled by soaking the TMS-MCM-48 template into a carbon precursor solution of 80% divinylbenzene (DVB) with a free radical initiator, azobisisobutyronitrile (AIBN) (DVB–AIBN mole ratio ≅ 10). Dissolved oxygen was removed by several freeze–pump–thaw cycles. Polymerization was performed by heating to 70 °C overnight. The resulting polymer was heavily cross-linked in the template pores. The template–polymer composites were then heated under N_2 gas flow at a heating rate of 1 °C min^{-1} to 750–850 °C and then held under these conditions for 7–10 h to carbonize the polymer. Porous carbon was obtained after subsequent dissolution of the silica framework in 48% aq. HF. The same procedures were also performed on calcined silica MCM-48 without any surface modification. The yield of obtained carbons was about 70–80% in both cases.

XRD patterns were measured at various stages during the course of synthesis (Fig. 1). Two intense peaks with about equal intensity at 2θ = 1.6 and 2.7 in synthesized carbon materials indicate long-range ordering of highly ordered uniform mesopores. It is interesting to note that the first intense peak not seen in parent MCM-48 template occurs in the synthesized carbons. The peak was suggested to occur due to the phase transition of MCM-48 with *Ia*3*d* space group to a new cubic phase with $I4_132$ space group due to shrinkage of the carbon walls upon removal of the silica framework.[8] Surprisingly, the overall XRD intensity for TMS-MCM-48 porous carbon was about two times higher than ones for the parent calcined silica MCM-48 template and for the MCM-48 carbon. Elemental analysis of the porous carbon replica shows a C:H mole ratio of about 23 (C 98.01 and H 0.35 wt%). Energy dispersive X-ray spectrophotometer analysis determined by field emission scanning electron microscopy also indicated a predominantly strong carbon signal at 0.270 keV with a weak residual undissolved silica signal at 1.752 keV.

TEM images from the thin edges of the porous carbon molecular sieves show a regular array of holes separated by walls (Fig. 2). The TMS-MCM-48 porous carbon showed much

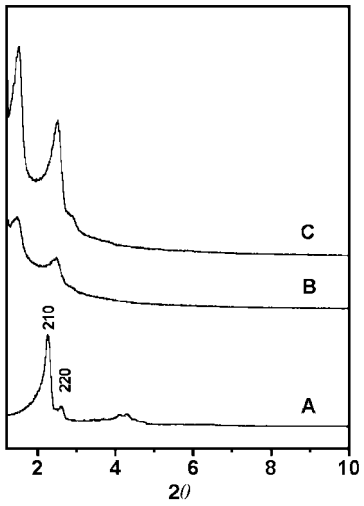

Fig. 1 X-Ray diffraction patterns of (a) calcined pure silica MCM-48 and mesoporous carbon obtained by using (b) silica MCM-48 and (c) TMS-MCM-48 as templates. These XRD patterns were obtained using a Rigaku D/MAX-III (3 kW). Each spectrum was measured under identical experimental conditions.

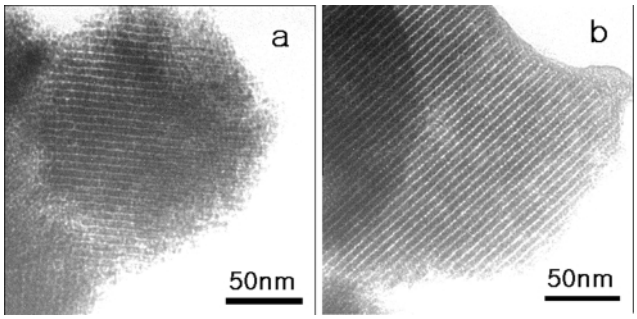

Fig. 2 Transmission electron micrograph (TEM) images of mesoporous carbon obtained by using (a) silica MCM-48 and (b) silica TMS-MCM-48 as templates.

better overall structural order than the MCM-48 porous carbon, which is also in good accordance with XRD results. The specific surface areas of the carbons were found to be 1200 ± 50 m^2 g^{-1} for nitrogen BET adsorption measurements. The pore size distribution data calculated from the adsorption branch of nitrogen adsorption–desorption curves by the BJH (Barrett–Joyner–Halenda) method showed that pores are uniform with quite narrow pore size distribution centered at 2.4 ± 0.2 nm.

Thermogravimetric (TG) weight change was recorded to study the thermal stability of carbons formed by carbonization of DVB in MCM-48 template under an O_2 atmosphere (Fig. 3). There was significant weight loss in a narrow temperature range at *ca.* 830 K for DVB carbon. The high temperature for DVB carbon, in good agreement with those for nanotubes and other graphitized carbons[14,15] indicates that the DVB carbon may have a graphitic nature. The corresponding TG temperature was near to 680 K for sucrose carbon in previous work.[8] This clearly indicates the DVB carbon with much improved thermal stability. Mechanical strength measured by monitoring XRD intensity changes after each pressurizing cycle of the pelletized carbon (100 mg and 1/2 inch diameter) for 1 min with gradually increasing pressure indicates that the DVB carbon was stable with no significant intensity change at pressures less than 4.0 ton cm^{-2} and above that, started decreasing its intensity slowly with 75% XRD intensity maintained at pressures of 4.8 ton cm^{-2} compared to the original intensity at atmospheric pressure. Calcined silica MCM-48 with high crystalline order and its silylated MCM-48 prepared here were stable at pressures of less than 2.4–2.7 ton cm^{-2} and *ca.* 3.0 ton cm^{-2}, respectively, but above these pressures, they started losing their crystallinity. This indicates that the mesoscopic porous carbon prepared here has much higher mechanical strength than the silica template.

In this work, we have obtained high quality mesoporous carbon with much better structural order for TMS-MCM-48 compared to those for MCM-48. This is unclear, but is perhaps due to the removal of oxygen sources in TMS-MCM-48 which are an effective quenching agent for DVB radical polymerization by replacing $Si(OH)_{1\text{ or }2}$ with $SiOSi(CH_3)_3$ *via* silylation. TMS-modified pores are also extremely hydrophobic compared to unmodified ones,[11,13] repelling more water molecules which can also be potential radical reaction quenchers and thus allowing more room for carbon precursors to fully fill the mesopore channels. Carbon prepared with phenol and formaldehyde was shown to have low thermal stability and lower structural ordering.[8] Also when we measure the XRD intensity ratios of the mesoporous carbon *versus* the parent calcined pure silica MCM-48 template as determined from a flat base line, our high quality carbon showed a much higher ratio of 2.2–2.5 than carbons prepared by carbonization of sucrose of about 1.3–1.6.[8] In addition, MCM-48 templated DVB carbon shows higher thermal stability than the corresponding sucrose carbon.

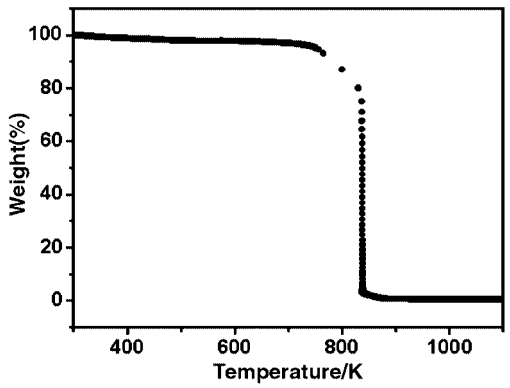

Fig. 3 Thermogravimetric weight change curve under an O_2 atmosphere for MCM-48 templated carbons prepared by the carbonization of DVB.

In summary, two major factors were considered in this work to improve the quality of mesoporous carbons: hydrophobicity of the template channels and the carbon precursor. The surface modification of the MCM-48 template and the use of DVB as a carbon precursor are considered to be a most efficient way of synthesizing highly ordered mesoporous carbons with greater structural integrity and thermal stability. We are currently carrying out further studies to evaluate this method which can be extended to the preparation of other high quality mesoporous carbons. We have synthesized carbons in the MCM-41 template using the same method. TEM pictures of the extracted carbon fibers showed continuous linear patterns due to carbon nanofibers, but in general not as orderly as the MCM-48 templated carbon because the fibers are not bound to each other in MCM-41. The highly ordered mesoporous carbon materials with superior structural integrity and thermal stability will find many new advanced applications in the future.

We thank the Korean Ministry of Science and Technology (I-01-03-A-073) and the Basic Science Institute (in Taejon) program (TEM images).

Notes and references

1 F. Rodriguez-Reinoso, in *Introduction to Carbon Technology*, ed. H. Marsh, E. A. Heintz and F. Rodriguez-Reinoso, Universidad de Alicante, Secretariado de Pub. Alicante, 1997, p. 35.
2 R. Ramkmar, S. Dheenadayalan and R. Pattabiraman, *J. Power Sources*, 1997, **69**, 75.
3 D. W. Breck, *Zeolite Molecular Sieves*, John Wiley, New York, 1974, ch. 8.
4 C. T. Kresege, M. E. Leonowizc, W. J. Roth, J. C. Vartuli and J. S. Beck, *Nature*, 1992, **359**, 710; M. W. Anderson, *Zeolites*, 1997, **19**, 220; P. Van Der Voort, M. Mathieu, F. Mess and E. F. Vansant, *J. Phys. Chem. B*, 1998, **102**, 8847; A. Corma, *Chem. Rev.*, 1997, **97**, 2373.
5 P. Enzel and T. Bein, *Chem. Mater.*, 1992, **4**, 819.
6 T. Kyotani, T. Nagai, S. Inoue and A. Tomita, *Chem. Mater.*, 1997, **9**, 609.
7 S. A. Johnson, E. S. Brigham, P. J. Olliver and T. E. Mallouk, *Chem. Mater.*, 1997, **9**, 2448.
8 R. Ryoo, S. H. Joo and S. Jun, *J. Phys. Chem. B*, 1999, **103**, 7743; M. Kruk, M. Jaroniec, R. Ryoo and S. H. Joo, *J. Phys. Chem. B*, 2000, **104**, 7960.
9 J. W. Lee, S. H. Yoon, T. H. Hyeon, S. M. Oh and K. B. Kim, *Chem. Commun.*, 1999, 2177.
10 R. Ryoo, S. H. Joo and J. M. Kim, *J. Phys. Chem. B*, 1999, **103**, 7435.
11 T. Kimura, S. Saeki, Y. Sugahara and K. Kuroda, *Langmuir*, 1999, **15**, 2794; F. D. Juan and E. Ruiz-Hitzky, *Adv. Mater.*, 2000, **12**, 430.
12 G. Socrates, *Infrared Characteristic Group Frequencies: Tables and Charts*, John Willey, New York, 1994, 2nd edn., ch. 18.
13 J. Chen, Q. Li, R. Xu and F. Xiao, *Angew. Chem., Int. Ed. Engl.*, 1995, **34**, 2694.
14 A. G. Rinzler, J. Liu, H. Dai, P. Nokolaev, C. B. Huffman, F. J. Rodriguez-Marcuas, P. J. Boul, A. H. Lu, D. Heymann, D. T. Colbert, R. S. Lee, J. E. Fisher, A. M. Rao, P. C. Eklund and R. E. Smalley, *Appl. Phys. A*, 1998, **67**, 29.
15 A. C. Dillon, T. Gennett, K. M. Jones, J. L. Alleman, P. A. Parilla and M. J. Heben, *Adv. Mater.*, 1999, **11**, 1354.

ChemComm

A fluorescent metal sensor based on macrocyclic chelation†

Gérard Klein, Daniel Kaufmann, Stefan Schürch and Jean-Louis Reymond*

Departement für Chemie und Biochemie, Universität Bern, Freiestrasse 3, 3012 Bern, Switzerland. E-mail: jean-louis.reymond@ioc.unibe.ch

Received (in Cambridge, UK) 15th January 2001, Accepted 14th February 2001
First published as an Advance Article on the web 6th March 2001

The ethylenediamine functionalized quinacridone derivatives 3a–c display an orange fluorescence ($\lambda_{em\,(max)}$ = 558 nm) which is quenched upon addition of coordinating metal ions by formation of a macrocyclic chelate bringing metal ion and fluorophore in close proximity to one another.

A number of small-molecule fluorescent sensors for metal ions have been developed in recent years, and find applications in trace-ion analysis and imaging. Fluorescence modulation upon metal binding is commonly observed whenever a fluorophore interacts directly with a non-bonding electron pair belonging to a metal-chelating group, typically placed one (phenols and anilines) or two (benzylic heteroatoms) bonds away from the fluorophore. This design forms the basis for the vast majority of fluorescent metal sensors described to date,[1–3] and usually implies that the metal sensors also operate as pH sensors. Herein we report a new type of fluorescent sensor in which a fluorescence quenching effect is obtained by formation of a macrocyclic metal chelate bringing metal ion and fluorophore in close proximity to one another. There is no direct interaction between the chelating group and the fluorophore, which avoids pH sensing.

Our sensor design is based on quinacridone **1**, a red organic pigment used in the dye industry and structurally related to acridone (Scheme 1).[4] A pair of chelating groups, such as ethylenediamines, are attached *via* a linker to each nitrogen atom of the symmetrical quinacridone. The linker is chosen long enough such that the protonation state of the chelating groups does not influence the fluorophore. Most importantly, the long linker now also allows a coordinating metal ion to bind simultaneously at both groups by forming a macrocyclic chelate in which the metal is in close proximity to the quinacridone chromophore. Such an arrangement should result in fluorescence quenching, in particular with energy-transfer quenching metal ions such as copper and nickel.[5]

Double alkylation of quinacridone **1** with dibromoalkanes gives dibromides **2a–c**. Further reaction with excess ethylenediamine then leads to ligands **3a–c** (Scheme 1). All ligands are obtained as trifluoroacetate salts after purification by reverse-phase HPLC.

As expected, the fluorescence spectra of ligands **3a–c** is independent of pH, with < 20% variation in intensity between pH 2 and pH 10. Fluorescence is directly proportional to concentration (0.1–100 μM, pH 7.2 or 9.0), showing that the ligands are not susceptible to auto-quenching. At pH 7.2, addition of Cu^{2+} to ligands **3a–c** induces almost complete quenching of fluorescence (98% quenching, $EC_{50} \approx 0.5$ μM at 1 μM ligand). There is no response with other divalent metal ions such as Hg^{2+}, Ni^{2+}, Co^{2+}, Zn^{2+}, Mg^{2+}, Ba^{2+}, Ca^{2+}, Mn^{2+}, Fe^{2+}, Pb^{2+}, Sr^{2+} (10^{-4} M of the chloride salts). At pH 9.0, quenching is observed for all three ligands with Cu^{2+} (Fig. 1), Ni^{2+} (96% quenching, $EC_{50} \approx 0.8$ μM), Co^{2+} (94% quenching, $EC_{50} \approx 8$ μM), and to a lesser extent with Hg^{2+} (70% quenching, $EC_{50} \approx 0.9$ μM) and Zn^{2+} (45% quenching, $EC_{50} \approx 0.7$ μM). The observed selectivity and pH-dependence of metal complexation with ligands **3a–c** corresponds to the stability constants of ethylenediamine metal complexes.[6] Fluorescence returns to its full intensity upon acidification of the metal–ligand solutions, as well as with high concentrations ($> 10^{-4}$ M) of Zn^{2+} or Hg^{2+}. In all cases the shape of the fluorescence spectrum is unaffected by quenching ($\lambda_{em\,(max)}$ = 558 nm). Remarkably, quenching has little effect on the visible absorbance spetrum or the wavelength of fluorescence emission. Thus solutions of free and complexed ligands **3a–c** show an indistinguishable red color in transparence. Under reflected light, however, the solutions of free ligands **3a–c** shine orange due to their fluorescence, while the metal-complexed ligands remain red (see ESI†).

Fluorescence titration curves at [L] = 1×10^{-5} M show a 1:1 stoichiometry of complexation for L = **3a–c** with Cu^{2+}, suggesting ML, M_2L_2 or M_nL_n modes of complexation.

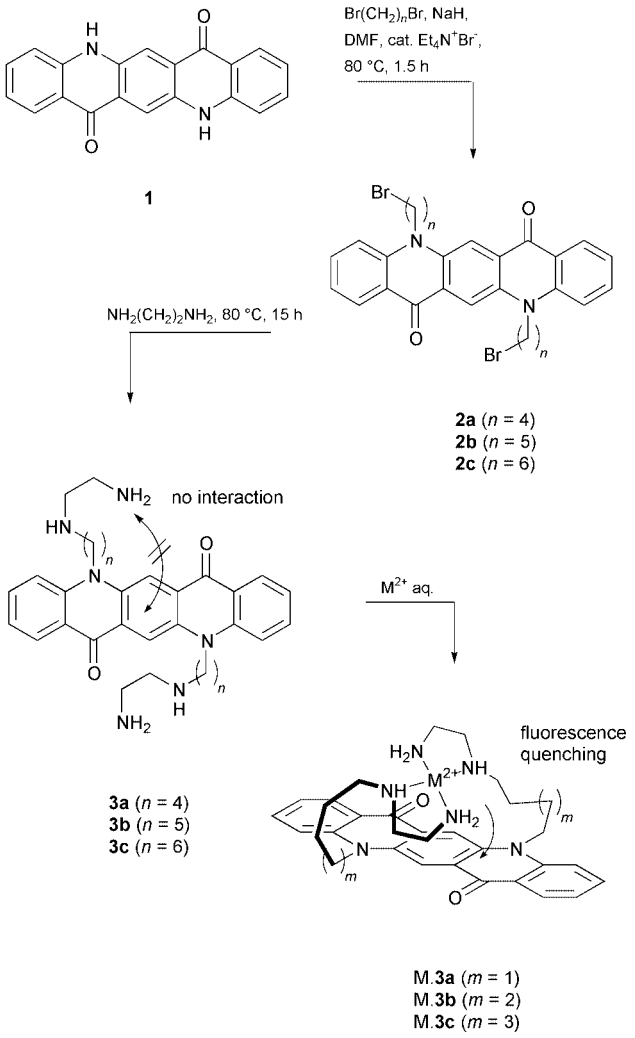

Scheme 1 Synthesis of ligands **3a–c** from quinacridone **1**. Complexation with coordinating metal ions (M = Cu, Hg, Zn, Ni, Co) leads to a macrocycle in which the metal ion is placed above the aromatic nucleus.

† Electronic supplementary information (ESI) available: electrospray MS data and photographs of solutions of ligand **3c** in the absence and presence of Cu^{2+}. See http://www.rsc.org/suppdata/cc/b1/b100535i/

DOI: 10.1039/b100535i

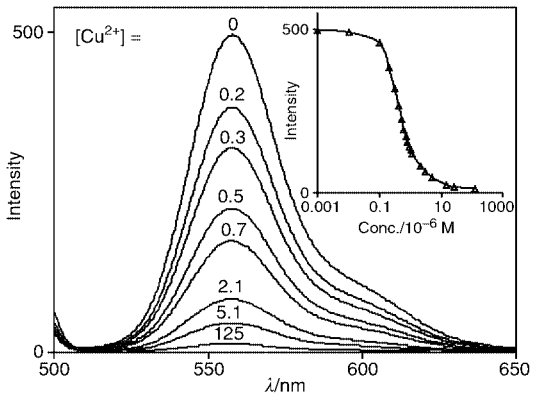

Fig. 1 Fluorescence emmission spectrum of 1×10^{-6} M ligand **3a** in the presence of increasing concentrations of Cu^{2+}. Insert: fluorescence intensity at λ_{em} = 558 nm as a function of copper concentration. Measured at 25 °C in H_2O–DMF 60 : 40, 1 mM Tris, pH 9.0, with λ_{ex} = 485 nm using a Perkin Elmer Luminescence spectrometer LS 50B.

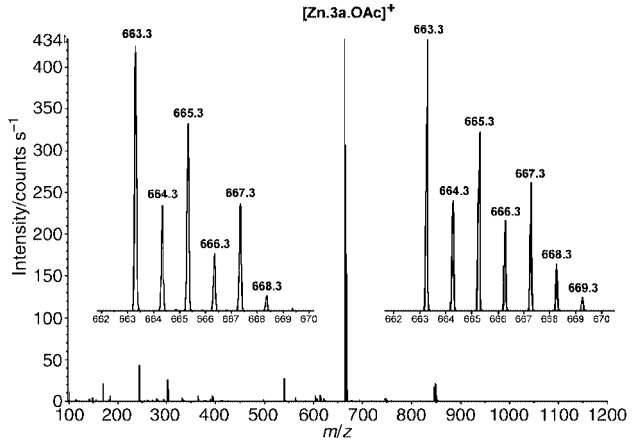

Fig. 2 Electrospray mass spectrum of the Zn.**3a** sample (10^{-3} M equimolar solution of **3a** and $Zn(OAc)_2$ in methanol). The spectrum exhibits an average mass resolving power of 10 000 (FWHM), which allows for full separation of the isotopic patterns. Insets show the measured (left) and calculated (right) pattern of the most abundant complex $[Zn.\mathbf{3a}.OAc]^+$, $C_{34}H_{46}N_6O_4Zn$, *m*/*z* = 663.264. Measured with a Sciex Q-Star Pulsar hybrid quadrupole-time-of-flight mass spectrometer (Applied Biosystems, Rotkreuz, Switzerland) equipped with a nanospray ion source (Protana, Odense, Denmark). A voltage of 1000 V was applied to the nanospray-needle and nitrogen was used as the drying gas.

Electrospray mass spectrometry shows that the ML complex is formed in equimolar solutions of metal ion and ligand **3a–c**. The ML complex disappears in favor of an M_2L species with excess metal [Fig. 2 and Table 1 (ESI)†].

In view of the MS-analysis, the fluorescence data is best interpreted in terms of the formation of an ML complex with a macrocyclic structure as shown in Scheme 1, where fluorescence is quenched by proximity of the coordinating metal.[7] The fact that quenching does not affect markedly either the aborbance (Fig. 2) or the fluorescence emmission spectrum is consistent with an energy-transfer mechanism for quenching. The quenching interaction disappears with the poor energy-transfer quenchers Zn^{2+} and Hg^{2+} when the M_2L complex is formed at high metal concentration, because the metal ions are not close enough to the fluorophore in this complex.[7] The continued quenching observed at high metal concentration with Cu^{2+}, Ni^{2+} or Co^{2+} can be explained by a transition to non-specific quenching by these strong energy-transfer quenchers.

The above experiments demonstrate that efficient fluorescent sensing of metal ions is possible by using a macrocyclic chelation effect. By contrast to standard metal sensors, there is no direct interaction between the metal-chelating groups and the fluorophore, which excludes pH-sensing. The fluorescence modulation obtained is directly visible by the eye since it occurs in the visible range. Remarkably, even weak quenching ions such as Hg^{2+} and Zn^{2+} produce an important fluorescence modulation by macrocyclic chelation. We are currently investigating the construction of macrocyclic chelation sensors with other fluorophores.

This work was supported by the Swiss National Science Foundation and the University of Bern. The authors thank Professor T. Ward for helpful discussions.

Notes and references

1 Reviews: A. P. de Silva, H. Q. N. Gunaratne, T. Gunnlaugsson, A. J. M. Huxley, C. P. McCoy, J. T. Rademacher and T. E. Rice, *Chem. Rev.*, 1997, **97**, 1515; A. W. Czarnik, *Chem. Biol.*, 1995, **2**, 423; A. W. Czarnik, *Acc. Chem. Res.*, 1994, **27**, 302; R. A. Bissell, A. P. de Silva, H. Q. N. Gunaratne, P. L. M. Lynch, G. E. M. Maguire, C. P. McCoy and K. R. A. S. Sandanayake, *Top. Curr. Chem.*, 1993, **168**, 223.

2 L. Fabbrizzi, M. Licchelli, P. Pallavicini, A. Perotti and D. Sacchi, *Angew. Chem., Int. Ed. Engl.*, 1994, **33**, 1975; L. Fabbrizzi, M. Licchelli, P. Pallavicini, A. Perotti, A. Taglietti and D. Sacchi, *Chem. Eur. J.*, 1996, **2**, 75; A. P. de Silva, H. Q. N. Gunaratne and C. P. McCoy, *J. Am. Chem. Soc.*, 1997, **119**, 7891; B. Ramachandran and A. Samanta, *Chem. Commun.*, 1997, 1037; G. E. Collins and L.-S. Choi, *Chem. Commun.*, 1997, 1135; J. Yoon, N. E. Ohler, D. H. Vance, W. D. Aumiller and A. W. Czarnik, *Tetrahedron Lett.*, 1997, **38**, 3845; U. Oguz and E. U. Akkaya, *Tetrahedron Lett.*, 1997, **38**, 4509; E. Brunet, M. T. Alonso, O. Juanes, R. Sedano and J. C. Rodriguez-Ubis, *Tetrahedron Lett.*, 1997, **38**, 4459; L. Prodi, F. Bolletta, N. Zaccheroni, C. I. F. Watt and M. J. Mooney, *Chem. Eur. J.*, 1998, **4**, 1090; L. Fabbrizzi, M. Licchelli, P. Pallavicini and L. Parodi, *Angew. Chem.*, 1998, **110**, 838; G. Hennrich, H. Sonnenschein and U. Resch-Genger, *J. Am. Chem. Soc.*, 1999, **121**, 5073; W.-S. Xia, R. H. Schmehl and C.-J. Li, *J. Am. Chem. Soc.*, 1999, **121**, 5599; H.-F. Ji, G. M. Brown and R. Dabestani, *Chem. Commun.*, 1999, 609; K. Rurack, M. Kollmannsberger, U. Retsch-Genger and J. Daub, *J. Am. Chem. Soc.*, 2000, **122**, 968; G. K. Walkup, S. C. Burdette, S. J. Lippard and R. Y. Tsien, *J. Am. Chem. Soc.*, 2000, **122**, 5644; L. Prodi, C. Bargossi, M. Montalti, N. Zaccheroni, N. Su, J. S. Bradshaw, R. M. Izatt and P. B. Savage, *J. Am. Chem. Soc.*, 2000, **122**, 6769; H.-F. Ji, R. Dabestani, G. M. Brown and R. A. Sachleben, *Chem. Commun.*, 2000, 833; W.-S. Xia, R. H. Schmehl and C.-J. Li, *Chem. Commun.*, 2000, 695; W.-S. Xia, R. H. Schmehl and C.-J. Li, *Eur. J. Org. Chem.*, 2000, 387.

3 Metal-sensors based on conformational changes affecting fluorescence: G. K. Walkup and B. Imperiali, *J. Am. Chem. Soc.*, 1996, **118**, 3053; G. K. Walkup and B. Imperiali, *J. Am. Chem. Soc.*, 1997, **119**, 3443; H. A. Godwin and J. M. Berg, *J. Am. Chem. Soc.*, 1996, **118**, 6415; A. Torrado, G. K. Walkup and B. Imperiali, *J. Am. Chem. Soc.*, 1998, **120**, 609; lipid aggregates: D. Y. Sasaki, D. R. Shnek, D. W. Pack and F. H. Arnold, *Angew. Chem.*, 1995, **107**, 995; dendrimers: V. Balzani, P. Ceroni, S. Gestermann, C. Kauffmann, M. Gorka and F. Vôgtle, *Chem. Commun.*, 2000, 853; perhydroanthracene: R. Krauss, H.-G. Weinig, M. Seydack, J. Bendig and U. Koert, *Angew. Chem.*, 2000, **112**, 1905.

4 For sensors for organic ligands using acridone see: J.-L. Reymond, T. Koch, J. Schröer and E. Tierney, *Proc. Natl. Acad. Sci. USA*, 1996, **93**, 4251; N. Bahr, E. Tierney and J.-L. Reymond, *Tetrahedron Lett.*, 1997, **38**, 1489; P. Geymayer, N. Bahr and J.-L. Reymond, *Chem. Eur. J.*, 1999, **5**, 1006; J. H. Rothman and W. C. Still, *Bioorg. Med. Chem. Lett.*, 1999, **9**, 509.

5 F. Bolletta, H. Costa, L. Fabbrizzi, M. Licchelli, M. Montalti, P. Pallavicini, L. Prodi and N. Zaccheroni, *J. Chem. Soc., Dalton Trans.*, 1999, 1381.

6 *Stability Constants Part 1, Organic Ligands*, Special Publication No. 6, The Chemical Society, London, 1957.

7 Molecular modelling (Spartan 5.1, semi-empirical calculations with PM3(tm)) shows that the metal ions (calculated for Cu^{2+} and Ni^{2+}) are placed at 5.5–6.5 Å above the quinacridone rings in all combinations of ligands **3a**, **3b** or **3c**, with tetrahedral, trigonal bipyramidal (+ 1 H_2O) or octahedral (+ 2 H_2O) coordination. In the M_2L complexes, the metal is placed on the side at 8.2 Å (with **3a**) to 11 Å (with **3c**) from the quinacridone.

Tandem reductive ring opening-retro-Bingel reactions of bismethano[60]fullerenes to give 1,2-dihydro[60]fullerylglycines

Glenn A. Burley,[a] Paul A. Keller,*[a] Stephen G. Pyne*[a] and Graham E. Ball[b]

[a] *Department of Chemistry, University of Wollongong, Wollongong, New South Wales, 2522, Australia. E-mail: Stephen_Pyne@uow.edu.au; Paul_Keller@uow.edu.au*
[b] *NMR Spectroscopy Unit, University of New South Wales, Sydney, New South Wales, 2052, Australia*

Received (in Cambridge) 17th January 2001, Accepted 12th February 2001
First published as an Advance Article on the web 6th March 2001

Bismethano[60]fullerene derivatives 1 and 3 give 1,2-dihydro[60]fullerylglycines 2 and 4 respectively by a novel tandem reductive ring opening-retro-Bingel reaction.

The addition of a single bis(ethoxycarbonyl)methylene unit [$C(CO_2Et)_2$] to [60]fullerene is readily achieved by treatment of C_{60} with diethyl bromomalonate under Bingel reaction conditions.[1] Sequential Bingel additions have been used to prepare the corresponding bis- and tris-adducts as mixtures of regioisomers.[2] The regiochemistry of these reactions however, improves as the fullerene becomes more substituted, as exemplified by the regioselective synthesis of $C_{60}[C(CO_2Et)_2]_6$ with the all-*e* addition pattern starting from *e-e-e*-$C_{60}[C(CO_2Et)_2]_3$.[3] The regioselective formation of bis- through to hexakis-adducts can now be realized using tethered-directed remote functionalization.[4] Anthracene and 9,10-dimethylanthracene have been employed as reversible covalent templates to regioselectively prepare tetrakis- and hexakis-derivatives ($C_{60}[C(CO_2Et)_2]_n$ n = 4,6).[5] Non-tethered bis-adducts ($C_{60}[C(CO_2Et)_2]_2$) can be isomerised under carefully controlled electrochemical conditions to afford predominantly a thermodynamically favoured mixture of bis-adducts ('walk-on-the-sphere rearrangements').[6] While one or more of the methano groups of higher adducts can be removed under reductive conditions (retro-Bingel reaction), either electrochemically[7] or chemically,[8,9] to give less substituted methano[60]fullerenes or C_{60} itself. The potential of using a malonate addend as a reversible directing group or a protecting group of more reactive double bonds on the fullerene sphere for the synthesis of functionalised fullerenes has been recently demonstrated.[7d,8]

Earlier we reported a method for preparing the protected cyclopropane amino acid fullerene derivative $C_{60}[C(N{=}CPh_2)(CO_2\,Bu^t)]$ from the reaction C_{60} and *tert*-butyl *N*-diphenylmethyleneglycinate under Bingel reaction conditions.[10] Treatment of this methano[60]fullerene derivative with sodium cyanoborohydride under protic conditions resulted in reduction of the C61 imino group and concomitant ring opening of the cyclopropane ring to give, after a further reduction step and protonolysis, the novel 1,2-dihydro[60]fullerylglycine derivative, $C_{60}H[C(NHCHPh_2)(CO_2Bu^t)]$.[10] More recently we have extended this study to the synthesis of the corresponding tethered *trans*-4 bismethano[60]fullerene derivative **1**.[11] Interestingly, the regiochemistry of this tethered reaction was different to that found using the analogous tethered bismalonate system. We report here our study on the reductive ring opening reactions of the bis-adduct **1** and that of its corresponding untethered diethyl ester analogue **3**.

Treatment of a solution of **1** in THF–MeOH at pH 4 with sodium cyanoborohydride at ambient temperature, as described by us previously,[10] resulted in only recovered starting material. However, after much experimentation, we discovered that treatment of a solution of **1** in DCM with 5 equiv. of boron trifluoride–diethyl ether, initially at 0 °C with warming to rt over 30 min (presumably to activate the imine by complexation to the imine nitrogen), followed by the addition of acetonitrile and 10 equiv. of sodium cyanoborohydride gave, after 90 min, a mixture of the 1,2-dihydro[60]fullerylglycine **2** and C_{60}. Separation of this mixture by column chromatography on silica gel gave pure samples of **2** and C_{60} in yields of 42 and 12%, respectively (Scheme 1).[12] These fullerene compounds arise formally from a tandem reductive ring opening-retro-Bingel reaction and a double retro-Bingel reaction, respectively. Interestingly, none of the double reductive ring-opened bisfullerylglycine adduct $\{C_{60}H_2[C(NHCHPh_2)(CO_2R)]_2\}$ was isolated. The structure of **2** was clearly evident from NMR spectroscopy. The UV-vis spectrum of **2** in DCM showed distinct absorbances at 430, 640 and 705 nm, similar to that found in the derivative $C_{60}H[C(NHCHPh_2)(CO_2Bu^t)]$.[10] The ^{1}H NMR spectrum of **2** revealed a one proton singlet at δ 6.84 that corresponded to the single fullerene proton (H_χ). An upfield shift of the aromatic protons of the benzhydryl moiety was consistent with the chemical transformation of the imine to the secondary amino functionality. The addend region of **2** revealed two doublets at δ 5.41 and 5.24 (J = 11.9 Hz) corresponding to the diastereotopic benzyl protons ($H_\delta/H_{\delta'}$). The other benzylic protons (H_ε) resonated as a two proton singlet at δ 5.08, whereas the two proton singlet at δ 3.40 was identified as corresponding to the methylene protons (H_ϕ). A singlet one proton resonance at δ 4.84 corresponded to the benzhydryl resonance (H_γ). A three proton coupled spin system was identified as H_α (δ 4.97, d, J 12.3 Hz), H_β (δ 5.24, d, J 2.5 Hz) and NH (δ 3.67, dd, J 12.3, 2.5 Hz).

The ^{13}C NMR spectrum of the fulleryl sp^2 region of **2**, like that of $C_{60}H[C(NHCHPh_2)(CO_2Bu^t)]$, revealed a structure lacking a plane of symmetry due to the newly formed stereogenic centre at C61. This centre gives rise to diastereotopic pairs of fulleryl sp^2 carbons that lie either side of the plane bisecting C1 and C2 of the fullerene sphere. A single set of fulleryl sp^3 resonances at C_χ (δ 58.9), and C_ω (δ 67.3) were observed in addition to resonances corresponding to the addend C_α (δ 70.4), C_β (δ 66.3) C_δ (δ 67.8), C_ε (δ 66.2), C_ϕ (δ 47.5) and C_γ (δ 66.5). These carbons were readily assigned from HSQC and HMBC experiments.

In principle, the product **2** could arise from the anionic intermediates **A** or **B**. The driving force for mono-elimination of the tether from **A** or **B** might be the relief of ring strain upon expulsion of one arm of the tether. In the case of **A**, a further driving force may be the conversion of a fulleryl dianion intermediate to a thermodynamic more stable fulleryl monoanionic system. Clearly the rate of mono-elimination of the

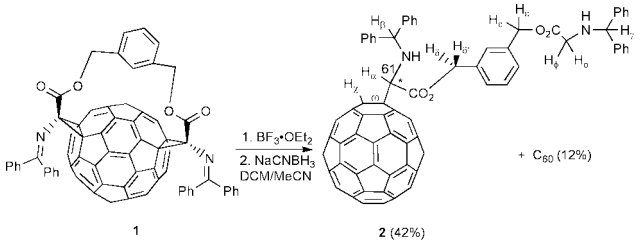

Scheme 1

DOI: 10.1039/b100655j

addend is much faster than the rate of elimination of the entire addend as indicated by the relative isolated yields of **2** and C_{60}.

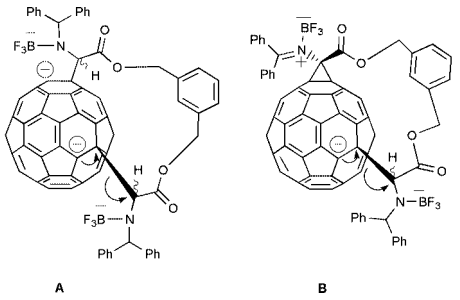

A B

To examine the influence of the tether on this ring opening-retro-Bingel reaction, the diethyl ester **3** was prepared from the base-catalysed trans-esterification of **1** with ethanol–THF–sodium carbonate as shown in Scheme 2. Treatment of **3** under similar reduction conditions to those described for **1** above also resulted in formation of a ring opened-retro-Bingel product, the ethyl ester **4**. This compound was obtained pure in 51% yield after column chromatography. A smaller amount of C_{60} (10%) was also isolated (Scheme 2). Compound **4** exhibited ^{1}H NMR and ^{13}C NMR resonances that were almost identical to those of $C_{60}H[C(NHCHPh_2)(CO_2Bu^t)]$[10] and **2**, except for those resonances associated with the different ester groups. The mono-ester **4** was also prepared in 58% yield from reductive ring opening of the methano[60]fullerene **5** (Scheme 3). In this case C_{60} (12%) and the reduced addend **6** (8%) were also isolated. The isolation of **6** supports our earlier proposed mechanism for these ring-opening reactions.[10,13]

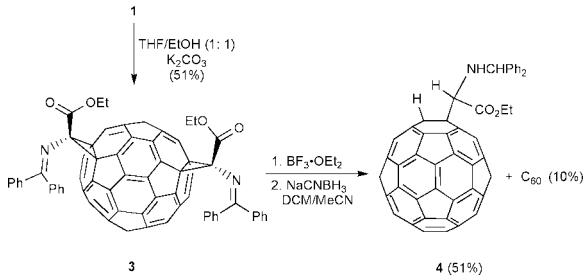

Scheme 2

Thus we have demonstrated a general method for reductive ring opening of [60]fullerenes having a fused cyclopropane imino ester moiety. Both bis- and monomethano[60]fullerenes of this type give 1,2-dihydro[60]fullerylglycines, the latter by a novel tandem reductive ring opening-retro-Bingel reaction. In light of these results it can be concluded that the presence of the tether is not the driving force for the mono-elimination of one of the addends. While C_{60} is formed in all of these reactions it is only a minor component and thus the rate of elimination of one of these addends from the bismethanofullerene derivatives appears to be higher than the corresponding elimination of both addends. These results suggest that a dianion like **A** may be an intermediate in the tandem reductive ring opening-retro-Bingel reactions of **1** and **3**.

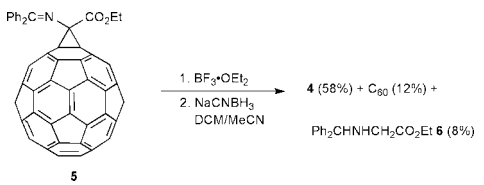

Scheme 3

The application of this chemistry to prepare more highly functionalised fullerenes is in progress. In principle, bis-cyclopropane imino esters can also function as directing and protecting groups for the synthesis of more highly functionalised fullerenes. For example, after the addition of further addends to the fullerene surface of **1** or **3** the bis-cyclopropane imino ester group could be then converted, under relatively mild conditions that would be compatible with a variety of other functional groups, to the mono-fullerylglycine moiety to give a variety of novel multifunctionalised fullerenes.

We thank the Australian Research Council for financial support and for a PhD scholarship to G. A. B.

Notes and references

1 C. Bingel, *Chem. Ber.*, 1993, **126**, 1957.

2 A. Hirsch, I. Lamparth and H. R. Karfunkel, *Angew. Chem., Int. Ed. Engl.*, 1994, **33**, 437.

3 A. Hirsch, I. Lamparth and T. Grösser, *J. Am. Chem. Soc.*, 1994, **116**, 9385.

4 F. Diederich and R. Kesinger, *Acc. Chem. Res.*, 1999, **32**, 537.

5 (*a*) I. Lamparth, C. Maichle-Mössmer and A. Hirsch, *Angew. Chem., Int. Ed. Engl.*, 1995, **34**, 1607; (*b*) R. Schwenninger, T. Müller and B. Kräutler, *J. Am. Chem. Soc.*, 1997, **119**, 9317; (*c*) X. Camps and A. Hirsch, *J. Chem. Soc., Perkin Trans. 1*, 1997, 1595.

6 (*a*) R. Kessinger, M. Gómez-López, C. Boudon, J.-P. Gisselbrecht, M. Gross, L. Echegoyen and F. Diederich, *J. Am. Chem. Soc.*, 1998, **120**, 8545; (*b*) L. E. Echegoyen, F. D. Djojo, A. Hirsch and L. Echegoyen, *J. Org. Chem.*, 2000, **65**, 4994.

7 (*a*) M. Keshavarz-K., B. Knight, R. C. Haddon and F. Wudl, *Tetrahedron*, 1996, **52**, 5149; (*b*) R. Kessinger, J. Crassous, A. Herman, M. Ruttimann, L. Echegoyen and F. Diederich, *Angew. Chem., Int. Ed.*, 1998, **37**, 1919; (*c*) N. S. Fender, B. Nuber, D. I. Schuster, S. R. Wilson and L. Echegoyen, *J. Chem. Soc., Perkin Trans. 2*, 2000, 1924; (*d*) R. Kessinger, N. S. Fender, L. E. Echegoyen, C. Thilgen, L. Echegoyen and F. Diederich, *Chem. Eur. J.*, 2000, **6**, 2184.

8 N. N. P. Moonen, C. Thilgen, L. Echegoyen and F. Diederich, *Chem. Commun.*, 2000, 335.

9 For a related study on other methano[60]fullerenes see: M. W. J. Beulen, L. Echegoyen, J. A. Rivera, M. A. Herranz, A. Martin-Domenech and N. Martin, *Chem. Commun.*, 2000, 917.

10 G. A. Burley, P. A. Keller, S. G. Pyne and G. E. Ball, *Chem. Commun.*, 1998, 2539.

11 G. A. Burley, P. A. Keller, S. G. Pyne and G. E. Ball, *Chem. Commun.*, 2000, 1717.

12 Synthesis of **2**: Boron trifluoride–diethyl ether (0.104 g, 732.80 μmol) was added dropwise over 1 min to a solution of **1**[11] (0.095 g, 73.19 μmol) in DCM (100 mL) at 0 °C. The reaction mixture was allowed to warm to rt over a 30 min period when MeCN (50 mL) was added. Sodium cyanoborohydride (0.046 g, 732.80 μmol) was added to the reaction mixture which was stirred for 90 min and then concentrated *in vacuo*. The reaction mixture was redissolved in chloroform (100 mL) and washed with saturated ammonium chloride solution (10 mL), followed by saturated sodium bicarbonate solution (10 mL). The organic layer was dried ($MgSO_4$) and concentrated *in vacuo*. Column chromatography, eluting with DCM–hexane (90:10) provided [60]fullerene (0.006 g, 12%) and **2** (0.043 g, 42%) as a brown amorphous solid. UV/vis (DCM) 330 nm (sh, 15000), 435 nm (3000). ^{1}H NMR ($CDCl_3$ CS_2 (80 : 40), 600 MHz): d 3.37 (s, 2H), 3.66 (dd, 1H, J = 12.3, 2.7 Hz), 4.84 (s, 1H), 4.98 (d, 1H, J = 12.3 Hz), 5.07 (s, 2H), 5.24 (d, 1H, J = 11.9 Hz), 5.28 (d, 1H, J = 2.7 Hz), 5.41 (d, 1H, J = 11.9 Hz), 6.84 (s, 1H), 7.19 (t, 2H, J = 7 Hz), 7.23–7.38 (m, 14H), 7.41 (t, 2H, J = 7.9 Hz), 7.47 (t, 2H, J = 7.6 Hz), 7.64 (d, 2H, J = 7.8 Hz), 7.74 (d, 2H, J = 7.8 Hz). ^{13}C NMR ($CDCl_3$ CS_2 (80 : 40), 125 MHz): δ 172.39, 172.31, 154.03, 152.99, 152.17, 151.05, 147.50, 147.20, 147.07, 146.97, 146.43, 146.43, 146.42, 146.38, 146.33, 146.25, 146.19, 146.18, 146.16, 145.88, 145.75, 145.71, 145.58, 145.44, 145.42, 145.35 (2 × C), 145.31, 145.22, 144.74, 144.68, 144.38, 144.35, 143.17, 143.13, 143.11, 142.63, 142.58, 142.56, 142.43, 142.23, 142.14, 142.09, 142.06, 142.04, 142.01, 141.72, 141.70, 141.54, 141.49, 141.47, 140.39, 140.37, 139.62, 139.23, 137.34, 136.43, 136.32, 136.14, 135.45, 129.32, 129.12, 129.07, 129.04, 128.91, 128.71, 128.04, 127.68, 127.29, 127.26, 70.38, 67.74, 67.32, 66.56, 66.35, 66.09, 58.87, 49.08. MS(ES): *m/z* 1327 (M + 23), 720 (C_{60}).

13 The reduced addend was not isolated from the reactions involving **1** and **3** because of the small scales of these reactions.

Self-inclusion and paraffin intercalation of the *p-tert*-butylcalix[4]arene host: a neutral organic clay mimic†

Eric B. Brouwer, Kostantin A. Udachin, Gary D. Enright, John A. Ripmeester,* Kristopher J. Ooms and Peter A. Halchuk

Steacie Institute for Molecular Sciences, National Research Council, Ottawa, Ontario, Canada K1A 0R6. E-mail: jar@ned1.sims.nrc.ca

Received (in Columbia, MO, USA) 6th November 2000, Accepted 18th January 2001
First published as an Advance Article on the web 6th March 2001

Two newly identified structures arise upon the crystallisation of the *p-tert*-butylcalix[4]arene host molecule from tetradecane: the guest-free, self-included host structure, and a 1:1 host–guest structure in which the paraffin guest is anchored in the bowl-shaped host cavity and intercalates layers of host molecules in a lamellar structure reminiscent of clays.

The crystal structures of inclusion compounds formed between the *p-tert*-butylcalix[4]arene host and small organic guest molecules have been studied extensively in order to understand guest-induced structural motifs, inclusion propensities and molecular recognition capabilities.[1] The bowl-shaped cavity of this relatively small supramolecular host molecule provides an excellent test site for isolating and probing the weak non-covalent host–guest interactions that prevail in much more complex supramolecular materials.[2] Essentially, three structural motifs have been observed with *p-tert*-butylcalix[4]arene inclusions with neutral guests: 1:1 and 2:1 host:guest structures,[3,4] and more recently, hydrogen-bonded structures formed with amine guests.[5] Herein we report two additional structures involving *p-tert*-butylcalix[4]arene that demonstrate the versatility of this host molecule to form multiple structural motifs under only slightly different synthetic conditions.

The host:guest ratio of compounds formed between linear hydrocarbon guests and *p-tert*-butylcalix[4]arene changes from 1:1 to 2:1 when the guest contains chains longer than six skeletal atoms, *e.g. n*-hexane or 1-chloropentane.[4,6] The longest paraffinic guest to form a 2:1 compound appears to be dodecane, with the alkane folded into a compact isomer in the double-sided host cavity.[6] With the next paraffin in the series, tetradecane, 2:1 host:guest inclusions no longer form, but rather two quite distinct motifs become apparent.

In the first instance, heating of *p-tert*-butylcalix[4]arene in a solution of tetradecane at 70 °C for three days yields guest-free crystals **1**,‡ since the solid-state ^{13}C CP MAS (cross-polarisation, magic angle spinning) NMR spectrum [Fig. 1(a)] of this compound shows tetradecane resonances to be absent. The multiplicity pattern of the host resonances is consistent with low-symmetry environments for the host molecule in the asymmetric unit.

The X-ray crystal structure of **1** (Fig. 2) shows that the host cavities are occupied by Bu^t groups of host molecules in the adjacent layer to form a self-included structure, such as seen with *p-tert*-butylcalix[5]arene.[7] The included Bu^t group is disordered over two positions with a site occupancy of 0.22/0.78. The shortest distance between the carbon atom of the included Bu^t group and the calixarene cavity wall is 3.4 Å. To transform the 1:1 structural motif, as seen with the pentane guest,[4] to the self-included bilayer structure, each calix is rotated off the 4-fold symmetry axis by 28° and moved towards the facing layer by 4.1 Å.

In the second instance, heating of the host molecule in tetradecane at 70 °C for eight days gives a structure with

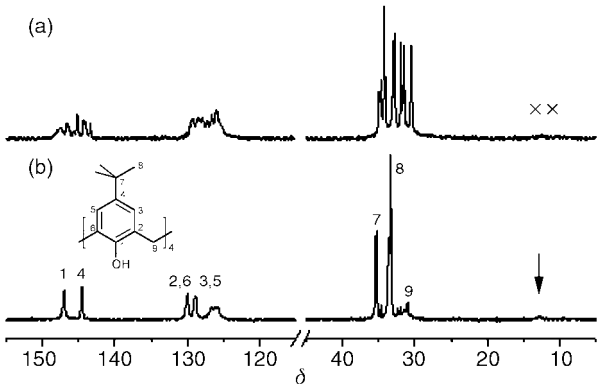

Fig. 1 Partial 50.3 MHz ^{13}C CP MAS NMR spectra: (a) self-included *p-tert*-butylcalix[4]arene **1**, (b) *p-tert*-butylcalix[4]arene–tetradecane inclusion/intercalation compound **1**·$C_{14}H_{30}$. Spinning sideband intensity is indicated by 'X'; the arrow indicates the tetradecane methyl resonance.

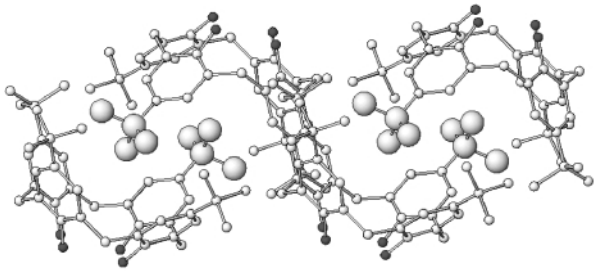

Fig. 2 Bilayer structure of the self-included *p-tert*-butylcalix[4]arene **1**. Hydrogen atoms are removed for clarity; oxygen atoms are black; cavity-filling *tert*-butyl carbons are shown at a larger radius for emphasis.

tetradecane present as guest‡ as indicated by the tetradecane resonances in the ^{13}C CP MAS NMR spectrum [Fig. 1(b)]. Whereas the guest methylene resonances are coincident with the host resonances, the tetradecane methyl line is distinct at δ 12.

Like inclusions formed with short-chain hydrocarbon guests,[2,4] the X-ray crystal structure of the second compound **1**·$C_{14}H_{30}$ shows a host:guest ratio of 1:1. The packing of the host layer (*ab* plane, $a \approx b$ with $\gamma \approx 90°$) is only slightly distorted from the tetragonal motif commonly observed in other 1:1 compounds. In all other aspects, the structure of the second compound is quite distinct. The most notable feature is the pillaring of the host layers by the guest molecules. The structural model from diffraction refines to give two coexisting structural schemes that are consistent with this pillaring. In the first, one end of the guest is tethered in a host cavity, and at the point where the chain leaves the cavity it bends into the interlamellar space in a pillaring fashion [Fig. 3(a)]. The second scheme has two guest positions. One guest has both ends of the molecule tethered in host cavities of two adjacent bilayers and the second occupies vacant interlamellar space between pillaring guests [Fig. 3(b)]. In both schemes the host positions are

† Issued as NRCC No. 43878.

DOI: 10.1039/b009133m

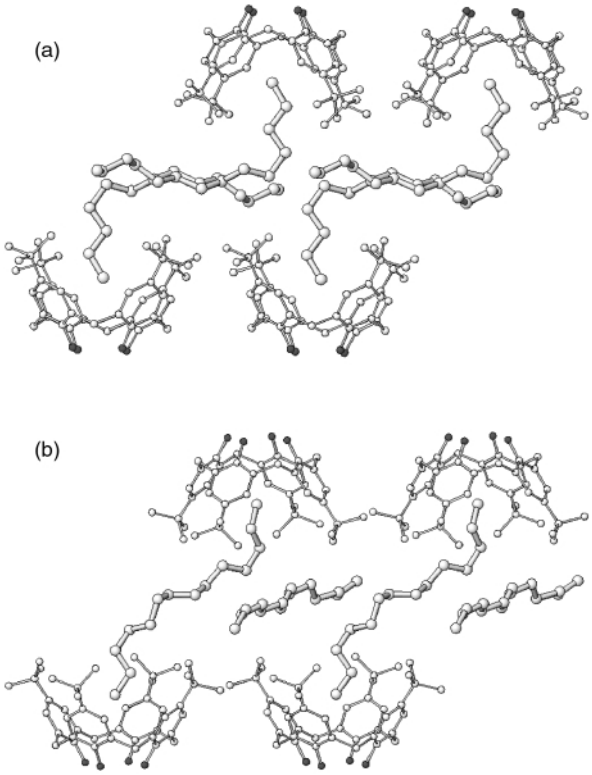

Fig. 3 Bilayer structure of the *p-tert*-butylcalix[4]arene–tetradecane inclusion/intercalation compound **1**·$C_{14}H_{30}$. (a) The end-to-interlayer spacing motif, (b) the end-to-end motif. Disordering in guest and host has been removed for clarity. Hydrogen atoms are removed for clarity; oxygen atoms are black.

identical, whereas the guest positions are disordered over two positions. The guest molecule in the interlayer space has a near all-*trans* conformation, but guest molecules that are included at either or both ends, are very different. All Bu^t groups in both structures are disordered over two positions with the site occupation *ca.* 0.5 , 0.4 to 0.6 and 0.3 to 0.7.

The bilayer structure of sodium calix[4]arenesulfonate, with the interlayer spacing occupied by water, has been compared to that of a clay.[8] The intercalated structure reported here shows a similar structure, although here it is a strictly neutral organic material, with lipophilic rather than hydrophilic regions. Examination of the bilayers of the 1:1 and 2:1 *p-tert*-butylcalix[4]arene–guest structural motifs suggests that the hydroxyl ends of the calixarenes are sufficiently polar to favour their mutual interaction in the bilayer, but allowing intercalation in the less polar interlamellar space. The present intercalated structure has well ordered layers separated by highly disordered interlayer regions giving a rather high diffraction *R*-value typical of clays. Clays also have the ability to tune the interlayer space by the intercalation of appropriate guests.[9] The *p-tert*-butylcalix[4]arene–tetradecane structure suggests that the distance between host bilayers may be tuned by intercalation of paraffins of appropriate length, and work to check this is currently in progress. Finally, noting that the self- and guest-included structures result from only slightly different crystallisation conditions, we anticipate that forming structures of *p-tert*-butylcalix[4]arene–tetradecane favouring only one of the two guest–host schemes (Fig. 3) may be possible by judicious choice of crystallisation conditions.

We have identified two new structural arrangements of supramolecular materials involving *p-tert*-butylcalix[4]arene. The self-included structure illustrates the collapsed lattice that likely occurs upon complete loss of guest from a *p-tert*-butylcalix[4]arene–guest inclusion compound. The structure formed with long paraffinic guests indicates synthetic access to a new class of calixarene-based lipophilic organic clay mimics. An upper limit to the length of the intercalating guests remains to be determined.

Notes and references

‡ *Crystal data*: **1**: $C_{44}H_{56}O_4$, M = 648.89, monoclinic, space group $P2_1/c$, a = 9.5878(5), b = 30.500(2), c = 13.541(1) Å, β = 109.852(1)°, U = 3724.5(4) Å^3, T = 173 K, Z = 4, D_c = 1.157 g cm^{-3}, μ(Mo-Kα) = 0.072 mm^{-1}, 43766 reflections measured, 9591 unique (R_{int} = 0.0343), R = 0.0414, R_w = 0.0984 [data $I > 2\sigma(I)$].

1·$C_{14}H_{30}$·$C_{44}H_{56}O_4$·$C_{14}H_{30}$, M = 847.27, triclinic, space group $P\bar{1}$, a = 12.647(3), b = 12.659(3), c = 17.565(4) Å, α = 96.23(1), β = 100.41(1), γ = 90.12(1)°, U = 2748.8(11) Å^3, T = 173 K, Z = 2, D_c = 1.024 g cm^{-3}, μ(Mo-Kα) = 0.062 mm^{-1}, 17876 reflections measured, 6465 unique (R_{int} = 0.125), R = 0.0889, R_w = 0.1975 [data $I > 2\sigma(I)$].

Both structures were solved using direct methods and refined by full-matrix least-squares on F^2 using SHELXTL.[10] CCDC 158144 and 158145. See http://www.rsc.org/suppdata/cc/b0/b009133m/ for crystallographic data in .cif or other electronic format.

1 C. D. Gutsche, *Calixarenes Revisited*, RSC, Cambridge, 1998.
2 E. B. Brouwer, K. A. Udachin, G. D. Enright and J. A. Ripmeester, *Chem. Commun.*, 1998, 587.
3 G. D. Andreetti, R. Ungaro and A. Pochini, *J. Chem. Soc., Chem. Commun.*, 1979, 1005.
4 E. B. Brouwer, J. A. Ripmeester and G. D. Enright, *J. Inclusion Phenom. Mol. Recognit. Chem.*, 1996, **24**, 1.
5 E. B. Brouwer, K. A. Udachin, G. D. Enright, C. I. Ratcliffe and J. A. Ripmeester, *Chem. Commun.*, 2000, 1905.
6 E. B. Brouwer, G. D. Enright, C. I. Ratcliffe, J. A. Ripmeester and K. A. Udachin, *Dynamic Structures of Host–Guest Systems*, in *Calixarenes 2001*, ed. Asfari, Böhmer, Harrowfield and Vicens, Kluwer, Dordrecht, 2001, pp. 296–311; K. A. Udachin, G. D. Enright, E. B. Brouwer and J. A. Ripmeester, *J. Supramol. Chem.*, submitted.
7 J. F. Gallagher, G. Ferguson, V. Böhmer and D. Kraft, *Acta Crystallogr., Sect. C*, 1994, **50**, 73.
8 A. W. Coleman, S. G. Bott, S. D. Morley, C. M. Means, K. D. Robinson, H. Zhang and J. L. Atwood, *Angew. Chem., Int. Ed. Engl.*, 1988, **27**, 1361.
9 R. M. Barrer and D. M. McLeod, *Trans. Faraday Soc.*, 1955, **51**, 1290; J. T. Kloprogge, *J. Porous Mater.*, 1998, **5**, 5.
10 G. M. Sheldrick, *Acta Crystallogr., Sect. A*, 1990, **46**, 467; G. M. Sheldrick, *Acta Crystallogr., Sect. A*, 1993, **49**, C467.

ChemComm

Homologous families of chloride-rich 4,4′-bipyridinium salt structures†

Ben Dolling, Amy L. Gillon, A. Guy Orpen,* Jonathan Starbuck and Xi-Meng Wang

School of Chemistry, University of Bristol, Cantock's Close, Bristol, UK BS8 1TS. E-mail: guy.orpen@bristol.ac.uk

Received (in Cambridge, UK) 27th November 2000, Accepted 2nd February 2001
First published as an Advance Article on the web 6th March 2001

New layer and three-dimensional 4,4′-bipyridinium salts of Cl^-, $[MCl_6]^{2-}$ (M = Os, Pt) and $[FeCl_5]^{2-}$ contain $NH\cdots(Cl)_2\cdots HN$ interactions which form hydrogen bonded ribbons which in turn give one-, two-, or three-dimensional periodic networks; two related families of homologous motifs are present in these salts together with those of square planar, polymeric and tetrahedral $[MCl_4]^{2-}$ (M = Pt, Pd, Mn, Cd, Pb, Co, Zn, Hg), planar $[Cu_2Cl_6]^{2-}$ and square pyramidal $[SbCl_5]^{2-}$ dianions.

In the search for reliable strategies for crystal synthesis by design a key goal is the identification and exploitation of robust synthons[1] to control the relative orientation of the molecular components of the solid. While such local interactions (such as hydrogen bonds) may be necessary they may not be sufficient to afford control over the crystal structure or even the periodic network formed by synthons. Various possibilities may exist in which the same synthons are present but different although related structures form. In this paper we explore the relationships between the structures formed by complex salts containing similar molecular components and having closely related hydrogen bond-based synthon networks.

We have shown that chlorometallate anions and other metal chloride complexes are good hydrogen bond acceptors.[2] This has enabled preparation of three classes of tetrachlorometallate salts of stoichiometry $[4,4'\text{-}H_2bipy][MCl_4]$.[3] For square planar anions $[MCl_4]^{2-}$ (M = Pt, Pd), linear hydrogen bonded ribbons of type **A** are formed (see Scheme 1). When M = Pb, Mn or Cd the $[MCl_4]^{2-}$ moiety is polymerised and the zig-zag edge-sharing octahedral chains formed are cross-linked by hydrogen bonds to form **A**-type periodic motifs. The third family of structures has tetrahedral anions $[MCl_4]^{2-}$ (M = Zn, Co, Hg). Here we report that the simplest chlorine-containing salt of $[4,4'\text{-}H_2bipy]^{2+}$, $[4,4'\text{-}H_2bipy]Cl_2$ **1** itself, has a structure which presages the NH···Cl motifs in a large number of more complex chlorometallate salts. These more complex structures may be regarded as part of homologous families of structures formally derived from that of the chloride salt.

Treatment of metal chloride salts with aqueous HCl solutions of 4,4′-bipyridine led to isolation of crystalline salts **2**–**4**‡ whose single crystal structures were determined.§ Crystals of **2** and **3** are strictly isostructural and, as expected, have metal ions in essentially regular octahedral coordination. Compound **4** contains the rare trigonal bipyramidal $[FeCl_5]^{2-}$ ion, which has not apparently previously been obtained from aqueous media.[4] Presumably its isolation in this case is due to its stabilisation in the solid state through the network of hydrogen bonds formed (see below). The bipyridinium ions $[4,4'\text{-}H_2bipy]^{2+}$ in **1**–**4** have normal geometries.

All of these structures contain motif **B**, in a doubled form, **C**, as do the $[4,4'\text{-}H_2bipy]$ salts of the tetrahedral $[MCl_4]^{2-}$ anions (M = Zn, Co, Hg) **5**–**7**.[3c] The dimensions of units **B** are given in Table 1 for **1**–**4** and **5**–**7**[3c] and $[4,4'\text{-}H_2bipy][PtCl_4]$ **8**.[3c] They show some variation in geometry, notably for **5**–**7**, in which one of the NH···Cl contacts is *ca.* 3 Å. In **1**, ribbons of type **D** are formed because interaction **C** is present at both ends of the bipyridinium ion. The same **D**-type ribbons are present in the

† Electronic supplementary information (ESI) available: synthesis details for **1**–**4**, crystal refinement details and colour structures for **1**, **2** and **4**. See http://www.rsc.org/suppdata/cc/b0/b009467f/

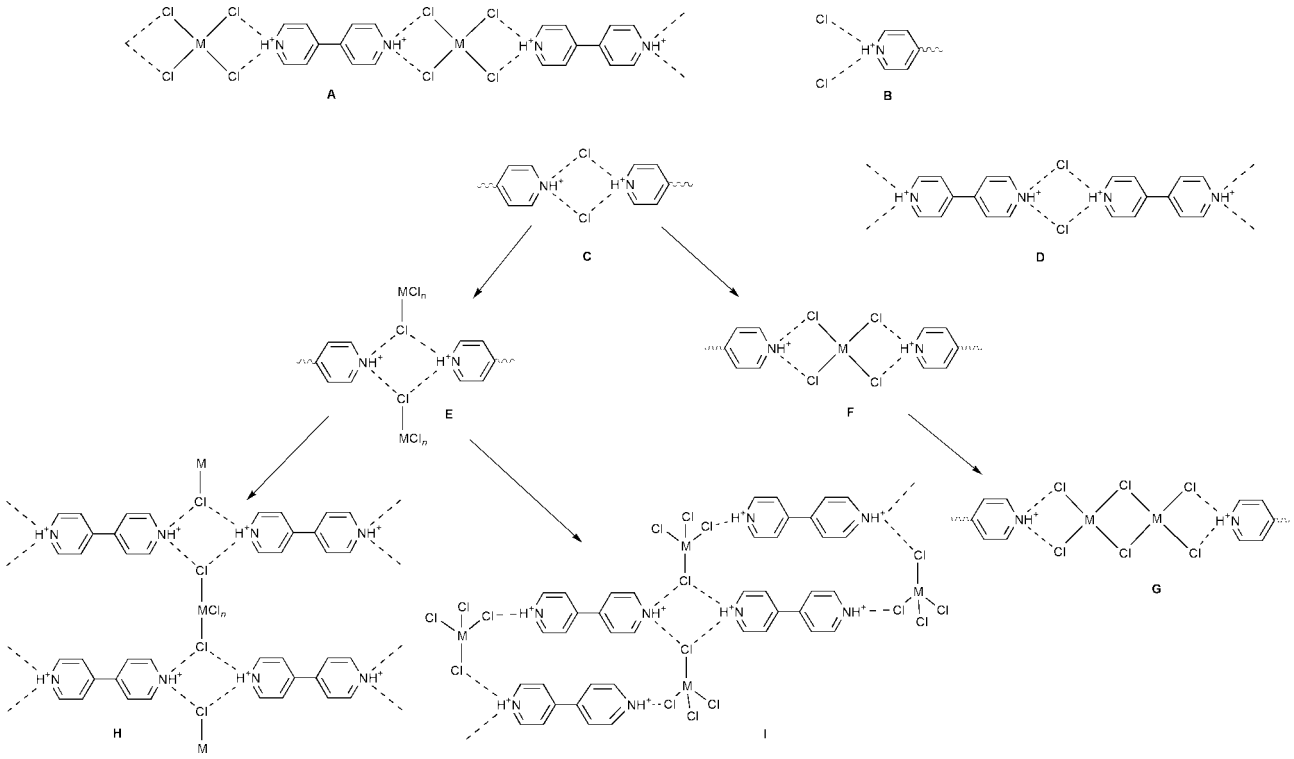

Scheme 1

DOI: 10.1039/b009467f

Table 1 Selected hydrogen bond[ab] lengths, angles and Cl···Cl distances in crystals of [4,4′-H_2bipy]Cl_2 **1** and [4,4′-H_2bipy][MCl_6] **2**, **3**, [4,4′-H_2bipy][MCl_5] **4**, [4,4′-H_2bipy][MCl_4] **5**–**8**† (see ref. 3*c*)

	1	**2** (M = Os)	**3** (M = Pt)	**4** (M = Fe)	**5** (M = Zn)	**6** (M = Co)	**7** (M = Hg)	**8** (M = Pt)
Cl···HN/Å	2.49, 2.51	2.59	2.59	2.54, 2.54	2.30,[c] 2.63, 3.04	2.32,[c] 2.63, 3.06	2.28,[c] 2.74, 2.93	2.40
M–Cl···HN/°	—	127	126	131, 135	116,[c] 91, 91	116,[c] 91, 91	112,[c] 88, 86	92
MCl···H–N/°	131, 132	143	144	137, 137	156,[c] 139, 123	156,[c] 140, 123	162,[c] 136, 125	136
Cl···Cl/Å	3.744	3.107	3.044	3.461	4.267	4.264	4.250	3.250

[a] Only Cl···HN contacts < 3.15 Å are listed.[2] Other hydrogen bonds (notably Cl···HC)[5] are omitted for brevity. [b] Values quoted for hydrogen bonds are based on hydrogen atom positions determined by X-ray diffraction. [c] Two-centre interaction, not involved in **C**-type interaction.

structures of **2**, **3** and **4** albeit in a form in which the chloride is also bonded to a metal ion (*i.e.* as in **E**). Ribbons **A** are present in [4,4′-H_2bipy][MCl_4] for M = Pt, Pd, Mn, Cd and Pb,[3c] in which the pair of Cl^- ions in **D** are replaced by a planar MCl_4 moiety (see **F**). In [4,4′-H_2bipy][Cu_2Cl_6][6] (see **G**) the planar anion contains two square planar metals and takes the place of the two chlorides in **D**. Therefore, **G** may be regarded as the next higher homologue in the sequence **D**, **F**, **G**.

In **2**–**4** ribbons of type **D** are cross-linked by the metal ions (see **E** and **H**) so that *trans* chlorides at the metal belong to different ribbons. In the isostructural salts **2** and **3** these chains are parallel and coplanar and therefore neutral layers are formed (see Fig. 1). These contain a (4,4) network[7] with motif **E** at the nodes and equal numbers of organic (bipyridyl) and inorganic (metal) connections. In **4** the trigonal bipyramidal $[FeCl_5]^{2-}$ dianions link ribbons inclined at 55° to one another and a three-dimensional structure results in which there are two sets of criss-cross **D**-type ribbons (see Fig. 2) with every second ribbon parallel and coplanar. The network formed here is of the rare $CdSO_4$ type in which nodes of square-planar connectivity (here motif **E**) are linked in a three-dimensional manner.[8,9] Salts **5**–**7** also contain motif **C** but as part of a double-stranded chain (see **I**) in which only one end of the dication is engaged in a **C**-type interaction, the other forming a short, two-centre hydrogen bond with just one chloride ligand (see ref. 3*c* for further details on this interaction). Finally, it is striking that of the two known polymorphs[10] of the [4,4′-H_2bipy] salt of the square pyramidal anion $[SbCl_5]^{2-}$ one has layers of form **H** and the other contains ribbons of type **A**.

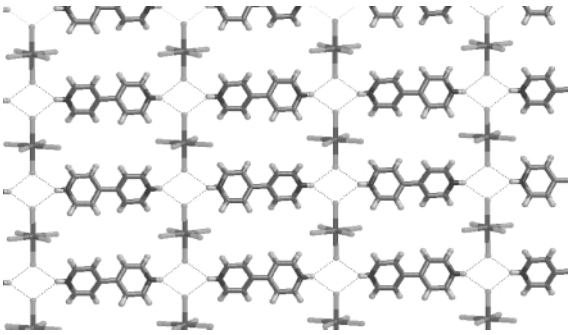

Fig. 1 A hydrogen bonded layer present within the crystal structure of [4,4′-H_2bipy][$OsCl_6$] **2**. Compound **3** is isostructural with **2**.

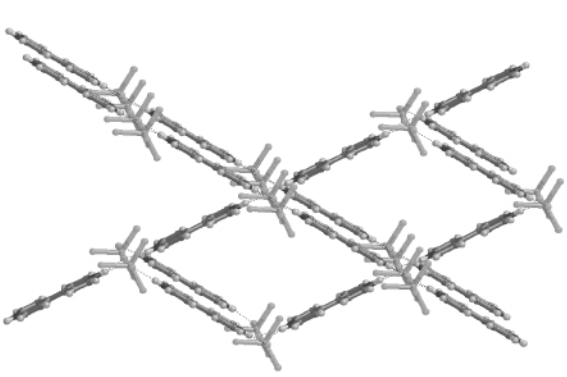

Fig. 2 A view of the crystal structure of [4,4′-H_2bipy][$FeCl_5$] **4**.

Indeed, all of the perchlorometallate [4,4′-H_2bipy] salts whose structures are known to us (as judged by the content of the current release of the Cambridge Structural Database[11] and as reported or cited here) incorporate motif **C**.

The recurrence of motif **C**, in periodic motif **D** and the derived **F**–**I** in this range of structures (and various analogous bromide salts)[3] implies that **C** is a robust feature of such salts.

Financial support of the EPSRC and the Royal Society (a Royal Society China Royal Fellowship for X.-M. W.) and the Leverhulme Trust (a Royal Society Leverhulme Trust Senior Research Fellowship for A. G. O.) is gratefully acknowledged.

Notes and references

‡ Full synthesis details and crystal refinement details for **1**–**4** are given as ESI.† *Synthesis* of **2**–**4**: a stoichiometric amount of 4,4′-bipy dissolved in aqueous HCl was added to an aqueous solution of the metal chloride in air, and crystalline samples grown from solution. In the case of **4** this yielded a mixture of iron(III) containing products, presumably as a result of aerial oxidation of the ferrous chloride used. A sample of crystalline **4** was obtained by hand selection of crystals.

§ *Crystal data*: for [4,4′-H_2bipy]Cl_2 **1**: $C_{10}H_{10}Cl_2N_2$, M = 229.1, monoclinic, space group $C2/c$ (no. 15), a = 12.687(4), b = 12.0981(19), c = 7.0707(17) Å, β = 112.565(18)°, U = 1002.2(4) Å^3, Z = 4, μ = 0.605 mm^{-1}, T = 173 K, 1151 unique data, $R1$ = 0.026. For [4,4′-H_2bipy][$OsCl_6$] **2**: $C_{10}H_{10}Cl_6N_2Os$, M = 561.10, orthorhombic, space group *Ibam* (no. 72), a = 7.3602(10), b = 12.8184(18), c = 15.606(2) Å, U = 1472.3(3) Å^3, Z = 4, μ = 9.734 mm^{-1}, T = 173 K, 883 unique data, $R1$ = 0.024. For [4,4′-H_2bipy][$PtCl_6$] **3**: $C_{10}H_{10}Cl_6N_2Pt$, M = 565.99, orthorhombic, space group *Ibam* (no. 72), a = 7.4757(17), b = 12.837(2), c = 15.362(2)Å, U = 1474.2(5) Å^3, Z = 4, μ = 10.590 mm^{-1}, T = 173 YK, 884 unique data, $R1$ = 0.017. For [4,4′-H_2bipy][$FeCl_5$] **4**; $C_{10}H_{10}Cl_5N_2Fe$, M = 391.30, orthorhombic, space group *Ama2* (no. 40), a = 16.651(2), b = 11.6816(15), c = 7.2764(10) Å, U = 1415.3(3) Å^3, Z = 4, μ = 1.990 mm^{-1}, T = 173 K, 1671 unique data, $R1$ = 0.029. CCDC 154205–154208. See http://www.rsc.org/suppdata/cc/b0/b009467f/ for crystallographic data in .cif or other electronic format.

1 G. R. Desiraju, *Angew Chem., Int. Ed. Engl.*, 1995, **34**, 2311; G. R. Desiraju, *Chem. Commun.*, 1997, 1475.
2 G. Aullón, D. Bellamy, L. Brammer, E. A. Bruton and A. G. Orpen, *Chem. Commun.*, 1998, 653.
3 (*a*) G. R. Lewis and A. G. Orpen, *Chem. Commun.*, 1998, 1873; (*b*) A. L. Gillon, A. G. Orpen, J. Starbuck, X.-M. Wang, Y. Rodríguez-Martín and C. Ruiz-Pérez, *Chem. Commun.*, 1999, 2287; (*c*) A. L. Gillon, G. R. Lewis, A. G. Orpen, S. Rotter, J. Starbuck, X.-M. Wang, Y. Rodríguez-Martín and C. Ruiz-Pérez, *J. Chem. Soc., Dalton Trans.*, 2000, 3897.
4 B. D. James, J. Liesegang, M. Bakalova, W. M. Reiff, B. W. Skelton and A. H. White, *Inorg. Chem.*, 1995, **34**, 2054.
5 C. B. Aakeroy. T. A. Evans, K. R. Seddon and I. Palinko, *New J. Chem.*, 1999, **23**, 145.
6 M. Bukowska-Strzyzewska and A. Tosik, *Pol. J. Chem.*, 1979, **53**, 2423.
7 S. R. Batten and R. Robson, *Angew. Chem., Int. Ed. Engl.*, 1998, **37**, 1460.
8 M. O'Keeffe, M. Eddouadi, H. Li, T. Reineke and O. M. Yaghi, *J. Solid State Chem.*, 2000, **152**, 3.
9 L. Carlucci, G. Ciani, P. Macchi and D. M. Proserpio, *Chem. Commun.*, 1998, 1837; K. N. Power, T. L. Hennigar and M. J. Zaworotko, *Chem. Commun.*, 1998, 595; O. M. Yaghi, H. Li and M. O'Keeffe, *Mater. Res. Soc. Symp. Proc.*, 1997, **453**, 127.
10 A. Lipka, *Z. Anorg. Allg Chem.*, 1980, **469**, 229; A. Lipka, *Z. Naturforsch., Teil B*, 1983, **38**, 1615.
11 F. H. Allen and O. Kennard, *Chem. Des. Automat. News*, 1993, **8**, 1; F. H. Allen and O. Kennard, *Chem. Des. Automat. News*, 1993, **8**, 31.

A coumarin-derivative dye sensitized nanocrystalline TiO_2 solar cell having a high solar-energy conversion efficiency up to 5.6%

Kohjiro Hara,[a] Kazuhiro Sayama,[a] Yasuyo Ohga,[b] Akira Shinpo,[b] Sadaharu Suga[b] and Hironori Arakawa*[a]

[a] *National Institute of Materials and Chemical Research (NIMC), 1-1 Higashi, Tsukuba, Ibaraki 305-8565, Japan. E-mail: h.arakawa@home.nimc.go.jp*

[b] *Hayashibara Biochemical Laboratories, Inc., 564-176 Fujita, Okayama 701-0221, Japan*

Received (in Cambridge, UK) 18th December 2000, Accepted 8th February 2001
First published as an Advance Article on the web 6th March 2001

It is found that newly synthesized coumarin derivatives work as highly efficient photosensitizers for dye-sensitized nanocrystalline TiO_2 solar cells producing a 5.6% solar-light-to-electricity conversion efficiency, the highest efficiency so far among organic dye-sensitized solar cells, with a short-circuit current density of 13.8 mA cm^{-2}, an open-circuit photovoltage of 0.63 V, and a fill factor of 0.63 under standard AM 1.5 irradiation (100 mW cm^{-2}).

Dye-sensitized solar cells have been extensively investigated since Grätzel and coworkers reported a highly efficient solar-energy-to-electricity conversion efficiency, η, of 10%.[1] Transition metal complexes, *e.g. cis*-di(thiocyanato)bis(4,4′-dicarboxy-2,2′-bipyridine)ruthenium(II) [$Ru(dcbpy)_2(NCS)_2$], have been mainly applied, so far, in dye-sensitized solar cells as photosensitizers.[1–4] Organic dyes have been also used as photosensitizers for dye-sensitized solar cells.[5–9] Recently we reported a dye-sensitized TiO_2 solar cell, using special merocyanine dye aggregates as the photosensitizer, which showed a highly efficient η of 4.2%.[7] This result encouraged us to look for more efficient organic dye photosensitizers for dye-sensitized TiO_2 solar cells.

Coumarin dyes, *e.g.* coumarin 343 (C343) (Scheme 1), are recognized as good organic dye photosensitizers, injecting electrons effectively into the conduction band of semiconductors.[10,11] For example, Murakoshi *et al.* observed an ultrafast electron injection (< 20 fs) from C343 into the conduction band of TiO_2.[11] The η values of nanocrystalline semiconductor solar cells using conventional coumarin dyes such as C343 as the photosensitizer is, however, much lower than that of solar cells sensitized by Ru complex photosensitizers because of the narrow absorption area in the visible region. A wide absorption range in the visible region for the coumarin dye is required to attain highly efficient solar-energy-to-electricity conversion. We have synthesized new coumarin derivatives which are able to absorb visible light from 400 up to 700 nm and prepared highly efficient dye-sensitized nanocrysalline TiO_2 solar cells using such new coumarin photosensitizers. The value of η increased up to 5.6%, the highest efficiency among organic dye-sensitized solar cells so far, using 2-cyano-5-(2,3,6,7-tetrahydro-1,1,7,7-tetramethyl-11-oxo-1*H*,5*H*,11*H*-[1]benzopyrano[6,7,8-*ij*]quinolizin-10-yl)penta-2,4-dienoic acid **2** as the photosensitizer. It should be noted that the photocurrent performance of a TiO_2 solar cell composed of this dye (compound **2**) is almost equal to that of the $Ru(dcbpy)_2(NCS)_2$ system.

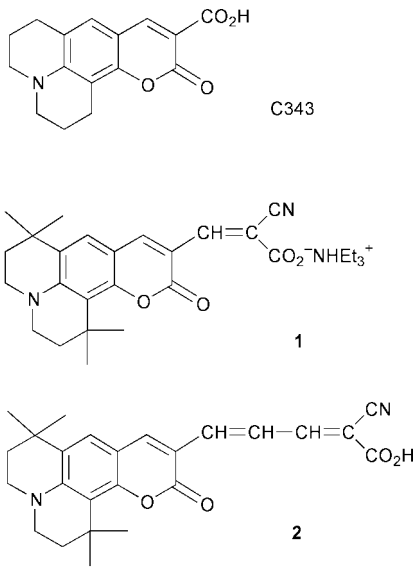

Scheme 1 Molecular structure of new coumarin derivatives.

Compound **1**† was synthesized by refluxing an acetonitrile solution containing 2,3,6,7-tetrahydro-1,1,7,7-tetramethyl-11-oxo-1*H*,5*H*,11*H*-[1]benzopyrano[6,7,8-*ij*]quinolizin-10-carbaldehyde **3** and cyanoacetic acid in the presence of piperidine, and purified by column chromatography using silica gel and a chloroform–methanol mixed solvent as the eluting solution. Recrystallization of **1** from acetonitrile solution in the presence of triethylamine afforded a red purple crystalline triethylammonium salt. 3-(2,3,6,7-Tetrahydro-1,1,7,7-tetramethyl-11-oxo-1*H*,5*H*,11*H*-[1]benzopyrano[6,7,8-*ij*]quinolizin-10-yl)propenal **4** was prepared from **3** by Wittig reaction and then Vilsmeier–Haack reaction. Compound **2**† was synthesized starting from **4** and cyanoacetic acid by a similar procedure for **1**. Resulting precipitates of **2** were dissolved in DMF and a bright purple crystalline compound was obtained upon recrystallization.

TiO_2 nanoparticles were prepared by hydrolysis of Ti tetraisopropoxide as described elsewhere.[12,13] TiO_2 thin films were prepared by screen printing on transparent conducting oxide (TCO, F-doped SnO_2) and then sintered at 500 °C for 1 h. Nanocrystalline TiO_2 films (10–13 μm thick) were coated with dyes by dipping the film in 3×10^{-4} mol dm^{-3} dye solutions in ethanol or *tert*-butyl alcohol–acetonitrile (1:1). The dye-coated TiO_2 electrode was incorporated into a thin-layer sandwich-type cell with a Pt sputtered TCO as the counter electrode, a spacer film, and an organic electrolyte solution to measure the solar cell performance. The electrolyte was 0.6 mol dm^{-3} 1,2-dimethyl-3-propylimidazolium iodide (DMPImI)–0.1 mol dm^{-3} LiI–0.05 mol dm^{-3} I_2 in methoxyacetonitrile. η Values for solar cells were measured using a standard AM 1.5 solar simulator and a digital sourcemeter.

Absorption spectra of C343, compounds **1** and **2** in ethanol and compound **2** adsorbed on a transparent TiO_2 film (4 μm thick) are shown in Fig. 1. The threshold wavelengths of absorption spectra for compounds **1** and **2** are 570 and 630 nm, respectively, while that for C343 was 500 nm, indicating that introducing the –CH=CH– unit into the coumarin framework expanded the conjugation in the dye resulting in wide absorption in the visible region. This wide absorption and red shift of absorption maximum in the visible region for photosensitizers is desirable for light harvesting of solar energy. The absorption spectrum of compound **2** adsorbed on a TiO_2 film is

DOI: 10.1039/b010058g

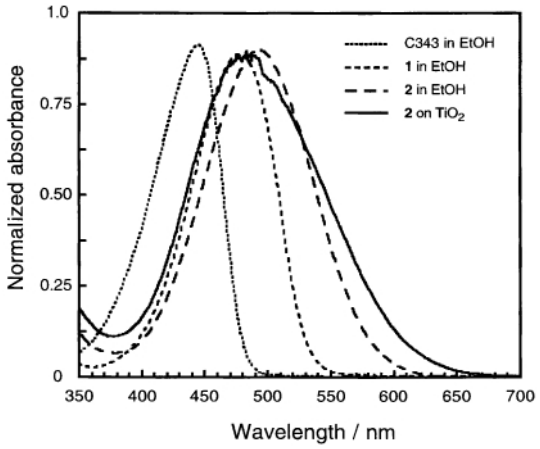

Fig. 1 Absorption spectra of C343, **1** and **2** in EtOH, and of **2** adsorbed on a TiO_2 film whose absorbance is normalized: (- - - - - -) C343, (– – –) **1** in ethanol, (— —) **2** in ethanol, (—) **2** adsorbed on TiO_2.

slightly expanded compared with that in ethanol. A long tail of absorption up to 670 nm was observed, indicating a strong electronic coupling between compound **2** and TiO_2. The absorption spectrum of compound **2** absorbed on TiO_2 films thicker than 10 μm gave an absorption band edge which tailed up to 750 nm, the deep purple film being similar to that of the Ru complex.

Fig. 2 shows typical action spectra of incident photon-to-current conversion efficiencies (IPCE) obtained from nanocrystalline TiO_2 solar cells sensitized by compound **2** as well as $Ru(dcpby)_2(NCS)_2(TBA)_2$. Visible light (400–750 nm) can be converted to current with a maximum of 76% at 470 nm by the solar cell composed of compound **2**, producing a large photocurrent.

Taking into consideration light absorption loss by TCO-coated glass, the light-to-current conversion efficiency is close to 100% from 450 to 550 nm. Both a large amount of compound **2** adsorbed on to a TiO_2 film (10 μm thick), 1×10^{-7} mol cm^{-2}, and the large absorption coefficient of dye (compound **2**) itself, *e.g.* 52 500 dm^3 mol^{-1} cm^{-1} at 504 nm in methnol, increased the light harvesting efficiency. The coverage of the TiO_2 surface with the dye was *ca.* 70% as derived from the roughness factor of the film, 1000, and the cross sectional area of one dye molecule, 1.2 nm^2. It should be noted that the IPCE performance of the solar cell with **2** is almost equal to that of the $Ru(dcbpy)_2(NCS)_2$ system, as shown in Fig. 2. The maximum short-circuit photocurrent density (J_{sc}) for a **2**-sensitized TiO_2 solar cell reached 15 mA cm^{-2} under AM 1.5 irradiation (100 mW cm^{-2}).

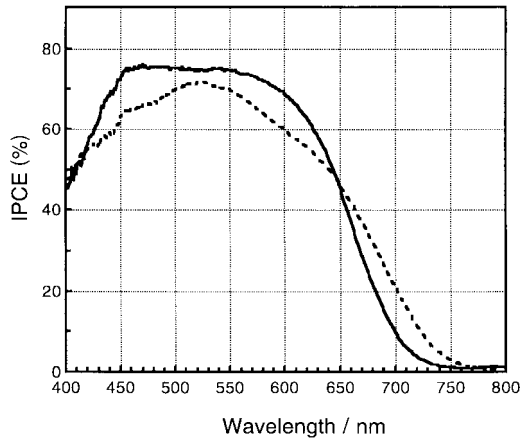

Fig. 2 Typical action spectra of incident photon-to-current conversion efficiencies (IPCE) obtained for nanocrystalline TiO_2 solar cells sensitized by **2** (—) and $Ru(dcbpy)_2(NCS)_2(TBA)_2$ (- - - -).

The lowest unoccupied molecular orbital (LUMO) of **2** (measured electrochemically) at −0.8 V *vs.* NHE, is able to inject electrons into the conduction band of the TiO_2 electrode (−0.5 V *vs.* NHE).[13] Good stability of the dye under irradiation for 2 days, with a turnover number of 100 000, was observed by a brief experiment using an opened cell, indicating effective cycling from the ground state of compound **2** to the oxidized form with efficient electron transfer from the dye to TiO_2 and from I^- ions to the oxidized dyes. Detailed investigation of the long term stability of the dye using a sealed cell will be carried out.

The maximum efficiency for the **2**-sensitized TiO_2 solar cell was 5.6% with a J_{sc} of 13.8 mA cm^{-2}, an open-circuit photovoltage (V_{oc}) of 0.63 V, and a fill factor (*ff*) of 0.63 under standard AM 1.5 irradiation, which is the highest solar cell performance, so far, among organic dye-sensitized solar cells. Our results strongly support the prospect for promising application of organic dye photosensitizers in dye-sensitized nanocrystalline semiconductor solar cells, and indicate the importance of molecular structure design for tuning photosensitizers to produce high efficiency dye-sensitized solar cells. If electron injection occurs through chemical bonding of the carboxyl group, the structures of compound **1** and **2**, whose carboxyl group is directly connected to the conjugated methine chain, is advantageous for improving the injection of electrons into semiconductors. In addition, the cyano group (–CN) connected to the methine chain and the carboxyl group might be effective for electron injection due to their strong electron acceptability. We are currently synthesizing new dyes absorbing in a wider visible region and studying solar cell performance and mechanisms in detail.

This work was supported by the Science and Technology Agency, Center of Excellence Development Project (COE project), Japan.

Notes and references

† Compound **1**: mp 186–192 °C, $\delta_H(CDCl_3)$: 1.28 (6H, s), 1.32 (9H, t), 1.54 (6H, s), 1.74 (2H, t), 1.80 (2H, t), 3.13 (6H, q), 3.23 (2H, t), 3.36 (2H, t), 7.19 (1H, s), 8.38 (1H, s), 8.75 (1H, s).

Compound **2**: MS (ESI) *m/z*: 419.1 (M + H), 436.0 (M + H_2O), 450.8 (M + CH_3OH), 482.9 (M + $2CH_3OH$), 490.8 (M + THF); mp 270–275 °C, $\delta_H(CDCl_3)$: 1.31 (6H, s), 1.53 (6H, s), 1.74–1.85 (4H, m), 3.41–3.49 (4H, m), 7.47 (2H, m), 7.75 (1H, dd), 8.08 (1H, d), 8.22 (1H, s).

1 M. K. Nazeeruddin, A. Kay, I. Rodicio, R. Humphry-Baker, E. Muller, P. Liska, N. Vlachopoulos and M. Grätzel, *J. Am. Chem. Soc.*, 1993, **115**, 6382.
2 M. K. Nazeeruddin, P. Péchy and M. Grätzel, *Chem. Commun.*, 1997, 1705.
3 H. Sugihara, L. P. Singh, K. Sayama, H. Arakawa, M. K. Nazeeruddin and M. Grätzel, *Chem. Lett.*, 1998, 1005.
4 A. Islam, H. Sugihara, K. Hara, L. P. Singh, R. Katoh, M. Yanagida, Y. Takahashi, S. Murata and H. Arakawa, *New J. Chem.*, 2000, **24**, 343.
5 K. Hara, T. Horiguchi, T. Kinoshita, K. Sayama, H. Sugihara and H. Arakawa, *Chem. Lett.*, 2000, 316.
6 K. Hara, T. Horiguchi, T. Kinoshita, K. Sayama, H. Sugihara and H. Arakawa, *Sol. Energy Mater. Sol. Cells*, 2000, **64**, 115.
7 K. Sayama, K. Hara, N. Mori, M. Satsuki, S. Suga, S. Tsukagoshi, Y. Abe, H. Sugihara and H. Arakawa, *Chem. Commun.*, 2000, 1173.
8 Z.-S. Wang, F.-Y. Li and C.-H. Huang, *Chem. Commun.*, 2000, 2063.
9 Z.-S. Wang, F.-Y. Li, C.-H. Huang, L. Wang, M. Wei, L.-P. Jin and N. Q. Li, *J. Phys. Chem.*, 2000, **104**, 9676.
10 J. M. Rehm, G. L. McLendon, Y. Nagasawa, K. Yoshihara, J. Moser and M. Grätzel, *J. Phys. Chem.*, 1996, **100**, 9577.
11 K. Murakoshi, S. Yanagida, M. Capel and E. W. Castner, Jr., in *Interfacial Electron Transfer Dynamics of Photosensitized Zinc Oxide Nanoclusters*, ed. M. Moskovits, ACS, Washington DC, 1997, pp. 221.
12 C. J. Barbé, F. Arendse, P. Comte, M. Jirousek, F. Lenzmann, V. Shklover and M. Grätzel, *J. Am. Ceram. Soc.*, 1997, **80**, 3157.
13 K. Kalyanasundaram and M. Grätzel, *Coord. Chem. Rev.*, 1998, **77**, 347.

ChemComm

Extended framework materials incorporating cyanide cluster complexes: structure of the first 3D architecture accommodating organic molecules†

Nikolaj G. Naumov,[a] Dmitriy V. Soldatov,[b] John A. Ripmeester,*[b] Sofia B. Artemkina[a] and Vladimir E. Fedorov[a]

[a] *Institute of Inorganic Chemistry, Russian Academy of Sciences, Novosibirsk 630090, Russia*
[b] *Steacie Institute for Molecular Sciences, National Research Council of Canada, Ottawa K1A 0R6, Canada. E-mail: jar@ned1.sims.nrc.ca*

Received (in Columbia, MO, USA) 25th September 2000, Accepted 18th January 2001
First published as an Advance Article on the web 6th March 2001

Hexadentate cluster anions $[Re_6S_8(CN)_6]^{4-}$ coordinate to Mn(II) centers to give a neutral 3D coordination network topologically related to the structure of Prussian Blue; the residual space is filled with isopropyl alcohol molecules, both ligated to Mn(II) and guest-solvated.

For three centuries, polydimensional metal cyanides have intrigued chemists with their diversity and unique properties.[1] Representatives include the oldest synthetic coordination compound Prussian Blue‡[2,3] which gives rise to a wide family of 'blues' and 'greens',[1–4] Hofmann and related clathrates,[5] and inclusion compounds formed by cadmium cyanide.[6] Today, cyanide complexes are important elements in crystal engineering.[7] Very recently, the cyanide cluster complexes $[Re_6X_8(CN)_6]^{4-}$ (X = S, Se, Te)[8] capable of acting as octahedral hexadentate ligands have become available. The first structural studies were performed for salts (usually hydrated) of these cluster anions, where pure ionic packing or H-bonded systems were found.[8] Incorporation of M(II) cations (Mn, Fe, Co, Zn, Cd)[9–12] resulted in layered coordination polymers. With M(II) (Mn, Co, Ni) and tetrapropylammonium cations 0D, 1D and 2D structures were obtained.[13] Salts reported with negatively charged 3D coordination frameworks include $Cs_2Mn_3[Q]_2\cdot 15H_2O$ [Q = $Re_6Se_8(CN)_6$], $(H_3O)_2Co_3[Q]_2\cdot 14.5H_2O$,[14] Cs_2[*trans*-$Fe(H_2O)_2]_3[Q]_2\cdot 18H_2O$ and its Mn, Co, Ni and Cd analogs,[9] $(H_3O)_2Zn_3[Q]_2\cdot 20H_2O$[15] and others,[11,12,16] with plenty of water molecules as well as metal or H_3O^+ cations filling the space of the open pore system.

In the course of our efforts to design novel porous materials with a high propensity for absorbing organic species[17] we have exploited cyanide cluster complexes as prospective building units. For this purpose the capability of the cluster anions to create weakly charged or electrically neutral 3D-bonded networks seems essential. The 3D phase $[Zn(H_2O)]_2[Re_6S_8(CN)_6]\cdot 7H_2O$ has been reported[9] but is of low inclusion capacity as it contains two interpenetrating neutral frameworks. Dehydrated $Ga_4[Re_6Se_8(CN)_6]_3\cdot xH_2O$ and $Fe_4[Re_6Te_8(CN)_6]_3\cdot xH_2O$,[16] $[Cd_2(H_2O)_4][Re_6S_8(CN)_6]_3\cdot 14H_2O$,[18] have been reported to absorb alcohols; $[Co_2(H_2O)_4][Re_6S_8(CN)_6]\cdot 10H_2O$ and $[Co(H_2O)_3]_4[Co_2(H_2O)_4][Re_6Se_8(CN)_6]_3\cdot 44H_2O$ have demonstrated vapochromic behavior during exposure to organic solvents. Structural studies showing included organic species are not available so far, however. We report here, for the first time, on a 3D polymer formed from Mn(II) cations bound to $[Re_6S_8(CN)_6]^{4-}$ cluster anions in molar ratio of 2:1 where the residual space is filled with organic molecules, in this case isopropyl alcohol.

Red octahedral crystals of the compound were grown in the course of slow diffusion of isopropyl alcohol vapor into a solution of 70 mg $K_4[Re_6S_8(CN)_6]$ [0.04 mmol; see ref. 8(*c*) for synthesis], 25 mg $MnSO_4\cdot 5H_2O$ (0.10 mmol), and 7 mL of water. A single crystal was maintained inside a sealed capillary filled with supernatant solution and studied by X-ray diffraction.§ The chemical formula derived therefrom was $\{[Mn(Pr^iOH)_2(H_2O)]_2[Re_6S_8(CN)_6]\}\cdot 2Pr^iOH$. A fine crystalline product was prepared by mixing saturated solutions of 170 mg $K_4[Re_6S_8(CN)_6]$ (0.1 mmol) and of 70 mg $MnSO_4\cdot 5H_2O$ (*ca.* 0.3 mmol) in water–isopropyl alcohol (1:3 v/v). A powder diffractogram of the bulky fresh product corresponded well to that calculated from single-crystal X-ray diffraction data, but the elemental analysis was not satisfactory because the compound readily lost isopropyl alcohol when exposed to air. The position of the ν(CN) band at 2143 cm^{-1} in the IR spectrum (in liquid paraffin) corresponded to a bridging cyanide group, values close to 2134–2138 cm^{-1} were found previously for cyanides bridging the 'Re_6S_8' core with Mn(II), Fe(II), Co(II) and Cd(II).[10]

The geometry of the anion fragment $[Re_6S_8(CN)_6]^{4-}$ found in the structure [Fig. 1(a)] is similar to those previously reported.[9–11,13,18] The Re_6 cluster is an almost ideal octahedron with Re–Re distances of 2.598–2.602 Å, the sulfur atoms capping each triangular face at Re–S distances of 2.399–2.414 Å. Six cyanide ligands coordinate to rhenium atoms through carbon with C–N distances of 2.117–2.118 Å, sticking out in pairs in a mutually perpendicular fashion.

The Mn(II) center has an 'N_3O_3' octahedral environment [Fig. 1(b)]. Three mutually perpendicular bonds extend to cyanide nitrogens, connecting each center to three neighboring cluster anions with Mn–N distances of 2.16–2.19 Å. The coordination octahedron is completed by three oxygen atoms from one water [at 2.220(7) Å] and two isopropyl alcohol molecules [2.230(7) and 2.259(6) Å for molecules A and B, respectively]. There is one further isopropyl alcohol molecule which is not chemically bound to the metal center, as it is H-bonded to ligand water with an O(water)–O(Pr^iOH) distance of 2.65(2) Å.

In the crystal structure, two Mn(II) centers are located about the inversion center, with an Mn–Mn distance of ≈5.3 Å. Isopropyl alcohol molecules attached to one center penetrate between isopropyl alcohol molecules attached to another center. The resulting packing associate $\{[Mn(Pr^iOH)_2(H_2O\cdots$

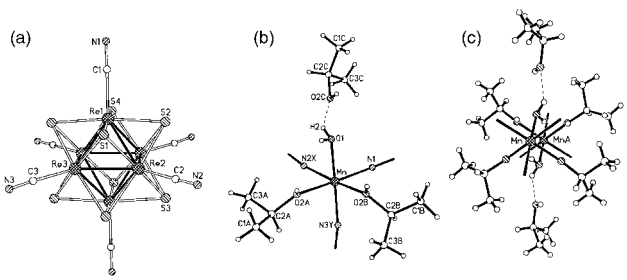

Fig. 1 The structure of the $[Re_6S_8(CN)_6]^{4-}$ cluster anion (a), coordination environment of Mn(II) (b), and the $\{[Mn(Pr^iOH)_2(H_2O\cdots Pr^iOH)]_2\}^{4+}$ associate. Hydrogen bonds are shown with dashes. N2X and N3Y arise from N2 and N3 atoms through $(-1/2 + x, 1/2 - y, 1 - z)$ and $(3/2 - x, -y, -1/2 + z)$ operations, respectively; the MnA atom rises from Mn through centrosymmetry.

† Published as NRCC No. 43879.

DOI: 10.1039/b008040n

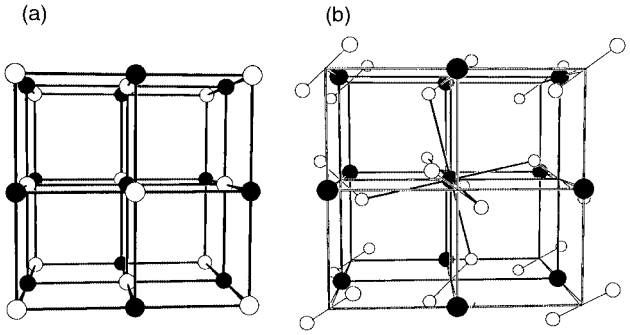

Fig. 2 3D coordination motif in Prussian Blue (a) [one unit cell is shown; black spheres show Fe(III) and open spheres show Fe(II) cations] compared to the 3D framework of the title compound (b) (one unit cell, schematic drawing: black spheres replace the cluster anions [Fig. 1(a)] and pairs of open spheres connected by single lines represent the associates [Fig. 1(c)]; coordination to manganese atoms is shown by solid lines for only the central cyanide cluster.

$Pr^iOH)]_2\}^{4+}$ is shown in Fig. 1(c). It should be noted that this fragment is complementary to the $[Re_6S_8(CN)_6]^{4-}$ cluster as it bears an equal but opposite charge and possesses six octahedrally disposed acceptor coordination sites (three about each Mn).

The 3D coordination framework in the structure shows profound parallels with the main structural motif of Prussian Blue; the latter is shown in Fig. 2(a).[2,3] In the structure of our work the $[Re_6S_8]^{10-}$ and $\{[Mn(Pr^iOH)_2(H_2O\cdots Pr^iOH)]_2\}^{4+}$ units play the role of Fe centers of two different types; each unit has six neighbors of another type attached approximately octahedrally through six cyanide bridges [Fig. 2(b)]. The unit cell of Prussian Blue is cubic with an *a*-parameter of 10.2 Å. The inner space within the smaller cubes is large enough to accommodate alkali metal cations and water molecules. The 3D framework of our structure also has a cubic motif distorted to orthorhombic. But the average unit cell parameter of 16.8 Å is dramatically larger than that in Prussian Blue. From the estimated volume of the $\{Mn_2[Re_6S_8(CN)_6]\}$ the framework occupies not more than 34% of the overall structure, with the residual empty space of 3120 Å^3 concentrated mainly in the eight smaller cubes of the unit cell. Moreover, the neutral charge of the framework makes it more hydrophobic. Such factors explain the filling of the inner space with isopropyl alcohol molecules, both as ligands and as solvating species. A cut-away layer of the 3D framework is shown in Fig. 3(a) and the packing of isopropyl alcohol solvate species inside the smaller cubes is shown in Fig. 3(b).

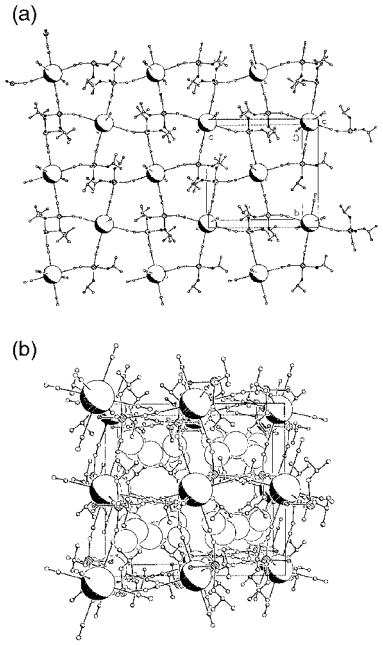

Fig. 3 Cut-away layer of the 3D framework in the title material (a) (coordinated water and isopropyl alcohol molecules are also shown) and packing of guest-solvated isopropyl alcohol molecules (van der Waals dimensions) in the small cube cavities (b). For clarity, cluster cores Re_6S_8 are replaced with 1.5 Å spheres.

Prussian Blue and related compounds form an extensive class of 3D coordination polymers revealing a remarkable stability of the main architecture and the ability to include small molecules and cations. This study demonstrates how utilization of cluster cyanides makes it possible to design analogous polymers but displaying a propensity to include species of larger size and lower polarity, thus making these useful materials for absorbing common organics.

D. V. S. is grateful for support in the form of a Visiting Fellowship.

Notes and references

‡ Discovered in 1704 by a Berlin painter [see ref. 1(*a*)].

§ *Crystal data* for $\{[Mn(Pr^iOH)_2(H_2O)]_2[Re_6S_8(CN)_6]\}\cdot 2Pr^iOH$: $C_{24}H_{52}Mn_2N_6O_8Re_6S_8$, M = 2036.3, orthorhombic, a = 16.501(3), b = 16.633(3), c = 17.208(3) Å, U = 4723(2) Å^3, T = 298 K, space group *Pbca* (no. 61), Z = 4, D_c = 2.86 g cm^{-3}, μ(Mo-Kα) = 16.2 mm^{-1}, 51564 reflections collected, 5961 unique (R_{int} = 0.066) which were used in solution and refinement. The final R-values were 0.053 (all data) and 0.033 [for 4397 intense ($I > 2\sigma_I$) data]. CCDC 149441. See http://www.rsc.org/suppdata/cc/b0/b008040n/ for crystallographic data in .cif or other electronic format.

1 (*a*) W. P. Fehlhammer and M. Fritz, *Chem. Rev.*, 1993, **93**, 1243; (*b*) K. R. Dunbar and R. A. Heintz, *Prog. Inorg. Chem.*, 1997, **45**, 283.
2 J. F. Keggin and F. D. Miles, *Nature*, 1936, **137**, 577.
3 H. J. Buser, A. Ludi, W. Petter and D. Schwarzenbach, *Chem. Commun.*, 1972, 1299.
4 (*a*) K. A. Hofmann, H. Arnoldi and H. Hiendlmaier, *Ann.*, 1907, **352**, 54 (*Chem. Abstr.* 1907, **1**, 1269); (*b*) *Handbook of Chemical Synonyms and Trade Names*, ed. W. Gardner, E. I. Cooke and R. W. I. Cooke, CRC Press, Boca Raton, FL, 1978, p. 584.
5 (*a*) K. A. Hofmann and F. A. Kuspert, *Z. Anorg. Allg. Chem.*, 1897, **15**, 204; (*b*) T. Iwamoto, *J. Inclusion Phenom.*, 1996, **24**, 61.
6 (*a*) T. Iwamoto, S. Nishikiori, T. Kitazawa and H. Yuge, *J. Chem. Soc., Dalton Trans.*, 1997, 4127; (*b*) B. F. Abrahams, B. F. Hoskins, J. Liu and R. Robson, *J. Am. Chem. Soc.*, 1991, **113**, 3045.
7 (*a*) T. Iwamoto, in *Comprehensive Supramolecular Chemistry*, ed. D. D. MacNicol, F. Toda and R. Bishop, Pergamon, Oxford, 1996, vol. 6; pp. 643–690; (*b*) R. Robson, in *Comprehensive Supramolecular Chemistry*, ed. D. D. MacNicol, F. Toda and R. Bishop, Pergamon, Oxford, 1996, vol. 6; pp. 733–755.
8 (*a*) Yu. V. Mironov, A. V. Virovets, V. E. Fedorov, N. V. Podberezskaya, O. V. Shishkin and Yu. T. Struchkov, *Polyhedron*, 1995, **14**, 3171; (*b*) Yu. V. Mironov, J. A. Cody, T. A. Albrecht-Schmitt and J. A. Ibers, *J. Am. Chem. Soc.*, 1997, **119**, 493; (*c*) N. G. Naumov, A. V. Virovets, N. V. Podberezskaya and V. E. Fedorov, *J. Struct. Chem.*, 1997, **38**, 857; (*d*) H. Imoto, N. G. Naumov, A. V. Virovets, T. Saito and V. E. Fedorov, *J. Struct. Chem.*, 1998, **39**, 720.
9 L. G. Beauvais, M. P. Shores and J. R. Long, *Chem. Mater.*, 1998, **10**, 3783.
10 N. G. Naumov, A. V. Virovets, Yu. I. Mironov, S. B. Artemkina and V. E. Fedorov, *Ukr. Khim. Zh.*, 1999, **65** (N5), 21.
11 L. G. Beauvais, M. P. Shores and J. R. Long, *J. Am. Chem. Soc.*, 2000, **122**, 2763.
12 M. V. Bennett, M. P. Shores, L. G. Beauvais and J. R. Long, *J. Am. Chem. Soc.*, 2000, **122**, 6664.
13 (*a*) N. G. Naumov, S. B. Artemkina, A. V. Virovets and V. E. Fedorov, *Solid State Sci.*, 1999, **1**, 473; (*b*) N. G. Naumov, S. B. Artemkina, A. V. Virovets and V. E. Fedorov, *J. Solid State Chem.*, 2000, **153**, 195.
14 N. G. Naumov, A. V. Virovets, M. N. Sokolov, S. B. Artemkina and V. E. Fedorov, *Angew. Chem., Int. Ed.*, 1998, **37**, 1943.
15 N. G. Naumov, A. V. Virovets and V. E. Fedorov, *Inorg. Chem. Commun.*, 2000, **3**, 71.
16 M. P. Shores, L. G. Beauvais and J. R. Long, *J. Am. Chem. Soc.*, 1999, **121**, 775.
17 (*a*) D. V. Soldatov, J. A. Ripmeester, S. I. Shergina, I. E. Sokolov, A. S. Zanina, S. A. Gromilov and Yu. A. Dyadin, *J. Am. Chem. Soc.*, 1999, **121**, 4179; (*b*) D. V. Soldatov and J. A. Ripmeester, *Chem. Mater.*, 2000, **12**, 1827.
18 M. P. Shores, L. G. Beauvais and J. R. Long, *Inorg. Chem.*, 1999, **38**, 1648.

ChemComm

Formation of folded complexes retaining intramolecular H-bonding in the extraction of nickel(II) by phenolic oxime and aliphatic diamine ligands

Victoria M. Hultgren (née Jones),[a] Ian M. Atkinson,[b] Roy L. Beddoes,[a] David Collison,*[a] C. David Garner,*[c] Madeleine Helliwell,[a] Leonard F. Lindoy*[d] and Peter A. Tasker*[e]

[a] *Department of Chemistry, The University of Manchester, Oxford Road, Manchester, UK M13 9PL. E-mail: david.collison@man.ac.uk*
[b] *School of Biomedical and Molecular Sciences, James Cook University, Townsville, Queensland 4811, Australia*
[c] *School of Chemistry, The University of Nottingham, University Park, Nottingham, UK NG7 2RD*
[d] *School of Chemistry, University of Sydney, Sydney NSW 2006, Australia*
[e] *Department of Chemistry, University of Edinburgh, West Mains Road, Edinburgh, UK EH9 3JJ*

Received (in Cambridge, UK) 20th November 2000, Accepted 16th February 2001
First published as an Advance Article on the web 7th March 2001

Solvent extraction of Ni^{II} by phenolic oximes is enhanced significantly by addition of aliphatic diamines; octahedral [Ni(II)(phenolate-oxime)$_2$(diamine)] complexes have been characterised that contain a novel folded conformation, retaining intramolecular hydrogen bonding between the two oxime ligands.

Hydrometallurgical processes based on solvent extraction are becoming increasingly important[1] in the recovery of metals. Approximately 20% of the worldwide production of copper now involves solvent extraction using phenolic oximes (H_2SaloxR, Scheme 1) derived from salicylaldehydes (R = H) or *o*-ketophenols (R = alkyl). These reagents are able to transfer Cu^{II} from acidic sulfate media containing a high concentration of Fe^{III}.[2,3] An important aspect of the chemistry involved in this solvent extraction is the formation of square-planar [Cu(HSaloxR)$_2$] complexes, stabilised by interligand hydrogen bonding (Scheme 1).[4]

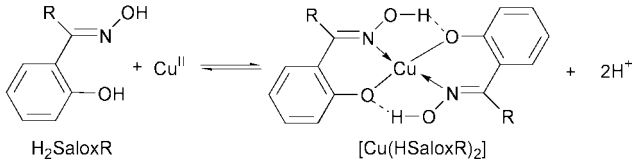

Scheme 1 The 'pH-swing' equilibrium for the acid leach/solvent extraction/electrowinning circuits for copper production; the phenolic oximes (H_2SaloxR) are derived from a salicylaldehyde (R = H) or an *o*-ketophenol (R = alkyl).[2,3]

Phenolic oxime reagents (H_2SaloxR) are not effective extractants for nickel in commercial solvent extraction processes because their $pH_{1/2}$ (the pH for 50% loading of the extractant as [Ni(HSaloxR)$_2$]) values are not sufficiently low to allow recovery from acidic feeds and the kinetics of the extraction process tend to be poor.[3] We have investigated the use of aliphatic acyclic polyamines (B) as agents for enhancing the solvent extraction of Ni^{II} by phenolic oximes. This approach was based on earlier observations that the extraction of Ni^{II} from aqueous media is enhanced when combinations of ligands are used, *e.g.* salicylic acid plus an aliphatic acyclic diamine[5] or salicylaldoxime plus a monodentate *N*-heterocycle.[6]

The extraction experiments accomplished and the results obtained are summarised in Table 1. The extent of the extraction of Ni^{II}, from H_2O into CH_2Cl_2, was significantly greater for H_2SaloxH plus a diamine, as compared with the extent of extraction by either reagent alone. The addition of a diamine (B) to a mixture of Ni^{II} and H_2SaloxH would be expected to favour extraction of the Ni^{II}, since B will act as a base and displace the equilibrium of Scheme 1 and, therefore, increase the amount of [Ni(HSaloxH)$_2$] **1** formed. However, the improvement in the efficiency of the extraction that we have observed may also involve two other contributing effects.

Firstly, we have obtained evidence for ligand assembly[7] between H_2SaloxH and representatives of the diamines listed in Table 1. In particular, the isolation and crystallographic characterisation of [(H_2SaloxH)$_2$(Me_4en)], plus ^{1}H NMR spectra recorded for a combination of these two reagents in $CDCl_3$ solution,[8] clearly demonstrate that H_2SaloxH and Me_4en form a 2:1 assembly. This ligand assembly would make a favourable contribution to the entropy of formation of [Ni(HSaloxH)$_2$(Me_4en)] **2** and related complexes.[7]

Secondly, the addition of each of the diamines (B) to a solution of **1** in CH_2Cl_2 (1:1) produced a colour change from the dark green of **1** to a shade of blue or red, depending upon the nature of B, and produced 1:1 complexes, [Ni(HSaloxH)$_2$B].† These processes have been followed by UV–VIS–NIR spectroscopy and the general result obtained is exemplified in Fig.1, for the addition of aliquots of pn to a solution of **1** in CH_2Cl_2. In each case, a stepwise increase in the absorbance at *ca.* 900 nm was observed, together with a concomitant decrease in the absorbance and a slight shift to higher energy in the λ_{max} at *ca.* 600 nm. An isosbestic point was observed in each titration, consistent with the reaction proceeding by a simple process. The variation of the absorbance at λ_{max} of 600 and 900 nm with the reagent ratio indicated that **1** and B interact with a 1:1 stoichiometry.

Isolation and recrystallisation of the solids formed by reacting [Ni(HSaloxR)$_2$] and B (1:1) in CH_2Cl_2 produced crystalline materials of composition [Ni(HSaloxR)$_2$B]. The compounds for which R = H, B = Me_4en (**2**)‡ or pn and R =

Table 1 Percentage of Ni^{II} extracted from an aqueous medium into CH_2Cl_2 using a base (B) plus salicylaldoxime (H_2SaloxH)[a]

Diamine (B)	B alone (2 mM)	H_2SaloxH + B (1 mM)	H_2SaloxH + B (2 mM)	H_2SaloxH + B (3 mM)
N,*N*-Me_2en	11	100	100	100
N,*N*'-Me_2en	16	98	100	100
pn	19	93	94	93
N,*N*'-Me_2pn	32	98	100	100
Me_4en	37	59	86	100

[a] The extraction experiments were carried out using mechanically-shaken and stoppered vials containing $Ni(NO_3)_2 \cdot 6H_2O$ (1 mM) in H_2O (5 cm^3) and H_2SaloxH (2 mM) and B (1–3 mM) in CH_2Cl_2 (5 cm^3). Each system was equilibrated for 4 h at 25 °C and the concentration of nickel in the aqueous phase was then determined by atomic absorption spectroscopy. H_2SaloxH (2 mM) alone extracted 13% of the Ni^{II}. Each of the reported values is an average of three experiments and has an estimated error of ±3%. Abbreviations for B: *N*,*N*-Me_2en = *N*,*N*-dimethylethylenediamine; *N*,*N*'-Me_2en = *N*,*N*'-dimethylethylenediamine; pn = 1,3-diaminopropane; *N*,*N*'-Me_2pn = *N*,*N*'-dimethyl-1,3-diaminopropane; Me_4en = *N*,*N*,*N*',*N*'-tetramethylethylenediamine.

DOI: 10.1039/b009267n

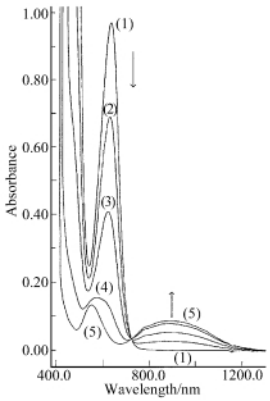

Fig. 1 The VIS–NIR absorption spectra for the addition of four [(2)–(5)] successive aliquots (2.4 mM) of pn to [Ni(HSaloxH)$_2$] (10 mM) in CH_2Cl_2; (1) is the spectrum of [Ni(HSaloxH)$_2$] prior to the addition of pn.

Me, B = *N*,*N*'-Me$_2$en have been characterised by X-ray crystallography.[8] Each compound is comprised of neutral mononuclear complexes with the Ni^{II} in a distorted octahedral environment, as exemplified by the molecular structure of **2** (Fig. 2). Each oxime is bound to the Ni^{II} *via* the phenolate *O*-atom and the oxime *N*-atom, to give a six-membered chelate ring that spans adjacent (*cis*) sites, and the diamine acts as a bidentate *cis*-*N*,*N*-chelate. Each [Ni(HSaloxR)$_2$B] compound that has been characterised by X-ray crystallography contains complexes exclusively in the form of the coordination isomer of the type shown in Fig. 2. An important structural feature of this isomer is that it involves retention of hydrogen bonding between the oximic hydroxyl groups and the phenolate oxygens. This type of hydrogen bonding is well established; *e.g.* in **1**[9] and [Cu(HSaloxH)$_2$],[4] it stabilises the *planar* complex (see Scheme 1). However, the [Ni(HSaloxR)$_2$B] complexes reported herein are the first examples that manifest the corresponding *folded* interligand, intramolecular H-bonding. Thus, in the octahedral [Ni(HSaloxR)$_2$B] complexes, *cis*-chelation of the diamine results in a folding about the phenolate–phenolate axis and the oxime N-atoms rotate to become mutually *cis*; the phenolate O-atoms remain mutually *trans*, but the O–Ni–O angle is reduced from 180 to 168.4(1)°. In **2**, the distances O1···O4 [2.670(4) Å] and O2···O3 [2.627(4) Å] are slightly (*ca.* 0.15 Å) longer than the corresponding distances in **1** (average 2.52 Å).[9] This difference is consistent with the increased span of the intramolecular H-bonding required to accommodate six-coordinate, high-spin, Ni^{II}, as compared to the planar four-coordinate, low-spin, Ni^{II} present in **1**.[10] Consistent with this view, the Ni–O and Ni–N$_{ox}$ bonds are longer by *ca.* 0.25 and 0.30 Å, respectively, in **2** than in **1**.[9] The oxime hydrogen atoms in **1** were located by Fourier techniques and the length of the hydrogen bonds to the phenolic oxygens (H2$_O$···O3 and H4$_O$···O1) are 1.70 and 1.88 Å, respectively. Given the importance of intramolecular H-bonding in stabilising [Cu(HSaloxR)$_2$] complexes, thereby aiding the efficacy and selectivity of the process employed for the commercial extraction of Cu^{II},[2,3] it is of considerable interest to observe that a similar, *but folded*, arrangement is present in the octahedral [Ni(HSaloxR)$_2$B] complexes.

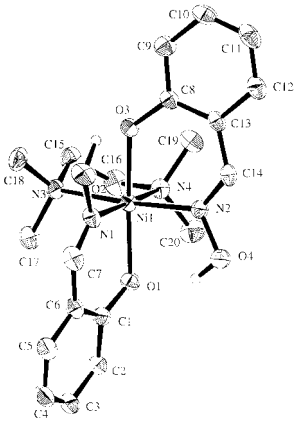

Fig. 2 ORTEP view and atomic labelling scheme for [Ni(HSaloxH)$_2$(Me$_4$en)]. Selected bond lengths (Å): Ni1–N1 2.065(4), Ni1–N2 2.057(3), Ni1–N3 2.171(4), Ni1–N4 2.170(4), Ni1–O1 2.050(3), Ni1–O3 2.041(3); selected interbond angles (°): O1–Ni1–O3 168.4(1), O1–Ni1–N1 85.4(1), O1–Ni1–N2 86.5(1), O1–Ni1–N3 97.7(1), O1–Ni1–N4 93.5(1), O3–Ni1–N1 85.8(1), O3-Ni1–N2 86.3(1), O3–Ni1–N3 90.1(1), O3–Ni1–N4 95.9(1), N1–Ni1–N2 91.7(1), N1–Ni1–N3 92.1(1), N1–Ni1–N4 175.0(1), N2–Ni1–N3 174.6(1), N2–Ni1–N4 93.1(1), N3–Ni1–N4 83.2(1); selected non-bonded distances (Å): O4···O4 3.175(7), O2···O3 2.627(4), O4···O1 2.670(4).

We consider that: (i) the displacement of the equilibrium of Scheme 1 by the presence of the basic diamine; (ii) the possible operation of a ligand 'assembly effect';[7] and (iii) the formation of [Ni(HSaloxR)$_2$B] with retention of the intramolecular H-bonding, could each contribute to the significant increase in the amount of Ni^{II} extracted by a combination of a phenolic oxime and a diamine, as compared with the amount of Ni^{II} extracted by either reagent alone.

We thank EPSRC and Avecia (formerly Zeneca Specialties) for the provision of a CASE studentship and travel funds to V. M. H. We also acknowledge the Australian Research Council for support.

Notes and references

† [Ni(HSaloxH)$_2$][9] (0.043 g, 0.13 mmol) was dissolved in CH_2Cl_2 (5 cm^3) and Me$_4$en (20 μL, 0.13 mmol) added, producing an instantaneous change from green to blue. The solution was stirred for 10 min at RT, then layered with *n*-hexane (5 cm^3) and left to evaporate in air. The blue product was washed with a small amount of *n*-hexane and dried *in vacuo*. Yield 65%. $C_{20}H_{28}N_4O_4Ni$: found (calc.): C 53.6 (53.7), H 6.4 (6.3), N 12.6 (12.5), Ni 12.6 (13.1)%. VIS–NIR (refl.) λ_{max}/nm (rel. abs.) 975.2 (0.14), 583.2 (0.15). μ_{eff} at RT 3.13 μ_B. IR (KBr)/cm^{-1} 1644w δ_{OH}, 1597s $\nu_{C=C}$, 1544m $\nu_{C=N}$, 1189m, 907s ν_{N-O}, 1292s, 995s ν_{C-O}.

‡ *Crystal data* for $C_{20}H_{28}N_4O_4Ni$: M = 447.17, monoclinic, space group $P2_1/c$ (no. 14), a = 9.529(2) b = 14.329(3) c = 15.944(4) Å, β = 97.14(2)°, U = 2160.9(9) Å^3, T = 294(1) K, Z = 4, μ(Cu-Kα) = 15.72 cm^{-1}, 3590 reflections measured, 3366 unique, 2597 for $I > 2.50\sigma(I)$ (R_{int} = 0.085) on a Rigaku AFC5R, which were used in all calculations. The final $R1$ = 0.058, wR = 0.067. The structure was solved by direct methods with SIR92[11] and expanded using Fourier techniques.[12,13] Non-hydrogen atoms were refined anisotropically and hydrogen atoms were placed in idealised positions (C–H = 0.95 Å), except for the four (O–H) that were found by difference Fourier analysis. All of the hydrogen atoms were refined isotropically to convergence, then fixed for the final rounds of refinement. The maximum and minimum peaks in the final difference Fourier map were 0.77 and −0.80 e Å^{-3}, respectively. CCDC 154046. See http://www.rsc.org/suppdata/cc/b0/b009267n/ for crystallographic data in .cif or other electronic format.

1 F. Habashi, *A Textbook of Hydrometallurgy*, Metallurgie Extractive Quebec, Enr., Sainte-Foy, Quebec, 1993.
2 A. W. Ashbrook, *Coord. Chem. Rev.*, 1975, **16**, 285.
3 J. Szymanowski, *Hydroxyoximes and Copper Hydrometallurgy*, CRC Press, Boca Raton, FL, 1993, p. 1.
4 M. A. Jarski and E. C. Lingafelter, *Acta Crystallogr.*, 1964, **17**, 1109.
5 J. Aggett and G. A. Woollard, *J. Inorg. Nucl. Chem.*, 1981, **43**, 2959.
6 A. P. Rao and S. P. Dubey, *J. Inorg. Nucl. Chem.*, 1972, **34**, 2041.
7 K. R. Adam, I. M. Atkinson, S. Farquhar, A. J. Leong, L. F. Lindoy, M. S. Mahinay, P. A. Tasker and D. Thorp, *Pure Appl. Chem.*, 1998, **70**, 2345.
8 V. M. Hultgren (née Jones), R. L. Beddoes, D. Collison, C. D. Garner, M. Helliwell and P. A. Tasker, *J. Chem. Soc., Dalton Trans.*, in preparation.
9 L. L. Merritt Jr., C. Guare and A. E. Lessor Jr., *Acta Crystallogr.*, 1956, **9**, 253; R. C. Srivastava, E. C. Lingafelter and P. C. Jain, *Acta Crystallogr.*, 1967, **22**, 922.
10 K. Hendrick, P. A. Tasker and L. F. Lindoy, *Prog. Inorg. Chem.*, 1985, **33**, 1.
11 SIR92: A. Altomare, M. Cascarano, C. Giacovazzo and A. Guagliardi, *J. Appl. Crystallogr.*, 1993, **26**, 343.
12 DIRDIF94: P. T. Beurskens, G. Admiraal, G. Beurskens, W. P. Bosman, R. de Gelder, R. Israel and J. M. M. Smits, 1994, The DIRDIF-94 program system, Technical Report of the Crystallography Laboratory, University of Nijmegen, The Netherlands.
13 teXsan: Crystal Structure Analysis Package, Molecular Structure Corporation The Woodlands, TX, 1985 & 1992.

Spontaneous crystallization of zincophosphate sodalite by means of dry substrate grinding

Stanisław Kowalak,* Aldona Jankowska and Elżbieta Baran

Faculty of Chemistry, A. Mickiewicz University, Poznań, Poland. E-mail: skowalak@main.amu.edu.pl

Received (in Cambridge, UK) 10th January 2001, Accepted 16th February 2001
First published as an Advance Article on the web 7th March 2001

Zincophosphate sodalites can be obtained by simple grinding of the substrate salts [$ZnCl_2$, $Zn(NO_3)_2$, Na_2HPO_4, Na_2CO_3] in a mortar, provided that at least one of the applied salts contains crystallization water.

The hydrothermal synthesis of zeolites or zeolite-like materials usually comprises forming an initial gel and its subsequent crystallization often at enhanced temperature and sometimes for extended times. Stucky and coworkers[1,2] demonstrated the unusual possibility to obtain faujasite (FAU) or sodalite (SOD) (zincophosphate, zincoarsenate, zincoantimonate) structures by means of spontaneous crystallization upon mixing aqueous solutions of the substrates at low temperatures. The above zeolite-like materials have been extensively studied by several research groups.[3] Such spontaneous crystallization can be useful for encapsulation of certain compounds inside the inner cages upon their formation. Our earlier attempts to prepare ultramarine analogs by introduction and further transformation of sodium polysulfides inside zincophosphate sodalite prepared according to the Stucky recipe[1] have not been successful[4] because of the low stability of the crystalline structure. The crystallization of zincophosphate with sodium polysulfide present in the initial mixture did not lead to formation of the sodalite structure. Another attempt to introduce polysulfides into the zincophosphate upon crystallization comprised simple grinding of the substrates without any water. Although mixtures containing polysulfides did not form a sodalite, it was interesting that a blank sample containing no sulfides formed the sodalite structure merely by grinding of the substrates.

The following study presents series of syntheses of zincophosphate sodalite by means of spontaneous, *dry* crystallization. The following principal substrates have been applied: $ZnCl_2$, $Zn(NO_3)_2{\cdot}6H_2O$, Na_2HPO_4, $Na_3PO_4{\cdot}12H_2O$, NaOH, Na_2CO_3, $Na_2CO_3{\cdot}12H_2O$ (all supplied by POCh, Poland). In some cases additional compounds (such as KBr, NaCl, CdS, elemental S) were admitted to the initial mixtures. The Zn/P ratio was always 0.85 and Na/Zn was 3.5, *i.e.* similar to that applied by Stucky and coworkers for synthesis of the SOD structure.[1,2] NaOH applied in preliminary experiments was replaced by sodium carbonate because of easier grinding of the latter. The procedure comprised grinding of the substrate mixture (usually *ca.* 2 g) in a ceramic mortar for *ca.* 10 min, then washing of the products with water and drying at 60 °C. The sequence of admittance of the substrates to the mixture varied. The obtained samples were characterized by means of XRD, IR, DTA, DTG and SEM.

The grinding of the mixture [*e.g.* $Zn(NO_3)_2{\cdot}6H_2O$, Na_2HPO_4, Na_2CO_3] led to release of water from the hydrated salts which made the sample wet. The evolution of CO_2 on grinding was noticeable due to Na_2CO_3 decomposition in the presence of Zn salts. Table 1 indicates the composition and sequence of adding the substrates as well as the structure and pH of the first drops of the filtrate on washing. Fig. 1 indicates high crystallinity SOD structures of the samples obtained from mixtures of Na_2HPO_4, Zn salts and Na_2CO_3 provided that one of components contains crystallization water. The as-made samples (before washing) usually contain a noticeable amount of NaCl or $NaNO_3$ (indicated in Fig. 1 for the sample ZnP-1*), which can then be washed out. It is remarkable that the sequence of substrate admittance affects the crystallinity and purity of the products. The sample obtained by merging all the substrates together (ZnP-0) contains more hopeite impurities than the samples ZnP-2 and ZnP-1, where either acidic (Zn) or alkaline (Na_2CO_3) components are admitted last. The SOD structure does not appear if Na_3PO_4 is used as the P source. The sequence of admittance as well as the P source influence the pH of the resulted products. It is likely that the pH of the mixture is an important factor for obtaining the SOD structure. The best results were achieved at pH ~ 7. The value of pH was as high as 11–12 for the samples prepared from Na_3PO_4 (with a similar molar ratio). The SOD structure was not formed on grinding when anhydrous salts were used (*e.g.* sample ZnP-4*), however, this sample attained the SOD structure upon washing with water

Table 1 Results of *dry* crystallization of zincophosphates

Sample	Substrates (order of admission)	pH	Structure
ZnP-SOD[1]	H_3PO_4 + NaOH + $Zn(NO_3)_2$ + H_2O	7.5	SOD + H
ZnP-0	Na_2HPO_4 + Na_2CO_3 + $Zn(NO_3)_2{\cdot}6H_2O$; all substrates mixed together	6.8	SOD + H
ZnP-1*	Na_2HPO_4 + Na_2CO_3 + $Zn(NO_3)_2{\cdot}6H_2O$		SOD + $NaNO_3$
ZnP-1	Na_2HPO_4 + Na_2CO_3 + $Zn(NO_3)_2{\cdot}6H_2O$	6.8	SOD
ZnP-2	Na_2HPO_4 + $Zn(NO_3)_2{\cdot}6H_2O$ + Na_2CO_3	6.8	SOD
ZnP-3	Na_2CO_3 + $Zn(NO_3)_2{\cdot}6H_2O$ + Na_2HPO_4	6.5	SOD + H
ZnP-4*	Na_2HPO_4 + Na_2CO_3 + $ZnCl_2$		NaCl
ZnP-4	Na_2HPO_4 + Na_2CO_3 + $ZnCl_2$	6.5	SOD
ZnP-5*	Na_2HPO_4 + $Na_2CO_3{\cdot}10H_2O$ + $ZnCl_2$	8.2	NaCl + SOD
ZnP-6*	$Na_3PO_4{\cdot}12H_2O$ + $Zn(NO_3)_2{\cdot}6H_2O$	12	$NaNO_3$
ZnP-7*	$Na_3PO_4{\cdot}12H_2O$ + $ZnCl_2$	11	NaCl

* The as made samples (not washed); H-hopeite; the pH was measured for the first drops of the filtrate on washing.

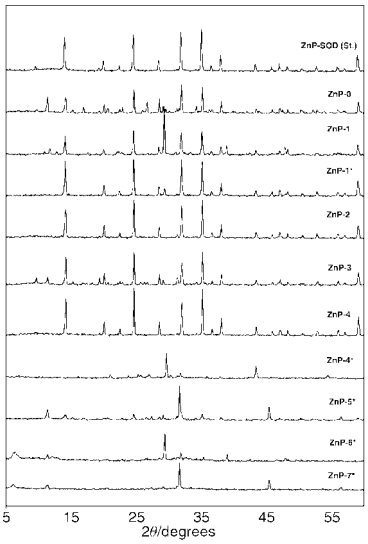

Fig. 1 XRD patterns of indicated samples. ZnP-SOD (St) indicates the sample prepared according to the Stucky recipe.[1] Samples indicated by asterisks were not washed before the diffraction measurements.

DOI: 10.1039/b100434b

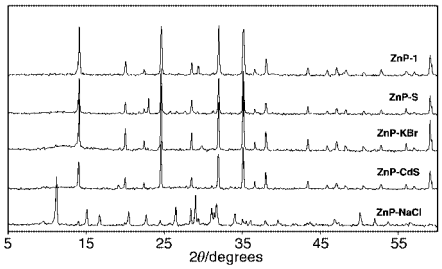

Fig. 2 XRD patterns of the indicated samples.

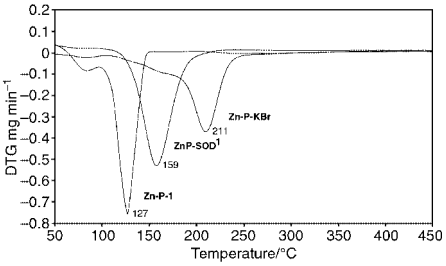

Fig. 4 Typical DTG curves (in air) for the indicated samples.

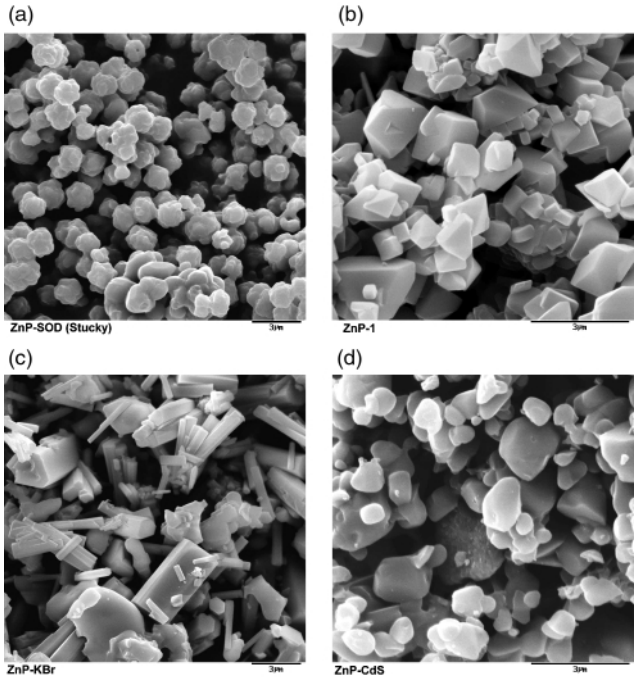

Fig. 3 SEM pictures of (a) sodium zincophospate sodalite prepared according to Stucky;[1] (b) sample ZnP-1; (c) sample ZnP-KBr; (d) sample ZnP-CdS.

(ZnP-4). The sodalite structure has also been attained when some additional compounds were admitted (KBr, S, CdS, see Table 2), whereas other salts (*e.g.* NaCl, Na_2S_n) impeded formation of the SOD structure (Fig. 2). No bromide was detected in the sample prepared with KBr, although its presence affected the morphology of the product (Fig. 3). The size of crystallites obtained using this *dry* method (*ca.* 2 μm) was similar to those prepared from solution as well as aluminosilicate sodalite (Fig. 3). CdS is most likely encapsulated inside the sodalite cages and only at high CdS loading (CdS/Zn > 0.2) do the SEM images indicate the presence of sulfide particles on the surface of sodalite crystallites.

The thermal properties of the samples obtained by grinding [examined by thermal (DTA) and gravimetric (TG, DTG) analyses (Fig. 4)] indicate the most significant effects attributed to removal of water. The dehydration temperatures differed for the samples prepared from different substrates or in the presence of additional components (*e.g.* KBr). It is interesting that regardless of the differences in dehydration temperatures, the amount of water removed is always the same (*ca.* 10%), which corresponds to empirical formula of the products: $NaZnPO_4{\cdot}H_2O$. For sample ZnP–CdS the weight loss on heating to 200 °C is only *ca.* 5%. This lower content of water results from encapsulation of CdS. The XRD data of the samples calcined at 200 °C indicate decomposition of the structure after removal of water which is not regenerated upon contact with atmospheric moisture.

Table 2 Syntheses with additional compounds (main procedure as for ZnP-1)

Sample	Additional reagents	Remarks
ZnP-S	S dissolved in CS_2 (Zn/S = 1,33)	SOD, yellow
ZnP-KBr	KBr ground with mixture (Zn/KBr = 0,35)	SOD, no Br^-
ZnP-CdS	CdS powder ground with mixture (Zn/CdS = 0,04)	SOD, yellow
ZnP-NaCl	NaCl (Zn/NaCl = 0,7)	Poor crystallinity

Another series of experiments with anhydrous substrate salts ground with a small admixture of various polar reagents such as ethanol, phenol, amines, acetone, nitrobenzene, acetonitrile, DMSO, DMF or liquid ammonia sometimes resulted in crystalline structures analogous to zeolites.[5]

The present preliminary results indicate a great affinity of zinc salts and phosphates to form a sodalite crystalline structure. Spontaneous crystallization of the sodalite structure can take place even upon grinding of substrate salts. The *dry* crystallization, however, requires some water, which is supplied from crystallization water present in at least one of the components of the substrate mixture. The sequence of adding the mixture components as well as the pH of the mixture affects the results of the syntheses. It seems that some additional compounds (*e.g.* S, CdS) can be encapsulated into the sodalite cages on *dry* crystallization. The admittance of a small amount of polar reagents (other than water) to an anhydrous substrate mixture can sometimes result in structures similar to zeolites.

Notes and references

1 W. T. A. Harrison, T. E. Gier, K. L. Moran, J. M. Nicol, H. Eckert and G. D. Stucky, *Chem. Mater.*, 1991, **3**, 27.
2 T. E. Gier and G. D. Stucky, *Nature*, 1991, **349**, 508.
3 W. T. A. Harrison, T. E. Gier, J. M. Nicol and G. D. Stucky, *J. Solid State Chem.*, 1995, **114**, 249; M. J. Castagnola and P. K. Dutta, *Microporous Macroporous Mater.*, 1998, **20**, 149; X. Bu, T. E. Gier, P. Feng and G. D. Stucky, *Microporous Macroporous Mater.*, 1998, **20**, 371; H. Y. Ng and W. T. A. Harrison, *Microporous Macroporous Mater.*, 1998, **23**, 197; R. W. Broach, R. L. Bedard and S. G. Song, *Chem. Mater.*, 1999, **11**, 2076.
4 S. Kowalak, M. Stróżyk, M. Pawłowska, M. Miluśka and J. Kania, *Stud. Surf. Sci. Catal.*, 1997, **105**, 237.
5 S. Kowalak and A. Jankowska, study in progress.

An unusual abrupt thermal spin-state transition in $[FeL_2][BF_4]_2$ [L = 2,6-di(pyrazol-1-yl)pyridine]†

Joanne M. Holland,[a] Judith A. McAllister,[bc] Zhibao Lu,[d] Colin A. Kilner,[a] Mark Thornton-Pett[a] and Malcolm A. Halcrow*[a]

[a] *School of Chemistry, University of Leeds, Woodhouse Lane, Leeds, UK LS2 9JT. E-mail: M.A.Halcrow@chem.leeds.ac.uk*
[b] *Department of Chemistry, University of Cambridge, Lensfield Road, Cambridge, UK CB2 1EW*
[c] *Interdisciplinary Research Centre in Superconductivity, University of Cambridge, Madingley Road, Cambridge, UK CB3 0HE*
[d] *Centre for Self-Organising Molecular Systems, School of Chemistry, University of Leeds, Woodhouse Lane, Leeds, UK LS2 9JT*

Received (in Cambridge, UK) 29th January 2001, Accepted 15th February 2001
First published as an Advance Article on the web 7th March 2001

The complex $[Fe(L^1H)_2][BF_4]_2$ exhibits an abrupt thermal spin-crossover which may be mediated by an order–disorder transition of the BF_4^- anions.

The spin-crossover phenomenon in Fe(II) complexes continues to be well studied,[1] reflecting their potential applicability as bistable materials for information storage.[2] For such applications, a thermally induced spin-state transition must occur over as small a temperature range as possible, and should exhibit a hysteresis loop.[2] These properties reflect intermolecular cooperativity within the sample, and are most often associated with a concomitant crystallographic phase transition and/or loss of long-range ordering. However, there are isolated examples where this is not the case, and intermolecular cooperativity in a thermal spin–spin transition is instead mediated by covalent pathways,[3] or *via* intermolecular hydrogen-bonding,[4] π–π interactions[5,6] or van der Waals contacts.[7] Following our studies of the electronic structures and solid state fluxionality of $[Cu(L^1R)_2]^{2+}$ (R = H, mesityl),[8–10] we wished to examine the Fe(II) complex chemistry of L^1R. This was of particular interest since several salts of $[Fe(L^2)_2]^{2+}$ {a structural isomer of $[Fe(L^1H)_2]^{2+}$} exhibit both thermal and light-induced spin-state transitions, whose physics has been extensively studied.[11]

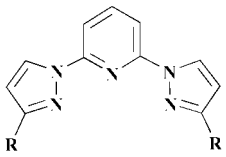

L^1R

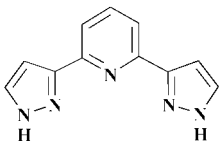

L^2

Complexation of $Fe(BF_4)_2 \cdot 6H_2O$ with 2 mol equivalents of L^1H[12] in acetone affords a mustard precipitate of $[Fe(L^1H)_2][BF_4]_2$ **1** in 70% yield, which can be recrystallised from MeCN–Et_2O.‡ Variable-temperature magnetic susceptibility measurements§ from polycrystalline **1** demonstrated a transition between high-spin ($S = 2$, $\chi_mT = 3.6$–3.7 cm^3 K mol^{-1}[13]) and low-spin ($S = 0$, $\chi_mT \leqslant 0.3$ cm^3 K mol^{-1}[13]) states centred at $T = 259$ K, with a transition width of 3 K and a 3 K hysteresis loop (Fig. 1). This change is reflected in the colour of the compound, which changes sharply from mustard yellow to dark brown upon cooling; this change is reversible upon rewarming to room temperature. Differential scanning calorimetry (DSC) experiments§ of **1** confirmed these results, showing a first-order transition centred at 260 K, with a hysteresis width of 4 K. Values of $\Delta H = 17.2(2)$ kJ mol^{-1} and $\Delta S = 66.2(8)$ J mol^{-1} K^{-1} for the transition were derived from the DSC data.

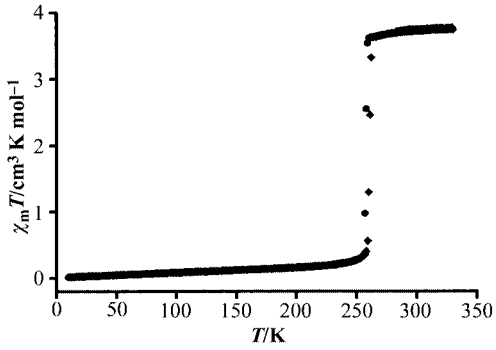

Fig. 1 Plot of χ_mT *vs.* T for polycrystalline **1** in cooling (●) and warming (◆) modes.

The temperature of the transition was also confirmed by measuring the crystallographic unit cell in the range 240–300 K, which demonstrated a discontinuity within the range 259–261 K in cooling and warming modes. No hysteresis was detected by this method, although this might reflect the less accurate temperature control at the diffractometer, which is estimated at ±2 K. There is no change in space group ($P2_1$) at these temperatures; rather, the transition is characterised by a decrease of 0.55 Å in the crystallographic *c*-direction, an increase of 0.05 Å in *b*, and an increase of 2.0° in β as the temperature is lowered (see ESI†). The decrease in unit cell volume associated with the phase transition (ignoring thermal contraction effects) is 35(5) Å^3 or 2.6%, the latter being a typical value for a spin state transition in an Fe(II) complex.[14] The temperature of the crystal can be cycled across the transition several times, although the crystal begins to decay noticeably after *ca.* five cycles.

Four datasets were collected from the complex, at 375, 290, 240 and 150 K.¶ The molecular structures of the complex dication at 290 and 375 K are crystallographically indistinguishable, as are the structures at 240 and 150 K (see ESI†). Therefore, only the structure analyses at 290 and 240 K will be discussed in detail. At both temperatures the six-coordinate Fe(II) ion in **1** has approximate local D_{2d} symmetry, with Fe–N bond lengths that are typical of a high-spin (290 K) and low-spin (240 K) Fe(II) centre (Fig. 2).[15] At 240 K the Fe–N distances are shorter than at 290 K by an average of 0.215(10) Å, which is a typical value for a high- to low-spin transition involving a Fe(II) complex with a hexa-nitrogen donor set.[15] As a result, the average ligand bite angle has increased at 240 K [80.0(3)°] compared to 290 K [73.47(18)°].

† Electronic supplementary information (ESI) available: tabulated and plotted unit cell dimensions for **1** between 240–300 K; tabulated magnetic susceptibility data between 10–330 K. See http://www.rsc.org/suppdata/cc/b1/b100995h/

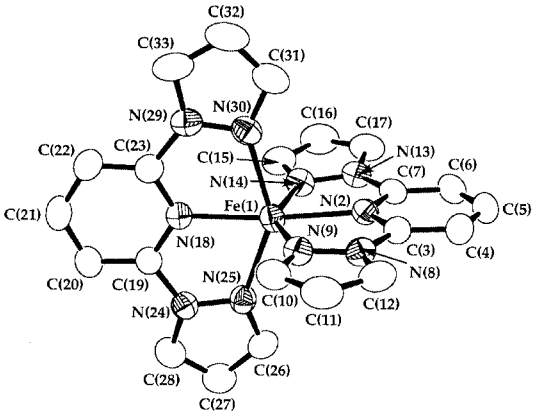

Fig. 2 View of the $[Fe(L^1H)_2]^{2+}$ dication in the crystal of **1** at 290 K, showing the atom numbering scheme employed for the complex cation. Thermal ellipsoids are at the 35% probability level. For clarity, all H atoms have been omitted. The complex at 240 K is visually indistinguishable. Selected distances (Å) and angles (°) at 290 K: Fe(1)–N(2) 2.1248(19), Fe(1)–N(9) 2.193(2), Fe(1)–N(14) 2.175(3), Fe(1)–N(18) 2.127(2), Fe(1)–N(25) 2.184(3), Fe(1)–N(30) 2.185(3); N(2)–Fe(1)–N(9) 73.47(8), N(2)–Fe(1)–N(14) 73.65(9), N(2)–Fe(1)–N(18) 173.15(10), N(2)–Fe(1)–N(25) 113.14(9), N(2)–Fe(1)–N(30) 100.21(10), N(9)–Fe(1)–N(14) 147.08(9), N(9)–Fe(1)–N(18) 104.24(8), N(9)–Fe(1)–N(25) 98.46(9), N(9)–Fe(1)–N(30) 92.88(9), N(14)–Fe(1)–N(18) 108.21(9), N(14)–Fe(1)–N(25) 95.95(9), N(14)–Fe(1)–N(30) 91.12(10), N(18)–Fe(1)–N(25) 73.44(9), N(18)–Fe(1)–N(30) 73.31(10), N(25)–Fe(1)–N(30) 146.58(9). Selected distances (Å) and angles (°) at 240 K: Fe(1)–N(2) 1.893(3), Fe(1)–N(9) 1.979(3), Fe(1)–N(14) 1.968(3), Fe(1)–N(18) 1.905(3), Fe(1)–N(25) 1.981(4), Fe(1)–N(30) 1.975(4); N(2)–Fe(1)–N(9) 80.22(14), N(2)–Fe(1)–N(14) 80.05(14), N(2)–Fe(1)–N(18) 178.25(18), N(2)–Fe(1)–N(25) 101.75(15), N(2)–Fe(1)–N(30) 98.34(15), N(9)–Fe(1)–N(14) 160.26(13), N(9)–Fe(1)–N(18) 100.50(14), N(9)–Fe(1)–N(25) 92.92(14), N(9)–Fe(1)–N(30) 92.24(14), N(14)–Fe(1)–N(18) 99.21(14), N(14)–Fe(1)–N(25) 91.57(15), N(14)–Fe(1)–N(30) 90.11(15), N(18)–Fe(1)–N(25) 79.83(15), N(18)–Fe(1)–N(30) 80.06(15), N(25)–Fe(1)–N(30) 159.82(13).

To conclude, we have shown that crystalline **1** undergoes a cooperative spin-state transition centred at 260(1) K, which does not involve a crystallographic phase change. It is not clear what mediates the cooperativity of this transition. However, one possibility is implied by the isomorphous complex $[Cu(L^1H)_2][BF_4]_2$ **2**, in which pseudo-Jahn–Teller cooperativity is mediated by rotation of the BF_4^- anions in the crystal.[10] It is therefore intriguing that there is an apparent change in the anion motion in **1** across the spin-state transition. At 290 K, all F atoms in both BF_4^- anions are badly disordered, implying that there is essentially free rotation of the near-spherical anions within their lattice cavity. In contrast, at 240 K one F atom in each ion appears to be crystallographically ordered, so that the anions are now disordered by rotation about one B–F bond. Experiments to further define the influence of anion motion on the spin-crossover in **1**, and to determine the magnetic properties of other $[Fe(L^1R)_2]^{2+}$ complexes, are in progress.

We would like to thank The Royal Society (M. A. H.), the EPSRC (J. A. M., Z. L.) and the University of Leeds for funding.

Notes and references

‡ *Analytical data* for **1**: Found C, 40.7; H, 2.8; N, 21.2. Calc. for $C_{22}H_{18}B_2F_8FeN_{10}$: C, 40.5; H, 2.8; N, 21.5%.

§ Susceptibility measurements were carried out in an applied field of 1000 G, with the sample being poised at each temperature for 1 min before measurement. DSC experiments were run using a temperature ramp of 10 °C min^{-1}.

¶ Four datasets were collected for **1** ($C_{22}H_{18}B_2F_8FeN_{10}$, M_r = 651.93, monoclinic, $P2_1$, Z = 2).

Crystal data: at 375 K: a = 8.5301(3), b = 8.5518(4), c = 19.1757(5) Å, β = 94.9043(24)°, U = 1393.70(9) $Å^3$, μ(Mo-Kα) = 0.628 mm^{-1}; 15873 measured reflections, 6039 independent, R_{int} = 0.035; $R(F)$ = 0.045, $wR(F^2)$ = 0.120, Flack parameter −0.001(17). The F atoms of both BF_4^- anions were badly disordered at this temperature. Each anion was modelled using three different disorder orientations, in a 0.50 : 0.25 : 0.25 occupancy ratio. All B–F distances were restrained to 1.37(2) Å, and non-bonded F···F distances within each disorder orientation to 2.24(2) Å. All non-H atoms with occupancy ⩾0.5 were refined anisotropically.

At 290 K: a = 8.4947(2), b = 8.5070(2), c = 19.0535(6) Å, β = 95.7050(18)°, U = 1370.07(6) $Å^3$, μ(Mo-Kα) = 0.639 mm^{-1}; 15406 measured reflections, 5442 independent, R_{int} = 0.043; $R(F)$ = 0.040, $wR(F^2)$ = 0.110, Flack parameter 0.022(15). Refinement details as for the 375 K structure.

At 240 K: a = 8.4977(3), b = 8.5665(3), c = 18.4299(8) Å, β = 98.0931(12)°, U = 3128.25(9) $Å^3$, μ(Mo-Kα) = 0.659 mm^{-1}; 10234 measured reflections, 5538 independent, R_{int} = 0.045; $R(F)$ = 0.046, $wR(F^2)$ = 0.124, Flack parameter 0.006(19). Both BF_4^- anions were disordered by rotation about one B–F bond. The disordered F atoms of the two anions were modelled over three orientations, with 0.50 : 0.25 : 0.25 and 0.40 : 0.30 : 0.30 occupancy ratios. All B–F distances were restrained to 1.39(2) Å, and non-bonded F···F distances within each disorder orientation to 2.27(2) Å. All non-H atoms with occupancy >0.5 were refined anisotropically.

At 150 K: a = 8.4575(2), b = 8.5233(2), c = 18.3756(4) Å, β = 98.2896(13)°, U = 1310.78(5) $Å^3$, μ(Mo-Kα) = 0.668 mm^{-1}; 19914 measured reflections, 5715 independent, R_{int} = 0.038; $R(F)$ = 0.031, $wR(F^2)$ = 0.079, Flack parameter −0.009(10). No disorder was detected at this temperature, and no restraints were applied. All non-H atoms were refined anisotropically.

CCDC 158392–158395. See http://www.rsc.org/suppdata/cc/b1/b100995h/ for crystallographic data in .cif or other electronic format.

1 H. A. Goodwin, Y. Garcia and P. Gütlich, *Chem. Soc. Rev.*, 2000, **29**, 419.
2 O. Kahn, *Science*, 1998, **279**, 44.
3 Y. Garcia, O. Kahn, L. Rabardel, B. Chansou, L. Salmon and J.-P. Tuchagues, *Inorg. Chem.*, 1999, **38**, 4663.
4 L. Wiehl, G. Kiel, C. P. Köhler, H. Spiering and P. Gütlich, *Inorg. Chem.*, 1986, **25**, 1565.
5 J.-F. Létard, P. Guionnieau, L. Rabardel, J. A. K. Howard, A. E. Goeta, D. Chasseau and O. Kahn, *Inorg. Chem.*, 1998, **37**, 4432.
6 P. Guionnieau, J.-F. Létard, D. S. Yufit, D. Chasseau, G. Bravic, A. E. Goeta, J. A. K. Howard and O. Kahn, *J. Mater. Chem.*, 1999, **9**, 985.
7 E. W. Müller, H. Spiering and P. Gütlich, *Chem. Phys. Lett.*, 1982, **93**, 567; B. Gallois, J.-A. Real, C. Hauw and J. Zarembowitch, *Inorg. Chem.*, 1990, **29**, 1152.
8 N. K. Solanki, E. J. L. McInnes, F. E. Mabbs, S. Radojevic, M. McPartlin, N. Feeder, J. E. Davies and M. A. Halcrow, *Angew. Chem., Int. Ed.*, 1998, **37**, 2221.
9 A. J. Bridgeman, M. A. Halcrow, M. Jones, E. Krausz and N. K. Solanki, *Chem. Phys. Lett.*, 1999, **314**, 176.
10 M. A. Leech, N. K. Solanki, M. A. Halcrow, J. A. K. Howard and S. Dahaoui, *Chem. Commun.*, 1999, 2245.
11 T. Buchen, P. Gütlich, K. H. Sugiyarto and H. A. Goodwin, *Chem. Eur. J.*, 1996, **2**, 1134 and references therein.
12 D. L. Jameson and K. A. Goldsby, *J. Org. Chem.*, 1990, **55**, 4992.
13 C. J. O'Connor, *Prog. Inorg. Chem.*, 1982, **29**, 203.
14 Y. Garcia, P. Guionneau, G. Bravic, D. Chasseau, J. A. K. Howard, O. Kahn, V. Ksefontov, S. Reiman and P. Gütlich, *Eur. J. Inorg. Chem.*, 2000, 1531 and references therein.
15 E. König, *Prog. Inorg. Chem.*, 1987, **35**, 527.

ChemComm

Low temperature electrochemical synthesis of titanium nitride

Lucy E. Griffiths,[a] Martin R. Lee,[b] Andrew R. Mount,[a] Hiroshi Kondoh,[c] Toshiaki Ohta[c] and Colin R. Pulham*[a]

[a] *Department of Chemistry, The University of Edinburgh, The King's Buildings, West Mains Road, Edinburgh, Scotland, UK EH9 3JJ. E-mail: C.R.Pulham@ed.ac.uk*
[b] *Department of Geology and Geophysics, The University of Edinburgh, Grant Institute, West Mains Road, Edinburgh, Scotland, UK EH9 3JW*
[c] *Department of Chemistry, Graduate School of Science, The University of Tokyo, 7-3-1 Hongo, Bunkyo-ku, Tokyo 113-0033, Japan*

Received (in Cambridge, UK) 19th January 2001, Accepted 20th February 2001
First published as an Advance Article on the web 7th March 2001

Electrochemical oxidation of a titanium electrode in a solution of potassium amide in liquid ammonia resulted in the deposition of titanium nitride either as a thin film or as nanoparticles.

Titanium nitride is a technologically important material that exhibits excellent chemical stability, good wear resistance, and high electrical conductivity. As a thin film, titanium nitride finds uses as a hard coating for cutting tools,[1] as a diffusion barrier for microelectronic devices,[2] as an optical coating,[3] and as a gold-coloured surface for jewellery.[4] Conventional routes to thin films of TiN include heating titanium metal in a stream of ammonia,[5] reactive sputtering,[6] and chemical vapour deposition.[7] Many of these techniques require high temperatures and/or expensive equipment or precursors. Electrochemical synthesis is therefore an alternative route that has attracted significant interest. Previous studies have included anodisation of titanium in acetonitrile at an applied cell voltage of up to 1500–3000 V,[8] and nitridation of a titanium anode in an acetonitrile solution containing a primary amine and tetrabutylammonium bromide followed by heating at high temperatures.[9] Each of these routes produces TiN films, but incorporation of carbon-containing impurities is significant. A reduction in the level of carbon incorporation has been achieved by the use of NH_4Br–NH_3 electrolyte solutions. This resulted in an uncharacterised powder which on calcining at 1100 °C under flowing ammonia produced either small particles of TiN or could be used to coat substrates with TiN after calcining.[10] Electrochemical surface nitriding of titanium in a molten LiCl–KCl eutectic melt has been shown to produce TiN films, but the operating temperature of this process is 450 °C.[11] Titanium nitride powders have also attracted interest in the field of powder technology as precursors for the fabrication of sintered compact or thin films. A route describing the production of TiN particles by galvanostatic electrolysis using a titanium plate in a solution of *n*-butylamine in acetonitrile has recently been reported, but post-processing by heating to 200–1000 °C in the presence of ammonia was invariably required in order to generate TiN.[12]

In this work we describe an electrochemical process that operates at or below ambient temperatures to give, in one step, thin films or particles of TiN. Furthermore, the nature of the process favours nitride formation, with no incorporation of carbon, oxygen or halogen. This is because it involves liquid ammonia solutions containing the basic electrolyte KNH_2 rather than organic solvents containing the acidic NH_4Cl or NH_4Br electrolytes used previously.[9,10,12]

The apparatus for the electrochemical experiments is described below.† Sweeping the titanium electrode potential at sweep rates of 50–100 mV s^{-1} between 0.00 V and a negative potential limit, in excess of −1.50 V, produced a reduction current of several mA. During the reverse sweep to 0.00 V in the cyclic voltammogram (CV), an associated oxidation peak was observed at *ca.* −750 mV. On continued cycling, this oxidation peak was observed to diminish as the reduction wave shifted to more negative potentials. The CV recorded after 30 min showed little decrease in the negative sweep and no oxidation peak in the positive sweep at these potentials. It seems likely that this reduction reaction involves the reduction of the native titanium(IV) oxide with the loss of oxide from the titanium surface. The oxidation peak then corresponds to the reformation of the oxide surface. On repeated cycling, a fraction of the reduced oxide is lost to the bulk solution by diffusion. Thus the cycling eventually results in the production of an oxide-free titanium surface.

On stepping the potential of the cleaned titanium electrode from 0.00 to +3.00 V, a large positive current of several mA was initially observed, indicative of electrode oxidation, which fell slowly with time. Increasing the electrode potential (first to +4.00 V, then to +5.00 V) resulted in increases in the oxidation current, as did increasing the temperature of the solution from −78 to −33 °C, with no sign of gas evolution at the electrode. Stirring of the solution did not increase the current, indicating that the current is not limited by mass transport of solution species to the electrode. These results are consistent with the growth of a surface nitride film on the electrode surface by an oxidation that involves liquid ammonia and/or amide. Removal of the titanium electrode and washing with water revealed a golden coloured film.

CV sweeps to oxidising potential for clean titanium also showed an oxidation current due to nitride film growth. Each cycle resulted in the progressive shift of this oxidation current to more positive potentials. The increase by >1.00 V in the oxidative potential limit of this electrode, whilst retaining a similar pseudocapacitance, indicates that the deposited film is relatively inert and is conducting; this is a strong indication that the film is titanium nitride. The observed increase in current on raising the temperature of the ammonia solution from −78 to −33 °C allows one to calculate an activation energy for the process in the order of +20 kJ mol^{-1}. Extrapolation to 25 °C would predict an approximately 50-fold increase in the current compared with the current passed at −78 °C. For this reason, a pressure cell was constructed such that liquid ammonia at 25 °C could be safely contained. The predicted increase in current was indeed observed, but in this case small particles of a yellow–brown material grew on the surface of the titanium electrode. Evidence that these particles were electrically conducting was provided by the observations that (i) the particles grew as 'tendrils' towards the counter electrode, and (ii) when dislodged from the electrode surface by gentle tapping the current *decreased*, indicating a reduction of electrically conducting surface area. The small size of the particles caused them to be readily oxidised to TiO_2 in the presence of air and aqueous base. Hence it was essential to remove excess KNH_2 by washing the particles with portions of liquid ammonia, followed by removal of the last traces of ammonia *in vacuo* before handling in air. Glancing angle X-ray powder diffraction of the film and particles showed no peaks, but did show significant background scattering indicative of an amorphous or nano-crystalline phase.

DOI: 10.1039/b100713k

Attempts to anneal the film at 800 °C under argon resulted in some degree of sharpening, but were not conclusive. Subsequent characterisation involved a range of techniques that required as little processing of the film as possible.

The electrodeposited film showed a transition from metallic to superconducting behaviour at *ca.* 4.5 K in a field of 100 G; the magnitude of the transition, when correlated with the charge passed during synthesis, further indicated that titanium nitride was the major product of reaction. The temperature of the transition also suggested that the stoichiometry of the TiN_x film is such that x is very close to 1.[13]

The SEM-EDX spectrum also pointed to a nitride-containing film. Not surprisingly given the nature of the sample (TiN on bulk Ti) the spectrum was dominated by the strong Ti Kα line, but clearly discernible was the N 2p line (adjacent to the Ti Lα line). Quantitative assessment of the stoichiometry was not possible owing to the considerable contribution to the intensity from the titanium substrate. It is significant, however, that no peaks corresponding to either oxygen or potassium contaminants were observed.

Conclusive evidence for the identification of both the film and powder as TiN was provided by the Raman spectra. These display three broad bands, the positions of which were in extremely good agreement both with spectra described in the literature,[14] and with spectra obtained from authentic stoichiometric TiN powder. Previous Raman studies have shown that the relative intensities of the Raman bands at 550 and 235 cm^{-1} depend upon the stoichiometry of the titanium nitride.[14] The band at lower energy is ascribed to nitrogen vacancies in the lattice and its intensity relative to the band at 550 cm^{-1} increases rapidly with increasing nitrogen deficiency. When compared with published spectra, the Raman spectra of both film and powder suggest a value of x for the TiN_x that is close to unity.

Analysis of the films by X-ray photoelectron spectroscopy (XPS) was dominated by strong peaks for titanium (2p) and oxygen (1s) characteristic of TiO_2. This was not entirely unexpected given that several months elapsed between preparation and examination by XPS and points to aerial oxidation of the TiN film at its surface. After argon ion sputtering to an approximate depth of 50 nm, the Ti 2p peak shifted to a lower binding energy and a N 1s peak appeared at 397.2 eV, indicative of stoichiometric TiN.[15] The N 1s peak persisted to a depth of ~600 nm into the sample consistent with the expected film thickness based on the amount of charge passed. Transmission electron microscopy showed aggregates of approximately spherical particles of diameter *ca.* 5–10 nm (Fig. 1).

Electron diffraction from these particles produced distinct rings with the occasional appearance of spots. The separation of these rings corresponds to *d*-spacings in good agreement with those reported for the osbornite phase of TiN.[16]

We have demonstrated in this work that electrochemical oxidation of a titanium electrode in liquid ammonia/KNH_2 at temperatures between −78 and 25 °C, results in the deposition of TiN either as a thin film or as nanoparticles depending on the current density. A key step in the production of coherent thin films has been found to be repeated cycling of the titanium electrode to negative potentials such that a substantial negative current is observed. In this way, the native oxide layer is removed, thereby facilitating growth of chemically pure TiN when the electrode is subsequently held at positive potential. Furthermore, there is no requirement for post-processing of the films or particles at elevated temperatures. Preliminary results using other metal electrodes (*e.g.* Ta, Mo and W) suggest that this process is a general low-temperature route to metal nitrides.

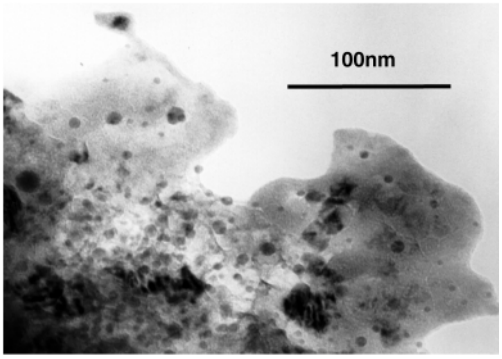

Fig. 1 TEM image of TiN particles mounted in epoxy resin.

We thank the EPSRC for a studentship (L. E. G.) and the British Council for a Monbusho Research Fellowship (L. E. G.). We dedicate this communication to the memory of the late Dr Marten Barker—a major contributor to the field of metal nitride chemistry.

Notes and references

† All operations were performed under dry, oxygen-free nitrogen. Saturated solutions of KNH_2 in liquid NH_3 at −78 °C were prepared by the addition of oxide-free potassium metal to dry liquid NH_3. Electrochemical experiments were performed using a three-electrode system; working electrode Ti foil (area ≈ 1 cm^2), counter electrode Pt coil (area >> 1 cm^2), pseudo-reference electrode (PRE) bright Pt wire. All potentials are reported with respect to this PRE. Electrochemical experiments at 25 °C involved a pressurised Pyrex vessel.

1 R. Bühl, H. K. Pulker and E. Moll, *Thin Solid Films*, 1981, **80**, 265.
2 G. I. Grigorov, K. G. Grigorov, M. Stayanova, J. L. Vignes, J. P. Langeron and P. Denjean, *Appl. Phys. A*, 1993, **57**, 195.
3 E. Velkonen, T. Karlsson, B. Karlsson and B. O. Johansson, *Proc. SPIE 1983 Int. Conf.*, 1983, **401**, 41.
4 B. Zega, M. Kornmann and J. Amiquet, *Thin Solid Films*, 1977, **54**, 577.
5 L. E. Toth, *Refractory Materials Vol. 7: Transition Metal Carbides and Nitrides*, Academic Press, New York, 1971.
6 O. Auciello, T. Barnes, S. Chevacharoenkul, A. F. Schreiner and G. E. McGuire, *Thin Solid Films*, 1989, **181**, 65.
7 T. Gerfin and K.-H. Dahmen, in *CVD of Non-Metals*, ed. W. S. Rees Jr., VCH, Weinheim, 1996, pp. 155–170.
8 J. Schrekenback, F. Schlottig, D. Dietrich, A. Hofman and G. Marx, *Appl. Surf. Sci.*, 1995, **90**, 129.
9 C. Rüssel, *Chem. Mater.*, 1990, **2**, 1941.
10 C. B. Ross, T. Wade and R. M. Crooks, *Chem. Mater.*, 1991, **3**, 768; T. Wade and R. M. Crooks, *Chem. Mater.*, 1996, **8**, 832.
11 T. Goto, M. Tada and Y. Ito, *Electrochim. Acta*, 1994, **8**, 1107; T. Nishikiori, T. Nohira, T. Goto and Y. Ito, *Electrochem. Solid State Lett.*, 1999, **2**, 278.
12 K. Nakajima and S. Shimada, *J. Mater. Chem.*, 1998, **8**, 955.
13 F. Lefloch, C. Hoffmann and O. Demolliens, *Physica C*, 1999, **319**, 258.
14 W. Spengler, R. Kaiser, A. N. Christensen and G. Müller-Vogt, *Phys. Rev. B*, 1978, 1095; R. D. Vispute, J. Narayan and Jagannadham, *J. Electron. Mater.*, 1996, **25**, 151.
15 M. J. Vasile, A. B. Emerson and F. A. Baiocchi, *J. Vac. Sci. Technol. A.*, 1990, **8**, 99.
16 N. Schönberg, *Acta Chem. Scand.*,1954, **8**, 213.

ChemComm

A linearly coordinated Hg(0) trapped in a gold(I) metallocryptand cage

Vincent J. Catalano,*[a] Mark A. Malwitz[a] and Bruce C. Noll[b]

[a] *Department of Chemistry, University of Nevada, Reno, NV 89557, USA. E-mail: vjc@unr.edu*
[b] *Department of Chemistry, University of Colorado, Boulder, CO 80309, USA*

Received (in Irvine, CA, USA) 10th January 2001, Accepted 16th February 2001
First published as an Advance Article on the web 7th March 2001

Hg(0) is effectively encapsulated through strong, closed-shell metallophilic interactions by Au(I)-based metallocryptands using the multidentate P_2phen [2,9-bis(diphenylphosphino)-1,10-phenanthroline] ligand; synthesis, characterization and X-ray crystallography are presented.

Even though elemental mercury has found numerous uses and applications in many fields of chemistry, the coordination chemistry of Hg(0) remains extremely limited, and no stable compounds are known where a Hg(0) atom is coordinated to ligands forming a classical coordination compound. Rather, Hg(0) is often found as part of an electron-rich transition metal cluster[1,2] or as an adduct to the face of *triangulo* clusters.[3,4] For example, Puddephatt and coworkers[5] reported the reversible addition of Hg(0) to the trigonal face of $[Pt_3(\mu\text{-CO})(\mu\text{-dppm})_3]^{2+}$ (dppm = $Ph_2PCH_2PPh_2$) to form mixed-metal clusters that contain naked, triply bridging Hg(0) atoms. Similarly, Venanzi and coworkers[6] demonstrated that the addition of elemental Hg to $[Pt_3(\mu\text{-CO})_3(PPhPr^i_2)_3]$ produces a cluster containing two Pt_3 triangles bridged by a Hg_2 unit. More recently, Puddephatt and coworkers[7,8] extended this motif to generate cage complexes based on the triangular Pt_3 core that are capable of encapsulating metal ions including Hg(0) or Tl(I).

We too, have been investigating the encapsulation of metal ions by inorganic cage complexes denoted as metallocryptands and found a similar affinity for the incarceration of metals with s^2 electronic configurations.[9,10] Recently, we demonstrated that the Au(I)-based metallocryptand employing the ligand 2,9-bis-(diphenylphosphino)-1,10-phenanthroline (P_2phen) is a selective host for Tl(I) ion, and the resulting $[Au_2Tl(P_2phen)_3]^{3+}$ complex is intensely luminescent.[11] We have now extended this concept to the encapsulation of elemental Hg and report the structure of the resulting metallocryptate containing an Hg(0) atom in an unusually low coordination mode.

As shown in Scheme 1, the yellow $[Au_2Hg(P_2phen)_3](PF_6)_2$ **1** is readily prepared by reacting a chloroform solution containing 3 equivalents of colorless P_2phen with 2 equivalents of Au(tht)Cl (tht = tetrahydrothiophene) and a single drop of elemental mercury.† The chloride salt can be metathesized to the PF_6^- salt using excess $NaPF_6$. Alternatively, **1** can be synthesized by Hg(0) addition to the two-coordinate, gold macrocycle,[11] $[Au_2(P_2phen)_2](PF_6)_2$, and the free ligand in chlorocarbon solution. The $^{31}P\{^1H\}$ spectrum (CD_3CN) of **1** displays a singlet at δ 34.8 with ^{199}Hg satellites ($^2J_{PHg}$ 48 Hz, ^{199}Hg is 16.8% abundant, I = 1/2) and a heptet at δ −143.7 that integrates for two PF_6^- anions. The $^{199}Hg\{^1H\}$ NMR spectrum (Fig. 1) displays a septet at δ –1199.8 ($^2J_{HgP}$ 48 Hz) indicating a single Hg environment coupled to six chemically equivalent

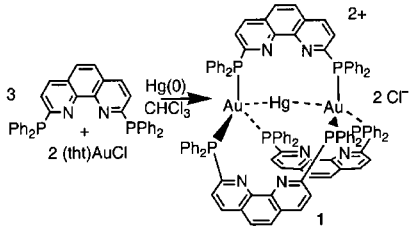

Scheme 1

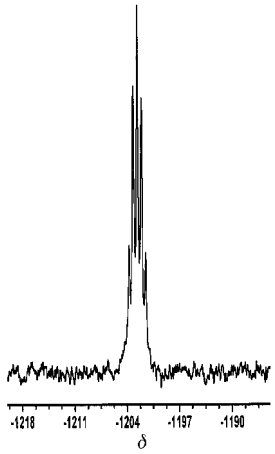

Fig. 1 89.312 MHz $^{199}Hg\{^1H\}$ NMR spectrum of $[Au_2Hg(P_2phen)_3](PF_6)_2$ in CD_3CN at 25 °C.

phosphorus atoms. For comparison, the phosphine environment in **1** is slightly more shielded than that observed in either $[Au_2Tl(P_2phen)_3](PF_6)_3$ or $[Au_2Na(P_2phen)_3](PF_6)_3$ which show resonances at δ 45.7 and 45.5, respectively. As probed by $^{31}P\{^1H\}$ NMR spectroscopy, the Hg atom appears to interact with the AuP_3 center in a fashion similar to the corresponding Tl(I) containing species, as the $^2J_{HgP}$ coupling constant in **1** is closely related to the $^2J_{TlP}$ of 186 Hz observed in $[Au_2Tl(P_2phen)_3](PF_6)_3$ by the simple ratio of the gyromagnetic ratios for ^{199}Hg and ^{205}Tl. Further, $^2J_{HgP}$ coupling constants ranging from 41 to 70 Hz were reported for Hg(0) trapped in the hexaplatinum clusters.[7] No comparable ^{199}Hg NMR chemical shifts could be found for genuine Hg(0) complexes. However, a chemical shift of δ −1310 was reported[12] for the low valent Hg cluster, $[Hg_4](AsF_6)_2$. The chemical shift dispersion for ^{199}Hg is quite large (> 5000 ppm) and is very sensitive to ligation, concentration and temperature.[13] Consistent with other metallocryptates[9] the ^1H NMR spectrum displays single resonances for the three magnetically distinct phenanthroline protons. These signals are only minimally shifted (±0.06 ppm) relative to the uncoordinated ligand. However, two sets of resonances corresponding to phenyl ring protons are observed in the metallocryptate suggesting that two phenyl ring environments exist: one along the metal–metal axis and one equatorial to this axis.

The structure of **1** as determined by X-ray diffraction‡ is presented in Fig. 2. The structure contains two trigonally-coordinated Au(I) centers capping a D_3 symmetric cage containing an Hg(0) atom. As can be seen in Fig. 2 the overall geometry of the complex is helical; however the bulk material is racemic as dictated by the centrosymmetric space group. The helicity is reflected in the large P(1)–Au(1)–Au(2)–P(2), P(3)–Au(1)–Au(2)–P(4) and P(5)–Au(1)–Au(2)–P(6) torsion angles of 91.2, 89.1 and 91.9°, respectively. This twisting of the trigonal planes compresses the metallocryptate to accommodate the requisite Au(1)···Au(2) separation of 5.546(1) Å. No attempt was made to resolve **1** into its chiral components.

The Au(1)–Hg(1) and Au(2)–Hg(1) separations are nearly identical at 2.7847(4) and 2.7804(4) Å, respectively. The three-

DOI: 10.1039/b100432h

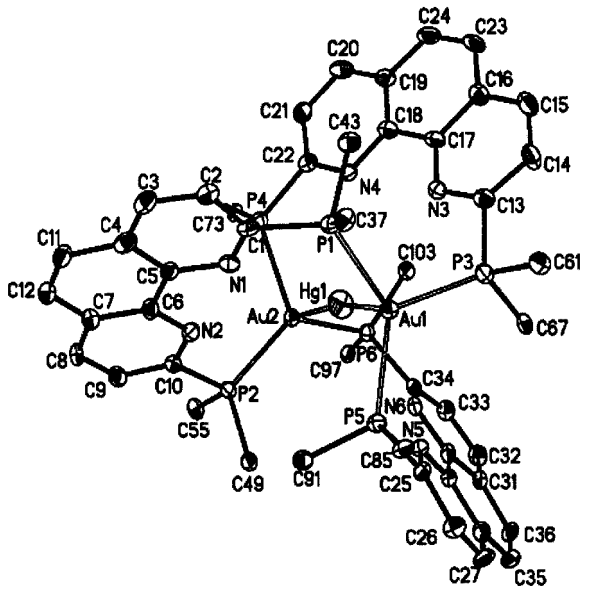

Fig. 2 Thermal ellipsoid plot for the cation of **1**. Hydrogen atoms and phenyl rings are removed for clarity. Selected distances (Å) and angles (°): Au1–Hg1 2.7847(4), Au2–Hg1 2.7807(4), Hg1–N1 3.589(2), Hg1–N2 3.636(2), Hg1–N3 3.374(2), Hg1–N4 3.378(2), Hg1–N5 3.659(2), Hg1–N6 3.604(2); Au1–Hg1–Au2 170.48(1), P1–Au1–P3 113.01(6), P1–Au1–P5 124.49(6), P3–Au1–P5 1217.63(6), P2–Au2–P4 116.01(6), P2–Au2–P6 125.32(5), P4–Au2–P6 113.44(6), P1–Au1–Hg1 98.14(4), P3–Au1–Hg1 94.74(4), P5–Au1–Hg1 98.90(4), P2–Au2–Hg1 98.61(4), P4–Au2–Hg1 95.72(4), P6–Au2–Hg1 98.31(4).

atom linkage is slightly bent with an Au(1)–Hg(1)–Au(2) angle of 170.48(1)°. The two Au atoms are distorted from their respective trigonal coordination planes towards the Hg atom by *ca*. 0.3 Å each. The Hg–N separations range from 3.374(1) to 3.659(1) Å (av. Hg–N 3.540 Å) and are considered non-interacting indicating that the attractive Au–Hg interaction is responsible for maintaining this assembly. The freedom of the Hg atom to move about the cage is reflected by its larger thermal ellipsoid as compared to the Au atoms, a trend noted in other metallocryptands.

The attractive Au–Hg interactions observed here can be rationalized using a simplified molecular orbital approach discussed elsewhere.[10] Although considered formally non-bonding, the metal–metal separations reported here are shorter than the sum of the respective covalent radii (Au = 1.34, Hg = 1.49 Å) indicating a significant attraction between these closed-shell metals. Similar associations with other closed-shell metal ions have been observed in other metallocryptates[9] and in the related trigonally coordinated Pt(0) and Pd(0) phosphine complexes.[14]

The Hg–Au separations described here are shorter than those found in $[Pt(AuPPh_3)_8(Hg)_2]^{4+}$ [3.0070(5) and 3.0011(5) Å][15] and those found in $[(PPh_3)Pt(AuPPh_3)_6(HgNO_3)](NO_3)$ [2.945(3)–3.636(2) Å].[16] Interestingly, in the former complex the Hg is added as Hg(II) while the latter complex is formed by the addition of Hg(0) to $[(PPh_3)Pt(AuPPh_3)_6](NO_3)$. However, to the best of our knowledge there are no reports of a genuine Hg(0) atom coordinating to two Au(I) centers in a linear fashion.

The electronic absorption spectrum (CH_2Cl_2) of **1** shows absorptions attributable to ligand π–π* transitions between 230 and 280 nm, a broad, unresolved band centered *ca*. 360 nm, and a low energy absorption at 390 nm which may be attributed to the $M_{d\sigma^*} \rightarrow M_{p\sigma^*}$ transition. Compound **1** is weakly emissive, and excitation into the low energy manifold produces an emission band centered at 580 nm. A similar, yet significantly more intense emission is observed in the isoelectronic Tl(I) containing species $[Au_2Tl(P_2phen)_3]^{3+}$ which was assigned to a metal-centered phosphorescence process. Unlike $[Au_2Tl(P_2phen)_3]^{3+}$ compound **1** exhibits an electrochemical oxidation (CH_2Cl_2, irreversible) at *ca*. 1.25 V *vs*. Ag/AgCl. No reversible reductions were observed out to the solvent limit.

The successful encapsulation of Hg(0) by the gold-based metallocryptand further demonstrates the applicability of these inorganic cage complexes as effective probes of closed-shell metal–metal interactions. This methodology may be applied to other d^{10}-based metallocryptands including Pd(0) and Pt(0) where similar metal–metal interactions are expected. Further, by careful ligand manipulation it may be possible to induce a stronger coordination environment around the encapsulated Hg(0) atom. We are actively pursuing these species.

Acknowledgment is made to the National Science Foundation (CHE-9624281) and to the Donors of The Petroleum Research Fund, administered by the American Chemical Society for their generous financial support of this research.

Notes and references

† *Preparation*: $[Au_2Hg(P_2phen)_3](PF_6)_2$ **1**: a 25 mL Erlenmeyer flask was charged with 0.0308 g (5.61 mmol) of 2,9-bis(diphenylphosphino)-1,10-phenanthroline (P_2phen) and 0.100 g (5.61 mmol) of $[Au_2(P_2phen)_2](PF_6)_2$ dissolved in 8 mL of MeCN. To the pale yellow solution was added an excess amount of elemental mercury. This mixture was placed in an ultrasonic cleaner for *ca*. 5 min producing a lemon-yellow solution. The solution was decanted away from excess mercury and filtered through a short pad of Celite. Precipitation with Et_2O afforded a lemon-yellow solid. Yield: (63%).

$C_{108}H_{78}N_6Au_2F_{12}HgP_8 \cdot 2CH_3CN$. Calc. C, 51.38; H, 3.18; N, 3.81. Found: C, 51.22; H, 3.43; N, 3.83%. ^{1}H NMR (300 MHz, CD_3CN, 25 °C): δ 8.330 (d, *J* 8.0 Hz), 8.055 (s), 7.526 (d, *J* 8.42 Hz), 7.501 (m), 7.413 (m), 7.135 (m), 6.740 (m), 6.254 (m), 5.809 (m); ^{31}P{^{1}H} (121 MHz, CD_3CN, 25 °C): δ 34.78 [s br (d, $^2J_{HgP}$ 48 Hz)]; ^{199}Hg{^{1}H} (89.312 MHz, CD_3CN, 25 °C): δ −1199.8 (hept, $^2J_{PHg}$ 48 Hz)

‡ *Crystal data*: $C_{112}H_{78}Au_2F_{12}HgN_8P_8$, **1**·2$CH_3CN$ *M* = 2606.11, monoclinic, space group $P2_1/n$, *a* = 17.6778(5), *b* = 29.5895(9), *c* = 19.4103(6), β = 91.686(1) Å, *V* = 10148.7(5) Å^3, *T* = 135 K, *Z* = 4, μ(Mo-Kα) = 4.595 mm^{-1}, 99 405 reflections measured, 23 285 unique (R_{int} = 0.0452) were used in all calculations. The final *R*1 (all data) was 0.0819 and *wR2* (all data) was 0.1097 [*R*1 = 0.0487 ($I > 2\sigma I$)]. Single crystals of $[Au_2Hg(P_2phen)_3](PF_6)_2 \cdot 2CH_3CN$ were grown by slow diffusion of diethyl ether into an acetonitrile solution of the complex. A suitable crystal was mounted in inert oil in the N_2 cold stream of a Bruker SMART diffractometer. The data ($2.68 < 2\theta < 55.00°$) were corrected for absorption using SADABS, and the structure was solved by direct methods and refined by full-matrix least squares. CCDC 156335. See http://www.rsc.org/suppdata/cc/b1/b100432h/ for crystallographic data in .cif or other electronic format.

1 L. H. Gade, *Angew. Chem., Int. Ed. Engl.*, 1993, **32**, 24 and references therein.
2 L. H. Gade, B. F. G. Johnson, J. Lewis, G. Conole and M. McPartlin, *J. Chem. Soc., Dalton Trans.*, 1992, 3249.
3 Y. Yamamoto, H. Yamazaki and T. Sakurai, *J. Am. Chem. Soc.*, 1982, **104**, 2329.
4 A. D. Burrows and D. M. Mingos, *Coord. Chem. Rev.*, 1996, **154**, 19.
5 G. Schoettel, J. J. Vittal and R. J. Puddephatt, *J. Am. Chem. Soc.*, 1990, **112**, 6400.
6 A. Albinati, A. Moor, P. S. Pregosin and L. M. Venanzi, *J. Am. Chem. Soc.*, 1982, **104**, 7672.
7 L. Hao, J. J. Vittal and R. J. Puddephatt, *Organometallics*, 1996, **15**, 3115.
8 L. Hao, J. J. Vittal and R. J. Puddephatt, *Inorg. Chem.*, 1996, **35**, 269.
9 V. J. Catalano, B. L. Bennett, R. Yson and B. C. Noll, *J. Am. Chem. Soc.*, 2000, **122**, 10 056.
10 V. J. Catalano, B. L. Bennett and B. C. Noll, *Chem. Commun.*, 2000, 1413.
11 V. J. Catalano, B. L. Bennett, H. M. Kar and B. C. Noll, *J. Am. Chem. Soc.*, 1999, **121**, 10 235.
12 R. J. Gillespie, R. Granger, K. R. Morgan and G. J. Schrobilgen, *Inorg. Chem.*, 1984, **23**, 887.
13 B. Wrackmeyer and R. Contreras, in *Annual Reports on NMR Spectroscopy*, ed. G. A. Webb, Academic Press, London, 1992, vol. 24, pp. 267–329.
14 V. J. Catalano, B. L. Bennett, S. Muratidis and B. C. Noll, *J. Am. Chem. Soc.*, 2001, **123**, 173.
15 J. J. Bour, W. v. d. Berg, P. P. J. Schlebos, R. P. F. Kanter, M. F. J. Schoondergang, W. P. Bosman, J. M. M. Smits, P. T. Beurskens, J. J. Steggerda and P. van der Sluis, *Inorg. Chem.*, 1990, **29**, 2971.
16 R. A. T. Gould and L. H. Pignolet, *Inorg. Chem.*, 1994, **33**, 40.

ChemComm

Preparation and pervaporation properties of a MEL-type zeolite membrane

Vu A. Tuan, Shiguang Li, Richard D. Noble and John L. Falconer*

Department of Chemical Engineering, University of Colorado, Boulder, CO 80309-0424, USA.
E-mail: john.falconer@colorado.edu

Received (in Irvine, CA, USA) 19th October 2000, Revised manuscript received 19th January 2001, Accepted 13th February 2001
First published as an Advance Article on the web 7th March 2001

A boron-substituted ZSM-11 (Si/B = 100, MEL structure) membrane was prepared and shown to selectively permeate methyl ethyl ketone, propan-1-ol, and propan-2-ol from aqueous solutions.

Zeolite membranes have the potential to continuously separate mixtures by both adsorption and molecular sieving because the zeolite pores are of molecular size. Most previous studies of zeolite membranes have focused on MFI (silicalite-1 and ZSM-5) membranes.[1,2] The MFI zeolites have a system of straight channels (pore size: 0.53 × 0.56 nm) interconnected by zigzag channels (pore size: 0.51 × 0.55 nm). Isomorphous substitution has been shown to be an effective method for modifying the MFI structure, and membranes with B substituted into the MFI framework membranes had higher n-C_4H_{10}/i-C_4H_{10} gas-phase selectivities than Al-ZSM-5 membranes.[3] In the current study, a B-ZSM-11 membrane was prepared that exhibited better pervaporation properties for organic/water mixtures than obtained for ZSM-5 membranes that were prepared by the same procedures. The ZSM-11 zeolite pore size is similar to that for ZSM-5, but it has intersecting straight channels (pore size: 0.54 × 0.53 nm).

The B-ZSM-11 membrane was prepared by *in situ* crystallization onto a tubular porous stainless steel support (500 nm pore size, Mott Corporation). The MEL structure can be hydrothermally synthesized from gels containing NaOH. den Exter[4] claimed that the MEL structure could not be synthesized as a pure phase, however, and they obtained a mixture of MFI and MEL structures.[4] Sano[5] prepared Al-ZSM-11 films on nonporous Teflon slabs, but did not show that these films were continuous membranes; no separations were reported for these films.

We prepared an alkali-free, ZSM-11 membrane that contained boron in the structure (Si/B = 100), and XRD of powder collected from the bottom of the tube indicated a MEL structure (Fig. 1). All peaks match those reported by Szostak[6] for MEL crystals, and no additional peaks were observed.

The synthesis was similar to alkali-free, MFI zeolite membranes, which showed higher separation selectivities than MFI membranes prepared from synthesis gels containing NaOH.[3] The molar composition of the gel was: 2.5 TBAOH : 0.195 $B(OH)_3$: 19.5 SiO_2 : 450 H_2O, where TBAOH (tetrabutylammonium hydroxide) was used as template, and silica sol (Ludox-AS40) was the Si source. Hydrothermal synthesis was carried out at 403 K for 72 h, and two synthesis layers were required. After synthesis, the membrane was washed, dried, and calcined at 753 K for 8 h with heating and cooling rates of 0.015 and 0.018 K s^{-1}, respectively.

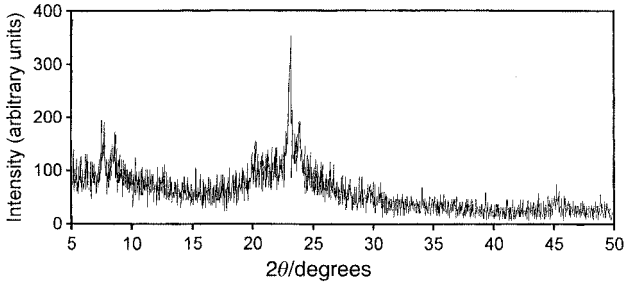

Fig. 1 XRD spectrum of the powder collected from the bottom of a B-ZSM-11 zeolite membrane.

The B-ZSM-11 membrane was used for separation of organic/water mixtures by pervaporation, using an apparatus described previously.[7] The membrane was calcined at 673 K for 3 h prior to each run at a given liquid feed composition in order to ensure that no species remained from previous experiments. The feed concentrations were 5 wt% organic. The permeate vapor was condensed by a liquid-nitrogen trap, and the downstream pressure was maintained below 0.5 kPa. The flux was measured by weighing the permeate, and permeate concentrations were measured by off-line GC.

Fig. 2 shows the steady-state total flux and the MEK/water separation selectivity as a function of temperature. A maximum flux of 0.69 kg m^{-2} h^{-1} and a maximum separation selectivity of 224 were obtained at 333 K. As the temperature increased, the fluxes increased because the diffusion rates increased, and the MEK diffusion rate increased slightly faster than the water diffusion rate. Since pure water permeated faster than pure MEK (Fig. 2), and the ideal MEK/water selectivity was *ca.* 0.8; the high MEK/water selectivity was due to the preferential adsorption of MEK. The separation selectivity was higher than the vapor–liquid equilibrium selectivity, which was 90 at 333 K.

Smetana *et al.*[8] separated a MEK/water mixture using a silicalite membrane and obtained a maximum MEK/water selectivity of 146 at 307 K with a MEK flux of 0.25 kg m^{-2} h for a 5 wt% MEK feed. Their results were similar to those measured for a silicalite-filled silicone composite membrane reported by Devine *et al.*[9] The ZSM-11 membrane has a similar flux and a higher selectivity.

Table 1 shows the pervaporation results for separation of propan-1-ol and propan-2-ol from aqueous solutions through the B-ZSM-11 membrane at 333 K. For comparison, fluxes and

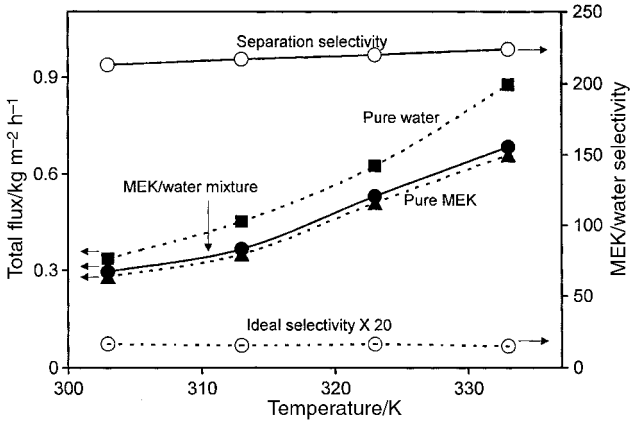

Fig. 2 Total flux and MEK/water selectivity as a function of temperature for pervaporation of a 5 wt% MEK aqueous solution through a B-ZSM-11 membrane. The flux of pure water and pure MEK are also shown. The ideal selectivity is the ratio of the fluxes.

DOI: 10.1039/b008547m

Table 1 Comparison of pervaporation results through B-ZSM-11 and B-ZSM-5 membranes for propanol/water mixtures at 333 K

Feed solution	Membrane	Total flux/ kg m^{-2} h^{-1}	Separation selectivity
Propan-1-ol/water	B-ZSM-11	0.25	25
	B-ZSM-5	0.072	7.8
Propan-2-ol/water	B-ZSM-11	0.31	16
	B-ZSM-5	0.068	7.0

selectivities are presented for a B-ZSM-5 membrane.[3] Both membranes had two zeolite layers prepared by similar procedures, but the fluxes and separation selectivities for the B-ZSM-11 membrane are approximately three times higher. Both propan-1-ol/water and propan-2-ol/water separation selectivities are higher than their ideal selectivities (0.21 and 0.18, respectively), and this indicates separations is due to preferential adsorption.

For MFI zeolites, the surface changes from hydrophobic (silicalite-1) to hydrophilic (Al-ZSM-5) when Si is replaced by Al in the framework. However, the substitution of B instead of Al in both MFI and MEL frameworks apparently does not make the membrane hydrophilic since high organic/water selectivities were obtained for the boron-substituted membranes, and the separations were due to preferential adsorption.

Notes and references

1 T. Sano, M. Hasegawa, Y. Kawahami, Y. Kiyozumi, H. Yanagishita, D. Kitamoto and F. Mizukami, *Stud. Surf. Sci. Catal.*, 1994, **84**, 1175.
2 Y. Yan, M. E. Davis and G. R. Gavalas, *Ind. Eng. Chem. Res.*, 1995, **34**, 1652.
3 V. A. Tuan, R. D. Noble and J. L. Falconer, *AIChE J.*, 2000, **46**, 1201.
4 M. J. den Exter, Ph.D. Dissertation, Delft University of Technology, Delft, The Netherlands, 1996.
5 T. Sano, *Recent Res. Dev. Pure Appl. Chem.*, 1998, **2**, 31.
6 R. Szostak, *Molecular Sieves*, van Nostrand, New York, 1989.
7 Q. Liu, R. D. Noble, J. L. Falconer and H. H. Funke, *J. Membr. Sci.*, 1996, **117**, 163.
8 J. F. Smetana, J. L. Falconer and R. D. Noble, *J. Membr. Sci.*, 1996, **114**, 127.
9 K. M. Devine, A. J. Meier and C. S. Slate, *Proc. 7th Int. Conf. Pervaporation Processes in the Chemical Industry*, 1995, p. 339.

Typeset and printed by Black Bear Press Limited, Cambridge, England

Nanometer space resolved photochemistry

Steven De Feyter,[a] Johan Hofkens,[a] Mark Van der Auweraer,[a] Roeland J. M. Nolte,[b] Klaus Müllen[c] and F. C. De Schryver*[a]

[a] *Katholieke Universiteit Leuven (K.U.Leuven), Department of Chemistry, Celestijnenlaan 200 F, B-3001 Heverlee, Belgium. E-mail: frans.deschryver@chem.kuleuven.ac.be*
[b] *University of Nijmegen, Department of Organic Chemistry, NSR Center, Toernooiveld, 6525 ED Nijmegen, The Netherlands*
[c] *Max-Planck-Institut für Polymerforschung, Ackermannweg 10, D-55021, Mainz, Germany*

Received (in Cambridge, UK) 23rd November 2000, Accepted 31st January 2001
First published as an Advance Article on the web 23rd February 2001

The development of scanning probe techniques has opened new ways to visualize and gain insight in chemical and physical processes with unprecedented spatial resolution. Scanning near-field optical microscopy combining high spatial topographic resolution and optical resolution surpassing the diffraction limit, has been applied for structure determination and manipulation studies of organic materials. With scanning tunnelling microscopy, photo-induced chemical reactions have been studied at the liquid/solid interface with subnanometer resolution.

Introduction

The birth of scanning probe techniques revolutionized the way small objects or domains can be visualized. Common to all scanning probe techniques is a tiny probe, which scans a surface at a very small distance from it and the interaction between probe and object is translated into a signal. The ultimate control in positioning has been achieved by using piezoelectric elements. Since the invention of the scanning tunnelling microscope (STM),[1] several experimental schemes have been developed which allow detection of a great variety of interactions between probe and surface. Among those techniques, scanning near-field optical microscopy (SNOM)[2,3] takes a special place due to its optical resolution below the diffraction limit.

In STM, a metallic tip is brought very close to a conductive substrate and by applying a voltage between both conductive media, a tunnelling current may result (Fig. 1A). The exponential distance dependence of the tunnelling current provides excellent means to control the distance between the probe and the surface. Very high resolution (atomic) can be achieved but in general, the use of this probe technique is limited to conductive substrates. In contrast, in atomic force microscopy (AFM) forces exerted by the sample on the tip are recorded and several detection schemes are possible. In addition, modification of tips with carbon nanotubes leads to supertips with enhanced spatial and mechanical properties[4] and chemically modified AFM tips provide chemical contrast and can allow the measurement of binding forces.[5]

SNOM combines both the possibilities of AFM and optical microscopy. On the one hand, it allows for probing the surface and obtaining information on the topography. On the other hand, in aperture SNOM, the probe contains an aperture and the sample can be illuminated very locally (Fig. 1B). The diameter of the aperture at the end of the probe is typically of the order of 50–100 nm and therefore the illuminating spot is not diffraction limited. Both transmission and fluorescence in combination with polarization provide appropriate contrast mechanisms. The high sensitivity of this technique has been demonstrated by its ability to detect even single molecules.[6,7]

Frans De Schryver obtained his doctoral degree at K.U.Leuven in 1964 and returned as staff member to his Alma Mater after a two-year postdoctoral stay as a Fulbright fellow at the University of Arizona with Speed Marvel. He became a Full Professor in 1975 working in the field of photochemistry and photophysics. He received a Humboldt research award in 1993 and stayed with G. Wegner and J. P. Rabe at the Max-Planck-Institute for Polymer Research in Mainz. As a result of this stay he combined space and time resolution in the study of organic molecules. He received the Porter medal in 1998 and the Havinga medal and Forster memorial lecture award in 1999.

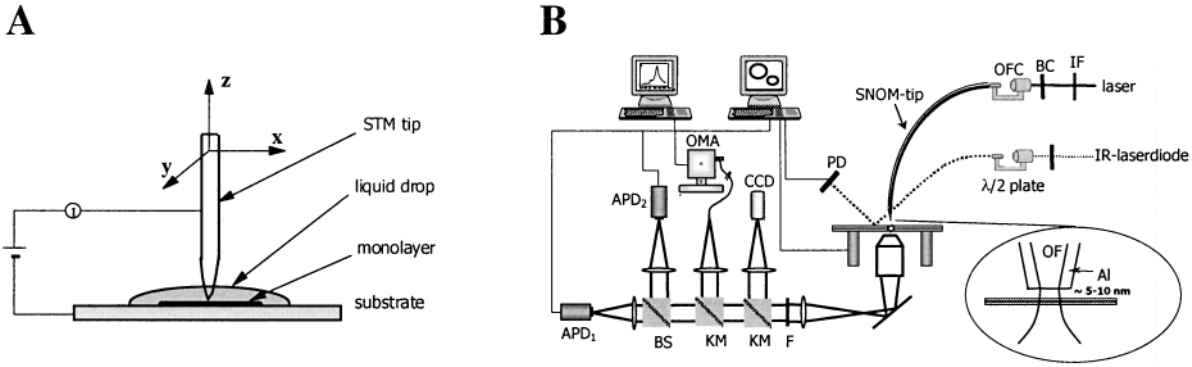

Fig. 1 (A) Scheme of a STM-setup. Note that during the experiments the tip is partially immersed in the fluid layer. (B) Scheme of the SNOM-setup. IF = interference filter, BC = Berek's compensator, OFC = optical fiber coupler, OF = optical fiber, PD = photodiode, F = filter, KM = kinematic mirror, BS = beam splitter, CCD = charge coupled device, APD = avalanche photodiode, OMA = optical multichannel analyser.

The high-resolution qualities of these techniques in addition to their local probing character make them very useful tools for the study of surface phenomena in various research fields. In our research group these techniques have been used to study several photo-induced processes at surfaces. In the first section here we will demonstrate how SNOM is useful in characterising and modifying the optical properties of materials on a sub-micrometer size. In the second, we will exemplify the use of STM for studying photo-induced reactions at the liquid/solid interface.

Scanning near-field optical microscopy

There are a number of excellent reviews on SNOM,[8–12] and its applications in the study of organic materials.[11,13–16] The reader is referred to these reports for detailed information on the technique and some of its applications. We focus on some of our results on the use of SNOM for the study of organic fluorescent materials and photo-induced local modifications in thin films or on substrates.

Single objects

Latex beads

As stated in the introduction, SNOM allows study of the optical properties of materials with subwavelength resolution. Thin poly(vinyl alcohol) (PVA) polymer films containing dye-labelled 100 nm beads were investigated.[17,18]

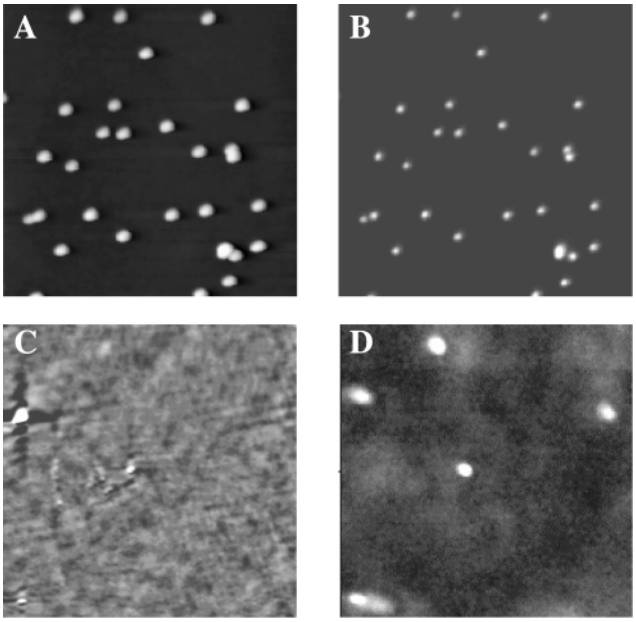

Fig. 2 SNOM image sets taken from a *ca*. 50 nm thin film (A topography, B fluorescence) and a *ca*. 10 μm thick film (C topography, D fluorescence) consisting of *ca*. 100 nm dye-labeled latex particles embedded in a PVA matrix. Image sizes: $10 \times 10\ \mu m^2$. The excitation wavelength is 488 nm for set A, B and 458 nm for set C, D.

Fig. 2 comprises a topographic (A) and a fluorescence map (B) of a thin polymer film (*ca*. 50 nm as measured by AFM) consisting of dye-labelled latex particles embedded in a PVA matrix. The image set was acquired while the polymer film was irradiated through the aperture probe at an excitation wavelength of 488 nm.[18] Based on their measured size the bead-like structures in the topography images can be attributed to single latex particles. The pattern of the black–white contrast in the topographic images corresponds to a diameter of 109 nm. In the fluorescence map in Fig. 2B, the particles displayed in the topographic image can be correlated with distinct spots of a fluorescence intensity exceeding the background intensity. Note that the size of the fluorescence spots is substantially smaller than the features in the topography image. In the latter, the signal is derived from the interaction of the tip end (including the Al coating surrounding the aperture) and the sample surface, while for the fluorescence measurement, the dimension of the aperture itself determines the optical resolution. The latex particles were also embedded in a film a few μm thick.[17] Fig. 2C,D shows one image set representing on the left side the topography and on the right side the fluorescence map. Where the topography shows only structures with a height substantially less than the size of a latex particle, fluorescence spots of high intensity appear in the fluorescence maps. Only some of these spots correlate with the topographic information. This finding reveals a unique capability of SNOM. In contrast to most scanning probe microscopies, SNOM is able to probe subinterface properties occurring in spatial domains that are located a few 10 nm beneath a sample–air interface. The luminescence properties of these domains can be addressed by the collimated radiation field generated by the aperture probe.

In order to gain insight in the distribution of functional groups and the distance between these functional groups in latex beads, energy transfer in latex beads has been investigated. Therefore, the shell of latex beads (core = polystyrene, shell = poly(acrylate) (PA), diameter *ca*. 100 nm) has been covalently labelled with two different dyes, Bodipy and TMR (Fig. 3). The beads are dispersed in a 10 nm thin PVA matrix. The spectral overlap between the emission spectrum of Bodipy (energy donor) and the absorption spectrum of TMR (energy acceptor) allows for efficient energy transfer between those dyes within individual latex beads. The energy transfer process has been 'visualized' by recording the wavelength dependent fluorescence intensity of individual beads obtained upon excitation of the Bodipy chromophores for different label concentrations. The fluorescence maps and spectra clearly show efficient excitation energy transfer within a single latex bead and energy transfer is more pronounced when the relative distances between donor and acceptor decrease. The efficiency of the energy transfer ranges from 85 to 57%, depending on the dye concentration (Fig. 3A). No significant differences have been found between different beads. When those beads are dispersed in a poly(acrylate) matrix, which has a lower T_g compared to PVA, the excitation energy transfer efficiency decreases (74% relative to 85%) and this is more pronounced (62%) when the samples are annealed (Fig. 3B). This has been attributed to 'swelling' of the PA latex shell, resulting in an increase of the distance between chromophores and a decrease in energy transfer efficiency.

SNOM not only allows investigation of photophysical properties of chromophore labelled latex beads, but also permits the visualization of a phototransformation leading to bleaching.[17] The latex particles in the topographic image of Fig. 4A are clearly correlated with fluorescence structures in the corresponding fluorescence map (Fig. 4B). The torus-like shaped fluorescence structures do not directly reflect the dye distribution on the particles, but result from the overlap of the intensity distribution of the radiation field beneath the aperture. In the course of the photobleaching experiment, the SNOM probe was positioned above the particle on the right, and the particle was raster-scanned while the particle was irradiated with the 458 nm light emanating from the probe. After 2 h, almost no fluorescence is observed from the denoted position in the fluorescence map (Fig. 4D), where the probe illuminated the latex particle. However, the topography image (Fig. 4C) indicates that the particle was not removed or destroyed during scanning. This experiment demonstrates that a photochemical reaction can be induced upon irradiation with the SNOM probe and that the photochemical reaction induced by the optical near-field is restricted to a nanometer length scale. Local photobleaching has also been demonstrated in molecular systems,[19] supramolecular systems[20] and polymers.[21]

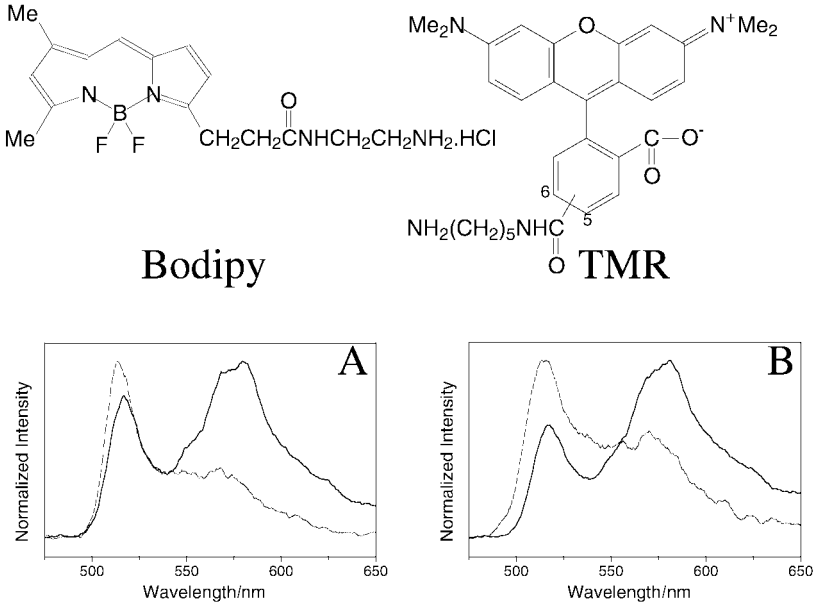

Fig. 3 Chemical structures of Bodipy [λ_{max}(em) = 514 nm] and TMR [λ_{max}(em) = 572 nm]. Normalized fluorescence spectra obtained on single beads. (A) High (black) and low (gray) label concentrations of Bodipy/TMR. The polymer film is PVA. (B) Beads with high label concentration dispersed in PVA-matrix (black) and PA-matrix (gray). The excitation wavelength is 458 nm.

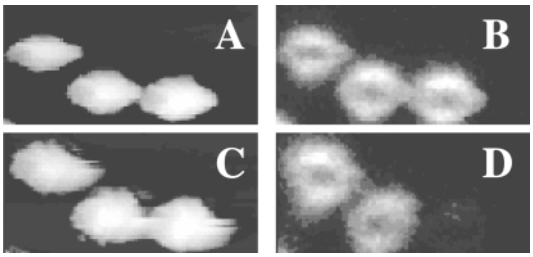

Fig. 4 SNOM image sets comprising the topographic images (A, C) and the fluorescence maps (B, D) of a section of a thin film, before and after photobleaching the right latex bead, respectively.

Supramolecular structures

Porphyrin rings

In addition to the study of single objects, SNOM also helps to visualize parts of supramolecular structures. The formation of ring-like structures has been observed in the evaporation process of organic solutions containing a broad range of materials including metal particles,[22] polymers,[23] proteins[24] and organic molecules.[25–27] In particular, the deposition of these solutions on a substrate lead to micron scale ring-shaped arrangements of the solute/dispersed materials. Using SNOM, a deeper insight into the morphology and the local optical properties of solvent-evaporated porphyrin thin films has been reached. In particular, the effects of the concentration of the starting solution on the film morphology have been investigated.

Evaporation of a 10^{-6} M solution of PtP (Fig. 5A) in $CHCl_3$ on glass yielded symmetric rings for which the topography and fluorescence images are highly correlated.[25]

The ring diameter ranges between 100 nm and 10 μm, while the height of the rims, determined from the SNOM topographic image, varies between 10 and 300 nm. The fluorescence intensity measured inside the rings equalled the background value indicating the absence of porphyrin material at these positions. The use of a more dilute solution (10^{-7} M) resulted in the formation of incomplete ring-shaped assemblies that were made up from individual isolated structures which were observed both in the topography and the fluorescence image (Fig. 6B). In these conditions the rings had smaller diameters and the heights of the beads that comprise most of the rings were substantially smaller than the heights of the well formed rings prepared from more concentrated solutions.

A further characterization of the films in terms of the local optical properties and molecular organization was performed using fluorescence polarization imaging. From these data it

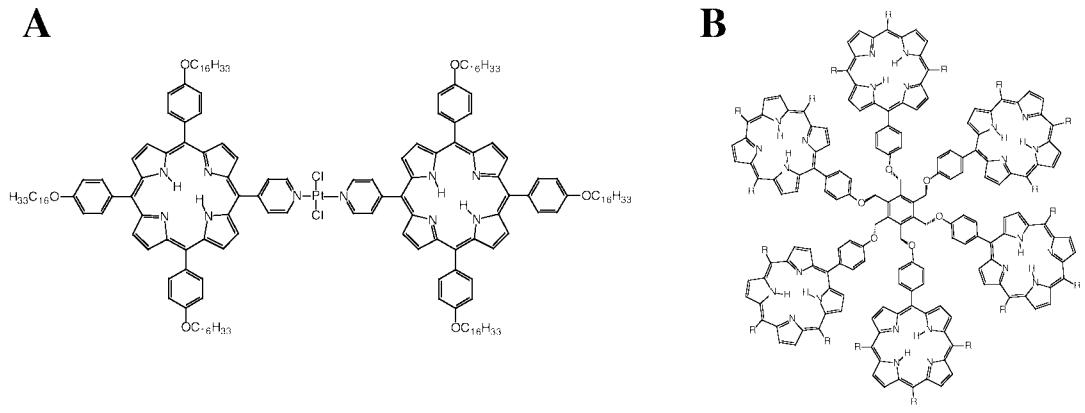

Fig. 5 Schematic representation of PtP (A) and BP_6 (B).

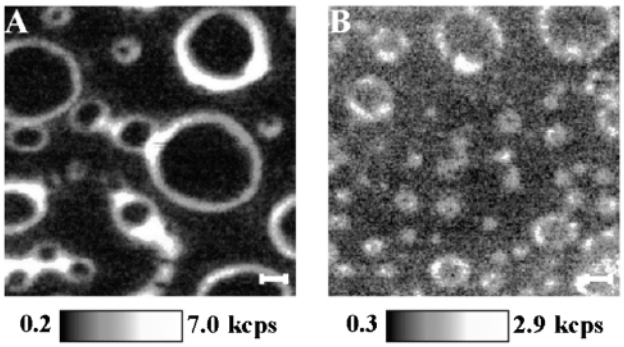

Fig. 6 SNOM fluorescence images of evaporated films of PtP/$CHCl_3$ solutions on glass. The scale bars represent 1 μm. (A, B) Fluorescence image taken on a sample prepared by solvent casting of a 10^{-6} M (A), and a 10^{-7} M (B) solution.

could be stated that in these films small, organized aggregates are present which, by using linearly polarized light for excitation, can be photoselected and that these aggregates show polarized emission. The length of these aggregates, as determined from the line profiles taken in the fluorescence polarization images, varies between 50 nm and *ca.* 300 nm. Annealing of the PtP ring samples leads to an increase in size, density and ordering of the aggregates.

Similar experiments were performed using samples prepared by evaporation of a $BP_6/CHCl_3$ (Fig. 5B) solution. For the samples studied before annealing, the images corresponding to the different polarization configuration were identical (images are not presented). On the other hand, the annealed samples exhibit strong polarization contrast. When the fluorescence intensity distributions in the rings are compared to what was found for PtP, a much smoother profile is observed. For the BP_6 samples the intensity distribution depends over a longer range on the excitation polarization with parallel emission polarization. When the excitation polarization is oriented horizontally in the image (Fig. 7B) the upper and lower parts of the rings have a relative higher intensity than the left and the right parts of the rings. Turning the excitation polarization 90 degrees (Fig. 7C) results in higher fluorescence intensity for the left and right parts of the ring. The different intensity distributions are not observed in the images taken with the excitation and the emission polarization oriented perpendicular with respect to each other. The observed fluorescence pattern can only be explained if there is a preferential orientation of the molecules in the rings. This would lead to a specific orientation of the absorption dipoles in the ring. Using polarized excitation results in a preferential absorption of the excitation light at the positions where the polarization and the absorption dipole of the chromophore are parallel. This results in higher fluorescence intensity at the respective positions. If the molecules are schematically presented as disks the orientation should be preferentially perpendicular to the sample plane. A possible arrangement of the disks in the rings could be one with the planes parallel or perpendicular to the radial of the ring.

These rings have been mechanically manipulated at the submicron scale with AFM. This manipulation was carried out by implementing an interface, called the nanoManipulator, on a combined AFM–confocal microscope.[28] A small amount of the fluorescent material from the ring could be displaced with the AFM tip. A special tool (sweep mode), in which the AFM tip is moved very fast perpendicular to the direction of the desired manipulation which creates a virtually broader tip, allowed a modification of 130 nm (Fig. 8A). The resolution attainable in these kinds of experiments could go down below 100 nm and is primarily determined by the tip and sample geometry. Besides the possibility of mechanically manipulating porphyrin rings using the force applied by an AFM tip, it is feasible to manipulate or modify locally the optical properties of these rings in terms of tip-induced photobleaching using the light coming from a SNOM-tip.[28] In such an experiment the dimensions of the manipulated area are related to the size of the SNOM probe used in the experiment (Fig. 8B).

J-Aggregates in polyelectrolyte layers

As an alternative to Langmuir–Blodgett (LB) film deposition,[29,30] self-assembly techniques based on covalent or coordination chemistry were developed.[31,32] In the beginning of the 1990s, Decher *et al.* demonstrated the alternate adsorption of cationic and anionic polyelectrolytes as a novel technique for the preparation of molecular multilayers.[33] This method was applied for the layer by layer fabrication of alternate assemblies containing J-aggregates[34,35] of a cyanine dye. J-Aggregates act as a multi-charged supramolecular ensemble, which promises a strong adsorption. Only a few papers report local properties of J-aggregates on a nanometer scale. The group of Barbara has applied SNOM to the investigation of J-aggregates, examining J-aggregates of 1,1′-diethyl-2,2′-cyanine iodide, pseudoisocyanine (PIC) which were formed in a solution with poly(vinyl sulfate) (PVS) and spin-coated onto quartz substrates.[20,36,37]

We have used SNOM for the investigation of J-aggregates of 3,3-disulfopropyl-5,5′-dichloro-9-ethylthiacarbocyanine (THIATS), formed in a layer by layer self-assembled multilayer when alternating with the cationic polyelectrolyte, poly-(allylamine) (PAH) The influence of the top layer and of ageing of the samples was studied.

Fluorescence images were obtained for a freshly deposited sample [glass/poly(styrene sulfonate] (PSS)/PAH/THIATS/PAH). The micrographs were obtained by excitation at 514 nm and collecting the total fluorescence. In the fluorescence micrograph, very short organized structures with an enhanced

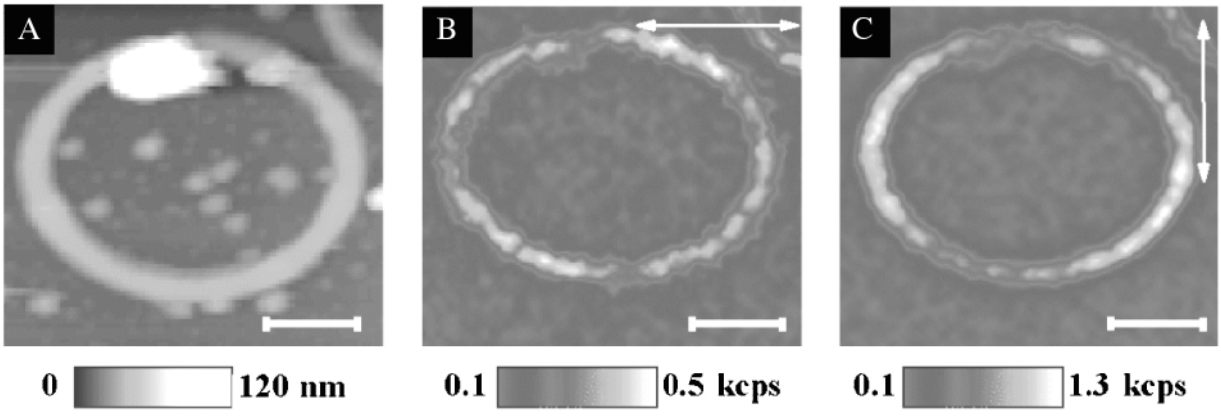

Fig. 7 A set of SNOM topographic and fluorescence polarization images acquired from a sample prepared by evaporation of a 10^{-6} M $BP_6/CHCl_3$ solution on glass after annealing in an oven at 75 °C for several days. The white scale bar on each image represents 1 μm. The orientation of the excitation polarization is indicated with the white arrows on the images. All fluorescence images are acquired with a parallel polarization configuration.

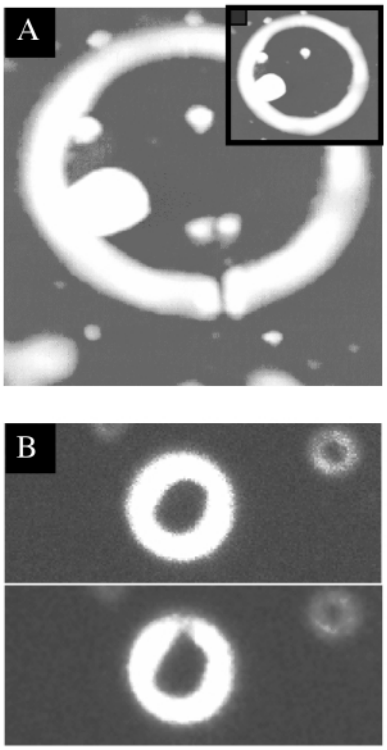

Fig. 8 (A) Mechanical and (B) optical manipulation of porphyrin rings at the submicrometer scale. (A) AFM image. The modification (cut through the ring) is around 130 nm. The insert is the intact ring before manipulation. (B) SNOM fluorescence images of a porphyrin ring before (upper half) and after (lower half) local photobleaching with a SNOM tip, leading to a modification of 280 nm wide.

fluorescence can be observed (Fig. 9A). Annealing of this sample at 70 °C induced structures in the fluorescence micrograph which resemble a needle-like pattern (Fig. 9B). The structures in the freshly deposited sample can be the nucleating sites for this pattern. The needle-like pattern was also observed in the fluorescence micrographs obtained for a multilayer which was kept at room temperature for 45 days after deposition (Fig. 9C). This suggests that a re-orientation and redistribution of the dye molecules into microcrystals does not happen immediately after deposition but that ageing of the sample is needed to obtain the needle-like pattern in the fluorescence micrograph. High-resolution images (not shown) reveal that the experimental width of the needles, measured in near-field, is about 80 nm, which corresponds to the lateral optical resolution of the experiment. The length of the needles exceeds a micron. We attribute the formation of needle-like structures to the PAH layer on top of the dye layer which must induce a redistribution and re-orientation of the dye molecules into microcrystals. The smoothness of topography suggests that the height of the microcrystals is small compared to the thickness of one polymer layer.[38,39]

In order to investigate to what extent the crystallites observed in the fluorescence image are oriented, polarized fluorescence images were obtained. Fig. 10 displays fluorescence images for a sample with PAH as top layer and for which the time between the deposition and the measurements was 45 days. Image 10A, B, C and D are the micrographs with 0°–0°, 0°–90°, 90°–0°, 90°–90° orientation of the polarizer and analyser, respectively. For different orientations of the emission polarizers different image contrasts were obtained. Fluorescence micrographs, obtained with the same orientation of the analyser but with different orientations of the polarizer, show the same fluorescent structures. The image contrast is furthermore independent of the excitation polarization at a fixed emission polarization. This indicates that the absorbing species is oriented randomly and that no photoselection occurs. One should realise that 514 nm, where the excitation occurs, is far from the absorption maximum of the J-aggregates situated at 623 nm. At 514 nm absorption is probably mainly due to residual monomers and sandwich dimers which transfer their excitation energy to the J-aggregates.

With a 'horizontal' orientation of the analyser, the emission of 'vertically' oriented needles was enhanced, while with a 'vertical' orientation of the analyser, the emission of 'horizon-

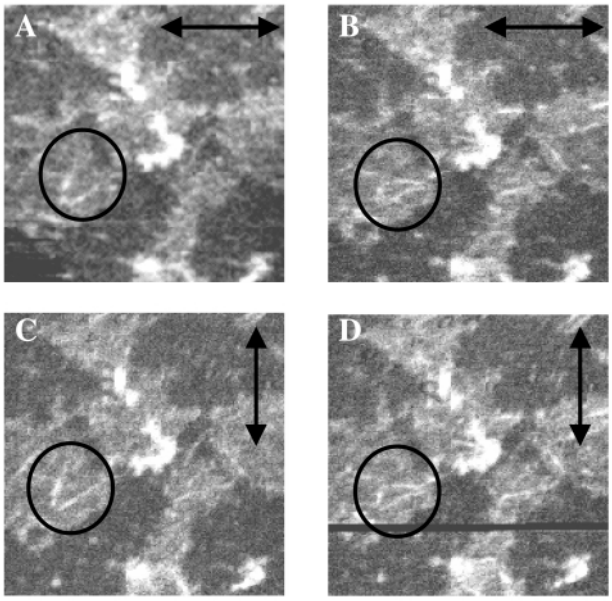

Fig. 10 Polarized SNOM measurements of a THIATS-containing multilayer covered by a layer of poly(allylamine) (PAH): Fluorescence micrographs with 0°–0° (A), 0°–90° (B), 90°–0° (C), 90°–90° (D) orientation of the excitation polarizer and fluorescence emission analyser respectively. The arrows indicate the excitation polarization. Excitation occurred at 514 nm.

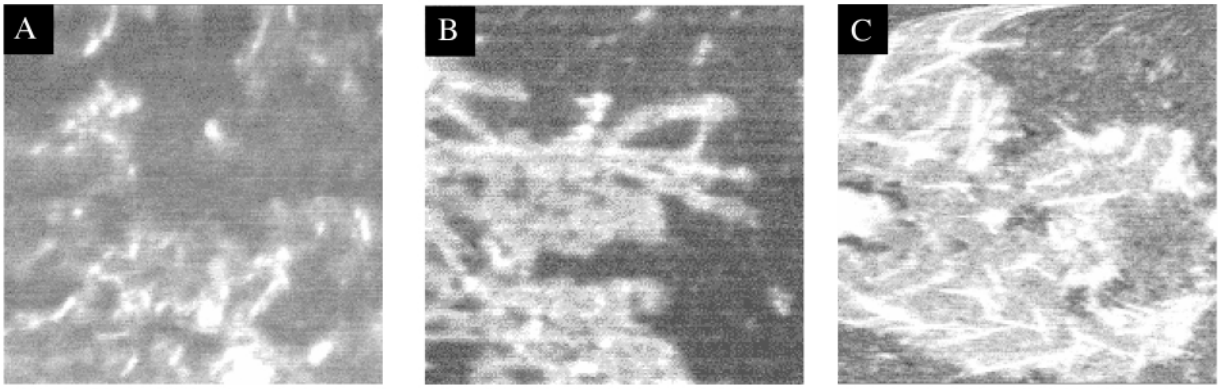

Fig. 9 SNOM fluorescence micrographs of a 10 μm × 10 μm sample with a PAH top layer: fresh sample (A), annealed sample (B), aged sample (C). Bright areas correspond to high fluorescence while dark areas correspond to low fluorescence relatively to each other.

tally' oriented needles was enhanced. This indicates that the transition dipoles of the emitting species have an orientation, which is highly correlated over several hundreds of nanometers to several microns. Furthermore in the 'horizontally' oriented needles, the emission dipole of the dye molecules will be oriented preferentially 'vertical' and *vice versa*. Needle-like structures, which are oriented at an angle of 45°, are visible in all the fluorescence micrographs. In Fig. 10, the area where the influence of the polarizers is clearly visible is marked with a white circle.

Excitation of residual monomers and dimers at 514 nm resulted in J-aggregate emission, which is polarized. The emission dipole of the dye molecules is oriented perpendicular to the needles. If a 2-D brickstone arrangement[40,41] is assumed for the aggregates their maximum π–π-interactions will occur perpendicular to the transition dipole and in the plane of the aggregate. Also the largest plane of the molecule is that parallel to both the long and the short axis. Hence packing along this plane will both be characterized by the largest π–π-interactions and reduce the hydrophobic interaction to a maximal extent. Therefore, the maximum growth rate of the microcrystals will be observed in those directions.

Scanning tunnelling microscopy and photochemistry

Where optical detection with SNOM is still limited to tens of nm, STM allows us to increase further the spatial resolution. In the last two decades, STM has proven to be a very valuable tool for the structure determination of surfaces at subnanometer resolution. The use of this technique is not restricted to a low temperature UHV environment but it has a wider application field and has also been applied successfully under ambient conditions and even in liquids. Moreover, the use of STM has been extended to the study of organic molecules physisorbed on conductive substrates at the liquid/solid interface.[42–47] In our research group, topics such as structure,[48] chirality,[49–51] dynamics[52–56] and light-induced reactions[57–59] are studied in physisorbed organic monolayers at the liquid/solid interface under ambient conditions.[60] The samples are prepared by applying a drop of a solution containing the compound under investigation on the basal plane of a freshly cleaved piece of highly oriented pyrolytic graphite (HOPG). The molecules are adsorbed on the graphite surface by physisorption. Adsorbate–substrate and adsorbate–adsorbate interactions lower the molecular mobility. This decrease in mobility (dynamics) is important for successful high resolution imaging with STM, which is often realized, in our group, by using molecules which display high affinity for the graphite substrate, for instance by having long alkyl chains. Intermolecular hydrogen bonding stabilises the two-dimensional network formed by the physisorbed molecules studied. In contrast to Langmuir–Blodgett films of fatty acids and their salts, the molecules are in most cases oriented parallel to the graphite substrate. It is important to note that during the measurements, the STM tip is immersed in the solution on top of the monolayer and that during the measurement molecules in the physisorbed monolayer might undergo desorption–adsorption dynamics. The presence of the solvent layer has some advantages. On one hand, it allows for the repair of defects in the monolayer by the desorption–adsorption dynamics and on the other hand, it lowers the force of the STM tip on the monolayer during scanning.

Using this experimental approach, we have investigated some photochemical reactions at the liquid/graphite interface. The aim of these studies was to demonstrate the feasibility of using STM for the study of photo-induced processes and on the other hand to learn more about these processes by STM.

A reversible reaction: *trans–cis* isomerization

With the aim of imaging the starting material and the reaction product of a reversible photoreaction, the *cis–trans* isomerization of an azo isophthalic acid derivative was investigated.[58] Upon irradiation with light of an appropriate wavelength, the *trans* to *cis* isomerization can be induced.

To achieve an efficient conversion of the *trans* to the *cis* isomer, the irradiation wavelength should match the absorption maximum of the *trans* isomer. The absorption maximum of the *cis* and *trans* isomer is situated at 317 and 360 nm, respectively. Upon irradiation at 366 nm, a photostationary mixture with a high *cis* isomer content is reached. When kept in the dark at room temperature the *cis* isomer spontaneously converts to the thermodynamically more stable *trans* isomer. For the STM experiments, an almost saturated solution of the azo compound in undecan-1-ol was applied on the surface of a freshly cleaved HOPG piece (Fig. 11). The solvent undecan-1-ol was selected

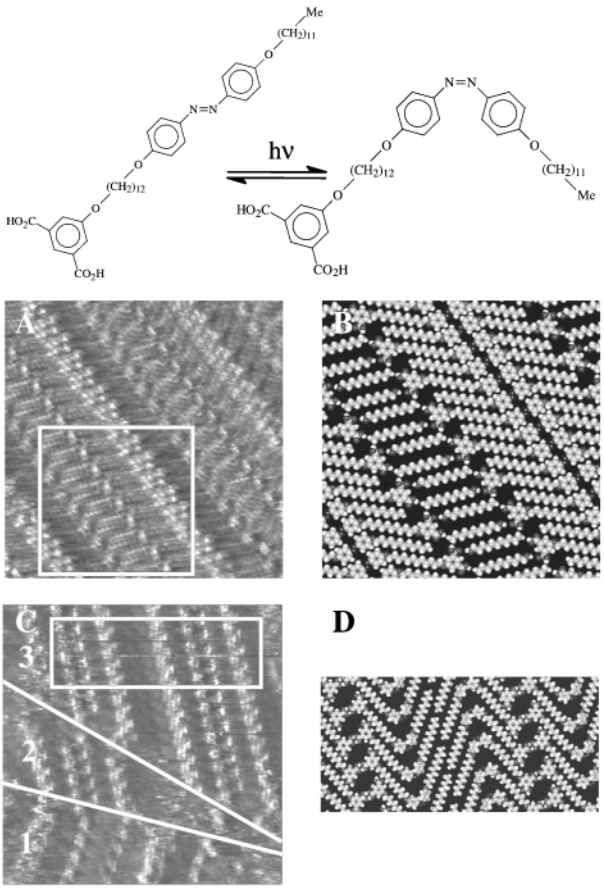

Fig. 11 *Cis* and *trans* isomer, reagent and product of a reversible photo-induced reaction. (A) STM image of an ordered monolayer of *trans* formed by physisorption from undecan-1-ol. Image size is 13 × 13 nm². White corresponds to the highest and black to the lowest measured tunnelling current in the image. (B) Molecular model for the two-dimensional packing of *trans*. The molecular model represents the area indicated in the STM image. (C) After illumination, STM image of an ordered monolayer of coexisting *cis*- and *trans*-domains. The domain boundaries are indicated by white lines. Image size is 13.4 × 13.4 nm². The molecular order in domain 1 corresponds to *trans*. The molecular order in domain 2 and 3 can be correlated with *cis*.

for its high boiling point (the solvent layer stays on top of the monolayer for several hours); in addition the solvent competes for intermolecular hydrogen bonding of the solute molecules which might disfavour physisorption.

Fig. 11A and 11B show an STM image and model of a monomolecular layer of the *trans*-form physisorbed from undecan-1-ol and shielded from light. The images are recorded in the constant height mode and the contrast is a function of the tunnelling probability as a function of *xy* coordinates. Bright and dark features in the images reflect a high and low tunnelling probability, respectively. Distinct bright spots corresponding to the isophthalic acid groups are easily recognized in the image. The somewhat broader bright bands represent the azobenzene moieties; in addition, the alkyl chains can be recognized in the image. Undecan-1-ol molecules are co-deposited in lamellae

separating lamellae of the azo-compound. Fig. 11C shows an STM image of a monolayer obtained by physisorption from a photostationary mixture after illumination of the solution in a cuvette (*ex situ*) at 366 nm. In addition to the regular monolayer structure characteristic for *trans* (domain 1), a new monolayer structure appeared which was not observed for *trans* monolayers (domains 2 and 3). Therefore, the patterns observed in these two domains must originate from a different molecular arrangement. Again, the bright spots correspond to the isophthalic acid groups and the broader bright bands to the azobenzene moieties. The measured lamellar distances and the observed molecular packing correspond to a monolayer of self-assembled *cis* isomers without solvent co-deposition. The absence of solvent co-deposition is probably due to the spatial orientation of the acid functions in the molecular arrangement of the *cis* isomer. It was not possible to form adlayers, which show solely *cis* structure. This can be attributed to the photostationary character of the mixture and to the larger affinity of *trans* compared to *cis* to form monolayers on the graphite surface. During imaging, the *cis* domains disappear with time. Finally, only *trans* domains could be observed, illustrating the reversibility of the reaction at the liquid/graphite interface. Similarly, *trans–cis* isomerization could be induced and their respective domains imaged by irradiating *in situ* a droplet of the *trans* isomer dissolved in undecan-1-ol directly on the graphite surface.

A possible mechanism for replacement of physisorbed 'reactant' molecules by the 'product' initiated by *in situ* illumination is the following. Irradiation of the system will lead to a change of the equilibrium composition and a concentration gradient in the supernatant solution. A decrease in *trans* concentration will induce desorption and enhance the adsorption of *cis* molecules. In addition, the isomerization reaction could also occur on the graphite surface itself and initiate the *cis*-product domain formation although this is expected to contribute only to a minor extent due to steric hindrance. During imaging (illumination off), these *cis* domains disappear with time until finally only *trans* isomer domains remain, due to the thermal back reaction (*cis* to *trans*).

The *cis–trans* isomerization has also been studied for another isophthalic acid derivative where one of the phenyl groups of the azobenzene moiety is the isophthalic acid group. Also for this compound the reaction could be visualized, however only after illumination *ex situ*.[60]

An irreversible reaction

In addition to a reversible *cis–trans* isomerization, an irreversible photoreaction was studied: the phototransformation of 10-diazo-2-hexadecylanthrone to 2-hexadecyl-9,10-anthraquinone.[57] Irradiation leads to the dissolution of the highly ordered molecular pattern of the reactant, starting at a domain boundary. When the irradiation is stopped, the highly ordered pattern reappeared and recrystallization of the reactant molecules occurred. As described in the previous section, the desorption must be the result of the formation of a concentration gradient induced by illumination. When irradiation is stopped, the system relaxes and the 2D crystal is reformed. Only when all reactant was transformed to product, which occurred after several illumination cycles were monolayers of 2-hexadecyl-9,10-antraquinone formed. Both phototransformations are believed to take place predominantly in the supernatant solution.

A topochemical reaction

To demonstrate the possibility of reactivity *within* the physisorbed monolayer, the study of a topological reaction was considered: the photopolymerization of a diacetylene[59] for which it is known that the relative orientation of the diacetylene monomer groups is critical as is shown in numerous studies in 3D crystals. The molecule chosen in this study is the diacetylene containing isophthalic acid derivative (Fig. 12).

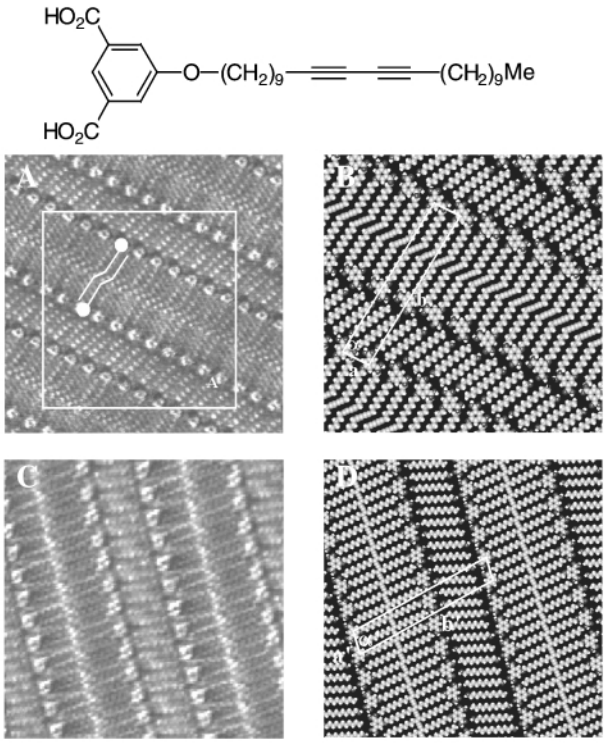

Fig. 12 Molecular structure of 5-(10,12-tricosadiinyloxy)isophthalic acid. (A) STM image of a physisorbed monolayer monomer from a solution in undecan-1-ol. Image size is 12.7 × 12.7 nm². The orientation of two molecules is indicated with a stick model. (B) Corresponding molecular model of the area indicated in the STM image in (A). (C) STM image of a polymerized monolayer structure. Image size is 10.8 × 10.8 nm². (D) Molecular model of the imaged area in (C).

This compound forms a physisorbed monolayer spontaneously at the liquid/graphite interface from a undecan-1-ol solution (Fig. 12A). The structure consists of lamellae of the diacetylene derivative alternated by solvent lamellae. The diacetylene moieties appear as bright spots in the middle of the lamellae. Within a lamella, the distance between isophthalic acid groups is 9.44 ± 0.09 Å. The alkyl chains are lying parallel to the substrate in the direction of one of the main graphite axes, and the orientation is modelled in Fig. 12B. After *in situ* illumination (254 nm, no scanning) of the monolayer film on graphite, the surface was re-examined, using the same scanning parameters as prior to the illumination, and again monolayer structures are observed (Fig. 12C). Isophthalic acid groups and solvent molecules are well resolved. The contrast in the middle of a lamella can be described by a series of bright spots, clearly distinct from the individual acetylene units, which suggests that the monolayer structure might be polymerized along the lamella direction. The most important change in the monolayer structure, however, is the change in spacing between the isophthalic acid groups. The distance was determined to be 9.81 ± 0.05 Å, in contrast to the unpolymerized repeating distance of 9.44 ± 0.09 Å. A molecular model for a polymerized monolayer structure is shown in Fig. 12D. The experimental value of 9.81 Å for the isophthalic acid group distance is in perfect accordance with the value of 9.82 Å obtained in a model optimized for the polymer chain. Consequently, the repeating distance in the polymer backbone is 4.91 Å which is in agreement with the three-dimensional crystal structure data of polymerized diacetylenes.[61] The structural parameters, describing the orientation of adjacent diacetylene units in unpolymerized monolayers, correspond to those values for which it was shown experimentally by X-ray crystallography of 3-D samples that crystallized diacetylene monomers could polymerize.[61]

Conclusions

The invention and development of scanning probe microscopy techniques has opened new ways to study surface phenomena with unprecedented resolution. The strength of these techniques is the very local nature of the probing mode and their general applicability even under ambient conditions, combined with the very high resolution. Both STM and SNOM have proven to be valuable tools in the study of thin organic films and photo-induced modifications on a very small scale. STM is for these kinds of systems used for the observation of the reactions while SNOM can optically modify material in an active way. Both techniques will continue to contribute in an important way to the study of photo-induced modifications on surfaces.

Acknowledgements

We thank the DWTC, through IUAP-IV-11, the F.W.O.-Vlaanderen and ESF SMARTON for financial support. We also gratefully thank Dr K. Grim, Dr P. Vanoppen, Dr K. Jeuris, A. Gesquière, M. Abdel-Mottaleb, E. Rousseau and P. Foubert for their substantial input in the realization of the experiments. S.D.F. and J.H. thank the Fund for Scientific Research–Flanders (FWO) for a postdoctoral fellowship. The collaborations were made possible thanks to the TMR project SISITOMAS.

Notes and references

1 G. Binnig and H. Rohrer, *Helv. Phys. Acta*, 1982, **55**, 726.
2 U. Dürig and D. W. Pohl, *J. Appl. Phys.*, 1986, **59**, 3318.
3 E. Betzig, A. Lewis, A. Harootunian, M. Isaacson and E. Kratschmer, *Biophys. J.*, 1986, **49**, 269.
4 H. J. Dai, J. H. Hafner, A. G. Rinzler, D. T. Colbert and R. E. Smalley, *Nature*, 1996, **384**, 147.
5 S. S. Wong, E. Joselevich, A. T. Woolley, C. L. Cheung and C. M. Lieber, *Nature*, 1998, **394**, 52.
6 E. Betzig and R. J. Chichester, *Science*, 1993, **262**, 1422.
7 J. A. Veerman, M. F. Garcia-Parajo, L. Kuipers and N. F. van Hulst, *J. Microsc.-Oxford*, 1999, **197**, 477.
8 E. Betzig and J. K. Trautman, *Science*, 1992, **257**, 189.
9 H. Heinzelmann and D. W. Pohl, *Appl. Phys. A.*, 1994, **59**, 89.
10 D. Courjon and C. Banier, *Rep. Prog. Phys.*, 1994, **57**, 989.
11 R. C. Dunn, *Chem. Rev.*, 1999, **99**, 2891.
12 B. Hecht, B. Sick, U. P. Wild, V. Deckert, R. Zenobi, O. J. F. Martin and D. W. Pohl, *J. Chem. Phys.*, 2000, **112**, 7761.
13 D. A. Vanden Bout, J. Kerimo, D. A. Higgins and P. F. Barbara, *Acc. Chem. Res.*, 1997, **30**, 204.
14 P. F. Barbara, D. M. Adams and D. B. O'Connor, *Annu. Rev. Mater. Sci.*, 1999, **29**, 433.
15 P. Zhang, R. Kopelman and W. Tan, *Solid State Mater. Sci.*, 2000, **25**, 89.
16 R. Zenobi and V. Deckert, *Angew. Chem., Int. Ed.*, 2000, **39**, 1746.
17 M. Rücker, P. Vanoppen, F. C. De Schryver, J. J. Ter Horst, J. Hotta and H. Masuhara, *Macromolecules*, 1995, **28**, 7530.
18 K. Jeuris, P. Vanoppen, F. C. De Schryver, J. W. Hofstraat, L. G. J. van der Ven and J. W. van de Velde, *Macromolecules*, 1998, **31**, 8579.
19 A. K. Kirsch, V. Subramaniam, A. Jenei and T. M. Jovin, *J. Microsc.*, 1999, **194**, 448.
20 D. A. Higgens and P. F. Barbara, *J. Phys. Chem.*, 1995, **99**, 3.
21 J. A. DeAro, R. Gupta, A. J. Heeger and S. K. Buratto, *Synth. Met.*, 1999, **102**, 865.
22 P. C. Ohara, J. R. Heath and W. M. Gelbaert, *Langmuir*, 1998, **14**, 3418.
23 L. Zhou, P. C. Zhang, P. K. H. Ho, G. Q. Xu, S. F. Y. Li and L. Chan, *J. Mater. Sci. Lett.*, 1996, **15**, 2080.
24 U. Thiele, K. Mertig and W. Pompe, *Phys. Rev. Lett.*, 1998, **80**, 2869.
25 J. van Esch, M. F. Roks and R. J. M. Nolte, *J. Am. Chem. Soc.*, 1986, **108**, 6093; A. P. H. J. Schenning, D. H. W. Hubert, M. C. Feiters and R. J. M. Nolte, *Angew. Chem., Int. Ed. Engl.*, 1994, **23**/**24**, 2468.
26 J. Hofkens, L. Latterini, H. Faes, P. Vanoppen, K. Jeuris, S. De Feyter, J. Kerimo, P. F. Barbara, F. C. De Schryver, A. E. Rowan and R. J. M. Nolte, *J. Phys. Chem.*, 1997, **49**, 10 558.
27 H. A. M. Biemans, A. E. Rowan, A. Verhoeven, P. Vanoppen, L. Latterini, J. Foekema, A. P. H. J. Schenning, E. W. Meijer, F. C. De Schryver and R. J. M. Nolte, *J. Am. Chem. Soc.*, 1998, **120**, 11 054.
28 P. Foubert, P. Vanoppen, M. Martin, T. Gensch, J. Hofkens, A. Helser, A. Seeger, R. M. Taylor, A. E. Rowan, R. J. M. Nolte and F. C. De Schryver, *Nanotechnology*, 2000, **11**, 16.
29 I. Langmuir, *J. Am. Chem. Soc.*, 1917, **39**, 1848.
30 K. B. Blodgett, *J. Am. Chem. Soc.*, 1935, **57**, 1007.
31 L. Netzer and J. Sagiv, *J. Am. Chem. Soc.*, 1983, **105**, 647.
32 G. Cao, H. G. Hong and T. E. Mallouk, *Acc. Chem. Res.*, 1992, **25**, 420.
33 G. Decher, J. D. Hong and J. Schmitt, *Thin Solid Films*, 1992, **210**/**211**, 831.
34 G. Scheibe, *Angew. Chem.*, 1939, **52**, 633.
35 E. E. Jelley, *Nature*, 1936, **138**, 1009.
36 D. A. Higgins, P. J. Reid and P. F. Barbara, *J. Phys. Chem.*, 1996, **100**, 1174.
37 D. A. Higgins, J. Kerimo, D. A. Vanden Bout and P. F. Barbara, *J. Am. Chem. Soc.*, 1996, **118**, 4049.
38 G. Decher and J. Schmitt, *Prog. Colloid Polym. Sci.*, 1992, **89**, 160.
39 M. Lösche, J. Schmitt, G. Decher, W. G. Bouwman and K. Kjaer, *Macromolecules*, 1998, **31**, 8893.
40 V. Czikkely, H. D. Forsterling and H. Kuhn, *Chem. Phys. Lett.*, 1970, **6**, 11.
41 H. Asanumo, K. Ogawa, H. Fukunaga, T. Tani and J. Tanaka, *Proceedings ICPS '98: International Congress on Imaging Science*, University of Antwerp: Belgium, 1998.
42 J. S. Foster and J. E. Frommer, *Nature*, 1988, **333**, 542.
43 G. C. McGonigal, G. C. Bernhardt and D. J. Thomson, *Appl. Phys. Lett.*, 1990, **57**, 28.
44 J. P. Rabe and S. Buchholz, *Science*, 1991, **253**, 424.
45 J. Frommer, *Angew. Chem., Int. Ed. Engl.*, 1992, **31**, 1298.
46 D. M. Cyr, B. Venkataraman and G. W. Flynn, *Chem. Mater.*, 1996, **8**, 1600.
47 L. C. Giancarlo and G. W. Flynn, *Annu. Rev. Phys. Chem.*, 1998, **49**, 297.
48 A. Gesquière, M. M. S. Abdel-Mottaleb, S. De Feyter, F. C. De Schryver, F. Schoonbeek, J. van Esch, R. M. Kellogg, B. L. Feringa, A. Calderone, R. Lazzaroni and J. L. Brédas, *Langmuir*, 2000, **16**, 10 385.
49 S. De Feyter, A. Gesquière, P. C. M. Grim, F. C. De Schryver, S. Valiyaveettil, C. Meiners, M. Sieffert and K. Müllen, *Langmuir*, 1999, **15**, 2817.
50 S. De Feyter, P. C. M. Grim, M. Rücker, P. Vanoppen, C. Meiners, M. Sieffert, S. Valiyaveetiil, K. Müllen and F. C. De Schryver, *Angew. Chem., Int. Ed. Engl.*, 1998, **37**, 1223.
51 S. De Feyter, A. Gesquière, F. C. De Schryver, C. Meiners and K. Müllen, *Langmuir*, 2000, **16**, 9887.
52 A. Stabel, R. Heinz, F. C. De Schryver and J. P. Rabe, *J. Phys. Chem.*, 1995, **99**, 505.
53 A. Stabel, H. Heinz, J. P. Rabe, G. Wegner, F. C. De Schryver, D. Corens, W. Dehaen and C. Süling, *J. Phys. Chem.*, 1995, **99**, 8690.
54 A. Gesquière, M. Abdel-Mottaleb and F. C. De Schryver, *Langmuir*, 1999, **15**, 6821.
55 A. Gesquière, M. Abdel-Mottaleb, S. De Feyter, F. C. De Schryver, M. Sieffert, K. Müllen, A. Calderone, R. Lazzaroni and J. L. Brédas, *Chem. Eur. J.*, 2000, **6**, 3739.
56 S. De Feyter, K. Grim, J. van Esch, R. M. Kellogg, B. L. Feringa and F. C. De Schryver, *J. Phys. Chem. B*, 1998, **102**, 8981.
57 R. Heinz, A. Stabel, J. P. Rabe, G. Wegner, F. C. De Schryver, D. Corens, W. Dehaen and C. Süling, *Angew. Chem., Int. Ed. Engl.*, 1994, **33**, 2080.
58 P. Vanoppen, P. C. M. Grim, M. Rücker, S. De Feyter, G. Moessner, S. Valiyaveettil, K. Müllen and F. C. De Schryver, *J. Phys. Chem.*, 1996, **100**, 19636.
59 P. C. M. Grim, S. De Feyter, A. Gesquière, P. Vanoppen, M. Rücker, S. Valiyaveettil, G. Moessner, K. Müllen and F. C. De Schryver, *Angew. Chem., Int. Ed. Engl.*, 1997, **36**, 2601.
60 S. De Feyter, A. Gesquière, M. M. Abdel-Mottaleb, P. C. M. Grim, F. C. De Schryver, C. Meiners, M. Sieffert, S. Valiyaveettil and K. Müllen, *Acc. Chem. Res.*, 2000, **33**, 520.
61 V. Enkelmann, *Adv. Polym. Sci.*, 1984, **63**, 91.

One-pot ruthenium catalyzed synthesis of spiro[pyrrolidin-2-one] derivatives by a [2 + 2 + 1] cycloaddition of ketimines, carbon monoxide and ethylene†‡

Angela Göbel and Wolfgang Imhof*

Institut für Anorganische und Analytische Chemie der Friedrich-Schiller-Universität Jena, August-Bebel-Str. 2, 07743 Jena, Germany. E-mail: cwi@rz.uni-jena.de

Received (in Liverpool, UK) 10th October 2000, Accepted 13th February 2001
First published as an Advance Article on the web 8th March 2001

The reaction of chiral *N*,*N*′-bis(aryl)tetrahydropyrrolo-[2,1-*c*][1,4]oxazine-3,4-diylidenediamines with carbon monoxide and ethylene in the presence of a catalytic amount of $Ru_3(CO)_{12}$ leads to the formation of spiro-lactams by a formal [2 + 2 + 1] cycloaddition reaction, whereas the imine double bond next to the oxazine nitrogen atom remains unreacted; the same spiro-lactams may be synthesized if iron carbonyl complexes of the *N*,*N*′-bis(aryl)tetrahydropyrrolo-[2,1-*c*][1,4]oxazine-3,4-diylidenediamines are introduced as the starting compounds.

Spiro-lactams have been described as the key intermediates in the total synthesis of several natural products[1] *e.g.* cephalotaxine or aldosterone antagonists, where the lactam ring system is attached to the D-ring of a steroid core.[2] Spiro[pyrrolidine-3,3′-indole] and spiro[pyrrolidine-3,3′-oxindole] derivatives are known as natural products with high cytostatic potential.[3] On the other hand, Murai *et al.* have synthesized functionalized γ-butyrolactones by a formal [2 + 2 + 1] cycloaddition reaction from a ketone, ethylene and CO.[4] It has also been described that the reaction of CO and/or olefins with unsaturated imines catalyzed by $Ru_3(CO)_{12}$ proceeds *via* C–H activation steps in the β-position with respect to the C–N double bond, followed by insertion reactions of CO and the olefins into the carbon metal bond. These reactions lead to functionalized imines or in some cases *via* intramolecular cyclization reactions to dihydropyrrol-2-one or dihydrobenzoisoindol-1-one derivatives, respectively.[5] Similar reactions have also been reported starting from N-heterocyclic compounds or aromatic ketones, respectively.[6]

If the cycloaddition reaction described by Murai and coworkers were also to work in the case of ketimines as starting compounds, one would formally end up with spiro-lactams if the organic substituents R and R′ of the ketimines formed a cyclic moiety (Scheme 1).

In addition, it would be of interest to perform this reaction with chiral ketimines in order to achieve stereoselective reactions, which in most cases are necessary in the synthesis of natural products. Therefore we chose the chiral *N*,*N*′-bis(aryl)-tetrahydropyrrolo[2,1-*c*][1,4]oxazine-3,4-diylidenediamines, which may be easily prepared from *N*,*N*′-bis(aryl)oxalimidoyl chlorides, and *S*-prolinol[7] as the starting compounds. In our earlier work we were able to show that these ligands react with $Fe_2(CO)_9$ to produce dinuclear iron carbonyl complexes in which the $Fe_2(CO)_6$ moiety is coordinated to the diimine ligand in an unsymmetrical fashion.[7c] One of the iron atoms is coordinated by both imine nitrogen atoms *via* their lone pairs whereas the second metal is coordinating the imine double bond next to the oxazine oxygen atom in side-on fashion (Scheme 2). This unsymmetrical coordination mode of a 1,4-diazadiene ligand has also been described in the literature.[8]

Scheme 2 shows the reaction of the diimine ligands **1**–**3** with CO and ethylene in the presence of a catalytic amount of $Ru_3(CO)_{12}$ to produce the spiro-lactams **4**–**6**. This reaction may be described as a formal [2 + 2 + 1] cycloaddition reaction of a ketimine with CO and ethylene to give a pyrrolidin-2-one system. Remarkably, only one of the imine moieties of the starting compounds does react. The cycloaddition only takes place at the C–N double bond neighboring the oxazine oxygen atom. This imine moiety is also the one that coordinates the second iron atom in a side-on fashion if **1**–**3** are reacted with stoichiometric amounts of $Fe_2(CO)_9$ (Scheme 2).[7c] So the reaction discriminates between the two imine subunits of the starting material whereas in principle both should be reactive.

Crystallization from toluene produced crystals of one of the diastereomers of **4** suitable for X-ray structure analysis.[9] The result is depicted in Fig. 1. The molecular structure shows the tetrahydropyrrolo[2,1-*c*][1,4]oxazine system which was already present in **1**. Now one of the former imine carbon atoms is the spiro-atom to which the pyrrolidone ring formed by the cycloaddition is attached (C6). The bonds from the pyrrolidone nitrogen atom (N2) towards the surrounding carbon atoms are in the single bond size-range with the bond to the carbonyl carbon atom (C10) being slightly shorter due to partial delocalization of π-electron density from the C–O double bond to the nitrogen. The bonds of C8 and C9 which represent the former ethylene molecule are also clearly single bonds. As expected, the planes through the oxazine and the pyrrolidone ring systems show a

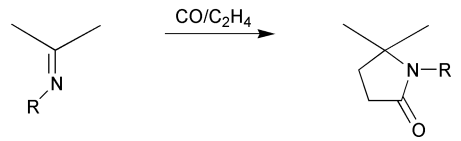

Scheme 1

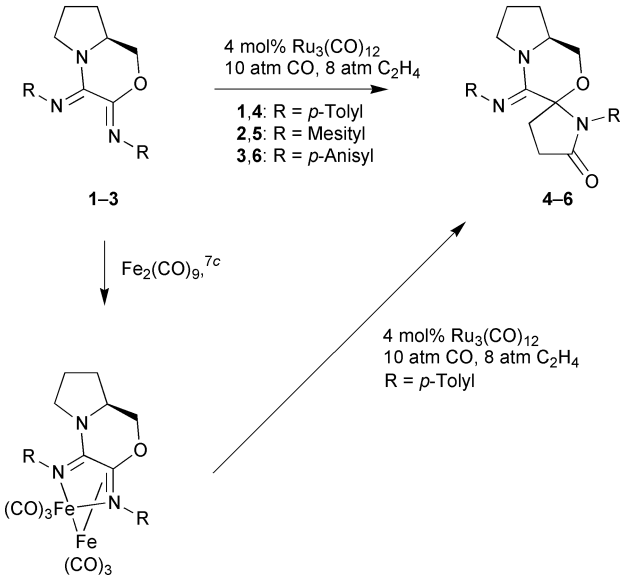

Scheme 2

† Electronic supplementary information (ESI) available: experimental details. See http://www.rsc.org/suppdata/cc/b0/b008290m/

‡ Dedicated to Prof. Ernst-Gottfried Jäger on the occasion of his 65th birthday.

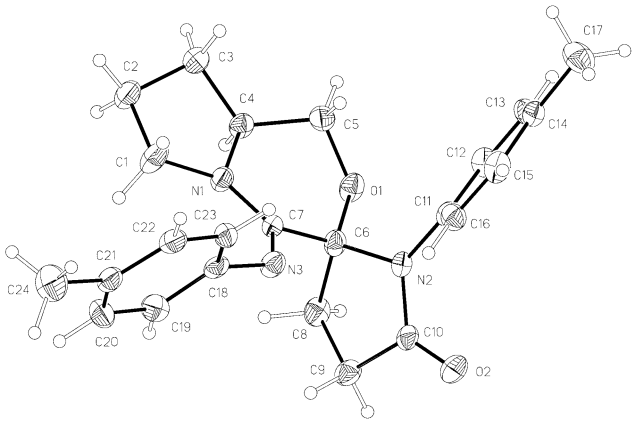

Fig. 1

nearly perpendicular arrangement. The second imine function of **1** did not react with CO and/or ethylene and thus the bond N3–C7 still shows a value typical for a double bond. **4** crystallizes in the chiral space group $P2_12_12_1$, so that in this crystal only the stereoisomer shown in Fig. 1 is present in which the *S*-configuration of prolinol still is preserved and the spiro-carbon atom (C6) shows a *R*-configuration.

NMR spectra of the crude reaction mixture of **4** show the presence of two isomers in a 1.5 : 1 ratio. The HMBC spectrum of the reaction mixture clearly proves that these isomers are diastereomers corresponding to the two different configurations possible at the new stereogenic center at C6. The spectra only show crosspeaks between the two different spiro-carbon atoms and the corresponding methylene protons at C5 (Fig. 1). If the second isomer was a regioisomer in which the reaction had taken place at the imine double bond next to the oxazine nitrogen atom, one would also expect to observe crosspeaks between the methylene moiety at C5 and the imine carbon atom next to the oxazine oxygen atom which then would have been preserved.

In the case of **4** the diastereomers may be separated by crystallization. NMR spectra of the crystals that were characterized also by X-ray diffraction show only one set of signals corresponding to the diastereomer which is the major component of the crude reaction mixture. The carbon resonances of the tetrahydropyrrolo[2,1-*c*][1,4]oxazine moiety do not differ very much from the corresponding signals in **1**,[6] with the exception, of course, of C6, which now is observed at δ = 94.3. The resonances of C8 and C9 give rise to signals at δ = 29.6 and 35.6, respectively.

The resonances of the second diastereomer show nearly identical chemical shifts compared to the one shown in Fig. 1. The most significant differences are the signals corresponding to the spiro-atom itself, which now is observed at δ = 95.5 and the resonances of the carbon atoms of C8 and C9, which are observed at δ = 35.5 and 21.3, respectively. The same observations can be made in the NMR spectra of the mixtures of diastereomers of **5** and **6**. For all compounds **4**–**6** the diastereomer which shows the signal of the spiro-carbon atom at higher field is the major component of the product mixture.

As mentioned previously, the reaction of **1**–**3** with $Fe_2(CO)_9$ yields dinuclear iron carbonyl complexes in which the two imine subunits are differently coordinated to the organometallic fragments (Scheme 1).[7c] In these complexes the imine double bond that is next to the oxazine oxygen atom is the one that is coordinated to both iron centers, whereas the other imine subunit is only bound to one $Fe(CO)_3$ moiety. So we tried to react the complex derived from **1** with CO and ethylene in the presence of a catalytic amount of $Ru_3(CO)_{12}$ under the same conditions as for the free ligands **1**–**3**. This reaction results in the quantitative formation of **4** also as a mixture of diastereomers in the same ratio as if the starting compound was **1**. This shows that the unsymmetrical coordination mode in the dinuclear iron complexes may well be of some relevance in the catalytic cycle leading to the spiro-lactams **4**–**6** and may also be responsible for the observed regioselectivity.

The authors gratefully acknowledge financial support by the Deutsche Forschungsgemeinschaft (SFB 436) and the fruitful cooperation with Professor R. Beckert, Institute of Organic Chemistry and Macromolecular Chemistry, Friedrich-Schiller-University, Jena.

Notes and references

1 (*a*) G. Stork, A. Brizzolara, H. Landesmann, J. Szmuszkovicz and R. Terrell, *J. Am. Chem. Soc.*, 1963, **85**, 207; (*b*) A. P. Stoll, T. J. Petcher and H. P. Weber, *Helv. Chim. Acta*, 1979, **62**, 1223; (*c*) P. D. Bailey, K. M. Morgan, D. I. Smith and J. M. Vernon, *Tetrahedron Lett.*, 1994, **35**, 7115; (*d*) T. Nagasaka, H. Sato and S. Saeki, *Tetrahedron: Asymmetry*, 1997, **8**, 191.

2 (*a*) L. N. Nysted and R. R. Burtner, *J. Org. Chem.*, 1962, **27**, 3175; (*b*) A. A. Patchett, F. Hofman, F. F. Giarusso, H. Schwam and G. E. Arth, *J. Org. Chem.*, 1962, **27**, 3822.

3 (*a*) P. L. Dupont, J. Lamotte-Brasseur, O. Dideberg, H. Campsteyn and M. Vermeire, *Acta Crystallogr. Sect. B*, 1977, **33**, 1801; (*b*) J. Leclercq, M.-W. De Pauw-Gillet, R. Bassleer and L. Angenot, *J. Ethnopharmacol.*, 1986, **15**, 305; (*c*) G. A. Cordell ed., *The Alkaloids: Chemistry and Biology*, Academic, San Diego, 1998, Vol. 5; (*d*) P. B. Alper, C. Meyers, A. Lerchner and D. R. Siegel and E. M. Carreira, *Angew. Chem.*, 1999, **111**, 3379.

4 N. Chatani, M. Tobisu, T. Asaumi, Y. Fukumoto and S. Murai, *J. Am. Chem. Soc.*, 1999, **121**, 7160.

5 (*a*) F. Kakiuchi, M. Yamauchi, N. Chatani and S. Murai, *Chem. Lett.*, 1996, 111; (*b*) T. Fukuyama, N. Chatani, F. Kakiuchi and S. Murai, *J. Org. Chem.*, 1997, **62**, 5647; (*c*) T. Morimoto, N. Chatani and S. Murai, *J. Am. Chem. Soc.*, 1999, **121**, 1758; (*d*) D. Berger and W. Imhof, *Chem. Commun.*, 1999, 1457; (*e*) D. Berger and W. Imhof, *Tetrahedron*, 2000, **56**, 2015.

6 (*a*) E. J. Moore, W. R. Pretzer, T. J. O'Connell, J. Harris, L. LaBounty, L. Chou and S. S. Grimmer, *J. Am. Chem. Soc.*, 1992, **114**, 5888; (*b*) S. Murai, F. Kakiuchi, S. Seine, Y. Tanaka, A. Kamatani, M. Sonoda and N. Chatani, *Pure Appl. Chem.*, 1994, **66**, 1527; (*c*) S. Murai, F. Kakiuchi, S. Sekine, Y. Tanaka, A. Kamatani, M. Sonoda and N. Chatani, *Nature*, 1993, **366**, 529; (*d*) F. Kakiuchi, S. Sekine, Y. Tanaka, A. Kamatani, M. Sonoda, N. Chatani and S. Murai, *Bull. Chem. Soc. Jpn.*, 1995, **66**, 62; (*e*) F. Kakiuchi, Y. Yamamoto, N. Chatani and S. Murai, *Chem. Lett.*, 1995, 681; (*f*) M. Sonoda, F. Kakiuchi, N. Chatani and S. Murai, *J. Organomet. Chem.*, 1995, **504**, 151; (*g*) M. Sonoda, F. Kakiuchi, A. Kamatani, N. Chatani and S. Murai, *Chem. Lett.*, 1996, 109; (*h*) F. Kakiuchi, M. Yamauchi, N. Chatani and S. Murai, *Chem. Lett.*, 1996, 111; (*i*) S. Murai, N. Chatani and F. Kakiuchi, *Bull. Chem. Soc. Jpn*, 1997, **69**, 589; (*j*) M. Sonoda, F. Kakiuchi, N. Chatani and S. Murai, *Bull. Chem. Soc. Jpn.*, 1997, **70**, 3117; (*k*) N. Chatani, T. Fukuyama, F. Kakiuchi and S. Murai, *J. Am. Chem. Soc.*, 1996, **118**, 493; (*l*) N. Chatani, Y. Ie, F. Kakiuchi and S. Murai, *J. Org. Chem.*, 1997, **62**, 2604; (*m*) T. Fukuyama, N. Chatani, J. Tatsumi, F. Kakiuchi and S. Murai, *J. Am. Chem. Soc.*, 1999, **120**, 11 522; (*n*) J. W. Szewczyk, R. L. Zuckerman, R. G. Bergman and J. A. Ellman, *Angew. Chem.*, 2001, **113**, 222.

7 (*a*) D. Lindauer, R. Beckert, T. Billert, M. Döring and H. Görls, *J. Prakt. Chem.*, 1995, **337**, 508; (*b*) D. Lindauer, *PhD Thesis, Jena University*, 1995; (*c*) W. Imhof, A. Göbel, R. Beckert and T. Billert, *J. Organomet. Chem.*, 1999, **590**, 104.

8 (*a*) R. Zoet, G. van Koten, F. Muller, K. Vrieze, M. van Wijnkoop, K. Goubitz, C. J. G. van Halen and C. H. Stam, *Inorg. Chim. Acta*, 1988, **149**, 193; (*b*) R. Zoet, J. T. B. Jastrzebiski, G. van Koten, T. Mahabiersing, K. Vrieze, D. Heijdenrijk and C. H. Stam, *Organometallics*, 1988, **7**, 2108; (*c*) M. J. A. Kraakman, K. Vrieze, H. Kooijman and A. L. Spek, *Organometallics*, 1992, **11**, 3760; (*d*) H.-W. Frühauf, A. Landers, R. Goddard and C. Krüger, *Angew. Chem.*, 1978, **90**, 56; (*e*) M. J. A. Kraakman, C. J. Elsevier, V. W. de Haar, K. Vrieze and A. L. Spek, *Inorg. Chim. Acta*, 1993, **203**, 157.

9 *Crystal and intensity data for* **4**: 183 K, yellow crystal, crystal size 0.3 × 0.1 × 0.02 mm, orthorhombic, a = 8.2350(4), b = 11.1009(6), c = 23.009(2) Å, V = 2103.4(2) Å^3, Z = 4, F(000) = 832, ρ_{calc} = 1.230 g cm^{-3}, spacegroup $P2_12_12_1$, abs. coeff. 0.079 mm^{-1}, θ limit 3.55–27.51°, ϕ- and ω-scan, 11462 refl. measured, 4734 independent refl., 3079 obs. refl. $F_o^2 > 2\sigma(F_o^2)$, 268 parameters, GOF = 1.069, R_1 = 0.0830, wR_2 = 0.1507, final diff. map electron density [e Å^{-3}] 0.214. CCDC 151894. See http://www.rsc.org/suppdata/cc/b0/b008290m/ for crystallographic files in .cif format.

ChemComm

Synthesis of novel dendrimers having a thermally reactive fluorescent core, and their thermal behavior

Hideo Tokuhisa, Emiko Koyama, Yoshinobu Nagawa and Kazuhisa Hiratani*

National Institute for Advanced Interdisciplinary Research, Tsukuba, Ibaraki 305-8562, Japan.
E-mail: hiratani@nair.go.jp

Received (in Cambridge, UK) 13th November 2000, Accepted 15th February 2001
First published as an Advance Article on the web 8th March 2001

Fluorescent poly(benzyl ether) dendrimers containing an isobutenyl and two naphthoate units at the core have been synthesized; thermal reaction (tandem Claisen rearrangement) of the dendrimers took place quantitatively, resulting in the complete quenching of the fluorescence.

In recent years, dendrimers have been extensively employed for both basic and applied studies, principally owing to their well defined structures that enable functional groups to be accurately placed in dendrimer frameworks.[1] In particular, the light-harvesting function of dendrimers, one of the most unique and attractive dendritic effects, has recieved great attention in terms of biomimetic systems for photosynthesis.[2,3] Here we propose a fluorescent-controllable system using novel dendrimers with a reactive, fluorescent core that performs successive Claisen rearrangements.[4] Thermal Claisen rearrangement of high-generation dendrimers is expected to switch the emission property from 'on' to 'off' with a high contrast.

Dendrimers **2**–**4** were synthesized (Scheme 1) by a simple esterification of the corresponding dendritic wedges HO[G-*n*] with acid chloride **6** using triethylamine as base, and were isolated by preparative gel permeation chromatography (GPC), in moderate yields (18–69%). Polyether dendritic wedges HO[G-*n*] were obtained by following the convergent-growth method reported by Hawker and Fréchet.[5] However, esterification of the dendritic wedge HO[G-4] remarkably decreased the yield to 2.5% possibly due to the steric hindrance around the reactive site under these conditions. Hence, for the synthesis of the dendrimer **5**, we applied a divergent/convergent joint approach: **6** was first esterified with 3,5-dihydroxybenzylalcohol using pyridine to give **7** in 34% yield, followed by the etherification with a twice molar excess of the dendritic wedge Br[G-3] to obtain dendrimer **5** in 55% yield (Scheme 1). All dendrimers were characterized by ^{1}H and ^{13}C NMR, IR and MALDI-TOF mass spectra.†

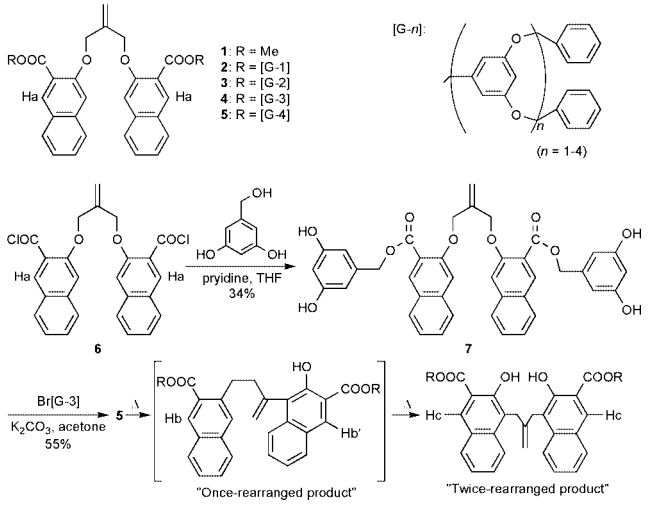

Scheme 1

The absorption spectra of compounds **1**–**5** in CH_2Cl_2 are shown in Fig. 1, with spectral data summarized in Table 1. There are two clear absorption bands in all the spectra: one in the UV region (265–300 nm), due mainly to the dendritic wedges and the other in the near-UV region (305–385 nm), due only to the naphthyl moiety in the core. As the aromatic building unit of the dendritic wedges increases, the molar extinction coefficient (ε) at 280 nm increases almost proportionally, while the absorption at 345 nm remains unchanged, as expected, confirming the structure of the compounds (Scheme 1).

In order to investigate the light-harvesting effect of the dendrimers, steady-state emission spectra of the different generation dendrimers in CH_2Cl_2 were measured and the fluorescent quantum yields are summarized in Table 1. As the generation increases, there is a monotonic increase of the fluorescence intensity at 400 nm from the focal point upon excitation at 280 nm, where the dendritic wedges absorbed mostly in higher generation dendrimers. On the other hand, direct excitation of the naphthyl core at 345 nm gave a fluorescence at 400 nm without much difference in the quantum yields, 19–24% (Table 1). These results evidently demonstrate that this enhanced fluorescence is caused by an efficient energy transfer from the dendritic wedges to the naphthyl core in the higher generation dendrimer, in other words, the larger dendrimers serve as better antennae to collect photons, in accord with the report of Aida and coworkers on the light-harvesting effect of a poly(benzyl ether) dendron.[2] However, the energy transfer efficiency of the higher generation dendrimers **4** and **5**

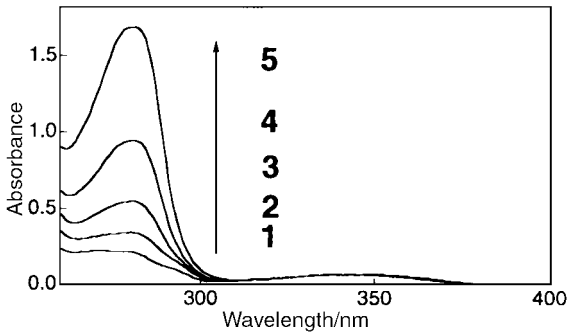

Fig. 1 UV–VIS absorption spectra of dendrimers **1**–**5** in CH_2Cl_2. The spectra are normalized to 1.98×10^{-5} M concentration.

Table 1 Extinction coefficients at 280 and 345 nm, and fluorescent quantum yields around 400 nm upon excitation at 280 and 345 nm

	280 nm		345 nm	
Compound	10^{-4} ε/ M^{-1} cm^{-1}	Φ_{fl}	10^{-3} ε/ M^{-1} cm^{-1}	Φ_{fl}
1	1.07	0.18	3.25	0.19
2	1.72	0.20	3.53	0.21
3	2.75	0.19	3.48	0.23
4	4.78	0.16	3.37	0.23
5	8.50	0.12	3.12	0.24

DOI: 10.1039/b009071i

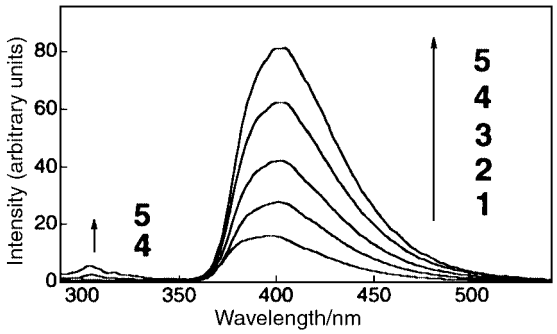

Fig. 2 Steady-state fluorescence spectra of dendrimers **1**–**5** in CH_2Cl_2 upon excitation at 280 nm. The spectra are normalized to 0.99×10^{-6} M concentration.

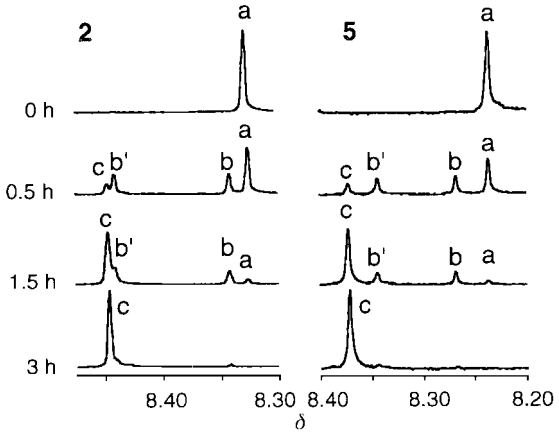

Fig. 3 ^{1}H NMR spectra of dendrimers **2** and **5** during the course of tandem Claisen rearrangement. Signals a, b, b′ and c arise from H_a, H_b, $H_{b'}$, and H_c in the naphthoates (Scheme 1).

decreases somewhat, taking into account the fact that the residual fluorescence at 308 nm from the dendritic wedges was observed and even increased for **5**. There are some reports on the loss in energy transfer efficiency for higher generation dendrimers, probably due to many factors based on Förster's mechanism.[3,6] We believe that the relatively small spectral overlap between the fluorescence of the dendritic wedges and the absorption of the core might be one of the key factors to decrease the energy transfer efficiency, although more data is required to discuss this point fully. Another noteworthy finding is that there was no red-shifted emission due to the excimer, expected to be formed between the two neighboring chromophores, in any spectra of the dendrimers in CH_2Cl_2. By contrast, the model compound **1** in the solid state showed a broad excimer emission around 500 nm while no additional signal or peak shift appeared for **5**, which suggests that inter- rather than intramolecular interactions between the chromophores cause excimer formation; the dendritic wedge of **5** shields the focal point so effectively as to prevent intermolecular collision.

We compared tandem Claisen rearrangement of the core unit among the dendrimers to investigate the steric effect on the reaction. Almost quantitative tandem Claisen rearrangement of all the dendrimers took place over 3 h in the absence of solvent at 150 °C. Indeed the rearrangement occurred even at 105 °C though 3 days were required to complete the reaction. Fig. 3 shows ^{1}H NMR spectra of dendrimers **2** and **5** during the course of tandem Claisen rearrangement at 150 °C. Surprisingly, there was no significant difference in the progress of the thermal reaction between the smaller and larger dendrimers. Indeed, the rate constants for this process were determined on the basis of the reasonable assumption that the rearrangement is a first-order successive reaction, to give almost identical rate-constants at 150 °C: $k_1 = 6 \times 10^{-4}$ s^{-1}, $k_2 = 4 \times 10^{-4}$ s^{-1} for **2**; $k_1 = 6 \times 10^{-4}$ s^{-1}, $k_2 = 5 \times 10^{-4}$ s^{-1}, for **5**. These results show that even for the dendrimer with 32 benzyl groups at the periphery there is no steric hindrance and enough space to form a chair- or boat-like conformation, thought to be adopted for the [3,3] sigmatropic rearrangement.[7]

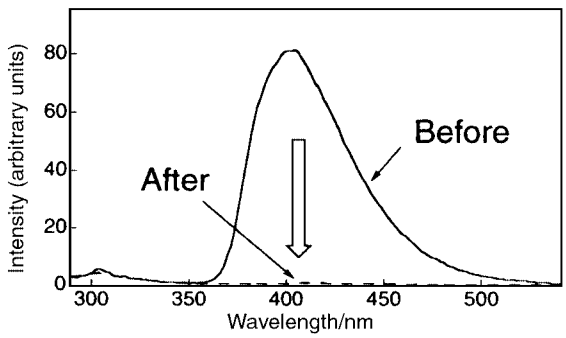

Fig. 4 Steady-state fluorescence spectra of dendrimer **5** in CH_2Cl_2 upon excitation at 280 nm before and after tandem Claisen rearrangement. The spectra are normalized to 0.99×10^{-6} M concentration.

Finally, the fluorescence spectra of the dendrimer **5** were compared before and after the rearrangement (Fig. 4). Interestingly, tandem Claisen rearrangement of the dendrimer resulted in complete quenching of the fluorescence around 400 nm with no change in the fluorescence at 308 nm arising from the dendritic wedge. We observed similar phenomena in the other dendrimers **1**–**4**. This indicates that the high generation dendrimers have potential to realize thermo- or photo-induced fluorescent images with high contrast.

In conclusion, we have demonstrated the light-harvesting effect of the fluorescent dendrimers having a reactive core for tandem Claisen rearrangement and their quenching by heating. Our finding that there is no steric hindrance on tandem Claisen rearrangement at the core of the dendrimers encourages us to incorporate other reactive groups into the core moiety such as carbamoyl, urea-type units in order to endow the dendrimer with new functions.

Notes and references

† *Selected data: for* **2**: δ_H (500 MHz, $CDCl_3$): 4.81 (s, 4H), 4.96 (s, 8H), 5.28 (s, 4H), 5.49 (s, 2H), 6.54 (t, *J* 2.2 Hz, 2H), 6.68 (d *J* 2.2 Hz, 4H), 7.20 (s, 2H), 7.27–7.38 (m, 22H), 7.45 (t, *J* 8.1 Hz, 2H), 7.66 (d, *J* 8.1 Hz, 2H), 7.78 (d, *J* 8.1 Hz, 2H), 8.33 (s, 2H); MS (MALDI-TOF) m/z calc. for $C_{68}H_{56}O_{10}$ $[M + Na]^+$ 1056.2, found 1055.0. For **3**: δ_H (500 MHz, $CDCl_3$): 4.78 (s, 4H), 4.88 (s, 8H), 4.96 (s, 16H), 5.26 (s, 4H), 5.47 (s, 2H), 6.50 (t, *J* 2.3 Hz, 2H), 6.53 (t, *J* 2.3 Hz, 4H), 6.63 (d, *J* 2.3 Hz, 8H), 6.65 (d, *J* 2.3 Hz, 4H), 7.17 (s, 2H), 7.27–7.38 (m, 42H), 7.42 (m, 2H), 7.63 (d, *J* 8.3 Hz, 2H), 7.74 (d, *J* 8.0 Hz, 2H), 8.31 (s, 2H); MS (MALDI-TOF) *m*/*z* calc. for $C_{124}H_{104}O_{18}$ $[M + Na]^+$ 1905.1, found 1904.1. For **4**: δ_H (500 MHz, $CDCl_3$): 4.73 (s, 4H), 4.82 (s, 8H), 4.86 (s, 16H), 4.94 (s, 32H), 5.22 (s, 4H), 5.44 (s, 2H), 6.47–6.52 (m, 14H), 6.59–6.63 (m, 28H), 7.13 (s, 2H), 7.25–7.39 (m, 84H), 7.59 (d, *J* 8.1 Hz, 2H), 7.68 (d, *J* 8.1 Hz, 2H), 8.28 (s, 2H); MS (MALDI-TOF) *m*/*z* calc. for $C_{236}H_{200}O_{34}$ $[M + Na]^+$ 3603.1, found 3602.2. For **5**: δ_H (500 MHz, $CDCl_3$): 4.67 (s, 4H), 4.74 (s, 8H), 4.79 (s, 16H), 4.82 (s, 32H), 4.90 (s, 64H), 5.17 (s, 4H), 5.41 (s, 2H), 6.46–6.49 (m, 30H), 6.57–6.59 (m, 60H), 7.07 (s, 2H), 7.21–7.32 (m, 164H), 7.53 (d, *J* 8.1 Hz, 2H), 7.61 (d, *J* 8.1 Hz, 2H), 8.24 (s, 2H); MS (MALDI-TOF) *m*/*z* calc. for $C_{460}H_{392}O_{66}$ $[M + Na]^+$ 6999.0, found 6995.9.

1 M. Fischer and F. Vögtle, *Angew. Chem., Int. Ed.*, 1999, **38**, 885; C. Z. Chen and S. L. Cooper, *Adv. Mater.*, 2000, **12**, 843; A. W. Bosman, H. M. Janssen and E. W. Meijer, *Chem. Rev.*, 1999, **99**, 1665; V. Balzani, S. Campagna, G. Denti, A. Juris, S. Serroni and M. Venturi, *Acc. Chem. Res.*, 1998, **31**, 26; F. Zeng and S. C. Zimmerman, *Chem. Rev.*, 1997, **97**, 1681.

2 T. Sato, D.-L. Jiang and T. Aida, *J. Am. Chem. Soc.*, 1999, **121**, 10658.

3 A. Adronov and J. M. J. Fréchet, *Chem. Commun.*, 2000, **18**, 1701.

4 K. Hiratani, T. Takahashi, K. Kasuga, H. Sugihara, K. Fujiwara and K. Ohashi, *Tetrahedron Lett.*, 1995, **36**, 5567; K. Hiratani, H. Uzawa, K. Kasuga and H. Kambayashi, *Tetrahedron Lett.*, 1997, **38**, 8993.

5 C. J. Hawker and J. M. J. Fréchet, *J. Am. Chem. Soc.*, 1990, **112**, 7638.

6 C. Devadoss, P. Bharathi and J. S. Moore, *J. Am. Chem. Soc.*, 1996, **118**, 9635.

7 R. P. Lutz, *Chem. Rev.*, 1984, **84**, 205.

Nanofiltration-coupled catalysis to combine the advantages of homogeneous and heterogeneous catalysis

Koen De Smet, Sven Aerts, Erik Ceulemans, Ivo F. J. Vankelecom* and Pierre A. Jacobs

Centre for Surface Chemistry and Catalysis, Faculty of Agricultural and Applied Biological Sciences, Katholieke Universiteit Leuven, Kardinaal Mercierlaan 92, 3001 Leuven, Belgium. E-mail: ivo.vankelecom@agr.kuleuven.ac.be

Received (in Cambridge, UK) 12th December 2000, Accepted 21st February 2001
First published as an Advance Article on the web 8th March 2001

In a hybrid process that combines nanofiltration with homogeneous catalysis, the best possible reaction rates, chemoselectivities and enantioselectivities are obtained in a continuous operation mode while recycling the catalyst.

In industrial processes, heterogeneous catalysts are generally preferred as they facilitate removal of the catalyst after reaction[1] and allow a continuous operation mode. On the other hand, preparing a heterogeneous catalyst can be tedious and might demand a high preparative effort. In certain cases, mass or heat transfer limitations in the solid state catalyst may lead to decreased activities, and homogeneous reactions generally show higher chemo- and enantio-selectivities.[2]

In the reported hybrid process (Fig. 1), a reaction takes place in a continuously stirred tank reactor, thus reaching activities and selectivities as in homogeneous reactions. The liquid is contacted with a nanofiltration (NF) membrane that allows products to permeate but rejects the dissolved catalyst. This set-up is made possible by the recent development of solvent resistant NF membranes.[3] They have a molecular weight cut-off (MWCO) in the range of 200–700 Da and working conditions below 40 °C and 35 bar.

In related work by Giffels *et al.*,[4] the same membranes are used but they behave only like ultrafiltration membranes under the reaction conditions applied. This implies that an enlargement of their oxazaborolidines is still necessary to have them rejected by the membrane. Derivatisation of the catalyst in order to enlarge it—*e.g.* by linking it to polymers or by forming dendrimers—is avoided in our experiments by operating the membrane filtration under true nanofiltration conditions. The catalysts are thus retained by the membrane without the need to derivatise them first, and they can be used off the shelf in the form in which they are readily available.

In particular, chiral catalysts are among the preferred systems for this hybrid membrane/catalysis process due to their extremely high cost and their sensitivity towards traditional heterogenisation methods. Furthermore, most of these catalysts contain transition metal complexes with a molecular weight above 500 Da and high activities and selectivities under moderate reaction conditions. In the reported set-up, the hydrogen pressure needed for the hydrogenation of the substrates, forms—without any additional cost or equipment—the driving force for the membrane permeation. The whole hybrid process is operated in such a way that a sufficient amount of product with high purity is yielded in the catalytic process, while a good rejection of the the catalyst and reasonable fluxes are preserved in the NF.

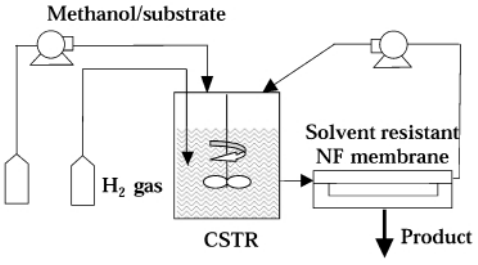

Fig. 1 Reactor set-up for NF-coupled catalysis.

The continuous enantioselective hydrogenation of dimethyl itaconate (DMI) with Ru–BINAP (MW 929 Da) and of methyl 2-acetamidoacrylate (MAA) with Rh–EtDUPHOS (MW 723 Da) (Fig. 2) were selected because of the excellent performance[5] of these catalysts and their industrial relevance.[6] Several ways to heterogenise these complexes have been reported already[7–9] but most did not equal the performance of the homogeneous catalyst, either in ee, activity or in the range of possible substrates.

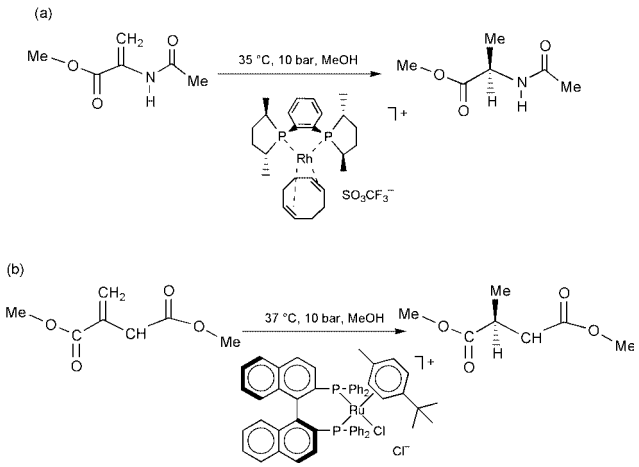

Fig. 2 Reactions with (a) Rh–EtDUPHOS and (b) Ru–BINAP.

Because the membrane fluxes in the NF part of the process are coupled *via* the hydrogen pressure to the reaction rates during catalysis, the reaction rate and enantiomer excess were determined first in a batch-wise reference reaction at pressures that fall within the range for nanofiltration (Table 1).

The homogeneous reactions were carried out in magnetically stirred 10 ml autoclaves. 0.35 g (2.5 mM) MAA was dissolved in 9 ml MeOH and flushed with N_2 before adding 1.7 mg Rh–EtDUPHOS (2.35 μM). For the homogeneous reaction with Ru–BINAP, 0.6 g (4 mM) DMI was dissolved in 9 ml MeOH, flushed with N_2 and subsequently mixed with 4.3 mg (4.6 μM) catalyst. The results[10] are shown in Fig. 1. For the hydrogenation of DMI with Ru–BINAP, no literature data could be found. The enantiomer excess and the activity for reactions with Rh–EtDUPHOS were lower than reported in the literature.[11]

Table 1 Hydrogenations of MAA and DMI with, respectively, Rh–EtDUPHOS and Ru–BINAP

	Substrate/ catalyst	Pressure/ bar	*T*/°C	TOF/ h^{-1}	Ee (%)
Rh–EtDUPHOS[a]	2000	2	22	> 2000	99.4
Rh–EtDUPHOS	1050	4	30	703	95
Ru–BINAP	850	10	37	330	93

[a] Burk *et al.*[11]

Table 2 Methanol fluxes at different temperatures and pressures for MPF-60 membranes (KOCH)

Pressure/bar	*T*/°C	Flux/kg m^{-2} h^{-1}
10	30	1.2
	40	1.6
	50	2.6
	60	3.2
15	30	1.7

This is believed to be due to a less thorough pre-treatment of solvents and reagents as compared with literature.

A NF membrane generally does not discriminate between reactants and hydrogenated products, given their negligible difference in MW, shape or polarity. This means that the conditions that determine the membrane flux—such as membrane type, membrane area, applied pressure gradient, temperature and type of solvent[12]—can be adjusted to the catalytic conditions that determine the conversion of the reactant. Methanol fluxes through the NF membrane (KOCH, MPF-60), are given in Table 2 for different temperatures and pressures: as expected, higher temperature and pressure are tools used to increase the flux through the membrane and thus realise a shorter residence time (τ) for a given reactor volume.

The continuous reactions were carried out in a stirred 100 ml autoclave containing an MPF-60 membrane at the bottom. The permeate was collected in a cooled flask (−78 °C). Both feed and permeate were analysed by GC and AAS to determine retention (retained concentration/feed concentration) of reactants, products and catalyst. For the hydrogenation of DMI with Ru–BINAP at 37 °C and 10 bar, the feed solution (C_0 = 0.4 μM) was pumped at a rate of 3.6 ml h^{-1} to the reaction mixture (V = 14 ml, C_0 = 0.4 μM and 33.7 mg Ru–BINAP). The hydrogenation of MAA was performed at 35 °C and 10 bar (V = 16 ml, C_0 = 0.13 μM and 8.5 mg Rh–EtDUPHOS) with the feed solution (C_0 = 0.13 μM) added at a rate of 3.5 ml h^{-1}.

To fully prove the concept, activities should remain unchanged after several refreshments of the reactor volume and the complex should be retained sufficiently. The hydrogenation of DMI shows a constant enantiomer excess as a function of time (Fig. 3). The very small decrease in conversion, becoming apparent after several hours, can be ascribed to the incomplete rejection of Ru–BINAP (> 98%). Nevertheless, this nanofiltration-coupled catalysis allowed the continuous hydrogenation of ten reactor volumes—as indicated by the vertical lines on the graph—with an enantiomer excess of 93%, which equals those reached under homogeneous conditions. For the hydrogenation of MAA with Rh–EtDUPHOS (Fig. 4), the decrease in enantiomer excess and conversion in the long term is slightly more significant. Since the 97% retention of this complex cannot alone account for this effect, a slow deactivation of the catalyst—possibly due to oxidation of the phosphine ligand—is assumed but still needs further investigation. The total TONs for the hydrogenation with Ru–BINAP and Rh–EtDUPHOS are, respectively, 1950 and 930.

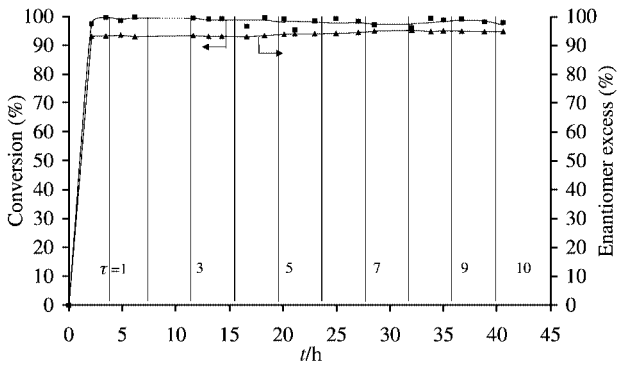

Fig. 3 Conversion and enantiomer excess as a function of time for the continuous NF-coupled hydrogenation with Ru–BINAP.

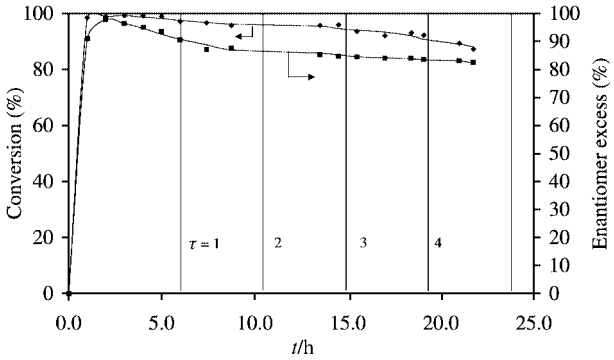

Fig. 4 Conversion and enantiomer excess as a function of time for the continuous NF-coupled hydrogenation with Rh–EtDUPHOS.

These two continuous reactions demonstrate the general concept of this hybrid process to perform homogeneous reactions in a continuous mode whenever the membrane is able to retain the catalyst and does not retain the products. Even though the system is limited by working conditions—like solvent, temperature and pressure—it is believed that the concept can be applied in many different types of reaction and for a wide range of catalysts and substrates, especially in the field of fine chemical synthesis.

This work was supported by the Belgian Federal Government in the frame of an IAP-PAI grant on Supramolecular Catalysis. K. D. S. acknowledges 'het Vlaams Instituut voor de bevordering van het wetenschappelijk-technologisch onderzoek in de industrie' (IWT) for a grant as doctoral research fellow. I. F. J. V. acknowledges a fellowship as Post-doctoral Researcher from the Fund for Scientific Research (FWO).

Notes and references

1 E. Lindner, T. Schneller, F. Auer and H. A. Mayer, *Angew. Chem., Int. Ed.*, 1999, **38**, 2154.
2 I. F. J. Vankelecom and P. A. Jacobs, in *Immobilisation of Chiral Catalysts*, ed. D. De Vos, I. F. J. Vankelecom and P. A. Jacobs, VCH Weinhein, 2000, ch. 2, pp. 19–42.
3 KOCH International B.V., Membrane Systems Division.
4 G. Giffels, J. Beliczey, M. Felder and U. Kragl, *Tetahedron: Asymmetry*, 1998, **9**, 691: S. Rissom, J. Beliczey, G. Giffels, U. Kragl and C. Wandrey, *Tetrahedron: Asymmetry*, 1999, **10**, 923.
5 S. Akutagawa, *Appl. Catal.*, 1995, **128**, 171
6 S. C. Stinson, *C&EN*, September 1998, pp. 83–104.
7 D. J. Bayston, J. L. Fraser, M. R. Ashton, A. D. Baxter, M. E. C. Polywka and E. M. Moses, *J. Org. Chem.*, 1998, **63**, 3137.
8 R. ter Halle, B. Colasson, E. Schulz, M. Spagno and M. Lemaire, *Tetrahedron Lett.*, 2000, **41**, 643.
9 K. T. Wan and M. E. Davis, *Nature*, 1994, **370**, 449; I. F. J. Vankelecom, D. Tas, R. F. Parton, V. Van de Vyver and P. A. Jacobs, *Angew. Chem.*, 1996, **108**, 1445; I. F. J. Vankelecom, A. Wolfson, S. Geresh, M. Landau, M. Gottlieb and M. Hershkovitz, *Chem. Commun.*, 1999, **23**, 2407.
10 The GC analysis was carried out on a Chiraldex G-TA (Chrompack) with N_2 as carrier, whereas MAA reactions were analysed on a Chirasil-DEX CD (Chrompack) column with H_2 as carrier. The amount of catalyst in the permeate was determined by measuring the Ru concentration by atomic absorption spectroscopy (Varion Techtron AA6) at 349.9 nm and the Rh concentration at 343.5 nm.
11 M. J. Burk, J. E. Feaster, W. A. Nugent and R. L. Harlow, *J. Am. Chem. Soc.*, 1993, **115**, 10 125.
12 D. R. Machado, D. Hasson and R. Semiat, *J. Membr. Sci.*, 1999, **163**, 93; D. R. Machado, D. Hasson and R. Semiat, *J. Membr. Sc.*, 1999, **166**, 63; J. A. Whu, B. C. Baltzis and K. K. Sirkar, *J. Membr. Sci.*, 2000, **170**, 159.

ChemComm

Preparation of resin-bound amine *N*-oxides and demonstration of their use in synthetic carbonyl cluster chemistry†

Nicholas E. Leadbeater* and Cornelia van der Pol‡

Department of Chemistry, King's College London, Strand, London, UK WC2R 2LS
E-mail: nicholas.leadbeater@kcl.ac.uk

Received (in Cambridge, UK) 15th January 2001, Accepted 21st February 2001
First published as an Advance Article on the web 13th March 2001

The preparation of two polymer-supported amine *N*-oxides is presented and their application as an improved methodology for synthetic metal carbonyl cluster chemistry is illustrated.

Amine *N*-oxides are readily deoxygenated by metal carbonyls. This mild reaction offers a general method for the activation of the complexes towards the substitution of a carbonyl with another ligand, avoiding the extreme temperatures and pressures normally required for direct substitution of carbonyl groups.[1,2] The main disadvantage of this route when applied to metal carbonyl clusters is that, in the case of unstable or highly-reactive complexes, it is often hard to remove all traces of amine *N*-oxide from the product. This has the drawback that, in subsequent reactions, a trace of *N*-oxide left in the starting material mixture can affect the reaction chemistry leading either to unwanted by-products or totally altering the course of the reaction.[3]

Within the organic chemistry community there is increasing interest in the development of polymer-supported catalysts and reagents for use in the synthesis of target molecules.[4] One of the key advantages of immobilizing a catalyst or reagent on a polymer support is the ease of separation from the product mixture at the end of a reaction and hence the greatly simplified work-up needed. To date, synthetic inorganic and organometallic chemists do not seem to have taken advantage of using supported complexes in their chemistry. Here, we report the simple synthesis of two polymer-bound amine *N*-oxides and demonstrate their use and applicability in organometallic cluster chemistry through the synthesis of the ruthenium and osmium trinuclear cluster complexes $M_3(CO)_{12-n}(MeCN)_n$ (M = Ru, Os; n = 1, 2).[5] The use of a supported *N*-oxide, as reported here, is significant since the cluster complexes can be prepared and purified very easily. These complexes have proven very useful as starting materials for a range of interesting cluster chemistry studies since their first reports in the early 1980s.[6,7]

The desired polymer-supported amine *N*-oxides were prepared in two steps from Merrifield's resin using modified literature procedures (Scheme 1).[8,9] Attention was focused on polymer-supported 'benzylpiperidine *N*-oxide' **1** and polymer-supported 'diethylbenzylamine *N*-oxide' **2**.§ The final loading of *N*-oxide on the polymer support was calculated at *ca.* 0.9–1.0 mmol g resin^{-1}. Like their homogeneous analogues, **1** and **2** are hygroscopic and are best stored under a blanket of dry nitrogen. Before use, water was removed by warming the beads gently (to no more than 35 °C) under vacuum.

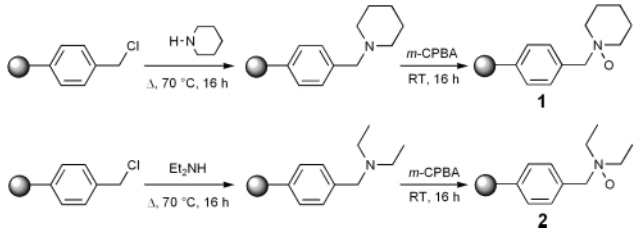

Scheme 1 The synthesis of polymer-supported *N*-oxides **1** and **2**.

The applicability and activity of the resin-bound amine *N*-oxides **1** and **2** were assessed initially by using them in the synthesis of the mono- and bis-acetonitrile-substituted clusters $Ru_3(CO)_{11}(MeCN)$ **3a** and $Ru_3(CO)_{10}(MeCN)_2$ **4a** following the method of Johnson and Lewis (Scheme 2).[10]¶ Product yields are shown in Table 1.

The selectivity for **3a** or **4a** depends primarily upon the acetonitrile : $Ru_3(CO)_{12}$ ratio and upon the amine *N*-oxide : $Ru_3(CO)_{12}$ ratio but it is almost impossible to obtain 100% pure **3a** *via* any amine *N*-oxide route. In polymer-supported reagent chemistry it is often the case that a slight excess of the resin-bound species is required since not all the active sites on the polymer are readily accessible. However, in order to form the monosubstituted complex **3a** we prefer to use exactly one equivalent of **1** or **2**. Although traces of $Ru_3(CO)_{12}$ may then be present in the product, this compound is much less reactive and therefore less likely to perturb subsequent reactions than is **4a**, the impurity found if excess amine *N*-oxide is used.

The bis-substituted cluster is prepared in good yield using 2.5 equivalents of **1** or **2**. Again, the product can be easily separated from the amine *N*-oxide by filtering off the supported reagent.

We studied the effect of temperature on the synthesis of **3a** and **4a** using **1** and **2** and found that it is essential to perform the addition of the amine *N*-oxide at or below 0 °C. This is of interest when compared with other reports of resin-bound reagents which suggest that reactions that need low temperatures when using homogeneous reagents can often be performed at room temperature using heterogeneous analogues because of the rate retarding effects of immobilization.

We find that a small quantity of a ruthenium complex remains attached to the beads, even after thorough washing. One possibility is that a small proportion of the $Ru_3(CO)_{12}$ becomes tethered to the resin through more than one point of attachment. This is certainly possible given the close proximity of the amine *N*-oxide sites on the supported complex and the flexibility of the resin backbone. Once attached in this way, it may be difficult for the ruthenium complex formed to be removed from the support. This impacts on the recylability of the resins but work is currently underway to alleviate this problem by removal of the trace metal before re-loading the resin with *N*-oxide.

As a continuation of our studies, we used the resin-bound *N*-oxides for the synthesis of $Os_3(CO)_{11}(MeCN)$ **3b** and $Os_3(CO)_{10}(MeCN)_2$ **4b** (Scheme 2).[11] The *mono*-substituted complex was prepared by adding one equivalent of **1** or **2** to a dichloromethane–acetonitrile solution of $Os_3(CO)_{12}$. Yields are shown in Table 1. Again, although traces of $Os_3(CO)_{12}$ are

Table 1 Product yields

Product	Yield using **1** (%)	Yield using **2** (%)
$Ru_3(CO)_{11}(MeCN)$ **3a**	83	84
$Ru_3(CO)_{10}(MeCN)_2$ **4a**	85	92
$Os_3(CO)_{11}(MeCN)$ **3b**	80	85
$Os_3(CO)_{10}(MeCN)_2$ **4b**	73	86

† Electronic supplementary information (ESI) available: experimental details. See http://www.rsc.org/suppdata/cc/b1/b100494h/
‡ Study placement student from Hogeschool van Utrecht, The Netherlands.

DOI: 10.1039/b100494h

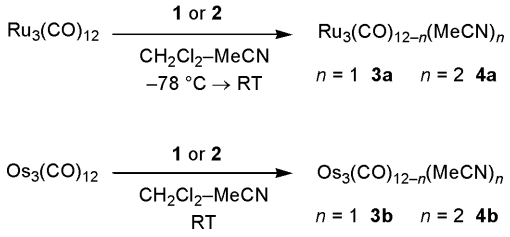

Scheme 2 The use of **1** and **2** in synthetic cluster chemistry.

present in the product, this is less likely to be problematic in subsequent reactions than is **4b**. The bis-substituted cluster is formed in good yield when three equivalents of **1** or **2** are added to a dichloromethane–acetonitrile solution of $Os_3(CO)_{12}$.

With both the ruthenium and osmium clusters we find that **2** is a better reagent than **1**, giving higher yields and a more selective reaction. This could be due to the difference in steric bulk of the two amine oxides, the environment around the active centres in **2** being less crowded as compared with that around **1**. This is of key importance when considering the need for close encounter in the reaction between the clusters and the amine *N*-oxide.

In conclusion, the results presented here illustrate the applicability of **1** and **2** as reagents for the synthesis of substituted carbonyl clusters. They are particularly useful in the case of **3a** and **4a**, both of which are easily decomposed and where removal of the amine *N*-oxide from the reaction mixture is essential before performing further reactions.

We believe that it will be possible to use **1** and **2** as reagents for further chemistry and work is currently under way to confirm this assertion.

Experimental methods and spectroscopic data are presented as ESI.†

The Royal Society is thanked for a University Research Fellowship (N. E. L.). King's College London is thanked for funding.

Notes and references

§ Addition of an excess of amine (piperidine or diethylamine) to Merrifield's solid-phase resin (polystyrene crosslinked with 2% divinylbenzene; *ca.* 4.3 mmol Cl g resin^{-1}) in dioxane followed by heating overnight gives the resin-bound amine equivalent. Treatment of the resin-bound amines in chloroform with *m*-chloroperbenzoic acid at 0–25 °C gave the desired amine *N*-oxide.

¶ A dichloromethane–acetonitrile solution of $Ru_3(CO)_{12}$ was cooled to −78 °C before adding the resin-bound amine *N*-oxide. The reaction mixture was then allowed to warm up to room temperature. Filtration of the solution to remove the resin-bound reagent followed by removal of the solvent leads to isolation of the product. The exploratory reactions were performed using *ca.* 20 mg $M_3(CO)_{12}$ but can easily be scaled up to prepare larger quantities of product.

1 A. Albini, *Synthesis*, 1993, 263.
2 T. Y. Luh, *Coord. Chem. Rev.*, 1984, **60**, 255.
3 L. P. Clarke, P. R. Raithby and G. P. Shields, *Polyhedron*, 1997, **16**, 3775.
4 See, for example: J. H. Clark, A. P. Kybett and D. J. Macquarrie, *Supported reagents: Preparation and Applications*, VCH, New York, 1992.
5 Kerr *et al.* have recently reported the use of supported *N*-oxides in the cobalt mediated Pauson–Khand reaction. See: D. S. Brown, E. Campbell, W. J. Kerr, D. M. Lindsay, A. J. Morrison, K. G. Pike and S. P. Watson, *Synlett*, 2000, 1573.
6 See, for example: *Metal Clusters in Catalysis*, ed. B. C. Gates, L. Guczi and H. Knözinger, Elsevier, New York, 1986; *Metal Clusters in Chemistry*, ed. P. Braunstein, L. A. Oro and P. R. Raithby, Wiley-VCH, Weinheim, 1999.
7 A database search shows more than 300 publications citing these reagents since 1981.
8 N. W. Hird, K. Irie and K. Nagai, *Tetrahedron Lett.*, 1997, **38**, 7111.
9 J. C. Craig and K. K. Purushothaman, *J. Org. Chem.*, 1970, **35**, 1721.
10 G. A. Foulds, B. F. G. Johnson and J. Lewis, *J. Organomet. Chem.*, 1985, **296**, 147.
11 B. F. G. Johnson, J. Lewis and D. A. Pippard, *J. Chem. Soc., Dalton Trans.*, 1981, 407.

Highly selective separation of n-hexane from branched, cyclic and aromatic hydrocarbons using B-ZSM-5 membranes

Sabina K. Gade, Vu A. Tuan, Christopher J. Gump, Richard D. Noble and John L. Falconer*

Department of Chemical Engineering, University of Colorado, Boulder, CO 80309-0424, USA.
E-mail: john.falconer@colorado.edu

Received (in Irvine, CA, USA) 12th January 2001, Accepted 13th February 2001
First published as an Advance Article on the web 13th March 2001

Boron-modified ZSM-5 zeolite membranes were effective for separating n-alkanes from 2,2-dimethylbutane, benzene and cyclohexane in binary mixtures, and enhanced selectivity was seen when both benzene and cyclohexane were mixed with n-hexane.

Zeolite membranes have high potential for separations owing to their unique pore structures and adsorption properties, and their superior thermal, mechanical and chemical properties. Zeolite membranes have been prepared with different zeolite structures, but the MFI structure has been studied most extensively. The MFI structure can be modified by isomorphous substitution of Si by trivalent elements into the zeolite framework. The zeolite surface can change from hydrophobic (silicalite) to hydrophilic (Al-ZSM-5) and from non-acidic (silicalite) to strongly acidic (Al-ZSM-5). Recently, we reported that B-ZSM-5 membranes have superior separation properties over silicalite or ZSM-5 with Al, Ge or Fe substitution.[1,2] For example, a B-ZSM-5 membrane had an n-C_4H_{10}/i-C_4H_{10} separation selectivity of 60 at 473 K. Here we report the separation of binary mixtures of n-hexane with branched, cyclic and aromatic hydrocarbon vapors using B-ZSM-5 membranes. The ternary n-hexane–benzene–cyclohexane mixture was also separated.

The B-ZSM-5 membranes used in this study were prepared by *in situ* crystallization from alkali-free gels onto tubular porous supports (stainless steel: 500 nm diameter pores, Mott Metallurgical; α-alumina: 200 nm diameter pores, US Filter). The molar gel composition was 4.44 TPAOH : 19.46 SiO_2 : 1.55 $B(OH)_3$: 500 H_2O, where TPAOH (tetrapropylammonium hydroxide) was used as the template. This corresponds to a Si : B ratio in the gel of 12.5. A previous study[2] has shown that the Si : B ratio in the zeolite is similar to that in the synthesis gel. Details of membrane preparation were reported elsewhere.[1] Membranes prepared for this study were characterized by single gas permeation and n-butane/i-butane ideal selectivity at 473 K. The results were similar to previous membranes that were characterized by SEM and XRD.[1] The SEM photos showed a continuous, intergrown layer that was 85–100 μm thick and was composed of randomly oriented crystals 5–10 μm in diameter. The XRD pattern of the membrane matched the MFI structure. The peak intensities in the patterns of all membranes were high and the background was low indicating a high degree of crystallinity.

Vapor permeation rates were measured in a continuous flow system that was described in detail elsewhere.[3] The hydrocarbon liquid was evaporated into a helium stream that flowed through the inside of the tubular membrane. The membrane was located in a stainless steel module that was heated by heating tapes. The binary hydrocarbon feeds were approximately 50 : 50, and the feed stream was *ca*. 10% hydrocarbon and 90% helium. Both sides of the membrane were at atmospheric pressure, and the He sweep gas provided a driving force across the membrane by removing the permeating components. The permeate stream was analyzed by a GC equipped with a flame ionization detector. A log-mean pressure driving force was used to calculate permeances, and permselectivity was calculated as the ratio of the permeances.

Fig. 1 shows that n-hexane can be separated from 2,2-dimethylbutane (DMB) using B-ZSM-5 membranes on α-alumina and stainless steel supports. The separation selectivities were highest (> 2000) at 373 K and they decreased with increasing temperature. The selectivity may decrease at high temperature because zeolite and non-zeolite pores expand with temperature. Since DMB (0.62 nm kinetic diameter) is larger than the MFI zeolite pore diameter, as measured by XRD (0.53–0.56 nm), its flux is expected to increase more with a slight increase in pore size. Even at 523 K, the stainless steel-supported membrane separated the n-hexane–DMB mixture with selectivity of 72.

The B-ZSM-5 membranes had much higher separation selectivities than a silicalite-1 membrane prepared by the same procedure (Fig. 2). The DMB permeances were lower and the n-hexane permeances were higher in the B-ZSM-5 membrane. The lower DMB permeances may be due to the narrowing of zeolite pores because either B^{3+} is smaller than Si or extra-framework boron deposited in the pores. According to the Pauling rule, B^{3+} cations are less stable in the framework due to their small size and they are partially removed from the framework during calcination. The gel composition for a B-ZSM-5 membrane is different from that for a silicalite-1 membrane and that could also change the quality of the membrane and reduce the number of non-zeolite pores.

Selectivities for n-hexane–DMB of 600–2000 at 360–373 K were reported by Coronas *et al.*[4] and Gump *et al.*,[5] but preferential adsorption of n-hexane rather than molecular sieving was responsible. In contrast, Ginoir-Fendler *et al.*[6] and Flanders *et al.*[3] observed selectivities of 1000 at 363 K and 70–250 at 473 K and separation was not due to preferential adsorption. Vroon *et al.*[7] obtained a selectivity of 600 at 300 K and of 2000 at 473 K. The separation selectivities were only 25–120 at 300 K for other ZSM-5 membranes.[8,9]

Separation of n-alkanes from cyclic and aromatic compounds has been studied less. Funke *et al.*[10] obtained a separation

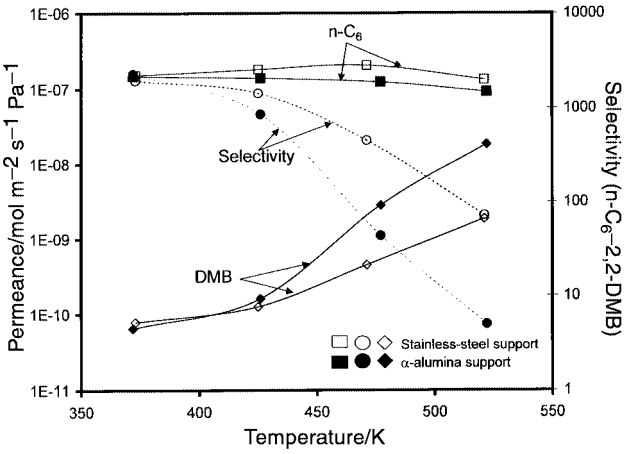

Fig. 1 n-Hexane–2,2-DMB permeances and separation selectivities as a function of temperature for B-ZSM-5 membranes on alumina and stainless steel.

Table 1 Permeances and separation selectivities for 50:50 n-hexane–organic mixtures through supported B-ZSM-5 membranes

	α-Alumina support			Stainless steel support		
	Permeance/mol m^{-2} s^{-1} Pa^{-1} (±15%)		Selectivity (±20%) n-Hexane–organic	Permeance/mol m^{-2} s^{-1} Pa^{-1} (±10%)		Selectivity (±14%) n–Hexane–organic
Organic	n-Hexane × 10^7	Organic × 10^{10}		n-Hexane × 10^7	Organic × 10^{10}	
DMB	1.5	0.65	2280	1.5	0.78	1950
Cyclohexane	2.4	3.3	720	1.3	2.2	570
Benzene	2.4	5.5	440	1.0	2.6	370
Benzene + cyclohexane (50:50)	2.2	2.8	790	1.5	1.8	800

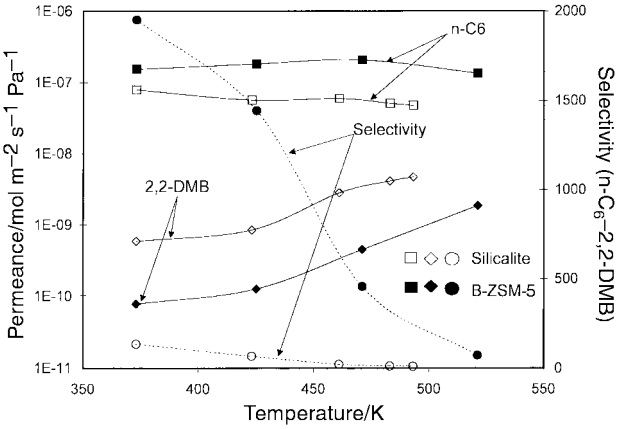

Fig. 2 n-Hexane–2,2-DMB permeances and separation selectivities as a function of temperature for silicalite-1 and B-ZSM-5 membranes on stainless steel.

selectivity of 25 at 373 K for a n-hexane–cyclohexane (50:50) mixture. Our B-ZSM-5 membranes had n-hexane–cyclohexane separation selectivities of 570 and 720 at 373 K (Table 1). Kita *et al.*[11] reported that a Y-type membrane separated n-hexane from benzene with a selectivity of 260 at 373 K. The n-hexane–benzene separation selectivities for B-ZSM-5 at 373 K were 370 on stainless steel and 440 on α-alumina supports. The B-ZSM-5 membrane also separated n-C_5 to n-C_8 alkanes from benzene, and the selectivities changed significantly with carbon number and temperature. At 373 K, the selectivities decreased from 660 to 16 as the carbon number of the alkane increased. In contrast, at 473 K, selectivities increased from 11 to 524 as the carbon number increased. For separations at 373 K, benzene permeances were almost constant but n-alkane permeances decreased as their carbon number increased. Apparently the coverages for all the alkanes were close to saturation at 373 K, so they all effectively inhibited benzene permeances. The benzene permeances in the mixtures were lower than the permeance of pure benzene. The diffusion rate of the alkane decreased with increasing carbon number, probably due to an increase in adsorption strength, and thus the selectivity decreased with carbon number. In contrast, at 473 K, the alkane permeances were almost constant because the permeances of the longer alkanes increased more with temperature. The benzene permeances at 473 K *decreased* as the alkane carbon number increased because the longer alkanes adsorbed more strongly and thus had higher coverages than the shorter alkanes. Thus, the longer alkanes more effectively blocked benzene and therefore the alkane–benzene selectivity was higher for the longer alkanes.

The separation selectivities of the ternary n-hexane–cyclohexane–benzene mixture (50:25:25) were 790–800 at 373 K, which are *significantly higher than those observed for the binary mixtures* (Table 1). The cyclohexane plus benzene permeances were lower than in the binary mixture, whereas the n-hexane permeances were similar. This increase in selectivity in the ternary mixture may be the result of competition for adsorption sites in the zeolite.

In summary, B-ZSM-5 zeolite membranes separated n-alkanes from branched, cyclic and aromatic hydrocarbons with high selectivities at elevated temperatures.

We gratefully acknowledge support by the NSF/IUCRC for Membrane Applied Science and Technology (MAST).

Notes and references

1 V. A. Tuan, J. L. Falconer and R. D. Noble, *AIChE J.*, 2000, **46**, 1201.
2 V. A. Tuan, R. D. Noble and J. L. Falconer, *Micropor. Mesopor. Mater.*, 2000, **41**, 269.
3 C. L. Flanders, V. A. Tuan, R. D. Noble and J. L. Falconer, *J. Membr. Sci.*, 2000, **176**, 43.
4 J. Coronas, R. D. Noble and J. L. Falconer, *Ind. Eng. Chem. Res.*, 1998, **37**, 166.
5 C. J. Gump, R. D. Noble and J. L. Falconer, *Ind. Eng. Chem. Res.*, 1999, **38**, 2775.
6 A. Ginoir-Fendler, J. Peureux, H. Mozzanega and J. A. Dalmon, *Stud. Surf. Sci. Catal.*, 1996, **101**, 127.
7 Z. A. E. P. Vroon, K. Keizer, M. J. Gilde, J. Verweij and A. J. Burgraaf, *J. Membr. Sci.*, 1996, **113**, 293.
8 T. Matsufuji, K. Watanabe, N. Nishiyama, Y. Egashira, M. Matsukata and K. Ueyama, *Ind. Eng. Chem. Res.*, 2000, **39**, 2434.
9 S. Kallus, P. Langlois, G. E. Romanos, T. Sterioti, E. S. Kikkinides and N. K. Kanellopoulos, *Stud. Surf. Sci. Catal.*, 2000, **128**, 467.
10 H. H. Funke, A. M. Argo, J. L. Falconer and R. D. Noble, *Ind. Eng. Chem. Res.*, 1997, **36**, 137.
11 H. Kita, K. Fuchida, T. Horita, H. Asamura and K. Akamoto, *Proc. 6th International Conference on Inorganic Membranes*, Montpellier, France, 2000, p. 58.

ChemComm

Over one hundred solvates of sulfathiazole†

Ann L. Bingham,[a] David S. Hughes,[a] Michael B. Hursthouse,*[a] Robert W. Lancaster,[b] Stewart Tavener[c] and Terence L. Threlfall*[c]

[a] *Chemistry Dept., University of Southampton, Southampton, UK SO17 1BJ. E-mail: mbh@soton.ac.uk*
[b] *Glaxo Wellcome R&D, Stevenage, Herts, UK SG2 9NY*
[c] *Chemistry Dept., University of York, York, UK YO10 5DD*

Received (in Cambridge, UK) 28th November 2000, Accepted 22nd February 2001
First published as an Advance Article on the web 13th March 2001

The sulfadrug sulfathiazole forms an extensive family of solvates and adducts, the crystal structures of which show a large variety of hydrogen-bonded frameworks.

In a recent communication, Nangia and Desiraju[1] analysed the relative solvate-forming propensities of fifty common solvates, and highlighted the need for systematic studies of the formation and structure of solvates. We have been engaged in such a study, largely based on one compound, the sulfadrug sulfathiazole, I,

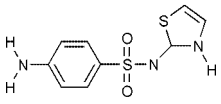

I

with remarkable solvate forming abilities, which developed out of a detailed reinvestigation of the polymorphism of this compound[2]. We present here a preliminary report of our findings.

The sulfadrugs show extensive polymorphism.[2,3] They also crystallise erratically from solution, despite the contrary impression that might be gained from the literature. In the search for reliable crystallisation procedures for sulfathiazole polymorphs, several less common solvents were tried and in quite a number of cases solvates were obtained. This was surprising, since the only well-defined solvate encountered in over 40 papers[4] during 60 years of investigation was that from dioxane.[5] Shirotani *et al.*[6] have described 3 further solvates of sulfathiazole, but their work seems to have been subsequently overlooked. In the belief that a detailed preparative and structural study of solvate formation may give an insight into the crystallisation behaviour of the parent materials, we have explored this topic further. The first solvate we produced was that from cyclohexanone. Reasoning from the analogy between the structures of dioxane and cyclohexanone, we tried numerous other 6- and 5-membered saturated heterocyclic and carbocyclic rings possessing at least one polar group, the function of the latter being presumed to involve hydrogen bonding with one of the 5 acceptors and 3 donors in the sulfathiazole molecule. Single crystal X-ray determinations however showed a remarkable variety of structures with varying propensity for hydrogen bonding between the sulfathiazole and the solvent guest. The study was extended to a wider range of solvents with different molecular shapes and sizes, different polarities and different functional groups, and also to the preparation of mixed crystals with partners that are solids at ambient temperature. The solvates are easily made by crystallisation from the appropriate solvent, sometimes with the help of chloroform as a crystallisation aid. Sulfathiazole has a solubility at elevated temperatures of around 10% in typical solvate-forming solvents. It is very soluble (30–60%) in more polar solvents such as dimethylformamide or tetramethylurea but generally fails to form solvents from such solutions. It has a limited solubility in solvents of low polarity and usually only sulfathiazole polymorphs crystallise from these solutions. Surprisingly, we found that molecules with long aliphatic hydrocarbon chains can form solvates provided a solvatophilic group such as lactone or lactam is present. The two-component solid–solid adduct crystals can be made by fusion or sometimes by crystallisation of the components using an inert solvent. The presence of a third component is detrimental on thermodynamic grounds,[7] but in practice, as noted above for chloroform, may be favourable for kinetic reasons.

More than 100 solvates plus many related 2-component systems containing sulfathiazole have now been made, including inter-sulfa-drug combinations such as sulfapyridine with sulfathiazole.‡ All have been characterised by near- and mid-infrared spectroscopy, powder XRD and hot-stage microscopy, and studied, in some cases also by DSC/TGA, solid state NMR, Raman spectroscopy and microscopy. The crystal structures of more than 60 solvates and adducts have so far been determined; others are in progress. The existence of such a large collection of data allows a unique opportunity for the comparative investigation of the structural and spectral characteristics and of the factors determining solvate formation. Detailed consideration of this is beyond the scope of a Communication, and is the central theme of a series of full papers, now in preparation. However, the results obtained can be usefully summarised as follows.

No solvent containing an aromatic carbocyclic group has given a solvate. Virtually every saturated carbocycle or heterocycle of appropriate polarity, and of ring size 3 to 8 produces a solvate. Only the behaviour of aliphatic solvates is difficult to predict, although polarity can be distinguished as a key factor. A wide range of groups including cyano, ester, ether. keto, sulfonyl, and amido groups are capable of providing the necessary polar characteristics. A hydroxy group generally seems to be detrimental to solvate formation, although a very unstable solvate has been made from *n*-propanol. The identification of the latter solvate together with that of acetonitrile raises the question as to whether many of the outcomes of sulfathiazole polymorph preparation procedures are mediated by the intervention of unstable solvates. Competitive experiments, in which sulfathiazole is crystallised from mixed solvates, have shown a stability sequence of lactams > lactones > cyclic carbonates > cyclic ketones, which parallels the order of solvent polarity. The relative stabilities of adducts with different sized rings have not been determinable so far because the crystalline product from these competition reactions has often not been one of the expected products. Some of these may be polymorphs of solvates, since DSC shows that some of the solvates are di- or tri-morphic. (Fig. 1.) The infrared spectra of the solvates are almost always close to that of the highest melting polymorph I (mp 203 °C), (the structure of which contains two crystallographically independent molecules, and which we regard as a sulfathiazole solvate of sulfathiazole), and unlike those of the three mutually similar low-melting polymorphs, even though the solvates always desolvate to the lower melting polymorphs, especially polymorph IV.§ This may be explained by the fact that in the structures so far determined the

† Electronic supplementary information (ESI) available: solvates and adducts of sulfathiazole. See http://www.rsc.org/suppdata/cc/b0/b009540k/

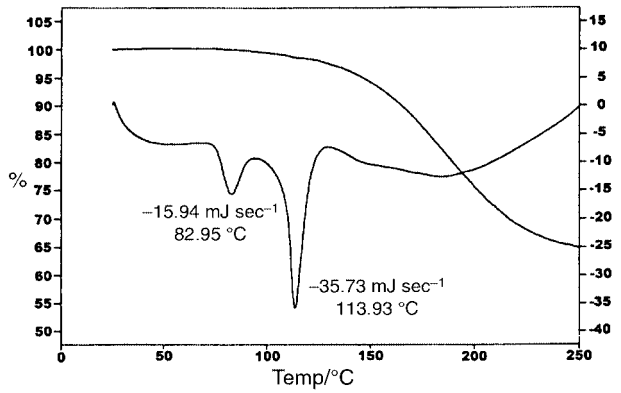

Fig. 1 DSC and TGA traces of the sulfathiazole-ε-caprolactone adduct. The endotherms without mass loss indicate phase transitions to new polymorphs, confirmed by hot-stage microscopy.

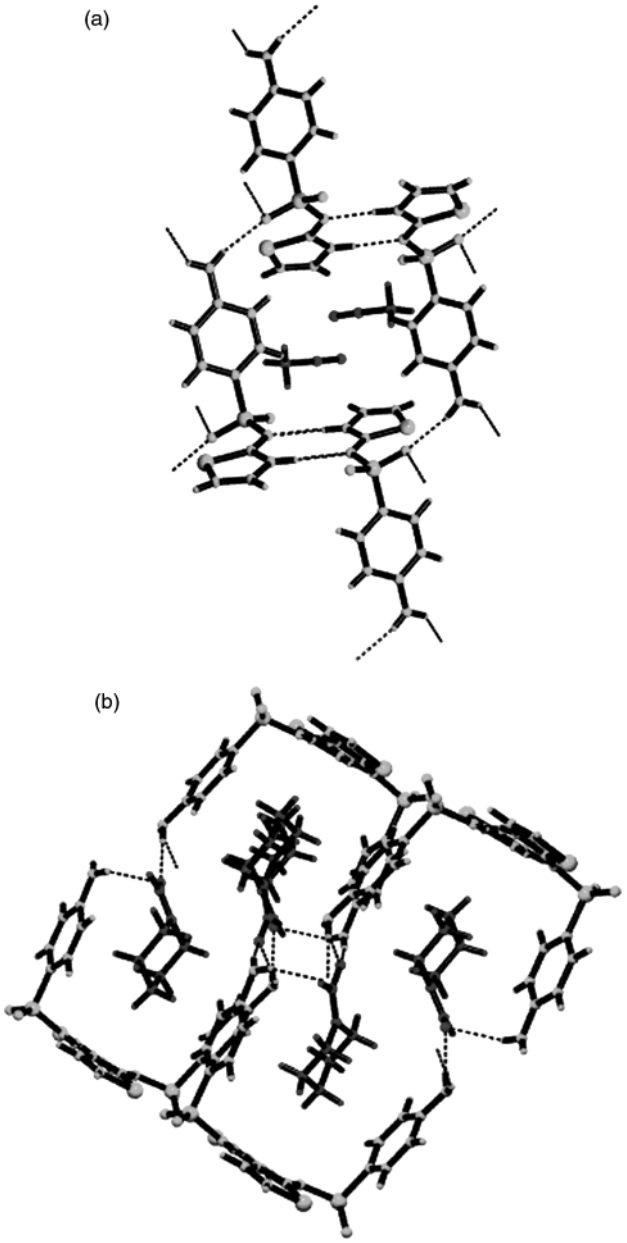

Fig. 2 (a) Detail from the crystal structure of the 1:1 adduct sulfathiazole–acetonitrile—a clathrate. (b) Detail from the crystal structure of the 1:1 adduct sulfathiazole–*N*-formylpiperidine—a co-crystal.

close amido–imido dimer present in sulfathiazole polymorph I but not in any of the others, features extensively in the solvate structures. The similarity of IR spectra for systems that are found to have quite different crystal structures is explained in terms of the presence of similar H-bonding associations but different supramolecular assemblies.

Terminology for the description of solid state molecular structures is unsatisfactory, even for single component systems.[8,9] Consideration of the multitude of structures displayed by the solvates listed in Nangia and Desiraju's paper raises the question as to whether nomenclature is even less adequate for the greater complexity resulting from two-component systems.

On the basis of the structure determinations so far completed in our study, we identify two types of structure which might provide a more generally useful classification—a) *clathrates*, or, more generally *inclusion phases*, in which the main function of the guest molecule is cavity filling, with or without additional weak H-bonding, in a host molecule assembly having a channel, layer or 3D framework structure, and b) *co-crystals* in which the partner molecule forms an essential part of the hydrogen bonded framework. In each class we have also found salts where proton transfer has occurred from the sulfathiazole molecule to a basic function on the guest. An example of each of the two main structure types is shown in Figs. 2a and 2b.¶

Multiple solvates have been reported for a variety of compounds, but these invariably show a large degree of isostructurality.[10] By contrast, our study has shown that sulfathiazole would appear to show more solid state structural versatility than any other organic molecule. We are investigating why this might be the case and whether other compounds form huge numbers of overlooked solvates or whether sulfathiazole is unique. To this end, the solvate forming propensities of other sulfadrugs are being examined. Preliminary experiments indicate that sulfapyridine forms many solvates, but not so extensively as sulfathiazole, and often with different solvates. The host–solvent relationship appears to be a very specific one even for such closely related hosts as the sulfadrugs, as might be expected from the huge variety of structures displayed by the sulfadrug polymorphs.

Notes and references

‡ A list of the solvates and adducts prepared so far, is given in the Supplementary Material.

§ The numbering scheme used here for the five fully characterised polymorphs is that described in D. C. Apperley, R. A. Fletton, R. K. Harris, R. W. Lancaster, S. Tavener and T. L. Threlfall, *J. Pharm. Sci.*, 1999, **88**, 1275.

¶ *Crystal data:* compound **1**, sulfathiazole–acetonitrile, $[C_9H_9N_3O_2S_2][C_2H_3N]$ M_r = 296.37, monoclinic, a = 10.741(2), b = 7.592(2), c = 16.748(3) Å, β = 103.99(3)°, U = 1325.2(5) Å^3, space group $P2_1/c$, Z = 4, T = 150 K. Reflections measured 5364 (θ_{max} = 25.35°, 82.6% complete), observed [$I > 2\sigma(I)$] 1997, R_{int} = 0.15. R = 0.059, ωR_2 = 0.111, 211 parameters. Compound **2**, sulfathiazole–*N*-formylpiperidine, $[C_9H_9N_3O_2S_2][C_6H_{11}NO]$ M_r = 368.47, triclinic, a = 10.539(2), b = 12.189(2), c = 13.981(3), α = 95.29(30), β = 107.38(3), γ = 90.63(3)°, U = 1705.3(6) Å^3, space group $P\bar{1}$, Z = 2, T = 150 K. Reflections measured 10626, θ_{max} 24.97°, 91.7% complete), observed 2877, Rint = 0.044. R = 0.0450, ωR_2 = 0.0955, 557 parameters. CCDC 154065 and 154066. See http://www.rsc.org/suppdata/cc/b0/b009540k/ for crystallographic data in .cif or other electronic format.

1 T. Nangia and G. R. Desiraju, *Chem Commun.*, 1995, 605
2 M. Kuhnert-Brandstaetter, *Thermomicroscopy in the Analysis of Pharmaceuticals*, Pegamon Press, Oxford, 1974.
3 S. Yang and J. K. Guillory, *J. Pharm. Sci.*, 1972, **61**, 26.
4 A. Burger and R. D. Dialer, *Pharm. Acta Helv.*, 1983, **58**, 72.
5 F. V. Babilev, V. K. Bel'skii, Y. A. Simonov and A. P. Arzamastev, *Khim-Pharm. Zh.*, 1987, **21**, 1275.
6 K.-I. Shirotani, E. Suzuki and K. Sekiguchi, *Chem. Pharm. Bull.*, 1983, **31**, 2085.
7 D. J. W. Grant and T. Higuchi, *Solubility Behaviour of Organic Compounds, Techniques in Chemistry*, Vol. XXI. ed. Weissberger, Wiley, New York, 1990.
8 T. L. Threlfall, *Analyst*, 1995, **120**, 2435.
9 W. B. Jensen, *J. Chem. Ed.*, 1998, **75**, 817.
10 K. Nakano, K. Sada and M. Miyata, *Chem. Commun.*, 1996, 989.

ChemComm

Tandem ring-closing metathesis–radical cyclization based on 4-(phenylseleno)butanal and methyl 3-(phenylseleno)propanoate — a route to bicyclic compounds

Derrick L. J. Clive* and Hua Cheng

Chemistry Department, University of Alberta, Edmonton, Alberta, Canada T6G 2G2

Received (in Corvallis, OR, USA) 4th January 2001, Accepted 7th February 2001
First published as an Advance Article on the web 13th March 2001

α,ω-(Phenylseleno) carbonyl compounds, such as 4-(phenylseleno)butanal (1) and methyl 3-(phenylseleno)propanoate (2), are easily converted by anionic reactions into substances that undergo sequential ring-closing metathesis and radical cyclization, affording bicyclic products.

The usefulness of radical cyclization is often determined by the ease with which the cyclization substrates can be made. In this regard, the nature of the homolyzable group is, of course, important, because this determines the stages at which it may be introduced. In particular, early introduction can avoid the extra steps involved in replacing a non-homolyzable group by one that is homolyzable. For radical generation, phenyl selenides have the distinct advantage that the PhSe group is usually inert to basic or nucleophilic reagents[1] and, among the common transformations, care need be exercised only in the choice of oxidizing agent[2,3] when selenium is present. We have found that the PhSe group is compatible with the Grubbs catalyst $(Cy_3P)_2Cl_2Ru{=}CHPh$,[4–8] and we report that α,ω-(phenylseleno) carbonyl compounds, such as 4-(phenylseleno)butanal (**1**[9]) and methyl 3-(phenylseleno)propanoate (**2**[10]) are useful for the

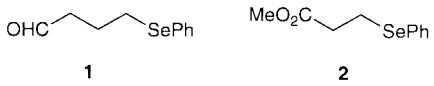

construction of substances that undergo sequential ring-closing metathesis[11] and radical cyclization. The PhSe group allows the use of anionic chemistry that would not be suitable in the

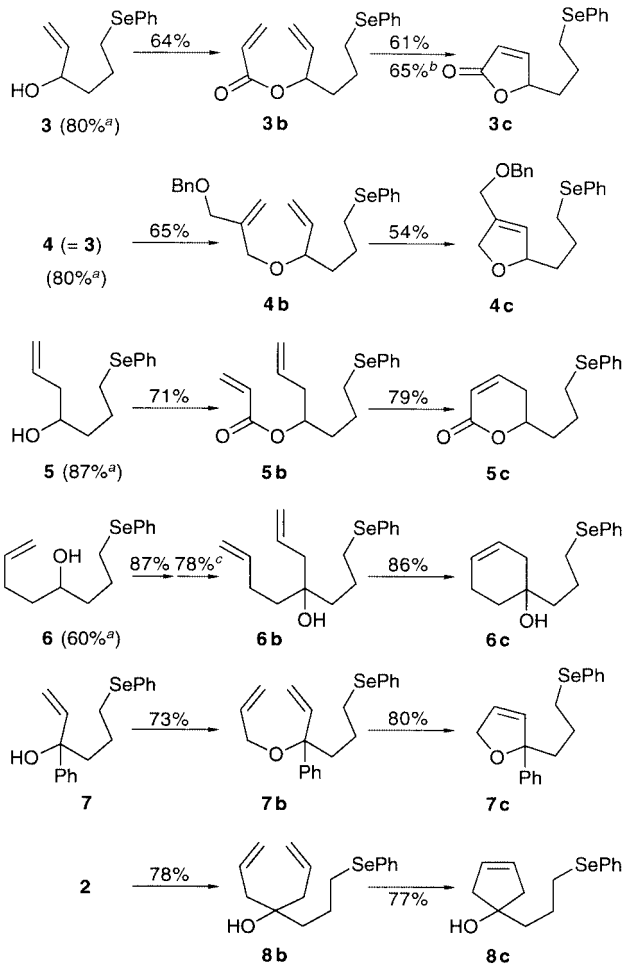

Scheme 1 (*a*) Yield from **1**. (*b*) Corrected for recovered **3b**. (*c*) First yield is for the oxidation of **6** to the corresponding ketone; second yield for reaction of the ketone with allylmagnesium bromide.

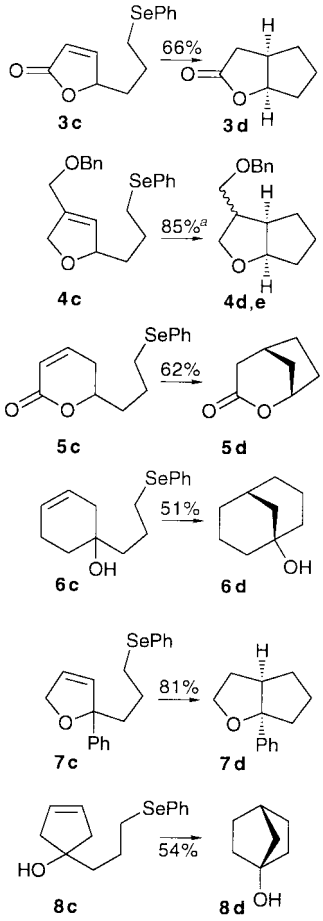

Scheme 2 (*a*) Yield of more polar isomer [(3α,3aβ,6aβ)-stereochemistry] 60%; yield of less polar isomer [(3α,3aα,6aα)-stereochemistry] 25%.

DOI: 10.1039/b100336b

presence of halogen or carboxy groups as the eventual source of radicals.[12] Several publications have reported that the catalyst is usually not compatible with sulfide substrates.[4,5]

The starting materials **3b**–**8b** (Scheme 1) for the metathesis–radical closure sequence were made as follows. Aldehyde **1** was converted into alcohols **3** (80%), **5** (87%), and **6** (60%) (Scheme 1) by reaction with vinyllithium, allylmagnesium bromide, and but-3-enylmagnesium bromide, respectively. Reaction of **1** with phenyllithium (50%), oxidation, using pyridine·SO_3 in DMSO[2] (87%), and treatment of the resulting ketone with vinyllithium afforded alcohol **7** (85%).

The alcohols **3**, **5**, **6** and **7** were easily converted into substrates for ring-closing metathesis by simple ionic reactions. Acylation of **3** and **5** with acryloyl chloride (Et_3N, DMAP, CH_2Cl_2) gave **3b** (64%) and **5b** (71%), respectively (Scheme 1), and the ethers **4b** (65%) and **7b** (73%) were made by alkylation (NaH, THF) of **3** with 2-chloromethyl-3-[(phenylmethyl)-oxy]prop-1-ene[13,14] and of **7** with allyl bromide, respectively.

The metathesis substrate **6b** was prepared by oxidation of **6** (87%), again using the pyridine·SO_3–DMSO system—which is an excellent reagent for selective oxidation of phenylseleno alcohols—and treatment with allylmagnesium bromide (78%).

The bis-allyl selenide **8b** was obtained directly from ester **2** by the action of allylmagnesium bromide (78%).

Each of the bis-olefins shown in Scheme 1 underwent ring-closing metathesis in the presence of $(Cy_3P)_2Cl_2Ru$=CHPh (8–12 mol%; 22% for **3b**), and the products were isolated by flash chromatography. The reactions were usually run in PhH at 50 °C for 12 h [**4b**, **6b** (65 °C), **7b**, **8b** (refluxing PhH,[15] 8 h)], or in refluxing CH_2Cl_2 in the presence of Ti(OPr-*i*)$_4$,[16] (42 h,[17] **3b**, 8 h, **5b**). In the case of the acrylates (**3b**, **5b**), Ti(OPr-*i*)$_4$ must be added to complex the ester carbonyl and prevent unproductive complexation of carbenoid intermediates.[18]

The radical cyclization step (see Scheme 2), leading to **3d**, **4d**,**e**, **5d**–**8d**, was carried out under standard conditions by syringe pump addition (over *ca*. 10 h) of a PhH solution of Bu_3SnH (1.4–2.2 equiv., 0.01–0.08 M) and AIBN (0.2–0.4 equiv., 0.006–0.03 M) to a refluxing solution (0.01–0.02 M) of the substrate (1 equiv.) in the same solvent. In the case of **6c** we isolated only the product of 6-*exo* cyclization, and not the isomeric alcohol resulting from 7-*exo* closure.[19]

The above experiments establish that the PhSe group, which serves as a very convenient radical source, can be introduced at an early stage in synthetic routes that involve ionic reactions and that end with sequential application of two powerful bond-forming processes, ring-closing metathesis and radical cyclization.

All new compounds were characterized spectroscopically, including high resolution mass measurements.

Acknowledgment is made to the Natural Sciences and Engineering Research Council of Canada and to Merck Frosst for financial support.

Notes and references

1 A. Y. Mohammed and D. L. J. Clive, *J. Chem. Soc., Chem. Commun.*, 1986, 588.

2 *Cf.* J. R. Parikh and W. von E. Doering, *J. Am. Chem. Soc.*, 1967, **89**, 5505.

3 Other oxidation methods: (*a*) R. Baudat and M. Petrzilka, *Helv. Chim. Acta*, 1979, **62**, 1406; (*b*) D. H. R. Barton, D. J. Lester, W. B. Motherwell and M. T. B. Papoula, *J. Chem. Soc., Chem. Commun.*, 1980, 246; (*c*) G. H. Posner and M. J. Chapdelaine, *Tetrahedron Lett.*, 1977, 3227; (*d*) M. Shimizu, H. Urabe and I. Kuwajima, *Tetrahedron Lett.*, 1981, **22**, 2183; (*e*) J. Lucchetti and A. Krief, *C. R. Acad. Sci., Ser. C*, 1979, **288**, 537.

4 Sulfides and disulfides have been subjected to ring-closing metathesis, using a *molybdenum* catalyst; in some experiments a ruthenium catalyst [$(Cy_3P)_2Cl_2Ru$=CHCH=CPh_2] was unsatisfactory (Ref. 5), as was $(Cy_3P)_2Cl_2Ru$=CHPh (Ref. 6).

5 *E.g.* (*a*) S.-Y. Shon and T. R. Lee, *Tetrahedron Lett.*, 1997, **38**, 1283; (*b*) S. K. Armstrong and B. A. Christie, *Tetrahedron Lett.*, 1996, **37**, 9373.

6 A. G. M. Barrett, M. Ahmed, S. P. Baker, S. P. D. Baugh, D. C. Braddock, P. A. Procopiou, A. J. P. White and D. J. Williams, *J. Org. Chem.*, 2000, **65**, 3716.

7 For a rare example of ring-closing metathesis of a sulfide, using $(Cy_3P)_2Cl_2Ru$=CHPh, see: A. G. M. Barrett, S. P. D. Baugh, D. C. Braddock, K. Flack, V. C. Gibson, M. R. Giles, E. L. Marshall, P. A. Procopiou, A. J. P. White and D. J. Williams, *J. Org. Chem.*, 2000, **63**, 7893.

8 For an extensive table of functional group-catalyst compatibility, see: S. K. Armstrong, *J. Chem. Soc., Perkin Trans. 1*, 1998, 371.

9 (*a*) D. L. J. Clive and R. J. Bergstra, *J. Org. Chem.*, 1990, **55**, 1786; (*b*) C. Bigogno, B. Danieli, G. Lesma and D. Passarella, *Heterocycles*, 1995, **41**, 973.

10 K. Hiroi, J. Abe, K. Suya, S. Sato and T. Koyama, *J. Org. Chem.*, 1994, **59**, 203.

11 For one of several recent reviews, see: R. H. Grubbs and S. Chang, *Tetrahedron*, 1998, **54**, 4413.

12 For synthesis of bridgehead bicyclic sultams by tandem ring-closing metathesis–radical cyclization (in which the radical is derived from a halomethylsulfonyl group), see: L. A. Paquette and S. M. Leit, *J. Am. Chem. Soc.*, 1999, **121**, 8126.

13 T. Konosu, Y. Furukawa, T. Hata and S. Oida, *Chem. Pharm. Bull.*, 1991, **39**, 2813.

14 In the alkylation with this reagent, NaI was added to generate the iodide *in situ*.

15 Reaction was very slow in refluxing CH_2Cl_2. *Cf.* A. Fürstner, O. R. Thiel, L. Ackermann, H.-J. Schanz and S. P. Nolan, *J. Org. Chem.*, 2000, **65**, 2204.

16 A solution of the substrate was refluxed in the presence of Ti(OPr-*i*)$_4$ before adding the Grubbs catalyst.

17 A fresh portion of catalyst was added after 30 h.

18 (*a*) A. Fürstner and K. Langemann, *J. Am. Chem. Soc.*, 1997, **119**, 9130; (*b*) A. K. Gosh, J. Cappiello and D. Shin, *Tetrahedron Lett.*, 1998, **39**, 4651.

19 *Cf.* A. L. J. Beckwith, *Tetrahedron*, 1981, **37**, 3073.

Intermolecular hydrogen binding of a chiral host and a prochiral imidazolidinone: enantioselective Norrish–Yang cyclisation in solution

Thorsten Bach,*[a] Tobias Aechtner[a] and Bernhard Neumüller†[b]

[a] *Lehrstuhl für Organische Chemie I, Technische Universität München, D-85747 Garching, Germany. E-mail: thorsten.bach@ch.tum.de*

[b] *Fachbereich Chemie, Philipps-Universität, D-35032 Marburg, Germany*

Received (in Cambridge, UK) 19th December 2000, Accepted 21st February 2001
First published as an Advance Article on the web 13th March 2001

The Norrish–Yang cyclisation of a prochiral imidazolidinone which was conducted in the presence of a chiral host afforded enantiomerically enriched (up to 26% *ee*) 1,3-diazabicyclo[3.3.0]octanones in good yields (73–86%) with a distinct preference for the *exo*-diastereoisomer (dr = 77/23–90/10).

The photochemical cyclisation of ketones *via* intramolecular hydrogen abstraction and subsequent ring closure is termed Norrish–Yang cyclisation.[1] It is a valuable C–C-bond forming reaction in the course of which two new stereogenic centres are formed. The facial diastereoselectivity of the reaction has been extensively studied[2,3] and applications of the Norrish–Yang cyclisation to natural product synthesis have been reported.[4] For the photocyclisation of amino acid derivatives a remarkable chirality transfer has been observed.[5] Enantioselective variants of the Norrish–Yang cyclisation have been investigated in the solid phase employing either precursors that crystallize in chiral space groups[6] or inclusion compounds of a prochiral substrate and a chiral host.[7] We have now attempted to achieve an enantioselective Norrish–Yang cyclisation in the liquid phase mediated by a chiral complexing agent[8] and report on the preliminary results of this work. The chiral host compounds **1** and **2** can be readily prepared from trimesic acid (1,3,5-

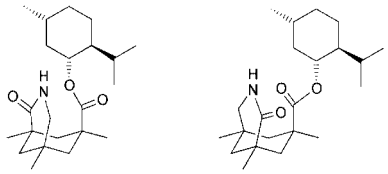

1 **2**

benzenetricarboxylic acid) *via* the well-known all-*cis*-1,3,5-trimethylcyclohexane-1,3,5-tricarboxylic acid (Kemp's triacid).[9,10] They are diastereomeric due to the chiral menthyl residue and can be separated by flash chromatography.

Lactams are attached to the host **1** or its diastereoisomer **2** *via* the carbonyl group and *via* the NH-group by two hydrogen bonds.[11] The lactam is fixed by the two-point binding in a chiral environment with the result that formerly enantiotopic faces become diastereotopic. As the menthyl residue acts simply as a sterically bulky substituent hosts **1** and **2** are expected to behave as if they were enantiomers. The prochiral imidazolidin-2-one **3** was selected as Norrish–Yang cyclisation substrate. It exhibits a lactam binding site which should allow for an association with the host compounds. The compound was readily prepared from the parent imidazolidin-2-one by monoacetylation,[12] 1,4-addition to phenyl vinyl ketone and deprotection. Upon irradiation (Rayonet RPR 3000 Å or Original Hanau TQ 150/duran filter) the ketone yielded four products which are depicted in Scheme 1.

The results of the preliminary study conducted with the easily accessible hosts **1** and **2** are summarized in Table 1. In general,

† To whom inquiries about the X-ray analysis should be addressed at the Philipps-Universität Marburg.

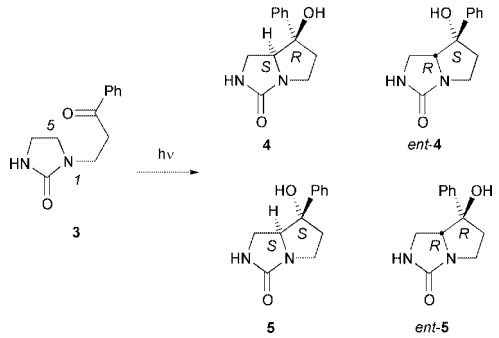

3 **4** ***ent*-4** **5** ***ent*-5**

Scheme 1 Possible stereoisomers obtained from the Norrish–Yang cyclisation of imidazolidin-2-one **3**.

the conversion is complete and the yield of photocyclisation products are high (73–86%). The *exo*-isomers **4** and *ent*-**4** are the preferred diastereoisomers formed in toluene solution (entries 2–14)[13] whereas the *endo*-isomers **5** and *ent*-**5** are favored in the polar protic solvent *tert*-BuOH. It is reasonable to assume that *tert*-BuOH increases the size of the substituent OH by coordination[1,2] and leads to a reversal of the steric demand from Ph > OH to OH > Ph. The *exo*/*endo*-selectivity did not change (entries 3/7/11, 4/8/12, *etc*.) upon variation of the temperature. Contrary to that, the enantioselectivity was significantly influenced by this variation. The increase from 5% *ee* at 30 °C (entry 4) to 26% *ee* at −45 °C (entry 12) observed with 2.5 equiv. of host **1** exemplifies the typical temperature dependence which is partially due to an increased association. The increase in enantioselectivity upon increasing the host concentration (entries 3/4, 5/6, 7/8, *etc*.) undermines the crucial

Table 1 Norrish–Yang cyclisation of imidazolidinone **3** in the presence of hosts **1** and **2**

Entry	Host	Equiv.	Temp./°C	Yield (%)[a]	*exo*/*endo*[b]	Ee (%)[c]
1	—[d]	—	30	75	38/62	—
2	—	—	30	73	88/12	—
3	**1**	1	30	82	90/10	3
4	**1**	2.5	30	86	88/12	5
5	**2**	1	30	73	88/12	−4
6	**2**	2.5	30	82	89/11	−7
7	**1**	1	−10	86	78/22	7
8	**1**	2.5	−10	77	77/23	16
9	**2**	1	−10	73	85/15	−6
10	**2**	2.5	−10	73	80/20	−15
11	**1**	1	−45	77	81/19	11
12	**1**	2.5	−45	77	79/21	26
13	**2**	1	−45	82	79/21	−14
14	**2**	2.5	−45	77	84/16	−25

[a] Yield of isolated product after chromatographic purification. [b] The ratio of the two diastereoisomers (**4** + *ent*-**4**)/(**5** + *ent*-**5**) was determined by ^{1}H-NMR spectroscopy of the crude product mixture. [c] The ee of the major *exo*-diastereoisomer was determined as (**4** − *ent*-**4**):(**4** + *ent*-**4**) by chiral HPLC (eluent: H_2O–MeCN = 95:5 → 90:10; column: Macherey-Nagel EC 200/4 nucleodex beta-OH). [d] *tert*-BuOH was used as the solvent.

DOI: 10.1039/b100300n

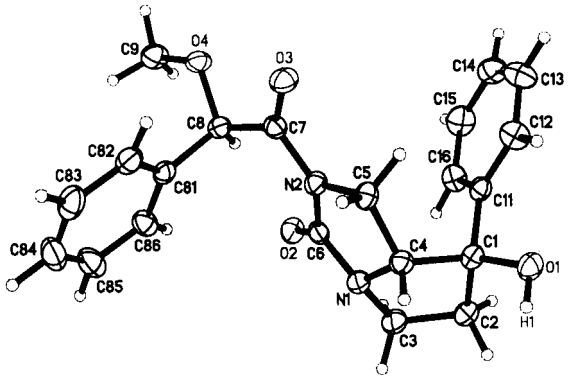

Fig. 1 A molecule of compound **6** in the crystal.

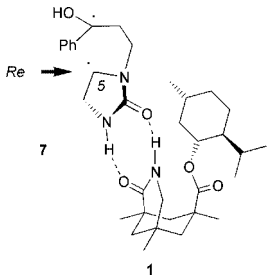

Fig. 2 The differentiation of enantiotopic sites at the C-5 radical center in the 1,4-biradical intermediate **7** associated to host **1**.

role the association plays in the enantioselective photocyclisation under scrutiny. The earlier assumption that the hosts **1** and **2** should behave as if they were enantiomers was proven experimentally. The opposite enantiomer was formed upon replacement of **1** with **2** (entries 3/5, 4/6, 5/7, etc.) resulting in a negative ee value. The minor diastereoisomers **5** and *ent*-**5** behaved similar to the major diastereoisomers with regard to the ee.

The absolute configuration of the major enantiomer *ent*-**5** obtained from the irradiation of compound **3** in the presence of host **2** was elucidated by single crystal X-ray crystallography. To this end, it was converted into its *N*-acyl derivative **6** by a sequence of *O*-silylation, *N*-acylation with (*R*)-(−)-*O*-methylmandelic acid chloride and desilylation.[14]

If host **2** delivers *ent*-**5** as major enantiomer host **1** delivers **5** with opposite optical rotation as was experimentally confirmed. The C–C-bond formation step which is decisive for the absolute configuration of products occurs from the C-5 *Re*-face of a 1,4-biradical intermediate **7** depicted in Fig. 2. The shielding of the *Si*-face by the menthyl group of host **1** is apparent although it is certainly not optimal. It is an obvious conclusion from this mechanistic picture that the absolute configuration of the major enantiomer **4** is also determined in the complex **7**–**1** (Fig. 2) and that the stereogenic centres within the imidazolidinone ring of diastereoisomers **4** and **5** have identical (*S*)-configuration. This assignment has already been implemented in Scheme 1.

Our preliminary study unequivocally demonstrates that a differentiation between the enantiotopic faces of radical centres are possible upon association to hosts of type **1**. Based on this observation enantioselective radical type cyclization reactions at chiral hosts are conceivable. Further studies are under way which will address this question in detail.

This work was supported by the *Deutsche Forschungsgemeinschaft* (Ba 1372/4-2) and by the *Fonds der Chemischen Industrie*.

Notes and references

1 Reviews: (*a*) P. J. Wagner, R. G. Weiss and H.-G. Hennig, in *Handbook of Photochemistry and Photobiology*, ed. W. M. Horspool and P.-S. Song, CRC Press, Baton Rouge, 1995, pp. 449–500; (*b*) P. J. Wagner and B.-S. Park, *Org. Photochem.*, 1991, **11**, 227; (*c*) P. Margaretha, in *Methoden der Organischen Chemie (Houben-Weyl) 4te Aufl.*, Band E 17e, ed. A. de Mejiere, Thieme, Stuttgart, 1997, pp. 71–75.

2 Substrate-induced diastereoselectivity: (*a*) U. Lindemann, G. Reck, D. Wulff-Molder and P. Wessig, *Tetrahedron*, 1998, **54**, 2529; (*b*) P. Wessig and J. Schwarz, *Helv. Chim. Acta*, 1998, **81**, 1803; (*c*) U. Lindemann, D. Wulff-Molder and P. Wessig, *Tetrahedron: Asymmetry*, 1998, **9**, 4459; (*d*) A. G. Griesbeck, H. Heckroth and J. Lex, *Chem. Commun.*, 1999, 1109 and refs. cited therein.

3 Auxiliary-induced diastereoselectivity: P. Wessig, P. Wettstein, B. Giese, M. Neuburger and M. Zehnder, *Helv. Chim. Acta*, 1994, **77**, 829 and refs. cited therein.

4 Examples: (*a*) T. Sugimura and L. A. Paquette, *J. Am. Chem. Soc.*, 1987, **109**, 3017; (*b*) G. A. Kraus and L. Chen, *J. Am. Chem. Soc.*, 1990, **112**, 3464.

5 (*a*) S. Sauer, A. Schumacher, F. Barbosa and B. Giese, *Tetrahedron Lett.*, 1998, **39**, 3685; (*b*) B. Giese, P. Wettstein, C. Stähelin, F. Barbosa, M. Neuburger, M. Zehnder and P. Wessig, *Angew. Chem.*, 1999, **111**, 2722; *Angew. Chem. Int. Ed. Engl.*, 1999, **38**, 2586.

6 Selected references: (*a*) M. Leibovitch, G. Olovsson, J. R. Scheffer and J. Trotter, *J. Am. Chem. Soc.*, 1998, **120**, 12 755; (*b*) T. Asahi, M. Nakamura, J. Kobayashi, F. Toda and H. Miyamoto, *J. Am. Chem. Soc.*, 1997, **119**, 3665; (*c*) E. Cheung, M. R. Netherton, J. R. Scheffer and J. Trotter, *J. Am. Chem. Soc.*, 1999, **121**, 2919.

7 Selected references: (*a*) H. Aoyama, M. Sakamoto, K. Kuwabara, K. Yoshida and Y. Omote, *J. Am. Chem. Soc.*, 1983, **105**, 1958; (*b*) F. Toda, H. Miyamoto and R. Matsukawa, *J. Chem. Soc. Perkin Trans. 1*, 1992, 1461; (*c*) F. Toda, K. Tanaka, O. Kakinoki and T. Kawakami, *J. Org. Chem.*, 1993, **58**, 3783; (*d*) F. Toda, H. Miyamoto and K. Kanemoto, *Chem. Commun.*, 1995, 1719.

8 Reviews: (*a*) S. R. L. Everitt and Y. Inoue, in *Molecular and Supramolecular Photochemistry: Organic Molecular Photochemistry*, Vol. 3, ed. V. Ramamurthy and K. S. Schanze, Dekker, New York, 1999, pp. 71–130; (*b*) Y. Inoue, *Chem. Rev.*, 1992, **92**, 741; (*c*) H. Rau, *Chem. Rev.*, 1983, **83**, 535.

9 J. G. Stack, D. P. Curran, S. V. Geib, J. Rebek, Jr. and P. Ballester, *J. Am. Chem. Soc.*, 1992, **114**, 7007.

10 T. Bach, H. Bergmann and K. Harms, *Angew. Chem.*, 2000, **112**, 2391; *Angew. Chem., Int. Ed.*, 2000, **39**, 2302.

11 T. Bach, H. Bergmann and K. Harms, *J. Am. Chem. Soc.*, 1999, **121**, 10 650.

12 (*a*) H. K. Hall, Jr. and A. K. Schneider, *J. Am. Chem. Soc.*, 1958, **80**, 6409; (*b*) H. Kohn, M. J. Cravey, J. H. Arceneaux, R. L. Cravey and M. R. Willcott, III, *J. Org. Chem.*, 1977, **42**, 941.

13 Representative procedure: A solution of the substrate **3** (0.1 mmol, 21.8 mg) and the chiral host **1** (0.25 mmol, 91.0 mg) in 20 ml of toluene was degassed for 30 min by a continuous stream of argon. The mixture was subsequently irradiated in a liquid cooled merry-go-round apparatus at −45 °C until the reaction was complete according to TLC (12 h). After evaporation of the solvent the diastereomeric ratio (dr) was determined from the crude product by integration of appropriate ^{1}H-NMR signals. The residue was purified by flash chromatography (eluent: EtOAc–MeOH = 98 : 2). The host **1** (R_f = 0.46; pentane–*tert*-butyl methyl ether = 25 : 75) was recovered and the products **4**/*ent*-**4** (R_f = 0.50; EtOAc–MeOH = 80 : 20) and **5**–*ent*-**5** (R_f = 0.52; EtOAc–MeOH = 80 : 20) were separated. The total yield was 16.8 mg (77%). The collected fractions of compounds **4**–*ent*-**4** were evaporated and the enantiomeric excess was determined by chiral HPLC (Table 1).

14 *Crystal data:* for **6**: chemical formula: $C_{21}H_{22}N_2O_4$, formula weight: 366.44 g mol^{-1}, crystal system: orthorhombic, unit cell dimensions: a = 894.6(1); b = 1250.0(1); c = 1635.0(1) pm, volume: 1828.3(3) × 10^{-30} m^3, temperature: 213 K, space group symbol: $P2_12_12_1$, number of molecules in unit cell: Z = 4, absorption coefficient: 7.6 cm^{-1}, reflections collected: 3696, independent reflections: 3399 [R_{int} = 0.0238], R index (all data): wR_2 = 0.0925, R index conventional [$I > 2\sigma(I)$]: R = 0.0343. CCDC 156228. See http://www.rsc.org/suppdata/cc/b1/b100300n/ for crystallographic data in .cif or other electronic format.

ChemComm

A three-dimensional heterogeneous DNA sensing surface formed by attaching oligodeoxynucleotide-capped gold nanoparticles onto a gold-coated quartz crystal

Shubo Han, Jianqiao Lin, Munlika Satjapipat, Alfred J. Baca and Feimeng Zhou*

Department of Chemistry and Biochemistry, California State University, Los Angeles, Los Angeles CA 90032, USA. E-mail: fzhou@calstatela.edu

Received (in Cambridge, UK) 9th January 2001, Accepted 21st February 2001
First published as an Advance Article on the web 13th March 2001

Exposing oligodeoxynucleotide (ODN)-capped Au nanoparticles to a quartz crystal under shear oscillation resulted in the formation of a uniform monolayer containing these nanoparticles or multilayers with islands of the ODN-capped nanoparticles, which, in turn, improved the extent of DNA hybridization.

The development of sensitive and sequence-specific assays of nucleic acids in samples of biological origins has recently been a research area under active pursuit. Thiolated single-stranded oligodeoxynucleotides (HS-ss-ODNs) immobilized onto gold films[1–9] or gold nanoparticles[10] have received a great deal of attention. The use of DNA-capped gold nanoparticles was also shown as an attractive route for enhancing the sensitivities of several important techniques. For instance, a probe/target/probe-nanoparticle sandwich and a dendritic structure based on ODN-capped gold nanoparticles were developed by Zhou *et al.*[11] and by Willner and coworkers,[12] respectively, to amplify the weak quartz crystal microbalance (QCM), or more accurately, the thickness-shear mode sensor (TSM)[5,6] signals inherent in conventional ODN probe/ODN target hybridization based on the use of HS-ss-ODNs. The employment of gold nanoparticles in conjunction with other techniques [*e.g.* atomic force microscopy (AFM) and surface plasmon resonance spectroscopy[13,14]] were also demonstrated to improve other analytical 'figure of merits', such as selectivity and dynamic range.

We report here a simple procedure for attaching ODN-capped gold nanoparticles onto thin gold films for subsequent hybridization with target DNA molecules. The procedure is devised on the basis of a serendipitous discovery we made in performing a sandwich DNA assay described in ref. 11. We found that ODN-capped gold nanoparticles can be rapidly adsorobed onto a thin, polished gold film that is part of a quartz crystal undergoing shear oscillation (8 MHz fundamental frequency). Curve 1 in Fig. 1 depicts the dramatic frequency decrease resulting from attaching 30-mer-capped gold nanoparticles (*ca.* 890 Hz) upon injecting buffer solutions containing these ODN-capped nanoparticles. The attachment of the ODN-capped gold nanoparticles onto the gold-coated crystal must have arisen from the well known non-specific interaction between the DNA bases and the gold surface,[1,2] since the ODN-capped gold nanoparticles do not possess any affinity for the Au surface with a monolayer coverage of hexanethiol SAM (Curve 2), and the gold nanoparticles alone do not appear to adhere to the gold film (Curve 3). We believe that the shear motion of the thin gold film greatly facilitated a surface rearrangement of the adsorbed ODN-capped gold nanoparticles to form a robust film. The formation of the ODN-capped gold nanoparticle film appears to proceed layer-by-layer. AFM images revealed that a compact monolayer of the ODN-capped gold nanoparticle assembly was produced (Fig. 2a) after *ca.* 100 s of exposure of the crystal to an ODN-capped Au nanoparticle solution. The surface morphology of the crystal surface becomes much more uniform as the ODN-capped nanoparticles are within a smaller size distribution than the gold grains originally present at the crystal (not shown). Thus the surface of crystal was not rougher than the original polished gold film, suggesting that mass changes described below are unlikely to be caused by the effects due to the porosity and/or roughness of the new surface. Extensive exposure of the crystal surface under the shear motion to the solution, on the other hand, leads to the formation of multilayers of ODN-capped gold nanoparticles (Fig. 2b). Individual gold nanoparticles with a size around 13–15 nm can be resolved. Upon exposure for an extended period of time (*e.g.* 8000 s), a purple thin film can actually be visualized. Also notice that, beyond the first layer, it appears that the ODN-capped gold nanoparticles tend to agglomerate preferentially at certain sites to produce islands. These islands, together with the nanoparticle

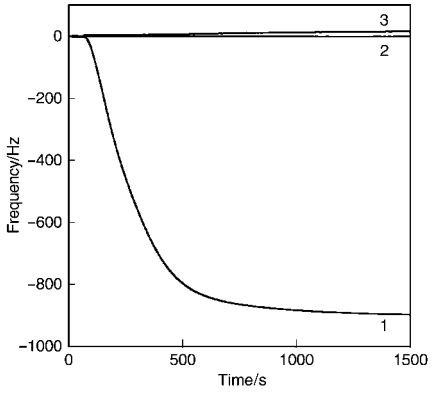

Fig. 1 QCM responses to the injections of 100 μL solutions containing Au nanoparticles and Au particles capped with HS-ss-DNA of different numbers of DNA bases. Curve 1 shows the response at the crystal surface to the injection of the Au nanoparticles capped with the 30-mer probe with the sequence of 5′-AGAGGATCCCCGGGTACCGAGCTC-GAATTC$(CH_2)_6$SH-3′. This sequence is complementary to the 47-mer target 5′-GAATTCGAGCTCGGTACCCGGGGATCCTCTACTGGCC-GTCGTTTTAC-3′ used in the follow-up hybridization experiment (shown in Fig. 3). Curves 2 and 3 correspond to the responses to a 0.15 μM 30-mer-capped Au nanoparticle at a crystal modified with a hexanethiol SAM and to a 0.15 μM Au nanoparticle solution at a crystal, respectively.

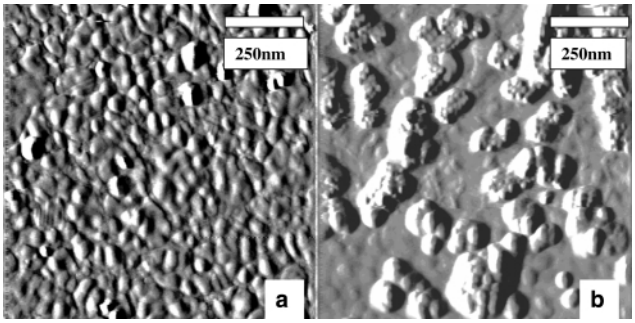

Fig. 2 AFM images of (a) a gold film covered with the 30-mer-capped gold nanoparticle assembly formed by exposing the gold film to the DNA-capped Au nanoparticle solution for 100 s, and (b) a gold film modified with the 30-mer-capped nanoparticle assembly formed upon an 8000 s exposure.

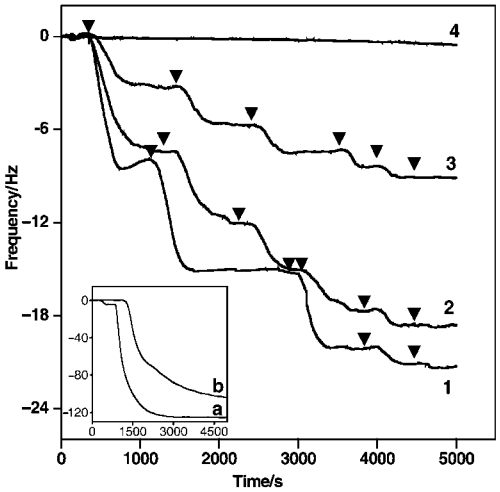

Fig. 3 QCM responses acquired after the injections of a 47-mer target (5′-GAATTCGAG CTCGGTACCCGGGGATCCTCTACTGGCCGTCGT-TTTAC-3′) at a crystal covered with a 30-mer-capped Au nanoparticle assembly (Curve 1), the 47-mer target at a crystal covered with a 16-mer (5′-$HS(CH_2)_6$GTAAAACGACGGCCAG3′)-capped Au nanoparticle assembly (Curve 2), the 47-mer target at a crystal covered with a sub-monolayer of 30-mer SAM (Curve 3), and a 47-mer target (5′-CTTGGAGAGCTCGG-TACCCGGGGATCCTCTACTGGCCGTCGTTTTAC-3′) with six of the bases mismatching the bases on the 30-mer probe that had been immobilized onto the gold nanoparticles (Curve 4). Inset: (a) hybridization of the 47-mer target with the 16-mer probe and the frequency change in a subsequent injection of the 30-mer-capped gold nanoparticle solution, and (b) the frequency change upon injecting the 30-mer-capped gold nanoparticle solution into the QCM cell housing a crystal covered with only the 16-mer probe. Arrows indicate the injection points.

terraces that are not covered, thus provide a unique 3-D ODN-capped gold nanoparticle assembly with many sites for DNA hybridization. Fig. 3 shows DNA hybridization at crystals covered with different ODN-capped gold nanoparticles (Curves 1 and 2) and the comparison of the results with those acquired at crystals modified with only HS-ss-ODN (Curve 3). As can be seen, the five consecutive injections of a 3.35 μg mL^{-1} 47-mer target solution resulted in a cumulative frequency decrease of *ca.* 22 Hz at a crystal covered with 30-mer-capped gold nanoparticles, whereas the injections of the same target solution at a crystal modified with 16-mer-capped gold nanoparticles produced a 19 Hz change. Both frequency decreases are greater than those observed from multiple injections of the target solution into a QCM housing a 30-mer SAM (*ca.* 9 Hz in Curve 3). Therefore, it seems that more probe molecules are present at the films containing ODN-capped gold nanoparticles since more target molecules can be detected at such films. Previous studies of gold films covered with different ODNs have shown that the surface density of a thiolated 32-mer is slightly less than 1.8×10^{-11} mol cm^{-2}.[3] We measured, with an inductively coupled plasma-atomic emission spectrometer, the average gold : sulfur ratio on the 30-mer-capped Au nanoparticles to be 1 : 87. Using a diameter of 13 nm for the Au nanoparticles,[14] we calculated the surface density to be 2.7×10^{-11} mol cm^{-2}. These values correspond to sub-monolayer coverages (*e.g.* 2.7×10^{-11} mol cm^{-2} corresponds to *ca.* 49% coverage)[9] and are consistent with those reported in many previous papers.[1,2,4-9] Obviously, the surface density associated with the sub-monolayer of HS-ss-ODN film would not lead to an extensive DNA hybridization at the surface. This contention is in line with the weak QCM signals observed by many research groups[11,15,16] without post-hybridization treatment or target derivatization. Thus, the formation of a multilayer of ODN-capped gold nanoparticles provides a unique means to increase the total number of probes per unit area by converting the ODN assembly at a 2-D surface to a 3-D network. Another implication of the incomplete HS-ss-ODN surface coverage at gold is that the non-specific interaction between ODN and the bare gold regions could lead to an overestimate of the DNA hybridization when ODN-capped gold nanoparticles were employed to amplify hybridization signals. Indeed, when we performed the sandwich assay using the 16-mer probe on the gold surface and the 30-mer-capped gold nanoparticle as the second probe for signal amplification of the hybridized 47-mer target, most of the frequency decrease appears to result from the non-specific adsorption of the gold nanoparticles onto the gold regions that were not occupied by the 16-mer. As seen in the inset of Fig. 3, Curve a, which shows the frequency change associated with the typical 'sandwich assay',[11] and Curve b, which shows the non-specific adsorption of the 30-mer probes immobilized to the nanoparticles onto the gold surface that has a partial coverage of 16-mer probes, have yielded similar frequency changes. In Curve a, the first step (*ca.* 4.5 Hz) corresponds to the hybridization of the 47-mer target with the 16-mer probe and the second step (*ca.* 126 Hz) is due to the combined effect of non-specific adsorption (*ca.* 108 Hz in Curve b) and the legitimate hybridization of the 30-mer on the gold nanoparticles with the surface-confined 47-mer target.

The comparison between the signal intensities of Curves 1 and 2 indicates that longer ODN probes would cause a larger extent of hybridization. While the longer probes tend to coil more extensively, and consequently impose a greater hindrance to target hybridization, the difference in binding energy between the two different strands should be more predominant for these short ODNs. To ensure that mass changes shown in Curves 1 and 2 in Fig. 3 did not originate from non-specific target adsorption onto the ODN-capped gold nanoparticles films, we conducted a control experiment. The absence of any appreciable frequency change at the 30-mer-capped gold nanoparticle film upon the injections of a target with six mismatched bases confirms that non-specific adsorption did not occur (Curve 4).

In closing, we have developed a method to modify a crystal surface with oligonucleotide-functionalized gold nanoparticles. The attachment of the ODN-capped gold nanoparticles increases the total number of ss-ODN probes available for DNA hybridization. An important point that merits attention is that caution should be exercized when ODN-capped gold nanoparticles are used in connection with the sandwich assay by QCM since non-specific adsorption of the DNA-functionalized gold nanoparticles could lead to an overestimate of the signal enhancement.

Notes and references

1 R. Levicky, T. M. Herne, M. J. Tarlov and S. K. Satija, *J. Am. Chem. Soc.*, 1998, **120**, 9787.
2 A. B. Steel, T. M. Herne and M. J. Tarlov, *Anal. Chem.*, 1998, **70**, 4670.
3 A. B. Steel, R. L. Levicky, T. M. Herne and M. J. Tarlov, *Biophys. J.*, 2000, **79**, 975.
4 D. N. Furlong, F. Caruso, E. Rodda, K. Niikura and Y. Okahata, *Anal. Chem.*, 1997, **69**, 2043.
5 B. A. Cavic, G. L. Hayward and M. Thompson, *Analyst*, 1999, **124**, 1405.
6 M. Thompson and L. M. Furtado, *Analyst*, 1999, **124**, 1133.
7 J. Wang, P. E. Nielsen, M. Jiang, X. Cai, J. R. Fernades, D. H. Grant, M. Ozsoz, A. Beglieter and M. Mowart, *Anal. Chem.*, 1997, **69**, 5200.
8 A. J. Thiel, A. G. Frutos, C. E. Jordan, R. M. Corn and L. M. Smith, *Anal. Chem.*, 1997, **69**, 4948.
9 S. O. Kelley, J. K. Barton, N. M. Jackson and M. G. Hill, *Bioconjugate Chem.*, 1997, **8**, 31.
10 C. A. Mirkin, *Inorg. Chem.*, 2000, **39**, 2258 and references therein.
11 X.-C. Zhou, S. J. O'Shea and S. F. Y. Li, *Chem. Commun.*, 2000, 953.
12 F. Patolsky, K. T. Ranji, A. Lichtenstein and I. Willner, *Chem. Commun.*, 2000, 1025.
13 L. A. Lyon, M. D. Musick, P. C. Smith, B. D. Reiss, D. J. Pena and M. J. Natan, *Sens. Actuators, B*, 1999, **54**, 118.
14 S. Han, J. Lin, F. Zhou and R. L. Vellanoweth, *Biophys. Biochem. Res. Commun.*, 2000, **279**, 265.
15 F. Patolsky, A. Lichtenstein and I. Willner, *J. Am. Chem. Soc.*, 2000, **2000**, 418.
16 E. Huang, M. Satiapipat, S. Han and F. Zhou, *Langmuir*, 2001, **17**, 1215.

ChemComm

First synthesis of a phosphonothiashikimic acid derivative†

Montserrat Heras, Mihaela Gulea and Serge Masson*

Laboratoire de Chimie Moléculaire et Thioorganique (UMR CNRS, 6507), ISMRA-Université de Caen et CNRS, 6 boulevard du Maréchal Juin, F-14050 Caen, France. E-mail: serge.masson@ismra.fr

Received (in Cambridge, UK) 30th January 2001, Accepted 21st February 2001
First published as an Advance Article on the web 13th March 2001

A new phosphono and thio analogue of shikimic acid ester has been synthesised from a thiopyranic derivative obtained *via* a [4 + 2] cycloaddition involving a phosphonodithioformate as heterodienophile.

Shikimic acid[1] **I** (Scheme 1) is an important intermediate in the biosynthesis of aromatic amino acids from carbohydrates in plants and microorganisms. Therefore, increasing effort has been directed towards the synthesis of its analogues as potential enzyme inhibitors in this biological pathway. Several modifications of the shikimic acid structure were described, including the functionalisation of the cyclohexene ring,[2] the substitution of the carboxylic function by a phosphono group[3] (phosphono shikimic acid **II**) or the replacement of the methylene group involved in the shikimate pathway by a sulfur atom (thiashikimic acid **III**). We report here the first synthesis of a new racemic derivative of compound **IV** which is both a phosphono and thio analogue of shikimic acid.

As for the preparation of thiashikimic acid ester,[4] we used a hetero Diels–Alder cycloaddition for the first step of our synthesis (Scheme 2). However, instead of the unknown and probably very unstable thioaldehyde-phosphonate (analogue of a thioxoacetate) we used a very stable and readily accessible phosphonodithioformate **1** (very recently described by our group as a new heterodienophile[5]). Although relatively slow (7 days), the reaction of (*E*,*E*)-1,4-diacetoxybutadiene with this dithioester in refluxing THF led to the functionalized dihydrothiopyranic derivative **2** as a mixture of diastereomers **2a** and **2b** in a 2 : 1 ratio and 87% yield (use of a Lewis acid to accelerate the reaction[5] was excluded because it induced some undesirable degradation of the cycloadduct). These isomers were easily separated by chromatography on silica gel. By comparison with the reaction of the thioxoacetate,[4] we could expect for the major isomer **2a** (58%) resulting from a preferential phosphonyl-*endo* cycloaddition, a *cis* configuration as far as the two acetoxy and the phosphono groups are concerned. The structures assumed for **2a** and **2b** were indeed found in accordance with the observed coupling constants between phosphorus and protons on C_3 and C_6: large equatorial–equatorial or axial–axial coupling (torsion angle $\Phi \sim 0$ or $\sim 180°$) and almost null equatorial–axial coupling ($\Phi \sim 90°$)[6] (Scheme 3).

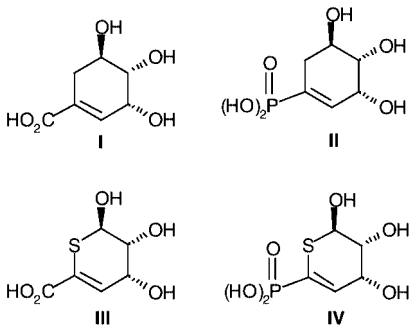

Scheme 1

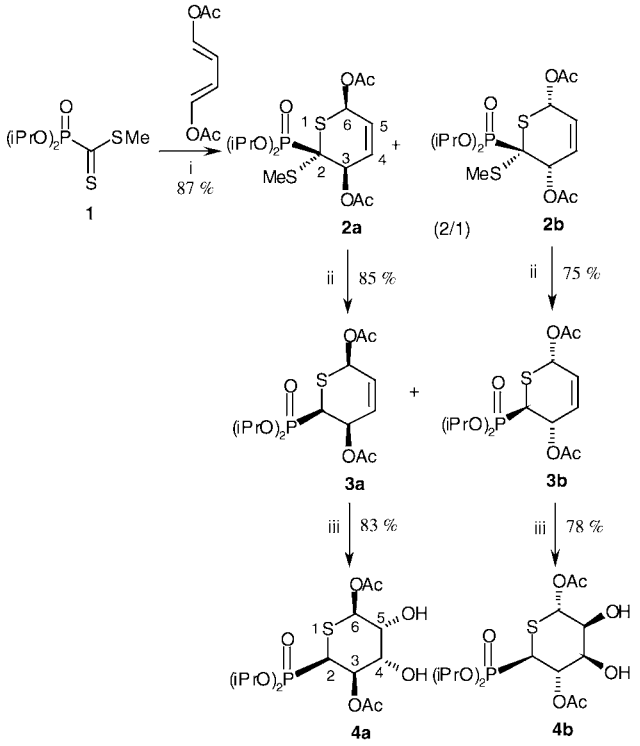

Scheme 2 *Reagents and conditions*: i: THF, rt, 7 d; ii: Bu_3SnH–AIBN, refluxing benzene, 2 h; iii: OsO_4–Py, rt, 2 h.

Each isomer was then desulfanylated using Bu_3SnH–AIBN in refluxing benzene and, as expected from our preliminary study,[5] the heterocyclic sulfur atom is not affected by the reaction. A mixture of 2,3-*cis* **3a** and 2,3-*trans* **3b** isomers was respectively obtained in a 2 : 1 ratio from **2a** (85%) and in a 5 : 3 ratio from **2b** (75%). The favoured formation of isomer **3a** could be explained by the preferential reduction of the anomeric radical on the opposite side to the C_3 acetoxy groups through an axial attack.[7] The stereochemistry of these diastereomers was deduced from the $^3J_{H2–H3}$ = 6.1 (for **3a**) and 10.7 Hz (for **3b**) coupling constants.

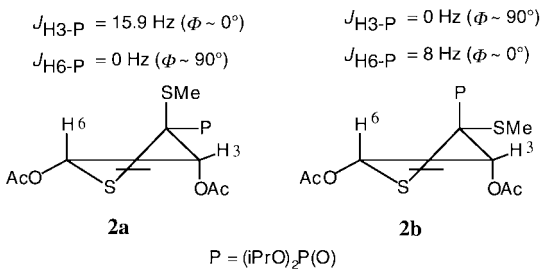

Scheme 3 Relative configurations of cycloadducts **2** (one conformer of each isomer is represented).

† Electronic supplementary information (ESI) available: experimental. See http://www.rsc.org/suppdata/cc/b1/b101050f/

DOI: 10.1039/b101050f

After separation of these isomers by flash column chromatography on silica gel they were dihydroxylated by osmium tetroxide in pyridine. Compound **3a** gave the corresponding *cis*-diol **4a** (83%) as a single isomer, by attack from the less hindered side of the molecule. Under the same conditions, the dihydroxylation of isomer **3b** gave diol **4b** (78%). To avoid the possible 1,2-migration of an acetyl group[4] from O–C_3 to O–C_4, diols **4a** and **4b** were protected as acetylated derivatives **5a** and **5b** before performing a basic elimination of acetic acid (Scheme 4). From tetraacetate **5a**, this 1,2-elimination occurred in hot pyridine to give the phosphonothiashikimic derivative **6** in 57% yield after purification. As expected, for the epimer **5b**, in which the relevant proton and acetoxy group are not in a *trans* configuration, the elimination failed in similar conditions. However, using a stronger base (NaH in THF), **5b** led to the same expected compound **6** in 43% yield. In this way, both *Diels–Alder* isomeric cycloadducts were used for the synthesis of the target molecule **6**. The observed *J* values ($^3J_{H5–H6}$ = 4.6, $^3J_{H5–H4}$ = 3.3 Hz) for the acetoxy derivative of phosphonoshikimate **6** are consistent with the attributed structure and in good agreement with that of its carboxylic analogue.[4]

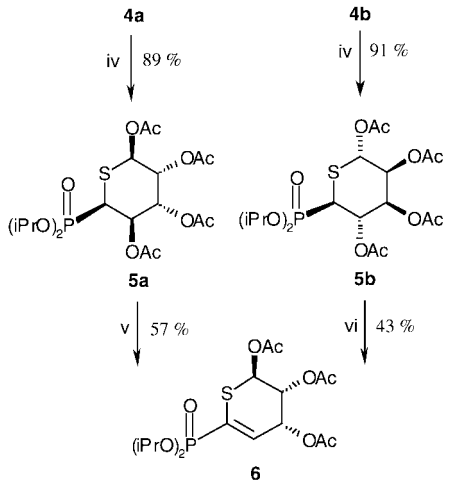

Scheme 4 *Reagents and conditions*: iv: $(AcO)_2O$–Py, 80 °C, 12 h; v: Py, reflux, 36 h; vi: 3 equiv. NaH, THF, rt, 36 h.

The search of an efficient enantioselective version of this synthesis is now under investigation. Besides, the preparation of other thiapyranic derivatives, from the phosphonodithioformate **1** and various functionalized dienes by the same sequence, cycloaddition–desulfanylation–dihydroxylation, are in progress and will be the subject of a full publication.

We thank the Réseau Inter-Régional Normand de Chimie Organique Fine (RINCOF, Contrat de Plan Etat-Bassin Parisien-Régions Haute-Normandie-Basse-Normandie) for financial support to M. Heras.

Notes and references

1 Review: S. Jiang and G. Singh, *Tetrahedron*, 1998, **54**, 4697.
2 (*a*) S. Jiang, G. Singh, D. J. Boam and J. R. Coggins, *Tetrahedron: Asymmetry*, 1999, **10**, 4087; (*b*) J. K. Sutherland, W. J. Watkins, J. P. Bailey, A. K. Chapman and G. M. Davies, *J. Chem. Soc., Chem. Commun.*, 1989, 1385; (*c*) J. K. Sutherland, R. C. Whitehead and G. M. Davies, *J. Chem. Soc., Chem. Commun.*, 1993, 464.
3 S. Mirza and J. Harvey, *Tetrahedron Lett.*, 1991, **32**, 4111.
4 D. Adam, A. A. Freer, N. W. Isaacs, G. W. Kirby, A. Littlejohn and M. S. Rahman, *J. Chem. Soc., Perkin Trans. I*, 1992, 1261.
5 B. Heuze, R. Gasparova, M. Heras and S. Masson, *Tetrahedron Lett.*, 2000, **41**, 7327.
6 E. Ôhler, E. Haslinger and E. Zbiral, *Chem. Ber.*, 1982, **115**, 1028 and references therein.
7 For examples of selective axial trapping of anomeric radicals see: (*a*) M. Gulea, J. M. Lopez-Romero, L. Fensterbank and M. Malacria, *Org. Lett.*, 2000, **2**, 2591; (*b*) B. Giese, *Angew. Chem., Int. Ed. Engl.*, 1989, **28**, 969; (*c*) H. Togo, W. He, Y. Waki and M. Yokoyama, *Synlett*, 1998, 700.

Preparation of π-conjugated polymer-protected gold nanoparticles in stable colloidal form

Yong Zhou, Hideaki Itoh, Takashi Uemura, Kensuke Naka* and Yoshiki Chujo*

Department of Polymer Chemistry, Graduate School of Engineering, Kyoto University, Yoshida, Sakyo-ku, Kyoto, 606-8501, Japan. E-mail: ken@chujo.synchem.kyoto-u.ac.jp

Received (in Cambridge, UK) 17th January 2001, Accepted 21st February 2001
First published as an Advance Article on the web 13th March 2001

π-Conjugated polymer-protected gold nanoparticles of narrow size distribution in stable colloidal form have been prepared *via* reduction of $HAuCl_4$ by a π-conjugated poly(dithiafulvene) having electron donating properties.

Recently, hybrid systems consisting of inorganic nanoparticles with π-conjugated polymers as supporting matrices were found to display various interesting characteristics, particularly in the areas of dielectric properties, energy storage, catalytic activity, and magnetic susceptibility. The reason is that π-conjugated polymers as one-dimensional semiconductors have the advantage of being easy to process to form large-area devices. Their energy gaps and ionization potentials can readily be tuned by chemical modification of the polymer chains. The process of charge transfer at the contact between a metal nanoparticle and an organic (or polymeric) semiconductor plays an important role in many areas of technology.[1] The electronic structure of the polymer chain strongly influences the characteristic of the metal nanoparticles.[2,3]

This communication describes the first example of stable colloidal forms of nanocomposites consisting of metal nanoparticles protected with a π-conjugated polymer. Reduction of metal ions by the π-conjugated polymer leads to metal nanoparticles with the resulting oxidized polymer protecting the metal nanoparticles. It has already been reported that reduced forms of polymers such as polypyrrole and polyaniline are converted to the respective oxidized forms with simultaneous *in situ* reduction of metal ions, Pd(II) and Au(III) to their elemental forms.[4–6] However, these composites could not be dispersed in any solvents. Here we used a π-conjugated polymer containing the strong electron-donating dithiafulvene unit in the main chain, which was synthesized recently by our group.[7] We found that gold colloidal particles were formed with narrow size distribution *via* reduction of $HAuCl_4$ by the π-conjugated poly(dithiafulvene) (PDF). The oxidized polymer then protected and stabilized the gold nanoparticles.

In a typical preparation of π-conjugated polymer-protected gold nanoparticles, PDF† (5.44 mg, 2.86×10^{-5} mol by repeating unit) was dissolved in 5 ml of a dimethyl sulfoxide (DMSO) solution of $HAuCl_4$ (5×10^{-6} mol). The reaction mixture was stirred for 24 h at room temperature. The reaction mixture changed gradually from yellow to purple with stirring. A similar solution in the absence of PDF was also stirred for 24 h at room temperature. The solution remained yellow. These results indicate the reduction of $HAuCl_4$ to gold nanoparticles by PDF. The resulting DMSO solution of the polymer-protected gold nanoparticles was stable without precipitation for more than a month at room temperature under air. The sample showed film-forming properties when the DMSO solution was cast onto a glass slide.

Fig. 1(a) shows a transmission electron microscopy (TEM) image of the produced π-conjugated PDF-protected gold nanoparticles, which was deposited on a grid from a DMSO solution. It can be seen that spherical gold nanoparticles were produced with narrow size distribution and high dispersion. The histogram of the size distribution is shown in Fig. 1(b), which was obtained directly from an enlarged TEM image by counting 300 particles. The average size of the particles was 6 nm.

Fig. 2 shows the UV–VIS absorption spectrum of the PDF-protected gold nanoparticles in DMSO. An absorption band appears at 550 nm. It can be concluded that the band results from the surface plasmon resonance of the gold nanoparticles. A π–π* transition absorption band of PDF was observed around 400 nm.[7] The surface plasmon resonance band of gold colloids is calculated theoretically to be at 510–525 nm in an aqueous system.[8] It is clear that the absorption band of the PDF-protected gold nanoparticles was strongly red shifted compared with the theoretical value. It is well known that, for spherical

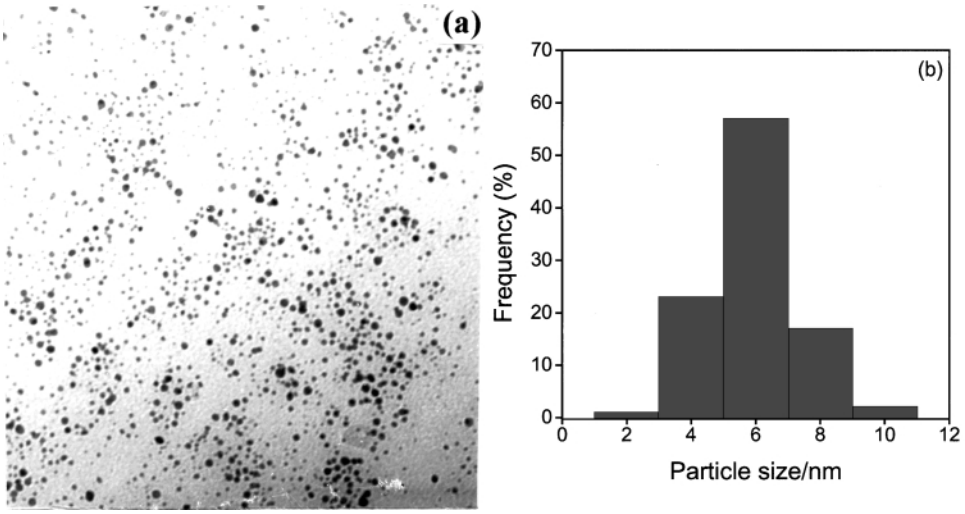

Fig. 1 (a) TEM image of the π-conjugated PDF-protected gold nanoparticles; (b) Histogram of the size distribution of the π-conjugated PDF-protected gold nanoparticles.

DOI: 10.1039/b100636n

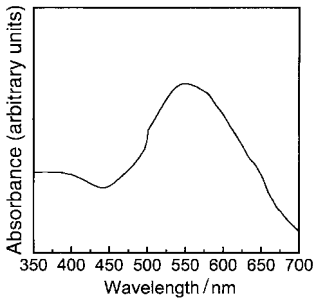

Fig. 2 UV–VIS absorption spectrum of the PDF-protected gold nanoparticles in DMSO.

colloidal metals of size 3–20 nm, there is not a strong dependence of the absorption spectrum on particle size.[8] This is because, for particle sizes below *ca*. 20 nm diameter the quadrupole and higher-order term in the Mie summation become significant.[9] In the present case, since the gold nanoparticles were of average size 6 nm, the red shift was not due to the size effect. However, the surrounding medium affects the absorption peak position of the metal nanoparticle by varying the interface conditions.[10] In this case, to study the influence of DMSO on the surface plasmon resonance band of the gold colloid, we used $NaBH_4$ as the reducing reagent and polyvinylpyrrolidone (PVP) as the protecting polymer for reduction of $HAuCl_4$ in DMSO. The absorption band of the gold nanoparticles of size 14 nm produced by this system was located at *ca*. 520 nm *i.e.* with no red shift. These results indicate that the red shift originated from the influence of the oxidized PDF. When protected by the oxidized PDF, the work function of the gold particle will decrease compared to that *in vacuo*, which lowers the energy of the surface resonance state,[11] leading to the red shift of the absorption band.[12]

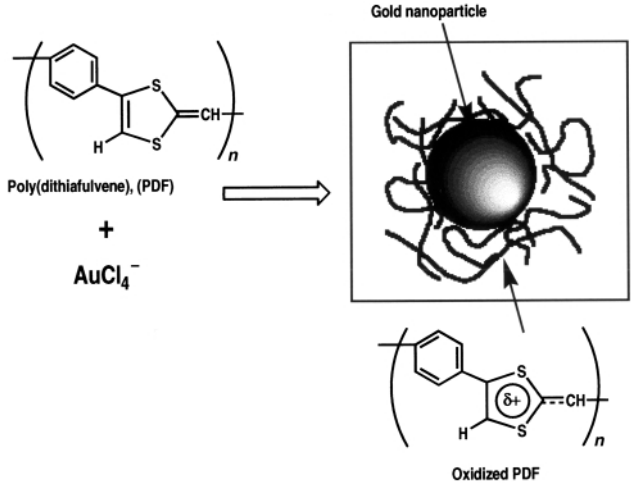

Fig. 3 Schematic illustration of the formation of the PDF-protected gold nanoparticles.

In conclusion, π-conjugated polymer-protected gold nanoparticles of narrow size distribution have been prepared in stable colloidal form *via* reduction of $HAuCl_4$ by the π-conjugated electron-donating PDF. Formation of the gold nanoparticle by the π-conjugated PDF is schematically shown in Fig. 3. The oxidized π-conjugated PDF induced a strong red shift of the absorption spectrum of the gold nanoparticles.

We thank Dr M. Tsujii, Dr S. Yamamoto and Professor T. Fukuda (Kyoto University) for the TEM micrographs. We also thank Dr T. Sato (Kyoto University) for helpful discussions.

Notes and references

† PDF was prepared from 1, 4-diethynylbenzene according to our previous report.[7] The number-average molecular weight (M_n) of PDF used here was 5440 as determined by ^{1}H NMR spectroscopy.

1 J. C. Scott and G. G. Malliaras, *Chem. Phys. Lett.*, 1999, **299**, 115.
2 K. V. Sarathy, K. S. Narayan, J. Kim and J. O. White, *Chem. Phys. Lett.*, 2000, **318**, 543.
3 T. Hertel, E. Knoesel, M. Wolf and G. Ertl, *Phys. Rev. Lett.*, 1996, **76**, 535.
4 S. W. Huang, K. G. Neoh, C. W. Shih, D. S. Lim, E. T. Kang, H. S. Han and K. L. Tan, *Synth. Met.*, 1998, **96**, 117.
5 K. G. Neoh, K. K. Tan, P. L. Goh, S. W. Huang, E. T. Kang and K. L. Tan, *Polymer*, 1999, **40**, 887.
6 S. W. Huang, K. G. Neoh, E. T. Kang, H. S. Han and K. L. Tan, *J. Mater. Chem.*, 1998, **8**, 1743.
7 K. Naka, T. Uemura and Y. Chujo, *Macromolecules*, 1999, **32**, 4641.
8 J. A. Creighton and D. G. Eadon, *J. Chem. Soc., Faraday Trans.*, 1991, **87**, 3881.
9 M. Kerker, *The Scattering of Light and Other Electromagnetic Radiation*, Academic Press, New York, 1969, p. 38.
10 S. Underwond and P. Mulvaney, *Langmuir*, 1994, **10**, 3427.
11 M. Wolf, E. Knoesel and T. Hertel, *Phys. Rev. B*, 1996, **54**, R5295.
12 N. Sandhyarani and T. Pradeep, *J. Mater. Chem.*, 2000, **10**, 981.

Peripherally-substituted polydimethylsiloxane phthalocyanines: a novel class of liquid materials

Eva M. Maya,*[ab] James S. Shirk,[a] Arthur W. Snow[a] and Gerald L. Roberts[b]

[a] *Naval Research Laboratory, Washington DC 20375-5342, USA. E-mail: emaya@ccf.nrl.navy.mil*
[b] *George Mason University, Department of Chemistry, 4400 University Drive, Fairfax, Virginia 22030-4444, USA*

Received (in Irvine, CA, USA) 16th January 2001, Accepted 13th February 2001
First published as an Advance Article on the web 13th March 2001

Isotropic liquid phthalocyanine compounds with peripheral polydimethylsiloxane oligomer substitution were synthesized and found to have a unique combination of thermorefractive and nonlinear optical properties along with unusual metal substitution reactivity and aggregation behavior.

Polydimethylsiloxane oligomer substitution at the periphery of a phthalocyanine ring generates a liquid material with exceptional optical properties and chemical behavior. This material is designed to have the rheological and thermorefractive properties of a silicone fluid[1] and the nonlinear optical properties characteristic of the phthalocyanine chromophore.[2] Structure **1** in Scheme 1 combines these molecular features coupled through an aromatic ether linkage. The motivation for this design is to combine two mechanisms important to an optical limiting application[2] into a single compound: a large fluence dependent, refractive index;[1] and a reverse saturable optical absorption.[2] The aromatic ether linkage further incorporates an enhanced photo-oxidative stability. Cloaking of the phthalocyanine ring in a silicone covering has important implications for the chemistries of aggregation and metal substitution. To our knowledge, no examples of peripheral silicone substituted phthalocyanines have been previously reported. In this communication we report synthesis and preliminary characterization of a new class of liquid phthalocyanine (Pcs) materials.

Two routes for the synthesis of the lead and metal-free phthalocyanine compounds are depicted in Scheme 1. Starting reagents for both routes are prepared in the first step. The butyl capped hydrosilyl terminated poly(dimethylsiloxane) (PDMS) oligomer (**2**) (DP = 9 in this example) is synthesized by an anionic ring opening polymerization of hexamethylcyclotrisiloxane.[3] The allylphenoxyphthalonitrile (**3**) is prepared by a nitroaromatic displacement reaction of 4-nitrophthalonitrile[4] with 2-allylphenol. In the preferred route, the PDMS oligomer is first coupled to the allylphenoxyphthalonitrile by a hydrosilylation reaction. Next the allylphenoxyphthalonitrile–PDMS adduct (**4**) is cyclotetramerized in the presence of lead oxide to yield the phthalocyanine **1a**. The alternate route is to first conduct the cyclotetramerization yielding the tetrakis(allylphenoxy)phthalocyanine (**5**) then to perform the hydrosilylation to yield the phthalocyanine product (**1**). This route has the disadvantage of a more arduous purification (as a consequence of a required large excess of **2** to ensure a quantitative conversion of the allyl groups) and the use of a heterogeneous non-acidic hydrosilylation catalyst (to avoid displacement of a labile metal from the phthalocyanine cavity).

Structures **1**–**5** are consistent with spectroscopic characterization.† The phthalocyanine materials have both a mixed isomer and polydisperse character. The phthalocyanine forming reaction produces a statistical mixture of four possible isomers.[5] The polydispersity is a result of the manner in which the butyl capped PDMS oligomer (**2**) is prepared.[6] These features are regarded as advantages in discouraging liquid crystal formation. In an analogous phthalocyanine system with polyethylene oxide oligomer substituents it was found that a monodisperse system is liquid crystalline[7] while that with a polydisperse system is an isotropic liquid.[8] Liquid crystallinity is detrimental for applications where optical transparency is required.

The PDMS chains determine the liquid character of these materials, which are viscous liquids at room temperatures. The glass transition temperatures, *T*g, for the Pb (**1a**), H_2 (**1b**) phthalocyanine compounds and the phthalonitrile precursor (**4**) are 3, 16, and 14 °C respectively. This narrow range of glass transition temperatures is a consequence of the dominant effect of the siloxane chains. A similar trend of a slightly increasing *T*g, when progressing from lead to metal-free phthalocyanine with epoxy substituted phthalocyanine glasses, has previously been observed.[9] This trend correlates with a greater tendency of the metal-free phthalocyanine to aggregate relative to the lead phthalocyanine.[10] At rt these phthalocyanine materials will fill short length (~4 μm) optical cells by capillary action over several hours. At elevated temperatures (~100 °C) the viscosity

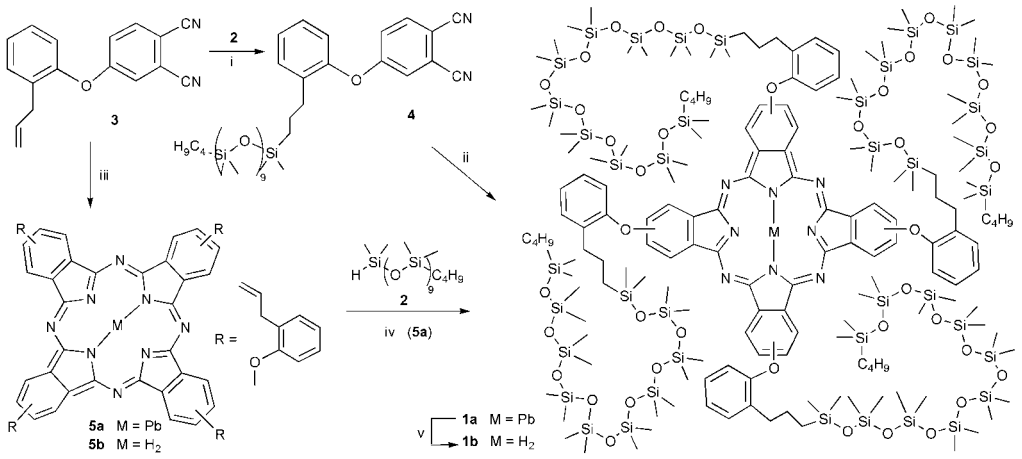

Scheme 1 *Reagents and conditions*: i, 3 drops of 0.1 N solution of $H_2PtCl_6 6H_2O$ in isopropanol, 60 °C, 1 h; ii, PbO, 165 °C, 16 h; iii, PbO or hydroquinone, 165–180 °C, 16 h; iv, 8 drops of platinium-divinyl tetramethyldisiloxane complex, toluene, 20 h; v, toluene, F_3CCOOH, 10 min.

is much lower, the aggregation is reduced (spectroscopic detection), and the filling of the cell is much more rapid.

The refractive index of a thin film of the lead phthalocyanine compound (**1a**) was measured by ellipsometry and also by measuring the angle of total internal reflection for a thin film on a prism of known refractive index. Over a temperature range of 24 to 95 °C the refractive index at 1550 nm decreased from 1.492 to 1.465. This corresponds to a decrease of $4 \pm 1 \times 10^{-4}$ per degree Centigrade and correlates well with the dn/dT reported (4×10^{-4} °C^{-1}) for linear dimethylsiloxane oligomers.[1] This decrease also indicates that the temperature dependence of the refractive index of silicone substituted phthalocyanines is dominated by PDMS chains. Relative to other polymers, polydimethylsiloxane has an exceptionally large dn/dT,[11] and this combination with the phthalocyanine structure demonstrates a successful coupling of this property and this chromophore.

Z-scan and optical limiting measurements were performed on the lead phthalocyanine compound (**1a**) to characterize the nonlinear optical properties. The Z-scan of a 20.2 mM sample of **1a** in a 50.5 μm sample cell at 532 nm is shown in Fig. 1. The material is a strong reverse saturable absorber at 532 nm. An estimate of the excited state cross section from this Z-scan and from a nonlinear transmission experiment on the same sample gave a value of the excited state cross section of ~20 times that of the ground state at 532 nm. This implies that the material is a very good reverse saturable absorber. The nonlinear absorbing properties are similar to those found in lead tetrakis(cumylphenoxy)phthalocyanine, $PbPc(CP)_4$.[12] The strong nonlinear absorption, in combination with the large dn/dT reported above, makes this a superior optical limiter material.

Finally, the silicone chains covering the phthalocyanine chromophore impart some unusual chemical behavior, particularly with regard to metal substitution reactions and aggregate formation. When the siloxane–phthalonitrile precursor (**4**) is subjected to the Linstead conditions of lithium pentoxide–pentan-1-ol for conversion to lithium phthalocyanine,[13] a product with a Q-band diagnostic of the dilithium substituted phthalocyanine (675 nm) is obtained. However, it is very difficult to displace the normally very labile lithium with protons. Normally, this occurs under very mild acidic conditions. We find that normal and progressively more severe acid exchange conditions were unsuccessful.‡ Treatment with concentrated HCl and heating resulted in conversion being first observed at 90 °C which became quantitative after 2 h at this temperature. However, once the lithium ion is displaced by the proton, subsequent metal ion substitution reactions proceed under normal conditions.§

The other aspect of unique chemical behavior is in the aggregation tendency. Phthalocyanine compounds aggregate as a concentration dependent association of phthalocyanine rings. The dimerization constant is a useful measure of this aggregation tendency. Typical dimerization constants for phthalocyanine compounds range from 10^4 to 10^6 M^{-1}.[14] Preliminary analysis of concentration dependence of the Q-band absorption using a monomer–dimer equilibrium model indicates that the dimerization constant for **1b** is 150 ± 100 M^{-1}. This is significantly less than the range for phthalocyanine dimerization constants mentioned above. We attribute this result to the nature of the siloxane chain and the ortho substitution of the phenylene ether linkage to the phthalocyanine ring.

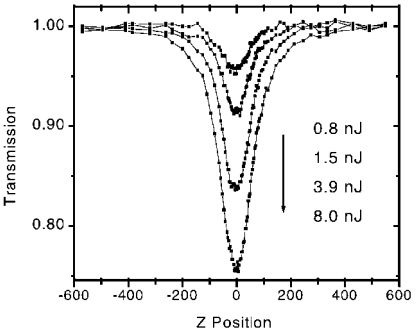

Fig. 1 A Z-scan of a 20.2 mM sample of **1a** at increasing input energy.

In summary, the incorporation of PDMS oligomers as phthalocyanine peripheral substituents combines the desirable rheological and refractive properties of a silicone fluid with the nonlinear optical properties associated with the phthalocyanine. The long silicone substituents further impart unique chemical behavior with respect to the phthalocyanine synthesis and aggregation.

Dr John Callahan is gratefully acknowledged for recording the mass spectra, and the Office of Naval Research is acknowledged for financial support.

Notes and references

† *Selected data* for **1a**; λ(toluene)/nm 721, 648, 365; ν(NaCl)/cm^{-1} 2959 (CH), 1608 and 1492 (C–C), 1253 ($SiCH_3$), 1091 and 1014 (SiOSi), 800 (SiC). For **1b** λ(toluene)/nm 703, 666, 638, 605, 346; ν(NaCl)/cm^{-1} 3295 (NH), 2959 (CH), 1615 and 1479 (C–C), 1259 ($SiCH_3$), 1091 and 1027 (SiOSi), 807 (SiC); m/z 4500–2200 consists of peaks separated by 74 amu due to $-Si(CH_3)_2O-$ degradation which is common to mass spectra of PDMS oligomers.[6] For **2**: δ_H($CDCl_3$, 300 MHz)/ppm 0.04–0.07 (54H, br s, $SiCH_3$), 0.19 (6H, m, $SiCH_3$), 0.53 (2H, m, $SiCH_2$), 0.89 (3H, t, CH_3), 1.32 (4H, m, CH_2), 4.70 (1H, sept, SiH); ν(NaCl)/cm^{-1} 2972 (CH), 2132 (SiH), 1272 ($SiCH_3$), 1098 and 1027 (SiOSi), 800 (SiC). For **3**: δ_H($CDCl_3$, 300 MHz)/ppm 3.23 (2H, d, CH_2), 4.95 (2H, dd, $=CH_2$), 5.78 (1H, m, =CH), 6.95 (1H, d, H_{arom}), 7.12–7.33 (5H, m, H_{arom}), 7.68 (1H, d, H_{arom}); δ_C($CDCl_3$, 75 MHz) 34.0, 108.5, 114.9 and 115.4 (CN), 116.7, 117.6, 120.8, 120.9, 121.0, 126.7, 128.5, 131.6, 132.4, 135.3, 135.4, 151.1, 161.7; ν(NaCl)/cm^{-1} 3082 ($=CH_2$), 2229 (CN), 1615 (C=C), 1595 and 1486 (C–C), 1246; For **4**: δ_H($CDCl_3$, 300 MHz)/ppm 0.012–0.064 (60H, m, $SiCH_3$), 0.51 (4H, m, $SiCH_2$), 0.86 (3H, t, CH_3), 1.29 (4H, m, CH_2), 1.58 (2H, m, CH_2), 2.49 (2H, t, CH_2), 6.95 (1H, d, H_{arom}), 7.14–7.31 (5H, m, H_{arom}), 7.68 (1H, d, H_{arom}); ν(NaCl)/cm^{-1} 2966 (CH), 2229 (CN), 1602 and 1492 (C–C), 1254 ($SiCH_3$), 1098 and 1033 (SiOSi), 806 (SiC); For **5a** λ(toluene)/nm 721, 650, 346; ν(NaCl)/cm^{-1} 3076 ($=CH_2$), 2919 (CH), 1638 (C=C), 1608, 1485 (C–C), 1239. For **5b** λ(toluene)/nm 703, 667, 639, 605, 350; ν(NaCl)/cm^{-1} 3295 (NH), 3075 ($=CH_2$), 1638 ($CH=CH_2$), 1611 and 1467(C–C), 1228; δ_H($CDCl_3$, 300 MHz)/ppm −4.1 (s, NH), 3.6 (m, CH_2), 5.1 (m, $=CH_2$), 6.1 (m, CH=), 6.8–7.7 (m, H_{arom}); m/z 1091.

‡ Unsuccessful lithium displacement conditions: aliquot addition of trifluoroacetic acid (10 min); second aliquot addition of trifluoroacetic acid (30 min); aliquot addition of conc. HCl (10 min).

§ Copper and lead ions were substituted into the metal-free phthalocyanine using the acetate salts and refluxing for 2 h in pentan-1-ol–THF.

1 J. Dugas, P. Michel, L. Martin and J. M. Cariou, *Appl. Opt.*, 1986, **25**, 3807.
2 H. S. Nalwa and J. S. Shirk, in *Phthalocyanines: Properties and Applications*, ed. C. C. Leznoff and A. B. P. Lever, VCH, NY, 1996, vol. 4, p. 79–181.
3 A. T. Holohan, M. H. George, J. A. Barrie and D. G. Parker, *Macromol. Chem. Phys.*, 1994, **195**, 2965.
4 T. M. Keller, T. R. Price and J. R. Griffith, *Synthesis*, 1980, **8**, 613.
5 M. Hanack, G. Schmid and M. Sommerauer, *Angew. Chem., Int. Ed. Engl.*, 1993, **32**, 1422.
6 S. K. Pollack and A. M. Morgan, *ACS Polymer Preprints*, 2000, **41**, 631.
7 N. B. McKeown and J. Painter, *J. Mater. Chem.*, 1994, **4**, 1153; G. J. Clarkson, B. M. Hassan, D. R. Maloney and N. B. McKeown, *Macromolecules*, 1996, **29**, 1854.
8 A. W. Snow, J. S. Shirk and R. G. S. Pong, *J. Porphyrins Phthalocyanines*, 2000, **4**, 518.
9 R. D. George, A. W. Snow, J. S. Shirk, S. R. Flom and R. G. S. Pong, *Mater. Res. Soc. Symp. Proc.*, 1995, **374**, 275.
10 A. W. Snow and N. L. Jarvis, *J. Am. Chem. Soc.*, 1984, **106**, 4706.
11 R. S. Moshrefzadeh, M. D. Radcliffe, T. C. Lee and S. K. Mohapatra, *J. Lightwave Technol.*, 1992, **10**, 420; J. M. Cariou, J. Dugas, L. Martin and P. Michel, *Appl. Opt.*, 1986, **25**, 334; R. M. Waxler, D. Horowitz and A. Feldman, *Appl. Opt.*, 1979, **18**, 101.
12 J. S. Shirk, R. G. S. Pong, F. J. Bartoli and A. W. Snow, *Appl. Phys. Lett.*, 1993, **63**, 1880.
13 P. A. Barret, C. E. Dent and R. P. Linstead, *J. Chem. Soc.*, 1938, 1157.
14 R. D. George, A. W. Snow, J. S. Shirk and W. R. Barger, *J. Porphyrins Phthalocyanines*, 1998, **2**, 1 and references therein.

ChemComm

Wet chemical synthesis of silver nanorods and nanowires of controllable aspect ratio†

Nikhil R. Jana,* Latha Gearheart and Catherine J. Murphy*

Department of Chemistry and Biochemistry, University of South Carolina, 631 Sumter Street, Columbia, SC 29208, USA. E-mail: murphy@mail.chem.sc.edu; jana@mail.chem.sc.edu

Received (in Cambridge, UK) 15th January 2001, Accepted 15th February 2001
First published as an Advance Article on the web 13th March 2001

Using a seed-mediated growth approach in a rodlike micellar media, silver nanorods of varied aspect ratio were prepared from nearly spherical 4 nm silver nanoparticles.

The physical and photophysical properties of metals on the nanometer scale are influenced by the shape of the nanoparticle.[1] Well defined silver nanorods and nanowires are desirable for their optical and electronic properties.[2,3] However, preparation of silver nanoparticles by chemical reduction methods generally yields a wide range of sizes and morphologies.[4] Silver nanorods and nanowires have been prepared by ultraviolet irradiation–photoreduction,[5] solid–liquid phase arc-discharge,[6] a pulsed sonochemical method,[7] templated by DNA,[8] with a carbon nanotube template,[9] in mesoporous silica,[10] in polymer films,[11] and in membrane templates.[12] Here, a new strategy is applied. A preformed silver seed was used to promote silver growth in solution, by chemical reduction of a silver salt. The presence of a rodlike micelle in solution promoted silver rod formation. We have been able to reproducibly make silver nanorods of aspect ratio 2.5–15 (10–15 nm short axes) and nanowires of 1–4 micrometer length with 12–18 nm short axes, and effectively separate the rods or wires from spheres and other shapes by centrifugation. Our method is not electrochemical and requires no nanoporous membrane, and thus may be more amenable to large-scale preparation of these materials.

The Ag seeds, 4 nm in diameter on average, were prepared by chemical reduction of $AgNO_3$ by $NaBH_4$ in the presence of trisodium citrate to stabilize the nanoparticles.‡ To make nanorods§ and wires¶ of varying aspect ratio, $AgNO_3$ was reduced by ascorbic acid in the presence of seed, the micellar template cetyltrimethylammoniun bromide (CTAB), and NaOH. The seed concentration and base concentration relative to the Ag^+ concentration are key to making larger aspect-ratio nanomaterials. CTAB is also necessary to produce a high yield of rods. Rods and wires can be separated from spheres by centrifugation.‖

The electronic absorption spectra of silver nanorod solutions show the conventional 400 nm peak observed for spherical silver nanoparticles and another peak at longer wavelengths, due to the longitudinal plasmon band of rod-shaped particles (ESI†).[1a,c,13–15] Decreasing the amount of seed in the nanorod preparation led to a further red shift of longer-wavelength longitudinal plasmon bands in the nanorod products, implying that the silver rods increased in average aspect ratio as the seed concentration decreased. Our optical data are in accord with what others have observed for metallic nanorods for transverse and longitudinal plasmon bands.[1a,c,13–15] In the absence of CTAB, spheroidal nanorods (aspect ratio < 2.5) were unstable and reverted to spheres (as judged by the disappearance of the long-wavelength absorption band) within 10 min. In the absence of seed, silver ion reduction by ascorbic acid in the presence of CTAB yielded only a few rods, which varied in aspect ratio.

Transmission electron microscopy (TEM) was performed on centrifuged solutions that had additional long wavelength peaks in their optical absorption spectra.** Figs. 1 and 2 show micrographs of particles prepared from 4 nm seeds after shape separation. The elongated rods shown in Fig. 1 were of uniform length (42 ± 3 nm) and aspect ratio (3.5). Interestingly, these rods self-assemble in a manner resembling a two-dimensional smectic liquid crystal upon gradual solvent evaporation. Depending on seed concentration, rods of aspect ratio 10–15 can also be seperated.§¶‖ Fig. 2 shows a micrograph of silver nanowires, 1–4 μm long with aspect ratio 50–350, mostly separated from spherical side-products. EDAX analysis of the samples confirmed that the particles were silver (not silver oxide) with a considerable amount of CTAB still present.

The only difference between the preparation of nanorods and the preparation of nanowires was the relative amount of NaOH in solution. For the nanorods, the pH of the reaction solution was slightly higher than the pK_a of the second proton of ascorbic acid (≈ 11.8), suggesting that the ascorbate dianion is a significant component of the solution. In the case of the nanowires, the pH of the solution was slightly lower than this pK_a, sugggesting that the monoanion of ascorbic acid (first $pK_a \approx 4.1$) is predominant in solution. It is reasonable that silver ion complexes of these two different forms of the reducing agent, in conjunction with their complexation with the cationic CTAB and silver seed in solution, are important in nanorod and nanowire formation. Mechanistic studies are in progress. Nonetheless, our new wet chemical synthetic method of silver

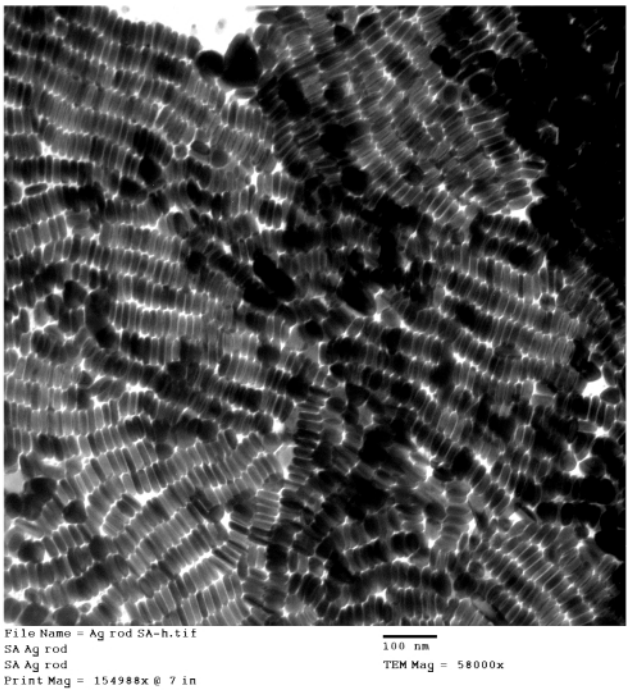

Fig. 1 TEM image of shape-separated silver nanorods from a preparation with 0.06 mL seed; scale bar = 100 nm.

† Electronic supplementary information (ESI) available: UV–VIS spectra of silver nanorods. See http://www.rsc.org/suppdata/cc/b1/b100521i/

DOI: 10.1039/b100521i

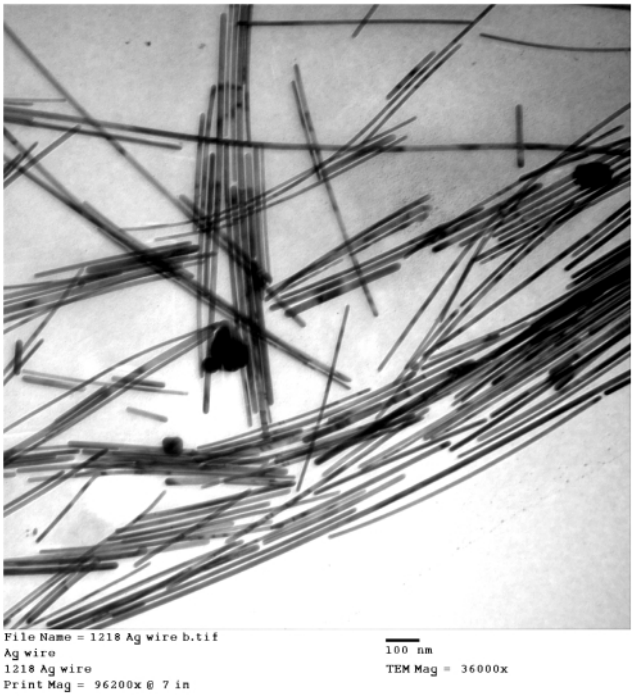

Fig. 2 TEM image of shape-separated silver nanowires; scale bar = 100 nm.

nanorods and nanowires is relatively simple to perform, and requires no nanoporous membrane.

Notes and references

‡ Preparation of 4 nm seed: a 20 mL solution with a final concentration of 0.25 mM $AgNO_3$ and 0.25 mM trisodium citrate in water was prepared. While stirring vigorously, 0.6 mL of 10 mM $NaBH_4$ was added all at once. Stirring was stopped after 30 s. This seed was used 2 h after preparation but could not be used after 5 h, as a thin film of particles appeared at the water surface. According to transmission electron microscopy, seed diameters were 4 ± 2 nm. For capping action of citrate see: A. Henglein and M. Giersig, *J. Phys. Chem. B*, 1999, **103**, 9533.

§ Procedure for Ag rods: first, six sets of solutions were prepared containing 0.25 mL of 10 mM $AgNO_3$, 0.50 mL of 100 mM ascorbic acid, and 10 mL of 80 mM CTAB. Next, a varied amount of 4 nm seed solution (2 mL, 1 mL, 0.5 mL, 0.25 mL, 0.125 mL or 0.06 mL) was added. Finally, 0.10 mL of 1 M NaOH was added to each set. NaOH must be added last to obtain the desired nanorods in decent yield. After adding the NaOH, the solution was gently shaken just enough to mix the NaOH with the rest of the solution. Within 1–10 min a color change occurred varying from red, to brown, to green depending on seed concentration. Each solution contained a mixture of rods and spheres with the aspect ratio of the rods increasing with decreasing seed concentration.

¶ Procedure for Ag wires: a solution containing 2.5 mL of 10 mM $AgNO_3$, 5.0 mL of 100 mM ascorbic acid and 93 mL of 80 mM CTAB was prepared. Next, 2.5 mL of the 4 nm seed solution was added. Finally, 0.5 mL of 1 M NaOH was added. After adding the NaOH, the solution was gently shaken just enough to mix the NaOH with the rest of the solution. A yellow color appeared within 15 min.

‖ Rods were concentrated and partially separated from spheres and surfactant by centrifugation. For solutions containing 0.25 mL of seed or more, 10 mL of solution was centrifuged at 6000 rpm for 30 min. The supernatant, containing mostly small spheres and platelets, was removed and the solid, containing some platelets and more rods with aspect ratio of 3–4, were redispersed in 0.5 mL of deionized water. For solutions containing 0.125 mL or 0.06 mL of seed, 10 mL of the solution was centrifuged at 2000 rpm for 6 min. The supernatant, containing short rods, spheres, and platelets, was separated from the solid which contained rods of aspect ratio 3–4 and a few larger rods (aspect ratio 10–15). Wires were partially separated from spheres and surfactant by centrifugation. For wires, 10 mL of the solution was centrifuged at 6000 rpm for 30 min. The supernatant was removed and the precipitate, containing silver nanowires, was redispersed in 0.5 mL of deionized water.

** All TEM grids were prepared from the solutions that were separated by centrifugation. 1.5 μL of solution was added to each grid. The grids and a small beaker of water were placed under a glass dish. The beaker of water provided a water vapor atmosphere to allow for slow drying (1–2 h) of the rod or wire solutions on the grid.

1 (*a*) J. A. Creighton and D. G. Eadon, *J. Chem. Soc., Faraday Trans.*, 1991, **87**, 3881; (*b*) S. Nie and S. R. Emory, *Science*, 1997, **275**, 1102; (*c*) S. Link and M. A. El-Sayed, *J. Phys. Chem. B*, 1999, **103**, 8410; (*d*) Z. L. Wang, *J. Phys. Chem. B*, 2000, **104**, 1153.
2 J. L. Yao, G. P. Pan, K. H. Xue, D. Y. Wu, B. Ren, D. M. Sun, J. Tang, X. Xu and Z. Q. Tian, *Pure Appl. Chem.*, 2000, **72**, 221.
3 J. T. Hu, T. W. Odom and C. M. Lieber, *Acc. Chem. Res.*, 1999, **32**, 435; W. P. McConnell, J. P. Novak, L. C. Brousseau, R. R. Fuierer, R. C. Tenent and D. L. Feldheim, *J. Phys. Chem. B*, 2000, **104**, 8925.
4 S. Sánchez-Cortés, J. V. García-Ramos and G. Morcillo, *J. Colloid Interface Sci.*, 1994, **167**, 428; C. H. Monro, W. E. Smith, M. Garner, J. Clarkson and P. C. White, *Langmuir*, 1995, **11**, 3712; U. Nickel, A. Z. Castell, K. Poppl and S. Schneider, *Langmuir*, 2000, **16**, 9087.
5 Y. Zhou, S. H. Yu, C. Y. Wang, X. G. Li, Y. R. Zhu and Z. Y. Chen, *Adv. Mater.*, 1999, **11**, 850.
6 Y. Zhou, S. H. Yu, X. P. Cui, C. Y. Wang and Z. Y. Chen, *Chem. Mater.*, 1999, **11**, 545.
7 J. Zhu, S. Liu, O. Palchik, Y. Koltypin and A. Gedanken, *Langmuir*, 2000, **16**, 6396.
8 E. Braun, Y. Eichen, U. Sivan and G. Ben-Yoseph, *Nature*, 1998, **391**, 775.
9 J. Sloan, D. M. Wright, H. G. Woo, S. Bailey, G. Brown, A. P. E. York, K. S. Coleman, J. L. Hutchison and M. L. H. Green, *Chem. Commun.*, 1999, 699.
10 M. H. Huang, A. Choudrey and P. Yang, *Chem. Commun.*, 2000, 1063.
11 S. Bhattacharrya, S. K. Saha and D. Chakravorty, *Appl. Phys. Lett.*, 2000, **76**, 3896.
12 V. M. Cepak and C. R. Martin, *J. Phys. Chem. B*, 1998, **102**, 9985.
13 B. M. I. van der Zande, M. R. Bohmer, L. G. J. Fokkink and C. Schonenberger, *Langmuir*, 2000, **16**, 451.
14 Y. Y. Yu, S. S. Chang, C. L. Lee and C. R. C. Wang, *J. Phys. Chem. B*, 1997, **101**, 6661.
15 C. A. Foss, G. L. Hornyak, J. A. Stockert and C. R. Martin, *J. Phys. Chem.*, 1994, **98**, 2963.

Synthesis, characterization and C–H activation reactivity of bis(ethylene) boratabenzene rhodium complexes†

David H. Woodmansee, Xianhui Bu and Guillermo C. Bazan*

Departments of Chemistry and Materials, University of California, Santa Barbara, CA 93106, USA. E-mail: bazan@chem.ucsb.edu

Received (in Irvine, CA, USA) 16th November 2000, Accepted 13th February 2001
First published as an Advance Article on the web 13th March 2001

Reaction of Li[C_5H_5B–Ph] with [$RhCl(C_2H_4)_2]_2$ gives [C_5H_5B–Ph]$Rh(C_2H_4)_2$ 1 in 91% yield; similarly, Li[C_5H_5B–NMe_2] with [$RhCl(C_2H_4)_2]_2$ gives [C_5H_5B–NMe_2]$Rh(C_2H_4)_2$ 2 in 85% yield; single crystal X-ray analysis studies of 1 and 2 show a molecular geometry analogous to those of the Cp and Cp* complexes; the use of 1 and 2 in promoting alkane boration was evaluated against the activity of Cp*$Rh(C_2H_4)_2$ 3; the boratabenzene complexes 1 and 2 show faster initiation, but yield less thermally stable catalysts than 3.

Advances in the chemistry of homogeneous transition metal complexes containing boratabenzene (Bb) ligands[1] have shown that it is possible to control the catalytic activity at the metal by choice of the boron substituent.[2] The dependence of significant elementary reactions on the electron density at the metal and how these parameters change as a function of Bb structure have also been studied.[3] Dialkylaminoboratabenzene is a considerably stronger donor than phenylboratabenzene, and both are considerably weaker than the isoelectronic cyclopentadienyl (Cp) or pentamethylcyclopentadienyl (Cp*) ligands.[4] Given a Cp or Cp*-based catalyst, it is possible to obtain a nearly isostructural complex by Bb substitution, however these species will display slightly different catalytic cycles.[5]

Cp* complexes of Group 9 metals have been intensely studied in C–H activation reactions.[6] Recently, Iverson and Smith[7] and Hartwig and coworkers[8] have demonstrated that complexes such as Cp*$Ir(PMe_3)H(Cy)$ (Cy = *c*-C_6H_{11}), Cp*$Rh(C_2H_4)_2$[9] **3** and Cp*Rh(η^4-C_6Me_6) mediate the selective functionalization of unactivated alkanes. In particular, the rhodium complexes are highly effective in catalyzing the reaction of 4,4,4′,4′,5,5,5′,5′-octamethyl-2,2′-bi-1,3,2-dioxaborolane (pinBBpin) to 2-(1-octyl)-4,4,5,5-tetramethyl-1,3,2-dioxaborolane.[8] The importance of alkane functionalization is well appreciated and motivates considerable research.[10]

In view of the interest in these reactions, we decided to investigate whether boratabenzene complexes could participate in C–H activation processes. Three-center–two-electron interactions of type **A**[11] are known, which could weaken the M–H bond strength. It is also expected[12] that the nitrogen on aminoboratabenzene ligands will coordinate to Lewis acids, as in **B**. Precoordination of a diborane or a borane–hydride would

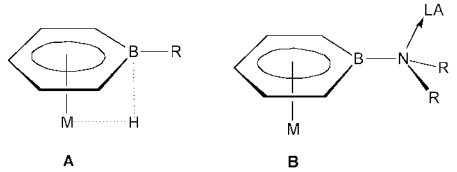

increase the local concentration of reactant near the vicinity of the metal center. Finally it is anticipated that in cycles that involve oxidative addition/reductive elimination sequences, the Bb counterparts will show more facile reductive elimination steps.[13]

In this contribution we report the synthesis and characterization of [C_5H_5B–Ph]$Rh(C_2H_4)_2$ **1** and [C_5H_5B–NMe_2]$Rh(C_2H_4)_2$ **2**. Phenyl and dimethylamino functionalities were chosen because they correspond to the weakest and strongest donors, respectively.[3] We also show that **1** and **2** can be used to catalyze C–H activation processes, that the boron substituent influences the reactivity of rhodium and that the relative stabilities of the resulting Bb catalysts are lower than that of the Cp* counterpart.

Reaction of Li[C_5H_5B–Ph][14] with [$RhCl(C_2H_4)_2]_2$, followed by standard workup, provides **1** in 85% yield as a red–orange powder [eqn. (1)].[15] A similar protocol, starting with Li[C_5H_5B–NMe_2], gives **2** in 91% yield.

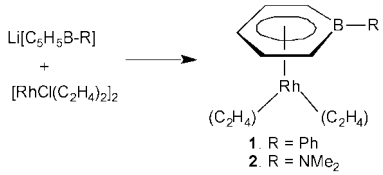

(1)

Single crystal X-ray diffraction studies of **1** (Fig. 1) and **2** (Fig. 2)‡ confirm the isostructural relationship to **3**.[16] Three independent molecules are present in the unit cell of **2**, which differ slightly on the rotation of the Bb ring relative to the '$Rh(C_2H_4)_2$' base. The B–Rh distance is shorter for **1** (2.398 Å for **1**; av. = 2.516 Å for **2**) and the B–N distances in the three molecules of **2** are consistent with B–N π-bonding.[17] Interestingly, in both **1** and **2**, the Bb ring is rotated such that the boron atom sits above one of the ethylene ligands.

The ^{1}H NMR signals of the ethylene ligands in **1** and **2** show variable temperature behavior. Two doublets are observed at the

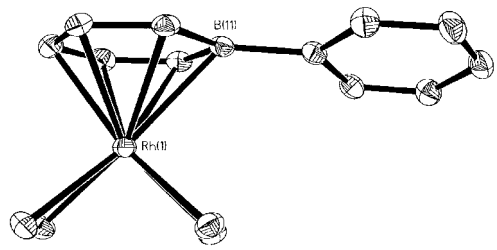

Fig. 1 ORTEP drawing of **1**; hydrogen atoms omitted for clarity.

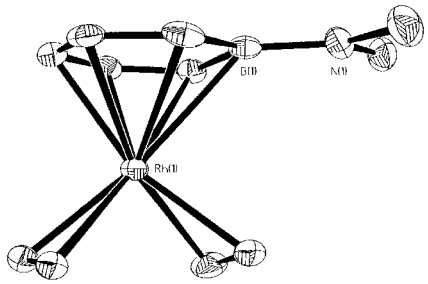

Fig. 2 ORTEP drawing of one of the three independent molecules in the crystal of **2**; hydrogen atoms omitted for clarity.

† Electronic supplementary information (ESI) available. Complete details for experimental procedures. See http://www.rsc.org/suppdata/cc/b0/b009246k/

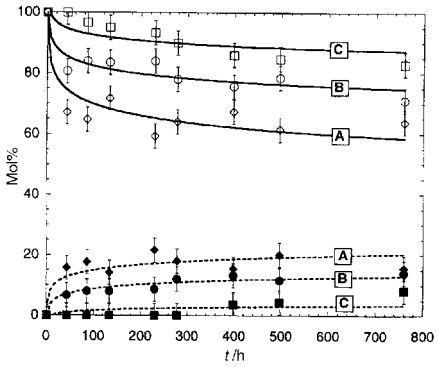

Fig. 3 Mol% of boron present as pinBBpin (——) and pinB–octyl (- - - -) as a function of time for reactions at 50 °C, containing (a) **1**, (b) **2** and (c) **3**; the lines are included to aid the eye.

low-temperature limit, which coalesce into a single resonance as the temperature increases. These data indicate facile ethylene rotation about the axis joining the metal to the center of the C=C bond. This propeller-like motion is well known in the cyclopentadienyl counterparts such as **3**[18] and its rate depends on the back-bonding ability of the metal.[19] From ^{1}H NMR coalescence experiments, $\Delta G^{\ddagger}$ = 60(3) kJ mol^{-1} (T_c = 311 K) for **1** and 50(3) kJ mol^{-1} (T_c = 265 K) for **2**. Both barriers are lower than that observed for **3** (71.5 kJ mol^{-1} at 340 K),[19] and are consistent with less efficient back bonding to ethylene in the Bb complexes.

To compare how **1** and **2** catalyze C–H activation reactions relative to **3**, we examined the boration of octane[20] with pinBBpin [eqn. (2)], under the reagent ratios and conditions established by Hartwig and coworkers.[8] The progress of the reactions was monitored by ^{11}B NMR spectroscopy against an internal standard [B(C_6F_5)$_3$ inside a capillary]. Product identity was further confirmed by use of GC–MS analysis.

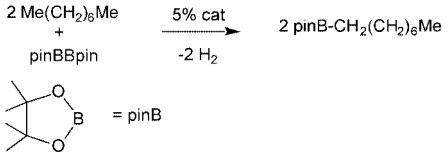

(2)

Fig. 3 shows the consumption of pinBBpin as a function of time using **1**, **2** or **3** with octane as the solvent at 50 °C, together with the molar percent of pinB–octyl. Mass balance is compensated by the formation of pinB–H (not shown). The reaction with **1** is most active at initial reaction times, followed by those of **2** and then **3**. As the reaction progresses, the activity quickly shuts down for the three cases. For **1**, the reaction yield of pinB–octyl is *ca*. 20% (assuming that one mole of pinBBpin yields two moles of pinB–octyl),[8] while for **3** the yield is only 7%. When the reaction temperature is 95 °C, the reactions mixtures containing **1** and **2** become inactive after 24 h and achieve only 15% conversion (Fig. 4). For the Cp* counterpart, the reaction continues until all starting material is consumed. The addition of mercury (300 and 3250 equiv. relative to Rh) does not affect the course of the reaction and suggests that the reactions are mediated by homogenous species.[21]

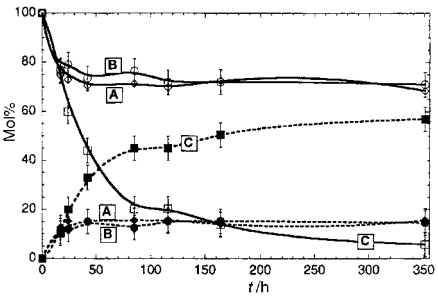

Fig. 4 Mol% of boron present as pinBBpin (——) and pinB-octyl (- - - -) as a function of time for reactions at 95 °C, containing (a) **1**, (b) **2** and (c) **3**; the lines are included to aid the eye.

In summary, we have shown that Bb complexes are capable of participating in catalytic C–H functionalization reactions. Under specific conditions these Bb complexes can initiate the reaction more quickly than their Cp* analogs. However, Bb compounds are less thermally stable and degrade before the reaction in eqn. (2) reaches completion. Compounds such as **1** and **2** may provide catalytic C–H activation possibilities for reactions that require milder conditions.

We are grateful to the Department of Energy, the ACS PRF and Equistar Chemicals LP for financial assistance.

Notes and references

‡ *Crystal data*: for **1**: $C_{15}H_{18}BRh$, M = 312.01, orthorhombic, $P2_12_12_1$, T = 293(2) K, λ = 0.71073 Å, a = 7.490(2), b = 8.566(2), c = 20.509(5) Å, V = 1315.8(5) Å^3, Z = 4, D_c = 1.575 Mg m^{-3}, μ = 1.271 mm^{-1}, reflections collected 7954, independent reflections 3001 [R(int) = 0.0459], final R indices [$I > 2\sigma(I)$]: $R1$ = 0.0266, $wR2$ = 0.0505, largest diff. peak, hole: 0.816, −0.447 e Å^{-3}.

For **2**: $C_{11}H_{19}BNRh$, M = 278.99, monoclinic, $P2_1/c$, T = 293(2) K, λ = 0.71073 Å, a = 7.101(4), b = 17.021(8), c = 29.49(2) Å, β = 94.873(9)°, V = 3551(3) Å^3, Z = 12, D_c = 1.565 Mg m^{-3}, μ = 1.404 mm^{-1}, reflections collected 30927, independent reflections 6270 [R(int) = 0.1217], final R indices [$I > 2\sigma(I)$]: $R1$ = 0.0374, $wR2$ = 0.0541, largest diff. peak, hole 0.529, 0.427 e Å^{-3}. CCDC 154632 and 154633.

1 G. E. Herberich and H. Ohst, *Adv. Organomet. Chem.*, 1986, **25**, 199; A. J. Ashe III, S. Al-Ahmad and X. G. Fang, *J. Organomet. Chem.*, 1999, **581**, 92.
2 G. C. Bazan, G. Rodriguez, A. J. Ashe III, S. Al-Ahmad and C. Müller, *J. Am. Chem. Soc.*, 1996, **118**, 2291; G. C. Bazan, G. Rodriguez, A. J. Ashe III, S. Al-Ahmad and J. W. Kampf, *Organometallics*, 1997, **16**, 2492; J. S. Rogers, G. C. Bazan and C. K. Sperry, *J. Am. Chem. Soc.*, 1997, **119**, 9305; R. W. Barnhart, G. C. Bazan and T. Mourey, *J. Am. Chem. Soc.*, 1998, **120**, 1082.
3 R. A. Lee, R. J. Lachicotte and G. C. Bazan, *J. Am. Chem. Soc.*, 1998, **120**, 6037; G. C. Bazan, W. D. Cotter, Z. J. A. Komon, R. A. Lee and R. J. Lachicotte, *J. Am. Chem. Soc.*, 2000, **122**, 1371.
4 G. E. Herberich, C. Engelke and W. Pahlmann, *Chem. Ber.*, 1979, **112**, 607.
5 H. Bönnemann, *Angew. Chem., Int. Ed. Engl.*, 1985, **24**, 248.
6 B. A. Arndtsen, R. G. Bergmann, T. A. Mobley and T. H. Peterson, *Acc. Chem. Res.*, 1995, **28**, 154; R. H. Crabtree, *Chem. Rev.*, 1995, **95**, 2599.
7 C. N. Iverson and M. R. Smith III, *J. Am. Chem. Soc.*, 1999, **121**, 7696.
8 H. Chen, S. Schlecht, T. C. Semple and J. F. Hartwig, *Science*, 2000, **287**, 1995.
9 K. Moseley, J. W. Kang and P. M. Maitlis, *J. Chem. Soc.*, 1970, 2875.
10 W. D. Jones, *Science*, 2000, **287**, 1942; K. M. Waltz, C. N. Muhoro and J. F. Hartwig, *Organometallics*, 1999, **18**, 3383; R. H. Carbtree, *Chem. Rev.*, 1985, **85**, 245; in *Activation and Functionalization of Alkane*, ed. C. L. Hill, Wiley, New York, 1989; A. E. Shilov and G. B. Shul'pin, *Chem. Rev.*, 1997, **97**, 2879; R. A. Periana, D. J. Taube, S. Gamble, H. Taube, T. Satoh and H. Fujii, *Science*, 1998, **280**, 560; S. S. Stahl, J. A. Labinger and J. E. Bercaw, *Angew. Chem., Int. Ed.*, 1998, **37**, 2180.
11 G. E. Herberich, B. D. Hessner and D. P. J. Köffer, *J. Organomet. Chem.*, 1989, **362**, 243; C. K. Sperry, W. D. Cotter, R. A. Lee, R. J. Lachicotte and G. C. Bazan, *J. Am. Chem. Soc.*, 1998, **120**, 7791.
12 J. S. Rogers, R. J. Lachicotte and G. C. Bazan, *J. Am. Chem. Soc.*, 1999, **121**, 1288.
13 A. J. Ashe III, S. Al-Ahmad, J. W. Kampf and V. G. Young, *Angew. Chem., Int. Ed. Engl.*, 1997, **36**, 2014; C. K. Sperry, G. C. Bazan and W. D. Cotter, *J. Am. Chem. Soc.*, 1999, **121**, 1513.
14 A. J. Ashe III and P. Shu, *J. Am. Chem. Soc.*, 1971, **93**, 1804.
15 For the synthesis of boratabenzene–rhodium(cyclooctadiene) complexes see: G. E. Herberich, H. J. Becker, K. Carsten, C. Engelke and W. Koch, *Chem. Ber.*, 1976, **109**, 2382.
16 R. Blom, D. W. H. Rankin, H. E. Robertson and R. N. Perutz, *J. Chem. Soc. Dalton Trans.*, 1993, 1983; M. Arthurs, C. Piper, D. A. Morton-Blake and M. G. B. Drew, *J. Organomet. Chem.*, 1992, **429**, 257.
17 P. Paetzold, *Adv. Inorg. Chem.*, 1987, **31**, 123.
18 R. Cramer, *J. Am. Chem. Soc.*, 1964, **86**, 217.
19 R. Cramer and J. Mrowca, *Inorg. Chim. Acta*, 1971, **5**, 528.
20 Purified according to: D. D. Perrin and W. L. F. Armarego, *Purification of Laboratory Chemicals*, Pergamon Press, Oxford, 1988.
21 D. R. Anton and R. H. Crabtree, *Organometallics*, 1983, **2**, 855; K. S. Weddle, J. D. Aiken III and R. G. Finke, *J. Am. Chem. Soc.*, 1998, **120**, 5653.

A new heptadentate tripodal ligand leading to a gadolinium complex with an improved relaxation efficiency

Yann Bretonnière,[a] Marinella Mazzanti,*[a] Jacques Pécaut,[b] Frank A. Dunand[c] and André E. Merbach[c]

[a] *Laboratoire de Reconnaissance Ionique et Matériaux Moléculaires, Service de Chimie Inorganique et Biologique, UMR 5046, Département de Recherche Fondamentale sur la Matière Condensée, CEA-Grenoble, 38054 Grenoble, Cedex 09, France. E-mail: mazzanti@drfmc.ceng.cea.fr*

[b] *Laboratoire de Chimie de Coordination, Service de Chimie Inorganique et Biologique, UMR 5046, Département de Recherche Fondamentale sur la Matière Condensée, CEA-Grenoble, 38054 Grenoble, Cedex 09, France.*

[c] *Institut de Chimie Minérale et Analytique, Université de Lausanne, BCH, CH-1015 Lausanne, Switzerland*

Received (in Cambridge, UK) 17th January 2001, Accepted 21st February 2001
First published as an Advance Article on the web 13th March 2001

The new heptadentate tripodal ligand tpaa containing three pyridinecarboxylate binding units reacts with Gd(III) in water to give a thermodynamically stable complex which displays high relaxivity.

In recent years there has been a rapid growth in the field of coordination chemistry of lanthanides(III) with polydentate ligands.[1,2] This development has been mainly spurred by the application of gadolinium complexes as magnetic resonance imaging (MRI) contrast agents[3–5] and of europium or terbium complexes as luminescent probes in time-resolved fluoroimmunoassays.[6,7] The key property of an efficient contrast agent is its ability to enhance the nuclear magnetic relaxation rate of solvent water protons. This can be achieved by the presence of a high number of inner sphere water molecules in combination with fast water exchange, long rotational correlation times and long electronic relaxation times. The current approach to achieve higher relaxivity consists in increasing the rotational correlation time (τ_R) by increasing the molecular weight of the contrast agent through the formation of macromolecular complexes by covalent or non-covalent linkage of Gd(III) chelates to large biomolecules. However the effective enhancement of the rotational correlation time attainable in these systems is limited by the residence lifetime (τ_M) of the coordinated water molecule. The relatively long τ_M of Gd complexes of octadentate ligands such as the currently approved contrast agents $[Gd(dtpa)(H_2O)]^{2-}$ and $[Gd(dota)(H_2O)]^{-}$† appears to be related to the dissociative exchange mechanism of the water molecule. This prevents dendrimeric Gd(III) derivatives[8] and non-covalent adducts of Gd(III) chelates with large bio-molecules[9] from attaining their potential relaxation enhancement.

Heptadentate ligands allow the coordination of two water molecules in the inner sphere of the metal and consequently yield higher relaxivity with respect to Gd(III) complexes of octadentate ligands. In addition Gd(III) complexes containing heptadentate[10,11] or hexadentate ligands[12] have shown faster water-exchange rates than complexes with octa-coordinating ligands. In spite of this, heptadentate ligands have seldom been used in the design of Gd(III) based contrast agents.[5]

Here we report the synthesis of the new tripodal ligand, tpaa (containing three pyridinecarboxylate arms connected to a nitrogen atom)‡ which acts an an heptadendate chelator thus allowing the coordination of at least two water molecules in its lanthanide(III) complexes. Moreover the ligand tpaa leads to an uncharged Gd(III) complex which should show reduced potential for osmotic cell damage.

As shown in Scheme 1, H_3tpaa **2** was prepared by hydrolysis of the heptadentate ligand tpa(trisamide) **1**, obtained from the condensation of the 6-aminomethyl derivative and the 6-chloromethyl derivative of 2-(*N*,*N*-diethylcarboxamido)pyridine in the presence of K_2CO_3. The protonation constants of H_3tpaa were determined by potentiometry [pK_{a1} = 2.5(2), pK_{a2} = 3.3(1), pK_{a3} = 4.11(6), pK_{a4} = 6.78(4)]. The $[Gd(tpaa)(H_2O)]_2$ complex **3**§ was obtained as colorless crystals suitable for X-ray diffraction¶ by slow evaporation of a 1 : 1 solution of $GdCl_3$ and H_3tpaa in water. Fig. 1 shows the structure of **3** in which two Gd(III) centers are joined by two bridging oxygens from the monodentate carboxylate groups of two different tpaa ligands to form a dimeric complex. The metal ion is nine-coordinated by four nitrogens and three carboxylate oxygens of tpaa, one water molecule and a carboxylate oxygen of the neighboring complexed ligand. The coordination geometry can be described as a distorted tricapped trigonal prism in which O(1), N(2) and N(3) occupy the capping positions in the rectangular faces. The average Gd–N(pyridyl) distance [2.56(4) Å] is shorter than the average Gd–N(tert) distances found in the neutral nonadentate complexes $(Gd(do3ma)(H_2O)]_2$[13]† (2.66 Å) and [Gd(dtpa-bea)(H_2O)][14]† [2.70(3) Å], while the distance Gd–N(apical) [2.7886(19) Å] in **3** is 0.222 Å longer than the sum of the ionic radii of Gd and N, probably due to the oligomerization. The Gd–O(water) distance [2.399(2) Å] is shorter than those found in the dimeric 9-coordinate complex $[Gd(do3ma)(H_2O)]_2$[13]† [2.451(5) and 2.56(4) Å] and in the eight-coordinate complex $[Gd(tren\text{-}Me\text{-}3,2\text{-}hopo)(H_2O)_2]$[15]† [2.446(5) and 2.436(4) Å], but is similar to the Gd–O(water) distances in the monomeric nine-coordinate complex [Gd(dtpa-bea)(H_2O)] [2.42(3) Å].[14] The tendency of the $[Gd(tpaa)(H_2O)_2]$ complex to oligomerize in the solid state, and in the conditions generated in the electrospray analysis arises from the presence of a relatively exposed metal face due to the flexibility of the unhindered tpaa ligand. This property of aminocarboxylate to oligomerize in water has only been observed before in the presence of macrocyclic ligands.

In order to avoid toxicity, Gd(III) complexes are required to be highly thermodynamically (and preferably also kinetically) stable for application as contrast agents. Potentiometric data

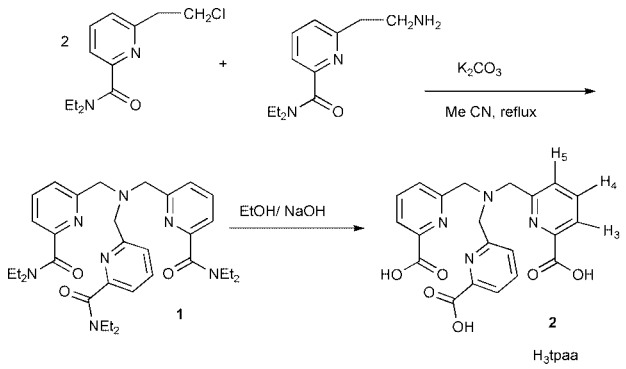

Scheme 1

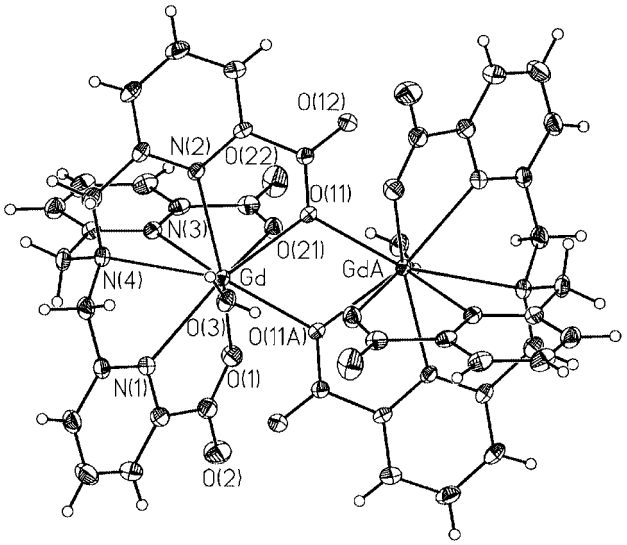

Fig. 1 Crystal structure of $[Gd(tpaa)(H_2O)]_2{\cdot}7H_2O$ **3** with thermal ellipsoids at 30% probability. Selected bond lengths (Å): Gd···GdA 4.125, Gd–O(11) 2.,4726(17), Gd–O(11A) 2.4010(15), Gd–O(1) 2.4414(17), Gd–O(21) 2.3783(17), Gd–O(3) 2.399(2), Gd–N(1) 2.546(2), Gd–N(2) 2.6051(19), Gd–N(3) 2.531(2), Gd–N(4) 2.7886(19) (symmetry transformation used to generate equivalent atoms A: $-x + 1$, $-y$, $-z$).

obtained by titration of 1:1 metal:H_3tpaa mixtures in the pH range 2.8–8 can be satisfactorily fitted to eqn. (1) leading to a

$$Gd^{3+} + tpaa^{3-} \rightleftharpoons [Gd(tpaa)] \quad \log\beta_{GdL} = 10.2(2) \qquad (1)$$

pM value of 11.2 for Gd(III) {$-\log[M]_{free}$ at pH 7.4, $[M]_{total}$ = 1 μM, $[tpaa]_{total}$ = 10 μM} which indicates a reasonable physiological stability of $[Gd(tpaa)(H_2O)]_2$ as compared to the lowest pGd value (15.8) found in commercially used MRI agents.[5] Only a small decrease of the physiological stability is observed for the Gd complex of the less rigid podate tpaa with respect to Gd complexes containing macrocyclic heptadentate ligands such as do3a (14.5).[5] Moreover we expect that the stability and the solubility of the gadolinium complex could be improved by suitable substitution of the pyridine rings.

The relaxivity r_{1p} is a critical property of a potential contrast agent which represents the increase in the water proton nuclear magnetic relaxation rate per millimolar concentration of the paramagnetic compound. At 60 MHz, r_{1p} was measured to be 13.3 $mM^{-1}\ s^{-1}$ at 25 °C (9.37 $mM^{-1}\ s^{-1}$ at 37 °C) for **3**. This value is higher than those found in the mono-aquo complexes $[Gd(dtpa)(H_2O)]^{2-}$ or $[Gd(dota)(H_2O)]^{-}$ (4.3 $mM^{-1}\ s^{-1}$ at 25 °C) and than the values found in bis-aquo complexes containing macrocyclic heptadentate ligands such as $[Gd(do3a)(H_2O)_2]$† (6.1 $mM^{-1}\ s^{-1}$ at 25 °C) and $[Gd(pcta[12])(H_2O)_2]$† (6.9 mM s^{-1} at 25 °C).[10,11] This high value cannot simply be explained by the presence in aqueous solution of two water molecules coordinated to the Gd(III) ion (each molecule makes a contribution to the relaxivity of *ca.* 2.5 $mM^{-1}\ s^{-1}$). A preliminary study of the temperature dependence of the relaxivity indicates that the inner sphere water molecules are involved in a fast exchange with the bulk water, in agreement with what is expected for complexes containing heptadentate ligands. More detailed NMR studies are in progress in order to elucidate the origin of this high relaxivity.

In summary we have described a new type of heptadentate ligand which leads to a gadolinium complex with unusually high relaxivity and fast water exchange.

Moreover the straightforward introduction of substituents on the pyridine rings allows us to envisage ligands with a higher water solubility, containing functional groups capable of non-covalent or covalent interactions with slowly moving substrates such as proteins or polysaccharides. This could lead to contrast agents with longer rotational correlation times and consequently higher relaxivities or to increased specific tissue affinity.

This work was supported by the Commissariat à l'Energie Atomique. We thank Colette Lebrun for help in recording the mass spectra.

Notes and references

† H_4dota = 1,4,7,10-tetraazacyclododecane-*N*,*N*′,*N*″,*N*‴-tetraacetic acid, H_5dtpa = diethylenetriaminepentaacetic acid, H_3dtpa-bea = dtpa-bis(ethylamide), H_3pcta[12] = 3,6,9,15-tetraazabicyclo[9.3.1]pentadeca-1(15),11,13-triene-3,6,9-triacetic acid, H_3tren-Me-3,2-hopo = tris[(3-hydroxy-1-methyl-2-oxo-1,2-didehydropyridine-4-carboxamido)ethyl]amine, H_3do3ma = (1*R*,4*R*,7*R*)-α,α′,α″-trimethyl-1,4,7,10-tetraazacyclododecane-1,4,7-triacetic acid, H_3do3a = 1,4,7,10-tetraazacyclododecane-1,4,7-triacetic acid.

‡ H_3tpaa = α,α′,α″nitrilo(6-methyl-2-pyridinecarboxylic acid). The synthesis of tris[6-(2-*N*,*N*-diethylcarbamoyl)pyridyl)methyl]amine **1** will be described in detail elsewhere. Anal. Calc. for $H_3tpaa{\cdot}1.6\ H_2O$ ($C_{21}H_{15.2}N_4O_{7.6}$): C, 55.9; H, 4.7; N, 12.4; O, 26.9. Found: C, 55.9; H, 4.8; N, 12.25; O, 27.0%. δ_H(400 MHz, DMSO-d_6, 298 K). 7.92 (H4, t, 3H), 7.89 (H3/5, dd, 3H, *J* 7.2, 1.8 ż), 7.82 (H3/5, dd, 3H, *J* 7.2, 1.8 Hz), 3.93 (CH_2, s, 6H); δ_C(400 MHz, DMSO-d_6, 298 K), 165.9 (CO_2), 158.9, 147.6, 137.6, 125.9, 122.8, 59.2 (CH_2). ES^+-MS: *m/z* 423 $[LH_3 + H]^+$, 445 $[LH_3 + Na]^+$, 461 $[LH_3 + K]^+$, 401 $[LH_3 + Na - CO_2]^+$; 417 $[LH_3 + K - CO_2]^+$ ES^-: *m/z* 459 $[LH_3 + K - 2H]^-$; 421 $[LH_3 - H]^-$; 415 $[LH_3 + K - 2H - CO_2]^-$; 322 $[LH_3 + K - C_7H_7NO_2]^-$.

§ *Experimental*: stoichiometric amounts of H_3tpaa (30 mg, 0.07 mmol) and of $GdCl_3{\cdot}6H_2O$ (26.4 mg, 0.07 mmol) were dissolved in boiling water (10 mL). Slow cooling followed by slow evaporation of the resulting solution yielded the gadolinium complex $[Gd(tpaa)(H_2O)]_2{\cdot}7H_2O$ as colorless crystals (35 mg, yield 75%). ES^+-MS (based on the most abundant isotope of GD): *m/z* 578 $[Gd(tpaa) + H]^+$, 590 $[Gd(tpaa - CO_2)OH + K]^+$, 616 $[Gd(tpaa) + K]^+$, 763 $[Gd(tpaa) + KCl + K]^+$, 1154 $\{[Gd(tpaa)]_2 + H\}^+$, 1193 $\{[Gd(tpaa)]_2 + K\}^+$.

¶ *Crystal data*: $[Gd(tpaa)(H_2O)]_2{\cdot}7H_2O$ **3**, $C_{42}H_{48}N_8O_{21}Gd_2$, *M* = 1315.38, orthorhombic, *Pbcn*, *a* = 13.0347(15), *b* = 15.6221(17), *c* = 23.506(4) Å, *V* = 4786.5(12) $Å^3$, *Z* = 4, D_c = 1.825 g cm^{-3}, μ = 2837 mm^{-1}. 5943 independent reflections (θ_{max} = 29.12°) were collected at 298 K. Refinement using the SHELXTL 5.05 package on all data converged at R_1 = 0.0234, *wR*2 = 0.0496. Data were collected using a Bruker SMART CCD area detector three-circle diffractometer (Mo-Kα radiation, λ = 0.71073 Å, graphite monochromator). CCDC 157262. See http://www.rsc.org/suppdata/cc/b1/b100657f/ for crystallographic data in .cif or other electronic format.

1 D. Parker and J. A. G. Williams, *J. Chem. Soc., Dalton Trans.*, 1996, 3613.
2 C. Piguet and J.-C. G. Bünzli, *Chem. Soc. Rev.*, 1999, **28**, 347.
3 R. B. Lauffer, *Chem. Rev.*, 1987, **87**, 901.
4 S. Aime, M. Botta, M. Fasano and E. Terreno, *Chem. Soc. Rev.*, 1998, **27**, 19.
5 P. Caravan, J. J. Ellison, T. J. McMurry and R. B. Lauffer, *Chem. Rev.*, 1999, **99**, 2293.
6 G. Mathis, *Clin. Chem.*, 1995, **41**, 1391.
7 *Bioanalytical Applications of Labeling Technologies*, ed. I. Hemmilä, T. Stahlberg and P. Mottram, Wallac-Oy, Turku, Finland, 1994.
8 E. Toth, D. Pubanz, S. Vauthey, L. Helm and A. Merbach, *Chem. Eur. J.*, 1996, **2**, 1607.
9 S. Aime, M. Botta, M. Fasano, G. S. Crich and E. Terreno, *J. Biol. Inorg. Chem.*, 1996, **1**, 312.
10 S. Aime, M. Botta, G. S. Crich, G. B. Giovenzana, R. Pagliarin, M. Sisti and E. Terreno, *Magn. Reson. Chem.*, 1998, **36**, S200.
11 S. Aime, M. Botta, G. S. Crich, G. B. Giovenzana, G. Jommi, R. Pagliarin and M. Sisti, *Inorg. Chem.*, 1997, **36**, 2992.
12 S. Hajela, M. Botta, S. Giraudo, J. Xu, K. N. Raymond and S. Aime, *J. Am. Chem. Soc.*, 2000, **122**, 11 228.
13 S. I. Kang, R. S. Ranganathan, J. E. Enswiler, K. Kumar, J. Gougoutas, M. F. Malley and M. F. Tweedle, *Inorg. Chem.*, 1993, **32**, 2912.
14 M. S. Konings, W. C. Dow, D. B. Love, K. N. Raymond, S. C. Quay and S. M. Rocklage, *Inorg. Chem.*, 1990, **29**, 1488.
15 J. Xu, S. J. Franklin, D. W. Whisenhunt, Jr and K. N. Raymond, *J. Am. Chem. Soc.*, 1995, **117**, 7245.

A first synthesis of (±)-2,3-dihydroxytrinervitanes†

Masahiro Hoshikawa, Kana Hayashi, Makoto Yagi and Tadahiro Kato*

Department of Chemistry, Faculty of Science, Science University of Tokyo, 1-3 Kagurazaka, Shinjuku-ku, Tokyo 162-8601, Japan. E-mail: tkato@chm1srv1.ch.kagu.sut.ac.jp

Received (in Cambridge, UK) 19th December 2000, Accepted 27th February 2001
First published as an Advance Article on the web 14th March 2001

The total synthesis of 2,3-dihydroxytrinervitanes, 1a and 1b, was performed from secotrinervitane-type allyl chloride 2

More than two decades ago, characterization of 2,3-dihydroxytrinervitanes **1a** and **1b** (Fig. 1) was reported as the typical defensive substances from several species of termite soldiers inhabiting the tropics.[1] In spite of their unique structure and interesting biological activity, the total synthesis of **1a** and **1b** remained unpublished.[2]

We have been greatly interested in the biogenetic-type synthesis of diterpenoids secreted by termites and have explored the synthetic route of trinervitane **3** and kempane **5** skeletons through the intermediate, allyl chloride **2**, as illustrated in Scheme 1.[3] Our further effort led to completion of the synthesis of trinervitanes **1a** and **1b** as a *dl*-form. This paper reports the result of our study.

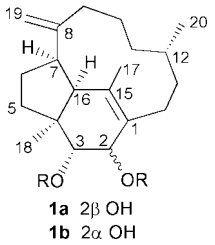

Fig. 1 Structure of 2β- and 2α-trinervitanes.

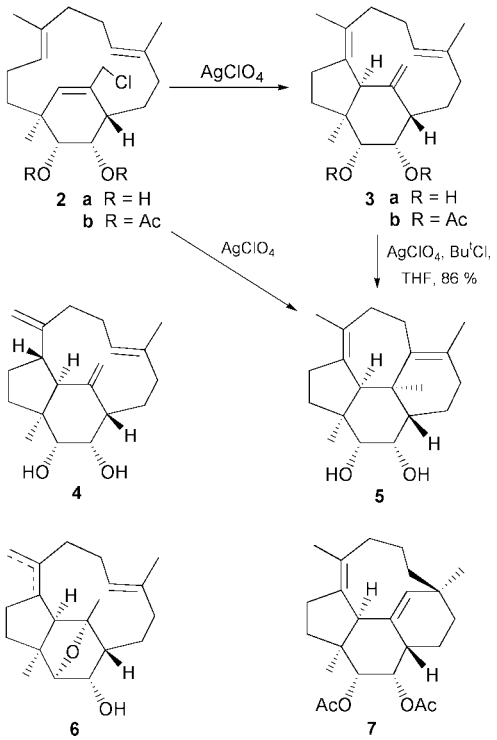

Scheme 1 Construction of trinervitane **3** and kempane **5** skeletons.

As reported previously,[4] the desired trinervitanes **3a** and **4** were provided in 68 and 5% yields, respectively, with accompanying formation of etheric compound **6** as unpurified minor product when **2a** was submitted to the reaction with $AgClO_4$ in THF at −20 °C. This ring-closure reaction depends largely on the reaction temperature, *i.e.* a completely different tetracyclic kempane diol **5** was formed in 50% yield when the reaction of **2a** with $AgClO_4$ was carried out at +20 °C. Treatment of **3a** at rt with $HClO_4$ in THF, prepared *in situ* by the reaction of *tert*-butyl chloride and $AgClO_4$, gave the kempane diol **5** in high yield. Based on this evidence, we first attempted to improve the yield of **3**.‡ We were surprised to find that completely different tetracyclic diacetate **7**[5] was isolated in high yield when diacetate **2b**, quantitatively prepared from **2a**, was treated with $AgClO_4$ in THF at rt. Eventually, **2b** was converted into **3b** in 91% yield by treatment with $AgClO_4$ (1.2 eq.) in the presence of pyridine (1.5 eq.) at rt.

The next step was focused on the regio- and face-selective hydrogenation of triene **3a** possessing three different types of double bonds. The PtO_2-catalyzed hydrogenation in MeOH afforded a 7:3 mixture of 11,12-dihydro derivatives, revealing the two remaining double bonds at 7(8) and 15(17) positions are inert under the employed conditions. The separation of the reduction products was unsuccessful at this stage since it forms prism-shaped mixed crystals, mp 92–94 °C and HPLC of the mixture showed the single peak under several conditions. As regards the reasonable conformation of the macro ring of the triene **3**, two gross structures are possible as shown in Fig. 2. The plane of the 11(12) double bond is perpendicular to the cyclohexane ring in one conformation (*perpendicular* conformation: PC) and horizontal in the other conformation (*horizontal* conformation: HC). The hydrogenation may occur from the opposite faces depending on the conformation, that is, the perpendicular conformation gives the 12β-methyl product by selective H_2 addition from the α-side. The horizontal conformation leads to the 12α-Me isomer by the preferential β-face attack, the opposite α-face being partly masked by the 15(17) double bond. The existence of **3a** as the horizontal conformation was deduced by the fact that **3a** is easily convertible to the cyclized products **5** and **7** under protonic conditions as mentioned in Scheme 1. The detailed NOESY experiments in the NMR spectrum of **3a** supported this deduction. Expecting the conformational change of the methylenecyclohexane moiety of **3a**, the five-membered carbonate ring was introduced at the 2 and 3 positions with carbonyldiimidazole to give **3c**. The 0.2 ppm up-field shift of 11-H of **3c** was observed, indicating the change of the chair-type cyclohexane ring of **3a** to the twisted form, in which the 15(17)

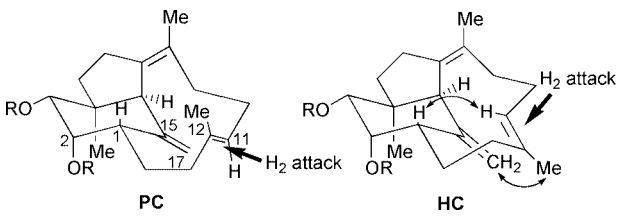

Fig. 2 Possible conformations of the triene **3**.

DOI: 10.1039/b010175n

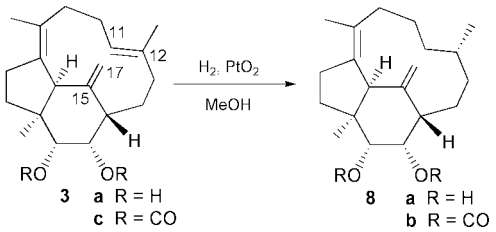

Scheme 2 Hydrogenation of triene **3**.

double bond locates more closely to the plane of the 11(12) double bond. The hydrogenation of **3c** in CH_2Cl_2 provided a 6:1 mixture of C_{12}-stereoisomers (Scheme 2). It was luckily found that both stereoisomers of the carbonate **8b** were easily separable by flash chromatography, affording the corresponding reduction products suitable for X-ray crystallographic analyses. The X-ray analyses demonstrated unequivocally the major product possessed 12α-Me configuration.

After removal of the carbonyl group of **8b**, the diol **8a** was treated with MOMCl (2 eq.) and diisopropylethylamine (4 eq.) in CH_2Cl_2 for 3 h at rt to furnish the 3-MOM ether **8c** in 74% yield accompanied with the 2-MOM ether (13%) and 2,3-diMOM ether **8d** (7%). The unnecessary minor products were converted to **8c** by hydrolysis (2 M HCl in MeOH), followed by etherification with MOMCl under the same conditions. The PCC oxidation of **8c** proceeded smoothly to give the corresponding ketone **9** in 91% yield (Scheme 3). For the isomerization of **9** to the conjugated enone **10**, we had to attempt several basic conditions[6] before finding the successful conditions of DBU in refluxing toluene for a week (89% yield). The convex face selective oxidation of **10c**, obtained from **10a** by the usual procedures, took place exclusively with MCPBA, affording the epoxide **11** in quantified yield.

The ring-opening conditions of the epoxide **11** were quite restricted since the 16-proton is labile under acidic and basic conditions. Of the reagents we examined TMSCl at −10 °C was the only choice and it gave a 1:1 mixture of **12** and its isomer **13** in 30% respective yields.[7] The hydrogenation of **12** afforded, as expected, a single product **14** (85%), the stereochemistry of the 7-position being assigned based on the convex selectivity as in the case of epoxidation of **10c**. The dehydration of the *tert*-alcohol **14** furnished a *ca.* 5:3:1 mixture of **10c**, **15** and trisubstituted isomer in total 83% yield. After separation with $AgNO_3$–SiO_2 column chromatography, **15** was reduced with LAH, giving an easily separable 1:1 mixture of 2,3-dihydroxytrinervitanes, **1a** and **1b**. The chemical shifts and coupling constants in the proton NMR of the synthetic materials were in complete accord with the reported values[1b] within experimental deviation due to the applied instruments.

Thus, we have accomplished the total synthesis of 2,3-dihydroxytrinervitanes in *dl*-form. Our recent study[8] on the enantiometrically pure synthetic intermediate may enable us to perform the enantiospecific synthesis of **1a** and **1b**.

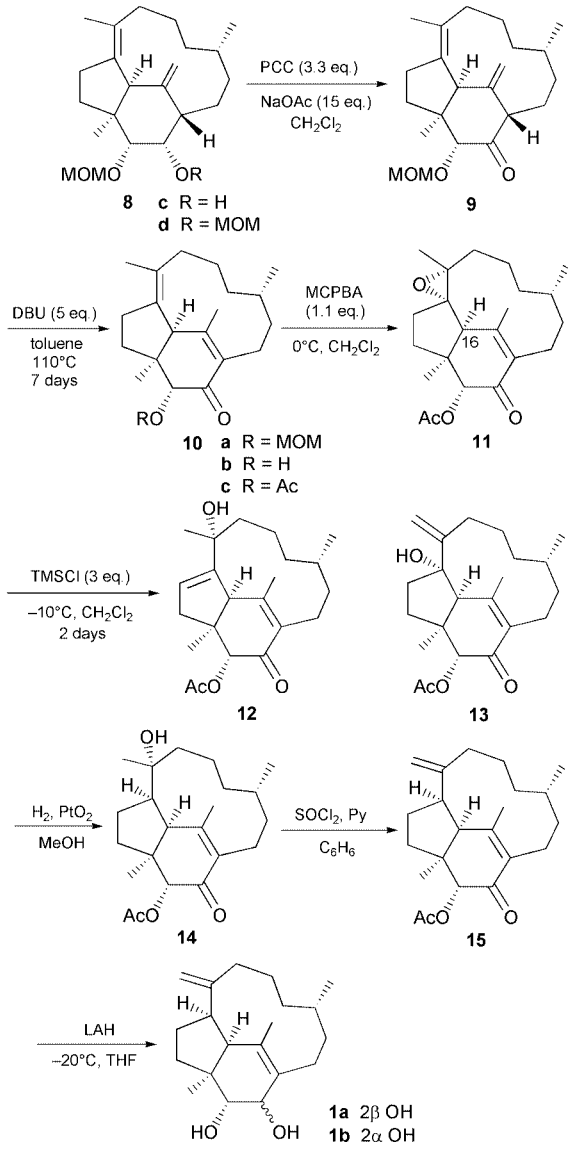

Scheme 3 Synthesis of (±)-trinervitanes **1a** and **1b**.

Notes and references

† This is Part 61 of Cyclization of Polyenes; for part 60, see ref. 3.
‡ The IR, ^1H and ^{13}C NMR and mass spectra were in agreement with all the new compounds.

1 Isolation; (*a*) G. D. Prestwich, S. P. Tanis, F. G. Pilkiewicz, I. Miura and K. Nakanishi, *J. Am. Chem. Soc.*, 1976, **98**, 6062; (*b*) J. Vrkoc, M. Budesinsky and P. Sedmera, *Collect. Czech. Chem. Commun.*, 1978, **43**, 2478. X-ray; G. D. Prestwich, S. P. Tanis, J. P. Springer and J. Clardy, *J. Am. Chem. Soc.*, 1976, **98**, 6061.

2 Synthesis of 2,3-deoxytrinervitane; M. Kodama, M. Matsushita, S. Yoshio, K. Tanimoto, E. Noda, H. Hioki and Y. Fukuyama, *The 39th Symposium on Natural Products*, 1997, **39**, 289.

3 T. Kato, T. Hirukawa, T. Suzuki, M. Tanaka, M. Hoshikawa, M. Yagi, M. Tanaka, S. Takagi and N. Saito, *Helv. Chim. Acta*, in press, 2001, and references cited therein.

4 T. Kato, M. Tanaka, M. Hoshikawa and M. Yagi, *Tetrahedron Lett.*, 1998, **39**, 7553.

5 Diol prepared from deprotection of **7**; ^1H NMR (400 MHz, $CDCl_3$) δ 1.08 (s, Me(20)), 1.18 (s, Me(18)), 1.57 (s, Me(19)), 3.19 (s, H-C(16)), 3.49 (br s, H-C(3)), 3.84 (br s, H-C(2)), 5.56 (s, H-C(17)); ^{13}C NMR (100 MHz, $CDCl_3$) δ 22.6 (q, C(18)), 22.7 (q, C(19)), 23.4 (t, C(14)), 24.2 (t, C(10)), 28.7 (q, C(20)), 30.0 (t, C(6)), 32.0 (t, C(13)), 34.0 (t, C(9)), 37.8 (t, C(5)), 39.3 (s, C(12)), 39.3 (d, C(1)), 45.6 (t, C(11), 46.5 (s, C(4)), 59.2 (d, C(16)), 72.7 (d, C(3)), 74.7 (d, C(2)), 132.2 (s, C(8)), 136.2 (s, C(7)), 137.1 (s, C(15)) and 139.6 (d, C(17)).

6 Isomerization was unsuccessful under the following conditions; i) Bu^{t}OK, THF, reflux, ii) NaH, THF, iii) NaH, DMSO, reflux, iv) LDA.

7 Hydroboration–oxidation of **10** took place at the undesired position, affording the 8(19)-dihydro-7-hydroxy derivative of **13**. All the trials of dehydration of the 7,8-diol of **10**, obtained by OsO_4 oxidation, gave only hopeless results.

8 T. Kato, S. Ebihara, T. Furukawa, H. Tanahashi and M. Hoshikawa, *Tetrahedron: Asymmetry*, 1999, **10**, 3691.

ChemComm

Intramolecular carbonyl olefination of esters. Regioselective preparation of enol ethers of cyclic ketones by the titanocene(II)-promoted reaction of alkyl ω,ω-bis(phenylthio)alkanoates

Md. Abdur Rahim, Hironori Sasaki, Jun Saito, Tooru Fujiwara and Takeshi Takeda*

Department of Applied Chemistry, Tokyo University of Agriculture and Technology, Koganei, Tokyo 184-8588, Japan. E-mail: takeda-t@cc.tuat.ac.jp

Received (in Cambridge, UK) 19th December 2000, Accepted 21st February 2001
First published as an Advance Article on the web 14th March 2001

The treatment of alkyl ω,ω-bis(phenylthio)alkanoates with $Cp_2Ti[P(OEt)_3]_2$ produced enol ethers of 5-, 6-, 7-, and 9-membered cyclic ketones.

Intramolecular reactions of phosphorous ylides and related α-phosphorous carbanions with ketones and aldehydes have been used by a number of workers for the preparation of cycloalkenes, including complex natural products.[1] However, intramolecular carbonyl olefinations of esters using the phosphorous carbanions are generally unsuccessful because these reactions end up with the formation of acylation products.[2] Only the preparation of certain five- and six-membered cyclic compounds, in which the formation of a double bond is facilitated by π-conjugation with a carbonyl group or an aromatic ring, has been achieved.[3] Transition metal–carbene complexes and related reagents have been employed for this transformation. Stille and Grubbs have described the formation of titanium–carbene complexes by the ring-opening metathesis of strained norbornylene derivatives and their intramolecular reaction with an ester carbonyl.[4] Although tungsten–carbene complex promoted transformation of benzyl 2-benzylhex-5-enoate into 3-benzyl-2-benzyloxycyclopentene *via* olefin metathesis–carbonyl olefination was reported, the experimental details including the yield of the product were not disclosed.[5] Mortimore and Kociénski reported the cyclization of 4,4-dibromobutyl benzoate utilizing a $TiCl_4$–Zn–TMEDA system.[6] The olefination product, 6-phenyl-3,4-dihydro-2*H*-pyran, however, was obtained in only a poor yield. The intramolecular McMurry coupling of keto esters is regarded as a formal intramolecular olefination of esters, and various cyclanones have been prepared by this method.[7] Although this reaction is useful for the preparation of furans and benzofurans,[8] its application to the synthesis of alicyclic vinyl ethers has yet to appear. Formal intramolecular carbonyl olefination consisting of the intermolecular carbonyl olefination of esters and subsequent ring closing metathesis has been employed for the synthesis of cyclic vinyl ethers.[9] The studies described above indicate that the intramolecular carbonyl olefination of esters still remains a problem to be solved.

Recently we reported a new method for carbonyl olefination using a thioacetal–$Cp_2Ti[P(OEt)_3]_2$ **1** system.[10] Since this reaction is useful for the olefination of esters, we have studied its application to the synthesis of cyclic vinyl ethers. Unfortunately the attempt to prepare monocyclic vinyl ethers by

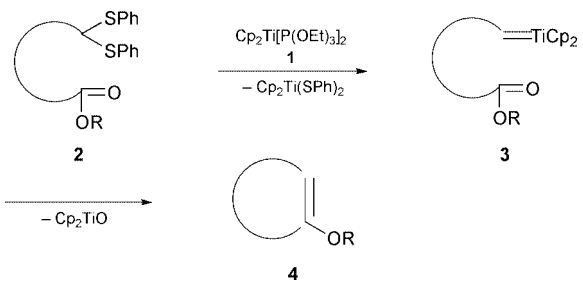

Scheme 1

Table 1 Intramolecular carbonyl olefination of alkyl ω,ω-bis(phenylthio)alkanoates **2**

Entry	Ester **2**	Temp. (Time/h)	Product **4** (Yield/%)
1	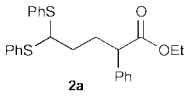 **2a**	reflux (2)	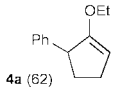 **4a** (62)
2	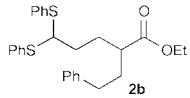 **2b**	15 °C (3)	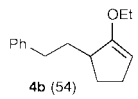 **4b** (54)
3	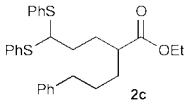 **2c**	rt (3)	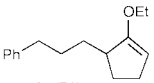 **4c** (71)
4	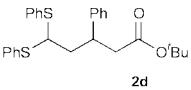 **2d**	rt (5)	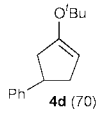 **4d** (70)
5	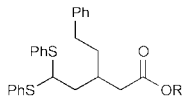 **2e**: R = Et	reflux (2)	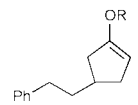 **4e** (44)
6	**2f**: R = Bu^t	rt (3)	**4f** (75)
7	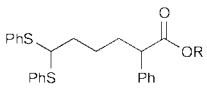 **2g**: R = Et	reflux (3)	 **4g** (53)
8	**2h**: R = Bu^t	reflux (3)	**4h** (56)
9	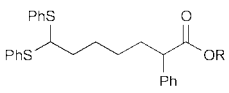 **2i**: R = Me	reflux (3)	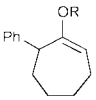 **4i** (68, 73[a])
10	**2j**: R = Pr^i	reflux (3)	**4j** (67)
11	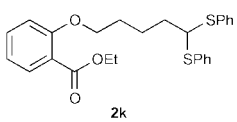 **2k**	rt (3)	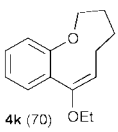 **4k** (70)
12	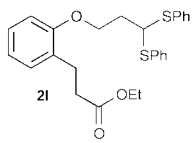 **2l**	rt (5)	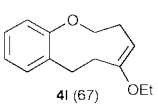 **4l** (67)

[a] The reaction was performed on a 5 mmol scale.

DOI: 10.1039/b010156g

the titanocene(II)-promoted olefination of ω,ω-bis(phenylthio)alkyl alkanoates was unsuccessful owing to the concomitant formation of oligomers.[11] Herein we describe the intramolecular reaction of alkyl ω,ω-bis(phenylthio)alkanoates **2**. This reaction proceeds by way of the titanium–carbene complexes **3** to produce a wide variety of vinyl ethers of cyclic ketones **4** without formation of any oligomer (Scheme 1).

When methyl 2-phenyl-7,7-bis(phenylthio)heptanoate **2i** was treated with the low-valent titanium species **1** (4 equiv.) at room temperature for 1 h, the complete disappearance of the starting material was observed. Column chromatography using basic alumina gave the cyclic vinyl ether **4i** in 59% yield. The cyclization of **2i** in refluxing THF produced **4i** in better yield (Table 1, Entry 9). In a similar manner, the enol ethers of five-, six-, and seven-membered cyclic ketones were obtained in good yields by the reaction of alkyl α-substituted ω,ω-bis(phenylthio)alkanoates. The substituent α to the carbonyl group is not crucial for the present olefination. The reactions of the esters carrying a substituent at the β-position also produced the corresponding cyclic compounds **4d**–**f**.† It was found that the *tert*-butyl esters gave better yields than the corresponding ethyl esters in these reactions (see Entries 5 and 6). In some case, we observed the partial isomerization of the initial olefination product to the tetrasubstituted cycloalkene. This isomerization, however, was absolutely depressed when the reaction was carried out at 15 °C (Entry 2).

The advantage of the present preparation is that the starting materials are easily prepared by the use of organosulfur building blocks. Thus the esters **2k** and **l** were obtained by the Williamson ether synthesis utilizing ω,ω-bis(phenylthio)alkanols and were transformed into the nine-membered cyclic vinyl ethers **4k** and **l** with high stereoselectivity. The *E*-configuration of their double bonds was determined by NOESY.

All the experiments described above were carried out on a small scale (0.5 mmol). Since an intramolecular reaction generally requires high dilution conditions to prevent the competitive intermolecular reaction, decrease in the yield is sometimes a serious problem upon scale up. We examined a gram-scale reaction of **2i** to confirm the synthetic utility of the present reaction. Using a slightly modified procedure,[12] the cycloheptene **4i** was obtained in better yield (73%) than for the smaller scale reaction (Entry 9).

In conclusion, we have established the first versatile method for the regioselective preparation of vinyl ethers of cyclic ketones by the intramolecular carbonyl olefination of esters. Further study on the application of this methodology to the synthesis of a variety of heterocycles is currently in progress.

This work was supported by a Grant-in-Aid for Scientific Research from the Ministry of Education, Science, Sports, and Culture, of Japanese Government (No. 11119214 and 11440213).

Notes and references

† *A typical experimental procedure*: to 6 ml of a THF solution of the titanocene(II) reagent **1,** prepared from titanocene dichloride (498 mg, 2.0 mmol), magnesium turnings (58 mg, 2.4 mmol), triethyl phosphite (0.69 ml, 4.0 mmol), and finely powdered molecular sieves 4 Å (200 mg),[13] was added 10 ml of a THF solution of **2f** (237 mg, 0.50 mmol) dropwise over 20 min at room temperature under argon. After stirring for 3 h, the reaction was quenched by addition of 1 M NaOH (20 ml). The insoluble materials were filtered off through Celite and washed with ether (10 ml). The layers were separated, and the aqueous layer was extracted with ether (3 ×30 ml). The combined organic extracts were washed with 1 M NaOH (20 ml) and dried over K_2CO_3. After removal of the solvent, the residue was chromatographed over alumina gel (deactivated with 5% of H_2O; eluted with 1% triethylamine in hexane) to afford 92 mg (75%) of **4f**.

1 K. B. Becker, *Tetrahedron*, 1980, **36**, 1717; B. E. Maryanoff and A. B. Reitz, *Chem. Rev*., 1989, **89**, 863.
2 For example, see H. O. House and H. Babad, *J. Org. Chem.*, 1963, **28**, 90.
3 P. J. Murphy and S. E. Lee, *J. Chem. Soc., Perkin Trans. 1*, 1999, 3049.
4 J. R. Stille and R. H. Grubbs, *J. Am. Chem. Soc.*, 1986, **108**, 855; J. R. Stille, B. D. Santarsiero and R. H. Grubbs, *J. Org. Chem.*, 1990, **55**, 843.
5 G. C. Fu and R. H. Grubbs, *J. Am. Chem. Soc.*, 1993, **115**, 3800.
6 M. Mortimore and P. Kociénski, *Tetrahedron Lett.*, 1988, **29**, 3357.
7 J. E. McMurry and D. D. Miller, *J. Am. Chem. Soc.*, 1983, **105**, 1660; J. E. McMurry and D. D. Miller, *Tetrahedron Lett.*, 1983, **24**, 1885; M. Iyoda, T. Kushida, S. Kitami and M. Oda, *J. Chem. Soc., Chem. Commun.*, 1987, 1607.
8 A. Banerji and S. K. Nayak, *J. Chem. Soc., Chem. Commun.*, 1990, 150; A. Fürstner, D. N. Jumbam and H. Weidmann, *Tetrahedron Lett.*, 1991, **32**, 6695; A. Fürstner and A. Hupperts, *J. Am. Chem. Soc.*, 1995, **117**, 4468.
9 O. Fujimura, G. C. Fu and R. H. Grubbs, *J. Org. Chem.*, 1994, **59**, 4029; K. C. Nicolaou, M. H. D. Postema, E. W. Yue and A. Nadin, *J. Am. Chem. Soc.*, 1996, **118**, 10 335; K. C. Nicolaou, M. H. D. Postema and C. F. Claiborne, *J. Am. Chem. Soc.*, 1996, **118**, 1565.
10 Y. Horikawa, M. Watanabe, T. Fujiwara and T. Takeda, *J. Am. Chem. Soc.*, 1997, **119**, 1127; T. Takeda, M. Watanabe, N. Nozaki and T. Fujiwara, *Chem. Lett.*, 1998, 115; M. A. Rahim, H. Taguchi, M. Watanabe, T. Fujiwara and T. Takeda, *Tetrahedron Lett.*, 1998, **39**, 2153; T. Takeda, M. Watanabe, M. A. Rahim and T. Fujiwara, *Tetrahedron Lett.*, 1998, **39**, 3753; T. Fujiwara, N. Iwasaki and T. Takeda, *Chem. Lett.*, 1998, 741.
11 M. A. Rahim, T. Fujiwara and T. Takeda, *Tetrahedron*, 2000, **56**, 763.
12 For the preparation of the titanocene(II) reagent **1** on a large scale, see T. Fujiwara, K. Yanai, K. Shimane, M. Takamori and T. Takeda, *Eur. J. Org. Chem.*, 2001, 155.
13 T. Fujiwara, Y. Kato and T. Takeda, *Tetrahedron*, 2000, **56**, 4859.

First isolation of *N*-alkoxyaminyl radicals

Yozo Miura* and Tatsuya Tomimura

Department of Applied Chemistry, Faculty of Engineering, Osaka City University, Sumiyoshi-ku, Osaka 558-8585, Japan. E-mail: miura@a-chem.erg.osaka-cu.ac.jp

Received (in Cambridge, UK) 17th January 2001, Accepted 22nd February 2001
First published as an Advance Article on the web 14th March 2001

***N*-(*tert*-Butoxy)-*N*-(2,4-diaryl-6-*tert*-butylphenyl)aminyls have been isolated; this is the first isolation of *N*-alkoxyaminyl radicals.**

Although a variety of *N*-alkoxyalkylaminyl (RṄOR),[1–3] *N*-alkoxyvinylaminy[4] and *N*-alkoxyarylaminyl radicals (ArṄOR)[1,2,5–10] have been investigated for a long period and persistent *N*-alkoxyaminyls have been found, there are no reports of isolation of *N*-alkoxyaminyls. This is in contrast to the chemistry of thioaminyl radicals (RṄSR). In the case of thioaminyls a variety of radicals have been isolated and their X-ray crystallographic and magnetic studies have been carried out.[11,12] Isolable stable free radicals have attracted much attention as spin sources or building blocks of organic magnetic materials.[13,14] In this communication we report on the first isolation of *N*-alkoxyarylaminyl radicals and their characterization.

N-(*tert*-Butoxy)-*N*-(2,4-diphenyl-6-*tert*-butylphenyl)aminyl (**1a**) was prepared by treating the lithium salt of 2,4-diphenyl-6-*tert*-butylaniline with two equiv. of *tert*-butyl peroxybenzoate

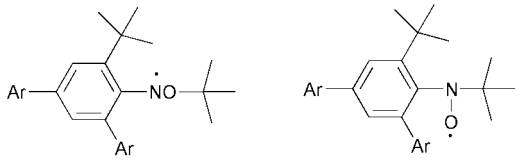

1 **2**

a Ar = Ph
b Ar = 4-FC_6H_4
c Ar = 4-ClC_6H_4
a-d_{10} Ar = C_6D_5

at −78 °C in THF.[15] The reaction mixture showed a deep red colour, and TLC analysis indicated formation of a red coloured product, along with the presence of the unreacted starting aniline and some minor products. Separation of the red zone by column chromatography (silica gel, 3 : 1 hexane–benzene) gave **1a** in 24% yield. In the same manner, **1b** and **1c** were isolated in 17 and 20% yields, respectively. Recrystallization of the isolated radical solid from MeOH afforded red plates (**1a**, **c**) or red needles (**1c**). The structures of radicals were confirmed by the IR spectra and elemental analyses. In the IR spectra no NH absorption was observed and the elemental analyses were in satisfactory agreement with the calculations in all cases. For **1a** single crystal X-ray crystallographic analysis was performed.

N-Alkoxyarylaminyls **1** were stable in solution, even in the presence of atmospheric oxygen and, although **1a** was heated at 80 °C in degassed benzene for 10 d, 80% of the radical survived and no rearrangement to the corresponding aminoxyl **2** was observed.[8,16] These observations indicate that **1** is an oxygen insensitive and thermally stable radical.

Since **1a** gave a single crystal suitable for the X-ray crystallographic analysis on recrystallization from MeOH, we performed an X-ray crystallographic study on **1a**.† The ORTEP drawing of the molecular structure is shown in Fig. 1. The X-ray crystallographic data shows the following structural characteristics. The N and O atoms are coplanar with the benzene ring A within 0.05 Å. While benzene ring C makes a dihedral angle of 41.5° with benzene ring A, benzene ring B makes a dihedral angle of 86.0° with benzene ring A, indicating that there is a large steric congestion around the radical center. Accordingly, it is likely that delocalization of the unpaired electron spin onto benzene ring B is very or negligibly small, and this means that the benzene ring B plays an important role in steric protection, but does not contribute to electronic stabilization of the radical. Since the N–O bond has the character of a two center–three electron bond where the unpaired electron is accommodated in the anti-bonding orbital,[17] its bond length in **1** [1.358(2) Å] is somewhat shorter than typical N(sp^2)–O bonds (1.397 Å).[18]

The EPR parameters are summarized in Table 1. All the EPR spectra of **1** were a simple 1 : 1 : 1 triplet signal (a_N = 0.997–1.01 mT, g = 2.0041–2.0042) with a large peak-to-peak linewidth (ΔH_{pp}) of 0.31–0.33 mT, and no hyperfine couplings due to protons were observed. The large ΔH_{pp} is attributed to the presence of many unresolved protons with very small

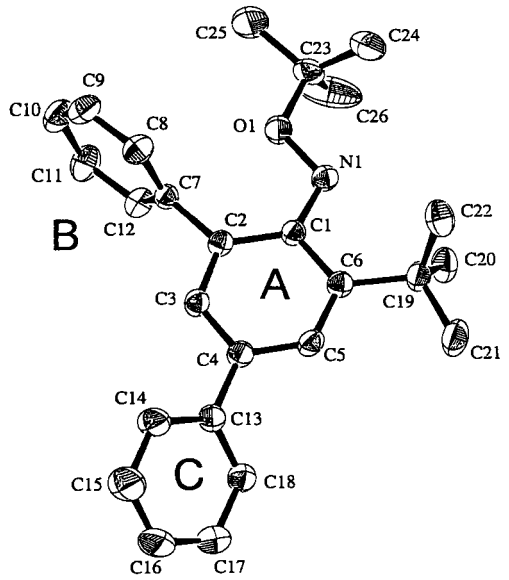

Fig. 1 ORTEP drawing of **1a**. Selected bond lengths and angles and torsion angles are as follows: C1–N1 1.368(3) and N1–O1 1.358(2) Å; C1–N1–O1 111.1(2) and N1–O1–C(23) 113.1(2)°; C2–C1–N1–O1 6.8(3), C6–C1–N1–O1 −175.4(2) and C1–N1–O1–C23 −173.9(2)°.

Table 1 EPR and UV-Vis spectroscopic data for **1**, **3** and **4** in benzene at 20 °C

Radical	a_N/mT	g	λmax/nm (ε/l mol^{-1}cm^{-1})
1a	1.01	2 .0042	545 (1230), 334 (28 600)
1b	0.997	2.0041	545 (1270), 334 (27 200)
1c	0.999	2.0042	553 (1120), 342 (29 900)
1a-d_{10}[ab]	1.00	2.0042	—
3	1.27	2.0062	—
4	0.987	2.0038	—

[a] The hyperfine coupling constants are determined by computer simulation. [b] a_H for the anilino *meta* protons (2H) is 0.170 mT.

DOI: 10.1039/b100698n

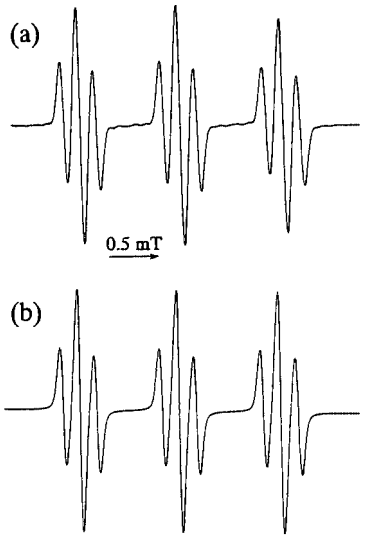

Fig. 2 EPR spectrum of **1a**-d_{10} in benzene at 20 °C. (a) Observed spectrum; (b) computer simulated spectrum.

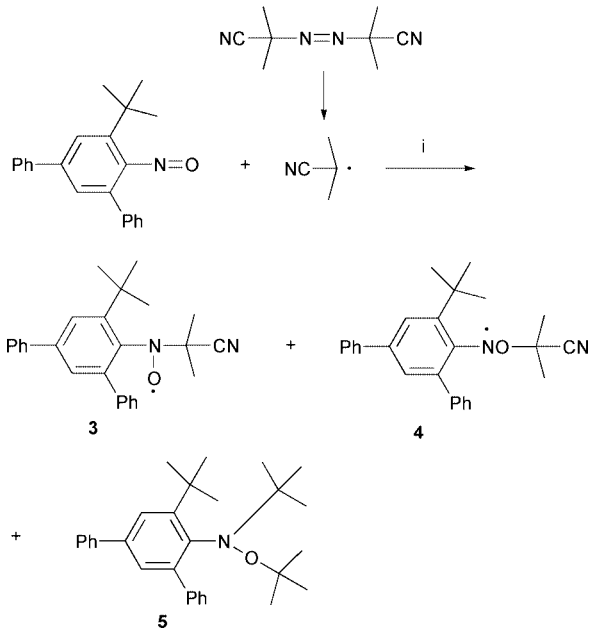

Scheme 1

hyperfine coupling constants. To reduce the ΔH_{pp} values, the two benzene rings of **1a** were deuterated. The deuterated radical **1a**-d_{10} was prepared from (2,4-diphenyl-d_5)-6-*tert*-butylaniline and *tert*-butyl peroxybenzoate in the same manner as for that of **1a**. As shown in Fig. 2, the EPR spectrum of **1a**-d_{10} is split into 1 : 2 : 1 triplets of a 1 : 1 : 1 triplet, and computer simulation gave a_N = 1.00 mT and a_H (2H) = 0.170 mT. The protons giving a_H of 0.170 mT are assigned to the anilino *meta* protons.

To compare the a_N and g values of **1** with those for the corresponding aminoxyls **3** was generated by addition of the 2-cyanoprop-2-yl radical to 2,4-diphenyl-6-*tert*-butylnitrosobenzene (Scheme 1). After a mixture of 2,4-diphenyl-6-*tert*-butylnitrosobenzene and 1,1′-azobis(propane-2-carbonitrile) in benzene was heated at 80 °C for 1 h, EPR spectra of the solution were measured at 20 °C. The spectra showed the presence of **3** and **4** in a ratio of *ca.* 3 : 1. While the a_N and g values for **3** are 1.27 mT and 2.0062, those for **4** are 0.989 mT and 2.0038, indicating that a_N of **3** are much larger than those for **1** or **4**, as well as the g value. Although **4** could be isolated as a red oil with a spin concentration of 89% in 3.9% yield by column chromatography, **3** could not be isolated in pure form. Since **5** is the main product and its mobility (R_f) in column chromatography was almost the same as that of **3**, **3** was separated as a mixture with **5**.

The UV-Vis spectra were measured using benzene as the solvent. The data are listed in Table 1. A λmax at 545–553 nm with ε of 1120–1270 l mol^{-1}cm^{-1} is observed, which is attributable to the characteristic red colours of **1**.

Notes and references

† Crystal data for **1a**: $C_{26}H_{30}ON$, M = 372.53, orthorhombic, a = 36.9243(9), b = 11.2495(3), c = 10.9599(3) Å, V = 4552.5(5) Å^3, T = 296 K, space group *Pbca* (# 61), Z = 8, μ(Mo-Kα) = 0.65 cm^{-1}, 13507 reflections measured, 5112 unique (R_{int} = 0.017) which were used in all calculations. R = 0.078, R_w = 0.116, GOF = 1.57. CCDC 159014. See http://www.rsc.org/suppdata/cc/b1/b100698n/ for crystallographic files in .cif format.

1 W. C. Danen and F. A. Neugebauer, *Angew. Chem., Int. Ed. Engl.*, 1975, **14**, 783.
2 W. C. Danen, C. T. West and T. T. Kensler, *J. Am. Chem. Soc.*, 1973, **95**, 5716.
3 H. Woynar and K. U. Ingold, *J. Am. Chem. Soc.*, 1980, **102**, 3813.
4 W. Ahrens, K. Wieser and A. Berndt, *Tetrahedron Lett.*, 1973, 3141.
5 A. T. Balaban, P. T. Frangopol, M. Frangopol and N. Negoita, *Tetrahedron*, 1967, **23**, 4661.
6 S. Terabe and R. Konaka, *J. Chem. Soc., Perkin Trans. 2*, 1973, 369.
7 N. Negoita, R. Baican and A. T. Balaban, *Tetrahedron Lett.*, 1973, 1877.
8 W. Ahrens and A. Berndt, *Tetrahedron Lett.*, 1973, 4281.
9 R. A. Kaba and K. U. Ingold, *J. Am. Chem. Soc.*, 1976, **98**, 7375.
10 M. Negareche, M. Boyer and P. Tordo, *Tetrahedron Lett.*, 1981, **22**, 2879.
11 Y. Miura, in *Trends Org. Chem.*, 1997, **6**, 197; Y. Miura, in *Recent Res. Dev. Org. Chem.*, 1998, vol. 2, 251–268.
12 Y. Miura, T. Tomimura and Y. Teki, *J. Org. Chem.*, 2000, **65**, 7889 and references cited therein.
13 *Magnetic Properties of Organic Materials*, ed. P. M. Lahti, Marcel Dekker, New York and Basel, 1999.
14 Proceedings of the 6th International Conference on Molecule-Based Magnets, ed. O. Kahn, *Mol. Cryst. Liq. Cryst.*, 1999, **334**, 1–712; **335**, 1–706.
15 A. C. M. Meesters and M. H. Benn, *Synthesis*, 1978, 679.
16 R. West and P. Boudjouk, *J. Am. Chem. Soc.*, 1973, **95**, 3983.
17 N. C. Baird, *J. Chem. Educ.*, 1977, **54**, 291.
18 F. H. Allen, O. Kennard, D. G. Watson, L. Brammer, A. G. Orpen and R. Taylor, *J. Chem. Soc., Perkin Trans. 2*, 1987, S1.

ChemComm

A solvothermal route to capped CdSe nanoparticles

Ujjal K. Gautam,[a] Michael Rajamathi,[b] Fiona Meldrum,[c] Peter Morgan[d] and Ram Seshadri[a]

[a] *Solid State and Structural Chemistry Unit, Indian Institute of Science, Bangalore 560 012 India. E-mail: seshadri@sscu.iisc.ernet.in*
[b] *Department of Chemistry, St. Joseph's College, Bangalore 560 025, India*
[c] *Department of Chemistry, Queen Mary and Westfield College, University of London, Mile End Road, London, UK E1 4NS. E-mail: f.c.meldrum@qmw.ac.uk*
[d] *Rockwell Science Center, 1049 Camino Dos Rios, Thousand Oaks, CA 91360, USA. E-mail: pemorgan@rsc.rockwell.com*

Received (in Cambridge, UK) 23rd November 2000, Accepted 28th February 2001
First published as an Advance Article on the web 14th March 2001

We present a convenient and safe one-pot route to capped 3 nm CdSe nanoparticles making use of common starting materials and inexpensive, low-boiling solvents under solvothermal conditions; H_2Se required for the reaction is generated *in situ* through the aromatization of tetralin by Se.

In semiconductor nanocrystals of materials such as CdSe, the happy union of bulk and molecular properties results in a rich photophysics that is not only interesting in its own right, but also lends itself to a number of applications.[1] One such application is the use of CdSe nanocrystals as fluorescent probes in biological imaging.[2] The key to all semiconductor nanoparticle research is the ability to prepare stable (typically through surface passivation – also referred to as capping) monodisperse particles that have very few defects. A number of techniques have been used to achieve this and have recently been reviewed in this journal.[3] Perhaps most widely used is the method introduced by Bawendi and coworkers[4] which involves the reaction of an organocadmium precursor with an Se source in a high temperature solvent such as trioctyl phosphine oxide (TOPO), which also doubles as a capping agent.

We have been interested in the preparation of chalcogenide nanoparticles from inexpensive starting materials of low toxicity. Cadmium stearate is easy to prepare† and dissolves in organic solvents such as toluene, in which it is known to react with H_2Se to yield chalcogenides. Since relatively high temperatures are required to prepare defect-free, monodisperse nanoparticles, we have carried out the synthesis in toluene using stainless steel bombs. H_2Se is not easily handled under these conditions, so we have employed the aromatization of tetralin to naphthalene by elemental Se in order to prepare H_2Se *in situ*. The addition of small amounts of dodecanethiol as a capping agent results in 3 nm nanoparticles with a narrow size distribution. The dark solution obtained from the reaction precipitates solid products when the solvent polarity is increased through the addition of propan-2-ol. The precipitated solid easily redissolves in toluene forming bright orange solutions.

Our procedure is inspired by the simple method of Mitchell and Morgan[5] who prepared $CuCr_2Se_4$ in mineral oil at 330 °C using stearate salts as the metal source and the aromatization of sitosterol as the H_2Se source. Qian and coworkers[6] have recently reported the preparation of 7 nm CdSe nanoparticles under solvothermal conditions using ethylenediamine at 120 °C.

Fig. 1 displays a TEM image of the nanoparticles. While a few large particles (*ca.* 10 nm) are occasionally seen, the vast majority of the particles are smaller; with a mean diameter of 3.0 nm and a standard deviation of 0.16 nm (*ca*. 5% of the mean). The powder XRD profile of the nanoparticles acquired in transmission mode is displayed in Fig. 2(a). We find that the profile is well fitted by the Rietveld[7] method to the cubic (a = 6.01(1) Å) zinc blende structure rather than the usual hexagonal wurtzite structure. Stacking 3 nm × 3 nm slabs of CdSe along the c axis in hexagonal and cubic (in different proportions) arrangements permits simulations using the DIFFaX[8] program, which confirms a cubic zinc blende structure relatively free from hexagonal defects. The Rietveld fit and cubic and hexagonal DIFFaX simulations (using a correlation length of about 3 nm in the c direction) are also displayed in Fig. 2(a).

The UV–VIS absorption spectrum in toluene [Fig. 2(b)] shows absorption peaks at 514 and 412 nm, consistent with quantum confinement. Bawendi, Steigerwald and Brus[9] have discussed the correlation of absorption spectra and particle diameter for various nanoparticles. According to their correlation, the particle size corresponding to the spectrum in Fig. 2(b) is close to about 2.5 nm and not 3.0 nm as obtained here from TEM. The discrepancy could arise from (i) the different crystal structure obtained in the present case and (ii) the difficulty in estimating sizes from the very small, low-contrast particles seen in the TEM image. Toluene solutions of the nanoparticles also show strong photoluminescence as seen from the emission spectrum displayed in Fig. 2(b) as a dashed line.

The presence of the thiol capping was verified from C–H stretches in the FTIR spectrum, as well as by thermogravimetry in air. We observe a weight loss of 35% before 400 °C which, if ascribed to the thiol cap, suggests that for 3 nm particles there is one thiol molecule for every 22 Å^2 of nanoparticle surface.

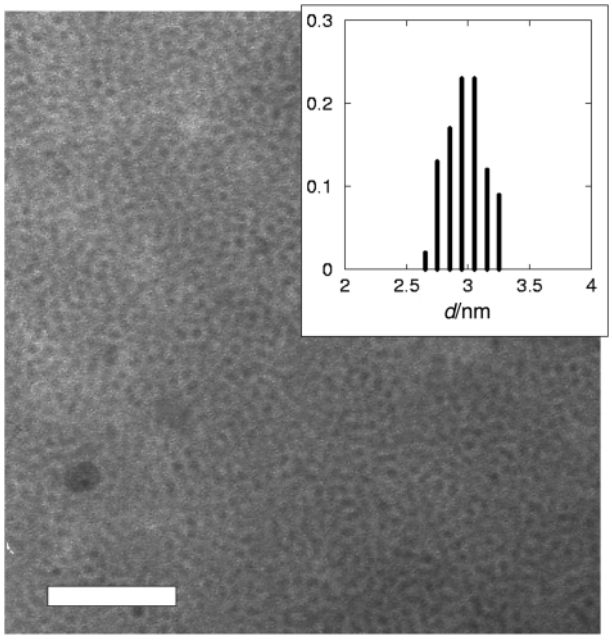

Fig. 1 TEM image of a relatively dense arrangement of CdSe nanoparticles showing a tendency to close packing in the plane (bar = 50 nm). The inset shows a histogram of particle sizes.

DOI: 10.1039/b009394g

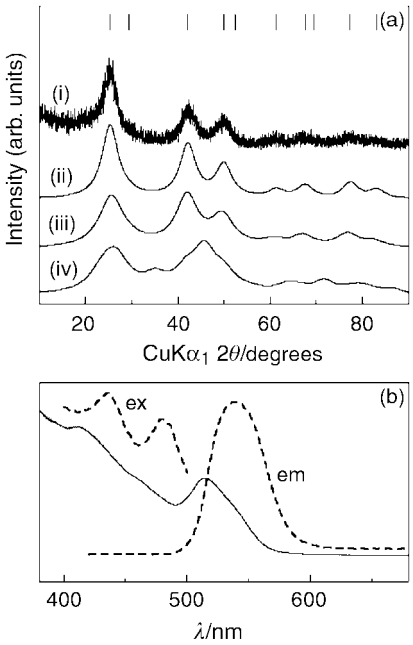

Fig. 2 (a) (i) Powder XRD pattern of CdSe compared with (ii) the background-subtracted Rietveld fit (R_{Bragg} = 6.4%), (iii) DIFFaX simulation of 3 nm cubic zinc blende stacking of CdSe, and (iv) DIFFaX simulation of a 3 nm hexagonal wurtzite stacking of CdSe. The vertical lines at the top are expected peak positions for the cubic zinc blende structure. (b) UV–VIS absorption spectrum of the nanoparticles in toluene. Dashed lines display luminescence spectra: emission (em) following excitation at 400 nm, and excitation (ex) following emission at 540 nm.

Energy dispersive X-ray analysis (EDAX) suggested that the Cd : Se ratio is nearly 1 : 1 (within 4%). When S is included in the analysis, the atomic ratios of S : Cd : Se are close to 20 : 40 : 40 (within a 5% error). Using a model of 3 nm particles with a thiol every 22 Å² of surface, we obtain a calculated S : Cd : Se of 120 : 260 : 260 (atoms) in reasonable agreement with the EDAX.

In conclusion, we present a new and convenient route to prepare large quantities of capped CdSe nanoparticles. The route can easily be extended to other nanoparticle chalcogenides of interest. The major advantages of the present route are that (i) there is no need to handle materials under inert conditions, (ii) inexpensive solvents can be used, and (iii) volatile, toxic organometallics can be avoided. Our method yields cubic (rather than hexagonal) CdSe nanoparticles, perhaps as a result of the autogenous pressure that develops during the preparative procedure.

This work has been supported by the Department of Science and Technology, India.

Notes and references

† Cadmium stearate [$Cd(St)_2$], prepared from the reaction of $Cd(OH)_2$ with molten stearic acid, could be reprecipitated from toluene and analyzed by FTIR and gravimetry. In a typical reaction 1.36 g (2 mmol) of [$Cd(St)_2$], 0.158 g (2 mmol) of Se, 0.2 g (1.5 mmol) of tetralin and 0.1 g (0.5 mmol) of dodecanethiol were taken in 50 ml of toluene in a stainless steel bomb (*ca.* 70% filling, Teflon gasket) and placed in an oven that had been preheated to 250 °C. After 5 h the bomb was removed and cooled to room temperature. The solid product obtained by precipitation as mentioned in the text was dried at 50 °C in air overnight. XRD patterns were acquired on a STOE STADI-P diffractometer in transmission geometry using a 0.02° step scan. Samples were prepared for TEM by placing a drop of the toluene solution of CdSe nanoparticles on a carbon-coated, Formvar-covered Cu TEM grid and subsequently drawing off excess solution. The grids were examined using a JEOL 2000EX TEM operating at 120 kV. The EDAX analysis used a Link ISIS system attached to a JEOL JSM 5600LV scanning electron microscope. UV–VIS spectra were recorded on a Hitachi U3000 spectrophotometer and photoluminescence on a Perkin Elmer L50 B spectrometer.

1 M. Nirmal and L. Brus, *Acc. Chem. Res.*, 1999, **32**, 407.
2 W. C. W. Chan and S. Nie, *Science*, 1998, **281**, 2016; M. Bruchez, Jr., M. Moronne, P. Gin, S. Weiss and A. P. Alivisatos, *Science*, 1998, **281**, 2013.
3 M. Green and P. O'Brien, *Chem. Commun.*, 1999, 2235.
4 C. B. Murray, D. J. Norris and M. G. Bawendi, *J. Am. Chem. Soc.*, 1993, **115**, 8706.
5 P. W. D. Mitchell and P. E. D. Morgan, *J. Am. Ceram. Soc.*, 1974, **57**, 278.
6 Y. Xie, W. Z. Wang, Y. T. Qian and X. M. Liu, *J. Solid State Chem.*, 1999, **47**, 82.
7 Rietveld refinements made use of version 1.20 of the XND Rietveld code: J.-F. Bérar, *Proceedings of the IUCr Satellite Meeting on Powder Diffractometry, Toulouse*, France, July, 1990; J.-F. Bérar and P. Garnier, II APD Conference, NIST (US), Gaithersburg, MD, May, 1992, NIST Special Publication, 1992, **846**, 212.
8 DIFFaX version 1.801, M. M. J. Treacy, J. M. Newsam and M. W. Deem, *Proc. R. Soc. London Ser. A*, 1991, **433**, 499.
9 M. G. Bawendi, M. L. Steigerwald and L. E. Brus, *Annu. Rev. Phys. Chem.*, 1990, **41**, 477.

ChemComm

Dioxygen mediated oxo-transfer to an amine and oxidative *N*-dealkylation chemistry with a dinuclear copper complex

Christiana Xin Zhang,[a] Hong-Chang Liang,[a] Eun-il Kim,[a] Qing-Fen Gan,[a] Zoltán Tyeklár,[a] Kin-Chung Lam,[b] Arnold L. Rheingold,[b] Susan Kaderli,[c] Andreas D. Zuberbühler[c] and Kenneth D. Karlin*[a]

[a] *Department of Chemistry, The Johns Hopkins University, Baltimore, MD 21218, USA. E-mail: karlin@jhu.edu*
[b] *Department of Chemistry, University of Delaware, Newark, DE 19716, USA*
[c] *Institut für Anorganische Chemie, University of Basel, CH-4056 Basel, Switzerland*

Received (in Irvine, CA, USA) 8th November 2000, Accepted 15th February 2001
First published as an Advance Article on the web 14th March 2001

Reaction of dioxygen with a dinuclear copper(I) complex of a new binucleating ligand is described, wherein a peroxo–dicopper(II) (Cu_2–O_2) intermediate leads to an oxo-transfer reaction to give an *N*-oxide of an *N*-benzyl internal ligand substrate; additionally observed regioselective oxidative *N*-dealkylation chemistry occurs.

Copper(I)–dioxygen reactivity studies,[1–6] particularly those involving actual substrate oxidations, are of interest as models for metalloproteins which effect oxidative transformations,[4,5,7,8] and may serve in the development of oxidation reagents. One type of chemistry which we have extensively examined involves O_2-binding and reactivity in the dinuclear complexes where two copper(I) ions each coordinate to a bis[(2-(2-pyridyl)ethyl]amine (PY2) tridentate moiety which is linked through the alkylamino nitrogens by a $–(CH_2)_n–$ (n = 3–5) (**N*n***),[9,10] or *m*-xylyl group (**XYL**);[5,11] in the former case reversible O_2-binding occurs, while in the latter situation, the Cu_2–O_2 intermediate effects xylyl aromatic hydroxylation chemistry. In our continuing effort to investigate the behavior of Cu_2–O_2 species and their reactivities toward internal substrates, we report here the use of a new ligand analogue **D**, with similarities to **N*n*** and **XYL** ligands, but possessing an *N*-benzyl internal moiety. We describe the nature of the O_2-binding to form Cu_2–O_2 species in the dicopper(I) complex of **D**, and novel oxo-transfer and oxidative *N*-dealkylation chemistry. Such reactions occur in copper proteins (*e.g.* peptidylglycine monooxygenase, PHM)[8,12] and heme cytochrome P-450 monooxygenases.[13]

The copper(I) complex $[Cu^I_2(\mathbf{D})]^{2+}$ (**1**) was synthesized by reaction of 2 equiv. of $[Cu^I(MeCN)_4]^+$ with **D**.† An X-ray structure of **1** was obtained (Fig. 1).‡ While both copper(I) ions possess distorted tetrahedral tetracoordination, the binding is highly unsymmetrical; Cu1 ligates to its PY2 tridentate plus the central benzylamine nitrogen atom N7. The other Cu atom (Cu2) has instead as its fourth ligand a perchlorate oxygen atom O5. We have previously observed related asymmetry utilizing trinucleating ligands, either for tricopper(I)[14] or tricopper(II)[15] complexes, wherein three copper ions bind a tridentate chelate, but only one coordinates to a similarly 'central' amine nitrogen. The copper ion moieties are well separated in **1**, with Cu1···Cu2 = 5.43 Å.

At −80 °C in dichloromethane, the dicopper(I) complex $[Cu^I_2(\mathbf{D})]^{2+}$ **1** reacts with excess dioxygen to give a Cu_2O_2 species $[Cu^{II}_2(\mathbf{D})(O_2)]^{2+}$ **2** which gradually decomposes (*vide infra*). Stopped-flow kinetic results show that the reversible (k_1/k_{-1}) formation of species **2** is first order in both **1** and O_2 with k_1 = (10 ± 0.3) $M^{-1}s^{-1}$ (183 K) [$\Delta H^{\ddagger}$ = (15.8 ± 0.8) kJ mol^{-1}, $\Delta S^{\ddagger}$ = (−135 ± 4) J K^{-1} mol^{-1} (183–206 K)}. The UV–VIS spectrum of **2** [λ_{max} = 360 (ε 12 500), 514 nm (ε 1220 dm^3 mol^{-1} cm^{-1})] shows features which are very similar to the Cu_2–O_2 peroxo–dicopper(II) complexes established with **XYL**[6,16] and **N*n***[9] ligands, $[Cu_2(\mathbf{XYL})(O_2)]^{2+}$ and $[Cu_2(\mathbf{N}n)(O_2)]^{2+}$, respectively, indicating that **2** also possesses a μ-η²:η² side-on peroxodicopper(II) core.

As mentioned, an *N*-benzyl moiety was designed into **D** as a potential oxidizable site. Indeed, analysis of products obtained when O_2 is reacted with $[Cu^I_2(\mathbf{D})]^{2+}$ **1** at 0 °C reveals that the *N*-oxide **D**–**O** is obtained (Scheme 1); a labeling experiment shows that the O atom is derived from dioxygen, suggesting an oxygen atom transfer reaction has occurred.§ However, $[Cu^{II}_2(\mathbf{D})(O_2)]^{2+}$ (**2**) is not directly responsible for the formation of **D**–**O**, since if it is allowed to stand at −80 °C, whereupon decomposition occurs, no **D**–**O** forms [kinetics of decomposition: k_2 = (4.5 ± 0.9) × 10^{-4} s^{-1} at 183 K; $\Delta H^{\ddagger}$ = (44 ± 2)

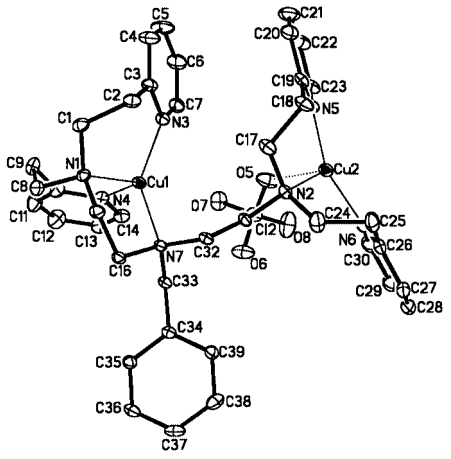

Fig. 1 ORTEP diagram of the cationic portion of complex **1**. Selected bond lengths (Å): Cu1···Cu2 5.432, Cu1–N1 2135(3), Cu1–N3 1.979(3), Cu1–N4 2.024(3), Cu1–N7 2.106(3), Cu2–N2 2.252(3), Cu2–N5 1.927(3), Cu2–N6 1.925(3), Cu2–N6 1.925(3), Cu2–O5 2.551(3).

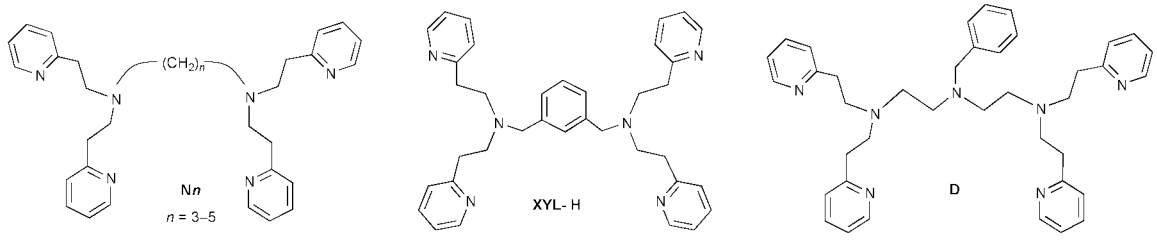

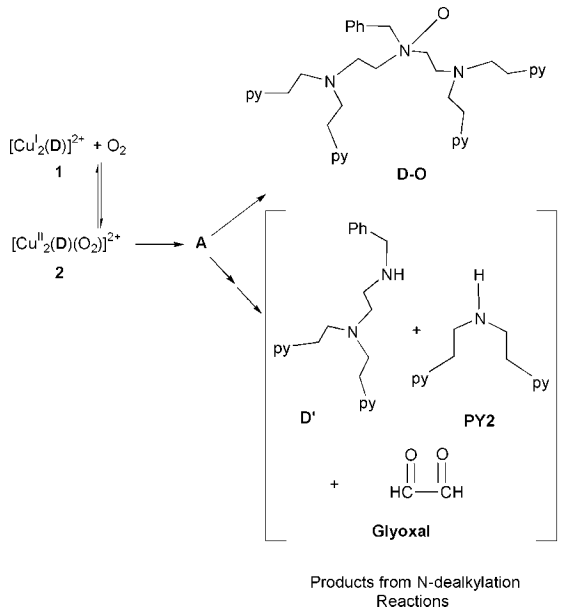

Scheme 1

kJ mol^{-1}, $\Delta S^{\ddagger}$ = (62 ± 8) J K^{-1} mol^{-1} (198–293 K)]. We suggest that the oxo-transfer reaction, having a relatively large activation energy (*i.e.* higher temperatures are required to see **D**–**O** product), is effected by a very reactive intermediate (**A**; Scheme 1) derived from **2**, which is formed in steady state. Direct formation of the different oxidation products, *i.e.* without formation of intermediate **A**, can be ruled out by the observation that the overall rate constant k_1k_2/k_{-1} shows a perfectly linear Eyring plot between 198 and 293 K. Differentiation between the various oxidation products thus must occur after the rate determining step k_2.

When the oxygenation of [Cu$^{I}_2$(**D**)]$^{2+}$ **1** is carried out at room-temperature and for longer reaction times (> 12 h), additional products derived from oxidative *N*-dealkylation chemistry are produced. **D′** is the amine byproduct from the hydroxylation of one of the non-benzylic methylene carbons adjacent to the middle nitrogen. The other fragment expected from this *N*-dealkylation, an aldehyde, is not isolable; it is further oxidized to yield glyoxal and **PY2** (Scheme 1). Overall, **D′**, glyoxal and **PY2** form in excellent yield and material balance.¶ The fact that this chemistry requires reaction times much longer than the lifetime of the peroxo species [Cu$^{II}_2$(**D**)(O$_2$)]$^{2+}$ **2** ($t_{1/2}$ = 0.01 s at 298 K) indicates that as for the **D**–**O** formation, **2** is not responsible for the oxidative *N*-dealkylation; in another case, a Cu$_2$-O$_2$ intermediate *is* known to effect such reactivity.[17] Here, other complexes derived from the decomposition of **2**, perhaps Cu^{II}–OH–Cu^{II} or Cu^{II}–O–Cu^{II} species, may be responsible. We note that anaerobic addition of 2 [Cu(H$_2$O)$_6$](ClO$_4$)$_2$ and base to **D**, followed by heating, does lead to similar oxidative *N*-dealkylation chemistry. The oxidative *N*-dealkylation chemistry here appears to be regioselective, as benzaldehyde (which would form by oxidation at the most easily oxidizable methylene group) is formed in trace amounts only.

In conclusion, a new dicopper(I) compound, **1**, has been synthesized with a built-in substrate and dissimilar copper(I) environments. [Cu$^{I}_2$(**D**)]$^{2+}$ **1** reacts with dioxygen yielding a peroxo species [Cu$^{II}_2$(**D**)(O$_2$)]$^{2+}$ **2** which decomposes leading to two different ligand transformation reactions: (1) a reactive species, which derives from **2**, is competent to effect an oxo-transfer reaction to give the *N*-oxide **D**–**O**. This appears to be a rare known copper–dioxygen mediated amine to *N*-oxide transformation. (2) With higher temperatures and over longer time periods, the Cu$_2$–O$_2$ species transforms to copper(II) products which effect biomimetic regioselective oxidative *N*-dealkylation chemistry. Additional studies will be directed towards further structural and mechanistic understanding of the chemistry described.

We are grateful to the National Institutes of Health (K. D. K., GM28962) and the Swiss National Science Foundation (A. D. Z.) for support of this research.

Notes and references

† Reaction of **D** with 2 equiv. of [Cu(MeCN)$_4$](ClO$_4$) gave **1**(ClO$_4$)$_2$, for which satisfactory C, H and N analyses were obtained.

‡ *Crystal data* for $C_{39}H_{47}Cl_2Cu_2N_7O_8\cdot 3CH_2Cl_2$. M = 1194.59, triclinic, $P\bar{1}$, a = 10.5816(2), b = 14.8247(2), c = 18.0045(2) Å, α = 112.4800(3), β = 97.2565(2), γ = 94.2666(2)°, V = 2565.53(6) Å^3, Z = 2, T = 173 K, $R(F)$ = 0.0469, $R(wF^2)$ = 0.1084. After accounting for the diCu cation and two ClO$_4^-$, a large void space of 644.8 Å^3 containing numerous, but chemically ill defined, difference peaks was resolved using SQUEEZE (A. Spek, PLATON library), which determined the presence of a total of 241 electrons, or *ca.* six molecules of the recrystallization solvent CH_2Cl_2 per unit cell. Due the collective nature of this treatment of solvent, the atom list does not contain individual atomic contributions. All other software was contained in the SHELXTL (5.1) library (G. Sheldrick, Bruker AXS, Madison, WI). CCDC 150146. See http://www.rsc.org/suppdata/cc/b0/b009053k/ for crystallographic data in .cif or other electronic format.

§ When the oxygenation reaction of **1** was carried out at 0 °C in CH_2Cl_2 for 10 min, **D**–**O** was isolated after workup in 47% yield. With an $^{18}O_2$ reaction, an ^{18}O atom is incorporated into **D**–^{18}**O** with 92% efficiency. *Characterization* of **D**–**O**: ^{1}H NMR ($CDCl_3$) δ 2.92 (m, 20H), 3.08 (m, 4H), 4.17 (s, 2H), 7.11–7.14 (m, 8H), 7.40–7.60 (m, 9H), 8.45 (d, 4H); positive ion FAB-MS: **D**–**O** *m/z*: 630.4 (MH$^+$), **D**–^{18}**O** *m/z*: 632.4 (MH$^+$).

¶ Organic products were isolated and characterized from the oxygenation reaction of **1** in DMF at room temperature over 12 h: **D′** (71%) ^{1}H NMR ($CDCl_3$) δ 2.54 (t, 2H), 2.73 (t, 2H), 2.88 (m, 8H), 3.58 (s, 2H), 7.05–7.12 (m, 4H), 7.26–7.36 (m, 5H), 7.50–7.53 (m, 2H), 8.43 (d, 2 H) positive ion FAB-MS *m/z*: 361 (MH$^+$); **PY2** (51%) ^{1}H NMR ($CDCl_3$) δ 2.47 (s, 1H), 3.0-3.3 (m, 8H), 7.13–7.20 (m, 4H) 7.40–7.60 (m, 2H), 8.45 (d, 2H) positive ion FAB-MS *m/z*: 228 (MH$^+$); glyoxal (51.7%, isolated and quantified as its 2,4-dinitrophenylhydrazone) ^{1}H NMR (DMSO-d$_6$) δ 7.96 (d, 2H), 8.47 (q, 2H), 8.88 (s, 2H), 11.89 (s, 2H).

1 S. Schindler, *Eur. J. Inorg. Chem.*, 2000, 2311.
2 M. Suzuki, H. Furutachi and H. Okawa, *Coord. Chem. Rev.*, 2000, **200**–**202**, 105.
3 A. G. Blackman and W. B. Tolman, *Struct. Bonding (Berlin)*, 2000, **97**, 179–211.
4 C. X. Zhang, H.-C. Liang, K. J. Humphreys and K. D. Karlin, in *Copper–Dioxygen Complexes and Their Roles in Biomimetic Oxidation Reactions*, ed. L. Simandi, Dordrecht, The Netherlands, 2001.
5 K. D. Karlin and A. D. Zuberbühler, in *Formation, Structure and Reactivity of Copper Dioxygen Complexes*, ed. J. Reedijk and E. Bouwman, New York, 1999.
6 K. D. Karlin, S. Kaderli and A. D. Zuberbühler, *Acc. Chem. Res.*, 1997, **30**, 139.
7 E. I. Solomon, U. M. Sundaram and T. E. Machonkin, *Chem. Rev.*, 1996, **96**, 2563.
8 J. P. Klinman, *Chem. Rev.*, 1996, **96**, 2541.
9 H.-C. Liang, K. D. Karlin, R. Dyson, S. Kaderli, B. Jung and A. D. Zuberbühler, *Inorg. Chem.*, 2000, in press.
10 E. Pidcock, H. V. Obias, M. Abe, H.-C. Liang, K. D. Karlin and E. I. Solomon, *J. Am. Chem. Soc.*, 1999, **121**, 1299.
11 E. Pidcock, H. V. Obias, C. X. Zhang, K. D. Karlin and E. I. Solomon, *J. Am. Chem. Soc.*, 1998, **120**, 7841.
12 N. J. Blackburn, F. C. Rhames, M. Ralle and S. Jaron, *JBIC*, 2000, **5**, 341.
13 M. Sono, M. P. Roach, E. D. Coulter and J. H. Dawson, *Chem. Rev.*, 1996, **96**, 2841.
14 K. D. Karlin, Q.-F. Gan, A. Farooq, S. Liu and J. Zubieta, *Inorg. Chim. Acta*, 1989, **165**, 37.
15 S. T. Frey, H. H. J. Sun, N. N. Murthy and K. D. Karlin, *Inorg. Chim. Acta*, 1996, **242**, 329.
16 K. D. Karlin, M. S. Nasir, B. I. Cohen, R. W. Cruse, S. Kaderli and A. D. Zuberbühler, *J. Am. Chem. Soc.*, 1994, **116**, 1324.
17 S. Mahapatra, J. A. Halfen and W. B. Tolman, *J. Am. Chem. Soc.*, 1996, **118**, 11 575.

ChemComm

Influence of pore wall thickness on the steam stability of Al-grafted MCM-41

Robert Mokaya

School of Chemistry, University of Nottingham, University Park, Nottingham, UK NG7 2RD. E-mail: r.mokaya@nottingham.ac.uk

Received (in Cambridge, UK) 29th January 2001, Accepted 27th February 2001
First published as an Advance Article on the web 14th March 2001

Mesoporous aluminosilicate MCM-41 with improved steam stability may be prepared by grafting Al onto pure silica MCM-41 materials that possess thick pore walls.

Mesostructured aluminosilicates are currently attracting considerable research interest due to their potential use as heterogeneous catalyst.[1,2] Their main attraction is a well ordered mesostructure with uniform pores whose size is much larger than that of channels present in traditional microporous zeolites. They are therefore able to catalyse chemical transformations involving molecules too large to fit the pore channels of zeolites. The use of mesoporous aluminosilicates such as Al-MCM-41, in for example the cracking of heavy fractions in petroleum refining, is however hampered by their inadequate hydrothermal stability, which is lower than that of zeolites.[1,3] There have been several recent studies aimed at improving the hydrothermal stability of mesoporous aluminosilicates in boiling water and/or under steaming conditions.[4–7] It has been shown that Al-MCM-41 materials prepared *via* grafting routes are extremely stable in boiling water.[4–6] Directly prepared Al-MCM-41 has also been shown to exhibit considerable hydrothermal stability especially at relatively low Al contents.[8,9] More recently Liu *et al*. have shown that steam stable mesostructured aluminosilicates may be prepared using zeolite type seeds.[7] It has recently been suggested that a possible route to steam stable Al-MCM-41 is *via* the preparation of materials with thick pore walls.[1,3] However an attempt to prepare such steam stable (thick walled) Al-MCM-41 *via* direct (mixed-gel) synthesis was unsuccessful.[1,3] The direct mixed gel synthesis of Al-MCM-41 is known to be unpredictable and therefore it is to be expected that any attempt to carefully control the pore wall thickness will present considerable challenges. The pore wall thickness of pure silica MCM-41 can, on the other hand, be readily controlled by careful choice of synthesis conditions.[10,11] Here we report on the influence of pore wall thickness on the steam stability of Al-grafted MCM-41 and show that the stability of these materials can be remarkably improved by using thick-walled pure silica MCM-41 as 'starting material'. The improvement in structural steam stability is accompanied by a higher retention of acidity which is important for the use of these materials as solid acid catalysts. Mesostructured aluminosilicates prepared *via* grafting routes offer distinct advantages over directly synthesised materials with respect to accessibility to active (Al) sites and structural ordering;[12] their stabilisation is therefore desirable. Furthermore their preparation is not restricted by 'template synthesis' which can be expensive, irreproducible and in some cases inimical to the incorporation of Al. The starting point for Al-grafted materials is the purely siliceous mesoporous silica, which may take any form (hexagonal, cubic, lamellar) and can be prepared *via* a range of inexpensive synthesis routes employing cationic, neutral, non-ionic or even non-surfactant templates and cheap sources of silica.[13]

In order to vary the pore wall thickness of the starting pure silica MCM-41 materials, three different crystallisation regimes were used. This was achieved by varying the crystallisation temperature and duration. In brief the three purely siliceous MCM-41 materials were prepared by dissolving tetramethylammonium hydroxide (TMAOH) and cetyltrimethyammonium bromide (CTAB) in distilled water by stirring at 35 °C. The silica source, fumed silica (sigma), was then added to the solution under stirring for 1 h. After further stirring for 1 h the resulting synthesis gel of composition SiO_2:0.25 CTAB:0.2 TMAOH:40 H_2O was left to age for 20 h at room temperature following which the gel was transferred to a Teflon-lined autoclave and heated as follows; at 150 °C for 48 h (standard Si-MCM-41, designated sample A),[9] 140 °C for 96 h (sample B) and 145 °C for 96 h (sample C). In each case the solid product was obtained by filtration, washed with distilled water, dried at room temperature and calcined in air at 550 °C for 8 h. Al-grafted MCM-41 materials were prepared at a target bulk Si/Al ratio of 13 as previously described using aluminium chlorhydrol as the grafting reagent.[14] In all cases the final bulk Si/Al ratio was very close to the expected value and the proportion of tetrahedrally coordinated Al was similar. The Al-grafted samples were designated Al-MCM41-A, Al-MCM41-B and Al-MCM41-C where A, B and C represent the pure silica MCM-41 material from which they were derived. Hydrothermal stability was tested by heat treatment at 800 or 900 °C for 4 h in a flow of nitrogen saturated with water vapour at room temperature.

The textural parameters of the Al-grafted materials before and after hydrothermal treatment are given in Table 1. The basal spacing increases from sample Al-MCM41-A to Al-MCM41-C; this is consistent with previous results, which show that crystallisation at higher temperature and/or longer time favours larger basal spacing.[10,11] The surface area decreases from sample Al-MCM41-A to Al-MCM41-C while the pore volume remains constant. This is accompanied by an increase in pore size and pore wall thickness as shown in Table 2. The data in Table 2 is calculated using two methods, so as to clearly demonstrate the variation in pore wall thickness. Powder XRD and N_2 sorption isotherms obtained for the Al-grafted materials before hydrothermal treatment are given in Figs. 1 and 2 respectively. In all three cases well ordered aluminosilicate materials were obtained as indicated by the XRD patterns. All the samples also exhibit a N_2 sorption isotherm with a well developed step in the relative pressure (P/P_o) range 0.2–0.5 characteristic of capillary condensation into uniform mesopores.

Figs. 1 and 2 show the powder XRD patterns and N_2 sorption isotherms of the Al-grafted materials after hydrothermal treatment at 800 and 900 °C for 4 h. All the samples are

Table 1 Textural properties and acidity of the studied materials

Sample	d_{100}/Å	Surface area/ $m^2\ g^{-1}$	Pore volume/ $cm^3\ g^{-1}$	Acidity/ mmol $H^+\ g^{-1}$
Al-MCM41-A	42.2	907	0.78	0.83
steamed 800 °C	39.4	785	0.58	0.41
steamed 900 °C	35.0	224	0.19	0.16
Al-MCM41-B	50.7	749	0.76	0.82
steamed 800 °C	47.3	674	0.64	0.48
steamed 900 °C	41.8	258	0.27	0.18
Al-MCM41-C	55.6	734	0.78	0.84
steamed 800 °C	51.4	727	0.88[a]	0.71
steamed 900 °C	45.7	501	0.48	0.40

[a] Includes some textural mesoporosity.

DOI: 10.1039/b100997o

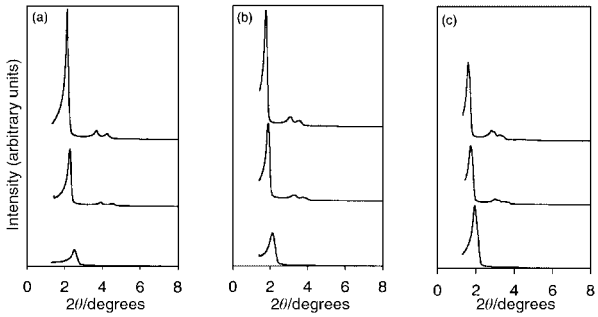

Fig. 1 Powder XRD patterns of Al-grafted MCM-41 samples, (a) Al-MCM41-A, (b) Al-MCM41-B and (c) Al-MCM41-C, before (top) and after hydrothermal treatment at 800 °C (middle) and 900 °C (bottom). The intensity scale is the same for all samples.

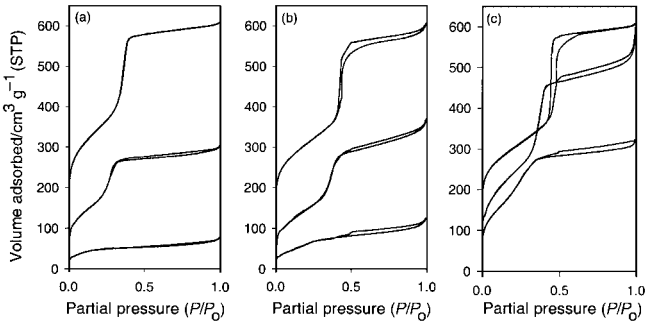

Fig. 2 Nitrogen sorption isotherms of Al-grafted MCM-41 samples, (a) Al-MCM41-A, (b) Al-MCM41-B and (c) Al-MCM41-C, before (top) and after hydrothermal treatment at 800 °C (middle) and 900 °C (bottom).

Table 2 Comparison of pore diameter and corresponding pore wall thickness for Al-grafted materials

	Pore diameter/Å			Wall thickness/Å	
Sample model	a_o	$4V/S$	Geometric model[a]	$4V/S$	Geometric model[a]
Al-MCM41-A	48.7	34.4	38.1	14.3	10.6
Al-MCM41-B	58.5	40.6	45.6	17.9	12.9
Al-MCM41-C	64.2	42.5	50.2	21.7	14.0

[a] Pore diameter (PD) was calculated based on a geometric model according to the equation:[16] PD = $cd(\rho V_p/1 + \rho V_p)^{1/2}$, where c = 1.213, ρ (density of silica walls) = 1.6 g cm^{-3},[17] and d is basal spacing (d_{100}) and V_p is mesopore volume; a_o = the lattice parameter from the d_{100} spacing using the formula $a_o = 2d_{100}/\sqrt{3}$; wall thickness = a_o − PD.

relatively stable at 800 °C. The decrease in pore volume after treatment at 800 °C is 26% for sample Al-MCM41-A and 16% for sample Al-MCM41-B. In contrast the mesopore volume of sample Al-MCM41-C remains virtually unchanged while its total pore volume increases due to the presence of textural mesoporosity. The surface area follows the same trend. These observations imply that hydrothermal stability at 800 °C is, to some extent, influenced by the pore wall thickness. The influence of pore wall thickness is more clearly illustrated after the more severe hydrothermal treatment at 900 °C. From Fig. 1 and 2 it is clear that sample Al-MCM41-A, which has the thinnest pore walls, is severely degraded after treatment at 900 °C. The N_2 sorption isotherm of the resulting material exhibits virtually no mesoporous character. The surface area and pore volume decrease by 75%. Sample Al-MCM41-B shows better retention of structural ordering after treatment at 900 °C compared to sample Al-MCM41-A; its surface area and pore volume are reduced by *ca.* 65% although it still exhibits a N_2 sorption isotherm with some mesoporous character. When subjected to similar treatment, sample Al-MCM41-C shows considerable retention of structural ordering; the XRD pattern of Al-MCM41-C steamed at 900 °C is comparable to that of the parent material and its N_2 sorption isotherm still exhibits a relatively sharp mesopore filling step. The surface area and pore volume are reduced by only 32 and 38% respectively. It appears therefore that the steam stability of the Al-grafted MCM-41 materials increases with increasing pore wall thickness. It is worth pointing out that the steam stability of the pure silica 'starting' samples was very poor (in any case lower than that of the Al-grafted materials) and increased only marginally with increasing pore wall thickness. The surface area of pure silica samples A, B and C, after steam treatment at 900 °C for 4 h, was 69, 105 and 150 m^2 g^{-1} while the pore volume was 0.12, 0.15 and 0.21 cm^3 g^{-1}, respectively. The improved stability exhibited by the Al-grafted samples with thicker pore walls is therefore due to a combination of the strengthened framework and the presence of Al in the framework.[15] On stability of the core silica framework, we further note that the extent of silica condensation in the as-synthesised pure silica samples increased with pore wall thickness.[10] Consequently on calcination, the more polymerised (thicker walled) samples undergo less 'forced' condensation thus resulting in fewer strained siloxane bonds within the core silica framework. The greater stability of the thicker walled Al-grafted samples is accompanied by better retention of acidity as indicated by the data (determined using thermally programmed desorption of cyclohexylamine as previously described[4]) in Table 1. In brief samples saturated with cyclohexylamine (CHA) were pre-treated at 80 °C for 2 h and cooled under nitrogen prior to thermogravimetric analysis.[4] The weight loss between 300 and 450 °C was used to compute the acid content in mmol CHA g^{-1} assuming that each base molecule interacts with one acid site. Better retention of acidity may be an indication of lower levels of dealumination in the thicker walled Al-grafted samples. The findings reported here open new opportunities for the preparation of steam stable Al-MCM41 given that there are other methods that can be used to stabilise the pure silica starting material prior to Al grafting.

I am grateful to the EPSRC for an Advanced Fellowship.

Notes and references

1 A. Corma, *Chem. Rev.*, 1997, **97**, 2373.
2 S. Biz and M. L. Occelli, *Catal. Rev.-Sci. Eng.*, 1998, **40**, 329.
3 A Corma, M. S. Grande, V. Gonzalez-Alfaro and A. V. Orchilles, *J. Catal.*, 1996, **159**, 375.
4 R. Mokaya, *Angew. Chem., Int. Ed.*, 1999, **38**, 2930.
5 S. C. Shen and S. Kawi, *Chem. Lett.*, 1999, 1293.
6 R. Mokaya and W. Jones, *Chem. Commun.*, 1998, 1839.
7 Y. Liu, W. Zhang and T. J Pinnavaia, *J. Am. Chem. Soc.*, 2000, **122**, 8791.
8 S. C. Shen and S. Kawi, *J. Phys. Chem. B*, 1999, **103**, 8870.
9 R. Mokaya, *J. Phys. Chem. B*, 2000, **104**, 8279.
10 R. Mokaya, *J. Phys. Chem. B*, 1999, **103**, 10 204.
11 A. Sayari, P. Liu, M. Kruk and M. Jaroniec, *Chem. Mater.*, 1997, **9**, 2499; C.-F Cheng, W. Zhou and J. Klinowski, *J. Chem. Phys. Lett.*, 1996, **263**, 247.
12 R. Mokaya and W. Jones, *Chem. Commun.*, 1997, 2185; R. Ryoo, S. Jun, J. M. Kim and M. J. Kim, *Chem. Commun.*, 1997, 2225.
13 J. Y. Ying, C. P. Mehnert and M. S. Wong, *Angew. Chem., Int. Ed.*, 1999, **38**, 56; S. S. Kim, T. R. Pauly and T. J. Pinnavaia, *Chem. Commun.*, 2000, 1661; J. M. Kim and G. D. Stucky, *Chem. Commun.*, 2000, 1159.
14 R. Mokaya and W. Jones, *J. Mater. Chem.*, 1999, **9**, 555.
15 J. M. Kim, J. H. Kwak, S. Jun and R. Ryoo, *J. Phys. Chem.*, 1995, **99**, 16 742.
16 M. Kruk, M. Jaroniec and A. Sayari, *J. Phys. Chem. B*, 1997, **101**, 583; M. Kruk, M. Jaroniec and A. Sayari, *Langmuir*, 1997, **13**, 6267.
17 N. Floquet, J. P. Coulomb, S. Giogio, Y. Grillet and P. L. Llewellyn, *Stud. Surf. Sci. Catal.*, 1998, **117**, 583.

Engineering the haem monooxygenase cytochrome P450$_{cam}$ for monoterpene oxidation

Stephen G. Bell, Rebecca J. Sowden and Luet-Lok Wong*

Department of Chemistry, Inorganic Chemistry Laboratory, University of Oxford, South Parks Road, Oxford, OX1 3QR UK. E-mail: luet:wong@chem.ox.ac.uk; Fax: +44-(0)1865-272690; Tel: +44-(0)1865-275963

Received (in Liverpool, UK) 15th December 2000, Accepted 5th March 2001
First published as an Advance Article on the web 16th March 2001

Monooxygenated terpenes are fine fragrance and flavouring chemicals, and active site mutants of the haem monooxygenase cytochrome P450$_{cam}$ which were designed to have improved complementarity between the substrate binding pocket and the monoterpenes (+)-α-pinene (1) and *S*-limonene (2) have been shown to have greatly enhanced activity for the oxidation of these two substrates, and the major products, verbenol and isopiperitenol from (1) and (2) respectively, were formed with high regioselectivity and near-total stereoselectivity.

Terpenes have the general formula $(C_5H_8)_n$ and are biosynthesized from isoprene units.[1] Terpenoid compounds, which mainly comprise the parent terpenes and their oxidation products such as the epoxides, alcohols, aldehydes and ketones, constitute one of largest class of organic compounds in biological systems. Many mono- and sesqui-terpenoid compounds are sought-after fragrances and flavourings due to their distinctive and pleasant odours.[2,3] For example isopiperitenol and carveol, which are intermediates in the biosynthesis of terpenoid compounds that give the characteristic flavours of different species of mint, are formed by the oxidation of (*S*)-limonene by highly specific cytochrome P450 enzymes in the plants.[4,5] As a result of their desirable properties, monooxygenated terpenoids are amongst some of the highest added value fine chemicals. Therefore the one step synthesis of these compounds by direct oxidation of the readily available parent terpenes could have important applications in synthesis. We report here the engineering of the haem monooxygenase cytochrome P450$_{cam}$ for the oxidation of the monoterpenes (+)-α-pinene (**1**) and (*S*)-limonene (**2**).

Cytochrome P450$_{cam}$ catalyses the oxidation of the bicyclic compound D-(+)-camphor to 5-*exo*-hydroxycamphor, the first step in the camphor metabolism pathway of the soil bacterium *Pseudomonas putida*.[6,7] The mechanism, structure, and substrate binding of P450$_{cam}$ have been extensively studied.[8] Since the bicyclic compound (**1**) is structurally related to camphor (Fig.1), we made the reasonable assumption that the two molecules might be bound in similar orientations within the P450$_{cam}$ active site. From the crystal structure the camphor carbonyl group forms a hydrogen bond with Y96 and is in van der Waals contact with F87.[9] Since this carbonyl group is absent from (**1**), the Y96F mutation should improve the binding of (**1**) by removing the polar phenol side-chain,[10] while the larger side-chain of the F87W mutation should improve the enzyme–substrate fit. The C_{10} methyl group of camphor contacts V247. Since the allylic methyl group of (**1**) is in a different position in the molecule, the V247L mutation should also improve the enzyme–substrate complementarity. The mutants Y96F, F87W–Y96F, Y96F–V247L and Y96F–F87W–V247L of P450$_{cam}$ were therefore examined for the binding and oxidation

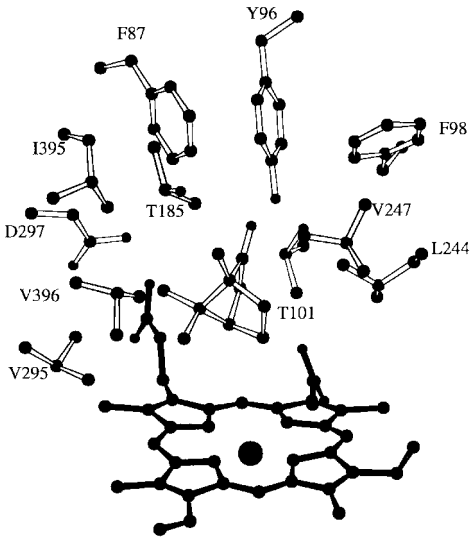

Fig. 1

Table 1 Binding and oxidation of (+)-α-pinene (**1**) and (*S*)-limonene (**2**) by wild-type (WT) cytochrome P450$_{cam}$ and active site mutants

	WT	Y96F	F87W–Y96F	Y96F–V247L	F87W–Y96F–V247L
(+)-α-Pinene (1)					
% High spin haem	85	95	95	95	75
K_D (μM)	1.10	0.15	0.08	0.14	0.30
NADH turnover rate[a]	81.5	147	171	298	129
Product formation rate[a]	18.6	56	96	271	65
Coupling efficiency[c]	23%	38%	56%	91%	51%
(*S*)-limonene (2)					
% High spin haem	20	40	40	60	10
K_D (μM)	5.20	0.55	2.10	1.08	—[d]
NADH turnover rate[a]	4.0	52	100	301	119
Product formation rate[b]	0.2	15.7	31	187	45
Coupling efficiency[c]	5.1%	30%	31%	62%	38%

[a] Given as nanomoles of NADH consumed per nanomole of P450$_{cam}$ per minute. [b] The total amount (in nanomoles) of product formed per nanomole of P450$_{cam}$ per minute. [c] The coupling efficiency is the ratio of the total amount of products formed to the amount of NADH consumed and is expressed as a percentage. [d] Due to the small spectral changes the substrate binding constant could not be reliably determined.

DOI: 10.1039/b100290m

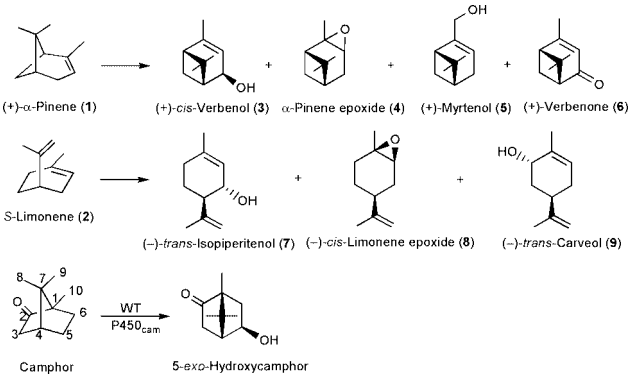

Scheme 1

of (**1**). The monocyclic compound (**2**) could also be bound in a similar orientation to camphor if it adopted the slightly higher energy conformation shown in Fig.1, and these mutants may also have higher activities for the oxidation of (**2**).

The substrate binding and catalytic parameters for the oxidation of (**1**) and (**2**) by wild-type $P450_{cam}$ and the mutants are given in Table 1. The monocyclic (**2**) was a very poor substrate for the wild-type compared to camphor (K_D = 0.25μM, rate = 400 min^{-1} under identical conditions, 100% coupling efficiency). However, the bicyclic (**1**) was bound much more tightly and oxidised at a faster rate with higher coupling than (**2**), in all likelihood reflecting the closer structure of (**1**) to camphor. As predicted the Y96F mutation strengthened the binding and also increased the rate and coupling for the oxidation of both substrates, particularly for (**2**). The addition of the F87W or V247L mutation further enhanced both the binding and oxidation activity for (**1**), suggesting improved enzyme–substrate fits in the F87W–Y96F and Y96F–V247L double mutants. Interestingly (**1**) was bound more tightly by the Y96F and these two double mutants than camphor was by the wild-type, and the fast substrate oxidation rate of 271min^{-1} and near total coupling efficiency of the Y96F–V247L double mutant almost matched the camphor oxidation activity of wild-type $P450_{cam}$. For (**2**) the addition of the F87W and V247L mutations slightly weakened substrate binding but substantially increased the rate and coupling, and so although (**2**) was less tightly bound it was located closer to the haem resulting in more efficient substrate oxidation. The F87W–Y96F–V247L triple mutant showed weaker monoterpene binding and lower activity compared to the double mutants, probably due to steric hindrance between (**1**) and (**2**) and the much smaller active site cavity in this mutant.

Since camphor is selectively oxidised at C_5 to give the *exo* alcohol, the major products from the proposed binding orientation of (**1**) should be (+)-*cis*-verbenol (**3**) and α-pinene epoxide (**4**) (Fig.1, Scheme1). GC co-elution experiments showed that (**3**) was indeed the major product (> 60%) for all the $P450_{cam}$ enzymes. The *cis* and *trans* isomers of (**4**) were minor products (total < 8%), and the enzymes showed little selectivity between the two. In addition (+)-myrtenol (**5**), which arose from oxidation of the allylic methyl group, and verbenone (**6**), the further oxidation product of (**3**), were also formed (Scheme 1). The most active mutant Y96F–V247L gave 70% (**3**) and 7% each of (**5**) and (**6**), while the less active triple mutant F87W–Y96F–V247L was the most selective, giving 85% (**3**).

The selectivity for the oxidation of (**2**) was more sensitive to the mutations. Chiral-phase GC analysis showed that the main products were (−)-*trans*-isopiperitenol (**7**), (−)-*cis*-limonene epoxide (**8**), and (−)-*trans*-carveol (**9**) (Scheme1). All the $P450_{cam}$ enzymes had very high diastereoselectivity (> 95% by GC) for the formation of all these products. Mutants containing the F87W mutation were more selective for (**7**) (82% for both the F87W–Y96F and F87W–Y96F–V247L mutants). The most active mutant Y96F–V247L gave 70% (**7**) but also the highest proportion (16%) of (**9**), while the less active wild-type and Y96F mutant gave the most epoxide (17 and 26% respectively). The predicted major product from the proposed binding orientation was (−)-*cis*-isopiperitenol, and some (*S*)-limonene epoxide was also expected. The observation of the *trans* isomer (**7**) and also some carveol product suggested that the more conformationally mobile (**2**) did not adopt the camphor binding orientation, and that there were multiple substrate binding modes. We note that the P450 enzyme from peppermint oxidises (**2**) with total selectivity to give the *trans*-isopiperitenol (**7**), while the spearmint enzyme gives only *trans*-carveol (**9**).[11,12]

In summary the results suggest that the strategy of designing mutations based on the structure of the monoterpenes and potential side-chain/substrate contacts to improve the enzyme–substrate fit was very successful in promoting monoterpene oxidation by $P450_{cam}$. In addition, with some further selectivity engineering, $P450_{cam}$ variants may have applications in the biotransformation of terpenes in fine chemical synthesis. Finally, since not all of the limonene and pinene oxidation products have been utilised by nature, the oxidation of these and indeed other terpenes by engineered P450 enzymes could give rise to novel fragrances and flavourings or new biologically active compounds.

We thank the Higher Education Funding Council for England for support of this work, and the referees for helpful comments. SGB thanks the Biotechnology and Biological Sciences Research Council, UK, and RJS the Engineering and Physical Sciences Research Council, UK, for studentships.

Notes and references

1 J. Gershenzon and R. B. Croteau, *Lipid Metab. Plants*, 1993, 339.
2 S. Arctander, *Perfume and Flavor Materials of Natural Origin*, Allured, Wheaton IL, 1960.
3 B. V. Charlwood and K. A. Charlwood, *Monoterpenoids*, 1991, **7**, 43; B. M. Fraga, *Sesquiterpenoids*, 1991, **7**, 45.
4 F. Karp, C. A. Mihaliak, J. L. Harris and R. B. Croteau, *Arch. Biochem. Biophys.*, 1990, **276**, 219.
5 C. Haudenschild, M. Schalk, F. Karp and R. B. Croteau, *Arch. Biochem. Biophys.*, 2000, **379**, 127.
6 I. C. Gunsalus and G. C. Wagner, *Methods Enzymol.*, 1978, **52**, 166.
7 S. G. Sliga and R. I. Murray, in *Cytochrome P450: Structure, Mechanism and Biochemistry*, ed. P. R. Ortiz de Montellano, Plenum, New York, 1st edn., 1986.
8 E. J. Mueller, P. J. Loida and S. G. Sligar, in *Cytochrome P450: Structure, Mechanism and Biochemistry*, ed. P. R. Ortiz de Montellano, Plenum, New York, 2nd edn., 1995.
9 T. L. Poulos, B. C. Finzel and A. J. Howard, *J. Mol. Biol.*, 1987, **195**, 687.
10 W. M. Atkins and S. G. Sligar, *J. Biol. Chem.*, 1988, **263**, 18842.
11 R. B. Croteau and J. Gershenzon, *Recent Adv. Phytochem.*, 1994, **28**, 193.
12 M. Schalk and R. B. Croteau, *Proc. Natl. Acad. Sci. USA*, 2000, **97**, 11948.

Neutral and cationic yttrium alkyl complexes with linked 1,4,7-triazacyclononane-amide monoanionic ancillary ligands: synthesis and catalytic ethene polymerisation†‡

Sergio Bambirra, Daan van Leusen, Auke Meetsma, Bart Hessen* and Jan H. Teuben

Centre for Catalytic Olefin Polymerisation, Stratingh Institute of Chemistry and Chemical Engineering, University of Groningen, Nijenborgh 4, 9747 AG Groningen, The Netherlands. E-mail: hessen@chem.rug.nl

Received (in Cambridge, UK) 30th January 2001, Accepted 20th February 2001
First published as an Advance Article on the web 14th March 2001

Yttrium dialkyl complexes [*N*,*N*′-R_2-tacn-*N*″-$(CH_2)_2NBu^t$]-$Y(CH_2SiMe_3)_2$ (R = Me, Pr^i; tacn = 1,4,7-triazacyclononane) were prepared; when activated with $[PhNMe_2H][B(C_6F_5)_4]$ these complexes form cationic alkyl species that are active ethene polymerisation catalysts.

Cationic group 4 metal alkyl species with linked dianionic cyclopentadienyl-amide ancillary ligands, such as $[C_5Me_4SiMe_2NBu^t]M(alkyl)^+$ **A** (M = Ti, Zr), are highly efficient

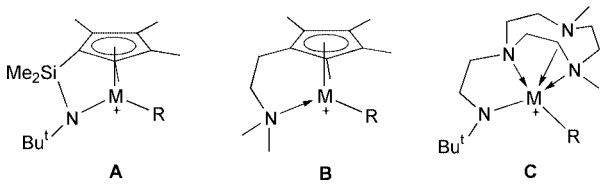

catalysts for the polymerisation of alkenes.[1] The isoelectronic group 3 metal alkyl complexes with these ligands are neutral, and much less effective in alkene polymerisation.[2] One approach that might allow the generation of cationic group 3 metal alkyl species is to replace either one of the monoanionic moieties of the ancillary ligand (amide or cyclopentadienyl) by a neutral functionality. A recent patent showed that replacement of the amide group by an amine donor can lead to $[C_5Me_4CH_2CH_2NMe_2]M(alkyl)^+$ **B**, (M = Sc) species that are active in catalytic alkene polymerisation.[3] We have designed a ligand in which an amido functionality is attached to a substituted 1,4,7-triazacyclononane (tacn) group, and that allowed us to generate cationic tacn-amide group 3 metal alkyl complexes of type **C**. These species were found to be highly active in the catalytic polymerisation of ethene.

1,4,7-Triazacyclononane ligands have been successfully used as 6-electron *fac*-tridentate ligands on a wide range of transition metals, and various neutral and anionic tacn derivatives have appeared in the literature recently.[4] The new tacn-amine derivatives *N*,*N*′-R_2-tacn-*N*″-$(CH_2)_2NBu^tH$ (R = Pr^i, **1**; Me, **2**) were prepared in two steps from the known corresponding *N*,*N*′-dialkyl-1,4,7-triazacyclononanes[5] (Scheme 1). Reaction of these *N*,*N*′-dialkyltriazacyclononanes with *N*-*tert*-butylchloroacetamide in refluxing actonitrile, with a catalytic amount of NaI, yielded the corresponding *N*-*tert*-butyl-(4,7-dialkyl-1,4,7-triazacyclonon-1-yl)acetamides. These were then reduced with $LiAlH_4$ in refluxing diglyme and purified, after hydrolysis and acid–base extraction, by Kugelrohr distillation (**2**) or column chromatography (**1**).

Reaction of the amine **1** with the yttrium trialkyl $Y(CH_2SiMe_3)_3(thf)_2$[6] in C_6D_6 results in formation of $SiMe_4$, free thf, and the yttrium dialkyl complex [*N*,*N*′-Pr^i_2-tacn-*N*″-$(CH_2CH_2)NBu^t]Y(CH_2SiMe_3)_2$ **3**, (Scheme 1), as seen by NMR spectroscopy. The same reaction in pentane solvent (0.5 mmol scale), followed by crystallization, yielded analytically pure, white crystalline **3**. The isolated yield (28%) was rather modest, mainly due the high solubility of the product. An X-ray structure determination of **3**§ confirmed its identification as a monomeric, thf-free yttrium dialkyl (Fig. 1). As expected, the three nitrogens of the tacn moiety are bound in *fac* arrangement to the metal centre. There is considerable asymmetry in the structure of the complex, as seen *e.g.* in the angle N(1)–Y–C(19) 113.8(2)° *vs.* N(1)–Y–C(23) 95.9(2)°, and the groups are

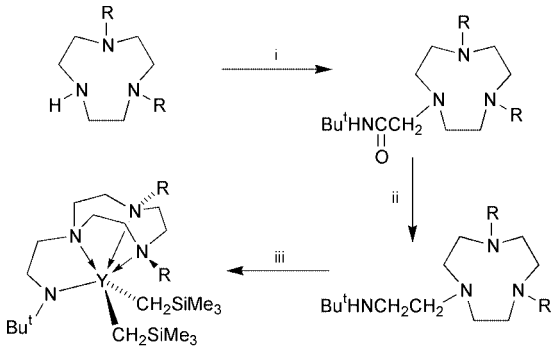

Scheme 1 *Reagents and conditions*: i, *N*-*tert*-butylchloroacetamide, MeCN, cat. NaI, reflux, 1 h; ii, $LiAlH_4$, diglyme, reflux, 3 h (**2**) or 100 h (**1**), followed by hydrolysis and acid–base extraction; iii, $Y(CH_2SiMe_3)_3(thf)_2$, pentane, 14 h, 20 °C.

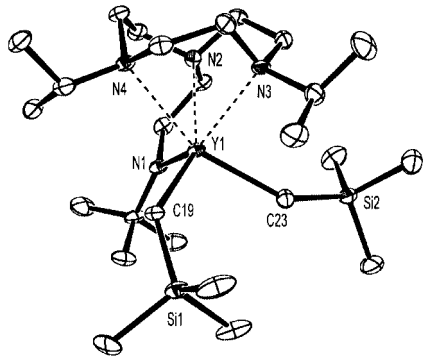

Fig. 1 Molecular structure of **3** (hydrogen atoms omitted for clarity, unlabeled atoms are carbon, thermal ellipsoids drawn at 30% probability level). Selected interatomic distances (Å) and angles (°): Y–N(1) 2.231(5), Y–N(2) 2.541(5), Y–N(3) 2.618(5), Y–N(4) 2.740(5), Y–C(19) 2.476(5), Y–C(23) 2.421(7); C(19)–Y–C(23) 101.1(2), N(1)–Y–N(2) 72.4(2), N(2)–Y–N(3) 68.8(2), N(2)–Y–N(4) 65.5(2), N(3)–Y–N(4) 68.9(2), N(3)–Y–C(23) 86.7(2), N(4)–Y–C(19) 82.7(2), Y–C(19)–Si(1) 134.2(3), Y–C(23)–Si(2) 145.4(4).

† Electronic supplementary information (ESI) available: experimental, spectroscopic and polymerization details. See http://www.rsc.org/suppdata/cc/b1/b101012n/

‡ Netherlands Institute for Catalysis Research (NIOK) publication no. RUG 01-4-01.

Table 1 Catalytic ethene polymerisation with **3** and **4** in conjunction with $[PhNMe_2H][B(C_6F_5)_4]$ activator[a]

Dialkyl	T/°C	PE yield/g	Productivity/ 10^3 kg(PE) mol(Y)$^{-1}$ h^{-1} bar^{-1}	10^{-3} M_w	M_w/M_n
4	30	5.62	0.70	471	4.0
4	50	9.40	1.18	325	4.9
4	80	14.30	1.79	98	6.0
3[b]	30	11.95	0.96	—[c]	—[c]

[a] *Conditions:* toluene solvent (150 ml), 10 μmol Y dialkyl complex, 10 μmol activator, 5 bar ethene pressure, 10 min run time. [b] 15 min run time. [c] Not determined.

arranged in such a way as to prevent the eclipsing of the ligand Pr^i and Y–alkyl groups. The Y–N distances for the tacn nitrogens span a considerable range, the shortest being the distance to the bridgehead nitrogen Y–N(2), 2.541(5) Å, and the longest the Y–N(4) distance, 2.740(5) Å, N(4) being practically *trans* to C(23). This asymmetry appears to be retained in solution, as the ambient temperature ^{1}H and ^{13}C NMR spectra show resonances consistent with an asymmetric species (*e.g.* four resonances for the diastereotopic CH_2SiMe_3 methylene protons).[7] The alkyl methylene carbon resonances are found at δ 33.7 and 31.0, with rather large $^1J_{YC}$ coupling constants (*ca.* 38 Hz) and relatively small $^1J_{CH}$ coupling constants of 95 Hz.

Reaction of the amine **2** with $Y(CH_2SiMe_3)_3(thf)_2$ in pentane yielded the corresponding dialkyl complex [*N*,*N*′-Me$_2$-tacn-*N*″-(CH$_2$CH$_2$)NBu^t]Y(CH$_2$SiMe$_3$)$_2$ **4**, analytically pure in 86% isolated yield. The smaller size of the alkyl substituents makes the complex more fluxional, as the room temperature ^{1}H NMR spectrum of **4** shows broad resonances consistent with a species with an average C_s symmetry. Cooling a toluene-d_8 solution of **4** to −60 °C slows down this dynamic process, revealing spectra with four Y–alkyl methylene and two Y–C resonances, again consistent with an asymmetric ground state structure.[8]

The dialkyl complex **4** reacts cleanly with the Brønsted acid $[PhNMe_2H][B(C_6F_5)_4]$[9] in C_6D_5Br solvent to give $SiMe_4$, free $PhNMe_2$, and an ionic species formulated as {[*N*,*N*′-Me$_2$-tacn-*N*″-(CH$_2$CH$_2$)NBu^t]Y(CH$_2$SiMe$_3$)}[B(C$_6$F$_5$)$_4$] **6**.[10] The ^{1}H NMR spectrum shows a single resonance at δ −1.06 for the YCH_2 group (J_{YH} not resolved), and the ^{13}C NMR YCH_2 resonance at δ 37.0 (J_{YC} 40.7 Hz), shifted downfield and with a larger J_{YC} relative to the dialkyl **4**. The ionic species **6** is thermally relatively stable, and remains essentially unchanged over 1 h at ambient temperature in bromobenzene solution. In contrast, reaction of the dialkyl complex **3** with $[PhNMe_2H][B(C_6F_5)_4]$ leads to rapid formation of propene and 2 equiv. of $SiMe_4$ (as seen by ^{1}H NMR spectroscopy), and an ill-defined yttrium species. Apparently, an Pr^i substituent on the ancillary ligand is metallated on one of its methyl groups, followed by elimination of propene. When the reaction is performed in the presence of an excess of d_8-thf, the cationic alkyl species is trapped before ligand metallation occurs, giving a species formulated (based on its ^{1}H NMR characteristics) as {[*N*,*N*′-Pr$^i_2$-tacn-*N*″-(CH$_2$CH$_2$)NBu^t]Y(CH$_2$SiMe$_3$)(d_8-thf)}-[B(C$_6$F$_5$)$_4$] (**5**·d_8-thf), with YCH_2 resonances at δ −1.29 and −1.35 (dd, $^2J_{HH}$ 11.0 Hz, J_{YH} 3.0 Hz).[11]

Ethylene homopolymerisation experiments (toluene solvent) showed that the dialkyls **3** and **4**, in combination with the Brønsted acid activator $[PhNMe_2H][B(C_6F_5)_4]$, yield active ethene polymerisation catalysts, with observed productivities up to 1.79×10^3 kg(PE) mol(Y)$^{-1}$ h^{-1} bar^{-1}. Relatively short run times (10–15 min) were chosen to minimise inhomogeneity and mass transfer effects. Over the run period the catalysts show a modest (25–30%) decrease in ethene uptake rate. The results listed in Table 1 show that the productivity of the Me$_2$-tacn system is enhanced by increasing the reaction temperature, but that the polydispersity of the polyethene produced also increases substantially. One possible explanation for this is that the initial cationic alkyl catalyst is thermally transformed into another species that is also active in the polymerisation of ethene, thus leading to bimodal product distributions. The polymerisation behaviour of this type of catalyst and its dependence on various parameters (ligand substitution pattern, activator species, *etc.*) is subject of further study.

In conclusion, we have prepared new yttrium dialkyl species with monoanionic tetradentate triazacyclononane-amide ancillary ligands. Reactions of these dialkys with $[PhNMe_2H][B(C_6F_5)_4]$ generate the ionic species **5**·thf-d_8 and **6**, rare examples of spectroscopically characterised cationic group 3 metal alkyls.[12] These cationic alkyl species are active catalysts for the polymerisation of ethene.

This investigation was supported by ExxonMobil Chemical Company.

Notes and references

§ *Crystallographic data* for **3**: $C_{26}H_{61}N_4Si_2Y$, M = 574.87, triclinic, space group $P\bar{1}$, a = 9.815(1), b = 9.859(1), c = 17.291(1) Å, α = 95.60(1), β = 90.68(1), γ = 98.63(1)°, U = 1645.7(4) Å^3, T = 130 K, Z = 2, D_c = 1.160 g cm^{-3}, μ = 18.6 cm^{-1}, Enraf-Nonius CAD4-F diffractometer, λ(Mo-Kα) = 0.71073 Å, 6433 unique reflections, final residuals $wR(F^2)$ = 0.1800, $R(F)$ = 0.0731 for 3940 reflections with $F_o \geq 4\sigma(F_o)$ and 311 parameters. CCDC 157466. See http://www.rsc.org/suppdata/cc/b1/b101012n/ for crystallographic data in .cif or other electronic format.

1 For a recent review of this chemistry, see: A. L. McKnight and R. M. Waymouth, *Chem. Rev.*, 1998, **98**, 2587.

2 P. J. Shapiro, E. E. Bunel, W. P. Schaefer and J. E. Bercaw, *Organometallics*, 1990, **9**, 867; P. J. Shapiro, W. D. Cotter, W. P. Schaefer, J. A. Labinger and J. E. Bercaw, *J. Am. Chem. Soc.*, 1994, **116**, 4623; K. C. Hultzsch, P. Voth, K. Beckerle, T. P. Spaniol and J. Okuda, *Organometallics*, 2000, **19**, 228.

3 J. A. M. Canich, T. D. Schaffer, J. N. Christopher and K. R. Squire, *World Pat.*, WO0018808, 2000, (Exxon).

4 For recent examples of functionalised 1,4,7-triazacyclononane ligands and metal complexes thereof, see: S. E. Watkins, X. Yang, D. C. Craig and S. B. Colbran, *Chem. Commun.*, 1999, 1539; L. M. Berreau, J. A. Halfern, V. G. Young, Jr., and W. B. Tolman, *Inorg. Chem.*, 1998, **37**, 1091; C. Stockheim, L. Hoster, T. Weyhermüller, K. Wieghardt and B. Nuber, *J. Chem. Soc., Dalton Trans.*, 1996, 4409; D. A. Robson, L. H. Lees, P. Mountford and M. Schröder, *Chem. Commun.*, 2000, 1269; M. A. H. Male, M. E. G. Skinner, P. J. Wilson, P. Mountford and M. Schröder, *New J. Chem.*, 2000, **24**, 575; B. Quian, L. M. Henling and J. C. Peters, *Organometallics*, 2000, **19**, 2805, and references therein.

5 C. Fassbeck and K. Wieghardt, *Z. Anorg. Allg. Chem.*, 1992, **608**, 60.

6 M. F. Lappert and R. Pearce, *J. Chem. Soc., Chem. Commun.*, 1973, 126.

7 *Selected NMR data* for **3**: ^{1}H NMR (500 MHz, C_6D_6) δ −0.26 (dd, J_{HH} 10.5, J_{YH} 3.3 Hz, 1H, YC*H*H), −0.53 (dd, J_{HH} 10.8, J_{YH} 2.1 Hz, 1H, YC*H*H), −0.83 (dd, J_{HH} 10.8, J_{YH} 3.0 Hz, 1H, YCH*H*), −1.00 (dd, J_{HH} 10.8, J_{YH} 2.1 Hz, 1H, YCH*H*). ^{13}C NMR (125.7 MHz, C_6D_6) δ 33.7 (dt, J_{YC} 36.9, J_{CH} 95.1 Hz, YCH_2), 31.0 (t, J_{YC} 38.7, J_{CH} 95.0 Hz, YCH_2).

8 *Selected NMR data* for **4**: ^{1}H NMR (500 MHz, −60 °C, C_7D_8) δ −0.62 (d, J_{HH} 11.0 Hz, 1H, YC*H*H), −0.86 (d, J_{HH} 11.0 Hz, 1H, YC*H*H), −0.94 (d, J_{HH} 11.0 Hz, 1H, YCH*H*), −1.06 (d, J_{HH} 10.5 Hz, 1H, YCH*H*). The J_{YH} coupling on the YCH_2 protons is unresolved. ^{13}C NMR (125.7 MHz, −60 °C, C_7D_8) δ 29.8 (dt, J_{YC} 35.4, J_{CH} 93.3 Hz, YCH_2), 28.5 (dt, J_{YC} 38.9, J_{CH} 97.3 Hz, YCH_2).

9 G. G. Hlatky, H. W. Turner and R. R. Eckman, *J. Am. Chem. Soc.*, 1989, **111**, 2728.

10 *NMR data* for the cation of **6**: ^{1}H NMR (500 MHz, −30 °C, C_6D_5Br) δ 2.58–2.22 (m, 16H, NCH_2), 2.18 (s, 6H, NMe), 1.09 (s, 9H, Bu^t), 0.11 (s, 9H, CH_2SiMe_3), −1.06 (br, 2H, YCH_2). ^{13}C{^{1}H} NMR (125.7 MHz, C_6D_5Br, −30 °C) δ 60.09 (NCH_2), 56.05 (NCH_2), 53.33 (CMe_3), 53.75 (NCH_2), 51.78 (NCH_2), 46.51 (NMe), 46.16 (NCH_2), 37.02 (d, $^1J_{YC}$ 40.7 Hz, YCH_2), 30.17 (CMe_3), 4.31 (SiMe).

11 *NMR data* for the cation of **5**·thf-d_8: ^{1}H NMR (500 MHz, −30 °C, C_6D_5Br–thf-d_8) δ 3.48 (sept, J_{HH} 6.0 Hz, 1H, C*H*Me$_2$), 3.40 (t, J_{HH} 13.0 Hz, 1H, NCH_2), 2.79–2.75 (m, 2H, NCH_2), 2.68–2.59 (m, 3H, NCH_2), 2.55–2.48 (m, 2H, NCH_2), 2.42–2.29 (m, 3H, NCH_2), 2.25–2.17 (m, 3H, NCH_2), 1.27 (br, 1H, CHMe_2), 1.18 (d, J_{HH} 6.0 Hz, 6H, CHMe_2), 1.15 (s, 9H, Bu^t), 0.84 (d, J_{HH} 5.5 Hz, 3H, CHMe_2), 0.80 (d, J_{HH} 5.5 Hz, 3H, CHMe_2), 0.09 (s, 9H, Me_3SiCH_2), −1.29 (dd, J_{HH} 11.0, J_{YH} 3.0 Hz, 1H, YC*H*H), −1.35 (dd, J_{HH} 11.0, J_{YH} 3.0 Hz, 1H, YCH*H*).

12 L. W. M. Lee, W. E. Piers, M. R. J. Elsegood, W. Clegg and M. Parvez, *Organometallics*, 1999, **18**, 2947; L. Lee, D. J. Berg, F. W. Einstein and R. J. Batchelor, *Organometallics*, 1997, **16**, 1819; S. Haleja, W. P. Schaefer and J. E. Bercaw, *J. Organomet. Chem.*, 1997, **532**, 45.

ChemComm

Competitive intramolecular nucleophilic aromatic substitution: a new route to coumarins

Concepción Alonso, Marilyn M. Olmstead, Michael H. Nantz and Mark J. Kurth*

Department of Chemistry, University of California, One Shields Avenue, Davis, CA 95616 USA. E-mail: mjkurth@ucdavis.edu

Received (in Corvallis, OR, USA) 10th November 2000, Accepted 17th January 2001
First published as an Advance Article on the web 14th March 2001

4-Hydroxy-3-(2′-pyridyl)coumarins (4) (R = 6-Cl, H, 6-NO_2, 8-NO_2) were prepared in moderate to good yields by the intramolecular nucleophilic aromatic substitution reaction of β-ketoesters (I) in refluxing xylenes; evidence for the reversible formation of benzo[*c*]quinolizinium III from I (X = 4-Cl), with eventual formation of 4 (R = 6-Cl), is also presented.

Cystic fibrosis (CF) results from defects in the gene encoding a cyclic adenosine monophosphate-dependent chloride ion channel known as the cystic fibrosis transmembrane conductance regulator[1] (CFTR) and is characterized by defective chloride transport across epithelia of the airways, exocrine ducts, and intestine as well as viscous epithelial mucous secretions.[2] Becq's recent report[3] that the benzo[*c*]quinolizinium derivative MPB-07 (**II**, Fig. 1) activates wild-type CFTR membrane protein[4] in a variety of cell systems, coupled with our interests[5] in developing small molecule drugs capable of modulating chloride-selective ion channels,[6] led us to explore the use of 3-oxo-2-(2′-pyridyl)(*o*-halophenyl)propanoates as precursors to CFTR-active compounds. The synthesis of benzo[*c*]quinolizinium salts *via* an intramolecular cyclization reported by Fozard and Bradsher[7] led us to consider cyclization of **I** to MPB-07 analog **III** by an intramolecular *ipso* substitution reaction. We report here a wider perspective on the intriguing and useful intramolecular nucleophilic aromatic substitution chemistry of these α-(2-pyridyl)-β-ketoesters.

Our work started with *C*-acylation of benzyl 2-(2-pyridyl)acetate (**1**, Scheme 1),† in turn generated by the transesterification of methyl 2-(2-pyridyl)acetate with lithium benzoxide.[8] Generation of the lithium salt of **1** and subsequent treatment with various *o*-halobenzoyl chlorides gave the corresponding 3-oxo-2-(2′-pyridyl)(*o*-halophenyl)propanoates (**2**). Yields for **1** → **2** are generally moderate (60–75%) for a variety of halobenzoyl chlorides.

Heating **2a** in xylenes at reflux for 2 h delivered a crystalline product which we initially assumed was benzo[*c*]quinolizinium salt **III** (82% yield, Scheme 2). However, single crystal X-ray crystallographic analysis‡ (Fig. 2) revealed that the product was in fact isolated as the neutral benzo[*c*]quinolizine **3a** replete with 1-carboalkoxy and 2-oxo substituents on the newly formed ring. The observation that **2a** → **3a** *via* **III**, which was consistent with the results reported by Fozard and Bradsher for cycloquaternization of *cis*-2′-chloro-2-stilbazole, suggested that *ipso* substitution in our 3-oxo-2-(2′-pyridyl)(*o*-halophenyl)propanoate series would provide a general route to the benzo[*c*]quinolizine ring system.

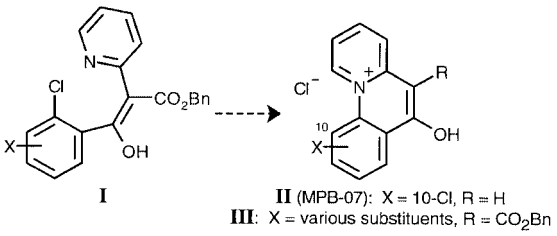

Fig. 1 3-Oxo-2-(2′-pyridyl)(*o*-halophenyl)propanoates as precursors to benzo[*c*]quinolizinium derivatives.

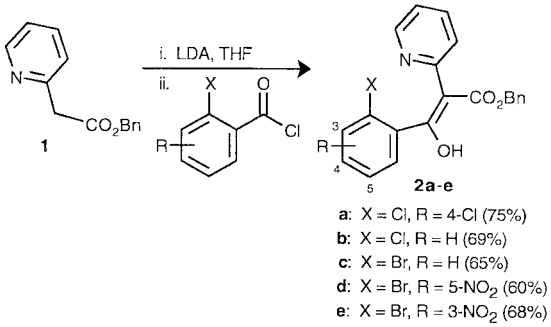

Scheme 1 Preparation of 3-oxo-2-(2′-pyridyl)(*o*-halophenyl)propanoates.

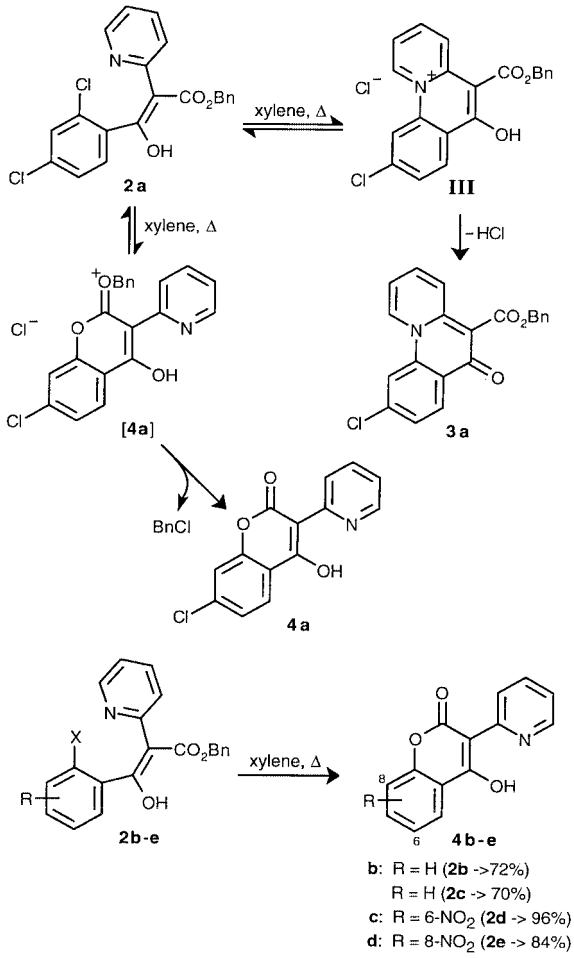

Scheme 2 Intramolecular *ipso* substitution in 3-oxo-2-(2′-pyridyl)(*o*-halophenyl)propanoates.

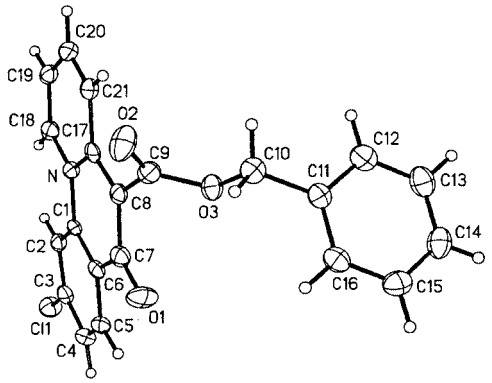

Fig. 2 X-Ray crystallographic structure of **3a**.

However, the next substrate investigated, **2b**, underwent ring-closing *ipso* substitution with loss of the benzyl ester moiety.† On closer inspection, it became apparent that *ipso* substitution of the *o*-chloro substituent in **2b** had occurred *via* nucleophilic attack of the carboalkoxy giving 4-hydroxycoumarin **4b** as the sole isolated product (72%). We speculate that **2** exists in a highly enolized, hydrogen-bonded (N···H–O) conformation[9] which biases the system to intramolecular carboalkoxy—rather than pyridyl—nucleophilic attack resulting in **2b** → **4b**. In the case of **2a**, the *p*-chloro substituent apparently deactivates the ring toward nucleophilic attack to the extent that only the 2-pyridyl moiety is nucleophilic enough to participate in *ipso* substitution, leading to formation of **3a**.

These observations led us to speculate that benzo[*c*]quinolizine **3a** might represent the kinetic product in this reaction and raised the question whether further heating of the **2a** → **3a** reaction mixture might lead to formation of the corresponding 4-hydroxycoumarin derivative. This would presumably occur by reversion of **III** to **2a** by intermolecular *ipso* attack by chloride followed by slow intramolecular ring-closing by carboalkoxy *ipso* attack to [**4a**]. Once formed, irreversible loss of BnCl from [**4a**] would deliver **4a**. To test this idea, the **2a** → **3a** reaction was performed in toluene-d_8 (110 °C) and intermittently monitored by ^{1}H-NMR. As anticipated, we observed the fairly rapid formation of **3a** (**2a** consumed in 72 h) followed by its slow disappearance and matched by the slow appearance of both benzyl chloride and 4-hydroxycoumarin **4a** (intermittent monitoring over 12 d). Moreover, when the laboratory scale reaction of compound **2a** was performed in refluxing xylene, formation of benzo[*c*]quinolizine **3a** was detected early on (monitored by TLC). Continued heating for 10 d afforded 4-hydroxycoumarin **4a** in 65% yield.

Three additional 3-oxo-2-(2′-pyridyl)(*o*-halophenyl)propanoates were also investigated (**2c**–**e**). In each of these, the *o*-halo substituent was a bromine and, in two of these, a strongly activating nitro group was incorporated at C5 (**2d**) or C3 (**2e**). In each of these cases, only carboalkoxy nucleophilic attack was observed. The yields for **2** → **4** are generally quite good (70–96%), with the more electron deficient C-ring systems affording higher yields.

The method reported here provides a general and useful route for the production of 4-hydroxy-3-(2′-pyridyl)coumarin derivatives. While both pyridyl and carboalkoxy moieties can participate in this reaction, reversible formation of the benzo-[*c*]quinolizinium coupled with irreversible loss of benzyl chloride during coumarin formation leads to the exclusive formation of the 4-hydroxy-3-(2′-pyridyl)coumarin derivative.

We thank the National Science Foundation and Cystic Fibrosis Foundation for financial support of this research as well as the National Science Foundation CRIF program (CHE-9808183) for Varian Inova 400 MHz and Mercury 300 MHz NMR instrument purchases. C. A. thanks the Departamento de Educación, Universidades e Investigación del Gobierno Vasco (Spain) for a Postdoctoral Fellowship.

Notes and references

† *General procedure for C-acylation of benzyl 2-(2′-pyridyl)acetate* (**1**): to a cold (0 °C) solution of diisopropyl amine (0.33 mL, 2.4 mmol) in dry ethyl ether (6.0 mL) under inert atmosphere was added dropwise n-BuLi (1.63 M in hexane, 1.47 mL, 2.4 mmol). The mixture was cooled to −78 °C and a solution of phenylmethyl 2-(2′-pyridyl)acetate (0.456 g, 2.0 mmol) in dry ethyl ether (2.0 mL) was added dropwise. This mixture was stirred at −78 °C for 60 min at which time a solution of the appropriate benzoyl chloride (2.0 mmol) in dry ethyl ether (1.0 mL) was added dropwise. Stirring was continued at 0 °C for an additional 30 min at which time the reaction was treated with 1 M aq. HCl and extracted with CH_2Cl_2. The organic layer was dried ($MgSO_4$), concentrated, and the oily residue was recrystallized from hexane.

General procedure for 4-hydroxycoumarin formation (**2** → **4**): a solution of phenylmethyl 3-aryl-3-oxo-2-(2′-pyridyl)propanoate **2** (0.2 mmol) in xylenes (2.0 mL) was stirred at reflux under N_2 for 2 h. After removal of the solvent in vacuum, the 4-hydroxycoumarin product was purified by silica gel chromatography (hexanes : EtOAc).

‡ *Crystallographic data*: **3a** (R = −C_6H_5) $C_{21}H_{14}ClNO_3$, M = 363.78, triclinic, space group $P\bar{1}$, a = 7,1272(9), b = 9.5407(12), c = 13.1738(10) Å, α = 77.273(8), β = 79.502(9), γ = 68.701(10)°, U = 808.95(16) Å^3, Z = 2, μ = 2.280 mm^{-1}, T = 133(2) K, a unique data set of 2105 independent reflections was collected, $R1$ = 0.0355 for all data. CCDC 152984. See http://www.rsc.org/suppdata/cc/b0/b009172n/ for crystallographic data in .cif or other electronic format.

1 A. L. Gibson, L. M. Wagner, F. S. Collins and D. L. Oxender, *Science*, 1991, **254**, 109.
2 J. R. Riordan, J. M. Rommens, B. S. Kerem, N. Alon, R. Rozmahel, Z. Grzelezak, J. Zielenski, S. Lok, N. Plavsic, J. L. Chou, M. L. Drumm, M. C. Iannuzzi, F. S. Collins and L. C. Tsui, *Science*, 1989, **245**, 1059.
3 F. Becq, Y. Mettey, M. A. Gray, L. J. Galietta, R. L. Dormer, M. Merten, T. Metaye, V. Chappe, C. Marvingt-Mounir, O. Zegarra-Moran, R. Tarran, L. Bulteau, R. Dérand, M. M. C. Pereira, M. A. McPherson, C. Rogier, M. Joffre, B. E. Argent, D. Sarrouilhe, W. Kammouni, C. Figarella, B. Verrier, M. Gola and J.-M. Verfond, *J. Biol. Chem.*, 1999, **274**, 27 415.
4 J. R. Riordan, J. M. Rommens, B. S. Kerem, N. Alon, R. Rozmahel, Z. Grzelczak, J. Zeilenski, S. Lok, N. Plavsic, J. Chou, M. L. Drumm, M. C. Iannuzzi, F. S. Collins and L. C. Tsui, *Science*, 1989, **245**, 1066; B. Kerem, J. M. Rommens, J. A. Buchanan, D. Markiewicz, T. K. Cox, A. Chakravarti, M. Buchwald and L. C. Tsui, *Science*, 1989, **245**, 1073.
5 M. Eda, M. J. Kurth and M. H. Nantz, *J. Org. Chem.*, 2000, **65**, 5131; M. J. Haddadin, M. J. Kurth and M. Olmstead, *Tetrahedron Lett.*, 2000, **41**, 5613.
6 M. Li, J. D. MacCann, M. P. Anderson, J. P. Clancy, C. M. Liedtke, A. C. Nairn, P. Greengard and M. J. Welssch, *Science*, 1989, **244**, 1353.
7 A. Fozard and C. K. Bradsher, *J. Org. Chem.*, 1966, **31**, 2346.
8 B. M. Bhawal, S. P. Khanapure and E. R. Biehl, *Synthesis*, 1991, 113.
9 Remarkably, the enolic proton in **2a** appears as a singlet at 18.4 ppm ($CDCl_3$) which we believe is indicative of a pyridine H-bonded conformation.

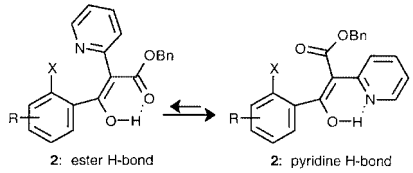

Direct production of hydrogen from ethanolic aqueous solutions over oxide catalysts†

Jordi Llorca, Pilar Ramírez de la Piscina,* Joaquim Sales and Narcís Homs*

Departament de Química Inorgànica, Facultat de Química, Universitat de Barcelona, C/ Martí i Franqués 1-11, 08028 Barcelona, Spain. E-mail: pilar.piscina@qi.ub.es

Received (in Cambridge, UK) 8th January 2001, Accepted 1st March 2001
First published as an Advance Article on the web 16th March 2001

Steam-reforming of ethanol over ZnO gives highly effective production of CO-free H_2: 5.1 mol of H_2 per mol of reacted ethanol is formed at 723 K under 100% ethanol conversion.

There is growing interest in the use of H_2 as an alternative fuel mainly due to environmental aspects.[1,2] Alcohols could constitute a good supply of hydrogen, as they are efficient H_2-reservoirs and could avoid the difficulty of H_2-distribution. In this context, many efforts have been applied to the production of hydrogen from steam-reforming of methanol by using methanol synthesis-based catalysts;[3–5] however, there are fewer papers dealing with ethanol steam-reforming.[6] However, two considerations point to ethanol as an alternative to methanol: (i) the yield of H_2 is higher, (ii) ethanol is a renewable material which can be easily obtained from biomass. As regards the use of supported catalysts in the steam-reforming of ethanol, mainly copper- and cobalt-based catalysts have been studied.[7–9] In both cases the behaviour of supported catalysts was strongly affected by the support used. However, their role remains unclear and no exhaustive studies of transformations of ethanol over individual inorganic oxides under ethanol steam-reforming conditions have been reported.

Here we report the behaviour of several oxides, with a wide range of redox and acid–base properties, in the steam-reforming of ethanol. A high H_2O:ethanol ratio was used to explore the possibility of using ethanol as obtained from biomass (aqueous solutions of concentration *ca.* 15% in ethanol are obtained from sugar cane or starch-rich grains). In some cases total conversion of ethanol and high selectivity to the reforming reaction were attained.

The following oxides with the indicated BET surface area were used: MgO (prepared by adding ammonia to a $MgCl_2$ solution, 110 $m^2\ g^{-1}$), γ-Al_2O_3 (Girdler, 188 $m^2\ g^{-1}$), SiO_2 (Degussa–Hüls, 200 $m^2\ g^{-1}$), TiO_2 (Degussa–Hüls, 45 $m^2\ g^{-1}$), V_2O_5 (Merck, 22 $m^2\ g^{-1}$), ZnO (1) (Asturienne New Jersey, 11 $m^2\ g^{-1}$), ZnO (2) (prepared by decomposition of $3ZnO{\cdot}2ZnCO_3{\cdot}3H_2O$, 100 $m^2\ g^{-1}$), La_2O_3 (Merck, 11 $m^2\ g^{-1}$), CeO_2 (Aldrich, 17 $m^2\ g^{-1}$), Sm_2O_3 (Merck, 9 $m^2\ g^{-1}$). Steam-reforming of ethanol was carried out between 573 and 723 K, at atmospheric pressure, using a 1:13:70 C_2H_5OH:H_2O:Ar stream (molar ratio) and 0.1 g of the appropriate oxide diluted with inactive SiC, under a gas hourly space velocity (GHSV) of 5000 h^{-1}. After periods of 2 h at each temperature, the temperature was increased consecutively from 573 to 623, 673 and 723 K; at the final temperature the reaction was conducted over a period of 20 h. Products were analysed on-line by gas chromatography. Hydrogen was analysed with a TCD using Ar as a carrier gas, CO and CO_2 were analysed with an FID after passing through a methanizer, and hydrocarbons as well as oxygenated products were separated with a capillary column and analysed with an FID.

Conversion of ethanol increased with temperature for all samples (see Fig. 1). However, significant differences between

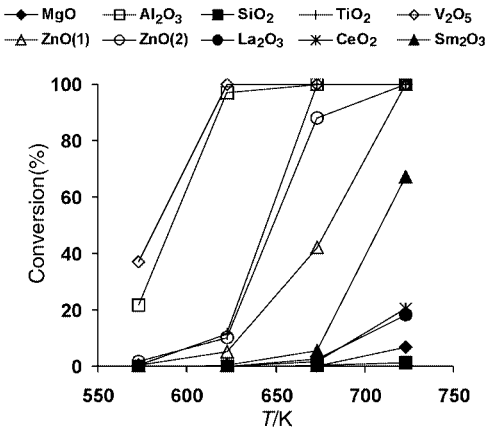

Fig. 1 Ethanol conversion as a function of temperature for different oxides. Reaction conditions: total pressure 1 atm, $C_2H_5OH:H_2O:Ar = 1:13:70$ (molar ratio), GHSV = 5000 h^{-1}.

them in terms of activity, stability and selectivity were found. The temperature required for total conversion was lower for V_2O_5 and γ-Al_2O_3 (623 K) than for the other oxides, and even at 723 K, conversions of $< 10\%$ were obtained over MgO and SiO_2 and were *ca.* 20% over La_2O_3 and CeO_2. A comparison between conversion values, after 20 h of reaction at 723 K and initial values (after 2 h of reaction at 723 K), shows a high deactivation process for TiO_2 and Sm_2O_3. Conversion diminished from 100% to 3.9% for TiO_2 and from 67.2% to 37.9% for Sm_2O_3. After reaction these two oxides appeared black, and carbon deposition during reaction could be responsible for the drop in activity. Table 1 shows the product selectivity and the ethanol conversion values after 20 h at 723 K (GHSV = 5000 h^{-1}) under the steam-reforming conditions mentioned above for catalysts with conversion $> 5\%$. The values of selectivity obtained with the different catalysts can be explained in terms of the contribution of the following reactions: ethanol steam-reforming (1), ethanol decomposition to CH_4 (2), ethanol dehydration (3), ethanol dehydrogenation (4), ethanol decomposition to acetone (5) and water–gas shift reaction (WGSR) (6).

$$CH_3CH_2OH + 3H_2O \rightarrow 2CO_2 + 6H_2 \quad (1)$$

$$CH_3CH_2OH \rightarrow CO + CH_4 + H_2 \quad (2)$$

$$CH_3CH_2OH \rightarrow C_2H_4 + H_2O \quad (3)$$

$$CH_3CH_2OH \rightarrow CH_3CHO + H_2 \quad (4)$$

$$2CH_3CH_2OH \rightarrow CH_3COCH_3 + CO + 3H_2 \quad (5)$$

$$CO + H_2O \rightarrow CO_2 + H_2 \quad (6)$$

Negligible steam-reforming of ethanol was observed over MgO and γ-Al_2O_3. Over γ-Al_2O_3 only the dehydration of ethanol to ethylene was observed and over MgO high selectivity to acetaldehyde was obtained. These findings are consistent with the acidic and basic characteristics of γ-Al_2O_3 and MgO respectively,[10] which in addition do not have redox properties.

† Dedicated to Professor Rafael Usón on the occasion of his 75th birthday.

DOI: 10.1039/b100334h

Table 1 Catalytic performance on a C_2H_5OH–H_2O–Ar ($C_2H_5OH:H_2O = 1:13$ molar ratio) stream at 723 K and atmospheric pressure

Sample	GHSV/h^{-1}	Conv.(%)	Product selectivity[a] (%)								mol H_2/ mol EtOH	mol CO_2/ mol EtOH
			H_2	CO	CO_2	CH_4	C_2H_4	C_3H_6	CH_3CHO	CH_3COCH_3		
MgO	5000	6.9	45.9	—	0.4	0.9	6.8	1.7	44.3	—		
Al_2O_3	5000	100	—	—	—	—	100	—	—	—		
V_2O_5	5000	100	36.7	1.1	19.1	1.2	33.3	0.4	8.2	—		
ZnO (1)	5000	100	61.4	—	18.5	1.1	1.7	0.5	10.2	6.6		
ZnO (2)	5000	100	64.6	—	21.1	0.7	0.6	0.3	0.2	12.5		
La_2O_3	5000	19.9	44.4	—	17.7	4.5	33.0	0.4	—	—		
CeO_2	5000	24.4	52.4	0.2	15.9	1.1	18.9	0.1	—	11.4		
Sm_2O_3	5000	37.9	32.0	—	11.9	0.9	53.3	0.5	—	1.4		
ZnO (2)	2300	100	60.4	—	20.2	0.5	1.0	0.2	2.6	15.1	1.6	0.5
ZnO (2)	3800	100	63.2	—	21.0	0.4	1.0	0.2	3.4	10.8	2.0	0.7
ZnO (2)	9900	100	65.0	—	21.8	0.3	1.1	0.2	5.9	5.8	2.4	0.8
ZnO (2)	19000	100	72.0	—	23.8	0.3	1.6	0.2	0.9	1.2	4.3	1.4
ZnO (2)	22000	100	73.4	—	24.3	0.5	1.0	0.1	0.4	0.3	5.1	1.7

[a] Water not included.

The product distribution for the remaining oxides indicates that the steam-reforming of ethanol took place. However, all samples in Table 1 except zinc oxides, showed significant yields in the dehydration of ethanol. For V_2O_5 the production of ethylene can be related to its acidic properties.[10,11] On the other hand, the dehydration of ethanol over La_2O_3 and Sm_2O_3 has been proposed to occur over basic centres,[11] with the production of ketones from alcohols also related to basic centres in the oxides. The high conversion values and high selectivity to CO_2 and H_2 obtained over ZnO (1) and ZnO (2) is of note. Over these oxides the main reactions under the experimental conditions used were the decomposition of ethanol to acetone, the reforming of ethanol and the WGSR. The decomposition of ethanol to acetone is well documented over ZnO-based catalysts.[12,13] This takes place *via* several successive reactions such as dehydrogenation and aldol condensation over basic centres. The performance of ZnO in the steam-reforming of ethanol could be a consequence of its basic and redox characteristics. The basic properties should be related to the dehydrogenation of ethanol to acetaldehyde and then, its specific redox characteristics could help to aid the steam-reforming reaction.

The yield of acetone is expected to be affected by the contact time. A deeper study of the transformations of ethanol over ZnO (2) as a function of contact time indicated that it is possible to have a very high yield in the reforming of ethanol and to minimize the yield of all the other ethanol transformations. Table 1 also compiles some results obtained for GHSV ranging from 22 000 to 2300 h^{-1}. Different space velocities were obtained by dilution of the C_2H_5OH–H_2O mixture (1 : 13 molar ratio) with Ar, after each change the system was stabilised for 2 h and then the products were analysed. In all cases total conversion of ethanol was obtained and no CO was detected (detection limit of CO 17 ppm). When the reaction was conducted at 22 000 h^{-1}, only 2.3% of the total products were other than H_2 or CO_2. Under these conditions, values of 5.1 mol H_2 and 1.7 mol CO_2 per mol of reacted ethanol were recorded representing 85% of the theoretical values that can be obtained from ethanol reforming. This finding, together with the absence of CO production (or at least < 17 ppm) indicate that a ZnO-based catalytic system may be used for H_2 production for fuel cells. Moreover, at a practical level, bioethanol could be used as raw material.

We thank CICYT (MAT1999-0477) and Generalitat de Catalunya (1999 SGR-00044) for financial support.

Notes and references

1 J. N. Armor, *Appl. Catal. A*, 1999, **176**, 159.
2 M. A. Peña, J. P. Gomez and J. L. G. Fierro, *Appl. Catal. A*, 1996, **144**, 7.
3 J. P. Breen and J. R. H. Ross, *Catal. Today*, 1999, **51**, 521.
4 S. Velu, K. Suzuki and T. Osaki, *Chem. Commun.*, 1999, 2341.
5 N. Takezawa and N. Iwasa, *Catal. Today*, 1997, **36**, 45.
6 X. Verykios, *WO Pat.*, 99/61369, 1999 and references therein.
7 F. Haga, T. Nakajima, H. Miya and S. Mishima, *Catal. Lett.*, 1997, **48**, 223.
8 N. Iwasa and N. Takezawa, *Bull. Chem. Soc. Jpn.*, 1991, **64**, 2619.
9 J. C. Amphlett, S. Leclerc, R. F. Mann, B. A. Peppley, P. R. Roberge, paper no. 98-269, *Proc. Intersoc. Energy Convers. Eng. Conf., 33rd*, Colorado Springs, USA, 1998.
10 H. H. Kung, *Stud. Surf. Sci. Catal.*, 1989, **45**, 146.
11 K. Tanabe, M. Misono, Y. Ono and H. Hattori, *Stud. Surf. Sci. Catal.*, 1989, **51**, 215.
12 T. Nakajima, T. Yamaguchi and K. Tanabe, *J. Chem. Soc., Chem. Commun.*, 1987, 394.
13 R. Sreerama Murthy, P. Patnaik, P. Sidheswaran and M. Jayamani, *J. Catal.*, 1988, **109**, 298.

ChemComm

An expeditious solvent-free route to ionic liquids using microwaves

Rajender S. Varma* and Vasudevan V. Namboodiri

Clean Processes Branch, National Risk Management Research Laboratory, US Environmental Protection Agency, MS 443, 26 W. Martin Luther King Drive, Cincinnati, OH 45268, USA. E-mail: Varma.Rajender@epa.gov

Received (in Corvallis, OR, USA) 9th February 2001, Accepted 22nd February 2001
First published as an Advance Article on the web 20th March 2001

A microwave-assisted preparation of a series of ambient temperature ionic liquids, 1-alkyl-3-methylimidazolium (AMIM) halides, that proceeds *via* efficient reaction of 1-methylimidazole with alkyl halides/terminal dihalides under solvent-free conditions, is described.

In addition to their role in electrochemistry[1] (electrolytes for battery, fuel cells *etc.*), heavy metal ion extraction,[2] phase transfer catalysis, and polymerization,[3] ionic liquids are emerging as a set of new green solvents, mainly as a replacement for conventional volatile organic solvents.[4] The use of a large excess of conventional volatile solvents required to run a chemical reaction is of ecological and economic concern. Ambient temperature ionic liquids encompassing 1,3-dialkylimidazolium cations (**A**) have shown great promise as an attractive alternative to conventional solvents.[5] The important properties of these ionic liquids are low volatility, negligible vapor pressure, ease of handling, accelerated reaction rates, potential for recycling, and compatibility with various organic compounds and organometallic catalysts.[6] Also, the products from reactions conducted in ionic liquids can be extracted very easily using various organic solvents. The preparation of 1,3-dialkylimidazolium halides *via* the conventional heating method in refluxing solvents requires several hours to afford reasonable yields and also uses a large excess of alkylhalides/organic solvents as the reaction medium.[7] In view of the emerging importance of the ionic liquids as reaction media[8] and our general interest in MW-assisted chemical processes,[9] we decided to explore the synthesis of ionic liquids using microwave (MW) irradiation under solvent-free conditions. Herein, we report an efficient method for the preparation of ionic liquids using microwave irradiation as the energy source by simple exposure of neat reactants in open containers to microwaves using an unmodified household MW oven. This solvent-free approach requires only a few minutes of reaction time in contrast to several hours needed under conventional heating conditions which uses an excess of reactants.

In an unmodified household MW oven it is not possible to vary the MW power. The reduction in power level simply entails that it operates at its full power but for a reduced period of time. A recently introduced household MW oven (Panasonic) equipped with inverter technology provides a realistic control of the microwave power to a desirable level. We examined the effect of microwave power on a set of reactions using 1-butyl bromide (1-BuBr) and 1-methylimidazole (MIM) as reactants (Table 1).† Upon microwave irradiation, the ionic liquid starts forming which increases the polarity of the reaction medium thereby increasing the rate of microwave absorption. The formation of ionic liquid could be monitored visibly in the reaction when it turns from clear solution to opaque and finally clear. It is observed that at elevated power levels evaporation of alkyl halide and partial decomposition/charring of the ionic liquid occurs possibly due to the localized heating of the ionic liquid, which eventually results in lower yields. To circumvent this problem, we conducted the reaction with intermittent heating and mixing at a moderate power level to provide better yields and cleaner ionic liquid formation.‡ After the first irradiation for 30 s at 240 W (~bulk temperature 70–100 °C) the homogeneity of the reaction mixture changes due to formation of a small amount of ionic liquid. The reaction mixture is then taken out, mixed again for 10 s and then heated at the same power level for an additional 15 s. This step is repeated until the formation of a clear single phase ionic liquid product. At this stage, the unreacted starting materials are removed by washing with ether and the product dried under vacuum at 80 °C.

A series of ionic liquids prepared by microwave heating and the protocol is then compared with the similar preparation using conventional heating (oil bath at 80 °C). The comparative results are summarized in Table 2. Most of the halides used in this study have higher boiling points and are converted efficiently to ionic liquids under microwave irradiation. The relatively less reactive and low boiling reactants such as butyl chloride and 2-bromobutane (entries 1 and 4, Table 2) incurred loss due to evaporation and hence are used in excess quantity. The reactivity trend of halides is found to be in the order $I^- > Br^- > Cl^-$. Due to the high reactivity of the iodides excellent yields are obtained in all cases with minimum exposure time. The conventional methods reported in the literature generally use a large excess of alkyl halide–THF as solvents. The present method is eco-friendly and uses only stoichiometric amounts of reactants.

The preparation of ionic liquids bearing polycations are of recent synthetic interest.[10] We have prepared novel dicationic compounds (**B**) utilizing alkyl dihalides. The butyl and hexyl dicationic salts (entries 11–15, Table 2) are solids at rt. The corresponding octyl analogues with bromide/chloride as the anions are viscous liquids (entries 16 and 17, Table 2) whereas the iodo compound (entry 18, Table 2) is a solid. From the NMR data the dicationic salts generated from chloro and bromoalkanes (entries 11, 13, 14 and 16, Table 2) are slightly contaminated with the corresponding monocationic intermediate (< 5%). However, the diiodoalkanes, being reactive, afforded pure products. The purity of ionic salts prepared *via* microwave heating are found to be superior to those prepared *via* conventional heating methods, presumably due to inefficient mixing in the later, once the solid product (**B**) begins to form.§

The thermogravimetric analyses (TGA) and differential scanning calorimetry (DSC) data show that all ionic liquids

Table 1 Optimization of reaction conditions for preparation of ionic liquid using microwaves

No.	1-BuBr/ mmol	MIM/ mmol	MW-Power/W	Time/s	Yield (%)
1	1	1	120	60	42
2	1	1	120	120	62
3[a]	1	1	240	120	78
4[a]	1	1	360	60	76
5[a]	1	1	360	60	76
6	1	1	240	30 + 15 + 15 + 15	81
7[b]	1.1	1	240	30 + 15 + 15 + 15	86
8[b]	1.2	1	240	30 + 15 + 15 + 15	86

[a] Partial decomposition occurred at high power or extended irradiation time. [b] The reaction mixture was thoroughly mixed on a vortex mixer prior to irradiation.

DOI: 10.1039/b101375k

Table 2 Preparation of ionic liquids based on alkylimidazolium halides

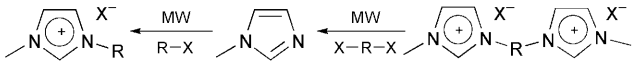

A B

Where X = Cl, Br, I

Entry	Alkylhalide (RX)	RX-mmol	MIM-mmol	MW-Time/s	Yield[a] (%)	Yield[b] (%) (time/h)
1	1-chlorobutane	4	2	30 + 15 + 15 + 15 + 15	76	50 (5)
2	1-bromobutane	2.2	2	30 + 15 + 15 + 15	86	76 (5)
3	1-iodobutane	2.2	2	30 + 10 + 10 + 10	92	93 (3)
4	2-bromobutane	4	2	30 + 15 + 15 + 15 + 15	71	61 (5)
5	1-chlorohexane	2.2	2	30 + 15 + 15 + 15 + 15	81	53 (5)
6	1-bromohexane	2.2	2	30 + 15 + 15 + 15	89	78 (5)
7	1-iodohexane	2.2	2	30 + 10 + 10 + 10	93	89 (3)
9	1-iodoheptane	2.2	2	30 + 10 + 10 + 10	94	95 (3)
10	1-bromooctane	2.2	2	30 + 15 + 15 + 15	91	73 (5)
11	1,4-dibromobutane	1	2.2	30 + 15 + 15 + 15	81	76 (5)
12	1,4-diiodobutane	1	2.2	15 + 15 + 10 + 10	91	89 (3)
13	1,6-dichlorohexane	1	2.2	30 + 15 + 15 + 15 + 15	82	56 (5)
14	1,6-dibromohexane	1	2.2	30 + 15 + 10 + 10	92	72 (5)
15	1,6-diiodohexane	1	2.2	15 + 15 + 10 + 10	85	97 (3)
16	1,8-dichlorooctane	1	2.2	30 + 15 + 15 + 15 + 15	78	72 (5)
17	1,8-dibromooctane	1	2.2	30 + 15 + 15 + 15	92	76 (5)
18	1,8-diiodooctane	1	2.2	15 + 15 + 10 + 10	94	93 (3)

[a] Using MW at power 240 W. [b] Using alternative heating method (oil bath at 80 °C). Entry, mp; 11, 67–69 °C; 12, 110–112 °C; 13, 85–87 °C; 14, 112–116 °C; 15, 149–150 °C; 18, 120–123 °C.

(Table 2) are pure and are free of any starting materials. These studies also establish that the compounds are thermally stable up to 280 °C and then start decomposing with complete decomposition occurring above 300 °C.¶

In conclusion, a solvent-free MW-assisted protocol is developed for the synthesis of ionic liquids in open containers using an unmodified household microwave oven. Essentially, the ionic liquids can be generated *in situ* and subsequent reactions conducted in the same pot.

The authors wish to thank Mr Ballard Mullins for the TGA and DSC analyses. V.V.N. is a postgraduate research participant at the National Risk Management Laboratory administered by the Oak Ridge Institute for Science and Education through an interagency agreement between the US Department of Energy and the US Environmental Protection Agency.

Notes and references

† In a typical reaction, 1-bromobutane (2.2 mmol) and MIM (2 mmol) are placed in a test tube, mixed thoroughly on a vortex Mixer (Fisher, Model 231) and the mixture is heated intermittently in an unmodified household MW oven (Panasonic NN-S740WA-1200W) at 240 W (30 s irradiation with 10 s mixing) until a clear single phase is obtained. The bulk temperature recorded is in the range 70 to 100 °C. The resulting ionic liquid is then cooled, washed with ether (3 × 2 mL) to remove unreacted starting materials and product dried under vacuum at 80 °C to afford 86% of 1-butyl-3-methylimidazolium bromide, ^{1}H NMR (250 MHz; D_2O), δ_H: 0.72 (t, CH_3), 1.15 (m, CH_2), 1.81 (m, CH_2), 3.71 (s, N-CH_3), 4.09 (m, N-CH_2), 7.38 (s, NCH), 7.43 (s, NCH), 8.7 (s, N(H)CN); ^{13}C NMR δ_C: 12.89 (t, CH_2), 19.02 (m, CH_3), 31.51 (m, CH_2), 35.86 (N-CH_2), 49.51 (N-CH_3), 122.40 (NCH), 123.73 (NCH), 136.21 (N(H)CN). An experiment on a relatively large scale (22 mmol of 1-bromobutane and 20 mmol of MIM) afforded 87% yield.

‡ There are commercial microwave devices available that provide adequate mixing and control of reaction parameters such as temperature, pressure *etc.* For description see details at sites: http://www.cem.com; http://www.microcure.com and http://www.personalchemistry.com

§ The NMR spectra of the samples are recorded on a Brucker 250 MHz spectrometer using D_2O as solvent and CD_3OD/$CDCl_3$ as the standards. The new compounds are characterized by elemental analyses, ^{1}H and ^{13}C NMR. The data for a representative dicationic compound, entry 15, δ_H (250 MHz; D_2O) 1.29 (m, CH_2), 1.82 (m, CH_2), 3.71 (s, N-CH_3), 4.14 (m, N-CH_2), 7.38 (s, NCH), 7.43 (s, NCH), 8.7 (s, NC (H)N); δ_c: 24.99 (t, CH_2), 29.17 (m, CH_3), 36.18 (N-CH_2), 49.57 (N-CH_3), 122.35 (NCH), 123.64 (NCH), 135.97 (NC (H)N), (Calc. for $C_{14}H_{24}N_4I_2$: C, 33.49; H, 4.82; N, 11.16; Found. C, 33.69; H, 4.93; N, 11.68%).

¶ The TGA of the sample is performed by heating from 25 to 500 °C at a rate of 10 °C min^{-1} and DSC is conducted from 25 to 450 °C at a heating rate of 10 °C min^{-1}.

1 J. S. Wilkes, J. A. Levinsky, R. A. Wilson and C. L. Hussey, *Inorg. Chem.*, 1982, **21**, 1263.
2 S. Dai, Y. H. Ju and C. E. Barnes, *J. Chem. Soc., Dalton Trans.*, 1999, 1201; A. E. Visser, R. P. Swatloski and R. D. Rogers, *Green Chemistry*, 2000, **2**, 1; A. E. Visser, R. P. Swatloski, W. M. Reichert, R. D. Rogers, R. Mayton, S. Sheff, A. Wierzbicki and J. H. Davis, Jr., *Chem. Commun.*, 2001, 135.
3 A. J. Carmichael, D. M. Haddleton, S. A. F. Bon and K. R. Seddon, *Chem. Commun.*, 2000, 1237.
4 T. Welton, *Chem. Rev.*, 1999, **99**, 2701.
5 J. S. Wilkes and M. J. Zaworotko, *J. Chem. Soc., Chem. Commun.*, 1992, 965.
6 J. D. Holbrey and K. R. Seddon, *Clean Products and Processes*, 1999, **1**, 223; J. G. Huddleston, H. D. Willauer, R. P. Swatloski, A. E. Visser and R. D. Rogers, *Chem. Commun.*, 1998, 1765.
7 P. Volker, W. Bohm and W. A. Herrmann, *Chem. Eur. J.*, 2000, **6**, 1017.
8 For the recent commentary on the general utility of ionic liquids see: M. Freemantle, *Chem. Eng. News*, 1 January, 2001, p. 21; M. Freemantle, *Chem. Eng. News*, 15 May, 2000, p. 37; H. Carmichael, *Chem. Ber.*, January 2000, p. 36.
9 R. S. Varma, in *Green Chemistry: Challenging Perspectives*, ed. P. Tundo and P. T. Anastas, Oxford University Press, Oxford, 2000, pp. 221–244; R. S. Varma, *J. Heterocycl. Chem.*, 1999, **35**, 1565; R. S. Varma, *Green Chemistry*, 1999, **1**, 43.
10 S. I. Lall, D. Mancheno, S. Castro, V. Behaj, J. I. Cohen and R. Engel, *Chem. Commun.*, 2000, 2413.

ChemComm

Synthesis and biological evaluation of a PtdIns(3,4,5)P_3 affinity matrix

Gavin F. Painter,[a,b] Jan. W. Thuring,[a,b] Ze-Yi Lim,[a] Andrew B. Holmes,*[a,b] Phillip T. Hawkins[c] and Leonard R. Stephens[c]

[a] *Cambridge Centre for Molecular Recognition, Department of Chemistry, University of Cambridge, Lensfield Road, Cambridge, UK CB2 1EW. E-mail: abh1@cam.ac.uk; Fax: +44 1223 336362; Tel: +44 1223 336404*

[b] *Melville Laboratory, Department of Chemistry, University of Cambridge, Pembroke Street, Cambridge, UK CB2 3RA. E-mail: abhl@cam.ac.uk; Fax: +44 1223 334866; Tel: +44 1223 334370*

[c] *Babraham Institute, Department of Signalling, Inositide Laboratory, Cambridge, UK CB2 4AT*

Received (in Cambridge, UK) 9th February 2001, Accepted 27th February 2001
First published as an Advance Article on the web 20th March 2001

New PtdIns(3,4,5)P_3 binding proteins have been identified utilising PtdIns(3,4,5)P_3 modified affinity matrix 1 which was synthesised from *myo*-inositol derivative 2, phosphoramidite 9 and an agarose based solid support.

The role of *myo*-inositol phospholipids in cell signalling systems is well established.[1–4] One such signal transduction mechanism involves the *in vivo* production of PtdIns(3,4,5)P_3 *via* phosphorylation of PtdIns(4,5)P_2 mediated by PI3K.[5] Although PtdIns(3,4,5)P_3 binding proteins are known,[6] many of the cellular processes downstream of PI3K activation do not yet have a defined lipid binding protein mapped above them. For this reason we embarked on the preparation and evaluation of an affinity matrix based on PtdIns(3,4,5)P_3.

The phospholipid was attached to an agarose matrix by an amide linkage formed between a carboxylic acid-terminated side chain on the agarose and a 3-(ω-aminoacyl)glycerol derivative on the phospholipid (Scheme 1). The phospholipid **11** was prepared by coupling the alcohols **2**[7] and **3** (from the commercially available (*S*)-(+)-1,2-*O*-isopropylideneglycerol **4**) through a phosphodiester linkage.

We initially protected the primary alcohol **4** as the *tert*-butyldiphenylsilyl ether, but encountered difficulties in its removal at a later stage of the synthesis. A more efficient process involved 4-methoxybenzylation of the primary alcohol **4** (Scheme 2),[8] followed by acetonide removal to give the PMB-ether **5** (PMB = *p*-methoxybenzyl). Selective esterification of the primary alcohol in **5** with the Cbz-protected (Cbz = benzyloxycarbonyl) ω-amino acid **6**, followed by palmitoylation of the secondary alcohol **7** gave the diester **8**. Oxidative removal (CAN) of the PMB protecting group and phosphitylation of **3** with BnOP(N^iPr_2)$_2$[9] gave the phosphoramidite **9**.†

The lipid side chain, in the form of the phosphoramidite **9**, was then coupled with the enantiomerically pure alcohol (−)-**2** to afford the perbenzylated compound **10** (Scheme 3). Reductive debenzylation was readily effected using H_2 (50 psi) in the presence of Pd-black and $NaHCO_3$ in ^{t}BuOH–H_2O (6:1) as the solvent, to afford the amine **11** in good yield.† This was then coupled with the *N*-hydroxysuccinimide (NHS) activated ester resin, Affi-Gel 10,‡ to afford the PtdIns(3,4,5)P_3 modified matrix **1**. Excess resin (*ca*. 5 equiv.) was required to ensure the complete consumption of the amine which was determined by a negative Kaiser test.§

Pilot experiments showed that PKB (25 μM) [a known[6,10] PtdIns(3,4,5)P_3 binding protein] would bind to the matrix **1** and could be completely displaced by 10 μM D,D-PtdIns(3,4,5)P_3¶ but not at all by 10 μM L,L-PtdIns(3,4,5)P_3, thus establishing the potential specificity of the matrix. When applied to a pig neutrophil cytosol a number of proteins have been identified that bind to the resin **1** in a PtdIns(3,4,5)P_3 sensitive manner.

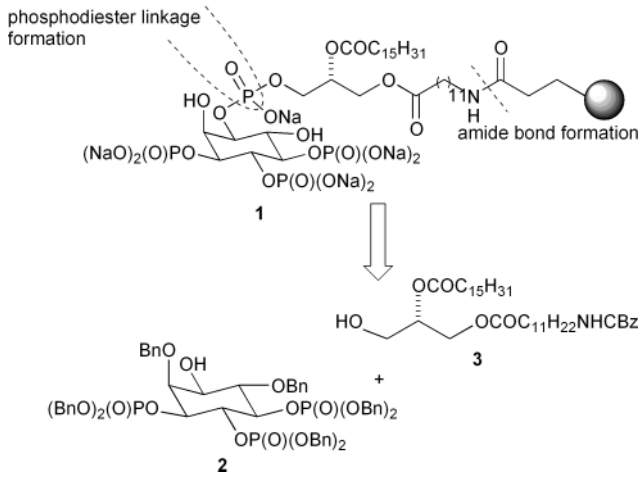

Scheme 1

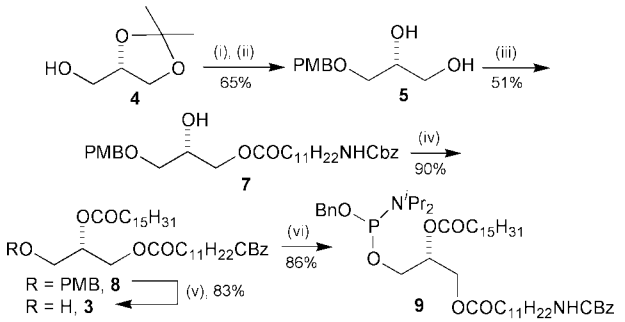

Scheme 2 *Reagents and conditions*: i, NaH, *p*-MeOC$_6$H$_4$CH$_2$Cl (PMBCl), DMF; ii, PTSA, MeOH; iii, HOOC$_{11}$H$_{22}$NHCBz **6**, DCC, DMAP, CH_2Cl_2; iv, palmitoyl chloride, DMAP, pyridine, CH_2Cl_2; v, CAN, MeCN–H_2O (4:1); vi, BnOP(N^iPr_2)$_2$, 1*H*-tetrazole, CH_2Cl_2.

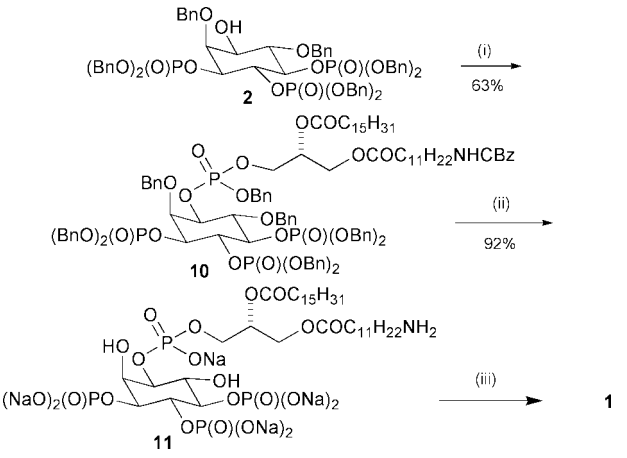

Scheme 3 *Reagents and conditions*: i, 1*H*-tetrazole, **9**, CH_2Cl_2, then MCPBA; ii, Pd-black, H_2 (50 psi), ^{t}BuOH–H_2O (6:1), $NaHCO_3$; iii, Affi-Gel 10, $NaHCO_3$, H_2O.

DOI: 10.1039/b101320n

Several novel proteins were identified and the full biological results will be disclosed in a separate publication. One of these proteins was subsequently shown to be identical to the recently characterised protein, DAPP1, possessing a Src homology (SH2) domain and a pleckstrin homology (PH) domain. This novel protein had been independently identified from a database search by comparison of the PH domain sequences with known PtdIns(3,4,5)P_3 binding proteins.[11] The fact that the 'functional screen assay' identified several proteins including DAPP1, which is involved in endosomal trafficking or sorting,[12] is noteworthy and exemplifies the strength of the approach. Very recently biotinylated PtdIns(3,4,5)P_3 has been used as an affinity ligand for the purification of recombinant PtdIns(3,4,5)P_3 binding proteins.[13]

In summary we have demonstrated a synthesis of a PtdIns(3,4,5)P_3-modified matrix and demonstrated its use as a tool for the identification of proteins binding to PtdIns(3,4,5)P_3.[14] The flexible nature of the methodology and the biological success of resin **1** warrants further investigation into the preparation and biological evaluation of other D-3 phosphorylated *myo*-inositol phospholipid modified matrices.[15]

We thank the BBSRC, the Cambridge Commonwealth Trust, the CVCP (ORS to Z.-Y. L), Astra-Zeneca and Tan Kar Kee Foundation, Singapore (Z.-Y. L.) for financial support, and the EPSRC for provision of the Swansea Mass Spectrometry Service. We thank Dr Corinne Kaye for helpful advice on the use of agarose supports.

Notes and references

† All new compounds exhibited spectroscopic and analytical data in accord with the assigned structure. *Selected data* (*J* values in Hz) for **9**: $[\alpha]_D^{22}$ + 7.0 (*c* 1.9 in $CHCl_3$); δ_H (250 MHz, $CDCl_3$), 7.38–7.28 (10 H, m, Ph), 5.20–5.10 (1 H, m), 5.10 (2 H, br s, OCH_2Ph), 4.80–4.60 (3 H, m), 4.36 (1 H, m), 4.12 (1 H, m), 3.85–3.55 (4H, m), 3.18 [2 H, dt, (apparent quartet), *J* 6.7, 6.7, CH_2CH_2NH], 2.29 (4 H, two overlapping t, *J* 7.3), 1.64–1.40 (6 H, m), 1.30–1.20 (38 H, m), 1.18 (6 H, d, *J* 6.8, 2 × Me), 1.17 (6 H, d, *J* 6.8, 2 × Me), 0.87 (3 H, t, *J* 6.9, Me); δ_P (101.25 MHz, $CDCl_3$), 149.2, 149.1; *m/z* (FIB) [Found: $(M + Na)^+$ 921.6022. $C_{52}H_{87}N_2O_8PNa$ requires 921.6098]. For **11**: $[\alpha]_D^{22}$ +3.0 (*c* 0.1 in H_2O); ν_{max} (KBr/cm^{-1}) 3403, 2920, 2850, 1742, 1238, 1094; δ_H (250 MHz, D_2O), 5.25 (1 H, br s), 4.45–3.80 (10 H, m), 2.95–2.85 (2 H, m), 2.40–2.25 (4 H, m), 1.65–1.05 (44 H, m), 0.85–0.70 (3 H, m); δ_P (101.25 MHz, D_2O), 5.81, 4.79, 3.55, 0.80; *m/z* (−ve FAB) 1142 [$(M - Na)^-$, 25%], 1119 (50), 1098 (100), 1076 (90).

‡ Affi-Gel 10 was purchased from BioRad.

§ The matrix **1** was constructed by reacting 60 μmol of *N*-hydroxysuccinimide activated resin (4 mL) with 12.2 μmol of the amine **11** in the presence of 122 μmol $NaHCO_3$ at 0 °C overnight.

¶ D,D-PtdIns(3,4,5)P_3 refers to the dipalmitoyl analogue of PtdIns(3,4,5)P_3 containing the 1(D)-*myo*-inositol ring stereochemistry and *sn*-2-diacylglycerol side chain; L,L-PtdIns(3,4,5)P_3 refers to the enantiomer.

1 C. L. Carpenter and L. C. Cantley, *Curr. Opin. Cell Biol.*, 1996, **8**, 153.
2 A. Toker, M. Meyer, K. K. Reddy, J. R. Falck, R. Aneja, S. Aneja, A. Parra, D. J. Burns, L. M. Ballas and L. C. Cantley, *J. Biol. Chem.*, 1994, **269**, 32 358.
3 M. J. Berridge, *Nature*, 1993, **361**, 315.
4 L. R. Stephens, T. R. Jackson and P. T. Hawkins, *Biochem. Biophys. Acta*, 1993, **1179**, 27.
5 C. P. Downes and A. N. Carter, *Cell. Signalling*, 1991, **3**, 501.
6 P. R. Shepherd, D. J. Withers and K. Siddle, *Biochemical J.*, 1998, **333**, 471.
7 G. F. Painter, S. J. A. Grove, I. H. Gilbert, A. B. Holmes, P. R. Raithby, M. L. Hill, P. T. Hawkins and L. R. Stephens, *J. Chem. Soc., Perkin Trans. 1*, 1999, 923.
8 J. Chen, A. A. Profit and G. D. Prestwich, *J. Org. Chem.*, 1996, **61**, 6305.
9 C. E. Dreef, C. J. J. Elie, P. Hoogerhout, G. A. van der Marel and J. H. van Boom, *Tetrahedron Lett.*, 1988, **29**, 6513.
10 S. R. James, C. P. Downes, R. Gigg, S. J. A. Grove, A. B. Holmes and D. R. Alessi, *Biochem. J.*, 1996, **315**, 709.
11 S. Dowler, R. A. Currie, C. P. Downes and D. R. Alessi, *Biochem. J.*, 1999, **342**, 7.
12 K. Anderson, P. Lipp, M. Bootman, S. H. Ridley, J. Coadwell, L. Rönnstrand, J. Lennartsson, A. B. Holmes, G. F. Painter, J. Thuring, Z.-Y. Lim, H. Erdjument-Bromage, A. Grewal, P. Tempst, L. R. Stephens and P. T. Hawkins, *Curr. Biol.*, 2000, **10**, 1403.
13 D. S. Wang, T. T. Ching, J. St. Pyrek and C. S. Chen, *Anal. Biochem.*, 2000, **208**, 301.
14 P. Hawkins, L. Stephens, S. Ridley, K. Anderson, J. Coadwell, K. Davidson, A. Eguinoa, A. McGregor, M. Manifava, N. Ktistakis, G. Painter, J. Thuring, M. Cooper, Z.-Y. Lim, A. Holmes, S. Dove, R. H. Michell, A. Grewal, H. Erjument-Bromage and P. Tempst, *Nature Cell Biol.*, manuscript in preparation.
15 Z.-Y. Lim, J. W. Thuring, A. B. Holmes, M. Manifava and N. T. Ktistakis, manuscript submitted for publication.

ChemComm

Silica-bound copper(II) triazacyclononane: a robust material for the heterogeneous hydrolysis of a phosphodiester

Brett R. Bodsgard and Judith N. Burstyn*

Department of Chemistry, University of Wisconsin, Madison, Wisconsin 53706, USA. E-mail: burstyn@chem.wisc.edu

Received (in Irvine, CA, USA) 28th June 2000, Revised manuscript received 16th January 2001, Accepted 13th February 2001
First published as an Advance Article on the web 16th March 2001

Copper(II) triazacyclononane, a catalyst for the hydrolysis of phosphate esters, has been covalently immobilized onto a silica surface and the resulting compound is a robust material that can effect heterogeneous phosphodiester hydrolysis.

The exceptional stability of phosphodiesters makes their cleavage a challenging task: at neutral pH and 25 °C, the half-life for the hydrolysis of dimethyl phosphate is estimated to be 130 000 years.[1] It is well documented, however, that a large range of metal ions and metal complexes are able to dramatically increase the rate of hydrolysis of phosphodiesters in aqueous solutions.[2] We have shown that in aqueous solution dichloro(1,4,7-triazacyclononane)copper(II) ($Cu[9]aneN_3Cl_2$) catalytically hydrolyzes the activated phosphodiester, bis(4-nitrophenyl)phosphate (BNPP).[3] A drawback of these homogeneous catalysis reactions is the inability to recover and reuse the catalyst. A heterogeneous catalyst, however, formed by immobilization of the active complex onto a solid support, can be easily separated from the reaction products and recycled continuously. Here we report the synthesis and characterization of silica-bound $(Cu[9]aneN_3)^{2+}$ and its reaction chemistry with BNPP.

Silica-bound $(Cu[9]aneN_3)^{2+}$ was prepared by a rhodium-catalyzed hydrosilation reaction between *N*-(4-but-1-enyl)-1,4,7-triazacyclononane[4] and hydride-modified silica,[5] both of which were prepared according to literature procedures. The chosen method of immobilization was favored because it produced more uniform and hydrolytically stable silicon–alkyl group linkages.[6] Conventional methods usually involve immobilization through an amide bond, which is not appropriate because $(Cu[9]aneN_3)^{2+}$ has been shown to hydrolyze amides.[7] *N*-(4-but-1-enyl)-1,4,7-triazacyclononane and hydride-modified silica were refluxed in toluene in the presence of Wilkinson's catalyst $[RhCl(PPh_3)_3]$ for 3 days, covalently linking the macrocycle to the silica surface (Scheme 1).[8] Unreacted hydrides were blocked with ethyl groups by charging the flask with ethylene (1 atm) and vigorously stirring the reaction solution for 15 h at room temperature.[9] After thorough washes with toluene, dioxane, and acetone, silica-bound triazacyclononane **1**, a pale yellow solid, was collected and dried at room temperature.

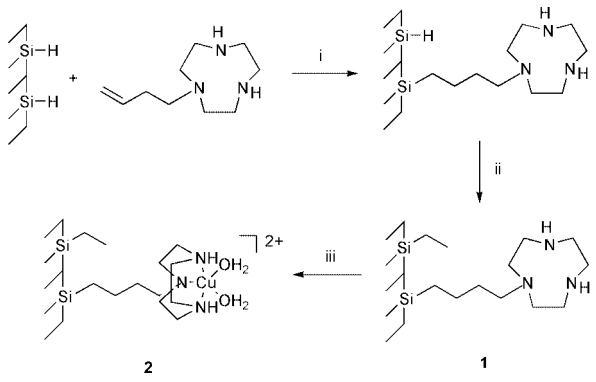

Scheme 1 *Reagents and conditions*: i, $RhCl(PPh_3)_3$, toluene, reflux, 3 days; ii, C_2H_4, $RhCl(PPh_3)_3$, toluene, 25 °C, 15 h; iii, $Cu(NO_3)_2$ (aq).

Characterization of **1** reveals that the silica surface has been modified with an organic layer. Elemental analysis was performed on **1**, yielding the following mass percentages: C 5.14%, H 1.54% and N 1.11%.[10] Based on the nitrogen value, it was calculated that the surface concentration of triazacyclononane was 0.264 mmol (g silica)$^{-1}$. Additionally, it was estimated that, of the original hydrides present on the silica surface, 24% had reacted with the *N*-(4-but-1-enyl)-1,4,7-triazacyclononane. Both of these values agree well with other reported values for silica-bound macrocycles.[11]

Metallation of **1** was achieved by mixing an aqueous solution of copper(II) nitrate with **1** and stirring vigorously for 30 min. The yellow material quickly became blue. The solid was isolated by filtration over a glass frit and was repeatedly washed with water until the washings were colorless. Finally, the material was washed twice with methanol and allowed to air dry, resulting in a pale blue solid, silica-bound copper(II) triazacyclononane **2**. EPR spectroscopy was used to probe the copper(II) environments in **2**. Spectra were recorded at both room temperature and 77 K.[12] The 77 K spectrum of **2** showed the characteristics of an axially symmetric d^9 copper complex.[13] The room temperature spectrum of **2** (Fig. 1) was essentially identical to its 77 K spectrum. A broadened spectrum was not observed, revealing that spin–spin interactions between the copper centers are minor or non-existent. Therefore, the conclusion can be drawn that the copper complexes anchored to the silica surface are well separated and non-interacting. This result demonstrates that dimerization of $(Cu[9]aneN_3)^{2+}$, an occurrence that contributes to rate reduction in the hydrolysis of phosphodiesters in aqueous solution,[3] will not be a factor for reactions with **2**.

Kinetic experiments showed that **2** was effective at hydrolyzing BNPP. Typical experiments began with the addition of 60 mg **2** to 50 mM HEPES [*N*-(2-hydroxyethyl)piperazine-*N*′-ethanesulfonic acid] buffer at pH 7.8. The solution was stirred

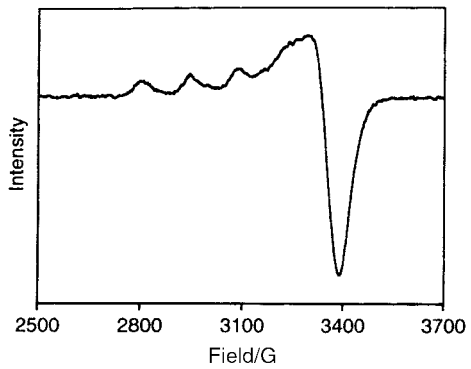

Fig. 1 X-Band EPR spectrum of **2** (undiluted powder sample). The spectrum was recorded at 298 K, 101 mW microwave power, 3.2×10^5 receiver gain, 5.88 G modulation amplitude, 9.6469 GHz microwave frequency, 100 kHz modulation frequency and a 163.84 ms time constant, using 10 averaged scans, each containing 4096 data points; $g_\perp = 2.065$, $g_\parallel = 2.283$, $A = 143$ G.

DOI: 10.1039/b005264g

vigorously for 15 min to wet the solid, followed by addition of 5 mM BNPP, to a total reaction volume of 3 mL. The solution was allowed to stir in the dark at 25 °C and was monitored by visible spectrophotometry, following the absorption at 400 nm due to the hydrolysis product 4-nitrophenolate.[14] Fig. 2(a) shows a plot of concentration of 4-nitrophenolate *vs.* time for a typical reaction. The plot shows an extended induction period where no hydrolysis was observed, and then a linear increase in product formation followed by a second linear region of product formation at a slower rate. The slowing of the reaction at relatively low (20%) conversion suggests that product inhibition may be significant. When **2** was allowed to stir with the buffer for 5 days prior to the addition of substrate, a significantly reduced induction period was observed, indicating that solvation of the solid surface is a limitation in this system. Negligible BNPP hydrolysis was observed in the absence of **2** or in the presence of **1** at the same temperature and pH over a two week period.

The same portion of **2** can be reused to hydrolyze additional samples of BNPP. In an initial reaction cycle, 60 mg **2** was combined with 5 mM BNPP in 50 mM HEPES, pH 7.8, as above. After *ca.* 700 h, by which time the reaction was proceeding at the slower rate, **2** was isolated from the suspension and repeatedly washed with 1 mL aliquots of 50 mM HEPES buffer (pH 7.8) until the washings were colorless (at least five washings). Fresh HEPES and BNPP (identical concentrations as in cycle 1) were added to **2** and the 4-nitrophenolate concentration was monitored as a function of time. In the second cycle, hydrolysis was again observed, following the same reaction profile as the first cycle with the exception of a shorter induction period (data not shown). This same portion of **2** was recycled a third time following the same procedure as for the second cycle, and identical hydrolytic activity was observed.

When **2** was recycled while the hydrolysis rate was maximal, after *ca.* 150 h, the higher reaction rate could be maintained through repeated reaction cycles. In the first reaction cycle 60 mg **2** and 5 mM BNPP were reacted at 25 °C, pH 7.8 (50 mM HEPES) for 300 h, and slow hydrolysis was observed. After isolation and washing by the procedure described above, **2** was combined with fresh substrate and buffer under the same conditions as in the first cycle. The reaction was followed for *ca.* 150 h. The rate of hydrolysis in the second cycle was significantly greater than in the first. The recycling procedure was repeated through 12 cycles over the course of 3 months: Fig. 2(b) shows data for cycles 1, 4 and 7. Cycles 1–5 proceeded with progressively increasing reaction rates. Once the maximal rate was achieved at cycle 5, all subsequent cycles exhibited the same rate of reaction. The maximal observed rate of hydrolysis was 7.5×10^{-10} M s^{-1}; this rate is significantly faster than the uncatalyzed rate, which cannot be measured at room temperature and neutral pH. These data reveal that if **2** is isolated, washed and recycled while reacting at its maximal rate, the high rate can be maintained through repeated cycles for an extended period of time.

The data presented herein demonstrate effective heterogeneous hydrolysis of a phosphodiester promoted by a surface-immobilized copper(II) macrocycle, $(Cu[9]aneN_3)^{2+}$. Importantly, **2** can be reused over many months to hydrolyze additional portions of BNPP, and a higher reaction rate can be maintained at low percentage conversion to product. The hydrophobic nature of the material is likely responsible for the long induction period and work is currently underway to promote the silica–substrate interaction.

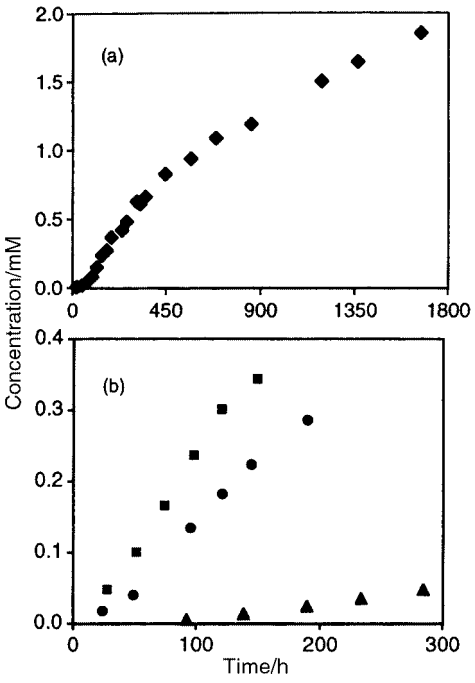

Fig. 2 (a) Single reaction time course. Plot of concentration of 4-nitrophenolate *vs.* time for **2**-mediated hydrolysis of BNPP. Reactions were carried out at pH 7.8, maintained by 50 mM HEPES, and 25 °C. The substrate (5 mM BNPP) was added to 60 mg **2**, and a suspension was maintained by constant stirring. Aliquots were clarified by centrifugation and filtration for absorbance measurements. (b) Multiple cycle, initial rate time course. Plot of concentration of 4-nitrophenolate *vs.* time for **2**-mediated hydrolysis of BNPP: see (a) for conditions. Each reaction after cycle 1 was allowed to proceed to *ca.* 6% conversion to product before recycling; (▲) cycle 1, (●) cycle 4, (■) cycle 7.

Notes and references

1 A. Radzicka and R. Wolfenden, *Science*, 1995, **267**, 90.
2 J. A. Connolly, J. H. Kim, M. Banaszczyk, M. Drouin and J. Chin, *Inorg. Chem.*, 1995, **34**, 1094; Y. Gultneh, Allwar, B. Ahvazi, D. Blaise, R. J. Butcher, J. Jasinski and J. Jasinski, *Inorg. Chim. Acta*, 1996, **241**, 31; B. K. Takasaki and J. Chin, *J. Am. Chem. Soc.*, 1993, **115**, 9337; J. Chin, *Acc. Chem. Res.*, 1991, **24**, 145.
3 K. A. Deal and J. N. Burstyn, *Inorg. Chem.*, 1996, **35**, 2792.
4 L. J. Farrugia, P. A. Lovatt and R. D. Peacock, *Inorg. Chim. Acta*, 1996, **246**, 343.
5 Triethoxysilane and silica gel (Baker 60–200 mesh) were refluxed in a solution of HCl and dioxane for 1 h; see: C. Chu, E. Jonsson, M. Auvinen, J. J. Pesek and J. E. Sandoval, *Anal. Chem.*, 1993, **65**, 808.
6 B. Lynch, J. D. Glennon, C. Troltzsch, U. Menyes, M. Pursch and K. Albert, *Anal. Chem.*, 1997, **69**, 1756.
7 E. L. Hegg and J. N. Burstyn, *J. Am. Chem. Soc.*, 1995, **117**, 7015.
8 Modeled after hydrosilation reactions in: J. E. Sandoval and J. J. Pesek, *Anal. Chem.*, 1991, **63**, 2364.
9 Ethylene consumption was indicated by the inrush of air as flask was opened.
10 Elemental analysis was performed by Galbraith Laboratories, Inc., Knoxville, TN.
11 V. Dudler, L. F. Lindoy, D. Sallin and C. W. Schlaepfer, *Aust. J. Chem.*, 1987, **40**, 1557; C. Gros, F. Rabiet, F. Denat, S. Brandès, H. Chollet and R. Guilard, *J. Chem. Soc., Dalton Trans.*, 1996, 1209.
12 Electron paramagnetic resonance was performed on a Bruker EPR 300E spectrometer. All measurements were taken at X-band, and the frequency was measured with an EIP model 625 frequency counter.
13 The X-band EPR spectrum of **2** (undiluted powder sample) was recorded at 77 K, 15.98 mW microwave power, 1.6×10^3 receiver gain, 18.593 G modulation amplitude, 9.2215 GHz microwave frequency, 100 kHz modulation frequency, and a 163.84 ms time constant, using 10 averaged scans, each containing 4096 data points: $g_\perp = 2.064$, $g_\parallel = 2.285$, $A = 148$ G.
14 Aqueous solutions were prepared with water purified by passage through a Millipore purification system. Kinetic measurements were made in 1.00 cm pathlength quartz cells with the use of a Hitachi U-3210 UV/visible spectrophotometer. Correction for the spontaneous hydrolysis of BNPP was accomplished by direct difference to a reference cell identical in all respects except lacking **2**. The concentration of 4-nitrophenolate produced was calculated from the extinction coefficient (18 700 M^{-1} cm^{-1}). Concentrations were corrected for the degree of ionization of the 4-nitrophenol at the pH and reaction temperature; see: A. E. Martell and R. M. Smith, *Critical Stability Constants*, Plenum Press, New York, 1977.

ChemComm

Design, machine synthesis, and NMR-solution structure of a β-heptapeptide forming a salt-bridge stabilised 3_{14}-helix in methanol and in water†

Per I. Arvidsson, Magnus Rueping and Dieter Seebach*

Laboratorium für Organische Chemie der Eidgenössischen Technischen Hochschule, ETH-Zentrum, Universitätstrasse 16, CH-8092 Zürich, Switzerland. E-mail: seebach@org.chem.ethz.ch

Received (in Cambridge, UK) 31st January 2001, Accepted 28th February 2001
First published as an Advance Article on the web 12th March 2001

Salt-bridge formation may be used to stabilise the 3_{14}-helical conformation of β-peptides in aqueous solution, as shown by a 2D-NMR spectroscopic investigation.

The design, synthesis, and characterisation of artificial molecules capable of forming specific and predictable secondary structures offer new possibilities in the field of molecular recognition, catalysis, and protein folding.[1] Thus, it is not surprising that unnatural oligomers like β-peptides have received considerable attention, since these molecules are able to form stable secondary structures with as few as six residues.[2] Although we are starting to understand some of the factors influencing the folding of these molecules, much work remains until we are able to correctly predict how a particular sequence of unconstrained building blocks will fold, especially in aqueous media. To investigate if salt-bridge formation can be used to stabilise β-peptidic secondary structures we set out to synthesise the β-heptapeptide **1** (Fig. 1).

The sequence of **1** was selected based on the following design principles: (*i*) we expect an *all*-β^3 peptide to form a 3_{14}-helix[2]; (*ii*) use of charged residues will ensure high water solubility; (*iii*) residues with positively and negatively charged side-chains should be positioned in an *i*/*i* + 3 disposition so that they are in juxtaposition on the ternary 3_{14}-helix, allowing for the two desired salt-bridges to be formed; (*iv*) β^3-HOrnithine rather than β^3-HLysine residues were chosen since this brings the charges closer together and less entropy is lost upon salt-bridge formation; (*v*) one side of the helix is covered by aliphatic side-chains to allow for intramolecular hydrophobic interactions, Fig. 1.

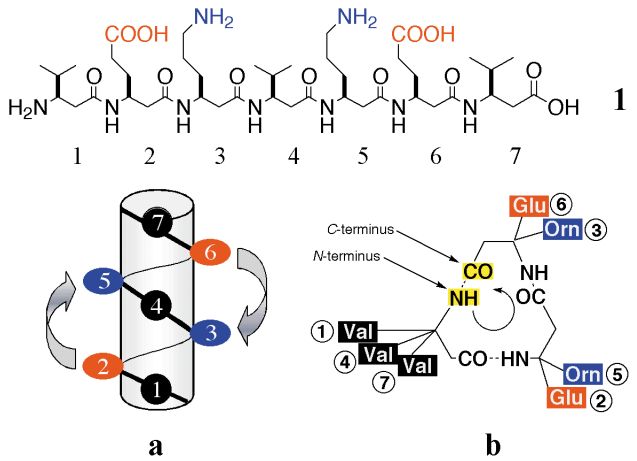

Fig. 1 Molecular formula of the β-heptapeptide **1** and schematic representations of a linear 3_{14}-helical structure from the side (**a**) and from top (**b**). Colour-code: Black = hydrophobic residues, Blue = positively charged residues, and Red = negatively charged residues.

† Electronic supplementary information (ESI) available: NMR spectroscopy and conc. dependent CD-spectra of **1**. See http://www.rsc.org/suppdata/cc/b1/b101085i/

The *all*-β^3-heptapeptide **1** was synthesised on *Wang* resin (0.25 mmol scale) using the standard *FastMoc* chemistry as implemented in an Applied Biosystem 433A automated peptide synthesiser. The protocol involved 45 min coupling times with four equiv. of the HBTU–HOBt activated β-amino acid (Fmoc-β^{3}HVal-OH, Fmoc-β^{3}HOrn(Boc)-OH, and Fmoc-β^{3}HGlu(OtBu)-OH prepared by Arndt-Eistert homologation),[3] 5 × 10 min deprotection, including NMP–DCM washings. The crude peptide was isolated in 78% purity, after TFA mediated removal of the protecting groups and cleavage from the resin. Purification by reverse phase HPLC (C18 column; MeCN–water gradient containing 0.1% TFA) afforded the pure peptide **1** in 65% yield, as characterised by its electrospray mass spectrum and complete assignment of the 500 MHz ^{1}H NMR spectrum. The main impurity (10%) was also isolated and characterised as *N*-Fmoc **1**, thus confirming previous observations that the standard Fmoc-cleavage, with 20% piperidine, is insufficient for complete Fmoc removal of β-peptides with chain-lengths exceeding six amino acids.[4] To the best of our knowledge, this is the first time a β-peptide was synthesised with standard coupling conditions on an automated synthesiser, suggesting that automated synthesis may be successfully applied for β-peptides of longer sequences and combinatorial libraries, especially if the deprotection protocol is modified according to our recently improved conditions.[4]

β-Peptide **1** exhibits excellent solubility in both water and MeOH. The far-UV circular dichroism (CD) spectra of **1** in MeOH and aqueous solution are shown in Fig. 2. As expected, the CD spectrum in MeOH displays a minimum at *ca*. 216 nm and a maximum at *ca*. 198 nm, characteristic of a 3_{14}-helix with (*M*)-chirality. Remarkably, when one compares the mean molar ellipticity of all β^3-peptides synthesised in our laboratory to date this peptide exhibits the strongest ellipticity of all in MeOH solution. The CD spectra recorded in aqueous solution also show the typical pattern of a 3_{14}-helical conformation.[4] Furthermore, the pH dependence study in Fig. 2 suggests that the two salt-bridges successfully increase the stability of the

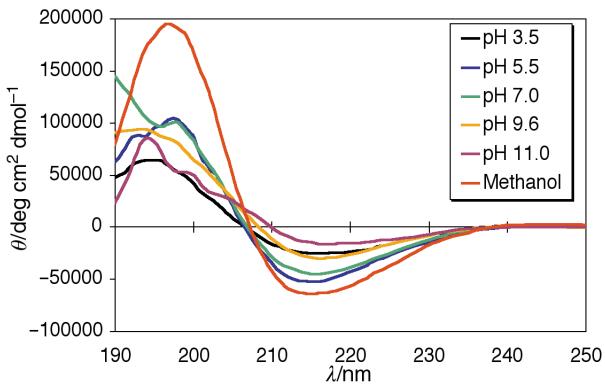

Fig. 2 CD-spectra of **1** in MeOH solution (red) and in aqueous solutions at different pH values (all measurements were done at 0.2 mM). The minimum near 215 nm, considered characteristic of a (*M*) 3_{14}-helical structure, shows maximal intensity at pH 5.5 (blue) consistent with a salt-bridge stabilisation.

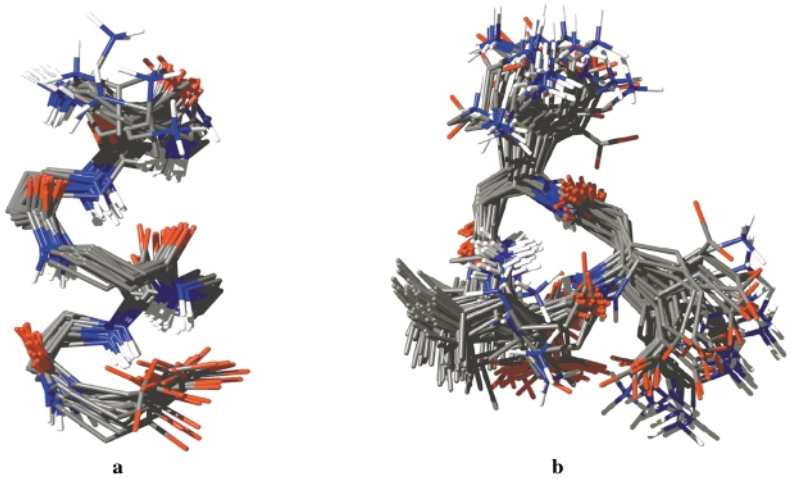

Fig. 3 Solution structure of the β-heptapeptide **1** in MeOH represented as a bundle of 25 lowest-energy structures obtained by simulated annealing, using NMR dihedral-angles and NOE-distance restraints, in the XPLOR programme. View along the (*M*) 3_{14}-helical axis with side-chains omitted (**a**), and top-view with side-chains (**b**).

helix since the strongest molar ellipticity is observed at pH 5.5, *i.e.* the pH value where the ornithine residues are expected to be protonated and the glutamic acid residues are still deprotonated. The CD spectra displayed only a slight change in the range 0.02 to 2 mM (see supporting information †), suggesting that no aggregation takes place in this concentration range. This observation is surprising if one considers the amphiphilic nature of the helix, and raises the question how to distribute the side-chains in order to achieve self-aggregation of 3_{14}-helical structures.

A detailed 2D-NMR spectroscopic study was undertaken to obtain high-resolution data on the actual conformation of **1** in water and in MeOH. The MeOH spectrum, recorded at 500 MHz, showed good separation of all signals and allowed complete assignment of all ^{1}H resonances in their respective spin system using DQF-COSY and TOCSY techniques; HSQC and HMBC experiments could then be used for sequence assignment. The large ^3J(NH; C(β)-H) coupling constants establish that the NH and C(β)-H protons are in an anti-periplanar arrangement. The diastereotopic CH_2(α) protons were assigned assuming that the axial protons exhibit a large, and the lateral protons a small, coupling with C(β), which is in agreement with the stronger NOEs observed from H-C(β) to the lateral H-C(α) protons than to the axial H-C(α) protons. ROESY spectra were acquired at three different mixing times (80, 150, and 300 ms), and a total of 72 NOEs were extracted from the spectra with mixing time 300 ms. Integration of the cross peak volumes followed by calibration allowed classification of the NOEs in three distance categories with the following upper bound distance limits: strong < 3.0 Å, medium < 3.5 Å, and weak < 4.5 Å. These distance restraints, together with 6 (NH, C(β)-H) dihedral angle restraints, derived from the coupling constants, were subjected to simulated annealing following the XPLOR protocol. The calculation produced a set of 25 structures with lowest restraint violations. These structures show a well-defined left-handed 3_{14}-helical conformation, Fig. 3. The side chains of β^3-HGlu and β^3-HOrn are on top of each other, thus allowing the designed salt bridges to form.

The NMR spectra recorded in aqueous solution at pH 5.5 showed more spectral overlap. Although it was possible to assign all resonances using a combination of the TOCSY, HMBC, and HSQC spectra, integration of the cross-peak volumes in the ROESY spectra was severely hampered by overlap. Nevertheless, the following NOEs could be unambiguously assigned: NH(2) and NH(4) to H-C(β) *i*+2 and *i*+3; NH(2) to NH(3); NH(3) to side chain protons of residue 6; H-C(β) of residue 4 to the lateral H-C(α) proton on residue 1. A qualitative treatment of these key NOEs, together with the large ^3J(NH; C(β)-H) coupling constants observed, imply the 3_{14}-helical conformation. Furthermore, no NOEs violating this conformation were observed. Based on the NMR spectroscopic data and the characteristic CD-spectra we conclude that the main conformation of β-peptide **1** is a 3_{14}-helix in MeOH as well as in water. Thus, since this is the first time a high resolution method supports the folding of a β-peptide without covalent constrains in water,[5] this study demonstrates that salt-bridge formation constitutes a valuable tool for the design of stabilised unnatural secondary structures in aqueous media.

P. I. A. gratefully acknowledges a postdoctoral fellowship from the Swedish Foundation for International Cooperation in Research and Higher Education (STINT). B. Brandenberg is acknowledged for recording the NMR-spectra.

Notes and references

1 S. H. Gellman, *Acc. Chem. Res.*, 1998, **31**, 173; A. E. Barron and R. N. Zuckermann, *Curr. Opin. Chem. Biol.*, 1999, **3**, 681; K. D. Stigers, M. J. Soth and J. S. Nowick, *Curr. Opin. Chem. Biol.*, 1999, **3**, 714.

2 D. Seebach and J. L. Matthews, *Chem. Commun.*, 1997, 2015; W. F. DeGrado, J. P. Schneider and Y. Hamuro, *J. Peptide Res.*, 1999, **54**, 206; K. Gademann, T. Hintermann and J. V. Schreiber, *Curr. Med. Chem.*, 1999, **6**, 905.

3 J. Podlech and D. Seebach, *Liebigs Ann.*, 1995, 1217; G. Guichard, S. Abele and D. Seebach, *Helv. Chim. Acta*, 1998, **81**, 187; S. Abele, G. Guichard and D. Seebach, *Helv. Chim. Acta*, 1998, **81**, 2141.

4 R. E. Marti, K. H. Bleicher and K. W. Bair, *Tetrahedron Lett.*, 1997, **38**, 6145; J. V. Schreiber and D. Seebach, *Helv. Chim. Acta*, 2000, **83**, 3139; D. Seebach, J. V. Schreiber, P. I. Arvidsson and J. Frackenpohl, *Helv. Chim. Acta*, 2001, **84**, 271.

5 D. H. Appella, J. J. Barchi, S. R. Durell and S. H. Gellman, *J. Am. Chem. Soc.*, 1999, **121**, 2309; B. W. Gung and D. Zou, *J. Org. Chem.*, 1999, **64**, 2176; D. Seebach, A. Jacobi, M. Rueping, K. Gademann, M. Ernst and B. Jaun, *Helv. Chim. Acta*, 2000, **83**, 2115.

ChemComm

X-ray crystal structure of a locked nucleic acid (LNA) duplex composed of a palindromic 10-mer DNA strand containing one LNA thymine monomer†

Martin Egli,*[a] George Minasov,[b] Marianna Teplova,[a] Ravindra Kumar[c] and Jesper Wengel[c]

[a] *Department of Biological Sciences, Vanderbilt University, Nashville, Tennessee 37235, USA, E-mail: martin.egli@vanderbilt.edu*
[b] *Department of Molecular Pharmacology and Biological Chemistry, Northwestern University Medical School, Chicago, Illinois 60611, USA*
[c] *Department of Chemistry, University of Southern Denmark, DK-5230 Odense M, Denmark*

Received (in Cambridge, UK) 27 November 2000, Accepted 22nd February 2001
First published as an Advance Article on the web 14th March 2001

Locked nucleic acid (LNA), a recently introduced nucleic acid analogue with a bicyclic 2′-*O*,4′-*C*-methylene linked furanose sugar, exhibits enhanced affinities for DNA and RNA relative to the corresponding oligodeoxyribonucleotides and oligoribonucleotides; we report the first crystal structure of an LNA unit incorporated in an oligonucleotide duplex. The structure at 1.4 Å resolution of the DNA–LNA decamer duplex with one LNA thymine monomer per strand provides a detailed view of the conformation and hydration of locked nucleic acid residues in a duplex A-form.

LNA (Fig. 1), exhibits stability of self-pairing that significantly exceeds those observed with DNA and RNA.[1–3] The UV melting temperatures of mixed DNA–LNA[1,4] and RNA–LNA[5] strands paired to DNA or RNA are increased by between 4 to 9 °C per modified residue compared to the corresponding unmodified duplexes. Increased RNA affinity, higher nuclease resistance and the observation that RNAs targeted by mixed DNA–LNA oligonucleotides are degraded by RNase H render LNA a promising third-generation antisense modification.[6]

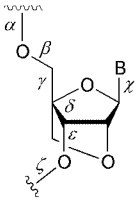

Fig. 1 Structure of LNA; torsion angles are labeled.

NMR solution structures of DNA–LNA[7–9] and RNA–LNA[10] duplexes containing either single or multiple LNA residues in one strand demonstrated the preference of the locked sugar for a C3′-*endo* conformation. Based on these experiments it was concluded that enthalpic (improved stacking) and entropic factors (conformational preorganization) may account for the unprecedented gains in the thermodynamic stabilities of LNA-modified duplexes. In order to examine the detailed conformation of LNA residues and the hydration of the bicyclic sugar moiety, we determined the single crystal structure of the DNA–LNA decamer duplex [GCGTA**T**$^{\mathbf{L}}$ACGC]$_2$ with a single LNA thymine **T**$^{\mathbf{L}}$ at high resolution.

The mixed DNA–LNA decamer was synthesized‡ using phosphoramidite chemistry as previously described[1] and purified to >98%. The modified decamer crystallizes§ in the A-form, the right-handed duplex geometry presumably preferred by an LNA–LNA duplex. The crystallographic model was refined¶ with simulated annealing and force field methods, using an initial orientation from Molecular Replacement.¶ The decamer duplex exhibits an average helical rise of 2.95 Å and the average values for helical twist and inclination are 31.2 and 17.8°, respectively. An overview of the crystal data and refinement parameters is shown in Table 1 and final electron density maps around LNA residues are depicted in Fig. 2.

The sugar conformations of the two locked thymines 6 and 16 are both C3′-*endo* (Fig. 3) and the respective values for the pseudorotation[17] angle *P* are 16.9 and 18.3° (calculated with the program CURVES[18]). All deoxyriboses in the decamer exhibit C3′-*endo* puckers and the average value of their *P* angles (17.9°; excluding the two LNA residues) is very similar to those of the modified thymines. Thus, the bicyclic sugar moieties fit seamlessly into an A-form double helix and the additional restraints appear to lock them in an A-type pucker.

In addition to the sugar–phosphate backbone torsion angle δ that is a characteristic of the ribose conformation (Fig. 1), the five other backbone torsions adopt values that are also consistent with the standard *sc*$^-$, *ap*, *sc*$^+$, *sc*$^+$, *ap*, *sc*$^-$ genus (α to ζ) of A-form double helices. A comparison of the backbone

Table 1 Crystal data and refinement parameters

Space group	orthorhombic $P2_12_12_1$
Unit cell constants [Å]	a = 26.14, b = 43.96, c = 45.80
Temperature [K]	110
Wavelength [Å]	0.93218
Beamline /detector	APS DND-CAT 5-ID/ MARCCD
Resolution [Å]	1.40
No. of unique reflections	10,950
Data completeness (all/last shell) [%]	99.7/96.7
R_{sym} (all/last shell) [%]	4.9/26.0
No. of nucleic acid atoms	408
No. of water molecules	127
R-work/*R*-free [%]	16.7/17.4
r.m.s for bonds/angles from standards Å/°]	0.009/1.51

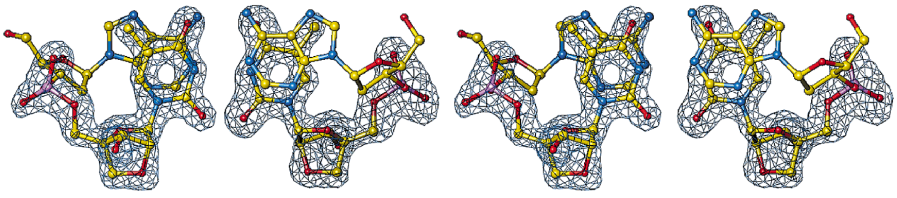

Fig. 2 Stereo drawing of the simulated annealing omit electron density (3σ-level) around modified residues **T**$^{\mathbf{L}}$6 and **T**$^{\mathbf{L}}$16 in the [(dA5p**T**$^{\mathbf{L}}$6)- (dA15p**T**$^{\mathbf{L}}$16] base pair step. Atoms are colored yellow, red, blue and magenta for carbon, oxygen, nitrogen and phosphorus, respectively.

DOI: 10.1039/b009447l

torsions in the modified thymines with those in the rest of the duplex does not manifest any notable deviations. Therefore the bicyclic modification in LNA is fully compatible with the A-form geometry adopted by both DNA and RNA. Similarly, the glycosidic torsion angles in both LNA residues are in the standard *anti* geometry and no significant changes appear to result from the chemical modification in the local helical parameters, such as slide and x- and y-displacement (Fig. 3).

Our findings here based on X-ray crystallographic data are consistent with those obtained from NMR solution studies of DNA and RNA duplexes with either single or multiple LNA residues in one of the strands.[7–10] According to those experiments, the exceptional thermodynamic stability gains seen with LNA-modified duplexes (both in the DNA and the RNA contexts) are a result of the conformational preorganization of modified single strands for the duplex state (entropic contribution) as well as of the improved stacking both in the single- and double-stranded states (enthalpic contribution).

Unlike 2′-deoxyribose sugars which lack a functionality for hydrogen bond formation at the C2′-position, the locked sugars contain a hydrogen bond acceptor in the form of O2′ (Fig. 1). In the crystal structure both 2′-oxygens are engaged in hydrogen bonds to water molecules (Fig. 3). Extensive hydration of individual hydrogen bond acceptors and donors in oligonucleotides is often accompanied by an increased thermodynamic stability of the corresponding duplexes (see, for example, references 19 and 20). However, it is difficult to draw conclusions as to the role of sugar hydration in the overall stability of LNA-modified DNA duplexes or all-LNA duplexes. The arrangement of water molecules around locked sugars observed here is reminiscent of the solvation in the case of the 2′-oxygen in 2′-*O*-methyl RNA.[21,22] Duplexes of 2′-*O*-methylated oligoribonucleotides exhibit thermodynamic stabilities that are increased by about 1 °C per modified residue relative to RNA. However, the precise contribution of hydration to the stability increase in the case of 2′-*O*-methyl RNA is not understood.

Our study provides a first look at the conformational properties of LNA in a crystal structure at relatively high resolution. The main characteristics of the structure are the standard A-type conformation induced by LNA residues and the capacity of the 2′-oxygen that is part of the bicyclic sugar framework to engage in a least two hydrogen bonds to water molecules. Circular dichroism spectra (CD) of LNA–LNA duplexes in solution indicated that such duplexes appear to adopt a conformation that closely resembles the A-form geometry of RNA–RNA duplexes. However, these spectra also manifested subtle differences between the two species (data not shown). The present analysis of a duplex with only a single LNA residue per strand does not provide any insight into potential conformational differences between LNA and RNA duplexes. Attempts to determine a crystal structure of a completely modified LNA–LNA duplex are underway.

This work was supported by the NIH (GM-55237 to M. E.). We thank the Danish Natural Science Research Council and the Danish Technical Research Council for financial support, Ms Britta M. Dahl for oligonucleotide synthesis and Dr Christopher J. Wilds for discussions. The DNDCAT Synchrotron Research Center at the APS, Argonne, IL, is supported by E. I. DuPont de Nemours & Co., The Dow Chemical Company, the NSF and the State of Illinois.

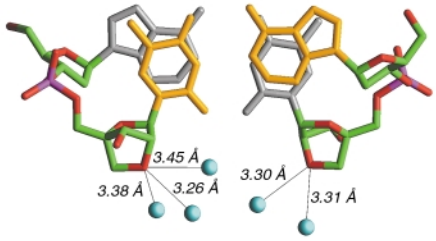

Fig. 3 The [**T**$^{\mathbf{L}}$pdA]$_2$ base pair step viewed approximately along the helical axis. Atoms of the upper and lower base pairs are shown in yellow and gray, respectively. Atoms of the sugar–phosphate backbone are colored green, red and magenta for carbon, oxygen and phosphorus, respectively. Water molecules within hydrogen bonding distance of O2′ atoms from **T**$^{\mathbf{L}}$ residues 6 (left) and 16 (right) are drawn as cyan spheres and hydrogen bonds are drawn as thin solid lines with their lengths indicated.

Notes and references

† Coordinates and structure factors have been deposited in the Protein Data Bank (pdb code 1i5w).

‡ The decamer was synthesized on a 2 μmole scale and the trityl-on strand was purified by RP-HPLC (C4, triethylammonium acetate pH 7–acetonitrile). Following detritylation the unprotected oligonucleotide was HPLC-purified a second time and then desalted.

§ Crystallization conditions were screened with a commercial sparse matrix kit (Nucleic Acid Miniscreen, Hampton Research, Laguna Niguel, CA), using the hanging drop vapor diffusion technique. Crystals suitable for diffraction experiments were obtained under the following conditions: 2 μl of a 2.8 mM decamer solution (single strand) were mixed with 2 μl buffer solution (10% 2-methylpentane-2,4-diol (MPD), 40 mM sodium cacodylate pH 6, 12 mM spermine tetrahydrochloride and 80 mM potassium chloride) and equilibrated against 1 ml of a 35% (v/v) MPD reservoir solution. A crystal was mounted in a nylon loop and shock-frozen in liquid nitrogen. Diffraction data were collected on the insertion device beamline (5-ID) of the DuPont-Northwestern-Dow Collaborative Access Team at the Advanced Photon Source (APS), Argonne National Laboratory (Argonne, IL). A total of 300 frames at high and low resolution ranges were recorded and reflections were integrated and merged in the DENZO/SCALEPACK suite.[11] A summary of amount and quality of the data is given in Table 1.

¶ The structure of the LNA-modified decamer was determined by the Molecular Replacement method using an A-form search model and the program AMORE.[12] The initial model was refined with the program CNS[13] setting aside 10% of the reflections for calculating the free R-factor.[14] Standard bond lengths and angles constraints[15] were employed for the DNA portion of the model and the geometric parameters for LNA residues were calculated with the program CHEM3D (CambridgeSoft Corporation, Cambridge, MA). The individual duplex models and the resulting Fourier electron density maps were visualized with the program TURBO-FRODO[16] on Silicon Graphics computers. Final refinement parameters and average root mean square (r.m.s.) deviations for bonds and angles from standard values are listed in Table 1. CCDC 156032.

1 A. A. Koshkin, S. K. Singh, P. Nielsen, V. K. Rajwanshi, R. Kumar, M. Meldgaard, C. E. Olsen and J. Wengel, *Tetrahedron*, 1998, **54**, 3607.
2 J. Wengel, *Acc. Chem. Res.*, 1999, **32**, 301.
3 S. Obika, D. Nanbu, Y. Hari, J. Andoh, K. Morio, T. Doi and T. Imanishi, *Tetrahedron Lett.*, 1998, **39**, 5401.
4 S. K. Singh, P. Nielsen, A. A. Koshkin and J. Wengel, *Chem. Commun.*, 1998, 455.
5 S. K. Singh and J. Wengel, *Chem. Commun.*, 1998, 1247.
6 C. Wahlestedt, P. Salmi, L. Good, J. Kela, T. Johnsson, T. Hökfelt, C. Broberger, F. Porreca, J. Lai, K. Ren, M. Ossipov, A. Koshkin, N. Jacobsen, J. Skouv, H. Oerum, M. H. Jacobsen and J. Wengel, *Proc. Natl. Acad. Sci. U.S.A.*, 2000, **97**, 5633.
7 C. B. Nielsen, S. K. Singh, J. Wengel and J. P. Jacobsen, *J. Biomol. Struct. Dyn.*, 1999, **17**, 175.
8 M. Petersen, C. B. Nielsen, K. E. Nielsen, G. A. Jensen, K. Bondensgaard, S. K. Singh, V. K. Rajwanshi, A. K. Koshkin, B. M. Dahl, J. Wengel and J. P. Jacobsen, *J. Mol. Recogn.*, 2000, **13**, 44.
9 K. E. Nielsen, S. K. Singh, J. Wengel and J. P. Jacobsen, *Bioconj. Chem.*, 2000, **11**, 228.
10 K. Bondensgaard, M. Petersen, S. K. Singh, V. K. Rajwanshi, R. Kumar, J. Wengel and J. P. Jacobsen, *Chem. Eur. J.*, 2000, **6**, 2687.
11 Z. Otwinowski and W. Minor, *Methods Enzymol.*, 1997, **276**, 307.
12 J. Navaza, *Acta Cryst. A*, 1994, **50**, 157.
13 A. T. Brünger, Crystallography & NMR System (CNS), Version 0.9, Yale University, New Haven, CT, 1998.
14 A. T. Brünger, *Nature*, 1992, **355**, 472.
15 G. Parkinson, J. Vojtechovsky, L. Clowney, A. T. Brünger and H. M. Berman, *Acta Cryst. D*, 1996, **52**, 57.
16 C. Cambillau and A. Roussel, Turbo Frodo, Version OpenGL.1, Université Aix-Marseille II, Marseille, France, 1997.
17 C. Altona and M. Sundaralingam, *J. Am. Chem. Soc.*, 1972, **94**, 8205.
18 R. Lavery and H. Sklenar, *J. Biomol. Struct. Dyn.*, 1989, **6**, 655.
19 M. Egli, N. Usman and S. Portmann, *Biochemistry*, 1996, **32**, 3221.
20 V. Tereshko, S. Gryaznov and M. Egli, *J. Am. Chem. Soc.*, 1998, **120**, 269.
21 P. Lubini, W. Zürcher and M. Egli, *Chem. Biol.*, 1994, **1**, 39.
22 D. A. Adamiak, J. Milecki, M. Popenda, R. W. Adamiak, Z. Dauter and W. R. Rypniewski, *Nucleic Acids Res.*, 1997, **25**, 4599.

ChemComm

Synthesis of unsymmetrical ethers and branched olefins from alcohols over a novel $(HO)_3ZrO_3SO–CH_2CH_2–OSO_3Zr(OH)_3$-derived catalyst

J. G. C. Shen,[a] T. H. Kalantar,[b] Q. Ma,[a] R. G. Herman[a] and K. Klier*[a]

[a] *Department of Chemistry and Zettlemoyer Center for Surface Studies, 6 East Packer Avenue, Lehigh University, Bethlehem, PA 18015, USA. E-mail: kk04@lehigh.edu*

[b] *M. E. Pruitt Research Center, Dow Chemical Co., Midland, MI 48674, USA*

Received (in Cambridge, UK) 3rd January 2001, Accepted 28th February 2001
First published as an Advance Article on the web 16th March 2001

A novel disodium 1,2-ethanediol bis(hydrogen sulfate) salt precursor-based solid acid catalyst is demonstrated to have significantly enhanced activity and high selectivity in producing methyl isobutyl ether (MIBE) or isobutene from a methanol–isobutanol mixture.

Methanol and isobutanol are the predominant products formed from CO/H_2 synthesis gas over alkali-promoted Cu/ZnO-based (low temperature) catalysts[1,2] and copper-free (high temperature) catalysts.[3,4] Since the two alcohols are produced together, their direct coupling to synthesize ethers for a number of applications is of interest. One such ether is the unsymmetrical methyl isobutyl ether (MIBE) which has desirable characteristics as a fuel additive (cetane number = 53),[5] and thus, can be employed as an additive to or as a neat fuel to substitute for current diesel fuels.[6,7] MIBE from direct coupling of methanol–isobutanol [eqn. (1)] was investigated over a number of solid acid catalysts.[8]

$$(CH_3)_2CHCH_2OH + CH_3OH \rightarrow (CH_3)_2CHCH_2OCH_3 + H_2O \quad (1)$$

Improvement of yields, particularly over inorganic oxides, was found to be desirable. Furthermore, if new catalysts were found for selectively converting isobutanol to isobutene, eqn. (2),

$$(CH_3)_2CHCH_2OH \rightarrow (CH_3)_2C{=}CH_2 + H_2O \quad (2)$$

a chemical route to isobutene from natural gas or coal-derived synthesis gas would be provided.[5] Such a process would alleviate isobutene dependence on petroleum feedstock. Kinetic analyses,[8b,9] together with theoretical calculations,[10] suggest that the mechanism of reaction 1 is the S_N2 pathway involving competitive adsorption of reactants on proximal dual Brønsted acid sites on the catalyst surface, while that of process 2 has been proposed to be an E2 reaction.[8] Reactions 1 and 2 are a specific implementation of a general class of dehydrocondensations and dehydrations occurring in a mixture of a light alcohol and a heavier C_2-branched primary alcohol.

In the present work, we studied a novel heterogeneous catalyst derived from a $(HO)_3Zr–O_3SOCH_2CH_2OSO_3–Zr(OH)_3$ precursor which gave rise to proximal strong surface acid functionalities $(HOSO_2O–Zr–O–)_2$, as prompted by the requirement to activate the two alcohols.[8,10] High resolution X-ray photoelectron, near-infrared, and ^{13}C magic angle spinning nuclear magnetic resonance spectra confirmed the composition, structure and physicochemical properties of the catalyst. The results show that the 1,2-ethanediol bis(hydrogen sulfate) moiety was successfully grafted onto the surface of zirconium hydroxide, as will be reported elsewhere in detail.[11] The main features of the preparation sequence are presented in Scheme 1.

Here, the disodium 1,2-ethanediol bis(hydrogen sulfate) salt precursor $(NaOSO_3CH_2)_2$ **1** was converted to the ammonium form $(NH_4OSO_3CH_2)_2$ **2** by exchange over a catex column, an aqueous solution of compound **2** was combined with a zirconium hydroxide suspension to form the derivative $(–O_xZr–OSO_3CH_2)_2$ **3**, which was calcined in air at 773 K to remove the $–(CH_2CH_2)–$ residues, resulting in the surface-derivatized

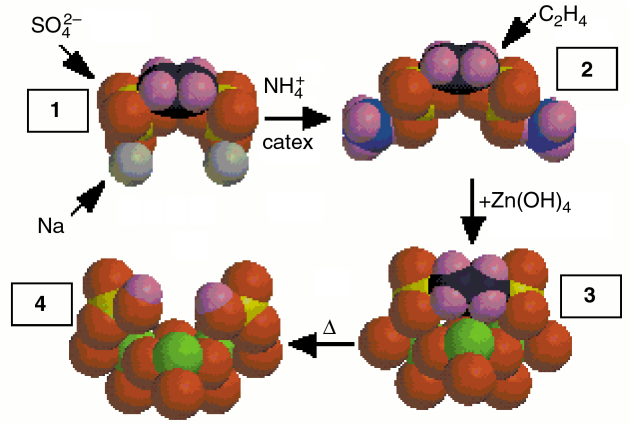

Scheme 1 Atom colour codes are as follows: C, black; H, pink; O, red; S, yellow; N, blue, Zr, green; Na, gray.

species $(–O_xZr–OSO_3H)_2$ **4** with proximal acid sites. Upon calcination, this catalyst exhibited a surface sulfate-to-zirconium surface mol ratio of 0.84, corresponding to 0.72 mmol surface S/g catalyst, and all its carbon was removed. Thus the final composition corresponds to the formula $(HSO_4)_{0.84}$-$ZrO_{2,surf}$ on the surface of pure zirconia. This material simultaneously possessed a high thermal stability.

The dehydration of methanol–isobutanol (2-methyl-1-propanol, 99.9+%, Alfa) was investigated in a downflow stainless steel tubular reactor with controls of temperature (398–508 K), total pressure ($101.3–3.1 \times 10^3$ kPa, 1 atm = 101.325 kPa) and Bu^iOH/MeOH molar ratio (0/100–50/50) in a carrier gas of 5% N_2 diluted in He. Steady state activities were achieved within 2 h of initiation of alcohol injection or after altering a reaction variable such as temperature or pressure. Testing of the $(HO)_3Zr–O_3SOCH_2CH_2OSO_3–Zr(OH)_3$-derived catalyst under each condition was carried out for 8–12 h. No catalyst deactivation was observed over several hundred hours of testing.

At 448 K, the MIBE yield was 0.087 mol/kg cat/h (Table 1), which represented an enhancement of 78% compared with 0.049 mol/kg cat/h over previously reported SO_4^{2-}/ZrO_2,[9] and

Table 1 Product space time yields (mol/kg cat/h) in the reaction of MeOH/Bu^iOH (8.97 : 8.97 kPa) at 3.44 mol/kg cat/h alcohols, 16 mol/kg cat/h carrier gas and 101.3 kPa total pressure over $(HO)_3Zr–O_3SOCH_2CH_2OSO_3–Zr(OH)_3$-derived catalyst

T/K	MIBE	Isobutene	DME	DIBE	MTBE	DTBE
398	0.002	—	—	—	—	—
423	0.020	—	—	0.008	—	—
448	0.087	1.430	—	0.005	—	0.003
448[a]	0.049	1.290[c]	0.103	—	0.007	—
448[b]	0.029	0.378[c]	0.034	0.015	0.014	0.016

[a] SO_4^{2-}/ZrO_2 catalyst. [b] H-montmorillonite catalyst. [c] Butene included isobutene, *n*-butene, *cis*- and *trans*-2-butene.

Table 2 Product space time yields (mol/kg cat/h) and selectivity (%) in the reaction of MeOH/Bu^{i}OH (2:1 molar ratio) at 15.6 mol/kg cat/h alcohols, 186 mol/kg cat/h carrier gas and 498 K over the $(HO)_3Zr–O_3SOCH_2CH_2OSO_3–Zr(OH)_3$-derived catalyst

Total pressure/kPa	MeOH pressure/kPa	Bu^{i}OH pressure/kPa	MIBE	Isobutene	DIBE	DTBE	MIBE selectivity	Isobutene selectivity
101.3	5.2	2.6	0.156	3.525	—	—	4.2	95.8
691.0	35.7	17.8	0.393	3.201	—	—	10.9	89.1
1036.5	53.5	26.7	0.521	2.972	—	0.012	14.9	84.8
1727.5	89.1	44.6	0.557	2.197	—	0.006	20.2	79.6
2418.5	124.8	62.4	0.675	1.473	—	0.007	31.3	68.4
3109.5	160.5	80.2	0.702	0.335	0.015	0.007	66.3	31.6

of 200% compared with H-montmorillonite catalyst.[9] The isobutene yield of 1.43 mol/kg cat/h, also at 448 K, represented an increase of 11 and ~280% over the SO_4^{2-}/ZrO_2 and H-montmorillonite catalysts, respectively.[9] Other products involved dimethyl ether (DME) and traces of di-isobutyl ether (DIBE), di-*tert*-butyl ether (DTBE), methyl *tert*-butyl ether (MTBE) and octenes.

Table 2 demonstrates that MIBE yields increased, whereas isobutene yields decreased, with total alcohol pressure increasing from 7.8 to 240.7 kPa. For example, 0.156 mol/kg cat/h MIBE at 7.8 kPa kept increasing with pressure to 0.702 mol/kg at 240.7 kPa, while isobutene at 7.8 kPa (3.525 mol/kg cat/h) exhibited a decreasing trend to 0.335 mol/kg cat/h at 240.7 kPa. The data in Table 2 are consistent with the Langmuir–Hinshelwood kinetic laws,[8b] $v_{MIBE} = k_4K_Mp_MK_Bp_B/(1 + K_Mp_M + K_Bp_B)^2$ and $v_{Isobutene} = k_3K_Bp_B/(1 + K_Bp_B + K_Mp_M)^2$, which were derived on the basis of the reactions (1) and (2) occurring on the dual acid sites.[8b] The values of constants fitting the data of Table 2 were k_3 = 33.1 mol/kg cat/h, k_4 = 3.2 mol/kg cat/h, K_M = 0.035 kPa^{-1} and K_B = 0.086 kPa^{-1}.

Here, the ratio K_B/K_M = 2.46 shows that isobutanol adsorbed preferentially on the acid sites, agreeing with its greater basicity over methanol.[8b,12] When the partial pressure of isobutanol was increased in the range of 0–1.6 kPa while maintaining the partial pressure of methanol constant at 8.97 mPa, the MIBE space time yield increased from zero to 0.057 mol/kg cat/h, while the DME decreased from 0.040 mol/kg cat/h to zero. This distribution of DME and MIBE can be reasonably explained by kinetics previously observed on other catalysts,[8b] with $K_B > K_M$. The experimental data also show increasing yields of isobutene with increased molar ratio of Bu^{i}OH/MeOH. In addition, the enhancement of selectivity toward isobutene from 0% at 398 K to 94% at 448 K (Table 1) results from the increase of K_B/K_M with increasing temperature. The isobutanol dehydration to isobutene competed with MeOH/Bu^{i}OH coupling to MIBE. At relatively high temperatures, a large ratio of K_B/K_M resulted in an enhancement of the $\theta_{Bu^iOH}/\theta_{MeOH}$ ratio (θ, surface coverage), and favored the dehydration of the adsorbed isobutanol to isobutene [eqn. (2)]. The apparent activation energy for the formation of each product was determined from Arrhenius plots, yielding 22 kcal mol^{-1} for MIBE and 24 kcal mol^{-1} for isobutene. The activation energy of 19 kcal mol^{-1} for DME was obtained by theoretical calculations.[10]

The kinetic behavior of eqn. (1) showed that isobutanol partial pressure (p_B) promoted the MeOH/Bu^{i}OH coupling to MIBE, whereas the kinetic behavior of eqn. (2) indicated that increasing isobutanol pressure (p_B) very strongly suppressed its dehydration, and the kinetic order became negative at high p_B.[9] At low alcohol partial pressures, high selectivity of isobutene is ascribed to a significant fraction of unoccupied acid sites on the surface of the $(HSO_4)_2–2ZrO_2$ catalyst. These free acid sites are considered to promote the dehydration of adsorbed isobutanol to isobutene according to the dual site elimination mechanism of eqn. (2), whereby one site adsorbs the reacting alcohol and the second site is an acceptor for the product water.[8b,9] At high alcohol partial pressures, the fraction of acid sites occupied by alcohol molecules approaches unity, and the catalyst favors MIBE formation. The ratio of MIBE/isobutene increased with increasing alcohol pressure even at constant p_B/p_M. Moreover, the effect of pressure was found to be reversible, *i.e.* when alcohol pressure was decreased to its original value, isobutene production increased and MIBE decreased to their original rates.

The butene formed over the present $(HSO_4)_{0.84}–ZrO_{2,surf}$ catalyst was pure isobutene, whereas over other catalysts such as H-montmorillonite and H-ZSM-5, products involved isobutene, significant amounts of *n*-butene, and *cis*- and *trans*-2-butene. The highly concentrated Brønsted acid sites on this catalyst effectively catalyzed removal of OH from the alcoholic carbon and of H from the neighboring carbon, and resulted in isobutene formation. On the other hand, the single Brønsted acid site on the surface of other catalysts was associated with carbenium ion chemistry,[13] which leads to butene rearrangement in isobutanol dehydration.[13,14]

In conclusion, the novel heterogeneous catalyst derived from the $(HO)_3Zr–O_3SOCH_2CH_2OSO_3–Zr(OH)_3$ precursor effectively catalyzes MIBE formation at high pressures and favored isobutene production at low pressures.

Financial support from the US Department of Energy (DE-FG26-98FT40113-1) is appreciated. Special thanks go to Dr A. C. Miller at Lehigh University for the HR-XPS analyses.

Notes and references

1 (*a*) K. Klier, in *Catalysis on the Energy Scene*, ed. A. Kaliaguine and A. Mahay, Elsevier, Amsterdam, 1984, p. 439; (*b*) K. Klier, R. G. Herman and C. W. Young, *Preprints, Div. Fuel Chem., ACS*, 1984, **29(5)**, 273; (*c*) G. A. Vedage, P. B. Himelfarb, G. W. Simmons and K. Klier, *ACS Symp. Ser.*, 1985, **279**, 295.

2 (*a*) J. G. Nunan, C. E. Bogdan, K. Klier, K. J. Smith, C. W. Young and R. G. Herman, *J. Catal.*, 1989, **116**, 195; (*b*) J. G. Nunan, R. G. Herman and K. Klier, *J. Catal.*, 1989, **116**, 222.

3 E. Tronconi, N. Ferlazzo, P. Forzatti and I. Pasquon, *Ind. Eng. Chem. Res.*, 1987, **26**, 2122.

4 E. Tronconi, L. Lietti, P. Forzatti and I. Pasquon, *Appl. Catal.*, 1989, **47**, 317.

5 R. G. Herman, K. Klier, O. C. Feeley and M. A. Johansson, *Prep. Div. Fuel Chem. ACS*, 1994, **39(2)**, 343.

6 T. H. Fleisch and P. C. Meurer, *Fuel Technol. Management*, 1996, **6(4)**, 54.

7 Y. Ohno, T. Shikada, T. Ogawa, M. Ono and M. Mizuguchi, *Prep. Div. Fuel Chem. ACS*, 1997, **42(2)**, 705.

8 (*a*) J. Nunan, K. Klier and R. G. Herman, *J. Chem. Soc., Chem. Commun.*, 1985, 676; (*b*) J. G. Nunan, K. Klier and R. G. Herman, *J. Catal.*, 1993, **139**, 406; (*c*) O. C. Feeley, Q. Sun, R. G. Herman, M. A. Johansson, L. Lietti and K. Klier, *Catal. Lett.*, 1995, **35**, 13.

9 K. Klier, R. G. Herman, M. A. Johansson and O. C. Feeley, *Prep. Div. Fuel Chem. ACS*, 1992, **37(1)**, 236.

10 K. Klier, H. H. Kwon, R. G. Herman, R. A. Hunsicker, Q. Ma and S. J. Bollinger, in *12th International Congress on Catalysis*, ed. A. Corma, F. V. Melo, A. Mendioroz and F. L. S. Fierro, Elsevier, Amsterdam, 2000, p. 3447.

11 J. G. C. Shen, T. H. Kalantar, R. G. Herman, K. Klier and J. E. Roberts, to be submitted.

12 J. Long and B. Munson, *J. Am. Chem. Soc.*, 1973, **95**, 2427.

13 O. C. Feeley, M. A. Johansson, R. G. Herman and K. Klier, *Prep. Div. Fuel Chem. ACS*, 1992, **37(4)**, 1817.

14 S. Kotsarenko and L. V. Malysheva, *Kinet. Catal.*, 1983, **24**, 877.

On the option of generating novel type surfaces with multiphilic ligands within the cavity of a giant metal–oxide based wheel type cluster: chemical reactions with well-defined nanoobjects

Achim Müller,*[a] Samar K. Das,[a] Christoph Kuhlmann,[a] Hartmut Bögge,[a] Marc Schmidtmann,[a] Ekkehard Diemann,[a] Erich Krickemeyer,[a] Josef Hormes,[b] Hartwig Modrow[b] and Matthias Schindler[b]

[a] *Lehrstuhl für Anorganische Chemie I, Fakultät für Chemie, Universität Bielefeld, Postfach 100131, D-33501 Bielefeld, Germany. E-mail: a.mueller@uni-bielefeld.de*

[b] *Physikalisches Institut, Universität Bonn, D-53115 Bonn, Germany*

Received (in Cambridge, UK) 9th January 2001, Accepted 21st February 2001
First published as an Advance Article on the web 16th March 2001

The reaction of an aqueous solution of sodium molybdate with cysteine hydrochloride acting as educt and reducing agent at rather low pH values (≈ 1.5) results in the formation of $Na_3[Mo_{154}O_{462}H_{14}(H_2O)_{48}(HO_2C–(NH_3^+)HC–CH_2–S–S–CH_2–CH(NH_3^+)–COO^-)_{11}]\cdot x\ H_2O$ 1 ($x \approx 250$) containing nanosized ring-shaped clusters which capture the oxidation product of cysteine, *i.e.* the diprotonated cystine ligands (H_2cystine$^+$) at the inner wall of their cavities; interestingly, the multiphilic ligands containing different types of functional groups (two $–NH_3^+$, one $–CO_2^-$, one $–CO_2H$ and one –S–S–) attach to the inner wall of the cluster through one of the two carboxylate groups thereby demonstrating the possibility to generate novel type surfaces within the cavity of a nanostructured ring-shaped cluster.

The design of multifunctional and especially of well ordered micro- and meso-porous materials which can incorporate guest molecules is a challenging task of modern chemistry.[1–3] Guests which may be reversibly and specifically bound at different appropriate sites of the host are of special interest. In particular this type of interaction may be significant for the synthesis of specially designed porous materials and may play a key role in catalysis and especially in separation methods. Polyoxometalates, formed by self-assembly processes are ideal systems in this respect as they can form crystalline materials with well-defined cavities and pores.[4]

Our recent interests in this field include the design of cavities within networks built up by giant wheel type species which can be opened and closed again as required.[5,6] Here we report a novel compound, in which cystine ligands (H_2cystine$^+$) are coordinated at the inner wall of a relevant nanosized car-tire shaped cluster anion.

If an aqueous acidified solution of Na_2MoO_4 is reduced with cysteine at *ca.* 55 °C, blue crystals of **1** precipitate after 1–2 days.† Compound **1** was characterized by elemental analysis‡ (including cerimetric titration to determine the formal number of Mo^V centers), thermogravimetry (for the determination of the crystal water content), bond valence sum (BVS) calculations[7] (to determine the positions of the H_2O ligands and to distinguish between Mo^{VI} and Mo^V centers), spectroscopic methods (IR, resonance-Raman, UV–VIS, XANES)§ and finally by single crystal X-ray structure analysis.¶ For the synthesis of **1**, cysteine acts as reducing agent at rather low pH values (≈ 1.5) resulting in the formation of the mixed-valent $\{Mo_{154}\}$ type cluster with 28 Mo^V centers (formal consideration) while the protonated form of the oxidized product, *i.e.* cystine, gets coordinated to the inner surface of the giant cluster through one of its carboxylate ends (Scheme 1).

The single crystal X-ray structure of **1** revealed the tetradecameric ring-shaped structure (Fig. 1) of the anion **1a** of **1**, which can be compared to that of the related parent host anion **2a**[5e] by substituting $2 \times 11 = 22$ H_2O ligands with 11 cystine (H_2cystine$^+$, see Scheme 1). According to the related building-block principle, **1a** and **2a** can be formulated generally as $[\{Mo_2\}_{14}\{Mo_8\}_{14}\{Mo_1\}_{14}]$ or specifically as $[\{(O)_2{=}Mo^{VI}(\mu\text{-}O)L_iMo^{VI}{=}(O)_2\}_{14}\{Mo^{VI/V}_8O_{26}(\mu_3\text{-}O)_2H(H_2O)_3\text{-}Mo^{VI/V}\}^{3-}_{14}]^{3-}$ **1a** and $[\{(O)_2{=}Mo^{VI}(H_2O)(\mu\text{-}O)(H_2O)Mo^{VI}{=}(O)_2\}^{2+}_{14}\{Mo^{VI/V}_8O_{26}(\mu_3\text{-}O)_2H(H_2O)_3Mo^{VI/V}\}^{3-}_{14}]^{14-}$ **2a** (ΣL_i = 11 μ-$HO_2C–(NH_3^+)HC–CH_2–S–S–CH_2–CH(NH_3^+)–CO_2^-$ + 6 H_2O).

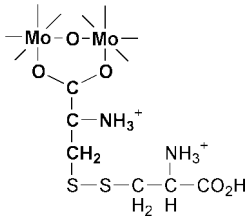

Scheme 1 Atoms found in the crystal structure shown in bold.

While the basic $\{Mo_8\}$ and $\{Mo_1\}$ units are identical in both clusters, this is not the case for all of the $\{Mo_2\}$ groups because of the substitution of some H_2O ligands. The complete structure of the cystine ligands is—as expected—not found in the crystal structure due to the related high degree of disorder of the long chains which show an extreme flexibility and are attached to the inner wall through one of the two 'carboxylate ends'.‖ However, the experimental results of numerous carbon, hydrogen, nitrogen and sulfur analyses‡ together with spectroscopic data establish the fact that the cystine ligands are intact. The

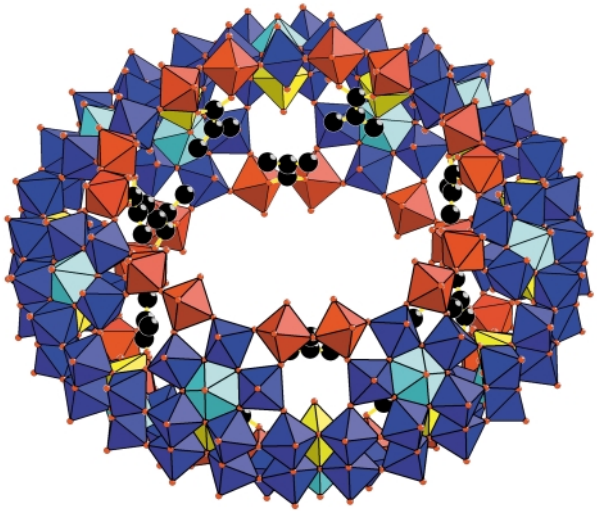

Fig. 1 Inclined view into the giant wheel type cluster anion **1a** in crystals of **1** in polyhedral (polyoxomolybdate part) and partly in ball-and-stick representation ($\{Mo_2\}$: red; $\{Mo_8\}$: blue (central pentagonal bipyramids: cyan); $\{Mo_1\}$: yellow; oxygen: small red circles; carbon and (disordered) nitrogen: enlarged black circles).

DOI: 10.1039/b100362n

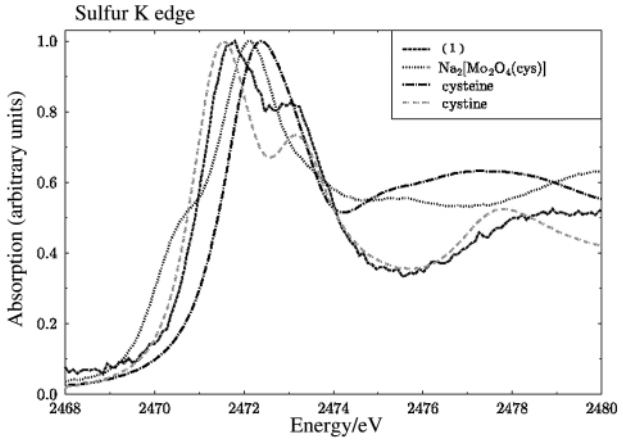

Fig. 2 S K-edge XANES spectra.

abundance of coordinated H_2cystine$^+$ is mainly supported by the IR and XANES spectral studies. In particular, a comparison of the S K-edge spectra of **1** (Fig. 2) and authentic cystine with those of cysteine and a cysteine molybdenum complex provides clear support for the presence of the former ligands. The absorptions at *ca.* 2472 eV are assigned to excitations of S 1s electrons to the first unoccupied electronic states of either the complexes or the free ligands. In the case of the complexes there are also unoccupied states centered on the molybdenum–oxygen part, but these are spatially significantly separated. Therefore, only ligand-internal transitions exhibit higher probabilities. The patterns for cystine and cysteine however, free or complexed, differ characteristically. The IR spectrum proves the abundance of cystinium cations which is indicated by the presence of a medium intensity band at 1495 cm^{-1} assigned to the $\delta(NH_3^+)$ mode of the cation as well as by the characteristic ν(C=O) band at 1730 cm^{-1} of the $-CO_2H$ group.[8] The diprotonation of the cystine ligands is supported by the experimental results of Na analyses since each replacement of a H_2O ligand by H_2cystine$^+$ reduces the negative charge of the original cluster **2a** by one unit. (However, the presence of one monoprotonated instead of diprotonated cystine in connection with four instead of three (highly disordered) Na^+ cations could not be excluded.) The resulting low charge is consistent with the very low solubility of **1**.

The 11 H_2cystine$^+$ ligands, coordinated to $\{Mo_2\}$ units through their carboxylate functions, are located quite disordered near the inner wall of the cavity (Fig. 1). Such a situation is also suggested by molecular modelling using the MM+ force field approach.** When all positions known from the crystal structure determination are kept fixed the remaining energy hypersurface turns out to be rather flat.

To summarize the interesting aspects: it is possible to place molecules at the inner wall of the cavity of a giant metal–oxide based wheel type cluster by replacing H_2O ligands. With the use of ambiphilic and/or multiphilic ligands, new characteristic surface structures inside the cavity can be generated. This process, which has been employed here with the cystine attached to the inner wall, creates an interesting type of (inner) surface with $-NH_3^+$, $-CO_2H$ and $-S-S-$ functions, which we are currently attempting to construct. This type of research work has special relevance for the construction of novel silica hybride materials containing these types of clusters.

Notes and references

† To an aqueous solution (35 mL) of $Na_2MoO_4 \cdot 2H_2O$ (3.0 g, 12.4 mmol) and hydrochloric acid (25 mL, 1.1 M) in a 100 mL Erlenmeyer flask, L-cysteine hydrochloride monohydrate (0.41 g, 2.3 mmol) was added and the reaction medium was stirred for 5 min at room temperature. The yellow color, which developed immediately after addition of cysteine, changed to bright green within 2–3 min and after a further 5 min to blue–grey. The suspension was subsequently heated in an oil bath at 55 °C under constant stirring for 2 h (flask covered with a watch glass) resulting in a dark blue solution which was kept at 20 °C for another 2 h. The amorphous blue material, separated after this time, was filtered off and the blue filtrate was kept at room temperature for 2 d in a 100 mL Erlenmeyer flask at 15–20 °C (note: the storing temperature should not exceed 20 °C). The precipitated blue crystals were filtered from the mother-liquor, washed with cold water and dried at room temperature. Yield: 0.9 g (≈ 37% based on Mo).

‡ Anal. Calc. for $C_{66}H_{753}Mo_{154}N_{22}Na_3O_{804}S_{22}$ (M = 30272.96): C, 2.62; H, 2.51; N, 1.02; S, 2.33; Na, 0.23. Found: C, 2.7; H, 2.4; N, 1.0; S, 2.4; Na, 0.3%.

§ *Selected spectroscopic data* for **1**: IR (KBr pellet) (ν/cm^{-1}): 1730w {ν(C=O)}, 1607m {$\nu_{asym}(CO_2^-) + \delta(H_2O)$}, 1494m {$\delta(NH_3^+)$}, 1412w, 1346w, 1135w, 991m, 975m, 905wm {ν(Mo=O)}, 861w, 755bw, 630s, 558s. Resonance-Raman (KBr dilution, λ_e = 1064 nm) (ν/cm^{-1}): 800s, 534s, 460s, 325s, 214s. VIS–NIR (water) (λ_{max} /nm): 748 (IVCT), 1072 (IVCT).

¶ *Crystal data* for **1**: $C_{66}H_{753}Mo_{154}N_{22}Na_3O_{804}S_{22}$, M = 30272.96 g mol^{-1}, monoclinic, space group $C2/m$, a = 36.243(2), b = 42.788(2), c = 31.541(1) Å, β = 107.886(1)°, U = 46549(4) Å^3, Z = 2, D_c = 2.160 g cm^3, μ = 2.156 mm^{-1}, $F(000)$ = 29176, crystal size = 0.40 × 0.20 × 0.20 mm. Crystals of **1** were removed from the mother liquor and immediately cooled to 183(2) K on a Bruker AXS SMART diffractometer (three circle goniometer with 1 K CCD detector, Mo-Kα radiation, graphite monochromator). Hemisphere data were collected in ω at 0.3° scan width in three runs with 606, 435 and 230 frames (ϕ = 0, 88 and 180°) at a detector distance of 5 cm. A total of 138023 reflections (1.50 < Θ < 27.06°) were collected of which 50782 unique reflections (R_{int} = 0.072) were used. An empirical absorption correction using equivalent reflections was performed with the program SADABS. The structure was solved with the program SHELXS-97 and refined using SHELXL-93 to R = 0.065 for 25857 reflections with $I > 2\sigma(I)$; max./min. residual electron density 2.141 and −1.701 e Å^{-3}. (SHELXS/L, SADABS from G. M. Sheldrick, University of Göttingen 1993/1997; structure graphics with DIAMOND 2.1 from K. Brandenburg, Crystal Impact GbR, 1999.) CCDC 154874. See http://www.rsc.org/suppdata/cc/b1/b100362n/ for crystallographic data in .cif or other electronic format.

‖ In the meantime we have isolated and characterized (including crystal structure determination) an analogous compound with valine amino acid ligands—also attached to the inner wall of the ring *via* the carboxylate oxygen atoms—which show the same type of disorder.

** Molecular modelling was performed with the Hyperchem 6 Pro program from Hypercube Inc. employing the MM+ force field. The parameters implemented in this program were used without change.

1 *Multifunctional Mesoporous Inorganic Solids*, ed. C. A. C. Sequeira and M. J. Hudson, Kluwer, Dordrecht, 1993; *Comprehensive Supramolecular Chemistry, Vol. 6, Solid-state Supramolecular Chemistry: Crystal Engineering* and *Vol. 7, Solid-state Supramolecular Chemistry: Two- and Three-dimensional Inorganic Networks*, ed. J. L. Atwood, J. E. D. Davies, D. D. MacNicol, F. Vögtle and J-M. Lehn, Pergamon/Elsevier, Oxford, 1996.

2 G. Férey and A. K. Cheetham, *Science*, 1999, **283**, 1125; H. Li, A. Laine, M. O'Keeffe and O. M. Yaghi, *Science*, 1999, **283**, 1145.

3 M. E. Davis, *Chem. Eur. J.*, 1997, **3**, 1745 and references therein.

4 A. Müller, F. Peters, M. T. Pope and D. Gatteschi, *Chem. Rev.*, 1998, **98**, 239.

5 (*a*) A. Müller, E. Krickemeyer, J. Meyer, H. Bögge, F. Peters, W. Plass, E. Diemann, S. Dillinger, F. Nonnenbruch, M. Randerath and C. Menke, *Angew. Chem., Int. Ed. Engl.*, 1995, **34**, 2122; (*b*) A. Müller, E. Krickemeyer, H. Bögge, M. Schmidtmann, C. Beugholt, P. Kögerler and C. Lu, *Angew. Chem., Int. Ed.*, 1998, **37**, 1220; (*c*) A. Müller, M. Koop, H. Bögge, M. Schmidtmann and C. Beugholt, *Chem. Commun.*, 1998, 1501; (*d*) A. Müller, S. K. Das, H. Bögge, C. Beugholt and M. Schmidtmann, *Chem. Commun.*, 1999, 1035; (*e*) A. Müller, S. K. Das, V. P. Fedin, E. Krickemeyer, C. Beugholt, H. Bögge, M. Schmidtmann and B. Hauptfleisch, *Z. Anorg. Allg. Chem.*, 1999, **625**, 1187; (*f*) A. Müller, S. Q. N. Shah, H. Bögge and M. Schmidtmann, *Nature*, 1999, **397**, 48.

6 A. Müller, E. Krickemeyer, H. Bögge, M. Schmidtmann and F. Peters, *Angew. Chem., Int. Ed.*, 1998, **37**, 3360; A. Müller, V. P. Fedin, C. Kuhlmann, H. Bögge and M. Schmidtmann, *Chem. Commun.*, 1999, 927; A. Müller, S. Polarz, S. K. Das, E. Krickemeyer, H. Bögge, M. Schmidtmann and B. Hauptfleisch, *Angew. Chem., Int. Ed.*, 1999, **38**, 3241.

7 I. D. Brown, in *Structure and Bonding in Crystals*, ed. M. O'Keeffe and A. Navrotsky, Academic Press, New York, 1981, vol. II, pp. 1–30.

8 K. Nakamoto, *Infrared and Raman Spectra of Inorganic and Coordination Compounds*, Wiley-Interscience, New York, 4th edn., 1986.

9 S. Polarz, B. Smarsly, C. Göltner and M. Antonietti, *Adv. Mater.*, 2000, **12**, 1503.

Generation of cluster capsules (I_h) from decomposition products of a smaller cluster (Keggin-T_d) while surviving ones get encapsulated: species with core–shell topology formed by a fundamental symmetry-driven reaction

Achim Müller,* Samar K. Das, Hartmut Bögge, Marc Schmidtmann, Alexandru Botar and Adrian Patrut

Lehrstuhl für Anorganische Chemie I, Fakultät für Chemie, Universität Bielefeld, Postfach 100131, D-33501 Bielefeld, Germany. E-mail: a.mueller@uni-bielefeld.de

Received (in Cambridge, UK) 27th November 2000, Accepted 19th February 2001
First published as an Advance Article on the web 19th March 2001

A novel and fundamental reaction system of matter following a type of 'supramolecular Darwinism' leads to the formation of giant spherical nano-sized cluster capsules as kinetically controlled destination having the highest possible symmetry (I_h) and formed directly from the decomposition products of the well known but less symmetrical Keggin anions (T_d) in aqueous medium in the presence of Fe^{III}– acting as a type of environmental influence–under conditions where Keggin anions are known to be extremely stable; remarkably the remaining non-decomposed Keggin anions finally get (non-covalently) encapsulated protected by the formed spherical capsules of the new supramolecular compound $[PMo_{12}O_{40} \subset \{(Mo^{VI})Mo^{VI}_5\}_{12}\ Fe^{III}_{30}O_{252}(H_2O)_{102}(MeCO_2)_{15}]\cdot xH_2O$ 1 ≡ 1a $\cdot xH_2O$ ($x \approx 120$).

The fact that self-assembly processes–based on simple (mainly highly symmetrical) building blocks or preorganized units–preferentially lead to higher symmetrical reaction products is an interesting phenomenon, *e.g.* in cluster chemistry which has not been explored in detail until now. Examples are the well known Keggin type anions, like $[PMo_{12}O_{40}]^{3-}$ (T_d) formed from molybdate and phosphate, models for the Fe_4S_4 type ferredoxin, like $[Fe_4S_4(SH)_4]^{2-}$ (T_d), the molybdenum-oxide-based giant wheels ($\approx D_{7d}$) as well as spheres (I_h). Therefore, the question arises as to why highest (possible) symmetrical species are the targets, and furthermore, whether we can elucidate this phenomenon or solve the problem by means of a model reaction system. In a novel fundamental type of reaction, which can be related to a type of '*Supramolecular Darwinism*' (see below), it can be shown that tetrahedral Keggin anions 'lose–at least partly–the competition' with higher symmetrical, *i.e.* icosahedral capsule type species as kinetic target in aqueous solution even under conditions where they are quantitatively formed. The formation of the latter occurs at the expense of the former.

In the presence of Fe^{III} ($FeCl_3\cdot 6H_2O$), *i.e.* formally in a kind of 'environmental attack', the Keggin anions[1] decompose in solution with the formation of the pentagonal $\{(Mo^{VI})Mo^{VI}_5O_{21}\}$ type building blocks which get linked by $\{Fe^{III}(H_2O)_2\}^{3+}$ groups. This leads finally to the formation of novel composites consisting of discrete icosahedral nanocluster capsules with the encapsulated Keggin anions $[PMo_{12}O_{40}]^{3-}$, which are abundant in the new compound $[PMo_{12}O_{40} \subset \{(Mo^{VI})Mo^{VI}_5\}_{12}Fe^{III}_{30}O_{252}(H_2O)_{102}(MeCO_2)_{15}]\cdot xH_2O$ **1** ≡ **1a**$\cdot xH_2O$ ($x \approx 120$).† Upon drying, **1** shows a fast solid-state reaction with the consequence that the composites **1a** get covalently linked leading to the formation of $\{PMo_{12}O_{40} \subset H_4[(Mo^{VI})Mo^{VI}_5\}_{12}Fe^{III}_{30}O_{254}(H_2O)_{98}(MeCO_2)_{15}]\cdot xH_2O$ **2** ≡ **2a**$\cdot xH_2O$ ($x \approx 60$), see refs. 2–4. This condensation process is only important in the present context as the relevant dry (!) product can be more easily structurally characterized compared to **1**. Using Fe^{II} instead of Fe^{III} the related compounds $[H_yPMo_{12}O_{40} \subset \{(Mo^{VI})Mo^{VI}_5\}_{12}Fe^{III}_{30}O_{252}(H_2O)_{102}(MeCO_2)_{15}]\cdot xH_2O$ **3** ≡ **3a** $\cdot xH_2O$ ($x \approx 120$) and $\{H_yPMo_{12}O_{40} \subset H_4\{(Mo^{VI})Mo^{VI}_5\}_{12}Fe^{III}_{30}O_{254}(H_2O)_{98}(MeCO_2)_{15}\}\cdot xH_2O$ **4** ≡ **4a**$\cdot xH_2O$ ($x \approx 60$) are obtained which contain the one- or two-electron reduced Keggin anions $[H_yPMo_{12}O_{40}]^{3-}$.‡ Compound **4** can be obtained not only by the present new fundamental type of reaction but also in a facile synthesis starting from the simple ingredients phosphate, molybdate, acetate, and Fe^{II}.[2]

Compound **2** with the cross-linked composites having core–shell topology and partly also **1**, *i.e.* the 'corresponding' non-dried crystals, were characterized by elemental analyses, thermogravimetry (to determine the crystal water content), single-crystal X-ray structure analysis§ [including the calculation of bond valence sums in order to distinguish between (terminal) O and OH_2 ligands] and spectroscopic methods (IR, Raman, UV–VIS, NIR) as well as magnetic measurements.¶ Whereas the complete structural characterization of **4**, obtained with another reaction, has already been reported (see ref. 2), the corresponding non-dried new compound **3** was characterized, like **1**, spectroscopically and by its crystal data (see below).‖ Compounds **1** and **3** with discrete cluster units (space group $P2_1/n$) as well as **2** and **4** with their corresponding layer structures (space group *Cmca*) are isostructural and have, as expected, practically the same unit cell dimensions. The crystal structures of **2** and **4** show the icosahedral capsule/nucleus type composites, abundant in **1** and **3,** cross-linked to 2D type assemblies *via* the formation of four Fe^{III}–O–Fe^{III} bonds per unit (see footnote ‖). Whereas the capsules of **1** and **2** have, as mentioned above, non-covalently bonded classical non-reduced Keggin anions $[PMo_{12}O_{40}]^{3-}$ (Fig. 1) those of **3** and **4** have the reduced Keggin anions $[H_yPMo_{12}O_{40}]^{3-}$ encapsulated. The acetate ligands, which are highly disordered, are located inside the spheres and coordinate as bidentate ligands bridging Mo and Fe sites. As the non-dried compounds **1** and **3** with the discrete cluster composites and different electron populations have, as expected, the same space group and practically the same unit cell dimensions as the compound $[\{(Mo^{VI})Mo^{VI}_5\}_{12}Fe^{III}_{30}O_{252}(MeCO_2)_{10}\{Mo_2O_7(H_2O)\}\{H_2Mo_2O_8(H_2O)\}_3(H_2O)_{91}]\cdot xH_2O$ **5** ($x \approx 140$) containing the same $\{(Mo)Mo_5O_{21}\}_{12}Fe_{30}$ cluster capsules without Keggin ions, and for which the complete single crystal X-ray analysis has been performed,[8] **1** and **3** can easily be identified from the relevant crystal data.§ (Note that in the present case the non-dried crystals of **1** and **3** do not diffract sufficiently.)

The important result of this investigation is that the Keggin ions are not stable in the presence of Fe^{III} (or Fe^{II} and air) as they decompose, while $\{(Mo^{VI})Mo^{VI}_5O_{21}\}$ type pentagons are formed which are subsequently linked by $\{Fe^{III}(H_2O)_2\}^{3+}$ groups. The remarkable fact is that the remaining non-decomposed Keggin ions (reduced or not reduced) appear in the reaction product encapsulated. Interestingly, the Keggin ions even seem to accelerate the formation of their cage around them as templates. This models the observation that assembly processes of simple linkable units lead preferably to highly symmetrical species. The process can be correlated with a general symmetry formalism or symmetry-evolution principle for a quasi isolated (!) system; in this respect, the second law of thermodynamics and the symmetry-evolution principle are isomorphic (see ref. 6). The degree of symmetry cannot decrease as the system evolves, but either remains constant or

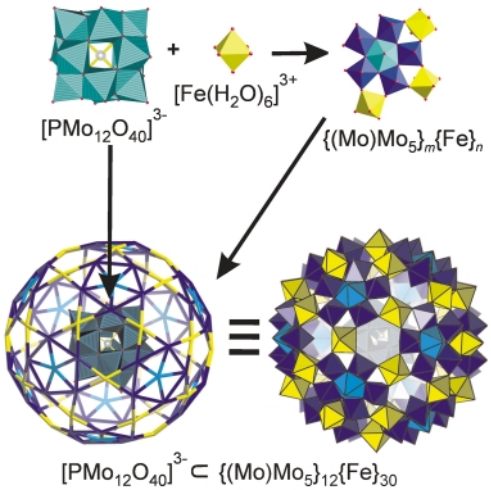

Fig. 1 Reaction scheme showing the decomposition of a part of the Keggin anions (top left, polyhedral representation) in the presence of Fe^{III} forming thereby fragments of the type $\{(Mo)Mo_5\}_m\{Fe\}_n$ which function as building blocks (top right, polyhedral representation) and leading finally to the formation of the $\{(Mo)Mo_5\}_{12}\{Fe\}_{30}$ type cage (bottom left with wire-frame representation of the capsule's metal atoms in blue and yellow (Fe part), and bottom right with polyhedral representation of the capsule), which subsequently encapsulates the remaining non-decomposed Keggin anions (polyhedral representation) to form the supramolecular species with core-shell topology: guest ⊂ (pentagon)$_{12}$(linker)$_{30}$ ≡ $[PMo_{12}O_{40}\subset\{(Mo)Mo_5O_{21}\}_{12}Fe_{30}(H_2O)_{102}(MeCO_2)_{15}]$ (colour code $MoO_{6/7}$ polyhedra: blue/turquoise, FeO_6 octahedra: yellow).

increases. (The effect is at least as symmetric as the cause.) This corresponds to the fact that causal relations exist between states of cause subsystems and states of effect subsystems, while states of the subsystems are determined by the states of the whole system. In other words, equivalent initial states must evolve into equivalent final states (see also ref. 5).

To express the related general aspect: two competing molecular systems model a type of '*Supramolecular Darwinism*' principle.** Spherical shell type molecules with highest possible (icosahedral) symmetry are for symmetry reasons the kinetically controlled destination and best adapted to the environment.

Notes and references

† *Syntheses*: **1**: to an aqueous solution (60 mL) of $H_3[PMo_{12}O_{40}]\cdot xH_2O$ (4.0 g, 2.2 mmol), $MeCO_2H$ (15 mL, 100%) and $FeCl_3\cdot 6H_2O$ (2.5 g, 9.2 mmol) 20 mL of NaOH solution (1 M) was added. The resulting clear brownish solution was kept in an open beaker for one week at 20 °C. Yellow plates of **1** precipitated during this time.

2: The wet crystals of **1** were filtered off, washed with water and kept at room temp. The condensation reaction was complete after *ca*. 1 h. Yield: 1.0 g (17.5% based on the starting Keggin type compound). (Note: single crystals suitable for X-ray structure analysis were obtained under more dilute conditions.)

3: To an aqueous solution (25 mL) of $H_3[PMo_{12}O_{40}]\cdot xH_2O$ (5.0 g, 2.7 mmol) and $MeCO_2H$ (10 mL, 100%), $FeCl_2\cdot 4H_2O$ (1.0 g, 5 mmol) was added (colour change to blue–green). 15 mL of NaOH solution (1 M) was subsequently added and the resulting clear solution was kept in an open flask for 2 weeks at 20 °C while greenish plates precipitated.

4: The wet crystals of **3** were filtered off, washed with water and kept at room temp. for the solid-state condensation reaction. Yield: 0.25 g (3.5% based on the starting Keggin type compound).

‡ For **3** or **4** it is difficult to distinguish between a one- and two-electron reduced system (even to position the electrons) which is mainly due to the presence of a large number (12 + 102) of metal atoms in connection with apparent analytical problems and due to disorder phenomena.

§ *Unit cell parameters for* **1**: monoclinic, space group $P2_1/n$, a = 26.548(4), b = 34.737(9), c = 28.910(4) Å, β = 97.194 (3)°, U = 26 452 (30) Å^3.

Crystal data for **2**: $C_{30}H_{365}Fe_{30}Mo_{84}O_{482}P$, M = 18 205.65, orthorhombic, space group *Cmca*, a = 36.847(1), b = 34.936(1), c = 34.859(1) Å, U = 44 874(3) Å^3 , Z = 4, D_c = 2.695 g cm^{-3}, μ = 3.328 mm^{-1}, F(000) = 34 896, crystal size = 0.22 × 0.12 × 0.02 mm. Dry crystals of **2** were measured at 183(2) K on a Bruker AXS SMART diffractometer (Mo-Kα, graphite monochromator). A total of 113 792 (1.71 < θ < 25.0°) reflections were collected of which 20 083 unique reflections (R_{int} = 0.155) were used. The structure was solved using the program SHELXS-97 and refined using the program SHELXL-97 to R = 0.073 for 10 583 reflections with $I > 2\sigma(I)$. Several crystal water molecules could not be located due to their disorder. For the encapsulated Keggin ion only the central P atom and (partly disordered) Mo atoms (but not the O atoms because of the disorder) could be detected for which the occupancy factors, however, add up to 12. These data together with the analysis, vibrational spectrum and the employed pH support the presence of a complete Keggin anion rather than a lacunary type one. Due to the disorder and related basic analytical problems in connection with the error limit of the number of acetate ligands, differently protonated Keggin ions cannot be completely excluded. CCDC 153129. See http://www.rsc.org/suppdata/cc/b0/b009518b/ for crystallographic data in .cif or other electronic format.

Unit cell parameters for **3**: monoclinic, space group $P2_1/n$, a = 26.388(8), b = 34.698(3), c = 28.852(1) Å, β = 96.958(4)°; U = 26 224(36) Å^3.

¶ *Selected physical and spectroscopic data* for **2**: IR (KBr pellet) (ν/cm^{-1}): 1618m {δ(H_2O)}, 1535m {$\nu_{as}(CO_2)$}, 1422m {$\nu_s(CO_2)$}, 1068w {ν_{as}(PO)}, 960m {ν(Mo=O)}, 775s, 623s, 567m, 433w. Raman (KBr dilution, λ_e = 1064 nm) (ν/cm^{-1}): 950s {ν(Mo=O)}, 836w, 512w, 371w, 241w. UV–VIS (solid state reflectance spectrum) λ_{max}/nm: *ca*. 285 (sh), *ca*. 370 (br). The magnetic susceptibility data are identical to those of **4** (see ref. 2).

‖ The crystals have to be taken from the corresponding mother-liquors and immediately investigated, because **2** and **4** with the characteristic layer structures are formed very fast even at room temperature due to a classical inorganic condensation process (see refs. 3 and 4). In the present case this corresponds to the following process (in schematic representation) which

$$\underset{\mathbf{A}}{-Fe^{III}(OH_2) + (H_2O)Fe^{III}-} \xrightarrow{-H^+} \underset{\mathbf{B}}{-Fe^{III}(OH) + (H_2O)Fe^{III}-} \xrightarrow{-H^+/-H_2O} \underset{\mathbf{C}}{-Fe^{III}-O-Fe^{III}-}$$

takes place after the capsules come closer together due to partial loss of crystal water. The related steps can be observed easily through the shrinking of the unit cell volumes. **A** denotes here the discrete composites and **C** the final product. Under the present mild conditions the content of each capsule remains of course unchanged.

** The term Darwinism is not only used in the literature in the sense of Darwin's *The Origin of Species by Means of Natural Selection*, but also for non-biological systems under (dissipative) stationary non-equilibrium conditions: (H. Haken uses it in his synergetics approach: H. Haken, *Synergetics*, Springer, Berlin, 1983; see especially: H. Haken, *Erfolgsgeheimnisse der Natur—Synergetik: Die Lehre vom Zusammenwirken*, Rowohlt, Reinbek, Hamburg, 1995, pp. 91, 94, 289 and H. Haken and A. Wunderlin, *Die Selbststrukturierung der Materie*, Vieweg, Braunschweig, 1991, p. 448 and additionally E. Ben-Jakob and H. Levine, *Nature*, 2001, **409**, 985 ['Pattening *via* competition']). In classical chemical reactions in general, a 'competition' between (molecular) species can be addressed. However, this is hardly detectable, in contrast to the present case where the different (kinetic) stabilities of two species can easily be referred to / explained by their different symmetry.

1 M. T. Pope and A. Müller, *Angew. Chem., Int. Ed. Engl.*, 1991, **30**, 34; J. N. Barrows and M. T. Pope, *Adv. Chem. Ser.*, 1990, **226**, 403.
2 A. Müller, S. K. Das, P. Kögerler, H. Bögge, M. Schmidtmann, A. X. Trautwein, V. Schünemann, E. Krickemeyer and W. Preetz, *Angew. Chem., Int. Ed.*, 2000, **39**, 3413; see also: J. Uppenbrink, A Soupçon of Phosphate, *Science* (Highlights, Editors' Choice), 2000, **290**, 411.
3 A. Müller, E. Krickemeyer, S. K. Das, P. Kögerler, S. Sarkar, H. Bögge, M. Schmidtmann and Sh. Sarkar, *Angew. Chem., Int. Ed.*, 2000, **39**, 1612.
4 A. Müller, S. K. Das, E. Krickemeyer, P. Kögerler, H. Bögge and M. Schmidtmann, *Solid State Sci.*, 2000, **2**, 847.
5 I. S. Dimitriev, *Symmetrie in der Welt der Moleküle*, VEB Deutscher Verlag für Grundstoffindustrie, Leipzig, 1987 (Chapter: Symmetrie und chemische Reaktion).
6 J. Rosen, *Symmetry in Science: An Introduction to the General Theory*, Springer, New York, 1995.

ChemComm

Visualisation of counter-rotating ring currents in kekulene

Erich Steiner,[a] Patrick W. Fowler,*[a] Leonardus W. Jenneskens*[b] and Angela Acocella[a]

[a] *School of Chemistry, University of Exeter, Stocker Road, Exeter, UK EX4 4QD. E-mail: P.W.Fowler@ex.ac.uk*
[b] *Debye Institute, Department of Physical Organic Chemistry, Utrecht University, Padualaan 8, 3584 CH Utrecht, The Netherlands. E-mail: jennesk@chem.uu.nl*

Received (in Cambridge, UK) 5th December 2000, Accepted 26th February 2001
First published as an Advance Article on the web 19th March 2001

Current-density maps for kekulene 1 computed using an *ab initio* all-electron distributed-origin method show global diamagnetic and paramagnetic circulations around outer and inner perimeters ('rim' and 'hub'), subsuming six local benzenoid diamagnetic π circulations, in qualitative agreement with the Hückel–London π model, but in contradiction of an [18]-in-[30] concentric-annulene description of 1.

Even before its synthesis in 1978 the cyclic polyacene kekulene (**1**, $C_{48}H_{24}$),[1] which consists of twelve annelated benzene rings, was already a subject of debate. Qualitative considerations suggest that **1** may be represented either as a D_{6h} Clar structure containing six benzenoid sextets[2] (**1a**) or an [18]annulene-within-a-[30]annulene corresponding to superposition of two D_{3h} Kekulé resonance structures (**1b**, Fig. 1). The proposal[3] that circularly conjugated **1** possesses superaromaticity, *i.e.* enhanced stabilisation energy, led to controversy[4] resolved by a recent *ab initio* study.[5] A comparison of the computed geometric, energetic and magnetic properties[6] of **1** with those of anthracene, phenanthrene, 1,2:7,8-dibenzanthracene and [18]annulene, showed no enhanced stabilisation energy, diamagnetic exaltation or magnetic anisotropy, all as would be expected from the qualitative graph theoretical analysis,[4] indicating that **1** is not superaromatic, and is realistically described by the D_{6h} structure **1a**.[5] These conclusions are compatible with the single-crystal X-ray structure of **1**. They also match the ^{1}H NMR data: the downfield-shifted $\delta(^1H)$ of the inner protons [H(3); 10.45/10.47][7] differs markedly from that of the corresponding protons in [18]annulene (−3.0[8]), as expected from the positive (paramagnetic; 5.0[5]) and negative (diamagnetic; −13.4[5]) NICS[6] values calculated for the geometric centres of **1** and [18]annulene, respectively (**III**, Fig. 1).

In a recent paper[9] the general picture of the 'annulene-within-an-annulene' model[10] for planar coronene (**2**, $C_{24}H_{12}$) and bowl-shaped corannulene (**3**, $C_{20}H_{10}$) was rejected on the basis of direct computation using *ab initio* all-electron distributed-origin methods and mapping of the current densities induced by a uniform magnetic field.† For **2** and **3**, two strong counter-rotating ring currents, a diamagnetic (anti-clockwise) and paramagnetic (clockwise) circulation around the rim and hub, respectively, were found.

To address the question of the electronic structure of kekulene **1**, *ab initio* all-electron current-density maps were calculated using the same distributed-origin methods.† Here we report the results, which support the Clar and Hückel pictures (*cf.* **1a**, Fig. 1).

The geometry of **1** was optimised using the 6-31G** basis set;[11] the planar, structure of **1** [D_{6h} symmetry (**1a**)] agrees with single-crystal X-ray data (Table 1).[3,5,7]

Fig. 2 shows the computed current-density maps† of **1a** for (a) the σ, (b) π and (c) total (σ + π) electrons at $1a_0$ above the molecular plane. The σ map demonstrates the characteristic superposition of diamagnetic circulations centred on σ bonds, giving rise to a cumulative net central paramagnetic circulation within each hexagonal ring. The π map shows a pattern of current density dominated by intense diamagnetic and paramagnetic circulations around outer and inner perimeters ('rim' and 'hub'), respectively. Residual benzenoid diamagnetic circulations within the central hexagons of the anthracene-like sub-units, are also visible (**1a**; rings **I**, Fig. 1). No diamagnetic circulations are observed in the hexagons at the six corner positions (**1a**; rings **II**, Fig. 1). This pattern is reminiscent of the computed *ab initio* current-density maps for anthracene and phenanthrene.[12] Thus, when placed in a perpendicular magnetic field, **1** has induced counter-rotating ring currents with a diamagnetic rim and a paramagnetic hub, in flat contradiction of the prediction of the [18]annulene-within-a-[30]annulene model, which would give diamagnetic rim and hub ring currents.[4]

The quality of the current-density maps is established by the calculated CTOCD-PZ2 integrated magnetic properties,† which are consistent with available experimental[7] and previous *ab initio* data acquired using different methods.[5]

The computed magnetic anisotropy $\Delta\xi$ (−153.9 a.u.) of **1a**, which tends to correlate[9] with the conventional exaltation of *isotropic* magnetic susceptibility Λ,[13] is *ca.* 10 times that of benzene. Thus, the CTOCD results support the conclusion that **1a** is not superaromatic.[3–5] The calculated $\Delta\xi$ is in qualitative agreement with an estimate of Λ (178×10^{-6} cm^3 mol^{-1} [14]).

The mean absolute shielding (σ) at the geometric centres of the distinct rings (**1a**; **I** 14.6, **II** 8.0 and **III** −3.2, Fig. 1), which with the required sign change are NICS[6] values (**I** −10.8, **II** −4.3 and **III** 5.0[5]), are consistent with the sense and strength of the calculated current densities (Fig. 2).

The computed mean absolute shieldings of the protons positioned on rim [H(1)/H(2)] and hub [H(3)] show good agreement with experiment (Table 1). The substantial downfield shift of H(3) with respect to H(1) [$\Delta\delta$ 1.62 (2.08/2.02[7])]

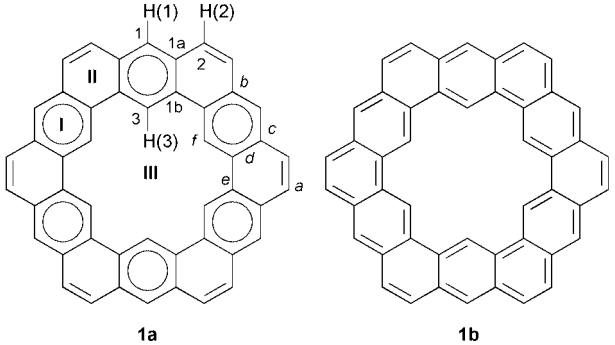

Fig. 1 Alternative Clar (**1a**) and Kekulé (**1b**) structures for **1**.

Table 1 Computed bond lengths (in Å) and shifts $\delta(^1H)$ and $\delta(^{13}C)$ for **1**

Bond[a]	6-31G**[b,c]	Atom[a]	$\delta(^1H)_{calc}$[b]	$\delta(^{13}C)_{calc}$
a	1.339 [1.347–1.351]	1	8.07 [8.37/8.45]	127.6
b	1.453 [1.438–1.449]	1a	—	131.5
c	1.394 [1.391–1.397]	1b	—	130.1
d	1.410 [1.415–1.421]	2	7.58 [7.95/8.01]	127.4
e	1.466 [1.453–1.461]	3	9.69 [10.45/10.47]	117.6
f	1.383 [1.381–1.390]			

[a] See **1a**, Fig. 1. [b] $\delta(^1H)_{calc} = 30.8 - 10^{-6}\sigma(^1H)$ and $\delta(^{13}C)_{calc} = 185.6 - 10^{-6}\sigma(^{13}C)$.† Experimental values in square brackets.[7] [c] See ref. 3.

DOI: 10.1039/b009763m

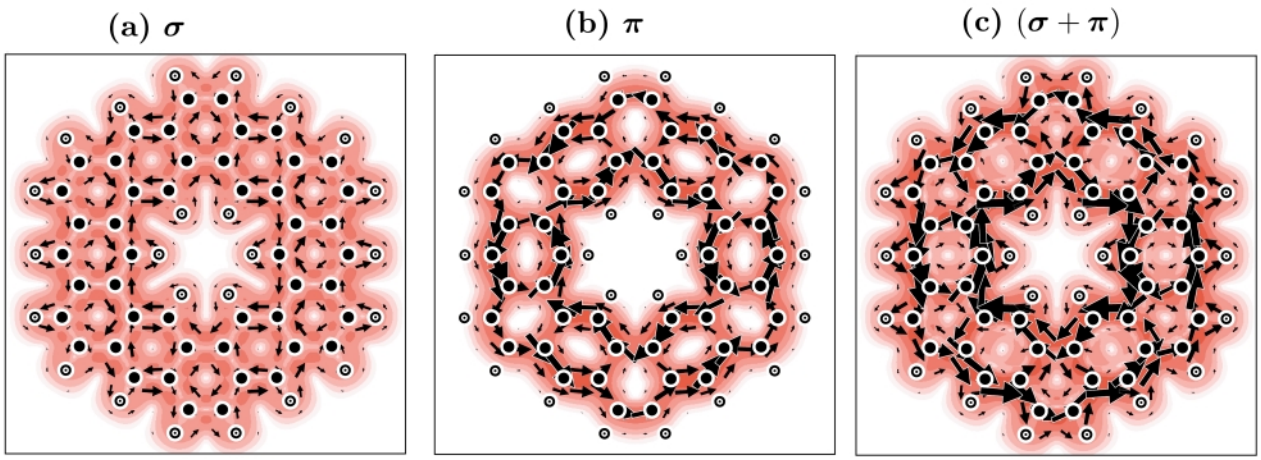

Fig. 2 Computed current-density maps of **1** [(a) σ, (b) π and (c) σ + π electrons].

and H(2) [$\Delta\delta$ 2.11 (2.50/2.46[7])] is in line with the strong paramagnetic hub ring current along the hub. Unfortunately, the extreme insolubility of **1** thwarted acquisition of its ^{13}C NMR spectrum. The $\delta(^{13}C)$ values of **1** compare with those of the corresponding position in anthracene and phenanthrene. We note that for C(3) an upfield shift of *ca.* 5 ppm is predicted (Table 1).

It is interesting to compare the results with the predictions of two simple models for the response of **1** to a uniform magnetic field. The annulene-within-an-annulene[10] picture of **1** (*cf.* **1b**, Fig. 1) considers the 48π-electron system as two separate $4n$ + 2 circuits, an outer 30π and an inner 18π cycle. As *disjoint* aromatic monocycles, each would therefore carry a uniform induced diamagnetic ring current, and hence **1** would have *con-rotating* currents. In contrast, when the Hückel–London model[15] is applied of **1**, a more complex pattern of induced currents in all 60 bonds is predicted. Application of symmetry constraints and current conservation at each vertex of the graph (as in electrical circuits[16]) shows that in fact all bond currents are functions of just three independent parameters, which govern the inner, outer and radial current flow. In the simplest version, where all bonds have equal resonance integrals, counter-rotating circulations on rim and hub are predicted,[4] in qualitative agreement with the *ab initio* π map, though with much weaker currents in the radial bonds connecting inner and outer perimeters (Fig. 3). If the resonance integral of the radial bonds is reduced to zero, the interior current slows down and reverses recovering the (physically incorrect) annulene-within-an-annulene model.‡

We gratefully acknowledge travel grants from the Council for Chemical Sciences of the Netherlands Organisation for Scientific Research and the British Council and thank the European Union TMR Network scheme, contract FMRX-CT097-0126 (support for A. A., University of Bologna).

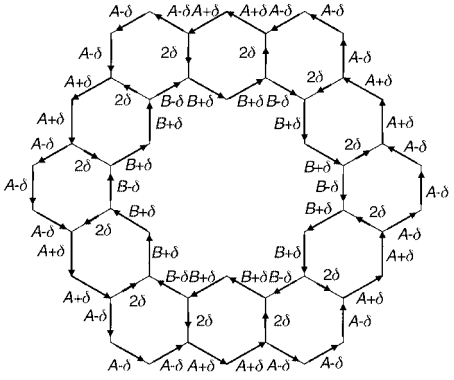

Fig. 3 Induced bond currents in the Hückel–London π model of **1**.‡

Notes and references

† For procedures see ref. 9.

‡ With all bond lengths set to 1.4 Å, perimeter resonance integrals set to the benzene β, and integrals for radial bonds to β', the variation $1 \geqslant \beta'/\beta \geqslant 0$ covers the range from **1** to a fully decoupled [18]-in-[30] annulene. All current strength parameters (Fig. 3) are monotonic: $1.18 \leqslant A \leqslant 3.64$, $0.18 \leqslant \delta \leqslant 0$, $0.99 \geqslant B \geqslant -2.24$, in units of the benzene ring current. The hub has a paramagnetic current for $0.424 < \beta'/\beta$, a diamagnetic current for $\beta'/\beta < 0.407$.

1 H. A. Staab and F. Diederich, *Angew. Chem., Int. Ed. Engl.*, 1978, **17**, 372; H. A. Staab and F. Diederich, *Chem. Ber.*, 1983, **116**, 3487.
2 E. Clar, *Polycyclic Hydrocarbons*, Academic Press Inc., London, 1964.
3 J. Cioslowski, P. B. O'Connor and E. D. Fleischmann, *J. Am. Chem. Soc.*, 1991, **113**, 1086; Z. Zhou, *J. Phys. Org. Chem.*, 1995, **8**, 103.
4 For an opposing view: J.-I. Aihara, *J. Am. Chem. Soc.*, 1992, **114**, 865. J.-I. Aihara, *J. Chem. Soc., Faraday Trans.*, 1995, **91**, 237.
5 H. Jiao and P. von R. Schleyer, *Angew. Chem., Int. Ed. Engl.*, 1996, **35**, 2383.
6 P. von R. Schleyer, C. Maerker, A. Dransfeld, H. Jiao and N. J. R. van Eikema Hommes, *J. Am. Chem. Soc.*, 1996, **118**, 6137; see also: U. Fleischer, W. Kutzelnigg, P. Lazzeretti and V. Mühlenkamp, *J. Am. Chem. Soc.*, 1994, **116**, 5298.
7 H. A. Staab, F. Diederich, C. Krieger and D. Schweitzer, *Chem. Ber.*, 1983, **116**, 3504.
8 F. Sondheimer, *Acc. Chem. Res.*, 1972, **5**, 81.
9 E. Steiner, P. W. Fowler and L. W. Jenneskens, *Angew. Chem., Int. Ed.*, 2001, **40**, 362.
10 For a review: R. Benshafrut, E. Shabtai, M. Rabinovitz and L. T. Scott, *Eur. J. Org. Chem.*, 2000, 1091 and references therein.
11 CADPAC: R. D. Amos and J. E. Rice, *The Cambridge Analytical Derivatives Package*, Issue 4.0, 1987.
12 E. Steiner and P. W. Fowler, *Int. J. Quantum Chem.*, 1996, **60**, 609; A. Ligabue, U. Pincelli, P. Lazzeretti and R. Zanasi, *J. Am. Chem. Soc.*, 1999, **121**, 5513.
13 H. J. Dauben, J. D. Wilson and J. L. Laity, *Diamagnetic Susceptibility Exaltations as a Criterion of Aromaticity*, in *Nonbenzenoid Aromatics*, ed. J. P. Snyder, Academic Press, New York, vol. 2, 1971.
14 G. Ege and H. Volger, *Z. Naturforsch., Teil B*, 1972, **27**, 918.
15 A. Pasquarello, M. Schluter and R. C. Haddon, *Phys. Rev. A.*, 1993, **47**, 1783; A. Ceulemans, L. F. Chibotaru and P. W. Fowler, *Phys. Rev. Lett.*, 1998, **80**, 1861.
16 G. Kirchoff, *Ann. Phys. Chem.*, 1847, 497–508; N. L. Biggs, E. K. Lloyd and R. J. Wilson, *Graph Theory 1736–1936*, Clarendon Press, Oxford, 1998, ch. 8.

ChemComm

Hop, skip or jump? Proton transport in the $CaZrO_3$ perovskite oxide

M. Saiful Islam,*[a] R. Andrew Davies[a] and Julian D. Gale[b]

[a] *Department of Chemistry, University of Surrey, Guildford, UK GU2 7XH. E-mail: m.islam@surrey.ac.uk*
[b] *Department of Chemistry, Imperial College of Science, Technology and Medicine, London, UK SW7 2AY*

Received (in Cambridge, UK) 29th January 2001, Accepted 2nd March 2001
First published as an Advance Article on the web 19th March 2001

***Ab initio* simulations of the $CaZrO_3$ proton conductor predict that the transport mechanism involves proton transfer between adjacent oxygen ions (but predominantly inter-octahedra), and that the energetics of proton–dopant binding is favourable in accord with spectroscopic evidence.**

Metal oxides with the ABO_3 perovskite structure have received considerable attention as solid-state proton conductors,[1,2] with a range of promising electrochemical applications including fuel cells, gas sensors and hydrogen pumps. Most attention has focused on cerates[3] and zirconates[4] which possess varying levels of proton conductivity. An important example is the development of a potentiometric sensor for hydrogen in molten metal based upon doped $CaZrO_3$ as the proton-conducting electrolyte.[5] The $CaZrO_3$ material is typically acceptor-doped with trivalent ions (*e.g.* In^{3+}) at the Zr^{4+} site, which is crucial to proton dissolution.

It is acknowledged that the macroscopic behaviour of materials is often controlled by fundamental mechanisms acting on the microscopic scale. However, the information derived from most conductivity experiments is not sufficient to identify the precise mechanistic features of proton transport. There is also conflicting debate as to whether there is any significant interaction between the dopant ion and the protonic defect (hydroxyl ion at oxygen site), which may lead to defect clustering or proton 'trapping'.

In an attempt to gain further insight into these problems we have investigated the important $CaZrO_3$ material using quantum mechanical techniques based upon density functional theory (DFT), which are increasingly powerful tools for exploring solid-state properties. This preliminary account builds upon our previous atomistic modelling and X-ray absorption (EXAFS) studies, where we have already obtained valuable microscopic information on the defect chemistry of perovskite-type oxides.[6,7] Here we focus, for the first time, on the distorted orthorhombic phase of $CaZrO_3$, which extends earlier simulation work on ideal cubic perovskites.[8]

The present account of the computational techniques will be brief since more detailed reviews are given elsewhere.[9,10] The calculations are performed within the DFT framework, with the exchange-correlation energy being treated using the generalised-gradient approximation. The particular implementation of DFT employed here combines a plane-wave basis set with the total energy pseudopotential method (as embodied in the CASTEP code[9]) which is ideally suited to calculations on periodic systems. Our simulations are based upon ultrasoft pseudopotentials with the Brillouin zone sampled according to the Monkhorst–Pack scheme.[11] The DFT-pseudopotential approach can be utilised to perform *ab initio* dynamics which essentially combines the solution of the electronic structure with classical molecular dynamics (MD) for the nuclei. The MD simulations, which are highly computationally demanding, used a periodically repeated system of $Ca_4Zr_4O_{12}H$, a time-step of 0.5 fs and a total duration of 4000 time-steps at a temperature of 1000 K within the NVT ensemble; full computational details will be reported in ref. 12. It is worth noting that *ab initio* techniques of this kind have been applied successfully to other oxides including studies of molecular absorption on surfaces[13] and lithium intercalation.[14]

Table 1 Calculated and experimental structural parameters of orthorhombic $CaZrO_3$

	Experimental[a]	Calculated
Unit cell parameters		
a/Å	5.5912	5.5895
b/Å	8.0171	8.0550
c/Å	5.7616	5.7667
Mean bond lengths and angles		
Zr–O (×6)/Å	2.0964	2.1052
Ca–O (×4)/Å	2.3817	2.3742
Ca–O (×4)/Å	2.7616	2.7680
Ca–O (×4)/Å	3.5101	3.5345
Zr–O(1)–Zr/°	145.76	143.46
Zr–O(2)–Zr/°	146.50	146.35

[a] Ref. 15.

The starting point for this study, prior to the introduction of the proton, was the simulation of the equilibrium bulk structure. The perovskite structure of $CaZrO_3$ is built upon a framework of corner-linked ZrO_6 octahedra with the calcium ion in a 12-coordinate site. The orthorhombic structure (space group *Pcnm*) exhibits significant tilting of the octahedra from the ideal cubic configuration.[15] The calculated and experimental lattice parameters, bond lengths and bond angles are listed in Table 1. Examination of the values shows good agreement between experimental and simulated structures, with $< 0.5\%$ deviation in the cell parameters and bond lengths. In addition, the appreciable tilting of the ZrO_6 octahedra (and the corresponding Zr–O–Zr bending) are correctly reproduced.

Of primary interest here is the information on the microscopic mechanism revealed by the MD calculations. Graphical analysis of the evolution of the system with time shows a number of proton 'hopping' events during the simulation run. Fig. 1 presents 'snapshots' of one of these proton hops between neighbouring oxygen ions of connecting octahedra, illustrating initial and barrier (transition) states. This confirms that proton conduction occurs *via* a simple transfer of a lone proton from one oxygen ion to the next (Grötthuss mechanism), with no evidence for the migration of hydroxyl ions ('vehicle' mechanism) on the present timescale.

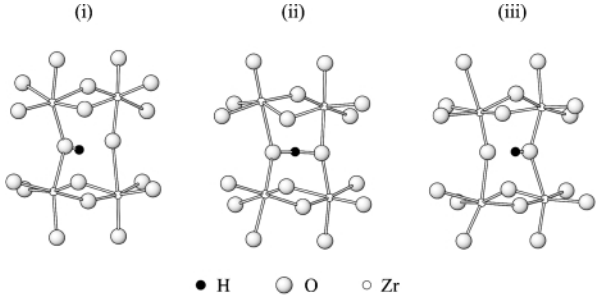

Fig. 1 Sequence of three snapshots from *ab initio* MD simulations showing inter-octahedra proton hopping in orthorhombic $CaZrO_3$ (the Ca ions are omitted for clarity).

We also find rapid rotational and stretching motion of the O–H group, which allows the reorientation of the proton towards the next oxygen ion before the transfer process. However, the simulations reveal predominantly inter-octahedra proton hopping, rather than within octahedra. This diffusion path is influenced by the ZrO_6 tilting within the orthorhombic structure which leads to short oxygen–oxygen separations between the vertices of adjacent octahedra (shown in Fig. 1). These results are consistent with the observation that proton mobility is lower in perovskite structures deviating strongly from cubic.[1,2] There is also considerable lattice vibrational dynamics with large amplitudes of vibration of the oxygen ions. In particular, for each hopping event the O(H)–O distance shortens from equilibrium values (of *ca*. 2.7–2.9 Å) to <2.4 Å so as to facilitate proton transfer; this suggests that migration is 'phonon-assisted'. We note that recent simulations of zeolites have found similar coupling between proton motion and framework dynamics.[16]

The interaction between oxygen ions and the proton is probed further by analysis of the electron density distribution (illustrated in Fig. 2 as a contour map for the inter-octahedra path). The barrier state displays a symmetric density distribution, in which there is equal hydrogen bonding to the two adjacent oxygen ions (leading to a shorter oxygen–oxygen distance). This confirms that the proton is not transferred through a totally 'free' state, so that all the OH bonds are never completely broken. Although additional analysis of the wavefunction would be useful, it is apparent that the host lattice exhibits localised spherical-like density about the nuclei indicative of the largely ionic character.

In an attempt to probe the question of proton–dopant association, we have undertaken a series of calculations on defect pairs ($OH_O^{\bullet}M'_{Zr}$) comprised of a hydroxyl ion and a neighbouring dopant substitutional; here we employed a slightly larger periodically-repeated system corresponding to $Ca_8Zr_7MO_{24}H$ in order to achieve a lower dopant content. Attention was focused on three commonly used dopants in $CaZrO_3$, namely Sc^{3+}, Ga^{3+} and In^{3+}. The binding energies were derived with respect to the two isolated defects where a negative value indicates the system is bound.

The resulting energies (reported in Table 2) predict that all the hydroxyl–dopant pairs are favourable configurations, with the lowest value for Ga^{3+}. Although there are no experimental data on $CaZrO_3$ for direct comparison, the calculated values are in accord with proton 'trapping' energies of *ca*. -0.2 and -0.4 eV for Sc-doped $SrZrO_3$ and Yb-doped $SrCeO_3$ respectively, derived from recent muon spin relaxation (μSR) and quasi-elastic neutron scattering (QENS) experiments.[17] These studies postulate that in the course of their diffusion, protons are temporarily trapped at single dopant ions. The present calculations therefore predict possible trapping effects and the presence of proton–dopant pairs in the $CaZrO_3$ material. It is noted, however, that defect pairs do not necessarily preclude the presence of isolated protons and dopant ions, since clusters will be in equilibrium with single defects. This picture can be viewed as analogous to oxygen ion conductivity in fluorite oxides and the well-known importance of dopant–vacancy interactions.[18]

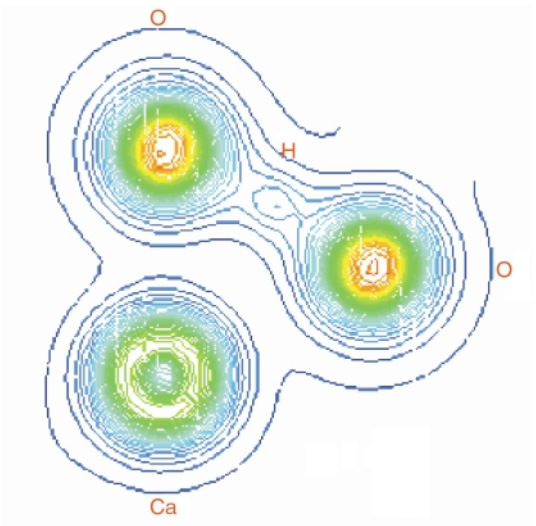

Fig. 2 Electronic charge density of the barrier (transition) state for inter-octahedra proton transfer in the plane defined by Ca, O and H (colour scale: high to low density is red to blue).

Table 2 Binding energies of hydroxyl–dopant pairs ($OH_O^{\bullet}M'_{Zr}$) at nearest-neighbour sites

Dopant	E_{bind}/eV[a]
Sc^{3+}	−0.31
Ga^{3+}	−0.18
In^{3+}	−0.30

[a] 1 eV ≡ 96.486 kJ mol^{-1}.

In summary, our *ab initio* simulation study has allowed us to gain significant insight as to the proton migration mechanism and proton–dopant binding in the $CaZrO_3$ orthorhombic perovskite at the microscopic level. This forms part of the continuing effort to improve our understanding of proton transport, a key phenomenon in a variety of systems that range from inorganic solids to biomolecules. Further simulation work is in progress and it is hoped that the present study prompts new experimental investigations in this area using, for example, neutron scattering or muon spin techniques.

We wish to thank the EPSRC for funding this work, the Royal Society for a University Research Fellowship (J. D. G.) and the Computational Chemistry Working Party for the use of the supercomputer facilities at the Rutherford Appleton Laboratory, UK.

Notes and references

1 H. Iwahara, *Solid State Ionics*, 1999, **125**, 271; K. D. Kreuer, *Chem. Mater.*, 1996, **8**, 610.
2 T. Norby and Y. Larring, *Curr. Opin. Solid State Mater. Sci.*, 1997, **2**, 593; A. S. Nowick, Y. Du and K. C. Liang, *Solid State Ionics*, 1999, **125**, 303.
3 R. C. T. Slade, S. D. Flint and N. Singh, *J. Mater. Chem.*, 1995, **4**, 509; D. Shima and S. M. Haile, *Solid State Ionics*, 1997, **97**, 443; K. S. Knight, *Solid State Ionics*, 2000, **127**, 43.
4 L. van Rij, L. Winnubst, L. Jun and J. Schoonman, *J. Mater. Chem.*, 2000, **10**, 2515; B. Groß, J. Engeldinger, D. Grambole, F. Hermann and R. Hempelmann, *Phys. Chem. Chem. Phys.*, 2000, **2**, 297.
5 T. Yajima, K. Koide, H. Takai, N. Fukatsu and H. Iwahara, *Solid State Ionics*, 1995, **79**, 333.
6 R. A. Davies, M. S. Islam and J. D. Gale, *Solid State Ionics*, 1999, **126**, 323; M. Cherry, M. S. Islam, J. D. Gale and C. R. A. Catlow, *J. Phys. Chem.*, 1995, **99**, 14614.
7 M. S. Islam, *J. Mater. Chem.*, 2000, **10**, 1027; M. S. Islam and S. D'Arco, *Chem. Commun.*, 1996, 2291; L. J. Winch and M. S. Islam, *J. Chem. Soc., Chem. Commun.*, 1995, 1595.
8 W. Münch, K. D. Kreuer, G. Seifert and J. Maier, *Solid State Ionics*, 2000, **136–137**, 183; F. Shimojo, K. Hoshino and H. Okazaki, *J. Phys. Condens. Matter*, 1998, **10**, 285.
9 M. C. Payne, M. P. Teter, D. C. Allan, T. A. Arias and J. D. Joannopoulos, *Rev. Mod. Phys.*, 1992, **64**, 1045.
10 M. J. Gillan, in *Computer Simulation in Materials Science*, ed. M. Meyer and V. Pontikis, Kluwer, Dordrecht, 1991.
11 H. J. Monkhorst and J. D. Pack, *Phys. Rev. B*, 1976, **13**, 5188.
12 M. S. Islam, R. A. Davies and J. D. Gale, *Chem. Mater.*, 2001, in press.
13 P. J. D. Lindan, J. Muscat, S. Bates, N. M. Harrison and M. J. Gillan, *Faraday Discuss.*, 1997, **106**, 135.
14 J. S. Braithwaite, C. R. A. Catlow, J. H. Harding and J. D. Gale, *Phys. Chem. Chem. Phys.*, 2000, **2**, 3841; G. Ceder, Y. M. Chiang, D. R. Sadoway, M. K. Aydinol, Y. I. Jang and B. Huang, *Nature*, 1998, **392**, 694.
15 H. J. A. Koopmans, G. M. H. van de Velde and P. J. Gellings, *Acta Crystallogr., Sect. C*, 1983, **39**, 1323.
16 E. Fois and A. Gamba, *J. Phys. Chem. B*, 1999, **103**, 1794.
17 R. Hempelmann, M. Soetratmo, O. Hartmann and R. Wappling, *Solid State Ionics*, 1998, **107**, 269; C. Karmonik and R. Hempelmann, *Phase Transitions*, 1996, **58**, 175.
18 C. R. A. Catlow, *J. Chem. Soc., Faraday Trans.*, 1990, **86**, 1167.

Synthesis, crystal structure and theoretical studies of the first *endo*:*endo*-2,4-diphosphabicyclo[1.1.0]butane†

Cameron Jones,* Jamie A. Platts* and Anne F. Richards

Department of Chemistry, University of Wales, Cardiff, PO Box 912, Park Place, Cardiff, UK CF10 3TB. E-mail: jonesca6@cardiff.ac.uk

Received (in Cambridge, UK) 29th January 2001, Accepted 27th February 2001
First published as an Advance Article on the web 16th March 2001

The reaction of $PbCl_2$ with *Z*-[CyP=C(Bu^t)MgCl(OEt$_2$)] (Cy = cyclohexyl) affords the first example of an *endo*:*endo*-2,4-diphosphabicyclo[1.1.0]butane, $Cy_2P_2C_2Bu^t_2$, which displays unusual spectroscopic and geometric properties, the origins of which have been explored by theoretical calculations.

Because of their unusual properties and application to organic transformations, strained hydrocarbon rings and cages have been the subject of intense investigation.[1] In recent years this attention has extended to the phosphorus substituted analogues of these systems, often with remarkable results.[2] For example, Niecke *et al.* have succeeded in preparing several stable, crystalline, diradical 1,3-diphosphacyclobutanediyls **I**.[3] Thermal valence isomerisations of these have yielded 1,2-dihydro-

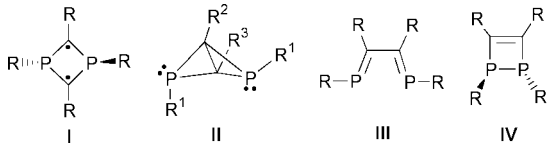

I II III IV

1,2-diphosphetes **IV**[4] whilst a photolytic isomerisation has yielded the only example of a 2,4-disphosphabicyclo[1.1.0]butane **II** (R^1 = Mes* ($C_6H_2Bu^t_3$-2,4,6), R^2 = $SiMe_3$, R^3 = H, **1**) which has *exo*:*endo*-phosphorus substituents.[3] Indeed, compound **1** can itself thermally valence isomerise to the corresponding 1,4-diphosphabutadiene **III**. The relative stabilities of these isomers have been calculated to be in the order **I** < **II** < **III** < **IV**.[3–5] Compounds of the general type **III** and **IV** are now relatively common and have found a number of applications as building blocks in organophosphorus and organometallic chemistry, and as ligands in the formation of novel coordination compounds.[2,6] Despite this, examples of **I** and **II** are very rare and their preparation can be challenging. We have developed a high yielding stereospecific route to a range of phosphavinyl Grignard reagents, *e.g. Z*-[CyP=C(Bu^t)MgCl(OEt$_2$)] (Cy = cyclohexyl) **2**,[7] which we saw as potential precursors to $P_2C_2R_4$ heterocycles such as **I** and **II** *via* oxidative coupling reactions. The results of our endeavours in this area are reported herein.

† Electronic supplementary information (ESI) available: calculation data and atomic coordinates for compounds **4**–**6**. See http://www.rsc.org/suppdata/cc/b1/b100993l/

Treatment of an ethereal solution of $PbCl_2$ with 2 equivalents of **2** at −78 °C led to the deposition of lead metal and the stereoselective formation of the diphosphabicyclo[1.1.0]butane **3** in 60% yield (Scheme 1). The reaction also occurs with $SnCl_2$ though in lower (30%) yield. The mechanism of this reaction presumably involves an organolead intermediate, *Z,Z*-[Pb{C(Bu^t)=PCy}$_2$], though this could not be detected when the reaction was followed by ^{31}P NMR spectroscopy. The formation of **3** contrasts with the reaction between **2** and Me_2SnCl_2 which does not lead to an oxidative coupling but to *Z,Z*-[Me_2Sn{C(Bu^t)=PCy}$_2$] as the major product.[8] Interestingly, **3** was found to be remarkably stable (mp 118 °C) and did not valence isomerise in refluxing toluene over 10 h or when treated with UV light (*cf.* the facile thermal isomerisation of **1**).

Most of the spectroscopic data‡ for **3** are consistent with its proposed structure. However, its ^{31}P{^{1}H} NMR spectrum displays a singlet at δ 12 ppm which is far removed from the expected region (upfield of δ −80 ppm, *e.g.* δ −83 and −84 ppm for **1**) for three-membered phosphirane rings[2,9] but close to values normally observed for examples of **I**.[3,4] In addition, the signal for the framework carbon atoms appears as a triplet at δ 60.3 ppm, $^1J_{PC}$ 52 Hz, which is significantly downfield of the values for **1**, δ 28.3 ppm, and phosphirane rings in general.[9] We hoped to shed light on these apparent inconsistencies by carrying out density functional studies[10] on the three possible stereoisomers of tetramethyl-2,4-disphosphabicyclo[1.1.0]butane. A summary of the results of this preliminary investigation is shown in Table 1.

It is clear that the *endo*:*endo* isomer is the thermodynamically least favourable of the three isomers but probably forms in the case of **3** due to stereochemical constraints on the coupling reaction. The calculated ^{31}P NMR shift for **4** is close to the experimental value for **3** and more than 100 ppm downfield of the values for **5**, **6** and the experimentally observed compound **1**.[3] Unfortunately there are no known examples of *exo*:*exo* diphosphabicyclobutanes for purpose of comparison. An explanation for the low field ^{31}P and ^{13}C NMR shifts for **3**

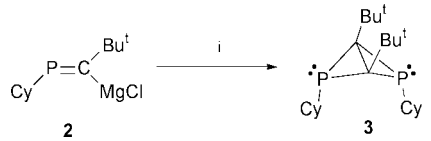

2 3

Scheme 1 *Reagents and conditions:* i, 1/2 $PbCl_2$, Et_2O, −78 °C, $-MgCl_2$, $-Pb_{(s)}$

Table 1 Calculations on tetramethyl-2,4-diphosphabicyclo[1.1.0]butane isomers

	Endo:*endo* (C_2) **4**	*Exo*:*exo* (C_{2v}) **5**	*Endo*:*exo* (C_s) **6**
Relative energy/kJ mol^{-1}	25.5	6.5	0.0
^{31}P NMR/ppm	19 (12)[a]	−171	−104, −143 (−83, −84)[b]
Fold angle (PCCP)/°	131.7 (131.6)[a]	109.5	117.5 (117)[a]
C_{ring}–C_{ring}/Å	1.53 (1.54)[a]	1.48	1.50 (1.51)[b]
Σ angles on P/°	275.6 (280.2)[a]	247.3	266.3, 251.0 (257.1, 253.8)[b]

Geom. calculations: B3LYP/6-31 + G(d,p); energy and NMR calculations: B3LYP/6-311++G(d,p).[10] [a] Experimental values for **3**. [b] Experimental values for **1**.[3]

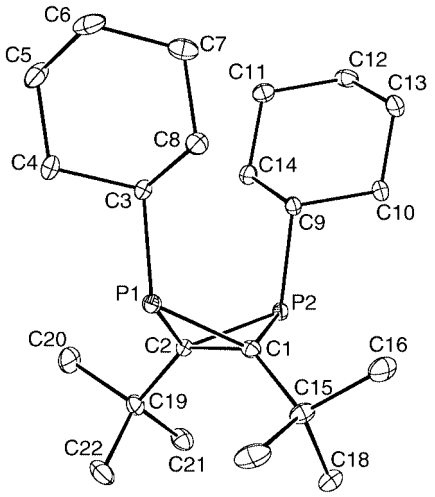

Fig. 1 Molecular structure of **3**. Selected bond lengths (Å) and angles (°): P(1)–C(1) 1.833(3), P(1)–C(2) 1.826(3), P(1)–C(3) 1.875(3), P(2)–C(1) 1.819(3), P(2)–C(2) 1.832(3), P(2)–C(9) 1.859(3), C(1)–C(2) 1.543(4); C(2)–P(1)–C(1) 49.89(13), C(2)–P(1)–C(3) 113.03(13), C(1)–P(1)–C(3) 117.25(13), C(1)–P(2)–C(2) 50.01(13), C(1)–P(2)–C(9) 112.39(13), C(2)–P(2)–C(9) 116.47(13), C(15)–C(1)–C(2) 138.0(3), C(19)–C(2)–C(1) 138.0(3).

may be drawn from its geometry (Fig. 1).§ The fold angle between its two PCC rings is in good agreement with theoretical calculations on **4** and markedly greater than in **1**,[3] **5** and **6**. There is a concomitant loss of pyramidalisation of its P- and framework C-centres relative to **1** and **6** and a lengthening of the transannular bond. Thus it is possible that the bonding in the P_2C_2 frameworks of the *endo*:*endo* isomers, **3** and **4**, lies closer to that reported for partially delocalised 1,3-diphosphacyclobutanediyls than does the bonding in the *endo*:*exo* isomers, **1** and **6**. In this context it is noteworthy that the two general valence isomers **I** and **II** have been described as bond stretch or orbital isomers.[3,4]

We are currently carrying out more extensive calculations to determine the nature of any bonding differences in **4**–**6**. We are also further investigating valence isomerisations of **3** and related compounds, in addition to exploring the versatility of **2** as a synthon in the formation of other strained organophosphorus heterocycles and cages. The results of these studies will appear in forthcoming publications.

We gratefully acknowledge financial support from the EPSRC (studentship for A. F. R) and for access to the UK Computational Chemistry Facility.

Notes and references

‡ *Spectroscopic data* for **3**: $^{31}P\{^1H\}$ NMR (145.8 MHz, C_6D_6) δ 12 (s, PCy); ^1H NMR (400 MHz, C_6D_6) δ 1.17 (s, 18H, Bu^t), 0.80–1.75 (m, 22H, Cy); ^{13}C NMR (100.6 MHz, C_6D_6, 298 K) δ 24.9 (CH_2), 26.1 (CH_2, $^3J_{PC}$ 6 Hz), 30.3 (CH_2, $^2J_{PC}$ 11 Hz), 30.9 (C(CH_3)$_3$, $^3J_{PC}$ 7 Hz), 31.5 (CH, $^1J_{PC}$ 62, $^3J_{PC}$ 11 Hz), 32.5 (C(CH_3)$_3$, $^2J_{PC}$ 14 Hz), 60.3 (PCP, $^1J_{PC}$ 52 Hz); IR ν/cm^{-1} 1458m, 1376m, 1259m, 847m, 802m, 720 m; MS APCI *m*/*z* (%): 366 (M^+, 100); satisfactory elemental analysis obtained.

§ *Crystal data* for **3**: $C_{22}H_{40}P_2$ M = 366.48, orthorhombic, space group $P2_12_12_1$, a = 9.945(2), b = 14.071(3), c = 16.065(3) Å, V = 2248.1(8) Å^3, Z = 4, D_c = 1.083 g cm^{-3}, F(000) = 808, μ(Mo-Kα) = 1.95 cm^{-1}, 150(2) K, 2303 unique reflections, R (on F) 0.0417, wR (on F^2) 0.1223 ($I > 2\sigma I$).

CCDC 157235. See http://www.rsc.org/suppdata/cc/b1/b100993l/ for crystallographic data in .cif or other electronic format.

1 M. D. Levin, P. Kaszynski and J. Michl, *Chem. Rev.*, 2000, **100**, 169 and references therein.
2 K. B. Dillon, F. Mathey and J. F. Nixon, in *Phosphorus: The Carbon Copy*, Wiley, Chichester, 1998, and references therein.
3 E. Niecke, A. Fuchs and M. Nieger, *Angew. Chem., Int. Ed.*, 1999, **38**, 3028 and references therein.
4 O. Schmidt, A. Fuchs, D. Gudat, M. Nieger, W. Hoffbauer, E. Niecke and W. W. Schoeller, *Angew. Chem., Int. Ed.*, 1998, **37**, 949.
5 W. W. Schoeller and U. Tubbesing, *Chem. Ber.*, 1996, **129**, 419.
6 C. Charrier, N. Maigrot, F. Mathey, F. Robert and Y. Jeanin, *Organometallics*, 1986, **5**, 623.
7 D. E. Hibbs, C. Jones and A. F. Richards, *J. Chem. Soc., Dalton Trans.*, 1999, 3531.
8 C. Jones and A. F. Richards, *J. Chem. Soc., Dalton Trans.*, 2000, 3233.
9 F. Mathey and M. Regitz, in *Comprehensive Heterocyclic Chemistry II*, Pergamon, Oxford, 1996.
10 Full details of calculations have been submitted as supplementary material (ESI).†

ChemComm

Polarity and hydrogen-bonding of ambient to near-critical water: Kamlet–Taft solvent parameters

Jie Lu, James S. Brown, Charles L. Liotta and Charles A. Eckert*

Schools of Chemical Engineering, Chemistry and Biochemistry, and Specialty Separations Center, Georgia Institute of Technology, Atlanta, GA 30332-0100, USA. E-mail: cae@che.gatech.edu

Received (in Corvallis, OR, USA) 9th January 2001, Accepted 20th February 2001
First published as an Advance Article on the web 16th March 2001

The Kamlet–Taft solvent parameters π^*, α, and β of saturated liquid water have been determined from 25 to 275 °C based on solvatochromic measurements and indicate that the polarity and hydrogen-bonding of water are highly tunable properties with temperature.

Nearcritical water (NCW) is an environmentally benign solvent and alternative reaction medium, which can simultaneously solubilize organics and ionics[1] because the dielectric constant of water decreases significantly at elevated temperatures (for example, ε = 23.5 at 275 °C).[2] In addition, the ionization constant of water increases several orders of magnitude from ambient to nearcritical conditions,[3] providing hydronium and hydroxide ions that can act as modest acid or base catalysts in chemical reactions.[4,5] Interest in NCW as a reaction medium has prompted study of the solvent properties of water at elevated temperature.[6,7] However, to date our understanding of the solvent properties of NCW has been inadequate for correlating and predicting chemical reactions and other physicochemical processes.

Kamlet–Taft solvent parameters π^*, α, and β have been related to a variety of configurational properties in solution: solubilities, partition coefficients, thermodynamic and kinetic properties of chemical reactions, *etc.*, based on successful treatments of solvent effects by linear solvation energy relationship (LSER) theory,[8]

$$XYZ = (XYZ)_0 + s\pi^* + a\alpha + b\beta$$

where π^*, α and β are the parameters for dipolarity/polarizability, hydrogen bond donating ability and hydrogen bond accepting ability, respectively. XYZ and $(XYZ)_0$ are the solvent-dependent physicochemical properties in a given solvent and in a reference solvent (gas or inert solvent). *s*, *a*, and *b* are solvent-independent coefficients indicating the susceptibility of the corresponding parameters to the solvent property. Based on the LSER theory, the π^*, α, and β solvent parameters of water can be used to correlate and predict processes occurring in NCW. In this work, we report the solvatochromic parameters of saturated liquid water in the temperature range 25–275 °C.

A high-pressure titanium optical cell equipped with sapphire windows (Insaco Inc., PA, 0.50 inches diameter, 0.25 inches thick) sealed with gold gaskets (Aldrich, 99.99%) was constructed to measure the solvatochromic parameters of NCW from ambient to nearcritical conditions. The path length of the cell is 10.5 mm at rt and the internal volume is 17.7 cm^3.

Some of the indicators used decompose in water at elevated temperatures. When decomposition products contain similar chromophores to those of indicators, an undesirable spectral shift can result. In order to avoid errors associated with decomposition of solvatochromic indicators, the cell was first loaded with water (Aldrich, HPLC grade, deoxygenated with N_2 before being used) and heated to the desired temperature. Then a small amount of concentrated indicator solution was injected into the cell through a sample loop. Temperature equilibrium was restored within 10 s. Multiple spectra were measured in less than five minutes before significant decomposition could take place. A Hewlett-Packard 8450 UV-Vis spectrophotometer was used to perform the spectroscopic measurements and data processing.

The π^* parameters were determined based on the UV-Vis spectral shift of 4-nitroanisole (Aldrich, 97%). Cyclohexane and dimethyl sulfoxide at ambient conditions were used as reference solvents, the π^*s of which are 0.0 and 1.0, respectively.

The spectral shift of the dichloro-substituted betaine dye (2,6-dichloro-4-(2,4,6-triphenyl-1-pyridinio)phenolate, Fluka, HPLC grade) was measured to obtain α parameters instead of commonly used betaine dye. To function as an effective solvatochromic indicator, a betaine dye must remain deprotonated. The p*K*a of the betaine dye (E_T(30) dye) is 8.6,[9] while that of dichloro-substituted betaine dye (E_T(33) dye) is 4.8. The latter is less basic and a more suitable indicator for this study due to the increased ionization constant of water at nearcritical conditions. The E_T(30) values of water were obtained from the established correlation between E_T(30) and E_T(33).[9] The calculation of α is based on the correlation with E_T(30) and π^*, which is deduced from the correlation of literature data of 16 compounds.[10] 4-nitroaniline (Aldrich, 99+%) and *N*,*N*-dimethyl-4-nitroaniline (Acros) were used to obtain the β based on the solvatochromic comparison method.[11]

The π^* values of water are shown at different temperatures from 25 to 275 °C in Fig. 1. The dipolarity/polarizability of water decreases continuously with increasing temperature. At 275 °C, water has a polarity comparable to that of acetic acid at rt. This trend is consistent with the decrease in the dielectric constant of water with temperature as observed by Uematsu and Franck.[2]

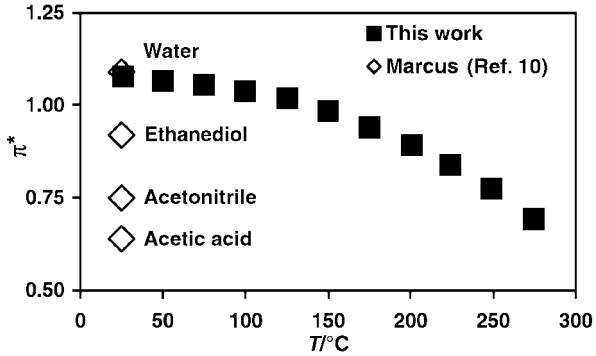

Fig. 1 π^* for nearcritical water as a function of temperature.

α indicates the hydrogen bond donating ability of a solvent. The α values of saturated liquid water as a function of temperature are shown in Fig. 2. The hydrogen bond donating ability of water decreases at elevated temperature and changes from that of ambient water to ambient methanol-like and then to ambient ethanol-like when we raise the temperature from 25 to 275 °C.

β indicates the hydrogen bond accepting ability of a solvent. The β values of water are shown in Fig. 3. Although various values of β are reported in the literature, this result at rt is consistent with that of Taft *et al.*, who attributed it to water-

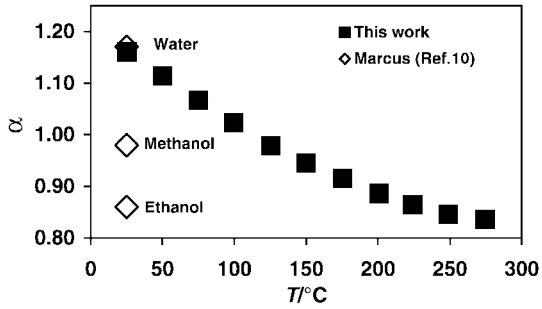

Fig. 2 α for nearcritical water as a function of temperature.

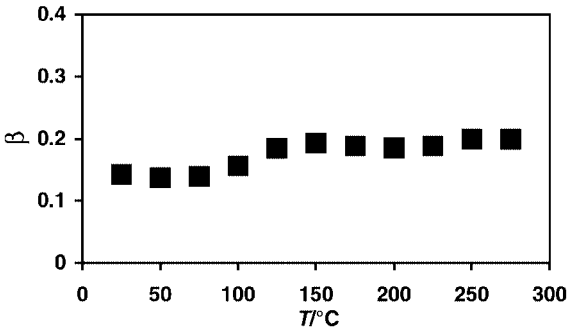

Fig. 3 β for nearcritical water as a function of temperature.

solvent clusters.[12] In contrast to the π^* and α of water, the β actually increases slightly with increasing temperature. The slight increase of β may be brought about by the breakdown of the hydrogen-bonding network of water at elevated temperature, which makes the oxygen atom of the water molecule more accessible as a hydrogen bond acceptor.[13] Bennett and Johnston measured the solvatochromism behavior of organic probes in near- and supercritical water, and observed similar large changes in polar and hydrogen-bonding interactions as the temperature was increased from ambient to 250 °C.[6]

In summary, the large dipolarity/polarizability, π^*, and hydrogen bond donating ability, α, of ambient water decrease significantly with increasing temperature. The hydrogen bond accepting ability, β, remains low and relatively constant throughout the entire temperature range studied. NCW is a benign and promising reaction medium for the replacement of organic solvents. The Kamlet–Taft parameters we report in this work provide a powerful tool for describing varied physicochemical processes in NCW.

The authors are grateful for the financial support of the National Science Foundation (CTS-9613063) and the Environmental Protection Agency (R-825325 and R-82813001-0). We would like to thank Brandon Eason, Kevin West, and David Bush for valuable suggestions and discussions.

Notes and references

1 J. S. Brown, J. P. Hallett, D. Bush, C. L. Liotta and C. A. Eckert, *J. Chem. Eng.*, 2000, **45**, 846.
2 M. Uematsu and E. U. Franck, *J. Phys. Chem.*, 1980, **9**, 1291.
3 W. L. Marshall and E. U. Franck, *J. Phys. Chem.*, 1981, **10**, 295.
4 K. Chandler, F. Deng, A. K. Dillow, C. L. Liotta and C. A. Eckert, *Ind. Eng. Chem. Res.*, 1997, **36**, 5175.
5 Y. Ikushima, K. Hatakeda, O. Sato, T. Yokoyama and M. Arai, *Angew. Chem., Int. Ed.*, 1999, **38**, 2910.
6 G. E. Bennett and K. P. Johnston, *J. Phys. Chem.*, 1994, **98**, 441.
7 W. L. Marshall and E. U. Franck, *J. Phys. Chem.*, 1981, **10**, 295.
8 J. -L Abboud, M. J. Kamlet and R. W. Taft, *Prog. Phys. Org. Chem.*, 1981, **13**, 485.
9 M. A. Kessler and O. S. Wolfbeis, *Chem. Phys. Lipids*, 1989, **50**, 51.
10 Y. Marcus, *Chem. Soc. Rev.*, 1993, 409.
11 C. Reichardt, *Chem. Rev.*, 1994, **94**, 2319.
12 R. W. Taft, M. H. Abraham, R. M. Doherty and M. J. Kamlet, *Nature*, 1985, **313**, 384.
13 Y. Ikushima, K. Hatakeda, N. Saito and M. Arai, *J. Chem. Phys.*, 1998, **108**, 5855.

Novel dendron-stabilized gold nanoparticles with high stability and narrow size distribution†

Min-Kyu Kim,[a] You-Moon Jeon,[a] Woo Sung Jeon,[a] Hee-Joon Kim,[a] Seung Gab Hong,[b] Chan Gyung Park[b] and Kimoon Kim*[a]

[a] *National Creative Research Initiative Center for Smart Supramolecules and Department of Chemistry, Division of Molecular and Life Sciences, Pohang University of Science and Technology, San 31 Hyojadong, Pohang 790-784, Republic of Korea. E-mail: kkim@postech.ac.kr*

[b] *Center for Advanced Aerospace Materials, Pohang University of Science and Technology, San 31 Hyojadong, Pohang 790-784, Republic of Korea*

Received (in Cambridge, UK) 16th January 2001, Accepted 28th February 2001
First published as an Advance Article on the web 21st March 2001

Dendron-stabilized gold nanoparticles synthesized with Fréchet-type dendrons possessing a single thiol group at the focal point have small cores (average diameters of 2.4–3.1 nm) with narrow size distribution and remarkably high stability; in particular, the nanoparticles synthesized with the second generation dendron has an almost monodisperse core (2.4 ± 0.2 nm).

The chemistry of metal nanoparticles is one of the rapidly emerging research fields because of their potential applications to sensor devices, catalysis, nanoelectronics and many other area.[1] In particular, synthesis of large quantities of monodisperse nanoparticles of diameter < 10 nm is important for many of their applications. Following the seminal work of Schiffrin and coworkers[2] on stable gold clusters coated with alkanethiolate monolayers, many monolayer-stabilized gold nanoparticles have been reported.[3] Among them, dendrimer-stabilized gold nanoparticles, in which dendrimers play dual roles as a stabilizer and a permselective organic shell, have drawn considerable attention: early examples include gold colloids coated with poly(amidoamine) (PAMAM) dendrimers containing terminal amines.[4,5] However, they are only stable in solution and in the presence of excess of free dendrimers owing to the low affinity of the terminal amine groups for gold. Subsequently, PAMAM dendrimers partially functionalized with thiol groups have been used to enhance the stability of the dendrimer-stabilized gold nanoparticles.[6] Despite the enhanced stability, however, the resulting gold nanoparticles exhibit a rather broad size distribution because the degree of functionalization of the dendrimers is difficult to control precisely. Herein we report a new strategy where dendrons with a single thiol group at the focal point are used as a stabilizer and a permselective organic shell is employed to produce Au nanoparticles. This affords highly stable Au nanoparticles with smaller cores (ave. diam., 2.4–3.1 nm) and narrower size distribution. In fact, the nanoparticles synthesized with the second generation dendron has an almost monodisperse core (2.4 ± 0.2 nm). To our knowledge, this is the first set of examples of dendron-stabilized metal nanoparticles.[7]

First, second and third generation dendron-thiols (**D1**, **D2**, and **D3**, respectively; Scheme 1)[8] were prepared from the reaction of the corresponding Fréchet-type dendron-bromides[9] with thioacetic acid, followed by reduction with $LiAlH_4$.† Dendron-stabilized gold nanoparticles (**D1–Au**, **D2–Au**, and **D3–Au**) were synthesized by the two-phase method reported by Schiffrin with some modification.[2] More specifically, a two-phase mixture containing $HAuCl_4$ in water and tetraoctylammonium bromide in toluene was stirred, the organic layer separated and treated with dendron-thiol (dendron-thiol : Au = 2 : 1) and finally allowed to stir vigorously with an aqueous solution of $NaBH_4$ which afforded the crude product. Purification of the crude products by several cycles of precipitation–filtration–dissolution from toluene–ethanol solution yields **D1–Au** and **D2–Au** as black powders, and **D3–Au** as a black waxy powder. All of the nanoparticles are soluble in common organic solvents such as toluene, acetone, dichloromethane, chloroform or THF. They are remarkably stable both in solution, as well as in the solid state. Little decomposition or aggregation occurs even after several months in solution, as judged by their solubilities and UV–VIS spectra. Furthermore, these nanoparticles remain unchanged after standing overnight at elevated temperatures (at 50 °C in solution and at 160 °C in the solid state). The origin of the remarkable stabilities of these dendron-stabilized Au nanoparticles remains to be established.

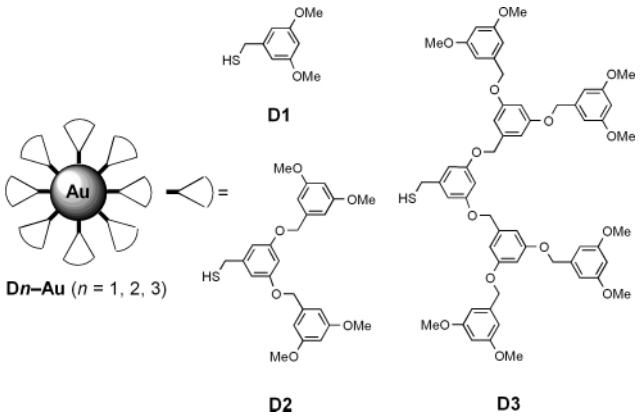

Scheme 1 Schematic illustration of dendron-stabilized Au nanoparticles.

The core size and size distribution of the dendron-stabilized Au nanoparticles were examined by high resolution transmission electron microscopy (HR-TEM) (Fig. 1). In general, the present Au nanoparticles have a narrower size distribution than most of the previously known alkanethiolate-,[3a] arylthiolate-,[3b] or dendrimer-stabilized gold nanoparticles.[4–6] For example, **D1–Au**, having an average core size of 2.8 ± 0.3 nm, shows a narrower size distribution compared with the gold nanoparticles prepared with arylthiols of similar sizes.[3b] Most remarkably, **D2–Au** is nearly monodisperse with an average core size of 2.4 ± 0.2 nm. The core size and dispersity are not significantly affected by use of different molar ratios of **D2** : $HAuCl_4$ such as 0.5 and 6. Such monodispersity is seldom observed in unfractionated metal nanoparticles.[10] On the other hand, **D3–Au** has a larger and less narrow-disperse core (3.1 ± 0.6 nm) compared with **D1–Au** and **D2–Au**. The larger core size of **D3–Au** over those of **D1–Au** and **D2–Au** is in contrast to the earlier observation that the cores of dendrimer-stabilized Au nanoparticles decrease in size and dispersity with increasing dendrimer generation.[4,5] At present, we do not understand why

† Electronic supplementary information (ESI) available: synthetic procedures and characterization data for dendron-thiols (**D1**–**D3**) and their gold nanoparticles. See http://www.rsc.org/suppdata/cc/b1/b100575h/

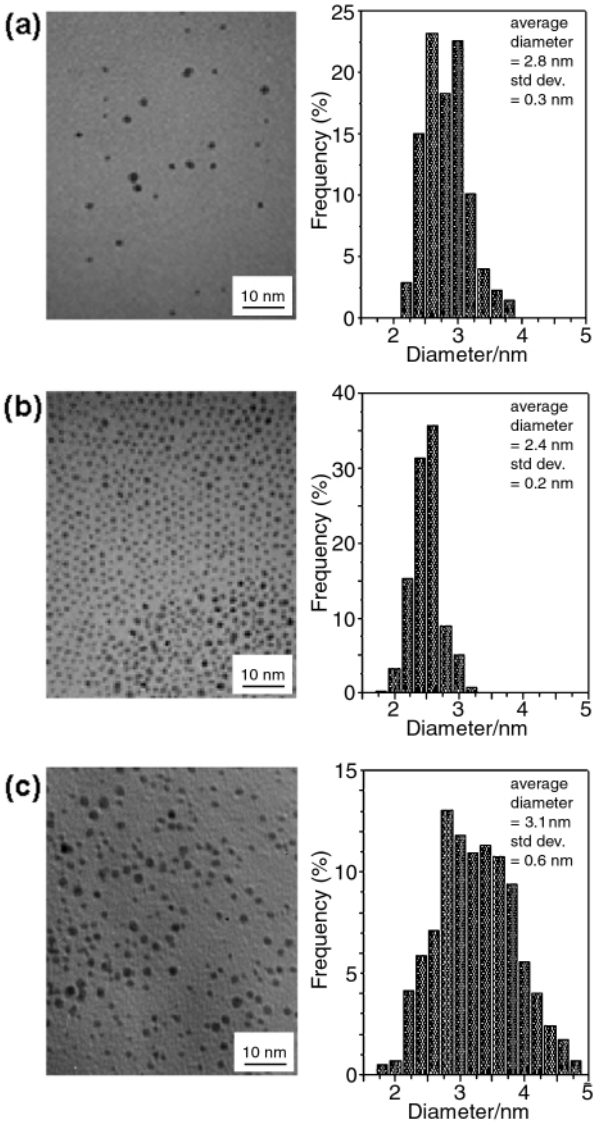

Fig. 1 TEM micrographs and histograms of size distribution for the dendron-stabilized Au nanoparticles: (a) **D1–Au**, (b) **D2–Au** and (c) **D3–Au**. The average core sizes and distribution were determined by counting 345 (**D1–Au**), 598 (**D2–Au**) and 819 (**D3–Au**) particles.

there is apparently no correlation between dendron generation and particle size. However, we suspect that the second generation dendron **D2** may have a 'magic' size to protect Au particles with the particular size leading to monodispersity. We are currently investigating in depth the effect of dendron size on the size and dispersity of Au nanoparticles. As seen in Fig. 2, **D1–Au** and **D3–Au** exhibit a typical surface plasmon (sp) band at 530–540 nm in their UV–Vis spectra, whereas **D2–Au** displays a very weak sp band, which is consistent with its smaller particle size and narrower distribution.[11] Further characterization of the dendron-stabilized Au nanoparticles is in progress.

In summary, we present the first dendron-stabilized Au nanoparticles synthesized with Fréchet-type dendrons possessing a single thiol group at the focal point, which have remarkably high stability and narrow size distribution. Particularly, the results on **D2–Au** suggest that this method may

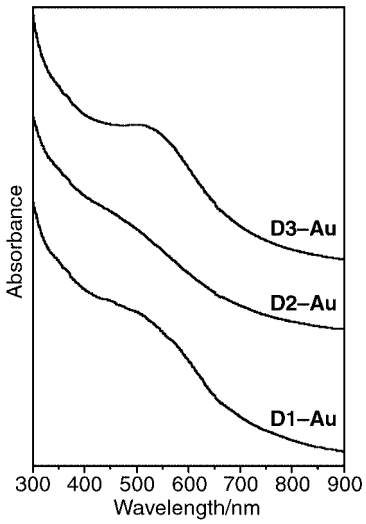

Fig. 2 UV–Vis spectra of the dendron-stabilized Au nanoparticles in THF.

provide a convenient way to synthesize stable, monodisperse Au nanoparticles with small cores. Furthermore, this work should be easily expanded to the synthesis of other dendron-stabilized metal nanoparticles which may find useful applications in many areas including chemical sensing and catalysis.

We gratefully acknowledge Creative Research Initiative Program of the Korean Ministry of Science and Technology for support of this work, Brain Korea 21 Program of the Korean Ministry of Education for graduate studentships to M.-K. K., and Professor P. K. Bharadwaj for reading the manuscript.

Notes and references

1 A. C. Templeton, W. P. Wuelfing and R. W. Murray, *Acc. Chem. Res.*, 2000, **33**, 27; A. N. Shipway, E. Katz and I. Willner, *ChemPhysChem.*, 2000, **1**, 18.
2 M. Brust, M. Walker, D. Bethell, D. J. Schiffrin and R. Whyman, *J. Chem. Soc., Chem. Commun.*, 1994, 801.
3 (*a*) M. J. Hostetler, J. E. Wingate, C.-J. Zhong, J. E. Harris, R. W. Vachet, M. R. Clark, J. D. Londono, S. J. Green, J. J. Stokes, G. D. Wignall, G. L. Glish, M. D. Porter, N. D. Evans and R. W. Murray, *Langmuir*, 1998, **14**, 17; (*b*) S. Chen and R. W. Murray, *Langmuir*, 1999, **15**, 682; (*c*) T. G. Schaaff, G. Knight, M. N. Shafigullin, R. F. Borkman and R. L. Whetten, *J. Phys. Chem. B*, 1998, **102**, 10 643; (*d*) S. Chen and K. Kimura, *Langmuir*, 1999, **15**, 1075; (*e*) L. O. Brown and J. E. Hutchison, *J. Am. Chem. Soc.*, 1997, **119**, 12 384.
4 K. Esumi, A. Suzuki, N. Aihara, K. Usui and K. Torigoe, *Langmuir*, 1998, **14**, 3157; K. Esumi, A. Suzuki, A. Yamahira and K. Torigoe, *Langmuir*, 2000, **16**, 2604.
5 M. E. Garcia, L. A. Baker and R. M. Crooks, *Anal. Chem.*, 1999, **71**, 256.
6 V. Chechik and R. M. Crooks, *Langmuir*, 1999, **15**, 6364.
7 After submission of this paper, a report on Au nanoparticles stabilized with 4-pyridone-based dendrons was published: R. Wang, J. Yang, Z. Zheng, M. D. Carducci, J. Jiao and S. Seraphin, *Angew. Chem., Int. Ed.*, 2001, **40**, 549.
8 Y. Takaguchi, S. Suzuki, T. Mori, J. Motoyoshiya and H. Aoyama, *Bull. Chem. Soc. Jpn.*, 2000, **73**, 1857.
9 C. J. Hawker and J. M. J. Fréchet, *J. Am. Chem. Soc.*, 1990, **112**, 7638; R. Sadamoto, N. Tomioka and T. Aida, *J. Am. Chem. Soc.*, 1996, **118**, 3978.
10 Dendrimer-encapsulated Pd and Pt nanoparticles were reported to be almost monodisperse (1.4 ± 0.2 nm): M. Zhao and R. M. Crooks, *Angew. Chem., Int. Ed.*, 1999, **38**, 364.
11 M. M. Alvarez, J. T. Khoury, T. G. Schaaff, M. N. Shafigullin, I. Vezmar and R. L. Whetten, *J. Phys. Chem. B*, 1997, **101**, 3706.

ChemComm

Pd-catalyzed synthesis of arylacetic acid derivatives from boronic acids†

Lukas J. Gooßen*

Max-Planck-Institut für Kohlenforschung, Kaiser-Wilhelm-Platz 1, D-45470 Mülheim an der Ruhr, Germany. E-mail: goossen@mpi-muelheim.mpg.de; Fax: +49-208-306-2985; Tel: +49-208-306-2392

Received (in Cambridge, UK) 23rd January 2001, Accepted 22nd February 2001
First published as an Advance Article on the web 21st March 2001

A palladium(0)-catalyzed cross-coupling reaction between arylboronic acids or esters and α-bromoacetic acid derivatives is described which allows the synthesis of various functionalized arylacetic acid derivatives under mild conditions.

Methylenecarboxy groups are key functionalities in many biologically active compounds such as the antiinflammatory and analgesic drugs Indomethacin or Aclofenac.[1] A mild and efficient procedure for the introduction of the methylenecarboxy group into functionalized molecules is thus of great interest. Traditional syntheses involve multistep procedures that are often incompatible with sensitive functionalities.[2] Alternatively, transition metal-catalyzed cross-coupling reactions between aryl halides and Reformatsky reagents,[3] tin,[4] copper,[5] and other enolates,[6] or ketene acetals have been employed.[7] Some electrochemical syntheses have also been reported.[8] However, especially for applications in combinatorial chemistry, most of these syntheses are quite inconvenient due to the instability or toxicity of the reagents or the required bases.

We imagined that the inverse approach of combining an arylmetal species with an α-halocarbonyl derivative might be an interesting alternative, especially for substrates containing sensitive functions such as enolizable keto-groups. Due to their easy handling and long shelf life, arylboronic acid derivatives would be the starting materials of choice, particularly for small-scale reactions. Arylboronic esters have recently become widely accessible from aryl halides by *in situ* coupling reactions that tolerate many functional groups.[9,10] In order to permit an application of the outlined coupling reaction in drug discovery, it is of utmost importance to overcome the necessity of using highly toxic reagents such as thallium carbonate.[11] Initial studies were carried out with phenylboronic acid and ethyl bromoacetate (Scheme 1).

Under standard Suzuki conditions using tetrakis(triphenylphosphine)palladium and potassium carbonate in DMF,[12] only trace amounts of the expected product **3** were detected. Instead, redox reactions between the arylboronic acid and ethyl bromoacetate predominated, leading to large amounts of biphenyl **4** and benzene **5**. This is not surprising since similar systems have purposely been used in the synthesis of symmetrical biaryls.[13] We have now discovered that the selectivity of the reaction can be completely inverted when bulky, moderately electron-donating phosphines are employed as ligands on palladium. Selected results are shown in Table 1.

Changing the ligand from triphenylphosphine to tri(*o*-tolyl)phosphine significantly improves the selectivity towards the desired coupling product and allows smooth conversions even at room temperature. In order to determine the origin of this effect, we varied both the steric and the electronic properties of the ligand (entries 1–9). Tri(*m*-tolyl)phosphine gives only poor selectivities, which led us to conclude that the steric bulk of the tri(*o*-tolyl)phosphine is responsible for the good selectivities. Additionally, the lower selectivities observed for tri(*o*-ethylphenyl)-, tri(*m*-xylyl)-, tri(mesityl)-, and di-*tert*-butylbiphenyl-2-ylphosphine indicate that the ligand must not be too electron-rich. These combined requirements are best fulfilled with tri(1-naphthyl)phosphine, and indeed, this ligand leads to enhanced product selectivity. Chelating phosphines such as (±)-BINAP totally inhibited the reaction, suggesting that the catalytic cycle proceeds through mono-ligated palladium complexes.

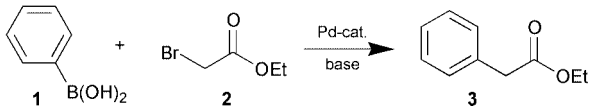

Scheme 1 Coupling of benzeneboronic acid and ethyl bromoacetate.

† Dedicated to Professor K. B. Sharpless on the occasion of his 60th birthday.

Both palladium(II) acetate and tris(dibenzylideneacetone) dipalladium(0) can be used as palladium(0) precursors and show no significant differences in activity (entries 3, 14). However, the amount of biaryl formed is slightly higher when palladium(II) acetate is used. This suggests that the boronic acid initially acts as a reducing agent for the palladium(II). Since a slight excess of boronic acid is usually added, this reaction has no influence on the isolated yields.

The choice of the base also affects the product selectivity (entries 3, 10, 11 and 8, 15). Both K_2CO_3 and K_3PO_4 are equally suitable as bases. However, at room temperature, shorter reaction times were often observed with potassium phosphate. KF was inferior for most substrates since larger amounts of the reduction products were formed. Only in the case of some electron-poor boronic acids did KF become the base of choice (see also Table 2). Other bases, for instance triethylamine, were significantly less active. Best results were obtained with excess amounts of base.

THF proved to be by far the most effective solvent. In acetonitrile, the reaction was much slower and the use of more polar solvents, *e.g.* DMF, drastically decreased the amount of isolable products. This could indicate that hydrolysis of the ester occurs. In THF, however, the presence of small quantities of

Table 1 Effects of the reaction conditions on the product distribution

	Ligand	Conv. (%)	**3**[a] (%)	**4**[a] (%)	**5**[a] (%)
1	PPh_3	95	34	38	< 5
2	P(*m*-Tol)$_3$	75	3	23	75
3	P(*o*-Tol)$_3$	100	86	12	< 1
4	P(*o*-EtPh)$_3$	100	51	19	10
5	P(*m*-Xyl)$_3$	100	80	15	5
6	P(Mes)$_3$	80	80	15	5
7	P(*t*-Bu)$_2$Biph	100	67	31	2
8	P(Nap)$_3$	100	88	7	5
9	BINAP	< 5	—	< 1	< 1
10[b]	P(*o*-Tol)$_3$	100	78	15	7
11[c]	P(*o*-Tol)$_3$	100	36	20	28
12[d]	P(*o*-Tol)$_3$	90	14	6	< 1
13[e]	P(*o*-Tol)$_{33}$CN	82	35	6	< 1
14[f]	P(*o*-Tol)$_3$	100	89	10	< 1
15[g]	P(Nap)$_3$	100	91	7	2

Conditions: 3 mol% $Pd(OAc)_2$, 9 mol% ligand, 5 equiv. base, 2 equiv. H_2O, THF, 20 °C. [a] Selectivities determined by GC. [b] KF as base. [c] NEt_3 as base. [d] In DMF. [e] In acetonitrile. [f] $(dba)_3Pd_2$ instead of $Pd(OAc)_2$. [g] K_3PO_4 as base.

DOI: 10.1039/b100834j

Table 2 Pd-catalyzed synthesis of arylacetic acid derivatives

Comp.	Ar	X	Method A Yield (%)[a]	Method B Yield (%)[a]
3a	Phenyl	OEt	85 (90)	87 (91)
3b	*o*-Tolyl	OEt	90 (90)	75 (79)
3c	1-Naphthyl	OEt	80 (84)	68 (70)
3d	*p*-MeO-Phenyl	OEt	84 (85)	76 (79)
3e	*p*-Acetylphenyl	OEt	79 (80[c]	60 (65)
3f	*p*-Tolyl	OEt	90 (93)	
3g	*m*-Chlorophenyl	OEt	70 (75)[b]	
3h	*p*-Formylphenyl	OEt	67 (74)[c]	
3i	*m*-Nitrophenyl	OEt	40 (40)[b]	
3k	*m*-AcNH-Phenyl	OEt	63 (70)	
3l	2-Thienyl	OEt	33 (33)[b]	
3m	2-Fluorophenyl	OEt	31 (42)[c]	
6	Phenyl	$N(C_5H_{10})$	81 (89)	
7	Phenyl	$O(C_4H_8)Br$	72 (90)	68 (72)

Conditions: (A) 1.2 equiv. arylboronic acid, 3 mol% $Pd(OAc)_2$, 9 mol% $P(Nap)_3$, 5 equiv. K_3PO_4, 2 equiv. H_2O, 20 °C, THF; (B) 1.2 equiv. pinacol boronate, 3 mol% $Pd(OAc)_2$, 9 mol% $P(Nap)_3$, 5 equiv. K_3PO_4, 2 equiv. H_2O, 20 °C, THF. [a] Isolated yields (GC-determined yields in parentheses). [b] KF instead of K_3PO_4. [c] K_2CO_3 instead of K_3PO_4

water had no adverse effect on the reaction outcome so that special drying of the solvent and the reagents is not required.

The generality and selectivity of the reaction were investigated using a number of arylboronic acids **1a**–**m** in combination with several alkyl halides (Scheme 2).

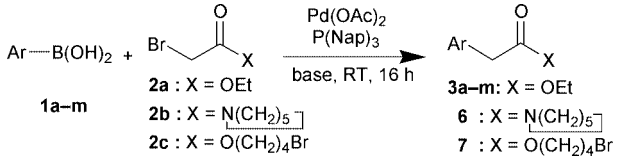

Scheme 2 Pd-catalyzed synthesis of arylacetic acid derivatives.

As can be seen in Table 2 (Method A), most substrates give good yields. Electron-poor and electron-rich compounds are equally suitable for the transformation. Even sterically hindered compounds (*o*-tolylboronic acid) or substrates that are sometimes problematic in palladium-catalyzed reactions (nitro- or heteroarenes) were successfully employed. Moreover, products containing enolizable keto-groups are readily formed without any signs of side products arising from undesired aldol condensations.

Besides ethyl bromoacetate (**2a**), other bromoacetates (**2c**) or -amides (**2b**) can be used. The high selectivity of the transformation is demonstrated by the formation of compound **7**‡ (Table 2): the arylation of 4-bromobutyl bromoacetate (**2c**) takes place exclusively α to the carbonyl group even though a primary alkyl bromide functionality is present.

Many functionalized pinacol boronates§ (**10**) are conveniently accessible from aryl halides (**8**) and bispinacol diboron[9] or pinacol borane (**9**).[10] We thus considered it to be important to extend our reaction to this substrate class (Scheme 3).

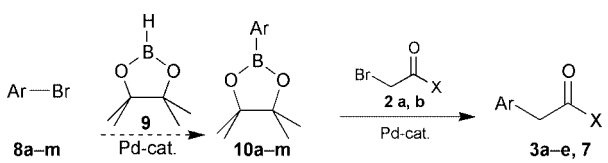

Scheme 3

We were pleased to find that the best conditions for the conversion of the boronic acids turned out also to be optimum conditions for pinacol boronate and that the reaction usually gives similar yields for both starting materials (Table 2, 'method B').

In summary, the disclosed palladium-catalyzed cross-coupling reaction between arylboronic acids or esters and α-bromoacetic esters or α-bromoacetic amides represents a mild and general approach to arylacetic acid derivatives. The simple reaction protocol which involves only air-stable chemicals and does not require absolutely dry solvents makes this reaction a valuable alternative to the existing protocols, especially for applications in combinatorial chemistry and drug discovery.

I thank M. Rössig and A. Söthe for technical assistance and Professor Dr M. T. Reetz for generous support and constant encouragement.

Notes and references

‡ *Synthesis of 4-bromobutyl phenylacetate* (**7**): A 100 mL flask was charged with palladium acetate (67.3 mg, 0.30 mmol), tri-1-naphthylphosphine (371 mg, 0.90 mmol), 4-bromobutyl bromoacetate (**2b**) (2.74 g, 10.0 mmol) and an excess of potassium phosphate (10.61 g, 50.0 mmol). The reaction vessel was purged with argon, a solution of benzeneboronic acid (1.46 g, 12.0 mmol) in THF (40 ml) was added and the reaction mixture was stirred at 20 °C overnight. The reaction slurry was then poured into water (300 mL) and extracted 3× with 100 mL portions of dichloromethane. The combined organic layers were dried over $MgSO_4$, filtered, and the volatiles were removed *in vacuo*. The residue was purified by fractional distillation. A colorless oil (2.41 g, 89%) boiling at 91 °C/0.01 mbar was collected and identified as the desired product. ^{1}H NMR (300 MHz, $CDCl_3$, 25 °C, TMS): δ = 7.33–7.26 (m, 5H), 4.12 (t, ^3J (H,H) = 6 Hz, 2H), 3.62 (s, 2H), 3.38 (t, ^3J (H,H) = 6 Hz, 2H), 1.87 (m, 2H), 1.79 (m, 2H) ppm; ^{13}C NMR (75 MHz, $CDCl_3$, 25°C, TMS): δ = 171.5, 134.0, 129.2, 128.6, 127.1, 63.8, 41.4, 32.9, 29.2, 27.2 ppm; MS (70 eV): *m/z* (%): 270(6) [M^+], 191(4), 179(4), 136(23), 91(100); HRMS: calcd. for $C_{12}H_{15}BrO_2$ [M^+]: 270.02555; found: 270.02546; anal. calcd. for $C_{12}H_{15}BrO_2$ (271.16): C, 53.16; H, 5.58; N, 0.0; found: C, 52.96; H, 5.65; N, 0.0. The reactions in Table 1 and Table 2 were performed at least twice on 1 mmol scale using 0.05 mL tetradecane as an internal GC standard. The products were isolated by column chromatography (SiO_2, hexane–ethyl acetate 10 : 1) and characterized by means of ^{1}H and ^{13}C NMR as well as by GC-MS.

§ The IUPAC name for pinacol boronates and pinacol borane is 2,3-boranediyldioxy-2,3-dimethylbutane.

1 T. Y. Shen, *Angew. Chem.*, 1972, **84**, 512; *Angew. Chem., Int. Ed. Engl.*, 1972, **11**, 460.

2 For common methods such as the hydrolysis of benzylnitriles, the carbonylation of benzyl halides, or the Willgerodt reaction of acetophenones see: J. March, *Advanced Organic Chemistry*, Wiley, New York, 4th Edn., 1992, pp. 1281–1282; further methods: (*a*) T. Zincke, *Chem. Ber.*, 1869, **2**, 738; (*b*) R. Quelet and J. Gavarret, *Bull. Soc. Chim. Fr.*, 1950, 1075; (*c*) J. B. Woell and H. Alper, *Tetrahedron Lett.*, 1984, **25**, 3791; (*d*) Prileshajew, *Zh. Russ. Fiz.-Chim. O-va*, 1910, **42**, 1395.

3 (*a*) W. W. Leake and R. Levine, *J. Am. Chem. Soc.*, 1959, **81**, 1627; (*b*) J. F. Fauvarque and A. Jutand, *J. Organomet. Chem.*, 1979, **177**, 273; (*c*) F. Orsini and F. Pelizzoni, *Synth. Comm.*, 1987, **17**, 1389.

4 M. Kosugi, Y. Negishi, M. Kameyama and T. Migita, *Bull. Chem. Soc. Jpn.*, 1985, **58**, 3383.

5 K. Okuro, M. Furuune, M. Miura and M. Nomura, *J. Org. Chem.*, 1993, **58**, 7606.

6 (*a*) M. van Leeuwen and A. McKillop, *J. Chem. Soc., Perkin Trans. 1*, 1993, 2433; (*b*) M. F. Semmelhack, B. P. Chong, R. D. Stauffer, T. D. Rogerson, A. Chong and L. D. Jones, *J. Am. Chem. Soc.*, 1975, **97**, 2507; (*c*) S. G. Lias and P. Ausloos, *J. Am. Chem. Soc.*, 1977, **99**, 4833; (*d*) M. Kawatsura and J. F. Hartwig, *J. Am. Chem. Soc.*, 1999, **121**, 1473.

7 (*a*) C. Carfagna, A. Musco and C. Sallese, *J. Org. Chem.*, 1991, **56**, 261; (*b*) T. Sakamoto, Y. Kondo, K. Masumoto and H. Yamanaka, *Heterocycles*, 1993, **36**, 2509; (*c*) F. Agnelli and G. A. Sulikowski, *Tetrahedron Lett.*, 1998, **39**, 8807.

8 (*a*) J. Chaussard, J.-C. Folest, J.-Y. Nédélec, J. Périchon, S. Sibille and M. Troupel, *Synthesis*, 1990, 369; (*b*) M. Durandetti, J.-Y. Nédélec and J. Périchon, *J. Org. Chem.*, 1996, **61**, 1748; (*c*) J.-C. Folest, J. Périchon, J. F. Fauvarque and A. Jutand, *J. Organomet. Chem.*, 1988, **342**, 259.

9 (*a*) T. Ishiyama, M. Murata and N. Miyaura, *J. Org. Chem.*, 1995, **60**, 7508; (*b*) T. Ishiyama, Y. Itoh, T. Kitano and N. Miyaura, *Tetrahedron Lett.*, 1997, **38**, 3447.

10 (*a*) M. Murata, T. Oyama, S. Watanabe and Y. Masuda, *J. Org. Chem.*, 1997, **62**, 6458; (*b*) M. Murata, T. Oyama, S. Watanabe and Y. Masuda, *J .Org. Chem*, 2000, **65**, 164.

11 M. Sato, N. Miyaura and A. Suzuki, *Chem. Lett.*, 1989, 1405.

12 N. Miyaura and A. Suzuki, *Chem. Rev.*, 1995, **95**, 2457.

13 (*a*) S. Yamaguchi, S. Ohno and K. Tamao, *Synlett*, 1997, **10**, 1199; (*b*) M. Moreno-Manas, M. Perez and R. Pleixats, *J. Org. Chem.*, 1996, **61**, 2346.

ChemComm

Enantioselective total synthesis of the phytotoxic lactone herbarumin I

Alois Fürstner* and Karin Radkowski

Max-Planck-Institut für Kohlenforschung, D-45470 Mülheim/Ruhr, Germany.
E-mail: fuerstner@mpi-muelheim.mpg.de; Fax: +49 208 306 2994; Tel: +49 208 306 2342

Received (in Cambridge, UK) 5th February 2001, Accepted 5th March 2001
First published as an Advance Article on the web 21st March 2001

A concise total synthesis of the potent herbicide herbarumin I (1) is presented based on an (*E*)-selective RCM reaction forging the 10-membered ring of this macrolide.

Bioassay guided fractionation of a culture broth of the fungus *Phoma herbarum* recently led to the discovery of two novel nonenolides. Named herbarumin I (**1**) and herbarumin II (**2**), these lactones were found to exhibit significant phytotoxic

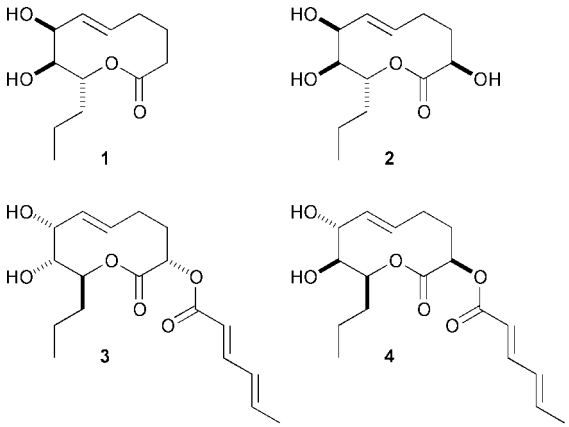

effects in an assay monitoring the radicle elongation of *Amaranthus hypochondriacus* seedlings, with IC_{50} values being as low as 5.43×10^{-5} for compound **1**.[1] This level of activity together with the fact that closely related compounds such as pinolidoxin (**3**)[2] and lethaloxin (**4**)[3] also exert significant phytotoxicity renders this class of compounds promising new lead structures in the search for novel herbicidal agents. Described below is the first total synthesis of a member of this family of natural products.

Our approach to herbarumin I (**1**) as the most active compound of this series is guided by the perception that the stereochemistry of its three contiguous chiral centers is matched by the pattern displayed by D-ribose. Therefore, the D-ribonolactone acetonide derivative **5** was chosen as a well accessible starting material which is converted on a multigram scale into tosylate **6** (Scheme 1).[4] Subsequent treatment with NaOMe in THF leads to product **7** *via* transesterification followed by spontaneous closure of the epoxide ring once the alkoxide at O-4 is liberated.[5] This compound is then exposed to the cuprate reagent formed from EtMgBr and CuBr·Me_2S in THF,[6] thus providing lactone **8** in 60% yield.† DIBAL-H reduction followed by reaction of the resulting lactol **9** with methylenetriphenylphosphorane in the presence of catalytic amounts of quinuclidine[7] delivers alcohol **10** in good yield, which is esterified with hex-5-enoic acid in the presence of DCC and DMAP to afford diene **11**. This sets the stage for the crucial macrocyclization reaction *via* ring closing olefin metathesis (RCM).

During the last decade, olefin metathesis has evolved into a versatile and practical tool for advanced organic chemistry.[8] Despite the impressive number of applications of this reaction to the synthesis of structurally diverse carbo- and heterocycles, it must be kept in mind that the formation of medium sized rings by this method still poses considerable challenges.[9,10] Because of the inherent ring strain, eight- to eleven-membered cycloalkenes are particularly prone to the reverse process, *i.e.* to ring opening metathesis (ROM) or ring opening metathesis polymerization (ROMP).

It has been shown, however, that this problem can be circumvented in many cases by incorporating suitable conformational control elements forcing the substrate to adopt a suitable conformation for ring closure. This facilitates RCM and stabilizes the product formed against the competing ROMP

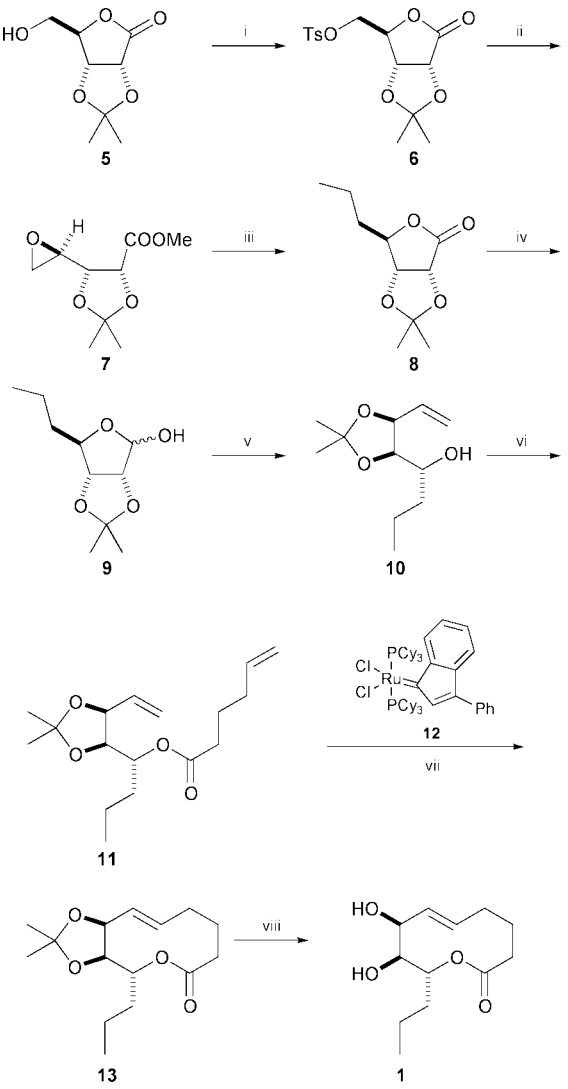

Scheme 1 *Reagents and conditions*: i, tosyl chloride, pyridine, −20 °C, 16 h, 77%; ii, NaOMe, THF, 0 °C → rt, 16 h, 62%; iii, EtMgBr (3 eq.), CuBr·Me_2S (3 eq.), THF, −78 °C → rt, 16 h, 60%; iv, DIBAL-H, CH_2Cl_2, −78 °C, 2 h, 97%; v, $Ph_3P{=}CH_2$ (2 eq.), quinuclidine (0.2 eq.), THF, reflux, 30 min, 77%; vi, hex-5-enoic acid, DCC, DMAP, CH_2Cl_2, rt, 4 d, 84%; vii, catalyst **12** (10 mol%), CH_2Cl_2, reflux, 7 h, 69%; viii, aq. HCl (1 M), THF, 50 °C, 16 h, 90%.

DOI: 10.1039/b101148k

pathway. The isopropylidene acetal of compound **11** may act as such a temporary constraint which adequately shapes this particular diene and simultaneously confers bias upon the stereochemistry of the newly formed double bond.[11]

We were pleased to find that this is indeed the case. Treatment of compound **11** with catalytic amounts of the ruthenium indenylidene complex **12**[12] in refluxing CH_2Cl_2 affords the desired ten-membered lactone **13** as the only product in 69% isolated yield. Although applications of RCM to the synthesis of medium-sized and macrocyclic cycloalkenes are frequently plagued by the formation of *E*/*Z*-mixtures,[8,13] compound **13** was obtained as a single diastereoisomer which was assigned the *E*-configuration based on detailed NMR investigations.‡ This particular example also nicely features the excellent application profile of the ruthenium complex **12** which is equipotent or even superior to the more popular Grubbs carbene $(Cy_3P)_2(Cl)_2Ru{=}CHPh$[14] yet easier to make from stable and commercially available precursors.[12]

Final cleavage of the acetal group with dilute aq. HCl occurs uneventfully and provides herbarumin I **1** in 90% yield as a low melting solid. Although the $[\alpha]_D$ value of the synthetic sample deviates from the reported one to some extent,§ there is no doubt as to the constitution and configuration of this compound since the high resolution NMR spectra (Bruker DMX 600) as well as the IR and MS data are in excellent agreement with the proposed structure and perfectly match those reported in the literature.§

In summary, a concise total synthesis of the potent phytopathogenic macrolide herbarumin I is presented. The approach using D-ribonolactone as a convenient source of chirality is based on a highly efficient and diastereoselective RCM reaction for the formation of the ten-membered ring of the target, which is delivered in enantiomerically pure form in only 8 steps starting from **5** in ~11% overall yield. Extensions of this methodology to other members of this series of herbicidal agents are underway and will be disclosed in the near future.

Generous financial support by the Deutsche Forschungsgemeinschaft (Leibniz award) and the Fonds der Chemischen Industrie is gratefully acknowledged. We thank Dr R. Mynott and C. Wirtz for their help with the interpretation of the NMR spectra of compound **13**.

Notes and references

† Competitive attack of bromide ions on epoxide **7** could not be fully supressed; small amounts of 5-bromo-2,3-isopropylidene-D-ribono-1,4-lactone thus formed are separated by flash chromatography. In this context it should also be noted that all attempts to prepare compound **8** more directly by reaction of tosylate **6** with various ethyl donors (Et_2CuLi or EtMgBr + $CuBr{\cdot}Me_2S$) turned out to be low yielding and could not compete with the route depicted in Scheme 1.

‡ NMR investigations at this stage are hampered by the fact that compound **13** exists in two slowly interconverting conformers in solution. The assignment of the stereochemistry of the double bond, however, is unambiguous and is ultimately corroborated by the successful completion of the synthesis, providing synthetic **1** which exhibits a coupling constant of ^3J = 15.8 Hz for the vicinal olefinic protons. Details on the structural assignment of **13** will be reported in a forthcoming full paper.

§ Synthetic **1**: $[\alpha]_D^{20}$ +10.8° (*c* 0.51, EtOH); ref. **1**: $[\alpha]_D$ +28.0° (*c* 0.1, EtOH). Spectroscopic data of synthetic **1**: IR: 3450, 3033, 2960, 2929, 2872, 1716, 1631, 1203, 1058, 982 cm^{-1}; ^1H NMR (600 MHz, $CDCl_3$) δ 5.58 (ddd, 1H, *J* = 15.8, 1.7, 1.0 Hz, H-6), 5.49 (dddd, 1H, *J* = 15.8, 10.3, 4.0, 2.3 Hz, H-5), 4.92 (td, 1H, *J* = 9.6, 2.6 Hz, H-9), 4.40 (quint., 1H, *J* = 2.3 Hz, H-7), 3.48 (dd, 1H, *J* = 9.8, 2.3 Hz, H-8), 2.39 (br s, 1H, −OH), 2.38 (br d, 1H, *J* = 12.3 Hz, H-4a), 2.30 (ddd, 1H, *J* = 14.0, 5.8, 2.4 Hz, H-2a), 2.14 (br s, 1H, −OH), 1.98 (ddd, 1H, *J* = 14.0, 12.9, 2.0 Hz, H-2b), 1.92 (m, 1H, H-4b), 1.87 (m, 1H, H-3a), 1.86 (m, 1H, H-10a), 1.71 (m, 1H, H-3b), 1.54 (ddt, 1H, *J* = 14.4, 9.7, 4.8 Hz, H-10b), 1.35 (m, 1H, H-11a), 1.27 (m, 1H, H-11b), 0.89 (t, 3H, *J* = 7.3 Hz, −Me); ^{13}C NMR (75 MHz, $CDCl_3$) δ 176.3, 130.7, 124.7, 73.6, 73.3, 70.1, 34.4, 33.7, 33.3, 24.6, 17.9, 13.8; MS (EI): *m*/*z* (rel. intensity): 228 (3, $[M^+]$), 200 (5), 144 (10), 143 (40), 126 (16), 125 (100), 97 (33), 95 (12), 86 (29), 84 (11), 83 (24), 81 (12), 79 (19), 70 (19), 69 (14), 57 (52), 55 (28); MS (ESI): 251 ($[M + Na]^+$), 479 ($[2M + Na]^+$).

1 J. F. Rivero-Cruz, G. Garcia-Aguirre, C. M. Cerda-Garcia-Rojas and R. Mata, *Tetrahedron*, 2000, **56**, 5337.
2 L. de Napoli, A. Messere, D. Palomba, V. Piccialli, A. Evidente and G. Piccialli, *J. Org. Chem.*, 2000, **65**, 3432. Note that the stereochemistry at C-2 of compound **3** has not yet been unequivocally determined. According to the conclusions reached in ref. 1, however, this center is likely (*S*)-configurated as shown in the inserted structure.
3 A. Arnone, G. Assante, M. Montorsi, G. Nasini and E. Ragg, *Gazz. Chim. Ital.*, 1993, **123**, 71. Note that only the relative stereochemistry of compound **4** has been established so far.
4 L. Hough, J. K. N. Jones and D. L. Mitchell, *Can. J. Chem.*, 1958, **36**, 1720.
5 (*a*) R. W. Hoffmann and W. Ladner, *Chem. Ber.*, 1983, **116**, 1631; (*b*) See also: R. M. Ortuno, R. Merce and J. Font, *Tetrahedron*, 1987, **43**, 4497.
6 H. Takahata, Y. Uchida and T. Momose, *J. Org. Chem.*, 1995, **60**, 5628.
7 W. V. Dahlhoff, *Liebigs Ann. Chem.*, 1992, 109.
8 (*a*) A. Fürstner, *Angew. Chem.*, 2000, **112**, 3140; *Angew. Chem., Int. Ed.*, 2000, **39**, 3012; (*b*) R. H. Grubbs and S. Chang, *Tetrahedron*, 1998, **54**, 4413; (*c*) M. Schuster and S. Blechert, *Angew. Chem.*, 1997, **109**, 2124; *Angew. Chem., Int. Ed. Engl.*, 1997, **36**, 2036; (*d*) R. Roy and S. K. Das, *Chem. Commun.*, 2000, 519; (*e*) A. Fürstner, *Top. Catal.*, 1997, **4**, 285; (*f*) S. K. Armstrong, *J. Chem. Soc., Perkin Trans. 1*, 1998, 371.
9 M. E. Maier, *Angew. Chem.*, 2000, **112**, 2153; *Angew. Chem., Int. Ed.*, 2000, **39**, 2073.
10 Syntheses of ten-membered rings by RCM are still scarce; for leading references see: (*a*) A. Fürstner and T. Müller, *Synlett.*, 1997, 1010; (*b*) S. Chang and R. H. Grubbs, *Tetrahedron Lett.*, 1997, **38**, 4757; (*c*) K. Gerlach, M. Quitschalle and M. Kalesse, *Synlett*, 1998, 1108; (*d*) B. E. Fink, P. R. Kym and J. A. Katzenellenbogen, *J. Am. Chem. Soc.*, 1998, **120**, 4334; (*e*) T. Oishi, Y. Nagumo and M. Hirama, *Chem. Commun.*, 1998, 1041; (*f*) M. Quitschalle and M. Kalesse, *Tetrahedron Lett.*, 1999, **40**, 7765; (*g*) M. Delgado and J. D. Martin, *J. Org. Chem.*, 1999, **64**, 4798; (*h*) S. J. Bamford, K. Goubitz, H. L. van Lingen, T. Luker, H. Schenk and H. Hiemstra, *Perkin Transactions 1*, 2000, 345; (*i*) K. Nakashima, R. Ito, M. Sono and M. Tori, *Heterocycles*, 2000, **53**, 301.
11 For a recent example showing the dramatic influence of protecting groups on the stereochemical course of RCM see: A. Fürstner, O. R. Thiel and G. Blanda, *Org. Lett.*, 2000, **2**, 3731.
12 (*a*) The preparation is described by Hill, although the structure was erroneously assigned as an allenylidene complex, *cf.*: K. J. Harlow, A. F. Hill and J. D. E. T. Wilton-Ely, *J. Chem. Soc., Dalton Trans.*, 1999, 285; (*b*) The correct phenylindenyl structure has been revealed in: L. Jafarpour, H.-J. Schanz, E. D. Stevens and S. P. Nolan, *Organometallics*, 1999, **18**, 5416; (*c*) The catalytic activity has been demonstrated by: A. Fürstner, A. F. Hill, M. Liebl and J. D. E. T. Wilton-Ely, *Chem. Commun.*, 1999, 601; (*d*) For applications in total synthesis see: A. Fürstner and O. R. Thiel, *J. Org. Chem.*, 2000, **65**, 1738; (*e*) A. Fürstner, J. Grabowski, C. W. Lehmann, T. Kataoka and K. Nagai, *ChemBioChem*, 2001, **2**, 60.
13 For a complementary approach delivering (*Z*)-cycloalkenes stereoselectively see: (*a*) A. Fürstner and G. Seidel, *Angew. Chem.*, 1998, **110**, 1758; *Angew. Chem., Int. Ed.*, 1998, **37**, 1734; (*b*) A. Fürstner, C. Mathes and C. W. Lehmann, *J. Am. Chem. Soc.*, 1999, **121**, 9453; (*c*) A. Fürstner, O. Guth, A. Rumbo and G. Seidel, *J. Am. Chem. Soc.*, 1999, **121**, 11108; (*d*) A. Fürstner, K. Grela, C. Mathes and C. W. Lehmann, *J. Am. Chem. Soc.*, 2000, **122**, 11 799; (*e*) A. Fürstner, K. Radkowski, J. Grabowski, C. Wirtz and R. Mynott, *J. Org. Chem.*, 2000, **65**, 8758; (*f*) A. Fürstner and A. Rumbo, *J. Org. Chem.*, 2000, **65**, 2608.
14 P. Schwab, R. H. Grubbs and J. W. Ziller, *J. Am. Chem. Soc.*, 1996, **118**, 100.

Continuous platinum-catalyzed enantioselective hydrogenation in 'supercritical' solvents

Roland Wandeler, Niklaus Künzle, Michael S. Schneider, Tamas Mallat and Alfons Baiker*

Laboratory of Technical Chemistry, Swiss Federal Institute of Technology, ETH-Zentrum, CH-8092 Zürich, Switzerland. E-mail: E-mail:baiker@tech.chem.ethz.ch; Fax: +41 1 6321163; Tel: +41 1 6323153

Received (in Cambridge, UK) 15th January 2001, Accepted 6th March 2001
First published as an Advance Article on the web 21st March 2001

Hydrogenation of ethyl pyruvate in 'supercritical' ethane in a fixed bed reactor over cinchona-modified Pt/Al_2O_3 affords good ee at an exceptionally high rate, whereas in carbon dioxide the catalytic performance under similar conditions is inferior.

Application of supercritical (sc) fluids as solvents and reactants has great potential for optimizing chemical reactions.[1–3] The continuous hydrogenation of organic compounds in sc CO_2 or propane has recently been reported by Poliakoff and co-workers.[4] Here we show the first example of a continuous asymmetric hydrogenation in a 'sc' fluid. The well studied enantioselective hydrogenation of ethyl pyruvate (EP)[5] over cinchonidine (CD)-modified Pt/Al_2O_3 has been chosen as a model reaction (Scheme 1) to demonstrate the feasibility of the process. A crucial point is that trace amounts of the chiral modifier have to be fed continuously to the reactor in order to maintain a good ee with time-on-stream.[6] We show that the application of 'sc'ethane as a solvent affords a remarkable increase in reaction rate compared to the best conventional solvent, toluene. Note that the widely used term supercritical is deprived of any meaning in multi-component systems since phase separation is still possible at conditions beyond the mixture critical point or the critical point of the pure components.[7] For convenience, 'sc' is used here in quotes for the solvent-rich phase at temperatures exceeding its mixture critical point, irrespective of further liquid phases present.

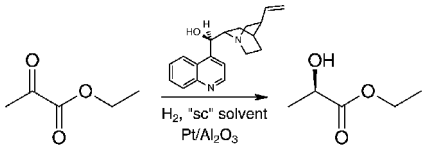

Scheme 1

Catalytic studies were carried out in a continuous stainless steel tubular fixed-bed reactor with 12.5 mm inner diameter.[6] A mechanical mixture of 100 mg 5 wt% Pt/Al_2O_3 (Engelhard 4759, metal dispersion: 0.27) and 900 mg Al_2O_3 (110 m^2 g^{-1} surface area) as diluent was employed, resulting in a catalyst bed length of 15 mm. The catalyst was prereduced *in situ* at 400 °C in H_2. A flow of 1.0 ml min^{-1} EP (Fluka, 97%) was mixed with ethane (99.5%) or CO_2 (99.995%) and H_2 (99.999%) in a static mixer before entering the reactor. CD (Fluka, > 98%) was fed together with EP (Fluka, 97%) at a molar ratio EP : CD of 2500 : 1. The corresponding solution was prepared immediately before the reaction and kept cool and in the dark to minimize side-reactions. Conversion and ee were determined by GC analysis without derivatization. Chemoselectivity to ethyl lactate was always 100%. Enantiomeric excess is defined as $([R] - [S])/([R] + [S])$.†

Preliminary studies using CO_2 and ethane as solvents indicated that the latter is a better solvent for EP hydrogenation. Fig. 1 shows the changes in conversion and ee induced during continuous hydrogenation of EP when the solvent is changed from dense CO_2 to ethane. Note the prominent increase in reaction rate and enantioselectivity with ethane. A similar but

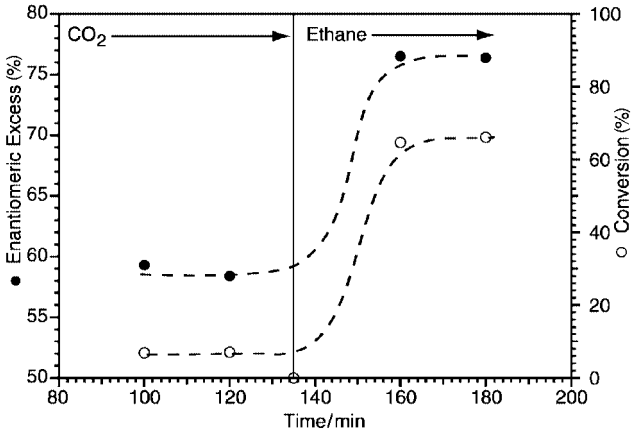

Fig. 1 Conversion (○) and ee (●) of EP hydrogenation in dense CO_2 and ethane at 30 °C and 100 bar. Molar ratio of solvent : EP : H_2 = 500 : 1 : 10. EP-flow was 4.3 mmol min^{-1}.

reversed behaviour was observed when the sequence of solvents was changed. The poor performance in CO_2 is not completely understood yet. A possible explanation is partial poisoning of the platinum catalyst due to the formation of CO *via* the reverse water gas shift reaction ($CO_2 + H_2 \rightleftharpoons CO + H_2O$).[8] As a consequence of these comparative studies further investigations were performed in ethane.

Careful consideration of the phase behavior under reaction conditions is critical for understanding the outcome of the reaction. The phase behavior of the system under reaction conditions was investigated in a computer controlled high-pressure view cell of variable volume (23–63 ml), equipped with on-line digital video imaging and recording. The magnetically stirred cell consisted of a horizontal cylinder equipped with a sapphire window covering the entire diameter and an opposite, horizontally moving piston equipped with another sapphire window for illumination of the system. The basic setup of the computer-based approach and video imaging has been described before.[9]

The reaction mixture ethane–EP–H_2 exhibited a three-phase LLV equilibrium (EP–rich liquid, ethane-rich liquid and ethane–H_2-rich gaseous phase) at 30 and 40 °C. The upper two ethane-rich phases critically merged at around 40 °C and 70 bar. Beyond this upper critical endpoint of the coexistence of the ethane-rich phases, the system exhibited a two-phase equilibrium of a liquid EP-rich phase and a dense fluid ('sc') ethane-rich phase, continuously blending to one phase with increasing pressure. The pressure required for this transition depended strongly on temperature (20–50 °C) and H_2 concentration (1–9%) in the system. A similar phase behavior was found in the system ethane–ethyl lactate–H_2 as well as in the system ethane–ethyl pyruvate–ethyl lactate–H_2. On this basis we assume that the whole conversion range can be well modelled by the ethane–EP–H_2 system discussed above.

At low H_2 concentration, the transition from a multiphase to a homogeneous fluid phase (single phase) was accompanied by a pronounced increase in EP conversion (Fig. 2, k = 2). In

DOI: 10.1039/b100511l

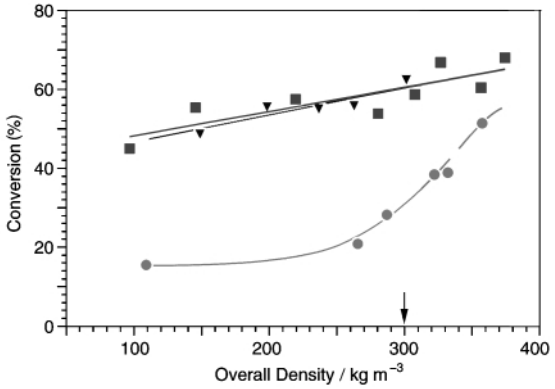

Fig. 2 Conversion of EP at 40 °C as a function of overall density at various H_2 concentrations. Ethane : EP : H_2 molar ratio = 200 : 1 : *k*, (○) *k* = 2, (■) *k* = 10, (▼) *k* = 20. Arrow marks density required for merging of fluid phases to homogeneous phase.

contrast, at higher H_2 concentration the conversion changed continuously with density, irrespective of changes in phase behavior. This behavior clearly corroborates the often made assumption that a homogeneous fluid phase affords remarkably higher reaction rates, which only holds true under conditions where mass transfer of the limiting reactant is enhanced due to elimination of phase boundaries. Enantiomeric excess to (*R*)-ethyl lactate was in the range 55–75%, depending on the temperature and H_2 concentration. Representative results illustrating the influence of pressure and reactant ratio (H_2 : EP) at 40 °C are listed in Table 1. Note that full conversion could easily be attained by increasing the contact time. Lower conversions are shown here to illustrate the effect of reaction conditions on reaction rate (conversion).

The continuous enantioselective hydrogenation in 'sc' ethane afforded a remarkably fast reaction with good ee. At best, a TOF of 15 s^{-1} was obtained at 70% conversion and ambient temperature. Using toluene as solvent provided the highest TOF of 1.8 s^{-1} under otherwise comparable conditions and optimal H_2 concentration. The process in 'sc' ethane furthermore facilitated an easy and complete separation of the solvent from the reactants by simple expansion of the reaction mixture.

Table 1 Conversion, ee and number of phases present at different pressures and feed compositions, for the enantioselective hydrogenation of EP in dense ethane at 40°C

Feed ratio	*p*/bar	Number of phases	ee (%)	Conv. (%)
	62	3	66	49
H_2 : EP = 20	88	2	65	55
	114	1	63	59
	62	3	68	20
H_2 : EP = 2	88	1	71	37
	114	1	72	50

The phase behavior of the system can be understood in terms of immiscibility of the EP-rich and ethane-rich dense phases at intermediate temperature. The solubility of EP in the ethane-rich dense phase depends mainly on the density of this phase in the temperature range investigated.[10] In fact, complete solvation of EP occurred at a density of around 300 kg m^{-3} (indicated in Fig. 2) for all temperatures and H_2 concentrations, resulting in a saturated ethane-rich dense phase under these conditions. The higher the H_2 concentration in the system, the higher was the pressure required to achieve a density of 300 kg m^{-3} and thus complete solubility of EP in the dense ethane-rich phase. Note that coexistence of two phases was observed at values well above the critical parameters of ethane (ethane, T_c = 32.2 °C, p_c = 48.8 bar). This observation illustrates the danger of assuming that the phase behavior of a multi-component system is similar to that of the pure solvent.

In conclusion, we have shown the feasibility of continuous enantioselective hydrogenation of an α-ketoester in dense ('sc') ethane by continuous dosing of a minute quantity of the chiral modifier CD. High reaction rates combined with good enantioselectivity and easy separation of products are beneficial features of this process.

Financial support by the 'Bundesamt fuer Energie' and by the 'Kommission für Technologie und Innovation' (KTI) is gratefully acknowledged.

Notes and references

† Safety note: the experiments described in this paper involve the use of relatively high pressure and require equipment with the appropriate pressure rating.

1 P. G. Jessop, T. Ikariya and R. Noyori, *Chem. Rev.*, 1999, **99**, 475.
2 A. Baiker, *Chem. Rev.*, 1999, **99**, 453.
3 P. G. Jessop and W. Leitner (Eds.), *Chemical Synthesis Using Supercritical Fluids*, Wiley-VCH, Weinheim, 1999.
4 M. G. Hitzler and M. Poliakoff, *Chem. Commun.*, 1997, 1667; M. G. Hitzler, F. R. Smail, S. K. Ross and M. Poliakoff, *Org. Process Res. Dev.*, 1998, **2**, 137.
5 A. Baiker, *J. Mol. Catal. A*, 1997, **115**, 473; A. Baiker, *J. Mol. Catal. A*, 2000, **163**, 203.
6 N. Künzle, R. Hess, T. Mallat and A. Baiker, *J. Catal.*, 1999, **186**, 239.
7 J. S. Rowlinson and F. L. Swinton, *Liquids and Liquid Mixtures*, Butterworth & Co Ltd, London, 3rd edn., 1982.
8 B. Minder, T. Mallat, K. H. Pickel, K. Steiner and A. Baiker, *Catal. Lett.*, 1995, **34**, 1.
9 R. Wandeler and A. Baiker, *Chimia*, 1999, **53**, 566.
10 J. Chrastil, *J. Phys. Chem.*, 1982, **86**, 3016.

Typeset and printed by Black Bear Press Limited, Cambridge, England

ChemComm
FEATURE ARTICLE

Catalytically active centres in porous oxides: design and performance of highly selective new catalysts

John Meurig Thomas*[ab] and Robert Raja[ac]

[a] *Davy Faraday Research Laboratory, The Royal Institution of Great Britain, 21 Albemarle Street, London, UK W1X 4BS. E-mail: robert@ri.ac.uk*
[b] *Department of Materials Science and Metallurgy, University of Cambridge, Pembroke Street, Cambridge, UK CB2 3QZ*
[c] *Department of Chemistry, University of Cambridge, Lensfield Road, Cambridge, UK CB2 1EW*

Received (in Cambridge, UK) 9th January 2001, Accepted 15th February 2001
First published as an Advance Article on the web 29th March 2001

Active centres have been designed on high-area, molecular sieve catalysts which, *inter alia*, can convert n-alkanes to n-alkanols and n-alkanoic acids, cyclohexane to cyclohexanol, cyclohexanone and adipic acid, and n-hexane to adipic acid all using either oxygen or air as oxidants. A number of one-step processes and solvent-free chemical conversions, of paramount importance in the development of clean technology, are also described with catalysts designed (i) to oxidise *p*-xylene to terephthalic acid aerobically, (ii) to effect Baeyer–Villiger reactions with oxygen, and (iii) for the conversion of cyclohexanone to ε-caprolactam under mild conditions. The inner surfaces of mesoporous silicas may also be atomically engineered so as to yield high-performance epoxidation of alkenes at Ti^{IV}-centred active sites, as well as enantioselective hydrogenations of organic species using constrained chiral catalysts.

John Meurig Thomas began his academic career at the University of Wales, first at Bangor then at Aberystwyth where he was Head of Chemistry from 1969 to 1978. He then became Head of the Department of Physical Chemistry, University of Cambridge and Professorial Fellow at Kings College. He succeeded George Porter as Director of the Royal Institution and the Davy Faraday Research Laboratory (1986–1991), where he still does most of his experimental work. His researches have covered wide areas of solid state, surface and materials chemistry, and heterogeneous catalysis and he has received numerous medals and awards for his various contributions. Ten years ago he was knighted for services to chemistry and the popularisation of science. In 1993 he became Master of the oldest college in Cambridge, Peterhouse. In 1999, he was the (first) recipient of the American Chemical Society award for creative research in homogeneous and heterogeneous catalysis.

Robert Raja received his Masters degree in Chemistry at the Birla Institute of Technology and Science and completed his Ph.D. on zeolite mimics of enzymes with Paul Ratnasamy at the National Chemical Laboratory, Pune, India (1997). He was Royal Commission of 1851 Exhibitioner at the Davy Faraday Research Laboratory of the Royal Institution of Great Britain (1997–1999) and is currently a Peterhouse Senior Research Associate at the Department of Chemistry, Cambridge University, working jointly with Brian F. G. Johnson and John Meurig Thomas. His research interest focuses on designing novel microporous and mesoporous catalysts for environmentally benign selective oxidation and hydrogenation processes. He is the author of 30 research publications and is the co-inventor of five International Patents.

1 Introduction

Important milestones in our understanding of catalytically active centres were reached in the mid-1960s with Phillips's determination, by X-ray crystallography, of the structure of lysozyme,[1] and Blow's elucidation, also by X-ray diffraction, of the structure of chymotrypsin,[2] and in particular of the precise environment of the catalytic pockets within these solid enzymes. Not only did knowledge of the structure of the active centres suggest a convincing mechanism for the mode of action of these two catalysts, it transformed the world of enzymology. Ever since that time, protein engineers[3] have become increasingly expert at designing new biological catalysts principally because they know (a) what the precise, atomically-resolved structure of the active centre is in many wild enzymes, and (b) the atomic changes that should be made in the vicinity of the active centre so as to enhance either the enzyme's activity, its selectivity, or both.

It is not possible to use the X-ray approach of protein crystallographers in the study of solid (low surface-area) inorganic heterogeneous catalysts, principally because the bulk of the catalyst contributes vastly more to the diffraction of the X-rays than do the minute numbers of active centres distributed in a random manner at the exterior surface of the solid. When, however, highly microporous or mesoporous solids such as those that possess channels, cavities or cages with diameters in the ranges 4–14 Å (micro) and 15–250 Å (meso) are used as catalyst supports, the atomic structures of the implanted active centres may be retrieved by X-ray-based methods but this time by the use of X-ray absorption fine-structure spectroscopy (XAFS) rather than by X-ray diffraction.[4–8] XAFS as a technique yields detailed local structural information even when the catalyst is non-crystalline.[7–9]

Microporous and mesoporous hosts (see below) may have internal surface areas that are so large—in excess of 1000 $m^2\ g^{-1}$—that, effectively, these solids are best envisaged as possessing three-dimensional surfaces. Either by heterogenizing well-defined organometallic precursors on mesoporous hosts, or by preparing microporous hosts that contain within them adroitly placed potentially active centres, advantage may be taken of special *in situ* methods, described fully elsewhere,[5–9] to determine in atomic detail the nature of the catalytically active sites prior to and during the course of the chemical transformation. Armed with this knowledge, one is in a far better position chemically to modify variants of the original catalysts and thereby to enhance their performance. Knowledge of the atomic architecture of the active centre also facilitates interpretative mechanisms of the catalytic path, a task nowadays greatly aided by invoking reliable computational procedures either of the atomistic or electronic kind. Table 1

takes cognizance of all the above points, and also emphasizes other practical desiderata pertaining to porous (open-structure) oxide catalysts discussed herein.

Table 1 Desiderata for engineered porous oxide catalysts

High activity, high selectivity, longevity and durability
Freedom from restrictions imposed by diffusional considerations (reactants and products)
Capable of facilitating regio-selective, shape-selective and enantioselective processes
Should operate under mild conditions and be environmentally, economically and atom efficient
Should be able to facilitate an increasing number of solvent-free conversions
Possession of isolated, well-defined (single-site) active centres, the atomic architecture of which may be delicately modified
Capability of yielding detailed mechanistic understanding of catalytic action
Between them certain microporous (3.5–14.5 Å apertures) and mesoporous (15–250 Å) oxides satisfy all these desiderata

Close to a half of the elements of the Periodic Table are capable of being incorporated into the framework structures—generally in tetrahedral, but more frequently nowadays in six- or five-fold coordination—of the ever-growing families of microporous and mesoporous materials. In the case of microporous solids, the largest two sub-families are the aluminosilicates and **al**umino**p**h**o**sphates (AlPOs). These are essentially three-dimensional networks of corner-sharing SiO_4 and AlO_4 tetrahedra and of AlO_4 and PO_4 tetrahedra, respectively. Heteroatoms, especially those known to exhibit powerful catalytic properties such as Co^{III}, Mn^{III}, Fe^{III}, Ti^{IV}, may be incorporated substitutionally at regular framework sites. (They may, as in the case of cobalt or manganese, be easier to introduce during preparation as Co^{II} or Mn^{II} ions: they are later convertible, by calcination *in situ*, for example, into their higher-valent forms, Co^{III} and Mn^{III}.) Mesoporous solids, on the other hand, are generally easier to prepare in their pristine state (as SiO_2, GeO_2, TiO_2, *etc*.), and heteroatoms, which serve as the loci of catalytic action, are grafted onto the inner surfaces of the mesopores after synthesis, as described in Section 3 below.

2 Specific examples of designed, characterized and proven microporous catalysts

Although the main thrust of our work is to arrive at new solid inorganic catalysts by engineering appropriate active centres through the principles of solid-state and surface chemistry, we especially aim to produce those catalysts that are important in the context of *clean technology*. The intellectual challenge is to devise strategies for such environmentally desirable objectives as:

- the development of one-step processes and/or solvent-free chemical conversions; and
- to produce oxidation catalysts that use air or oxygen as the oxidant.

In describing below the progress that we have made towards these goals we also recall the salient features of those currently favoured, important processes that need to be replaced either because of their expense, and/or inconvenience, or because they are environmentally (or otherwise) unacceptable.

We now proceed to highlight our work on:

A the selective oxidation of cyclohexane in air to cyclohexanol, cyclohexanone and adipic acid;
B regio- and shape-selective oxyfunctionalization of n-alkanes in air to yield n-alkanols and n-alkanoic acids;
C conversion of n-hexane to adipic acid in air;
D aerobic oxidation of *p*-xylene to terephthalic acid;
E Baeyer–Villiger reactions using oxygen as the oxidant for conversion of (i) ketones to lactones and (ii) alkenes to epoxides;
F solid-acid-catalyzed dehydrations and oligomerizations, and
G ammoximation of cyclohexanone to yield the oxime and caprolactam.

For a majority of these conversions it has been shown[8,10,11] that free radicals participate in a crucial, spatially constrained manner. One of the key features of our approach[12,13] to the design of the necessary catalysts is to insert (implant) transition metal ions in high oxidation states into the framework of the microporous oxide. These serve as free radical initiators (see, for example, Section E below), but the mean-free path of the radicals is necessarily small (owing to the microporosity of the solid) so that only a limited number of reactions may ensue. Moreover, by astute choice of the dimensions of the pores of the molecular sieve oxide within which the transition metal ion active centres are placed, one may harness the advantages of shape selectivity, whereby only molecules of certain sizes and shapes may reach, or diffuse away from, the active centres. In some instances, where the siting of active centres and the access to them of reactant molecules are sharply defined, it becomes possible to effect regio-selective as well as shape-selective conversions.[10]

A The selective oxidation of cyclohexane to cyclohexanol, cyclohexanone and adipic acid

Apart from its intrinsic importance in the chemistry of C–H activation,[14] the selective oxidation of cyclohexane to yield cyclohexanol and cyclohexanone is the centre-piece of the commercial production of nylon. Many key precursors and products in the polymer industry are generated in costly and polluting processes that also involve the selective oxidation of cyclohexane (Scheme 1).[15] Intermediates such as cyclohexanol

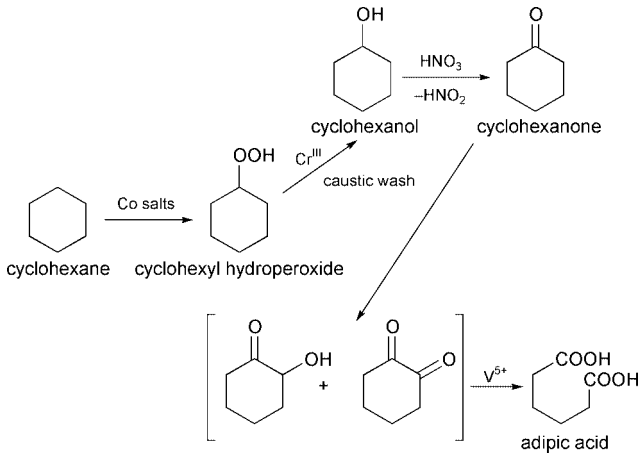

Scheme 1

and cyclohexanone, which, together, are known as K-A oil, are the stepping stones for the production of caprolactam (Scheme 2), which is the monomer for nylon 6, and adipic acid (AA) which is the building block for a series of synthetic polyamide fibres such as nylon 66 and polyurethane resins. Alternate synthetic routes have been developed, such as the one-step oxidation of cyclohexane with either alkyl hydroperoxide as oxidant and a catalyst consisting of cobalt salts,[16,17] or dioxygen as oxidant and a cobalt acetate catalyst in acetic acid.[18] More recent industrial syntheses include homogeneously catalyzed hydrocarboxylation or carboalkoxylation of butadiene.

Because the free radicals generated in the autoxidation of cyclohexane are constrained in space within the interior of the

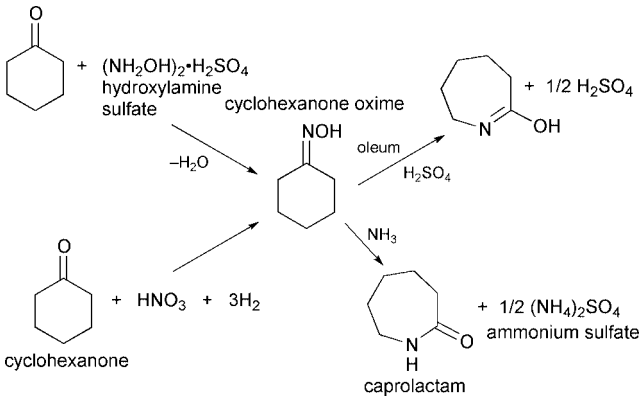

Scheme 2

high-area porous catalysts chosen by us, we opted to prepare three distinct kinds of MeAlPO molecular sieve catalysts for this oxidation: $Co^{III}(Mn^{III})$AlPO-36,[19] $Fe^{III}(Mn^{III})$AlPO-5,[20] and Fe^{III}AlPO-31[21] (see Fig. 1).

When a few percent of Al^{III} ions in AlPO-36 (pore aperture 6.5 × 7.5 Å) are replaced by Co^{III} (or Mn^{III}) ions it becomes[19] a good catalyst for cyclohexane oxidation in O_2, the principal products being cyclohexanol and cyclohexanone and small quantities of adipic acid (AA). XAFS measurements show that, in CoAlPO-36, only 50% of the Co^{II} ions present in the framework in the as-prepared state may be raised to the Co^{III} state by calcining in air. In FeAlPO-5, however, (pore aperture 7.3 × 7.3 Å) all of the iron ions are found (by XAFS) to be in the Fe^{III} state. Indeed, this active site (Fe^{III} in the framework) has an immediate environment almost indistinguishable from that of Fe^{III} in FeZSM-5 (Fig. 2) in which again the Fe^{III} resides in the framework.

We argued that there was merit in designing a MeAlPO molecular sieve catalyst in which the active sites (either Fe^{III} or Mn^{III}) are the same as, but the pores are significantly smaller than, those of MeAlPO-5 analogues. This would mean that, of the reaction intermediates formed within the pores of the catalyst, those that are more sinuous (like AA) would diffuse out readily. MeAlPO-31, in the form of Fe^{III}AlPO-31, was therefore selected by us.[21] In effect, we capitalize here on 'product shape-

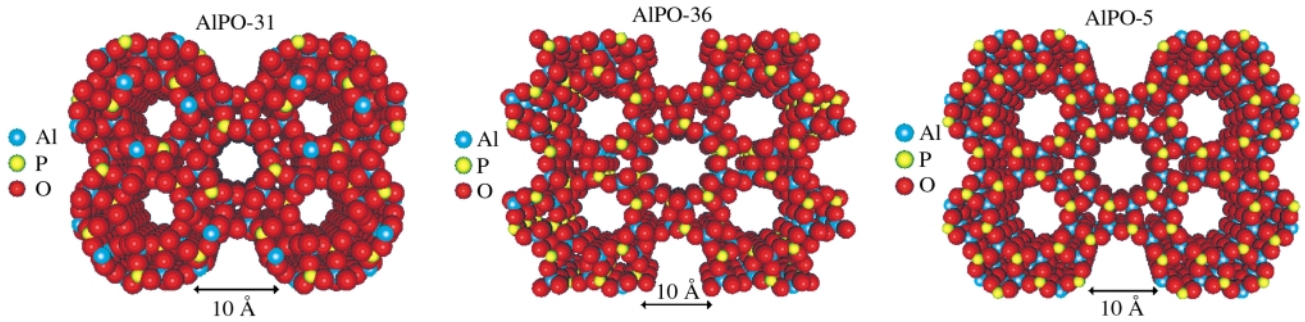

Fig. 1 Computer graphic representation of the framework structures of the three aluminophosphate molecular sieves used in this work. In the active microporous catalysts a small fraction of the Al^{III} framework ions is replaced by either Co^{III} or Mn^{III} or Fe^{III} ions, which function as the active centres (see text). Diameters of the apertures are: AlPO-31, 5.4 Å; AlPO-36, 6.5 × 7.5 Å; and AlPO-5, 7.3 Å.

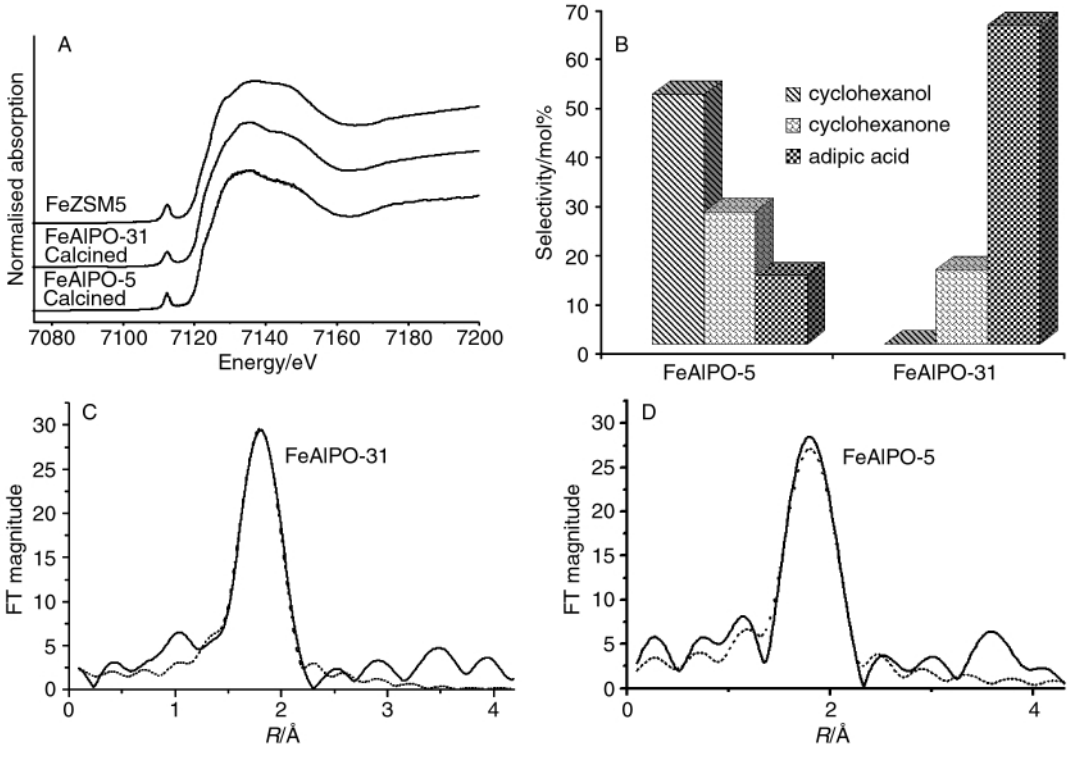

Fig. 2 (A) X-Ray absorption near-edge (XANES) spectra of as-synthesized FeZSM-5 (with framework-substituted Fe^{III} ions) and of calcined FeAlPO-31 and FeAlPO-5. Note the similarities in pre-edge intensities. (B) Bar chart contrasting the product selectivities (at T = 373 K, 24 h contact time) of the three principal, selective oxidation products with these two catalysts. (C) and (D) Associated Fourier transform of calcined FeAlPO-31 and FeAlPO-5, respectively (the solid and the dashed curves represent the experimental and calculated data, respectively.

selectivity' (in the same sense as described by Weisz[22] for acid-catalyzed dehydrations of alkanols)—only those products with appropriate molecular dimensions may diffuse easily out of the pores, whereas larger ones formed in the course of the reaction are trapped inside on account of their significantly retarded diffusion. Qualitatively, we may envisage the free radical and molecular intermediates cyclohexanol, cyclohexanone, formed from cyclohexyl hydroperoxide (cHHP) or 2-hydroxycyclohexanone and 1,2-cyclohexanedione, to be held in the vicinity of the active site until oxidation proceeds further to yield the more mobile and desired linear product AA (see Fig. 3). Because of the more puckered walls of AlPO-31 compared with AlPO-5, and the significantly reduced pore diameter (5.4 Å), we have the constrained environment required for the favoured production of AA (see Fig. 2).

B Regio- and shape-selective oxyfunctionalization of n-alkanes in air

Although linear alkanes are readily oxidized to completion (burnt) at elevated temperatures, they are among the most difficult to oxyfunctionalize at lower temperatures. It is widely acknowledged that the controlled oxyfunctionalization of linear alkanes is one of the major challenges of modern catalysis; and particularly desirable products are those that have been terminally oxidized (hexanoic acid, for example), since these serve as feedstocks for the chemical and pharmaceutical industries. A gleam in the eye of the expert catalyst scientist is to arrive at a catalyst that regiospecifically functionalizes n-alkanes using either air or dioxygen as the oxidant.[23] We have succeeded in doing this (for n-alkane C_nH_{2n+2}, n = 6–8, 10, 12) using a carefully designed MeAlPO molecular sieve.[8,10,11,24] Moreover, we have very recently demonstrated how, by judicious modification of the siting of single-site active centres within the same kind of catalyst Co^{III}AlPO-18, it also becomes possible to achieve double terminal oxyfunctionalization, thereby enabling n-hexane to be converted in air to AA (see below).

We are certain that Me^{III} ions (substituting for Al^{III} ones, in the MeAlPO-18) are a *sine qua non* for the catalytic oxidation of the hydrocarbon. If, for example, Mg^{II} or Zn^{II} ions (or Co^{II} or Mn^{II} ions) are present in place of Me^{III} ions in the MeAlPO, no oxidation ensues.

To achieve single, terminal methyl group attack, one harnesses the fact that the Me^{III} ion active site must, during reaction, be readily accessed in a preferential manner by the terminal methyl group of the alkane. One must also ensure that the alkane can gain entry into the interior of the MeAlPO catalyst only by an 'end-on' approach (Fig. 4), otherwise oxyfunctionalization of the CH_2 groups at C_2 and C_3 will occur. [It must be remembered that, all the while during the oxidation, the catalyst and alkanes are swathed in molecular oxygen (Fig. 4) as the latter is so small that it readily reaches the Me^{III} and other sites within the molecular sieve catalyst.)

CoAlPO-18 or MnAlPO-18 catalysts are very effective in the regioselective oxidation of n-alkanes. Apart from the qualitative arguments given above for facilitating terminal attack, the quantitative results of energy-minimization (see Fig. 5) yield further insights into, and a deeper understanding of, the regiospecificity.

The computation, which combines Monte Carlo, molecular dynamics and docking procedures,[25] reveals that the terminal methyl group is significantly closer to a tetrahedral framework site than either C_2 or C_3 carbons in the alkane chain. Moreover, the end of the alkane becomes slightly bent, and all this favours oxidation of the terminal (mainly) and penultimate carbon atoms, just as is seen in the experimental results (Fig. 6).

The so-called primary selectivity index (defined as the ratio of concentration of primary products to secondary/tertiary products normalized for the respective number of hydrogens in the alkane molecule) is superior for the Co^{III}AlPO-18 and Mn^{III}AlPO-18 catalysts than for all previously reported[14,26] inorganic heterogeneous catalysts, even though the latter use sacrificial oxidants such as iodosylbenzene[27] and not air or O_2. It is to be noted[10] that some 70% of the products of oxidation of n-octane after 24 h are the result of oxyfunctionalization of the terminal methyl group for Co^{III}AlPO-18 (60% for Mn^{III}AlPO-18). Octanoic acid, octan-1-al and octan-1-ol, in descending order, are the principal products of oxyfunctionalization of n-octane.

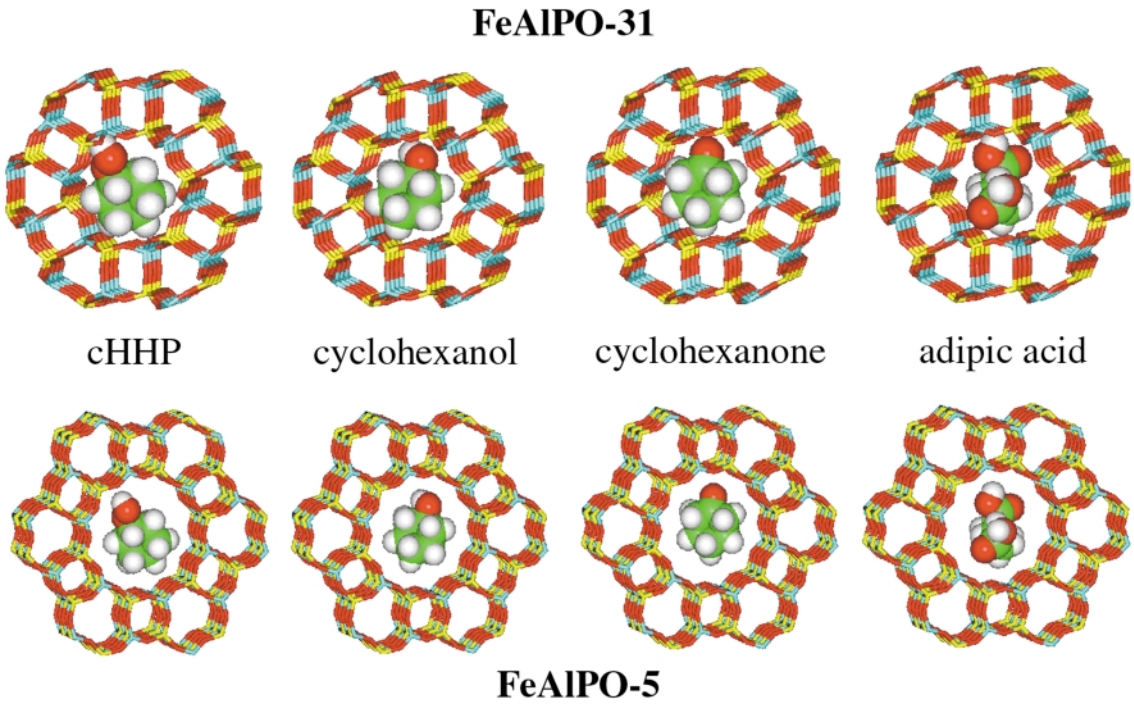

Fig. 3 In the autocatalytic oxidation of cyclohexane in air, the main products are cyclohexyl hydroperoxide (cHHP), cyclohexanol, cyclohexanone and adipic acid (AA). In the larger (7.3 Å) FeAlPO-5 catalyst, all products diffuse out freely, whereas in the smaller pore (5.4 Å) FeAlPO-31 catalyst, diffusion out of the solid is much easier for the sinuous adipic acid molecule than for the other three, which fit rather tightly within the pores. This product shape-selectivity explains the results shown in Fig. 2B.

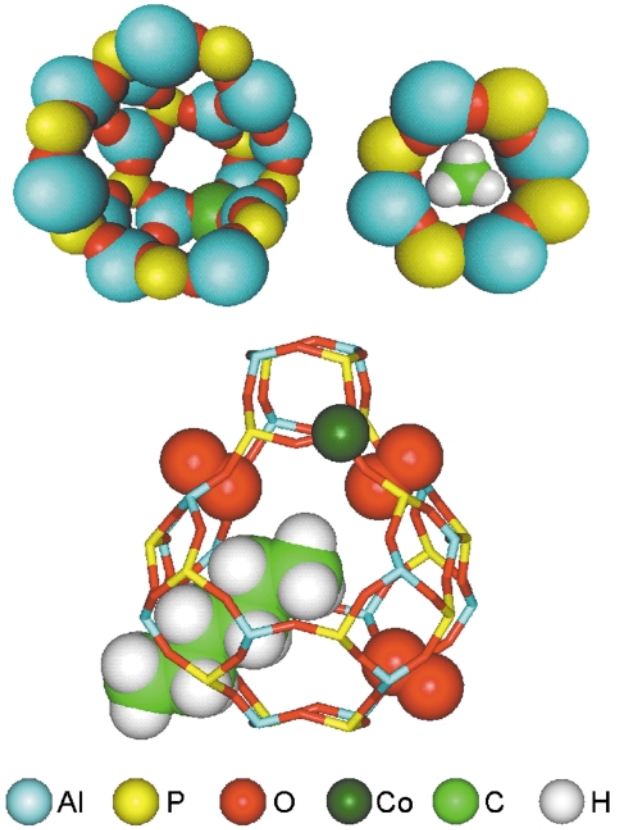

Fig. 4 Views of (left) interior of the chabazitic cage in the Co^{III}AlPO-18 catalyst, with the end-on approach of the alkane to the active site emphasized (top right). At the bottom is another view showing the approach to the Co^{III} active site of n-hexane into the chabazitic cage. Oxygen molecules freely enter the cage *via* the other openings.

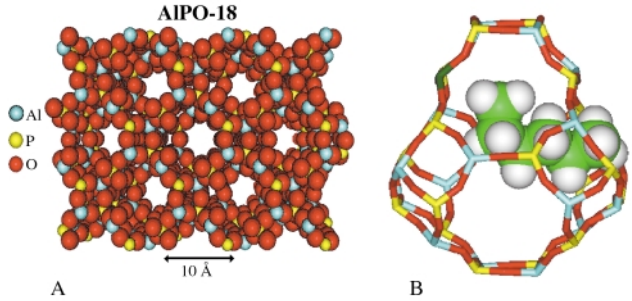

Fig. 5 (A) Computer graphic view of the framework structure of AlPO-18. Each of the intersecting pores, whose openings are shown here, has an array of side pockets possessing a so-called chabazitic structure shown in B. (B) Energy-minimized configuration adopted by n-hexane at 0 K inside the chabazitic cage of the AlPO-18 framework. This configuration was derived from a calculation that combines Monte Carlo, molecular dynamics and docking procedures as described in ref. 25. Note that the terminal methyl group (C_1) is significantly closer to a tetrahedral framework site (and hence to the Me^{III} active centre) than either C_2 or C_3.[10]

C Converting n-hexane to adipic acid (AA) in air

To achieve oxyfunctionalization at both (methyl) ends of n-hexane, a sufficiently large number of framework Co^{III} ions needs to be accommodated on the inner walls of the CoAlPO-18 catalyst in such a manner that two framework Co^{III} ions should be separated by *ca.* 7–8 Å from one another. With the composition $Co_{0.1}Al_{0.9}PO_4$ for the CoAlPO-18 structure (*i.e.* with a Co : P ratio of 0.1, instead of 0.04, as above) there is a high probability for there being two (separated) Co^{III} ions in each cage of the AlPO-18 structure, and for these two ions to be situated opposite one another as shown in Fig. 7.

Fig. 8 summarizes the results of the selective oxidation experiments and, in particular, highlights the contrast in catalytic performance—especially in regard to production of

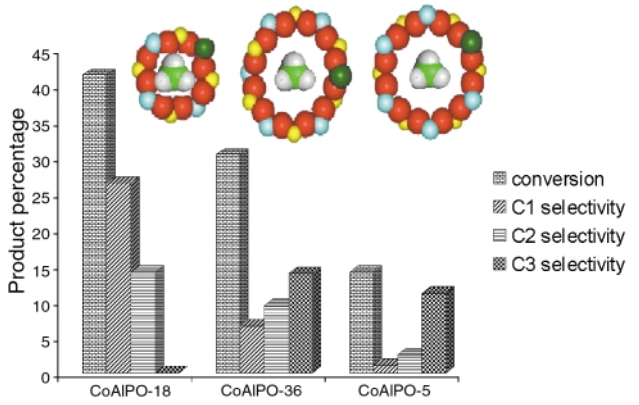

Fig. 6 Bar chart showing the regio-selective oxyfunctionalization of n-hexane when exposed to air and a Co^{III}AlPO-18 catalyst. 65% of the products are oxyfunctionalized at the terminal methyl (C_1), and 34% at the penultimate methylene (C_2) carbons, in marked contrast to what occurs under identical conditions (373 K, 1.5 MPa, 24 h) with CoAlPO-36 and CoAlPO-5 catalysts.

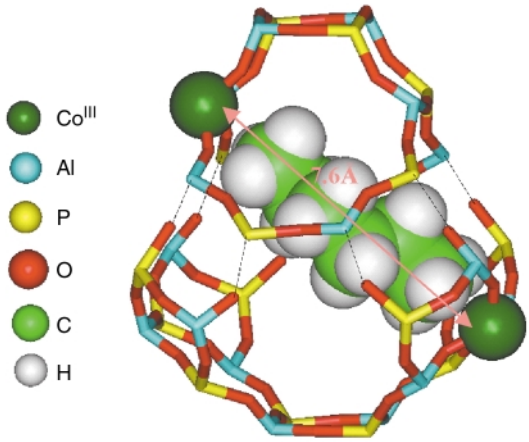

Fig. 7 With two Co^{III} ions at the opposite vertices of the chabazitic cage in CoAlPO-18 (as occurs when the composition is close to $Co_{0.1}Al_{0.9}PO_4$), their separation distance (*ca.* 7.6 Å) is similar to that which separates the two terminal methyl groups in n-hexane. This maximizes the occurrence of oxyfunctionalization of the alkane to form adipic acid (see text and Fig. 8)

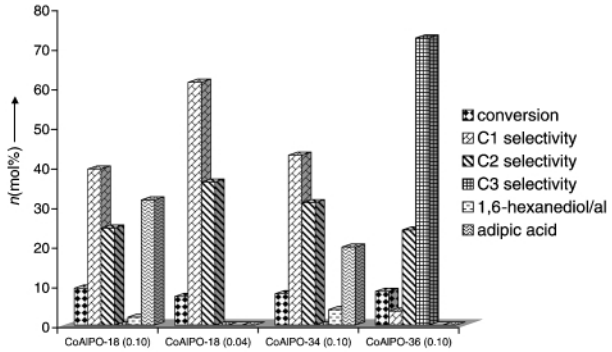

Fig. 8 A low ratio of Co : P (*e.g.* 0.04) in the CoAlPO-18 catalyst yields essentially no adipic acid, whereas a high one (*ca.* 0.10) yields substantial quantities. The closely similar CoAlPO-34 catalyst (which is structurally identical to CoAlPO-18 in its chabazitic cages and pore dimensions) also yields adipic acid with a high (0.10) Co : P ratio. CoAlPO-36, on the other hand, which has no chabazitic cages and has larger pores than CoAlPO-18 or CoAlPO-34, and which therefore exerts no shape selectivity, produces no adipic acid.

adipic acid—of low and high Co : P ratios for CoAlPO-18 (*i.e.* 0.04 and 0.10, respectively). It is to be noted that CoAlPO-34, which is very similar structurally to CoAlPO-18 (they each have chabazitic cages), exhibit broadly similar catalytic performance

when the Co : P ratio is 0.10. But CoAlPO-36, which has a much larger pore aperture (6.5 × 7.5 Å) is markedly different from both CoAlPO-18 and CoAlPO-34.

Detailed kinetic studies (described elsewhere[10,28]) are also informative, especially when compared with those reported earlier for CoAlPO-18 with a Co : P ratio of 0.04. With a Co : P ratio of 0.10, for both CoAlPO-18 and CoAlPO-34 catalysts, hexan-1-ol is the major product during the initial stages of the reaction, but this is subsequently converted to hexan-1-al and hexanoic acid. After 5 h, hexane-1,6-diol, hexane-1,6-dial and traces of adipic acid appear in the reaction mixture as well as the three principal products (hexan-1-ol, hexan-1-al and hexanoic acid) observed earlier.[10]

It is noteworthy that there is no decrease in the hexanoic acid selectivity, but at prolonged contact times (10–24 h) there is a steady decrease in the concentration of both hexane-1,6-diol and hexane-1,6-dial, and a concomitant build-up in the production of AA. Evidently, the production of AA arises as a result of the further oxidation of the hexane-1,6-diol and hexane-1,6-dial. Further, when hexanoic acid was taken as the substrate (instead of n-hexane), using CoAlPO-18 (0.10) as catalyst, we did not observe any conversion to AA. With a Co : P ratio of 0.04, the CoAlPO-18 catalyst, under identical conditions, does not produce hexane-1,6-diol or hexane-1,6-dial or any detectable AA. This active adipic acid-producing CoAlPO-18 catalyst, with a Co : P ratio of 0.10, is remarkably stable and there is no leaching of the cobalt ions (see Section 4) during catalysis.

D Terephthalic acid from *p*-xylene

Textile and synthetic fibres such as saturated polyesters (Terylene) are made from terephthalic acid, which is currently produced commercially by the oxidation of *p*-xylene using aggressive reagents such as bromine, and acetic acid as solvent (Scheme 3).[15] In 1992, the worldwide demand for terephthalic

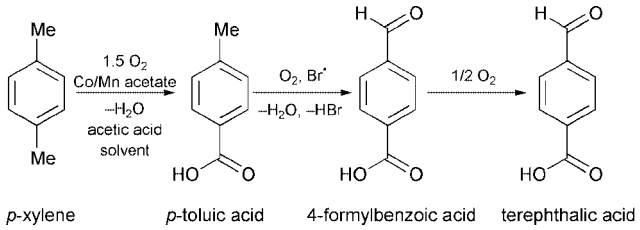

Scheme 3

acid was 12.6 × 10^6 tonnes and textile and industrial fibres accounted for 75% of this demand.[29] Various salts of cobalt and manganese can be used as homogeneous catalysts and the bromine source is usually HBr, NaBr or tetrabromoethane. The highly corrosive bromine–acetic acid environment requires the use of titanium-lined equipment.

Our approach to the design of suitable catalysts for this important reaction again relies on the use of a microporous molecular sieve in which the active sites are Co^{III} or Fe^{III} ions in framework sites substituting for Al^{III} ions. These catalysts operate under solvent-free conditions without the need for corrosive activators and solvents such as bromine or acetic acid. Their mode of operation also relies on shape-selective, free-radical processes of a spatially constrained kind. Moreover, all such oxidation catalysts designed by us require only benign oxidants (dioxygen or air), and consist of inexpensive, readily preparable, $Co^{III}(Fe^{III})$–AlPO-36 or $Co^{III}(Fe^{III})$–AlPO-5.

Our molecular sieve catalysts are effective for the aerobic oxidation of *p*-xylene, the main products being toluic acid, 4-formylbenzoic acid (4-carboxybenzaldehyde) and terephthalic acid, leaving the benzene ring virtually untouched. 4-Formylbenzoic acid is a troublesome impurity and, because of its structural similarity to terephthalic acid, it co-crystallizes with the latter and becomes trapped and inaccessible for completion of the oxidation.[30] We find that AlPO-36-based catalysts, containing up to 10 atom% of transition metal ions (Co^{III}, Mn^{III}, Fe^{III}, *etc*.), suppress the formation of 4-formylbenzoic acid and increase the selectivity for terephthalic acid. As in the case of Co^{III}AlPO-18, containing *ca*. 10 atom% of Co^{III} ions in the framework (see Section C), one might envisage oxyfunctionalization occurring simultaneously at both methyl ends of *p*-xylene, which could well be the reason for the higher selectivity of the Co^{III}AlPO-36 (0.10) catalyst for terephthalic acid (see Fig. 9) compared to Co^{III}AlPO-36 (0.04).[31] Owing to the low solubility of terephthalic acid in *p*-xylene (and since no co-solvents are used) most of it precipitates as it forms.[32]

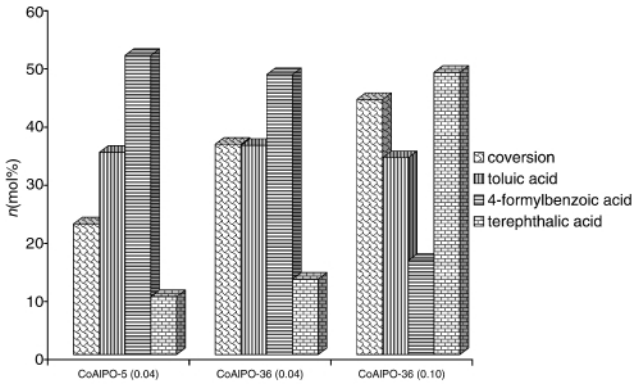

Fig. 9 CoAlPO-36, with a high Co : P ratio (*ca*. 0.10) is a good catalyst for the aerial oxidation of *p*-xylene to terephthalic acid (see text).

E Baeyer–Villiger reactions using oxygen as the oxidant

A reaction of great commercial importance is that devised more than a century ago by Baeyer and Villiger[33] who showed how cyclic ketones could be converted into lactones using a powerful oxidant, such as peroxomonosulfuric acid, H_2SO_5, otherwise known as Caro's acid. This reaction plays a central role in applications that span antibiotics, steroids and numerous aspects of agrochemistry. For environmental and other reasons the use of H_2SO_5, or alternatives such as (the potentially explosive) 90% H_2O_2, is frowned upon (where not banned); and some have turned to the use of milder forms of H_2O_2 in the presence of inorganic materials such as methyl-trioxorhenium.

Our approach (Fig. 10) relies[34] on Mn^{III} (or Co^{III})-framework-substituted MeAlPOs, in which air (or O_2) and a

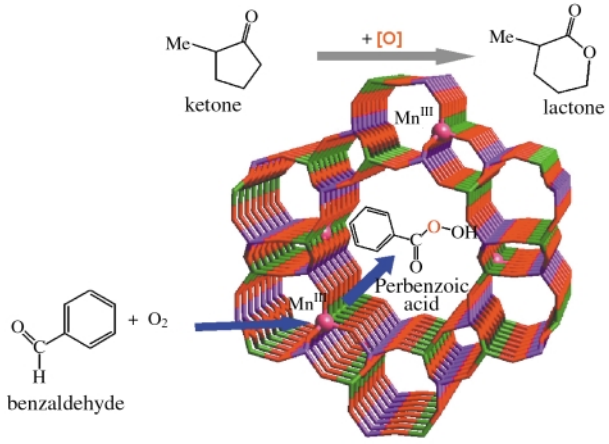

Fig. 10 Graphical representation of a Mn^{III}AlPO-36 molecular sieve catalyst showing the Baeyer–Villiger oxidation of a cyclic ketone to the corresponding lactone. In place of the conventional aggressive oxidants such as H_2SO_5, here, perbenzoic acid is formed *in situ* from benzaldehyde in the presence of O_2 assisted by the Mn^{III} active sites. (After Thomas *et al.*[15])

sacrificial aldehyde are used. These constituents produce *in situ*, a percarboxylic acid (*e.g*. perbenzoic acid), and this functions as

an environmentally successful oxygen donor to convert the ketone to the corresponding lactone. [A similar approach, again using a sacrificial aldehyde, serves to epoxidize a range of alkenes in O_2 (air), with the same kind of molecular sieve catalyst employing a Mn^{III} (or Co^{III}) active site in its framework.[35]]

Insofar as catalytic epoxidations are concerned, as with Baeyer–Villiger reactions with ketones, the centre-piece of our heterogeneous catalytic conversion is MeAlPO-36 (with Me ≡ Mn^{III} and Co^{III}). In both cases, we exploit the easy autoxidation of aldehydes to promote the *in situ* formation of peroxy acids.[36]

Benzaldehyde molecules may freely enter the large internal areas of MeAlPO-36 thereby generating[37] first PhCO· and then PhCOOO· radicals, which, from the sequence of steps shown below, lead to the formation of perbenzoic acid and the alkene

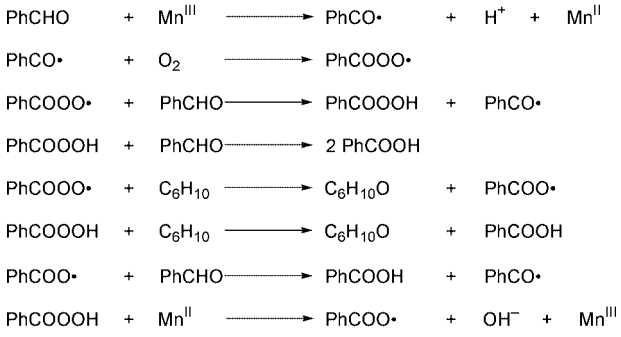

oxide—in our case[35] cyclohexene oxide. This free-radical-based epoxidation of cyclohexene [and other alkenes such as α-(+)-pinene, *R*-(+)-limonene and styrene] is mechanistically quite distinct from the radical-free epoxidation of alkenes using alkyl hydroperoxides and titanosilicate catalysts (which is described in Section 3A, below).

F Solid acid-catalyzed reactions

As described elsewhere,[38] solid acid catalysts are urgently required in the petrochemical and other industries to replace such environmentally aggressive and widely used liquid acids as HF, H_3PO_4 and H_2SO_4. Following the lead given by the Union Carbide group[39] on the use of metal-ion- and silicon (framework)-substituted AlPOs as Brønsted acid catalysts, our colleague Jiesheng Chen and one of us[40] found that many MeAlPO-18 molecular sieves (M ≡ Zn^{II}, Mg^{II}, Co^{II}, Ni^{II}, *etc.*) were extremely effective, shape-selective catalysts for the dehydration of methanol to olefins. Moreover, they could be readily prepared in a state of high phase purity.[40] Such are the dimensions of the cavities and locations of the active sites—loosely attached protons to framework oxygen atoms in the vicinity of the metal ions (Me) {or of the Si^{IV} ions that substitute for framework P^V ions}[41] as shown in Fig. 11—that there is room inside this molecular sieve acid catalyst for the production of only ethene, propene and traces of butene. Because of the spatial restrictions, no aromatic molecules, such as those produced using H^+-ZSM-5 catalysts, can be formed. This is an example of transition-state shape-selectivity.

Success in designing shape-selective, microporous solid-acid catalysts consists in building a molecular sieve, the pore apertures and cage dimensions of which function as spatial constraints for the production of bulky hydrocarbons, but which still favour the generation of the light olefins alluded to above. By careful choice of structure-directing agents (SDAs), a new, shape-selective, microporous MAlPO solid acid catalyst, known as DAF-4, having a framework structure essentially the same as that of the naturally occurring zeolitic mineral levyne was produced.[42] In its Co^{II}-substituted form, DAF-4 transforms methanol with greater than 75% conversion at 350 °C into

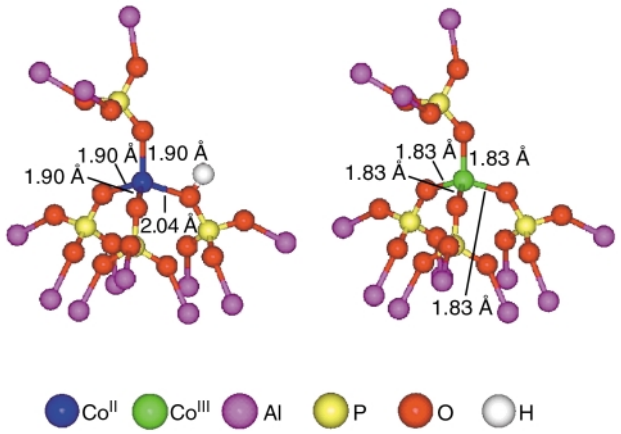

Fig. 11 The Brønsted acid active centre in Co^{II}AlPO-18 consists of the Co^{II} ion (shown in blue) together with its nearby proton (white) loosely bound to an adjacent framework oxygen. (When this acid catalyst is calcined in oxygen, the Co^{II} ion is converted to Co^{III} which is the redox active centre.[5])

ethene and propene, with a selectivity of *ca.* 60% and *ca.* 20% for the two alkenes, respectively.

There are many points of similarity between catalytic reactions in microporous sieves on the one hand and enzymatic reactions on the other, shape-selectivity being the most prominent common feature. Further points of comparison have been made in a recent study[43] with Harris and his group involving the (solid)-acid-catalyzed oligomerization or cyclo-dimerisation of 3-hydroxy-3-methylbutan-2-one, hereafter abbreviated as HMB.

HMB is a stable liquid at ambient temperature. In acidic solutions, however, HMB readily undergoes reaction to generate a variety of products including the cyclic dimer (see Scheme 4) and the dehydrated reactant $MeCOC(Me)=CH_2$. The

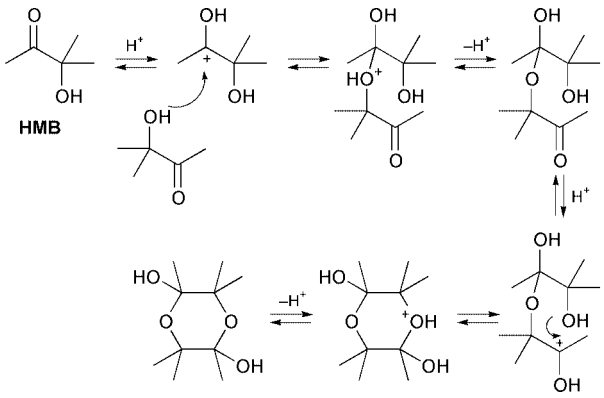

Scheme 4

precise nature and distribution of the products varies significantly depending on the solvent and conditions used for the proton-catalyzed solution-state reaction. However, when HMB is incorporated within the channels of a synthetic zeolite, ferrierite, only one product (established by ^{13}C solid state MAS NMR) is observed together with some unreacted HMB. A plausible mechanism for the Brønsted acid-catalyzed cyclo-dimerisation is shown in Scheme 4. Harris and coworkers[43] have recently made a comparison of the proton-catalyzed bimolecular reaction observed in the cyclo-dimerization of HMB and other monomers with the mode of action of triosephosphate isomerase.

G Ammoximations: ε-caprolactam from cyclohexanone

For completeness, we should also mention the ability possessed by our designed Me^{III}AlPO-36 and Me^{III}AlPO-5 molecular sieve catalysts in effecting ammoximations. The reaction of

cyclohexanone with hydroxylamine (in its sulfate or phosphate form) is the best known method for the production of cyclohexanone oxime, and its subsequent Beckmann rearrangement to ε-caprolactam is an important, industrially used reaction. About 90% of ε-caprolactam world-wide is produced by using the above-mentioned conventional cyclohexanone process. However, large-scale industrial processes for the production of ε-caprolactam (monomer for nylon 6), employing cyclohexanone as the starting material, invariably produce large quantities of ammonium sulfate as by-products (see Scheme 2), which are undesirable. In 1990, the world-wide production of ε-caprolactam reached 3 million metric tons.

Fig. 12 summarizes the results of our ammoximation experiments using cyclohexanone in the presence of ammonia

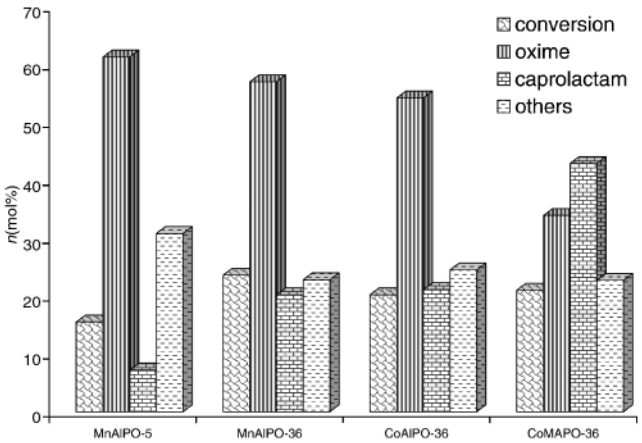

Fig. 12 Bar chart showing the relative performance of various transition metal ion (framework)-substituted molecular sieve catalysts in the conversion of cyclohexanone to its corresponding oxime and ε-caprolactam. The best catalyst is the bifunctional one (CoMAPO-36) which has both redox- and Brønsted acid-active sites.

and H_2O_2 [O_2 or *tert*-butyl hydroperoxide (TBHP) can also be used as oxidants], and MnAlPO-5 or Mn(Co)-AlPO-36 as catalysts, to produce the corresponding cyclohexanone oxime and ε-caprolactam. The ketone (cyclohexanone) is first oxidized in the presence of the 'redox' (Co^{III}, Mn^{III}) ions and ammonia to the oxime (cyclohexanone oxime). The Brønsted acid sites in the molecular sieves catalyze the subsequent Beckmann rearrangement of cyclohexanone oxime to ε-caprolactam. Interestingly, the (deliberate) introduction of acid centres (in the form of Mg^{II} or Zn^{II}, during synthesis, and typified by CoMAPO-36 in Fig. 12), further enhanced the selectivity for ε-caprolactam, thereby bringing out the bifunctional ability possessed by our catalysts.

3 Atomically engineered active sites in mesoporous solids

Here we demonstrate how to design and characterize high-performance catalysts for four distinct categories of reaction: the epoxidation of alkenes, solvent-free hydrogenations of unsaturated organic species, a novel kind of enantioselective hydrogenation, and selective oxidation (including oxidative dehydrogenation). Since these conversions employ mesoporous catalysts (with pore diameters upwards of 30 Å), quite bulky organic molecules (many of which could not gain access to the active centres inside the microporous catalysts discussed so far in this review) may be processed. Moreover, all the desiderata enumerated in Table 1, with the exception of regio- and shape-selective processes that are easier to effect with microporous, molecular sieve catalysts are achievable with mesoporous silicas onto the three-dimensional surface areas of which active sites have been grafted as described below.

A Titanosilicate epoxidation catalysts

The catalytic conversion of propylene to propylene oxide over Ti/SiO_2 catalysts in the presence of *tert*-butyl hydroperoxide (TBHP) is an industrially important epoxidation that accounts for an annual production of more than a million tons of propylene oxide worldwide.[23] From the outset,[44] there has been much speculation as to both the nature of the active site and the mechanism of this reaction and other selective oxidations effected by titanium-centred catalysts.[45] Five years ago, one of us and his colleagues set out[46] to prepare single-site, Ti^{IV}-centred, silica-based catalysts by reacting titanocene dichloride in the presence of triethylamine with the silanol groups that line (see Fig. 13) the inner walls of mesoporous silica. After

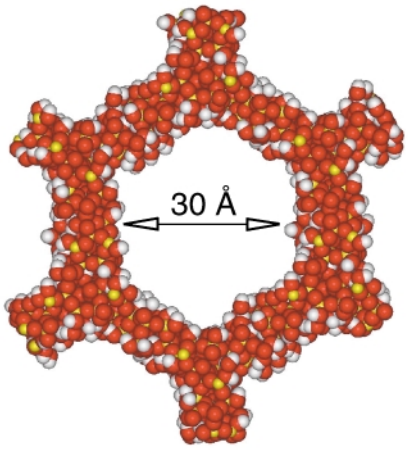

Fig. 13 Computer graphic representation of a single mesopore in MCM-41 silica (red, oxygen; yellow, silicon; white, hydrogen).

subsequent calcining in oxygen, all the organic residue in the silica-bound titanocene was driven off; and XAFS analysis showed that the structure of the active site is as shown in Fig. 14.

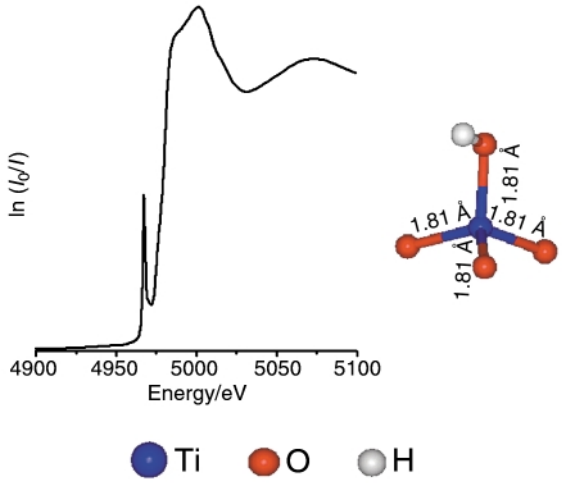

Fig. 14 Ti K-edge XANES of a Ti↑MCM-41 epoxidation catalyst after calcination. Both the XANES and EXAFS data (latter not shown) point to the tripodally attached titanyl group as the (Ti^{IV}-centred) active site.[47]

Both the XANES and EXAFS results for this catalyst revealed that isolated Ti^{IV}-centred active sites, composed of a tripodally-linked titanol groups, abound on the catalyst surface. There are no signs of Ti–O–Ti linkages, nor of any titanyl (T=O) groups of the kind proposed[44] earlier, either of a three- or five-coordinated kind. Detailed comparisons (of XAFS data) with several other local Ti^{IV}-centred oxygen environments leave no doubt[47–49] that the active sites in our highly active (so-called[48] Ti↑MCM-41) catalyst are four-coordinated. There are no 6-coordinated Ti^{IV}-centred sites present in the as-prepared catalyst. Thomas and Sankar also recorded[7,47,49] XAFS data

during the course of operation of the Ti ↑ MCM-41 catalyst in the epoxidation of cyclohexene to its epoxide with TBHP, a convenient test reaction. Significantly, the coordination shell of the original, 4-coordinated Ti^{IV} active sites expands to six during catalysis. And, whereas four of the surrounding oxygens are at distances strictly comparable to those in the pristine active site, in the reactive state there are two additional oxygens situated further away. This fact flatly contradicts the mechanism of epoxidation proposed earlier:[44] a more realistic picture is one in which, just prior to the act of epoxidation, the Ti^{IV}-centred active site is in six-fold coordination. This is compatible with the radical-free picture of epoxidation that we established previously.[48] Our method of preparing highly active titanosilicate catalysts from a titanocene precursor has been shown[50] recently to be ideally suited for the one-pot conversion of citronellal into isopulegol epoxide (see Scheme 5).

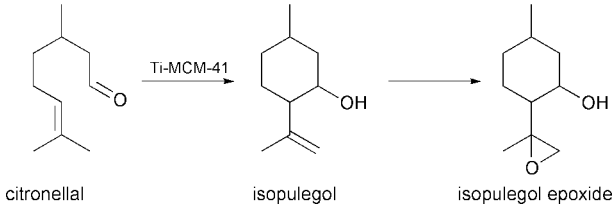

Scheme 5

Knowing the structure of the active site, we may set about boosting its catalytic activity by altering its immediate environment. This can be done by replacing[51] one of the silicons in the tripodally attached Ti^{IV} centre by germanium. The resulting catalyst, with a modified active site, exhibits an activity for the epoxidation of cyclohexene that surpasses that of the original catalyst, which, in turn, is superior to that of the catalyst prepared according to the procedure employed for the industrial preparation. There is clearly a favourable electronic influence in proceeding from ⩾$(SiO)_3$Ti–OH to ⩾$(SiO)_2$(GeO)Ti–OH.

It is a fortunate fact that titanosilsesquioxanes,[52] in which the Ti occupies one of the eight vertices of the cube formed by alkyl-substituted Si_7O_{11} moieties, are soluble in organic solvents, and that they also function as good, homogeneous epoxidation catalysts.[53] Moreover, the immediate environment of the Ti^{IV}-centred active sites in these soluble catalysts may also be readily probed using the XAFS technique.

Significantly, the performance of the heterogeneous and homogeneous Ti^{IV}-centred epoxidation catalysts are quantitatively very similar,[54] both in the un-enhanced and promoted states, caused by juxtaposing germanium in place of silicon. Furthermore, the fact that the turnover frequency in absolute terms (number of moles of the alkene epoxidized by the active site in unit time) is essentially the same for the heterogeneous as it is for the homogeneous (titanosilsesquioxane) catalyst lends independent proof (beyond the structural one based on EXAFS) that our designed titanosilicate catalysts are indeed 'single-site' ones.

B Engineered active centres for selective hydrogenations: encapsulated bimetallic nanocatalysts for solvent-free reactions

An inherent advantage possessed by mesoporous silicas, of the type exemplified in Fig. 13, is that it is readily possible to insert into such pores mixed-metal carbonylates that are quite bulky, or to graft onto their inner walls carefully constructed, chirally biased large metal complexes. In a collaboration with Johnson and his coworkers, we have capitalised upon this fact. In particular, we have inserted[55] cluster carbonylate salts such as $[Ru_6C(CO)_{16}CuCl]_2[PPN]_2$, where PPN stands for bis-(triphenylphosphino)iminium, into MCM-41 silica. These salts can be shown by *ex situ* HREM studies[55] to be encapsulated in a spatially uniform manner along the inner surfaces of the mesopores. (The Si–OH groups undergo hydrogen-bonding with the O–C–M bond of the carbonyls). *In situ* XAFS and FTIR studies are used to chart the progressive conversion, by gentle thermolysis, of the carbonylate salts into the denuded, bimetallic (carbided) nanoparticle catalysts. Separate Cu and Ru K-edge XAFS studies, for example, yield[55] a good picture of the active nanoparticle catalyst (*ca.* 15 Å diameter), which has a composition $Cu_4Ru_{12}C_2$. (They exhibit high turnover frequencies for hex-1-ene, diphenylacetylene, stilbene, *cis*-cyclooctene, D-limonene and 1,5,9-cyclododecatriene.)

In a further collaboration with Johnson and his group, a number of solvent-free selective hydrogenations of polyenes using a bimetallic Ru_6Sn nanoparticle catalyst have been highlighted[56] (see Fig. 15 and 16). The selective hydrogenation

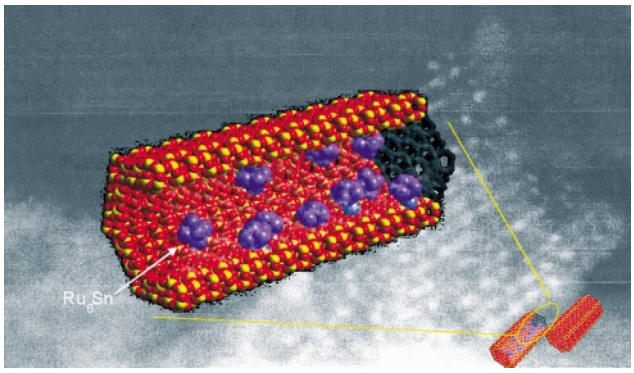

Fig. 15 Clusters of Ru_6Sn, anchored at the inner surfaces of mesoporous silica (MCM-41) function as powerful catalysts in the solvent-free selective hydrogenation of a variety of polyenes. In the background electron micrograph the linearly arranged white spots demarcate the anchored bimetallic clusters (diameter *ca.* 10 Å).[15]

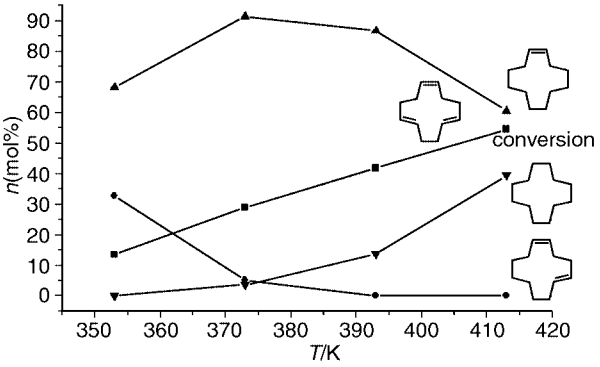

Fig. 16 The influence of temperature on the activity and selectivity of an anchored Ru_6Sn nanoparticle catalyst in the selective hydrogenation of 1,5,9-cyclododecatriene.[56]

of polyenes such as 1,5,9-cyclododecatriene is quite an important procedure in the synthesis of organic and polymeric intermediates such as laurolactam, 12-aminododecanoic acid and dodecanedioic acid, which are important monomers for nylon 12, nylon 612, copolyamides, polyesters and for various materials used as coatings (see Scheme 6). Hitherto, Raney nickel, Pd, Pt, Co, and mixed transition metal complexes have been used for these hydrogenations, and all the reactions entail the use of organic solvents (such as n-heptane or benzonitrile) and often in the presence of efficient hydrogen donors (such as 9,10-dihydroanthracene). Our procedures emphasize that there are solvent-free routes available for such processes.

C Constrained chiral catalysts for enantioselective hydrogenation

The large diameters of mesoporous silica permit the direct grafting of complete chiral metal complexes on to the inner walls by functionalizing the pendant surface silanols with organic groups such as alkyl halides, amines, carboxylates and

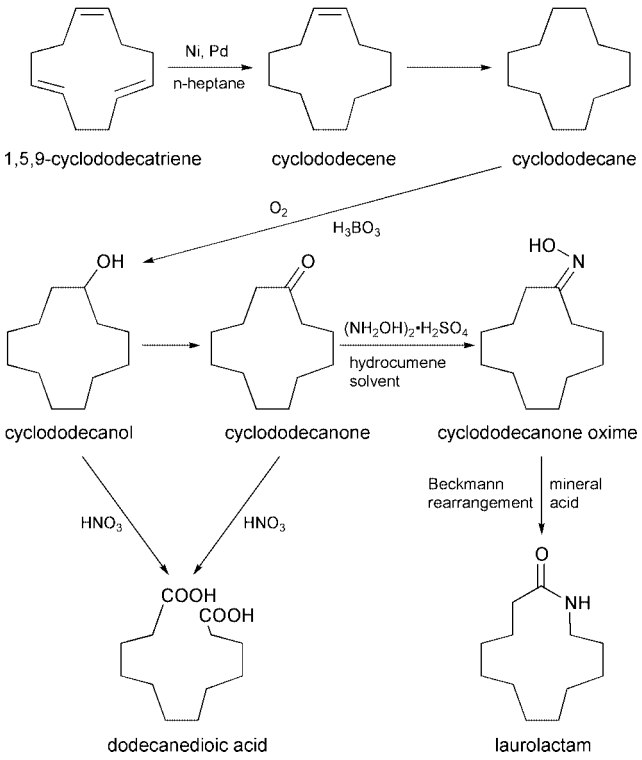

Scheme 6

phosphanes. As pointed out by our colleague Maschmeyer,[57] this opens routes to the preparation of novel catalysts consisting of quite large concentrations of accessible, well-spaced and structurally well-defined active centres. As detailed elsewhere,[8,57,58] chiral chelate ligands based on 1,1′-bis(diphenylphosphino)ferrocene (dppf) are particularly attractive for tethering on to mesoporous silica; and the superior performance of the chiral, heterogenized catalyst compared with the unconfined homogeneous analogue in the allylic amination (Tsuji–Trost) reaction between cinnamyl acetate and benzylamine has been described.[58]

We have recently demonstrated[59] that this kind of confined dppf catalyst displays remarkable increases in both enantioselectivity and activity in the one-step hydrogenation of ethyl nicotinate to ethyl nipecotinate (see Scheme 7) when compared to an analogous homogeneous compound. Some of the key points to note here are as follows:

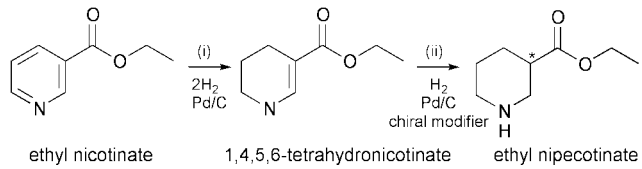

Scheme 7

- the previously available[60] procedure for producing the biologically relevant nipecotinate entailed a two-step process (Scheme 7) and the use of a chiral modifier, such as dihydrocinchonidine, in one of the steps;
- confinement is a crucial step in producing the enantioselective, anchored ferrocenyl precursor that is prepared as outlined in Scheme 8;
- when exactly the same ferrocenyl precursor is attached in a spatially unconstrained fashion to a silsesquioxane, thereby producing a homogeneous catalytic analogue of the chiral catalyst confined within mesoporous silica, no enantioselectivity results (Fig. 17);
- to maximize the efficiency of such confined chiral catalysts the exterior surfaces of the mesoporous silica are first reacted with dichlorodiphenylsilane, so as to ensure that anchoring of the dppf precursor occurs only at the interior faces of the siliceous support.[58]

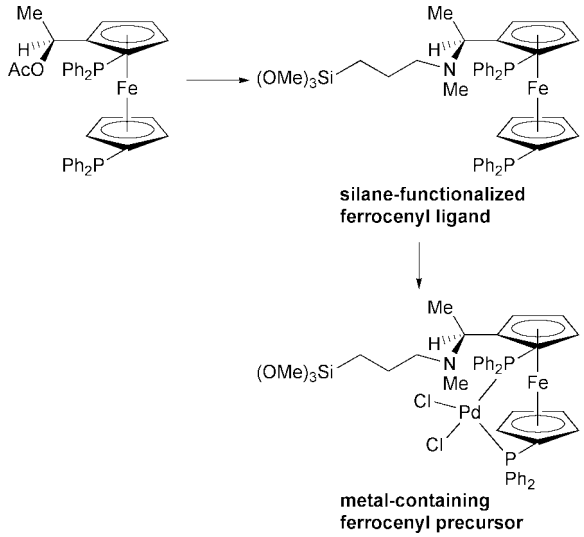

Scheme 8

It is to be emphasized that the enantioselectivity that we achieve in this approach (with constrained chiral catalysts) is somewhat different from that which was introduced by Corma[61] but quite distinct from that used by Hutchings.[62]

D Selective oxidations and oxidative dehydrogenations

Here we illustrate briefly the merits of engineering well-defined active centres at mesoporous silica surfaces for the purposes of (i) oxidatively dehydrogenating methanol at Mo^{VI}-centred sites; and (ii) selectively oxidizing hydrocarbons grafted at vanadyl centres and an anchored oxo-centred Co^{III} acetate oligomer.

Just as $Ti(\eta^5\text{-}C_5H_5)_2Cl_2$ serves as an excellent means of introducing isolated Ti^{IV}-centred, catalytically active sites on a silica support (for epoxidation and other conversions[50]), so also does[63] $Mo(\eta^5\text{-}C_5H_5)_2Cl_2$ function as a similar precursor for the creation of Mo^{VI}-centred sites for the oxidative dehydrogenation of methanol to produce formaldehyde. Mo K-edge XAFS shows that, at low loadings, isolated, tetrahedrally-bound MoO_4 species are generated on the surface; however, these bipodally attached oxo–molybdenum species are held less strongly to the silica support than the tripodal Ti^{IV} centres described earlier.

Designed vanadium-centred active sites situated at the inner surface of mesoporous siliceous hosts (as well as at amorphous, microporous mixed-metal oxides of the types described by Maier *et al.*[64]) are catalysts, under mild conditions, for both the epoxidation of alkenes (typified by cyclohexene) and the selective oxidation of alkanes (typified by cyclohexane). XAFS studies proved invaluable in determining the nature of these active sites (see Fig. 18), the performance of which could be boosted[65] by juxtaposing methyl groups (to enhance the hydrophobicity) in the immediate vicinity of the vanadyl active centre.

In homogeneous mixtures of Co^{III} acetates rich in acetic acid, such as those used commercially in the selective oxidation of cyclohexane, many oligomers of the cobalt salt are present. By isolating and testing the catalytic activity of each separate oligomer it was found that the trimer displayed exceptional selectivity in oxidizing the CH groups of adamantane.[66] Specimens of the trimer were accordingly tethered to the inner walls of mesoporous silica, and the resulting uniform heterogeneous catalyst exhibited high activity in the solvent-free oxidation of cyclohexane to cyclohexanol and cyclohexanone using the sacrificial oxidant TBHP.[17] Moreover, *in situ* XAFS measurements showed that significant structural changes occurred in the tethered trimer during the initial period of induction prior to the onset of catalysis. There is reason to

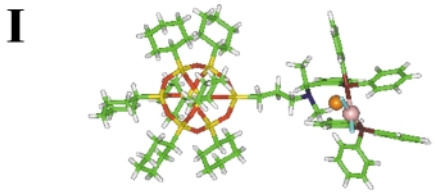

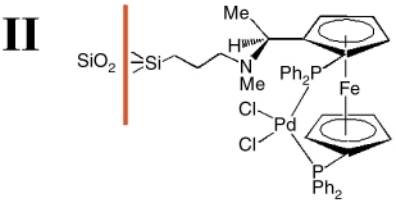

Dppf–ferrocenyl–diamine–Pd catalyst	Substrate (reactant)	*t*/h	Conv. (%)	ee (%)
Homogeneous (**I**)	Ethyl	72	15.9	—
	nicotinate	120	27.2	—
Tethered silica (**II**)	Ethyl	72	12.6	2
	nicotinate	120	19.2	2
Tethered to MCM-41 and confined inside mesopore (**III**)	Ethyl	48	35.5	17
	nicotinate	72	53.7	20

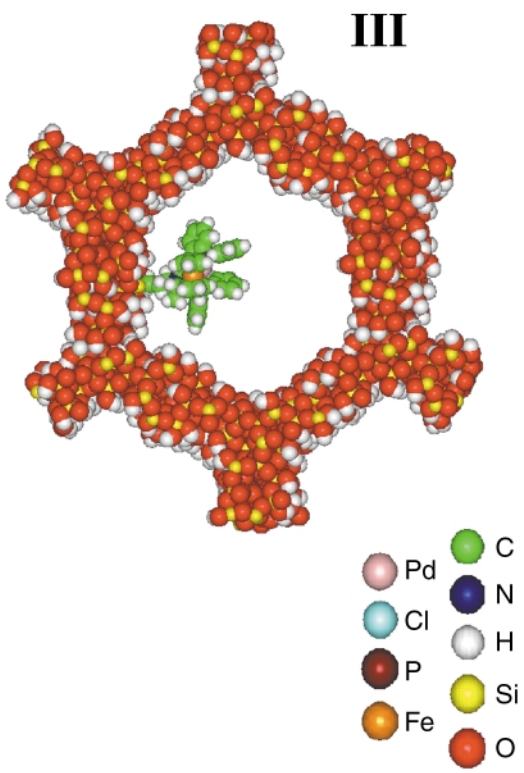

Fig. 17 Depiction of the catalytically active centre attached to a soluble silsesquioxane moiety **I** (top left) to a non-porous silica particle **II**, and bound in a constrained manner inside mesoporous silica **III** (right). The table (bottom left) shows that a significant measure of enantiomeric excess (ee) and substantial conversions are obtained only when the dppf–ferrocenyl–Pd-catalyst is in a constrained environment within the mesopore.

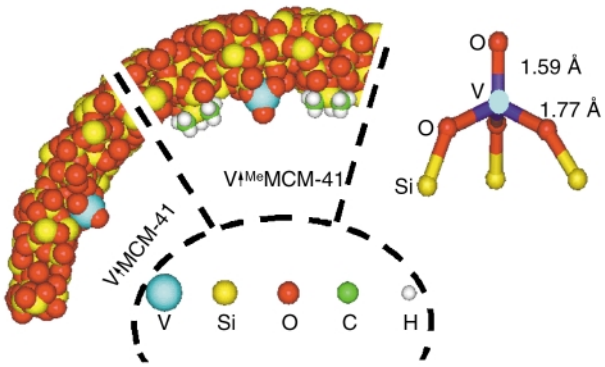

Fig. 18 A vanadyl active centre: (left) grafted onto a mesoporous silica; (centre) surrounded by nearby surface methyl groups to boost hydrophobicity; and (right) model, with bond distances derived from XAFS spectra (not shown), of the four-coordinated vanadium ion.[65]

believe[67] that certain metal complexes anchored to the inner walls of mesoporous silica may function as effective oxidation catalysts.

E Other related reactions

The atomic engineering of active centres on silica surfaces described above is part of a widely-applicable approach used previously by us[17,38,66,68] and others, especially by Basset and his group in their pioneering work[69] on surface organometallic chemistry. Basset *et al.*[70–73] have, for example, shown how various kinds of C–C bond cleavage and formation (involving hydrogenolysis or metathesis of alkanes) may proceed smoothly at tantalum hydride centres that are either monopodally or bipodally anchored to silica surfaces.

Among the principles that we seek to emphasize in this review are the twin advantages in using (a) synchrotron radiation for the *in situ* and *ex situ* characterisation[47] of the precise nature of the engineered active centres, and (b) well-defined mesoporous silicas with their high internal surface areas and adjustable pore diameters.

4 The stability of our catalysts

When we began our studies of MeAlPO selective oxidation catalysts, many practitioners who had earlier studied such solids predicted that we would run into insurmountable obstacles largely because of the tendency for the framework ions that constitute the active sites to be leached out of the molecular sieves during reaction. It is undoubtedly true that such solids do tend to suffer leaching if aggressive solvents (such as acetic acid) are used. But, from the outset, our aim was to achieve desirable chemical conversions in a solvent-free manner. By simply using the reactants (such as n-alkanes and oxygen as oxidant) we found that our microporous, molecular sieve catalysts ($Me^{III}AlPO$-*n* with $Me \equiv Fe^{III}$, Co^{III} or Mn^{III}) remained intact even after repeated use, provided that the overall conversion in the oxidations was kept relatively low (*ca.* 10–12%). This level of conversion avoids leaching by the polar products of the reaction (such as the n-alkanoic acids).

One recommended experimental test designed to ascertain whether the catalysis is truly heterogeneous or merely apparently so entails filtering off the 'active' solid catalyst from the reaction mixture (when hot) and then determining whether the reactants are still catalytically converted (by leached out active entities) in the residual liquid. Whenever we have carried out such tests they have always been negative: no reaction ensues in the absence of the solid molecular sieve catalyst [a striking example is shown in Fig. 2b of ref. 10(a)].

There is another incontrovertible procedure[20] to test whether the catalysis is truly heterogeneous or only apparently so because leached out ions are retained within the liquid phase that closely adheres to the molecular sieve. This is the one which involves taking an equimolar mixture of n-hexane and cyclohexane and subjecting it to aerobic oxidation over a $Co^{III}AlPO$-18 (or $Mn^{III}AlPO$-18) catalyst. There is, unsurprisingly, no conversion whatsoever of the cyclohexane molecule

as it is too large to gain access into the interior of the MeAlPO-18 where the vast majority of the active sites are located. The conversion of the n-hexane, however, is, as expected, to be quite substantial (there being good selectivity for terminally oxy-functionalised products). However, when the same reactant mixture is dissolved in acetic acid, the Co^{III}AlPO-18 catalyst gives rise to considerable oxidation of both cyclohexane and n-hexane. Moreover, C_2 and C_3 alcohols and ketones are now the main products (not the C_1 alcohols or acids) from n-hexane. Clearly, acetic acid as a solvent results in homogeneous as well as heterogeneous catalysis.

Other work (as yet unpublished) using CrAlPO-5 as a molecular sieve catalyst has likewise been found to facilitate genuine heterogeneous conversions (such as the decomposition of cyclohexyl hydroperoxide) of organic chemical compounds.

Leaching has to be considered as a factor also in the epoxidation and other oxidative reactions catalyzed by mesoporous silica on to which Ti^{IV} or Mo^{VI} centres have been grafted. Whereas tripodally attached Ti^{IV} ions stand up well to continued use as epoxidation catalysts with reagents such as TBHP,[54] detailed investigations[52c,53a] with model silsesquioxanes show that bipodally or monopodally attached Ti^{IV} ions are less securely held and tend to be leached out during reaction. Moreover, in the case of dipodally attached Mo^{VI} ions, leaching is quite appreciable, making the molybdenocene-derived Mo/SiO_2 catalyst[63] analogue of Ti/SiO_2 less effective in oxidative dehydrogenation reactions.

Acknowledgements

We thank the EPSRC (for a rolling grant to J. M. T.), The Commissioners of the Royal Commission of 1851 for an Exhibition (to R. R.), and our colleagues, especially Drs Sankar, Bell, Lewis, Maschmeyer, Professor B. F. G. Johnson and Professor C. R. A. Catlow and their groups, for their valuable stimuli.

References

Based on the opening plenary lecture given by John Meurig Thomas at Materials Discussion No. 3, 26–29 September, 2000, University of Cambridge, UK.

1 D. C. Phillips, *Proc. Natl. Acad. Sci. USA*, 1967, **57**, 484.
2 D. M. Blow, *Acc. Chem. Res.*, 1976, **9**, 145.
3 C. Branden and J. Tooze, *Introduction to Protein Structure*, Garland, New York, 2nd edn., 1998.
4 J. W. Couves, J. M. Thomas, D. Waller, R. H. Jones, A. J. Dent, G. E. Derbyshire and G. N. Greaves, *Nature*, 1991, **354**, 465.
5 J. M. Thomas and G. N. Greaves, *Science*, 1994, **265**, 1675; J. M. Thomas, G. N. Greaves, G. Sankar, P. A. Wright, J. Chen, A. J. Dent and L. Marchese, *Angew. Chem., Int. Ed. Engl.*, 1994, **33**, 1871.
6 J. M. Thomas, *Chem. Eur. J.*, 1997, **3**, 1557.
7 J. M. Thomas and G. Sankar, *Top. Catal.*, 1999, **8**, 1.
8 J. M. Thomas, *Angew. Chem., Int. Ed. Engl.*, 1999, **38**, 3588.
9 J. M. Thomas and W. J. Thomas, *Heterogeneous Catalysis: Principles and Practices*, Wiley-VCH, Weinheim, 1997, ch. 3.
10 (*a*) J. M. Thomas, R. Raja, G. Sankar and R. G. Bell, *Nature*, 1999, **398**, 227; (*b*) R. Raja, J. M. Thomas, G. Sankar and R. G. Bell, *Stud. Surf. Sci. Catal.*, 2000, **130A**, 2313.
11 J. M. Thomas, R. Raja, G. Sankar and R. G. Bell, *Acc. Chem. Res.*, 2001, **34**, in press.
12 Our EXAFS studies establish beyond doubt the oxidation state of the framework-substituted transition-metal ions that function as the catalytically active centres.
13 P. A. Barrett, G. Sankar, C. R. A. Catlow and J. M. Thomas, *J. Phys. Chem. A.*, 1996, **100**, 8977.
14 P. A. MacFaul, D. D. M. Wayner and K. U. Ingold, *Acc. Chem. Res.*, 1998, **31**, 159; J. M. Thomas, *Nature*, 1985, **314**, 669; *Activation and Functionalization of Alkanes*, ed. C. L. Hill, Wiley, Chichester, 1989, ch. 6–8, 16; C. A. Tolman, J. D. Druliner, M. J. Nappa and N. Herron, in *Activation and Functionalization of Alkanes*, C. L. Hill, ed., Wiley, Chichester, 1989, pp. 303–360; N. Herron and C. A. Tolman, *J. Am. Chem. Soc.*, 1987, **109**, 2837.
15 J. M. Thomas, R. Raja, G. Sankar, B. F. G. Johnson and D. W. Lewis, *Chem. Eur. J.*, 2001, **7**, in press.
16 E. P. Talsi, V. D. Chinakov, V. P. Babenko, V. N. Sidelnikov and K. I. Zamaraev, *J. Mol. Catal. A.*, 1993, **81**, 215.
17 T. Maschmeyer, R. D. Oldroyd, J. M. Thomas, G. Sankar, I. J. Shannon, J. A. Klepetko, A. F. Masters, J. K. Beattie and C. R. A. Catlow, *Angew. Chem., Int. Ed. Engl.*, 1997, **36**, 1639.
18 K. Tanaka, *Chem. Technol.*, 1974, **9**, 555.
19 G. Sankar, R. Raja and J. M. Thomas, *Catal. Lett.*, 1998, **55**, 15.
20 R. Raja, G. Sankar and J. M. Thomas, *J. Am. Chem. Soc.*, 1999, **121**, 11926.
21 M. Dugal, G. Sankar, R. Raja and J. M. Thomas, *Angew. Chem., Int. Ed.*, 2000, **39**, 2310.
22 P. B. Weisz, W. O. Haag and R. M. Lago, *Nature*, 1984, **309**, 589.
23 R. Murugavel and H. W. Roesky, *Angew. Chem., Int. Ed. Engl.*, 1997, **36**, 477.
24 R. Raja and J. M. Thomas, *Chem. Commun.*, 1998, 1841.
25 C. M. Freeman, C. R. A. Catlow, J. M. Thomas and S. Brode, *Chem. Phys. Lett.*, 1991, **186**, 137.
26 B. R. Cook, T. J. Reinert and T. S. Suslick, *J. Am. Chem. Soc.*, 1986, **108**, 7281; D. Mansuy, *Pure Appl. Chem.*, 1987, **59**, 759.
27 J. A. Smegal and C. L. Hill, *J. Am. Chem. Soc.*, 1983, **105**, 3515.
28 R. Raja, G. Sankar and J. M. Thomas, *Angew. Chem., Int. Ed. Engl.*, 2000, **39**, 2313.
29 Food and beverage containers, which constituted the fastest growing segment, accounted for 13% while other applications include film for audio, video and photography, high-performance molding resins, industrial coatings, electrical insulating varnishes, aramid fibres, plasticizers and adhesives.
30 Industrial purification procedures are quite expensive and often involve the hydrogenation of 4-formylbenzoic acid to the more soluble toluic acid, which can be further oxidized to terephthalic acid.
31 Further work is in progress to clarify this point.
32 This is then further esterfied with a BF_3–MeOH mixture, to yield dimethyl terephthalate.
33 A. Baeyer and V. Villiger, *Ber. Dtsch. Chem. Ges.*, 1899, **32**, 3625.
34 R. Raja, J. M. Thomas and G. Sankar, *Chem. Commun.*, 1999, 525.
35 R. Raja, G. Sankar and J. M. Thomas, *Chem. Commun.*, 1999, 829; A wide range of linear and cyclic alkenes such as hex-1-ene, cyclohexene, α-(+)-pinene, (*R*)-(+)-limonene and styrene were oxidized to their corresponding epoxides in high yields.
36 T. Mukaiyama, in *The Activation of Dioxygen and Homogeneous Catalytic Oxidation*, ed. D. H. R. Barton, A. E. Mantell and D. T. Sawyer, Plenum, New York, 1993, p. 133.
37 H. F. W. J. van Breukelan, M. E. Gerrisen, V. M. Ummels, J. S. Broes and J. H. C. van Hoof, *Stud. Surf. Sci. Catal.*, 1996, **105**, 1029.
38 J. M. Thomas, *Philos. Trans. R. Soc. A*, 1990, **333**, 173; J. M. Thomas, *Sci. Am.*, 1992, **266**, 112.
39 See for example, J. A. Rabo, *Proc. 10th Intl. Congr. Catalysis*, L. Guczi, ed. F. Solymosi and P. Tetanyi, Buadpest, Akademia Kaio, 1992, p. 1 and references therein.
40 J. Chen and J. M. Thomas, *J. Chem. Soc., Chem. Commun.*, 1994, 603.
41 J. Chen, J. M. Thomas, P. A. Wright and R. P. Townsend, *Catal. Lett.*, 1994, **28**, 241.
42 P. A. Barrett, R. H. Jones, J. M. Thomas, G. Sankar, I. J. Shannon and C. R. A. Catlow, *Chem. Commun.*, 1996, 2001; J. M. Thomas and D. W. Lewis, *Z. Phys. Chem.*, 1997, **4**, 29.
43 S.-Ok, S. Kitchen, K. D. M. Harris, M. Dugal, G. Sankar and J. M. Thomas, *Catal. Lett.*, in press.
44 R. A. Sheldon, *J. Mol. Catal. A.*, 1983, **20**, 1; K. A. Jorgenson, *Chem. Rev.*, 1989, **89**, 431.
45 M. Taramasso, G. Perego and B. Notari, *US Pat.*, 4410501, 1983; B. Notari, *Adv. Catal.*, 1996, **41**, 253; D. Gleeson, G. Sankar, C. R. A. Catlow, J. M. Thomas, G. Spano, S. Bordiga, A. Zecchina and C. Lamberti, *Phys. Chem. Chem. Phys.*, 2000, **2**, 4812.
46 T. Maschmeyer, F. Rey, G. Sankar and J. M. Thomas, *Nature*, 1995, **378**, 159.
47 J. M. Thomas and G. Sankar, *Acc. Chem. Res*, 2001, **34**, in press; J. M. Thomas and G. Sankar, *J. Synchrotron Radiat.*, 2001, **8**, 55.
48 R. D. Oldroyd, J. M. Thomas, T. Mascmeyer, P. A. MacFaul, D. W. Snelgrove, K. U. Ingold and D. D. M Wayner, *Angew. Chem., Int. Ed. Engl.*, 1996, **35**, 2787.
49 J. M. Thomas, *Faraday Discuss.*, 1996, **105**, 1.
50 M. Guidotti, G. Moretti, R. Psaro and N. Ravasio, *Chem. Commun.*, 2000, 1789.
51 R. D. Oldroyd, G. Sankar and J. M. Thomas, *Chem. Commun.*, 1997, 2025.
52 (*a*) F. J. Feher, S. L. Gonzales and J. W. Ziller, *Inorg. Chem.*, 1988, **27**, 3440; (*b*) R. Murugavel, A. Voigt, M. G. Walwalker and H. W. Roesky,

Chem. Rev., 1996, **96**, 2205; (*c*) H. C. L. Abbenhuis, S. Krijnen and R. A. van Santen, *Chem. Commun.*, 1997, 331.
53 (*a*) M. C. Klunduk, T. Maschmeyer, J. M. Thomas and B. F. G. Johnson, *Chem. Eur. J.*, 1999, **5**, 1481; (*b*) M. Crocker, R. H. M. Herold and A. G. Orpen, *Chem. Commun.*, 1997, 2411.
54 J. M. Thomas, G. Sankar, M. C. Klunduk, M. P. Attfield, T. Maschmeyer, B. F. G. Johnson and R. G. Bell, *J. Phys. Chem. B.*, 1999, **103**, 8809.
55 D. S. Shephard, T. Maschmeyer, G. Sankar, J. M. Thomas, D. Ozkaya, B. F. G. Johnson, R. Raja, R. D. Oldroyd and R. G. Bell, *Chem. Eur. J.*, 1998, **4**, 1214; W. Zhou, J. M. Thomas, D. S. Shephard, B. F. G. Johnson, D. Ozkaya, T. Maschmeyer, R. G. Bell and Q. Ge, *Science*, 1998, **280**, 705.
56 S. Hermans, R. Raja, J. M. Thomas, B. F. G. Johnson, G. Sankar and D. Gleeson, *Angew. Chem., Int. Ed. Engl.*, 2001, **40**, in press.
57 T. Maschmeyer, *Unpublished Presentation at the Annual Progress Meeting at the Davy–Faraday Research Laboratory*, 17 March, 1995; J. M. Thomas, *Faraday, Discuss.*, 1995, **100**, C9; J. M. Thomas, T. Maschmeyer, B. F. G. Johnson and D. S. Shephard, *J. Mol. Catal. A.*, 1999, **141**, 139.
58 B. F. G. Johnson, S. A. Raynor, D. S. Shephard, T. Maschmeyer, J. M. Thomas, G. Sankar, S. Bromley, R. D. Oldroyd, L. F. Gladden and M. D. Mantle, *Chem. Commun.*, 1999, 1167.
59 S. A. Raynor, J. M. Thomas, R. Raja, B. F. G. Johnson, R. G. Bell and M. D. Mantle, *Chem. Commun.*, 2000, 1925.
60 H.-U. Blaser, H. Honig, M. Studer and C. Wedemeyer-Exl, *J. Mol. Catal. A*, 1999, **139**, 253.
61 A. Corma, M. Iglesias, C. del Pino and F. Sànchez, *Proc. 10th Int. Cong. Catal.*, Elsevier, Amsterdam, 1993, p. 2293.
62 G. J. Hutchings, *Chem. Commun.*, 1999, 301.
63 I. J. Shannon, T. Maschmeyer, R. D. Oldroyd, G. Sankar, J. M. Thomas, H. Pernot, J. P. Balikdjian and M. Che, *J. Chem. Soc., Faraday Trans.*, 1998, **94**, 1495.
64 W. F. Maier, J. A. Martens, S. Klein, J. Heilmann, R. Parton, K. Vercruysse and P. A. Jacobs, *Angew. Chem., Int. Ed. Engl.*, 1996, **35**, 180.
65 R. D. Oldroyd, G. Sankar, J. M. Thomas, M. Hunnius and W. F. Maier, *J. Chem. Soc., Faraday Trans.*, 1998, **94**, 3177.
66 T. Maschmeyer, J. M. Thomas and A. F. Masters, in *New Trends in Materials Chemistry*, A. K. Cheetham and C. R. A. Catlow, ed., NATO ASI, 1997, **498**, 461.
67 M. Dugal, R. Raja, G. Sankar and J. M. Thomas, work in progress.
68 J. M. Thomas, *J. Mol. Catal. A.*, 1999, **146**, 77.
69 J. M. Basset, J. P. Candy, A. Chopin, B. Didillon, F. Quignand and A. T. Théolier, in *Perspectives in Catalysis*, ed. J. M. Thomas and K. I. Zamaraev, Blackwell Sci. Pub., Oxford, 1992, p. 125.
70 V. Vidal, A. T. Théolier, J. Thivolle-Cazat and J. M. Basset, *Science*, 1997, **276**, 99.
71 V. Vidal, A. T. Théolier, J. Thivolle-Cazat and J. M. Basset, *J. Chem. Soc., Chem. Commun*, 1995, 991.
72 M. Chabanas, V. Vidal, C. Copéret, J. Thivolle-Cazat and J. M. Basset, *Angew. Chem., Int. Ed.*, 2000, **39**, 1962.
73 O. Maury, G. Saggio, A. T. Théolier, M. Taoufik, V. Vidal, J. Thivolle-Cazat and J. M. Basset, *Comptes Rendes*, 2000, **3**, 583.

ChemComm

Liposome made of imidazolyl-substituted porphyrin as a single component

Naoto Nagata, Shin-ichi Kugimiya and Yoshiaki Kobuke*

Graduate School of Materials Science, Nara Institute of Science and Technology, CREST, Japan Science and Technology Corporation (JST), 8916-5 Takayama, Ikoma City, 630-0101, Japan. E-mail: kobuke@ms.aist-nara.ac.jp

Received (in Cambridge, UK) 27th November 2000, Accepted 8th March 2001
First published as an Advance Article on the web 29th March 2001

5,15-Bis(imidazol-4-yl)-10,20-bis(ω-carboxyalkyloxyphenyl)porphyrin 2 was assembled in water to form liposomal dispersions, whose structure were confirmed by DLS, AFM, TEM measurements as well as entrapment of a hydrophilic fluorescent probe.

Solar energy conversion is undertaken efficiently in chloroplasts or photosynthetic bacterial membranes, where chlorophylls or bacteriochlorophylls are arranged in well-organized structures of fixed distances and orientations. Examples are found in photosynthetic bacterial light-harvesting complexes where a large number of bacteriochlorophylls are arranged in a macro-ring form by coordination of imidazolyl side chains from transmembrane α-helices.[1] We have been interested in constructing light harvesting systems from chromophore assemblies without use of peptides.[2] Recently, we found that 5,15-bis(4-dodecyloxyphenyl)-10,20-bis(imidazol-4-yl)porphyrin **1** was assembled through imidazolyl–imidazolyl hydrogen bonds in non-polar media and that the assembly could perform more or less antenna functions.[3] Following on from this, large porphyrin assemblies were planned, to be organized into the form of liposomes by their own combined intermolecular interactions. For this purpose, a bis(imidazolyl)porphyrin **2** having two meso-ω-carboxyalkoxyphenyl substituents was designed and prepared according to Lindsey's procedure[4] from imidazol-4(5)-yl-2,2′-dipyrrylmethane and ethyl 12-(4-formylphenoxy)dodecanoate, followed by hydrolysis.[5]

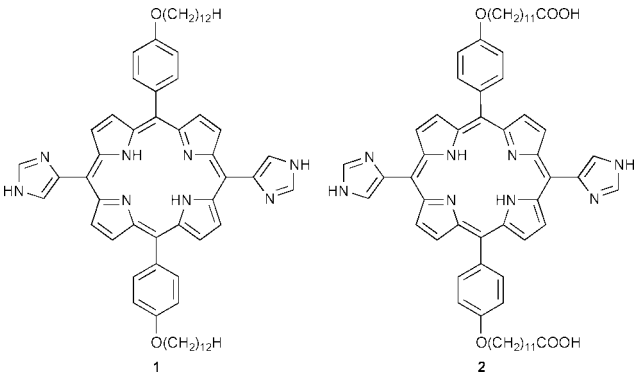

1 2

Compound **2** was dispersed in water by sonication and subjected to gel filtration column separation to isolate the fraction corresponding to small unilamellar vesicles.[6] Dynamic light scattering (DLS) measurement[7] of the dispersion of **2** elucidated a mean diameter of 27 ± 8 nm. The aqueous sample was then applied on a smooth mica plate and dried in air. Fig. 1(a) shows a top view of atomic force microscope (AFM) measurement and 1(b) the side view along the line in 1(a). The observed full widths at the baseline level were 36, 32 and 38 nm for (A), (B) and (C), respectively. These values are larger than those estimated from DLS measurements because of the geometrical tip/sample convolution effect.[8] Fig. 1(c) shows a TEM image of the liposome dispersions. Many particles with diameters in the range 20–30 nm are observed, along with some aggregates that may have formed through drying under vacuum. These images confirm the size distribution obtained by the DLS measurement.

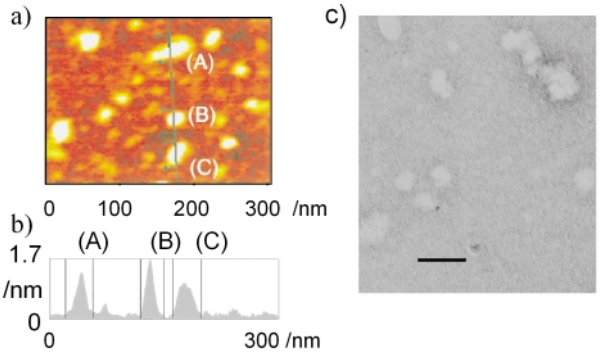

Fig. 1 AFM image of dispersion prepared from **2** developed on mica. a) A top view and b) a cross-section along the line in a). c) TEM image of negatively stained samples of dispersion from **2** with uranyl acetate. (bar = 50 nm).

The size of the system is apparently larger than that of spherical micellar aggregates in the range 2–4 nm[9] and coincides with the typical range for small unilamellar vesicles, 20–30 nm. Definitive evidence of vesicle formation, however, would be obtained by proving the presence of an interior aqueous phase and showing it to be capable of keeping polar solutes inside the vesicle. Therefore, a hydrophilic fluorescent probe, pyranine, was co-sonicated with **2** and the dispersion was isolated by Sephadex G-50 gel filtration.[10] Because of the strong absorption of porphyrin **2** and diffraction from the dispersion, no absorption of pyranine was detected in the UV-Vis spectrum. However, the presence of pyranine in the fraction from a gel filtration column was detected by its fluorescence spectra as shown in Fig. 2(a). The fluorescence intensity was low, due to self-quenching at the relatively high initial concentration of 0.3 mM. Fig. 2(b) and (c) show the emission from pyranine after 24 h and 40 h, respectively, from the gel filtration. The intensity gradually increased in a slow time-course and reached a saturation value only after 40 h. In a separate experiment, the fluorescence intensity of pyranine was increased 3× by the addition of 0.1 ml of a 0.1% aqueous solution of Triton X-100. Adsorption of pyranine on the liposomal membrane surface is unfavorable because both components are negatively charged, but in order to safely exclude that possibility the liposome was prepared without the

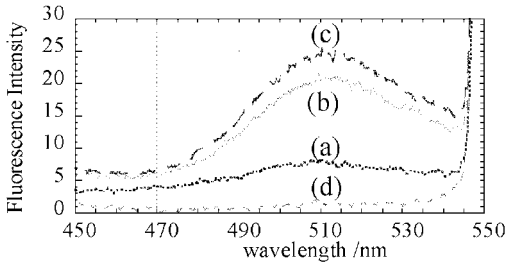

Fig. 2 Fluorescence spectra of porphyrin dispersion co-sonicated with pyranine, λ_{EX} = 280 nm. (a) Just after gel filtration (Sephadex G-50). (b) The same after 24 h and (c) 40 h. (d) Same as (a) without co-sonication, but after treatment with 0.3 mM pyranine, followed by gel filtration.

DOI: 10.1039/b009458g

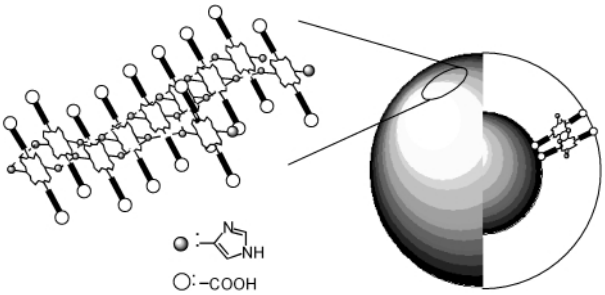

Fig. 3 Schematic representation of the liposome structure of **2** in aqueous solution.

addition of pyranine and than subjected to gel filtration. The resulting liposome fraction was immersed in a 0.3 mM pyranine solution. The liposome fraction, gel-filtered again, gave no fluorescence emission of pyranine (Fig. 2(d)). These results clearly indicate that the membrane can hold the entrapped pyranine and release it slowly to the exterior, when the fluorescence intensity is increased by liberation from the concentration quenching.

Based on these observations, the dispersions are concluded to be liposomes that contain an interior aqueous phase and provide a barrier toward the release of the hydrophilic solute entrapped. Their size corresponds to small unilamellar vesicles. A schematic representation of liposome formation from **2** is shown in Fig. 3. The liposomes we report on here are made only of bis(imidazolyl)porphyrin **2** without any phospholipid such as lecithin. To the best of our knowledge, Fuhrhop and coworkers reported only one example of liposome formation from porphyrins in the literature.[11] In their report, tetrakis[(bixinylamino)-*o*-phenyl]porphyrin was stabilized by side chain polymerization. In our system, the primary driving force for the formation of membrane aggregates comes from hydrophobic and ionic interactions of the amphiphilic compound in water.

The absorption spectrum of **2** dispersed in water (λ_{max} = 426 nm with the bandwidth at the half-height(hbw) of 91 nm resembled that of **1** in cyclohexane (λ_{max} = 432.5 nm and hbw_{Soret} = 86 nm). Both Soret bands were significantly broadened compared to that of **1** in methanol (λ_{max} = 417 nm and hbw_{Soret} = 40 nm). Analysis of ^{1}H-NMR and UV spectral studies shows bisimidazolylporphyrin **1** to assemble into primarily a slipped cofacial orientation through imidazole–imidazole hydrogen bonds in non-polar solvents such as cyclohexane, toluene or $CDCl_3$, but not methanol.[3] Similar structure formation is expected for the dispersion of **2** in water by hydrogen bond networks in the aggregate assembled by hydrophobic interactions. A further stabilization may be provided by hydrogen bond networks by imidazolyl substituents and π–π interactions of porphyrins assembled in the central belt part of the membrane and therefore favoured by an entropy term. The low permeability of entrapped pyranine across the liposomal membrane suggests that a strong hydrogen bond network has been constructed in the central region of the membrane. The liposomal membrane seems rather stiff as judged from AFM and TEM images since the liposomes maintained convex structures even under dry or vacuum conditions, respectively. The symmetrical structure of two carboalkoxyphenyl-substituted porphyrins may not be ideal for the formation of liposomes of small curvatures. However, a membrane-penetrating lipid, glycerol dialkylglycerol tetraether from thermophilic archaebacteria,[12] provides a convincing example of stable liposome formation from such symmetrical transmembrane lipids.

Porphyrins assembled in liposomal membranes are interesting materials in view of testing functions of light harvesting, light-induced charge separation and electron transfer across the membrane. Research targets along these lines are currently under active investigation.

The authors thank Dr M. Iwano (NAIST) and Mr N. Ohkubo (Seiko Instruments Co.) for the measurement of TEM images and AFM images, respectively.

Notes and references

1 G. McDermott, S. M. Prince, A. A. Free, A. M. Hawthornthwaite-Lawless, M. Z. Papiz, R. J. Cogdell and N. W. Isaacs, *Nature*, 1995, **374**, 517; J. Koepke, X. Hu, C. Muenke, K. Schulten and H. Michel, *Structure*, 1996, **4**, 581.

2 I. V. Rubtsov, Y. Kobuke, H. Miyaji and K. Yoshihara, *Chem. Phys. Lett.*, 1999, **308**, 323.

3 N. Nagata, S. Kugimiya and Y. Kobuke, *Chem. Commun.*, 2000, 1389.

4 C.-H. Lee and J. S. Lindsey, *Tetrahedron*, 1984, **39**, 11 427.

5 5,15-Bis[4-(11-carboxyl)undecyloxyphenyl]-10,20-bis(imidazol-4-yl)-porphyrin **2**: ^{1}H NMR (600 MHz, TFA-D, 40 °C) δ = 9.63 (2H, s, imidazole), 8.91 (2H, s, imidazole), 9.05 (4H, br, pyrrole$^{\beta}$H), 8.85 (4H, br, pyrrole$^{\beta}$H), 8.57 (4H, d, J = 8.1 Hz, phenoxy), 7.79 (4H, d, J = 8.1 Hz, phenoxy), 4.56 (4H, br, O$^{\alpha}$CH$_2$), 2.57 (2H, m, $-^{\beta}$CH$_2-$), 2.16 (4H, br, $-$CH$_2$CO$_2$H), 1.80–1.33 (32H, s, $-$(CH$_2$)$_9-$). UV-vis(CHCl$_3$) λ_{max}/nm: 417, 519, 550, 590, 654. Mass (MALDI-TOF, α-CHCA) m/z 1023.42 (M + H), Calcd ($C_{62}H_{70}N_8O_6$): 1022.54.

6 Preparation of liposomes: bis(imidazolyl)porphyrin **2** (0.5 mg, 0.48 μmol) was dissolved in MeOH (5 mL). After evaporation of the solvent, the sample was dried under vacuum at rt for 6 h. The thin porphyrin film thus obtained was dispersed in a solution of pyranine (0.5 mg) dissolved in 3 mL of distilled water. The dispersion was sonicated in a cold room at 4 °C using a horn-type sonicator (TOMY SEIKO, UR-200) for 5 min (level 4) and left at 4 °C for 10 min cooling. This procedure was repeated 4×. The dispersions free from external pyranine were isolated through a Sephadex G-50 gel filtration column (ø 2 × 20 cm).

7 Dynamic light scattering (DLS) measurement was carried out by DLS-6000 (Photal, Co.). The atomic force microscope (AFM) image of the dispersion of **2** on a mica plate was obtained on a SPI 3800N (Seiko Instruments Co.) according to a dynamic force mode with a Si cantilever (a spring constant of 56 N m^{-1}, tip curvature radius of 10 nm).

8 J. Yang, T. Laurion, T.-C. Jao and J. H. Fendler, *J. Phys. Chem.*, 1994, **98**, 9391.

9 J. H. Fendler, *Membrane Mimetic Chemistry*, John Wiley & Sons, Inc., 1982. Radius of DTAB micelle was reported as 1.67 nm, H. L. Tavernier, A. V. Barzykin, M. Tachiya and M. D. Fayer, *J. Phys. Chem. B*, 1998, **102**, 6078.

10 M. Merritt, M. Lanier, G. Deng and S. L. Regen, *J. Am. Chem. Soc.*, 1998, **120**, 8494.

11 T. Komatsu, E. Tsuchida, C. Böttcher, D. Donner, C. Messerschmidt, U. Siggel, W. Stocker, J. P. Rabe and J.-H. Fuhrhop, *J. Am. Chem. Soc.*, 1997, **119**, 11660.

12 H. Komatsu and P. L.-G. Chong, *Biochemistry*, 1998, **37**, 107.

Is ferrocene more aromatic than benzene?†

Matthew Laskoski, Winfried Steffen, Mark D. Smith and Uwe H. F. Bunz*

Department of Chemistry and Biochemistry, The University of South Carolina, Columbia, SC 29208, USA. E-mail: bunz@mail.chem.sc.edu

Received (in Columbia, MO, USA) 30th November 2000, Accepted 30th January 2001
First published as an Advance Article on the web 22nd March 2001

A combination of Pd-catalyzed arene–alkynyl couplings and $Cu(OAc)_2$-promoted internal alkyne dimerization furnishes novel ferrocene-based dehydroannulenes in high yield.

The notion of aromaticity in sandwich and half-sandwich complexes dates back to their observed Friedel–Crafts reactivity and was computationally explored by Bursten and Fenske, leading to the concept of metalloaromaticity,[1] reinforced both by Mitchell's[2] fundamental experiments utilizing chromotrene, cymantrene, and ruthenocene-fused dimethyldihydropyrenes and Schleyer's recent NICS calculations on organometallic π-complexes.[3] While there is little doubt that ferrocene is aromatic, its *degree* of aromaticity is less clear (more or less aromatic than benzene?), and experimental measures are lacking, due to the specific problem of *making* suitable ferroceno-fused dehydroannulenes or dehydrobenzoannulenes.[2] We present herein the synthesis and characterization of ferrocene-based benzodehydro[14]annulenes (**8**,**9**), a ferrocene-based dehydro[14]annulene (**10**), as well as the hitherto unknown 1,2-benzo-3,4,7,8,9,10,13,14-hexadehydro[14]annulene **13**.

The fusion of a [14]dehydroannulene to any π-system offers the unique opportunity to elucidate the (relative) aromaticity of the latter by examining (a) the ^{1}H NMR chemical shifts and b) the coupling constants of the vinylic H-5,6 protons in the dehydroannulene. According to both Mitchell[2] as well as to Günther and Scott,[4] the disruption of aromaticity under increasing bond fixation can lead to an increase in the observed $^3J_{HH}$ values of the coupling constants[4] and an upfield shift of the vinylic protons.[5] Dehydroannulenes **10** and **13** allow to directly compare the effects of benzo-*vs*. ferroceno-annelation onto an aromatic [14]dehydroannulene, which should be a measure of the relative aromaticity of ferrocene *vs*. that of the epitome of aromaticity, benzene.

Vollhardt and coworkers and others[6,7] developed a powerful route to hexadehydro[14]annulenes. Pd-catalyzed coupling of two C_4-fragments to an unsaturated 2,5-hexadiyne, a C_6-fragement (**1**, **11**) is followed by an internal Glaser[8] type cyclization, which leads to dehydro[14]annulene-derivatives. While originally reported for the synthesis of *benzo*dehydroannulenes we have exploited this concept to make **8**–**10** and **13** (Scheme 1).[9] Starting from 1,2-diethynylferrocene[10] (**1**), Pd/Cu-catalyzed coupling with **2**–**4** furnishes the open tetraynes **5**–**7** in yields of 30–96% (ESI)†. The relatively low yield of **5** is probably due to the electron-donating character of the iodide **2**. The coupling products **5**–**7** are stable oils, which were purified by column chromatography. Removal of the trimethylsilyl groups by potassium carbonate or NBu_4F proceeds smoothly and in high yields. Efficient, copper-catalyzed ring closure by $Cu(OAc)_2$ in acetonitrile[8] furnishes the cycles **8**–**10** in 50–62%

† Electronic supplementary information (ESI) available: experimental including details of preparation and spectroscopic characterization of all new compounds. See http://www.rsc.org/suppdata/cc/b0/b009696m/

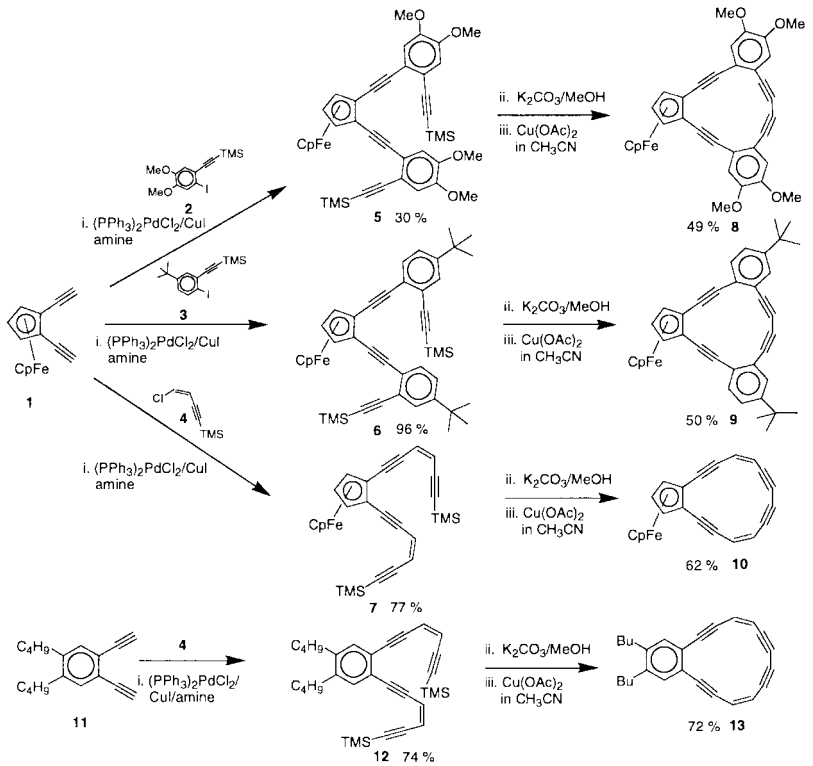

Scheme 1

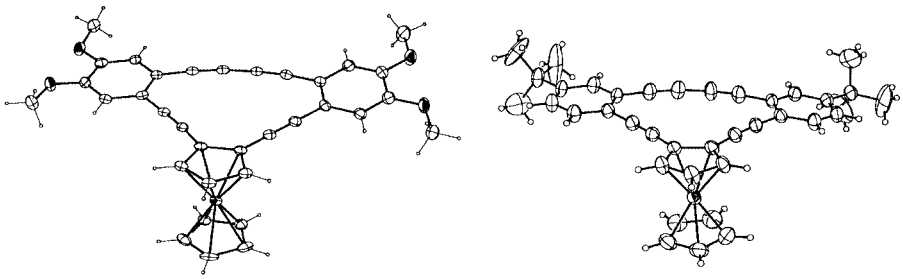

Fig. 1 ORTEP of the organometallic dehydroannulenes **8** and **9**

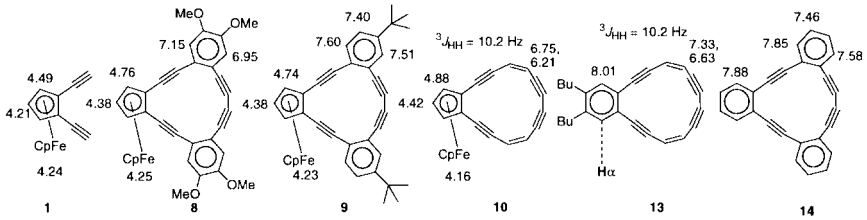

Scheme 2

yield as sole isolable products. The remainder of these reactions is black, insoluble, and intractable, a consequence of the partial oxidative decomposition of the ferrocene nuclei by the Cu^{II} salts, and low yields in the copper-catalyzed homocoupling reactions of ethynylated ferrocene derivatives have been observed earlier.[10,11] If instead of **1**, 1,2-diethynyl-4,5-dibutylbenzene **11** is coupled to **4**, we obtain the novel hexadehydrobenzo[14]annulene **13** in an overall yield of 53% after Cu-catalyzed coupling.[8] The material is orange–yellow and stable in dilute solution, but unstable as a solid at ambient temperature. Surprisingly, this is the first reported hexadehydrobenzo[14]annulene.

The cycles **8** and **9** are stable in the solid state and crystallize well from hexane–dichloromethane mixtures to give a specimen suited for single-crystal X-ray analysis.‡ Fig. 1 shows the ORTEPs of **8** and **9**. The bond angles and bond lengths are in excellent agreement with the expected values showing distinct bond alternation between triple, double and single bonds. The large hydrocarbon ligand is planar, as expected for a [14]-dehydroannulene. In the solid state, the diyne units of the cycles do not show unusual contacts, and we did not observe solid-state polymerization of these dehydroannulenes.

Most interesting with respect to ferrocene's aromaticity are the ^{1}H NMR spectra of **8**–**10**. Comparison of the ^{1}H NMR spectrum of Vollhardt's cyclyne (**14**)[5,6] and that of the benzo–fused dehydro[14]annulene **13** allows extraction of the relative aromaticity of ferrocene with respect to benzene. When the ^{1}H NMR spectrum of **14** is compared to that of **9**, a small upfield shift is observed for H_α (the protons adjacent to the dehydro[14]annulene), suggesting that, if no other effects are present, ferrocene has a similar, or bigger localizing influence on the dehydroannulenic core than benzene (Scheme 2). This measure is clear but relatively indirect. A proton attached to the reporter annulene would increase the effect, and thus the compounds **10** and **13** offer a much more direct comparison. The ^{1}H NMR spectrum of the benzo compound **13** shows two doublets at δ 7.33 and 6.63, while in the ^{1}H NMR spectrum of **10** the *same* vinylic protons appear at δ 6.75 and 6.21, respectively. In the same wake we can compare the ^{1}H NMR spectrum of **7** (open, non-aromatic) to that of **10** (closed) and the ^{1}H NMR spectrum of **12** to that of **13**. Upon conversion of **7** $\rightarrow$**10** the annulenic vinyl protons experience a modest downfield shift ($\Delta\delta_{\text{vinyl-H}}$ = 0.40 and 0.77) and the vinylic $^3J_{HH}$ coupling decreases slightly by ΔJ_{HH} = 0.7 Hz, while for the conversion of **12** $\rightarrow$ **13** the shift of the vinyl protons is much bigger ($\Delta\delta_{\text{vinyl-H}}$ = 0.78 and 1.32 respectively). Here the coupling constant decreases by ΔJ_{HH} = 0.8 Hz. These data show that upon ring closure to **10** the downfield shift of the vinyl protons is relatively small, while the downfield shift in the ^{1}H NMR spectra, when closing the benzo-fused ring (**12** $\rightarrow$ **13**), is almost twice of these values. Consequently a benzene ring disturbs the aromaticity of the fused dehydro[14]annulene *less* than a ferrocene ring. Both sets of data suggest, that in the ferrocene case there is a stronger localization of the dehydro[14]annulene than for benzo-fused **13**, and thus ferrocene is *more* aromatic than benzene by this measure. These arguments are in line with Mitchell's findings.[2] In future we will report the electrochemistry, Bergman rearrangement and the products of the pyrolysis of the ferrocene-fused dehydroannulenes **8**–**10**.

U. H. F. B., W. S. and M. L. thank the National Science Foundation (CAREER award, CHE 9981765, 2000–2004). U. H. F. B. is Camille Dreyfus Teacher-Scholar (2000–2004).

Notes and references

‡ *Crystal data*: CCDC 157834 and 157835. See http://www.rsc.org/suppdata/cc/b0/b009696m/ for crystallographic data in .cif or other electronic format.

1 B. E. Bursten and R. F. Fenske, *Inorg. Chem.*, 1979, **18**, 1760.
2 R. H. Mitchell, Y. Chen, N. Khalifa and P. Zhou, *J. Am. Chem. Soc.*, 1998, **120**, 1785; for other interesting organometallic dehydroannulenes, see: P. R. Sharp, *J. Am. Chem. Soc.*, 2000, **122**, 9880; S. S. H. Mao, F. Q. Liu and T. D. Tilley, *J. Am. Chem. Soc.*, 1998, **120**, 1193.
3 P. v. R. Schleyer, B. Kiran, D. V. Simion and T. S. Sorensen, *J. Am. Chem. Soc.*, 2000, **122**, 510.
4 L. T. Scott, M. A. Kirms, H. Günther and H. Puttkammer, *J. Am. Chem. Soc.*, 1983, **105**, 1372.
5 A. J. Matzger and K. P. C. Vollhardt, *Tetrahdron Lett.*, 1998, **39**, 6791 and references therein.
6 K. P. Baldwin, A. J. Matzger, D. A. Scheiman, C. A. Tessier, K. P. C. Vollhardt and W. J. Youngs, *Synlett*, 1995, 1215; for a general treatise of cyclic oligophenylacetylenes, see: M. M. Haley, J. J. Pak and S. C. Brand, *Top. Curr. Chem.*, 1999, **201**, 82.
7 For a similar route to important cage-type phenyleneethynylenes, see: Y. Rubin, T. C. Parker, S. I. Khan, C. L. Holliman and S. W. McElvany, *J. Am. Chem. Soc.*, 1996, **118**, 5308.
8 F. Vögtle and R. Berscheid, *Synthesis*, 1992, 58; P. Siemsen, R. C. Livingston and F. Diederich, *Angew. Chem.*, 2000, **39**, 2633.
9 For cyclobutatdiene containing dehydro[14]annulenes, see: U. H. F. Bunz, G. Roidl and R. D. Adams, *J. Organomet. Chem.*, 2000, **600**, 56.
10 U. H. F. Bunz, *J. Organomet. Chem.*, 1995, **494**, C8; U. H. F. Bunz, G. Roidl, M. Altmann, V. Enkelmann and K. D. Shimizu, *J. Am. Chem. Soc.*, 1999, **121**, 10719.
11 Z. Yuan, G. Stringer, I. R. Jobe, D. Kreller, K. Scott, L. Koch, N. J. Taylor and T. B. Marder, *J. Organomet. Chem.*, 1993, **452**, 115.

Superior performance of *ex*-framework FeZSM-5 in direct N_2O decomposition in tail-gases from nitric acid plants

J. Pérez-Ramírez,* F. Kapteijn, G. Mul and J. A. Moulijn

Industrial Catalysis, DelftChemTech, Delft University of Technology, Julianalaan 136, 2628 BL Delft, The Netherlands. E-mail: j.perezramirez@tnw.tudelft.nl

Received (in Cambridge, UK) 29th January 2001, Accepted 7th March 2001
First published as an Advance Article on the web 22nd March 2001

Isomorphous substitution of Fe in the MFI framework and extraction by steaming leads to a highly active and stable catalyst for N_2O decomposition in tail-gas from nitric acid plants.

Nitrous oxide (N_2O) has been identified as a greenhouse gas and a contributor to the destruction of ozone in the stratosphere.[1,2] At present, emission from nitric acid plants is the most important environmentally harmful source of N_2O in the chemical industry, since abatement technologies for the other major industrial source, *i.e.* adipic acid plants, have been successfully developed.[2] The direct catalytic decomposition of N_2O into N_2 and O_2 is an attractive *end-of-pipe* solution to reduce N_2O emissions, but none of the catalysts proposed in the literature show a good activity and stability in N_2O decomposition in the presence of high concentrations of O_2, NO_x and H_2O.[2,3] FeZSM-5 is an interesting system because N_2O conversion shows anomalous behaviour in the presence of these tail-gas components.[4] Different preparation methods have been reported to optimize the catalytic performance of FeZSM-5, not only in N_2O decomposition,[5,6] but also in de-NO_x HC-SCR and selective oxidations.[7–9] In this study, an *ex*-framework FeZSM-5 catalyst is shown to be very active and stable in direct N_2O decomposition in simulated tail-gas from nitric acid plants, compared to FeZSM-5 catalysts prepared by sublimation and (aqueous and solid) ion-exchange methods.

Isomorphously substituted FeZSM-5 was synthesized hydrothermally using TPAOH as the template.[10] The as-synthesized sample was calcined in air at 823 K for 10 h and was converted into the H-form by three consecutive exchanges with a NH_4NO_3 solution (0.1 M) for 12 h and subsequent air calcination at 823 K for 5 h (FeZSM-5*c*). Finally, the catalyst was activated in flowing steam at ambient pressure (water partial pressure of 300 mbar and 30 ml min^{-1} of N_2 flow) at 873 K during 5 h (*ex*-FeZSM-5). Other FeZSM-5 catalysts were prepared by liquid (aqueous) ion-exchange with $Fe(NO_3)_3{\cdot}9H_2O$ (*lie*-FeZSM-5) and solid-ion exchange with $FeCl_2{\cdot}4H_2O$ (*sie*-FeZSM-5), following standard procedures described in the literature.[5,8] NH_4-ZSM-5 (P&Q Corporation) was used as the support. *Sub*-FeZSM-5 was prepared by sublimation of $FeCl_3$ on H-ZSM-5 (Degussa).[7] The reaction was carried out in a six-flow reactor system,[11] by passing a mixture of N_2O (4.5 mbar), O_2 (70 mbar), NO (1 mbar) and H_2O (15 mbar) in He at a flow rate of 50–100 ml min^{-1} over 50 mg of catalyst (125–200 μm). Total pressure was 3 bar and space velocities (*GHSV*) of 36 000–120 000 h^{-1} were applied. Before reaction, the catalysts were pretreated in He at 723 K for 1 h. The product gases were analyzed with a chemiluminescence NO_x analyzer and by GC equipped with a thermal conductivity detector, using a PoraplotQ column and a Molsieve 5A column.

Table 1 shows the characterization results and the specific activity per mol of iron (turnover frequency, TOF) of the different catalysts. Fig. 1 shows that *sub*-FeZSM-5 and *ex*-FeZSM-5 induce similar absolute N_2O conversion levels in a N_2O–He feed and significantly higher levels than the exchanged catalysts. *sie*-FeZSM-5 is more active than *lie*-FeZSM-5. Calculation of the TOF at 700 K (Table 1) shows that the specific activity per mol of iron is more than 4, 7 and 10 times higher for *ex*-FeZSM-5 than for *sie*-FeZSM-5, *sub*-FeZSM-5 and *lie*-FeZSM-5, respectively. Electron microscopy reveals a very dispersed and homogeneous distribution of FeO_x clusters of 1–2 nm in *ex*-FeZSM-5 (see graphical abstract and Table 1), denoted as micro-aggregates here. The other preparation methods fail to lead to a homogeneous distribution of the iron species in the catalyst, as revealed by the broad FeO_x cluster size distribution indicated in Table 1. Activation of the calcined sample (FeZSM-5*c*) with steam at 873 K is crucial to create active Fe-species in *ex*-FeZSM-5, as can be concluded by comparison of the activity curves of both samples in Fig. 1. The steam treatment induces the migration of iron towards extra-framework positions by cleavage of Si-O-Fe bonds, as revealed by UV–VIS spectroscopy,[10] producing the FeO_x micro-aggregates. This treatment also leads to dealumination of the zeolite framework and formation of a secondary network of larger pores.

The performance of *ex*-FeZSM-5 in different feed mixtures containing N_2O and O_2, NO_x and/or H_2O is shown in Fig. 2. These gases are present in tail-gases from nitric acid plants. *ex*-FeZSM-5 shows a substantial N_2O conversion above 700 K in

Table 1 Data of catalysts used

Catalyst	Si/Al[a]	Fe[a]/wt%	ΔL[b]/nm	10^{-4} TOF[c]/s^{-1}
ex-FeZSM-5	31.3	0.64	1–2	48.6
sie-FeZSM-5	37.5	1.50	5–15	10.5
lie-FeZSM-5	37.5	1.46	7–25	4.7
sub-FeZSM-5	14.0	5.0	3–12	6.5

[a] Determined by ICP-OES and AAS. [b] FeO_x cluster size distribution (determined by TEM). [c] Mol of N_2O converted per mol of Fe ions s^{-1}, determined at 700 K after 1 h time on stream; feed composition: 4.5 mbar N_2O in He, total pressure 3 bar, GHSV = 36 000 h^{-1}.

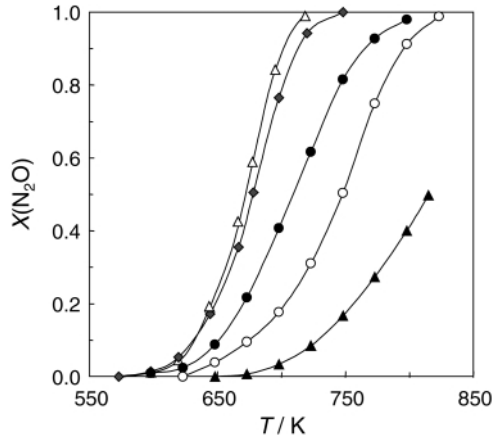

Fig. 1 N_2O conversion as a function of temperature over (◆) *ex*-FeZSM-5, (▲) calcined FeZSM-5*c*, (●) *sie*-FeZSM-5, (○) *lie*-FeZSM-5 and (△) *sub*-FeZSM-5. Feed composition: 4.5 mbarN_2O in He; total pressure 3 bar; GHSV = 36 000 h^{-1}.

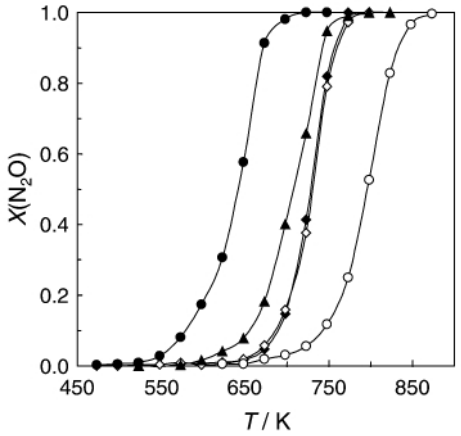

Fig. 2 N_2O conversion as a function of temperature in different feed compositions: (◆) 4.5 mbarN_2O, (◇) 4.5mbarN_2O + 70 mbarO_2, (●) 4.5 mbarN_2O + 1 mbarNO, (○) 4.5 mbarN_2O + 15 mbarH_2O, (▲) 4.5 mbarN_2O + 70 mbarO_2 + 1 mbarNO + 15 mbarH_2O; balance He; total pressure 3 bar; GHSV = 60 000 h^{-1}.

a N_2O–He feed. Addition of O_2 to the feed hardly affects the activity, while NO enhances the reaction rate considerably. Apparently, molecular oxygen does not dissociate over FeZSM-5 and does not compete with N_2O for active sites. NO scavenges adsorbed O* (deposited by N_2O decomposition), forming NO_2 and regenerates the active site. Water severely inhibits the reaction, probably by hydroxylation of the active sites and adsorption in the zeolite channels. Nevertheless, in the complete gas mixture (N_2O + O_2 + NO_x + H_2O), *ex*-FeZSM-5 still shows a significantly higher activity than in N_2O alone. The promoting effect of NO is thus stronger than the inhibition by H_2O. This extraordinary behaviour distinguishes FeZSM-5 from other N_2O decomposition catalysts (usually based on noble metals like Rh or Ru), since these are severely inhibited by NO_x (*via* surface nitrite/nitrate formation) and H_2O.[2,3,12,13] The remarkable behaviour of *ex*-FeZSM-5 is not limited to its activity, but also includes stability. N_2O conversion over *ex*-FeZSM-5 exhibits a remarkable stability in the complete feed mixture at different space velocities, ranging from 36 000 to 120 000 h^{-1} (Fig. 3). *sub*-FeZSM-5 shows slight deactivation at 36 000 h^{-1}. Significant deactivation was observed for the *sie*-FeZSM-5 and *lie*-FeZSM-5 catalysts, further increasing the differences in performance of the catalysts.

The differences in activity and stability of the different FeZSM-5 samples can be related to the preparation method, which lead to different constitutions of the catalysts with respect

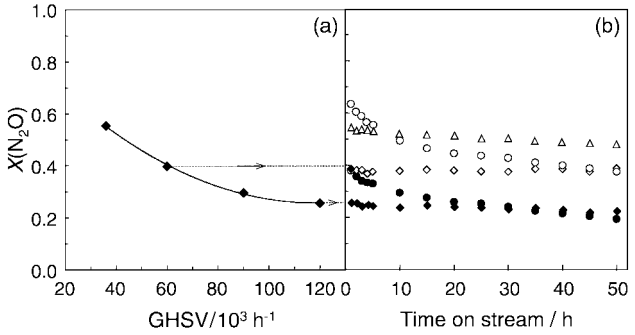

Fig. 3 N_2O conversion as a function of (a) the space velocity (GHSV) over *ex*-FeZSM-5 and (b) time-on-stream over (◇) *ex*-FeZSM-5 (60 000 h^{-1}, 700 K), (◆) *ex*-FeZSM-5 (120 000 h^{-1}, 700 K), (●) *sie*-FeZSM-5 (36 000 h^{-1}, 725 K) (○) *lie*-FeZSM-5 (36 000 h^{-1}, 775 K) and (△) *sub*-FeZSM-5 (36 000 h^{-1}, 700 K). Feed composition: 4.5 mbar N_2O + 70 mbar O_2 + 1 mbar NO + 15 mbar H_2O, balance He. Total pressure 3 bar.

to dispersion, morphology, and structure of the active sites. A comparison of the FeO_x cluster size and TOF suggests a correlation (Table 1): the TOF increases with decreasing average FeO_x cluster size. The FeO_x micro-aggregates observed by TEM in *ex*-FeZSM-5 represent a large fraction of the total amount of Fe in the sample (*ca*. 70%), as estimated by ^{57}Fe Mössbauer spectroscopy. Sublimation and ion-exchange lead to a significantly lower relative amount of small clusters than the *ex*-framework method. In general, for other FeZSM-5 catalysts, the identification of the active species is difficult, due to the inhomogeneous nature of the catalysts. Isolated Fe^{3+} ions, binuclear and multinuclear complexes, small iron–oxide clusters, and large iron-oxide particles have been identified.[5–10] Large FeO_x particles at the external surface of the zeolite are widely accepted to be inactive in the de-NO_x HC-SCR.[5,7,8] This could also explain the lower activity of ion-exchanged catalysts compared to *ex*-FeZSM-5 in N_2O decomposition. *sub*-FeZSM-5 possesses small FeO_x clusters (*ca*. 3 nm), which may account for the high activity observed, but this catalyst also contains a significant fraction of large FeO_x particles (*ca*. 12 nm). A contribution of other iron species in the zeolites to the N_2O decomposition activity can not be excluded. We are currently further investigating the structure of the active sites in the different samples and the reason for the high stability of the *ex*-framework catalyst. We are also addressing the effect of the pore size distribution and extra framework aluminum formed in the steaming procedure of *ex*-FeZSM-5 on the activity.

The temperature of the exhaust in nitric acid plants, which ranges from 500 to 773 K depending on the plant operation, is of utmost importance for the feasibility of an *end-of-pipe* catalytic solution. Large modern dual-pressure plants, with tail-gases in the range 723–773 K, contribute to *ca*. 75% of the total N_2O emission. Nitric acid production facilities in the Netherlands (high-temperature tail-gases) contribute to 25 kton y^{-1}, *i.e. ca*. 6% of the global N_2O emission related to nitric acid plants (*ca*. 400 kton y^{-1}).[14] The use of *ex*-FeZSM-5, which shows stable N_2O conversion (> 90%) at 725 K and 60 000 h^{-1}, appears quite viable. This technology can contribute to greenhouse gas abatement in a cost-attractive way, since *ex*-FeZSM-5 does not contain any expensive noble metal. For low temperature tail-gases (500–525 K), typical in low (single or dual)-pressure plants, *ex*-FeZSM-5 would additionally require extra-heat exchange to preheat the feed mixture, or the addition of hydrocarbon as reducing agent.

Notes and references

1 H. Rodhe, *Science*, 1990, **248**, 1217.
2 G. Centi, S. Perathoner and F. Vanazza, *CHEMTECH*, 1999, **12**, 48.
3 F. Kapteijn, J. Rodríguez-Mirasol and J. A. Moulijn, *Appl. Catal. B*, 1996, **9**, 25.
4 F. Kapteijn, G. Marbán, J. Rodríguez-Mirasol and J. A. Moulijn, *J. Catal.*, 1997, **167**, 256.
5 M. Kögel, R. Mönnig, W. Schwieger, A. Tissler and T. Turek, *J. Catal.*, 1999, **182**, 470.
6 G. Centi and F. Vanazza, *Catal. Today*, 1999, **53**, 683.
7 H-Y. Chen and W. M. H. Sachtler, *Catal. Today*, 1998, **42**, 73.
8 R. Joyner and M. Stockenhuber, *J. Phys. Chem. B*, 1999, **103**, 5963.
9 G. I. Panov, A. K. Uriarte, M. A. Rodkin and V. I. Sobolev, *Catal. Today*, 1998, **41**, 365.
10 A. Ribera, I. W. C. E. Arends, S. de Vries, J. Pérez-Ramírez and R. A. Sheldon, *J. Catal.*, 2000, **195**, 287.
11 J. Pérez-Ramírez, R. J. Berger, G. Mul, F. Kapteijn and J. A. Moulijn, *Catal. Today*, 2000, **60**, 290.
12 J. Oi, A. Obuchi, G. R. Bamwenda, A. Ogata, H. Yagita, S. Kushiyama and K. Mizuno, *Appl. Catal. B*, 1997, **12**, 277.
13 G. Centi, A. Galli, B. Montanari, S. Perathoner and A. Vaccari, *Catal. Today*, 1997, **35**, 113.
14 C. Kroeze, *Nitrous oxide emission inventory and options for control in the Netherlands*, Report nr.773001004, National Institute for Public Health and the Environment, Bilthoven, Netherlands, 1994.

ChemComm

A general, two-directional synthesis of *C*-(1→6)-linked disaccharide mimetics: synthesis from non-carbohydrate based starting materials

Michael Harding and Adam Nelson*

School of Chemistry, University of Leeds, Leeds, UK LS2 9JT

Received (in Cambridge, UK) 6th February 2001, Accepted 1st March 2001
First published as an Advance Article on the web 26th March 2001

The enantiomerically enriched diol 1,4-di(furan-2-yl)butane-1,4-diol (*R*,*R*)-1, synthesised either by Sharpless kinetic resolution or asymmetric reduction of the corresponding diketone, was a key intermediate in the stereodivergent synthesis of diastereoisomeric *C*-(1→6)-linked disaccharides. Two-directional stereoselective functionalisation steps, for example *syn*- and/or *anti*-selective dihydroxylation reactions, were exploited in the stereoselective synthesis of five diastereoisomeric *C*-linked disaccharides.

Libraries of stereo- and regioisomeric oligosaccharides and carbohydrate mimetics can probe large areas of conformational space, and can be used to identify unnatural ligands for carbohydrate receptors.[1] *C*-Linked glycosides are a particularly interesting class of carbohydrate mimetic which are resistant to enzymatic degradation, have potential as inhibitors of glycosidases and glycosyl transferases[2] and often have biological activity[3] and conformational properties[4] which are similar to natural oligosaccharides. Established methods for the preparation of stereoisomeric *C*-linked di- and trisaccharides often rely on the separation of the stereoisomers which result from unselective functionalisation reactions; this approach has been exploited in the synthesis of *C*-linked analogues of disaccharides formed from D- and L-hexoses, and *C*-linked trisaccharides which are potential ligands for cell surface proteins.[5]

In this communication, we describe the preparation of some *C*-linked analogues of some (1→6)-linked disaccharides from the racemic difuryl diol *rac*-**1**, prepared by unselective reduction of the corresponding diketone. Sharpless kinetic resolution[6] of *rac*-**1** returned (*R*,*R*)-**1** in 38% yield and 85% ee. An alternative approach[7] involved asymmetric reduction of the corresponding diketone using borane–dimethyl sulfide complex and 10 mol% of Corey's CBS catalyst **8** to give the diol **1** as a 85 : 15 mixture of diastereoisomers in 80% yield; (*R*,*R*)-**1** had > 98% ee. Oxidative ring expansion of the furan rings of (*R*,*R*)-**1**, using $VO(acac)_2$/^{t}BuOOH, and acetalisation, gave the dipyranone **2** as a 75 : 25 mixture of anomers (Scheme 1), which were reduced with $NaBH_4$ to give the separable diols **3**.

The C_2-symmetric diol **3** was a key intermediate in our divergent synthesis of *C*-linked disaccharides. For example, dihydroxylation of both of the alkenes of **3** under Upjohn conditions (cat. OsO_4–NMO) occurred opposite[8] to the adjacent hydroxy groups to give, after acetylation, the hexaacetate **4** as a > 95 : 5 mixture of diastereoisomers. This two-directional approach[9] is very efficient indeed: in just two steps, six new stereogenic centres have been introduced in the reaction sequence **2**→**4** with almost complete stereocontrol. The di-THP **4** is a protected *C*-linked disaccharide mimetic in which *C*-6 of the one of the rings has been replaced with a methoxy group.

In a similar manner, the diastereomeric diol **5**, synthesised by Mitsunobu inversion of **3** and hydrolysis, was converted into the protected *C*-linked disaccharides **6** and **7**. Hence, double dihydroxylation of **5** opposite to[8] the axial hydroxy groups gave, after acetylation, the protected *C*-linked disaccharides **6** and **9** in 53 and 23% yield respectively. Alternatively, directed[10] double dihydroxylation of **5** under Donohoe's reaction conditions gave, after acetylation, the hexaacetate **7** in 78% yield. The ability to choose at a late stage which diasteroisomer is synthesised is an exceptionally valuable feature of a general synthesis of stereoisomeric analogues.

A two-directional synthetic strategy[9] does not, of course, restrict our approach to the synthesis of C_2-symmetric mim-

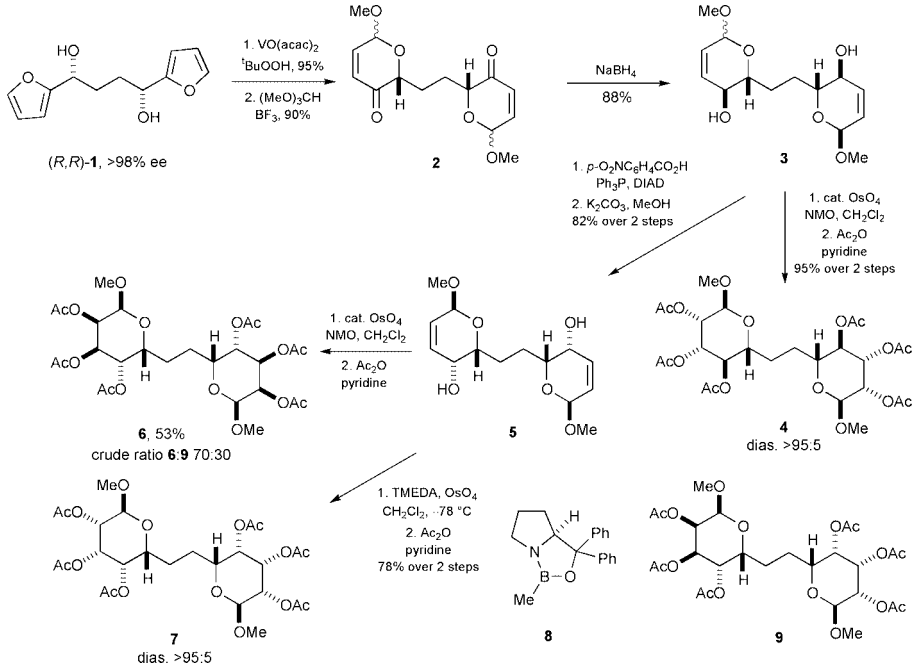

Scheme 1

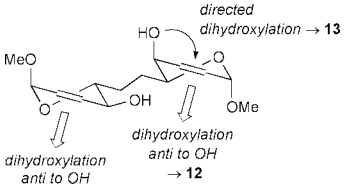

Fig. 1

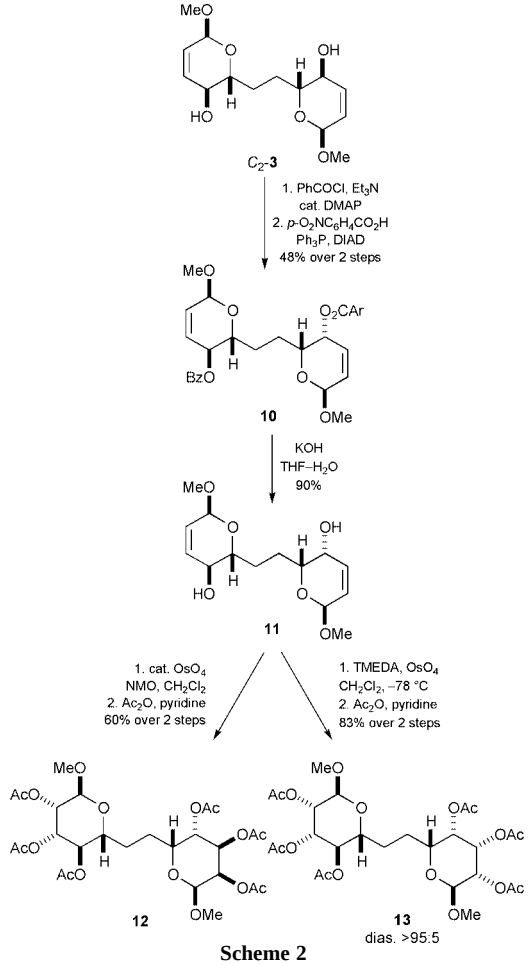

Scheme 2

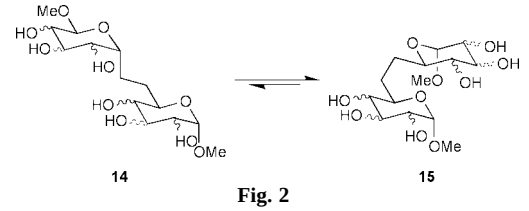

Fig. 2

etics. For example, benzoylation of one of the homotopic alcohols of **3**, inversion of the remaining alcohol and hydrolysis, gave **11** in which the dihydropyran rings had been stereochemically differentiated (Scheme 2). Dihydroxylation of **11**, *anti* to both of the hydroxy groups[8] (Fig. 1) gave the protected carbohydrate mimetic **12**.

More remarkably, the diol **11** could be elaborated in a two-directional fashion such that the stereochemical outcome of dihydroxylation was different in each of the rings. The diol **11** has both an axial and an equatorial hydroxy group; the dihydroxylation of **11** under Donohoe's conditions (TMEDA, OsO_4, CH_2Cl_2, −78 °C) was directed[10] by the axial alcohol but occurred *anti* to the equatorial alcohol (Fig. 1) to give, after acetylation, the protected disaccharide mimetic **13** in 83% yield.

The stereoisomeric compounds **4**, **6**, **7**, **9**, **12** and **13** can be considered to be protected versions of either *C*-α(1→6)- or *C*-β(1→6)-linked disaccharides (see Fig. 2). Although the free *C*-disaccharides are likely to predominantly populate the conformation **15** which resembles a β-linked disaccharide formed from a D and an L sugar (see Table 1), higher energy conformations can often be stabilised by complexation with a carbohydrate receptor.[4b] The conformations **14** mimic α(1→6)-linked disaccharides formed from two natural sugars (see Table 1).

Table 1 Classification of *C*-linked disaccharide mimetics

Compound	Parent α-linked disaccharide(s)	Parent β-linked disaccharide(s)
4	D-Alt-α(1→6)-D-Man	L-Gal-β(1→6)-D-Man
6	D-Gal-α(1→6)-D-Gul	L-Alt-β(1→6)-D-Gul
7	D-All-α(1→6)-D-Tal	L-Tal-β(1→6)-D-Tal
9	D-Gal-α(1→6)-D-Tal or D-All-α(1→6)-D-Gul	L-Alt-β(1→6)-D-Tal or L-Tal-β(1→6)-D-Gul
12	D-Gal-α(1→6)-D-Man or D-Alt-α(1→6)-D-Gul	L-Alt-β(1→6)-D-Man or L-Gal-β(1→6)-D-Gul
13	D-All-α(1→6)-D-Man or D-Alt-α(1→6)-D-Tal	L-Tal-β(1→6)-D-Man or L-Gal-β(1→6)-D-Tal

We believe that our work is the first synthesis of *C*-linked disaccharides entirely from non-carbohydrate based precursors, though Vogel has reported the use of a non-carbohydrate based template to introduce one of the sugar rings.[11] Most other syntheses rely on the coupling of sugar derivatives.[12–15] A particular merit of our approach, which makes it amenable to the synthesis of libraries of stereoisomeric carbohydrate mimetics, is that several diastereomeric *C*-linked disaccharides may be prepared by minor variation of a general reaction sequence. There are 136 possible stereoisomeric carbohydrate mimetics **14** (ignoring anomers); we have reported the stereoselective synthesis of five of these mimetics, and their enantiomers could have been synthesised by using the enantiomeric reagent in the enantioselective step.

We thank the Leverhulme Trust for a grant to the University of Leeds, the Royal Society for funds for chiral HPLC equipment, AstraZeneca and Pfizer for strategic research funding and Robert Hodgson for helpful discussions.

Notes and references

1 R. Liang, L. Yan, J. Loebach, M. Ge, Y. Uozumi, K. Sekanina, N. Horan, J. Gildersleeve, C. Thompson, A. Smith, K. Biswas, W. C. Still and D. Kahne, *Science*, 1996, **274**, 1520.
2 Y. Du, R. J. Linhardt and I. R. Vlahov, *Tetrahedron*, 1998, **54**, 9913.
3 J. Wang, P. Kovác, P. Sinäy and P. J. Glaudemans, *Carbohydr. Res.*, 1998, **308**, 191.
4 See: (*a*) Y. Wang, P. G. Goekjian, D. M. Ryckman, W. H. Miller, S. A. Babirad and Y. Kishi, *J. Org. Chem.*, 1992, **57**, 482; (*b*) J. F. Espinosa, E. Montero, A. Vian, J. L. García, H. Dietrich, R. R. Schmidt, M. Martín-Lomas, A. Imberty, F. J. Canada and J. Jiménez-Barbero, *J. Am. Chem. Soc.*, 1998, **120**, 1309.
5 (*a*) R. W. Armstrong and D. P. Sutherlin, *Tetrahedron Lett.*, 1994, **35**, 7743; (*b*) D. P. Sutherlin and R. W. Armstrong, *J. Org. Chem.*, 1997, **62**, 5267.
6 Y. Kobayashi, M. Kusakabe, Y. Kitano and F. Sato, *J. Org. Chem.*, 1988, **53**, 1586.
7 D. J. Aldous, W. M. Dutton and P. G. Steel, *Tetrahedron: Asymmetry*, 2000, **11**, 2455.
8 J. K. Cha, W. J. Christ and Y. Kishi, *Tetrahedron*, 1984, **40**, 2247.
9 C. Poss and S. L. Schreiber, *Acc. Chem. Res.*, 1994, **27**, 9.
10 T. J. Donohoe, P. R. Moore, M. J. Waring and N. J. Newcombe, *Tetrahedron Lett.*, 1997, **38**, 5027.
11 (*a*) R. Ferritto and P. Vogel, *Tetrahedron: Asymmetry*, 1994, **5**, 2077; (*b*) R. M. Bimwala and P. Vogel, *J. Org. Chem.*, 1992, **57**, 2076.
12 F. K. Griffin, D. E. Paterson and R. J. K. Taylor, *Angew. Chem., Int. Ed.*, 1999, **38**, 2939.
13 (*a*) A. Dondoni, H. M. Zuurmond and A. Boscarato, *J. Org. Chem.*, 1997, **62**, 8114; (*b*) O. R. Martin and W. Lai, *J. Org. Chem.*, 1993, **58**, 176.
14 W. R. Kobertz, C. R. Bertozzi and M. D. Bednarski, *J. Org. Chem.*, 1996, **61**, 1894.
15 M. H. D. Postema and D. Calimente, *Tetrahedron Lett.*, 1999, **40**, 4755.

Solid phase synthesis of aryl-ether dendrimers

Andrea Basso,[a] Brian Evans,[b] Neil Pegg[b] and Mark Bradley*[a]

[a] *Department of Chemistry, University of Southampton, Highfield, Southampton, UK SO17 1BJ. E-mail: MB14@soton.ac.uk*

[b] *Glaxo Wellcome Research and Development, Gunnels Wood Road, Stevenage, UK SG1 2NY*

Received (in Cambridge, UK) 2nd January 2001, Accepted 7th March 2001
First published as an Advance Article on the web 26th March 2001

Solid phase chemistry can be used to prepare, in excellent yield and purity, a range of Fréchet-type aryl-ether dendrimers, for use in either dendrimer conjugation studies, resin loading enhancement or the wedge based synthesis of larger dendrimers.

Over the past few years we have shown that resin-bound polyamidoamine (PAMAM) dendrimers are readily synthesized[1,2] and are inert under a broad range of chemical conditions[3] such as coupling reactions, nucleophilic displacements or borohydride reductions. However, synthetic patterns requiring the use of strong reducing agents or strong bases have to be avoided. In the area of solution dendrimer synthesis Fréchet[4] has reported the construction of arylether dendrimers *via* the alkylation of bromobenzylic dendrimeric fragments with 3,5-dihydroxybenzyl alcohol, with which he also introduced the concept of convergent dendrimer synthesis. Since polyether dendrimers are substantially more chemically inert than the PAMAM dendrimers and because of the problems associated with solution dendrimer synthesis, the solid-phase synthesis of Fréchet-type aryl-ether dendrimers (Fig. 1) was targeted both as a means of resin loading enhancement as well as a convenient approach to dendrimer *wedge*[4] synthesis. Since the building blocks originally used by Fréchet were considered to be unsuitable for solid-phase synthesis, 3,5-bis(acetoxymethyl)-phenol (**1**) was used and was prepared by modification of the literature procedure.[5,6] The presence of a phenolic group and of two acetyl-protected primary alcohols allowed the synthesis of the dendrimer *via* a two-step iterative procedure, consisting of a Mitsunobu condensation followed by ester hydrolysis. The synthesis was first carried out using an analytical construct,[7] consisting of glycine attached to the TFA-cleavable Rink linker[8] allowing ready characterisation of the intermediates and optimisation of the Mitsunobu condensations and ester hydrolysis. Compound **2**, obtained in two steps from **1**, was coupled onto Gly-Rink-PS resin under standard conditions (Scheme 1) to give **3**.

Hydrolysis of **3** followed by Mitsunobu condensation with (**1**) afforded Generation 2.0 dendrimer after TFA cleavage. The most efficient conditions for the hydrolysis were found to be Bu_4NOH(aq)–THF 1:3, while the Mitsunobu reaction was performed with DIAD–PPh_3† in THF. Generation 3.0 and 4.0 dendrimers were synthesized using the same procedure and the crude HPLC trace of Generation 3.0 dendrimer is shown in Fig. 2.[9] Dendrimers were subsequently synthesized directly on hydroxymethylpolystyrene **4** (Scheme 2), which was obtained from commercial Merrifield resin (1% DVB, 0.93 mmol g^{-1}, 90–106 μm) *via* displacement of the chloride with caesium acetate in DMF and hydrolysis of the resulting ester with Bu_4NOH(aq) in THF. This was extended to give dendrimer resin **6** as shown in Scheme 2.

The loading of resin **4** was determined to be 0.82 mmol g^{-1} (0.44 nmol $bead^{-1}$). Synthesis of generation 3.0 dendrimer resin gave a resin with a loading of 2.85 mmol g^{-1} (3 nmol

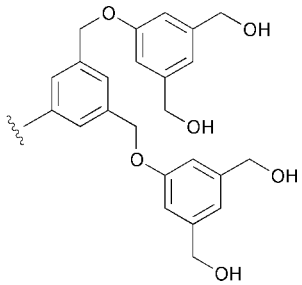

Fig. 1 Fréchet-type aryl-ether dendrimer fragment.

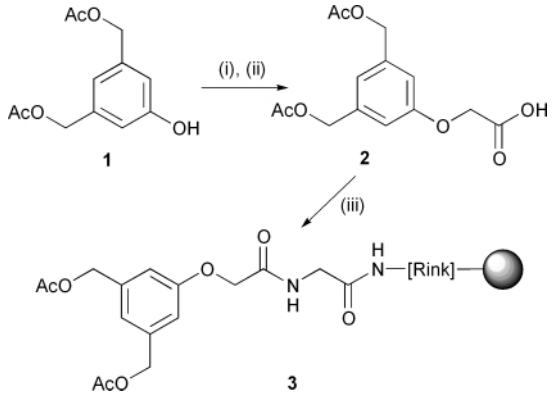

Scheme 1 (i) *tert*-Butylbromoacetate, K_2CO_3, CH_3CN; (ii) TFA, DCM (2:3), (iii) H-Gly-Rink-PS, DIC,† HOBt, DMF.

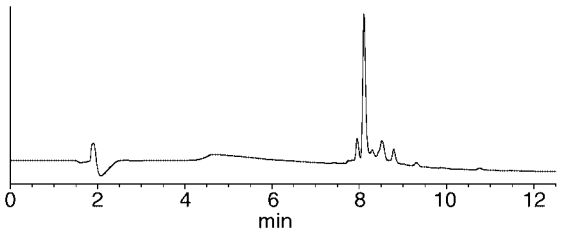

Fig. 2 HPLC trace of polyether dendrimer Generation 3.0.

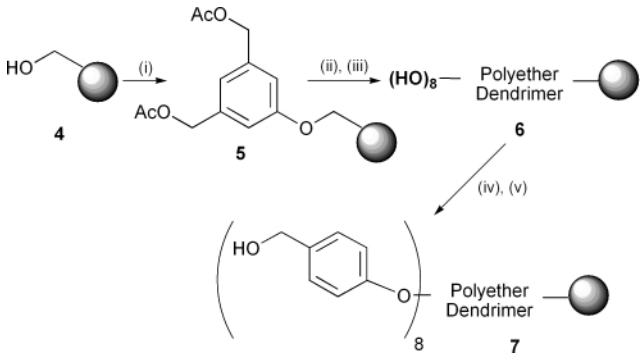

Scheme 2 (i) **(1)**, DIAD, PPh_3, THF; (ii) Bu_4NOH (aq), THF (1:3); (iii) Repeat twice (i) and (ii), (iv) methyl-4-hydroxybenzoate, DIAD, PPh_3, THF; (v) $LiAlH_4$, THF.

DOI: 10.1039/b100003i

Table 1 Bead diameter (μm) in different solvents (average of 10 beads)

	Dry	DCM	DMF	MeOH	H_2O	THF
4	90	165	155	95	95	175
6	110	145	185	105	110	150
$(Ac)_8$-6	115	195	190	110	115	190

bead^{-1}) (7 times that of the initial resin). Since the synthesis of this dendrimer involved 7 distinct Mitsunobu condensations and 14 distinct ester hydrolyses and the final loading was 86% of that expected this implies that each reaction had proceeded to 99.3% completion. The swelling properties of this resin were analyzed and compared with those of hydroxymethylpolystyrene and are summarized in Table 1.

The diameter of the dry resin beads increased by about 25% after the dendrimerisation process. Acetyl-protected dendrimer resin had the same swelling trend as the hydroxymethylpolystyrene **4**, while resin **6** presented some interesting features with apolar solvents like DCM and THF. In these solvents the resin swelled much less than the parent acetyl-protected resin and also less than resin **4**, due to the high density of hydroxy groups. The two resins **4** and **6** were also compared in terms of reaction kinetics. Fmoc-Ala-OH was coupled onto the two resins and Fmoc and quantitative ninhydrin tests were carried out with samples removed over 2 h. Differences in reactivity were found to be negligible.

To prove the versatility of this new resin, methyl 4-hydroxybenzoate was coupled *via* a Mitsunobu condensation on to resin **6** and the resin-bound methyl ester was then reduced with $LiAlH_4$ (Scheme 2). This two-step procedure was found to be an efficient alternative method to introduce the Wang linker onto a polystyrene support. The polyether dendrimer resin was perfectly stable to $LiAlH_4$ reduction and the final loading of the dendrimer–Wang resin **7** was found to be 2.3 nmol bead^{-1}. The utility of resin **7** was demonstrated by synthesising the hexapeptide Leu-Enkephaline-Lys. Following cleavage with TFA–H_2O 95:5 and purification, the peptide was isolated in 66% yield, relative to the loading of resin **4**.

In conclusion, we have demonstrated that the polyether dendrimer resin can be conveniently and efficiently synthesised on hydroxymethyl polystyrene resins and that the final loading is sufficient for multiple single-bead screenings and is inert under severe chemical conditions. Moreover we have shown that polyether dendrimers can be conveniently synthesised on the solid phase. No purification of the intermediates (usually a non-trivial step, taking in account the molecular weight and character of these molecules) is required to obtain highly pure compounds. The *wedges* synthesised on solid phase could be used to assemble bigger fragments according to the convergent dendrimer methodology outlined by Fréchet.

We thank the BBSRC for funding (ROPA).

Notes and references

† DIAD = diisopropylazodicarboxylate. DIC = diisopropylcarbodiimide.

1 V. Swali, N. J. Wells, G. J. Langley and M. Bradley, *J. Org. Chem.*, 1997, **62**, 4902.
2 N. J. Wells, A. Basso and M. Bradley, *Biopolymers (Peptide Science)*, 1998, **47**, 381.
3 (*a*) A. Basso, B. Evans, N. Pegg and M. Bradley, *Tetrahedron Lett.*, 2000, **41**, 3763; (*b*) A. Basso, B. Evans, N. Pegg and M. Bradley, *Eur. J. Org. Chem.*, 2000, **23**, 3887.
4 C. J. Hawker and J. M. J. Fréchet, *J. Chem. Soc., Chem. Commun.*, 1990, 1010.
5 3,5-Bis(methoxycarbonyl)phenol was protected as the *tert*-butyldimethylsilyl ether before reduction with $LiAlH_4$. After acetylation of the primary alcohols, silyl protection was removed with TFA–H_2O 9:1.
6 P. R. Ashton, D. W. Anderson, C. L. Brown, A. N. Shipway, J. F. Stoddart and M. S. Tolley, *Chem. Eur. J.*, 1998, **4**, 781.
7 S. C. Mckeown, S. P. Watson, R. A. E. Carr and P. Marshall, *Tetrahedron Lett.*, 1999, **40**, 2407.
8 For a review on linkers and cleavage strategies, see: F. Guiller, D. Orain and M. Bradley, *Chem. Rev.*, 2000, **100**, 2091.
9 NMR of Generation 3.0 dendrimer: DMSO-d_6: $\delta(^1H)$ = 7.30 (s, 1H, ArH Gen 1.0), 7.24 (s, 2H, ArH Gen 2.0), 7.19 (br s, 6H, ArH Gen 1.0 and 2.0), 7.06 (br s, 2H, NH_2), 6.97 (s, 4H, ArH Gen 3.0), 6.95 (s, 8H, ArH Gen 3.0), 5.22 (s, 4H, CH_2 Gen 1.0), 5.17 (s, 8H, CH_2 Gen 2.0), 4.68 (s, 2H, O-CH_2-CO), 4.55 (s, 16H, CH_2 Gen 3.0), 3.85 (br s, 2H, NH-CH_2-CO); $\delta(^{13}C)$: 171.1, 168.3, 159.0, 158.8, 158.4, 144.3, 139.5, 139.3, 120.0, 119.3, 117.4, 113.8, 113.5, 111.4, 69.5, 69.3, 67.4, 63.2, 41.8; *m/z* (TOF LD$^+$): 1107.5 (100%, $(M + Na)^+$), 1123.4 (30%, $(M + K)^+$).

Steric activation of chelate catalysts: efficient polyketone catalysts based on four-membered palladium(II) diphosphine chelates

Stephen J. Dossett,*[a] Amy Gillon,[b] A. Guy Orpen,[b] James S. Fleming,[b] Paul G. Pringle,*[b] Duncan F. Wass[a] and Matthew D. Jones[a]

[a] *BP, Chertsey Road, Sunbury-on-Thames, Middlesex, UK TW16 7LN*
[b] *School of Chemistry, University of Bristol, Cantock's Close, Bristol, UK BS8 1TS. E-mail: paul.pringle@bristol.ac.uk*

Received (in Cambridge, UK) 18th December 2000, Accepted 6th February 2001
First published as an Advance Article on the web 26th March 2001

Palladium(II) complexes of ligands of the type $Ar_2PCH_2PAr_2$ and $Ar_2PN(Me)PAr_2$ (Ar = *ortho*-substituted phenyl group) are very efficient catalysts for copolymerisation of CO and C_2H_4.

The perfectly alternating polyketone made by palladium(II)-catalysed copolymerisation of CO and alkenes [eqn. (1)] has

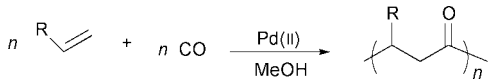

(1)

numerous potential applications.[1] Several types of palladium(II) chelates have been reported to be catalysts[1,2] but diphosphine chelates outperform all others in terms of activity and selectivity. Drent *et al.*[1] have shown that the CO/C_2H_4 copolymerisation catalytic activity of palladium(II) complexes of diphosphines of the type $Ar_2P(CH_2)_nPAr_2$ is a sensitive function of the backbone chain length, *n*, and the aryl group, Ar.

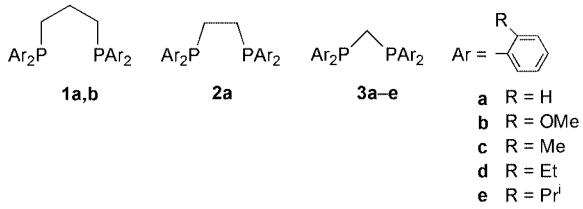

Thus it was shown that the 6-membered chelate derived from **1a** was an order of magnitude more active than the 5-membered analogue from **2a** and that the 4-membered chelate from **3a** was essentially inactive. It was also disclosed that the complex of **1b**, containing *ortho*-methoxy substituents, gave a polymer of significantly greater molecular weight than that obtained with the complexes of unsubstituted ligand **1a**.[3] The catalyst sensitivity to chelate ring size might be rationalised in terms of bite angle effects.[4] However, we show here that the activity of 4-membered Pd–P–C–P chelates is dramatically increased by the presence of bulky *ortho* substituents on the aryl groups and that polymerisation rates comparable to, or even exceeding, the best commercial catalysts are obtained with 4-membered Pd–P–N–P chelates.[5,6]

The diphosphine ligands **3b–e** were made from bis(dichlorophosphino)methane[7] according to eqn. (2) and fully

(2)

characterised. The catalysts were tested for the production of ethene/propene/CO terpolymer over a 3 h period at 50 barg and 70 °C in dichloromethane using tris(pentafluorophenyl)borane promoter. In Table 1, the polymer yield is a measure of the productivity of the catalysts over 3 h. The polymerisation rate and catalyst half-life, as determined by fitting first order curves to the cumulative gas uptake profiles, are also given in Table 1. The borane activation method was reported recently and involves the transfer of a pentafluorophenyl group from boron to palladium to form a cationic $Pd–C_6F_5$ complex which is the catalytically active species.[6] The catalysts were formed by the reaction of palladium acetate and ligand *in situ* or using pre-formed palladium acetate complexes. The results obtained in terms of rate and productivity are the same (within the accuracy of our measurements) for both of these methods, indicating that the same catalytic species is formed in both cases (see Table 1, entries 3 and 4).

Polydispersities are consistently around the value of 2, as expected for a single site catalyst, and termonomer incorpora-

Table 1 Copolymerisation of CO and C_2H_4 results

Entry	Ligand[a]	Yield/g	Rate[b]/ g gPd^{-1} h^{-1}	Half-life[b]/ min	M_w	M_n	PDI	C_3H_6 incorp. (%)
1	**3a**[d]	0.2	[c]	[c]	58000	24000	2.4	6.0
2	**3b**[d]	1.5	1029	44	81000	31000	2.6	6.0
3	**3c**	2.8	2020	38	78000	42000	1.9	6.6
4	**3c**[d]	3.0	2185	35	71000	42000	1.7	6.3
5	**3d**[d]	5.0	2776	53	98000	50000	2.0	6.5
6	**3e**[d]	25.1	9396	165	278000	107000	2.6	5.0
7	**3e**[e]	0.3	[c]	[c]	17000	13000	1.3	7.1
8	**5a**	0.4	[c]	[c]	[f]	[f]	[f]	[f]
9	**5b**	12.0	4800	160	103000	43000	2.4	3.6[g]
10	**5c**	7.7	3454	144	282000	113000	2.5	3.6[g]
11	**5d**	10.4	4029	152	639000	179000	3.6	3.7[g]
12	**5e**	17.0	11517	134	888000	355000	2.5	3.7[g]
13	**5e**[e]	0.2	[c]	[c]	20000	9300	2.1	4.9[g]

[a] Polymerisation conditions: 50 barg C_2H_4/CO, 20.0 g C_3H_6, CH_2Cl_2 diluent, 70 °C for 3 h using $B(C_6F_5)_3$ promoter (0.2 mmol). Catalyst solution formed *in situ* with $Pd(OAc)_2$ (0.01 mmol) and ligand (0.01 mmol). [b] Determined by fitting first order curve to cumulative gas uptake profile. [c] Rate too low to be determined. [d] Conditions as above, except $[Pd(OAc)_2(ligand)]$ (0.01mmol) complex was pre-formed. [e] Conditions as above, except methanol diluent and $HBF_4·OMe_2$ promoter (0.05 mmol). [f] Only oligomeric products were formed. [g] 12.0 g Propene used.

tion is largely unaffected by ligand structure. However, other aspects of the polymerisations are very sensitive to the structure of the ligand. Generally, polymerisation rate, catalyst stability and polymer molecular weight all increase with increasing steric bulk of the aryl *ortho* substituent (entries 1–6). These effects are very pronounced with the *o*-isopropylphenyl derivative **3e** (entry 6) where, compared with the *o*-ethylphenyl derivative **3d** (entry 5), the productivity has increased 5-fold and the molecular weight has doubled. Polymerisation under the methanolic conditions described by Drent[1] gave only a very low rate (entry 7), showing the importance of the activation method used. Indeed, even dppm (**3a**) produces polymer under our conditions, albeit in very low yield (entry 1). Derivative **3b** (entry 2), bearing polar methoxy substituents, gives some improvement over the performance of **3a**; however, productivity is less than one third that of the sterically similar *ortho* ethyl compound **3d**.

The correlation between the steric bulk of the *ortho* substituents and the catalytic performance of the 4-membered chelates led us to investigate further the source of this steric activation by carrying out solid state and solution structural studies of model chelates of general structure **4** (M = Pd, X = Cl, OAc; M = Pt, X = Cl). Most enlightening to the catalysis

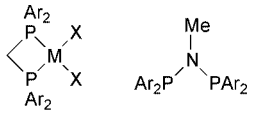

4a–e **5a–e**

discussed here is the structure of the chelate complex **4e** (M = Pt, X = Cl), a model for the very active catalyst system derived from **3e**. The crystal structure of **4e** was determined (as its dichloromethane solvate) and is shown in Fig. 1.† It shows a flat 4-membered chelate ring with, as a consequence, isoclinal aryl groups, two of which have *ortho*-isopropyl groups orientated so as to block the axial sites at the metal. The NMR spectra for **4e** show that this species is fluxional. The ^{31}P NMR spectrum of **4e** in $CDCl_3$ at +20 °C is a singlet at −64.5 ppm [^1J(PtP), 3130 Hz] but this signal broadens as the temperature is lowered and at −60 °C, there appears to be a 1 : 1 mixture of two species which give rise to an AB pattern [δ_A −65.4, $^1J(PtP_A)$ 3045 Hz, δ_B −66.1, $^1J(PtP_B)$ 3337 Hz, $^1J(P_AP_B)$ 48 Hz] and a singlet [δ_C −68.4, ^1J(PtP) 3195 Hz]. The ^{1}H NMR signals for the isopropylgroups of **4e** are broad at ambient temperatures and at −60 °C this signal is resolved into overlapping complex multiplets. The ^{1}H and ^{31}P NMR spectra for the parent dppm complex **4a** (M = Pt, X = Cl) are invariant with temperature and therefore the changes in the NMR spectra with temperature

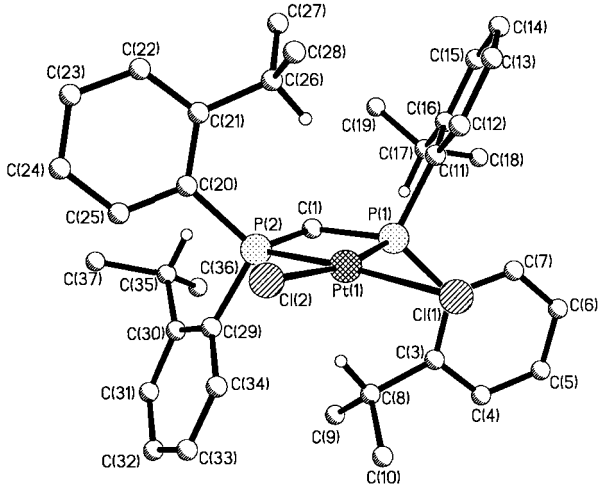

Fig. 1 Molecular structure and numbering scheme for **4b**. All but tertiary isopropyl hydrogen atoms have been omitted for clarity. Important molecular bond lengths (Å) and angles (°): Pt(1)–P(1) 2.2301(9), Pt(1)–P(2) 2.2202(9), Pt(1)–Cl(1) 2.3627(9), Pt(1)–Cl(2) 2.3465(9); P(1)–Pt(1)–P(2) 75.96(3), P(1)–C(1)–P(2) 94.54(13).

observed with **4e** are associated with the presence of the bulky *ortho* substituents. Thus we tentatively assign the fluxionality of **4e** to interconversion of symmetrical and unsymmetrical rotamers arising from restricted rotation around the aryl–P bond.

The success of bulky diarylphosphinomethane ligands prompted us to investigate other one-atom backbone diphosphines in which similar steric effects may be observed. Amino-bridged diphosphines offered such a suitably versatile ligand architecture. Although the chemistry of the simple ligands based on this structural motif has been studied,[8] the synthesis of bulky derivatives **5b–e** and their use in catalysis has not been explored. The methylamino-bridged diphosphines (**5a–e**) were made according to eqn. (3) and fully characterised.

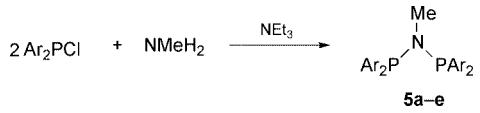

(3)

5a–e

The palladium(II) complexes of ligands **5a–e** were tested for polymerisation activity as before (entries 8–13) and the results largely parallel those obtained with (**3a–e**). Thus, polymerisation rate, catalyst stability and polymer molecular weight all increase with increasing steric bulk of the aryl *ortho* substituent (entries 8–13) and methanolic conditions give only very low activity (entry 13). In this case, the *ortho*-methoxy derivative **5b** (entry 9) shows comparable productivity to the ethyl derivative **5d**, albeit to give a lower molecular weight material. The N_1-backbone chelates are consistently superior to their C_1-backbone analogues and the polymerisation rate of the most active catalyst in this family, **5e**, exceeds that of even dppp (**1a**) under our conditions.[6] The molecular weight of the polymer produced by this system is also extremely high compared with other polyketone catalysts.[1,3,6]

Our studies have shown that 4-membered palladium(II) diphosphine chelates, hitherto considered to be inefficient polyketone catalysts, are in fact very active when sterically demanding derivatives are used.

Notes and references

† *Crystal data* for **4b**·CH_2Cl_2: $C_{38}H_{48}Cl_4P_2Pt$, M = 903.59, monoclinic, space group $P2_1/c$ (no. 14), a = 12.942(2), b = 12.338(2), c = 23.711(7) Å, β = 98.64(2)°, U = 3743.1(15) Å^3, Z = 4, μ = 4.146 mm^{-1}, T = 173 K, 8581 unique data, $R1$ = 0.0220.

CCDC 155957. See http://www.rsc.org/suppdata/cc/b0/b010063n/ for crystallographic files in .cif or other electronic format.

1 E. Drent and P. H. M. Budzelaar, *Chem. Rev.*, 1996, **96**, 663 and references therein; E. Drent, J. A. M. vanBroekhoven and P. H. M. Budzelaar, *Recl. Trav. Chim.*, 1996, **115**, 263; W. P. Mul, H. Oosterbeek, G. A. Beitel, G. J. Kramer and E. Drent, *Angew. Chem., Int. Ed.*, 2000, **39**, 1848; E. Drent, *Eur. Pat. Appl.*,1984, EP121965 (to Shell).

2 S. Doherty, G. R. Eastham, R. P. Tooze, T. H. Scanlan, D. Williams, M. R. J. Elsegood and W. Clegg, *Organometallics*, 1999, **18**, 3558; B. Milani and G. Mestroni, *Comments on Inorg. Chem.*, 1999, **20**, 301; K. Nozaki, T. Hiyama, S. Kacker and I. T. Horvath, *Organometallics*, 2000, **19**, 2031; C. Gambs, S. Chaloupka, G. Consiglio and A. Togni, *Angew. Chem., Int. Ed.*, 2000, **39**, 2486; K. Vrieze, J. H. Groen, J. G. P. Delis, C. J. Elsevier and P. W. N. M. vanLeeuwen, *New. J. Chem.*, 1997, **21**, 807.

3 J. A. M. van Broekhoven and R. L Wife, *Eur. Pat. Appl.*, 1988, EP257663 (to Shell).

4 P. W. N. M van Leeuwen and P. Diekes, *J. Chem Soc., Dalton Trans.*, 1999, 1519.

5 For first disclosure of these catalysts see: S. J. Dossett, *World Pat. Appl.*, 1997, 97/37765 (to BP Chemicals); S. J. Dossett, *World Pat Appl.*, 2000, 00/06299 (to BP Chemicals); S. J. Dossett J. S. Fleming and P. G. Pringle, *World Pat. Appl.*, 2000, 00/03803 (to BP Chemicals).

6 G. K. Barlow, J. D. Boyle, N. A. Cooley, T. Ghaffar and D. F. Wass, *Organometallics*, 2000,**19**, 1470 and references therein.

7 S. Heitkamp, H. Sommer and O. Stelzer, *Inorg. Synth.*, 1989, **27**, 120.

8 M. S. Balakrishna, V. Sreenivasa Reddy, S. S. Krishnamurthy, J. F. Nixon and J. C. T. R. Burkett St. Laurent, *Coord. Chem. Rev.*, 1994, **129**, 1.

A novel reaction on a Mo_2N/γ-Al_2O_3 catalyst: low-temperature isomerization of but-1-ene

Zili Wu, Can Li,* Pinliang Ying, Zhaobin Wei and Qin Xin*

State Key Laboratory of Catalysis, Dalian Institute of Chemical Physics, Chinese Academy of Sciences, PO Box 110, Dalian 116023, China. E-mail: xinqin@ms.dicp.ac.cn; canli@ms.dicp.ac.cn

Received (in Cambridge, UK) 17th January 2001, Accepted 9th February 2001
First published as an Advance Article on the web 26th March 2001

An Mo_2N/γ-Al_2O_3 catalyst is found to catalyze the double-bond migration (DBM) of adsorbed but-1-ene below 201 K by *in situ* FT-IR spectroscopy, resembling the behavior of Group VIII metals in the isomerization of butenes.

Recently, molybdenum nitrides have attracted much attention because they show catalytic properties resembling Group VIII metals in a number of reactions involving hydrogen,[1] such as hydrotreating (HDS and HDN), hydrogenolysis, hydrogenation and NH_3 synthesis. However, these studies were concentrated on passivated nitride catalysts. It is known that the passivation procedure causes a dramatic change in the nitride surface, *i.e.* from nitride to oxygen-covered nitride. Therefore, the surface of the passivated catalyst has been modified by the oxygen and it does not reflect the case of the fresh nitride catalyst. Recent study[2] has shown that the reduced, passivated and nitrided Mo_2N/γ-Al_2O_3 catalysts show very different IR spectra of adsorbed CO, indicating quite different properties of the surface sites of the two catalysts. It is therefore reasonable to deduce that the fresh molybdenum nitride may show different catalytic behaviour in some reactions compared with the reduced, passivated one. Here, such an example is presented: the double-bond migration (DBM) of but-1-ene is found, by *in situ* FT-IR spectroscopy, to proceed on an Mo_2N/γ-Al_2O_3 catalyst below 201 K, but not on a reduced, passivated one even at room temperature (RT).

The preparation of the passivated Mo_2N/γ-Al_2O_3 (10 mass% Mo) catalyst is described elsewhere.[3,4] XPS data show that Mo^{6+}, Mo^{4+} and $Mo^{\delta+}$ ($0 < \delta < 4$) cations, with a binding energy of Mo $3d_{5/2}$ at 232.6, 230.7 and 229.0 eV, respectively, are present for the passivated sample. This is consistent with the unsupported Mo nitrides,[4] indicating the formation of the Mo_2N phase on the γ-Al_2O_3 support. Previous XRD results[5] also show that the Mo_2N phase is formed and well dispersed on the support of the Mo_2N/γ-Al_2O_3 catalysts with low Mo loading.

For the IR study, a passivated sample was renitrided in a quartz IR cell in flowing NH_3. The sample renitrided in the IR cell is denoted Mo_2N/γ-Al_2O_3 or nitrided sample, whereas the passivated sample treated with H_2 at 773 K for 2 h is denoted as reduced, passivated Mo_2N/γ-Al_2O_3. Haddix *et al.*[6] have reported that an air-exposed γ-Mo_2N sample can be renitrided by simply treating it in flowing NH_3 at 973 K, and that the procedure did not affect the BET surface area, the crystal structure and the H_2 uptake characteristics. So it can be deduced that the surface of our nitrided sample is in the Mo_2N form. IR spectra were collected on a Fourier transform infrared spectrometer (Nicolet Impact 410) with a resolution of 4 cm^{-1}.

Fig. 1(a)–(e) shows the IR spectra recorded from the adsorption and reaction of but-1-ene on the Mo_2N/γ-Al_2O_3 catalyst below RT. Shown in Fig. 1(a), the IR spectra of adsorbed but-1-ene at 150 K are characterized by bands of ν(CH) at 3070 cm^{-1}, ν(C=C) at 1631 cm^{-1} and CH vibrations in the 3000 and 1400 cm^{-1} regions. The band at 1631 cm^{-1} is attributed to weakly π-adsorbed but-1-ene on the support of the Mo_2N/γ-Al_2O_3 sample. Another band of ν(C=C) at 1597 cm^{-1} can be attributed to σ-bonded but-1-ene on the Mo sites,[7] indicating some chemical changes of adsorbed butenes on the surface of Mo_2N/γ-Al_2O_3 even at quite low temperature. With increased temperatures, the following spectra changes are observed.

(1) At 181 K, the decrease in the amount of adsorbed but-1-ene is evidenced by the decrease in the ν(CH) band at 3070 cm^{-1}, which is accompanied by the appearance of a new band at 3005 cm^{-1}. The change in the ν(C=C) region is also obvious. The intensity ratio of the two bands at 1631 and 1597 cm^{-1} is smaller than that in Fig. 1(a), namely, more σ-bonded but-1-ene is formed with the decrease of π-adsorbed but-1-ene on the surface. Meanwhile, an additional small band at 1619 cm^{-1} appears.

(2) Further increase of the temperature to 201 K causes substantial changes in the IR spectra, where all the characteristic bands of the adsorbed but-1-ene disappear: bands at 3070 and 1631 cm^{-1} disappear and the band at 1597 cm^{-1} decreases in intensity. Concomitantly, new bands appear and increase in intensity: one ν(CH) band at 3005 cm^{-1}, two bands in ν(C=C) region at 1619 and 1614 cm^{-1}, indicating the formation of new adsorbed species from but-1-ene.

(3) At 256 K, shown in Fig. 1(e), the band at 1619 cm^{-1} becomes dominant in the ν(C=C) region and the band at 1597 cm^{-1} is very weak. This IR spectrum is completely different from that of the adsorbed but-1-ene [Fig. 1(a)], suggesting that a reaction of but-1-ene on the Mo_2N/γ-Al_2O_3 catalyst occurs.

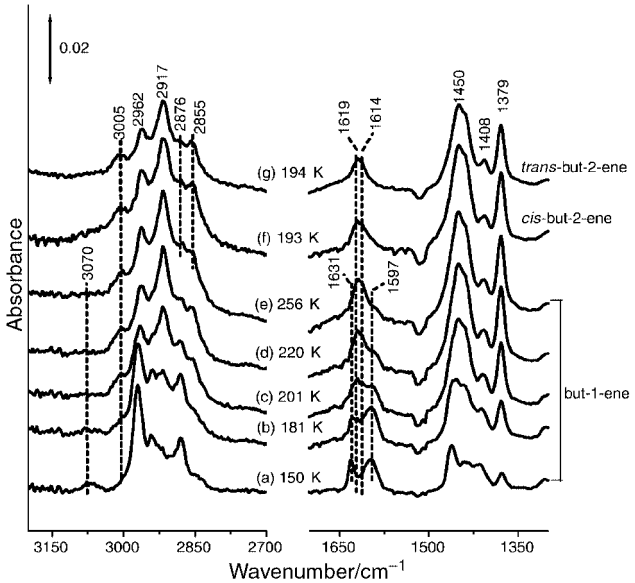

Fig. 1 IR spectra of but-1-enes and but-2-enes adsorbed on to a Mo_2N/γ-Al_2O_3 catalyst at 145 K and recorded at elevated temperatures: but-1-ene at (a) 150 K; (b) 181 K; (c) 201 K; (d) 220 K; (e) 256 K; *cis*-but-2-ene at (f) 193 K; *trans*-but-2-ene at (g) 194 K. In the IR study, the passivated sample was heated from RT to 623 K in 30 min, then to 723 K in 100 min, further from 723 K to 873 K in 75 min, and finally held for 60 min. The renitrided sample was then evacuated at 773 K for 60 min and subsequently cooled to 145 K, a small amount of but-1-ene (*ca.* 0.05 Torr) was introduced and then the temperature was gradually increased to RT.

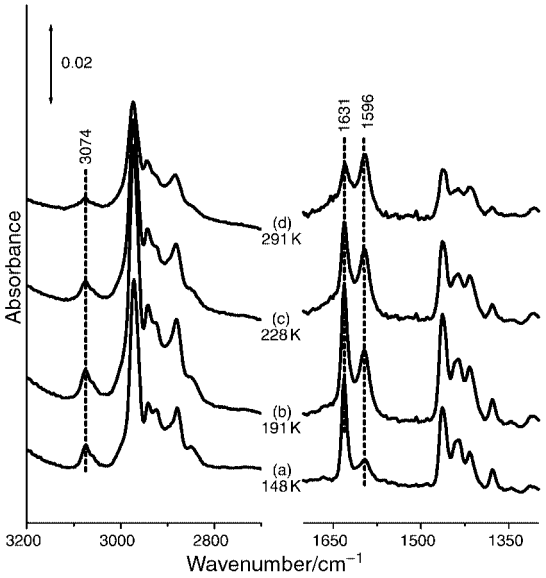

Fig. 2 IR spectra of but-1-ene adsorbed on to a reduced, passivated Mo_2N/γ-Al_2O_3 catalyst initially at (a) 145 K and then increased to (b) 192 K, (c) 231 K and (d) 291 K. The IR procedure for the reduced, passivated sample is similar to that of the nitrided sample.

A similar experiment of but-1-ene adsorption on nitrided γ-Al_2O_3 shows no evident changes in the IR spectra, confirming that the changes in but-1-ene adsorbed on the Mo_2N/γ-Al_2O_3 catalyst are mainly associated with the surface of Mo_2N.

The most likely products formed from the reaction of but-1-ene on the Mo_2N/γ-Al_2O_3 catalyst at such low temperatures are regarded as being the isomers *cis*- and *trans*-but-2-ene. IR spectra of the adsorbed *cis*- and *trans*-but-2-ene on the Mo_2N/γ-Al_2O_3 catalyst at about 193 K are shown respectively in Fig. 1(f) and 1(g) for a comparison with those of the reaction products from the adsorption of but-1-ene [Fig. 1(e)]. In the ν(CH), ν(C=C) and δ(CH) regions, the three spectra show similar contours to each other, implying similar surface species. Hence, it is clear that the adsorbed species produced from the reaction of but-1-ene on the Mo_2N/γ-Al_2O_3 catalyst are a mixture of *cis*- and *trans*-but-2-ene.

The adsorption of but-1-ene was also carried out on the reduced, passivated Mo_2N/γ-Al_2O_3 catalyst. As exhibited in Fig. 2, IR spectra of adsorbed but-1-ene at 145 K [Fig. 2(a)] presents similar contours to those from the Mo_2N/γ-Al_2O_3 catalyst at 150 K [Fig. 1(a)]. However, a further increase of temperatures does not cause changes in the spectra: IR bands at 3074, 1631 and 1596 cm^{-1}, characteristic bands of adsorbed but-1-ene, are still evident even at 291 K and no new bands appear. It is obvious that adsorbed but-1-ene does not convert to its isomers on the reduced, passivated Mo_2N/γ-Al_2O_3 catalyst.

The DBM of butenes has been widely investigated on a variety of catalysts, including solid acid catalysts,[8] base catalysts[9] and noble metal catalysts.[10,11] Only a few studies[12] reported the isomerization properties of reduced, passivated nitride catalysts, and there is no such study on fresh nitrides. Until now, this is the first study reporting the low-temperature isomerization of but-1-ene on a nitrided Mo catalyst. For the Mo_2N/γ-Al_2O_3 catalyst, the surface oxygen sites have been eliminated during the renitridation procedure and the surface Mo sites are in a low valence state (*ca*. 0–2).[2] It can be deduced[13] that the acidity of the nitrided Mo catalyst is quite weak. Therefore, the DBM of but-1-ene may not proceed *via* the same mechanism as that on reduced, passivated nitrides where the activity is attributed to the surface oxide sites as a consequence of the passivation procedure.[12]

A separate coadsorption experiment of CO with but-1-ene on the Mo_2N/γ-Al_2O_3 catalyst showed that preadsorbed CO greatly inhibits the isomerization of but-1-ene, and also that adsorbed but-1-ene significantly influences CO adsorption on Mo sites,[3] suggesting that the DBM of but-1-ene takes place on the same surface sites as for CO adsorption, mostly the $Mo^{\delta+}$ ($0 < \delta < 2$) cus (coordinatively unsaturated sites). Hence, it is likely that the Mo_2N/γ-Al_2O_3 catalyst behaves in a similar way to noble metal catalysts where but-1-ene isomerization also takes place on metal sites. The mechanism of the reaction can be referred from the literature[10] where the paths for an addition–abstraction (AD–AB) mechanism (alkyl–reversal) and an abstraction–addition (AB–AD) mechanism (π-allylic intermediate) are reported. Rooney and Webb[10] suggested that, in the isomerization of *n*-butenes on metal catalysts, the alkyl intermediates prevail at low temperatures whereas allylic intermediates participate to a greater extent in the surface processes as temperature is increased. Therefore, for low-temperature DBM of but-1-ene on the Mo_2N/γ-Al_2O_3 catalyst, it is reasonable to deduce that the mechanism of this reaction resembles one of the two mechanisms proposed on noble metal catalysts, most possibly the AD–AB mechanism (alkyl intermediate).

In conclusion, a novel reaction, low-temperature isomerization of but-1-ene, is found on the Mo_2N/γ-Al_2O_3 catalyst using IR spectroscopy. The reduced, passivated Mo_2N/γ-Al_2O_3 catalyst does not catalyze this reaction even at RT. The isomerization reaction is proposed to proceed *via* an alkyl intermediate on the surface $Mo^{\delta+}$ ($0 < \delta < 2$) cus on the nitrided Mo sample. This mechanism is quite different from that of the passivated nitride catalyst in isomerization reactions but is similar to that of Group VIII metals. The results manifest the unique catalytic properties of fresh nitride catalysts and urge more attention to be focussed on fresh nitrides, which may catalyze some new reactions.

This work was supported financially by the National Nature Science Foundation of China (NSFC, No. 29625305).

Notes and references

1 S. T. Oyama, *Catal. Today*, 1992, **15**, 179.
2 S. Yang, C. Li, J. Xu and Q. Xin, *J. Phys. Chem. B*, 1998, **102**, 6986.
3 Z. Wu, Z. Hao, P. Ying, C. Li and Q. Xin, *J. Phys. Chem. B*, 2000, **104**, 12275.
4 Z. Wu, Y. Chu, S. Yang, Z. Wei, C. Li and Q. Xin, *J. Catal.*, 2000, **194**, 23.
5 C. Sayag, G. Bugli, P. Havil and G. Djéga-Mariadassou, *J. Catal.*, 1997, **167**, 372.
6 G. W. Haddix, J. A. Reimer and A. T. Bell, *J. Catal.*, 1987, **108**, 50.
7 N. Sheppard and C. De La Cruz, *Adv. Catal.*, 1996, **41**, 1.
8 J. N. Kondo, L. Shao, F. Wakabayashi and K. Domen, *J. Phys. Chem.*, 1997, **101**, 9314.
9 M. P. Rosynek, J. S. Fox and J. L. Jensen, *J. Catal.*, 1981, **71**, 64.
10 J. J. Rooney and G. Webb, *J. Catal.*, 1964, **3**, 488.
11 D. Yoon, M. X. Yang and G. A. Somorjai, *J. Catal.*, 1998, **176**, 35.
12 M. K. Neylon, S. Choi, H. Kwon, K. E. Curry and L. T. Thompson, *Appl. Catal., A: General*, 1999, **183**, 253.
13 M. Nagai, Y. Goto, A. Irisawa and S. Omi, *J. Catal.*, 2000, **191**, 128.

Area correction of multi-atom–acceptor hydrogen bond frequency distributions

Zbigniew Ciunik*[a] and Gautam R. Desiraju*[b]

[a] *Faculty of Chemistry, University of Wrocław, 14 F. Joliot-Curie St., 50-383 Wrocław, Poland. E-mail: ciunik@wchuwr.chem.uni.wroc.pl*

[b] *School of Chemistry, University of Hyderabad, Hyderabad 500 046, India. E-mail: desiraju@uohyd.ernet.in*

Received (in Columbia, MO, USA) 15th November 2000, Accepted 25th February 2001
First published as an Advance Article on the web 26th March 2001

Frequency distributions of hydrogen bond trajectories for X–H···Ph interactions (X = O, N, C) need to be corrected for the finite area of the acceptor moiety and once this correction has been performed, it is seen that the donor groups have a distinct tendency to interact with the centroid of the aromatic ring.

Statistical analysis of experimental and theoretical data is very important for a correct interpretation of several chemical phenomena. Hydrogen bonds are typically described in terms of various parameters (lengths, angles) obtained from crystal structure determinations. These parameters are most simply depicted as histograms. However, such simple methods of analysis can be sometimes misleading.[1] For example, it was found that a distribution of hydrogen bond angles, θ, in O–H···O hydrogen bonds is in the range 120–180° with a maximum at around 160°. Such an observation suggests that hydrogen bonds in crystals are non-linear.[2] This is, however, inconsistent with theoretical predictions in the gas phase, say for the water–water dimer. The reason for this seeming contradiction is the failure to take into account a geometrical factor that seriously influences the crystal statistics. The number of hydrogen bonds with angle θ is proportional to $\sin\theta$ for purely geometrical reasons, there being a greater probability of finding such interactions on the rims of cones of increasing solid angles. A simple procedure, namely the use of $N/\sin\theta$ instead of N (where N is the number of hydrogen bonds in the interval θ to $\theta + \Delta\theta$) in the histograms, effectively resolves this contradiction. This is known today as the *cone correction* and is illustrated in Fig. 1(a). This correction is used widely in the interpretation of hydrogen bonds and occurs as a standard procedure in the program VISTA that is a part of the Cambridge Structural Database (CSD).[3]

Recent work on weak X–H···Ph hydrogen bonds has led to only a limited consensus concerning the nature of these interactions.[4] Some authors have held that the donor group X–H interacts with the centroid of the aromatic ring.[5–8] Others have stated that donors interact with one or more of the ring carbon atoms.[9–11] However, neither of these conclusions has been unambiguously substantiated. During our own studies of X–H···Ph (X = O, N, C) interactions, we realised that the frequency distributions of these interactions must be corrected for the fact that the acceptor, being of a multiatom type, has a finite area. Therefore the numbers of observed trajectories of the

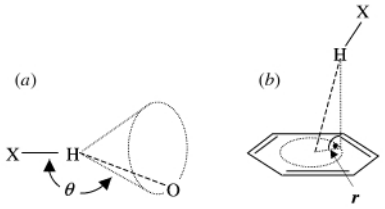

Fig. 1 Schematic diagrams for geometrical corrections of hydrogen bond metrics. (a) Cone correction for hydrogen bond angles θ. (b) Area correction for hydrogen bond offsets r.

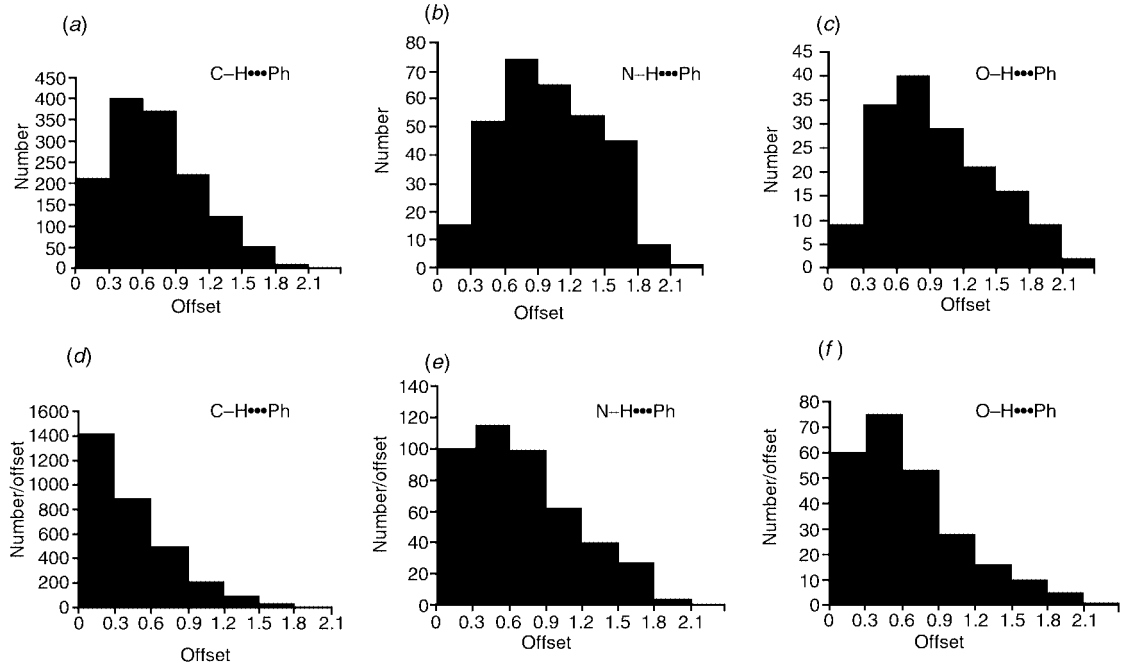

Fig. 2 Histograms of offsets r for X–H···Ph hydrogen bonds: Uncorrected (a) C–H···Ph, (b) N–H···Ph and (c) O–H···Ph; corrected (d) C–H···Ph, (e) N–H···Ph and (f) O–H···Ph. Offsets are in Å.

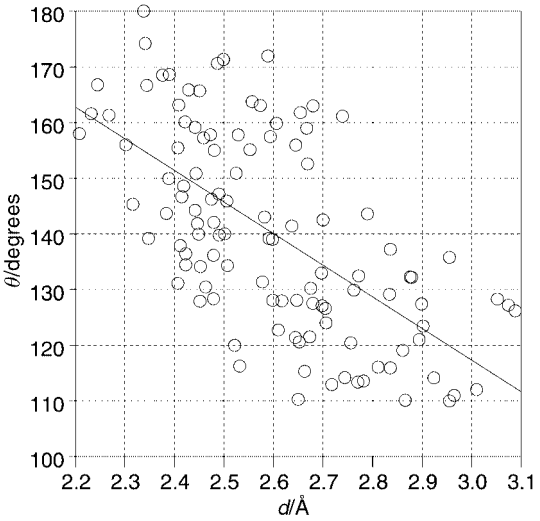

Fig 3 d–θ scatterplot for O–H···Ph hydrogen bonds with $r \leqslant 1.2$ Å, assuming that the ring centroid is the point acceptor. Notice the inverse correlation typical of hydrogen bonds.

donor onto the acceptor are a result of both chemical and geometrical factors. Simply put, an interaction X–H···Ph has an offset r which is the distance from the ring centroid to the projection of the H-atom position on the plane of the ring. This is shown in Fig. 1(b). The number of hydrogen bonds with offset r is proportional to $2\pi r$ for geometrical reasons and accordingly, histograms of N (where N is the number of offsets in the range r and $r+\Delta r$) must be replaced by N/r before they become chemically meaningful. So, we would like to term this procedure an *area correction* to match the term *cone correction* used in θ histograms.

Fig. 2(a), (b) and (c) are uncorrected histograms of X–H···Ph offsets for C–H···Ph, N–H···Ph and O–H···Ph hydrogen bonds ($d \leqslant 3.10$ Å, $\theta \geqslant 110°$) from 769, 649 and 431 appropriately retrieved crystal structure data in the CSD.† The histograms contain 1379, 314 and 160 hydrogen bonds respectively. Figs. 2(d), (e) and (f) are the respective corrected histograms.‡ The correction is carried out within ranges of 0.3 Å; the range from 0.0 to 0.3 Å is corrected by a factor of 1/(0.15), the range between 0.3 and 0.6 Å is corrected by a factor of 1/(0.45), and so on. The uncorrected histograms seem to indicate no particular offset preference. However, all three area corrected histograms show a preference for hydrogen bonds to a phenyl ring to be directed at or near the centre of the ring. For C–H···Ph interactions, this preference is clear. For N–H···Ph and O–H···Ph interactions, there is a maximum around 0.3 Å from the centroid. However, the number of observations in these latter cases is insufficient to draw fine distinctions.§ What *is* important is that the preference for a centroid or a close-to-centroid approach is seen in all cases.

To examine this matter further, we obtained the scatterplot of the hydrogen bond angle θ *vs.* the hydrogen bond distance d, assuming the centroid to be the point acceptor site for the 112 O–H···Ph hydrogen bonds with offsets < 1.20 Å (Fig. 3). This scatterplot (correlation coefficient -0.63) shows the typical inverse length–angle correlation that arises from the electrostatic nature of hydrogen bonds,[4] and indicates that the centroid may be reasonably approximated as the acceptor site in these interactions. The corresponding C–H···Ph scatterplot is fuzzier but this is not unexpected.

In summary, we conclude that this area correction for phenyl ring acceptors should be used in all relevant analyses of hydrogen bonds formed to such multiatom acceptors.

We thank the DST–KBN for travel support to Z. C. under Indo-Polish grant INT/POL/008.00 and Dr A. Nangia for helpful discussions and comments.

Notes and references

† CSD (release: April 2000, 215 403 hits). Data were retrieved using the following overall criteria for all structures: 'no polymers'; 'no disorder'; 'error free structures'; 'atom coordinates present'; H···Ph(centroid) distances shorter than 3.5 Å and $R \leqslant 0.05$. Two additional criteria were used: 'no ions' for the N–H···Ph contacts (to eliminate the $>$N–H$^+$ donors); $T \leqslant$ 120 K for the C–H···Ph contacts. For polynuclear ring acceptors, the offsets were calculated only with respect to the phenyl ring towards which the donor is oriented.

‡ Histograms were prepared using program Microsoft Excel.

§ Unsurprisingly, the exact profiles of the N–H···Ph and O–H···Ph histograms near the centroid depend on the range within which the area correction is performed (0.2, 0.3 Å). This is not the case for the C–H···Ph histogram, because the number of observations (1379) is satisfactorily large.

1 R. Balasubramanian, R. Chidambaram and G. N. Ramachandran, *Biochim. Biophys. Acta*, 1970, **221**, 196.
2 J. Kroon and J. A. Kanters, *Nature*, 1974, **248**, 367.
3 F. H. Allen and O. Kennard, *Chem. Des. Autom. News*, 1993, **8**, 31.
4 G. R. Desiraju and T. Steiner, *The Weak Hydrogen Bond in Structural Chemistry and Biology*, Oxford University Press, 1999.
5 J. F. Malone, C. M. Murray, M. H. Charlton, R. Docherty and A. J. Lavery, *J. Chem. Soc., Faraday Trans.*, 1997, **93**, 3429.
6 N. N. L. Madhavi, A. K. Katz, H. L. Carrell, A. Nangia and G. R. Desiraju, *Chem. Commun.*, 1997, 1953.
7 D. Braga, F. Grepioni and E. Tedesco, *Organometallics*, 1998, **17**, 2669.
8 Z. Ciunik, S. Berski, Z. Latajka and J. Leszczynski, *J. Mol. Struct.*, 1998, **442**, 125.
9 M. Nishio, M. Hirota and Y. Umezawa, *The CH/π interaction. Evidence, Nature and Consequences*. Wiley, New York, 1998.
10 Y. Umezawa, S. Tsuboyama, H. Takahashi, J. Uzawa and M. Nishio, *Tetrahedron*, 1999, **55**, 20 047.
11 Y. Umezawa, S. Tsuboyama, H. Takahashi, J. Uzawa and M. Nishio, *Bioorg. Med. Chem.*, 1999, **7**, 2021.

A structurally characterised, naked sp^3-hybridised carbanion in the zwitterionic imido complex [Ti(NBu^t){C(Me$_2$pz)$_3$}Cl(THF)] (HMe$_2$pz = 3,5-dimethylpyrazole)†

Sally C. Lawrence, Michael E. G. Skinner, Jennifer C. Green and Philip Mountford*

Inorganic Chemistry Laboratory, South Parks Road, Oxford, UK OX1 3QR.
E-mail: philip.mountford@chem.ox.ac.uk; Fax: +44 1865 272690

Received (in Cambridge, UK) 8th January 2001, Accepted 27th February 2001
First published as an Advance Article on the web 26th March 2001

Reaction of the tris(3,5-dimethylpyrazolyl)methane complex [Ti(NBu^t){HC(Me$_2$pz)$_3$}Cl$_2$] with MeLi or LiNPr$^i_2$ in tetrahydrofuran (THF) gives the zwitterionic titanium imido derivative [Ti(NBu^t){C(Me$_2$pz)$_3$}Cl(THF)] 2 which contains the first structurally authenticated, naked sp^3-hybridised carbanion; the molecular and electronic structures of 2 are described.

The tris(pyrazolyl)hydroborate ligands are important face-capping, anionic, six-electron donor ligands in inorganic and organometallic coordination chemistry.[1] Their neutral analogues, the tris(pyrazolyl)methanes are considerably less well developed.[2] We are interested in the use of tris(pyrazolyl)-methanes in our ongoing program in early transition metal imido chemistry.[3] Target complexes of the type [Ti(NR)-{tris(pyrazolyl)methane}Cl$_2$] are isolobal analogues of the group metallocenes [M(η-C$_5$R$_5$)$_2$Cl$_2$] (M = Ti, Zr) which are in turn a very important class of single-site olefin polymerisation catalysts;[4] no tris(pyrazolyl)methane-supported imido complexes have been described previously. As part of these studies we found a unique example of a stabilised, naked *sp*^{3}-hybridised carbanion as described below.

Reaction of [Ti(NBu^t)Cl$_2$(py)$_3$][5] with HC(Me$_2$pz)$_3$ (HMe$_2$pz = 3,5-dimethylpyrazole) in CH_2Cl_2 afforded the tris(3,5-dimethylpyrazolyl)methane complex [Ti(NBu^t){HC-(Me$_2$pz)$_3$}Cl$_2$] **1** in 80% yield after the addition of hexane (Scheme 1).‡ Reaction of **1** with one equivalent of MeLi (initially in a failed attempt to alkylate titanium) or LiN(Pr^i)$_2$ in THF leads to smooth removal of the apical proton of HC(Me$_2$pz)$_3$ and formation of the diamagnetic compound [Ti(NBu^t){C(Me$_2$pz)$_3$}Cl(THF)] **2** in *ca.* 60% yield. Reaction of **2** in benzene with HCl (1 equivalent) reforms **1**; the corresponding reaction of **2** with DCl forms [Ti(NBu^t){DC-(Me$_2$pz)$_3$}Cl$_2$] **1-d** with deuterium enrichment occuring exclusively at the apical carbon of the tridentate ligand.

Crystallization of **2** from toluene at 5 °C gave diffraction-quality crystals.§ The molecular structure of **2** is shown in Fig. 1 together with selected bond lengths and angles. Fourier difference syntheses revealed the positions of all hydrogen atoms of the {C(Me$_2$pz)$_3$}$^-$ ligand; none was located for the apical carbon C(24). A formal negative charge is assigned to this atom as illustrated in Scheme 1; the Ti centre thus has a formal charge of +4 in line with the observed diamagnetism. The N–C–N angles subtended at C(24) lie in the range 108.3(3)–109.6(3)°, consistent with this atom being formally sp^3 hybridised. In general, the distances and angles for **2** are comparable with those of previously reported titanium imido and tris(pyrazolyl)methane complexes.[2,3,6] The solution ^{1}H and ^{13}C NMR data for **2** support the solid state structure.

The {C(Me$_2$pz)$_3$}$^-$ ligand in [Ti(NBu^t){C-(Me$_2$pz)$_3$}Cl(THF)] **2** is analogous to the hydroborate relative {HB(Me$_2$pz)$_3$}$^-$. We have previously reported a series of titanium imido complexes with tris(pyrazolyl)hydroborate li-

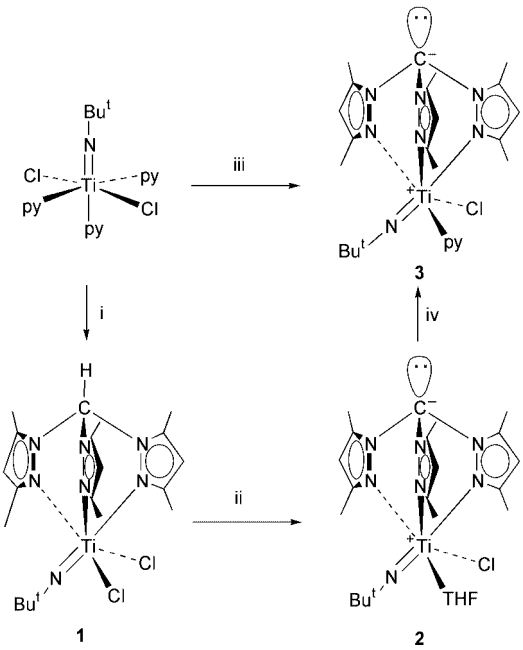

Scheme 1 *Reagents and conditions*: i HC(Me$_2$pz)$_3$, CH_2Cl_2, rt, 1 h, 80%; ii MeLi or LiN(Pr^i)$_2$, THF, −80 °C to rt, 2–4 h, 60–62%; iii LiC(Me$_2$pz)$_3$, THF, −80 °C to rt, 16 h, 50%; iv pyridine (1 equiv.), C_6D_6, rt, 20 min, > 95%.

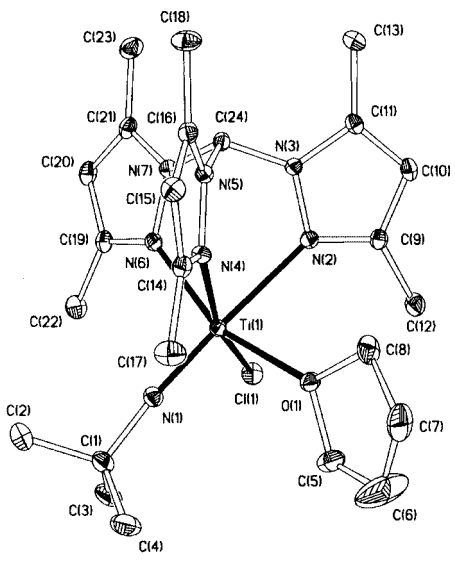

Fig. 1 Displacement ellipsoid (20%) plot of [Ti(NBu^t){C-(Me$_2$pz)$_3$}Cl(THF)] **2**. Hydrogen atoms and toluene of crystallization are omitted for clarity. For selected bond lengths see Table 1.

† Electronic supplementary information (ESI) available: isosurface for the HOMO of **2a**. See http://www.rsc.org/suppdata/cc/b1/b100315l/

Table 1 Comparison of selected bond distances (Å) for [Ti(NH){HC(pz)$_3$}Cl$_2$] **1a**, [Ti(NPBu^t){C(Me$_2$pz)$_3$}Cl(THF)] **2**, [Ti(NH){C(pz)$_3$}Cl(OH$_2$)] **2a** and [Ti(NH){HB(pz)$_3$}Cl(OH$_2$)] **4**. For the Ti–N$_{pyrazole}$ distances 'A', 'B' and 'C' refer to the nitrogens *trans* to imide, Cl and O (or Cl for **1a**), respectively

	1a	**2**	**2a**	**4**
Ti=N$_{imide}$	1.711	1.713(3)	1.71	1.70
Ti–O	—	2.152(3)	2.15	2.08
Ti–Cl	2.40	2.394(1)	2.41	2.37
Ti–N$_{pyrazole(A)}$	2.44	2.358(3)	2.36	2.30
Ti–N$_{pyrazole(B)}$	2.28	2.191(4)	2.22	2.17
Ti–N$_{pyrazole(C)}$	2.28	2.169(3)	2.16	2.11

gands. The Ti=N$_{imide}$, Ti–Cl and Ti–N$_{pyrazolyl}$ distances in **2** are comparable to those of tris(pyrazolyl)hydroborate analogues.

DFT (density functional theory) calculations[8] were used to optimise the geometry of [Ti(NH){C(pz)$_3$}Cl(OH$_2$)] **2a** as a model for [Ti(NBu^t){C(Me$_2$pz)$_3$}Cl(THF)] **2**, and to determine its electronic structure.¶ Comparative calculations were also carried out for the tris(pyrazolyl)hydroborate species [Ti(NH){HB(pz)$_3$}Cl(OH$_2$)] **4** and for C_s symmetric [Ti(NH){HC(pz)$_3$}Cl$_2$] **1a** (as a model for [Ti(NBu^t){HC(Me$_2$pz)$_3$}Cl$_2$] **1**). Table 1 compares selected bond distances for **1a**, **2**, **2a** and **4**. There is very good agreement between those of the real compound **2** and of its model **2a**. The N–C$_{apical}$–N angles in **1a** (110–111°) are comparable to those of **2a** (108–109°) in line with the sp^3 hybridisation of the apical carbon; in **4** the N–B–N angles lie in the range 107–109°.

The highest occupied molecular orbital (HOMO) for [Ti(NH){C(pz)$_3$}Cl(OH$_2$)] **2a** is based predominantly on the {C(pz)$_3$}$^-$ apical carbon and has a computed energy of −5.14 eV; the isosurface is shown in Fig. 2.† There is an energy separation of 2.00 eV between this MO and the lowest unoccupied molecular orbital (LUMO) which is Ti 3d in character. The calculations support our proposal that **2** and **3** are zwitterionic Ti(IV) complexes that contain naked, formally sp^3-hybridised apical carbanions; an alternative interpretation of **2** and **3** as antiferromagnetically coupled Ti(III) complexes with an apical carbon-based radical can be discounted. There is a net atomic charge (calculated from the Voronoi Deformation Density[8]) of −0.13 e for the apical carbon in **2a** whereas the corresponding atomic charge in **1a** is 0.11 e; the atomic charges for Ti in **1a**, **2a** and **4** are 0.29, 0.32 and 0.29 e, respectively. The molecular and electronic structures for [Ti(NH){C(pz)$_3$}Cl(OH$_2$)] **2a** and [Ti(NH){HB(pz)$_3$}Cl(OH$_2$)] **4** confirm the analogy between {C(R$_3$pz)$_3$}$^-$ and {HB(R$_3$pz)$_3$}$^-$.

The apical carbon in [Ti(NBu^t){C(Me$_2$pz)$_3$}Cl(THF)] **2** is the first example of any naked, sp^3-hybridised carbanion.[6] Formally sp^2-hybridised carbanions are very well-established in the literature and for such species the planar geometry around the carbanion assists resonance stabilization.[6,9] Previous reports have shown that the apical carbon of the free or complexed parent tris(pyrazolyl)methane can be deprotonated (and, in many instances, functionalised this way),[10] but no carbanionic species have been structurally characterised.

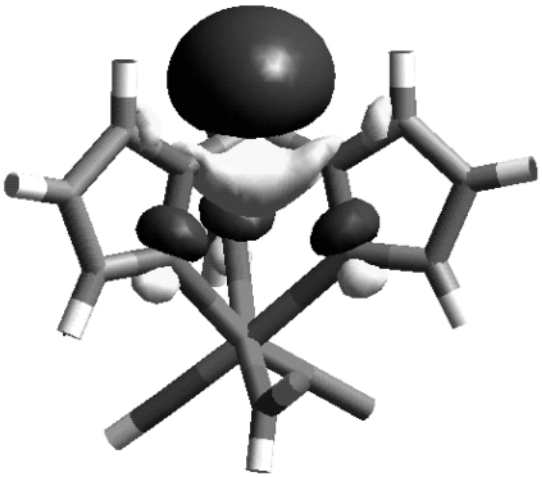

Fig. 2 Isosurface for the highest occupied molecular orbital of **2a**.

The anionic {C(Me$_2$pz)$_3$}$^-$ is potentially a new ligand in transition metal chemistry, not least because of the improved, multi-gram synthesis now available for HC(Me$_2$pz)$_3$.[2b] The methyl substituents in the 5-position of the pyrazolyl rings clearly offer significant protection of the carbanionic carbon in **2**. Moreover, it is possible to cleanly deprotonate HC(Me$_2$pz)$_3$ itself (*i.e.* without prior complexation to a metal centre) by reaction with MeLi in THF to form benzene-soluble LiC(Me$_2$pz)$_3$ **5** in quantitative isolated yield. The anionic apical carbon in **5** is confirmed by reaction with D$_2$O to generate DC(Me$_2$pz)$_3$ with deuterium enrichment exclusively in the apical position. We have established the potential use of LiC(Me$_2$pz)$_3$ **5** as a reagent (*via* salt-elimination type reactions) and source of anionic {C(Me$_2$pz)$_3$}$^-$. Thus, reaction of [Ti(NBu^t)Cl$_2$(py)$_3$] with LiC(Me$_2$pz)$_3$ **5** in THF forms [Ti(NBu^t){C(Me$_2$pz)$_3$}Cl(py)] **3** in good yield (Scheme 1). A survey of the syntheses and chemistry of a range of zwitterionic complexes with the anionic {C(Me$_2$pz)$_3$}$^-$ ligand and its homologues is currently underway.

This work was supported by the EPSRC and Royal Society. S. C. L. is the recipient of a European Scatcherd Scholarship. We thank Professor D. L Reger for his improved synthesis of HC(Me$_2$pz)$_3$ prior to publication, and Professor S. Trofimenko for helpful comments.

Notes and references

‡ Satisfactory characterising data have been obtained for all the new compounds.

§ *Crystal data* for **2**: $C_{24}H_{38}ClN_7OTi\cdot0.5C_7H_8$, M = 570.04, monoclinic, $C2/c$, a = 23.894(2), b = 13.8900(9), c = 20.0340(9) Å, β = 114.882(3)°, U = 6031.85 Å^3, Z = 8, T = 150 K, μ = 0.40 mm^{-1}, 5737 independent reflections (R_{merge} = 0.042), 3675 [$I > 3\sigma(I)$] used in refinement, final R indices: R = 0.0412, R_w = 0.0573.

CCDC 15549. See http://www.rsc.org/suppdata/cc/b1/b100315l/ for crystallographic data in .cif or other electronic format.

¶ Calculations were performed using the density functional methods of the Amsterdam Density Functional (ADF) code Version 2000.02.[8]

1 S. Trofimenko, *Scorpionates. The Coordination Chemistry of Polypyrazolylborate Ligands*, Imperial College Press, London, 1999.
2 For leading references see the following and references therein: (*a*) D. L. Reger, C. A. Little, A. L. Rheingold, M. Lam, T. Concolino, A. Mohan and G. J. Long, *Inorg. Chem.*, 2000, **39**, 4674; (*b*) D. L. Reger, T. C. Grattan, K. J. Brown, C. A. Little, J. J. S. Lamba, A. L. Rheingold and R. D. Sommer, *J. Organomet. Chem.*, 2000, **607**, 120.
3 See the following and references therein: N. A. H. Male, M. E. G. Skinner, S. Y. Bylikin, P. J. Wilson, P. Mountford and M. Schröder, *Inorg. Chem.*, 2000, **39**, 5483; M. E. G. Skinner, D. A. Cowhig and P. Mountford, *Chem. Commun.*, 2000, 1167; P. Mountford, *Chem. Commun.*, 1997, 2127 (Feature Article).
4 C. Janiak, in *Metallocenes: synthesis, reactivity, applications*, ed. A. Togni and R. L. Halterman, Wiley-VCH, New York, 1998, vol. 2; pp. 547.
5 A. J. Blake, P. E. Collier, S. C. Dunn, W.-S. Li, P. Mountford and O. V. Shishkin, *J. Chem. Soc., Dalton Trans.*, 1997, 1549.
6 The United Kingdom Chemical Database Service, D. A. Fletcher, R. F. McMeeking and D. Parkin, *J. Chem. Inf. Comput. Sci.*, 1996, **36**, 746.
7 S. C. Dunn, P. Mountford and O. V. Shishkin, *Inorg. Chem.*, 1996, **35**, 1006.
8 C. Fonseca Guerra, J. G. Snijider, G. te Velde and E. J. Baerends, *Theor. Chem. Acc.*, 1998, **99**, 391.
9 See the following and references therein: C. Eaborn, A. Farook, P. B. Hitchcock and J. D. Smith, *Organometallics*, 1998, **17**, 3135; M. T. Reetz, S. Hütte and R. Goddard, *Eur. J. Org. Chem.*, 1999, 2475.
10 P. K. Byers and F. G. A. Stone, *J. Chem. Soc., Dalton Trans.*, 1991, 93; M. A. Esteruelas, L. A. Oro, R. M. Claramunt, C. Lopéz, J. L. Lavandera and J. Elguero, *J. Organomet. Chem.*, 1989, **366**, 245; W. Kläui, M. Berghahn, G. Rheinwald and H. Lang, *Angew. Chem., Int. Ed.*, 2000, **39**, 2464.

ChemComm

Variation of the energy gap in fullerene-based dendrons: competitive *versus* sequential energy and electron transfer events

José L. Segura,[a] Rafael Gómez,[a] Nazario Martín,*[a] Chuping Luo,[b] Angela Swartz[b] and Dirk M. Guldi*[b]

[a] *Departamento de Química Orgánica, Facultad de Ciencias Químicas, Universidad Complutense, E-28040-Madrid, Spain. E-mail: nazmar@eucmax.sim.ucm.es*

[b] *Radiation Laboratory, University of Notre Dame, IN 46556, USA. E-mail: guldi.1@nd.edu*

Received (in Cambridge, UK) 9th January 2001, Accepted 15th February 2001
First published as an Advance Article on the web 29th March 2001

Artificial molecular models, based on rigid dendrimeric *meta*-substituted phenylenevinylene moieties bearing different electron donating groups and the electron acceptor C_{60}, were probed in an effort to gain control over a sequential *versus* a competitive scenario in energy and electron transfer events.

The design of supramolecular ensembles for use in energy conservation and conversion is a long-standing objective.[1] Understanding the complexity of efficient energy migration and unidirectional electron transfer occurring, for example, in the photosynthetic reaction center[2] offers powerful guidelines for developing artificial devices. A particularly challenging aspect is to explore the role of a sequence *versus* a competition in energy/electron transfer reactions, especially upon altering the energy gaps.

The choice of the connecting spacer in donor–bridge–acceptor (D–B–A) assemblies is fundamental, since it ensures the control over distance, angle and coupling between the donor and acceptor. These parameters govern in large character, rate and efficiency of long distance energy and/or electron transfer processes.[3,4] Dendritic structures provide key criteria such as rigidity and conjugation, which, most importantly, can be chemically fine-tuned.[5] In turn, these unique molecular architectures emerged as versatile building blocks for the preparation of artificial systems.[6]

Previous work has focused mainly on encapsulating flexible dendron units.[7] The flexibility prohibits, however, a detailed comprehension of effects stemming from donor–acceptor separation and/or orientation, which drew our attention to the unique features of a stiff dendritic macromolecule.[8]

Here we report on the synthesis and photophysical studies of D–B–A systems in which four dibutylaniline (**8a**) or dodecyloxynaphthalene (**8b**) electron donors are located at the peripheral positions of well-defined phenylenevinylene-based dendrons and an acceptor fullerene at the focal point of the dendrimer.

Yu and coworkers[9a] and Meier and Lehman[9b] have reported synthetic routes towards formyl-substituted rigid poly(phenylenevinylene) dendrimers starting from different AB_2 type building blocks. A remarkable advantage of the convergent route, presented here is the use of a nitrile group in the readily available AB_2 starting material **1**.[10] This functionality remains unaffected during the Arbuzov and the Wittig–Horner reaction (*i.e.* with aldehydes **3a**,**b**) to yield bisphosphonate **2** and the first-generation dendrons **4a**,**b** with an *all-trans* configuration, respectively.

Subsequent treatment of the nitrile-substituted systems **4a,b** with DIBAL-H in dichloromethane transforms them in good yield to the corresponding formyl-substituted analogues **5a**,**b**. In the next step, a second Wittig–Horner reaction of **5a**,**b** with bisphosphonate **2** affords the nitrile-substituted second-generation dendrons **6a**,**b**. Additional DIBAL-H treatment allowed us to prepare the formyl functionalized dendrons **7a**,**b**. Dyads **8a,b** have been prepared in good yields (30%) by 1,3-dipolar cycloaddition of the respective rigid dendron (**7a**,**b**) to C_{60} in the presence of sarcosine in refluxing toluene (Fig. 1).[11]

The redox properties of the fullerene-containing dendrons **8a,b** were studied by cyclic voltammetry in toluene/acetonitrile (4 : 1 v/v) solutions and revealed several oxidation and reduction steps. In particular, anodic processes with peaks at 0.72 V (**8a**) and 1.30 V (**8b**) refer to the oxidation of the dibutylaniline and dodecyloxynaphthalene moieties, respectively. In the cathodic region three quasireversible reduction waves were recorded (**8a**: −0.65; −1.07, −1.70 V, **8b**: −0.64, −1.03; −1.62 V), which correspond to the stepwise reduction of the fullerene moiety and resemble those observed for a fulleropyrrolidine reference.

Replacement of the poly(arylenevinylene) cores (**8b**) with the analogous dibutylaniline functionalities (**8a**) imposes important consequences on the dendron's physico-chemical properties: red-shifted ground-state maxima in combination with better electron donor character create quite different energy gaps between the dendron's singlet excited state and that of the $C_{60}^{\bullet-}$–dendron$^{\bullet+}$ radical pair in **8a** and **8b**.

In general, the strongly fluorescing dendrons **7a** and **6b** with quantum yields as high as 0.47, give rise to an almost entirely quenched emission in dyads **8a** and **8b** (Table 1). For example, in non-polar toluene the dendrimer emission in the visible (400–450 nm) is reduced by more than two orders of magnitude.

From this observation we reach the conclusion that in toluene the dendrimer singlet excited state in **8a**,**b** undergoes a rapid singlet–singlet energy transfer to the energetically lower-lying

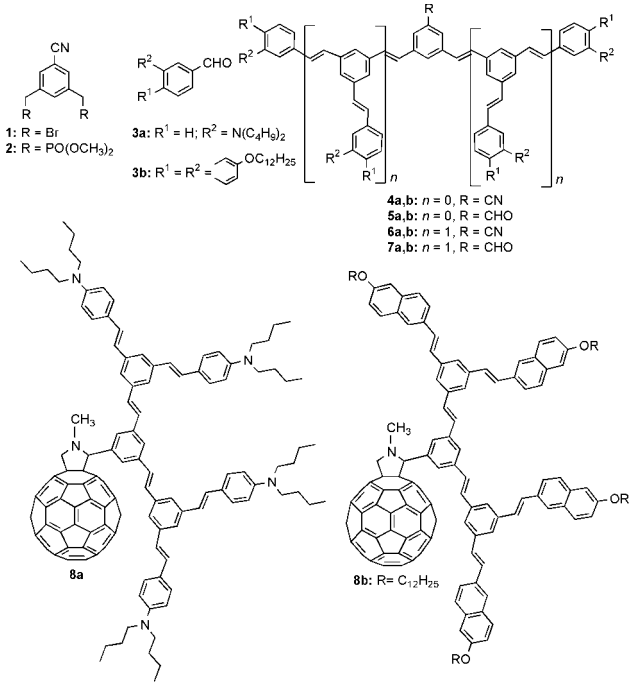

Fig. 1

Table 1 Photophysical properties of dendrons **6b**/**7a** and dyads **8a**/**8b**

	6b	7a	8b	8a
Dendron				
Φ_{FL} (toluene)	0.47[e]	0.31[f]	3.15×10^{-3}[e]	2.5×10^{-3}[f]
Φ_{FL} (THF)			3.07×10^{-3}[e]	2.2×10^{-3}[f]
τ_{FL} (toluene)/ns	1.99[e]	2.05[f]		
$\tau_{singlet}$ (toluene)/ns	1.97	2.01		
$-\Delta G_{ET}°$[a]/eV			1.34	1.67
λ[a]/eV			1.49	1.42
$-\Delta G_{EnergyT}°$/eV			1.24	0.99
Fullerene				
Φ_{FL}[b] (toluene)			5.4×10^{-4}	3.9×10^{-4}
Φ_{FL}[b] (THF)			4.0×10^{-4}	0.6×10^{-4}
Φ_{FL}[b] (BzCN)			3.0×10^{-4}	0.4×10^{-4}
τ_{FL}[b] (toluene)/ns			1.51	1.48
$\tau_{singlet}$[c] (toluene)/ns			1.49	1.40
$\tau_{singlet}$[c] (THF)/ns			1.51	0.16
$\tau_{singlet}$[c] (BzCN)/ns			1.42	0.09
$\Phi_{triplet}$[d] (toluene)			0.60	0.29
$\Phi_{triplet}$[d] (THF)			0.43	—[g]
$\Phi_{triplet}$[d] (BzCN)			0.30	—[g]
$-\Delta G_{ET}°$[a]/eV			0.10	0.68

[a] In benzonitrile; radius: (r_+) dibutylaniline = 3.7 Å; (r_+) naphthalene = 3.5 Å; (r_-) fullerene = 4.4 Å; donor–acceptor separation: (r_{D-A}) **8a** = 16.7 Å; (r_{D-A}) **8b** = 19.1 Å. [b] Measured at the 715 nm maximum, excitation at dendron ground state maximum. [c] Measured at the 880 nm maximum. [d] Measured at the 700 nm maximum. [e] Measured at the 413 nm maximum; excitation at 340 nm. [f] Measured at the 450 nm maximum; excitation at 380 nm. [g] Radical pair.

fullerene singlet (Fig. 2). Evidence that this energy transfer indeed takes place, comes from a set of decisive emission and excitation measurements.

The species evolving from energy transfer, namely, the fullerene singlet excited state (1.76 eV), has been identified *via* the characteristic fluorescence pattern[12] of a fulleropyrrolidine produced in nearly comparable quantum yields. Importantly, the complementary excitation spectrum of the fullerene emission in **8a**,**b** is virtually identical with the ground-state absorption and the excitation spectra of the reference compounds. To further test the above assignment, that is, a rapid singlet–singlet energy transfer, transient absorption spectroscopy was deemed necessary. Despite the unequivocal and nearly quantitative excitation (355 nm) of the dendrimer moieties no spectral evidence for the dendrimer's singlet–singlet absorption (*ca.* 650 nm) was found after the 18 ps laser pulse. Instead the spectral features are identical with the texture of the fullerene singlet excited state. Specifically, a characteristic maximum at 880 nm is a clear attribute of the fullerene singlet–singlet absorption. The rise time of the 880 nm absorption, representing the actual energy transfer event in **8a**,**b**, is, however, masked by the instrument response time and, therefore, prevents a meaningful kinetic analysis of the intramolecular reaction. On a longer time-scale the fate of the fullerene singlet excited state is identical to that known for a fulleropyrrolidine: intersystem crossing, driven by a strong spin-orbit coupling, governs the transformation (*ca.* 6.0×10^8 s^{-1}) of the singlet into the triplet excited state. The latter was identified by a long-lived (*ca.* 20 μs) and strongly absorbing triplet–triplet maximum (700 nm).

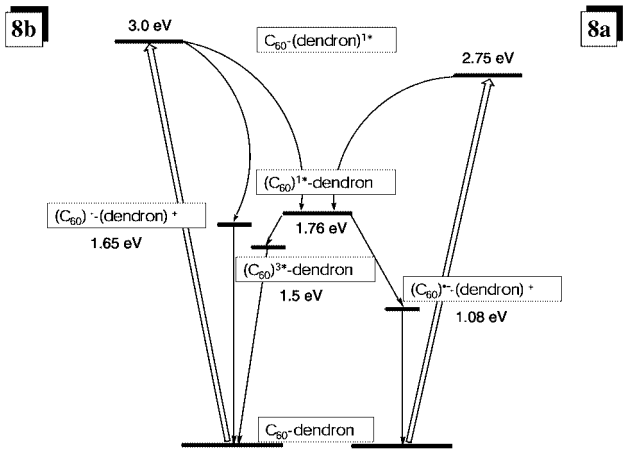

Fig. 2

Upon probing more polar THF and benzonitrile, the fullerene fluorescence in **8b** reveals a gradual decrease of up to 50%, while the dendron emission continued to be almost unchanged relative to that in toluene. This observation is consistent with an assumption that implies an energy transfer scenario, which is in competition with an activated electron transfer. Crucial support for this competitive synopsis evolves from the fullerene singlet lifetimes (Table 1), which are, despite the emission quenching, identical to those of a fulleropyrrolidine in all the solvents investigated.

8a, on the other hand, reveals much stronger reductions of the fullerene emission (up to 94%). Most importantly, much shorter lifetimes of the fullerene singlet excited state, the product of the initial energy transfer, were seen. This suggests, in sharp contrast to **8b**, a sequential energy and electron transfer starting from the initially excited dendron. In its final instance this sequence generates restrictively a radical pair, $C_{60}^{\cdot-}$–dendron$^{\cdot+}$.

Formation of the charge-separated state was established for both donor–acceptor systems by means of transient absorption spectroscopy. The fullerene π-radical anion displayed its typical near-IR absorption at 1000 nm, while the one-electron oxidized forms of the donors were evidenced through their absorption in the visible with λ_{max} *ca.* 480 nm (**8a**) and 540 nm (**8b**). It is important to note that for the dibutylaniline-containing dyad **8a** the radical pair, with lifetimes of 350 ns and 725 ns, in THF and benzonitrile, respectively is the sole product, corroborating the sequence of energy and electron transfer. Quite different is the situation for the poly(arylenevinylene) derivative **8b**: both energy transfer and electron transfer products were noted as superimposed spectral features.

This work has been supported by the DGESIC of Spain (Project PB98-0818) and by the European Comission (Contract JOR3CT980206). Part of this work has been supported by the Office of Basic Energy Sciences of the US Department of Energy. This is document NDRL-4286 from the Notre Dame Radiation Laboratory.

Notes and references

1 M. R. Wasielewski, *Chem. Rev.*, 1992, **92**, 435; M.-J. Blanco, M. C. Jiménez, J.-C. Chambron, V. Heitz, M. Linke and J.-P. Sauvage, *Chem. Soc. Rev.*, 1999, **28**, 293.
2 W. F. J. Vermaas, *Science*, 1994, **263**, 1511; M. A. Stefen, K. Q. Lao and S. G. Boxer, *Science*, 1994, **264**, 810.
3 M. A. Fox and M. Chanon, *Photoinduced Electron Transfer*, Elsevier, Amsterdam, 1988.
4 M. H. B. Stowell, T. M. McPhillips, D. C. Rees, S. M. Soltis, E. Abresch and G. Feher, *Science*, 1997, **276**, 812.
5 For a review on light-harvesting dendrimers, see: A. Adronov and J. M. J. Fréchet, *Chem. Commun.*, 2000, 1701.
6 A. Adronov, S. L. Gilat., J. M. J. Frechet, K. Ohta, F. V. R. Neuwahl and G. R. Fleming, *J. Am. Chem. Soc.*, 2000, **122**, 1175 and references therein.
7 J.-F. Nierengarten, *Chem. Eur. J.*, 2000, **6**, 3667.
8 Z. Xu and J. S. Moore, *Acta Polym.*, 1994, **45**, 83; C. Devadoss, P. Bharathi and J. S. Moore, *J. Am. Chem. Soc.*, 1996, **118**, 9635; A. G. Avent, P. R. Birkett, F. Paolucci, S. Roffia, R. Taylor and N. K. Wachter, *J. Chem. Soc., Perkin Trans. 2*, 2000, 1409.
9 (*a*) S. K. Deb, T. M. Maddux and L. Yu, *J. Am. Chem. Soc.*, 1997, **119**, 9079; (*b*) H. Meier and M. Lehmann, *Angew. Chem. Int. Ed.*, 1998, **37**, 643.
10 G. J. Bodwell, J. N. Bridson, T. J. Houghton and B. Yarlagadda, *Tetrahedron Lett.*, 1997, **38**, 7475.
11 M. Prato and M. Maggini, *Acc. Chem. Res.*, 1998, **31**, 519.
12 D. M. Guldi and M. Prato, *Acc. Chem. Res.*, 2000, **33**, 695.

ChemComm

Synthesis of a novel mesoporous iron phosphate

Xuefeng Guo, Weiping Ding,* Xueguang Wang and Qijie Yan*

Department of Chemistry, Nanjing University, Nanjing, 210093, P. R. China. E-mail: qyan@nju.edu.cn and dingwp@nju.edu.cn

Received (in Cambridge, UK) 17th January 2001, Accepted 2nd March 2001
First published as an Advance Article on the web 29th March 2001

A novel mesoporous iron phosphate, possessing a specific surface area of 254 m^2 g^{-1} and average pore diameter of 2.6 nm, is synthesized using a fluoride route.

Since the discovery of M41s silica molecular sieves in 1992,[1] mesoporous materials, possessing remarkably large internal surface areas and narrow pore size distributions, have attracted considerable attention for their great potential application as catalysts, absorbents, and host materials. Several supermolecular assembly pathways have also been developed and extended to synthesize a variety of mesoporous metal oxides[2] and aluminophosphates.[3–6] Compared to those successes, however, only a few preparative approaches have been reported for the preparation of mesoporous transition metal phosphates.[7–10]

Iron phosphate has been reported as a good catalyst for selective oxidation reactions, *e.g.* oxidative dehydrogenation of isobutyric acid to methacrylic acid, a versatile raw material for various polymers,[11] and partial oxidation of methane or ethane to oxygenates.[12] Iron phosphates with novel mesostructure would be interesting in terms of structure and catalytic performance. Huang *et al.*[13] have reported microporous iron phosphate with an open framework and a cell volume of 2957.5 Å^3 and expected it to be a novel catalyst. The preparation of mesoporous iron phosphate, however, has not been reported so far, although the preparation of mesoporous aluminium phosphate has been reported. Considering the similarity between iron and aluminium in their chemical properties, the preparation of mesoporous iron phosphate should be feasible. Unfortunately, despite substantial effort we failed to synthesize mesoporous iron phosphate using similar methods reported for the preparation of mesoporous aluminium phosphate.

Using a series of surfactants and different experimental conditions, we have finally prepared some mesostructural lamellar and porous iron phosphates. Here we report our successful synthesis and characterization of ordered mesoporous iron phosphate with an average pore size of 2.6 nm.

In a typical sample preparation route, 8.08 g $Fe(NO_3)_3$ was dissolved in 80 g distilled water and 7.16 g Na_2HPO_4, dissolved in 80 g distilled water, was added with stirring. The resulting $FePO_4$ precipitate was recovered by centrifugation and washed by distilled water. The precipitate was suspended in 20 g distilled water, followed by dropping 1.32 g HF (40 wt%) into the suspension with vigorous stirring. When a transparent solution was obtained, 2.88 g sodium dodecyl sulfate (surfactant), dissolved in 10 g water, was added to the solution with stirring at room temperature for 30 min. The resultant mixture was heated to 60 °C and held for 2.5 h. After cooling to room temperature, a light yellow precipitate was observed in the solution which was recovered by centrifugation, followed by repeated washing with water and acetone. The resultant solid was dried at room temperature.

Removal of the surfactant species from the as-synthesized solid was carried out by anion exchange in a manner similar to that reported by Holland *et al.*[14] for the preparation of mesoporous aluminophosphate. The as-synthesized solid (0.7 g) was mixed with a 0.05 M ethanol solution of sodium acetate (50 ml) with stirring at room temperature for 40 min. The solid was then recovered by centrifugation, washed thoroughly using ethanol and dried at room temperature. XRD (Rigaku D/Max-RA diffractometer), TEM (JEOL-200CX; 160 kV), FTIR (Nicolet 170SX FTIR spectrometer) and nitrogen sorption (Micromeritics ASAP 2000 sorption analyzer) were used to characterize the resultants.

A strong absorption peak at *ca.* 1252 cm^{-1}, characteristic of $(ROSO_3)^-$, was observed in the FTIR spectra of the surfactant containing sample which vanished after acetate-treatment, indicating no residual dodecyl sulfate species in the acetate-treated sample. This appears to suggest the complete removal of the surfactant in the sample. X-Ray diffraction patterns of as-synthesized sample and acetate-treated sample are shown in Fig. 1. Both patterns show a sharp diffraction peak (100) at low angle ($2\theta \approx 2.4$ and 2.3°, for the surfactant containing and acetate-treated samples, respectively). The low-angle diffraction peaks suggest a mesoporous structure of the obtained iron phosphate samples. The slight shift to higher angle for the acetate-treated sample reveals slight contraction of mesostructure of iron phosphate upon surfactant removal. A TEM photograph, (Fig. 2) confirms the mesoporous structure of the acetate-treated samples. The isothermal N_2 sorption data of the

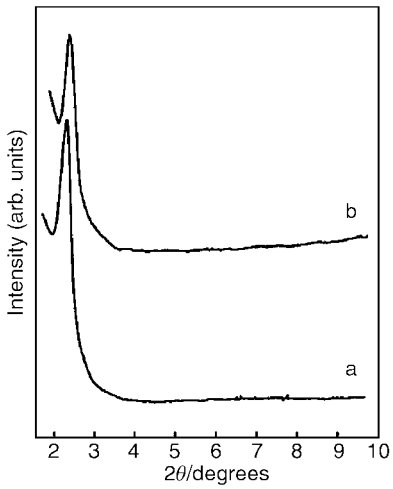

Fig. 1 XRD patterns of the as-synthesized sample (a) and acetate-treated sample (b).

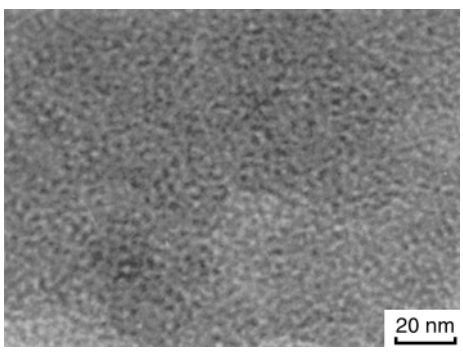

Fig. 2 TEM image of mesoporous iron phosphate after surfactant extraction.

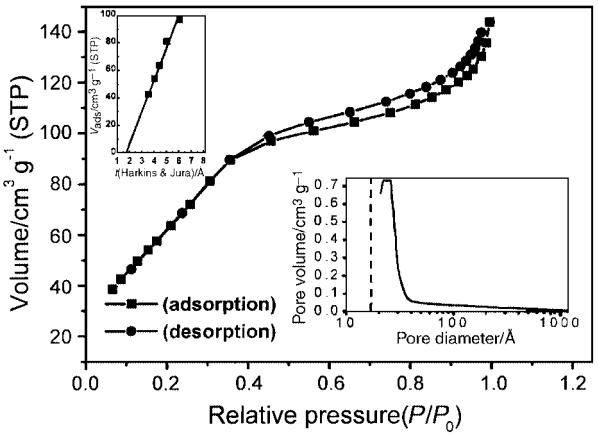

Fig. 3 Nitrogen adsorption–desorption isotherm of acetate-treated sample measured at 77 K, insets show pore diameter distribution of the sample (right) and *t*-plot (left).

acetate-treated sample at 77 K are shown in Fig. 3. The type-IV isotherm with a small hysteresis loop is similar to that of mesoporous zirconium phosphate reported in ref. 7. Quantitative calculation shows the acetate-treated mesoporous iron phosphate possesses a BET surface area of *ca*. 254 m^2 g^{-1} and a pore volume of 0.21 cm^3 g^{-1}, similar to documented non-silicate mesoporous solids, and narrow a distribution of pore diameter centered at 2.6 nm (Fig. 3, right inset). The linear *t*-plot suggests the sample possess uniform pores (Fig. 3, left inset). With the unit cell dimension ($a_0 = 2d_{100}/\sqrt{3}$) and the pore diameter, the wall thickness can be calculated as *ca*. 1.6 nm, much thicker than that of typical siliceous MCM41 (*ca*. 1.0 nm). The greater molecular weight and much thicker walls of the pores should be responsible for the lower BET specific surface area on comparing the mesoporous iron phosphate to M41s mesoporous silica.

We have attempted many routes other than *via* HF but all gave layer structures rather than an ordered mesoporous structure. Fluorides other than HF, *e.g*., ammonium fluoride and sodium fluoride, were tested but failed to give mesoporous iron phosphate. It appears HF plays an important role in the mesoporous iron phosphate synthesis. Undissociated HF molecules (aqueous HF is a weak acid with p$K_a \approx 4$) may react with iron phosphate to form ion pairs, as shown in Scheme 1. F ions

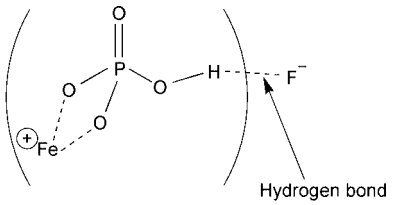

Scheme 1 The effect of fluoride on the charge density of Fe–P–O clusters.

bonding to [Fe–P-O–H]$^+$ *via* hydrogen bonding so adjusting the charge density of [Fe–P-O–H]$^+$ allow matching of the surface charge of the surfactant micelles, resulting in the formation of hexagonal mesoporous iron phosphate.

In conclusion, a novel mesoporous iron phosphate has been synthesized for the first time using a fluoride route. After removal of surfactant by acetate-exchange, mesoporous iron phosphate with a surface area of 254 m^2 g^{-1} and average pore size of 2.6 nm was obtained.

Notes and references

1 C. T. Kresge, M. E. Leonowicz, W. J. Roth, J. C. Vartuli and J. S. Beck, *Nature*, 1992, **359**, 710.
2 D. M. Antonelli and J. Y. Ying, *Angew. Chem., Int. Ed. Engl.*, 1996, **35**, 426.
3 A. Sayari, V. R. Karra, J. S. Reddy and I. L. Moudrakovski, *Chem. Commun.*, 1996, 411.
4 P. Y. Feng, Y. Xia, J. L. Feng, X. H. Bu and G. D. Stuky, *Chem. Commun.*, 1997, 949.
5 T. Kimura, Y. Sugahara and K. Kuroda, *Chem. Mater.*, 1999, **11**, 508.
6 Y. Z. Khimyak and J. Klinowski, *J. Chem. Soc., Faraday Trans.*, 1998, **94**, 2241.
7 J. Jiménez-Jiménez, P. Maireles-Torres, P. Olivera-Pastor, E. Rodríguez-Castellón, A. Jiménez-López, D. J. Jones and J. Rozière, *Adv. Mater.*, 1998, **10**, 812.
8 T. Abe, A. Taguchi and M. Iwamoto, *Chem. Mater.*, 1995, **7**, 1429.
9 T. Doi and T. Miyake, *Chem. Commun.*, 1996, 1635.
10 M. Roca, J. E. Haskouri, S. Cabrera, A. Beltrán, J. Alamo, D. Beltrán, M. D. Marcos and P. Amorós, *Chem. Commun.*, 1998, 1883.
11 J. M. Millet, *Catal. Rev-Sci.Eng.*, 1998, **40**, 1.
12 Y. Wang and K. Otsuka, *J. Catal.*, 1997, **171**, 106.
13 C. Y. Huang, S. L. Wang and K. H. Lii, *J. Porous Mater.*, 1998, **5**, 147.
14 B. T. Holland, P. K. Isbester, C. F. Blanford, E. J. Munson and A. Stein, *J. Am. Chem. Soc.*, 1997, **119**, 6796.

A photoresponsive laser dye containing photochromic dithienylethene units

Tsuyoshi Kawai,[a] Takatoshi Sasaki[a] and Masahiro Irie*[ab]

[a] *Department of Chemistry and Biochemistry, Graduate School of Engineering, Kyushu University, 6-10-1 Hakozaki, Higashi-ku, Fukuoka 812-8581, Japan. E-mail: tkawai@cstf.kyushu-u.ac.jp*

[b] *CREST, Japan Science and Technology Corporation, 6-10-1 Hakozaki, Higashi-ku, Fukuoka 812-8581, Japan*

Received (in Cambridge, UK) 8th January 2001, Accepted 20th February 2001
First published as an Advance Article on the web 29th March 2001

A novel molecule, containing two photochromic dithienylethene moieties linked to a fluorescent bis(phenylethynyl)anthracene residue has been prepared, and shows a reversible change in its fluorescence quantum yield from 0.001 to 0.83, and a corresponding increase in laser emission intensity, on exposure to UV light.

Dithienylethenes are the most promising photochromic compounds among various photochromic compounds for the photoelectronic applications, such as optical memory media and photoswitching devices, because of their fatigue resistant and thermally irreversible properties.[1–4] Although several dithienylethene derivatives have been reported to exhibit reversible fluorescence intensity changes upon photoisomerization,[5–11] the fluorescence quantum yields (Φ_{fl}) of the molecules were relatively small. In the present work, a highly fluorescent dithienylethene was prepared and its photoresponsive laser emission was demonstrated.

9,10-Bis(2-phenylethynyl)anthracene was chosen as the fluorescence unit, because its Φ_{fl} is high (Φ_{fl} = 1) and its emission spectrum overlaps with the characteristic absorption band of the closed-ring isomer of 1,2-bis(2,5-dimethyl-3-thienyl)perfluorocyclopentene.[12] The two photochromic dithienylethene units, 1-(2,5-dimethyl-3-thienyl)-2-(2,4-dimethyl-5-bromo-3-thien-yl)perfluorocyclopentene, were connected to the fluorescent unit, 9,10-bis(4-bromo-phenylethynyl)anthracene by Pd(0) catalyzed cross-coupling reaction to obtain **1a** shown in Scheme 1. The molecular structure and purity of **1a** were confirmed by elemental analysis, ^{1}H-NMR and mass analysis.[13]

Fig. 1 shows optical absorption spectral change of **1a** in THF solution upon photoisomerization. By irradiation with 313 nm light the absorption bands at 340 nm decreased along with the increase of a new absorption band between 500 and 650 nm. The original absorption spectrum was recovered by irradiation with visible light (λ > 500 nm). Fig. 1 also shows the absorption spectrum of the isolated photo-product. It should be noted that there was only one photo-product in the HPLC analysis although **1** has two dithienylethene units. On the basis of the ^{1}H-NMR, the photo-product was assigned to the ring closed form **1b** in which one of the two dithienylethene units is in the closed-ring form.[13] Upon excitation of **1b**, excitation energy transfer from the excited open-ring unit to the closed-ring unit is considered to suppress further photo-cyclization of **1b**.

Fig. 1(b) shows the fluorescence emission spectrum of **1** in THF solution. The emission profile is similar to that of the bis(phenylethynyl)anthracene unit. The fluorescence intensity decreased upon irradiation with 313 nm light and almost disappeared in the isolated **1b**. The original emission spectrum

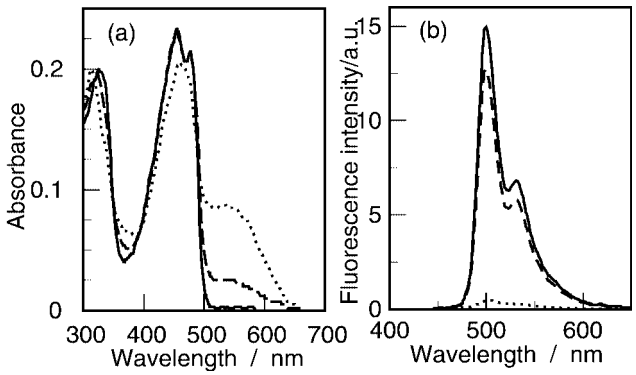

Fig. 1 (a) Absorption spectra of **1a** (solid line), **1b** (dotted line) and the photostationary state under irradiation with 313 nm light (broken line) in THF solution (**1a**: ε_{455nm} = 50500 M^{-1} cm^{-1}). (b) Fluorescence spectra of **1a** (solid line), **1b** (dotted line) and the photostationary state under irradiation with 313 nm light (broken line) in THF solution (excitation wavelength = 450 nm). (Irradiation of 313 nm light induces both cyclization and cycloreversion reactions.)

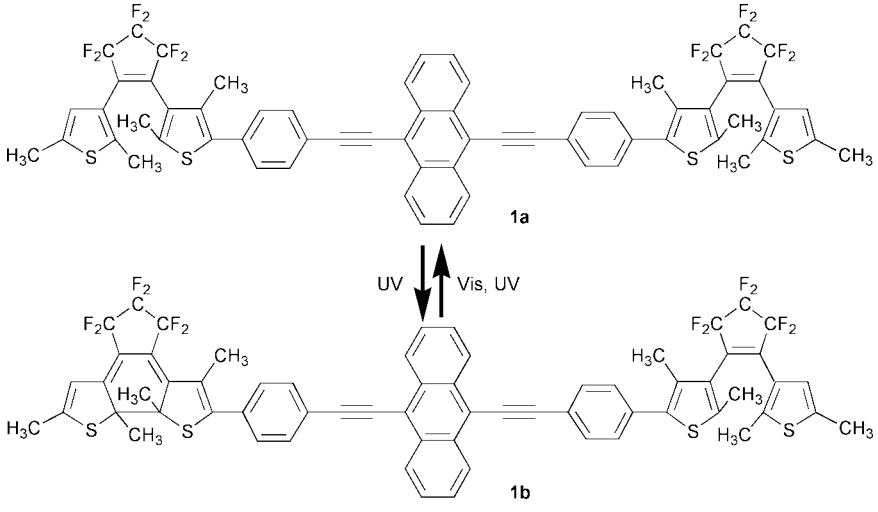

1a **1b**

Scheme 1

DOI: 10.1039/b100330p

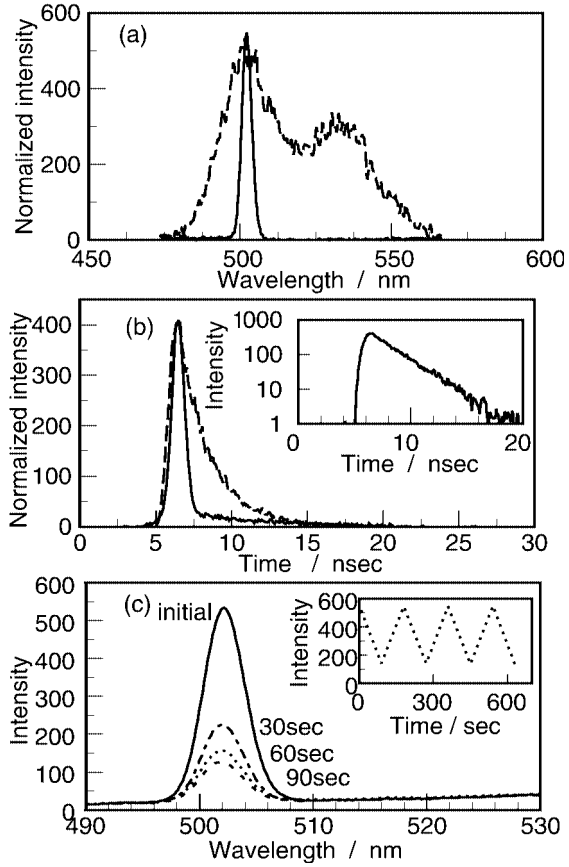

Fig. 2 Wavelength domain (a) and time domain (b) emission profiles of **1a** in (solid line) and outside (broken line) of the laser cavity. (Inset of (b): logarithmic decay of the spontaneous emission.) (c) Emission spectra of **1a** in the laser cavity, before UV irradiation (solid line), and after UV light irradiation for 30, 60 and 90 s (PSS). (Inset of (c): repetitive change of laser intensity with the alternative irradiation cycles of UV and visible light.)

was recovered by visible light irradiation. The fluorescence quantum yields, ϕ_{fl}, of **1a** and **1b** were determined, by using 9,10-bis(phenylethynyl)anthracene as a reference, to be ϕ_{fl} = 0.83 and $\phi_{fl} < 0.001$, respectively.

The strong fluorescence quenching in **1b** is attributed to the efficient energy transfer from the excited bis(phenylethynyl)anthracene to the closed-ring dithienylethene unit. Because of spectral overlapping of the emission band of **1a** at about 530 nm and the absorption band of **1b**, the excited state of the bis(phenylethynyl)anthracene unit is quenched by the closed-ring unit. The residual weak emission observed in isolated **1b** was considered to be the emission from a small amount of **1a** which was formed from **1b** during the fluorescence measurement.

The laser emission experiment of **1a** was carried out as follows. THF solution of **1a** (0.1 mM) in a quartz cuvette (10 × 10 mm) was placed in the cavity of a dye laser system (Laser Photonics, DL2S), which is composed of a front highly reflective mirror, a back grating reflector and a cylindrical lens for focusing the pumping beam from a pulsed N_2 laser (Hamamatsu Photonics, LN-203). The excitation laser power, the pulse width, the wavelength and the repetition frequency were 0.1 mJ, 600 psec, 337.1 nm, and 10 Hz, respectively. The solution was stirred during the measurements. The emission was detected with a gated streak-scope system (Hamamatsu Photonics, C4334-01, C5094 and C4792). The emission from the laser cavity was detected by an analog integration mode, while its spontaneous emission was detected by a single-photon counting mode. Fig. 2(a) and (b) show emission spectra and the decay profile of **1a** placed inside and outside of the laser cavity, respectively. The emission of **1a** in the laser cavity showed a symmetrical narrow peak and any Stokes line typical for the spontaneous emission was not observed. The spontaneous emission decayed exponentially with a single lifetime of about 1.8 nsec, as shown in the inset of Fig. 2(b), while the emission from the laser cavity was dumped immediately with the excitation light pulse. The narrow and symmetrical emission profiles in the wavelength and the time domains are typical for the laser emission. Characteristic threshold of the laser emission was observed at about 0.08 mJ.

As shown in Fig. 2(c), the laser emission intensity dramatically decreased by irradiation with 313 nm light and it was recovered to the initial value by irradiation with visible light (λ > 500 nm). The reversible intensity change was observed for several tenth cycles. The emission power remained stable after standing in the absence of UV light.

In conclusion, a photochromic dithienylethene having bis(phenylethynyl)anthracene changed the fluorescence intensity by photoisomerization of the dithienylethene units (between ϕ_{fl} = 0.83 and < 0.001). The dye exhibited a laser emission and the emission intensity was reversibly switched by alternative irradiations with 313 nm light and λ > 500 nm light.

This work was partly supported by CREST (Core Research for Evolution Science and Technology) of Japan Science and Technology Corporation (JST) and also by Grant-in-Aid for Scientific Research on Priority Areas ('Molecular Synchronization', #11167263) from the Ministry of Education, Science, Sports and Culture, Japan.

Notes and references

1 M. Irie and M. Mohri, *J. Org. Chem.*, 1988, **53**, 803.
2 M. Irie and K. Uchida, *Bull. Chem. Soc. Jpn.*, 1998, **71**, 985.
3 M. Irie, *Chem.Rev.*, 2000, **100**, 1685.
4 T. Kawai, T. Koshido and K. Yoshino, *Appl. Phys. Lett.*, 1995, **67**, 795.
5 K. Koshido, T. Kawai and K. Yoshino, *Synth. Met.*, 1995, **73**, 257.
6 G. M. Tsivgoulis and J.-M. Lehn, *Angew.Chem., Int.Ed.Engl.*, 1995, **34**, 1119.
7 G. M. Tsivgoulis and J.-M. Lehn, *Chem. Eur. J.*, 1996, **2**, 1399.
8 Y. Kaneuchi, T. Kawai, M. Hamaguchi, K. Yoshino and M. Irie, *Jpn. J. Appl. Phys.*, 1997, **36**, 3736.
9 A. Fernandez-Acebes and J.-M. Lehn, *Adv. Mater.*, 1998, **10**, 1519.
10 M. Takeshita and M. Irie, *Chem.Lett.*, 1998, 1123.
11 K. Kasatani, S. Kambe and M. Irie, *J. Photochem. Photobio. A: Chem.*, 1999, **122**, 11.
12 S. Kobatake, T. Yamada, K. Uchida and M. Irie, *J. Am. Chem. Soc.*, 1999, **121**, 2380.
13 **1a**: Anal. Found: C, 65.48; H, 3.98%. Calcd. for $C_{64}H_{42}F_{12}S_4$: C, 65.86; H, 3.63%. ^{1}H NMR (200 MHz, $CDCl_3$) δ = 2.05 (s, 6H), 2.07 (s, 6H), 2.29 (s, 6H), 2.40 (s, 6H), 6.65 (s, 2H), 7.47 (d, 4H, J = 7.8 Hz), 7.67 (m, 4H), 7.80 (d, 4H, J = 7.8 Hz), 8.70 (m, 4H), MS (m/z) = 1166 (M^+). **1b**: ^{1}H NMR ($CDCl_3$) δ = 2.05 (s, 3H), 2.07 (s, 3H), 2.16 (s, 3H), 2.19 (s, 3H), 2.22 (s, 3H), 2.23 (s, 3H), 2.29 (s, 3H), 2.40 (s, 3H), 6.07 (s, 1H), 6.65 (s, 1H), 7.46 (d, 2H, J = 7.8 Hz), 7.52 (d, 2H, J = 7.8 Hz), 7.64–7.72 (m, 4H), 7.77–7.86 (m, 4H), 8.65–8.75 (m, 4H), MS (m/z) = 1166 (M^+).

A new templating method for three-dimensional mesopore networks

J. C. Jansen,[a] Z. Shan,[a] L. Marchese,[b] W. Zhou,[c] N. v. d. Puil[d] and Th. Maschmeyer*[a]

[a] *Laboratory of Applied Organic Chemistry and Catalysis, Julianalaan 136, 2628 BL Delft, Delft University of Technology, The Netherlands. E-mail: Th.Maschmeyer@tnw.tudelft.nl*
[b] *Dipartimento SCA, Università del Piemonte Orientale C.so Borsalino 54, 15100 Alessandria and Dipartimento di Chimica IFM, Universitá di Torino v.P. Giuria, 7, 10125, Torino, Italy*
[c] *School of Chemistry, University of St. Andrews, St. Andrews, Fife, UK KY16 9ST*
[d] *ABB-Lummus Global Inc., 1515 Broad Street, Bloomfield NJ 07003, USA*

Received (in Cambridge, UK) 30th January 2001, Accepted 8th March 2001
First published as an Advance Article on the web 30th March 2001

A new templating method using small, inexpensive non-surfactant chemicals has been developed facilitating the synthesis of hydrothermally stable foam-like mesopore networks with high surface areas.

Porous materials are of fundamental importance in science and technology.[1] Various templates are employed to direct the synthesis of uniform micro-, meso- and macro-pores. Principally, three types of templating have been reported thus far, *i.e* templating by individual molecules giving rise to micropores, by micelles giving rise to mesopores and by emulsions or latex particles giving rise to macropores.[2–5]

Here, we report a new templating method for well defined mesoporous (siliceous) oxides (denoted as TUD-1, Fig. 1),[6] in which small, non-surfactant templates direct the formation of mesosized structural features during the polycondensation of inorganic species upon temperature increase during synthesis. The key to a successful formation of mesopores is the careful control of the intermolecular interaction among organic templates and inorganic species, *i.e.* matching the type of template molecule with the temperature regime used. With a system initially composed of three different components, (*i.e.* water, silica source and template) taking account of the change in the nature of interactions between the different constituents with temperature, we were able to synthesize a new material that is characterized by well-defined pores with an easily tunable mesopore size distribution (25–250 Å in diameter), three-dimensional connectivities (foam-type structure), high surface areas (up to *ca*. 1000 m^2 g^{-1}), and high thermal and hydrothermal stability (negligible degradation at 650 °C for 12 h or boiling in water for 2 h, little degradation after heating to 1000 °C for 2 h or boiling in water for 17 h).

The starting point of our investigation was the desire to examine whether large pores in structured silicas might be templated, not by micelles or by very large and complex organic molecules, but by aggregates of simpler molecules. Following some preliminary investigations, triethanolamine was selected as a small, inexpensive and stable organic template with a high boiling point (*ca*. 340 °C) and good miscibility towards water, alkoxysilanes (Si-source) and the silica species generated by their hydrolysis. The new methodology also allows the facile introduction of catalytic sites (acid, base, redox) as well as micropores during the initial synthesis stage.

In the first step, a homogeneous mixture is obtained by mixing tetraethylorthosilicate (TEOS), triethanolamine (TEA) and water at room temperature.† After aging and drying in air, this mixture solidified and formed a homogeneous gel, the X-ray powder diffraction pattern of which showed no discernible peak. We interpret these data as deriving from a largely hydrogen-bonded siliceous composite polymer: the initial hydrolysis of TEOS was followed by the partial condensation of the resulting silanol species with each other and with some of the TEA, forming mixtures of mono- and oligomeric silatrane complexes and of various silica species (by ^{1}H, ^{13}C and ^{29}Si solution and MAS NMR). Hydrothermal treatment of this material changed its structure from amorphous to mesostructured. Finally, TUD-1 was obtained as a white mesoporous solid by the removal of the template either *via* Soxhlet extraction or *via* calcination. The circumstance that the mesopore range obtained is found to be directly proportional to the heating time (see Fig. 2) allowed for a very convenient, direct control of the mesopore size distributions of TUD-1. Interestingly, the porous structure can also be created without hydrothermal treatment, by employing careful calcination instead (for which a low ramp rate of *ca*. 1 °C min^{-1} is required). Hydrothermal treatment at moderately high temperature or thermal treatment (calcination) with a low ramp rate is necessary, because the condensation reactions of the various silica species are not completed after the gel formation.

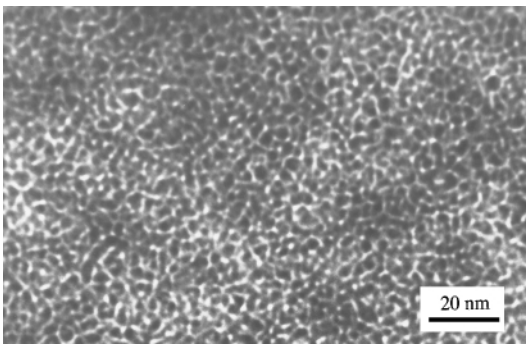

Fig. 1 High resolution transmission microscopy (HRTEM) image of the regular, mesoporous foam-like structure of TUD-1.

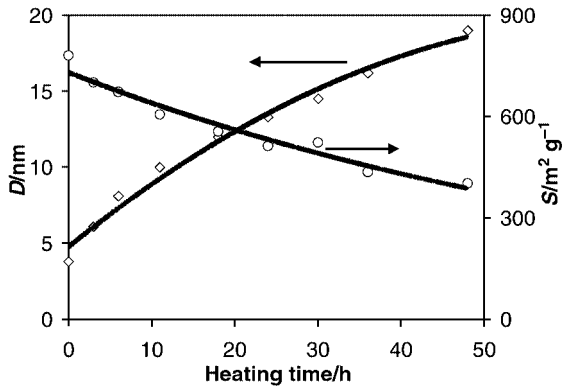

Fig. 2 Typical graph obtained when tuning the mesoporosity by variation of the heating time during hydrothermal treatment (in this case a homogeneous synthesis mixture with a molar composition of TEOS: 0.5TEA: 0.1TEAOH: $11H_2O$ was, after drying at 98 °C for 24 h, heated in an autoclave to 190 °C for different times). *D* is the mesopore diameter at maximum peak height calculated using the BJH model based on nitrogen desorption branch; *S* is the mesopore surface area calculated using the t-plot method.

At low temperatures (up to 100 °C) and after substantial loss of volatile components (water and ethanol, up to 70 wt%), the strengths of the various interactions between TEA, the various types of silatrane complexes and the silica oligomers are similar enough to form a homogeneous mixture without mesostructure. However, at elevated temperatures the silica oligomers condense extensively and the silatrane complexes partially or fully hydrolyze due to the more labile nature of Si–alkoxy bonds as compared to Si–siloxy bonds. The TEA is then largely expelled from the silica network and separate silica and template phases begin to form. The coalescence of the resulting silica particles further separates the phases on a mesoscale. This micro-syneresis (resulting in a solid–liquid mixture) gradually forces the TEA into meso-sized aggregates, templating the mesopores.

X-Ray diffraction patterns of TUD-1 show only one peak at low angle (scanning from 0.5–40° in 2θ), indicating it is a mesostructured material. Nitrogen adsorption isotherms revealed reproducible surface areas of between 500 and 1000 $m^2\ g^{-1}$ and pore volumes of between 0.6 and 1.7 $cm^3\ g^{-1}$, depending on the synthesis conditions. When employing hydrothermal treatment, the pore volume and wall thickness of TUD-1 increased with time, with a corresponding decrease in surface area, demonstrating that the pore formation is a dynamic process, consistent with the model proposed above.

We attempted to visualise the mesopore connectivity by HRTEM using Pt wires as a contrast agent.[7] The resulting images are consistent with a 3-D connectivity, but not sufficient to prove this. The synthesis of an inverse structure of TUD-1 out of carbon (using the methodology of Ryoo[8]) yielded a nanoscale carbonaceous network (surface area $>1000\ m^2\ g^{-1}$, tunable mesopore size),‡ showing a similar image of a foam-like mesopore structure (Fig. 3). This result excludes one- or two-dimensional pore connectivities in TUD-1, as otherwise the resultant carbonaceous mesopore network would collapse upon the removal of silica. Thus, we were able to show that TUD-1 contains three-dimensional pore networks.

Hence, siliceous TUD-1, with its inherent possibility of a bimodal pore distribution (*vide supra*), offers a wide scope for chemical applications as most procedures commonly employed to impart functionality on silica can be used. For example, it is very straightforward to prepare highly dispersed metal particles on TUD-1. Furthermore, ^{29}Si CP-MAS NMR measurements of a typical TUD-1 sample before and after calcination reveal the presence a substantial Q_3 signal, allowing for functionalization *via* grafting onto the pendant silanol groups lining the mesopore walls.[9]

In addition, metals such as, *e.g.* titanium, zirconium or vanadium can be grafted *via* complexation with the TEA onto the surface of the mesopore wall, providing a 'one-pot' grafting methodology.[10]

In a similar vein, functionalized surfaces are easily fashioned in a one-pot procedure by the inclusion of a certain amount of functional siloxy precursor (*e.g.* $NH_2(CH_2)_3Si(OEt)_3$) into the synthesis gel.[11] Moreover, strong acid sites (by NH_3-TPD) can be prepared that are located in the micropores, whereas the mesopores can be made mildly acidic, offering a wide scope for application in acid catalyzed reactions.

Full results on acid site functionalizations, one-pot surface functionalizations, metal particle and metal oxide impregnations/immobilizations and related catalytic tests will be published shortly.

This work was financially supported by ABB Lummus Global, IN, USA. We thank Mr J. Groen for the gas adsorption measurements.

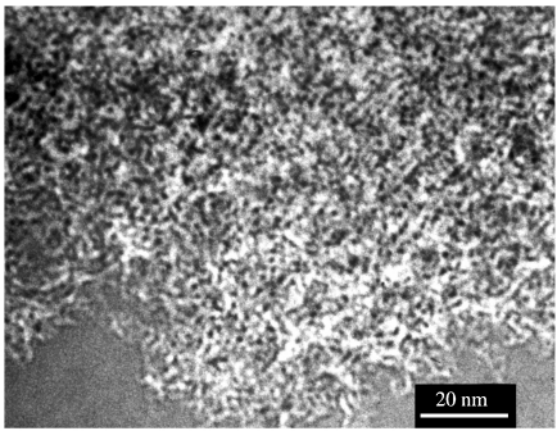

Fig. 3 Mesoporous carbon templated by TUD-1 silica, yielding an 'inverse' TUD-1 structure.

Notes and references

† Tetraethyl orthosilicate (TEOS), triethanolamine (TEA) and water were combined at room temperature in ratios of 1:0.25–2:10–40 to obtain a homogeneous mixture. This mixture solidified after aging at room temperature for 6–24 h and subsequent heating to 96–100 °C for 12–24 h in air, forming a homogeneous gel. This gel was transferred into an autoclave and heated at *ca*. 150–200 °C for between 0 and 3 days. Finally it was calcined at 600 °C for 10 h with a ramp rate of *ca*. 1 °C min^{-1} in air, or extracted in a Soxhlet apparatus using ethanol for 3 days to obtain the final mesoprous materials. Micropores could also be introduced by addition of traditional zeolite templates, *e.g.* tetraethylammonium hydroxide, with a ratio of 0.1–0.3 with respect to Si in the final synthesis mixture.

‡ The carbonaceous network templated by TUD-1 shows a bimodal mesopore system due to structure transformation. The sizes of these two mesopores can be tuned in ranges of 3.5–5.0 and 15–25 nm, respectively, depending on the original TUD-1 sample. Full details will be published shortly.

1 J. M. Thomas, *Nature*, 1994, **368**, 289.
2 A. Corma, *Chem. Rev.*, 1997, **97**, 2373.
3 C. T. Kresge, M. E. Leonowicz, W. J. Roth, J. C. Vartuli and J. S. Beck, *Nature*, 1992, **359**, 710.
4 S. D. Sims, D. Walsh and S. Mann, *Adv. Mater.*, 1998, **10**, 151; A. Imhof and D. J. Pine, *Nature*, 1997, **389**, 948.
5 Q. Huo, D. I. Margolese, U. Ciesla, P. Feng, T. E. Gier, P. Sieger, R. Leon, P. M. Petroff, F. Schüth and G. D. Stucky, *Nature*, 1994, **368**, 317; H. Yang, N. Coombs and G. A. Ozin, *Nature*, 1997, **386**, 692; S. S. Kim, W. Zhang and T. J. Pinnavaia, *Science*, 1998, **282**, 1302.
6 Z. Shan, Th. Maschmeyer and J. C. Jansen (Delft University of Technology, ABB Lummus Global Inc.) *World Pat.*, WO 00/15551, 2000.
7 C. H. Ko and R. Ryoo, *Chem. Commun.*, 1996, 2467.
8 R. Ryoo, S. H. Joo and S. Jun, *J. Phys. Chem. B*, 1999, **103**, 7743.
9 Th. Maschmeyer, F. Rey, G. Sankar and J. M. Thomas, *Nature*, 1995, **378**, 159; K. Moller and Th. Bein, *Chem. Mater.*, 1998, **10**, 2950.
10 Z. Shan, E. Gianotti, J. C. Jansen, J. A. Peters, L. Marchese and Th. Maschmeyer, *Chem. Eur. J*, 2001, **7**, 1437.
11 J. H. Clark and D. J. Macquarrie, *Chem. Commun.*, 1998, 853.

Antibody catalyzed modification of amino acids. Efficient hydrolysis of tyrosine benzoate†

Fabio Benedetti,*[a] Federico Berti,*[a] Alfonso Colombatti,[b] Massimiliano Flego,[a] Lucia Gardossi,[c] Paolo Linda[c] and Silvia Peressini[a]

[a] *Dipartimento di Scienze Chimiche, Università di Trieste, Via Giorgieri 1, I-34127 Trieste, Italy. E-mail: berti@dsch.univ.trieste.it; Fax: + 39 40 6763903*
[b] *Dipartimento di Scienze e Tecnologie Biomediche, Università di Udine, and CRO – IRCSS, Aviano, P.le Kolbe 4, I-33100, Udine, Italy*
[c] *Dipartimento di Scienze Farmaceutiche, Università di Trieste, P.le Europa 1, I-34127 Trieste, Italy*

Received (in Cambridge, UK) 11th January 2001, Accepted 8th March 2001
First published as an Advance Article on the web 29th March 2001

Esterase antibody 522c2, the first example of a catalytic antibody specifically programmed to control the reactivity of functional groups on the side chain of tyrosine, accelerates the hydrolysis of benzoate esters of L-tyrosine and tyrosine-containing dipeptides by a factor of 10^4 and is moderately active against other benzoate esters.

The control of reactivity of functional groups on the side chains of amino acids and peptides is a potentially attractive field for applications of catalytic antibodies.[1] The selective modification of amino acid side chains in peptides and proteins is important for many areas of chemistry, from organic synthesis to the irreversible inhibition of enzymes and the improvement of pharmacokinetic properties of peptide drugs.[2] However, the high level of control over chemo- and regioselectivity which is required for these transformations is not easily obtained by chemical or enzymatic approaches.[3]

While a number of antibody catalyzed reactions taking place on amino acid substrates have been described, there are no examples to date dealing specifically with the reactivity of amino acid side-chains. In this communication we describe the activity of esterase antibody 522C2, the first catalytic antibody specifically designed to hydrolyze an ester group on the tyrosine phenolic side chain. As benzoate is a common modifier and protecting group in amino acid and peptide chemistry, we chose the hydrolysis of tyrosine benzoate **1** as the target reaction (Scheme 1).

Hapten **2**, a classical phosphonate transition state analog, was synthesized by a conventional approach,[4] *via* the corresponding monoester monochloride.† The carboxylate group of tyrosine

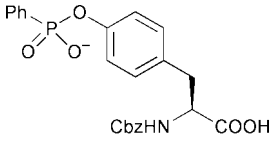

2

was used to conjugate directly the phosphonate to cationised bovine serum albumin (cBSA)†. We reasoned that holding the hapten in close contact with the carrier protein surface would result in a relatively 'open' antigen binding site, able to recognize and hydrolize the substrate also when tyrosine is part of a peptide chain. For this reason the use of a linker between the hapten and the carrier was avoided.

The cBSA conjugate was used to immunize three Balb/c mice following a standard protocol.[5] Hybridomas obtained from the

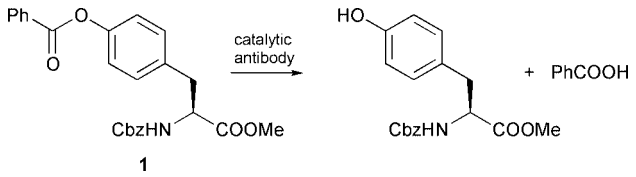

1

Scheme 1

fusion of spleen cells were selected on the basis of the affinity of the antibodies for an ovalbumin (OVA) conjugate of **2** and cloned. Only three good binders for the hapten **2** were obtained, but two of the selected antibodies (517A41 and 522C2) exhibited catalytic activity for the hydrolysis of benzoate **1** after purification by protein G and ion exchange chromatography.† Antibody 517A41 was only a weak catalyst (k_{cat}/k_0 = 148), while 522C2 accelerated the hydrolysis of **1** by a factor of over 10^4 and was selected for further studies (Table 1). After the preliminary kinetic assay, carried out on the antibody isolated from hybridoma supernatants, 522C2 was subcloned and larger quantities of the antibody were obtained from ascitic fluids. A fully functional Fab fragment was also obtained by papain digestion and purification by gel exclusion and ion exchange chromatography. The observed catalytic activity was always reproducibile and did not depend on the antibody's preparation.

The kinetic parameters for the catalyzed hydrolysis of ester **1** were calculated at pH 8 in TRIS buffer at 25 °C (k_{cat} = 0.063), and at pH 7.5 in PBS at 30 °C (k_{cat} = 0.017), showing in both cases a rate enhancement factor in excess of 10^4 (Table 1).† This allows the observation of a net enhancement of more than 150-fold in the initial rates of hydrolysis under typical experimental conditions (5 μM antibody, 50 μM substrate **1**), in spite of the rather high value of K_M (370–500 μM), which does not allow the maximum rate to be reached within the solubility limit of this substrate.

The antibody is inhibited by an equimolar amount of the phosphonate **2**. The apparent dissociation constant of the antibody–hapten complex obtained by a competitive ELISA assay[6] ($K_{d,app}$ = 75 nM) is in reasonable agreement with the upper limit for the inhibition constant ($K_i \leq$ 100 nM) estimated from kinetic measurements. Inhibition by the hapten demonstrates that the catalyzed process takes place in the antibody combining site and is not due to interactions between the substrate and the protein surface. Nonspecific interactions of this type can indeed be observed when the hydrolysis of **1** is carried out in the presence of BSA or unrelated mouse IgGs, but result in a modest acceleration by a factor of less than 1.5 in the initial rates (at 5 μM protein and 50 μM substrate **1**).

For an antibody accelerating a reaction by simple transition state complementarity, it has been derived that $K_M/K_i = k_{cat}/k_0$.[7] In the case of 522C2, the values of k_{cat}/k_0 (11 000) and K_M/

† Electronic supplementary information (ESI) available: the synthesis and characterization of compound **2**, preparation of the immunogenic conjugate, preparation and purification of monoclonal antibodies, experimental details for kinetic studies and Lineweaver-Burk plots. See http://www.rsc.org/suppdata/cc/b1/b100450f/

Table 1 Kinetic parameters for the 522C2 catalyzed hydrolysis of tyrosine benzoate and other esters

Substrate	k_0/s^{-1}	k_{cat}/s^{-1}	K_M (μmol dm^{-3})	k_{cat}/k_0	k_{cat}/K_M (dm^3 s^{-1} mol^{-1})	$k_{cat}/K_M k_0$ (dm^3 mol^{-1})
(*S*)-**1**[a]	5.06×10^{-6}	0.063	500	12 400	126	2.5×10^7
(*S*)-**1**[b]	1.53×10^{-6}	0.017	370	11 100	45.9	3.0×10^7
(*S*)-**1**[b,c]	1.53×10^{-6}	0.020	410	13 100	48.8	3.2×10^7
3a[b]	8.16×10^{-6}				44.9	5.5×10^6
3b[b]	1.04×10^{-4}				35.4	3.4×10^5
3c[b]	4.49×10^{-5}				8.5	1.9×10^5
3d[b]	1.94×10^{-4}				—	—
5[b]	2.90×10^{-6}				0.39	1.4×10^6
6[d]	5.70×10^{-8}	5.5×10^{-4}	460	9 700	1.2	2.1×10^7
7[d]	8.21×10^{-8}	7.5×10^{-4}	650	9 100	1.2	1.4×10^7

[a] TRIS 10 mM, pH 8, dioxane 10%, 25 °C. [b] PBS, pH 7.5, 10% dioxane, 30 °C. [c] Fab fragment. [d] PBS, pH 7.5, 30% DMSO, 30 °C.

$K_{d,app}$ (4900) indicate that selective recognition of the transition state significantly contributes to the catalytic activity. Thus 522C2 behaves similarly to other ester hydrolyzing antibodies for which oxyanion stabilization has been recognized as the main source of catalytic activity.[8]

Antibody 522C2 is highly specific for the *S*-enantiomer of tyrosine benzoate, mirroring the configuration of the hapten, and no acceleration over background is observed in the hydrolysis of the corresponding *R*-ester. While displaying such a high enantiospecificity, antibody 522C2 is able to hydrolyze a number of simplified esters **3** in which tyrosine is replaced by *p*-nitrophenol. Solubility, and the high values of K_M for these substrates, restrict the accessible substrate concentrations to a range in which [*S*] << K_M. Therefore, second order rate constants, corresponding to k_{cat}/K_M ratios assuming Michaelis–Menten behaviour, were obtained for this set of esters and the ratio $k_{cat}/K_M \cdot k_0$ (catalytic proficiency) was chosen to compare the efficiency of the antibody on these substrates (Table 1).[9]

Data in Table 1 show that one order of magnitude in the catalytic proficiency is lost on going from *N*-Cbz-tyrosine benzoate **1** to *p*-nitrophenyl benzoate **3a**. This decrease in the catalytic activity of the antibody is paralleled by its affinity for the corresponding phosphonates. In fact, while the tyrosine phosphonate **2**, as we have seen, is a strong binder, the simple phenyl phenylphosphonate **4** does not inhibit 522C2. This

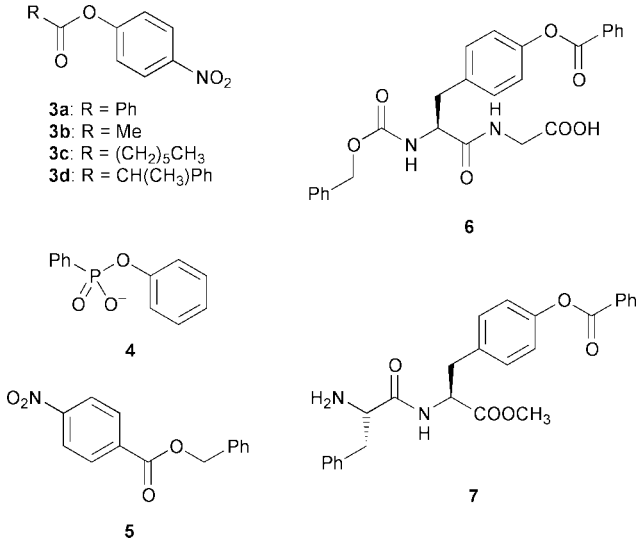

indicates that in the substrate **1** and hapten **2** the region of the molecule corresponding to the protected α-amino acid group plays a significant role in recognition by the antibody.

Replacing the benzoyl group by aliphatic residues, as in the hydrolysis of esters **3b** and **3c**, results in a further decrease of catalytic proficiency by one order of magnitude (Table 1). The catalytic activity is completely lost when branching is introduced in the ester **3d**. Surprisingly however, antibody 522C2 shows good efficiency in the hydrolysis of benzyl *p*-nitrobenzoate **5**.

It is noteworthy that the substrate selectivity exhibited by 522C2 is reversed with respect to that displayed by a hydrolytic enzyme such as α-chymotrypsin. This protease is known to hydrolyze esters with a broad specificity. However, under similar conditions, the acceleration in the hydrolysis of *p*-nitrophenyl ester **3a** is six times higher than the acceleration in the hydrolysis of tyrosine ester **1**. Another major difference between α-chymotrypsin and 522C2 is represented by the pre-steady state burst which is observed with the enzyme but not with 522C2, in agreement with the mechanism proposed for the antibody.

Finally, the activity of 522C2 was also tested on the dipeptides **6** and **7** (Table 1). 522C2 retains most of its catalytic activity on both the dipeptide benzoates even in the presence of 30% DMSO, which is necessary for solubility. Replacement in **7** of the *N*-Cbz protecting group with the somewhat isosteric residue of phenylalanine does not lead to a loss of activity.

In conclusion, 522C2 is an efficient and selective catalyst for the hydrolysis of (*S*)-tyrosine benzoate and retains its activity when the substrate is part of a simple dipeptide. This preliminary result is promising in view of a possible extension of this approach to the selective deprotection of tyrosine benzoate in more complex peptide structures, which would be a valuable application and is currently being investigated.

We are grateful to CNR (Progetto Finalizzato Biotecnologie) and to MURST (Programma PRIN) for financial support.

Notes and references

1 D. Hilvert, *Annu. Rev. Biochem.*, 2000, **69**, 751; G. M. Blackburn and A. Garçon, in *Biotechnology*, ed. D. R. Kelly, Wiley-VCH, Weinheim, 2nd edn., vol. 8b, 2000, p. 403; J. D. Stevenson and N. R. Thomas, *Nat. Prod. Rep.*, 2000, **17**, 535; J. L. Reymond, *Top. Curr. Chem.*, 1999, **200**, 59; G. M. Blackburn, A. Datta, H. Denham and P. Wentworth Jr., *Adv. Phys. Org. Chem.*, 1998, **31**, 249.

2 S. P. Vyas, P. Venugopalan, A. Sood and N. Mysore, *Pharmazie*, 1997, **52**, 339; D. K. Clodfelter, A. H. Pekar, D. M. Rebhun, K. A. Destrampe, H. A. Havel, S. R. Myers and M. L. Brader, *Pharmacol. Res.*, 1998, **15**, 254; M. Baudys, D. Letourneur, F. Liu, D. Mix, J. Jozefonvicz and S. W. Kim, *Bioconjugate Chem.*, 1998, **9**, 176.

3 B. T. Miller, *Biochem. Biophys. Res. Commun.*, 1996, **218**, 377; R. D. Lundbald, *Techniques in Protein Modification*, CRC Press, Boca Raton, 1995; A. W. Yem, H. A. Zurcher-Neely, K. A. Richard, N. D. Staite, R. L. Heinrikson and M. R. Deibel, *J. Biol. Chem.*, 1989, **264**, 17691; L. Gardossi, D. Bianchi and A. Klibanov, *J. Am. Chem. Soc.*, 1991, **113**, 6328.

4 M. F. Hersman and L. F. Audrieth, *J. Org. Chem.*, 1958, **23**, 1889.

5 E. Harlow and D. Lane, *Antibodies, a Laboratory Manual*, Cold Spring Harbor Laboratory, 1988, p. 139.

6 B. Friguet, A. F. Chaffotte, L. Djavadi-Ohaniance and M. E. Goldberg, *J. Immunol. Methods*, 1985, **77**, 305.

7 J. D. Stewart and S. J. Benkovic, *Nature*, 1995, **375**, 388.

8 J. L. Buchbinder, R. C. Stephenson, T. S. Scanlan and R. J. Fletterick, *J. Mol. Biol.*, 1998, **282**, 1033; J. B. Charbonnier, B. Gigant, B. Golinelli-Pimpaneau and M. Knossow, *Biochimie*, 1997, **79**, 653; G. MacBeath and D. Hilvert, *Chemistry & Biology*, 1996, **3**, 433.

9 A. R. Radzicka and R. A. Wolfenden, *Science*, 1995, **267**, 90; C. L. Lo, P. Wentworth, K. W. Jung, J. Yoon, J. A. Ashley and K. D. Janda, *J. Am. Chem. Soc.*, 1997, **119**, 10 251.

Design and synthesis of novel tubular and cage structures based on thiazole-containing macrolactams related to marine cyclopeptides

Gerald Pattenden* and Toby Thompson

School of Chemistry, The University of Nottingham, University Park, Nottingham, UK NG7 2RD. E-mail: gp@nottingham.ac.uk; Fax: +44 (0)115 951 3535; Tel: +44 (0)115 951 3530

Received (in Cambridge, UK) 13th February 2001, Accepted 8th March 2001
First published as an Advance Article on the web 29th March 2001

Tubular and cage structures, *i.e.* 16 and 18, have been synthesised from modified cyclic peptides following selective cyclotrimerisations of L-ornithine and L-glutamic acid thiazole amino acids under high dilution conditions.

Marine organisms, especially sea-squirts, have delivered an astonishing variety of novel cyclopeptide alkaloids which accommodate thiazole and oxazole rings derived from unusual amino acids, *e.g.* trunkamide **1**,[1] ascidiacyclamide **2**.[2] The

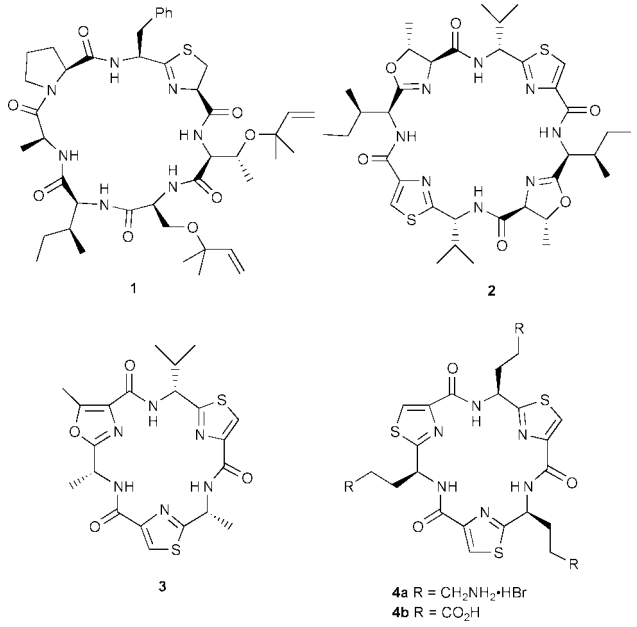

sequence of alternating heterocyclic rings and amino acid units which characterise these structures has led to speculation that the metabolites may have a role to play *in vivo* as metal transport agents, and/or that metals may act as templates in their biological assembly from constituent amino acids/heterocyclic rings.[3] In previous studies we have examined the self assembly and metal-templated cyclooligomerisations of amino acid based thiazoles and oxazoles, culminating in the syntheses of novel cyclotetramers and cyclotrimers,[4] and also in the total synthesis of the natural cyclopeptide dendroamide A **3**.[5] In a continuation of this work we have now investigated the syntheses of the cyclopeptide scaffolds **4a** and **4b**, containing additional amino and carboxylic acid functionality respectively, with a view to examining their applications in the synthesis of 'cage-' and 'tube-' like structures for possible use as membrane ion channel mimics and for the development of macromolecular devices and scaffolds for protein mimics. Thus, in this *Communication* we describe concise syntheses of **4a** and **4b**[6] and their conversion into the tubular polyamide **16** and into the cage structure **18**.[7,8]

Each of the substituted thiazoles **4a** and **4b** was prepared by routes developed in our laboratories and based on well-established literature precedent. Thus, protection of the C-5 amino group of L-ornithine **5** as its *Z*-carbamate followed by Boc protection of the C-2 amino function first led to the carboxylic acid **6**. Amidation of **6** followed by treatment with Lawesson's reagent [2,4-bis(4-methoxyphenyl)-1,3,2,4-dithiaphosphetane-2,4-disulfate] next produced the thioamide **7**. A Hantzsch thiazole ring forming reaction between **7** and ethyl bromopyruvate[9] then gave the substituted thiazole **8** which, on saponification of the ethyl ester and removal of the Boc protection, gave the L-ornithine based thiazole amino acid **9** with ⩾95% ee (Scheme 1).[10]

The corresponding L-glutamic acid based thiazole **14** was prepared from L-glutamic acid 5-methyl ester **10** following Boc protection and coupling with DL-serine benzyl ester benzenesulfonate leading to the dipeptide **11**. After conversion of **11** into the thioamide **12**, cyclodehydration in the presence of Burgess' reagent [methyl(carboxysulfamoyl)triethylammonium hydroxide, inner salt][11] next produced the corresponding thiazoline which was immediately converted into the thiazole **13** upon treatment with $BrCCl_3$–DBU at 0 °C.[12] Debenzylation of **13** under catalytic transfer hydrogenation conditions[13] and Boc deprotection finally gave the free thiazole amino acid **14** with ⩾95% ee (Scheme 2).

When the L-ornithine amino acid thiazole **9** was treated with pentafluorophenyl diphenylphosphinate (FDPP) in the presence of *i*-Pr_2NEt in DMF under high dilution, selective cyclooligomerisation took place to give the cyclic trimer **15a** in 11% yield. In a similar manner, cyclooligomerisation of the L-glutamic acid based thiazole **14** under the same conditions led cleanly to the C_3-symmetric cyclic trimer **15b** in 41% yield (Scheme 3). After removal of the amine protection in **15a** and saponification of the methyl ester groups in **15b**, activation of the tris-carboxylic acid **4b** with FDPP and *i*-Pr_2NEt followed by treatment with the tris-amine **4a** under high dilution in DMF led to the formation of the tubular structure **16** as a powder in 30% yield (Scheme 4).† Mass spectometry indicated the presence of a monomeric product. This was reinforced by the NMR spectroscopic data for

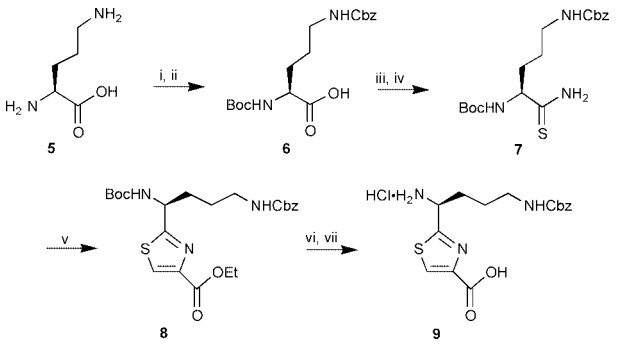

Scheme 1 *Reagents and conditions*: i, $CuCO_3$, H_2O, 30 min, then ZCl, NaOH, 1 h, then EDTA, 2 M HCl, 2 h, 88%; ii, $(Boc)_2O$, NaOH, THF–H_2O, 12 h, 71%; iii, isobutyl chloroformate, NMM (*N*-methylmorpholine), THF, NH_3 (g), −5 °C, 1 h, 99%; iv, Lawesson's reagent, THF, 24 h, 99%; v, ethyl bromopyruvate, $KHCO_3$, DME, −15 °C, then TFAA, collidine, DME, −15 °C, 79%; vi, NaOH, THF–H_2O, 18 h, 97%; vii, 4 M HCl, dioxane, 12 h, 98%.

DOI: 10.1039/b101417j

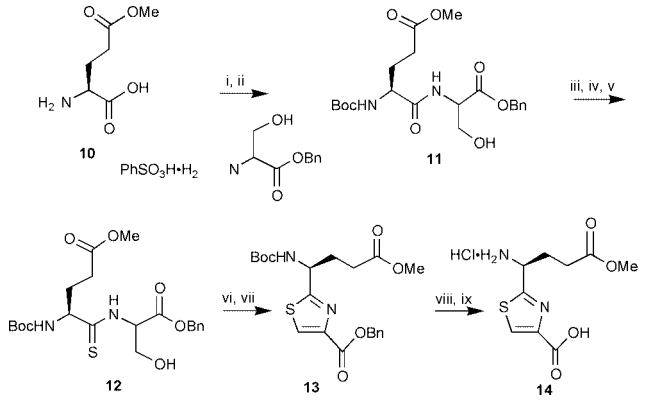

Scheme 2 *Reagents and conditions*: i, $(Boc)_2O$, Et_3N, THF–H_2O, 24 h, 90%; ii, HOBt, EDCI·HCl, NMM, CH_2Cl_2, 0 °C, 30 min, then DL-serine benzyl ester benzenesulfonate, NMM, 0 °C → RT, 48 h, 94%; iii, TBDMSCl, Et_3N, DMAP, CH_2Cl_2, 14 h, 86%; iv, Lawesson's reagent, C_6H_6, 80 °C, 14 h, 94%; v, TBAF, THF, 0 °C, 3 h, 91%; vi, Burgess' reagent, THF, 65 °C, 30 min; vii, $CBrCl_3$, DBU, CH_2Cl_2, 0 °C, 4 h, 63% over two steps; viii, NH_4HCO_2, 10% Pd/C, EtOH, 78 °C, 24 h, 70%; ix, 2 M HCl, dioxane, 24 h, 60%.

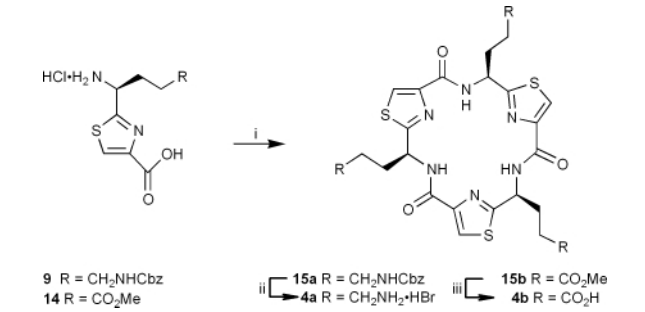

Scheme 3 *Reagents and conditions*: i, FDPP, *i*-Pr_2NEt, DMF, (**15a** 3 d, 11%; **15b** 9 d, 41%); ii, 33% HBr–AcOH, 6 h, 77%; iii, NaOH, THF–H_2O, 12 h, 98%.

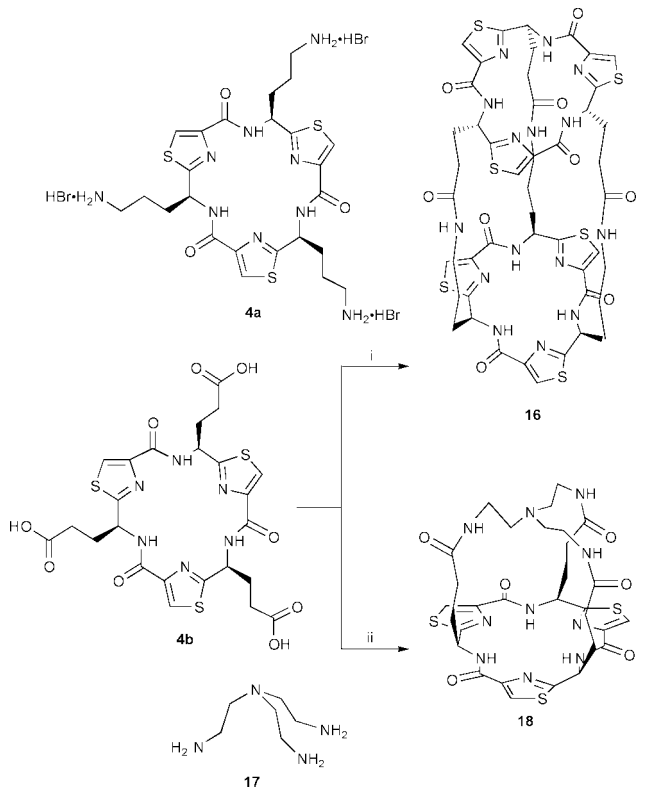

Scheme 4 *Reagents and conditions*: i, FDPP, *i*-Pr_2NEt, **4a**, DMF, 10 d, 30%; ii, FDPP, *i*-Pr_2NEt, **17**, DMF, 3 d, 40%.

16 which were consistent with those expected for a C_3-symmetric polymacrocycle. Most notably, two singlet peaks at δ 8.13 and δ 8.11 were observed in the ^{1}H NMR spectrum corresponding to the two sets of thiazole protons. Additionally, NMR signals were observed relating to the amide N–H (δ 8.47 and δ 8.43) and the α-carbon protons (δ 5.68 and δ 5.58) within the macrocyclic rings.

A corresponding condensation between the L-glutamic acid trimer **4b** and tris(aminoethyl)amine **17** in the presence of FDPP–Pr_2NEt led to isolation of the cage structure **18**, also as a solid, in 40% yield.‡ Again, mass spectrometry established that formation of the desired monomer had occurred. Additionally, the ^{1}H NMR spectrum confirmed the structure of **18** as C_3-symmetric with peaks at δ 8.89 and δ 8.11 relating to the ring N–H and thiazole protons with a signal at δ 6.26 corresponding to the three side-chain amide protons. The applications of the C_3-symmetric cyclic trimers **4a** and **4b** and their relatives in asymmetric and library synthesis, and also in molecular recognition phenomena, will be described in future publications.

We thank Dr Luis Castro for his interest in this study and Merck Sharp and Dohme for financial assistance. We also thank Dr Kate Jolliffe for preliminary work with the synthesis of the L-ornithine thiazole.

Notes and references

† **16**: mp 236–237 °C (decomp.) (from $CHCl_3$–MeOH–Et_2O); $[\alpha]_D^{294}$ −38.4° [*c* = 0.5, ($CHCl_3$–MeOH 3:1)]; IR (cm^{-1}): 3401, 3007, 2930, 1668, 1541; δ_H (500 MHz, $CDCl_3$) 8.47 (3H, m), 8.43 (3H, dd, *J* = 8.1 and 3.0 Hz), 8.13 (3H, s), 8.11 (3H, s), 5.68 (3H, m), 5.58 (3H, m), 3.67–3.01 (6H, m), 2.68–2.32 (9H, m), 2.31–2.12 (9H, m), 2.02–1.91 (3H, m), 1.57–1.51 (3H, m); δ_C [125 MHz, ($CDCl_3$)] 173.2 (s), 169.7 (s), 159.7 (s), 159.6 (s), 148.8 (s), 148.7 (s), 124.4 (d), 124.3 (d), 51.4 (d), 50.4 (d), 39.7 (t), 35.9 (t), 34.3 (t), 32.0 (t), 25.9 (t); HRMS (ES) *m/z* 1196.2198; calcd. for $C_{48}H_{51}S_6N_{15}O_9Na$ ([M + Na]$^+$): 1196.2216.

‡ **18**: mp 281–282 °C (decomp.) (from $CHCl_3$–MeOH–Et_2O); $[\alpha]_D^{294}$ −26.4° [*c* = 0.5, ($CHCl_3$–MeOH 3:1)]; IR (cm^{-1}): 3399, 3007, 1672, 1543; δ_H (360 MHz, $CDCl_3$) 8.89 (3H, d, *J* = 9.5 Hz), 8.11 (3H, s), 6.26 (3H, br s), 5.94 (3H, d, *J* = 9.1 Hz), 3.40 (3H, m), 3.12 (3H, m), 2.67–2.41 (12H, m), 2.32–2.24 (3H, m), 2.18–2.08 (3H, m); δ_C [90.5 MHz, ($CDCl_3$–CD_3OD 9:1)] 173.0 (s), 167.8 (s), 159.3 (s), 148.8 (s), 123.8 (d), 53.0 (t), 48.5 (d), 37.0 (t), 31.8 (t), 28.9 (t); HRMS (ES) *m/z* 751.1917; calcd. for $C_{30}S_3N_{10}O_6H_{36}Na$ ([M + Na]$^+$): 751.1879.

1 Y. Hamamoto, M. Endo, T. Nakagawa, T. Nakanishi and K. Mizukawa, *J. Chem. Soc., Chem. Commun.*, 1983, 323.
2 D. J. Baume, B. F. Bowden, A. R. Carroll, J. C. Coll, C. M. Ireland, J. K. MacLeod and T. M. Zabriskie, *Aust. J. Chem.*, 1996, **49**, 659.
3 J. P. Michael and G. Pattenden, *Angew. Chem., Int. Ed. Engl.*, 1993, **32**, 1.
4 A. Bertram, J. S. Hannam, K. A. Jolliffe, F. González-Lopez de Turisó and G. Pattenden, *Synlett*, 1999, 1723; A. J. Blake, J. S. Hannam, K. A. Jolliffe and G. Pattenden, *Synlett*, 2000, 1515.
5 A. Bertram and G. Pattenden, *Synlett*, 2000, 1519.
6 For contemporaneous studies see: D. Mink, S. Mecozzi and J. Rebek, Jr., *Tetrahedron Lett.*, 1998, **39**, 5709; G. Haberhauer, L. Samogyi and J. Rebek, Jr., *Tetrahedron Lett.*, 2000, **41**, 5013.
7 For contemporaneous studies see: T. D. Clark, L. K. Buehler and M. R. Ghadiri, *J. Am. Chem. Soc.*, 1998, **120**, 651.
8 Following completion of this manuscript, complementary related studies were described by Fairlie *et al.*: Y. Singh, N. Sokolenko, M. J. Kelso, L. R. Gahon. G. Abbenante and D. P. Fairlie, *J. Am. Chem. Soc.*, 2001, **123**, 333.
9 M. W. Bredenkamp, C. W. Holzapfel and W. J. van Zyl, *Synth Commun.*, 1990, **20**, 2235; E. Aguilar and A. I. Meyers, *Tetrahedron Lett.*, 1994, **35**, 2473.
10 Enantiomeric excess was determined by ^{19}F NMR spectroscopy following Boc deprotection and formation of the respective Mosher's amides: H. S. Mosher and J. A. Dale, *J. Am. Chem. Soc.*, 1973, **95**, 512.
11 P. Wipf and P. C. Fritch, *Tetrahedron Lett.*, 1994, **35**, 5397.
12 D. R. Williams, P. D. Lowder, Y. G. Gu and D. A. Brooks, *Tetrahedron Lett.*, 1997, **38**, 331.
13 T. Bieg and W. Szeja, *Synthesis*, 1985, 76.

ChemComm

The effect of bulky substituents on the olefin polymerisation behaviour of nickel catalysts bearing [P,O] chelate ligands

Vernon C. Gibson,* Atanas Tomov, Andrew J. P. White and David J. Williams

Department of Chemistry, Imperial College of Science, Technology and Medicine, Exhibition Road, South Kensington, London, UK SW7 2AY. E-mail: v.gibson@ic.ac.uk

Received (in Cambridge, UK) 19th February 2001, Accepted 7th March 2001
First published as an Advance Article on the web 29th March 2001

Incorporation of bulky substituents adjacent to the oxygen donor site of [P,O]Ni catalysts affords dramatic increases in olefin polymerisation activities

Nickel catalysts have provided some of the most significant advances in late transition metal olefin polymerisation catalysis and have given some of the most promising results with regard to polar monomer incorporation into polyolefinic materials.[1–4] One of the earliest systems to be investigated was the nickel-ylide oligomerisation system (**1**) introduced by Keim *et al.*[5] and subsequently developed by the groups of Starzewski[6] and Klabunde[7] for olefin polymerisation and copolymerisation. However the intrinsic activities of these catalysts are not high.

Bulky substituents have been shown to have a strong influence on the activities and selectivities of α-diimine[8] and salicylaldimine[9] nickel catalysts, yet the influence of sterically demanding groups has not been fully explored in the [P,O]Ni system. Several sites around the ligand are amenable to modification (see **2** below†): (i) the tertiary phosphine substituents (R^1), (ii) the backbone carbon substituent (R^2) adjacent to the phosphine donor, and (iii) the backbone carbon substituent (R^3) adjacent to the enolate oxygen. It was also recognised that an alternative approach to changing the steric influence at the enolate oxygen site is to exchange the oxo group for the isoelectronic [NR] unit. Here, we describe a series of new nickel catalysts containing [P,O] chelate ligands which reveal a dramatic enhancement in ethylene polymerisation activities, in some cases in excess of two orders of magnitude, on introduction of bulky substituents, especially at the site adjacent to the oxygen donor group.

The phosphorus ylide ligand precursors **3**–**5** (Scheme 1) were

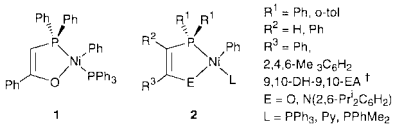

synthesised *via* modified literature procedures.[10,11] The ligand precursors **6**–**8** were prepared *via* Diels–Alder addition of crotonic acid or fumaric acid to anthracene, followed by conversion to the acyl chloride and subsequent treatment with benzylidenetriphenylphosphorane. For **8**, the bis(acyl chloride) is used to introduce the pendant phosphonium group. The catalysts **3a**–**8a** were then generated *in situ* by treatment of $Ni(cod)_2$ with the phosphorus ylide ligand precursor. *In situ* $^{31}P\{^1H\}$ NMR studies show that oxidative addition of **3**–**8** to the Ni(0) species occurs very rapidly in the presence of an olefin to form [P,O]Ni chelates.

Complexes containing these chelate ligands were also synthesised and isolated‡ from the corresponding ligand precursors and $Ni(cod)_2$ in the presence of an auxiliary ligand, typically triphenyl- or dimethylphenyl-phosphine, or pyridine. A crystal structure of the complex **6b**§ containing the ligand from catalyst system **6a** and the stabilising triphenylphosphine ligand is shown in Fig. 1. Complex **6b** crystallises with two independent molecules **A** and **B** in the asymmetric unit both of which have very similar conformations, the differences being in the relative orientations of the phenyl substituents. The geometry at nickel is only very slightly distorted square planar, the nickel and the four coordinated atoms being coplanar to within *ca.* 0.028 Å in both molecules. The plane of the C(43) phenyl ring is, in both molecules, oriented almost orthogonally

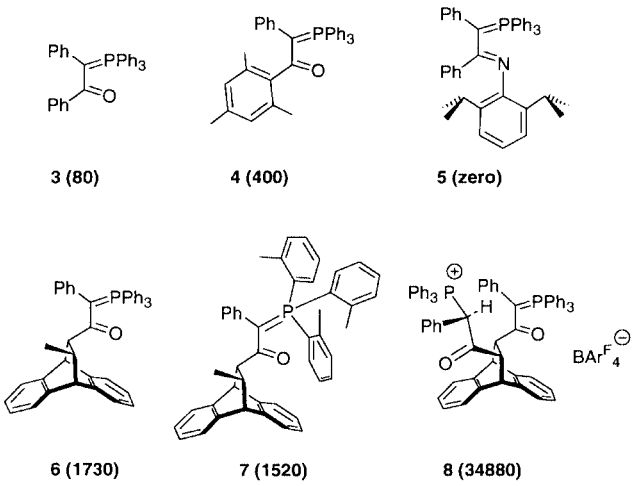

Scheme 1 Ligand precursors (LP) used in the corresponding *in situ* catalyst systems LP/$Ni(cod)_2$/olefin, **3a**–**8a** (olefin = ethylene, propylene or hex-1-ene) and their catalytic activities (g $mmol^{-1}$ h^{-1}) for ethylene polymerisation; BAr^F_4 = $[3,5\text{-}(CF_3)_2C_6H_3]B$.

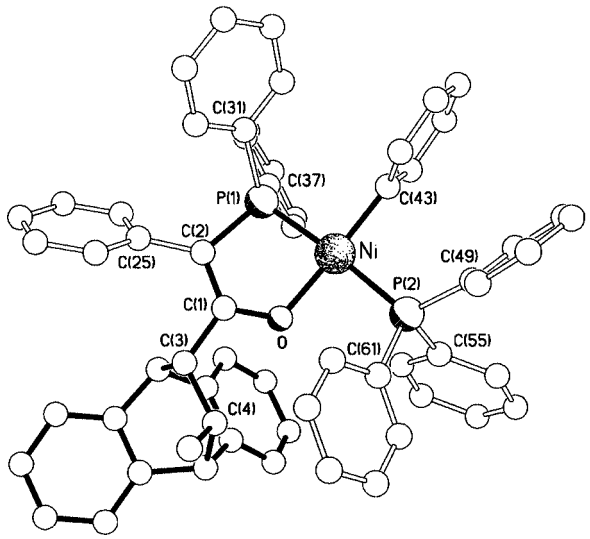

Fig. 1 One of the pair of crystallographically independent molecules present in the structure of **6b**. Selected bond lengths (Å) (data for molecule **B** are given in square brackets); Ni–O 1.901(2) [1.906(2)], Ni–P(1) 2.165(1) [2.174(1)], Ni–P(2) 2.212(1) [2.223(1)], Ni–C(43) 1.921(1) [1.928(1)], P(1)–C(2) 1.784(3) [1.775(3)], O–C(1) 1.309(4) [1.308(4)], C(1)–C(2) 1.374(4) [1.368(4)].

DOI: 10.1039/b101582f

to this plane. The *cis* angles at nickel are in the ranges 85.74(6)–93.03(7) and 85.43(6)–93.27(6)° in **A** and **B**, respectively, within each case the most acute angle being associated with the bite of the chelating ligand. The Ni–P(1) distance is, in both molecules, 0.05 Å shorter than that to P(2), indicating possibly an extension of the clear pattern of bond delocalisation, that extends from O through to P(1) *via* C(1) and C(2), to include the metal centre. The chelate ring has a slightly folded envelope conformation with the phosphorus atom lying 0.28 Å (molecule **A**) and 0.13 Å (molecule **B**) out of the plane of the remaining four atoms which are coplanar to within 0.007 Å (molecule **A**) and 0.009 Å (molecule **B**). The C(25) phenyl substituent is rotated by *ca.* 55° (**A**) and 68° (**B**) out of the plane of the chelate ring. The O–C(1)–C(3)–C(4) torsion angle is, in both molecules, small (*ca.* 6 and 15° in **A** and **B**, respectively), possibly as a consequence of a C(4)–H···O intramolecular hydrogen bond (the H···O distances are 2.24 and 2.26 Å in **A** and **B**, respectively).

The activities of these neutral catalysts for ethylene polymerisation and the results of product analyses are collected in Table 1. The ligand precursor **3**, and its triphenylphosphine stabilised nickel complex have been described earlier as precursors to ethylene polymerisation catalysts.[3,12] The catalytic performance of **3**/Ni(cod)$_2$ (**3a**) was used as a benchmark for the present study. Polymerisations were carried out both on *in situ* generated catalysts, which do not require the presence of a phosphine scavenger, and on the tertiary-phosphine stabilised pre-catalysts in the presence of Ni(cod)$_2$. Approximately the same activities are found in both cases and the resultant polymers also possess similar properties. In all cases, the polyethylene is essentially linear with number average molecular weights in the range 3000–10 000 and with molecular weight distributions in the range 2.0–3.7. It can be seen that there is an increase in activity upon introduction of a mesityl unit on the carbon adjacent to the enolate oxygen (**4a** *cf.* **3a**). Surprisingly, the activity falls to zero when the oxo group is exchanged for a N(diisopropylphenyl) unit (**5a**). A dramatic increase in activity is found upon introduction of the bulky anthracenyl-derived substituent (**6a**–**8a**), particularly for the phosphonium-containing catalyst **8a** which achieves an activity of almost 35 000 g mmol^{-1} h^{-1}. Comparison of **6a** with **7a** indicates that there is no beneficial effect on activity of increasing the size of the phosphorus substituents.

Another interesting feature of the neutral nickel complexes bearing bulky [P,O] ligands is their ability to oligomerise propylene and hex-1-ene. While co-polymerisations of ethylene with higher α-olefins by nickel phosphinoenolate complexes have been reported,[7] there have been no reports of propylene or hex-1-ene oligomerisations using these or related catalysts. Our attempts to oligomerise propylene with **3a** resulted in formation of only traces of propylene dimers. However **6a**, dissolved in toluene, oligomerised propylene at 4 bar and 70 °C with an activity of 1350 g mmol^{-1} h^{-1} to give a Schultz–Flory distribution (K = 0.64) of C_6–C_{48} olefins. Catalyst **8a** oligomerises propylene with a similar activity to give oligomers with a similar product distribution. Both catalysts homo-oligomerise hex-1-ene to C_{12}–C_{36} oligomers with relatively low activities. Thus, for example, catalyst **6a** shows an activity of 15 g mmol^{-1} h^{-1} for hex-1-ene oligomerisation.

The increase in activity is clearly linked to the introduction of the bulky anthracenyl-derived substituent next to the oxygen donor site. Possible effects of this are to protect the electrophilic nickel centre from binding potentially poisoning donor groups and/or to disfavour the coordination of Lewis acids at the oxygen site, especially another nickel centre which can result in ligand migration and formation of a catalytically inactive bis(chelate) species. Co-polymerisations of ethylene with hydrocarbon and polar co-monomers are presently under investigation.

BP Chemicals Ltd is thanked for financial support. Drs G. Audley and J. Boyle are thanked for GPC and NMR measurements, respectively.

Table 1 Results of ethylene polymerisation using catalytic systems **3a**–**8a** in toluene at 70 °C[a]

Cat. system	Ligand amount/ μmol	Mole ratio Ni/L	Ethylene pressure/ bar	PE yield/g	Activity[b]/ g mmol^{-1} h^{-1}	M_n	M_w/M_n
3a	20.0	5	1	0.4	80	6000	2.3
4a	5.0	5	1	0.5	400	4200	2.4
6a	4.4	5	1	1.9	1730	5200	3.6
6b	10.0[c,d]		1	3.2	1280[e]	5100	3.7
7a	10.0	5	1	3.8	1520	3500	2.0
8a	2.5	12	4	21.8	34880	5000	3.6
8a	2.4	12	2	18.3	30500	5200	3.5
8a[f]	2.7	12	4	10.0	14800	9900	5.4[g]

[a] Polymersations carried out in Schlenk tubes or Fisher–Porter bottles, over 15 min. [b] Based on concentration of ligand precursor. [c] 5 equivalents Ni(cod)$_2$ used as phosphine scavenger. [d] Conc. of Ni complex **6b**. [e] g mmol[Ni]$^{-1}$ h^{-1}. [f] Polymerisation carried out at 50 °C. [g] Bimodal molecular weight distribution.

† 9,10-Dihydro-9,10-ethanoanthracene.

‡ For example, synthesis of **6b**: a solution of 0.50 g (1.82 mmol) bis(*cis,cis*-cycloocta-1,5-diene)nickel(0), 1.09 g (1.82 mmol) *rac-trans*-11-(1-phenyl-1-triphenylphosphoranylideneacetyl)-12-methyl-9,10-dihydro-9,10-ethanoanthracene and 0.48 g (1.82 mmol) triphenylphosphine in toluene (50 ml) was stirred at room temperature for 24 h and at 50 °C for 1 h. The solvent was removed *in vacuo* and the residue was dissolved in toluene (7–8 ml). Addition of *n*-heptane (15–20 ml) gave a yellow precipitate which was filtered, washed with *n*-heptane and dried *in vacuo*. Yield, 1.10 g (66%), Anal. Found: C, 79.56; H, 5.64. $C_{61}H_{50}NiOP_2$ requires C, 79.66; H, 5.64%. ^{1}H NMR (250 MHz, C_6D_6): δ 0.72 (3H, d, J 6.72 Hz, CH_3), 2.17 (1H, m, CH), 2.79 (1H, m, CH), 3.53 (1H, d, J 1.70 Hz, CH), 4.24 (1H, d, J 1.70 Hz, CH), 6.40 (2H, t, Ar), 6.52 (1H, t, Ar), 6.72 (3H, m, Ar), 6.82–6.92 (8H, m, Ar), 6.92–7.09 (14H, m, Ar), 7.11–7.21 (10H, m, Ar), 7.30–7.34 (3H, m, Ar), 7.88–7.95 (2H, m, Ar). ^{31}P{^{1}H} NMR (101 MHz, C_6D_6): δ 22.01 (d, J 281.5 Hz, PPh_3), 33.58 (d, J 281.5 Hz, PPh_2). (+) FAB MS: m/z 918 (M^+), 841 ($M - Ph^+$), 656 ($M - PPh_3^+$).

§ *Crystal data* for **6b**·0.5C_7H_{16}: $C_{61}H_{50}OP_2Ni$·0.5C_7H_{16}, M = 969.8, monoclinic, $P2_1/n$ (no. 14), a = 22.153(2), b = 10.861(1), c = 42.785(4) Å, β = 90.68(1)°, V = 10293(2) Å^3, Z = 8 (2 independent molecules), D_c = 1.252 g cm^{-3}, μ(Cu-Kα) = 14.5 cm^{-1}, T = 203 K, orange–yellow prismatic needles; 15157 independent measured reflections, F^2 refinement, R_1 = 0.050, wR_2 = 0.122, 11797 independent observed reflections [$|F_o| > 4\sigma(|F_o|)$, $2\theta \leqslant 120°$], 1067 parameters. CCDC 158572. See http://www.rsc.org/suppdata/cc/b1/b101582f/ for crystallographic data in .cif or other electronic format.

Notes and references

1 G. J. P. Britovsek, V. C. Gibson and D. F. Wass, *Angew. Chem., Int. Ed.*, 1999, **38**, 429.
2 S. D. Ittel, L. K. Johnson and M. Brookhart, *Chem. Rev.*, 2000, **100**, 1169.
3 U. Klabunde, R. Mulhaupt, T. Herskovitz, A. H. Janowicz, J. Calabrese and S. D. Ittel, *J. Polym. Sci. Polym. Chem. Ed.*, 1987, **25**, 1989.
4 S. Mecking, *Angew. Chem., Int. Ed.*, 2001, **40**, 534.
5 W. Keim, F. H. Kowaldt, R. Goddard and C. Krüger, *Angew. Chem., Int. Ed. Engl.*, 1978, **17**, 466.
6 K. A. O. Starzewski and J. Witte, *Angew. Chem., Int. Ed. Engl.*, 1985, **24**, 599.
7 U. Klabunde and S. D. Ittel, *J. Mol. Catal.*, 1987, **41**, 123.
8 L. K. Johnson, C. M. Killian and M. Brookhart, *J. Am. Chem. Soc.*, 1995, **117**, 6414.
9 T. R. Younkin, E. F. Conner, J. I. Henderson, S. K. Friedrich, R. H. Grubbs and D. A. Bansleben, *Science*, 2000, **287**, 460.
10 H. J. Bestmann and B. Arnason, *Chem. Ber.*, 1962, **95**, 1513.
11 P. Braunstein, J. Pietsch, Y. Chauvin, S. Mercier, L. Saussine, A. DeCian and J. Fischer, *J. Chem. Soc., Dalton Trans.*, 1996, 3571.
12 W. Barnet, R. Bauer, H. Chung, W. Keim and P. Glockner (Shell Oil Co.), *US Pat.*, 3 686 159, 1972.

Highly luminous substituted bipyrroles

Chi-Ming Che,*[a] Chun-Wai Wan,[a] Wei-Zhu Lin,[a] Wing-Yiu Yu,[a] Zhong-Yuan Zhou,[b] W.-Y. Lai[c] and S.-T. Lee[c]

[a] *Department of Chemistry, The University of Hong Kong, Pokfulam Road, Hong Kong, China. E-mail: cmche@hku.hk*

[b] *Open Laboratory of Chirotechnology, Department of Applied Biology and Chemical Technology, The Hong Kong Polytechnic University, Hunghom, Hong Kong, China*

[c] *Centre of Super-Diamond and Advanced Film and Department of Physics and Materials Science, City University of Hong Kong, Tat Chee Avenue, Hong Kong, China*

Received (in Cambridge, UK) 4th December 2000, Accepted 27th February 2001
First published as an Advance Article on the web 29th March 2001

Two functionalized bipyrroles, 3,3′,5,5′-tetraethoxycarbonyl-4,4′-dipropyl-2,2′-bipyrrole 1 and 3,3′,5,5′-tetraethoxycarbonyl-4,4′-diphenyl-2,2′-bipyrrole 2, are highly luminescent materials at room conditions; they show UV emission at λ_{max} = 416 (1) and 414 nm (2) with quantum yields close to unity in the solid state; the molecular structure of 2 shows a coplanar structure stabilized by intramolecular hydrogen bonds, and the molecules are self-assembled along the crystallographic *c* axis by π-stacking interaction to form a one-dimensional chain; electroluminescence of 1 is evaluated.

The chemical, physical and electronic properties of conducting conjugated organic polymers such as poly(*p*-phenylenevinylenes)[1] and polythiophenes[2] have been widely exploited for the past decade, and recently some of these materials have been successfully developed for application in molecular electronics and light-emitting diode (LED) devices. However, among the numerous conducting polymers prepared to date, polypyrroles are the most extensively studied.[3] Apparently, polypyrroles possess a number of features that are attractive to materials science such as environmental stability, good redox properties and high electrical conductivity. Several applications based on polypyrroles including supercapacitors, electrochemical sensors, anti-static coating and drug delivery systems have been resulted.[4] Apart from these applications, to our knowledge, there are no reports describing highly luminescent poly/oligopyrroles at ambient conditions in the literature. Herein, we present the first report on UV photoluminescence of two functionalized bipyrrole compounds, namely 3,3′,5,5′-tetraethoxycarbonyl-4,4′-dipropyl-2,2′-bipyrrole **1** and 3,3′,5,5′-tetraethoxycarbonyl-4,4′-diphenyl-2,2′-bipyrrole **2** (Fig. 1). Blue luminous materials for application in blue-light emitting devices has recently been receiving widespread interest in materials science. We[5] and others[6] have reported that metal complexes of some *N*-heterocycles such as 7-azaindole, di-2-pyridylamine and 2,6-bis(2-pyridylamino)pyridine are strongly luminescent in the UV region; some of them have shown promising results as light-emitters for LED fabrication.[5b]

As reported by Nonell *et al.*,[7] **1** and **2** were prepared by the copper-mediated dehalogenated coupling of the iodopyrroles. The crude products were recrystallized by slow solvent evaporation of a CH_2Cl_2–MeOH mixture to afford colorless needle-shaped crystals.† As depicted in Fig. 2(a), the bipyrrole **2** adopts a near planar structure in a transcoid configuration, where the carbonyl functions of the carboxylate substituents are hydrogen bonded with the pyrrolic NH groups [N(1)···O(1A) 2.651 Å; N(1)···O(4) 2.486 Å]. It should be noted that the interannular torsion angle of unsubstituted 2,2′-bipyrrole for the most stable conformation is about 30° along the principal molecular axis according to theoretical models and some physical measurements.[8] In this work, we found that the coplanar conformation of **2** is essentially stabilized by intramolecular hydrogen bonding. Indeed, several studies by Brédas *et al.* have pointed out that coplanarity of the polyaromatic materials would permit better π-conjugation, thereby lowering the ionization potential and band gap of the compounds.[9] It is also suggested that coplanar conformation of polypyrroles

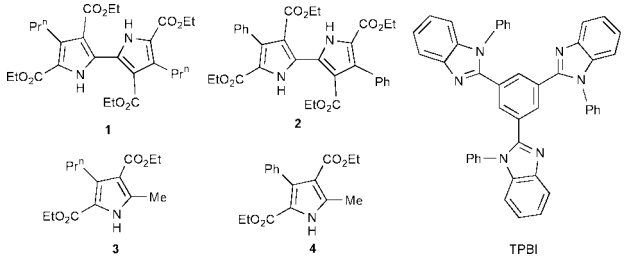

Fig. 1 Functionalized bipyrroles: 3,3′,5,5′-tetraethoxycarbonyl-4,4′-dipropyl-2,2′-bipyrrole **1** and 3,3′,5,5′-tetraethoxycarbonyl-4,4′-diphenyl-2,2′-bipyrrole **2**.

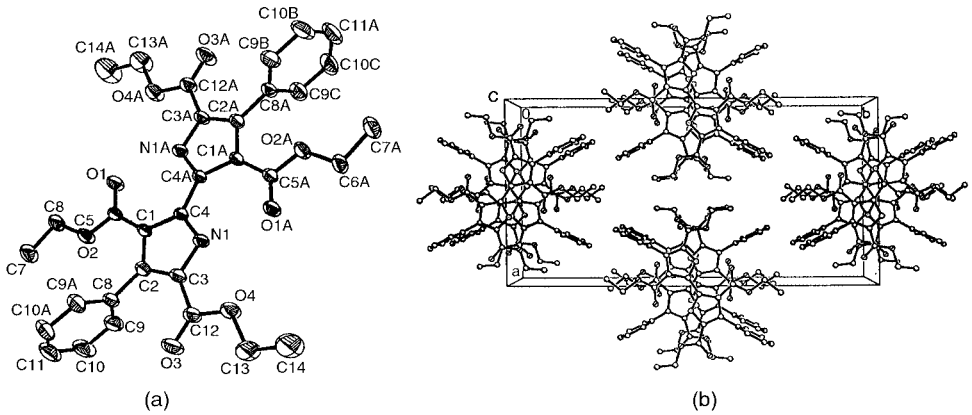

Fig. 2 (a) Perspective view of molecular structure and (b) crystal packing diagram of **2**.

Table 1 Photophysical data for bipyrroles **1** and **2**

	UV–VIS λ_{max}/nm (ε/dm^3 mol^{-1} cm^{-1})[a]	Emission maxima λ_{max}/nm (298 K)			Lifetime[e]	
		Solid state	CH_2Cl_2	Φ_{em}[b]	Solid state	Solution[f]
1	250 (38020) 350 (30940)	416	415	0.56[c]	2.0	2.7
2	290 (21020) 346 (34950)	414, 431(sh)	401	0.87[c]	0.63, 3.39	0.3, 2.5
3	271 (16780)	—[d]	313	0.0016		
4	275 (16820)	—[d]	360	0.0175		

[a] In CH_2Cl_2 at 298 K. [b] In degassed CH_2Cl_2 [c] Excited at 345 nm. [d] Intensity too weak to measure. [e] Excited at 266 nm ps pulses (T = 300 K). [f] In degassed CH_2Cl_2 (1 mM).

could facilitate intrachain mobility of charge defects such as polarons or bipolarons.[9b,c] By comparing the absorption spectra with those of the mono-pyrrole analogues (2,4-diethoxycarbonyl-5-methyl-3-propylpyrrole **3** and 2,4-diethoxylcarbonyl-5-methyl-3-phenylpyrrole **4**),[10] the absorptions for the bipyrroles are significantly red-shifted (see Table 1) due to the extended π-conjugation of the molecules.

The phenyl rings are oriented perpendicular to the bipyrrole plane, and the four carboxylate groups are arranged in a spiral arrangement along the principal C_2 axis of the molecule. The respective O(1)–C(5) and O(3)–C(12) distances of 1.212(1) and 1.187(1) Å are consistent with a C=O formulation, and the C(1)–C(5) [1.457(1) Å], C(3)–C(12) [1.473(2) Å] and C(4)–C(4A) [1.462(2) Å] distances are slightly shorter than a typical C–C (sp^3-hybridized) single bond, suggesting the presence of a partial double bond character. The molecule appears to form a one-dimensional chain along the crystallographic *c* axis *via* intermolecular π-stacking interaction [see Fig. 2(b)], the interplanar separation is *ca.* 3.8 Å [N(1)–N(1′) 3.669 Å and C(1)–C(1′) 3.723 Å].

The absorption and emission data of the bipyrroles are shown in Table 1. Their absorption spectra are featured by two absorption bands (250 and 350 nm for **1**; 290 and 346 nm for **2**), presumably arisen from π–π* transitions. Importantly, both compounds are strongly luminous at around 400 nm. In CH_2Cl_2 solution, the emission quantum yields (Φ_{em}) of **1** and **2** are 0.56 and 0.87, respectively, and their solid state quantum yields are unity within the experimental error. We observed a large Stokes shift with a magnitude of *ca.* 4500 cm^{-1} for the emission from the lowest singlet π–π* transition of the bipyrroles, which suggests a significant structural distortion of the excited state from the ground state structure. For better understanding the nature of emission, we have examined the emission of the bipyrroles using picosecond laser spectrophotometer. The luminescent lifetimes are listed in Table 1. The short lifetimes suggest that the emissions are due to fluorescence arising from the singlet π–π* transitions. Upon cooling the solid sample of **1** to 15 K, a vibronically structured emission was identified with a peak splitting of *ca.* 1080 cm^{-1}, which corresponds to the skeletal vibration of the bipyrrole. The measured luminescence lifetime was found to be 5.9 ns.

The transient luminescence trace of **2** monitored at 420 nm revealed two decay processes with lifetimes being 0.63 and 3.39 ns in the solid state, and 0.3 and 2.5 ns in solution. For **1**, however, there is only a single exponential decay with lifetime being 2.0 and 2.7 ns in the solid state and CH_2Cl_2 solution, respectively. We propose that the short luminescence decay [*i.e.* lifetime = 0.3 ns (solution) and 0.63 ns (solid)] for **2** may have originated from the rapid excited state energy transfer between the bipyrrole ring(s) and the phenyl substituent(s).[11]

The electroluminescence (EL) of the bipyrrole **1** has been evaluated. A film of **1** (20 or 50 nm) was obtained by vapor deposition onto a glass substrate pre-coated with indium–tin oxide and 4,4′-bis[*N*-(1-naphthyl)-*N*-phenylamino)biphenyl (NPB; thickness = 80 nm). To achieve better contact between the emitter layer (*i.e.* **1**) and the Mg : Ag cathode, a layer of TPBI (40 or 20 nm, see Fig. 1 for structure) was evaporated on top of the bipyrrole layer. When the LED was forward biased with the ITO electrode at positive polarity, EL with a blue–green color was observed. The EL spectrum shows a prominent band at 440 nm, which is red–shifted from the solid state emission of **1** (blue color, λ_{max} = 415 nm). It should be noted that the PL spectrum of the bipyrrole film is essentially identical with the solid state emission of **1**. The reasons underlying the red-shift of the EL remain unclear. The maximum luminance of 750 cd m^{-2} with maximum efficiency being 0.9 cd A^{-1} was attained at 14 V.

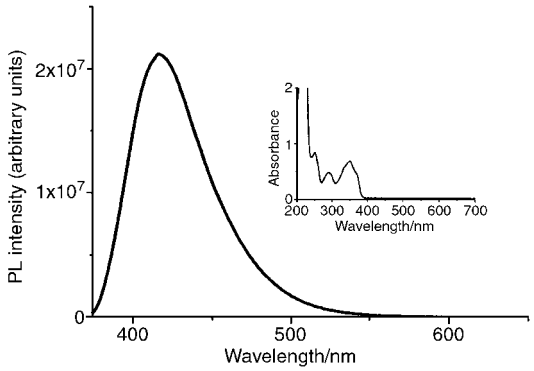

Fig. 3 Emission and absorption (inset) spectra of **1** in CH_2Cl_2 solution at 298 K.

We acknowledge the support from The University of Hong Kong and the Hong Kong Research Grants Council.

Notes and references

† *X-Ray crystallography*: the intensity data were collected on a Bruker CCD diffractometer with graphite-monochromated Mo-Kα radiation (λ = 0.71073 Å) at room temperature. All the calculations were performed by using SHELXTL-PL version 5.10 package on a HP computer. The structure was solved by the direct methods and refined by the full-matrix least-squares methods. *Crystal data* for **2**: colorless needle, dimensions 0.22 × 0.08 × 0.08 mm, $C_{32}H_{32}N_2O_8$, M_r = 572.60, orthorhombic, space group = *Ibam*, a = 14.363(2), b = 27.535(4), c = 7.272(1) Å, V = 2876.2(7) Å^3, Z = 4, D_c = 1.322 g cm^{-3}, F(000) = 1208; μ(Mo-Kα)/mm^{-1} = 0.577, 9113 reflections were collected, of which 1742 with $|F_o| > 2.0\sigma(|F_o|)$ were observed; R_1 = 0.054; wR_2 = 0.15. CCDC 156695. See http://www.rsc.org/suppdata/cc/b0/b009687n/ for crystallographic files in .cif format.

1 A. Kraft, A. C. Grimsdale and A. B. Holmes, *Angew. Chem., Int. Ed.*, 1998, **37**, 402 and references therein.

2 J. Roncali, *Chem. Rev.*, 1992, **92**, 711; G. Schopf and G. Kossmehl, *Adv. Polym. Sci.*, 1997, **129**, 1.

3 J. Simonet and J. R. Berthelot, *Prog. Solid State Chem.*, 1991, **21**, 1; D. L. Wise, G. E. Winek, D. J. Trantolo, T. M. Cooper and J. D. Gresser, in *Electrical and Optical Polymer Systems*, Marcel Dekker, Inc., New York, 1998, vol. 17.

4 B. Scrosati, *Applications of Electroactive Polymers*, Chapman & Hall, London, 1993; J. Rodriguez, H. J. Grande and T. F. Otero, in *Handbook of Organic Conductive Molecules and Polymers*, ed. H. S. Nalwa, John Wiley & Sons, New York, 1997, p. 415.

5 (*a*) C.-F. Lee, K.-F. Chin, S.-M. Peng and C.-M. Che, *J. Chem. Soc., Dalton Trans.*, 1993, 467; (*b*) Y. Ma, H.-Y. Chao, Y. Wu, S.-T. Lee, W.-Y. Yu and C.-M. Che, *Chem. Commun.*, 1998, 2491; (*c*) K.-Y. Ho, W.-Y. Yu, K.-K. Cheung and C.-M. Che, *Chem. Commun.*, 1998, 2101; (*d*) K.-Y. Ho, W.-Y. Yu, K.-K. Cheung and C.-M. Che, *J. Chem. Soc., Dalton Trans.*, 1999, 1581.

6 S.-F. Liu, Q. Wu, H. L. Schmider, H. Aziz, N.-X. Hu, Z. Popovic and S. Wang, *J. Am. Chem. Soc.*, 2000, **122**, 3671; W. Yang, H. Schmider, Q. Wu. Y.-S. Zhang and S. Wang, *Inorg. Chem.*, 2000, **39**, 2397.

7 S. Nonell, N. Bou, J. I. Borrell, J. Teixido, A. Villanueva, A. Juarranz and M. Canete, *Tetrahedron Lett.*, 1995, **36**, 3405.

8 C. Gatti, G. Frigerio, T. Benincori, E. Brenna, F. Sannicoló, G. Zotti, S. Zecchin and G. Schiavon, *Chem. Mater.*, 2000, **12**, 1490 and references therein.

9 (*a*) J. L. Brédas, R. Silbey, D. S. Boudreaux and R. R. Chance, *J. Am. Chem. Soc.*, 1983, **105**, 6555; (*b*) J. L. Brédas and G. B. Street, *Acc. Chem. Res.*, 1985, **18**, 309; (*c*) J. L. Brédas, G. B. Street, B. Themans and J. M. Andre, *J. Chem. Phys.*, 1985, **83**, 1323; (*d*) J. L. Brédas and A. J. Heeger, *Macromolecules*, 1990, **23**, 1150.

10 For preparation, see: A. C. Braithwaite and T. N. Waters, *J. Inorg. Nucl. Chem.*, 1973, **35**, 3223.

11 T. Sato, K. Hori, M. Fujitsuka, A. Watanabe, O. Ito and K. Tanaka, *J. Chem. Soc., Faraday Trans.*, 1998, **94**, 2355.

Polymer site–site interactions: mechanistic implication in the solid-phase Zincke reaction

Masahiro Eda[a] and Mark J. Kurth*[b]

[a] *Department of Chemistry, University of California, One Shields Avenue, Davis, CA 95616-5295, USA. E-mail: mjkurth@ucdavis.edu*

[b] *Welfide Corporation, 2-25-1, Shodai-Ohtani, Hirakata, Osaka, Japan 573-1153*

Received (in Corvallis, OR, USA) 8th December 2000, Accepted 30th January 2001
First published as an Advance Article on the web 29th March 2001

Mechanistic aspects of the solid-phase Zincke reaction have been investigated using Wang resins; a proton transfer mechanism is proposed which obviates the need for covalent bond site–site interactions.

In 1903, Zincke reported the ring opening-reaction of 2,4-dinitrophenylpyridinium chloride (**1**) with aniline to give 5-anilino-*N*-phenyl-2,4-pentadienylideniminium chloride (**3**, R = Ph; Scheme 1)[1] which underwent ring reclosure to give *N*-phenylpyridinium chloride (**4**, R = Ph).[1] This process, known as the Zincke reaction, is now the standard route to *N*-arylpyridinium salts which cannot be formed by direct reaction of electrophiles with pyridine.[2] The Zincke mechanism had previously been divided into ring-opening[3] (**1** → **3**) and ring-closing[4] (**3** → **4**) stages until Ise and co-workers determined the complete process for **1** → **4** as shown in Scheme 1.[5] In this mechanism, excess amine (RNH_2) assists in proton transfer and reacts twice with **1** to deliver intermediate **3**.

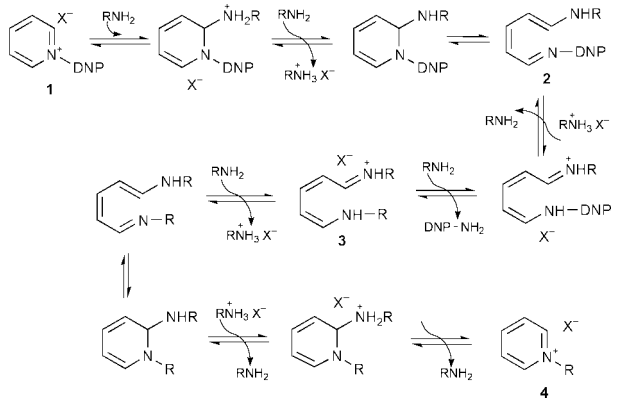

Scheme 1

We recently reported[6] a solid-phase (SP) variant of the Zincke reaction, which according to Ise's mechanism, would require two kinds of resin-bound amine interactions — 'proton transfer site–site interactions' and 'covalent bond site–site interactions' (Scheme 2). However, an intriguing question arises as to whether the SP Zincke reaction proceeds *via* **3** as formation of this intermediate requires covalent bond site–site interactions between two resin-bound amines. Since the amine moiety (RNH_2) is attached to resin in the SP system, formation of the SP aminopentadienylideniminium (**3′**; Scheme 3) and subsequent re-closure to the SP Zincke product (**4′**) would seem to be inefficient because each covalent bond site–site interaction generates a new crosslink which would reduce resin mobility[7] and hinder formation of SP intermediate **3′**. Moreover, most SP aminopentadienylideniminiums (**3′**) would not be able to negotiate the six membered transition-state required for electrocyclic ring closing.

We reasoned that conversion of Zincke salt to Zincke product (**1′** → **4′**; Scheme 3) by a process which avoids the intermediacy of aminopentadienylideniminiums would be more likely in the SP reaction. To probe this, we have carried out more detailed studies of the SP Zincke reaction and report our findings here.

Three crucial factors mediate site–site interactions in SP reactions: (i) crosslinking density, (ii) functional group loading, and (iii) solvent properties.[8] Therefore, we have compared Zincke reactions using Wang resins (both 1%- and 2%-crosslinked; Novabiochem) at a variety of amine loading levels.[9] Wang resin (**5**) was loaded[10] with a mixture of Fmoc–amino alcohol and a suitable amount of *n*-propanol to provide resin **6** (Scheme 4). The actual amino loading of **7** was determined by UV spectrophotometric analysis of the Fmoc decomposition product.

Reaction of amino resin **7a** (100 mg) with Zincke salt **8a**[11] (5 eq. relative to **7a**'s amine loading) both with and without TEA (10 μL) or 2,4-dinitroaniline (DNP–NH_2, 13 mg) in solvent (toluene or *n*-butanol, 2 mL) at 80 °C for 35 h gave SP Zincke product **9a**. Cleavage of the Wang tether in **9a** using 10% TFA in CH_2Cl_2 solution gave Zincke product **10**. The overall yield of **7a** → **10** was determined by HPLC analysis [Symmetry® C_{18}, 4.6 × 150 mm, linear gradient elution of 10–100% MeOH–phosphoric acid buffer solution (pH 7.0) for 20 min; flow rate 1 mL min^{-1}; detection, 220 nm, **10**: t_R = 9.32 min]. Fig. 1 shows the relationship between resin **7a**'s amine loading and the yield of Zincke product **10**. Running SP reactions with TEA increases product yield at all loading levels for either degree of crosslinked resin. Addition of DNP–NH_2 causes no yield improvement (*i.e.* product yield with and without DNP–NH_2 were similar) suggesting that DNP–NH_2 (formed *in situ*) does not assist proton transfer in **7a** → **9a**. In contrast, TEA does play an important role in assisting proton transfer so that **7a** → **9a** proceeds primarily *via* the process outlined in Scheme 4.

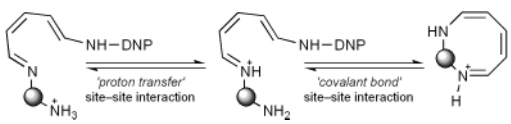

Scheme 2

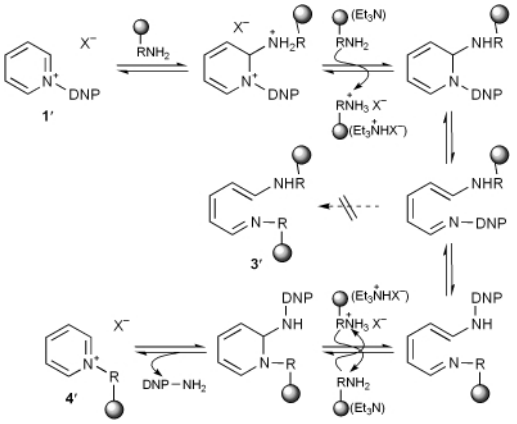

Scheme 3

DOI: 10.1039/b009886h

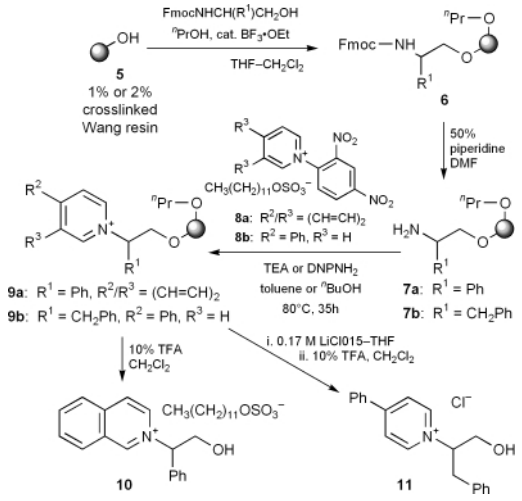

Scheme 4

Relative to *n*-butanol (effective solution-phase solvent),[11] toluene is the solvent of choice for SP Zincke reactions due to its ability to swell the resin.[12] Unfortunately, these distinct solvent requirements make meaningful rate comparisons between solution (24 h, 118 °C)[2b,11] and SP (35 h, 80 °C) unworkable.

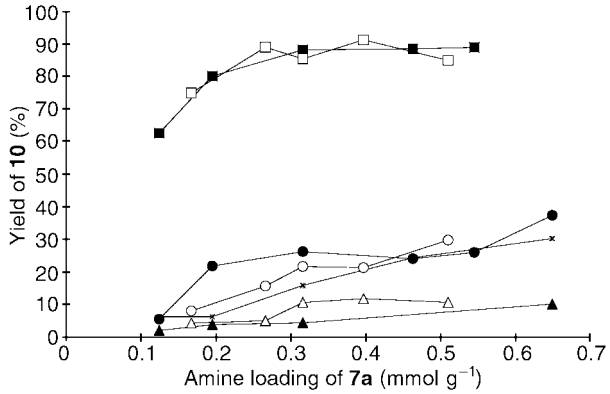

Fig. 1 Plotted yield of **10** *versus* the amine loading of **7a**: 1% crosslinked (●), 2% crosslinked (○), 1% crosslinked + TEA (■), and 2% crosslinked + TEA (□) in toluene, and 1% crosslinked (▲) and 2% crosslinked (△) in *n*-butanol; 1% crosslinked + DNP–NH_2 (⁎) in toluene.

We also studied the more reactive combination of SP amine **7b** condensing with Zincke salt **8b**[6] to give SP Zincke product **9b**. Subsequent treatment of **9b** with LiCl, followed by cleavage, liberated **11** as the chloride salt. The relationship between amine loading in starting resin **7b** and yield of **11** is shown in Fig. 2. Again, reactions in the presence of TEA resulted in good product yields. In reactions without TEA, yield improvement was observed with resin loadings for **7b** of >0.3 mmol g^{-1}. This result—namely, that effective site–site interactions occur at loadings >0.3 mmol g^{-1}—is in agreement with Patchornik's report that 0.1–0.3 mmol g^{-1} loadings can be employed successfully in syntheses requiring effective site-isolation.[13] The fact that SP Zincke reactions proceed in good yield at resin loadings of $\leqslant 0.3$ mmol g^{-1}—even at lower loading such as 0.09 mmol g^{-1}—in the presence of TEA indicates that this reaction can progress from Zincke salt **1′** to SP Zincke product **4′** without the formation of intermediate **3′**. No amine site–site interactions are required if TEA is present to negotiate proton transfer and direct conversion of **1′** to **4′**. However, reactions run without added TEA on resin with loadings of >0.3 mmol g^{-1} experience significant proton transfer site–site interaction as evidenced by the increased yield.

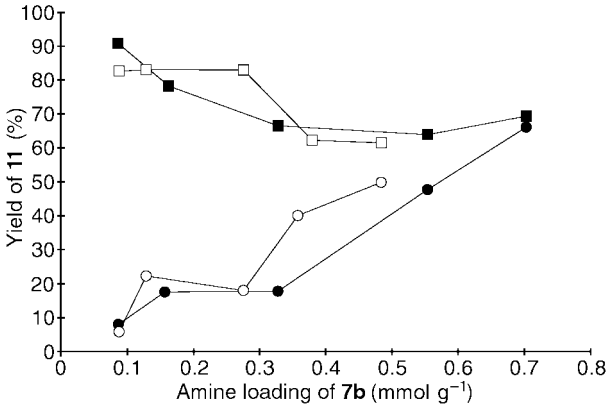

Fig. 2 Plotted yield of **11** *versus* the amine loading of **7b**: 1% crosslinked (●), 2% crosslinked (○), 1% crosslinked + TEA (■), and 2% crosslinked + TEA (□) in toluene.

The yields of Zincke product from 1%- and 2%-crosslinked Wang resin are generally equivalent (see Fig. 1). Indeed, solvent swelling ratios (*s*) for 1%- and 2%-DVB–styrene beads are quite similar (s = 5.13 and 4.52 in toluene, respectively)[14] which suggests that these crosslink densities are not sufficiently disparate to cause differential site–site interactions.

In summary, we have analyzed the SP Zincke mechanism under a variety of resin loadings and reaction conditions. We conclude that while **3′** may be involved to some limited extent in this SP Zincke transformation, a proton transfer mechanism provides the more likely reaction path for conversion of polymer-supported amine (●–RNH_2) to polymer-supported Zincke product (**4′**; Scheme 3). Addition of TEA greatly facilitates the SP Zincke reaction by involvement of Et_3N–$Et_3N{\cdot}HX$ in several key SP proton transfer steps.

The National Science Foundation and the Cystic Fibrosis Foundation supported this research; the NMR spectrometers used were funded in part by a grant from NSF (CHE-9808183).

Notes and references

1 (*a*) Th. Zincke, *Justus Liebigs Ann. Chem.*, 1903, **330**, 361; (*b*) Th. Zincke, G. Heuser and W. Moller, *Justus Liebigs Ann. Chem.*, 1904, **333**, 296.
2 (*a*) A. N. Kost, S. P. Gromov and R. S. Sagitullin, *Tetrahedron*, 1981, **37**, 3423; (*b*) Y. Genisson, C. Marazano, M. Mehmandoust, D. Gnecco and B. C. Das, *Synlett*, 1992, 431.
3 (*a*) E. Van den Dunghen, J. Nasielski and P. Van Laser, *Bull. Soc. Chim. Belg.*, 1957, **66**, 661; (*b*) J. Kavalek and V. Sterba, *Collect. Czech. Chem. Commun.*, 1973, **38**, 3506.
4 (*a*) E. N. Marvell, G. Caple and I. Shahidi, *J. Am. Chem. Soc.*, 1970, **92**, 5641; (*b*) E. N. Marvell and I. Shahidi, *J. Am. Chem. Soc.*, 1970, **92**, 5646; (*c*) E. N. Marvell, G. Caple and I. Shahidi, *Tetrahedron Lett.*, 1967, **3**, 277.
5 S. Kunugi, T. Okubo and N. Ise, *J. Am. Chem. Soc.*, 1976, **98**, 2282.
6 M. Eda, M. J. Kurth and M. H. Nantz, *J. Org. Chem.*, 2000, **65**, 5131.
7 P. Hodge and E. Khoshdel, *React. Polym.*, 1985, **3**, 143.
8 P. Hodge, *Chem. Soc. Rev.*, 1997, **26**, 417.
9 The maximum loading of commercially available 2%-crosslinked Wang resin is 0.91 mmol g^{-1}. Therefore, we used 1%-crosslinked resin with 1.2 mmol g^{-1} functionalization to give comparable loadings.
10 S. Hanessian and F. Xie, *Tetrahedron Lett.*, 1998, **39**, 733.
11 D. Barbier, C. Marazano, B. C. Das and P. Potier, *J. Org. Chem.*, 1996, **61**, 9596.
12 Toluene swells Wang resin 2.3 times more than *n*-butanol.
13 A. Patchornik and M. A. Kraus, *J. Am. Chem. Soc.*, 1970, **92**, 7587.
14 Z. Y. Ding, J. J. Aklonis and R. Salovey, *J. Polym. Sci.-Part B: Polym. Phys.*, 1991, **29**, 1035.

ChemComm

Rapid hydroformylation of alkyl acrylates in supercritical CO_2

Yulai Hu,[a] Weiping Chen,[a] Anna M. Banet Osuna,[a] Alison M. Stuart,[b] Eric G. Hope[b] and Jianliang Xiao*[a]

[a] *Leverhulme Centre for Innovative Catalysis, Department of Chemistry, University of Liverpool, Liverpool, UK L69 7ZD. E-mail: j.xiao@liv.ac.uk*

[b] *Department of Chemistry, University of Leicester, Leicester, UK LE1 7RH*

Received (in Cambridge, UK) 30th January 2001, Accepted 8th March 2001
First published as an Advance Article on the web 29th March 2001

Fast and regioselective hydroformylation of alkyl acrylates can readily be accomplished in supercritical CO_2 ($scCO_2$), which promotes the reaction probably *via* specific solvent–solute interactions.

The hydroformylation of acrylic esters produces bifunctional compounds, which can be converted into synthetically useful intermediates such as malonic acid and 1,4-dicarboxylic acid derivatives and butyrolactones. In the past three decades or so, a number of publications have appeared, directed towards effecting the reaction with acceptable rates and regioselectivities.[1–10] In this context, catalysts based on various rhodium-ligand combinations have been examined. However, in common organic solvents and regardless of the ligands that have been tested, the reaction is in general slow and high temperature and/or high pressure are often required.[1,6,7,9,10] For example, in the hydroformylation of ethyl acrylate in ethylbenzene, complete conversion, corresponding to an average turnover frequency (TOF) of 413 h^{-1}, of the olefin was only achieved in 5 h reaction time at 150 °C and *ca*. 100 bar syngas using $[RhCl(CO)_2]_2$ in the presence of bis(diphenylphosphino)butane (DPPB).[1] While milder reaction conditions are possible with phosphite[4] and phosphanobornadiene ligands,[2] the TOFs were very low. Much improved rates have recently been obtained when the reaction is run under organo-aquo biphasic conditions or when a 'supported aqueous phase' catalyst is used.[5,8] However, low solubilities of the less hydrophilic acrylates in water limit the applicability of the biphasic systems and, in the case of the latter, it was shown that even a slight alteration in the water content in the supported aqueous phase could sharply reduce the activity of the catalyst. We report herein that fast and selective hydroformylation of alkyl acrylates can readily be effected in $scCO_2$ in the presence of $[Rh(acac)(CO)_2]$ and the fluoroalkylated phosphine ligand P(*p*-$C_6H_4C_6F_{13})_3$ (Scheme 1).[11]

We first tested this ligand in the hydroformylation of butyl acrylate in toluene and compared the results obtained with three other ligands, PPh_3, DPPB and P(*p*-$C_6H_4OMe)_3$, of which the first two are frequently used and DPPB is one of the most effective ligands in liquid solvents.[1,5,7] The reaction was performed using a combination of $[Rh(acac)(CO)_2]$ and 10 equiv. of a phosphine ligand as catalyst precursor in an autoclave at 80 °C and 20 bar H_2–CO (1:1) with the initial olefin concentration being 0.28 M. All the reactions were run for 1 h and were homogeneous throughout. The results are summarized in Table 1. Consistent with previous findings, DPPB stands out as the most effective ligand in terms of the average TOF to aldehydes given in Table 1. With PPh_3 and the relatively electron-rich P(*p*-$C_6H_4OMe)_3$, the expected aldehydes could barely be detected. With the electron-deficient P(*p*-$C_6H_4C_6F_{13})_3$, a TOF of 85 was observed. Increasing the syngas pressure to 50 bar led to some increase in TOF to 122, which is still significantly lower than the value of 304 with DPPB. Judging from these values, it is clear that hydroformylation of acrylates in normal organic solvents by arylphosphines, including the most effective DPPB, will be of little practical value.

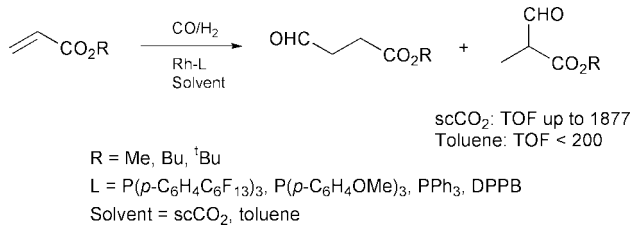

Scheme 1

Table 1 Hydroformylation of butyl acrylate by Rh-L in toluene[a]

L	Pressure/ bar	Conv. (%)[b]	Ald. (%)[c]	TOF/h^{-1}[d]
PPh_3	20	< 1		
P(*p*-$C_6H_4OMe)_3$	20	< 1		
P(*p*-$C_6H_4C_6F_{13})_3$	20	2.1	99.8	85
P(*p*-$C_6H_4C_6F_{13})_3$	50	2.7	99.8	122
DPPB	20	7.6	99.9	304

[a] Reactions were carried out at L–$[Rh(acac)(CO)_2]$ = 10, olefin–rhodium = 4000, olefin concentration = 0.28 mol dm^{-3}, 80 °C and indicated H_2–CO (1:1) pressure in 20 mL of toluene for 1 h, with product analysed by GC. [b] Conversion of the acrylates. [c] Selectivity to branched aldehydes. The linear aldehydes were not detected by GC. The hydrogenated product, propionates, accounts for the product balance. [d] Average turnover frequency: mole of aldehyde formed per mole of catalyst per hour.

Having determined the activity of the Rh-P(*p*-$C_6H_4C_6F_{13})_3$ catalyst in toluene, we then applied the same catalyst to the hydroformylation of methyl, butyl and ^{t}butyl acrylates in $scCO_2$ (Scheme 1).† The reactions were carried out for 1 h and the detailed procedure has been described before.[11] Table 2 summarises the results obtained in $scCO_2$ and those in toluene under the same temperature, pressure and olefin concentrations. In all these reactions, the linear aldehydes could not be detected by GC, which is in line with the literature that the hydroformylation of acrylates usually affords branched aldehydes as the dominant product.[1–10] The ratio of the hydrogenated product, propionates, was somewhat higher in $scCO_2$ (*ca*. 2.5%) than in toluene (< 0.5%). However, of much more significant

Table 2 Hydroformylation of acrylates by Rh-P(*p*-$C_6H_4C_6F_{13})_3$ in $scCO_2$ and toluene[a]

Substrate	Solvent	[Olefin][b]	Conv. (%)[c]	Ald. (%)[d]	TOF/ h^{-1}[e]
Methyl acrylate	$scCO_2$	0.45	40.8	97.6	1593
Butyl acrylate	$scCO_2$	0.28	42.9	97.5	1671
^{t}Butyl acrylate	$scCO_2$	0.28	46.9	97.4	1827
Methyl acrylate	Toluene	0.45	2.3	99.6	92
Butyl acrylate	Toluene	0.28	2.1	99.8	84
^{t}Butyl acrylate	Toluene	0.28	4.8	99.6	191

[a] Reactions were carried out at P(*p*-$C_6H_4C_6F_{13})_3$–$[Rh(acac)(CO)_2]$ = 10, olefin–rhodium = 4000, 80 °C, 180 bar CO_2 and 20 bar H_2–CO (1:1) for 1 h. [b] Olefin concentration: mol dm^{-3}. [c] Conversion of the acrylates. [d] Selectivity to branched aldehydes. The linear aldehydes were not detected by GC. The hydrogenated product propionates accounts for the product balance. [e] Average turnover frequency.

DOI: 10.1039/b101043n

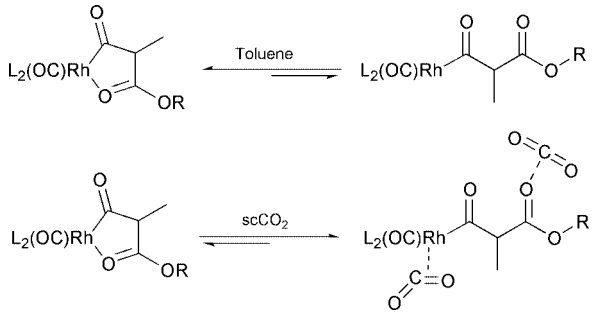

Scheme 2

interest is the observation that, in $scCO_2$, the average TOFs for the formation of aldehydes ranged from 1593 to 1827 h^{-1}, whereas in toluene the TOFs were less than 200 h^{-1}. In both solvents, the fastest rates were derived from the sterically most demanding ^{t}butyl acrylate. Thus, by simply changing the reaction medium from toluene to $scCO_2$, the TOF values increased *ca*. 10–20 fold. Such dramatic enhancement in reaction rates by $scCO_2$ has rarely been observed before,[11–14] although the high miscibility of various gases with CO_2 and its excellent transport properties have often been suggested to be impetus for fast reactions.[15] One of the best-known examples, where greatly improved rates were achieved, is the hydrogenation of CO_2 by a Ru-PMe_3 catalyst, the high rates being partly attributed to the high concentration of the gaseous reagents.[15] In the present study, the enhanced TOFs are less likely to be primarily due to a high concentration of syngas in $scCO_2$, since more than doubling the pressure for the hydroformylation of butyl acrylate in toluene led to a TOF of only 122 h^{-1} (Table 1), far less than that of 1671 h^{-1} obtained in $scCO_2$ at 20 bar.

A further demonstration of the rate enhancement aforesaid is the hydroformylation of a mixture of butyl acrylate and dec-1-ene in $scCO_2$. The reaction was run under identical conditions to those for butyl acrylate itself, except with the concentration of the olefin reduced by *ca*. half (0.12 M for both dec-1-ene and butyl acrylate). The TOFs observed for butyl acrylate and dec-1-ene were 1511 and 379 h^{-1}, respectively. This is remarkable, considering that in the absence of the acrylate the average TOF for dec-1-ene (0.22 M initial concentration) was 2794 h^{-1} under otherwise identical reaction conditions.[11] In a similar experiment in toluene, the TOF was found to be 56 for the acrylate and 24 h^{-1} for dec-1-ene, while in the absence of the acrylate the TOF for the latter olefin (0.28 M) rose to 901. Evidently, the Rh-P(*p*-$C_6H_4C_6F_{13})_3$ catalyst is considerably more chemoselective towards the less reactive acrylates, but it is only in $scCO_2$ where it becomes highly active as well.

The significant enhancement in hydroformylation rates for the acrylates in $scCO_2$ might be accounted for by specific solvent–solute interactions. The low rates observed in common organic solvents are generally believed to be a result of the formation of thermodynamically stable five or six-membered rings (Scheme 2, where only the intermediate leading to branched product is shown).[7,8] The rate determining step of the hydroformylation has therefore been suggested to be the dissociation of the chelated carbonyl species to give a coordinatively unsaturated intermediate that is active towards the oxidative addition of H_2.[8] We suggest that, in $scCO_2$, the equilibrium position is shifted in favour of the key unsaturated intermediate as a result of a carbonyl–CO_2 donor–acceptor interaction as shown in Scheme 2. Previous spectroscopic studies have already shown that carbonyl groups can act as Lewis bases and interact with CO_2 acting as a Lewis acid.[16] In addition, coordination of CO_2 to the rhodium atom of the unsaturated intermediate and other oxygen atoms is possible, which would further shift the equilibrium to the right.[17] A similar model involving H_2O and hydrogen bonding was earlier proposed to account for the increase in rates in the hydroformylation of acrylates in the presence of water.[5,8]

In summary, we have shown that the hydroformylation of alkyl acrylates, although sluggish in conventional organic solvents, can readily be effected in $scCO_2$. In such reactions, CO_2 acts not only as a solvent but may also function as an electron acceptor, interacting with and stabilizing key carbonyl intermediates and thus promoting the overall reaction. Such specific solvent–solute interactions have rarely been exploited in catalysis in $scCO_2$ but could provide a unique means for tuning chemical activity and selectivity in synthesis in $scCO_2$.

We thank the EPSRC (Y. H., W. C.), the Royal Society (A. M. S., E. G. H.) and the LCIC (A. M. B. O., J. X.) for financial support.

Notes and references

† **CAUTION**: When working with high-pressure equipment, appropriate safety devices, including but not limited to pressure relief mechanisms and blast shields, should be used.

1 M. Tanaka, T. Hayashi and I. Ogata, *Bull. Chem. Soc. Jpn.*, 1977, **50**, 2351.
2 D. Neibecker and R. Réau, *Angew. Chem., Int. Ed. Engl.*, 1989, **28**, 500.
3 I. Amer and H. Alper, *J. Am. Chem. Soc.*, 1990, **112**, 3674.
4 H. Yamashita, B. L. Roan, T. Sakakura and M. Tanaka, *J. Mol. Catal.*, 1993, **81**, 255.
5 G. Fremy, E. Monflier, J. F. Carpentier, Y. Castanet and A. Mortreux, *Angew. Chem., Int. Ed. Engl.*, 1995, **34**, 1474.
6 G. Fremy, Y. Castanet, R. Grzybek, E. Monflier, A. Mortreux, A. M. Trzeciak and J. J. Ziolkowski, *J. Organomet. Chem.*, 1995, **505**, 11.
7 C. W. Lee and H. Alper, *J. Org. Chem.*, 1995, **60**, 499 and references therein.
8 G. Fremy, E. Monflier, J. F. Carpentier, Y. Castanet and A. Mortreux, *J. Mol. Catal.*, 1998, **129**, 35.
9 H. K. Reinius, R. H. Laitinen, A. O. I. Krause and J. T. Pursiainen, *Catal. Lett.*, 1999, **60**, 65.
10 H. K. Reinius and A. O. I. Krause, *J. Mol. Catal.*, 2000, **158**, 499.
11 A. M. B. Osuna, W. Chen, E. G. Hope, R. D. W. Kemmitt, D. R. Paige, A. M. Stuart, J. Xiao and L. Xu, *J. Chem. Soc., Dalton Trans.*, 2000, 4052.
12 D. Koch and W. Leitner, *J. Am. Chem. Soc.*, 1998, **120**, 13398.
13 I. Bach and D. J. Cole-Hamilton, *Chem. Commun.*, 1998, 1463.
14 N. J. Meehan, A. J. Sandee, J. N. H. Reek, P. C. J. Kamer, P. W. N. M. van Leeuwen and M. Poliakoff, *Chem. Commun.*, 2000, 1497.
15 P. G. Jessop, T. Ikariya and R. Noyori, *Chem. Rev.*, 1999, **99**, 475.
16 S. G. Kazarian, M. F. Vincent, F. V. Bright, C. L. Liotta and C. A. Eckert, *J. Am. Chem. Soc.*, 1996, **118**, 1729.
17 C. S. Pomelli, J. Tomasi and M. Solà, *Organometallics*, 1998, **17**, 3164.

One-step, solid-state reaction to the synthesis of copper oxide nanorods in the presence of a suitable surfactant

Wenzhong Wang[ab] Yongjie Zhan[a] and Guanghou Wang*[ab]

[a] *National Laboratory of Solid State Microstructures & Department of Physics, Nanjing University, Nanjing 210093, P. R. China. E-mail: wangqun@netra.nju.edu.cn*

[b] *Structure Research Laboratory, University of Science and Technology of China, Hefei, Anhui 230026, P. R. China*

Received (in Cambridge, UK) 11th October 2000, Accepted 8th March 2001
First published as an Advance Article on the web 29th March 2001

A novel and simple one-step, solid-state reaction in the presence of a suitable surfactant has been developed to synthesize uniform copper oxide nanorods with average diameters of *ca.* 8 nm and lengths of up to 400 nm.

One-dimensional nanostructural materials are currently the focus of considerable interest. Many methods have been used for the preparation of nanorods or nanowires.[1–6] However, to our knowledge, complex process control, high reaction temperatures or long synthesis time may be required for these approaches. Here we report a novel and simple one-step, solid-state reaction in the presence of a suitable surfactant, polyethylene glycol (PEG) 400, for preparation of copper oxide nanorods. This method requires no complex apparatus and techniques. The process is carried out in air at room temperature and the synthetic time is very short.

Transition metal oxide-containing glasses are of interest due to their possible technological application in electrical and optical switching devices. Copper oxide is a p-type semiconductor and it is useful for the preparation of organic catalysts. Great attention has been devoted to metal–organic chemical vapor deposition (MOCVD) processes for the fabrication of copper oxides. Interest has been spurred on by the applications of these materials for the vapor phase deposition of high-T_c superconducting films.[7–10] Applications of copper oxides have recently been extended to gas sensors.[11–13]

The procedure employed by us for preparing copper oxide nanorods is as follows. In a typical synthesis, 5.045 g of $CuCl_2 \cdot 2H_2O$ and 3 g of NaOH were ground for 5 min each before mixing together, 6 ml of polyethylene glycol (PEG) 400 was then added to the mixture. After 30 min of grinding, the mixture was washed in an ultrasonic bath three times with distilled water and then with EtOH to remove the PEG. Finally, the product was dried in air at 60 °C for 3 h.

X-Ray powder diffraction (XRD) was carried out on a Rigaku D_{max} γ_A X-ray diffractometer with Cu-Kα radiation (λ = 0.154178 nm). Transmission electron microscopy (TEM) micrographs were taken using a JEM-200CX transmission electron microscope, with an accelerating voltage of 200 kV.

Fig. 1 shows the XRD pattern of a sample of the copper oxide nanorods prepared by the one-step, solid-state reaction in the presence of a suitable surfactant, PEG 400. Powder XRD peaks of the copper oxide are consistent with the data of the JCPDS file.[14] The peaks at 2θ values of 32.530, 35.408, 38.728, 45.200, 48.856, 53.525, 58.627, 60.266, 67.976, 74.940 and 81.273° correspond to the crystal planes of 110, 002, 111, 112, 202, 020, 202, 113, 220(312), 004, 313 of crystalline copper oxide, respectively.

The TEM image of the copper oxide sample of Fig. 1 is shown in Fig. 2, which reveals that the copper oxide powders consist of uniform nanorods. It can be seen that the nanorods have average diameters of *ca*. 8 nm and lengths of up to 400 nm. The formation of a rod shape of copper oxide is speculated to be due to the surfactant assemblage because PEG in water can form a chain structure.[15]

In summary, a novel and facile method has been developed to synthesize copper oxide nanorods. This relatively fast reaction gives nanorods or nanometric powders with potentially broad applications in the synthesis and in the shape control of nanometric powders.

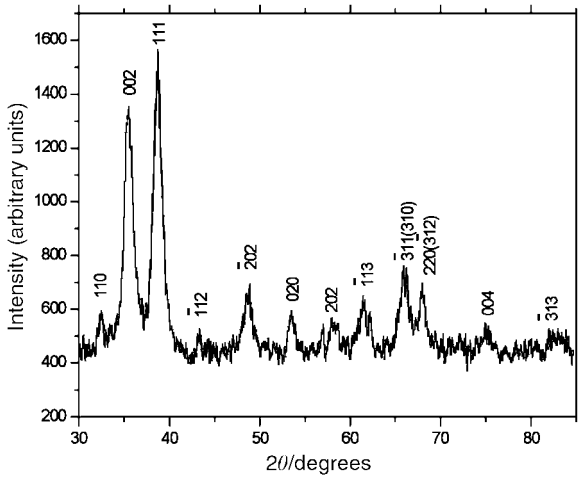

Fig. 1 XRD pattern of a copper oxide nanorod sample produced by a one-step, solid-state reaction in the presence of a suitable surfactant at room temperature.

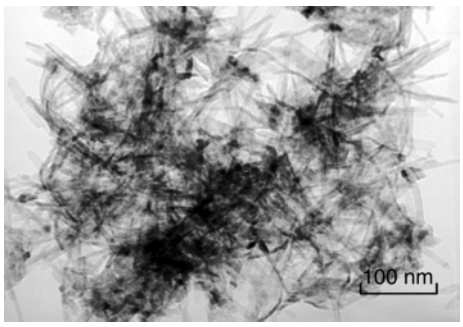

Fig. 2 TEM image of the copper oxide nanorod sample shown in Fig. 1.

This work was supported by the National Natural Science Foundation of P. R. China (No. 29890210, 10023001, 10074024).

Notes and references

1 H.-P. Lin and C.-Y. Mou, *Science*, 1996, **273**, 765.
2 H.-P. Lin, S. Cheng and C.-Y. Mou, *Chem. Mater.*, 1998, **10**, 581.
3 S. A. Davis, S. L. Burkkett, N. H. Mendeison and S. Mann, *Nature*, 1997, **385**, 420.
4 M. Zhang, Y. Bando, K. Wada and K. Kurashima, *J. Mater. Sci. Lett.*, 1999, **18**, 1911.
5 B. Cheng, W. Q. Jiang, Y. R. Zhu and Z. Y. Chen, *J. Mater. Sci. Lett.*, 2000, **19**, 503.
6 S. A. Sapp, B. B. Larshmi and C. R. Mortiu, *Adv. Mater.*, 1999, **11**, 402.

7 J. G. Bednorz and K. A. Muller, *Z. Phys., B*, 1986, **64**, 189.
8 A. D. Berry, K. D. Gaskill, R. T. Holm, E. J. Cukauskas, R. Kaplan and R. L. Henry, *Appl. Phys. Lett.*, 1988, **52**, 1743.
9 G. Malandrino, G. G. Condorelli, G. Lanza and I. L. Fragala, *J. Alloys Compd.*, 1997, **251**, 314.
10 G. Malandrino, G. G. Condorelli, G. Lanza, I. L. Fragala, U. Scottidi Uccio and M. Valentino, *J. Alloys Compd.*, 1997, **251**, 332.
11 T. Ishihara, M. Higuchi, T. Takagi, M. Ito, H. Nishiguchi and T. Takita, *J. Mater. Chem.*, 1998, **8**, 2037.
12 T. Ishihara, K. Kometani, M. Hashida and Y. Takita, *J. Electrochem. Soc.*, 1991, **138**, 173.
13 J. Tamaki, K. Shimanoe, Y. Yamada, Y. Yamamoto, N. Miura and N. Yamazoe, *Sens. Actuators B*, 1998, **49**, 121.
14 Joint Committee on Powder Diffraction Standards, *Diffraction Data File, No.5-661, JCPDS International Center for Diffraction Data*, Peensylvania, 1991.
15 J.-H. Sun, Y-J. Gong, W.-H. Fan, D. Wu and Y.-H. Sun, *Chem. J. Chin. Univ.*, 2000, **21**, 95.

Platinum(II) nicotinamide complexes as receptors for oxo-anions†

Chantelle R. Bondy,[a] Philip A. Gale*[b] and Stephen J. Loeb*[a]

[a] *School of Physical Sciences, Chemistry and Biochemistry, University of Windsor, Windsor, ON, Canada N9B 3P4. E-mail: loeb@uwindsor.ca*

[b] *Department of Chemistry, University of Southampton, Southampton, UK SO17 1BJ. E-mail: philip.gale@soton.ac.uk*

Received (in Cambridge, UK) 11th February 2001, Accepted 13th March 2001
First published as an Advance Article on the web 30th March 2001

The coordination of four *n*-butylnicotinamide ligands to a platinum(II) centre provides a facile method of organizing amide H-bond donors for anion binding; the PF_6^- complex is an effective receptor for a variety of oxo-anions.

The coordination of anionic guest species by hydrogen bond donating receptors is an area of supramolecular chemistry that continues to attract attention.[1] A large number of the anion receptors reported so far are 'built' upon organic scaffolds such as calixarenes.[2] However, the preparation of these types of receptors can often be synthetically challenging, a fact that prompted us to look for alternative means of arranging hydrogen bond donating groups. It occurred to us that some easy to prepare metal ligand complexes could be exploited as simple pieces of inorganic molecular scaffolding.[3] We initially chose to study square planar platinum(II) complexes due to their relative inertness towards ligand substitution and nicotinamide ligands due to their ease of synthesis. The homoleptic $[PtL_4]^{2+}$ complex cation is an ideal candidate to act as an anion receptor as it provides both hydrogen bond donating amides[4] and an electrostatic contribution from the metal centre. As a first test of this strategy, the complex $[Pt(L)_4]^{2+}$ (L = *n*-butylnicotinamide), **1**, has been synthesised as the PF_6^- salt and shown to act

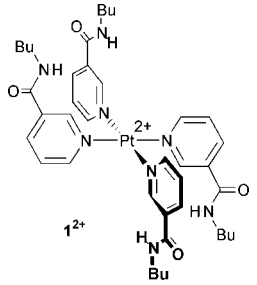

as a polydentate anion receptor both in solution and in the solid state.†

The *n*-butylnicotinamide ligand was prepared from the nicotinamide ethylester and *n*-butylamine by standard methods.[5] The Pt^{II} complex was prepared by reacting 1 equiv. of $PtCl_2(EtCN)_2$ with 4 equiv. of ligand and 2 equiv. of $AgPF_6$ in MeCN solution.[6] After filtration to remove AgCl and evaporation of the solvent, crude $\mathbf{1}[PF_6]_2$ was recrystallized from $MeCN/Et_2O$ and isolated in 87% yield.‡ The material produced in this fashion was determined to be analytically pure and subsequently used in all anion receptor studies. Recrystallization of $\mathbf{1}[PF_6]_2$ from a CH_2Cl_2/Pr^i_2O solvent mixture produced crystals of $\mathbf{1}[PF_6]_2{\cdot}2CH_2Cl_2$ suitable for an X-ray structure determination.§

Fig. 1 shows a ball and stick representation of the X-ray structure of $\mathbf{1}[PF_6]_2{\cdot}2CH_2Cl_2$. By drawing an analogy to calix[4]arene nomenclature, there are four conformations (cone, partial cone, 1,3- and 1,2-alternate) possible for **1** due to facile

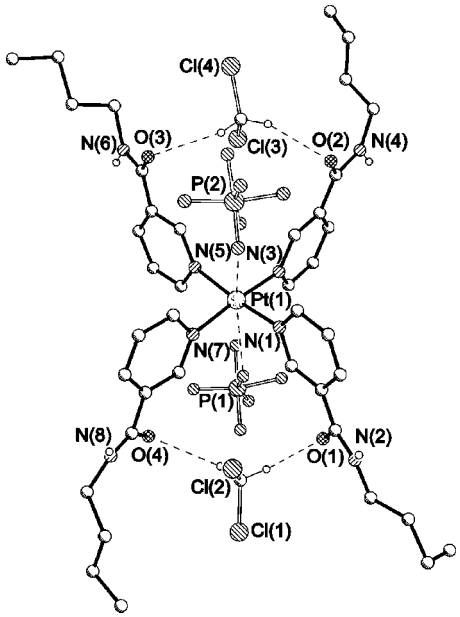

Fig. 1 X-Ray structure of $\mathbf{1}[PF_6]_2{\cdot}2CH_2Cl_2$ showing the basic numbering scheme. C–H···O distances (Å) and angles (°): H(50A)···O(4) 2.40, C(50)–H(50A)···O(4) 113; H(50B)···O(1) 2.43, C(50)–H(50B)···O(1) 118; H(60A)···O(2) 2.42, C(60)–H(60A)···O(2) 115; H(60B)···O(3) 2.47, C(60)–H(60B)···O(3) 125. Pt···F distances (Å) and angles (°): Pt(1)···F(1) 3.42, Pt(1)···F(1)–P(1) 147; Pt(1)···F(8) 3.28, Pt(1)···F(1)–P(1) 155.

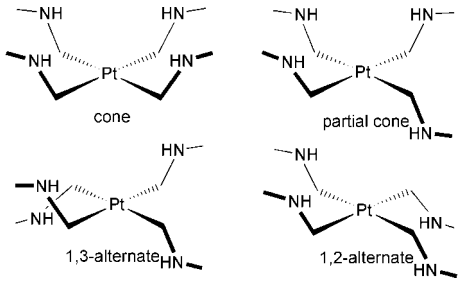

rotation about the Pt–N bonds.[7] In the solid state, the four nicotinamide ligands adopt a centrosymmetric 1,2-alternate conformation which places two amide hydrogen bonding sites in a *cis* orientation on each side of the metal square plane. Interestingly, the amide NH groups do not interact with the PF_6^- anions which are situated above and below the Pt^{II} metal centre presumably to maximize electrostatic interactions and cation–anion crystal packing. In fact, it is the amide C=O groups which are involved in hydrogen bonding to the methylene hydrogens of the CH_2Cl_2 solvent molecules. It was therefore assumed that (i) the PF_6^- anions would not be competitive for the binding of the oxo-anions used in this study[8] and (ii) a 2:1 anion:host ratio is certainly possible and may predominate.

The ability of $\mathbf{1}[PF_6]_2$ to function as a receptor for oxo-anions in solution was determined by measuring association constants, K_a, in various solvents by ^1H NMR spectroscopic titration

† Electronic supplementary information (ESI) available: titration plots for $[PtL_4][PF_6]_2$ with various oxo-anions. See: http://www.rsc.org/suppdata/cc/b1/b101440o/

DOI: 10.1039/b101440o

Table 1 Association constants, K_a, for $\mathbf{1}^{2+}$ with various oxo-anions

Anion[a]	Solvent	K_a/M^{-1}
$CF_3SO_3^-$	CD_3CN	129
ReO_4^-	CD_3CN	150
NO_3^-	CD_3CN	K_1 = 562, K_2 = 132
HSO_4^-	CD_3CN/DMSO-d_6 3:1 *v/v*	149
$CH_3CO_2^-$	CD_3CN/DMSO-d_6 3:1 *v/v*	Precipitate[b]
$H_2PO_4^-$	CD_3CN/DMSO-d_6 1:9 *v/v*	Precipitate[b]
$CH_3CO_2^-$	CD_3CN/DMSO-d_6 1:9 *v/v*	K_1 = 230, K_2 = 491

[a] Anion added as the tetrabutylammonium salt. [b] Precipitation occurred during the titration. The precipitate re-dissolved upon further addition of anions, however the titration profile could not be fitted satisfactorily (see ESI†).

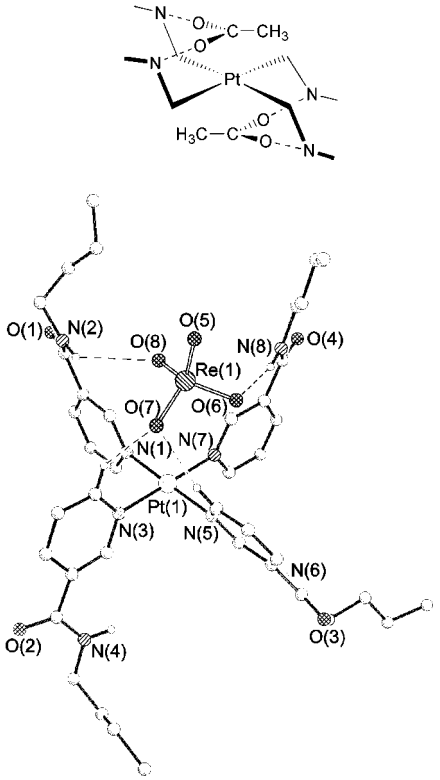

Fig. 2 X-Ray structure of the $[\mathbf{1}(ReO_4)]^+$ cation showing the basic numbering scheme. N–H···O distances (Å) and angles (°): H(2A)···O(8) 2.79, N(2)–H(2A)···O(8) 137; H(8A)···O(6) 2.13, N(8)–H(8A)···O(6) 168; H(11A)···O(7) 2.50, C(11)–H(11A)···O(7) 142; H(21A)···O(7) 2.37, C(21)–H(21A)···O(7) 171. Pt···O distances (Å) and angles (°): Pt(1)···O(6) 4.20, Pt(1)···O(6)–Re(1) 86; Pt(1)···O(7) 4.11, Pt(1)···O(7)–Re(1) 89; Pt(1)···O(8) 4.16, Pt(1)···O(8)–Re(1) 87. Pt(1)···Re(1) 4.42.

techniques. The results reported in Table 1 for $CF_3SO_3^-$, ReO_4^-, NO_3^-, HSO_4^-, $H_2PO_4^-$ and $CH_3CO_2^-$, show that receptor **1** is capable of acting as an effective host for oxo-anions. There appears a certain amount of selectivity towards planar bidentate anions such as NO_3^- and $CH_3CO_2^-$ and these are bound in a 1:2 receptor:anion ratio. This can be attributed to a shape specific match between two *cis* amido groups and a bidentate anion. In particular, the binding of acetate ion is relatively strong even in the very polar 9:1 DMSO/MeCN mixture. The fact that K_2 is greater than K_1 infers that binding of the first anion has a positive allosteric effect, which favours binding of the second.

The tetrahedral or pseudo-tetrahedral oxo-anions ReO_4^-, $CF_3SO_3^-$ and HSO_4^- are more weakly bound and solution evidence supports a simpler 1:1 receptor:anion ratio or at least a situation in which K_1 can be reliably obtained but K_2 is too small to be measurable. The 1:1 host:anion binding observed for the weakly coordinated ReO_4^-, $CF_3SO_3^-$ and HSO_4^- anions is supported by the X-ray structure§ of $\mathbf{1}[ReO_4]_2$ shown in Fig. 2. In particular, it can be seen that in order to try and maximise hydrogen bonding to a single ReO_4^- anion with 3-fold symmetry the relatively acidic nicotinamide CH's from the ligands on the opposite side of the square plane contribute to binding the anion. To do this, the complex must distort significantly from centrosymmetry, a fact that presumably disfavours the interaction with a second anion resulting in the observation of 1:1 binding in solution.

Although solubility problems and thus the need to vary solvent systems prohibited a direct comparison of all the available anions, there is sufficient evidence to suggest that this new type of anion receptor is worthy of further study. The results presented herein suggest that future re-design of this type of host might produce anion receptors with high selectivity and binding strength based on a simple inorganic scaffold.

S. J. L. thanks the Natural Science and Engineering Research Council of Canada for financial support. P. A. G. thanks the Royal Society for a University Research Fellowship and the RSC for an International Journals Grant.

Notes and references

‡ *Selected data* for $\mathbf{1}[PF_6]_2$: ^{1}H NMR (CD_3CN): δ 9.36 (s, 4H, Ar), 8.94 (d, 4H, Ar, ^2J 5.7 Hz), 8.23 (d, 4H, Ar, ^2J 8.1 Hz), 7.62 (t, 4H, Ar, ^2J 5.7 Hz, 8.1 Hz), 7.36 (s, 4H, NH), 3.36 (q, 8H, NCH_2), 1.58 (q, 8H, CH_2), 1.39 (q, 8H, CH_2), 0.94 (t, 12H, CH_3), *Determination of* association constants: in a typical run, anion portions were added to the host solution (1×10^{-2} M) in aliquots of 0.1 to 5 equiv. and 0.5 to 7 equiv. K_a values were determined using EQNMR.[9]

§ *Crystal data*: for $\mathbf{1}[PF_6]_2 \cdot 2CH_2Cl_2$: $C_{42}H_{60}Cl_4F_{12}N_8O_4P_2Pt$, M = 1367.81, monoclinic, space group *Cc*, a = 16.2726(4), b = 8.9587(2), c = 39.2903(5) Å, β = 96.253(1)°, U = 5693.7(2) Å^3, T = 293(2) K, Z = 4, μ = 2.793 mm^{-1}, 5449 independent reflections (R_{int} = 0.0159). $R1$ = 0.0310, $wR2$ = 0.0802, ($I > 2\sigma I$), $R1$ = 0.0369, $wR2$ = 0.0844, (all data), goodness-of-fit = (F^2) = 1.033. For $\mathbf{1}[ReO_4]_2$: $C_{56}H_{42}N_8O_{12}PtRe_2$, M = 1586.47, triclinic, space group $P\bar{1}$, a = 10.182(1), b = 14.618(1), c = 17.408(2) Å, α = 72.888(3), β = 88.487(3), γ = 71.773(2)°, U = 2346.0(6) Å^3, T = 293(2) K, Z = 2, μ = 8.203 mm^{-1}, 6103 independent reflections (R_{int} = 0.0719). $R1$ = 0.0698, $wR2$ = 0.1518, ($I > 2\sigma I$), $R1$ = 0.1062, $wR2$ = 0.1714, (all data), goodness-of-fit = (F^2) = 1.028. Data were collected on a Bruker SMART CCD instrument and solutions performed using the SHELXTL 5.03 Program Library, Siemens Analytical Instrument Division, Madison, WI, USA, 1997. CCDC 158329 and 158330. See http://www.rsc.org/suppdata/cc/b1/b101440o/ for crystallographic data in .cif or other electronic format.

1 P. A. Gale, *Coord. Chem. Rev.*, 2000, **199**, 181; 2001, **213**, 79; P. D. Beer and P. A. Gale, *Angew. Chem., Int. Ed.*, 2001, **40**, 486; J. L. Sessler and W. E. Allen, *Chemtech*, 1999, **29**, 16; F. P. Schmidtchen and M. Berger, *Chem. Rev.*, 1997, **97**, 1609; P. D. Beer and D. K. Smith, *Prog. Inorg. Chem.*, 1997, **46**, 1; J. L. Atwood, K. T. Holman and J. W. Steed, *Chem. Commun.*, 1996, 1401; K. Kavallieratos, S. R. de Gala, D. J. Austin and R. H. Crabtree, *J. Am. Chem. Soc.*, 1997, **119**, 2325; A. P. Davis, J. F. Gilmer and J. J. Perry, *Angew. Chem., Int. Ed. Engl.*, 1996, **35**, 1312; *Supramolecular Chemistry of Anions*, ed. A. Bianchi, K. Bowman-James and E. García-España, Wiley-VCH, New York, 1997.

2 B. R. Cameron and S. J. Loeb, *Chem. Commun.*, 1997, 573; P. D. Beer, M. G. B. Drew, C. Hazlewood, D. Hesek, J. Hodacova and S. E. Stokes, *J. Chem. Soc., Chem. Commun.*, 1993, 229; I. Stibor, D. S. M. Hafeed, P. Lhotak, J. Hodacova, J. Koca and M. Cajan, *Gazz. Chim. Ital.*, 1997, **127**, 673; N. Pelizzi, A. Casnati, A. Friggeri and R. Ungaro, *J. Chem. Soc., Perkin Trans. 2*, 1998, 1307; P. D. Beer, P. A. Gale and D. Hesek, *Tetrahedron Lett.*, 1995, **36**, 767.

3 For a recent example of this basic concept see: L. A. Uppadine, M. G. B. Drew and P. D. Beer, *Chem. Commun.*, 2001, 291.

4 S. Valiyaveettil, J. F. J. Engbersen, W. Verboom and D. N. Reinhoudt, *Angew. Chem., Int. Ed.*, 1993, **32**, 900; A. P. Bisson, V. M. Lynch, M. K. C. Monahan and E. V. Anslyn, *Angew. Chem., Int. Ed. Engl.*, 1997, **36**, 2340.

5 J. March, *Advanced Organic Chemistry, Reactions, Mechanisms and Structures*, Wiley-Interscience, New York, 1992, p. 421.

6 V. Yu. Kukushkin, A. Oskarsson and L. I. Elding, *Inorg. Synth.*, 1997, **31**, 279.

7 Variable temperature ^{1}H NMR spectra showed no evidence of the different conformations in solution. This is presumably a result of facile interconversion *via* rotation about Pt–N bonds.

8 For an example of an encapsulated PF_6^- anion see: D. A. McMorran and P. J. Steel, *Angew. Chem., Int. Ed. Engl.*, 1997, **36**, 2340.

9 M. J. Hynes, *J. Chem. Soc., Dalton Trans.*, 1993, 311.

Unprecedented formation of lactone derivatives in thiacalix[4]arene series

Pavel Lhoták,*[a] Miroslav Dudicč,[a] Ivan Stibor,[a] Hana Petříčková,[b] Jan Sýkora[b] and Jana Hodačová[c]

[a] *Department of Organic Chemistry, Institute of Chemical Technology, Technická 5, 166 28, Prague 6, Czech Republic. E-mail: lhotakp@vscht.cz*

[b] *Department of Solid State Chemistry, Institute of Chemical Technology, Technická 5, 166 28, Prague 6, Czech Republic*

[c] *Institute of Organic Chemistry and Biochemistry, Academy of Sciences of the Czech Republic, Flemingovo 2, 166 10, Prague 6, Czech Republic*

Received (in Cambridge, UK) 25th January 2001, Accepted 8th March 2001
First published as an Advance Article on the web 30th March 2001

Distal bis(carboxymethyloxy) derivatives of thiacalix[4]arene were found to undergo an unprecedented intramolecular cyclisation to yield lactone compounds 5a or 5b, the structure of lactones possessing nine-membered ring was proved by X-ray crystallography; inherent chirality of new compounds was demonstrated using separation on a chiral HPLC column.

The well-established chemistry of calix[*n*]arene family[1,2] was recently 'rejuvenated' by the discovery of so called thiacalix-[4]arenes.[3] The presence of sulfur atoms instead of methylene groups makes thiacalix[4]arenes **1a** and **1b** very interesting molecules with some novel features compared with the chemistry of 'classical' calixarenes (Scheme 1). Thus, the preparation of appropriate tetrasulfoxide[4] or tetrasulfone[4a,5] derivatives proceed very easily by direct oxidation of sulfur. Unfortunately, the employment of thiacalix[4]arenes as building blocks or molecular scaffolds in supramolecular chemistry is still rather restricted by almost unknown chemistry of these compounds and the lack of general derivatization methods. As we found recently, simple tetraalkylated products[6] exhibit interesting conformational behaviour[7] that differ to a high degree from that of 'classical' calix[4]arene derivatives. In this paper we report on another example of different chemical behaviour of thiacalix[4]arene derivatives.

During our attempts at the preparation of diamides by the reaction of acyl chlorides **4a** or **4b** with various aromatic amines we isolated substantial amounts of unknown byproduct. Surprisingly, as we found, the same type of compounds can be prepared in high yields using the reaction of **4a** or **4b** in the presence of triethylamine in tetrahydrofuran. Thus, the stirring of **4a** (prepared from **3a** by the reaction with oxalyl chloride) with 6 eq. of Et_3N in THF at rt leads to the main product **5a** in 69% yield.[8] The ^{1}H NMR spectrum of this compound (see ESI†) exhibits two singlets of Bu^t groups (0.88 and 1.40 ppm) and four doublets with characteristic meta coupling (J ~ 2.2 to 2.7 Hz) in the aromatic region. Together with two doublets possessing typical geminal coupling constants (J ~ 12 Hz) at 4.63 and 5.52 ppm it reflects C_2 symmetry of the whole molecule. This was confirmed also by ^{13}C NMR where the expected 18 signals were recognised. The above-mentioned findings can be explained by structure **5a** formed by the intramolecular reaction of acyl chloride with the neighbouring hydroxy group.

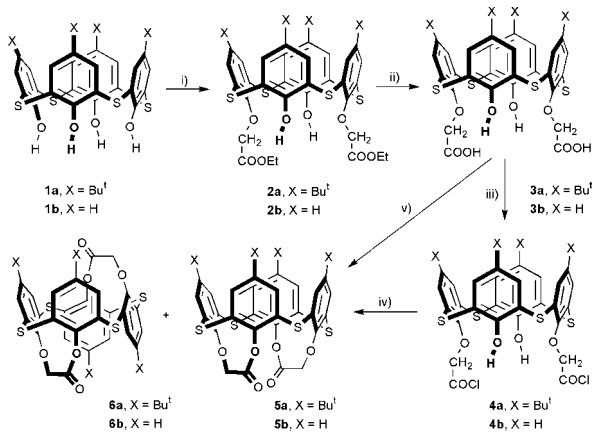

Scheme 1 i) $BrCH_2COOEt$, acetone–K_2CO_3; ii) KOH, H_2O–EtOH; iii) $(COCl)_2$, CH_2Cl_2; iv) NEt_3, CH_2Cl_2; v) P_2O_5, CH_2Cl_2.

As we found, the same product can be prepared directly from diacid **3a** by reaction with a dehydration agent. Thus heating of **3a** with acetanhydride led to **5a** in 50% yield while stirring the same acid with P_2O_5 in DCM solution gave **5a** in 66% yield, in both cases accompanied by 10% of byproduct **6a**. The splitting pattern and the number of signals in the ^{1}H NMR spectrum of **6a** is identical with that of **5a**. On the other hand, there is a dramatic change in the chemical shifts of methylene groups where corresponding protons are shifted up-field by 1.5 and 1.1 ppm respectively if compared with **5a**. This indicates a strong anisotropic shielding effect of aromatic units in good agreement with the proposed *1,2-alternate* conformation. Albeit all our attempts to grow suitable crystals for X-ray analysis have failed, molecular modelling (MOPAC) confirmed the close proximity of C–H bonds and the plane of inverted aromatic units (see ESI). Interestingly, the corresponding derivative **6b** has not been observed in similar reactions of **3b**.

Bis(carboxymethyloxy) derivatives **3a** and **3b** adopt a *cone* conformation both in the solution (proved by NMR) and in the solid state (X-ray crystallography). On the other hand, the formation of the *1,2-alternate* product **6a** requires a previous rotation of the CH_2COOH substituent through the cavity which was never observed in the chemistry of 'classical' calixarenes. As we found very recently,[9] in contrast to 'classical' calix[4]arene the propyl groups are not bulky enough to fully prevent such a rotation in the thiacalixarene series. Because the steric requirements of the carboxymethyl groups are apparently comparable or even lower than those of propyl, anticipated rotation of this group seems to be feasible.

The above described behaviour, the formation of lactones **5** or **6**, was observed only in the case of thiacalix[4]arene derivatives. The same reactions carried out with 'classical' calix[4]arene never gave similar cyclic products, probably due to the better preorganisation of thiacalixarene moiety for intramolecular cyclisation (bigger cavity).

The structure of **5a** possessing nine-membered lactone rings was unequivocally demonstrated using a single crystal X-ray diffraction[10] (suitable single crystals were obtained by slow evaporation of EtOAc–CH_2Cl_2 solution). The presence of two bridges induces the distortion of the *cone* conformation and impresses an effective C_2 symmetry to the whole structure (Fig. 1). Four sulfur atoms are placed in the corners of a lozenge with shorter (S2–S4) and longer (S1–S3) diagonals being 6.9 and 8.3 Å, respectively. Two opposite aromatic rings are tilted outwards while the other two units are almost coplanar thus closing the cavity for potential inclusion of solvent molecule. As follows

DOI: 10.1039/b100906k

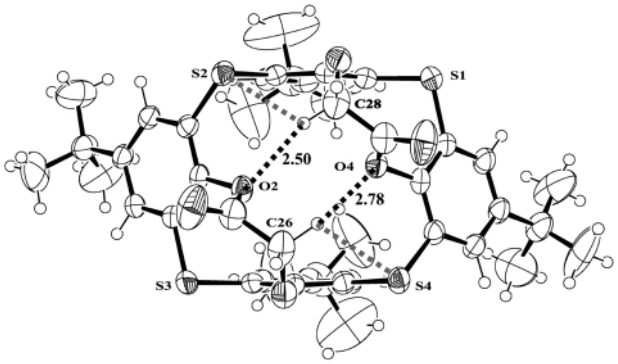

Fig. 1 X-ray structure (ORTEP drawing) of **5a** with indicated intramolecular hydrogen bonds.

from Fig. 1, the structure is supported by intramolecular hydrogen bonds (HBs) between lactone methylene hydrogens (H261, H282) and neighbour oxygen atoms O2, O4 with possible contribution of sulfur bridges S2, S4 (all distances shorter than 3 Å).

A very interesting feature of the derivative **5a** is represented by its molecular packing. The thiacalix[4]arene moieties are arranged along the *y* axis in such a way that they create an infinite network of molecules held together by the non-classical intermolecular hydrogen bonds. Every carbonyl oxygen is in a close contact with at least two hydrogen atoms of *tert*-butyl groups from a neighbouring thiacalix[4]arene unit (see ESI) with distances of 2.49 and 2.84 Å (two other hydrogens are slightly further than 3.0 Å). To the best of our knowledge such an arrangement has never been described in the calix[4]arene chemistry (Cambridge Structural Database).

Lactone **5b** also possesses very unusual crystal packing.[11] As is obvious from Fig. 2, derivative **5b** creates a kind of dimer with a net of close contacts between carbonyl oxygen and neighbour CH_2 groups of lactone functions (hydrogen bonds with the H···O=C distances 2.64–2.85 Å). These dimers are then interconnected by several additional HBs between carbonyl oxygens and aromatic hydrogens from neighbouring calixarene units (Ar–H···O=C distances ~2.70 Å). The network of molecules is held together by the intermolecular π–π interactions between the aromatic rings (upper rims) of thiacalix[4]arenes (Fig. 2). The average distance of the two coplanar rings (3.5 Å) is very similar to that in other thiacalixarene derivatives (3.41 Å) as described very recently.[14]

The inherent chirality of the new compounds was demonstrated using HPLC chromatography on a chiral column (*R*,*R*)-Wheelk-O 1, which is designed for the separation of systems possessing π–π and/or HB interactions. The column proved to be highly suitable for separating lactones **5a** and **5b**, especially because of the possibility of using chlorinated solvents which is important for the solubilization of the compounds. Thus, derivative **5b** exhibits base-line separation with retention times 24.9 and 26.5 min for appropriate enantiomers (see ESI).

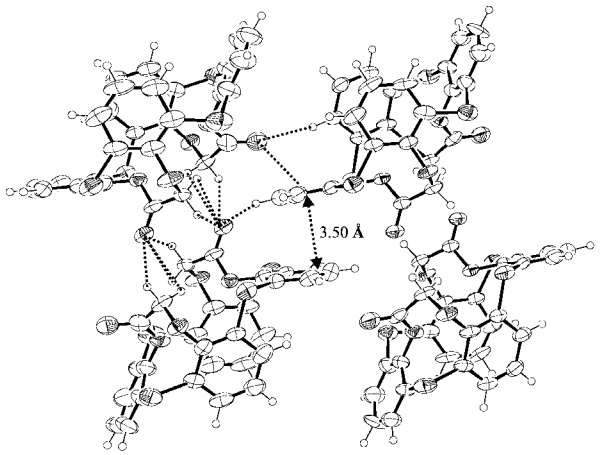

Fig. 2 Crystal packing of **5b** demonstrating intermolecular hydrogen bonding network, all indicated contacts are shorter than 3.00 Å.

In conclusion, bis(carboxymethyloxy) derivatives of thiacalix[4]arene were found to undergo an unprecedented intramolecular cyclisation to yield nine-membered lactone compounds **5a** or **5b**. The X-ray diffraction of these compounds revealed an interesting molecular packing, held together by the combination of π–π and HB interactions. The inherent chirality of the new compounds was demonstrated through separation on a chiral HPLC column.

Notes and references

† Electronic supplementary information (ESI) available: Figs. S1–S4 and experimental details. See http://www.rsc.org/suppdata/cc/b1/b100906k/

1 For books on calixarenes see: (*a*) *Calixarenes: A Versatile Class of Macrocyclic Compounds*; eds. J. Vicens and V. Böhmer, Kluwer, Dordrecht, 1991; (*b*) C. D. Gutsche, *Calixarenes Revisited: Monographs in Supramolecular Chemistry*, Vol 6., ed. J. F. Stoddart, The Royal Society of Chemistry, Cambridge, 1998.

2 For recent reviews on calixarene see: (*a*) A. Ikeda and S. Shinkai, *Chem. Rev.*, 1997, **97**, 1713; (*b*) V. Böhmer, *Angew. Chem., Int. Ed. Engl.*, 1995, **34**, 713.

3 H. Kumagai, M. Hasegawa, S. Miyanari, Y. Sugawa, Y. Sato, T. Hori, S. Ueda, H. Kamiyama and S. Miyano, *Tetrahedron Lett.*, 1997, **38**, 3971.

4 (*a*) N. Iki, H. Kumagai, N. Morohashi, K. Ejima, M. Hasegawa, S. Miyanari and S. Miyano, *Tetrahedron Lett.*, 1998, **39**, 7559; (*b*) N. Iki, F. Narumi, T. Fujimoto, N. Morohashi and S. Miyano, *J. Chem. Soc., Perkin Trans. 2*, 1998, 2745; (*c*) G. Mislin, E. Graf, M. W. Hosseini, A. DeCian and J. Fischer, *Tetrahedron Lett.*, 1999, **40**, 1129; (*d*) N. Morohashi, N. Iki, Ch. Kabuto and S. Miyano, *Tetrahedron Lett.*, 2000, **41**, 2933.

5 G. Mislin, E. Graf, M. W. Hosseini, A. DeCian and J. Fischer, *J. Chem. Soc., Chem. Commun.*, 1998, 1345.

6 P. Lhoták, M. Himl, S. Pakhomova and I. Stibor, *Tetrahedron Lett.*, 1998, **39**, 8915.

7 J. Lang, H. Dvořáková, I. Bartošová, P. Lhoták, I. Stibor and R. Hrabal, *Tetrahedron Lett.*, 1999, **40**, 373.

8 Preparation of **5a**, **5b** and **6a** see ESI†.

9 J. Lang, J. Vlach, H. Dvořáková, P. Lhoták, M. Himl, R. Hrabal and I. Stibor, *J. Chem. Soc., Perkin Trans. 2*, in press.

10 Crystallographic data for **5a**: $C_{44}H_{48}O_6S_4$: M = 801.100 g mol^{-1}, monoclinic system, space group $P2_1/c$, a = 20.044(1), b = 10.731(1), c = 20.490(1) Å, β = 102.17(1)°, Z = 4, V = 4308.2(5) Å^3, D_c = 1.2351 g cm^{-3}, μ(Cu Kα) = 2.39 mm^{-1}, crystal dimensions of 0.6 × 0.3 × 0.2 mm. Data were measured at 293 K on an Enraf–Nonius CAD4 diffractometer with graphite monochromated Cu-Kα radiation. The structure was solved by direct methods[12] and anisotropically refined by full matrix least-squares on F[13] to final R = 0.0756 and R_w = 0.0828 using 5629 independent reflections (θ_{max} = 67.94°). Lactone methylene hydrogens were found from difference Fourier maps, the other hydrogen atoms were located from expected geometry and were not refined. Psi scan was used for the absorption correction.

11 Crystallographic data for **5b**: $C_{28}H_{16}O_6S_4$, M = 576.671 g mol^{-1}, monoclinic system, space group $P2_1/c$, a = 19.670(8), b = 9.503(2), c = 28.757(3) Å, β = 103.22(2)°, Z = 8 (2 in asymmetric unit), V = 5232(2) Å^3, D_c = 1.464 g cm^{-3}, μ(Cu Ka) = 3.705 mm^{-1}, crystal dimensions of 0.5 × 0.3 × 0.2 mm. Data were measured at 293 K on an Enraf–Nonius CAD4 diffractometer with graphite monochromated Cu-Kα radiation. The structure was solved by direct methods[12] and anisotropically refined by full matrix least-squares on F[13] to final R = 0.0818 and R_w = 0.0733 using 3906 independent reflections (θ_{max} = 64,94°). Lactone methylene hydrogens were found from difference Fourier maps, the other hydrogen atoms were located from expected geometry and were not refined. Psi scan was used for the absorption correction. CCDC 157253 and 157254. See http://www.rsc.org/suppdata/cc/b1/b100906k/ for crystallographic files in .cif format.

12 A. Altomare, G. Cascarano, G. Giacovazzo, A. Guagliardi, M.C. Burla, G. Polidori and M. Camalli, (1994) SIR92, A program for automatic solution of crystal structures by direct methods. *J. Appl. Cryst.*, 1994, **27**, 435.

13 D. J. Watkin, C. K. Prout, R. J. Carruthers and P. Betteridge, 1996, CRYSTALS Issue 10, Chemical Crystallography Laboratory, Oxford, UK.

14 P. Lhoták, L. Kaplánek, I. Stibor, J. Lang, H. Dvořáková, R. Hrabal and J. Sýkora, *Tetrahedon Lett.*, 2000, **41**, 9339.

ChemComm

Tweezers hosts for intercalation of Lewis base guests: Tuning physico-chemical properties of cofacial porphyrin dimers

Julie Brettar, Jean-Paul Gisselbrecht, Maurice Gross* and Nathalie Solladié*

Laboratoire d'Electrochimie et de Chimie Physique du Corps Solide, Université Louis Pasteur et CNRS, 4 rue Blaise Pascal, 67000 Strasbourg, France. E-mail: nsolladie@chimie.u-strasbg.fr; gross@chimie.u-strasbg.fr, nsolladie@chimie.u-strasbg.fr

Received (in Cambridge, UK) 10th January 2001, Accepted 8th March 2001
First published as an Advance Article on the web 30th March 2001

The synthesis and both spectroscopic and electrochemical studies of a bis-porphyrinic tweezer are reported, as well as the insertion of Lewis base guests into the host bis-porphyrinic cavity, monitored through physico-chemical characteristics.

In natural photosynthetic systems, the energy contained in a single photon is transferred in a very short time and with minimal loss from the point where it is absorbed to where it is needed.[1]

Increased efforts have been developed towards understanding this great efficiency and many multi-porphyrinic devices have been synthesized as potential models of the natural system.[2] One possible approach for the preparation of such devices is to force the cofacial orientation of the porphyrins *via* the use of a rigid spacer.[3] With the aim of identifying an optimized spacer for the construction of photonic and electronic wires, we first focused on the study of a cofacial porphyrin dimer.[4] We now report how the insertion of a pyrazine molecule into the cavity of a Zn(II) porphyrin dimer through host–guest interactions causes an electronic coupling between the two porphyrin chromophores.

A 1,8-diethynylanthracenic spacer has been chosen for its expected ability to hold two chromophores in a cofacial orientation and for synthetic reasons as well. Indeed, the use of a Sonogashira coupling reaction between the diacetylene **1** and the iodoporphyrin **2**[5] allowed the efficient synthesis of dimer **3a** in four steps starting from commercially available compounds (Fig. 1).[6] The free-base dimer **3b** was obtained in 89% yield by demetallation of the two porphyrins under acidic conditions.[7]

UV-visible spectra of the reference porphyrins, the Zn(II) and free-base 5,10,15,20-tetra(3,5-di-*tert*-butylphenyl)porphyrins **4a**–**b**, and both dimers **3a** and **3b** were recorded in CH_2Cl_2 solutions. Only a small blue shift (2 nm for free-base compounds and 3 nm for metallated porphyrins) as well as a tiny broadening of the Soret band could be noticed from the monomer to the dimer, indicating that almost no coupling exists between the two porphyrins.

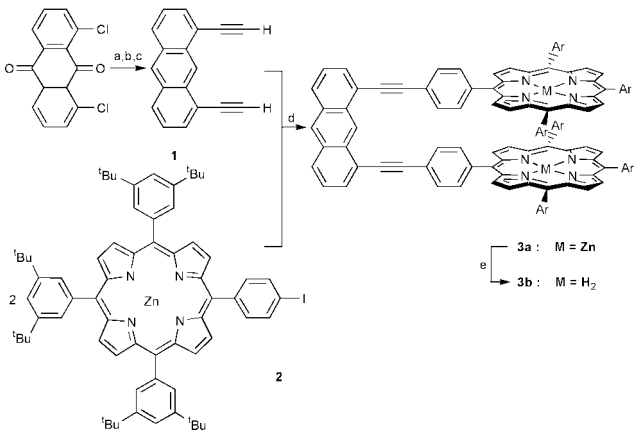

Fig. 1 (a) Zn, NH_3aq., then HCl, *i*-PrOH, 36%; (b) TMSCCMgBr, PPh_3, $Ni(acac)_2$, THF, reflux, 75%; (c)K_2CO_3, THF–CH_3OH 85:15, 61%; (d) $Pd(PPh_3)_2Cl_2$, CuI, NEt_3, 63%; (e) TFA in CH_2Cl_2, 89%. Ar = 3,5-di-*tert*-butylphenyl.

Fluorescence measurements were carried out in CH_2Cl_2 on both dimers **3a**–**b**, and also on the spacer **1** and on the reference porphyrins **4a**–**b**. Upon almost selective excitation of the anthracene moiety at 267 nm in the free-base dimer **3b**, only the fluorescence of the two porphyrins could be detected, indicating a total quenching of the emission from the anthracenic moiety. The assumption of an energy transfer from anthracene to the adjacent porphyrins was corroborated by the registration of the excitation spectrum of the dimer **3b**, which matches the absorption of the multicomponent system. A similar energy transfer from anthracene towards the adjacent chromophores was also observed upon irradiation of the Zn(II) dimer **3a** but the quantum yield was smaller and the fluorescence of the anthracenic sub-unit still remains the main deactivation pathway.

We investigated also the possible generation of host–guest complexes between the Zn(II) bis-porphyrin **3a** and small bidentate ligands bearing two nitrogen atoms.[4] Pyrazine and DABCO (1,4-diazabicyclo[2.2.2]octane) were chosen as first examples because of their fairly different p*K*a values (respectively 0.6 and 3). The coordination was monitored by ^{1}H NMR and UV-visible absorption spectroscopies in order to determine, in particular, the stoichiometry of the complexes, and the effects of such coordination on the characteristics of the porphyrin dimer.

The complexation was first studied by ^{1}H NMR (300 MHz) titration of dimer **3a** with pyrazine in $CDCl_3$. Upon addition of increasing amounts of pyrazine to a 2.10^{-3} M solution of porphyrin dimer **3a**, changes in the chemical shifts were observed up to a concentration of pyrazine equal to one equiv. of **3a** and no further changes beyond. This strongly suggests that a 1:1 complex was created between pyrazine and porphyrin dimer **3a**. Further indications on this complexation were obtained from UV-visible spectrophotometric titrations of a 2.10^{-5} M solution of dimer **3a** in CH_2Cl_2 with pyrazine (Fig. 2): such a titration of **3a** with pyrazine resulted in significant red-shift of the Soret and Q bands in the porphyrins,[8] and the titration curves obtained from absorption changes at 562 nm (Q band) exhibited a sharp saturation beyond the concentrations ratio 1:1 for pyrazine–**3a**. The titration data and the observed isosbestic points clearly indicated the existence of an equilibrium between two defined species, thus leading to the conclusion that a 1:1 complex was formed between dimer **3a** and pyrazine, with an association constant of $10^{5.6}$ M^{-1}.[9] In contrast, there was no experimental evidence of any appreciable complex formation between the reference porphyrin **4a** and pyrazine at such low concentrations by either UV-visible or ^{1}H NMR spectroscopies. These results clearly indicated that the pyrazine molecule was inserted into the cavity of the porphyrin dimer **3a**, yielding a 1:1 host–guest complex.

Titration of **3a** with DABCO and the absence of complexation between the latter and the reference porphyrin **4a** until a

DOI: 10.1039/b100423i

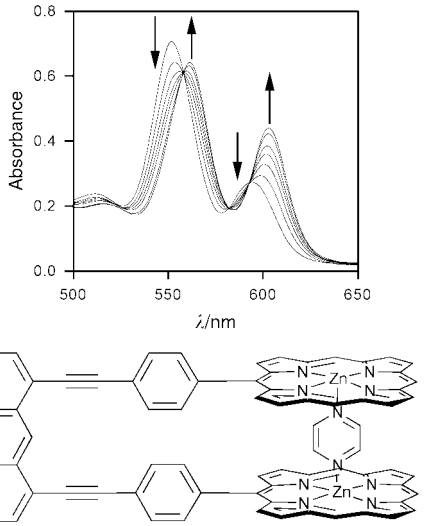

Fig. 2 UV-vis spectroscopic titration of **3a** with pyrazine in CH_2Cl_2 at rt. Spectral change of **3a** on addition of pyrazine at rt: [**3a**] $= 2.10^{-5}$ M, concentrations ratio = [pyrazine]:[**3a**] = 0; 0.2, 0.4, 0.6, 0.8, 1, 2. 3,5-Di-*tert*-butylphenyl substituents on the porphyrins have been omitted for clarity.

concentrations ratio of DABCO–**4a** = 10:1, produced similar conclusions as above with pyrazine. A 1:1 host–guest complex was created by insertion of one DABCO molecule into the cavity of each porphyrin dimer **3a**, with an association constant of 10^7 M^{-1}.[9]

Electrochemical studies were carried out on a glassy carbon working electrode in CH_2Cl_2 + 0.1 M Bu_4NPF_6. Cyclic voltammetry exhibited, for the porphyrin dimer **3a**, two reversible oxidation steps as well as a third, irreversible oxidation and three reversible reduction steps at respectively −2.30 (2e$^-$), −2.10 (1 e$^-$), −1.86 (2 e$^-$), +0.32 (2 e$^-$), +0.64 (2 e$^-$) and +0.95 V *vs.* Fc^+/Fc. Assignments of the different steps were made by comparison with the redox pattern of the building blocks, namely anthracene **1** and porphyrin **4a**, whose redox characteristics are summarised in Table 1.

Analysis of the electrochemical results revealed that the reversible one electron reduction of **3a** at −2.10 V and the irreversible oxidation at +0.95 V *vs.* Fc^+/Fc occur on the anthracene linker. The remaining four electron transfers each involve two one-electron reversible transfers occurring on the two porphyrin units. The peak shape and characteristics of the cyclic voltammograms indicated that the two porphyrins behave in **3a** as independent redox centers as expected from the large ring–ring distance (*ca.* 5.8 Å, according to molecular modelling). Such a distance makes unlikely any interaction between the two porphyrin rings.

In the presence of increasing amounts of pyrazine, the cyclic voltammograms of **3a** were modified up to a pyrazine–**3a** ratio of 1, in agreement with the UV-visible titrations. The resulting complex gave well resolved cyclic voltammograms where the first oxidation and the first reduction steps each became split into two distinct one-electron reversible steps at respectively −1.87 and −1.95 V *vs.* Fc^+/Fc and +0.28 and +0.40 V vs. Fc^+/Fc.[10] Such a behavior is characteristic of a porphyrin–porphyrin interaction. This experimental observation unambiguously indicated that it is possible to modify the electron transfer pattern of the dimer **3a** by host–guest interactions, as documented for instance in the present paper, by intercalating one pyrazine molecule into the cavity of the bis-porphyrinic tweezer **3a**. Both spectroscopic and electrochemical studies on the complexation of either pyrazine or DABCO Lewis bases by the porphyrin dimer **3a** revealed that no further spectral or voltamperogram changes occurred beyond a concentrations ratio Lewis base–**3a** = 1:1.

Table 1 Redox potentials in CH_2Cl_2 + 0.1 M Bu_4NPF_6 obtained by cyclic voltammetry on a glassy carbon working electrode. All potentials are given *vs.* ferrocene used as internal standard. Pyrazine is not electroactive in the available potential range

Species	Reduction *E* (V *vs.* Fc^+/Fc)				Oxidation *E* (V *vs.* Fc^+/Fc)		
1	−2.08 (1 e$^-$)						+0.97 (irrev.)
4a	−2.25 (1 e$^-$)		−1.85 (1 e$^-$)	+0.35 (1 e$^-$)		+0.67 (1 e$^-$)	
3a	−2.30 (2 e$^-$)	−2.10 (1 e$^-$)	−1.86 (2 e$^-$)	+0.32 (2 e$^-$)		+0.64 (2 e$^-$)	+0.96 (irrev.)
3a + **pyrazine**	−2.07 (1 e$^-$)	−1.95 (1 e$^-$)	−1.87 (1 e$^-$)	+0.28 (1 e$^-$)	+0.40 (1 e$^-$)	+0.75 (2 e$^-$)	+0.95 (irrev.)

The above results clearly indicated that each bidentate Lewis base (pyrazine and DABCO) was inserted into the cavity of the porphyrin dimer **3a**, generating a 1:1 host–guest complex. The enhanced stability observed in the complexation of the bidentate bases by the dimer **3a** (if compared with the complexation of the same bases by the reference porphryin **4a**) may be ascribed to the preorganization of the Zn(II) bis-porphyrin **3a**. The spectrometric and electrochemical results revealed that the 1:1 host–guest complex generated between **3a** and the pyrazine molecule enabled the two porphyrins to undergo an electronic coupling. Such changes in the spectroscopic and electrochemical properties of cofacial porphyrin dimers by host–guest interactions pave the way towards self-coordinated molecular systems with predictable spectral and redox characteristics. Work is in progress on this subject.

This work was supported by the CNRS.

Notes and references

1 J. Barber and B. Andersson, *Nature*, 1994, **370**, 31; W. Kühlbrandt, *Nature*, 1995, **374**, 497; G. McDermott, S. M. Prince, A. A. Freer, A. M. Hawthornthwaite-Lawless, M. Z. Papiz, R. J. Cogdell and N. W. Isaacs, *Nature*, 1995, **374**, 517; T. Pullerits and V. Sundström, *Acc. Chem. Res.*, 1996, **29**, 381.

2 R. W. Wagner, T. E. Johnson and J. S. Lindsey, *J. Am. Chem. Soc.*, 1996, **118**, 11 166 and references cited therein; D. L. Officer, A. K. Burrell and D. C. W. Reid, *J. Chem. Soc., Chem. Commun.*, 1996, 1657; M. S. Vollmer, F. Würthner, F. Effenberger, P. Emele, D. U. Meyer, T. Stümpfig, H. Port and H. C. Wolf, *Chem. Eur. J.*, 1998, **4**, 260; A. Osuka and H. Shimidzu, *Angew. Chem., Int. Ed. Engl.*, 1997, **36**, 135.

3 C. K. Chang and I. Abdalmuhdi, *J. Org. Chem.*, 1983, **48**, 5388; J. P. Fillers, K. G. Ravichandran, I. Abdalmuhdi, A. Tulinsky and C. K. Chang, *J. Am. Chem. Soc.*, 1986, **108**, 417; T. Nagata, A. Osuka and K. Maruyama, *J. Am. Chem. Soc.*, 1990, **112**, 3054; J. P. Collman, J. E. Hutchison, M. Angel Lopez, A. Tabard, R. Guilard, W. K. Seok, J. A. Ibers and M. L'Her, *J. Am. Chem. Soc.*, 1992, **114**, 9869; H. A. Staab and T. Carell, *Angew. Chem., Int. Ed. Engl.*, 1994, **33**, 1466; J. P. Collman, D. A. Tyvoll, L. Leng Chng and H. T. Fish, *J. Org. Chem.*, 1995, **60**, 1926.

4 C. A. Hunter, M. N. Meah and J. K. M. Sanders, *J. Am. Chem. Soc.*, 1990, **112**, 5773; I. P. Danks, I. O. Sutherland and C. Hong Yap, *J. Chem. Soc., Perkin Trans. 1*, 1990, 421; Y. Kuroda, K. Sugou and K. Sasaki, *J. Am. Chem. Soc.*, 2000, **122**, 7833; M. R. Johnston, M. J. Gunter and R. N. Warrener, *Chem. Commun.*, 1998, 2739; V. V. Borovkov, J. M. Lintuluoto and Y. Inoue, *Org. Lett.*, 2000, **2**, 1565; X. Huang, B. Borhan, B. H. Rickman, K. Nakanishi and N. Berova, *Chem. Eur. J.*, 2000, **6**, 216.

5 N. Solladié and M. Gross, *Tetrahedron Lett.*, 1999, **40**, 3359.

6 H. O. House, D. Koepsell and W. Jaeger, *J. Org. Chem.*, 1973, **38**, 1167; H. E. Katz, *J. Org. Chem.*, 1989, **54**, 2179.

7 R. W. Wagner, T. E. Johnson and J. S. Lindsey, *J. Am. Chem. Soc.*, 1996, **118**, 11 166.

8 C. A. Hunter and L. D. Sarson, *Angew. Chem., Int. Ed. Engl.*, 1994, **33**, 2313; C. C. Mak, N. Bampos and J. M. K. Sanders, *Angew. Chem., Int. Ed.*, 1998, **37**, 3020; N. Armaroli, F. Diederich, L. Echegoyen, T. Habicher, L. Flamigni, G. Marconi and J.-F. Nierengarten, *New J. Chem.*, 1999, 77.

9 J. R. Miller and G. D. Dorough, *J. Am. Chem. Soc.*, 1952, **74**, 3977; P. Hambright, *J. Chem. Soc., Chem. Commun.* 1967, 470; C. H. Kirksey, P. Hambright and C. B. Storm, *Inorg. Chem.*, 1969, **8**, 2141.

10 Y. Le Mest, M. L'Her and J.-Y. Saillard, *Inorg. Chim. Acta*, 1996, **248**, 181.

Enantioselective synthesis of bicyclic compounds *via* catalytic 1,4-addition-ring closing metathesis†

Robert Naasz, Leggy A. Arnold, Adriaan J. Minnaard and Ben L. Feringa*

Department of Organic and Molecular Inorganic Chemistry, Stratingh Institute, University of Groningen, Nijenborgh 4, NL-9747 AG Groningen, The Netherlands. E-mail: Feringa@chem.rug.nl; Fax: +(50)3634296

Received (in Cambridge, UK) 8th January 2001, Accepted 8th March 2001
First published as an Advance Article on the web 30th March 2001

A novel three step asymmetric annulation procedure comprises a tandem catalytic enantioselective 1,4-addition-allylic substitution, Grignard addition and ring closing metathesis (RCM) sequence to provide [6,6], [7,6], [8,6] and [6,7] bicyclic products with ee's of 93–97% in which the size of both rings can easily be varied independent of each other.

Novel routes to carbobicyclic compounds in enantiomerically pure form continue to offer a synthetic challenge since numerous products including terpenes and steroids show this structural feature. A classical example is found in the synthesis of (±)-D-homo-19-nortestosterone starting from the readily available Wieland–Miescher ketone for which an asymmetric synthesis proceeds *via* the Hajos–Parrish version of the Robinson annulation.[1,2] In the pursuit of novel catalytic asymmetric annulation strategies we focus on the construction of enantiomerically pure carbobicyclic products with various ring sizes.[3]

Since the pioneering work by the groups of Grubbs and Schrock, ring closing metathesis (RCM) has become a powerful tool for the synthesis of a variety of cyclic structures.[4] Especially for medium sized and macrocyclic ring systems, which are difficult or even impossible to make by other methods, RCM proved to be highly valuable.[5] As a result of the remarkable tolerance of the Grubbs catalyst towards various functional groups, RCM is increasingly applied in natural product synthesis.[6]

We envisioned that by making use of a combination of RCM and the copper–phosphoramidite based catalytic enantioselective 1,4-addition developed in our laboratories, a variety of enantiomerically pure bicyclic products would become readily accessible. In these bicyclic products both ring sizes can easily be varied, independent of each other. The following considerations were made: (i) cyclic enones with different ring sizes and substituents can be employed in the catalytic 1,4-addition with enantioselectivities generally exceeding 96% in the products. These products can subsequently act as templates onto which a second ring can be annulated.[7] (ii) The use of RCM for this annulation would make different ring sizes in the second ring possible.[8]

To examine the viability of this approach we synthesized 2-allyl-3-alkylcycloalkanones **2a–f** by a tandem 1,4-addition-allylic substitution reaction.[3,9]

As is shown in Scheme 1 the zinc enolate resulting from the catalytic 1,4-addition of dialkylzinc reagent to cycloalkenones in the presence of phosphoramidite ligand (*S*,*R*,*R*)-**3** (1 mol%) and $Cu(OTf)_2$ (0.5 mol%) was trapped stereo- and regioselectively by the Pd–allyl complex *in situ* generated from allyl acetate and a catalytic amount of $Pd(PPh_3)_4$, giving disubstituted cycloalkanones **2a–f** in good yields and with ee's ranging from 93 to 97% (Table 1). Furthermore a *trans–cis* ratio of 9 : 1 or higher is observed in all cases except for **2e** (entry 5).[10] In the case of **2b** and **2d** complete diastereoselectivity towards the *trans* isomer is found.

† Electronic supplementary information (ESI) available: NMR spectra and detailed explanation. See http://www.rsc.org/suppdata/cc/b1/b100283j/

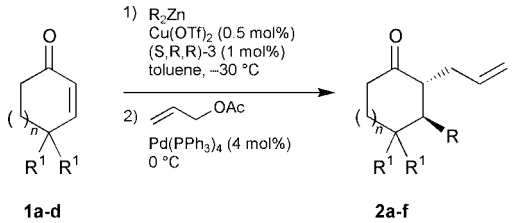

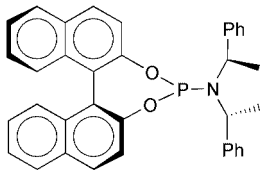

(S,R,R)-**3**

Scheme 1

Table 1 Tandem-1,4-addition-allylic substitution to cyclic enones.

Entry	Enone	*n*	R^1	R		C.y. **2** (%)[a]	ee **2** (%)[b]	*trans–cis*[c]
1	**1a**	1	H	Et	**2a**	88	96	9 : 1
2	**1b**	2	H	Et	**2b**	86	—[d]	—[e]
3	**1c**	3	H	Et	**2c**	79	97	196 : 1
4	**1d**	1	Me	Et	**2d**	82	—[d]	—[e]
5	**1a**	1	H	Me	**2e**	92	96	5.3 : 1
6	**1a**	1	H	Bu	**2f**	83	93	9 : 1

[a] Isolated yield after column chromatography. [b] Determined by chiral GC (Chiraldex G-TA). [c] Determined by GC. [d] Not determined. [e] Only *trans* detected.

By introducing a second terminal alkene moiety *via* the 1,2-addition of suitable Grignard reagents such as vinyl-, allyl- and butenylmagnesium halides to **2a–f**, the corresponding dienes **4a–h** are formed which are next converted to carbobicyclic structures **6a-h** by RCM as is shown in Scheme 2.

Table 2 summarizes the results of this new enantioselective method for the preparation of carbobicyclic structures. As expected, a reasonable selectivity was observed for the addition

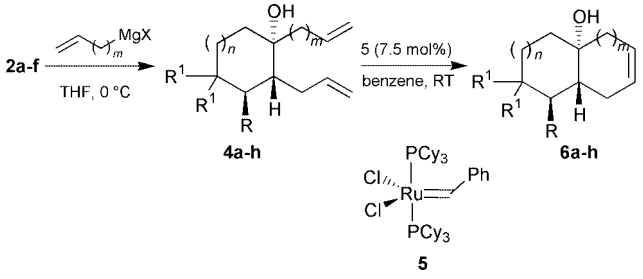

Scheme 2

DOI: 10.1039/b100283j

Table 2 Grignard addition and RCM

Entry		R	R[1]	*n*	*m*		C.y. **4**[a] (%)	ee **4**[b] (%)		Ring system	C.y. **6**[d] (%)	ee **6**[b] (%)
1	**2a**	Et	H	1	1	**4a**	92	—[c]	**6a**	[6,6]	60	96
2	**2b**	Et	H	2	1	**4b**	68[d]	96	**6b**	[7,6]	100	96
3	**2c**	Et	H	3	1	**4c**	95	97	**6c**	[8,6]	43	97
4	**2d**	Et	Me	1	1	**4d**	70	—[c]	**6d**	[6,6]	79	97
5	**2e**	Me	H	1	1	**4e**	82	—[c]	**6e**	[6,6]	46	96[e]
6	**2f**	Bu	H	1	1	**4f**	92	—[c]	**6f**	[6,6]	68	93
7	**2a**	Et	H	1	0	**4g**	64	—[c]	**6g**	[6,5]	—[f]	—
8	**2a**	Et	H	1	2	**4h**	98	—[c]	**6h**	[6,7]	65	96

[a] Isolated yield as a mixture of diastereomers. [b] Determined by chiral GC (Chiraldex G-TA). [c] Not determined. [d] Isolated yield of all-*trans* isomer after column chromatography. [e] Determined by chiral HPLC after conversion into the *p*-nitrobenzoate ester. [f] Only a small amount (< 10%) of *cis*-fused **6g** was detected by GC.

of the Grignard reagents to **2a**–**f** in all cases and the major isomer results from the attack of the Grignard reagent *trans* to the allyl group leading to the all-*trans* isomer as the major product (Scheme 2). Addition of allylmagnesium chloride (*m* = 1, entry 1) to a 90 : 10 *trans–cis* mixture of **2a** yields three out of four possible diastereomers of **4a** in a ratio of 74:16:10 as judged by GC. This result is explained as follows: addition of the Grignard reagent to the *trans* compound (2*R*,3*S*)-**2a** proceeds preferably *trans* to the allyl group but not with complete selectivity accounting for 74% (1*R*,2*R*,3*S*)-1,2-diallyl-3-ethylcyclohexanol (**4a**) and 16% (1*S*,2*R*,3*S*)-**4a**. The relative configuration of the major isomer was determined by COSY, HSQC and NOESY NMR experiments on the *p*-nitrobenzoate ester of **6a**.† Addition to the minor *cis* compound (2*S*,3*S*)-**2a** accounts for the 10% of another isomer of **4a**, most probably (1*S*,2*S*,3*S*)-**4a**.

In the case of *trans*-**2b** the ratio of *trans* and *cis* addition is 80:20 and pure *trans*-**4b** (68%) could be isolated by column chromatography. The addition to *trans*-**2c** proceeds with a moderate selectivity giving a *trans*:*cis* ratio of 63 : 37. Addition of butenylmagnesium bromide (*m* = 2) to a 9 : 1 *trans–cis* mixture of **2a** in THF at 0 °C required transmetallation to the organocerium reagent to prevent enolization and to give complete conversion to **4h** as a mixture of 3 isomers (87 : 12 : 1) with (1*R*,2*R*,3*S*)-**4h** as the major product (entry 8).[11]

All dienes **4a**–**h** readily undergo ring closure in benzene in the presence of 7.5 mol% of Grubbs catalyst **5**, except for **4g**. In the latter case formation of only a small amount of **6g** was observed (entry 7). GC analysis revealed that only the *cis* isomer of **4g** had been converted. The *trans*-fused 5,6-ring system is not formed, most probably due to the strain in such a system.[12] Formation of a six membered ring (entries 1–6) proceeded well in all cases as 100% conversion was observed, indicating that both *cis*- and *trans*-fused ring systems are readily formed. Isomerically pure *trans*-diene **4b** provided the 7,6-bicyclic product in 100% isolated yield. In all other cases the major isomer of the resulting carbobicyclic products from this annulation protocol was isolated in moderate to good yield by simple chromatographic procedures with ee's ranging from 93 to 97%. For example, (1*S*,9*R*,9a*R*)-**6a** could be isolated in 60% yield. Annulation of a seven membered ring by RCM was also successful as (1*S*,4a*R*,9a*R*)-**6h** with an ee of 96% was isolated in 65% yield (entry 8).

In conclusion, new methodology for the synthesis of enantiomerically pure carbobicyclic compounds has been developed, based on an enantioselective tandem 1,4-addition–allylic substitution, Grignard addition and RCM three step sequence. In contrast to most methodologies for asymmetric annulations, which are restricted to specific ring sizes, the method presented here gives high enantioselectivities for the construction of a variety of bicyclic structures. Products with [6,6], [7,6], [8,6] and [6,7] carbobicyclic skeletons and different alkyl substituents have been prepared with ee's ranging from 93–97%.

This work was supported by the Dutch Foundation for Scientific Research (NWO).

Notes and references

1 R. K. Boeckman, Jr., *J. Am. Chem. Soc.*, 1974, **96**, 6179; G. Stork and J. Singh, *J. Am. Chem. Soc.*, 1974, **96**, 6181.

2 Z. G. Hajos and D. R. Parrish, *J. Org. Chem.*, 1974, **39**, 1615; Z. G. Hajos and D. R. Parrish, *Org. Synth.*, 1984, **63**, 26; P. Buchsacher and A. Fürst, *Org. Synth.*, 1984, **63**, 37.

3 R. Naasz, L. A. Arnold, M. Pineschi and B. L. Feringa, *J. Am. Chem. Soc.*, 1999, **121**, 1104

4 Recent reviews on RCM: A. Fürstner, *Angew. Chem., Int. Ed.*, 2000, **39**, 3013; R. H. Grubbs and S. Chang, *Tetrahedron*, 1998, **54**, 4413.

5 For examples ranging from 5- to 19-membered rings see: A. Fürstner and L. Ackermann, *Chem. Commun.*, 1999, 95; 72-membered ring: K. Akawa, T. Eguchi and K. Kakinuma, *J. Org. Chem.*, 1998, **63**, 4741.

6 Recent examples A. Fürstner, T. Gastner and H. Weintritt, *J. Org. Chem.*, 1999, **64**, 2361; M. T. Crimmins and A. L. Choy, *J. Am. Chem. Soc.*, 1999, **121**, 5653; M. Scholl and R. H. Grubbs, *Tetrahedron Lett.*, 1999, **40**, 1425; K. C. Nicolaou, J. Y. Xu, S. Kim, J. Pfefferkorn, T. Oshima, D. Vourloumis and S. Hosokawa, *J. Am. Chem. Soc.*, 1998, **120**, 8661.

7 B. L. Feringa, *Acc. Chem. Res.*, 2000, **33**, 346; L. A. Arnold, R. Imbos, A. Mandoli, A. H. M. De Vries, R. Naasz and B. L. Feringa, *Tetrahedron*, 2000, **56**, 2865; B. L. Feringa, M. Pineschi, L. A. Arnold, R. Imbos and A. H. M. De Vries, *Angew. Chem., Int. Ed. Engl.*, 1997, **36**, 2620; A. H. M. De Vries, A. Meetsma and B. L. Feringa, *Angew. Chem., Int. Ed. Engl.*, 1996, **35**, 2374; For a recent general review on enantioselective conjugate additions: M. P. Sibi and S. Manyem, *Tetrahedron*, 2000, **56**, 8033.

8 For examples of other annulations using RCM: S. C. Cho, P. H. Dussault, A. D. Lisec, E. C. Jensen and K. W. Nickerson, *J. Chem. Soc., Perkin Trans. 1*, 1999, 193; J. S. Clark, G. P. Trevitt, D. Boyal and B. Staman, *Chem. Commun.*, 1998, 2629; S. Hölder and S. Blechert, *Synlett*, 1996, 505; A. Fürstner and K. Langemann, *J. Org. Chem.*, 1996, **61**, 8746; C. A. Tarling, A. B. Holmes, R. E. Markwell and N. D. Pearson, *J. Chem. Soc., Perkin Trans. 1*, 1999, 1695.

9 M. Kitamura, T. Miki, K. Nakano and R. Noyori, *Tetrahedron Lett.*, 1996, **37**, 5141.

10 The relative configuration of the major isomer of **2a** has previously been determined: M. Kitamura, T. Miki, K. Nakano and R. Noyori, *Bull. Chem. Soc. Jpn.*, 2000, **73**, 999.

11 For general information on the preparation and addition of organocerium componds see: N. Takeda and T. Imamoto, *Org. Synth.*, 1998, **76**, 228.

12 D. J. Holt, W. D. Bark, R. R. Jenkins, D. L. Davies, S. Garratt, J. Fawcett, D. R. Russell and S. Ghosh, *Angew. Chem., Int. Ed.*, 1998, **37**, 3298; B. Schmidt and T. Sattelkau, *Tetrahedron*, 1997, **53**, 12 991; S. J. Miller, S.-H. Kim, Z.-R. Chen and R. H. Grubbs, *J. Am. Chem. Soc.*, 1995, **117**, 2108; S. J. Miller and R. H. Grubbs, *J. Am. Chem. Soc.*, 1995, **117**, 5855.

ChemComm

Racemisation and rearrangement of 1,2-dihydro-1,3,5-triazines: a novel reversible thermal electrocyclic reaction†

Gordon Lowe,* Carolyn Carr and Rachel Quarrell

The Dyson Perrins Laboratory, Department of Chemistry, Oxford University, South Parks Road, Oxford, UK OX1 3QY. E-mail: gordon.lowe@chem.ox.ac.uk

Received (in Cambridge, UK) 7th February 2001, Accepted 8th March 2001
First published as an Advance Article on the web 30th March 2001

Chiral 1,2-diaryl-1,2-dihydro-4,6-diamino-1,3,5-triazines undergo facile racemisation by a reversible thermal electrocyclic reaction mechanism; the transient intermediate can lead, after tautomerisation, to rearranged racemic 2-aryl-1,2-dihydro-4-amino-6-anilino-1,3,5-triazines.

Cycloguanil **1a** (**1**, $R^1 = R^2 = Me$) is a potent inhibitor of *Plasmodium falciparum* dihydrofolate reductase (*pf*DHFR). It has been extensively employed (usually as the prodrug

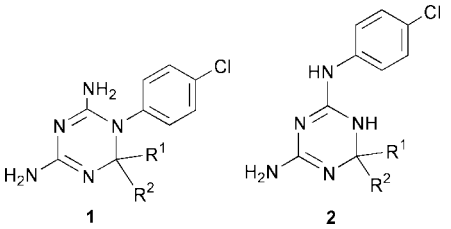

1 **2**

proguanil) alone or in combination with other drugs, as a prophylactic agent and for the treatment of malaria. As a result, malaria parasites resistant to the drug have emerged and compromised its clinical utility.[1] Analysis of DHFR sequences of several resistant *P. falciparum* isolated from different geographical origins revealed that resistance to cycloguanil is associated with point mutations in the DHFR gene.[2,3] The importance of residue 16 in *pf*DHFR for binding cycloguanil has been investigated using mutants obtained *via* a synthetic gene.[1]

Recently, a three-dimensional homology model of *pf*DHFR was constructed to aid understanding of the structural basis of antifolate resistance in malaria.[4] This study led to the hypothesis that resistance of the A16V+S108T mutant of *pf*DHFR to cycloguanil is due to a steric clash between one of the methyl groups of cycloguanil and Val-16 of the mutant *pf*DHFR, and that mutation of residue 108 (S108T) reinforces this steric constraint. Support for this hypothesis was obtained by testing both the wild-type and A16V+S108T mutant *pf*DHFRs against cycloguanil analogues devoid of one or both methyl groups.[4] By replacing one of the C2 methyl groups in cycloguanil by hydrogen and the other by an aryl group **1b** (**1**, $R^1 = H$, $R^2 = Ph$) the inhibitory activity against the A16V+S108T mutant *pf*DHFR is restored to the level obtained with cycloguanil against the wild-type *pf*DHFR.[5] Unlike cycloguanil (**1a**), these analogues (**1b**) possess a chiral centre and only one of the enantiomers is likely to have significant inhibitory activity against the A16V+S108T mutant of *pf*DHFR.

Previous attempts to resolve racemates of **1c** (**1**, $R^1 = H$, $R^2 =$ alkyl) as diastereoisomeric salts using chiral acids have failed.[6] 1,2-Dihydro-1,3,5-triazines should be capable of thermal electrocyclic ring-opening by a disrotatory pathway; there are, however, two such pathways. Steric considerations normally determine the preferred pathway[7] and since N lacks configurational stability, enantiomer **I** will ring-open by an anticlockwise rotation about the C2–N1 bond, while enantiomer **III** will open by a clockwise rotation about the C2–N1 bond leading to the sterically least-hindered common intermediate **II** (Scheme 1). Since intermediate **II** can ring close by either a clockwise or anticlockwise disrotatory pathway at C2, the product will be racemic.

The temperature at which pericyclic reactions occur is influenced by steric factors and heteroatomic substitutents.[7,8] The electrocyclic ring closure of *trans*-2, *cis*-4, *trans*-6-octatriene to *cis*-5,6-dimethyl-1,3-cyclohexa-1,3-diene occurs at 132 °C with a $t_{0.5}$ = 4.3 h.[9] 1-Aryl-1,2-dihydro-4,6-diamino-1,3,5-triazines are synthesised from aryl biguanides and a carbonyl compound in refluxing ethanol under acidic conditions.[10] Since there is no accumulation of the Schiff base intermediate it may be reasonably assumed that the ring closure is not rate determining and could occur at or close to room temperature. If the ring-opening also occurs at or close to room temperature this would provide an explanation for the failure to resolve racemates of **1c** by the crystallisation of diastereoisomeric salts.

When α- or β-cyclodextrin was added to a solution of racemic **1d** (**1**, $R^1 = H$, $R^2 = p\text{-}ClC_6H_4$), resonances of the enantiomeric dihydrotriazines were seen to separate in the 500 MHz ^1H NMR spectrum. The effect of increasing the concentration of β-cyclodextrin on the ^1H NMR spectrum of racemic **1d** is shown in Fig. 1. This demonstrates that the enantiomers have sufficient lifetime at room temperature to be observed on the NMR time-scale and therefore in principle should be resolvable. The *p*-chlorophenyl groups are expected to bind within the β-cyclodextrin cavity and it is noticeable that their chemical shifts are most sensitive to the presence of β-cyclodextrin (Fig. 1). Only at a high molar ratio (17 : 1) of β-cyclodextrin to racemic **1d** are the enantiomeric C2–H resonances resolved.

In view of the ability of β-cyclodextrin to selectively shift the resonances of the enantiomers of **1d** in the NMR spectrum, we

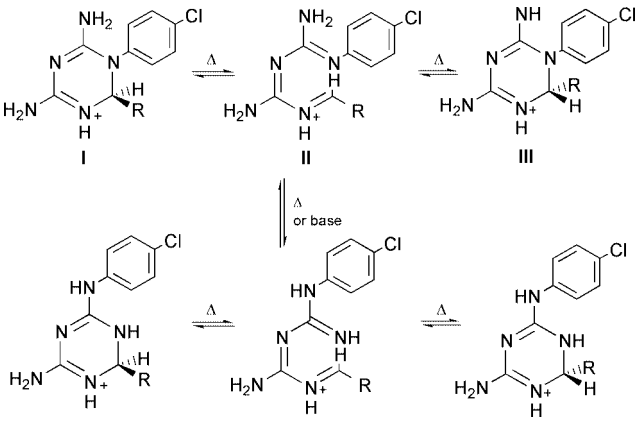

Scheme 1 Proposed mechanism for the racemisation and rearrangement of 1,2-disubstituted-1,2-dihydro-4,6-diamino-1,3,5-triazines.

† Electronic supplementary information (ESI) available: Arrhenius plot for racemisation of enantiomers of **1d**. See http://www.rsc.org/suppdata/cc/b1/b101245m/

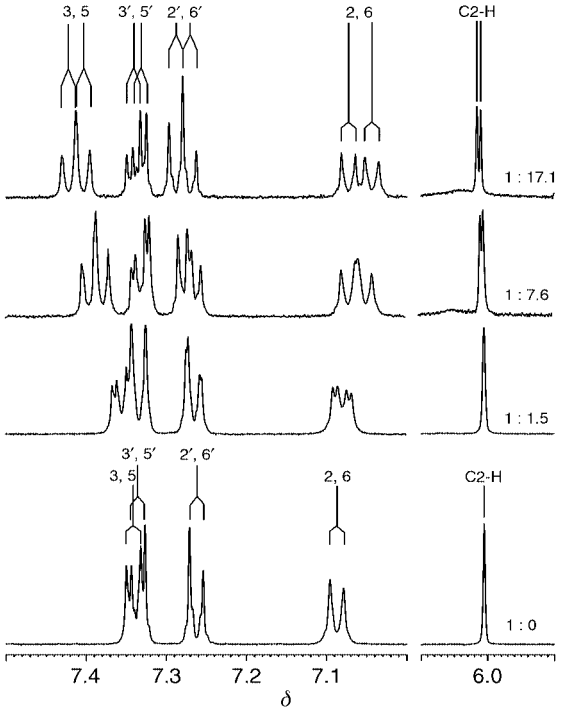

Fig. 1 ^{1}H NMR spectra of racemic **1d** hydrochloride (**1**, R^1 = H, R^2 = *p*-ClC_6H_4) in D_2O in the presence of an increasing concentration of β-cyclodextrin. The molar ratio of **1d** hydrochloride to β-cyclodextrin is shown on the right of each spectrum. 1- and 2-*p*-ClC_6H_4 substituents are designated unprimed and primed, respectively. The assignments were made by NOE experiments.

sought to separate the enantiomers of **1d** by HPLC on a column with β-cyclodextrin covalently attached to the silica support (Shodex Orpak CDBS-453; 4.6 × 150 mm). A solvent system was found[11] which would resolve the racemate and this system worked well at 10 °C. The CD spectra of the resolved enantiomers of **1d** were of similar shape but of opposite sign.

By incubating a solution of each enantiomer in a temperature controlled heating block and measuring the proportion of the two enantiomers (by HPLC on the β-cyclodextrin column) as a function of time, the rate of racemisation of the enantiomers of **1d** was determined. Racemisation of the enantiomers obeyed a first order rate law and the data were plotted using the equation $\ln x_e/(x_e - x) = 2kt$ where x is the amount of the initial enantiomer that was converted to the other enantiomer at time t, and x_e is the amount converted at equilibrium (*i.e.* $x_e = 0.5$).[12] The rate constants were determined between 40 and 60 °C at 5 °C intervals. The activation energy (E_a = 165 kJ mol^{-1}) was obtained from the slope of the Arrhenius plot (ESI†) from which the enthalpy of activation ($\Delta H^{\ddagger}$ = 162 kJ mol^{-1}) and the entropy of activation ($\Delta S^{\ddagger}$ = +176 J K^{-1} mol^{-1}) were calculated.

The relatively high enthalpy of activation is understandable since the stable 1,2-dihydro-4,6-diamino-1,3,5-triazine ring is being disrupted by breaking a single bond and forming a double bond. Moreover, the ring-opened intermediate **II** (Scheme 1) has more degrees of freedom than the cyclic 1,2-dihydro-1,3,5-triazine and hence the entropy of activation should be positive as observed. The balance of these two competing factors leads to a relatively small Gibbs function of activation and hence a fast ring-opening reaction. Thus, although it has now been possible to resolve a racemic 1,2-diaryl-1,2-dihydro-4,6-diamino-1,3,5-triazine, its half life is too short to make it worthwhile resolving these materials since as prophylactic agents they will circulate in the blood (at 37 °C) for several days.

Cycloguanil **1a** as its hydrochloride salt undergoes rearrangement to 2,2-dimethyl-4-amino-6-*p*-chloroanilino-1,2-dihydro-1,3,5-triazine **2a** (**2**, $R^1 = R^2$ = Me) on heating to its melting point (bath temperature 245 °C). As its free base in aqueous solution the rearrangement occurs at a much lower temperature (< 100 °C); the reaction is catalysed by base.[6,13] In dimethyl sulfoxide we observed rearrangement of the racemic **1d** hydrochloride (*ca.* 12 mM) at 60 °C with a half-life of *ca.* 10 days. Addition of an equimolar amount of KCl decreased the half-life to about 8 days. We propose that in dimethyl sulfoxide the chloride ion (which is essentially unsolvated in this solvent) acts as a general base and catalyses the tautomerisation of the acyclic intermediate **II** (Scheme 1). Support for this proposal was provided by the observation that addition of an equimolar amount of KF to a dimethyl sulfoxide solution of racemic **1d** hydrochloride (*ca.* 12 mM) markedly accelerates the rearrangement, the half-life at 60 °C now being about 14 min.[14] When an enantiomer of **1d** is treated under the same conditions the rearranged product **2b** (**2**, R^1 = H, R^2 = *p*-ClC_6H_4) is racemic. Thus the rearrangement and the racemisation of 1-aryl-2-substituted-1,2-dihydro-4,6-diamino-1,3,5-triazines can be envisaged as occurring by the common intermediate **II** (Scheme 1).

The reversible thermal electrocyclic reaction of 1,2-dihydro-1,3,5-triazines has not been recognised previously. Since 1,2-diaryl-1,2-dihydro-4,6-diamino-1,3,5-triazines are potent inhibitors of mutant *pf*DHFRs found in resistant strains of the malaria parasite *Plasmodium falciparum*,[5] binding to the target enzyme can be expected to perturb the enantiomer ratio in favour of the more effective inhibitor. Thus the facile reversible thermal electrocyclic reaction reported here renders unnecessary the resolution of these materials for therapeutic use.

Notes and references

1 W. Sirawaraporn, T. Sathitkul, R. Sirawaraporn, Y. Yuthavong and D. V. Santi, *Proc. Natl. Acad. Sci. USA*, 1997, **94**, 1124.
2 D. S. Peterson, W. K. Milhous and T. E. Wellems, *Proc. Natl. Acad. Sci. USA*, 1990, **87**, 3018.
3 L. K. Basco, P. H. Eldin de Pecoulas, C. M. Wilson and J. Le Bras, *Mol. Biochem. Parasitol.*, 1995, **69**, 135.
4 G. Rastelli, W. Sirawaraporn, P. Sompornpisut, T. Vilaivan, S. Kamchonwongpaisan, R. Quarrell, G. Lowe, Y. Thebtaranonth and Y. Yuthavong, *Bioorg. Med. Chem. Lett.*, 2000, **8**, 1117.
5 Y. Yuthavong, T. Vilaivan, N. Chareonsethakul, S. Kamchonwongpaisan, W. Sirawaraporn, R. Quarrell and G. Lowe, *J. Med. Chem.*, 2000, **43**, 2738.
6 H. C. Carrington, A. F. Crowther and G. J. Stacey, *J. Chem. Soc.*, 1954, 1017; T. Vilaivan, personal communication.
7 R. B. Woodward and R. Hoffmann, *The Conservation of Orbital Symmetry*, Verlag Chemie GmbH, Academic Press Inc., 1970, p. 38.
8 D. A. Evans and A. M. Golob, *J. Am. Chem. Soc.*, 1975, **97**, 4765.
9 E. N. Marvell, G. Caple and B. Schatz, *Tetrahedron Lett.*, 1965, 385.
10 E. J. Modest and P. Levine, *J. Org. Chem.*, 1956, **21**, 14.
11 Solvent system: H_2O–MeCN–buffer (10:10:80 v/v) buffer = 1 M NaCl or 1 M NH_4Cl; NH_4Cl was used to prepare samples for chiroptical measurements, and removed before these were taken.
12 K. J. Laidler, *Chemical Kinetics*, Harper & Row, New York, 1987, p. 29.
13 E. J. Modest, *J. Org. Chem.*, 1956, **21**, 1.
14 The rate is sensitive to trace amounts of water in the DMSO as is the line-width of the ^{19}F NMR signal of the fluoride ion.

Synthesis of a double-activated switchable molecule *via* ruthenium–acetylide barbituric derivatives

Jean-Luc Fillaut,* Matthew Price, Andrew L. Johnson and Johann Perruchon

Institut de Chimie de Rennes, Laboratoire 'Organométalliques et Catalyse', UMR 6509 CNRS - Université de Rennes 1, Campus de Beaulieu, 35042 Rennes, France. E-mail: jean-luc.fillaut@univ-rennes1.fr

Received (in Cambridge, UK) 19th October 2000, Accepted 8th March 2001
First published as an Advance Article on the web 30th March 2001

Ruthenium–σ-acetylide derivatives connected to barbituric acceptors through a π-conjugated bridge define a series of molecular systems presenting highly tunable properties.

Several molecular systems capable of performing elementary tasks on the molecular level have been synthesized in recent years.[1] In most cases, the molecular device obeys a binary rule; *i.e.* an input provides a positive or negative output response.[2] This ability to switch on/off a function through an external parameter (light, electron transfer, chemical reaction) defines the concept of a molecular switch. Another objective is the building of molecules which exhibit useful electronic/photonic functions that can be externally controlled.[3] With this in mind, organometallic and coordination compounds are currently the subject of considerable investigations.[4] Transition metal complexes with η^1-alkynyl ligands ($L_nMC{\equiv}CR$) attract particular interest, mostly as precursors of molecules containing a linear array of delocalized π-systems between two different functionalities.[5]

In this context, we set out to investigate metal–alkynyl donor–acceptor systems, as prototypes for molecular materials possessing switchable properties, through chemical or redox modifications. We now describe the design and synthesis of ruthenium(II)–alkynyl, connected to a barbituric acceptor, selected for its ability in stabilizing charge delocalized canonical structures through an heteroaromatic limit form, as a first example of this concept.

Knoevenagel condensation of **1**[6] (Scheme 1) with barbituric acid yields the target compound **2a** as an air-stable blue powder. Its structure was confirmed by spectrometric methods.† The UV–VIS spectra of complexes **1** and **2a**, characterized by intense ($\varepsilon \approx 1.2$–2×10^4 M^{-1} cm^{-1}) MLCTs at λ_{max} = 410 and 547 nm, respectively, in THF [Fig. 1(*a*)] proved the donor–acceptor nature of these systems.

Complex **2a** possesses three independant sites for successive protonation–deprotonation sequences (Scheme 2), which permit us to modulate the donor–acceptor coupling in **2a**, alternatively at the donor or at the acceptor head, as depicted through dramatic colour changes. The protonation on the β-carbon of transition metal acetylide complexes leading to their

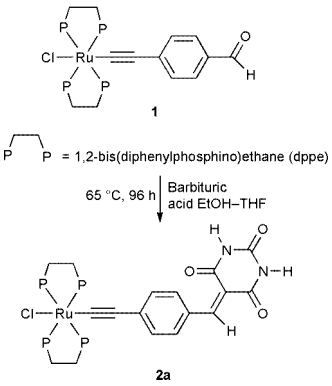

Scheme 1 Synthesis of the barbituric derivative **2a**.

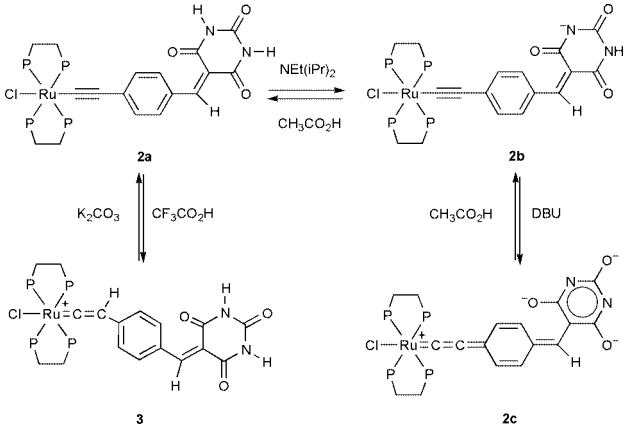

Scheme 2

corresponding vinylidene is a well-known process.[7,8] Addition of an excess of a strong acid (HCl, CF_3CO_2H) to **2a** was therefore monitored by ^{31}P NMR: a significant shift of the signal for the 4 equivalent phosphorus nuclei from 48.6 to 39.6 ppm was observed. This latter value is consistent with the formation of a *trans*-chlororuthenium–vinylidene cationic complex **3** (Scheme 2).[9] The presence of a quintuplet ($^4J_{[P,H]}$ = 3 Hz) at 3.96 ppm in the ^1H NMR spectrum of **3** is also in agreement with such a Ru=C=C*H* cationic fragment.

Simultaneously a rapid colour change from purple to red (λ_{max} = 495 nm, $\varepsilon = 1.7 \times 10^4$ M^{-1} cm^{-1}) [Fig. 1(*b*)] was observed. This reveals the weakening of the donor–acceptor electronic coupling arising from an alteration of the metal–acetylide moiety. This hypothesis was confirmed by electrochemical studies on the Ru^{2+}/Ru^{3+} redox couple. Complex **2a** presents a reversible oxidation wave in its cyclic voltammogram [Fig. 2(*a*)] at $E_{1/2}$ = 560 mV *vs.* SCE, in CH_2Cl_2,‡ assigned to the Ru(II)/(III) oxidation. The addition of a slight excess of trifluoroacetic acid to **2a** resulted in the total disappearance of the initial anodic wave, as expected for a vinylidene derivative [see Fig. 2(*a*,*b*)]. As the CV for **2a** reappears upon addition of K_2CO_3 to **3**, complete reversibility and high speed switching were observed for both the protonation (acetylide to vinylidene) and deprotonation (vinylidene to acetylide) reactions.

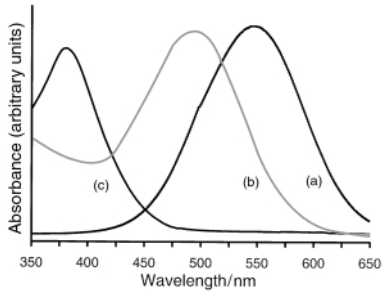

Fig. 1 Absorption spectra of **2** in THF: (*a*) pure **2a**; (*b*) after addition of 1 equiv. of CF_3CO_2H to **2a**; (*c*) after addition of 2 equiv. of DBU to **2a**.

DOI: 10.1039/b100384b

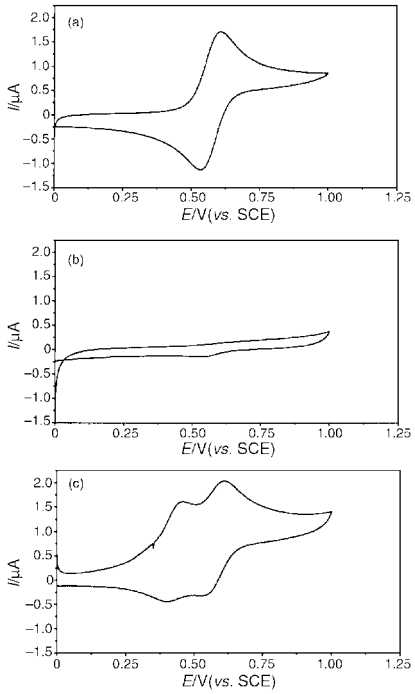

Fig. 2 Cyclic voltammograms‡ of **2a** in CH_2Cl_2, at a scan rate of 200 mV s^{-1}: (*a*) pure **2a**; (*b*) after addition of 1 equiv. of CF_3CO_2H on **2a**; (*c*) after addition of 1 equiv. of DBU on **2a** (see text).

On the other hand, the addition of a strong base (KOH, DBU (DBU = 1,8-diazabicyclo[5.4.0]undec-7-ene)), to **2a** induces an immediate colour change from purple to pale yellow (λ_{max} = 380 nm, $\varepsilon = 1.5 \times 10^4$ M^{-1} cm^{-1}) [Fig. 1(*c*)]. A minor variation of the ^{31}P NMR shift for the phosphorus ligands, from 48.6 to 49.5 ppm, is observed. This process is perfectly reversible, upon addition of a weak acid (CH_3CO_2H). Both these observations are consistent with the weakening of the acceptor strength of the barbituric moiety as a result of its deprotonation. This hypothesis was ascertained by monitoring the modifications of the Ru(II)/(III) oxidation wave of **2a**, upon sequential addition of DBU. This resulted in the growth of a new anodic wave, at a less positive potential ($E_{1/2}$ = 460 mV *vs.* SCE, in CH_2Cl_2), in accord with the formation of a more electron rich species, whereas the initial wave ($E_{1/2}$ = 560 mV *vs.* SCE) was progressively disappearing [Fig. 2(*c*): for instance, these concomitant reversible waves were observed upon addition of 1 equiv. DBU].

Two equivalents of base were necessary to afford complete conversion from the purple compound **2a** to its yellow analogue. This process was therefore monitored by ^1H NMR spectroscopy. As expected, complete disappearance of both the NH (at 8.2 and 7.9 ppm) and a significant shift of the ethylenic CH signal (from 8.5 to 8.1 ppm) at the barbituric head resulted from the addition of 2 equiv. of DBU. Addition of 1 equiv. of base gave an unclear outcome (partial disappearance and broadening of the most significant signals of **2a**). At this stage, two ^{31}P NMR signals were observed at 48.6 and 49.5 ppm, which indicated that the deprotonation process was not complete. This process was monitored, by ^1H NMR, upon addition of a large excess of the less basic *N*-ethyldiisopropylamine. The initial signals for the NH groups disappeared, but only slight variations were observed for the ethylenic proton, at 8.5 ppm, and the aromatic system, at 8.2 and 6.4 ppm. Neither colour change (UV–VIS spectra) nor electrochemical potential shift for the oxidation of **2** were observed. Finally, complete conversion from **2a** into its yellow analogue were obtained when 1 equiv. of DBU was added to the solution containing the weaker base. We assume then that a double NH deprotonation at the barbituric head[9] is necessary to induce considerable electronic changes (Scheme 2: **2b** represents one of the ketoenolic forms of the monodeprotonated species whereas **2c** is a conceivable mesomeric form of the bi-deprotonated derivative).

This second mode of switching is different from the first one which acts more specifically on the metal–acetylide moiety. The synthesis of complex **2a** has therefore proven an effective strategy for designing highly sensitive derivatives, whose properties are adjustable alternatively at the donor or at the acceptor head. On the other hand, such a switching mode could permit us to control the hydrogen binding ability of the barbituric head, either by deprotonation on this residue or by protonation on the ruthenium moiety.

This research was supported by the CNRS, the MENRT, and the Socrates-Erasmus Program (financial support to M. P. from the University of Edinburgh).

Notes and references

† *Selected values for* **2a**: ^1H NMR ($CDCl_3$, ppm) δ 8.46 (s, 1 H, =CH), 8.20 and 6.47 (dd, 4 H, *J* 8.5 Hz, aromatic), 8.03 and 7.88 (brs, 2 × 1 H, NH), 7.4–6.9 (m, 40 H, aromatic of the dppe), 2.65 (m, 8 H, CH_2); ^{31}P NMR ($CDCl_3$, ppm) δ 48.7 (s, $RuPPh_2$); $^{13}C\{^1H\}$ NMR ($CDCl_3$, 75.47 MHz, ppm) δ 163.9, 161.5 and 148.9 (C=O); 159.1 (CH), 158.6 (Ru–*C*≡C), 138.8–123.2 (C aromatics), 126.9 (Ru–C≡*C*); 110.3 (Cq. barbituric), 30.5 (CH_2, dppe); IR (CH_2Cl_2, cm^{-1}) ν 2038 (C≡C); MS (FAB) *m/z* 1172.1895 $[M]^+$, calcd. 1172.1901.

‡ The electrochemistry of **2a** was carried out at 298 K in a standard three-electrode system (platinum working/auxiliary electrode and SCE reference electrode) using a 0.1 M dm^{-3} $[Bu^n_4N][PF_6]$–CH_2Cl_2 solution as electrolyte.

1 V. Balzani, M. Gomez-Lopez and J. F. Stoddart, *Acc. Chem. Res.*, 1998, **31**, 405; A. Credi, M. Montaldi, V. Balzani, S. J. Langford, F. M. Raymo and J. F. Stoddart, *New J. Chem.*, 1998, 1061; J.-P. Sauvage, *Acc. Chem. Res.*, 1998, **31**, 611. For examples of multimode switching, see: L. Gobbi, P. Seiler and F. Diederich, *Angew. Chem., Int. Ed.*, 1999, **38**, 674; J. Achatz, C. Fischer, J. Salbeck and J. Danb, *J. Chem. Soc., Chem. Commun.*, 1991, 504.

2 J.-M. Lehn, *Supramolecular Chemistry, Concepts and Perspectives*, VCH, Weinheim, 1995.

3 T. Gunnlaugsson, D. A. MacDonail and D. Parker, *Chem. Commun.*, 2000, 93.

4 L. Fabbrizi, M. Licchelli and P. Pallavicini, *Acc. Chem. Res.*, 199, **32**, 846.

5 P. F. H. Schwab, M. D. Levin and J. Michl, *Chem. Rev.*, 1999, **99**, 1863; S. Le Stang, F. Paul and C. Lapinte, *Organometallics*, 2000, **19**, 1035; J. Gil-Rubio, M. Laubender and H. Werner, *Organometallics*, 2000, **19**, 1365.

6 D. Touchard, A. Daridor and P. H. Dixneuf, unpublished results: **1** was synthesized from ethynylbenzaldehyde[8] following a general procedure previously described[9] with specific modifications.

7 D. Touchard, P. Haquette, S. Guesmi, L. Le Pichon, A. Daridor, L. Toupet and P. H. Dixneuf, *Organometallics*, 1997, **16**, 3640.

8 C. Bianchini, P. Innocenti, A. Meli, M. Perruzini and F. Zanobini, *Organometallics*, 1990, **9**, 2514.

9 S. Aoki, M. Shiro, T. Koika and E. Kimura, *J. Am. Chem. Soc.*, 2000, **122**, 576.

Synthesis of organometallic dendrimers by ligand exchange reactions: reversible bonding of dendrons to a core in transition metal acetylide dendrimers

Kiyotaka Onitsuka, Asako Iuchi, Masanori Fujimoto and Shigetoshi Takahashi*

The Institute of Scientific and Industrial Research, Osaka University, 8-1 Mihogaoka, Ibaraki, Osaka 567-0047, Japan. E-mail: takahashi@sanken.osaka-u.ac.jp

Received (in Cambridge, UK) 19th February 2001, Accepted 9th March 2001
First published as an Advance Article on the web 30th March 2001

Ligand exchange reactions of chloride ligands on a trinuclear palladium acetylide core with platinum acetylide dendrons having a 4-pyridyl group at a focal point result in the quantitative formation of novel organometallic dendrimers, which easily revert to the core and the dendrons by treatment with Bu_4NCl.

Dendrimers are three-dimensional macromolecules with regularly hyperbranched structures, and have a wide range of potential applicable to the development of new materials.[1] In recent years, attention has shifted towards dendritic molecules containing metal centers since they exhibit characteristic properties such as redox behavior and catalysis.[2] Previously we have synthesized novel organometallic dendrimers composed of platinum acetylide units.[3,4] On the other hand, configurational and constitutional changes in a dendritic molecule responding to simple external stimuli are of interest for the practical application of dendrimers.[5,6] Thus, we engaged in the construction of organometallic dendrimers containing switchable metal components by adopting coordination bonds. Herein we report the syntheses of novel organometallic dendrimers in which platinum–acetylide dendrons are reversibly bonded to a palladium acetylide core.

It is well known that halide ligands on transition metal atoms are reversibly substituted for neutral ligands such as phosphine and pyridine. We have therefore designed platinum–acetylide dendrons having a 4-pyridyl group at a focal point and have achieved successful preparation by a convergent method as shown in Scheme 1. Reaction of the platinum acetylide complex **1** with 1,3,5-triethynylbenzene derivative **2**, which has two terminal acetylenes and one pyridylethynyl group, in the presence of a Cu(I) catalyst gave the first generation dendron **GD1** in 74% yield. Similar reactions of diplatinum **3** and hexaplatinum complexes **5**, which were prepared as reported previously,[4] with **4** gave second and third generation dendrons **GD2** and **GD3** in 60 and 44% yield, respectively (Scheme 2). Trace analysis on these reactions by GPC showed that sharp peaks due to **GD2** with a higher molecular weight relative to those of **3** and **4** grew with consumption of the substrates. Purification by column chromatography on alumina followed by reprecipitation from CH_2Cl_2–hexane gave a single product which was confirmed by GPC analysis. Although no molecular ion peaks of these dendrons except for **GD1** were detected in the mass spectrum, full characterization was performed by means of NMR spectral analyses. For example, the ^{31}P NMR spectrum of **GD3** exhibited two singlet signals at δ 11.0 and 10.8 in a 4 : 3 integral ratio. The former was assignable to the phosphine on the platinum atoms bound to the *p*-methoxyphenylethynyl groups on the surface of the dendron, whereas the latter was due to the phosphines on inner platinum atoms. In the ^1H NMR spectrum, a sharp signal due to methoxy protons appeared at δ 3.78 with twelve-fold intensity of those of the signals due to α- and β-protons of pyridyl groups at the focal point.

We then examined the synthesis of dendrimers by the ligand exchange reaction of the trinuclear platinum–acetylide complex

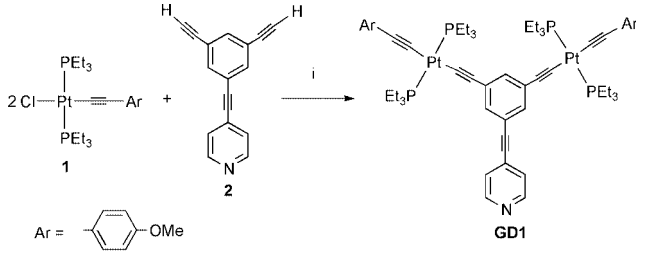

Scheme 1 *Reagents and conditions*: i, Cu(I) cat., Et_2NH, room temp., 1 d, 74%.

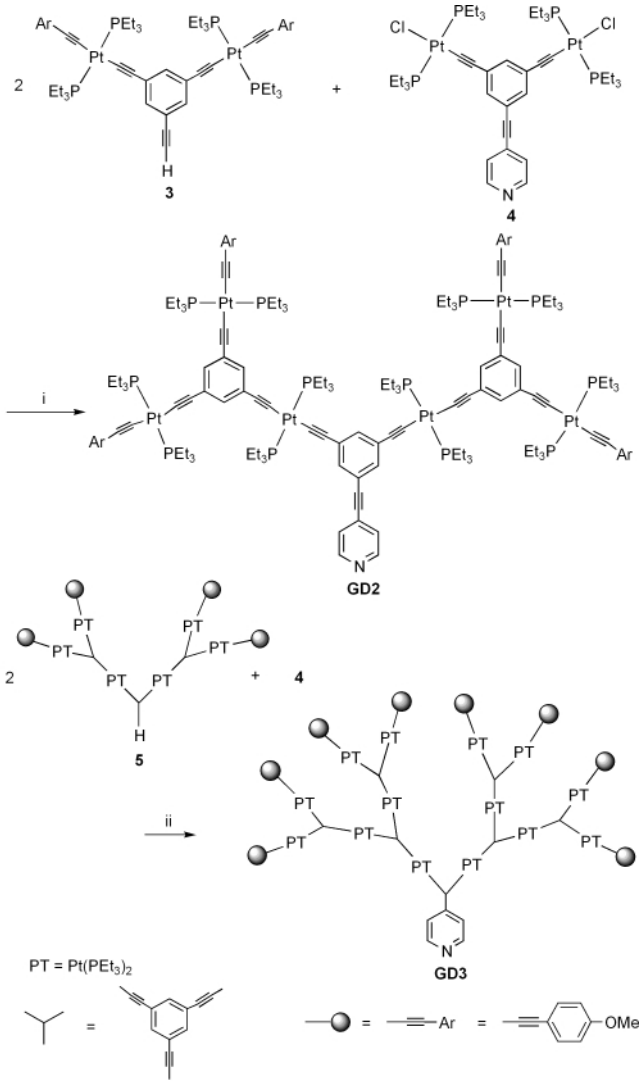

Scheme 2 *Reagents and conditions*: i, Cu(I) cat., Et_2NH, room temp., 3 h, 60%; ii, Cu(I) cat., Et_2NH, room temp., 3 h, 44%.

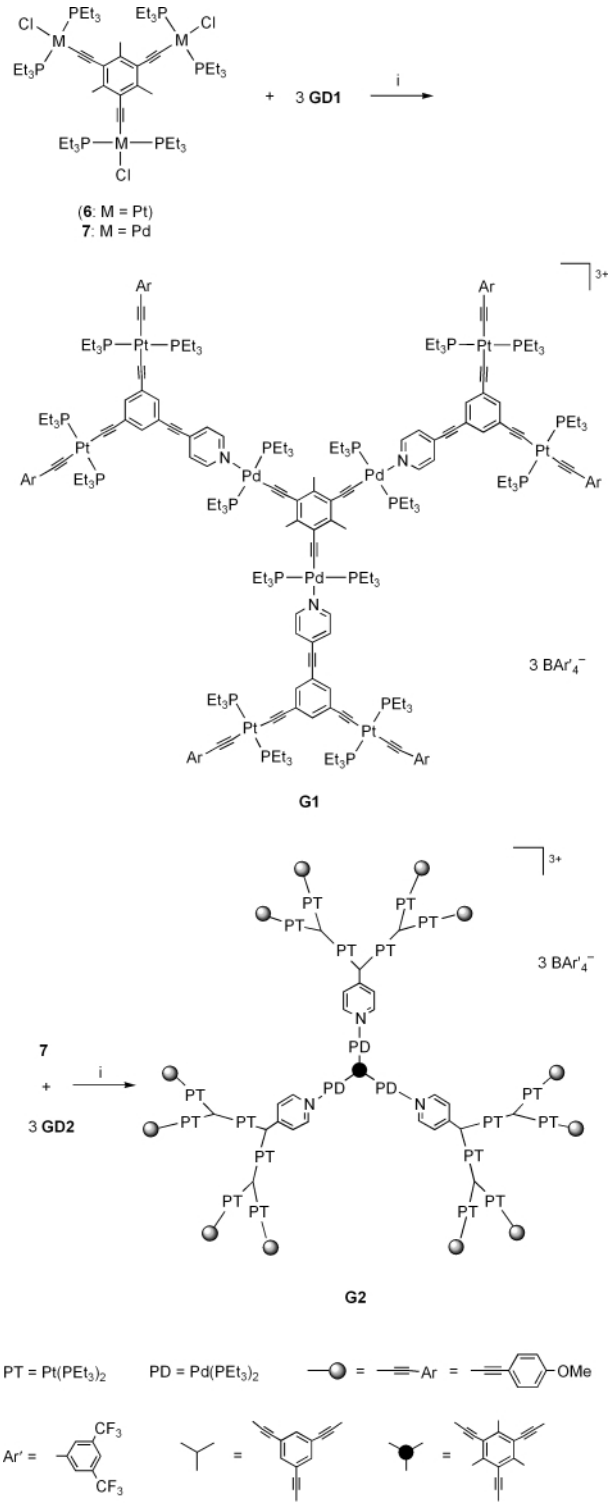

Scheme 3 *Reagents and conditions*: i, 3.3 $NaBAr'_4$, benzene, room temp., 30 min, quantitative yields.

6 with dendrons.[7] Although chloride ligands on complex **6** are easily replaced with pyridine in the presence of KPF_6, the reaction of complex **6** with **GD1** allowed only partial ligand exchange to give a mixture of the desired dendrimer and other complexes having one or two **GD1** in the molecule. Therefore, the core was changed to a palladium–acetylide complex **7** and it was found that the treatment with **GD1** in the presence of $NaBAr'_4$ (Ar′ = 3,5-$(CF_3)_2C_6H_3$) resulted in complete ligand exchange and produced the first generation dendrimer **G1** in a quantitative yield (Scheme 3). Similarly, the second generation dendrimer **G2** was also prepared by the reaction of **7** with **GD2** in quantitative yield. However, no exchange of chloride ligand with **GD3** took place and third generation dendrimer **G3** did not form at all. The difference in reactivity between **GD2** and **GD3** may arise from the steric effect of **GD3**.

The absence of structural defects in dendrimers **G1** and **G2** was confirmed by spectral analysis. A singlet signal assignable to PEt_3 on palladium was observed at δ 32.2 in the ^{31}P NMR spectrum of **G2** while the spectrum of **7** showed a signal at δ 32.7. The ^1H NMR spectrum of **G2** exhibited a sharp singlet at δ 2.87 due to the methyl protons of the central mesitylene moiety while the methyl signal of **7** was observed at δ 3.14. In the ^1H NMR spectrum of **G2** the integral ratio of the central methyl signal relative to that of the methoxy protons situated at the surface was 1 : 4. These data clearly suggest that all chloride ligands on palladium were replaced with the pyridyl groups of **GD2**, and are consistent with the structure of **G2**.

Treatment of dendrimer **G1** with excess Bu_4NCl in benzene led to the quantitative formation of core **7** and dendron **GD1** (Scheme 4). Similar treatment of dendrimer **G2** regenerated **7** and **GD2** in quantitative yield. These results suggest that the bonding of dendrons **GD1** and **GD2** to core **7** can be reversibly controlled by the ligand exchange reaction. Quantitative formation of **G1** and dissociation into **7** and **GD1** were repeated up to three times by successive treatment of $NaBAr'_4$ and Bu_4NCl, respectively. These results show the first examples of morphology control in dendrimers by chemical stimuli other than light.[6]

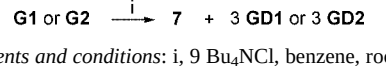

Scheme 4 *Reagents and conditions*: i, 9 Bu_4NCl, benzene, room temp., 30 min, quantitative yields.

This work was supported by Grant-in-Aid for Scientific Research on Priority Areas, (No. 11136224 'Metal-assembled Complexes') from the Ministry of Education, Science, Sports and Culture. We thank The Material Analysis Center, ISIR, Osaka University, for support of spectroscopic and elemental analyses.

Notes and references

1 D. A. Tomalia, A. M. Naylor and W. G. A. Goddard III, *Angew. Chem., Int. Ed. Engl.*, 1990, **29**, 138; J. Issberner, R. Moors and F. Vögtle, *Angew. Chem., Int. Ed. Engl.*, 1994, **33**, 2413; A. W. Bosman, H. M. Janssen and E. W. Meijer, *Chem. Rev*., 1999, **99**, 1665; A. Adronov and J. M. J. Fréchet, *Chem. Commun.*, 2000, 1701.

2 M. A. Hearshaw and J. R. Moss, *Chem. Commun.*, 1999, 1; I. Cuadrado, M. Morán, C. M. Casado, B. Alonso and J. Losada, *Coord. Chem. Rev.*, 1999, **193–195**, 395; G. R. Newkome, E. He and C. N. Moorefield, *Chem. Rev.*, 1999, **99**, 1689.

3 N. Ohshiro, F. Takei, K. Onitsuka and S. Takahashi, *Chem. Lett.*, 1996, 871; N. Ohshiro, F. Takei, K. Onitsuka and S. Takahashi, *J. Organomet. Chem.*, 1998, **569**, 195.

4 K. Onitsuka, M. Fujimoto, N. Ohshiro and S. Takahashi, *Angew. Chem., Int. Ed.*, 1999, **38**, 689.

5 A. Archut, G. C. Azzellini, V. Balzani, L. De Cola and F. Vögtle, *J. Am. Chem. Soc.*, 1998, **120**, 12187.

6 M. Smet, L.-X. Liao, W. Dehaen and D. V. McGrath, *Org. Lett.*, 2000, **2**, 511; Y. Takaguchi, S. Suzuki, T. Mori, J. Motoyoshiya and H. Aoyama, *Bull. Chem. Soc. Jpn.*, 2000, **73**, 1857.

7 K. Onitsuka, H. Ogawa, T. Joh and S. Takahashi, *Chem. Lett.*, 1988, 1855.

Self-discrimination of the racemic ligands in the self-assembly of $[\{(dppp)Pt(L)\}_2]^{4+}$

Tae Woo Kim,[a] Myoung Soo Lah[b] and Jong-In Hong*[a]

[a] *School of Chemistry and Molecular Engineering, Seoul National University, Seoul 151-747, Korea. E-mail: jihong@plaza.snu.ac.kr*

[b] *Department of Chemistry, College of Science, Hanyang University, Ansan, Kyunggi-Do 425-791, Korea*

Received (in Cambridge, UK) 8th January 2001, Accepted 12th March 2001
First published as an Advance Article on the web 30th March 2001

Self-assembly of the racemic ligands, (*R*)- and (*S*)-1,1′-binaphthyl bis(isonicotinate) and Pt^{II} shows that the (*S*)-ligand stereospecifically recognises the (*R*)-ligand to give rise to an achiral heterodimeric complex.

Recently much progress has been achieved on the metal-assisted self-assembly of independent ligands.[1] A supramolecular assembly is manufactured from the information embedded in each preprogrammed molecular component.[2] The information stored in the rigid and chiral ligand systems can be used in the selective recognition of their partners in order to produce highly ordered supramolecular complexes from ligand mixtures in solution. In principle, the simplest situation arises from racemic ligands in which two extreme cases are possible. One is called ligand self-recognition, where each enantiomeric ligand selectively recognises itself to give a homochiral complex,[3] and the other is known as ligand self-discrimination, in which one enantiopure ligand specifically perceives its enantiomer to generate an achiral complex. There have been several examples of self-recognition of achiral and chiral ligands.[3,4] However, there exist few reports of ligand self-discrimination in which two different ligands form a heterodimeric complex.[5] Herein we report a system that exhibits ligand self-discrimination in which the complex of racemic ligands with metal ions produces only an achiral 2:2 complex.

The design of the ligand L (Fig. 1) satisfies three requirements needed for ligand self-discrimination: restricted rotational degrees of freedom, a divergent array of two pyridyl groups for preclusion of intramolecular ligation of a single metal, and ligand chirality. These requirements are fulfilled by the incorporation of chiral 1,1′-binaphthol into the ligand backbone. Both the racemic ligand (^{rac}L) and the enantiomerically pure ligands (^{S}L, ^{R}L) are readily prepared by ester condensation of the appropriate 1,1′-binaphthol and the acid chloride of isonicotinic acid. An equimolar mixture of $(dppp)M(OTf)_2$ (M = Pd^{II}, Pt^{II}) and L (^{S}L, ^{R}L, ^{rac}L) in acetone-d_6 was tested for the ligand chirality-induced self-discrimination process.†

^{1}H NMR titration spectra of ^{rac}L with $(dppp)Pd(OTf)_2$ in acetone-d_6 show a highly symmetric single set of signals at a 2:2 metal:ligand ratio. Addition of more $(dppp)Pd(OTf)_2$ to this 2:2 complex does not result in the generation of any new sets of signals, indicating the formation of a single metal complex. In contrast, ^{1}H NMR titrations of ^{S}L with $(dppp)Pd(OTf)_2$ show complicated sets of resonances. The differences between ^{1}H NMR titrations of ^{rac}L and ^{S}L, respectively, with $(dppp)Pd(OTf)_2$ imply that ^{S}L prefers to form an achiral, heterodimeric complex exclusively with ^{R}L, [(eqn. (1)] rather than a homochiral complex [eqn. (2)]. Interestingly, ^{1}H NMR titrations of L (^{rac}L or ^{S}L) with $(dppp)Pt(OTf)_2$ in acetone-d_6 do not produce any distinction between ^{rac}L and ^{S}L. It is reported that the Pt^{II} complex has the same coordination geometry as the Pd^{II} complex but the former cannot rapidly reach thermodynamic equilibrium at ambient temperature compared with the latter.[6] In fact, heating an equimolar mixture of ligand and $(dppp)Pt(OTf)_2$ results in the generation of a similar ^{1}H NMR pattern to that of the Pd^{II} complex. The single set of ^{1}H NMR resonances of the racemic complex compared with those of the enantiopure complex indicates that this system is an example of self-discrimination of the racemic ligands: ^{S}L stereospecifically recognises its counterpart, ^{R}L (Fig. 2).

$$^{S}L + {}^{R}L \xrightarrow{2\ (dppp)M^{2+}} [\{(dppp)M^{S}L\}\{(dppp)M^{R}L\}] \quad (1)$$

$$^{S}L \xrightarrow{(dppp)M^{2+}} [\{(dppp)M^{S}L\}_2]^{4+} + [\{(dppp)M^{S}L\}_3]^{6+} + \cdots \quad (2)$$

Careful interpretation of the HH-COSY of the achiral heterodimeric complex, $[\{(dppp)Pd\}_2(^{S}L)(^{R}L)]^{4+}$ reveals that

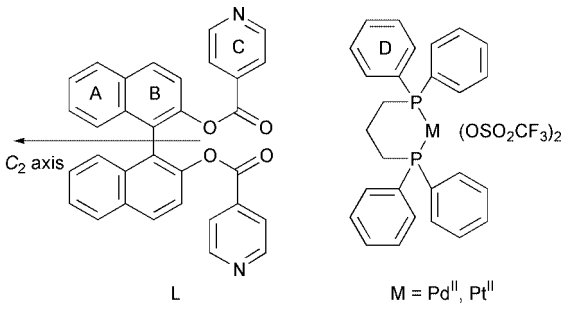

Fig. 1 Nomenclature of the ligands and metal complexes used in this work.

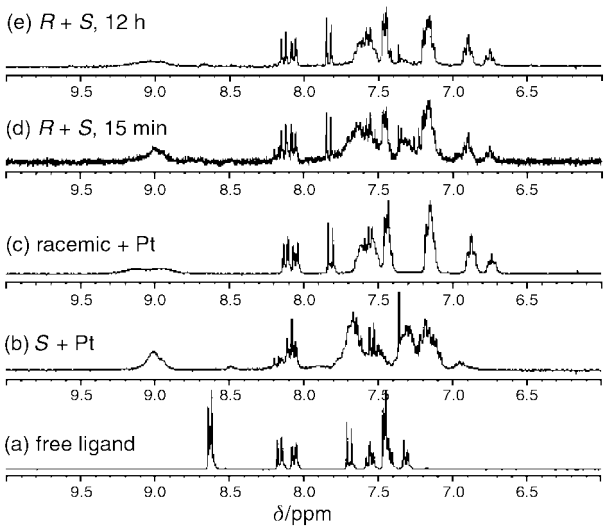

Fig. 2 Partial ^{1}H NMR spectra (300 MHz, acetone-d_6, aromatic protons) of (a) ligand L, (b) the complex of equimolar amounts of Pt^{II} and ^{S}L, (c) the complex of equimolar amounts of Pt^{II} and ^{rac}L. Monitoring of the reorganization of an equimolar mixture of 1:1 $Pt^{II}/^{S}$L and 1:1 $Pt^{II}/^{R}$L complexes (d) after 15 min and (e) after 12 h at 25 °C.

the signals for the four identical phenyl units of free dppp are split into two different sets. L has no symmetry plane due to its C_2 dissymmetry induced by 1,1′-binaphthol. Incorporation of the dissymmetric ^{S}L and ^{R}L into $[\{(dppp)Pd\}_2(^S L)(^R L)]^{4+}$ should break one symmetry plane of dppp which includes two P atoms and bisects two adjacent phenyl rings. This intriguing phenomenon constitutes strong evidence for the formation of $[\{(dppp)Pd\}_2(^S L)(^R L)]^{4+}$ in solution. In fact, the solubility of the enantiopure complex is different from that of the racemic complex: the enantiopure complex generally shows enhanced solubility in various solvent systems. In acetone solution, measurements of molecular weight by vapor pressure osmometry (VPO)[7] give M^N (number averaged molecular weight) = 4000 g mol^{-1} for an equimolar complex of ^{S}L and (dppp)Pd(OTf)$_2$, and M^N = 3400 g mol^{-1} for an equimolar complex of ^{S}L and (dppp)Pt(OTf)$_2$.‡ Calculated molecular weights of the 2:2 complex are 2627 and 2804 g mol^{-1} for $[\{(dppp)Pd\}_2(^S L)_2](OTf)_4$ and $[\{(dppp)Pt\}_2(^S L)_2](OTf)_4$, respectively. Thus, VPO measurements show that the formation of homodimeric structures is excluded in the enantiopure case.

The crystal structure of an equimolar complex of (dppp)Pt(OTf)$_2$ with ^{rac}L supports the interpretation of the solution behavior of the complex.§ As expected from the ^{1}H NMR titrations, the racemic ligands generate a heterodimeric species, $[\{dppp)Pt\}_2(^S L)(^R L)]$ (Fig. 3). A crystal structure shows two crystallographically independent but chemically identical complexes in the unit cell. Both of them have crystallographic inversion centers with a C_{2h} point group. There are many existing reports on the formation of planar rectangular boxes by metal-assisted self-assembly.[8] However, this complex has a particularly interesting structural variation from its predecessors. It forms a folded rectangular box: the two planes, N(2)–Pt(1)–N(1) and N(2A)–Pt(1A)–N(1A) are separated on the different spaces, making two steps of stairs. A rectangular cavity (6.8 × 7.2 Å) is in the center of the complex. Two triflate anions, captured in the center of the cavity, are in extensive van der Waals contact with the pyridyl groups of the ligand and are also in van der Waals contact with each other (F2A–F2A: 2.79, 2.91 Å). The remaining two triflate counter anions are in short contact with Pt(II) metal ions *via* an oxygen atom.

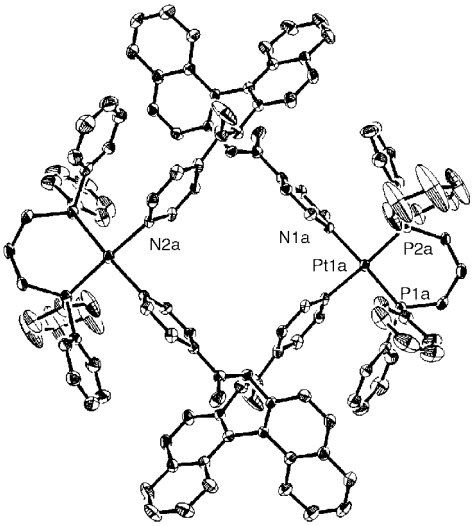

Fig. 3 An ORTEP representation of the structure of $[\{(dppp)Pt\}_2(^S L)(^R L)]^{4+}$ perpendicular to the Pt–Pt vector (30% probability thermal ellipsoids). Selected average distances (Å) and angles (°): Pt–P 2.260, Pt–N 2.098; P–Pt–P 90.76, N–Pt–N 85.14, *cis* P–Pt–N 92.02, *trans* P–Pt–N 176.61. (Because of two independent but chemically identical complexes in the unit cell, average values are reported.)

It turns out that the racemic ligands combine to generate an achiral 2:2 complex with Pd^{II} or Pt^{II}, whereas the enantiopure ligands are not assembled into an entropically favorable homodimer, presumably due to the unfavorable strain energy involved in the formation of a homodimer. The destabilization of the homochiral dimer will be reduced by reorganization to less strained oligomeric complexes. In order to identify the reorganisation behavior of the homochiral complex, the ^{1}H NMR signal changes of a 1:1 mixture of equimolar ^{R}L/(dppp)Pt(OTf)$_2$ and ^{S}L/(dppp)Pt(OTf)$_2$ complexes are monitored (Fig. 2). The convergence into the racemic complex suggests that the reorganisation process is reversible in dynamic equilibrium and that the heterodimeric complex represents a thermodynamically stable product.

We thank Professor Moon Geun Choi for the X-ray crystallographic data collection. Financial support from CMDS (KOSEF) is gratefully acknowledged. T. W. K. thanks the Ministry of Education for the BK 21 fellowship.

Notes and references

† *Selected data* for $[\{(dppp)Pt(^{rac}L)\}_2](OTf)_4$: ^{1}H NMR (500 MHz, acetone-d_6, 25 °C): δ 2.3 (br, 4H, CH_2-CH_2-CH_2), 3.3 (br, 8H, PCH_2), 6.73 (t, J 7.5 Hz, 4H, D^1-H), 6.89 (t, J 7.2 Hz, 8H, D^2-H), 7.11–7.17 (m, 4 + 8 + 4H, A-H + D^1-H + D^2-H), 7.40–7.44 (m, 8 + 4H, C-H + A-H), 7.50–7.57 (m, 8 + 4H, D^2-H + A-H), 7.59 (br, 8H, D^1-H), 7.81 (d, J 9.0 Hz, 4H, B-H), 8.05 (d, J 8.2 Hz, 4H, A-H), 8.16 (d, J 9.1 Hz , 4H, B-H), 9.01 (br, 8H, C-H); ESIMS: m/z = 2655.3 (found), 2655 (calc. for major isotope peak for $[(C_{32}H_{20}N_2O_4)_2(C_{27}H_{26}P_2Pt)_2(CF_3O_3S)_3]^+$); 1252.4 (found), 1253 (calc. for major isotope peak for $[(C_{32}H_{20}N_2O_4)_2(C_{27}H_{26}P_2Pt)_2(CF_3O_3S)_2]^{2+}$).

‡ In acetone solution at 25 °C, the racemic complex crystallized out to inhibit the measurement of molecular weight by VPO, and polystyrene M_W = 2360 (M_N = 2250 in VPO, M_N = 2180 in GPC) was used as calibration standard.

§ *Crystal data* for $[\{(dppp)Pt(^{rac}L)\}_2](OTf)_4$ (0.27 × 0.42 × 0.73 mm, white transparent crystal): $C_{122}F_{12}H_{92}N_4O_{20}P_4S_4Pt_2$, M = 2804.39, triclinic, $P\bar{1}$, a = 15.714(3), b = 21.797(4), c = 22.380(5) Å; α = 68.33(3), β = 78.78(3), γ = 79.56(3)°; V = 6937(2) Å^3, Z = 2, D_c = 1.530 g cm^{-3} (including solvent), μ(Mo-Kα, λ = 0.71073 Å) = 2.211 mm^{-1}, $2\theta_{max}$ = 52.9°; 37 830 measured reflections, 27 063 unique of which 19 580 observables [$I > 2\sigma(I)$]. The structure was solved by direct methods and refined by full-matrix least squares calculations with SHELX-97. The final $R1$ = 0.0522 for 19 580 reflections of $I > 2\sigma(I)$, $R1$ = 0.0830, $wR2$ = 0.1388 for all 27 063 reflections; measurements: Siemens SMART CCD equipped with a graphite crystal incident-beam monochromator *L*p.

CCDC 150517. See http://www.rsc.org/suppdata/cc/b1/b100329l/ for crystallographic data in .cif or other electronic format.

1 M. Fujita, in *Comprehensive Supramolecular Chemistry*, ed., J.-P. Sauvage and M. W. Hosseini, Pergamon, Oxford, 1996, vol. 9, pp. 253–282.
2 J.-M. Lehn, *Supramolecular Chemistry: Concepts and Perspectives*, VCH, Weinheim, 1995.
3 M. A. Masood, E. J. Enemark and T. D. P. Stack, *Angew. Chem., Int. Ed.*, 1998, **37**, 928.
4 (*a*) M. Albrecht, M. Schneider and H. Röttele, *Angew. Chem., Int. Ed. Engl.*, 1999, **38**, 557; (*b*) D. L. Caulder and K. N. Raymond, *Angew. Chem., Int. Ed. Engl.*, 1997, **36**, 1440; (*c*) R. Krämer, J.-M. Lehn and A. Marquis-Rigault, *Proc. Natl. Acad. Sci. USA*, 1993, **90**, 5394.
5 (*a*) B. Hasenknopf, J.-M. Lehn, G. Baum and D. Fenske, *Proc. Natl. Acad. Sci. USA*, 1996, **93**, 1397; (*b*) M. Kitamura, S. Okada, S. Suga and R. Noyori, *J. Am. Chem. Soc.*, 1989, **111**, 4028.
6 M. Fujita, F. Ibukuro, K. Yamaguchi and K. Ogura, *J. Am. Chem. Soc.*, 1995, **117**, 4175.
7 (*a*) J. R. Fredericks and A. D. Hamilton, in *Comprehensive Supramoleclar Chemistry*, ed., J.-P. Sauvage and M. W. Hosseini, Pergamon, Oxford, 1996, vol. 9, p. 568; (*b*) C. T. Seto and G. M. Whitesides, *J. Am. Chem. Soc.*, 1993, **115**, 905.
8 (*a*) M. Fujita, J. Yazaki and K. Ogura, *J. Am. Chem. Soc.*, 1990, **112**, 5645; (*b*) M. Fujita, S. Nago, M. Iida, K. Ogata and K. Ogura, *J. Am. Chem. Soc.*, 1993, **115**, 1574; (*c*) K. Onitsuka, S. Yamamoto and S. Takahashi, *Angew. Chem., Int. Ed.*, 1999, **38**, 174; (*d*) C. A. Hunter and L. D. Sarson, *Angew. Chem., Int. Ed.*, 1994, **33**, 2313.

ChemComm

t-BuOK-Catalyzed addition of ketones and nitriles to vinylic silanes, phosphines and thio derivatives

Tanasri Bunlaksananusorn, Alain Louis Rodriguez and Paul Knochel*

Fachbereich Chemie, Ludwig-Maximilians-Universität München, Butenandstr. 5-13, Haus F, D-81377 München, Germany. E-mail: Paul.Knochel@cup.uni-muenchen.de; Fax: 0049-089-2180-7680; Tel: 0049-089-2180-7681

Received (in Cambridge, UK) 13th February 2001, Accepted 13th March 2001
First published as an Advance Article on the web 30th March 2001

Catalytic amounts of *t*-BuOK in DMSO allow the smooth addition of nitriles and in some cases of ketones to vinylsilanes, phosphines or thio derivatives in good yields.

The conjugate addition of metalated nitriles **1** or ketones **2** to activated alkenes of type **3** (Z = electron-withdrawing group) is a well-known reaction (Michael addition).[1] Stabilized nucleophiles like enolates usually do not add to moderately activated vinylic derivatives of type **3** (Z = SiR_3, SR or PR_2).

Only highly reactive organolithiums add to these moderately active Michael-acceptors.[2] Recently, we have found that potassium enolates of ketones or nitriles generated catalytically using *t*-BuOK in DMSO or *N*-methylpyrrolidinone (NMP) have a high nucleophilicity in these solvents and add readily to various styrenes in good yields, allowing a unique catalytic phenylethylation reaction.[3] Herein, we wish to report that a range of nitriles add to vinylic silanes **3a** and **3b**, diphenylvinylphosphine (**3c**), phenyl vinyl thioether (**3d**) and phenyl vinyl sulfoxide (**3e**) in the presence of a catalytic amount of *t*-BuOK (20 mol%) in DMSO leading to the corresponding Michael-adducts **4a–g** and **4i–4k** in 60–88% yield (Scheme 1, Table 1). Thus, 2-phenylbutyronitrile **1a** (entry 1 of Table 1) adds to triphenylvinylsilane (**3a**) within 12 h at 40 °C in the presence of *t*-BuOK (20 mol%) in DMSO leading to the addition product **4a** in 60% yield. The related cyclohexanecarbonitrile (**1b**) adds to **3a** even at rt (12 h) affording the adduct **4b** in 76% yield (entry 2). Triethoxyvinylsilane (**3b**) adds similarly valeronitrile (**1d**), secondary nitriles **1a** and α-tetralone (**2a**) at 40 °C. In this case potassium ethoxide (20 mol%) is used as a catalyst in NMP. This avoids alkoxide exchanges at silicon and leads to the functionalized alkyltriethoxysilanes **4c–e** and **5d** in 65–86% yield (entries 3–5 and entry 15). These products may be interesting precursors for the preparation of functionalized silicones. This result shows that a variety of potassium alkoxides can certainly be used in this catalytic addition reaction. Vinylic phosphines only reluctantly undergo the addition of nucleophiles[2g] and, usually, efficient additions only are observed to vinylic phosphine oxide derivatives or alkenylphosphonium salts.[4] Under our reaction conditions, various nitriles add to diphenylvinylphosphine (**3c**) very smoothly (25 °C, 1 h) leading to the expected products **4f–g** in 81–88% yield and the double addition product **4h** in 80% yield. Interestingly, ketones like α-tetralone (**2a**), camphor (**2b**) and cyclohexanone (**2c**) also undergo an efficient Michael addition at 40 °C (12 h) leading to the ketophosphines **5a**, **5b** and **5c** in respectively 80, 72 and 65% yields (entries 12, 13 and 14). In the case of **5b** only the *endo*-isomer is produced.[5] Finally, nitriles like **1a** or **1b** add also to phenyl vinyl thioether (**3d**) affording the Michael-adducts **4i–j** (entries 9 and 10) in 75–78% yield. The corresponding sulfoxide (**3e**) adds nitrile **1a** under similar conditions (40 °C, 1 h) furnishing the sulfoxide **4k** in 82% yield (entry 11).

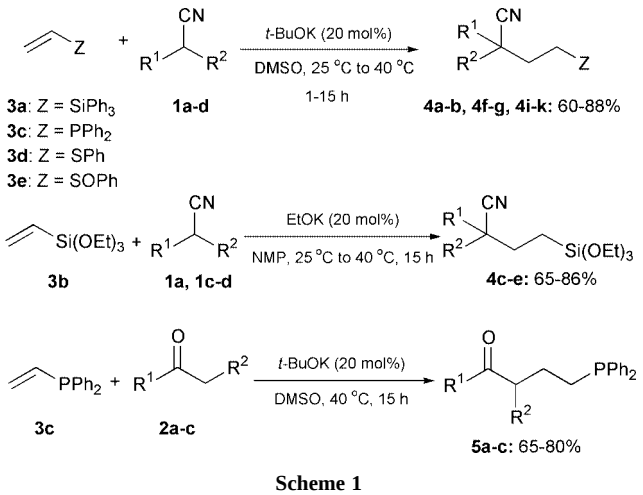

Scheme 1

In summary, we have described a new *t*-BuOK-catalyzed addition of nitriles to various moderately active Michael-acceptors allowing the preparation of new functionalized silanes, phosphines and thioethers. In the case of diphenylvinylphosphine (**3c**) the addition of ketones also proceeds well. We are currently exploring the application of this reaction for the preparation of new chiral ligands for metal catalysis.[6]

We thank the Deutsche Forschungsgemeinschaft (Leibniz program) and the Humboldt Foundation for a scholarship to A. R. We also thank the BASF AG (Ludwigshafen), Chemetall GmbH (Frankfurt) and Degussa-Hüls AG (Hanau) for the generous gift of chemicals.

Notes and references

1 (*a*) M. E. Jung, in *Comprehensive Organic Synthesis*, ed. B. M. Trost, I. Fleming and M. F. Semmelhack, 1991, vol. 4, p. 1; (*b*) P. Perlmutter, *Conjugate Addition Reactions in Organic Synthesis*, Pergamon Press, 1992.

2 (*a*) L. F. Casan and H. G. Brooks, *J. Am. Chem. Soc.*, 1952, **74**, 4582; (*b*) D. Seebach, R. Bürstinghaus, B. T. Gröbel and M. Kolb, *Liebigs Ann. Chem.*, 1977, 830; (*c*) T. H. Chan, E. Chang and E. Vinokur, *Tetrahedron Lett.*, 1970, 1137; (*d*) J. Yoshida, S. Nakatani and S. Isoe, *J. Org. Chem.*, 1989, **54**, 5655; (*e*) N. H. Andersen, P. F. Duffy, A. D. Denniston and D. B. Grotjahn, *Tetrahedron Lett.*, 1978, **19**, 4315; (*f*) D. Seebach, *Synthesis*, 1969, 17; (*g*) M. S. Rahman, J. W. Steed and K. K. Hii, *Synthesis*, 2000, 1320.

3 A. L. Rodriguez, T. Bunlaksananusorn and P. Knochel, *Org. Lett.*, 2000, **21**, 3285.

4 R. M. Cory, D. M. T. Chan, Y. M. A. Naguib, M. H. Rastall and R. M. Renneboog, *J. Org. Chem.*, 1980, **45**, 1852.

5 The relative stereochemistry of the *endo*-configuration has been established by NOESY experiment.

6 Typical procedure: preparation of 2-ethyl-2-phenyl-4-diphenylphosphinobutanenitrile (**4f**): To a stirred solution of *tert*-butoxide (45 mg, 0.4 mmol) in DMSO (2 mL) was successively added, under argon, 2-phenylbutyronitrile (**1a**; 290 mg, 2 mmol) and diphenylvinylphosphine (**3c**, 420 mg, 2 mmol). The reaction was stirred for 1 h at rt. Water (3 mL) and CH_2Cl_2 (25 mL) were added, and the resulting solution was washed with brine, dried ($MgSO_4$) and concentrated under reduced pressure. The crude product was purified by flash chromatography (silica gel, 5% ether–pentane) to give the desired product **4f** (630 mg, 88% yield).

Table 1 Nitriles **4a**–**k** and ketones **5a**–**d** obtained by the *t*-BuOK-catalyzed addition of nitriles and ketones to the vinylic silanes, phosphines, thioethers and sulfoxides **3a**–**e** in DMSO

Entry	Carbonyl compound	Activated alkene	Product of type **4** or **5**	Yield (%)[a]
1	**1a**	**3a**	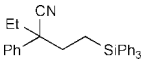 **4a**	60
2	**1b**	**3a**	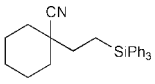 **4b**	76
3	**1a**	**3b**	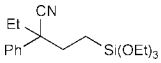 **4c**	86[b]
4	**1c**	**3b**	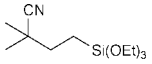 **4d**	85[b]
5	**1d**	**3b**	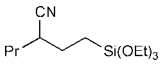 **4e**	65[b]
6	**1a**	**3c**	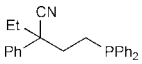 **4f**	88
7	**1c**	**3c**	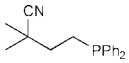 **4g**	81
8	**1d**	**3c**	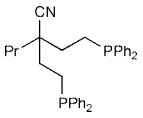 **4h**	80
9	**1a**	**3d**	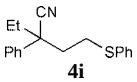 **4i**	78
10	**1b**	**3d**	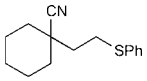 **4j**	75
11	**1a**	**3e**	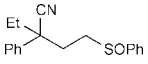 **4k**	82
12	**2a**	**3c**	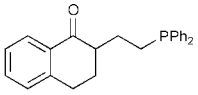 **5a**	80
13	**2b**	**3c**	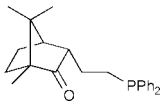 **5b**	72
14	**2c**	**3c**	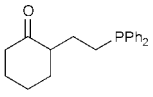 **5c**	65
15	**2a**	**3b**	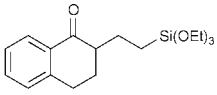 **5d**	65[b]

[a] Yield of analytically pure products; [b] EtOK (20 mol%) in NMP was used.

Axial guanine binding to a diplatinum(III) core

Gunnar Kampf,[a] Michael Willermann,[a] Ennio Zangrando,[b] Lucio Randaccio[b] and Bernhard Lippert*[a]

[a] *Fachbereich Chemie, Universität Dortmund, 44221 Dortmund, Germany. E-mail: lippert@pop.uni-dortmund.de*
[b] *Dipartimento di Scienze Chimiche, Universitá di Trieste, 34127 Trieste, Italy*

Received (in Cambridge, UK) 2nd February 2001, Accepted 12th March 2001
First published as an Advance Article on the web 30th March 2001

The preparation, crystal structure and NMR spectroscopic properties of a cisplatin-derived diplatinum(III) complex is reported which contains two bridging 1-methylcytosinato nucleobases in mutual *head–tail* orientation and in addition two axially bound 9-ethylguanine nucleobases.

Reactions of di-, rather than mononuclear metal antitumor complexes with nucleobases or DNA, in which the integrity of the dimetal core is retained, have recently attracted attention. Examples are nucleobase adducts of dinuclear Pt(II) complexes with flexible aliphatic (**i**)[1] or rigid heterocyclic linkers (**ii**),[2] and

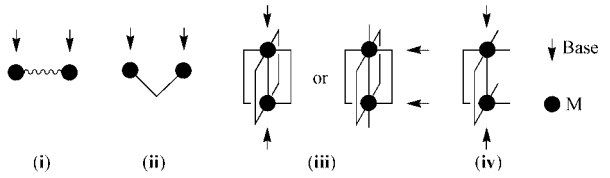

'lantern' type dirhodium(II) tetracarboxylates (**iii**).[3] In the latter case nucleobase binding can occur both through the axial positions[4] or with replacement of two bridging ligands.[5] Here we report on a diplatinum(III) complex (**iv**) which binds two guanine nucleobases with high efficiency through the two axial positions of the dimetal core. The novelty of (**iv**) relates to Pt binding through guanine-N^7, a pattern ruled out in the case of dimetal tetracarboxylates (**iii**) because of repulsive interactions between O^6 of guanine and the four oxygen donor atoms in the metal plane.[6] In contrast, axial binding of adenine nucleobases (*via* N^7) was rationalized on the basis of favourable H bonding interactions with the MO_4 plane.[3–5] The observation by Aoki *et al.*[7] on axial theophylline-N^7 binding to a mixed-valence tetrakis(μ-acetamidato)rhodium(II)-rhodium(III) cation was a logical consequence of the partial replacement of O atoms by NH functions and the possibility of interligand H bond formation. Consistent with this view, the presence of three H donor sites (NH, two NH_3) in the MN_4 faces of the diplatinum(III) core applied in this study proved particularly advantageous for guanine binding.

The title compound was prepared as follows: The diplatinum(II) precursor *cis*-[{$Pt(NH_3)_2$(μ-mcyt-N^3-N^4)}$_2$]$^{2+}$ (**1**)[8] con-

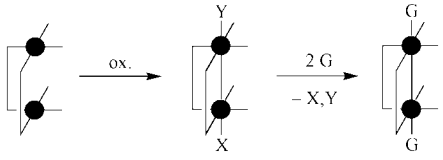

taining two bridging 1-methylcytosinato (mcyt) model nucleobases in *head–tail* arrangement was oxidized to the diplatinum(III) complex *cis*-[X$Pt(NH_3)_2$(μ-mcyt-N^3-N^4)$_2$-$Pt(NH_3)_2$Y](Z)$_n$ (**2**).[9] Subsequently, the axial ligands X and Y were replaced by 9-ethylguanine (Hetgua) by adding this nucleobase to an aqueous solution of **2** (pH ≃ 2) to give *cis*-[{$Pt(NH_3)_2$(Hetgua-N^7)(mcyt-N^3-N^4)}$_2$]$^{4+}$ (**3**). The cation of the title compound **3** $[ClO_4]_4 \cdot 5H_2O$[10,11] is depicted in Fig. 1. Salient structural features are as follows: the Pt–Pt bond length of 2.5868(8) Å is in the typical range for single bonds of diplatinum(III) complexes derived from cisplatin.[12] The two Pt planes form an angle of 20.3(1)°, and the torsional angle about the Pt–Pt vector is 26.9(2)° (N(3C)–Pt–Pt–N(4C)) and 33.2(2)° (N2–Pt–Pt–N1). Pt–N distances in the Pt plane are normal [Pt–N(4C), 2.002(5); Pt–N(3C), 2.043(5); Pt–N(2), 2.056(5) Å] or only slightly elongated [Pt–N(1), 2.070(5) Å]. However, the Pt–N^7 bond [2.189(6) Å] is markedly longer than those typically seen in Pt(II)[13] and Pt(IV)[14] complexes of guanine. The guanine ligand is oriented in such a way, that O^6 escapes any steric clash with O^2 of the mcyt ligand by H bond formation with the two NH_3 groups (N1···O6G, 2.854(8); N2···O6G, 3.101(7) Å; angles: N1–H1A···O6G, 159.8(4); N2–H2B···O6G, 144.2(4)°].

Compound **3** is stable in aqueous solution for at least 7 d. The ^{195}Pt NMR signal at −816 ppm is consistent with a Pt(III) oxidation state and the singlet indicates that the two Pt centers have identical environments. A ^{195}Pt ^{1}H HMQC experiment reveals ^4J coupling between ^{195}Pt and H5 of mcyt (9.2 Hz), ^5J coupling between ^{195}Pt and H6 of mcyt (8.3 Hz), as well as ^3J coupling between ^{195}Pt and H8 of Hetgua (5.2 Hz). While coupling with the cytosine protons are in the expected range,[15] it is noted that ^3J coupling to guanine H8 is rather small as compared to guanine bases bonded to Pt(II) (20–32 Hz[16]) and even to Pt(IV) (12 Hz[14]). It is a consequence of the apparent weak binding of the axial guanine ligands. This situation contrasts the strong binding of a single, C^5 bonded 1-methyluracilyl entity to a diplatinum(III) core,[17] which has some

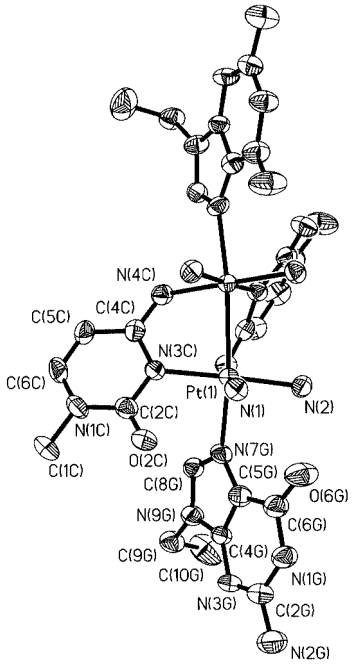

Fig. 1 Crystal structure of cation of *cis*-[{$Pt(NH_3)_2$(Hetgua-N^7)(mcyt-N^3-N^4)}$_2$][$ClO_4]_4 \cdot 5H_2O$(**3**).

structural similarity with the present case as it is another example of a diplatinum(III) complex carrying a nucleobase in an axial position.

The affinity of **2** for the guanine model nucleobase is retained in reactions with the corresponding nucleoside 2′-deoxyguanosine and the nucleotide 5′-dGMP. Binding occurs rapidly, as evident from ^{1}H NMR spectroscopy. Doubling of most resonances is consistent with formation of diastereomers upon combination of the chiral *head–tail* species **2** with the chiral nucleoside/nucleotide.[15] The guanosine adduct is stable in aqueous solution for approximately 1 d, whereas the 5′-GMP compound is stable for at least one week (*e.g.* ^{195}Pt NMR resonance at δ −804 ppm for 5′-dGMP complex). Afterwards the ^{1}H NMR spectra of both species become quite complicated. It is unclear at present whether oxidative degradation processes of either the purine skeleton and/or the sugar moieties take place similarly to the situations encountered with Au(III)[21] and high valent Mn,[22] Ni,[23] or Ru[24] species.

Attempts to bind model nucleobases other than guanine, *e.g.* 1-methylcytosine, 1-methyluracil or 9-methyladenine to **2** under comparable conditions, failed. Thus **2** appears to be highly selective for guanine nucleobases. Whether this feature may be exploited to generate a chemical probe for guanine in nucleic acids remains to be seen.

This work was supported by the Vigoni programme and the Fonds der Chemischen Industrie.

Notes and references

1 N. Farrell, Y. Qu, U. Bierbach, M. Valsecchi and E. Menta, in *Cisplatin: Chemistry and Biochemistry of a Leading Anticancer Drug*, ed. B. Lippert, VCHA, Zürich and Wiley-VCH, Weinheim, 1999, p. 479.

2 S. Komeda, H. Ohishi, H. Yamane, M. Harikawa, K.-I. Sakaguchi and M. Chikuma, *J. Chem. Soc., Dalton Trans.*, 1999, 2959.

3 J. M. Asara, J. S. Hess, E. Lozada, K. R. Dunbar and J. Allison, *J. Am. Chem. Soc.*, 2000, **122**, 8, and references therein.

4 J. R. Rubin, T. P. Haromy and M. Sundaralingam, *Acta Crystallogr.*, 1991, **C47**, 1712.

5 C. A. Crawford, E. F. Day, V. P. Saharan, K. Folting, J. C. Huffman, K. R. Dunbar and G. Christou, *Chem. Commun.*, 1996, 1113; K. R. Dunbar, J. H. Matonic, V. P. Saharan, C. A. Crawford and G. Christou, *J. Am. Chem. Soc.*, 1994, **116**, 2201.

6 An example of an unsubstituted guanine dianion binding to a tetrakis(phosphato) bridged diplatinum(III) species has been reported which, however, is not relevant to this discussion as binding to Pt occurs through N^9: R. El-Mehdawi, F. R. Fronczek and D. M. Roundhill, *Inorg. Chem.*, 1986, **25**, 3714. Similar arguments apply to N^9 bonded theophylline and caffeine complexes of tetrakis(acetato)dirhodium(II) complexes: K. Aoki and H. Yamazaki, *J. Chem. Soc., Chem. Commun.*, 1980, 186.

7 K. Aoki, M. Hoshino, T. Okada, H. Yamazaki and H. Sekizawa, *J. Chem. Soc., Chem. Commun.*, 1986, 314.

8 R. Faggiani, B. Lippert, C. J. L. Lock and R. A. Speranzini, *J. Am. Chem. Soc.*, 1981, **103**, 1111.

9 **2a**: X = NO_2^-, Y = H_2O, Z = ClO_4^-, n = 3; **2b**: X = Y = ONO_2^-, Z = NO_3^-, n = 2; **2c**: X = Y = H_2O, Z = ClO_4^-, n = 4. All three compounds have been characterized by X-ray crystallography. Details will be reported elsewhere. Oxidation of **1** was achieved by any of the following oxidants: HNO_3, $HClO_4$, or $K_2S_2O_8$. In a typical experiment, **1** (82.26 mg; 0.095 mmol) is dissolved in concentrated $HClO_4$ (1.5 ml), the orange solution then diluted with 3.5 ml H_2O and allowed to slowly evaporate. Orange crystals of **2a** are collected in *ca.* 72% yield. ^{1}H NMR (200 MHz, D_2O, δ/ppm) of **2a**: 7.35 (d, ^3J = 7.4 Hz H6), 7.31 (d, ^3J = 7.4 Hz H6), 6.04 (d, ^3J = 7.4 Hz H5), 5.91 (d, ^3J = 7.4 Hz H5), 3.40 (s, CH_3), 3.33 (s, CH_3). ^{195}Pt-NMR (42.998 MHz, D_2O δ/ppm): −1000, −445.

10 Synthesis:10.9 mg (0.06 mmol) of 9-ethylguanine is added to a solution of 32.9 mg (0.03 mmol) of **2a** in water (1 ml). Upon slow evaporation compound **3** crystallizes and is collected as several fractions to give 26 mg (0.017 mmol, 58% yield) **3**. Anal. calcd. for **3**, $C_{24}H_{52}N_{20}O_{25}Cl_4Pt_2$ (1552.84 g mol^{-1}): C 18.57; H 3.38, N 18.04%; found: C 18.8, H 3.1, N 18.2%.

11 Crystal data for **3**: $C_{24}H_{52}N_{20}O_{25}Cl_4Pt_2$ M_r = 1552.84, monoclinic, space group $C2/m$, a = 17.574(4), b = 20.356(4), c = 13.815(3), β = 91.69(3), V = 4940(2) Å^3, Z = 8, D_c = 2.088 g cm^{-3}, μ(Mo-Kα) = 5.978 mm^{-1}, T = 293(2) K, Enraf–Nonius–KappaCCD[18] with graphite monochromator, φ-scans, 6661 independent reflections, R_{int} = 0.044, structure solved by standard Patterson methods[19] and refined by full matrix least squares on F^2 using SHELXL-97[20]. All non-hydrogen atoms were refined anisotropically. Hydrogens were placed at calculated positions and not further refined. One perchlorate is heavily disordered. 368 refined parameters gave R_1 = 0.0428 and wR_2 = 0.1104 for 4665 reflections with $I \geqslant 2\sigma(I)$ and R_1 = 0.0673 and wR_2 = 0.1163 for all data, minimum and maximum features in difference Fourier map were 2.61 and −2.19 e Å^{-3} (near Cl3). CCDC 157798.

12 B. Lippert, *Prog. Inorg. Chem.*, 1989, **37**, 1.

13 E. Zangrando, F. Pichierri, L. Randaccio and B. Lippert, *Coord. Chem. Rev.*, 1996, **156**, 275.

14 G. Frommer, H. Preut and B. Lippert, *Inorg. Chim. Acta*, 1992, **193**, 111.

15 T. Wienkötter, M. Sabat, G. Fusch and B. Lippert, *Inorg. Chem.*, 1995, **34**, 1022.

16 G. Raudaschl and B. Lippert, *Inorg. Chim. Acta*, 1983, **80**, L49.

17 H. Schöllhorn, U. Thewalt and B. Lippert, *J. Chem. Soc., Chem. Commun.*, 1986, 258.

18 NONIUS BV, KappaCCD package, Röntgenweg 1, P.O.Box 811, 2600 AV Delft, Netherlands; Z. Otwinowsky and Minor, *Processing of X-ray Diffraction Data Collected in Oscillation Mode*, Methods in Enzymology, ed., C. W. Carter, Jr. and R. M. Sweet, Academic Press, 1996, **276**, 307.

19 G. M. Sheldrick, *Acta Crystallogr., Sect. A*, 1990, **46**, 467.

20 G. M. Sheldrick, SHELXL-97, Program for crystal structure refinement, University of Göttingen, Germany, 1997.

21 A. Schimanski, E. Freisinger, A. Erxleben and B. Lippert, *Inorg. Chim. Acta*, 1998, **283**, 223.

22 G. Pratviel, J. Bernadou and B. Meunier, *Angew. Chem., Int. Ed. Engl.*, 1995, **34**, 746 and refs. cited.

23 H.-C. Shih, N. Tang, C. J. Burrows and S. E. Rokita, *J. Am. Chem. Soc.*, 1998, **120**, 3284.

24 P. J. Carter, C.-C. Cheng and H. H. Thorp, *Inorg. Chem.*, 1996, **35**, 3348.

Preparation of 1,5-dinitrenonaphthalene in cryogenic matrices†

Tadatake Sato,* Hiroyuki Niino, Sundaram Arulmozhiraja, Masahiro Kaise and Akira Yabe

National Institute of Materials and Chemical Research (NIMC), Higashi 1-1, Tsukuba, Ibaraki 305-8565, Japan. E-mail: sato-tadatake@aist.go.jp

Received (in Cambridge, UK) 24th October 2000, Accepted 9th March 2001
First published as an Advance Article on the web 30th March 2001

1,5-Dinitrenonaphthalene was prepared in two cryogenic matrices by photolysis of 1,5-diazidonaphthalene; the cryogenic matrices were an argon matrix at 11 K and a glassy 2-methyltetrahydrofuran matrix at 77 K; the photolysis was analyzed by UV-VIS, FT-IR, and ESR matrix isolation spectroscopies.

Dinitrenes have been intensively studied to examine the magnetic properties of the building blocks in molecule-based magnetic materials.[1] The two nitreno groups in dinitrenes are triplet centers and provide important insight into intramolecular interelectronic exchange interaction. Some dinitrenes exist in the quinonoidal form, where, for each nitreno group, one of the unpaired electrons of the nitrogen atom forms a π bond with a π electron of the adjacent carbon atom.[2,3] Hence, these dinitrenes are not high-spin molecules but diradicals with two localized electrons in a singlet ground state. Even though they are not very attractive as organic magnetic materials for technical applications, these dinitrenes are important species for the study of interelectronic interaction in organic diradicals.[4] In these quinonoidal dinitrenes, electronic interaction between the radical centers is explained by spin polarization,[2] an important interelectronic exchange mechanism. The quinonoidal dinitrenes have been studied to understand the relationship between their interelectronic exchange interaction and their chemical structure.[1] However, frequently there are complicating structural ambiguities, such as twisting of the aromatic system in biphenyl[5,6] or *E–Z* iosmerization in stilbene.[2] Connecting two nitreno groups to a condensed polycyclic aromatic hydrocarbon, where structural ambiguity is excluded, should make it easier to study the relationship between structure and interelectronic interaction and could lead to a clearer understanding of this relationship, Here, we studied 1,5-dinitrenonaphthalene, where two nitreno groups were connected to a rigid naphthalene structure, by low temperature matrix isolation spectroscopies.

Crystallites of 1,5-diazidonaphthalene **1** were vaporized at 45 °C and codeposited with argon (99.9999%) onto a CsI plate at 11 K. Matrix-isolated **1**, which showed structured UV-VIS absorption bands in the 300–340 nm region (Fig. 1) and major IR bands at 2116, 1409, 1294, 781, and 707 cm^{-1}, was photolyzed by XeCl excimer laser pulses (λ = 308 nm, 1 Hz, 1.2 mJ cm^{-2} $pulse^{-1}$, τ = 20 ns). The photolysis was simultaneously monitored by FT-IR and UV-VIS spectroscopies.[7] Upon irradiation at 308 nm, the UV-VIS and IR absorption bands ascribed to **1** decreased rapidly, while some new bands appeared. These new bands behaved differently during irradiation: in the UV-VIS absorption spectra, the weak absorption bands at 581, 565, 541, 535, 391, and 372 nm disappeared after prolonged irradiation, while the absorption bands at 470, 442, and 415 nm increased continuously during the irradiation (Fig. 1). A similar behavior was observed in the FT-IR spectra, with some new bands disappearing and others growing continuously during irradiation. The former bands were ascribed to mononitrene **2** in the triplet state, showing good agreement with the theoretical IR spectrum calculated at the UB3LYP/6-31G* level.† Meanwhile, the FT-IR spectrum obtained upon irradiation with 330 shots (Fig. 2(a)) did not contain the characteristic IR band of the azido group (2116 cm^{-1}). Thus, the resulting product was formed by elimination of two nitrogen molecules from **1** (Scheme 1). This product (**3**) showed a prominent IR band at 750 cm^{-1} and others at 507, 1033, 1161, 1212, 1279, 1393, 1466, and 1506 cm^{-1}. These bands were ascribed to a single photoproduct from the dynamic behavior in intensity during irradiation.[8] Moreover, the dynamic behavior of the IR spectra corresponded to that of the

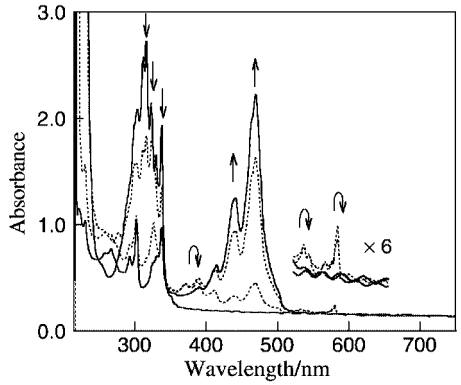

Fig. 1 UV-VIS absorption spectra of **1** photolyzed by XeCl excimer laser pulses (0, 30, 140, and 3440 shots) in an argon matrix. Arrows show the dynamic behavior in intensity of peaks during irradiation.

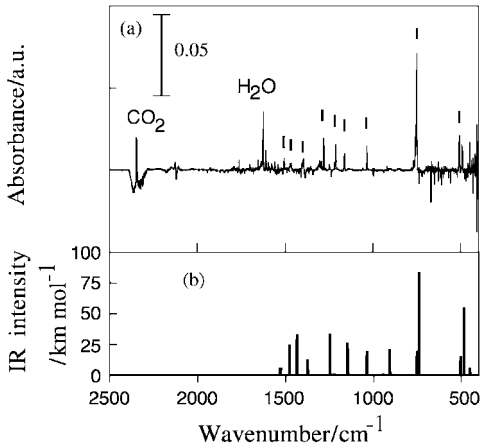

Fig. 2 (a) FT-IR spectrum observed upon irradiation with 330 shots and (b) theoretical IR spectrum of **3** (open-shell singlet state).

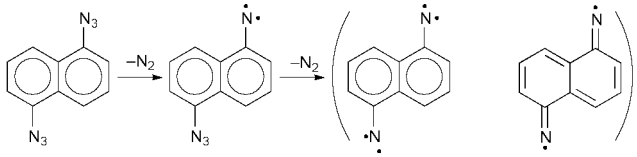

Scheme 1

† Electronic supplementary information (ESI) available: experimental details and computational study of the dinitrenes. See http://www.rsc.org/suppdata/cc/b0/b008560j/

DOI: 10.1039/b008560j

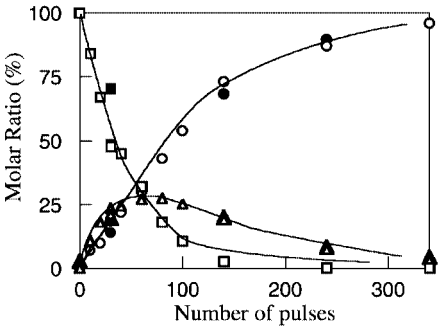

Fig. 3 Dynamic behavior of the intensities in the UV-VIS and FT-IR bands ascribed to **1** (solid squares, 339 nm; open squares, 1409 cm^{-1}), **2** (solid triangles, 581 nm; open triangles, 769 cm^{-1}), and **3** (solid circles, 470 nm; open circles: 750 cm^{-1}).

UV-VIS spectra during the whole irradiation as shown in Fig. 3. This behavior of the UV-VIS and IR bands ascribed to **1**, **2**, and **3** revealed a typical consecutive reaction, that is, consecutive elimination of two nitrogen molecules from **1**.[9] No IR bands ascribable to other species were observed under the present conditions. The observed FT-IR spectrum was compared with the theoretical IR spectrum of 1,5-dinitrenonaphthalene. For the quinonoidal dinitrenes reported as far, the ground state is the singlet diradical state which lies slightly below the triplet state: their energy gaps between singlet and triplet states ($\Delta E_{S\text{-}T}$) are rather small (< 1 kcal mol^{-1}).[2,3] The state order of the dinitrene with different spin multiplicities was often difficult to reproduce in the computational study,[10] since the theoretical calculations for singlet-diradicals show much difficulty because of their multireference character. It has recently been reported that calculations using the symmetry-broken spin-unrestricted DFT method give reasonable solutions for such diradicals.[10–12] Moreover, this method can afford reasonable solutions even for larger molecules. Therefore, preliminary calculations for the singlet, triplet, and quintet states of **3** were carried out at the UB3LYP/6-31G* level. Fig. 2(b) shows the theoretical IR spectrum of the singlet state. The theoretical calculation underestimated the wavenumbers of the IR bands by ~125 cm^{-1}. The deviation was larger than that shown normally in the calculations at this computational level. The deviations would be due to the spin contamination: the results on **3** showed the spin squared expectation ($< S^2 >$) value of 1.78, indicating the admixture of the triplet and quintet states. In the symmetry-broken spin-unrestricted calculations, the $< S^2 >$ value of the singlet diradical should be 1.0.[11] Although deviations in wavenumber were shown, the observed spectral feature was well described by comparison of those with other spin multiplicities (see ESI†). Moreover, the observed UV-VIS spectra indicated the quinonoidal structure as followed. (1) The UV-VIS bands (470, 442, and 415 nm) of **3** corresponded to that of the 1,5-naphthoquinone derivative (475 and 458 nm) which should have a similar electronic structure to the quinonoidal dinitrene.[13] (2) The INDO/S computation[14] based on the quinonidal geometry of singlet diradical predicts major UV-VIS bands at 468 and 460 nm, that are in agreement with the experimental results. Thus, it is concluded that the photoproduct prepared from **1** was 1,5-dinitrenonaphthalene, which was the quinonoidal singlet diradical in the ground state. The dinitrene **3** was formed by elimination of two nitrogen molecules from **1** without the rearrangement observed for 1- or 2-azidonaphthalenes.[15]

UV-VIS spectroscopy revealed that a similar photolysis occurred for **1** in a glassy 2-methyltetrahydrofuran (MTHF) matrix at 77 K upon a Xe lamp irradiation through a band-pass glass filter ($350 < \lambda < 380$ nm). Under these conditions, ESR spectroscopy (X band) was used to analyze the photolysis of a MTHF solution of **1** (4.6 mM). Upon irradiation, ESR signals at 622 and 611 mT, ascribed to triplet mononitrenes,[16] were observed in addition to the typical impurity signal in the $g = 2$ region. Signals ascribable to a dinitrene with higher spin multiplicity were not observed. The absence of the signals indicated that the ground state of **3** was a singlet diradical. Minato and Lahti[2] and Nimura and others[3] report that 1,4-dinitrenobenzene **4** and several other quinonoidal dinitrenes show ESR signals ascribable to thermally populated excited triplet states. The reason for the absence of such signals can be explained as follows: since 1,5-dinitrenonaphthalene has a larger $\Delta E_{S\text{-}T}$ than **4** and the other quinonoidal dinitrenes, the population of the thermally-excited triplet state is too low to detect. The DFT calculations support our interpretation of the reason why the quinonoidal triplet ESR signals are difficult to detect.† Moreover, theoretical calculations with higher levels by Serwinski *et al.* also support our interpretation.[17]

In conclusion, 1,5-dinitrenonaphthalene was formed by the consecutive elimination of nitrogen molecules from 1,5-diazidonaphthalene upon irradiation at 308 nm in low-temperature matrices. On the basis of matrix isolation spectroscopies and theoretical calculations, we confirmed that the dinitrene formed was a quinonoidal singlet diradical with a relatively large $\Delta E_{S\text{-}T}$. Further study on other dinitrenonaphthalenes is in progress.

We are grateful to Professor Paul M. Lahti (University of Massachusetts) and Professor Hideo Tomioka (Mie University) for helpful discussions.

Notes and references

1 S. Nimura and A. Yabe, *Molecular Magnetism of Organic Molecules and Materials*, ed. P. M. Lahti, Marcel Dekker, New York, p. 127, 1999 and references therein.
2 M. Minato and P. M. Lahti, *J. Am. Chem. Soc.*, 1997, **119**, 2187.
3 S. Nimura, O. Kikuchi, T. Ohana, A. Yabe, S. Kondo and M. Kaise, *J. Phys. Chem. A*, 1997, **101**, 2083.
4 For instance, A. Rajca, S. Rajca and J. Wongsriratanakul, *Chem. Commun.*, 2000, 1021, and references therein.
5 C. Ling and P. M. Lahti, *Chem. Lett.*, 1993, 769.
6 T. Ohana, M. Kaise, S. Nimura, O. Kikuchi and A. Yabe, *Chem. Lett.*, 1993, 765.
7 The sample chamber has two pairs of windows: KBr windows for IR measurement and quartz windows for UV-VIS measurement. Therefore, UV-VIS and FT-IR spectra of the same sample matrix can be simultaneously observed.
8 The photoproduct **3** was generated upon irradiation at 308 nm and photolyzed at 248 nm. The dynamic behavior of these bands was analyzed for its generation and decomposition. All of these bands showed similar dynamic behavior.
9 The dynamic behavior in absorbance was scaled to express the molar ratio in the matrix. The molar ratios (%) of **1** and **2** to initial **1** were estimated from the absorbance of the IR bands due to the azido groups in each compound on the basis of their theoretical IR intensities (1929 and 923 km mol^{-1} for **1** and **2**, respectively). The residual portion was allocated to **3** because no other species was detected under the present conditions. The absorbance of the UV-VIS bands are scaled to fit the dynamics in absorbance of the IR bands.
10 P. M. Lahti, A. S. Ichimura and J. A. Sanborn, *J. Phys. Chem. A*, 2001, **105**, 251.
11 J. Gräfenstein, A. M. Hjerpe, E. Kraka and D. Cremer, *J. Phys. Chem. A*, 2000, **104**, 1748.
12 G. Orlova and J. D. Goddard, *J. Chem. Phys.*, 2000 **112**, 10 085, and references therein.
13 H. L. K. Schmand, H. Kratzin and P. Boldt, *Liebigs Ann. Chem.*, 1976, 1560.
14 The INDO/S calculation was done using a WinMOPAC program package (ver. 2.0.2) on a personal computer.
15 I. R. Dunkin and P. C. P. Thomson, *J. Chem. Soc., Chem. Commun.*, 1980, 499.
16 The signal was observed at 622 mT initially, which was ascribed to **2**; this signal corresponds to a zero field splitting of $|D/hc| = 0.918$ cm^{-1}. This signal decreased upon irradiation, while the signal at 611 mT increased. The latter signal was ascribed to 1-amino-5-nitrenonaphthalene by the literature (T. Harder, J. Bendig and G. Sholz, *J. Am. Chem. Soc.*, 1996, **118**, 2497).
17 P. R. Serwinski, R. Walton, J. A. Sanborn, P. M. Lahti, T. Enyo, D. Miura, H. Tomioka and A. Nicolaides, *Org. Lett.*, in press.

ChemComm

Pillar-shaped structures and patterns of three-dimensional carbon nanotube alignments

Xianbao Wang, Yunqi Liu* and Daoben Zhu*

Center for Molecular Science, Institute of Chemistry, Chinese Academy of Sciences, Beijing 100080, P. R. China. E-mail: liuyq@infoc3.icas.ac.cn

Received (in Cambridge, UK) 8th January 2001, Accepted 16th March 2001
First published as an Advance Article on the web 30th March 2001

Pillar-shaped structures and patterns of three-dimensional multi-walled carbon nanotube arrays have been synthesized by pyrolysis of iron(II) phthalocyanine.

Alignments of carbon nanotubes (CNTs) are particularly important for fabricating functional devices such as field emitters[1–4] and nanoelectronics[5,6] as well as ultrahydrophobic materials.[7] Two-dimensional (2D) aligned nanotubes were obtained previously by using chemical vapor deposition (CVD) over catalyst embedded in mesoporous silica[4,8] or on quartz substrate[9] and over laser-patterned catalysts.[10] Recently, Ren *et al.*[11,12] have reported the synthesis of self-aligned 2D nanotubes on glass substrates by using plasma-enhanced CVD, although this method suffered from complex pre-synthesis manipulations. However, to our knowledge, preparation of three-dimensional (3D) CNT alignments has not been reported. Here, we have developed a simple method for a large-scale synthesis of 3D aligned CNTs normal to the quartz substrate surface without any pre- or post-synthesis manipulations.

A typical experimental procedure was as follows:[13] a clean quartz glass plate ($4 \times 2 \times 0.1$ cm) was placed in a flow reactor consisting of a quartz tube and a furnace fitted with an independent temperature controller. A flow of Ar–H_2 (1 : 1, v/v, 20 cm^3 min^{-1}) was then introduced into the quartz tube during heating. After the central region of the furnace reached 950 °C, a quartz boat with 0.5 g of iron(II) phthalocyanine was placed in the region where the temperature was 550 °C. After 5 min heating, CNTs grew in a direction normal to the substrate surface. The CNT samples were examined by scanning electron microscopy (SEM, JEOL JSM-6301F) to characterize their profile, alignment and uniformity. Transmission electron microscopy (TEM, Hitachi H-800, 100 kV) was used to determine the diameters and microstructure of the CNTs. X-Ray photoelectron spectroscopy (XPS) analyses of the samples were performed on a VG ESCALAB 220-IXL spectrometer using an Al-Kα X-ray source (1486.6 eV).

Fig. 1 shows SEM images of 3D regular arrays of nanotubes aligned along the direction perpendecular to the substrate surface. As can be seen in Fig. 1(a), a few pillar-shaped structures of CNTs grow out from the 2D alignments in a well distributed mode. At high magnification, the SEM image [Fig. 1(b)] clearly shows that the pillar-shaped structures dispersed in the middle of the 2D CNT alignments. The CNT posts with a diameter of *ca*. 3.4 μm are 7.8 μm higher than the 2D nanotube alignments, whose height is typically 6 μm from the quartz substrate. The structure is reminiscent of papillose epidermal cells of lotus leaf surfaces that provide very effective water-repellent and anti-adhesive properties against particulate contamination, denoted self-cleaning ability.

A high magnification SEM image (Fig. 2) of an individual nanotube post shows that it is a tubular bundle with a diameter of 2.8 μm and a height of 5.5 μm. A TEM investigation (inset) reveals that the nanotubes composing 3D alignments are bamboo-like multiwalled nanotubes[15] with a diameter of *ca*. 50 nm. The alignment is partially preserved despite the sonication of the raw material in ethanol before deposition of the nanotubes onto the holey carbon film TEM grid. This clearly indicates that the nanotubes of 3D alignments are densely packed and held together by van der Waals interactions.

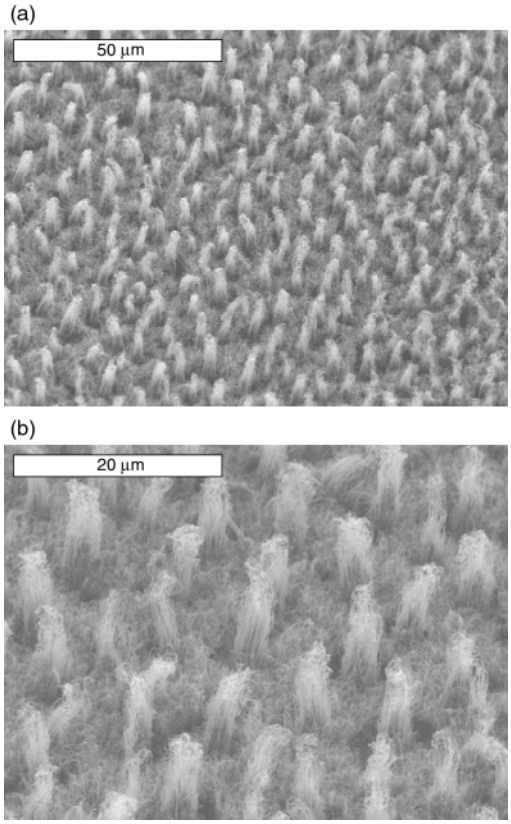

Fig. 1 SEM images of 3D regular arrays of nanotubes aligned along the direction perpendecular to the substrate surface: (a) an oblique 45° of pillar-shaped CNT alignments. (b) a high magnification image of nanotube posts.

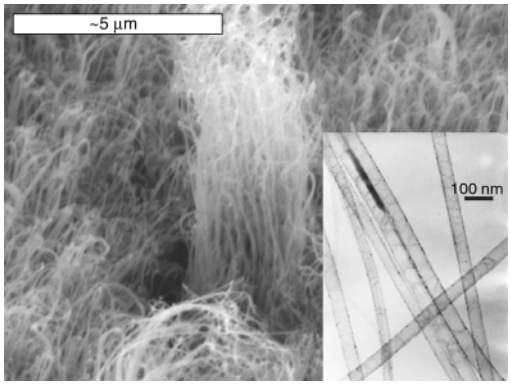

Fig. 2 SEM images of an individual nanotube post from an oblique 45^0 (inset, a TEM image of CNTs).

DOI: 10.1039/b100326g

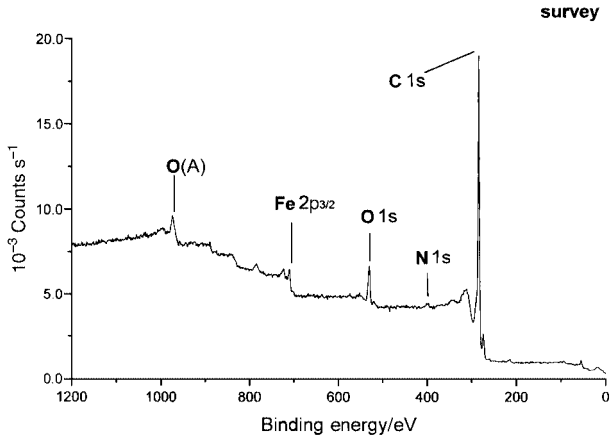

Fig. 3 A wide survey XPS spectrum of the carbon nanotubes.

Fig. 3 shows a wide survey XPS spectrum of the nanotubes. A sharp peak at 284.5 eV corresponds to a π* feature associated with sp^2 hybridized carbon. This observation confirms that the nanotubes mainly contain carbon. Besides carbon (93.30 atom%), nitrogen (0.96 atom%) and iron (0.74 atom%), oxygen (5.00 atom%) is also present in the surface of the nanotubes, which may arise from air absorbed on the nanotubes. A split in the π*-type peak of the N 1s spectrum (not shown) reveals the presence of two peaks at 399.3 and 401.1 eV, corresponding to sp^2 pyridine-like N and sp^3 bridgehead-type N incorporated into the graphitic network, respectively.[16] The 399.3 eV feature is due to pyridinic nitrogen present at the nanotube end, while the peak centered at 401.1 eV corresponds to trivalent nitrogen replacing the carbon in the hexagonal structure.[17] The substitutional N in a graphite sheet strongly favours the formation of pentagons and heptagons, which is responsible for the bamboo-like morphologies.[15]

In addition to the pillar-shaped 3D nanotube alignments, most interesting patterns made of nanotubes arrays, such as ring-like castles [Fig. 4(a)] and a 490 μm long crucian carp without a tail and fins [Fig. 4(b)], were observed under similar experimental conditions. Although the growth mechanism for these patterns is not clear at the present stage, we think that the substrate should be responsible for their formation. Apart from this, both the strong van der Waals interactions between the tubes and the high surface density of the growing nanotubes serve as additional factors for the constituent nanotube to be "uncoiled" and allow the aligned nanotubes to develop on the quartz substrate.

In conclusion, we report the pillar-shaped fabrication and the most interesting patterns of 3D CNT alignments by pyrolysis of iron(II) phthalocyanine. The nanotube alignments have been identified as promising candidates for field emitters in applications such as flat panel displays. Moreover, we can find innumerable technical applications in the field of biomimetic materials if the ultrahydrophobic property of the pillar-shaped 3D alignments of CNTs can be transferred to artificial surfaces (*e.g.* cars, facades, foils). Further efforts should concentrate on the understanding the growth mechanism and controlled synthesis of the 3D regular arrays of the nanotubes.

We gratefully acknowledge financial support from the National Nature Science Foundation of China (NSFC) and the Chinese Academy of Sciences.

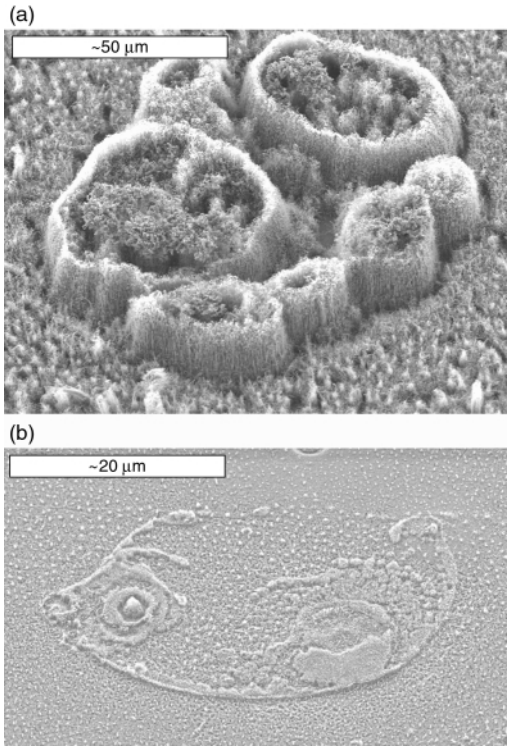

Fig. 4 SEM images of 3D nanotube patterns: (a) ring-like castles. (b) A 490 μm long crucian carp without a tail and fins.

Notes and references

1 W. A. de Heer, A. Chatelain and D. Ugarte, *Science*, 1995, **270**, 1179.
2 A. G. Rinzler, J. H. Hafner, P. Nikolaev, L. Lou, S. G. Kim, D. Tomanek, P. Nordlander, D. Colbert and R. S. Smalley, *Science*, 1995, **269**, 1550.
3 Y. Chen, D. T. Show and L. Guo, *Appl. Phys. Lett.*, 2000, **76**, 2469.
4 S. Fan, M. G. Chapline, N. R. Franklin, T. W. Tombler, A. M. Cassell and H. Dai, *Science*, 1999, **283**, 512.
5 P. G. Collins, A. Zettle, H. Bando, A. Thess and R. E. Smalley, *Science*, 1997, **278**, 100.
6 S. J. Tans, A. R. M. Vershuerent and C. Dekker, *Nature*, 1998, **393**, 49.
7 D. Öner and T. J. McCarthy, *Langmuir*, 2000, **16**, 7777.
8 W. Z. Li, S. S. Xie, L. X. Qian, B. H. Chang, B. S. Zou, W. Y. Zhou, R. A. Zhao and G. Wang, *Science*, 1996, **274**, 1701.
9 C. N. R. Rao, R. Sen, B. C. Satishkumar and A. Govindaraj, *Chem. Commun.*, 1998, **15**, 1525.
10 M. Terrones, N. Grobert, J. Olivares, J. P. Zhang, H. Terrones, K. Kordatos, W. K. Hsu, J. P. Hare, P. D. Townsend, K. Prassides, A. K. Cheetham, H. W. Kroto and D. R. M. Walton, *Nature*, 1997, **388**, 52.
11 Z. F. Ren, Z. P. Huang, J. W. Xu, J. H. Wang, P. Bush, M. P. Siegal and P. N. Provencio, *Science*, 1998, **282**, 1105.
12 Z. P. Huang, J. W. Xu, Z. F. Ren, J. H. Wang, M. P. Siegal and P. N. Provencio, *Appl. Phys. Lett.*, 1998, **73**, 3845.
13 X. B. Wang, Y. Q. Liu and D. B. Zhu, *Appl. Phys. A*, 2000, **71**, 347.
14 W. Barthlott and C. Neinhuis, *Planta*, 1997, **202**, 1.
15 X. B. Wang, W. P. Hu, Y. Q. Liu and D. B. Zhu, *Carbon*, 2001, in press.
16 M. Terrones, P. Redlich, N. Grobert, S. Trasobares, W. Hsu, H. Terrones, Y. Zhu, J. P. Hare, C. L. Reeves, A. K. Cheetham, M. Rühle, H. W. Kroto and D. R. M. Walton, *Adv. Mater.*, 1999, **11**, 655.
17 M. Nath, B. C. Satishkumar, A. Govindaraj, C. P. Vinod and C. N. R. Rao, *Chem. Phys. Lett.*, 2000, **322**, 333.

cis-Fused γ-lactones from simple precursors *via* β-lactone rearrangements

T. Howard Black,*† Douglas C. Smith,‡ Shane A. Eisenbeis, Karen A. Peterson and Mark S. Harmon

Department of Chemistry, Eastern Illinois University, Charleston, IL 61920 USA. E-mail: thblack@eiu.edu

Received (in Corvallis, OR, USA) 2nd January 2001, Accepted 3rd March 2001
First published as an Advance Article on the web 3rd April 2001

***cis*-Fused bicyclic γ-lactones were prepared in a three step sequence, featuring the stereospecific rearrangement of spiro bicyclic β-lactones; the dependence of the β- to γ-lactone ring expansion on the relative stabilities of the intermediate carbocations was also investigated.**

We have previously demonstrated that β-lactones, such as **1**, undergo ring expansion towards more highly or equally substituted carbon atoms, *via* carbocation rearrangements, to afford γ-lactones **2** (Scheme 1).[1] Moreover, it has also been determined that this ring expansion requires that both migrating bonds bear an antiperiplanar relationship with respect to one another to effect γ-lactone formation.

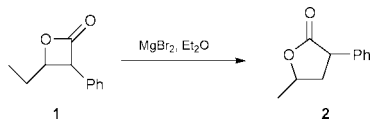

Scheme 1

In an effort to further explore the scope and limitations of this very useful transformation, we examined the rearrangement of β-lactones derived from cyclic ketones, carefully selected in order to most accurately ascertain how structural variations within the spiro-bound carbocycle would affect β- to γ-lactone ring expansion reactions.

Scheme 2 depicts the method by which butyrolactones were prepared from simple carbonyl precursors.[2] In this study, the dianion of either isobutyric acid or acetic acid was condensed with cyclic ketones **3** to afford the corresponding β-hydroxy acids **4** in fair to good yields.[3] These acids were subsequently treated with $PhSO_2Cl$ in pyridine for 12 h at 0 °C to provide, in good to excellent yields, spiro bicyclic β-lactones **5**. Treatment of **5** with freshly prepared $MgBr_2$[4] in anhydrous diethyl ether initiated their rearrangement to the fused γ-lactones **6** or, in one case, the corresponding β,γ-unsaturated carboxylic acid **7**.[5] These results are summarized in Table 1.

The pivotal event in this transformation is the rearrangement of one intermediate tertiary carbocation to another tertiary carbocation; this is followed by annulation to form the γ-lactone ring. The *cis* fusion of these systems, although predicted on

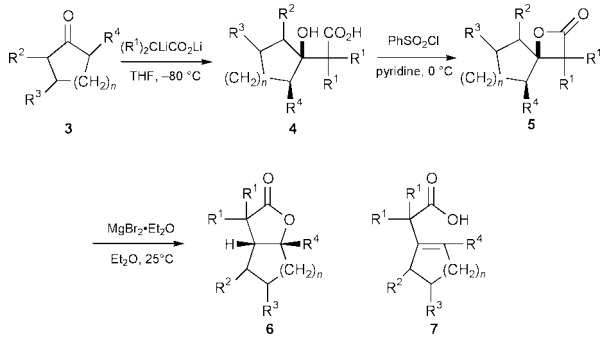

Scheme 2

† Camille and Henry Dreyfus Scholar, 1993–1995.
‡ Camille and Henry Dreyfus Fellow, 1993–1995.

Table 1 Structural and yield data for Scheme 2

						Isolated yield (%)			
Suffix	**3***n*	R^1	R^2	R^3	R^4	**4**	**5**	**6**	**7**
a	1	CH_3	H	H	CH_3	67	85	88	0
b	2	CH_3	H	H	CH_3	63	93	73	0
c	2	H	H	H	CH_3	78	82	84	0
d	2	CH_3	H	H	OCH_3	89	73	85	0
e	2	CH_3	Benzo fused		H	79	67	0	57

mechanistic grounds, could not be determined spectroscopically *a priori*; thus, stereochemical assignment of these compounds was made by analogy to compounds previously reported in the literature. Accordingly, the known[6] γ-lactone **6c** was prepared from the dianion of acetic acid and 2-methylcyclohexanone, **3c**, in 54% overall yield (three steps). This compound was found to have physical and spectral characteristics identical to those previously reported for the *cis* isomer.[4] Moreover, this analog permitted unequivocal stereochemical determination spectroscopically through the use of NOE techniques; these results are summarized in Fig. 1. Irradiation of the methyl group in Fig. 1 led to an NOE enhancement of 7.2% for the adjacent bridgehead proton, while reciprocal irradiation of the bridgehead proton led to an NOE enhancement of 3.7% for the adjacent methyl group. Therefore, compounds **6a,b,d** were also assigned a *cis* ring fusion by analogy.

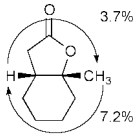

Fig. 1

In only one instance was a fused bicyclic butyrolactone not produced. The rearrangement of spiro bicyclic β-lactone **5e**, derived from α-tetralone, to such an entity, would have required the rearrangement of a tertiary benzylic carbocation to a secondary homobenzylic species. As this is obviously a thermodynamically unfavorable process, elimination occurred instead to provide exclusively β,γ-unsaturated carboxylic acid **7e**.[7]

An interesting observation noted during this investigation was the migration of a hydride, in place of an available methoxy group, in the **5d** to **6d** transformation. Reetz has demonstrated heteroatom migration preferentially to hydride in β-lactone ring expansions, when single bond rotation allows for ready alignment of either.[8] However, in β-lactone **5d**, only the hydrogen is situated in the required antiperiplanar alignment with the lactone ring oxygen; thus, exclusive migration of the hydride occurs in high yield. These reactions are illustrated in Scheme 3. The success of the transformation of **5d** to **6d** bodes very well for future applications as an alternative route for the preparation of γ-*exo*-enol lactones,[9] which are common structural units in natural products possessing a variety of applications.[10] Moreover, this strategy also allows for an alternative preparation[11] of 1,4-dicarbonyl compounds, which are useful

DOI: 10.1039/b100261a

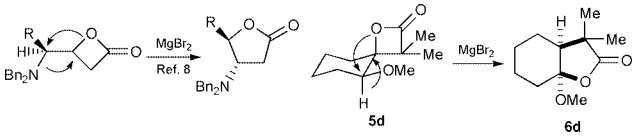

Scheme 3

synthons in natural products synthesis. Future studies of the generality of this procedure are planned, employing different heteroatom substituents in various conformations, to determine the scope and limitations of this potentially very useful new protocol.

In summary, the ability of β-lactones to rearrange to their corresponding butyrolactone derivatives depends upon both the relative stability of the two involved intermediate carbocations and the ability of the migrating bonds to achieve an anti-periplanar relationship. This method has also proved to be very efficient for the preparation of a variety of *cis* fused bicyclic lactones, and provides easy access to these important structural subunits.

We wish to thank Dr Ellen Keiter of Eastern Illinois University and Dr Dean Carlson of Purdue University for their assistance in determining the relative stereochemistry of the bicyclic γ-lactones. Additionally, we would like to thank the Petroleum Research Fund (administered by the ACS), the National Science Foundation (CHE-9203760), the Camille and Henry Dreyfus Foundation, and the National Institutes of Health (GM52677-01) for their financial support; as well as the NSF ILI program for funds with which to purchase a GCMS (USE-9251113) and a QE 300 NMR spectrometer (CHE-8815619).

Notes and references

1 (*a*) T. H. Black and W. J. DuBay, *Tetrahedron Lett.*, 1987, **28**, 4787; (*b*) T. H. Black and J. D. Fields, *Synth. Commun.*, 1988, **18**, 125. See also ref. 2.
2 T. H. Black, W. J. DuBay III and P. S. Tully, *J. Org. Chem.*, 1988, **53**, 5922. All precursors were purchased from Aldrich Chemical Co., Inc.
3 These acids were routinely recrystallized (ethyl acetate) prior to lactonization, so that only the predominant (shown) stereoisomer was carried on. In early experiments, the *erythro*:*threo* isomer ratio was determined to be at least 95:5.
4 Note: it is important to use freshly prepared $MgBr_2$ to effect this rearrangement. This is most readily accomplished by treating 1,2-dibromoethane with magnesium metal in anhydrous ether for approximately 1 h prior to the addition of the β-lactone substrate. Employing either commercial $MgBr_2$ or its diethyl ether complex results in considerably lower yields of the γ-lactone.
5 Titanium tetrachloride is the only other Lewis acid found to mediate this transformation, although its much greater acidity occasionally causes undesired side reactions; see T. H. Black, J. A. Hall and R. G. Sheu, *J. Org. Chem.*, 1988, **53**, 2371.
6 (*a*) R. A. Bunce, R. E. Drumright and V. L. Taylor, *Synth. Comm.*, 1989, **19**, 2423; (*b*) G. H. Lee, E. B. Choi, E. Lee and C. S. Pak, *J. Org. Chem.*, 1994, **59**, 1428.
7 Similar behavior has been observed previously; see T. H. Black, S. A. Eisenbeis, T. S. McDermott and S. L. Maluleka, *Tetrahedron*, 1990, **46**, 2307.
8 M. T. Reetz, A. Schmitz and X. Holdgrun, *Tetrahedron Lett.*, 1989, **30**, 5421.
9 M. Yamamoto, *J. Chem. Soc., Perkin Trans. 1*, 1981, 582.
10 (*a*) R. Kazlauskas, P. T. Murphy, R. J. Quinn and R. J. Wells, *Tetrahedron Lett.*, 1977, 37; (*b*) J. A. Pettus Jr., R. M. Wing and J. J. Sims, *Tetrahedron Lett.*, 1977, 41.
11 (*a*) H. Kunz and M. Lindig, *Chem. Ber.*, 1983, **116**, 220; (*b*) C. Brückner and H.-U. Reissig, *J. Org. Chem.*, 1988, **53**, 2440; (*c*) K. Griesbaum, H.-J. Greunig, W. Volpp and I.-C. Jung, *Chem. Ber.*, 1991, **124**, 947.

Au nanoparticle- and silver-enhancement reaction-amplified microgravimetric biosensor

Xiaodi Su,*[a] Sam Fong Yau Li [b] and S. J. O'Shea[a]

[a] *Institute of Materials Research & Engineering, No. 3, Research Link, Singapore 117602. E-mail: xd-su@imre.org.sg*
[b] *Department of Chemistry, National University of Singapore, 10 Kent Ridge Crescent, Singapore 119260*

Received (in Cambridge, UK) 6th December 2000, Accepted 13th March 2001
First published as an Advance Article on the web 3rd April 2001

An ultrasensitive microgravimetric biosensor has been developed incorporating Au nanoparticle-amplified sandwiched immunoassay and silver enhancement reaction; Au nanoparticle-promoted silver(I) reduction and silver metal deposition result in *ca.* two orders of magnitude improvement in human IgG quantification.

The use of gold nanoparticles as a signal amplifier has attracted increasing interest in biosensor development. For example, in surface plasmon resonance[1–3] and microgravimetric quartz crystal microbalance (QCM)[4] based protein binding assay and DNA hybridization assay, mass coupling of functional Au nanoparticles results in a tens- to hundreds-fold sensitivity increase. However, the use of primary Au nanoparticles is not the end of the amplification. Efforts have been made to realize ultrasensitive biosensing by means of sequent amplification routes of, for example, multilayered[5] or dendritic-type Au nanoparticles.[6] In the latter example (microgravimetric DNA sensor), the primary Au nanoparticle amplification (*ca.* 10-fold) is followed by a secondary dendritic-type Au nanoparticle interaction. A total of 30-fold signal enhancement is achieved through the stepwise amplification.

Immunogold silver staining (IGSS) has been widely used in histochemical microscopy studies,[7] where functional Au nanoparticles act as catalysts to reduce silver ions to metallic silver. The autometallographic silver deposition procedure enlarges the size and darkens the color of the particles, such that protein-, antibody- or DNA-conjugated Au particles become visible under electron- or light-microscope. Most recently, this amplification strategy has been adopted in a pioneering study of scanometric DNA array quantification.[8] The incorporation of Au nanoparticle labeling and silver staining amplification results in two orders of magnitude improvement in detection sensitivity when compared with a conventional fluorophore system. Based on the similar amplification routes, a silicon-based flexural plate wave sensor has been developed.[9] The mass loading caused by Au particle-catalyzed deposition of metallic silver leads to a five orders of magnitude improvement in cancer antigen detection. In addition to the Au conjugate-promoted silver staining reaction, enzyme conjugate-catalyzed precipitation processes have also been applied for signal amplification in QCM and electrochemical sensors.[10,11]

Using an Au conjugate as a biocatalytic probe, we present herein an ultrasensitive microgravimetric QCM biosensor, in which primary Au nanoparticle-amplified sandwiched-immunoassay is followed by a silver staining reaction. The sensor elements are 10 MHz AT-cut quartz crystals coated with silver electrodes. An immunochemical molecular recognition event between anti-human IgG (a-h IgG) and human IgG (h IgG) is chosen to illustrate the sandwich procedure and, sequentially, the silver enhancement reaction (Scheme 1). It can be seen the proposed assay starts from the shielding of the metal electrode by polystyrene treatment. As reported in our previous study,[12] deposition of a polystyrene film (from a 5 mg ml^{-1} toluene solution) shields the silver electrode from undesirable oxidation and, in addition, provides a substrate for biomolecular immobilization. In this study, to evaluate the coverage of the polymer film further, the silver enhancement reagent [a freshly prepared 1:1 mixture of the silver enhancement solution A

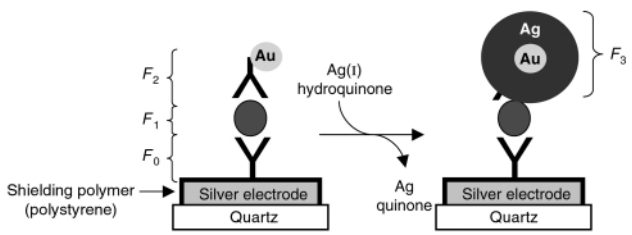

Scheme 1 Schematic illustration of the Au nanoparticle-based, sandwiched immunoassay and silver staining amplification.

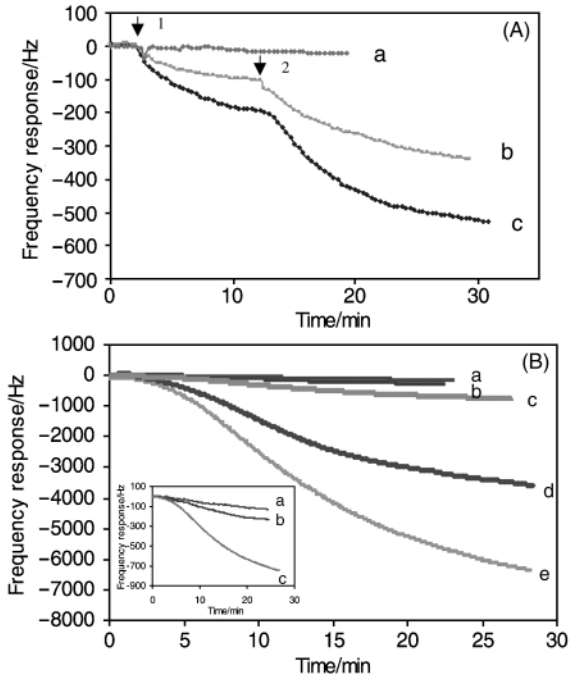

Fig. 1 (A) Frequency response of a-h IgG-modified sensors upon the application of h-IgG (10 μg ml^{-1}, curve b; 20 μg ml^{-1}, curve c) at arrow 1 and, sequentially, F_c specific a-h IgG:Au at arrow 2. Curve a is obtained when the modified sensor was exposed to the Au conjugate directly without h IgG application. (B) Frequency response of sandwiched complex coated sensors upon the exposure to silver enhancement reagent. Curves a and b are the background signals obtained in the absence of Au conjugate and h IgG incubation, respectively, in the sandwiched procedures; curves c, d and e represent h IgG concentrations of 0.5, 10 and 20 μg ml^{-1}, respectively.

DOI: 10.1039/b009768n

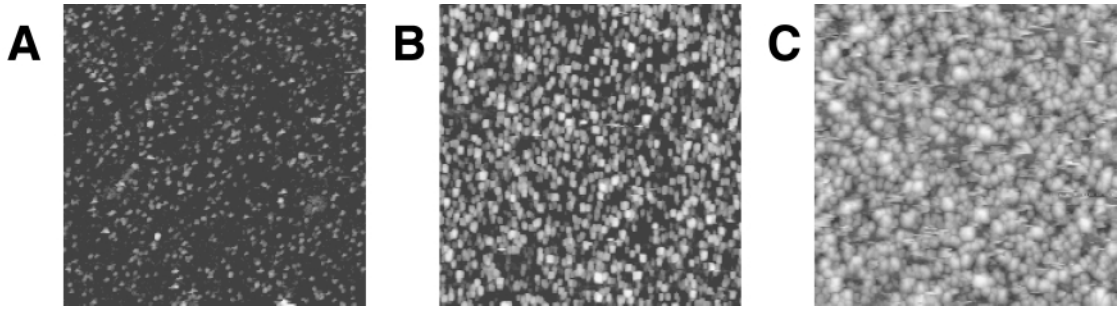

Fig. 2 AFM images (1 μm × 1 μm) of anti-h IgG/h-IgG (20 μg ml^{-1})/a-h IgG:Au coated surfaces before exposure (A), and after 10 min (B) and 30 min (C) exposure to silver enhancement solution.

(silver salt) and solution B (hydroquinone initiator) from Silver Enhancer Kit, SE-100 (Sigma)] was applied to the treated surface. After 30 min of reaction, no darkening of the surface was observed and the resonant frequency of the sensor remained unchanged. Thus it can be assumed that, after shielding by polystyrene, none of the metal electrode is exposed to serve as a nucleation site for silver ion reduction. This is essential for the proposed assay.

After polystyrene coating, the sensor surfaces were exposed to 0.5 mg ml^{-1} of a-h IgG (γ-chain specific, Sigma) in PBS buffer, pH 7.4. Through 1 h of incubation at 37 °C, the antibody molecules were firmly immobilized through passive adsorption and hydrophobic interaction. After blocking the non-occupied binding sites (2% BSA incubation for 15 min), the modified surfaces (with resonant frequency F_0) were exposed to h IgG (purified from serum, Sigma) and, when equilibrated, to 10 nm Au-conjugated a-h IgG (F_c-specific, Sigma). As a result, the analyte (h IgG) was sandwiched between bound antibodies and Au-conjugated antibodies. Fig. 1(A) shows the frequency responses of the sandwich procedures. The binding of h IgG with bound a-h IgG leads to a smooth frequency decrease to F_1. Complete binding is achieved within *ca*. 10 min. The following Au conjugate application results in further frequency response to F_2 after a longer duration of about 20 min. The total frequency changes caused by the sandwich procedures (F_0–F_2) are three- to four-fold greater than those obtained by direct analyte binding (F_0–F_1). The lower response of the Au conjugates may arise from steric inhibition of the huge molecules (it has been estimated that a 10 nm Au particle conjugates with seven IgG molecules). If the a-h IgG-modified sensor was exposed to Au-conjugated a-h IgG directly without analyte application, no frequency response was detectable [curve a in Fig. 1(A)]. This confirms that the binding of the Au-conjugate is attributable to the primary amplification for h IgG determination in the sandwich assay.

This is not the end of the amplification. Upon formation of the sandwiched immunocomplex, the sensor surfaces are coated with Au nanoparticles, which serve as nucleation sites to catalyze silver ion reduction. Fig. 1(B) shows the frequency responses of the sandwiched-immunocomplex-coated surfaces upon application of the silver enhancement solution. The deposition of metallic silver on the surface of the bound Au particle boosts the signal further to F_3 (Scheme 1). To optimize the signal and to reduce the silver staining background, after the sandwich reactions the sensors were rinsed thoroughly using deionized water to remove all salt content so as to avoid the auto-nucleation of silver. In addition, a five-fold diluted silver enhancement solution was optimal in reducing the staining background obtained in the absence of Au-conjugated antibodies [curve (a) in Fig. 1(B)] or h IgG [curve (b) in Fig. 1(B)]. These results confirm that neither significant nonspecific silver staining nor nonspecific Au particle binding occurs. Under the optimal conditions, the enormous frequency changes caused by silver metal deposition on a-h IgG/h IgG/a-h IgG:Au-coated sensors (F_2–F_3) are reflective of h IgG at different concentrations [curves c–e in Fig. 1(B)]. The incorporated primary and secondary amplified signals (F_0–F_3) are proportional to h IgG concentrations with ΔF(Hz) = $317C_{IgG}$(μg ml^{-1}) + 256, r^2 = 0.962. This is about two orders of magnitude more sensitive than that of direct assay.[12] It is also interesting to note that Fig. 2(B) reveals the mechanism of Au-promoted silver(I) reduction: within the first 5 min, the reduction is slow; after 5 min, significant reduction appears; and at *ca*. 30 min the reduction tends to be complete.[7]

The above observations are further proved by atomic force microscopy (AFM) studies. AFM images(1 μm × 1 μm) acquired for a-h IgG/h IgG/a-h IgG:Au-coated surfaces before [Fig. 2(A)] and after exposure to the silver enhancement solution [Fig. 2(B) and 2(C)] were obtained using a TMX 2000 Explorer System (TopoMetrix, Santa Clara, CA) operated under ambient conditions. Si_3N_4 cantilevers with V-shaped tips (20–50 nm radius of curvature) were used for measurement in contact mode. Although the observed particle size may deviate from the actual value because of the intrinsic curvature of the tip,[13] the deposition of metallic silver on the surface of the Au particles is still clearly evident.

In conclusion, we have developed an ultrasensitive QCM biosensor which combines metal electrode shielding, Au nanoparticle-amplified sandwiched-assay and a silver enhancement reaction. Based on this method, the detection sensitivity of the microgravimetric sensor is no longer subject to the mass of the analyte molecules. Since the proposed assay relies on the shielding of the metal electrode, the advanced electrode shielding technique remains a challenge. For example, functionalization of a polystyrene film may combine electrode protection with covalent DNA molecule immobilization in one preparation step, such that the proposed assay can be extended to ultrasensitive DNA analysis. In addition, this study suggests the possibility of utilizing the silver enhancement reaction for quantification in chip-based biosensing.

Notes and references

1 L. He, M. D. Musick, S. R. Nicewarner, F. G. Salinas, S. J. Benkovic, M. J. Natan and C. D. Keating, *J. Am. Chem. Soc.*, 2000, **122**, 9071.
2 L. A. Lyon, M. D. Musick and M. J. Natan, *Anal. Chem.*, 1998, **70**, 5177.
3 L. A. Lyon, M. D. Musick, P. C. Smith, B. D. Reiss, D. J. Pena and M. J. Natan, *Sens. Actuators B*, 1999, **54**, 118.
4 X. C. Zhou, S. J. O'Shea and S. F. Y. Li, *Chem. Commun.*, 2000, 953.
5 T. A. Taton, R. C. Mucic, C. A. Mirkin and R. L. Letsinger, *J. Am. Chem. Soc.*, 2000, **122**, 6305.
6 F. Patolsky, K. T. Ranjit, A. Lichtenstein and I. Willner, *Chem. Commun.*, 2000, 1025.
7 G. W. Hacker, in *Colloidal Gold: Principles, Methods, and Applications*, ed. M. A. Hayat, Academic Press, San Diego, CA, 1989, vol. 1. chap. 10.
8 T. A. Taton, C. A. Mirkin and R. L. Letsinger, *Science*, 2000, **289**, 1757.
9 A. W. Wang, R. Kiwan, R. M. White and R. L. Ceriani, *Sens. Actuators, B*, 1998, **49**, 13.
10 A. Bardea, E. Katz and I. Willner, *Electroanalysis*, 2000, **12**, 1097.
11 R. C. Richard and M. D. Ward, *J. Am. Chem. Soc.*, 1988, **110**, 8623.
12 X. D. Su, H. T. Ng, C. C. Dai, S. J. O'Shea and S. F. Y. Li, *Analyst*, 2000, **125**, 2268.
13 A. Doron, E. Joselevich, A. Schlittner and I. Willner, *Thin Solid Films*, 1999, **340**, 183.

Carbonyl and olefin reactivities for the Baylis–Hillman reaction of fluorocarbonyls

P. Veeraraghavan Ramachandran,* M. Venkat Ram Reddy and Michael T. Rudd

H. C. Brown and R. B. Wetherill Laboratories of Chemistry, Purdue University, West Lafayette, Indiana 47907-1393, USA. E-mail: chandran@purdue.edu

Received (in Corvallis, OR, USA) 10th November 2000, Accepted 6th March 2001
First published as an Advance Article on the web 4th April 2001

The product formation and yields for the Baylis–Hillman reaction of fluorine-containing carbonyl compounds depend on a balance between the reactivities of the carbonyl and olefin partners.

It is well established that the biological properties of medicinal compounds can often be influenced by fluorine substitution.[1] The physical properties of several electronic and optical devices also depend immensely on the structure of fluoroorganic molecules.[2] Fluorine substitution provides organic chemists with an opportunity to study an extreme case of electronic effect in reactions.[1,2] As part of our ongoing projects in fluoroorganic chemistry,[3] we examined the Baylis–Hillman (BH) reaction[4] of activated olefins with fluoro-aldehydes and -ketones in the

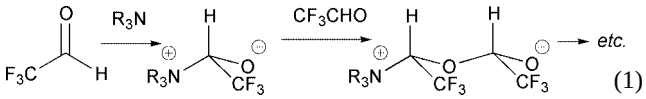

(1)

presence of 10 mol% of 1,4-diazabicyclo[2.2.2]octane (DABCO). Herein we report a fascinating relation between the reactivities of the carbonyl and olefin partners for the BH reaction of fluorocarbonyls; a match providing optimum yields of the products, whereas a mismatch resulting in the decomposition or side reaction of the faster reacting partner.

Acrolein (**1a**), methyl vinyl ketone (**1b**), ethyl acrylate (**1c**) and acrylonitrile (**1d**) were the olefins chosen for the reaction. Initially we studied the reaction of fluoral (**2**) with **1a**–**d**. Upon mixing **2** with **1a** at rt under neat conditions, in the presence of 10% DABCO, polymerization of both reactants occurred. Both of these are known to polymerize in the presence of amines [eqn. (1)].[5,6] We then carried out the reaction in THF and obtained a very low yield of the expected product along with the polymerized starting materials. With the hope of arresting the polymerization, we lowered the reaction temperature to −25 °C and obtained a 40% yield of the product, **3a** [eqn. (2)]. However,

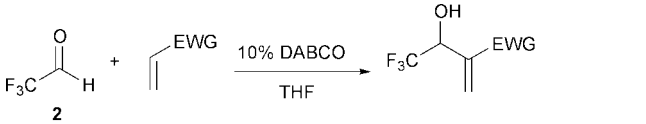

(2)

we could not suppress the polymerization completely. Further lowering the temperature had a deleterious effect since polymerization of both reactants was faster than the BH reaction at this temperature.

Reaction of **2** with **1b** provided the product **3b** in 35% yield under neat conditions, at rt, 1 h. Surprisingly, the yield in THF at −25 °C was 65%! [eqn. (2)]. However, the reaction of **1c** provided only a 20% yield of the product **3c** at rt under neat conditions [eqn. (2)]. Decreasing the reaction temperature suppressed the BH reaction completely and only the polymer of fluoral was obtained. Olefin **1d** did not yield any BH product **3d** at room or lower temperature.

Reaction of 2,2,3,3,4,4,4-heptafluorobutanal (**4**), the fluorinated homolog of **2**, showed identical reaction patterns with slightly improved yields of the products. Thus, while **1a** and **1b** provided 50 and 70% yield, respectively, of products at −25 °C, **1c** provided 22% yield of the product **5c** and **1d** failed to provide any product at rt.

The dissimilarity in product yields from activated olefins of differing reactivity captivated us. We considered a less reactive perfluorinated aldehyde that does not undergo polymerization in the presence of a 3°-amine and tested pentafluorobenzaldehyde (**6**) with **1a**–**d**. While the reactions of **1b**–**d** were complete under neat condition at rt within 2–4 d, **1a** polymerized. However, it reacted in THF at 0 °C within 15 min providing 95% yield of the product [eqn. (3)].

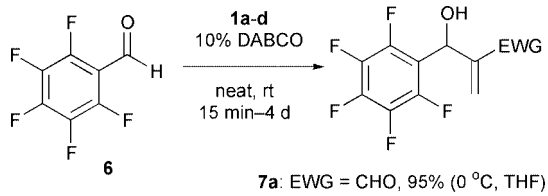

(3)

7a: EWG = CHO, 95% (0 °C, THF)
7b: EWG = COMe, 70%
7c: EWG = CO_2Et, 70%
7d: EWG = CN, 75%

Ordinary ketones undergo Baylis-Hillman reaction occasionally under high pressures[4] and activated carbonyls, such as α-keto esters and hexafluoroacetone undergo relatively fast reaction.[7,8] 1,1,1-Trifluoroacetone (**8**) is known to trimerize in the presence of amines.[9] However, our partial success with **2** persuaded us to carry out its reaction at low temperatures. In fact, we obtained only 10–12% yield of the products **9a** with **1a** in THF at −25 °C, and **9d** with **1d** at rt. Olefins **1b** and **1c** failed to provide any product with **8**. We isolated a polymeric material in both of these cases.

To avoid the polymerization initiated by abstraction of the α-hydrogen atom, we focused our attention on aromatic trifluoromethyl ketones. The treatment of 2,2,2-trifluoroacetophenone (**10**) with two equiv. of **1a**, under neat conditions, at rt did not provide any product. Decreasing the reaction temperature to −25 °C yielded 15% of acrolein dimer along with its polymer. Olefin **1b** also did not provide any of the expected BH products at rt, although we obtained a 30% yield of the dimer. Lowering the temperature resulted only in the suppression of the dimerization. In contrast, a slow reaction (7 d) between **10** and **1c** resulted in 70% yield of the expected allylic alcohol **11c**. The reaction with **1d** was faster, complete within 24 h, and provided 94% yield of the product **11d** [eqn. (4)].

2-(Trifluoroacetyl)thiophene (**12**) provided similar results. On testing with **1a**–**d**, it underwent reaction only with **1c** within 7 d providing the product **13c** in 65% yield, and with **1d**, within 24 h, providing the product allylic alcohol **13d** in 82% yield [eqn. (4)].

DOI: 10.1039/b009177b

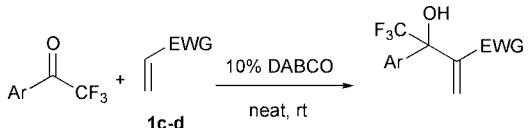

10: Ar = Ph
12: Ar = 2-Thiophene

11c: Ar = Ph; EWG = CO_2Et, 70%
11d: Ar = Ph; EWG = CN, 94%
13c: Ar = 2-Thiophene; EWG = CO_2Et, 65%
13d: Ar = 2-Thiophene; EWG = CN, 82%

(4)

2,3,4,5,6-Pentafluoroacetophenone (**14**) behaved like an ordinary ketone, failing to react with any of the four activated olefins.

In conclusion, we have studied the effect of fluorine substitution in the Baylis–Hillman reaction. A series of novel functionalized fluorinated allyl alcohols have been synthesized during this study, enriching fluoroorganic chemistry.[10] We have successfully obtained products even from amine-sensitive carbonyls as well as olefins by controlling the reaction conditions. This is the first report of a Baylis–Hillman reaction at such low temperatures (−25 °C).

When the fluorocarbonyls are extremely reactive, capable of reacting with themselves in the presence of an amine (*e.g.* fluoral, heptafluorobutanal), the olefin has to be very reactive as well (*e.g.* acrolein, methyl vinyl ketone) to obtain the products. A mismatch as in the case of relatively less reactive ethyl acrylate and acrylonitrile results in the polymerization of these fluoroaldehydes. The reaction of a less reactive fluorocarbonyl, such as pentafluorobenzaldehyde, is effective with both highly reactive and moderately reactive olefins. Decreasing the reactivity of the fluorocarbonyl further (*e.g.* 2,2,2-trifluoroacetophenone) provides good yield of products only with the less reactive olefins (*e.g.* ethyl acrylate and acrylonitrile). Ring-fluorination of aromatic ketones does not sufficiently activate the carbonyl for the reaction. It appears that a match between the reactivities of the fluorocarbonyl and olefin partners is essential for obtaining reasonable yield of the products in the Baylis–Hillman reaction.[11]

The financial assistance from Eastman Kodak Company is gratefully acknowledged.

Notes and references

1 For several recent reviews see: *Biomedical Frontiers of Fluorine Chemistry*, ed. I. Ojima, J. R. McCarthy, and J. T. Welch, ACS Symposium Series, **639**, American Chemical Society, Washington DC, 1996.
2 For several recent reviews see: (*a*) *Asymmetric Fluoroorganic Chemistry*, ed. P. V. Ramachandran, ACS Symposium Series, **746**, American Chemical Society, Washington, DC, 2000; (*b*) For a review on the effect of fluorine on OH, NH, and CH acidities, see: M. Schlosser, *Angew. Chem., Int. Ed.*, 1998, **37**, 1497.
3 (*a*) P. V. Ramachandran, B. Gong and H. C. Brown, *J. Org. Chem.*, 1995, **60**, 61; (*b*) H. C. Brown, G. M. Chen, M. P. Jennings and P. V. Ramachandran, *Angew. Chem., Int. Ed.*, 1999, **38**, 2052; (*c*) P. V. Ramachandran, M. P. Jennings and H. C. Brown, *Org. Lett.*, 1999, **1**, 1399.
4 For a recent review see: D. Basavaiah, P. D. Rao and R. S. Hyma, *Tetrahedron*, 1996, **52**, 8001.
5 W. K. Busfield and E. Whalley, *Polymer*, 1966, **7**, 541.
6 N. Yamashita, M. Yoshihara and T. Maeshima, *J. Macromol. Sci., Chem.*, 1973, **7**, 569.
7 (*a*) C. Grundke and H. M. R. Hoffman, *Chem. Ber.*, 1987, **120**, 1461; (*b*) D. Basavaiah, T. K. Bharathi and V. V. L. Gowriswari, *Tetrahedron Lett.*, 1987, **28**, 4351.
8 A. S. Golubev, M. V. Galakhov, A. F. Kolomiets and A. V. Fokin, *Izv. Akad. Nauk Ser. Khim.*, 1992, 2763.
9 M. M. Dhingra and K. R. Tatta, *Org. Mag. Res.*, 1977, **9**, 23.
10 For a review on fluorinated allylic alcohols as building blocks, see: T. Allmendinger, C. Angst and H. Karfunkel, *J. Fluorine Chem.*, 1995, **72**, 247.
11 The reaction of methyl vinyl ketone with fluoral is representative. 2,2,2-Trifluoroacetaldehyde (0.49 g, 5 mmol) was added, at −25 °C, to a stirred solution of methyl vinyl ketone (0.70 g, 10 mmol, 0.83 mL) in THF (5 mL). DABCO (0.056 g, 0.5 mmol) in 0.5 mL THF was added to this and was stirred at this temperature for an additional hour. The solvent was evaporated under vacuum, and the crude reaction mixture was purified by silica gel chromatography (hexanes–ethyl acetate 9:1) to yield 0.55 g (65%) of the pure product.

ChemComm

Photocontrolled self-assembly of molecular switches

Linda N. Lucas,[a] Jan van Esch,*[a] Richard M. Kellogg[b] and Ben L. Feringa*[a]

[a] *University of Groningen, Organic and Molecular Inorganic Chemistry, Stratingh Institute, Nijenborgh 4, 9747 AG, Groningen, The Netherlands. E-mail: Esch@chem.rug.nl; Feringa@chem.rug.nl*

[b] *Syncom BV, Kadijk 3, 9747 AT, Groningen, The Netherlands*

Received (in Liverpool, UK) 1st February 2001, Accepted 1st March 2001
First published as an Advance Article on the web 3rd April 2001

A new self-assembling system is developed, based on dithienylcyclopentene photochromic switches, which forms extended aggregates in solution and for which the viscosity can be changed by light.

The self-assembly of small functional molecules into supramolecular structures comprises a powerful approach towards the development of new materials and devices of nanoscale dimensions,[1,2] and the control of these organisational processes by chemical or physical elements is a major challenge. A promising approach towards such responsive or smart materials is the integration of an addressable function, *e.g.* photochromic moieties,[3] into the supramolecular building blocks, which would offer the possibility to alter the self-assembly process of the individual molecules or change the properties of the supramolecular arrays by means of light.[4]

Here we report on a new self-assembling system based on diarylethene photochromic switches,[3] which forms extended aggregates in solution, and the viscosity of which can be changed by light. Diarylethene and particularly dithienylcyclopentene molecular switches[3,5] are a distinct class of photochromic compounds that can undergo a reversible ring-closure reaction upon irradiation with UV- and visible-light, respectively, which is accompanied by a pronounced change of the electronic properties and conformational flexibility: in the open form (**1o**) the two thienyl moieties are not conjugated and can rotate around the bond connecting them with the cyclopentene ring, whereas in the ring-closed form (**1c**) the conjugation extends throughout the molecule and the rotational freedom is lost (Scheme 1). In this study, the geometrical change accompanying the photochemical transformation is exploited to change the self-assembling properties of **1**, and hence the macroscopic properties of the system. The dithienylcyclopentenes used here offer two distinct features when compared to the commonly used azostilbenes:[4] (i) the photochemically induced ring-closure reaction of dithienylcyclopentenes involves geometrical transformation which is clearly different from the *cis–trans* isomerization, and (ii) the activation energy for thermal interconversion between the open and closed form is large.[3] The use of dithienylcyclopentenes in switchable supramolecular systems will therefore expand the scope of available transformations and will lead to thermally bistable systems (Scheme 1).

In order to promote the formation of supramolecular assemblies in solution by hydrogen bonding, a dithienylcyclopentene-switch has been extended with amide groups (Scheme 1). The 1,2-bis(5′[(alkylamino)carbonyl]-2′-methylthien-3′-yl)cyclopentenes (**1o** and **2o**) were synthesised in a two-step procedure starting from 1,2-bis(5′-formyl-2′-methylthien-3′-yl)cyclopentene.[6] Oxidation with Ag_2O provided the corresponding diacid, which was next converted to amides **1o** and **2o** by first activating the carboxylic acid with 2-chloro-4,6-dimethoxytriazine, followed by a reaction of the activated ester with the corresponding amine. Compounds **1o** and **2o**† were obtained in 33 and 30% overall yield, respectively, after column chromatography starting from the dialdehyde.

The gelation behaviour of **1o** was studied in various solvents of different polarity.[7] It was found that **1o** did not form gels with any of the solvents investigated, but with apolar solvents, like cyclohexane, dodecane and benzene, clear viscous solutions were formed at concentrations well above 5 mM, indicating that aggregation of **1o** occurs.[8] The ^{1}H NMR spectra of **1o** in C_6D_6 show a gradual down field shift of δ_{NH} from 5.26 to 5.56 ppm, and an increase of the line width with increasing concentration, indicating that **1o** forms highly dynamic aggregates through hydrogen bonding between the amide groups at higher concentrations. Together with the observation that the results are not changed by prolonged aging of the samples, this also indicates that the aggregates formed by **1o** are equilibrium structures. Fitting of the data to a cooperative aggregation model[9] revealed that the dimerization constant K_2 = 81 ± 3 M^{-1}, and the association constant for the formation of higher order aggregates K_N = 787 ± 19 M^{-1}. Apparently, the formation of higher order aggregates by bisamide **1o** is highly favored over the formation of dimers in apolar solvents like benzene. Viscosity measurements‡ were performed with a 14.6 mM solution of **1o** in benzene at different shear rates. As is clear from the data shown in Fig. 1, the viscosity decreases with increasing shear rate, indicating that solutions of **1o** behave as a non-Newtonian liquid. Although the molecular interpretation of this phenomenon is not yet clear, similar shear-thinning effects have been observed in helical self-assembled polymers consisting of small hydrogen bonding subunits.[8] It should be noted that dissolution of **2o** does not result in gel formation, nor does it cause a significant increase of the viscosity of the solvent.[10] Moreover, the ^{1}H NMR spectra of **2o** in C_6D_6 show only minor

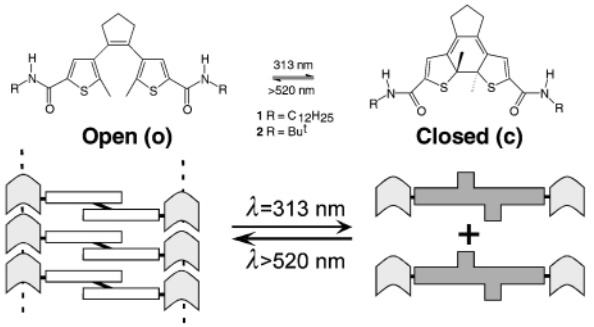

Scheme 1 Photoswitching of diarylethene **1o** and **2o** and thereby controlling the extent of self-assembly of **1** by photochemical switching.

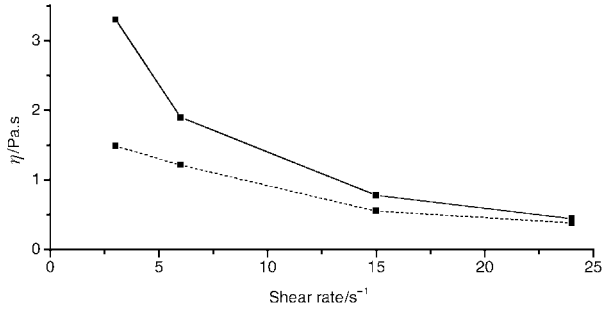

Fig. 1 Viscosity of 14.6 mM solution of **1o** in benzene before (—) and after irradiation (···) (**1o**/**1c** = 4).

DOI: 10.1039/b101231m

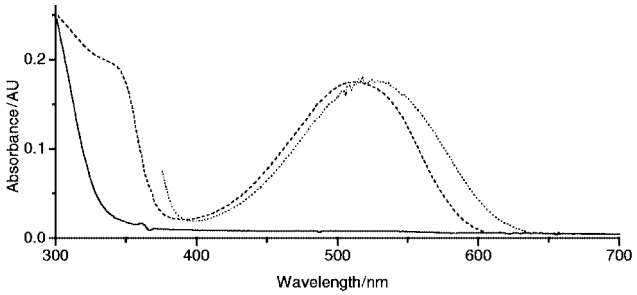

Fig. 2 UV–VIS spectra of a solution of **1o** in benzene (0.29 mM) before (—) and after irradiation (---) at 313 nm for 20 min and of a viscous solution of **1o** in benzene (11.7 mM) after irradiation (···) for 10 min at 313 nm.

shifts (< 0.05 ppm) upon increasing the concentration from 2 to 22 mM, indicating that the sterically more demanding *tert*-butyl groups effectively prevent aggregation of **2o** by intermolecular hydrogen bonding.

The photochromic behaviour§ of a dilute solution of **1o** in benzene (0.29 mM) was followed by UV spectroscopy as is depicted in Fig. 2. Upon irradiation of the solution of **1o** at 313 nm, a new absorption band at 514 nm appeared due to the formation of the conjugated closed form **1c**. From ^{1}H NMR data it was deduced that the photostationary state consists of a mixture of **1o** and **1c** in a molar ratio of **1o**/**1c** = 0.43. Irradiation at λ > 520 nm causes a complete conversion to the initial state consisting of pure **1o**, and this switching process between **1o** and **1c** could be repeated several times without showing any degradation. It is interesting to note that switching between **1o** and **1c** is not prohibited by formation of intra-molecular hydrogen bonds as has previously been reported for carboxylic acid derivatives of diarylethene switches,[11] although it cannot be excluded that such an intra-molecular hydrogen bond between the two amide groups is present. Also irradiation of a concentrated viscous solution of **1o** in benzene (11.7 mM) leads to the appearance of an absorption band at longer wavelength, characteristic for the formation of the closed form. The absorption maximum of **1c** shows a small red shift to 524 nm and is slightly broadened compared to the measurements at low concentrations, indicative of a weak exciton coupling between the chromophores in the aggregates. The switching process is also fully reversible in these concentrated solutions and can be repeated several times, although at very long irradiation times (> 20 h) some decomposition (< 5%) takes place.[12] The viscous solution needs, however, considerably longer irradiation times (6 h) to reach the photo-stationary state compared to monomeric solutions of **1o** (< 0.5 h), but quantitative analysis of the kinetics is not yet possible in our experimental set-up due to inner filter effects and an inhomogeneous optical field.

Most remarkably, even at relatively low conversions of **1o** to **1c** (**1o**/**1c** = 4) there is a clear decrease of the viscosity compared to benzene solutions of pure **1o**, demonstrating that the viscosity of solutions of **1** can be controlled by light (Fig. 1).[13] In order to determine whether this photo-induced viscosity change is due to a change of the aggregate properties like stiffness, or to a change of the extent of aggregation of **1**, the photoconversion of viscous benzene solutions of **1o** (7.32 mM in C_6D_6) was followed by ^{1}H NMR. Irradiation of a solution of **1o** at 313 nm caused the appearance of a second set of NH and CH_3 signals, which can be assigned to the closed form **1c**.§ After 50 min irradiation the NH signal of **1c** appears as a shoulder upfield from the NH signal of **1o**. After longer irradiation times both the NH signals of **1o** and **1c** are shifted upfield compared to the NH signal of pure **1o** (5.53 ppm) and after 6 h they have reached a constant position at 5.39 ppm. Although these results do not rule out any mesoscopic changes of the aggregates due to irradiation, they clearly indicate that photoconversion of **1o** to **1c** causes a decrease of the extent of aggregation. After 6 h irradiation a photostationary state was reached with the ratio **1o**/**1c** = 0.5 (determined from the integration of the CH_3 signals of **1o** and **1c** at, respectively, 1.76 and 2.16 ppm), which is comparable to the photostationary state of monomeric **1**. Irradiation at λ > 520 nm causes a complete conversion to **1o** with the NH signal again appearing at 5.53 ppm. Apparently, both the photoswitching and the aggregation of **1** are completely reversible. For comparison, similar experiments were carried out with C_6D_6 solutions of **2o**. Irradiation of 22 mM solutions of **2o** also resulted in two NH signals at 5.37 and 5.44 ppm, which can be assigned to **2o** and **2c** respectively, but for this compound the NH signals did not shift with increasing conversion of **2o** to **2c**. Also the viscosity measurements did not reveal a significant change of the viscosity due to photoswitching of **2**.

In conclusion, the bis-amide photochromic switch **1** self-assembles in apolar solvents through a cooperative association mechanism, and forms extented aggregates, resulting in highly viscous solutions. Most remarkably, the reversible photoswitching of **1** from the open form to the closed form causes a change of the extent of aggregation, which is accompanied by a decrease of the viscosity. These changes can be attributed to different molecular properties like shape and conformational freedom of the open and closed form of diarylethene switch **1**, and it is expected that this feature of diarylethene switches can be employed to control other macroscopic properties like gel formation by light as well.

We are grateful for a fellowship to J. van Esch from the Royal Academy of Science of the Netherlands (KNAW), and we thank ir. V. W. A. Verhoeven for this help with the viscosity measurements.

Notes and references

† Compounds **1o** and **2o** were fully characterised showing spectroscopic and analytical data in accordance with the structure shown.

‡ Viscosity measurements were performed on a Brabender Rheotron, with a cone/plate geometry (cone angle 3°), and ^{1}H NMR experiments were performed on a Varian VXR-300 spectrometer, using 0.15–22 mM benzene solutions of **1** or **2**. All measurements have been carried out at room temperature. For a more detailed survey about viscosity measurements the following reference is recommended: A. Dinsdale and F. Moore, *Viscosity and its Measurement*, Chapmann and Hall, London, 1962.

§ The samples were irradiated in a 1 mm quartz cuvet for UV–VIS measurements and in 5 mm pyrex tubes for NMR experiments, using a 200 W mercury lamp with a 313 nm band-pass or a 520 nm high-pass filter.

1 J.-M. Lehn, *Supramolecular Chemistry*, VCH, Weinheim, 1995; D. Philp and J. F. Stoddart, *Angew. Chem., Int. Ed. Engl.*, 1996, **35**, 1154.
2 J. W. Steed and J. L. Atwood, *Supramolecular Chemistry*, Wiley, Chichester, 2000.
3 *Photochroism: Memories and Switches*, guest editor M. Irie, *Chem. Rev.*, 2000, **100**, 1683.
4 F. Würthner and J. Rebek Jr., *J. Chem. Soc., Perkin Trans. 2*, 1995, 1727; F. Würthner and J. Rebek, Jr., *Angew. Chem., Int. Ed. Engl.*, 1995, **34**, 446; J. Rosengaus and I. Willner, *J. Phys. Org. Chem.*, 1995, **8**, 54; K. Murata, M. Oaki, T. Nishi, A. Ikeda and S. Shinkai, *J. Chem. Soc., Chem. Commun.*, 1991, 1715; M. S. Vollmer, T. D. Clark, C. Steinem and M. R. Ghadiri, *Angew. Chem., Int. Ed.*, 1999, **38**, 1598.
5 L. N. Lucas, J. van Esch, R. M. Kellogg and B. L. Feringa, *Chem. Commun.*, 1998, 2313.
6 S. L. Gilat, S. H. Kawai and J.-P. Lehn, *Chem. Eur. J.*, 1995, **1**, 275; J. M. Endtner, F. Effenberger, A. Hartschuh and H. Port, *J. Am. Chem. Soc.*, 2000, **12**, 3037.
7 P. Terech and R. G. Weiss, *Chem. Rev.*, 1997, **97**, 3133; J. H. van Esch and B. L. Feringa, *Angew. Chem., Int. Ed.*, 2000, **39**, 2263.
8 J. H. K. K. Hirschberg, L. Brunsveld, A. Ramzi, J. A. J. M. Vekemans, R. P. Sijbesma and E. W. Meijer, *Nature*, 2000, **407**, 167.
9 J. Jadżyn, M. Stockhausen and B. Żywucki, *J. Phys. Chem.*, 1987, **91**, 754; M. Akiyama and T. Ohtari, *Spectrochim. Acta, Part A*, 1994, **50**, 317; M. de Loos, J. van Esch, R. M. Kellogg and B. L. Feringa, *Angew. Chem., Int. Ed.*, 2001 **40**, 613.
10 The viscosity of **2o** at shear rates 3 s^{-1} and 24 s^{-1} is 0.0009 and 0.0000 Pa.s, respectively; for **2c** 0.0012 and 0.0004 Pa.s, respectively.
11 M. Irie, O. Miyatake, K. Uchida and T. Eriguchi, *J. Am. Chem. Soc.*, 1994, **116**, 9894.
12 See also: M. Irie, T. Lifka, K. Uchida, S. Kobatake and Y. Shindo, *Chem. Commun.*, 1999, 747.
13 M. Irie, A. Menju and K. Hayashi, *Macromolecules*, 1979, **12**, 1176; M. Irie, Y. Hirano, S. Hashimoto and K. Hayashi, *Macromolecules*, 1981, **14**, 262.

En route to the first stereoselective synthesis of axially chiral biscarbazole alkaloids†

Gerhard Bringmann,* Stefan Tasler, Heike Endress and Jörg Mühlbacher

Institut für Organische Chemie, Universität Würzburg, Am Hubland, 97074 Würzburg, Germany. E-mail: bringman@chemie.uni-wuerzburg.de; Fax: +49 931 888 4755; Tel: +49 931 888 5323

Received (in Cambridge, UK) 7th February 2001, Accepted 16th March 2001
First published as an Advance Article on the web 3rd April 2001

The first stereoselective synthesis of an axially chiral biscarbazole has been achieved, by application of the 'lactone concept'.

Axially chiral biaryl natural products are of increasing importance, but the phenomenon of atropisomerism is often neglected—even nowadays.[1] A typical example is, *e.g.* the class of biscarbazoles,[1,2] which consists of eleven *C,C*- and three *N,C*-coupled alkaloids. All of the *C,C*-bonded representatives should have a configurationally stable biaryl axis, which was, however, not recognized during structural elucidation. The first biscarbazole for which axial chirality was demonstrated, was bismurrayaquinone-A (**1**, Fig. 1):[3] after racemate resolution of synthetic **1**, the absolute configuration at the axis was attributed by quantum chemical circular dichroism (CD) calculations. Racemate resolutions succeeded also for murrastifoline-F[4] and for clausenamine-A (**2**, $R^1 = R^3 = OMe$, $R^2 = H$).[5]

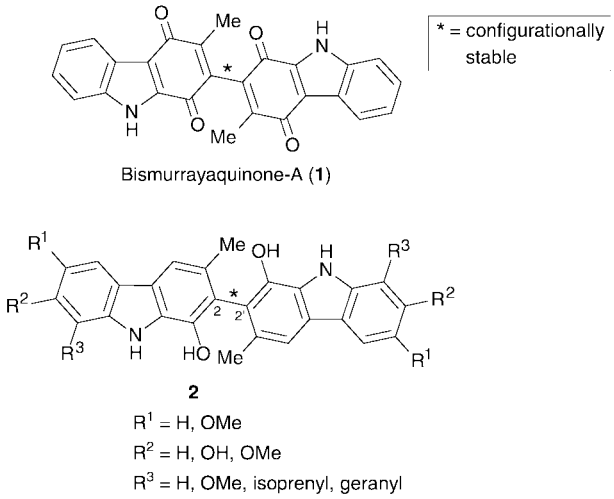

Fig. 1 Bismurrayaquinone-A (**1**) and the general structure of other 2,2′-coupled biscarbazole alkaloids.

No *stereoselective* approaches to biarylic biscarbazoles have so far been described. As a most rewarding synthetic target for a first atropo-enantioselective access we chose the 2,2′-coupled biscarbazole core **2** ($R^1 = R^2 = R^3 = H$, Fig. 1), since it constitutes the basic framework of five naturally occurring alkaloids, bismurrayaquinone-A (**1**), bismurrayafolines-B, -C, and -D, and clausenamine-A (all represented by the general structure **2**). Such a synthesis would also permit investigations on the (possibly divergent) bio-activities of the atropo-enantiomers of the respective natural products.[6] In this paper, we present the first stereoselective preparation of an axially chiral 2,2′-biscarbazole core related to **2**.

† Novel Concepts in Directed Biaryl Synthesis, part 95; for part 94, see G. Bringmann, A. Wuzik, J. Kümmel and W. A. Schenk, *Organometallics*, 2001, in press.

For the atropo-selective construction of the biaryl axis, we chose the 'lactone concept',[7] with biaryl lactone **9** (Scheme 1) as the crucial intermediate. Since it is configurationally unstable at the axis due to the ester bridge, it should permit an atroposelective ring cleavage with chiral nucleophiles in a dynamic kinetic resolution, giving rise to—then configurationally stable—atropisomers. The synthesis of lactone **9** required the preparation of the bromoacid **5** and the phenolic component **7**.

Exploratory work rapidly showed the necessity of protecting the base-sensitive and electron-pushing endocylic nitrogen, to avoid side reactions on the NH function or, due to its electronic impact, on the isocyclic ring. Such a protective group should, in the first instance, be robust to survive the scheduled reaction conditions, thus avoiding the need to establish different protective groups for each single step. For this purpose, the stable (and small) methyl group was chosen at this point, even though it bears the inherent problem of being cleavable only enzymically[8] or under extreme conditions,[9] which were not expected to be tolerated by the dimeric target structures of type **2**. For a first exploration of the synthetic concept, this disadvantage seemed acceptable.

The synthesis of the bromoacid **5** started from the phenolic carbazole ester **3**[10] (Scheme 1). Regioselective bromination at the 2-position was achieved by the DoM (= Directed *ortho*-Metalation)[11] strategy. The MOM (= methoxymethyl) function was introduced using MOMCl,[12] followed by *N*-methylation with dimethyl sulfate. $LiAlH_4$ reduction gave **4** as a DoM-suited substrate, which afforded 2-bromination in an excellent yield and with complete regioselectivity upon treatment with *n*BuLi and $(CBrCl_2)_2$. Conversion of this bromoalcohol into the corresponding acid **5** succeeded by Swern and $NaClO_2$ oxidation, giving the first coupling portion in as much as 52% overall yield from carbazole **3**.

The phenolic 'half' **7** was synthesized from murrayafoline-A (**6**),[10] by *N*-methylation with dimethyl sulfate and BBr_3-mediated *O*-demethylation. The crude 1-hydroxycarbazole **7** thus obtained was taken directly for esterification with bromoacid **5** with DCC and DMAP, giving ester **8** in 86% yield.

The intramolecular biaryl coupling of **8** was the most tricky and yield-limiting step of the synthesis. Among different reagents and conditions tested, the best result was obtained using 1.5 equiv. $Pd(OAc)_2$ and 3.0 equiv. PPh_3 for 1.5 h at 120 °C. The biscarbazole lactone **9** was isolated in 35% yield, along with 20–30% of the corresponding hydrodebromination product. This—compared to other lactone syntheses[7]—moderate coupling yield, which is in agreement with that for similar coupling substrates with an *ortho*-'OCH' unit next to the palladation site,[13] is disappointing at first sight; still, it opens up the first stereoselective access to an axially chiral biscarbazole core.

For the atroposelective ring cleavage of the configurationally unstable lactone **9**, a CBS reduction was attempted first, since it had given excellent chemical and optical yields in similar conversions.[7] In this case, however, apparently due to the significantly decreased reactivity of the ester group by the

DOI: 10.1039/b101241j

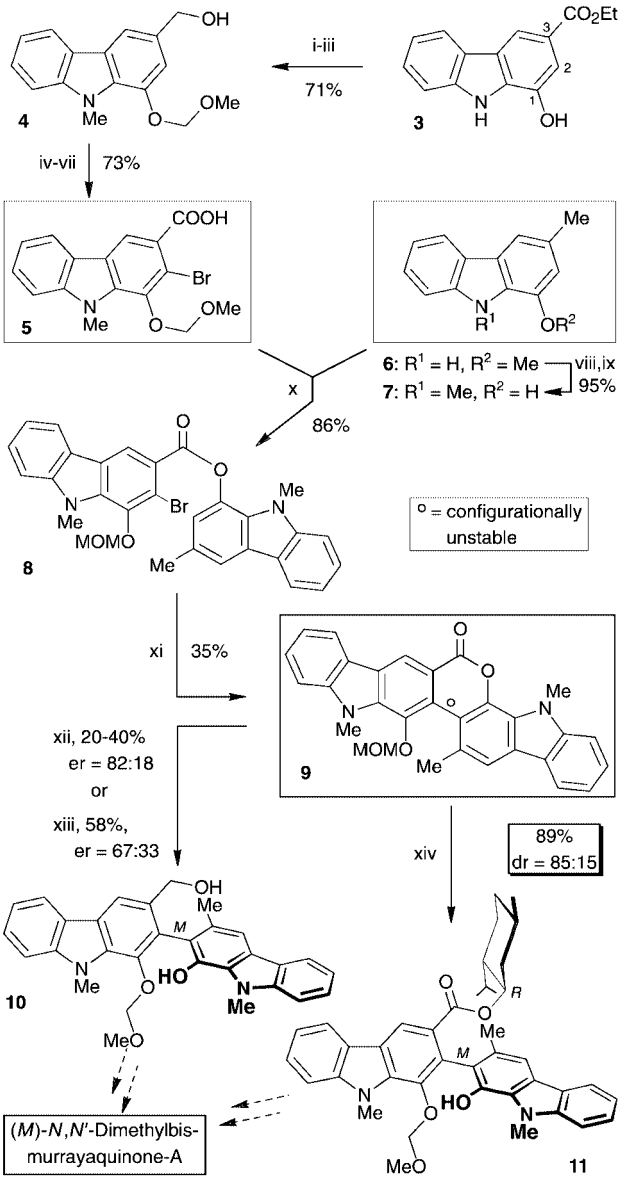

Scheme 1 *Reagents and conditions*: i, MOMCl, K_2CO_3, acetone, rt, 3 h, 79%; ii, Me_2SO_4, K_2CO_3, acetone, reflux, 15 h, 92%; iii, $LiAlH_4$, Et_2O, 0 °C, 3 h, 97%; iv, *n*BuLi, benzene, rt, 1 h; v, $(CBrCl_2)_2$, Et_2O, rt, 3.5 h, 90% (two steps); vi, DMSO, $(COCl)_2$, NEt_3, CH_2Cl_2, rt, 3.5 h, 83%; vii, $NaClO_2$, H_2NSO_3H, HOAc, H_2O, dioxane, rt, 24 h, 98%; viii, Me_2SO_4, 5 M KOH, CH_2Cl_2, $PhCH_2(nBu)_3NCl$, rt, ultrasound, 2 h, 97%; ix, BBr_3, CH_2Cl_2, rt, 5 h, 98%; x, DCC, DMAP, CH_2Cl_2, rt, 5 h; xi, $Pd(OAc)_2$, PPh_3, DMA, 120 °C, 1.5 h; xii, (*R*)-2-methyl-CBS-oxazaborolidine (Aldrich), BH_3·THF, THF, 0 °C to rt, 24 h; xiii, (*M*)-BINAL-H, THF, −20 °C, 16 h; xiv, lithiated (1*R*)-mentholate, toluene, 0 °C, 7 h. MOMCl: chloromethyl methyl ether.

electron-donating carbazole nitrogen, the reduction took place in only up to 40% yield, leading to the (*M*)-enantiomer of diol **10** with a maximum er of 82 : 18. Slightly better chemical yields were attained with (*M*)-BINAL-H (58%), but with an er of only 67 : 33, again in favor of (*M*)-**10**. The best results with respect to chemical yields and 'asymmetric inductions' were achieved with lithium (1*R*)-mentholate as a chiral *O*-nucleophile,[7] giving **11** in 89% yield and a dr of 85 : 15.

The attribution of the newly created axial configurations of the ring cleavage products was achieved by a combination of CD spectroscopy and quantum chemical CD calculations.[14,15] The CD spectrum for the main enantiomer of diol **10** was measured on line by LC-CD analysis on a chiral phase (Chiralcel OD-H) and matched very well the CD spectrum quantum chemically calculated for the (*M*)-enantiomer—here based on a molecular dynamics (MD) simulation[15]—clearly showing it to be (*M*)-configured, in agreement with the stereochemical outcome of many other cleavage reactions on similar lactone substrates.[7]

The purification of the main atropo-diastereomeric product **11** of the mentholate ring opening, by preparative HPLC on a chiral phase (Chiralcel OD), gave the first atropisomerically pure biscarbazole stereoselectively synthesized. The phenolic part of this pure main isomer proved to be highly sensitive to autoxidation during removal of the HPLC solvent in the presence of air oxygen to yield the corresponding quinone. The CD spectrum of its $LiAlH_4$ reduction product showed strong similarities with that of (*M*)-**10**, revealing the main atropisomer of **11** to be likewise (*M*)-configured, as was to be expected in analogy to numerous related lactone cleavage reactions.[7]

Since first attempts to adopt this reaction sequence for the atroposelective biscarbazole synthesis to substrates with an *N*-benzyl group as an eventually removable protective group for the carbazole nitrogen gave promising results, the final steps for the synthesis of an—unnatural—*N*,*N*′-dimethyl analog of bismurrayaquinone-A were not performed for the *N*-methyl protected model biscarbazole **11**.

The presented pathway provides the first stereoselective synthetic access to atropisomerically pure axially chiral biscarbazoles and defines the strategy for the now scheduled synthesis of the corresponding genuine alkaloids. The electronically exceptional conditions within the carbazole core as compared to those of the other biaryl systems previously prepared, made the realization of the lactone concept much harder than expected. That these problems could be overcome, succeeding in the preparation of an enantiomerically pure biscarbazole, demonstrates the value of the applied method.

This work was funded by the Deutsche Forschungsgemeinschaft (SFB 347) and by the Fonds der Chemischen Industrie. The authors thank K. Messer for skillful help on LC-CD analyses and Dr A. Wuzik for inspiring discussions.

Notes and references

1 G. Bringmann, C. Günther, M. Ochse, O. Schupp and S. Tasler, in *Prog. Chem. Org. Nat. Prod.*, ed. W. Herz, H. Falk, G. W. Kirby, R. E. Moore and C. Tamm, Springer, Wien, 2001, vol. 82, in press.
2 H. Furukawa, *Trends Heterocycl. Chem.*, 1993, **3**, 185; C. Ito, Y. Thoyama, M. Omura, I. Kajiura and H. Furukawa, *Chem. Pharm. Bull.*, 1993, **41**, 2096.
3 G. Bringmann, A. Ledermann, M. Stahl and K.-P. Gulden, *Tetrahedron*, 1995, **51**, 9353.
4 G. Bringmann, S. Tasler, H. Endress, J. Kraus, K. Messer, M. Wohlfarth and W. Lobin, *J. Am. Chem. Soc.*, 2001, **123**, 2703.
5 G. Lin and A. Zhang, *Tetrahedron*, 2000, **56**, 7163.
6 For biological activities of biscarbazole alkaloids, see: G. Bringmann, A. Ledermann, J. Holenz, M.-T. Kao, U. Busse, H. G. Wu and G. François, *Planta Med.*, 1998, **64**, 54; M. Itoigawa, Y. Kashiwada, C. Ito, H. Furukawa, Y. Tachibana, K. F. Bastow and K.-H. Lee, *J. Nat. Prod.*, 2000, **63**, 893; and ref. 5
7 G. Bringmann, M. Breuning and S. Tasler, *Synthesis*, 1999, 525.
8 N. Miyata, H. Kiuchi and M. Hirobe, *Chem. Pharm. Bull.*, 1981, **29**, 1489; W. Yang, T. Jiang, D. Acosta and P. J. Davis, *Xenobiotica*, 1993, **23**, 973.
9 N. V. Moskalev and E. E. Sirotkina, *Chem. Heterocycl. Comp.*, 1987, **23**, 275; N. P. Buu-Hoi and G. Saint-Ruf, *J. Chem. Soc. (C)*, 1966, 924; J. I. G. Cadogan, H. S. Hutchison and H. McNab, *Tetrahedron*, 1992, **48**, 7747.
10 G. Bringmann, S. Tasler, H. Endress, K. Peters and E.-M. Peters, *Synthesis*, 1998, 1501.
11 V. Snieckus, *Chem. Rev.*, 1990, **90**, 879.
12 For a preparation of MOMCl avoiding carcinogenic impurities, see: J. S. Amato, S. Karady, M. Sletzinger and L. M. Weinstock, *Synthesis*, 1979, 970.
13 G. Dyker, *Angew. Chem., Int. Ed.*, 1999, **38**, 1698; G. Bringmann, T. Pabst, P. Henschel, J. Kraus, K. Peters, E.-M. Peters, D. S. Rycroft and J. D. Connolly, *J. Am. Chem. Soc.*, 2000, **122**, 9127; A. V. R. Rao, T. K. Chakraborty and S. P. Joshi, *Tetrahedron Lett.*, 1992, **33**, 4045.
14 G. Bringmann and S. Busemann, in *Natural Product Analysis*, ed. P. Schreier, M. Herderich, H. U. Humpf and W. Schwab, Vieweg, Wiesbaden, 1998, pp. 195–212.
15 G. Bringmann, C. Günther, J. Mühlbacher, M. D. L. P. Gunathilake and A. Wickramasinghe, *Phytochemistry*, 2000, **53**, 409.

Ordered SBA-15 mesoporous silica containing phosphonic acid groups prepared by a direct synthetic approach

Robert J. P. Corriu,*[a] Lucien Datas,[b] Yannick Guari,[a] Ahmad Mehdi,[a] Catherine Reyé[a] and Chloé Thieuleux[a]

[a] *Laboratoire de Chimie Moléculaire et Organisation du Solide, UMR 5637 CNRS, Université de Montpellier II, Sciences et Techniques du Languedoc, Place E. Bataillon, F-34095 Montpellier Cedex 5, France. E-mail: corriu@crit.univ-montp2.fr*

[b] *Sercice commun de Microscopie Electronique TEMSCAN, Université paul Sabatier, 118 route de Narbonne 31062 Toulouse Cedex 4, France*

Received (in Cambridge, UK) 15th January 2001, Accepted 13th March 2001
First published as an Advance Article on the web 3rd April 2001

Highly ordered hydrothermally stable SBA-15 mesoporous silica containing phosphonic acid groups are synthesised for the first time by using amphiphilic block copolymers as the structure-directing agents.

Surfactant-templated mesoporous hybrid materials constitute a very exciting field in materials chemistry.[1–8] This class of materials has numerous potential applications[9–12] due to their high surface areas and their narrow pore size distributions as well as the diversity of the functional groups which they can contain. Recently Stucky *et al.*[8] have published the preparation of ordered SBA-15 mesoporous silica containing sulfonic acid groups using the direct synthetic approach. That prompted us to report in this paper the results that we obtained by the same route concerning the preparation and the physicochemical characteristics of periodic hybrid mesoporous materials containing phosphonic acid groups based on the co-condensation of tetraethylorthosilicate (TEOS) and an appropriate organotrimethoxysilane in the presence of triblock copolymers as the structure-directing agent under acidic conditions.

First we prepared SBA-15 mesoporous silica containing phosphonic acid diethyl ester groups. In a typical experiment 4.0 g of $EO_{20}PO_{70}EO_{20}$ was dissolved in an aqueous HCl solution (160 ml, pH ≈ 1.5). This solution was added to a mixture of 8.4 g of TEOS and of 1.4 g of trimethoxysilylpropyldiethylphosphonate **1** at ambient temperature. The mixture was stirred for 3 h giving rise to a microemulsion. After heating this perfectly transparent solution at 60 °C, a small amount of NaF (75.4 mg) was added with stirring to induce hydrolysis and polycondensation. The mixture was stirred at 60 °C for 48 h. The resulting solid was filtered off and washed. The surfactant was then removed by hot ethanol extraction in a Soxhlet apparatus affording the $X[PO(OEt)_2]$ material in 95% yield. The molar composition of the reaction mixture was: 0.04 F^-: 1 TEOS: 0.11 **1**: 0.02 P 123: 0.12 HCl: 220 H_2O. Some relevant physicochemical data for $X[PO(OEt)_2]$ are given in Table 1. The CP MAS ^{31}P NMR spectrum of $X[PO(OEt)_2]$ displays one sharp signal ($\Delta\nu_{1/2}$ = 720 Hz) which was attributed to the phosphonic acid diethyl ester group. Further indication of the presence of diethyl ester group was given by CP MAS ^{13}C NMR spectroscopy with the signal at 63 ppm attributed to $PO(OCH_2)$ groups. From elemental analysis, the content of functional groups was found to be of 1.33 mmol g^{-1} while the theoretical value was 1.29. The powder X-ray pattern (Fig. 1*a*) exhibits an intense diffraction peak corresponding to d_{100} spacing and two weak peaks (d_{110} 61.5 Å and d_{200} 52.5 Å) which are characteristic of a 2D hexagonal structure. Interestingly, no significant change was observed for the XRD pattern recorded eight months later of the material which was stored in air (Fig. 1*b*), indicating a very stable structure. Further evidence for a highly ordered 2D hexagonal structure was provided by the transmission electron microscopy (TEM) images shown in Fig. 2. The N_2 adsorption–desorption isotherm for $X[PO(OEt)_2]$ is displayed in Fig. 3. The sample showed type IV isotherm, characteristic of mesoporous materials with a narrow pore size distribution.

Two routes gave rise to mesoporous silica containing phosphonic acid groups. In both cases, silylation of SiOH groups was first achieved by treating the mesoporous solid with Me_3SiCl in toluene heated under reflux for 12 h in order to avoid side reactions between the phosphonic acid groups and the surface SiOH. Acid catalysed hydrolytic desalkylation[13] was then accomplished by treating the resulting solid $X_{Si}[PO(OEt)_2]$ with a 12 M aqueous solution of HCl for 24 h under reflux (route

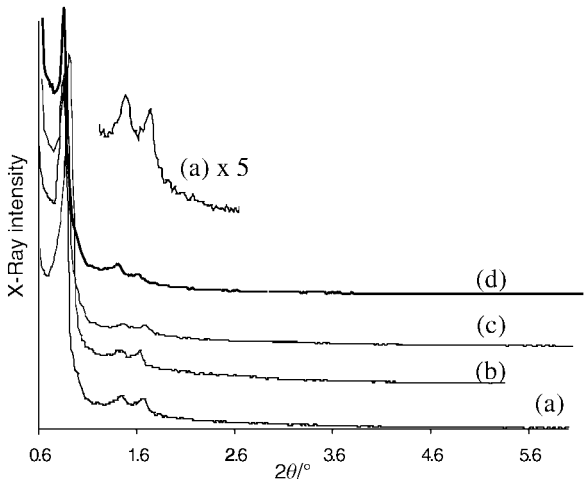

Fig. 1 XRD patterns for (*a*) $X[PO(OEt)_2]$; (*b*) for $X[PO(OEt)_2]$ after eight months; (*c*) for $X_{Si}aPO(OH)_2$; (*d*) for $X_{Si}bPO(OH)_2$.

Table 1 Physicochemical properties of mesoporous SBA-15 silica containing phosphonic acid diethyl ether or phosphonic acid groups

Sample	CP MAS ^{31}P NMR δ/ppm	Mmol g^{-1} (theor. value)	S_{BET}/m^2 g^{-1}	D_p[c]/Å	V_p/cm^3 g^{-1}	d_{100}/Å	Wall[d] thickness/Å
$X[PO(OEt)_2]$	33.5	1.33[a] (1.29)	696	75	1.03	106	47
$X_{Si}a[PO(OH)_2]$	32.5	1.08[b]	618	70	1.03	105	52
$X_{Si}b[PO(OH)_2]$	33.2	1.08[b]	580	71	0.89	105	51

[a] Calculated from elemental analysis. [b] Calculated from acid–base titration. [c] Calculated from the adsorption branch. [d] Calculated from a − pore size ($a_0 = 2d_{100}/\sqrt{3}$.

DOI: 10.1039/b100515o

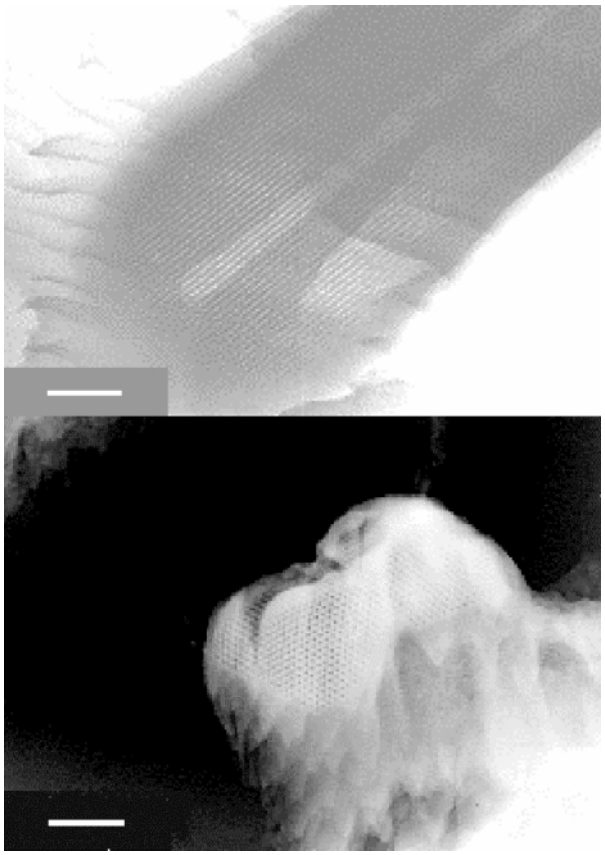

Fig. 2 TEM images of the X[PO(OEt)$_2$] material: (bottom) in the direction perpendicular to the pore axis; (top) in the direction of the pore axis. The images were recorded on a JEOL JEM 200CX transmission electron microscope. Scale bar = 100 nm.

a) giving rise to $X_{Si}a[PO(OH)_2]$. The second route (route b) consisted of the preparation of the bis(trimethylsilyl)phosphonate which can then be smoothly converted to phosphonic acid on contact with neutral H_2O at room temperature[14] thus avoiding the harsh reaction conditions of preparation of $X_{Si}a[PO(OH)_2]$. For this purpose, refluxing $X_{Si}[PO(OEt)_2]$ with 2 equiv. of Me_3SiBr in toluene for 24 h afforded $X_{Si}b[PO(OH)_2]$ after addition of H_2O. Some relevant physicochemical data for both materials are given in Table 1. It is worth noting that all the data are very similar. The CP MAS ^{31}P NMR spectra of both materials display only one sharp signal ($\Delta\nu_{1/2}$ = 640 Hz), indicating the absence of reaction between the phosphonic acid groups and the surface SiOH. Though the ^{31}P NMR chemical shift of the PO(OH)$_2$ groups is unfortunately very close to that of PO(OEt)$_2$ groups, evidence for the complete formation of phosphonic acid groups in both cases was given by CP MAS ^{13}C NMR spectroscopy with the disappearance of the signal attributed to the PO(OCH$_2$) groups. Furthermore, the exact amount of phosphonic acid groups was measured by acid–base titration. For this determination, the materials were first placed in an aqueous Li_2CO_3 solution (pH 8) in which an ion exchange occurred quantitatively (^{31}P NMR, δ 26 ppm ($\Delta\nu_{1/2}$ = 320 Hz), Li/P ratio, 1.95 from elem. anal.). The filtrate was then treated with an excess of an aqueous HCl solution. From the acid–base conductimetric titration, the amount of PO(OH)$_2$ groups per gram was found to be 1.08 mmol g^{-1} taking into account the same titration from $X_{Si}[PO(OEt)_2]$ as a blank. The N_2 adsorption–desorption isotherms are of type IV in both cases with a very similar narrow pore size distribution (Fig. 3). Figs. 1*c* and 1*d* show the powder X-ray patterns of respectively $X_{Si}a[PO(OH)_2]$ and $X_{Si}b[PO(OH)_2]$. They are very similar to

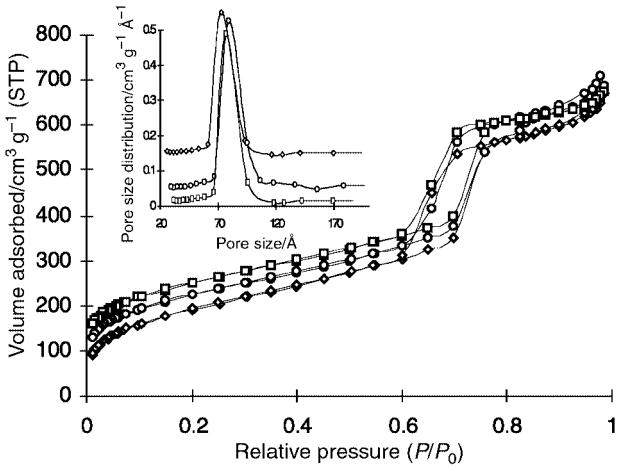

Fig. 3 Nitrogen adsorption–desorption isotherm and BJH pore size distribution plot (inset) of XPO(OEt)$_2$ (□), $X_{Si}aPO(OH)_2$ (○) and $X_{Si}bPO(OH)_2$ (◇). To allow a better comparison, the data for $X_{Si}aPO(OH)_2$ and XPO(OEt)$_2$ were shifted by 50 and 100 cm^3 g^{-1} respectively.

that of X[PO(OEt)$_2$] (Fig. 1*a*) indicating that the mesoscopic ordering completely survives both post syntheses. Thus, it can be concluded that the structures of these materials are hydrothermally stable as $X_{Si}a[PO(OH)_2]$ was treated with a 12 M HCl aqueous solution heated under reflux for 24 h. This is a specificity of SBA-15 materials.[8,15,16] They are also stable under basic conditions (pH 8). Finally, phosphonic acid groups are interesting in that they allow the incorporation of numerous transition metals which should have good potential in catalysis. As example, we show that treatment of $X_{Si}a[PO(OH)_2]$ with a THF solution of nickel acetylacetonate (2 equiv. per PO(OH)$_2$ group) heated under reflux for 12 h yielded quantitatively the nickel salts (one signal at 22 ppm in CP MAS ^{31}P NMR).

In summary, we have developed two routes in several steps giving rise to the same highly ordered mesoporous hybrid materials containing free phosphonic acid groups. This study constitutes, to the best of our knowledge, the first example of ordered mesoporous silica containing such a functional group.

Notes and references

1 R. Richer and L. Mercier, *Chem. Commun.*, 1998, 1775.
2 S. R. Hall, C. E. Fowler, B. Lebeau and S. Mann, *Chem. Commun.*, 1999, 201.
3 M. H. Lim and A. Stein, *Chem. Mater.*, 1999, **11**, 3285.
4 D. J. Macquarie, D. B. Jackson, J. E. G. Mdoe and J. H. Clark, *New J. Chem.*, 1999, **23**, 529.
5 R. J. P. Corriu, A. Mehdi and C. Reyé, *C.R. Acad. Sci. Paris, Sér. IIc*, 1999, 35.
6 L. Mercier and T. J. Pinnavaia, *Chem. Mater.*, 2000, **12**, 188.
7 R. J. P. Corriu, C. Hoarau, A. Mehdi and C. Reyé, *Chem. Commun.*, 2000, 71.
8 D. Margolese, J. A. Melero, S. C. Christiansen, B. F. Chmelka and G. D. Stucky, *Chem. Mater.*, 2000, **12**, 2448.
9 W. Zhang, J. Wang, P. T. Tanev and T. J. Pinnavaia, *Chem. Commun.*, 1996, 979.
10 W. Zhang, M. Froba, J. Wang, P. T. Tanev, J. Wong and T. J. Pinnavaia, *J. Am. Chem. Soc.*, 1996, **118**, 9164.
11 L. Mercier and T. J. Pinnavaia, *Adv. Mater.*, 1997, **9**, 500.
12 X. Feng, G. E. Fryxell, L.-Q. Wang, A. Y. Kim, J. Liu and K. M. Kemner, *Science*, 1997, **276**, 923.
13 G. M. Kosolopoff, in *Organophosphorus Compounds*, Wiley, Inc., New York, 1950.
14 C. E. McKenna, M. T. Higa, N. H. Cheung and M.-C. McKenna, *Tetrahedron Lett.*, 1977, **2**, 155.
15 D. Zao, Q. Huo, J. Feng, B. F. Chmelka and G. D. Stucky, *J. Am. Chem. Soc.*, 1998, **120**, 6024.
16 D. Zao, J. Feng, Q. Huo, N. Melosh, G. H. Fredrickson, B. F. Chmelka and G. D. Stucky, *Science*, 1998, **279**, 548.

Oxidation of chiral 9-fluorinated substrates by castor stearoyl-ACP Δ^9 desaturase yields novel products

Behnaz Behrouzian,[a] Brian Dawson,[b] Peter H. Buist*[c] and John Shanklin*[a]

[a] *Brookhaven National Laboratory, Department of Biology, Upton, NY 11973, USA. E-mail: shanklin@bnl.gov*
[b] *Research Services Division, Health Products and Food Branch, Health Canada, Tunney's Pasture, Ottawa, Ontario, Canada, K1A 0L2*
[c] *Carleton University, Department of Chemistry, 1125 Colonel By Drive, Ottawa, Ontario, Canada, K1S 5B6*

Received (in Corvallis, OR, USA) 21st December 2000, Accepted 1st March 2001
First published as an Advance Article on the web 3rd April 2001

Desaturation of (*S*)-9-fluorostearoyl-ACP using stearoyl-ACP Δ^9 desaturase yielded mainly (*E*)-9-fluoroalk-9-enic product, while desaturation of (*R*)-9-fluorostearoyl-ACP gave the novel (*Z*)-9-fluoroalk-9-ene and (*Z*)-9-fluoroalk-10-ene.

The O_2-dependent conversion of stearoyl acyl carrier protein (ACP) **1** to oleyl-ACP **2** is a remarkable example of a highly

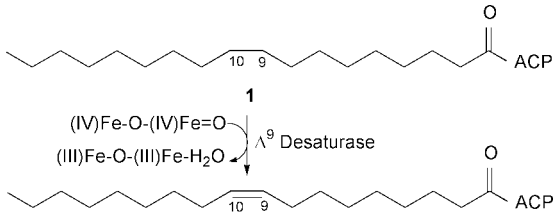

chemo-, regio- and stereoselective enzymatic process.[1] The enzyme responsible for this fascinating reaction, stearoyl-ACP Δ^9 desaturase, has been isolated from castor seed and is the only protein of its type to be thoroughly characterized. The X-ray crystallographic structure of this protein confirmed the presence of a non-heme diiron oxidant which is strategically located at the centre of a narrow, hydrophobic pocket.[2] The amino acid co-ordination of the catalytic diiron centre and the fold of the protein are very similar to that found in methane mono-oxygenase—an enzyme which converts methane and other small alkanes to the corresponding alcohol.[3] It has long been suggested that desaturation and hydroxylation reactions are closely related[4a] and that precise control of substrate conformation and oxidant location may play an important role in determining reaction outcome.[1,4b] We decided to probe the catalytic versatility of the stearoyl-ACP Δ^9 desaturase by challenging this enzyme with a substrate bearing a potentially non-oxidizable, CHF-group at C-9. The availability of chiral 9-hydroxystearic acid derived from natural sources offered a convenient synthetic entry into this project. Here, we report the results of this study.

Each enantiomer† of methyl 9-fluorostearate, (9*S*)-**3** and (9*R*)-**3**, was incubated separately as the ACP derivative (200 nmol) with freshly prepared Δ^9 desaturase (14 nmol) and required cofactors in a total volume of 250 μl for 30 min.[6] The reaction was quenched by addition of THF and the thioester fraction was reduced ($NaBH_4$) to give the corresponding terminal alcohols. These products were analyzed directly by ^{1}H-decoupled ^{19}F NMR and by GC/MS (60 m SP-23 capillary column) as the tetramethylsilyl derivatives.

We were somewhat surprised to observe that very little starting material could be detected in the extracts of both incubations, indicating that both (*S*)- and (*R*)-9-fluorostearates could function as substrates under these conditions (Fig. 1). No obvious inhibitory effects were noted and the product profile did not appear to change as a function of % conversion. The major product formed in the desaturation of (9*S*)-**3** was, after reductive workup, (*E*)-9-fluorooctadec-9-en-1-ol **4** (Scheme 1 and Fig. 1a)‡—identical in all respects (MS, ^{1}H-decoupled ^{19}F NMR, GC rt of TMS derivative) to a sample derived by LAH reduction of previously identified, methyl (*E*)-9-fluorooctadec-9-enoate.[7] Interestingly, this material was accompanied by a small (4–7% of the total products) but reproducible amount of a *threo*-9,10-fluorohydrin **5** (MS: *m/z* 215 $(C_9H_{18}OTMS)^+$, ^{1}H-decoupled ^{19}F NMR: δ −195.25).§ Notably, no products attributable to 9,9-fluorohydrin formation (9-keto- or its reduction product, 9-hydroxystearoyl alcohol) were observed.

Desaturation of the ACP derivative of (9*R*)-**3**, yielded two major novel fluorinated olefinic products, **6** and **7** (Scheme 1 and Fig. 1b).‡ **6** was determined to be the geometric isomer of **4** on the basis of its GC retention time (*ca*. 0.2 min shorter than the corresponding (*E*)-product), similar mass spectrum (*m/z* 358 M^+, 343 $(M - CH_3)^+$, 338 $(M - HF)^+$, 323 $[(M - CH_3) - HF]^+$) and ^{1}H-decoupled ^{19}F NMR chemical shift (δ −110.45 ppm; lit. (*Z*)-7-fluorotetradec-7-ene (δ −110.37 ppm)).[8] The second novel product **7** was identified as (*Z*)-9-fluorooctadec-

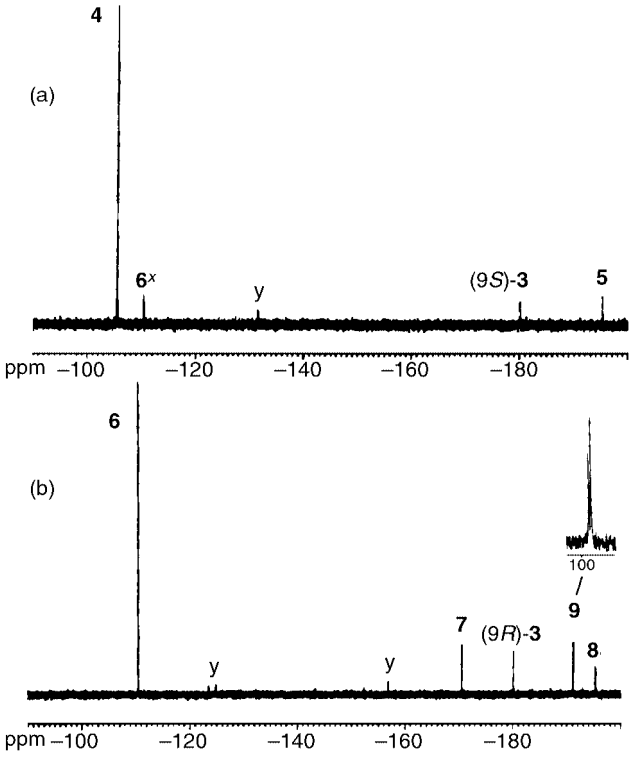

Fig. 1 ^{1}H-decoupled ^{19}F NMR (376.5 MHz) of products obtained from desaturation of (a), (9*S*)-**3**; (b), (9*R*)-**3**. Unidentified, minor peaks of variable intensity are marked with a 'y'. *x* Product derived from a minor amount of (*R*)-9-fluorostearoyl-ACP—the levels of this diastereomer appear to be enhanced relative to the (*S*)-9-fluoro-isomer in the ACP synthase-mediated acylation reaction as was previously noted in preliminary studies using racemic 9-fluorostearate as substrate.

DOI: 10.1039/b100035g

10-en-1-ol by comparison of its GC retention time and ^{1}H-decoupled ^{19}F NMR chemical shift (δ −170.54) with those of (*Z*)-8- and (*Z*)-11-fluorooctadec-9-en-1-ol (δ −170.61 and −170.34, respectively).¶ In addition, a mixture of stereoisomeric hydroxylated products (Scheme 1) was also observed in the product profile: *threo*- **8** (*m*/*z* 215 $(C_9H_{18}OTMS)^+$, ^{1}H-decoupled ^{19}F NMR: δ −195.27) and *erythro*-9,10-fluorohydrin **9** (*m*/*z* 215 $(C_9H_{18}OTMS)^+$; ^{1}H-decoupled ^{19}F NMR: δ −191.18 (.23)‖).

The formation of **4** with 'normal' regio- and stereochemistry *via* desaturation of (9*S*)-**3** indicates that this substrate can adopt the required gauche conformation for what is thought to be a diiron(IV)oxo-mediated, *syn*-dehydrogenation process.[7] However, when removal of the hydrogen occupying the '*pro-R*' position at C-9 is blocked by fluorine substitution as in (9*R*)-**3**, substantial reorientation of substrate occurs and two 'novel' olefinic products (**6**, **7**) are produced as depicted in Scheme 1. There is some precedent for a substrate-induced shift in the regiochemistry of desaturation,[6] but the observation of a switch in stereochemical outcome as displayed by the production of **6**, was completely unexpected. In a previous series of experiments, incubation of racemic 9-fluorostearoyl substrate with a structurally unrelated yeast Δ^9 desaturase produced only the anticipated methyl (*E*)-9-fluorooctadec-9-enoate.[7]

A small amount of hydroxylated materials *is* observed in the product profile of both fluorosubstrates (9*S*)-**3**, (9*R*)-**3**. These compounds do not appear to be formed by hydration of the corresponding fluoroolefins during the workup§ and thus it is tempting to attribute the formation of these products to an MMO-type hydroxylation reaction.[9] It is interesting to note that the stereochemistry of these compounds is dependent on the chirality of the fluorosubstrate: exclusively *threo*-product (**5**) was obtained from (9*S*)-**3**, while a mixture of *threo*- and *erythro*-fluorohydrins (**8**, **9**)‖ was formed from a conformationally distorted (9*R*)-**3** (Scheme 1). Experiments to further investigate the origin of these novel hydroxy products are in progress.

In summary, we have demonstrated a remarkably high preference for the catalysis of dehydrogenation rather than oxygen transfer by stearoyl-ACP Δ^9 desaturase. In addition, valuable new insights into the enantioselectivity of oxidative attack have been obtained.

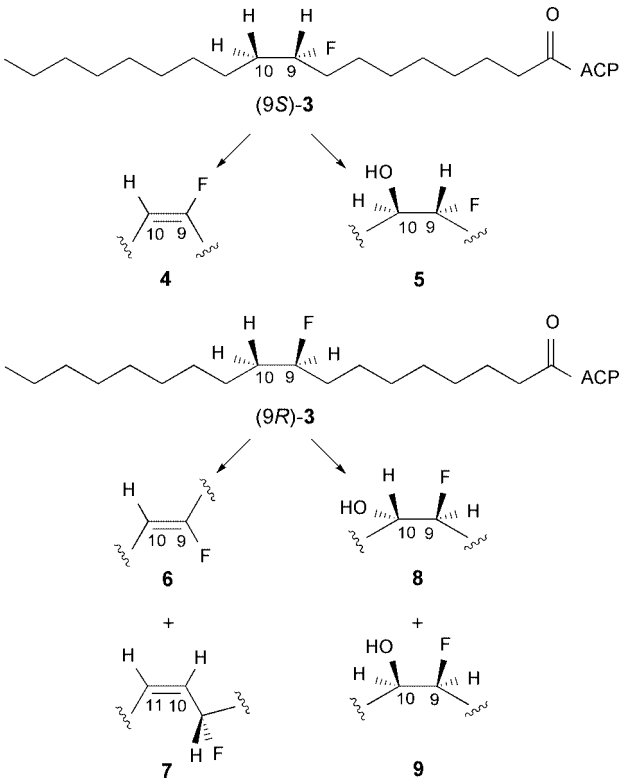

Scheme 1

This work was supported by an NSERC PDF (B. B.), an NSERC operating grant (P. H. B.) and the Office of Basic Energy Research of the US Department of Energy (J. S.). The technical assistance of Jamie Cote, Christine Caputo and Christopher Savile (Carleton University) in the synthesis of substrate analogues is gratefully appreciated.

Notes and references

† Methyl (*S*)-9-fluorostearate was synthesized *via* extraction of dimorphecolic ((*R*)-9-hydroxyoctadec-10,12-enoic) acid from *Dimorphoteca* seeds[5a] followed by reduction of double bonds using H_2/Pt and fluorination of the resultant methyl (*R*)-9-hydroxystearate with diethylaminosulfur trifluoride (DAST).[5b] The corresponding (*R*)-9-fluoro-enantiomer was prepared by inverting the stereogenic center of methyl (*R*)-9-hydroxystearate using the Mitsunobu reaction[5c] followed by fluorination using DAST. The absolute configuration of the methyl (*R*)- and (*S*)-9-hydroxystearates was confirmed using standard methods;[5d] the % ee of the alcohols (and hence that of the final fluorinated products[7]) was estimated to be more than 98%.[5d] The ACP derivatives of each enantiomer were prepared according to established enzymatic methods.[5e]

‡ The position of the double bond in **4**, **6** and **7** was confirmed by the results of a labelling experiment in which [10,10-$^2H_2$]-(*R*,*S*)-9-fluorostearoyl-ACP was converted to olefinic products with the concomitant loss of one deuterium: *m*/*z* 359 M^+, 344 $(M - CH_3)^+$, 339 $(M - HF)^+$, 324 $[(M - CH_3) - HF]^+$). The deuterated substrate was prepared from [1,1-$^2H_2$]-bromononane *via* a modification of a published procedure.[7] Since the allylic fluoride **7** is partially hydrolyzed to a pair of corresponding isomeric allylic alcohols (*m*/*z* 329 $[C_{11}H_{19}(OTMS)_2]^+$, 227 $(C_{10}H_{18}OTMS)^+$) during the work-up procedure ($NaBH_4$), the ratio of **6**/**7** is highly variable and ranges from 1 to 3 as measured by GC/MS. The recovery of total products and remaining substrate was estimated to be *ca*. 70–90% of theoretical.

§ The structural assignments were consistent with data obtained using readily available synthetic 9(10),10(9)-fluorohydrins.[7] Control experiments showed that the observed fluorohydrin products did not arise by hydration of fluoroolefins and *vice versa*: (a) no olefinic products were detected when the workup conditions of desaturase assay were simulated using synthetic fluorohydrin; (b) no fluorohydrin was detected as by-products of (*R*,*S*)-8- and (*R*,*S*)-11-fluorostearoyl-ACP desaturation; (c) no fluorohydrin was detected when a typical desaturase assay spiked with (*Z*)-9-fluorooctadec-9-en-1-ol was worked up. Under the same conditions, 9-ketostearoyl alcohol was reduced to the corresponding alcohol. (The detection limits in these control experiments was *ca*. 0.1% of total products.)

¶ Prepared by desaturation of the corresponding (*R*,*S*)-8- and (*R*,*S*)-11-fluorostearoyl-ACP substrates using castor stearoyl-ACP Δ^9 desaturase. The substrates were prepared by standard methods.[7]

‖ The *erythro*-9,10-fluorohydrin fraction appeared to contain some regioisomeric *erythro*-10,9-fluorohydrin as determined by ^{19}F NMR and GC ret. time, the appearance of a diagnostic cleavage ion in the mass spectrum (*m*/*z* 303 $(C_9H_{17}(OTMS)_2)^+$ and use of samples spiked with a synthetic standard of regioisomers (see footnote §). This result does not appear to be an artifact of the workup; fluorine scrambling may be due to a reversible elimination/addition of HF or direct fluorine migration[10] in the unsolvated environment of the active site.

1 J. Shanklin and E. B. Cahoon, *Annu. Rev. Plant. Physiol. Plant. Mol. Biol.*, 1998, **49**, 611.
2 Y. Lindqvist, W. Huang, G. Schneider and J. Shanklin, *EMBO J.*, 1996, **15**, 4081.
3 B. G. Fox, J. Shanklin, J. Ai, T. M. Loehr and J. Sanders-Loehr, *Biochemistry*, 1994, **33**, 12 776.
4 (*a*) K. Bloch, *Acc. Chem. Res.*, 1969, **2**, 193; (*b*) P. Broun, J. Shanklin, E. Whittle and C. Somerville, *Science*, 1998, **282**, 1315.
5 (*a*) C. R. Smith, T. L. Wilson, E. H. Melvin and I. A. Wolff, *J. Am. Chem. Soc.*, 1960, **82**, 1417; (*b*) W. J. Middleton, *J. Org. Chem.*, 1975, **4**, 574; (*c*) Y. Mitsunobu, *Org. Synth.*, 1981, 1; (*d*) P. E. Sonnet, S. F. Osman, H. C. Gerard and R. L. Dudley, *Chem. Phys. Lipids*, 1994, **69**, 121; (*e*) C. O. Rock and J. L. Garwin, *J. Biol. Chem.*, 1979, **254**, 7123.
6 J. A. Broadwater, B. J. Laundre and B. G. Fox, *J. Inorg. Biochem.*, 2000, **78**, 7.
7 P. H. Buist, B. Behrouzian, K. A. Alexopoulos, B. Dawson and B. Black, *J. Chem. Soc., Perkin. Trans. 1*, 1997, 2617.
8 M. Shimizu and H. Yoshioka, *Tetrahedron Lett.*, 1989, **30**, 967.
9 A. L. Feig and S. L. Lippard, *Chem. Rev.*, 1994, **94**, 759.
10 T. T. Tidwell, in *Progress in Carbocation Chemistry*, ed. X. Creary, JAI Press, London, 1989, vol. 1, pp. 1–44.

Sol–gel preparation of macroporous silica films by templating with polystyrene microspheres

Alexander N. Khramov and Maryanne M. Collinson*

Department of Chemistry, Kansas State University, 111 Willard Hall, Manhattan, KS 66506-3701, USA. E-mail: mmc@ksu.edu

Received (in Irvine, CA, USA) 29th September 2000, Accepted 27th February 2001
First published as an Advance Article on the web 3rd April 2001

Polystyrene microspheres have been used as templating entities to fabricate thin macroporous silicate films with controllable porosity for catalysis and chemical sensing-related applications.

The fabrication of microporous and mesoporous silica has received considerable attention due to the need to develop more efficient and stable materials for applications in catalysis, separations, coatings and chemical sensing.[1,2] Among various strategies for the preparation of porous materials, template-based sol–gel processing has rapidly gained popularity.[1] In this approach, the silicate matrix is assembled around a suitable template. Upon removal of the template, cavities with a specific size and shape remain in the cross-linked host.[1]

A wide variety of templates has been used to prepare materials with pore sizes that range from a few nanometers to several microns.[1,2] Examples used in the fabrication of porous silica materials include organic molecules,[3,4] latex spheres,[5,6] organic ligands,[7,8] bridged template ligands,[9–11] emulsion droplets,[12] and surfactants.[13–18] To date, most investigations have focused on the formation of *micropores* ($d < 2$ nm) or *mesopores* ($2 < d < 50$ nm) into bulk silica solids or thick membranes with a specific focus on the preparation of 3D arrays. Relatively little attention has been focused on the generation of *macroporosity* ($d > 50$ nm) in thin films, particularly those that allow for easy transport through the film.

In chemical sensing, thin films (typically < 1 μm) prepared using sol–gel technology are most often utilized due to their short path length for diffusion that decreases response times and improves recovery rates.[19,20] Sol–gel-derived thin films, however, are inherently much less porous than corresponding silica monoliths as gelation and evaporation occur simultaneously.[21,22] The ability to engineer porosity into these materials will clearly improve their performance in analytical science.

In this work, a new approach is described for the preparation of macroporous thin silica films whose pores are open on both sides and enable efficient transport of reagents through the film. This approach utilizes polystyrene microspheres as the templating entities to fabricate thin *macroporous* sol–gel-derived films with controllable porosity. A mild chemical treatment is used to completely remove the polystyrene template without destruction of the film. The morphology and properties of the templated silica films have been examined using a combination of microscopic, spectroscopic and electrochemical methods.

In these experiments, the silica sol was prepared by mixing tetramethoxysilane (TMOS) with water and 0.1 M hydrochloric acid followed by stirring for 5–10 min. The mole ratio of $Si:H_2O:HCl$ was 1 : 9 : 0.003. The original aqueous suspension of polystyrene microspheres (PSMS, Interfacial Dynamics, 8% wt/v surfactant-free, sulfated) was sonicated for 5 min prior to use. The sample solutions of PSMS suspension were prepared by mixing the original suspension with water and 10 mM sodium dodecyl sulfate followed by sonication for 2 min. The aged (3 days) silica sol was then added to a PSMS suspension in a ratio of 1 : 2 (v/v). The final mixture was vigorously stirred and again sonicated for 1 min and the resultant suspension was cast on the surface of a glassy carbon electrode or on a silicon substrate at *ca.* 7000 rpm using an in-house built rotator. The thin films were allowed to dry overnight under room conditions (45–55% RH, ambient temperature). The polystyrene microspheres were removed from the dense silica framework by soaking the film in chloroform for two hours.

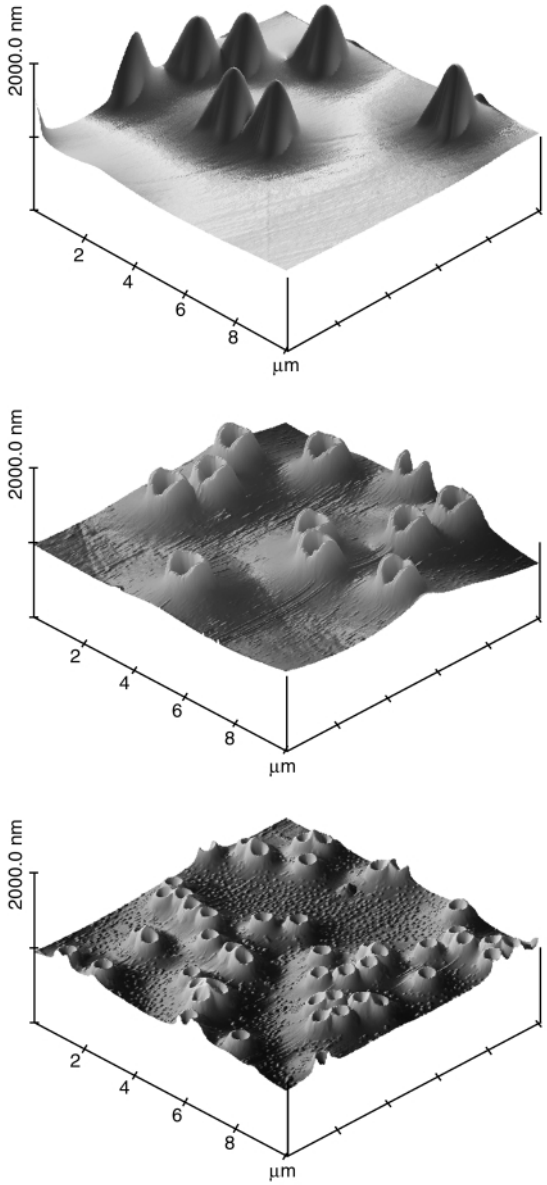

Fig. 1 10 μm × 10 μm AFM images of silicate films prepared from a sol containing 1.0 μm polystyrene microspheres, 1.3% wt/v before (top) and after (middle) chloroform treatment. (Bottom) macroporous silica film formed after removal of polystyrene microspheres from the composite film prepared with a sol containing 2.5% wt/v of 0.5 μm polystyrene microspheres.

DOI: 10.1039/b008035g

Fig. 1 (top and middle) shows AFM images of the composite silica films prepared with 1 μm diameter PSMS particles before and after chloroform treatment. As can be seen in the top panel of Fig. 1, the polystyrene particles embedded within the silicate film appear as the 'hills' randomly distributed through the topography of the film. Evaluation of the height of the embedded particles gives a value close to the diameter of the bare particle whereas the width is estimated to be approximately twice that of the particle. Upon formation of the film, the silica likely pulls away from the polystyrene microsphere exposing the top of the particle and building up around the sides.

After exposure to chloroform for two hours, the AFM images show craters that are visibly open with an inside top diameter close to the width of the polystyrene particle, Fig. 1 (middle). A blow up of the cross-section of a cavity formed from a 0.5 μm polystyrene microsphere is shown in Fig. 2. As can be seen, the shape of the cavity mimics the shape of the bottom half of the polystyrene particle. Part of the electrode underneath the polystyrene microsphere becomes exposed after removal of the particle. The size of the cavity can be changed by changing the diameter of the polystyrene microsphere template. Likewise, the number density of the cavities in the film can be increased *via* changes in the amount of polystyrene particles added to the sol. Fig. 1 (bottom) shows an AFM image of a templated film prepared from a sol containing 2.5% of 0.5 μm polystyrene microspheres. As can be seen, there are significantly more cavities in the films with an inner diameter close to the size of the polystyrene particle.

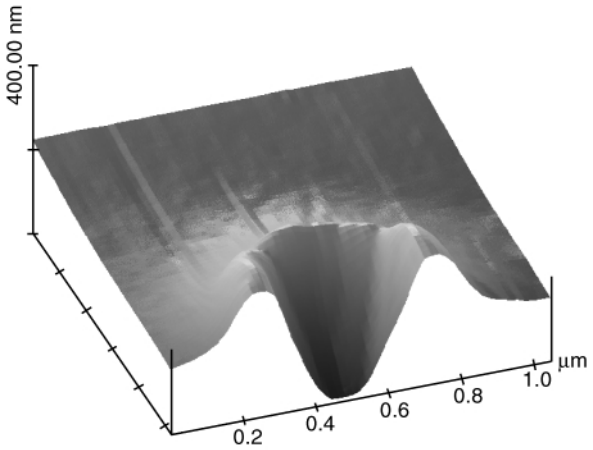

Fig. 2 Cross-section AFM image of an individual hole formed from a 0.5 μm polystyrene microsphere.

In order to verify that the films are open on both sides and allow for easy transport of reagents, electrochemical probe experiments were conducted. In these experiments, the silicate film cast on an electrode surface is placed in a solution containing an electroactive 'probe' molecule. If the probe molecule is able to reach the underlying electrode surface *via* diffusion through a defect site or a template induced cavity, Faradaic current will be observed. Fig. 3 shows the cyclic voltammograms of 1 mM ruthenium hexaammine $[Ru(NH_3)_6^{3+}]$ at the silicate film both before and after template removal. Prior to treatment in chloroform, no Faradaic current can be seen with any of the electroactive probes. This is consistent with our prior work that has shown that films fabricated with a silica sol prepared *via* the acid-catalyzed hydrolysis of tetramethoxysilane are compact and essentially defect-free.[23] After the polystyrene spheres are removed from the dense matrix, however, sigmoidal shaped CVs are obtained for $Ru(NH_3)_6^{3+}$ due to electron transfer at the electrode–solution interface produced by the template. The magnitude of the Faradaic current increases upon increasing the number density of cavities within the film.

In summary, a relatively simple approach is described to engineer porosity in otherwise dense silica films. The size and number density of the pores thus produced can be easily varied over a large range *via* judicious selection of the size of the polystyrene microsphere template and its concentration in the sol. The template is removed *via* chemical means, otherwise temperature sensitive reagents can also be entrapped within the silicate framework. It is envisioned that this approach can be utilized to prepare more porous sol–gel-derived materials for chemical sensing- and catalysis-related applications or serve as a unique way to fabricate ultra-small reaction vessels for small volume chemistry related applications.

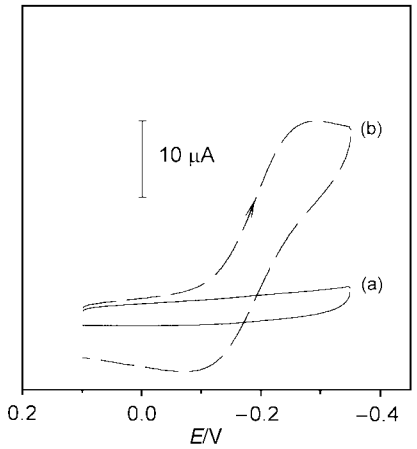

Fig. 3 Cyclic voltammograms of 1 mM ruthenium hexaammine in 0.1 M KNO_3 at a polystyrene templated film (a) before and (b) after chloroform treatment. Films were prepared from a silica sol containing 0.5 μm polystyrene microspheres, 1.3% wt/v. Scan rate 100 mV s^{-1}.

We gratefully acknowledge support of this work by the National Science Foundation.

Notes and references

1 N. K Raman, M. T Anderson and C. J Brinker, *Chem. Mater.*, 1996, **8**, 1682.
2 M. M. Collinson, *Crit. Rev. Anal. Chem.*, 1999, **29**, 289.
3 Y. Wei, J. Xu, H. Dong, J. H. Dong, K. Qiu and S. A. Jansen-Varnum, *Chem. Mater.*, 1999, **11**, 2023.
4 J. L. Hedrick, C. J. Hawker, M. Trollsas, J. Remenar, D. Y. Yoon and R. D. Miller, *Mater. Res. Soc. Symp. Proc.*, 1998, **519**, 65.
5 M. Klotz, A. Ayral, C. Guizard and L. Cot, *Bull. Korean Chem. Soc.*, 1999, **20**, 879.
6 B. Gates, Y. Yin and Y. Xia, *Chem. Mater.*, 1999, **11**, 2827.
7 N. K. Raman and C. J. Brinker, *J. Membr. Sci.*, 1995, **209**, 273.
8 Y. Lu, G. Cao, R. P. Kale, S. Prabakar, G. P. Lopez and C. J. Brinker, *Chem. Mater.*, 1999, **11**, 1223.
9 S. T. Hobson and K. J. Shea, *Chem. Mater.*, 1997, **9**, 616.
10 P. Chevalier, R. J. P. Corriu, P. Delord, J. J. E. Moreau and M. W. C. Man, *New J. Chem.*, 1998, 423.
11 D. W. Schaefer, G. B. Beaucage, D. A. Loy, T. A. Ulibarri, E. Black, K. J. Shea and R. J. Buss, *Mater. Res. Soc. Symp. Proc.*, 1996, **435**, 301.
12 A. Imhof and D. J. Pine, *Nature*, 1997, **389**, 948.
13 C. T. Kresge, M. E. Leonowicz, W. J. Roth, J. C. Vartuli and J. S. Beck, *Nature*, 1992, **359**, 710.
14 J. S. Beck, J. C. Vartuli, W. J. Roth, M. E. Leonowicz, C. T. Kresge, K. D. Schmitt, C. T.-W. Chu, D. H. Olson, E. W. Sheppard, S. B. McCullen, J. B. Higgins and J. L Schlenker, *J. Am. Chem. Soc.*, 1992, **114**, 10 834.
15 S. A. Bagshaw, E. Prouzet and T. J. Pinnavaia, *Science*, 1995, **269**, 1242.
16 M. H. Huang, B. S. Dunn, H. Soyez and J. I. Zink, *Langmuir*, 1998, **14**, 7331.
17 J. E. Martin, M. T. Anderson, J. Odinek and P. Newcomer, *Langmuir*, 1997, **13**, 4133.
18 S. H. Tolbert, T. E. Schaffer, J. Feng, P. K. Hansma and G. D. Stucky, *Chem. Mater.*, 1997, **9**, 1962.
19 O. Lev, M. Tsionsky, L. Rabinovich, V. Glezer, S. Sampath, I. Pankratov and J. Gun, *Anal. Chem.*, 1995, **67**, 22A.
20 D. Avnir, *Acc. Chem. Res.*, 1995, **28**, 328.
21 J. Brinker and G. Scherer, *Sol–Gel Science*, Academic Press, New York, 1989.
22 G. C. Frye, A. J. Ricco, S. J. Martin and C. J. Brinker, *Mater. Res. Soc. Symp. Proc.*, 1998, **121**, 349.
23 M. M. Collinson, C. G. Rausch and A. Voight, *Langmuir*, 1997, **13**, 7245.

ChemComm

Phage display selection of peptides possessing aldolase activity

Fujie Tanaka and Carlos F. Barbas III*

The Skaggs Institute for Chemical Biology and the Department of Molecular Biology, The Scripps Research Institute, 10550 North Torrey Pines Road, La Jolla, California 92037, USA. E-mail: carlos@scripps.edu; Fax: +1-858-784-2583; Tel: +1-858-784-9098

Received (in Corvallis, OR, USA) 10th January 2001, Accepted 1st March 2001
First published as an Advance Article on the web 3rd April 2001

Peptides catalyzing retro-aldol reactions were selected from a phage display peptide library using 1,3-diketones designed for the covalent selection of an enamine-based reaction mechanism.

The folded states of enzymes are key to their catalytic activity since structure can be used productively to modify the chemical reactivity of amino acid side chains, for example with electrostatic or hydrophobic effects, to build isolated reaction vessels, and to stabilize transition states of reactions. Small peptides are limited in their potential to catalyze reactions since they typically do not adopt well-defined structures. While the design of folded peptides has advanced tremendously in recent years, design at the level of catalysis is a challenging task. Rationally designed small catalytic peptides (14–42 amino acid residues peptides) have been reported that catalyze the decarboxylation of oxaloacetic acid,[1] ester hydrolysis,[2] and transesterifications.[2] Rational design, however, is limited in throughput.[1b] The combination of rational design with library based methods may be an attractive approach to catalyst development. Phage display allows for libraries of greater than 10^9 peptides to be probed for function, but this approach has not been used to select for catalytic peptides.[3] Here we report the applicability of a mechanism-based covalent selection of catalytic peptides *in vitro*. Peptides possessing aldolase activity (aldolase peptides) that use an enamine-type mechanism were selected by reaction of peptide phage with 1,3-diketones that have been employed for the induction of aldolase antibodies[4] (Scheme 1).

Amine catalyzed decarboxylation and aldol reactions share imine and enamine intermediates on their reaction coordinates. Accordingly, enzyme and antibody catalysts of these reactions are generally bifunctional catalysts capable of accelerating both decarboxylation and aldol reactions.[5] In order to select aldolase peptides that use an imine–enamine reaction mechanism, we sought to exploit mechanistic homology by using as our starting point an 18-residues peptide (YLK-18-opt)[1b] that catalyzes the decarboxylation of oxaloacetic acid. This peptide contains multiple lysyl residues that are key to its activity. To evolve the catalytic activity of this peptide, a 6-amino acid residue library was appended to the C-terminus of the peptide and the library was displayed on phage.[6] The phage display peptide library YKLLKELLAKLKWLLRKLXXXXXX (X = any of the natural 20 amino acids) was selected by three rounds of reaction with 1,3-diketones, **1**-BSA[4a] (bovine serum albumin) and

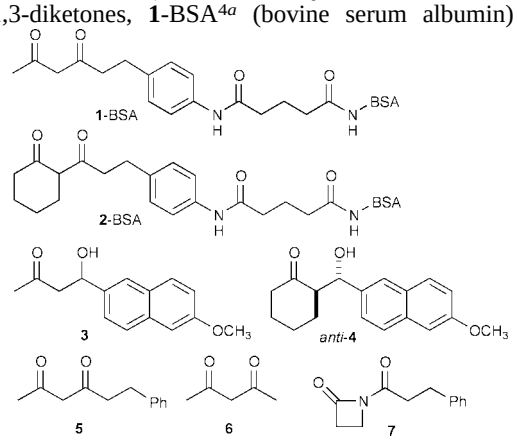

2-BSA.[4c] Screening of selected phage by ELISA identified clones that bound to **1**- and **2**-BSA. The two most reactive peptides as judged by ELISA, FT-YLK-3 and FT-YLK-4, were chemically synthesized (C-terminal amide). Both peptides catalyzed the retro-aldol reactions of fluorogenic substrates (±)-**3**[4b] and (±)-*anti*-**4**[4c] in 5% CH_3CN–42.5 mM Na phosphate (pH 7.5). Since the solubility of the peptide FT-YLK-4 was low in buffer (around neutral pH) and prevented exact kinetic analyses, FT-YLK-3 was characterized in detail.

YLK-18-opt	YKLLKELLAKLKWLLRKL-NH_2
FT-YLK-3	YKLLKELLAKLKWLLRKLLGPTCL-NH_2
FT-YLK-4	YKLLKELLAKLKWLLRKLSDHLCL-NH_2
FT-YLK-3-R5	YRLLRELLARLRWLLRRLLGPTCL-NH_2
FT-YLK-3-23S	YKLLKELLAKLKWLLRKLLGPTSL-NH_2

The catalyzed reaction displayed saturation kinetics as described by the Michaelis–Menten equation. The parameters of FT-YLK-3 and of the template peptide YLK-18-opt are shown in Table 1.[7] The K_m values were in mM range. The rate acceleration above the buffer catalyzed background reaction (k_{cat}/k_{uncat}) of the selected peptide FT-YLK-3 was 1400 and 500 for (±)-**3** and (±)-*anti*-**4**, respectively, and was superior to the template peptide YLK-18-opt. FT-YLK-3 demonstrated moderate enantioselectivity in the retro-aldol reaction of **3**. Studies performed using FT-YLK-3 (100 μM) and each of the enantiomers of **3** (1 mM) in 10% CH_3CN–40 mM Na phosphate (pH 7.5), revealed that the ratio of the initial velocities of FT-YLK-3-catalyzed reactions of (*R*)-**3**:(*S*)-**3** was 1.8:1.0.[8]

In order to probe the catalytic mechanism of the peptide, reactivity and mutational studies were performed. The catalyzed reaction was inhibited by the addition of diketone **5**. When FT-YLK-3 (100 μM) was mixed with diketone **5** (2 mM) at pH 7.5 for 2.5 h at rt and the retro-aldol activity assessed with (±)-**3** (1.2 mM) in 5% CH_3CN–42.5 mM Na phosphate (pH 7.5), the velocity of the retro-aldol reaction was < 15% that observed in the absence of **5**. Further, FT-YLK-3 formed a UV-observable enaminone with pentane-2,4-dione (**6**) when FT-YLK-3 (100 μM) was mixed with **6** (5 mM) as indicated by the appearance of a new absorption at 318 nm.[4] The pH profile of the velocity of the enaminone formation indicates that FT-YLK-3 has a pK_a

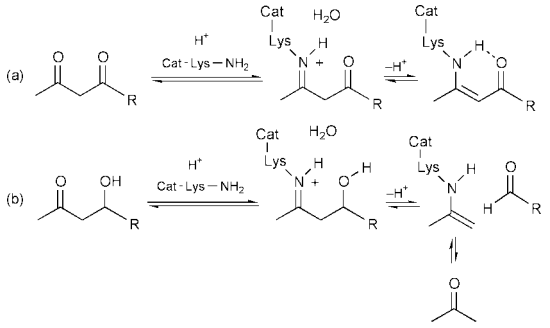

Scheme 1 (a) Enaminone formation of peptide catalyst (Cat) with 1,3-diketone. (b) An enamine mechanism for the retro-aldol reaction.

DOI: 10.1039/b100479b

Table 1 Kinetic parameters of the retro-aldol reactions[a]

	(±)-**3**			(±)-*anti*-**4**		
Peptide	K_m, mM	k_{cat}, min^{-1}	k_{cat}/k_{uncat}	K_m, mM	k_{cat}, min^{-1}	k_{cat}/k_{uncat}
YLK-18-opt	1.8	2.1×10^{-4}	540	0.9	4.1×10^{-4}	170
FT-YLK-3	1.8	5.6×10^{-4}	1400	1.1	1.2×10^{-3}	500

[a] Reaction conditions: [peptide] 100 μM, 5% CH_3CN–42.5 mM Na phosphate (pH 7.5) for (±)-**3** and, 5% DMSO–42.5 mM Na phosphate (pH 7.5) for (±)-*anti*-**4**, 25 °C. The first-order kinetic constant of the background reaction (k_{uncat}) was 3.9×10^{-7} for (±)-**3** and 2.4×10^{-6} min^{-1} for (±)-*anti*-**4**. The reaction was followed by monitoring the increase in fluorescence (λ_{ex} 330 nm, λ_{em} 452 nm).

lower than that typical of a lysine ε-amino group or a N-terminal amino group. The lowest pK_a is approximately 5.5. These results are consistent with peptide catalysis of the retro-aldol reaction using an enamine mechanism and chemically reactive amino group(s).

Since the low pK_a nucleophilic amino group of LysH93 of aldolase antibodies 38C2 and 33F12 can be specifically covalently modified with lactam **7**,[9] FT-YLK-3 was treated with **7** to further study amino group reactivity. FT-YLK-3 (100 μM) was mixed with **7** (1 mM) and analyzed by MALDI-mass at 30 min, 2 h, and 6 h. Analysis indicated a time-dependent modification at multiple sites. At 30 min, 0–4 additions of **7** per molecule of FT-YLK-3 were observed while 1–5 and 1–7 modifications were observed at 2 and 6 h, respectively. In addition to lysine and a free amino terminus, FT-YLK-3 contains tyrosine, threonine, and cysteine residues that can react with **7**. Even with consideration of labeling at these 3 additional potential modification sites, the results suggest that more than one reactive amino group is labeled.[10]

To examine the effect of the lysyl residues, all five lysyl residues in FT-YLK-3 were replaced by arginine residues. Peptide FT-YLK-3-R5 displayed less than 5% of the catalytic activity of FT-YLK-3 with (±)-**3**. This result is also consistent with catalytic role for the ε-amino groups of the lysine residues of FT-YLK-3. In addition, 1 mM of lysine, arginine, tyrosine, proline, and mixtures of these amino acids, or lysyl-lysine did not catalyze the retro-aldol reactions described above as assayed in 5% CH_3CN-42 mM Na phosphate (pH 7.5).

Since no additional amino functionalities were selected in FT-YLK-3, improvement of the catalytic activity of the peptide may originate from structural changes to the peptide and/or the addition of factors such as acid–base catalysis and transition state stabilization. The CD specta of FT-YLK-3 and YLK-18-opt (100 μM) in 45 mM Na phosphate buffer (pH 7.5) at 25 °C are shown in Fig. 1. For FT-YLK-3 the mean residue ellipticity at 208 and 222 nm were -3.04×10^4 and -2.47×10^4 deg cm^2 dmol^{-1}, respectively.[11] The CD spectra indicate that the peptide adopts an α-helical structure with an α-helical content of ~70%.[12] The template peptide YLK-18-opt showed a much reduced α-helical content under the same conditions, ~20%.[13] These results suggest that selection of the 6 amino acid residue C-terminal extension in FT-YLK-3 stabilizes the α-helical conformation of the peptide. MALDI mass analysis of FT-YLK-3 revealed the peptide forms a covalent dimer though a monomer was the main species detected after storage in the buffer used for kinetic studies. The dimer of FT-YLK-3 formed by a disulfide linkage did not preferentially form. The role of the Cys residue was assessed by synthesis of the Ser analog FT-YLK-3-23S. FT-YLK-3-23S catalyzed the retro-aldol reactions described above and the velocity of the catalyzed reaction of (±)-**3** (2 mM) was 75% that of FT-YLK-3. The ratio of the mean residue ellipticity of FT-YLK-3-23S at 208 and 222 nm were 0.8 and this ratio is the same as that observed in FT-YLK-3. The α-helix content of FT-YLK-3-23S was ~50%. The reduction in α-helical of FT-YLK-3-23S was correlated with a reduction in retro-aldolase activity. These results suggest that improved catalytic activity is intimately linked with stabilization of the conformation of the peptide.

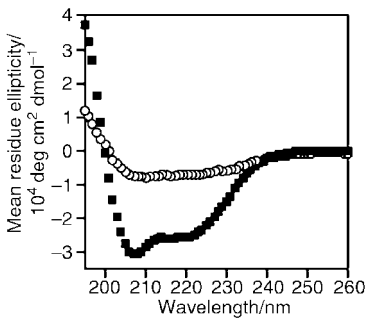

Fig. 1 CD spectra of peptides FT-YLK-3 (solid square) and YLK-18-opt (open circle). The CD spectra were recorded in 45 mM Na phosphate buffer (pH 7.5) at 25 °C at a peptide concentration of 100 μM.

In this study, we demonstrate that phage display and a compound designed to covalently trap catalysts that operate by a predefined mechanism can be used to directly select for small structured peptides that catalyze the aldol reaction. The coupling of phage display with this type of selection strategy provides a direct selection for peptide folding. For the aldolase peptide reported here, folding and catalytic activity were intimately linked.

This study was supported in part by the NIH (CA27489) and The Skaggs Institute for Chemical Biology.

Notes and references

1 (*a*) K. Johnsson, R. F. Allemann, H. Widmer and S. Benner, *Nature*, 1993, **365**, 530; (*b*) E. Perez-Paya, R. A. Houghten and S. E. Blondell, *J. Biol. Chem.*, 1996, **271**, 4120; (*c*) M. Allert, M. Kjellstrand, K. Broo, A. Nilsson and L. Baltzer, *J. Chem. Soc., Perkin Trans. 2*, 1998, 2271.

2 K. S. Broo, H. Nilsson, J. Nilsson and L. Baltzer, *J. Am. Chem Soc.*, 1998, **120**, 10 287 and refs. therein.

3 Complex schemes for phage display selection based on catalytic activity have recently been proposed: H. Pedersen, S. Holder, D. P. Sutherlin, U. Schwitter, D. S. King and P. G. Schultz, *Proc. Natl. Acad. Sci. USA*, 1998, **95**, 10 523; S. Demartis, A. Huber, F. Viti, L. Lozzi, L. Giovannoni, P. Neri, G. Winter and D. Neri, *J. Mol. Biol.*, 1999, **286**, 617.

4 (*a*) J. Wagner, R. A. Lerner and C. F. Barbas III, *Science*, 1995, **270**, 1797; (*b*) G. Zhong, R. A. Lerner and C. F. Barbas III, *Angew. Chem., Int. Ed.*, 1999, **38**, 3738; (*c*) F. Tanaka, R. A. Lerner and C. F. Barbas III, *J. Am. Chem. Soc.*, 2000, **122**, 4835.

5 R. D. Kobes and E. E. Dekker, *Biochem. Biophys. Res. Commun.*, 1967, **27**, 607; H. Nishihara and E. E. Dekker, *J. Biol. Chem.*, 1972, **247**, 5079; C. J. Vlahos and E. E. Dekker, *J. Biol. Chem.*, 1986, **261**, 11 049; R. Björnestedt, G. Zhong, R. A. Lerner and C. F. Barbas III, *J. Am. Chem. Soc.*, 1996, **118**, 11 720.

6 NNK codon mixture was used to encode 20 amino acids in the library. The phage display library was selected using pComb3 system: *Phage Display: A Laboratory Manual*, ed. C. F. Barbas III, D. R. Burton, J. K. Scott and G. J. Silverman, Cold Spring Harbor Laboratory Press, Cold Spring Harbor, New York, 2001.

7 The concentration of the peptide was determined by amino acid analysis.

8 The purity of the enantiomeric substrates that were used in the reactions is as follows: (*R*)-**3**, 99.5% ee; (*S*)-**3**, 98% ee.

9 F. Tanaka, R. A. Lerner and C. F. Barbas III, *Chem. Commun.*, 1999, 1383.

10 The order of the reactivity of the 5 lysyl residues of the peptide was not determined.

11 The mean residue ellipticity of FT-YLK-3 was calculated as the monomer.

12 P. Korsgren, P. Ahlberg and L. Baltzer, *J. Chem. Soc., Perkin Trans 2*, 2000, 643.

13 The α-helical content of YLK-18-opt is concentration dependent. See ref. 1*b*.

ChemComm

A new selenium-transferring reagent—triphenylphosphine selenide

Martin Bollmark[a] and Jacek Stawinski*[ab]

[a] *Department of Organic Chemistry, Arrhenius Laboratory, Stockholm University, S-106 91 Stockholm, Sweden*
[b] *Institute of Bioorganic Chemistry, Polish Academy of Sciences, Noskowskiego 12/14, 61-704 Poznan, Poland. E-mail: js@organ.su.se*

Received (in Cambridge, UK) 29th January 2001, Accepted 13th March 2001
First published as an Advance Article on the web 3rd April 2001

Triphenylphosphine selenide and its polymer-supported counterpart are found to be efficient selenium-transferring reagents for the conversion of H-phosphonate diesters and phosphite triesters into the corresponding phosphoroselenoate derivatives.

In the last two decades organoselenium chemistry became a rapidly expanding field of organic chemistry as various selenium-based reagents have enabled chemists to perform important synthetic transformations simply and in high yields.[1]

In 1957 Schwarz and Foltz[2] found that selenium is an essential nutrient for mammals (previously known as Factor 3 present in yeast) and prevents dietary necrotic degeneration of liver, heart and other organs. This unexpected nutritional role of selenium[3] has been a powerful incentive to study the biochemistry of organoselenium compounds.[4] Kindled by hopes of finding novel, useful theraputic properties, selenium has been incorporated into various biologically important compounds,† *e.g.* carbohydrates,[5] lipids,[6,7] nucleosides[8] and oligonucleotides.[9–11]

Organoselenophosphorus compounds are usually prepared[12] *via* P^{III} intermediates (*e.g.* phosphite triesters,[9,10,13] H-phosphonate-[6,11] or H-phosphonothioate[11] diesters), with a crucial step involving an oxidative transfer of selenium to phosphorus. As a source of electrophilic selenium in such transformations elemental selenium[6,14,15] and potassium selenocyanate,[10,13,16] are most commonly used. However, the low reactivity of these reagents and serious problems in their application in solid phase synthesis, led to the development of two selenizing agents soluble in organic solvents, 3*H*-1,2-benzothiaselenol-3-one (BTSe),[11] and bis(di-*O*,*O*-isopropyl phosphinothionyl)diselenide.[17]

To expand this short list of available selenizing reagents, we have embarked on investigations of a selenium exchange phenomenon between phosphine selenides and various P^{III} compounds as a viable route to selenophosphates. The rationale behind this was the observation that selenium-transfer from tertiary phosphine selenides to tertiary phosphines,[18] in contradistinction to phosphine sulfides, occurs readily at ambient temperature to produce an equilibrium mixture of the corresponding P^{III} and P^{V} species, as shown in Scheme 1.

Although established in a general sense, this reaction has not been recognised as a possible way of synthesising selenophosphorus compounds.

To find out if the selenium exchange process also occurs readily between phosphine selenides and other P^{III} compounds, we first investigated the reaction of triphenylphosphine selenide (TPPSe, **1**) with triethyl phosphite. Triphenylphosphine selenide **1**[14,16] seemed most attractive as a possible source of electrophilic selenium, since it is a stable, crystalline, inexpensive, commercial reagent, with good solubility in organic solvents.‡

Scheme 1

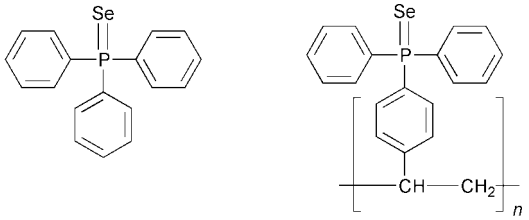

TPPSe **1** PS-TPPSe **2**

Thus, triethyl phosphite in chloroform was treated with selenide **1** (1.1 equiv.) and progress of the reaction was followed by ^{31}P NMR spectroscopy. It was rewarding to find that transfer of selenium from **1** (δ_P = 36.5, $^1J_{PSe}$ = 640 Hz) to triethyl phosphite (δ_P = 139.0) occurred rapidly (within 5 min) and quantitatively with the formation of triethyl phosphoroselenoate§ (δ_P = 72.0, $^1J_{PSe}$ = 938 Hz) and triphenylphosphine (δ_P = −4.2). Encouraged by this result we assessed TPPSe as a selenizing reagent for dinucleoside phosphite **3**¶ (Scheme 2). The reaction of **3** with 1.1 equiv. of selenide **1** was only slightly slower than that with triethyl phosphite (completion within 20 min) and produced the expected phosphoroselenoate triester **4** as a *ca.* 1 : 1 mixture of diastereomers (δ_P = 74.6 and 74.2, $^1J_{PSe}$ = 969 and 970 Hz). Compound **4** was isolated by silica gel chromatography (*ca.* 70% yield) and its structure was confirmed by NMR spectroscopy and MALDI data.

Somewhat surprisingly, attempted selenization of diethyl H-phosphonate with selenide **1** (2 equiv.) failed as no selenium-transfer occurred within 24 h (^{31}P NMR spectroscopy) in pyridine or in chloroform in the presence of triethylamine (5 equiv.). However, the conversion of diethyl H-phosphonate (δ_P = 7.6) into the corresponding silyl phosphite‖ (δ_P = 128.5) furnished rapid (< 10 min) and clean selenization upon addition of selenide **1** (1.1 equiv.) with the formation of diethyl phosphoroselenoate diester (δ_P = 56.2, $^1J_{PSe}$ = 934 Hz). We also found that selenization of diethyl H-phosphonate with **1** (2 equiv.) in pyridine could be effected without presilylation, when diazabicyclo[5.4.0]undec-7-ene (DBU, 5 equiv.) was used as base (completion within 25 min).

The efficacy of this approach for selenization of nucleoside H-phosphonate diesters was evaluated by reacting dinucleoside H-phosphonate **5a** with TPPSe (1.1 equiv.) in pyridine in the

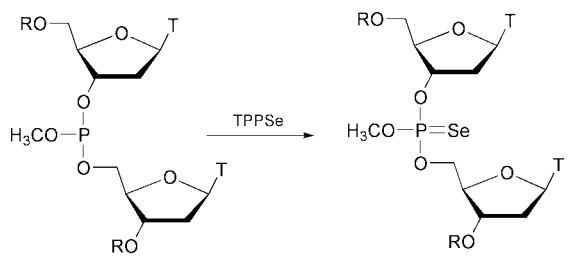

3 **4**

R = 4,4′-dimethoxytrityl
T = thymin-1-yl

Scheme 2

DOI: 10.1039/b101002f

presence of trimethylsilyl chloride (TMS-Cl, 6 equiv.) as a silylating agent (Scheme 3). The reaction was clean and went to completion within 15 min producing the silylated phosphoroselenoate **6a** (δ_P = 56.9 and 56.6) as the sole nucleotidic product. Similarly to diethyl H-phosphonate, selenization of H-phosphonate **5a** with **1** (1.1 equiv.) also occurred rapidly (< 5 min) and cleanly in pyridine in the presence of DBU (5 equiv.) as a base. The produced dinucleoside phosphoroselenoate **6a** was isolated from the reaction mixture by silica gel chromatography in *ca*. 90% yield and it was identical to **6a** prepared in another way.[11]

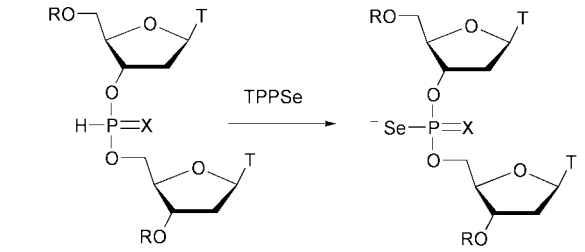

Scheme 3

The above conditions were also found to be most efficient for the preparation of phosphorothioselenoate **6b**[11] (δ_P = 104.2 and 103.8, $^1J_{PSe}$ 759.0 and 756.0 Hz) from the corresponding H-phosphonothioate **5a** (80% isolated yield).** Preliminary data from selenization of **5a** and **5b** containing different ratios of both diastereomers showed that selenide **1** furnished transfer of selenium to H-phosphonate and H-phosphonothioate diesters in a stereospecific manner (most likely with retention of configuration).

As the final part of these studies we also investigated the possibility of using a polymer-supported phosphine selenide **2** (PS-TPPSe) as a selenium-transferring reagent. Thus, a commercially available polystyryl diphenylphosphine resin was converted into selenide **2**†† and reacted with selected P^{III} derivatives. Preliminary ^{31}P NMR experiments showed that **2** can indeed act as an efficient selenium-transferring reagent. When triethyl phosphite was treated in dichloromethane with polymer-supported selenide **2** (4 equiv.), complete conversion to the corresponding phosphoroselenoate occurred within a few minutes. Also selenization of dinucleoside H-phosphonate **5a** with selenide **2** (3 equiv.) in the presence of DBU (5 equiv.) proceeded rapidly (> 5 min) producing the expected dinucleoside phosphoroselenoate **6a**.‡‡

In conclusion, we have developed a new and efficient method for the selenization of P^{III} compounds based on selenium exchange. Triphenylphosphine selenide **1**, which is proposed as a new source of electrophilic selenium in this method, is a stable, easy to handle, inexpensive and commercially available reagent, with good solubility in organic solvents. Efficiency of **1** as a selenium-transferring reagent was demonstrated by using it for the conversion of phosphite triesters and H-phosphonate diesters into the corresponding phosphoroselenoates, as well as in the transformation of H-phosphonothioate diesters into the phosphorothioselenoate derivatives. The reactions were fast and occurred under mild, homogeneous conditions. A polymer-supported counterpart of reagent **1**, triphenylphosphine selenide **2**, also showed favourable selenium-transferring properties. This reagent can be considered as an alternative to **1**, especially if separation problems arise.

We are indebted to Professor P. J Garegg for his interest in this work. Financial support from the Swedish Natural Science Research Council is gratefully acknowledged.

Notes and references

† Selenium compounds are generally toxic to animals. However, toxicity *per se* does not rule out a compound for drug use although it frequently prevents the administration of an effective dose that is also safe.

‡ Triphenylphosphine selenide **1** can also be easily prepared *via* selenization of triphenylphosphine in 1,4-dioxane with elemental selenium or according to the Nicpon and Meek procedure,[16] using KSeCN. Approximate solubility of **1** in organic solvents (solvent, mg mL^{-1}): acetonitrile, 6; THF, 80; pyridine 100; dichloromethane 130; chloroform, 230.

§ Identity of this and other phosphoroselenoates obtained in these studies (*e.g.* **4**, **6a**, **6b**) was confirmed by independent synthesis of these compounds *via* selenization of the corresponding P^{III} precursors with elemental selenium.

¶ Dinucleoside phosphite **4** was generated *in situ* from 5′-*O*-dimethoxytritylthymidin-3′-yl methyl *N*,*N*-bis(diisopropyl)phosphoramidite and 3′-*O*-dimethoxytritylthymidine in chloroform in the presence of tetrazole. Besides **4**, the reaction mixture contained *ca*. 10% hydrolysis products and *ca*. 5% of the unreacted phosphoramidite.

‖ Reaction in chloroform, using bis(trimethylsilyl)acetamide (BSA) and triethylamine.

** In a typical experiment, H-phosphonate **5a** or H-phosphonothioate **5b** (0.1 mmol) was dissolved in pyridine (4 mL) containing triphenylphosphine selenide **1** (2.0 equiv.), and DBU (5 equiv.) was added. After 5 min the reaction mixture was diluted with dichloromethane (20 mL), extracted with 0.5 M TEAB buffer (pH = 6.5, 4 × 50 mL) and the organic phase was subjected to silica gel chromatography using a stepwise gradient of methanol (0–2%) in chloroform containing 0.2% triethylamine. Yields: **6a** 90%, **6b** 80%.

†† Polymer-supported phosphine selenide **2** was synthesized by shaking in THF polystyryl diphenylphosphine resin with KSeCN (3 equiv.) for 4 h. After that time the ^{31}P NMR spectrum of the suspended polymer beads showed a complete disappearance of the broad signal at −5.4 ppm due to the phosphine and a new broad signal at 35.5 ppm due to phosphine selenide.

‡‡ *Ca*. 10% of the corresponding nucleoside 3′- and 5′-*H*-phosphonate monoesters were present in the reaction mixture, probably as a result of hydrolysis of **6a**.

1 *Organoselenium Chemistry*, ed. D. Liotta, John Wiley & Sons, New York, 1987; *Organoselenium Chemistry - A Practical Approach*, ed. T. G. Back, Oxford University Press, Oxford, 1999; *Organoselenium Chemistry: Modern Developments in Organic Synthesis*; ser. *Topics in Current Chemistry*, ed. W. Wirth, Springer, Berlin, 2000.
2 K. Schwarz and C. M. Foltz, *J. Am. Chem. Soc.*, 1957, **79**, 3292.
3 M. L. Scott, in *Organic Selenium Compounds: Their Chemistry and Biology*, ed. D. L. Klayman and W. H. H. Günther, Wiley-Interscience, New York, 1973, p. 629.
4 R. J. Shamberger, *Biochemistry of Selenium*, Plenum Press, New York & London, 1983.
5 M. Michalska, in *Biophosphates and Their Analogues—Synthesis, Structure, Metabolism and Activity*, ed. K. S. Bruzik and W. J. Stec, Elsevier Science Publishers B.V., Amsterdam, 1987, p. 211; D. Carriere, S. J. Meunier, F. D. Tropper, S. Cao and R. Roy, *J. Mol. Catal. A: Chem.*, 2000, **154**, 9.
6 I. Lindh and J. Stawinski, *J. Org. Chem.*, 1989, **54**, 1338.
7 S. D. Stamatov and S. Gronowitz, *Lipids*, 1993, **28**, 351.
8 G. Adiwidjaja, O. Schulze, J. Voss and J. Wirsching, *Carbohydr. Res.*, 2000, **325**, 107; N. D. P. Cosford and R. F. Schinazi, *J. Org. Chem.*, 1991, **56**, 2161.
9 M. Koziolkiewicz, B. Uznanski, W. J. Stec and G. Zon, *Chem. Scr.*, 1986, **26**, 251.
10 K. Mori, C. Boiziau, C. Cazenave, M. Matsukura, C. Subasinghe, J. S. Cohen, S. Broder, J. J. Toulme and C. A. Stein, *Nucleic Acids Res.*, 1989, **17**, 8207.
11 J. Stawinski and M. Thelin, *J. Org. Chem.*, 1994, **59**, 130.
12 J. Michalski and A. Markowska, in *Organic Selenium Compounds: Their Chemistry and Biology*, ed. D. L. Klayman and W. H. H. Günther, Wiley-Interscience, New York, 1973, p. 326.
13 W. J. Stec, G. Zon, W. Egan and B. Stec, *J. Am. Chem. Soc.*, 1984, **106**, 6077.
14 A. Michaelis and H. von Soden, *Ann.*, 1885, **229**, 295.
15 P. Pistschimuka, *J. Prakt. Chem.*, 1911, **84**, 746.
16 P. Nicpon and D. W. Meek, *Inorg. Chem.*, 1966, **5**, 1297.
17 J. Baraniak, D. Korczynski, R. Kaczmarek and W. J. Stec, *Nucleosides Nucleotides*, 1999, **18**, 2147.
18 D. H. Brown, R. J. Cross and R. Keat, *J. Chem. Soc., Dalton Trans.*, 1980, 871; D. H. Brown, R. J. Cross and R. Keat, *J. Chem. Soc., Chem. Commun.*, 1977, 708.

ChemComm

Fundamental design aspects of amphiphilic shell-crosslinked nanoparticles for controlled release applications

K. Shanmugananda Murthy, Qinggao Ma, Christopher G. Clark, Jr., Edward E. Remsen and Karen L. Wooley*

Department of Chemistry, Washington University, One Brookings Drive, CB 1134, St. Louis, MO 63130, USA. E-mail: klwooley@artsci.wustl.edu; Fax: +1 (314) 935 9844; Tel: +1 (314) 935 7136

Received (in Corvallis, OR, USA) 19th January 2001, Accepted 15th March 2001
First published as an Advance Article on the web 3rd April 2001

A unique method is developed for the controlled release of the hydrophobic polymer chains from the core of the shell crosslinked nanoparticles (SCKs) by selective cleavage of labile C–ON bonds present at the core–shell interface; this represents a methodology to probe the permeability of nanoscopic membranes and a means for applications in the controlled release of macromolecular species.

Polymeric nanoparticles, engineered with controlled composition, structure and dimensions, have attracted great interest in recent years for their potential applications in medicine and in nanotechnological devices, particularly as drug delivery vehicles.[1,2] Inspired by the nano-sized, amphiphilic core–shell structure of lipoproteins, shell crosslinked nanoparticles (SCKs) with a hydrophobic core, contained within a hydrogel network, were prepared by the self-assembly of amphiphilic block copolymers followed by intramicellar crosslinking between the polymeric chains located within the shell.[3] SCKs are characterized by their structural integrity and available functionality to attach receptor-recognizing ligands on the shell surface.[4] The control over size, shape and composition of these nanoparticles holds great potential in drug delivery applications.[5–7] The permeable crosslinked shell of the SCKs can act as a protective layer for the encapsulated guest molecules and determines the transport into and out of the core of these nanoparticles.[8] The polymer chains constituting the core can be selectively degraded and extracted to generate hollow nanospheres, which makes possible the loading of large quantities of guest molecules.[9]

SCKs with the core composed of bioactive polymeric chains, and covalently attached to the shell, through labile bonds at the core–shell interface, are expected to be of interest for the release of hydrophobic drugs, such as peptides.[2] Such SCKs may be useful as prodrugs with enhanced oral bioavailability for poorly absorbed drugs and may exhibit site-specificity and controlled release, the latter being controlled by the extent of crosslinking of the permeable shell membrane. Therefore, the porosity of these membrane networks, which are only a few nanometers in thickness, must be accurately evaluated. Herein, we report our preliminary results carried out on an SCK model system, based on poly(styrene)-*b*-poly(acrylic acid) (PS-*b*-PAA), possessing labile C–ON bonds present at the core–shell interface. The controlled release of the core PS chains is demonstrated, upon selective thermolytic cleavage of the C–ON bonds.

The synthetic approach for the preparation of the SCK nanoparticles from PS-*b*-PAA and the subsequent release of the PS chains from the core is presented in Scheme 1. SCKs possessing thermally labile C–ON bonds at the core-shell interface were prepared from the amphiphilic copolymer PS-*b*-PAA, which was designed to have a C–ON bond connecting the hydrophilic and hydrophobic blocks. The synthesis of PS-*b*-PAA utilized a combination of nitroxide mediated radical polymerization (NMRP) and atom transfer radical polymerization (ATRP)[10] from a bi-functional initiator, **1**.[11] The alkoxyamine group of **1** was utilized for polymerizing styrene by NMRP and the resulting PS with a terminal bromopropionyl ester group was then used as a macroinitiator for the ATRP of *tert*-butyl acrylate to obtain PS-*b*-P*t*BA.[12] The diblock was made amphiphilic by the hydrolysis of *tert*-butyl ester groups by reaction with TFA in CH_2Cl_2 at rt.[13]

Micellization of PS-*b*-PAA and subsequent shell crosslinking, using 2,2′-(ethylenedioxy)bis(ethylamine) as a crosslinker, were carried out according to the previously reported procedure.[3] To study the effect of shell crosslinking on the structure of the nanoparticles and, in particular, the shell permeability, polymeric micelles were crosslinked to different extents by adding stoichiometric ratios of diamine crosslinker to carboxylic acid moieties that would result in a maximum theoretical crosslinking of 20, 50 and 100%. Upon crosslinking, the C=O absorption band corresponding to free carboxylic acid groups (1710 cm^{-1}) decreased and the amide I and II bands (1650 and 1540 cm^{-1}) with intensity in proportion to the amount of added crosslinker appeared in the IR spectra of lyophilized samples of the SCKs. The effective Stokes, volume-weighted, mean hydrodynamic diameters (by dynamic light scattering (DLS) measurements) were 54 ± 3 nm for the micelles, and the SCKs were respectively, 55 ± 3, 28 ± 2 and 35 ± 3 nm for 20, 50 and 100% crosslinking.[14]

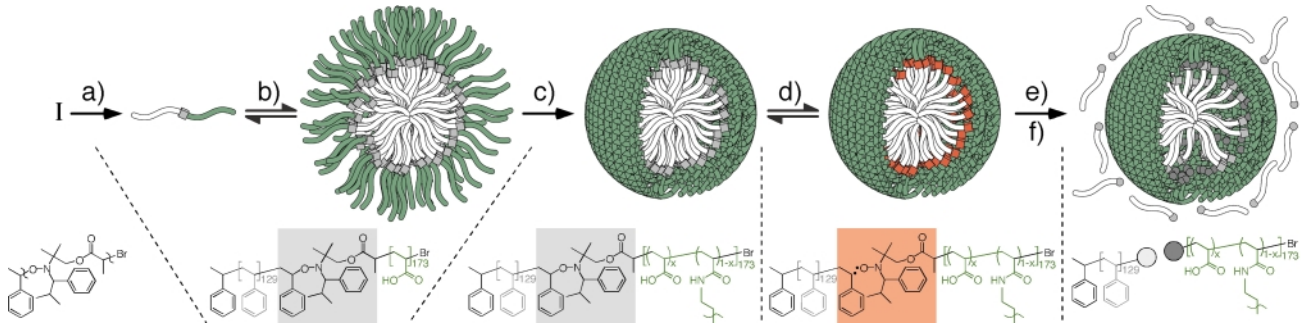

Scheme 1 The synthetic approach for the preparation of SCK nanoparticles by a combination of self-assembly and intramicellar crosslinking reactions followed by the subsequent release of core polymer chains upon the cleavage of C–ON bonds present at the core–shell interface. (a) *See* ref. 12 and 13; (b) and (c) *see* ref. 3; (d) thermolysis of C–ON bonds (125 °C, 24 h in water); (e) lyophilization and (f) resuspension in THF.

The irreversible termination of the PS· radicals, generated upon the thermal homolytic cleavage of the C–ON bonds at the core–shell interface[15] leads to the detachment of PS chains from the crosslinked shell. The addition of ascorbic acid during this process facilitates the irreversible termination of the carbon-centered radicals by reducing the aminoxyl counter radicals to the corresponding hydroxylamine.[16] Thermal decomposition studies were carried out first with the amphiphilic diblock copolymer PS-*b*-PAA, by heating at 125 °C for 24 h in a sealed Schlenk tube (in toluene–acetic acid, 80 : 20 v/v) in the presence and absence of ascorbic acid. The isolated PS (pure by ^{1}H NMR) accounted for 58.5% (ascorbic acid) and 20.7% (no ascorbic acid) of the theoretical amount of PS expected. The polydispersity index (PDI) decreased from 1.22 (for PS-*b*-PAA) to 1.10 (for the PS obtained upon decomposition). The GPC trace of the PS obtained was monomodal and the peak retention time coincided with that of the PS macroinitiator.

The amount of PS isolated (20.7% in 24 h) by the homolytic cleavage of C–ON bonds in PS-*b*-PAA was significant even in the absence of radical quencher, ascorbic acid. Hence, for simplicity, the cleavage of the C–ON bonds present at the core–shell interface of the SCKs were carried out by heating the aqueous solution of SCKs (125 °C in a sealed Schlenk tube for 24 h) in the absence of ascorbic acid. The kinetics of PS chains released from the core was followed by suspending the lyophilized SCKs in THF (at rt) with stirring and analyzing aliquots removed at different time intervals, after filtration through a 20 nm filter (Whatman), by GPC using a PS standard (M_n = 2450) of known weight as an internal reference. Representative GPC traces of PS released as a function of time, for SCKs with 20% crosslinking, are given in Fig. 1(a) and the data for % PS released as a function of time for SCKs with different extents of crosslinking are plotted in Fig. 1(b). In each case, the GPC retention time of the PS released and that of the PS macroinitiator was identical. Based on the nearly monodisperse GPC chromatograms of the released PS, it appears that bimolecular termination between the PS· radicals is not a major termination process. However, an alternative argument for the lack of observable PS dimer is that the molecular weight of the dimer may be sufficiently great as to prevent its permeation through the shell of the SCK. An inverse relationship was observed between the amount and rate of PS release with the extent of shell crosslinking. The amount of PS released (92 h) was 28.7, 6.8 and 3.5% for the SCKs with 20, 50 and 100% crosslinking, respectively.[17] The PS released during the initial period was rapid ('burst effect'), likely due to the increase in osmotic pressure with the addition of THF, followed by a decreasing rate of release, consistent with passive diffusion.

The amount of PS released from the nanoparticles was larger (28.7% in 92 h, 20% crosslinking) than that isolated (20.7%) from PS-*b*-PAA under similar decomposition conditions (125 °C, 24 h). A decreased efficiency of the recombination reactions between the PS· radicals in the core and the aminoxyl counter radicals located at the inner surface of the shell, leading to more dead PS chains, is consistent with the observed results for SCKs.

The experimental data reveal that the free PS chains, present in the core, can penetrate the hydrogel-like shell membrane. However, when the shell is highly crosslinked such penetration is inhibited. The controlled release of polymer chains from the core by adjusting the crosslink density of the shell opens the possibilities of designing polymeric nanoparticles with specific shell permeabilities, capable of delivery of large guests. This approach may provide a solution to some of the delivery problems posed by biologically active molecules, such as peptides and proteins, genes and oligonucleotides. The results of this study also provide a foundation for better understanding of the porosity of the crosslinked shell of SCKs.

Funding of this research, provided by National Science Foundation (DMR-9974457), is gratefully acknowledged.

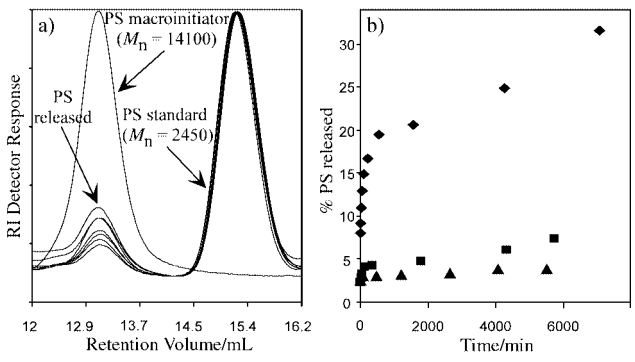

Fig. 1 (a) GPC traces of PS (M_n = 14100) released from the core of SCKs (20% crosslinking) as a function of time. The PS standard (M_n = 2450) provided concentration quantification. (b) Release kinetics of PS from the core of SCKs crosslinked to different extents (◆ 20%, ■ 50% and ▲ 100% crosslinking).

Notes and references

1 (*a*) J. L. West and N. J. Halas, *Curr. Opin. Biotechnol.*, 2000, **11**, 215; (*b*) K. Kataoka, in *Controlled Drug Delivery: the Next Generation*, ed. K. Park, American Chemical Society, Washington, DC, 1997, ch. 4.

2 (*a*) R. Langer, *Acc. Chem. Res.*, 2000, **33**, 94; (*b*) E. Allémann, J. C. Leroux and R. Gurny, *Ad. Drug Delivery Rev.*, 1998, **34**, 171.

3 H. Huang, T. Kowalewski, E. E. Remsen, R. Gertzmann and K. L. Wooley, *J. Am. Chem. Soc.*, 1997, **119**, 11 653.

4 J. Liu, Q. Zhang, E. E. Remsen and K. L. Wooley, *Biomacromolecules*, in press.

5 K. B. Thurmond II, E. E. Remsen, T. Kowalewski and K. L. Wooley, *Nucleic Acids Res.*, 1999, **27**, 2966.

6 Q. Zhang, E. E. Remsen and K. L. Wooley, *J. Am. Chem. Soc.*, 2000, **122**, 3642.

7 V. Bütün, N. C. Billingham and S. P. Armes, *J. Am. Chem. Soc.*, 1998, **120**, 12 135.

8 A. H. Baugher, J. M. Goetz, L. M. McDowell, H. Huang, K. L. Wooley and J. Schaefer, *Biophys. J.*, 1998, **75**, 2574.

9 (*a*) T. Sanji, Y. Nakatsuka, S. Ohnishi and H. Sakurai, *Macromolecules*, 2000, **33**, 8524; (*b*) H. Huang, E. E. Remsen, T. Kowalewski and K. L. Wooley, *J. Am. Chem. Soc.*, 1999, **121**, 3805.

10 (*a*) C. J. Hawker, *J. Am. Chem. Soc.*, 1994, **116**, 11 185; (*b*) K. A. Davis and K. Matyjasjewski, *Macromolecules*, 2000, **33**, 4039.

11 The initiator, **1**, was synthesized by reacting 1-hydroxy-2,2,5-trimethyl-3-(1-phenylethoxy)-4-phenyl-3-azahexane (HAA) with excess bromoisopropionyl bromide in the presence of triethylamine. The crude ester was purified by column chromatography eluting with hexane–ethylacetate (4 : 1). ^{1}H NMR ($CDCl_3$, 300 MHz, diastereomers) δ 7.5–7.1 (m, 20H), 5.0–4.8 (m, 2H), 4.5–2.3 (m, 8H), 2.0–1.8 (m, 8H), 1.66 (d, 3H, J = 6.6 Hz), 1.58 (d, 3H, J = 6.6 Hz), 1.37 (d, 3H, J = 6.3 Hz), 1.36 (d, 3H, J = 6.3 Hz), 1.26 (s, 3H,), 1.05 (s, 3H), 0.98 (d, 3H, J = 6.3 Hz), 0.61 (s, 3H,), 0.59 (d, 3H, J = 6.6 Hz), 0.26 (d, 3H, J = 6.6 Hz). HRMS mass calculated for $C_{25}H_{34}BrNO_3$ $[M + 1]^+$ 476.17, found 476.2. For the preparation of HAA *see* D. Benoit, V. Chaplinski, R. Braslau and C. J. Hawker, *J. Am. Chem. Soc.*, 1999, **121**, 3904.

12 Styrene (13.10 g, 0.126 mol), **1** (0.43 g, 9×10^{-4} mol) and acetic anhydride (0.19 g, 1.8×10^{-3} mol) were charged into a Schlenck tube and after three freeze–thaw cycles, the tube was sealed and the polymerization was carried out at 125 °C for 6 h. The bromopropionyl terminated PS (M_n (GPC) = 14100 g mol^{-1}, PDI = 1.11) was isolated by methanol precipitation and was then used as an initiator (4.00 g, 2.84 $\times 10^{-4}$ mol) for the ATRP of *tert*-butyl acrylate (8.75 g, 6.80×10^{-2} mol) in the presence of *N*,*N*′,*N*′,*N*″*N*″-pentamethyldiethylenetriamine (0.10 g, 5.80×10^{-4} mol) and CuBr (0.07 g, 4.70×10^{-4} mol) at 50 °C for 15 h.

13 To 6.05 g of PS-*b*-P*t*BA was added 150 mL of CH_2Cl_2 followed by 15.0 mL of TFA. The reaction mixture was stirred at 25 °C for 40 h, concentrated *in vacuo*, and precipitated (3×) in hexane from THF solution. The PS-*b*-PAA product was dried under vacuum.

14 The effect of shell crosslinking upon the hydrodynamic diameter is being studied in detail for these and other shell crosslinked nanostructures.

15 Model studies with ethyl 2-bromopropionate under similar reaction conditions gave no ester bond hydrolysis.

16 C. Li, J. He, L. Li and J. Cao, *Macromolecules*, 1999, **32**, 7012.

17 In a blank experiment, performed upon 20% crosslinked SCKs without heating, 3% of the PS chains were extracted (in 92 h) from the core, presumably these were macroinitiator contaminants.

Suzuki coupling with ligandless palladium and potassium fluoride

George W. Kabalka,* Vasudevan Namboodiri and Lei Wang

Departments of Chemistry and Radiology, University of Tennessee, Knoxville, TN, USA. E-mail: kabalka@utk.edu; Fax: +1(865)974-2997; Tel: +1(865)974-3260

Received (in Corvallis, OR, USA) 12th February 2001, Accepted 14th March 2001
First published as an Advance Article on the web 3rd April 2001

A ligandless palladium catalyzed Suzuki coupling reaction is described.

The palladium catalyzed carbon–carbon cross-couplings of organometallics with organoelectrophiles is an important synthetic reaction.[1] Most organometallic compounds are sensitive to air, moisture or are toxic and often will not tolerate functional groups which may be important in complex syntheses. Boronic acids constitute one of the few organometallic reagents that tolerate a wide range of functional groups, are available and generally environmentally benign. In addition, they are inert to air, resistant to heat, and can be recrystallized from water or alcohol.

The Suzuki reaction[2] which uses boron-containing precursors has gained considerable attention in recent years because a large number of functionally substituted boron-containing reagents are commercially available. The Suzuki reaction generally employs expensive organic solvents such as tetrahydrofuran as well as expensive complex palladium catalysts. These palladium reagents tend to be difficult to manipulate and recover. We recently reported an energy efficient modification of the Suzuki reaction using an alumina surface and palladium powder which solved some of these problems.[3,4]

Earlier studies revealed that potassium fluoride was an effective Suzuki base.[5] Therefore we selected KF as the base for the current study. We found that aromatic iodides readily couple with arylboronic acids in the presence of palladium powder when the reactions are carried out in methanol, Scheme 1. The initial results are summarized in Table 1. The reaction can be utilized to couple benzyl bromides with arylboronic acids but aryl bromides and aryl chlorides are ineffective substrates. Aliphatic boronic acids are also not reactive.

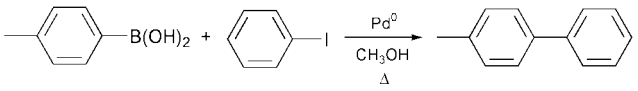

Scheme 1

Table 1 Suzuki coupling of tolylboronic acid with aryl iodides[a]

Boronic acid	Aryl iodide	Yield[b] (%)
4-Methylphenyl	1-Fluoro-2-iodobenzene	91
4-Methylphenyl	1-Iodo-4-nitrobenzene	94
4-Methylphenyl	2-Iodoaniline	77
4-Methylphenyl	4-Iodoacetophenone	93
4-Methylphenyl	4-Iodoanisole	83
4-Methylphenyl	2-Iodothiophene	93
4-Methylphenyl	2-Iodophenol	76
4-Methylphenyl	1-Fluoro-3-iodobenzene	98
4-Methylphenyl	4-Iodotoluene	89

[a] Reactions carried out utilizing 1.0 mmol of aryl iodide and 1.1 mmol of tolylboronic acid in refluxing methanol (5 mL) for 4 h in the presence of palladium powder. [b] Isolated yields.

Table 2 Suzuki coupling of arylboronic acids with aryl iodides[a]

Boronic acid	Aryl iodide	Yield[b] (%)
Naphthyl	Iodobenzene	90
Naphthyl	1-Iodo-4-nitrobenzene	89
Naphthyl	2-Iodoaniline	74
2-Methylphenyl	2-Iodothiophene	90
2-Methylphenyl	1-Iodo-4-nitrobenzene	93
2-Methylphenyl	Iodobenzene	97
3-Formylphenyl	2-Iodothiophene	98
3-Formylphenyl	1-Iodo-4-nitrobenzene	98

[a] Reactions carried out utilizing 1.0 mmol of aryl iodide and 1.1 mmol of arylboronic acid in refluxing methanol (5 mL) for 4 h in the presence of palladium powder. [b] Isolated yields.

From the data in Tables 1 and 2, it would appear that the reaction is relatively insensitive to the electronic nature of substituents on the aromatic ring.

The synthesis of 4-methylbiphenyl is representative: palladium black (0.050 g), KF (0.380 g), *p*-methylphenylboronic acid (0.150 g, 1.10 mmol) and iodobenzene (0.204 g, 1.0 mmol) were added to a clean, dry, 50 mL round bottomed flask. Methanol (5 mL) was added to the mixture and the solution was refluxed for 4 h in the open air. After decanting the solution, the product was isolated *via* flash chromatography to yield 4-methylbiphenyl (92.2%); m.p. 44.0–45.5 °C, ^{1}H NMR ($CDCl_3$; δ ppm): 7.40 (m, 9 H), 2.37 (s, 3H).

It is important to note that the palladium metal can be recovered and recycled by a simple decantation of the reaction solution. In one series of experiments, we carried out eight consecutive preparations of 4-methylbiphenyl with no significant loss in product yields. In each case, the palladium powder was recovered by decantation, washed with methanol, and the experiment repeated. We made no effort to rigorously exclude water from the reactions. In fact, successful syntheses were achieved in 20% aqueous methanol.

We wish to thank the U.S. Department of Energy and the Robert H. Cole Foundation for their support of this research.

Notes and references

1 N. Miyaura and A. Suzuki, *Chem. Rev.*, 1995, **95**, 2457.
2 A. R. Martin and Y. Yang, *Acta Chem. Scand.*, 1999, **47**, 221.
3 G. W. Kabalka, R. M. Pagni and C. M. Hair, *Org. Lett.*, 1999, **1**, 1423.
4 S. V. Rajender and N. P. Kannan, *Tetrahedron. Lett.*, 1999, **40**, 439.
5 T. Ishiyama, H. Kizaki, T. Hayashi, A. Suzuki and N. Miyaura, *J. Org. Chem.*, 1998, **63**, 4726.

Cooperative cation and anion coordination by a bifunctional imidophosphorane ligand framework; syntheses and structures of [LiCl{Bu^{t}NHP)μ-NBu^t)$_2$PNH(2-py)}$_3$] and [{Bu^{t}NP(μ-NBu^t)$_2$PN(2-py)}Li$_2$·{Li(Bu^{t}N)$_2$P}]†

Andrew D. Bond, Emma L. Doyle, Sara J. Kidd, Anthony D. Woods and Dominic S. Wright*

Chemistry Department, University of Cambridge, Lensfield Road, Cambridge, UK CB2 1EW. E-mail: dsw1000@cus.cam.ac.uk

Received (in Cambridge, UK) 18th December 2000, Accepted 8th March 2001
First published as an Advance Article on the web 3rd April 2001

The neutral ligand [Bu^{t}NHP(μ-NBu^t)$_2$PNH(2-py)] and its dilithiate [{Bu^{t}NP(μ-NBu^t)$_2$PN(2-py)}Li$_2$] exhibit a parallel ability to coordinate cations and anions, as revealed in the structures of the tris-solvate [LiCl{Bu^{t}NHP(μ-NBu^t)$_2$PNH(2-py)}$_3$] 1 and the unusual co-complex [{Bu^{t}NP(μ-NBu^t)$_2$PN(2-py)}Li$_2$·{Li(Bu^{t}N)$_2$P}] 2.

In recent years the coordination chemistry of new ligand systems based on Group 15 element/nitrogen frameworks has been the focus of an increasing number of investigations.[1] The most intensively studied species of this class are $[E_2(NR)_4]^{2-}$ dianions, which have been prepared for all the Group 15 elements (E = P–Bi).[2–5] For the heavier congeners (As–Bi) the dianion frameworks are readily established by condensation reactions of the dimers $[Me_2NE(\mu\text{-}NR)]_2$ with primary amido lithium complexes ($[RNHLi]_n$).[3–5] However, the phosphorus analogues are obtained by metallation of the pre-formed acids $[RNHP(\mu\text{-}NR)]_2$ with organolithium reagents.[2] The structures of the resulting lithium cages are based on $[\{E_2(NR)_4\}Li_2]$ cubane units, generally being of the type $[\{E_2(NR)_4\}Li_2\cdot 2thf]$[2a,5] or $[\{E_2(NR)_4\}\ Li_2]_2$[2b,3,4] (depending on the presence or absence of thf solvation). We recently showed that the precursor [Bu^{t}NHP(μ-NBu^t)$_2$PCl] is useful in the synthesis of non-symmetrical dianions, the reaction of the former with [CyPHLi] (Cy = cyclohexyl)/Bu^{n}Li giving the bifunctional (hard/soft) dianion [Bu^{t}NP(μ-NBu^t)$_2$PPCy]$^{2-}$.[6]

Both NMR spectroscopic and analytical investigations revealed that the reaction of (2-py)NHLi with [Bu^{t}NHP(μ-NBU^t)PCl][6] does not yield the free ligand [Bu^{t}NHP(μ-NBu^t)PNH(2-py)] (py = pyridyl), rather the product is the lithium chloride complex [LiCl{Bu^{t}NHP(μ-NBu^t)PNH(2-py)}$_3$] (Scheme 1) (ESI†). Addition of Bu^{n}Li to a solution of **1** [prepared *in situ* from the 1:1 reaction of [Bu^{t}NHP(μ-NBu^t)PCl] with (2-py)NHLi] (1.6 equiv., respectively)] leads to precipitation of LiCl and the formation of [{BuNP(μ-NBu^t)$_2$PN(2-py)}Li$_2$·{Li(Bu^{t}N)$_2$P}] **2** (in 19% yield) (ESI†). A ^{31}P NMR study of the reaction mixture before and after the addition of Bu^{n}Li reveals that the production of **2** stems from the formation of $[Bu^tNHP(\mu\text{-}NBu^t)]_2$ as a significant byproduct in the synthesis of **1**. ^{31}P NMR studies also show that only the dilithiate $[\{Bu^tNP(\mu\text{-}NBu^t)_2PN(2\text{-}py)\}Li_2]_n$ is produced by lithiation of *pure* **1**. However, addition of $[\{P_2(NBu^t)_4\}_2Li_2]_2$ (the product of lithiation of $[Bu^tNHP(\mu\text{-}NBu^t)]_2$[2b]) to a solution of $[\{Bu^tNP(\mu\text{-}NBu^t)_2PN(2\text{-}py)\}Li_2]_n$ in the correct stoichiometric ratio gives **2**.‡ The formation of **2** can therefore be explained in both cases by symmetrical cleavage of the P_2N_2 ring units of $[\{P_2(NBu^t)_4\}_2Li_2]_2$ (Scheme 1). Of particular interest is the highly deshielded nature of the P centre of the $[(Bu^tN)_2P]^-$ anion in **2**, whose resonance is found at δ 395.3 (+25 °C). This value is considerably greater than observed for other $[(RP)_2N]^-$ anions (*ca.* δ 340–360).[2b,7] suggesting an even greater degree of charge separation within the anion backbone in **2** [*i.e.* N$^-$–P$^+$–N$^-$ rather than (N⋍P⋍N)$^-$]. The extent of this charge separation is probably related to the unusual coordination mode of the $[(Bu^tN)_2P]^-$ anion observed in the later structural characterisation of the complex (involving two N–Li bonds to each of the N centres of the anion, rather than only one as in all other previously characterised lithiates[2b,7]).

Confirmation of the structure proposed on the basis of spectroscopic and analytical studies is provided by a low-temperature X-ray crystallographic study of **1**.‡ This reveals that **1** is monomeric in the solid state, being composed of a lithium chloride unit which is coordinated by three neutral [Bu^{t}NHP(μ-NBu^t)PNH(2-py)] ligands (the molecules having exact C_{3v} symmetry about the Li–Cl bond axis) (Fig. 1). Although other tris-pyridine complexes of LiCl have been structurally characterised,[8] the 'cooperative' mode of coordination of the LiCl unit in **1** (by a combination of (pyridyl)N–Li bonding and H-bonding to the Cl$^-$ anion within the hydrophilic ligand cavity) is, to our knowledge, unprecedented for such an inorganic ligand system. This behaviour has closer parallels

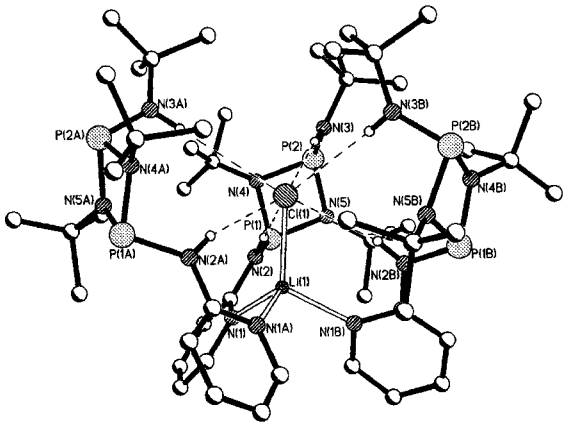

Fig. 1 Structure of the tris-solvate **1**: H-atoms (except those attached to N) have been omitted for clarity. Key bond lengths (Å) and angles (°); Li(1)–Cl(1) 2.325(9), N(1)–Li(1) 2.093(5), P(1)–N(2) 1.710(3), P(1)–N(4) 1.703(3), P(1)–N(5) 1.705(3), P(2)–N(3) 1.642(3), P(2)–N(4) 1.728(3), P(2)–N(5) 1.733(3), Cl(1)···H(2N) 2.65; [N(2)–H(2N)···Cl(1) 165.2], Cl(1)···H(3N) 3.18 [N(3)–H(3N)···Cl(1) 176.7], *exo*-N–P(1,2)–μ-N range 103.03(4)–104.9(2), N(4)–P(1)–N(5) 81.4(1), N(4)–P(2)–N(5) 80.0(1), P(1)–N(4)–P(2) 98.5(2), P(1)–N(5)–P(2) 98.2(2).

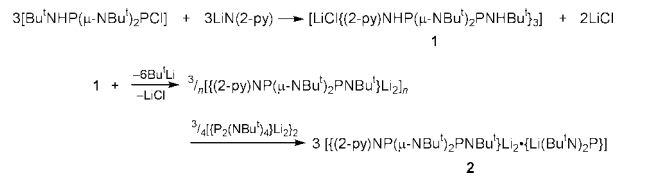

Scheme 1

† Electronic supplementary information (ESI) available: syntheses of **1** and **2**. See http://www.rsc.org/suppdata/cc/b0/b010093p/

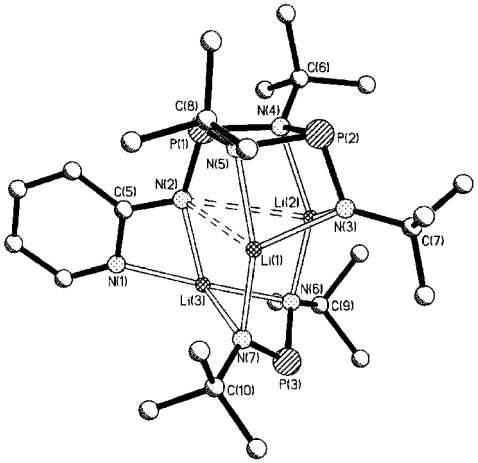

Fig. 2 Structure of the co-complex **2**; H-atoms have been omitted for clarity. Key bond lengths (Å) and angles (°); *dianion*: P(1)–N(2) 1.670(3), P(1)–N(4) 1.754(2), P(1)–N(5) 1.756(3), P(2)–N(3) 1.646(3), P(2)–N(4) 1.790(2), P(2)–N(5) 1.787(3); exo-N–P(1,2)–μ-N range 99.5(1)–101.2(1), N(4)–P(1)–N(5) 83.2(2), N(4)–P(2)–N(5) 81.3(1), P(1)–N(4)–P(2) 97.3(1), P(1)–N(5)–P(2) 97.4(1); *monoanion*: P(3)–N(6) 1.613(3), P(3)–N(7) 1.606(3); N(6)–P(3)–N(7) 102.0(1); Li–N *framework*: N(1)–Li(3) 2.002(6), N(2)–Li(3) 2.040(6), N(2)···Li(1) 2.523(7), N(2)···Li(2) 2.823(7), N(3)–Li(1) 2.085(6), N(3)–Li(2) 2.022(6), N(4)–Li(2) 2.152(6), N(5)–Li(1) 2.164(6), N(6)–Li(2) 2.087(6), N(7)–Li(1) 2.080(6), N(6)–Li(3) 2.087(6), N(7)–Li(3) 2.109(6).

with organic ligand frameworks such as the mode of coordination of HSO_4^- and $H_2PO_4^-$ ions by the tripodal naphthylurea receptor $N\{CH_2CH_2NHC(=O)NHC_{10}H_7\}_3$.[9] Judging by the lengths of the N–H···Cl interactions involved, the H-bonds with the NH(2-py) groups [Cl(1)···H(2N) 2.647(3) Å] are far more significant than those to the Bu^{t}NH groups [Cl(1)···H(3N) 3.177(3) Å]. This conclusion is confirmed by the variable-temperature ^{1}H NMR spectrum of the complex, in which the (2-py)NH proton resonance shifts from δ 6.40 at 20 °C to δ 5.60 at 40 °C with disruption of the N–H···Cl H-bonds. In comparison, the resonance for the Bu^{t}NH protons remains almost static (at δ 3.30).

The structure of **2**‡ consists of a co-complex of the anticipated pseudo-cubane [{Bu^{t}NP(μ-NBu^t)$_2$N(2-py)}Li$_2$] with a [(Bu^{t}N)$_2$P]Li monomer (Fig. 2). Alkali metal complexes containing [(RN)$_2$P]$^-$ anions have only been observed previously where sterically demanding organic substituents are present, which prevent dimerisation into [P$_2$(NR)$_4$]$^{2-}$ dianions (such as 2,4,6-Bu$^t_3$C$_6$H$_2$ or 1-adamantyl).[2b,7,10] Significantly, the steric demands of the Bu^t group alone are insufficient to prevent dimerisation in [{P$_2$(NBu^t)$_4$}Li]$_2$[2b] or its thf solvate [{P$_2$(NBu^t)$_4$}Li$_2$·2thf].[2a] Clearly, the disruption of this dimerisation and the 'trapping' of the [(Bu^{t}N)$_2$P]$^-$ anion in **2** stem from the ability of the supporting [{Bu^{t}NP(μ-NBu^t)$_2$PN(2-py)}Li$_2$] pseudo-cubane to coordinate cooperatively the cation and anion of the [(Bu^{t}N)$_2$P]Li monomer (behaviour which parallels that of the neutral [Bu^{t}NHP(μ-NBu^t)PNH(2-py)] ligand in **1**, *i.e.* the Li$^+$ cations now playing a similar role to the H atoms in anion coordination). A similar ability to form co-complexes of this type has also been observed for the Group 15 complex [{Sb(NCy)$_3$}$_2$Li$_6$][11] and the Group 16 complex [S(NBu^t)$_3$Li$_2$].[12]

Examination of the Li–N bond lengths found in the core of **2** reveals that chelation of Li(3) by the N(2-py) group plays a decisive role in stabilising the [(Bu^{t}N)$_2$P]Li monomer. In fact, bonding of the imido N centre of the N(2-py) group to the two Li$^+$ cations within the [{BuNP(μ-NBu^t)$_2$PN(2-py)}Li$_2$] fragment [N(2)–Li(1) 2.523(7), N(2)–Li(2) 2.823(7) Å] is almost completely sacrificed to allow effective coordination of Li(3) by the N(2-py) group [N(1)–Li(3) 2.003(6), N(2)–Li(3) 2.040(6) Å]. Thus, Li(1) and Li(2) only interact significantly with the terminal and μ-NBu^t groups of the [Bu^{t}NP(μ-NBu^t)$_2$PN(2-py)]$^{2-}$ dianion [N(3)–Li(1,2) mean 2.05, N(4,5)–Li(1,2) mean 2.16 Å], and these Li$^+$ cations are therefore primed (spacially and electronically) for coordination by the two N centres of the [(Bu^{t}N)$_2$P]$^-$ anion [Li(1,2)–N(7,6) 2.08 Å]. Although the P···N bond lengths within the [(Bu^{t}N)$_2$P]$^-$ anion [P(3)–N(6) 1.613(3), P(3)–N(7) 1.606(3) Å] are similar to those found in [(RN)$_2$P]Li complexes containing bulky substituents (*ca.* 1.58–1.60 Å),[2b,7] unlike the latter the PN$_2$Li ring in **2** is non-planar as a result of the interaction of the N atoms of the anion with Li(1) and Li(2). This is a unique coordination mode for any [(RN)$_2$P]$^-$ anion.[2b,7,10,13]

We gratefully acknowledge the EPSRC (A. D. B., E. L. D., S. J. K., A. D. W.) for financial support.

Notes and references

‡ *Crystal data*: for **1**; $C_{51}H_{99}ClLiN_{15}P_6$, M = 1150.66, rhombohedral, space group $R\bar{3}$, Z = 6, a = b = 22.563(2), c = 23.8030(10) Å, V = 10493.4(14) Å^3, μ(Mo-Kα) = 0.223 mm^{-1}, T = 230(2) K. Data were collected on a Nonius KappaCCD diffractometer. Of a total of 12953 reflections collected, 4938 were independent (R_{int} = 0.071). The structure was solved by direct methods and refined by full-matrix least squares on F^2. Final $R1$ = 0.066 [$I > 2\sigma(I)$] and $wr2$ = 0.232 (all data).[14] The H atoms attached to N(2) and N(3) were placed geometrically and allowed to ride during subsequent refinement. All of the Bu^t groups exhibit rotational disorder. This was modelled with 50% occupancy in each of the sites.

For **2**; $C_{25}H_{49}Li_3N_7P_3$, M = 561.44, monoclinic, space group $P2_1/n$, Z = 4, a = 17.1197(5), b = 10.5016(4), c = 18.8343(4) Å, β = 98.535(2)°, V = 3348.61(18) Å^3, μ(Mo-Kα) = 0.202 mm^{-1}, T = 180(2) K. Data were collected on a Nonius KappaCCD diffractometer. Of a total of 24258 reflections collected, 7577 were independent (R_{int} = 0.067). The structure was solved by direct methods and refined by full-matrix least squares on F^2. Final $R1$ = 0.0723 [$I > 2\sigma(I)$] and $wR2$ = 0.207 (all data).[14] The Bu^t groups attached to N(6) and N(7) exhibit disorder about the C–N bonds rotational axis. This was modelled with 50% occupancy in two sites. CCDC 155955 and 155956. See http://www.rsc.org/suppdata/cc/b0/b010093p/ for crystallographic data in .cif or other electronic format.

1 M. A. Beswick and D. S. Wright, *Coord. Chem. Rev.*, 1998, **176**, 373; M. A. Beswick, M. E. G. Mosquera and D. S. Wright, *J. Chem. Soc., Dalton Trans.*, 1998, 2437 and references therein.

2 (*a*) I. Schranz, L. Stahl and R. J. Staples, *Inorg. Chem.*, 1998, **37**, 1493; (*b*) J. K. Brask, T. Chivers, M. L. Krahn and M. Parvez, *Inorg. Chem.*, 1999, **38**, 290.

3 M. A. Beswick, E. A. Harron, A. D. Hopkins, P. R. Raithby and D. S. Wright, *J. Chem. Soc., Dalton Trans.*, 1999, 107.

4 R. A. Alton, D. Barr, A. J. Edwards, M. A. Paver, M.-A. Rennie, C. A. Russell, P. R. Raithby and D. S. Wright, *J. Chem. Soc., Chem. Commun.*, 1994, 1481.

5 D. Barr, M. A. Beswick, A. J. Edwards, J. R. Galsworthy, M. A. Paver, M.-A. Rennie, C. A. Russell, P. R. Raithby, K. L. Verhorevoort and D. S. Wright, *Inorg. Chim. Acta*, 1996, **248**, 9.

6 A. Bashall, B. R. Elvidge, M. A. Beswick, S. J. Kidd, M. McPartlin and D. S. Wright, *Chem. Commun.*, 2000, 1439.

7 E. Nieke, M. Frost, M. Nieger, V. von der Gönna, A. Ruban and W. W. Schoeller, *Angew. Chem., Int. Ed. Engl.*, 1994, **33**, 2111; R. Detsch, E. Nieke, M. Nieger and W. W. Schoeller, *Chem. Ber.*, 1992, **125**, 1119.

8 C. L. Raston, B. W. Skelton, C. R. Whittaker and A. H. White, *Aust. J. Chem.*, 1988, **41**, 341; C. L. Raston, B. W. Skelton, C. R. Whittaker and A. H. White, *J. Chem. Soc.*, 1988, 991.

9 H. Xie, S. Yi, X. Yang and S. Wu, *New. J. Chem.*, 1999, **23**, 1105; see also, *Supramolecular Chemistry of Anions*, ed. A. Bianchi, E. Carcía-España and K. Bowman-James, Wiley-VCH, Weinheim, 1997.

10 The only other complex containing a [(Bu^{t}N)$_2$P] ligand is [(Bu^{t}N)$_2$PSnMe$_2$Cl], M. Bürklin, E. Hanecker, H. Nöth and W. Storch, *Angew. Chem.*, 1985, **97**, 979; M. Bürklin, E. Hanecker, N. Nöth and W. Storch, *Angew. Chem., Int. Ed. Engl.*, 1985, **24**, 999.

11 A. J. Edwards, M. A. Paver, M.-A. Rennie, C. A. Russell, P. R. Raithby and D. S. Wright, *Angew. Chem.*, 1995, **107**, 1088; A. J. Edwards, M. A. Paver, M.-A. Rennie, C. A. Russell, P. R. Raithby and D. S. Wright, *Angew. Chem., Int. Ed. Engl.*, 1995, **34**, 1012.

12 R. Fleischer and D. Stalke, *Chem. Commun.*, 1998, 343; R. Fleischer, S. Freitag and D. Stalke, *J. Chem. Soc., Dalton Trans.*, 1998, 193.

13 For other main group and transition metal complexes containing [(RN)$_2$P]$^-$ ligands see, P. B. Hitchcock, H. A. Jasim, M. F. Lappert and H. D. Williams, *J. Chem. Soc., Chem. Commun.*, 1986, 1634; O. J. Scherer, E. Franke and J. Kaub, *Angew. Chem., Int. Ed. Engl.*, 1986, **25**, 96; U. Wirringer, H. Voelker, H. W. Roesky, Y. Schermolovich, L. Markovski, I. Uson, M. Noltemeyer and H.-G. Schmit, *J. Chem. Soc., Dalton Trans.*, 1995, 1951.

14 SHELXTL PC version 5.03, Siemens Analytical Instruments, Madison, WI, 1994.

Highly efficient C–C coupling reactions using metallated benzylphosphine complexes of palladium

Scott Gibson,*[a] Douglas F. Foster,[a] Graham R. Eastham,[b] Robert P. Tooze[b]† and David J. Cole-Hamilton*[a]

[a] *School of Chemistry, University of St Andrews, St Andrews, Fife, Scotland, UK KY16 9ST. E-mail: djc@st-and.ac.uk*

[b] *Ineos Acrylics, Wilton, Middlesbrough, Cleveland, UK TS90 8JE*

Received (in Cambridge, UK) 8th January 2001, Accepted 13th March 2001
First published as an Advance Article on the web 3rd April 2001

Phosphapalladacyclic complexes synthesised from *ortho*-bromobenzylphosphine ligands are effective catalysts for carbon–carbon bond forming reactions, exhibiting activity that compares with, and in several examples exceeds, that of existing systems.

Outstandingly active catalysts for the Heck (Scheme 1) and Suzuki (Scheme 2) coupling reactions using palladacyclic compounds have been reported by Herrmann *et al.* (**1**, turnover numbers (TON, mol (mol Pd)$^{-1}$) for Heck reactions up to 1 M),[1,2] Milstein and coworkers (**2**)[3] and Bedford and coworkers (**3**, TON for Heck up to 5.75 M, but substantial formation of polystyrene occurred and TON to product was not reported).[4]

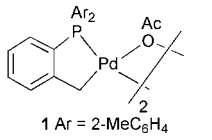

1 Ar = 2-MeC$_6$H$_4$

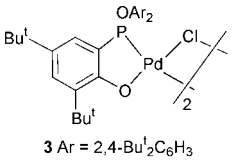

3 Ar = 2,4-Bu$^t_2$C$_6$H$_3$

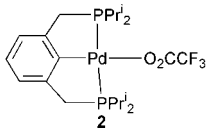

2

We were interested in whether the nature of the Pd–C bond was important in determining catalyst efficiencies, so we attempted the synthesis of a complex similar to that of Herrmann *et al*., but with a metallated benzyl ligand.

† Current address: ICI Synetix, PO Box 1, Belasis Avenue, Billingham, Cleveland, UK TS23 1LB.

Tertiary *o*-bromobenzylphosphine ligands **4** undergo metallation with [Pd$_2$(dba)$_3$] (dba = dibenzylideneacetone) to yield the palladacycle complexes **5** (Scheme 3) which also exhibit efficient cross-coupling catalytic activity. In common with the studies of Herrmann *et al.*, we have found that aryl groups on the phosphine moiety of the palladacyclic complex give superior catalytic performance than electron-donating alkyl groups,[5] so we have concentrated on complex **5a** (Table 1).

The reaction of 4-bromoacetophenone with *n*-butyl acrylate consistently resulted in reasonable yields of 85–90% when 2×10^{-4} mol% of **5a** was used. As expected, longer reaction times were required to achieve the same yield when a lower reaction temperature was used (entry 2). It is noted that higher

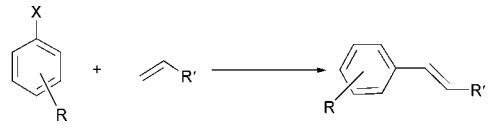

Scheme 1 Heck coupling reaction.

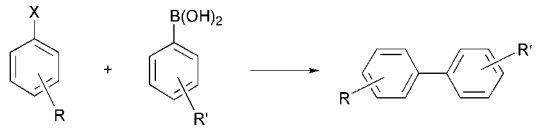

Scheme 2 Suzuki reaction.

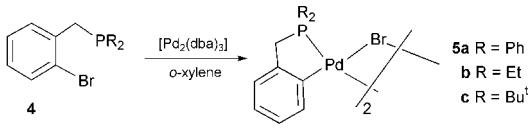

Scheme 3 Synthesis of new palladium metallocycles.

Table 1 Heck coupling reactions catalysed by new palladium complexes[a]

Entry	Aryl bromide	Alkene	[Pd](mol%)	*T*/°C	*t*/h	Conv (%)[b]	Yield (%)[c]	TON/mol product (mol Pd)$^{-1}$
1	4-Bromoacetophenone	Butyl acrylate	0.0002	170	20	85.5	85.1	425 300
2	4-Bromoacetophenone	Butyl acrylate	0.0002	130	143	88.9	88.4	442 250
3	4-Bromoacetophenone	Butyl acrylate	0.00002	160	48	63.2	49.3	2464 800
					144	81.6	71.8	3590 400
4	4-Bromoacetophenone	Butyl acrylate	0.000002	160	72	41.5	2.1	1037 500
5	4-Bromobenzaldehyde	Butyl acrylate	0.00001	150	96	37.2	37.2	3720 000
6	Bromobenzene	Butyl acrylate	0.004	130	175	84.5	84.5	21 100
7	4-Bromoanisole	Butyl acrylate	0.004	130	175	67.6	67.6	16 900
8	4-Bromo-*N*,*N*-dimethylaniline	Butyl acrylate	0.02	130	24	19.3	19.3	1 930
9	4-Bromoacetophenone	MMA[d]	0.002	130	48	96.4	96.4[e]	48 200
10	4-Bromophenol	Butyl acrylate	0.02	130	24	21.1	20.0	1 000
11	4-Bromoaniline	Butyl acrylate	0.02	130	48	97.6	2.0	97
12	2-Bromo-6-methoxynaphthalene	Ethene (20 bar)	0.05	140	11	68.0	68.0	1 360
13[f]	4-Bromoacetophenone	Butyl acrylate	0.02	130	24	98.6	98.1	4 900

[a] *Reaction conditions*: 50 mmol aryl bromide, 70–100 mmol alkene, 55 mmol NaOAc, 50 cm^3 *N*,*N*-dimethylacetamide. [b] Based on aryl bromide consumed determined by GC-MS. [c] Of product, determined by GC-MS. [d] Methyl methacrylate. [e] Three products formed. [f] Complex **5c** used.

DOI: 10.1039/b100328n

Table 2 Suzuki coupling reactions catalysed by new palladium complexes[a]

Entry	Aryl halide	[**5a**](mol%)	*T*/°C	*t*/h	Yield (%)[b]	TON/mol product (mol Pd)$^{-1}$
1	4-Bromoacetophenone	0.002	130	20	100	49 750
2	4-Bromoacetophenone	0.001	130	24	97	96 600
3	4-Bromoacetophenone	0.0002	130	24	67	334 500
4	4-Chloroacetophenone	0.02	130	48	0	0
5	4-Chlorobenzaldehyde	0.01[c]	130	24	27.2[d]	2 724

[a] *Reaction conditions*: 50 mmol aryl halide, 75 mmol phenylboronic acid, 100 mmol K_2CO_3, 150 cm^3 *o*-xylene. [b] Determined by GC-MS. [c] Catalyst **5c**. [d] Conversion is 83.4%, other products are 1-(4-chlorophenyl)-1-phenylmethanol (37.4%) and 1-4-biphenyl-1-phenylmethanol (19%).

temperature (170 °C, entry 1) is required to achieve activity comparable to the Herrmann system (1000 000 TON in 24 h at 130 °C),[5] but no additive/promoting salts (*e.g.* NBu_4Br) are required. In fact we have not observed any increase in activity or catalyst stability when such salts are added to our system. As the catalyst concentration is decreased, higher turnover numbers, in excess of 3×10^6, are achieved at the expense of product selectivity (entries 3 and 4). Indeed, when bromoacetophenone was used as the substrate, Michael addition to the alkene was a competing side reaction, which predominated with higher temperatures and lower catalyst concentration. The Michael addition is reversible so that the selectivity to the coupled product increases with time (Fig. 1). Michael addition was not observed when 4-bromobenzaldehyde was used (entry 5), as the aldehyde proton is less acidic than the α protons of the acetophenone, and a TON of 3.7×10^6 was achieved with good selectivity. There is also evidence to suggest that complex **5a** is deactivated more quickly due to palladium metal aggregation when higher catalyst concentrations are used, resulting in incomplete reaction. Product decomposition at prolonged high reaction temperatures has also proven a problem with certain substrates.

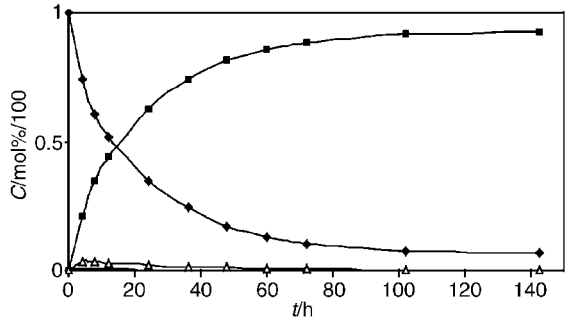

Fig. 1 Diagram of the concentration (*C* in mol%/100) *vs*. reaction time of the Heck reaction of 4-bromoacetophenone (◆) with *n*-butyl acrylate at 130 °C to form *n*-butyl (*E*)-4-acetylcinnamate (■): catalyst **5a** (0.0001 mol%, 0.0002 mol% Pd). Michael addition by-products (△) and (□) are also formed.

Non-activated and deactivated (electron donating) substrates, such as bromobenzene, 4-bromoanisole and 4-bromo-*N*,*N*-dimethylaniline (entries 6–8) require higher catalyst concentrations and reaction times to obtain reasonable yields, but the turnover numbers compare favourably with other palladacyclic systems.[5] Even 4-bromophenol reacted to give 20% of *n*-butyl-(*E*)-4-hydroxycinnamate, but 4-bromoaniline gave almost exclusively Michael addition products. The industrially important reaction of ethene with 2-bromo-6-methoxynaphthalene also occurs with excellent selectivity and good activity (entry 12).

Although the observations of Herrmann that aryl donating groups on the phosphino moiety give higher activity than alkyl groups have been confirmed, complex **5c** catalyses the coupling of 4-bromoacetophenone and *n*-butyl acrylate with excellent selectivity when 0.02 mol% Pd is used (entry 13).

In addition to being an effective Heck catalyst, complex **5a** also exhibits catalytic activity towards the Suzuki coupling, and, to a lesser extent, the Stille coupling (35% yield from 4-bromoacetophenone and Me_3PhSn in 6 h at 110 °C, 3528 turnovers) and the hydroarylation reaction[6] (57% conversion of norbornene to phenylnorbornane using **5a** and bromobenzene in 12 h at 130 °C, 9500 turnovers).

The Suzuki reaction is the coupling of aryl halides with arylboronic acids (Scheme 2). It is mechanistically similar to the Heck reaction, and both the Herrmann[1b] and Bedford[7] complexes have also been reported as active catalysts for this reaction. Some results for the coupling of alkyl halides with phenylboronic acid are displayed in Table 2.

Excellent conversions and selectivities are observed with catalyst concentrations down to 0.001 mol% Pd, after which longer reaction times are required. In contrast to the results of Bedford and coworkers, little activity is observed when toluene is used as the reaction solvent (Bedford obtains 1000 000 TON in toluene in 2.25 h).[7] No activity is observed with aryl chlorides when using complex **5a**, but using the more electron donating **5c** activities higher than those reported by Fu and coworkers[8] using Pd/PBu^t_3 complexes (maximum TON = 200) or than those recently reported by Beller and coworkers[9] using unmetallated monophosphine palladium complexes (maximum TON < 2000) are obtained in the coupling of 4-chlorobenzaldehyde with phenylboronic acid. The major side products of this reaction are 1-(4-chlorophenyl)-1-phenylmethanol and 1-(4-biphenyl)-1-phenylmethanol. Since the latter arises from coupling of the Suzuki product to the boronic acid, the overall turnovers to Suzuki products are *ca.* 4600, which is similar to the best results obtained by Buchwald using di-*tert*-butylphosphinobiphenyl.[10] Other highly active catalysts for Suzuki coupling, which have been reported since the submission of this communication, show very low activities for coupling of chloroaromatics with aryl boronic acids.[11,12]

In conclusion, we have developed an underligated palladium catalyst system that shows comparable activity to existing palladacycle systems but does not require promoting salts. By making the P atom strongly electron donating (Bu^t_2P groups), a catalyst which shows very high activity for coupling of Suzuki chloroaromatic compounds is obtained.

Notes and references

1 W. A. Herrmann, C. Brossmer, K. Ölefe, C.-P. Reisinger, T. Priermeier, M. Beller and H. Fischer, *Angew. Chem., Int. Ed. Engl.*, 1995, **34**, 1844.
2 M. Beller, H. Fischer, W. A. Herrmann, K. Ölefe and C. Brossmer, *Angew. Chem., Int. Ed. Engl.*, 1995, **34**, 1848.
3 M. Ohff, A. Ohff, M. E. van der Boom and D. Milstein, *J. Am. Chem. Soc.*, 1997, **119**, 11 687.
4 D. A. Albisson, R. B. Bedford and P. N. Scully, *Tetrahedron Lett.*, 1998, **39**, 9793.
5 W. A. Herrmann, C. Brossmer, C.-P. Reisinger, T. H. Riermeier, K. Ölefe and M. Beller, *Chem. Eur. J.*, 1997, **3**, 1357.
6 J. M. Brunel, A. Heumann and G. Buono, *Angew. Chem., Int. Ed.*, 2000, **39**, 1946
7 D. A. Albisson, R. B. Bedford, S. E. Lawrence and P. N. Scully, *Chem. Commun.*, 1998, 2095.
8 A. F. Littke, C. Y. Dai and G. C. Fu, *J. Am. Chem. Soc.*, 2000, **122**, 4020.
9 M. G. Andreu, A. Zapf and M. Beller, *Chem. Commun.*, 2000, 2475.
10 J. P. Wolfe, R. A. Singer, B. H. Young and S. L. Buchwald, *J. Am. Chem. Soc.*, 1999, **121**, 9550.
11 R. B. Bedford and S. L. Welch, *Chem. Commun*, 2001, 129.
12 M. Feuerstein, D. Laurenti, C. Bougeant, H. Doucet and M. Santelli, *Chem. Commun.*, 2001, 325.

ChemComm

Continuous flow homogeneous catalysis: hydroformylation of alkenes in supercritical fluid–ionic liquid biphasic mixtures

Murielle F. Sellin, Paul B. Webb and David J. Cole-Hamilton*

School of Chemistry, University of St. Andrews, St. Andrews, Fife, Scotland, UK, KY16 9ST. E-mail: djc@st-and.ac.uk

Received (in Cambridge, UK) 30th January 2001, Accepted 13th March 2001
First published as an Advance Article on the web 3rd April 2001

Rhodium complexes of [1-propyl-3-methylimidazolium]$_2$ [PhP($C_6H_4SO_3$-3)$_2$] dissolved in the ionic liquid, 1-butyl-3-methylimidazolium hexafluorophosphate catalyse the hydroformylation of oct-1-ene at a constant rate for > 20 h in a continuous flow process in which the substrate, gases and products are transported in and out of the reactor dissolved in $scCO_2$; < 1 ppm rhodium is present in the collected product.

Rhodium catalysts show very high activity and good regioselectivity under mild operating conditions for the hydroformylation of long chain hydrocarbons, but have not yet been commercialised for linear alkenes with > 6 C atoms because of problems associated with the separation of the low volatility product aldehydes from the thermally sensitive catalyst.[1] Instead, the less efficient cobalt based catalysts are still in use for the synthesis of soap and detergent range alcohols.[2] Various new ways are being investigated to ovecome this separation problem but the ideal system would provide a continuous flow process in which the advantages of reactions in the homogeneous phase (all catalytic sites equally accessible, high activity and high selectivity) could be combined with transport of the substrate, CO and H_2 into the solution and transport of the product aldehyde from the solution. This would mimic the systems currently in use for hydroformylation of propene and ethene.[1] As part of our on going studies on the use of supercritical fluids in homogeneous catalysis,[3–5] we have recently reported such a system,[5] where the catalyst is dissolved in a triaryl phosphite and the reactants are introduced dissolved in $scCO_2$, which is also used to remove the products from the reaction; both the ligand and the catalyst have low solubility in $scCO_2$. The initially high activity and selectivity to the desired linear aldehyde are gradually lost because the phosphite slowly dissolves in the $scCO_2$ and is removed from the system; it is also degraded by water.[5]

For a continuous flow system, an involatile solvent, which is insoluble in $scCO_2$ and contains a polar (preferably ionic) catalyst would be ideal and these properties are met by ionic liquids.[6] Previous attempts to carry out hydroformylation in room temperature ionic liquids using rhodium complexes of sulfonated triphenylphosphine ligands, showed rather low conversions,[7] perhaps because of the low solubility of permanent gases in the ionic liquid. Somewhat improved conversions could be obtained if other solvents (THF, toluene or water) were added. Even so, conversions were only of the order of 30%.[7] More recently, such reactions have been successfully carried out in ionic liquids using rhodium complexes of cobaltocenium based diphosphine ligands.[8]

A recent report has shown that $scCO_2$ is highly soluble in certain ionic liquids (up to 0.6 mol fraction), whilst the ionic liquid is insoluble in $scCO_2$.[9] Since $scCO_2$ is fully miscible with permanent gases and is a good solvent for alkenes and aldehydes, we reasoned that $scCO_2$ might help transport the permanent gases into the ionic liquid and could then also act as the transport medium for a flow system. A very recent paper shows that $scCO_2$ can extract a wide range of organic compounds from ionic liquids of this type.[10] We now report results of a study of the hydroformylation of alkenes in supercritical fluid–ionic liquid biphasic mixtures.

Table 1 shows results obtained from the hydroformylation of hex-1-ene in the ionic liquid, 1-butyl-3-methylimidazolium hexafluorophosphate using triphenylphosphite as the rhodium based ligand.† As with other ligands,[7] the results obtained in the pure ionic liquid are poor with a selectivity to aldehyde of only 15.7%, and the linear : branched (l:b) ratio is low at 2.4 although all of the hex-1-ene is converted. The main products arise from aldol condensation of the product aldehydes. On adding $scCO_2$, the rate of reaction falls, but the selectivity to aldehyde increases to 82.3% and the l:b ratio to 6:1. Using toluene as solvent, the rate and selectivity to aldehydes are high, but the l:b ratio is low (2.5).

In view of the success of the reaction in the biphasic system, we carried out similar reactions of hex-1-ene or non-1-ene, flushing the products from the reactor with $scCO_2$ at the reaction temperature and pressure at the end of the reaction and decompressing into a second autoclave held at low temperature.[4,5] After all the product had been removed by this flushing process, the reactor was cooled, depressurised and recharged with fresh substrate, CO, H_2 and CO_2. Several repetitive uses of the same catalyst show that it retains activity and selectivity for 2–3 runs, but then loses both. Visual inspection shows that the catalyst solution has become black and ^{31}P NMR studies show the presence of $O_2PF_2^-$ and $P(OPh)_nF_{3n}$ (n = 1–2). These products arise from reaction of the PF_6^- with water, releasing HF, which then attacks the phosphite.

Because of the water sensitivity of the ligands in this system, we investigated sulfonated triphenylphosphines, for which both the ligands and the rhodium complexes are insoluble in $scCO_2$. Complexes derived from the sodium salts of mono- and trisulfonated triphenylfosphine show low activity, at least in the case of the trisulfonate because of low solubility in the ionic liquid. We, therefore, synthesised [$Ph_2PC_6H_4SO_3$]-[BMIM] and used it together with [$Rh_2(OAc)_4$] as the catalyst precursor for the hydroformylation of non-1-ene in the $scCO_2$–[BMIM]PF_6 biphasic system with flushing of the products from the reactor with $scCO_2$. Fig. 1 shows that the activity of a rhodium catalyst derived from this ligand remains high for 12 runs (tunrover number = 160–320 h^{-1}) and the l:b ratio is acceptable. Rhodium leaching is not observed (< 0.003%) for

Table 1 Hydroformylation of hex-1-ene catalysed by [$Rh_2(OAc)_4$]/$P(OPh_3)$[a]

Solvent	Co-solvent	Conversion (%)	Aldehyde selectivity (%)	l:b
Toluene		> 99	83.9	2.5
[BMIM]PF_6		> 99	15.7[b]	2.4
[BMIM]PF_6	$scCO_2$[c]	40	83.5	6.1

[a] [$Rh_2(OAc)_4$] (10 mg, 4.5×10^{-5} mol), $P(OPh_3)$ (0.2 g, 6.7×10^{-3} mol), hex-1-ene (2 cm^3, 1.8×10^2 mol), 4 cm^3 of solvent, 70 bar CO/H_2, 100 °C, 1 h. [b] The majority of the product is condensed aldehydes. [c] Total pressure = 230 bar.

DOI: 10.1039/b101046h

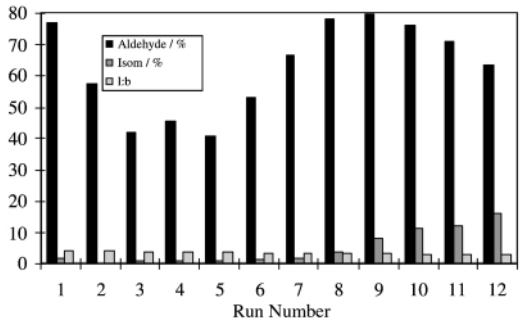

Fig. 1 Repetitive use of a catalyst synthesised *in situ* from $[Rh_2(OAc)_4]$ (10.3 mg, 4.7 $\times$ 10^{-5} mol Rh) and $[BMIM][Ph_2P(C_6H_4SO_3)]$ (0.33 g, 0.7 mmol) for the hydroformylation of non-1-ene (2 cm^3) in $[BMIM]PF_6$ (4 cm^3), CO/H_2 40 bar, total pressure 185 bar, 100 °C, 1 h. The products were flushed from the reactor using $scCO_2$ at the reaction temperature and pressure after each run. The reactor was then depressurised, recharged, repressurised and reheated.

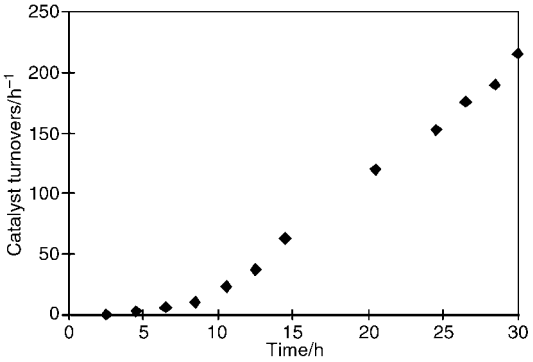

Fig. 3 Catalyst turnovers during the continuous flow hydroformylation of oct-1-ene (0.03 cm^3 min^{-1}, 1.91 $\times$ 10^{-4} mol min^{-1}) catalysed by $[Rh_2(OAc)_4]$ (10 mg, 4.5 $\times$ 10^{-5} mol Rh)/$[PMIM][PhP(C_6H_4SO_3)_2]$ (0.47 g, 7.1 $\times$ 10^{-4} mol) dissolved in the ionic liquid, $[BMIM]PF_6$ (6 cm^3). CO/H_2 (0.45 dm^3 min^{-1}), 200 bar total pressure, 100 °C.

the first 9 runs. Throughout the series of runs, the l:b ratio falls slowly (from 3.7 to 2.5), isomerisation increases and, after the ninth run, Rh leaching becomes significant. ^{31}P NMR studies of the organic phase show no P resonances confirming that the phosphine is not leaching, but the ^{31}P NMR spectrum of the ionic liquid after the 12th run shows only PF_6^- and $[Ph_2P(O)C_6H_4SO_3][BMIM]$. The rhodium leaching after run 9 can then be attributed to the ligand oxidation so that the active species is $[RhH(CO)_4]$, which is soluble in $scCO_2$ and which is known to give more isomerisation and lower l:b ratios than phosphine coordinated systems.[1] Isomerisation increases and l:b ratio decreases with increased recycling of the catalyst as a result of the increased ligand oxidation. The observed ligand oxidation may arise from contamination with air during the many openings of the reactor. However, the stability of the ligand framework towards degradation led us to select a similar ligand for continuous flow studies.

The apparatus used for the continuous flow reactions is shown in Fig. 2 and consists of separate feeds for the alkene, the CO and H_2 and the CO_2. These join above the reactor and pass through the ionic liquid before being removed from the reactor still in the $scCO_2$ undergoing a two stage decompression to recover the products, which are then analysed by GC. Fig. 3 shows the results of an experiment using $PhP(C_6H_4SO_3)_2]$-$[PMIM]_2$ (PMIM = 1-propyl-3-methylimidazolium) and $[Rh_2(OAc)_4]$ dissolved in $[BMIM]PF_6$, with the oct-1-ene substrate being transported into and the products being transported out of the reactor using $scCO_2$ as the transport vector. The experiment was carried out for 33 h and the linearity of the graph over 8–30 h shows that the catalyst is stable at least over this period of time.‡ The l:b ratio of the product aldehydes is 3.1 throughout the reaction, showing that ligand oxidation is not occurring. Rh analysis of the recovered products shows < 1 ppm of Rh in any of the samples (< 0.06% of the Rh loaded). GCMS and NMR analyses of the recovered liquid products show the presence only of the two aldehyde products and unreacted substrate, indicating that the continuous flow supercritical fluid–ionic liquid biphasic system provides a method for continuous flow homogeneous catalysis, with built in separation of the products from both the catalyst and the reaction solvent, and that this is possible even for relatively low volatility products. The only related system to have been reported uses a catalyst supported on a sol–gel silica operating as a heterogeneous catalyst again with the transporting agent being $scCO_2$.[11] Since submission of this paper, two other relevant papers have appeared. Asymmetric hydrogenation has been carried out in an ionic liquid, with the product being removed by flushing with $scCO_2$[12] and hydrogenation of alkenes or of CO_2, the latter in the presence of triethylamine, has been carried out in an ionic liquid–$scCO_2$ biphasic system with flushing of the products from the reactor with $scCO_2$ and reuse of the catalyst up to four times.[13]

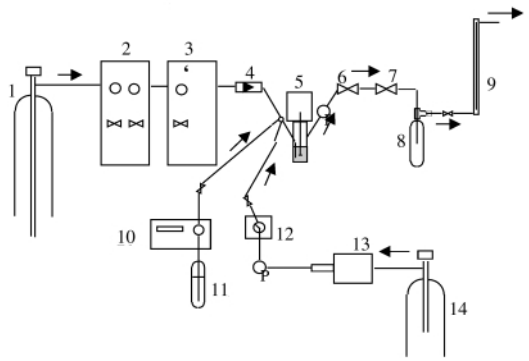

Fig. 2 Reactor for continuous flow hydroformylation. 1 CO_2 supply, 2 Liquid CO_2 pump, 3 Pressure regulator, 4 Non-return valve, 5 Autoclave with magnetically driven paddle stirrer, 6 1st expansion valve, 7 2nd expansion valve, 8 Collection vessel, 9 Flow metre, 10 Liquid substrate pump, 11 Liquid substrate supply, 12 CO/H_2 dosimeter, 13 Gas booster, 14 CO/H_2 supply.

We thank the EC TMR programme (M. F. S.) and the EPSRC (P. B. W.) for Fellowships.

Notes and references

† We have shown that triphenylphosphite complexes of rhodium are active and selective for hydroformylation in $scCO_2$ whilst also being insoluble.[5]
‡ In more recent studies we have shown that aldehydes can be produced at a constant rate and selectivity (l:b = 3.8) for 72 h.

1 C. H. Frohning and Ch. W. Kohlpaintner, in *Applied Homogeneous Catalysis with Organometallic Compounds*, ed. B. Cornils and W. Herrmann, VCH, Weinheim, 1996, p. 29; *Rhodium Catalyzed Hydroformylation*, ed. P. W. N. M. van Leeuwen and C. Claver, Kluwer, Dordrecht, 2000.
2 B. Cornils, in *New Synthesis with Carbon Monoxide*, ed. J. Falbe, Springer Verlag, Berlin, 1980, ch. 1.
3 I. Bach and D. J. Cole-Hamilton, *Chem. Commun.*, 1998, 1463.
4 R. J. Sowden, M. F. Sellin, N. De Blasio and D. J. Cole-Hamilton, *Chem. Commun.*, 1999, 2511.
5 M. F. Sellin and D. J. Cole-Hamilton, *J. Chem. Soc., Dalton Trans.*, 2000, 1681.
6 T. Welton, *Chem, Rev.*, 1999, **99**, 2071.
7 Y. Chauvin, L. Mussmann and H. Olivier, *Angew. Chem., Int. Ed. Engl.*, 1996, **34**, 2698.
8 C. C Brasse, U. Englert, A. Salzer, H. Waffenschmidt and P. Wasserscheid, *Organometallics*, 2000, **19**, 3818.
9 L. A. Blanchard, D. Hancu, E. J. Beckman and J. F. Brennecke, *Nature*, 1999, **399**, 28.
10 L. A. Blanchard and J. F. Brennecke, *Ind. Eng. Chem. Res.*, 2001, **40**, 287.
11 N. J. Meehan, A. J. Sandee, J. N. H. Reek, P. C. J. Kamer, P. W. N. M. van Leeuwen and M. Poliakoff, *Chem. Commun.*, 2000, 1497.
12 R. A. Brown, P. Pollet, E. McKoon, C. A. Eckert, C. L. Liotta and P. G. Jessop, *J. Am. Chem. Soc.*, 2001, **123**, 1254.
13 F. Liu, M. B. Abrams, R. T. Baker and W. Tumas, *Chem. Commun.*, 2001, 433.

Electrophoretic assembly of nanozeolites: zeolite coated fibers and hollow zeolite fibers†

C. Ke,[a] W. L. Yang,[b] Z. Ni,[a] Y. J. Wang,[a] Y. Tang,*[a] Y. Gu[a] and Z. Gao[a]

[a] *Department of Chemistry, Fudan University, Shanghai 200433, P. R. China. E-mail: yitang@fudan.edu.cn*
[b] *Department of Macromolecular Science and Key Laboratory of Molecular Engineering of Polymers of Ministry of Education, Fudan University, Shanghai 200433, P. R. China*

Received (in Cambridge, UK) 20th December 2000, Accepted 16th March 2001
First published as an Advance Article on the web 3rd April 2001

Zeolite coated fibers with compact and full deposits have been fabricated by electrophoretic deposition of nanozeolites onto carbon fibers, whereafter hollow zeolite fibers have been obtained by calcination to remove the substrates.

Zeolites have been widely used in various fields as a class of crystalline materials with unique properties such as large microporosity, molecular sieving behavior and high hydrothermal stability. Construction of zeolite coated fibers and hollow zeolite fibers with designed structures has attracted considerable attention due to their fast diffusion and low pressure drop while maintaining high catalytic efficiency.[1–3] Although several methods have been put forward to prepare these materials, such as *in situ* soft solution process,[1] *in situ* zeolite deposition[2] and seed film method,[3] they all suffer from the drawback that the film thickness and the zeolite particle size are difficult to control. In addition, it is difficult for the last two methods to avoid the zeolites crystallizing concurrently in the synthesis solution. To overcome the limitations above, the layer-by-layer (LbL) technique has been utilized recently to prepare hollow zeolite fibers in our laboratory.[4] The products prepared by LbL are expected to be more favorable for mass transfer due to their solely nanozeolite composed walls whose thickness is convenient to control.

Electrophoretic deposition (EPD) is another effective and controllable method to assemble charged colloid particles.[5–13] The advantages of the EPD process are twofold: one is the fine uniformity of the deposition, the other is the easy manipulation and convenient control of the process.[7,8] The performance of the EPD method has made it an attractive route to effectively manufacture ordered structures of colloidal systems, such as micrometer-sized silica colloids, polystyrene latexes,[5,6,9,10] nanometer-sized gold colloids,[7,11] and submicron ceramic powders.[12,13] The EPD technique is also used to modify electrodes.[14–16] A Pt disk electrode modified with a large crystal zeolite/polymer coating of *ca.*11 micron thickness was obtained by the high-voltage (200 V) EPD technique in organic solution.[15,16] Recently, nanozeolites have proved to be efficient 'building blocks' to construct hierarchical structures for their colloidal character and surface charge.[4,17,18] Here, exploiting the characteristic properties of nanozeolites, the EPD technique has been used for the first time to fabricate zeolite coated carbon fibers (ZCFs) and hollow zeolite fibers (HZFs) with ultra-thin walls of nanozeolite under low voltage (1–3 V) in aqueous solution.

The preparation of ZCFs was operated in an electrophoretic cell, where a cathodic carbon fiber (*ca.* 7 μm diameter, 2 cm length) bundle was centered in a cylindrical platinum container (*ca.* 2.75 cm diameter) which served as the anode. In this arrangement, voltages were controlled by a CHI660 Electrochemical Workstation. Nanocrystals of silicalite-1 (95 ± 10 nm diameter, determined by DLS) were prepared and purified by a literature method.[19] Suspensions for EPD experiments were obtained by dispersing the nanosilicalite-1 in distilled water to a concentration of *ca.* 1.5 wt%. The pH of the suspension was adjusted with 0.1 M HCl. Prior to use, the carbon fibers were cleaned according to the literature.[3] To yield HZFs, ZCFs were heated to 873 K at a heating rate of 5 K min^{-1} in nitrogen and kept for 4 h, then calcined in air for 8 h at the same temperature to remove the substrates.

Dense and complete deposition of nanozeolites on carbon fibers is an essential requirement for the preparation of perfect ZCFs as well as intact HZFs by the EPD technique. The success of deposition relies on conditioning two sequential steps (i) the motion of particles towards the electrode and (ii) the formation of a coherent deposit on the electrode surface by overcoming the electrostatic repulsion arising from the similar charge of nanoparticles.[5,8] It has been suggested the latter step is induced by lateral interaction between the deposited particles caused by electrodynamic flows which result from distortions in the applied electric field and the passage of ionic current through the solution.[5,6,20] The modulation of the entire process thereby can be fulfilled by changing the particle charge and the field strength. Hence, the pH of the suspension and the voltage exerted on the electrophoretic cell are important variables.

At pH 6 the zeta potential of the nanosilicalite-1 particles was only +4.5 mV (DELSA 440SX), thus zeolite particles prefer to coalesce and form aggregates in solution during the EPD process. When the pH was adjusted to 4.5, there were largely uncoated areas on the carbon substrates. This can be explained by the electrical force driving nanoparticles towards the cathode being too weak to form complete and dense deposits although the zeta potential rose to +21.1 mV. The best result was obtained at pH 2.5 [Fig. 1(b)]. All longitudinal strips on the original carbon fibers [Fig. 1(a)] disappeared, implying that the deposits obtained at pH 2.5 [Fig. 1(b)] were compact and complete due to the high zeta potential of +46.8 mV. This result illustrates

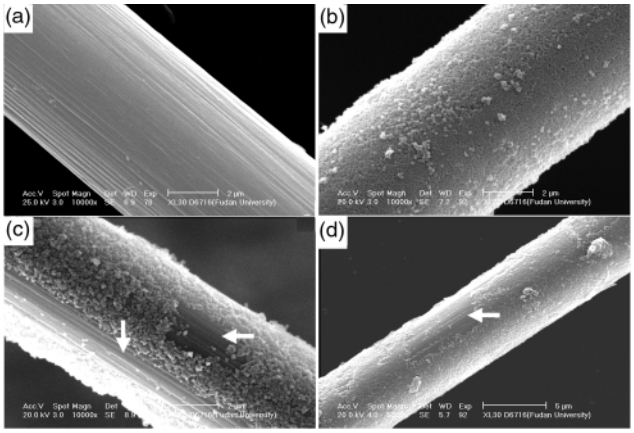

Fig. 1 SEM images of original carbon fibers (a) and zeolite coated fibers prepared under voltages of 2 V (b), 1 V (c) and 3 V (d) at pH 2.5 for 2 × 10 min.

† Electronic supplementary information (ESI) available. XRD patterns and other related SEM images of zeolite coated fibers and hollow zeolite fibers. See http://www.rsc.org/suppdata/cc/b0/b010197o/

DOI: 10.1039/b010197o

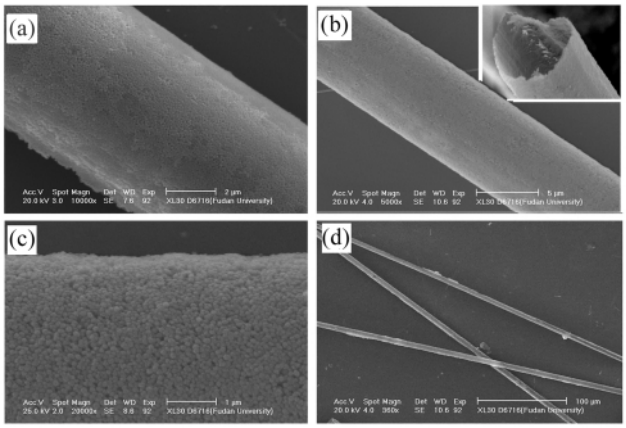

Fig. 2 SEM images of zeolite coated fibers (a) and hollow zeolite fibers (b, c, d) prepared at pH 2.5 and step voltage 1 V, 2 × 10 min; 2 V, 2 × 10 min; (c) and (d) are high and low magnification micrographs of (b), respectively.

how the particle mobility towards the cathode is largely enhanced as the zeta potential increases,[9] thereby facilitating the formation of complete deposits on the cathode. Upon applying different voltages, such as 1, 2 and 3 V, each for two cycles of 10 min (2 × 10 min), the deposit thickness increased with increased voltage. There were many bare areas when applying 1 V [see arrows in Fig. 1(c)] due to insufficient particles being deposited on the cathode. In addition, it is noticeable that most of the particles on the fibers assembled in large or small clusters, implying the existence of lateral motion of the particles on the electrode.[6] When 2 V was applied, the fibers were fully coated with nanozeolites as shown in Fig. 1(b), attributed to the improved rate of particle movement towards the cathode under increased electric field. At 3 V, although deposits on some areas of the fibers were thicker, some bare areas were found again [Fig. 1(d)]. The reason for this may be the production of hydrogen due to the electrolysis of water at the cathode which hinders the deposition or peels the deposited layer off the electrode.[21] Water electrolysis was also established by the current *vs.* time curve at 3 V. Unlike the monotonously decreasing current with time at 2 V this exhibited an increasing trend as well as fluctuation at 3 V. The EPD process at 2 V provides a feasible route to fabricate ZCFs with compact and complete deposits under appropriate conditions.

To fabricate ZCFs with denser and thicker coatings and further obtain intact HZFs, two improved processes have been adopted: (i) lengthening the deposition time from 2 V, 2 × 10 min to 2 V, 2 × 20 min, (ii) the application of a step voltage: 1 V, 2 × 10 min; 2 V, 2 × 10 min. Although both procedures improved the quality of deposits and produced intact HZFs after removal of the carbon substrates, the walls of fibers prepared by the latter method were more smooth and uniform. Fig. 2(a) shows that ZCFs prepared *via* the step voltage possessed even and dense zeolite films instead of the original texture of the carbon fibers [Fig. 1(a)]. After calcination the carbon substrates in the ZCFs were removed and hollow fibers with uniform walls were obtained [Fig. 2(b) and inset]. A micrograph of HZFs at high magnification [Fig. 2(c)] demonstrated the uniformity and compactness of the zeolite walls while a micrograph at low magnification [Fig. 2(d)] reveals the high fidelity of HZFs maintaining the original carbon fibrous morphology. The improvement under step voltage can be ascribed to better matching between the motion of nanozeolites towards the cathode and the lateral motion on the cathode.[5] The non-conducting nanozeolites deposited on the cathode under 1 V might reduce the voltage drop over the suspension,[8] so weakening the actual effect of the later application of 2 V so as to slow down the velocity towards the cathode.

The XRD spectrum of carbon substrates shows the pattern of an amorphous phase. However characteristic peaks of silicalite-1 occurred in patterns of ZCFs and only peaks ascribed to silicalite-1 appeared in patterns of HZFs. IR spectra of ZCFs and HZFs further confirm that the carbon fibers have been coated by nanozeolites and HZFs are solely composed of silicalite-1 particles.

Our research has shown that the EPD technique can be employed to assemble nanozeolite particles conveniently and effectively. Uniform zeolite coated fibers have been fabricated by this method and after removal of the substrates, hollow zeolite fibers with ultra-thin walls composed solely of nanozeolites can be obtained. Currently, the preparation of zeolite materials with other structures by electrophoretically assembling various nanozeolites and the applications of zeolite coated fibers as well as hollow zeolite fibers are under way in our laboratory.

This work is supported by the Major State Basic Research Development Program (Grant No. 2000077500), the NNSFC (Grant No. 29873011) and the Foundation for University Key Teacher by the Ministry of Education.

Notes and references

1 K. Okada, K. Kuboyama, T. Takei, Y. Kameshima, A. Yasumori and M. Yoshimura, *Microporous Mesoporous Mater.*, 2000, **37**, 99.
2 S. Mintova, V. Valtchev and B. J. Schoeman, *J. Mater. Sci. Lett.*, 1996, **15**, 840.
3 V. Valtchev, B. J. Schoeman, J. Hedlund, S. Mintova and J. Sterte, *Zeolites*, 1996, **17**, 408.
4 Y. J. Wang, Y. Tang, X. D. Wang, W. L. Yang and Z. Gao, *Chem. Lett.*, 2000, 1344.
5 M. Trau, D. A. Saville and I. A. Aksay, *Science*, 1996, **272**, 706.
6 M. Trau, D. A. Saville and I. A. Aksay, *Langmuir*, 1997, **13**, 6375.
7 S. Y. Zhao, S. B. Lei, S. H. Chen, H. Y. Ma and S. Y. Wang, *Colloid Polym. Sci.*, 2000, **287**, 682.
8 O. O. Van der Biest and L. J. Vandeperre, *Annu. Rev. Mater. Sci.*, 1999, **29**, 327.
9 M. Holgada, F. Garcia-Santamaria, A. Blanco, M. Ibisate, A. Cintas, H. Miguez, C. J. Serna, C. Molpeceres, J. Requena, A. Mifsud, F. Meseguer and C. Lopez, *Langmuir*, 1999, **15**, 4701.
10 R. C. Hayward, D. A. Saville and I. A. Aksay, *Nature*, 2000, **404**, 56.
11 M. Giersig and P. Mulvaney, *Langmuir*, 1993, **9**, 3408.
12 I. Zhitomirsky and L. Gal-Or, *Mater. Lett.*, 1999, **38**, 10.
13 I. Zhitomirsky, *Mater. Lett.*, 2000, **42**, 262.
14 C. Song and G. Villemure, *J. Electroanal. Chem.*, 1999, **462**, 143.
15 C. B. Ahlers and J. B. Talbot, *J. Electrochem. Soc.*, 1999, **146**, 3259.
16 C. B. Ahlers and J. B. Talbot, *Electrochem. Acta.*, 2000, **45**, 3379.
17 L. M. Huang, Z. B. Wang, J. Y. Sun, L. Miao, Q. Z. Li, Y. S. Yan and D. Y. Zhao, *J. Am. Chem. Soc.*, 2000, **122**, 3530.
18 X. D. Wang, W. L. Yang, Y. Tang, Y. J. Wang, S. K. Fu and Z. Gao, *Chem. Commun.*, 2000, 2161.
19 R. Ravishankar, C. Kirschhock, B. J. Schoeman, P. Vanoppen, P. J. Grobet, S. Storck, W. F. Maier, J. A. Martens, F. C. De Schryver and P. A. Jacobs, *J. Phys. Chem. B*, 1998, **102**, 2633.
20 Y. Solomentsev, M. Bohmer and J. L. Anderson, *Langmuir*, 1997, **13**, 6058.
21 M. Bohmer, *Langmuir*, 1996, **12**, 5747.

Mechanism of alkene aziridination in the [(biaryldiimine)Cu^{I}] catalyst system; precise substrate orientation *via* two-centre binding†

Kevin M. Gillespie, Edward J. Crust, Robert J. Deeth* and Peter Scott*

Department of Chemistry, University of Warwick, Coventry, UK CV4 7AL. E-mail: peter.scott@warwick.ac.uk; Fax: +44(0)24 7657 2710; Tel: +44(0)24 7652 3238

Received (in Cambridge, UK) 13th February 2001, Accepted 16th March 2001
First published as an Advance Article on the web 4th April 2001

The highly enantioselective (≤98%) aziridination of cinnamate esters is achieved using the title catalyst system *via* a concerted non-polar mechanism involving ancillary binding of carbonyl group to copper.

The addition of nitrenes RN: to alkenes is an attractive method for the synthesis of aziridines.[1] Evans' work[2] and particularly the asymmetric variant,[3] has inspired a number of groups to design chiral metal complex systems for this reaction.[4] The standard protocol uses an I^{III} iodinane such as PhINTs as the source of nitrene and a metal complex (most successfully of Cu) which acts as a transfer catalyst (Fig. 1). An early report provided powerful evidence for the presence of a discrete nitrenoid complex intermediate **I**.[5]

It has been noted that both Cu^{I} and Cu^{II} act as adequate precatalysts and that UV spectra of the Cu^{I} and Cu^{II}-derived reaction mixtures are indistinguishable in the Evans system.[2] Mechanistic evidence from Pérez relating to a tris(pyrazolyl)borate catalyst points clearly to Cu^{II}.[6] It is becoming clear, however, that the mechanism may be system-dependent; Norrby has very recently described detailed calculations on the Jacobsen system which indicate a route by which a Cu^{II} starting complex may enter the Cu^{I} manifold.[7] *In situ* UV spectra of our catalysts are consistent with operation in this lower oxidation state.

The Evans and Jacobsen systems appear to be complementary in that the former give excellent enantioselectivity for *trans* disubstituted alkenes,[3] while the latter are most efficient for *cis*.[5] We were thus rather surprised to find that [CuL(CH$_3$CN)$_2$] **1**, which is a very fast and selective precatalyst for *cis*-disubstituted alkenes,[8] also mediates the rapid aziridination of a range of *trans*-cinnamate esters with excellent enantioselectivity (Scheme 1, Table 1).

Data from competitive kinetic experiments based on eight cinnamate esters gave an excellent straight line Hammett plot, using simple σ_X constants, with slope $\rho = -0.65$ (Fig. 2). The low negative value of ρ indicates that the intermediate species is not dipolar, *i.e.* there is little build up of positive charge at the benzylic carbon in the rate- and selectivity-determining nitrene transfer step. Even so, we might expect a deviation from linearity in Fig. 2 for mesomerically electron-donating substituents (*e.g.* OMe), necessitating the use of σ^+ constants.[6,9] That this is *not* observed indicates that there is minimal through-conjugation between substituent X and the reaction centre. This is probably caused by disinclination of the system to become planar (*vide infra*). In any event, the behaviour is very different from that in the Pérez system for which a two-term Hammett-type equation incorporating σ^+ and Jackson's $\sigma\cdot$ constants[10] was required to fit the data.[6] Finally in this regard we note that the

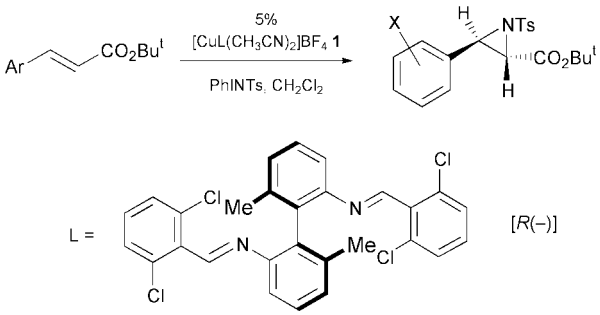

Scheme 1 Catalytic synthesis of cinnamate esters using **1**.

Table 1 Enantioselective aziridination of cinnamate esters *etc*.

Entry	X (See Scheme 1)[a]	Yield[b]	ee[c]
1	H	77	89
2	4-MeO	67	93
3	4-Me	82	88
4	3-Me	56	96
5	4-F	45	98
6	4-Cl	89	92
7	4-Br	59	98
8	3-NO_2	32	96
9	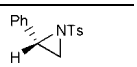	99	34[d]
10	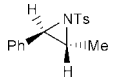	88	28[d,e]

[a] Absolute configurations of all cinnamate products were [2*S*, 3*R* (−)] as inferred by comparison of relative retention times of the enantiomers with those of entry 1 for which the configuration is known.[3] [b] Isolated yield of pure aziridine. [c] Ee determined by HPLC (Chiralcel OD 15 cm × 0.46 cm i.d. hexane : propan-2-ol (various ratios). [d] Ee determined by ^{1}H NMR using [Eu(hfc)$_3$]. [e] *Trans* : *cis* ratio 97 : 3. [e] Ee given for *trans* product.

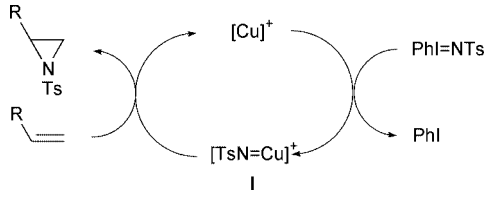

Fig. 1 Cycle for the Cu-catalysed aziridination of alkenes with PhINTs.

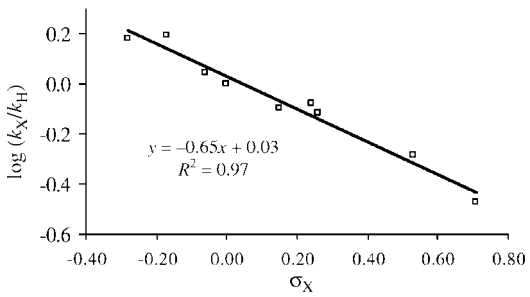

Fig. 2 Hammett plot for the reaction in Scheme 1.

† Electronic supplementary information (ESI) available: experimental and theoretical details. See http://www.rsc.org/suppdata/cc/b1/b101415n/

DOI: 10.1039/b101415n

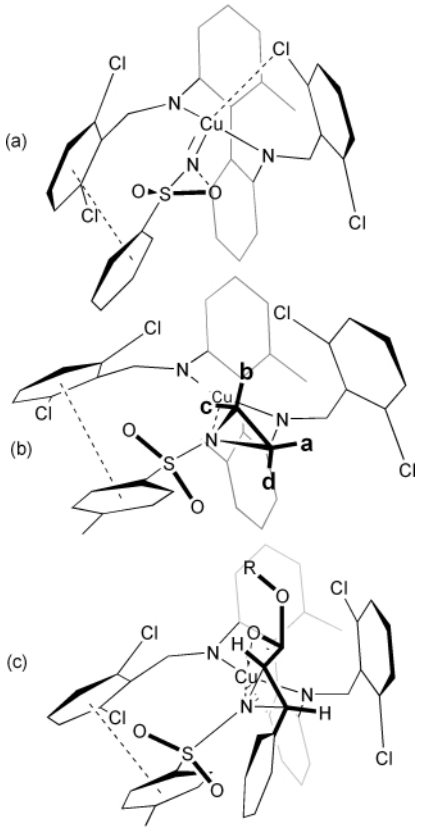

Fig. 3 Based on calculated (DFT) structures of (a) catalyst [CuL(NTs)] **2**, (b) aziridine complex **3** and (c) cinnamate ester aziridine complex.

presence of significant radical character in our rate- (and selectivity-) determining step is strongly opposed by the absence of detectable levels of *cis* cinnamate aziridines in the product mixtures. Our catalysts clearly operate *via* a concerted mechanism; both C–N bonds are formed at approximately the same time.

Armed with this experimental data we set out to investigate the structure of the relevant catalytic intermediates using Density Functional Theory (DFT).† A fully optimised DFT structure of the precatalyst **1** was found to be essentially superimposable on the molecular structure.[8] The proposed catalyst species arising from the removal of the CH_3CN groups and addition of the nitrene NTs *i.e.* [CuL(NTs)] **2** was minimised successfully. One of two similar structures located† is shown in Fig. 3(a). The tosyl group is oriented such that the arene forms what may be a planar π stacking interaction with one of the dichlorophenyl groups. Interestingly, coordination of one of the sulfonyl O atoms to the nitrene N has occurred, thus forming a three-membered ring.‡ Although we do not wish to assert that this interaction plays an important part in the catalysis, it does indicate that the N atom is highly electrophilic, as expected from the negative value of ρ above. The TsN–Cu distance of 1.80 Å in **2** indicates multiple metal–ligand bond character.

Insights into the interactions between the catalyst and alkene were obtained by computing the structure of a complex with ethylene bound to the nitrene N.[7] The aziridine complex [CuL($TsNC_2H_4$)] **3** thus obtained [Fig. 3(b)] has a TsN→Cu distance of 1.93 Å. The alignment of the alkene fragment in this species is controlled by the chiral ligand *via* the orientation of the tosyl group as described above.

The energetic consequences of adding substituents to the alkene were assessed by optimising the structures for three orientations of styrene bound to N; that with a phenyl group in site **a** was not considered viable since it is severely hindered by a dichlorophenyl group. The structures with phenyl in sites **b**–**d** have the same energies within *ca*. 10 kJ mol^{-1}, and this is consistent with the modest enantioselectivity for aziridination of this alkene (entry 9). The stereochemical preference for the cinnamate esters is more clear cut however. Placing a $–CO_2Me$ group in site **b** facilitates coordination of the carbonyl oxygen to the otherwise three-coordinate copper [Fig. 3(c)]; this is not feasible at sites **c** and **d**.§ The interaction contributes *ca*. 20 kJ mol^{-1} to the stability of the structure, and, assuming that this energetic preference is reflected at the transition state for alkene binding (which seems likely given the concerted mechanism) it readily explains the excellent selectivity observed. The absolute sense of asymmetric induction is as predicted by this model.

Two compelling pieces of circumstantial evidence further support our proposed mode of enantioselection. Firstly, the cinnamate phenyl group must be placed in site **d**, and our calculations indicate that its achievement of coplanarity with the alkene unit (and thus through-conjugation, *vide supra*) is hampered by steric effects [Fig. 3(c)]. Secondly, we note that while Evans' bis(oxazoline) system was highly selective for aziridination of both cinnamates *and trans*-β-methylstyrene, **1** performed very poorly with the latter (entry 10). With no suitable coordinating group, this alkene shows little preference for either of the two possible diastereomeric orientations, *viz*. Me and Ph at sites **b** and **d**.

Hence the observed enantioselectivity for aziridination of cinnamate esters with precatalyst **1** arises in two-centre binding of the substrate. While being somewhat unexpected, it is related to well documented examples of η^2 substrate binding at catalytic metal centres.[11]

P. S. wishes to thank EPSRC for a postdoctoral fellowship (to K. M. G). R. J. D. acknowledges the EPSRC UK Computational Chemistry Facility for computing resources.

Notes and references

‡ In contrast, Norrby[7] found that in calculations based on the Jacobsen system, η^2-*N,O* coordination at Cu of N–SO_2Me was found throughout. We were unable to locate such a structure here.

§ In the catalyst structure there is weak dative coordination of an aryl C atom at this site [see Fig. 3(a)].

1 D. Tanner, *Angew. Chem., Int. Ed. Engl.*, 1994, **35**, 599; E. N. Jacobsen, *Aziridination*, in *Comprehensive Asymmetric Catalysis*, ed. E. N. Jacobsen, A. Pfaltz and H. Yamamoto, Springer, Hamburg, 1999.

2 (*a*) D. A. Evans, K. A. Woerpol, M. M. Hinman and M. M. Faul, *J. Am. Chem. Soc.*, 1991, **113**, 726; (*b*) D. A. Evans, M. M. Faul and M. T. Bilodeau, *J. Org. Chem.*, 1991, **56**, 6744; (*c*) D. A. Evans, K. A. Woerpol and M. J. Scott, *Angew. Chem., Int. Ed. Engl.*, 1992, **31**, 430; (*d*) D. A. Evans, M. M. Faul and M. T. Bilodeau, *J. Am. Chem. Soc.*, 1994, **116**, 2742.

3 D. A. Evans, M. M. Faul, M. T. Bilodeau, B. J. Anderson and D. M. Barnes, *J. Am. Chem. Soc.*, 1993, **115**, 5328.

4 M. Shi, N. Itoh and Y. Masaki, *J. Chem. Res. M.*, 1996, 1946; H. Nishikori and T. Katsuki, *Tetrahedron Lett.*, 1996, **37**, 9245; A. M. Harm, J. G. Knight and G. Stemp, *Synlett*, 1996, 677.

5 (*a*) Z. Li, K. Cosner and E. N. Jacobsen, *J. Am. Chem. Soc.*, 1993, **115**, 5326; (*b*) Z. Li, R. W. Quan and E. N. Jacobsen, *J. Am. Chem. Soc.*, 1995, **117**, 5889; (*c*) R. W. Quan, Z. Li and E. N. Jacobsen, *J. Am. Chem. Soc.*, 1996, **118**, 8156.

6 M. M. Díaz-Requejo, P. J. Pérez, M. Brookhart and J. L. Templeton, *Organometallics*, 1997, **16**, 4399.

7 P. Brandt , M. J. Södergren, P. G. Andersson and P. O. Norrby, *J. Am. Chem. Soc.*, 2000, **122**, 8013.

8 C. J. Sanders, K. M. Gillespie, D. Bell and P. Scott, *J. Am. Chem. Soc.*, 2000, **122**, 7132.

9 P. Müller, C. Baud and Y. Jacquier, *Can. J. Chem.*, 1998, **76**, 738.

10 S. Dinçtürk and R. A. Jackson, *J. Chem. Soc., Perkin Trans. 2*, 1981, 1127.

11 J. S. Johnson and D. A. Evans, *Acc. Chem. Res.*, 2000, **33**, 325; S. Feldgus and C. R. Landis, *J. Am. Chem. Soc.*, 2000, **122**, 12 714.

Typeset and printed by Black Bear Press Limited, Cambridge, England

CHEMCOMM
Feature Article
www.rsc.org/chemcomm

Luminescent carbon-rich rhenium(I) complexes

Vivian Wing-Wah Yam

Department of Chemistry, The University of Hong Kong, Pokfulam Road, Hong Kong, P. R. China. E-mail: wwyam@hku.hk

Received (in Cambridge, UK) 16th August 2000, Accepted 16th February 2001
First published as an Advance Article on the web 16th March 2001

The synthesis and luminescence behaviour of carbon-rich rhenium(I) complexes containing rigid-rod sp carbon chains are reported. Perturbation of the luminescence properties through structural variation of the ancillary ligands and the carbon chain length has been achieved. Utilization of the alkynylrhenium(I) system for mixed-metal complex formation is also described.

Introduction

The constant search for new advanced materials with new and improved properties has led to a variety of investigations into inorganic/organometallic molecular materials.[1] It is well known that the properties of materials may be modified dramatically by seemingly subtle changes in chemical structure, thus the possibility of using organometallic or metal-containing structural moieties to prepare molecular materials with interesting and possibly useful characteristics is an attractive option. With metal-containing materials, a wide variety of transition metals with different nature, coordination geometry, coordination number, and oxidation states, and hence the number of d electrons, can be employed. These together with the wide diversity of ligand systems and variation would provide an extremely important and rich area of research in the field of materials science. Recently, there has been a growing interest in the chemistry of carbon-rich metal-containing systems, in particlar those with long sp carbon chains.[1d–f] The alkynyl group, with its linear geometry, the rigidity of its structure, its extended π-electron delocalization and its ability to interact with metal centres *via* p_π–d_π overlap which can effectively strengthen the metal–carbon bonds, would render it an attractive building block for the construction of carbon-rich metal-containing materials which may possess potential applications as nonlinear optical materials, molecular wires, and molecular electronics. Despite the growing interest and extensive studies in metal acetylides, relatively less attention was focused on the luminescence behaviour of this class of compounds. In this context, we have directed our research efforts specifically to the design and synthesis of luminescent metal acetylides which we believe, with a careful design and judicious choice of metal and ligand systems, can be employed as versatile building blocks for the construction of luminescent molecular and oligomeric materials.

Early work on metal acetylides dated back to as early as 1960 when copper and mercury acetylides in polymeric form were reported and were proposed to have a linear geometry.[2] However, these materials were found to be intractable which precluded their purification and characterization. In the late 1970s, Hagihara and coworkers reported the first soluble polyynes containing platinum and palladium metal atoms in the main chain.[3a,b] Subsequent work by the same group had resulted in general synthetic routes to group 10 metal-containing one-dimensional polyynes.[3] Recent works by the groups of Lewis[4] and Marder[5] and others[6] have developed new routes to incorporate group 8, 9 and 10 metals into the polyyne backbone. Despite all these important contributions, studies on these polymeric systems present several difficulties, such as the exact arrangement of the structure, the molecular weight distribution, linear chains *vs.* side chains, heterogeneity of the samples, reproducibility and many others, which would render a direct understanding of the structure–property relationship and the fundamental understanding on the spectroscopic origin of these chromophores less straightforward and less amenable to study.

In order to provide a more thorough and fundamental understanding on the structure–property relationship and the spectroscopic origin of these carbon-rich metal-containing materials, it is therefore crucial to design and synthesize discrete C_n-containing and C_n-bridged metal-based molecular materials and to study their chemical and physical properties.[7]

In this article, the focus will be directed towards the rhenium(I) acetylide system and our recent efforts to design luminescent carbon-rich rhenium(I) complexes with extended carbon chains. Application of these rhenium(I) acetylides as metalloligands to generate mixed-metal luminescent molecular materials will also be described.

Mononuclear rhenium(I) acetylides

The first report on the synthesis, molecular structures and chemistry of rhenium(I) acetylide complexes dates back to 1968 when Bruce *et al.* reported the synthesis of $[Re(CO)_5(C{\equiv}CR)]$ (R = Ph or C_6F_5)[8] from the reaction of $[Re(CO)_5Cl]$ and the corresponding lithiated acetylide. Later on, Beck and coworkers reported the synthesis, molecular and electronic structures of a series of mononuclear and dinuclear pentacarbonylrhenium(I) acetylide complexes $[Re(CO)_5(C{\equiv}CR)]$ (R = CH_3, $SiMe_3$, H)

Vivian W. W. Yam was born in Hong Kong in 1963. She graduated with her first class honours BSc degree in 1985 from The University of Hong Kong. After this she obtained her PhD degree under the supervision of Professor Chi-Ming Che on high-valent metal–oxo chemistry from the same university in 1988. After spending two years as a lecturer in the Department of Applied Science at the City Polytechnic of Hong Kong (now City University of Hong Kong), she moved back to The University of Hong Kong as a lecturer in 1990. She was appointed to a Senior Lectureship in 1995, Readership in 1997, and the Chair of Chemistry in 1999. She is now also the Head of the Chemistry Department. Her research interests include inorganic/organometallic photophysics and photochemistry, polynuclear metal complexes and clusters with special emphasis on metal acetylides, chalcogenides and chalcogenolates, supramolecular chemistry, inorganic/organometallic molecular functional materials for spectrochemical and luminescence sensing and molecular recognition, optoelectronics, photoswitching and molecular devices.

DOI: 10.1039/b006694j

and $[(CO)_5Re–C\equiv C–Re(CO)_5]$.[9] Reactions of these complexes with other transition metal centres with different coordination geometry have also been studied.[10] Recently, the syntheses of rhenium(I) polyyne complexes such as $[Re(Cp)(NO)(PPh_3)\{(C\equiv C)_nR\}]$ (R = Me, $SiMe_3$, H, Ph, 1-naphthyl, n = 1–5) and $[Cp(NO)(PPh_3)Re(C\equiv C)_nReCp(NO)(PPh_3)]$ (n = 2, 4, 6, 8, 10), have been reported by Gladysz and coworkers.[11] The chemical properties and the electrochemical behaviour of these complexes and the mixed-metal systems prepared from such complexes with terminal acetylides have also been studied.[11*f,g,i*,12] The synthesis and molecular structures of metal clusters containing rhenium(I) acetylide units have also been described.[13]

In view of the well documented metal-to-ligand charge transfer (MLCT) excited state chemistry of rhenium(I) α,α′-diimine complexes,[14] in which the first report on their luminescence behaviour appeared in 1974 when the photophysical properties of $[Re(CO)_3(phen)Cl]$ were described and a metal-to-ligand charge-transfer (MLCT) excited state assignment was proposed by Wrighton and Morse,[14*a*] together with the interesting structural characteristics of rhenium(I) acetylides, the photophysical and photochemical studies of mononuclear and polynuclear luminescent organometallic rhenium(I) α,α′-diimines, especially those containing an acetylide moiety, should represent a challenging area of research. In addition, incorporation of strong σ-donating acetylide ligands would raise the energy of the d–d states of the rhenium(I) centre and thereby improve the population of the MLCT state.

In 1995 we reported the synthesis of the first luminescent rhenium(I) acetylide complexes.[15*a*] A series of mononuclear rhenium(I) acetylides, $[Re(CO)_3(^tBu_2bpy)(C\equiv CR)]$ (R = ^{t}Bu **1**, $SiMe_3$ **2**, Ph **3**, C_6H_4OMe-4 **4**, C_6H_4-Et-4 **5**, C_6H_4Ph-4 **6**, 4-pyridyl **7**, $C_6H_4C\equiv CH$-4 **8**, $^nC_6H_{13}$ **9**, $^nC_8H_{17}$ **10**, $^nC_{10}H_{21}$ **11**, H **12**), have been synthesized (Scheme 1) by the reaction of $[Re(CO)_3(^tBu_2bpy)Cl]$ with LiC≡CR in diethyl ether (prepared *in situ* by the reaction of ^{n}BuLi with the corresponding RC≡CH), which were subsequently characterized and their photophysical properties studied.[15,16] Fig. 1 shows the perspective drawing of **1**. In general, the electronic absorption spectra of these complexes in acetone show an intense low energy absorption band at *ca*. 391–440 nm, attributable to a MLCT $[d_\pi(Re) \rightarrow \pi^*(^tBu_2bpy)]$ transition.

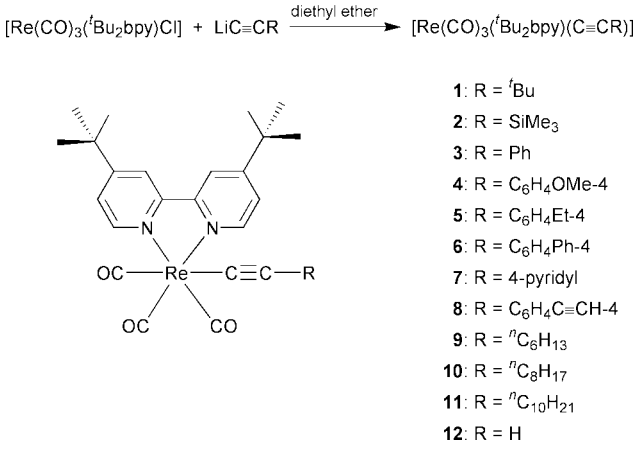

Scheme 1

A red shift of this MLCT absorption band relative to that of the chloro counterpart $[Re(CO)_3(^tBu_2bpy)Cl]$ has been observed. This finding has been ascribed to the presence of a more electron-rich rhenium(I) centre in the acetylide complexes as a result of the stronger σ-donating ability of the acetylides than the chloro ligand. The MLCT absorption energies have also been found to follow the order: **11** ≈ **10** ≈ **9** < **1** ≈ **4** ≈ **5** ≈ **3** < **2** < **12**, in line with the σ-donating ability of the acetylides:

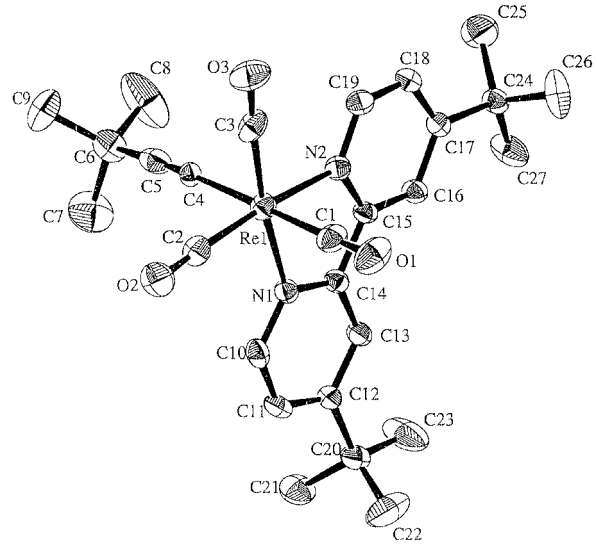

Fig. 1 The perspective drawing of **1**. Hydrogen atoms have been omitted for clarity. Reproduced with permission from ref. 15(*a*).

–C≡C^{n}C$_{10}$H$_{21}$ ≈ –C≡C^{n}C$_8$H$_{17}$ ≈ –C≡C^{n}C$_6$H$_{13}$ > –C≡C^{t}Bu ≥ –C≡CC$_6$H$_4$OMe-4 ≈ –C≡CC$_6$H$_4$Et-4 > –C≡CPh > –C≡CSiMe$_3$ > –C≡CH. This is also in agreement with the fact that a more electron-donating acetylide would render the rhenium(I) centre more electron rich and thereby decrease the MLCT transition energy. Similar observations have also been reported in the photoelectron spectroscopic studies of the $[FeCp(CO)_2(C\equiv CR)]$ (R = H, Ph, ^{t}Bu)[17] and in the $[W(\equiv CH)(dmpe)_2X]$ (X = C≡CPh, C≡CSiMe$_3$, C≡CH) systems.[18] This low energy absorption of the rhenium(I) acetylides is also found to be sensitive to the polarity of the solvent. For example, the absorption maximum of **1** in MeOH at 391 nm is red-shifted to 464 nm in *n*-hexane. This further supports the MLCT assignment of the low energy absorption as similar solvatochromic shifts are commonly observed for rhenium(I) α,α′-diimine complexes.[14*i,l*,19]

Attempts to synthesize rhenium(I) acetylide complexes with α,α′-diimine ligands other than that of 4,4′-di-*tert*-butyl-2,2′-bipyridine using the method described above were unsuccessful, yielding intractable solids in all cases. The use of LiC≡CR has limited the choice of the solvents employed, and in most cases the starting precursor complexes $[Re(CO)_3(N\text{-}N)Cl]$, unlike the 4,4′-di-*tert*-butyl-2,2′-bipyridine analogue $[Re(CO)_3(^tBu_2bpy)Cl]$, are insoluble or very sparingly soluble in the solvents used. Thus an improved route was developed which precluded the necessity of employing lithiated reagents. By refluxing a mixture of $[Re(CO)_3(bpy)Cl]$, RC≡CH, AgOTf and Et_3N in THF (Scheme 2), a series of $[Re(CO)_3(bpy)(C\equiv CR)]$

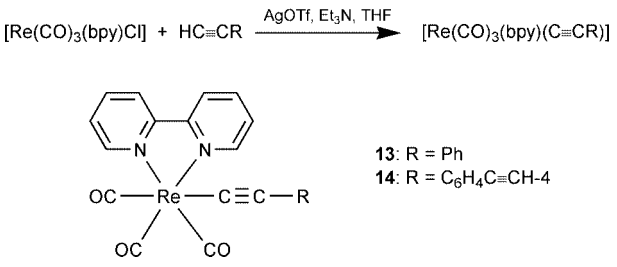

Scheme 2

were obtained in reasonable yield (R = Ph **13**, $C_6H_4C\equiv CH$-4 **14**).[20] It has been found that both the absorption and emission of the 2,2′-bipyridine counterparts occur at a lower energy than the $^tBu_2bpy$ analogues with the same acetylide ligand. This

observation further supports the involvement of the π* orbital of the α,α′-diimine ligands in the MLCT excited state of the complexes while the possibility of a MLCT [d_π(Re) → π*(C≡C)] excited state has been ruled out as an opposite trend in the absorption energies would be observed.

Upon excitation at λ > 350 nm, these mononuclear rhenium(I) acetylide complexes all show intense and long-lived orange–red luminescence in the solid state and in solutions, with lifetimes in the microsecond to sub-microsecond range. Unlike other rhenium(I)–alkyl or –aryl complexes which only emit at low temperature and undergo photodissociation reactions readily upon excitation into their σ(M–C) → π*(N–N) transition bands,[19,21] these rhenium(I) acetylide complexes are emissive in solutions at room temperature and are fairly photostable. With reference to other luminescent rhenium(I) α,α′-diimine systems,[14] the origin of the emission has been ascribed to a ^{3}MLCT [d_π(Re) → π*(N–N)] excited state; the lifetimes of which are also in the range typically found for this class of excited states.[14] The emission of the rhenium(I) acetylide complexes has also been found to occur at a lower energy relative to that of [Re(CO)$_3$(N–N)Cl]. Besides, the MLCT emission energies of the rhenium(I) α,α′-diimine complexes with different acetylide ligands also show a similar trend as observed in the electronic absorption spectra. In general, more electron-donating acetylides give a lower energy MLCT emission band and this is consistent with the σ- and π-donating ability of the acetylide moieties. The emission spectra of the starting material, [Re(CO)$_3$(^{t}Bu$_2$bpy)Cl], **1** and **12** are shown in Fig. 2. However, unlike other rhenium(I) α,α′-diimine

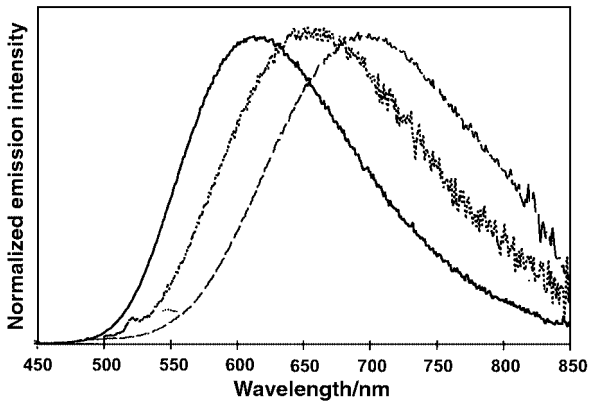

Fig. 2 The emission spectra of [Re(CO)$_3$(^{t}Bu$_2$bpy)Cl] (—), **1** (----) and **12** (·····) in degassed THF at 298 K.

complexes whose luminescence properties are strongly dependent on the solvent,[14*i*,*l*,19] the emission energies of these rhenium(I) acetylides are not very sensitive to the solvent polarity. On the other hand, these luminescent rhenium(I) acetylides have also been found to exhibit interesting rigidochromism. For example, the orange–red emissions of **9** (λ_{em} = 690 nm) and **12** (λ_{em} = 660 nm) in a EtOH–MeOH (4:1, v/v) solution at 298 K are blue-shifted to λ_{em} = 560 and 545 nm for **9** and **12**, respectively, in a 77 K glass of the same solvent mixture. Such luminescence rigidochromism has also been reported in other Re(I) α,α′-diimine systems.[14*a*,*i*,19]

Recently, we have extended our work to the use of the diynyl and triynyl units as ligands for the extension of the carbon chain. A series of mononuclear luminescent rhenium(I) α,α′-diimine complexes containing a diynyl moiety, [Re(CO)$_3$(^{t}Bu$_2$bpy)(C≡C–C≡CH)] **15** and [Re(CO)$_3$(^{t}Bu$_2$bpy)(C≡C–C≡CPh)] **16**, and triynyl moiety, [Re(CO)$_3$(^{t}Bu$_2$bpy)(C≡C–C≡C–C≡CPh)] **17**, [Re(CO)$_3$(^{t}Bu$_2$bpy)(C≡C–C≡C–C≡CSiMe$_3$)] **18** and [Re(CO)$_3$(Me$_2$bpy)(C≡C–C≡C–C≡CSiMe$_3$)] **19**, have been synthesized (Scheme 3) and characterized in our laboratory.[22] Reaction of [Re(CO)$_3$(^{t}Bu$_2$bpy)Cl],[14*a*] KF, AgOTf and Me$_3$SiC≡C–C≡CSiMe$_3$ in MeOH under reflux conditions afforded [Re(CO)$_3$(^{t}Bu$_2$bpy)(C≡C–C≡CH)] **15**, while reaction of [Re(CO)$_3$(^{t}Bu$_2$bpy)Cl], AgOTf, NEt$_3$ and PhC≡C–C≡CH in refluxing THF gave [Re(CO)$_3$(^{t}Bu$_2$bpy)(C≡C–C≡CPh)] **16**. The perspective drawing of **15** is shown in Fig. 3.

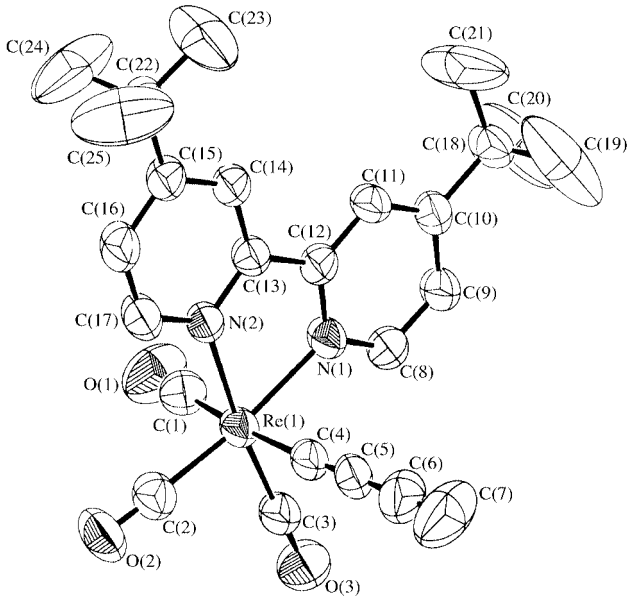

Fig. 3 The perspective drawing of **15**. Hydrogen atoms have been omitted for clarity. Reproduced with permission from ref. 22(*a*).

The triynyl complexes were synthesized by the heterocoupling reactions of [Re(CO)$_3$(N–N)(C≡C–C≡CH)] with the corresponding RC≡CH in the presence of a copper(I) catalyst and a base.[22*b*] Reaction of [Re(CO)$_3$(^{t}Bu$_2$bpy)(C≡C–C≡CH)] **15**,[22*a*] PhC≡CH and Cu(OAc)$_2$ in pyridine under reflux conditions afforded [Re(CO)$_3$(^{t}Bu$_2$bpy)(C≡C–C≡C–C≡CPh)] **17**, while reaction of [Re(CO)$_3$(N–N)(C≡C–C≡CH)], IC≡C-SiMe$_3$, piperidine and CuI in THF at room temperature gave [Re(CO)$_3$(N-N)(C≡C–C≡C–C≡CSiMe$_3$)] (N–N = ^{t}Bu$_2$bpy **18**; N–N = Me$_2$bpy **19**).

In THF, complexes **15** and **16** show intense absorption bands at *ca.* 404 and 416 nm, respectively, similarly assigned as the spin-allowed MLCT [d_π(Re) → π*(^{t}Bu$_2$bpy)] transition. The lower MLCT absorption energy for **16** than **15** is consistent with the better σ- and π- donating abilities of PhC≡C–C≡C than HC≡C–C≡C,[17,18,23] which render the Re(I) centre more electron-rich, and raise the Re d_π orbital energy, similar to that observed in the related mono-alkynyl system [Re(CO)$_3$(^{t}Bu$_2$bpy)X],[15] in which the MLCT absorption band occurs at higher energy for X = HC≡C than for X = PhC≡C.

Similarly, in the triynyl series, the intense absorption bands of **17** (426 nm), **18** (412 nm) and **19** (420 nm), in THF have been tentatively assigned as the d_π(Re) → π*(^{t}Bu$_2$bpy or Me$_2$bpy) MLCT transition. Similar to the monoynyl and diynyl systems, the lower MLCT absorption energy for **17** than **18** is again consistent with the better π-donating abilities of PhC≡C–C≡C–C≡C than Me$_3$SiC≡C–C≡C–C≡C, which render the Re(I) centre more electron-rich, and raise the Re d_π orbital energy.

Excitation of **15** and **16** both in the solid state and in solutions at room temperature at λ > 400 nm resulted in strong orange luminescence, attributed to the ^{3}MLCT phosphorescence. The excitation spectra of **15** and **16** in THF show an excitation band at *ca.* 400 and 410 nm, respectively, which closely resembles that of the MLCT absorption maxima. The slightly lower MLCT emission energy of **16** than **15** in THF is in line with the stronger σ- and π-donating abilities of the phenyldiynyl unit than the butadiynyl ligand, *i.e.* PhC≡C–C≡C **16** (625 nm) < HC≡C–C≡C **15** (620 nm). Similar trends have been observed in

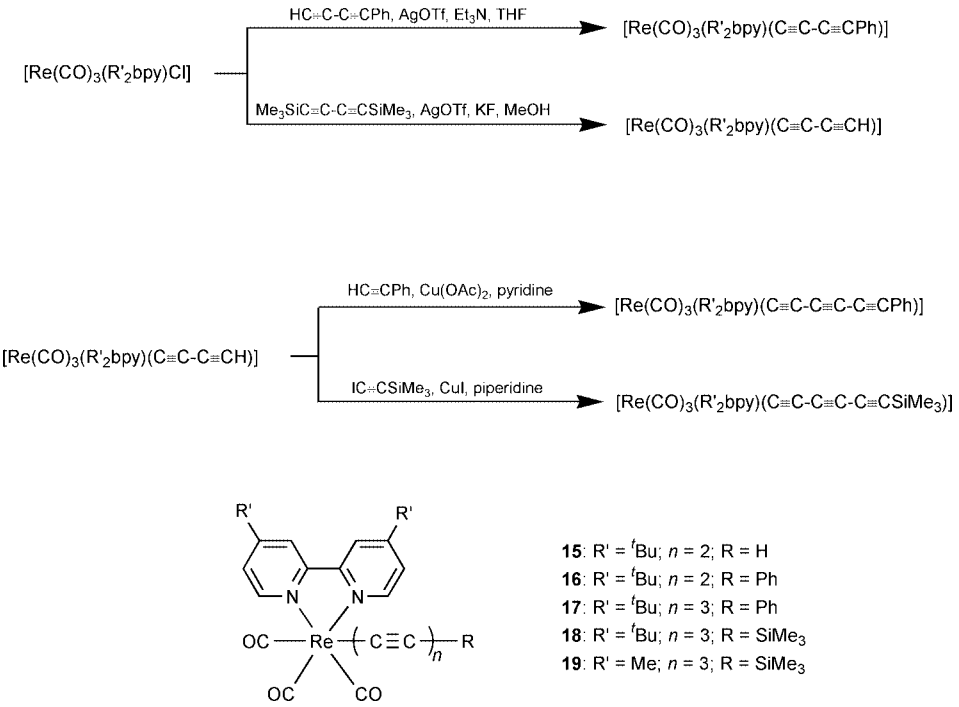

15: R' = ^{t}Bu; *n* = 2; R = H
16: R' = ^{t}Bu; *n* = 2; R = Ph
17: R' = ^{t}Bu; *n* = 3; R = Ph
18: R' = ^{t}Bu; *n* = 3; R = $SiMe_3$
19: R' = Me; *n* = 3; R = $SiMe_3$

Scheme 3

the monoacetylide analogues [PhC≡C **3** (688 nm) < HC≡C **12** (670 nm)].[15]

Similarly, excitation of the triynyl complexes **17**–**19** both in the solid state and in solutions at room temperature at λ > 400 nm resulted in strong orange luminescence, attributed to the ^{3}MLCT phosphorescence. All the lifetimes of the diynyl and triynyl complexes were in the microsecond to sub-microsecond range; as are typically found for ^{3}MLCT states of rhenium(I) systems.[14] The lower MLCT emission energy of **17** than **18** in THF is again in line with the stronger π-donating abilities of the phenyltriynyl unit than the trimethylsilyltriynyl ligand, *i.e.* PhC≡C–C≡C–C≡C **17** (620 nm) < Me_3SiC≡C–C≡C–C≡C **18** (596 nm). Both **17** and **18** emit at higher energies than their respective monoynyl and diynyl counterparts, *i.e.* in the [Re(CO)$_3$(^{t}Bu$_2$bpy)X] system, the emission energies in THF follow the order: PhC≡C–C≡C–C≡C **17** (620 nm) > PhC≡C–C≡C **16** (625 nm) > PhC≡C **3** (688 nm); Me_3SiC≡C–C≡C–C≡C **18** (596 nm) > Me_3SiC≡C **2** (670 nm). Fig. 4 shows the

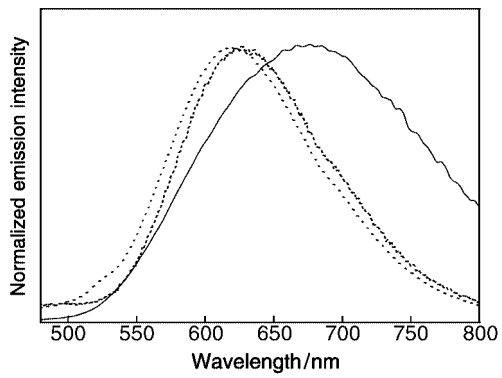

Fig. 4 The emission spectra of **3** (—), **16** (----) and **17** (·····) in THF solution at 298 K.

emission spectral trend of the complexes as a function of the acetylenic carbon chain length. The observation of a blue shift in emission energies upon increasing the number of the C≡C units disfavours an assignment of a ^{3}MLCT {d_π(Re) → π*[(C≡C)$_n$R]} or a metal-perturbed ^{3}IL {π[(C≡C)$_n$R] → π*[(C≡C)$_n$R]} origin (*n* = 1, 2, 3) and is suggestive of an assignment of a ^{3}MLCT [d_π(Re) → π*(^{t}Bu$_2$bpy)] origin. Preliminary molecular orbital studies using Extended Hückel molecular orbital (EHMO) theory on **17** and its diynyl analogue [Re(CO)$_3$(^{t}Bu$_2$bpy)(C≡C–C≡CPh)] **16** show that in both the diynyl and triynyl systems, the LUMO mainly consists of π*(^{t}Bu$_2$bpy) character while the HOMO is mainly dominated by the antibonding character of the Re–(C≡C)$_n$Ph (*n* = 2, 3) moiety resulted from the overlap of the d_π(Re) and π[(C≡C)$_n$Ph] orbitals, which is supportive of a d_π(Re) → π*(^{t}Bu$_2$bpy) MLCT character for the electronic transition. An increase in the HOMO–LUMO energy gap has also been observed on extending the C≡C unit from the diynyl to the triynyl species, in which the LUMO energies remain more or less the same while the HOMO energies decrease with an increasing number of C≡C units. The observed trend of a higher MLCT emission energy in the triynyl system than the diynyl and hence the monoynyl systems, in line with EHMO studies, may originate from a decreased overlap integral between the d_π(Re) and the triynyl π(RC≡CC≡CC≡C) orbitals than that of d_π(Re) and the π(RC≡CC≡C) and π(RC≡C) orbitals resulting from the delocalization of electron density across the C$_n$ unit, despite the better energy match between π(RC≡CC≡CC≡C) and the d_π(Re) orbital, *i.e.* the overlap of the more closely energy-matched d_π(Re) and π(RC≡CC≡CC≡C) orbitals does not necessarily raise the d_π(Re) orbital to an energy higher than that for the diynyl and monoynyl cases, and may give rise to the anomalous energy trend in which the MLCT emission energy is in the order: PhC≡C–C≡C–C≡C > PhC≡C–C≡C > PhC≡C. An alternative rationale for the increased MLCT energies upon increasing the number of the C≡C units is that given the similar σ-donating properties of the monoynyl, diynyl and triynyl unit,[17,23] the much better π-accepting ability of RC≡C–C≡C–C≡C than RC≡C–C≡C which in turn is better than RC≡C may become the dominating factor, stabilizing the Re d_π orbitals to a greater extent, and hence gives rise to a higher energy ^{3}MLCT [d_π(Re) → π*(^{t}Bu$_2$bpy or Me$_2$bpy)] emission. However, in view of the much less importance of the d_π(Re)–π*[(C≡C)$_n$R] interaction, as reflected from EHMO studies, such possibilities are not favoured.

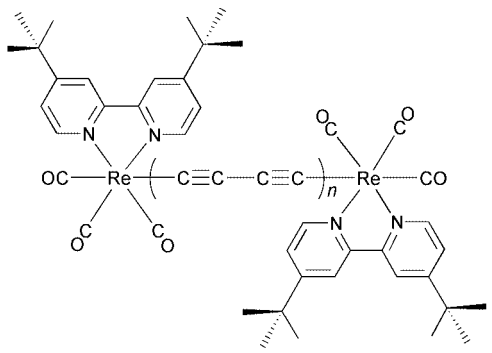

20: n = 1
21: n = 2
22: n = 3

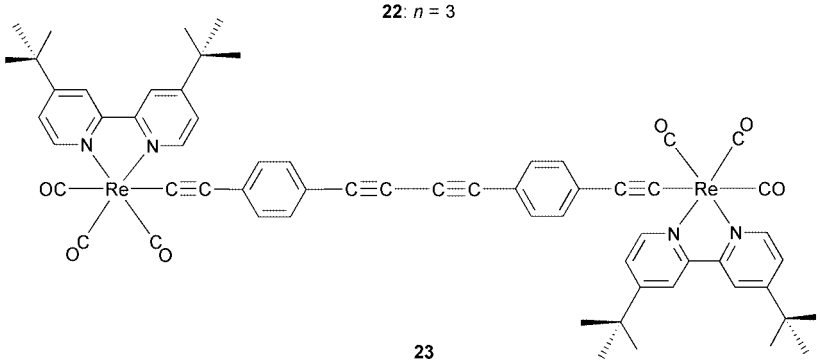

23

Dinuclear rhenium(I) acetylides

Besides mononuclear complexes, dinuclear rhenium(I) α,α′-diimine complexes with a bridging acetylide ligand, [(^{t}Bu$_2$bpy)-(CO)$_3$Re–C≡C–C≡C–Re(CO)$_3$(^{t}Bu$_2$bpy)] **20**,[15b] [(^{t}Bu$_2$bpy)-(CO)$_3$Re–C≡C–C≡C–C≡C–C≡C–Re(CO)$_3$(^{t}Bu$_2$bpy)] **21**, [(^{t}Bu$_2$bpy)(CO)$_3$Re–C≡C–C≡C–C≡C–C≡C–C≡C–C≡C–Re-(CO)$_3$(^{t}Bu$_2$bpy)] **22** and [(^{t}Bu$_2$bpy)(CO)$_3$Re–C≡C-C$_6$H$_4$–(C≡C-4)–C≡C–C$_6$H$_4$–(C≡C-4)–Re(CO)$_3$(^{t}Bu$_2$bpy)] **23**, have also been synthesized by homo-coupling reactions involving the respective [(^{t}Bu$_2$bpy)(CO)$_3$Re–(C≡C)$_n$H] complexes in the presence of Cu(OAc)$_2$ and pyridine. The perspective view of **20** is depicted in Fig. 5. Upon photoexcitation, complex **20** exhibits long-lived luminescence at *ca.* 660–690 nm which has been proposed to originate from a ^{3}MLCT [d_π(Re) → π*(^{t}Bu$_2$bpy)] excited state. Upon excitation at λ > 430 nm, complex **23** emits at *ca.* 640 nm which is at a slightly higher energy than that of the mononuclear counterpart **8** (λ_{em} = 670 nm). The solid-state emission spectra of **23** at 298 and 77 K show vibronically structured emission band with vibrational progressional spacings of *ca.* 1500 and 2000 cm^{-1}, typical of ground-state aromatic ν(C⋍C) and acetylide ν(C≡C) stretching frequencies, respectively.

Mixed-metal acetylides

In order to further explore the possibility of utilizing the rhenium(I) acetylides as versatile building blocks in molecular architecture, we have successfully synthesized mixed-metal acetylide complexes using the 'metal complex as ligand' or the so-called metalloligand approach. The first approach we employed was to utilize the [Re(CO)$_3$(bpy)(C≡CPh)] **13** complex as an η^2-ligand towards Cu(I) and Ag(I) ions.[24] Reaction of [Re(CO)$_3$(bpy)(C≡CPh)] **13** with [Cu(MeCN)$_4$]PF$_6$ in THF at room temperature afforded [{η^2-Re(CO)$_3$-(bpy)(C≡CPh)}$_2$Cu]PF$_6$ **24**. Similarly, reaction of [Re(CO)$_3$-(bpy)(C≡CPh)] with [Ag(MeCN)$_4$]PF$_6$ under similar conditions gave the analogue, [{η^2-Re(CO)$_3$(bpy)(C≡CPh)}$_2$Ag]PF$_6$ **25**. The perspective drawings of the complete cations of **24** and **25** are shown in Figs. 6 and 7, respectively. The slightly longer C≡C bond distances in **24** [1.20(1)–1.23(1) Å] and **25** [1.199(8)–1.203(8) Å] relative to the [Re(CO)$_3$(bpy)(C≡CPh)] **13** precursor [1.199(9) Å], together with the bond weakening observed in IR spectroscopy where lower ν(C≡C) values have been observed for **24** (2029 cm^{-1}) and **25** (2033 cm^{-1}) than [Re(CO)$_3$(bpy)(C≡CPh)] **13** (2083 cm^{-1}), are consistent with the π-coordination mode of the alkynyl group to the d^{10} metal centres.

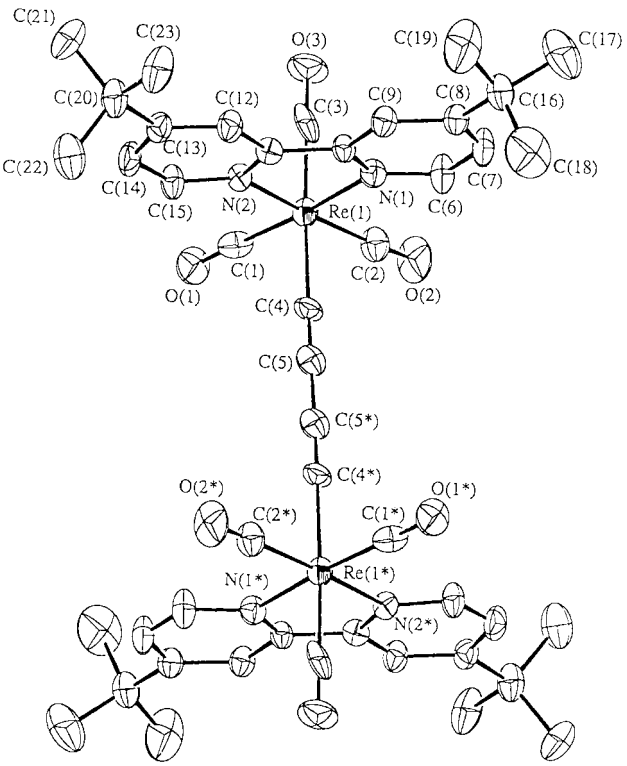

Fig. 5 The perspective drawing of **20**. Hydrogen atoms have been omitted for clarity. Reproduced with permission from ref. 15(*b*).

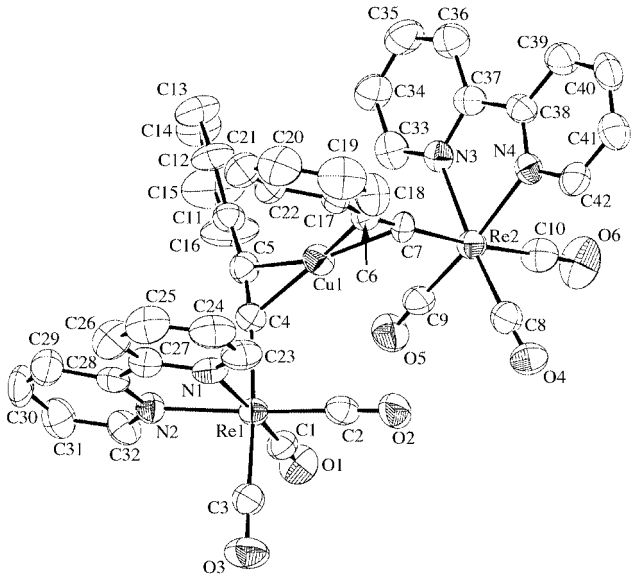

Fig. 6 The perspective drawing of the complex cation of **24**. Hydrogen atoms have been omitted for clarity. Reproduced with permission from ref. 24.

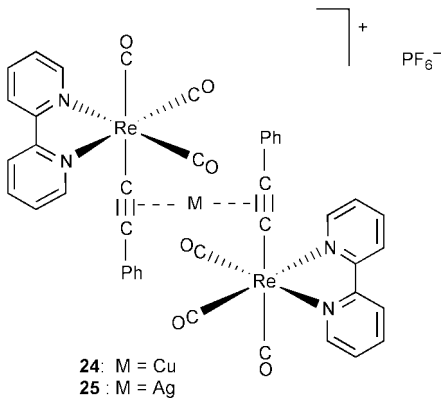

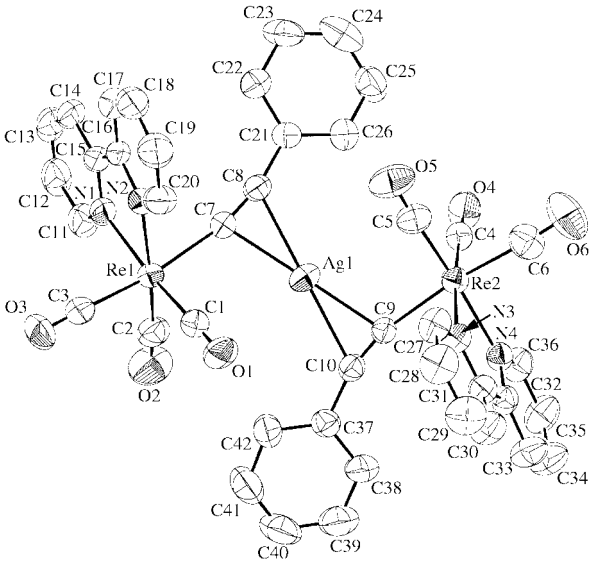

Fig. 7 The perspective drawing of the complex cation of **25**. Hydrogen atoms have been omitted for clarity. Reproduced with permission from ref. 24.

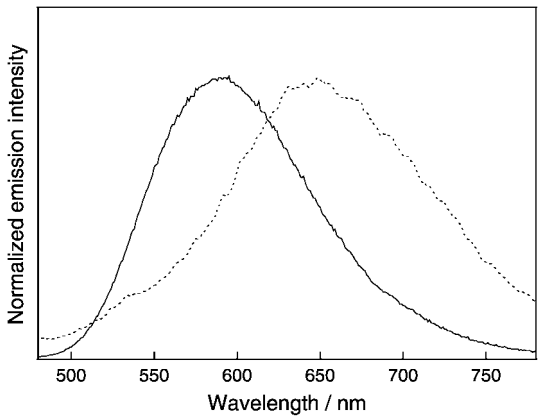

Fig. 8 The emission spectra of **13** (·····) and **24** (—) in degassed CH_2Cl_2 at 298 K.

The electronic absorption spectra of **24** and **25** show an intense MLCT absorption band at *ca.* 396 nm in dichloromethane solution. The shift of the MLCT absorption to the blue relative to that of $[Re(CO)_3(bpy)(C{\equiv}CPh)]$ **13** (420 nm) is in line with the lower-lying d_π(Re) orbital in **24** (396 nm) and **25** (396 nm), resulted from the reduced π-donating ability of the acetylide ligand upon π-coordination to the d^{10} metal ions.

Excitation of **24** and **25** also resulted in orange ^{3}MLCT phosphorescence. Similar to the absorption studies, the emissions of **24** (590 nm) and **25** (600 nm) in CH_2Cl_2 are shifted to higher energies compared to that of $[Re(CO)_3(bpy)(C{\equiv}CPh)]$ **13** (654 nm). Fig. 8 shows the emission spectra of **13** and **24** in degassed CH_2Cl_2 at 298 K. Such a trend is consistent with an assignment of a ^{3}MLCT [d_π(Re) → π*(bpy)] emission origin and disfavours the assignment of a ^{3}MLCT [d_π(Re) → π*(C≡CPh)] origin, since the acetylide becomes a poorer π-donor upon coordination to Cu(I) and Ag(I), lowering the energy

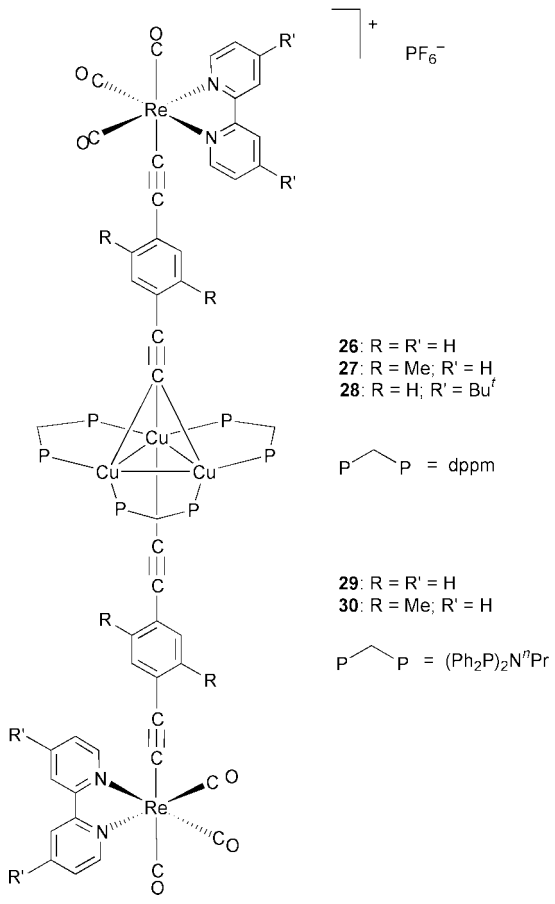

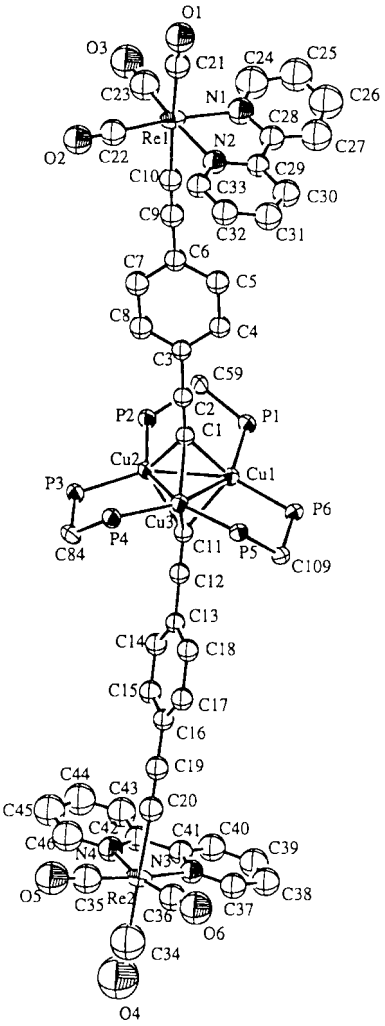

Fig. 9 The perspective drawing of the complex cation of **26**. Hydrogen atoms have been omitted for clarity. Reproduced with permission from ref. 26.

of the Re d_π orbitals, and hence leading to a higher energy ^{3}MLCT [d_π(Re) → π*(bpy)] emission.

A second approach was to utilize the rhenium(I) acetylides with terminal –C≡CH groups as the metalloligand. Recent works by us have shown that luminescent copper(I) acetylides are also promising building blocks for the construction of rigid-rod oligomeric and polymeric materials.[25] As a further step towards this goal, a series of pentanuclear mixed-metal copper(I)–rhenium(I) acetylide complexes $[Cu_3(\mu\text{-P–P})_3\{\mu_3\text{-}\eta^1\text{-C}\equiv\text{C–C}_6H_2R_2\text{-2,5-C}\equiv\text{C-4–Re(N–N)(CO)}_3\}_2]^+$ [P–P = dppm, N–N = bpy, R = H **26**, Me **27**; P–P = dppm, N–N = ^{t}Bu$_2$bpy, R = H **28**; P–P = $(Ph_2P)_2N^n$Pr, N–N = bpy, R = H **29**, Me **30**] have been synthesized and their luminescence properties studied.[26] The perspective view of the complex cation of **26** is displayed in Fig. 9. The electronic absorption spectra of these complexes reveal, in addition to the high energy intraligand (IL) absorption bands at *ca*. 250–300 nm and the vibronically structured bands at *ca*. 348–378 nm, a lower-energy absorption at *ca*. 440 nm, which is assigned to a MLCT [d_π(Re) → π*(N–N)] transition. All the complexes display strong orange luminescence upon photoexcitation. The low energy emission bands at *ca*. 600–660 nm have been suggested to arise from a ^{3}MLCT [(d_π(Re) → π*(N–N)] excited state. The energy trend of this low energy emission is in line with the π* orbital energies of the diimine ligands. The complexes with more electron-rich $(Ph_2P)_2N^n$Pr phosphine ligands are found to emit at slightly lower energy than that of the dppm counterparts. This can be rationalized by the fact that the more electron-donating $(Ph_2P)_2N^n$Pr phosphines would render the copper(I) centres more electron rich, and in turn destablilize the Re(I) d_π orbitals and therefore the ^{3}MLCT [d_π(Re) → π*(N–N)] emission occurs at lower energy.

Conclusion

It is interesting to realize that the rhenium(I) acetylide system offers, indeed, a very versatile and powerful building block for the construction of various luminescent rigid-rod and mixed-metal carbon-rich complexes. By careful planning and the judicious choice of the diimine ligands, the acetylide ligands, the extension of the C≡C units, the nature of the heterometals in the mixed-metal complexes, and the spectator ligands on the heterometal centres, one could readily tune the spectroscopic and emission properties of the systems. An interesting observation is the blue shift in the emission energy upon extending the carbon chain in these complexes, which differs from the common concept of tuning the emission energy to the red by extending the number of acetylenic units in organic polyynes. Besides, the tuning of emission energies by π-coordination of the rhenium–acetylide moiety to d^{10} metal ions or σ-coordination of the acetylide to the trinuclear copper(I) diphosphine units using the metalloligand approach would represent a new concept in the design of luminescent molecular materials. All these examples demonstrate the importance and versatility of systematic structural variation in elucidating the spectroscopic origins of these systems and the flexibility of emission energies tuning simply by changing the nature of the excited state through perturbations on the metal and ligand orbital energies.

Acknowledgements

Financial support from the Research Grants Council and The University of Hong Kong is gratefully acknowledged. The author is also indebted to her students and coworkers, whose names appear in the references. Special thanks are due to Dr K. M. C. Wong for his help in the preparation of the manuscript and to Dr K. K. Cheung for his help in solving the X-ray crystal structures.

References

1 See, for recent reviews: (*a*) *Inorganic Materials*, ed. D. W. Bruce and D. O'Hare, Wiley, London, 1992; (*b*) R. J. Puddephatt, *Chem. Commun.*, 1998, 1055; (*c*) P. F. H. Schwab, M. D. Levin and J. Michl, *Chem. Rev.*, 1999, **99**, 1863; (*d*) H. Lang, *Angew. Chem., Int. Ed. Engl.*, 1994, **33**, 547; (*e*) U. H. F. Bunz, *Angew. Chem., Int. Ed. Engl.*, 1996, **35**, 969; (*f*) M. I. Bruce, *Coord. Chem. Rev.*, 1997, **166**, 91.

2 V. V. Korshak, A. M. Sladkov and Y. P. Kurdryavtsev, *Vysokomol. Soedin.*, 1960, **2**, 1824; A. S. Hay, *J. Org. Chem.*, 1960, **25**, 1275.

3 (*a*) K. Sonogashira, S. Takahashi and N. Hagihara, *Macromolecules*, 1977, **10**, 879; (*b*) S. Takahashi, M. Kariya, T. Yakate, K. Sonogashira and N. Hagihara, *Macromolecules*, 1978, **11**, 1063; (*c*) K. Sonogashira, S. Kataoka, S. Takahashi and N. Hagihara, *J. Organomet. Chem.*, 1978, **160**, 319; (*d*) S. Takahashi, E. Murata, M. Kariya, K. Sonogashira and N. Hagihara, *Macromolecules*, 1979, **12**, 1016; (*e*) K. Sonogashira, K. Ohga, S. Takahashi and N. Hagihara, *J. Organomet. Chem.*, 1980, **188**, 237.

4 S. J. Davies, B. F. G. Johnson, M. S. Khan and J. Lewis, *J. Chem. Soc., Chem. Commun.*, 1991, 187; B. F. G. Johnson, A. K. Kakkar, M. S. Khan and J. Lewis, *J. Organomet. Chem.*, 1991, **409**, C12; M. S. Khan, N. A. Pasha, A. K. Kakkar, P. R. Raithby, J. Lewis, K. Fuhrmann and R. H. Friend, *J. Mater. Chem.*, 1992, **2**, 759; M. S. Khan, A. K. Kakkar, N. J. Long, J. Lewis, P. R. Raithby, P. Nguyen, T. B. Marder, F. Wittmann and R. H. Friend, *J. Mater. Chem.*, 1994, **4**, 1227; R. D. Markwell, I. S. Butler, A. K. Kakkar, M. S. Khan, Z. H. Al-Zakwani and J. Lewis, *Organometallics*, 1996, **15**, 2331; N. Chawdhury, A. Köhler, R. H. Friend, M. Younus, N. J. Long, P. R. Raithby and J. Lewis, *Macromolecules*, 1998, **31**, 722.

5 H. B. Fyfe, M. Mlekuz, D. Zargarian, N. J. Taylor and T. B. Marder, *J. Chem. Soc., Chem. Commun.*, 1991, 188; H. B. Fyfe, M. Mlekuz, G. Stringer, N. J. Taylor and T. B. Marder, *Inorganic and Organometallic Polymers with Special Properties*, ed. R. M. Laine, NATO ASI Series, Kluwer Acad. Publ., Dordrecht, The Netherlands, 1992, vol. 206, p. 331.

6 K. C. Sturge, A. D. Hunter, R. McDonald and B. D. Santarsiero, *Organometallics*, 1992, **11**, 3056; H. Nishihara, T. Shimura, A. Ohkubo, N. Matsuda and K. Aramaki, *Adv. Mater.*, 1993, **5**, 752.

7 R. Nast, *Coord. Chem. Rev.*, 1982, **47**, 89; M. I. Bruce, *Chem. Rev.*, 1991, **91**, 197; H. Lang, K. Köhler and S. Blau, *Coord. Chem. Rev.*, 1995, **143**, 113; F. Paul and C. Lapinte, *Coord. Chem. Rev.*, 1998, **178**–**180**, 431; R. Ziessel, M. Hissler, A. El-ghayoury and A. Harriman, *Coord. Chem. Rev.*, 1998, **178**–**180**, 1251.

8 M. I. Bruce, D. A. Harbourne, F. Waugh and F. G. A. Stone, *J. Chem. Soc. A*, 1968, 356.

9 M. Appel, J. Heidrich and W. Beck, *Chem. Ber.*, 1987, **120**, 1087; W. Beck, B. Niemer, J. Breimair and J. Heidrich, *J. Organomet. Chem.*, 1989, **372**, 79; J. Heidrich, M. Steimann, M. Appel, W. Beck, J. R. Phillips and W. C. Trogler, *Organometallics*, 1990, **9**, 1296.

10 T. Weidmann, V. Weinrich, B. Wagner, C. Robl and W. Beck, *Chem. Ber.*, 1991, **124**, 1363; S. Mihan, T. Weidmann, V. Weinrich, D. Fenske and W. Beck, *J. Organomet. Chem.*, 1997, **541**, 423; S. Mihan, K. Sünkel and W. Beck, *Chem. Eur. J.*, 1999, **5**, 745.

11 (*a*) A. Wong and J. A. Gladysz, *J. Am. Chem. Soc.*, 1982, **104**, 4948; (*b*) J. J. Kowalczyk, A. M. Arif and J. A. Gladysz, *Organometallics*, 1991, **10**, 1079; (*c*) D. R. Senn, A. Wong, A. T. Patton, M. Marsi, C. E. Strouse and J. A. Gladysz, *J. Am. Chem. Soc.*, 1988, **110**, 6096; (*d*) J. A. Ramsden, F. Agbossou, D. R. Senn and J. A. Gladysz, *J. Chem. Soc., Chem. Commun.*, 1991, 1360; (*e*) Y. Zhou, J. W. Seyler, W. Weng, A. M. Arif and J. A. Gladysz, *J. Am. Chem. Soc.*, 1993, **115**, 8509; (*f*) J. W. Seyler, W. Weng, Y. Zhou and J. A. Gladysz, *Organometallics*, 1993, **12**, 3802; (*g*) M. Brady, W. Weng and J. A. Gladysz, *J. Chem. Soc., Chem. Commun.*, 1994, 2655; (*h*) T. Bartik, B. Bartik, M. Brady, R. Dembinski and J. A. Gladysz, *Angew. Chem., Int. Ed. Engl.*, 1996, **35**, 414; (*i*) M. Brady, W. Weng, Y. Zhou, J. W. Seyler, A. J. Amoroso, A. M. Arif, M. Böhme, G. Frenking and J. A. Gladysz, *J. Am. Chem. Soc.*, 1997, **119**, 775.

12 W. Weng, T. Bartik and J. A. Gladysz, *Angew. Chem., Int. Ed. Engl.*, 1994, **33**, 2199; W. Weng, T. Bartik, M. Brady, B. Bartik, J. A. Ramsden, A. M. Arif and J. A. Gladysz, *J. Am. Chem. Soc.*, 1995, **117**, 11922.

13 A. A. Koridze, O. A. Kizas, N. E. Kolobova, V. N. Vinogradova, N. A. Ustynyuk, P. V. Petrovskii, A. I. Yanovsky and Y. T. Struchkov, *J. Chem. Soc., Chem. Commun.*, 1984, 1158; A. D. Shaposhnikova, R. A. Stadnichenko, G. L. Kamalov, A. A. Pasynskii, I. L. Eremenko, S. E. Nefedov, Y. T. Struchkov and A. I. Yanovsky, *J. Organomet. Chem.*, 1993, **453**, 279.

14 (*a*) M. S. Wrighton and D. L. Morse, *J. Am. Chem. Soc.*, 1974, **96**, 998; (*b*) V. Balzani and F. Scandola, *Supramolecular Photochemistry*, Ellis-Horwood, Chichester, 1991; (*c*) K. Kalyanasundaram, *Photochemistry of Polypyridine and Porphyrin Complexes*, Academic Press, London, 1992; (*d*) O. Horváth and K. L. Stevenson, *Charge Transfer Photochemistry of Coordination Compounds*, VCH, New York, 1993; (*e*) S. M. Fredericks, J. C. Luong and M. S. Wrighton, *J. Am. Chem. Soc.*, 1979, **101**, 7415; (*f*) J. V. Caspar, B. P. Sullivan and T. J. Meyer, *Inorg. Chem.*, 1984, **23**, 2104; (*g*) B. P. Sullivan, C. M. Bolinger, D. Conrad, W. J. Vining and T. J. Meyer, *J. Chem. Soc., Chem. Commun.*, 1985, 1414; (*h*) G. T. Tapolsky, R. Duesing and T. J. Meyer, *J. Phys. Chem.*, 1989, **93**, 3885; (*i*) A. J. Lees, *Chem. Rev.*, 1987, **87**, 711; (*j*) S. V. Wallendael, R. J. Shaver, D. P. Rillema, B. J. Yoblinski, M. Stathis and T. F. Guarr, *Inorg. Chem.*, 1990, **29**, 1761; (*k*) T. J. Meyer, *Acc. Chem. Res.*, 1989, **22**, 163; (*l*) B. P. Sullivan, *J. Phys. Chem.*, 1989, **93**, 24.

15 (*a*) V. W. W. Yam, V. C. Y. Lau and K. K. Cheung, *Organometallics*, 1995, **14**, 2749; (*b*) V. W. W. Yam, V. C. Y. Lau and K. K. Cheung, *Organometallics*, 1996, **15**, 1740.

16 V. C. Y. Lau, Ph.D Thesis, The University of Hong Kong, 1997.

17 D. L. Lichtenberger, S. K. Renshaw and R. M. Bullock, *J. Am. Chem. Soc.*, 1993, **115**, 3276; D. L. Lichtenberger, S. K. Renshaw, A. Wong and C. D. Tagge, *Organometallics*, 1993, **12**, 3522.

18 J. Manna, S. J. Geib and M. D. Hopkins, *J. Am. Chem. Soc.*, 1992, **114**, 9199.

19 D. J. Stufkens, *Comments Inorg. Chem.*, 1992, **13**, 359.

20 K. M. C. Wong, Ph.D Thesis, The University of Hong Kong, 1998.

21 J. C. Luong, R. A. Faltynek and M. S. Wrighton, *J. Am. Chem. Soc.*, 1979, **101**, 1597; L. A. Lucia, R. D. Burton and K. S. Schanze, *Inorg. Chim. Acta*, 1993, **208**, 103.

22 (*a*) V. W. W. Yam, S. H. F. Chong and K. K. Cheung, *Chem. Commun.*, 1998, 2121; (*b*) V. W. W. Yam and S. H. F. Chong, *Organometallics*, 2000, **19**, 5092.

23 J. Manna, K. D. John and M. D. Hopkins, *Adv. Organomet. Chem.*, 1995, **38**, 79.

24 V. W. W. Yam, S. H. F. Chong, K. M. C. Wong and K. K. Cheung, *Chem. Commun.*, 1999, 1013.

25 V. W. W. Yam, K. K. W. Lo, W. K. M. Fung and C. R. Wang, *Coord. Chem. Rev.*, 1998, **171**, 17; V. W. W. Yam and K. K. W. Lo, *Chem. Soc. Rev.*, 1999, **28**, 323.

26 V. W. W. Yam, W. K. M. Fung, K. M. C. Wong, V. C. Y. Lau and K. K. Cheung, *Chem. Commun.*, 1998, 777.

CHEMCOMM Communication
www.rsc.org/chemcomm

The first isolable dialkyl iodophosphates

Christopher M. Timperley* and Matthew J. Waters

Defence Science and Technology Laboratory, Chemical and Biological Defence Sector, Porton Down, Salisbury, Wiltshire, UK SP4 0JQ. E-mail: cmtimperley@dera.gov.uk

Received (in Cambridge, UK) 30th January 2001, Accepted 16th March 2001
First published as an Advance Article on the web 5th April 2001

The synthesis and characterization of the first dialkyl iodophosphates to be isolated in a pure state is described; $(CF_3CH_2O)_2P(O)I$ and $[(CF_3)_2CHO]_2P(O)I$ have electronegative fluoro-ester groups and can be distilled under vacuum.

The study of derivatives of phosphoric acid is one of the oldest branches of organic chemistry. In 1868, Wichelhaus isolated the first member of the dialkyl halophosphate series, diethyl chlorophosphate $(CH_3CH_2O)_2P(O)Cl$.[1] Later work led to the fluorophosphate $(CH_3CH_2O)_2P(O)F$[2] and the bromophosphate $(CH_3CH_2O)_2P(O)Br$; the latter is unstable and decomposes after 3 days at room temperature.[3] The corresponding iodophosphate $(CH_3CH_2O)_2P(O)I$, like all known iodophosphates, decomposes extremely easily and has not been obtained out of solution.[4–6] In continuation of our studies on fluoroalkyl phosphoryl compounds,[7,8] we now describe the synthesis and characterization of the first isolable dialkyl iodophosphates (and the first such molecules containing fluoro-ester groups). Our results indicate that the presence of electronegative fluorine atoms[9] significantly enhances thermal stability.

We prepared bis(fluoroalkyl) phosphites **1a** and **1b** in good yield by treating the intermediate from tertiary butanolysis of phosphorus trichloride, namely $Cl_2P(O)H$, with two molar equivalents of trifluoroethanol or hexafluoroisopropanol (Scheme 1).† The synthesis of compound **1a** this way was reported by Gibbs and Larsen; modification of their procedure[10] gave the new phosphite **1b**. Both bis(fluoroalkyl) phosphites can be stored in glass vials in a refrigerator for many months without change.

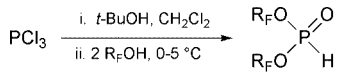

$R_F = CF_3CH_2$ δ_P 7.0 **1a** 89%
$(CF_3)_2CH$ δ_P 7.9 **1b** 71%

Scheme 1

Treatment of bis(trifluoroethyl) phosphite **1a** with a solution of iodine in toluene,[11] with argon blowing through the mixture to help remove hydrogen iodide, gave iodophosphate **2a** (Scheme 2). It was purified by vacuum distillation (bp 40 °C/0.02 mmHg).‡ This is the first time iodination of a dialkyl phosphite has permitted the isolation of a pure iodophosphate: the reaction with diethyl phosphite is complicated by dealkylation of diethyl iodophosphate by hydrogen iodide, and pure product cannot be obtained.[4] The greater ease of dealkylation of the $CH_3CH_2O–$ group compared to the $CF_3CH_2O–$ group is because the ethoxy oxygen is more basic than the trifluoroethoxy oxygen, and thus more easily converted into a

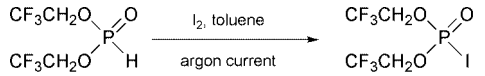

1a δ_P -47.7 **2a** 46%

Scheme 2

leaving group by protonation, and also because the α-carbon of the $CH_3CH_2O–$ group is a softer acid than that of the $CF_3CH_2O–$ group, making it more vulnerable to attack by iodide ion, itself a soft base.

Iodination of bis(hexafluoroisopropyl) phosphite **1b**, without argon blowing through the reaction mixture, gave a 1 : 2 ratio of iodophosphate **2b** and iodo acid **3** (Scheme 3), as shown by multinuclear NMR experiments. The iodo acid arises from dealkylation of the iodophosphate by resident hydrogen iodide; the by-product $(CF_3)_2CHI$ was not detected, but most likely escaped due to its volatile nature.

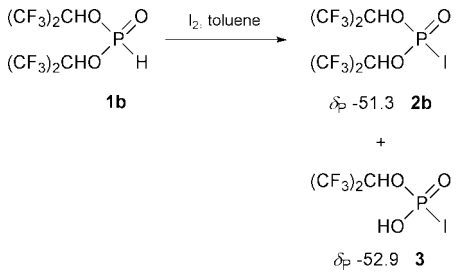

1b δ_P -51.3 **2b** + δ_P -52.9 **3**

Scheme 3

Although bis(fluoroalkyl) iodophosphates resist dealkylation more than their unfluorinated counterparts, hydrogen iodide formation is best avoided during their synthesis. Treatment of bis(hexafluoroisopropyl) phosphite **1b** with *N*-iodosuccinimide (NIS), a convenient source of 'positive' iodine, led to good conversion to the iodophosphate, as shown by GC-MS analysis of the reaction mixture (Scheme 4). Iodophosphate **2b** was purified by vacuum distillation (bp 46 °C/2 mmHg).§

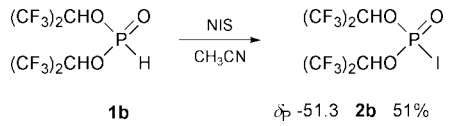

1b δ_P -51.3 **2b** 51%

Scheme 4

Iodophosphates **2a–b** are pale yellow liquids that deposit traces of black solid on storage in a refrigerator. In line with other dialkyl halophosphates,[1] the iodophosphates might be expected to be colourless. The yellow colour is probably attributable to contamination by iodine vapour during distillation; the deposit during storage is assumed to be precipitated iodine. The phosphorus chemical shifts in deuteriochloroform for bis(trifluoroethyl) iodophosphate **2a** and bis(hexafluoroisopropyl) iodophosphate **2b** are −47.7 and −51.3 ppm. Values for $(CH_3CH_2O)_2P(O)I$ and $(CCl_3CH_2O)_2P(O)I$ in chloroethane are −41 and −50 ppm respectively.[6]

In summary, we have developed routes to two dialkyl iodophosphates that comprise the first such species to have been isolated and characterized properly. This discovery, which lags behind the first isolation of a pure dialkyl phosphorochloridate by over 130 years, opens up new frontiers in organic phosphorus and iodine chemistry. Further studies relating to the synthesis of

a range of bis(fluoroalkyl) phosphites and their reactions with halogens will be reported in due course.

We thank the Ministry of Defence UK for funding the work.

Notes and references

† *Materials and methods:* trifluoroethanol and hexafluoroisopropanol were purchased from Apollo Scientific Ltd UK. Analytical information was obtained using documented instrumentation and techniques: see C. M. Timperley, M. Bird, I. Holden and R. M. Black, *J. Chem. Soc., Perkin Trans. 1*, 2001, 26. NMR data were recorded in $CDCl_3$ solution.

‡ *Bis(trifluoroethyl) iodophosphate* **2a**: a solution of iodine (5.08 g, 0.02 mol) in toluene (100 cm^3) was added dropwise to bis(trifluoroethyl) phosphite (4.92 g, 0.02 mol) in toluene (75 cm^3) at 0–5 °C with stirring and passage of argon through the solution. After addition, the purple solution was left for 2 h. Residual iodine was removed by filtration through a small plug of silica gel. Removal of toluene and double distillation of the residue gave **2a** as a pale yellow liquid (3.42 g, 46%). Bp 40 °C/0.02 mmHg. δ_H (500 MHz) 4.45 (4H, m, OCH_2); δ_C (125 MHz) 121.4 (dq, J = 13 and 278 Hz, CF_3), 69.4 (dq, J = 5 and 37 Hz, OCH_2); δ_F (470 MHz) −74.1 (6F, t, J = 7 Hz, CF_3); ν_{max}/cm^{-1} (film) 1454, 1421, 1296 (P=O), 1174, 1070, 962, 883, 849; *m/z* (CI) 373 (M + 1), 353 (M − F), 245 (M − I); HRMS (+ve ion EI): Calc. for $C_4H_4F_6IO_3P$ 371.939 ([M − HF]$^+$ = 351.933), found 351.933 (error 0.7).

§ *Bis(hexafluoroisopropyl) iodophosphate* **2b**: a solution of *N*-iodosuccinimide (2.62 g, 11.65 mmol) in acetonitrile (20 cm^3) was added dropwise by cannula to a stirred solution of bis(hexafluoroisopropyl) phosphite (4.45 g, 11.65 mmol) in acetonitrile (30 cm^3). After 2 h, GC-MS analysis showed good conversion to product. Removal of solvent and double distillation of the oily residue gave **2b** as a pale yellow liquid (3 g, 51%). Bp 46 °C/2 mmHg. δ_H (500 MHz) 5.28 (2H, dsep, J = 5 Hz, OCH); δ_C (125 MHz) 119.9 (dq, J = 6 and 282 Hz, CF_3), 71.9 (dsep, J = 7 and 37 Hz, OCH); δ_F (470 MHz) −72.3 (6F, m, CF_3), −73.2 (6F, m, CF_3); ν_{max}/cm^{-1} (film) 1379, 1300 (P=O), 1280–1205 (strong bands), 1117, 1068, 904, 879, 854; *m/z* (CI) 509 (M + 1), 489 (M − F), 381 (M − I); HRMS (+ve ion EI): Calc. for $C_6H_2F_{12}IO_3P$ 507.933 ([M − HF]$^+$ = 487.927), found 487.926 (error 1.6).

1 Refer to G. M. Kosolapoff, *Organophosphorus Compounds*, John Wiley & Sons, New York, 1950, p. 242.

2 Diethyl fluorophosphate $(CH_3CH_2O)_2P(O)F$ was first prepared in 1932 by W. Lange and G. von Krüger, *Chem. Ber*., 1932, **65**, 1598. For a review of the history of this 'nerve agent', see C. M. Timperley, *Highly Toxic Fluorine Compounds*, in: R. E. Banks (Ed.), *Fluorine Chemistry at the Millennium: Fascinated by Fluorine*, Elsevier, Oxford, UK, 2000, pp. 499–538.

3 H. Goldwhite and B. C. Saunders, *J. Chem. Soc*., 1955, 3564.

4 H. McCombie, B. C. Saunders and G. J. Stacey, *J. Chem. Soc*., 1945, 921.

5 A. Skowronska, M. Pakulski, J. Michalski, D. Cooper and S. Trippett, *Tetrahedron Lett*., 1980, **21**, 321.

6 Although the synthesis of $(CH_3CH_2O)_2P(O)I$ and the chloro analogue $(CCl_3CH_2O)_2P(O)I$ have been prepared by iodination of the respective trialkyl phosphites at −40 °C, their purification and full characterization has not been carried out. See J. Michalski, M. Pakulski and A. Skowronska, *J. Chem. Soc., Perkin Trans. 1*, 1980, 833.

7 C. M. Timperley, J. F. Broderick, I. Holden, I. J. Morton and M. J. Waters, *J. Fluorine Chem*., 2000, **106**, 43.

8 C. M. Timperley, I. Holden, I. J. Morton and M. J. Waters, *J. Fluorine Chem*., 2000, **106**, 153.

9 The hexafluoroisopropoxy group is more electron-withdrawing than the trifluoroethoxy group: pK_a values for $(CF_3)_2CHOH$ and CF_3CH_2OH are 9.3 and 12.4 respectively (compare these with 17.1 for isopropanol and 15.9 for ethanol). See M. Hudlicky, *Chemistry of Organic Fluorine Compounds*, Ellis Horwood, London, 2nd Edition, 1992, p. 550.

10 D. E. Gibbs and C. Larsen, *Synthesis*, 1984, 410. The reaction mixture from tertiary butanolysis of phosphorus trichloride was left for 1 h at 0–5 °C and hexafluoroisopropanol was added dropwise over 30 mins. After standing for 12 h at rt, the mixture was heated under reflux for 3 h, the solvent removed and the residue distilled to give bis(hexafluoroisopropyl) phosphite **1b** as a mobile colourless liquid (71%). Bp 62 °C/8 mmHg.

11 The solubility of iodine in g kg^{-1} of solvent at 25 °C decreases in the order: toluene 1875 > diethyl ether 337 > benzene 164; see *Kirk-Othmer Encyclopedia of Chemical Technology*, Wiley, New York, 3rd Edition, 1978, vol. 13, p. 652. Toluene is therefore the best choice of solvent for the iodination reaction.

CHEMCOMM Communication
www.rsc.org/chemcomm

Photoreactions of *N*-alkoxy-4-(*p*-chlorophenyl)thiazole-2(3*H*)-thiones with L-cysteine derivatives in aqueous solutions

Jens Hartung,* Rainer Kneuer and Kristina Špehar

Institut für Organische Chemie, Universität Würzburg, Am Hubland, D-97074 Würzburg Germany. E-mail: hartung@chemie.uni-wuerzburg.de; Fax: +49 (0)931 / 888 4606

Received (in Cambridge, UK) 1st February 2001, Accepted 16th March 2001
First published as an Advance Article on the web 17th April 2001

Photolysis of substituted *N*-alkoxythiazolethiones 1 in aqueous solvents furnishes alkoxyl radicals 2 which, upon stereoselective 5-*exo-trig* cyclization, are trapped by water soluble thiols (L-cysteine, L-cysteine ethyl ester, or the reduced form of glutathione, GSH) to afford disubstituted tetrahydrofurans 3 in synthetically useful yields and with satisfactory to excellent diastereoselectivities.

Oxygen radicals are transients in a number of biosyntheses of structurally diverse secondary metabolites.[1–3] In view of the significance of such transformations it is surprising to note that only a limited number of laboratory studies have been performed under biomimetic conditions in order to explore the properties of proposed O-radical key intermediates in water.[4,5] Major drawbacks for adapting standard radical procedures from organic to aqueous solvents originate from an insolubility of the selected reagents such as the radical precursor itself and the trapping reagent, for instance Bu_3SnH.[6] Therefore, we have investigated the feasibility of stereoselective alkoxyl radical reactions in homogeneous and heterogeneous aqueous solvents under neutral (*i.e.* non-oxidative) conditions and disclose our latest results in this communication.

N-Alkoxy-4-(*p*-chlorophenyl)thiazole-2(3*H*)-thiones **1a–d** were selected as O-radical precursors. Thione **1b** had been prepared previously.[6] Heterocycles **1a**, **1c–d** are new compounds which were obtained from the corresponding alkyl chloride (**1a**) or tosylates (**1c**, **1d**) and *N*-hydroxy-*p*-chlorophenylthiazole-2(3*H*)-thione tetraethylammonium salt according to standard procedures.[6]† Thiones **1a–d** themselves are poorly soluble in water. Therefore, all photoreactions of **1** with polar thiols were performed in two phase systems ($C_6H_5CF_3$–H_2O) or in homogeneous mixtures of 1,4-dioxane (hereafter dioxane) and water. Thiols of different polarity and molecular size were selected as hydrogen atom donor: L-cysteine, L-cysteine ethyl ester (as its hydrochloride, L-CysOEt·HCl) and the reduced form of glutathione (GSH, γ-L-glutamyl-L-cysteinylglycine).[7] The selection of $C_6H_5CF_3$ as organic solvent, which is less toxic than benzene, was based on the necessity of direct comparison of the newly obtained data with those from photoreactions of thiones **1** using Bu_3SnH as state of the art reagent.‡ Thus, a solution of 1-phenyl-5-methylhexenoxythiazolethione **1a** and L-CysOEt·HCl in a mixture of $C_6H_5CF_3$–H_2O was treated with a 2 M solution of NaOH and was photolyzed at room temperature in a Rayonet photoreactor (λ_{max} = 350 nm). After complete consumption of **1a**, the pH of the aqueous phase is adjusted to 2 in order to extract residual hydrogen donor into the aqueous phase. The organic layer affords upon workup 68% of 2,5-*trans*-disubstituted tetrahydrofuran **3a** (entry 1, conditions 1, *cis*:*trans* = 30:70) (Scheme 1).‡§

Alternatively we found that tetrahydrofuran **3a** could be prepared in similar yields from thione **1a** in a homogeneous mixture of dioxane and water by application of L-CysOEt·HCl as hydrogen atom donor and neat Na_2CO_3 as base (entry 1, conditions 2, 64%, *cis*:*trans* = 30:70). Other organic cosolvents such as CH_3CN, acetone, or MeOH, were found to be inferior to dioxane. In a third experiment, 53% of tetrahydrofuran **3a** was obtained from the photoreaction of thiazolethione **1a** and GSH in dioxane–H_2O (entry 1, conditions 3, 53%, *cis*:*trans* = 30:70). These findings indicate, that efficient stereoselective alkoxyl radical cyclizations in homogeneous aqueous solvents are feasible. However, it is essential to use 10 equiv. of L-cysteine derivatives as hydrogen atom donors at the given concentration level, since lower thiol strengths lead to the formation of alkoxyl radical-derived alcohols besides the corresponding carbonyl compounds in 1:1 molar ratios. Compared to the corresponding Bu_3SnH-mediated reactions the yields decrease only slightly whereas stereoselectivities are not affected by the change in solvent.‡

The best conditions 1–3 (Scheme 1) were subsequently applied for experiments using 2-phenylpentenyloxythiazolethione **1b** (entry 2) and derivatives **1c–d** (entries 3–4). Photoreactions using 2-substituted 4-pentenyloxythiazolethiones **1b** and **1c** afforded *cis*-2,4-disubstituted tetrahydrofurans **3b** and **3c** as major products which is in line with the general guidelines of stereoselective 5-*exo-trig* alkoxyl cyclizations[8–10] and with the Beckwith–Houk model[11] for carbon radical ring closure reactions (entries 2 and 3). The observed high stereoselectivity for the formation of 4-*tert*-butyl-2-methylte-

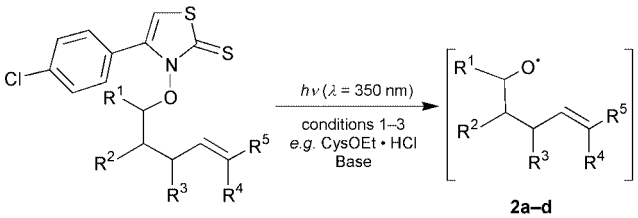

1a–d **2a–d**

1–3	R^1	R^2	R^3	$R^4 = R^5$
a	Ph	H	H	Me
b	H	Ph	H	H
c	H	*t* Bu	H	H
d	H	H	*t* Bu	H

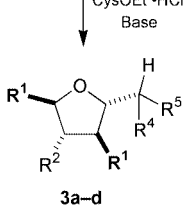

3a–d

Entry	1	Yields **3a–d** [%] (*cis* : *trans*)		
		conditions 1 [a]	conditions 2 [b]	conditions 3 [c]
1	**1a**	68 (30 : 70)	64 (30 : 70)	53 (30 : 70)
2	**1b**	50 (88 : 12)	52 (88 : 12)	34 (88 : 12)
3	**1c**	71 (90 : 10)	66 (90 : 10)	60 (90 : 10)
4	**1d**	68 (<2 : >98)	64 (<2 : >98)	47 (<2 : >98)

Scheme 1 Stereoselective synthesis of disubstituted tetrahydrofurans **3** from *N*-alkoxythiazolethiones **1** and L-cysteine derivatives. L-CysOEt HCl = L-cysteine ethyl ester hydrochloride, GSH = γ-L-glutamyl-L-cysteinylglycine. [a] Conditions 1: $C_6H_5CF_3$–H_2O = 4/1 (v/v), 2 M NaOH, L-CysOEt HCl. [b] Conditions 2: dioxane–H_2O = 4/1 (v/v), L-CysOEt HCl, Na_2CO_3. [c] Conditions 3: dioxane–H_2O = 4/1 (v/v), GSH.§

DOI: 10.1039/b101097m

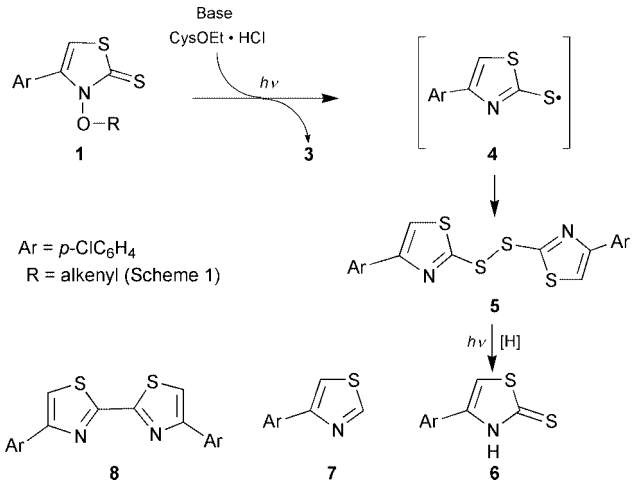

Scheme 2 Formation of thiazoles **5**–**8** from *N*-alkoxythiazolethiones **1**.

trahydrofuran **3c** from the corresponding alkenoxyl radical **2c** (entry 3, *cis*:*trans* = 90:10) is considered to originate from beneficial steric effects of the *tert*-butyl substituent. This interpretation is supported by a noteworthy 2,3-*trans*-selectivity for the formation of 3-*tert*-butyl-2-methyltetrahydrofuran **3d** from the corresponding thiazolethione **1d** (entry 4).[7,10,11]

According to the data which are reported in Scheme 1 it is obvious that heterogeneous and homogeneous conditions 1 and 2 (Scheme 1), which demand L-CysOEt·HCl as hydrogen atom donor and a suitable base, are superior to the GSH for preparing tetrahydrofurans **3** from thiones **1**. It is worth mentioning, that GSH requires the presence of water in order to deliver its hydrogen atom to cyclized *O*-radicals, although GSH is partially soluble in pure dioxane. Similar observations were made for free amino acid L-cysteine as hydrogen atom donor which affords almost identical yields and selectivities of **3** as GSH does (not shown in Scheme 1). Further, syntheses of tetrahydrofurans **3** fail if photolyses of thiones **1** and GSH are performed in heterogeneous mixtures. For example, the photoreaction of radical precursor **1b** and GSH in $C_6H_5CF_3$–H_2O affords 2-phenylpent-4-en-1-ol (34%) and the corresponding aldehyde 2-phenylpent-4-enal (21%) as sole products.

In almost every photochemical run, formation of a colorless to yellowish precipitate was observed. This material was soluble in acetone, but less soluble in diethyl ether. It was shown to be a mixture of strongly UV-absorbing compounds which were characterized as different primary and secondary photoproducts presumably of the starting thiones **1** (Scheme 2). Expected addition products of either glutathionyl or cysteinyl radicals to the thiocarbonyl group in parent thiones **1a–d** were surprisingly absent in the reaction mixtures.[6] According to control experiments it is likely that the disulfide **5** is formed as primary product which then undergoes further absorption of UV light to afford both 4-(*p*-chlorophenyl)thiazole-2(3*H*)-thione (**6**) and thiazole **7** besides the bisthiazole **8**. Evidence for this assumption is derived from products obtained after photodecomposition of disulfide **5** at λ = 350 nm in dioxane–water (4:1, v/v) which affords 43% of thiazole **7** and 16% of thiazolethione **6**. It is interesting to note that the thiazole-derived photoproducts **5**–**8** (Scheme 2) are identical to those isolated from photochemical studies using the parent acid of **1**, *i.e.* *N*-hydroxy-4-(*p*-chlorophenyl)thiazolethione, as hydroxyl radical source for DNA-strand break in photobiological studies.[12]

In conclusion, we have demonstrated that L-cysteine-derivatives, *e.g.* L-CysOEt, or the tripeptide GSH can be applied as useful radical traps for the stereoselective formation of disubstituted tetrahydrofurans **3** *via* an alkoxyl radical pathway in aqueous solvents. These investigations point to the feasibility of *O*-radical reactions using *N*-alkoxythiazole-2(3*H*)-thiones, *e.g.* derivatives of **1**, under biomimetic conditions. Further work is in progress in order to pursue *O*-radical chemistry in water as the sole solvent.

This work was generously supported by the Deutsche Forschungsgemeinschaft (Project Ha1705/3–2). Also, we express our gratitude to Dipl.-Chem. Philipp Schmidt for providing samples of thiazolethione **1a** and Dr Hideki Okamoto for helpful discussions.

Notes and references

† Satisfactory analytical data were obtained for all new compounds in this study: thiazolethiones **1a**, **1c**, and **1d**, and tetrahydrofurans **3c** and **3d**.

‡ For comparison, yields of tetrahydrofurans **3** from photoreactions of **1** and Bu_3SnH in $C_6H_5CF_3$ were determined. Figures in brackets denote the *cis*–*trans* ratios: **3a**: 93% (30:70), **3b**: 60% (88:12), **3c**:97% (90:10), **3d**:88% (<2:>98).

§ In a typical run thiazolethione **1** (1 mmol) was dissolved in the organic solvent ($C_6H_5CF_3$ or 1,4-dioxane, 20 ml). L-CysOEt·HCl (10 mmol) and a base (9 mmol, see Scheme 1), or GSH, or L-cysteine (10 mmol) were dissolved in water (5 mL). Both solutions were combined while stirring to afford the reaction mixture which was photolyzed at ambient temperature in a Rayonet® photoreactor (λ = 350 nm). Upon complete consumption of **1** (*ca.* 30 min), the colorless to yellowish precipitate was filtered-off and the remaining solution was worked up as follows. For reactions with CysOEt in $C_6H_5CF_3$–H_2O, 2 M HCl was added with agitation to adjust to pH 2 in the aqueous phase. Subsequently, phases were separated and the aqueous layer was extracted with diethyl ether (2 × 10 mL). The combined organic phases were dried with $MgSO_4$ and concentrated *in vacuo*. The product **3** was purified by column chromatography (SiO_2, petroleum ether–Et_2O = 2:1, v/v). If dioxane is used as solvent, the organic solvent is first evaporated from the reaction mixture. Subsequently, diethyl ether was added (20 mL) to the aqueous phase and tetrahydrofurans **3** were isolated as described above.

1 J. Hartung and R. Kneuer, *Eur. J. Org. Chem.*, 2000, 1677.
2 D. C. Ayres and J. D. Loike, *Lignans—Chemical, Biological, and Clinical Properties*, Cambridge University Press, Cambridge, 1990, pp 269–302
3 V. Ullrich and R. Brugger, *Angew. Chem.*, 1994, **106**, 1987; *Angew. Chem., Int. Ed. Engl.*, 1994, **33**, 1911.
4 E. J. Corey, C. Shih, N. Y. Shih and K. Shimoji, *Tetrahedron Lett.*, 1984, **25**, 5013.
5 N. A. Porter, M. O. Funk, D. Gilmore, R. Isaac and J. Nixon, *J. Am. Chem. Soc.*, 1976, **98**, 6000.
6 J. Hartung, M. Schwarz, I. Svoboda and H. Fuess, *Eur. J. Org. Chem.*, 1999, 1275.
7 H. Strittmatter, A. Dussy, U. Schwitter and B. Giese, *Angew. Chem.*, 1999, **111**, 238; *Angew. Chem., Int. Ed. Engl.*, 1999, **38**, 135.
8 J. Hartung and F. Gallou, *J. Org. Chem.*, 1995, **60**, 6706.
9 J. Hartung, M. Hiller and P. Schmidt, *Chem. Eur. J.*, 1996, **2**, 1014.
10 J. Hartung, *Eur. J. Org. Chem.*, 2001, 619.
11 B. Giese, N. Porter and D. P. Curran, *Stereochemistry of Radical Reactions*, VCH, Weinheim, 1995.
12 W. Adam, J. Hartung, H. Okamoto, C. R. Saha-Möller and K. Špehar, *Photochem. Photobiol.*, 2000, **72**, 619.

CHEMCOMM Communication
www.rsc.org/chemcomm

Influence of water on the chirality of camphorsulfonic acid-doped polyaniline

Veronica Egan, Robert Bernstein, Laura Hohmann, Thu Tran and Richard B. Kaner*

Department of Chemistry & Biochemistry and Exotic Materials Institute, University of California, Los Angeles, Los Angeles, CA 90095-1569, USA. E-mail: kaner@chem.ucla.edu

Received (in Irvine, CA, USA) 2nd November 2000, Accepted 20th March 2001
First published as an Advance Article on the web 5th April 2001

Polyaniline doped with *R*-(−)- or *S*-(+)-camphorsulfonic acid produces an inexpensive chiral substrate; the presence or absence of water can be used to invert the dopant-induced circular dichroism (CD) absorbance at 450 nm, shedding light on conflicting literature reports.

Chiral polyaniline has potential applications in molecular recognition and enantiomeric separations.[1–3] In searching the literature of chiral camphorsulfonic acid-doped polyaniline, we discovered that alternating directions have been reported for the main dopant-induced circular dichroism (CD) absorbance peak centered at 450 nm. For example, when doped with *S*-(+)-camphorsulfonic acid, the CD absorbance at 450 nm is sometimes reported to be in the positive direction,[3–6] whereas at other times it is reported to be in the negative direction.[1,5–9] If chiral polyaniline is to be useful as an active material in sensors and separations[1,2] this phenomenon needs to be understood. Here, we demonstrate that the chirality of polyaniline is critically dependent upon the water content of the polymer before exposure to the chiral acid dopant.

Polyaniline is a simple conjugated polymer, which can be polymerized *via* either chemical[10] or electrochemical oxidation of aniline.[11] Aniline is an inexpensive achiral molecule heavily used in the dye industry.[12] The half-oxidized emeraldine base form of polyaniline can be readily doped to the conducting emeraldine salt form when mixed with a strong acid (Scheme 1).

Emeraldine base doped with either enantiomer of camphorsulfonic acid produces a chiral form of polyaniline.[1,4,6] Since camphorsulfonic acid is only optically active below 300 nm, the doping-induced peak at 450 nm can be attributed exclusively to chiral polyaniline, and therefore, this absorbance can be used to monitor chirality in the polymer. Here, the emeraldine base form of polyaniline was chemically synthesized according to a literature procedure[10,13] and camphorsulfonic acid doping in *N*-methylpyrrolidinone was carried out using a 2:1 mass (5:1 molar) ratio of emeraldine base to camphorsulfonic acid.†

To study the effects of water upon chiral polyaniline, one sample of emeraldine base was placed in a 60 °C oven for four days and allowed to dry thoroughly, while a second sample from the same batch was soaked in deionized water for four days followed by brief vacuum filtration. The dry (3–5% water content determined by thermogravimetric analysis) and wet (>50% water content determined by thermogravimetric analysis) emeraldine base samples were then doped with either *S*-(+)- or *R*-(−)-camphorsulfonic acid in *N*-methylpyrrolidinone and CD spectra obtained. Surprisingly, a CD peak at 450 nm could be induced to give either a positive or a negative signal simply by thoroughly wetting or drying the emeraldine base polyaniline prior to doping with *S*-(+)-camphorsulfonic acid in *N*-methylpyrrolidinone (see Fig. 1): the dry sample doped with *S*-(+)-camphorsulfonic acid results in the positive CD peak; the wet sample doped with *S*-(+)-camphorsulfonic acid gives the negative CD peak. Tests performed on different batches of wet and dry emeraldine base all exhibited the same trends in CD direction at 450 nm. Therefore, the water content of the emeraldine base prior to doping with camphorsulfonic acid has a dramatic affect upon the chirality of the doped polyaniline.

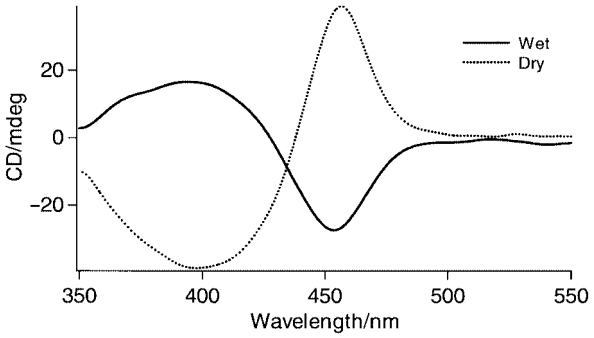

Fig. 1 Resulting CD spectra of polyaniline dried prior to doping with *S*-(+)-camphorsulfonic acid in *N*-methylpyrrolidinone (Dry) and wetted prior to doping with *S*-(+)-camphorsulfonic acid in *N*-methylpyrrolidinone (Wet).

Wet and dry emeraldine base samples doped with *R*-(−)-camphorsulfonic acid in *N*-methylpyrrolidinone gave exactly analogous, but inverted, CD results (see Fig. 2). Note that the direction of the CD peak at 450 nm induced with *R*-

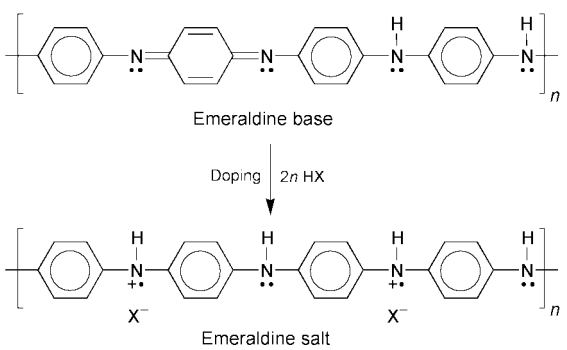

Scheme 1 Fully doped polyaniline; molar ratio of emeraldine base to dopant acid (HX) is 2:1.

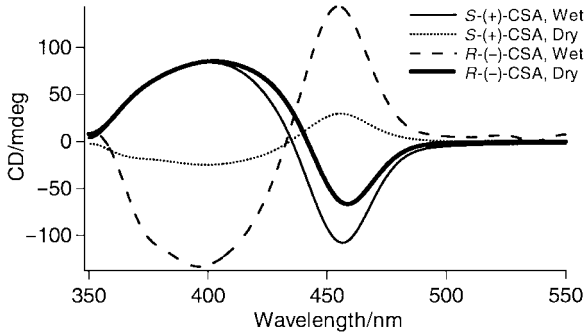

Fig. 2 Resulting CD spectra of polyaniline doped with *R*-(−)- or *S*-(+)-camphorsulfonic acid after exposure to either drying or wetting conditions prior to doping in *N*-methylpyrrolidinone.

Table 1 Effects of water on the chirality of camphorsulfonic acid-doped polyaniline in *N*-methylpyrrolidinone

Condition of emeraldine base prior to doping with camphorsulfonic acid	CD direction at 450 nm	
	S-(+)-Camphorsulfonic acid	*R*-(−)-Camphorsulfonic acid
Wet	−	+
Dry (60 °C)	+	−
Dry (60 °C) → Wet	−	+
Wet → Dry (60 °C)	+	−
Wet → vacuum dried, room temperature	+	−

(−)-camphorsulfonic acid for wet polyaniline is now in the positive direction, whereas the dry sample is now in the negative direction. Therefore, polyaniline can be readily manipulated to produce the same form of optically active polyaniline when doped with opposite enantiomers. The direction of the CD signal is dependent upon both the condition of the emeraldine base prior to doping, and upon which enantiomer is used for doping. Additionally, all of the solutions were cast as thin, doped emeraldine films onto quartz plates and CD spectra obtained. All the samples gave the same CD peak direction at 450 nm as when in solution. Therefore, this phenomenom exists regardless of whether the sample is in solution or in the solid state.

In order to rule out that the drying temperature caused a chemical change to the emeraldine base structure, a sample of polyaniline dried at 60 °C for a four-day period was subsequently soaked in deionized water to produce the wet form of emeraldine base. The sample was then doped with *S*-(+)-camphorsulfonic acid in *N*-methylpyrrolidinone overnight and analyzed by CD. The resulting CD peak at 450 nm was negative which is the same CD direction observed for unheated, wet polyaniline doped with *S*-(+)-camphorsulfonic acid (see Table 1). To further rule out heating at 60 °C as the cause for the reversal in chirality, water elimination *via* vacuum drying at room temperature was substituted for oven drying. A sample of wet emeraldine base was dried for seven days under vacuum at room temperature and then doped with *S*-(+)-camphorsulfonic acid in *N*-methylpyrrolidinone. The resulting CD direction–positive at 450 nm–was the same as for emeraldine base dried at 60 °C. When the inverse experiment was performed, *i.e.* using wet emeraldine base dried in a 60 °C oven for several days, a positive CD signal at 450 nm was obtained after doping with *S*-(+)-camphorsulfonic acid. This is the same direction as observed for emeraldine base dried at 60 °C as summarized in Table 1. Thus, polyaniline behaves according to the last environment that it is exposed to. This indicates that water is the causal factor rather than a chemical reaction (*e.g.* cross-linking) of the polyaniline itself or involving some impurity. This also demonstrates that the process is fully reversible prior to doping.

The above temperature experiments were also performed with *R*-(−)-camphorsulfonic acid instead of the *S*-(+)-form. A sample of emeraldine base polyaniline dried at 60 °C for a four-day period was subsequently soaked in deionized water and doped with *R*-(−)-camphorsulfonic acid in *N*-methylpyrrolidinone overnight. A second emeraldine base sample was first soaked in water and then dried in a 60 °C oven before doping with *R*-(−)-camphorsulfonic acid. Additionally, wet emeraldine base polyaniline that was dried at room temperature under vacuum was also doped with *R*-(−)-camphorsulfonic acid. All samples were analyzed with CD and the results are summarized in Table 1. The *R*-(−)-camphorsulfonic acid-doped polyaniline behaves analogously to *S*-(+)-camphorsulfonic acid doped polyaniline except that all CD directions at 450 nm are now inverted.

The discovery that water can cause a reversal in chirality, and its ability to make polyaniline doped with opposite enantiomers appear to have the same chiral configuration based on CD is significant because it could explain the observed inversion of expected chiralities reported in the literature.[3,7,14] For example, Wallace and coworkers have shown that chiral polyaniline doped with the same enantiomer of camphorsulfonic acid prepared electrochemically produces an inverted CD peak at 450 nm to that produced chemically.[3,5,7] Their electrochemically prepared chiral polyaniline when doped with *S*-(+)-camphorsulfonic acid produces a negative 450 nm peak, whereas their chemically generated polyaniline doped with *S*-(+)-camphorsulfonic acid in *N*-methylpyrrolidinone produces a positive CD peak at this wavelength. The authors conclude that there must be different configurations for the electrochemically and chemically prepared chiral polyanilines.[5] However, since the electrochemically prepared chiral polyaniline was electropolymerized in an aqueous solution and its CD is similar in direction to the wet polyaniline described here, it is likely that the water used in the electrochemical process contributes to the chiral configuration of the polyaniline.

Thus, the CD spectra of *S*-(+)- and *R*-(−)-camphorsulfonic acid doped polyanilines in *N*-methylpyrrolidinone can appear identical depending upon the water content of the emeraldine base prior to doping. This process is fully reversible before doping and is simply a function of the water content and is not related to the drying temperature.

This work was supported by the University of California Campus Laboratory Collaboration program (CLC).

Notes and references

† All samples were made with 60 mg of polyaniline and 30 mg (1.3×10^{-4} mole) of camphorsulfonic acid in 4 mL of *N*-methylpyrrolidinone. The mixtures were shaken and allowed to dope for at least four hours and then filtered through cotton. Each sample for CD analysis consisted of 40 μL of a stock solution that was diluted with 150 μL of *N*-methylpyrrolidinone. Films were prepared by placing a few drops of solution onto quartz plates that were dried at 60 °C for two hours. All CD analyses were carried out using a Jasco J715 CD Spectropolarimeter and a Fast Fourier Transform to filter out high frequency noise. Owing to the difficulty of completely dissolving polyaniline in *N*-methylpyrrolidinone, the concentrations, and therefore the CD intensities, vary from sample to sample. The CD spectra presented in Fig. 2 for *S*-(+)- and *R*-(−)-camphorsulfonic acid-doped polyaniline used polymer powder from the same synthesis, whereas the analogous spectra for *S*-(+)-camphorsulfonic acid- doped polyaniline in Fig. 1 used polymer powder from a different synthetic batch.

1 H. L. Guo, C. M. Knobler and R. B. Kaner, *Synth. Met.*, 1999, **101**, 44.
2 H. L. Guo, C. M. Knobler and R. B. Kaner, *U.S. Patent Pending*.
3 M. R. Majidi, L. A. P. Kane-Maguire and G. G. Wallace, *Polymer*, 1995, **36**, 3597.
4 E. E. Havinga, M. M. Bouman, E. W. Meijer, A. Pomp and M. M. J. Simenon, *Synth. Met.*, 1994, **66**, 93.
5 I. D. Norris, L. A. P. Kane-Maguire and G. G. Wallace, *Macromolecules*, 1998, **31**, 6529.
6 L. A. P. Kane-Maguire, A. G. MacDiarmid, I. D. Norris, G. G. Wallace and W. G. Zheng, *Synth. Met.*, 1999, **106**, 171.
7 M. R. Majidi, L. A. P. Kane-Maguire and G. G. Wallace, *Polymer*, 1994, **35**, 3113.
8 M. R. Majidi, L. A. P. Kane-Maguire and G. G. Wallace, *Polymer*, 1996, **37**, 359.
9 M. R. Majidi, L. A. P. Kane-Maguire and G. G. Wallace, *Aust. J. Chem.*, 1998, **51**, 23.
10 Y. Cao, A. Andreatta, A. J. Heeger and P. Smith, *Polymer*, 1989, **30**, 2305.
11 D. Chinn, J. Dubow, J. Li, J. Janata and M. Josowicz, *Chem. Mater.*, 1995, **7**, 1510.
12 S. Buvdavari, in *The Merck Index*, Rahway, New York, 1989.
13 W. S. Huang, B. D. Humphrey and A. G. MacDiarmid, *J. Chem. Soc., Faraday Trans.*, 1986, **82**, 2385.
14 V. Aboutanos, L. A. P. Kane-Maguire and G. G. Wallace, *Synth. Met.*, 2000, **114**, 313.

CHEMCOMM Communication
www.rsc.org/chemcomm

A remarkable water-soluble (molecular) alloy with two tuneable solid-to-solid phase transitions

Dario Braga,*[a] Gianna Cojazzi,[b] Demis Paolucci[a] and Fabrizia Grepioni*[c]

[a] *Department of Chemistry G. Ciamician, University of Bologna, 40126 Bologna, Italy. E-mail: dbraga@ciam.unibo.it*
[b] *Centro CNR per la Fisica delle Macromolecole c/o Dipartimento di Chimica G. Ciamician, Università di Bologna, Via Selmi 2, 40126 Bologna, Italy*
[c] *Department of Chemistry, University of Sassari, 07100 Sassari, Italy. E-mail: grepioni@ssmain.uniss.it*

Received (in Cambridge, UK) 23rd February 2001, Accepted 20th March 2001
First published as an Advance Article on the web 17th April 2001

The organometallic cations $[(\eta^5\text{-}C_5H_5)_2Co]^+$ and $[(\eta^5\text{-}C_5H_5)_2Fe]^+$ are fully miscible in the solid state and form the mixed crystalline material $[(\eta^5\text{-}C_5H_5)_2Co_xFe_{1-x}][PF_6]$, which undergoes two fully reversible phase transitions that can be tuned by varying the molar ratio of the two cations; the water-soluble organometallic salt thus possesses the behaviour of a molecular alloy.

Crystal polymorphism is the property of a substance to exist in different crystalline phases resulting from different arrangements of the molecules in the solid state.[1,2] Polymorphic modifications of the same substance may differ markedly in chemical and physical properties such as diffraction pattern and solid state spectroscopy. We are investigating polymorphism and solid state dynamic behaviour in a systematic manner, with a focus on organometallic systems.[3] In particular, we are interested in obtaining new crystal forms by non-solution methods (*e.g.* grinding,[4] seeding,[5] desolvation[6]) and in controlling the interconversion between polymorphs and between pseudo-polymorphs. The study of polymorphism falls into the mainstream of (molecular) crystal engineering.[7]

In this context, we have recently investigated by single crystal and powder X-ray diffraction as well as by calorimetric methods the phase transition behaviour of the crystalline salts $[(\eta^5\text{-}C_5H_5)_2M][PF_6]$ (M = Co, Fe).[8] The two crystalline materials are isomorphous at room temperature and undergo two fully reversible solid-to-solid phase transitions on changing the temperature. A RT $\rightleftharpoons$ LT transition occurs on cooling the room temperature phases below 252 (M = Co) and 213 K (M = Fe), whereas a RT $\rightleftharpoons$ HT transition is observed on heating the crystalline materials above 314 (M = Co) and 347 K (M = Fe). Hence, the main difference between the two materials arises from the interval of thermal stability of the intermediate RT phase (*ca.* 62 K for M = Co and 134 K for M = Fe). The relationship between the three solid phases is shown in Fig. 1.

The close structural similarity between the two complexes of $[(\eta^5\text{-}C_5H_5)_2M]^+$ (M = Co, Fe) prompted us to explore the possibility of growing crystals from solutions containing mixtures of the two cations. We were seeking answers to the following questions: (i) would the two cations form co-crystals or separate out in crystals of the two salts? (ii) In the former case, could we expect to be able to control the phase transition behaviour by varying the $[(\eta^5\text{-}C_5H_5)_2Co]^+$:$[(\eta^5\text{-}C_5H_5)_2Fe]^+$ molar ratio? In this design we were also helped by the large difference in colour: $[(\eta^5\text{-}C_5H_5)_2Co][PF_6]$ is bright yellow, and $[(\eta^5\text{-}C_5H_5)_2Fe][PF_6]$ is deep blue.

We have discovered that, in the solid state, the two cations are fully miscible in the whole range of composition and that the composition is the same as that of the *water solutions* from which the mixed-crystals are precipitated, *e.g.* the mixed salts can be formulated as $[(\eta^5\text{-}C_5H_5)_2Co_xFe_{1-x}][PF_6]$ (with $0 < x < 1$). Moreover, the phase transition behaviour depends linearly on the composition. The temperatures at which the two solid-to-solid phase transitions occur vary regularly, as a direct function of the molar ratio, between the two extremes defined by the homo-cationic crystals.

Mixed crystals were precipitated from water solutions containing $[(\eta^5\text{-}C_5H_5)_2Co]^+$:$[(\eta^5\text{-}C_5H_5)_2Fe]^+$ in the molar ratios: 90:10, 75:25, 50:50 and 25:75. The pure Co and Fe compounds have closely similar unit cell dimensions [data at room temperature for Co/Fe: a = 13.355(3)/13.408(6), b = 9.441(8)/9.530(2), c = 9.427(6)/9.482(2) Å, β = 92.87(4)/93.17(3)°, V_{cell} = 1187(1)/1209(1) Å^3];[8] hence one could expect the mixed crystals to obey Vegard's rule of linear change in lattice dimensions with composition.[9a] Since deviations from this behaviour are known[9b] the diffraction patterns for all the bulk precipitates were measured to ensure that only the same phase as that of the starting materials had formed. The colours of the precipitates were also very indicative of the formation of mixed-crystals since $[(\eta^5\text{-}C_5H_5)_2Co_x\text{-}Fe_{1-x}][PF_6]$ are green and the colour changes from green to

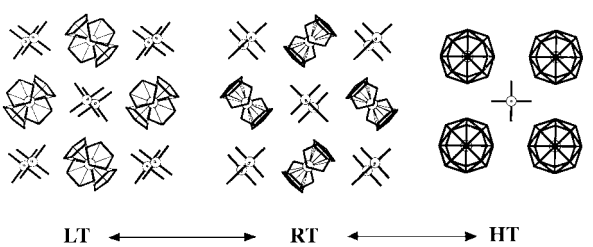

Fig. 1 The relationship between the ion arrangements in $[(\eta^5\text{-}C_5H_5)_2M][PF_6]$ (M = Co, Fe) in their (a) low, (b) room and (c) high temperature phases; in the case of M = Fe also the anions are orientationally disordered in the high temperature phase.

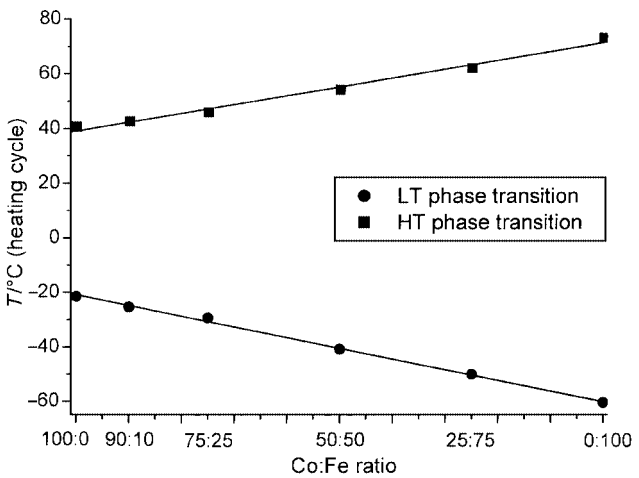

Fig. 2 The temperature variation of the RT $\rightleftharpoons$ LT and RT $\rightleftharpoons$ HT transitions with $[(\eta^5\text{-}C_5H_5)_2Co]^+$ and $[(\eta^5\text{-}C_5H_5)_2Fe]^+$ in the molar ratios 100:0, 90:10, 75:25, 50:50, 25:75, 0:100.

DOI: 10.1039/b101749g

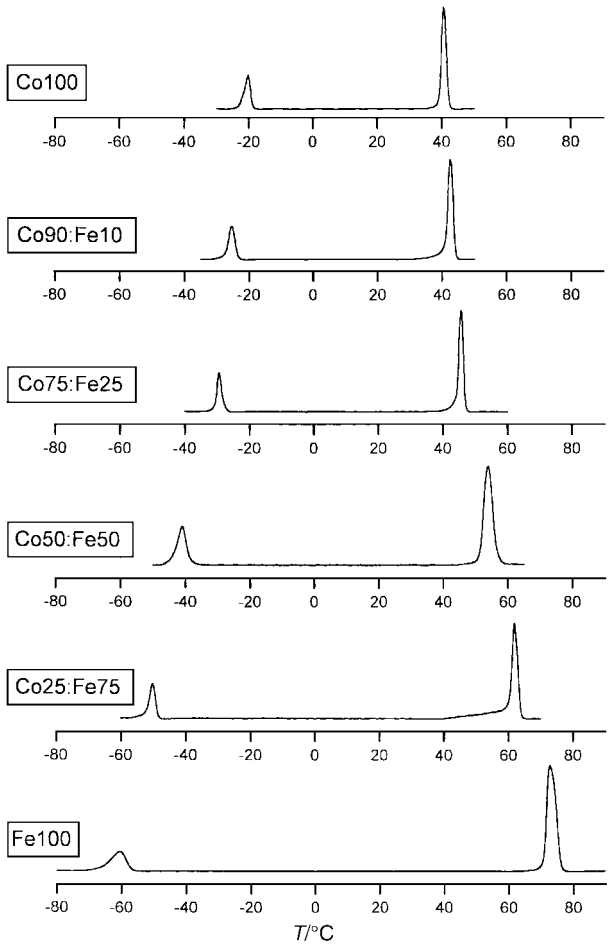

Fig. 3 DSC thermograms (heating cycle) showing how the RT ⇌ LT and RT ⇌ HT transitions 'diverge' from the values observed in the case of $[(\eta^5\text{-}C_5H_5)_2Co]^+$ as the percentage of $[(\eta^5\text{-}C_5H_5)_2Fe]^+$ in the mixture is increased. (For the sake of clarity and comparison, all baselines have been subtracted from the DSC thermograms.)

blue–green with the increasing molar fraction of the Fe component. Each mixed salt powder was subjected to a full cycle of differential calorimetry measurements (DSC), both in the cooling and in the heating regimes, to measure the temperatures of the two solid-to-solid phase transitions. The temperature variation of the RT ⇌ LT and RT ⇌ HT transitions with composition is shown in Fig. 2 (for the heating cycle). A comparison of the DSC thermograms is shown in Fig. 3: note how the peaks corresponding to the RT ⇌ LT and RT ⇌ HT transitions diverge as the percentage of $[(\eta^5\text{-}C_5H_5)_2Fe]^+$ is increased. As in the cases of the pure materials the two processes are fully reversible.[10]

In conclusion, we have been able to *tune* the phase transition behaviour of the crystalline material $[(\eta^5\text{-}C_5H_5)_2Co_x\text{-}Fe_{1-x}][PF_6]$ by varying the $[(\eta^5\text{-}C_5H_5)_2Co]^+$:$[(\eta^5\text{-}C_5H_5)_2Fe]^+$ molar ratio, because the $[(\eta^5\text{-}C_5H_5)_2Co]^+$ and $[(\eta^5\text{-}C_5H_5)_2Fe]^+$ cations form fully miscible solid solutions. The linear response of physical properties with composition is typical of inorganic alloys[11] and of crystals constructed by almost isostructural species (*e.g.* naphthalene and 1,2,4,5-tetrachlorobenzene, or 2-chloronaphthalene and 2-bromonaphthalene)[11] but, to the best of our knowledge, it has never been reported for organometallic molecular salts. Thus, the mixed-crystal $[(\eta^5\text{-}C_5H_5)_2Co_xFe_{1-x}][PF_6]$, though being composed of molecular ions and soluble in water, possesses the features of a random A_xB_{1-x} alloy.

We plan to explore the behaviour of the salts $[(\eta^5\text{-}C_5H_5)_2M][PF_6]$ (M = Co, Fe) on changing the counterions, *i.e.* by doping the crystals with isostructural anions such as $[AsF_6]^-$ and $[SbF_6]^-$, and/or by using other isoelectronic, quasi-isomorphous, organometallic salts, *e.g.* $[(\eta^5\text{-}C_5H_5)(\eta^6\text{-}C_6H_6)Ru][PF_6]$ (one phase transition RT ⇌ HT at 332.5 K)[12] or $[(\eta^6\text{-}C_6H_6)_2Cr][PF_6]$ (no phase transition between 200 and 373 K).[8]

We thank M.U.R.S.T. (projects *Supramolecular Devices* and *Solid Supermolecules*), the Universities of Bologna (project *Innovative Materials*) and Sassari for financial support, and C. Righetti for helping us with some of the DSC measurements. We thank C. Aakeröy for asking one of us (D. B.) a stimulating question on the occasion of a talk at the University of Strasbourg, and J. Dunitz and J. Bernstein for useful suggestions.

Notes and references

1 W. C. McCrone, in *Polymorphism in Physics and Chemistry of the Organic Solid State*, ed. D. Fox, M. M. Labes and A. Weissemberg, Interscience, New York, 1965; vol. II, p. 726; T. L. Threlfall, *Analyst*, 1995, **120**, 2435.

2 J. Bernstein and A. T. Hagler, *J. Am. Chem. Soc*., 1978, **100**, 673; J. Dunitz and J. Bernstein, *Acc. Chem. Res*., 1995, **28**, 193; J. Dunitz, *Acta Crystallogr., Sect. B*, 1995, **51**, 619; J. Bernstein, R. E. Davis, L. Shimoni and N. L. Chang, *Angew. Chem., Int. Ed. Engl*., 1995, **34**, 1555; N. Bladgen and R. J. Davey, *Chem. Br*., 1999, **35**, 44.

3 D. Braga, *Chem. Rev*., 1992, **92**, 369; D. Braga and F. Grepioni, *Chem. Soc. Rev*., 2000, **29**, 229.

4 D. Braga, F. Grepioni and L. Maini, *Chem. Commun*., 1999, 937.

5 D. Braga, G. Cojazzi, L. Maini, M. Polito and F. Grepioni, *Chem. Commun*., 1999, 1949.

6 D. Braga, G. Cojazzi, A. Abati, L. Maini, M. Polito, L. Scaccianoce and F. Grepioni, *J. Chem. Soc., Dalton Trans*., 2000, 3969.

7 See, for general entries: *Crystal Engineering: from Molecules and Crystals to Materials*, ed. D. Braga, F. Grepioni and A. G. Orpen, Kluwer Academic Publishers, Dordrecht, 1999; 'Proceedings of the Dalton Discussion on Inorganic Crystal Engineering', *J. Chem. Soc., Dalton Trans*., 2000, pp. 3705–3998 the whole issue; D. Braga and F. Grepioni, *Acc. Chem. Res*., 2000, **33**, 601.

8 F. Grepioni, G. Cojazzi, S. M. Draper, N. Scully and D. Braga, *Organometallics*, 1998, **17**, 296.

9 (*a*) L. Vegard and H. Dale, *Z. Kristallogr*., 1928, **67**, 148; (*b*) D. T. Hodul and M. J. Sienko, *Inorg. Chem*., 1981, **20**, 3655.

10 For the general preparation procedure for the salts $[(\eta^5\text{-}C_5H_5)_2M][PF_6]$ (M = Co, Fe) see ref. 8. Powder diffractograms were collected on a Philips PW-1100 automated diffractometer (Cu-Kα, graphite monochromator). DSC thermograms were measured on a Perkin-Elmer DSC-7 apparatus in sealed aluminium pans, at the scanning rate of 5.0 °C min^{-1} (for Co:Fe 90:10, 75:25 and the pure Co salt) and 10.0 °C min^{-1} (for Co:Fe 50:50, 25:75 and the pure Fe salt). Correspondence between solution and solid chemical compositions was demonstrated by the absence of any trace of starting material in the DSC plots after crystallization. Mechanical mixing of the two species by *grinding* together powders of the two crystalline materials in different molar ratios yielded mixtures that showed the features of both crystals, *i.e.* the presence of four peaks in the DSC resulting from the superimposition of the DSC plots of the pure samples.

11 A. I. Kitaigorodsky, *Mixed Crystals*, Springer Verlag Series in Solid-State Sciences 33, Springer-Verlag, Berlin, 1984.

12 F. Grepioni, G. Cojazzi, D. Braga, E. Marseglia, L. Scaccianoce and B. F. G. Johnson, *J. Chem. Soc., Dalton Trans*., 1999, 553.

CHEMCOMM Communication
www.rsc.org/chemcomm

A novel radical cyclization of 2-bromoindoles. Synthesis of hexahydropyrrolo[3,4-*b*]indoles

Gordon W. Gribble,* Heidi L. Fraser and Jeanese C. Badenock

Department of Chemistry, Dartmouth College, Hanover, NH 03755-3564, USA.
E-mail: grib@dartmouth.edu

Received (in Corvallis, OR, USA) 16th February 2001, Accepted 14th March 2001
First published as an Advance Article on the web 17th April 2001

Hexahydropyrrolo[3,4-*b*]indoles 6, 10, and 13 are obtained from 2-bromo-3-carboxamides 5, 9, and 12, respectively, by a 1,5-radical translocation process followed by 5-*endo-trig* cyclization to the indole C-2 position.

We wish to describe a new synthesis of hexahydropyrrolo[3,4-*b*]indoles from 2-bromoindole-3-carboxamides involving sequential indole C-2 radical generation, 1,5-hydrogen atom abstraction, and 5-*endo-trig* cyclization to the indole C-2 position. In connection with our interest in pyrrolo[3,4-*b*]indoles[1] and indolo[2,3-*a*]quinolizidines,[2] we envisioned the free radical sequence shown in Scheme 1 as an attractive route to these ring systems.

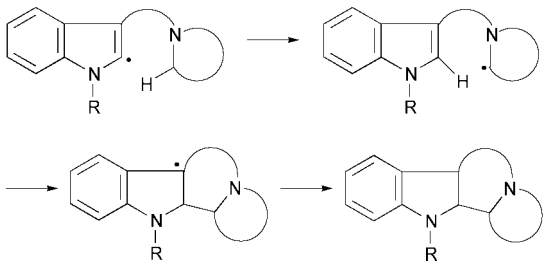

Scheme 1

We herein report the viability of this sequence for the synthesis of hexahydropyrrolo[3,4-*b*]indoles. The radical precursor 2-bromoindole **5** was prepared as shown in Scheme 2. Indole (**1**) was converted to amide **3** in two steps as previously described.[3] Subsequent *N*-methylation and C-2 bromination using the conditions described by Bergman[4] for *N*-carboxyindole afforded **5**† in excellent overall yield. An X-ray crystal structure determination confirmed the structure of **5**.[5]

The radical cyclization was performed by the slow addition over 36 h of a degassed solution of tri-*n*-butyltin hydride and catalytic AIBN in toluene to a refluxing solution of bromoindole **5** in toluene. This resulted in the formation of the desired

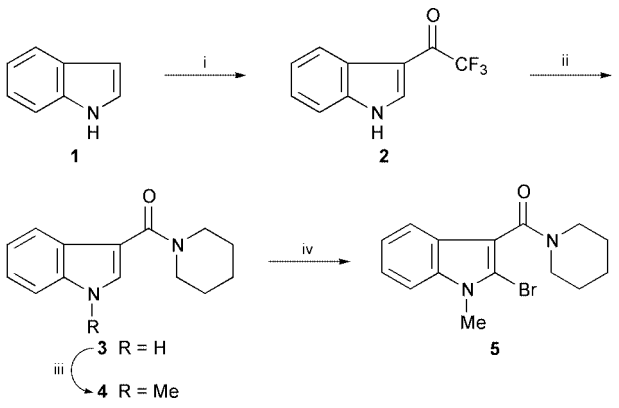

Scheme 2 *Reagents and conditions*: i, $(CF_3CO)_2O$, Et_2O, 0 °C (87%); ii, BuLi, piperidine, THF, 0 °C (97%); iii, NaOH, EtOH, MeI, acetone, rt (99%); iv, Bu^{t}Li, THF, $BrCl_2CCCl_2Br$, −78 °C to rt (88%).

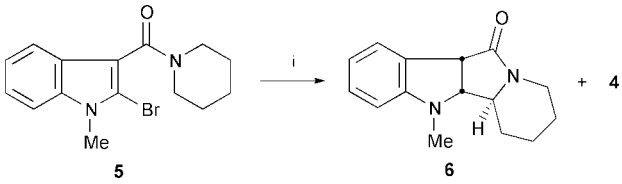

Scheme 3 *Reagents and conditions*: i, Bu_3SnH, AIBN, toluene, reflux, 36 h (**6**, 54%; **4**, 42%).

dihydroindole **6**† (54%), along with the reduction product **4** (42%) (Scheme 3). The structure of **6** is fully supported by spectral and analytical data, including an X-ray crystal structure determination.[5]

We believe that this reaction involves the sequence (1) generation of the expected C-2 radical, (2) 1,5-H atom abstraction to give the α-amidoyl radical, (3) 5-*endo-trig* cyclization to the indole double bond, and (4) hydrogen abstraction to give indoline **6**. The first two steps in this process have been termed 'radical translocation' by Snieckus and Curran.[6] Attempts to improve the yield of **6** relative to reduction product **4** using other radical generation methods have not been successful. Treatment of indoline **6** with DDQ (CH_2Cl_2, rt) gave indole **7** in 50% yield (Scheme 4).

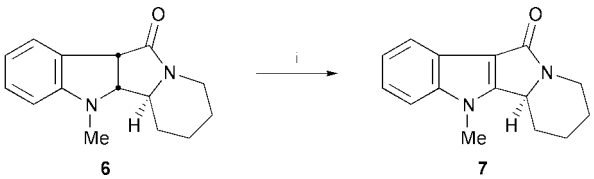

Scheme 4 *Reagents and conditions*: DDQ, CH_2Cl_2, rt, 18 h (50%).

As summarized in Scheme 5 we have applied this radical cyclization to several other substrates (**9**, **12**, **15**) and two of these afforded the expected cyclized pyrrolo[3,4-*b*]indoles **10** and **13**. However, only reduction product **14** was obtained from **15**.

Amides **8**,† **11**,† and **14**,† were synthesized by *N*-methylation of the corresponding indole-3-carboxamides[3] in 97, 77, and 80% yields, respectively, as illustrated in Scheme 2 for **4**. The usual bromination procedure afforded the 2-bromoindoles **9**,† **12**,† and **15**† in excellent yields. The structures of **9**, **12**, and **15** were confirmed by X-ray crystallography.[5]

Although radical cyclizations to the indole C-2 position are precedented[7] and the generation of indole C-2 radicals has been described by Jones,[8,9] our work is the first example of a 1,5-hydrogen atom transfer reaction of a 2-bromoindole-3-carboxamide and subsequent 5-*endo-trig* cyclization to the indole double bond. Following the completion of our initial work, Jones reported[9] a similar 1,5-H atom abstraction from the radical derived from 2-bromo-3-formyl-*N*-(4-phenylbutyl)indole and subsequent radical translocation and 5-*exo-trig* cyclization to the indole C-2 position. Jones has also recently described[10] a radical translocation sequence leading to indole C-3 5-*exo-trig* cyclization. Some other hydrogen atom abstrac-

DOI: 10.1039/b101859k

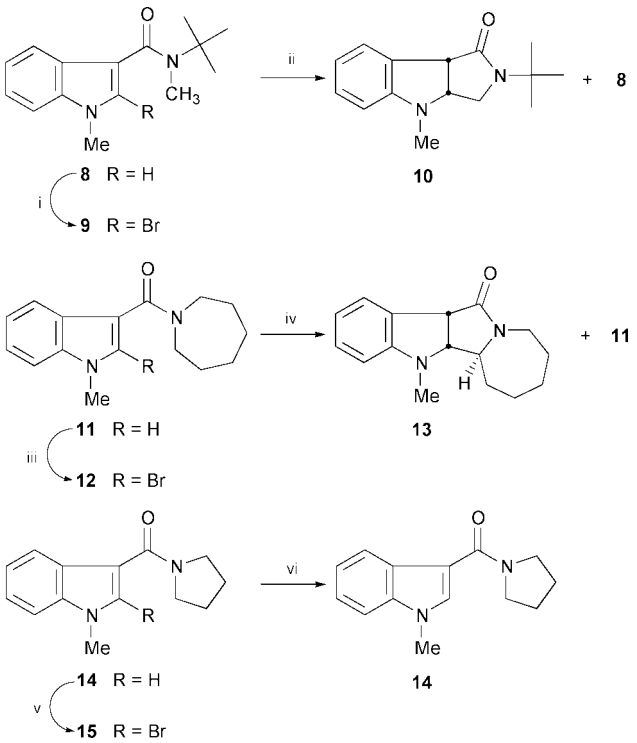

Scheme 5 *Reagents and conditions*: i, Bu^{t}Li, THF, $BrCl_2CCCl_2Br$, −78 °C to rt (86%); ii, Bu_3SnH, AIBN, toluene, reflux, 48 h (**10**, 51%; **8**, 22%); iii, Bu^{t}Li, THF, $BrCl_2CCCl_2Br$, −78 °C to rt (90%); iv, Bu_3SnH, AIBN, toluene, reflux, 72 h (**13**, 51%; **11**, 30%); v, Bu^{t}Li, THF, $BrCl_2CCCl_2Br$, −78 °C to rt (94%); vi, Bu_3SnH, AIBN, toluene, reflux, 72 h.

tion–translocation of α-amidoyl radical schemes not involving indoles have been reported.[6,11] While we favor the direct 5-*endo-trig* radical cyclization pathway shown in Scheme 1, of which there are precedents,[12,13] a 4-*exo-trig* cyclization to a spiro β-lactam intermediate followed by a 1,2-alkyl migration (ring expansion), as suggested by a referee, cannot be ruled out. However, such 1,2-alkyl shifts for radicals are rare[14] and the migration terminus is a nucleophilic carbon-centered radical. Moreover, based on the work of Ikeda,[13] we would have expected to isolate spiro β-lactams if a 4-*exo-trig* radical cyclization pathway was operating.

We thank the National Institutes of Health (GM58601) for support and Drs Mukund Sibi, Jack Li, and Larry Yet for helpful discussion.

Notes and references

† *Selected physical and spectroscopic data*: **4**: mp 103–104 °C; δ_H (300 MHz, $CDCl_3$) 7.59–7.63 (m, 2H), 7.33–7.36 (m, 1H), 6.98–7.13 (m, 2H), 3.78 (s, 3H), 3.53–3.57 (t, 4H, J = 5.4 Hz), 1.38–1.61 (m, 6H); δ_C (500 MHz, $CDCl_3$, −50 °C) 166.3, 135.7, 131.6, 125.3, 121.9, 120.4, 120.2, 110.2, 109.7, 48.8, 43.2, 33.3, 26.6, 25.4, 24.4; IR ν(KBr)/cm^{-1} 2934, 2850, 1611; *m*/*z* 242 (M$^+$), 228, 158 (100%), 131, 103, 77 (Calc. for $C_{15}H_{18}N_2O$: C, 74.35; H, 7.49; N, 11.56. Found: C, 74.23; H, 7.51; N, 11.50%). **5**: mp 105–107 °C; δ_H (300 MHz, $CDCl_3$) 7.46–7.49 (m, 1H), 7.07–7.26 (m, 3H), 3.73 (br s, 5H), 1.59 (m, 8H); δ_C (500 MHz, $CDCl_3$, −50 °C) 164.5, 135.6, 125.0, 122.1, 120.6, 118.6, 113.9, 110.7, 109.5, 48.2, 42.7, 31.4, 26.6, 25.4, 24.1; IR ν(KBr)/cm^{-1} 2934, 2845, 1622, 1522, 1428; *m*/*z* 320 (M$^+$), 236 (100%), 209, 158, 129; HRMS: calc. *m*/*z* 320.0524, found *m*/*z* 306.0517. **6**: mp 120–121 °C; δ_H (300 MHz, $CDCl_3$) 7.40 (d, 1H, J = 7.3 Hz), 7.13 (t, 1H, J = 8.0 Hz), 6.70 (td, 1H, J' = 1.0 Hz, J'' = 7.3 Hz), 6.42 (d, 1H, J = 7.7 Hz), 4.14 (dd, 2H, J' = 4.5 Hz, J'' = 13.2 Hz), 4.08 (d, 1H, J = 9.4 Hz), 3.84 (dd, 1H, J' = 2.1 Hz, J'' = 9.4 Hz), 2.86 (s, 3H), 2.64 (td, 1H, J' = 3.4 Hz, J'' = 12.8 Hz), 1.95 (m, 2H), 1.48 (m, 3H); δ_C ($CDCl_3$) 170.6, 151.0, 128.6, 125.1, 124.9, 118.0, 106.1, 69.2, 62.9, 48.9, 40.6, 33.4, 26.7, 24.6, 23.9; IR ν(film)/cm^{-1} 2922, 2856, 2344, 1678, 1606, 1489; *m*/*z* 242 (M$^+$), 158, 131 (100%), 103, 77; HRMS: calc. *m*/*z* 242.1420, found *m*/*z* 242.1421; (Calc. for $C_{15}H_{18}N_2O$: C, 74.34; H, 7.49; N, 11.57. Found: C, 74.12; H, 7.41; N, 11.54%). **8**: mp 165–166 °C; δ_H (300 MHz, $CDCl_3$) 7.68–7.71 (dd, 1H, J' = 1.39 Hz, J'' = 7.31 Hz), 7.46 (s, 1H), 7.19–7.35 (m, 3H), 3.81 (s, 3H), 3.06 (s, 3H), 1.57 (s, 9H); δ_C ($CDCl_3$) 169.4, 136.8, 132.4, 126.1, 122.4, 121.2, 121.0, 114.4, 109.9, 56.4, 35.5, 33.4, 28.1; IR ν(KBr)/cm^{-1} 3458, 3113, 2975, 1627 (Calc. for $C_{15}H_{20}N_2O$: C, 73.74; H, 8.25; N, 11.47. Found: C, 73.67; H, 8.30; N, 11.44%). **9**: mp 105–106 °C; δ_H (300 MHz, $CDCl_3$) 7.57–7.71 (dt, 1H, J' = 1.2 Hz, J'' = 8.0 Hz), 7.14–7.34 (m, 3H), 3.76 (s, 3H), 2.96 (s, 3H), 1.57 (s, 9H); δ_C ($CDCl_3$) 167.1, 136.4, 125.8, 122.5, 121.0, 119.6, 114.7, 114.2, 109.5, 56.5, 34.2, 31.5, 28.0; IR ν(film)/cm^{-1} 3456, 3052, 2979, 1627 (Calc. for $C_{15}H_{19}BrN_2O$: C, 55.74; H, 5.92; N, 8.67; Br, 24.72. Found: C, 56.13; H, 5.94; N, 8.64; Br, 24.42%). **11**: mp 111–112 °C; δ_H (300 MHz, $CDCl_3$) 7.80–7.83 (dt, 1H, J' = 1.1 Hz, J'' = 7.0 Hz), 7.13–7.28 (m, 4H), 3.70 (s, 3H), 3.63–3.67 (t, 4H, J = 5.9 Hz), 1.57–1.74 (m, 8H); δ_C (500 MHz, $CDCl_3$, −45 °C) 166.9, 135.7, 129.8, 126.2, 121.8, 120.8, 120.1, 110.1, 109.3, 49.0, 45.6, 33.0, 29.3, 28.2, 27.2, 26.0; IR ν(film)/cm^{-1} 3053, 2932, 1605 (Calc. for $C_{16}H_{20}N_2O$: C, 74.97; H, 7.86; N, 10.93. Found: C, 74.90; H, 7.93; N, 10.79%). **12**: mp 125–126 °C; δ_H (300 MHz, $CDCl_3$) 7.46 (d, 1H, J' = 7.1 Hz), 7.10–7.27 (m, 4H), 3.73 (s, 3H), 3.40–3.70 (m, 4H), 1.52–1.87 (m, 8H); δ_C ($CDCl_3$) 166.0, 136.3, 125.6, 122.5, 120.8, 119.0, 113.0, 112.9, 109.5, 49.4, 45.9, 31.4, 29.5, 27.9, 27.4, 26.4; IR ν(film)/cm^{-1} 3053, 2933, 1618; *m*/*z* 334 (M$^+$), 255, 236 (100%), 130, 103, 77 (Calc. for $C_{16}H_{19}BrN_2O$: C, 57.32; H, 5.71; N, 8.36; Br, 23.83. Found: C, 57.57; H, 5.69; N, 8.35; Br, 23.54%). **14**: mp 110–113 °C; δ_H (300 MHz, $CDCl_3$) 8.15 (d, 1H, J' = 7.5 Hz), 7.38 (s, 1H), 7.34–7.21 (m, 3H), 3.81 (s, 3H), 3.69 (m, 2H), 1.95 (m, 2H); δ_C (500 MHz, $CDCl_3$, −40 °C) 165.0, 135.9, 130.7, 127.0, 122.3, 121.8, 120.8, 110.2, 109.2, 48.9, 46.3, 33.3, 26.4, 24.2; IR ν(film)/cm^{-1} 2942, 2872, 1590; *m*/*z* 228 (M$^+$), 158 (100%), 130, 103, 77. **15**: mp 100–105 °C; δ_H (300 MHz, $CDCl_3$) 7.54 (d, 1H, J = 8.1 Hz), 7.29 (d, 1H, J = 8.3 Hz), 7.23 (td, 1H, J' = 7.6 Hz, J'' = 1.0 Hz), 7.15 (td, 1H, J' = 7.6 Hz, J'' = 1.2 Hz), 3.76 (s, 3H), 3.74 (t, 2H, J = 6.6 Hz), 3.41 (t, 2H, J = 6.6 Hz), 2.00 (m, 2H), 1.87 (m, 2H); δ_C ($CDCl_3$) 164.7, 136.2, 125.1, 122.5, 121.0, 120.8, 119.7, 119.4, 109.6, 48.3, 45.8, 31.5, 25.9, 24.6; IR ν(KBr)/cm^{-1} 3456, 2922, 2856, 1733, 1622; *m*/*z* 308 (M$^+$), 262, 236, 192 (100%), 158, 129; HRMS: calc. *m*/*z* 306.0368, found *m*/*z* 306.0367.

1 E. T. Pelkey and G. W. Gribble, *Chem. Commun*., 1997, 1873; G. W. Gribble, E. T. Pelkey and F. L. Switzer, *Synlett*, 1988, 1061; G. W. Gribble, E. T. Pelkey, W. M. Simon and H. A. Trujillo, *Tetrahedron*, 2000, **56**, 10133.

2 G. W. Gribble, *J. Org. Chem*., 1972, **37**, 1833; G. W. Gribble, J. L. Johnson and M. G. Saulnier, *Heterocycles*, 1981, **16**, 2109.

3 H. L. Hassinger, R. M. Soll and G. W. Gribble, *Tetrahedron Lett*., 1998, **39**, 3095.

4 J. Bergman and L. Venemalm, *J. Org. Chem*., 1992, **57**, 2495.

5 J. P. Jasinski, J. C. Badenock, H. L. Fraser and G. W. Gribble, unpublished results.

6 V. Snieckus, J.-C. Cuevas, C. P. Sloan, H. Liu and D. P. Curran, *J. Am. Chem. Soc*., 1990, **112**, 896.

7 For recent examples, see G. A. Kraus and H. Kim, *Synth. Commun*., 1993, **23**, 55; S. Caddick, K. Aboutayab, K. Jenkins and R. I. West, *J. Chem. Soc., Perkin Trans. 1*, 1996, 675; F. E. Ziegler and M. Belema, *J. Org. Chem*., 1997, **62**, 1083; C. J. Moody and C. L. Norton, *J. Chem. Soc., Perkin Trans. 1*, 1997, 2639; W. Zhang and G. Pugh, *Tetrahedron Lett*., 1999, **40**, 7591; S.-F. Wang, C.-P. Chuang and W.-H. Lee, *Tetrahedron*, 1999, **55**, 6109; L. D. Miranda, R. Cruz-Almanza, M. Pavón, Y. Romero and J. M. Muchowski, *Tetrahedron Lett*., 2000, **41**, 10 181.

8 A. P. Dobbs, K. Jones and K. T. Veal, *Tetrahedron*, 1998, **54**, 2149.

9 A. Fiumana and K. Jones, *Tetrahedron Lett*., 2000, **41**, 4209.

10 S. T. Hilton, T. C. T. Ho, G. Pljevaljcic and K. Jones, *Org. Lett*., 2000, **2**, 2639; S. T. Hilton, T. C. T. Ho, G. Pljevaljcic, M. Schulte and K. Jones, *Chem. Commun*., 2001, 209.

11 A. L. J. Beckwith and J. M. D. Storey, *J. Chem. Soc., Chem. Commun*., 1995, 977; T. Sato, Y. Kugo, E. Nakaumi, H. Ishibashi and M. Ikeda, *J. Chem. Soc., Perkin Trans. 1*, 1995, 1801; M. Ikeda, Y. Kugo and T. Sato, *J. Chem. Soc., Perkin Trans. 1*, 1996, 1819; J. Rancourt, V. Gorys and E. Jolicoeur, *Tetrahedron Lett*., 1998, **39**, 5339; J. M. D. Storey, *Tetrahedron Lett*., 2000, **41**, 8173.

12 For leading references to 5-*endo-trig* radical cyclizations, see S. Bogen, M. Gulea, L. Fensterbank and M. Malacria, *J. Org. Chem*., 1999, **64**, 4920; J. Cassayre, B. Quiclet-Sire, J.-P. Saunier and S. Z. Zard, *Tetrahedron Lett*., 1998, **39**, 8995.

13 H. Ishibashi, N. Nakamura, K. Ikeda, M. Okada, H. Ishibashi and M. Ikeda, *J. Chem. Soc., Perkin Trans. 1*, 1992, 2399; T. Sato, N. Machigashira, H. Ishibashi and M. Ikeda, *Heterocycles*, 1992, **33**, 139.

14 B. Giese, *Radicals in Organic Synthesis: Formation of Carbon–Carbon Bonds*, Pergamon, Oxford, 1986, pp. 19–20; J. Fossey, D. Lefort and J. Sorba, *Free Radicals in Organic Chemistry*, Wiley, Chichester, 1995, pp. 161–165.

CHEMCOMM Communication
www.rsc.org/chemcomm

Induced assembly of a catenated chain of edge-sharing silver(I) dodecahedra with embedded acetylide by silver(II)-tmc (tmc = 1,4,8,11-tetramethyl-1,4,8,11-tetraazacyclotetradecane)

Quan-Ming Wang and Thomas C. W. Mak*

Department of Chemistry, The Chinese University of Hong Kong, Shatin, New Territories, Hong Kong SAR, P.R. China. E-mail: tcwmak@cuhk.edu.hk

Received (in Cambridge, UK) 6th December 2000, Accepted 12th March 2001
First published as an Advance Article on the web 9th April 2001

In the mixed-valent complex $[Ag^{II}(tmc)(BF_4)][Ag^{I}_6(C_2)(CF_3CO_2)_5(H_2O)]\cdot H_2O$, a $[Ag^{II}(tmc)(BF_4)]^{+1}_{\infty}$ cationic column induces the assembly of a novel, anionic zigzag chain constructed from edge-sharing of silver(I) triangulated dodecahedra each enclosing a C_2^{2-} species.

Recent studies have furnished convincing spectroscopic and structural evidence for the existence of argentophilicity,[1–4] namely the d^{10}–d^{10} closed-shell attraction[5] that promotes the aggregation of silver(I) centers. Our efforts in this direction have yielded a series of novel double,[2] triple[3] and quadruple[4] salts containing Ag_2C_2 as a component, in which the C_2^{2-} species (commonly known as the acetylide dianion, IUPAC name acetylenediide) is fully encapsulated in a variety of silver polyhedra. In these silver acetylide-containing systems, bridging anionic ligands such as fluoride, nitrate, trifluoroacetate and triflate have been used to connect the $C_2@Ag_n$ (n = 6–9) units into layers and three-dimensional networks. A natural sequel is to investigate the effect of co-existing metal ions on the assembly of polyhedral silver(I) cages, and for this purpose we choose the macrocyclic *N*-donor ligand 1,4,8,11-tetramethyl-1,4,8,11-tetraazacyclotetradecane (tmc) for *in situ* generation of $[Ag^{II}(tmc)]$. A decided advantage of this strategy is to avoid the introduction of a different metal, which may cause complications such as competition with silver(I) for ligand binding or precipitation of undesirable products. Proceeding in this way, we have successfully isolated a novel, mixed-valent silver complex $[Ag^{II}(tmc)(BF_4)][Ag^{I}_6(C_2)(CF_3CO_2)_5(H_2O)]\cdot H_2O$ **1**, which represents the first example of an acetylide-containing, one-dimensional coordination polymer composed of edge-sharing $C_2@Ag_8$ cages.

Compound **1** was obtained by dissolving freshly prepared Ag_2C_2 in an aqueous solution of CF_3CO_2Ag and $AgBF_4$, to which tmc was then added.† The propensity of divalent silver to act as an oxidizing agent is well documented,[6] and this unusual oxidation state can be stabilized by macrocyclic ligands, especially aza-crowns and nitrogen heterocycles.[7] In the present instance, the addition of tmc led to disproportionation of silver(I) to give elemental silver and complexed silver(II). X-Ray structural analysis‡ indicated that the square planar $[Ag^{II}(tmc)]^{2+}$ cation (mean atomic deviation from least squares plane 0.06 Å) exhibits disorder, being a superposition of two distinct *RSSR* and *RSRS* configurations[8] in a 2:1 ratio. For *RSSR*, the four methyl groups of tmc are arranged in two pairs, one on each side of the AgN_4 plane [Fig. 1(a)]; this conformation is also designated as Type III for the possible stereoisomeric forms of tmc.[8] For *RSRS*, all four methyl groups lie on the same side of the AgN_4 plane, corresponding to the Type I conformation [Fig. 1(b)]. The Ag–N bond lengths in the range 2.180(8)–2.206(8) Å are in agreement with 2.195 Å found in $[Ag^{II}(tmc)](ClO_4)_2$.[9] Weak axial interactions of the d^9 silver(II) center, which is subjected to Jahn–Teller distortion, with adjacent BF_4^- ligands at Ag7–F1, 2.972 Å and Ag7–F2′ (1 + x, y, z), 2.934 Å serve to link the complexed Ag(II) cations into a $[Ag^{II}(tmc)(BF_4)]^{+1}_{\infty}$ column running parallel to the *a* axis [Fig. 2(a)]. The Ag–F distances fall within the range 2.60–3.02 Å for CF–Ag contacts in some silver(I) complexes containing fluorinated organic ligands.[10]

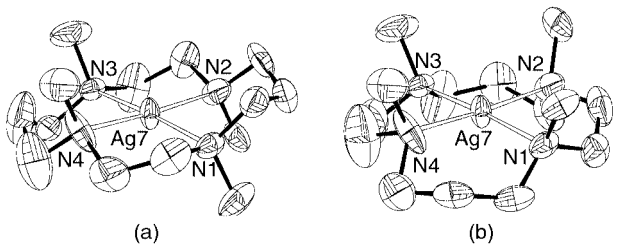

Fig. 1 Disordered $[Ag^{II}(tmc)]^{2+}$ cation involving superposition of two conformations of the tmc ligand: (a) Type III (*RSSR*) and (b) Type I (*RSRS*) in a ratio of 2:1. Both types share the same set of N atoms and two methyl groups. Thermal ellipsoids are drawn at the 30% probability level. Selected bond lengths (Å): Ag7–N1 2.196(7), Ag7–N2 2.206(8), Ag7–N3 2.184(7), Ag(7)–N4 2.180(8).

Induced by the presence of such a cationic column, a parallel polymeric anionic chain [Fig. 2(b)] is assembled from the Ag(I), C_2^{2-} and $CF_3CO_2^-$ species. The building block of its backbone is an unprecedented triangulated dodecahedron as shown in Fig. 3. Atom sets Ag1–Ag2–Ag3–Ag4 and Ag5–Ag5a–Ag6–Ag6b are each coplanar within 0.088 and 0.109 Å, respectively, making a dihedral angle of 80.2°. This dodecahedron can be regarded as the fusion of two sets of tetrahedra, elongated Ag2–Ag3–Ag5a–Ag6 and flattened Ag1–Ag4–Ag5–Ag6b. The C_2^{2-} species retains its triple bond character with C–C bond length 1.17(1) Å. In contrast, much longer C–C bond distances are found for interstitial C_2 units in organometallic compounds, such as 1.39(2) Å in $[Co_9(C_2)(CO)_{19}]^{2-}$ and 1.48(2) Å in

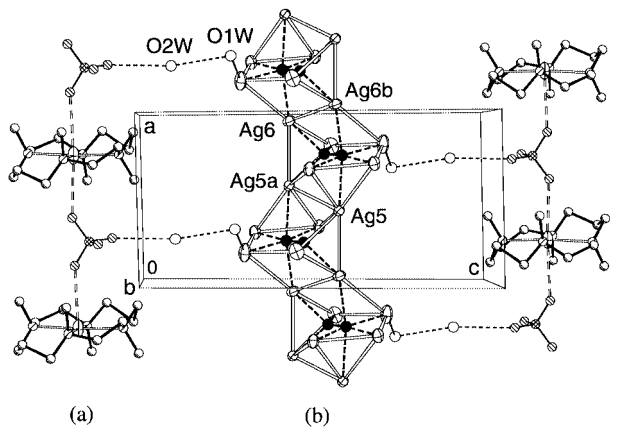

Fig. 2 Crystal structure of **1**. Hydrogen bonds are shown as dashed lines, and trifluoroacetate ligands have been omitted for clarity. (a) A column-like $[Ag^{II}(tmc)(BF_4)]^{+1}_{\infty}$ cationic column. The disordered $[Ag^{II}(tmc)]^{2+}$ cation is represented by its major configuration, and the weak axial $Ag^{II}\cdots F$ interactions are shown by dashed open lines. (b) Polymeric $[Ag^{I}_6(C_2)(CF_3CO_2)_5(H_2O)]^{-1}_{\infty}$ zigzag chain formed from edge-sharing of silver dodecahedra. The mid-points of the Ag5–Ag5a and Ag6–Ag6b bonds are located at inversion centers.

DOI: 10.1039/b009765i

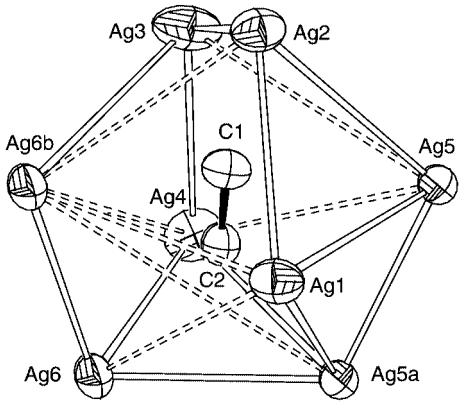

Fig. 3 Silver(I) triangulated dodecahedron with an encapsulated C_2^{2-} anion. Ag···Ag distances longer than 3.4 Å (twice the van der Waals radius of silver) are represented by broken open lines. Thermal ellipsoids are drawn at the 30% probability level. Symmetry codes: (a) $-x+1, -y+1, -z+1$; (b) $-x+2, -y+1, -z+1$.

$[Rh_{12}(C_2)(CO)_{25}]$.[11,12] The present C_2^{2-} ion has σ-type interactions with all seven silver(I) atoms at Ag–C = 2.172(8)–2.497(9) Å. The Ag···Ag distances lie in the range 2.818–3.366(1) Å, which is suggestive of significant argentophilic interactions.[1–4] The dodecahedra share edges of the type Ag5–Ag5a and Ag6–Ag6b to generate a chain-like structure [Fig. 2(b)]. An alternative description is that the silver atoms of type Ag5 and Ag6 construct a nearly planar zigzag chain with type Ag1, Ag2, Ag3 and Ag4 silver atoms hitched to it through the binding of C_2^{2-} anions. The aqua ligand O1W is coordinated to Ag3 at 2.426(7) Å, while one μ_3 and four μ_2 trifluoroacetate ligands chelate Ag···Ag edges or act as bridges between silver polyhedra. The Ag–O bond distances are in the range 2.208(7)–2.546(6) Å. The crystal structure of **1** is composed of a parallel packing of $[Ag^{I}_6(C_2)(CF_3CO_2)_5(H_2O)]^{-1}_{\infty}$ anionic zigzag chains and $[Ag^{II}(tmc)(BF_4)]^{+1}_{\infty}$ cationic columns, with lattice water molecule O2W forming hydrogen bonds with O1W and a F atom of the tetrafluoroborate group (Fig. 2).

The silver polyhedra with embedded C_2^{2-} that have been found so far are all single cages except for the face-sharing double cage in the quadruple salt $2Ag_2C_2{\cdot}3AgCN{\cdot}15CF_3CO_2Ag{\cdot}2AgBF_4{\cdot}9H_2O$.[4] The single cages are either connected by bridging ligands or directly linked through vertex sharing into two- or three-dimensional networks. Compound **1** represents the first example of a chain-like structure constructed from edge-sharing $C_2@Ag_8$ polyhedra.

Metal–macrocyclic complexes have been employed as templating agents in the synthesis of inorganic polymers and oligomers, two recent examples being the utilization of crown-ether complexes for generating one- and two-dimensional cadmium–thiocyanate coordination solids[13] and thio-crown-ether complexes for extended polyiodide networks.[14] Very recently, crown ethers have been used to isolate discrete clusters containing a $C_2@Ag_7$ unit in our laboratory.[15] In the present work, the unique capability of the tetraaza macrocyclic ligand to generate and stabilize a higher oxidation state of silver was exploited, and the resulting Ag(II)–tmc complex then utilized as a template to induce the formation of the $C_2@Ag_8$ dodecahedra and their inter-linkage into a silver(I) polymeric zigzag chain. Further investigation of the structural diversity of silver acetylide-containing systems and the role played by various metal–macrocycle templates is in progress.

This project is supported by Hong Kong Research Grants Council Earmarked Grant CUHK 4268/00P.

Notes and references

† Ag_2C_2 was prepared as described previously.[2] **CAUTION**: thoroughly dried Ag_2C_2 detonates easily upon mechanical shock or heating, and only a small quantity should be used in any chemical reaction.

Synthesis of **1**: Ag_2C_2 was added to 1 mL of a concentrated aqueous solution of $AgCF_3CO_2$ and $AgBF_4$ (molar ratio *ca.* 1 : 1) in a plastic beaker with stirring until saturated. Excess Ag_2C_2 was filtered off, and 45 mg of tmc were added to the filtrate. The colorless solution turned rapidly to dark red along with the precipitation of black metallic silver, which was removed by filtration. The red filtrate was allowed to stand without disturbance, and dark-red block-like crystals of **1** were obtained in *ca.* 40% yield after several days. Compound **1** is relatively stable in the dark but readily decomposes in common solvents such as water and ethanol.

‡ *Crystal data* for **1**: $C_{26}H_{36}Ag_7F_{19}N_4O_{12}$, M = 1723.49, triclinic, space group $P\bar{1}$ (no. 2), a = 8.1641(3), b = 16.9942(7), c = 17.4266(8) Å, α = 71.826(1), β = 89.518(1), γ = 85.287(1)°, V = 2289.1(2) Å^3, Z = 2, D_c = 2.501 Mg m^{-3}, $F(000)$ = 1642, μ(Mo-Kα) = 3.066 mm^{-1}; 15581 reflections measured, 10862 unique (R_{int} = 0.0244), final $R1$ = 0.055, $wR2$ = 0.143 for 6130 observed reflections [$I > 2\sigma(I)$]. Data collection was performed at 293 K on a Bruker SMART 1000 CCD diffractometer using frames of oscillation range 0.3°, with 2.5° < θ < 28°.

CCDC 153551. See http://www.rsc.org/suppdata/cc/b009765i/ for crystallographic data in .cif or other electronic format.

1 G.-C. Guo and T. C. W. Mak, *Angew. Chem., Int. Ed.*, 1998, **37**, 3183; M. A. Omary, T. R. Webb, Z. Assefa, G. E. Shankle and H. H. Patterson, *Inorg. Chem.*, 1998, **37**, 1380; M. A. Rawashdeh-Omary, M. A. Omary and H. H. Patterson, *J. Am. Chem. Soc.*, 2000, **122**, 10 371; C.-M. Che, M.-C. Tse, M. C. W. Chan, K. K. Cheung, D. L. Phillips and K.-H. Leung, *J. Am. Chem. Soc.*, 2000, **122**, 2464.

2 G.-C. Guo, Q.-G. Wang, G.-D. Zhou and T. C. W. Mak, *Chem. Commun.*, 1998, 339; G.-C. Guo, G.-D. Zhou and T. C. W. Mak, *J. Am. Chem. Soc.*, 1999, **121**, 3136; G.-C. Guo, G.-D. Zhou, Q.-G. Wang and T. C. W. Mak, *Angew. Chem., Int. Ed.*, 1998, **37**, 630.

3 Q.-M. Wang and T. C. W. Mak, *J. Am. Chem. Soc.*, 2000, **122**, 7608.

4 Q.-M. Wang and T. C. W. Mak, *J. Am. Chem. Soc.*, 2001, **123**, 1501.

5 P. Pyykkö, *Chem. Rev.*, 1997, **97**, 597; M. Jansen, *Angew. Chem., Int. Ed. Engl.*, 1987, **26**, 1098.

6 H. N. Po, *Coord. Chem. Rev.*, 1976, **20**, 171.

7 K. B. Mertes, *Inorg. Chem.*, 1978, **17**, 49.

8 T. W. Hambley, *J. Chem. Soc., Dalton Trans.*, 1986, 565; V. J. Thom, C. C. Fox, J. C. A. Boeyens and R. D. Hancock, *J. Am. Chem. Soc.*, 1984, **106**, 5947; J. C. A. Boeyans and S. M. Dobson, in *Stereochemical and stereophysical behaviour of macrocycles*, ed. I. Bernal, Elsevier, Amsterdam, 1987, ch. 1, pp. 34, 55, 63.

9 H. N. Po, E. Brinkman and R. J. Doedens, *Acta Crystallogr., Sect C*, 1991, **47**, 2310.

10 H. Plenio and R. Diodone, *Chem. Ber.*, 1996, **129**, 1211; R. Uson, J. Fornies, M. Tomas, J. Casas, F. A. Cotton, L. R. Falvello and R. Llusar, *Organometallics*, 1988, **7**, 2279; R. Uson, J. Fornies, M. Tomas, F. A. Cotton and L. R. Falvello, *J. Am. Chem. Soc.*, 1984, **106**, 2482; P. M. Jeffries, S. R. Wilson and G. S. Girolami, *J. Organomet. Chem.*, 1993, **203**, 449; E. Hartmann and J. Strähle, *Z. Anorg. Allg. Chem.*, 1990, **583**, 31.

11 S. Martinengo, L. Noziglia, A. Fumagalli, V. G. Albano, D. Braga and F. Grepioni, *J. Chem. Soc., Dalton Trans.*, 1998, 2493.

12 V. G. Albano, P. Chini, S. Martinengo, M. Sansoni and D. Strumolo, *J. Chem. Soc., Dalton Trans.*, 1978, 459.

13 H. Zhang, X.-M. Wang, K.-C. Zhang and B. K. Teo, *Coord. Chem. Rev.*, 1999, **183**, 157.

14 A. J. Blake, F. A. Devillanova, R. O. Gould, W.-S. Li, V. Lippolis, S. Parsons, C. Radek and M. Schröder, *Chem. Soc. Rev.*, 1998, **25**, 195.

15 Q.-M. Wang and T. C. W. Mak, *Angew. Chem., Int. Ed.*, 2001, **40**, 1130.

CHEMCOMM Communication
www.rsc.org/chemcomm

Hexagonal mesostructured chalcogenide frameworks formed by linking $[Ge_4Q_{10}]^{4-}$ (Q = S, Se) clusters with Sb^{3+} and Sn^{4+}

Krishnaswamy K. Rangan,[a] Pantelis N. Trikalitis,[a] Thomas Bakas[b] and Mercouri G. Kanatzidis*[a]

[a] *Department of Chemistry, Michigan State University, East Lansing, Michigan 48824, USA. E-mail: kanatzid@cem.msu.edu*
[b] *Department of Physics, University of Ioannina, Greece*

Received (in Cambridge, UK) 4th January 2001, Accepted 8th March 2001
First published as an Advance Article on the web 9th April 2001

The synthesis and properties of new hexagonal ordered mesostructured phases of framework containing adamantane $[Ge_4Q_{10}]^{4-}$ (Q = S, Se) clusters linked by Sb^{3+} and Sn^{4+} ions and templated with cetylpyridinium surfactant are reported.

Mesoporous non-oxidic semiconductor materials have the potential to combine electronic and optical properties with shape selectivity.[1–3] However this potentially large class of materials remains an underdeveloped area. Chalcogenide analogs to mesostructured silicates[4,5] are still scarce because their synthesis remains a challenge although progress in this area has been reported recently.[6–8] We are exploring the use of cetylpyridinium bromide (CPBr) surfactant in the synthesis of mesostructured chalcogenido frameworks. We recently reported that hexagonally ordered metal germanium sulfides form with $[Ge_4S_{10}]^{4-}$ anions and tetrahedral cations and show intense photoluminescence.[9] In order to probe whether the stability of the phases depends on the coordination properties of the linking metal ion, we explored ions that generally do not adopt tetrahedral coordination such as Sb^{3+}, Bi^{3+}, Sn^{2+}, Pb^{2+}, or are capable of several coordination environments *e.g.* Sn^{4+}. We find that many of these in fact fail to produce hexagonal mesostructures under our synthetic conditions. Namely, Bi^{3+}, Sn^{2+} and Pb^{2+} form highly disordered phases.[10] Only Sb^{3+} and Sn^{4+} form readily hexagonal sulfido and selenido frameworks of the type $CP_2M_xGe_4Q_{10+y}$ and are described here. The Sb/Ge_4Se_{10} analog features the smallest semiconductor energy gap reported so far in this class of materials.

The $CP_2M_xGe_4Q_{10+y}$ phases (denoted as CPMGeQ where M = Sb^{3+}, Sn^{4+} and Q = S, Se) were synthesized by the addition of a formamide (FM) solution of Sb^{3+} or Sn^{4+} in to a solution of supramolecularly organized $[Ge_4Q_{10}]^{4-}$ and CP surfactants in warm FM. In a typical experiment, $K_4Ge_4Q_{10}$ (1 mmol) and 4 g cetylpyridinium bromide monohydrate ($CPBr{\cdot}H_2O$) were dissolved in 20 mL of FM. On adding 1 mmol of SbI_3 or SnI_4 in 10 mL of FM to this solution precipitation occurs immediately. The mixtures were aged for 24 h at 80 °C, filtered, washed with hot FM and methanol and dried under vacuum. The sulfide phases were yellow and the selenides were brown in color. The elemental C, H, N and EDS analyses of these phases are given in Table 1. These analyses did not show potassium or halide ions in the products. Thermal gravimetric analyses (TGA) are in agreement with the C, H, N analyses results (see Table 1). The results suggest chemical formulae $CP_2Sb_{1.3}Ge_4S_{11}$, $CP_2Sn_{1.6}Ge_4S_{11.8}$, $CP_2Sb_{1.5}Ge_4Se_{11.5}$ and $CP_2Sn_{1.7}Ge_4Se_{12.3}$ for the mesophases. The compositions observed are similar to those reported for $CTA_2M_2Ge_4S_{10}$ (M = Ni^{2+}, Zn^{2+}, Co^{2+}, Cu^{2+})[11] and $CPM^{III}GeS$ (M^{III} = Ga and In) phases.[9] The charge balance of the CP^+ and Sb^{3+}/Sn^{4+} cations in the compounds is presumably achieved by both $Ge_4Q_{10}^{4-}$ clusters and Q^{2-}

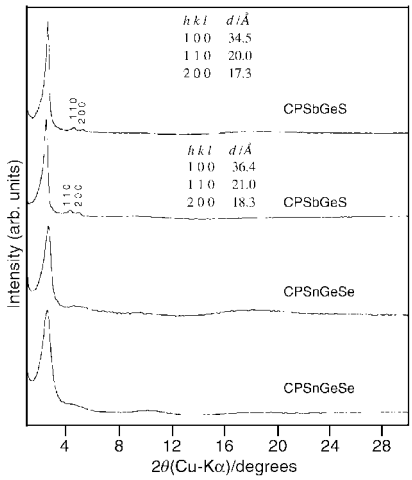

Fig. 1 X-Ray diffraction patterns of the CPMGeQ phases.

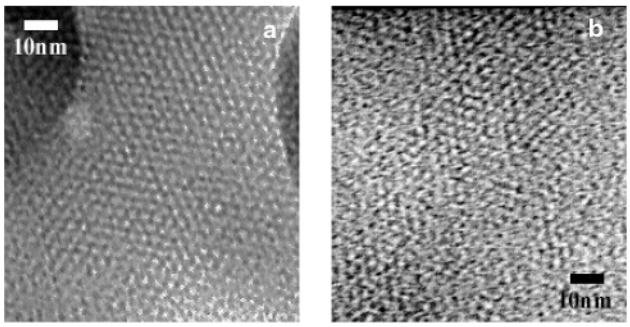

Fig. 2 TEM image of (a) CPSbGeS and (b) CPSnGeS looking down the pore channel axis. High resolution transmission electron micrographs were acquired with a JEOL 120CX instrument equipped with a CeB_6 filament and operating at 120 keV.

Table 1 Elemental analysis, powder XRD data and band gaps of CPMGeQ phases

Mesophase	Band gap/eV (colour)	C, H, N analyses (%)	Atom ratio[a] M:Ge:Q	Powder XRD data d/Å	Powder XRD data a_H[b]/Å	TGA wt. loss (%)
CPSbGeS	2.69 (yellow)	36.5, 5.8, 2.1	1.3:4:11.0	34.5, 20.0, 17.3	40.0(6)	44.5
CPSnGeS	2.89 (yellow)	33.0, 5.3, 2.0	1.6:4:11.8	34.2, 19.9, 17.2	39.7(6)	41.1
CPSbGeSe	1.74 (brown)	27.7, 4.5, 1.6	1.5:4:11.5	36.4, 21.0, 18.3	42.2(6)	34.8
CPSnGeSe	2.02 (brown)	21.5, 3.5, 1.4	1.7:4:12.3	35.9, 20.3	41.3(6)	31.4

[a] EDS data normalized with Ge atom ratio. [b] Maximum estimated error.

DOI: 10.1039/b100222h

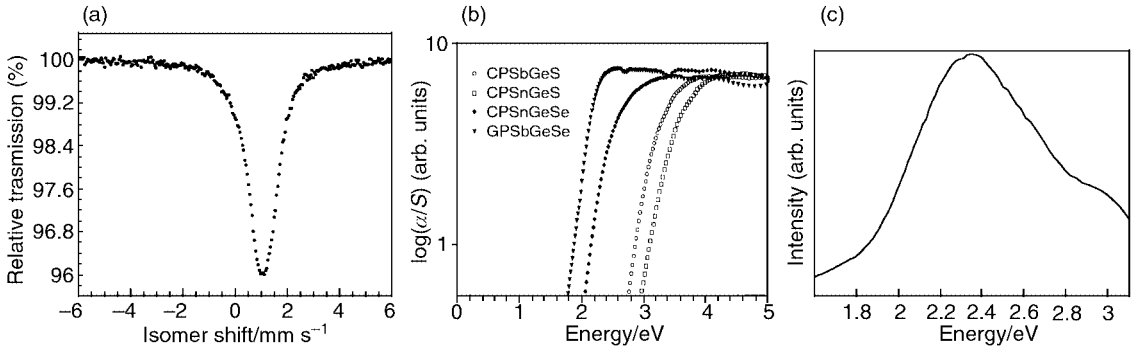

Fig. 3 (a) ^{119}Sn Mössbauer spectra (85 K) of CPSnGeS. The IS value (mm s^{-1}) is referenced to $BaSnO_3$. (b) Solid state optical absorption spectra of CPMGeQ compounds and (c) photoluminescence spectrum of CPSbGeS at 77 K.

anions.[12] Such framework materials incorporating mixed $[Ge_4S_{10}]^{4-}/[S^{2-}]$ species have already been observed in the crystal structure of TMACuGS-2 (TMA = tetramethylammonium).[13]

Powder X-ray diffraction (XRD) patterns of the CPSbGeQ phases (Fig. 1) show a strong peak followed by two weak reflections at $2 < 2\theta < 6°$, similar to those of hexagonal mesoporous silica.[4] The three peaks could be indexed in a hexagonal unit cell as (100), (110) and (200) reflections with a_H lattice parameter of 40.0(6) and 42.2(6) Å for the sulfide and selenide phases, respectively. The presence of well defined higher order (110) and (200) reflections in the XRD patterns of CPSbGeQ indicate that the pores of the inorganic framework posses long range hexagonal order. In the CPSnGeQ phases, the first strong peak could be indexed as the (100) reflection of hexagonal lattice with a_H parameter of 39.7(6) and 41.3(6) Å for CPSnGeS and CPSnGeSe respectively. However, the higher order (110) and (200) reflections are not well resolved giving a broad peak at $3 < 2\theta < 6°$. This is attributed to the smaller coherence lengths of the hexagonal regions arising from disordered pore regions occurring in between. This is observed in the TEM images discussed below.

The pore organization of CPSbGeQ phases was readily observed by transmission electron microscopy (TEM). Fig. 2(a) shows typical TEM image of CPSbGeS with the uniform hexagonal arrangement of pores occupied by the assembly of CP molecules. The pore to pore separations are in good agreement with those obtained from the powder XRD data. Fig. 2(b) shows a characteristic TEM image of CPSnGeS down the pore channel axis. In this case (and in CPSnGeSe), the TEM image shows that the hexagonal domains are smaller (< 30 nm) and separated by disordered domains with worm-holes. This is consistent with the powder XRD patterns discussed above.

IR spectroscopy of the CPMGeQ phases shows the fingerprint pattern of the adamantane Ge_4Q_{10} clusters. For example, CPSbGeS showed broad bands at 470, 426, 383 and 302 cm^{-1}. The band at 426 cm^{-1} corresponds to the terminal sulfur stretching modes of the adamantane Ge_4S_{10} cluster bonded to metal cations and that at 383 cm^{-1} is due to vibrations of the inner cage Ge_4S_6.[14] These bands occur at 307 and 285 cm^{-1} in the corresponding Se phase.

The oxidation state of Sn in CPSnGeQ was probed with ^{119}Sn Mössbauer spectroscopy, a powerful tool for the characterization of tin compounds. The observed spectra show one type of Sn present in the structure with isomer shift (IS) and quadrupole splitting of 1.11, 0.45 mm s^{-1} for CPSnGeS and 1.49, 0.40 mm s^{-1} for CPSnGeSe, respectively, Fig. 3(a). These values are fully consistent with a Sn^{4+} oxidation state and confirm that no reduction of the metal has taken place.[15]

Optical absorption spectroscopy of the mesostructured chalcogenides show well defined sharp band gaps in the range 1.7–2.8 eV [Fig. 3(b), Table 1]. These energies lie in the same range as several useful semiconductors such as CdS, CdSe, GaP *etc*. Therefore, these materials may be potentially interesting, for a number of opto-electronic investigations. CPSnGeQ phases have higher band gaps than the corresponding Sb^{3+} phases. The band gaps for the selenium compounds generally occur at lower energies than those of the corresponding sulfur analogs. Accordingly, CPSbGeSe showed the lowest band gap (1.74 eV) in the CPMGeQ systems reported here.

The CPSbGeS phase shows intense photoluminescence (PL) when excited with light above the band gap. [Fig. 3(c)]. With an excitation line of 3.48 eV (356 nm) green emission was observed at 77 K, with a maximum at 2.35 eV (528 nm).[16] The PL originates most likely from the pyridinium chromophore[17] but it is believed to involve the inorganic framework as well. This is because each component alone (surfactant or framework) is not capable of producing the observed response. Typically the pyridinium chromophore alone emits at much higher energy 2.87 eV (432 nm). Further, removal of the pyridinium group at 250 °C under vacuum, resulted in the loss of PL property. Because both the organic and the inorganic components are required for green emission, the reported materials are true nanocomposites.

The support of this research by NSF-CRG grant CHE 99-03706 is gratefully acknowledged. This work made use of the SEM and TEM facilities of the Center for Advanced Microscopy, MSU.

Notes and references

1 R. W. J. Scott, M. J. MacLachlan and G. A. Ozin, *Curr. Opin. Solid State Mater. Sci*., 1999, **4**, 113.
2 S. Dhingra and M. G. Kanatzidis, *Science*, 1992, **258**, 1769.
3 H. Li, A. Laine, M. O'Keeffe and O. M. Yaghi, *Science*, 1999, **283**, 1145.
4 C. T. Kresge, M. E. Leonowicz, W. J. Roth, J. C. Vartuli and J. S. Beck, *Nature*, 1992, **359**,710.
5 Q. Huo, D. I. Margolese, U. Ciesla, P. Feng, T. E. Gier, P. Sieger, R. Leon, P. M. Petroff and G. D. Stucky, *Nature*, 1994, **368**, 317; P. T. Tanev, M. Chibwe and T. J. Pinnavaia, *Nature*, 1994, **368**, 321.
6 M. Wachhold, K. K. Rangan, M. Lei, M. F. Thorpe, S. J. L. Billinge, V. Petkov, J. Heising and M. G. Kanatzidis, *J. Solid State Chem*., 2000, **152**, 21.
7 M. J. MacLachlan, N. Coombs and G. A. Ozin, *Nature*, 1999, **397**, 681.
8 P. V. Braun, P. Osenar and S. I. Stupp, *Nature*, 1996, **380**, 325.
9 K. K. Rangan, P. N. Trikalitis and M. G. Kanatzidis, *J. Am. Chem. Soc*., 2000, **122**, 10 230.
10 The disordered phases have nominal composition of $CP_2Bi_2Ge_4S_{17}$, $CP_{2.5}Sn^{II}_3Ge_4S_{13}$ and $CP_{1.5}Pb_3Ge_4S_{16}$.
11 M. J. MacLachlan, N. Coombs, R. L. Bedard, S. White, L. K. Thompson and G. A. Ozin, *J. Am. Chem. Soc*., 1999, **121**, 12 005.
12 The source of Q^{2-} (Q = S, Se) ions could be adventitious K_2Q present in the starting material $K_4Ge_4Q_{10}$ or fragmentation of $[Ge_4Q_{10}]^{4-}$ clusters. The lack of a characteristic signature for Q^{2-} makes it difficult to detect and characterize these species by standard techniques.
13 K. Tan, Y. Ko, J. B. Parise and A. Darovsky, *Chem. Mater*., 1996, **8**, 448.
14 O. Achak, J. Y. Pivan, M. Maunaye, M. Loüer and D. Loüer, *J. Solid State Chem*., 1996, **121**, 473.
15 P. E. Lippens, *Phys. Rev. B*, 1999, **60**, 4576.
16 In contrast CPSnGeSe and CPSbGeSe do not show PL at 77 K suggesting that the lower band gap frameworks quench the PL.
17 The PL may originate from the pyridinium chromophore of the surfactant, yet excitation spectra show that PL is observed even with excitation energies below the π–π transition of pyridinium.

CHEMCOMM Communication
www.rsc.org/chemcomm

Synthesis of aza-*C*-galacto disaccharides from C1-substituted galactals

Xuhong Cheng, Govindaraj Kumaran and David R. Mootoo*

Department of Chemistry, Hunter College/CUNY, 695 Park Avenue, New York, New York 10021, USA. E-mail: dmootoo@shiva.hunter.cuny.edu

Received (in Corvallis, OR, USA) 15th February 2001, Accepted 13th March 2001
First published as an Advance Article on the web 17th April 2001

C1-substituted galactals are transformed *via* the double reductive amination on their 1,5-diketone derivatives, to aza-β-*C*-galacto-disaccharides.

Interest in polyhydroxylated azaheterocycles as biochemical tools and therapeutic agents has been extensively documented.[1] Attention has focused on their potent activity as glycosidase inhibitors.[1,2] Guidelines for the design of glycone specific glycosidase inhibitors are well known, but models for aglycone specific inhibitors,[2] or for mimetics associated with other carbohydrate mechanisms are not as well developed.[3] Structures with a high degree of structural complexity, for example as found in disaccharide analogues, are of interest as probes of recognition specificity.[2a,b] Of these, *C*-disaccharides (*e.g.* **1**, **2**) have the added benefit of stability towards chemical and enzymic hydrolysis. We and others have shown that C1-substituted glycals **3** are attractive precursors to *C*-disaccharides **1**.[4–6] Herein, we illustrate the versatility of such C1 substituted glycals, by the synthesis of the novel, biologically interesting aza-β-*C*-galactosides **4**–**6**. N-linked lipid iminocyclitols related to **4** have recently shown potential as inhibitors of gp-120/galactosylceramide binding.[3c] Azasugar **5** is an analog of the ubiquitous lactose subunit and **6** is a potential mimetic of a recently discovered selectin antagonist.[7]

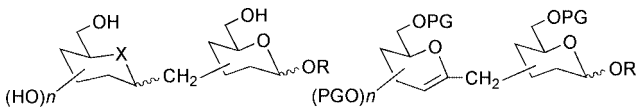

1 X = O *C*-Disaccharide
2 X = NH Aza-*C*-Disaccharide
3

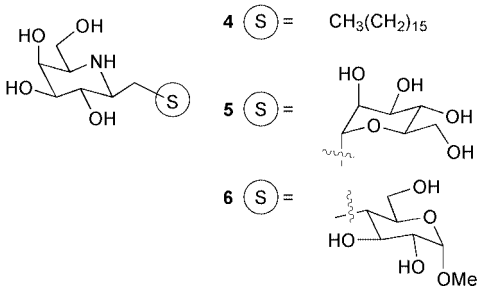

We envisaged a route to aza-*C*-disaccharides which is based on the stereoselective double reductive amination on a complex diketone **7** (Scheme 1).[8] Our optimism was guided by several examples of highly stereoselective double reductive aminations in polyhydroxylated dicarbonyl substrates.[9] An attractive aspect of this approach is the introduction of the amine in a single operation at a relatively late stage in the synthesis, thereby reducing protecting group inefficiencies. In addition the synthetic precursors are C1-substituted glycals which may be assembled *via* convergent syntheses, and therefore appropriate for complex disaccharide structures. Prompted by a recent report of a similar double reductive amination strategy to aza-β-(1 → 6)-*C*-disaccharides,[10] we describe a preliminary account of our results. In the former case, the diketone substrates were prepared from 'disaccharide' ketal precursors, obtained *via* the

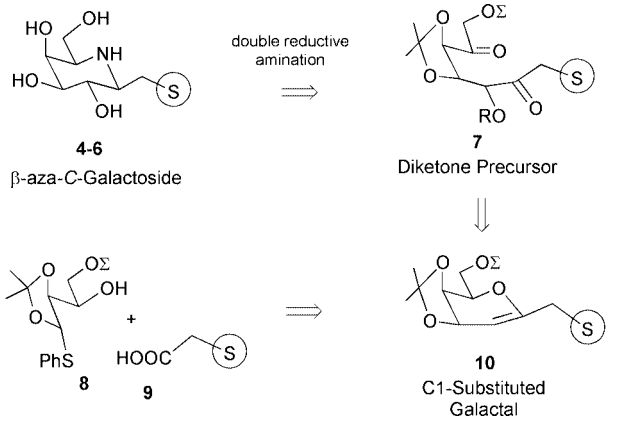

Scheme 1

addition of monosaccharide lithio acetylides to pyranolactones. While applicable to 1 → 6 type disaccharide systems, this type of organometallic coupling strategy is not generally applicable to methylene linked structures (*e.g.* 1 → 2, 1 → 3 and 1 → 4 linked disaccharide analogues). By comparison, the diketones in our approach are obtained through dihydroxylation of C1-substituted glycals (*e.g.* **10**). Such glycals may be obtained through our oxocarbenium ion cyclization methodology, starting from the ester derived from the 1-thio-1,2-isopropylidene acetal (TIA)-alcohol **8** and the acid partner **9**,[4] or *via* other protocols.[6] The esterification reaction used for the 'glycone'–'aglycone' coupling is experimentally straightforward and allows access to C1-pyrano substituted glycals (and hence *C*-disaccharide derivatives) with intersaccharide linkers of any length.

The methodology was first applied to the galactal **11** (Scheme 2). Dihydroxylation of **11** with osmium tetroxide–NMNO proceeded with complete α-selectivity to provide lactol **12** in 80% yield. Selective acetylation of **12** and PCC oxidation of the monoacetate **13** led to the diketone **14** in 78% overall yield from **12**. Treatment of **14** with 1.5 equiv. of $NaCNBH_3$, 1.2 equiv. of ammonium formate in anhydrous methanol in the presence of freshly activated 4 Å molecular sieves afforded the

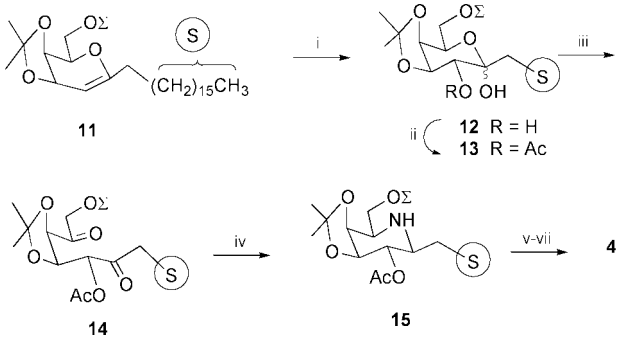

Scheme 2 (i) OsO_4, NMNO, acetone, 80%; (ii) Ac_2O, DMAP, EtOAc, 95%; (iii) PCC, CH_2Cl_2, NaOAc; Celite, 4 Å MS, 82%; (iv) $NaCNBH_3$, NH_4HCO_2, 4 Å MS, anhyd. MeOH, 72%; (v) NaOMe, MeOH; (vi) Bu_4NF, THF; (vii) HCl, MeOH, 58% over three steps.

DOI: 10.1039/b101598m

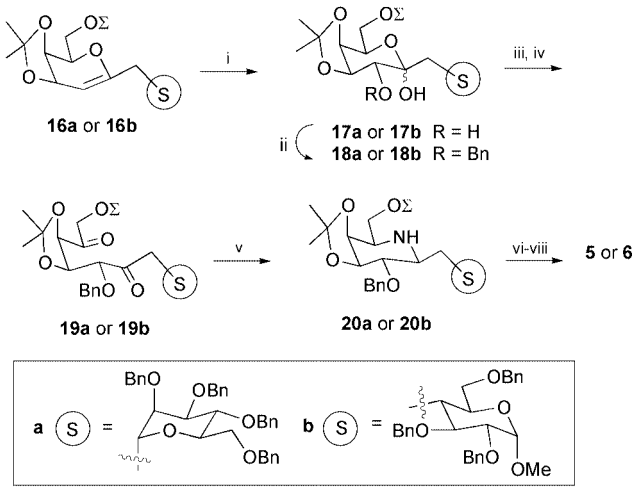

Scheme 3 (i) OsO_4, NMNO, acetone, **17a** (81%), or K_3FeCN_6, DBU, acetone, **17b** (83%); (ii) BnBr, AgOTf, CH_2Cl_2, **18a** (87%), **18b** (62%); (iii) $NaBH_4$, EtOH; (iv) Swern's Ox. **19a** (60%), **19b** (64%), over two steps; (v) $NaCNBH_3$, NH_4HCO_2, 4 Å MS, anhyd. MeOH, **20a** (72%), **20b** (68%); (vi) Bu_4NF, THF; (vii) HCl, MeOH; (viii) H_2, Pd/C, EtOH, HCOOH, **5** (67%), **6** (60%) over three steps.

aza-β-*C*-galactoside **15** as a single stereoisomer in 72% yield.[11] The stereochemistry of **15** was assigned on the basis of *J* values ($J_{1,2}$ = 9.9, $J_{2,3}$ = 7.7, $J_{3,4}$ = 5.1, $J_{4,5}$ = 2.2 Hz) and observation of 1% NOE effects between H1, and H3 and H5 respectively.[12] Removal of protecting groups in **15** under standard conditions provided the desired aza-β-*C*-galactoside **4** in 58% overall yield from **15**.[13]

Dihydroxylation of galactal **16a** (Scheme 3) under the aforementioned conditions produced a single ketal **17a** in 80% yield. These conditions led to lower yields for the reaction of the gluco linked galactal **16b**. However use of potassium ferricyanide instead of NMNO as co-oxidant in the presence of DBU led to high yield of the desired hydroxy ketal **17b**.[14] Although the secondary alcohols in **17a,b** could be selectively converted to their acetate derivatives, this protecting group proved to be incompatible with subsequent steps. Compounds **17a,b** were therefore converted to the respective benzyl ethers **18a,b**. Unlike the case for ketal **12**, direct oxidation of **18a,b** to the requisite diketones was not successful. Diketones **19a,b** were eventually obtained *via* a two step reduction–oxidation procedure on **18a,b**. Treatment of **19a,b** under reductive amination conditions provided the *C*-aza derivatives **20a,b** in 72 and 64% yields respectively. The stereochemistry in **20a,b** was assigned from NOESY experiments in a similar fashion as described for **15**. Standard deprotection procedures on **20a** and **20b** provided the desired β-aza-*C*-disaccharides **5** and **6** respectively.[15]

The high stereoselectivity of these double reductive aminations is consistent with the model developed by Stevens for the hydride reduction of six membered cyclic iminium ions.[16] Thus preferred α-face reduction on imium ions like **21** and **22** would

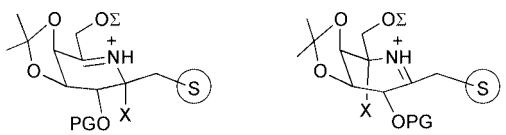

lead to the observed β-aza-*C*-galacto motif. The observation of the same sense of stereochemical bias in gluco and manno type diketones, supports this stereochemical model.[8c,10] Therefore, given the availability of C1-substituted glucals and galactals, and the amenability of such compounds to conversion to different C2 substituted ketals, the methodology described herein is expected to provide access to a wide variety of aza-β-*C*-glycosides. These directions are currently being explored.

We thank the National Institutes of Health (NIH), General Medical Sciences (GM 57865) for their support of this research. 'Research Centers in Minority Institutions' award RR-03037 from the National Center for Research Resources of the NIH, which supports the infrastructure (and instrumentation) of the Chemistry Department at Hunter, is also acknowledged.

Notes and references

1 For recent reviews: (*a*) N. Asano, R. J. Nash, R. J. Molyneux and G. W. J. Fleet, *Tetrahedron: Asymmetry*, 2000, **11**, 1645; (*b*) P. Sears and C. H. Wong, *Angew. Chem., Int. Ed. Eng*., 1999, **38**, 2300.

2 (*a*) T. D. Heightman and A. T. Vasella, *Angew. Chem., Int. Ed*., 1999, **38**, 750; (*b*) L. A. G. M. van den Broek, in *Carbohydrates in Drug Design*, ed. Z. J. Witczak and K. A. Nieforth, Marcel Dekker, Inc., New York, 1997, pp. 471–493; (*c*) G. Legler, in *Carbohydrate Mimics: Concepts and Methods*, ed Y. Chapleur, Wiley-VCH, New York, 1998, pp. 461-490; (*d*) B. Ganem, *Acc. Chem. Res*., 1996, **29**, 340.

3 (*a*) C.-H. Wong, R. L Halcomb, Y. Ichikawa and T. Kajimoto, *Angew. Chem., Int. Ed. Engl*., 1995, **34**, 521; (*b*) T. D. Butters, L. A. G. M. van den Broek, G. W. J. Fleet, T. M. Krulle, M. R. Wormald, R. A. Dwek and F. M. Platt, *Tetrahedron: Asymmetry*, 2000, **11**, 113; (*c*) K. T. Weber, D. Hammache, J. Fantini and B. Ganem, *Biorg. Med. Chem. Lett*., 2000, **10**, 1011.

4 N. Khan, X. Cheng and D. R. Mootoo, *J. Am. Chem. Soc*., 1999, **121**, 4918.

5 T. Eisele, M. Ishida, G. Hummel and R. Schmidt, *Liebigs Ann*., 1995, 2113.

6 M. H. D. Postema, D. Calimente, L. Liu and T. L. Behrmann, *J. Org. Chem*., 2000, **65**, 6061.

7 K. Hiruma, T. Kajimoto, G. Weitz-Schmidt, I. Ollmann and C.-H. Wong, *J. Am. Chem. Soc*., 1996, **118**, 9265.

8 For other approaches to aza-*C*-disaccharides: (*a*) B. A. Johns, Y. T. Pan, A. D. Elbein and C. R. Johnson, *J. Am. Chem. Soc*., 1997, **119**, 4856; (*b*) C. Marquis, S. Picasso and P. Vogel, *Synthesis*, 1999, 1441; (*c*) O. R. Martin and O. M. Saavedra, *J. Org. Chem*., 1996, **61**, 6987; O. R. Martin, in *Carbohydrate Mimics: Concepts and Methods*, ed Y. Chapleur, Wiley-VCH, New York, 1998, pp. 259–282.

9 For other stereoselective double reductive aminations on dicarbonyl substrates: (*a*) K. Abe, T. Okumura, T. Tsugoshi and N. Nakamura, *Synthesis*, 1984, 597; (*b*) W. Zou and W. A. Szarek, *Carbohydr. Res*., 1993, **242**, 311; (*c*) E. W. Baxter and A. B. Reitz, *J. Org. Chem*., 1994, **59**, 3175; (*d*) H. Zhao and D. R. Mootoo, *J. Org. Chem*., 1996, **61**, 6762.

10 M. A. Leeuwenburgh, S. Picasso, H. S. Ovekleeft, G. A. van der Marel, P. Vogel and J. H. van Boom, *Eur. J. Org. Chem*., 1999, 1185.

11 Anhydrous conditions were required for optimal yields in the reductive amination reactions. See ref. 8c for the same observation.

12 The coupling constants are similar to those expected for 3,4-*O*-isopropylidene-β-*O*-galactosides. For example, see: P. L. Barili, G. Catelani, F. D'Andrea and E. Mastrorilli, *J. Carbohydr. Chem*., 1997, **16**, 1001.

13 For **4**: clear oil; ^{1}H NMR (500 MHz, CD_3OD) δ0.90 (t, J = 7.0 Hz, 3H), 1.30 (m, 28H), 1.50 (m, 2H), 1.62 (m, 1H), 1.94 (m, 1H), 2.78 (m, 1H), 3.15 (t, J = 6.5 Hz, 1H), 3.42 (dd, J = 3.0, 8.5 Hz, 1H), 3.62 (t, J = 10.0 Hz, 1H), 3.78 (m, 2H), 4.00 (br s, 1H). ^{13}C NMR (75 MHz, CD_3OD) δ 14.6, 23.9, 26.8, 30.6, 30.7, 30.9, 31.1, 32.0, 32.2, 60.9, 61.2, 61.5, 68.9, 71.7, 75.6. FAB HRMS calcd for $C_{23}H_{48}NO_4$ (M + H) 402.3583, found 402.3584.

14 M. Minamoto, K. Yamamoto and J. Tsuji, *J. Org. Chem*., 1990, **55**, 766.

15 For **5**: white powder; ^{1}H NMR (500 MHz, D_2O) δ2.05 (m, 1H), 2.32 (br d, J = 15.5 Hz, 1H), 3.29 (br t, J = 9.5 Hz, 1H), 3.45 (t, J = 6.5 Hz, 1H), 3.63 (dd, J = 3.0, 9.5 Hz, 1H), 3.68–3.90 (m, 9H), 4.15 (br s, 1H), 4.20 (m, 1H). ^{13}C NMR (90 MHz, D_2O) δ 28.7, 59.0, 59.7, 60.1, 66.8, 68.0, 69.5, 70.4, 70.5, 73.2, 74.9, 76.0. FAB HRMS calcd for $C_{13}H_{26}NO_9$ (M + H) 340.1608, found 340.1608. For **6**: ^{1}H NMR (500 MHz, D_2O) δ1.29 (m, 1H), 1.67 (m, 1H), 2.09 (br d, J = 16.0 Hz, 1H), 2.44 (t, J = 10.0 Hz, 1H), 2.83 (t, J = 6.5 Hz, 1H), 3.36 (t, J = 10.0 Hz, 1H), 3.41 (s, 3H), 3.50–3.70 (m, 6H), 3.83 (m, 2H), 4.01 (d, J = 3.0 Hz, 1H), 4.83 (d, J = 3.5 Hz, 1H). ^{13}C NMR (90 MHz, D_2O) δ 31.6, 42.6, 55.1, 58.2, 59.3, 61.6, 61.9, 69.5, 71.9, 72.1, 72.3, 72.6, 75.0, 99.6. ESMS: 354.2 (M + H).

16 R. V. Stevens, *Acc. Chem. Res*., 1984, **17**, 289.

CHEMCOMM Communication
www.rsc.org/chemcomm

C–F bond activation of perfluoroalkenes by ruthenium phosphine hydride complexes: X-ray crystal structures of *cis*-Ru(dmpe)$_2$F(F···HF) and [Ru(dcpe)$_2$H]$^+$[(CF$_3$)$_2$C=C(O)CF$_2$CF$_3$]$^-$

Matthew S. Kirkham, Mary F. Mahon and Michael K. Whittlesey*

Department of Chemistry, University of Bath, Claverton Down, Bath, UK BA2 7AY. E-mail: m.k.whittlesey@bath.ac.uk

Received (in Cambridge, UK) 8th December 2000, Accepted 20th March 2001
First published as an Advance Article on the web 6th April 2001

The reaction of (CF$_3$)$_2$C=C(F)CF$_2$CF$_3$ or CF$_3$CF=CF$_2$ with Ru(dmpe)$_2$H$_2$ affords the bifluoride fluoride complex *cis*-Ru(dmpe)$_2$F(F···HF), whereas reaction with Ru(dcpe)$_2$H$_2$ yields the cation [Ru(dcpe)$_2$H]$^+$ with [(CF$_3$)$_2$C=C(O)CF$_2$CF$_3$]$^-$ as the anion.

Considerable advances have been made in the past few years on the activation of carbon–fluorine bonds and there is now a wide range of both early and late transition metal complexes available that can be employed in this regard.[1] Among these studies, several metal hydride complexes stand out due to their ability to cleave both saturated and unsaturated perfluorocarbons under very mild conditions.[2] Indeed, Rh(PMe$_3$)$_4$H has proved sufficiently active to bring about the catalytic hydrogenation of C$_6$F$_6$ to C$_6$F$_5$H with only very mild heating.[3] In most of these cases, C–F activation is accompanied by elimination of HF, which provides a strong thermodynamic driving force for the reaction, to give metal hydride products.

We have previously reported that *cis*-Ru(dmpe)$_2$H$_2$ (**1**, dmpe = Me$_2$PCH$_2$CH$_2$PMe$_2$) activates the C–F bond in C$_6$F$_6$ at −78 °C to give *trans*-Ru(dmpe)$_2$(C$_6$F$_5$)H, thus releasing HF, which subsequently reacts with **1** to form the bifluoride hydride complex *trans*-Ru(dmpe)$_2$H(FHF), **2**.[4] This facile C–F activation by Ru(dmpe)$_2$H$_2$ prompted us to investigate its reactivity with other unsaturated fluorocarbons. Thus, we now report that **1** reacts with (CF$_3$)$_2$C=C(F)CF$_2$CF$_3$ or CF$_3$CF=CF$_2$ to give the bifluoride fluoride complex, *cis*-Ru(dmpe)$_2$F(F···HF), **3**, in preference to a hydride product. In contrast, Ru(dcpe)$_2$H$_2$ [dcpe = (C$_6$H$_{11}$)$_2$PCH$_2$CH$_2$P(C$_6$H$_{11}$)$_2$] reacts with the same perfluoroalkenes to give the 16-electron hydride species [Ru(dcpe)$_2$H]$^+$ and a perfluoroenolate anion.

Treatment of a benzene or THF solution of **1** with (CF$_3$)$_2$C=C(F)CF$_2$CF$_3$ (ratio 1 : 1) at room temperature results in the rapid formation of **2** and *cis*-Ru(dmpe)$_2$F(F···HF) **3** (ratio *ca.* 1 : 4) as shown by multinuclear NMR spectroscopy.† The ^{1}H NMR spectrum of **3** in C$_6$D$_6$ exhibited a doublet at δ 14.2 with a $^1J_{HF}$ coupling constant of 328 Hz. The corresponding ^{19}F NMR spectrum displayed a doublet at δ −174 with the same coupling constant and two broad multiplets at δ −343 and −362 corresponding to the two types of Ru–F bond. The ^{31}P{^{1}H} NMR spectrum of **3** showed a complex multiplet at δ 57 and an 'apparent' quintet signal at δ 42. The latter was assigned to the mutually *trans* P atoms which show similar couplings to both *cis*-P and *cis*-F atoms. GC–MS analysis of the fluoro-organic products showed that a mixture of four compounds with *m*/*z* 246 [*i.e.* replacement of 3F by 3H in (CF$_3$)$_2$C=C(F)CF$_2$CF$_3$] was formed, although it has not proved possible to characterise this mixture any further using multinuclear NMR.

When the same reaction was conducted in the presence of ten equivalents of Et$_3$N, the formation of **2** was completely suppressed, allowing the isolation of **3**. The X-ray crystal structure determination of **3**‡ (Fig. 1) shows the *cis* disposition of the two fluoride ligands and a strong hydrogen bonding interaction between one of them and the HF moiety. The Ru–FHF bond length is significantly lengthened [2.168(3) Å] compared to the unperturbed Ru–F bond [2.101(3) Å]. Both Ru–F distances are noticeably longer than those found in the difluoride complex *cis*-Ru(dppp)$_2$F$_2$ (dppp = Ph$_2$PCH$_2$CH$_2$CH$_2$PPh$_2$) (average 2.06 Å), which is the only other well characterised ruthenium fluoride complex that is not stabilised by carbonyl ligands.[5] A comparison of the F···F distance in **3** and related complexes reveals that the value of 2.292(8) Å is slightly longer than that in the bifluoride complex **2** [2.276(8) Å][4] but considerably shorter than the corresponding distances in M(PMe$_3$)$_4$H$_2$F(FHF)[6] [M = Mo, 2.351(8) Å; M = W, 2.390(13) Å] or Pd(PPh$_3$)$_2$(Ph)FHF (2.36 Å).[7] The M–F···F unit is bent in all of these cases with an angle at the metal-bound fluorine in the range 129–157°. The Ru–F···F angle in **3** is 142°. These data suggest that Ru(dmpe)$_2$F(F···HF) is most accurately described as a bifluoride fluoride complex in the solid state, although in solution the magnitude of J_{HF} points to a weakening of the Ru–F···H--F interaction.

A change of the chelating phosphine from dmpe to dcpe results in a dramatic change in the reactivity at the metal centre which allows the fate of the fluorocarbon to be more accurately determined. Although Ru(dcpe)$_2$H$_2$ shows no reaction towards C$_6$F$_6$, even upon heating to 80 °C, addition of an equimolar amount of (CF$_3$)$_2$C=C(F)CF$_2$CF$_3$ in benzene gives orange crystals in 31% yield at room temperature overnight. A single crystal X-ray diffraction study confirmed these crystals to be [Ru(dcpe)$_2$H]$^+$[(CF$_3$)$_2$C=C(O)CF$_2$CF$_3$]$^-$, **4**, (Fig. 2).‡ While the gross structure is similar to that reported by Winter and Hornung for the [BPh$_4$] salt,[8] there are some differences between the structural parameters in our structure which we attribute to crystal packing effects. In the perfluoroenolate anion, lengthening of the C=C bond [1.426(9) Å] and shortening of the C–O bond [1.228(7) Å] suggest delocalisation of charge across the C=C–O unit.[9] Formation of [(CF$_3$)$_2$C=C(O)CF$_2$CF$_3$]$^-$ arises from hydrolysis by adventitious water, since addition of excess water (10 equivalents) to a

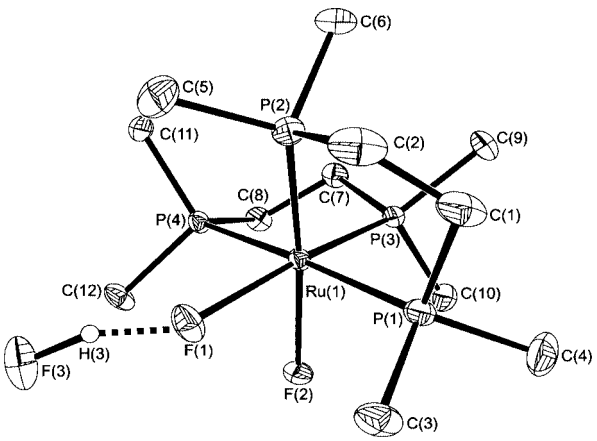

Fig. 1 ORTEX view of the molecular structure of **3**. Ellipsoids are shown at the 30% level. Principal bond lengths (Å) and angles (°): Ru–F(1) 2.168(3), Ru–F(2) 2.101(3), F(1)–F(3) 2.292(8); F(3)–F(1)–Ru 141.8(2), F(1)–Ru–F(2) 85.4(1).

DOI: 10.1039/b009862k

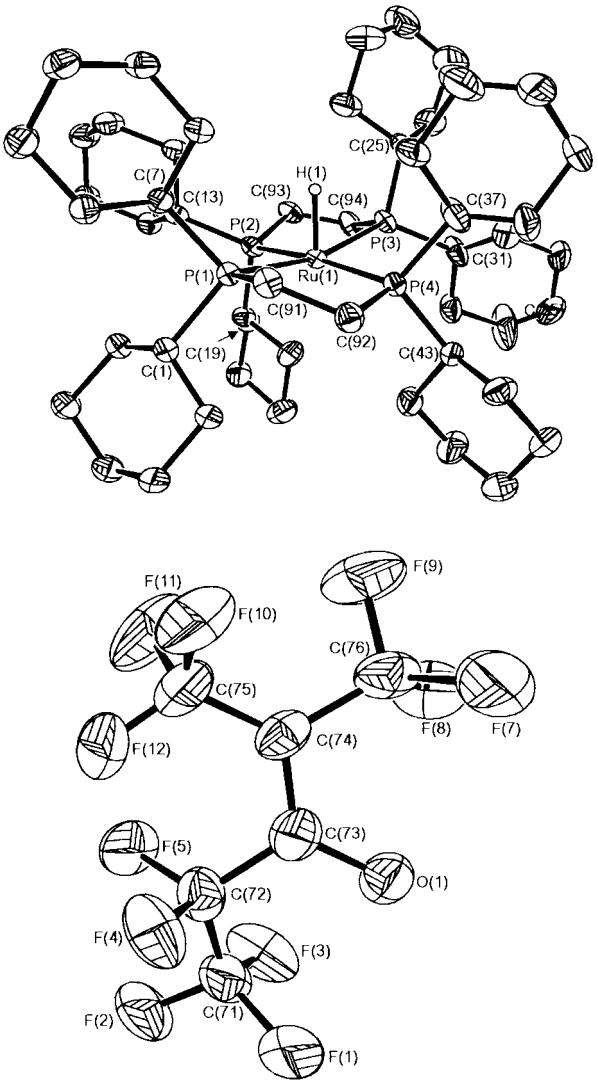

Fig. 2 ORTEX view of the molecular structure of **4**. Ellipsoids are shown at the 30% level. Selected bond distances (Å) and angles (°): C(72)–C(73) 1.514(10), C(73)–C(74) 1.426(9), C(73)–O(1) 1.228(7); P(2)–Ru–P(3) 81.62(4), P(1)–Ru–P(4) 83.56(4).

1 : 1 mixture of $Ru(dcpe)_2H_2$ and $(CF_3)_2C{=}C(F)CF_2CF_3$ affords **4** in quantitative yield in 12 hours. The $^{31}P\{^1H\}$ NMR spectrum† of **4** in d_8-THF displayed a singlet at δ 73.4 whereas the proton NMR showed a high field quintet at $\delta -31.9$ (J 19.22 Hz), in agreement with the reported values for $[Ru(dcpe)_2H]^+$.[8] The ^{19}F NMR spectrum of **4** showed the expected four resonances for the anion.[10]

Addition of hexafluoropropene to the dihydride complexes resulted in very similar reactivity to that seen with $(CF_3)_2C{=}C(F)CF_2CF_3$. Addition of 1 atmosphere of $CF_3CF{=}CF_2$ to a THF solution of **1** resulted in the formation of **3** as the only inorganic product. Analysis of the fluoro-organic products by ^{19}F NMR revealed the presence of both *Z*- and *E*-$CF_3CF{=}CFH$ and $CF_3CF{=}CH_2$ in a ratio 4 : 1 : 3. Addition of $CF_3CF{=}CF_2$ to a THF solution of $Ru(dcpe)_2H_2$ gave $[Ru(dcpe)_2H]^+$ with $[(CF_3)_2C{=}C(O)CF_2CF_3]^-$ unexpectedly present as the anion.

In summary, we have shown that the pathways for C–F bond activation of perfluoroalkenes by $Ru(P{-}P)_2H_2$ is highly dependent upon the phosphine substituents. The mechanism(s) surrounding the formation of **3** and **4** are presently under investigation.

We thank EPSRC and the University of Bath for financial support, Johnson Matthey plc for the loan of $RuCl_3$ and Dr Michael Rüf of Bruker AXS GmbH Analytical X-Ray Systems for collecting data on compound **3**. We thank Dr Trevor Dransfield (University of York) for GC–MS measurements and wish to acknowledge Professors R. N. Perutz (University of York) and W. D. Jones (University of Rochester) for helpful discussions.

Notes and references

† *Selected spectroscopic data* for **3**: NMR (400 MHz, d_6-benzene, 298 K): ^1H, δ 14.20 (d, J_{HF} 328 Hz, 1H, HF). $^{31}P\{^1H\}$, δ 56.8 (m), 42.2 (quin, J_{PP} = J_{PF} 23 Hz). ^{19}F, $\delta -342.75$ (m, RuF), -362.42 (m, RuF). IR (C_6D_6, cm^{-1}) 2452, 1915 (ν FHF). C, H analysis fitted $Ru(dmpe)_2F_2$, probably due to facile loss of HF upon heating. Anal. calc. for $C_{12}H_{32}F_2P_4Ru$: C, 32.80; H, 7.34. Found: C, 32.55; H, 7.28%. For **4**: NMR (400 MHz, d_8-THF, 298 K): ^1H, $\delta -31.87$ (quin, J_{HP} 19.22 Hz, 1H, Ru–H). $^{31}P\{^1H\}$, δ 73.4 (s). ^{19}F, $\delta -45.5$ (qt, J_{FF} 10.73, J_{FF} 19.57, 3F, CF_3), -51.3 (q, J_{FF} = 10.73, 3F, CF_3), -77.8 (s, 3F, CF_3), -113.6 (q, J_{FF} 19.57, 2F, CF_2). FAB-MS: m/z 947 ($[Ru(dcpe)_2H]^+$). Anal. calc. for $C_{58}H_{97}F_{11}OP_4Ru$: C, 55.98; H, 7.86. Found: C, 56.10; H, 8.12%.

‡ *Crystal data*: for $[Ru(dmpe)_2F(F{\cdots}HF)]$ **3**: $C_{12}H_{33}F_3P_4Ru$, M = 459.33, monoclinic, space group Cc, a = 9.071(1), b = 17.621(2), c = 13.805(2) Å, β = 106.061(2)°, U = 1965.2(4) Å^3, T = 133 K, Z = 4, μ(Mo-Kα) = 0.71073 mm^{-1}, 5399 data were collected on a Bruker SMART 1000 CCD diffractometer of which 4105 were unique (R_{int} = 0.0221), 3938 had $F_o > 4\sigma(F_o)$, $5.22 < 2\theta < 56.64°$, no absorption correction was applied. Structure solved by direct methods using SHELXS[11] and all non-hydrogen atoms refined anisotropically using full-matrix least squares on F^2 (SHELXL-97).[12] Hydrogen atoms included at calculated positions throughout except for H(3) which was located and positionally refined. R_1 = 0.0322 (for 4σ data), wR_2 = 0.0775, S = 1.005 (for all data).

For $[Ru(dcpe)_2H]^+[(CF_3)_2C{=}C(O)CF_2CF_3]^-{\cdot}2C_6H_6$ **4**: $C_{70}H_{109}F_{11}OP_4Ru$, M = 1400.52, triclinic, space group $P\bar{1}$, a = 12.386(3), b = 13.661(4), c = 21.907(6) Å, α = 106.14(2), β = 93.17(2), γ = 93.83(2)°, U = 3542.23(17) Å^3, T = 170 K, Z = 2, μ(Mo-Kα) = 0.838 mm^{-1}, 33863 data were collected on a Nonius Kappa CCD area detector of which 10742 were unique (R_{int} = 0.0441), 8993 had $F_o > 4\sigma(F_o)$, $7.04 < 2\theta < 47.64°$, no absorption correction was applied. Structure solved by direct methods using SHELXS[11] and all non-hydrogen atoms refined anisotropically using full-matrix least squares on F^2 (SHELXL-97).[12] Hydrogen atoms included at calculated positions throughout except for H(1) which was located and positionally refined. R_1 = 0.0571 (for 4σ data), wR_2 = 0.1511, S = 1.041 (for all data).

CCDC 154917 and 154918. See http://www.rsc.org/suppdata/cc/b0/b009862k/ for crystallographic data in .cif or other electronic format.

1 J. L. Kiplinger, T. G. Richmond and C. E. Osterberg, *Chem. Rev.*, 1994, **94**, 973; J. Burdenuic, B. Jedlicka and R. H. Crabtree, *Chem. Ber./Recl.*, 1997, **130**, 145; T. G. Richmond, in *Topics in Organometallic Chemistry, Activation of Unreactive Bonds and Organic Synthesis*, ed. S. Murai, Springer-Verlag, New York, 1999; T. G. Richmond, *Angew. Chem., Int. Ed.*, 2000, **39**, 3241.
2 S. T. Belt, M. Helliwell, W. D. Jones, M. G. Partridge and R. N. Perutz, *J. Am. Chem. Soc.*, 1993, **115**, 1429; B. L. Edelbach and W. D. Jones, *J. Am. Chem. Soc.*, 1997, **119**, 7734; B. L. Edelbach, A. K. F. Rahman, R. J. Lachicotte and W. D. Jones, *Organometallics*, 1999, **18**, 3170; B. J. Kraft, R. J. Lachicotte and W. D. Jones, *J. Am. Chem. Soc.*, 2000, **122**, 8559.
3 M. Aizenberg and D. Milstein, *J. Am. Chem. Soc.*, 1995, **117**, 8674.
4 M. K. Whittlesey, R. N. Perutz and M. H. Moore, *Chem. Commun.*, 1996, 787; M. K. Whittlesey, R. N. Perutz, B. Greener and M. H. Moore, *Chem. Commun.*, 1997, 187.
5 P. Barthazy, R. M. Stoop, M. Worle, A. Togni and A. Mezzetti, *Organometallics*, 2000, **19**, 2844.
6 V. J. Murphy, T. Hascall, J. Y. Chen and G. Parkin, *J. Am. Chem. Soc.*, 1996, **118**, 7428; V. J. Murphy, D. Rabinovich, T. Hascall, W. T. Klooster, T. F. Koetzle and G. Parkin, *J. Am. Chem. Soc.*, 1998, **120**, 4373.
7 D. C. Roe, W. J. Marshall, F. Davidson, P. D. Soper and V. V. Grushin, *Organometallics*, 2000, **19**, 4575.
8 R. F. Winter and F. M. Hornung, *Inorg. Chem.*, 1997, **36**, 6197; The X-ray structure of the PF_6 salt has recently been reported: A. Martelletti, V. Gramlich, F. Zürcher and A. Mezzetti, *New J. Chem.*, 1999, 189.
9 D. J. Burton, Z.-Y. Yang and W. Qui, *Chem. Rev.*, 1996, **96**, 1641.
10 T. Martini and C. Schumann, *J. Fluorine Chem.*, 1976, **8**, 535; V. F. Snegirev, K. N. Makarov and I. L. Knunyants, *J. Fluorine Chem.*, 1981, **17**, 441.
11 G. M. Sheldrick, *Acta. Crystallogr., Sect. A*, 1990, **46**, 467.
12 G. M. Sheldrick, University of Göttingen, Göttingen, Germany, 1997.

CHEMCOMM
Communication
www.rsc.org/chemcomm

A low band gap conjugated metallopolymer with nickel bis(dithiolene) crosslinks

Christopher L. Kean and Peter G. Pickup*

Department of Chemistry, Memorial University of Newfoundland, St. John's, Newfoundland, Canada A1B 3X7. E-mail: ppickup@mun.ca

Received (in Cambridge, UK) 16th January 2001, Accepted 16th March 2001
First published as an Advance Article on the web 6th April 2001

A low band gap conjugated metallopolymer has been prepared by the electrochemical polymerization of bis[1,2-di(2-thienyl)-1,2-ethenedithiolene]nickel.

The incorporation of transition metal complexes into conjugated organic polymers offers a new dimension for the development of advanced electronic, catalytic, and sensing materials.[1,2] Dithiolene complexes[3] are attractive building blocks for such systems because of their aromaticity, and the ease of reduction (n-doping) of the aromatic system. The observation of superconductivity[4] and non-linear optical properties[5,6] in metal dithiolene salts provides great incentive for their hybridization with conjugated polymers.[2]

We report here on a dithiolene based conjugated metallopolymer prepared by the electrochemical polymerization of bis[1,2-di(2-thienyl)-1,2-ethenedithiolene]nickel **1**.[7] The extensive conjugation of this complex, and the electron donating effect of the peripheral thiophenes make it an attractive unit for constructing intrinsic (neutral) molecular conductors.[8]

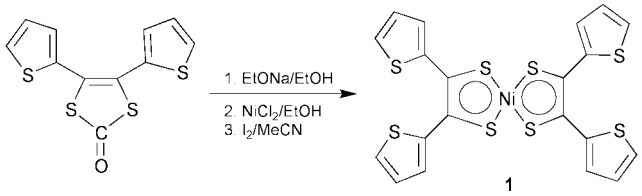

Fig. 1(a) shows a cyclic voltammogram of **1**† in solution. Reversible waves appear at formal potentials (*vs.* SSCE) of $E^{\circ\prime}(-1 \leftrightarrow -2) = -0.66$ V, $E^{\circ\prime}(0 \leftrightarrow -1) = +0.13$ V, $E^{\circ\prime}(+1 \leftrightarrow 0) = 1.08$ V, and an irreversible oxidation (not shown) begins at *ca.* +1.26 V. The first two waves have been assigned as reductions of the aromatic metal dithiolene unit to the anion and dianion by analogy with the electrochemistry of other ditholene complexes.[9] The third wave ($E^{\circ\prime} = +1.08$ V) must then be due to oxidation of the complex to the cation. The reversibility of this wave suggests that the positive charge is localized on the metal dithiolene unit. However, since cycling into this wave leads to deposition of a polymer on the electrode surface, there is presumably some delocalization onto the peripheral thiophene rings. Cycling into the forth (irreversible) wave at higher potentials leads to more rapid polymer deposition and therefore this wave must correspond to oxidation of one or more of the thiophene rings.

Fig. 1(b) show cyclic voltammograms of a poly-**1** coated electrode‡ in the absence of **1** in solution. The new broad wave starting at +0.5 V is characteristic in both shape and position of a conjugated oligothiophene backbone, and provides clear evidence that anodic polymerization of **1** has occurred at the vacant α-positions of the thiophenes. The oxidation current increases sharply at potentials higher than the limit of +1 V used for Fig. 1(b), and this leads to loss of the polymer's electrochemistry, which is again consistent with an oligothiophene-based material. The two Ni–dithiolene based waves seen for the monomer (at −0.66 and +0.13 V) are both retained by the polymer, indicating that the Ni–dithiolene center remains intact. The anodic shifts of these waves (to −0.49 and +0.19 V) are due primarily to the change in junction potential (*ca.* 80 mV) on changing the electrolyte to MeCN + Et_4NClO_4. Their broadening and splitting into multiple overlapping waves can be attributed to the variety of slightly different Ni sites that would arise from factors such as coupling of different combinations of the four peripheral thiophenes, different conjugation lengths, and defects causes by the reaction of peripheral thiophenes with trace water in the solvent. The unusual voltammetric wave shapes observed for the polymer and the apparent lack of reversibility are presumably due to ion transport effects which commonly produce complex voltammetric behaviours for polymer films.

Fig. 2 shows electronic absorption spectra of **1** in solution, and a poly-**1** film on an indium/tin oxide electrode at various

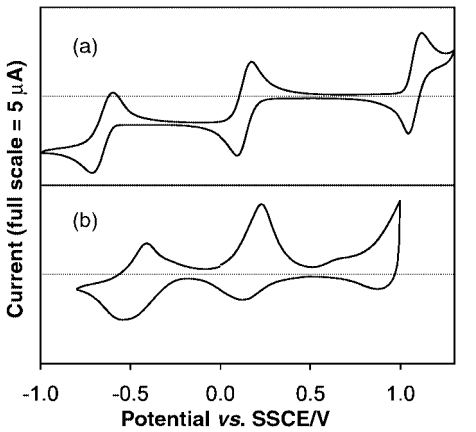

Fig. 1 Cyclic voltammetry (100 mV s^{-1}) of: (a) **1** in CH_2Cl_2 containing 0.1 mol dm^{-3} Bu_4NPF_6; (b) a poly-**1** coated Pt electrode in acetonitrile containing 0.1 mol dm^{-3} Et_4NClO_4.

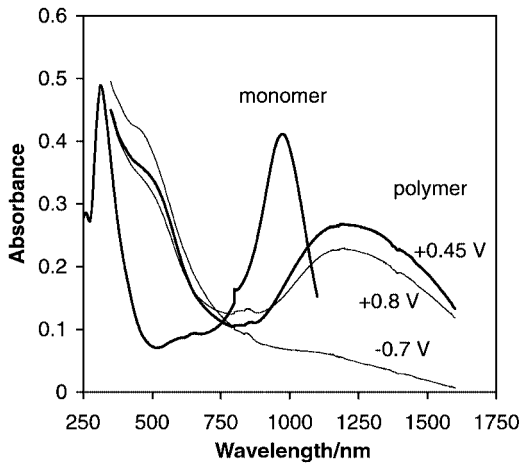

Fig. 2 Electronic absorption specta of **1** in CH_2Cl_2 and a poly-**1** coated indium/tin oxide electrode at the indicated potentials in acetonitrile containing 0.1 mol dm^{-3} Et_4NClO_4.

DOI: 10.1039/b100598g

potentials. Comparing the monomer spectrum with that of the polymer at +0.45 V (same oxidation state), it is seen that the monomer π–π^* absorbance at 973 nm is shifted significantly to higher wavelength (1193 nm) in the polymer, which is consistent with the increase in energy of the HOMO that would result from its extended delocalization in the polymer and is evidenced by the decrease in potential of the thiophene based electrochemistry in Fig. 1. The new absorbance seen as a shoulder at *ca*. 450 nm for the polymer is consistent with an expected π–π^* transition for a conjugated oligothiophene-like backbone.

Partial oxidation of the polymer (at +0.8 V) causes a partial bleaching of the complexes π–π^* absorbance and an increase in absorbance at *ca*. 800 nm. These changes are consistent with partial depletion of the π band, and the formation of polaron or bipolaron states within the polymer's band-gap. Reduction of the polymer at -0.7 V causes bleaching of the Ni complex's π–π^* absorbance, consistent with the filling of its LUMO (π^*) band.

Preliminary conductivity measurements by impedance spectroscopy and using an interdigitated array electrode indicate that the electronic conductivity associated with the 0/-1 mixed valent state is *ca*. 10^{-6} S cm^{-1}, and that oxidation (p-doping) of the backbone at +1 V increases the conductivity to *ca*. 10^{-4} S cm^{-1}. Although these conductivities are disappointing, they should be regarded as lower limits that can be improved by optimization of the film forming procedure. The band gap of poly-**1**, estimated from the onset of the 1193 nm absorbance, is < 0.8 eV (*ca*. 0.35 eV based on the difference between $E^{0\prime}(0 \leftrightarrow -1)$ and the onset of the backbone oxidation at *ca*. +0.54 V), which offers significant promise for the development of intrinsic conductors.

The presence of four peripheral thiophene rings on **1** presumably results in a highly crosslinked polymer without extended linear chains. Better electronic conductivities may therefore be achieved by using **1** as a crosslinking agent in a linear polymer (*e.g*. by copolymerization with bithiophene), or by use of similar complexes with fewer thiophene substituents. Both of these approaches are currently being explored.

This work was supported by the Natural Sciences and Engineering Research Council of Canada and Memorial University.

Notes and references

† **1** was prepared (in *ca*. 25% yield following CH_2Cl_2/silica column chromatography) by the reaction of 4,5-dithiophen-2-yl-1,3-dithiol-2-one[10] with NaOEt in EtOH, followed by addition of $NiCl_2$ in EtOH. The product was precipitated with Et_4NBr, dissolved in acetonitrile and oxidized to **1** with I_2. δ_H(500 MHz, CD_2Cl_2, ppm *vs*. TMS): 7.59 (1H, dd, *J* 5.7 and 1.4 Hz), 7.29 (1H, dd, J = 4.6 and 1.4 Hz), 7.07 (1H, dd). MS: *m*/*z* 566 (M, 0.3%), 256 (36%), 190 (100%). Elemental analysis. Calc. for $C_{20}H_{12}S_8Ni$:C, 42.33; H, 2.13; S, 45.20. Found: C, 42.09; H, 2.16; S, 44.49%.

‡ Films of poly-**1** on electrodes were prepared by constant potential (+1.2 V) electrolysis of a solution of **1** in CH_2Cl_2 containing 0.1 mol dm^{-3} Bu_4NPF_6.

1 P. G. Pickup, *J. Mater. Chem*., 1999, **8**, 1641.
2 R. P. Kingsborough and T. M. Swager, *Prog. Inorg. Chem*., 1999, **48**, 123.
3 U. T. Mueller-Westerhoff and B. Vance, in *Comprehensive Coordination Chemistry*, ed. G. Wilkinson, R. D. Gillard and J. A. McCleverty, Pergamon, Oxford, 1987, vol. 12, pp. 595–631.
4 M. N. Collomb, A. Deronzier, K. Gorgy and J. C. Lepretre, *New. J. Chem*., 2000, **24**, 455.
5 I. Malfant, N. Cordente, P. G. Lacroix and C. Lepetit, *Chem. Mater*., 1998, **10**, 4079.
6 C. T. Chen, T. Y. J. Lin, C. H. Chen and K. J. Lin, *J. Chin. Chem. Soc*., 2000, **47**, 197.
7 W. Freyer, *Z. Chem*., 1984, **24**, 32.
8 A. Kobayashi, H. Tanaka, M. Kumasaki, H. Torii, B. Narymbetov and T. Adachi, *J. Am. Chem. Soc*., 1999, **121**, 10
9 J. A. McCleverty, *Prog. Inorg. Chem*., 1968, **10**, 49.
10 E. G. Cammisa, *Synthesis of Low Band Gap Polymers*, M.Sc. thesis, Memorial University of Newfoundland, St. John's, Canada, 2000.

CHEMCOMM Communication
www.rsc.org/chemcomm

Application of the 'resin-capture–release' methodology to macrocyclisation *via* intramolecular Suzuki–Miyaura coupling

Virginie Lobrégat,[a] Gilles Alcaraz,*[a] Hugues Bienaymé[b] and Michel Vaultier*[b]

[a] *S.E.S.O. UMR-CNRS 6510, Université de Rennes 1-Beaulieu, F-35042 Rennes, France. E-mail: michel.vaultier@univ-rennes1.fr*
[b] *Rhône-Poulenc Industrialisation BP 62, F-69192, Saint-Fons, France. E-mail: hugues.bienaymé@crit.rhone-poulenc.com*

Received (in Cambridge, UK) 5th February 2001, Accepted 19th March 2001
First published as an Advance Article on the web 9th April 2001

Aryl boronic acids can be trapped by an ammonium hydroxide-form Dowex® Ion Exchangers resin (D-OH$^-$) leading to polymer-ionically bound borates and cyclized, when properly designed, into macroheterocycles under Suzuki–Miyaura coupling conditions.

Biarylcyclopeptides are important targets[1] since such compounds are potentially promising therapeutic agents.[2] The solid phase synthesis of macrocyclic systems involving a transition metal catalysed C–C bond formation is a current challenge investigated with polymer-covalently bound precursors.[3] However, such synthetic strategies involving an aryl–aryl coupling at a final stage are scarse. To the best of our knowledge, only one example describing the synthesis of a β-turn mimic *via* a Suzuki–Miyaura ring-closing reaction has been reported.[4] These approaches generally required sophisticated multistep synthesis on the solid support prior the crucial C–C bond formation.

In this context, we thought that the application of the 'resin-capture–release' hybrid technique[5] to the generation of polymer supported borate species bearing a remote aryl halide moiety followed by a releasing cyclisation under Suzuki–Miyaura's conditions could bring an efficient and easy solution to the synthesis of biarylic macrocyles. In order to check this idea, we developed a simple resin-capture method to immobilize arylboronic acids species by reaction with macroporous ammonium hydroxide-form Dowex® Ion Exchangers resin (D-OH$^-$) as B^{IV}-arylborates. The simple addition of a dilute THF solution of boronic acids **1** onto D-OH$^-$ resin resulted in the quaternization of the boron atom, leading to the formation of the corresponding immobilized hydroxyborate adduct **2** (Scheme 1).

Loading of the resin was easily achieved and controlled with **1a–d** featuring various functionalities. In all cases, about 75% of the given theoretical capacity (*ca.* 1.6 mmol g^{-1} of dry resin) can be reached.[6] The strength of this ionic linkage was evaluated by submitting the phenylhydroxyborate resin **2a** (as a representative example) to continuous extraction with Soxhlet apparatus. With water as solvent, only 10% leaching of **1a** from **2a** was observed after 72 h while no leaching could be detected after 18 h using THF. Another interesting feature is that despite their total insolubility, resins **2** can be readily analysed by standard ^{11}B NMR spectroscopic methods as a heterogeneous suspension in classical solvents. The NMR spectra of such

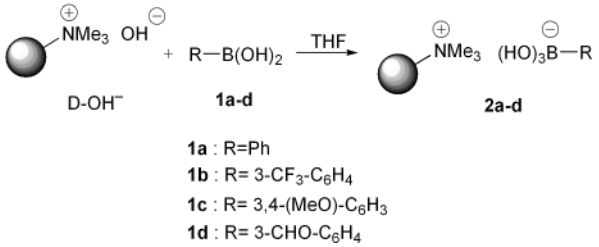

Scheme 1 Resin-capture of arylboronic acids.

Table 1 ^{11}B NMR chemical shifts for **1** and **2**

	δ^{11}B/ppm		
1a:	28.7 (THF–C_6D_6)	**2a**:	2.9 (D_2O)-$\nu_{1/2}$ = 339 Hz
1b:	28.5 (d_6-DMSO)	**2b**:	1.8 (D_2O)-$\nu_{1/2}$ = 225 Hz
1c:	28.8 (d_6-DMSO)	**2c**:	2.0 (D_2O)-$\nu_{1/2}$ = 345 Hz
1d:	29.3 (d_6-acetone)	**2d**:	2.0 (D_2O)-$\nu_{1/2}$ = 270 Hz

suspensions of resins **2** in D_2O for example are well-resolved ($\nu_{1/2}$ < 500 Hz) with ^{11}B chemical shifts observed in the expected region (typically δ ~2 ppm Table 1). Efficient Suzuki–Miyaura coupling reactions could be achieved with these immobilized arylhydroxyborates (Scheme 2). The reac-

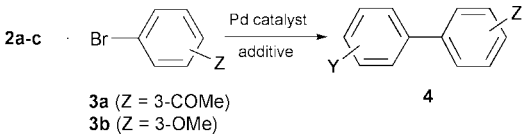

Scheme 2 *Reagents and conditions*: loading of 0.8 mmol g^{-1}, D-Br$^-$ (1 eq.), cat. $Pd(OAc)_2$ (2 mol%), H_2O, rt, 17 h.

tions leading to **4** were performed in water[7] in the presence of two bromoarenes bearing respectively an activating electron-withdrawing group (**3a**; Z = 3-COMe) and an electron-donating-group (**3b**; Z = 3-OMe) selected for their different reactivity towards the rate-determining oxidative addition step in the catalytic cycle.[8] The results reported in Table 2 verify this trend. In the case of **2c** (entries 5 and 6), the expected protodeboronation side-reaction occurs at the expense of the formation of **4**.

Table 2 Releasing Suzuki–Miyaura cross-coupling reaction

Entry	**2**	**3**	**4**[a]
1	**2a**	**3a**	86%
2	**2a**	**3b**	60%
3	**2b**	**3a**	75%
4	**2b**	**3b**	61%
5	**2c**	**3a**	38%(65%)[b]
6	**2c**	**3b**	22%

[a] Isolated yield respect to **3**. [b] Reaction carried out at 56 °C

We then developed an original route to build up precursors **5** (Scheme 3) containing both the arylboronic and bromoaryl moieties necessary to perform the macrocyclisation reaction using an expedient multicomponent one pot synthesis.[9] Compounds **5** were obtained in good yields by mixing 3-propanalbenzeneboronic acid, morpholine and the selected isocyanoacetamide[10] in MeOH. As described (*vide supra*), **5** was efficiently anchored and in addition purified as **6** at an optimized loading of *ca.* 0.15 mmol g^{-1} of dry resin. In the absence of added base, by mixing **6** (1 eq.) with quaternary

DOI: 10.1039/b101156l

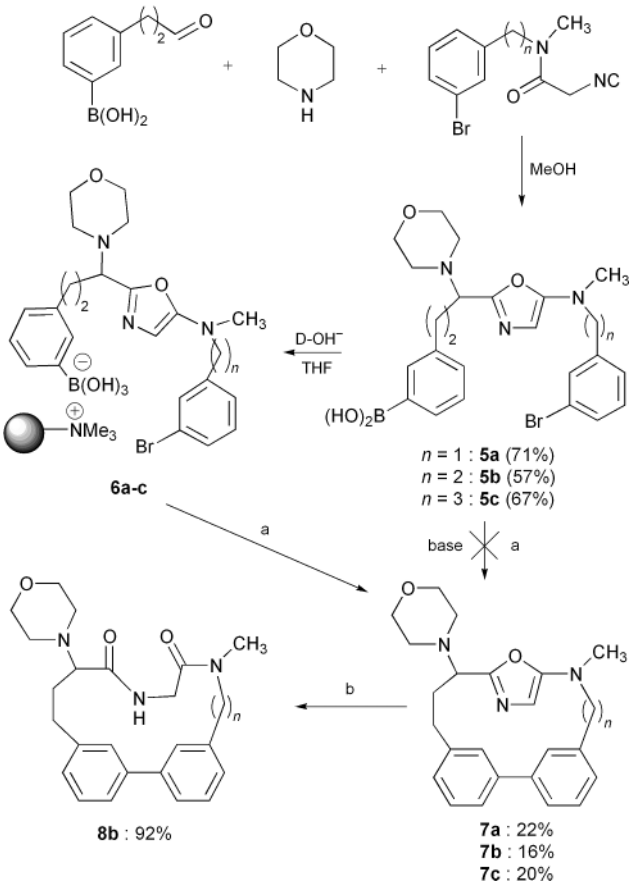

Scheme 3: *Reagents and conditions*: (a) D-Br$^-$ (1 eq.), cat. $Pd(OAc)_2$ (5 mol%), TPPDS (20 mol%), THF–H_2O (4:1), 40 °C, 40 h; (b) TFA (120 eq.), H_2O (30 eq.), rt, 2 h.

ammonium bromide-form Dowex® Ion Exchangers resin (D-Br$^-$), $Pd(OAc)_2$ (5 mol%) and triphenylphosphine disulfonic acid disodium salt (TPPDS, 20 mol%) in a THF–H_2O mixture at 40 °C, fourteen- to sixteen-membered macrocycles **7** were released and successfully isolated pure after a simple filtration–extraction sequence followed by a filtration through a pad of silica gel in 16–22% yield. For comparison, when compounds **5** were submitted to identical conditions in THF solution, macroheterocycles **7** were not obtained (Scheme 2).

HRMS and collected NMR data are in agreement with the proposed structures which have been confirmed by an X-ray diffraction study performed on **7b**[11] Under acidic conditions the oxazole **7b** could be ring-expanded into the corresponding biarylcyclopeptide **8b**[11] in 92% yield, thus opening the way to a general and efficient synthesis of this class of macroheterocycles.

Notes and references

1 For a review, see: A. V. Rama Rao, M. K. Gurjar, K. L. Reddy and A. S. Rao, *Chem. Rev*., 1995, **95**, 2135.

2 (*a*) R. Kannan and D. H. Williams, *J. Org. Chem*., 1987, **52**, 5435; (*b*) U. Schmidt, R. Meyer, V. Leitenberger, A. Lieberknecht and H. Griesser, *J. Chem. Soc., Chem. Commun*., 1991, 275; (*c*) U. Schmidt, R. Meyer, V. Leitenberger, A. Lieberknecht and H. Griesser, *J. Chem. Soc., Chem. Commun*., 1992, 951; (*d*) A. G. Brown, M. J. Crimmin and P. D. Edwards, *J. Chem. Soc., Perkin Trans. 1*, 1992, 123.

3 (*a*) M. Hiroshige, J. R. Hauske and P. Zhou, *J. Am. Chem. Soc*., 1995, **117**, 11590; (*b*) K. C. Nicolaou, N. Winssinger, J. Pastor, S. Ninkovic, F. Sarabia, Y. He, D. Vourloumis, Z. Yang, T. Li, P. Glannakakou and E. Hamel, *Nature*, 1997, **387**, 268; (*c*) K. C. Nicolaou, N. Winssinger, J. Pastor and F. Murphy, *Angew. Chem., Int. Ed*., 1998, **37**, 2534.

4 (*a*) W. Li and K. Burgess, *Tetrahedron Lett*., 1999, **40**, 6527; (*b*) N. Miyaura and A. Suzuki, *Chem. Rev*., 1995, **95**, 2457.

5 (*a*) A. Kirschning, H. Monenschein and R. Wittenberg, *Chem. Eur. J*., 2000, **6**, 4445; (*b*) J. G. Keay and E. F. V. Scriven, *Chem. Ind*., 1994, **53**, 339; (*c*) S. Khound and P. J. Das, *Tetrahedron*, 1997, **53**, 9749.

6 The loading is determined by differential weighing between the quantity of **1** initially introduced and recovered after several washings of the resin.

7 D. Badone, M. Baroni, R. Cardamone, A. Ielmini and U. Guzzi, *J. Org. Chem*., 1997, **62**, 7170.

8 A. Suzuki, in *Metal-catalyzed Cross-coupling Reactions*, eds. F. Diederich and P. J. Stang, Wiley-VCH, Weinheim, 1998, p.55.

9 For recent references on multicomponent reactions see: (*a*) A. Dömling and I. Ugi, *Angew. Chem., Int. Ed*., 2000, **39**, 3168; (*b*) H. Bienaymé, C. Hulme, G. Oddon and P. Schmitt, *Chem. Eur. J*., 2000, **6**, 3321.

10 Efficient synthesis of these compounds have been developed in our laboratory: V. Lobrégat, Ph.D thesis, University of Rennes, 2000.

11 Selected physical data: **7b** mp (Et_2O) 176 °C, ^{1}H NMR (200 MHz, $CDCl_3$) δ 5.91 (s, oxazolic-CH); ^{13}C NMR (50.33 MHz, $CDCl_3$) δ 98.8 (oxazolic-*C*H), 123.7, 124.1, 127.2, 127.3, 127.8, 128.5, 128.9, 130.4 (8 × aryl-*C*H), 138.8, 140.8, 141.5, 141.7 (4 × aryl-C_{IV}), 151.4, 156.6 (2 × oxazolic-C_{IV}), HRMS [M$^{+\cdot}$] calcd. for $C_{25}H_{28}N_3O_2$: *m*/*z* 403.2260. Found: 403.2275. **8b** ^{13}C NMR (50.33 MHz, $CDCl_3$) δ 41.5 (NH-CH_2-CO), 70.2 (N-*C*H-CO), 139.0, 140.7, 141.1, 142.4 (4 × aryl-C_{IV}), 168.3 (NH-CH_2-*C*O), 172.0 (NH-*C*O), HRMS [M$^{+\cdot}$] calcd. for $C_{25}H_{31}N_3O_3$: *m*/*z* 421.2365. Found: 421.2380.

CHEMCOMM Communication
www.rsc.org/chemcomm

Photo-switching spin pairs—synergy between LIESST effect and magnetic interaction in an iron(II) binuclear spin-crossover compound†

Guillaume Chastanet,[a] Ana B. Gaspar,[b] José Antonio Real*[b] and Jean-François Létard*[a]

[a] *Institut de Chimie de la Matière Condensée de Bordeaux, Laboratoire des Sciences Moléculaires, UPR CNRS No. 9048, 87 Av. du Doc. A. Schweitzer, 33608 Pessac, France. E-mail: letard@chimsol.icmcb.u-bordeaux.fr*

[b] *Departament de Química Inorgánica/Institut de Ciencia Molecular, Universitat de València, Dr. Moliner 50, 46100 Burjassot, València, Spain*

Received (in Cambridge, UK) 10th January 2001, Accepted 22nd March 2001
First published as an Advance Article on the web 6th April 2001

The decrease of the magnetic response under irradiation at very low temperature was interpreted as a new evidence of synergy between magnetic interaction and spin transition in an iron(II) binuclear SC compound.

The design and the synthesis of polynuclear complexes with versatile chemical and physical properties are of current interest in the areas of molecule-based electronic, photochemistry and magnetism. The goal is to develop novel materials whose properties can be controlled by the input of external information. In this context, particular interest has been focused on iron(II) spin-crossover (SC) compounds because they can be considered among the best examples of switchable coordination molecules. A reversible transition between the paramagnetic high-spin state (HS, $S = 2$) and the diamagnetic low-spin state (LS, $S = 0$) can be induced by a change in temperature, pressure or by light irradiation.[1] This latter effect opens some interesting perspectives to design optical switches. In 1984, Decurtins *et al.* discovered that by irradiation with green light the SC compound $[Fe(ptz)_6](BF_4)_2$ (ptz = 1-propyltetrazole) at 20 K could be converted from the stable LS state to the metastable HS state.[2] Later, Hauser reported the reverse-LIESST effect, wherein red light is used to convert back the compound into the LS state.[3]

Up to now, most of the SC compounds exhibiting LIESST properties are assemblies of monomeric units with through-space rather than through-bond interactions. Allowing SC centers to communicate by chemical bridges, *i.e.* oligomeric or polymeric species, is an important strategy to explore and enhance cooperativity of a given system.[4,5] Along this line, binuclear compounds of formula $[\{Fe(L)(NCX)_2\}_2(bpym)]$ (L = bpym (2,2′-bipyrimidine), bt (2,2′-bithiazoline) and X = S, Se) represent one of the most unusual family in the SC field. These compounds are the simplest example of polynuclear SC complexes exhibiting a rich variety of magnetic regimes. Further, they are the only iron(II) example where the interplay between both spin crossover and intramolecular magnetic exchange phenomena are present in the same molecule. In $[\{Fe(bpym)(NCS)_2\}_2(bpym)]$ the two iron(II) ions are in the HS state and couple antiferromagnetically through the bridge bpym ($J = -4.1$ cm^{-1} in the zero-field Hamiltonian $H = -JS_AS_B$) giving an $S = 0$ ground pair state HS–HS at low temperature.[6] In contrast, $[\{Fe(bpym)(NCSe)_2\}_2(bpym)]$ shows a one-step transition involving 50% of iron atoms at $T_c = 125$ K,[7] whereas an almost complete two-step spin transition in the range 160–210 K takes place for $[\{Fe(bt)(NCS)_2\}_2(bpym)]$.[8] This behavior was interpreted in terms of the occurrence of LS–LS ↔ LS–HS ↔ HS–HS pair spin states in each binuclear unit.[8] The stabilisation of the LS–HS mixed spin pair was assigned to the synergy effect between anticooperative intramolecular and cooperative intermolecular interactions.

Recently, we have reported the unusual photomagnetic behavior stemming from the interplay between spin-crossover and magnetic coupling phenomena.[9] At low temperature, light switches $[\{Fe(bt)(NCS)_2\}_2(bpym)]$ from the $S = 0$ spin state of the LS–LS pair to the $S = 0$ spin state of the HS–HS pair. Warming the sample first reveals the latent magnetic coupling between the HS iron(II) ions as the $S = 1$, 2, 3 and 4 excited states are populated, then switches off this virtual pair spin state at temperatures as high as 60 K where molecules have enough energy to overcome the barrier associated with the change of molecular geometry upon spin conversion. As a continuation of this study we have investigated the LIESST effect on $[\{Fe(bpym)(NCSe)_2\}_2(bpym)]$. As mentioned above, this compound exhibits an incomplete thermal spin transition interpreted in terms of HS–HS ↔ LS–HS conversion at 125 K (Fig. 1). The slight decrease of the magnetic response as T approaches absolute zero is due to zero-field splitting of the $S = 2$ spin state of the mixed-spin pair.

At 10 K, we observed that green light irradiation (530.9 nm, power 10 mW cm^{-2})[10] induces a decrease of $\chi_M T$ from 2.6 to 1.6 cm^3 K mol^{-1}. Similar behavior was recorded at 647–679, 759–799 and 830 nm. Usually, the observation of a decrease in the magnetic response under light irradiation is a signature of reverse-LIESST as the HS state is converted into the LS state. However, for $[\{Fe(bpym)(NCSe)_2\}_2(bpym)]$ this situation is no longer valid because of the occurrence of the unusual HS–LS state and the virtual excited HS–HS state which involves a latent antiferromagnetic interaction similar in magnitude as observed for $[\{Fe(bt)(NCS)_2\}_2(bpym)]$.[9] Hence, a decrease of the magnetic response should be expected upon irradiation.

Fig. 1 compares $\chi_M T$ *vs.* T (χ_M is the molar magnetic susceptibility and T the temperature) of the photoinduced

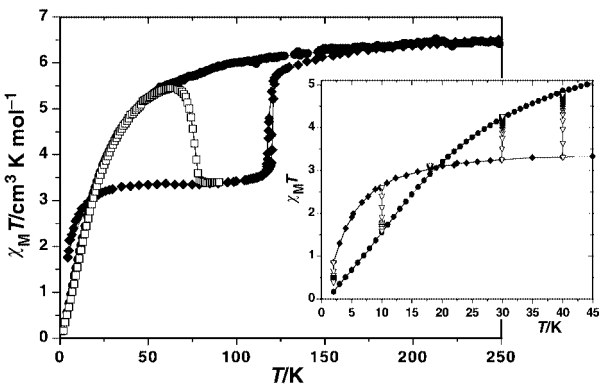

Fig. 1 $\chi_M T$ *vs.* T for (◆) $[\{Fe(bpym)(NCSe)_2\}_2(bpym)]$ and (●) $[\{Fe(bpym)(NCS)_2\}_2(bpym)]$. (□) refers to the warming mode of $[\{Fe(bpym)(NCSe)_2\}_2(bpym)]$ after the irradiation was applied for 1 h at 10 K, then turned off. Inset: data obtained with irradiation (▽) for 1 h at 2, 10, 17, 30 and 40 K.

† Dedicated to the memory of Olivier Kahn.

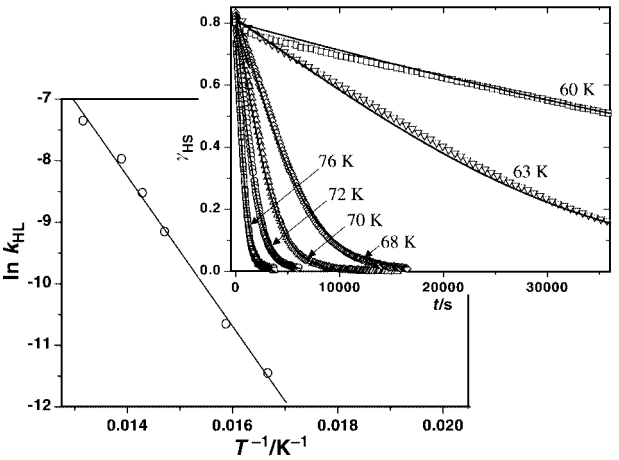

Fig. 2 Ln k_{HL} *vs.* 1/*T* curve of [{Fe(bpym)(NCSe)$_2$}$_2$(bpym)]. Inset: time dependence at various temperatures of the HS molar fraction generated by light irradiation at 10 K.

[{Fe(bpym)(NCSe)$_2$}$_2$(bpym)] with the binuclear [{Fe(bpym)(NCS)$_2$}$_2$(bpym)] compound containing two iron(II) ions in the HS–HS state in the whole temperature range.[6–8] Both magnetic responses are similar below 40 K. It is well known that the interaction parameter, *J*, in a coupled binuclear compound depends essentially on the nature of the chemical bridge. As for both compounds the bridging network is similar, in case of a quasi-quantitative LS–HS → HS–HS conversion (LIESST effect), the magnetic properties of [{Fe(bpym)(NCSe)$_2$}$_2$(bpym)] after irradiation and [{Fe(bpym)(NCS)$_2$}$_2$(bpym)] should be very similar. In contrast, a LS–LS population (reverse-LIESST) should lead to a diamagnetic ground state for [{Fe(bpym)(NCSe)$_2$}$_2$(bpym)] very different from the magnetic properties of [{Fe(bpym)(NCS)$_2$}$_2$(bpym)]. The data displayed on Fig. 1 are in favor of the first alternative.

Fig. 1 also shows the $\chi_M T$ value of [{Fe(bpym)(NCSe)$_2$}$_2$(bpym)] under light irradiation at 2, 10, 17, 30 and 40 K. In all cases, the photostationary point reached the $\chi_M T$ limit of [{Fe(bpym)(NCS)$_2$}$_2$(bpym)], confirming the HS–HS population.[11] What is remarkable is that at 17 K, both before and after irradiation, the compound has a similar magnetic response. This does not mean that the LIESST effect does not occur. In fact, we are faced with two totally different spin states. Before irradiation, the system acts as a HS–LS mixed-spin pair, resulting in a $S = 2$ spin state with a $\chi_M T$ value of 3 cm^3 K mol^{-1}. After irradiation, the two iron(II) are HS and coupled antiferromagnetically with a thermal population of the low-lying spin states, $S = 1$–4, located at energies $E(S) = -JS(S + 1)/2$ above the ground state $S = 0$. At 17 K, the population of the HS–HS pair, assuming a *J* factor of −4.1 cm^{-1} and a *g* value of 2.13, is 16% $S = 0$, 35% $S = 1$, 29% $S = 2$, 15% $S = 3$ and 5% $S = 4$. The resulting $\chi_M T$ value is then 3 cm^3 K mol^{-1} and similar to that of the HS–LS mixed-spin pair.

The kinetics of the relaxation were investigated from 2 K up to 75 K (Fig. 2). Below 55 K, the relaxation is very slow, for instance, at 10 K the magnetic response varies by *ca.* 0.01% in 13 h, which requires relaxation rates smaller than 10^{-6} s^{-1}. From 55 to 75 K, the dynamic of the relaxation is faster and falls within the time window of our set-up. This behavior matches the theory of HS → LS relaxation proposed by Buhks *et al.*[12] which predicts a temperature-independent relaxation rate, *i.e.* a tunneling process, at low temperature and an activation relaxation process at higher temperatures. The decays of the HS molar fraction, γ_{HS}, *vs.* time, at various temperatures, are also represented in Fig. 2; γ_{HS} is deduced from $[(\chi_M T)_{h\nu} - (\chi_M T)_{HS-LS}]/[(\chi_M T)_{AF} - (\chi_M T)_{HS-LS}]$.[13] An analysis of these data indicates that the relaxation curves can be satisfactorily fitted by a sigmoidal law.[14] This reflects a self-acceleration process as γ_{HS} decreases. The plot of ln k_{HL} *vs.* 1/*T* (Fig. 2) gives a straight line, with an activation energy $E_a = 850$ cm^{-1}, a pre-exponential factor $k_\infty = 6.6 \times 10^3$ s^{-1} and an additional activation energy associated to the cooperativity $E_a^* = 53$ cm^{-1}. Such parameters allow understanding of the shape of the T_c(LIESST) experiment[14] reported in Fig. 1. In the tunneling region where the kinetic of the relaxation back to the HS–LS state is very slow, the $S = 1$–4 spin states of the local HS–HS pair are progressively populated and $\chi_M T$ increases. Above 55 K, the relaxation process of the local HS–HS pair becomes thermally activated and a deviation appears with the magnetic properties of [{Fe(bpym)(NCS)$_2$}$_2$(bpym)]. The critical T_c(LIESST) temperature is found at 75 K.

In summary, this communication reports a new example of synergy between magnetic interaction and spin transition under light irradiation in an iron(II) binuclear SC compound. For the first time at very low temperature, the photoconversion of a LS–HS into a HS–HS pair, according to the LIESST effect, results in a decrease in the magnetic response. This behavior in the complex [{Fe(bpym)(NCSe)$_2$}$_2$(bpym)] arises from the conversion of the $S = 2$ initial state into an $S = 0$ low-lying spin state by light irradiation.

We are grateful for financial assistance from the European Commission for granting the TMR-Network 'Thermal and Optical Switching of Spin States (TOSS)', Contract No. ERB-FMRX-CT98-0199. Also we would like to thank the financial assistance of the Spanish DGICYT through Project PB97-1397 and of the PICASSO program.

Notes and references

1 P. Gütlich, A. Hauser and H. Spiering, *Angew. Chem., Int. Ed. Engl.*, 1994, **33**, 2024.
2 S. Decurtins, P. Gütlich, C. P. Köhler, H. Spiering and A. Hauser, *Chem. Phys. Lett.*, 1984, **105**, 1.
3 A. Hauser, *Chem. Phys. Lett.*, 1986, **124**, 543.
4 O. Kahn and C. Jay Martinez, *Science*, 1998, **279**, 44.
5 J. A. Real, E. Andrés, M. Carmen Muñoz, M. Julve, T. Granier, A. Bousseksou and F. Varret, *Science*, 1995, **268**, 265.
6 J. A. Real, I. Castro, A. Bousseksou, M. Verdaguer, R. Burriel, M. Castro, J. Linares and F. Varret, *Inorg. Chem.*, 1997, **36**, 455.
7 J. A. Real, J. Zarembowitch, O. Kahn and X. Solans, *Inorg. Chem.*, 1987, **26**, 2939.
8 J. A. Real, H. Bolvin, A. Bousseksou, A. Dworkin, O. Kahn, F. Varret and J. Zarembowitch, *J. Am. Chem. Soc.*, 1992, **114**, 4650.
9 J.-F. Létard, J. A. Real, N. Moliner, A. B. Gaspar, L. Capes, O. Cador and O. Kahn, *J. Am. Chem. Soc.*, 1999, **121**, 10 630.
10 Irradiation was carried out by using a Kr$^+$ laser or a diode laser (830 ± 15 nm). The measurements were performed on a very thin layer of powder sample. The weight was estimated by comparing the thermal SC curve with the curve recorded with an heavier and accurately weighed sample.
11 Result in agreement with applied-field Mössbauer spectroscopy used to detect coupled states of iron(II). V. Ksenofontov, H. Spiering, A. B. Gaspar, J. A. Real and P. Gütlick, International Conference on Molecular Magnets, San Antonio, TX, September 16–21, 2000.
12 E. Buhks, G. Navon, M. Bixon and J. Jortner, *J. Am. Chem. Soc.*, 1980, **102**, 2918.
13 $(\chi_M T)_{h\nu}$ represents the magnetic response reached after irradiation, $(\chi_M T)_{HS-LS}$ corresponds to the HS–LS mixed-spin pair and $(\chi_M T)_{AF}$ is calculated according to the Van Vleck equation with the zero-field spin Hamiltonian being expressed as $H = -JS_A \cdot S_B$; see O. Kahn, *Molecular Magnetism,* VCH, New York, 1993.
14 In the thermally activated domain the relaxation rate is given by $\partial\gamma_{LS}/\partial t = -k^*_{HL}\gamma_{LS}$ with $k^*_{HL} = k_{HL} \exp(-(E^*_a/kT)\gamma_{LS})$ and $k_{HL} = k_\infty \exp(-(E_a/kT))$; see A. Hauser, *Chem. Phys. Lett.*, 1992, **192**, 65.
15 T_c(LIESST) refers to the limit temperature where, in a SQUID magnetometer, the photoinduced HS information is erased. The procedure is reported in: J.-F. Létard, O. Capes, G. Chastanet, N. Moliner, S. Létard, J. A. Real and O. Kahn, *Chem. Phys. Lett.*, 1999, **313**, 115.

CHEMCOMM Communication
www.rsc.org/chemcomm

An unprecedented interpenetrating structure with two covalently bonded open-frameworks of different dimensionality

Jack Y. Lu* and Amy M. Babb

Department of Chemistry, University of Houston-Clear Lake, 2700 Bay Area Blvd., Houston, TX 77058, USA. E-mail: lu@ch.uh.edu

Received (in Cambridge, UK) 17th January 2001, Accepted 22nd March 2001
First published as an Advance Article on the web 6th April 2001

A chemical rearrangement under hydrothermal conditions resulted in an unprecedented interpenetrating structure with two covalently bonded open frameworks of different dimensionality: {[$Cu_2(IN)_4{\cdot}3H_2O$]·[$Cu_2(IN)_4{\cdot}2H_2O$]}·$3H_2O$ (IN = isonicotinate).

Interpenetrating network structures have been one of the fascinating subjects in crystal engineering of coordination polymers owing to their attractive new topologies and intriguing structural features.[1–8] Many of these structures have been reviewed recently.[9] Although interpenetrating networks consisting of chemically and topologically different components are rare, Robson and coworkers[10] reported interpenetrating nets of different topology where a single, rhombohedral α-polonium-related net interpenetrates with two types of hydrogen-bonded sheets, one consisting entirely of water and the other of F^- ions and water molecules, while Zaworotko and coworkers[11] synthesized the first example of interpenetrating covalent and non-covalent 2D networks. While some of the interpenetrating structures may be predictable, structural control of metal–organic reactions remains a great challenge, and often, unexpected structures may result. Here we report an unprecedented interpenetrating structure with two covalently bonded open frameworks of different dimensionality formed from a chemical rearrangement under hydrothermal conditions: {[$Cu_2(IN)_4{\cdot}3H_2O$]·[$Cu_2(IN)_4{\cdot}2H_2O$]}·$3H_2O$ (IN: isonicotinate) **1**.

The reaction of $Cu(NO_3)_2{\cdot}2.5H_2O$ with nicotinic acid and *trans*-1,2-bis(4-pyridyl)ethylene in a mole ratio of 1 : 1 : 1 under hydrothermal conditions at 140 °C for three days produced dark blue crystals of **1** in 59% yield suitable for single crystal X-ray diffraction analysis.† The structure consists of a covalently bonded three-dimensional (3D) open-channel network and a covalently bonded two-dimensional (2D) open-framework which are mutually interpenetrating. The 3D network contains three crystallographically distinct copper atoms (Fig. 1). Atom Cu(1) is square pyramidal coordinated by two pyridyl groups from two IN units and two carboxylate groups from the other two IN units in a monodentate fashion. A water molecule occupies the remaining site. Atoms Cu(2) and Cu(3) are in octahedral sites surrounded by two water molecules occupying the axial positions, with two pyridyls and two carboxylates from four IN units occupying the equatorial positions. Both Cu(2) and Cu(3) clearly show John–Teller distortion. The square pyramidal and octahedral Cu centers are linked by four two-connected tridentate IN units into a single-net 3D open-channel-network. The large rectangle in the open-channel-network consists of six Cu and six IN units (Fig. 1). The four Cu atoms at each corner of the rectangle display separations of 17.776 × 8.928 Å. The large rectangular channels in the 3D network extend into two directions, perpendicular to each other (Fig. 1). The topology of this 3D network is similar to a single net of tetragonal $CdSO_4$ type suggested by O'Keeffe *et al.*[12] The 2D open-framework consists of two independent copper atoms. Atoms Cu(4) and Cu(5) are in square pyramidal positions (Fig. 2). Each copper atom is coordinated by two carboxylate groups from two IN units in a monodentate fashion, and two pyridyl groups from the other two IN units. A water molecule occupies the remaining apical site. The square pyramidal copper atoms are linked by four two-connected tridentate IN units into a two-dimensional square grid network (Fig. 2). The Cu–Cu lengths in the square grid are 8.871 × 8.862 Å. The 3D and 2D open-frameworks interpenetrate to form an unprecedented mixed-

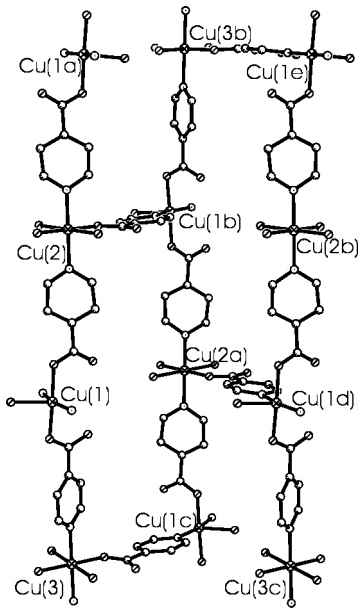

Fig. 1 View of the rectangular open framework in the 3D structure with copper atoms labeled and complete coordination shown.

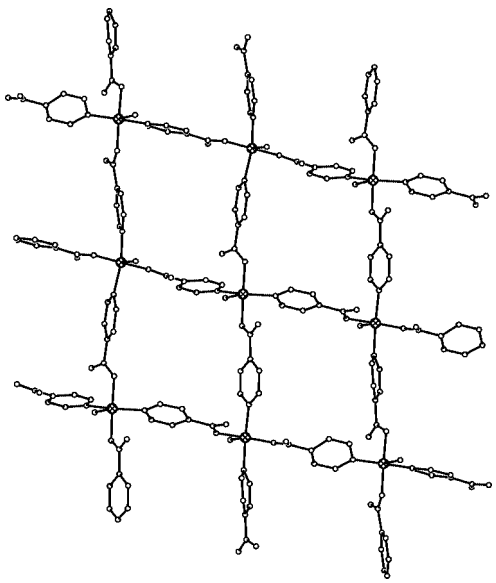

Fig. 2 View of a representative section of the 2D lattice. Note that all Cu atoms have square pyramidal coordination.

DOI: 10.1039/b100634g

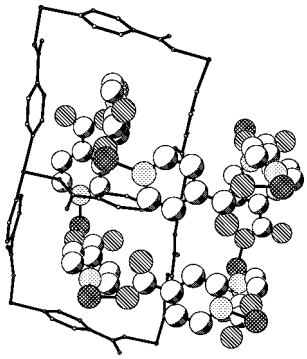

Fig. 3 Interlocked units in the interpenetrating structure. Only two of the four 2D square grids are shown for clarity.

2D–3D structure. The interpenetration is in such a way that each 3D closed-circuit displaying a 'table-frame' shape interlocks with four square grids of a 2D sheet (Fig. 3), so that each rectangular open-channel in the 3D network interpenetrates with two 2D sheets. Although several coordination polymers of isonicotinate and its derivatives have been reported, the structural feature in complex **1** has not been observed.[13] In spite of the interpenetrating networks in **1**, a dozen water molecules are included in a unit cell. Numerous hydrogen-bonding interactions found in the interpenetrating structure link the coordinating water molecules and the carboxylate groups of IN units between the 3D and 2D networks [O(9)···O(13) 2.864 Å, O(9)···O(15), 2.924 Å, O(11)···O(15) 2.865 Å, O(21)···O(4) 2.794 and 2.855 Å]. Thermal analysis indicated that the interpenetrating framework lost water molecules below 150 °C, and started to decompose at *ca*. 275 °C.

The reaction to prepare **1** was conducted *via* a self-assembly process under fairly mild hydrothermal conditions. The interpenetrating structure is stabilized owing to an unexpected chemical rearrangement of the ligand. While the reaction is fully reproducible, many attempts made to produce compound **1** from using isonicotinate instead of nicotinate as starting materials all failed.[14] The chemical rearrangement from nicotinate to isonicotinate under hydrothermal conditions is not well understood, while in other cases, rearrangements under hydrothermal conditions have been observed such as with 2,2-dipyridylamine.[15] The *trans*-1,2-bis(4-pyridyl)ethylene present in the reaction mixture is a necessary component for the preparation of compound **1**. Although the present research results might indicate that structural control of metal–organic reactions and prediction of interpenetrating networks under hydrothermal conditions could be a long-term challenging task in some cases, we are actively seeking clear directions from related investigations as well as searching for other unexpected structures under hydrothermal conditions.

We are grateful for financial support from the Welch Foundation. This work made use of MRSEC/TCSUH Shared Experimental Facilities supported by the National Science Foundation and the Texas Center for Superconductivity at the University of Houston.

Notes and references

† *Crystal data* for **1**: M = 1375.10, monoclinic, space group, $P2_1/c$; cell dimensions: a = 22.554(1), b = 11.462(1), c = 21.861 (1) Å, β = 105.645(1)°, U = 5441.6(4) Å^3, Z = 4, D_c = 1.678 g cm^{-3}, μ = 1.635 mm^{-1}, T = 223(2) K. Reflections collected: 25199; independent reflections: 8507 ($R_{(int)}$ = 0.0447). Final R indices [$I > 4\sigma(I)$]: R_1 = 0.0675, wR_2 = 0.1529. Several water molecules were disordered and hydrogen atoms on water molecules could not be located. Additionally, a few of the pyridyl rings were found to be disordered over two different orientations, and these were refined using distance constraints. CCDC 157033.

1 L. Carlucci, G. Ciani, D. M. Proserpio and S. Rizzato, *Chem. Commun*., 2000, 1319; L. Carlucci, G. Ciani and D. M. Proserpio, *New J. Chem*., 1998, 1319.
2 K. A. Hirsch, S. R. Wilson and J. S. Moore, *Chem. Commun*., 1998, 13.
3 T. M. Reineke, M. Eddaoudi, D. Moler, M. O'Keeffe and O. M. Yaghi, *J. Am. Chem. Soc*., 2000, **122**, 4843.
4 O. R. Evans, Z. Wang and W. Lin, *Chem. Commun*., 1999, 1903.
5 R. W. Gable, B. F. Hoskins and R. Robson, *J. Chem. Soc., Chem. Commun*., 1990, 1677.
6 L. R. Macgillivray, S. Subramanian and M. J. Zaworotko, *J. Chem. Soc., Chem. Commun*., 1994, 1325.
7 M. A. Withersby, A. J. Blake, N. R. Champness, P. A. Cooke, P. Hubberstey and M. Schröder, *J. Am. Chem. Soc*., 2000, **122**, 4044.
8 M. Fujita, Y. J. Kwon, O. Sasaki, K. Yamaguchi and K. Ogura, *J. Am. Chem. Soc*., 1995, **117**, 7287.
9 S. R. Batten and R. Robson, *Angew. Chem., Int. Ed*., 1998, **37**, 1460; M. J. Zaworotko, *Chem. Commun*., 2001, 1.
10 B. F. Hoskins, R. Robson and D. A. Slizys, *Angew. Chem., Int. Ed. Engl*., 1997, **36**, 2752.
11 K. Biradha, K. V. Domasevitch, B. Moulton, C. Seward and M. J. Zaworotko, *Chem. Commun*., 1999, 1327.
12 M. O'Keeffe and B. G. Hyde, *Crystal Structures I: Patterns and Symmetry*, Mineralogical Society of America, Washington, DC, 1996; M. O'Keeffe, M. Eddaoudi, H. Li, T. Reineke and O. M. Yaghi, *J. Solid State Chem*., 2000, **152**, 3; L. Carlucci, G. Ciani, P. Macchi and D. M. Proserpio, *Chem. Commun*., 1998, 1837.
13 See, for example: O. R. Evans, R.-G. Xiong, Z. Wang, G. K. Wong and W. Lin, *Angew. Chem., Int. Ed*., 1999, **38**, 536; R.-G. Xiong, S. R. Wilson and W. Lin, *J. Chem. Soc., Dalton Trans*., 1998, 4089.
14 Reactions using isonicotinate instead of nicotinate produced a mixed-ligand complex: unit cell dimensions: a = 11.839(1), b = 13.377(1), c = 28.522 (2) Å, β = 98.209(1)°. Reactions using only *trans*-1,2-bis(4-pyridyl)ethylene produced very different, poor quality red crystals the structure of which was not obtained.
15 J. Y. Lu, B. R. Cabrera, R.-J. Wang and J. Li, *Inorg. Chem*., 1998, **37**, 4480.

CHEMCOMM Communication
www.rsc.org/chemcomm

Acceleration in nitroxide mediated 'living' free radical polymerizations

Eva Harth, Brooke Van Horn and Craig J. Hawker*

Center for Polymeric Interfaces and Macromolecular Assemblies, IBM Almaden Research Center, 650 Harry Road, San Jose, CA, 95120-6099, USA. E-mail: hawker@almaden.ibm.com

Received (in Columbia, MO, USA) 6th February 2001, Accepted 21st March 2001
First published as an Advance Article on the web 9th April 2001

Intramolecular H-bonding has been shown to be a powerful tool in increasing the performance of alkoxyamine initiators for nitroxide mediated living free radical polymerizations.

The continued evolution of nanoscale science as a major research area has attracted significant attention in recent years.[1–3] In concert with this evolution, the field of polymer synthesis has witnessed an increase in sophistication with a wide range of new synthetic techniques being developed for the preparation of well defined, functionalized macromolecules. Prime examples are the preparation of dendritic macromolecules,[4,5] single site catalysts,[6–8] and the elucidation of a variety of different living free radical polymerization strategies.[9,10] These include nitroxide mediated,[11,12] atom transfer radical polymerization (ATRP),[13,14] and radical addition fragmentation/transfer procedures (RAFT).[15,16] While there are advantages and disadvantages to each procedure, our recent work has concentrated on nitroxide mediated processes since it has the potential to be the simplest of the three procedures.

A major recent advance in nitroxide mediated polymerizations has been the development of α-hydrido nitroxides, in which the presence of a hydrogen atom on the α-carbon leads to a significant increase in the range of vinyl monomers that undergo controlled polymerization.[17,18] While these new nitroxides, or their corresponding alkoxyamines such as **1**, can now be used to prepare poly(acrylates) with polydispersities in the range 1.05–1.10, the typical reaction times and temperatures (48 h at 125 °C) are still unacceptable for reactive monomers that may undergo unwanted side reactions. Also from an industrial point of view, reaction times of less than 6 h and temperatures of *ca.* 100 °C are more economically desirable.

In developing new nitroxides for living free radical polymerizations we were drawn to an observation from our initial work[19] in which the hydroxy-substituted alkoxyamine **2** was observed

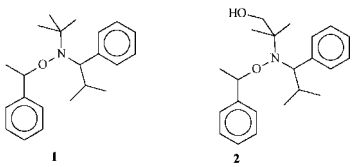

1 **2**

to yield slightly faster rates of polymerization when compared to the parent alkoxyamine **1**. While the effect was not dramatic it did correlate with the tendency of nitroxides to act as H-bond acceptors, thereby modifying their reactivity.[20] These observations, coupled with a seminal report by Studer[21] of enhanced dissociation rates for hydroxy-substituted alkoxyamines prompted an investigation into the influence of H-bonding on nitroxide mediated living free radical polymerizations. Since dissociation of **2** leads to the nitroxide **3** which is able to form a favored six-membered intramolecular H-bond (Fig. 1), it was decided to maximize the potential of this intramolecular H-bonding effect by examining the initiating ability of the tris-hydroxy derivative, **4**.

The synthesis of **4** starts from the cheap and readily available 2,2,2-tris(hydroxymethyl)nitromethane **5** which was protected

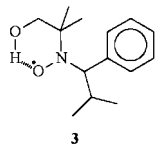

3

Fig. 1 Structure of proposed intramolecular H-bonding in nitroxide **3**.

as its ortho ester **6** before reductive coupling with isobutyryl aldehyde in the presence of zinc/HOAc to give the nitrone **7**. Reaction with phenyl magnesium bromide at reduced temperatures affords the protected nitroxide **8** which can then be coupled with styrene under catalytic Jacobsen's conditions[22] yielding the protected alkoxyamine **9**. Deprotection of either **8** or **9** could be accomplished under mild conditions with *p*-toluenesulfonic acid to give the corresponding tris(hydroxymethyl) derivatives, **10** and **4**, in essentially quantitative yields (Scheme 1).

The ability of **4** to mediate living free radical polymerization was initially examined using styrene as the monomer. Under identical conditions, the alkoxyamine initiator, **1** or **4**, was dissolved in 200 equivalents of styrene and heated at 125 °C under argon with samples being removed at various intervals. Comparison of the results showed an increase in the rate of polymerization for **4** of *ca.* 50% with high conversion being obtained in 3–4 h (*cf.* 5–6 h for **1**). More importantly, the increased rate of polymerization was accompanied by a decrease in polydispersity with values of between 1.07 and 1.09 typically being obtained (*cf.* 1.10–1.12 for **1**). This increased reactivity for **4** also allowed the polymerization temperature to

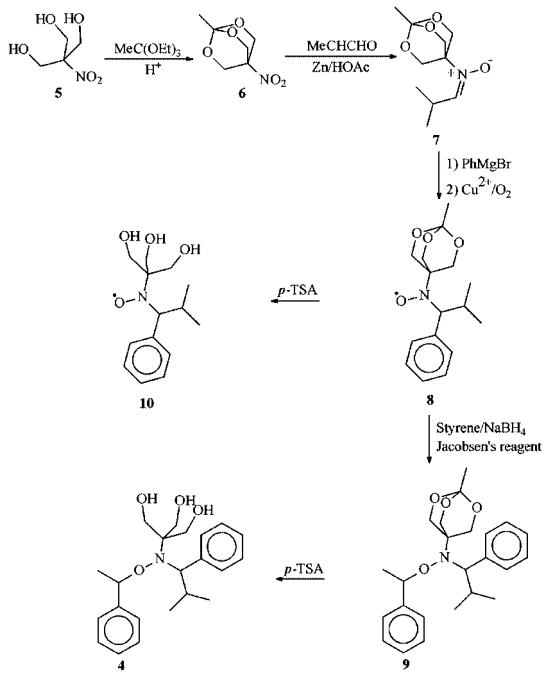

5 **6** **7** **8** **9** **10** **4**

Scheme 1

DOI: 10.1039/b102145c

be reduced while still maintaining acceptable polymerization times. For example, the polymerization of styrene at 85 °C for 48 h resulted in moderate conversions (50–55%) and low polydispersities (1.15–1.20). Extension of this work to 1,3-dienes such as isoprene also showed a similar trend, increased rate of polymerization and a reduction in polydispersity.[23]

A more significant result was observed when the polymerization of polar monomers was examined. For acrylates, the polymerization rate was increased by at least an order of magnitude by the use of the tris(hydroxymethyl) derivative, **4**. As can be seen in Fig. 2, the polymerization of *n*-butyl acrylate initiated by **4** in the presence of 5 mol% of the corresponding nitroxide **10** reaches 80% conversion after only 2 h at 120 °C, in direct contrast to **1** and 5 mol% of **12**, for which a conversion of only 6% is obtained. It should also be noted a loss of control did not accompany this increased rate of polymerization, narrow polydispersities in the region of 1.1 and controlled molecular weights were obtained with **4**. This improvement now permits acrylate monomers to be polymerized to high conversion under controlled living free radical conditions in only 2–3 h compared to 36–48 h for **1**. Attempts to perform the polymerization of acrylate monomers at lower temperatures were also successful with moderate conversions (*ca*. 40–50%) being obtained after heating at 100 °C for 24 h. At these lower temperatures, the unfunctionalized initiator **1** did not result in any detectable polymerization.

This anomalous behavior of acrylate monomers, when compared to styrene and 1,3-dienes, suggested that the increased efficiency of **4** was monomer dependent and to address this question the polymerization of acrylamides was examined. Interestingly, an increase in the rate of polymerization was again observed with **4** and high conversions were obtained after 7–8 h.[23] While not as dramatic an increase as for acrylates, it is significantly greater than the rate increase observed for styrene or isoprene.

The unique ability of the tris(hydroxymethyl) substitution pattern to facilitate nitroxide mediated polymerizations suggested that H-bonding might be a key feature. To elucidate the effect of H-bonding, similar experiments to those described above were performed with the protected alkoxyamine **9** which is not capable of forming H-bonds. Surprisingly, **9** proved to be a poor initiator for all the monomer families studied with high polydispersities and low polymerization rates being obtained in each case. For example, polymerization of 200 equivalents of styrene in the presence of **9** for 2 h at 125 °C resulted in only 19% conversion with high conversions requiring 16 h (*cf*. 3–4 h for **4** and 5–6 h for **1**). The polymers obtained were also poorly defined with polydispersities typically in the range of 1.4–1.5. Similar decreased rates of polymerization and levels of control were observed for other monomer families suggesting that the protected initiator **9** is a poor initiator for nitroxide mediated living free radical polymerizations. Since the substitution pattern in **4** is similar to **9**, the substantially improved performance of **4** is most likely a result of intramolecular H-bonding and not steric or electronic effects. Additional support for the importance of H-bonding comes from the kinetic observations of Marque[24] coupled with preliminary work from Matyjaszewski[25] using phosphonic acid derivatives of 2,2,6,6-tetramethylpiperidinyloxy, TEMPO.

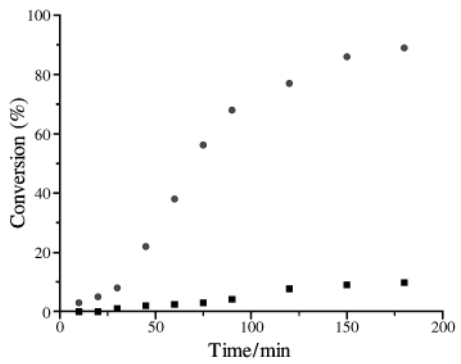

Fig. 2 Plot of percent monomer conversion *vs*. time for the polymerization of *n*-butyl acrylate (200 equivalents) in the presence of **4** (1.0 equivalent) and **10** (0.05 equivalents) (●) and **1** (1.0 equivalents) and **12** (0.05 equivalents) (■) at 125 °C.

In conclusion, intramolecular H-bonding has been shown to be a powerful tool in increasing the performance of alkoxyamine initiators for nitroxide mediated living free radical polymerizations. Increases in the rate of polymerization were observed for polar monomers such as acrylamides and especially acrylates, while only moderate improvements were obtained for non-polar monomers, such as styrene and isoprene. In each case, the degree of control during the polymerization was improved which led to lower polydispersities and a better correlation between experimental and theoretical molecular weights.

Financial support from the MRSEC Program of the NSF under Award Number DMR-9808677 for the Center for Polymeric Interfaces and Macromolecular Assemblies and the IBM Corporation is gratefully acknowledged.

Notes and references

1 J. N. Cha, G. D. Stucky, D. E. Morse and T. J. Deming, *Nature*, 2000, **403**, 289.
2 W. A. Petka, J. L. Harden, K. P. McGrath, D. Wirtz and D. A. Tirrell, *Science*, 1998, **281**, 389.
3 K. B. Thurmond, II, T. Kowalewski and K. L. Wooley, *J. Am. Chem. Soc*., 1997, **119**, 6656.
4 S. Hecht, N. Vladimirov and J. M. J. Fréchet, *J. Am. Chem. Soc*., 2001, **123**, 18.
5 A. P. H. J. Schenning, C. Elissen-Roman, J.-W. Weener, M. W. P. L. Baars, S. J. van der Gaast and E. W. Meijer, *J. Am. Chem. Soc*., 1998, **120**, 8199.
6 M. S. Sanford, M. Ulman and R. H. Grubbs, *J. Am. Chem. Soc*., 2001, **123**, 749.
7 M. Cheng, A. B. Attygalle, E. B. Lobkovsky and G. W. Coates, *J. Am. Chem. Soc*., 1999, **121**, 11 583.
8 S. A. Svejda, L. K. Johnson and M. Brookhart, *J. Am. Chem. Soc*., 1999, **121**, 10 634.
9 K. Matyjaszewski, in *Controlled radical polymerization*, ACS Symp. Ser. 685, ed. K. Matyjaszewski, American Chemical Society, Washington, DC, 1998, p. 1.
10 H. Fischer, *J. Polym. Sci., Polym. Chem*., 1999, **37**, 1885.
11 M. Rodlert, E. Harth, I. Rees and C. J. Hawker, *J. Polym. Sci., Polym. Chem*., 2000, **38**, 4749.
12 R. B. Grubbs, J. M. Dean, M. E. Broz and F. S. Bates, *Macromolecules*, 2000, **33**, 9522.
13 K. Matyjaszewski, D. A. Shipp, G. P. McMurtry, S. G. Gaynor and T. Pakula, *J. Polym. Sci., Polym. Chem*., 2000, **38**, 2023.
14 U. Uegaki, M. Kamigaito and M. Sawamoto, *J. Polym. Sci., Polym. Chem*., 1999, **37**, 3003.
15 R. T. A. Mayadunne, E. Rizzardo, J. Chiefari, J. Krstina, G. Moad, A. Postma and S. H. Thang, *Macromolecules*, 2000, **33**, 243.
16 C. P. R. Nair, P. Chaumont and D. Charmot, *J. Polym. Sci., Polym. Chem*., 1999, **37**, 2511.
17 D. Benoit, C. J. Hawker, E. E. Huang, Z. Lin and T. P. Russell, *Macromolecules*, 2000, **33**, 1505.
18 D. Benoit, S. Grimaldi, S. Robin, J.-P. Finet, P. Tordo and Y. Gnanou, *J. Am. Chem. Soc*., 2000, **122**, 5929.
19 D. Benoit, V. Chaplinski, R. Braslau and C. J. Hawker, *J. Am. Chem. Soc*., 1999, **121**, 3904.
20 A. L. J. Beckwith, V. W. Bowry and K. U. Ingold, *J. Am. Chem. Soc*., 1992, **114**, 4983.
21 A. Studer, *Angew. Chem., Int. Ed*., 2000, **6**, 1108.
22 J. Dao, D. Benoit and C. J. Hawker, *J. Polym. Sci., Polym. Chem*., 1998, **36**, 2161.
23 Polymerization of 200 equivalents of isoprene with **4** at 125 °C for 16 h resulted in 76% conversion, M_n = 14 000, polydispersity of 1.10, *cf*. 45% conversion, M_n = 8000, PD = 1.18 for **1**. Polymerization of 200 equivalents of *N,N*-dimethylacrylamide with **4** and **10** at 125 °C for 3 h resulted in 81% conversion, M_n = 15 000, polydispersity of 1.12, *cf*. 9% conversion, M_n = 1700, PD = 1.27 for **1** and **12**.
24 S. Marque, H. Fischer, E. Baier and A. Studer, *J. Org. Chem*., 2001, **66**, 1146.
25 K. Matyjaszewski, S. G. Gaynor, D. Greszta, D. Mardare, T. Shigemoto and J. S. Wang, *Macromol. Symp*., 1995, **95**, 217.

CHEMCOMM Communication
www.rsc.org/chemcomm

Zinc(II) driven intra-molecular electronic energy transfer in a supramolecular assembly held by coordinative interactions

Michela Di Casa, Luigi Fabbrizzi,* Maurizio Licchelli, Antonio Poggi, Antonella Russo and Angelo Taglietti

Dipartimento di Chimica Generale, Università di Pavia, Viale Taramelli 12, 27100 Pavia, Italy

Received (in Cambridge, UK) 1st February 2001, Accepted 22nd March 2001
First published as an Advance Article on the web 10th April 2001

In a MeOH solution the complex $[Zn^{II}(L)]^{2+}$ gives an adduct with the coumarin-343 anion and an electronic energy transfer process takes place from the fluorophore placed on the ligand L to the fluorescent anion, according to a mechanism which can be reversively switched OFF–ON following an acid–base input.

Photonic energy can be transferred from an excited fragment Fl_1 (adsorbing light at wavelength λ_1) to a proximate fragment Fl_2, which emits light at a distinctly higher wavelenth λ_2. A typical mechanism involves the occurrence of a double electron transfer process between Fl_1 and Fl_2, according to a circular pathway, and requires that the two fragments experience occasional van der Waals contacts so that their orbitals can overlap.[1] When Fl_1 and Fl_2 are (or belong to) distinct molecules, a large excess of one of the fluorophores is required in order to ensure the occurrence of the occasional contact: the electronic energy transfer (EET) has an intermolecular nature and the photophysical response (*e.g.* the increase of the fluorescence intensity, I_F, at λ_2) must follow Stern–Volmer behaviour. However, the process can also take place intramolecularly, if Fl_1 and Fl_2 are covalently linked by a relatively short spacer, which makes their encounter much more probable.[2] Intramolecular EET can also be achieved in supramolecular systems in which Fl_1 and Fl_2 belong to distinct moieties held together by non-covalent interactions (*e.g.* hydrogen bonding).[3] EET processes in supramolecular systems are of interest in the fast-growing area of molecular level devices, molecular computing and elementary nanotechnology.[4] We describe here an example of an intramolecular EET process in a system held together by metal–ligand interactions. Metal-mediated inter-component energy transfer has been observed in a few cases.[5] The involved metal is the Zn^{II} cation, which is photophysically inactive and plays an architectural role,[6] bringing Fl_1 and Fl_2 to a suitable distance for the occurrence of an efficient EET process. From this perspective, in the molecule **L** a tripodal tetramine platform

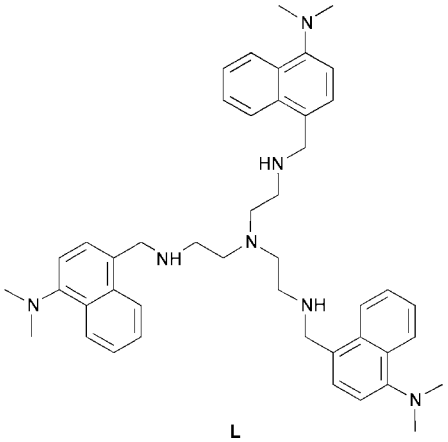

L

has been equipped with three equivalent luminescent fragments that absorb UV light (*N*,*N*-dimethylamine-1-naphthalene: Fl_1; absorption band centred at λ_{max} = 330 nm, emission band centred at λ_{max} = 424 nm).† On the other hand, the dye coumarin-343 was chosen as Fl_2, showing a strong emission at λ_{max} = 475 nm and containing a carboxylic function. Substantial overlap of the absorption band of Fl_1 and of the emission band of Fl_2 fulfils the prerequisite for the occurrence of an EET process.[7]

The tetramine **L** must be preliminarily organised through Zn^{II} coordination, according to a process which can be spectrofluorimetrically monitored. In particular, titration of an ethanolic solution of **L** with Zn^{II} induces an increase in the Fl_1 emission intensity, at 330 nm; a limiting value (2.5-fold enhancement) is achieved with the addition of one or more Zn^{II} equivalents. This behaviour is consistent (i) with the formation of a $[Zn^{II}(\mathbf{L})]^{2+}$ complex, and (ii) with the fact that Zn^{II} coordination prevents the occurrence of an electron transfer (eT) process from the proximate amine nitrogen atom to the photoexcited Fl_1 fluorophore—this eT process was responsible for partial quenching of the fluorescence. On formation of the $[Zn^{II}(\mathbf{L})]^{2+}$ complex, full emission of Fl_1 is restored.

Subsequently, an ethanolic solution of $[Zn^{II}(\mathbf{L})]^{2+}$ (1×10^{-5} mol dm^{-3}), irradiated at 330 nm, was titrated with a standard solution of Fl_2. Progressive addition of the titrating solution induced a progressive decrease in the emission band of Fl_1 and the development of an emission band at 475 nm, indicating Fl_2 sensitisation and the occurrence of an EET process involving Fl_1 and Fl_2 (see Fig. 1).

The fluorescence intensity, I_F, of the band at 424 nm *vs.* equiv. of Fl_2 profile (decreasing), as well as the I_F at 475 nm *vs.* equiv. of Fl_2 profile (increasing, see inset in Fig. 1) correspond to the formation of a 1:1 adduct between $[Zn^{II}(\mathbf{L})]^{2+}$ and coumarin-343. The log K values for the adduct formation equilibrium, calculated through non-linear, least squares treatment of the titration profiles, are 5.98 ± 0.04 (λ = 335 nm) and 6.01 ± 0.03 (λ = 475 nm). This behaviour can be explained considering that: (i) the tripodal tetramine **L** imposes a trigonal bipyramidal stereochemistry on the Zn^{II} ion, leaving one vacant axial position; in the absence of coordinating anions, this

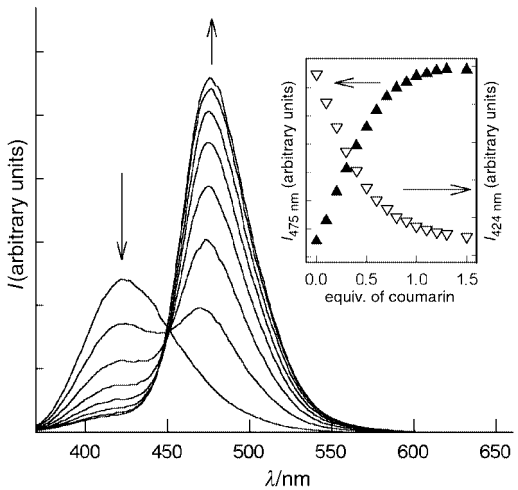

Fig. 1 Selected emission spectra recorded during the spectrofluorimetric titration of a MeOH solution of $[Zn^{II}(\mathbf{L})]^{2+}$ (1×10^{-5} M) with a standard MeOH solution of coumarin-343. The corresponding titration profiles (fluorescence intensity *vs.* equiv. of coumarin) are shown in the inset.

DOI: 10.1039/b101113h

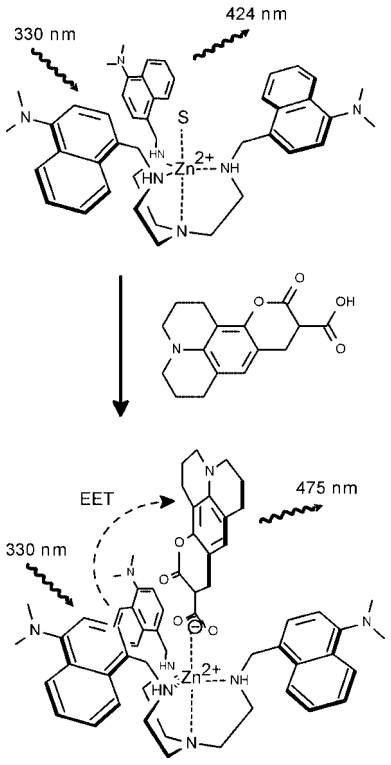

Scheme 1

position can be occupied by a solvent molecule; (ii) the CO_2H group of coumarin-343 deprotonates and the carboxylate fragment replaces the solvent molecule loosely bound in the axial position; (iii) coordination to the metal brings the photoexcited Fl_1 substituent close enough to Fl_2 to ensure the occurrence of an efficient EET process, thus leading to a substantial sensitisation of Fl_2 emission. Any intermolecular contribution to the process was found to be negligible at this low concentration scale of the reagents (10^{-5} mol dm^{-3}). The mechanism of the process is illustrated in Scheme 1.

Thus, the Zn^{II} ion acts as a glue, sticking together the two fluorogenic fragments. It should be noted that an energy transfer rate constant larger than 3.5×10^9 s^{-1} can be calculated from the equation $k_{EET} = (\Phi_0/\Phi - 1)/\tau^\circ$, where τ° is the lifetime of Fl_1 in the $[Zn^{II}(\mathbf{L})]^{2+}$ complex (2.6 ns), and Φ_0 and Φ are the values of the quantum yield of Fl_1, in the $[Zn^{II}(\mathbf{L})]^{2+}$ complex and in the $[Zn^{II}(\mathbf{L})(Fl_2)]^{+}$ adduct, respectively.[8]

When the titration experiment is repeated in the absence of the metal cation, no evidence of adduct formation is observed. In this case, a small development of the coumarin emission band at 475 nm occurs, while a small quenching of Fl_1 emission is observed. This behaviour is ascribed to intermolecular dynamic quenching *via* energy transfer, and was found to obey strictly the Stern–Volmer relationship along the investigated concentration range (up to 5×10^{-5} mol dm^{-3}).

In order to check the role of the metal cation in the EET process further, a solution containing equimolar amounts of ligand **L** and of coumarin-343 was titrated with a Zn^{2+} standard solution, whilst recording the emission spectra (λ_{exc} = 330 nm). Addition of the metal ion switches ON the electronic energy flow: the emission at 475 nm increases as Zn^{2+} is added, reaching a *plateau* with the addition of one equivalent of the metal ion. The $[Zn^{II}(\mathbf{L})(Fl_2)]^{+}$ ternary complex displays an interesting switching behaviour with respect to the addition of standard acid and base. In fact, when a methanolic solution of $[Zn^{II}(\mathbf{L})(Fl_2)]^{+}$ is titrated with triflic acid, the sensitised coumarin-343 emission decreases and completely disappears upon the addition of 4 equiv. acid (see Fig. 2). In other words, H^+ ions switches OFF the electronic energy flow between Fl_1 and Fl_2. This effect is due to the successful competition of the protons for the amine groups, which leads to demetallation and to the moving away of Fl_1 and Fl_2. The electronic energy flow can be switched ON again on titration with standard base. In

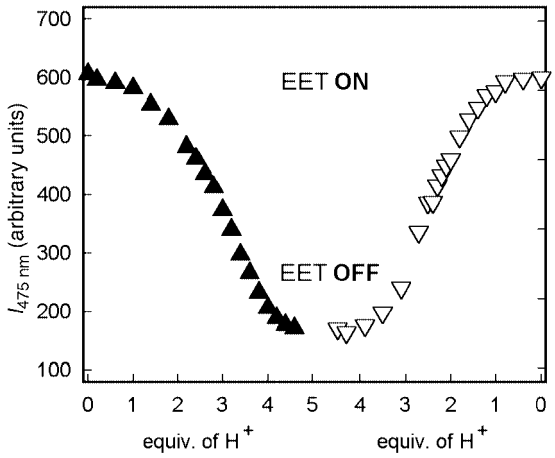

Fig. 2 The effect of an acid–base input on the emission of the $[Zn^{II}(\mathbf{L})(Fl_2)]^{+}$ system when excited at λ_{exc} = 330 nm.

particular, upon addition of an ethanolic solution of NaOH, the emission at 475 nm is progressively restored, to reach its original intensity after 4 equiv., thus ensuring the complete formation of the $[Zn^{II}(\mathbf{L})(Fl_2)]^{+}$ ternary complex. In this sense, the system under investigation shows some similarity to the *plug-and-socket* devices, recently introduced by Balzani and coworkers.[8] Analogy is not complete due to the fact that in the $[Zn^{II}(\mathbf{L})(Fl_2)]^{+}$ system we do not observe a penetration of the socket by the plug. In any case, previously reported examples were based on weak and reversible hydrogen bonding interactions. In the present study, we took profit from the distinctly stronger metal–ligand interaction, which ensures the formation of an especially stable adduct, thus guaranteeing a firm contact between the two photoactive components. Moreover, the lability of the Zn^{II} cation provides quick reversibility and a prompt ON–OFF response, following the acid–base stimulus.

This work has been supported by the Italian Ministry of University (MURST, Progetto: Dispositivi Molecolari) and the IHC European Project 'Molecular Level Devices and Machines'.

Notes and references

† *Preparation* of **L**: a solution of 4-dimethylamino-1-naphthaldehyde (9.1 mmol in 50 mL of MeOH) was added dropwise over 2 h under magnetic stirring to a solution of tris(2-aminoethyl)amine (3 mmol in 100 mL of MeOH). The reaction mixture was kept at 40 °C for 36 h, and then $NaBH_4$ was carefully added in small portions and the reaction was heated at 50 °C overnight. The solvent was then removed under reduced pressure and the resulting sticky solid was suspended in 100 mL of water. The aqueous phase was extracted with CH_2Cl_2 (3 × 50 mL). The organic phase was dried with $MgSO_4$ and the solvent distilled off, giving **L** as a light yellow oil, which was washed with several portions of diethyl ether. Yield: 67%. FAB MS *m*/*z*(%) 696 (100) M − H$^+$. ^{1}H NMR (400 MHz, $CDCl_3$): δ 8.25 (d, 3H, napththyl H), 8 (d, 3H, naphthyl H), 7.45 (m, 6H, naphthyl H), 7.25 (d, 3H, napththyl H), 6.9 (d, 3H, naphthyl H), 4.1 (s, 6H, HNCH_2-naphthyl), 3.0–2.5 (m, 30H, NCH_2CH_2NH and NCH_3).

1 N. J. Turro, *Modern Molecular Photochemistry*, University Science Book, Mill Valley, California, 1991.
2 V. Balzani and F. Scandola, *Supramolecular Photochemistry*, Ellis Horwood, Chichester, 1991; S. Speiser, *Chem. Rev*., 1996, **96**, 1953
3 M. Montalti, R. Ballardini, L. Prodi and V. Balzani, *Chem. Commun*., 1996, 2011; R. K. Castellano and M. D. Ward, *Chem. Soc. Rev*., 1997, **26**, 365; S. L. Craig, C. Nuckolls and J. Rebek, Jr., *J. Am. Chem. Soc*., 2000, **122**, 7876; S. Weidner and Z. Pikramenou, *Chem. Commun*., 1998, 1473; S. Encinas, N. R. M. Simpson, P. Andrews, M. D. Ward, C. M. White, N. Armaroli, F. Barigelletti and A. Houlton, *New J. Chem*., 2000, **12**, 987.
4 A. P. de Silva, H. Q. N. Gunaratne, T. Gunlaugson, A. J. M. Huxley, C. P. McCoy, J. T. Rademacher and T. E. Rice, *Chem. Rev*., 1997, **97**, 1515
5 S. I. Weissman, *J. Chem. Phys*., 1950, **18**, 1258; B. Alpha, J.-M. Lehn and G. Mathis, *Angew Chem., Int. Ed. Engl*., 1987, **26**, 266; C. A. Hunter and R. K. Hyde, *Angew. Chem., Int. Ed. Engl*., 1996, **35**, 1936.
6 G. De Santis, L. Fabbrizzi, M. Licchelli, A. Poggi and A. Taglietti, *Angew. Chem., Int. Ed. Engl*., 1996, **35**, 202.
7 A. Adronov, S. L. Gilat, J. M. J. Frechet, K. Ohta, F. V. R. Neuwahl and G. R. Fleming, *J. Am. Chem. Soc*., 2000, **122**, 1175
8 E. Ishow, A. Credi, V. Balzani, F. Spadola and L. Mandolini, *Chem. Eur. J*., 1999, **5**, 984

CHEMCOMM
Communication
www.rsc.org/chemcomm

Supramolecular tapes formed by a catanionic cyclodextrin in water

Bart Jan Ravoo, Raphael Darcy,* Antonino Mazzaglia, Darren Nolan and Kevin Gaffney

Department of Chemistry, National University of Ireland, University College Dublin, Belfield, Dublin 4, Ireland. E-mail: raphael.darcy@ucd.ie

Received (in Liverpool, UK) 12th December 2000, Accepted 22nd March 2001
First published as an Advance Article on the web 10th April 2001

A β-cyclodextrin substituted with amino and carboxymethyl groups on the primary and secondary side respectively, has a positively charged primary face and a negatively charged secondary face at neutral pH, and self-assembles in water into supramolecular tapes that are 50–300 nanometres wide and up to 20 micrometres long.

'Janus' cyclodextrins are cyclodextrins with distinctly different primary and secondary faces.[1] The preparation of such cyclodextrins is not trivial since it requires synthetic differentiation of the primary and secondary sides of the cyclodextrin molecule.[2] However, several types of Janus cyclodextrins have been prepared to date, all of which show interesting self-assembling properties. The largest class of Janus cyclodextrins comprises amphiphilic molecules in which one face of the cyclodextrin has been substituted with large hydrophobic groups while the other face is substituted with polar or ionic groups, or is left unsubstituted. Many of these cyclodextrins are very hydrophobic and insoluble in water. However, recent reports describe micelles as well as bilayer vesicles composed entirely of amphiphilic cyclodextrins.[3,4] A second group of Janus cyclodextrins contains thiol or sulfide substituents exclusively on one face of the molecule, which induce assembly into monolayers on gold surfaces.[5] Yet another class contains small hydrophobic substituents on one face and polar or ionic substituents, or none, on the other face. These molecules form dimers in several solvents.[6] Finally, cyclodextrins with polar or ionic substituents on one face of the molecule (and no substituents on the other face) can form dimers in polar solvents,[7] and even specific heterodimers between ionic cyclodextrins of opposite charge in water.[8] We now report a new Janus β-cyclodextrin **3** bearing amino groups on the primary face and carboxymethyl groups on the secondary face, to give a cyclic oligo-aminoacid structure designed to assemble in water by multiple ion-pairing.

Heptakis(6-azido-6-deoxy)-β-cyclodextrin **1**[9] was reacted with sodium iodoacetate in the presence of potassium *tert*-butoxide at 80 °C in DMF to yield 6-azido-6-deoxy-2-*O*-carboxymethyl-β-cyclodextrin **2**. This product was isolated by precipitation from water at pH 2. ^{1}H NMR (300 MHz, d_6-DMSO) showed a signal for the methylene protons of the carboxymethyl group at 4.35 ppm and separate signals for H_1' at 5.15 and H_1 at 4.92 ppm. According to the relative integration of these ^{1}H NMR signals, a reproducible average of five carboxymethyl groups was introduced in **2**. The resolution of the NMR spectra of **2** is poor due to a combination of aggregation and loss of molecular symmetry. Cyclodextrin **2** was then reduced to 6-amino-6-deoxy-2-*O*-carboxymethyl-β-cyclodextrin **3** by conventional phosphine reduction.[10] Product **3** was isolated by precipitation in water at pH 2 and purified by size exclusion chromatography. Despite our best efforts, the final product retained traces of phosphines. The structure of **3** (with five carboxymethyl groups on O-2) was confirmed by NMR. ^{1}H NMR (300 MHz, D_2O) shows a signal for the methylene protons of the carboxymethyl group at 4.28 ppm and signals for H_1' at 5.07 as well as H_1 at 5.30 ppm. ^{13}C NMR (500 MHz, D_2O) shows the carbonyl and the methylene carbon of the carboxymethyl group at 174.4 and 69.1 ppm, respectively, as well as C_2' at 80.0 and C_2 at 68.0 ppm. No shift was observed for C_3' relative to C_3, confirming substitution at O-2 instead of O-3, as anticipated for this type of reaction at the secondary side of cyclodextrins.[2] As for **2**, the resolution of the NMR spectra of **3** is poor due to a combination of aggregation and loss of molecular symmetry.

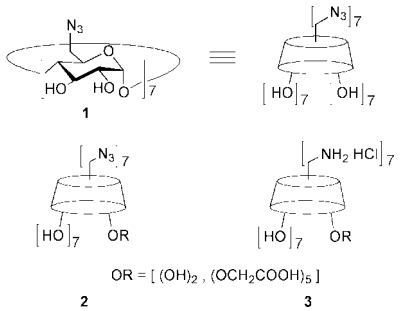

Cyclodextrin **3** readily dissolves in 10 mM HEPES buffer (pH 7.4) upon gentle agitation at rt. The solution (0.1–1.0 mg mL^{-1}) is not completely transparent. Using transmission electron microscopy (with either uranyl acetate or phosphotungstic acid as negative stain)[11] we observed that cyclodextrin **3** self-assembles into elongated tape-like structures (Figs. 1 and 2). The tapes are between 50 and 300 nanometres wide and up to 20 μm long, yet only several nanometres thick. They seem quite flexible, since multiple twists, bends and folds are observed. However, the tapes are also rather fragile, and readily break into smaller fragments during the preparation of samples for electron microscopy. A significant fraction of the cyclodextrin is present as amorphous aggregates. As expected, no tapes but only amorphous aggregates are observed when the pH is either reduced from 7.4 to 4, or increased from 7.4 to 10, or when 0.5 M NaCl is added to the cyclodextrin solution. At high and low pH, and also in the presence of more than 0.1 M NaCl,

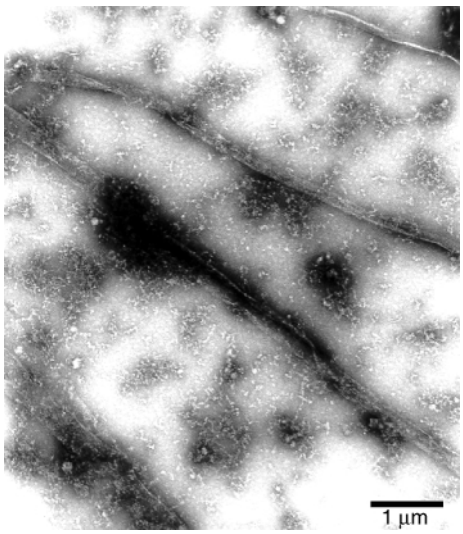

Fig. 1 Electron micrograph of cyclodextrin **3** in HEPES buffer (pH 7.4). Negative staining with 1% uranyl acetate.

DOI: 10.1039/b009908m

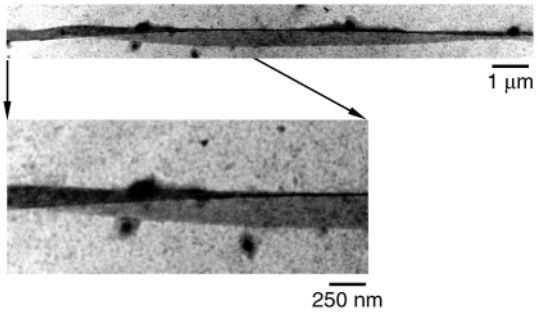

Fig. 2 Electron micrograph of cyclodextrin **3** in HEPES buffer (pH 7.4). Negative staining with 1% phosphotungstic acid.

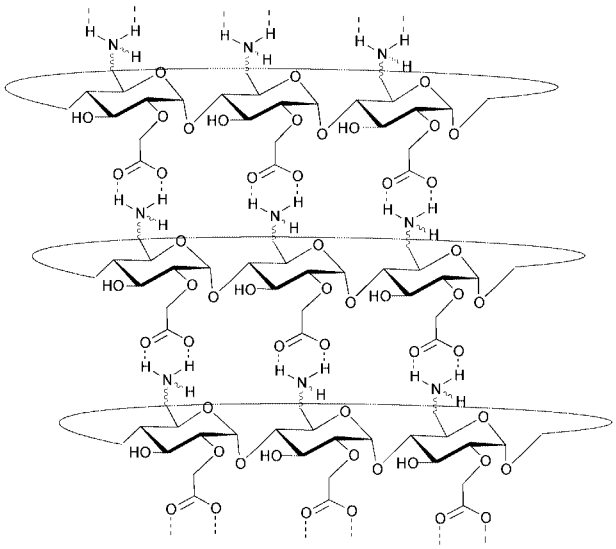

Fig. 3 Schematic illustration of the self-assembly of cyclodextrin **3**.

the solution of cyclodextrin **3** becomes completely transparent. Clearly, the elongated tapes at neutral pH and low ionic strength scatter visible light much more than the smaller, amorphous aggregates present at high and low pH, and at high ionic strength. The intensity of the scattered light at 400 nm as a function of NaCl concentration is constant up to 40 mM of added NaCl, and rapidly decreases at higher ionic strength. This demonstrates that the elongated tapes only form in aqueous solution of low ionic strength.

We propose that the elongated tapes result from ion-pairing of the catanionic cyclodextrin **3**. At neutral pH and low ionic strength, molecules of **3** assemble face to face, similar to the heterodimers described in the literature,[8] except that here each molecule has oppositely charged faces, so that the molecular pairing can continue indefinitely in two directions. The cyclodextrins can form an efficient intermolecular hydrogen bond network, with each molecule providing multiple NH hydrogen bond donor sites and CO hydrogen bond acceptor sites (Fig. 3). In this way they imitate the self-assembly of certain cyclic peptides to form nanotubes in water,[12] although here the protonated amino and carboxylate groups operate each on one side of the molecule, rather than alternately on the same side as do the hydrogen bonding NH and CO groups in the case of the peptides. The supramolecular structure adopted by cyclodextrin **3** is fundamentally different from previous examples of cyclodextrin self-assembly in polar solvents (including water), which have been induced by elongated guest molecules, namely the poly(rotaxanes)[13] and diphenylhexatriene inclusion compounds.[14]

The molecular faces of **3** may not perfectly superimpose. In crystal structures, cyclodextrins not only form channel structures, but also each molecular face can overlap with more than one other face to form cage structures.[15] Here, the molecules apparently assemble in three directions, two of which seem to be favoured over the third, as when bricks are used to form a wall. This would result in the formation of elongated tapes of variable width, but constant thickness. Further structural and computational investigations, as well as synthetic modifications, will contribute to a better understanding of the self-assembly of this novel catanionic Janus cyclodextrin.

A. M., K. G. and D. N. are grateful for financial support from SA Druggists International and Enterprise Ireland. B. J. R. is Schering-Plough (Avondale) Co. Newman Scholar in Organic Chemistry. The authors thank Dr D. Cottell for generous facilities in the Laboratory of Electron Microscopy at University College Dublin.

Notes and references

1 A. Marsh, E. G. Nolen, K. M. Gardinier and J. M. Lehn, *Tetrahedron Lett*., 1994, **35**, 397.
2 A. R. Kahn, P. Forgo, K. J. Stine and V. T. d'Souza, *Chem. Rev*., 1998, **98**, 1977.
3 R. Auzély-Velty, F. Djedaïni-Pilard, S. Désert, B. Perly and Th. Zemb, *Langmuir*, 2000, **16**, 3727.
4 B. J. Ravoo and R. Darcy, *Angew. Chem., Int. Ed*., 2000, **39**, 4324.
5 (*a*) M. T. Rojas, R. Königner, J. F. Stoddart and A. E. Kaifer, *J. Am. Chem. Soc*., 1995, **117**, 336; (*b*) G. Nelles, M. Weisser, R. Back, P. Wohlfahrt, G. Wenz and S. Mittler-Weher, *J. Am. Chem. Soc*., 1996, **118**, 5039; (*c*) M. W. J. Beulen, J. Bügler, M. R. de Jong, B. Lammerink, J. Huskens, H. Schönherr, G. J. Vancso, B. A. Boukamp, H. Wieder, A. Offenhäuser, W. Knoll, F. C. J. M. van Veggel and D. N. Reinhoudt, *Chem. Eur. J*., 2000, **6**, 1176; (*d*) G. Schmid and N. Beyer, *Eur. J. Inorg. Chem*., 2000, 835.
6 B. Hamelin, L. Jullien, A. Laschewsky and C. Herve du Penhoat, *Chem. Eur. J*., 1999, **5**, 546.
7 T. Kraus, M. Budešínský and J. Závada, *Eur. J. Org. Chem*., 2000, 3133.
8 (*a*) B. Hamelin, L. Jullien, F. Guillo, J. M. Lehn, A. Jardy, L. de Robertis and H. Driguez, *J. Phys. Chem*., 1995, **99**, 17 877; (*b*) L. Jullien, H. Cottet, B. Hamelin and A. Jardy, *J. Phys. Chem. B*., 1999, **103**, 10 866; (*c*) P. Schwinté, A. Holohan, R. Darcy and F. O'Keeffe, *J. Incl. Phenom. Macrocyclic Chem*., 1999, **35**, 657.
9 (*a*) A. Gadelle and J. Defaye, *Angew. Chem., Int. Ed. Engl*., 1991, **30**, 78; (*b*) H. Parrot-Lopez, C.-C. Ling, P. Zhang, A. Baszkin, G. Albrecht, C. de Rango and A. W. Coleman, *J. Am. Chem. Soc*., 1992, **114**, 5479.
10 F. Guillo, B. Hamelin, L. Jullien, J. Canceill, J. M. Lehn, L. de Robertis and H. Driguez, *Bull. Soc. Chim. Fr*., 1995, **132**, 857.
11 Samples for transmission electron microscopy were prepared on carbon/formvar coated 200 mesh copper grids, stained with uranyl acetate or phosphotungstic acid, and examined in a JEOL 2000 electron microscope operating at 80 kV.
12 J. D. Hartgerink, J. R. Granja, R. A. Milligan and M. R. Ghadiri, *J. Am. Chem. Soc*., 1996, **118**, 43.
13 (*a*) G. Wenz, *Angew. Chem., Int. Ed. Engl*., 1994, **33**, 803; (*b*) S. A. Nepogodiev and J. F. Stoddart, *Chem. Rev*., 1998, **98**, 1959.
14 (*a*) G. Pistolis and A. Malliaris, *J. Phys. Chem*., 1996, **100**, 15 562; (*b*) G. Pistolis and A. Malliaris, *J. Phys. Chem. B*., 1998, **102**, 1095.
15 G. A. Jeffrey and W. Saenger, *Hydrogen Bonding in Biological Structures*, Springer Verlag, Berlin, 1991, ch. 18.

CHEMCOMM Communication
www.rsc.org/chemcomm

Selective structure changes of core–shell gold–silver nanoparticles by laser irradiation: homogeneisation *vs.* silver removal

Jean-Pierre Abid,[a] Hubert H. Girault*[a] and Pierre F. Brevet[b]

[a] *Laboratoire d'Electrochimie, Ecole Polytechnique Federale de Lausanne, CH-1015 Lausanne, Switzerland. E-mail: girault@epfl.ch*

[b] *Laboratoire de Spectrometrie Ionique et Moleculaire, Universite Claude Bernard Lyon 1, Batiment Alfred Kastler, UMR 5579, 43 Boulevard du 11 Novembre 1918, F-69622 Villeurbanne Cedex, France*

Received (in Cambridge, UK) 24th January 2001, Accepted 13th March 2001
First published as an Advance Article on the web 17th April 2001

A method involving laser irradiation is shown to lead to selective modification of core–shell gold–silver nanoparticles.

In recent years, a large range of preparations have been proposed for the design of novel metallic nanoparticles. For both uncoated and passivated metallic nanoparticles like thioalkane or thionicotinamide-coated gold nanoparticles,[1,2] numerous chemical or physical procedures for their preparation have been published and compared,[3–6] in particular with respect to the size and shape distributions.[7] For spherical nanoparticles, a strong emphasis has always been given to the diameter of the particles and the width of the distribution around the mean diameter. These properties are usually assessed by UV–VIS absorption spectroscopy and Transmission Electron Microscopy (TEM). Routinely, particles with diameters between 5 and 25 nm with a standard deviation between 1 and 2 nm are reported. One general aim is to reduce even further the standard deviation of the size distribution since many physical properties of the particles are size dependent. This is true for the wavelength corresponding to the maximum of the absorption spectrum of the particles in solution and also for the hyperpolarisability of the particles.[8,9]

The control of the size distribution is not very efficient during nanoparticle formation when the metal salt reduction technique is used. However, this is probably the most widely used technique although it does not yield a very narrow distribution. Subsequent size separation processes are therefore required.[10] The search for a convenient way to narrow the size distribution for monodisperse aqueous solutions of nanoparticles is thus required and recently laser irradiation has been proposed with the report of both size reduction and shape changes of metal particles in solution.[2,11–13] Nevertheless, the physical mechanisms at work have not been fully elucidated although melting, photoejection of electrons and fragmentation have been observed depending on the laser irradiation conditions. In this work, we report the laser irradiation of core-shell gold–silver nanoparticles with a diameter *ca.* 23.4 nm and their subsequent changes for different laser fluences when pulses with a 5 ns duration at a 532 nm wavelength are used.

Silver coated gold nanoparticles were prepared by reduction of a gold tetrachloroaurate salt containing 10 mg of gold in 190 mL of water made up to 200 mL with 10 mL of a 38.8 mM sodium citrate solution.[14] The ruby red coloured solution was then cooled down to room temperature before being boiled again. Near the boiling point, silver nitrate was added to 60 mL of the gold solution in aliquots of 200 μL with the amount of silver adjusted to the desired mole fraction with respect to gold. The stoichiometric equivalents of citrate were added after each silver addition to ensure the complete reduction of the silver ions. Here we present the results for a solution with a mole fraction of gold of 0.60 although other ratios can be obtained by this preparation method. The size distribution of the solution was characterized by TEM on a Philips CM20 transmission electron microscope and UV–VIS absorbance spectra were recorded with a Varian 1E UV–VIS spectrophotometer. For the TEM measurements, a drop of the solution was deposited on a copper grid on a carbon film and dried under a N_2 atmosphere in a glove box. The size distribution was then deduced from the measurements of the diameter of 200 particles from 6 different batches. The average diameter measured was 23.4 nm with a standard deviation of 1.4 nm. The laser irradiation was performed with a nanosecond Continuum Minilite II Nd^{3+}–YAG laser, delivering pulses at a repetition rate of 10 Hz at 532 nm. The cross section of the irradiation beam was controlled with a 10 cm focal lens and measured to be 0.125 cm^2 at the entrance of the cell. At energies varying between 12 and 2 mJ per pulse, this corresponds to fluences between 96 and 16 mJ cm^{-2}, respectively. In all experiments, the nanoparticle solutions were used directly as prepared without further additions of others species such as oxidising agents. The volume of the aqueous solution of nanoparticles was maintained at 1.5 mL in a quartz cell. Irradiation times were varied but the results presented here all correspond to irradiation times of 60 minutes. The UV–VIS absorbance of the initial orange coloured solution of the nanoparticles consisting of a gold core with a silver outer-shell is presented in Fig. 1. The absorbance of the core–shell nanoparticle exhibits two surface plasmon resonances at 410 and 502 nm characteristic of this bimetallic phase system. It is important to realise though that one cannot attribute a particular band to the surface plasmon excitation of one single metal phase only. Indeed, from a Mie theory calculation for such a core–shell system, one calculates the absorption cross-section of the core–shell particle altogether. It can however be noticed that the absorption cross-section is always dominated by the gold core absorption at all wavelengths.[15] From the TEM measurements, no rod shaped particles were observed and therefore the particles are assumed spherical hereafter.

Upon 60 minutes of irradiation of the sample with 532 nm light at a high fluence of 96 mJ cm^{-2}, the UV–VIS absorbance spectrum is substantially modified, now presenting only one surface plasmon excitation located at 510 nm, see Fig. 2, which

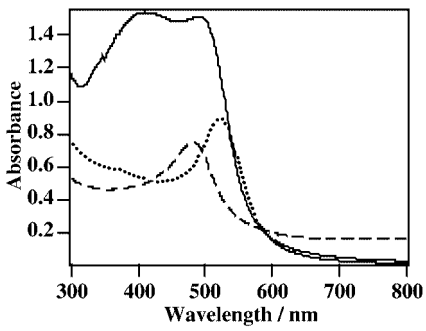

Fig. 1 UV–VIS spectra for Au 0.6 Ag 0.4 core–shell nanoparticles of different morphologies: mixed core–shell (solid line), homogeneous (dashed line) particles. The spectrum of pure gold is also given (dotted line).

DOI: 10.1039/b100856k

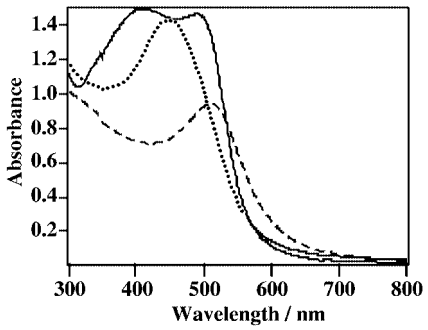

Fig. 2 Absorption spectra of Ag coated Au nanoparticles after irradiation with different fluences for 60 min: no irradiation (solid line), irradiation at low fluence (dotted line) and at high fluence (dashed line).

is a value very close to the position of the surface plasmon band for pure gold particles. From the TEM measurements of the irradiated samples, it appears that particles with diameters larger than 15 nm are not observed anymore whereas the number of particles with a diameter between 3 and 15 nm increased. When the solution is irradiated during an equal amount of time with a lower fluence of 16 mJ cm^{-2}, the absorbance spectrum is different with a single surface plasmon band observed located at a wavelength of 455 nm, see Fig. 2. This is the exact location of the surface plasmon band excitation for a mixed gold–silver nanoparticle with the same mole fraction of 0.6 for gold. Such a homogeneous particle can be produced by the simultaneous reduction by citrate of a mixed salt of sodium tetrachloroaurate and silver nitrate with an initial mole fraction of gold of 0.6. From the TEM measurements, the diameter of the particles ranged between 3 and 17 nm and no particles with a diameter larger than 17 nm were observed. These results at low fluence have recently been observed by Hodak *et al*.[16] The origin of the difference in the resulting UV–VIS absorbance spectra after irradiation is the result of the competition between two dominant processes: surface oxidation and melting. At low fluences with an irradiation wavelength of 532 nm, the absorption is preferentially localised into the gold core because of the smaller absorptivity of silver compared to the gold at this wavelength.[17] The plasmon excitation is the dominant process leading to a rapid phonon excitation through electron–phonon coupling in less than 1 ps and thermal relaxation within the nanosecond pulse duration by phonon–phonon coupling. This process induces the melting of the particle since internal temperatures reached are above the melting temperature for gold, the bulk value of which is 1339 K. However, this phenomenon occurs on a very short timescale since phonon–phonon equilibration with the surrounding medium is complete within 100 ps.[18] The internal diffusion process involving the mixing of the gold internal core and the outer silver shell must then be rapid, with a timescale of the same order of magnitude of 100 ps. It is likely that complete homogeneity is only obtained after a number of pulses.[16] In contrast, at high fluences, the process is different leading to the removal of the silver layer. Absorption of more than one photon is a process known to occur.[12] At high fluences with a wavelength of 532 nm, the process of the absorption of at least two photons, or an energy of more than 4.64 eV, a value above that of the work function of silver equal to 4.3 eV, induces the photooxidation of silver. The redox reaction is similar to an electrochemical anodic dissolution of silver ($E^0_{Ag^+/Ag}$) concomitant with the reduction of the electrolyte. The gold inner shell is not affected by photooxidation as the work function of gold is higher (5.2 eV). The process of evaporation of atoms of both silver or gold is highly unlikely from a physical statistics point of view and thus the successive absorption of photons with time intervals greater than 100 ps cannot be regarded as a dominant channel of relaxation. No pure silver particles were observed in solution after irradiation as seen from the absence of any plasmon band excitation around 400 nm. The silver cations formed therefore by photooxidation are not reduced again in solution to form silver nanoparticles.

The irradiation fluence was observed to change the shape as well as the diameter of the nanoparticles. This work demonstrates the possibility of the use of laser irradiation as a tool to selectively change the morphology of core–shell gold–silver nanoparticles.

This work is supported by the Swiss National Fund for Research under the grant n° 21-55762.98. We thank Valerie Devaud for her help , Juliette Rinuy, Dr Alastair Wark and Cyril Cayron for the TEM measurements and Paolo Galletto and Jean Lerme for fruitfull discussions.

Notes and references

1 M. Brust, J. Fink, D. Bethell, D. J. Schiffrin and C. Kiely, *J. Chem. Soc., Chem. Commun*., 1995, 1655.
2 H. Fujiwara, S. Yanagida and P. V. Kamat, *J. Phys. Chem. B*, 1999, **103**, 2589.
3 J. Turkevich, P. J. Stevenson and J. Hillier, *Discuss. Faraday Soc*., 1951, **11**, 55.
4 J. H. Fendler, *Chem. Rev*., 1987, **87**, 877.
5 L. Rodriguez-Sanchez, M. C. Blanco and M. A. Lopez-Quintela, *J. Phys. Chem. B*, 2000, **104**, 9683.
6 F. Mafune, J. Kohno, Y. Takeda, T. Kondow and H. Sawabe, *J. Phys. Chem. B*, 2000, **104**, 9111.
7 Y. Yu, S. Chang, C. Lee and C. R. C. Wang, *J. Phys. Chem. B*, 1997, **101**, 6661.
8 U. Kreibig and M. Vollmer, in *Optical Properties of Metal Clusters*, Springer, Berlin, 1995.
9 P. Galletto, P. F. Brevet, H. H. Girault, R. Antoine and M. Broyer, *Chem. Commun*., 1999, 581.
10 T. G. Schaaf, M. N. Shafigullin, J. T. Khoury, I. Vezmar, R. L. Whetten, W. G. Cullen and P. N. First, *J. Phys. Chem. B*, 1997, **101**, 7885.
11 A. Takami, H. Kurita and S. Koda, *J. Phys. Chem. B*, 1999, **103**, 1226.
12 P. V. Kamat, M. Flumiani and G. V. Hartland, *J. Phys. Chem. B*, 1998, **102**, 3123.
13 S. Link, C. Burda, B. Nikoobakht and M. A. El-Sayed, *J. Phys. Chem. B*, 2000, **104**, 6152.
14 R. G. Freeman, M. B. Hommer, K. C. Grabar, M. A. Jackson and M. J. Natan, *J. Phys. Chem*., 1996, **100**, 718.
15 C. F. Bohren and D. R. Huffman, in *Absorption and Scattering of Light by Small Particles*, Wiley, New York, 1983.
16 J. H. Hodak, A. Henglein, M. Giersieg and G. V. Hartland, *J. Phys. Chem*., 2000, **104**, 11 708.
17 A. M. Prokhorov, V. I. Konov, I. Ursu and I. N. Mihailescu, *Laser Heating of Metals*, Adam Hilger, 1990.
18 T. S. Ahmadi, S. L. Logunov and M. A. El-Sayed, *J. Phys. Chem*., 1996, **100**, 8053.

CHEMCOMM Communication
www.rsc.org/chemcomm

Solid-phase tandem radical addition–cyclisation reaction of oxime ethers

Hideto Miyabe, Kayoko Fujii, Hirotaka Tanaka and Takeaki Naito*

Kobe Pharmaceutical University, Motoyamakita, Higashinada, Kobe 658-8558, Japan. E-mail: taknaito@kobepharma-u.ac.jp

Received (in Cambridge, UK) 31st January 2001, Accepted 20th March 2001
First published as an Advance Article on the web 10th April 2001

The solid-phase tandem C–C bond-forming reactions of oxime ethers connected with α,β-unsaturated carbonyl groups proceeded effectively under iodine atom-transfer reaction conditions to give the azacycles or chiral oxacycles after cleavage of the resin.

Solid-phase radical reactions have been developed for an important carbon–carbon bond-forming method on solid support under mild reaction conditions.[1] We have recently demonstrated that triethylborane as a radical initiator has the potential to induce intermolecular and intramolecular radical reactions on solid support.[2] Moreover, the employment of triethylborane and its related radical initiator such as diethylzinc at low reaction temperature would facilitate the control of stereochemistry in solid-phase reactions.[3] Within our program directed towards solid-phase radical reactions, the development of solid-phase multi carbon–carbon bond-forming reactions and their stereocontrol is the new focus of our efforts. We now report the tandem radical addition–cyclisation reaction of oxime ethers anchored to a polymer support.

In our studies on the radical reaction of various oxime ethers in solution,[4] we have recently succeeded in the solution-phase tandem radical addition–cyclisation reaction of substrates having two different radical acceptors such as acrylate and aldoxime ether moieties.[5] On the basis of the results in the solution-phase reactions, we first examined the simple solid-phase tandem radical addition–cyclisation reaction of aldoxime ether **3** connected with the α,β-unsaturated carbonyl group.

Preparation of **3** anchored to a polymer support is shown in Scheme 1. Treatment of α-chloroacetaldoxime ether **1** with 2-aminoethanol followed by acylation with acryloyl chloride gave oxime ether **2**. To enhance the reactivity of resin-bound substrate, we introduced a temporary spacer by the reaction of **2** with glutaric anhydride. The oxime ether having the spacer moiety was attached to Wang resin by treatment with DCC in the presence of DMAP to give **3**. The loading level of Wang resin-bound oxime ether **3** was determined to be 0.81 mmol g^{-1} through quantification of nitrogen by elemental analysis.

To a flask containing aldoxime ether **3** and Pr^iI (30 equiv.) in toluene a commercially available 1.0 M solution of triethylborane in hexane was added three times (3 equiv. × 3) as a radical initiator at 100 °C (Scheme 1). The reaction mixture was stirred at 100 °C for 2 h, then the resin was filtered and successively washed with CH_2Cl_2, AcOEt, and MeOH. The cleavage of the resin by treatment with NaOMe gave the desired azacyclic product **5a** in 69% isolated yield. However, the radical cyclisation of oxime ether **3** at 25 °C did not proceed.[2b] Good chemical yields were also observed in the radical reaction using different radical precursors such as cyclohexyl, cyclopentyl, and *sec*-butyl iodides under the iodine atom-transfer reaction conditions. Moreover, it is noteworthy that this iodine atom-transfer radical reaction has a practical advantage over the reaction using toxic tin reagent. A remarkable feature of these reactions is the construction of two carbon–carbon bonds on solid support under mild reaction conditions without strictly anhydrous solvents and reagents. In this reaction, triethylborane would act as a reagent for trapping the intermediate aminyl radicals to regenerate an ethyl radical; therefore, more than a stoichiometric amount of triethylborane would be required (Scheme 2).

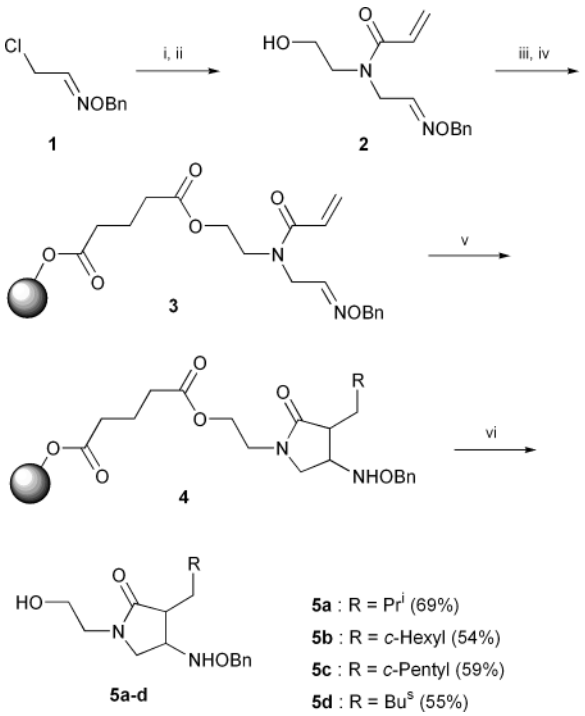

Scheme 1 *Reagents and conditions*: i, 2-Aminoethanol, 20 °C, 88%; ii, CH_2=CHCOCl, Na_2CO_3, acetone, H_2O, 0 °C, 87%; iii, Glutaric anhydride, Py, 80 °C, 93%; iv, Wang resin, DCC, DMAP, CH_2Cl_2, 20 °C; v, RI, Et_3B in hexane, toluene, 100 °C; vi, NaOMe, MeOH, THF, H_2O, 20 °C.

Stereocontrol in solid-phase radical reactions has been of great importance in SPOS (solid-phase organic synthesis). Based on the above results, we next examined the control of stereochemistry in the solid-phase tandem radical addition–cyclisation reaction. Preparation of **10** anchored to a polymer support is shown in Scheme 3. Monoacetylation of *p*-xylene glycol, mesylation of monool with mesyl chloride in the

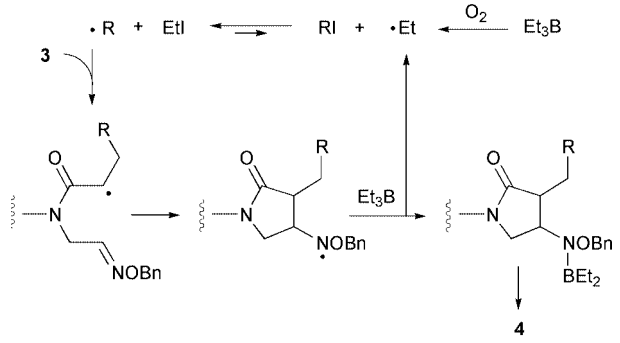

Scheme 2

DOI: 10.1039/b101074n

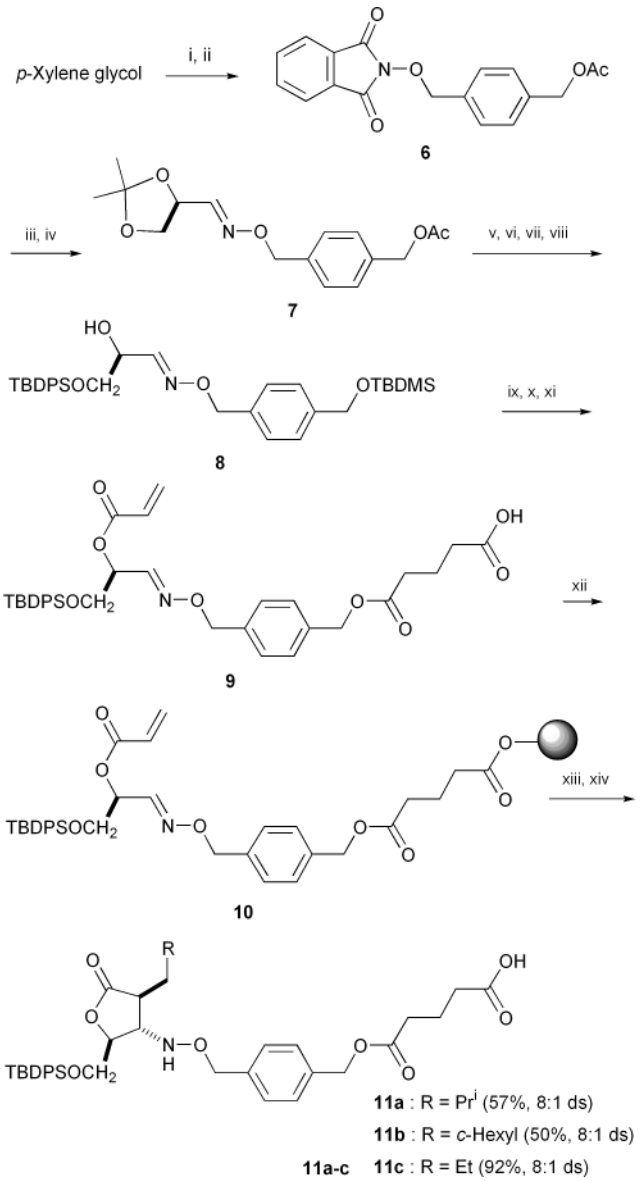

Scheme 3 *Reagents and conditions*: i, Bu^{n}Li, AcCl, THF, 0 °C, 65%; ii, MsCl, Et_3N, CH_2Cl_2, 0 °C and then *N*-hydroxyphthalimide, Et_3N, CH_2Cl_2, reflux, 71%; iii, $N_2H_4{\cdot}H_2O$, MeOH, 20 °C, 99%; iv, 2,3-isopropylidene-D-glyceraldehyde, Py, 25 °C, 73%; v, PPTS, MeOH, 65 °C, 74%; vi, TBDPSCl, imidazole, DMF, 20 °C, 75%; vii, K_2CO_3, aq. MeOH, 20 °C, 99%; viii, TBDMSCl, imidazole, DMF, 20 °C, 75%; ix, CH_2=CHCOCl, Et_3N, CH_2Cl_2, 0 °C, 65%; x, PPTS, MeOH, 65 °C, 80%; xi, glutaric anhydride, Py, 80 °C, 99%; xii, Wang resin, DCC, DMAP, CH_2Cl_2, 20 °C; xiii, Et_3B in hexane, RI:toluene = 4:1, 100 °C; xiv, TFA, CH_2Cl_2, 20 °C.

presence of triethylamine, and then treatment of the resulting mesylate with *N*-hydroxyphthalimide in one-pot afforded the imide **6** in 71% yield (Scheme 3). Treatment of **6** with hydrazine monohydrate and subsequent condensation of the resulting alkoxyamine with 2,3-isopropylidene-D-glyceraldehyde gave the chiral oxime ether **7**, which was easily converted to the secondary alcohol **8**. The reaction of **8** with acryloyl chloride followed by treatment with pyridinium toluene-*p*-sulfonate in MeOH gave deprotected benzyl alcohol, which was then treated with glutaric anhydride to give carboxylic acid **9** (Scheme 3). The carboxylic acid **9** was attached to Wang resin by treatment with DCC in the presence of DMAP in CH_2Cl_2 at 20 °C for 12 h to give the resin-bound oxime ether **10**.

The reaction of **10** with an ethyl radical proceeded effectively by treatment with triethylborane to give the chiral oxacycles **11c** in 92% yield after cleavage of the resin, which was carried out under acidic reaction conditions due to the base-sensitivity of **11c** (Scheme 3). However, the reactivity of chiral oxime ether **10** towards other alkyl radicals was quite different from that of oxime ether **3**. The treatment of **10** with Pr^{i}I (24 equiv. × 3) and triethylborane (6 equiv. × 3) in toluene at 100 °C gave a large amount of the ethylated product **11c** and a small amount of the isopropylated product **11a** after cleavage of the resin. This result suggests that, in this reaction, the addition of ethyl radical, generated from triethylborane, competes with the iodine atom-transfer process because triethylborane, having Lewis acidic character, probably coordinates the substrate on the polymer-support and is concentrated on the surface of the resin. A similar trend has been observed in our previous studies.[3] Selective formation of the desired isopropylated product **11a** was observed in the reaction of **10** (50 mg) using triethylborane (5.9 equiv. × 3) in Pr^{i}I–toluene (4:1, v/v, 5 mL) at 100 °C. Based on ^{1}H-NMR analysis, a 8:1 diastereomeric mixture of the isopropylated oxacyclic product **11a** was obtained in 54% isolated yield. Additionally, in the solid-phase reactions, the often tedious workup to remove excess reagents from the reaction mixture was eliminated simply by washing the resin with solvents. The addition of a bulky cyclohexyl radical proceeded in slightly low chemical efficiency under the same reaction conditions to give the alkylated product **11b** but with a similar diastereoselectivity.

In conclusion, we have demonstrated that tandem radical reactions are an excellent method for the stereoselective construction of multi carbon–carbon bonds on solid support.

This work was supported by research grants from the Ministry of Education, Science, Sports and Culture of Japan and the Science Research Promotion Fund of the Japan Private School Promotion Foundation. H. M. gratefully acknowledges financial support from the Takeda Science Foundation and the Fujisawa Foundation, Japan. This investigation was supported in part by the Memorial Foundation for Medical and Pharmaceutical Research.

Notes and references

1 (*a*) A. Routledge, C. Abell and S. Balasubramanian, *Synlett*, 1997, 61; (*b*) X. Du and R. W. Armstrong, *J. Org. Chem.*, 1997, **62**, 5678; (*c*) M. P. Sibi and S. V. Chandramouli, *Tetrahedron Lett.*, 1997, **38**, 8929; (*d*) X. Du and R. W. Armstrong, *Tetrahedron Lett.*, 1998, **39**, 2281; (*e*) S. Berteina and A. De Mesmaeker, *Tetrahedron Lett.*, 1998, **39**, 5759; (*f*) S. Berteina, S. Wendeborn and A. De Mesmaeker, *Synlett*, 1998, 1231; (*g*) Y. Watanabe, S. Ishikawa, G. Takao and T. Tour, *Tetrahedron Lett.*, 1999, **40**, 3411; (*h*) A.-M. Yim, Y. Vidal, P. Viallefont and J. Martinez, *Tetrahedron Lett.*, 1999, **40**, 4535; (*i*) S. Caddick, D. Hamza and S. N. Wadman, *Tetrahedron Lett.*, 1999, **40**, 7285; (*j*) X. Zhu and A. Ganesan, *J. Comb. Chem.*, 1999, **1**, 157; (*k*) E. J. Enholm, M. E. Gallagher, S. Jiang and W. A. Batson, *Org. Lett.*, 2000, **2**, 3355.

2 (*a*) H. Miyabe, Y. Fujishima and T. Naito, *J. Org. Chem.*, 1999, **64**, 2174; (*b*) H. Miyabe, H. Tanaka and T. Naito, *Tetrahedron Lett.*, 1999, **40**, 8387.

3 H. Miyabe, C. Konishi and T. Naito, *Org. Lett.*, 2000, **2**, 1443.

4 (*a*) T. Naito, *Heterocycles*, 1999, **50**, 505; (*b*) H. Miyabe, M. Torieda, K. Inoue, K. Tajiri, T. Kiguchi and T. Naito, *J. Org. Chem.*, 1998, **63**, 4397; (*c*) H. Miyabe, S. Kanehira, K. Kume, H. Kandori and T. Naito, *Tetrahedron*, 1998, **54**, 5883.

5 H. Miyabe, K. Fujii, T. Goto and T. Naito, *Org. Lett.*, 2000, **2**, 4071.

CHEMCOMM Communication
www.rsc.org/chemcomm

New discovery in the traditional Baylis-Hillman reaction of arylaldehydes with methyl vinyl ketone

Min Shi,* Chao-Qun Li and Jian-Kang Jiang

Laboratory of Organometallic Chemistry, Shanghai Institute of Organic Chemistry, Chinese Academy of Sciences, 354 Fenglin Lu, Shanghai 200032 China. E-mail: mshi@pub.sioc.ac.cn

Received (in Cambridge, UK) 31st January 2001, Accepted 13th March 2001
First published as an Advance Article on the web 10th April 2001

In the Baylis-Hillman reaction of arylaldehydes with methyl vinyl ketone, we found that, besides the normal Baylis-Hillman reaction product 1, the diadduct 2 can also be formed at the same time and the yield of 2 can reach 55% by increasing the amount of methyl vinyl ketone; but for acrylonitrile and methyl acrylate, only the normal Baylis-Hillman adduct was obtained; the substituent's effects were also examined and a plausible reaction mechanism was proposed for the formation of 2.

The Baylis-Hillman reaction has progressed,[1] and now includes a catalytic asymmetric version,[2] since Baylis and Hillman first reported the reaction of acetaldehyde with ethyl acrylate and acrylonitrile in the presence of catalytic amounts of 1,4-diazabicyclo[2,2,2]octane (DABCO) in 1972.[3] However, during our own investigation on this simple and useful reaction,[4] we found that, in the reaction of arylaldehydes with methyl vinyl ketone (MVK) catalyzed by DABCO, the reaction products are not as simple as those reported before. For example, using *p*-nitrobenzaldehyde (1.0 eq.) and MVK (2.0 eq.) as substrates in the presence of catalytic amounts of DABCO (0.1 eq.) in DMSO or DMF, we found that, besides the normal Baylis-Hillman reaction product **1a** compound **2a** was also formed at the same time as a *syn* and *anti* mixture (2 : 3)[5] (Scheme 1, Table 1, entries 1–3). If using *p*-dimethylaminopyridine (DMAP) as a Lewis base in DMSO or DMF, **1a** was exclusively obtained in high yields under the same reaction conditions (Scheme 1, Table 1, entries 4–5). However, in CH_2Cl_2 using DMAP as a Lewis base, **1a** and **2a** were formed along with **3a**, a Michael addition product of **1a** with MVK (Scheme 2).[6] At present, we do not understand why **3a** should be formed in CH_2Cl_2. Increasing the amount of MVK in the reaction system raised the yield of **2a**. Using 4.0 or 8.0 eq. of MVK, the yield of **2a** reached 53 and 55%, respectively (Table 1, entries 6 and 7). The reaction temperature slightly affected the yield of **2a** (Table 1, entries 8 and 9). At higher temperature, the dimer of MVK was formed as well.[7] The formation of **2a** indicates that another important reaction process can operate in the traditional Bayliss-Hillman reaction.

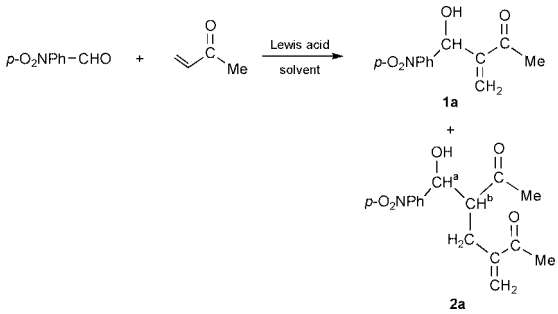

Scheme 1

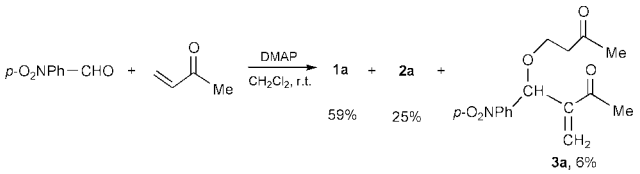

Scheme 2

For *m*-nitrobenzaldehyde, *p*-bromo or *p*-chlorobenzaldehyde and *trans*-cinnamaldehyde similar results were obtained (Scheme 3, Table 2, entries 3, 9, 11, 16). Using DMAP as a Lewis base, **1** was exclusively formed (Scheme 3, Table 2, entries 4, 10, 12, 17). For benzaldehyde or aliphatic aldehyde, only the corresponding normal Baylis-Hillman adducts **1** were formed under the same reaction conditions (Scheme 3, Table 2,

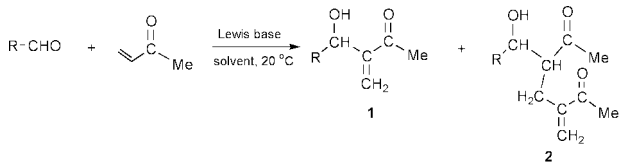

b: R = *m*-NO_2Ph, **c**: R = *o*-NO_2Ph, **d**: R = *p*-BrPh, **e**: R = *p*-ClPh, **f**: R = Ph, **g**: R = *p*-EtPh, **h**: R = PhCH=CH, **i**: R = $CH_3(CH_2)_3$.

Scheme 3

Table 1 Baylis-Hillman reactions of aldehydes (1.0 eq.) with methyl vinyl ketone (2.0 eq.) in the presence of Lewis base (0.1 eq.)

						Yield (%)[a]	
Entry	R	Lewis base	Solvent	Temp./°C	Time/h	**1a**	**2a**[e]
1	*p*-NO_2Ph	DABCO	DMSO	20	40	60	20
2	*p*-NO_2Ph	DABCO	DMF	20	40	63	23
3	*p*-NO_2Ph	DABCO	CH_2Cl_2	20	40	61	34
4	*p*-NO_2Ph	DMAP	DMSO	20	40	85	0
5	*p*-NO_2Ph	DMAP	DMF	20	40	83	0
6	*p*-NO_2Ph	DABCO	DMF[b]	20	60	41	53
7	*p*-NO_2Ph	DABCO	DMF[c]	20	60	41	55
8	*p*-NO_2Ph	DABCO	DMF[b]	−30	60	54	40
9[d]	*p*-NO_2Ph	DABCO	DMF[b]	70	60	37	56

[a] Isolated yields. [b] Mole ratio of aldehyde : MVK = 1 : 4. [c] Mole ratio of aldehyde : MVK = 1 : 8. [d] Dimer of MVK was formed. [e] *syn* : *anti* = 2 : 3.

Table 2 Baylis-Hillman reactions of aldehydes (1.0 eq.) with methyl vinyl ketone (2.0 eq.) in the presence of Lewis base (0.1 eq.)

					Yield (%)[a]	
Entry	R	Lewis base	Solvent	Time	**1**	**2**[d]
1	*m*-NO_2Ph	DABCO	DMSO	20	50	27
2	*m*-NO_2Ph	DABCO	DMF	20	50	27
3	*m*-NO_2Ph	DABCO	DMF[b]	20	50	41
4	*m*-NO_2Ph	DMAP	DMF	20	87	0
5	*o*-NO_2Ph	DABCO	DMF	50	83	0
6	*o*-NO_2Ph	DMAP	DMF	20	83	0
7	*o*-NO_2Ph	DMAP	CH_2Cl_2	40	81	0
8	*p*-BrPh	DABCO	DMF	140	57	25
9	*p*-BrPh	DABCO	DMF[b]	80	51	36
10	*p*-BrPh	DMAP	DMF	120	88	0
11	*p*-ClPh	DABCO	DMF[b]	160	62	33
12	*p*-ClPh	DMAP	DMF	60	67	0
13	Ph	DABCO	DMF	90	73	0
14	Ph	DMAP	DMF	130	54	0
15	*p*-EtPh	DMAP	DMF	7d	0	0
16	PhCH=CH	DABCO	DMF[b]	60	57	24
17	PhCH=CH	DMAP	DMF[b]	49	60	0
18[c]	$CH_3(CH_2)_3$	DABCO	DMF[b]	49	15	0

[a] Isolated yields. [b] Mole ratio of aldehyde : MVK = 1 : 4. [c] Dimer of MVK was formed. [d] *syn* : *anti* = 2 : 3.

entries 13, 18) and for *p*-ethylbenzaldehyde, no reaction occurred at all (Scheme 3, Table 2, entry 15). But surprisingly we found that, for *o*-nitrobenzaldehyde, the Baylis-Hillman adduct **1** was produced as the single product (Table 2, entries 4–6). This result suggested that the *o*-nitro group on the phenyl ring could block out the further reaction of **1** with MVK.

In the traditional Baylis-Hillman reaction for simple methyl vinyl ketone (MVK), this phenomenon has never been reported before. Only in the reaction of dicarbonyl compounds with acrylonitrile in the presence of DABCO, the diadduct, which was thought to be derived either from reaction of acrylonitrile dimer with starting material or from the conjugated addition of the anion derived from a second molecule of acrylonitrile to the Baylis-Hillman adduct, was obtained as a minor product.[8] In order to clarify the mechanism for the formation of **2a**, we carried out the reactions of **1a** (1.0 eq.) with MVK (2.0–8.0 eq.) and *p*-nitrobenzaldehyde (1.0 eq.) with MVK dimer (1.0 eq.) in the presence of catalytic amounts of DABCO (0.1 eq.), respectively (Scheme 4). We found that **2a** was indeed formed

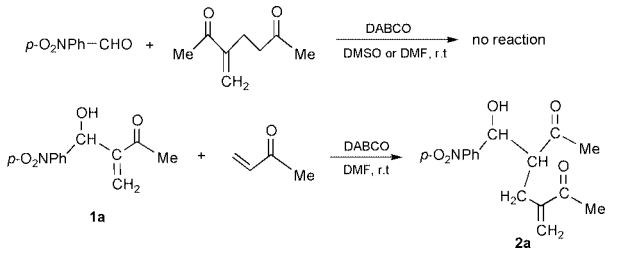

Scheme 4

from the reaction of **1a** with methyl vinyl ketone (MVK) in the presence of catalytic amounts of DABCO (0.1 eq.) as a *syn* and *anti* mixture (2 : 3), but that no reactions occurred between *p*-nitrobenzaldehyde and MVK dimer under the same reaction conditions (Scheme 4). The yield of **2a** can reach 41 or 48% if using 4.0 or 8.0 eq. of MVK, respectively. Thus, we can conclude that two reactions occur for the traditional Baylis-Hillman reaction of aryaldehydes with MVK. One is the normal Baylis-Hillman reaction which is the 1,2-addition of the anion derived from MVK to *p*-nitrobenzaldehyde. The other is the conjugated addition (Michael addition) of the anion derived from a second molecule of MVK to **1**.

In conclusion, we found that in the Baylis-Hillman reaction of arylaldehydes with methyl vinyl ketone, besides the normal Baylis-Hillman adduct **1**, diadduct **2** was also formed and was confirmed to be derived from the further reaction of **1** with MVK *via* a conjugated addition reaction. Efforts are underway to elucidate the mechanistic details of this reaction and to disclose the scope and limitations of this reaction. Work along this line is currently in progress.

We thank the State Key Project of Basic Research (Project 973) (No. G2000048007) and the National Natural Science Foundation of China for financial support. We also thank the Inoue Photochirogenesis Project (ERATO, JST) for chemical reagents.

Notes and references

1 E. Ciganek, *Org. React.*, 1997, **51**, 201; D. Basavaiah, P. D. Rao and R. S. Hyma, *Tetrahedron*, 1996, **52**, 8001; S. E. Drewes and G. H. P. Roos, *Tetrahedron*, 1988, **44**, 4653; L. J. Brzezinski, S. Rafel and J. M. Leahy, *J. Am. Chem. Soc.*, 1997, **119**, 4317; T. Miyakoshi and S. Saito, *Nippon Kagaku Kaishi*, 1983, 1623; *Chem. Abstr.*, 1984, **100**, 156191g; I. E. Marko, P. G. Giles and N. J. Hindley, *Tetrahedron*, 1997, **53**, 1015; H. Richter and G. Jung, *Tetrahedron Lett.*, 1998, **39**, 2729; A. G. M. Barrett, A. S. Cook and A. Kamimura, *Chem. Commun.*, 1999, 2533; E. P. Kunidig, L. H. Xu, P. Romanens and G. Bernardinelli, *Tetrahedron Lett.*, 1993, **34**, 7049; V. Aggarawal, A. Mereu, G. J. Tarver and R. MaCague, *J. Org. Chem.*, 1998, **63**, 7183; M. Kawamura and S. Kobayashi, *Tetrahedron Lett.*, 1999, **40**, 1539; T. Kataoka, T. Iwama, S.-i. Tsujiyama, T. Iwamura and S.-i. Watanaba, *Tetrahedron*, 1998, **54**, 11 813; T. Kataoka, T. Iwama, S. Kinoshita, Y. Tsujiyama, T. Iwamura and S. Watanabe, *Synlett.*, 1999, 197; T. Kataoka, T. Iwama, S. Tsujiyama, K. Kanematsu, T. Iwamura and S. Watanabe, *Chem. Lett.*, 1999, 257; T. Kataoka, T. Iwama and S. Tsujiyama, *Chem. Commun.*, 1998, 197; M. Ono, K. Nishimura, Y. Nagaoka and K. Tomioka, *Tetrahedron Lett.*, 1999, **40**, 1509; G. Li, H.-X. Wei, J. J. Gao and T. D. Caputo, *Tetrahedron Lett.*, 2000, **41**, 1; T. Kataoka, H. Kinoshita, T. Iwama, S.-i. Tsujiyama, T. Iwamura, S.-i. Watanabe, O. Muraoka and G. Tanabe, *Tetrahedron*, 2000, **56**, 4725; G. Li, J. Gao, H.-X. Wei and M. Enright, *Org. Lett.*, 2000, **2**, 617.

2 Y. Iwabuchi, M. Nakatani, N. Yokoyama and S. Hatakeyama, *J. Am. Chem. Soc.*, 1999, **121**, 10 219.

3 A. B. Baylis and M. E. D. Hillman, *Ger. Offen.*, 1972, **2**, 155, 113; *Chem. Abstr.*, 1972, **77**, 34174q; M. E. D. Hillman and A. B. Baylis, *US Pat.*, 1973, 3,743,669; K. Morita, Z. Suzuki and H. Hirose, *Bull. Chem. Soc. Jpn.*, 1968, **41**, 2815.

4 M. Shi and J.-K. Jiang, *Tetrahedron*, 2000, **56**, 4793; M. Shi, J.-K. Jiang and Y.-S. Feng, *Org. Lett.*, 2000, **2**, 2397.

5 The *syn* and *anti* ratio of **2a** was determined by the ^{1}H NMR spectral data based on the *J* value of H^a and H^b (Scheme 1) because the *anti*-isomer usually has bigger *J* value (for *anti*-**2a**: JH^aH^b = 6.3 Hz, for *syn*-**2a**: JH^aH^b = 2.8 Hz). The spectral data of **1a**: mp 76–77 °C; IR (KBr) ν 1658 cm^{-1} (C=O); ^{1}H NMR ($CDCl_3$, 300 MHz, TMS) δ 2.37 (3H, s, Me), 3.34 (1H, d, *J* = 5.3 Hz, OH), 5.69 (1H d, *J* = 5.3 Hz), 6.04 (1H, s), 6.28 (1H, s), 7.56 (2H, d, *J* 8.6 Hz, Ar), 8.25 (2H, d, *J* 8.6 Hz, Ar); MS (EI) *m*/*z* 220 (M^+ − 1, 20.9), 204 (M^+ − 17, 100), 174 (M^+ − 47, 88.1). The spectral data of *anti*-**2a**: a colorless oil; IR (KBr) ν 1709 and 1676 cm^{-1} (C=O); ^{1}H NMR ($CDCl_3$, 300 MHz, TMS) δ 2.07 (3H, s, Me), 2.37 (3H, s, Me), 2.52 (1H, dd, *J* = 13.8, 5.2 Hz, CH), 2.60 (1H, dd, *J* = 13.8, 7.9 Hz, CH), 3.15–3.25 (1H, m, CH), 3.76 (1H, d, *J* = 7.4 Hz, OH), 4.80 (1H, t, *J* = 6.3 Hz, CH), 5.92 (1H, s), 6.12 (1H, s), 7.55 (2H, d, *J* = 9.4 Hz, Ar), 8.22 (2H, d, *J* = 9.4 Hz, Ar); MS (EI) *m*/*z* 274 (M^+ − 18, 13.2), 232 (M^+ − 59, 24.5), 97 (M^+ − 194, 44), 43 (M^+ − 248, 100). The spectral data of *syn*-**2a**: a colorless oil; IR (KBr) ν 1709 and 1676 cm^{-1} (C=O); ^{1}H NMR ($CDCl_3$, 300 MHz, TMS) δ 2.04 (3H, s, Me), 2.25 (3H, s, Me) 2.52 (1H, dd, *J* = 13.8, 5.2 Hz, CH) 2.60 (1H, dd, *J* = 13.8, 7.9 Hz, CH), 3.15–3.25 (1H, m, CH), 3.67 (1H, d, *J* = 2.8 Hz, OH), 5.0 (1H, t, *J* = 2.8 Hz, CH), 5.73 (1H, s), 5.97 (1H, s), 7.53 (2H, d, *J* = 9.4 Hz, Ar), 8.20 (2H, d, *J* = 9.4 Hz, Ar); MS (EI) *m*/*z* 274 (M^+ − 18, 13.2), 232 (M^+ − 59, 24.5), 97 (M^+ − 194, 44), 43 (M^+ − 248, 100).

6 The spectral data of **3a**: a colorless oil; IR (KBr) ν 1712 and 1675 cm^{-1} (C=O); ^{1}H NMR ($CDCl_3$, 300 MHz, TMS) δ 2.15 (3H, s, Me), 2.78 (3H, s, Me), 2.69 (2H, t, *J* = 7.2 Hz, CH_2), 3.50–3.62 (1H, m, CH), 3.62–3.74 (1H, m, H), 5.4 (1H, s), 6.23 (1H, s), 7.53 (2H, d, *J* = 9.4 Hz, Ar), 8.20 (2H, d, *J* = 9.4 Hz, Ar); MS (EI) *m*/*z* 291 (M^+, 3.2), 274 (M^+ − 18, 10.5), 72 (M^+ − 219, 24.2), 43 (M^+ − 248, 100).

7 Dimer could be obtained from methyl vinyl ketone in the presence of DABCO. The ^{1}H NMR data of dimer: IR (KBr) ν 1714 and 1676 cm^{-1} (C=O); ^{1}H NMR ($CDCl_3$, 300 MHz) δ 2.07 (3H, s, Me), 2.29 (3H, s, Me), 2.40–2.54 (4H, m, CH_2), 5.80 (1H, s, CH), 6.0 (1H, s, CH); MS (EI) *m*/*z* 141 (MH^+, 0.84), 125 (M^+ − 15, 60), 97 (M^+ − 43, 100), 43 (M^+ − 97, 100).

8 G. M. Strunz, R. Bethell, G. Sampson and P. White, *Can. J. Chem.*, 1995, **73**, 1666.

CHEMCOMM Communication
www.rsc.org/chemcomm

Stereocontrolled synthesis of 2,4,5-trisubstituted tetrahydropyrans

Eiman H. Al-Mutairi,[a] Stuart R. Crosby,[a] Julia Darzi,[a] John R. Harding,[b] Rachael A. Hughes,[a] Clare D. King,[b] Thomas J. Simpson,[a] Robert W. Smith[a] and Christine L. Willis*[a]

[a] *School of Chemistry, University of Bristol, Cantock's Close, Bristol, UK BS8 1TS. E-mail: chris.willis@bristol.ac.uk*
[b] *AstraZeneca UK Ltd, Mereside, Alderley Park, Macclesfield, UK SK10 4TG*

Received (in Cambridge, UK) 13th February 2001, Accepted 12th March 2001
First published as an Advance Article on the web 11th April 2001

Cyclisation of homoallylic acetals under acidic conditions leads to the formation of 2,4,5-trisubstituted tetrahydropyrans with the creation of two new asymmetric centres with excellent stereocontrol. By varying the acid and the nucleophile, the reaction may be adapted for the preparation of 2,4,5-trisubstituted tetrahydropyrans with either a halide, alcohol, acetate or amide at C-4.

Substituted tetrahydropyrans are common features of many natural products and biologically active compounds and many strategies for their synthesis have been reported. One valuable approach to the preparation of tetrahydropyrans is a Prins type cyclisation in which treatment of a homoallylic acetal (or a mixture of a homoallylic alcohol and carbonyl compound) with acid leads to formation of an oxocarbenium cation intermediate which undergoes an intramolecular reaction with the alkene.[1] Upon cyclisation, the fate of the resulting carbocation intermediate is dependent upon the reaction conditions and substrates employed. Thus, Thompson and coworkers have shown that acetals derived from (*E*)- or (*Z*)-hex-3-en-1-ol cyclised in the presence of titanium tetrabromide or tetrachloride to give the *trans*- or *cis*-3-ethyl-4-halotetrahydropyrans respectively with good stereocontrol.[2] Prins type cyclisations have been widely used for the synthesis of 2,4,6-trisubstituted tetrahydropyrans[3] but examples of their use in the preparation of tetrahydropyrans with other substitution patterns has been rather more limited.[4] In this paper we describe a direct method for the preparation of 2,4,5-trisubstituted tetrahydropyrans from homoallylic acetals[5] which enables the creation of two asymmetric centres with excellent stereocontrol and in which a variety of functional groups may be introduced at C-4.

The substrate used for our initial cyclisation studies was the homoallylic acetal **2** which was readily prepared in 4 steps from ethyl 3-hydroxybutanoate **1** (readily available in both enantiomeric forms) by MEM (methoxyethoxymethyl) protection of the alcohol, DIBAL-H reduction to the aldehyde followed by Horner Wadsworth Emmons chain extension with triethyl phosphonoacetate and finally a further DIBAL-H reduction of the resultant (*E*)-α,β-unsaturated ester. In the first cyclisation study, homoallylic acetal **2** was treated with titanium tetrachloride in CH_2Cl_2 giving the 2,5-disubstituted 4-chlorotetrahydropyran **3** in 63% yield (Scheme 1). From the ^1H and ^{13}C-NMR spectra and NOE studies it was apparent that a single product had been isolated in which all three substituents were in an equatorial position.[6] When the primary alcohol of **2** was protected as the TBDPS ether **4**, the $TiCl_4$ mediated reaction gave an improved 74% yield of the cyclic product **5** again as a single diastereomer. By using other Lewis acids, further halides could be introduced at C-4 of the tetrahydropyran. Thus, treatment of **4** with titanium tetrabromide gave the 4-bromo derivative **6** in 85% yield and reaction of **2** with $BF_3{\cdot}Et_2O$ in CH_2Cl_2 gave a 55% yield of the 2,5-disubstituted 4-fluorotetrahydropyran **7**.

The synthetic utility of these cyclisations would be greatly extended if functional groups other than a halide could be introduced at C-4. Several methods have been reported for the introduction of oxygenated substituents at C-4 in Prins type

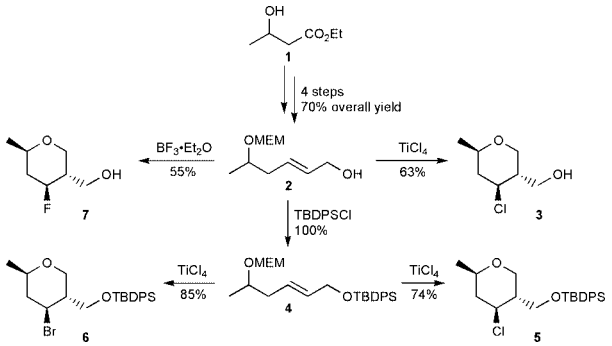

Scheme 1

cyclisations with varying success. These include the use of mercuric triflate,[7] scandium triflate,[8] $BF_3{\cdot}Et_2O$–AcOH,[3e,9] and TFAA–AcOH.[3f] We investigated a range of methods to cyclise homoallylic acetal **2** with the introduction of an oxygen nucleophile into C-4 of a tetrahydropyran. One of the more efficient procedures proved to be treatment of **2** with $BF_3{\cdot}Et_2O$ in the presence of AcOH as the nucleophile and TMSOAc to act as a fluoride trap to prevent competing formation of the 4-fluoro derivative **7**. Under these conditions, acetate **8** was obtained in 53% yield. Alternatively, treatment of **2** with anhydrous trifluoroacetic acid gave diol **9** in 72% yield after hydrolysis of the resultant 4-trifluoroacetate with potassium carbonate in MeOH, (Scheme 2). Again these reactions proceeded with good stereocontrol and only the all equatorial diastereomer was isolated.

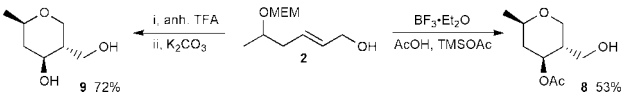

Scheme 2

To further examine the use of TFA for the cyclisation of homoallylic acetals to give 2,4,5-trisubstituted tetrahydropyrans, a series of substrates with a *cis* double bond and a SEM, MEM or MOM group were prepared from pent-4-yn-2-ol **10** (Scheme 3). The hydroxy group of **10** was converted to the acetal prior to reaction of the alkyne with butyllithium, $BF_3{\cdot}Et_2O$ and propylene oxide giving a mixture of diastereomeric alcohols **11**. Catalytic hydrogenation of **11** in the presence of Lindlar's catalyst gave the (*Z*)-alkenols **12** and then oxidation under Swern conditions gave the three required homoallylic acetals **13**. Treatment of the SEM acetal **13** with aqueous TFAA gave three products in which the tetrahydropyran **14** was formed in only 18% yield. The major products were the diastereomeric tetrahydrofurans **15** and **16** formed *via* rearrangement of the double bond into conjugation, hydrolysis of the acetal and an intramolecular conjugate addition to the resultant enone.

However, treatment of each of the acetals **13** with anhydrous TFA in dichloromethane gave, after hydrolysis of the initially formed trifluoroacetate, the 2,5-disubstituted-4-hydroxytetra-

DOI: 10.1039/b101414p

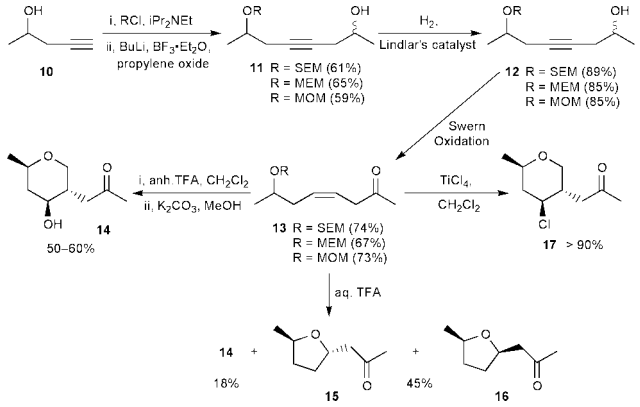

Scheme 3

hydropyran **14** in 50–60% yield with all three substituents again in an equatorial position. Interestingly the stereochemical outcome of this reaction differs from that reported for the cyclisation of MEM protected (*Z*)-hex-3-en-1-ol with $TiCl_4$ in which a *cis* relationship of the vicinal halide and alkyl group predominated.[2] In addition, Rychnovsky and co-workers have shown that although the $TiCl_4$ mediated cyclisation of an (*E*)-unsaturated homoallylic acetal gives an all equatorial 2,5,6-trisubstituted 4-chlorotetrahydropyran, the reaction on the analogous (*Z*)-isomer leads to a mixture of diastereomers in which the 4-chloro-5-alkyl substituents are *cis* in the major isomer.[9] Thus the MEM acetal **13** was cyclised using $TiCl_4$ and the product **17** was obtained in 92% yield again with all the substituents equatorial.

To the best of our knowledge Prins type cyclisations of homoallylic acetals to tetrahydropyrans have never been conducted in the presence of nitrogen nucleophiles although products from such reactions would be of great general value in synthesis. It would be expected that the acidic reaction conditions required for formation of the oxocarbenium cation would not be compatible with the use of amines as nucleophiles. Indeed we found this to be the case. However, on treatment of homoallylic acetal **4** with triflic acid in acetonitrile the 4-amido derivative **18** was obtained in excellent yield (Scheme 4).

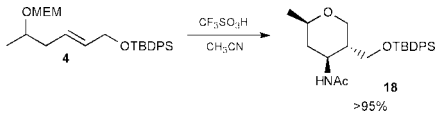

Scheme 4

In conclusion, Prins type cyclisation of homoallylic acetals provides a versatile approach to the synthesis of 2,4,5-trisubstituted tetrahydropyrans. Our initial investigations indicate that excellent stereocontrol may be achieved with both *cis* and *trans* alkenes giving the all equatorial product and this merits further investigation. By varying the acid and nucleophile a halide (bromide, chloride or fluoride), oxygenated group (hydroxy, ether or ester) or a nitrogen containing substituent may be introduced at C-4 of the tetrahydropyran.

We are grateful to the following for funding: AstraZeneca and the EPSRC (R. A. H.), Glaxo Wellcome (R. W. S.) and the BBSRC (S. C.).

Notes and references

1 Review: B. B. Snider, in *Comprehensive Organic Synthesis*, ed. B. M. Trost and I. Fleming, Pergamon Press, 1991, vol. 2, p. 527.
2 R. C. Winstead, T. H. Simpson, G. A. Lock, M. D. Schiavelli and D. W. Thompson, *J. Org. Chem.*, 1986, **51**, 275.
3 For example: (*a*) L. Coppi, A. Ricci and M. Taddei, *Tetrahedron Lett.*, 1987, **28**, 973; (*b*) Z. Y. Wei, J. S. Li and D. Wang, *Tetrahedron Lett.*, 1987, **28**, 3441; (*c*) L. Coppi, R. Ricci and M. Taddei, *J. Org. Chem.*, 1988, **53**, 913; (*d*) I. E. Marko and F. Chelle, *Tetrahedron Lett.*, 1997, **38**, 2895; (*e*) G. S. Vismanathan, J. Yang and C.-J. Li, *Org. Lett.*, 1999, **1**, 993; (*f*) S. D. Rychnovsky, G. Yang, Y. Hu and U. R. Khire, *J. Org. Chem.*, 1997, **62**, 3022; (*g*) S. D. Rychnovsky, Y. Hu and B. Ellsworth, *Tetrahedron Lett.*, 1998, **39**, 7271; (*h*) J. Yang, G. S. Viswanathan and C.-J. Li, *Tetrahedron Lett.*, 1999, **40**, 1627; (*i*) M. J. Cloninger and L. E. Overman, *J. Am. Chem. Soc.*, 1999, **121**, 1092.
4 For example: *3,4-Disubstitution*, P. R. Stapp, *J. Org. Chem.*, 1969, **34**, 479; *2,4-disubstitution*, I. T. Kay and E. G. Williams, *Tetrahedron Lett.*, 1983, **24**, 5915; C. Chen and P. S. Mariano, *J. Org. Chem.*, 2000, **63**, 3252; *2,5,6-trisubstitution*, P. Mohr, *Tetrahedron Lett.*, 1995, **36**, 2453; *2,3,4,5,6-pentasubstitution*, S. D. Rychnovsky and C. R. Thomas, *Org. Lett.*, 2000, **2**, 1217.
5 The only other example of the preparation of a 2,4,5-trisubstituted tetrahydropyran *via* a Prins cyclisation of a homoallylic acetal is that of I. T. Kay and D. Bartholomew, *Tetrahedron Lett.*, 1984, **25**, 2035.
6 All compounds were fully characterised, spectroscopic data for 4-chlorotetrahydropyran **3**: δ_H(300 MHz, $CDCl_3$) 1.22 (3H, d, *J* 6.3, 2-CH_3), 1.69 (1H, dt, *J* 13.0 and 11.5, 3-H_{ax}), 1.92 (1H, m, 5-H), 2.04 (1H, br s, OH), 2.21 (1H, ddd, *J* 13.0, 4.5 and 2.0, 3-H_{eq}), 3.40 (1H, t, *J* 12.0, 6-H_{ax}), 3.46 (1H, m, 2-H), 3.79 (2H, m, 5-CH_2OH), 4.03 (1H, dt, *J* 11.5 and 4.5, 4-H), 4.09 (1H, dd, *J* 12.0 and 4.5, 6-H_{eq}); δ_C(75 MHz, $CDCl_3$) 21.3 (2-CH_3), 44.2 (C-3), 47.0 (C-5), 57.6 (C-4), 61.0 (5-CH_2OH), 69.6 (C-6), 73.5 (C-2); *m*/*z* (CI) 167 and 165 (MH^+, 4 and 14%), 149 (5), 147 (15), 129 (75), 111 (48) and 85 (100). (Found: MH^+ 165.0685 $C_7H_{14}O_2Cl$ requires 165.0682).
7 M. Nishizawa, T. Shigaraki, H. Takao, H. Imagawa and T. Sugihara, *Tetrahedron Lett.*, 1999, **40**, 1153.
8 W.-C. Zhang, G. S. Viswanathan and C.-J. Li, *Chem. Commun.*, 1999, 291; W.-C. Zhang and C.-J. Li, *Tetrahedron*, 2000, **56**, 2403.
9 Y. Hu, D. J. Skalitzky and S. D. Rychnovsky, *Tetrahedron Lett.*, 1996, **37**, 8679.

CHEMCOMM Communication
www.rsc.org/chemcomm

Solid-phase synthesis of oxo(mercaptoacetylglycylglycylglycine)rhenate(v)

José Antonio Bravo,[a] Alex Gibson,[b] Karen Loughran[b] and Mark Bradley*[a]

[a] *Department of Chemistry, University of Southampton, Southampton, UK SO17 1BJ. E-mail: MB14@soton.ac.uk*
[b] *Nycomed Amersham PLC of Amersham Place, Little Chalfont, Buckinghamshire, UK HP7 9NA*

Received (in Cambridge, UK) 2nd January 2001, Accepted 7th March 2001
First published as an Advance Article on the web 11th April 2001

The solid phase synthesis of tetrabutylammonium oxo-(mercaptoacetylglycylglycylglycine) rhenate(v) has been achieved by utilising $ReOCl_3(PPh_3)_2$ as a stable source of Re(v) and provides a synthesis of bi-functional chelates for use in nuclear medicine.

Over the last 10 years, there has been tremendous progress in transferring solution-phase expertise into solid-phase organic synthesis (SPOS). Here, we wish to report the solid-phase synthesis of oxo(mercaptoacetylglycylglycylglycine)rhenate(v) ($ReOMAG_3$)[1] an analogue of ($^{99m}TcOMAG_3$) the widely used renal imaging agent. The advantages of a solid phase approach in this area being the relative ease of synthesis, the ability to directly load the resin with the metal agent of choice, and the prospect of making bead based libraries that can be readily screened using radioactivity to pinpoint the desired ligand. The physical properties of ^{186}Re (1.07 MeV beta max, 3.7 d half life, 137 keV gamma photons (9%) and ^{188}Re (2.12 MeV beta max, 0.9 d half life, 155 KeV gamma photons (15%)) have prompted nuclear medicine chemists to use $^{186/188}Re$-labelled bio-molecules[2] as therapeutic tools in the treatment of cancers. Another important driving force is that Re chemistry can provide a non-radioactive alternative to ^{99m}Tc, the most widely used radionuclide in diagnostic nuclear medicine, when studying the coordination chemistry of Tc.[3] This is due to the lanthanide contraction such that Re and Tc have very similar physical characteristics, although rhenium complexes are harder to reduce and kinetically more inert than those of technetium. In the indirect labelling method, a bifunctional chelate is first metallated and then conjugated to a monoclonal antibody capable of targeting a specific tumour-associated antigen. $ReOMAG_3$ has been the choice of preformed chelate by a number of groups.

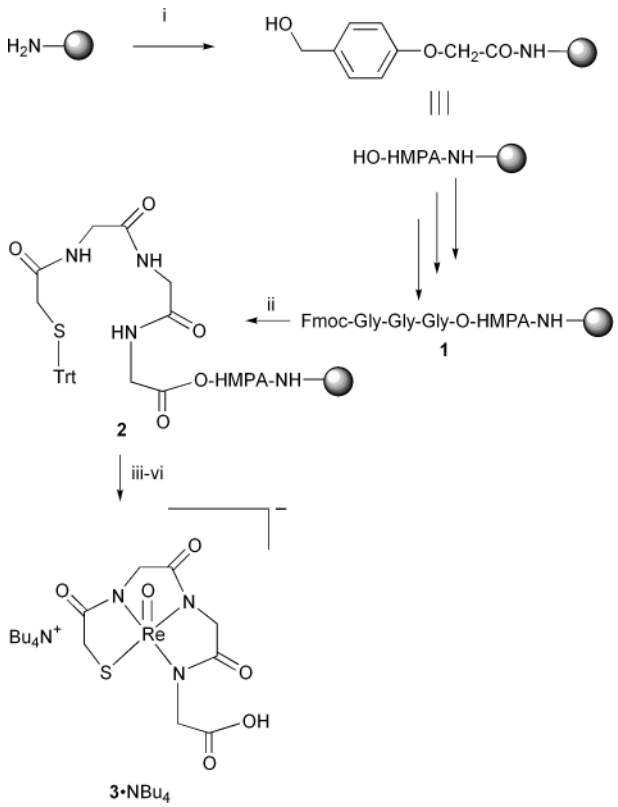

Scheme 1 Solid-phase synthesis of $ReOMAG_3$ (**3**). (i) 4-Hydroxymethylphenoxyacetic acid, DIC, HOBt, CH_2Cl_2–DMF (4 : 1), overnight; (ii) (a) 20% piperidine, DMF, (b) Trt-S-CH_2CO_2H, DIC, HOBt, CH_2Cl_2:DMF (4 : 1), 4 h; (iii) 2% TFA, 2% TIPS; (iv) $ReOCl_3(PPh_3)_2$, DBU, DMF, 18 h; (v) 60% TFA, 5% H_2O in CH_2Cl_2, 4 h; (vi) Bu_4NCl, H_2O–CH_2Cl_2.

4-Hydroxymethylphenoxyacetic acid (HMPA) (Scheme 1) was anchored onto TentaGel-S-NH_2 (130 μm, 0.29 mmol g^{-1}, Rapp Polymere) using equimolar amounts of HOBt and DIC.[4] The first Fmoc-Gly residue was attached using a similar procedure but with a catalytic amount of DMAP. Following standard Fmoc chemistry, Fmoc-triglycine (**1**) was synthesised on the solid support. After thoroughly drying the resin was deprotected and subjected to a quantitative ninhydrin test to give a loading of 0.17 mmol g^{-1} (theoretical loading 0.25 mmol g^{-1}). After Fmoc deprotection of **1**, tritylmercaptoacetic acid[5] was coupled to the resin using HOBt and DIC as coupling reagents. The free thiol group was obtained by treating the resin eight times with 2% TFA, 2% TIPS in DCM for 15 min each time. Shorter reaction times were not successful. The resin was then treated with $ReOCl_3(PPh_3)_2$[6] as the most efficient source of Re(v). Optimal conditions were a 1 : 2 molar ratio of Re-$OCl_3(PPh_3)_2$[6] with DBU in DMF for 18 h. The use of higher molar ratios or higher temperatures gave worse results. After

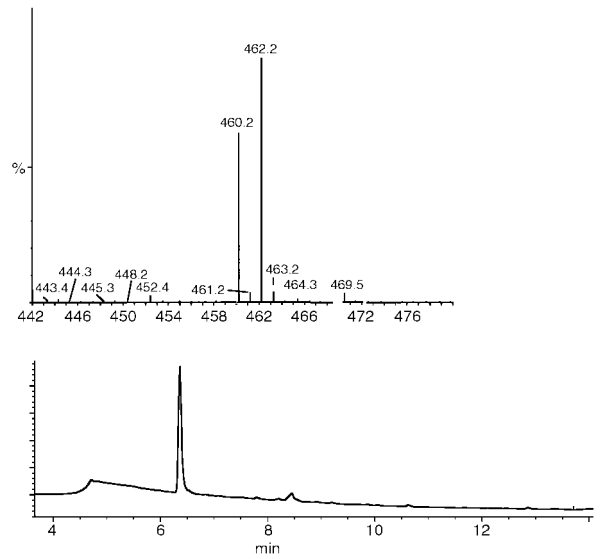

Fig. 1 MS and HPLC analysis of the solid-phase synthesis of $ReOMAG_3$.

DOI: 10.1039/b100004g

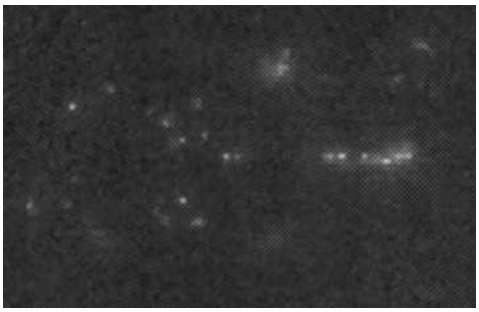

Fig. 2 Phosphoimager scan of resin-bound $^{99m}TcOMAG_3$.

TFA cleavage and counter ion exchange chromatography, $[Bu_4N][ReO(MAG_3)]$ (**3**·NBu_4) was obtained[7] in 91% purity (following RP-HPLC),[8] (Fig. 1). This compound showed identical RP-HPLC retention time, ESMS and IR to a sample prepared in solution following the procedure of Fritzberg *et al*.[9] The same series of reactions was also carried out successfully on aminomethylpolystyrene resin (1% DVB, 1.24 mmol g^{-1}).

To demonstrate the use of resin linked chelates for the screening of resin based libraries of MAG_3 derivatives, a solid phase labelling experiment using MAG_3 as a ligand for ^{99m}Tc was carried-out. In this fashion, Trt-$SMAG_3$ immobilized onto TentaGel-S-NH_2 *via* the HMPA linker was first submitted to trityl deprotection conditions as above and then to $^{99m}TcO_4^{2-}$, sodium gluconate and $SnCl_2$ in saline. After thorough washing of the resin, 45% of the radioactivity was retained. This resin was then swollen in water and carefully plated in a 1% agarose solution poured over a glass surface. Using automatic autoradiography or a Storm Phosphoimager it was possible to localize areas in the gel containing radioactive beads (Fig. 2).

A similar experiment where the thiol deprotection step was intentionally omitted resulted in no ^{99m}Tc complexation, as indicated by the absence of activity in the washed resin. Other controls such as acetylated TentaGel-S-NH_2 submitted to direct labelling conditions ($^{99m}TcO_4$ in saline) or to ligand exchange labelling conditions ($^{99m}TcO_4$, sodium gluconate and $SnCl_2$ in saline) showed no technetium complexation by the polymeric support.

In conclusion the synthesis of tetrabutylammonium oxo-(mercaptoacetylglycylglycylglycine)rhenate(v) has been achieved in high purity by using a preformed Re(v) complex as the source of Re(v). This opens the possibility of screening libraries of ligands for Re affinity and therefore new ligands for binding Tc for medicinal imaging applications.

Notes and references

1 For a solid-phase synthesis of other rhenium(v) oxo complexes see: Y. Shi and S. Sharma, *Bioorg. Med. Chem. Lett*., 1999, **9**, 1469.

2 W. A. Volker and T. J. Hoffman, *Chem Rev*., 1999, **99**, 2269.

3 For reviews see: K. Schwochau, *Angew. Chem., Int. Ed. Engl*, 1994, **33**, 2258; S. Jurisson and J. D. Lydon, *Chem. Rev*., 1999, **99**, 2205; S. Liu and D. S. Edwards, *Chem. Rev*., 1999, **99**, 2235

4 F. Albericio and G. Barany, *Int. J. Peptide Protein Res*., 1985, **26**, 92.

5 D. Brenner, A. Davison, J. Lister-James and A. G. Jones, *Inorg. Chem*., 1984, **23**, 3793.

6 N. P. Johnson, C. J. L. Lock and G. Wilkinson, *Inorg. Synth*., 1967, **9**, 145.

7 Typical procedure: *ca*. 30 mg of resin loaded with Trt-$SMAG_3$ was pre-swollen in CH_2Cl_2 (1mL) for 10 minutes in a peptide vessel. Solvent was removed by applying N_2 pressure. The resin was treated with a solution of 2% TFA, 2% TIPS in CH_2Cl_2 (*ca*. 10 mL × 15 min × 8 times). The resin was washed with CH_2Cl_2 and pre-swollen in DMF for 10 min. After removing excess solvent, a solution of $ReOCl_3(PPh_3)_2$ (23 mg, 28 μmol) and DBU (8.5 μL, 56 μmol) in DMF (3 mL) was added to the resin. After shaking on a mechanical shaker for 12 h at rt, the resin was filtrated and washed thoroughly with DMF, CH_2Cl_2, MeOH and Et_2O. The compound was cleaved from the resin with 60% TFA, 5% H_2O in CH_2Cl_2 for 4 h. TFA was removed *in vacuo* and the residue suspended in H_2O. Bu_4NCl (8 mg, 29 μmol) was added and the compound was extracted into CH_2Cl_2. Negative ESMS: m/z = 462 $[M]^-$. IR: 975 cm^{-1} (Re=O).

8 Analytical HPLC: chromatograms were obtained on a Hewlett Packard HP-1100 system equipped with a Phenomenex Prodigy C18 reverse phase column (3.0 mm × 150 mm). Solvents used were: A: 0.1% TFA in H_2O and B: 0.042% TFA in CH_3CN, gradient 0% B to 100% B over 20 min. The column effluent was monitored using a detector wavelength of 220 nm. The retention time of $ReOMAG_3$ was 6.4 min.

9 T. N. Rao, D. Adhikesavalu, A. Camerman and A. R. Fritzberg, *Inorg. Chim. Acta*, 1991, **180**, 63.

CHEMCOMM Communication
www.rsc.org/chemcomm

Novel acylation of a vinyl group by the reaction of an aldehyde and a vinylselenonium ylide

Shin-ichi Watanabe, Tomokazu Kusumoto, Chikayo Yoshida and Tadashi Kataoka*

Gifu Pharmaceutical University, 6-1 Mitahora-higashi 5-chome, Gifu 502-8585, Japan. E-mail: kataoka@gifu-pu.ac.jp; Fax: +81-58-237-5979; Tel: +81-58-237-3931

Received (in Cambridge, UK) 17th January 2001, Accepted 23rd March 2001
First published as an Advance Article on the web 11th April 2001

Vinylselenonium ylide, which was generated from (*Z*)-vinylselenonium salt with a base such as sodium or potassium hydride, reacted with aromatic aldehydes to produce the α,β-unsaturated ketones, which were obtained in better yields from the aldehydes with an electron-withdrawing group than from those with an electron-donating group.

Generally, vinylonium salts, for example vinylphosphonium,[1] sulfonium,[2] and selenonium[3] salts, are utilized as Michael acceptors against nucleophiles to produce saturated alkyl ylides, which are among the most important synthons of the C–C bond forming reaction. If the α-hydrogen of a vinylonium salt is abstracted by a base, a vinyl onium ylide is formed. There have been few reports about the reactivity of vinylphosphonium ylide, which reacts with carbonyl compounds to afford allene derivatives through the Wittig olefination.[4] However, reports on the reaction of other vinylonium ylides with carbonyl compounds have been lacking.

In the course of our studies on alkenylselenonium salts,[5] we have focused on the reactivity of vinylselenonium ylides with great interest. To our astonishment, the reactions of vinylselenonium ylides with aromatic aldehydes did not bring about the Wittig type reaction but caused an acylation reaction of a vinyl group. Although there have been a few reports on the efficient acylation of the vinyl group using aldehyde *via* alkoxyvanadium[6] or alkoxyzirconocene intermediates,[7] our reaction is quite different from these reactions which use an organometallic reagent. This transformation is a novel and original reaction, and would attract the interest of many chemists in the unprecedented behavior of vinyl ylides. We report herein the first example of acylation reactions of vinylselenonium ylides with aldehydes affording *trans*-chalcone derivatives efficiently *via* umpolung of a carbonyl group like the Lapworth condensation.[8]

Firstly, vinylselenonium salts bearing an α-hydrogen were prepared from the reactions of vinylsilanes with diphenyl selenoxide and Lewis acid in CH_2Cl_2 at rt by reference to the procedure for alkynylselenonium salts (Scheme 1).[9]† (*E*)-Trimethylstyrylsilanes **1a** and **1b** reacted cleanly in the presence of trifluoromethanesulfonic anhydride for 4 and 2 h to afford the vinylselenonium triflates **2a** and **2b** in 87% and 59% yield, respectively, with retention of configuration. The (*Z*) stereochemistry of **2b** was established by observation of the NOE enhancement (10%) between the α-vinylic proton and *ortho*-protons of the *Z*-aryl group.

Next, we investigated the reactions of vinylselenonium ylides with aldehydes (Scheme 2). The ylides were generated by the

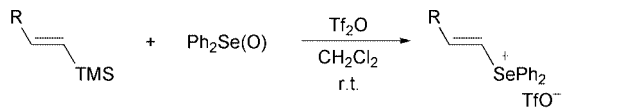

Scheme 1

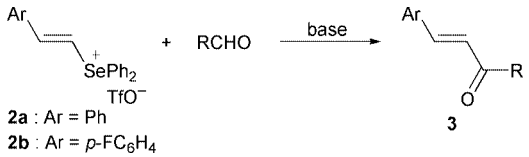

Scheme 2

reaction of vinylselenonium salts **2** with sodium hydride. The reaction of vinylselenonium salt **2a** (1 equiv.) with *p*-nitrobenzaldehyde (1 equiv.) in the presence of 1.3 equiv. of sodium hydride at 0 °C for 3 h in THF gave *p*-nitrophenyl styryl ketone **3a** in 65% yield but did not proceed at −78 °C. Since *p*-chlorobenzaldehyde gave *p*-chlorophenyl styryl ketone **3b** (11%) with recovery of the aldehyde (30%), 2 equiv. of sodium hydride were used and the yield of **3b** was improved up to 58%. However, the reactions with benzaldehyde or *p*-tolualdehyde gave complex mixtures including unreacted aldehyde, and α,β-unsaturated ketones were not isolated. To confirm the formation of the vinylselenonium ylide, vinylselenonium salt **2b** was stirred with 1 equiv. of sodium hydride in THF at 0 °C for 3 h without the aldehyde, followed by treatment with D_2O to afford a mixture of **2b** and **2b′** (**2b**:**2b′** = 9:16) in 40% yield. The mixture of **2b** and **2b′** was treated with sodium hydride in the presence of *p*-nitrobenzaldehyde under the same conditions as for the reaction of **2a** with *p*-nitrobenzaldehyde to give the compound **3c**, which contained no deuterium, in 49% yield (Scheme 3). This finding indicated that the above reactions proceeded *via* a vinylselenonium ylide. On the other hand, the reaction of vinylselenonium salt **2b** and benz(aldehyde-*d*) with sodium hydride in DMF at 0 °C for 4 h was conducted to trace the hydrogen atom of an aldehyde. 3-(4-Fluorophenyl)-1-phenylpropenone **3d** obtained in 14% yield did not contain any deuterium.

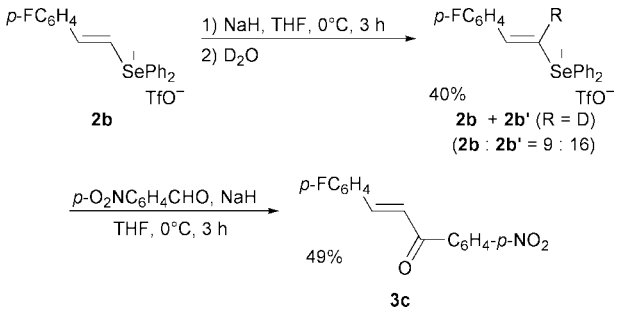

Scheme 3

On the basis of these results, we propose a plausible mechanism for the reactions of vinylselenonium salts with aldehydes (Scheme 4). Vinylselenonium ylide **4** is formed from the reaction of vinylselenonium salt **2** with sodium hydride followed by reaction with an aldehyde to produce betaine **5**. Deprotonation from the betaine **5** by a base gives rise to the β-elimination to generate allenoate ion **6**, which isomerizes to the α,β-unsaturated carbonyl compound **3**.

DOI: 10.1039/b100660f

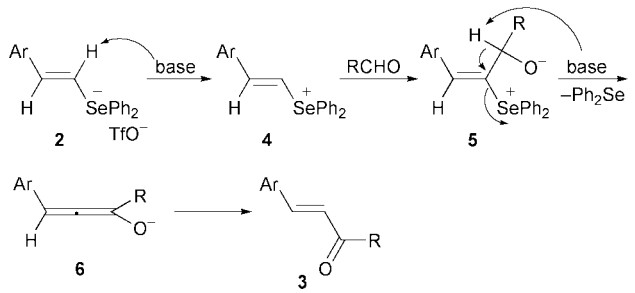

Scheme 4

Next, potassium hydride, as a stronger base than sodium hydride, was adopted in this reaction to improve the yield of compound **3** (Table 1).‡ The reaction of *p*-nitrobenzaldehyde with 2 equiv. of vinylselenonium salt **2a** in the presence of 3 equiv. of potassium hydride in THF at 0 °C for 0.5 h afforded the chalcone derivative **3a** in excellent yield (entry 1). The reactions of *p*-halobenzaldehydes also gave the corresponding α,β-unsaturated carbonyl compounds **3b** and **3e** in high yields compared with the reactions using sodium hydride (entries 2 and 3). Although no chalcone derivative had been obtained from the reaction of benzaldehyde or *p*-tolualdehyde using sodium hydride, *trans*-chalcone **3f** was given using potassium hydride in THF–DMSO (13 : 1) at −30 °C in up to 60% yield (entry 5); moreover, the reaction with *p*-tolualdehyde bearing the electron-donating group afforded chalcone derivative **3g** in moderate yield (entry 6).

Table 1 Reactions of vinylselenonium salt **2a** with aldehydes in the presence of KH[a]

Entry	RCHO	Conditions	Product (% yield)
1	*p*-$O_2NC_6H_4CHO$	KH, THF, O °C, 0.5 h	**3a** (94)
2	*p*-ClC_6H_4CHO	KH, THF, O °C, 0.5 h	**3b** (77)
3	*p*-BrC_6H_4CHO	KH, THF, O °C, 0.5 h	**3e** (76)
4	PhCHO	KH, THF, −10 °C, overnight	**3f** (43)
5		KH, THF–DMSO,[b] −30 °C, 2 h	**3f** (60)
6	*p*-MeC_6H_4CHO	KH, THF–DMSO,[b] −30 °C, 3.5 h	**3g** (49)

[a] **2a**: RCHO : KH = 2 : 1 : 3. [b] THF : DMSO = 13 : 1.

In conclusion, we have shown the first example of the reactions of vinylselenonium ylides with aldehydes, which proceed *via* the β-elimination of the adducts of the vinylselenonium ylides and the aldehydes because the selenonio group is a good leaving group to produce *trans*-chalcone derivatives. The results described in this paper implies that the vinylselenonium ylides would react with other carbonyl compounds differently from vinylphosphonium ylides, and we continue our study on the vinylselenonium ylides to exploit their new reactions.

This research was partially supported by the Ministry of Education, Science, Sports and Culture, Grant-in-Aid for Encouragement of Young Scientists, 2000, 11771388.

Notes and references

† *A typical example*: Trifluoromethanesulfonic anhydride (0.8 cm^3, 4.7 mmol) was added dropwise to a stirred solution of diphenyl selenoxide (1.1 g, 4.3 mmol) and (*E*)-trimethylstyrylsilane (0.84 g, 4.7 mmol) in dichloromethane (30 cm^3) at 0 °C. The mixture was stirred at rt for 4 h. After the solvent was evaporated under reduced pressure, the precipitate was washed several times with ether and recrystallised from CH_2Cl_2–Et_2O to afford 1.82 g (87%) of **2a** as colorless prisms: mp 113–114 °C; δ_H 7.41 (d, 1H, *J* 16.0), 7.50 (t, 2H, *J* 8.0), 7.63–7.71 (m, 9H), 7.73–7.90 (m, 6H); FABMS *m*/*z* 337 [M − TfO]$^+$; Found: C, 51.8; H, 3.5. $C_{21}H_{17}F_3O_3SSe$ requires C, 52.0; H, 3.5%.

‡ *A typical example*: Potassium hydride (12 mg, 0.3 mmol) was added to a stirred solution of vinylselenonium salt **2a** (97 mg, 0.2 mmol) and *p*-bromobenzaldehyde (19 mg, 0.1 mmol) in THF (3 cm^3) at 0 °C. The mixture was stirred at the same temperature for 0.5 h, poured into water and extracted with ethyl acetate. The extracts were washed with brine and dried over $MgSO_4$. After the solvent was evaporated under reduced pressure, the residue was separated by preparative TLC (hexane–AcOEt = 5 : 1) to give **3e** (22 mg, 76%) as colorless powder: δ_H 7.42–7.43 (m, 3 H), 7.48 (d, 1H, *J* 16.0), 7.64 (d, 4H, *J* 8.0), 7.82 (d, 1H, *J* 16.0), 7.89 (d, 2H, *J* 8.0); EIMS *m*/*z* 287 (M)$^+$; Found: C, 62.9; H, 4.0. $C_{15}H_{11}BrO$ requires C, 62.7; H, 3.9%.

1 H. J. Bestmann and R. Zimmerman, in *Comprehensive Organic Synthesis*, ed. B. M. Trost, Pergamon Press, Oxford, 1991, vol. 6, p. 171; E. E. Schweizer and G. J. O'Neill, *J. Org. Chem.*, 1965, **30**, 2082; K. Okuma, K. Ikari, M. Ono, Y. Sato, S. Kuge, H. Ohta and T. Machiguchi, *Bull. Chem. Soc. Jpn.*, 1995, **68**, 2313; F. Clerici, M. L. Gelmi, D. Pocar and R. Rondena, *Tetrahedron*, 1995, **51**, 9985; I. Burley and A. T. Hewson, *Tetrahedron Lett.*, 1994, **35**, 7099; Y. Shen and J. Yao, *J. Org. Chem.*, 1996, **61**, 8659.

2 A. C. Knipe, in *The Chemistry of the Sulphonium Group, Part 1*, ed. C. J. M. Stirling, Wiley, Chichester, 1981, p. 313.

3 Y. Watanabe, Y. Ueno and T. Toru, *Bull. Chem. Soc. Jpn.*, 1993, **66**, 2042.

4 H. J. Bestmann, *Angew. Chem., Int. Ed. Engl.*, 1977, **16**, 349; T. Minami, S. Shikita, S. So, M. Nakayama and I. Yamamoto, *J. Org. Chem.*, 1988, **53**, 2937; M. Arisawa and M. Yamaguchi, *J. Am. Chem. Soc.*, 2000, **122**, 2387.

5 S. Watanabe, K. Yamamoto, Y. Itagaki and T. Kataoka, *J. Chem. Soc., Perkin Trans. 1*, 1999, 2053; S. Watanabe, E. Mori, H. Nagai and T. Kataoka, *Synlett*, 2000, 49; S. Watanabe, E. Mori, H. Nagai, T. Iwamura, T. Iwama and T. Kataoka, *J. Org. Chem*, 2000, **65**, 8893; S. Watanabe, K. Yamamoto, Y. Itagaki, T. Iwamura, T. Iwama, T. Kataoka, G. Tanabe and O. Muraoka, *J. Chem. Soc., Perkin. Trans. 1*, **3**, 239.

6 T. Hirao, D. Misu and T. Agawa, *J. Am. Chem. Soc.*, 1985, **107**, 7179.

7 B. Zheng and M. Srebnik, *J. Org. Chem.*, 1995, **60**, 3278.

8 A. Lapworth, *J. Chem. Soc.*, 1903, **83**, 995.

9 T. Kataoka, S. Watanabe, M. Yamamoto, M. Yoshimatsu, G. Tanabe and O. Muraoka, *J. Org. Chem.*, 1998, **63**, 6382.

CHEMCOMM Communication
www.rsc.org/chemcomm

Characterisation of small molecule binding to DNA using a quartz crystal resonant sensor

Flavia Fucassi,[a] Karl D. Pavey,[a] Jillian E. Lowe,[a] Cedric J. Olliff,[a] Michael H. L. Green,[a] Frank Paul[b] and Peter J. Cragg*[a]

[a] *School of Pharmacy and Biomolecular Sciences, University of Brighton, Cockcroft Building, Moulsecoomb, Brighton, UK BN2 4GJ. E-mail: P.J.Cragg@bton.ac.uk*
[b] *Novel Methods Group, CASS, GlaxoSmithKline Pharmaceuticals, NFSP North, Harlow, Essex, UK CM19 5AW*

Received (in Cambridge, UK) 4th January 2001, Accepted 22nd March 2001
First published as an Advance Article on the web 12th April 2001

A new development in quartz crystal resonant sensor (QCRS) technology allows real-time analysis of binding by small molecules to DNA and has been tested using superoxide dismutase mimics.

Low molecular weight compounds interact with DNA in a variety of ways, from intercalation by π-stacking and hydrogen bonding to covalent bond formation.[1] The strength of the interaction is a good indication of each compound's binding mode with DNA and may be a direct indication of mutagenicity. We have developed a test based on the quartz crystal resonant sensor (QCRS) to measure DNA–analyte binding directly in real time. The QCRS is a robust sensor for which applications as diverse as volatile organic compound detection,[2] monitoring of antibody–antigen agglutination[3] and gene sensing have been found.[4] The technique uses surface modified piezoelectric quartz crystals to register the presence of chemical and biological species in the liquid phase *via* the change in resonant frequency as a function of analyte adhesion with time. Our method allows the determination of the type of interaction between DNA and small molecules, together with direct observation of any destructive effects such as DNA scission.† Briefly, thin film gold electrodes on the quartz crystals are coated with a bifunctional binder (NeutrAvidin™) followed by suitably functionalised DNA (Scheme 1). Solutions of small molecule analytes are then passed over the sensor in a flow-through cell and the frequency changes resulting from binding, due to the concomittant mass increase of the sensor, are monitored. The duration of the experiment makes the technique ideally suited to rapid screening of small molecule–DNA interactions. To confirm that the binding observed was indeed to DNA and not to one of the substrates on the QCRS, test runs were performed on partially modified sensors. Solutions of compounds were passed over crystals which had NeutrAvidin™, but no DNA, attached. Any observed frequency changes were short lived and final deviations from the base frequency were approximately 5% of the deviation shown when DNA was present. To ensure consistency all tests were carried out at the same flow rate (5 μl min^{-1}).

Analytes expected to bind to DNA in a variety of different ways were chosen to test the technique. Cisplatin **1** was chosen to probe strong, irreversible binding.[5] 5-Aminoacridine **2** and 9-amylaminoacridine **3**[6] were chosen to represent varying degrees of intercalation. Bleomycin **4** was included as an example of a well known DNA cleaving agent.[7]

To complement the behaviour of these analytes we also tested manganese(III) salen chloride **5**[8] and its 3,3′-methoxy analogue **6**.[9] These compounds act as successful superoxide dismutase mimics *in vivo* and have recently been shown to extend average lifespan in nematode worms, *Caenorhabditis elegans*.[10] Observation of the binding, if any, to DNA may reveal how they work and will represent a true trial of the system.

Fig. 1 shows that **1** took less than two minutes from injection to saturate the sensor and exhibited a drop in resonant frequency of 68 Hz. As expected, **2** bound slowly, taking about 8 min to saturate binding sites, and gave an overall frequency change of 8 Hz. The binding profile for **3** has a similar pattern to that of **2** but a greater frequency change (32 Hz) was observed due to the increased hydrogen bonding available to this compound. Compound **4** showed initial binding followed by a plateau which we speculate is due to a rearrangement process. The frequency then dropped again before finally rising after a further 8 minutes. This behaviour is consistent with cleavage of DNA and its subsequent removal from the surface of the sensor. Initial association rates calculated for each compound show a greater than 10-fold difference between cisplatin and 9-amylaminoacridine, and an additional 75-fold difference when compared with 5-aminoacridine (Table 1). Early literature studies involving acridines suggest that more than one site is involved in the intercalation process.[11] A mechanism published for proflavin suggested that its mechanism was distinct from either intercalation or electrostatic attraction.[12] It is thought unlikely that our observed responses are due solely to the binding of low molecular weight compounds to DNA. In particular, a degree of reorganisation is likely within the structure of the DNA that may cause frequency shifts due to viscoelastic interfacial changes additive to the initial mass change. Similar phenomena have been observed with ligands binding to RNA.[13,14]

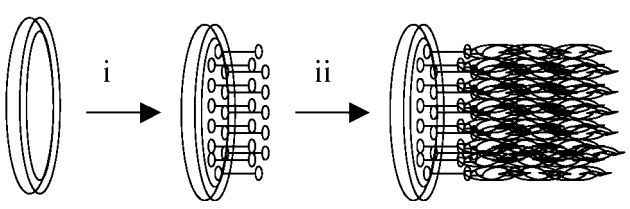

Scheme 1 Sensor preparation: i, surface modification of gold covered quartz crystal with NutrAvidin™; ii, addition of biotinylated DNA.

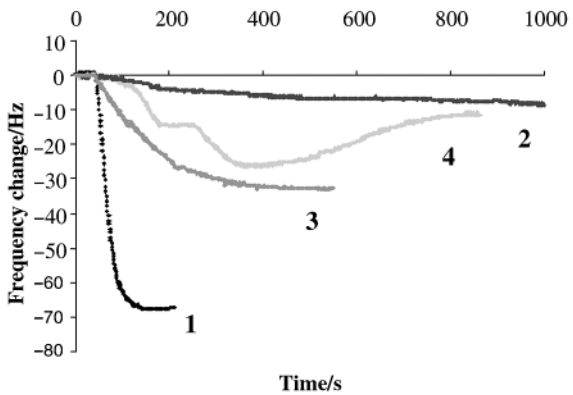

Fig. 1 Binding curves for compounds **1**, **2**, **3** and **4**.

DOI: 10.1039/b100175m

Table 1 Mass changes and initial binding rates for analytes

Compound	Mass change upon addition to sensor/μg[a]	Initial association rate/s^{-1}
Cisplatin **1**	0.60	1.54
5-Aminoacridine **2**	0.50	0.02
9-Amylaminoacridine **3**	0.60	0.14
Bleomycin **4**	0.56	0.20
[Mn(III)(salen)]$^+$ **5**	0.70	0.25
[Mn(III)(3,3′-methoxysalen)]$^+$ **6**	0.71	0.03

[a] Calculations assume saturation of compounds on DNA.

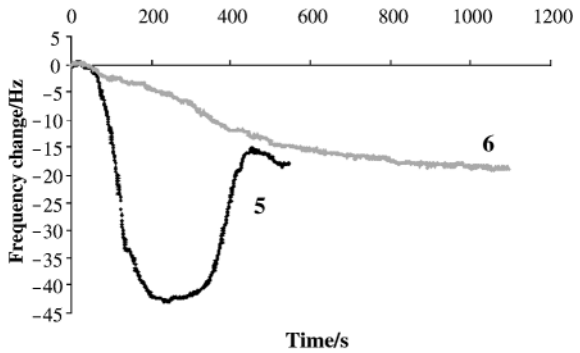

Fig. 2 Binding curves for compounds **5** and **6**.

It can be seen from Fig. 2 that **5** has a similar profile to that of **4** indicating initial strong binding to DNA followed by cleavage. To confirm this interpretation we stained the QCRS-tethered DNA with acridine orange. Fluorescence microscopy of the QCRS prior to addition of **5** showed a spatially homogeneous distribution of stained DNA across the sensor surface. Further microscopy of the eluent, following addition of **5**, showed that it contained acridine orange-stained DNA, confirming that **5** had pro-oxidant activity towards free DNA. Conversely the 3,3′-methoxy analogue, **6**, appeared to intercalate weakly, with a similar profile to the acridine derivatives, giving a maximum frequency drop of 20 Hz. Staining DNA with acridine orange prior to addition of **6** and examination of the eluent post addition indicated no significant cleavage. After 8 min the binding profile of **5** follows that of **6** indicating that they both act as weak intercalators in the long term.

Melov *et al*. have shown that both **5** and **6** extend lifespan of *C*. *elegans*; however, only **6** gives rise to re-emergent fertility in longer lived worms.[10] We conclude that the lack of pro-oxidant activity of **6**, as indicated by the QCRS, is responsible in part for its greater benefits.

It appears that both the magnitude of the frequency change and, more importantly, the binding profile due to each analyte are directly related to the type of analyte–DNA interaction. The QCRS is therefore an ideal technique to study the interactions of a wide variety of small molecules with DNA and other biological macromolecules.

This research has been supported by the A-T Children's Project and GlaxoSmithKline Pharmaceuticals.

Notes and references

† *Experimental conditions*: 8.6 mm diameter, 10 MHz AT-cut quartz crystals (Hi-Q International, Cambridge, UK) were furnished with 100 nm thick gold electrodes (19.5 mm^2 area), placed into an in-house fabricated flow-through liquid cell (20 μl volume) and connected to a novel gain control oscillator[15] designed specifically to work in liquid environments of high viscosity and density. Output from the crystals was monitored using a Fluka-6689 frequency counter capable of sub-single hertz resolution, data being collected once per second *via* Fluka Timeview software. Crystals were washed with HPLC grade ethanol prior to deposition of Neutr-Avidin™ (Pierce, IL, USA). The electrodes were coated with Neutr-Avidin™ by a single 20 μl injection of the binding agent (2 mg ml^{-1} in Sorensen's phosphate buffer) *via* an all PEEK™ Rheodyne MMB six-way valve into the running buffer until a stable baseline with noise below 0.2 Hz was observed. Once a stable signal had been obtained for the modified crystal, it was washed with biotinylated DNA (b-DNA, Vector Laboratories Ltd, Peterborough, UK) at 50 μg ml^{-1} in Sorensen's phosphate buffer (20 μl injection loop, 1 μg per injection). Washes were repeated until no further frequency change was observed in order to ensure that the sensor surface was saturated (*ca*. 2.5 μg of DNA on the surface). The b-DNA contained a range of lengths from 125 to 23 100 base pairs to ensure variation in potential binding sites for the analytes. Modified electrodes were exposed to solutions of the DNA binding agents (500 μM in phosphate buffer solution, Table 1, flow rate 5 μl min^{-1}, 22 ± 0.5 °C) and resultant frequency changes monitored for up to 20 min. Run-to-run reproducibility was better than 5% (N = 3) in all cases.

1 J. W. Steed and J. L. Atwood, *Supramolecular Chemistry*, Wiley, Chichester, 1st edn., 2000, pp. 77–81.
2 M. J. Swann, A. Glidle, L. Cui, J. R. Barker and J. M. Cooper, *Chem. Commun*., 1998, 2753.
3 K. D. Pavey, Z. Ali, C. J. Olliff and F. Paul, *J. Pharm. Biomed. Anal*., 1999, **20**, 241.
4 X. C. Zhou, S. J. O'Shea and S. F. Y. Li, *Chem. Commun*., 2000, 953.
5 S. F. Bellon, J. H. Coleman and S. J. Lippard, *Biochemistry*, 1991, **30**, 8026
6 J. P. Yeo, Ph.D. Thesis, University of Brighton, 1984.
7 B. Halliwell and J. M. C. Gutteridge, *Free radicals in biology and medicine*, Oxford University Press, Oxford, 3rd edn., 1999, pp. 711–715.
8 V. Pecoraro and W. M. Butler, *Acta Crystallogr., Sect. C*, 1986, **42**, 1151.
9 Prepared in the same manner as manganese(III) salen chloride, substituting *o*-vanillin for salicylaldehyde.
10 S. Melov, J. Ravenscroft, S. Malik, M. S. Gill, D. W. Walker, P. E. Clayton, D. C. Wallace, B. Malfroy, S. E. Doctrow and G. J. Lithgow, *Science*, 2000, **289**, 1567.
11 L. S. Lerman, *J. Mol. Biol*., 1961, **3**, 18
12 J. Ramstein and M. Leng, *Biophys. Chem*., 1975, **3**, 234.
13 B. A. Cavic, F. L. Chu, L. M. Furtado, G. L. Hayward, D. P. Mack, M. E. McGovern, H. Su and M. Thompson, *Faraday Discuss*., 1997, **107**, 159.
14 A. Janshoff, H.-J. Galla and C. Stenheim, *Angew. Chem., Int. Ed*., 2000, **39**, 4004.
15 *Br. Pat*., 9823410.7, 1999.

CHEMCOMM Communication
www.rsc.org/chemcomm

A new approach to superior optical limiting materials—planar 'open' heterothiometallic clusters†

Chi Zhang,*[abc] Yinglin Song,*[a] B. M. Fung,[b] Ziling Xue[d] and Xinquan Xin*[c]

[a] *Department of Applied Physics, Harbin Institute of Technology, Harbin 150001, P. R. China*
[b] *Department of Chemistry and Biochemistry, University of Oklahoma, Norman, Oklahoma 73019, USA. E-mail: czhang@chemdept.chem.ou.edu*
[c] *Department of Chemistry and State Key Laboratory of Coordination Chemistry, Nanjing University, Nanjing 210093, P. R. China*
[d] *Department of Chemistry, The University of Tennessee, Knoxville, Tennessee 37996-1600,USA*

Received (in Cambridge, UK) 9th January 2001, Accepted 20th March 2001
First published as an Advance Article on the web 12th April 2001

A new approach to superior optical limiting materials, utilizing planar 'open' skeleton heterothiometallic clusters, is reported by incorporating heavy atoms and altering cluster skeletons and is found to decrease the limiting thresholds to as low as 0.07 J cm^{-2}, among the best for OL materials.

Rapid recent developments of both high-power frequency-tunable lasers and optical signal detection techniques have led to increasing demands for broadband nonlinear optical materials.[1] These materials have been designed either to protect sensitive optical sensors such as the human eye from intense optical radiation[2] or to be used in optical computers and broadband communications for data acquisition, storage, transmission, and processing.[1,3] Over the past decades, research in the optical limiting (OL) materials has been largely focused on inorganic semiconductors, conjugated polymers, organic molecules, and organometallic compounds.[1–6] The general relationships between molecular structures and OL performance in various existing OL materials are, however, yet to be well established, and this has presented a difficult task in the effort to improve the OL properties through molecular structure design.[5d]

We have recently developed Mo(W)/S/Cu(Ag) heterothiometallic clusters as a new class of OL materials.[7] These clusters combine the advantages of inorganic heavy atoms, organic ligands, and versatile cluster structures. Studies have been conducted on the relationship between the structures and OL properties of these clusters with various skeleton shapes such as butterfly, nest, half-open cubane, trinuclear linear, cubane, hexagonal-prismatic, twin-nest, twenty-nuclear supercage and cluster polymer.[7,8] Unlike some traditional OL materials, the skeletons and constituent elements in these clusters were found to have considerable influence on their OL performance. Changes in cluster compositions (skeletal or terminal elements), such as incorporation of heavy atoms, generally enhance the OL performance of these clusters. Moreover, cubane-shaped and hexagonal-prismatic clusters show large OL effects.[7a,c] The OL effect of these two kinds of clusters are comparable to those of fullerene C_{60} and phthalocyanine derivatives, respectively, which are generally regarded to be among the best OL materials.[1,5,6] The enhancement in the OL properties of the hexagonal-prismatic clusters over the cubane-shaped clusters suggested that modification of cluster structures may further enhance their OL properties.

With these in mind, we have thus studied the OL properties of a series of planar clusters $[MS_4Cu_4X_2(py)_6]$ (X = I, M = W, **1**, Mo, **2**; X = Br, M = W, **3**, Mo, **4**; X = Cl, M = W, **5**, Mo, **6**) and $(Et_4N)_2[MS_4Cu_4(NCS)_4(2\text{-pic})_4]$ (M = W, **7**; Mo, **8**). The clusters **1**–**8** were all synthesized in our laboratories;[7b,8a] **1**–**6** were prepared from the reactions of $(NH_4)_2MS_4$, CuX and py† while **7** and **8** were obtained from the reactions of $(Et_4N)_2MS_4$ and CuSCN with 2-pic.[8a] The structures of **1**, **3** and **4** were determined by IR, elemental analyses and X-ray diffraction.‡

These clusters all have a pentanuclear planar 'open' structure with a $[MS_4Cu_4]$ aggregate of approximate D_{2d} symmetry (Scheme 2). Their electronic spectra show a relatively weak linear absorption in the VIS–NIR region.† The OL effects of clusters **1**–**8** in DMF solutions were measured with linear, polarized 8 ns duration laser pulses at 532 nm generated from a Q-switched frequency-doubled Nd:YAG laser.

The NLO process in these clusters can be approximately represented by eqn. (1)[6c]

$$\frac{dI}{dz} = -\left[\alpha_0 + \left\{\left(1 + K_\alpha \frac{I}{I_s}\right)\sigma_g N \Big/ \left(1 + \frac{I}{I_s}\right)\right\}\right] I \qquad (1)$$

where α_0 is the linear absorption coefficient of the solvent, σ_g is the absorption cross-section of the ground-state molecular solution, N is the concentration of the cluster sample solution, $I_s = h\gamma/\sigma_g\tau_{eg}$ is the saturable intensity, with τ_{eg} being the lifetime of the excited-state, and $K_\alpha = \sigma_e/\sigma_g$ is the ratio between the excited-state absorption cross-section and the ground-state absorption cross-section. The limiting thresholds of these clusters, which is defined here as the incident fluence at which the transmittance falls to 50% of the linear transmittance, were found to be 0.07, 0.08, 0.08, 0.10, 0.10 and 0.15 J cm^{-2}, respectively. Representative energy-dependent transmittance data for cluster **1**, shown in Fig. 1, shows a reduction in transmittance at high fluence. The limiting thresholds of **1**–**5** are comparable to those (*ca.* 0.1 J cm^{-2}) of phthalocyanine derivatives[6a,b] and hexagonal-prismatic $Mo_2Ag_4S_8(PPh_3)_4$,[7c] and, to our knowledge, among the lowest reported so far.[9] The limiting thresholds of **7** and **8** were found to be 0.3 and 0.5 J cm^{-2}, respectively, and higher than those of the neutral clusters $MS_4Cu_4X_2(py)_6$ (**1**–**6**) with halide and pyridine ligands.

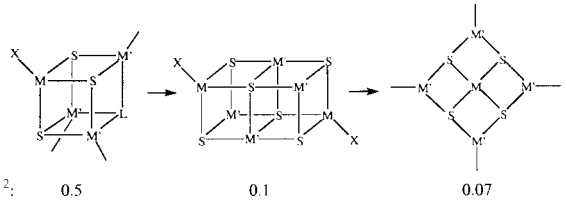

Scheme 1

† Electronic supplementary information (ESI) available: 1, Preparation and characterization of the planar 'open' heterothiometallic clusters; 2, molecular structures of clusters; 3, pump–probe experiment setup and results; 4, ground-state absorption spectra of clusters; 5, figures for *Z*-scan experiments under open-aperture configuration of clusters; 6, figures of energy-dependent transmittance of clusters; 7, Table 1: limiting thresholds of compounds. See http://www.rsc.org/suppdata/cc/b1/b100395j/

DOI: 10.1039/b100395j

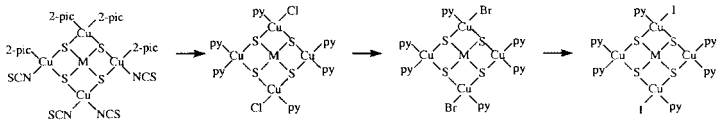

Scheme 2

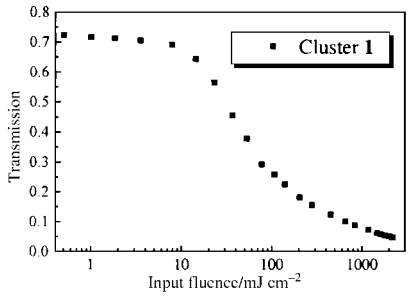

Fig. 1 The energy-dependent transmittance of **1**.

The alteration of the cluster skeleton (cubane-shaped → hexagonal-prismatic → pentanuclear planar) led to significant enhancements in OL properties of these clusters (Scheme 1). In addition, in the pentanuclear planar clusters, the substitution of light elements by heavy elements [Mo by W, and Cl or N (in SCN) by Br or I, respectively] further reduced the limiting thresholds (Scheme 2). The ESI gives a list of the limiting thresholds of these pentanuclear planar W(Mo)/S/Cu heterothiometallic clusters (**1**–**8**) and other OL materials reported earlier.†

Pump–probe measurements were conducted on clusters **1**–**8** to further investigate the physical origin of their optical nonlinearities.† A frequency-doubled Nd : YAG pulse laser with a 532 nm wavelength and 8 ns pulse width was used as a pump beam (pulse energy: 300 μJ). A CW He–Ne laser with 632.8 nm wavelength was used as a probe beam (optical power: 20 mW). The change of the probe beam intensity *vs*. the delay time was recorded after the pump beam by using BOXCAR. The optical nonlinearities of the clusters and fullerene C_{60} were studied using the same experimental setup. The pump–probe experimental results indicate that the optical nonlinearity responses of the clusters are similar to that of fullerene C_{60} which exhibits a typically excited-state nonlinearity.[5b] We can therefore reasonably conclude that the OL ability in clusters mainly arises from excited-state absorption processes. In the meantime, the results of *Z*-scan experiments[10] show that clusters **1**–**8** have remarkable and very strong nonlinear optical absorption effects.† The NLO absorptive experiment under an open-aperture configuration of **1** is depicted in Fig. 2. These NLO absorptive properties meet the essential requirements of ideal OL materials. We speculate that OL properties of **1**–**4** were enhanced in part by the planar skeleton and the heavy atoms in the clusters. The heavy atom effects of the planar 'open' structures in **1**–**4** may allow better spin–orbital couplings, and thus intersystem crossing at the excited states.[5d,7a] Large spin–orbital couplings might be beneficial if the nonlinear absorption of desired excited states are associated with the T_1–T_n electronic transitions as found for fullerene C_{60} and phthalocyanine systems.[5,6] In addition, the use of heavy atoms such as W and I may introduce more sublevels into the energy hierarchy, and provide more allowed electronic transitions for the initial excited state in **1**–**4**. The increased numbers of the allowed electronic transitions probably enhance the nonlinear absorption of the initial excited state to higher excited states. On the other hand, the planar clusters have higher symmetry than the cubane-shaped and hexagonal-prismatic clusters. The higher symmetry, as in the phthalocyanine systems,[5d] may decrease the probability of ground-state electronic transitions and give a smaller absorption cross-section σ_g and a larger σ_e/σ_g (K_α) ratio, which are obtained from the *Z*-scan measurements.

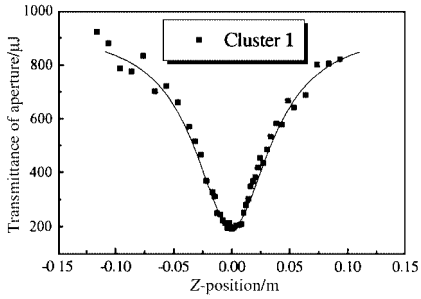

Fig. 2 The *Z*-scan experiment under an open-aperture configuration of **1**.

The current work showed that molecular engineering approaches such as incorporating heavy atoms and altering cluster skeletons are perhaps a promising research direction in search of better OL materials. Studies are under way to further probe the ultrafast OL mechanism of these planar 'open' heterothiometallic clusters **1**–**8** and to design and prepare better OL materials.

We thank the National Science Foundations of China and USA, Foundation of HIT.

Notes and references

‡ CCDC 156623–156625. See http://www.rsc.org/suppdata/cc/b1/b100395j/ for crystallographic data in .cif or other electronic format.

1 L. W. Tutt and T. F. Boggess, *Prog. Quantum. Electron.*, 1993, **17**, 299; J. Zyss, *Molecular Nonlinear Optics*, Academic Press, New York, 1994; H. S. Nalwa and S. Miyata, *Nonlinear Optics of Organic Molecules and Polymers*, CRC Press, New York, 1997.

2 *Conference on Lasers and Electro-Optics*, Technical Digest Series, Optical Society of America, Washington, DC, 1993; *MRS Symp. Proc.* (*Materials for Optical Limiting*), 1995, 374; *MRS Symp. Proc.* (*Materials for Optical Limiting II*), 1998, 479.

3 I. R. Whittall, A. M. McDonagh, M. G. Humphrey and M. Samoc, *Adv. Organomet. Chem.*, 1999, **43**, 349; S. P. Karna and A. T. Yeates, *Nonlinear Optical Materials*, American Chemical Society, Washington, DC, 1996.

4 J. L. Bredas, C. Adant, P. Tackx, A. Persoons and B. M. Pierce, *Chem. Rev.*, 1994, **94**, 243; N. J. Long, *Angew. Chem., Int. Ed. Engl.*, 1995, **34**, 21; W. Nie, *Adv. Mater.*, 1993, **5**, 520.

5 (*a*) L. W. Tutt and A. Kost, *Nature*, 1992, **356**, 224; (*b*) D. G. McLean, R. L. Sutherland, M. C. Brant, D. M. Brandelik, P. A. Fleitz and T. Pottenger, *Opt. Lett.*, 1993, **18**, 858; (*c*) Y. L. Song, G. Y. Fang, Y. X. Wang, S. T. Liu, C. F. Li, L. C. Song, Y. H. Zhu and Q. M. Hu, *Appl. Phys. Lett.*, 1999, **74**, 332; (*d*) Y. P. Sun and J. E. Riggs, *Int. Rev. Phys. Chem.*, 1999, **18**, 43.

6 (*a*) J. W. Perry, K. Mansour, I. Y. S. Lee, X. L. Wu, P. V. Bedworth, C. T. Chen, D. Ng, S. R. Mardar, P. Miles, T. Wada, M. Tian and H. Sasabe, *Science*, 1996, **273**, 1533; (*b*) J. W. Perry, K. Mansour, S. R. Marder, K. J. Perry, D. Jr. Alvarez and L. Choong, *Opt. Lett.*, 1994, **19**, 625; (*c*) C. F. Li, L. Zhang, M. Yang, H. Wang and Y. X. Wang, *Phys. Rev. A*, 1994, **49**, 1149.

7 (*a*) S. Shi, W. Ji, S. H. Tang, J. P. Lang and X. Q. Xin, *J. Am. Chem. Soc.*, 1994, **116**, 3615; (*b*) H. W. Hou, X. Q. Xin and S. Shi, *Coord. Chem. Rev.*, 1996, **153**, 25; (*c*) W. Ji, S. Shi, H. J. Du, P. Ge, S. H. Tang and X. Q. Xin, *J. Phys. Chem.*, 1995, **99**, 17 297.

8 (*a*) C. Zhang, Y. L. Song, G. C. Jin, G. Y. Fang, Y. X. Wang, S. S. S. Raj, H. K. Fun and X. Q. Xin, *J. Chem. Soc., Dalton Trans.*, 2000, 1317; (*b*) C. Zhang, Y. L. Song, Y. Xu, H. K. Fun, G. Y. Fang, Y. X. Wang and X. Q. Xin, *J. Chem. Soc., Dalton Trans.*, 2000, 2823, and references therein; (*c*) H. W. Hou, Y. T. Fan, C. X. Du, Y. Zhu, W. L. Wang, X. Q. Xin, M. K. M. Low, W. Ji and H. G. Ang, *Chem. Commun.*, 1999, 647.

9 Y. P. Sun and J. E. Riggs recently reported a limiting threshold in toluene solution of 0.05 J cm^{-2} for C_{60} for a linear transmittance of 55% [ref. 5(*d*)].

10 M. Sheik-Bahae, A. A. Said, T. H. Wei, D. J. Hagan and Van E. W. Stryland, *IEEE. J. Quantum Electron.*, 1990, **26**, 760.

CHEMCOMM
Communication
www.rsc.org/chemcomm

Electron beam induced *in situ* clusterisation of 1D $ZrCl_4$ chains within single-walled carbon nanotubes

Gareth Brown,[ab] Sam R. Bailey,[a] Jeremy Sloan,[ab] Cigang Xu,[a] Steffi Friedrichs,[a] Emmanuel Flahaut,[a] Karl S. Coleman,[a] John L. Hutchison,[b] Rafal E. Dunin-Borkowski[b] and Malcolm L. H. Green*[a]

[a] *Wolfson Catalysis Centre (Carbon Nanotechnology Group), Inorganic Chemistry Laboratory, University of Oxford, South Parks Road, Oxford, UK OX1 3QR. E-mail: malcolm.green@chem.ox.ac.uk*

[b] *Department of Materials, University of Oxford, South Parks Road, Oxford, UK OX1 3PH*

Received (in Cambridge, UK) 8th February 2001, Accepted 7th March 2001
First published as an Advance Article on the web 17th April 2001

Cluster formation can be induced *in situ* in SWNTs filled with $ZrCl_4$ by electron beam irradiation of SWNT/$ZrCl_4$ composites within a field emission gun transmission electron microscope (FEGTEM); the process represents a possible route to the synthesis of 1D-quantum dot arrays formed by related materials.

Single-walled carbon nanotubes (SWNTs)[1] can be filled by solution-deposition[2] or capillarity methods[3] similar to those used to fill multi-walled carbon nanotubes (MWNTs).[4,5] There is now considerable theoretical[6,7] and experimental[8–11] evidence indicating that doped SWNTs show enhanced conductive or opto-electronic properties compared to untreated tubules. In addition, as most SWNTs fall within a narrow 1.2–1.6 nm diameter range when formed by vaporisation of catalytically doped carbon,[12,13] their capillaries can template the formation of atomically thin crystals of tubule-specified diameters. Recently these have included 2×2 and 3×3 atomic layer thick KI crystals,[14,15] helical iodine chains,[9] 1D polyhedral chains of lanthanide halide crystals[16] and chains of fullerene or endofullerene molecules.[17–20] In this study, we show how discrete $ZrCl_x$ (with $0 \leqslant x < 4$) clusters of constrained diameters can be formed within SWNTs by electron-beam irradiation of tubules filled with $ZrCl_4$.

The SWNTs used in this work were prepared by a catalytic arc synthesis method.[13] $ZrCl_4$ was resublimed at 693 K under N_2 from the as-supplied product (Aldrich, 99.9%). As-prepared SWNT material was mixed with $ZrCl_4$ in a 1 : 1 ratio by mass under dry box conditions and ground thoroughly. Each sample was sealed under vacuum in a silica glass ampoule and heated at 2 K min^{-1} to 623 K in a tube furnace, held at that temperature for 1 h and then furnace cooled to room temperature. The specimen was characterised in a JEOL 3000F FEGTEM operated at 300 kV and equipped with a Gatan 794 (1 k $\times$ 1 k pixel) CCD camera. The beam density in imaging mode was *ca.* 5×10^5 e^- nm^{-2} s^{-1} which is equivalent to a current of *ca.*2.7 $\times$ 10^{-14} A. The chemical identity of the specimen was confirmed by energy-dispersive X-ray microanalysis (EDX) using a 0.5 nm diameter focussed electron probe, a LINK 'Pentafet' detector and an Oxford Instruments 'ISIS' 300 system.

When examined under the FEGTEM, both nanotube bundles and discrete SWNTs were observed to be filled continuously with 1D chains of $ZrCl_4$. EDX microanalysis performed on discrete filled SWNTs confirmed the chemical identity of the filling material. As a spread electron beam of specified electron density (see above) was held upon regions of filled SWNTs, the filling material underwent progressive changes in morphology as it segregated to form discrete clusters. The sequence of events was followed over periods of up to 20 min, after which the encapsulating SWNTs denatured.

Fig. 1 shows a sequence of ten FEGTEM images obtained over *ca.* 4 min. In the initial image **I**, two continuously filled SWNTs can be seen with the upper tubule being terminated by a cap visible on the right of the image. By image **II**, the filling in the bottom tubule has already segregated into three *ca.* 3–4 nm long clusters. By image **V**, the arrowed clusters have different lengths of 3, 2 and 4 nm, respectively. By image **VI**, the material in the topmost tubule had also segregated into two clusters (arrowed). By the final image **X**, discrete *ca.* 1 nm long clusters can be seen in the two nanotubes with the number of clusters in the bottom tubule increased from three (see image **V**) to four. It is important to note that during these initial transformations (*i.e.* before the denaturing of the SWNTs) the walls of the tubules remained relatively unchanged, indicating that no chemical interaction between the carbon walls and the filling material had occurred. A minimum length of *ca.* 1 nm for the clusters was eventually obtained after irradiation for *ca.* 8 min.

The microstructure of the filling material in image **I** is indistinct whereas several of the longer clusters in images **II**, **III** and **V** consist of 1D arrays of dark spots similar to those reported recently for lanthanide halides of the form $LnCl_3$ (Ln = La, Nd, Sm, Eu, Gd, Tb, Yb) formed within SWNTs.[16] In those structures, the dark spot arrays were attributed to 1D chains of edge-sharing $LnCl_6$ polyhedra, with the heavy Ln^{3+} cations dominating the image contrast over the less strongly scattering

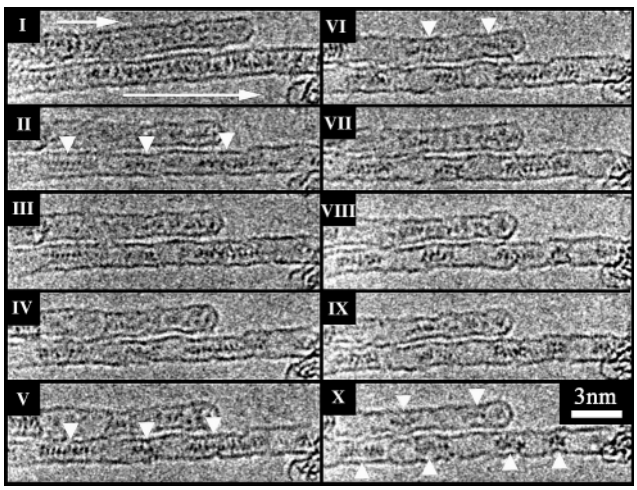

Fig. 1 Sequence of images **I** to **X** obtained at *ca.* 20 s intervals showing gradual clusterisation of $ZrCl_4$ within SWNTs induced by electron-beam irradiation within a FEGTEM. Image **I** shows two SWNTs continuously filled with $ZrCl_4$ (large arrows). After *ca.* 80 s (image **V**), filling in the bottom tubule has reformed into three distinct separated clusters (small arrows). After *ca.* 100 s (image **VI**) filling in the top tubule has segregated into two clusters. After 4 min (image **X**), the filling has segregated into a total of six distinct clusters (small arrows). In images **II**, **III** and **V**, distinct 1D arrays of dark spots are visible. Note 'bulging' either side of the central cluster in the lower SWNT in images **VI** and **VII**.

DOI: 10.1039/b101261o

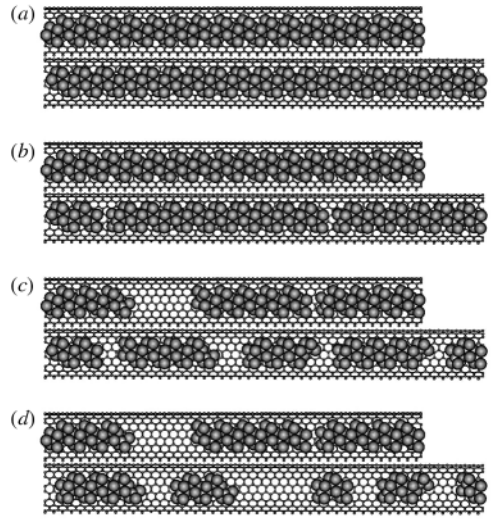

Fig. 2 Idealised structural representation of cluster formation within a pair of SWNTs. SWNTs continuously filled with $ZrCl_4$ (*a*) undergo beam irradiation until a break occurs in the filling after *ca.* 4–10 s (*b*). Either side of the break, the chains will terminate in reduced polyhedra. After 40–50 s, several long clusters are formed (*c*) and beam reduction continues until complete clusterisation occurs (*d*). This process may continue until all the chlorine is eliminated from the clusters.

Cl^- anions. It is therefore reasonable to assume that $ZrCl_4$, which forms an edge-sharing '*trans*' octahedral chain structure in the bulk,[21] forms similar 1D chains within SWNT capillaries and that the dark spots visible in images **I–X** in Fig. 1 correspond to more strongly scattering Zr^{4+} ions rather than to the weaker scattering Cl^- ions.

An additional interesting point is that the SWNTs distort during the clusterisation process. For example, in images **VI** and **VII** (Fig. 1) the lower tubule, which has a constant diameter of *ca.* 1.4 nm in the initial image (*i.e.* image **I**, Fig. 1), shows symmetric 0.1 nm 'bulges' either side of the central $ZrCl_x$ cluster. We believe that these 'bulges' are caused by complimentary ovaloid distortions in the SWNTs resulting from asymmetric distortions induced in the $ZrCl_x$ clusters by the beam rearrangement process. Such distortions will cause an apparent local variation in the SWNT diameter when viewed in projection in a FEGTEM.

Electron beam bombardment of MX_n halides at intermediate accelerating voltages (typically 100–400 kV) produces isolated stoichiometric Frenkel-type defects in bulk crystals.[22,23] However, in smaller volume halide crystallites (*ca.* 1 μm^3 particle size) elimination of halogen and the formation of surface metal occurs instead.[24] We propose therefore that the 1D $ZrCl_4$ chains undergo sequential elimination of chlorine to form clusters of $ZrCl_x$, of progressively lower stoichiometry (*i.e.* x decreases from 4 to 0), according to the schematic depiction in Fig. 2(*a*)–(*d*). Complete elimination of chlorine would result in the formation of metallic Zr clusters although we have not yet been able to verify this. Similarly, it has not been possible to determine the nature of the eliminated chlorine species (*i.e.* such as radicals, ions, charged molecular fragments, *etc.*). We assume that chlorine diffuses out of side-wall defects or open ends of SWNTs in the same way that gaseous endofullerene molecules have been demonstrated to diffuse into them.[19,20] As no significant damage to the SWNT walls was observed during clusterisation, carburisation of the clusters is not thought to occur, although surface reaction of the carbon with the eliminated chlorine species (see above) remains a possibility.

In conclusion, $ZrCl_4$ contained within SWNTs can be beam-reduced *in situ* to form $ZrCl_x$ clusters (with $0 \leqslant x < 4$) of controlled diameter. While beam-induced coalescence of fullerene molecules has been reported within SWNTs,[17,18] this is the first time that cluster segregation has been reported. If this phenomenon can be extended in a controlled way to bulk SWNT samples containing semiconducting or metallic species (or their precursors) then this may represent a route to the synthesis of one dimensional arrays of quantum dots within SWNTs. In addition, more detailed analytical studies of the clusterisation phenomena (*e.g.* high resolution EELS studies[20]) should lead to a better understanding of the mechanism of halide decomposition for these virtually 'all surface' crystals.

Financial support was provided by Petroleum Research Fund, administered by the American Chemical Society (grant No. 33765-AC5), the EPSRC (grant nos. GR/L59238 and GR/L22324) and Colebrand Ltd. for financial support. C. X. is grateful for a K. C. Wong Scholarship (University of Oxford), a Light Senior Scholarship (St Catherine's College, Oxford) and the Henry Lester trust. S. F. is indebted to BMBF and to the Fonds der Chemischen Industrie for additional financial support. J. S. and K. S. C. are indebted to the Royal Society.

Notes and references

1 S. Iijima and T. Ichihashi, *Nature*, 1993, **363**, 603.
2 J. Sloan, J. Hammer, M. Zweifka-Sibley and M. L. H. Green, *Chem. Commun.*, 1998, 347.
3 J. Sloan, D. M. Wright, H. G. Woo, S. Bailey, G. Brown, A. P. E. York, K. S. Coleman, J. L. Hutchison and M. L. H. Green, *Chem. Commun.*, 1999, 699.
4 P. M. Ajayan and S. Iijima, *Nature*, 1993, **361**, 333.
5 S. C. Tsang, Y. K. Chen, P. J. F. Harris and M. L. H. Green, *Nature*, 1994, **372**, 159.
6 D. Östling, D. Tománek and A. Rosén, *Phys. Rev. B*, 1997, **55**, 13 980.
7 F. J. García-Vidal, J. M. Pitarke and J. B. Pendry, *Phys. Rev. B*, 1998, 586 783.
8 R. S. Lee, H. J. Kim, J. E. Fischer, A. Thess and R. E. Smalley, *Nature*, 1997, **388**, 255.
9 L. Grigorian, K. A. Williams, S. Fang, G. U. Sumanasekera, A. L. Loper, E. C. Dickey, S. J. Pennycook and P. C. Eklund, *Phys. Rev. Lett.*, 1998, **80**, 5560.
10 G. Che, B. B. Lakshmi, C. R. Martin and E. R. Fisher, *Langmuir*, 1999, **15**, 750.
11 S. Liu, J. Zhu, Y. Mastai, I. Felner and A. Gedanken, *Chem. Mater.*, 2000, **12**, 2205.
12 P. Nikolaev, A. Thess, A. G. Rinzler, D. T. Colbert and R. E. Smalley, *Chem. Phys. Lett.*, 1997, **266**, 422.
13 C. Journet, W. K. Maser, P. Bernier, A. Loiseau, M. Lamy, M. L. de la Chapelle, S. Lefrant, P. Derniard and J. E. Fisher, *Nature*, 1997, **388**, 756.
14 J. Sloan, M. C. Novotny, S. R. Bailey, G. Brown, C. Xu, V. C. Williams, S. Freidrichs, E. Flahaut, R. L. Callendar, A. P. E. York, K. S. Coleman, M. L. H. Green, R. E. Dunin-Borkowski and J. L. Hutchison, *Chem. Phys. Lett.*, 2000, **329**, 61.
15 R. R. Meyer, J. Sloan, R. E. Dunin-Borkowski, A. I. Kirkland, M. C. Novotny, S. R. Bailey, J. L. Hutchison and M. L. H. Green, *Science*, 2000, **289**, 1324.
16 C. Xu, J. Sloan, G. Brown, S. R. Bailey, V. C. Williams, S. Friedrichs, K. S. Coleman, J. L. Hutchison, R. E. Dunin-Borkowski and M. L. H. Green., *Chem. Commun.*, 2000, 2427.
17 B. W. Smith, M. Monthioux and D. E. Luzzi, *Nature*, 1998, **396**, 323.
18 J. Sloan, R. E. Dunin-Borkowski, J. L. Hutchison, K. S. Coleman, V. C. Williams, J. B. Claridge, A. P. E. York, C. Xu, S. R. Bailey, G. Brown, S. Friedrichs and M. L. H. Green, *Chem. Phys. Lett.*, 2000, **316**, 191.
19 B. W. Smith, D. E. Luzzi and Y. Achiba, *Chem. Phys. Lett.*, 2000, **331**, 137.
20 K. Suenaga, M. Tence, C. Mory, C. Colliex, H. Kato, T. Okazaki, H. Shinohara, K. Hirahara, S. Bandow and S. Iijima, *Science*, 2000, **290**, 1331.
21 A. F. Wells, in *Structural Inorganic Chemistry*, Oxford University Press, Oxford, 5th edn., 1990, p. 424.
22 C. R. A. Catlow, K. M. Diller and L. W. Hobbs, *Philos. Mag. A*, 1980, **42**, 123.
23 M. L. Jenkins and M. A. Kirk, in *Characterisation of Radiation Damage by Transmission Electron Microscopy*, Institute of Physics, Bristol, 2000, p. 173.
24 G. C. Fryburg and R. A. Lad, *Surf. Sci.*, 1975, **48**, 353.

CHEMCOMM
Communication
www.rsc.org/chemcomm

{2Fe3S} clusters related to the di-iron sub-site of the H-centre of all-iron hydrogenases

Mathieu Razavet, Sian C. Davies, David L. Hughes and Christopher J. Pickett*

Department of Biological Chemistry, John Innes Centre, Norwich, UK NR4 7UH.
E-mail: chris.pickett@bbsrc.ac.uk

Received (in Cambridge, UK) 8th March 2001, Accepted 16th March 2001
First published as an Advance Article on the web 17th April 2001

The first synthetic {2Fe3S} clusters structurally related to the sub-site of the H-centre of the all-iron hydrogenases are described: tripodal dithiolate thioether ligands allow the synthesis of di-iron pentacarbonyls with differential (2:3) S ligation of the Fe atoms.

X-Ray crystallographic data for Fe-only hydrogenases isolated from *Desulfovibrio desulfuricans*[1] and *Clostridium pasteurianum*[2] together with IR evidence show that the active centre of the enzyme possesses an unprecedented {2Fe3S} sub-site at which CO and CN ligands are bound.[3] The two Fe atoms of the sub-site share two bridging sulfur ligands of a propanedithiolate or related unit[4] with one of the Fe atoms additionally sulfur ligated by a cysteinyl ligand bridged to a {4Fe4S} cluster, Fig. 1(a). Molecules with a {2Fe2S} propanedithiolate core and CO/CN ligation have been synthesised[5] which possess structural elements of the CO inhibited sub-site.[6] We now show that formal backbone modification of the propanedithiolate ligand allows access to carbonyls with a {2Fe3S} core with differential S-ligation of the iron atoms, Fig. 1(b).

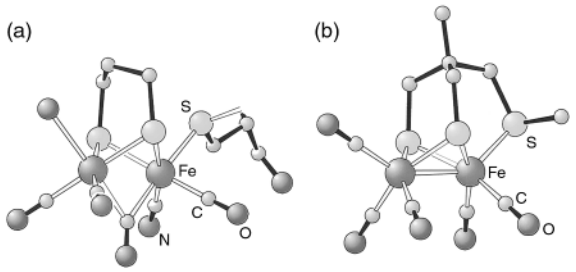

Fig. 1 (a) Proposed structure of the H-centre of Fe-only hydrogenases; this is a composite model combining features reported by Peters (PDB code 1FEH) and Nicolet (code 1HFE). (b) View of a molecule of the product **D**.

Two thiolate sulfur ligands of the tripodal thiolate **A**[7] are readily coupled with dimethyl disulfide with formation of a stable five-membered ring **B**, Scheme 1. This allows chemistry to be carried out on the unprotected thiol group. Reaction with MeI gives the thioether derivative, and subsequent reductive cleavage of the disulfide bond gives the backbone functionalised propanedithiol ligand **C**, Scheme 1.† The ligand reacts with $[Fe_3(CO)_{12}]$ to yield the {2Fe3S}-carbonyl **D** which has been fully characterised by X-ray crystallography, Fig. 1(b), and spectroscopy.‡

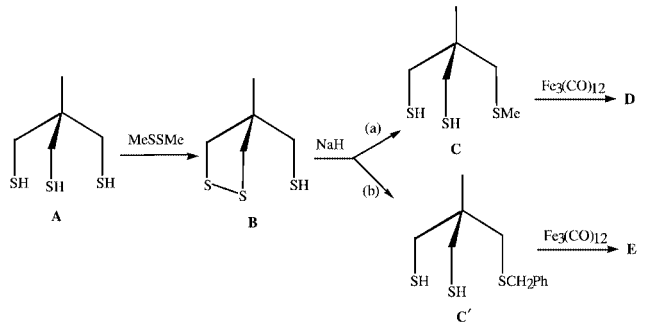

Scheme 1 Routes to ligands and complexes. *Reagents*: (a) i, MeI; ii, $LiAlH_4$; iii, H_2SO_4; (b) i, $PhCH_2Br$; ii, $LiAlH_4$; iii, H_2SO_4.

There are two independent molecules (plus their mirror image molecules) in crystals of **D**. The two molecules are essentially identical, and in each, the Fe–Fe distance is short, mean value 2.512(4) Å, indicative of an iron–iron bond. Each iron atom has five other contacts, in a square pyramidal coordination pattern, with the iron atom displaced (mean) 0.382(10) Å from the mean base plane towards the apical carbonyl ligand and 0.322(5) Å towards the thioether S atom. In each molecule, the normals to the square base planes are inclined at (mean) 74.7(6)° and the planes are hinged through the two bridging thiolate sulfur atoms of the S_3 ligands; the Fe–$S_{bridging}$ distances have a mean value of 2.254(1) Å. The third S atom, the thioether S, is coordinated to one of the iron atoms at a similar, mean distance of 2.254(3) Å and occupies the apical coordination site. Two carbonyl ligands occupy the base planes on each iron and one occupies the apical site of the second iron atom. The S_3 ligand thus lies atop the $Fe_2(CO)_5$ unit and is symmetrically arranged (with a pseudo-mirror plane through the iron atoms and the apical groups) except for the thioether methyl group which veers to one side or the other of the mirror plane. Both enantiomers are present in these centrosymmetric crystals.

The structural similarities between the enzyme sub-site and the model compound are evident from Fig. 1. The Fe···Fe bond distance in **D** and the average bridging Fe–S bond lengths are similar to those distances estimated from the protein crystallographic data, which are 2.6 and 2.3 Å, respectively[1,2] but the thioether Fe–S distance in **D** is shorter than the corresponding sub-site Fe–$S_{cysteine}$ distance in the enzyme which is *ca* 2.5 Å.

The benzyl analogue **E** is obtained by straightforward modification of the synthesis, Scheme 1. Its crystal structure, Fig. 2, confirms a conformation very similar to that of **D** with only very minor differences in bond angles and dimensions.‡

We have monitored the reaction of complex **D** with 2 equivalents of cyanide [K^+(18-crown-6) salt; MeCN]. This reveals its conversion within 30 min to a new species **F** which shows two distinct CN stretches, three terminal CO bands and a bridging CO band at 1780 cm^{-1}, Scheme 2. **F** is indefinitely stable in MeCN at 0 °C but on standing for 18 h at RT it slowly transforms to a new species **G** . The IR pattern and frequencies of **G** very closely resemble those of $[Fe_2(CO)_4(CN)_2$-

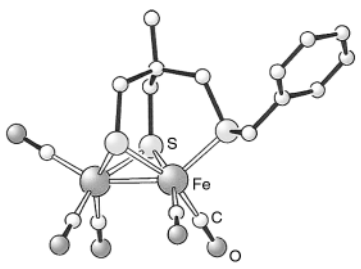

Fig. 2 View of the molecule of the product **E**.

DOI: 10.1039/b102244j

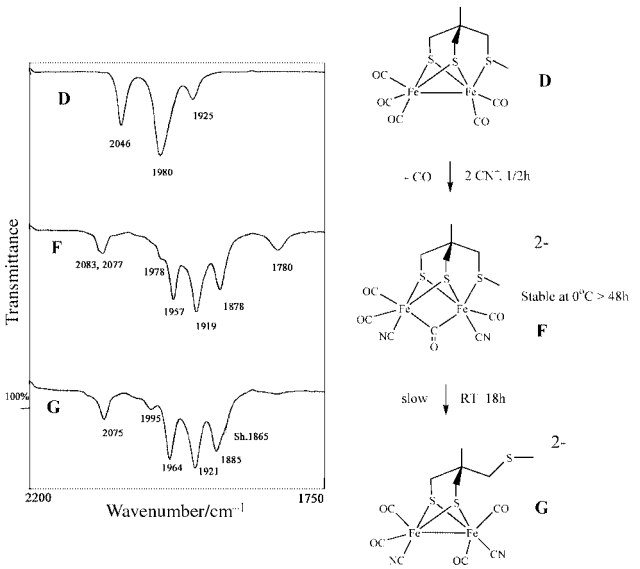

Scheme 2 Solution IR time course for reaction of **D** with cyanide in MeCN and proposed pathway to the species **F** and **G**.

$(SCH_2CH_2S)]^{2-}$,[5] showing a single ν(CN) at 2075 cm^{-1}, Scheme 2. FAB-MS of **G** shows a strong parent ion at 759 for {(K+18-crown-6)$[Fe_2(CO)_4(CN)_2\{MeSCH_2C(Me)(CH_2S)_2\}]$}. These preliminary results are consistent with the initial formation of a CO bridged di-cyanide species **F** which slowly isomerises to the metal–metal bonded terminal carbonyl species **G** with dissociation of the methyl thioether group, Scheme 2. This provides the first tentative evidence for the genesis of a model complex with all the principal structural features of the CO inhibited form of the natural sub-site: two cyanide groups, terminal and bridging CO ligands, and a {2Fe3S} core.§

Finally, we see in the preparation of **E** that a thiolate-*protected* rather than -*blocked* group can been introduced at one of the iron atoms: this or other S-protection/deprotection approaches should open up further chemistry of the synthetic sub-site.

We thank the BBSRC and the John Innes Foundation for supporting this work. Drs D. J. Evans and J. R. Sanders are thanked for helpful discussion.

Notes and references

† *Spectroscopic and analytical* data. $MeC(CH_2S)_2CH_2SH$: ^{1}H NMR (400 MHz, $C_6D_5CD_3$): δ 0.73 (3H, s, CH_3), 0.89 (1H, t, ^3J 9 Hz, SH), 2.07 (2H, d, ^3J 9 Hz, CH_2SH), 2.27 [2H, d, ^2J 11.2 Hz, (*CH*HSSC*H*H)], 2.48 [2H, d, ^2J 11.2 Hz, (CH*H*SSCH*H*)]. FTIR (KBr): ν(SH) 2551m, br cm^{-1}. EIMS: *m/z* 166 $\{M\}^+$, 133 $\{M - SH\}^+$, 119 $\{M - CH_2SH\}^+$. Microanal.: $C_5H_{10}S_3$, found(calc.): C, 36.48(36.12); H, 6.14(6.06); S, 57.6(57.9)%. Yield 91%.

$MeC(CH_2SH)_2CH_2SMe$: ^{1}H NMR (400 MHz, CD_2Cl_2): δ 1.03 (3H, s, CH_3), 1.32 (2H, t, ^3J 9 Hz, SH), 2.13 (3H, s, SCH_3), 2.63 (2H, s, CH_2SCH_3), 2.63 [4H, d, ^3J 9 Hz, (HSCH_2CCH_2SH)]. EIMS: *m/z* 182 $\{M\}^+$, 101 $\{CH_3C(CH_2)_2CH_2S\}^+$, 87 $\{CH_3C(CH_2)CH_2S\}^+$, 69 $\{CH_3C(CH_2)_3\}^+$, 61 $\{CH_3CCH_2\}^+$, 47 $\{CH_2SH\}^+$. Microanal.: $C_6H_{14}S_3$, found(calc.): C, 39.26(39.56); H, 7.70(7.59); S, 53.0(52.8)%. Yield 55%.

$MeC(CH_2SH)_2CH_2SCH_2Ph$: ^{1}H NMR (400 MHz, CD_2Cl_2): δ 0.90 (3H, s, CH_3), 1.11 (1H, t, ^3J 9 Hz, SH), 2.46 (2H, s, CH_2SCH_2Ph), 2.47 [4H, d, ^2J 9 Hz, (HSCH_2CCH_2SH)], 3.63 (2H, s, SCH_2Ph), 7.24 (5H, m, $SCH_2C_6H_5$). EIMS: *m/z* 258 $\{M\}^+$, 166$\{CH_3C(CH_2S)_2CH_2SH\}^+$, 133$\{CH_3C(CH_2S)_2CH_2\}^+$, 101$\{CH_3C(CH_2)_2CH_2S\}^+$, 91$\{CH_2Ph\}^+$, 69$\{CH_3C(CH_2)_3\}^+$. Yield 31%.

$[Fe_2(CO)_5\{MeSCH_2C(Me)(CH_2S)_2\}]$: ^{1}H NMR (400 MHz, CD_2Cl_2): δ 0.90 (3H, s, CH_3), 1.65 [2H, d, ^2J 14 Hz, (*H*HCCCH*H*)], 2.05 (2H, br, CH_2SCH_3), 2.23 [2H, d, ^2J 14 Hz, (H*H*CCC*H*H)], 2.64 (3H, s, SCH_3). FTIR (in CH_3CN): ν(CO) 1925w, 1979s, br and 2046s cm^{-1}. EIMS: *m/z* 432 $\{M\}^+$, 404$\{M - CO\}^+$, 376$\{M - 2CO\}^+$, 348$\{M - 3CO\}^+$, 320$\{M - 4CO\}^+$, 292$\{M - 5CO\}^+$, 180$\{MeC(CH_2S)_2CH_2SMe\}^+$, 176$\{Fe_2S_2\}^+$, 61 $\{CH_3CCH_2\}^+$. Microanal.: $C_{13}H_{12}O_5S_3Fe_2\cdot(0.1C_6H_{14})$ found(calc.): C, 31.60(31.59); H, 3.05(3.04); S, 20.8 (21.8)%. Yield 49% (recrystallised from hexane).

$[Fe_2(CO)_5\{PhCH_2SCH_2C(Me)(CH_2S)_2\}]$: ^{1}H NMR (400 MHz, CD_2Cl_2): δ 0.90 (3H, s, CH_3), 1.70 [2H, d, ^2J 14 Hz, (H*H*CCC*H*H)], 1.82 (2H, s, CH_2SCH_2Ph), 2.28 [2H, d, ^2J 14 Hz, (*H*HCCCH*H*)], 4.12 (2H, s, SCH_2Ph), 7.40 (5H, m, $SCH_2C_6H_5$). FTIR (in CH_3CN): ν(CO) 1925w, 1981s, br, 2046s and 2073vw cm^{-1}. EIMS: *m/z* 508 $\{M\}^+$, 480$\{M - CO\}^+$, 452$\{M - 2CO\}^+$, 424$\{M - 3CO\}^+$, 396$\{M - 4CO\}^+$, 368$\{M - 5CO\}^+$, 267$\{Fe_2SSCH_2Ph\}^+$, 231$\{Fe_2SCH_2C(Me)CH_2S\}^+$, 176$\{Fe_2S_2\}^+$, 91$\{CH_2Ph\}^+$. Microanal.: $C_{19}H_{16}O_5S_3Fe_2$, found(calc.): C, 40.26(40.16); H, 3.57(3.15); S, 15.9(18.9)%. Yield 73% (recrystallised from MeCN).

‡ *Crystal structure* analyses. $[Fe_2(CO)_5\{MeSCH_2C(Me)(CH_2S)_2\}]$: *crystal data:* $C_{11}H_{12}Fe_2O_5S_3$, M = 432.1, monoclinic, space group $P2_1/n$ (equiv. to no. 14), a = 18.467(2), b = 10.9622(12), c = 16.906(2) Å, β = 105.267(8)°, V = 3301.6(6) Å^3, Z = 8, D_c = 1.739 g cm^{-3}, $F(000)$ = 1744, T = 293 K, μ(Mo-Kα) = 21.5 cm^{-1}, λ(Mo-Kα) = 0.71069 Å.

Deep red, irregular fragment of a diamond-shaped plate crystal, sealed in a capillary. Preliminary photographic examination, then Nonius CAD4 diffractometer. 3528 Unique reflections to θ_{max} = 21°, the limit of measurable intensities; 2614 'observed' with $I > 2\sigma_I$. Corrections for slight deterioration, absorption (semi-empirical ψ-scan methods) and elimination of negative net intensities (Bayesian statistical methods). Structure determination by direct methods in SHELXS[8] (A), refinement by full-matrix least-squares methods, on F^2, in SHELXL[9] (B). Final wR_2 = 0.061, R_1 = 0.046 (B) for all 3528 reflections weighted $w = \sigma^{-2}(F_o^2)$; for the 'observed' data, R_1 = 0.028. Highest difference peaks (*ca.* 0.24 e Å^{-3}) close to a carbonyl ligand.

$[Fe_2(CO)_5\{PhCH_2SCH_2C(Me)(CH_2S)_2\}]$: *crystal data:* $C_{17}H_{16}Fe_2O_5S_3$, M = 508.2, triclinic, space group $P\bar{1}$ (no. 2), a = 9.8755(11), b = 11.3853(13), c = 10.3912(13) Å, α = 110.555(10), β = 92.983(9), γ = 104.374(9)°, V = 1047.2(2) Å^3, Z = 2, D_c = 1.612 g cm^{-3}, $F(000)$ = 516, T = 293(1) K, μ(Mo-Kα) = 17.1 cm^{-1}, λ(Mo-Kα) = 0.71069 Å.

Very thin, red-brown plate mounted on a glass fibre. Similar diffractometer procedure and processing, giving 3686 unique reflections to θ_{max} = 25° (2715 'observed' with $I > 2\sigma_I$). No deterioration correction necessary. Final wR_2 = 0.105 and R_1 = 0.053 (B) for all 3686 reflections weighted $w = [\sigma^2(F_o^2) + (0.0579P)^2]^{-1}$, with $P = (F_o^2 + 2F_c^2)/3$; for the 'observed' data only, R_1 = 0.037. Highest difference peaks (to *ca.* 0.4 e Å^{-3}) all in the cluster core region.

CCDC 156989 and 161064. See http://www.rsc.org/suppdata/cc/b1/b102244j/ for crystallographic data in .cif or other electronic format.

§ Well-resolved IR data for the *oxidised* CO inhibited H-centre have been reported recently by De Lacey *et al.*[10] giving: ν(CN) at 2096 and 2089 cm^{-1}; $\nu(CO_{terminal})$ at 2016, 1972 and 1963 cm^{-1}; and $\nu(CO_{bridging})$ at 1811 cm^{-1}. In this paramagnetic state the di-iron sub-site is magnetically described as a localised mixed-valence state, though critically whether Fe^{II}–Fe^{III} or Fe^{I}–Fe^{II} was undecided.[11] The data we have at hand for the Fe^{I}–Fe^{I} species **F** show: ν(CN) at 2083 and 2077 cm^{-1}; $\nu(CO_{terminal})$ at 1957, 1919 and 1878 cm^{-1}; and $\nu(CO_{bridging})$ at 1780 cm^{-1}. Thus $\Delta\nu(CO_{terminal})$ corresponds to 59, 53 and 85 cm^{-1} respectively with $\Delta\nu(CO_{bridge})$ = 31 cm^{-1}. These magnitudes are consistent with the oxidised CO-form of the sub-site having the Fe^{I}–Fe^{II} configuration (*i.e.* it is one-electron oxidised with respect to **F**) and lends support to the deduction of De Lacey *et al.* that proximal iron atom is in the Fe ^{II} state {$\Delta\nu$(CO) = 85 cm^{-1}} with the less perturbed distal iron atom {$\Delta\nu$(CO) = 59, 53 cm^{-1}} in the Fe^{I} state.

1 Y. Nicolet, C. Piras, P. Legrand, C. E. Hatchikian and J. C. Fontecilla-Camps, *Structure*, 1999, **7**, 13.
2 J. W. Peters, W. N. Lanzilotta, B. J. Lemon and L. C. Seefeldt, *Science*, 1998, **282**, 1853.
3 A. J. Pierik, M. Hulstein, W. R. Hagen, S. P. J. Albracht and K. A. Bagley, *Eur. J. Biochem.*, 1998, **258**, 572.
4 Y. Nicolet, B. J. Lemon, J. C. Fontecilla-Camps and J. W. Peters, *TIBS*, 138, **25**, 2000.
5 A. Le Cloirec, S. P. Best, S. Borg, S. C. Davies, D. J. Evans, D. L. Hughes and C. J. Pickett, *Chem. Commun.*, 1999, **22**, 2285; M. Schmidt, S. M. Contakes and T. B. Rauchfuss, *J. Am. Chem. Soc.*, 1999, **121**, 9736; E. J. Lyon, I. P. Georgakaki, J. H. Reibenspies and M. Y. Darensbourg, *Angew. Chem., Int. Ed.*, 1999, **38**, 3178.
6 B. J. Lemon and J. W. Peters, *Biochemistry*, 1999, **38**, 12 969.
7 C. Kolomyjec, J. Whelan and B. Bosnich, *Inorg. Chem.*, 1983, **22**, 2343.
8 G. M. Sheldrick, *Acta Crystallogr., Sect. A*, 1990, **46**, 467.
9 G. M. Sheldrick, SHELXL - Program for crystal structure refinement, University of Göttingen, Germany, 1993.
10 A. L. De Lacey, C. Stadler, C. Cavazza, E. C. Hatchikian and V. M. Fernandez, *J. Am. Chem. Soc.*, 2000, **122**, 11 232.
11 C. V. Popescu and E. Munck, *J. Am. Chem. Soc.*, 1999, **121**, 7877.

CHEMCOMM
Communication
www.rsc.org/chemcomm

Unexpected bonding similarities between the bridging metalloligands $[MoCp(CO)_3]^-$ and $[PtI(CO)_2(PPh_3)]^-$ acting as 4-electron donors in metal clusters. Crystal structures of $[Pt_2Mo(\mu\text{-}CO)_3(\mu\text{-}PPh_2)Cp(PPh_3)_2]$ and $[Pt_3(\mu\text{-}CO)_2(\mu\text{-}PPh_2)I(PPh_3)_3]$†‡

Christine Archambault,[a] Robert Bender,*[a] Pierre Braunstein,*[a] Salah-Eddine Bouaoud,[b] Djemel Rouag,[b] Stéphane Golhen[c] and Lahcène Ouahab[c]

[a] *Laboratoire de Chimie de Coordination, UMR 7513 CNRS, Institut Le Bel, Université Louis Pasteur, 4 rue Blaise Pascal, F-67070 Strasbourg Cedex, France. E-mail: braunst@chimie.u-strasbg.fr*
[b] *Institut de Chimie, Université de Constantine, route de AÏn el Bey, Constantine, Algeria*
[c] *Laboratoire de Chimie du Solide et Inorganique Moléculaire, UMR 6511 CNRS, Institut de Chimie, Université de Rennes 1, Campus de Beaulieu, 35042 Rennes Cedex, France*

Received (in Cambridge, UK) 13th February 2001, Accepted 22nd March 2001
First published as an Advance Article on the web 17th April 2001

Reactions of the diplatinum complex $[Pt_2(\mu\text{-}H)(\mu\text{-}PPh_2)I_2(PPh_3)_2]$ with the carbonylmetalates $[MCp(CO)_3]^-$ (M = Mo, W) or $[Co(CO)_4]^-$ afforded the new 44e clusters $[Pt_2M(\mu\text{-}CO)_3(\mu\text{-}PPh_2)Cp(PPh_3)_2]$ (M = Mo, 2; M = W, 3) and $[Pt_3(\mu\text{-}CO)_2(\mu\text{-}PPh_2)I(PPh_3)_3]$ 5, respectively, whose structures can be analysed as formed by a 26e $[Pt_2(\mu\text{-}PPh_2)(PPh_3)_2]^+$ cation and a bridging, 4e donor anion, $[MCp(CO)_3]^-$ in 2 and 3, or the new 18e fragment $[PtI(CO)_2(PPh_3)]^-$ in 5.

In the search for versatile synthetic methods, numerous metal–metal bonded complexes and clusters have been obtained by reaction of carbonylmetalates with mononuclear halide complexes,[1,2] whereas fewer studies have been concerned with dinuclear halide precursors.[3] The reactions of the diplatinum complex $[Pt_2(\mu\text{-}H)(\mu\text{-}PPh_2)I_2(PPh_3)_2]$ **1**, prepared by reaction of $[Pt_2(\mu\text{-}PPh_2)(\mu\text{-}o\text{-}C_6H_4PPh_2)(PPh_3)_2]$[4a] with 2 equiv. of HI in THF,[4b] with three different carbonylmetalates has now afforded clusters whose structures reveal an unexpected bonding similarity between the 18e metalloligands $[MCp(CO)_3]^-$ (M = Mo, W) and $[PtI(CO)_2(PPh_3)]^-$ which are best viewed as 4e donors towards a d^9–d^9 Pt(I)–Pt(I) unit.

Reaction of 1 equiv. of **1** with 3 equiv. of $[MCp(CO)_3]^-$ in thf afforded the mixed-metal clusters $[Pt_2M(\mu\text{-}CO)_3(\mu\text{-}PPh_2)Cp(PPh_3)_2]$ (M = Mo, **2**; M = W, **3**) (Scheme 1).§ Their $^{31}P\{^1H\}$ NMR spectra contain a triplet at low field for the μ-PPh_2 ligand and a doublet for terminal phosphines, both with satellites due to couplings with two Pt atoms. In addition, the pattern of the resonance of the phosphine ligands is typical for a P→Pt–Pt←P chain. An X-ray diffraction study of **2**¶ established that the metal atoms form an isosceles triangle with a Pt–Pt edge bridged by a PPh_2 group (Fig. 1). Two CO ligands occupy a semi-bridging position on the Pt–Mo edges and the third one is semi-triply bridging over the metallic face. This arrangement is reminiscent of that in the tetranuclear cluster $[Pt_2Mo_2(\mu\text{-}CO)_6Cp_2(PEt_3)_2]$ **4**,[5a] its palladium analogue,[5b] or in the trinuclear cluster $[Pd_2Mo(\mu\text{-}Cp)(\mu\text{-}CO)_3Cp(PPr^i_3)_2]$.[6] Each Pt atom is ligated by a PPh_3 ligand and the Mo atom by a η^5-cyclopentadienyl ligand. The metal–metal distances in **2** are comparable with those in **4**.[5a] The Pt–(μ-P)–Pt angle (69.55(4)°) is one of the narrowest for a PPh_2 group bridging a metal–metal bond. It is close to that in $[Pt_2(\mu\text{-}PPh_2)_2(PPh_3)_2]$ (*ca.* 69.0°)[7] but smaller than in $[Pt_2\{\mu\text{-}Co(CO)_3(PPh_3)\}(\mu\text{-}PPh_2)(PPh_3)_2]$ (72.41(8)°),[8] which is consistent with a longer Pt–Pt bond of 2.664(1) Å in the latter. The three P atoms are almost in the metal plane, at +0.140(2), +0.044(2) and +0.050(2) Å, respectively. The PPh_3 ligands are almost aligned with the Pt atoms.

The highest yields of clusters **2** and **3** were obtained with a ratio of three $[MCp(CO)_3]^-$ anions for one dinuclear complex **1**. Since one anion enters in the composition of the clusters, the other two are probably eliminated with other ligands of **1**, *i.e.* H and I.

Reaction of 3 equiv. of $[Co(CO)_4]^-$ with 1 equiv. of complex **1** unexpectedly afforded the new homonuclear triplatinum cluster $[Pt_3(\mu\text{-}PPh_2)(\mu\text{-}CO)_2I(PPh_3)_3]$ **5**§ instead of Pt–Co cluster(s). The $^{31}P\{^1H\}$ NMR spectrum contains three signals flanked by ^{195}Pt satellites. The singlet at δ 279.6 is assigned to a PPh_2 group bridging two equivalent Pt atoms and the doublet

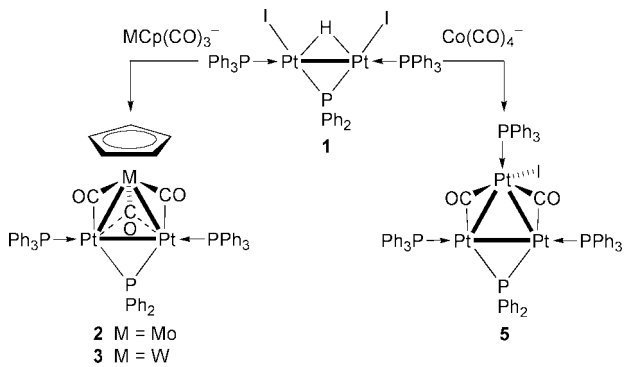

Scheme 1

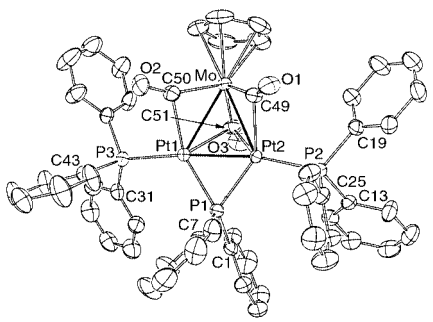

Fig. 1 Molecular structure of $[Pt_2Mo(\mu\text{-}CO)_3(\mu\text{-}PPh_2)Cp(PPh_3)_2]$ **2**. Selected interatomic distances (Å) and angles (°): Pt(1)–Pt(2) 2.6048(3), Pt(1)–Mo 2.7963(5), Pt(2)–Mo 2.8139(6), Pt(1)–P(1) 2.282(2), Pt(1)–P(3) 2.261(2), Pt(2)–P(1) 2.283(2), Pt(2)–P(2) 2.254(2); Pt(1)–Mo–Pt(2) 55.33(1), Mo-Pt(1)–Pt(2) 62.68(1), Mo–Pt(2)–Pt(1) 61.99(1), P(3)–Pt(1)–Pt(2) 174.78(4), P(2)–Pt(2)–Pt(1) 169.72(4), Pt(1)–P(1)–Pt(2) 69.55(4).

† Electronic supplementary information (ESI) available: preparation of **2**, **3** and **5**. See http://www.rsc.org/suppdata/cc/b1/b101410m/
‡ In memoriam Luigi M. Venanzi, who contributed so much to inorganic and cluster chemistry.

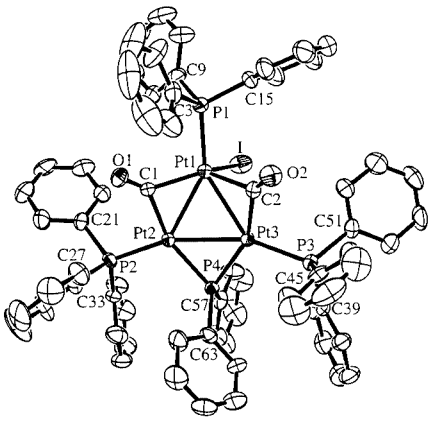

Fig. 2 Molecular structure of $[Pt_3(\mu\text{-}PPh_2)(\mu\text{-}CO)_2I(PPh_3)_3]$ **5**. Selected interatomic distances (Å) and angles (°): Pt(1)–Pt(2) 2.6832(13), Pt(1)–Pt(3) 2.694(2), Pt(2)–Pt(3) 2.736(2), Pt(1)–I 2.8165(17), Pt(1)–P(1) 2.268(3), Pt(2)–P(2) 2.238(3), Pt(3)–P(3) 2.256(3), Pt(2)–P(4) 2.279(3), Pt(3)–P(4) 2.273(3), Pt(2)–Pt(1)–Pt(3) 61.17(4), P(1)–Pt(1)–I 99.72(8), Pt(1)–Pt(2)–Pt(3) 59.62(5), P(2)–Pt(2)–Pt(3) 160.76(7), P(3)–Pt(3)–Pt(2) 159.33(7), Pt(3)–P(4)–Pt(2) 73.90(8).

at δ 33.8 to the phosphine ligands in the $Ph_3P\rightarrow Pt\text{–}Pt\leftarrow PPh_3$ moiety. These phosphines are coupled with a third phosphorus, which resonates as a triplet at δ 75.2. From the intensities of its ^{195}Pt satellites, it is deduced that this phosphine is coordinated to a Pt atom, which is itself linked to two equivalent Pt atoms. Cluster **5** should contain a triangle of Pt atoms, each bearing a phosphine ligand, with two Pt atoms being bridged by a PPh_2 group. An X-ray diffraction study¶ established the structure of **5** in which the shortest edge of the metal triangle, Pt(2)–Pt(3), is bridged by a PPh_2 group and the other two are each symmetrically bridged by a CO group (Fig. 2). A PPh_3 ligand is coordinated to each Pt atom and an iodine atom is bonded to Pt(1). The P(1)Pt(1)C(1)C(2)I atoms form the apices of a trigonal pyramid with P(1) in an apical position. The P(1)–Pt(1) bond makes angles of *ca*. 100° with the three basal bonds Pt(1)–I, Pt(1)–C(1) and Pt(1)–C(2).

Formation of **5** implies a complex reaction mechanism, where carbonyl groups have exchanged between cobalt and platinum, probably *via* a mixed Pt–Co complex. Fragmentation of the Pt_2 entity of complex **1** is required to form the Pt_3 framework and iodine could either remain on one of the Pt atoms or I^- attack an intermediate species. Complex reactions between Pt(II) halide complexes and $[Co(CO)_4]^-$ have been described from which heterometallic Pt–Co clusters with diverse Pt/Co compositions were isolated[9] and when the isoelectronic metalates $[Mn(CO)_5]^-$ or $[Fe(CO)_3(NO)]^-$ were used instead, no Pt–Mn or Pt–Fe clusters were observed, respectively, but rather $[Pt_5(CO)_6(PR_3)_4]$ which resulted from selective reductive carbonylation of the Pt(II) precursor complex.[10]

The 44e clusters **2** and **3** can formally be viewed as formed of two fragments, the cationic, 26-valence electrons (VE) entity $[Pt_2(\mu\text{-}PPh_2)(PPh_3)_2]^+$, which possesses two vacant fragment orbitals (2a′ and 2a″ in C_s symmetry)[11] and a bridging, 18-VE carbonylmetalate $[MCp(CO)_3]^-$. The HOMOs of the latter ($1a_1$ + 1e) can formally donate 4e to the dinuclear cation,[12] so that each Pt atom achieves its usual 16 VE count. The 44e count in cluster **5** is not unusual for Pt_3 clusters (with two 16e and one 18e metal centres), although the 42e alternative is more frequently encountered.[13] By analogy with the bonding behaviour of $[MCp(CO)_3]^-$, one can view the fragment $[PtI(CO)_2(PPh_3)]^-$ as a bridging group formally donating 4e to the $[Pt_2(\mu\text{-}PPh_2)(PPh_3)_2]^+$ cation, through two Pt–Pt bonds and two bridging CO groups, *i.e*. 2e to each Pt atom. In terms of electron counting, this makes these metalates behave remarkably similar to bridging halides or $\mu\text{-}PR_2^-$. To our knowledge, the anionic 18e complex $[PtI(CO)_2(PPh_3)]^-$ has not been isolated previously.

We are grateful to Professor J. Fischer and Dr A. DeCian for the crystal structure determination of **2** and thank the CNRS, the Ministère de la Recherche and the Ministère des Affaires Etrangères (Paris) and the Ministère des Affaires Etrangères (Alger) for support of the Strasbourg-Constantine Cooperation Project 96 MDU 371.

Notes and references

§ *Selected data*: **2**: IR (KBr) ν(CO)/cm^{-1}: 1830s, 1788s. FAB-MS (NBA matrix): *m*/*z* 1099.1 ($[Pt_2(\mu\text{-}PPh_2)(PPh_3)_2]^+$ = [M − $MoCp(CO)_3$]$^+$). ^{31}P{^{1}H} NMR (THF–C_6D_6): δ 283.3 (t, ^2J(P–P) 42, ^1J(Pt–P) 2738 Hz), 42.8 (d, ^2J(P–P) 42, ^1J(Pt–P) 4780, ^2J(Pt–P) 50, ^3J(P–P) 88 Hz).

3: IR (KBr) ν(CO)/cm^{-1}: 1830s, 1788s. FAB-MS (NBA matrix): *m*/*z* 1099.1 ($[Pt_2(\mu\text{-}PPh_2)(PPh_3)_2]^+$ = [M − $WCp(CO)_3$]$^+$). ^{31}P{^{1}H} NMR (THF–C_6D_6): δ 312.4 (t, ^2J(P–P) 43, ^1J(Pt–P) 2631 Hz), 44.1 (d, ^2J(P–P) 43, ^1J(Pt–P) 4832, ^2J(Pt–P) 87, ^3J(P–P) 87 Hz).

5: IR (KBr) ν(CO)/cm^{-1}: 1831s, 1789vs. ^{31}P{^{1}H} NMR ($CDCl_3$): δ 279.6 (s, ^1J(Pt–P) 2511 Hz), 75.2 (t, ^3J(P–P) 44, ^1J(Pt–P) 5809, ^2J(Pt–P) 505 Hz), 33.8 (d, ^3J(P–P) 44, ^1J(Pt–P) 4382, ^2J(Pt–P) 70, ^3J(P–P) 81 Hz).

¶ *Crystal data*: for **2**: single crystals were obtained by slow diffusion of diethyl ether into a solution of **2** in dichloromethane. $C_{56}H_{45}MoO_3P_3Pt_2\cdot H_2O$, M = 1363.04, triclinic, space group $P\bar{1}$, a = 12.053(1), b = 13.690(1), c = 17.292(3) Å, α = 109.271(6), β = 92.541(6), γ = 106.169(6)°, V = 2557.5(5) Å^3, Z = 2, D_c = 1.77 g cm^{-3}, μ = 5.886 mm^{-1}, T = 173 K, λ(Mo-Kα) = 0.70930 Å, 8988 data collected, 7078 data with $I > 3\sigma(I)$, θ min./max. = 2.5/24.92°, $R(F)$ = 0.023, $R_w(F)$ = 0.034, GOF = 1.095.

For **5**: single crystals were obtained by slow diffusion of hexane into a solution of **5** in toluene. $C_{68}H_{55}IO_2P_4Pt_3$, M = 1740.17, triclinic, space group $P\bar{1}$, a = 13.564(12), b = 14.954(6), c = 17.948(8) Å, α = 69.64(3), β = 75.44(4), γ = 63.98(4)°, V = 3046(3) Å^3, Z = 2, D_c = 1.897 g cm^{-3}, μ = 7.528 mm^{-1}, T = 253 K, λ(Mo-Kα) 0.71073 Å, 11189 data collected, 10693 data with $I > 2\sigma(I)$, R_1 = 0.0397, wR_2 = 0.0913. CCDC 158327 and 158328. See http://www.rsc.org/suppdata/cc/b1/b101410m/ for crystallographic data in .cif or other electronic format.

1 *Metal Clusters in Chemistry*, ed. P. Braunstein, L. A. Oro and P. R. Raithby, Wiley-VCH, Weinheim, vol. 1, 1999.
2 *Comprehensive Organometallic Chemistry II*, ed. E. W. Abel, F. G. A. Stone and G. Wilkinson, Pergamon, Oxford, vol. 10, 1995.
3 R. Bender, P. Braunstein, A. Tiripicchio and M. Tiripicchio-Camellini, *J. Chem. Soc., Chem. Commun*., 1984, 42; R. Bender, P. Braunstein and C. de Méric de Bellefon, *Polyhedron*, 1988, **7**, 2271; P. Braunstein, *New J. Chem*., 1994, **18**, 51.
4 (*a*) R. Bender, S.-E. Bouaoud, P. Braunstein, Y. Dusausoy, N. Merabet, J. Raya and D. Rouag, *J. Chem. Soc., Dalton Trans*., 1999, 735; (*b*) C. Archambault, R. Bender and P. Braunstein, unpublished results.
5 (*a*) R. Bender, P. Braunstein, J.-M. Jud and Y. Dusausoy, *Inorg. Chem*., 1984, **23**, 4489; (*b*) R. Bender, P. Braunstein, J.-M. Jud and Y. Dusausoy, *Inorg. Chem*., 1983, **22**, 3394.
6 H. Werner, P. Thometzek, C. Krüger and H.-J. Kraus, *Chem. Ber*., 1986, **119**, 2777.
7 N. J. Taylor, P. C. Chieh and A. J. Carty, *J. Chem. Soc., Chem. Commun*., 1975, 448.
8 R. Bender, P. Braunstein, B. Metz and P. Lemoine, *Organometallics*, 1984, **3**, 381.
9 J.-P. Barbier, P. Braunstein, J. Fischer and L. Ricard, *Inorg. Chim. Acta*, 1978, **31**, L361.
10 J.-P. Barbier, R. Bender, P. Braunstein, J. Fischer and L. Ricard, *J. Chem. Res. (S)*, 1978, 230; R. Bender, P. Braunstein, J. Fischer, L. Ricard and A. Mitschler, *Nouv. J. Chim*., 1981, **5**, 81.
11 L. Zhu and N. M. Kostic, *Organometallics*, 1988, **7**, 665.
12 P. Hofmann and H. R. Schmidt, *Angew. Chem., Int. Ed. Engl*., 1986, **25**, 837.
13 D. Imhof and L. M. Venanzi, *Chem. Soc. Rev*., 1994, **23**, 185; A. D. Burrows and D. M. P. Mingos, *Coord. Chem. Rev*., 1996, **154**, 19; M. T. Garland, K. Costuas, S. Kahlal and J.-Y. Saillard, *New J. Chem*., 1999, **23**, 509; W. Wang, P. J. Low, A. J. Carty, E. Sappa, G. Gervasio, C. Mealli, A. Ienco and E. Perez-Carreño, *Inorg. Chem*., 2000, **39**, 998.

CHEMCOMM Communication
www.rsc.org/chemcomm

Steam reforming of biomass-derived ethanol for the production of hydrogen for fuel cell applications

Athanasios N. Fatsikostas, Dimitris I. Kondarides and Xenophon E. Verykios*

Department of Chemical Engineering, University of Patras, GR-26500 Patras, Greece. E-mail: verykios@chemeng.upatras.gr

Received (in Cambridge, UK) 14th February 2001, Accepted 29th March 2001
First published as an Advance Article on the web 18th April 2001

Ni/La_2O_3 catalyst exhibits high activity and good long term stability for steam reforming of ethanol to hydrogen production and is a good candidate for ethanol reforming processors for fuel cell applications.

Fuel cells may be a promising alternative means of electricity generation for stationary decentralized applications. They offer significant advantages which include absence of pollutant emission, since they use hydrogen as the fuel, and high conversion efficiency, which may be even higher when they operate on the co-generation mode. In recent years, fuel cells have been seriously considered for electric vehicle operation, making possible so-called Zero Emission Vehicles.

An important source of hydrogen for stationary fuel cell applications is natural gas, while for transportation, methanol and gasoline are being considered. These fossil fuels do not address the issue of carbon dioxide emissions, however, which may only be addressed by the use of a renewable fuel as the hydrogen source. Ethanol can be produced renewably from several biomass sources, including energy plants, waste materials from agroindustries or forestry residue materials, or even organic fractions of municipal solid waste. Thus, in contrast to the fossil-fuel-based systems, the bioethanol-to-hydrogen-system has the significant advantage of being nearly CO_2 neutral, since the carbon dioxide produced is consumed for biomass growth, thus offering a nearly closed carbon loop. In addition, the use of ethanol offers important storage and handling safety advantages.

In the present communication, the catalytic steam reforming of ethanol for hydrogen production is discussed, with respect to catalyst performance characteristics. The steam reforming of ethanol for hydrogen production has been shown to be entirely feasible from a thermodynamic point of view.[1–3] An issue of major importance is then to develop highly active, selective and durable catalysts for the reaction. Although much work has been carried out on methanol reforming, only a limited number of reports have appeared in the literature dealing with the reforming of ethanol.[4–6] Here, we report results obtained over a Ni/La_2O_3 catalyst, which has been previously found to exhibit good performance characteristics under conditions of carbon dioxide reforming of methane to synthesis gas.[7] It is shown that under certain operating conditions, the Ni/La_2O_3 catalyst is very active and stable for the steam reforming of ethanol and is characterized by high selectivity toward hydrogen production.

The 17% Ni/La_2O_3 catalyst employed in the present study was prepared by the wet impregnation method using $Ni(NO_3)_2$ and La_2O_3 (Alfa Products) as starting materials, following a procedure that has been described in detail elsewhere.[7] Catalytic performance tests have been conducted in the temperature range 300–800 °C, over catalyst samples previously reduced *in situ* with hydrogen (500 °C, 2 h). In a typical experiment, a water–ethanol mixture (molar ratio 3:1) is pumped into a heated chamber and vaporized. The water–ethanol gas stream (160 cm^3 min^{-1}) is then fed to a quartz micro-reactor containing 100 mg of catalyst. The composition of the reactor effluent is analyzed by means of two gas chromatographs, connected in series: the first is equipped with two packed columns (Porapak, Carbosieve) and two detectors (TCD, FID) and uses He as carrier gas. Porapak is used for the separation of C_2H_5OH, H_2O, CH_3CHO, CH_4, C_2H_4 and C_2H_6. Carbosieve is used for the separation of CO, CO_2 and CH_4. The second gas chromatograph, which uses N_2 as carrier gas, is equipped with a Carbosieve column and a TCD detector and is solely used for the analysis of the produced hydrogen.

Typical experimental results obtained are presented in Fig. 1, in which the conversion of ethanol and the selectivities to various reaction products are shown as a functions of reaction temperature. At temperatures below 300 °C, steam reforming of ethanol does not occur appreciably. Instead, dehydrogenation of ethanol occurs to an appreciable extent producing acetaldehyde and hydrogen. Increasing reaction temperature results in a progressive decrease of selectivity toward acetaldehyde, which drops to zero at temperatures above 550 °C. In this temperature range the reforming reactions of both acetaldehyde and ethanol prevail. It is interesting to observe that no ethylene is detected in the reaction products, indicating that no dehydration of ethanol is taking place, as might be expected. This is due to the fact that this particular catalyst, which utilizes La_2O_3 as the carrier material, does not possess any acidic sites, which are required for the dehydration route. Steam reforming of ethanol takes place to a significant extent at temperatures above 400 °C, as evidenced by the sharp increase of ethanol conversion and by the increase of selectivities toward CO and H_2 (Fig. 1). By-products of the reaction are CO_2 and CH_4, which are formed by reaction of CO with water (shift reaction) and with hydrogen (methanation), respectively. Selectivities toward CO_2 and CH_4

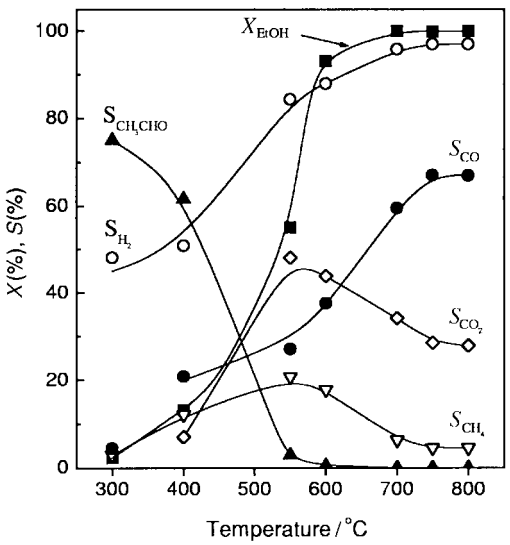

Fig. 1 Effect of reaction temperature on the conversion of ethanol (X_{EtOH}) and on selectivities toward acetaldehyde (S_{CH_3CHO}), carbon monoxide (S_{CO}), carbon dioxide (S_{CO_2}), methane (S_{CH_4}) and hydrogen (S_{H_2}), obtained over the 17% Ni/La_2O_3 catalyst. *Experimental conditions*: mass of catalyst: 100 mg; particle size: 0.25–0.50 mm; H_2O:EtOH molar ratio: 3:1; flow rate: 160 cm^3 min^{-1} (W/F = 0.0375 g s cm^{-3}); P = 1 atm.

DOI: 10.1039/b101455m

increase with increasing temperature and go through maxima at *ca.* 550 °C. Above this temperature, the reformation of methane with CO_2 and with H_2O becomes thermodynamically feasible, resulting in a decrease of the selectivities of both CH_4 and CO_2, since the Ni/La_2O_3 catalyst is known to be very active for these reforming reactions.[7] The observed decrease in the production of CO_2 may be due in part to the inverse shift reaction. At temperatures above 600 °C, the conversion of ethanol reaches 100% and the selectivity toward hydrogen exceeds 90% (Fig. 1). Under these conditions, the only undesirable product is methane, which competes with H_2 for hydrogen atoms. However, from a practical point of view, a small concentration of methane in the reformate may be tolerated since methane present at the exhaust of the fuel cell can be burned, along with unreacted hydrogen, to provide the heat necessary for the highly endothermic reforming reaction. In any event, conversion of methane *via* reforming with CO_2 and H_2O proceeds at higher reaction temperatures, resulting in increased yield of H_2 production.

The contact time dependence of the conversion of ethanol and of the selectivity toward reaction products, as well as the stability of the catalyst with time-on-stream were examined over a catalyst in which the active component (Ni/La_2O_3) was deposited on γ-Al_2O_3 pellets (Engelhard) of a surface area of 180 $m^2\ g^{-1}$. This type of catalyst formulation may be necessary for a practical application since La_2O_3 is hydroscopic and pellets made out of this material do not possess the necessary strength in the presence of steam, especially at low temperatures. This problem is avoided if lanthana is dispersed over the surface of materials which have the necessary strength, such as alumina pellets. For the experiment described here, the γ-Al_2O_3 pellets were impregnated with $La(NO_3)_3$ and then calcined in air at 900 °C for 30 h. The resulting material was then impregnated with $Ni(NO_3)_2$, dried at 110 °C for 24 h, reduced in H_2 at 500 °C for 5 h and crushed to particles of 0.25–0.50 mm in diameter.

The effect of contact time on the catalytic performance of the $(Ni/La_2O_3)/Al_2O_3$ catalyst at the reaction temperature of 750 °C is shown in Fig. 2, in which the conversion of ethanol and the selectivities towards various reaction products are plotted as functions of W/F. It is observed that for contact times >0.1 g s cm^3 the conversion of ethanol is 100% and the reaction is highly selective toward hydrogen ($>95\%$), the only unwanted by-product being methane ($<5\%$). As the contact time decreases, the conversion of ethanol progressively drops, accompanied by a decrease of the selectivity toward the reformation products (CO and H_2) and by an increase of the selectivity toward CO_2 and by-products, such as CH_3CHO, C_2H_4 and C_2H_6. It is interesting to observe that at low contact times (low ethanol conversion) appreciable amounts of ethylene are formed, obviously by dehydration of ethanol over acidic Al_2O_3 sites. This reaction did not occur measurably over the Ni/La_2O_3 catalyst which does not possess acidic sites.

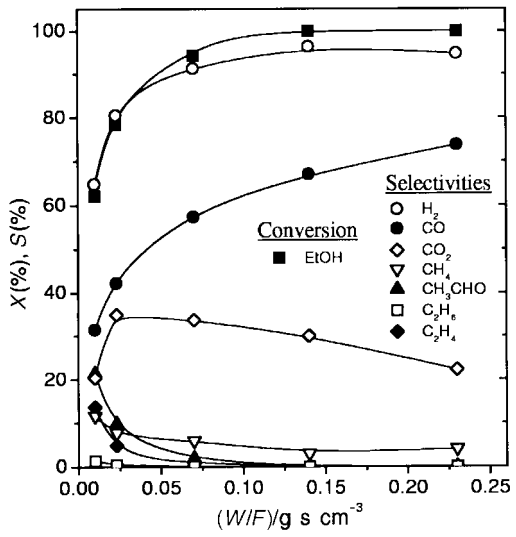

Fig. 2 Effect of space time (W/F) on the conversion of ethanol and on the selectivities toward reaction products, over the $(Ni/La_2O_3)/Al_2O_3$ catalyst. *Experimental conditions*: mass of catalyst: 100 mg; particle size: 0.25–0.50 mm; H_2O:EtOH molar ratio: 3:1; T = 750 °C; P = 1 atm.

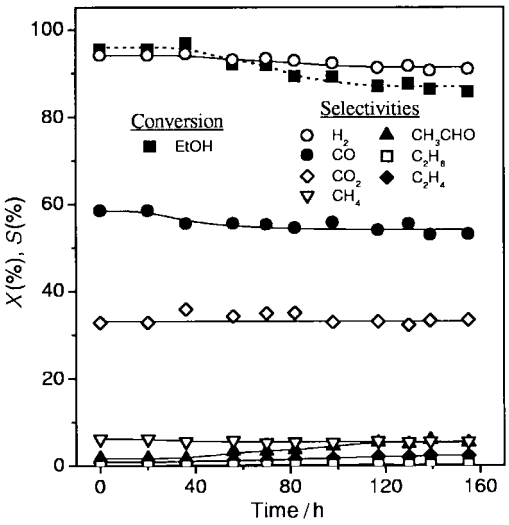

Fig. 3 Conversion of ethanol and selectivities toward reaction products as functions of time-on-stream, obtained over the $(Ni/La_2O_3)/Al_2O_3$ catalyst. *Experimental conditions*: mass of catalyst: 100 mg; particle size: 0.25–0.50 mm; H_2O:EtOH molar ratio: 3:1; flow rate: 87 $cm^3\ min^{-1}$ (W/F = 0.0690 g s cm^{-3}); T = 750 °C; P = 1 atm.

The stability of the $(Ni/La_2O_3)/Al_2O_3$ catalyst has been examined at 750 °C and the results are shown in Fig. 3, in which the alterations of activity and selectivity are plotted as functions of time-on-stream. Under the experimental conditions employed (see legend of Fig. 3), a small deactivation of the catalyst is observed during the first 80–100 h on stream, where conversion of ethanol drops from 95 to 88%, while further exposure of the catalyst to the reaction mixture does not result in further deactivation. It is interesting to observe that selectivity toward hydrogen does not change significantly and slightly decreases from the initial value of 94 to 91% after 155 h on stream. Selectivities toward the formation of other products, such as CO, CO_2, CH_4, CH_3CHO, C_2H_4 and C_2H_6 also stabilize after 100–120 h.

Summarizing, the present results reveal that the Ni/La_2O_3 catalyst, or the $(Ni/La_2O_3)/Al_2O_3$ pelleted form, exhibits high activity and, most importantly, good long term stability for steam reforming of ethanol to hydrogen production and is a good candidate to be used in ethanol reforming processors for fuel cell applications.

This work was funded in part by the Commission of the European Community, under contract ERK6-CT-1999-00012, and by the Hellenic General Secretariat of Research and Technology (EPET II).

Notes and references

1 K. Vasudeva, N. Mitra, P. Umasankar and S. C. Dhingra, *Int. J. Hydrogen Energy*, 1996, **21**, 13.
2 G. Maggio, S. Freni and S. Cavallaro, *J. Power Sources*, 1998, **74**, 17.
3 I. Fishtik, A. Alexander, R. Datta and D. Geana, *Int. J. Hydrogen Energy*, 2000, **25**, 31.
4 S. Cavallaro and S. Freni, *Int. J. Hydrogen Energy*, 1996, **21**, 465.
5 F. Haga, T. Nakajima, H. Miya and S. Mishima, *Catal. Lett.*, 1997, **48**, 223.
6 F. Marino, E. G. Cerella, S. Duhalde, M. Jobbagy and M. A. Laborde, *Int. J. Hydrogen Energy*, 1998, **23**, 1095.
7 Z. Zhang and X. E. Verykios, *J. Chem. Soc., Chem. Commun.*, 1995, 71.

CHEMCOMM
Communication
www.rsc.org/chemcomm

Converting a layer perovskite into a non-defective higher-order homologue: topochemical synthesis of $Eu_2CaTi_2O_7$

Raymond E. Schaak, Erin N. Guidry and Thomas E. Mallouk*

Department of Chemistry, The Pennsylvania State University, University Park, PA 16802, USA

Received (in Columbia, MO, USA) 15th November 2000, Accepted 15th March 2001
First published as an Advance Article on the web 17th April 2001

Topochemical reduction of $CaEu_2Ti_2O_8$, a new $n = 1$ mixed Ruddlesden–Popper/Dion–Jacobson phase prepared by divalent ion-exchange of $NaEuTiO_4$, yields the non-defective $n = 2$ Ruddlesden–Popper phase $Eu_2CaTi_2O_7$.

Transition-metal oxides that possess the perovskite structure are important materials that exhibit a wide range of useful properties, including ferroelectricity, superconductivity, colossal magnetoresistance, and catalytic activity. Layered perovskites that belong to the Ruddlesden–Popper,[1] $A_2[A'_{n-1}B_nO_{3n+1}]$, and Dion–Jacobson,[2] $A[A'_{n-1}B_nO_{3n+1}]$, families are known to possess similar properties, which often depend sensitively on the thickness of the perovskite block. As an example, the Curie temperature and magnetoresistive effects vary with increasing n (the number of octahedra that stack in the perovskite block) in the Ruddlesden–Popper manganate series $(La,Sr)_{n+1}Mn_nO_{3n+1}$.[3]

Many layered perovskites also undergo interlayer ion-exchange reactions, so they are ideal precursors to new metastable materials. For example, Dion–Jacobson phases that contain divalent interlayer cations,[4] as well as perovskite/copper-halide[5] and vanadate[6] intergrowths, can be synthesized at relatively low (< 500 °C) temperatures from layered perovskite precursors. Similarly, A-site defective three-dimensional perovskites can be synthesized by dehydrating proton-exchanged Ruddlesden–Popper phases,[7] and non-defective perovskites can be synthesized by topochemically reducing the appropriate Dion–Jacobson precursors.[8] In general, it is not possible to make these same ordered phases by direct, high temperature synthesis.

Since the electronic and magnetic properties of layered perovskites vary with the perovskite block thickness, the ability to convert among similar homologues in a series is a potentially useful tool for fine-tuning their properties. Recently, Gopalakrishnan and coworkers converted $HLnTiO_4$ (Ln = La, Nd, Sm, Gd), a family of $n = 1$ Ruddlesden–Popper phases, into $Ln_2\square Ti_2O_7$, an A-site defective $n = 2$ Ruddlesden–Popper series, by carefully dehydrating the $n = 1$ precursor.[9] The unique ordering of the lanthanide cations and the protons in $HLnTiO_4$ (or alkali cations in the parent phase $NaLnTiO_4$) in alternate rows imparts interlayer reactivity only to every other layer, which is necessary for the conversion from an $n = 1$ to an $n = 2$ phase.

Topochemical reduction is a powerful alternative to dehydration, because it can create *non-defective* condensed structures. One can envision a similar conversion reaction that transforms $NaLnTiO_4$ into a non-defective $n = 2$ phase (Fig. 1). $NaEuTiO_4$, the $n = 1$ Ruddlesden–Popper parent phase, contains the easily reducible Eu^{3+} cation, which converts to Eu^{2+} when heated in hydrogen. The concomitant loss of oxygen from the lattice is necessary for the topochemical collapse to occur. $NaEuTiO_4$ contains twice the number of interlayer Na^+ cations than are needed to fill the A-sites of a perovskite block, so divalent ion exchange must first be done to give the correct stoichiometry of interlayer cations, forming $A^{II}_{0.5}EuTiO_4$. Subsequent reduction can collapse the perovskite layers over the divalent A-site cations, resulting in the $n = 2$ Ruddlesden–Popper phase $A^{II}_{0.5}EuTiO_{3.5}$ (or $Eu_2A^{II}Ti_2O_7$).

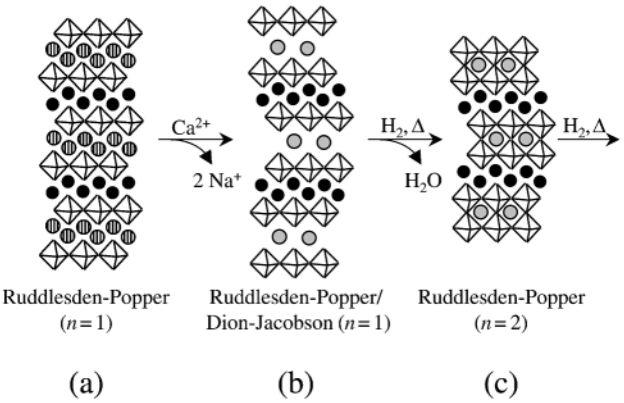

Fig. 1 Topochemical transformation of an $n = 1$ Ruddlesden–Popper phase into a non-defective $n = 2$ phase, which includes (a) $NaEuTiO_4$, (b) $CaEu_2Ti_2O_8$, and (c) $Eu_2CaTi_2O_7$.

$NaEuTiO_4$ was synthesized as reported in the literature[10] and reacted with 1 M $Ca(NO_3)_2$ for 1 week at 45 °C to form $Ca_{0.5}EuTiO_4$ (or $CaEu_2Ti_2O_8$). Energy-dispersive X-ray analysis (EDAX)[11] confirms that 85% of the sodium is replaced by calcium, which is consistent with the efficiencies of other aqueous and non-aqueous divalent ion-exchanges.[4,8] (Attempts at ion exchange using Sr^{2+} and Ba^{2+} resulted in significantly less exchange, presumably due to the size mismatch between Na^+ and the large divalent cations.) Fig. 2(b) shows the X-ray

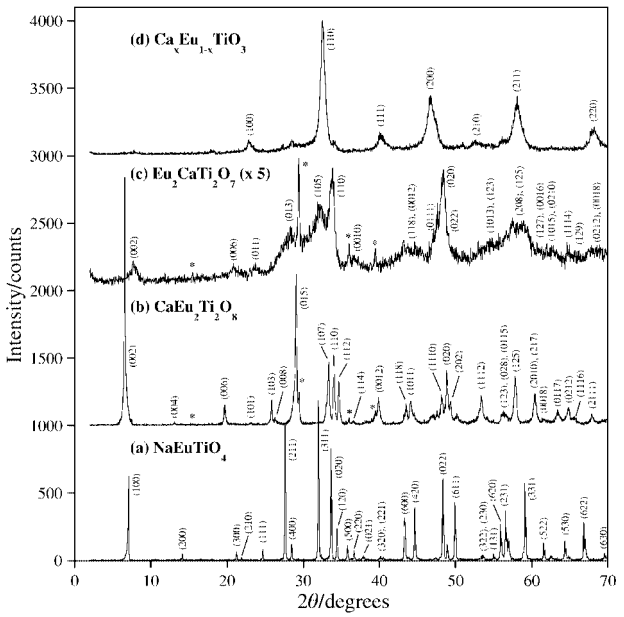

Fig. 2 XRD patterns for (a) $NaEuTiO_4$, (b) $CaEu_2Ti_2O_8$ formed by divalent ion exchange of $NaEuTiO_4$, (c) $Eu_2CaTi_2O_7$ synthesized under H_2 at 650 °C, and (d) $Ca_xEu_{1-x}TiO_3$, the thermodynamically stable product formed at 800 °C. A pyrochlore impurity is labeled with an asterisk in (b) and (c). Note that the vertical scale in (c) is expanded by a factor of 5.

DOI: 10.1039/b009230b

Table 1 Lattice parameters and selected data for layered perovskites

Compound	Description	Colour	Space group	Lattice parameters/Å
$NaEuTiO_4$	n = 1 RP	White	*Pbcm*[a]	a = 12.5471(2) b = 5.3307(2) c = 5.3328(1)
$CaEu_2Ti_2O_8$	n = 1 RP/DJ	White	*I*4/*mmm*	a = 3.7302(2) c = 27.125(3)
$Eu_2CaTi_2O_7$	n = 2 RP	Black	*I*4/*mmm*	a = 3.78(2) c = 24.2(3)

[a] The space group is taken from ref. 10.

diffraction (XRD)[12] pattern for $CaEu_2Ti_2O_8$. The proposed structural model of $CaEu_2Ti_2O_8$ contains alternating staggered and eclipsed layers, as shown in Fig. 1b. Thus, $CaEu_2Ti_2O_8$ can be considered as a mixed $n = 1$ Ruddlesden–Popper/Dion–Jacobson phase. After drying for 1 h at 400 °C to remove interlayer water, $CaEu_2Ti_2O_8$ was indexed on a tetragonal unit cell (Table 1) with a doubled c-axis due to the staggered alternate layers. A pyrochlore impurity is identified in Fig. 2(b), and $CaEu_2Ti_2O_8$ decomposes completely to CaO and pyrochlore-type $Eu_2Ti_2O_7$ upon further heating in air.

Interestingly, a related compound, $Ca_{0.43}Na_{0.14}LaTiO_4$ (prepared by Wiley and coworkers by divalent ion-exchange in anhydrous calcium nitrate),[4b] is also a mixed $n = 1$ Ruddlesden–Popper/Dion–Jacobson phase, but unlike $CaEu_2Ti_2O_8$, each layer remains staggered as in the parent $NaLaTiO_4$ phase. In this case, as well as for $ZnEu_2Ti_3O_{10}$ reported earlier,[8] aqueous ion exchanges give the perovskite sheets lateral mobility to adopt an eclipsed conformation, while ion-exchanges using anhydrous nitrates or molten chlorides retain the staggered symmetry of the parent crystal.

When $CaEu_2Ti_2O_8$ is heated in hydrogen to reduce Eu^{3+} to Eu^{2+} and remove oxygen from the lattice, the perovskite layers above and below the Ca^{2+} cations collapse, encasing Ca^{2+} in the A-sites of the two bridged perovskite slabs to form the $n = 2$ Ruddlesden–Popper phase $CaEu_2Ti_2O_7$, or $Eu_2CaTi_2O_7$ (written in the traditional form to emphasize the location of Eu^{2+} in the interlayer). Unfortunately, $Eu_2CaTi_2O_7$ [Fig. 2(c)] is a low temperature phase, since it decomposes to perovskite-type $Ca_xEu_{1-x}TiO_3$ [Fig. 2(d)] when heated above 650 °C in hydrogen. (While Eu^{3+} fits well in the rocksalt-type interlayer sites, Eu^{2+} is too large to adopt the same coordination, so the reduced structure is unstable.) As with the metastable $Ln_2{\square}Ti_2O_7$ series, a short reaction time is needed in order to isolate the topochemical product. Thus, $Eu_2CaTi_2O_7$ has a limited stability window and is formed only by heating $CaEu_2Ti_2O_8$ for 30 min in hydrogen at 625 °C. Below 600 °C, the reduction does not occur.

The XRD pattern of $Eu_2CaTi_2O_7$ is shown in Fig. 2(c). A highly crystalline pyrochlore impurity, which was a minor impurity phase in Fig. 2(b), remains unchanged upon heating in hydrogen. Thus, Fig. 2(c) can be indexed as a mixture of phases—a crystalline $Ca_xEu_{2-x}Ti_2O_7$ pyrochlore phase, and the $n = 2$ Ruddlesden–Popper phase $Eu_2CaTi_2O_7$, which is characterized by much broader peaks. The broad peaks and low intensity indicate that the product is not very crystalline and that the topochemical collapse introduces disorder over large regions. Although broad, all of the peaks can be indexed to a tetragonal unit cell consistent with that of an $n = 2$ Ruddlesden–Popper phase (Table 1). $Eu_2CaTi_2O_7$ appears to be isostructural with $K_2SrTa_2O_7$.[13] The a axis lattice parameter of $Eu_2CaTi_2O_7$ is contracted relative to $K_2SrTa_2O_7$ (a = 3.9768, c = 21.7062 Å, from ref. 13) and related $n = 2$ phases, while the c axis lattice parameter is significantly larger (Table 1), which is consistent with the size variations between Ti^{4+}/Ta^{5+} and Eu^{3+}/Eu^{2+}. The absence of a major peak around $2\theta = 41°$ in Fig. 2(c), which corresponds to the (111) cubic perovskite peak, indicates minimal decomposition to $Ca_xEu_{1-x}TiO_3$ (the thermodynamically stable phase upon further heating in hydrogen). Likewise, the presence of an intense low angle reflection, as well as higher-index peaks consistent with a tetragonal unit cell, indicates that a layered structure is retained.

The progression of low-angle XRD peaks for $NaEuTiO_4$, $CaEu_2Ti_2O_8$ and $Eu_2CaTi_2O_7$ (Fig. 2) shows the layer spacings expected for an $n = 1$ Ruddlesden–Popper phase, an $n = 1$ Ruddlesden–Popper/Dion–Jacobson intergrowth, and an $n = 2$ Ruddlesden–Popper phase, respectively. $CaEu_2Ti_2O_8$ has a larger layer spacing (13.56 Å) than $NaEuTiO_4$ (12.55 Å), which is consistent with the expected increase from the eclipsed perovskite slabs. Likewise, the decrease in the layer spacing for $Eu_2CaTi_2O_7$ (*ca.* 12.1 Å) relative to $CaEu_2Ti_2O_8$ can only be explained by the bridging of octahedra from the perovskite slabs. Reduction without topochemical collapse (*i.e.* an oxygen-deficient $n = 1$ phase) would result in a larger layer spacing than $CaEu_2Ti_2O_8$ (due to the larger Eu^{2+} cation), so the (002) peak would have shifted to lower angles instead of higher angles.

While the topochemical conversion of an $n = 1$ to a defective $n = 2$ Ruddlesden–Popper phase has already been demonstrated,[9] this work represents the first route to a non-defective higher order layered perovskite. This kind of topochemical reaction could have interesting implications for fine-tuning the properties of carefully designed magnetic and ferroic phases. Additionally, it is an important extension of the topochemical reduction reaction that converts layered perovskites into three-dimensional perovskites, since it involves lower-order Ruddlesden–Popper homologues and results in a two-dimensionally bonded product. Indeed, this work demonstrates that topochemical reduction can be viewed as a generalized approach for the rational synthesis of metastable non-defective perovskites.

This work was supported by National Science Foundation grant CHE-9529202. E. N. G. thanks the NSF Summer Program in Solid State Chemistry for support of her work at Penn State. This material is based upon work supported under a National Science Foundation Graduate Fellowship.

Notes and references

1 S. N. Ruddlesden and P. Popper, *Acta Crystallogr.*, 1957, **10**, 538; S. N. Ruddlesden and P. Popper, *Acta Crystallogr.*, 1958, **11**, 54; S. Uma, A. R. Raju and J. Gopalakrishnan, *J. Mater. Chem.*, 1993, **3**, 709.

2 M. Dion, M. Ganne and M. Tournoux, *Mater. Res. Bull.*, 1981, **16**, 1429; A. J. Jacobson, J. W. Johnson and J. T. Lewandowski, *Inorg. Chem.*, 1985, **24**, 3727; M. M. J. Treacy, S. B. Rice, A. J. Jacobson and J. T. Lewandowski, *Chem. Mater.*, 1990, **2**, 279.

3 Y. Moritomo, A. Asamitsu, H. Kuwahara and Y. Tokura, *Nature*, 1996, **380**, 141.

4 (*a*) K. Hyeon and S. Byeon, *Chem. Mater.*, 1999, **11**, 352; (*b*) R. A. McIntyre, A. U. Falster, S. Li, W. B. Simmons, Jr., C. J. O'Connor and J. B. Wiley, *J. Am. Chem. Soc.*, 1998, **120**, 217; (*c*) J. N. Lalena, B. L. Cushing, A. U. Falster, W. B. Simmons, Jr., C. T. Seip, E. E. Carpenter, C. J. O'Connor and J. B. Wiley, *Inorg. Chem.*, 1998, **37**, 4484.

5 T. A. Kodenkandath, J. N. Lalena, W. L. Zhou, E. E. Carpenter, C. Sangregorio, A. U. Falster, W. B. Simons, Jr., C. J. O'Connor and J. B. Wiley, *J. Am. Chem. Soc.*, 1999, **121**, 10 743.

6 J. Gopalakrishnan, T. Sivakumar, K. Ramesha, V. Thangadurai and G. N. Subbanna, *J. Am. Chem. Soc.*, 2000, **122**, 6237.

7 J. Gopalakrishnan and V. Bhat, *Inorg. Chem.*, 1987, **26**, 4301; P. J. Ollivier and T. E. Mallouk, *Chem. Mater.*, 1998, **10**, 2585; R. E. Schaak and T. E. Mallouk, *J. Solid State Chem.*, 2000, **155**, 46.

8 R. E. Schaak and T. E. Mallouk, *J. Am. Chem. Soc.*, 2000, **122**, 2798.

9 V. Thangadurai, G. N. Subbanna and J. Gopalakrishnan, *Chem. Commun.*, 1998, 1300.

10 K. Toda, Y. Kameo, S. Kurita and M. Sato, *Bull. Chem. Soc. Jpn.*, 1996, **69**, 349; K. Toda, Y. Kameo, S. Kurita and M. Sato, *J. Alloys Compd.*, 1996, **234**, 19.

11 EDAX data was recorded using a JEOL-JSM 5400 scanning electron microscope at the Electron Microscope Facility for the Life Sciences in the Biotechnology Institute at the Pennsylvania State University.

12 X-Ray diffraction patterns were obtained on a Philips X-Pert MPD diffractometer using monochromatized Cu-Kα (λ = 1.5418 Å) radiation.

13 T. A. Kodenkandath and J. B. Wiley, *Mater. Res. Bull.*, 2000, **35**, 1737.

CHEMCOMM Communication
www.rsc.org/chemcomm

Carbohydrate analogue polymers by ring opening metathesis polymerisation (ROMP) and subsequent catalytic dihydroxylation

Stefan Meier,[a] Harald Reisinger,[b] Rainer Haag,[b] Stefan Mecking,[b] Rolf Mülhaupt*[b] and Franz Stelzer[a]

[a] *Institut für Chemische Technologie organischer Stoffe der Technischen Universität Graz, Stremayrgasse 16, A-8010 Graz, Austria. E-mail: stelzer@ictos.tu-graz.ac.at; Fax: +433168738951*
[b] *Freiburger Materialforschungszentrum und Institut für Makromolekulare Chemie der Albert-Ludwigs-Universität Freiburg i.Br., Stefan-Meier-Straße 21, D-79104 Freiburg i.Br. Germany. E-mail: mulhaupt@uni-freiburg.de*

Received (in Cambridge, UK) 18th January 2001, Accepted 28th March 2001
First published as an Advance Article on the web 17th April 2001

Ring opening metathesis poymerisation (ROMP) followed by catalytic dihydroxylation affords macromolecules with 1,2-diol structures. These new macromolecular compositions represent *C*-glycoside analogues of ribofuranose polymers that are thermally and hydrolytically stable.

Carbohydrate–protein interactions play an important role in many biological processes. Polysulfates derived from carbohydrates were recognized as potent and selective inhibitors of the *in vitro* replication of HIV and other enveloped viruses. In the case of sulfated dextrans the activity strongly depended on the molar mass of the oligosaccharides.[1,2] The design of new carbohydrate-analogue polymers is of special interest in polymer chemistry and life sciences—applications range from drug systems to novel biocompatible materials and surface coatings. Ring-opening metathesis polymerisation (ROMP) offers attractive potential for the synthesis of well defined carbohydrate analogue polymers. The modern catalyst generations, developed by Schrock and Grubbs, tolerate polar groups and afford living polymerisation which is the key to molar mass control. Novel families of ROMP glycopolymers were prepared by Kiessling, Schrock, Grubbs and co-workers[3–7] using sugar-substituted derivatives of norbornene and 7-oxanorbornenes as monomers. Since conventional polysaccarides are prone to metabolic degradation by glycosidases due to their glycosidic linkages,[2] hydrolytically stable carbohydrate-analogue compounds without glycoside linkages in the backbone represent interesting candidates for biomedical applications (Fig. 1).

Here we present a versatile synthetic method for the preparation of novel polyribofuranose analogue polymers which do not contain glycoside linkages between the monomeric units in the polymer backbone that are prone to metabolic degradation by glycosidases. This should provide an oligosaccharide analogue structure with improved biocompatibility and longer half-life times. Initial research on related oligosaccharide-analogue polymers was reported by Clark and Lee[8] who used ROMP of 7-oxanorbornene diol derivatives. Since the double bonds of the polymer backbone were hydrogenated, the resulting saccharide-analogue polymers contained only two hydroxy groups per repeating unit. The objective of our research was the synthesis of polymers containing fully hydroxylated repeating units. These are pseudo-polyribofuranoses, with structures very similar to those of natural carbohydrates. The synthetic strategy displayed in Scheme 1 employs ROMP of dihydroxy-substituted bicyclic olefin monomers and subsequent dihydroxylation of the double bonds in the polymer backbone.

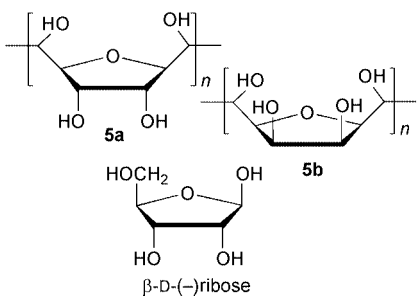

Fig. 1 Comparison between β-D-(−)ribose and the novel carbohydrate analogue polymers **5a**,**b**.

Both pure 2-*exo*, 3-*exo*-7-oxanorbornene diol **1a** and the corresponding *endo* isomer **1b** were synthesized according to a literature procedure.[9] Unfortunately, all attempts to perform ring-opening metathesis polymerisation in water, employing the water soluble Grubbs catalyst $RuCl_2(=CHPh)$-$[Cy_2PCH_2CH_2N(CH_3)_3{}^+Cl^-]_2$ **7** failed. Therefore, compounds **1a** and **1b** were transformed into their corresponding ketals **2a** and **2b** as reported by Schrock and co-workers.[10] ROMP in THF gave high yields (80–90%) using the well known Grubbs catalyst **6**. The monomer to catalyst ratio was varied in order to obtain polymers with different molecular masses. Properties of the obtained polymers are listed in Table 1. The resulting polymers **3a**,**b** were soluble in THF, acetone, $CHCl_3$ and CH_2Cl_2 but not in water or methanol. A polydispersity index M_w/M_n of 1.5, determined by size exclusion chromatography (SEC), reflects a relatively narrow molecular mass distibution (*cf.* Table 1). A significant difference was observed with respect to the *cis*/*trans* double bond ratio in **3a** and **3b**, respectively. The *cis* double bond content of **3a** was 30% compared to 80% for **3b**.

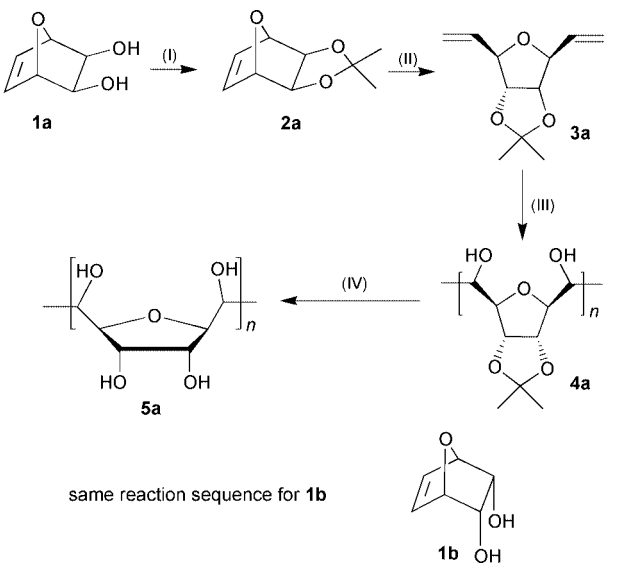

Scheme 1 Synthesis of the pseudo polyribofuranoses [**a** = *exo*, **b** = *endo*; (I), *cf.* ref. 10; (II), $RuCl_2(=CHPh)(PCy_3)_2$ (**6**), THF; (III), cat. OsO_4, NMO, acetone, H_2O, MeOH; (IV), CF_3CO_2H–H_2O (9 : 1 vol. ratio)].

DOI: 10.1039/b100680k

Table 1 Properties of **3a**,**b** and **4a**,**b**

	[M]/ [[Ru][a]	M_n/ g mol^{-1}[b]	PDI	T_g/°C[c]	σ_c/mol%[d]	σ_E/mol%[e]
endo	25	7 100	1.50	n.d	80	71
	50	12 200	1.50	155	82	71
	75	14 800	1.47	156	82	69
exo	50	19 300	1.42	85	33	n.d.
	75	33 900	1.42	86	34	n.d.
	100	36 600	1.51	86	30	n.d.

[a] Monomer to catalyst ratio. [b] Determined for **3a**,**b** in $CHCl_3$ against PS standard. [c] Obtained for **3a**,**b**. [d] Content of *cis* double bonds in **3a**,**b**. [e] Content of *erythro* diols in **4a**,**b**.

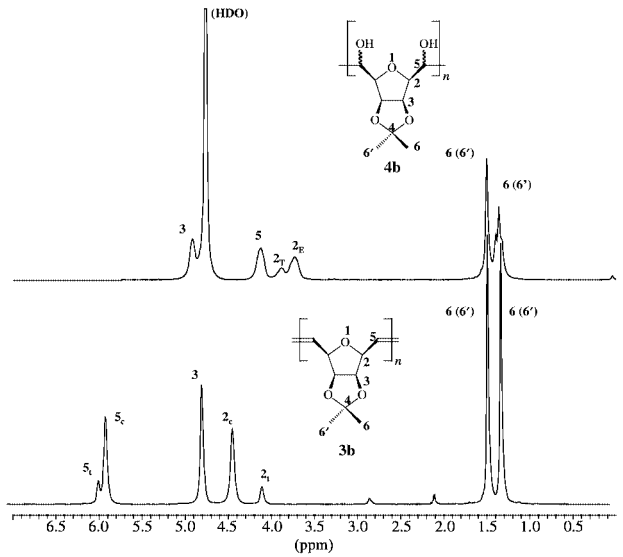

Fig. 2 ^{1}H NMR spectrum of **3b** (acetone-d6, 300 MHz) in comparison to **4b** (D_2O, 300 MHz).

The NMR-peaks were assigned based on COSY and DEPT-NMR techniques and by comparison with chemical shifts of related structures.[11] It is noteworthy that the *exo* and *endo* polymers also differ strongly in their glass transition temperatures (T_g) (**3a** T_g = 85 °C, **3b** T_g = 155 °C).

So far, typical polymer analogue reactions for the derivatisation of the double bonds produced by ROMP have employed sulfonation, hydrogenation, the formation of carbonamide[12] and epoxidation.[12,13] In order to produce the desired pseudo-polyribofuranose structures we decided to dihydroxylate the double bonds in the backbone of the ROMP polymers **3a**,**b**. To the best of our knowledge this is the first time that successful catalytic dihydroxylation of ROMP polymer has been achieved. While catalytic dihydroxylations are well known for many low molecular weight oligoalkenes[14a] it has rarely been successfully applied in polymer functionalisation.[14b]

It is even more surprising that for the ROMP polymer **3a/b** a quantitative conversion of all double bonds into 1,2-diol structures could be achieved. SEC measurements confirmed that polymer degradtion did not occur during dihydroxylation. In the ^{1}H NMR spectra displayed in Fig. 2 the signals at δ = 5.86 ppm and 5.94 ppm, which are assigned to the *cis* and *trans* double bonds of **3b**, completely disappeared after the dihydroxylation step. The signal for the protons in the 5 position was shifted to δ = 4.1 ppm. The signal for the proton in the allylic position to the *cis* and *trans* double bonds 2c, 2t were shifted from δ = 4.38 ppm and 4.04 ppm to 3.8 ppm and 3.6 ppm respectively. In accordance with the dihydroxylation of double bonds of low molecular weight compounds, the *cis* double bonds are converted selectively to *erythro* diols and the *trans* double bonds to the corresponding *threo* diols.[15] In the case of **3b** the dihydroxylation method described for oligoalkenes[14a] and polyalkenes[14b] was well suited to obtain the fully hydroxylated pseudo-polyribofuranose **4b** which was completely water and methanol soluble. However, it was not soluble in THF, acetone and other organic solvents. In the case of **3a** the fully dihydroxylated polymer **4a** was only partially soluble in water but fully soluble in methanol. Therefore methanol was added instead of water as medium for the dihydroxylation in order to achieve a quantitative conversion. After deprotection of the ketal groups of **4b** by means of CF_3COOH–H_2O (9 : 1 vol. ratio) a water insoluble polymer **5b** was obtained which formed fine needles after precipitation from solution. These needles were only soluble in DMF or DMSO. ^{1}H-NMR data showed that the polymer was fully deprotected, which was indicated by the lack of peaks in the region of δ = 1.0–1.7 ppm. The hydrolytic stability of this carbohydrate analogue polymer towards acidic media (see above) is much better with respect to that of natural carbohydrates containing acetal linkages in the backbone. The solubility behaviour of these new pseudo-furanose derivatives is very similar to that of *e.g.* cellulose (cellulose is water insoluble, methyl cellulose with up to 45% ether bonds is water soluble), thus indicating that the pseudo-polyribofuranoses are likely to exhibit superstructures *via* intermolecular hydrogen bonding. The structure–property relationships of these new polyribofuranose analogue compounds will be investigated in more detail.

The authors gratefully acknowledge financial support by the European Union (TMR-Project GLASSCYCLICS Contract No. FMRX-CT97-0116). We thank Sven Kasper and Christina Schmutz for technical assistance and Professor Walter Burchard for many helpful discussions relating to the characterization of polyhydroxy compounds.

Notes and references

1 Y. C. Lee and R. T. Lee, *Acc. Chem. Res.*, 1995, **28**, 321.
2 M. Witvrouw, J. Desmyter and E. DeClercq, *Antiviral Chem. Chemother.*, 1994, **5**, 345.
3 K. H. Mortell, M. Gingras and L. L. Kiessling, *J. Am. Chem. Soc.*, 1994, **116**, 12 053.
4 M. C. Schuster, K. H. Mortell, A. D. Hegeman and L. L. Kiessling, *J. Mol. Catal. A*, 1997, **116**, 209.
5 D. D. Manning, X. Hu, P. Beck and L. L. Kiessling, *J. Am. Chem. Soc.*, 1997, **119**, 3162.
6 K. Nomura and R. R. Schrock, *Macromolecules*, 1996, **29**, 540.
7 C. Fraser and R. H. Grubbs, *Macromolecules*, 1995, **28**, 7248.
8 M. B. Clark and T. R. Lee, *Polym. Prepr.*, 1998, **39**(1), 416.
9 H. Prinzbach, H. Bringmann, J. Markert, G. Fischer and L. Knothe, *Chem. Ber.*, 1986, **119**, 589.
10 G. C. Bazan, J. H. Oskam, H.-N. Cho, L. Y. Park and R. R. Schrock, *J. Am. Chem. Soc.*, 1991, **113**, 6899.
11 B. M. Novak and R. H. Grubbs, *J. Am. Chem. Soc.*, 1988, **110**, 960.
12 T. J. Boyd and R. R. Schrock, *Macromolecules*, 1999, **32**, 6608.
13 M. Lautens, A. S. Abd-El-Azis and G. Schmidt, *Macromolecules*, 1990, **23**, 2819.
14 (*a*) R. Haag, R. Zuber, S. Donon, C.-H. Lee, M. Noltemeyer, K. Johnson and A. de Meijere, *J. Org. Chem.*, 1998, **63**, 2544; (*b*) R. Haag, A. Sunder and J. F. Stumbé, *J. Am. Chem. Soc.*, 2000, **122**, 2954.
15 P. Hadwiger and A. E. Stütz, *Synlett*, 1999, **11**, 1787.

CHEMCOMM Communication
www.rsc.org/chemcomm

A new series of dendrimers with 4,4′-bipyridinium cores capable of fast electron transfer reactions

Rosa Toba,[a] José María Quintela,[a] Carlos Peinador,*[a] Esteban Román[b] and Angel E. Kaifer*[b]

[a] *Departamento de Química Fundamental, Universidade da Coruña, Campus A Zapateira, 15071 La Coruña, Spain*

[b] *Center for Supramolecular Science and Department of Chemistry, University of Miami, Coral Gables, FL 33124-0431, USA. E-mail: akaifer@miami.edu*

Received (in Columbia, MO, USA) 17th January 2001, Accepted 22nd March 2001
First published as an Advance Article on the web 17th April 2001

A new series of dendrimers containing a single 4,4′-bipyridinium (viologen) core has been synthesised and characterized that exhibit fast heterogeneous electron transfer reactions from the first to the third generation of dendritic growth.

Dendrimers with redox active cores have been proposed as promising materials for miniaturized information storage circuits.[1] Ideally, injecting/extracting electrons into or from the core of the dendrimer would be a simple way to store and/or read a bit of information in a single molecule. However, the redox active core must be surrounded by a considerable amount of inert material to prevent electronic 'cross-talk', that is, self-exchange electron transfer reactions between neighboring dendrimers that would lead to data losses in a two-dimensional storage array. To the best of the authors' knowledge, the isolation of the redox core by growing dendritic branches has always led to significantly decreased rates of heterogeneous electron transfer.[2] This trend has been clearly demonstrated with dendrimers synthesized around porphyrin,[3] ferrocene[4] and a variety of redox active, metal complex centers.[5] Here, we report the preparation and characterization of a new series of three dendrimers (compounds **1**–**3**, see structures below) containing a single 4,4′-bipyridinium (viologen) core residue covalently attached to two identical Fréchet-type dendrons[6] (first to third generation). The voltammetric behavior of these compounds reveals that the first one-electron reduction of the viologen core is reversible (fast) and rather insensitive to the size of the dendrons throughout the series, an unexpected finding from the available reports on related dendritic systems.[3–5]

The synthetic strategy for the preparation of the dendritic viologens utilized a convergent method. The benzyl bromide dendrons were prepared according to the procedure reported by Fréchet and Hawker.[7] Menschutkin reaction between 4,4′-bipyridine and two equivalents of the corresponding dendron bromides (DMF at 55 °C) afforded, after counterion exchange, the symmetrical dendrimers with a viologen unit at the core.† Their structure was confirmed by ^{1}H and ^{13}C NMR spectroscopies.‡ All compounds yielded satisfactory elemental analyses and exhibited very good correlation with the calculated molecular masses as evidenced by their FAB or MALDI-TOF mass spectra.‡

The influence of the dendritic structure on the electrochemical behavior of the core viologen units was investigated by cyclic voltammetry in acetonitrile solution. Typically, viologen derivatives exhibit two reversible reduction waves that correspond to the formation of a cation radical ($V^{2+} \rightarrow V^{+}$) and a neutral ($V^{+} \rightarrow V$) species.[8] The first reduction is generally very fast, and the second is often coupled to precipitation processes due to the uncharged nature of the fully reduced species, which is insoluble in solvents of intermediate to high polarity.[9] In agreement with the results reported for a different series of bipyridinium-based dendrimers,[10] we found (see Table 1) that the half-wave potentials ($E_{1/2}$) for the first reduction process shift to less negative values as the dendrimer generation increases. Analysis of the peak-to-peak potential splittings (ΔE_p) indicates that this electrochemical process is reversible at moderate scan rates for all dendrimers, even for the third generation compound **3**. However, some distortions associated with precipitation of the one-electron reduced species on the electrode surface are evident in the voltammograms for the

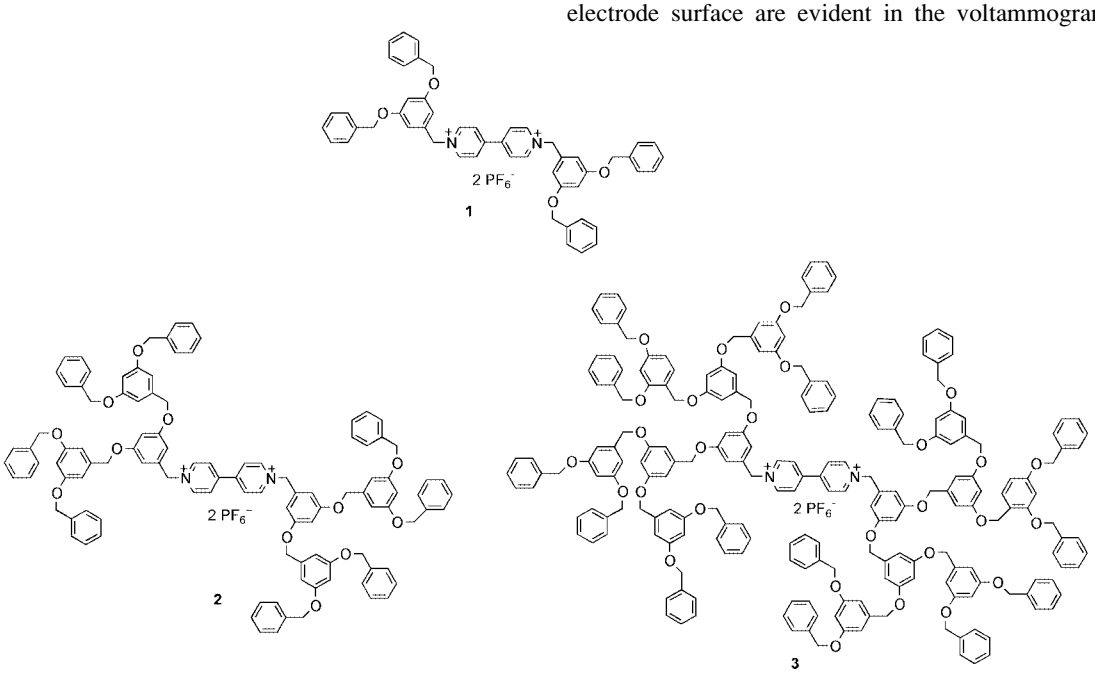

DOI: 10.1039/b102134f

Table 1 Half-wave potentials ($E_{1/2}$ in V *vs.* Ag/AgCl) and peak-to-peak potential splittings (ΔE_p in mV) for the first and second reduction of dendrimers **1–3** in CH_3CN at 25 °C

	Dendrimer **1**		Dendrimer **2**		Dendrimer **3**	
Electrochemical parameter[a]	$V^{2+} \rightarrow V^{+}$	$V^{+} \rightarrow V$	$V^{2+} \rightarrow V^{+}$	$V^{+} \rightarrow V$	$V^{2+} \rightarrow V^{+}$	$V^{+} \rightarrow V$
$E_{1/2}$	−0.316	−0.754	−0.309	−0.751	−0.274	−0.705
ΔE_p at 0.1 V s^{-1}	65	62	62	65	56	35
ΔE_p at 0.5 V s^{-1}	66	75	65	75	56	42
ΔE_p at 1.0 V s^{-1}	66	81	69	75	60	60
ΔE_p at 2.0 V s^{-1}	74	81	69	71	65	79
ΔE_p at 3.0 V s^{-1}	78	89	78	64	70	85

[a] All electrochemical parameters were measured with a glassy carbon working electrode immersed in 0.25 mM **1–3** + 0.1 M $TBAPF_6$ solutions in acetonitrile. The reported half-wave potential values were measured at 0.1 V s^{-1}.

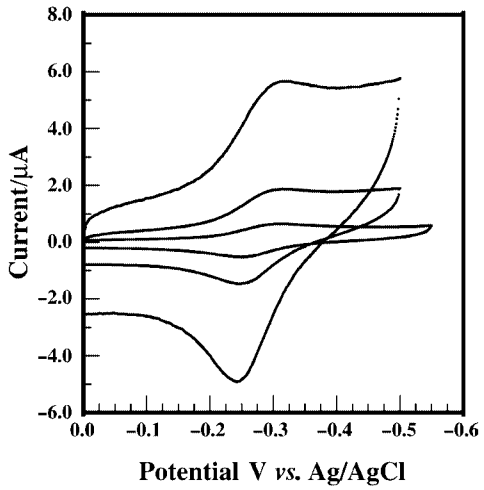

Fig 1 Cyclic voltammetric waves (at scan rates 0.1, 0.5 and 3.0 V s^{-1}) corresponding to the first one-electron reduction of dendrimer **3** (0.25 mM) in 0.1 M $TBAPF_6$–MeCN. Data were recorded with a glassy carbon working, platinum auxiliary and Ag/AgCl reference electrodes.

largest dendrimer (see Fig. 1). At faster scan rates (up to 3 V s^{-1}), our voltammetric data still reveal that the first reduction is quite fast (the largest ΔE_p value measured in these experiments was 78 mV). The distortions mentioned above precluded us from obtaining reliable values for the apparent heterogeneous rates of electron transfer.

The half-wave potentials corresponding to the second electron uptake exhibit the same trend, shifting to less negative values with increasing dendrimer generation. The kinetics of the electron transfer reaction appear to be fast, although very marked precipitation effects were observed. As was the case for the first reduction process, these effects were most visible for the third generation dendrimer **3**. Overall, the trend observed in the $E_{1/2}$ values reveals that the reduction process is thermodynamically more favored as the dendritic structure grows. We attribute this observation to the increasing hydrophobic character of the dendrimer core, which makes it progressively harder to solvate effectively the two positive charges of the viologen core. Therefore, reduction (partial or total elimination of the core charges) becomes more favorable with increasing dendrimer generation.

To our knowledge this is the first example of dendrimers containing a single electroactive core unit that shows relatively fast heterogeneous electron transfer reactions even in the third generation, as measured at scan rates as fast as 3 V s^{-1}. Taken together, these results open some interesting possibilities and suggest that dendrimers with viologen cores are promising in the search for electrochemically active dendrimers with practical applications. We are currently working on methods to immobilize these or similar dendrimers at interfaces in order to obtain electrochemical behavior that will not be affected by precipitation effects.

We are grateful to Xunta de Galicia (J. M. Q. and C. P., PGIDT00PXI10306PR) and NSF (AEK, CHE-9982014) for the support of this work. R. T. thanks the Xunta de Galicia for a graduate fellowship. E. R. thanks the University of Miami for a Maytag graduate fellowship.

Notes and references

† A solution of the dendron bromide (0.06 mmol) and 4,4′-bipyridine (4.7 mg, 0.03 mmol) in DMF (1 ml) was stirred under inert atmosphere at 55 °C for 24 h. After cooling to room temperature, the solvent was removed under reduced pressure and the residue dissolved in acetone (1 ml). An aqueous solution of NH_4PF_6 was added. The solvents were removed *in vacuo* and the solid triturated in water. The precipitate was filtered off, washed with water and diethyl ether. The resulting solid was purified by size-exclusion chromatography (Sephadex LH-20), eluting with MeCN to yield the pure dendrimer.

‡ Dendrimer **1**: Yield 90%; ^{1}H NMR (200 MHz, CD_3CN): δ 5.11 (s, 8H), 5.72 (s, 4H), 6.72–6.76 (m, 6H), 7.32–7.49 (m, 20H), 8.36 (d, 4H, ^3J (H, H) 6.8 Hz), 8.95 (d, 4H, ^3J (H, H) 6.8 Hz); ^{13}C NMR (50 MHz, CD_3CN): 65.5, 70.9, 103.9, 109.3, 128.3, 128.6, 128.9, 129.4, 135.5, 137.6, 146.4, 151.1, 161.5; FB MS: *m*/*z* 907 $(M - PF_6^-)^+$, 762 $(M - 2PF_6^-)^+$.

Dendrimer **2**: Yield 86%; ^{1}H NMR (200 MHz, CD_3CN): δ 5.03 (s, 24H), 5.68 (s, 4H), 6.56–6.67 (m, 18H), 7.30–7.38 (m, 40H), 8.18 (d, 4H, ^3J (H, H) 6.8 Hz), 8.82 (d, 4H, ^3J (H, H) 6.7 Hz); ^{13}C NMR (50 MHz, CD_3CN): 65.5, 70.6, 102.3, 104.1, 107.4, 109.4, 128.1, 128.5, 128.8, 129.4, 135.4, 137.9, 140.2, 146.3, 150.7, 160.9, 161.3; FAB MS: *m*/*z* 1756 $(M - PF_6^-)^+$, 1611 $(M - 2PF_6^-)^+$.

Dendrimer **3**: Yield 78%; ^{1}H NMR (200 MHz, CD_3CN): δ 4.84 and 4.95 (each s, 56H), 5.52 (s, 4H), 6.46–6.60 (m, 56H), 7.19–7.33 (m, 80H), 8.04 (d, 4H, ^3J (H, H) 6.7 Hz), 8.72 (d, 4H, ^3J (H, H) 6.8 Hz); ^{13}C NMR (50 MHz, CD_3CN): 65.5, 70.4, 70.7, 102.2, 102.4, 104.1, 107.5, 109.4, 127.9, 128.6, 128.9, 129.4, 135.4, 138.0, 140.2, 140.6, 146.3, 150.5, 160.8, 160.9, 161.4; MALDI-TOF MS: *m*/*z* 3308.4 $(M - 2PF_6^-)^+$.

1 C. B. Gorman, J. C. Smith, M. W. Hager, B. L. Parkhurst, H. Sierzputowska-Gracz and C. A. Haney, *J. Am. Chem. Soc.*, 1999, **121**, 9958.
2 A. E. Kaifer and M. Gómez-Kaifer, *Supramolecular Electrochemistry*, Wiley-VCH, Weinheim, 1999, ch. 16.
3 P. J. Dandliker, F. Diederich, A. Zingg, J.-P. Gisselbrecht, M. Gross, A. Louati and E. Sanford, *Helv. Chim. Acta*, 1997, **80**, 1773; K. W. Pollak, J. W. Leon, J. M. Fréchet, M. Maskus and H. D. Abruña, *Chem. Mater.*, 1998, **10**, 30.
4 Y. Wang, C. M. Cardona and A. E. Kaifer, *J. Am. Chem. Soc.*, 1999, **121**, 9765; C. M. Cardona, T. D. McCarley and A. E. Kaifer, *J. Org. Chem.*, 2000, **65**, 1857.
5 G. R. Newkome, R. Güther, C. N. Moorefield, F. Cardullo, L. Echegoyen, E. Pérez-Cordero and H. Luftmann, *Angew. Chem., Int. Ed. Engl.*, 1995, **34**, 2023; C. B. Gorman, B. L. Parkhust, W. Y. Su and K. Y. Chen, *J. Am. Chem. Soc.*, 1997, **119**, 1141; V. Balzani, S. Campagna, G. Denti, A. Juris, S. Serroni and M. Venturi, *Acc. Chem. Res.*, 1998, **31**, 26; F. Vögtle, M. Plevoets, M. Nieger, G. C. Azzellini, A. Credi, L. De Cola, V. De Marchis, M. Venturi and V. Balzani, *J. Am. Chem. Soc.*, 1999, **121**, 6290; G. R. Newkome, A. K. Patri and L. A. Godínez, *Chem. Eur. J.*, 1999, **5**, 1445.
6 Structurally related compounds have been used as 'rotaxane dumbbells', see: D. A. Amabilino, P. R. Ashton, V. Balzani, C. L. Brown, A. Credi, J. M. J. Fréchet, J. W. Leon, F. M. Raymo, N. Spencer, J. F. Stoddart and M. Venturi, *J. Am. Chem. Soc.*, 1996, **118**, 12 012.
7 C. J. Hawker and J. M. Fréchet, *J. Am. Chem. Soc.*, 1990, **112**, 7638.
8 C. L. Bird and A. T. Kuhn, *Chem. Soc. Rev.*, 1981, **10**, 49.
9 A. Mirzoian and A. E. Kaifer, *Chem. Eur. J.*, 1997, **3**, 1052.
10 S. Heinen and L. Walder, *Angew. Chem., Int. Ed.*, 2000, **39**, 806.

CHEMCOMM
Communication
www.rsc.org/chemcomm

Catalytic conversion of butadiene to ethylbenzene over the nanoporous nickel(II) phosphate, VSB-1

Jong-San Chang,[ab] Sang-Eon Park,*[b] Qiuming Gao,[a] Gérard Férey[c] and Anthony K. Cheetham*[a]

[a] *Materials Research Laboratory, University of California, Santa Barbara, CA 93106, USA. E-mail: cheetham@mrl.ucsb.edu*
[b] *Catalysis Center for Molecular Engineering, Korea Research Institute of Chemical Technology (KRICT), P.O. Box 107, Yusung, Taejon 305-606, Korea. E-mail: separk@pado.krict.re.kr*
[c] *Institut Lavoisier, UMR CNRS 173, Université de Versailles Saint Quentin, 45 avenue des Etats-Unis, 78035 Versailles Cedex, France.*

Received (in Irvine, CA, USA) 14th November 2000, Accepted 9th March 2001
First published as an Advance Article on the web 18th April 2001

The large-pore nickel(II) phosphate, VSB-1, shows excellent selectivity (> 80%) for the dehydrocyclodimerization of butadiene to ethylbenzene at 400 °C; conversion to 4-vinylcyclohexene and oligomeric byproducts is < 5% in each case.

The widespread utility of aluminosilicate zeolites in the field of shape-selective catalysis[1] has led to a quest for other families of nanoporous materials that might exhibit catalytic activity. In spite of the enormous amount of work that has been done in this area,[2] only two other families of materials, the aluminum phosphates[3] and the titanosilicates,[4] have yielded molecular sieves with exciting catalytic properties. For example, SAPO-34, an $AlPO_4$ with the chabazite structure, is being exploited for the conversion of methanol to olefins,[3] and the titanosilicate, TS-1, is a very effective for selective oxidations using hydrogen peroxide.[4] Attempts to make nanoporous transition metal phosphates have led to the discovery of many new phases, *e.g.* V–P–O,[5] Fe–P–O[6] and Co–P–O,[7] but, as is the case with most non-silicate open-frameworks, the poor thermal stability of these systems leads to the collapse of the pore structures on activation, thus rendering them unsuitable for applications that require porosity. Recently, however, we described the first example of an open-framework nickel phosphate, VSB-1 (Versailles/Santa Barbara-1),[8] whose porosity can be readily accessed by low temperature calcination. The structure is stable to *ca.* 550 °C. In the present work, we show that this phase is catalytically active in the dehydrocyclodimerization of butadiene to ethylbenzene.

VSB-1 was prepared as a green powder from a hydrothermal reaction at 180 °C for 6 d between nickel(II) chloride hexahydrate and phosphoric acid (85% by weight) in the presence of ammonium fluoride. Further details are given in ref. 8. This new material has a large unidimensional channel composed of 24 NiO_6 and PO_4 polyhedra, and the free diameter of the channel is estimated to be 8.8 Å (Fig. 1). Its surface area and chemical composition are 82 $m^2\ g^{-1}$ and $Ni_{18}(HPO_4)_{14}(OH)_3F_9(H_3O/NH_4)_4 \cdot 12H_2O$, respectively.[8] Zeolite NaX (Si : Al = 1.40, S_{BET} = 875 $m^2\ g^{-1}$), used for comparison of the catalytic activity, was obtained from Fluka Chemie AG.

The cyclodimerization of 1,3-butadiene to 4-vinylcyclohexene (VCH) and its dehydrogenation to ethylbenzene or styrene (Scheme 1) could provide an attractive route for styrene production and is regarded as an interesting alternative to the classical ethylbenzene dehydrogenation process.[9] VSB-1 and NaX were investigated for this reaction. The catalytic runs were carried out in a fixed-bed, vertical flow quartz reactor mounted inside a tubular furnace at 400 °C and atmospheric pressure. After the catalyst had been placed in the reactor it was heated up to 450 °C in an oxygen flow for 4 h for activation and to remove any adsorbed species. The reactor was then purged with helium for 1 h at the same temperature and cooled down to the desired reaction temperature. 1,3-Butadiene (99%, Matheson) was delivered with a constant flow (typically 3 ml gas min^{-1}) and preheated to 200 °C and mixed with helium (10 ml min^{-1}) in a baffled gas-phase mixer within an oven at 200 °C. Product gases were analyzed downstream by on-line gas chromatograph (HP 5890II) with a flame ionization detector (FID). The capillary column (J&W, DB-WAX) of the gas chromatograph allowed the separation of the products.

Fig. 2 shows the conversion of butadiene *via* Diels–Alder cyclodimerization at 400 °C over VSB-1 and NaX. The thermal (non-catalytic) conversion of butadiene to 4-vinylcyclohexene or ethylbenzene in a Pyrex-filled glass reactor under the same conditions as our catalyst testing was less than 1%. We find that NaX gives very high butadiene conversion, at least initially [Fig. 2(*b*)], but very poor selectivity for cyclodimerization (< 30%). The main products over NaX are oligomeric ones such as polyalkenes, presumably due to residual acidity in the zeolite at high temperatures.

According to our unpublished results, VSB-1 has much weaker acidity than zeolite NaX, so there is a reasonable expectation that oligomerization will be less than in the aluminosilicate. This behavior is confirmed in our experiments [Fig. 2(*a*)]. Steady state conversions are obtained after approximately 1 h and are sustained for at least 5 h. Although the activity of VSB-1 is relatively low, it exhibits high selectivity (> 90%) towards the cyclodimerization products, ethylbenzene and VCH. In particular, it is noted that VSB-1 shows remarkably high selectivity for ethylbenzene (82%). The

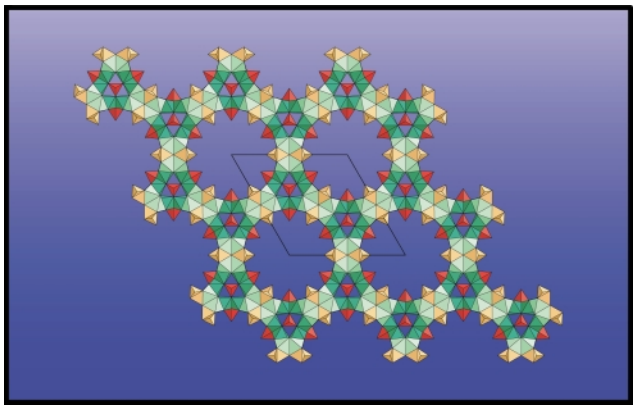

Fig. 1 A view of the structure of VSB-1 down [001]. NiO_6 octahedra and PO_4 tetrahedra are shown in green and red, respectively. The disordered sites are shown in light green and orange.

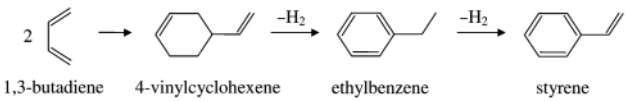

Scheme 1

DOI: 10.1039/b009160j

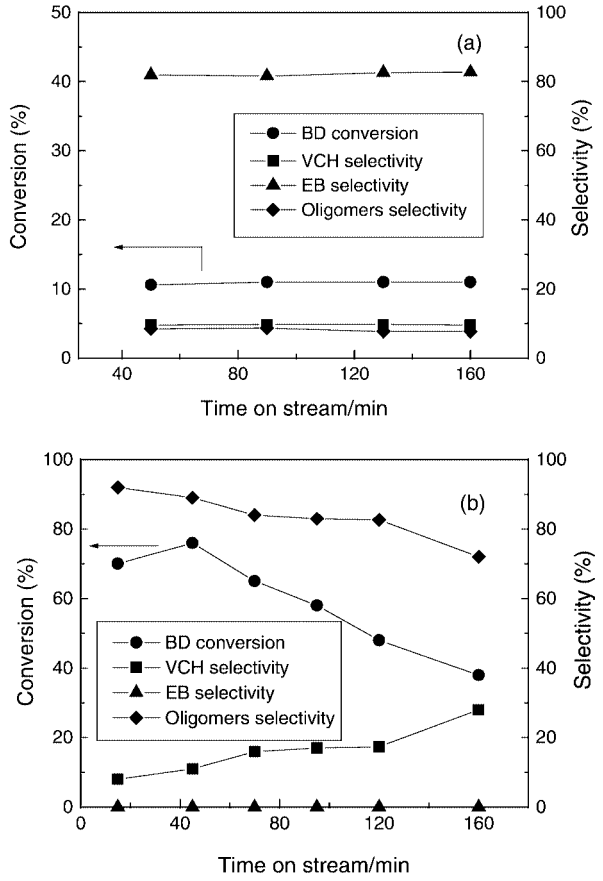

Fig. 2 The Diels–Alder cyclodimerization of 1,3-butadiene over (a) VSB-1 and (b) NaX. Reaction conditions: T = 400 °C, GHSV = 7800 h^{-1}, feed gas = 1,3-butadiene–helium (3/10). Notation: BD; 1,3-butadiene, VCH; 4-vinylcyclohexene, EB; ethylbenzene.

reaction certainly involves the cyclodimerization of butadiene to VCH followed by dehydrogenation to form ethylbenzene; that is, the whole process is better described as a dehydrocyclodimerization. In contrast, NaX did not produce any ethylbenzene or styrene. Interestingly, VSB-1 displays 2% selectivity to styrene at 425 °C (data not shown), but catalyst deactivation is observed at this temperature due to the deposition of oligomeric products.

The Diels–Alder cylcodimerization of 1,3-butadiene to VCH is a well-known thermally-initiated electrocyclic reaction, that is kinetically second-order in butadiene.[10] Neither acidic nor basic catalysts have been used successfully for this reaction.[11] In addition to homogeneous catalyst systems,[12] the cyclodimerization of butadiene has been found over large-pore molecular sieves such as CuY,[13] NaZSM-20,[11] NaBeta[11] and NaX.[13] The catalytic role of non-acidic zeolites in the Diels–Alder reaction has therefore been understood in terms of the ability of zeolites to concentrate hydrocarbons within their cavities.[11] Thus, by increasing the butadiene concentration inside the zeolitic pores relative to that in the external gas phase, the zeolite can enhance the rates of bimolecular reactions such as the Diels–Alder reaction. In the present work, the high selectivity of VSB-1 for the cyclodimerization may again be ascribed to the concentration effect within its large pore channel (8.8 Å). Moreover, the high selectivity towards ethylbenzene over VSB-1 points to the role of the Ni species within its open framework in the partial dehydrogenation step. This type of selectivity has been seen with other nanoporous materials containing transition metals, but not with acidic or basic catalysts. For example, a Ni-impregnated aluminum phosphate catalyst was reported to be active in the dehydrogenation of cyclohexane at 400 °C.[14]

Although the active sites for this reaction are unclear as yet, the high selectivity of VSB-1 for ethylbenzene highlights the bifunctional role of VSB-1. Another important feature of VSB-1 is its excellent stability. The catalytic performance is very stable over several hours, and, significantly, no appreciable deactivation is observed. The stability of VSB-1 is consistent with a previous report that it is thermally stable in air to 550 °C,[8] in contrast to most other open-framework transition metal phosphates. In the case of NaX, severe catalyst deactivation was noted as the reaction proceeded due to the formation and deposition of oligomeric cokes.

In summary, our work shows that the nanoporous nickel(II) phosphate, VSB-1, has some interesting catalytic properties, exhibiting good stability and high selectivity for ethylbenzene in the dehydrocyclodimerization of 1,3-butadiene. The catalytic performance is ascribed to the bifunctional role of VSB-1, *i.e.* the dehydrogenation ability of Ni species and the concentration effect of the nanoporous structure. Further studies are in progress to elucidate the active sites of VSB-1 for the cyclodimerization and dehydrogenation. In the light of earlier work that demonstrated the dehydrogenation of EB to styrene at temperatures as low as 250 °C,[15] we are also exploring the possibility that a single stage conversion of butadiene to styrene might be possible.

A. K. C. thanks the Foundation de 1'Ecole Normale Supérieure and the Région de 1'Ile de France for a Chaire Internationale de Recherche, Blaise Pascal. We also thank the CNRS for financial support and the provision of a Poste Rouge for Q. G. A Korea Science and Engineering Foundation Fellowship for J. S. C. is gratefully acknowledged. We also thank the Korean Ministry of Science and Technology (Institutional Research Program, KK-0005-F0) for supporting this work and Mr Y. S. Choi for experimental support.

Notes and references

1 M. E. Davis, *Chem. Eur. J.*, 1997, **3**, 1745 and references therein.
2 A. K. Cheetham, G. Férey and T. Loiseau, *Angew. Chem., Int. Ed.*, 1999, **38**, 3268; G. Férey and A. K. Cheetham, *Science*, 1999, **283**, 1125.
3 B. V. Vora, T. L. Marker, P. T. Barger, H. R. Nilsen, S. Kvisle and T. Fuglerud, in *Fourth International Natural Gas Conversion Symposium*, ed. M. de Pontes, R. L Espinoza, C. P. Nicolaides, J. H. Scholtz and M.S. Scurrell, Elsevier, Amsterdam, *Stud. Surf. Sci. Catal.*, 1997, **107**, 87.
4 B. Notari, *Adv. Catal.*, 1996, **41**, 253; R. J. Saxton, *Top. Catal.*, 1999, **43**, 9.
5 V. Soghomanian, Q. Chen, R. C. Haushalter, J. Subieta and J. O'Connor, *Science*, 1993, **259**, 1596; T. Loiseau and G. Férey, *J. Solid State Chem.*, 1994, **111**, 416.
6 D. R. Corbin, J. F. Whitney, W. C. Fultz, G. D. Stucky, M. M. Eddy and A. K. Cheetham, *Inorg. Chem.*, 1986, **25**, 2280; H. M. Lin, K.-H. Lii, W.-C. Jiang and S.-L. Wang, *Chem. Mater.*, 1999, **11**, 519.
7 J. Chen, R. H. Jones, S. Natarajan, M. B. Hursthouse and J. M. Thomas, *Angew. Chem., Int. Ed.*, 1994, **33**, 639; P. Feng, X. Bu, S. H. Tolbert and G. D. Stucky, *J. Am. Chem. Soc.*, 1997, **119**, 2497.
8 N. Guillou, Q. Gao, M. Nogues, R. E. Morris, M. Herview, G. Férey and A. K. Cheetham, *C. R. Acad. Sci. Paris*, 1999, **2**, 387.
9 D. A. Hucul, *US Patent*, 5 336, 822, 1994.
10 R. Hoffmann and R. B. Woodward, *J. Am. Chem. Soc.*, 1965, **87**, 4388; D. Rowley and H. Steiner, *Discuss. Faraday Soc.*, 1951, **10**, 198.
11 R. M. Dessau, *J. Chem. Soc., Chem. Commun.*, 1986, 1167.
12 P. Heimbach, P. W. Jolly and G. Wilke, *Adv. Organomet. Chem.*, 1970, **8**, 29.
13 I. E. Maxwell, R. S. Downing and S. A. J. van Langen, *J. Catal.*, 1980, **61**, 485; I. E. Maxwell, *Adv. Catal.*, 1982, **31**, 1.
14 S. A. El-Hakam, A. A. El-Khouly and A. S. Khder, *Appl. Catal. A: Gen.*, 1999, **185**, 247.
15 Y.-S. Choi, Y.-K. Park, J.-S. Chang, S.-E. Park and A. K. Cheetham, *Catal. Lett.*, 2000, **69**, 93; R. Neumann and I. Dror, *Appl. Catal. A: Gen.*, 1998, **172**, 67.

CHEMCOMM
Communication
www.rsc.org/chemcomm

Coexisting covalent and noncovalent nets: parallel interpenetration of a puckered rectangular coordination polymer and aromatic noncovalent nets

Susan A. Bourne,[b] Jianjiang Lu,[a] Brian Moulton[a] and Michael J. Zaworotko*[a]

[a] *Department of Chemistry, University of South Florida, 4202 E. Fowler Ave (SCA 400), Tampa, F 33620, USA. E-mail: xtal@usf.edu*
[b] *Department of Chemistry, University of Cape Town, Rondebosch 7700, South Africa*

Received (in Columbia, MO, UK) 20th February 2001, Accepted 21st March 2001
First published as an Advance Article on the web 18th April 2001

[Zn(*m*-isophthalate)(1,2-bis(4-pyridyl)ethane)]$_n$·*x*A (A = benzene, nitrobenzene, toluene, benzaldehyde, dioxane) represent the first examples of parallel interpenetration between noncovalent and metal–organic frameworks.

Crystal engineering[1] has provided chemists with a useful paradigm for the development of rational approaches to the design of solid-state structures that are based upon self-assembly of metal nodes and multifunctional ligands.[2] However, it has become clear that interpenetration[3] and supramolecular isomerism[4] are common phenomena in coordination polymers and that subtle factors such as choice of solvent and the presence of templates bring an added level of diversity and uncertainty to the outcome of a particular experiment. Batten and Robson[3] have delineated the modes in which coordination polymers can exhibit self-interpenetration and describe such systems in terms of 'nets' (*i.e.* a collection of nodes with some clearly defined connectivity or topology). We[5] recently suggested how topological considerations can be used to explain interpenetration of two very different types of net: 2-D square grids formed from octahedral metal ions coordinated to two linear bifunctional ligands such as 4,4′-bipyridine[6] and planar noncovalent nets comprising organic guest molecules.[7] That the square coordination polymer grids are flat ensures inclined interpenetration between the two types of network. Such 'hybrid' structures might bring with them the intriguing possibility of combining the structural and functional features of two very different types of molecular component.[8]

We report herein several structures† that exhibit the coexistence of coordination polymer and noncovalent nets *via* a parallel interpenetration mode that is possible because the coordination polymer exists as a novel, puckered 2-D grid. We also demonstrate that the absence of a suitable component for the noncovalent nets precludes formation of the 2-D coordination polymer, and rather affords a novel 3-D supramolecular isomer of the coordination polymer. Self-assembly of Zn(II) ions with 1,3-benzenedicarboxylate (bdc) and 1,2-bis(4-pyridyl)ethane (bpeta) in the presence of an appropriately sized guest affords a novel, puckered, rectangular grid structure, [Zn(bdc)(bpeta)]$_n$ **1**. **1** crystallizes from EtOH if benzene (**1a**), nitrobenzene (**1b**), toluene (**1c**), benzaldehyde (**1d**) or 1,4-dioxane (**1e**) are also present. However, if the solvent is changed to pure MeOH, MeOH/naphthalene or CH_2Cl_2, a different supramolecular isomer of **1** is formed—a 3-D structure, **2**—which can also be formulated as [Zn(bdc)(bpeta)]$_n$. The covalent network in **1a** is sustained by a tetrahedral Zn(II) ion coordinated to two bdc and two bpeta ligands. Four of these units give rise to a rectangular cavity incorporated in a (4,4)-network in which zinc ion serves as node. The tetrahedral geometry around the zinc ion causes adjacent rectangular cavities to fold with an angle of 99.94° between Zn ions, producing a 'puckered' layer of cavities, as shown in Fig. 1. Adjacent cavities have slightly different environments in that the orientation of the aromatic rings of the bdc units differs: in one (cavity A) the rings are coplanar with the plane of the

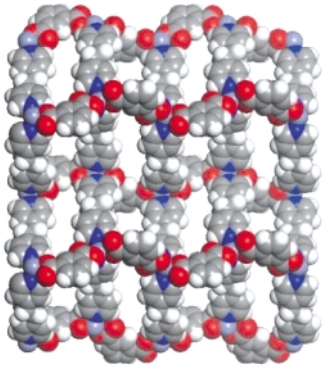

Fig. 1 Space-filling views of the puckered, rectangular, grid coordination polymer network in **1a**. The puckering of the (4,4)-network can be clearly seen and affords cavities and channels within the plane of the network.

cavity, while for the next cavity (B) opposite bdc moieties orient up and down with respect to the plane of the cavity. Effective dimensions for the cavities are 4.8 × 13.3 Å (for A) and 6.0 × 13.6 Å (for B). The bpeta ligands contain pyridyl rings that are only slightly twisted (torsion angle 167.7°) and these ligands are bowed when viewed down the Zn···Zn direction. The coordination polymer layers pack close to one another, with metal centres and cavities stacked above one another, when viewed down [1 0 0]. The interlayer separation is 9.672 Å and there are C–H···π and π···π interactions between layers (the C···$\pi_{centroid}$ distance is 3.532 Å and the $\pi_{centroid}$···$\pi_{centroid}$ distances are 3.611 and 3.705 Å, consistent with distances to be expected for such interactions).

The organic guest molecules in **1a**–**e** form what could be regarded as (6,3)-'puckered brick wall' networks that are sustained by noncovalent interactions (Fig. 2). Fig. 3 illustrates how two of the noncovalent networks engage in parallel interpenetration with the coordination polymers, thereby forming a structure that is similar to the laminated, self-interpenetrated structure exhibited by 1,3,5-benzenetricarboxylic acid and 4,4′-bipyridine.[9]

The critical influence of the solvent and organic components on the self-assembly process is clearly illustrated by the formation of **2**, which exhibits a dramatically different structure that can be described as a pseudo-tetrahedral framework

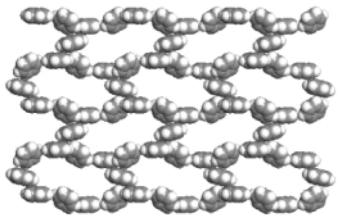

Fig. 2 A view of the noncovalent nets that are formed by benzene molecules in **1a**.

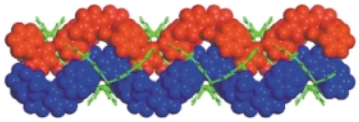

Fig. 3 An illustration of how two noncovalent networks (illustrated in space-filling mode) generate parallel interpenetration with one puckered rectangular grid (illustrated in stick mode) in **1a**.

because the tetrahedral Zn ions are linked by angular and linear spacer ligands. Zn···Zn separations in **2a** are 9.90 and 13.34 Å; this inequality in spacer length leads to a distortion of the diamondoid network that would otherwise be formed (Fig. 4). The large void generated within the pseudo-diamondoid cage is filled by the mutual interpenetration of three independent networks (Fig. 5). Guest molecules in **2a** occupy cavities between the metal-coordination networks, and are isolated from one another. Each cavity has a volume of 91 Å^3, and represents 4.4% of the unit cell volume. Thus the total volume occupied by guest molecules in this structure is only 17.6%.[10]

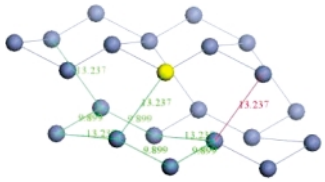

Fig. 4 The pseudo-diamondoid network in **2a**. The bridging ligands are omitted for clarity.

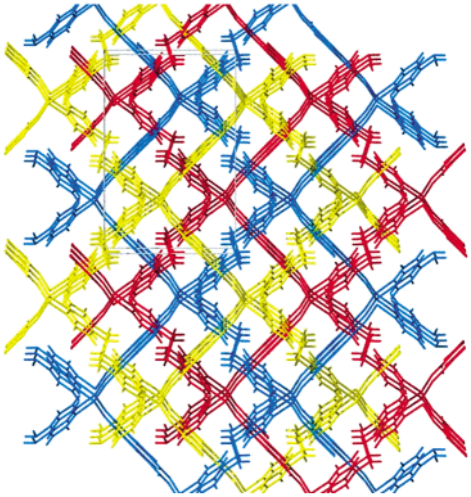

Fig. 5 An illustration of the three pseudo-diamondoid networks that interpenetrate in **2a**.

The existence of the novel supramolecular isomers **1** and **2** is not in itself surprising. However, that their existence appears to be closely linked to whether or not topologically complementary noncovalent nets can be formed provides insight into how chemists can control such supramolecular isomerism and in the process generate hybrid structures that are based upon very different molecular components.

Notes and references

† *Synthesis and data:* 2D-[Zn(bdc)(bpeta)]$_n$·x(A), **1**(**a**–**e**) and 3D-[Zn(bdc)(bpeta)]$_n$·(solvent), **2**(**a**,**b**), were prepared by dissolving $Zn(NO)_3·6H_2O$ (typical example: 0.149 g, 0.5 mmol) and 1,3-benzenedicarboxylic acid (0.166 g, 1 mmol) in ethanol and layering this with a solution of 1,2-bis(4-pyridyl)ethane (0.184 g, 1 mmol) in A. Colorless, rod-shaped crystals were formed at the solvent interface. Intensity data for **1a**–**e** and **2a**,**b** were collected at −100 °C on a Bruker SMART-APEX diffractometer using Mo-Kα radiation (λ = 0.7107 Å). The data were corrected for Lorentz and polarization effects and also for absorption using the SADABS program. Structures were solved using direct methods and refined by full-matrix least squares on $|F|^2$.[11] All non-hydrogen atoms were refined anisotropically and hydrogen atoms were placed in geometrically calculated positions and refined with temperature factors 1.2 × those of their parent atoms.

1b, **1c**, **1d** and **1e** are isostructural with **1a**: they crystallize in $P2_1/n$ with similar cell parameters, they have similar, but not identical, host:guest ratios [for **1a** and **1e** this is 1:2.5, for **1b**–**1d** (which encapsulate slightly larger guests) it is 1:2]; their interlayer separations are in the range 10.244–10.546 Å and they possess cavities with effective dimensions of *ca.* 5 × 13 Å (cavity type A) and *ca.* 5.5 × 14.5 Å (cavity type B). **1b**–**d** have Zn–Zn–Zn angles of 87–89°, while **1e** has an angle of 100.64°, which is closer to that observed in **1a**.

Crystal data for **1a**: monoclinic, $P2_1/n$, a = 9.672(1), b = 20.217(2), c = 14.977(2) Å, β = 93.545(2)°, V = 2923.2(5) Å^3, Z = 4, D_c = 1.384 g cm^{-3}, μ = 0.883 mm^{-1}, F(000) = 1268, $2\theta_{max}$ = 25°. Final residuals (for 377 parameters) were R_1 = 0.0406 and wR_2 = 0.0764 for 3242 reflections with $I > 2\sigma(I)$, and R_1 = 0.0680, wR_2 = 0.0817 for all 5077 data. Residual electron density was 0.75 and −0.48 e Å^{-3}. [Cell parameters for **1b**: a = 10.546(2), b = 18.400(3), c = 15.209(2) Å, β = 90.971(3)°, V = 2950.8(7) Å^3. Cell parameters for **1c**: a = 10.243(3), b = 18.317(5), c = 15.391(4) Å, β = 91.116(5)°, V = 2887(1) Å^3. Cell parameters for **1d**: a = 10.437(2), b = 18.516(4), c = 15.190(3) Å, β = 90.119(4)°, V = 2935(1) Å^3. Cell parameters for **1e**: a = 10.545(1), b = 20.202(2), c = 14.239(2) Å, β = 96.781(2)°, V = 3012.3(6) Å^3].

Crystal data for **2a**: orthorhombic, *Pnna*, a = 10.020(1), b = 15.195(5), c = 13.689(1) Å, V = 2084.1(4) Å^3, Z = 8, D_c = 1.589 g cm^{-3}, μ = 1.466 mm^{-1}, F(000) = 1016, $2\theta_{max}$ = 26°. Final residuals (for 138 parameters) were R_1 = 0.0444 and wR_2 = 0.1146 for 1934 reflections with $I > 2\sigma(I)$, and R_1 = 0.0483, wR_2 = 0.1167 for all 2151 data. Residual electron density was 0.72 and −0.58 e Å^{-3}. [Cell parameters for **2b**: a = 9.676(3), b = 15.470(5), c = 13.547(5) Å, V = 2028(1) Å^3].

High resolution thermogravimetric analysis (TA Instruments TGA 2950) shows a multi-step weight loss between ambient temperature and 200 °C, which can be attributed to the release of guest (for example, **1a**: observed mass loss 33.6%, calc. for 2.5 benzene 32.1%) followed by further thermal decomposition at 300–400 °C, apparently caused by destruction of the coordination polymer.

CCDC 153763–153769. See http://www.rsc.org/suppdata/cc/b1/b102153m/ for crystallographic data in .cif or other electronic format.

1 G. R. Desiraju, *Crystal Engineering: The Design of Organic Solids*, Elsevier, Amsterdam, 1989; G. M. J. Schmidt, *Pure Appl. Chem.*, 1971, **27**, 647.

2 L. Carlucci, G. Ciani and D. M. Proserpio, *Chem. Commun.*, 1999, 449; L. R. MacGillivray, R. H. Groeneman and J. L. Atwood, *J. Am. Chem. Soc.*, 1998, **120**, 2676; C. B. Aakeröy, A. M. Beatty and D. S. Leinen, *Angew. Chem., Int. Ed.*, 1999, **38**, 1815; H. J. Choi and M. P. Suy, *J. Am. Chem. Soc.*, 1998, **120**, 10 622; H. Li, M. Eddaoudi, M. O'Keeffe and O. M. Yaghi, *Nature*, 1999, **402**, 276; M. J. Zaworotko, *Chem. Commun.*, 2001, 1; M. A. Withersby, A. J. Blake, N. R. Champness, P. A. Cooke, P. Hubberstey, W.-S. Li and M. Schröder, *Inorg. Chem.*, 1999, **38**, 2259.

3 S. R. Batten and R. Robson, *Angew. Chem., Int. Ed.*, 1998, **37**, 1460.

4 T. L. Hennigar, D. C. Macquarrie, P. Losier, R. D. Rogers and M. J. Zaworotko, *Angew. Chem., Int. Ed. Engl.*, 1997, **36**, 972.

5 K. Biradha, A. Mondal, B. Moulton and M. J. Zaworotko, *J. Chem. Soc., Dalton Trans.*, 2000, 3837; K. Biradha, K. V. Domasevitch, B. Moulton, C. Seward and M. J. Zaworotko, *Chem. Commun.*, 1999, 1327.

6 R. W. Gable, B. F. Hoskins and R. Robson, *Chem. Commun.*, 1990, 1677; M. Fujita, Y. J. Kwon, S. Washizu and K. Ogura, *J. Am. Chem. Soc.*, 1994, **116**, 1151; T. Soma and T. Iwamoto, *Acta Crystallogr. Sect. C*, 1996, **52**, 1200; L. Carlucci, G. Ciani and D. M. Proserpio, *New J. Chem.*, 1998, 1319; J. Lu, T. Paliwala, S. C. Lim, C. Yu, T. Y. Niu and A. J. Jacobson, *Inorg. Chem.*, 1997, **36**, 923; D. Hagrman, R. P. Hammond, R. Haushalter and J. Zubieta, *Chem. Mater.*, 1998, **10**, 2091; M. L. Tong, X. M. Chen, X. L. Yu and T. C. W. Mak, *J. Chem. Soc., Dalton Trans.*, 1998, 5; R. H. Groeneman, L. R. MacGillivray and J. L. Atwood, *Chem. Commun.*, 1998, 2735; S. R. Batten, B. F. Hoskins and R. Robson, *Chem. Eur. J.*, 2000, **6**, 156;S. Kawata, S. Kitagawa, M. Kondo, I. Furuchi and M. Munakata, *Angew. Chem., Int. Ed. Engl.*, 1994, **33**, 1759.

7 K. Biradha, K. V. Domasevitch, C. Hogg, B. Moulton, K. N. Power and M. J. Zaworotko, *Crystal. Eng.*, 1999, **2**, 37.

8 E. Coronado, J. R. Galan-Mascaros, C. J. Gomez-Garcia and V. Laukhin, *Nature*, 2000, **408**, 447.

9 C. V. K. Sharma and M. J. Zaworotko, *Chem. Commun.*, 1996, 2655.

10 A. L. Spek, PLATON, Utrecht University, The Netherlands, 2000.

11 G. M. Sheldrick, SHELX-97. University of Gottingen, Germany, 1998.

CHEMCOMM Communication
www.rsc.org/chemcomm

Nanoballs: nanoscale faceted polyhedra with large windows and cavities

Brian Moulton, Jianjiang Lu, Arunendu Mondal and Michael J. Zaworotko*

Department of Chemistry, University of South Florida, 4202 E Fowler Ave (SCA 400), Tampa, FL 33620, USA. E-mail: xtal@usf.edu

Received (in Columbia, MO, USA) 11th March 2001, Accepted 21st March 2001
First published as an Advance Article on the web 18th April 2001

Self-assembly of molecular polygons by linking their vertices provides nanosized faceted polyhedra that are porous, contain chemically accessible sites on their facets, are chemically robust, neutral and soluble in common laboratory solvents.

In recent years chemists have developed synthetic design strategies that are based upon the concepts of self-assembly. This supramolecular approach to synthesis, a 'bottom-up'[1] approach to nanoscience, has afforded a new generation of discrete, high molecular weight compounds. These compounds are exemplified by nanoscale spheroid architectures that are based upon Platonic (regular) and Archimedean (semi-regular) solids.[2–9]

Nanoscale versions of Platonic and Archimedean solids have been prepared by one of two approaches: edge-sharing of molecular polygons,[7] or connection of appropriately designed molecular vertices by linear bifunctional rod-like ligands.[10] Edge-sharing of molecular polygons affords closed convex polyhedra whereas connection of vertices generates open structures that are the edge-skeletons of polyhedra. However, there exist other examples of uniform polyhedra[11,12] that to our knowledge remain unexplored in the context of synthetic chemistry. Uniform polyhedra include prisms and antiprisms, polyhedra having star faces and vertices, and polyhedra with both concave and convex faces.[13] In particular, there are nine uniform polyhedra that are closely related to Platonic and Archimedean solids but differ in that their convex faces can be constructed by linking the vertices of regular polygons. Such structures are termed faceted polyhedra[14] since they must contain both open (concave) and closed (convex) faces (*i.e.* faceting).

As revealed by Fig. 1 there are three faceted uniform polyhedra that can be generated by linking the vertices of squares and which one occurs will be strongly influenced by the angle subtended by the 'spacer' moiety that links the vertices: *cubohemioctahedron* (90°) < *small rhombihexahedron* (120°) < *small rhombidodecahedron* (144°). Therefore, judicious control of the angle subtended by the vertices of the squares should afford control over which polyhedron will result. The molecular squares that we have targeted for study are the previously reported metal-organic secondary building units[15] (SBUs) $M_2(RCO_2)_4$ **A**. **A** is illustrated in Fig. 2 and represents a ubiquitous SBU that is present in nearly 900 crystal structures in the Cambridge Structural Database (CSD).[16] It should be noted that it has already been demonstrated that use of polycarboxylate ligands in $M_2(RCO_2)_4$ (*e.g.* benzene-1,4-dicarboxylate[17] or benzene-1,3,5-tricarboxylate[18]) affords self-assembled infinite structures with predictable topology and relatively high thermal stability. It occurred to us that the angular bifunctional ligand benzene-1,3-dicarboxylate, bdc, which subtends an angle of 120°, offers the possibility of generating discrete nanoscale *small rhombihexahedra* or supramolecular isomers[19] in the form of novel infinite coordination polymers.

Nanoscale *small rhombihexahedra* **1**, are formed by layering methanolic $Cu(NO_3)_2$ and H_2bdc onto a solution of pyridine that contains templates such as nitrobenzene or 1,2-dichlorobenzene. Single crystals of $[(L)(S)Cu_2(bdc)_2]_{12}$, L = pyridine, S = methanol, **1a**, form within hours. Alternatively, microcrystals of **1a** can be obtained quantitatively by direct mixing of the above reagents. The crystal structure of **1a**† is illustrated in Fig. 3 and reveals that it can be described as being composed of vertex linked molecular squares (green) that self-assemble into *small rhombihexahedra*. **1a** contains pyridine ligands that are axially bonded to the metal ions that lie at the exterior surface and MeOH ligands at the interior surface metal binding sites. The internal cavity has a volume of *ca.* 1 nm^3 that is easily large enough to encapsulate C_{60}. To our knowledge, **1a** represents the largest spheroid structure that has yet been crystallographically characterized. It has a molecular volume of >10 nm^3 and a molecular weight of 6.80 kDa. **1** can also be formed for L = S = methanol, **1b**. Thus far we have isolated two crystalline phases that contain **1b**, a monoclinic and a cubic phase.†

An isomer of the *small rhombihexahedron* $[(MeOH)_2Cu_2(bdc)_2]_{12}$ **2** crystallizes under similar conditions with 2,6-dimethylpyridine, a non-coordinating base, present instead of pyridine. **2** is illustrated in Fig. 4 and the connectivity of the SBUs is different. **2** has a molecular weight of 6.23 kDa, a molecular volume of *ca.* 10 nm^3 and exhibits textbook hexagonal close packing. Molecular modelling indicates insignificant difference in terms of torsional strain between **1** and **2** (calculated using MSIs Cerius² Minimizer module).

1 and **2** are distinguished by the following features: they are neutral and soluble in organic solvents; they are chemically robust because of the stability of the square SBU (confirmed by high resolution mass spectrometry); they are likely to be chemically diverse because **A** exists for so many metals,

Fig. 1 The three types of faceted uniform polyhedra that can be generated by linking the vertices of squares only: *cubohemioctahedron*, *small rhombihexahedron* and *small rhombidodecahedron*.

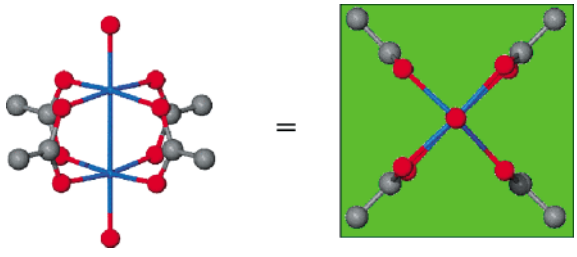

Fig. 2 The square SBU, $M_2(RCO_2)_4$ **A**, employed in this study. In the compounds described herein, **A** is schematically represented as a square (green).

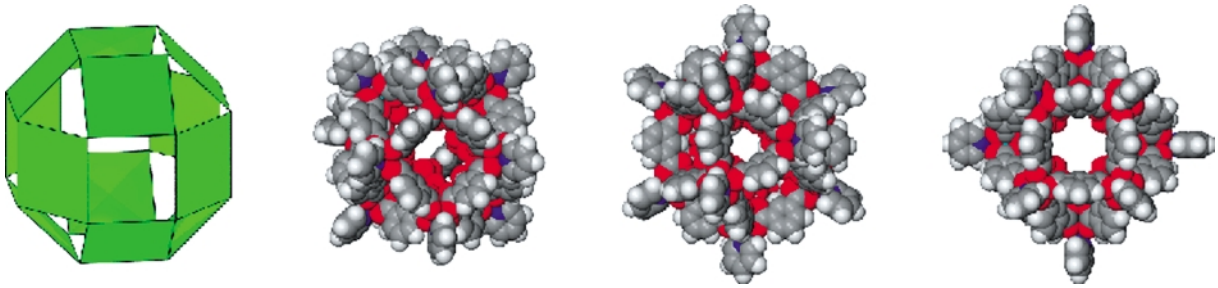

Fig. 3 Crystal structure of $[(L)(S)Cu_2(bdc)_2]_{12}$, L = pyridine, S = methanol, **1**. The schematic illustrates how linking of molecular squares generates the edge-skeleton of **1**. Note how the large bowl-shaped square and triangular windows provide access to the interior of **1**. Disordered solvent is found in these windows and in the 1 nm^3 internal cavity. There is high thermal motion and/or disorder in the ligands and the guest molecules but the structure of the core is well determined and unambiguous.

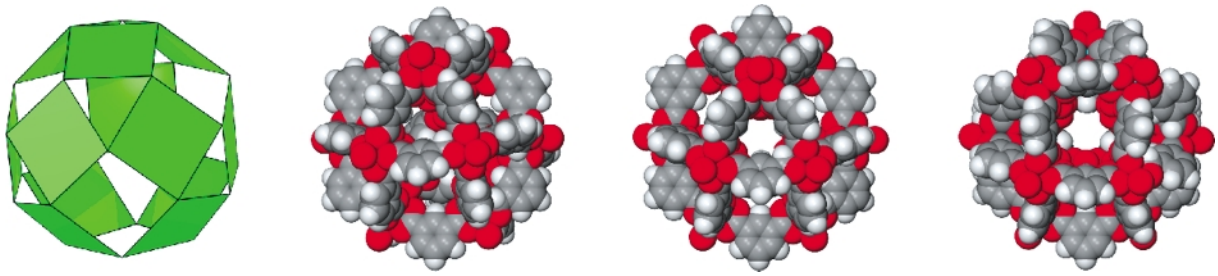

Fig. 4 Crystal structure of $[(S)_2Cu_2(bdc)_2]_{12}$, S = methanol, **2**. The schematic illustrates the subtle differences between the connectivity in **1** and **2**.

including magnetically active and catalytically active metals; they have both internal and external sites that are suitable for further chemical modification. Indeed, it is possible to envisage **1** and **2** as the building blocks for much larger structures by acting as the node of infinite networks[20] or as the core of mesoscale dendritic structures; their interior cavities can be accessed *via* triangular or square windows, which are bowl shaped and contain organic guests. Loss of coordinated molecules occurs at higher temperatures. Furthermore, judicious selection of angular spacers in the presence of molecular polygons should ultimately generate all nine faceted polyhedra and their structural isomers.

Notes and references

† *Crystallographic data:* intensity data for **1** and **2** were collected at 173 K on a Bruker SMART-APEX diffractometer using Mo-Kα radiation (λ = 0.7107 Å). The data were corrected for Lorentz and polarization effects and for absorption using the SADABS program. Structures were solved using direct methods and refined by full-matrix least squares on $|F|^2$.[11] All non-hydrogen atoms were refined anisotropically and hydrogen atoms were placed in geometrically calculated positions and refined with temperature factors 1.2 times those of their bonded atoms.

Crystal data: for **1a**: triclinic, $P\bar{1}$, a = 26.202(9), b = 27.756(10), c = 28.408(10) Å, α = 92.583(5), β = 96.393(5), γ = 92.643(5)°, V = 20 483(12) Å^3, Z = 2, D_c = 1.279 g cm^{-3}, μ = 1.29 mm^{-1}, F(000) = 7752, $2\theta_{max}$ = 37.88° ($-23 \leqslant h \leqslant 23$, $-25 \leqslant k \leqslant 25$, $-25 \leqslant l \leqslant 20$). Final residuals (for 2529 parameters) were $R1$ = 0.1386 for 10 314 reflections with $I > 2\sigma(I)$, and $R1$ = 0.2849, $wR2$ = 0.4220, GOF = 1.082 for all 31 316 data. Residual electron density: 0.93 and −0.51 e Å^{-3}.

For **1b** (monoclinic phase): monoclinic, $C2/c$, a = 33.933(7), b = 36.925(7), c = 29.577(6) Å, β = 93.4595(28)°, V = 36 991.0 Å^3, Z = 4, D_c = 1.353 g cm^{-3}, μ = 0.76 mm^{-1}, F(000) = 15 582, $2\theta_{max}$ = 34.61° ($-28 \leqslant h \leqslant 28$, $-30 \leqslant k \leqslant 30$, $-24 \leqslant l \leqslant 13$). Final residuals (for 823 parameters) were $R1$ = 0.1353 for 3512 reflections with $I > 2\sigma(I)$, and $R1$ = 0.3056, $wR2$ = 0.4226, GOF = 1.031 for all 11 089 data. Residual electron density: 0.66 and −0.44 e Å^{-3}.

For **1b** (cubic phase): cubic, $Im\bar{3}m$, a = 27.6895(17) Å, V = 21 229.8 Å^3, Z = 2, D_c = 1.016 g cm^{-3}, μ = 1.24 mm^{-1}, F(000) = 6454, $2\theta_{max}$ = 46.50° ($-30 \leqslant h \leqslant 27$, $-26 \leqslant k \leqslant 30$, $-29 \leqslant l \leqslant 30$). Final residuals (for 100 parameters) were $R1$ = 0.0784 for 996 reflections with $I > 2\sigma(I)$, and $R1$ = 0.1069, $wR2$ = 0.2953, GOF = 1.138 for all 1501 data. Residual electron density: 0.83 and −0.44 e Å^{-3}.

For **2**: hexagonal, $P6_3/m$, a = b = 28.6458(19), c = 28.1649(26), V = 20 015.2 Å^3, Z = 2, D_c = 1.222 g cm^{-3}, μ = 1.32 mm^{-1}, F(000) = 7326, $2\theta_{max}$ = 45.11° ($-21 \leqslant h \leqslant 30$, $-27 \leqslant k \leqslant 27$, $-22 \leqslant l \leqslant 30$). Final residuals (for 728 parameters) were $R1$ = 0.1116 for 4003 reflections with $I > 2\sigma(I)$, and $R1$ = 0.1837, $wR2$ = 0.3416, GOF = 1.317 for all 8931 data. Residual electron density: 1.16 and −1.53 e Å^{-3}.

CCDC 161338–161341. See http://www.rsc.org/suppdata/cc/b1/b102714j/ for crystallographic data in .cif or other electronic format.

1 R. Feynman, *Eng. Sci.*, 1960, 22.
2 G. W. Orr, L. J. Barbour and J. L. Atwood, *Science*, 1999, **285**, 1049.
3 L. R. MacGillivray and J. L. Atwood, *Nature*, 1997, **389**, 469.
4 B. Olenyuk, M. D. Levin, J. A. Whiteford, J. E. Shield and P. J. Stang, *J. Am. Chem. Soc.*, 1999, **121**, 10 434.
5 B. Olenyuk, J. A. Whiteford, A. Fechtenkotter and P. J. Stang, *Nature*, 1999, **398**, 796.
6 P. J. Stang, B. Olenyuk, D. C. Muddiman and R. D. Smith, *Organometallics*, 1997, **16**, 3094.
7 N. Takeda, K. Umemoto, K. Yamaguchi and M. Fujita, *Nature*, 1999, **398**, 794.
8 M. Fujita, D. Oguro, M. Miyazawa, H. Oka, K. Yamaguchi and K. Ogura, *Nature*, 1995, **378**, 469.
9 K. Umemoto, K. Yamaguchi and M. Fujita, *J. Am. Chem. Soc.*, 2000, **122**, 7150.
10 P. J. Stang and B. Olenyuk, *Acc. Chem. Res.*, 1997, **30**, 502.
11 M. J. Wenninger, *Polyhedron Models*, Cambridge University Press, Cambridge, 1989.
12 E. W. Weisstein, *The CRC Concise Encyclopedia of Mathematics*, CRC Press, Boca Raton, FL, 1999.
13 H. S. M. Coxeter, M. S. Longuet-Higgins and J. C. P. Miller, *Philos. Trans. R. Soc. London, A*, 1954, **246**, 401.
14 A. Holden, *Shapes, Space, and Symmetry*, Columbia University Press, New York, 1971.
15 O. M. Yaghi, H. L. Li, C. Davis, D. Richardson and T. L. Groy, *Acc. Chem. Res.*, 1998, **31**, 474.
16 F. H. Allen and O. Kennard, *Chem. Des. Autom. News*, 1993, **8**, 31.
17 M. Eddaoudi, H. L. Li and O. M. Yaghi, *J. Am. Chem. Soc.*, 2000, **122**, 1391.
18 S. S. Y. Chui, S. M. F. Lo, J. P. H. Charmant, A. G. Orpen and I. D. Williams, *Science*, 1999, **283**, 1148.
19 T. L. Hennigar, D. C. MacQuarrie, P. Losier, R. D. Rogers and M. J. Zaworotko, *Angew. Chem., Int. Ed. Engl.*, 1997, **36**, 972.
20 A. F. Wells, *Structural Inorganic Chemistry*, Oxford University Press, Oxford, 5th edn, 1984.

CHEMCOMM
Communication
www.rsc.org/chemcomm

Confinement of the ions [M⊂[2.2.2]cryptand]$^+$ and [cobalt(III)-bis(dicarbollide)]$^-$ in the divergent curved surfaces of a Ni(II) macrocycle

Michaele J. Hardie,† Nino Malic, Colin L. Raston*† and Brett A. Roberts

School of Chemistry, Monash University, Clayton, Melbourne, Victoria 3800, Australia

Received (in Columbia, MO, USA) 24th January 2001, Accepted 26th February 2001
First published as an Advance Article on the web 18th April 2001

Treatment of M[Co($C_2B_9H_{11}$)$_2$], M = Na or K, with [2.2.2]cryptand and 5,7,12,14-tetramethyldibenzo[*b*,*i*]-1,4,8,11-tetraazacyclotetradecinenickel(II) results in a 1:1:1 complex, assembled with the cobalticarborane anion snugly residing in the phenyl lined face of the Ni(II) macrocycle through C–H···N and C–H···π interactions, with the ensuing [M⊂[2.2.2]cryptand]$^+$ supercation residing in the smaller methyl faced cavity of the macrocycle.

The nickel(II) macrocycle 5,7,12,14-tetramethyldibenzo[*b*,*i*]-1,4,8,11-tetraazacyclotetradecinenickel(II) [Ni(TMTAA)] is a versatile receptor for neutral molecules, forming supramolecular host–guest complexes, as perched structures, with a range of globular cage molecules including C_{60}, *o*-carborane (icosahedral 1,2-$C_2B_{10}H_{12}$) and the phosphorus chalcogenides P_4(S or Se)$_3$,[1,2] and also for disc-shaped [$(H_2O)_2$∩18-crown-6][3] and torus shaped *cyclo*-octasulfur.[2] Ni(TMTAA) is a rigid, saddle-shaped macrocycle possessing two divergent concave surfaces which arise from the steric interactions of the methyl groups and the adjacent H-atoms on the aromatic rings. It can act as a heterotopic divergent receptor with C_{60}, or it can self-associate into dimers through the phenyl-lined face with the supermolecule acting as a homotopic divergent receptor for a range of molecules. A related macrocyle with two methyl groups on each of the aromatic rings (*trans* to the N-centres) forms 1:1 complexes with C_{60}[4] and C_{70}.[5]

We now report the formation of a multicomponent supramolecular array where the Ni(TMTAA) receptor acts as a divergent heterotopic receptor for globular-type ionic species, both the super-cationic and anionic species [M⊂[2.2.2]cryptate]$^+$, M = Na or K, and [Co($C_2B_9H_{11}$)$_2$]$^-$, Scheme 1. For the anion this takes on a novel C–H hydrogen bonding array with Ni(TMTAA), with a pre-programmed complementarity of curvature of the two interacting components, which is also the case for the cation to macrocycle interplay. The cobalticarborane or cobalt(III) bis(dicarbollide) is a weakly coordinating anion,[6] able to act as a soft anion in building up supramolecular architecture.[7]

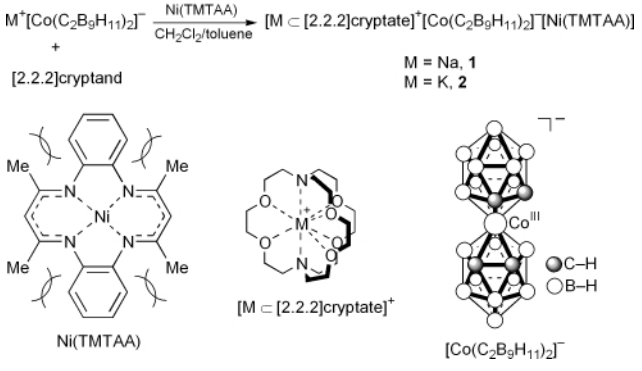

Scheme 1

Slow evaporation of CH_2Cl_2/toluene solutions containing a 1:1:1 mixture of sodium cobalticarborane, [2.2.2]cryptand and Ni(TMTAA) affords the complex [Na⊂[2.2.2]cryptate]$^+$-[Co($C_2B_9H_{11}$)$_2$]$^-$[Ni(TMTAA)], **1**, in high yield, Scheme 1.‡ The potassium analogue **2** was similarly prepared by first converting the sodium salt of the cobalticarborane to the potassium salt by treating a 1:1 mixture of sodium cobalticarborane and [2.2.2]cryptand with excess KPF_6. Both compounds were characterised by NMR and microanalysis and their structures in the solid state established from X-ray diffraction studies.§

Compounds **1** and **2** are isomorphous and isostructural, crystallising in the space group $P2_1/c$ with the asymmetric unit comprised of [M⊂[2.2.2]cryptate]$^+$, [Co($C_2B_9H_{11}$)$_2$]$^-$ and one Ni(TMTAA) molecule. Salient features of the structure are borne out in Fig. 1. There is a striking snug fit of the cobalticarborane in the phenyl-lined face of the macrocycle. Moreover, the pairs of C–H groups (one from each carborane ligand) are adjacent to each other in a staggered conformation, as established elsewhere for this anion,[7] such that the C–H groups from each carborane ligand furthest from each other form non-classical C–H···π hydrogen bonds to their closest aromatic ring, and the other C–H groups form weak hydrogen bonds to a N-centre. Associated distances for C–H···$\pi_{centroid}$ (C···$\pi_{centroid}$) are 2.60 (3.66) and 3.10 (4.14) Å for **1** and 2.72 (3.79) and 2.88 (3.94) Å for **2**. Distances for C–H···N (C···N) are 2.69 (3.63) and 2.46 (3.51) Å for **1** and 2.52 (3.56) and 2.73 (3.73) Å for **2**. The C–H···$\pi_{centroid}$ distances are comparable with those reported for complexes of cyclotriveratrylene and *o*-carborane.[8–11] *Ab initio* calculations for a C–H···π interaction

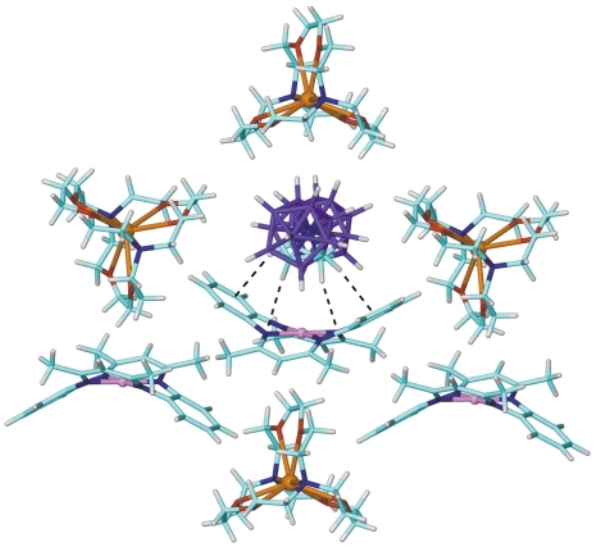

Fig. 1 Projection showing the interplay between the ions of [K⊂[2.2.2]cryptand]$^+$, [Co($C_2B_9H_{11}$)$_2$]$^-$ and Ni(TMTAA). Broken lines correspond to C–H···π and C–H···N hydrogen bonding interactions.

† Present address: School of Chemistry, University of Leeds, Leeds, UK LS2 9JT. E-mail: c.l.raston@chem.leeds.ac.uk

between the same carborane and benzene gave a C–H···π distance of 2.694 Å, and a weak energy of interaction of 2.72 kcal mol^{-1}.[8] The acidic C–H groups of carboranes also form hydrogen bonds to O-centres of 18-crown-6,[12] and to other hydrogen bond acceptors.[13] Recent studies have established that the cobalticarborane can form close inter-anion contacts associated with C–H···H–B interactions at 2.40 Å.[7]

The supercation [M⊂[2.2.2]cryptate]$^+$ also interacts with Ni(TMTAA), with one arm of the [M⊂[2.2.2]cryptate]$^+$ sitting in the methyl face of the macrocycle at the van der Waals limit, thereby maximising steric complementarity between the two curved surfaces. Thus, with the anion residing in the other face, Ni(TMTAA) acts as a divergent receptor for the ions as part of a linear array, Fig. 1. The other two arms of the supercation form a cavity in which the cobalticarborane anion sits, the closest B–H···O contacts being 3.40 Å. Related to this work is the binding of various metal ion complexes of [2.2.2]cryptand in bowl-shaped cavities of calix[4]resorcinarenes.[14]

The extended structure also has the aromatic protons of Ni(TMTAA) lying astride two arms of the cryptate, Fig. 1. This packing is more efficient for complex **2** compared with **1** which relates to the smaller size of the sodium cation (0.98 Å radius) with respect to the [2.2.2]cryptand cavity (approx. 1.4 Å radius).[15] Here the coordination environment is distorted, as evidenced by the N–Na–N angle at 168.57(7)° and acute O–Na–O angles at 57.78(6)–64.56(6)°. In contrast, the cavity is a better fit for the potassium cation (1.33 Å radius)[15] and the supercation approximates to D_{3h} symmetry (ignoring the ethylene linkages); the N–K–N angle is now 176.47(9)° and acute O–K–O angles more uniform at 57.36(10)–61.22(10)°. Metal to N- and O-centre distances in the supercations are unexceptional, Na–O 2.371(2)–2.919(2) Å, Na–N 2.668(2) and 3.014(2) Å, *cf.* K–O 2.730(3)–2.866(3) Å, K–N 2.993(4) and 3.014(4) Å.

UV–Vis experiments were conducted for Ni(TMTAA) *versus* [Na⊂[2.2.2]cryptand]$^+$[Co($C_2B_9H_{11}$)$_2$]$^-$ in dichloromethane, nitromethane and chlorobenzene, albeit without any evidence of complex formation in solution. Electrospray mass spectra were collected of the complex **2** in dichloromethane/methanol solution. However, no peaks corresponding to any multicomponent species in the gaseous phase were observed.

In conclusion, we have established a new class of compounds based on a divergent receptor for supercations and anions which show steric and electronic complementarity, with the success of the work in part attributed to the rigidity of the Ni(II) macrocycle receptor.

We are grateful to the Australian Research Council for support of this work.

Notes and references

‡ *Synthesis* of [M⊂[2.2.2]cryptand][Co($C_2B_9H_{11}$)$_2$][Ni(TMTAA)] M = Na, **1**: Na[Co($C_2B_9H_{11}$)$_2$] (20 mg, 57.7 μmol) and [2.2.2]cryptand (22 mg, 57.7 μmol) were dissolved in CH_2Cl_2 (3 ml), then Ni(TMTAA) (23 mg, 57.7 μmol) was added followed by toluene (3 ml), after it had dissolved. Slow evaporation of the solvent over several days yielded a purple–brown crystalline solid. Yield 48 mg (74%), mp. 275 °C, $C_{44}H_{80}B_{18}CoN_6NaNiO_6$ requires: C 47.0, H 7.17, N 7.47%. Found: C 47.14, H 7.16, N 7.55%. ^{1}H NMR ($CDCl_3$, 300 MHz) δ 2.07 (s, 12H, CH_3), 2.64 (t, ^3J 5.1 Hz, 12H, NCH_2), 3.58 (t, ^3J 5.1 Hz, 12H, NCH_2CH_2), 3.62 (s, 12H, OCH_2), 3.98 (br s, 4H, BCH), 4.84 (s, 2H, CH), 6.53–6.57 (m, 4H, ArH), 6.65–6.70 (m, 4H, ArH).

For M = K, **2**: Na[Co($C_2B_9H_{11}$)$_2$] (15 mg, 43.3 μmol), [2.2.2]cryptand (16 mg, 42.5 μmol) and KPF_6 (300 mg) were dissolved in acetone. The acetone was quickly evaporated and the residue extracted with CH_2Cl_2 and filtered, whereupon the CH_2Cl_2 filtrate was evaporated. The dissolution–evaporation–extraction procedure was then repeated with a further 300 mg KPF_6. To the final, orange-coloured CH_2Cl_2 extract (*ca.* 4 ml) was added Ni(TMTAA) (32 mg, 79.8 μmol) followed by an equal volume of toluene, and the solution allowed to evaporate slowly overnight. The resulting crystalline precipitate was filtered off, washed with toluene and air dried. Mp 287 °C, $C_{44}H_{80}B_{18}CoKN_6NiO_6$ requires: C 46.34, H 7.07, N 7.37%. Found: C 46.35, H 7.06, N 7.27%. ^{1}H NMR ($CDCl_3$, 300 MHz) δ 2.07 (s, 12H, CH_3), 2.53 (t, 4.8 Hz, 12H, NCH_2), 3.53 (t, 4.8 Hz, 12H, NCH_2CH_2), 3.60 (s, 12H, OCH_2), 4.00 (br s, 4H, BCH), 4.84 (s, 2H, CH), 6.53–6.57 (m, 4H, ArH), 6.65–6.70 (m, 4H, ArH).

§ *Crystal data* for compounds **1** and **2** (in parentheses): [Na,K⊂[2.2.2]cryptand][Co($C_2B_9H_{11}$)$_2$], $C_{44}H_{80}B_{18}CoNa[K]N_6NiO_6$, M_r = 1124.35 (1140.46), monoclinic, $P2_1/c$, a = 19.5377(2) [19.7345(2)], b = 18.2124(2) [18.1965(2)], c = 16.3576(2) [16.5687(3)] Å, β = 108.487(1) [108.493(1)]°, V = 5520.13(11) [5642.57(13)] Å^3, D_c = 1.353 [1.342] g cm^{-3}, μ = 0.702 (0.753) cm^{-1} (no correction), Z = 4, T = 123(1) K, 66247 (77324) reflections collected, 11964 (11034) unique reflections, R_{int} = 0.097 (0.138), $2\theta_{max}$ = 55 (52)° [7729 (6314) observed, $I > 2\sigma(I)$, 698 (698) parameters, no restraints, R_1 = 0.0499 (0.0552), wR_2 = 0.0982 (0.1350)], S = 1.043 (1.029). Enraf-Nonius KappaCCD diffractometer, Mo-Kα radiation, crystals mounted in oil: The non-hydrogen atoms were refined anisotropically and hydrogen atoms were included at geometrically estimated positions.

CCDC 160797–160798. See http://www.rsc.org/suppdata/cc/b1/b102140k/ for crystallographic data in .cif or other electronic format.

1 P. Andrews, J. L. Atwood, L. J. Barbour, P. J. Nichols and C. L. Raston, *Chem. Eur. J.*, 1998, **4**, 1384.
2 P. C. Andrews, P. D. Croucher, J. L. Atwood, L. J. Barbour, P. J. Nichols and N. O. Smith, *J. Chem. Soc., Dalton Trans.*, 1999, 2927.
3 K. Baranyai, P. J. Nichols and C. L. Raston, *Angew. Chem., Int. Ed.*, 2000, **39**, 1842.
4 P. D. Croucher, P. J. Nichols and C. L. Raston, *J. Chem. Soc., Dalton Trans.*, 1999, 279.
5 P. D. Croucher, J. M. E. Marshall, P. J. Nichols and C. L. Raston, *Chem. Commun.*, 1999, 193.
6 M. F. Hawthorne, D. C. Young, T. D. Andrews, D. V. Howe, R. L. Pilling, A. D. Pitts, M. Reintjes and L. F. Warren, *J. Am. Chem. Soc.*, 1968, **90**, 879; Z. Xie, T. Jelinek, R. Bau and C. A. Reed, *J. Am. Chem. Soc.*, 1994, **116**, 1907.
7 M. J. Hardie and C. L. Raston, *Angew. Chem., Int. Ed.*, 2000, **39**, 3835.
8 R. J. Blanch, M. Williams, G. D. Fallon, M. G. Gardier, R. Kaddour and C. L. Raston, *Angew. Chem., Int. Ed. Engl.*, 1997, **36**, 504.
9 M. J. Hardie, C. L. Raston and B. Wells, *Chem. Eur. J.*, 2000, **6**, 3293.
10 M. J. Hardie and C. L. Raston, *Eur. J. Inorg. Chem.*, 1999, 195.
11 P. C. Andrews, M. J. Hardie and C. L. Raston, *Coord. Chem. Rev.*, 1999, **189**, 169.
12 P. D. Godfrey, W. J. Grigsby, P. N. Nichols and C. L. Raston, *J. Am. Chem. Soc.*, 1997, **119**, 9283.
13 M. G. Davidson, T. G. Hibbert, J. A. K. Howard, A. MacKinnon and K. Wade, *Chem. Commun.*, 1996, 2285; G. Harakas, T. Vu, C. B. Knobler and M. F. Hawthorne, *J. Am. Chem. Soc.*, 1998, **120**, 6405; K. A. Lyssenko, M. Y. Antipin and V. N. Lebedev, *Inorg. Chem.*, 1998, **37**, 5834; M. J. Hardie, P. D. Godfrey and C. L. Raston, *Chem. Eur. J.*, 1999, **5**, 1828.
14 A. Lutzen, A. R. Renslo, C. A. Schalley, B. M. O'Leary and J. Rebek, *J. Am. Chem. Soc.*, 1999, **121**, 7455.
15 L. F. Lindoy, *The Chemistry of Macrocyclic Ligand Complexes*, Cambridge University Press, Cambridge, 1989, pp. 189.

Typeset and printed by Black Bear Press Limited, Cambridge, England

CHEMCOMM
Feature Article
www.rsc.org/chemcomm

Taxol, a molecule for all seasons

David G. I. Kingston

Department of Chemistry, M/C 0212, Virginia Polytechnic Institute and State University, Blacksburg, VA 24061, USA. E-mail: dkingston@vt.edu

Received (in Cambridge, UK) 3rd January 2001, Accepted 19th February 2001
First published as an Advance Article on the web 26th March 2001

The diterpenoid natural product taxol, first discovered in the 1960's has proved to be the most important new anticancer drug introduced in the last ten years. A brief history of taxol's development from laboratory curiosity to blockbuster drug is followed by a summary of its chemistry, including an overview of the six completed syntheses of taxol. The review concludes with a discussion of its bioactivity as a promoter of tubulin polymerization and as a drug.

Introduction

With the possible exception of Viagra, probably no new drug in the last 20 years has generated as much public interest and excitement as has taxol (paclitaxel or Taxol™, **1**).[1] This interest

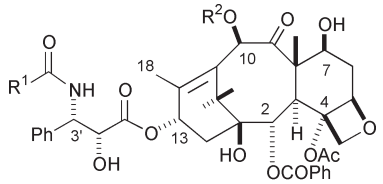

1 R^1 = Ph, R^2 = Ac
2 R^1 = Me_3CO, R^2 = H

was fueled primarily by taxol's excellent clinical activity against ovarian and breast cancers, but it was intensified by the severe supply problems that were in effect during the period leading up to its general clinical use. These problems were successfully solved, as will be described below, and taxol is now widely available and is the largest-selling anticancer drug of all time, with sales of over $1.5 billion in 1999.[2] This review will give a brief history of the development of taxol from a laboratory curiosity to a blockbuster drug, and will then describe some recent advances in the chemistry and biology of this fascinating compound.

History of taxol's development as an anticancer drug

Discovery of the bioactivity now known to be due to taxol was made in 1962, when Arthur Barclay, a botanist working for the US Department of Agriculture under contract to the US National Cancer Institute (NCI), made a collection of the stem and bark of *Taxus brevifolia* Nutt. in Washington State. These plant samples, along with many others, were duly extracted and tested for bioactivity, and in 1964 the extract from *T. brevifolia* was found to be cytotoxic to KB cells. The extract was assigned to Dr Monroe Wall at Research Triangle Institute, and taxol was isolated in 1967.[3] The structure was elucidated by a combination of X-ray studies of two degradation products and ^{1}H-NMR analysis of the intact molecule, and was published in 1971.[4]

Initial reaction to taxol as a potential anticancer drug was less than enthusiastic. Although it was clearly an active compound, with activity both in cell culture and also *in vivo* against various leukemias and the Walker 256 carcinosarcoma, its activity was only modest in these assays. To add to its problems, it was highly insoluble in water, and would thus clearly present formidable formulation problems, and it was isolated in only very modest yield from the bark of a relatively uncommon and slow-growing tree. Not a good outlook for a potential drug candidate!

Fortunately testing was carried out in some new *in vivo* bioassays that were introduced by NCI in the early 1970's, and it proved to be strongly active in a B16 mouse melanoma model. On the basis of this activity, and with enthusiastic support from Dr Matthew Suffness at NCI and Dr Monroe Wall, taxol was selected as a development candidate in 1977. Development of taxol as a drug was a challenging task because of the problems with solubility and supply noted earlier, and also because of its relatively low potency. The solubility problem was successfully overcome with a formulation in ethanol and Cremophor EL, and this turned out to be important in both negative and positive ways. On the negative side, the high levels of Cremophor required led to hypersensitivity reactions and almost led to the withdrawal of taxol from clinical trials. On the positive side, there is some evidence that Cremophor has a pharmaceutical effect over and above its surfactant properties, and may act to reverse multidrug resistance.[3]

Interest in taxol as a drug candidate was increased significantly when Susan Horwitz reported in 1979 that it had what was then a completely new mechanism of action, in that it promoted the assembly of the proteins α- and β-tubulin into microtubules.[5] A schematic representation of taxol's effect on the tubulin polymerization process is shown in Fig. 1.

Microtubules are required for chromosome segregation and for other operations such as intracellular transport and positioning of internal cellular organelles, and all of these activities require that the microtubules be in dynamic equilibrium with monomeric tubulins. Several compounds, including the clinically used drugs vinblastine (Velban™) and vincristine (Oncovin™), were known to operate as spindle poisons by *preventing* the assembly of tubulin into microtubules, but taxol was the first compound in which the activity was linked to *promotion* of microtubule assembly. This discovery proved to be important in maintaining interest in the development of taxol at a time when its initial clinical results were discouraging. Taxol's mechanism

David G. I. Kingston was born in London, and received his BA and PhD degrees (Lord Todd and D. W. Cameron) from Cambridge University in 1960 and 1964, respectively. After postdoctoral appointments at MIT and Cambridge, he moved to the USA, where he is currently a University Distinguished Professor at Virginia Polytechnic Institute and State University. In addition to his work on taxol, he is carrying out biodiversity conservation and drug discovery work in Suriname and Madagascar, and he also serves as one of several lay pastors in his local church, the Blacksburg Christian Fellowship.

DOI: 10.1039/b100070p

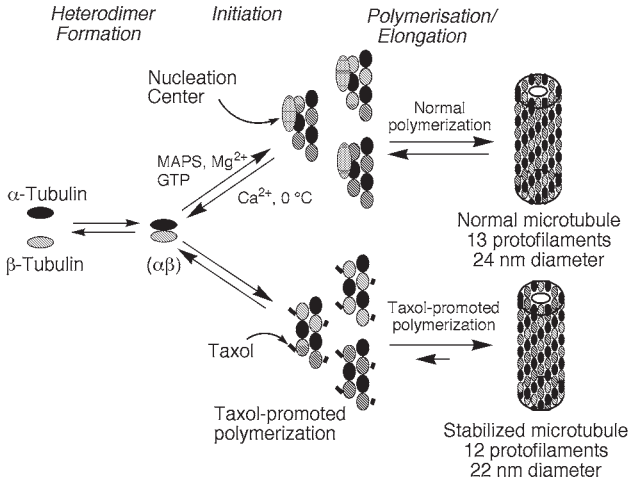

Fig. 1 Schematic representation of normal microtubule assembly (upper) and taxol-promoted microtubule assembly (lower).

of action, and specifically its binding to microtubules, will be discussed in more detail in a later section of this review.

Taxol went into Phase I clinical trials in 1984, and into Phase II trials in 1985. These trials were limited by the supply of the drug, but gave the first clear evidence of activity with clinically relevant responses in ovarian cancer and in breast cancer reported in 1989[6] and 1991[7] respectively. Taxol and its semisynthetic analog docetaxel (Taxotere™, **2**) are now used (either as single agents or in combination with other drugs such as cisplatin) for the treatment of ovarian cancer, breast cancer, and non-small-cell lung cancer.[8]

The taxol supply crisis and its solution

The recognition of taxol's clinical activity created a crisis in the supply of the drug, since at the time it was only available in low yield from the bark of *T. brevifolia*. Since this tree is relatively uncommon, occurring most abundantly in the old-growth forests of the Pacific Northwest of the USA, the prospects of the large-scale logging needed to supply taxol to the clinical market raised serious environmental concerns.[9]

The responsibility for solving this problem fell to the Bristol-Myers Squibb Company, which had obtained the rights to develop taxol from the NCI under a Cooperative Research and Development Agreement. The various options for increasing the supply included increased harvesting of *T. brevifolia* bark, the isolation of taxol from a renewable resource such as yew needles, the semisynthesis of taxol from other taxoids in yew, and bioproduction through plant tissue culture. Initial supplies of taxol for clinical use were obtained by increased harvesting of *T. brevifolia* bark. The real breakthrough came from a combination of Potier's discovery that needles of the English yew, *T. baccata*, contained substantial amounts of 10-deacetylbaccatin III (**3**), in addition to smaller amounts of baccatin III (**4**),[10] with Holton's discovery of an efficient semisynthesis of taxol from the protected baccatin III (**5**) through a β-lactam

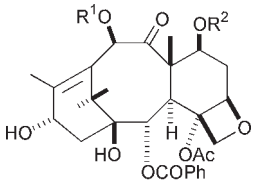

3 $R^1 = R^2 = H$
4 $R^1 = Ac$, $R^2 = H$
5 $R^1 = Ac$, $R^2 = SiEt_3$

intermediate; the details of this synthesis will be described later.[11] This invention was licensed to Bristol-Myers Squibb, and enabled the company to produce enough taxol to meet an escalating demand, with sales rising from about $400 million in 1994 to an estimated $1600 million in 2000.[2]

In addition to this and other semisynthetic routes, several workers have investigated the production of taxol by plant tissue culture methods, and at least two companies (Phyton Inc. and ESCA Genetics) have developed production methods.[12] Reported yields range from 0.012–0.05%, with specific production rates of 0.3 mg g^{-1} dry cell weight per day for up to 40 days.[13] These yields are close to those needed for commercially viable production, and it is thus quite probable that full-scale bioproduction of taxol will begin within the next few years, especially since Bristol-Myers Squibb signed agreements in 1998 with Phyton Inc. to commercialize Phyton's plant cell fermentation technology. The production of taxol by the fungus *Taxomyces andreanae* was reported by Stierle *et al*. in 1993, but the yield was extremely low (25–50 ng L^{-1}) and a large increase in this yield through strain improvement will be needed before a fungal culture method would be commercially viable. More recently Strobel and his coworkers have found that the fungus *Periconia* sp. isolated from *Torreya grandiflora* produces taxol at the 800 ng L^{-1} level when stimulated with benzoic acid.[14] Other sources of taxol have also been discovered, with one of the more interesting ones being hazelnut cultivars and their associated fungal endophytes.[15] Since taxol appears to be produced by the hazelnut cultivars as well as by their fungal endophytes, this is the first example of taxol being found in a plant outside the Taxaceae family.

The quest to understand taxol's structure–activity relationships

The chemistry of taxol has been thoroughly investigated by a large number of academic and industrial researchers, and this review will thus not attempt to provide a complete coverage. Readers interested in a more comprehensive review can consult any of the several available books[16–19] and reviews,[20–23] including a comprehensive forthcoming review.[24] This section will thus describe some of the early work from the author's laboratory, and will then summarize the major findings for each section of taxol's structure.

Early studies

Our work on taxol began in 1979 with a conversation between the author and Bob Holton, who at that time was a member of the Virginia Tech faculty. He had developed the outline of a synthetic approach to taxol, and we agreed that we would collaborate on this synthesis. He would start at the beginning in a 'bottom up' approach, while I would start with taxol and study its chemistry in a 'top down' approach. Since we did not have a supply of taxol, I decided to begin by looking at the possible conversion of *O*-cinnamoyltaxicin I triacetate (**6**), available by Lythgoe's procedure from taxine B (**7**)[25] into taxol or taxol-like compounds. I isolated about 100 mg of crude taxine B from yew bushes growing on the Virginia Tech campus, converted it into **6**, and did some preliminary work on forming the oxetane ring. At this point I also contacted Dr Matthew Suffness at the US National Cancer Institute, and was able to obtain a small amount of pure taxol, together with larger amounts of various side cuts from the large-scale purification of taxol for the pending clinical trials. With these extracts in hand the need for the conversion of **6** into taxol-like compounds was removed, and this aspect of the project was dropped. It was thus very gratifying to find that Scheeren,[26] Potier,[27] and Saicic[28] have all published conversions of taxine to taxol-like compounds within the last few years.

Bob Holton and I submitted a proposal to the National Institutes of Health in 1980 for funding of our joint approach to taxol, but there was little interest in the compound at that time

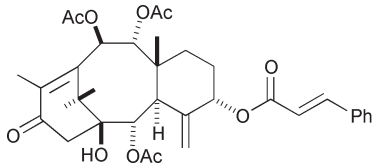

6

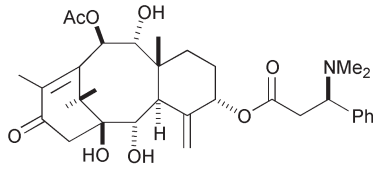

7

and the proposal was not funded. At this point we decided to try our luck at separate proposals, and so while Bob went back to NIH (where he eventually did get funded for his work) I chose to apply to the American Cancer Society. To their credit the reviewers at the ACS saw the value of studying the chemistry of taxol, and we received a modest grant in 1982.

Our basic approach in these early days, when little was known about the chemistry of taxol, was to try to modify its functional groups one at a time, to see whether they were individually necessary for the activity of the drug. We began by showing that the side-chain hydroxy group at the 2′-position was much more reactive to acetylation than that at the 7-position, and Susan Horwitz, with whom we had begun to collaborate, showed that the resulting taxol acetates still retained much of taxol's activity.[29] The reverse proved true on oxidation, however, and the 7-hydroxy group could be oxidized selectively to the corresponding 7-oxo derivative. This product proved to be unstable, and readily underwent β-elimination to give the ring-opened product **8**. Compound **8** turned out to be essentially non-cytotoxic, thus providing the first hint of the importance of the oxetane ring to taxol's activity.[30]

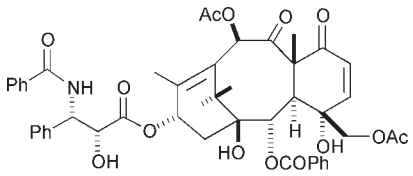

8

With a molecule as complex as taxol, not every experiment gave the expected result. Sometimes the unexpected results were useful, although more often they were not. One of the useful results came from our desire to reduce the C-9 keto group to an alcohol. Treatment of taxol with sodium borohydride left the keto group essentially untouched, but removed the side chain in good yield; the yield was later improved by the use of tetrabutylammonium borohydride in dichloromethane (Scheme 1).[31]

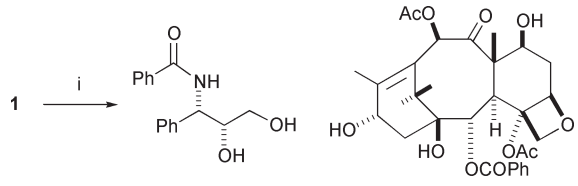

Scheme 1 *Reagents and conditions*: i, Bu_4NBH_4 (excess), CH_2Cl_2, rt, 24 h 98%.

This unexpected reduction of an ester in the presence of a keto group was due to the extremely hindered location of the 9-keto group and to the presence of an α-hydroxy group on the side chain. The reduction products were the diol **9** and baccatin III (**4**), and this formation of baccatin III from taxol or (equally well) from crude taxol–cephalomannine mixtures available from the National Cancer Institute gave us and other workers ready access to baccatin III.

Another surprising reaction was that of taxol with Meerwein's reagent, $Et_3O^+BF_4^-$. The reaction was originally carried out in an attempt to cleave the side-chain amide group, since it was known that amides react selectively with Meerwein's reagent in the presence of esters to yield imino ethers.[32] In the event, the amide group was unreactive but the oxetane ring underwent an assisted ring-opening to give compound **10**.[33] Compound **10**, like compound **8**, was essentially inactive in tubulin-assembly and cytotoxicity assays, thus emphasizing the importance of the oxetane ring to taxol's activity.

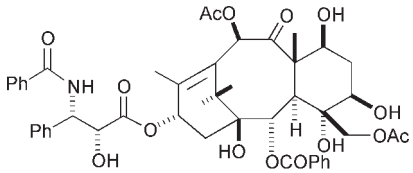

10

In the following sections the chemistry and structure–activity relationships of taxol will be summarized, with an emphasis on work carried out at Virginia Tech but including key results from other laboratories. The discussion will follow a clockwise route, starting with the 'northern hemisphere' and proceeding around the oxetane ring to the 'southern hemisphere' and thence to the side chain.

The northern hemisphere

The C-11–C-12 double bond in the A-ring of taxol is relatively unreactive, as indicated by the fact that hydrogenation of baccatin III gives a hexahydro product in which the C-2 benzoyl group is reduced to a cyclohexylcarbonyl group while the C-11–C-12 double bond is untouched.[34] Epoxidation of taxol with *m*-chloroperbenzoic acid also fails, but the epoxide **11** could be prepared by oxidation of 10-deacetoxytaxol; compound **11** turned out to be more active than taxol in a tubulin-assembly assay but less cytotoxic to B16 melanoma cells.[35]

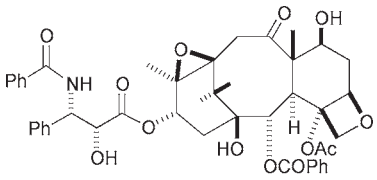

11

Interestingly the enol **12**, obtained by reduction of 7-(triethylsilyl)-13-oxobaccatin III with Zn–AcOH, is stable and can be acylated. Acylation with the oxazolidine **13** (Scheme 2) gave the isotaxol derivative **14**; compound **14** is slightly more cytotoxic than taxol.[36]

Allylic bromination of 7,13-di(triethylsilyl)baccatin III gave the bromide **15**, which gave the corresponding C-18 analogs on treatment with nucleophiles such as Me_2CuLi, NaN_3, Bu_4NOAc and KCN. Attachment of the taxol side chain and deprotection gave the C-18 analogs **16** (X = Me, N_3, OAc or CN), all of which were less cytotoxic than taxol, with the methyl derivative being the most active (Scheme 3).[37]

Taxol can be selectively deacetylated at C-10 to give 10-deacetyltaxol by treatment with hydrazine[38] or with sodium bicarbonate and hydrogen peroxide.[39] Deoxygenation of the 10-hydroxy group was originally achieved using Barton's xanthate chemistry,[40] but a simpler method was developed by treating taxol with samarium diiodide.[41,42] The resulting 10-deacetoxytaxol **17** had a similar cytotoxicity to taxol,[40] and

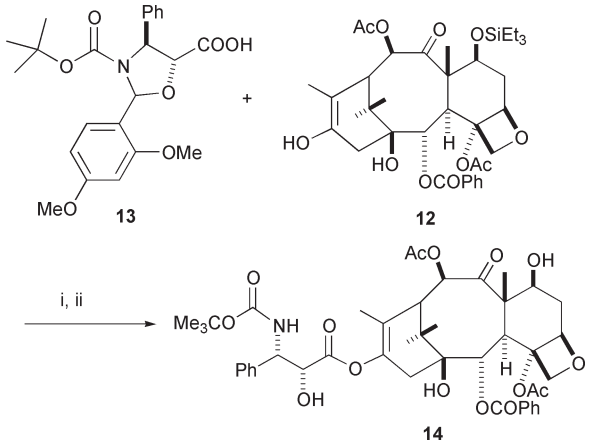

13 **12** **14**

Scheme 2 *Reagents and conditions*: i, DCC, DMAP; ii, AcOH–H_2O, rt, 4 days, 40% overall.

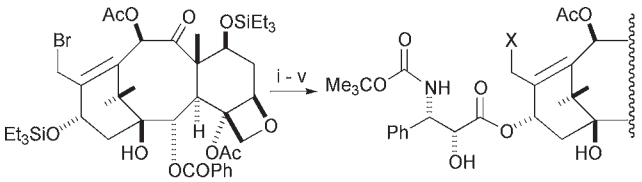

15 **16**

Scheme 3 *Reagents and conditions*: i, Me_2CuLi, THF, −78 °C; ii, HF–pyridine, rt; iii, TES-Cl, imidazole, DMF, 0 °C, 40%; iv, NaHMDS, THF, −78 °C, then β-lactam synthon; v, HF–pyridine, rt, 53%.

the same was true for the corresponding docetaxel analog **18**.[42]

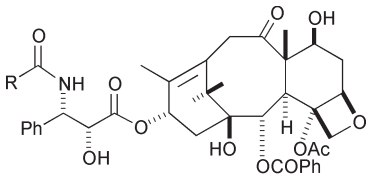

17 R = Ph
18 R = Bu^tO

Acylation of 10-deacetyltaxol at the C-10 position has yielded a number of useful analogs, including the dichloronicotinyl derivative **19** which is more cytotoxic than taxol

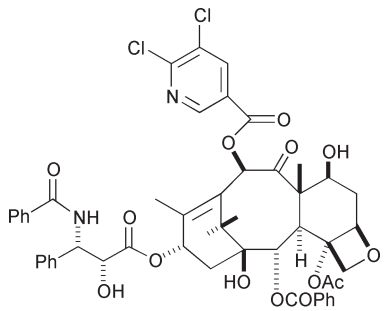

19

against both normal and drug-resistant MCF-7 cells.[43] Taxol analogs with isobutyl or isobutenyl substituents replacing the 3′-phenyl group and various C-10 acyl groups have been prepared by Ojima, and several of these have shown improved cytotoxicity against the resistant cell line MCF7-R.[44]

The C-7 hydroxy group can be removed selectively by the Barton xanthate deoxygenation route to give 7-deoxytaxol **20**, and the same intermediate can be used to convert 7-*epi*taxol to taxol.[45] 7-Deoxytaxol has the same cytotoxicity as taxol in the HCT116 cell line, suggesting that the 7-hydroxy group is not essential for taxol's activity.[45,46]

Although the 7-hydroxy group may not be necessary for taxol's activity, modifications at C-7 have yielded analogs with improved properties, and the thiomethyl derivative **21** has been selected by Bristol-Myers Squibb for development as a 'second-generation' taxol analog: it is currently in clinical trials, with preliminary reports that it is performing well.[47]

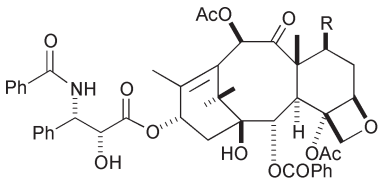

20 R = H
21 R = OCH_2SCH_3

Dehydration at C-7 can be accomplished by treatment of the 7-triflate derivative with a non-nucleophilic base such as DBU to give 6,7-dehydrotaxol (**22**),[38,48] which was slightly less cytotoxic than taxol to CA46 cells.[48] Osmylation of **22** gave the 6α,7α-diol **24**. Protection of **22** as its TBDMS ether gave **23**, which could be converted to the 2′-protected diol **25**; this was converted to the C-nortaxol analog **26** by reaction with lead tetraacetate and deprotection.[49] Compound **26** was significantly less cytotoxic than taxol, which is surprising given the very similar shapes of the two compounds. Diol **25** could also be converted to 6α-hydroxytaxol (**27**), which is the major human metabolite of taxol.[50] Although the yield was low, the starting material was recovered unchanged and could be recycled to effect a good overall conversion (Scheme 4).

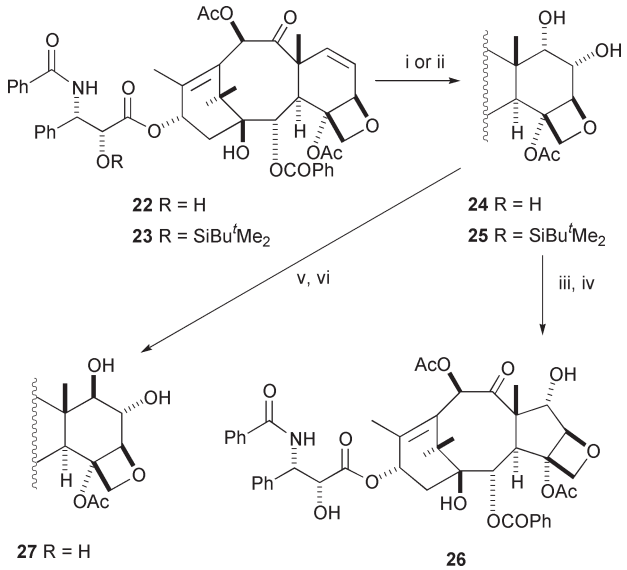

22 R = H
23 R = $SiBu^tMe_2$
24 R = H
25 R = $SiBu^tMe_2$
27 R = H
26

Scheme 4 *Reagents and conditions*: i, **22**, OsO_4, NMO, 25 °C, 9 h, 71% of **24**; ii, **23**, OsO_4, NMO, 25 °C, 9 h, 78% of **25**; iii **25**, $Pb(OCc)_4$, $NaHCO_3$, 2 h, 0 °C, 67%; iv, THF, HF–pyridine, 1.5 h, rt, 86% of **26**; v, DBU, PhMe, 80 °C, 12% (95% based on unrecovered starting material); vi, THF, HF–pyridine, 75%.

The oxetane ring

As noted earlier, opening of the oxetane ring to give compounds **8** or **10** essentially eliminated taxol's cytotoxicity and tubulin-assembly activity. The question thus arose as to the reason for this effect; putting the question another way, why is the oxetane ring necessary for taxol's activity? It is clearly not involved in any covalent binding to tubulin, since taxol can be exchanged with labeled taxol on tubulin, and we thus elected to test whether changing the size and electronegativity of the hetero-

atom had any effect. The sulfetane analog **29** was selected for study, and was prepared by reaction of the key intermediate **28** with Li_2S, followed by acylation at C-4, reaction with phenyllithium to open the cyclic carbonate, and deprotection (Scheme 5). Sulfetane **29** was significantly less active than taxol in both tubulin-assembly and cytotoxicity assays.[51]

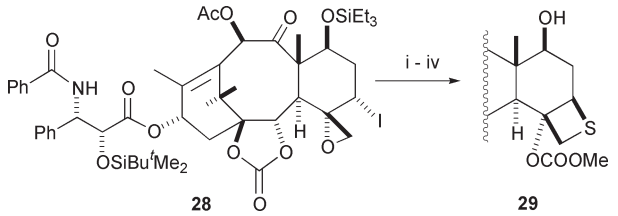

Scheme 5 *Reagents and conditions*: i, Li_2S, THF, rt, 28 h, then Im_2CO, imidazole, rt, 12 h, 56%; ii, LHMDS, THF, −78 °C (7 min), rt (1 min), −78 °C (2 min) then $ClCO_2Me$, 39%; iii, PhLi, THF, −78 °C, 3 min, 61%; iv, HF–pridine, rt, 9 h, 76%.

The reason for the lack of activity of **29** as compared with taxol, and the reason for the lack of activity of oxetane ring-opened analogs, has been discussed by Snyder on the basis of a minireceptor model of the binding site for taxol on tubulin.[52] These authors note that oxetane ring-opened analogs such as **8** and **11** also lack the C-4 acetate function, which has been shown to be necessary for activity, and conclude that hydrogen bond acceptor properties and the rigidification of the taxol ring system by the oxetane ring also play a role in stabilizing the taxol–tubulin complex. The lack of activity of the thietane analog **29** is explicable because the larger sulfur atom does not fit well in the binding site. The predictions of the Snyder model were supported by the observation that the cyclopropyl derivative **30** is almost as active as taxol in a tubulin assembly assay.[53]

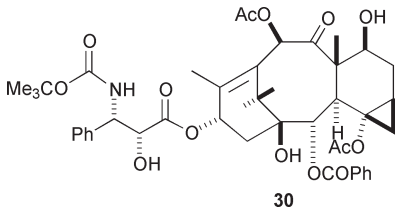

The southern hemisphere

The C-4 acetate function, or at least a C-4 acyl function, is necessary for activity, as mentioned above. Thus C-4 deacetyltaxol is significantly less active than taxol,[54] and 4-deacetoxytaxol is also much less active than taxol.[55] Some C-4 derivatives are more active than taxol, however, and the carbonate **31** is in clinical trials.[56,47]

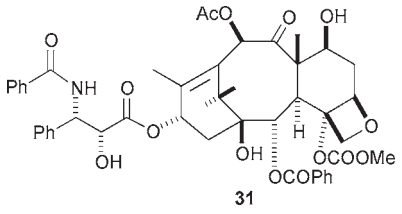

Modifications of the C-2 benzoate have yielded a number of interesting derivatives. The benzoyloxy group or a similar group is necessary for activity, since 2-debenzoyloxytaxol (**32**)[57] and 1-benzoyl-2-debenzoyloxytaxol (**33**)[58] are both inactive. Replacement of the C-2 benzoyl group with other acyl groups results in taxol analogs which can be significantly less active or more active than taxol.[59,60] Interestingly the difference in activity is modulated by the position of substituents on the benzene ring of substituted benzoyl groups; 2-*p*-azidobenzoyltaxol is essentially inactive, while 2-*m*-azidobenzoyltaxol is almost an order of magnitude more active than taxol.[59]

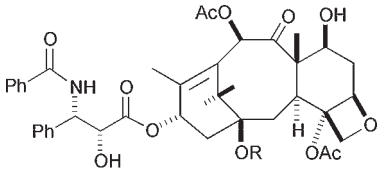

It has not proved possible to remove the C-1 hydroxy group by Barton deoxygenation or other deoxygenation methods; an attempt to do so led to formation of the C-2 deoxy product **33**.[58] Some C-1 deoxytaxol derivatives were, however, prepared from the natural product baccatin VI (**34**) by selective deacetylation and side-chain attachment (Scheme 6). The 1-deoxy-9-dihydrodocetaxel analog **35** was about one third as active as taxol in tubulin assembly and cytotoxicity assays.[61]

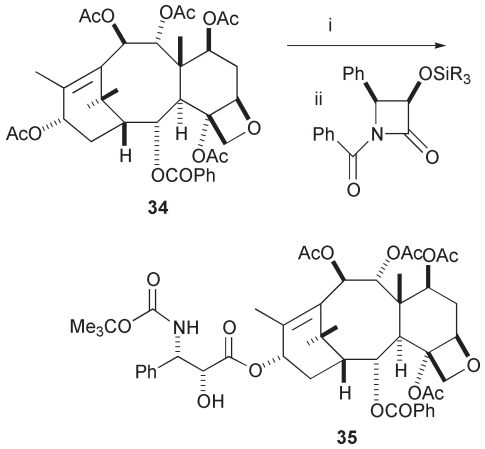

Scheme 6 *Reagents and conditions*: i, Red Al, THF, 77%; ii, NaH, THF, β-lactam, 0 °C–rt, 86%; HF–pyridine, −20 °C, 87%.

Analogs at the C-14 position have also been prepared by Ojima and Appendino from the naturally-occurring 14β-hydroxy-10-deacetylbaccatin III. The most interesting analogs have come from a series of compounds with a carbonate group linking the C-14 and C-1 hydroxy groups;[62] the derivative **36** is under development by Bayer as an orally active anticancer drug.[63]

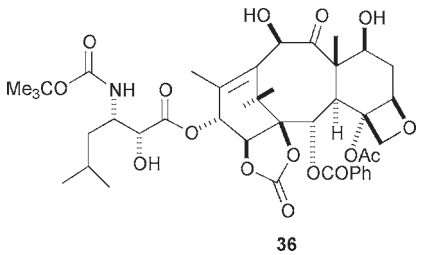

The side chain

Our work on the side chain has been concerned largely with finding direct methods for the conversion of taxol or its congener cephalomannine (**37**) into other N-acyl analogues. The initial success came with the finding that cephalomannine could be ozonized selectively in high yield to give the ketoamide **38** (Scheme 7). Acylation of **38** with a desired substituted benzoic acid gave the corresponding 2′-acyl derivative selectively, and this could be reacted with *o*-phenylenediamine under anhydrous acidic conditions to give an *N*-acyl analog of taxol. Reaction proceeds *via* the 2-aminoquinoxaline derivative **39**, which is cleaved under the acidic conditions to the free 3′-amine. This amine then undergoes a spontaneous *O* → *N* intramolecular acyl transfer reaction to give the final product **40**.[64]

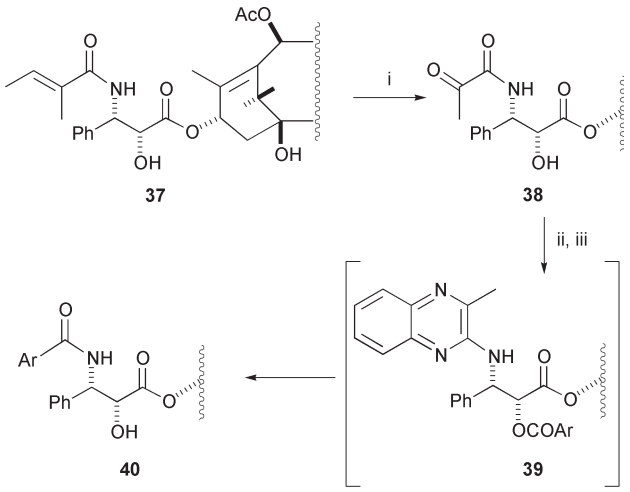

Scheme 7 *Reagents and conditions*: i, O_3, CH_2Cl_2, −78 °C, 30 min, 97%; ii, $ArCO_2OH$, DCC, 4-pyrrolidonopyridine, EtOAc, 2 h, 90%; iii, 4 Å sieves, PhH, *o*-phenylenediamine, *p*-TsOH (cat.), reflux, 12 h, 80%.

A second pathway was developed to convert taxol into docetaxel.[65] Protection of taxol as its 2′-(benzyloxycarbonyl)-7-(triethylsilyl) derivative was followed by reaction with di-*tert*-butyl dicarbonate and DMAP to give the imide **41**. Compound **41** was then converted into 10-acetyldocetaxel **42** by reaction with magnesium methoxide followed by HF–pyridine to deprotect the 7-position.

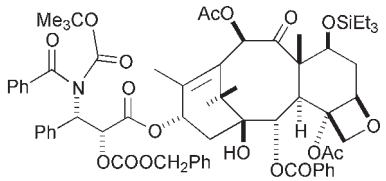

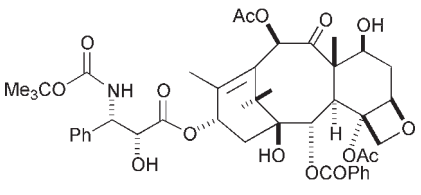

Many routes have been developed to prepare the taxol side chain and to attach it to a protected baccatin III derivative to prepare taxol or an analog thereof, and this chemistry has been reviewed.[11,66] Because of the congested position of the 13-hydroxy group of baccatin III, esterification with a simple protected taxol side chain is difficult and proceeds in only modest yield.[67] The most important synthetic methods are thus those which use a cyclically protected form of the taxol side chain, and these are the methods used commercially in the synthesis of taxol and docetaxel.

As mentioned earlier, taxol is prepared commercially by acylation of a 7-protected baccatin III derivative (**5**) with a β-lactam such as **43** (Scheme 8); the use of other β-lactams such as **44** yields docetaxel analogs.[11] The β-lactams needed for the synthesis of Scheme 8 are prepared by condensation of an enolate with an imine, but there have been many different approaches to the details of this synthesis. In Holton's original approach the β-lactam was prepared by a Staudinger reaction of acetyl glycolyl chloride with the imine from benzaldehyde and *p*-anisidine; this gave the desired *syn* lactam stereoselectively, but of course in racemic form.[11] Several enantioselective syntheses of suitably protected β-lactams have been developed, with Georg's route from Oppolzer's chiral auxiliary[68]

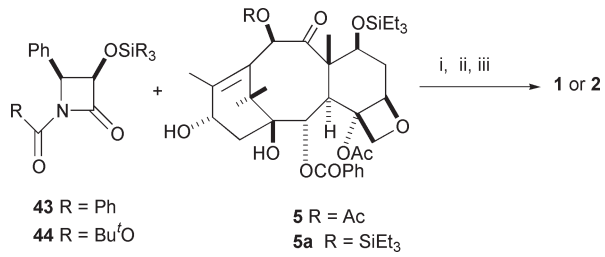

Scheme 8 *Reagents and conditions*: i, **5** (0.1 M in THF), *n*-BuLi, −45 °C; ii, **43** or **44** (0.2 M in THF), warm to 0 °C, 2 h, 95%; iii, HF–pyridine, MeCN, 98%.

(Scheme 9) and Ojima's synthesis from (1*R*,2*S*)-2-phenylcyclohexan-1-ol[69] (Scheme 10) being early and effective approaches.

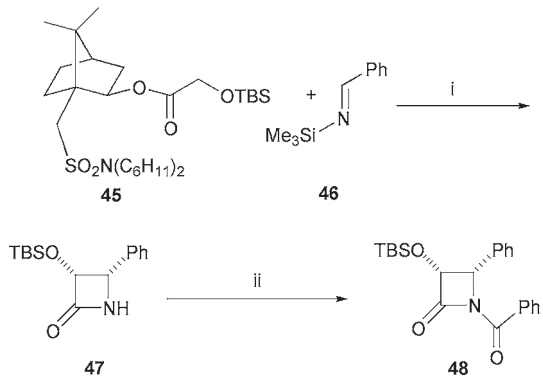

Scheme 9 *Reagents and conditions*: i, LDA, THF, 94%; ii, PhCOCl, CH_2Cl_2, Et_3N, DMAP, 96%, 93–97% ee.

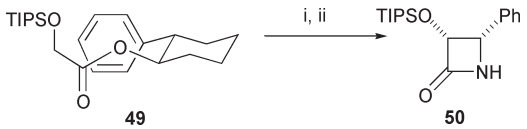

Scheme 10 *Reagents and conditions*: i, LDA; ii, PhCH=NTMS, 85%, 96% ee.

Other chiral syntheses of the β-lactam have been developed by Farina,[70] Commerçon,[71] and Fujisawa[72] from chiral imine precursors, by Holton[73] and by Palomo[74] from oxazolidinone auxiliaries, and by Lee by means of a Sharpless oxidation,[75] to name just a few. A convenient enzyme-catalyzed resolution of racemic β-lactam has also been published by Sih.[76]

The second major synthetic route is through an oxazolidine carboxylic acid intermediate. This pathway was originally developed by Commerçon and his co-workers, and is illustrated in Scheme 11 below.[77] The azido ester **51** can be prepared by

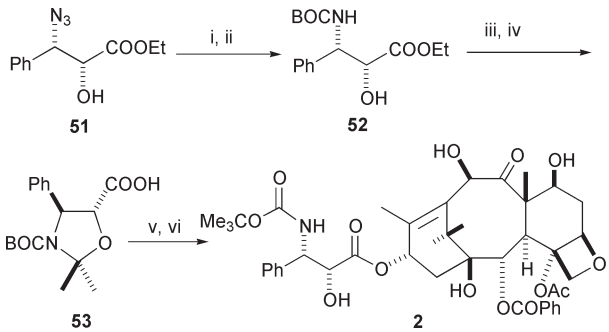

Scheme 11 *Reagents and conditions*: i, H_2, Pd/C; ii, $(BOC)_2O$, 65%; iii, $CH_2=C(OCH_3)CH_3$, PPTS; iv, LiOH, EtOH–H_2O, 99%; v, 7,10-diTroc-10-deactylbaccatin, III, DCC, DMAP, 99%; vi, HCO_2H, then $(BOC)_2O$, then Zn, AcOH, H_2O, 62%.

ring-opening of an epoxide derived from a Sharpless epoxidation,[78] by the Staudinger reaction previously mentioned,[71] or in

several other ways. Reduction and protection of **51** gave the carbamate **52**, which was converted to the oxazolidine **53** and thence to docetaxel (**2**). The weakness of the original approach lay in the deprotection and reprotection steps necessary to open the oxazolidine ring, but this weakness has been resolved in several ways. In one approach (Scheme 12) the trichloromethyl

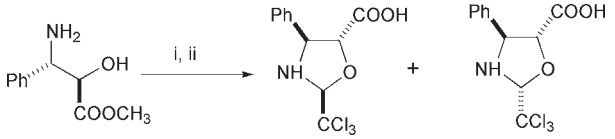

54 55 56

Scheme 12 *Reagents and conditions*: i, CCl_3CHO, PPTS; ii, LiOH, MeOH, then HCl.

oxazolidines **55** and **56** could be coupled directly with 7,10-ditrocbaccatin III without the necessity of protecting the nitrogen; the resulting coupled product was converted to docetaxel by treatment with zinc and acetic acid followed by N-acylation.[79] In a second approach from the same group it was found that the *p*-methoxybenzylidene oxazolidines **57** and **58**

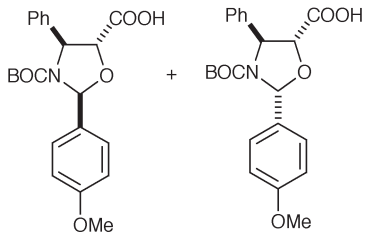

57 58

could be coupled with protected baccatin III derivatives in almost quantitative yield, and that the coupled products could then be treated with toluenesulfonic acid to remove the *p*-methoxybenzylidene group selectively;[80] this approach thus provides a very efficient route to docetaxel.

A third general approach is through an oxazoline intermediate. Coupling of the oxazoline **59** with 7-(triethylsilyl)baccatin III proceeded in excellent yield to give the coupled product **60**, which could be hydrolyzed to taxol in one step (Scheme 13).[81] The simplicity of this route has attracted several

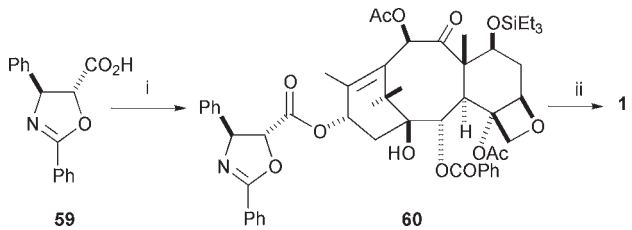

59 60

Scheme 13 *Reagents and conditions*: i, dry PhMe, 4-pyrrolidonopyridine (cat.), DCC, rt, 30 min, 95%; ii, 0.1 M HCl, 95 °C, 2 h, 75%.

syntheses of suitable oxazolines, including syntheses of racemic material from cinnamyl alcohol through addition of phenylselenyl triflate and azide ion[82,83] and a synthesis of chiral oxazolines from (L)-phenylglycine.[84] One unexpected synthesis of the oxazoline derivative **60** was derived from the dioxooxathiazolidine **61**, which gave **60** on coupling with 7-(triethylsilyl)baccatin III.[85]

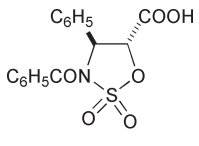

61

Many taxol analogs with modified side chains have been prepared in studies to find improved analogs of taxol. The best-known such compound is docetaxel (**2**), which was prepared early on by Potier and his colleagues and has entered clinical use.[86] The other noteworthy compound with a modified side chain is the 14β-hydroxytaxol derivative **36**, which as noted earlier is in clinical trials. The side chain of this compound differs from that of taxol by having an isobutyl group replacing the 3′-phenyl group and a *tert*-butoxycarbonyl group replacing the 3′-*N*-benzoyl group. Other analogs with modified side chains have been reviewed.[21,66]

Some taxol analogs with highly modified side chains are of interest because of the light they throw on the conformation of the side chain. Thus the methylated analog **62** is more cytotoxic than taxol to HCT116 colon carcinoma cells and has an increased binding affinity to tubulin.[87–89] Its enhanced potency may be due to a reduction in the degree of freedom of rotation of the C-2′–C-3′ bond, or possibly to an additional hydrophobic binding interaction of the methyl group with the microtubule binding site. The conformationally restricted analog **63** has

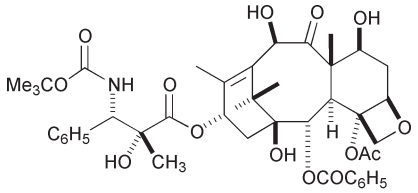

62

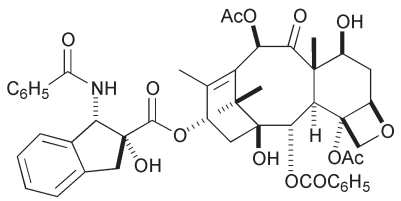

63

comparable cytotoxicity to taxol in several cell lines,[90] suggesting that the side chain may exist in an 'open' conformation rather than the hydrophobically collapsed conformation that has been proposed.[91]

The synthesis of taxol

The synthesis of taxol presented one of the more difficult challenges to synthetic chemists, both because of its complex ring system and because of its many chiral centers. It is a tribute to the current development of synthetic methodology that six independent syntheses have been achieved to date, using a variety of approaches.

Since baccatin III has been converted into taxol by many different routes, as noted earlier, a synthesis of baccatin III constitutes a synthesis of taxol. The six routes will not be discussed in detail because of space limitations, but a brief summary of each will be provided.

The first two syntheses were published essentially simultaneously in 1994 by Holton and Nicolaou. In the Holton synthesis (Scheme 14), the natural product β-patchoulene served as the starting material to generate the protected diol **64**. A clever ring-opening of the epoxide of **64** then gave the AB ring system **65**, and this was elaborated to the ABC system **67** through intermediate **66**. Final elaboration of ring D and functional group manipulations then gave baccatin III.[92]

In the Nicolaou synthesis (Scheme 15), the A and C ring precursors **68** and **69** were both made by Diels–Alder chemistry, and were then coupled by a Shapiro reaction and elaborated to the AC system **70**. A McMurry coupling of **70** generated the ABC system **71**, which was then converted to the ABCD system **72** and thence to baccatin III.[93]

The Danishefsky synthesis (Scheme 16) is the only one to date to start with a preformed D-ring. The key to the success of

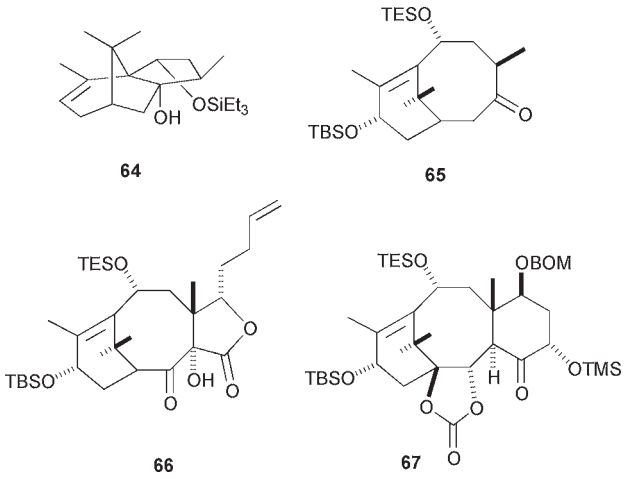

Scheme 14 The Holton synthesis.

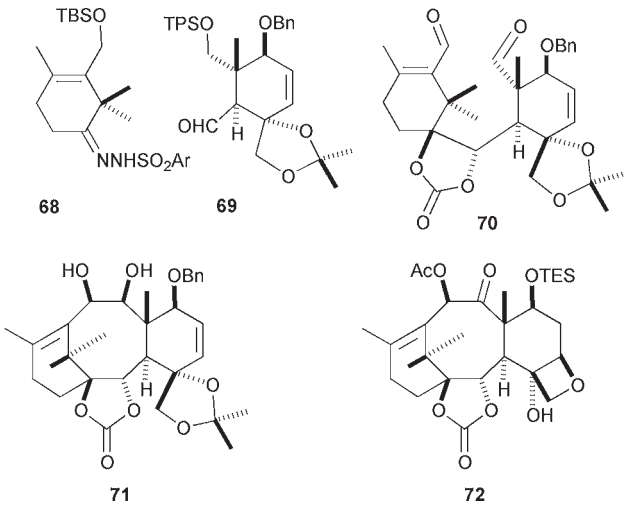

Scheme 15 The Nicolaou synthesis.

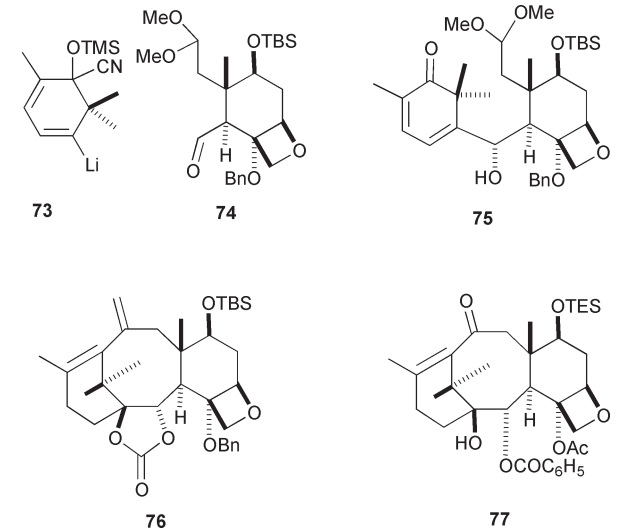

Scheme 16 The Danishevsky synthesis.

this approach was the protection of the C-4 hydroxy group as a benzyl ether rather than as an acetate, thus avoiding complications from neighbouring group participation by this group. The CD ring system **74** was prepared from the Wieland–Miescher ketone, and this was then coupled with the A-ring synthon **73** to give the A–CD unit **75**. Cyclization to the ABCD system **76** was achieved by the Heck reaction, and oxidation and functional group manipulations gave **77**, which was converted to baccatin III by appropriate oxidation chemistry.[94]

The Wender synthesis (Scheme 17), like the Holton synthesis, is of the form A → AB → ABC → ABCD, but it started

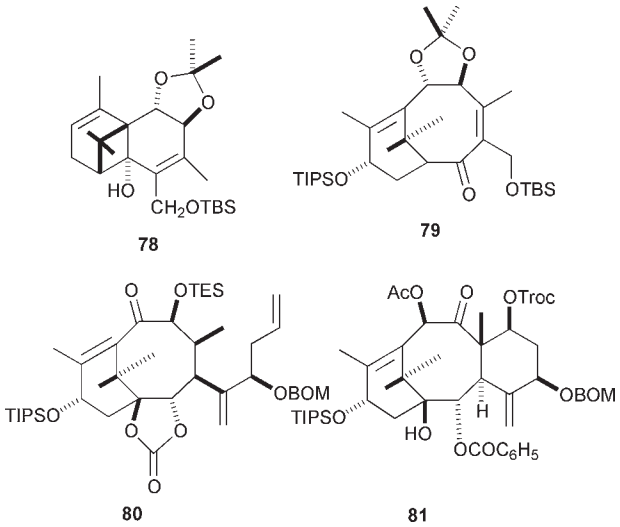

Scheme 17 The Wender synthesis.

from verbenone, which provided 10 of the 20 carbons of the baccatin III ring system. Some ingenious chemistry converted verbenone to intermediate **78**, which then underwent oxidative cleavage in a manner reminiscent of the conversion of **64** to **65** in the Holton synthesis. Intermediate **79** was then converted into **80** through elaboration of the C-3 position and aldol condensation, and the synthesis was completed by formation of the oxetane ring. The overall synthesis, at 37 steps from verbenone, is claimed to be the shortest recorded synthesis of taxol.[95]

The Kuwajima synthesis, first reported in 1998 with the full report appearing in 2000, uses the A + C → A–C → ABC → ABCD approach (Scheme 18).[96] The A-ring synthon **83** was

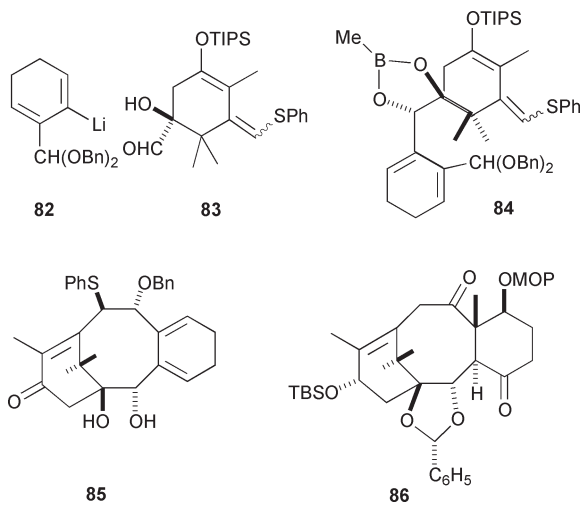

Scheme 18 The Kuwajima synthesis.

prepared in 16 steps from propargyl alcohol, and this was coupled with the C-ring synthon **82** to give the A–C adduct **84**. Adduct **84** was cyclized by a novel reaction to give **85**, and this was elaborated to **86**; the C-18 methyl group was introduced *via* a cyclopropane intermediate. Final incorporation of the oxetane ring gave baccatin III.

The final synthesis by Mukaiyama, reported in 1999 (Scheme 19), is unique in starting with the acyclic precursor **87** and cyclizing it to the stereochemically defined B-ring synthon **88**. Rings C and A (in that order) were then built onto ring B to

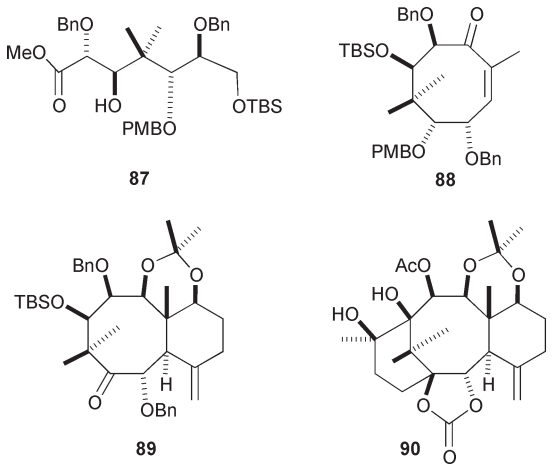

Scheme 19 The Mukaiyama synthesis.

give intermediate **89** and then **90**, and addition of ring D completed the synthesis.[97]

The bioactivity of taxol

As noted in the introduction to this review, taxol was discovered on the basis of the antileukemic and cytotoxic activities of *T. brevifolia* extracts, but its mechanism of action was found to be its ability to promote the assembly of tubulin into microtubules. In brief, taxol binds to the assembled microtubule with a stoichiometry of approximately 1 mole of taxol to 1 mole of tubulin dimer and stabilizes it to dissociation (Fig. 1). This binding occurs in the absence of any cofactors, and the resulting disruption of the equilibrium between tubulin and microtubules also disrupts cell division and ultimately leads to cell death by apoptosis.[98,99]

The binding of taxol to tubulin polymers and the associated interruption of the cell cycle was thought for a long time to be its only significant mechanism of action, but in recent years it has been increasingly clear that taxol can bring about apoptotic cell death by a second mechanism which is independent of mitotic arrest.[100,101] The protein Bcl-2 has been identified as a second taxol-binding protein[102] which undergoes dose-dependent hyperphosphorylation in the presence of taxol.[103] The situation is complex, however, since it has also been shown that Bcl-2 phosphorylation in the presence of taxol is linked to the latter's tubulin-assembly activity, and it has thus been proposed that taxol-promoted assembly of microtubules leads to Raf-1 activation and Bcl-2 phosphorylation, and thence to apoptosis.[104] The binding of taxol to tubulin is thus clearly biologically significant, and has been studied extensively by several methods. A detailed understanding of this binding has become much more achievable in recent years thanks to the work of Downing and his collaborators, who have reported the structure of tubulin at a resolution of 3.7 Å using electron crystallography on crystalline sheets formed in the presence of zinc.[105,106]

The interaction of taxol with tubulin

Several different methods have been used to study the interaction of taxol with tubulin. In studies by the photoaffinity labeling technique, various labeled taxol analogs have been used to study the location of the binding site of taxol on tubulin. Thus 3′-(*p*-azidobenzamido)taxol (**91**) photolabeled the N-terminal 31 amino acid unit of β-tubulin preferentially,[107] while 2-(*m*-azidobenzoyl)taxol (**92**) labeled a peptide containing amino acids 217–231 of β-tubulin,[108] and the photoaffinity probe **93** was shown to bind to Arg^{282} in β-tubulin.[109]

A second useful technique has been that of fluorescence spectroscopy. This technique has the significant advantage that

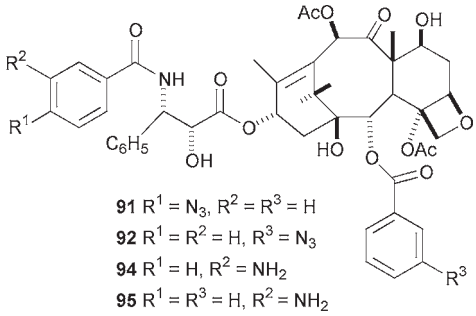

91 $R^1 = N_3$, $R^2 = R^3 = H$
92 $R^1 = R^2 = H$, $R^3 = N_3$
94 $R^1 = H$, $R^2 = NH_2$
95 $R^1 = R^3 = H$, $R^2 = NH_2$

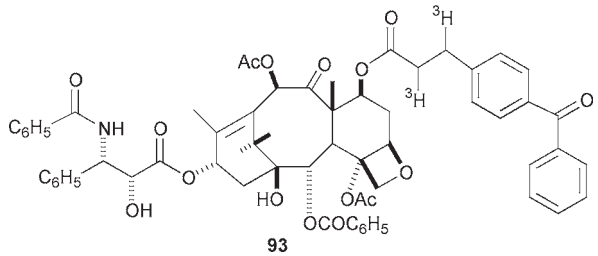

93

it is performed on systems in solution, thus avoiding potential problems with changes in shape on preparing solid samples for analysis. As one example, 2-(*m*-aminobenzoyl)taxol (**94**) gave solvent-dependent absorption and emission spectra. Using this information it was possible to show that the fluorophore binding site on the microtubule is in an environment of intermediate polarity, and also that tubulin has two binding sites for taxol, one high affinity site and one low affinity site.[110] Studies using fluorescence resonance energy transfer measurements showed that the distance between the taxol and colchicine binding sites is approximately 17 Å.[111] A recent paper describes results with the 3′-*N*-(*m*-aminobenzoyl)taxol **95**.[112] It was found that **95** bound to two types of site on the microtubules, with binding affinities of 61 nM and 3.3 μM. It bound to a single site on microtubules assembled from GDP-tubulin with a dissociation constant of 2.5 μM, and it bound to a single site on microtubules assembled from the GTP analog GMPCPP with a dissociation constant of 15 nM. It was thus proposed that although all the subunits of the microtubule at the steady state are the same 'GTP–tubulin–taxol', they are formed through two different pathways: either from taxol binding to a tubulin subunit before GTP hydrolysis (a high affinity binding) or taxol binding to a tubulin subunit after GTP hydrolysis (a low affinity binding). Studies with fluorescent taxol derivatives have also been carried out by others.[113,114]

A number of investigators have studied the NMR spectra of taxol in various solvents in an attempt to determine the solution conformation. In non-polar solvents such as chloroform taxol seems to exist primarily in a set of 'open' conformations in which the side chain is oriented away from the 2-benzoyl group,[115,116] but in polar aqueous solvents it adopts a set of 'hydrophobically collapsed' conformations in which the 3′-phenyl group is oriented towards the 2-benzoyl group.[91] Over-interpretation of these results in terms of a 'binding conformation' of taxol to tubulin is, however, dangerous, since taxol exists in chloroform (and presumably also in polar solvents) as a population of different conformations.[117] It is possible that taxol's relatively weak association with tubulin may be due in part to the presence of a large number of nonproductive conformers.

NMR studies of taxol bound to microtubules can be made using the technique of solid state magic angle spinning, and two such studies have been reported. In one study fluorine-containing taxol analogs were used to obtain an F–F distance of 6.5 Å in the difluoro analog **96**.[118,119] In the second study, internuclear distances between ^{13}C and F were obtained by the REDOR technique on the quadruply labeled analog **97**, and these results were coupled with fluorescence data to lead to the

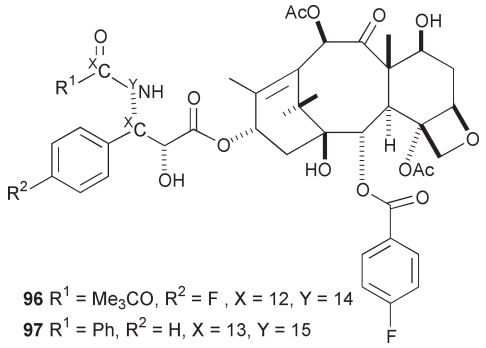

96 $R^1 = Me_3CO$, $R^2 = F$, X = 12, Y = 14
97 $R^1 = Ph$, $R^2 = H$, X = 13, Y = 15

proposal of structure **98** as the most probable conformation of taxol on tubulin.[120]

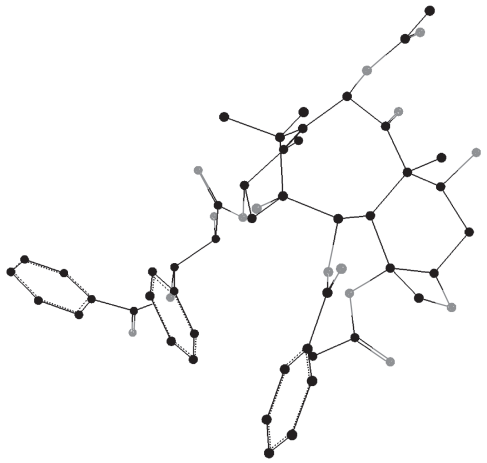

98

Taxol mimics

For many years taxol was the only compound known to promote the assembly of tubulin into microtubules, but over the past few years several other natural products have been discovered with the same or similar activity. The most important compounds of this class are the epothilones A (**99**) and B (**100**),[121,122] discodermolide (**101**),[123] and eleutherobin (**102**),[124,] but other compounds with this activity have also been discovered. These include rhazinilam,[125] which inhibits the disassembly of microtubules but has a different mechanism of action than taxol, laulimalide and isolaulimalide,[126] WS9885B,[127] and poly-isoprenylated benzophenones such as guttiferone E.[128] The naturally occurring 3(2*H*)-furanone derivative geiparvin has been found to counteract the microtubule-assembly effects of taxol, suggesting that it is a competitive inhibitor at the taxol-binding site of tubulin.[129]

The taxol pharmacophore

Much of the chemical work reported in the previous sections was carried out with a view to determining structure–activity relationships for taxol and its analogs and thus to defining the pharmacophore in chemical terms. Some of this work can be summarized as in Fig. 2 opposite, where the key structure–activity relationships of taxol are shown.

The discovery of the tubulin-assembly properties of the natural products referred to in the previous section opened up a second way of delineating the taxol pharmacophore, since comparisons could be made between the structures of taxol and of these taxol mimics. Various approaches to this important question have been made, with most studies concentrating on a

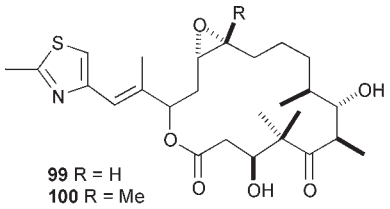

99 R = H
100 R = Me

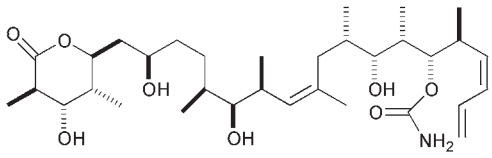

101

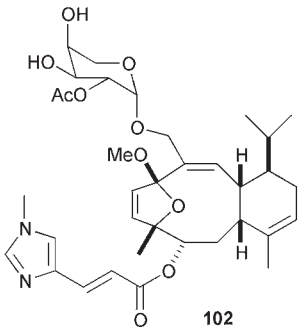

102

comparison of the structures and activities of taxol and its analogs and the epothilones.

In one approach various bridged analogs of taxol such as **103** were prepared by olefin methathesis.[130] Three related analogs

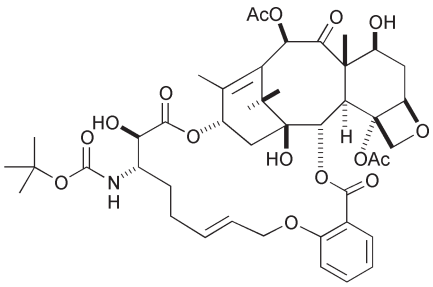

103

were found to be cytotoxic to the human breast cancer cell line MDA-435/LCC6-WT with IC_{50} values of less than 1 μM. These activities are significantly less than that of taxol in the same cell line (0.0031 μM), but the compounds also showed tubulin-assembly activity that was only only slightly less than that of taxol, so they are presumably binding to the same binding site as taxol. These data were used to support a model of the pharmacophore in which the aryl sector of epothilone overlaps the C-13 acyl side chain of taxol and in which the baccatin portion of the taxol molecule is relatively non-essential.

A second approach, developed by Giannakakou and his collaborators, was based on a comparison of the effects of taxol and various epothilone analogs on the polymerization of native tubulin and of modified tubulins carrying β-tubulin mutations near the taxol-binding site.[131] Two possible common overlaps of the epothilones and taxol were found. In the first the C-2 benzoyl group of taxol overlapped with much of the 1-methyl-2-thiazolyl side chain of the epothilones, while in the second the thiazole portion of the epothilones overlapped with the side chain of taxol.

A third approach deduced a different binding based on the finding that the side chain of taxol is not as essential for activity as was previously thought, since 2-(*m*-azidobenzoyl)baccatin III is significantly active as a promoter of tubulin polymeriza-

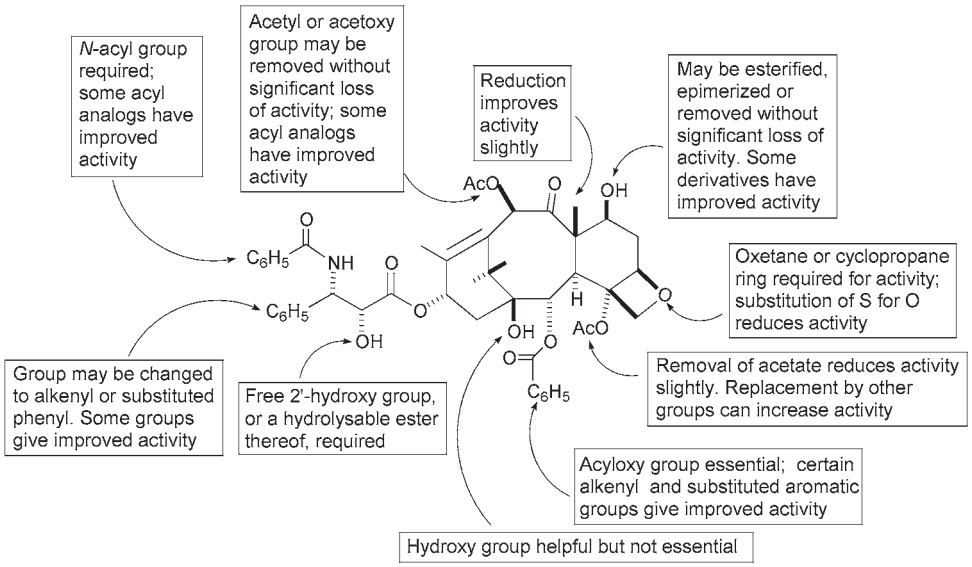

Fig. 2 Structure–activity relationships of taxol.

tion and is a competitive inhibitor of the binding of taxol to microtubules.[132] These studies led to the proposal of a pharmacophore model similar to the first binding mode of Giannakakou *et al*. A perceptive evaluation of the various models has been published.[133]

A different approach was taken by Snyder, who developed a minireceptor model for the binding of taxol and epothilone to the microtubule based on an analysis of tubulin-assembly data.[134] This model places the thiazole ring of the epothilones in the same region of the receptor as the side chain of taxol, consistent with the second binding mode of Giannakakou *et al*.[131] It also predicts much of the SAR data for taxol and the epothilones and appears to be an interesting first step towards the development of a full binding site model.

In summary, the taxol pharmacophore is still under development, with at least two rather different competing hypotheses, and further work will be needed to clarify the situation. It is reasonable however to expect that a final model of the taxol pharmacophore will eventually be developed and will be used in a predictive way to create new and improved taxol analogs.

Conclusion

The preceding review has just scratched the surface of the enormous amount of work that has been done on taxol. In addition to the chemical work summarized above, an enormous amount of work has been done on optimizing the clinical use of taxol in cancer treatment, and several recent reviews of this work have appeared.[8,135–137] The big question, of course, is what sort of difference have the taxoid drugs (taxol and docetaxel) made to cancer treatment? Have they improved cancer survival significantly? The literature on this subject is surprisingly sparse, in part because optimum combination therapies of the taxoids with other drugs are still being worked out; it is expected that such combinations will significantly enhance their use.[137] At present the taxoids are routinely used for the treatment of breast, lung, and ovarian carcinomas, and for AIDS-related Kaposi's sarcoma, and they have been called 'the most powerful compounds' (among the chemotherapeutic drugs introduced in the last decade).[135] In spite of the wide use of the taxoid drugs over the last decade, it appears that improvement in patient survival is modest at best. The greatest number of studies has been done with breast cancer, and for this disease Miller and Sledge state 'Combination therapy (of taxol or docetaxel with other drugs) has increased response rates but as yet has not improved the overall survival of patients with metastatic disease. Improved survival with the addition of paclitaxel to standard adjuvant therapy reported in a recent trial suggests the true impact of the taxanes has not yet been realized.'[137] A slightly more cautious view is expressed by Nabholtz and his colleagues 'However, the impact of taxanes on the natural history of breast cancer is yet to be defined, despite the trend of results suggesting that these agents have the potential for significant improvements in advanced and, most importantly, adjuvant therapy of breast cancer.'[136] A third evaluation was made by a panel of experts convened by the US National Institutes of Health in November 2000. The NIH Consensus Statement approved by this panel reads in part 'Currently available data are inconclusive and do not permit definitive recommendations regarding the impact of taxanes on either relapse-free or overall survival.'[138]

Although the impact of the taxoid drugs on patient survival is thus still a matter of research and debate, the outlook remains bright. The new analogs referred to earlier in this review will almost certainly improve patient survival, while increased understanding of the way taxol binds to tubulin and advances in such areas as drug targeting[139] will most probably lead to even better agents in the future. These factors thus suggest that taxol and its analogs will continue to be important cancer chemotherapeutic drugs well into the new millennium.

Acknowledgements

The work described above from the author's laboratory could not have been accomplished without a large group of talented and hard-working colleagues and collaborators, whose names are given in the references cited from my laboratory; I owe them all a great debt for their excellent work. The tubulin and REDOR studies described in the last section were done in collaboration with Dr Susan Bane (SUNY Binghamton) and Dr Jacob Schaefer (Washington University, St. Louis), and I am enormously grateful to them and their colleagues for these exciting results. I would like to pay especial tribute to Dr Matthew Suffness, who was a leading proponent of research on taxol within the National Cancer Institute, and who provided much help and encouragement to the author. His tragic early death in 1995 deprived the natural products community of a staunch supporter and a good friend. Financial support was provided by the American Cancer Society and by the National

Cancer Institute from grants CA48974, CA55731, and CA69571, and I am most grateful for this crucial component of our work.

References

1 The chemical compound **1** was named taxol by its discoverers in 1971. Unknown to them a French company had trademarked the name Taxol in the 1930's for a laxative product. Rights to this trademark were acquired by Bristol-Myers Squibb, who then applied it to their formulation of the chemical substance **1**. Because of the greater familiarity of most readers with the name taxol than the alternate USAN paclitaxel, the former will be used in this review. No infringement of the Bristol-Myers Squibb trademark is implied by this usage.
2 A. M. Thayer, *Chem. Eng. News*, 2000, **78**(45), 20.
3 M. Suffness and M. E. Wall, in *Taxol: Science and Applications*, ed. M. Suffness, CRC Press, Inc., Boca Raton, FL, 1995, p. 3.
4 M. C. Wani, H. L. Taylor, M. E. Wall, P. Coggon and A. T. McPhail, *J. Am. Chem. Soc*., 1971, **93**, 2325.
5 P. B. Schiff, J. Fant and S. B. Horwitz, *Nature*, 1979, **277**, 665.
6 W. P. McGuire, E. K. Rowinsky, N. B. Rosenshein, F. C. Grumbine, D. S. Ettinger, D. K. Armstrong and R. C. Donehower, *Ann. Intern. Med*., 1989, **111**, 273.
7 F. A. Holmes, R. S. Walters, R. L. Theriault, A. D. Forman, L. K. Newton, M. N. Raber, A. U. Buzdar, D. K. Frye and G. N. Hortobagyi, *J. Nat. Cancer Inst*., 1991, **83**, 1797.
8 J. Crown and M. O'Leary, *Lancet*, 2000, **355**, 1176.
9 M. Chase, *The Wall Street Journal*, 1991, **117**(69), 1.
10 G. Chauviere, D. Guénard, F. Picot, V. Senilh and P. Potier, *Acad. Sci. Paris, Serie II*, 1981, **293**, 501.
11 R. A. Holton, R. J. Biediger and P. D. Boatman, in *Taxol®: Science and Applications*, ed. M. Suffness, CRC Press, Boca Raton, FL, 1995, p. 97.
12 R. N. Patel, *Ann. Rev. Microbiol*., 1998, **98**, 361
13 M. Seki, C. Ohzora, M. Takeda and S. Furusaki, *Biotechnol. Bioengl*., 1997, **53**, 214.
14 J. Y. Li, R. S. Sidhu, E. J. Ford, D. M. Long, W. M. Hess and G. A. Strobel, *J. Ind. Microbiol. Biotechnol*., 1998, **20**, 259.
15 A. M. Hoffman, M. Ross, K. Weigandt, H. Gulati and W. Khan, Book of Abstracts, 219th ACS National Meeting, San Francisco, CA, March 26–30, 2000. Abstract Biol-127.
16 M. Suffness, ed., *Taxol®: Science and Applications*, CRC Press, Boca Raton, FL, 1995.
17 G. I. Georg, T. T. Chen, I. Ojima and D. M. Vyas (ed.), *Taxane Anticancer Agents*, ACS Symposium Series 583, American Chemical Society, Washington, DC, 1995.
18 W. P. McGuire and E. K. Rowinsky (ed.), *Paclitaxel in Cancer Treatment*, Dekker, New York, 1995.
19 V. Farina (ed.), *The Chemistry and Pharmacology of Taxol and its Derivatives*, Elsevier, New York, 1995.
20 D. G. I. Kingston, A. A. Molinero and J. M. Rimoldi, in *Progress in the Chemistry of Organic Natural Products*, ed. W. Herz, G. W. Kirby, R. E. Moore, W. Steglich and C. Tamm, Springer-Verlag, New York, 1993, p. 1.
21 G. I. Georg, T. C. Boge, Z. S. Cheruvallath, J. S. Clowers, G. C. B. Harriman, M. Hepperle and H. Park, in *The Medicinal Chemistry of Taxol*, ed. M. Suffness, Boca Raton, FL, 1995.
22 S. Lin and I. Ojima, *Expert Opin. Ther. Patents*, 2000, **10**, 1.
23 I. Ojima, S. D. Kuduk and S. Chakravarty, *Adv. Med. Chem*., 1999, **4**, 69.
24 D. G. I. Kingston, P. G. Jagtap, H. Yuan and L. Samala, in *Progress in the Chemistry of Organic Natural Products*, ed. W. Herz, G. W. Kirby, R. E. Moore, W. Steglich and C. Tamm, Springer-Verlag, New York, 2001, in press.
25 J. N. Baxter, B. Lythgoe, B. Scales, R. M. Scrowston and S. Trippett, *J. Chem. Soc*., 1962, 2964.
26 P. H. G. Wiegerinck, L. Fluks, J. B. Hammink, S. J. E. Mulders, F. M. H. de Groot, H. L. M. van Rozendaal and H. W. Scheeren, *J. Org. Chem*., 1996, **61**, 7092.
27 H. Poujol, A. A. Mourabit, A. Ahond, C. Poupat and P. Potier, *Tetrahedron*, 1997, **53**, 12 575.
28 R. N. Saicic and R. Matovic, *J. Chem. Soc., Perkin Trans. 1*, 2000, 59.
29 W. Mellado, N. F. Magri, D. G. I. Kingston, R. Garcia-Arenas, G. A. Orr and S. B. Horwitz, *Biochem. Biophys. Res. Commun*., 1984, **124**, 329.
30 N. F. Magri and D. G. I. Kingston, *J. Org. Chem*., 1986, **51**, 797.
31 N. F. Magri, D. G. I. Kingston, C. Jitrangsri and T. Piccariello, *J. Org. Chem*., 1986, **51**, 3239.
32 F. M. F. Chen and N. L. Benoiton, *Can. J. Chem*., 1977, **55**, 1433
33 G. Samaranayake, N. F. Magri, C. Jitrangsri and D. G. I. Kingston, *J. Org. Chem*., 1991, **56**, 5114.
34 G. Samaranayake, K. A. Neidigh and D. G. I. Kingston, *J. Nat. Prod*., 1993, **56**, 884.
35 G. C. B. Harriman, R. K. Jalluri, G. L. Grunewald, D. G. Vander Velde and G. I. Georg, *Tetrahedron Lett*., 1995, **36**, 8909.
36 R. C. Kelly, N. A. Wicnienski, I. Gebhard, S. J. Qualls, F. Han, P. J. Dobrowolski, E. G. Nidy and R. A. Johnson, *J. Am. Chem. Soc*., 1996, **118**, 919.
37 K. Uoto, I. Mitsui, H. Terasawa and T. Soga, *Bioorg. Med. Chem. Lett*., 1997, **7**, 2991.
38 R. A. Johnson, E. G. Nidy, P. J. Dobrowolski, I. Gebhard, S. J. Qualls, N. A. Wicnienski and R. C. Kelly, *Tetrahedron Lett*., 1994, **35**, 7893.
39 Q. Y. Zheng, L. G. Darbie, X. Cheng and C. K. Murray, *Tetrahedron Lett*., 1995, **36**, 2001.
40 A. G. Chaudhary and D. G. I. Kingston, *Tetrahedron Lett*., 1993, **34**, 4921.
41 R. A. Holton, C. Somoza and K.-B. Chai, *Tetrahedron Lett*., 1994, **35**, 1665.
42 G. I. Georg and Z. S. Cheruvallath, *J. Org. Chem*., 1994, **59**, 4015.
43 G. I. Georg, Y. Liu, S. M. Ali, T. C. Boge, J. Zygmunt and R. H. Himes, 219th ACS National Meeting, March 26–30, San Francisco, CA, 2000, Abstr. MEDI 72.
44 I. Ojima, J. C. Slater, E. Michaud, S. C. Kuduk, P.-Y. Bounaud, P. Vrignaud, M.-C. Bissery, J. M. Veith, P. Pera and R. J. Bernacki, *J. Med. Chem*., 1996, **39**, 3889.
45 A. G. Chaudhary, J. M. Rimoldi and D. G. I. Kingston, *J. Org. Chem*., 1993, **58**, 3798.
46 S.-H. Chen, S. Huang, J. Kant, C. Fairchild, J. Wei and V. Farina, *J. Org. Chem*., 1993, **58**, 5028.
47 J. F. Kadow, S.-H. Chen, P. Dextraze, C. R. Fairchild, J. Golik, S. B. Hansel, K. A. Johnston, R. A. Kramer, F. Y. Lee, B. H. Long, C. Ouellet, R. K. Perrone, W. C. Rose, G. E. Schulze, M. Xue, J.-M. Wei, M. D. Wittman, H. Wong, J. J. K. Wright, M. E. Zoeckler and D. M. Vyas, 219th ACS National Meeting, San Francisco, CA, 2001, Abstr. MEDI 298.
48 X. Liang, D. G. I. Kingston, C. M. Lin and E. Hamel, *Tetrahedron Lett*., 1995, **36**, 2901.
49 X. Liang, D. G. I. Kingston, B. H. Long, C. A. Fairchild and K. A. Johnston, *Tetrahedron*, 1997, **53**, 3441.
50 H. Yuan and D. G. I. Kingston, *Tetrahedron Lett*., 1998, **39**, 4967.
51 A. A. L. Gunatilaka, F. D. Ramdayal, M. H. Sarragiotto, D. G. I. Kingston, D. L. Sackett and E. Hamel, *J. Org. Chem*., 1999, **64**, 2694.
52 M. Wang, B. Cornett, J. Nettles, D. C. Liotta and J. P. Snyder, *J. Org. Chem*., 2000, **65**, 1059.
53 J. Dubois, S. Thoret, F. Guéritte and D. Guénard, *Tetrahedron Lett*., 2000, **41**, 3331.
54 K. A. Neidigh, M. M. Gharpure, J. M. Rimoldi, D. G. I. Kingston, Y. Q. Jiang and E. Hamel, *Tetrahedron Lett*., 1994, **35**, 6839.
55 M. D. Chordia, A. G. Chaudhary, D. G. I. Kingston, Y. Q. Jiang and E. Hamel, *Tetrahedron Lett*., 1994, **35**, 6843.
56 S.-H. Chen, J.-M. Wei, B. H. Long, C. A. Fairchild, J. Carboni, S. W. Mamber, W. C. Rose, K. Johnston, A. M. Casazza, J. F. Kadow, V. Farina, D. Vyas and T. W. Doyle, *Bioorg. Med. Chem. Lett*., 1995, **5**, 2741.
57 S.-H. Chen, J.-M. Wei and V. Farina, *Tetrahedron Lett*., 1993, **34**, 3205.
58 A. G. Chaudhary, M. D. Chordia and D. G. I. Kingston, *J. Org. Chem*., 1995, **60**, 3260.
59 (*a*) A. G. Chaudhary, M. M. Gharpure, J. M. Rimoldi, M. D. Chordia, A. A. L. Gunatilaka, D. G. I. Kingston, S. Grover, C. M. Lin and E. Hamel, *J. Am. Chem. Soc*., 1994, **116**, 4097; (*b*) D. G. I. Kingston, A. G. Chaudhary, M. D. Chordia, M. Gharpure, A. A. L. Gunatilaka, P. I. Higgs, J. M. Rimoldi, L. Samala, P. G. Jagtap, P. Giannakakou, Y. Q. Jiang, C. M. Lin, E. Hamel, B. H. Long, C. R. Fairchild and K. A. Johnston, *J. Med. Chem*., 1998, **41**, 3715.
60 (*a*) G. I. Georg, S. M. Ali, T. C. Boge, A. Datta, L. Falborg, H. Park, M. Mejillano and R. H. Himes, *Bioorg. Med. Chem. Lett*., 1995, **5**, 259; (*b*) K. C. Nicolaou, J. Renaud, P. G. Nantermet, E. A. Couladouros, R. K. Guy and W. Wrasidlo, *J. Am. Chem. Soc*., 1995, **117**, 2409.
61 D. G. I. Kingston, M. D. Chordia and P. G. Jagtap, *J. Org. Chem*., 1999, **64**, 1814.
62 I. Ojima, Y. H. Park, C.-M. Sun, I. Fenoglio, G. Appendino, P. Pera and R. J. Bernacki, *J. Med. Chem*., 1994, **37**, 1408.
63 M. I. Nicoletti, T. Colombo, C. Rossi, C. Monardo, S. Stura, M. Zucchetti, A. Riva, P. Morazzoni, M. B. Donati, E. Bombardelli, M. D'Incalci and R. Giavazzi, *Cancer Res*., 2000, **60**, 842.
64 A. A. L. Gunatilaka, M. D. Chordia and D. G. I. Kingston, *J. Org. Chem*., 1997, **62**, 3775.

65 P. G. Jagtap and D. G. I. Kingston, *Tetrahedron Lett*., 1999, **40**, 189.
66 P. G. M. Wuts, *Curr. Opin. Drug Disc. Devel*., 1998, **1**, 329.
67 J.-N. Denis, A. E. Greene, D. Guénard, F. Guéritte-Voegelein, L. Mangatal and P. Potier, *J. Am. Chem. Soc*., 1988, **110**, 5917.
68 G. I. Georg, Z. S. Cheruvallath, G. C. B. Harriman, M. Hepperle and H. Park, *Bioorg. Med. Chem. Lett*., 1993, **3**, 2467.
69 I. Ojima, I. Habus, M. Zhao, M. Zucco, Y. H. Park, C. M. Sun and T. Brigaud, *Tetrahedron*, 1992, **48**, 6985.
70 V. Farina, S. I. Hauck and D. G. Walker, *Synlett*, 1992, **1**, 761.
71 J. D. Bourzat and A. Commerçon, *Tetrahedron Lett*., 1993, **34**, 6049.
72 M. Shimizu, T. Ishida and T. Fujisawa, *Chem. Lett*., 1994, 1403.
73 R. A. Holton and J. H. Liu, *Bioorg. Med. Chem. Lett*., 1993, **3**, 2475.
74 C. Palomo, J. M. Aizpurua, J. I. Miranda, A. Mielgo and J. M. Odriozola, *Tetrahedron Lett*., 1993, **34**, 6325.
75 C. E. Song, S. W. Lee, E. J. Roh, S.-G. Lee and W.-K. Lee, *Tetrahedron: Asymmetry*, 1998, **9**, 983.
76 R. Brieva, J. Z. Crich and C. J. Sih, *J. Org. Chem*., 1993, **58**, 1068.
77 A. Commerçon, D. Bezard, F. Bernard and J. D. Bourzat, *Tetrahedron Lett*., 1992, **33**, 5185.
78 J.-N. Denis, A. E. Greene, A. A. Serra and M.-J. Luche, *J. Org. Chem*., 1986, **51**, 46.
79 E. Didier, E. Fouque and A. Commerçon, *Tetrahedron Lett*., 1994, **35**, 3063.
80 E. Didier, E. Fouque, I. Taillepied and A. Commerçon, *Tetrahedron Lett*., 1994, **35**, 2349.
81 D. G. I. Kingston, A. G. Chaudhary, A. A. L. Gunatilaka and M. L. Middleton, *Tetrahedron Lett*., 1994, **35**, 4483.
82 M. Tiecco, L. Testaferri, A. Temperini, L. Bagnoli, F. Marini and C. Santi, *Syn. Comm*., 1998, **28**, 2167.
83 M. Tiecco, L. Testaferri, A. Temperini, F. Marini, L. Bagnoli and C. Santi, *Synth. Commun*., 1999, **29**, 1773.
84 K.-Y. Lee, Y.-H. Kim, M.-S. Park and W.-H. Ham, *Tetrahedron Lett*., 1998, **39**, 8129.
85 E. Baloglu and D. G. I. Kingston, *J. Nat. Prod*., 1999, **62**, 1068.
86 D. Guénard, F. Guéritte-Voegelein and P. Potier, *Acc. Chem. Res*., 1993, **26**, 160.
87 J.-N. Denis, A. Fkyerat, Y. Gimbert, C. Coutterez, P. Mantellier, S. Jost and A. E. Greene, *J. Chem. Soc., Perkin Trans. 1*, 1995, 1811.
88 J. Kant, W. S. Schwartz, C. Fairchild, Q. Gao, S. Huang, B. H. Long, J. F. Kadow, D. R. Langley, V. Farina and D. Vyas, *Tetrahedron Lett*., 1996, **37**, 6495.
89 I. Ojima, T. Wang and F. Delaloge, *Tetrahedron Lett*., 1998, **39**, 3663.
90 L. Barboni, C. Lambertucci, R. Ballini, G. Appendino and E. Bombardelli, *Tetrahedron Lett*., 1998, **39**, 7177.
91 D. G. Vander Velde, G. I. Georg, G. L. Grunewald, C. W. Gunn and L. A. Mitscher, *J. Am. Chem. Soc*., 1993, **115**, 11 650.
92 (*a*) R. A. Holton, C. Somoza, H.-B. Kim, F. Liang, R. J. Biediger, P. D. Boatman, M. Shindo, C. C. Smith, S. Kim, H. Nadizadeh, Y. Suzuki, C. Tao, P. Vu, S. Tang, P. Zhang, K. K. Murthi, L. N. Gentile and J. H. Liu, *J. Am. Chem. Soc*., 1994, **116**, 1597; (*b*) R. A. Holton, H.-B. Kim, C. Somoza, F. Liang, R. J. Biediger, P. D. Boatman, M. Shindo, C. C. Smith, S. Kim, H. Nadizadeh, Y. Suzuki, C. Tao, P. Vu, S. Tang, P. Zhang, K. K. Murthi, L. N. Gentile and J. H. Liu, *J. Am. Chem. Soc*., 1994, **116**, 1599.
93 K. C. Nicolaou, Z. Yang, J. J. Liu, H. Ueno, P. G. Nantermet, R. K. Guy, C. F. Claiborne, J. Renaud, E. A. Couladouros, K. Paulvannan and E. J. Sorensen, *Nature*, 1994, **367**, 630.
94 S. J. Danishefsky, J. J. Masters, W. B. Young, J. T. Link, L. B. Snyder, T. V. Magee, D. K. Jung, R. C. A. Isaacs, W. G. Bornmann, C. A. Alaimo, C. A. Coburn and M. J. Di Grandi, *J. Am. Chem. Soc*., 1996, **118**, 2843.
95 (*a*) P. A. Wender, N. F. Badham, S. P. Conway, P. E. Floreancig, T. E. Glass, C. Granicher, J. B. Houze, J. Janichen, D. Lee, D. G. Marquess, P. L. McGrane, W. Meng, T. P. Mucciaro, M. Muhlebach, M. G. Natchus, H. Paulsen, D. B. Rawlins, J. Satkofsky, A. J. Shuker, J. C. Sutton, R. E. Taylor and K. Tommoka, *J. Am. Chem. Soc*., 1997, **119**, 2755; (*b*) P. A. Wender, N. F. Badham, S. P. Conway, P. E. Floreancig, T. E. Glass, J. B. Houze, N. E. Krauss, D. Lee, D. G. Marquess, P. L. McGrane, W. Meng, M. G. Natchus, A. J. Shuker, J. C. Sutton and R. E. Taylor, *J. Am. Chem. Soc*., 1997, **119**, 2757.
96 H. Kusama, R. Hara, S. Kawahara, T. Nishimori, H. Kashima, N. Nakamura, K. Morihira and I. Kuwajima, *J. Am. Chem. Soc*., 2000, **122**, 3811.
97 T. Mukaiyama, I. Shiina, H. Iwadare, M. Saitoh, T. Nishimura, N. Ohkawa, H. Sakoh, K. Nishimura, Y.-I. Tani, M. Hasegawa, K. Yamada and K. Saitoh, *Chem. Eur. J*., 1999, **5**, 121.
98 J. J. Manfredi and S. B. Horwitz, *Pharmacol. Ther*., 1984, **25**, 83.
99 S. B. Horwitz, M. W. Davidson and R. A. Holton, *Trends Pharmacol. Sci*., 1992, **13**, 134.
100 W. Fan, *Biochem. Pharmacol*., 1999, **57**, 1215.
101 T.-H. Wang, H.-S. Wang and Y.-K. Soong, *Cancer (N. Y.)*, 2000, **88**, 2619.
102 D. J. Rodi, R. W. Janes, H. J. Sanganee, R. A. Holton, B. A. Wallace and L. Makowski, *J. Mol. Biol*., 1999, **285**, 197.
103 C. D. Scatena, Z. A. Stewart, D. Mays, L. J. Tang, C. J. Keefer, S. D. Leach and J. A. Pietenpol, *J. Biol. Chem*., 1998, **273**, 30 777.
104 M. V. Blagosklonny, P. Giannakakou, W. S. El-Deiry, D. G. I. Kingston, P. I. Higgs, L. Neckers and T. Fojo, *Cancer Res*., 1997, **37**, 130.
105 E. Nogales, S. G. Wolf and K. H. Downing, *J. Struct. Biol*., 1997, **118**, 119.
106 E. Nogales, M. Whittaker, R. A. Milligan and K. H. Downing, *Cell*, 1999, **96**, 79.
107 S. Rao, N. E. Krauss, J. M. Heerding, C. S. Swindell, I. Ringel, G. A. Orr and S. B. Horwitz, *J. Biol. Chem*., 1994, **269**, 3132.
108 S. Rao, G. A. Orr, A. G. Chaudhary, D. G. I. Kingston and S. B. Horwitz, *J. Biol. Chem*., 1995, **270**, 20 235.
109 S. Rao, L. He, S. Chakravarty, I. Ojima, G. A. Orr and S. B. Horwitz, *J. Biol. Chem*., 1999, **274**, 37 990.
110 Y. Han, A. G. Ghaudhary, M. D. Chordia, D. L. Sackett, B. Perez-Ramirez, D. G. I. Kingston and S. Bane, *Biochemistry*, 1996, **35**, 14 173.
111 Y. Han, A. G. Malak, A. G. Chaudhary, M. D. Chordia, D. G. I. Kingston and S. Bane, *Biochemistry*, 1998, **37**, 6636.
112 Y. Li, J. Edsall, R. P. G. Jagtap, D. G. I. Kingston and S. Bane, *Biochemistry*, 2000, **39**, 616.
113 S. Sengupta, T. C. Boge, Y. Liu, M. Hepperle, G. I. Georg and R. H. Himes, *Biochemistry*, 1997, **36**, 5179.
114 J. F. Diaz, R. Strobe, Y. Engelborghs, A. A. Souto and J. M. Andreu, *J. Biol. Chem*., 2000, **275**, 26 265.
115 H. J. Williams, A. I. Scott, R. A. Dieden, C. S. Swindell, L. E. Chirlian, M. M. Francl, J. M. Heerding and N. E. Krauss, *Tetrahedron*, 1993, **49**, 6545.
116 H. J. Williams, A. I. Scott, R. A. Dieden, C. S. Swindell, L. E. Chirlian, M. M. Francl, J. M. Heerding and N. E. Krauss, *Can. J. Chem*., 1994, **72**, 252.
117 J. P. Snyder, N. Nevins, D. O. Cicero and J. Jansen, *J. Am. Chem. Soc*., 2000, **122**, 724.
118 I. Ojima, T. Inoue, J. C. Slater, S. Lin, S. D. Kuduk, S. Chakravarty, J. J. Walsh, T. Cresteil, B. Monsarrat, P. Pera and R. J. Bernacki, in *Asymmetric Fluoroorganic Chemistry: Synthesis, Applications and Future Development*, ed. P. V. Ramachandran, American Chemical Society, Washington, DC, 2000, p. 158.
119 I. Ojima, T. Inoue and S. Chakravarty, *J. Fluorine Chem*., 1999, **97**, 3.
120 Y. Li, B. Poliks, L. Cegelski, M. Poliks, Z. Cryczynski, G. Piszczek, P. Jagtap, G. D. R. Studelska, D. G. I. Kingston, J. Schaefer and S. Bane, *Biochemistry*, 2000, **39**, 281.
121 D. M. Bollag, P. A. McQueney, J. Zhu, O. Hensens, L. Koupal, J. Liesch, M. Goetz, E. Lazarides and C. M. Woods, *Cancer Res*., 1995, **55**, 2325.
122 R. J. Kowalski, P. Giannakakou and E. Hamel, *J. Biol. Chem*., 1997, **272**, 2534.
123 E. ter Haar, R. J. Kowalski, E. Hamel, C. M. Lin, R. E. Longley, S. P. Gunasekera, H. S. Rosenkranz and B. W. Day, *Biochemistry*, 1996, **35**, 243.
124 T. Lindel, P. R. Jensen, W. Fenical, B. H. Long, A. M. Casazza, J. Carboni and C. R. Fairchild, *J. Am. Chem. Soc*., 1997, **119**, 8744.
125 C. Dupont, D. Guénard, L. Tchertanov, S. Thoret and F. Guéritte, *Bioorg. Med. Chem*., 1999, **7**, 2961.
126 S. L. Mooberry, G. Tien, A. H. Hernandez, A. Plubrukarn and B. S. Davidson, *Cancer Res*., 1999, **59**, 653.
127 C. D. Vanderwal, D. A. Vosburg, S. Weiler and E. J. Sorensen, *Org. Lett*., 1999, **1**, 645.
128 D. Rouz, H. A. Hadi, S. Thoret, D. Guénard, O. Thoison, M. Päis and T. Sévenet, *J. Nat. Prod*., 2000, **63**, 1070.
129 A. Miglietta, C. Bocca, E. Gadoni, L. Gabriel, A. Rampa, A. Bisi, P. Valenti and P. Da Re, *Anti-Cancer Drug Design*, 1996, **11**, 35.
130 I. Ojima, S. Lin, T. Inoue, M. L. Miller, C. P. Borella, X. Geng and J. J. Walsh, *J. Am. Chem. Soc*., 2000, **122**, 5343.
131 P. Giannakakou, R. Gussio, E. Nogales, K. H. Downing, D. Zaharevitz, B. Bollbuck, G. Poy, D. Sackett, K. C. Nicolaou and T. Fojo, *Proc. Natl. Acad. Sci. USA*, 2000, **97**, 2904.
132 L. He, P. G. Jagtap, D. G. I. Kingston, H.-J. Shen, G. A. Orr and S. B. Horwitz, *Biochemistry*, 2000, **39**, 3972.
133 B. W. Day, *Trends Pharmacol. Sci*., 2000, **21**, 321.
134 M. Wang, X. Xia, Y. Kim, D. Hwang, J. M. Jansen, M. Botta, D. C. Liotta and J. P. Snyder, *Org. Lett*., 1999, **1**, 43.

135 E. A. Eisenhauer and J. B. Vermorken, *Drugs*, 1998, **55**, 5.
136 J.-M. Nabholtz, K. Tonkin, M. Smylie, H.-J. Au, M.-A. Lindsay and J. Mackey, *Expert Opin. Pharmacother.*, 2000, **1**, 187.
137 K. D. Miller and G. W. Sledge, Jr., *Cancer Invest.*, 1999, **17**, 121.
138 http://odp.od.nih.gov/consensus/cons/114/114_statement.htm
139 S. Lin and I. Ojima, *Expert Opin. Ther. Pat.*, 2000, **10**, 869.

CHEMCOMM
Communication
www.rsc.org/chemcomm

A highly selective host–guest system formed and stabilized due to concerted halogen···oxygen and C-H···O non-bonded interactions:† X-ray structures of racemic 1,2,3,4,5-penta-*O*-benzoyl-6-*O*-tosyl *myo*-inositol–dihalomethane (CH_2X_2, X = Cl and Br) inclusion complexes

Kana M. Sureshan,[a] Rajesh G. Gonnade,[b] Mysore S. Shashidhar*[a] Vedavati G. Puranik[b] and Mohan M. Bhadbhade*[b]

[a] *Division of Organic Chemistry (Synthesis), National Chemical Laboratory, Pune 41008, India*
[b] *Division of Physical Chemistry, National Chemical Laboratory, Pune 411008, India. E-mail: mohanb@sil.ncl.res.in*

Received (in Cambridge, UK) 13th February 2001, Accepted 28th March 2001
First published as an Advance Article on the web 20th April 2001

***myo*-Inositol derivative as a host assembles around crystallographic 2-fold axis selectively accommodating dihalomethanes as guests having a C_2 symmetry; formation of highly stable host–guest complexes is attributed to halogen···oxygen and C–H···O interactions.**

An intermolecular recognition process is a result of a number of non-covalent interactions that exist between the molecules.[1] Recently much effort has been concentrated upon recognizing and analyzing the nature of such interactions due to the demands of designing the functional molecular assemblies[2] which span wide areas—from molecular selectivity in separation techniques to drug–receptor interactions in drug design and to material science. In this paper we report a serendipitous discovery of highly selective encapsulation of dihalomethanes by the *myo*-inositol derivative **2**‡ (Scheme 1) due to halogen···oxygen interactions.

The compound **2**, which resisted crystallization in most of the common solvents like chloroform, ethyl acetate, carbon tetrachloride *etc*. readily formed good quality crystals when crystallized from dichloromethane. We further noted that this 'spontaneous' crystallization of **2** occurred only from dihalomethanes, (CH_2X_2, X = Cl, Br and I). So much was the dependence on CH_2X_2 in crystal formation that even their presence at 2.5% (v/v) along with other solvents induced crystallization of **2**. The presence of dihalomethanes in these crystals was revealed by elemental analysis§ and ^{1}H NMR spectroscopy. The DSC¶ of **3** and **4** indicated that dihalomethanes were retained in crystals close to their melting points (183–192 °C for **3** and 186–188 °C for **4**), suggesting a strong association of the guest molecules with the host.‖ The X-ray structures** of two inclusion complexes of **2** with dihalomethanes revealed that halogen···oxygen interactions, or what is termed as 'halogen bonding',[3] played a vital role in forming a stable host–guest assembly, a bonding recognized as a strong driving force in formation of co-crystals and controlling the construction of supramolecular architectures. It is thought that the remarkable specificity for dihalomethanes in the formation of crystals with **2** will have applications in the separation of halocarbon compounds, through the design of suitable organic hosts such as compound **2**.

View of the molecular packing of **3** down the *c*-axis (Fig. 1) clearly reveal the thorough open channels of dimensions ~6.5 × 4.5 Å formed by the host assembly containing the guest molecules. Amongst all possible host–guest interactions, notable ones are halogen···oxygen short contacts (Fig. 2) in **3** (Cl···O = 2.968 (9) Å) as well as in **4** (Br···O = 3.336 (7) Å) which are shorter than the sum of their van der Waal's radii (3.20 and 3.35 Å respectively). The short halogen···oxygen distances were analyzed earlier[4] to understand the exact nature and favored geometry of their interactions.[5] Although C–X···O linear geometry is suggested for stronger interactions, the present structure shows some deviation from linearity (139.5° (4) and 142.1° (2) for **3** and **4** respectively).[6] Even then it is striking that this 'halogen bonding' has induced the assembly of the host. However, solvent retention is a multi-point recognition phenomenon[7] as evidenced by other weak interactions between the CH_2X_2 guest molecules and the host, which certainly aid in the host–guest stabilization. For instance, there are C–H···O contacts[8] between the CH_2 hydrogens of the guest with the carbonyl oxygens O2 and O4 of the host in both **3** and **4**. The halogen atoms are also involved in weak C–H···X interactions with the phenyl C–H groups of the neighbouring assembly.

It is noteworthy that solvents CH_2Cl_2, CH_2Br_2 and CH_2I_2 readily form crystals with **2,** whereas halogenated solvents

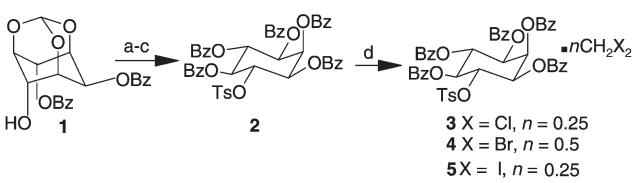

Scheme 1 (a) Pyridine–tosyl chloride, reflux 24 h; (b) pTsA·H_2O–methanol 60 °C, 24 h; (c) pyridine–benzoyl chloride, 0 °C to rt, 24 h, 89% (for 3 steps); (d) crystallization from CH_2X_2 or $CHCl_3$–CH_2X_2 mixture.

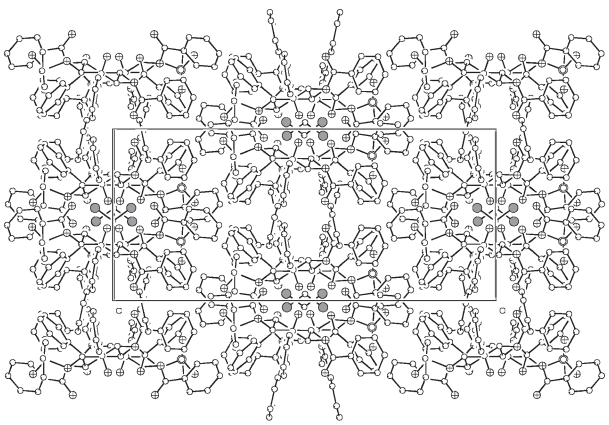

Fig. 1 Molecular packing of **3** viewed down the *c*-axis showing the open framework containing CH_2Cl_2 guest molecules. H-atoms are omitted for clarity. Atom code: ● chlorine, ⊕ oxygen, ○ carbon and ◎ sulfur.

† Electronic supplementary information (ESI) available: a table of intermolecular interactions. See http://www.rsc.org/suppdata/cc/b1/b101394g/

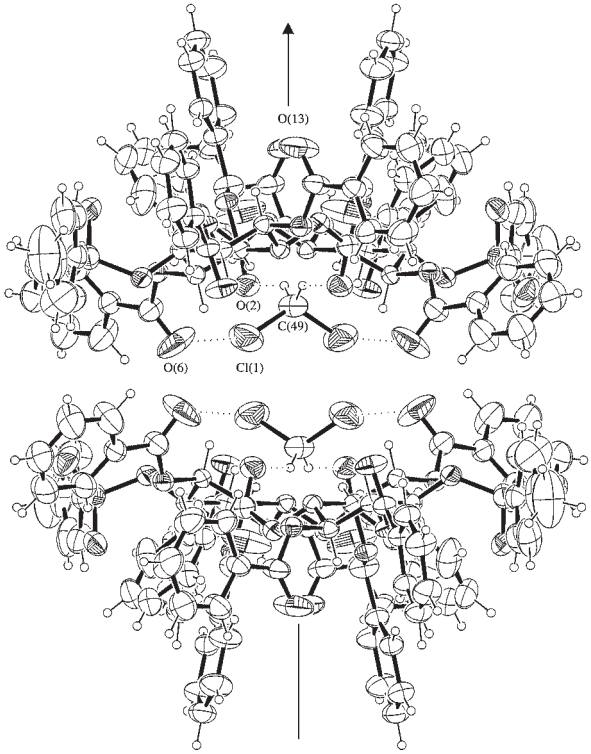

Fig. 2 Formation of an elliptical open channel with the guests in **3**; twofold related host–guest association showing Cl···O and significant C–H···O interactions. Ellipsoids are drawn at the 30% probability level for non-H atoms.

which lack C_2 symmetry (chloroform, methyl iodide) do not yield crystals. Clathrating hosts with open channel formation around the two fold symmetry axis have been reported,[9] but the inclusion of the guest was found to be non-specific, accommodating a wide range of guest molecules; whereas the host **2** is highly specific to dihalomethanes which occupy a crystallographic two-fold axis. But there seems to be a restriction on the steric size of the guest—only the guests having a C_2 symmetry of molecular diameter of ~6.0 Å such as CH_2X_2 are accommodated (to produce crystals), while the higher homologues like 1,2-dichloroethane or 1,2-dibromoethane are not. We believe that the guest induces the assembling process by bringing the second molecule of the host (related by a crystallographic two-fold axis) around it (Fig. 2) making strong halogen···oxygen contacts. The other half of the cavity is completed by the two host molecules related by a center of symmetry (Fig. 2). These two halves are cemented to each other by significant C–H···O interactions to complete the elliptical open framework. All the hydrophobic phenyl groups point outward while the hydrophilic carbonyl oxygens point toward the center of the cavity.

In summary, a novel host–guest assembly held together, notably by halogen···oxygen non-bonded contacts, has been prepared and characterized. Study of such systems, which lack polar groups (OH, COOH, NH_2 *etc*.) is essential to further extend our knowledge of weak interactions among molecules, which play a vital role in crystal growth, enzyme–substrate recognition and ligand–receptor binding.[10] The present adducts re-emphasize the role of 'halogen bonding' in self-assembly and molecular recognition. The work presented shows there is potential for the exploitation of these interactions in the separation of traces of dihalomethanes from other organic compounds or solvents.

This work was supported by the Department of Science and Technology, New Delhi. K. M. S. is the recipient of a Senior Research Fellowship from CSIR, New Delhi. We gratefully acknowledge Dr Michael Ruff from Bruker-axs for the X-ray data on SMART-1000 CCD diffractometer. We are highly indebted to Professors K. Venkatesan and Gautam Desiraju for their valuable constructive criticism and suggestions in this work.

Notes and references

‡ All the compounds in Scheme 1 are racemic. The dibenzoate **1** was prepared as reported earlier.[11] All the compounds gave satisfactory spectroscopic data (IR, ^{1}H and ^{13}C NMR) and elemental analysis.

§ Analytical data for **3**: calc. for $C_{48}H_{38}O_{13}S{\cdot}0.25CH_2Cl_2$: C, 66.13%; H 4.43%; found: C, 66.16%; H, 4.43%. **4**: calc. for $C_{48}H_{38}O_{13}S{\cdot}0.50CH_2Br_2$: C, 61.84%; H, 4.17%; found: C, 62.38%; H, 4.16%. **5**: Calc. for $C_{48}H_{38}O_{13}S{\cdot}0.25CH_2I_2$: C, 62.87%, H, 4.32%. found: C, 62.73%, H, 4.45%.

¶ The DSC was performed on a Perkin-Elmer DSC 7 instrument in open aluminium crucibles, sample wt. 5 mg (approx), heating rate of 10 K min^{-1}, and nitrogen as purge gas for all the measurements.

‖ Melting point of **2** without dihalomethane was 240–241 °C.

** Crystals of **3** and **4** are isomorphous. *Crystal data* for **3**: $C_{48}H_{38}O_{13}S{\cdot}0.25\ CH_2Cl_2$, M = 876.08, crystal dimensions 0.20 × 0.19 × 0.11 mm, monoclinic, space group $C2/c$, a = 26.771(4), b = 11.608(3), c = 30.783(6) Å, β = 105.176(6)°, V = 9232(3) Å^3, Z = 8, D_c = 1.261 g cm^{-3}, μ = 0.162 mm^{-1}, 22 898 reflection measured, 6618 unique [$I > 2\sigma(I)$], R value 0.056 (R_w = 0.1280). *Crystal data* for **4**: $C_{48}H_{38}O_{13}S{\cdot}0.50CH_2Br_2$, M = 941.77 crystal dimensions 0.24 × 0.22 × 0.16 mm, monoclinic, space group $C2/c$, a = 26.927(17), b = 11.716(8), c = 30.874(2) Å, β = 105.998(10)°, V = 9362.7(11) Å^3, Z = 8, D_c = 1.336 g cm^{-3}, μ(Mo-Kα) = 0.986 mm^{-1}, 26 695 reflections measured, 6718 unique [$I > 2\sigma(I)$], R value 0.0664 (R_w = 0.2172). Data of both the compound were collected on a Bruker SMART 1000 diffractometer (CCD) (Mo-Kα, λ = 0.71073 Å) at T = 293(2) K. All the data were corrected for Lorentzian, polarisation and absorption effects. SHELX-97[12] was used for structure solution and full-matrix least squares refinement on F^2. Hydrogen atoms were included in the refinement as per the riding model. CCDC 147891 and 147892. See http://www.rsc.org/suppdata/cc/b1/b101394g/ for crystallographic data in .cif and other electronic formats.

1 J.-M. Lehn, *Supramolecular Chemistry: Concepts and Perspectives*, VCH Verlag, Weinheim, 1995; J. Rebec, Jr., *Acc. Chem. Res*., 1999, **32**, 278; M. R. Caira and Nassimbeni, *Comprehensive Supramolecular Chemistry*, ed. J. L. Atwood, J. E. D. Davies, D. D. MacNicol and F. Vogtle, Elsevier, Oxford, 1996, vol. 6, pp. 825–850.
2 G. R. Desiraju, *Comprehensive Supramolecular Chemistry*, ed. J. L. Atwood, J. E. D. Davies, D. D. MacNicol and F. Vogtle, Elsevier, Oxford, 1996, vol. 6, pp. 1–22.
3 E. Corradi, S. V. Meilee, M. T. Messina, P. Metrangolo and G. Resnati, *Angew. Chem., Int. Ed*., 2000, **39**, 1782.
4 O. Hassel and C. Romming, *Quart. Rev. Chem. Soc*., 1962, **16**, 1; H. A. Bent, *Chem. Rev*., 1968, 587; J. D. Dunitz, *Mol. Cryst. Liq. Cryst*., 1996, **279**, 209; M. N. Sabesan and K. Venkatesan, *Acta Crystallogr., Sect. B*, 1971, **27**, 986; S. Barriga, L. S. Konstantinova, C. E. Marcos, O. A. Rakitin, C. W. Rees, T. Torroba, A. J. P. White and J. Williams, *J. Chem. Soc., Perkin Trans. 1*, 1999, 2237; F. H. Allen, J. P. M. Lommerse, V. J. Hoy, J. A. K. Howard and G. R. Desiraju, *Acta Crystallogr., Sect. B*, 1997, **53**, 1006; N. Ramasubbu, R. Parthasarathy and P. Murray-Rust, *J. Am. Chem. Soc*., 1986, **108**, 4308.
5 J. P. M. Lommerse, A. J. Stone, R. Taylor and F. H. Allen, *J. Am. Chem. Soc*., 1996, **118**, 3108.
6 P. Murray-Rust and W. D. S Motherwell, *J. Am. Chem. Soc*., 1979, **101**, 4374.
7 A. Nangia and G. R. Desiraju, *Chem. Commun*., 1999, 605.
8 G. R. Desiraju, *Acc. Chem. Res*., 1996, **29**, 441.
9 N. Z. Huang and T. C. W. Mak, *J. Chem. Soc., Chem. Commun*., 1982, 543.
10 V. Cody and P. Murray-Rust, *J. Mol. Struct*., 1984, **112**, 189.
11 T. Banerjee and M. S. Shashidhar, *Tetrahedron Lett*., 1994, **35**, 8053.
12 G. M. Sheldrick, SHELXL-97 program for crystal structure solution and refinement, University of Göttingen, Germany, 1997.

CHEMCOMM Communication
www.rsc.org/chemcomm

Photonic transduction of electrochemically-triggered redox-functions of polyaniline films using surface plasmon resonance spectroscopy

Vladimir Chegel,† Oleg Raitman, Eugenii Katz, Rachel Gabai and Itamar Willner*

Institute of Chemistry, The Hebrew University of Jerusalem, The Farkas Center for Light-Induced Processes, Jerusalem 91904, Israel. E-mail: willnea@vms.huji.ac.il

Received (in Cambridge, UK) 7th February 2001, Accepted 22nd March 2001
First published as an Advance Article on the web 20th April 2001

Surface plasmon resonance (SPR) spectroscopy is used to follow the swelling and shrinking processes of a polyaniline redox-active polymer; SPR provides a reading signal for the electrochemical stimuli that activate the polymer.

Phase transitions of polymers and signal-triggered swelling processes of polymers are subjects of extensive research efforts.[1,2] Volume changes of polymers are triggered by temperature,[3] pH,[4] solvent composition[5] and light.[6] Electrochemical activation of redox-polymers provides a means to stimulate swelling.[7] Recently the stress induced on an AFM cantilever as a result of the redox-activation of polyaniline was used to develop an electrofueled microdevice[8] that may act as a micro-robot or micro-pump. Surface plasmon resonance (SPR) has been recently applied to study interfacial phenomena associated with electrochemical transformations of thin films at electrode surfaces.[9] Here we describe the SPR transduction of the redox-activation of polyaniline films, and the accompanying swelling and shrinking processes using *in situ* electrochemical/SPR measurements.

Polyaniline was generated on a Au-covered glass-slide (*ca.* 0.64 cm^2) used for SPR-measurements (Bio-Suplar 2, Analytical μ-Systems, Germany) by the electropolymerization of aniline, 0.1 M, in an electrolyte solution composed of H_2SO_4, 0.1 M, and Na_2SO_4, 0.5 M, (applied potential 0.8 V *vs.* Ag-wire quasi-reference electrode for 5 s).[10] The resulting film obtained upon passing charge of 9.7 mC, that corresponds to the formation of *ca.* 10 μg of the polymer, was washed with background solution composed of H_2SO_4, 0.1 M, and Na_2SO_4, 0.5 M, to exclude from the cell the residual monomer. The polyanilin film can be reversibly oxidized and reduced, eqn. (1), and the polymer exists in the oxidized positively charged state, $(An^{2+})_n$, and reduced neutral state, $(An)_n$, at the potential 0.4 and 0.0 V, respectively.[12]

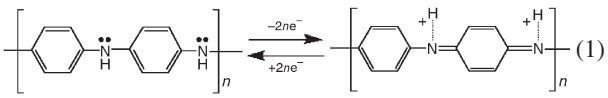

(1)

Fig. 1, inset (I), curve (x), shows the SPR spectrum of the bare Au-surface. The polyaniline film, $(An)_n$ was equilibrated at the potential 0.0 V in the electrolyte solution prior the SPR-measurements. Fig. 1, inset (I), curve (y), shows the spectrum of the polyaniline film assembled on the Au-surface immediately after the application of the potential corresponding to 0.4 V on the electrode resulting in the oxidation of the polymer layer. While the dots correspond to the experimental points, the solid line corresponds to the theoretical fitting[11,12] of the data according to the Fresnel equation. The derived film thickness corresponds to *ca.* 150 nm. Fig. 1(A), curves (a–e), shows the SPR spectra at the potential of 0.4 V, conditions that retain the polymer in its oxidized state, $(An^{2+})_n$. These spectra are time-dependent and a decrease of the reflectance minimum is observed, because of the polymer swelling.[13] The spectrum recorded 10 min after the application of the oxidizing potential of 0.4 V, Fig. 1(A), curve (e), corresponds to a polymer thickness of *ca.* 180 nm. Thus, the swelling process occurring at 0.4 V results in the increase of the polymer thickness by *ca.* 30 nm. It should be noted that the similar thickness change was observed by AFM upon the electrochemically-induced shrinking–swelling process of a polyaniline layer.[14] Fig. 1(A), curve (f), was recorded under conditions where the applied potential

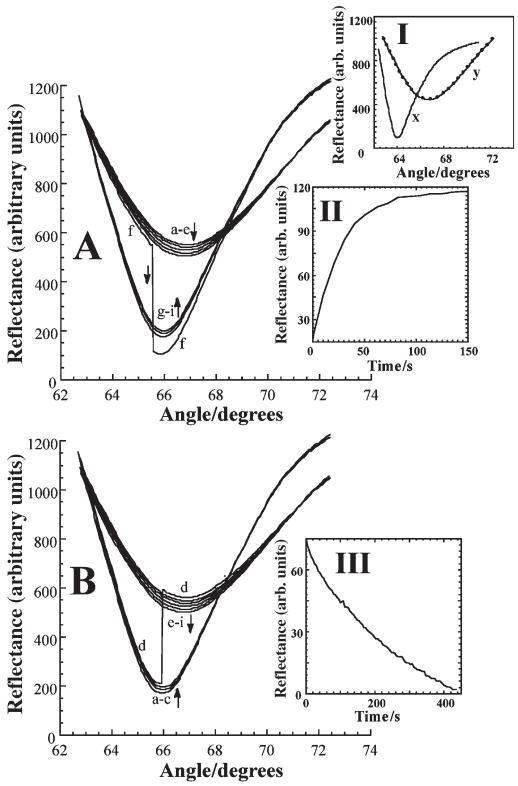

Fig. 1 SPR spectra measured for the polyaniline-modified Au-surface upon electrochemically-induced shrinking and swelling processes. (A) The polymer was equilibrated at 0.0 V for 5 min prior to the measurements. (a–e) The spectra measured after the potential was changed to 0.4 V. (f) The spectrum measured during the potential change to 0.0 V. (g–i) The spectra measured after the potential was changed to 0.0 V. (B) The polymer was equilibrated at 0.4 V prior to the measurements. (a–c) The spectra measured after the potential was altered to 0.0 V. (d) The spectra measured during the potential change to 0.4 V. (e–i) The spectra measured after the potential was changed to 0.4 V. Inset I: (x) The SPR spectrum for the bare Au-surface and (y) the SPR spectrum for the oxidized polymer film measured at 0.4 V (the dots show selected experimental points and the solid line is the best theoretical fit). Inset II: Time-dependent reflectance changes measured at a fixed angle of incidence (θ = 65°) immediately after the applied potential was changed from 0.4 to 0.0 V. Inset III: Time-dependent reflectance changes measured with the fixed angle of incidence (θ = 65°) immediately after the applied potential was changed from 0.0 to 0.4 V. All SPR measurements were performed in the background solution: H_2SO_4, 0.1 M, and Na_2SO_4, 0.5 M.

† Visiting scientist from the Institute of Physics of Semiconductors, National Academy of Sciences of Ukraine, Prospect Nauki, 45, Kiev, Ukraine.

DOI: 10.1039/b101243f

on the polymer-modified electrode was suddenly altered from 0.4 to 0.0 V. This spectrum shows the transition from the oxidized state of the polymer, $(An^{2+})_n$ to the reduced state, $(An)_n$. The instantaneous change in the spectrum mainly originates from the change of the refractive-index of the polymer as a result of its reduction. The subsequent SPR spectrum recorded at the potential of 0.0 V, Fig. 1(A), curve (g), shows a noticeable increase of the reflectance minimum after which only minor changes of the spectra were observed, Fig. 1(A), curves (h) and (i). These spectra changes can be attributed to the shrinking process of the reduced polymer and they reach a constant value after *ca*. 4 min. The main decrease in the polymer thickness as a result of the shrinking process occurs in the first minute after the potential change to 0.0 V, faster than the time-interval required to record the complete SPR spectrum. Thus, measurements with a fixed angle of incidence (θ = 65°) were applied to evaluate the kinetics of the shrinking process upon the potential change from 0.4 to 0.0 V, Fig. 1, inset II. The experimental results reveal a biexponential kinetics with rate constants corresponding to 9×10^{-3} and 5×10^{-4} s^{-1}. The fast and slow components exhibit the same population. The fast shrinking component may be attributed to the collapse of the hydrophobic polymer chains, formed upon reduction to a metastable configuration. The slow component is then attributed to the formation of an organized, densely-packed structure that expels the residual water. Similar biexponential dynamic changes were observed upon the compression of proteins.[15]

The second experiment was started by equilibration of the polymer-modified electrode at 0.4 V when the polymer is oxidized. The first SPR spectrum was recorded after the potential was shifted to 0.0 V, Fig. 1(B), curve (a). It should be noted that the time-scale of the measurements did not allow us to register the SPR spectrum characteristic of the metastable shrunken polymer film. The secondary slow kinetics of the shrinking process at the potential of 0.0 V is clearly visible in the SPR spectra, Fig. 1(B), curves (a–c). These changes reach a constant value after *ca*. 3 min. During the registration of the next spectrum, Fig. 1(B), curve (d), the applied potential was changed from 0.0 to 0.4 V. The immediate change of the SPR spectrum originates mainly from the change of the refractive-index of the polymer as a result of its oxidation. Continuous SPR measurements at the potential 0.4 V show the decrease of the polymer layer reflectance corresponding to the slow swelling process, Fig. 1(B), curves (d–i). The kinetics of the swelling process was recorded at a fixed angle of incidence (θ = 65°), Fig. 1, inset III. The kinetics of the swelling process corresponds to a first-order monoexponential process with a rate constant of 3×10^{-4} s^{-1}. It should be noted that upon redox-induced swelling and shrinking of the polymer film the uptake and release of counter-anions may change the conductivity of the film and thus may alter the reflectance. For redox-active films that lack swelling, *e.g*. Prussian blue, the reflectance changes due to ion transport are, however, minute.

The sequence of potential steps applied in the two experiments results in similar changes in the thickness values of the reduced or oxidized polymer films independently on the sequence of the reduction or oxidation steps that lead to a shrunken or swollen polymer film, respectively. Thus, the reversible transformation of the polymer layer between shrunken and swollen states with different thicknesses is possible. However, the complete shrinking–swelling cycle proceeds on the time scale of minutes. Realizing that the refractive index of the polymer undergoes very fast changes upon the reduction–oxidation process, one may use the polyaniline film as an interface for the reversible SPR transduction of electronic signals that actuate the polymer. Fig. 2(A) shows the chronoamperometric transients upon oxidation (0.4 V) and reduction (0.0 V) of the polyaniline layer. In this experiment, a potential-step that oxidizes $(An)_n$ to $(An^{2+})_n$ is applied. The polymer is not allowed to swell, and the opposite reductive potential-step is applied to generate the metastable $(An)_n$ that is oxidized again before it undergoes shrinking. By the cyclic application of the oxidative and reductive potential steps, the reversible SPR transduction of the polymer state is accomplished, Fig. 2(B).

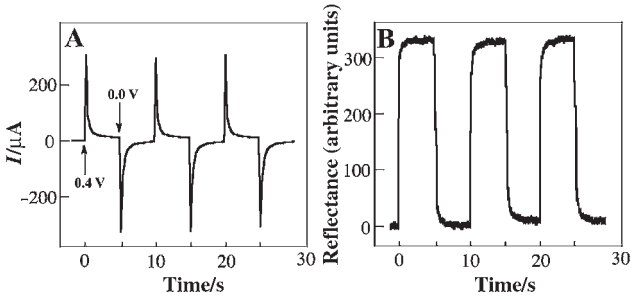

Fig. 2 (A) Multi-potential step chronoamperometric measurements corresponding to the oxidative and reductive transformations of the polyaniline layer. (B) Time-dependent reflectance changes measured at a fixed angle of incidence (θ = 65°) upon the multi-potential step experiment. The arrows show the time of the application of the oxidative (0.4 V) and reductive (0.0 V) potentials. The chronoamperometric and *in situ* SPR measurements were performed in a background electrolyte solution composed of H_2SO_4, 0.1 M, and Na_2SO_4, 0.5 M.

In conclusion, we have applied surface plasmon resonance spectroscopy for following the swelling and shrinking processes of a polyaniline redox-active film. SPR provides a reading signal for the electrochemical stimuli that activate the polymer.

Parts of this study were supported by the National Science Foundation Administered by the Israel Academy of Sciences and Humanities. The support of the Max-Planck Research Award for International Cooperation (I. W.) is gratefully acknowledged.

Notes and references

1 H. G. Schild, *Prog. Polym. Sci*., 1992, **17**, 163.
2 K. Dusek and D. Patterson, *J. Polym. Sci*., 1968, **A-2-6**, 1209.
3 A. Suzuki and T. Tanaka, *Nature*, 1990, **346**, 345.
4 M. Annaka and T. Tanaka, *Nature*, 1992, **355**, 430.
5 Y. Hirokawa and T. Tanaka, *J. Chem. Phys*., 1984, **81**, 6379.
6 (*a*) T. A. Smith, J. Hotta, K. Sasaki, H. Masuhara and Y. Itoh, *J. Phys. Chem*., 1999, **103**, 1660; (*b*) S. Juodkazis, N. Mukai, R. Wakaki, A. Yamaguchi, S. Matsuo and H. Misawa, *Nature*, 2000, **408**, 178.
7 (*a*) L. J. Kepley and A. J. Bard, *J. Electrochem. Soc*., 1995, **142**, 4129; (*b*) M. F. Suarez and R. G. Compton, *J. Electroanal. Chem*., 1999, **462**, 211.
8 R. Gabai, M. Lahav, E. Katz, I. Willner, C Durcan and M. Welland, submitted for publication.
9 (*a*) R. Georgiadis, K. A. Peterlinz, J. R. Rahn, A. W. Peterson and J. H. Grassi, *Langmuir*, 2000, **16**, 6759; (*b*) S. Koide, Y. Iwasaki, T. Horiuchi, O. Niwa, E. Tamiya and K. Yokoyama, *Chem. Commun*., 2000, 741.
10 (*a*) E. M. Genies and C. Tsintavis, *J. Electroanal. Chem*., 1985, **195**, 109; (*b*) M. K. Ram, M. Salerno, M. Adami, P. Faraci and C. Nicolini, *Langmuir*, 1999, **15**, 1252.
11 G. V. Beketov, Y. M. Shirshov, O. V. Shynkarenko and V. I. Chegel, *Sens. Actuators B*, 1998, **48**, 432.
12 The experimental SPR spectra of the polymer layer in the reduced and oxidized state were fitted to the theoretical curves based on five-phase Fresnel calculations using the Neelder–Mid algorithm of minimization. The computer fitting of the SPR spectra was performed primarily for the reduced state of the polyaniline layer using the known refractive index, n = 1.4, λ = 670 nm, (D. Mo, Y. Y. Lin, J. H. Tan, Z. X. Yu, G. Z. Zhou, K. C. Gong, G. P. Zhang and X.-F. He, *Thin Solid Films*, 1993, **234**, 468). The complex refractive-index of the oxidized state, $(An^{2+})_n$, was then calculated (n_{re} = 1.39, n_{im} = 0.46) by assuming the same polymer thickness immediately after the polyaniline film oxidation. The polymer film thickness in the oxidized state after the complete swelling was derived using the calculated values of the complex refractive index.
13 R. J. Green, S. Corneillie, J. Davis, M. C. Davies, C. J. Roberts, E. Schacht, S. J. B. Tendler and P. M. Williams, *Langmuir*, 2000, **16**, 2744.
14 R. Nyffenegger, E. Ammann, H. Siegenthaler, R. Kötz and O. Haas, *Electrochim. Acta*, 1995, **40**, 1411.
15 E. Zahavy, S. Rubin and I. Willner, *J. Chem. Soc., Chem. Commun*., 1993, 1753.

CHEMCOMM Communication
www.rsc.org/chemcomm

A novel group of allenic hydrocarbons from five Australian (Melolonthine) beetles†

Mary T. Fletcher,[a] Matthew J. McGrath,[a] Wilfried A. König,[b] Christopher J. Moore,[c] Bronwen W. Cribb,[d] Peter G. Allsopp[e] and William Kitching*[a]

[a] *Department of Chemistry, University of Queensland, Brisbane, Australia. E-mail: kitching@chemistry.uq.edu.au; Fax: +61 7 3365 4299; Tel: +61 7 3365 3925*
[b] *Institut für Organische Chemie, Universität Hamburg, Hamburg, Germany*
[c] *Department of Primary Industries, Brisbane, Australia*
[d] *Department of Zoology and Entomology, University of Queensland, Brisbane, Australia*
[e] *Bureau of Sugar Experiment Stations, Bundaberg, Australia*

Received (in Cambridge, UK) 26th February 2001, Accepted 28th March 2001
First published as an Advance Article on the web 20th April 2001

Allenic hydrocarbons, previously unknown as a molecular class from insects, are represented by $CH_3(CH_2)_n$-CH=•=CH-$(CH_2)_7CH_3$ (n = 11–15, 17, 19) in several Australian melolonthine scarab beetles and with demonstrated (*R*)-chirality when n = 11 and 13.

Melolonthine scarabs are pests of field crops and pastures,[1] and we have undertaken studies of the chemistry of certain sugarcane scarabs from north-eastern Australia. Cuticular hydrocarbons[2] from female adults were of surprisingly limited constitutional variation. In *Antitrogus consanguineus*, one component represents (GC analysis) *ca*. 50% of the cuticular hydrocarbons and this appeared to be a C-25 hydrocarbon with a molecular ion *m*/*z* 348 ($C_{25}H_{48}$), confirmed by GCMS-CI analysis. A minor component was the bis-homologue $C_{27}H_{52}$ (M^+, 376). On this basis, both incorporated two degrees of unsaturation.

A methoxymercuration–reductive demercuration ($NaBH_4$) protocol was conducted to locate the sites of unsaturation, with the resulting methyl ether groups guiding the mass spectral fragmentations.[3] This reaction provided a mixture of several mono- and bis-methyl ethers with the two most abundant bis-methyl ethers exhibiting identical mass spectra. These were deduced to be stereoisomers of 9,11-dimethoxypentacosane **1** on the basis of their fragmentations (Scheme 1). Two further components were similarly deduced to be mixtures of stereoisomers of 11-methoxypentacos-9-ene **2** and 9-methoxypentacos-10-ene **3**, resulting from initial mono-methoxymercuration and then reduction. This indicated that the C-25 hydrocarbon was $\Delta^{9,10}$-pentacosadiene **4** (Scheme 1). GC-MS analyses of the methyl ethers resulting from $NaBD_4$ reduction support these conclusions. In the case of bis-ethers **1**, two deuterium atoms were incorporated (*e*.*g*. M-15 at *m*/*z* 399 from *m*/*z* 397) but the ions at *m*/*z* 241 and 157 were unchanged. This confirms that both Hg atoms became attached to the central carbon of the allene (*i*.*e*. C-10), so that on reduction 10-$^2H_2$-**1** was formed.

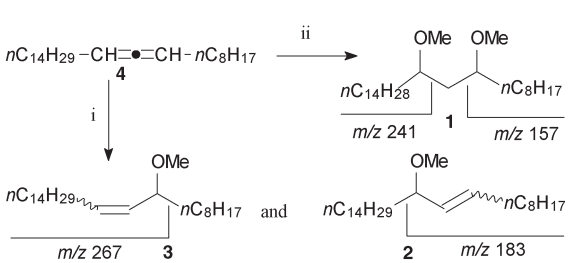

Scheme 1 *Reagents and conditions*: i, $Hg(OAc)_2$–MeOH then $NaBH_4$; ii, as for i (double addition/reduction).

† Electronic supplementary information (ESI) available: analytical data for **4**, **5**, **6** and **9**, and proposed McLafferty rearrangements for **4**. See http://www.rsc.org/suppdata/cc/b1/b101801i/

Similarly the minor C-27 component was concluded to be $\Delta^{9,10}$-heptacosadiene **5**, based on the formation of two isomers of 9,11-dimethoxyheptacosane, and also 9-methoxyheptacos-10-ene and 11-methoxyheptacos-9-ene. A more varied mixture of regioisomeric mono- and bis-methyl ethers would be anticipated from both conjugated and non-conjugated dienic hydrocarbons.

These conclusions were supported by diagnostic ions at *m*/*z* 166 and *m*/*z* 250 (for the C-25 compound) and *m*/*z* 166 and *m*/*z* 278 (for the C-27 compound), attributable to McLafferty rearrangement ions, known to appear in the mass spectra of acyclic allenes[4] (Scheme 2).

The major component was partially purified (HPLC:silica–hexane, *ca*. 0.3 mg). The ^1H NMR signal at δ 5.04 (br, m) correlated (HSQC) with the ^{13}C NMR signal at 90.8 ppm, (representing both sp^2-carbons), both signals being consistent with the allene structure. The signal for the central carbon of the allene group (expected ~200 ppm) was not discernible from this dilute sample.[5]

GCMS comparisons established that the C-25 allene **4** was also a minor cuticular component in two other sugarcane beetles, *Lepidiota negatoria* and *Dermolepida albohirtum*. Extracts from *D*. *albohirtum* and *L*. *picticollis* contained as a major component an allene with M^+ 320 ($C_{23}H_{44}$) and diagnostic ions at *m*/*z* 166 and *m*/*z* 222, again indicating 9,10-di-unsaturation. The $\Delta^{9,10}$-tricosadiene structure **6** was proposed for this constituent. When co-injected with a set of standard alkanes, the allenes **4**, **5** and **6** eluted just prior to the corresponding alkane and have equivalent chain lengths of 24.9, 26.9 and 22.9, respectively.

To confirm the identity of these three components, syntheses of **4**, **5** and **6** were then undertaken and a route was developed for delivery of both racemic and enantiomerically enriched systems. Key steps utilised were the 'acetylene zipper' reaction,[6] regioselective addition of $^nBu_3SnH$ to a propargylic alcohol, and *anti* elimination of $^nBu_3SnOMs$ (or $^nBu_3SnOAc$)[7] to install the propa-1,2-diene unit. This approach is shown in Scheme 3 for $\Delta^{9,10}$-pentacosadiene **4**.

Similar approaches furnished the racemic $\Delta^{9,10}$-tricosadiene **6** and $\Delta^{9,10}$-heptacosadiene **5**. GC-MS comparisons, including co-elution studies, established that the natural components were

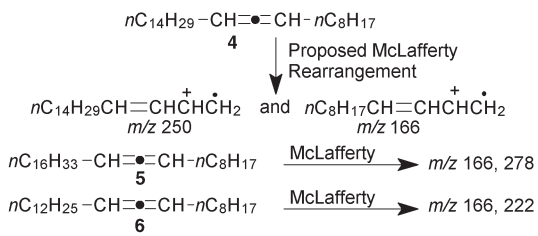

Scheme 2

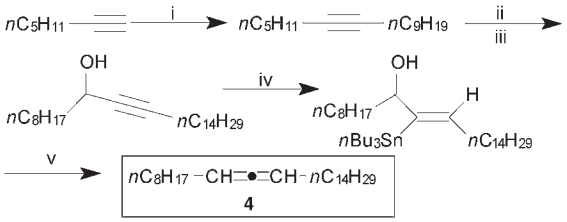

Scheme 3 *Reagents and conditions*: i, *n*BuLi, THF −78 °C/−40 °C then $nC_9H_{19}Br$, HMPA (97%); ii, KH, DAP (79%); iii, *n*BuLi, THF −78 °C/−40 °C then $nC_8H_{17}CHO$ (51%); iv, nBu_3SnH, AIBN 90 °C; v, MsCl, Et_3N (60% from alkynol).

6, **4** and **5**. In the case of the synthesised $\Delta^{9,10}$-pentacosadiene **4**, its ^1H and ^{13}C NMR spectra matched precisely the spectra of the natural component.

The chirality of the natural allenes was then addressed. The enantiomers of (±)-$\Delta^{9,10}$-tricosadiene **6** and (±)-$\Delta^{9,10}$-pentacosadiene **4** were base-line separated on a heptakis(6-*O*-*tert*-butyldimethylsilyl-2,3-di-*O*-methyl) β-cyclodextrin column, after *ca*. 160 min at 155 °C and *ca*. 200 min at 165 °C respectively. The natural $\Delta^{9,10}$-pentacosadiene (from *A*. *consanguineus*) was of high ee, and co-eluted with the first eluting enantiomer of the racemate. This applied also to $\Delta^{9,10}$-tricosadiene from *D*. *albohirtum*. The present allenes provide remarkable examples of the separation efficacy of these modified cyclodextrin phases.[8]

Nonracemic allenes of known predominating chirality were required next. The C-25 propargylic alcohol **7** (Scheme 4) was first oxidised to the ketone, and reduction with Me-CBS[9] afforded the (*S*)-alcohol **8** (80% ee, Mosher's ester analyses).[10] The predominant configuration was confirmed by converting the alcohol into decane-1,2-diol, whose rotation ($[\alpha]_D$ −7°; *c*, 0.12, MeOH) may be compared with that for the authentic (*S*)-isomer, ($[\alpha]_D$ −11.9°; *c*, 0.43, MeOH).[11] The (*S*)-propargylic alcohol **8** was then hydrostannylated, acetylated and treated with TBAF in DMSO to effect *anti*-elimination of $^nBu_3SnOAc$[12] and give the (*R*)-enantiomer, **9** ($[\alpha]_D$ −17° (*c*, 0.54, $CHCl_3$)[13] in 72% ee (enantioselective gas chromatography). Co-injection studies established that natural $\Delta^{9,10}$-pentacosadiene in *A*. *consanguineus* was predominantly the (*R*)-enantiomer (89% ee).

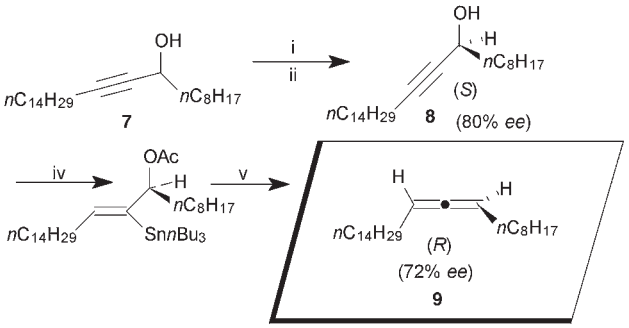

Scheme 4 *Reagents and conditions*: i, TPAP, NMO (82%); ii, (*S*)-MeCBS (2.5 equiv.) $BH_3{\cdot}SMe_2$ (5 equiv.) −30 °C 1 h (70%); iii, nBu_3SnH AIBN 90 °C neat; iv, Ac_2O, pyridine (14% from alkynol); v, TBAF, DMSO reflux (77%).

An analogous approach with (*S*)-tricosa-10-yn-9-ol (80% ee) provided predominantly (*R*)-$\Delta^{9,10}$-tricosadiene (77% ee, 36% from the alcohol). Natural $\Delta^{9,10}$-tricosadiene was then shown to be (*R*)-configured with 86% ee. Given the consistency of the location of the $\Delta^{9,10}$-propadiene unit, a predominating (*R*)-chirality is likely for $\Delta^{9,10}$-heptacosadiene, as well.

Examination of males of a further cane beetle species, *L*. *crinita* has revealed the presence of the higher allene, $\Delta^{9,10}$-hentriacontane, $C_{31}H_{60}$ (M^+ = 432 and McLafferty ions at *m*/*z* 334 and 166). A lower level component is $\Delta^{9,10}$-nonacosadiene, the C-29 allene (M^+ = 404, *m*/*z* 306 and 166). Co-occurring with the dominant C-25 allene in *A*. *consanguineus*, are much lower levels of the *even carbon numbered* $\Delta^{9,10}$-tetracosadiene (M^+ 334, *m*/*z* 246, 166) and $\Delta^{9,10}$-hexacosadiene (M^+ 362, *m*/*z* 264, 166), in the former case confirmed by synthesis.

All allenes identified have $\Delta^{9,10}$-unsaturation, and those odd numbered in carbon are considerably favoured. Administration of labelled potential precursors is being conducted to reveal possible routes to these hydrocarbons. As far as we are aware, allenic hydrocarbons were previously unknown from insects, although the male-produced pheromone of the dried bean beetle (*Acanthoscelides obtectus*) incorporates an allene moiety.[14] The biological role of these compounds is being investigated.

The authors are grateful to the Australian Research Council (SPIRT award) for support, to Professor R. W. Rickards for valuable suggestions, and to David Logan (BSES, Ayr, Australia) for provision of *D*. *albohirtum* specimens.

Notes and references

1 For a useful review see L. N. Robertson, P. G. Allsopp, K. J. Chandler and R. T. Mullins, *Aust. J. Agric. Res*., 1995, **46**, 1.
2 See, for example, A. G. Bagnères, J. L. Clément, M. S. Blum, R. F. Severson, C. Joulie and C. Lange, *J. Chem. Ecol*., 1990, **16**, 3213.
3 D. R. Nelson, C. L. Flatland and J. E. Baker, *Insect Biochem*., 1984, **14**, 435, and references therein.
4 J. R. Wiersig, A. M. H. Yeo and C. Djerassi, *J. Am. Chem. Soc*., 1977, **99**, 532.
5 For discussions of NMR spectra of allenes see: (*a*) D. H. Williams and I. Fleming, *Spectroscopic Methods in Organic Chemistry*, McGraw-Hill, London, 5th edn., 1995, pp. 157 and 163; (*b*) R. Steur, M. J. A. van Dongen, W. Dreuth, J. W. de Hann and L. J. M. van de Ven, *Tetrahedron Lett*., 1971, 3307.
6 (*a*) C. A. Brown and A. Yamashita, *J. Am. Chem. Soc*., 1974, **97**, 891; (*b*) J. C. Lindhort, G. L. van Mourik and H. J. J. Pabon, *Tetrahedron Lett*., 1976, 2565.
7 Y. Araki and T. Konoike, *Yuki Gosei Kagaku Kyokaishi*, 2000, **58**(10), 956. (*Chem Abs*., 133:321484).
8 J. Pietruzka, D. H. Hochmuth, B. Gehrcke, D. Icheln, T. Runge and W. A. Koenig, *Tetrahedron: Asymmetry*, 1992, 661.
9 E. J. Corey and C. J. Helal, *Angew. Chem., Int. Ed*., 1998, 1986.
10 G. R. Sullivan, J. A. Dale and H. S. Mosher, *J. Org. Chem*., 1973, **38**, 2143.
11 Y. Masooka, S. Masayuki and K. Mori, *Agric. Biol. Chem*., 1982, **46**, 2319.
12 Y. Araki and T. Konoike, *Tetrahedron Lett*., 1992, **33**, 5093.
13 Laevo-rotatory, non-cyclic, 1,3-dialkylallenes have the (*R*)-configuration. See for example, D. J Pasto and K. D. Sugi, *J. Org. Chem*., 1991, **56**, 4157, and references therein.
14 K. Mori, in *The Total Synthesis of Natural Products*, ed. J. Apsimon, John Wiley and Sons, New York, 1992, vol. 9, pp. 212–215.

CHEMCOMM Communication
www.rsc.org/chemcomm

Ionic liquids as catalytic green solvents for nucleophilic displacement reactions

Christy Wheeler,[a] Kevin N. West,[a] Charles L. Liotta[b] and Charles A. Eckert*[a]

[a] *School of Chemical Engineering, Georgia Institute of Technology, Atlanta, GA, 30332-0100, USA. E-mail: cae@che.gatech.edu*
[b] *School of Chemistry and Biochemistry, Georgia Institute of Technology, Atlanta, GA 30332-0400, USA*

Received (in Corvallis, OR, USA) 31st January 2001, Accepted 16th March 2001
First published as an Advance Article on the web 20th April 2001

We demonstrate the use of room-temperature ionic liquids as a catalytic, environmentally benign solvent for the cyanide displacement on benzyl chloride, replacing phase-transfer catalyzed biphasic systems and thus eliminating the need for a volatile organic solvent and hazardous catalyst disposal.

Ionic liquids have recently gained recognition as possible environmentally benign alternative chemical process solvents. Because of their vanishingly low vapor pressures, ionic species do not contribute to VOC emissions as do most organic solvents. Examples of their application in both reactions[1,2] and separations[3,4] have been demonstrated. Although many types of reactions have been investigated in ionic liquids, examples of nucleophilic substitution reactions are absent from the literature.

Nucleophilic displacement reactions are often carried out using phase-transfer catalysis (PTC) to facilitate the reaction between the organic reactants and the inorganic ionic salts that provide the nucleophiles.[5] The phase-transfer catalyst, often a tetraalkylammonium salt, acts as a shuttle for the reactant anion between a polar phase that contains the salt reactant and a non-polar phase that contains the organic reactant. This technique not only overcomes the problem of contacting the reactants, but also provides activation of the nucleophilic anion, since it is much less tightly bound to a tetraalkylammonium cation than it would be to a metal cation. In conventional PTC typical organic solvents are environmentally undesirable species such as methylene chloride or *o*-dichlorobenzene, and catalyst separation and recovery are significant challenges. With ionic liquids as both the solvent and the catalyst, there are zero VOCs, and it has been shown that product recovery is facile by CO_2 stripping.[3]

Because ionic liquids are comprised of bulky organic cations, they seem well suited for the types of reactions for which PTC is effective. There even exists the possibility that the solvent itself can act as a catalyst to activate the anion for reaction. The ionic liquid cation might not be as effective a catalyst as most PTCs; however, as a solvent, its high concentration should overcome this limitation, yielding a high reaction rate.

We chose the cyanide displacement on benzyl chloride to yield phenylacetonitrile, depicted in Scheme 1, as a model reaction. For the solvent, we selected the ionic liquid 1-*n*-butyl-3-methylimidazolium hexafluorophosphate (**1**), often called

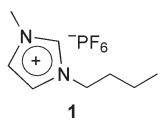

1

[bmim][PF_6]. The reaction was chosen because it has been well characterized in a variety of other systems. The choice of solvent was motivated by its being one of the most widely used, and therefore the most widely available, ionic liquids.

Scheme 1 Cyanide displacement on benzyl chloride.

These reactions were carried out in a 25 ml volumetric flask set in a recirculating heated bath and stirred with a magnetic stir bar. The concentration of benzyl chloride in the ionic liquid was 1 M, and the amount of potassium cyanide was three times the stoichiometric amount of benzyl chloride. While all of the benzyl chloride was visually observed to be soluble, solid potassium cyanide was present in the systems at all times. Before introduction of benzyl chloride, the salt was stirred overnight in the liquid so that the uniform particle sizes would form and the salt would reach an equilibrium concentration.[6] After the introduction of benzyl chloride, samples were drawn and dissolved in cold acetonitrile before being analyzed by HPLC equipped with a UV-Vis detector.

Reactions were carried out at 40, 60, and 80 °C, and conversion is plotted in Fig. 1. Reaction rates were high, with the reaction at 80 °C reaching complete conversion in less than half an hour. Although the reactions at 60 and 80 °C show the expected pseudo-first-order kinetic behavior (since the amount of cyanide available for reaction should be constant), the reaction at 40 °C appears to be zero order. This behavior indicates that mass transfer of potassium cyanide into the solvent is probably the rate-limiting step at the lower temperature, which is consistent with the fact that the viscosity of the ionic liquid is observed to decrease steeply with an increase in temperature. Although solid salt is always present in the reacting systems, the transfer into the liquid at higher temperatures is apparently faster than the reaction step itself, such that an equilibrium concentration of cyanide is achieved and pseudo-first-order behavior is exhibited.

The rate constants for each temperature are listed in Table 1. An effective activation energy of 19 kcal mol^{-1} is calculated using the data at 60 and 80 °C. Because the nature of the solvent changes with temperature, this activation energy includes several factors other than the temperature dependence of the intrinsic reaction rate, most especially the solubility of potassium cyanide.

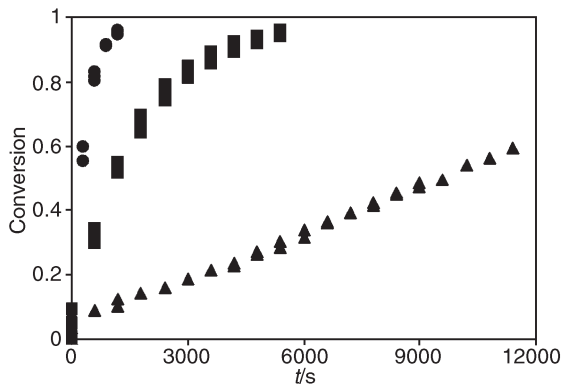

Fig. 1 Conversion of benzyl chloride to benzyl cyanide (● 80 °C, ■ 60 °C, ▲ 40 °C).

Table 1 Rate constants for reaction of benzyl chloride with potassium cyanide. Uncertainty is represented by 95% confidence intervals

Temperature/°C	Rate constant
40	[a](4.76 ± 0.12) × 10^{-5} mol L^{-1} s^{-1}
60	[b](5.45 ± 0.38) × 10^{-4} s^{-1}
80	[b](2.54 ± 0.10) × 10^{-3} s^{-1}

[a] Zero order. [b] Pseudo-first order.

Another reaction that has been demonstrated in a similar system is the base-promoted cyclo-alkylation of phenylacetonitrile with 1,4-dibromobutane, shown in Scheme 2. Kinetic data were not taken, but the reaction was complete in less than three hours. As in the previous example, the organic reactants were dissolved in the ionic liquid, and excess solid potassium hydroxide was present at all times.

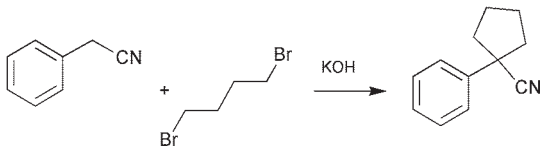

Scheme 2 Cyclo-alkylation of phenylacetonitrile with 1,4-dibromobutane.

Once the reaction is complete, we must turn our attention to product recovery and solvent recycle. As demonstrated by Blanchard *et al*., supercritical CO_2 can be incorporated to extract non-volatile organic compounds from ionic liquids.[3,7] Heating is sufficient to remove more volatile compounds from the solvent. Fig. 2 illustrates a proposed environmentally benign reaction and separation solvent system for reactions of organic compounds with inorganic salts. The low solubility of ionic liquids in water and in CO_2 allows for facile separation steps that should result in minimal solvent loss, although loss of ionic liquid in a water extraction must be considered when selecting the ionic liquid.

In conclusion, we have demonstrated the viability of ionic liquids as a solvent for reactions between organic compounds and inorganic salts. This opens many opportunities for environmentally friendly processing, especially when combined with the benign separations techniques that have already been demonstrated.

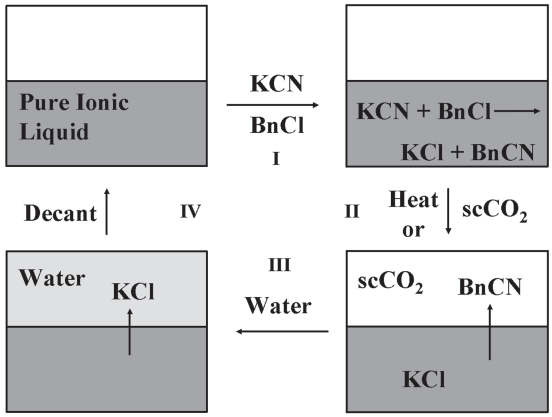

Fig. 2 A recyclable ionic liquid solvent system for nucleophilic substitution reactions. In step I, the reactants are added to the ionic liquid and the reaction is allowed to proceed. Step II involves the removal of the organic reactant *via* vaporization or supercritical fluid extraction. Washing with water, as in step III, will remove the salt product and after decantation, step IV, the purified ionic liquid is obtained and available for another reaction cycle.

We gratefully acknowledge the assistance of Ashley Wallin and Jessica Ryan in performing experiments. We also thank John Kantzes and Roger Moulton of SACHEM, Inc., in Austin, Texas, for provision of the ionic liquid.

Notes and references

1 Y. Deng, F. Shi, J. Beng and K. Qiao, *J. Mol. Catal. A: Chem.*, 2001, **165**, 33.
2 T. Welton, *Chem. Rev.*, 1999, **99**, 2071.
3 L. A. Blanchard and J. F. Brennecke, *Ind. Eng. Chem. Res.*, 2001, **40**, 287.
4 J. G. Huddleston, H. D. Williams, R. P. Swatloski, A. E. Visser and R. D. Rogers, *Chem. Commun.*, 1998, 1765.
5 C. M. Starks, C. L. Liotta and M. Halpern, *Phase-Transfer Catalysis*, Chapman and Hall, New York, 1994.
6 The [bmim][PF_6] was obtained from SACHEM, Inc., and used as received. Two separate bottles were used in these experiments, one labeled 97% pure, with the balance water, and the other without indication of water content. However, the results obtained with each were the same. The overnight heating of the solvent prior to reaction should allow the water content to come to an equilibrium level.
7 L. A. Blanchard, D. Hancu, E. J. Beckman and J. F. Brennecke, *Nature*, 1999, **399**, 28.

CHEMCOMM Communication
www.rsc.org/chemcomm

2-Azabicyclo[2.2.1]hept-5-enes from 7-azabicyclo[2.2.1]heptadienes by tandem intermolecular radical addition—homoallylic radical rearrangement

David M. Hodgson,*[a] Magnus W. P. Bebbington[a] and Paul Willis[b]

[a] *Dyson Perrins Laboratory, Department of Chemistry, University of Oxford, South Parks Road, Oxford, UK OX1 3QY. E-mail: david.hodgson@chem.ox.ac.uk*
[b] *AstraZeneca, R&D Charnwood, Bakewell Road, Loughborough, UK LE11 5RH*

Received (in Cambridge, UK) 2nd March 2001, Accepted 2nd April 2001
First published as an Advance Article on the web 20th April 2001

Addition of thiols to 7-azabicyclo[2.2.1]heptadienes such as 16 leads exclusively to 7-thio-substituted 2-azabicyclo[2.2.1]-hept-5-enes 17 in good yields *via* tandem intermolecular radical addition—homoallylic radical rearrangement.

Radical cyclisations and rearrangements are amongst the most powerful and versatile methods for the construction of mono and polycyclic systems.[1] Radical reduction of norbornenyl sbromide **1** or nortricyclyl bromide **4** is known to produce the same (~1:1) mixture of norbornene **2** and nortricyclene **3** (Scheme 1).[2] However, during the development of novel analgesics related to epibatidine by a strategy involving indirect skeletal interconversion of 7-aza to 2-azabicyclo[2.2.1]heptyl ring systems, we reported that radical deoxygenation of azanortricyclanol **5** delivers a single product **6**, even when R is potentially radical stabilising (*e.g.* Ar, Scheme 2).[3]

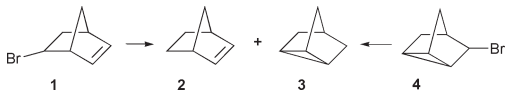

Scheme 1

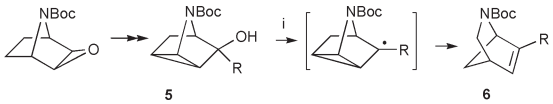

Scheme 2 *Reagents and conditions*: i, $ClCOCO_2Me$, DMAP, then Bu_3SnH, AIBN.

Following this demonstration of 'nitrogen-directed' radical rearrangement, we considered that a synthetically attractive direct skeletal interconversion might be possible by intermolecular radical addition–homoallylic radical rearrangement (Scheme 3). This would provide convergent access to synthetically important 2-azabicyclo[2.2.1]heptyl ring systems containing substitution not easily available by other methods.[4] Here we communicate our preliminary results concerning the realisation of this concept.

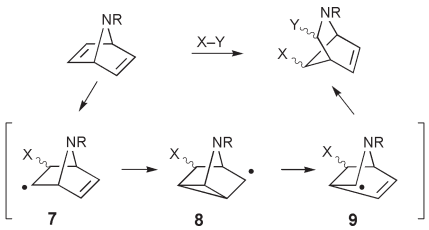

Scheme 3

Radical additions to norbornadiene **10** (and substituted norbornadienes), using thiols for example, have been well-studied and usually result in substituted nortricyclanes as the major products.[5] Consistent with these earlier studies, we found that addition of *p*-thiocresol to norbornadiene **10** (both 2 mol dm^{-3} in toluene) at 25 °C led preferentially to nortricyclyl sulfide **12**, with bicyclic sulfide **11** (*exo*- : *endo*-, 5:1)[6] being the only other product detected (**11**:**12**, ~1:3, Scheme 4).

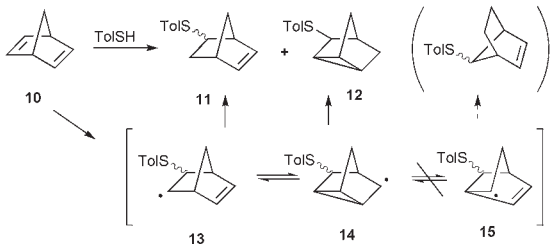

Scheme 4

Further experiments at increasing dilution indicated that the product ratio reached a constant level (**11**:**12**, ~ 1:6), once the concentration of each reactant was < 0.1 mol dm^{-3}. These latter results indicate attainment of equilibrium between the substituted norbornenyl and nortricyclyl radicals **13** and **14**. The presence of the sulfur substituent therefore leads to preferential cyclopropane opening in **14** back to **13** (rather than from **14** to **15**), with H-atom transfer to **14** to give nortricyclyl sulfide **12** being faster than H-atom transfer to **13** to give bicyclic sulfide **11**; hence the product profile observed does not reflect the **13**/**14** equilibrium position. This is in contrast to Scheme 1, where the rates of H-atom transfer to the norbornenyl and nortricyclyl radical intermediates leading to **2** and **3** are likely to be similar and therefore the product profile should reflect the ratio of radicals at equilibrium.

By comparison to the reactions of norbornadiene with thiols, the corresponding 7-aza systems such as **16** (available in two steps from the alkoxycarbonyl-protected pyrrole and tosyl ethyne)[7] behave in dramatically different fashion (Scheme 5, Table 1), but in accord with the earlier analysis (Scheme 3).

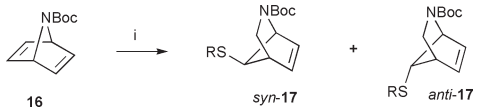

Scheme 5 *Reagents and conditions*: i, RSH (0.9 equiv.), benzene or toluene, 25 °C (R = aryl) or 80 °C (R = alkyl), 6–24 h.

Pleasingly, both aromatic and aliphatic thiols were found to react cleanly with only a slight excess (1.1 equiv.) of azadiene **16** in benzene or toluene (0.1 mol dm^{-3}) to give rearranged sulfides **17** in 6–72 h, depending on the reactivity of the thiol. In the case of the less reactive aliphatic thiols, heat was required for completion of the reaction in a satisfactory time. Aliphatic thiols are considerably poorer H-atom transfer agents than their aromatic counterparts.[8] This may explain the lower yields in these cases, as polymerisation could compete with atom

DOI: 10.1039/b101984h

Table 1 Thiol additions to 7-azabicyclo[2.2.1]heptadiene **16**

Thiol	T/°C	*t*/h	Yield (%)	*syn*-**17**:*anti*-**17**
TolSH[a]	20	24	92	3:1
PhSH	20	24	92	4:1
2,6-diMeC_6H_3SH	20	24	90	4:1
4-$NO_2C_6H_4SH$	20	72	50	7:1
Bu^nSH	80	6	59	2:1
Bu^tSH	80	24	48	5:1
$HO(CH_2)_3SH$	80	14	56	4:1

[a] TolSH with **16** (Boc = CO_2Me) at 20 °C for 4 h gave **17** (R = Tol, Boc = CO_2Me) in 66% yield (*syn*- : *anti*-, 4:1).

transfer. The major diastereoisomer in the reaction with *p*-thiocresol was shown by NOE analysis to be the *syn*-isomer arising from initial *exo*-attack of thiyl radical on azadiene **16**, and the predominant isomer obtained with the other thiols is assigned as *syn* by analogy. Evidence that the product sulfides **17** possess the rearranged 2-azabicyclo[2.2.1]hept-5-ene framework is, for example, that oxidation of **17** (R = Tol) using buffered peracetic acid (6 equiv., 25 °C, 18 h) gave in 91% yield the epimeric sulfones **17** (RS = Ts) with spectral data distinctly different from the 2-Ts-7-Boc-7-azabicyclo[2.2.1]hept-5-enes[9] that would be obtained from oxidation of the product of simple addition across one double bond in azadiene **16**. Subsequent desulfonylation of sulfones **17** (RS = Ts) with 6% sodium–amalgam (MeOH, 25 °C, 12 h) gave the known 2-azabicyclic alkene **6** (R = H)[3,10] in 33% yield as the only identifiable product.

Benzeneselenol shows similar behaviour with unsaturated systems to aromatic thiols, but is an order of magnitude superior as an H-atom transfer agent.[8] Under otherwise identical conditions to the earlier reactions of aromatic thiols (Table 1), it was found that benzeneselenol with azadiene **16** gives a small proportion (12%) of the selenide **18** arising from simple addition across one double bond, as well as the expected rearranged selenide **19** (81%, Scheme 6).

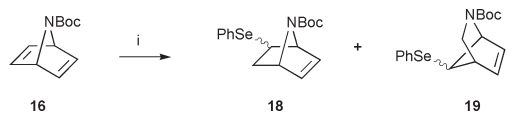

16 18 19

Scheme 6 *Reagents and conditions*: i, PhSeH (0.9 equiv.), benzene, 25 °C, 24 h.

This result allows an estimation of the rate constant for the rearrangement **7** → **9** (Scheme 3). Given that no products other than the 2-azabicyclic epimers **17** are observed in the addition of aromatic thiols, it seems probable that the rate constant for the rearrangement is between 1 and 2 orders of magnitude greater than the initial rate of H-atom transfer from the thiol. A thiol concentration of 0.1 mol dm^{-3} (typical in our studies) and an approximate second order rate constant for H-atom transfer of 10^8 mol^{-1} dm^3 s^{-1} (ref. 8), suggests a rate constant of $\approx 10^8$—10^9 s^{-1} for the rearrangement at 25 °C.

The absence of tricyclic products in any of the reactions with azadiene **16** suggests that the lifetime of the azatricyclic intermediate **8** is much shorter than that for either of the bicyclic intermediates **7** and **9** (Scheme 3). In kinetic studies of the nortricyclyl–norbornenyl radical rearrangement [**13** (Tos = H) and **14** (Tos = H), Scheme 4], the rates of ring opening and ring closure have been shown to be similar: $\approx 10^7$ s^{-1} at 25 °C.[11] In the azabicyclic system, however, it seems probable that the ring opening step (**8** → **9**) is significantly faster, with the transition state being lowered in energy by the stabilisation of the developing radical α- to nitrogen.[12] Rate constants for the ring opening of cyclopropyl methyl radicals to but-3-enyl radicals are known to be strongly influenced by substitution.[13]

In summary, we describe the first examples of free radical additions to 7-azanorbornadienes. The process demonstrates a new approach to the 2-azabicyclo[2.2.1]heptyl ring system by homoallylic radical rearrangement, which uses a nitrogen atom to promote and guide cyclopropane ring opening.[3,14] Extensions of the principle to other addition reactions, different ring systems and manipulation of the adducts towards targets of biological interest, are under investigation.

We thank AstraZeneca Pharmaceuticals and the EPSRC for an Industrial CASE award (to M. W. P. B.) and the EPSRC National Mass Spectrometry Service Centre for mass spectra. We also thank Professors S. J. Cristol and B. Giese for useful discussions and Dr B. Odell for expert assistance with structure elucidation using NMR.

Notes and references

1 *Radicals in Organic Synthesis*, ed. P. Renaud and M. P. Sibi, Wiley-VCH, Weinheim, 2001; B. Giese, B. Kopping, T. Göbel, J. Dickhaut, G. Thoma, K. J. Kulicke and F. Trach, *Org. React. (N. Y.)*, 1996, **48**, 301; A. L. J. Beckwith and K. U. Ingold, in *Rearrangements in Ground and Excited States*, ed. P. de Mayo, Academic, New York, 1980, vol. 1, pp. 161–310.
2 C. R. Warner, R. J. Strunk and H. G. Kuivila, *J. Org. Chem.*, 1966, **31**, 3381; T. A. Halgren, J. L. Firkins, T. A. Fujimoto, H. H. Suzukawa and J. D. Roberts, *Proc. Natl. Acad. Sci. U.S.A.*, 1971, **68**, 3216.
3 D. M. Hodgson, C. R. Maxwell and I. R. Matthews, *Synlett*, 1998, 1349.
4 D. Blondet and C. Morin, *Heterocycles*, 1982, **19**, 2155.
5 D. I. Davies, *Chem. Soc. Spec. Publ.*, 1970, **24**, 201; J. W. Wilt, in *Free Radicals*, ed. J. K. Kochi, Wiley, New York, 1973, vol. 1, pp. 333–501.
6 C. Maignan and R. A. Raphael, *Tetrahedron*, 1983, **39**, 3245.
7 H.-J. Altenbach, B. Blech, J. A. Marco and E. Vogel, *Angew. Chem., Int. Ed. Engl.*, 1982, **21**, 778.
8 M. Newcomb, *Tetrahedron*, 1993, **49**, 1151.
9 R. Leung-Toung, Y. Liu, J. M. Muchowski and Y.-L. Wu, *J. Org. Chem.*, 1998, **63**, 3235.
10 A. Kasyan, C. Wagner and M. E. Maier, *Tetrahedron*, 1998, **54**, 8047.
11 P. C. Wong and D. Griller, *J. Org. Chem.*, 1981, **46**, 2327.
12 D. J. Pasto, R. Krasnansky and C. Zercher, *J. Org. Chem.*, 1987, **52**, 3062.
13 D. C. Nonhebel, *Chem. Soc. Rev.*, 1993, **22**, 347.
14 J. H. Rigby and F. C. Pigge, *Tetrahedron Lett.*, 1996, **37**, 2201.

CHEMCOMM Communication
www.rsc.org/chemcomm

Solid-state ^{17}O NMR of thymine: a potential new probe to nucleic acid base pairing

Gang Wu,* Shuan Dong and Ramsey Ida

Department of Chemistry, Queen's University, Kingston, Ontario, Canada K7L 3N6. E-mail: gangwu@chem.queensu.ca; Fax: +1-613-533-6669

Received (in Corvallis, OR, USA) 4th January 2001, Accepted 29th March 2001
First published as an Advance Article on the web 24th April 2001

We report the first experimental solid-state ^{17}O NMR and theoretical (B3LYP/6-311++G) study of the ^{17}O electric-field-gradient and chemical shielding tensors in a free nucleic acid base, thymine.**

NMR spectroscopy is an important technique for studying structures of biological macromolecules. Most successful NMR applications have been based primarily on observation of spin-1/2 nuclei such as ^{1}H, ^{13}C and ^{15}N. Although oxygen is also an important element in biological molecules, ^{17}O (S = 5/2 and natural abundance = 0.037%) NMR studies are far less common.[1] To explore the potential of solid-state ^{17}O NMR spectroscopy in studying organic and biological compounds, we recently investigated a number of important oxygen-containing functional groups such as amides,[2] urea,[3] carboxylic acids,[4] phenols[4] and the oxonium ion.[5] Oxygen is also common in nucleic acids. Base pairing between nucleic acid molecules often directly involves oxygen atoms, *e.g.* G:C and A:U base pairing. To our knowledge, solid-state ^{17}O NMR has not been applied to compounds related to nucleic acids.

As a first step, we report solid-state ^{17}O NMR results for a free nucleic acid base, thymine; see Fig. 1. We synthesized [2-^{17}O]thymine and [4-^{17}O]thymine by acid-catalyzed exchange with $H_2{}^{17}O$ (40.9 atom% ^{17}O, ISOTEC, Miamisburg, Ohio) from 5-methyl-2-thiouracil and thymine, respectively. Solid-state ^{17}O NMR spectra were recorded on a Bruker Avance-500 spectrometer operating at 67.78 MHz for ^{17}O nuclei. Fig. 2 shows the experimental and simulated ^{17}O magic-angle spinning (MAS) NMR spectra of [2-^{17}O]thymine and [4-^{17}O]thymine. Analysis of these spectra yielded the following ^{17}O NMR parameters: O2, δ_{iso} = 200 ± 5 ppm, C_Q = 6.65 ± 0.02 MHz, η_Q = 1.00 ± 0.02; O4, δ_{iso} = 325 ± 5 ppm, C_Q = 8.40 ± 0.02 MHz, η_Q = 0.10 ± 0.02. Following the standard procedure,[2,6] we were also able to analyze the stationary ^{17}O NMR spectra shown in Fig. 2 and obtain the magnitude and relative orientation of the ^{17}O chemical shift (CS) tensors. The results are summarized in Table 1.

It can be seen from Table 1 that O2 and O4 exhibit drastically different ^{17}O NMR tensors. In particular, the amide-type oxygen, O4, shows a much larger C_Q, 8.40 MHz, than the urea-type oxygen, O2, 6.65 MHz. The difference between the ^{17}O CS tensors for O2 and O4 is also striking. The isotropic ^{17}O chemical shifts for O2 and O4 differ by 125 ppm. In addition, the span ($\Omega = \delta_{11} - \delta_{33}$) of the ^{17}O CS tensor for O4 is more than twice of that for O2. It is also apparent from Table 1 that, whereas the isotropic ^{17}O chemical shifts measured for O4 in the solid and solution states are essentially identical, the corresponding values for O2 differ by approximately 50 ppm! This is clearly a consequence of the strong intermolecular hydrogen-bonding interaction at O2 in crystalline thymine; see Fig. 1.

In order to evaluate quantitatively the influence of intermolecular hydrogen bonding interactions on the ^{17}O EFG and CS tensors in crystalline thymine, we chose to perform quantum chemical calculations using four different models. Model-I is simply an isolated thymine molecule. Model-II consists of two hydrogen-bonded thymine molecules, **1** and **2** as defined in Fig. 1. Model-III also consists of two thymine molecules, **1** and **3**. Model-IV is a trimeric cluster containing **1**, **2** and **3**. The experimental X-ray diffraction structure of thymine[7] was used in all the calculations. The positions of the hydrogen atoms were computed using the standard bond lengths and angles. The density functional theory (DFT) calculations were performed on a PC (400 MHz Pentium II processor, 128 MB RAM, 12 GB of

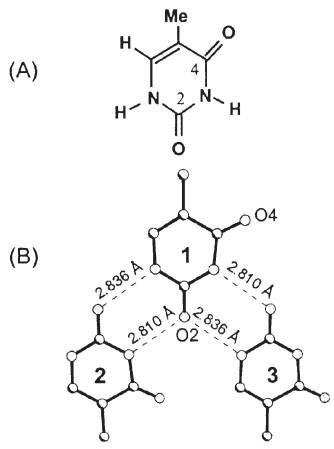

Fig. 1 (A) Chemical structure of thymine. (B) H-bond environment in crystalline thymine.[7] Thymine molecules are related by twofold screw axes. Hydrogen atoms are not shown for clarity.

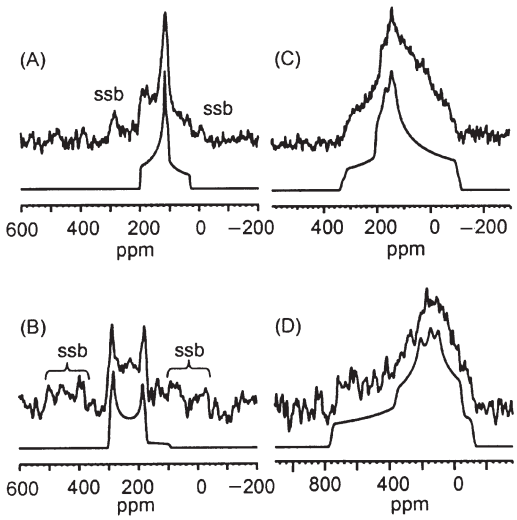

Fig. 2 Experimental (upper) and simulated (lower) ^{17}O MAS NMR spectra of (A) [2-^{17}O]thymine (3753 scans) and (B) [4-^{17}O]thymine (5236 scans). Experimental (upper) and simulated (lower) ^{17}O stationary NMR spectra of (C) [2-^{17}O]thymine (7400 scans) and (D) [4-^{17}O]thymine (5376 scans). The sample spinning frequency was 14.5 kHz. The B_1 field strength at the ^{17}O frequency was about 70 kHz. Spinning sidebands are marked as 'ssb'. A Hahn-echo pulse sequence was used in acquiring the stationary spectra. The recycle time was 10 s in all experiments.

DOI: 10.1039/b100337m

Table 1 Summary of experimental and theoretical (B3LYP/6-311++G**) ^{17}O NMR tensors in crystalline thymine

Compound	Model	δ_{iso}/ppm	δ_{11}/ppm	δ_{22}/ppm	δ_{33}/ppm	C_Q/MHz[a]	η_Q
[2-^{17}O]Thymine	I	298	441	406	48	8.42	0.55
	II	264	385	359	46	7.82	0.73
	III	250	365	344	40	7.72	0.79
	IV	226	327	306	45	7.12	0.99
	Exptl.	200 ± 2 (247.8)[b]	290 ± 5	270 ± 5	20 ± 5	6.65 ± 0.02	1.00 ± 0.02
[4-^{17}O]Thymine	I	387	698	487	−25	8.91	0.14
	II	399	685	480	−25	8.83	0.17
	III	380	734	496	−33	9.14	0.12
	IV	392	720	491	−34	9.08	0.15
	Exptl.	325 ± 2 (321.0)[b]	570 ± 5	360 ± 5	20 ± 5	8.40 ± 0.02	0.10 ± 0.02

[a] $C_Q = eQV_{zz}/h$ and $\eta_Q = (V_{xx} - V_{yy})/V_{zz}$. [b] Numbers in parentheses are the corresponding ^{17}O chemical shift values measured in DMSO solutions.

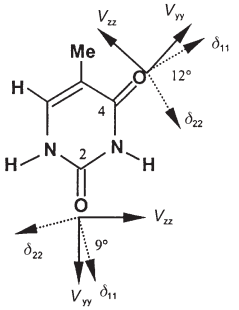

Fig. 3 Illustration of the orientations of the ^{17}O NMR tensors in thymine.

disk space) using Gaussian 98 program[8] with the standard 6-311++G** basis set and the B3LYP exchange functional.[9] The theoretical results are also presented in Table 1.

Close examination of the theoretical results reveals a remarkable difference between the ^{17}O NMR tensors for O2 and O4. In particular, both the ^{17}O quadrupole coupling tensor and the CS tensor at O2 exhibit a strong dependence on the cluster model used in the calculation, whereas the ^{17}O NMR tensors at O4 are essentially independent of the model. This clearly reflects the difference in the H-bond environment between O2 and O4. In the discussion that follows, we focus only on the ^{17}O NMR tensors for O2. As seen from Table 1, Model-I predicted Ω = 393 ppm and C_Q = 8.42 MHz for O2, which are considerably larger than the observed values, Ω = 270 ppm and C_Q = 6.65 MHz. When two H-bonds were considered in either Model-II or Model-III, smaller values were obtained for Ω and C_Q. When a complete H-bond network is included in the calculation (Model-IV), the theoretical results become much closer to the experimental values, Ω= 282 ppm and C_Q = 7.12 MHz. The observed decrease in the isotropic ^{17}O chemical shift (increase in *shielding*) from Models I to IV results mainly from the changes in δ_{11} and δ_{22}. The large difference between the isotropic ^{17}O chemical shifts measured in the solid state and in solution, 200 *vs*. 247.8 ppm, was well reproduced by the calculations of Model-I and Model-IV. The quadrupole coupling constant exhibits a reduction of approximately 1.3 MHz upon hydrogen bonding, the ^{17}O EFG tensor increases monotonically from Models I, II, III to IV. Finally, the agreement between the calculated results from Model-IV and the experimental data is reasonable; but it is also clear that all calculated ^{17}O NMR parameters are larger than the observed values by approximately 10%. These discrepancies are likely due to the limitation of the current theory.

Another piece of useful information from the quantum chemical calculations is the absolute orientations of ^{17}O NMR tensors in the molecular frame. As seen from Fig. 3, the *orientations* of the ^{17}O NMR tensors for O2 and O4 are similar, despite the large difference in the magnitude of the individual tensor components. It should be noted that the relative orientation between the ^{17}O EFG and CS tensors shown in Fig. 3 is in agreement with the experimental determination from the analysis of static ^{17}O NMR spectra.

In summary, we have presented the first solid-state ^{17}O NMR study of a free nucleic acid base. The present study demonstrates that it is feasible to obtain solid-state ^{17}O NMR spectra for ^{17}O-labeled nucleobases and that ^{17}O NMR *tensors* are excellent indicators of H-bond formation. These features are potentially useful for probing base pairing in nucleic acids. With the availability of very high magnetic fields (18.8 T or higher) and the advances in solid-state NMR methodology, it is anticipated that solid-state ^{17}O NMR will become a new addition to the arsenal for studying biological macromolecules.

G. W. thanks NSERC of Canada for research and equipment grants, Queen's University for a Chancellor's Research Award and the Government of Ontario for a Premier's Research Excellence Award. This research was partially supported by a grant from the Advisory Research Committee of Queen's University.

Notes and references

1 D. W. Boykin, *^{17}O NMR Spectroscopy in Organic Chemistry*, CRC Press, Boca Raton, Florida, 1991.
2 (*a*) G. Wu, K. Yamada, S. Dong and H. Grondey, *J. Am. Chem. Soc*., 2000, **122**, 4215; (*b*) K. Yamada, S. Dong and G. Wu, *J. Am. Chem. Soc*., 2000, **122**, 11 602.
3 S. Dong, R. Ida and G. Wu, *J. Phys. Chem. A*, 2000, **104**, 11 194.
4 S. Dong, K. Yamada and G. Wu, *Z. Naturforsch. A*, 2000, **55**, 21.
5 G. Wu, A. Hook, S. Dong and K. Yamada, *J. Phys. Chem. A*, 2000, **104**, 4102.
6 (*a*) J. T. Cheng, J. C. Edwards and P. D. Ellis, *J. Phys. Chem*., 1990, **94**, 553; (*b*) W. P. Power, R. E. Wasylishen, S. Mooibroek, B. A. Pettitt and W. Danchura, *J. Phys. Chem*., 1990, **94**, 591.
7 K. Ozeki, N. Sakabe and J. Tanaka, *Acta Crystallogr*., 1969, **B25**, 1038.
8 Gaussian 98, Revision A.6, M. J. Frisch, G. W. Trucks, H. B. Schlegel, G. E. Scuseria, M. A. Robb, J. R. Cheeseman, V. G. Zakrzewski, J. A. Montgomery, R. E. Stratmann, J. C. Burant, S. Dapprich, J. M. Millam, A. D. Daniels, K. N. Kudin, M. C. Strain, O. Farkas, J. Tomasi, V. Barone, M. Cossi, R. Cammi, B. Mennucci, C. Pomelli, C. Adamo, S. Clifford, J. Ochterski, G. A. Petersson, P. Y. Ayala, Q. Cui, K. Morokuma, D. K. Malick, A. D. Rabuck, K. Raghavachari, J. B. Foresman, J. Cioslowski, J. V. Ortiz, B. B. Stefanov, G. Liu, A. Liashenko, P. Piskorz, I. Komaromi, R. Gomperts, R. L. Martin, D. J. Fox, T. Keith, M. A. Al-Laham, C. Y. Peng, A. Nanayakkara, C. Gonzalez, M. Challacombe, P. M. W. Gill, B. Johnson, W. Chen, M. W. Wong, J. L. Andres, M. Head-Gordon, E. S. Replogle and J. A. Pople, Gaussian, Inc., Pittsburgh, PA, 1998.
9 (*a*) A. D. Becke, *Phys. Rev*., 1988, **A38**, 3098; (*b*) C. Lee, W. Yang and R. G. Parr, *Phys. Rev*., 1988, **B37**, 785; (*c*) A. D. Becke, *J. Chem. Phys*., 1993, **98**, 5648.

CHEMCOMM Communication
www.rsc.org/chemcomm

Evidence for weak base site participation in the vapour phase methylation of catechol over solid base catalysts

Venkataraman Vishwanathan,*[ab] Steven Ndou,[b] Lucky Sikhwivhilu,[b] Neville Plint,[b] K. Vijaya Raghavan[a] and Neil J. Coville*[b]

[a] *Indian Institute of Chemical Technology, Hyderabad 500-007, India*
[b] *Molecular Sciences Institute, School of Chemistry, University of the Witwatersrand, Johannesburg, Wits 2050, South Africa. E-mail: ncoville@aurum.chem.wits.ac.za*

Received (in Cambridge, UK) 15th February 2001, Accepted 2nd April 2001
First published as an Advance Article on the web 24th April 2001

The vapour phase alkylation of catechol over supported caesium catalysts gives good selectivity to guaiacol formation, and TPD studies indicate that this result can be correlated with the presence of weak basic sites on the catalyst.

Vapour phase alkylation of catechol is commercially important for the production of oxy-alkylated products, namely guaiacol and veratrole. These are synthetic intermediates used in the production of flavourings, fragrances and pharmaceuticals.[1] Studies on phenol alkylation have shown that product selectivity depends on the acid–base property of the catalyst surface.[2] The addition of metal ions to alumina is known to generate new active sites which are basic in nature.[3] Available literature on the vapour phase alkylation of catechol over solid base catalysts, though limited, suggests that the basic sites are primarily responsible for the formation of C-/O-alkylated products.[4,5] This is further supported by the report that CO_2 adsorption over the basic sites leads to catalyst deactivation.[6,7] However, there is no evidence to suggest that the weak sites over the base catalysts are primarily important for the formation of mono oxy-methylated products, in particular guaiacol. Here, for the first time, such a correlation is proposed, *i.e.* that a correlation exists between the weak base sites on a catalyst surface and selectivity to guaiacol.

The supported caesium catalysts were prepared by impregnating Al_2O_3, SiO_2 and TiO_2, all of commercial origin, with an appropriate amount of an aqueous solution of caesium hydroxide (10% Cs by mass). The resulting solids were dried and calcined in air at 673 K for 4 h. Temperature programmed desorption (TPD) was performed using CO_2 gas at a heating rate of 10 K min^{-1} in the temperature range 373–973 K.

The vapour phase alkylation of catechol with methanol was carried out in a vertical flow-type reactor at 623 K at atmospheric pressure (*ca.* 650 mm Hg). Before the start of the experiment, the catalyst (*ca.* 2 g) was activated in the reactor at 673 K for 1 h in nitrogen and then the solid was cooled to the reaction temperature. A pre-mixed catechol–methanol (1 : 3 w/w ratio) mixture was fed from the top of the reactor at a fixed rate of 5.1 ml min^{-1} (methanol-free catechol flow rate 0.95 mol h^{-1}) by means of a Sage syringe pump. After 1 h the liquid products were analysed by GC (FID) using a DB-1 capillary column. The reaction products were further confirmed by GC–MS (VG-11-250 data system) and ^{13}C NMR (Brucker AC-400) spectroscopy.

The reaction data for the vapour phase alkylation of catechol over unsupported and supported catalysts are shown in Table 1. The acidic oxides (Al_2O_3, SiO_2 and TiO_2) do not show much guaiacol formation. However, the basic oxide MgO shows a selectivity of 65% for guaiacol. This suggests that the basic sites on the catalyst *surface* are involved in the formation of guaiacol. It is interesting to note that caesium oxide alone shows a low activity and selectivity towards guaiacol formation. However, impregnation of caesium on to the acidic oxides (Al_2O_3, SiO_2 and TiO_2), increased the selectivity for guaiacol significantly. Both alumina and caesium-modified alumina show the highest reaction activity as compared to the other unsupported and supported oxides. This suggests that the stronger and larger number of acidic sites on the catalyst surface promotes more ring alkylation than side (O-) alkylation. In the case of both alumina and caesium-modified alumina a significant amount of polyalkylated products is also formed. The formation of phenol, and to a lesser extent diphenyl ether, indicates that both dehydration and ring alkylation are the two competitive

Table 1 Reaction data on unsupported and supported cesium catalysts

Catalyst	Activity mol h^{-1} g^{-1}	Selectivity (%) Guaiacol 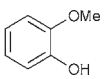	Veratrole 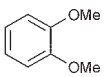	C-alkylated products[a]	Others[b]
TiO_2	0.718	10	2	36	42
Al_2O_3	2.341	18	3	73	6
SiO_2	0.133	20	43	33	4
MgO	0.106	65	15	15	5
Cs_2O	0.053	16	17	6	57
10 wt% Cs_2O/TiO_2	0.426	37	12	10	41
10 wt% Cs_2O/Al_2O_3	1.409	58	1	28	13
10 wt% Cs_2O/SiO_2	0.505	75	16	4	5

[a] 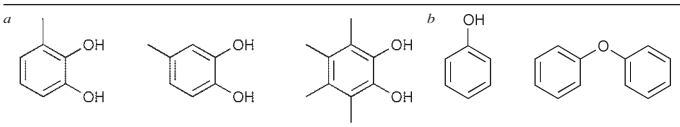
[b]

DOI: 10.1039/b101497h

reactions operating over the acidic sites. This is supported by the fact that both TiO_2 and $Cs–TiO_2$ show a significant amount of dehydrated products as compared with Al_2O_3 and $Cs–Al_2O_3$ catalysts.

The distribution of basic sites over unpromoted and promoted catalysts are shown in Fig. 1 and 2. The TPD profiles of CO_2 over Al_2O_3 and MgO (Fig. 1) show that although Al_2O_3 is more

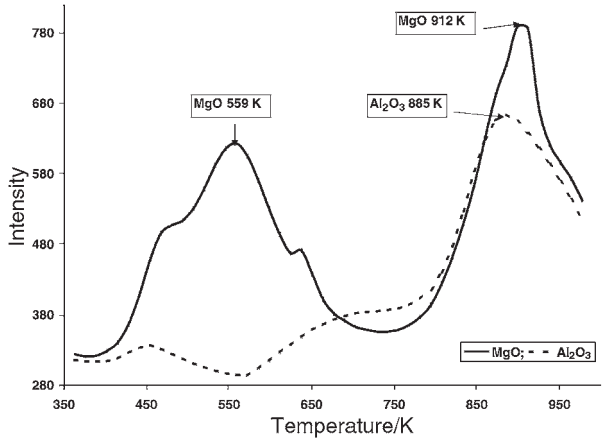

Fig. 1 CO_2 TPD profiles of MgO and Al_2O_3.

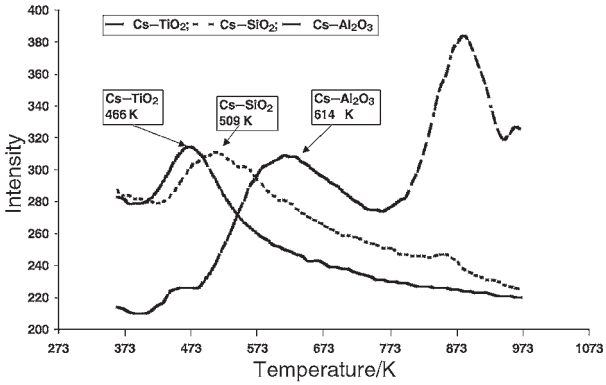

Fig. 2 CO_2 TPD profiles of Cs on TiO_2, SiO_2 and Al_2O_3.

acidic than MgO it also has a larger number of strong basic sites (885 K) with respect to MgO (912 K). The stronger basic sites on MgO at 912 K indicate that, apart from O^{2-} basic sites of MgO, the adjacent Mg^{2+} sites may also participate in CO_2 adsorption.[8] On the other hand, MgO has a greater number of weaker basic sites (559 K) than Al_2O_3. The fact that more guaiacol is formed on MgO than Al_2O_3 indicates that weaker basic sites may be primarily involved for the higher selectivity of guaiacol. Fig. 2 clearly demonstrates this finding. Here it is seen that addition of caesium to acidic supports transforms stronger base sites into weak sites, thus enhancing the selectivity for guaiacol. The higher selectivity for guaiacol at weaker basic sites over $Cs–SiO_2$ (75%) as compared with $Cs–Al_2O_3$ (58%) further supports the assumption that the formation of guaiacol is related to the strength and the number of the weak basic sites. However, in the case of $Cs–TiO_2$, the lower selectivity for guaiacol (37%) may suggest the possibility of an interaction between the promoter and titania, leading to compound formation.

In conclusion, it is evident from the foregoing results that the transformation of stronger basic sites to weaker ones upon addition of Cs_2O results in higher selectivity for guaiacol. Further work is in progress to explain the characteristic aspects of the title reaction in detail.

We wish to thank the University, THRIP and the NRF for financial support. The leave of absence granted by IICT, India, to V. V., to spend time at the University of the Witwatersrand, is acknowledged.

Notes and references

1 G. Dorothea, in *Phenol derivatives, Ullman Encyclopedia of Industrial Chemistry*, ed. E. Barabara, H. Stephen and S. Gail, VCH Verlagsgerellschaft, Weinhein, 1991, vol. A19, p. 354.
2 K. Tanabe and T. Nishizaki, *Proceedings of the 6th Congress on Catalysis*, London, 1977, vol. 2, p. 863.
3 K. Jurczyk and W. Kania, *Appl. Catal.*, 1989, **56**, 203.
4 S. Porchek, L. K. Minsker, R. Doeper and A. Renken, *Chem. Eng. Sci.*, 1996, **51**, 2933.
5 S. Porchek, R. Doeper and A. Renken, *Chem. Eng. Technol.*, 1994, **17**, 108.
6 Y. Fu, T. Baba and Y. Ono, *Appl. Catal., A: General*, 1998, **166**, 419.
7 Y. Fu, T. Baba and Y. Ono, *Appl. Catal., A: General*, 1998, **166**, 425.
8 H. Hattori, *Chem. Rev.*, 1995, **95**, 545.

CHEMCOMM Communication
www.rsc.org/chemcomm

Metallaboranes of the earlier transition metals. An *arachno* nine-vertex, nine-skeletal electron pair rhenaborane of novel shape: importance of total vertex connectivities in such systems

Sundargopal Ghosh, Arnold L. Rheingold*[a] and Thomas P. Fehlner*[b]

[a] *Department of Chemistry and Biochemistry, University of Delaware, Newark, DE 19716, USA. E-mail: arnrhein@udel.edu*
[b] *Department of Chemistry and Biochemistry, University of Notre Dame, Notre Dame, IN 46556, USA. E-mail: fehlner.1@nd.edu*

Received (in Irvine, CA, USA) 28th February 2001, Accepted 3rd April 2001
First published as an Advance Article on the web 24th April 2001

The synthesis and characterization of $Cp^*_2Re_2B_7H_{11}$ provides the first example of an open hypoelectronic metallaborane which is shown to possess an *arachno* geometry based on a total vertex connectivity identical with that of a canonical *arachno* nine-vertex, twelve-skeletal electron pair cluster.

Extensive catenation is a characteristic shared by the adjacent elements boron and carbon albeit expressed differently in structure, *e.g.* cages *vs.* rings and chains. The origin of the differences is well understood and the established relationship between geometry and the number of skeletal electron pairs (sep) for borane cages serves to provide interconnections between borane, heteroborane, carbocation, transition metal cluster and Zintl phase cluster chemistries.[1–6] The metal sites in a heteroborane, *e.g.* a metallaborane, perturb the borane bonding network and the structural response can be measured.[7,8] In an expression of the isolobal analogy, metallaboranes containing late transition metals frequently mimic simple main group fragments generating geometries that conform to the canonical structures associated with equivalent sep (the term cannonical refers to the set of shapes and associated sep's exhibited by the known boranes).[9,10]

The observations of Kennedy and coworkers of 'disobedient' metallaboranes[11] with *closo* geometries deviating from most spherical deltahedra (most homogeneous vertex connectivities)[12] have been interpreted in terms of a metal providing more orbitals to meet the $p + 1$ sep rule ('*isocloso*'–missing electrons localized on the metal)[13] or fewer electrons (p sep) demanding a skeletal shape with no borane analog ('*hypercloso*'–missing electrons delocalized over the skeleton).[14] Despite these contrasting analyses, what is clear is that the observed geometric structures are related by diamond–square–diamond (dsd) rearrangements.[15] Recently, we have described a homologous series of *closo*-metallaboranes, $Cp^*_2Re_2B_nH_n$ (n = 7–10, Cp^* = η^5-C_5Me_5), with $p - 2$ sep.[16] In addition, we completed a 10-atom, closed metallaborane series for sep running from $p + 1$ to $p - 2$.[17,18] These results demonstrate that the formal sep can vary widely from the canonical number and, as it decreases, the cluster shape deviates from that of a most spherical deltahedron. Taking the canonical shapes and sep's as the standard, we follow Corbett and designate these compounds as hypoelectronic.[19] Note that because hypoelectronic and canonical structures are related by dsd rearrangements, the total connectivity of the deltahedral framework is the same for a given value of p.

Kennedy and coworkers have also described examples of '*isonido*' metallaboranes ($p + 1$ sep) related to canonical *nido* geometries ($p + 2$ sep) in the same manner as '*isocloso*' are to *closo*.[11] For this reason we have sought examples of open clusters of the earlier metals in which the formal sep is even lower. Herein we describe an open rhenaborane with p sep and show how it can be classified as an *arachno* shape which normally requires $p + 3$ sep.

As previously reported, the reaction of BH_3·thf with $Cp^*_2Re_2H_4B_4H_4$ leads to the formation of $Cp^*_2Re_2B_7H_7$ and subsequent conversion to the higher analogs.[16,20,21] A minor product with an R_f higher than $Cp^*_2Re_2B_7H_7$ was greatly enhanced by using a lower borane to metallaborane ratio and reduced temperature and reaction time.† This new compound, **1**, has been isolated in modest yield and characterized spectroscopically and by a single crystal X-ray diffraction study.‡ The molecular mass corresponds to $Cp^*_2Re_2B_7H_{11}$ **1**, and the ^{1}H (temperature independent to −90 °C) and ^{11}B NMR spectra suggest two planes of symmetry. Besides the $BH_{terminal}$ protons (1 : 2 : 4) two equivalent BHB and two equivalent BHRh protons are also observed. A ^{1}H/^{11}B HETCOR experiment shows the latter four protons to be coupled exclusively to the four boron atoms equivalent in the NMR spectrum.

The framework structure of **1** only became clear when the solid state structure was determined (Fig. 1). Yet again an unanticipated shape is observed for a rhenaborane. **1** displays an open structure such that the edges defining the opening describe a boat shaped cyclohexane-like ring. Although the B–B and Re–B distances are comparable to those found in $Cp^*_2Re_2B_7H_7$[22,23] and higher homologues,[16] the ReRe distance is *ca.* 0.15 Å longer. On the other hand it is nearly the same as the W–W distance in $Cp^*_2W_2H_2B_7H_7$[20,21] and, thus, we suggest the presence of cross-cage metal–metal bonding in **1**. Based on the NMR results, the extra hydrogens can be placed on this skeleton in two ways as shown in Fig. 2(a) and (b). In (a) the ReH hydrogens lie in the plane of symmetry containing the two Re atoms and the unique B atom. In (b) they bridge two of the four

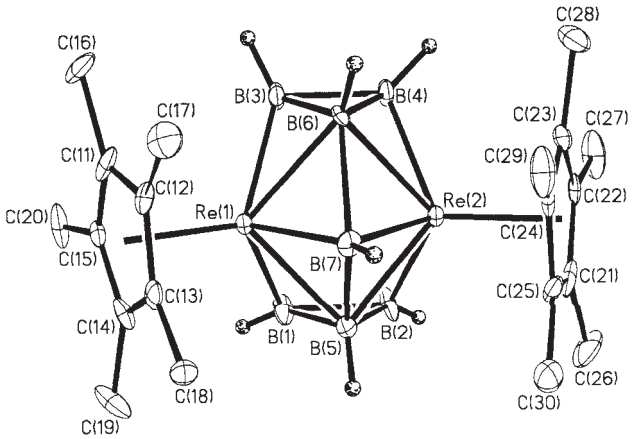

Fig. 1 Molecular structure and labelling diagram for $(Cp^*Re)_2B_7H_{11}$. Selected bond distances (Å) for one of two independent but chemically equivalent molecules: Re(1)–Re(2) 2.9744(5), Re(1)–B(1) 2.216(13), Re(1)–B(3) 2.221(13), Re(1)–B(5) 2.241(12), Re(1)–B(6) 2.271(11), Re(2)–B(2) 2.227(12), Re(2)–B(4) 2.211(12), Re(2)–B(5) 2.236(12), Re(2)–B(6) 2.258(13), Re(2)–B(7) 2.091(12), B(1)–B(2) 1.753(17), B(1)–B(5) 1.728(17), B(2)–B(5) 1.736(19), B(3)–B(4) 1.747(16), B(4)–B(6) 1.734(18), B(5)–B(7) 2.012(18), B(6)–B(7) 2.044(17).

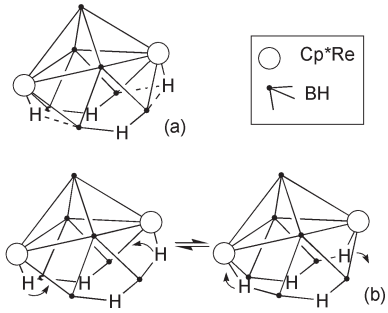

Fig. 2 Two possible placements of the four endo hydrogen atoms on **1**.

Re–B edges on the hexagonal opening thereby demanding a low barrier process for the exchange shown. We favor (b) as it is difficult to explain the observed coupling to boron with model (a).

As the Cp*Re fragment is a zero-electron fragment, the formal number of sep in **1** is 9; however, we find no way of connecting the geometry of **1** to either the canonical deltahedra or the observed deltahedra of $Cp^*_2Re_2B_nH_n$, (n = 7–10) by simple vertex removal. Therefore, we suggest an alternative approach which promises some generality. As already mentioned, the geometries adopted by $Cp^*_2Re_2B_nH_n$ (n = 7–10), have total vertex connectivities (tvc) equal to those of the canonical deltahedra, *e.g.* $Cp^*_2Re_2B_7H_7$ possesses two six-coordinate, two five-coordinate, five four-coordinate vertices (tvc = 42) whereas the canonical tricapped trigonal prism has six five-coordinate, three four-coordinate vertices (tvc = 42). An examination of the canonical *closo* series for p = 6–12 shows that the tvc increases monotonically in units of 6, *i.e.* tvc runs from 24 to 60.[16] This holds true for $Cp^*_2Re_2B_nH_n$ (n = 7–10) as well.[15] Likewise, if one uses Williams' preferred *nido* and *arachno* geometries,[24] one finds, that for *nido* cages, p = 6–11, tvc runs from 20 to 50 in units of 6 and for *arachno* cages, p = 6–10, tvc runs from 18 to 42 in units of 6. The assumption that tvc is conserved for *nido* and *arachno* structures, as already demonstrated for *closo* structures, yields a shape independent method for classifying non-canonical geometries.

Consider the new rhenaborane. **1** has an open structure with a tvc = 36. The canonical nine fragment *closo, nido* and *arachno* shapes have tvc's of 42, 38 and 36, respectively (Fig. 3). Thus, **1** is classified as a 9 sep *arachno* analog of a 12 sep canonical *arachno* borane. This parallels the relationship of 7 sep *closo* $Cp^*_2Re_2B_7H_7$ to a 10 sep *closo* canonical cage. The beauty of the approach is that it avoids the question of how many electrons a metal fragment actually contributes to cluster bonding ('*isocloso' vs. 'hypercloso'*) and suggests that, provided tvc is conserved, the shape adopted can be tailored to the electronic demands of the metal. The drawback is that, although this approach limits the number of shapes possible, it is not predictive. However, with the characterization of an increasing number of metallaboranes containing earlier metals, the role of the metal may eventually become sufficiently well defined to permit predictions as well as rationalizations.

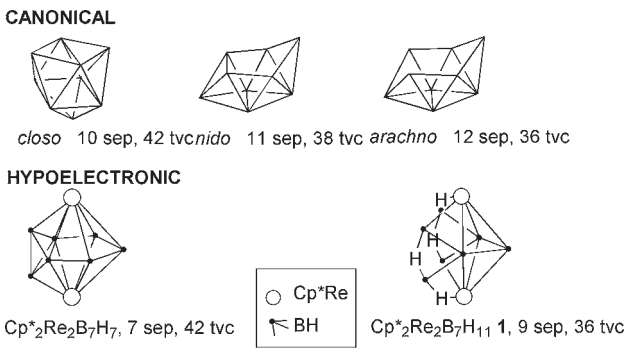

Fig. 3 Comparison of the canonical nine-atom *closo*, *nido* and *arachno* geometries with observed examples of *closo* and *arachno* hypoelectronic rhenaboranes with formal sep's three lower than the canonical values.

The generous support of the National Science Foundation is gratefully acknowledged.

Notes and references

† *Synthetic procedure* for **1**: to a 100 mL Schlenk tube, containing 0.15 g (0.21 mmol) of $(Cp^*ReH_2)_2B_4H_4$ in 15 mL of toluene was slowly added a three-fold excess of BH_3·thf. The reaction mixture was thermolysed for 15 h at 75 °C after which volatiles were removed *in vacuo*, the residue was extracted in hexane, and the extract filtered through Celite. After removal of solvent from the filtrate, the residue was chromatographed on silica gel TLC plates. Elution with hexane yielded four very closely spaced bands. The first yellow band to elute was $Cp^*_2Re_2B_7H_{11}$ **1** (0.026 g, 17%) and the subsequent bands were $(Cp^*Re)_2B_nH_n$ (n = 7–10).

Selected data for **1**: ν(hexane)/cm^{-1} 2498w, 2444w (B–H_{term}); δ_H(C_6D_6, 22 °C) 10.61 (pcq, 1BH_t), 7.51 (pcq, 4BH_t), 0.72 (pcq, 2BH_t), 0.04 (br, 2B–H–B), 1.76 (s, 30H, 2Cp*), −10.77 (s, 2Re–H–B); δ_B(C_6D_6, 22 °C, J/Hz) 98.1 (d, J_{BH} 162, 2B), 28.3 (d, J_{BH} 130, 4B), −7.2 (d, J_{BH} 141, 2B); HR-EIMS, m/z: $^{12}C_{20}{}^{1}H_{41}{}^{11}B_7{}^{187}Re_2$, calc. 732.2982, obs. 732.2948; isotope distribution corresponding to 7B, 2Re.

‡ *Crystal data* for $(Cp^*Re)_2B_7H_{11}$: M = 759.5, triclinic, $P\bar{1}$, yellow, a = 8.7967(2), b = 17.7865(3), c = 18.0509(4) Å, α = 111.5640(10), β = 102.924(2), γ = 99.4110(10)°, V = 2464.21 Å^3, Z = 4, Z' = 2, D_c = 2.046 g cm^{-3}, μ(Mo-Kα) = 98.2 cm^{-1}, $R(F)$ = 0.0485, $R(wF2)$ = 0.1372. Of 20 160 reflections collected, 8614 were independent. All non-hydrogen atoms were refined anisotropically. All Cp* hydrogen atoms were placed in idealized locations; the seven terminal B–H hydrogen atoms were located and refined. The four bridging hydrogen atoms were not located. CCDC 155582. See http://www.rsc.org/suppdata/cc/b1/b101918j/ for crystallographic data in .cif or other electronic format.

1 K. Wade, *Inorg. Nucl. Chem. Lett*., 1972, **8**, 559.
2 K. Wade, *New Sci*., 1974, **62**, 615.
3 K. Wade, *Adv. Inorg. Chem. Radiochem*., 1976, **18**, 1.
4 D. M. P. Mingos, *Nature (London)*, 1972, **236**, 99.
5 D. M. P. Mingos and D. J. Wales, *Introduction to Cluster Chemistry*, Prentice Hall, New York, 1990.
6 *Structural and Electronic Paradigms in Cluster Chemistry*, ed. D. M. P. Mingos, Springer, 1997, vol. 87.
7 T. P. Fehlner, *J. Chem. Soc., Dalton Trans*., 1998, 1525.
8 T. P. Fehlner, *Organometallics*, 2000, **19**, 2643.
9 J. D. Kennedy, *Prog. Inorg. Chem*., 1984, **32**, 519.
10 J. D. Kennedy, *Prog. Inorg. Chem*., 1986, **34**, 211.
11 J. D. Kennedy, in *The Borane, Carborane, Carbocation Continuum*, ed. J. Casanova, Wiley, New York, 1998, p. 85.
12 R. E. Williams, *Inorg. Chem*., 1971, **10**, 210.
13 J. D. Kennedy, *Inorg. Chem*., 1986, **25**, 111.
14 R. T. Baker, *Inorg. Chem*., 1986, **25**, 109.
15 R. L. Johnston, D. M. P. Mingos and P. Sherwood, *New J. Chem*., 1991, **15**, 831.
16 S. Ghosh, M. Shang, Y. Li and T. P. Fehlner, *Angew. Chem., Int. Ed*., 2001, **40**, 1125.
17 R. Littger, U. English, K. Ruhlandt-Senge and J. T. Spencer, *Angew. Chem., Int. Ed*., 2000, **39**, 1472.
18 X. Lei, M. Shang and T. P. Fehlner, *Organometallics*, 2001, **20**, 1479.
19 S. C. Sevov and J. D. Corbett, *Inorg. Chem*., 1991, **30**, 4875.
20 S. Ghosh, M. Shang and T. P. Fehlner, *J. Organomet. Chem*., 2000, **614–615**, 92.
21 S. Ghosh, X. Lei, M. Shang and T. P. Fehlner, *Inorg. Chem*., 2000, **39**, 5373.
22 A. S. Weller, M. Shang and T. P. Fehlner, *Chem. Commun*., 1998, 1787.
23 A. S. Weller, M. Shang and T. P. Fehlner, *Organometallics*, 1999, **18**, 853.
24 R. E. Williams, in *The Borane, Carborane, Carbocation Continuum*, ed. J. Casanova, Wiley-Interscience, New York, 1997, p. 3.

CHEMCOMM
Communication
www.rsc.org/chemcomm

Extremely high *trans* selectivity of Ti-MWW in epoxidation of alkenes with hydrogen peroxide

Peng Wu and Takashi Tatsumi*

Division of Materials Science & Chemical Engineering, Faculty of Engineering, Yokohama National University, 79-5 Tokiwadai, Hodogaya-ku, Yokohama 240-8501, Japan. E-mail: ttatsumi@ynu.ac.jp

Received (in Cambridge, UK) 13th February 2001, Accepted 16th March 2001
First published as an Advance Article on the web 24th April 2001

A novel titanosilicate with MWW topology, Ti-MWW, exhibits a behavior not observed on other titanosilicates such as TS-1, TS-2 and Ti-beta, in that it selectively epoxidizes *trans* isomers from a mixture of *cis*/*trans* alkenes with retention of stereochemistry.

The microporous titanosilicate TS-1 of MFI structure has attracted considerable attention of researchers since it is found to be an effective liquid-phase catalyst in the oxidation of various organic compounds using dilute hydrogen peroxide as an oxidant.[1] Ti-beta,[2,3] Ti-MOR[4] and Ti-ITQ-7[5] have also been prepared successfully with a purpose to make full use of various zeolite structures. Recently, we turned our attention to MWW zeolite (typically known as MCM-22[6]) because it has the structural diversity of supercages, 10-membered ring (MR) channels and side pockets, succeeding for the first time in preparing its titanosilicate derivative, Ti-MWW.[7]

In the epoxidation of lower olefins, Clerici *et al*. reported that TS-1 was more active for *cis*-but-2-ene than for *trans*-but-2-ene, which made TS-1 applicable to the production of epoxy derivatives with *cis*-configuration by starting from a mixture of alkenes containing *cis*/*trans* isomers.[8] We also observed that TS-1 was more selective for the *cis* isomers in the epoxidation of a *cis*/*trans* mixture of hex-2-enes.[9] The *cis*-selectivity of TS-1 is attributed to the higher reactivity of the *cis* isomer in epoxidation of various C_4 olefins.[1,8] However, we have discovered a totally opposite catalytic feature of Ti-MWW in the epoxidation of olefinic stereoisomers, which may bring about reconsideration of the stereoselectivity of titanosilicates in olefin epoxidation and give rise to investigation of the relationship between shape selectivity and microstructure of Ti active sites.

Ti-MWW was prepared by treating a Ti-containing lamellar precursor with MWW topology with acid solution, and subsequent calcination. The Ti-containing precursor was hydrothermally synthesized from fumed silica (Cab-o-sil M7D) and tetrabutyl orthotitanate in the presence of boric acid and using piperidine as a structure-directing agent (SDA) as reported in detail elsewhere.[7] Acid treatment with 2 M HNO_3 on the lamellar precursor removed extraframework Ti species together with some framework boron. The samples were then calcined in air at 803 K to burn off the organic SDA to obtain the Ti-MWW catalysts. The samples were proved to have the MWW topology by X-ray diffraction, and contain only isolated Ti species in the framework as evidenced by the predominant band at 220 nm in the UV–VIS spectrum (Fig. 1).

Other titanosilicates for control experiments, TS-1, TS-2, Ti-beta and Ti-MOR were prepared by a hydrothermal synthesis method or post-synthesis method using $TiCl_4$ vapor.[4] The liquid-phase oxidation of *cis*/*trans* mixtures of alkenes with hydrogen peroxide was carried out at 333 K in a round-bottom flask (20 ml) fitted with a condenser and a magnetic stirrer. For a typical run, a mixture of 0.05 g of catalyst, 10 mmol of alkenes, 10 mmol of hydrogen peroxide (31 wt% aqueous solution) and 10 mL of solvent was heated at a set temperature under vigorous agitation. The reaction mixture was analyzed using a gas chromatograph (Shimadzu 14 B) equipped with a 50 m OV-1 capillary column. The amount of hydrogen peroxide remaining in the reaction mixture was determined by titration with 0.1 M $Ce(SO_4)_2$ solution.

Table 1 shows the results of epoxidation of hex-2-ene isomers with a *cis*/*trans* ratio of 41 : 59 over various titanosilicates. The major products were 2,3-epoxyhexane with both *cis*- and *trans*-configurations. A small amount of diol product due to epoxide hydrolysis over acid sites was also obtained, especially for Ti-beta, owing to the rather strong acidity relating to the framework Al. The conversion of hex-2-enes depended greatly on the reaction conditions; Ti-MWW showed the highest specific catalytic activity in MeCN and higher efficiency in H_2O_2 utilization. What is more interesting is that Ti-MWW exhibited an extremely high selectivity for the epoxide with *trans*-configuration, while TS-1, TS-2, Ti-beta and Ti-MOR produced the *cis*-epoxide with a selectivity higher than the percentage of *cis*-isomer in the initial substrate. The selectivity of Ti-MWW for *trans*-epoxide was independent of its Ti content (entries 1–3) and the reaction time (entries 2 and 4) although the conversion increased with increase in Ti content. This unique property was not affected when using the protic solvent MeOH though the conversion was greatly decreased (entry 5). Furthermore, in the epoxidation of other olefins such as hept-2-enes, hept-3-enes and oct-2-enes all with a *cis*/*trans* ratio of 50 : 50, Ti-MWW showed a selectivity of 80, 72 and 81% for the corresponding *trans*-epoxides, respectively. All these findings allow us to draw the conclusion that Ti-MWW is a catalyst with a unique selectivity in the epoxidation of a mixture of *cis*/*trans* isomers.

Since the epoxidation of a mixture of *cis*/*trans* isomers is a competition reaction, the reaction of individual isomers would make the matter clearer. Fig. 2 compares Ti-MWW with TS-1 for the epoxidation of *cis*- and *trans*-oct-2-enes. Retention of seterochemical configuration was found for both Ti-MWW and TS-1, *i.e*. *cis*-oct-2-ene gave exclusively the *cis*-epoxide, and *trans*-oct-2-ene resulted in the *trans*-epoxide. This indicates no isomerization occurred during the reaction for both the substrate and epoxide. Ti-MWW exhibited the reactivity order of *trans*-oct-2-ene > *cis*-oct-2-ene, while TS-1 showed the reverse order. The higher reactivity of the *trans* isomer on Ti-MWW is

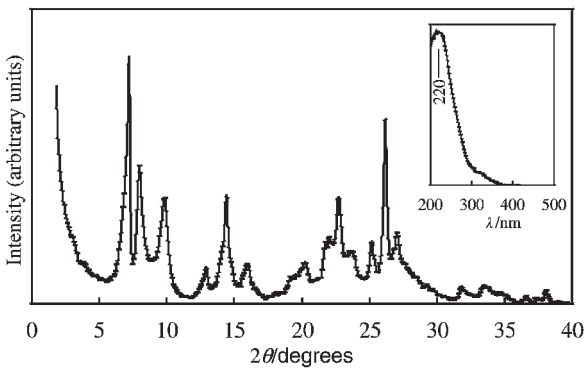

Fig. 1 X-Ray diffraction pattern and UV–VIS spectrum of Ti-MWW (Si : Ti = 64).

Table 1 Epoxidation of hex-2-ene isomers with hydrogen peroxide over various titanosilicates

				Prod. sel. (mol%)		Epoxide distribution (mol%)[a]		H_2O_2 (mol%)	
Entry	Cat.	Si/Ti	Conv. (mol%)	Epoxides	Diols	*cis*	*trans*	Conv.	Efficiency
1	Ti-MWW	146	16.4	97	3	20	80	18.4	89
2	Ti-MWW	64	37.6	99	1	17	83	39.6	95
3	Ti-MWW	46	50.8	99	1	19	81	66.1	92
4	Ti-MWW[b]	64	16.0	99	1	15	85	39.6	95
5	Ti-MWW[c]	64	9.3	98	2	18	82	9.6	97
6	TS-1	52	17.8	94	6	65	35	25.7	71
7	TS-1	42	29.1	96	4	66	34	32.5	89
8	TS-2	95	13.6	96	4	67	33	18.0	77
9	Ti-Beta	40	15.9	91	9	73	27	35.8	45
10	Ti-MOR	79	2.6	99	1	52	48	3.9	66

[a] Cat., 0.05 g; hex-2-enes (*cis*/*trans* = 41 : 59), 10 mmol; H_2O_2, 10 mmol; MeCN, 10 ml; temp., 333 K; time, 2 h. [b] The reaction time was 5 min. [c] MeOH used as solvent.

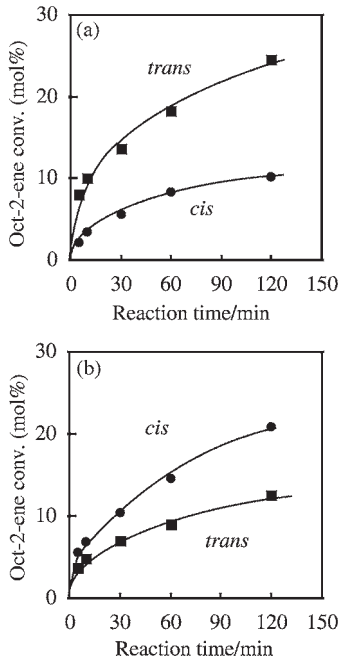

Fig. 2 Epoxidation of *cis* and *trans*-oct-2-ene over Ti-MWW (a) and TS-1 (b). Cat., 0.05 g; oct-2-ene, 10 mmol; H_2O_2, 10 mmol; MeCN, 10 mL; temp., 333 K.

thus consistent with its unique selectivity observed above in the reaction of mixtures.

Liquid-phase adsorption of a hex-2-ene mixture using the bulky solvent 1,3,5-triisopropylbenzene was carried out to investigate the different catalytic behavior between Ti-MWW and other titanosilicates. TS-1 adsorbed more selectively the *trans* isomer with smaller molecular size because of its medium pores of 10-MR. However, Ti-MWW, containing both 10-MR and 12-MR pores, exhibited similar adsorption phenomena to large-pore Ti-beta, that is, both adsorbents showed no obvious difference in the adsorption rate for the two isomers. Therefore, the high *trans* selectivity of Ti-MWW is not due to easier accommodation for the *trans* isomers.

Selective poisoning of the Ti sites in open space side pockets with 2,4-dimethylquinoline resulted in an unchanged conversion of hex-2-enes and the same *trans* selectivity for the epoxide, which indicates little contribution of the side pockets to the present epoxidation reactions. Therefore, the unique selectivity of Ti-MWW is presumed to originate mainly in its 10-MR channels and supercages, both restricted by 10-MR entrances. In particular, the 10-MR system of the MWW structure is defined by two-dimensional sinusoidal channels.[10] The unique tortuosity of the sinusoidal configuration would make the alkene molecules of *trans* configuration approach more easily to the Ti species than those of *cis* configuration, so resulting in higher *trans* selectivity. On the other hand, the channels of TS-1 and Ti-beta are suggested to favor the *cis* molecules approaching the Ti sites, owing to the characteristic tunnel-like channel structures. Further investigation in more detail is still required to clearly determine how the microstructure of Ti active sites affects the selectivity for substrates of different configurations. Nevertheless, the uniqueness of Ti-MWW strongly suggests the importance of considering 'steric compatability' between the substrate molecules and the Ti species when investigating shape selectivity.

As a result, this study clearly shows that Ti-MWW is an unusual catalyst in the oxidation of alkene stereoisomers, revealing a new concept of shape selectivity in constrained spaces in zeolite crystals.

Notes and references

1 M. Taramasso, G. Perego and B. Notari, *US Pat*., 4410501, 1983; G. Bellussi and M. S. Rigutto, *Stud. Surf. Sci. Catal*., 1991, **67**, 243; B. Norari, *Adv. Catal*., 1996, **41**, 253.

2 A. Corma, M. A. Camblor, P. Esteve, A. Martínez and J. Pérez-Pariente, *J. Catal*., 1994, **145**, 151.

3 N. Jappar, Q. Xia and T. Tatsumi, *J. Catal*., 1998, **180**, 132; T. Tatsumi and N. Jappar, *J. Phys. Chem*., 1998, **102**, 7126.

4 P. Wu, T. Komatsu and T. Yashima, *J. Catal*., 1997, **168**, 400; P. Wu, T. Komatsu and T. Yashima, *J. Phys. Chem. B*, 1998, **102**, 9297.

5 M. J. Díaz-Cabañas, L. A. Villaescusa and M. A. Camblor, *Chem. Commun*., 2000, 761.

6 M. E. Leonowicz, J. A. Lawton, S. L. Lawton and M. K. Rubin, *Science*, 1994, **264**, 1910.

7 P. Wu, T. Tatsumi, T. Komatsu and T. Yashima, *Chem. Lett*., 2000, 774; P. Wu, T. Tatsumi, T. Komatsu and T. Yashima, *J. Phys. Chem. B*, 2001, **105**, 2897.

8 M. G. Clerici and G. Bellussi, *Eur. Pat*. 315247 and 315248, 1988; M. G. Clerici and P. Ingallina, *J. Catal*, 1993, **140**, 71.

9 T. Tatsumi, M. Nakamura, K. Yuasa and H. Tominaga, *Chem. Lett*., 1990, 297.

10 S. L. Lawton, M. E. Leonowicz, P. D. Partridge, P. Chu and M. K. Rubin, *Microporous Mesoporous Mater*., 1998, **23**, 109.

CHEMCOMM Communication
www.rsc.org/chemcomm

First structural characterization of a mixed valent thallium(I/III) amide bearing an *n*-butylthallium(III) unit stabilized by a tripodal amido ligand

Christian H. Galka and Lutz H. Gade*

Laboratoire de Chimie Organométallique et de Catalyse, UMR 7513, Institut Le Bel, Université Louis Pasteur, 4, rue Blaise Pascal, 67000 Strasbourg, France. E-mail: gade@chimie.u-strasbg.fr

Received (in Cambridge, UK) 22nd January 2001, Accepted 10th April 2001
First published as an Advance Article on the web 24th April 2001

Lithiation of the tripodal amine HC{SiMe$_2$NH(*p*-Tol)}$_3$ with Bu^{n}Li in the presence of TlCl yielded the Tl(I/III) mixed valent complex [HC{SiMe$_2$N(*p*-Tol)}$_3$(TlBu^n)(Tl)] 2; an X-ray diffraction study established the central *n*-butyl–thallium(III) unit coordinated by the amido tripod in which two of the amido functions are additionally bridged by the Tl(I) atom.

The chemistry of formally closed shell low valent heavy p-block metals is characterized by unusual patterns of aggregation in the solid state through attractive metal–metal interactions.[1,2] We have recently begun to systematically investigate the structural chemistry of amidothallium(I) compounds in which the metal atoms occupy exposed positions thus making the molecules potential building blocks for larger aggregates.[3,4] The tripodal amido ligands developed by us were found to provide the platform for a whole series of polynuclear thallium(I) amides.[5,6] These are generally obtained by metal exchange reaction of the *in situ* generated or isolated lithium amides with TlCl in an ether or hydrocarbon solvent. In all cases the complete lithiation of the amine precursor was achieved before the metal exchange step. A simultaneous reaction of the alkyllithium reagent and thallium(I) chloride was expected to yield products which differ significantly from the compounds studied to date, and provide an entry into new types of mixed amido/alkylthallium complexes. Here, we report the remarkable first results of these variable metallation strategies.

Complete lithiation of the tripodal amine HC{SiMe$_2$NH(*p*-Tol)}$_3$ with Bu^{n}Li and subsequent reaction with either 3 molar equivalents of TlCl or 1 equivalent of $TlCl_3$ gave the Tl^{III} amide [HC{SiMe$_2$NH(*p*-Tol)}$_3$Tl] **1** which was characterized by elemental analysis as well as ^{1}H and ^{13}C NMR spectroscopy (Scheme 1).† However, upon carrying out the lithiation and transmetallation in one step by addition of 3 molar equivalents of *n*-butyllithium and thallium(I) chloride to the amine at

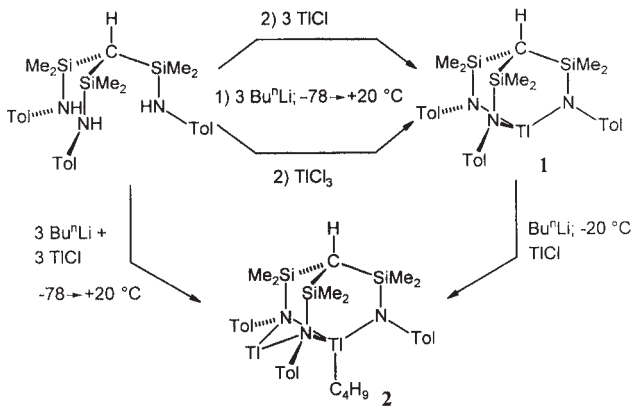

Scheme 1 Preparative routes leading to compounds **1** and **2**. In the conversion of **1** → **2** Bu^{n}Li probably first adds across one Tl^{III}–N bond alkylating the Tl^{III} centre. Subsequent Li–Tl^I exchange then gives **2**.

−78 °C in *n*-pentane and subsequent slow warming to ambient temperature over a period of 15 h a different type of compound was obtained as a yellow–orange crystalline solid **2**. The yield of the compound isolated in several preparations varied between 15 and 35% based on the amine starting material. The same material was isolated in higher yield (*ca.* 50%) upon reaction of **1** with 1 equivalent of *n*-butyllithium and transmetallation with TlCl. Its elemental analysis was consistent with two thallium atoms per ligand unit, and ^{1}H and ^{13}C NMR spectroscopy indicated that the product contained one residual *n*-butyl group.† A single crystal X-ray structure analysis confirmed the molecular structure of the Tl(III)/Tl(I) mixed metal complex **2** in which an *n*-butylthallium(III) unit is coordinated by the tripodal amido ligand while two of the donor atoms are bridged by a thallium(I) atom (Fig. 1).‡ The observation that the reaction of the lithium amide with TlCl exclusively leads to the Tl^{III} amide **1** which may be rationally converted to **2** by addition of Bu^{n}Li across a Tl^{III}–N bond and subsequent metal exchange (Scheme 1) suggests a formation of the *n*-butylthallium species along a similar route in the reaction of a mixture of Bu^{n}Li and TlCl with the amine.

Compound **2** is the first example of a structurally characterized long chain alkylthallium complex in contrast to the considerable number of methylthallium derivatives reported in the literature.[7] Such nonfunctionalized long chain alkylthallium species are thought to be thermally labile,[8] and it seems to be this particular coordination environment which renders **2** sufficiently stable to allow its isolation and characterization. The central thallium atom is not symmetrically coordinated by the ligand tripod due to the external bonding of the Tl(1) atom which not only draws the donor functions N(2) and N(3) together [N(2)–Tl(1)–N(3) 83.5(3)° in comparison to N(1)–Tl(1)–N(2) 99.3(3) and N(1)–Tl(1)–N(3) 104.7(3)°] but also induces an lengthening of the two Tl(1)–N bonds involved [Tl(1)–N(2) 2.321(7) Tl(1)–N(3) 2.326(7) Å in comparison to Tl(1)–N(1) 2.155(7) Å]. In contrast, the Tl–N bonds to monovalent Tl(2) are, as expected, significantly longer [Tl(2)–N(2) 2.694(7) and Tl(2)–N(3) 2.721(8)], in fact longer than those found in all thallium(I) amides hitherto investigated.[3–6,9] This may be a consequence of the extreme steric congestion in this part of the molecule in which the two heavy metal atoms are forced into close proximity by the bridging donor atoms; this leads to a remarkably short Tl(1)···Tl(2) contact of 3.3620(9) Å. The Tl(1)–C(40) bond length of 2.188(9) lies in the usual range of alkyl–Tl bonds in $TlMe_2$-complexes.[7]

The ^{1}H and ^{13}C NMR spectra of **2** recorded at 295 K in d_8-toluene are consistent with an effective threefold symmetry. The signals are broadened and coalesce upon cooling to 200 K, however, the rapid precipitation of the complex prohibited the detection of the low temperature limit. These observations suggest that the compound is fluxional with the 'external' Tl(I) atom exchanging between the different bridging positions. Such a 'rotation' of a monovalent metal atom coordinated to an amido tripod is reminiscent of the dynamic behaviour of the tripodal lithium triamidostannates investigated previously by us[10] and a similar dynamic behaviour has also been observed by Veith

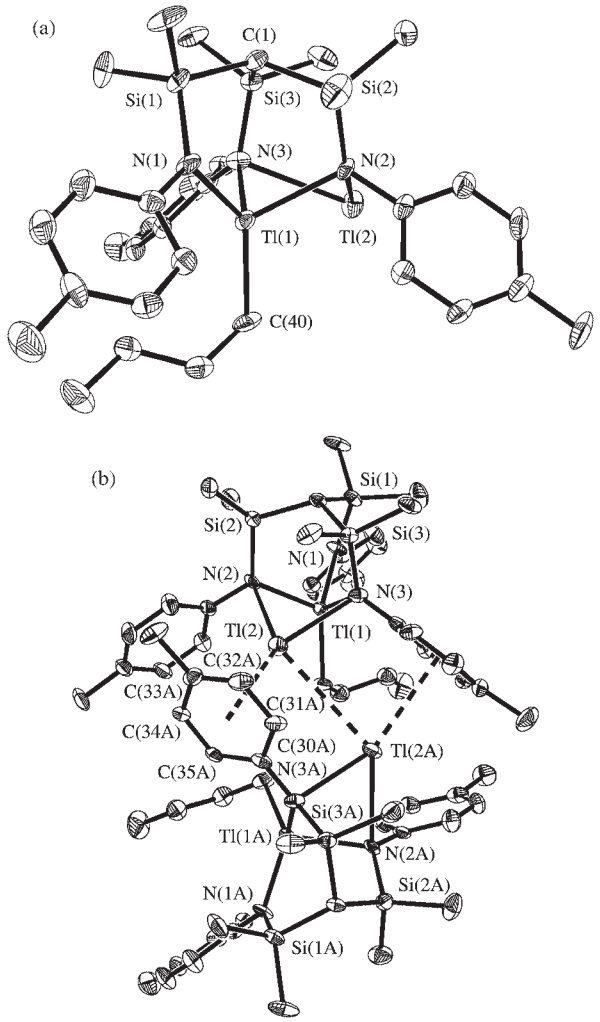

Fig. 1 (a) Molecular structure of $[HC\{SiMe_2N(p\text{-Tol})\}_3(TlBu^n)(Tl)]$ **2**. Selected bond lengths (Å) and interbond angles (°): C(1)–Si(1) 1.888(9), Si(1)–N(1) 1.733(8), Tl(1)–N(1) 2.155(7), Tl(1)–N(2) 2.321(7), Tl(1)–N(3) 2.326(7), Tl(2)–N(2) 2.694(7), Tl(2)–N(3) 2.721(8), Tl(1)–C(40) 2.188(9); Si(1)–C(1)–Si(2) 113.2(5), N(1)–Si(1)–C(1) 105.1(4), N(1)–Tl(1)–N(2) 99.3(3), N(1)–Tl(1)–N(3) 104.7(3), N(2)–Tl(1)–N(3) 83.5(3), N(2)–Tl(2)–N(3) 69.7(2), Tl(1)–N(2)–Tl(2) 83.8(2), Tl(1)–N(3)–Tl(2) 83.1(2), N(1)–Tl(1)–C(40) 131.9(3). (b) Dimeric aggregate of **2** in the solid state through π-arene–thallium contacts [Tl(2)–Tl(2A) 3.7615(13) Å].

et al. for a range of mixed Li–group 13 metal amido complexes.[11]

A closer inspection of the crystal structure of **2** revealed that the complex is aggregated in the form of weakly associated dimers [Fig. 1(b)]. This type of association occurs through weak π-arene–Tl(I) contacts[12] with, respectively one tolyl group of the neighbouring molecule: Tl(2)–C(Ar′) 3.26–3.51 Å; Tl(2)–centroid: 3.093 Å. This arrangement is supplemented by a relatively short intermetallic distance of Tl(2)–Tl(2′) 3.7615(13). While being significantly shorter than the sum of the van der Waals radii (4.0 Å) this Tl–Tl contact is nevertheless at the long end of the range found for such metal–metal contacts and therefore thought to play a secondary role.

We thank the Deutsche Forschungsgemeinschaft, the Fonds der Chemischen Industrie, and the CNRS (France) for funding.

Notes and references

† *Selected spectroscopic and analytical data*: for **1**: ^{1}H NMR (200.13 MHz, C_6D_6, 295 K) δ −0.78 (s, 1 H, CH), 0.51 [br s, 18 H, $Si(CH_3)_2$], 2.18 (s, 9 H, $C_6H_4CH_3$), 6.74 (d, 6 H, $^3J_{H2H3}$ 7.5 Hz, H^2, C_6H_4), 6.97 (d, 6 H, H^3, C_6H_4); {^{1}H} ^{13}C NMR (50.32 MHz, C_6D_6, 295 K) δ 8.4 [$Si(CH_3)_2$], 13.8 (CH), 20.6 ($C_6H_4CH_3$), 123.7 (C, C^4, C_6H_4), 129.3 (CH, C^2, C_6H_4), 131.3 (CH, C^3, C_6H_4), 153.8 (CN, C^1, C_6H_4); ^{29}Si {^{1}H} NMR (39.76 MHz, C_6D_6, 295 K) δ −4.1; $C_{28}H_{40}N_3Si_3Tl$ (707.29). Calc. C 47.55, H 5.70, N 5.94, Tl 28.90. Found: C 47.04, H 5.53, N 6.10, Tl 27.85%.

For **2**: ^{1}H NMR (400.13 MHz, C_6D_6, 295 K) δ −0.76 (br s, 1 H, CH), 0.44 [vbr s, 20 H, $Si(CH_3)_2$ + $Tl(CH_2)$], 0.49 [br s, 2 H, $Tl(CH_2CH_2)$], 0.57 [t, 2 H, $^3J_{H^aH^b}$ 7.1 Hz, H^a, $Tl((CH_2)_2CH_2)$], 0.97 [q, 3 H, H^b, $Tl((CH_2)_3CH_3)$], 2.16 (br s, 9 H, $C_6H_4CH_3$), 6.68–6.87 (br m, 6 H, H^2, C_6H_4), 6.93–7.06 (br m, 6 H, H^3, C_6H_4); {^{1}H} ^{13}C NMR (100.61 MHz, C_6D_6, 295 K) δ 6.7 [br d, $^3J_{TlC}$ 66 Hz, $Si(CH_3)_2$], 11.0 (CH), 11.6 [$Tl((CH_2)_3CH_3)$], 13.4 [br, $Tl(CH_2)$], 20.6 [$C_6H_4(CH_3)$], 30.2 [$Tl((CH_2)_2CH_2)$], 33.7 [br, $Tl(CH_2CH_2)$], 125.0 (br, C, C^4, C_6H_4), 128.3 (CH, C^2, C_6H_4), 130.2 (CH, C^3, C_6H_4), 150.4 (vbr, CN, C^1, C^6H_4; $C_{32}H_{49}N_3Si_3Tl_2{\cdot}0.5C_5H_{12}$ (1004.83). Calc. C 41.24, H 5.52, N 4.18, Tl 40.68. Found: C 41.14, H 5.33, N 3.99, Tl 41.12%.

‡ *Crystal data* for $[HC\{SiMe_2N(p\text{-Tol})\}_3(TlC_4H_9)(Tl){\cdot}0.5C_5H_{12}]$ **2**: $C_{32}H_{49}N_3Si_3Tl_2{\cdot}0.5C_5H_{12}$, orange blocks, crystal dimensions 0.6 × 0.4 × 0.3 mm, M = 1004.83, monoclinic, space group $C2/c$, a = 21.346(6), b = 14.4015(13), c = 26.384(10) Å, β = 107.869(14)°, U = 7719(4) Å^3, Z = 8, D_c = 1.729 g cm^{-3}, μ = 8.459 mm^{-1}, $F(000)$ = 3896, 7684 reflections collected ($2.00 < \theta < 24.99°$) at 193(2) K, 6781 independent (R_{int} = 0.0423), 5138 observed [$I > 2\sigma(I)$] 6781 used in the structure refinement; R_1 = 0.0471 [$I > 2\sigma(I)$], wR_2 = 0.1287 (all data), GOF = 1.069 for 382 parameters and 0 restraints, largest difference peak, hole = 2.214, −2.920 e Å^{-3}. The comparatively high residual electron density in **1** was in the vicinity of the thallium atoms.[13,14]

CCDC 157350. See http://www.rsc.org.suppdata/cc/b1/b100760m/ for crystallographic data in .cif or other electronic format

1 *Unkonventionelle Wechselwirkungen in der Chemie metallischer Elemente*, ed. B. Krebs, VCH, Weinheim, 1992; P. Pyykkö, *Chem. Rev*., 1997, **97**, 597; C. Janiak, *Coord. Chem. Rev*., 1997, **163**, 107.

2 G. Treboux and J.-C. Barthelat, *J. Am. Chem. Soc*., 1993, **115**, 4870; P. Schwerdtfeger, *Inorg. Chem*., 1991, **30**, 1660 and references therein.

3 K. W. Hellmann, L. H. Gade, I. J. Scowen and M. McPartlin, *Chem. Commun*., 1996, 2515; K. W. Hellmann, L. H. Gade, R. Fleischer and D. Stalke, *Chem. Commun*., 1997, 527.

4 Examples of structurally characterized Tl(I) amides: S. D. Waezsada, T. Belgardt, M. Noltemeyer and H. W. Roesky, *Angew. Chem., Int. Ed. Engl*., 1994, **33**, 1351; W. Frank, D. Kuhn, S. Müller-Becker and A. Ravazi, *Angew. Chem., Int. Ed. Engl*., 1993, **32**, 90; H. Schmidbaur, W. Bublak, B. Huber, J. Hofmann and G. Müller, *Chem. Ber*., 1989, **122**, 102; M. Veith, A. Spaniol, J. Pöhlmann, F. Gross and V. Huch, *Chem. Ber*., 1993, **126**, 2625; W. M. Boesveld, P. B. Hitchcock, M. F. Lappert and H. Nöth, *Angew. Chem., Int. Ed*., 2000, **39**, 222.

5 K. W. Hellmann, L. H. Gade, R. Fleischer and T. Kottke, *Chem. Eur. J*., 1997, **3**, 1801; K. W. Hellmann, L. H. Gade, A. Steiner, D. Stalke and F. Möller, *Angew. Chem., Int. Ed. Engl*., 1997, **36**, 160.

6 C. H. Galka, D. J. M. Trösch, M. Schubart, L. H. Gade, I. J. Scowen and M. McPartlin, *Eur. J. Inorg. Chem*., 2000, 2577.

7 F. Brady, K. Henrick, R. W. Matthews and R. G. Gillies, *J. Organomet. Chem*., 1980, **193**, 21; K. Henrick, R. W. Matthews and P. A. Tasker, *Inorg. Chem*., 1977, **16**, 3293; H. Gornitzka and D. Stalke, *Eur. J. Inorg. Chem*., 1998, 311; G. H. W. Milburn and M. R. Truter, *J. Chem. Soc. A*, 1967, 648; E. M. Váquez, A. Sánchez, J. S. Casas, J. Sordo and E. E. Castellano, *J. Organomet. Chem*., 1992, **438**, 29; G. M. Sheldrick and W. S. Sheldrick, *J. Chem. Soc. A*, 1970, 28; A. J. Canty, K. Mills, B. W. Skelton and A. H. White, *J. Chem. Soc., Dalton Trans*., 1986, 939.

8 Review: M. A. Paver, C. A. Russell and D. S. Wright, in *Comprehensive Organometallic Chemistry, Vol. 1*, ed. E. W. Abel, F. G. A. Stone and G. Wilkinson, Pergamon, Oxford, 2nd edn., 1995, p. 503. Examples of functionalized alkylthallium(III) complexes: A. Blaschette, P. G. Jones, A. Michalides and M. Näveke, *J. Organomet. Chem*., 1991, **415**, 25; J. Vicente, J.-A. Abad, G. Cara and P. G. Jones, *Angew. Chem., Int. Ed. Engl*., 1990, **29**, 1125.

9 K. W. Klinkhammer and S. Henkel, *J. Organomet. Chem*., 1994, **480**, 167 and references therein.

10 K. W. Hellmann, L. H. Gade, O. Gevert, P. Steinert and J. W. Lauher, *Inorg. Chem*., 1995, **34**, 4069; H. Memmler, U. Kauper, L. H. Gade, D. Stalke and J. W. Lauher, *Organometallics*, 1996, **15**, 3637.

11 M. Veith, M. Zimmer and S. Müller-Becker, *Angew. Chem., Int. Ed. Engl*., 1993, **32**, 1771.

12 C. H. Galka and L. H. Gade, *Inorg. Chem*., 1999, **38**, 1038 and references therein.

13 T. Kottke and D. Stalke, *J. Appl. Crystallogr*., 1993, **26**, 615; T. Kottke, R. J. Lagow and D. Stalke, *J. Appl. Crystallogr*., 1996, **29**, 465; D. Stalke, *Chem. Soc. Rev*., 1998, **27**, 171.

14 G. M. Sheldrick, *Acta Crystallogr., Sect. A*, 1990, **46**, 467; G. M. Sheldrick, SHELXS-97, Program for Crystal Structure Solution, Universität Göttingen, 1997; G. M. Sheldrick, SHELXL-97, Program for Crystal Structure Refinement, Universität Göttingen, 1997.

CHEMCOMM
Communication
www.rsc.org/chemcomm

Control of calcium carbonate morphology by transformation of an amorphous precursor in a constrained volume

Eva Loste and Fiona C. Meldrum*

Department of Chemistry, Queen Mary, University of London, Mile End Road, London, UK E1 4NS. E-mail: F.C.Meldrum@qmw.ac.uk

Received (in Cambridge, UK) 16th February 2001, Accepted 4th April 2001
First published as an Advance Article on the web 24th April 2001

Calcium carbonate crystals of defined morphology have been produced on transformation of an amorphous calcium carbonate precursor within a constrained volume.

The range of morphologies exhibited by inorganic crystals in biological systems is truly remarkable and provides a unique inspiration for synthetic crystal growth experiments.[1,2] Indeed, many biominerals display complex forms and curved surfaces that are as yet quite impossible to replicate in the laboratory. As an important step forward in understanding control of calcium carbonate growth *in vivo*, it has recently been demonstrated that certain biological calcite crystals actually comprise two mineral phases, calcite and amorphous calcium carbonate (ACC).[3–5] Examination of the mechanism of calcification in sea urchin embryos has further shown that in this organism, not only do ACC and calcite co-exist, but that ACC transforms into calcite over time.[3,4] The ACC therefore acts as a transient precursor to the more stable calcite phase,[3] and transformation of ACC to calcite within the constrained volume imposed by the spiculogenic cavity results in single crystals of calcite with a tri-radiate form and curved surfaces.

The role of ACC in the biological calcification process has not been entirely resolved, although it has been suggested that it may provide a temporary storage site in some organisms, or that in combination with a crystalline phase may provide a skeletal element with superior mechanical properties.[5,6] The experiments described here investigate whether ACC may also play an important role in morphological control. Indeed, it has been demonstrated that thin films of calcite can be formed in association with Langmuir monolayers *via* transformation of an ACC precursor film.[7] In common with the calcification mechanism active in sea urchins, in the current experiments ACC was contained within a restricted volume, and the morphological changes of the calcium carbonate particles on transformation to calcite were studied.

As a simple model system, 10 μm thick polycarbonate track-etch membranes were used as the crystallisation environment.[8] These membranes possess extremely regular cylindrical channels of diameter 3 μm, which are similar to the dimensions to sea urchin embryo spicules. ACC was precipitated in the membrane pores by placing a membrane between two half U-tube arms, and filling one tube with $CaCl_2$ solution and the other with Na_2CO_3 solution.† The experiments were carried out at 4–6 °C in order to stabilise ACC, by reducing the rate of transformation to calcite. Counter-diffusion of ions through the membrane pores resulted in precipitation of $CaCO_3$. The experimental conditions used generate ACC in bulk solution. Microscopic examination of the membrane after crystallisation revealed two populations of crystals. 15 μm crystals with intergrown, rhombohedral morphologies precipitated on the surface of the membrane. Particles were also observed within the membrane pores, and exhibited a circular cross section of the same dimensions as the membrane channel [Fig. 1(a)]. The morphologies of the intra-membrane crystals were further examined subsequent to dissolution of the membrane. Again, the two populations of crystals were observed but were readily distinguished on the basis of size and morphology. The intra-membrane crystals were of dimensions 3 × 10 μm and displayed cylindrical morphologies and curved surfaces, as shown in Fig. 1(b). Thus, both the size and shape of these crystals had been clearly dictated by the geometry of the membrane channels in which they had formed.

The crystals deposited on the membrane surface were adhered strongly to it, which compromised opportunities for *in situ* analysis of the intra-membrane crystals. To confirm that the intra-membrane crystals formed from an initial ACC phase, they were isolated by dissolution of the membrane at early stages of the experiment. Microscopic examination of the separated crystals clearly showed that the cylinders formed *via* an ACC precursor [Fig. 2(a)]. Spherical particles of diameter 0.5 μm, which are characteristic of ACC,[9,10] were observed to initially coat the walls of the pores, before filling in the entire volume and generating the final cylindrical form. Identical particles were produced in a control experiment by mixing the $CaCl_2$ and Na_2CO_3 solutions at low temperatures in the absence

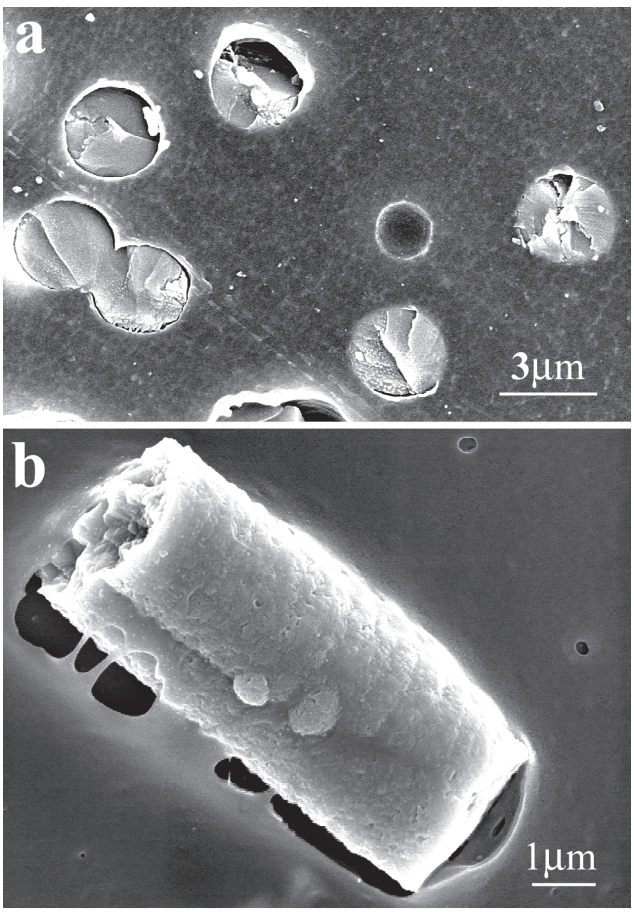

Fig. 1 (a) Calcium carbonate crystals grown within membrane pores. (b) Intra-membrane crystal isolated from the membrane, showing cylindrical morphology and dimensions identical to the membrane pores. Both images are of samples after 24 h.

DOI: 10.1039/b101563j

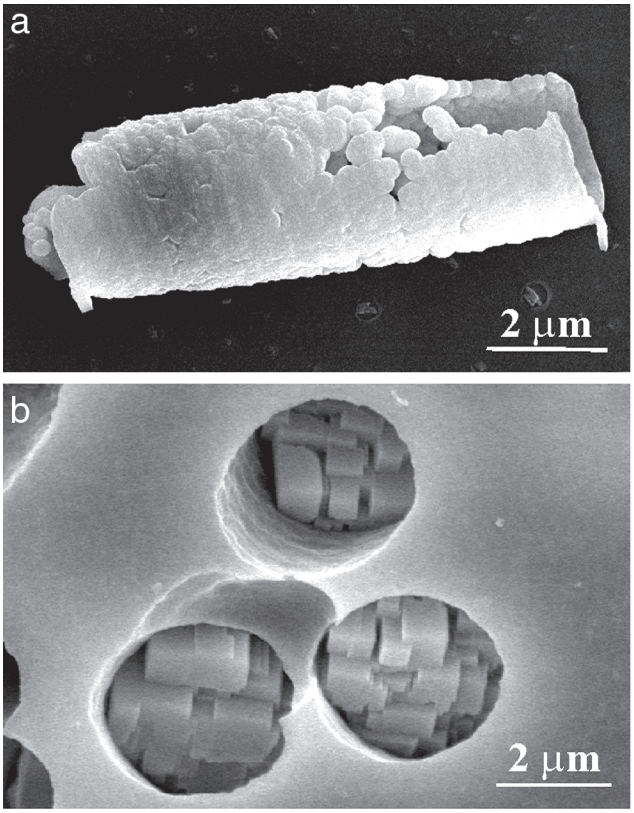

Fig. 2 (a) Intra-membrane particle, isolated after 15 min, showing its formation from spherical ACC particles. (b) Crystals grown within membrane pores showing crystalline faces characteristic of calcite (sampled after 24 h).

of the membrane, and were confirmed to be ACC using FTIR and XRD.

Comparison of the images of the intra-membrane particles at early stages [Fig. 2(a)], and after longer times [Fig. 1(b)] shows that the structure of the cylindrical particles alters with time. While the distinct spherical morphologies of the amorphous precursor particles are initially clearly observed within the cylindrical particle, continued incubation in solution results in transformation to a cylindrical particle with indentical overall morphology but with uniform structure. Examination of the ends of the mature cylindrical crystals frequently shows blocky crystal faces typical of rhombohedral calcite [Fig. 2(b)]. It has not as yet been impossible to conclusively identify the crystals as calcite, or to probe whether they are single crystal or polycrystalline as they are too small to investigate using standard laboratory XRD. However, selected area electron diffraction, carried out in a transmission electron microscope (TEM) was performed on the mature crystals in an attempt to obtain a diffraction pattern from a thinner edge area. Some diffraction patterns were obtained, all of which could be fitted to calcite. In addition, examination of the cylindrical particles between crossed polars in an optical microscope demonstrated that they were anisotropic, which again suggests crystallinity.

In order to investigate whether the precursor ACC phase was necessary for the precipitation environment to impose its structure on the final morphology of the crystal, the experiments were repeated at room, rather than low temperature. In the absence of the membrane, calcite precipitated immediately from solution. Precipitation within the membrane pores resulted in crystals of irregular, as opposed to cylindrical morphologies.

These experiments demonstrate that transformation of ACC within a constrained volume can produce a crystalline particle of morphology imposed by the environment. Both the ACC precursor phase and the constrained volume appear to be essential to this mechanism of morphology control. Biology obviously does not apply low temperature as a route to producing ACC. However, there is increasing evidence that organisms synthesise organic macromolecules specifically for stabilising ACC with respect to the thermodynamically stable phase calcite.[5,7,11] We therefore suggest that deposition of ACC within a vesicle may provide organisms with a route to producing crystals with elaborate forms and curved surfaces, such as the remarkable fenestrated calcitic skeletal plates of sea urchins.

We would like to thank the Department of Materials, Queen Mary, for access to electron microscope facilities.

Notes and references

† A polycarbonate track-etch membrane (pore diameter 3 μm) was placed between two, identical, half-U tube arms, which were clamped at the membrane position to form a U-tube. A small volume of cold water was introduced into the U-tube to wet the membrane. Equal volumes of 0.1 M solutions of Na_2CO_3 and $CaCl_2$ in Millipore water, which had been previously filtered and cooled to 4–8 °C were then simultaneously poured into each of the U-tube side-arms. The apparatus was placed in a refigerator at 4–6 °C for a period ranging from 15 min to 24 h. On completion of the experiment, the membrane was washed with water and was dried using compressed air. The $CaCO_3$ crystals produced in association with the membrane were examined using scanning electron microscopy (SEM) either *in situ* in the membrane, or after dissolution of the membrane in chloroform. All samples were Au-coated prior to examination in a JEOL 6300F scanning electron microscope (SEM), fitted with a field emission source and operating at 10 kV. Selected-area electron diffraction was also carried out on the $CaCO_3$ crystals after isolation from the membrane. A drop of an ethanolic solution of the isolated crystals were placed on a C-coated, Formvar-covered Cu TEM grid, and was examined in a JEOL 2010 transmission electron microscope (TEM) operating at 200 kV.

1 H. A. Lowenstam and S. Weiner, *On Biomineralization*, OUP, New York, 1989.
2 *Skeletal Biomineralization: Patterns, Processes and Evolutionary Trends, Vol. 2, Atlas and Index*, ed. J. G. Carter, Van Nostrand Reinhold, New York, 1990.
3 E. Beniash, J. Aizenberg, L. Addadi and S. Weiner, *Proc. R. Soc. London B*, 1997, **264**, 461.
4 E. Beniash, L. Addadi and S. Weiner, *J. Struct. Biol.*, 1999, **125**, 50.
5 J. Aizenberg, G. Lambert, L. Addadi and S. Weiner, *Adv. Mater.*, 1996, **8**, 222.
6 L. Addadi and S. Weiner, *Angew. Chem., Int. Ed. Engl.*, 1992, **31**, 153.
7 G. Xu, N. Yao, I. A. Aksay and J. T. Groves, *J. Am. Chem. Soc.*, 1998, **120**, 11977.
8 C. R. Martin, *Chem. Mater.*, 1996, **8**, 1739.
9 Y. Kojima, A. Kawanobe, T. Yasue and Y. Arai, *J. Ceram. Soc. Jpn.*, 1993, **101**, 1145.
10 L. Brecevic and A. E. Nielsen, *J. Cryst. Growth*, 1989, **98**, 504.
11 J. J. J. M. Donners, B. R. Heywood, E. W. Meijer, R. J. M. Nolte, C. Roman, A. P. H. J. Schenning and N. A. J. M. Sommerdijk, *Chem. Commun.*, 2000, 1937.

CHEMCOMM Communication
www.rsc.org/chemcomm

Glycosylation of the primary binding pocket of a subtilisin protease causes a remarkable broadening in stereospecificity in peptide synthesis

Kazutsugu Matsumoto,[a] Benjamin G. Davis*[b] and J. Bryan Jones*[c]

[a] *Department of Applied Chemistry and Biotechnology, Faculty of Engineering, Fukui University, Bunkyo 3-9-1, Fukui 910-8507, Japan*
[b] *Department of Chemistry, University of Durham, South Road, Durham, UK DH1 3LE. E-mail: Ben.Davis@durham.ac.uk*
[c] *Department of Chemistry, University of Toronto, 80 St. George St, Toronto, Ontario, Canada, M5S 3H6*

Received (in Liverpool, UK) 8th December 2000, Accepted 8th March 2001
First published as an Advance Article on the web 1st May 2001

Site-selective glycosylation at position 166 at the base of the primary specificity S_1 pocket in the serine protease subtilisin *Bacillus lentus* (SBL) created glycoproteins that are capable of catalyzing the coupling reactions of not only L- amino acid esters but also D-amino acid esters to give the corresponding dipeptides in good yields as a result of greatly broadened substrate specificities that can be rationalized by the interaction of the glycans acting as chiral auxiliaries in stereochemically mismatched pairs.

Enzymatic peptide coupling requires minimal protection of the substrate, proceeds under mild condition and without racemization.[1] In spite of these advantages, two major problems have limited the use of serine proteases in peptide synthesis. One is their efficient proteolytic (amidase) activity which causes hydrolysis of the coupled peptide product, and the other is their stringent structural and stereo-specificity which typically confines their use in synthesis to a limited range of L-amino acid substrates. Controlled site-selective glycosylation can be used to create glycosylated proteases with greatly improved esterase activities and enhanced esterase–amidase activity ratios (E/As) that are up to 8.4- and 17.2-fold enhanced over their unglycosylated wildtype (WT) counterparts, respectively.[2] By virtue of their higher esterase and lower amidase activities, these glycosylated enzymes are excellent candidates for efficient amide bond formation as they possess enhanced acylating properties and yet substantially reduced hydrolytic activity towards the peptide products of coupling. Moreover, these catalysts can be constructed on scales of hundreds of milligrams, thereby allowing their use in multigram scale syntheses. We reasoned that such glycosylated enzymes would not only be efficient catalysts for peptide ligation but that the presence of an internally bound carbohydrate might influence the stereospecificity of such ligations. Carbohydrates are effective chiral auxiliaries[3] and we wished to probe the effect of introducing the homochiral groups **a**–**d** (Scheme 1) into the primary binding region of an enzyme as a tactic for broadening substrate stereospecificity, perhaps by increasing the potential for stereochemically mismatched pairs.[4]

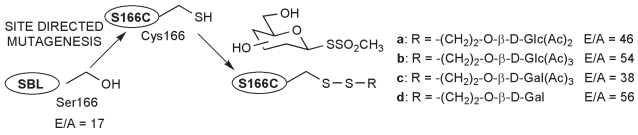

Scheme 1

Representative carbohydrates were attached to the interior of the primary S_1[5] binding pocket, which modulates P_1 specificity, of the serine protease subtilisin *Bacillus lentus* (SBL, EC 3.4.21.14) by site-selective glycosylation[2,6] at position 166. Gratifyingly, this also resulted in enhanced E/A values relative to unglycosylated SBL-WT (Scheme 1).[2]

Firstly, we probed the structural breadth of the P_1 specificity of S166C-S-**a**–**d** by examining the ligation of L-amino acids, (**1**)–(**3**) as acyl donors, with glycinamide (**7**) as an acyl acceptor (Scheme 2, Table 1)† using 1 mg ml^{-1} of active enzyme[7] in simple 1 : 1 water–DMF solutions. In accord with our goals of not reducing the existing substrate breadth of SBL, these results indicated that the introduction of carbohydrate groups **a**–**d** did not affect the essential, inherent ability of SBL to accept L-amino acids as acyl donors in peptide coupling reactions. Good

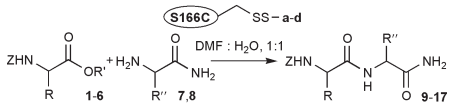

Scheme 2

Table 1 Glyco-SBL catalyzed peptide coupling reactions[a]

				Yield[b] (%) with				
Acyl donor	Acyl acceptor	Product	time/h	SBL-WT	S166C-**a**	S166C-**b**	S166C-**c**	S166C-**d**
Z-L-PheOBn (**1**)	$GlyNH_2$ (**7**)	*Z*-L-PheGlyNH_2 (**9**)	1	92	95	93	91	95
Z-L-AlaOBn (**2**)	**7**	*Z*-L-AlaGlyNH_2 (**10**)	5	91	85	77	92	83
Z-L-GluOMe(**3**)	**7**	*Z*-L-GluGlyNH_2 (**11**)	5	62	58	65	54	67
1	L-AlaNH_2 (**8**)	*Z*-L-Phe-L-AlaNH_2 (**12**)	24[c]	57	28	34	31	32
2	**8**	*Z*-L-Ala-L-AlaNH_2 (**13**)	24[c]	0	15	16	22	11
3	**8**	*Z*-L-Glu-L-AlaNH_2 (**14**)	24[c]	0	48	50	51	55
Z-D-PheOBn (**4**)	**7**	*Z*-D-PheGlyNH_2 (**15**)	48[d]	0	6	8	7	8
Z-D-AlaOBn (**5**)	**7**	*Z*-D-AlaGlyNH_2 (**16**)	48[d]	0	80	77	72	70
Z-D-GluOBn (**6**)	**7**	*Z*-D-GluGlyNH_2 (**17**)	48[d]	0	63	62	64	64

[a] DMF–water, 1 : 1, 0.1 M donor, 0.3 M acceptor, 0.036 mol% enzyme. Under the same conditions, spontaneous reaction did not occur. [b] Isolated yields. [c] 0.2 M acceptor. [d] Further 0.036 mol% added at 24 h.

DOI: 10.1039/b010021h

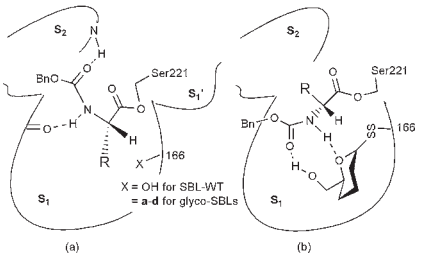

Fig. 1 Summarized representation of molecular mechanics analysis which showed different binding modes of (a) L-amino acids in SBL-WT or glyco-SBLs and (b) D-amino acids only in glyco-SBLs

to excellent yields of **9**, (91–95%), **10**, (77–92%), and fair yields of **11**, (54–67%) compared well, or were superior to, those for SBL-WT.

Our next goal was to investigate any secondary effects of S_1 pocket glycosylation upon P_1' specificity using the α-branched L-alaninamide (**8**) as a challenging acyl acceptor probe. The restricted S_1' specificity of the unglycosylated SBL-WT enzyme is demonstrated by its ability to catalyze only the coupling of **8** with the preferred L-phenylalaninate acyl donor **1**. Remarkably, in spite of the small S_1' pocket[8] all of the glyco-SBLs S166C-S-**a**–**d** were catalysts for the coupling of L-amino acids **1**–**3** with **8**. In the synthesis of **13**, low absolute yields were observed yet these represent a significant breakthrough in comparison with the absence of coupling activity prior to glycosylation. Excitingly, the yields of the coupling of **3** with **8** were similar to those obtained using unhindered **7** (48–55%). These results represent a dramatic improvement of the S_1' specificity of SBL. Interestingly, chemically-modified mutant enzymes bearing non-polar modifications at position 166 do not catalyze this ligation.[9] Possibly by exploiting polar interactions, we have obtained our goal of broadening substrate specificity, here of P_1' towards L-Ala to allow the synthesis of **12**–**14**, without diminishing the natural breadth of SBL. Indeed, previous molecular mechanics analysis of similarly internally glycosylated enzymes have indicated that such internally-bound carbohydrates may act as hydrogen-bonding motifs that give rise to enhanced kinetic parameters.[2]

Finally, we examined these powerful glyco-SBLs in the coupling of D-amino acids (**4**)–(**6**) as acyl donors with acyl acceptor **1**. The number of examples of enzyme catalyzed coupling of D-amino acids at the *C*-terminus of peptides by using D-amino acid acyl donors is vanishingly small and even then proceed with typically low efficiencies.[10] For example, to the best of our knowledge, yields above 10% for the incorporation of D-Glu have never been achieved.[9] Consistent with this, SBL-WT did not accept D-amino acids as acyl donors and starting materials **4**–**6** were recovered. In dramatic contrast, *all* of the glyco-SBLs S166C-S-**a**–**d** were able to catalyze the coupling of all three of these D-amino acid esters with acyl acceptor **1**. The reactions of **4** in all cases were slow and gave **15** in low yields, the best being 8% using S166C-S-**b**,**d**, and starting material **4** was recovered after 48 h in all cases. Peptide couplings of **5**, **6** with **7** proceeded more rapidly, and the yields were dramatically improved. In fact, the good yields of the D-dipeptide **17** (62–64%) were, surprisingly, superior to those found for coupling of L-Glu. Indeed, S166C-S-**c** showed a 1.2 : 1 stereochemical preference for D-glutamate **6** over L-glutamate **3**. Very high yields (up to 80%) of D-Ala dipeptide (**16**) were also observed.

Such is the remarkable nature of these broadened P_1 stereospecificities that we speculated that these glyco-SBLs may bind D-amino acids in a different mode from L-amino acids. Molecular mechanics analyses of SBL-WT and S166C-**a**–**d** with substrates **1**–**6** resulted in the models summarized in Fig. 1. In SBL-WT the normal binding mode for the acyl-enzyme intermediate, which is shown in Fig. 1(a), operates. The amino acid side chain (R) binds in the S_1 pocket with the reacting acyl group covalently linked to O_γ of the side chain of Ser221. This binding mode is not available to D-amino acids. In contrast, in the glyco-SBLs, Fig. 1(b), the presence of a homochiral auxiliary at position 166 with correct stereochemical disposition of its C-6 hydroxymethyl group and ring oxygen creates a hydrogen bond acceptor and donor motif which allows binding of the NHZ group in the S_1 pocket. Thus, glyco-SBLs may operate either by binding mode (a) *or* (b). However, in these glyco-SBLs, neither L-amino acids with the (a) mode nor D-amino acids with the (b) mode represent optimally matched diastereomeric pairs. This is consistent with their broadened specificity. By introducing a carbohydrate moiety at position 166 we have therefore tailored an enzyme with previously exclusive L-stereospecificity and excellent efficiency (matched pair) into an enzyme that has broadened L- and D-stereospecificity and reduced, but still good, efficiency due to mismatched pairing. This modified enzyme clearly has greater synthetic utility. This molecular mechanics analysis therefore raises the interesting possibility that the stereochemistry of the sidechain at 166 may influence stereospecificity through a double diastereoselective process. Further studies, including the synthesis of diastereomeric protein glycosylating reagents, to explore whether this is correct or whether location of just polar achiral groups at this position will have the same effect are now in progress. In addition, we are probing the precise effects of these modifications upon kinetic parameters k_{cat} and K_M using L- and D-amino acid substrates as both acceptors and donors in order to correlate the observed yield enhancements with true kinetic specificity.

In conclusion, glyco-SBLs S166C-S-**a**–**d** accept a wide range of substrates including D-amino acids as acyl donors and an α-branched acyl acceptor to give a variety of dipeptides, many in very high yields, that cannot be synthesized with SBL-WT. Furthermore, these dramatic improvements have been achieved without the loss of the natural ability of SBL to handle L-amino acids. It therefore represents a true broadening of synthetic utility and demonstrates that this site-selective glycosylation technology is a powerful tool for enhancing the application of enzymes in organic synthesis.

We acknowledge NSERC (Canada) and Genencor International, Inc for generous funding. We are also grateful to Genencor International, Inc., for providing WT- and S166C-SBL enzymes, and to Drs Rick Bott and Kanjai Khumtaveeporn for helpful discussions. We also thank the EPSRC (UK) for access to the Mass Spectrometry Service at Swansea and the Chemical Database Service at Daresbury.

References and notes

† Electronic supplementary information (ESI) available: detailed experimental procedures of peptide couplings and selected chemical data of the products. See http://www.rsc.org/suppdata/cc/b0/b010021m/

1 C.-H. Wong and G. M. Whitesides, *Enzymes in Synthetic Organic Chemistry*, Pergamon Press, Oxford, 1994, pp 41–130; K. Faber, *Biotransformations in Organic Chemistry*, 2nd ed. Springer-Verlag, Heidelberg, 1995, pp. 298–305 and references cited therein.
2 R. C. Lloyd, B. G. Davis and J. B. Jones, *Bioorg. Med. Chem.*, 2000, **8**, 1537.
3 H. Kunz and K. Ruck, *Angew. Chem., Int. Ed. Engl.*, 1993, **32**, 336.
4 S. Masamune, W. Choy, J. S. Peterson and L. R. Sita, *Angew. Chem., Int. Ed. Engl.*, 1985, **24**, 1.
5 Nomenclature according to I. Schechter and A. Berger, *Biochem. Biophys. Res. Commun.*, 1967, **27**, 152.
6 B. G. Davis, R. C. Lloyd and J. B. Jones, *J. Org. Chem.*, 1998, **63**, 9614; B. G. Davis and J. B. Jones, *Synlett*, 1999, 1495; B. G. Davis, M. A. T. Maughan, M. P. Green, A. Ullman and J. B. Jones, *Tetrahedron: Asymmetry*, 2000, **11**, 245; B. G. Davis, R. C. Lloyd and J. B. Jones, *Bioorg. Med. Chem.*, 2000, **8**, 1527; B. G. Davis, *Chem. Commun.*, 2001, 351.
7 Determined by titration with PMSF: C. Y. Hsia, G. Granshaw, C. Paech and C. J. Murray, *Anal. Biochem.*, 1996, **242**, 221.
8 For 3D-structure of SBL-WT see M. Knapp, J. Daubermann and R. R. Bott, RCSB-PDB entry *1jea*.
9 K. Khumtaveeporn, G. DeSantis and J. B. Jones, *Tetrahedron: Asymmetry*, 1999, **10**, 2563.
10 Y. Asano and T. L. Lübbehüsen, *J. Biosci. Bioeng.*, 2000, **89**, 295.

CHEMCOMM
Communication
www.rsc.org/chemcomm

Solid state supramolecular assemblies of charged supermolecules (Na[2.2.2]cryptate)$^+$ and anionic carboranes with host cyclotriveratrylene†

Michaele J. Hardie‡ and Colin L. Raston*‡

School of Chemistry, Monash University, Clayton, Melbourne, Victoria 3800, Australia

Received (in Cambridge, UK) 29th November 2000, Accepted 7th March 2001
First published as an Advance Article on the web 1st May 2001

The complex {(Na[2.2.2]cryptate)[CTV][Co($C_2B_9H_{11}$)$_2$]}$_2$(MeCN) (CTV = cyclotriveratrylene) features (Na[2.2.2]cryptate)$^+$∩CTV interplay as well as a closely packed chain of [Co($C_2B_9H_{11}$)$_2$]$^-$ counter-anions exhibiting dihydrogen bonding, and a similar cation–CTV assembly is found in (Na[2.2.2]cryptate)[CTV]($CHCl_3$)$_3$[$CB_{11}H_{12}$].

Cyclotriveratrylene (= CTV) **1** is a curved host molecule which forms ball-and-socket supermolecules with a number of large guest molecules such as fullerenes,[1,2] carborane,[2,3] and organometallic sandwich complexes;[4] and lattice inclusion structures with smaller organic guest molecules.[5] CTV can also be a π type donor ligand[6] or a chelating ligand for group 1 metals.[7] Chelating M(CTV) complexes feature polymeric or extended hydrogen bonded structures with solvent as intracavity CTV guest molecules and carborane $C_2B_{10}H_{12}$ or the anionic

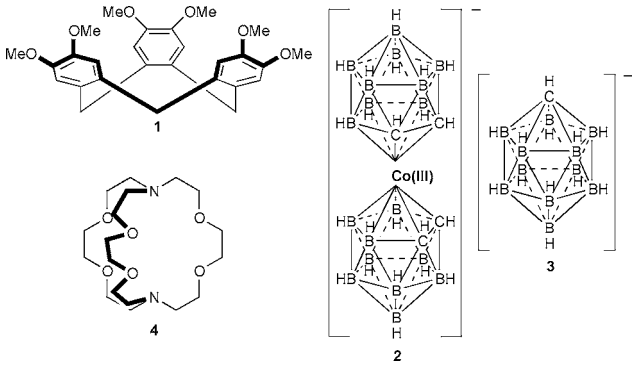

carboranes [Co($C_2B_9H_{11}$)$_2$]$^-$ **2** or [$CB_{11}H_{12}$]$^-$ **3** as lattice type guests.[7] The carboranes appear to play an important steric role in the stabilisation of the crystalline species. Entirely different host–guest and overall supramolecular behaviour between CTV and M$^+$(carborane)$^-$ is expected if M$^+$ is completely encapsulated by another host molecule such as [2.2.2]cryptand **4**, thus preventing the formation of M(CTV) chelate rings. This also introduces a large supercation (M[2.2.2]cryptate)$^+$ as a potential guest molecule for CTV, noting that the confinement of such species in container molecules is limited,[8] along with the large carborane anion. The crystalline complexes formed by (Na[2.2.2]cryptate)[Co($C_2B_9H_{11}$)$_2$] and (Na[2.2.2]cryptate)[$CB_{11}H_{12}$] with CTV are reported herein.

A yellow powder of (Na[2.2.2]cryptate)[Co($C_2B_9H_{11}$)$_2$] is obtained in high yields by mixing Na.**2** with **4** in aqueous solution. Combining this powder with 1 equivalent of CTV yields yellow–orange crystals of {(Na[2.2.2]cryptate)[CTV][Co($C_2B_9H_{11}$)$_2$]}$_2$(MeCN) **5** from MeCN–H_2O solution.† The structure was determined by single crystal X-ray diffraction techniques,§ and is shown in Fig. 1. Two cations, two **3** anions, two CTV hosts and one molecule of CH_3CN comprise the asymmetric unit. Each CTV molecule acts as a host for one molecule of (Na[2.2.2]cryptate)$^+$. There are two such (Na[2.2.2]cryptate)$^+$∩CTV supermolecules, each with a different orientation of the (Na[2.2.2]cryptate)$^+$ within the molecular cavity of the CTV, although both with hydrophobic ethylene groups within the CTV bowl. In one (Na[2.2.2]cryptate)$^+$∩CTV assembly the N–Na–N axis of the [2.2.2]cryptate is close to parallel with the plane formed by the three methylene carbons of the CTV. The distance between the Na and the centre of this plane is 7.66 Å and N–Na···plane centroid angles of 95.9 and 87.7° are observed. The other (Na[2.2.2]cryptate)$^+$∩CTV assembly is more skewed Na–N···centroid angles 64.9 and 114.9°. CTV molecules within the extended crystal lattice do not feature any π···π interactions, instead showing close contacts between the methylene groups of one CTV and methoxy oxygens of an adjacent molecule (C–H···O distances 2.3–2.4 Å).

The cobalticarborane anions stack in columns along the *b* axis, and are remarkably close given their electrostatic repulsion, with C–H···H–B separations under 2 Å, and closest C···B distance 3.65 Å. These distances are consistent with the formation of nonclassical H···H hydrogen bonds or dihydrogen bonds. Dihydrogen bonds have been previously reported for X–H···H–B (X = N, O) systems with similar H···H separations.[9] The C–H groups of carboranes are acidic and are known to form both classical hydrogen bonds,[10] and nonclassical C–H···π hydrogen bonds.[3,11] The anions are in one of two alternating orientations (Fig. 1) approximately perpendicular relative to one another. The torsion angle between the cobalticarborane vectors (vector defined as that between the two apical B positions *para* to the Co) is −65.9°. The anions are situated close to the methyl groups of the CTV, at closest B···C_{methyl} separation 3.71 Å. The siting of a carborane or anionic carborane near methyl groups or within methyl-lined cavities within a crystal lattice has also been observed in a number of other materials containing both carboranes and CTV[7] and is emerging as a structural trend.

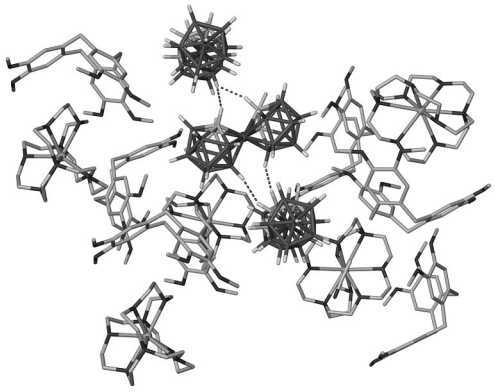

Fig. 1 Partial packing diagram from the crystal structure of {(Na[2.2.2]cryptate)[CTV][Co($C_2B_9H_{11}$)$_2$]}$_2$(MeCN) **5**. All C–H···B-H contacts < 2.3 Å between [Co($C_2B_9H_{11}$)$_2$]$^-$ anions consistent with dihydrogen bonds are shown as dashed lines.

† Electronic supplementary information (ESI) available: Synthesis of complexes **5** and **6** and discussion of structure solution and refinement for **5**. See http://www.rsc.org/suppdata/cc/b0/b009581h/

‡ Present address: School of Chemistry, University of Leeds, UK LS2 9JT. E-mail: c.l.raston@chem.leeds.ac.uk

Colourless crystals of (Na[2.2.2]cryptate)[CTV]-$(CHCl_3)_3[CB_{11}H_{12}]$ **6** grew from diffusion of hexane into a mixture of (Cs[2.2.2]cryptate)$[CB_{11}H_{12}]$, CTV and NaOH in $CHCl_3$–MeOH.† The structure was determined by single crystal X-ray diffraction techniques,§ and, as for complex **5**, features (Na[2.2.2]cryptate)$^+$∩CTV supermolecules as the primary host–guest species, [Fig. 2(a)]. The (Na[2.2.2]cryptate)$^+$ guest molecule is positioned in a more end-on fashion than was seen in **5**, with a longer Na-to-host centroid distance at 7.85 Å, and N–Na···centroid angles 55.0 and 134.8°. The CTV molecules also show secondary inclusion behaviour, with a molecule of $CHCl_3$ at distances consistent with the formation of bifurcated hydrogen bonds to each CTV dimethoxy group [Fig. 2(a)] at Cl_3C–H···OMe distances ranging from 2.23 to 2.52 Å (corresponding C···O separations 3.09 to 3.24 Å). Similar hydrogen bonding of $CHCl_3$ to two dimethoxy groups is observed in crystalline CTV$(CHCl_3)_2$.[5] Two of the $CHCl_3$ molecules have their donating C–H group in-plane with their respective acceptor dimethoxy groups, while the third binds in a different mode, with the C–H out-of-plane with the dimethoxy groups and the $CHCl_3$ molecule tilted in towards the molecular cavity of the CTV. One of the chlorines of this $CHCl_3$ is directed into the cleft of the (Na[2.2.2]cryptate)$^+$ guest molecule, shown in space filling representation in Fig. 2(b), hence both the CTV and the (Na[2.2.2]cryptate)$^+$ can be regarded as acting as host molecules for this $CHCl_3$.

As with complex **5**, the carborane anion is involved in hydrogen bonds *via* the acidic C–H. In **6** the $[CB_{11}H_{12}]^-$ anion forms a bifurcated hydrogen bond to two chlorine atoms of the out-of-plane $CHCl_3$ (Fig. 2). Notably, an identical reaction mixture with CH_2Cl_2, which is less likely to form hydrogen bonding interactions than $CHCl_3$, failed to produce crystalline products, indicating that these interactions are important in stabilising the crystalline product. The CTV molecules within the extended crystal lattice associate in pairs *via* a single, long π···π interaction, with coplanar aromatic rings at a centroid···centroid separation of 3.79 Å.

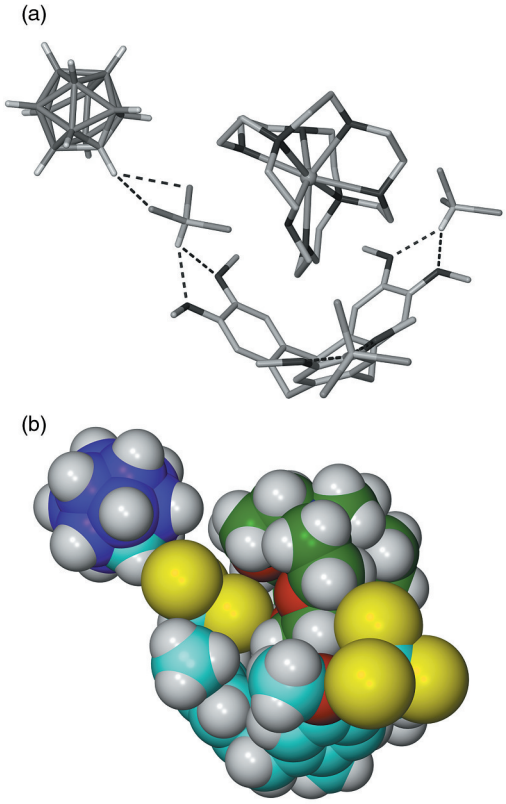

Fig. 2 Crystal structure of (Na[2.2.2]cryptate)[CTV]$(CHCl_3)_3[CB_{11}H_{12}]$ **6**. (a) Hydrogen bonding interactions between the molecular components (see text), only hydrogen positions on the $CHCl_3$ molecules and **3** anions are shown for clarity; (b) space filling representation, highlighting how a Cl from one $CHCl_3$ molecule is directed into the cleft of the (Na[2.2.2]cryptate)$^+$. Carbon atoms of [2.2.2]cryptate shown in green, others in blue.

The cation (Na[2.2.2]cryptate)$^+$, itself a host–guest complex, behaves as an intracavity guest for the host molecule CTV, while the bulky counter-anions $[Co(C_2B_9H_{11})_2]^-$ and $[CB_{11}H_{12}]^-$ are lattice counter-ions within the crystal packing. These and other carborane anions may be used to build up complicated supramolecular assemblies and generate new types of materials.

Support of this research from the Australian Research Council and helpful discussions with Dr Janet Scott are gratefully acknowledged.

Notes and references

§ *Crystal data*: X-ray data were collected at 123(1) K on an Enraf-Nonius KappaCCD single crystal diffractometer with Mo-Kα radiation (λ = 0.71073 Å). The structures were solved by direct methods with SHELXS-97 and refined by full-matrix least squares on F^2 using SHELXL-97. Carbon positions within carborane cages were assigned by an analysis of displacement parameters and bond lengths. All non-hydrogen atoms were refined anisotropically and hydrogens included at geometrically estimated positions, unless otherwise indicated. {(Na[2.2.2]cryptate)[CTV]-$[Co(C_2B_9H_{11})_2]\}_2(CH_3CN)$ **5**: $C_{100}H_{179}B_{36}Co_2N_5Na_2O_{24}$, M_r = 2388.48, monoclinic, space group $P2_1$, a = 16.5391(7), b = 12.7151(3), c = 29.6858(12) Å, β = 92.349(1), U = 6237.6(4) Å^3, Z = 2, D_c = 1.272 g cm^{-1}, μ = 0.341 mm^{-1} (no correction), yellow–orange needle, 0.33 × 0.12 × 0.05 mm, $2\theta_{max}$ = 50°, 36186 reflections measured, 19710 unique reflections (R_{int} = 0.107), 711 parameters, R_1 = 0.1270 (on 14445 observed data [$I > \sigma(I)$]), wR_2 = 0.2787 (all data), S = 1.061. The crystal was weakly diffracting, and the structure showed pseudosymmetry (see ESI†), with only the Na and Co refined anisotropically. (Na[2.2.2]cryptate)-[CTV]$(CHCl_3)_3[CB_{11}H_{12}]$ **6**: $C_{49}H_{81}B_{11}Cl_9N_2NaO_{12}$, M_r = 1351.11, monoclinic, space group $P2_1/n$, a = 13.5449(2), b = 25.3840(4), c = 19.4565(4) Å, β = 94.084(1), U = 6672.6(2) Å^3, Z = 4, D_c = 1.345 g cm^{-1}, μ = 0.440 mm^{-1} (no correction), colourless block, 0.30 × 0.28 × 0.23 mm, $2\theta_{max}$ = 52.0°, 38224 reflections measured, 13085 unique reflections (R_{int} = 0.076), 763 parameters, R_1 = 0.0603 (on 6971 observed data [$I > 2\sigma(I)$]), wR_2 = 0.1514 (all data), S = 1.031. CCDC 154067 and 154068. See http://www.rsc.org/suppdata/cc/b0/b009581h/ for crystallographic data in .cif or other electronic format.

1 J. L. Atwood, M. J. Barnes, M. G. Gardiner and C. L. Raston, *Chem. Commun*., 1996, 1449; J. L. Atwood, M. J. Barnes, R. S. Burkhalter, P. C. Junk, J. W. Steed and C. L. Raston, *J. Am. Chem. Soc*., 1994, **116**, 10 346; A. M. Bond, W. Miao, C. L. Raston, T. J. Ness, M. J. Barnes and J. L. Atwood, *J. Phys. Chem*., 2001 in press; H. Matsubara, A. Hasegawa, K. Shiwaku, K. Asano, S. Takahashi and K. Yamamoto, *Chem. Lett*., 1998, 923; H. Matsubara, S. Oguri, K. Asano and K. Yamamoto, *Chem. Lett*., 1999, 431.

2 M. J. Hardie, P. D. Godfrey and C. L. Raston, *Chem. Eur. J*., 1999, **5**, 1828.

3 R. J. Blanch, M. Williams, G. D. Fallon, M. G. Gardiner, R. Kaddour and C. L. Raston, *Angew. Chem., Int. Ed. Engl*., 1996, **36**, 504.

4 K. T. Holman, J. W. Steed and J. L. Atwood, *Angew. Chem., Int. Ed. Engl*., 1997, **36**, 1736.

5 J. W. Steed, H. Zhang and J. L. Atwood, *Supramol. Chem*., 1996, **7**, 37.

6 K. T. Holman, M. M. Halihan, J. W. Steed, S. S. Juisson and J. L. Atwood, *J. Am. Chem. Soc*., 1995, **117**, 7848.

7 M. J. Hardie, C. L. Raston and B. Wells, *Chem. Eur. J*., 2000, **6**, 3293; M. J. Hardie and C. L. Raston, *Angew. Chem., Int. Ed*., 2000, **39**, 3835; M. J. Hardie and C. L. Raston, *Crystal Growth Des*., 2001, **1**, 53.

8 A. Lützen, A. R. Renslo, C. A. Schalley, B. M. O'Leary and J. Rebek Jr., *J. Am. Chem. Soc*., 1999, **121**, 7455.

9 R. H. Crabtree, P. E. M. Seigbahn, O. Eisenstein, A. L. Rheingold and T. F. Koetzle, *Acc. Chem. Res*., 1996, **29**, 348; R. Custelcean and J. E. Jackson, *Angew. Chem., Int. Ed*., 1999, **38**, 1661.

10 D. Armspach, E. C. Constable, C. E. Housecroft, M. Neuburger and M. Zehnder, *New. J. Chem*., 1996, **20**, 331; M. G. Davidson, T. G. Hibbert, J. A. K. Howard, A. Mackinnon and K. Wade, *Chem. Commun*., 1996, 2285; G. Harakas, T. Vu, C. B. Knobler and M. F. Hawthorne, *J. Am. Chem. Soc*., 1998, **120**, 6405; K. A. Lyssenko, M. Y. Antipin and V. N. Lebedev, *Inorg. Chem*., 1998, **37**, 5834; O. Crespo, M. C. Gimeno and A. Laguna, *Polyhedron*, 1999, **18**, 1279.

11 M. J. Hardie and C. L. Raston, *Eur. J. Inorg. Chem*., 1999, 195.

CHEMCOMM Communication
www.rsc.org/chemcomm

Z-Contrast tomography: a technique in three-dimensional nanostructural analysis based on Rutherford scattering†

Paul A. Midgley,[a]* Matthew Weyland,[a] John Meurig Thomas*[ab] and Brian F. G. Johnson[c]

[a] *Department of Materials Science and Metallurgy, University of Cambridge, Pembroke Street, Cambridge, UK CB2 3QZ*
[b] *Davy Faraday Research Laboratory, Royal Institution of Great Britain, 21 Albermarle Street, London, UK W1X 4BS. E-mail: jmt@ri.ac.uk*
[c] *The University Chemical Laboratory, University of Cambridge, Lensfield Road, Cambridge, UK CB2 1EW*

Received (in Cambridge, UK) 26th February 2001, Accepted 9th April 2001
First published as an Advance Article on the web

A method for determining the three-dimensional structure of inorganic specimens using images formed from Rutherford scattered electrons, at a spatial resolution of 1 nm in all directions, is described and illustrated with results from a study of Pd–Ru bimetallic nanocatalysts supported on mesoporous silica: a 3D animation demonstrating the results may be viewed at *http://www-hrem.msm.cam.ac.uk/~mw259/Work/Tomo.html*

Though not universally acknowledged, the electron microscope is one of the most versatile and powerful instruments for the complete chemical analysis of any solid material. Not only can it cope with sample masses (10^{-18} g and less) that are far beyond the reach of X-ray analysis, it yields structural, mechanistic, compositional and electronic (valence states of ions and bonding between atoms) information on minute crystallographic phases that may contain hardly more than a dozen or so atoms. All this is possible because of the multiplicity of modes in which the microscope may be deployed. Thus it may give[1] bright field (BF) or dark field (DF) images (from forward scattered or Bragg scattered electrons, respectively) electron stimulated X-ray emission (XRE) spectra and elemental maps as well as electron energy loss spectra (EELS),[2] that can reflect such features as plasmon modes, the atomic coordination of light elements,[3] inter-atomic distances, d-electron population of transition metal ions and the momentum densities of electrons in amorphous solids.

Scanning transmission electron microscopy (STEM) is particularly useful in studies of nanoparticle catalysts supported within mesoporous silica because, by using a high angle annular dark field (HAADF) detector (see Fig. 1), which collects electrons that undergo Rutherford scattering, images can be acquired where the intensity is approximately proportional to Z^2 (Z is the atomic number of the scattering atom).[4] Fortunately many catalytically significant elements (Pd, Pt, Ru, Re, *etc*) have high Z, so that when they are supported on low Z material such as SiO_2 they are readily visible using HAADF detectors,[5] see Fig. 2. In addition the small probe sizes involved, *ca*. 0.8 nm in diameter, mean the resultant images have very high resolution. By also recording the electron-stimulated XRE from the nanoparticles their identity can be determined unambiguously (see, for example, ref. 4).

Valuable as the information yielded by STEM HAADF and XRE mapping undoubtedly is, especially in investigating nanocatalysts (and other nanoscientific problems), it is limited to providing 2D projections of 3D arrangements. The need exists to analyse, non-destructively, specimens fully in three dimensions especially if we seek to understand the factors responsible for the loss of activity, selectivity and stability of nanoparticle catalysts.

A suitable approach is electron tomography,[6] where the 3D structure is reconstructed from a tilt series of 2D projections. In practice this is achieved by tilting a specimen on one axis using the microscope goniometer and taking a micrograph at a range of tilts, typically every 1–2°, correcting for specimen move-

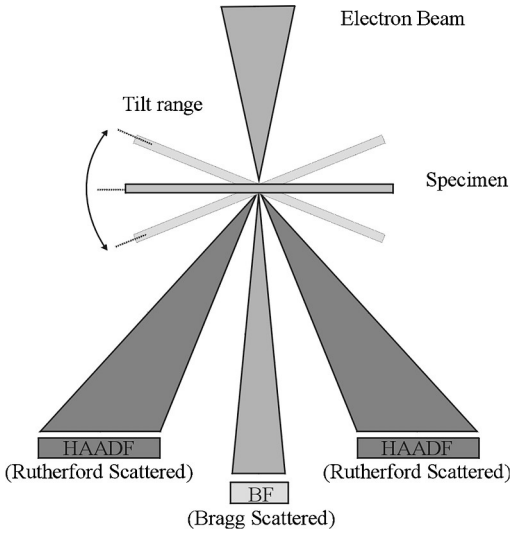

Fig. 1 Schematic of the detector layout in a scanning transmission electron microscope (STEM). The diameter of the tip of the electron beam is 0.8 nm.

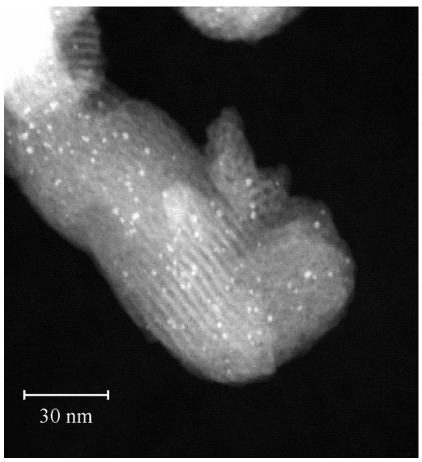

Fig. 2 HAADF image from a Pd–Ru nanocatalyst supported on mesoporous silica and mounted on a holey carbon grid. The mesopores (3 nm in diameter) and the nanocatalyst particles (1 nm in diameter) are clearly visible.

† Electronic supplementary information (ESI) available: 3D animations of a Pd–Ru bimetallic catalyst generated from a tomographic reconstruction of HAADF STEM images. See http://www.rsc.org/suppdata/cc/b1/b101819c/

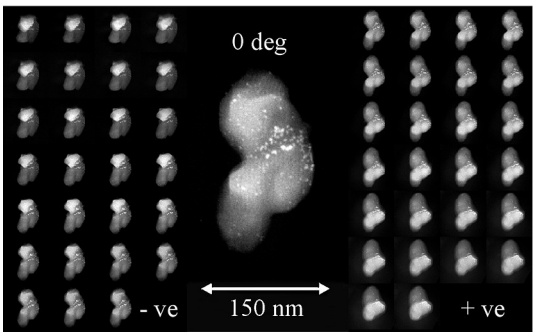

Fig. 3 Montage of the acquired tilt series showing all images and an enlargement of the zero tilt image.

ment, focus change and astigmatism throughout. In our case, the series is then processed offline using routines based on the Radon Fourier-slice theorem,[7] to reconstruct the full 3D structure.

In conventional electron tomography such a series is acquired using BF images dominated by Bragg-scattered electrons.[6] However, the large beam currents of conventional TEM means that such an approach cannot be used on specimens that are beam sensitive. The framework structure of mesoporous silica, for example, degenerates rather rapidly under TEM illumination and so is unsuitable for the prolonged acquisition times required for a tilt series. By using STEM, however, far smaller total beam exposure is involved. (Although the current density within the STEM probe is high, its energy can be dissipated to the surrounding (non-illuminated) areas unlike conventional static beam TEM). Another advantage arises from the scattering geometry in that HAADF imaging excludes almost all the electrons scattered coherently through low angles. This means that the resulting images are free from the misleading complications of electron phase contrast and, as such, they are 'true-projections' of the structure. As HAADF STEM images are formed primarily from incoherently scattered electrons, the combination of STEM HAADF imaging coupled with high operating voltages, to minimise inelastic interactions and thus ionisation damage, is an ideal basis for the tomography of catalysts.

We illustrate the power of HAADF STEM tomography by examining Pd–Ru bimetallic catalysts[8] supported on mesoporous silica. A HAADF tilt series was acquired on a CM300 field emission gun transmission electron microscope (FEGTEM), operating at 300 kV, in STEM mode using an on-axis Fischione HAADF detector. The series was acquired from +60° to −48° with an image every 2° giving a total of 55 images. These were spatially aligned using a cross-correlation algorithm applied sequentially to images stretched using an inverse cosine function that takes into account the variation in image width with tilt. After determining the tilt-axis for the data set, a 3D reconstruction was achieved using a weighted back-projection of consecutive 2D slices.[6a] The additional weighting function corrects for the relative oversampling of low frequencies when combining the image series from successive tilts.[6a]

The resultant reconstructions[9] have been displayed using multi-level voxel[10] projections, see Fig. 3. The multi-level voxel projection is achieved by contrast-selecting intensities from the reconstruction and assigning them definite colour and opacity values. This allows clear differentiation between the silica support (coloured grey) which has low intensity in the reconstruction from the low Z SiO_2, and the active nanoparticles (coloured red) which have high intensity in the reconstruction due to the high Z of the Pd/Ru. The reconstruction has sufficient resolution (1 nm^3) to allow a direct visualisation of the relative positions of mesopores and nanoparticles in all directions. Here we can show only 2D projections, but for the full 3D picture the reader may view an animation in the supplementary information (ESI†) on the RSC web site or at our web site.[11]

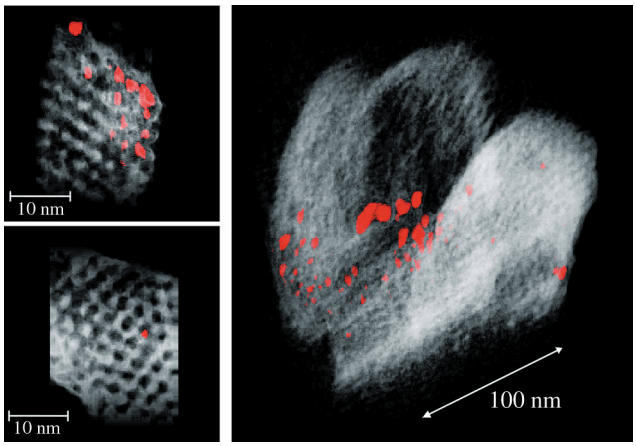

Fig. 4 Results from the tomographic reconstruction from the tilt series in Fig. 3. All images are multi-level voxel[10] red, green, blue, opacity (RGBO) projections. (a) and (b) are regions selected from the full reconstruction and (c) illustrates the reconstruction of nanoparticles and channels in multiple directions. The Pd–Ru particles are coloured red in all figures.

The reconstruction, as seen here or with the animations, reveals a number of important factors. On a practical level, it is clear that the silica framework has been reconstructed faithfully with essentially no beam damage even though long acquisition times are needed for the full series. The nanoparticles have a clear size distribution with larger particles sitting on the outside of the silica and smaller ones within the silica channels. The larger particles are those in which the original Pd_6Ru_6 metal clusters have coalesced. Those that have diameters >3 nm cannot be incorporated into the silica framework without severe disruption. Fig. 4(b) and the accompanying animation show a single nanoparticle anchored to the side of the wall of the silica channel exactly as suspected from other studies.[8] It is this type of nanoscale structural information, retrieved by non-destructive methods in contrast to atom-probe tomography,[12] coupled with bulk chemical analysis, which will be invaluable in developing and evaluating catalysts in the future.

Although we have demonstrated this technique primarily for the purposes of characterising supported catalysts, it has patently wide applications across the entire corpus of nanoscience and nanotechnology.

We acknowledge with thanks continued support from EPSRC (rolling grant to J. M. T.) and BNFL Research and Technology (studentship for M. W.).

Notes and references

1 J. M. Thomas, in *Inorganic Chemistry: Towards the 21st century*, ed M. H. Chisholm, ACS Publication 211, Washington, DC, 1983, p. 445.
2 J. M. Thomas, B. G. Willimas and T. G. Sparrow, *Acc. Chem. Res.*, 1985, **18**, 324.
3 R. D. Brydson, J. M. Thomas, H. Saur, W. Engel and E. Zeitler, *J. Chem. Soc., Chem. Commun.*, 1989, **15**, 1010.
4 D. Ozkaya, W. Zhou, J. M. Thomas, P. A. Midgley, V. J. Keast and S. Hermans, *Catal. Lett.*, 1999, **60**, 101.
5 M. M. J. Treacy and A. Howie, *J. Catal.*, 1980, **63**, 265.
6 (*a*) *Electron Tomography*, ed. J. Frank, Plenum Press, New York, 1992; (*b*) A. J. Koster, U. Ziese, A. J. Verkleij, A. H. Janssen and K. P. de Jong, *J. Phys. Chem. B*, 2000 **104**, 9368.
7 S. R. Deans, *The Radon Transform and Some of Its Applications*, John Wiley & Sons, New York, 1983.
8 (*a*) R. Raja, G. Sankar, S. Hermans, D. S. Shephard, T. Maschmeyer, S. Bromley, J. M. Thomas and B. F. G. Johnson, *Chem. Commun.*, 1999, **16**, 1571; (*b*) J. M. Thomas, *Angew Chem., Int. Ed.*, 1999, **38**, 3588.
9 All processing was undertaken using routines programmed in the IDL image processing language running on an IRIX operating system.
10 Voxel = a three dimensional pixel.
11 Department of Materials Science and Metallurgy Electron Microscopy Group: *http://www-hrem.msm.cam.ac.uk/~mw259/Work/Tomo.html*
12 M. K. Miller, *Atom-Probe Tomography: Analysis at the Atomic Level*, Kluwer Academic/Plenum Press, New York, 2000.

CHEMCOMM Communication
www.rsc.org/chemcomm

Noncovalent binding of the halogens to aromatic donors. Discrete structures of labile Br_2 complexes with benzene and toluene†

Aleksandr V. Vasilyev, Sergey V. Lindeman and Jay K. Kochi*

Department of Chemistry, University of Houston, Houston, Texas, 77204-5641, USA. E-mail: jkochi@pop.uh.edu

Received (in Columbia, MO, USA) 14th February 2001, Accepted 4th April 2001
First published as an Advance Article on the web 1st May 2001

Precise molecular structures resulting from the noncovalent interaction of Br_2 with benzene (and toluene) reveal the unusual localized bonding to *specific* (one or two) carbon centers in prereactive complexes leading directly to the transition states for electrophilic aromatic brominations.

Noncovalent interactions of benzene donors with a variety of small molecules including Brønsted acids (*e.g.* HF, HCl, $HOCH_3$), halogens (X_2 = F_2, Cl_2, Br_2, I_2) and Lewis acids (SO_2, NO, $AlCl_3$), *etc.* are under active investigation.[1,2] Molecular structures of these weak (intermolecular) complexes have been experimentally deduced with the aid of various spectroscopic techniques,[2,3] but their *fine structures* established by X-ray crystallographic methods are largely restricted to the halogen adducts.[4] Since the latter are prereactive intermediates critical to electrophilic aromatic halogenation,[5] it is important to establish the precise location of the noncovalently-bonded halogen relative to the aromatic ring. Unfortunately, the classic X-ray crystallography of the benzene complex of bromine by Hassel and Strømme at −40(−50) °C merely reveals the completely delocalized 'axial' orientation **A**, in which the Br–

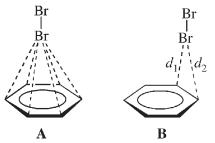

Br bond (2.28 Å) lies on the six-fold symmetry axis (at a bromine separation of 3.36 Å from the mean plane) of benzene.[6] (In other words, the six π electrons comprising the C–C bonds are all equally involved in the 'bonding' to bromine.) Moreover, the corresponding chlorine complex determined by the same workers at −90 °C shows these noncovalently bound crystals to be isomorphous with **A**[7] (which they also considered as further proof for their interesting axial model).

Although the axial model is generally accepted and widely cited, it is at variance with several (recent) theoretical studies which identify a significantly less symmetrical model **B**,[8,9] in which the more localized bonding locates the halogen directly above one C–C bond (*i.e.* η^2) or above a carbon atom (η^1).[10] Since a number of detailed IR studies[11,12] have been unable to resolve the ambiguity between the delocalized and localized models of halogen binding to benzene,[13] we sought the more definitive X-ray crystallographic analysis of the bromine complex with benzene as well as with toluene.

Owing to very weak intermolecular interactions, the requisite (1 : 1) bromine complexes with benzene and toluene for our studies were necessarily prepared *in situ* by (low-temperature) crystallization in a glass capillary.[6,7] Very careful temperature modulation was the critical factor in the successful growth of single crystals of the benzene and toluene complexes suitable for X-ray crystallography at −150 °C.†‡

In both the benzene and toluene complexes, dibromine is uniformly oriented perpendicular to the aromatic planes (with slight deviations α of typically $< 8°$); and the bromine approach occurs at a distance D = 3.01–3.17 Å which is significantly shorter than the sum of the van der Waals radii of 3.55 Å (see Table 1†).[14] Most importantly, the bromine does not coordinate to the benzene ring symmetrically—in striking contrast to the coaxial (delocalized) model **A** reported by Hassel and Strømme.[6] Instead, bromine is positioned over the rim (not above the center) of the benzene ring, being shifted by *ca.* 1.4 Å from the main symmetry axis (see Fig. 1 and δ in Table 1†). In all cases, there is an asymmetric coordination of bromine as given by the shortest Br···C distances d_1 and d_2 (see the localized structure **B**). However from the relative values of $(d_1^2 - D^2)^{1/2}$ and $(d_2^2 - D^2)^{1/2}$, we estimate the hapticity of coordination as: $\eta = 1 + 2(d_1^2 - D^2)^{1/2}/[(d_1^2 - D^2)^{1/2} + (d_2^2 - D^2)^{1/2}]$. Indeed, this evaluation leads to $\eta = 1$ if $d_1 = D$ ('over-atom' coordination) and $\eta = 2$ if $d_1 = d_2$ ('over-bond' coordination).

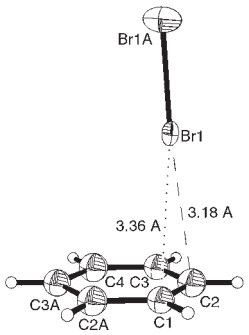

Fig. 1 ORTEP diagram showing the localized (over-atom/bond) coordination of Br_2 to benzene. Thermal ellipsoids of nonhydrogen atoms are shown at 50% probability level.

In the benzene/Br_2 complex, the calculated value of η = 1.52 (Table 1†) corresponds to coordination midway between the 'over-atom' and 'over-bond' configurations. In the toluene complex, the hapticities vary from 1.70 to 1.86 (in four non-equivalent moieties) and thus lie closer to the 'over-bond' coordination model. Moreover, the 'over-bond' coordinated bromine is remarkably shifted toward the *ortho-* or *para-*carbons (see Fig. 2) which correspond to the positions of highest electron density.

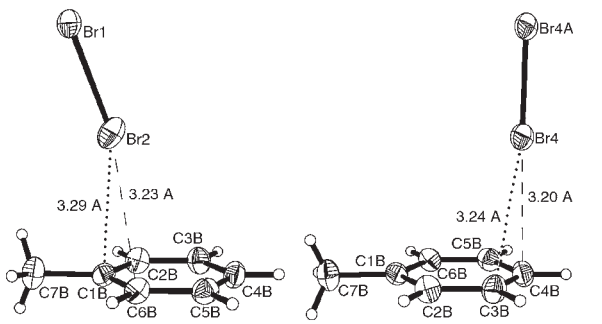

Fig. 2 Localized bonding of bromine to *ortho-* (left) and *para-* (right) centers of toluene in the charge-transfer complex.

† Electronic supplementary information (ESI) available: crystallization of $C_6H_6{\cdot}Br_2$ and $C_6H_5Me{\cdot}Br_2$, crystal data, and their principal geometric parameters. See http://www.rsc.org/suppdata/cc/b1/b102148f/

Such an experimental location of bromine is in a good agreement with the results of high level theoretical calculations which consistently discriminate against the symmetrical coaxial η^6-coordination, and favor both 'over-atom' and 'over-bond' (*i.e.* η^1 and η^2) coordinations without a significant energy barrier between them.[8,9,15] It is also noteworthy that the 'over-rim' coordination modes of Br_2 are highly reminiscent of those found in silver(I) complexes, as representing another general class of electron acceptors showing charge-transfer (non-covalent) binding to arene donors.[16,17]

The charge-transfer complex $[C_6H_6,Br_2]$ is presently the weakest EDA complex of dibromine studied in the solid state. Although the C···Br separation of 3.18 Å is 0.37 Å closer than the equilibrium van der Waals distance,[14] the contraction is perceptibly less than those previously reported in a series of complexes with slightly polarizable and weakly nucleophilic donors.[18] [For example, the X···Br distance contraction (relative to the corresponding equilibrium van der Waals separations) is 0.55 Å in the acetone/Br_2 complex (O···Br 2.82 Å),[20] 0.56 Å in the acetonitrile/Br_2 complex (N···Br 2.84 Å),[21] 0.57 Å in the $[Te_2Cl_{10}]^{2-}/Br_2$ complex (Cl···Br 3.03 Å),[22] and 0.60 Å in the $[Se_2Br_{10}]^{2-}/Br_2$ complex (Br···Br 3.10 Å).[22,23]] Moreover, the average C···Br separation of 3.156 Å in the toluene/Br_2 complex is somewhat shorter than that in the benzene complex, as expected from the better donor strength of toluene.[24]

The weak C(arene)···Br charge-transfer interaction is reflected in an almost unperturbed geometry of the coordinated dibromine. [The Br–Br bond length is actually very sensitive to coordination/polarization effects and readily elongates from 2.284 Å in the non-coordinated molecule (bond order $n = 1$) to 2.53 Å in $[Br_3]^-$ anion[25] (bond order $n = ½$).] As such, the Br–Br bond lengths of 2.301(2) Å in the benzene complex and an average of 2.302(1) Å in the toluene complex do not exhibit much elongation during complex formation. For comparison, the Br–Br bond lengths vary within a narrow range (2.28–2.33 Å) in the weakly coordinated acetone, acetonitrile, dioxane and methanol complexes.[20,21,26,27]

In the absence of significant polarization, dibromine can be coordinated equally well from either end (owing to the σ*-orbital which is localized at both bromine centers); and this explains why dibromine has often been found to be symmetrically coordinated to a pair of donor molecules (in a bridging manner), especially in complexes with weak donors.[4] In the benzene and toluene complexes, dibromine is also positioned symmetrically between the coordinated benzene rings forming infinite (weak) chains ···Ar···Br–Br···Ar···Br–Br···Ar··· through the crystal, and there are no specific interactions other than van der Waals contacts between the chains. Although the chains are highly symmetrical in the benzene/dibromine crystals—with two-fold axes (through the diagonals of the benzene rings and through the centers of the dibromine molecules) across the chains, the chains in the toluene/dibromine crystals are less so. Thus, two of the three dibromines (Br3–Br3A and Br4–Br4A) occupy inversion centers and are thus symmetrically coordinated, but the third dibromine (Br1–Br2) does not show crystallographic symmetry. Indeed, the latter exhibits some signs of larger polarization as a result of a less symmetric coordination (Table 1), and it has the shortest contact C···Br 3.053(4) Å as well as the longest Br–Br bond length 2.307(1) Å in the series. Interestingly, a similar asymmetric coordination of dibromine is found in the complex with methanol,[26] in which the O···Br distance is shorter (2.705 *vs.* 2.723 Å) and the Br–Br bond length is longer (2.324 *vs.* 2.303 Å) than those in the closely related (but symmetric) dioxane complex.[27] This structural effect predicts that polarization in isolated donor/acceptor dyads (as extant in dilute solutions) will be somewhat stronger than that observed in (crystalline) polymeric chains.

We thank the National Scientific Foundation and R. A. Welch Foundation for financial support.

Notes and references

‡ CCDC 162148 and 162149. See http://www.rsc.org/suppdata/cc/b1/b102148f/ for crystallographic data in .cif or other electronic format.

1 For example, an unusual number (3) of thematic issues of *Chem. Revs.* have been issued in the last dozen years: *viz.* 1988 (vol. **88**), 1994 (vol. **94**) and 2000 (vol. **100**); See, especially: K. S. Kim, P. Tarakeshwar and J. Y. Lee, *Chem. Rev.*, 2000, **100**, 4145.

2 *Molecular Interactions. From van der Waals to Strongly Bound Complexes*, ed. S. Scheiner, Wiley, New York, 1997; P. Hobza and R. Zahradnik, *Intermolecular Complexes*, Elsevier, New York, 1988; H. Ratajczak and W. J. Orville-Thomas, *Molecular Interactions*, Wiley, New York, vol. **1** (1980), vol. **2** (1981), vol. **3** (1982).

3 As observed variously in the gas phase, rare-gas matrix, solution, or the crystalline solid state.

4 O. Hassel and Chr. Rømming, *Quart. Rev. Chem. Soc.*, 1962, **26**, 1; O. Hassel, *Mol. Phys.*, 1958, **1**, 241.

5 M. J. S. Dewar, *The Electronic Theory of Organic Chemistry*, Clarendon Press, Oxford, 1958, p. 168; A. C. Legon, *Angew. Chem., Int. Ed.*, 1999, **38**, 2686; S. Fukuzumi and J. K. Kochi, *J. Am. Chem. Soc.*, 1981, **103**, 7240.

6 O. Hassel and K. O. Strømme, *Acta Chem. Scand.*, 1958, **12**, 1146 (in this temperature range, significant thermal motion caused a weak diffraction pattern and high angle reflections were absent).

7 O. Hassel and K. O. Strømme, *Acta Chem. Scand.*, 1959, **13**, 1781.

8 F. C. Grozema, R. W. J. Zijlstra, M. Swart and P. Th. Van Duijhen, *Int. J. Quantum Chem*, 1999, **75**, 709.

9 A. M. Mebel, H. L. Lin and S. H. Lin, *Int. J. Quantum Chem*, 1999, **72**, 307.

10 The descriptor η is the arene hapticity as defined by F. A. Cotton and G. Wilkinson, *Advanced Inorganic Chemistry*, Wiley, New York, 5th edn., 1988, p. 38; In structural comparisons discussed hereinafter, for convenience we make no distinction among the various halogens (Cl_2, Br_2 or I_2)

11 H. Bai and B. S. Ault, *J. Phys. Chem.*, 1990, **94**, 199; E. E. Ferguson, *J. Chem. Phys.*, 1956, **25**, 577; L. Fredin and B. Nelander, *J. Am. Chem. Soc.*, 1974, **96**, 1672.

12 S. A. Cooke, C. M. Evans, J. H. Holloway and A. C. Legon, *J. Chem. Soc., Faraday Trans.*, 1998, **94**, 2295; L. Fredin and B. Nelander, *Mol. Phys.*, 1974, **27**, 885; W. B. Person, C. F. Cook and H. B. Friedrich, *J. Chem. Phys.*, 1967, **46**, 2521.

13 See also: J. Collin and L. D'Or, *J. Chem. Phys.*, 1955, **23**, 397; H. B. Friedrich and W. B. Person, *J. Chem. Phys.*, 1966, **44**, 2161; G. DeBoer, J. W. Burnet, A. Fujimoto and M. A. Young, *J. Phys. Chem.*, 1996, **100**, 14 882; P. Y. Cheng, D. Zhong and A. H. Zewail, *J. Chem. Phys.*, 1996, **105**, 6216; J. T. Su and A. H. Zewail, *J. Phys. Chem. A*, 1998, **102**, 4082.

14 A. Bondi, *J. Phys. Chem.*, 1964, **68**, 441.

15 S. S. C. Ammal, S. P. Ananthavel, P. Venuvanalingam and M. S. Hegde, *J. Phys. Chem. A*, 1998, **102**, 532; A. Matsuzawa and Y. Osamura, *Bull. Chem. Soc. Jpn.*, 1997, **70**, 1531. However, see: G. Milano, G. Guerra and L. Cavallo, *Eur. J. Inorg. Chem.*, 1998, 1513; E. Kochanski and J. Prissette, *Nouv. J. Chem.*, 1980, **4**, 509; I. Jano, *Theor. Chim. Acta*, 1985, **66**, 341; E. G. Cook and J. C. Shug, *J. Chem. Phys.*, 1970, **53**, 723.

16 S. V. Lindeman, R. Rathore and J. K. Kochi, *Inorg. Chem.*, 2000, **39**, 5707.

17 The halogen/arene complexes have also been discussed as charge-transfer complexes. For reviews, see: J. Andrews and R. M. Keefer, *Molecular Complexes in Organic Chemistry*, Holden-Day, San Francisco, 1964; R. Foster, *Organic Charge-Transfer Complexes*, Academic, New York, 1969; S. Fukuzumi and J. K. Kochi, *J. Org. Chem.*, 1981, **46**, 4116.

18 According to Mulliken,[19] the dative contribution from $[Br_2^-,C_6H_6^+]$ plays a role in the noncovalent interaction. As such for charge-transfer complexes, the contraction is largely due to Coulombic and dispersion forces. See also: H. O. Hooper, *J. Chem. Phys.*, 1964, **41**, 599.

19 R. S. Mulliken, *J. Am. Chem. Soc.*, 1950, **72**, 600; R. S. Mulliken, *J. Am. Chem. Soc.*, 1952, **74**, 811; R. S. Mulliken and W. B. Person, *Molecular Complexes, A. Lecture and Reprint Volume*, Wiley, New York, 1969.

20 O. Hassel and K. O. Strømme, *Acta Chem. Scand.*, 1959, **13**, 275.

21 K.-M. Marstokk and K. O. Strømme, *Acta Crystallogr., Sect. B*, 1968, **24**, 713.

22 S. Hauge and K. Maroy, *Acta Chem. Scand.*, 1996, **50**, 1095.

23 V. Janickis, *Acta Chem. Scand.*, 1999, **53**, 188.

24 J. O. Howell, J. M. Goncalves, C. Amatore, L. Klasinc, R. M. Wightman and J. K. Kochi, *J. Am. Chem. Soc.*, 1984, **106**, 3968.

25 Cambridge Crystallographic Database, Release Fall 2000.

26 P. Groth and O. Hassel, *Acta Chem. Scand.*, 1964, **18**, 402.

27 O. Hassel and J. Hvoslef, *Acta Chem. Scand.*, 1954, **8**, 873.

CHEMCOMM
Communication
www.rsc.org/chemcomm

Insights into the chemical vapor deposition of GaN using the single-source precursor $Me_2N(CH_2)_3Ga(N_3)_2$: matrix isolation of $Ga(N_3)$

Jens Müller* and Sabine Bendix

Organometallics & Materials Chemistry, Anorganische Chemie II, Ruhr-Universität, 44780 Bochum, Germany. E-mail: jens.mueller@aci.ruhr-uni-bochum.de

Received (in Cambridge, UK) 2nd March 2001, Accepted 17th April 2001
First published as an Advance Article on the web 1st May 2001

The investigation of the pyrolysis of the single-source precursor $Me_2N(CH_2)_3Ga(N_3)_2$ 1 by matrix-isolation FTIR spectroscopy revealed monomeric $Ga(N_3)$ as a reactive intermediate.

The group 13 nitrides of Al, Ga and In and their ternary alloys $Al_xGa_yIn_zN$ ($x + y + z = 1$) are wide direct band gap materials with promising applications as new microelectronic and optoelectronic devices.[1] For example, blue-light emitting diodes and lasers based on gallium nitride can be constructed.[2] Usually, thin films of the nitrides can be epitaxially grown by chemical vapor deposition (CVD) from the trialkyl compounds MR_3 with a large excess of ammonia.[1,2] These organometallics are toxic, pyrophoric, and very sensitive to air and moisture and several efforts have been made to synthesize alternative precursors. If the element is equipped with a ligand that is capable of intramolecular coordination, then non-pyrophoric organometallics are accessible. In particular, the 3-dimethylaminopropyl ligand, $Me_2N(CH_2)_3$, has been successfully applied to various precursors: for example, the diazide $Me_2N(CH_2)_3Ga(N_3)_2$ **1** is a single-source precursor for the MOCVD of GaN.[3]

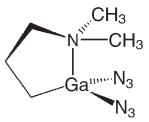

1

For a deeper understanding of a CVD process and a rational design of improved precursors, detailed knowledge of fragmentation mechanisms is needed. Recently, we started to investigate the fragmentation of intramolecularly coordinated alanes and gallanes of the type $Me_2N(CH_2)_3MX_2$ (X = Cl, Br, Me) using matrix isolation techniques.[4–7] In this procedure a carrier gas/precursor mixture is transported through a small pyrolysis tube and reactive intermediates produced by the fragmentation of the organometallic precursor are trapped on a CsI window at 15 K.

A series of high vacuum thermolysis experiments with the diazide **1** and argon as carrier gas was performed between ambient temperature and 800 °C.† Up to 450 °C compound **1** passes the thermolysis oven unchanged, but above this temperature new IR bands in the matrix IR spectra indicate the beginning of the fragmentation of **1**. Fig. 1 shows a typical IR spectrum of matrix-isolated products recorded after a thermolysis experiment at 520 °C (spectrum A). Under these conditions precursor **1** was completely fragmented; its typical IR absorptions could no longer be detected in argon matrices. In the common region of asymmetric stretching modes of azido groups two intense IR bands at 2135.4 and 2106.0 cm^{-1} were observed (Fig. 1A). The IR band at 2135.4 cm^{-1} unequivocally belongs to hydrazoic acid, HN_3, which has a well-known set of bands at 3316.7, 2286.2, 2135.4, 1264.1 and 1146.0.[8] That the second intense IR band, that at 2106.0 cm^{-1}, belongs to a second azide was revealed by photolysis experiments (Fig. 1B). Irradiation of the matrix-isolated thermolysis products with an Xe arc lamp for *ca*. 30 s selectively bleached the band at 2106.0 cm^{-1} plus an IR band at 1340.3 cm^{-1};‡ the frequencies, intensity pattern, and low half-band widths ($h_{\frac{1}{2}} < 2$ cm^{-1}) of these bands are indicative of a small molecular azide and we assign these two bands to the symmetric and asymmetric N_3 stretching mode of $Ga(N_3)$. The calculated harmonic frequencies and intensities [B3LYP/6-311+G(d)][9] of the two modes $\nu_{as}(N_3)$ [2230.7 cm^{-1}; 1080 km mol^{-1}] and $\nu_s(N_3)$ [1408.2 cm^{-1}; 249 km mol^{-1}] are in good agreement with our measured values. Recently, gallium(I) azide was observed for the first time by co-deposition matrix experiments of laser-ablated Ga atoms with nitrogen.[9] Among other Ga–N species, Zhou and Andrews identified $Ga(N_3)$ in excess of solid N_2 by IR bands at 2103.6 / 2096.8 cm^{-1} [$\nu_{as}(N_3)$] and 1331.3 / 1328.3 cm^{-1} [$\nu_s(N_3)$]; both bands were split by matrix site effects.[9] This assignment was strongly supported by nitrogen isotopic substitutions and DFT calculations. According to B3LYP/6-311+G(d) calculations, $Ga(N_3)$ is a C_s symmetrical molecule with a linear N_3 group and a Ga–N–N angle of 149.5°.[9] From the six normal modes only the two azide stretching vibrations and the Ga–N stretching mode are expected to have a sufficiently high transition moment to be detectable. The harmonic frequency of the Ga–N stretch was predicted at 384.3 cm^{-1} with an intensity of 133 km mol^{-1}, but it could not be detected in the laser-ablation experiments.[9]

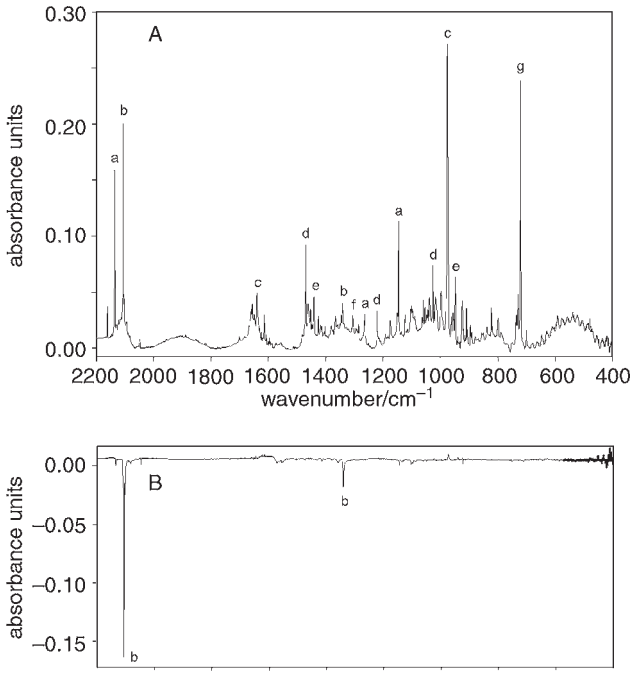

Fig. 1 A, products of thermolysis of **1** at 520 °C trapped in an excess of argon at 15 K; a: HN_3, b: $Ga(N_3)$, c: NH_3, d: $H_2C{=}NCH_3$, e: $H_2C{=}CH_2$, f: CH_4, g: HCN. B, difference IR spectrum obtained by photolysis of the product matrix A; negative IR bands indicate disappearing species.

DOI: 10.1039/b101987m

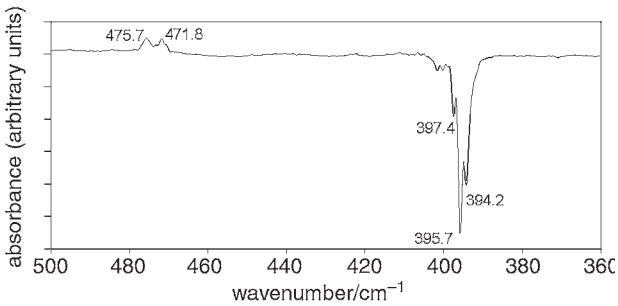

Fig. 2 Low-frequency region of the photolysis of the thermolysis products of **1** (see text for details).

We investigated the photolysis reaction of the thermolysis products of **1** in the frequency region 200–700 cm^{-1}. As depicted in Fig. 2 a set of three IR bands at 397.4, 395.7 and 394.2 cm^{-1}, disappears on irradiation. We assign this set to the missing ν(GaN) of $Ga(N_3)$. The experimental frequencies fit quite well to the predicted frequency of 384.3 cm^{-1}; the B3LYP method is known to underestimate low frequency modes.[10] Because of the natural abundance of the two isotopes, ^{69}Ga (60%) and ^{71}Ga (40%), two IR bands are expected for this vibrational mode. If we assign the most intense IR band at 395.7 cm^{-1} to $\nu(^{69}GaN)$ then the same mode for the ^{71}Ga isotope should occur at 393.9 cm^{-1} [B3LYP/6-311+G(d)], which is in good agreement with the measured band at 394.2 cm^{-1}. The appearance of three IR bands could be caused by an overlap of resonances of $Ga(N_3)$ in at least two different matrix sites: one site with 397.4 (^{69}Ga) and 395.7 cm^{-1} (^{71}Ga), and the other site with 395.7 (^{69}Ga) and 394.2 cm^{-1} (^{71}Ga). This interpretation is in accordance with the expected isotopic shifts, but the expected intensity pattern would be a little different from the observed one; the IR band at 395.7 cm^{-1} is expected to have a higher intensity. Furthermore, the IR band at 394.2 cm^{-1} shows a shoulder to its low frequency side indicating another overlap of IR bands.

GaN is the expected product of the photolysis of $Ga(N_3)$ in matrices. As a result of the photolysis reaction only two unresolved IR bands of low intensity at 475.7 and 471.8 cm^{-1} evolved (Fig. 2). Zhou and Andrews assigned an unresolved IR band at 484.9 cm^{-1} to GaN in N_2 matrices.[9] Because of a large mismatch between the calculated frequency (580.9 cm^{-1}) and the measured value, the authors interpreted the IR band at 484.9 cm^{-1} as being due to a GaN$\cdots$N$_2$ complex. We tentatively assign the two IR bands at 475.7 and 471.8 cm^{-1} to GaN, which might be perturbed by the N_2 molecule produced photochemically in the same matrix cage.

In addition to HN_3 and $Ga(N_3)$ the matrix containing the thermolysis products of **1** at 520 °C (Fig. 1) contained the well-known molecules NH_3, $H_2C{=}NCH_3$, $H_2C{=}CH_2$, CH_4 and HCN, which were identified by comparison with published data. With the exception of ammonia, all fragments have been found previously in similar thermolysis experiments with alanes and gallanes of the type $Me_2N(CH_2)_3MX_2$ (X = Cl, Br).[4,5]

Prior to our work, compound **1** was investigated by mass spectrometry[11] which is commonly used for *in situ* analysis of gas-phase species in CVD processes. Within this work $HGaN_6$, GaN_6, $HGaN_2$ and GaN_2 were identified close to the substrate surface. On the basis of the experimental data, however, the authors could not explain the formation of these species. Furthermore, it was not possible to distinguish between β-hydrogen elimination and homolysis of the Ga–C bond of **1**. The main aim of our investigation was to understand the fragmentation of the single-source precursor **1**. A β-hydrogen elimination of **1** would result in $HGa(N_3)_2$ and allyldimethylamine; this amine was not detected in any of our experiments. We checked independently that allyldimethylamine is stable under our applied thermolysis conditions.[4] This means that a β-hydrogen elimination can be excluded unequivocally for **1**.

We identified the monomeric hydrides HMX_2 in thermolysis reactions with alanes and gallanes of the type $Me_2N(CH_2)_3MX_2$ (X = Cl, Br).[4,5] Even though allyldimethylamine was not obtained in any of these experiments, the results were explained by β-hydrogen eliminations. We proposed that the temperatures needed for fragmentation reactions (> 800 °C) were so high that allyldimethylamine, formed as an intermediate, fragmented further to the obtained carbon-containing species. In order to prove this interpretation, we synthesized selectively deuterated starting compounds $Me_2NCH_2CD_2CH_2MBr_2$ (M = Al, Ga) and investigated them by matrix isolation techniques.[12] In none of the thermolysis experiments did we find the expected deuterates $DMBr_2$; only hydrides $HMBr_2$ were formed. That β-hydrogen elimination can occur for intramolecularly coordinated gallanes with high efficiency had been shown for the dimethyl derivative $Me_2NCH_2CD_2CH_2GaMe_2$.[7]

In summary, the following picture for the fragmentation of $Me_2N(CH_2)_3MX_2$ (X = Cl, Br, N_3) is in accordance with all experimental results. Homolysis of the M–C bond results in radicals of the type MX_2. These radicals presumably trap H atoms on their way to the matrix window. In the case of X = Cl or Br, the respective hydrides HMX_2 are stable enough to be detectable in an excess of solid argon. In the case of the azide **1** the proposed intermediate $HGa(N_3)_2$ eliminates HN_3 to give $Ga(N_3)$, an interpretation in accordance with the detected mixtures of HN_3 and $Ga(N_3)$.§ In terms of the CVD process with **1** as a single-source precursor, it is feasible that gallium(I) azide is a key intermediate in the GaN deposition.

This work was supported by the Fonds der Chemischen Industrie and by the Deutsche Forschungsgemeinschaft. We thank A. Devi (RUB) for the synthesis of **1** and R. A. Fischer (RUB) for his support.

Notes and references

† The matrix isolation apparatus is described in ref. 7. For the photolysis experiments a 150 W Xe arc lamp (XBO 150 W/4 in an Oriel arc lamp housing 66055-M) equipped with a cut-off filter for λ = 225 nm (Schott WG 225) was used.

‡ Because of matrix site effects, the intense band at 2106.0 cm^{-1} is accompanied by a low intensity band at 2102.7 cm^{-1}.

§ According to DFT type calculations at the BP/DZVP level of theory (R. Schmid, TU Munich, Germany) the free energy of activation (including zero point vibrational energy) at 600 K, for the elimination of $HGa(N_3)_2$ to HN_3 and $Ga(N_3)$ is 42.1 kcal mol^{-1}. This fragmentation is energetically preferred over an N_2 loss reaction.

1 A. C. Jones and P. O'Brien, *CVD of Compound Semiconductors*, VCH, Weinheim, 1997.
2 S. Nakamura and G. Fasol, *The Blue Laser Diode, GaN Based Light Emitters and Lasers*, Springer, Berlin, Heidelberg, 1997.
3 A. Miehr, M. R. Mattner and R. A. Fischer, *Organometallics*, 1996, **15**, 2053; A. Miehr, O. Ambacher, W. Rieger, T. Metzger, E. Born and R. A. Fischer, *Chem. Vap. Deposition*, 1996, **2**, 51; R. A. Fischer, A. Miehr, E. Herdtweck, M. R. Mattner, O. Ambacher, T. Metzger, E. Born, S. Weinkauf, C. R. Pulham and S. Parsons, *Chem. Eur. J.*, 1996, **2**, 1353; A. Devi, W. Rogge, A. Wohlfart, F. Hipler, H. W. Becker and R. A. Fischer, *Chem. Vap. Deposition*, 2000, **6**, 245.
4 J. Müller and B. Wittig, *Eur. J. Inorg. Chem.*, 1998, 1807.
5 J. Müller and H. Sternkicker, *J. Chem. Soc., Dalton Trans.*, 1999, 4149.
6 J. Müller, H. Sternkicker, U. Bergmann and B. Atakan, *J. Phys. Chem. A*, 2000, **104**, 3627.
7 J. Müller, B. Wittig and S. Bendix, *J. Phys. Chem. A*, 2001, **105**, 2112
8 D. W. Ball, Z. H. Kafafi, L. Fredin, R. H. Hauge and J. L. Margrave, *A Bibliography of Matrix Isolation Spectroscopy: 1954–1985*, Rice University Press, Houston, TX, 1988.
9 M. Zhou and L. Andrews, *J. Phys. Chem. A*, 2000, **104**, 1648.
10 A. Y. Timoshkin, H. F. Bettinger and H. F. Schaefer III, *J. Am. Chem. Soc.*, 1997, **119**, 5668.
11 J. Schäfer, J. Wolfrum, R. A. Fischer and H. Sussek, *Chem. Phys. Lett.*, 1999, **300**, 152.
12 J. Müller, B. Wittig and S. Bendix, unpublished results.

CHEMCOMM Communication
www.rsc.org/chemcomm

Formation and electrochemical desorption of stable and electroactive self-assembled monolayers (SAMs) of oligothiophene–fulleropyrrolidine dyads

Sheng-Gao Liu,[ac] Corinne Martineau,[b] Jean-Manuel Raimundo,[b] Jean Roncali*[b] and Luis Echegoyen*[a]

[a] *Department of Chemistry, University of Miami, FL 33143, USA. E-mail: echegoyen@miami.edu*
[b] *Ingénierie Moléculaire et Matériaux Organiques, UMR CNRS 6501, Université d'Angers, 2 Bd Lavoisier, 49045 Angers Cedex, France*
[c] *National Renewable Energy Laboratory, 1617 Cole Blvd., Golden, CO 80401-3393, USA*

Received (in Columbia, MO, USA) 17th January 2001, Accepted 21st March 2001
First published as an Advance Article on the web 1st May 2001

Stable, electroactive SAMs of oligothiophene–fulleropyrrolidine dyads have been prepared by spontaneous adsorption; electro-oxidation of the oligomeric system results in desorption.

Self-assembled monolayers (SAMs) provide unique opportunities to develop chemically tailored surfaces with specific chemical and physical properties.[1,2] Besides the considerable amount of work devoted to the development of selective electrochemical sensors,[1,2] SAMs have attracted increasing interest due to potential use in molecular electronics.[3]

In this context, there have been several reports concerning the preparation and characterization of SAMs derived from various kinds of linear π-conjugated oligomers on gold surfaces.[3–5] However, until now, all of these monolayers were prepared from oligomeric systems possessing one or two terminal alkanethiol groups eventually connected to the conjugated system *via* a flexible alkyl spacer. Recently, this approach has been successfully applied to the preparation of SAMs of C_{60}-derivatized oligothiophenes.[5] On the other hand, despite some theoretical controversy, the adsorption of thiophene onto Au(111) was recently demonstrated.[6]

Here, we show for the first time that stable SAMs can be produced on Au(111) surfaces by spontaneous adsorption of C_{60}-derivatized, π-conjugated oligomers of the thiophene and thienylenevinylene[7] series. Although the fulleropyrrolidine group represents a very convenient electroactive probe, its role in the process of SAM formation is not clearly elucidated at the present time.

Compounds **1**–**6** (Chart 1) were newly synthesized by reacting the appropriate carbaldehyde with C_{60} in the presence of *N*-methylglycine according to the methodology of Prato and coworkers[8] with a slight modification as reported for the synthesis of C_{60}–thiophene dyads by ourselves.[9] All new compounds were fully characterized by the usual spectroscopic and analytical techniques giving satisfactory results.†

SAMs were prepared by dipping ultra-clean, spherical, gold (99.9999%) bead electrodes‡ for 24–72 h in 1 mM *o*-dichlorobenzene (ODCB) solutions of compounds **1**–**6**. The electrodes were then thoroughly rinsed with ODCB and CH_2Cl_2, dried under an argon flow and immersed in 0.05 M Bu_4NPF_6–ODCB for electrochemical characterization. Sonication in ODCB did not remove the SAMs, indicating that the compounds are chemically adsorbed and not simply physisorbed.

The cyclic voltammogram (CV) of a SAM of **3** (Fig. 1) shows two well-resolved reversible cathodic waves with $E^0_1 = -0.65$ V and $E^0_2 = -1.04$ V corresponding to the first two one-electron reductions of the C_{60} fragment.[10] Scanning the potential to −1.8 V (*vs.* Ag/AgCl) allowed the observation of the reversible third reduction at −1.57 V (not shown in Fig. 1 due to an impurity present in OBCD at around −1.2 V). Within

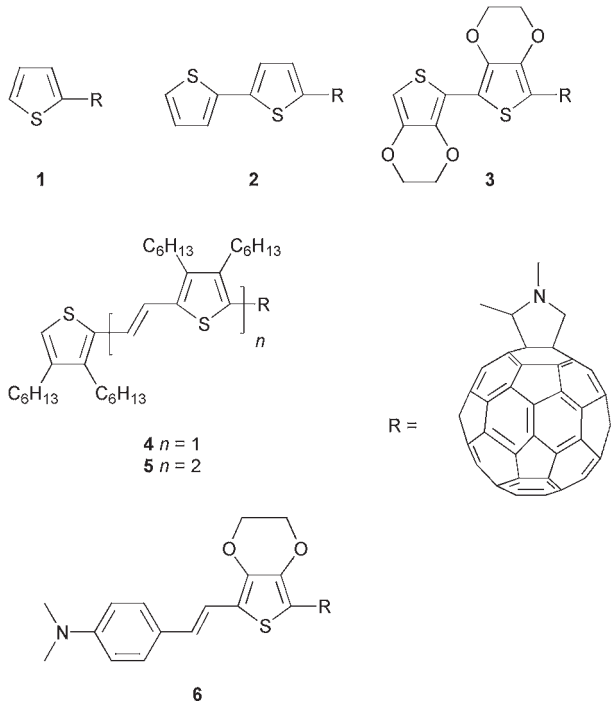

Chart 1

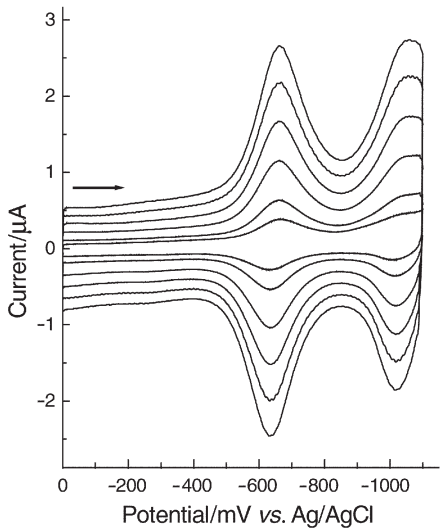

Fig. 1 CVs of a SAM of **3** in 0.05 M Bu_4NPF_6–ODCB system, scan rates between 100 (smallest current) and 1000 (largest current) mV s^{-1}.

DOI: 10.1039/b102132j

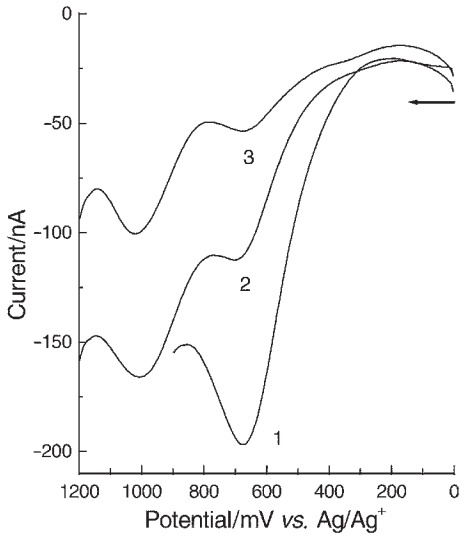

Fig. 2 Repetitive oxidation of a SAM of **3** by Osteryoung square-wave voltammetry in 0.05 M Bu_4NPF_6–ODCB system using a sweep width of 25 mV, frequency of 15 Hz, step potential of 4 mV, and a quiet time of 2 s.

the range of scan rates investigated (100–1000 mV s^{-1}), peak currents increased linearly with the scan rate while the peak potentials and peak-to-peak separations (ΔE_p) (19 and 27 mV for the first and the second reductions, respectively) were independent of scan rate. These characteristics together with the Gaussian shape of the CV waves are typical for surface-confined electroactive species.

Further confirmation of the formation of a surface-attached monolayer on the gold surface was obtained by analyzing the CV response of the $Ru(NH_3)_6^{3+/2+}$ couple at a bare gold electrode and at an electrode modified by a SAM of **3**. The CV recorded in the first case exhibits a reversible redox couple with $E^0 = -0.16$ V and $\Delta E_p = 63$ mV at 100 mV s^{-1}. In contrast, the CV recorded at the modified electrode reveals a drastic decrease of the intensity of the cathodic peak currents together with a *ca*. 50 mV negative shift of the E_{pc} and almost disappearance of the corresponding anodic wave. These results indicate that electron transfer at the interface between the modified gold surface and the solution redox species is severely hindered by the presence of the insulating monolayer.

SAM formation was investigated for the other compounds. Similar results were obtained for compounds **2**, **4** and **5**, but the surface coverage (Γ) decreased from 2.1×10^{-10} mol cm^{-2} for **3** to about 1.1×10^{-10}, 0.4×10^{-10} and 0.3×10^{-10} mol cm^{-2} for **2**, **4** and **5**, respectively.§ It is noteworthy that these Γ values are significantly larger than those reported for SAMs of C_{60}-derivatized oligothiophenes prepared *via* thiol attachment.[5] On the other hand, and despite many attempts using many different conditions (solvent, concentration, time of immersion), no SAM formation could be detected for compounds **1** and **6**.

SAMs derived from compounds **2**–**5** were stable under repetitive cycling in the negative potential region (up to −1.8 V *vs*. Ag/AgCl) and no modification of the CV response was observed after several weeks of storing the modified electrodes under ambient conditions. However, application of a positive potential corresponding to the first oxidation of the oligomeric π-conjugated system produces the rapid desorption of the SAMs (Fig. 2). Desorption was confirmed by the simultaneous disappearance of the fullerene-based reduction peaks. This behavior, which contrasts strikingly with the oxidative stability of SAMs derived from oligothiophenes attached *via* an alkanethiol,[4] suggests that the electron density of the sulfur atom, which depends on the redox state of the π-conjugated oligomer, could play an important role in the adsorption–desorption process.

To summarize, we have demonstrated that stable, electroactive SAMs of dyads involving fulleropyrrolidine and thiophene-based, π-conjugated oligomers can be readily formed on a gold surface and that these SAMs can be easily desorbed by electro-oxidation of the π-conjugated system. Although these preliminary results pose intriguing questions regarding the relationships between the process of SAM formation and the structural variables of the molecules (C_{60} group, substitution of the thiophene ring, presence of a free α-position at the terminal thiophene ring, chain length of the oligomeric system, *etc*.), the unique combination of properties exhibited by this new class of SAMs can open interesting perspectives in the field of thiophene-based molecular electrochemical and electronic devices.

S. G. L. and L. E. acknowledge the National Science Foundation for financial support of this work (CHE-9816503 and DMR-9803088). S. G. L. also thanks Dr Brian A. Gregg at the National Renewable Energy Laboratory (NREL) for partial support during the writing stages of the work at NREL.

Notes and references

† *Selected data* for **2**: Mp. > 250 °C. ^{1}H NMR (CS_2/C_6D_6): δ 7.12 (d, ^3J 3.7 Hz, 1H), 6.97 (dd, ^3J 5.0 Hz, ^3J 1 Hz, 1H), 6.96 (dd, ^3J 3.5 Hz, ^3J 1 Hz, 1H), 6.90 (d, ^3J 3.5 Hz, 1H), 6.79 (dd, ^3J 5.0 Hz, ^3J 3.7 Hz, 1H), 5.06 (s, 1H), 4.78 (d, ^3J 9.5 Hz, 1H), 4.09 (d, ^3J 9.5 Hz, 1H), 2.78 (s, 3H). MALDI-TOF mass spectrum: calc. for $C_{71}H_{11}NS_2$: *m*/*z* 941.03; found: 940.0 ($M - H^+$). Anal. calc. for $C_{71}H_{11}NS_2$: C 90.53, H 1.18, N 1.49, S 6.81. Found: C 90.19, H 1.54, N 1.53, S 6.56%.

‡ The geometric area (A) of the gold bead electrodes was determined from the slopes of the linear plot of the cathodic peak current *versus* the square root of the scan rate obtained for the diffusion-controlled reduction of $Ru(NH_3)_6^{3+}$, *i.e*., A = slope/$((2.69 \times 10^5) \times 1 \times D_0)^{1/2} \times C_0)$). A diffusion coefficient (D_0) of 7.5×10^{-6} cm^2 s^{-1} (at 25 °C in 0.1 M NaCl) was used (see: C. M. Yip and M. D. Ward, *Langmuir,* 1994, **10**, 549). Typical values for the geometric area of the electrode varied between 0.02 and 0.03 cm^2.

§ Surface coverage (Γ) of the SAMs was calculated by integration of the cathodic current during the first CV scan.

1 A. Kumar, N. L. Abbott, E. Kim, H. A. Biebuyck and G. M. Whitesides, *Acc. Chem. Res*., 1995, **28**, 219; L. M. Goldenberg, M. R. Bryce and M. C. Pettey, *J. Mater. Chem*., 1999, **9**, 1957; A. S. Flinck, F. C. J. L. van Veggel and D. N. Reinhoudt, *Adv. Mater*., 2000, **12**, 1315.

2 S.-G. Liu, H.-Y. Liu, K. Bandyopadhyay, Z.-Q. Gao and L. Echegoyen, *J. Org. Chem*., 2000, **65**, 3292; K. Bandyopadhyay, L.-H. Shu, H.-Y. Liu and L. Echegoyen, *Langmuir*, 2000, **16**, 2706.

3 J. M. Tour, L. Jones, D. L. Pearson, J. J. S. Lamba, T. P. Burgin, G. M. Whitesides, D. L. Allara, A. N. Parikh and S. V. Atre, *J. Am. Chem. Soc*., 1995, **117**, 9529; M. A. Reed, C. Zhou, C. J. Muller, T. P. Burgin and J. M. Tour, *Science*, 1997, **278**, 252; C. Kergueris, J.-P. Bourgoin, S. Palacin, D. Esteve, C. Urbina, M. Magoga and C. Joachim, *Phys. Rev. B*, 1999, **59**, 12 505.

4 R. Michalitsch, A. Elkassmi, P. Lang, A. Yassar and F. Garnier, *J. Chim. Phys*., 1998, **95**, 1339.

5 D. Hirayama, T. Yamashiro, K. Takimiya, Y. Aso, T. Otsubo, H. Norieda, H. Imahori and Y. Sakata, *Chem. Lett*., 2000, 570.

6 M. H. Dishner, J. C. Hemminger and F. J. Feher, *Langmuir*, 1996, **12**, 6176.

7 J. Roncali, *Acc. Chem. Res*., 2000, **33**, 147.

8 M. Maggini, A. Karlsson, G. Scorrano, G. Sandonà, G. Farnia and M. Prato, *J. Chem. Soc., Chem. Commun*., 1994, 589.

9 S.-G. Liu, L.-H. Shu, J. Rivera, H.-Y. Liu, J.-M. Raimundo, J. Roncali, A. Gorgues and L. Echegoyen, *J. Org. Chem*., 1999, **64**, 4884.

10 L. Echegoyen and L. E. Echegoyen, *Acc. Chem. Res*., 1998, **31**, 593.

CHEMCOMM Communication
www.rsc.org/chemcomm

Asymmetric synthesis of novel polyhydroxylated derivatives of indolizidine and quinolizidine by intramolecular 1,3-dipolar cycloaddition of *N*-(3-alkenyl)nitrones†

Piotr Gębarowski and Wojciech Sas*

Warsaw University of Technology, Faculty of Chemistry, ul. Noakowskiego 3, 00 664 Warszawa, Poland. E-mail: sas@ch.pw.edu.pl

Received (in Cambridge, UK) 31st January 2001, Accepted 10th April 2001
First published as an Advance Article on the web 1st May 2001

Reaction of 3-*O*-benzyl-1,2-*O*-isopropylidene-1,5-pentadialdo-α-D-xylofuranose with *N*-(1,1-dimethylbut-3-enyl)-hydroxylamine followed by intramolecular 1,3-dipolar cycloaddition yields 7-oxa-1-azabicyclo[2.2.1]heptane derivative 4, which is easily converted into novel polyhydroxylated quinolizidine 6 and indolizidine 8.

Polyhydroxylated derivatives of indolizidine and quinolizidine (frequently named as azasugars) are powerful glycosidase inhibitors and potential therapeutics.[1] Consequently, these compounds are targets of intensive synthetic studies.

Many syntheses of azasugars use derivatives of natural sugars as starting materials.[1] Based on our experience in intramolecular 1,3-dipolar cycloaddition of *N*-(3-alkenyl)nitrones[2,3] we envisaged that this reaction, proceeding with high regio- and diastereoselectivity,[4] might be a useful tool for conversion of sugar dialdehydes, with one carbonyl group masked, into bicyclic azasugars **E** (Fig. 1).

We reasoned that the nitrone **C**, attained from the protected cyclic or acyclic sugar dialdehydes **A** and *N*-homoallylhydroxylamine **B**, (a sugar ring in Fig. 1 is symbolised by the dashed bow) might undergo intramolecular 1,3-dipolar cycloaddition to give the **7**-oxa-1-azabicyclo[2.2.1]heptane derivative **D** with high stereoselectivity induced by the sugar moiety.‡ Subsequent unmasking of the carbonyl function, which could be combined with a modification of the sugar residue (*e.g.* shortening of the carbon skeleton by a diol cleavage), followed by hydrogenolysis of the N–O bond accompanied by intramolecular reductive amination would complete the synthesis of the target derivative **E**.

We describe herein the transformation of the cyclic sugar dialdehyde 1,2-*O*-isopropylidene-1,5-pentadialdo-α-D-xylofuranose **1**,[5] readily available from α-D-glucose, into the novel polyhydroxylated quinolizidine **6** and indolizidine **8**, possessing a tertiary carbon at an α position to nitrogen, to illustrate the usefulness of the proposed method for the bicyclic azasugar preparation (Scheme 1).

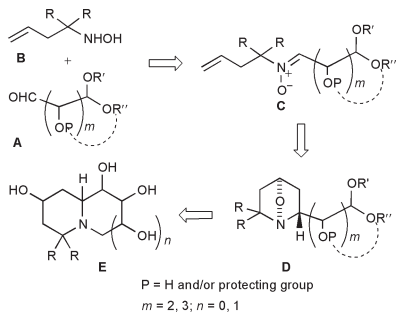

Fig. 1 General approach for asymmetric synthesis of bicyclic azasugars **E** by intramolecular 1,3-dipolar cycloaddition of *N*-(3-alkenyl)nitrones.

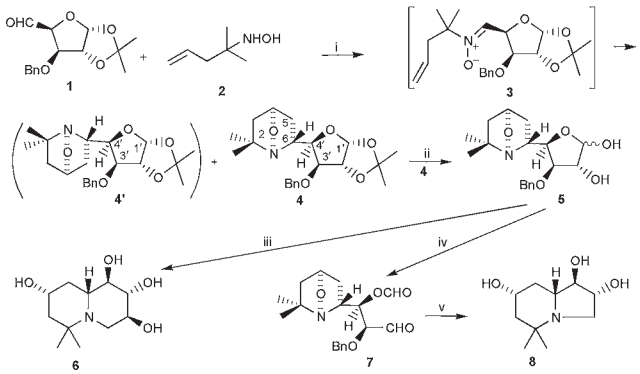

Scheme 1 *Reagents and conditions*: i, toluene, argon, 85–90 °C, 43 h, 52%; ii, 5% HCl aq., rt, 2 d, 96%; iii, H_2 (10 bar), Raney-Ni, MeOH, 75–80 °C, 21 h, 70% based on **4**; iv, $NaIO_4$, MeOH–H_2O, 0 °C; v, H_2 (10 bar), Raney-Ni, MeOH, rt, 24 h then 45 °C, 24 h, 55% based on **4**.

The *N*-homoallylhydroxylamine **2**, necessary for the preparation of **4**, was obtained from the aluminium amalgam reduction of 4-methyl-4-nitropent-1-ene (readily accessible from palladium(0)-catalysed *C*-allylation of 2-nitropropane[6]).[3] The aldehyde **1** heated with **2** in toluene, under argon, gave *N*-(3-alkenyl)nitrone **3** (Scheme 1), which *in situ* underwent intramolecular 1,3-dipolar cycloaddition. Although the possibility exists for formation of two adducts **4** and **4′**, we separated only one diastereoisomer **4** in 52% yield.§ Its structure was determined from ^{1}H NMR spectra and molecular modelling (AM1). The coupling constant between H_6 and $H_{4'}$ was very helpful for configurational assignment; the value of this constant, $^3J_{6,4'}$ = 9.9 Hz, is characteristic for protons in an antiperiplanar arrangement. Molecular modelling revealed that only for the adduct **4** did the lowest energy minimum correspond to the conformation in which H_6 and $H_{4'}$ are antiperiplanar.

The conversion of **4** into quinolizidine **6** was straightforward. Removal of isopropylidene protection by acidic hydrolysis gave cleanly the derivative **5**, which was hydrogenated in the presence of Raney-nickel to afford directly the quinolizidine **6** in 70% yield based on **4**. The structure of **6** from its ^{1}H NMR spectrum is consistent with the structure of **4**. Thus the heterobicyclic system adopts a structure close to *trans*-decaline and all hydroxy groups occupy equatorial positions.

The preparation of the indolizidine **8** was also easy. In this case the carbon skeleton of **5** was cut down by sodium periodate 1,2-diol cleavage to give the aldehyde **7**, which also without purification was hydrogenated in the presence of the nickel catalyst to yield **8** in 55% yield, based on **4**.

In conclusion, it has been shown that the intramolecular 1,3-dipolar cycloaddition of *N*-(3-alkenyl)nitrones, obtained from *N*-homoallylhydroxylamines and sugar dialdehydes, is very useful for the synthesis of polyhydroxylated derivatives of both quinolizidine and indolizidine. Further studies on improve-

† Electronic supplementary information (ESI) available: configurational assignment of the adduct **4** and experimental details of preparation and characterisation of **6** and **8**. See http://www.rsc.org/suppdata/cc/b1/b101057n/

ment and extension of this approach for the synthesis of bicyclic azasugars are in progress.

Notes and references

‡ To our best knowledge the intramolecular 1,3-dipolar cycloaddition reaction of *N*-(3-alkenyl)nitrones, obtained from non-racemic chiral aldhydes, has never been investigated.

§ All new compounds were fully characterised by ^{1}H and ^{13}C NMR, IR spectroscopy, high resolution mass spectrometry and optical rotation. Compound **4**: The aldehyde **1**[5] (0.58 g, 2.09 mmol) and the hydroxylamine **2**[3] (obtained from 0.50 g, 4.0 mmol of 4-methyl-4-nitropent-1-ene) were heated in toluene (4 cm^3), under argon, at 85–90 °C for 43 h. Chromatographic purification (silica gel, hexane–ethyl acetate, 5 : 1 → 2 : 1, v/v) furnished **4** (0.38 g, 52%) as white crystals, mp 91–92 °C (hexane); δ_H (500 MHz, $CDCl_3$): 1.12 (s, 3H, CH_3), 1.20 (s, 3H, CH_3), 1.24 (d, *J* 11.3 Hz, 1H, H_{3en}) 1.29 (s, 3H, CH_3), 1.46 (s, 3H, CH_3), 1.66 (dd, *J* 11.8, 7.8 Hz, 1H, H_{5en}), 1.75 (ddd, *J* 11.3, 5.4, 2.5 Hz, 1H, $H_{3'}$), 1.99 (m, 1H, $H_{5'}$), 3.86 (ddd, *J* 9.9, 7.8, 3.9 Hz, 1H, H_6), 4.07 (dd, *J* 9.9, 3.1 Hz, 1H, $H_{4'}$), 4.22 (d, *J* 3.1 Hz, 1H, $H_{3'}$), 4.59 (d, *J* 3.9 Hz, 1H, $H_{2'}$), 4.67 (AB, Δ 0.06, *J* 11.8 Hz, 2H, CH_2Ph), 4.83 (t, *J* 5.3 Hz, 1H, H_4), 5.88 (d, *J* 3.9 Hz, 1H, $H_{1'}$), 7.2–7.37 (m, 5H, C_6H_5); δ_C (50 MHz, $CDCl_3$): 24.43, 26.25, 26.70, 31.27, 36.81, 46.86, 57.41, 65.82, 72.21, 81.76, 82.64, 83.25, 104.70, 111.49, 127.64, 127.71, 128.37; ν cm^{-1}: 3068, 3032, 2980, 1452, 1372, 1076; HRMS *m*/*z* calc. for $C_{20}H_{26}NO_5$ $(M\text{-}CH_3)^+$ 360.1811, found 360.1791; $[\alpha]_D^{20}$ −40.5 (*c* 0.4, CH_2Cl_2).

1 *Iminosugars as Glycosidase Inhibitors, Nojirimycin and Beyond*, ed. A. E. Stuetz, Wiley–VCH, Weinheim, 1999; N. Asano, R. J. Nash, R. J. Molyneux and G. W. J. Fleet, *Tetrahedron: Asymmetry*, 2000, **11**, 1645.

2 A. Budzińska, M. Bukowska and W. Sas, *Tetrahedron Lett*., 1999, **40**, 565.

3 A. Budzińska and W. Sas, *Tetrahedron*, 2000, **57**, 2021.

4 W. Oppolzer, S. Siles, R. L. Snowden, B. H. Bakker and M. Petrzilka, *Tetrahedron*, 1985, **41**, 3497; P. G. M. Wuts and Y.-W. Jung, *J. Org. Chem*., 1988, **53**, 1957; B. H. Norman, Y. Gareau and A. Padwa, *J. Org. Chem*, 1991, **56**, 2154.

5 D. J. Mincher and G. Show, *J. Chem. Soc., Perkin Trans. 1*, 1984, 1279.

6 P. Aleksandrowicz, H. Piotrowska and W. Sas, *Tetrahedron*, 1982, **38**, 1321.

CHEMCOMM Communication
www.rsc.org/chemcomm

5-*Exo-dig,* 5-*exo-trig* cascade radical cyclisation on sugar-furanose templates: entry to angularly fused oxa- and dioxa-triquinane skeletons

Mukund K. Gurjar,* S. V. Ravindranadh and Punit Kumar

National Chemical Laboratory, Pune 411 008, India. E-mail: gurjar@dalton.ncl.res.in

Received (in Cambridge, UK) 20th February 2001, Accepted 10th April 2001
First published as an Advance Article on the web 1st May 2001

Serial radical cyclisation on sugar-furanose templates to create angularly fused oxa- and dioxa-triquinane skeletons has been described, the salient feature of this approach being to incipiently generate a tertiary radical from cyclopropylmethyl bromide with simultaneous release of allyl group and to subsequently incorporate it in the triquinane system.

Ever since their isolation, the angularly fused triquinanes have attracted intense attention of synthetic organic chemists as challenging targets.[1] Structural complexity associated with significant biological activity has necessitated development of very many approaches for their synthesis.[2] Among them, the radical cascade reactions are by far the most elegant and efficient approaches as significantly demonstrated by the work of Curran and others.[3] Bis-annulated sugars are also useful synthons for triquinane synthesis. For example, Fraser-Reid and coworkers[4] have performed some novel transformations mediated by serial radical cyclization of pyranose based sugar synthons[5] to create pyranosin diquinanes, elaborated to naturally occurring triquinanes.

We feel that radical cascade reactions on furanose ring systems of sugar derivatives would be interesting to explore primarily to understand the stereo-chemical behavior but more importantly to obtain synthons potentially useful for angularly fused, unknown and structurally novel oxa-triquinanes. The direct approach for oxa-triquinane would be to trigger a cascade of radical reactions by generating tertiary radicals on synthons with prefabricated radical acceptors (Scheme 1). Realistically, formation of a tertiary radical is a difficult proposition because its precursor, namely tertiary halide or tertiary thiocarbamate, is not easily accessible by conventional methods. However, the indirect formation of a tertiary radical with concomitant installation of an allylic side chain as radical acceptor, by our recently developed approach[6] of radical ring opening of spirocyclopropyl methyl bromide, could constitute an elegant and ideal proposition for this endeavor. This study forms the basic premise of this communication.

1,2:5,6-Di-*O*-isopropylidene-α-D-glucofuranose (**1**) was converted into the 3,3-spiro cyclopropylmethanol derivative (**2**) in five steps (Scheme 2).[7] It was then exposed to 0.8% sulfuric acid in methanol at rt to give the triol derivative whose oxidative cleavage with $NaIO_4$ absorbed on silica gel[8] in CH_2Cl_2 yielded the aldehyde (**3**). Compound **3** was immediately treated with

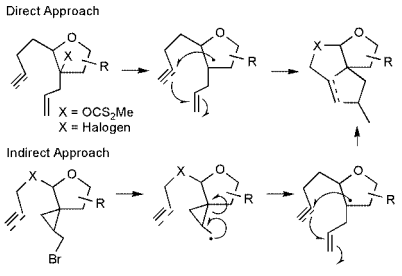

Scheme 1

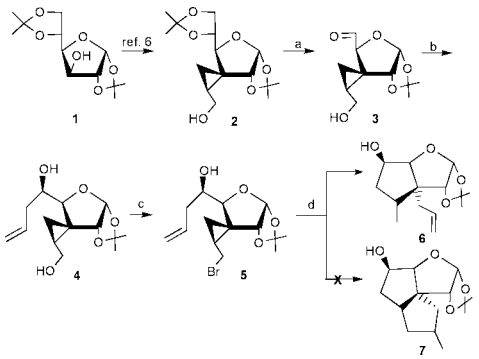

Scheme 2 *Reagents and conditions*: (a) (i) 0.8% H_2SO_4, MeOH, rt, 10 h; (ii) silica gel adsorbed $NaIO_4$, CH_2Cl_2, 15 min, 78% (two steps); (b) allyl bromide, Zn, aq. NH_4Cl, THF, 0 °C, 6 h, 72%; (c) PPh_3, CBr_4, pyridine, CH_2Cl_2, rt, 1 h, 83%; (d) TBTH, AIBN (cat), $C_6H_5CH_3$, 100 °C, 1 h, 70%.

Zn, allyl bromide under aqueous Barbier conditions[9] to give a predominantly (90%) and chromatographically separable allyl addition product (**4**) whose stereochemical assignment was based on literature precedents.[10] Compound **4** upon treatment with CBr_4–PPh_3 in CH_2Cl_2 in the presence of pyridine at rt gave the corresponding bromo derivative (**5**). Treatment of **5** with tri-*n*-butyl tin hydride (TBTH), AIBN in toluene (0.05 M) at 100 °C gave a single product whose fused bicyclic structure (**6**) was assigned on the basis of NMR and MS studies. Presence of compound **7** was not noticed. The formation of **6** indicated premature termination of serial radical cyclisation after the first *exo-trig* addition. This abrupt termination could be attributed to the poor reactivity of the methyl radical.[11] In order to circumvent this problem, we sought to explore the vinyl radical primarily for its pronounced reactivity coupled with the ease with which it could be generated.[12]

Accordingly, **3** was subjected to Barbier reaction in aqueous conditions with Zn and propargyl bromide to afford **8** as an exclusive product. The transformation of **8** into **9** was carried out as described earlier (Scheme 3).

The radical reaction of **9** with TBTH and AIBN (cat.) in dry toluene (0.05 M) at 100 °C gave the angularly fused oxa-triquinane derivatives **10a** and **10b,** whose formation was attributed to 5-*exo-dig*, 5-*exo-trig* serial cyclisations. The structure of the product was thoroughly investigated by high resolution ^1H NMR, ^{13}C NMR, MS and elemental analysis. The ^1H and ^{13}C NMR spectra indicated that it was a 8.5 : 1.5 mixture of diastereomers **10a** and **10b**. However, COSY and NOSY

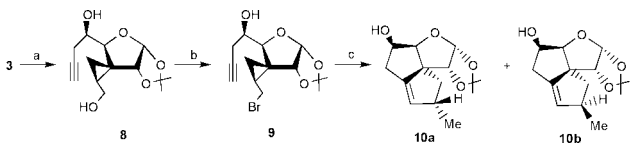

Scheme 3 *Reagents and conditions*: (a) HC≡C–CH_2Br, Zn, aq. NH_4Cl, THF, 0 °C, 6 h, 74%; (b) PPh_3, CBr_4, pyridine, CH_2Cl_2, rt, 1 h, 80%; (c) TBTH, AIBN (cat), $C_6H_5CH_3$, 100 °C, 1 h, 74%.

DOI: 10.1039/b101641p

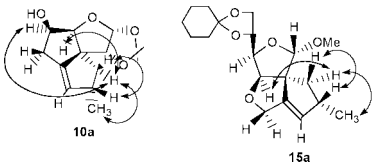

Fig. 1 NOSY studies.

studies (Fig. 1) on the major diastereomer **10a** revealed the absolute stereochemistry of the methyl group as indicated.[12]

We also synthesized starting from 1,2:5,6-di-*O*-cyclohexylidene-α-D-glucofuranose (**10**) the 2,2-spirocyclopropyl methyl bromide derivative **14** *via* intermediates **11**–**13** as shown in Scheme 4. Subsequent radical cascade reaction of **14** with TBTH and AIBN (cat.) in toluene at 100 °C gave the fused ring derivatives **15a** and **15b**. The ^{1}H and ^{13}C NMR spectra of the product showed to be a 8:2 mixture of diastereomers. The COSY and NOSY studies (Fig. 1) predicted the stereochemistry of the methyl group of the major product **15a** as indicated.[13]

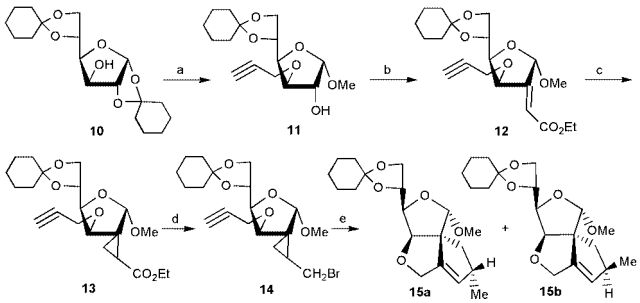

Scheme 4 *Reagents and conditions*: (a) (i) NaH, HC≡C–CH_2Br, DMF, 0 °C, 90%; (ii) H_2SO_4, MeOH, Δ, chromatography, 65%; (b) (I) IBX, DMSO, rt, 10 h; (ii) PPh_3=$CHCO_2Et$, C_6H_6, 80 °C, 2 h, 74% (two steps); (c) Me_2SOCH_3I, NaH, DMSO, rt, 3 h, 55%; (d) (i) DIBAL-H, CH_2Cl_2, 78 °C, 0.5 h, 87%; (ii) PPh_3, CBr_4, pyridine, rt, 82%; (e) TBTH, AIBN (cat), $C_6H_5CH_3$, 100 °C, 1 h, 80%.

In conclusion, we have developed a one pot, stereoselective 5-*exo-dig*, 5-*exo-trig* cascade radical cyclization utilizing the incipiently formed *C*-allyl radical leading to useful and structurally novel oxa-triquinane system.

S. V. R. thanks CSIR, New Delhi for a research fellowship.

Notes and references

1 L. A. Paquette and A. M. Doharty, *Polyquinane Chemistry*, Verlag, New York, 1987.

2 T. Hudlicky, G. Sinai-Zingde, M. G. Natchus, B. C. Ranu and P. Papadopolous, *Tetrahedron*, 1987, **43**, 5685; P. A. Wender and S. K. Singh, *Tetrahedron Lett.*, 1985, **26**, 5987; E. J. Enholm and Z. J. Jia, *J. Org. Chem.*, 1997, **62**, 174; J. Tormo, A. Moyano, M. A. Pericas and A. Riera, *J. Org. Chem.*, 1997, **62**, 4851; C.-K. Sha, K. C. Santhosh and S.-H. Lhi, *J. Org. Chem.*, 1998, **63**, 2699; J. Seo, H. Fain, J. B. Blanc and J. Montgomery, *J. Org. Chem.*, 1999, **64**, 6060; J. M. MacDougall and H. W. Moore, *J. Org. Chem.*, 1999, **64**, 7445; S. K. Verma, E. B. Fleischer and H. W. Moore, *J. Org. Chem.*, 2000, **65**, 8564; J. M. MacDougall and H. W. Moore, *J. Org. Chem.*, 1997, **62**, 4554; F. C. Watson and J. D. Kilburn, *Tetrahedron Lett.*, 2000, 10 341; N. M. H. Frost and G. Pattenden, *Tetrahedron Lett.*, 2000, **41**, 403; Y. K. Rao and M. Nagarajan, *J. Org. Chem.*, 1989, **54**, 5678.

3 D. P. Curran and S.-C. Kuo, *J. Am. Chem. Soc.*, 1986, **108**, 1106; D. P. Curran and S.-C. Kuo, *Tetrahedron*, 1987, **43**, 5653; A. I. Meyers and B. A. Lefker, *Tetrahedron*, 1987, **43**, 5663; H. M. R. Hoffmann, *Angew. Chem., Int. Ed. Engl.*, 1992, **31**, 1332; C. P. Jasperse, D. P. Curran and T. L. Fevig, *Chem. Rev.*, 1991, **91**, 1237.

4 R. Tsang and B. Fraser-Reid, *J. Am. Chem. Soc.*, 1986, **108**, 2116; J. K. Dickson, Jr., R. Tsang, J. M. Llera and B. Fraser-Reid, *J. Org. Chem.*, 1989, **54**, 5350; H. Pak, J. K. Dickson and B. Fraser-Reid, *J. Org. Chem.*, 1989, **54**, 5357; B. Fraser-Reid and R. Tsang, *Strategies and Tactics in Organic Synthesis*, T. Lindberg (ed.), Academic Press, New York, 1989; Vol. 2, 123; J. K. Dickson, Jr. and B. Fraser-Reid, *J. Chem. Soc., Chem. Commun.*, 1990, 1440; H. Pak, I. I. Canalda and B. Fraser-Reid, *J. Org. Chem.*, 1990, **55**, 3009.

5 R. Nouguier, C. Lesueur, E. De Reggi and M. P. Bertrand, *Tetrahedron Lett.*, 1990, **31**, 3541; C. Lesueur, R. Nouguier, M. P. Bertrand, P. Hoffmann and A. De Mesmaeker, *Tetrahedron*, 1994, **50**, 5369.

6 M. K. Gurjar, S. V. Ravindranadh and S. Karmakar, *Chem. Commun.*, 2001, 241.

7 M. K. Gurjar, B. V. N. B. S. Sharma and B. V. Rao, *J. Carbohydr. Chem.*, 1998, **17**, 1107.

8 Y.-L. Zhong and T. K. M. Shing, *J. Org. Chem.*, 1997, **62**, 2622.

9 S. Hanessian, H. Park and R. Y. Yang, *Synlett*, 1997, 351; S. Hanessian, H. Park and R. Y. Yang, *Synlett*, 1997, 353.

10 Z. Pakulski and A. Zamoski, *Tetrahedron*, 1997, **53**, 2653.

11 A. L. J. Beckwith, D. H. Roberts, C. H. Schiesser and A. Wallner, *Tetrahedron Lett.*, 1985, **26**, 3349.

12 G. Stork and N. H. Baine, *J. Am. Chem. Soc.*, 1982, **104**, 2321; G. Stork and R. Mook, Jr., *Tetrahedron Lett.*, 1986, **27**, 4529; A. L. J. Beckwith and D. M. O'Shea, *Tetrahedron Lett.*, 1986, **27**, 4525.

13 NMR data for **10a**: ^{1}H (500 MHz): δ 0.98 (d, 3 H, J = 7.2 Hz), 1.26 (t, 1 H, J = 10.8 Hz), 1.34, (s, 3 H), 1.47, (s, 3 H), 1.80 (m, 1 H) 2.50 (dd, 1 H, J = 5.4, 12.7 Hz), 2.67 (dd, 1 H, J = 3.6, 10.8 Hz), 2.95 (brs, 1 H), 3.72 (m, 1 H), 4.24 (d, 1 H, J = 4.0 Hz), 4.28 (d, 1 H, J = 3.0), 5.41 (s, 1 H), 5.74 (d, 1 H, J = 3.0 Hz); ^{13}C (125 MHz): δ 19.98, 27.27, 27.59, 33.99, 40.51, 42.70, 65.52, 74.79, 85.75, 87.75, 106.55, 112.59, 132.33, 144.66. NMR data for **15a**: ^{1}H (500 MHz): δ 1.09 (d, 3 H, J = 7.5 Hz), 1.3–1.75 (m, 10 H), 1.49 (t, 1 H, J = 12.7 Hz), 2.72 (dd, 1 H, J = 5.0, 12.7 Hz), 3.41 (brs, 1 H), 3.37 (s, 3 H), 3.90 (dd, 1H, J = 2.6, 7.6 Hz), 3.98 (dd, 1 H, J = 4.5, 7.6 Hz), 4.06 (ddd, 1 H, J = 1.5, 3.0, 11.3 Hz), 4.11–4.17 (m, 2 H), 4.29 (brd, 1 H, J = 10.6 Hz), 4.39 (m, 1 H), 4.69 (s, 1 H), 5.46 (s, 1 H); ^{13}C (125 MHz): δ 20.11, 23.85, 24.04, 25.17, 34.83, 36.55, 40.93, 44.99, 54.88, 65.86, 66.73, 71.34, 73.23, 81.79, 85.14, 108.32, 109.59, 128.59, 148.36.

CHEMCOMM Communication
www.rsc.org/chemcomm

Polar host–guest assembly mediated by halogen···π interaction: inclusion complexes of 2,4,6-tris(4-halophenoxy)-1,3,5-triazine (halo = chloro, bromo) with trihalobenzene (halo = bromo, iodo)

Ram K. R. Jetti,[a] Ashwini Nangia,*[a] Feng Xue[b] and Thomas C. W. Mak*[b]

[a] *School of Chemistry, University of Hyderabad, Hyderabad 500 046, India. E-mail: ansc@uohyd.ernet.in*

[b] *Department of Chemistry, The Chinese University of Hong Kong, Shatin, New Territories, Hong Kong SAR, P. R. China. E-mail: b005783@mailserv.cuhk.edu.hk*

Received (in Columbia, MO, USA) 15th February 2001, Accepted 5th April 2001
First published as an Advance Article on the web 1st May 2001

Crystallization of four isomorphous host–guest complexes in the polar space group $P6_3$ is ascribed to the recurring halogen(guest)···π(host) interaction.

Self-assembly of chiral crystals from achiral components[1] is a current endeavor in crystal engineering with applications in asymmetric synthesis and materials science. Crystallization of achiral or racemic molecules in acentric space groups is relevant not only for the design of functional solids, such as host–guest,[2] nonlinear optics,[3] but also has implications in our fundamental understanding of spontaneous resolution during crystallization.[4] In this context, it was recently noted by some of us[5] that co-crystallization of 2,4,6-tris(4-chlorophenoxy)-1,3,5-triazine **1** and 1,3,5-tribromobenzene (TBB) from an equimolar mixture

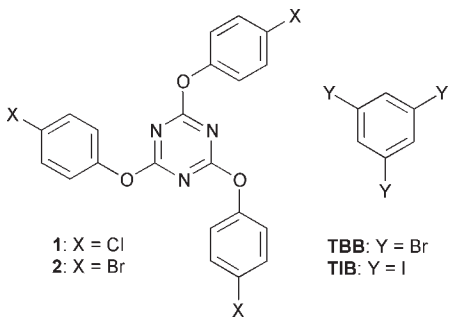

of benzene and ethyl acetate afforded a 1:1 complex, **1**·TBB, that belongs to the non-centrosymmetric space group $P6_3$. In **1**·TBB, the triazine molecules form a hexagonal network *via* the robust Cl···Cl trimer synthon. Tribromobenzene guest molecules located in the channels are bonded *via* C–Br···π and C–H···π interactions[6] to the C=C bond mid-point of the host phenyl ring rather than to the ring centroid, as ascertained by neutron diffraction.[5] In this paper we demonstrate the structural significance of halogen···π interactions[7] in inducing polar aggregation of molecules in the solid state. The description of space groups using terms such as (non)centrosymmetric, acentric, chiral and polar has been clarified in the crystallographic literature.[8]

Crystallization of chlorotriazine **1** and 1,3,5-triiodobenzene (TIB) from PhH–EtOAc afforded crystals of **1**·TIB (1:1) in space group $P6_3$.† The TIB guest species are accommodated in an open hexagonal network formed by a triangulo halogen synthon (Cl···Cl 3.56 Å, 107.0°, 167.0°) of triazine host molecules (Fig. 1). The hexahost framework of **1** and **2** with trihalobenzene guests is virtually identical to the intermolecular interaction network observed in their channel inclusion complexes with other guest species: benzene, hexamethylbenzene (HMB), hexachlorobenzene (HCB), trinitromesitylene (TNM), 1,3,5-trinitrobenzene (TNB), mesitylene (MES), 2,4,6-collidine (CLN) and hexamethylphosphoramide (HMPA).[9] However, the latter host–guest structures are centrosymmetric (space group

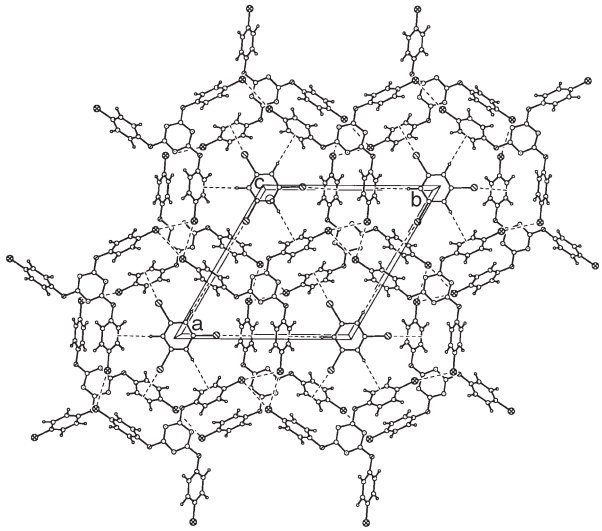

Fig. 1 Hexa-host network in **1**·TIB assembled through Cl···Cl triangulo synthon. TIB guest molecules are bonded *via* C–I···π and C–H···π interactions. Notice the herringbone motif between host phenoxy rings of adjacent channels.

$P6_3/m$) with the triazine core lying on a crystallographic mirror plane. Thus inclusion of trihalobenzene guests in the hexagonal nanotubes induces significant structural changes in the mutual orientation of host phenyl rings. Yet there is minimal change in the lattice parameters of **1**·TBB and **1**·TIB compared to the centrosymmetric structures (Table 1). Adjacent phenoxy rings are parallel in the $P6_3/m$ structures while they are twisted by an angle (τ) of 51.3° and 54.3° to each other in **1**·TBB and **1**·TIB. As a result of phenyl group tilting, away from the halogen and closer to the hydrogen, the guest molecules form short C–I···π

Table 1 Crystal data of some isomorphous complexes of **1** and **2** with various guests in $P6_3/m$ and $P6_3$ space groups

	Host/guest	Space group	Z	$a = b$ (Å)	c (Å)
2·CLN[a]	1:1	$P6_3/m$	2	15.468(2)	7.087(1)
1·½HCB[b]	2:1	$P6_3/m$	2	15.435(2)	6.876(1)
1·½HMB[b]	2:1	$P6_3/m$	2	15.411(2)	6.867(1)
2·½HMB[b]	2:1	$P6_3/m$	2	15.554(4)	6.951(3)
1·½TNB[b]	2:1	$P6_3/m$	2	15.255(2)	7.005(2)
2·½TNM[b]	2:1	$P6_3/m$	2	15.719(2)	7.034(1)
1·½HMPA[b]	2:1	$P6_3/m$	2	15.234(2)	6.880(1)
1·TBB[c]	1:1	$P6_3$	2	15.166(6)	6.743(2)
1·TIB[d]	1:1	$P6_3$	2	15.482(1)	7.011(1)
2·TBB[d]	1:1	$P6_3$	2	15.442(1)	6.991(1)
2·TIB[d]	1:1	$P6_3$	2	15.627(2)	7.046(1)

[a] Ref. 9*a*. [b] Ref. 9*b*. [c] Ref. 5 (neutron data). [d] This paper.

DOI: 10.1039/b102150h

(3.43 Å, 158.3°; Σ vdW radii = 2.0 + 1.7 = 3.7 Å) and long C–H···π (3.00 Å, 177.4°) interactions with different C=C bonds of the host phenyl ring.‡ Three such sinusoidal motifs stabilize the polar host–guest architecture (Fig. 2). The C–I···π interaction is polarization-induced, such that the C–I$^{\delta(+)}$ vector points towards the mid-point of a $\pi^{\delta(-)}$ bond, and is reminiscent of the type II halogen···halogen interaction[9] between host molecules. In effect, a slice of the host–guest layer in **1**·TIB is stabilized by Cl···Cl, C–I···π and C–H···π interactions (Table 2). The halogen···π radial motif in **1**·TIB channel resembles the Cl···π interaction observed recently in the pseudo-threefold cavity of calix[6]pyrrole with 2,2,2-trichloroethanol guest.[10] The interplay of numerous weak interactions, aryl–aryl, C–H···N, aryl–halogen and inter-halogen, resulting in microcavities that are tailored to the guest structure has been noted in a halogenated tweezer host molecule.[11]

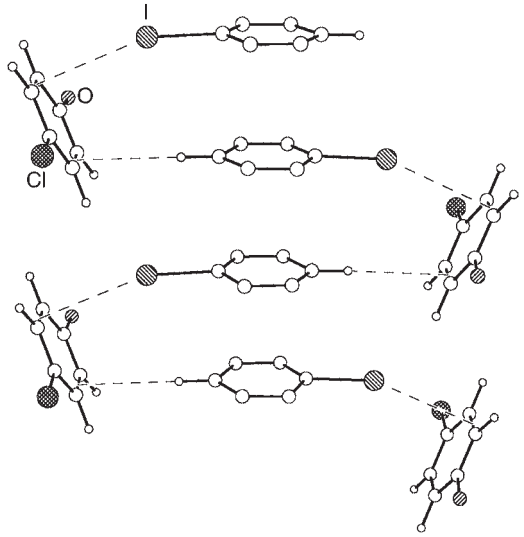

Fig. 2 Sinusoidal chain of C–I···π and C–H···π interactions in **1**·TIB that result in polar crystallization. Three such motifs rotated by 120° stabilize the host–guest channel architecture. Molecular fragments are truncated for clarity.

The 1:1 inclusion complexes of tribromobenzene and triiodobenzene with 2,4,6-tris(4-bromophenoxy)-1,3,5-triazine **2**, **2**·TBB and **2**·TIB respectively,† are isostructural with the corresponding inclusion complexes of **1** (Table 1). The mutual orientation of host phenyl rings and metrics of C–Br/I···π and C–H···π interactions are given in Table 2. Although the exact reasons as to why achiral or racemic molecules adopt non-centrosymmetric crystal packing are difficult to dissect,[1,4] the present case of four isomorphous structures offers a clue. Three polar chains of C–Br/I···π and C–H···π guest–host interactions rotated by 120° to each other stabilize the hexagonal nanotubes. The crystal structure would be centrosymmetric if such motifs in adjacent chains run anti-parallel and non-centrosymmetric if they are aligned in the same direction. The polarity of one nanotube is transmitted to adjacent channels *via* the edge-to-face[12] herringbone packing between host phenoxy rings related by a two-fold screw axis. Since inclusion complexes of **1** and **2** with many other guests are all centrosymmetric,[9] polar aggregation with TBB and TIB species in space group $P6_3$ appears to be guest-induced. Thus, the halogen- and hydrogen-bonded synthon in Fig. 2 is the minimum ensemble necessary to amplify polarity in the three-dimensional crystal, in other words it is a supramolecular chiron.[13] The mechanism for polar crystallization with flexible hosts **1** and **2** (guest–host X···π interaction) is conceptually different from the phenomenon for parallel alignment of D–π–A chromophores in the constrained channel of perhydrotriphenylene (guest–guest D···A interaction).[3]

Table 2 Metrics of intermolecular interactions in inclusion complexes of **1** and **2** in space group $P6_3$. See chemical diagram for labels X, Y and text for definition of torsion angle τ

	1·TBB[a]	**1**·TIB[b]	**2**·TBB[b]	**2**·TIB[b]
X···X (Å)	3.441(3)	3.56	3.51	3.55
C–X···X (°)	164.9, 104.9	167.0, 107.0	164.9, 104.9	165.3, 105.3
τ, π–π (°)	51.3	54.3	51.6	55.9
Y···π (Å)	3.353(4)	3.43	3.51	3.49
C–Y···π (°)	158.1(2)	158.3	157.1	158.0
H···π[c] (Å)	2.817(9)	3.00	2.94	3.03
C–H···π (°)	174.0(9)	177.4	176.4	175.2

[a] Ref. 5, neutron data. [b] X-ray data, this study. [c] C–H distance neutron-normalised to 1.083 Å.

We thank the Department of Science and Technology, Government of India (SP/S1/G29/98) and the Hong Kong Research Grants Council (CUHK 4206/99P) for research funding. R. K. R. J. thanks the CSIR for fellowship support.

Notes and references

† *Crystal data*: **1**·TIB ($C_{21}H_{12}Cl_3N_3O_3{\cdot}C_6H_3I_3$, M = 916.47). Hexagonal, $a = b$ = 15.4817(6), c = 7.0107(4) Å, $\alpha = \beta = 90$, $\gamma = 120°$, V = 1455.22(12) Å^3, D_c = 2.092 Mg m^{-3}, T = 294 K, space group $P6_3$ (no. 173), Z = 2, μ(Mo-K$_a$) = 0.3532 mm^{-1}, 8911 reflections measured, 1979 unique (R_{int} = 0.0253) which were used in all calculations. Final R = 0.0249 (obs.), 0.0335 (all); $wR(F^2)$ = 0.0616 (obs.), 0.0635 (all). **2**·TBB ($C_{21}H_{12}Br_3N_3O_3{\cdot}C_6H_3Br_3$, M = 908.88). Hexagonal, $a = b$ = 15.4420(13), c = 6.9909(7) Å, $\alpha = \beta = 90$, $\gamma = 120°$, V = 1443.7(2) Å^3, D_c = 2.091 Mg m^{-3}, T = 294 K, space group $P6_3$ (no. 173), Z = 2, μ(Mo-K$_a$) = 0.8378 mm^{-1}, 4453 reflections measured, 1715 unique, (R_{int} = 0.1359) which were used in all calculations. Final R = 0.0706 (obs.), 0.0771 (all); $wR(F^2)$ = 0.1681 (obs.), 0.1732 (all). **2**·TIB ($C_{21}H_{12}Br_3N_3O_3{\cdot}C_6H_3I_3$, M = 1049.85). Hexagonal, $a = b$ = 15.6268(16), c = 7.0464(10) Å, $\alpha = \beta = 90$, $\gamma = 120°$, V = 1490.2(3) Å^3, D_c = 2.340 Mg m^{-3}, T = 294 K, space group $P6_3$ (no. 173), Z = 2, μ(Mo-K$_a$) = 0.7203 mm^{-1}, 10 527 reflections measured, 2406 unique, (R_{int} = 0.0415) which were used in all calculations. Final R = 0.0269 (obs.), 0.0385 (all); $wR(F^2)$ = 0.0602 (obs.), 0.0644 (all). For structure solution and refinement methods, see ref. 8. CCDC reference numbers 161765–161767. See http://www.rsc.org/suppdata/cc/b1/b102150h/ for crystallographic files in .cif format.

‡ C–I···π and C–H···π geometries are longer and bent when measured to phenyl ring centroid (3.58 Å, 139.0°; 3.67 Å, 163.8°) because the guest molecule lies about 1 Å below the *sym*-triazine host.

1 (*a*) K. Tanaka, D. Fujimoto, T. Oeser, H. Irngartinger and F. Toda, *Chem. Commun.*, 2000, 413; (*b*) K. Tanaka, D. Fujimoto, A. Altruether, T. Oeser, H. Irngartinger and F. Toda, *J. Chem. Soc., Perkin Trans. 2*, 2000, 2115.
2 K. Biradha, C. Seward and M. J. Zaworotko, *Angew. Chem., Int. Ed.*, 1999, **38**, 492.
3 P. J. Langley and J. Hulliger, *Chem. Soc. Rev.*, 1999, **28**, 279.
4 M. Lahav and L. Leiserowitz, *Angew. Chem., Int. Ed.*, 1999, **38**, 2533.
5 C. K. Broder, J. A. K. Howard, D. A. Keen, C. C. Wilson, F. H. Allen, R. K. R. Jetti, A. Nangia and G. R. Desiraju, *Acta Crystallogr.*, 2000, **B56**, 1080.
6 G. R. Desiraju and T. Steiner, *The Weak Hydrogen Bond in Structural Chemistry and Biology*, OUP, Oxford, 1999.
7 I. Csöregh, E. Weber, T. Hens and M. Czugler, *J. Chem. Soc., Perkin Trans. 2*, 1996, 2733.
8 (*a*) J. P. Glusker and K. N. Trueblood, *Crystal Structure Analysis. A Primer*, OUP, Oxford, 2nd ed., 1985; (*b*) J. P. Glusker, M. Lewis and M. Rossi, *Crystal Structure Analysis for Chemists and Biologists*, VCH, New York, 1994; (*c*) C. Hammond, *The Basics of Crystallography and Diffraction*, OUP, Oxford, 1997; (*d*) J. D. Dunitz, *X-ray Analysis and the Structure of Organic Molecules*, VCH, Weinheim, 2nd ed., corrected reprint, 1995.
9 (*a*) R. K. R. Jetti, F. Xue, T. C. W. Mak and A. Nangia, *Cryst. Eng.*, 1999, **2**, 215; (*b*) R. K. R. Jetti, P. K. Thallapally, F. Xue, T. C. W. Mak and A. Nangia, *Tetrahedron*, 2000, **56**, 6707.
10 B. Turner, A. Shterenberg, M. Kapon, K. Suwinska and Y. Eichen, *Chem. Commun.*, 2001, 13.
11 A. Noman, M. M. Rahman, R. Bishop, D. C. Craig and M. L. Scudder, *Chem. Commun.*, 1999, 2389.
12 I. Dance and M. Scudder, *Chem. Eur. J.*, 1996, **2**, 481.
13 S. Hanessian, R. Saladino, R. Margarita and M. Simard, *Chem. Eur. J.*, 1999, **5**, 2169.

CHEMCOMM Communication
www.rsc.org/chemcomm

Towards hydroperoxovanadium complexes: the X-ray crystal structure of a peroxovanadium(v) complex containing a $V(O_2)(RCO_2H)(H_2O)_2$ cluster with hydrogen bond inter-linkages†

Marian Časný and Dieter Rehder*

Chemistry Department, University of Hamburg, D-20416 Hamburg, Germany. E-mail: rehder@xray.chemie.uni-hamburg.de

Received (in Cambridge, UK) 30th January 2001, Accepted 22nd March 2001
First published as an Advance Article on the web 3rd May 2001

The molecular structure of the oxo-peroxovanadium complex $[VO(O_2)(bpaH)]ClO_4{\cdot}2H_2O$, containing the new ligand *N,N*-bis(2-pyridylmethyl)-β-alanine (bpaH) reveals tight binding of the carboxylic acid function to the vanadium centre through its doubly bonded oxygen; the carboxylic acid proton mediates hydrogen bonding interactions comprising the peroxo group and the two waters of crystallisation, thus providing the basis for the potential formation of a hydroperoxo species.

Authentic peroxovanadium complexes as well as peroxovanadium complexes generated *in situ* have been employed as catalysts and in stoichiometrically conducted reactions as oxo transfer reagents for alcohols, arenes, alkenes and thioethers.[1,2] Likewise, the bromination of functionalised arenes is carried out by peroxovanadium complexes, or by vanadium compounds in the presence of H_2O_2.[3,4] Peroxovanadium intermediates have also been proposed for the enzymatic conversion of halide to hypohalous acid (or another Hal^+ species) by vanadate-dependent algal and fungal haloperoxidases in the presence of peroxide,[4–7] an assumption which has been fortified by the structural characterisation of the peroxo form of chloroperoxidase from the fungus *Curvularia inaequalis*.[8] Both the *in vitro* and *in vivo* oxidation of halide such as bromide is facilitated by an increase of the electrophilicity at the reaction site, *i.e.* by the intermediate formation of a hydroperoxo complex (Fig. 1, left) in the case of the peroxo ligand representing the reaction site,[4,5,9] a suggestion which finds support in the fact that (i) protons are consumed in these reactions,[9] (ii) alkylperoxo complexes are often more effective than the parent peroxides,[1] (iii) the cationic hydroperoxo–oxovanadium moiety is on a lower energy level (more stable) than the corresponding peroxo–oxovanadium species,[10] and (iv) a hydroperoxo form of the active site vanadium in bromoperoxidase from the marine alga *Ascophyllum nodosum* is quite within the bounds of probability as based on ^{17}O NMR evidence.[10] The asymmetric side-on coordination of RO_2^- has previously been reported for $[VO(O_2)(HO_2)(bipy)]$ (bipy = 2,2′-bipyridyl[12a]), $[VO(H_2O)(tBuO_2)(dipic)]$ (dipic = dipicolinate(2−))[12b] and $[\{VO(O_2)_2\}(\mu\text{-}\eta^1,\eta^2\text{-}O_2)\{VO(O_2)H_2O\}]^{2-}$.[13] Based on kinetic investigations, hydroperoxo intermediates have also been made plausible in oxo transfer reactions to metal-centred thiolates using $[VO(O_2)_2(pic)]^{2-}$,[14] and peroxidative halogenations with $[VO(O_2)(bpg)]$ (bpgH = *N,N*-bis(2-pyridylmethyl)glycine).[5,9] An additional point of considerable interest in the context of peroxovanadium complexes is their ability to inhibit phosphotyrosine phosphatases and thus act as insulin mimetics.[15]

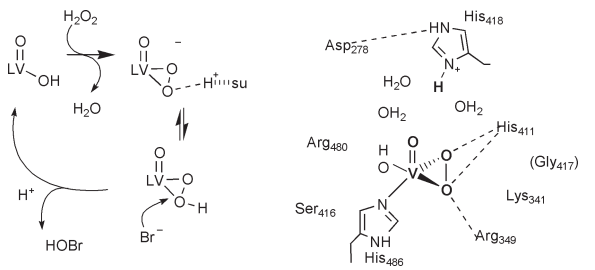

Fig. 1 Left: proposed mechanism for bromide oxidation (su = supporting group). Right: active site of the peroxo form of vanadate-dependent bromoperoxidase from *A. nodosum*, based on the structure of the native *A. nodosum* enzyme[18] and the peroxo form of the *C. inaequalis* peroxidase.[8] Potential mediators for proton transfer are His418, His411 and Asp278.

In the present work we report on a peroxovanadium complex giving rise to a tight hydrogen bonding network in which three different functionalities participate, *viz.* a coordinated and protonated carboxylate, two inter-lattice water molecules and the peroxo ligand. Hence a complex which may represent a preformed hydroperoxo species, or a compound which is able to rapidly and reversibly provide a proton for a hydroperoxo intermediate in catalytic turnover. Our complex thus models a situation which, in the haloperoxidases, is represented by aspartate or the distal histidine plus water molecules at the active site of the enzyme (Fig. 1, right). Aspartate as a mediator for proton-transfer has also been reported for vanadate-incorporated phytase,[16] a semi-synthetic vanadium peroxidase.[17]

The new ligand *N,N*-bis(2-pyridylmethyl)-β-alanine (bpaH) was synthesised† (Scheme 1) by modifying the procedure described for *N,N*-bis(2-pyridylmethyl)-glycine (bpgH).[19] The complex $[VO(O_2)(bpaH)]ClO_4{\cdot}2H_2O$ was obtained† by adding the ligand to an aqueous solution of $K[VO_3]$, followed by treatment with H_2O_2 and finally with dilute $HClO_4$ to adjust the solution to pH 1.7. Orange-coloured crystals were obtained from the ethanolic solution in the cold.

The molecular structure‡ of the compound is shown in Fig. 2; hydrogen bonding interactions have been indicated by dashed lines. The basic structure of the cation $[VO(O_2)(bpaH)]^+$ is a pentagonal bipyramid, with the peroxo ligand (O1 and O2) and the three nitrogens (N1, N2 and N3) of bpaH in the plane, and the oxo group O3 and carboxylic acid oxygen O4 in the apical positions. The ligand bpaH coordinates to the vanadium forming one six-membered and two five-membered chelate rings. The two pyridines are in the equatorial plane. The five atoms in the equatorial plane are nearly coplanar; the vanadium

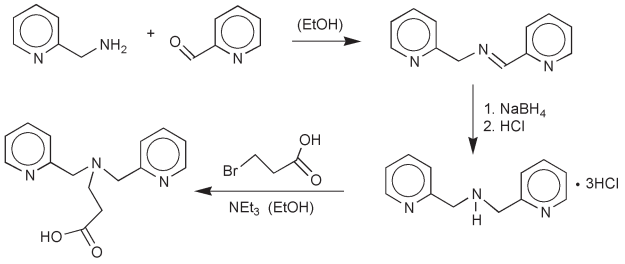

Scheme 1

† Electronic supplementary information (ESI) available: synthesis of bpaH and $[VO(O_2)(bpaH)ClO_4{\cdot}nH_2O$. See http://www.rsc.org/suppdata/cc/b1/b101010g/

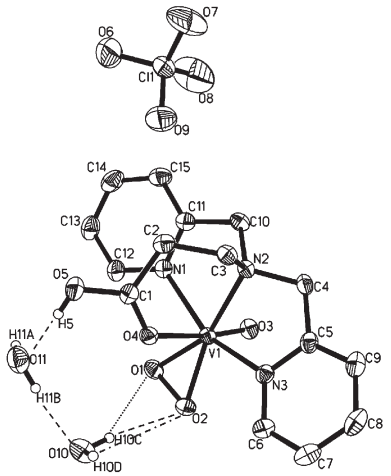

Fig. 2 Molecular structure of $[VO(O_2)bpaH]ClO_4{\cdot}2H_2O$ at the 50% probability level, including the hydrogen bonds (dashed lines). Selected bond lengths (Å) and angles (°): V–O1 1.8734(16), V–O2 1.8827(16), V–O3 1.5877(15), V–O4 2.2095(16), V–N1 2.132(2), V–N2 2.192(2), V–N3 2.133(2), O1–O2 1.422(2), C1–O4 1.222(3), C1–O5 1.302(3), O5–H5 0.8201(10); O1–V–N1 81.68(8), O1–V–O2 44.48(7), O2–V–N3 81.83(8), N1–V–N2 75.53(7), N2–V–N 374.13(7), O3–V–O4 172.25(7). Hydrogen bonds (Å): O1···H10C–O10 3.250, O2···H10C–O10 2.995, O2···H10D–O10 2.806, O5–H5···O11 2.550, O11–H11B···O10 2.711, O11–H11A···O6 (perchlorate) 2.993.

centre is displaced from this plane by 0.2163(8) Å towards the oxo group. The unusual coordination mode of the carboxylic acid function – through the doubly bonded oxygen O4 – has been described previously for a number of dipicolinato complexes of copper,[20] iron[21] and zinc[22] with bond lengths ranging from 2.3 to 2.5 Å (as compared to *ca*. 2.1 Å for the corresponding bond lengths of *de*protonated carboxylic acid functions). The angle O3–V–O4, 172.25°, only slightly deviates from linearity. The bond V–O4 [d = 2.2095(16) Å] is thus surprisingly strong, even more as it is subject to the *trans* effect exerted by the oxo group. It compares to the V–O (carboxylate) distances of 2.144 and 2.045 Å for the carboxylato group *trans* and *cis* to V=O, respectively, in $[VO(L)H_2O(O_2)]^-$ (H_2L = carboxymethylhistidine),[23] d[V–O (carboxylate)] = 2.138 Å for the *trans*-standing carboxylate in $[VO(O_2)(bpg)]$,[9] and d[V-O(carboxylate)] between 2.01 and 2.04 Å in other peroxovanadium complexes containing supporting ligands with *cis*-standing carboxylato functions.[24,25] The complex is the first example of a cationic monoperoxo–oxovanadium complex with an N_3O donor set. Other cationic vanadium complexes which have been described so far contain two NO donor sets ($[VO(O_2)(picolinamide)_2]^+$),[26] or one or two N_2 sets ($[VO(O_2)$-$(phen)(H_2O)_2]^+$;[27] $[VO(O_2)L_2]^+$, L = phen, bipy[28]).

The uncoordinated OH of the carboxylic acid group of $[VO(O_2)(bpaH)]^+$ links a water of crystallisation (O11) *via* a strong hydrogen bond of 2.550 Å, which in turn hydrogen binds to the perchlorate anion and a second water of crystallisation, O10. Two hydrogen bonds of weak to medium strength keep this water in the proximity of the coordinated peroxo group.§ Although only O2 of the peroxide is involved in this H-bonding network to a sizable extent, there are no significant differences in the V–O (peroxide) bond lengths. Bonding parameters [d(V–O1) 1.8734(16), d(V–O2) 1.8827(16) Å; angle O1–V–O2 = 44.48(7)°] are comparable to those in other peroxovanadium complexes;[9,13,23–25,29] the O–O bond length, 1.421(3), is in-between the margins noted for $[V_2O_2(O_2)_4H_2O]^{2-}$ [13] and $[VO(O_2)(tp)(pz)]$ (tp = tris(pyrazolyl)borate, pz = pyrazole).[30]

This special arrangement of carboxylic acid, water and peroxide provides a basis for a mechanism for rapid – and reversible – transfer of a proton to the activated (by coordination to vanadium) peroxo function, and hence a mechanism by which the electrophilicity of this site can be adapted to an appropriate substrate to be oxidised, such as bromide; *cf*. Fig. 1.

Notes and references

‡ *Crystal data*: $C_{15}H_{21}ClN_3O_{11}V$, M = 505.74, monoclinic, space group $C2/c$, a = 31.612(7), b = 7.1835(17), c = 21.290(16) Å, β = 123.274(4)°, V = 4042.1(16) Å^3, T = 293(2) K, Z = 8, μ(Mo-Kα) = 0.69 mm^{-1}. Independent reflections 4382 (R_{int} = 0.0265), final R values [$I > 2\sigma(I_0)$] R_1 = 0.0408, $wR2$ = 0.1005. CCDC 157361. See http://www.rsc.org/suppdata/cc/b1/b101010g/for crystallographic data in .cif or other electronic format.

§ Additional hydrogen bonding contacts exist between the peroxo group and the neighbouring pyridines of the ligand bpaH, *viz*. O1 and H12 (2.749 Å), and O2 and H6 (2.771 Å).

1 V. Conte, F. Di Furia and G. Licini, *Appl. Catal., A*, 1997, **157**, 335.
2 F. Van der Velde, I. C. W. E. Arends and R. A. Sheldon, *J. Inorg. Biochem.*, 2000, **80**, 81.
3 M. Bhattacharjee, S. Ganguly and J. Mukherjee, *J. Chem. Res. (S)*, 1995, 80.
4 M. J. Clague, N. L. Keder and A. Butler, *Inorg. Chem.*, 1993, **32**, 4754.
5 B. J. Hamstra, G. J. Colpas and V. L. Pecoraro, *Inorg. Chem.*, 1998, **37**, 949.
6 J. Mukherjee, S. Ganguly and M. Bhattacharjee, *Indian. J. Chem., Sect. A*, 1996, **35**, 471.
7 A. Butler and A. H. Baldwin, *Struct. Bonding (Berlin)*, 1997, **89**, 109.
8 A. Messerschmidt, L. Prade and R. Wever, *Biol. Chem.*, 1997, **378**, 309.
9 G. J. Colpas, B. J. Hamstra, J. W. Kampf and V. L. Pecoraro, *J. Am. Chem. Soc.*, 1996, **118**, 3469.
10 V. Conte, O. Bortolini, M. Carraio and S. Moro, *J. Inorg. Biochem.*, 2000, **80**, 41.
11 M. Časný, D. Rehder, H. Schmidt, H. Vilter and V. Conte, *J. Inorg. Biochem.*, 2000, **80**, 157.
12 (*a*) H. Szentivanyi and R. Stomberg, *Acta Chem. Scand. Ser. A*, 1984, **38**, 101; (*b*) H. Minoun, P. Chaumette, M. Mignard, L. Saussine, J. Fischer and R. Weiss, *Nouv. J. Chim.*, 1983, **7**, 467.
13 V. Suchá, M. Sivák, J. Tyršelová and J. Marek, *Polyhedron*, 1997, **16**, 2837.
14 A. F. Ghiro and R. C. Thomson, *Inorg. Chem.*, 1990, **29**, 4457.
15 B. I. Posner, R. Faure, J. W. Burgess, A. P. Bevan, D. Lachance, G. Zhang-Sun, I. George Fantus, J. B. Ng, D. A. Hall, B. Soo Lum and A. Shaver, *J. Biol. Chem.*, 1994, **269**, 4596.
16 D. Kostrewa, F. Grüninger-Leitch, C. D'Arcy, D. Mitchell and A. P. G. M. Van Loon, *Nat. Struct. Biol.*, 1997, **4**, 185.
17 F. Van der Velde, L. Könemann, F. Van Rantwijk and R. A. Sheldon, *Chem. Commun.*, 1998, 189.
18 M. Weyand, H.-J. Hecht, M. Kieß, M.-F. Liaud, H. Vilter and D. Schomburg, *J. Mol. Biol.*, 1999, **293**, 595.
19 D. D. Cox, S. J. Benkovic, L. M. Bloom, F. C. Bradley, M. J. Nelson, L. Que, Jr. and D. E. Wallick, *J. Am. Chem. Soc.*, 1988, **110**, 2026.
20 M. Biagini-Cingi, A. Chiesi-Villa, C. Guastini and M. Nardelli, *Gazz. Chim. Ital.*, 1972, **102**, 1026.
21 P. Laine, A. Gourdon and J.-P. Launay, *Inorg. Chem.*, 1995, **34**, 5138; P. Laine, A. Gourdon, J.-P. Launay and J.-P. Tuchagues, *Inorg. Chem.*, 1995, **34**, 5150.
22 K. Hakansson, M. Lindahl, G. Svensson and J. Albertsson, *Acta Chem. Scand.*, 1993, **47**, 449.
23 K. Kanamori, K. Nishida, N. Miyata and K.-I. Okamoto, *Chem. Lett.*, 1998, 1267.
24 M. Kaliva, T. Giannadaki, C. P. Raptopoulos, A. Tzerzis and A. Salifoglou, *Inorg. Chem.*, in the press; M. Tsaramyrsi, D. Kavousanaki, C . P. Raptopoulou, A. Terzis and T. Salifoglou, *Inorg. Chim. Acta*, in press.
25 M. Sivák, V. Suchá, L. Kuchta and J. Marek, *Polyhedron*, 1999, **18**, 93; L. Kuchta, M. Sivák, J. Marek, F. Pavelčik and M. Časný, *New J. Chem.*, 1999, 43.
26 M. Sivák, M. Mad'arova, J. Marek and J. Benko, *Chem. Listy*, 2000, **94**, 906.
27 V. K. Borzunov, V. S. Sergienko and M. A. Porai-Koshits, *Koord. Chimia*, 1993, **19**, 782.
28 V. S. Sergienko, V. K. Borzunov and M. A. Porai-Koshits, *Zh. Neorg. Khim.*, 1992, **37**, 1062.
29 F. W. B. Einstein, R. J. Batchelor, S. J. Angus-Dunne and A. S. Tracey, *Inorg. Chem.*, 1996, **35**, 1680.
30 M. Kosugi, S. Hikichi, M. Akita and Y. Moro-oka, *J. Chem. Soc., Dalton Trans.*, 1999, 1369.

CHEMCOMM Communication
www.rsc.org/chemcomm

Propeller-shaped molecules with giant off-resonance optical nonlinearities

Jérémie Brunel,[a] Isabelle Ledoux,[b] Joseph Zyss[b] and Mireille Blanchard-Desce*[c]

[a] *Département de Chimie, Ecole Normale Supérieure, 24 rue Lhomond, 75231 Paris Cedex 05, France*
[b] *Laboratoire de Photonique Quantique et Moléculaire, ENS Cachan, 61 avenue du Président Wilson, 94235 Cachan, France*
[c] *Synthèse et Electrosynthèse organiques (CNRS, UMR 6510), Université de Rennes 1, Campus de Beaulieu, Bât. 10A, 35042 Rennes cedex, France. E-mail: Mireille.Blanchard-Desce@univ-rennes1.fr*

Received (in Cambridge, UK) 13th February 2001, Accepted 17th April 2001
First published as an Advance Article on the web 2nd May 2001

Propeller-shaped molecules based on a triphenylbenzene crux bearing three oligomeric phenylenevinylene branches have been designed; very large first-order hyperpolarisabilities (up to $\|\beta\|$ = 800 10^{-30} esu) were obtained while maintaining wide transparency in the visible region by taking advantage and boosting of intramolecular charge transfer between the centre and the periphery.

Molecular nonlinear optics (NLO) has attracted increasing interest over the past twenty years,[1] owing to numerous applications in various fields such as telecommunications, optical data storage and information processing.[2] A substantial effort has been devoted to the design of molecules with enhanced NLO responses. Molecular engineering of conjugated one-dimensional (1D) compounds has been particularly successful, leading to push–pull compounds displaying giant off-resonance first-order (β)[3] and/or second-order (γ)[4] hyperpolarisabilities. Yet it became increasingly clear over recent years that multidimensional and multipolar structures offer challenging possibilities.[5] Lehn, Zyss and coworkers have opened a pioneering route towards octupolar molecules.[6] Such 2D or 3D structures take benefit from the tensorial nature of β, and potentially lead to very large β[7] and γ[8] values but most often at the expense of significantly reduced transparency in the visible region.[9] In order to achieve an improved nonlinearity–transparency trade-off, we have prepared nanoscale propeller-shaped molecules whose design is based on the grafting of three extended blades bearing an electron-withdrawing or an electron-releasing tip on a triphenylbenzene crux (Scheme 1). Oligomeric phenylenevinylene rods were selected to ensure effective electronic conjugation and preserve transparency. The triphenylbenzene core maintains a large distance between the conjugated branches, thus preventing sterical hindrances.

Based on this strategy, we have prepared homologous molecules with radius varying between 1.4 and 2.5 nm. The first generation (n = 1) was prepared from 1,3,5-tris(4-formylphenyl)benzene (**C_0**[10]) *via* either a triple Wittig or Wittig–Horner–Emmons reaction whereas the second generation (n = 2) was obtained from **C_1** *via* a triple Wittig–Horner–Emmons condensation with extended conjugated aldehydes X–Ph–CH=CH–Ph–CHO. The key reagent **C_1** was synthesized from **C_0** in a three-step procedure (Scheme 1). The conjugated aldehydes were primarily prepared in nearly quantitative yield by reacting terephthalaldehyde mono(diethyl acetal) with one equivalent of phosphonium salt X–Ph–CH_2–$P(Ph)_3I$ (X = $N(nC_6H_{13})_2$,[4b] or X = OnC_8H_{17}) or of diethyl 4-(methylsulfonyl)benzyl phosphonate (X = SO_2CH_3) followed by acid-catalysed hydrolysis. Molecules **1**–**6** were characterised by NMR spectroscopy, elemental analysis and/or high-resolution mass spectra, in agreement with the assigned structures.

All molecules show good transparency in a wide range of the visible region and an intense absorption in the near UV–blue visible region whose position is dependent on both the nature of the peripheral groups and the length of the transmitter system (Table 1). As expected, a red shift of the absorption band is observed with increasing electron-withdrawing or electron-releasing strength of the end groups. Interestingly, a bathochromic shift of the absorption band is obtained with increasing solvent polarity (Fig. 1a) and a noticeably more pronounced positive solvatochromism is observed in emission (Fig. 1b), indicative of a polar excited state. Such characteristic behaviour hints to significant charge redistribution taking place upon excitation, consistent with a multidimensional intramolecular charge transfer (MDICT) occurring between the core and the peripheral groups. The large Stokes shift values (4050

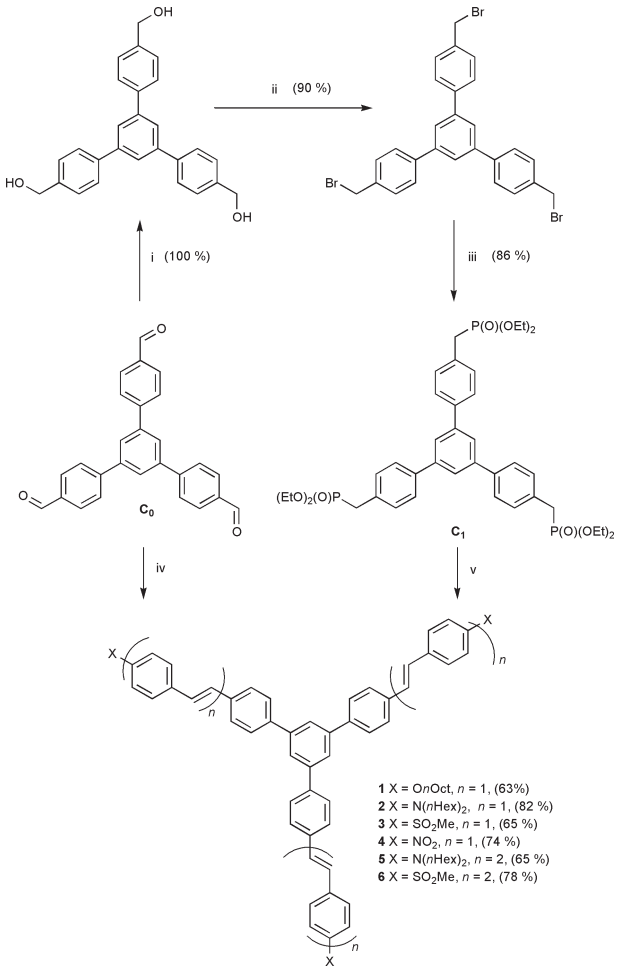

Scheme 1 *Reagents and conditions*: i: KBH_4 (1 equiv.), EtOH, 4 h, rt; ii: HBr conc. (10 equiv.), 5 h, reflux; iii: $P(OEt)_3$ (5 equiv.), 24 h, reflux; iv: compounds **1** and **2**: X–Ph–CH_2–$P(Ph)_3I$ (3.3 equiv.), KOtBu (3.5 equiv.), CH_2Cl_2, 4 h, rt; compounds **3** and **4**: X–Ph–CH_2–$P(O)(OEt)_2$ (3.3 equiv.), NaH (3.5 equiv.), THF, 4 h, rt; v: compounds **5** and **6**: X–Ph–CH=CH–Ph–CHO (3.3 equiv.), KOtBu (3.5 equiv.), CH_2Cl_2, 5 h, rt.

DOI: 10.1039/b101425k

Table 1 Linear and nonlinear optical properties of nanoscale propeller-shaped molecules derived from triphenylbenzene

	λ_{max}(abs)[a] /nm	$\Delta\tilde{\nu}$[b]/cm^{-1}	λ_{HLS}/nm	β_{HLS}[a]/ 10^{-30} esu	$\|\beta\|$[c]/ 10^{-30} esu	$\|\beta(0)\|$[d]/ 10^{-30} esu
1	344	170	1064	5	16	8
2	387	790	1064	29	94	50
3	342	510	1064	30	97	51
4[e]	385[e]	1060	1340	70	227	140
5	407	—	1340	150	486	278
6	377	1830	1340	250	810	510
***p*NA**	348	—	1064	10	32	12

[a] In chloroform. [b] Absorption solvatochromic shift = $1/\lambda_{max}$(toluene) $-1/\lambda_{max}$(DMSO). [c] The modulus $\|\beta\| = \sqrt{\sum_{ijk}\beta_{ijk}^2}$ is derived from β_{HLS} according to $\|\beta\| = \sqrt{\frac{21}{2}}\,\beta_{HLS}$ for molecules with C_{3h} symmetry, and to $\|\beta\| = \beta_{zzz} = \sqrt{\frac{35}{6}}\,\beta_{HLS}$ for 1D dipolar chromophores such as *p*-nitroaniline (*p*NA). [d] Static values are calculated using a two-level dispersion factor.[6b] [e] In DMSO.

cm^{-1} for molecule **2** in chloroform, and 8500 cm^{-1} for molecule **4** in DMSO) corroborate that important nuclear reorganisation is taking place after excitation, prior to emission as a result of significant electronic redistribution.

The first hyperpolarisabilities β have been determined by performing harmonic light scattering (HLS) experiments which yield the HLS molecular averaged hyperpolarisability $\sqrt{\langle\beta^2\rangle} = \beta_{HLS}$.[11] HLS experiments were performed at 1.064 or 1.34 μm in order to locate the second harmonic signal in the transparency region of the chromophores and to avoid contamination by two-photon fluorescence.[12] Comparison of homologous molecules bearing electron-releasing (**1**,**2**) or electron-withdrawing (**3**,**4**) end groups clearly shows that increasing the donating or accepting strength of the three terminal substituents results in a significant enhancement of β (Table 1), providing evidence that MDICT strongly influences the nonlinear responses. Following this observation, increasing the distance between the core and the periphery appeared as a rational way to boost the nonlinear responses. This strategy proved particularly successful: molecule **5** was found to exhibit a $\|\beta(0)\|$ value about six times larger than molecule **2**, whereas molecule **6** exhibits a first-order hyperpolarisability *one order of magnitude larger* than its shorter analogue **3**, while increasing by no more than 36% in weight and maintaining suitable transparency in the visible region. This is particularly advantageous in terms of efficiency-transparency trade-off: molecule **6** exhibits a $\|\beta(0)\|$ value about forty times larger than the prototypical push–pull compound *p*-nitroaniline (*p*NA), with a molecular weight no more than eight times larger.

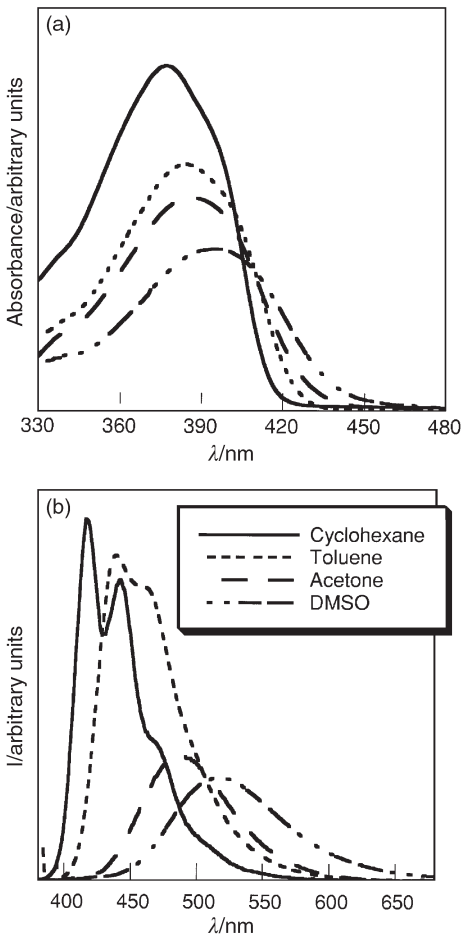

Fig. 1 Solvatochromic absorption (a) and emission (b) behaviour of molecule **2**.

Finally, by grafting either electron-donating or electron-withdrawing groups on the edges of conjugated blades branched on a triphenylbenzene crux, propeller-shaped molecules exhibiting high NLO properties and wide transparency in the visible range have been designed. Optimization leads to compounds presenting an improved transparency–nonlinearity trade-off ($\|\beta(0)\|$ = 500 10^{-30} esu, λ_{max} = 377 nm) as compared to tris-donor tris-acceptor octupolar 2D molecules. In addition, the superlinear dependence of β on size and their particular concave shape makes elongated analogues attractive candidates for incorporation in polymeric materials.

Notes and references

1 See for instance the special issue of *Chemical Physics* devoted to molecular nonlinear optics: *Chem. Phys*., 1999, 245, for current trends in molecular NLO.

2 D. A. Parthenopoulos and P. M. Rentzepis, *Science*, 1989, **245**, 842; Y. Shi, C. Zhang, H. Zhang, J. H. Bechtel, L. R. Dalton, B. H. Robinson and W. H. Steier, *Science*, 2000, **288**, 119.

3 M. Blanchard-Desce, V. Alain, P. V. Bedworth, S. R. Marder, A. Fort, C. Runser, M. Barzoukas, S. Lebus and R. Wortmann, *Chem. Eur. J*., 1997, **3**, 1091; V. Alain, M. Blanchard-Desce, I. Ledoux and J. Zyss, *Chem. Commun*., 2000, 353.

4 V. Alain, L. Thouin, M. Blanchard-Desce, U. Gubler, C. Bosshard, P. Günter, J. Muller, A. Fort and M. Barzoukas, *Adv. Mater*., 1999, **11**, 1210; V. Alain, S. Rédoglia, M. Blanchard-Desce, S. Lebus, K. Lukaszuk, R. Wortmann, U. Gubler, C. Bosshard and P. Günter, *Chem. Phys*., 1999, **245**, 51.

5 M. S. Wong, C. Bosshard, F. Pang and P. Günter, *Adv. Mater*., 1996, **8**, 677; S. Yokoyama, T. Nakahama, A. Otomo and S. Mashiko, *J. Am. Chem. Soc*., 2000, **122**, 3174.

6 I. Ledoux, J. Zyss, J. S. Siegel, J. Brienne and J.-M. Lehn, *Chem. Phys. Lett*., 1990, **172**, 440; J. Zyss, *J. Chem. Phys*., 1993, **98**, 6583.

7 C. Lambert, E. Schmälzin, K. Meerholz and C. Bräuchle, *Chem. Eur. J*., 1998, **4**, 512; C. Lambert, W. Gaschler, E. Schmälzin, K. Meerholz and C. Bräuchle, *J. Chem. Soc., Perkin, Trans., 2*, 1999, 577; M. Blanchard-Desce, J.-B. Baudin, L. Jullien, R. Lorne, O. Ruel, S. Brasselet and J. Zyss, *Opt. Mat*., 1999, **12**, 333; J. J. Wolff, F. Siegler, R. Matschiner and R. Wortmann, *Angew. Chem., Int. Ed*., 2000, **39**, 1436.

8 D. R. Greve, S. S. Schouchgaard, T. Geisler, J. C. Petersen and T. Bjørnholm, *Adv. Mater*., 1997, **9**, 1113; A. M. McDonagh, M. G. Humphrey, M. Samoc, B. Luther-Davis, S. Houbrechts, T. Wada, H. Sasabe and A. Persoons, *J. Am. Chem. Soc*., 1999, **121**, 1405.

9 C. Dhenault, I. Ledoux, I. D. W. Samuel, J. Zyss, M. Bourgault and H. Le Bozec, *Nature*, 1995, **374**, 339; B. del Rey, U. Keller, T. Torres, G. Rojo, F. Agulló-López, S. Nonell, C. Martí, S. Brasselet, I. Ledoux and J. Zyss, *J. Am. Chem. Soc*., 1998, **120**, 12 808.

10 E. Weber, M. Hecker, E. Koepp and W. Orlia, *J. Chem. Soc., Perkin, Trans. 2*, 1988, 1251.

11 R. W. Terhune, P. D. Maker and C. M. Savage, *Phys. Rev. Lett*., 1965, **14**, 681; K. Clays and A. Persoons, *Phys. Rev. Lett*., 1991, **66**, 2980.

12 M. C. Flipse, R. de Jonge, R. H. Woudenberg, A. W. Marsman, C. A. van Walree and L. W. Jenneskens, *Chem. Phys. Lett*., 1995, **245**, 297; I. D. Morrison, R. G. Denning, W. M. Laidlaw and M. A. Stammers, *Rev. Sci. Instrum*., 1996, **67**, 1445.

CHEMCOMM Communication
www.rsc.org/chemcomm

Direct resolution of C_{76} enantiomers by HPLC using an amylose-based chiral stationary phase

Chiyo Yamamoto,[a] Tomoko Hayashi,[a] Yoshio Okamoto,*[a] Shingo Ohkubo[b] and Tatsuhisa Kato[bc]

[a] *Department of Applied Chemistry, Graduate School of Engineering, Nagoya University, Chikusa-ku, Nagoya 464-8603, Japan. E-mail: okamoto@apchem.nagoya-u.ac.jp*
[b] *The Graduate University for Advanced Studies, Myodaiji, Okazaki 444-8585, Japan*
[c] *Institute for Molecular Science, Myodaiji, Okazaki 444-8585, Japan*

Received (in Cambridge, UK) 1st March 2001, Accepted 17th April 2001
First published as an Advance Article on the web 2nd May 2001

A chiral fullerene C_{76} was directly resolved by high-performance liquid chromatography (HPLC) using a chiral stationary phase, amylose tris(3,5-dimethylphenylcarbamate), bonded onto silica gel and the mirror-imaged CD spectra of the enantiomers were in good pattern agreement with those of the previous report.

In 1993, Hawkins and Meyer reported the kinetic resolution of C_{76} enantiomers by asymmetric osmylation,[1] and this method was successfully applied to the resolution of other chiral fullerenes, C_{78} and C_{84}.[2] However, direct resolution of chiral fullerenes by HPLC with a chiral column appears very difficult judging from the tiny structural differences in the C_{76} enantiomers as pointed out by Hawkins and has so far been unsuccessful,[1] although chiral fullerene C_{60} derivatives with achiral substituents have been successfully resolved into enantiomers using chiral stationary phases (CSPs) based on a cellulose derivative[3] and a tetranitrofluorenylidene derivative.[4]

Phenylcarbamate derivatives of polysaccharides, particularly cellulose and amylose, show high chiral recognition abilities when used as CSPs for HPLC.[5–7] Among the many derivatives, 3,5-dimethylphenylcarbamates of cellulose[8] and amylose[9] are very useful CSPs with an excellent ability of resolving a wide range of racemates. These CSPs have been prepared by coating or adsorbing the polysaccharide derivatives on silica gel, and therefore cannot be used with solvents such as $CHCl_3$ and THF that dissolve or swell the derivatives. On the other hand, amylose tris(3,5-dimethylphenylcarbamate) (Chiralpak AD) bonded to silica gel only at its terminal residue has been prepared *via* enzymatic polymerization, and can be used with $CHCl_3$ and THF.[10]

In the present study, we succeeded in the first direct HPLC resolution of the smallest chiral fullerene C_{76} on the chemically bonded Chiralpak AD using a hexane–$CHCl_3$ (80 : 20) mixture as the eluent.

The racemic C_{76} sample was isolated as a chlorobenzene solution by HPLC and identified by mass spectroscopy. The concentration of the solution was estimated to be *ca.* 0.36 mM l^{-1} based on the UV spectrum measurement.[11] The chemically bonded Chiralpak AD column was prepared by our group in Nagoya.[10] Chromatographic resolution was performed on a modified JASCO PU-980 chromatograph equipped with a UV and CD dual detector (JASCO CD-1595) and a recycle valve unit (HV-1592-01). The racemic C_{76} solution (100 μl) was injected into the chromatographic system with a Rheodyne Model 7125 injector. A hexane–$CHCl_3$ (80 : 20) mixture was used as the eluent at a flow rate 1.0 ml min^{-1}. UV spectra were measured in hexane–$CHCl_3$ and toluene solutions using a JASCO Ubest V-570 spectrophotometer. The CD spectra of the C_{76} enantiomers in hexane–$CHCl_3$ and toluene were taken on a JASCO J-720 L apparatus with a 0.2 cm quartz cell at ambient temperature.

When the resolution of the racemic C_{76} sample was examined on the commercial Chiralcel OD and Chiralpak AD columns using a hexane–propan-2-ol mixture as the eluent, the elution of the sample was not clearly observed probably because of very low solubility of C_{76} in this eluent which resulted in a very long retention time. This forced us to use chiral columns that can be used with a $CHCl_3$ eluent system. We then examined the resolution on the chemically bonded Chiralpak AD and Chiralcel OD phases using the hexane–$CHCl_3$ eluent, and found that Chiralpak AD had better resolution. The results of the resolution are shown in Fig. 1. Both the UV and CD signals were monitored by the dual detector. The UV signal always showed a single peak sometimes with a shoulder, while the CD signal monitored at 400 nm showed the first (+) peak followed by the second (–) peak. This indicates that a low degree of resolution was attained and in the first cycle two (+) peaks were clearly observed. The reason for the appearance of the two peaks is not immediately clear, but may be due to sample overloading. Very low loading capacity of the column seems to indicate that chiral recognition of the C_{76} enantiomers may be performed at specific chiral sites containing multi amylose chains. In all the recycle separations, only the front main part of the (+) fraction was recycled, and the late main portion of the (–) fraction was collected during each recycle. Therefore, as the number of recycles increased the UV intensity decreased, and after 8 recycles, almost no (–) peak was observed. After 5 recycles, the intensity ratio of the UV and CD detection at the peak top became almost constant. These results suggest that the (+) isomer after 8 recycles may have a higher enantiomeric excess (ee).

The HPLC analysis of the (+) and (–) fractions resolved by the recycling are shown in Fig. 2. The (+) fraction shows a very good agreement between the UV and CD curves indicating that this fraction has a high enantiomeric purity. On the other hand, the (–) fraction shows a small (+) peak besides a main (–) peak, indicating lower enantiomeric purity of this fraction.

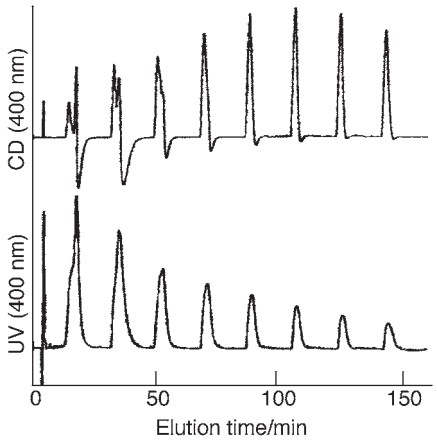

Fig. 1 Chromatographic recycled resolution of C_{76} on chemically bonded Chiralpak AD column. Column, 25 × 0.46 cm (id); eluent, hexane–$CHCl_3$ (80 : 20); flow rate, 1.0 ml min^{-1}.

DOI: 10.1039/b101972b

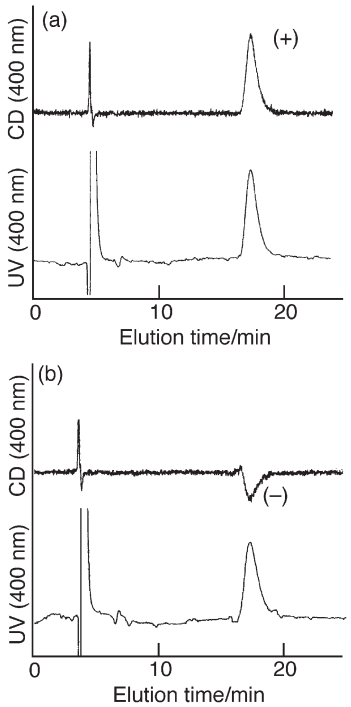

Fig. 2 HPLC chromatograms of the first (a) and the second (b) eluted enantiomers isolated after recycled resolution of C_{76}. (Column, chemically bonded Chiralpak AD; eluent, hexane–$CHCl_3$ (80:20); flow rate, 1.0 ml min^{-1}.)

Fig. 3 shows the CD spectra of the obtained C_{76} enantiomers in hexane–$CHCl_3$. When the solvent was replaced with toluene, almost identical spectra were observed. The spectral pattern is very similar to that for the C_{76} isolated by kinetic resolution,[1] but the intensity for the (+) fraction in this study is about 1.6 times greater than that for the above C_{76} which has been expected to have nearly 100% enantiomeric purity.[1] This means that our C_{76} would impossibly have over 100% ee based on the reported data. Since we used the same UV data[11] to estimate the C_{76} concentration,[12] the sample isolated in ref. 1 might have a lower enantiomeric purity, or the UV and CD measurements in ref. 1 might contain some error. Therefore, the reason for this disagreement in the CD data is not clear at this stage.

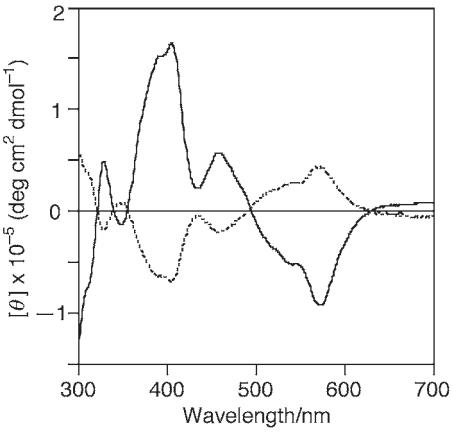

Fig. 3 CD spectra of C_{76} (first eluted enantiomer, solid line; second eluted enantiomer, dotted line) in toluene.

This work was partially supported by Grant-in-Aids for Scientific Research on Priority Areas No. 10208103.

Notes and references

1 J. M. Hawkins and A. Meyer, *Science*, 1993, **260**, 1918.
2 J. M. Hawkins, M. Nambu and A. Meyer, *J. Am. Chem. Soc.*, 1994, **116**, 7642.
3 M. Taki, S. Sugita, Y. Nakamura, E. Kasashima, E. Yashima, Y. Okamoto and J. Nishimura, *J. Am. Chem. Soc.*, 1997, **119**, 926.
4 B. Gross, V. Schurig, I. Lamparth and A. Hirsch, *J. Chromatogr. A*, 1997, **791**, 65.
5 Y. Okamoto and E. Yashima, *Angew. Chem., Int. Ed.*, 1998, **37**, 1020.
6 E. Yashima, C. Yamamoto and Y. Okamoto, *Synlett*, 1998, 344.
7 E. Yashima and Y. Okamoto, *Bull. Chem. Soc. Jpn.*, 1995, **68**, 3289.
8 Commercial name: Chiralcel OD (Daicel).
9 Commercial name: Chiralpak AD (Daicel).
10 N. Enomoto, S. Furukawa, Y. Ogasawara, H. Akano, Y. Kawamura, E. Yashima and Y. Okamoto, *Anal. Chem.*, 1996, **68**, 2798.
11 R. Ettl, I. Chao, F. Diederich and R. L. Whetten, *Nature*, 1991, **353**, 149.
12 The concentration of the isolated samples was estimated in a 2.0 mm cell based on ε = 28150 at 330 nm in ref. 11. The concentration of the first eluted enantiomer of C_{76} was 7.76×10^{-5} M and the CD intensity at 330 nm was 7.5 mdegree.

CHEMCOMM Communication
www.rsc.org/chemcomm

Promoting effect of CeO_2 in a Cu/CeO_2 catalyst: lowering of redox potentials of Cu species in the CeO_2 matrix

Parthasarathi Bera,[a] Sagar Mitra,[b] S. Sampath[b] and M. S. Hegde*[a]

[a] *Solid State and Structural Chemistry Unit, Indian Institute of Science, Bangalore-560012, India. E-mail: mshegde@sscu.iisc.ernet.in*
[b] *Department of Inorganic and Physical Chemistry, Indian Institute of Science, Bangalore-560012, India*

Received (in Cambridge, UK) 13th February 2001, Accepted 17th April 2001
First published as an Advance Article on the web 2nd May 2001

The promoting effect of CeO_2 in a Cu/CeO_2 catalyst for CO oxidation and NO reduction compared to CuO and Cu/ZrO_2 is deduced to be based on lowering of redox potentials of copper species in the Cu/CeO_2 matrix in relation to CuO and Cu/ZrO_2.

CeO_2 is an active support for precious metal as well as base metal catalysts and is widely used as a promoter for three way catalysts (TWCs). The promoting effect of CeO_2 is largely attributed to enhancement of metal dispersions, surface segregation of active metal, oxide ion defects for oxygen mobility and oxygen storage capacity (OSC).[1–5] Enhancement of catalytic activity by CeO_2 is observed in terms of reduction in the reaction temperature and decrease in activation energy. Complete CO oxidation over pure CeO_2 occurs above 500 °C while the temperature is brought down to 150 °C over Cu/CeO_2.[6–8] In contrast, 100% CO conversion occurs at 225 °C over bulk CuO. There seems to be an electronic interaction between Cu and CeO_2 which plays a vital role for the lowering of the reaction temperature and enhancement of the catalytic activity. Similar effects are also seen over Pt/CeO_2 and Pd/CeO_2 catalysts.[9] Several studies exist on the metal–support interaction and its effects on catalytic activity.[10–12] However, the exact nature of the interaction between metal ions and CeO_2 is not yet fully understood. We consider it worthwhile to investigate the Cu–CeO_2 interaction by electrochemical methods which can provide the redox properties of Cu species in a CeO_2 matrix. Here, we report for the first time, cyclic voltammetry and temperature programmed reaction (TPR) studies of a Cu/CeO_2 catalyst in comparison with CuO and Cu/ZrO_2. We show that the redox potentials of the Cu^{2+}/Cu^{+} and Cu^{+}/Cu^{0} couples in a CeO_2 matrix are lower than those in CuO and ZrO_2 matrices. The catalytic properties are consistent with the electrochemical behavior.

5% Cu/CeO_2 catalyst was prepared by the solution combustion method.[8] For the preparation of 5% Cu/ZrO_2 by this method, carbohydrazide (CH) was used as the fuel along with zirconyl nitrate and copper carbonate at 400 °C. X-Ray diffraction studies have shown that Cu^{2+} ions are substituted for Ce^{4+} to lead to a $Ce_{1-x}Cu_xO_{2-\delta}$ solid solution. Cu is in a +2 oxidation state as seen from X-ray photoelectron spectroscopy of the Cu 2p core level region as well as by electron paramagnetic resonance (EPR) spectra of Cu/CeO_2.[8]

Electrochemical studies were carried out with a CH-660A Electrochemical Analyzer (CH Instruments, USA) using a three-electrode cell configuration. The working electrodes were made by mixing 65 wt% graphite and 35 wt% Cu based materials. The mixture was ground thoroughly and 10 mm pellets of 1.5 mm thickness were prepared and subsequently mounted on a glass tube using conductive silver paint (Eltecks Corporation, India). Cu wire was used as the current collector. The electrode was polished to give a shining mirror finish using fine grade emery (SiC) paper. The counter electrode used was a Pt foil and saturated calomel electrode (SCE) was used as the reference electrode. The electrolyte solution was 0.05 M sodium sulfate (Na_2SO_4). The electrolyte was degassed by bubbling with N_2 prior to the measurement. In most cases the electrodes were cycled from +1.6 to −0.8 V at different scan rates. All experiments were performed at ambient temperature (*ca.* 25 °C).

The gas–solid reactions were carried out in a home-made TPR system equipped with a quadrupole mass spectrometer QXK300 (VG Scientific Ltd., England) using a packed bed tubular reactor.[8,9] Typically 0.1–0.2 g of the catalyst was loaded in a quartz tube reactor of 20 cm length and 6 mm diameter and the reactor was heated from 30 to 750 °C at a rate of 15 °C min^{-1}. The reactant gases were passed over the catalyst at a flow rate of 25 μmol s^{-1}.

The cyclic voltammogram of the Cu/CeO_2 electrode in 0.05 M Na_2SO_4 solution is shown in Fig. 1. The voltammogram obtained for the CuO electrode is also shown for comparison. The voltammograms consist of two cathodic and two anodic peaks for both bulk CuO and 5% Cu/CeO_2 samples in the scan range of 1.6 to −0.8 V *vs.* SCE. The Ce^{4+}/Ce^{3+} redox couple is not observed in the potential range studied. Similar voltammograms were observed for 5% Cu/ZrO_2 (not shown). The first peak labeled A is attributed to the reduction of Cu(II) to Cu(I) and the second peak B is due to reduction of Cu(I) to Cu(0) in all three cases.[13] The reduction potential values of $Cu^{2+} \rightarrow Cu^{+}$

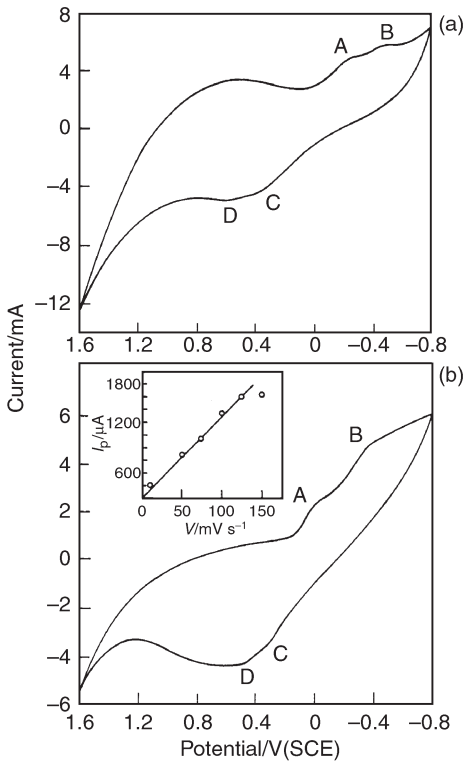

Fig. 1 Cyclic voltammograms of Cu species in (a) CuO and (b) 5% Cu/CeO_2 in 0.05 M Na_2SO_4 electrolyte at a scan rate of 50 mV s^{-1} (inset: peak current *vs.* scan rate relationship for peak B).

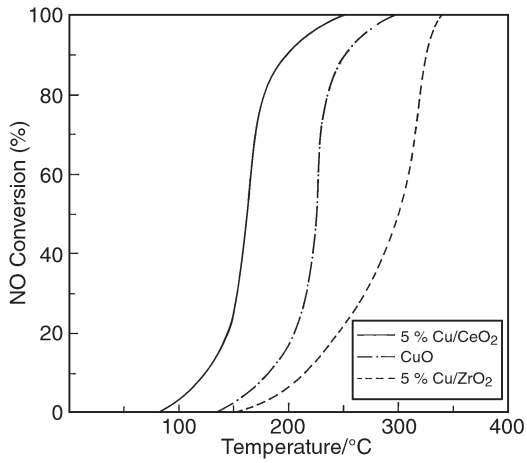

Fig. 2 NO conversion (%) over different Cu based catalysts for NO + NH_3 reaction.

and $Cu^{+} \rightarrow Cu^{0}$ in the CeO_2 matrix are −0.12 and −0.40 V, respectively, whereas the values for the CuO and Cu/ZrO_2 electrodes are −0.28, −0.50 and −0.38, −0.55 V, respectively. Oxidation potential values for $Cu^{0} \rightarrow Cu^{+}$ (peak C) and $Cu^{+} \rightarrow Cu^{2+}$ (peak D) in CeO_2 substrate are +0.25 and +0.50 V which are lower than those observed with CuO (+0.36 and +0.60 V) and Cu/ZrO_2 (+0.40 and +0.73 V) electrodes. The potential values indicate that Cu species in a Cu/CeO_2 matrix require less energy to be reduced and oxidized than in the case of pure CuO and Cu/ZrO_2 matrices. The plot of the second peak [B in Fig. 1(b)] as current (I_p) *vs*. scan rate (V) is shown as an inset in Fig. 1(b) for the Cu/CeO_2 system in 0.05 M Na_2SO_4 solution. The linear relationship indicates that the redox active species is surface confined.

NO conversions (%) for the NO + NH_3 reaction over 5% Cu/CeO_2, CuO and 5% Cu/ZrO_2 as a function of temperature are shown in Fig. 2. It is clear that complete NO conversion occurs at 250 °C over 5% Cu/CeO_2 whereas this requires 350 °C over 5% Cu/ZrO_2 with the reaction temperature over CuO lying in between. The reaction temperatures over these catalysts also follows the same trend for NO + CO and CO + O_2 reactions.

NO reduction by NH_3 involves electron transfer from NH_3 to NO. NH_3 is adsorbed on a Cu^{2+} site partially reducing the Cu^{2+} ion. This charge can be transferred to Ce^{4+} which can be picked up by NO to give [N] + [O]. Based on the electronic interaction between Ce 4f, O 2p and Cu 3d orbitals, electron transfer can be facilitated in Cu/CeO_2 as follows:

$$-Ce^{4+}-O^{2-}-Cu^{2+}- + e \rightleftharpoons -Ce^{4+}-O^{2-}-Cu^{+}- \rightleftharpoons -Ce^{3+}-O^{2-}-Cu^{2+}- \rightleftharpoons -Ce^{4+}-O^{2-}-Cu^{2+}- + e$$

Such a scheme involves the redox couples Cu^{2+}/Cu^{+} and Ce^{4+}/Ce^{3+}. These couples are available only for Cu/CeO_2 and not for CuO and Cu/ZrO_2 systems. A decrease in redox potentials of Cu species in Cu/CeO_2 as revealed in the voltammograms provides direct evidence of the promoting action of CeO_2. This will result in a decrease in the energy required for the electron transfer from NH_3 to NO and consequently a decrease in reaction temperature.

In conclusion, we have shown the correlation of catalytic properties of Cu/CeO_2 with the electrochemical behavior of the Cu species. The promoting action of CeO_2 is thus deduced to be *via* the lowering of redox potentials of Cu^{2+} ions in the CeO_2 matrix.

We thank Professor S. Vasudevan, Department of Inorganic and Physical Chemistry, Indian Institute of Science, Bangalore for useful discussions. One of the authors (P. B.), thanks the Council of Scientific and Industrial Research (CSIR), Government of India, for the award of a research fellowship. The Department of Atomic Energy (DAE), Government of India is gratefully acknowledged.

Notes and references

1 K. C. Taylor, *Catal. Rev.-Sci. Eng*., 1993, **35**, 457.
2 J. T. Kummer, *J. Phys. Chem*., 1986, **90**, 4747.
3 H. C. Yao and Y.-F. Y. Yao, *J. Catal*., 1984, **86**, 254.
4 J. G. Nunan, H. J. Robota, M. J. Cohn and S. A. Bradley, *J. Catal*., 1992, **133**, 309.
5 C. de Leitenburg, A. Trovarelli, F. Zamar, S. Maschio, G. Dolcetti and J. Llorca, *J. Chem. Soc., Chem. Commun*., 1995, 2181.
6 W. Liu, A. F. Sarofim and M. Flytzani-Stephanopoulos, *Chem. Eng. Sci*., 1994, **49**, 4871.
7 W. Liu and M. Flytzani-Stephanopoulos, *J. Catal*., 1995, **153**, 304.
8 P. Bera, S. T. Aruna, K. C. Patil and M. S. Hegde, *J. Catal*., 1999, **186**, 36.
9 P. Bera, K. C. Patil, V. Jayaram, G. N. Subbanna and M. S. Hegde, *J. Catal*., 2000, **196**, 293.
10 A. Tschöpe, M. L. Trudeau and J. Y. Ying, *J. Phys. Chem. B*, 1999, **103**, 8858.
11 A. Martínez-Arias, R. Cataluña, J. C. Conesa and J. Soria, *J. Phys. Chem. B*, 1998, **102**, 809.
12 A. Martínez-Arias, M. Fernández-García, J. Soria and J. C. Conesa, *J. Catal*., 1999, **182**, 367.
13 J. Xiao and G. Villmure, *Clays Clay Miner*., 1998, **46**, 195.

CHEMCOMM Communication
www.rsc.org/chemcomm

Complete characterisation of a Sb_2O_3/(21,−8)SWNT inclusion composite

Steffi Friedrichs,[a] Rüdiger R. Meyer,[b] Jeremy Sloan,*[ac] Angus I. Kirkland,[b] John L. Hutchison[c] and Malcolm L. H. Green[a]

[a] *Wolfson Catalysis Centre (Carbon Nanotechnology Group), Inorganic Chemistry Laboratory, South Parks Road, Oxford, UK OX1 3QR. E-mail: jeremy.sloan@chem.ox.ac.uk*
[b] *Department of Materials Science & Metallurgy, Pembroke Street, Cambridge, UK CB2 3QZ*
[c] *Department of Materials, Parks Road, Oxford, UK OX1 3PH*

Received (in Cambridge, UK) 13th March 2001, Accepted 12th April 2001
First published as an Advance Article on the web 2nd May 2001

The structure of a one-dimensional crystal of Sb_2O_3 encapsulated within a single-walled carbon nanotube and conformation of the latter have been solved simultaneously by high resolution transmission electron microscopy.

In this paper we report the characterisation of a one-dimensional crystal of Sb_2O_3, incorporated within a helical (21, −8) single-walled carbon nanotube (SWNT) achieved by object wave restoration from a focal series of high resolution transmission electron microscopy (HRTEM) images.† Within the nanocrystal, the atomic thickness in projection of individual antimony columns was determined and a substantial lattice contraction of the crystal along the tube axis observed. A simultaneous analysis of asymmetric fringe contrast in the tube walls provides convincing evidence for the chiral conformation of the nanotube.

SWNTs were produced using a metal catalysed arc synthesis technique similar to a method previously reported[1] and filled by capillary wetting.[2] Energy dispersive X-ray microanalysis (LINK 'ISIS' system) performed with a 0.5 nm electron probe confirmed the chemical identity of the filling material. HRTEM simulations, giving the complex wave function of the objects in question, were performed using a standard multislice algorithm[3,4] utilising a code provided by Kirkland.[5]

Fig. 1(a) shows the experimental restored HRTEM phase image of a 1.45 nm diameter SWNT containing an encapsulated single crystal of Sb_2O_3. The right tube wall displays a periodic lattice spacing of 0.224 nm, whereas the contrast variations on the left wall are effectively random. The observed periodic spacing on the right wall corresponds to the centre-to-centre spacing ($1.5d_{C–C}$ = 0.216 nm) between neighbouring 'zigzag' rows of carbon atoms in the SWNT wall lattice viewed in projection. The visibility of these spacings is determined by the SWNT conformation, the tilt angle of the cylinder relative to the electron beam and the HRTEM resolution (*ca.* 0.16 nm).

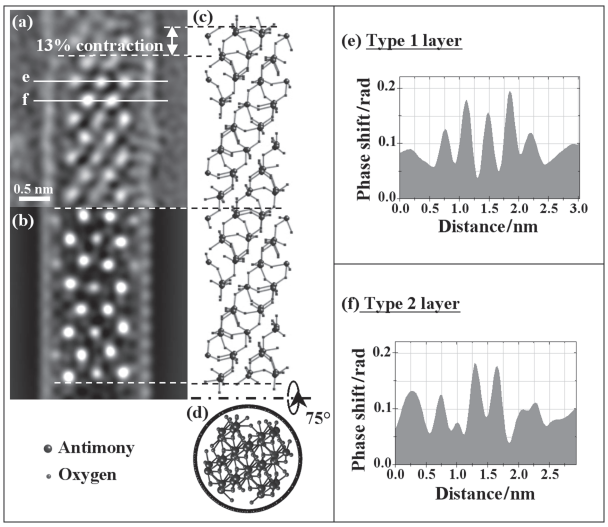

Fig. 1 Composite diagram showing the experimental restored phase image (a), the simulated phase image (b) and the structural model in the observed projection (c) and in end-on view (d), single pixel line profiles through type 1 (e) and type 2 (f) layers, respectively.

Fig. 2 illustrates the relationship between the observed wall periodicity, nanotube conformation and tilt angle together with corresponding simulations. Atomic coordinates for (*n, m*) nanotubes were generated by mapping the strip $\{\boldsymbol{r} \mid 0 \leq \boldsymbol{r} \cdot \boldsymbol{C}_h < |\boldsymbol{C}_h|^2\}$ of an unrolled hexagonal graphene lattice (with a carbon–carbon distance $d_{C–C}$ = 1.44 nm and lattice vectors $\boldsymbol{a}_1$, $\boldsymbol{a}_2$) onto a cylinder surface (Fig. 2). The structure of the SWNT is uniquely defined by the integers (*n,m*) with $n > 0$ and $-n/2 < m \leqslant n$‡ *via* the chiral vector $\boldsymbol{C}_h = n\boldsymbol{a}_1 + m\boldsymbol{a}_2$.[6] (*n*,0) and (*n*,*n*) represent the non-chiral zigzag and armchair configurations, respectively. All other (*n,m*) nanotubes are chiral with (*n* + *m*, −*m*) being the mirror image of (*n,m*).

The three differing conformation SWNTs shown in Fig. 2 (*i.e.* the (10,10) tubule in (a), the (18,0) tubule in (b) and the

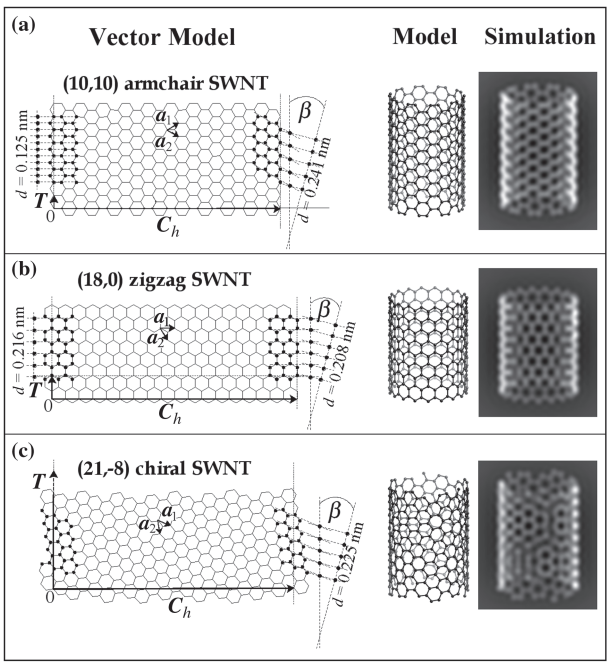

Fig. 2 (a)–(c) Schematic illustrations of the observable resolution of lattice fringes along SWNT walls of armchair, zigzag and chiral conformations, depending on the conformation, and the tilt angle β. The left column shows the unrolled graphene sheet, illustrating how the orientation of the chiral vector $\boldsymbol{C}_h$ w.r.t. the unit vectors $\boldsymbol{a}_1$ and $\boldsymbol{a}_2$ defines the rolling of a strip of the width $|\boldsymbol{C}_h|$ into a nanotube of a specific conformation and diameter. The middle column displays a modeled fraction of the SWNT, tilted by β = 15° out of the image-plane. The right column shows simulated phase images of the displayed models.

DOI: 10.1039/b102348a

(21,−8) tubule in (c)) all have diameters close to the *ca*. 1.4 nm diameter SWNT shown in Fig. 1(a).

As illustrated on the right sides of the vector models, contrast on the right tube wall is only observable when the 'zigzag' rows of carbon atoms are well aligned to the projection direction, *i.e.* when the difference $\delta_r = |\alpha - (-\beta)|$ between the chiral angle $\alpha = \angle(C_h,\boldsymbol{a}_1) = \arctan(\sqrt{3}m/(2n + m))$ and the tilt angle β of the tube axis out of the image plane is small. Similarly, contrast on the left wall is observed when $\delta_l = |\alpha - \beta|$ is small. As the numbers of atoms in projection on the tube wall is small, strong contrast will be visible for values of δ of up to 10° and the observed spacing will be given by $1.5d_{C-C}\cos\beta/\cos\alpha$ (Fig. 2(c)). For achiral tubes $\delta_l = \delta_r$ for any tilt angle and the contrast will therefore be equal on both walls. For $\beta = 0$ strong contrast will be visible on both walls of a zigzag-nanotube, whereas for the armchair tube, the difference $\delta = 30°$ is too large for an observation of any contrast due to the projection of the spacing between zigzag rows. Instead, the relevant projected spacing is that of $\sqrt{3}a/2 = 0.125$ nm between hexagon edges and centres (Fig. 1(b), left), which is too small to be resolved. For the chiral (21, −8) tube shown in Fig. 1(c), strong contrast is observed on the right wall when the top end of the tube is tilted towards the viewer. By measurement of the change in defocus along the tube, it was established that the top end of the tube was higher in the electron beam path and hence this tube must also have negative chirality.

The orientation of the incorporated crystal fraction can best be matched to an approximately $\langle 1\ 0\ -1 \rangle$ projection through a fragment of Sb_2O_3 derived from the orthorhombic valentinite structure, believed to be the high pressure form of Sb_2O_3.[7] The bulk valentinite structure consists of infinite double chains of SbO_3 units, running parallel to $\langle 0\ 0\ 1 \rangle$. In these double chains each Sb atom within the infinite Sb_2O_3 chains is coordinated by three oxygen atoms, one of which bridges between two Sb atoms.[7] The other cubic senarmonite form of antimony oxide consists of molecular Sb_4O_6 units.[8] Fig. 1(c) shows the proposed structure model (Fig. 1(d), end-on view) of the Sb_2O_3/SWNT composite.

The white spots in the reconstructed phase image represent atomic columns of antimony only in projection. The oxygen-sublattice could not be resolved, due to the weak scattering properties of oxygen and the staggering of the oxygen atoms in projection. Multislice simulations of the restored phase of Sb_2O_3 lattice fractions of appropriate thickness confirmed that the phase contrast due to the oxygen sublattice is negligible compared to that due to the antimony sublattice.

In the observed Sb_2O_3/SWNT composite the $\langle 4\ -1\ 2 \rangle$ Sb_2O_3 crystal direction, which subtends an angle of 78.3° with the optimum $\langle 1\ 0\ -1 \rangle$ viewing direction, is aligned along the tube axis. Therefore, the tube inclination of $\beta = 15°$, applied to the model and simulation in order to account for the observed contrast within the tube wall, is plausible as a small deviation from this viewing direction will not alter significantly the observed contrast of the crystal. Other preferred orientations of Sb_2O_3 were also observed but these always conformed to fragments of the valentinite strucure rather than senarmonite.

The repeating structural motif of the imaged encapsulated Sb_2O_3 crystal can be described as an alternating sequence of a layer containing three columns of Sb atoms (type 1 layer) followed by a layer containing two columns of Sb atoms (type 2 layer) arranged perpendicular to the long axis of the tube (Fig. 1(a)). Within each layer, the intensities due to the individual antimony columns vary in a complex fashion. The line profile through a type 1 layer (Fig 1(e)) shows a stacking pattern of 3–2–3 Sb atoms in projection. By contrast the line profile though a type 2 layer (Fig. 1(f)) gives two peaks of equal intensity approximately equivalent to the higher peak within the three-member layer indicating Sb columns three atoms in thickness. The multislice simulation in Fig. 1(b) also shows weak contrast close to the tube walls, resulting from single atom columns at the edge of the encapsulated crystal fragment. These were added to the periphery of the crystal model in order to account for corresponding weak peaks at these sites in the obtained phase image. However, the intensity of these peaks are not significantly higher than the background noise and it is impossible to assign these peaks to single-atom columns without a more accurate analysis of the phase contrast. The proposed model therefore consists of a Sb_2O_3 crystal fragment with sequences of 3–2–3 and (1–)3–3(–1) layers repeating every fourth equivalent layer along the $\langle 4\ -1\ 2 \rangle$ direction (Fig. 1(c)).

Since the oxygen sublattice was not resolvable, the oxygen coordination is predicted from the bulk valentinite structure. However, in order to fit the modeled Sb_2O_3 crystal into a 1.4 nm diameter SWNT, some oxygen atoms on the crystal surface were omitted. This can be justified in terms of an anticipated reduction in coordination at the Sb_2O_3/SWNT interface (*cf.* 2 × 2 and 3 × 3 KI crystals formed in SWNTs[9,10]).

Significant lattice distortions were observed in the Sb_2O_3 crystal. A comparison with the bulk structure of valentinite, shows that the encapsulated crystal displays a longitudinal contraction of 13% along the $\langle 4\ -1\ 2 \rangle$ axis (Fig. 1(a)–(c)). A similar contraction was also observed in a 3 × 3 KI crystal encapsulated within a SWNT.[9] In the Sb_2O_3/SWNT composite, lattice measurements from line traces show an average spacing of *ca*. 0.552 nm between type 1 or type 2 rows respectively, whereas in bulk Sb_2O_3 equivalent rows are spaced at *ca*. 0.638 nm. The observed lattice contraction may be caused by local interactions between the Sb_2O_3 crystal and the SWNT walls although the wall periodicity of a chiral nanotube cannot be commensurate with a periodic crystal over the long range, as was noted previously.[11] Additional distortions may be caused by the reduction in coordination at the Sb_2O_3/SWNT interface.

A more detailed account of this work is in press.[12]

We acknowledge the Petroleum Research Fund, administered by the American Chemical Society (Grant No. 33765-AC5), the EPSRC (Grant Nos. GR/L59238 and GR/L22324) and Colebrand Ltd. for financial support. S. F. is also indebted to BMBF and Fonds der Chemischen Industrie while J. S. is indebted to the Royal Society.

Notes and references

† The product was examined at 300 kV in a JEOL JEM-3000F FEGTEM (C_S = 0.57 nm; point resolution = 0.16 nm). Through focal series of individual filled nanotubes were acquired at a microscope magnification of ×600,000 using a GATAN 794 (1 k × 1 k pixel) CCD camera. From these focal series, the image wave was obtained using a Wiener filter restoration with abberations in the individual images.[11]

‡ The lower limit for *m* used here differs from the definition given in ref. 6, to ensure that the chiral angle α lies in the range $-30 < \alpha \leqslant 30°$.

1 C. Journet, W. K. Maser, P. Bernier, A. Loiseau, M. L. de la Chapelle, S. Lefrant, P. Deniard, R. Lee and J. E. Fischer, *Nature (London)*, 1997, **388**, 756.
2 J. Sloan, D. M. Wright, H.-G. Woo, S. Bailey, G. Brown, A. P. E. York, K. S. Coleman, J. L. Hutchinson and M. L. H. Green, *Chem. Commun.*, 1999, 699.
3 J. M. Cowley and A. F. Moodie, *Acta. Crystallogr.*, 1957, **10**, 609.
4 P. Goodman and A. F. Moodie, *Acta. Crystallogr., Sect. A*, 1974, **30**, 280.
5 E. J. Kirkland, in *Advanced Computing in Electron Microscopy*, Plenum Press, New York, 1998.
6 R. Saito, C. Dresselhaus and M. S. Dresselhaus, *Physical Properties of Carbon Nanotubes*, Imperial College Press, London, 1998.
7 C. Svensson, *Acta Crystallogr., Sect. B*, 1974, **30**, 458.
8 C. Svensson, *Acta Crystallogr. Sect. B*, 1975, **31**, 2016.
9 R. R. Meyer, J. Sloan, R. E. Dunin-Borowski, A. I. Kirkland, M. C. Novotny, S. R. Bailey, J. L. Hutchison and M. L. H. Green, *Science*, 2000, **289**, 1324.
10 J. Sloan, M. C. Novotny, S. R. Bailey, G. Brown, C. Xu, V. C. Williams, S. Friedrichs, E. Flahaut, R. L. Callendar, A. P. E. York, K. S. Coleman, M. L. H. Green, R. E. Dunin-Borkowski and J. L. Hutchison, *Chem. Phys. Lett.*, 2000, **329**, 61.
11 J. Sloan, J. Cook, M. L. H. Green, J. L. Hutchison and R. Tenne, *J. Mater. Chem.*, 1997, **7**, 1089.
12 S. Friedrichs, J. Sloan, J. L. Hutchinson, M. L. H. Green, R. R. Meyer and A. I. Kirkland, *Phys. Rev. B*, 2001, in press.

CHEMCOMM Communication
www.rsc.org/chemcomm

Perfectly polar assembly of molecular dipoles in crystals of Zn(II)(DMAP)(acac)$_2$: a case of self-poling†

S. Philip Anthony and T. P. Radhakrishnan*

School of Chemistry, University of Hyderabad, Hyderabad – 500 046, India.
E-mail: tprsc@uohyd.ernet.in

Received (in Cambridge, UK) 7th February 2001, Accepted 3rd April 2001
First published as an Advance Article on the web 2nd May 2001

Molecular dipoles assemble with a perfectly polar alignment in the crystals of the title complex and the hierarchy of intermolecular interactions in the lattice adheres to the requirements of a previously reported stochastic model for the production of polarity in supramolecular assemblies.

Molecular materials with a polar organization of the constituent dipoles are of great current interest because a variety of technologically important solid state properties such as pyroelectricity, piezoelectricity and nonlinear optical (NLO) effects may be realized in them.[1] Such materials would be the basis for the development of novel electro-optic (EO) and photorefractive devices[2] and nanoscale components such as molecular rectifiers.[3] Parallel alignment of molecular dipoles embedded in polymer films is achieved through electric field poling.[4] Non-centrosymmetric lattices are not common in molecular crystals;[5] special design strategies are often employed to induce noncentrosymmetricity.[6] Still rarer are highly polar molecular crystals with molecular dipoles aligned parallel to a single axis. Marder *et al.* have developed the 'salt methodology' wherein the anion sheets provide the driving force favoring a net polar alignment of cation sheets;[7] the well-known NLO crystal DAST has molecular dipoles in the crystal *ab* plane oriented at *ca.* 20° on either side of the *a* axis.[7b] Optimal chromophoric orientation for EO applications has been achieved through co-crystallization approaches by Bosshard and coworkers.[8] Another successful strategy is the inclusion of polar guest molecules in channels of host molecules developed by Hulliger *et al.*[9] The latter have also carried out stochastic modeling of the growth of polar bulk structures.[10] One of the significant conclusions from their study is that polarity in supramolecular assemblies is a tunable property controlled by the energetics of intermolecular interactions in different directions. While bonding interactions are required to assemble chains or sheets of polar molecules aligned along the direction of polarity evolution, the lateral interactions are required to be non-bonding recognitions to achieve 3-D polar alignment. The low density of the active molecules in two-component salts, co-crystals and the host–guest inclusion materials leads to less effective utilization of the bulk material to achieve the desired solid state effects. If molecular design involves a dipolar backbone with an optimal decoration that dictates weak or non-bonding lateral recognition, the assembly should lead to a polar crystal lattice with a higher density of the active species, a situation ideally suited for EO applications.[11] A potential candidate would be a 'screw'-shaped molecule with a dipolar axis and a 'head' which curtails lateral interactions without obstructing 1-D head-to-tail Coulombic interactions. We have realized this paradigm in the perfectly polar lattice of (4-dimethylaminopyridyl)bis(acetylacetonato)zinc(II) (ZNDA); DMAP–Zn forms the polar entity and the acac ligands the 'head'. This material also possesses good thermal stability and transparency.

ZNDA was synthesized by the direct replacement of the water molecule in Zn(acac)$_2$·H$_2$O by DMAP. Colorless crystals could be grown from methanol. X-Ray analysis revealed the orthorhombic space group F*dd*2 with half a molecule in the asymmetric unit;[12] C_2 rotation generates the other half. Zinc and the coordinated pyridine nitrogen, the *para* carbon and dimethylamino nitrogen atoms on DMAP lie on special positions on the *c*-axis. Zn(II) has distorted square-pyramidal coordination with normal bond parameters;[13] Fig. 1 shows clearly the 'screw'-shaped structure. The molecules pack into a perfectly polar lattice with the dipoles aligned along the *c* axis (Fig. 2) by virtue of the special position of Zn and DMAP. The origin of this organizational motif may be sought in the interplay of intermolecular interactions in the ZNDA lattice.

ZNDA is expected to have a sizeable dipole moment due to the push–pull nature of the DMAP–Zn(II) combination; AM1 calculation[14] on the molecular geometry from the crystal structure gives a value of 8.919 D. The electrostatic interaction between the dipoles directs the head-to-tail chain formation along the *c* axis. This is augmented by weak intermolecular H-bonds[15] between the carbon atoms of the dimethylamino groups of the DMAP ligand and oxygen atoms of the acac ligand of neighboring molecules ($r_{C7\cdots O12}$ = 3.679 Å; $\theta_{C7-H7B\cdots O12}$ = 158.7°). A further network of weak intermolecular H-bonds ($r_{C4\cdots O8}$ = 3.612 Å, $\theta_{C4-H4\cdots O8}$ = 139.6°; $r_{C7\cdots O8}$ = 3.526 Å,

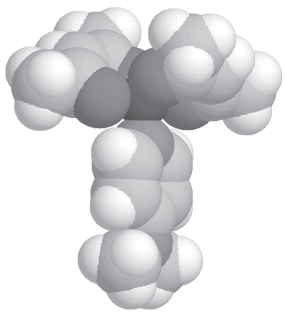

Fig. 1 Space-filling model of the molecular structure of ZNDA determined from single crystal X-ray analysis.

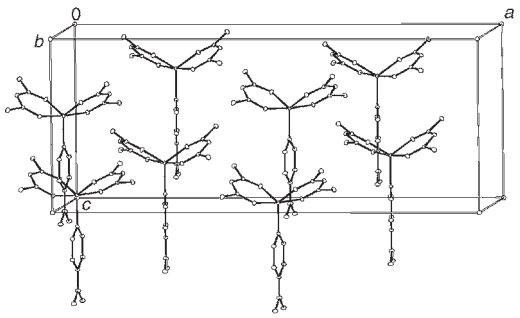

Fig. 2 View of the unit cell of ZNDA viewed approximately along the *b* axis; H atoms are omitted for clarity.

† Electronic supplementary information (ESI) available: synthesis characterization and crystal structure details of ZNDA and brief structural details of 4-morpholinopyridyl analog of ZNDA. Colour version of the space filling model of the structure of ZNDA. See http://www.rsc.org/suppdata/cc/b1/b101248g/

DOI: 10.1039/b101248g

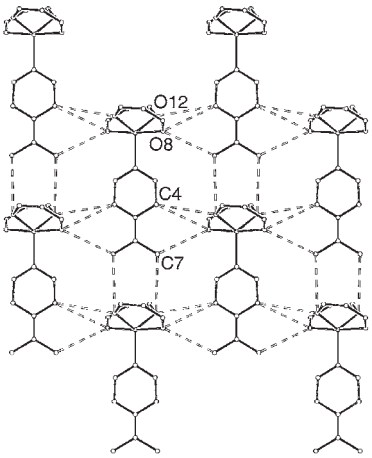

Fig. 3 Non-covalent interactions (dashed bonds) in the sheets of ZNDA molecules in the *bc* plane; all H atoms and methyl carbon atoms of the acac ligand are omitted for clarity.

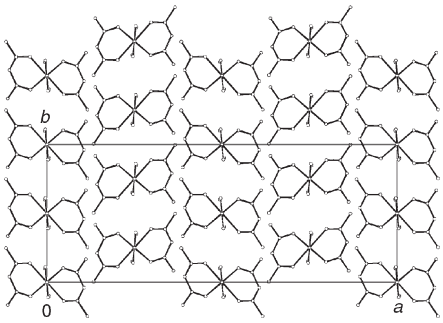

Fig. 4 Projection of the crystal lattice of ZNDA onto the *ab* plane; H atoms are omitted for clarity.

$\theta_{C7\text{-}H7A\cdots O8}$ = 155.6°; $r_{C4\cdots O12}$ = 3.585 Å, $\theta_{C4\text{-}H4\cdots O12}$ = 151.0°) between DMAP and acac binds the ZNDA molecules into a sheet parallel to the *bc* plane (Fig. 3). The sheets are well separated in the *a*-direction with a distance of *ca.* 7 Å between adjacent DMAP planes (Fig. 4). Neither strong nor even the weak bonding interactions present within the sheets are observed between the sheets. Thus the 3-D lattice structure of ZNDA is built from electrostatic interactions along the *c* axis and weak non-covalent interactions within the *bc* plane leading to sheet structures with no bonding recognition between the sheets in the *a* direction. This bulk organization[16] is in perfect accord with the Hulliger model for the generation of polarity in supramolecular systems.

The polar arrangement in molecular lattices is of interest in NLO applications. We have measured the second harmonic generation (SHG) from microcrystalline powders of ZNDA using the Kurtz–Perry technique.[17] SHG comparable to that of urea is observed. The low SHG is due to the small hyperpolarizability (AM1/TDHF[18] calculation on the molecular geometry from crystal structure gives a static hyperpolarizability of 4.4 × 10^{-30} esu) and the non-optimal molecular orientation in the crystals, for phase-matched SHG.[19] Large single crystals or oriented crystalline films have to be fabricated to carry out EO studies. Our current efforts are directed towards these goals. The good thermal stability (mp = 240 °C) and damage-free sublimation coupled with the large transparency range (λ_{max} = 282 nm, $\lambda_{cut\text{-}off}$ = 330 nm for methanol solutions) of ZNDA make it a promising candidate for further explorations.

In conclusion, the perfectly polar lattice of ZNDA, a case of self-poled assembly of molecular dipoles, reveals a hierarchy of intermolecular interactions in different directions in line with the requirements put forth in the stochastic model for the generation of polar supramolecular assemblies.

Financial support from the DST (Swarnajayanti Fellowship) and the use of the National Single Crystal Diffractometer Facility funded by the DST at the School of Chemistry, University of Hyderabad are gratefully acknowledged.

Notes and references

1 *Handbook of Laser Science and Technology*, ed. M. J. Weber, Supplement 2: Optical Materials, CRC Press, Boca Raton, FL, 1995; *Nonlinear Optical Properties of Organic Molecules and Crystals*, ed. D. S. Chemla and J. Zyss, Academic Press, New York, 1989, vol. 1, 2.

2 C. Bosshard and P. Günter, in *Nonlinear Optics of Organic Molecular and Polymeric Materials*, ed. S. Miyata and H. S. Nalwa, CRC Press, Boca Raton, FL, 1997, p. 391; W. E. Moerner and S. M. Silence, *Chem. Rev.*, 1994, **94**, 127.

3 A. S. Martin, J. R. Sambles and G. J. Ashwell, *Phys. Rev. Lett.*, 1993, **70**, 218.

4 *Poled Polymers and their Applications to SHG and EO Devices*, ed. S. Miyata and H. Sasabe, Gordon and Breach, Amsterdam, 1997.

5 The latest update (5.2) of the Cambridge Crystallographic Database shows 23.9% of the entries to be non-centrosymmetric.

6 C. Bosshard, R. Spreiter, U. Meier, I. Liakatas, M. Bösch, M. Jäger, S. Manetta, S. Follonier and P. Günter, in *Crystal Engineering: From Molecules and Crystals to Materials*, ed. D. Braga and F. Grepioni, Kluwer, Dordrecht, 1991, p. 261.

7 (*a*) S. R. Marder, J. W. Perry and W. P. Schaefer, *Science*, 1989, **245**, 626; (*b*) S. R. Marder, J. W. Perry and C. P. Yakymyshyn, *Chem. Mater.*, 1994, **6**, 1137.

8 M. S. Wong, F. Pan, M. Bösch, R. Spreiter, C. Bosshard, P. Günter and V. Gramlich, *J. Opt. Soc. Am. B*, 1998, **15**, 426.

9 J. Hulliger, O. König and R. Hoss, *Adv. Mater.*, 1995, **7**, 719; R. Hoss, O. König, V. Kramer-Hoss, U. Berger, P. Rogin and J. Hulliger, *Angew. Chem., Int. Ed. Engl.*, 1996, **35**, 1664; O. König, H.-B. Bürgi, T. Armbruster, J. Hulliger and T. Weber, *J. Am. Chem. Soc.*, 1997, **119**, 10 632; A. Quintel, J. Hulliger and M. Wübbenhorst, *J. Phys. Chem. B*, 1998, **102**, 4277.

10 J. Hulliger, P. J. Langley, A. Quintel, P. Rechsteiner and S. W. Roth, in *Supramolecular Engineering of Synthetic Metallic Materials*, ed. J. Veciana, C. Rovira and D. B. Amabilino, Kluwer, Dordrecht, 1999, p. 67; J. Hulliger, S. W. Roth, A. Quintel and H. Bebie, *J. Solid State Chem.*, 2000, **152**, 49.

11 A similar model has been proposed in: J. Hulliger, P. J. Langley and S. W. Roth, *Cryst. Eng.*, 1998, **1**, 177.

12 *Crystal data*: $C_{8.5}H_{12}NO_2Zn_{0.5}$; orthorhombic, space group *Fdd*2; *a* = 28.057(4), *b* = 11.363(2), *c* = 11.3253(17) Å; *Z* = 16; μ(Mo-Kα) = 1.383 mm^{-1}; no. of reflections ($I \geqslant 2\sigma_I$) = 1353; no. of parameters = 117; *R* = 0.0257; wR^2 = 0.0626; GOF = 1.064. CCDC 160057. See http://www.rsc.org/suppdata/cc/b1/b101248g/ for crystallographic data in .cif or other electronic format.

13 E. L. Lippert and M. R. Truter, *J. Chem. Soc.*, 1960, 4996; C. Zhang, R. Chadha, H. K. Reddy and G. N. Schrauzer, *Inorg. Chem.*, 1991, **30**, 3865.

14 M. J. S. Dewar, E. G. Zoebisch, E. F. Healy and J. J. P. Stewart, *J. Am. Chem. Soc.*, 1985, **107**, 3902.

15 G. R. Desiraju, *Acc. Chem. Res.*, 1996, **29**, 441.

16 We have also observed similar perfectly polar organization and hierarchy of intermolecular interactions in crystals of (4-morpholinopyridyl)bis(acetylacetonato)zinc(II) (see ESI†).

17 S. K. Kurtz and T. T. Perry, *J. Appl. Phys.*, 1968, **39**, 3798; for details of our procedure, see: P. Gangopadhyay and T. P. Radhakrishnan, *Chem. Mater.*, 2000, **12**, 3362.

18 M. Dupuis and S. Karna, *J. Comput. Chem.*, 1991, **12**, 487.

19 J. Zyss and J. L. Oudar, *Phys. Rev. A*, 1982, **26**, 2028.

CHEMCOMM Communication
www.rsc.org/chemcomm

Hydrothermally stable restructured mesoporous silica

Robert Mokaya

School of Chemistry, University of Nottingham, University Park, Nottingham, UK NG7 2RD. E-mail: r.mokaya@nottingham.ac.uk

Received (in Cambridge, UK) 20th February 2001, Accepted 17th April 2001
First published as an Advance Article on the web 2nd May 2001

Pure silica mesoporous materials that exhibit remarkable hydrothermal stability may be prepared by restructuring calcined MCM-41 *via* secondary synthesis involving extended recrystallisation.

Mesoporous silicas, such as MCM-41, are potentially useful as sorbents, heterogeneous catalysts and as hosts for the preparation of composite materials for advanced applications.[1] The preparation of mesoporous silicas which exhibit good hydrothermal stability (in hot water and under steaming conditions) is one of the most important requirements with respect to their use. To date, most of the work reported on the hydrothermal stability of mesoporous silicas has dealt with stability in boiling water.[2–6] This is mainly because stability in hot aqueous solutions is considered essential to ensure succesful post-synthesis modifications such as grafting and ion-exchange. Recent advances indicate that the hydrothermal stability of pure silica MCM-41 in boiling water can be improved by a variety of methods which include repeated pH adjustment and/or stabilisation *via* salt effects during synthesis,[2,5,7] restructuring of the as-synthesised material,[3,6] or the preparation of materials with thicker and more polymerised pore walls.[4] Stabilisation *via* a pore wall thickening approach appears to be the most straightforward, but no appropriate synthesis strategies for the control of wall thickness have so far been reported. Here we report on the remarkable steam and boiling water stability of restructured pure silica MCM-41 materials that are prepared *via* a seeded crystallisation route. The restructured materials are prepared *via* a route which involves the use of calcined MCM-41 as 'silica source' for secondary synthesis which is performed over extended periods of time. By extending the time allowed for high temperature recrystallisation during the secondary synthesis step it is possible to systematically increase the pore wall thickness. We believe that the remarkable stability observed here is due to a combination of thicker pore walls and a less strained silica framework. Restructuring during the extended 'recrystallisation' may act to heal any defects and relieve strains in the parent MCM-41 framework.

The parent MCM-41 was prepared using a normal procedure as follows: tetramethylammonium hydroxide (TMAOH) and cetyltrimethylammonium bromide (CTAB) were dissolved in distilled water by stirring at 35 °C to give a clear solution. The silica source, fumed silica (Sigma), was then added to the template solution under stirring for 1 hour. After further stirring for 1 h to allow the silica to be fully dispersed, the resulting synthesis gel of composition SiO_2:0.25CTAB:0.2 TMAOH:40 H_2O was left to age for 20 h at room temperature following which the gel was transferred to a Teflon-lined autoclave and heated at 150 °C for 48 h. The solid product was obtained by filtration, washed with distilled water, dried in air at room temperature and calcined in air at 550 °C for 8 h to yield the parent MCM-41. For restructuring, a synthesis gel of molar ratio as above was assembled except that the parent MCM-41 was used as the 'silica source'.[8–10] The experimental procedures were exactly as described above except that during the secondary synthesis the heating at 150 °C was performed for 96, 140 or 168 h. The restructured samples were designated MCM-41(RX) where X is the crystallisation time in hours, *i.e.* MCM-41(R96), MCM-41(R140) and MCM-41(R168) for 96, 140, 168 h, respectively. Hydrothermal stability was tested by heat treatment at 900 °C in a flow of nitrogen saturated with water vapour at room temperature.

The textural parameters of the parent and restructured MCM-41 materials before and after hydrothermal treatment are given in Table 1. First we note that the basal spacing of the restructured materials remains much the same despite the differences in the time allowed for recrystallisation. This is in contrast with previous results, which show that increasing the crystallisation time during high temperature (≥150 °C) synthesis of MCM-41 favours larger basal spacing.[13,14] The most likely explanation for the non-changing basal spacing observed here is that the structural backbone of the parent MCM-41 is maintained during the recrystallisation.[8–10] The main event during the recrystallisation may therefore involve further growth or linking of the existing parent MCM-41 particles as previously described.[4,9] We note that this is a strong indication of the previously proposed seeding mechanism.[8–10] The surface area and pore volume of the restructured materials gradually decrease with increasing recrystallisation time. The decrease in surface area and pore volume is presumably due to the formation of thicker pore walls; it is envisaged that the wall thickening occurs within the existing pores of the parent MCM-41.[4,9] This then causes the pore size to decrease as shown in Table 1. The pore wall thickness calculated for the materials increases by more than 50% from 10.0 Å for the parent MCM-41 to 11.4, 13.9 and 15.2 Å for MCM-41(R96), MCM-41(R140) and MCM-41(R168), respectively. This clearly represents a systematic increase in pore wall thickness of pure silica MCM-41 by simply changing the recrystallisation time. It is worth pointing out that the emphasis here is on the increase (*i.e.* >50%) rather than the actual pore wall thickness values, which can vary depending on the calculation method.[4] Powder XRD patterns of the parent and restructured MCM-41 materials are shown in Fig. 1A. In all cases well ordered materials were obtained as indicated by the XRD patterns which show an intense (100) diffraction peak and at least two higher order peaks. In contrast to extended direct synthesis, no significant

Table 1 Textural properties of the study materials

Sample	d_{100}/Å	Surface area/m^2 g^{-1}	Pore volume/cm^3 g^{-1}	Pore size[a]/Å
MCM-41	47.3	943	0.95	44.6
Steamed	37.6	131	0.17	
Refluxed		231	0.33	
MCM-41(R96)	48.1	806	0.83	44.1
Steamed	45.1	626	0.55	
Refluxed		669	0.83	
MCM-41(R140)	49.8	690	0.68	43.6
Steamed	47.4	650	0.63	
Refluxed		639	0.69	
MCM-41(R168)	49.2	613	0.59	41.6
Steamed	47.0	546	0.53	
Refluxed		552	0.62	

[a] Pore size was determined by applying a geometric model.[11] 1.6 g cm^{-3} was used as density of the silica walls.[12]

DOI: 10.1039/b101665m

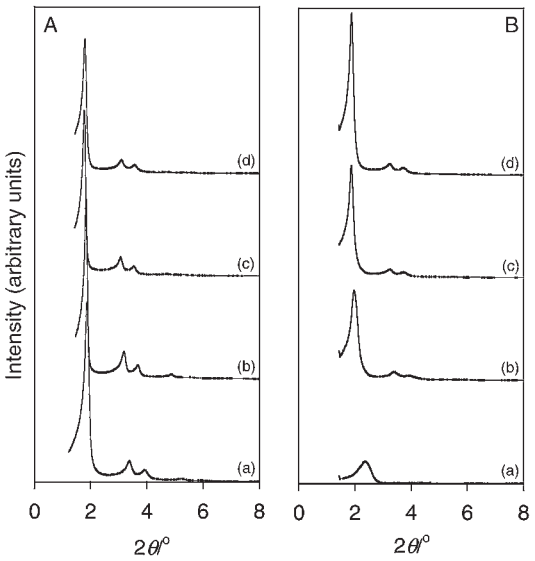

Fig. 1 Powder XRD patterns of (a) parent pure silica MCM-41, and restructured (b) MCM-41(R96), (c) MCM-41(R140) and (d) MCM-41(R168) materials before (A) and after (B) hydrothermal treatment at 900 °C under a flow of N_2 saturated with water vapour at room temperature. The intensity scales are the same for A and B.

diminution of structural ordering is observed even after recrystallisation for 168 h.[14]

Fig. 1B shows the powder XRD patterns of the parent MCM-41 and restructured materials after hydrothermal treatment at 900 °C. The parent sample is severely degraded after the hydrothermal treatment at 900 °C; the XRD pattern of the steamed parent sample exhibits only a weak (basal) 100 peak and no higher order peaks. The N_2 sorption isotherm of the steamed parent MCM-41 (not shown) exhibited virtually no mesoporous character and its surface area and pore volume reduced by more than 80% as shown in Table 1. We note that these observations are consistent with previous results on the steam stability of pure silica MCM-41 materials. For example, Chen *et al*. observed degradation of conventionally synthesised Si-MCM-41 after treatment at 850 °C in water vapour (8 Torr)[15] while materials prepared *via* repeated pH adjustment were severely degraded after 2 h at 800 °C in a flow of O_2 saturated with water vapour at room temperature.[7] In the present study steam stability was remarkably improved after restructuring. Fig. 1B indicates a much higher steam stability for the restructured samples compared with the parent MCM-41. It is also apparent from Fig. 1 that the stability of the restructured samples is higher for materials that have been recrystallised for longer periods of time. Indeed, for sample MCM-41(R168) there is virtually no change in the XRD pattern after the hydrothermal treatment at 900 °C. The N_2 sorption isotherms of the restructured samples (not shown) exhibit a sharp mesopore filling step characteristic of well ordered MCM-41 materials. The restructured samples are able to retain much of their original surface area and pore volume after steaming as indicated in Table 1. Sample MCM-41(R96) retains 78 and 66% of its original surface area and pore volume, respectively. Samples recrystallised for 140 and 168 h retain *ca*. 90% of their surface area and pore volume. These small reductions in surface area and pore volume observed for the steamed, restructured samples contrast sharply with the > 80% decrease for the parent MCM-41 material. Furthermore, the stability of the restructured framework is illustrated by the small lattice contractions observed for MCM-41(R140) and MCM-41(R168), *i.e*. only *ca*. 5% reduction in basal spacing compared with 20% contraction for the parent MCM-41.

We also investigated the stability of the restructured MCM-41 samples in boiling water. This was performed by refluxing the samples for 24 h in distilled water at a solid : liquid ratio of 1 g per litre. The trends observed in 'boiling water' stability were similar to those discussed above for steamed samples; the restructured samples retained their structural integrity while the parent MCM-41 sample was severely degraded. The surface area of the refluxed parent sample decreased by 75% compared with a reduction of typically < 17% for the restructured samples (see Table 1). Interestingly, the pore volume of the restructured samples was virtually unchanged after refluxing. (It is worth noting that MCM-41 materials prepared *via* repeated pH adjustment undergo severe degradation after 12 h in boiling water.[2] Restructuring of as-synthesised MCM-41 in the mother-liquor or water can yield slightly more stable materials which are nevertheless considerably degraded after 22 h in boiling water).[3] We also note that the restructured materials exhibit good thermal stability in static air; after calcination at 1000 °C for 6 h the parent MCM-41 was completely destroyed (its surface area reduced to 24 $m^2\ g^{-1}$) while MCM-41(R96) and MCM-41(R168) retained some structural ordering and surface area of 244 and 401 $m^2\ g^{-1}$ respectively. It appears therefore that the restructured materials reported here are exceptionally stable and in any case more hydrothermally stable than any previously reported MCM-41 with the possible exception of those stabilised with the addition of salts during synthesis.[5] Stabilisation in the present case is achieved *via* thicker and more polymerised pore walls which provide a silica framework which has fewer defects compared with that of the parent MCM-41. A higher extent of silica condensation in the restructured materials was confirmed by the proportion of fully condensed silica species in the as-synthesised samples; $Q^4 : Q^3$ ratios obtained from ^{29}Si MAS NMR analysis were in the range 3.5–4.5 for the restructured samples, compared with 1.5 for the parent MCM-41 material. It is likely that the restructuring, in addition to increasing pore wall thickness and silica condensation, also serves to heal any defects present in the parent material. The restructured materials therefore undergo little forced silica condensation during calcination thereby resulting in stabilised and less strained silica frameworks. This is consistent with the observation that on calcination, the restructured samples undergo virtually no lattice contraction, compared with a 9% decrease in the lattice size of the parent MCM-41 sample. It is also possible that the large particle size of the restructured materials contributes to their hydrothermal stability.[9]

The author is grateful to the EPSRC for an Advanced Fellowship.

Notes and references

1 J. Y. Ying, C. P. Mehnert and M. S. Wong, *Angew. Chem., Int. Ed*., 1999, **38**, 56.
2 R. Ryoo and S. Jun, *J. Phys. Chem. B*, 1997, **101**, 317.
3 M. Kruk, M. Jaroniec and A. Sayari, *Microporous Mesoporous Mater*., 1999, **27**, 219.
4 R. Mokaya, *J. Phys. Chem. B*, 1999, **103**, 10 204.
5 D. Das, C. M. Tsai and S. Cheng, *Chem. Commun*., 1999, 473.
6 L. Chen, T. Horiuchi, T. Mori and K. Maeda, *J. Phys. Chem. B*, 1999, **103**, 1216.
7 J. M. Kim, J. H. Kwak, S. Jun and R. Ryoo, *J. Phys. Chem*., 1995, **99**, 16 742.
8 R. Mokaya, W. Zhou and W. Jones, *Chem. Commun*., 1999, 51.
9 R. Mokaya, W. Zhou and W. Jones, *J. Mater. Chem*., 2000, **10**, 1139.
10 W. Zhou, R. Mokaya, S. Zhiping and T. Maschmeyer, *Prog. Nat. Sci*., 2001, **11**, 33.
11 M. Kruk, M. Jaroniec and A. Sayari, *J. Phys. Chem. B*, 1997, **101**, 583; M. Kruk, M. Jaroniec and A. Sayari, *Langmuir*, 1997, **13**, 6267.
12 N. Floquet, J. P. Coulomb, S. Giogio, Y. Grillet and P. L. Llewellyn, *Stud. Surf. Sci. Catal*., 1998, **117**, 583.
13 C.-F. Cheng, W. Zhou and J. Klinowski, *Chem. Phys. Lett*., 1996, **263**, 247.
14 R. Mokaya, *Microporous Mesoporous Mater*., 2001, **44–5**, 119.
15 C. Y. Chen, H.-X. Li and M. E. Davis, *Microporous Mater*., 1993, **2**, 17.

CHEMCOMM Communication
www.rsc.org/chemcomm

Incorporation of [U-^{13}C]glycerol defines plausible early steps for the biosynthesis of methylenomycin A in *Streptomyces coelicolor* A3(2)†

Gregory L. Challis*‡ and Keith F. Chater

Department of Genetics, John Innes Centre, Colney Lane, Norwich, UK NR4 7UH. E-mail: greg.challis@bbsrc.ac.uk; Fax: +44 (0)1603 450045; Tel: +44 (0)1603 450000

Received (in Cambridge, UK) 19th February 2001, Accepted 4th April 2001
First published as an Advance Article on the web 2nd May 2001

Incorporation of [U-^{13}C]glycerol into the linear plasmid-encoded secondary metabolite methylenomycin A, both intact and indirectly *via* metabolism to acetyl CoA, was observed in *Streptomyces coelicolor* suggesting plausible early biosynthetic steps for this unusual antibiotic.

Methylenomycins A and B, **1** and **2** respectively,[1] are the most well studied members of a small group of cyclopentanone antibiotics produced by various *Streptomyces* spp. Other members of this group include xanthocidin,[2] vertimycin,[3]

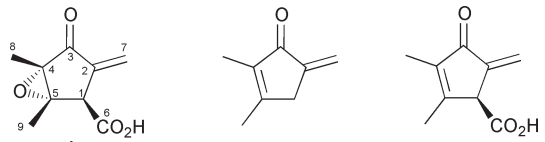

pentenomycin,[4] and sarkomycin,[5] which is an antitumour agent that has been used clinically in Japan. The *mmy* cluster of genes encoding methylenomycin biosynthesis and its regulation, as well as self-resistance, is localised on a large linear plasmid that is not essential for growth in *Streptomyces coelicolor* A3(2) and a large circular plasmid in *Streptomyces violaceoruber*.[5] Recently, the entire *mmy* cluster of *S. coelicolor* has been sequenced.[6] As a first step towards understanding how the enzymes encoded by this cluster assemble **1** and **2** we have reinvestigated the primary metabolic origins of these antibiotics.

Previous investigations showed that radiolabelled desepoxy-4,5-didehydro methylenomycin A **3**, which is also a metabolite of *S. coelicolor*, is incorporated into **1**.[7] Thus epoxidation of **3** appears to be the final step in the biosynthesis of **1**, whereas **2** probably derives from spontaneous decarboxylation of **3**. Additional experiments using radiolabelled precursors showed significant incorporation of acetate, pyruvate, succinate, aspartate and glycine into the carbon atoms of **1**.[8] Intact incorporation of acetate into C-4, C-8 and C-1, C-6 of **1** was deduced by ^{13}C NMR analysis of a sample isolated from a culture of *S. coelicolor* fed with [1,2-$^{13}C_2$]acetate (Scheme 1).[8]

Scheme 1

To further investigate the primary metabolic origins of the carbon atoms in **1**, the incorporation of [U-^{13}C]glycerol was examined.§ Surprisingly, the results of this experiment were inconsistent with the previously reported incorporation of [1,2-^{13}C]acetate into C-4, C-8 of **1**. The original interpretation of the acetate incorporation experiment depended on the assignment of the signal at 13.8 ppm in the ^{13}C NMR spectrum of **1** to the C-5 methyl substituent. This assignment was made on the basis of an apparent ^4J coupling between the C-5 methyl group and the hydrogen atom attached to C-1 in the ^{1}H NMR spectrum, in conjunction with heteronuclear decoupling experiments.[8] To resolve the conflict we measured the HMBC spectrum of **1**, which unambiguously showed that the signals at 13.8 and 8.2 ppm in the ^{13}C NMR spectrum are due to the C-4 and C-5 methyl groups, respectively (Fig. 1).

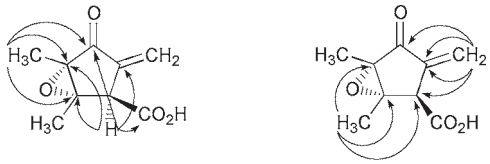

Fig. 1 Summary of HMBC correlations observed for **1**.

These assignments forced us to conclude that [1,2-^{13}C]acetate is incorporated intact into C-5, C-9 and C-1, C-6, rather than C-4, C-8 and C-1, C-6 as previously reported.[8] Consistent with this reinterpretation, the ^{13}C NMR spectrum of **1** isolated from the glycerol feeding experiment showed indirect incorporation of [U-^{13}C]glycerol into C-5, C-9 and C-1, C-6 presumably by catabolism *via* pyruvate to [1,2-^{13}C]acetyl CoA. In addition, double doublets centred on the signals for C-3 and C-8 were also observed in the spectrum, demonstrating that these carbons are coupled ($^2J_{C-C}$ = 3.4 Hz; Fig. 2), which is consistent with intact incorporation of [U-^{13}C]glycerol into C-3, C-4 and C-8. Such intact incorporation of glycerol is relatively unusual and has only been reported for four other microbial secondary metabolites.[9] The results of the glycerol incorporation experiment are summarised in Scheme 2.

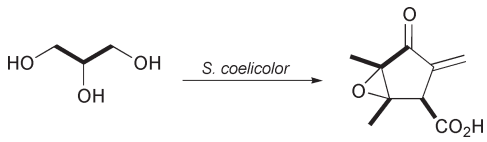

Scheme 2

On the basis of these results, we propose a pathway for the biosynthesis of **1** in *S. coelicolor* involving nucleophilic addition of C-2 of lactate (X = H, Y = OH) or of a glycolytic intermediate such as glyceraldehyde-3-phosphate (X = OPO_3^{2-}, Y = H) to C-3 of acetoacetyl ACP. This pathway, which is mechanistically distinct from those proposed for the incorporation of glycerol into other metabolites,[9] is consistent with the presence of the *mmyA* and *mmyC* genes in the methylenomycin cluster, which encode homologues of an ACP and ketoacyl synthase III (KAS III), respectively.[6] However, reduction of acetoacetyl ACP to 3-hydroxybutyryl ACP followed by nucleophilic displacement of the hydroxy group with C-2 of lactate or glyceraldehyde-3-phosphate cannot be

† Electronic supplementary information (ESI) available: HMBC, ^{1}H and ^{13}C NMR spectra of methylenomycin A. See http://www.rsc.org/suppdata/cc/b1/b101615f/

‡ Current address: Department of Chemistry, University of Warwick, Coventry, UK CV4 7AL. E-mail: g.l.challis@warwick.ac.uk; Fax +44 (0)2476 524112; Tel: +44 (0)2476 523653.

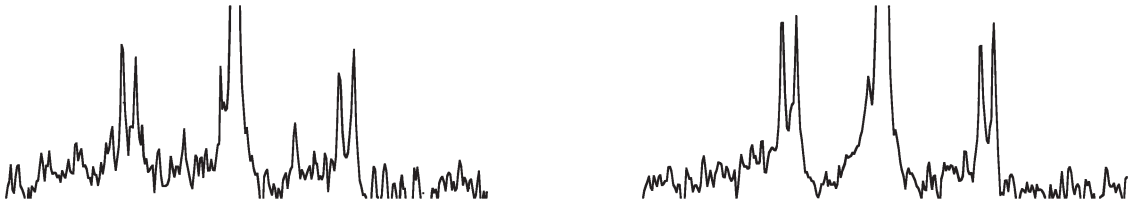

Fig. 2 Sections of the ^{13}C NMR spectrum of **1** isolated from cultures of *S. coelicolor* fed with [U-^{13}C]glycerol showing double doublets flanking the C-3 (left; 196.4 ppm) and C-8 (right; 8.2 ppm) resonances. While the larger splitting in each is due to ^{1}J coupling between C-3 or C-8 and C-4, the smaller splitting of 3.4 Hz in both is due to ^{2}J coupling between C-3 and C-8, consistent with intact incorporation of [U-^{13}C]glycerol into C-3, C-4 and C-8 of **1**.

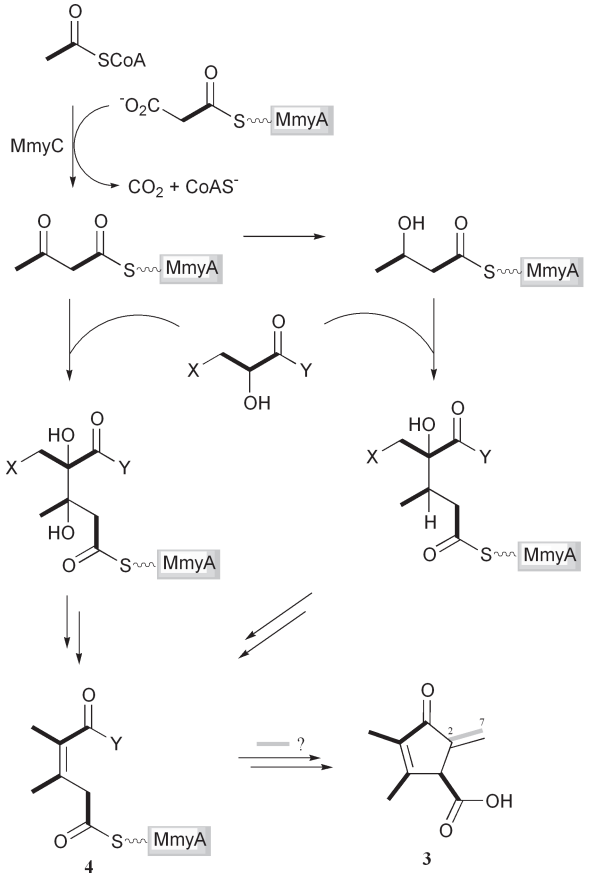

Scheme 3

ruled out.[10] In either case, several alternating dehydrations and enoyl reductions of the product would yield the common intermediate **4** (Scheme 3).

Conversion of **4** to the known biosynthetic intermediate **3** would require condensation with unknown precursors of C-2 and C-7 and hydrolysis of the thioester linkage to the ACP MmyA. Previous experiments eliminated the possibility that C-2 and C-7 are derived either from actetate as an intact two-carbon unit or from two *S*-adenosylmethionine methyl groups.[8] However, radioactivity from [2-^{14}C]glycine, has been shown to incorporate into **1** and this amino acid could therefore act as either an intact two-carbon precursor of C-2, C-7 or as a one-carbon donor for C-2 and C-7 *via* metabolism to methylene tetrahydrofolate.[8] To test this hypothesis we examined the incorporation of [1,2-$^{13}C_2$]glycine into **1**. To our surprise, there was no incorporation of ^{13}C into C-2 or C-7, instead approximately equal labelling of individual molecules at either C-5 and C-9, or C-1 and C-6 was observed. This result can be explained by transfer of ^{13}C-2 from one molecule of [1,2-$^{13}C_2$]glycine to another by serine hydroxymethyltransferase to give [U-^{13}C]serine, which is then metabolised to [1,2-$^{13}C_2$]acetyl CoA *via* pyruvate and incorporated into **1**. Thus, we have ruled out the derivation of C-2 and C-7 from intact glycine or from two one-carbon units donated by methylene tetrahydrofolate. Further experiments will be required to identify the cryptic two-carbon precursor of C-2 and C-7.

In conclusion, intact and indirect incorporation of [U-^{13}C]glycerol has elucidated the metabolic origins of the majority of carbon atoms in **1** and has defined plausible early steps for the biosynthesis of this metabolite in *S. coelicolor* A3(2).

Financial support by the Wellcome Trust (grant no. 053086) is gratefully acknowledged. We thank A. C. Foster and Professor S. V. Ley (University of Cambridge) for recording NMR spectra.

Notes and references

§ A solution of 50 mg of labelled glycerol in water was added to a 3-day-old 500 ml culture of *S. coelicolor* U9 grown in complete medium at 28 °C from spores as in ref. 8. After 24 h further incubation, the culture was filtered, and the filtrate was adjusted to pH 2 with 6 M HCl and extracted with an equal volume of ethyl acetate. **1** was purified from the organic extract by flash column chromatography (silica, AcOH–PhMe 1:9) and analysed by ^{13}C NMR spectroscopy at 100 MHz.

1 T. Haneishi, N. Kitahara, Y. Takiguichi, M. Arai and S. Sugawara, *J. Antibiot*., 1974, **27**, 386 and references therein; L. F. Wright and D. A. Hopwood, *J. Gen. Microbiol*., 1976, **95**, 96.
2 T. Sakurai, Y. Iiamura and K. Asahi, *Agric. Biol. Chem*., 1970, **34**, 325.
3 K. Umino, T. Furumai, N. Matsuzawa, Y. Awataguchi, Y. Ito and T. Okuda, *J. Antibiot*., 1973, **26**, 506.
4 H. Umezawa, T. Takeuchi and K. Nitta, *J. Antibiot*., 1953, **6**, 101.
5 K. F. Chater and C. J. Bruton, *EMBO J*., 1985, **4**, 1893 and references therein.
6 Genbank Accession number: AJ276673.
7 U. Hornemann and D. A. Hopwood, *Tetrahedron Lett*., 1978, 2977.
8 U. Hornemann and D. A. Hopwood, in *Antibiotics IV*, ed. J. W. Corcoran, Springer Verlag, Berlin Heidelberg, 1981, pp. 123.
9 N. Khaleeli, R. F. Li and C. A. Townsend, *J. Am. Chem. Soc*., 1999, **121**, 9223 and references therein; J. J. Lee, J. P. Lee, P. J. Keller, C. E. Cottrell, C. Chang, H. Zahner and H. G. Floss, *J. Antibiot*., 1986, **39**, 1123; S. Sakuda, A. Higashi, S. Tanaka, T. Nihira and Y. Yamada, *J. Am. Chem. Soc*., 1992, **114**, 663; Y. Sekiyama, H. Araya, K. Hasumi, A. Endo and Y. Fujimoto, *Tetrahedron Lett*., 1998, **39**, 6223.
10 Similarly the dehydration of 3-hydroxybutyryl ACP to give crotonyl ACP followed by conjugate nucleophilic addition of C-2 of lactate or glyceraldehyde-3-phosphate can not be ruled out, although it gives the same product.

CHEMCOMM Communication
www.rsc.org/chemcomm

Preparation of monodispersed nanocrystalline CeO_2 powders by microwave irradiation

Xue-Hong Liao,†[a] Jian-Min Zhu,[b] Jun-Jie Zhu,*[a] Jing-Zhong Xu[a] and Hong-Yuan Chen[a]

[a] *Department of Chemistry, Laboratory of Mesoscopic Materials and State Key Laboratory of Coordination Chemistry, Nanjing University, Nanjing, 210093, P. R. China. E-mail: gxyz@nju.edu.cn*
[b] *National Laboratory of Solid State of Microstructures, Nanjing University, Nanjing, 210093, P. R. China*

Received (in Cambridge, UK) 29th January 2001, Accepted 17th April 2001
First published as an Advance Article on the web 2nd May 2001

Monodispersed nanocrystalline CeO_2 powders of size *ca.* 2.0 nm displaying quantum size effects have been prepared by microwave irradiation in an aqueous solution containing $(NH_4)_2Ce(NO_3)_6$, PEG and NaAc.

Ceria (CeO_2) is a rare earth oxide with a high refractive index and a very sharp fundamental absorption edge and is a semiconductor with a band gap of 3.2 eV. It is also a highly efficient UV absorber and is used as an additive to glass (2–4% CeO_2) to protect light-sensitive materials, as a coating for corrosion protection of metals, as an oxidation catalyst, and as a counter electrode for electrochromic devices[1] as proposed recently. It is currently also being used as an oxygen ion conductor in solid oxide fuel cells (SOFCs), electrolyzers, oxygen pumps and amperometric oxygen monitors owing to its high oxygen ion conductivity.[2] Many studies have been conducted to prepare fine CeO_2 powders by using urea-based homogeneous precipitation,[3] hexamethylenetetramine-based homogeneous precipitation,[4] hydrothermal synthesis,[2] or cathodic electrogeneration of base.[5] Transparent colloidal solutions of ultrafine ceria particles were also directly obtained by Masashi *et al*,[6] by the reaction of cerium metal in 2-methoxyethanol at 200–300 °C. However, the preparation of nanocrystalline CeO_2 is very difficult using conventional conditions, and it is thus a challenge to find a novel approach to prepare the nanocrystalline oxide.

Since 1986, microwave irradiation has found a number of applications as a heating method in chemistry. As a quick, simple and energy efficient method, microwave synthesis has been developed, and is widely used for the synthesis of zeolites and ceramic materials.[7–11] Compared with conventional methods, microwave synthesis has the advantages of very short reaction times, production of small particles with a narrow particle size distribution, and high purity. Jansen *et al.* suggested that these advantages could be attributed to fast homogeneous nucleation and ready dissolution of the gel.[7] Unfortunately the exact nature of the interaction of the microwaves with the reactants during the synthesis of materials is somewhat uncertain and speculative. However, it is well known that the interaction between dielectric materials, liquids or solids, and the microwaves leads to what is generally known as dielectric heating in which electric dipoles in such materials respond to the applied electric field. In liquids, this constant reorientation leads to a friction between the molecules, which subsequently generates heat.[12] Many microwave phenomena are poorly understood such as non-thermal effects and the superheating effect.[2,13] In this study, a novel method for the preparation of ultrafine nanocrystalline cerium oxide is reported. Monodispersed nanocrystalline CeO_2 powders were successfully prepared by microwave irradiation by means of hydrolysis of $(NH_4)_2Ce(NO_3)_6$ in an aqueous solution containing poly(ethylene glycol)-2000 (PEG) and NaAc. Analysis of the results showed that the resulting CeO_2 powders were well crystallized, of *ca.* 2 nm size and showing a large quantum size effect.

An aqueous solution of 1 wt% PEG, 0.01 mol L^{-1} $(NH_4)_2Ce(NO_3)_6$ and 1 wt% NaAc was exposed to microwave radiation at a power level of 30% (the microwave operating in a 30 second cycles, on for 9 s, and off for 21 s at a total power of 650 W for 10 min), and then cooled to room temperature.‡ The resulting precipitate was centrifuged, washed with distilled water and dried in air. The final yellow product was collected for characterization.

The obtained powders were characterized by X-ray powder diffraction (XRD) (Fig. 1). The XRD pattern of the as-prepared product showed the presence of broad peaks, which corresponded to the (111), (220), (311) planes for a cubic fluorite structure.[14] The broadness of the peaks indicated that the crystallite size was very small. The microstructure of the sample was examined by high-resolution transmission electron microscopy (HRTEM). Typical TEM and HRTEM images of the sample are shown in Fig. 2(a) and (b). It is clear that as-prepared CeO_2 powders are crystalline with *ca.* 2 nm particle size (HRTEM image). In addition monodispersed nanocrystals were observed.

The UV–VIS absorption spectrum of the product dispersed in toluene is shown in Fig. 3 and shows a very large shift compared with the pure bulk crystal. The band gap E_g was 4.25 eV as calculated by the direct conversion method (in Fig. 4).[15] This is 1.0 eV larger than that of the pure bulk crystal (E_g = 3.19 eV).[1] The increase in the magnitude of the band gap is a consequence of the quantum size effect.

The proposed mechanism of microwave heating hydrolysis synthesis of CeO_2 nanoparticles may be as follows: first, hydrated Ce^{4+} ions can form complexes with H_2O molecules or OH^- ions. Polymers of this hydroxide, $Ce(H_2O)_x(OH^-)_y^{(4-y)+}$, can then serve as the precursors of the oxide. The starting precipitate from the Ce(IV) salt may be formed by nucleation of hydrated $Ce(H_2O)_x(OH^-)_y^{(4-y)+}$ so leading to very fine precursors for the final oxide. In aqueous solution, H_2O as a polar molecule tends to take protons away from coordinated hydroxide and the reaction equation can be expressed by eqn. (1).[2]

$$Ce(H_2O)_x(OH^-)_y^{(4-y)+} + H_2O \rightarrow CeO_2{\cdot}nH_2O + H_3O^+ \quad (1)$$

Compared with conventional heating methods, microwave heating presents a more rapid and simultaneous nucleation due

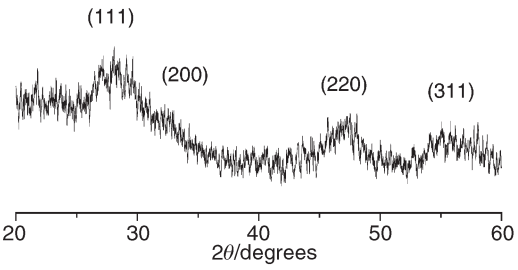

Fig. 1. XRD pattern of the as-prepared product.

† Permanent address: Huanggang Normal University, Huangzhou, 438000, Hubei, P. R. China.

DOI: 10.1039/b101004m

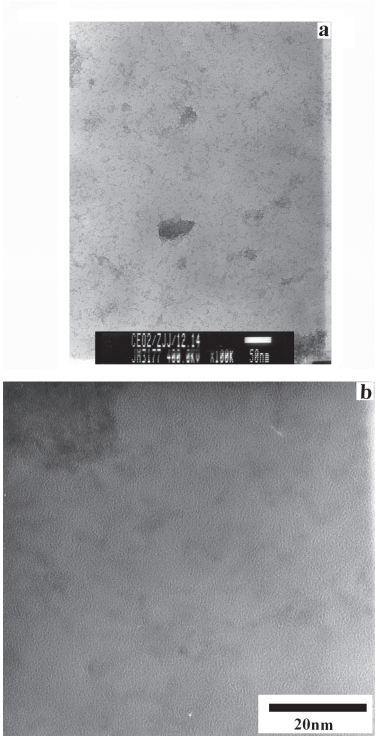

Fig. 2. TEM (a) and HRTEM (b) images of the as-prepared product.

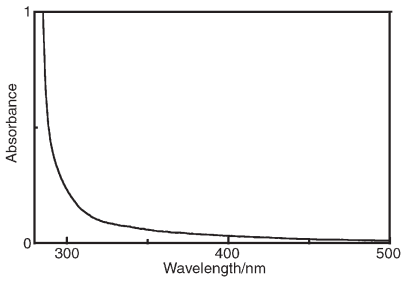

Fig. 3. UV–VIS absorbance spectrum of a toluene suspension containing 0.1046 g L^{-1} of the as-prepared product.

to the fast and homogeneous heating effects of microwaves. Moreover, uniform small particles can be synthesized due to the simultaneous nucleation and homogeneous heating. In addition, PEG, as a dispersion stabilizer, can inhibit segregation so as to obtain homogeneous precipitation. Use of PEG is a general method to synthesize nanocrystalline oxides with some nanocrystalline oxides such as TiO_2 and SnO_2 being successfully prepared *via* this route.

In conclusion, a microwave heating hydrolysis method has been successfully used for the preparation of ultrafine nanocrystalline CeO_2 powders. The advantage of this process is that it is fast, simple and energy efficient. It is predicted that upscaling of the process may lead to large quantities of nanosized CeO_2 crystallites. It also represents a general method to obtain other oxide nanocrystals.

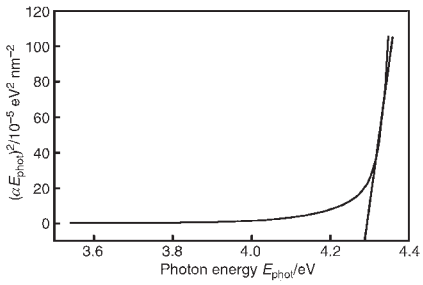

Fig. 4. Plot of $(\alpha E_{phot})^2$ *vs.* E_{phot} for direct transitions, where α is the absorption coefficient and E_{phot} the photon energy. The band gap E_g is obtained by extrapolation to $\alpha = 0$. The data are replotted from Fig. 3.

This work is supported by the National Natural Science Foundation of China and Ministry of Education of China.

Notes and references

‡ A 650 W microwave oven (Sanle General Electric Corp. Nanjing, China) was used for the refluxing system. Powder X-ray diffraction (XRD) patterns were recorded on Shimadzu XD-3A X-ray diffractometer (Cu-Kα radiation, $\lambda = 0.15418$ nm). HRTEM images of the products were obtained with a JEOL-4000EX high-resolution transmission electron microscope (HRTEM) with a 400 kV accelerating voltage. UV–VIS absorption spectra were recorded on a Shimadzu UV-Visible 3100 spectrophotometer.

1 Z. C. Orel and B. Orel, *Phys. Status Solidi B*, 1994, **186**, K33.
2 M. Hirano and E. Kato, *J. Am. Ceram. Soc.*, 1996, **79**, 777.
3 X. Chu, W. Chung and L. D. Schmidt, *J. Am. Ceram. Soc.*, 1993, **76**, 2115.
4 P. L. Chen and I. W. Chen, *J. Am. Ceram. Soc.*, 1993, **76**, 1577.
5 Y. C. Zhou, R. J. Phillips and J. A. Switzer, *J. Am. Ceram. Soc.*, 1995, **78**, 981.
6 I. Masashi, K. Minoru and I. Tomoyuki, *Chem. Commun.*, 1999, 957.
7 J. C. Jansen, A. Arafat, A. K. Barakat and H. Van Bekkum, in *Synthesis of Microporous Materials*, ed: M. L. Occelli and H. Robson, Van Nostrand Reinhold, New York, 1992, p. 507.
8 X. C. Xu, W. S. Yang, J. Liu and L. W. Lin, *Adv. Mater.*, 2000, **3**, 195.
9 O. Palchik, J. J. Zhu and A. Gedanken, *J. Mater. Chem.*, 2000, **10**, 1251.
10 J. J. Zhu, O. Palchik, S. G. Chen and A. Gedanken, *J. Phys. Chem. B*, 2000, **104**, 7344.
11 O. Palchik, I. Felner, G. Kataby and A. Gedanken, *J. Mater. Res.*, 2000, **15**, 2176.
12 K. J. Rao, B. Vaidhyanathan, M. Gaguli and P. A. Ramakrishnan, *Chem. Mater.*, 1999, **11**, 882.
13 R. Roy, *J. Solid State Chem.*, 1994, **111**, 11.
14 Joint Committee of Powder Diffraction Standards. Card No. 4-0593.
15 S. Tsunekawa, T. Fukuda and A. Kasuya, *J. Appl. Phys.*, 2000, **87**, 1318.

Typeset and printed by Black Bear Press Limited, Cambridge, England

CHEMCOMM
Feature Article
www.rsc.org/chemcomm

Solving the riddle of the intradiol and extradiol catechol dioxygenases: how do enzymes control hydroperoxide rearrangements?

Timothy D. H. Bugg* and Gang Lin

Department of Chemistry, University of Warwick, Coventry CV4 7AL

Received (in Cambridge, UK) 12th January 2001, Accepted 7th March 2001
First published as an Advance Article on the web 20th April 2001

Metallo-enzymes catalyse a rich variety of biochemical reactions, some of which have little or no precedent in laboratory chemistry.[1] Studies of such enzyme-catalysed reactions have benefited greatly in recent years from the pace of new protein X-ray crystallographic structures, but a detailed understanding of enzyme-catalysed reactions at the molecular level has required an interplay between structural studies, mechanistic studies, and small molecule model studies. This article will describe recent studies on an intriguing and long-standing puzzle in mechanistic enzymology, that of the non-haem iron-dependent catechol dioxygenases.[2]

Discovery of the catechol dioxygenases

A number of soil bacteria, especially *Pseudomonas*, have the metabolic capability to degrade aromatic compounds and utilise these compounds as the sole carbon source for growth.[3] A key step in these catabolic pathways is the oxidative cleavage of catechol, or substituted catechols, to give acyclic products. Two families of dioxygenase enzyme were discovered by O. Hayaishi which can catalyse the oxidative cleavage of catechol, both families utilising dioxygen as a substrate (see Scheme 1).[4–6] The intradiol dioxygenases, typified by catechol 1,2-dioxygenase (or pyrocatechase), cleave the carbon–carbon bond between the phenolic hydroxy groups to yield muconic acid as product, and require Fe^{3+} as a cofactor.[4] The extradiol dioxygenases, typefied by catechol 2,3-dioxygenase (or meta-pyrocatechase), cleave the carbon–carbon bond adjacent to the phenolic hydroxy groups to yield 2-hydroxymuconaldehyde as product, and require Fe^{2+} as a cofactor.[5]

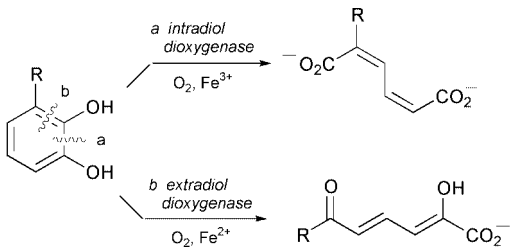

Scheme 1 Reactions catalysed by intradiol and extradiol dioxygenases.

Unlike the cytochrome P450-dependent oxygenases, which were discovered at this time, the metal co-factors were utilised as non-haem iron by these enzymes. Hayaishi was able to demonstrate, using $^{18}O_2$ labelling experiments, that catechol 1,2-dioxygenase incorporated both atoms of oxygen from dioxygen into the reaction products,[4] hence the designation as a dioxygenase. The mechanism invoked by Hayaishi to explain these results was that a four-membered dioxetane ring was formed during the reaction (see Scheme 2), which fragmented to form the reaction products.[6]

The reason for the different metal ion requirement of the two families of enzyme, however, remained a mystery. The intradiol dioxygenases were entirely selective for Fe^{3+}, and were inactivated by treatment with reducing agents; while the extradiol dioxygenases were entirely selective for Fe^{2+}, and were inactivated by treatment with oxidising agents. Each family of enzyme was quite specific for the production of their respective reaction product with a range of substrates. Furthermore, although catechol is well known to be sensitive to aerial oxidation, oxidative cleavage of catechol was a reaction unprecedented in organic chemistry.

X-Ray crystallography of catechol dioxygenases

Although the catechol dioxygenases were demonstrated by Hayaishi to be crystalline enzymes,[4] it was not until 1988 that the first X-ray structure of a catechol dioxygenase, the intradiol-cleaving protocatechuate 3,4-dioxygenase from *Pseudomonas putida*, was solved by Ohlendorf *et al.*[7] The enzyme consists of two subunits, in an oligomeric $(\alpha\beta Fe)_{12}$ structure (see Fig. 1**B**). The non-haem iron(III) cofactor was found to be ligated by four amino acid sidechains: the imidazole sidechains of His-460 and His-462, and the phenolic sidechains of Tyr-408 and Tyr-447 (see Fig. 1**D**). A fifth water ligand completes a trigonal bipyramidal structure. The two tyrosinate ligands are thought to stabilise the iron(III) cofactor and give the enzyme its characteristic deep red colour due to ligand-to-metal charge transfer interactions.[7] X-ray structures of protocatechuate 3,4-dioxygenase from *Pseudomonas aeruginosa* and *Acinetobacter* sp. ADP1 have also been solved.[8,9]

Recently another member of the intradiol dioxygenase family, catechol 1,2-dioxygenase from *Acinetobacter* sp. ADP1, has also been solved.[10] This enzyme consists of an α_2 homodimer with one iron(III) cofactor per subunit. The tertiary structure of the 1,2-CTD enzyme is similar to that found in 3,4-PCD, although 1,2-CTD contains a novel helical zipper motif at the interface of the two subunits, and contains two molecules of bound phospholipid (see Fig. 1**A**). The active site of 1,2-CTD contains a very similar arrangement of iron(III) ligands: Tyr-200 and His-226 are the axial ligands, and Tyr-164, His-224 and a water molecule are the equatorial ligands (see Fig. 1**C**).[10]

Structural elucidation of the iron(II)-dependent extradiol dioxygenases has proved more challenging, due largely to the facile oxidation of the cofactor. By carrying out the enzyme purification and crystallisation under an anaerobic atmosphere, Han *et al.* were in 1996 able to solve the structure of 2,3-dihydroxybiphenyl 1,2-dioxygenase (BphC) from *Pseudomonas* LB400,[11] a strain capable of degrading chlorinated biphenyls. The tertiary structure of the enzyme consists of two similar $\beta\alpha\beta\beta\beta$ domains, only one of which contains an iron(II) cofactor (see Fig. 2**A**). A funnel-shaped cavity leads to the active site, where the iron(II) centre is ligated by three amino acid sidechains: His-146, His-210 and Glu-260 (see Fig. 2**D**).[11] This His_2Glu/Asp motif is found in a number of other non-haem iron(II)-dependent oxygenases, including the α-ketoglutarate

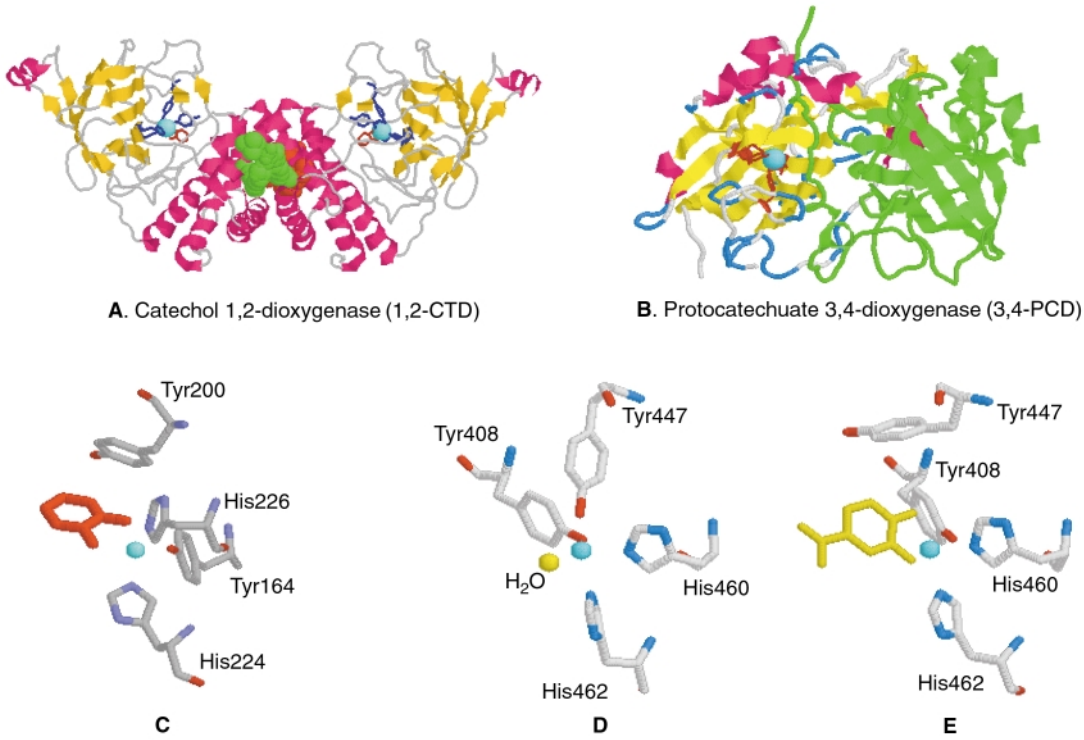

Fig. 1 X-Ray crystal structures of intradiol catechol dioxygenases. **A**. Catechol 1,2-dioxygenase (1,2-CTD) from *Acinetobacter* sp. ADP1,[10] showing iron(III) cofactor, ligands, and bound substrate. Bound phospholipid in shaded green (PDB accession number 1DLT). **B**. Protocatechuate 3,4-dioxygenase (3,4-PCD) from *Pseudomonas putida*,[7] showing α and β subunits (β subunit in green), iron(III) cofactor, ligands (PDB accession number 2PCD). **C**. Active site of 1,2-CTD,[10] showing iron(III) cofactor, ligands, and bound catechol substrate (in red). D. Active site of 3,4-PCD,[7] showing iron(III) cofactor and ligands. **E**. Active site of 3,4-PCD co-crystallised with analogue 2-hydroxyisonicotinic acid *N*-oxide (in yellow),[17] illustrating the movement of Tyr-447 (PDB accession number 3PCL).

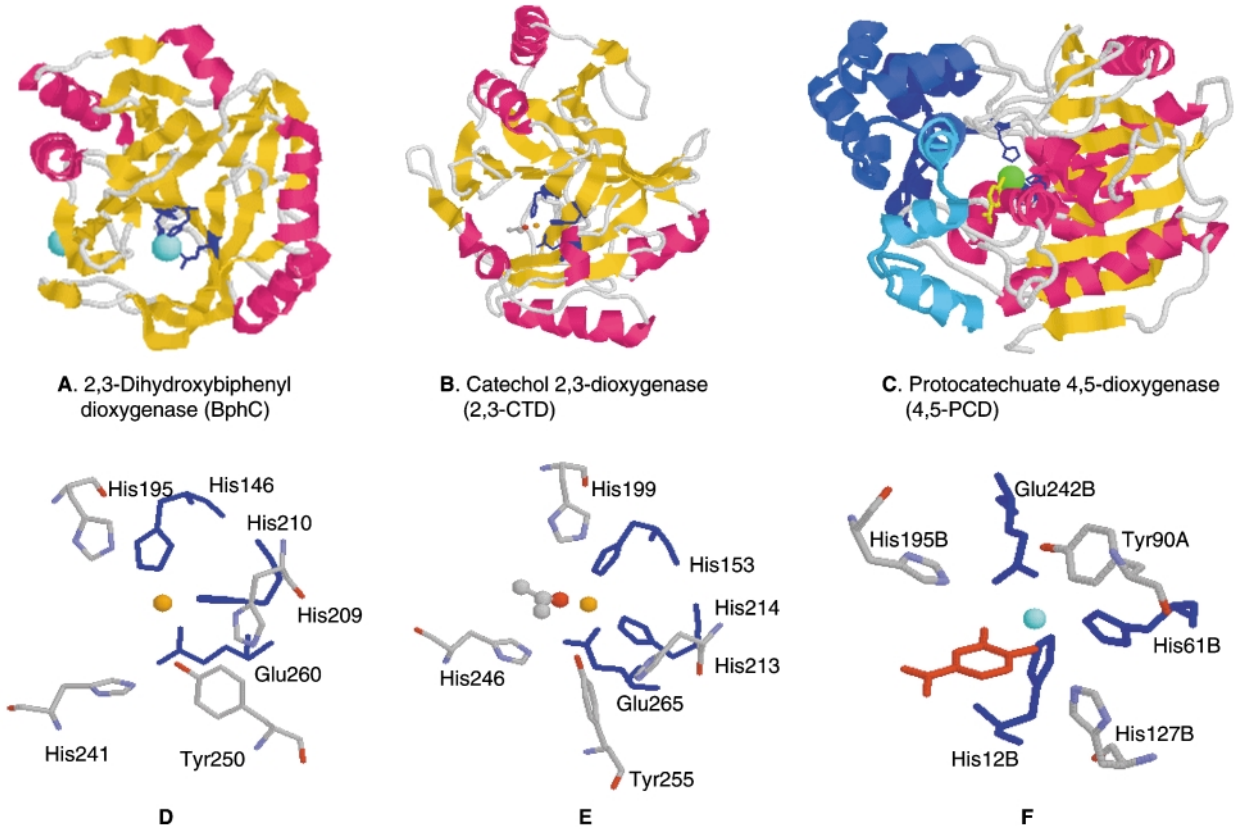

Fig. 2 X-Ray crystal structures of extradiol catechol dioxygenases. **A**. 2,3-Dihydroxybiphenyl 1,2-dioxygenase (BphC) from *Pseudomonas* LB400,[11] showing iron(II) cofactor and ligands (PDB accession number 1HAN). **B**. Catechol 2,3-dioxygenase (2,3-CTD) from *Pseudomonas putida mt-2*,[14] showing the iron(II) cofactor, ligands, and a molecule of acetone bound to the iron centre (PDB accession number 1MPY). **C**. Protocatechuate 4,5-dioxygenase (LigAB) from *Sphingomonas paucimobilis* SYK-6,[15] showing α and β subunits (α subunit in blue), iron(II) cofactor, ligands, and bound substrate (PDB accession number 1B4U). **D**. Active site of BphC,[11] showing iron(II) cofactor, ligands (in blue), and nearby active site residues. **E**. Active site of 2,3-CTD,[14] showing iron(II) cofactor, ligands (in blue), bound acetone molecule, and nearby active site residues. **F.** Active site of LigAB,[15] showing iron(II) cofactor, ligands (in blue), bound substrate protocatechuic acid (in red), and nearby active site residues.

dependent dioxygenases and isopenicillin N synthase.[12] The crystal structure of BphC from *Pseudomonas* KKS102 has also been solved with bound substrate, yielding a similar co-ordination geometry; however the crystallised form of the enzyme contains iron(III) rather than iron(II).[13]

The crystal structures of three other extradiol dioxygenases have now been solved. In 1998 Kita *et al.* reported the structure of catechol 2,3-dioxygenase from *Pseudomonas putida mt-2*, an α_4 tetramer.[14] The subunit structure is very similar to that of BphC, and the iron(II) cofactor is bound by His-153, His-214 and Glu-265 (see Fig. 2**B**,2**E**).[14] In 1999 Sugimoto *et al.* reported the structure of protocatechuate 4,5-dioxygenase from *Sphingomonas paucimobilis* SYK-6, which is composed of an $\alpha_2\beta_2$ tetramer.[15] This enzyme has no sequence similarity to BphC, yet the disposition of iron(II) ligands is very similar: the metal centre is co-ordinated by His-12, His-61 and Glu-242 (see Fig. 2**C**,2**F**).[15] In 2000 Titus *et al.* reported the structure of human homogentisate dioxygenase, a non-haem iron(II)-dependent dioxygenase involved in the mammalian degradation of L-phenylalanine and L-tyrosine.[16] This enzyme bears no sequence similarity to the bacterial extradiol catechol dioxygenases, yet its active site features are very similar: the iron(II) cofactor is bound by His-335, Glu-341 and His-371.[16]

Thus, the solution of several X-ray structures has shown that each family of catechol dioxygenases has a specific set of amino acid ligands for the non-haem iron cofactor. The iron(III) cofactor of the intradiol dioxygenases is ligated by two tyrosine residues and two histidine residues, whereas the iron(II) cofactor of the extradiol dioxygenases is ligated by two histidine residues and one glutamic acid residue. Yet how does this small difference in co-ordination chemistry relate to the choice of reaction pathway? The active site structures do not reveal obvious differences which would explain why one yields the intradiol cleavage product and the other the extradiol cleavage product.

Furthermore, recent structures of co-crystals of protocatechuate 3,4-dioxygenase have demonstrated that the axial tyrosine ligand, Tyr-447, swings away from the iron(III) centre upon binding of substrate analogues, leaving only three amino acid ligands for the iron(III) centre (see Fig. 1**E**).[17] The riddle of the intradiol *vs.* extradiol dioxygenases therefore becomes more intriguing: why Fe^{3+} and a His_2Tyr_2 motif (one of which appears to dissociate during the reaction) for intradiol cleavage, and why Fe^{2+} and a His_2Glu motif for extradiol cleavage?

Evidence for 1,2 (Criegee) rearrangements in the catechol dioxygenases

The catalytic mechanism proposed by Hayaishi involved the formation of a cyclohexadienone hydroperoxide in both the intradiol and extradiol dioxygenases, followed by the formation of a four-membered dioxetane ring.[4] Once formed, the strained dioxetane would readily undergo retro[2+2] cleavage to give the acyclic products, with complete incorporation of both atoms of oxygen from dioxygen (see Scheme 2). There was, however, some disquiet about this mechanism: the formation of dioxetanes was thought to be a highly endothermic process, and their breakdown should be accompanied by luminescence, which is not observed for the catechol dioxygenases.[18] Indeed, the only well-characterised example of a dioxetane intermediate in an enzyme-catalysed reaction was the firefly luciferase reaction, in which decomposition of a dioxetane intermediate yields the luminescence characteristic of the firefly.[19]

An alternative mechanism involves a 1,2-rearrangement of the intermediate hydroperoxide. It is well precedented that alkyl hydroperoxides can undergo migration of a carbon substituent onto the neighbouring electron-deficient oxygen, with loss of the second oxygen atom *via* heterolytic O–O cleavage (see Scheme 3). In the case of an alkyl hydroperoxide this is known as a Criegee rearrangement.[20] This type of 1,2-rearrangement is

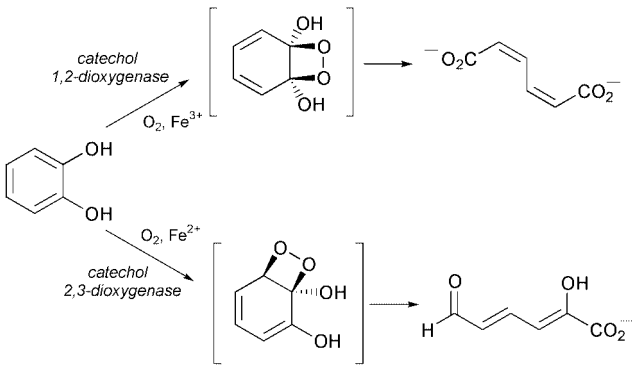

Scheme 2 Dioxetane intermediates proposed by Hayaishi for the catechol dioxygenases.

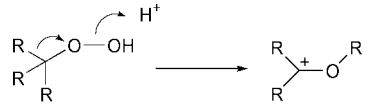

Scheme 3 1,2-Rearrangement of a hydroperoxide.

also commonly observed during the Baeyer–Villiger oxidation of ketones,[21] where an intermediate hydroperoxide is formed upon attack of hydrogen peroxide or a peracid on a ketone.

For intradiol cleavage, upon formation of a cyclohexadienyl hydroperoxide, migration of the adjacent acyl group (acyl migration) would yield muconic anhydride as an intermediate, which would undergo hydrolysis to give the product muconic acid. $^{18}O_2$ labelling studies on catechol 1,2-dioxygenase from *Pseudomonas arvilla* have revealed that the intradiol cleavage products contain 99% incorporation of a single atom of ^{18}O, and 74% incorporation of a second atom of ^{18}O, with 24% incorporation of only one atom of ^{18}O (see Scheme 4).[22] These

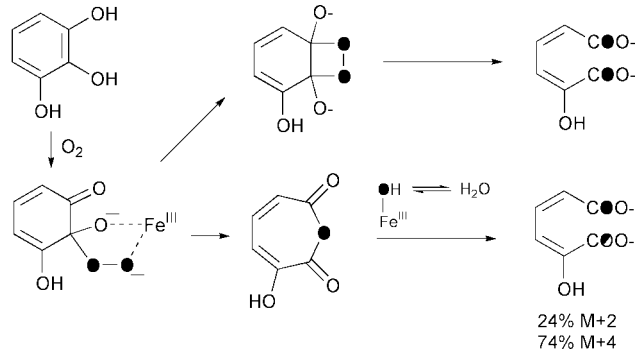

Scheme 4 $^{18}O_2$ labelling studies on the reaction of pyrogallol with catechol 1,2-dioxygenase from *Pseudomonas arvilla*.

data are not consistent with a dioxetane intermediate, but could be explained by a Creigee rearrangement to give an anhydride intermediate, followed by the partial exchange of the iron(III) ^{18}O-hydroxide with solvent water.[22] Interestingly, no single atom isotope incorporation is observed with the natural substrate catechol, implying a lack of exchange or a more efficient hydrolysis of the anhydride intermediate.[22] Model reactions for intradiol cleavage (see below) have in some cases yielded muconic anhydrides as reaction products, again consistent with a 1,2-rearrangement.

In the case of extradiol cleavage, there are two possible cyclohexadienyl hydroperoxides which could undergo 1,2-rearrangements. The first possibility is that proximal hydroperoxide (**1**) is formed, as for intradiol cleavage, which undergoes migration of the adjacent alkene (alkenyl migration) to give an α-keto-lactone intermediate, which then undergoes hydrolysis by iron(II) hydroxide to give 2-hydroxymuconate semi-aldehyde. The second possibility is that a distal hydro-

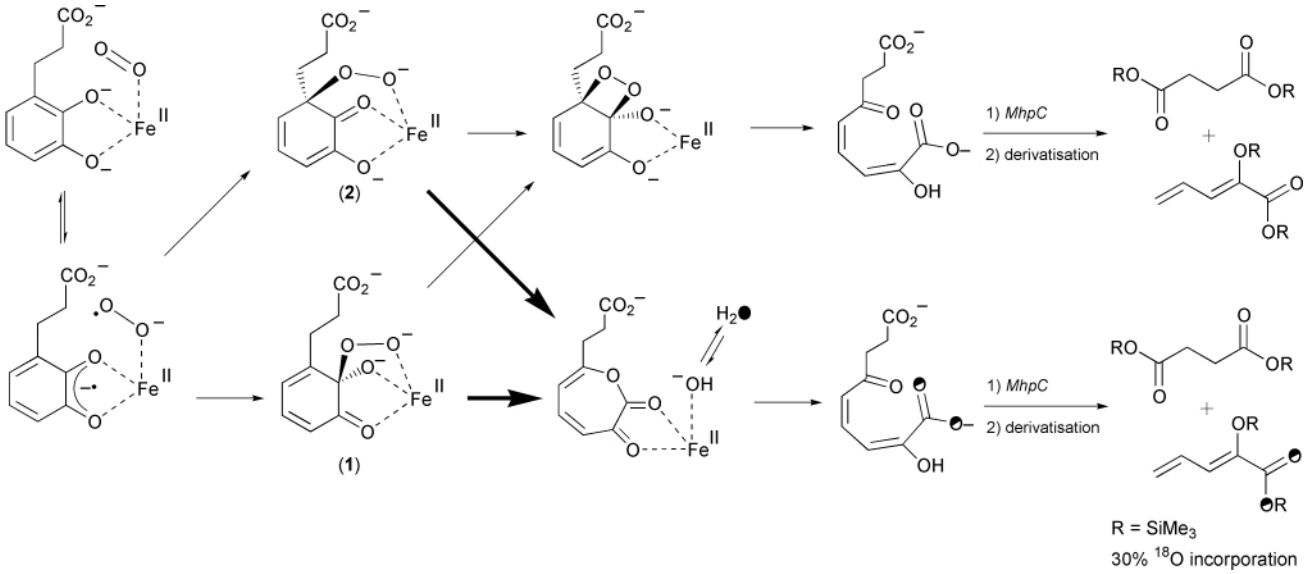

Scheme 5 Mechanistic schemes for MhpB-catalysed reaction showing ^{18}O labelling pattern.

peroxide (**2**) is formed, which undergoes 1,2-rearrangement *via* acyl migration to give the same α-keto-lactone intermediate (see Scheme 5). $^{18}O_2$ labelling studies carried out on *E. coli* 2,3-dihydroxyphenylpropionate 1,2-dioxygenase (MhpB) revealed that although both the acid and ketone carbonyls could be labelled with ^{18}O from $^{18}O_2$, upon reaction in $H_2{}^{18}O$ the carboxylate position was labelled to the extent of 30%, consistent with the formation of an α-keto lactone intermediate, and exchange of iron(II) hydroxide with solvent ^{18}O-labelled water (see Scheme 5).[23] The enzyme was also found to catalyse the hydrolysis of a saturated seven-membered lactone analogue (**3**; see Scheme 6).[23] These studies implicate a lactone intermediate arising from Criegee rearrangement in the extradiol cleavage reaction mechanism.

Thus, evidence from ^{18}O labelling experiments and model studies has revealed that both intradiol and extradiol cleavage reactions involve 1,2-rearrangements taking place on cyclohexadienyl hydroperoxide reaction intermediates, in close proximity to the non-haem iron cofactors.

Formation of cyclohexadienyl hydroperoxides *via* single electron transfers

The formation of cyclohexadienyl hydroperoxides is implicated in both intradiol and extradiol cleavage reactions from the studies discussed above. How are they formed? What are the differences between the Fe^{3+}-based intradiol reaction and the Fe^{2+}-based extradiol reaction?

There are several clues from known chemistry that single electron transfers may be involved in each case. First of all, it is well established that the triplet ground state of dioxygen is forbidden to react with paired-electron reagents, however it can react with radical species, and it can accept one electron from certain transition metal ions to form the much more reactive superoxide species.[24] Indeed, there are many examples of divalent transition metals (*e.g.* Fe^{II}, Co^{II}, Ir^{II}) which can form stable metal(III)-superoxide complexes upon reaction with dioxygen.[24] The next clue is that catechol readily undergoes single electron oxidation, *via* a stable semiquinone intermediate, to an *ortho*-quinone species (see Scheme 7). Thus, a redox-active metal such as iron could mediate one-electron transfers between catechol and dioxygen.

There are specific examples from transition metal chemistry which suggest that this may be the case. The X-ray crystal structure of a rhodium(III)–triphos–catecholate complex (**4**) with dioxygen synthesised by Bianchini *et al.* shows that dioxygen is bound as superoxide, and that catechol is bound as

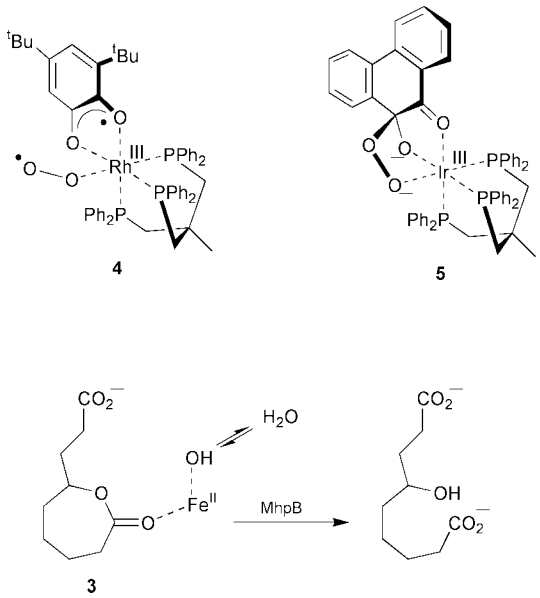

Scheme 6 Lactone hydrolysis catalysed by MhpB.

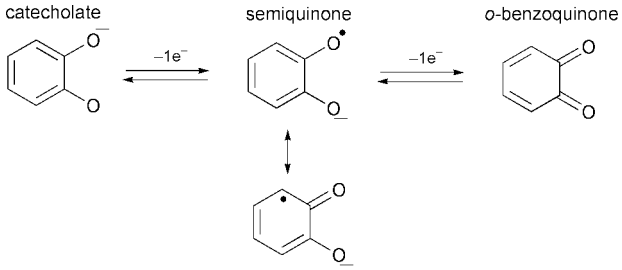

Scheme 7 Single electron oxidation of catechol.

its semiquinone.[25] This metal–semiquinone–superoxide complex could be formed by one-electron transfer from Rh^{III} to dioxygen, followed by one-electron transfer from catechol to Rh^{II}. The X-ray structure of the corresponding iridium(III) complex (**5**) shows a C–O bond formed between the catechol ring and dioxygen,[26] indicating that C–O bond formation between metal-bound semiquinone and metal-bound superoxide is feasible, to give a cyclohexadienyl hydroperoxide. A similar cyclohexadienyl hydroperoxide has been reported for a

Rh^{III} complex, formed by reaction of $Rh^{I}(PPh_3)_3Cl$ with 9,10-phenanthrenequinone.[27] One final clue for the involvement of superoxide is the existence of a model reaction for catechol cleavage involving treatment of catechol in DMSO with solid potassium superoxide, which gives a 5–10% yield of 2-hydroxymuconic semialdehyde, the extradiol cleavage product.[28]

EPR spectroscopic studies have shown that the iron(III) cofactor of the intradiol dioxygenase family ligates to the catechol hydroxy groups, by displacement of a bound water molecule; however no transient iron(II) intermediates are detectable during turnover.[29,30] EPR spectroscopic studies of the NO complex of the extradiol dioxygenase protocatechuate 4,5-dioxygenase have shown that the iron(II) cofactor binds both catecholic hydroxy groups, and binds NO; however no iron(III) intermediates could be detected during turnover.[31] Thus, EPR spectroscopy has provided no experimental evidence for the involvement of one-electron transfers in the catechol dioxygenase reactions. However, if the one-electron transfers were very fast, then no build-up of intermediates would be observable.

The existence of carbon-centred radicals in enzyme-catalysed reactions has been probed in several cases using 'radical trap' substrates containing a cyclopropyl group adjacent to the radical-bearing carbon atom.[32] Formation of the radical intermediate would then lead to an extremely rapid opening of the cyclopropane ring, yielding a new reaction product or leading to enzyme inactivation. A cyclopropyl-containing substrate analogue (**6**) was synthesised as a substrate for 2,3-dihydroxyphenylpropionate 1,2-dioxygenase (MhpB) from *E. coli*.[33] Both *cis*- and *trans*-substituted cyclopropyl analogues were found to be efficiently processed by the enzyme. However, when the products were analysed by further enzymatic degradation, it was found that isomerisation of the cyclopropyl ring substituents had occurred: processing of the *trans*-substituted substrate gave 94% *trans*-product and 6% *cis*-product; while processing of the *cis*-substituted substrate gave only 10% of the *cis*-product, and 90% of the *trans*-product (see Scheme 8). Having established that epimerisation *via* solvent exchange was not occurring, the only reasonable explanation of these results is that a radical-mediated reversible opening of the cyclopropyl ring is taking place.[33] Since the equilibrium position of ring-closed *vs.* ring-opened product is governed by the stability of ring-closed *vs.* ring-opened products, the reversible ring opening can be explained by the high stability of the initial semiquinone radical. These data provide some experimental evidence for a transient iron(II)–semiquinone–superoxide intermediate in the extradiol catechol dioxygenase reaction mechanism.

Evidence from model studies of intradiol cleavage also suggests the involvement of one-electron transfers. Analysis of a Fe^{III}tris(2-pyridylmethyl)amine complex (**7**), which showed high activity for intradiol catechol cleavage, by X-ray crystallography and ^{1}H NMR spectroscopy revealed a very strong iron–catecholate interaction, and increased semiquinone character in the bound substrate.[34,35] It was therefore proposed that formation of a transient Fe^{II}–semiquinone intermediate preceded reaction with dioxygen (see Scheme 9).[35] Since no

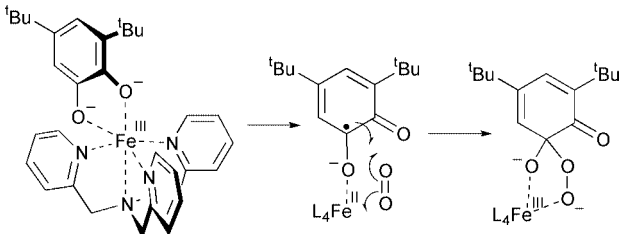

Scheme 9 Semiquinone activation proposed for intradiol cleavage.

binding of O_2 or NO to the iron(III) centre of the intradiol dioxygenases has been observed by EPR spectroscopy,[29,30] it is proposed that the iron(II)-bound semiquinone reacts directly with dioxygen, without prior binding of dioxygen to the iron centre.[35]

Thus, both intradiol and extradiol dioxygenases utilise single electron transfers to form a cyclohexadienyl hydroperoxide intermediate, although the order of steps is different in the two enzymes. In the extradiol dioxygenase active site single electron transfer from iron(II) to dioxygen is followed by single electron transfer from catechol to iron(III), to give a transient iron(II)–semiquinone–superoxide intermediate, which then undergoes C–O bond formation. In the intradiol dioxygenase active site single electron transfer from catechol to iron(III) gives an iron(II)-semiquinone intermediate which reacts directly with dioxygen to form the C–O bond. Both families make use of the

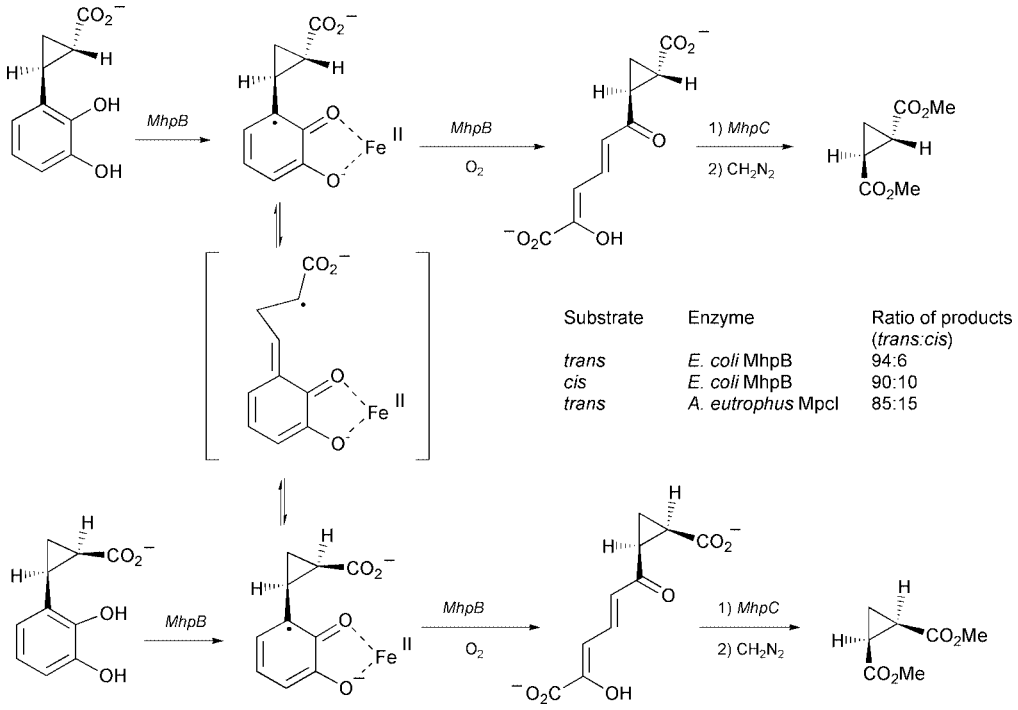

Scheme 8 *Cis–trans* isomerisation of a cyclopropyl radical trap (**6**) catalysed by extradiol dioxygenase MhpB.

single electron redox chemistry of iron and catechol, but *via* a different sequence.

Evidence for a proximal hydroperoxide in the extradiol catechol dioxygenases

Returning to the cyclohexadienyl hydroperoxide intermediate formed after the single electron redox chemistry described above, there is one important issue to be resolved. The extradiol cleavage mechanism could proceed *via* either of two possible cyclohexadienyl hydroperoxides (Scheme 5). As discussed in Section 3, either a proximal hydroperoxide could undergo alkenyl migration to give an α-keto-lactone, or a distal hydroperoxide could undergo acyl migration to give the same α-keto-lactone. Which is it?

Several pieces of circumstantial evidence favour the intermediacy of a proximal hydroperoxide, rather than a distal hydroperoxide. Inspection of models reveals that the geometry required to form the distal hydroperoxide is rather strained, and inspection of the X-ray structures of BphC also indicates that reaction at the proximal position of the substrate is more readily achievable than reaction at the distal position.[11,13] The iridium(III) model complex (**5**) containing a cyclohexadienyl hydroperoxide also exhibits a proximal hydroperoxide.[26]

More definitive evidence has been obtained for the extradiol dioxygenase 2,3-dihydroxyphenylpropionate 1,2-dioxygenase (MhpB) from *E. coli*. It was known from structure–activity relationships that MhpB would process substrates containing a diverse range of functional groups at the 3-position (*e.g.* alkyl, –CH=CHCO$_2$H, –OCH$_2$CO$_2$H) with comparable efficiency, which is hard to reconcile with the formation of a distal hydroperoxide at the 3-position.[33] A series of analogues of the proximal and distal hydroperoxides were synthesised, in which the –OOH functional group was replaced by –CH$_2$OH, and the cyclohexadienyl ring simplified to a cyclohexanone ring.[36] These 'carba' analogues are shown in Fig. 3. It was found that the carba analogue **7** of the distal hydroperoxide showed no inhibition of MhpB at 10 mM concentration. However, analogues **9** and **10** of the proximal hydroperoxide did show modest competitive inhibition of MhpB, with K_i values of 4.9 mM and 0.7 mM respectively. In contrast, the methyl-substituted analogue **8** showed no enzyme inhibition. Analysis by ^{1}H NMR spectroscopy revealed that in **9** and **10** the hydroxymethyl substituent is positioned in an axial oritentation with respect to the cyclohexanone ring, whereas in **8** the hydroxymethyl group was equatorial (see Fig. 3).[36] These data provided some experimental evidence in support of a proximal hydroperoxide, and furthermore indicated that the conformation adopted by the hydroperoxide was of importance, an axial hydroperoxide being required at the extradiol dioxygenase active site.

This result has an important consequence for the reaction mechanisms of both families of enzyme, namely that both reactions converge on the same proximal cyclohexadienyl hydroperoxide intermediate (see Fig. 4). In the case of the intradiol dioxygenases, this intermediate undergoes acyl migration to give a muconic anhydride, whereas in the extradiol dioxygenases the proximal hydroperoxide undergoes alkenyl migration to give an α-keto-lactone. Therefore, in spite of the differences in the early steps of the reaction mechanism, the inescapable conclusion is that the choice of intradiol *vs.* extradiol reaction pathways is controlled by the choice of acyl *vs.* alkenyl migration of a reactive proximal hydroperoxide intermediate. How might this choice of 1,2-rearrangements be controlled?

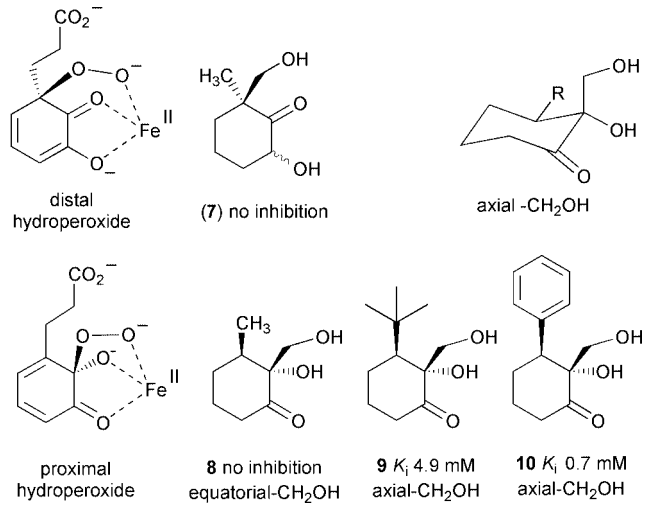

Fig. 3 Carba analogues of proximal and distal hydroperoxide reaction intermediates, tested as inhibitors for 2,3-dihydroxyphenylpropionate 1,2-dioxygenase (MhpB) from *Escherichia coli*.[36]

Acyl *vs.* alkenyl migration in hydroperoxide rearrangements

In order to address the question of acyl *vs.* alkenyl migration, we must first look at examples of hydroperoxide rearrangements in organic chemistry. This section will describe instructive examples from Criegee rearrangments and Baeyer–Villiger oxidations.

The first example which provides a good model for the desired proximal hydroperoxide occurs in the Baeyer–Villiger oxidation of 1,2-diketones, in which anhydride products are formed in a range of examples.[21] Thus, upon attack of peroxide or a peracid upon one ketone centre, an intermediate α-ketohydroperoxide is formed, which undergoes acyl migration (see Scheme 10). This example provides clear precedent for the acyl migration step of intradiol cleavage, to give an anhydride

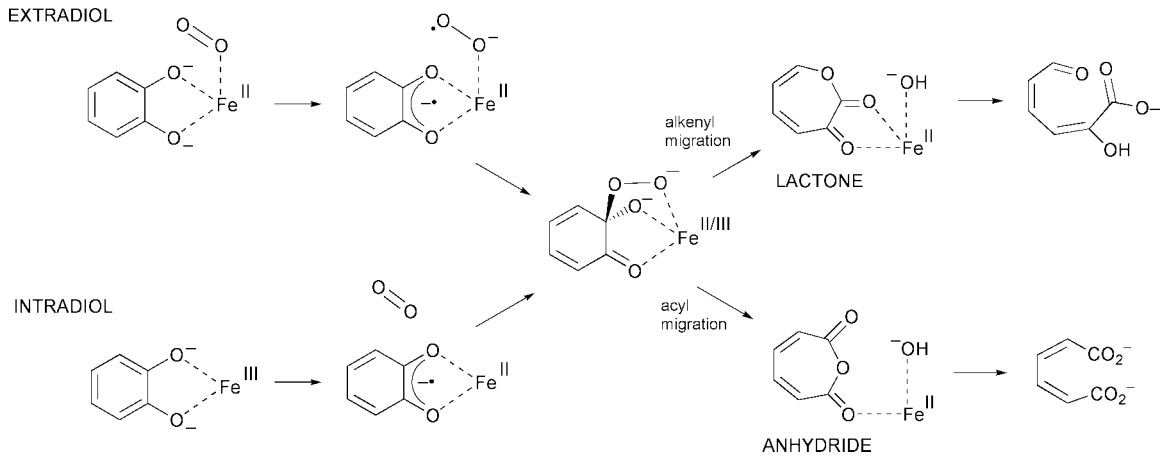

Fig. 4 Proposed mechanistic convergence of the catalytic mechanisms of the extradiol and intradiol catechol dioxygenases onto a common proximal hydroperoxide intermediate, and their divergence *via* alkenyl or acyl migration to give extradiol or intradiol reaction products.

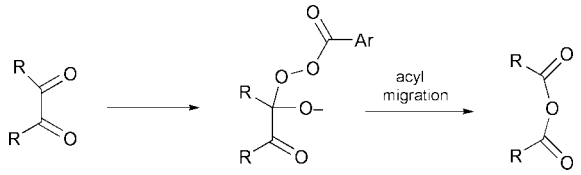

Scheme 10 Baeyer–Villiger oxidation of 1,2-diketones.

product. However, the mechanism of acyl migration may not be as straightforward as it seems. Baeyer–Villiger oxidation of ^{17}O-labelled benzil gave anhydride product containing ^{17}O in the bridging position, not consistent with a direct migration of an acyl group (see Scheme 11).[37] A mechanism was proposed

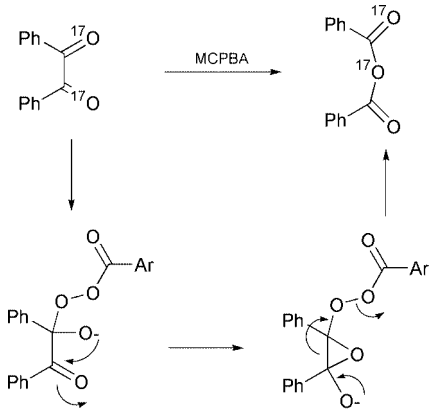

Scheme 11 Epoxide mechanism proposed for Bayer–Villiger oxidation of benzil.

involving attack of the alkoxide ion upon the adjacent ketone, to form a 1,2-epoxide, followed by C–C fragmentation to give the anhydride product (see Scheme 11).[37] It is known that the presence of electron-withdrawing groups reduces migratory aptitude in Baeyer–Villiger oxidations,[38] therefore the facile migration of an electron-deficient acyl group in this case could be rationalised by this alternative mechanism.

One recent observation suggests that such a mechanism might operate in the acyl migration of cyclohexadienyl hydroperoxides. Treatment of 6-alkyl-6-acetoxycyclohexa-2,4-dienones with carbonate buffer in water–methanol leads to a rapid C–C cleavage reaction, resulting in the production of acyclic esters (see Scheme 12). Studies of the mechanism of this

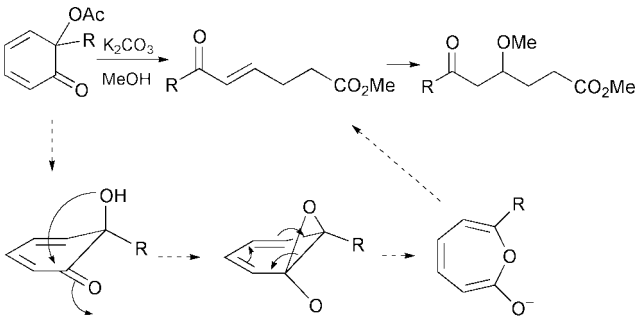

Scheme 12 Solvolytic C–C cleavage of 6-alkyl-6-acetoxycyclohexadienones (R = CH_3, Ph).

C–C cleavage reaction indicate that hydrolysis of the acetyl group is essential for ring cleavage, hence that a mechanism involving attack of the tertiary alcohol on the adjacent ketone, followed by a benzene oxide–oxepin interconversion, may mediate ring cleavage in this system (see Scheme 12). This mechanism provides an alternative pathway for acyl migration in the intradiol dioxygenase reaction.[39]

Recent work by Goodman and Kishi provides clear examples of alkenyl migration: treatment of a cyclohexenyl hydroperoxide with trifluoroacetic anhydride yields products arising from alkenyl migration in preference to alkyl migration (see Scheme 13A).[40] In cases where the hydroperoxide group is positioned on a bicyclic carbon skeleton, as shown in Scheme 13B, the choice of migrating group is determined by stereoelec-

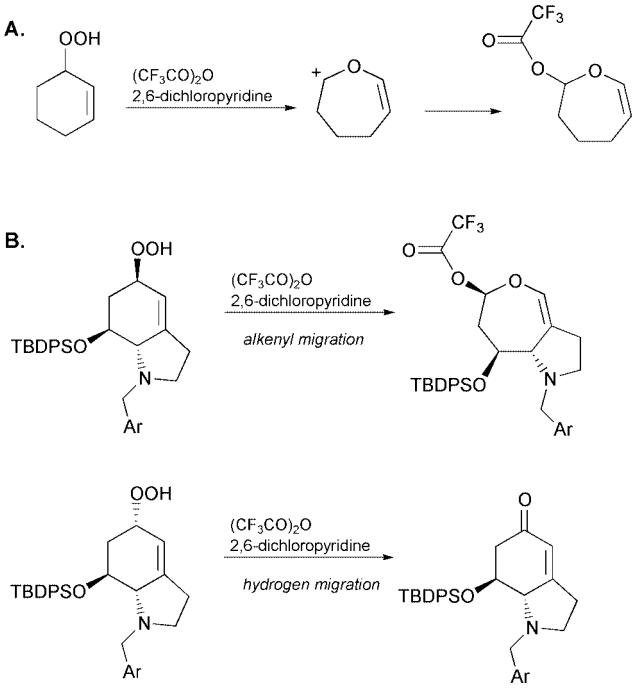

Scheme 13 Alkenyl migration of a cyclohexyl hydroperoxides.

tronic factors: the group which preferentially migrates is the one which is positioned anti-periplanar to the O–O bond which is being broken,[40] as one might expect from stereoelectronic arguments.[41]

This idea provides an attractive rationalisation of the results obtained using the carba-analogues of proximal hydroperoxide intermediates in the MhpB-catalysed reaction.[36] If the hydroperoxide functional group is positioned axially with respect to the cyclohexadienone ring, and is ligated to the iron(II) centre, then the O–O bond will be aligned in an antiperiplanar geometry with the C–C bond to the neighbouring alkenyl group which migrates in the extradiol reaction (see Fig. 5A). Thus, one factor

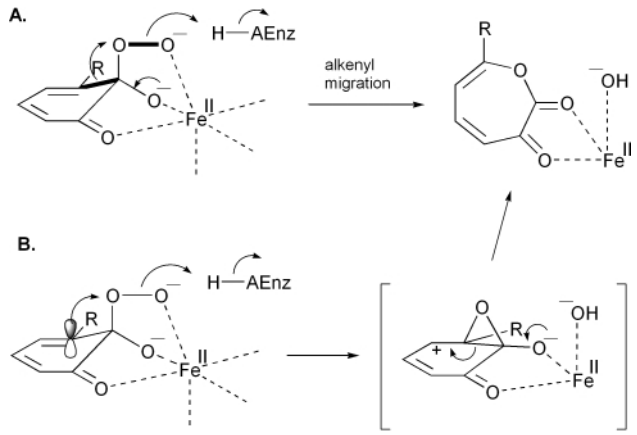

Fig. 5 Two possible mechanisms for alkenyl migration in the extradiol dioxygenase reaction pathway. **A**. σ bond migration of an axial hydroperoxide. **B**. π participation mechanism.

which could control the acyl *vs.* alkenyl migration of a common hydroperoxide intermediate is the conformation of the bound intermediate and hence precise positioning of the O–O bond.

Further reactions of alkenyl hydroperoxides provide an alternative mechanism for alkenyl migration. Nishinaga *et al.* have reported that treatment of a tributyl-substituted cyclohexadienone hydroperoxide with acetyl chloride–pyridine leads to the formation of two epoxides (see Scheme 14).[42] These

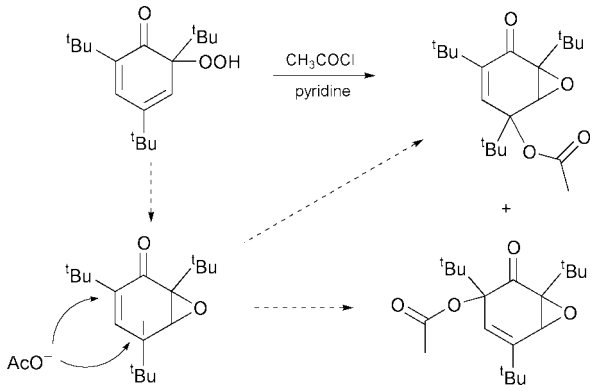

Scheme 14 Epoxide formation in cyclohexadienyl hydroperoxide rearrangement.

epoxides could be formed by nucleophilic participation of the neighbouring alkene to form an epoxide intermediate containing an allylic carbocation, which could be quenched by acetate. Note that in this case the *tert*-butyl substituent will ensure that the hydroperoxide is held axially with respect to the ring, which would bring the hydroperoxide in close proximity to the π system of the neighbouring diene. Further examples of the reaction of polyunsaturated fatty acid hydroperoxides to form epoxides have also been reported by Corey *et al.* (see Scheme 15).[43,44] Again an adjacent diene is present, so that the intermediate carbocation arising from nucleophilic participation would be a stabilised allylic carbocation.

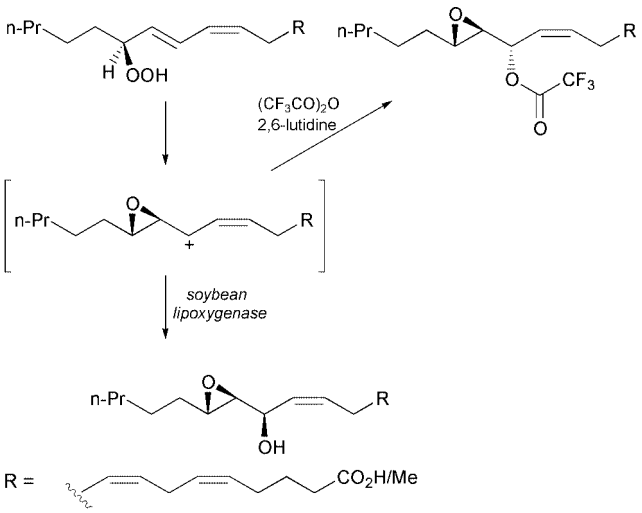

Scheme 15 Epoxide formation in polyunsaturated fatty acid hydroperoxide rearrangement.

This π participation mechanism could be applied to the alkenyl migration step of the extradiol reaction pathway.[36] If the hydroperoxide functional group is held axially with respect to the cyclohexadienone ring, then the π system of the diene would overlap with the σ* orbital of the O–O bond, leading to the formation of a transient epoxide species bearing an adjacent allylic carbocation, which would rapidly undergo C–C fragmentation to give the α-keto-lactone (see Fig. 5B). Thus, there are two subtly different mechanisms for alkenyl migration of an axial proximal hydroperoxide: either σ bond migration of an antiperiplanar alkenyl group, or π participation of the adjacent diene.

In conclusion, there are literature examples of both acyl migration and alkenyl migration in hydroperoxide 1,2-rearrangements in organic chemistry. The control of migratory group *via* stereoelectronic factors would provide an attractive means by which an enzyme active site might dictate intradiol *vs.* extradiol cleavage. However, the examples in this Section lack one crucial feature of the enzyme-catalysed reactions: the proximity of the non-haem iron centre, whose effects upon intradiol *vs.* extradiol cleavage will be discussed next.

Transition metal-based model reactions for oxidative catechol cleavage

Since the discovery of the catechol dioxygenases, many attempts have been made to mimic these reactions non-enzymatically. The intriguing iron cofactor specificity of the catechol dioxygenase suggested that the iron cofactor played a major role in the active site chemistry, hence most attempts have involved metal ion complexes of catechol substrates. Does the character of the iron centre control the choice of cleavage pathways?

Model systems for intradiol cleavage

The first model system for intradiol cleavage was an Fe^{III}–nitrilotriacetate complex **11**, which was reported to convert 3,5-di-*tert*-butylcatechol catalytically over a period of 4 days in the presence of oxygen to give the furanone derivative **12** in 80% yield.[45,46] An X-ray crystal structure of this complex showed the catechol substrate bound in bidentate fashion, with the geometry around the central Fe^{III} close to octahedral.[46] Labelling studies with $^{18}O_2$ on this system revealed the incorporation of one atom of $^{18}O_2$ into furanone **12**, consistent with the existence of an anhydride intermediate as shown in Scheme 16.[46]

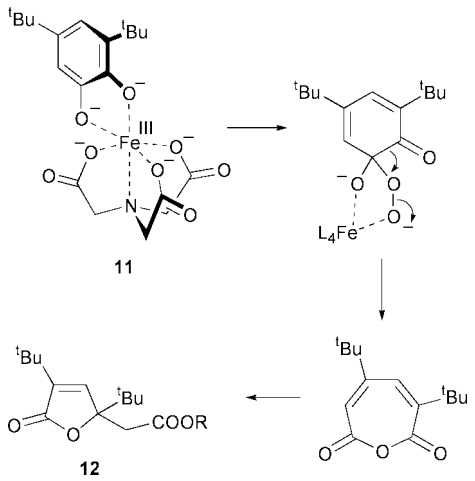

Scheme 16 Intradiol cleavage catalysed by Fe^{III}(NTA) complex **11**.

Subsequent studies using a range of iron(III) complexes showed a correlation between the reactivity of the Fe^{III}–ligand system and the Lewis acidity of the metal centre, which could be quantitatively assessed by measuring the redox potential for the catechol-to-semiquinone oxidation.[47] Of the complexes studied, the Fe^{III}–nitrilotriacetate complex **11** showed the highest reactivity, and the highest redox potential of +59 mV (and hence the highest affinity of the catechol ligand for the Fe^{III} centre).[47]

Further studies by Que and co-workers led to the discovery of more reactive Fe^{III} complexes,[34,35] the most active of which was Fe^{III}–tris(2-pyridylmethyl)amine **13**. This complex was found to react with dioxygen within minutes to form furanone **12** in 98% yield, at a rate of 15 M^{-1} s^{-1}, approximately 1000-fold faster than complex **11**. Analysis of complex **13** by X-ray crystallography and ^{1}H-NMR spectroscopy revealed a very strong iron–catecholate interaction, and increased semiquinone character in the bound substrate. It was therefore proposed that formation of a transient Fe^{II}–semiquinone intermediate preceded reaction with dioxygen, as shown previously in Scheme 9. Each of these tetradentate ligands **13**–**16**, when complexed to Fe^{III}, showed activity for intradiol cleavage, revealing that two easily accessible *cis* coordination sites are needed for coordination of the catecholate ligand and its subsequent reaction with dioxygen. The order of reactivity of the coordinated 3,5-di-*tert*-butylcatecholate ligand $(dbc)^{2-}$ was in the order $[Fe(\mathbf{13})(dbc)]^+$ > $[Fe(\mathbf{14})(dbc)]^+$ > $[Fe(\mathbf{15})(dbc)]^+$ > $[Fe(\mathbf{16})(dbc)]^+$, and is correlated to the Lewis acidity of the iron(III) centre.[34,35,45]

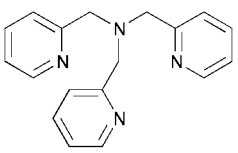

(**13**;TPA)

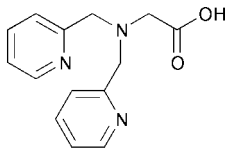

(**14**;BPG)

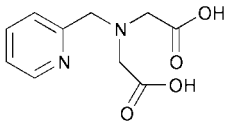

(**15**;PDA)

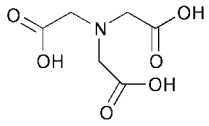

(**16**;NTA)

Girerd and co-workers have investigated the structures and reactivity of Fe^{III} complexes of **17**–**20** with 3,5-di-*tert*-butylcatechol, which all formed [Fe(L)(dbsq)] complexes with

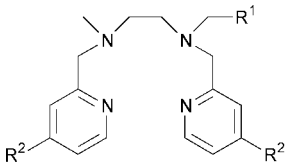

17 R^1 = H, R^2 = H
18 R^1 = H, R^2 = Cl
19 R^1 = 2-pyridyl, R^2 = H

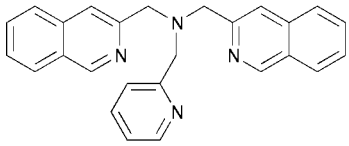

20

significant semiquinone character.[48] Reactivity for intradiol cleavage was found to correlate inversely with the λ_{max} value, the order of reactivity being **13** (874 nm) > **17** (935 nm) > **18** (941 nm) > **19** (957 nm).[48]

In most studies, 3,5-di-*tert*-butylcatechol has been used as a model substrate in functional investigations, however Krebs and co-workers have reported studies of iron(III) complexes of bis[(2-pyridyl)methyl][(1-methylimidazole-2-yl)methyl]amine **21** with a series of catechols.[49] The position of the ligand-metal

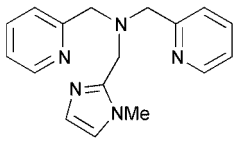

21

charge-transfer (LMCT) bands were observed to shift to lower energies by varying the substituents on the catecholate from electron-withdrawing to electron-donating. The reaction with dioxygen exhibits pseudo-first-order kinetics, and the order of activity correlates with the energy of the lower energy LMCT band of the complexes: electron-donating substituents on the catechol result in a higher dioxygenase activity.[49]

Palaniandavar *et al*. have studied a series of iron(III) complexes of tetradentate tripodal ligands **22**–**24**, and found that not only the phenolate-to-iron(III) charge transfer band but also the L^{2-}/dbc^{2-} to Fe^{III} charge transfer band is remarkably sensitive to the primary ligand environment.[50] The simultaneous appearance of the dbc^{2-} to Fe^{III} charge transfer band, the dbsq/dbc redox wave, and the lowering of the Fe^{III}/Fe^{II} redox potential on adding $dbcH_2$, even in the absence of added base, demonstrate the spontaneous deprotonation of the catechol substrate on binding to iron(III). Thus it is suggested that one function of the iron(III) center is to promote the loss of both protons of the substrate.[50]

Attempts to mimic the ligating abilities of histidine in the active site of the enzyme have been reported, by introducing benzimidazole moieties into a tripodal ligand.[51] Ligands **25**,**26** showed intradiol cleaving activity when complexed to Fe^{III}, the

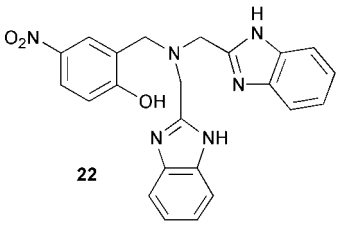

22

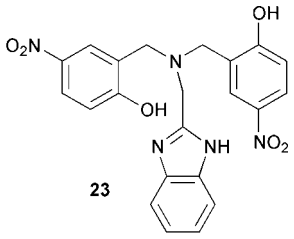

23

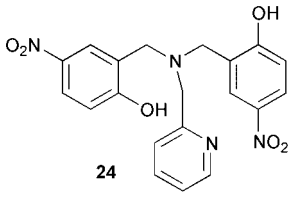

24

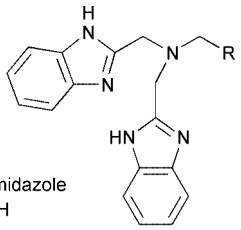

25 R = benzimidazole
26 R = CH_2OH

reaction rate depending on the steric and electronic properties of the coordinating ligand moieties.[51] Funabiki *et al*. have reported the first example of the oxidative cleavage of 3- and 4-chlorocatechols with dioxygen by an Fe^{III}(tpa) complex.[52] 4-Chlorocatechol was oxygenated at 25 °C in acetonitrile under an oxygen atmosphere by the iron complex prepared *in situ* by mixing $FeCl_3$ and tris(2-pyridylmethyl)amine (tpa), giving rise to intradiol cleavage products as shown in Scheme 17.[52]

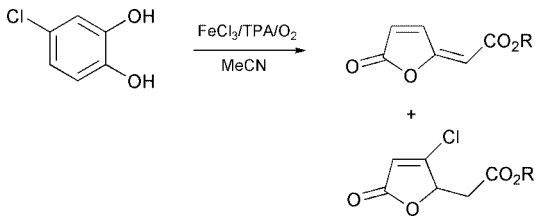

Scheme 17

Finally, Kruger *et al*. have reported a highly reactive and catalytically active model system by using *N*,*N*′-dimethyl-2,11-diaza[3,3](2,6)pyridinophane (**27**, L-N_4Me_2) as a macro-

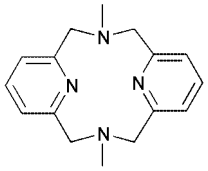

27

cyclic ligand.[53] For catalytic reaction, two equivalents of a base are needed per iron(III). With 1% of the iron(III) catalyst, a yield of 54% of muconic anhydride was obtained after a reaction time of 30 h.[53]

In summary, intradiol cleavage activity is observed with a number of tetradentate nitrogen ligands, complexed to Fe^{III}. High activity is correlated with Lewis acidity of the Fe^{III} centre, and semiquinone character of the bound catechol substrate. The tetradentate co-ordination geometry of these systems parallels the tetradentate Fe^{III} co-ordination state in the intradiol dioxygenase active sites (see Fig. 1).

Model systems for extradiol cleavage

Although most of model reactions for catechol oxidative cleavage perform intradiol cleavage, there are a few examples of oxidative cleavage by synthetic iron complexes to give 2-pyrone products which are believed to be of extradiol origin, although they are lacking one carbon atom. Funabiki *et al.* found that $FeCl_2/FeCl_3$ complexes with bipyridine/pyridine prepared *in situ* cleave 3,5-di-*tert*-butylcatechol to give a mixture of 2-pyrones, which incorporate ^{18}O label from $^{18}O_2$.[54] The 2-pyrones are proposed to derive from decarbonylation of the α-keto-lactone extradiol cleavage intermediate.[54]

Dei *et al*. found that the complex [Fe^{II}(TACN)(dbc)]Cl (**28**) yielded 2-pyrones upon exposure to O_2 in 35% yield (see Scheme 18).[55] Que *et al*. used the same complex to give an

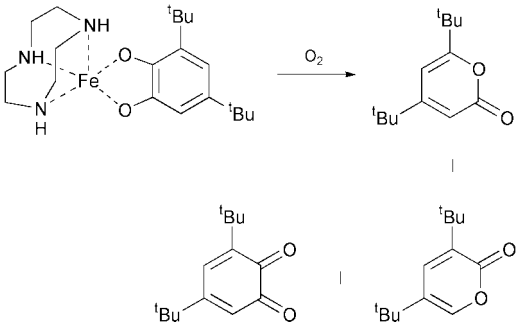

Scheme 18

almost quantitative yield of 2-pyrones using a modified procedure with additional base/ligand in favor of extradiol cleavage.[56] Moro-oka *et al*. found that oxygenation of the square pyramidal complex [Fe^{III}(hydrotris(3,5-diisopropyl-1-pyrazoyl)borate)(dbc)]Cl (**29**) results in the formation of 2-pyrones and an intradiol-derived anhydride (see Scheme 19).[57] They report that a related complex which adopts a

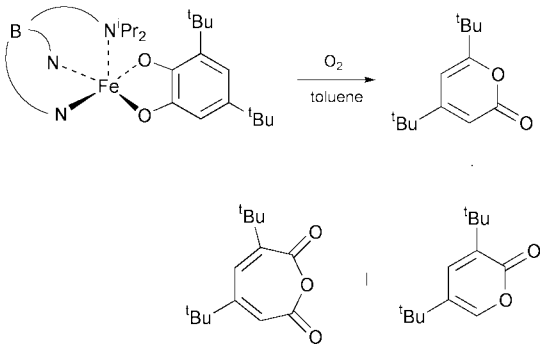

Scheme 19

trigonal bipyramidal geometry gives no 2-pyrone products, therefore a vacant co-ordination site appears to be required for oxygen activation.[57]

We have reported that the oxygenation of catechol by O_2 in the presence of $FeCl_2$ or $FeCl_3$, 1,4,9-triazacyclononane (TACN), and pyridine in methanol gives the authentic extradiol product 2-hydroxymuconic semi-aldehyde methyl ester in 50% yield.[58] In this model system $FeCl_2$–TACN shows higher selectivity for extradiol:intradiol cleavage (7 : 1) compared with $FeCl_3$–TACN (2 : 1), as shown in Scheme 20. Extradiol cleavage is only observed with the facial N_3-tridentate ligand TACN, and not with N,O-macrocycles, nor with N-substituted TACN macrocycles. We have found that this model reaction is highly regioselective for proximal 2,3-extradiol cleavage over distal 1,6-extradiol cleavage when using 3-methylcatechol (35 : 1), or 4-methylcatechol (> 99), or 3-(2,3-dihydroxyphenyl)propionic acid (> 99 : 1) as substrates.[59] The reaction proceeds in the absence of pyridine using monosodium

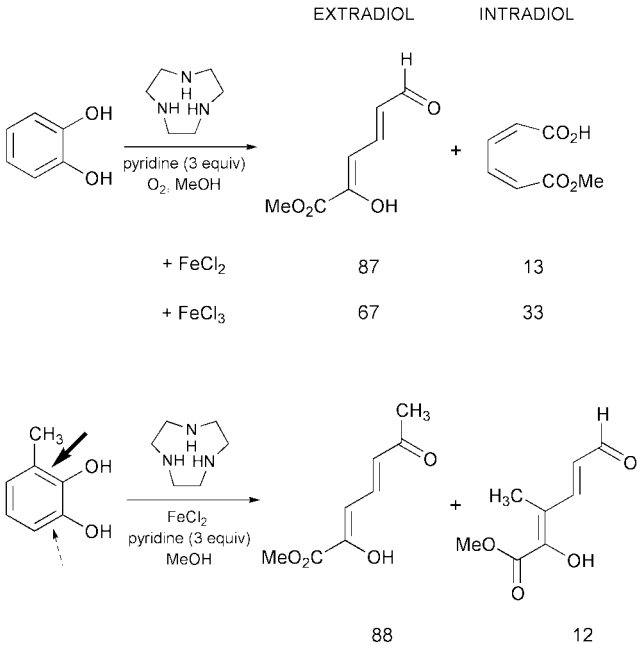

Scheme 20 $FeCl_2$–TACN model reaction for extradiol cleavage.

catecholate, but not disodium catecholate, implying that catechol binds to the iron centre as the monoanion,[59] the same conclusion reached from EXAFS studies on the 2,3-CTD–catechol complex.[60]

Studies of the mechanism of the $FeCl_2$–TACN model reaction have shown that the role of pyridine is two-fold: one equivalent of pyridine is required as a base to generate catechol monoanion, but one equivalent of pyridinium chloride is subsequently required as a proton donor to assist the Criegee rearrangement for extradiol cleavage.[59] Cleavage in the presence of methanol, ethanol or isopropanol yields the respective various alkyl esters of 2-hydroxymuconic semialdehyde, implying the intermediacy of a 7-membered α-keto-lactone, as for the enzymatic reaction.[59] The close similarities of regioselectivity and substrate selectivity between this model reaction and the *E. coli* MhpB-catalysed enzymatic reaction suggest that they follow a similar mechanism.

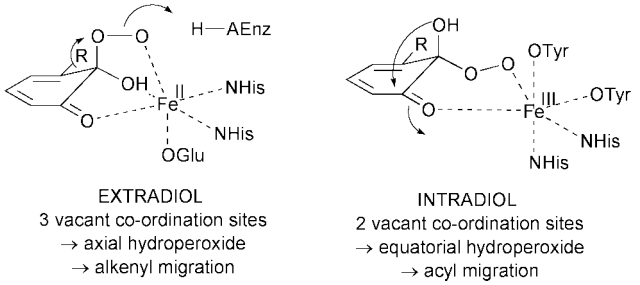

Scheme 21 Axial/equatorial hypothesis for extradiol/intradiol dioxygenase selectivity.

In summary, model systems for extradiol cleavage have proved more elusive, but extradiol cleavage is observed for a tridentate macrocyclic ligand, complexed with Fe^{II}, which shows high selectivity and appears to follow the same mechanism as the enzyme-catalysed reaction. It is interesting to note that both Fe^{II} and Fe^{III} are capable of extradiol cleavage in this system, but that Fe^{II} shows higher rate and selectivity, providing some insight into why Fe^{II} is found as the cofactor in the extradiol dioxygenases. The two-fold role of pyridine in this model reaction also suggests a role for an active site base, and a proton donor, in the extradiol dioxygenase active sites. All of the extradiol dioxygenases which have been structurally elucidated have, as well as the iron(II) ligands, an additional histidine residue near to the substrate binding site, and a

tyrosine–histidine pair which could function as a proton donor (see Fig. 2).

A hypothesis for extradiol *vs*. intradiol selectivity

At this point the reader will see that the choice of intradiol *vs*. extradiol reaction pathway will be influenced strongly by the co-ordination chemistry of the metal centre, but that the choice of acyl *vs*. alkenyl migration which ultimately dictates the reaction products will also be influenced by stereoelectronic factors, notably the positioning of the hydroperoxide O–O bond. In this section we will present a hypothesis which may rationalise the selectivity shown by the extradiol and intradiol dioxygenases using a stereochemical model.

In Section 5 we reached the important conclusion that, although there is a different order of initial events in the intradiol *vs*. extradiol reaction mechanisms, the two reaction mechanisms converge on a common proximal hydroperoxide intermediate. The choice of intradiol *vs*. extradiol reaction pathways is then determined by acyl *vs*. alkenyl migration rearrangements of this hydroperoxide intermediate. In Section 6 we saw that there is chemical precedent for both acyl migration and alkenyl migration, but that the choice of migratory group may be governed by stereoelectronic factors. In Section 7 we saw that the co-ordination chemistry of the metal centre is also important for choice of reaction pathway: tetradentate iron(III) complexes are effective catalysts for intradiol cleavage, but that the more elusive extradiol cleavage reaction can be catalysed by a facial tridentate iron(II) complex. These co-ordination states mimic the situation observed in the respective dioxygenase active sites.

Our hypothesis to rationalise these observations is that there are two stable conformations for the proximal hydroperoxide intermediate: one in which the hydroperoxide group is situated in a pseudo-axial orientation, and one in which the hydroperoxide is situated in a pseudo-equatorial orientation. In the extradiol dioxygenase active site the His_2Glu motif provides three protein ligands for iron(II) (as found in the TACN model reaction). Assuming that the iron(II) centre can access an octahedral co-ordination geometry during the catalytic cycle, then it is able to bind substrates and reaction intermediates *via* three co-ordination sites. It is therefore able to bind the proximal hydroperoxide intermediate in a tridentate fashion, and hence access the conformation in which hydroperoxide is pseudo-axial. In this conformation the hydroperoxide group is optimally aligned for alkenyl migration (*via* either σ bond migration or π participation) and hence undergoes extradiol cleavage.

In the intradiol dioxygenase active site the His_2Tyr_2 motif provides four protein ligands for iron(III) (as found in the tetradentate iron(III) models). Assuming that the iron(III) centre can access an octahedral co-ordination geometry during the catalytic cycle, then it is able to bind substrates and reaction intermediates *via* only two co-ordination sites. Bidentate co-ordination of the proximal hydroperoxide is not able to access the pseudo-axial hydroperoxide conformation, but instead binds as the pseudo-equatorial conformation, which then undergoes acyl migration. Why should an equatorial hydroperoxide promote acyl migration? One argument is that acyl migration is the 'default' option, as shown by the Baeyer–Villiger oxidation of 1,2-diketones. Alternatively, the axial hydroxy group is well positioned to attack the neighbouring ketone, which could initiate acyl migration *via* electrocyclic ring opening.[39]

The weakness in this argument in the latter case is that the axial tyrosine ligand (Tyr-447) of 3,4-PCD has been shown to swing away from the iron(III) centre upon substrate binding, leaving only three protein ligands.[17] However, presumably Tyr-447 is re-ligated to the iron(III) centre at the end of the catalytic cycle, so it is not clear whether it remains dissociated from the iron(III) centre throughout the reaction cycle, or becomes re-attached at some point. The observation that the majority of intradiol catalysts are tetradentate iron(III) complexes suggests that the availability of only two co-ordination sites may be a feature of the intradiol reaction.

Would this model explain the other amino acid sidechains found in the extradiol and intradiol active sites? Studies of the TACN extradiol model reaction imply a requirement for one base for substrate ligation, and one proton donor to assist alkenyl migration. In each of the extradiol active sites (see Fig. 2) there is a nearby histidine residue which could function as a base (His195 in BphC is situated 4.0 Å from the iron(II) centre),

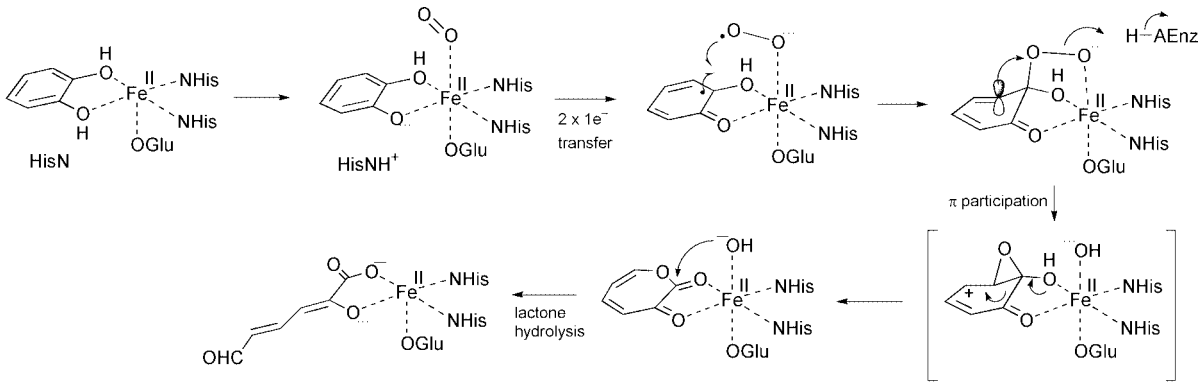

Fig. 6 Proposed catalytic mechanism for extradiol catechol cleavage, *via* an axial proximal hydroperoxide intermediate.

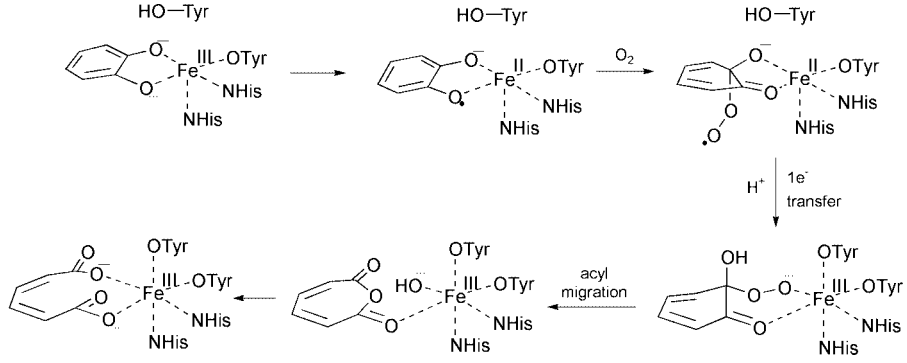

Fig. 7 Proposed catalytic mechanism for intradiol catechol cleavage, *via* an equatorial proximal hydroperoxide intermediate.

and also a nearby tyrosine–histidine pair which could function as a proton donor (Tyr250 in BphC is situated 3.8 Å from the iron(II) centre, with nearby His-241). The active sites of 3,4-PCD and 1,2-CTD (see Fig. 1) are, apart from the iron(III) ligands, notable for the absence of acid/base or polar amino acid sidechains, suggesting that the intradiol reaction requires relatively little catalytic assistance by the enzyme, consistent with the observation that a wide variety of tetradentate model systems are able to catalyse intradiol cleavage.

The overall catalytic mechanisms proposed for extradiol and intradiol cleavage are shown in Fig. 6 and 7. For extradiol cleavage, an active site base is required to generate the catechol mono-anion, and a proton donor is required to assist alkenyl migration. The iron(II) centre is able to activate both catechol and dioxygen, mediate one-electron transfers, assist alkenyl migration *via* Lewis acid catalysis, and activate Fe^{II}-hydroxide for lactone hydrolysis. For intradiol cleavage, substrate deprotonation appears to be driven by the stronger Lewis acidity of iron(III), which then activates the substrate for reaction with dioxygen, then mediates acyl migration, and assists hydrolysis of muconic anhydride. Both families of enzyme demonstrate the range of chemical functions carried out by non-haem iron in enzyme catalysis. A combination of mechanistic enzymology and small molecule model studies, in combination with protein crystallography, are now beginning to provide a rationalisation of how Nature has evolved two catalytic strategies for this difficult transformation, and the subtle chemical factors which control the choice of reaction pathway.

Acknowledgements

Studies in the author's laboratory have been supported by BBSRC and AstraZeneca Pharmaceuticals.

References

1 'Bioinorganic Enzymology', *Chem. Rev.*, whole issue (no. 7), 1996, **96**, 2237.
2 For a previous review of the catechol dioxygenases see: T. D. H. Bugg and C. J. Winfield, *Nat. Prod. Rep.*, 1998, **15**, 513; L. Que, Jr. and R. Y. N. Ho, *Chem. Rev.*, 1996, **96**, 2607.
3 S. Dagley, *Essays Biochem.*, 1975, **11**, 81.
4 O. Hayaishi, M. Katagiri and S. Rothberg, *J. Am. Chem. Soc.*, 1955, **77**, 5450.
5 Y. Kojima, N. Itada and O. Hayaishi, *J. Biol. Chem.*, 1961, **236**, 2223.
6 O. Hayaishi, *Bacteriol. Rev.*, 1966, **30**, 720.
7 D. H. Ohlendorf, J. D. Lipscomb and P. C. Weber, *Nature*, 1988, **336**, 403.
8 D. H. Ohlendorf, A. M. Orville and J. D. Lipscomb, *J. Mol. Biol.*, 1994, **244**, 586.
9 M. W. Vetting, C. A. Earhart and D. H. Ohlendorf, *J. Mol. Biol.*, 1994, **236**, 372.
10 M. W. Vetting and D. H. Ohlendorf, *Structure*, 2000, **8**, 429.
11 S. Han, L. D. Eltis, K. N. Timmis, S. W. Muchmore and J. T. Bolin, *Science*, 1995, **270**, 976.
12 E. L. Hegg and L. Que, Jr., *Eur. J. Biochem.*, 1997, **250**, 625.
13 T. Senda, S. Sugiyama, H. Narita, T. Yamamoto, K. Kimbara, M. Fukuda, M. Sato, K. Yano and Y. Mitsui, *J. Mol. Biol.*, 1996, **255**, 735.
14 A. Kita, S. I. Kita, I. Fujisawa, K. Inaka, T. Ishida, K. Horiike, M. Nozaki and K. Miki, *Structure*, 1998, **7**, 25.
15 K. Sugimoto, T. Senda, H. Aoshima, E. Masai, M. Fukuda and Y. Mitsui, *Structure*, 1999, **7**, 953.
16 G. P. Titus, H. A. Mueller, J. Burgner, S. Rodriguez de Cordoba, M. A. Penalva and D. E. Timm, *Nature Struct. Biol.*, 2000, **7**, 542.
17 A. M. Orville, J. D. Lipscomb and D. H. Ohlendorf, *Biochemistry*, 1997, **36**, 10 052.
18 G. Hamilton, in *Molecular Mechanisms of Oxygen Activation*, ed. O. Hayaishi, Academic Press, New York, 1974, pp. 443–444.
19 F. McCapra, *Acc. Chem. Res.*, 1976, **9**, 201; E. Conti, N. P. Franks and P. Brick, *Structure*, 1996, **4**, 287.
20 T. H. Lowry and K. S. Richardson, in *Mechanism and Theory in Organic Chemistry*, Harper & Row, New York, 1976, pp. 327–332.
21 For a comprehensive review of the Baeyer–Villiger oxidation see: G. R. Krow, *Org. React.*, 1993, **43**, 251.
22 R. J. Mayer and L. Que, Jr., *J. Biol. Chem.*, 1984, **259**, 13056.
23 J. Sanvoisin, G. J. Langley and T. D. H. Bugg, *J. Am. Chem. Soc.*, 1995, **117**, 7836.
24 E. Lee-Ruff, *Chem. Soc. Rev.*, 1977, **6**, 195.
25 C. Bianchini, P. Frediani, F. Laschi, A. Meli, F. Vizza and P. Zanello, *Inorg. Chem.*, 1990, **29**, 3402.
26 P. Barbaro, C. Bianchini, C. Mealli and A. Meli, *J. Am. Chem. Soc.*, 1991, **113**, 3181.
27 S. Dutta, S. M. Peng and S. Bhattacharya, *Inorg. Chem.*, 2000, **39**, 2231.
28 R. Müller and F. Lingens, *Z. Naturforsch.*, 1989, **44c**, 207.
29 J. W. Whittaker and J. D. Lipscomb, *J. Biol. Chem.*, 1984, **259**, 4476.
30 J. W. Whittaker and J. D. Lipscomb, *J. Biol. Chem.*, 1984, **259**, 4487.
31 D. M. Arciero and J. D. Lipscomb, *J. Biol. Chem.*, 1986, **261**, 2170.
32 C. J. Suckling, *Angew. Chem., Intl. Ed. Engl.*, 1988, **27**, 537; D. C. Nonhebel, *Chem. Soc. Rev.*, 1993, **22**, 348.
33 E. L. Spence, G. J. Langley and T. D. H. Bugg, *J. Am. Chem. Soc.*, 1996, **118**, 8336.
34 D. D. Cox and L. Que, Jr., *J. Am. Chem. Soc.*, 1988, **110**, 8085.
35 H. G. Jang, D. D. Cox and L. Que, Jr., *J. Am. Chem. Soc.*, 1991, **113**, 9200.
36 C. J. Winfield, Z. Al-Mahrizy, M. Gravestock and T. D. H. Bugg, *J. Chem. Soc., Perkin Trans. 1*, 2000, 3277.
37 P. M. Cullis, J. R. P. Arnold, M. Clarke, R. Howell, M. De Mira, M. Naylor and D. Nicholls, *J. Chem. Soc., Chem. Commun.*, 1987, 1088.
38 M. F. Hawthorne and W. D. Emmons, *J. Am. Chem. Soc.*, 1958, **80**, 6398.
39 K. L. Eley, P. J. Crowley and T. D. H. Bugg, *J. Org. Chem.*, 2001, **66**, 2091.
40 R. M. Goodman and Y. Kishi, *J. Org. Chem.*, 1994, **59**, 5125; *J. Am. Chem. Soc.*, 1998, **120**, 9392.
41 P. Deslongchamps, *Stereoelectronic Effects in Organic Chemistry*, Pergamon Press, Oxford, 1983, pp. 182–190.
42 A. Nishinaga, K. Nakamura, T. Shimizu and T. Matsuura, *Tetrahedron Lett.*, 1979, 2165.
43 E. J. Corey, W. G. Su and M. M. Mehrotra, *Tetrahedron Lett.*, 1984, **25**, 5123.
44 E. J. Corey and M. M. Mehrotra, *Tetrahedron Lett.*, 1983, **24**, 4921.
45 M. G. Weller and V. Weser, *J. Am. Chem. Soc.*, 1982, **104**, 1433.
46 L. S. White, P. V. Nilsson, L. H. Pignolet and L. Que, Jr., *J. Am. Chem. Soc.*, 1984, **106**, 8312.
47 L. Que, Jr., R. C. Kolanczyk and L. S. White, *J. Am. Chem. Soc.*, 1987, **109**, 5373.
48 P. Mialane, L. Tchertanov, F. Banse, J. Sainton and J. J. Girerd, *Inorg. Chem.*, 2000, **39**, 2440
49 M. Duda, M. Pascaly and B. Krebs, *J. Chem. Soc., Chem. Commun.*, 1997, 835.
50 R. Viswanathan, M. Palaniandavar, T. Balasubramanian and T. P. Muthiah, *Inorg. Chem.*, 1998, **37**, 2943.
51 M. Pascaly, C. Nazikkol, F. Schweppe, A. Wiedemann, K. Zurlinden and B. Krebs, *Z. Anorg. Allg. Chem.*, 2000, **626**, 50.
52 T. Funabiki, T. Yamazaki, A. Fukui, T. Tanaka and S. Yashida, *Angew. Chem., Intl. Ed. Engl.*, 1998, **37**, 4513.
53 W. O. Koch and H. J. Kruger, *Angew. Chem., Int. Ed. Engl.*, 1995, **34**, 2671.
54 T. Funabiki, A. Mizoguchi, T. Sugimoto, S. Tada, M. Tsugi, H. Sakamoto and S. Yoshica, *J. Am. Chem. Soc.*, 1986, **108**, 2921.
55 A. Dei, D. Gatteschi and L. Pardi, *Inorg. Chem.*, 1993, **32**, 1389.
56 M. Ito and L. Que, Jr., *Angew. Chem., Intl. Ed. Engl.*, 1997, **36**, 1342.
57 T. Ogihara, S. Hikichi, M. Akita and Y. Moro-oka, *Inorg. Chem.*, 1998, **37**, 2614.
58 G. Lin, G. Reid and T. D. H. Bugg, *Chem. Commun.*, 2000, 1119.
59 G. Lin, G. Reid and T. D. H. Bugg, *J. Am. Chem. Soc.*, 2001, in press.
60 L. Shu, Y. M. Chiou, A. M. Orville, M. A. Miller, J. D. Lipscomb and L. Que, Jr., *Biochemistry*, 1995, **34**, 6649.

CHEMCOMM Communication
www.rsc.org/chemcomm

Thermochromism of overcrowded bistricyclic aromatic enes (BAEs). A theoretical study†

P. Ulrich Biedermann,[ab] John J. Stezowski[c] and Israel Agranat*[a]

[a] *Department of Organic Chemistry, The Hebrew University of Jerusalem, Jerusalem 91904, Israel. E-mail: isria@vms.huji.ac.il; Fax: +972-2-6511907*
[b] *Institut für Organische Chemie, Universität Stuttgart, Pfaffenwaldring 55, 70569 Stuttgart, Germany*
[c] *Department of Chemistry, University of Nebraska-Lincoln, Lincoln NE-68588-0304, USA*

Received (in Cambridge, UK) 26th February 2001, Accepted 4th April 2001
First published as an Advance Article on the web 9th May 2001

A criterion for thermochromism has been derived from *ab initio* DFT B3LYP/6-31G* calculations of the *anti*-folded, *syn*-folded and twisted conformations of thermochromic and non-thermochromic overcrowded bistricyclic aromatic enes (BAEs) 1–8: the thermochromic species is the twisted conformation, a necessary condition being a small energy difference, < 30 kJ mol^{-1}, between the global minimum *anti*-folded and the thermochromic conformations.

Four score and a dozen years ago the phenomenon of thermochromism—reversible change of color with change of temperature—was revealed in bianthrone (**1**),[1] a leading overcrowded bistricyclic aromatic ene (BAE).[2] The BAEs are attractive substrates for the study of the conformational behavior of overcrowded ethylenes and for the interplay of strain and delocalization effects.[2] Thermochromic and photochromic BAEs and related overcrowded enes serve as candidates for chiroptical molecular switches and molecular motors.[3] Derivatives of **1** are topologically related to hypericin, wide spread in St. Johns Wort, an important remedy for depression.[4]

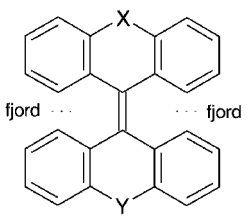

BAE

	X	Y
1	CO	CO
2	O	O
3	S	S
4	—	—
5	CH=CH	CH=CH
6	—	O
7	—	CO
8	O	CO

The thermochromism of **1** and related BAEs in solution has been attributed to a thermal equilibrium between two distinct and interconvertible conformers ($\mathbf{A} \overset{kT}{\longleftrightarrow} \mathbf{B}$),[5] where **A** is the room temperature, *anti*-folded (**a**), yellow conformer and **B** is the thermochromic, green–blue conformer. It is generally agreed that the thermochromic, piezochromic, and photochromic[6] **B** forms are identical. The prerequisites for thermochromism in BAEs have been a controversial issue.[7] Zwitterionic valence isomers, diradicals, thermally populated triplets, Woodward and Wasserman's electrocyclized isomer, planar, twisted, and double chair conformations have been suggested as the **B** form.[7] Previous studies applying various force fields[6a] and the semiempirical MINDO/3,[8] AM1,[9] and PM3[2c,d] methods failed to rationalize thermochromism in the BAEs series. Although PM3 calculations of the dynamic stereochemistry of BAEs agreed with experiment, they failed to rationalize the thermochromic behavior.[2c,d] We report here a theoretical approach, applying *ab initio* Hartree-Fock (HF) and Density Functional Theory (DFT), with the objective of determining whether a given BAE should be thermochromic.

The homomerous BAEs bianthrone (**1**), dixanthylene (**2**), dithioxanthylene (**3**), bifluorenylidene (**4**), bisdibenzocycloheptenylidene (**5**), and the heteromerous BAEs fluorenylidene-xanthene (**6**), fluorenylidene-anthrone (**7**), and xanthylidene-anthrone (**8**) were subjected to *ab initio* HF/6-31G* and DFT B3LYP/6-31G*[10] calculations using Gaussian 94.[11] All geometries were fully optimized subject to symmetry constraints as indicated. Minima and transition states were verified by computing vibrational frequencies at HF/STO-3G, and B3LYP/STO-3G optimized geometries. The following conformations were calculated: homomerous BAEs **1**–**5**, D_2 twisted (**t**), C_{2h} *anti*-folded (**a**) and C_{2v} *syn*-folded (**s**); **8**, C_2 twisted (**t**), C_s *anti*-folded with uneven degrees of folding (**au**), and C_s *syn*-folded with uneven degrees of folding (**su**); **6** and **7**, C_2 twisted (**t**), C_s *anti*-folded with uneven degrees of folding (**au**). Table 1 gives the calculated B3LYP/6-31G* and HF/6-31G* relative energies (ΔE_{rel}) of the optimized conformations. The experimental enthalpy values of the thermochromic **B** form, $\Delta H_{A\rightarrow B}$, and some geometrical parameters are also included.

According to the B3LYP/6-31G* results, three types of conformational behavior appear:

Table 1 Calculated and experimental relative energies of BAEs[a]

		Twist[b] ω^d	Fold[b] φ^e	HF[c] ΔE_{rel}	B3LYP[b] ΔE_{rel}	Exptl. $\Delta H_{A\rightarrow B}$
1	**a**-C_{2h}	0.0	41.5	0.0	0.0	
1	**t**-D_2	55.0	4.4	66.4	12.0	12.6[5f,13]
1	**s**-C_{2v}	0.0	42.5	45.3	43.4	
2	**a**-C_{2h}	0.0	40.9	0.0	0.0	
2	**t**-D_2	49.7	2.7	71.1[f]	24.4	23.4[5c]
2	**s**-C_{2v}	0.0	42.5	41.2	38.1	
3	**a**-C_{2h}	0.0	49.5	0.0	0.0	
3	**s**-C_{2v}	0.0	51.9	38.2	35.0	
3	**t**-D_2	57.8	8.0	159.5[f]	86.6	
4	**t**-D_2	34.0	2.4	0.0	0.0	
4	**a**-C_{2h}	0.0	23.5	33.4	39.0	
4	**s**-C_{2v}	0.0	20.5	73.1[f]	74.3[g]	
5	**a**-C_{2h}	0.0	52.4	0.0	0.0	
5	**s**-C_{2v}	0.0	55.6	20.4	19.9	
5	**t**-D_2	65.9	22.6	268.0[f]	166.9[f]	
6	**t**-C_2	42.2	3.9/3.8	0.0	0.0	
6	**au**-C_s	0.0	47.2/15.1	−22.5	4.5	
7	**t**-C_2	44.1	6.5/4.5	0.0	0.0	
7	**au**-C_s	0.0	47.2/16.4	−24.1	5.5	
8	**au**-C_s	0.0	42.1/40.3	0.0	0.0	
8	**t**-C_2	53.3	2.2/4.2	60.6	10.8	14.6[5c]
8	**su**-C_s	0.0	44.4/40.2	43.0	41.3	

[a] Energies in kJ mol^{-1}; the conformations are minima unless noted otherwise. [b] B3LYP/6-31G*. [c] HF/6-31G*. [d] Pure twist of the central ethylene bond: $\omega = \frac{1}{2}(\tau_{C9a\text{-}C9\text{-}C9'\text{-}C9a'} + \tau_{C8a\text{-}C9\text{-}C9'\text{-}C8a'})$. [e] Folding of the tricyclic moieties defined by the dihedral φ of the least-squares-planes of the aromatic rings. [f] Transition state. [g] Second order saddle point.

† Electronic supplementary information available: semiempirical and *ab initio* total energies of BAEs, calculated and experimental relative energies of BAEs, selected B3LYP/6-31G* geometric parameters and frontier orbital energies. See http://www.rsc.org/suppdata/cc/b1/b101797g/

 DOI: 10.1039/b101797g

Type 1: BAEs **1**, **2**, and **8** have *anti*-folded global minima **a**. For **1** and **2**, *anti*-folded conformations were found in the X-ray crystal structures, which correspond to the respective **A** forms.[2b,c] The twisted conformations **t** are only ΔE_{rel}(**1**) = 12.0 kJ mol^{-1}, ΔE_{rel}(**2**) = 24.4 kJ mol^{-1}, and ΔE_{rel}(**8**) = 10.8 kJ mol^{-1} higher in energy and thus may be populated thermally. The DFT calculated energies are in very good agreement with the experimentally determined enthalpies of the blue–green thermochromic **B** forms:[12] $\Delta H_{A\rightarrow B}$(**1**) = 12.6 kJ mol^{-1},[5f,13] $\Delta H_{A\rightarrow B}$(**2**) = 20.5,[5b] or 23.4[5c] kJ mol^{-1}, and $\Delta H_{A\rightarrow B}$(**8**) = 14.6 kJ mol^{-1}.[5c] The *syn*-folded conformations of **1**, **2**, and **8** are considerably higher in energy (ΔE_{rel}(**s**) = 38 to 43 kJ mol^{-1}). While the *anti*- and *syn*-folded conformations are colorless or pale yellow, the high twist in the central double bond reduces the π-overlap causing a substantial red shift and smaller HOMO–LUMO gaps in twisted conformations. This rationalizes the color change observed in thermochromic BAEs. Even a small population of the twisted conformation at elevated temperatures leads to a striking change of the visible color from yellow to green or blue-green (Fig. 1).

Type 2: BAEs **3** and **5** also adopt *anti*-folded conformations as global minima. However, in these cases the *syn*-folded conformations **s** are more stable than the twisted conformations **t**. The B3LYP/6-31G* conformational energies are ΔE_{rel}(**s**) = 35.0 and 19.9 kJ mol^{-1}, while ΔE_{rel}(**t**) = 86.6 and 166.9 kJ mol^{-1} for **3** and **5** (in **5**, **t** is a transition state). The twisted conformations cannot be populated in thermal equilibrium, explaining the absence of thermochromism in these compounds.

Type 3: BAEs **4**, **6**, and **7** have twisted global minima. This is in accord with the deep color of the three BAEs (thermochromic **B** form) at room temperature. The *anti*-folded conformation of **4** is considerably higher in energy, ΔE_{rel}(**a**) = 39.0 kJ mol^{-1}, while the folded conformations of **6** and **7** are only ΔE_{rel}(**au**) = 4.5 and 5.5 kJ mol^{-1} higher than the twisted conformations. Thus, the folded conformations of **6** and **7** may easily be populated. Packing effects may favor the folded conformations.[14] Indeed, yellow crystals with folded conformations have been observed in **6** and **7**.[2b,14]

The relative B3LYP/6-31G* conformational energies ΔE_{rel}(**t**) agree within ±4 kJ mol^{-1} with the experimental $\Delta H_{A\rightarrow B}$ of the thermochromic species. On the other hand, the Hartree-Fock results show substantial, systematic deviations from the experimental data. For HF/6-31G*, the average absolute error is 50 kJ mol^{-1}. The conformational energies of the twisted thermochromic **B** conformers are systematically overestimated by the HF calculations. According to the HF/6-31G* results, **s** is more stable than **t** in **1**, **2**, and **8**, leading to a Type 2 conformational behavior (non-thermochromic). Furthermore, at HF/6-31G*, **6** and **7** would have folded global minima and should be yellow at room temperature.

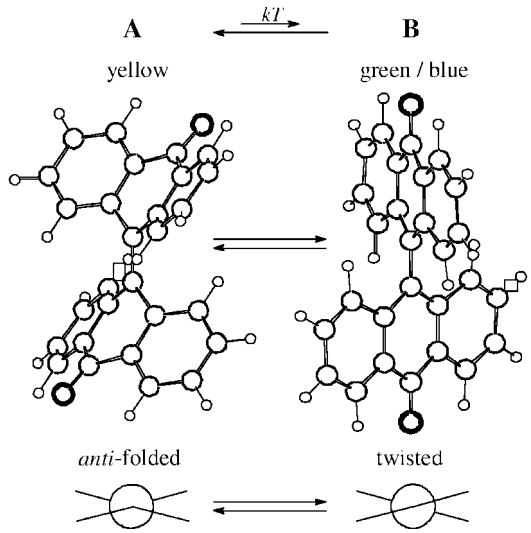

Fig. 1 The mechanism of thermochromism of BAEs using 3D structures of bianthrone (**1**) calculated at B3LYP/6-31G*.

The unique molecular architecture of BAEs gives rise to three conformations, *anti*-folded, *syn*-folded and twisted. Each conformation represents a different compromise between π-delocalization and steric strain. The bridges **X** and **Y** play an important role in the relative stability of the three conformations, leading to thermochromism in favorable cases.

In conclusion, the following necessary conditions for the thermochromic behavior of BAEs are deduced: (i) the global minimum of a thermochromic BAE is *anti*-folded (**a**) or unevenly *anti*-folded (**au**), whereas the thermochromic conformation is twisted (**t**); (ii) the energy difference between these conformations is small: (E(**t**) − E(**a**)) < 30 kJ mol^{-1}. While previous theoretical studies and *ab initio* Hartree-Fock calculations are flawed, giving conformational energies of twisted conformations that are systematically too high, inclusion of electron correlation *via* the DFT method solves this difficulty. The B3LYP/6-31G* ΔE_{rel}(**t**) and the experimental $\Delta H_{A\rightarrow B}$ of the thermochromic species agree within ±4 kJ mol^{-1}.

Notes and references

1 H. Meyer, *Monatsh. Chem.*, 1909, **30**, 165; H. Meyer, *Ber. Dtsch. Chem. Ges.*, 1909, **42**, 143.

2 (*a*) J. Sandström, *The chemistry of double-bonded functional groups*, Supplement A3, S. Patai, Ed., Wiley, 1997, p. 1253; (*b*) G. Shoham, S. Cohen, M. R. Suissa and I. Agranat, *Molecular Structure: Chemical Reactivity and Biological Activity*, J. J. Stezowski, J.-L. Huang, M.-C. Shao, Eds., IUCr Crystallographic Symposia 2, Oxford University Press, Oxford, 1988, p. 290; (*c*) P. U. Biedermann, J. J. Stezowski and I. Agranat, *Advances in Theoretically Interesting Molecules*, Vol. 4, R. P. Thummel Ed., JAI Press, Stamford, CT, 1998, p 245; (*d*) P. U. Biedermann, J. J. Stezowski and I. Agranat, *Eur. J. Org. Chem.*, 2001, 15.

3 B. L. Feringa, A. M. Schoevaars, W. F. Jager, B. de Lange and N. P. M. Huck, *Enantiomer*, 1996, **1**, 325; N. Koumura, R. W. J. Zijlstra, R. A. van Delden, N. Harada and B. L. Feringa, *Nature*, 1999, **401**, 152; B. L. Feringa, R. A. van Delden, N. Koumura and E. M. Geertsema, *Chem. Rev.*, 2000, **100**, 1789.

4 K. Linde, G. Ramirez, C. D. Mulrow, A. Pauls W. Weidenhammer and D. Melchart, *Brit. Med. J.*, 1996, **313**, 253; M. Philipp, R. Kohnen and K.-O. Hiller, K. Linde and M. Berner, *Brit. Med. J.*, 1999, **319**, 1534.

5 (*a*) W. T. Grubb and G. B. Kistiakowsky, *J. Am. Chem. Soc.*, 1950, **72**, 419; (*b*) W. Theilacker, G. Kortüm and G. Friedheim, *Ber. Dtsch. Chem. Ges.*, 1950, **83**, 508; (*c*) Y. Hirschberg and E. Fischer, *J. Chem. Soc.*, 1953, 629; (*d*) G. Kortüm, *Angew. Chem.*, 1958, **70**, 14; (*e*) Z. R. Grabowski and M. S. Balasiewicz, *Trans. Faraday Soc.*, 1968, **64**, 3346; (*f*) Y. Tapuhi, O. Kalisky and I. Agranat, *J. Org. Chem.*, 1979, **44**, 1949.

6 E. Fischer, *Rev. Chem. Intermed.*, 1984, **5**, 393; K. A. Muszkat, *The chemistry of quinonoid compounds*, Vol. 2, S. Patai, Z. Rappoport, Eds., Wiley, 1988, p. 203; W. H. Laarhoven, in: *Photochromism, Molecules and Systems*, H. Dürr and H. Bouas-Laurent Eds., Elsevier, Amsterdam, 1990, p. 970.

7 J. H. Day, *Chem. Rev.*,1963, **63**, 65; G. Kortüm, *Ber. Bunsen-Ges. Phys. Chem*, 1974, **78**, 391; R. B. Woodward and E. Wasserman, *J. Am. Chem. Soc.*, 1959, **81**, 5007.

8 O. Kikuchi and Y. Kawakami, *J. Mol. Struct. (Theochem)*, 1986, **137**, 365.

9 P. Sommer-Larsen, T. Bjørnholm, M. Jørgensen, K. Lerstrup, P. Frederiksen, K. Schaumburg, K. Brunfeldt, K. Bechgaard, S. Roth, J. Poplawski, H. Byrne, J. Anders, L. Eriksson, R. Wilbrandt and J. Frederiksen, *Mol. Cryst. Liq. Cryst.*, 1993, **234**, 89.

10 A. D. Becke, *J. Chem. Phys.*, 1993, **98**, 5648; C. Lee, W. Yang and R. G. Parr, *Phys. Rev. B*, 1988, **37**, 785; B. Miehlich, A. Savin, H. Stoll and H. Preuss, *Chem. Phys. Lett.*, 1989, **157**, 200.

11 Gaussian 94, Revision E.2, M. J. Frisch, J. A. Pople *et al.*, Gaussian, Inc., Pittsburgh PA, 1995.

12 The contributions of the zero-point corrections and thermal corrections to enthalpy to the relative conformational energies (conversion of ΔE_{rel} to ΔH) are insignificant (less than ±2 kJ mol^{-1} at B3LYP/STO-3G) and therefore neglected.

13 Earlier experimental values for $\Delta H_{A\rightarrow B}$(**1**) are: 11.3,[5e] 13.0,[5a] 13.8,[5a] 16.3,[5a] 14.2,[5b] 14.2,[5d] and 14.6 kJ mol^{-1}.[5c] $\Delta E_{rel}^{B3LYP/6-31G*}$ agrees best with the more recent lower experimental values.[5e,5f]

14 A. Levy, P. U. Biedermann and I. Agranat, *Org. Lett.*, 2000, **2**, 1811.

CHEMCOMM Communication
www.rsc.org/chemcomm

Synthesis of α-acetoxy and formyloxy ketones by thallium(III) promoted α-oxidation

Jong Chan Lee,* Yong Suk Jin and Ju-Hee Choi

Department of Chemistry, Chung-Ang University, Seoul 156-756, Korea. E-mail: jclee@cau.ac.kr; Fax: +82-2-825-4736; Tel: +82-2-824-7863

Received (in Cambridge, UK) 7th March 2001, Accepted 17th April 2001
First published as an Advance Article on the web 9th May 2001

Treatment of ketones with thallium(III) triflate in amide solvents at 60 °C for 30 min followed by addition of small amounts of H_2O cleanly provided the corresponding α-acyloxy ketones.

The α-hydroxy ketone subunit is found in a variety of biologically interesting natural products.[1] The formate and acetate groups can serve as useful protective groups for the hydroxy functions in α-hydroxy ketones.[2,3] The α-acetoxy ketones can be prepared *via* various ways which include the reaction of α-bromo ketones with carboxylate ions,[4] the oxidation of morpholine enamine with thallium(III) triacetate,[5] anodic oxidation of enol acetates in acetic acid,[6] and $Cu(acac)_2$ catalyzed insertion reactions of α-diazo ketones with carboxylic acids.[7] In addition, it has been reported that the solvolytic reaction of α-keto triflate in acetic acid or formic acid can provide corresponding α-acyloxy ketones,[8] but potential difficulties in preparing α-triflyloxy ketone precursors (*e.g.* α-triflyloxy propiophenone) limits their further synthetic applications. There exist only a few methods that deal with the direct preparation of α-acetoxy ketones from ketones. These involve the oxidation of ketones with lead tetraacetate,[9] the oxidation of ketones with manganese(III) acetate in acetic acid,[10] and the oxidation of aromatic ketones with hypervalent iodine reagent followed by solvolysis in acetic acid in the presence of silver carbonate.[11] Although many procedures have been reported for the preparation of α-acetoxy ketones, relatively little is known for the preparation of α-formyloxy ketones. The only reported method involves anodic oxidation of enol carbonate in DMF–$LiClO_4$.[12] To the best of our knowledge, no general method for the one-pot conversion of ketones to their corresponding α-formyloxy ketones has been reported.†

We now report a new and highly efficient preparation method for the α-formyloxy ketones and α-acetoxy ketones. This methodology is based on the hydrolysis of iminium salt intermediates **3** formed by the reaction of α-triflyloxy ketone with amide solvent. Initial treatment of ketones with thallium(III) triflate, formed *in situ* by the reaction of thallium(III) acetate with trifluoromethanesulfonic acid, in DMF at 60 °C followed by addition of small amounts of H_2O cleanly provided the α-formyloxy ketones in excellent yields. The probable mechanism is shown in Scheme 1. The thallium(III) organosulfonate mediated α-sulfonyloxylation of ketones is well established.[13] Therefore, the reaction of ketones with thallium(III) triflate at room temperature for 10 min should provide α-triflyloxy ketone intermediates **2** which undergoes rapid solvolytic reaction with DMF at 60 °C for 20 min to give iminium salts **3**. These intermediates are instantaneously hydrolysed to give desired α-formyloxy ketones in the presence of H_2O. Although the utility of DMF as a formate anion equivalent for the preparation of alkyl formates has been reported,[14] application of this method for the α-formyloxylation of ketones is unprecedented. Among the ketones examined, aliphatic ketones such as acetone and pentan-3-one gave complex product mixtures under the present reaction conditions. In the case of cyclopentanone, α-formyloxy cyclopentanone was detected in 98% yield as judged by GC analysis but a number of attempts to isolate pure α-formyloxy cyclopentanone by column chromatographic separation failed owing to the decomposition of the compounds. When the present reaction conditions were applied to cyclohexanone, a mixture of α-hydroxy cyclohexanone and α-formyloxy cyclohexanone was obtained in a ratio of 84 : 16 as indicated by GC, probably due to the highly unstable preformed α-formyloxy cyclohexanone undergoing further hydrolysis.

When the same reaction protocol used in α-formyloxylation of ketones was conducted in *N*,*N*-dimethylacetamide instead of DMF, α-acetoxylation of ketones took place remarkably well to give uniformly high yields of α-acetoxy ketones with all of the ketones examined. The representative results are summarized in Table 1. It is important to note that the solvolytic reaction of iminium salts in DMF was carried out at 60 °C to obtain the best results. Elevated temperature gave a number of side products. The intermediates iminium salts **3** were not stable enough to be isolated.

We have also studied the cleavage reactions of α-formyloxy and α-acetoxy ketones to their corresponding α-hydroxy ketones. We found the lithium hydroxide in aqueous solution to be suitable for the cleavage of the formyl and acetyl groups. Treatment of isolated α-formyloxy ketones or α-acetoxy ketones in THF–H_2O (3 : 1, v/v) solution of lithium hydroxide at room temperature for 2 min afforded the corresponding α-hydroxy ketones **5** in excellent yields ranging from 95 to 98%.

In conclusion, the facile conversion of ketones to the α-formyloxy ketones and α-acetoxy ketones has been accomplished in excellent yield. The present approach provides efficient entry for installation of α-acyloxy moieties into ketones and their clean deprotection should find wide applica-

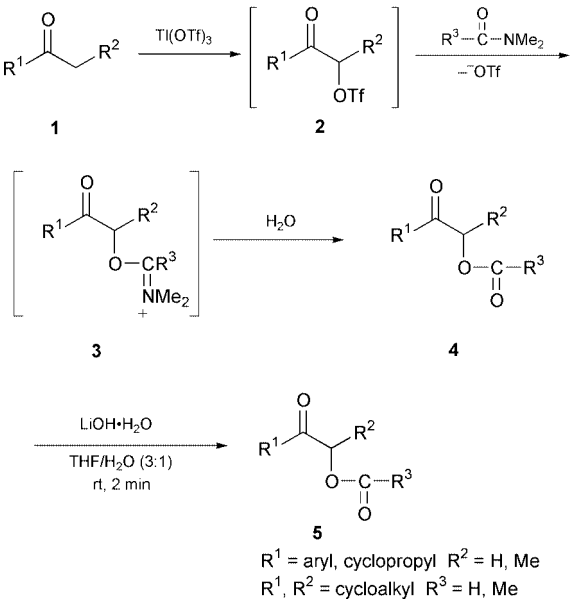

Scheme 1

 DOI: 10.1039/b102192n

Table 1 Conversion of ketones to α-formyloxy ketones

Entry	Ketones	% Yield[a] of α-formyloxy ketones	% Yield[a] of α-acetoxy ketones
1	$PhCOCH_3$	94	96
2	p-$CH_3C_6H_4COCH_3$	92	92
3	p-$CH_3OC_6H_4COCH_3$	97	98
4	p-$ClC_6H_4COCH_3$	90	90
5	$PhCOCH_2CH_3$	96	97
6	p-$CH_3C_6H_4COCH_2CH_3$	91	93
7	p-$CH_3OC_6H_4COCH_2CH_3$	97	98
8	p-$PhCH_2OC_6H_4COCH_2CH_3$	99	99
9	Cyclopropyl methyl ketone	99[b]	99[b]
10	Cyclopentanone	99[c]	99
11	Cyclohexanone	—[d]	99
12	Indan-1-one	98	99
13	2-Acetylthiophene	97	98

[a] Isolated yields. [b] The acyloxylation occurred at methyl position. [c] GC yield. [d] α-Hydroxy ketone was obtained as a major product.

tions in the construction of α-hydroxy ketone subunit in natural product synthesis.

The authors would like to thank the KOSEF (1999-2-121-001-5) for financial support.

Notes and references

† **Caution**: *Thallium compounds are highly toxic; they should therefore be handled with extreme caution and all operations must be carried out in an efficient fume hood.* The experimental procedure for the preparation of α-formyloxy acetophenone is representative. To thallium(III) acetate (0.572 g, 1.5 mmol) in DMF (5 mL) was added trifluoromethanesulfonic acid (0.675 g, 4.5 mmol) at rt under nitrogen with stirring for 10 min. To the reaction mixture acetophenone (0.120 g, 1.0 mmol) was added and stirred at 60 °C for 20 min. After reaction, the temperature was brought down to rt, H_2O (1 mL) was added and stirred for an additional 10 min. The reaction mixture was diluted with CH_2Cl_2 (30 mL), washed with saturated $NaHCO_3$ aqueous solution, water, and dried over $MgSO_4$. Evaporation of solvent, followed by short column chromatography on silica gel (ethyl acetate–hexane 1:2) yielded the α-formyloxy acetophenone.

1 B. Raduchel, *Synthesis*, 1980, 292.
2 (*a*) M. L. Wolfrom, A. Thompson and E. F. Evans, *J. Am. Chem. Soc.*, 1945, **67**, 1793; (*b*) C. Fenselau, *Steroid Reactions*, ed. C. Djerassi, Holden-Day, San Francisco, 1963, pp. 537–591.
3 For reviews about esters as hydroxy functional groups, see: (*a*) T. W. Green and P. G. M. Wuts, *Protective Groups in Organic Synthesis*, Wiley, New York, 1991, pp. 87–104; P. J. Kocienski, *Protecting Groups*, Thieme, Stuttgart, 1994, pp. 22–29.
4 (*a*) P. A. Levine and A. Walti, *Org. Synth.*, Coll. Vol. II, 1943, 4843; (*b*) E. B. Reid, R. B. Fortenbauch and H. R. Patterson, *J. Org. Chem.*, 1950, **15**, 579.
5 M. E. Kuehne and T. J. Giacobbe, *J. Org. Chem.*, 1968, **33**, 3359.
6 T. Shono, Y. Matsumura and Y. Nakagawa, *J. Am. Chem. Soc.*, 1975, **97**, 6144.
7 T. Shinada, T. Kawakami, H. Sakai, I. Takada and Y. Ohfune, *Tetrahedron Lett.*, 1998, **39**, 3757.
8 X. Creary, *J. Am. Chem. Soc.*, 1984, **106**, 5568.
9 D. J. Rawilson and G. Sosnovsky, *Synthesis*, 1973, 567.
10 A. S. Demir, N. Camkerten, H. Akgun, C. Tanyeli, A. S. Mahasneh and D. S. Watt, *Synth. Commun.*, 1990, **20**, 2279.
11 J. C. Lee and T. Hong, *Synth. Commun.*, 1997, **27**, 4085.
12 F. Barba, M. G. Quintanilla and G. Montero, *J. Org. Chem.*, 1995, **60**, 5658.
13 (*a*) M. S. Khanna, C. P. Garg and R. P. Kapoor, *Tetrahedron Lett.*, 1992, **33**, 1495; (*b*) M. S. Khanna, C. P. Garg and R. P. Kapoor, *Synlett*, 1992, 393.
14 (*a*) R. K. Boeckman and B. Ganem, *Tetrahedron Lett.*, 1974, 913; (*b*) J. Barluenga, P. J. Campos, E. Gonzalez-Nunez and G. Asensio, *Synthesis*, 1985, 426; (*c*) I. Fernandez, B. Garcia, S. Munoz, J. R. Pedro and R. Salud, *Synlett*, 1993, 489; (*d*) S. C. Suri, S. I. Rodgers, K. V. Radhakrishnan and V. Nair, *Synth. Commun.*, 1996, **26**, 1031.

CHEMCOMM Communication
www.rsc.org/chemcomm

2-Phenyl-*N*-tosylazetidine as a formal 1,4 dipole precursor†‡

Ioana Ungureanu, Philippe Klotz, Angèle Schoenfelder and André Mann*

Laboratoire de Pharmacochimie de la Communication Cellulaire, UMR 7081, Faculté de Pharmacie, 74 route du Rhin, BP 24, F-67401 Illkirch, France. E-mail: Andre.mann@pharma.u-strasbg.fr; Fax: +3(0)3 90 24 43 10; Tel: +33 (0)3 90 24 42 27

Received (in Cambridge, UK) 5th February 2001, Accepted 7th March 2001
First published as an Advance Article on the web 9th May 2001

_N_-Tosyl-2-phenylazetidine 1 in the presence of $BF_3{\cdot}Et_2O$ reacts as a formal 1,4 dipole with various activated or non activated alkenes.

Recently we reported that phenyl-*N*-tosylaziridines, in the presence of Lewis acids generate a double *exo* stabilized 1,3 dipole, suitable for [3 + 2] dipolar cycloadditions.[1] If the concept of dipole with *exo* stabilisation could be extended to phenyl-*N*-tosylazetidine **1**,[2,3] a zwitterionic or 1,4 dipole **1′** would be produced. Herein we present evidences for the existence of **1′** and several examples of its utilisation in [4 + 2] cycloaddition reactions (Scheme 1).

If azetidin-2-ones have received considerable attention, activity on the related azetidines has been less fevered.[4–6] As the benzylic C–N bond in **1** can be regioselectively broken,[7] we speculated that conditions might be found to open the azetidine ring and to realize complete charge separation, producing a transient dipole **1′**. This putative 1,4 dipole **1′** can be described as follows:[8] **1′** is a dipole of zwitterionic type according to the Huisgen's classification[3] with the two charges stabilized in an *exo* manner by the benzyl and tosyl groups. Indeed 1,4 dipole **1′**, if opposed to olefins, could represent a device to realise a formal *carboamination* for the rapid construction of azaheterocycles (Scheme 1).

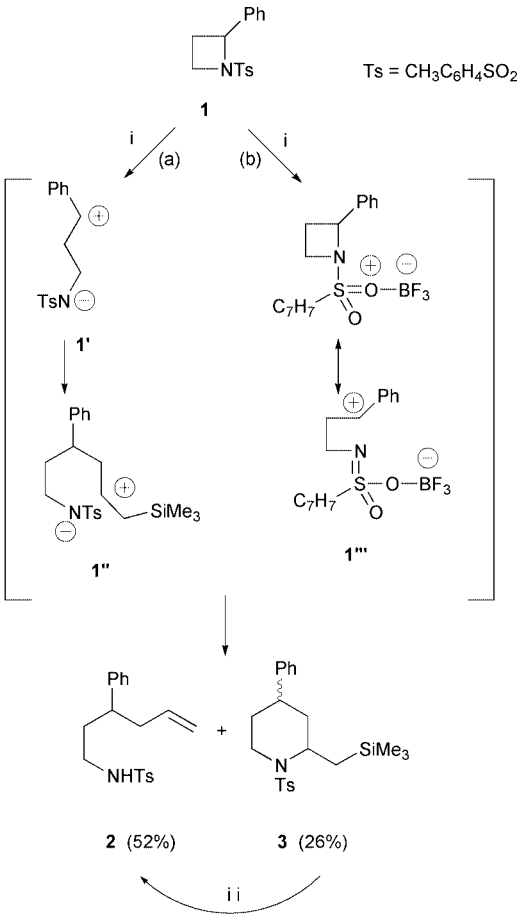

Scheme 1 *Reagents and conditions*: (i) allyltrimethylsilane $BF_3{\cdot}Et_2O$, −78 °C, CH_2Cl_2; (ii) TBAF, THF (95%).

For the generation of the dipole **1′** we expected that a Lewis acid might cause the desired charge separation.[1] To trap both the benzylic carbocation and the amide function in the elusive dipole **1**, we chose allyltrimethylsilane as a 'probe'.[9] Indeed, azetidine **1** reacts with allyltrimethylsilane in the presence of $BF_3{\cdot}Et_2O$. The obtained allylated product **2** and silylated piperidine **3** may have a common intermediate, a 1,6 zwitterion **1″**. If desired, the conversion of piperidine **3** to allylamine **2** can be performed in refluxing THF with TBAF [pathway (a) in Scheme 1]. However, a slightly different mechanism can also be proposed: BF_3 activates the oxygen (or nitrogen atom) of the sulfonamide function, the formed intermediate **1‴** is then ready for a nucleophilic attack at the benzylic cation operated by allylsilane and subsequent intramolecular capture or desilylation of the newly formed cation can then produce either **2** or **3** [pathway (b) in Scheme 1]. If from a theoretical point of view there is a great difference between a naked dipole such as **1′** and a more conventional zwitterion such as **1‴**, in practice the observed reactivity of **1** is best explained using the simplified intermediate **1′**.

According to our previous experience, dihydropyran (DHP) seems to be a better reagent than allylsilane for a dipole 'capture'.[1,10] Indeed in the presence of $BF_3{\cdot}Et_2O$ and a threefold excess of DHP, **1** is quantitatively transformed into three adducts **4a**, **4b** and **5**, but the chemical events are more complex than expected. A [4 + 2] cycloaddition takes place. The formation of the adducts **4a** (*exo*), **4b** (*endo*) and **5**, a di-substituted tetrahydropyridine with a pyranyl appendage, are accounted for by Scheme 2a. The structure of **4a** was obtained by a single crystal X-ray analysis.[11]

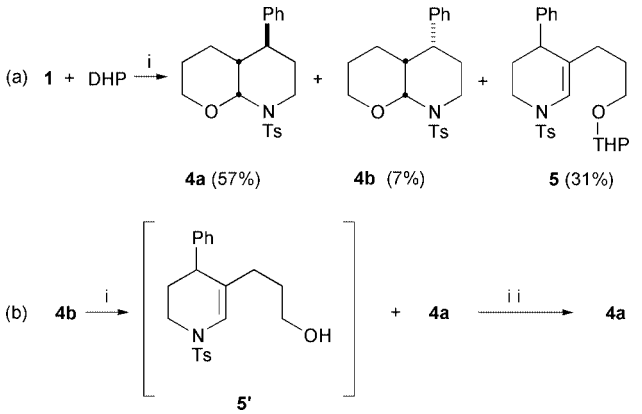

Scheme 2 *Reagents and conditions*: DHP, $BF_3{\cdot}Et_2O$, −78 °C, CH_2Cl_2; (ii) pTSA, toluene, reflux.

† This paper is dedicated to Professor Camille-Georges Wermuth.

‡ Electronic supplementary information (ESI) available: experimental details and characterization for key intermediates, including the ORTEP figures of the X-ray structures for compounds **4a** and **10**. See http://www.rsc.org/suppdata/cc/b1/b101168p/

 DOI: 10.1039/b101168p

The formation of **5** is best explained in the following way: under the reaction conditions the pyranyl ring in **4a** and/or **4b** is opened through an immonium/enamine acid catalysed process and the transiently formed alcohol **5′** is trapped by the excess of DHP present in the reaction mixture. In fact we suspect that the major pathway which produces **5** is the transformation of **4b**. Indeed in complementary experiments, we verified the stability of the two cycloadducts **4a** and **4b** in presence of $BF_3{\cdot}Et_2O$ at −78 °C. After 30 min **4a** was recovered unchanged, while **4b** was completely transformed into **4a** and **5′**, as shown by the analysis of the crude reaction mixture by NMR. Now if heated in toluene in the presence of pTSA, the mixture of **4a** and **5′** is totally converted to **4a** (Scheme 2b). Therefore it can be concluded that the reaction between **1** and DHP is a sequence of equilibria, the thermodynamic bicycle **4a** surviving under the reaction conditions, whereas **4b** evolves to **5** *via* **5′**. It should be noted that only the *cis* aza, oxo [4.4.0] bicycle was observed because the geometrical condition required for a maximal anomeric effect is accomplished only in a *cis* aza, oxo [4.4.0] bicycle.[12] Finally, it has to be emphasized that the chemical potentialities of **4a** as N,O acetal are considerable.[13]

Another question which was addressed: does **1′** react with simple non-activated double bonds? We selected commercially available exomethylene cycloalkanes (cyclobutane, pentane, and cyclohexane) as partners for **1**. In this case the formation of spiropiperidines was precisely anticipated. Indeed the adducts isolated and characterised were respectively the spiro compounds **6**, **7** and **8** (Scheme 3). These results confirm nicely the reactivity of **1** as a formal 1,4 dipole in [4 + 2] cycloaddition to olefins and are in line with the results obtained with the corresponding aziridine.[1] This sequence constitutes a new and rapid entry to spiropiperidine rings.

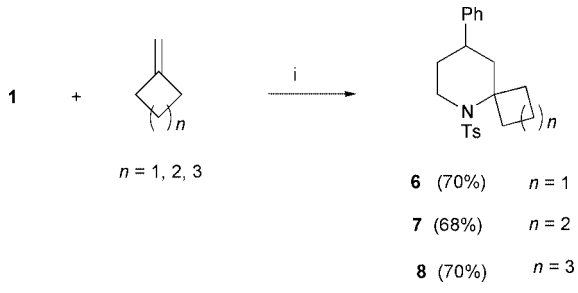

Scheme 3 *Reagents and conditions*: $BF_3{\cdot}Et_2O$, −78 °C, CH_2Cl_2.

The results from using cycloalkenes (cyclopentene, cyclohexene, cycloheptene) as 'dipolarophiles' were a surprise: cycloalkenes reacted with azetidine **1** in the presence of $BF_3{\cdot}Et_2O$, but no trace of the expected [4 + 2] cycloaddition products was observed. A complete NMR analysis of the obtained products showed the exclusive formation of spiro-pyrrolidines **9**–**11**. The single crystal X-ray analysis of **10**[14] confirmed the structural assignment made by NMR (Scheme 4). These unexpected results are best explained if the two following arguments are considered: hydride shift is assumed to provide the intermediate with the more stable tertiary (carbocation in respect to the secondary) and the formation of **9**–**11** is accounted for by the preferential formation of five over six-membered rings. These results are in sharp contrast with those for the corresponding aziridine where [3 + 2] cycloaddition was always the major pathway.[1]

Finally the formation of spiro-pyrrolidines results from a formal [4 + 1] cycloaddition of dipole **1′**. The hydride shift can be seen as additional proof for a stepwise, not concerted, mechanism of cycloaddition reactions of **1** on non-activated 1,2 disubstituted double bonds. *To the best of our knowledge no examples of such a reaction have been reported.* This sequence is a new entry to spiro-pyrrolidines, which constitute the core of some natural products.[15]

In summary, in this work we demonstrate that the 1,4 dipole **1′** with double *exo* stabilisation is accessible from azetidine **1**; **1′** reacts under mild conditions with several olefins to produce spiro-pyrrolidines or -piperidines by [4 + 2] or formal [4 + 1] cycloadditions; **1′** reacts with DHP to produce aza oxo [4.4.0] bicycles which are valuable intermediates. Finally, azetidine **1** allows, in one chemical step, a new and unique entry to azaheterocycles.

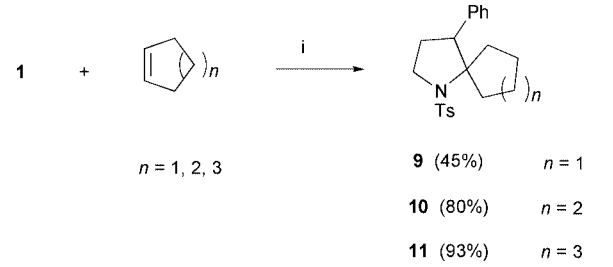

Scheme 4 *Reagents and conditions*: $BF_3{\cdot}Et_2O$, −78 °C, CH_2Cl_2.

Notes and references

1 I. Ungureanu, P. Klotz and A. Mann, *Angew. Chem., Int. Ed.*, 2000, **39**, 4615; I. Ungureanu, C. Bologa, S. Chayer and A. Mann, *Tetrahedron Lett.*, 1999, **40**, 5315.

2 W. Carruthers, *Cycloaddition Reactions in Organic Synthesis*, Pergamon Press, Oxford, 1990, pp 269–331.

3 R. Huisgen, *Angew. Chem.*, 1963, **13**, 604.

4 For reviews see: N. De Kimpe, in *Comprehensive Heterocyclic Chemistry II*, ed. A. Padwa, Elsevier, Oxford, 1996, Vol. 1B, Chapter 1.18, pp 507–589.

5 R. T. Schuman, R. B. Rothenberger, C. S. Campbell, G. F. Smith and D. S. Jefford-Moore, *J. Med. Chem.*, 1995, **38**, 4446.

6 B. Alcaide, P. Almendros, C. Aragoncilla and N. R. Salgado, *J. Org. Chem.*, 1999, **64**, 9596, and references cited therein; N. De Kimpe, K. A. Tehrani and G. Fonck, *J. Org. Chem.*, 1996, **61**, 6500.

7 E. Testa, L. Fontanella and V. Aresi, *Liebigs Ann. Chem.*, 1964, **676**, 160; W. J. Gensler and R. W. Koehler, *J. Org. Chem.*, 1962, **27**, 2754.

8 Other reported 1,4 dipoles: A. Padwa and M. A. Semones, *Tetrahedron Lett.*, 1996, **37**, 335; A. Ohta, F. Okazaki, Y. Yamanoi, M. A. Maede, Y. Oyagi, T. Kurihata and G. L. Pang, *Chem. Pharm. Bull.*, 1995, **43**, 705; H. Gotthardt and K. H. Schenk, *Angew. Chem., Int. Ed. Engl.*, 1985, **24**, 608; S. Levinger and S. Shatzwiller, *Tetrahedron*, 1977, **34**, 563.

9 K. Miura, T. Hondo, T. Nakagawa, T. Takahashi and A. Hosomi, *Org. Lett.*, 2000, **2**, 385; M. R. Schneider, P. Klotz, I. Ungureanu, A. Mann and C. G. Wermuth, *Tetrahedron Lett.*, 1999, **40**, 3873; C. W. Roberson and K. A. Woerpel, *J. Org. Chem.*, 1999, **64**, 1434; S. R. Angle and N. A. El-Said, *J. Am. Chem. Soc.*, 1999, **121**, 10 211; M. D. Groaning, G. P. Brengel and A. I. Meyers, *J. Org. Chem.*, 1998, **63**, 5517; M. R. Schneider, A. Mann and M. Taddei, *Tetrahedron Lett.*, 1996, **37**, 8493; C. E. Masse and J. S. Panek, *Chem. Rev.*, 1995, **95**, 1293.

10 F. Cardona, S. Valenza, A. Goti and A. Brandi, *Tetrahedron Lett.*, 1997, **38**, 8097; T. Iwashita, T. Kusumi and H. Kaskisawa, *J. Org. Chem.*, 1982, **47**, 230.

11 The X-ray structure and coordinates for compound **4a** have been deposited at the Cambridge Crystallographic Database, CCDC 142897. See http://www.rsc.org/suppdata/cc/b1/b101168p/ for crystallographic files in .cif format. *Crystal data* for **4a**: $C_{21}H_{25}NO_3S$, M = 371.50, triclinic, space group: $P\bar{1}$, a = 7.6170 (4), b = 11.0840 (6), c = 12.3600 (6) Å, U = 982.9 Å^3, T = 294 K, Z = 2, μ(Mo-K) = 0.184 mm^{-1}, 8028 measured reflections, 2079 unique (R_{int} = 0.04). The final $wR(F2)$ was 0.057 (all data).

12 P. Duhamel, A. Deyne, G. Dujardin, G. Plé and J.-M. Poirier, *J. Chem. Soc., Perkin Trans. 1*, 1995, 2103; P. Deslongchamps, *Stereoelectronic Effects in Organic Chemistry*, Pergamon Press, Oxford, 1983, pp 101–160.

13 For an excellent review on acylimonium chemistry see: W. N. Speckamp and M. J. Moolenaar, *Tetrahedron*, 2000, **51**, 3817.

14 The X-ray structure and coordinates for compound **10** have been deposited at the Cambridge Crystallographic Database, CCDC 142898. See http://www.rsc.org/suppdata/cc/b101168p/ for crystallographic files in .cif format. *Crystal data for* **10**: $C_{22}H_{27}NO_2S$, M = 369.59, monoclinic, space group P 1 21/n 1, a = 9.4881 (3), b = 18.6503 (8), c = 11.1767 (5) Å, U = 1937.2 Å^3, T = 293 K, Z = 4, μ(Mo-Kα) = 0.184 mm^{-1}, 10796 measured reflections, 3037 unique (R_{int} = 0.04). The final $wR(F2)$ was 0.067 (all data).

15 M. K. Werner, J. M. Santos and S. M. Weinreb, *J. Org. Chem.*, 1999, **64**, 4865; W. H. Pearson, N. S. Barta and J. W. Kampf, *Tetrahedron Lett.*, 1997, **38**, 3369; A. J. C. Blackman, C. Li, D. C. R. Hockless, B. W. Skelton and A. H. White, *Tetrahedron*, 1993 **49**, 8645.

CHEMCOMM Communication
www.rsc.org/chemcomm

1,9-Dihydro-3-phenyl-4*H*-pyrazolo[3,4-*b*]quinolin-4-one, a novel fluorescent probe for extreme pH measurement

Meihong Su, Yong Liu, Huimin Ma,* Quanli Ma, Zhihua Wang, Junlin Yang and Meixiang Wang*

Center for Molecular Sciences, Institute of Chemistry, Chinese Academy of Sciences, Beijing 100080, China. E-mail: mhmliang@public.bta.net.cn

Received (in Cambridge, UK) 21st February 2001, Accepted 19th April 2001
First published as an Advance Article on the web 10th May 2001

The synthesis of 1,9-dihydro-3-phenyl-4*H*-pyrazolo[3,4-*b*]quinolin-4-one and its pH-dependent fluorescent properties for extreme pH measurement are presented.

The accurate measurement of pH is very important because it usually plays a key role in a variety of systems. The most popular and direct device for pH measurement is the glass pH electrode. However, the known limitations of the glass pH electrodes (*e.g.* its electrical interference or mechanical damage to small cells, and the presence of acid error and especially alkaline error[1]) make them unsuitable for certain applications: intracellular pH and microscopy studies as well as the measurements of extreme pH values below 1 or above 9. In contrast to the electrochemical methods, optical measurements, based on fluorescent probes that are either protonated or deprotonated, have no such drawbacks.[2] Moreover, fluorescent measurements are convenient to microscopy studies, and can reflect the H^+ distribution and change within cells.[3] It is not surprising, therefore, that the researches on pH-dependent fluorescent probes have received a great attention,[4] particularly on the probes which are pH-sensitive to the near neutral pH value of normal body fluids for the point of biological application. To the best of our knowledge, however, relatively less attention was paid on the fluorescent probes which are pH-sensitive in the lower pH region (pH < 5) or the higher pH region (pH > 9), though in some cases pH changes (*e.g.* within the stomach) can enter the extreme pH ranges.[1,5] It is also a challenge to design a fluorescent probe with linear response over a broad range, because pH measurement can be accurately made only over a range of about two pH units, *i.e.* p*K*a ± 1. Although some attempts have been made to broaden the response range of pH measurement by using a mixture of multiple pH indicators,[6] this makes the system rather complex. Another feasible approach to the problem is to develop a probe with multiple steps of H^+ binding.[7] Unfortunately, the typically used pH-dependent groups such as –COOH, –OH, *etc*., have a high affinity for common metal ions, thus resulting in complexation and nonspecific response of the probe to H^+.

The objective of this research was to design a novel fluorescent probe which is both pH-selective and pH-sensitive for extreme pH ranges, by assembling several electronegative atoms in the different positions of a highly conjugated molecule. Scheme 1 shows the synthetic route to such a fluorescent probe, 1,9-dihydro-3-phenyl-4*H*-pyrazolo[3,4-*b*]quinolin-4-one **5**.[8] The reaction of 2-benzoylketene dithioacetal **1**[9] with **2** gave methylthio-substituted quinolone **3**. Upon treatment with hydrazine, **3** was converted quantitatively to hydrazone **4** which was then transformed into the designed product **5** by further heating in pyridine.

In order to increase the selectivity for H^+, the use of carboxyl which is easy to complex with metal ions was avoided. pH-dependent amino groups, though they are also strong ligands for metal ions, were mainly chosen as H^+ receptors because of their convenient arrangement in synthesis and the wealth of proton binding data available.[10] The arrangement of multiple H^+ receptors is conducive to obtaining a broad pH response range, and three nitrogen atoms and one oxygen atom were set in the probe **5**. To achieve the fluorescent response to extreme pH values, the environmental difference among the electronegative atoms in the conjugated molecule should be as large as possible. The potential binding sites for H^+ in **5** were therefore placed in quite different environments. Particularly following the known data,[11] one nitrogen atom [*e.g.* N(9)] was arranged in an electron-deficient position and another one N(1) in an electron-rich position, expecting the generation of considerably different p*K*a values. In addition, for improved selectivity, the arrangement of all the electronegative atoms in the structure should not provide a suitable cavity or a convenient formation of five- and six-membered ring complexes for metal ions. As shown in Scheme 1, the prepared probe **5** does not possess any favorable complexation sites for metal ions. The benzene ring in the position 3 of the probe would render a steric hindrance for any possible complexation of either the adjacent oxygen or nitrogen atom with metal ions.

The experimental results showed that the probe has a notable fluorescence quantum yield of φ_{base} = 0.14 in basic media (pH = 13.0) or φ_{acid} = 0.12 in acidic media (pH = 1.0) with an appreciable fluorescence lifetime of 11.12 ± 0.04 ns,[12] and its fluorescence spectra are highly dependent on pH (Fig. 1). Titration of fluorescence intensity with pH gave two p*K*a values of 2.61 and 12.44 (Fig. 1, insets),[13] which correspond to the protonations of the two nitrogen atoms N(9) and N(1) in the probe, respectively. It is understandable that only two of the electronegative atoms exhibit pH-sensitivity, because the basicity of the other two (one nitrogen and one oxygen) is largely weakened by their lone electron pairs participating in the system conjugation. As a result, the probe is capable of measuring the extreme pH values over the two pH ranges of 1.8–3.4 and 11.6–13.3, respectively. Further, the probe was stable and no obvious changes in fluorescence were observed within 5 months at rt. It should be pointed out that the probe is unsuitable for neutral pH measurements, since a nonlinear response of fluorescence intensity to pH was observed in that region.

To test the selectivity of the probe, the effects of various diverse ions upon the emission spectra were examined. The results showed that the selectivity of this probe for H^+ over other

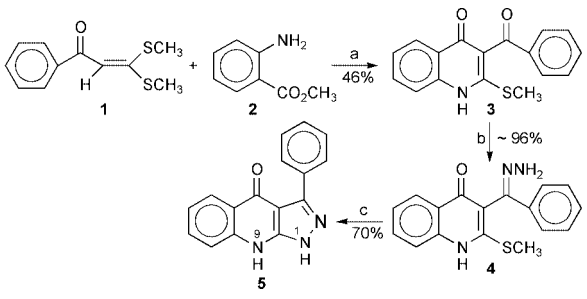

Scheme 1 *Reagents and conditions*: (a) propanoic acid, reflux 48 h; (b) hydrazine hydrate (30%), ethanol reflux; (c) anhydrous pyridine, argon protection, reflux 60 h.

 DOI: 10.1039/b101685g

Table 1 The tolerable concentration of foreign ions for the measurement of pH[a]

M^{n+}	Ca^{2+}	Cu^{2+}	Fe^{2+}	Fe^{3+}	K^+	Mg^{2+}	Mn^{2+}	Zn^{2+}	NO_3^-	PO_4^{3-}	CO_3^{2-}	SO_4^{2-}
$c/10^{-4}$ M[b]	10	10	0.70	0.40	20	0.80	40	2.6	0.50	2.0	0.20	4.0
$c/10^{-5}$ M[c]	20	4.5	3.6	3.4	20	0.32	0.20	2.2	1.0	1.0	8.3	20

[a] The tolerable concentration was estimated by the criterion at which a species gave a relative error of no more than 5% in the analytical signal (fluorescence intensity) of the probe (2.0×10^{-3} g dm^{-3}) in the presence of 0.1 M NaCl. [b] Measured in acid medium (pH = 2.0). [c] Measured in basic medium (pH = 12.0).

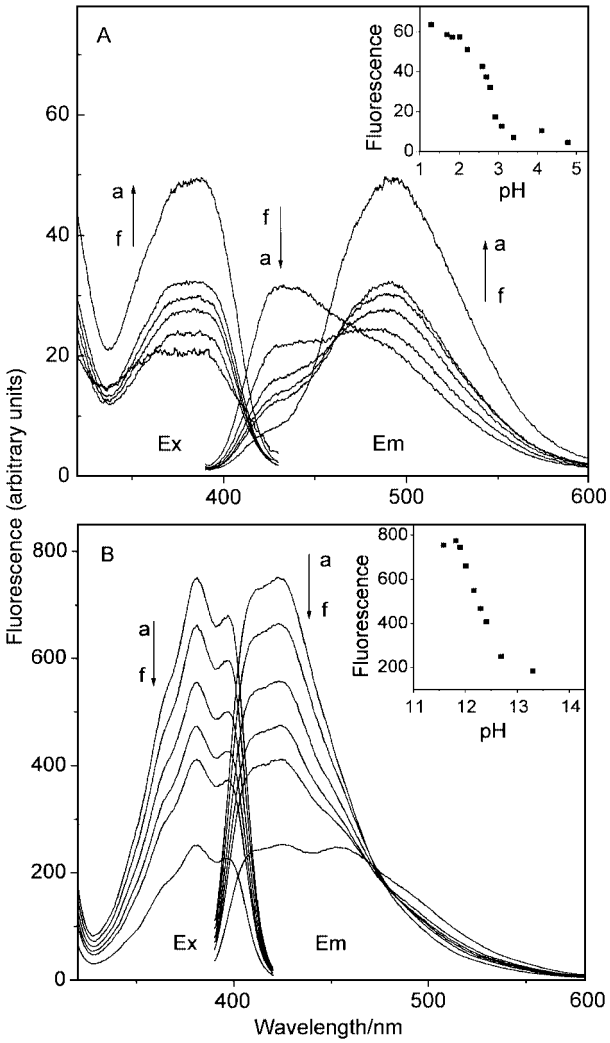

Fig. 1 pH-dependence of the fluorescence spectra of **5** (5×10^{-3} g dm^{-3}) in 0.1 M NaCl at various pH values (A): 1.29 (a), 2.59 (b), 2.72 (c), 2.81 (d), 3.09 (e), 3.41 (f); and (B): 11.82 (a), 12.01 (b), 12.17 (c), 12.29 (d), 12.41 (e), 12.69 (f). Different pH values were obtained by adding small amounts of 0.1 M HCl or NaOH to the solution. The excitation was at 385 nm for both of the emission spectra (Em) of (A) and (B); the emission was at 493 and 433 nm for the excitation spectra (Ex) of (A) and (B), respectively. Inset shows the variation of fluorescence emission intensity with pH at 493 (A) and 433 nm (B), respectively.

ions (Table 1) is of specificity, making it very useful for accurate measurement of extreme pH values.

The mechanism of the probe's fluorescence response to pH is complex due to the influence of protonation/deprotonation and the possible presence of enol–amide tautomerism, but it may be interpreted largely according to photoinduced electron transfer (PET) principle, which has been widely used to design a variety of fluorescent ion sensing molecules.[14] Nitrogen atoms often serve as both H^+ receptors and electron donors in the PET process. In acid media, the probe **5** has a longer fluorescence emission of 493 nm at the optimal excitation of 385 nm (Fig. 1A), and the H^+ binding equilibrium of the N(9) atom yields an isosbestic point at 462 nm. Further protonation of the probe may inhibit the related PET, resulting in fluorescence enhancement (Fig. 1, curve a). On the other hand, the deprotonation of the N(1) atom in basic media presumably revives the corresponding PET, causing fluorescence quenching at 433 nm (Fig. 1B).

In summary, a novel fluorescent pH probe **5** has been prepared by arranging several electronegative atoms in the different environments of a conjugated molecule. Although this probe is far from being an ideally broad pH sensor, it greatly complements glass pH electrodes. Further work in this area would be beneficial to designing more excellent fluorescent pH probes.

Financial supports from the NNSF of China and the CMS fund of CAS are acknowledged.

Notes and references

1 G. Mattock and G. R. Taylor, *pH Measurement and Titration*, Heywood, London, 1961.
2 C. Chan, W. Lo and K. Wong, *Biosensors Bioelectron.*, 2000, **15**, 7.
3 A. Srivastava and G. Krishnamoorthy, *Anal. Biochem.*, 1997, **249**, 140.
4 J. R. Lakowicz, *Principles of Fluorescence Spectroscopy*, 2nd Edn., Kluwer Academic/Plenum Publishers, New York, 1999.
5 S. Ohkuma and B. Poole, *Proc. Natl. Acad. Sci. USA*, 1978, **75**, 3327.
6 J. Lin and D. Liu, *Anal. Chim. Acta*, 2000, **408**, 49.
7 O. S. Wolfbeis and H. Marhold, *Fresenius Z. Anal. Chem.*, 1987, **327**, 347.
8 All new compounds **3**–**5** were fully characterized on the basis of their spectral (NMR, IR, MS) data and C–H–N analysis. *Selected data* for **5**: δ_H (300 MHz, 340 K, DMSO-d_6) 11.8 (1H, s, NH), 8.32 (2H, d, *J* 7.1), 8.19 (1H, d, *J* 7.9), 7.58 (1H, t, *J* 7.3), 7.37–7.47 (4H, m), 7.14 (1H, t, *J* 7.5); ν_{max} (KBr)/cm^{-1} 3132, 3059, 1631, 1573; EI mass spectrum (relative intensity), *m*/*z* 261 (100, M^+), 260 (45); Anal. Calcd for $C_{16}H_{11}N_3O$: C, 73.55; H, 4.24; N, 16.08. Found: C, 73.35; H, 4.40; N, 16.01%.
9 Z. T. Huang and Z. R. Liu, *Synth. Commun.*, 1989, **19**, 943.
10 R. A. Bissell, A. P. de Silva, H. Q. N. Gunaratne, P. L. M. Lynch, G. E. M. Maguire, C. P. McCoy and K. R. A. S. Sandanayake, *Top. Curr. Chem.*, 1993, **168**, 223.
11 D. D. Perrin, B. Dempsey and E. P. Serjeant, *pKa Prediction for Organic Acids and Bases*, Chapman and Hall, London and New York, 1981.
12 (*a*) Fluorescence quantum yield φ was determined according to the equation: $\varphi = \varphi_R F/F_R A_R/A$, where *F* is the integrated intensity, *A* is the absorbance and the subscript R refers to the reference fluorophore of quinine sulfate (1.0×10^{-6} g dm^{-3} in 0.05 M H_2SO_4). Fluorescence measurements were performed on a HITACHI F-4500 spectrofluorimeter; (*b*) Fluorescence lifetime in neutral medium (pH = 6.6) was obtained at 25 °C with a single photon-counting apparatus (HORIBA NAES-1100 time-resolved spectrofluorimeter).
13 pK_a was calculated by the equation: pK_a = pH ± lg [$(F_{max} - F)/(F - F_{min})$]. See: R. A. Bissell, A. P. de Silva, H. Q. N. Gunaratne, P. L. M. Lynch, G. E. M. Maguire and K. R. A. S. Sandanayake, *Chem. Soc. Rev.*, 1992, **21**, 187.
14 M. Ayadim, J. L. H. Jiwan, A. P. De Silva and J. Ph. Soumillion, *Tetrahedron Lett.*, 1996, **37**, 7039.

CHEMCOMM
Communication
www.rsc.org/chemcomm

Rhodium-catalyzed formation of boron–nitrogen bonds: a mild route to cyclic aminoboranes and borazines

Cory A. Jaska, Karen Temple, Alan J. Lough and Ian Manners*

Department of Chemistry, University of Toronto, 80 St. George Street, Toronto, Ontario, Canada M5S 3H6. E-mail: imanners@alchemy.chem.utoronto.ca

Received (in Cambridge, UK) 13th March 2001, Accepted 12th April 2001
First published as an Advance Article on the web 10th May 2001

Secondary amine–borane adducts $R_2NH{\cdot}BH_3$, which are stable to H_2 elimination below 100 °C, undergo efficient catalytic dehydrocoupling at 25–45 °C in the presence of Rh^I or Rh^{III} complexes to quantitatively form cyclic aminoboranes $[NR_2–BH_2]_2$ (1: R = Me or 2: *cyclo*-C_4H_8); under similarly mild conditions, the analogous adducts $NH_3{\cdot}BH_3$ and $MeNH_2{\cdot}BH_3$ yield borazines $[RN–BH]_3$ (3: R = H or 4: R = Me) in yields limited by intermolecular coupling reactions.

The application of transition metal catalysis to organic synthesis is of enormous current importance. In contrast, the development of analogous methods for the formation of homonuclear or heteronuclear bonds between main group elements is relatively unexplored. Nevertheless, the discovery of new synthetic methods, which can complement the classical reactions used in main group chemistry such as salt eliminations, is likely to be of key future importance for the general development of molecular and macromolecular p-block chemistry. Recent work has focused on catalytic dehydrocoupling routes[1] and the well-established catalytic dehydropolymerization of silanes, germanes and stannanes represents a key advance.[2–6] More recently, homodehydrocoupling chemistry has been extended to include P–P bond formation[7] and catalytic heterodehydrocoupling reactions to form B–Si,[8] Si–P,[9] Si–N,[10] and Si–O bonds[11,12] have also been reported. Recently, we reported the first examples of the transition metal-catalyzed formation of P–B bonds.[13] Thus, dehydrocoupling of phosphine–borane adducts at 60–130 °C in the presence of a range of precatalysts (*e.g.* Rh^I complexes) was found to provide a new route to phosphinoborane rings, chains and macromolecules.[13,14] In this preliminary communication we report well-characterized examples of the use of catalytic dehydrocoupling to form new boron–nitrogen bonds under mild conditions.[15]

Amine–borane adducts undergo thermally-induced dehydrocoupling at elevated temperatures to afford mixtures of small rings such as cyclic aminoboranes and borazines. For example, dimethylamine–borane, $Me_2NH{\cdot}BH_3$, eliminates hydrogen at 130 °C to quantitatively yield the cyclic dimer $[Me_2N–BH_2]_2$ **1**.[16] However, when a solution of $Me_2NH{\cdot}BH_3$ in toluene was treated with *ca.* 0.5 mol% of $[Rh(1,5\text{-cod})(\mu\text{-Cl})]_2$ (1,5-cod = 1,5-cyclooctadiene) or $RhCl_3{\cdot}3H_2O$ at 25 °C for 48–60 h, the quantitative formation of the cyclic aminoborane **1** was detected by ^{11}B NMR spectroscopy. The reaction time was reduced to 24 h when the temperature was raised to *ca.* 45 °C or the amount of catalyst increased to 5 mol%. The iridium complex $[Ir(1,5\text{-cod})(\mu\text{-Cl})]_2$ also catalyzed the dehydrocoupling reaction but this precatalyst (*ca.* 0.5 mol%) proved less active with the reaction time for quantitative conversion to **1** increasing to 72 h at 45 °C. Significantly, prolonged heating of neat $Me_2NH{\cdot}BH_3$ in the absence of catalyst over a period of 7 days at 45 °C resulted in the quantitative recovery of unreacted adduct, which clearly demonstrated the catalytic effect of the Rh and Ir complexes.

Cyclic aminoborane **1** was isolated as a colorless, extremely volatile yet air-stable crystalline solid.† The ^1H-coupled ^{11}B NMR spectrum showed a triplet at δ 4.75 ($^1J_{BH}$ 110 Hz), which was consistent with the coupling of two hydrogens to the boron centre. While ^1H and ^{13}C NMR spectra were also consistent with the proposed product, single-crystal X-ray diffraction‡ provided definitive confirmation (Fig. 1).[17] Notably, the B–N bond lengths of **1** (1.595(4) Å) closely match those of the analogous cyclic trimer $[Me_2N–BH_2]_3$ (1.61(4) Å)[18] and moreover, are in the range observed for amine–boranes (*ca.* 1.58 Å). The four-membered ring appears to be strained with bond angles deviating significantly from the tetrahedral ideal with values of 93.7(2) and 86.3(2)° for the N(1)–B(1)–N(1A) and B(1)–N(1)–B(1A) angles, respectively.

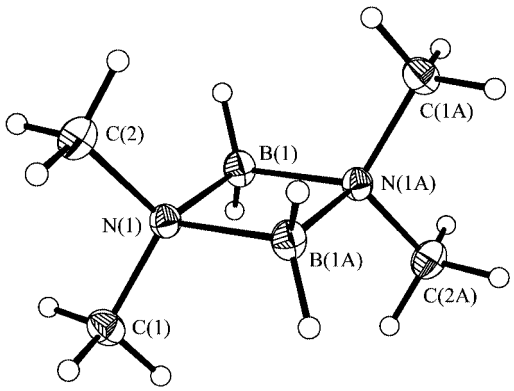

Fig. 1 Molecular structure of **1**. Selected bond lengths (Å) and angles (°): N(1)–B(1) 1.596(4), N(1A)–B(1) 1.595(4), N(1)–C(1) 1.478(4); N(1)–B(1)–N(1A) 93.7(2), B(1)–N(1)–B(1A) 86.3(2).

The formation of the cyclic dimer **1** *via* metal-catalyzed dehydrocoupling of a secondary amine–borane adduct represents a new, mild route to boron–nitrogen rings. We found that the strategy can be extended to other adducts such as pyrrolidine–borane, $(CH_2)_4NH{\cdot}BH_3$. Thus, the addition of catalytic (*ca.* 0.5 mol%) amounts of $[Rh(1,5\text{-cod})(\mu\text{-Cl})]_2$ or $RhCl_3{\cdot}3H_2O$ to a solution of the adduct (toluene, 25 °C, 24 h) similarly led to the quantitative formation of the cyclic aminoborane **2** (Scheme 1). Cyclic **2** was also characterized by multinuclear NMR spectroscopy† and by single-crystal X-ray diffraction.[19]

The catalytic dehydrocoupling methodology is not restricted to secondary amine–borane adducts. Thus, in the presence of $[Rh(1,5\text{-cod})(\mu\text{-Cl})]_2$ (1.5 mol%), the parent ammonia–borane adduct $NH_3{\cdot}BH_3$ was found to eliminate *two* equivalents of hydrogen to form borazine **3** (diglyme or tetraglyme, 45 °C, 72 h) by ^{11}B NMR (Scheme 2).[20] However, isolation from the reaction mixture by vacuum fractionation proved difficult; pure

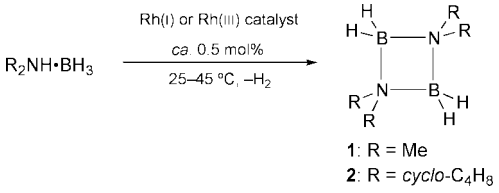

Scheme 1

 DOI: 10.1039/b102361f

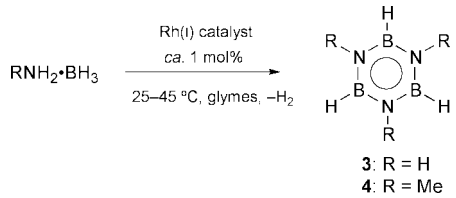

Scheme 2

3 was isolated in only *ca.* 10 % yield† with the major products being non-volatile, oligomeric species.[21,22]

Current preparations of borazine (*e.g.* from $NaBH_4$ and $(NH_4)_2SO_4$) require rather forcing conditions (elevated temperatures of 140–160 °C),[23] and, in our hands, are aggravated by similar difficulties in isolation. If optimized, the metal-catalyzed route may be advantageous, which is potentially significant as borazine and borazine oligomers have been shown to be useful precursors to cyclolinear polymers, boron nitride ceramics and nanotubes.[24–27]

In an attempt to minimize the intermolecular dehydrocoupling reactions, we also investigated the catalytic elimination of H_2 from *N*-methylamine–borane adduct. Indeed, we found that $MeNH_2{\cdot}BH_3$ undergoes dehydrocoupling in the presence of $[Rh(1,5\text{-cod})(\mu\text{-Cl})]_2$ (5 mol%), under similarly mild conditions (monoglyme or diglyme, 45 °C, 60 h) to afford *N*-trimethylborazine **4** by ^{11}B NMR. Pure **4** was isolated† in moderate yield (*ca.* 35–40%) by vacuum fractionation.[21,22] Previously developed routes to **4** typically involve high temperature dehydrogenation reactions such as the thermolysis of $MeNH_2{\cdot}BH_3$ at 100 °C to give the cyclic trimer $(MeNH{-}BH_2)_3$, followed by further pyrolysis at 200 °C.[28] Interestingly, through monitoring of the Rh catalyzed reaction by ^{11}B NMR, dehydrocoupling to form the cyclic aminoborane $(MeNH{-}BH_2)_3$ was found to occur first ($\delta -5.1$, $^1J_{BH}$ 108 Hz; lit. $\delta -5.4$, $^1J_{BH}$ 107 Hz),[29] followed by further loss of hydrogen to yield **4**. The isolation of a *ca.* 50% yield of non-volatile residue, indicates that intermolecular coupling also occurs in this case.[22] This process may involve catalytic dehydrocoupling of the intermediate $(MeNH{-}BH_2)_3$.

In summary, amine–borane adducts undergo B–N bond formation reactions under mild conditions in the presence of rhodium dehydrocoupling precatalysts (Schemes 1 and 2). Future work will involve an expansion of the scope of this new chemistry, which offers the prospect of improved routes to B–N compounds, and mechanistic investigations.

This research was supported by the Natural Science and Engineering Research Council of Canada (NSERC) and the Petroleum Research Fund (PRF) administered by the ACS. C. A. J. would like to thank the University of Toronto for a U of T Open Fellowship and K. T. thanks NSERC for a Postgraduate Scholarship (1997–2001). We would also like to acknowledge Professor William E. Buhro and Carolyn R. Jones from the Department of Chemistry, Washington University for many helpful discussions.

Notes and references

† *Selected spectroscopic data*: for **1**: yield (isolated) (0.18 g, 62%). ^1H NMR (300 MHz, $CDCl_3$): δ 3.2–2.0 (q, br, BH_2), 2.42 (s, CH_3). $^{13}C\{^1H\}$ NMR (75 MHz, $CDCl_3$): δ 52.0 (s, CH_3). ^{11}B NMR (160 MHz, $CDCl_3$): δ 4.75 (t, $^1J_{BH}$ 110 Hz, BH_2). For **2**: yield (isolated) (1.22 g, 73%). ^1H NMR (300 MHz, $CDCl_3$): δ 3.2–2.0 (q, br, BH_2), 2.84 (t, br, NCH_2CH_2), 1.70 (m, NCH_2CH_2). $^{13}C\{^1H\}$ NMR (75 MHz, $CDCl_3$): δ 60.1 (s, NCH_2CH_2), 23.7 (s, NCH_2CH_2). ^{11}B NMR (160 MHz, $CDCl_3$): δ 2.56 (t, $^1J_{BH}$ 110 Hz, BH_2). For **3**: yield (isolated) (0.57 g, *ca.* 10%). ^1H NMR (300 MHz, C_6D_6): δ 5.54 (t, br, NH), 4.45 (q, br, BH). ^{11}B NMR (160 MHz, C_6D_6): δ 30.2 (d, $^1J_{BH}$ 141 Hz, BH). For **4**: yield (isolated) (0.39 g, 40%). ^1H NMR (300 MHz, C_6D_6): δ 4.65 (q, br, BH), 2.96 (s, CH_3). $^{13}C\{^1H\}$ NMR (75 MHz, C_6D_6): δ 38.5 (s, CH_3). ^{11}B NMR (160 MHz, C_6D_6): δ 33.2 (d, $^1J_{BH}$ 132 Hz, BH). EI-MS (70 eV): 122 ($M^+ - H$, 100%).

‡ *Crystal data* for **1**: $C_4H_{16}B_2N_2$, M = 113.81, triclinic, space group $P\bar{1}$, a = 5.8330(7), b = 6.0290(10), c = 6.2400(10) Å, α = 80.372(8)°, β = 81.533(10)°, γ = 65.942(8)°, U = 196.80(5) Å^3, Z = 1, D_c = 0.960 Mg m^{-3}, μ = 0.055 mm^{-1}, $F(000)$ 64, T = 103(1) K, λ(Mo-Kα) = 0.71070 Å, crystal size 0.30 × 0.30 × 0.25 mm, 895 independent reflections, 3782 collected. Goodness-of-fit on F^2 = 1.162, final R indices [$I > 2\sigma(I)$], R_1 = 0.0963, wR_2 = 0.2866. Refinement was by full-matrix least squares on F^2 using all data. All hydrogens were included in calculated positions and refined isotropically.

CCDC 160965. See http://www.rsc.org/suppdata/cc/b1/b102361f/ for crystallographic data in .cif or other electronic format.

1 For a recent review, see: F. Gauvin, J. F. Harrod and H.-G. Woo, *Adv. Organomet. Chem.*, 1998, **42**, 363.
2 C. Aitken, J. F. Harrod and E. Samuel, *J. Am. Chem. Soc.*, 1986, **108**, 4059.
3 T. D. Tilley, *Acc. Chem. Res.*, 1993, **26**, 22.
4 J. A. Reichl and D. H. Berry, *Adv. Organomet. Chem.*, 1998, **43**, 197.
5 T. Imori, V. Lu, H. Cai and T. D. Tilley, *J. Am. Chem. Soc.*, 1995, **117**, 9931.
6 For a related example of demethanative coupling of germanes, see: S. M. Katz, J. A. Reichl and D. H. Berry, *J. Am. Chem. Soc.*, 1998, **120**, 9844.
7 N. Etkin, M. C. Fermin and D. W. Stephan, *J. Am. Chem. Soc.*, 1997, **119**, 2954.
8 Q. Jiang, P. J. Carroll and D. H. Berry, *Organometallics*, 1993, **12**, 177.
9 R. Shu, L. Hao, J. F. Harrod, H. G. Woo and E. Samuel, *J. Am. Chem. Soc.*, 1998, **120**, 12 988.
10 J. He, H. Q. Lui, J. F. Harrod and R. Hynes, *Organometallics*, 1994, **13**, 336.
11 Y. Li and Y. Kawakami, *Macromolecules*, 1999, **32**, 6871.
12 R. Zhang, J. E. Mark and A. R. Pinhas, *Macromolecules*, 2000, **33**, 3508.
13 H. Dorn, R. A. Singh, J. A. Massey, A. J. Lough and I. Manners, *Angew. Chem., Int. Ed. Engl.*, 1999, **38**, 3321.
14 H. Dorn, R. A. Singh, J. A. Massey, J. M. Nelson, C. A. Jaska, A. J. Lough and I. Manners, *J. Am. Chem. Soc.*, 2000, **122**, 6669.
15 To our knowledge, no examples of transition metal catalyzed dehydrocoupling routes to B–N bonds have appeared in the open literature. A patent (see Y. Blum and R. M. Laine, *US Pat.*, 4,801,439 1989) claims the catalytic formation of partially characterized mixtures of B–N compounds (including borazines) and insoluble polymeric products by the dehydrocoupling of mixtures of primary amines and $Me_3N{-}BH_3$ over extended periods of time at elevated temperatures. The conditions for the examples cited, typically 30–80 h, *ca.* 60 °C, in the presence of $Ru_3(CO)_{12}$, are also more forcing than with the Rh catalysts used in this communication.
16 A. B. Burg and C. L. Randolph Jr., *J. Am. Chem. Soc.*, 1949, **71**, 3451.
17 The crystal structure of **1** has been performed previously, but was only published as part of a dissertation by P. J. Schapiro from Cornell University (*Dissertation Abstr.*, 1962, **22**, 2607). This structure was found to have a different space group (*C*2/*m*) and unit cell dimensions than the one presented here.
18 L. M. Trefonas and W. N. Lipscomb, *J. Am. Chem. Soc.*, 1959, **79**, 4435.
19 C. A. Jaska, K. Temple, A. J. Lough and I. Manners, unpublished results.
20 Blank reactions performed in the absence of catalyst showed no dehydrocoupling products under the same conditions. Pure **3** and **4** were obtained through vacuum fractionation using traps at −45, −78 and −196 °C.
21 For an example of the trap-to-trap vacuum fractionation set-up for product purification, see: T. Wideman, P. J. Fazen, A. T. Lynch, K. Su, E. E. Remsen and L. G. Sneddon, *Inorg. Synth.*, 1998, **32**, 232.
22 The non-volatile residue was analyzed by ^{11}B NMR spectroscopy. Several distinct resonances were observed in the region δ = 26–36 suggesting further coupling. See, for comparison: P. J. Fazen, E. E. Remsen, P. J. Carroll, J. S. Beck, A. R. McGhie and L. G. Sneddon, *Chem. Mater.*, 1995, **7**, 1942.
23 T. Wideman and L. G. Sneddon, *Inorg. Chem.*, 1995, **34**, 1002.
24 R. T. Paine and L. G. Sneddon, *Chemtech*, 1994, **24**, 29.
25 P. J. Fazen, J. S. Beck, A. T. Lynch, E. E. Remsen and L. G. Sneddon, *Chem. Mater.*, 1990, **2**, 96.
26 T. Wideman and L. G. Sneddon, *Chem. Mater.*, 1996, **8**, 3.
27 O. R. Lourie, C. R. Jones, B. M. Bartlett, P. C. Gibbons, R. S. Ruoff and W. E. Buhro, *Chem. Mater.*, 2000, **12**, 1808.
28 T. C. Bissot and R. W. Parry, *J. Am. Chem. Soc.*, 1955, **77**, 3481.
29 C. K. Narula, J. F. Janik, E. N. Duesler, R. T. Paine and R. Schaeffer, *Inorg. Chem.*, 1986, **25**, 3346.

CHEMCOMM
Communication
www.rsc.org/chemcomm

Synthesis of spiro- and fused heterocycles by palladium catalysed carbo- and heteroannulation cascades of allenes

Ronald Grigg,* Ines Köppen, Marcello Rasparini and Visuvanathar Sridharan

Molecular Innovation, Diversity and Automated Synthesis (MIDAS) Centre, School of Chemistry, Leeds University, Leeds, UK LS2 9JT. E-mail: R.Grigg@chem.leeds.ac.uk

Received (in Cambridge, UK) 5th March 2001, Accepted 23rd April 2001
First published as an Advance Article on the web 10th May 2001

Two novel palladium catalysed cascade processes involving the generation of a (π-allyl)palladium intermediate from allenes in an intra- or intermolecular fashion, followed by regioselective intramolecular nucleophilic addition of amines, alcohols or malonates provide spiro- or linear fused heterocycles in good yield.

The importance and versatility of palladium catalysed processes involving allenes for the construction of carbon–carbon and carbon–heteroatom bonds is amply documented in a recent review.[1]

We have demonstrated that allenes are powerful relay switches in palladium catalysed polycomponent (poly)-cyclisation anion capture cascades.[2] Reaction of aryl/vinyl palladium(II) intermediates with allene leads to the formation of (π-allyl)palladium species able to undergo a wide range of transformations including attack by nucleophiles,[3] electrophiles[4] or transmetallation.[5]

The tactical combination of these transformations in an inter- and/or intramolecular fashion[6] enables expeditious increments of the molecular complexity of the products that are limited only by the ingenuity of the chemist.

We now report two novel palladium catalysed cascades ('Class 1' and 'Class 2') characterised by intramolecular anion capture[2] as the termination step. Both cascades are initiated by oxidative addition of Pd(0) into an Ar–I bond. In the 'Class 1' process this step is followed by an *exo-trig* cyclisation, intermolecular allene insertion and intramolecular capture of the resultant (π-allyl)palladium complex with a tethered nucleophile (amine or malonate anion) (Scheme 1a). This cascade results in the formation of three bonds and a spiro-fused ring system.

In the 'Class 2' process the (π-allyl)palladium complex is generated by an *exo-dig* cyclisation of the Ar–Pd species onto a proximal 1,2-dienamide. Subsequent interception of the resulting (π-allyl)palladium(II) species by a nucleophile leads to bicyclic lactams with formation of two rings and two new bonds (Scheme 1b).

The substrates for 'Class 1' process (Y = NR, $C(CO_2Me)_2$) were prepared in two steps by displacement of the allylic chlorides **1** or **3** with amines or dimethyl malonate (Scheme 2).

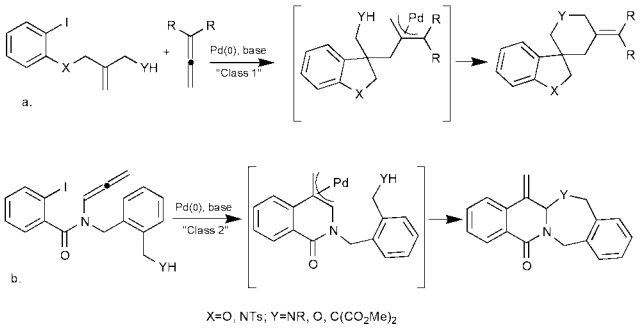

Scheme 1

Substrates **2a–c** and **4a–b** were then reacted with allene (1.0 bar) or 3-methylbuta-1,2-diene (dimethylallene) in the presence of a base and Pd(0) to afford the spirocyclic products in good yield[7] (Table 1). When dimethylallene was employed, exclusive formation of the regioisomer arising from attack at the less hindered end of the (π-allyl)palladium moiety was observed in all the cases.

We then focused our attention on a fully intramolecular process: a scaffold precursor **7** was synthesised in 57% overall yield from 2-bromobenzaldehyde (Scheme 3).

The formyl group was then exploited for the introduction of the desired nucleophiles (Scheme 4). The *N*-propargyl amides were then isomerised to the relatively labile *N*-allenyl amides

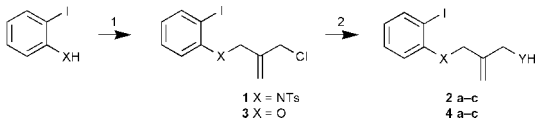

Scheme 2 *Reagents and conditions*: (1) 2-iodo-*N*-tosylaniline, NaH, 3-chloro-2-chloromethylpropene, DMF, rt, 48 h, 95% or 2-iodophenol, 3-chloro-2-chloromethylpropene, K_2CO_3, MeCN, reflux, 2 h, 91%; (2) primary amine (see Table 1), K_2CO_3, MeCN, reflux, 18 h (**2a**, 64%; **2b** 54%; **4a**, 61%, **4b**, 60%) or dimethyl malonate, K_2CO_3, CH_3CN, reflux, 18 h (**2c**, 80%, **4c**, 84%).

Table 1 Class 1 processes

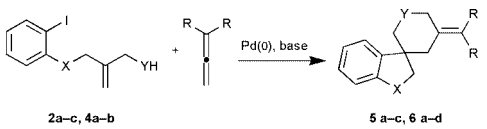

Entry	X	Y	R	Base[a]	Product	Yield (%)[b]
1 (**2a**)	NTs	*N*-Cyclopropyl	H	K_2CO_3	**5a**	59
2 (**2b**)	NTs	NBn	H	K_2CO_3	**5b**	54
3 (**2b**)	NTs	NBn	Me	K_2CO_3	**5c**	56
4 (**2c**)	NTs	$C(CO_2Me)_2$	H	Cs_2CO_3	**5d**	66
5 (**2c**)	NTs	$C(CO_2Me)_2$	Me	Cs_2CO_3	**5e**	72
6 (**4a**)	O	NBn	H	K_2CO_3	**6a**	55
7 (**4a**)	O	NBn	Me	K_2CO_3	**6b**	59
8 (**4b**)	O	*N*-Cyclopropyl	H	K_2CO_3	**6c**	65
9 (**4b**)	O	*N*-Cyclopropyl	Me	K_2CO_3	**6d**	66

[a] For experimental, see ref. 7. [b] Isolated analytically pure products.

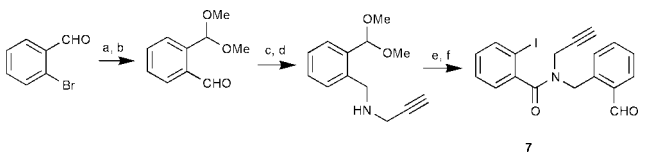

Scheme 3 *Reagents and conditions*: (1) MeOH, $CH(OMe)_3$, Dowex 50W X8-200, reflux, 18 h, 92%; 2) THF, *n*-BuLi, −78 °C, 30 min, then DMF, −78 °C to rt, 98%; (3) propargylamine, $MgSO_4$, DCM, 100%; (4) MeOH, $NaBH_4$, 0 °C, 95%; (5) 2-iodobenzoyl chloride, TEA, DCM, 0 °C to rt, 69%; (6) Montmorillonite K10, DCM, rt 10 min, 97%.

 DOI: 10.1039/b102046n

Table 2 Class 2 processes

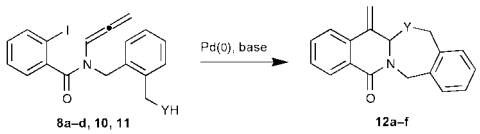

Entry	Y	Base[a]	Time (h)	Product	Yield (%)[d]
1 (**8a**)	NBn	K_2CO_3	24	**12a**	63
2 (**8b**)	*N*-Cyclopropyl	K_2CO_3	24	**12b**	55
3 (**8c**)	*N*-(1-Phenyl)ethyl	Ag_2CO_3	24	**12c**[b]	52
4 (**8d**)	*N*-(1-Naphthalen-1-yl)ethyl	Ag_2CO_3	24	**12d**[c]	54
5 (**10**)	O	Cs_2CO_3	48	**12e**	50
6 (**11**)	$C(CO_2Me)_2$	Cs_2CO_3	48	**12f**	45

[a] For experimental, see ref. 8. [b] 1.2 : 1 mixture of diasteroisomers (HPLC). [c] 1.5 : 1 mixture of diastereoisomers (^{1}H NMR). [d] Isolated analytically pure products.

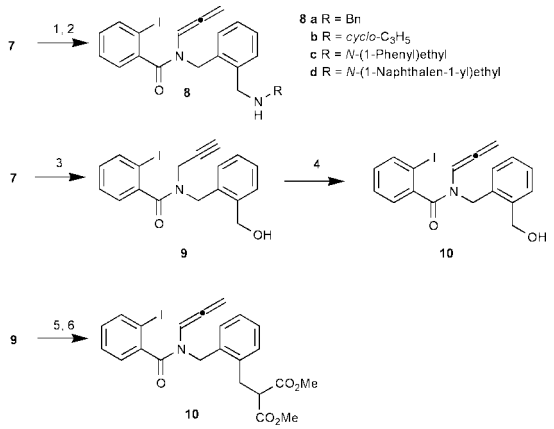

Scheme 4 *Reagents and conditions*: (1) Primary amine, $MgSO_4$, DCM, then MeOH, $NaBH_4$ 0 °C, 10 min, (**8a**, 85%, **8b**, 76%, **8c**, 71%, **8d**, 84%); (2) THF, *t*-BuOK (1.0 eq.), 0 °C, 1 min; (3) MeOH, $NaBH_4$ 0 °C, 10 min, 87%; (4) THF, *t*-BuOK (2.0 eq.), 0 °C, 1 min; (5) MsCl, TEA, DCM, 0 °C then DMF, sodium dimethyl malonate, 0 °C to rt, 60%; (6) THF, *t*-BuOK (2.0 eq.), 0 °C, 1 min.

immediately prior to the last Pd(0) catalysed step. The best conditions employed *t*-BuOK (1.1 eq. or 2.1 eq. when alcohols or malonates were used) in THF at 0 °C for 1 min. The transformation is nearly instantaneous and longer reaction times result in further isomerisation to *N*-prop-1-ynyl amides and to the formation of alcoholysis products.

All the substrates **8a**–**d** and **10**–**11** cyclised in 24–48 h in toluene at 50 °C in the presence of Pd(0) and an inorganic base[8] (Table 2).

We employed two chiral amines (**8c** and **8d**) in order to establish if the stereocenter α- to the nitrogen is able to induce a diastereofacial preference during the nucleophilic attack on the (π-allyl)palladium complex. When K_2CO_3 was employed, in both the cases a 1 : 1 mixture of diasteroisomers was obtained. Little improvement was achieved using Ag_2CO_3 (entry 3) or by increasing the steric hindrance around the nitrogen (entry 4). However, the two diasteroisomers were easily separated by crystallisation from EtOH.

A stronger base (entry 11) and longer reaction times were required (entry 10) for the less nucleophilic alcohol and malonate moieties.

In conclusion we have shown that this methodology permits access to unusual spiro- and fused heterocyclic frameworks.

We thank Leeds University and the EU for support.

Notes and references

1 R. Zimmar, C. U. Dinesh, E. Nandanan and F. A. Khan, *Chem. Rev.*, 2000, **100**, 3067.
2 R. Grigg and V. Sridharan, *J. Organomet. Chem.*, 1999, **576**, 65.
3 R. Grigg, V. Sridharan and L.-H. Xu, *J. Chem. Soc., Chem. Commun.*, 1995, 1903.
4 X. Gai, R. Grigg, S. Collard and J. Muir, *Chem. Commun.*, 2000, 1765.
5 U. Anwar, R. Grigg, M. Rasparini, V. Savic and V. Sridharan, *Chem. Comm.*, 2000, 645.
6 For a recent example of an intramolecular (π-allyl)palladium capture: L. E. Overman and M. D. Rosen, *Angew. Chem., Int. Ed.*, 2000, **39**, 4596.
7 Typical experimental conditions for 'Class 1' process: substrate (0.3 mmol), allene (1.0 bar, 100 ml one-neck pressure dram vessel) or dimethylallene (4.0 eq.), base (2.0 eq.), tri(2-furyl)phosphine (0.2 eq.), $Pd(OAc)_2$ (0.1 eq.), toluene (5.0 ml), 110 °C, 18 h.
8 Typical experimental conditions for 'Class 2' process: substrate (1.0 mmol), base (2.0 eq.), tri(2-furyl)phosphine (0.2 eq.), $Pd(OAc)_2$ (0.1 eq.), toluene (5 ml), 50 °C, 24–48 h.

CHEMCOMM
Communication
www.rsc.org/chemcomm

Tandem cationic cyclisation–aziridinium ion formation–nucleophilic ring opening: new methodology for the stereocontrolled synthesis of substituted pyrrolidines

Mark A. Graham,[a] Alan H. Wadsworth,[b] Mark Thornton-Pett[a]† and Christopher M. Rayner*[a]

[a] *School of Chemistry, University of Leeds, Leeds, UK LS2 9JT. E-mail: chrisr@chem.leeds.ac.uk*
[b] *GlaxoSmithKline Medicines Research Centre, Gunnels Wood Road, Stevenage, Hertfordshire, UK SG1 2NY*

Received (in Cambridge, UK) 6th March 2001, Accepted 12th April 2001
First published as an Advance Article on the web 11th May 2001

A novel tandem cationic cyclisation–aziridinium ion formation–nucleophilic ring opening procedure has been developed which provides powerful new methodology for the stereocontrolled synthesis of a wide variety of substituted pyrrolidines from acyclic precursors. The intermediate bicyclic aziridinium ions can be isolated and their structure has been confirmed by X-ray crystallography.

Saturated nitrogen heterocycles, including pyrrolidines and piperidines, occur in a wide variety of natural products and biologically active compounds.[1] Their synthesis has attracted much attention over the years, and methods which allow the construction of polysubstituted compounds with stereochemical control are particularly valuable.[2] Our research group has been involved in developing new chemistry of aziridinium ion intermediates, and alongside other workers in the field,[3] have shown them to be versatile, yet underused intermediates in synthetic organic chemistry.[4] Bicyclic aziridinium ions such as (**2**) have been known for some time, and are usually generated from the corresponding pyrrolidine-2-methanols or 3-hydroxypiperidines or halide derivatives thereof.[5] The reaction of these bicyclic aziridinium ions with nucleophiles is very useful synthetically, and is also of mechanistic interest as both pyrrolidine or piperidine products can be formed depending on the regioselectivity of the aziridinium ion cleavage reaction. However this methodology is limited due to the availability of suitable precursors, which are usually derived from proline or piperidine derivatives.

We have recently reported mechanistic and synthetic studies on the Lewis acid mediated nucleophilic cleavage of α-amino acetals.[6] In the course of this work we chose to investigate a range of substitution patterns, including *N*,*N*-diallylamines which were of interest as deprotection could be readily achieved under mild conditions to give the free primary amine.[7] At low temperatures, acetal substitution occurs,[6] however if the intermediate is allowed to warm to rt prior to addition of a nucleophile, then the final product is the substituted pyrrolidine (**3**) *as a single diastereoisomer* (Scheme 1). This can be rationalised by a cationic cyclisation of an *N*-allyl group onto the α-oxocarbenium ion, generated by cleavage of acetal (**1**). The nitrogen atom then intercepts the developing cationic centre directly forming the bicyclic aziridinium ion (**2**), followed by regioselective ring opening by the nucleophile.

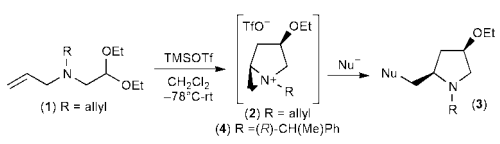

Scheme 1

† Author to whom communications regarding X-ray crystallography should be addressed.

The rearrangement to form the aziridinium ion proceeds in high yield, and such intermediates can be observed by ^{1}H NMR prior to addition of the nucleophile. Alternatively, they can be isolated as crystalline tetraphenylborate salts by addition of $NaBPh_4$ to an acetone solution of the triflate salts (**2**) followed by addition of ether to induce precipitation. The aziridinium ions isolated in this way, can be stored indefinitely, and are particularly attractive synthetic intermediates. This also allowed the use of X-ray crystallography to unambiguously determine the relative stereochemistry of the aziridinium ion (**4**) (Fig. 1) derived from *R*-(+)-α-methylbenzylamine, obtained by fractional crystallisation of the crude product mixture.[8]

Previous studies on the reactivity of bicyclic aziridinium ions such as (**2**) suggested that the regioselectivity of the ring opening reaction may be a problem, particularly if pyrrolidines were desired. However, we found that this was generally not the case (Table 1), and that a range of synthetically useful nucleophiles could be employed, leading to the synthesis of a diverse range of 1,2,4-trisubstituted pyrrolidines. Only in the case of oxygen nucleophiles were significant quantities of piperidine products formed, and in such cases, this could be improved by using more reactive synthetic equivalents.

Although these results were encouraging, the methodology did not offer the opportunity for control of absolute stereochemistry unless a resolution was used. We therefore also investigated more complex examples derived from substituted α-amino acetals which overcame this limitation. Examples are shown in Scheme 2.[6,9] In general, good selectivity is observed, which is essentially independent of nucleophile, consistent with the aziridinium ion intermediates (**7**) and (**10**). Importantly, even a substituent as small as a methyl group still allows for a good degree of stereocontrol for formation of aziridinium ion (**10**).

The observed stereocontrol can be rationalised by assuming all substitutents adopt a pseudo-equatorial position in a chair-like transition state in the cyclisation reaction (Fig. 2).

The remaining limitation on this chemistry lies in the nature of the acetal chosen. Although methyl and ethyl acetals are readily accessible, they do not allow for ready deprotection in the presence of sensitive functionality to give the more useful alcohol substituent. To address this problem we synthesised the

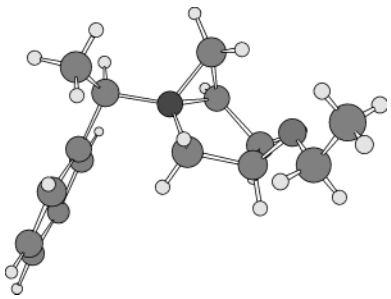

Fig. 1 X-Ray crystal structure of (**4**) (BPh_4 omitted for clarity).

 DOI: 10.1039/b102124i

benzyl acetal (**12**). This underwent smooth cyclisation with comparable efficiency and selectivity to other acetals (Scheme 3), and the product benzyl ether (**13**) should now be capable of hydrogenolysis, which would also allow concomitant N-deprotection to the parent substituted 3-hydroxypyrrolidine.

In summary, we have developed a novel tandem cationic cyclisation–aziridinium ion formation–nucleophilic ring opening procedure which provides powerful new methodology for the stereocontrolled synthesis of a wide variety of substituted pyrrolidines.[9] We are currently investigating this reaction further to determine its generality, and to exploit its potential in natural product synthesis. The results of these studies will be reported in due course.

Table 1 Nucleophilic opening of bicyclic aziridinium ions

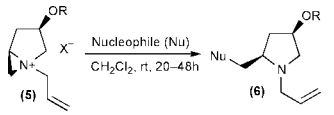

Entry	R	X[a]	Nucleophile	Product	Yield[b]
1	Me	BPh_4^-	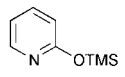	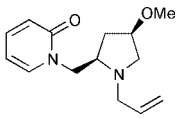	81%
2	Et	TfO^-	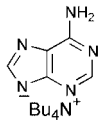	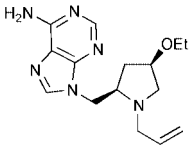	65%[c]
3	Et	BPh_4^-	$^nBu_2CuLi$	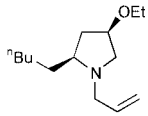	56%[c]
4	Me	BPh_4^-		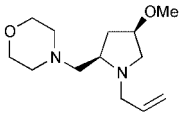	77%
5	Me	TfO^-		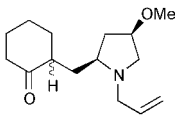	67%[d]
6	Me	BPh_4^-	NaOH	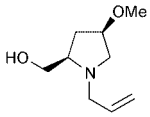	61% (<10%)
7	Me	TfO^-	MeONa	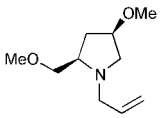	41% (20%)
8	Me	TfO^-	MeOH		68%[e]
9	Me	BPh_4^-	AcONa	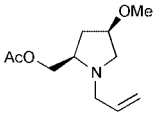	31% (28%)

[a] TfO^- counterion indicates aziridinium ion is generated *in situ*, whereas BPh_4^- counterion indicates preformed salt is used. [b] Yields for X = TfO^- are from the aminoacetal precursor, for X = BPh_4^-, yields are from the purified bicyclic aziridium ion salt; yields in parentheses are for isomeric piperidine. [c] CH_2Cl_2 exchanged for THF prior to addition of nucleophile. [d] 1:1 Mixture of diastereoisomers. [e] 55:45 Mixture of pyrrolidine and piperidine.

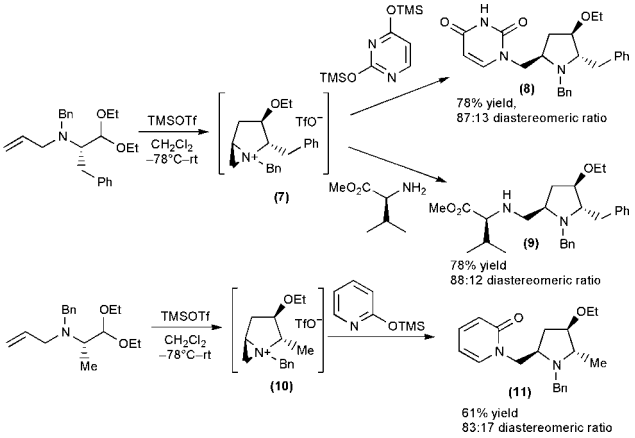

Scheme 2

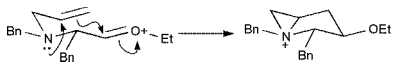

Fig. 2

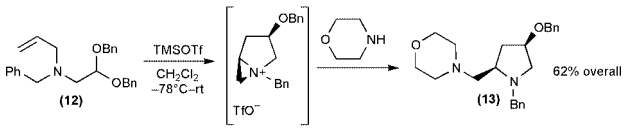

Scheme 3

We wish to thank the EPSRC and GlaxoSmithKline (Stevenage) for an Industrial CASE award.

Notes and references

1 See for example: A. A. Watson, G. W. J. Fleet, N. Asano, R. J. Molyneux and R. J. Nash, *Phytochemistry*, 2001, **56**, 265; D. O'Hagan, *Nat. Prod. Rep.*, 1997, 637.

2 A. Mitchinson and A. Nadin, *J. Chem. Soc., Perkin Trans. 1*, 2000, 2862 and references cited therein. For other recent examples see: D. W. Knight and R. Salter, *Tetrahedron Lett.*, 1999, **40**, 5915; A. M. Palmer and V. Jager, *Synlett*, 2000, 1405; I. A. O'Neil, E. Cleator, N. Hone, J. M. Southern and D. J. Tapolczay, *Synlett*, 2000, 1408.

3 See for example: T. H. Chuang and K. B. Sharpless, *Org. Lett.*, 1999, **1**, 1435 and references cited therein.

4 C. M. Rayner, *Synlett*, 1997, 11.

5 J. Cossy, C. Dumas and D. G. Pardo, *Eur. J. Org. Chem.*, 1999, 1693; K. A. Tehrani, K. van Syngel, M. Boelens, J. Contreras, N. De Kimp and D. W. Knight, *Tetrahedron Lett.*, 2000, **41**, 2507; L. Poitout, Y. Le Merrer and J. C. Depezay, *Tetrahedron Lett.*, 1996, **37**, 1613.

6 M. A. Graham, A. H. Wadsworth, M. Thornton-Pett, B. Carrozzini, G. L. Cascarano and C. M. Rayner, *Tetrahedron Lett.*, 2001, **42**, 2865. This paper also contains details of methods used for synthesis of appropriate precursors.

7 P. J. Kocienski, *Protecting Groups*, Thieme, 1994; see also ref. 4*b*.

8 Only one other X-ray crystal structure of an aziridinium ion has been reported, see: E. Pombo-Villar, J. Boelsterli, M. M. Cid, J. France, B. Fuchs, M. Walkinshaw and H. P. Weber, *Helv. Chim. Acta*, 1993, **76**, 1203. *Crystal data* for (**4**): $C_{39}H_{42}BNO$, M = 551.55, triclinic, a = 9.0282(2), b = 9.7091(2), c = 10.3036(2) Å, U = 791.07(3) Å^3, α = 114.3040(10), β = 97.6460(10), γ = 99.5540(10)°, T = 150 K, space group $P1$, Z = 1, λ(Mo-Kα) = 0.71073 Å, 8491 reflections measured, 5075 unique (R_{int} = 0.0392) which were used in all calculations. μ = 0.067 mm^{-1}, $R_1[I > 2\sigma(I)]$ = 0.0417, final $wR(F^2)$ was 0.1043 (all data). CCDC 160870. See http://www.rsc.org/suppdata/cc/b1/b102124i/ for crystallographic files in .cif format.

9 All new compounds have been characterised by ^{1}H and ^{13}C NMR, IR, MS and gave satisfactory elemental analysis. Stereochemical assignments for compounds (**8**), (**9**) and (**11**) were confirmed by NOE experiments; no attempt has been made to assign the stereochemistry of the minor diastereoisomeric products.

CHEMCOMM
Communication
www.rsc.org/chemcomm

A one-step synthesis of a free base secochlorin from a 2,3-dimethoxy porphyrin†

Jonathan L. Sessler,* Sergiy V. Shevchuk, Wyeth Callaway and Vincent Lynch

Department of Chemistry and Biochemistry, Institute for Cellular and Molecular Biology, The University of Texas at Austin, Austin, TX 78712-1167, USA. E-mail: sessler@mail.utexas.edu; Fax: 1-512-471-7550

Received (in Corvallis, OR, USA) 7th March 2001, Accepted 5th April 2001
First published as an Advance Article on the web 10th May 2001

The synthesis and X-ray structure of a C_2 symmetric secochlorin 2, obtained by a photosensitized oxidative ring opening of a 2,3-dimethoxy porphyrin, is described.

Photodynamic therapy (PDT), a promising treatment for a number of medical disorders, relies on selectively retained photosensitizers that are able to produce an efficient cytotoxic response upon activation with light. Currently, several porphyrin- or expanded porphyrin-type macrocycles are in advanced clinical testing or recently approved as PDT photosensitizers.[1] A range of other pyrrolic macrocycles are also being considered as photosensitizers, among them secochlorins.[1a] The first secochlorin to be characterized structurally was obtained as the result of an unexpected oxidative ring-opening of a corrinato nickel(II) salt.[2] Secochlorin diketones and dialdehydes have also been obtained from an analogous oxidative cleavage involving the corresponding nickel(II) chlorin diols.[3–5] As yet, however, these compounds have not been prepared in their non-metalated forms. On the other hand, several synthetic, structural, and spectroscopic studies of free base secoporphyrazines have been reported in recent years. For instance, a secoporphyrazine was formed as a minor side product during the synthesis of magnesium(II) porphyrazine as the result of the Linstead macrocyclization of 2,3-bis(dimethylamino)-2(*Z*)-butenedinitrile.[6] The same compound was also obtained in high yield by subjecting simple free base porphyrazine to manganese dioxide-mediated oxidation.[7] This latter method was further extended to core-metalated (*e.g.* Zn^{II}) and unsymmetrical free base porphyrazines. We now report the synthesis of the C_2 symmetric free base secochlorins **1** and **2** obtained in the form of their bis(methyl esters) as a result of an oxidative ring opening of dimethoxy-substituted porphyrins. To the best of our knowledge, compounds **1** and **2** represent the first example of a non-porphyrazine derived secochlorin to be characterized structurally in its free base form.

The porphyrin **3** containing a 3,4-dimethoxypyrrole unit was chosen as the starting material for the present secochlorin synthesis. This choice reflects the fact that attempts to prepare **3** from the readily available tripyrrane precursor 2,5-bis[(5-formyl-3-(3-hydroxypropyl)-4-methylpyrrol-2-yl)methyl]-3,4-diethylpyrrole[8] and 3,4-dimethoxypyrrole[9] using the standard '3 + 1' approach[10] gave rise not only to the expected porphyrin but also to secochlorin **1** as a minor side product. The chemical composition of **1** was inferred from CI mass-spectrometric analysis. Unfortunately, it proved impossible to separate the secochlorin from the major reaction product, porphyrin **3**, by column chromatography unless the side chain 3-hydroxypropyl groups were acetylated. This done, however, the desired separation was easily effected to give **2** in low (~5%) yield.

The interesting nature of **1** and its acetylated derivative **2**, led us to seek a more efficient synthesis. Here, we were inspired by the realization that **1** could have arisen from an air-based oxidation of the dominant 2,3-dimethoxyporphyrin product **3**. Based on such thinking, we considered that treating porphyrins, such as **3**, with singlet oxygen would effect conversion into the corresponding secochlorin. On a more practical level, we also thought it might prove useful to start with the bis-acetoxy porphyrin **4**, rather than **3**, so as to simplify purification of the corresponding secochlorin **2**, assuming it were to be produced. Accordingly, as shown in Scheme 1, porphyrin **4** (*ca.* 0.1 mol dm^{-3}) was dissolved in O_2-saturated methanol containing Rose Bengal (*ca.* 150 mg l^{-1}) and subject to irradiation using a 250 W projection lamp as a light source for *ca.* 10 h. Under these conditions, wherein singlet oxygen is the dominant oxidant,[11] the C_2 symmetric secochlorin was obtained in *ca.* 70% yield.

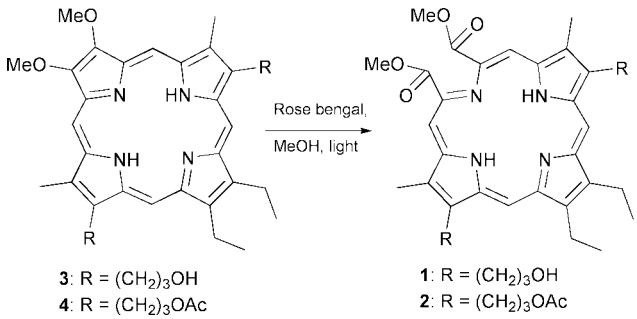

Scheme 1

UV-vis spectral analysis revealed that the Soret band of secochlorin **2** is red-shifted by approximately 11 nm as compared to porphyrin **4** (Fig. 1). More significant spectral changes were observed in the so-called Q-band region of the visible-spectrum. In particular, compound **2** was found to display a broad Q-type absorption band at 678 nm that is *ca.* 50 nm red-shifted compared to what is observed for the corresponding porphyrin **4**. This red-shifting of the lowest energy transition makes secochlorin **2** potentially interesting as a PDT photosensitizer.

Proton NMR spectroscopic studies of **2** and **4** revealed,‡ in accord with expectations, that the OCH_3 signal is shifted upfield

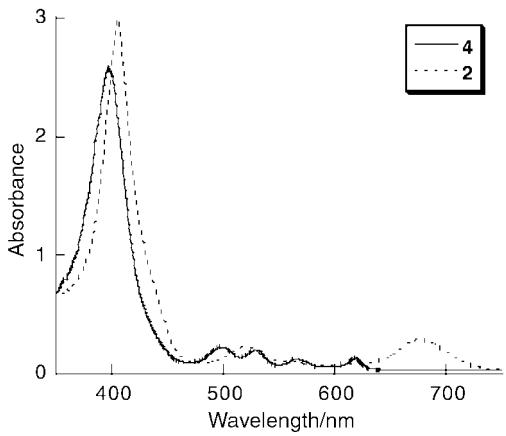

Fig. 1 Absorption spectra of porphyrin **4** and secochlorin **2**. CH_2Cl_2 solutions, room temperature.

† Electronic supplementary information (ESI) available: experimental details. See http://www.rsc.org/suppdata/cc/b1/b102139g/

 DOI: 10.1039/b102139g

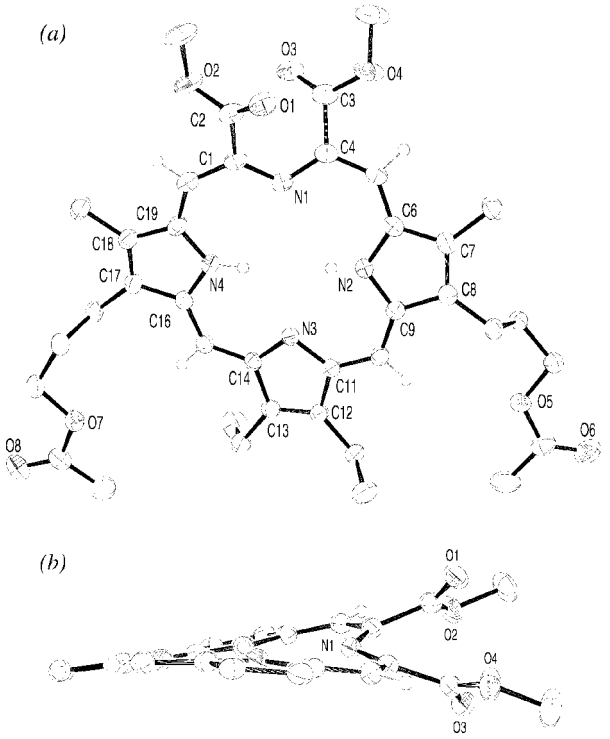

Fig. 2 Crystal structure of **2** showing a partial atom labelling scheme: *(a)* top and *(b)* side view. In the latter view, the pyrrole alkyl substituents are not shown on *(b)*. Thermal ellipsoids are scaled to the 50% probability level.

by *ca*. 0.6 ppm in secochlorin **2** (δ = 4.20 ppm) as compared to where it is seen in the case of porphyrin **4** (signal observed at 4.78 ppm). Presumably, it is the result of significant structural differences between **4** and **2**. Whereas the methoxy groups of **4** are bound directly to one of the porphyrin pyrroles, and hence in electronic contact with the main aromatic periphery, the methoxy groups of **2** are further removed from the principal secochlorin conjugation pathway. Further, they are tied up as ester groups. Separate from this, the four *meso*-carbon protons of porphyrin **4** were found to resonate as one singlet at 10.06 ppm, whereas in the case of **2** the corresponding protons resonate at slightly higher field and appear as two singlets (*i.e.* at 9.65 and 9.70 ppm, respectively).

A single-crystal X-ray diffraction analysis of **2** was also performed.§ This analysis confirmed the proposed secochlorin structure. In particular, it revealed that, on going from **4** to **2**, the dimethoxypyrrolic unit of porphyrin **4** gets transformed into a bis(methyl ester) moiety, without the connectivity of the macrocycle being otherwise modified (Fig. 2). The carbon–carbon bond lengths of the bis(methyl ester) unit [C1–C2 1.513(2), C3–C4 1.513(3) Å] are somewhat longer than the bond lengths in the pyrrole subunits [C6–C7 1.429(2), C8–C9 1.435(2), C11–C12 1.461(2), C13–C14 1.459(2), C16–C17 1.431(2), C18-C19 1.437(2) Å]. The C–N–C bond angle of the bis(methyl ester) [∠C1–N1–C4 120.24(14)°] was found to be significantly different from the bond angles seen for the pyrrolic units [∠C6–N2–C9 110.3(2)°, ∠C11–N3–C14 104.62(13)°, ∠C19–N4–C16 110.0°] and somewhat bigger than found for *meso*-tetraphenylsecochlorinato nickel(II)[6] [∠C1–N1–C4 114.3(3)°].

In summary, the synthesis of a novel secochlorin system by oxidative ring opening of a porphyrin is described. This convenient method, based on the singlet oxygen mediated ring opening of a 2,3-dimethoxyporphyrin, offers the prospect of allowing a range of new secochlorins to be prepared and isolated in their free base forms. Current work is focused on exploring the metallation chemistry of these new systems.

Support for this work came from the National Institute of Health (grant CA 68682 to J. L. S.) and Pharmacyclics, Inc.

Notes and references

‡ *Spectroscopic data* for **2**: ^{1}H NMR ($CDCl_3$), δ, ppm: −2.18 (s, 2H, NH), 1.79 (t, 6H, C*H*$_3$CH$_2$), 2.17 (s, 6H, pyrrole-C*H*$_3$), 2.51 (p, 4H, CH$_2$C*H*$_2$CH$_2$), 3.48 (s, 6H, C*H*$_3$COOCH$_2$), 3.83 (q, 4H, pyrrole-C*H*$_2$CH$_3$), 4.04 (t, 4H, pyrrole-C*H*$_2$CH$_2$CH$_2$), 4.20 (s, 6H, COOC*H*$_3$), 4.36 (t, 4H, C*H*$_2$OOCCH$_3$), 9.65 (s, 2H, *meso*-H), 9.70 (s, 2H, *meso*-H); ^{13}C NMR ($CDCl_3$), δ, ppm: 11.4, 18.3, 19.5, 21.1, 22.6, 31.4, 52.3, 63.8, 99.2, 99.6, 133.5, 134.7, 136.5, 137.5, 142.9, 143.2, 143.7, 167.2, 171.2. UV/vis (DCM), λ_{max}, nm: 402, 519, 677. CI-MS (M^+): 687. Anal. Calcd. for $C_{38}H_{46}N_4O_8$, %: C, 66.45; H, 6.75; N, 8.16; Found, %: C, 66.32; H, 6.80; N, 8.14. *Spectroscopic data* for **4**: ^{1}H NMR ($CDCl_3$): δ −3.78 (s, 2H, NH pyrrole), 1.88 (t, 6H, C*H*$_3$CH$_2$), 2.17 (s, 6H, pyrrole-C*H*$_3$), 2.63 (p, 4*H*, CH$_2$C*H*$_2$CH$_2$), 3.66 (s, 6H, C*H*$_3$COOCH$_2$), 4.01 (q, 4H, pyrrole-C*H*$_2$CH$_3$), 4.21 (t, 4H, pyrrole-C*H*$_2$CH$_2$CH$_2$), 4.40 (t, 4H, C*H*$_2$OCOOCH$_3$), 4.78 (s, 6H, OC*H*$_3$), 10.06 (s, 4H, *meso*-H); ^{13}C NMR ($CDCl_3$), δ, ppm: 11.4, 14.1, 18.5, 21.1, 22.6, 29.4, 31.7, 62.6, 96.3, 96.6, 99.2, 133.3, 134.6, 136.9, 137.2, 144.0, 145.0, 167.3, 171.2. UV/vis (DCM), λ_{max}, nm: 394, 497, 530, 565, 619. CI-MS (M^+): 655. Anal. Calcd. for $C_{38}H_{46}N_4O_6$, %: C, 69.70; H, 7.08; N, 8.56; Found, %: C, 69.82; H, 7.10; N, 8.54.

§ *Crystallographic data* for **2** (dark plates and prisms, 0.35 × 0.30 × 0.10 mm): $C_{38}H_{46}N_4O_8$, M = 686.79, triclinic, a = 9.7740(3), b = 12.2750(4), c = 16.3590(5) Å, α = 69.217(2), β = 84.584(2), γ = 82.626(2)°, T 123(2) K, U = 1817.27(10) Å^3, Z = 2, μ (Mo-Kα) = 0.088 mm^{-1}, 13040 reflections collected, 8267 independent reflections (R_{int} = 0.029), 5372 with $I \geqslant 2\sigma(I)$, R_1 = 0.0498, 0.0941 (all data), $wR(F^2)$ = 0.0981, 0.114 (all data). CCDC 160558. See http://www.rsc.org/suppdata/cc/b1/b102139g/ for crystallographic files in .cif format.

1 (*a*) E. D. Sternberg, D. Dolphin and C. Brückner, *Tetrahedron*, 1998, **54**, 4151; (*b*) T. D. Mody, *J. Porphyrin Phthalocyanines*, 2000, **4**, 362; (*c*) R. K. Panday, *J. Porphyrin Phthalocyanines*, 2000, **4**, 368; (*d*) I. J. MacDonald and T. J. Dougherty, *J. Porphyrin Phthalocyanines*, 2001, **5**, 105.

2 C. K. Chang, W. Wu, S.-S. Chern and S.-M. Peng, *Angew. Chem., Int. Ed. Engl.*, 1992, **31**, 70.

3 K. R. Adams, R. Bonnett, P. J. Burke, A. Salgado and M. Asunción Vallés, *J. Chem. Soc., Chem. Commun.*, 1993, 1860.

4 K. R. Adams, R. Bonnett, P. J. Burke, A. Salgado and M. Asunción Vallés, *J. Chem. Soc., Perkin Trans. 1*, 1997, 1769.

5 C. Brückner, E. D. Sternberg, L. K. MacAlpine, S. J. Rettig and D. Dolphin, *J. Am. Chem. Soc.*, 1999, **121**, 2609.

6 N. S. Mani, L. S. Beall, A. J. P. White, D. J. Williams, A. G. M. Barrett and B. M. Hoffman, *J. Chem. Soc., Chem. Commun.*, 1994, 1943.

7 A. G. Montablan, S. J. Lange, L. S. Beall, N. S. Mani, D. J. Williams, A. J. P. White, A. G. M. Barrett and B. M. Hoffman, *J. Org. Chem.*, 1997, **62**, 9284.

8 J. L. Sessler, T. D. Mody, G. W. Hemmi and V. Lynch, *Inorg. Chem.*, 1993, **32**, 3175.

9 A. Merz and T. Meyer, *Synthesis*, 1999, 94.

10 See for example: (*a*) K. M. Smith, *Strategies for the Synthesis of Octaalkylporphyrin Systems*, in *The Porphyrins Handbook*, K. M. Kadish, K. M. Smith and R. Guilard, Eds., Academic Press, San Diego, 2000; (*b*) J. L. Sessler, J. W. Genge, A. Urbach and P. Sansom, *Synlett*, 1996, 187; (*c*) A. Boudif and M. Momente, *J. Chem. Soc., Perkin Trans. 1*, 1996, 1235; (*d*) T. D. Lash, *Chem. Eur. J.*, 1996, **2**, 1197.

11 Rose Bengal is frequently used as a sensitizer to produce, upon irradiation, singlet oxygen in alcoholic solutions. See: A. A. Frimer, *Singlet O_2*, Boca Raton, Fla., 1985.

CHEMCOMM
Communication
www.rsc.org/chemcomm

Al distribution in ZSM-5 zeolites: an experimental study

J. Dědeček, D. Kaucký and B. Wichterlová

J. Heyrovský Institute of Physical Chemistry, Academy of Sciences of the Czech Republic, Dolejškova 3, CZ-182 23 Prague 8, Czech Republic. E-mail: wichterl@jh-inst.cas.cz

Received (in Cambridge, UK) 29th November 2000, Accepted 19th April 2001
First published as an Advance Article on the web 10th May 2001

Al atoms are not randomly distributed in ZSM-5 zeolites but their distribution is affected by the Si/Al composition and the synthesis procedure.

Zeolites with low concentration of aluminium in the framework (Si/Al > 8), such as *e.g.* those with the ZSM-5 structure, constitute a basis for catalysts of high significance in both acid–base and redox catalysis. Because of the low aluminium content, local Si–Al sequences described as 'Al pairs' [Al–O–$(Si–O)_{1,2}$–Al] and 'single' Al atoms [Al–O–$(Si–O)_{\geqslant 3}$–Al] that are far apart, are present in their frameworks.[1] Therefore, with divalent cations complete ion exchange is not possible.[2] Spatial distribution of the Si–Al sequences also leads to variations in the aluminium distribution in the zeolite channel system. As the occurrence and distribution of Al in the zeolite framework controls the presence, distribution and properties of catalytically active sites, *i.e.* of protonic and metal ion sites, the distribution of aluminium in the framework is very important for the catalytic properties of these materials. The presence of Al pairs is necessary for the exchange of divalent cations,[3] and the geometry of zeolite rings accommodating Al pairs affects coordination of the cations in zeolites.[3] However, no method is available for determination of the distribution of Al in silicon-rich zeolites. ^{29}Si MAS NMR can distinguish only Al–O–Si–O–Al pairs (representing only a minority of the Al pairs, < 5% Al, in ZSM-5[4]), while Al–O–$(Si–O)_2$–Al sequences cannot be distinguished from single Al atoms. Also ^{27}Al MAS NMR spectroscopy cannot provide such information. The theoretical approach using Monte Carlo simulation, based on the premise that Al distribution in zeolites is random, or quantum chemical studies modeling small clusters thus face severe limitations. Moreover, they cannot reflect the potential dynamic effect occurring during zeolite synthesis.

We suggest an indirect method for the estimation of the number of Al pairs and single Al atoms present in zeolites and of the distribution of Al pairs in framework local structures (cationic sites) in the zeolite channels. The method is based on monitoring of the distribution of bare divalent Co(II) ions, coordinated exclusively to framework oxygen atoms, at the cationic sites of dehydrated Co-zeolites exchanged to the maximum degree. To balance the positive charge of these bare divalent cations, two negative AlO_2^- charges are required at the cationic site. The d–d transitions of bare Co(II) ions in the Vis region reflect their coordination at the local geometry of the framework cationic sites. Three different cationic sites denoted as α, β and γ were suggested for bare Co(II) ions in mordenite, ferrierite and ZSM-5 structures.[5–7] In the case of the ZSM-5 matrix, Co(II) ions in the α site, characterized by a single band at 15 100 cm^{-1}, represent the Co(II) ions located above four framework oxygens forming a plane in the deformed six-membered ring composed of two five-membered rings. The Co(II) ions in the β site are located in another type of deformed six-membered ring, and their spectrum is composed of four bands at 16 000, 17 150, 18 600 and 21 200 cm^{-1}. The Co(II) ions in the 'boat shaped' γ site lead to a doublet of bands at 20 100 and 22 000 cm^{-1}. A schematic representation of these cationic sites is given in Fig. 1, (for details see ref. 7). Quantitative analysis of the corresponding Co(II) spectra provided the concentration and distribution of the Co(II) ions in the individual cationic sites of pentasil ring zeolites. Because bare Co(II) ions must be balanced by two framework AlO_2^- tetrahedra, the distribution of the bare Co(II) ions among the cationic sites in Co-ZSM-5 with maximum loading of the exchanged bare Co ions reflects the distribution of Al pairs [Al–O–$(Si–O)_{1,2}$–Al] at different cationic sites. Therefore, the bare Co(II) ions with characteristic spectral features can serve as probes for the distribution of Al pairs in zeolites.

To guarantee that the monitored Co(II) ions are counter ions to Al pairs, they should be present in the form of bare cations bound only to framework oxygens without coordinating extraframework ligands. This was confirmed by the NIR–Vis–UV spectra of dehydrated Co-ZSM-5 and supported by FTIR and EXAFS results. The absence of Co(II) ions coordinated to weak extraframework ligands, such as water or OH groups, was evidenced by the absence of the combination vibration bands around 5200 cm^{-1} (water) and 7200 cm^{-1} (water and OH). Also the band at 3650–3660 cm^{-1}, which reflects OH groups bound to Co or extraframework Al, was not found in the IR spectra of Co-ZSM-5 as well as in those of parent Na-ZSM-5. The latter information together with the ^{27}Al MAS NMR of Na-ZSM-5, indicating only T_d coordinated aluminium, evidenced that all aluminium was present in the zeolite frameworks. Coordination of the Co(II) ion to strong ligands such as an extraframework oxygen atom (Co–O–Co species) lead to intense charge transfer bands, which, however, are not found in the UV spectral region. Moreover, EXAFS results on Co-ZSM-5/A (Si/Al 14.1) showed Co(II) ions coordinated only to framework oxygens, and Co–O–Co type bonding was not detected.[8] Thus, the NIR–Vis–UV spectra can be used to provide evidence for the dominant presence of bare Co(II) ions in dehydrated Co-zeolites and for the estimation of the concentration and distribution of the Co(II) ions at the cationic sites.

The concentration of Al pairs in ZSM-5/A and B series† was obtained from the above described quantitative analysis of the Co(II) VIS spectra of Co-ZSM-5 zeolites with maximum loading of bare Co(II) ions (see ref. 7 and above). The effect of the procedure of zeolite synthesis and of the framework aluminium content in the ZSM-5 matrix (expressed as Si/Al ratio) on the relative concentration of Al pairs in α, β and γ sites (derived from absolute concentrations) is depicted in Fig. 2. The sum of the concentrations of Al pairs in α, β and γ sites

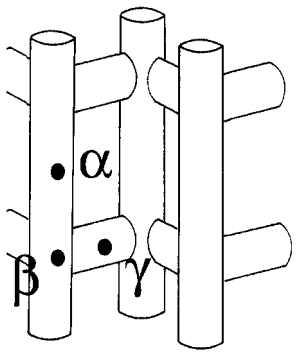

Fig. 1 Position of α, β and γ sites of the Co(II) ions in ZSM-5.

 DOI: 10.1039/b009589n

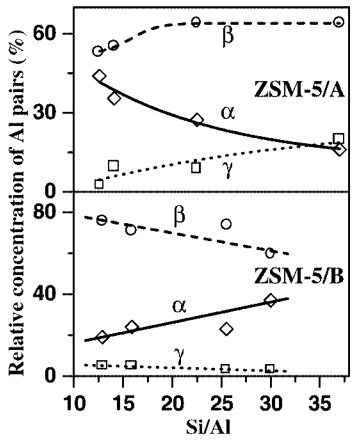

Fig. 2 Effect of Si/Al on relative concentration of Al pairs in α (——), β (– – –) and γ (···) sites for ZSM-5/A and /B.

represents the total concentration of Al pairs in the zeolite framework. The concentration of single Al atoms can be obtained as a difference between the total framework Al concentration (from bulk analysis, note that the extraframework Al species were not detected) and the concentration of Al pairs. The effect of the procedure of zeolite synthesis and of the framework aluminium content on the relative concentration of Al pairs and single Al atoms is described in Fig. 3. It is evident that the total concentration of Al pairs and single Al atoms as well as the relative concentration of Al pairs at the α, β and γ

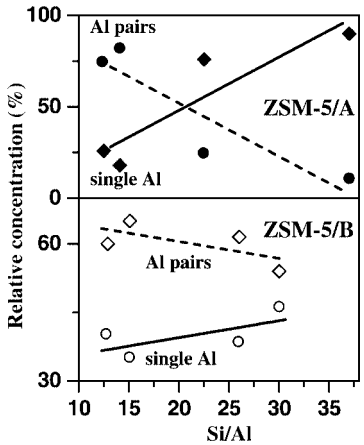

Fig. 3 Effect of Si/Al on relative concentration of single Al atoms (——) and Al pairs (– – –) for ZSM-5/A and /B.

cationic sites depend dramatically on the Si/Al composition and on the synthesis procedure.

The assumption of random or statistically controlled distribution of aluminium[1] cannot explain the dramatic differences in the Al distribution in zeolites synthesized under different conditions, and the dependence of the relative concentration of Al pairs in the α, β and γ sites on the Si/Al ratio. The results imply that the aluminium distribution in ZSM-5 is not random and not controlled exclusively by statistical rules. Preferences for the formation of single Al atoms and Al pairs in specific framework local structures play a significant role during zeolite synthesis and depend on the synthesis conditions.

It can be concluded that the Al distribution in silicon-rich molecular sieves is not random, but depends on the chemical composition of the zeolite and on the conditions of synthesis. The bare Co(II) ions detected by Vis spectroscopy represent a powerful tool for investigation of the Al distribution in silicon-rich zeolites. This provides a potential (i) for investigation of the relation between the activity of catalysts based on silicon-rich zeolites and the aluminium distribution in their framework, and (ii) for controlling the Al distribution in the framework of these zeolites by variation of synthesis procedures.

Financial support by the Grant Agency of the Czech Republic under the project # 104/00/0640 and by the EC COST program, project # D15/0014/00-OC D15.20 is gratefully acknowledged.

Notes and references

† ZSM-5 zeolites were prepared by two types of synthesis procedure. ZSM-5/A (Si/Al 12.5, 14.1, 22.5, 37) was provided by Slovnaft, Slovakia and ZSM-5/B (Si/Al 12.9, 15.9, 25.5, 30) was provided by the Research Institute of Inorganic Chemistry, Inc., Czech Republic. The parent Na-zeolites were ion-exchanged three times with 0.1 M $Co(NO_3)_2$ at ambient temperature. Dehydration of the samples was conducted at 770 K for 3 h under a dynamic vacuum up to 10^{-5} Torr.

1 N. O. Gonzales, A. K. Chakkraborty and A. T. Bell, *Catal. Lett.*, 1998, **50**, 135.
2 A. M. McAleer, L. V. C. Rees and A. K. Nowak, *Zeolites*, 1991, **11**, 329.
3 B. Wichterlová, J. Děrdeček and Z. Sobalík, *Catalysis by Unique Metal Ion Structures in Solid Matrices. From Science to Application*, ed. G. Centi, B. Wichterlová and A. Bell, Kluwer Academic Publishers, Dordrecht, 2001, p. 31–53.
4 G. C. Gobbi, G. J. Kennedy and C. A. Fyfe, *Chem. Lett.*, 1983, 1551.
5 J. Děrdeček and B. Wichterlová, *J. Phys. Chem. B*, 1999, **103**, 1462.
6 D. Kaucký, J. Děrdeček and B. Wichterlová, *Microporous Mesoporous Mater.*, 1999, **31**, 75.
7 J. Děrdeček, D. Kaucký and B. Wichterlová, *Microporous Mesoporous Mater.*, 2000, **35**–**36**, 483.
8 L. Drozdová, R. Prins, J. Děrdeček, Z. Sobalík and B. Wichterlová, *J. Phys. Chem. B*, submitted.

CHEMCOMM
Communication
www.rsc.org/chemcomm

'Chemical co-substrate rescue' of phytanoyl-CoA 2-hydroxylase mutants causing Refsum's Disease

Mridul Mukherji,[a] Nadia J. Kershaw,[a] Colin H. MacKinnon,[a] Ian J. Clifton,[a] Anthony S. Wierzbicki,[b] Christopher J. Schofield*[a] and Matthew D. Lloyd*[a]

[a] *The Oxford Centre for Molecular Sciences and The Dyson Perrins Laboratory, South Parks Road, Oxford, UK OX1 3QY, E-mail: matthew.lloyd@chem.ox.ac.uk, christopher.schofield@chem.ox.ac.uk*
[b] *Department of Chemical Pathology, King's, Guy's & St. Thomas' Medical School, St. Thomas' Hospital Campus, Lambeth Palace Road, London, UK SE1 7EH*

Received (in Cambridge, UK) 30th January 2001, Accepted 19th April 2001
First published as an Advance Article on the web 10th May 2001

The *in vitro* catalytic activity of two clinically observed mutants of phytanoyl-CoA 2-hydroxylase, an iron(II)/2-oxoglutarate-dependent oxygenase causing Refsum's Disease, was partially rescued by the use of alternatives to the natural cosubstrate, 2-oxoglutarate; this is the first demonstration of 'chemical co-substrate rescue' of mutations to an enzyme causing human disease.

Phytanic acid in the human diet is derived from the phytol sidechain of chlorophyll, but the presence of a 3-methyl group prevents its degradation *via* the fatty acid β-oxidation pathway. Instead, a preliminary pathway effects α-oxidation of phytanic acid, excising a methylene group to give pristanic acid.[1,2] Within this pathway, hydroxylation of phytanoyl-CoA to 2-hydroxyphytanoyl-CoA is catalysed by phytanoyl-CoA 2-hydroxylase (PAHX),[3,4] an iron(II) and 2-oxoglutarate-dependent oxygenase (Scheme 1).[5] Mutations to PAHX cause *ca.* 45% of adult Refsum's Disease (ARD) with other cases being associated with a second locus.[6]

Two common point mutations in human PAHX, R275W and R275Q, are present at an allele frequency of 3/40 (7.5%) and 5/40 (12.5%), respectively, in Dutch/Scandanavian patients with ARD.[3,7] Sequence analyses revealed that Arg-275 is conserved in all reported PAHX enzymes and closely related sequences. Analysis of the sequences in the light of crystal structures[8,9] for two other 2-oxoglutarate oxygenases suggested that Arg-275 binds the 5-carboxylate of the co-substrate *via* an electrostatic interaction.[8] We postulated that the PAHX R275Q and R275W mutants were inactive due to defective 2-oxoglutarate binding or utilisation, and that it may be possible to rescue their activity using alternative co-substrates.

The two clinically observed mutants of Arg-275 in human PAHX (R275Q and R275W)[3,7] and a further mutant R275A, made for comparison, were constructed by site-directed mutagenesis. The desired proteins were expressed *via* standard techniques in recombinant *E. coli* and purified as mature (*i.e.* without their peroxisomal targeting sequences) enzymes to > 95% homogeneity (by SDS-PAGE analysis). Mutations were confirmed by DNA sequencing and ESI MS analyses. Analysis of the secondary structure by circular dichroism suggested that all mutants had a similar overall structure to the wild-type enzyme.

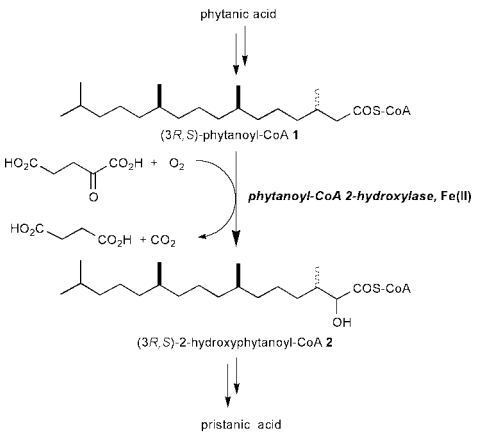

Scheme 1 The role of phytanoyl-CoA 2-hydroxylase in the peroxisomal degradation of phytanic acid.

Activity of the wild-type enzyme and mutants was assayed by conversion of phytanoyl-CoA to 2-hydroxyphytanoyl-CoA.[10] Assays were performed (at least in triplicate) according to a modified version of a published procedure[11] and included ATP to obtain maximum activity.[12] The activity was further enhanced *ca.* two-fold by the use of tris(carboxyethyl)phosphine (TCEP) in place of the previously used dithiothreitol (DTT).[11] Two concentrations of 2-oxoacid (2 and 60 mM) were used in order to facilitate detection of low levels of activity. Assay mixtures for the analogues contained: 50 mM Tris-HCl, pH 7.5, 1 mM $FeSO_4$, 50 μM synthetic (3*RS*,7*R*,11*R*)-phytanoyl-CoA, 0.44 mM β-cyclodextrin, 100 μM TCEP, 10 mM ascorbate, 4 mM ATP and *ca.* 20 μg enzyme (2 mM 2-oxoacid) or 10 μg enzyme (60 mM 2-oxoacid). Reactions were quenched with 250 mM EDTA after incubation for 60 min (2 mM 2-oxoacid) or 5 min (60 mM 2-oxoacid). Samples were centrifuged and analysed by HPLC using a Hypersil C_{18} column (250 × 4.6 mm) monitoring at 254 nm.[11]

Using the natural co-substrate, 2-oxoglutarate, the activity of the two clinically observed mutants was < 0.5% of that of the wild-type enzyme (Table 1). A range of 2-oxoacids was tested in an attempt to restore the activity of the mutants. Homogentisate, 4-hydroxyphenylpyruvate, indole-3-pyruvate, 2-mercaptosuccinate all gave specific activities of < 0.2 nmol min^{-1} mg^{-1} with wild-type enzyme and all mutants. The activity of the R275Q and R275W mutants was significantly 'rescued' compared to the wild-type activity with 2-oxoglutarate as a co-substrate using certain 2-oxoacids at a concentration of 60 mM (Table 1). Optimum rescue of mutants with hydrophobic/aliphatic residues in place of Arg-275 is achieved using 2-oxoacids with side-chains of 2–4 carbon atoms or equivalent length side-chains. Effective examples are in the use of 2-oxobutyrate with R275Q mutant (Table 1, entry 4) and 2-oxo-5-thiahexanoate with the R275W mutant (Table 1, entry 9). The latter case is striking because 2-oxo-5-thiahexanoate cannot be substituted for 2-oxoglutarate (< 0.5%) in assays with the wild-type enzyme. The dramatic change in co-substrate selectivity resulting from PAHX Arg-275 mutations may be useful for the clinical identification of these particular mutants using a modified assay with alternative 2-oxoacids.

Even higher levels of rescue were obtained in the case of the R275A mutant where most of the hydrophobic analogues tested (Table 1, entries 3–9), led to 22–28% rescue at 60 mM. An exception was 2-oxooctanoic acid (Table 1, entry 10), which was inactive with the wild-type enzyme, and all mutants assayed, presumably due to its carbon chain being too large to

 DOI: 10.1039/b101039p

Table 1 Specific activities of (3*RS*,7*R*,11*R*)-phytanoyl-CoA hydroxylation as catalysed by mature recombinant wild-type and mutant PAHX enzymes in the presence of various 2-oxoacids (nmol min^{-1} mg^{-1} protein). Assays were carried out with 2 mM or 60 mM 2-oxoacid

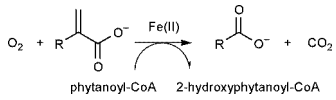

PAHX mutant	R275 (wild-type)		R275A		R275Q		R275W	
2-oxoacid/mM	2	60	2	60	2	60	2	60
1. 2-oxoglutarate R = $(CH_2)_2CO_2^-$	265	885	2.63	128	0.59	< 0.2	< 0.2	< 0.2
2. 2-oxoadipate R = $(CH_2)_3CO_2^-$	129	235	3.14	57.0	< 0.2	< 0.2	< 0.2	< 0.2
3. pyruvate R = CH_3	6.8	78.6	8.7	201	< 0.2	54.0	0.6	11.0
4. 2-oxobutyrate R = CH_2CH_3	2.1	69.4	5.7	250	2.7	106	0.9	55.2
5. 2-oxovalerate R = $(CH_2)_2CH_3$	1.6	40.1	4.8	210	3.0	71.6	1.93	63.9
6. 2-oxoisovalerate R = $CH(CH_3)_2$	0.65	45.3	4.30	192	1.52	72.2	0.49	17.0
7. 2-oxocaproate R = $(CH_2)_3CH_3$	0.7	20.1	5.3	235	1.33	42.4	2.4	66.2
8. 2-oxoisocaproate R = $CH_2CH(CH_3)_2$	0.8	17.8	4.8	217	1.9	45.4	2.2	56.2
9. 2-oxo-5-thiahexanoate R = $(CH_2)_2SCH_3$	< 0.2	< 0.2	4.8	226	1.6	52.8	2.6	98.2
10. 2-oxooctanoic acid R = $(CH_2)_5CH_3$	N/D	< 0.2	N/D	< 0.2	N/D	< 0.2	N/D	< 0.2

be accommodated in the proper orientation in the active site. The R275A mutant was also less selective than the wild-type or other tested mutants, presumably due to a relaxation of steric and electrostatic constraints reflecting the presence of a small, hydrophobic and neutral side-chain.

2-Oxoacids are metabolically related to proteinogenic amino acids *via* transamination reactions. Several of the 2-oxoacids which rescue the activity of the clinically observed R275W and R275Q mutants are thus accessible *via in vivo* amino acids, *e.g.* 2-oxovalerate from valine and 2-oxo-5-thiahexanoate from methionine. Thus, certain forms of ARD might be treated *via* dietary supplements containing the appropriate amino acids. Maple syrup urine disease is caused by a deleterious accumulation of excess 2-oxacids, and is treated, in the reverse of this proposed therapy, by a diet low in branched-chain amino acids.[13] Restoration of complete wild-type activity may not be required, as 5% of wild-type activity is apparently sufficient to effectively correct inherited homocystinuria[14] with vitamin B6.

To our knowledge the only other example of the rescue of enzyme activity with a modified co-substrate has involved the elegant use of ATP analogues to study *in vivo* activity of

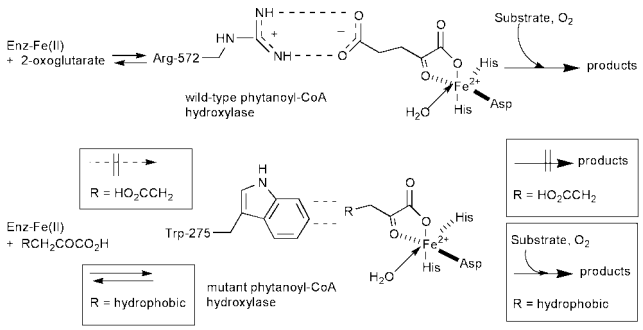

Scheme 2 'Chemical co-substrate rescue' of a PAHX mutant as exemplified for R275W. R = hydrophobic/aliphatic group. Wild-type enzyme showing interaction of guanidino group of Arg-275 and 5-carboxylate of 2-oxoglutarate (above). Unfavourable interaction between aromatic sidechain of Trp-275 and 5-carboxylate of 2-oxoglutarate; rescue of activity *via* hydrophobic interactions in 2-oxoacid binding site (below). The relative arrangement of the iron ligands is that of deacetoxycephalosporin C synthase (DAOCS).[8]

kinases.[15] The *in vitro* work that is reported here is the first demonstration of the 'chemical co-substrate rescue' of mutations in an enzyme (Scheme 2) implicated in a human disease. *In vivo* studies directed towards demonstrating the technique in cell lines are in progress.

Notes and references

1 D. Steinberg, in *'Refsum Disease', The metabolic and molecular basis of inherited metabolic disease*, ed. C. R. Scriver, A. L. Beaudet, W. S. Sly and D. Valle, New York, 1995.
2 N. M. Verhoeven, R. J. A. Wanders, B. T. Poll-The, J. M. Saudbubray and C. Jakobs, *J. Inherit. Metab. Dis.*, 1998, **21**, 697.
3 S. J. Mihalik, J. C. Morrell, D. Kim, K. A. Stackster, P. A. Watkins and S. J. Gould, *Nat. Genet.*, 1997, **17**, 185.
4 G. A. Jansen, R. Ofman, S. Ferdinandusse, L. IIjlst, A. O. Muisers, O. H. Skjeldal, O. Stokke, C. Jakobs, G. T. N. Besley, J. E. Wraith and R. J. A. Wanders, *Nature Genet.*, 1997, **17**, 190.
5 A. G. Prescott and M. D. Lloyd, *Nat. Prod. Rep.*, 2000, **17**, 367.
6 A. S. Wierzbicki, J. Mitchell, M. Lambert-Hammill, M. Hancock, J. Greenwood, M. C. Sidey, J. de Belleroche and F. B. Gibberd, *Eur. J. Hum. Genet.*, 2000, **8**, 649.
7 G. A. Jansen, E. M. Hogenhout, S. Ferdinandusse, H. R. Waterham, R. Ofman, C. Jakobs, O. H. Skjeldal and R. J. A. Wanders, *Hum. Mol. Gen.*, 2000, **9**, 1195.
8 K. Valegård, A. C. Terwisscha van Scheltinga, M. D. Lloyd, T. Hara, S. Ramaswamy, A. Perrakis, A. Thompson, H.-J. Lee, J. E. Baldwin, C. J. Schofield, J. Hajdu and I. Andersson, *Nature*, 1998, **394**, 805.
9 Z.-H. Zhang, J. Ren, J. K. Stammers, J. E. Baldwin, K. Harlos and C. J. Schofield, *Nat. Struct. Biol.*, 2000, **7**, 127.
10 M. Mukherji, N. J. Kershaw, I. J. Clifton, C. J. Schofield, A. S. Wierzbicki and M. D. Lloyd, *manuscript in preparation.*
11 S. J. Mihalik, A. M. Rainville and P. A. Watkins, *Eur. J. Biochem.*, 1995, **232**, 545.
12 K. Croes, V. Foulon, M. Casteels, P. P. Van Veldhoven and G. P. Mannaerts, *J. Lipid Res.*, 2000, **41**, 629.
13 S. E. Snyderman, P. M. Norton, E. Roitman and L. Holt, *Pediatrics*, 1964, **34**, 454.
14 J. P. Kraus, M. Janosik, V. Kozich, R. Mandall, V. Shih, M. P. Sperandeo, G. Sebastio, R. de Franchis, G. Andria, L. A. Kluijtmans, H. Blom, G. H. Boers, R. B. Gordon, P. Kamoun, M. Y. Tsai, W. D. Kruger, H. G. Koch, T. Ohura and M. Gaustadnes, *Hum. Mut.*, 1999, **13**, 362.
15 Y. Liu, K. Shah, F. Yang, L. Witucki and K. M. Shokat, *Chem. Biol.*, 1998, **5**, 91.

CHEMCOMM
Communication
www.rsc.org/chemcomm

Conversion of the carboxy group of sialic acid donors to a protected hydroxymethyl group yields an efficient reagent for the synthesis of the unnatural beta-linkage

Xin-Shan Ye, Xuefei Huang and Chi-Huey Wong*

Department of Chemistry and The Skaggs Institute for Chemical Biology, The Scripps Research Institute, 10550 North Torrey Pines Road, La Jolla, CA 92037, USA. E-mail: wong@scripps.edu

Received (in Corvallis, OR, USA) 5th March 2001, Accepted 4th April 2001
First published as an Advance Article on the web 10th May 2001

New sialyl donors with a protected hydroxymethyl group at the anomeric center are over 1000 times more reactive than the normal ester containing sialylation reagent and give excellent yield (> 90%) with unusually high β-stereoselectivity in sialylation.

N-Acetylneuraminic acid (sialic acid) residues are often located at the non-reducing end of glycoconjugates, and play important roles in many biological recognition events such as cancer metastasis and bacterial or viral infection.[1,2] The synthesis of sialyl glycoconjugates, however, remains a challenge.[3]

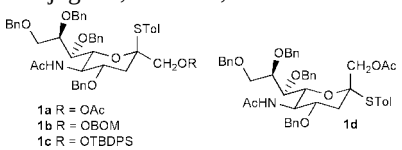

In a typical sialylation reaction, the electron withdrawing carboxy group at the anomeric center of sialic acids significantly destabilizes the oxonium ion forming transition state thus lowering the reactivity of sialyl donors towards nucleophiles. Furthermore, the steric hinderance at the anomeric center leads to elimination and low yields of sialylation. Various methods have been developed to overcome these problems, including, for example, introduction of an additional *N*-acetyl moiety,[4,5] installation of an anchimeric assisting group at the C3 position[5–8] or a carboxy equivalent at the anomeric center.[9,10] The latter approach includes utilizing a less electron withdrawing furyl substituent as the carboxy surrogate.[9] This method, however, failed to yield any disaccharides with secondary sugar alcohols. Increased reactivities towards *N*-iodosuccinimide (NIS) have also been observed with the reduced 2,3-didehydro sialic acid derivatives, but these reactions gave very low yields (~ 20%).[10]

To tackle the aforementioned problems, we converted the carboxy group of sialic acid to the hydroxymethyl group and prepared derivatives **1a**–**1d** for investigation (Scheme 1). The peracetylated sialic acid **3**[11] was treated with *p*-thiocresol to give thio-sialic acid **4b** in 75% yield together with 20% of the α isomer **4a**. The protective groups of **4b** were exchanged for benzyl groups to give compound **5** in two steps in 55% yield. Reduction of the ester moiety was accomplished with $LiBH_4$ in 90% yield to give the hydroxymethyl sialic acid derivative **2**, the hydroxy group of which was protected with the acetyl, benzyloxymethyl (BOM) or *tert*-butyldiphenylsilyl (TBDPS) group to give sialyl donors **1a**–**1c**. The α sialyl donor **1d** was prepared from **4a** in a similar manner as the β sialyl donor **1a**.

The relative reactivity values (RRV) of known and new sialic acid donors **1a**–**1d**, **2**, **4b** and **5** were measured as previously described[12] and shown in Table 1. Compared to the benzyl protected sialic acid **5**, over *three orders of magnitude* increase in RRV was observed with all the reduced sialic acid derivatives **1a**†–**1d** and **2** (RRV for **1a**, **1b**, **1c**, **1d** and **2** are 4.0×10^4, 2.3×10^5, 7.8×10^4, 8.0×10^4 and 3.3×10^5 respectively). The reactivities of all these reduced sialic acids (**1a**–**1d** and **2**) are

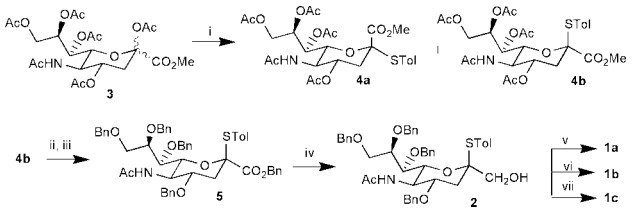

Scheme 1 *Reagents and conditions*: (i) *p*-Thiocresol, $BF_3{\cdot}Et_2O$, CH_2Cl_2, 20% for **4a**, 75% for **4b**; (ii) NaOMe, MeOH, 100%; (iii) NaH, BnBr, DMF, 55%; (iv) $LiBH_4$, THF, MeOH, 90%; (v) Ac_2O, pyridine, 96%; (vi) BOMCl, Pr^i_2NEt, CH_2Cl_2, 86%; (vii) TBDPSCl, imidazole, DMF, 96%.

comparable to or even higher than perbenzylated L-fucose **6** which was the most reactive thioglycoside measured previously.[12]

With the RRV values in hand, sialylation of donors **1a**–**1d** was performed. The TBDPS protected sialyl donor **1c** failed to undergo glycosylation with galactose acceptor **7**, presumably due to the large TBDPS group. With the smaller acetyl protective group, donor **1a** underwent smooth sialylation with galactose acceptor **7** to give disaccharides **8** and **9** in 95% yield (**8**:**9** = 15:1) in acetonitrile using dimethyl(methylthio)sulfonium triflate (DMTST) as the promoter[13,14] (Scheme 2a). No elimination product was isolated. The hydroxymethyl moiety of the products can be subsequently unmasked after sialylation and selectively oxidized to the carboxy group in three high yielding steps as demonstrated by transformation of compound **8** to **10** (Scheme 2b) and **9** to **12** (Scheme 2c). However, quite unexpectedly the predominant product **8** formed in the sialylation contains a β linkage between the two monosaccharides. The near zero $^3J_{C1,H3a}$ value in the EXCIDE[5,15] spectra of **8** and **11**‡

Table 1 Relative reactivity values (RRV) of various thio-glycosides[a]

Compound	RRV	Compound	RRV
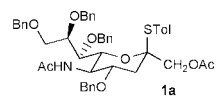 **1a**	4.0×10^4	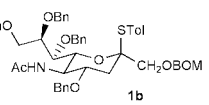 **1b**	2.3×10^5
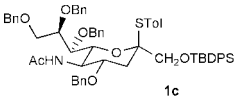 **1c**	7.8×10^4	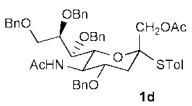 **1d**	8.0×10^4
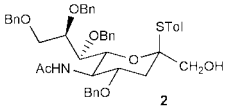 **2**	3.3×10^5	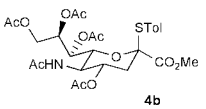 **4b**	2.55
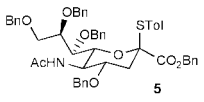 **5**	48.4	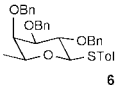 **6**	7.2×10^4

[a] The RRV is based on the reactivity of 1-thiotolyl-2,3,4,6-tetraacetyl-β-D-mannopyranoside.

 DOI: 10.1039/b102166b

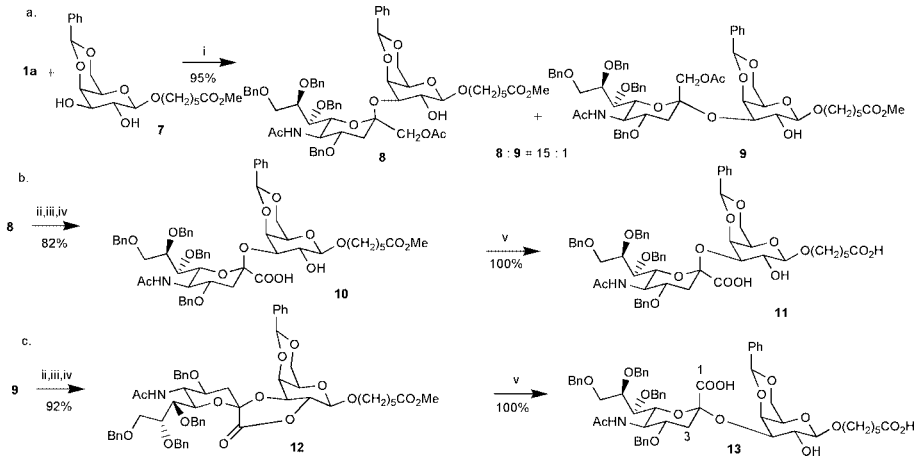

Scheme 2 *Reagent and conditions*: (i) DMTST, molecular sieves, CH_3CN, −40 °C to rt, overnight; (ii) NaOMe, MeOH, rt, 1 h; (iii) $PhI(OAc)_2$, TEMPO, rt, 12 h; (iv) $NaClO_2$, 2-methylbut-2-ene, rt, 4 h; (v) NaOH, H_2O, rt, 1 h.

indicated the β-configuration, while the $^3J_{C1,H3a}$ value of **13**§ was determined to be 6.1 Hz indicating its α-configuration. Comparison of the chemical shifts of H_{3eq} of compound **11** (2.64 ppm) and **13** (2.72 ppm)[16] further confirmed the assignment following the empirical rules of chemical shift.[4] The stereoselectivity does not vary much with different acceptors. Sialylation of various acceptors such as isopropyl alcohol **14**, lactose derivative **15** as well as primary alcohol **16**, glucosamine **17** and galactose **18**, with donor **1a** using DMTST as the promoter, gave predominantly the β-linked disaccharide[17] (β : α > 10 : 1) in high yields (> 90%). The exception was the sialic

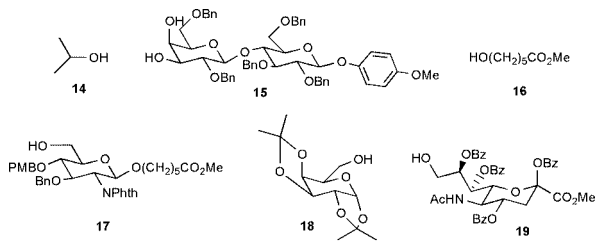

acid derivative **19** which gave a ratio of 3 : 1 favoring β-disaccharide in 90% total yield. Sialylations in solvents such as ether, toluene and dichloromethane gave even more β anomer than those performed in acetonitrile. The acetonitrile effect[18] could not significantly alter the anomeric selectivity. Sialylation of galactose **7** with the BOM protected donor **1b** or α sialyl donor **1d** gave the product with similar yield and stereoselectivity to those with donor **1a**.

Sialylations with promoters other than DMTST were also tested. MeOTf[19] failed to activate sialyl donor **1a** while with PhSOTf[20] only the β isomer was isolated when galactose **18** was sialylated with **1a**. The use of NIS and triflic acid (TfOH) improved the α-selectivity (α : β = 1 : 2.5) when galactose acceptor **7** was sialylated with **1a** in 90% total yield.

In conclusion, it has been demonstrated that the reactivity of sialic donors can be dramatically increased by reducing the carboxy group at the anomeric center to the hydroxymethyl moiety. Subsequent sialylation with these novel sialyl donors proceeded in excellent yield (> 90%) but with unusually high β stereoselectivity, probably due to a significant anomeric effect. The hydroxymethyl moiety can be easily oxidized to the carboxy group in high yield. The high reactivity of sialyl donors could find uses in the preparation of enzymatically stable unnatural oligosaccharides containing β-sialic acid. Oligosaccharides with unnatural glycosidic linkage could have important biological implications, as illustrated in the study of CD-1 mediated T-cell activation.[21] The new glycosylation reagents can also be utilized in programmable one-pot synthesis, where the sialylation reaction often has to be the first and most reactive as sialic acid is often located at the non-reducing end of bio-active oligosaccharides.[12] Introduction of a C-3 auxiliary may give the α-linkage.

This work was supported by the National Institutes of Health (GM-44154). We thank Dr Zhiyuan Zhang for helpful discussions.

Notes and references

† *Selected data* for **1a**: ^{1}H NMR (400 MHz, $CDCl_3$) δ 7.03 (d, J = 7.9 Hz, 2H), 5.06 (d, J = 8.5 Hz, 1H), 3.69 (dd, J = 3.8, 10.4 Hz, 1H), 2.26 (s, 3H), 2.20 (dd, J = 3.7, 13.5 Hz, 1H), 1.92 (dd, J = 11.0, 13.4 Hz, 1H); ^{13}C NMR (100 MHz, $CDCl_3$) δ 170.44, 170.15, 88.86, 69.17, 68.18, 51.77, 35.62, 23.69, 21.07, 20.66; HRMS (M + Cs) calcd for $C_{48}H_{53}O_8NSCs$ 936.2546, found 936.2577.

‡ *Selected data* for **11**: ^{1}H NMR (400 MHz, CD_3OD) δ 5.32 (s, 1H), 2.66 (dd, J = 4.4, 13.2 Hz, 1H), 2.16 (t, J = 7.6 Hz, 2H), 1.77 (s, 3H), 1.72 (dd, J = 11.3, 13.2 Hz, 1H); ^{13}C NMR (100 MHz, $CDCl_3$) δ 174.36, 170.04, 102.54, 101.90, 100.26, 69.93, 69.19, 68.84, 52.04, 51.60, 35.92, 33.69, 28.65, 25.36, 24.25, 23.22; $^3J_{C1,H3a} \sim 0$ Hz; HRMS (M − H + 2 Na^+) calcd for $C_{58}H_{65}O_{16}NNa_2$ 1054.4196, found 1054.4202.

§ *Selected data* for **13**: ^{1}H NMR (600 MHz, CD_3OD) δ 5.32 (s, 1H), 2.72 (dd, J = 3.7, 12.6 Hz, 1H), 2.16 (t, J = 7.2 Hz, 2H), 1.94 (s, 3H), 1.88 (t, J = 12.6 Hz, 1H); ^{13}C NMR (150 MHz, $CDCl_3$) δ 182.25, 174.40, 172.78, 103.45, 101.61, 101.28, 69.84, 68.80, 50.95, 38.15, 35.95, 29.43, 26.48; $^3J_{C1,H3a}$ = 6.1 Hz; HRMS (M − H + 2 Na^+) calcd for $C_{58}H_{65}O_{16}NNa_2$ 1054.4196, found 1054.4175.

1 M. P. DeNinno, *Synthesis*, 1991, 583.
2 K. Okamoto and T. Goto, *Tetrahedron*, 1990, **46**, 5835.
3 G.-J. Boons and A. V. Demchenko, *Chem. Rev.*, 2000, **100**, 4539.
4 A. V. Demchenko and G.-J. Boons, *Chem.-Eur. J.*, 1999, **5**, 1278.
5 N. Hossain and G. Magnusson, *Tetrahedron Lett.*, 1999, **40**, 2217.
6 J. C. Castro-Palomino, Y. E. Tsvetkov and R. R. Schmidt, *J. Am. Chem. Soc.*, 1998, **120**, 5434.
7 T. Ercegovic and G. Magnusson, *J. Org. Chem.*, 1995, **60**, 3378.
8 Y. Ito and T. Ogawa, *Tetrahedron*, 1990, **46**, 89.
9 S. J. Danishefsky, M. P. DeNinno and S.-H. Chen, *J. Am. Chem. Soc.*, 1988, **110**, 3929.
10 E. Kirchner, F. Thiem, R. Dernick, J. Heukeshoven and J. Thiem, *J. Carbohydr. Chem.*, 1988, **7**, 453.
11 A. Marra and P. Sinay, *Carbohydr. Res.*, 1989, **187**, 35.
12 Z. Zhang, I. R. Ollmann, X.-S. Ye, R. Wischnat, T. Bassov and C.-H. Wong, *J. Am. Chem. Soc.*, 1999, **121**, 734.
13 T. Murase, H. Ishida, M. Kiso and A. Hasegawa, *Carbohydr. Res.*, 1988, **184**, c1.
14 O. Kanie, M. Kiso and A. Hasegawa, *J. Carbohydr. Chem.*, 1988, **7**, 501.
15 H. Hori, T. Nakajima, Y. Nishida, H. Ohrui and H. Meguro, *Tetrahedron Lett.*, 1988, **29**, 6317.
16 Comparison of H_{3eq} chemical shifts must be based on the free acid forms **11** (2.64 ppm) and **13** (2.72 ppm). The formation of lactone **12** caused an upfield shift of H_{3eq} to 2.60 ppm while the chemical shift of H_{3eq} of **10** remained 2.64 ppm.
17 The stereochemistry of the disaccharides was determined by measuring $^3J_{C1,H3a}$ from the EXCIDE spectra as described for compounds **8**, **11** and **13**.
18 I. Braccini, C. Derouet, J. Esnault, C. Herve du Penhoat, J.-M. Mallet, V. MIchon and P. Sinay, *Carbohydr. Res.*, 1993, **246**, 23.
19 H. Lonn, *J. Carbohydr. Chem.*, 1987, **6**, 301.
20 V. Martichonok and G. M. Whitesides, *J. Org. Chem.*, 1996, **61**, 1702.
21 S. A. Porcelli and R. L. Modlin, *Annu. Rev. Immunol.*, 1999, **17**, 297.

CHEMCOMM
Communication
www.rsc.org/chemcomm

Cholesterol-armed cyclen–Na^+ complex as a chiral, helicated amphiphile for supramolecular architecture: self-aggregation and chirality induction in aqueous solution

Satoshi Shinoda,[a] Tsuyoshi Okazaki,[a] Tomoko Nishimura,[a] Kenzi Hori[b] and Hiroshi Tsukube*[a]

[a] *Department of Chemistry, Graduate School of Science, Osaka City University, Sugimoto, Sumiyoshi-ku, Osaka 558-8585, Japan. E-mail: tsukube@sci.osaka-cu.ac.jp*

[b] *Department of Applied Chemistry and Chemical Engineering, Faculty of Engineering, Yamaguchi University, Ube 755-0031, Japan*

Received (in Cambridge, UK) 14th February 2001, Accepted 20th April 2001
First published as an Advance Article on the web 10th May 2001

An octadentate Na^+ complex of chiral cholesterol-armed cyclen has a quadruple helicated structure and forms a stable self-aggregate in aqueous solution which offers chirality induction of achiral 5-dimethylaminonaphthalen-1-ylsulfonylglycine anion.

Several kinds of transition and lanthanide metal complexes are recognized as useful building blocks for supramolecular architecture,[1] because of their well-defined coordination topology, high thermodynamic stability and inert kinetics. In contrast, alkali metal complexes usually have versatile coordination structures, low stability and rapid kinetics, and hence their use for this purpose is limited. We demonstrate here that an octadentate Na^+ complex of chiral cholesterol-armed cyclen **1** forms a stable self-aggregate in aqueous solution which provides a unique microenvironment for chirality induction of achiral 5-dimethylaminonaphthalen-1-ylsulfonylglycine anion (DNS-Gly^-).[2] The employed cyclen **1**–Na^+ complex is a new type of chiral amphiphile furnished with three functional components (Fig. 1):[3] ester-armed cyclen as a twisted octadentate ligand;[4] four cholesterol groups as chiral and hydrophobic walls;[5] and the Na^+ ion as a charged group of amphiphile.[6] Since this Na^+ complex exhibits unexpectedly high stability and inert kinetics (log$K$ = 11.2 in C_2D_5OD), its self-aggregate is expected to offer three different levels of chirality in the aqueous solution: (1) chirality of cholesterol moieties; (2) helicity on asymmetrically twisted octadentate Na^+ complex; and (3) integrated chirality of highly structured Na^+ complexes on a supramolecular scale.

A series of metal complexes with tetra-armed cyclens are known to have C_4 symmetry in which four sidearms are arranged as a quadruple helicate *via* twisted square-antiprismatic coordination.[7] Actually, cyclen **2**–NaCl complex gave ^{13}C NMR signals for two carbons of the cyclen ring separately resonating at 51.50 and 49.51 ppm in $CDCl_3$ at 295 K, while a single signal was observed at 55.12 ppm for N-CH_2-CO-carbons of four sidearms. Although the enantiomerization can proceed either by a rotation of the four sidearms or an inversion of the cyclen cycle,[8] these observations indicated that cyclen **2**–Na^+ complex maintained unique quadruplicated helical structures in the solution (Fig. 1). Chiral cyclen **1**–NaCl complex similarly exhibited two separate ^{13}C NMR signals for cyclen ring carbons at 53.01 and 48.46 ppm, though each cholesterol moiety on the cyclen arm has several asymmetric carbons. As reported in some Na^+ complexes with chiral tetra-armed cyclens,[9] cyclen **1**–Na^+ complex is thought to have only a single C_4 orientation in which four chiral cholesterol moieties are arranged in an asymmetrically helicated fashion.

Cholesterol-armed cyclen **1**–NaCl complex spontaneously aggregated in an aqueous ethanol solution (H_2O–EtOH = 80/20, v/v; pH = 7.2, bis-tris-HCl)[10] and gave no precipitate from its aqueous solution after 10 days. The critical aggregation concentration was estimated as 4.0×10^{-6} mol dm^{-3} by fluorescence titrations, which was much smaller than those of common micelle-forming surfactants. Dynamic light scattering experiments showed that the aggregate had a mean hydrodynamic radius of 600 Å, and a TEM picture taken after treatment of uranyl acetate also indicated that it was of similar size (Fig. 2). Interestingly, this self-aggregate accommodated DNS-amino acid anions in the hydrophobic domains. When an excess of self-aggregate was added to an aqueous ethanol

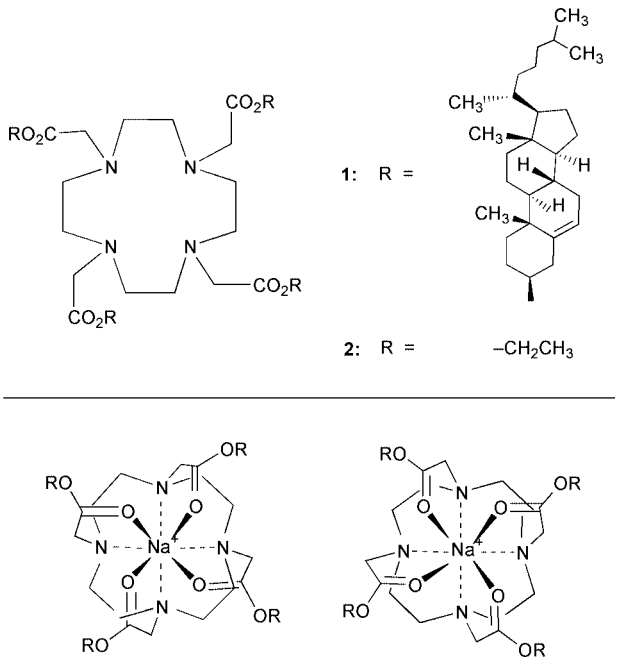

Fig. 1 Armed cyclens and quadruplicated helical structures of their Na^+ complexes.

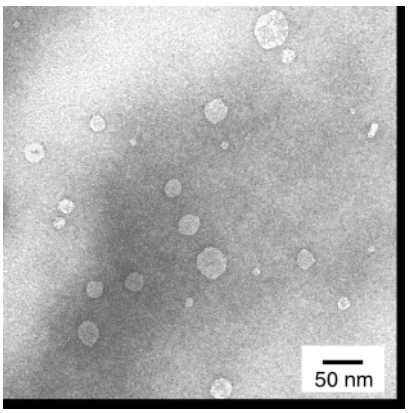

Fig. 2 TEM Picture of dispersed self-aggregates of cyclen **1**–NaCl complexes.

 DOI: 10.1039/b101438m

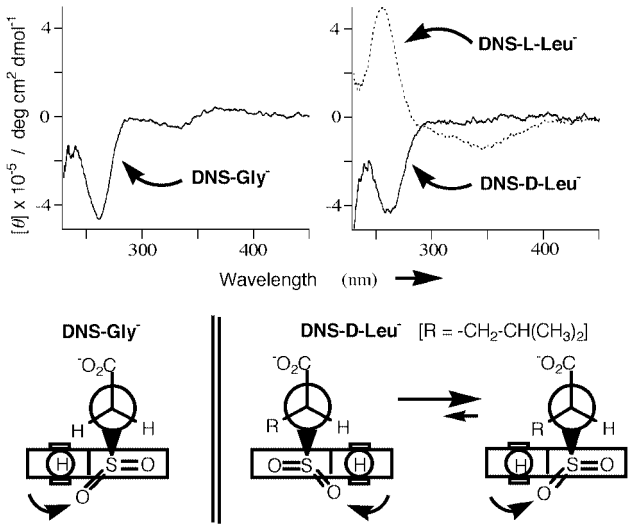

Fig. 3 CD Spectra and preferred conformations of dansyl-glycine (DNS-Gly) and dansyl-leucine (DNS-Leu) anions incorporated in self-aggregate of cyclen **1**–NaCl complexes. [**1**–NaCl] = 3.0×10^{-5} mol L^{-1}; [DNS-Gly$^-$] = 5.0×10^{-5} mol L^{-1}; [DNS-Leu$^-$] = 6.5×10^{-5} mol L^{-1}. The indicated CD spectra of DNS-D- and L-Leu anions were corrected by subtraction of those in the bulk aqueous phases.

solution of DNS-L-leucine anion (DNS-L-Leu$^-$), the fluorescence maximum of the guest anion shifted from 538 nm to 507 nm and the intensity was enhanced 6.5-fold. Cholesteryloxycarbonyl-4-methylmorpholine was examined for comparison. This also formed a water-soluble aggregate in the presence of Na^+ ion, but the resulting aggregate rarely accommodated DNS-amino acid anions. Therefore, the assembling of four cholesterol moieties on the octadentate Na^+ complex platform provided an effective microenvironment for inclusion of DNS-amino acid anions in the aqueous solution.

The self-aggregate of cyclen **1**–NaCl complexes further offered chirality induction of achiral anion substrates upon inclusion. Typically, DNS-Gly$^-$ was incorporated in the self-aggregate and exhibited a negative CD signal around 280 nm (Fig. 3). Both sign and intensity of the observed CD spectrum were similar to those of DNS-D-Leu$^-$ recorded in the self-aggregate, indicating that the conformation of DNS-Gly$^-$ was asymmetrically fixed as true in DNS-D-Leu$^-$ system. Such chirality induction phenomena were reported when the degree of freedom of achiral molecules was severely restricted in the solids, membranes, micelles and inclusion compounds.[11] Polonski *et al.* reported that the CD signal observed with chiral DNS-amino acid originated from unsymmetrical twisting of the sulfonamide group in relation to the naphthalene plane under the influence of hydrogen atom in the *peri*-position (Fig. 3).[12] Since the preferred conformation of DNS-D-Leu$^-$ was determined by the steric problem around the S=O bond rather than the *peri*-positioned hydrogen atom, the negative CD signal was indicative of 'anti-clockwise' conformation. The obtained CD results suggested that the 'anti-clockwise' conformation of DNS-Gly$^-$ was more stable than the 'clockwise' one, when this achiral anion was incorporated in the self-aggregate.

We demonstrated above that the self-aggregate of cyclen **1**–NaCl complexes having an asymmetrically helicated structure allowed chirality induction of the achiral guest anion upon inclusion. Since there are many structural variations in the armed cyclen–alkali metal complexes, their characteristic coordination chemistry provides further possibilities in the development of supramolecular architecture with fascinating functions.

The authors are grateful to Professors Takeshi Nagasaki of Osaka City University and Atsushi Yoshizawa of Hirosaki University for valuable comments on characterizations of the self-aggregate. This research was supported in a part by a Grant-in-Aid for Scientific Research from the Ministry of Education, Science, Culture and Sports, Japan.

Notes and references

1 S. Leininger, B. Olenyuk and P. J. Stang, *Chem. Rev.*, 2000, **100**, 853; G. F. Swiegers and T. J. Malefetse, *Chem. Rev.*, 2000, **100**, 3483.
2 Molecular recognition in aqueous solutions by self-aggregated amphiphiles: K. Ariga and T. Kunitake, *Acc. Chem. Res.*, 1998, **31**, 371; P. Grandimi, F. Mancin, P. Tecilla, P. Scrimin and U. Tonellato, *Angew. Chem., Int. Ed.*, 1999, **38**, 3061; S. Kolusheva, T. Shahal and R. Jelinek, *J. Am. Chem. Soc.*, 2000, **122**, 776.
3 This was prepared in a similar manner to that of cyclen **2**–NaCl complex (see Ref. 4) and fully characterized as **1**–NaCl·$5H_2O$.
4 H. Tsukube, Y. Mizutani, S. Shinoda, T. Okazaki, M. Tadokoro and K. Hori, *Inorg. Chem.*, 1999, **38**, 3506.
5 A. P. Davis, R. P. Bonar-Law and J. K. M. Sanders, *Comprehensive Supramolecular Chemistry*, Pergamon Press, Oxford, 1996, Vol. 4, p. 257.
6 Alkali metal complexes with cholesterol-functionalized crown ethers were reported to form vesicles, channels and gel materials: S. Shinkai and K. Murata, *J. Mater. Chem.*, 1998, **8**, 485.
7 L. L. Chappell, D. A. Voss, W. D. W. Horrocks and J. R. Morrow, *Inorg. Chem.*, 1998, **37**, 3989; C. L. Maupin, D. Parker, J. A. G. Williams and J. P. Riehl, *J. Am. Chem. Soc.*, 1998, **120**, 10 563; R. Dhillon, S. F. Lincoln, S. Madbak, A. K. W. Stephens, K. P. Wainwright and S. L. Whitbread, *Inorg. Chem.*, 2000, **39**, 1855.
8 F. A. Dunand, S. Aime and A. E. Merbach, *J. Am. Chem. Soc.*, 2000, **122**, 1506.
9 R. S. Dickens, J. A. K. Howard, C. L. Maupin, J. M. Moloney, D. Parker, R. D. Peacock, J. P. Riehl and G. Siligardi, *New J. Chem.*, 1998, 891; L. J. Govenlock, J. A. K. Howard, J. M. Moloney, D. Parker, R. D. Peacock and G. Siligardi, *J. Chem. Soc., Perkin Trans. 2*, 1999, 2415.
10 This complex exhibited no mesogenic property in the solid state.
11 F. Toda, H. Miyamoto, S. Kikuchi, F. Nogami and R. Kuroda, *J. Am. Chem. Soc.*, 1996, **118**, 11 315; D. Tickle, A. George, K. Jennings and P. Camilleri, *J. Chem. Soc., Perkin 2*, 1998, 467; K. Yamada, Y. Kobori and H. Nagasawa, *Chem. Commun.*, 2000, 97.
12 T. Polonski, A. Chimiak and M. Kochman, *Tetrahedron*, 1974, **30**, 641.

CHEMCOMM
Communication
www.rsc.org/chemcomm

A structural model of the ferrichrome type siderophore: chiral preference induced by intramolecular hydrogen bonding networks in ferric trihydroxamate†

Kenji Matsumoto, Tomohiro Ozawa, Koichiro Jitsukawa, Hisahiko Einaga and Hideki Masuda*

Department of Applied Chemistry, Faculty of Engineering, Nagoya Institute of Technology, Showa-ku, Nagoya 46-8555, Japan. E-mail: masuda@ach.nitech.ac.jp; Fax: +81-52-735-5228; Tel: +81-52-735-5228

Received (in Cambridge, UK) 8th January 2001, Accepted 19th April 2001
First published as an Advance Article on the web 10th May 2001

Tris{2-[(*N*-acetyl-*N*-hydroxy)-D-alanylamino]ethyl}amine (*R*-TAAE) has been synthesized as a chiral trihydroxamate artificial siderophore with hydrogen bonding networks, whose crystal structure of the iron(III) complex revealed Λ configuration induced by interstrand hydrogen bonding networks and steric repulsion by optically active amino acid residues.

Siderophores are low molecular weight iron(III)-sequestering agents produced by bacteria and fungi that form very stable iron(III) complexes.[1,2] A large number of siderophores form chiral complexes, because the ferric siderophore complexes are absorbed by microorganisms through specific receptors that recognize the absolute configuration of complexes on the cell membrane.[1,2] The absolute configurations of iron(III)–siderophore complexes have been determined *via* X-ray crystallography and circular dichroism (CD). For example, ferrichrome, a trishydroxamate siderophore, and enterobactin, a triscatecholate iron carrier, form complexes with a left-handed (Λ) and right-handed (Δ) helicity, respectively.[3–5] The chirality of siderophore–iron complexes differs, although they are induced by the same optically active L-amino acid. In order to examine the factors responsible for determining the chirality of siderophores, many analogues have been synthesized. Shanzer and coworkers have reported that intramolecular hydrogen bonds in chiral siderophore analogues are important for the chiral preference and stability of complexes.[6] However, crystal structures of chiral siderophore analogue complexes with such hydrogen bonds have not been reported yet. Recently, we reported a crystal structure of a racemic mixture of iron(III)–tris{2-[(*N*-acetyl-*N*-hydroxy)glycylamino]ethyl}-amine (TAGE, Scheme 1) and observed a triple-stranded helix with both *intra- and interstrand* hydrogen bonding networks.[7] Such a triple helix structure is expected to induce a pronounced difference between diastereomers by introduction of a sterically hindered chiral group. Next, tris{2-[(*N*-acetyl-*N*-hydroxy)-D-alanylamino]ethyl}amine (*R*-TAAE, Scheme 1) was synthesized as a chiral trihydroxamate artificial siderophore, where chiral centers are introduced in the TAGE ligand by replacing the Gly residues with D-Ala residues. Here, on the basis of the crystal structure and CD data of the iron(III) complex with *R*-TAAE, we describe the influence of the intramolecular hydrogen bonding networks on the chiral preference of the iron(III) complex of artificial siderophores.

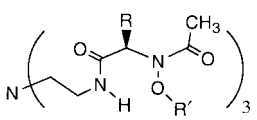

R = H, R′ = H : TAGE
R = Me, R′ = H : *R*-TAAE
R = H, R′ = Bn : TABGE
R = Me, R′ = Bn : *R*-TABAE

Scheme 1 TREN based trihydroxamate ligands with hydrogen bonding networks.

The ligand *R*-TAAE was synthesized according to a modification of a previously published method.[8] The iron(III) complex of *R*-TAAE (**1**) was prepared by reaction of Fe(acetylacetonato)$_3$ with *R*-TAAE in a biphasic ethyl acetate–water solution.[9] The crude complex was dissolved in an ethyl acetate solution containing a small amount of methanol, and then after slowly concentrating the solution for a few weeks, a deep-red colored single crystal of **1** suitable for X-ray diffraction analysis was obtained.‡

Initially the space group of the single crystal of **1** could not be distinguished from either $P4_12_12$ or $P4_32_12$ due to the enantiomorphous relationship between the two space groups. From the configuration of the ligand (*R*), the anomalous dispersion effect with Cu Kα radiation, and the difference in R_w values for Λ(*R*,*R*,*R*) and Δ (*S*,*S*,*S*) forms, 3.2 and 8.5, respectively, the space group and the absolute configuration of **1** were eventually determined to be $P4_12_12$ and Λ(*R*,*R*,*R*), respectively. The absolute configuration of **1** is identical to that of ferrichrome, although the chirality of the ligand differs from ferrichrome with Λ(*S*,*S*,*S*). As shown in Fig. 1, the iron ion has a distorted octahedral geometry with three hydroxamates and the overall structure is twisted with a pseudo-3-fold axis.

The average bond lengths between the iron(III) atom and the coordinating *N*-hydroxy O(N) and carbonyl O(C) atoms are Fe–O(N) = 1.970(7) and Fe–O(C) = 2.035(8) Å. The average

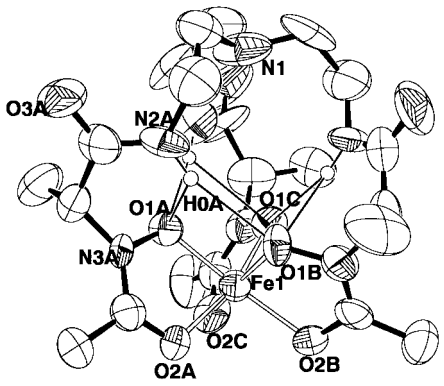

Fig. 1 Crystal structure of **1** showing the atom numbering schemes. Selected bond lengths (Å) and angles (°): Fe–O(1A) = 1.973(7), Fe–O(1B) = 1.964(7), Fe–O(1C) = 1.973(8), Fe–O(2A) = 2.029(8), Fe–O(2B) = 2.038(8), Fe–O(2C) = 2.037(8), O(1A)–Fe–O(2A) = 78.8(3), O(1B)–Fe–O(2B) = 78.8(3), O(1C)–Fe–O(2C) = 79.0(3). Intra- and interstrand hydrogen bond distances (Å): N(2A)···O(1A) = 2.78(1), N(2B)···O(1B) = 2.82(1), N(2C)···O(1C) = 2.92(1), N(2A)···O(1B) = 3.25(1), N(2B)···O(1C) = 3.17(1), N(2C)···O(1A) = 3.12(1).

† Electronic supplementary information (ESI) available: UV-vis and CD spectra of **1** and details of the determination of the absolute configuration and the space group of **1** are deposited as supporting information. See http://www.rsc.org/suppdata/cc/b1/b100306m/

 DOI: 10.1039/b100306m

O(N)–Fe–O(C) bond angle is 78.9(3)°. These values are quite comparable to those for natural trihydroxamate siderophores[2,3] and Fe^{III}TAGE.[7] The twist angle[10] determined for **1** is 44.0°. This is slightly larger than those of natural siderophores (ferrichrome = 42.5, ferricrocin = 40.4°)[2d] and is comparable to the calculated value (45.7°). As the difference between the observed and calculated twist angles is caused by deviation from the idealized C_3 symmetry,[2d] these findings reflect the difference in the symmetries of ligands. The average distances between amide nitrogen and coordinating *N*-hydroxy oxygens are 2.84 and 3.18 Å between intrastrands and interstrands, respectively. These values are slightly shorter than those observed for Fe^{III}TAGE (2.88 and 3.20 Å),[7] indicating that the intramolecular hydrogen bonding networks are enhanced by the introduction of optically active D-Ala to the ligand TAGE. The formation of such a strong intramolecular hydrogen bond is also supported by the ^{1}H NMR data of the benzyl-protected precursor of *R*-TAAE (*R*-TABAE, Scheme 1). The NMR data revealed a pronounced anisotropy in the benzyl protons ArCH_2 and tris(2-aminoethyl)amine (TREN) backbone protons NCH_2CH_2NH in $CDCl_3$ but not in DMSO-d_6. This anisotropy is evidently due to the restriction of rotation induced by intramolecular hydrogen bonding networks.[6b] On the other hand, such anisotropy was not observed for TABGE (a similar precursor of TAGE, Scheme 1) in both $CDCl_3$ and DMSO-d_6.

In aqueous solution at pH 7.4, the UV-vis spectrum of **1** showed a characteristic absorption band at 420 nm corresponding to the tris(hydroxamato)iron(III) complex. This indicates that the structure of **1** determined by X-ray crystallography is maintained in an aqueous solution. The CD spectrum of **1** exhibited positive and negative Cotton effects at 444 ($\Delta\varepsilon$ = +1.0) and 358 nm ($\Delta\varepsilon$ = −0.8). These values are qualitatively similar to those determined from the solution and crystalline CD spectra of ferrichrome,[3] indicating that, like ferrichrome, the absolute configuration of **1** is Λ in both the solution and solid states.

Consequently, the observed chiral preference of **1**, crystalline and in solution, is reasonably explained as a result of the orientation of the triple helix induced by intramolecular hydrogen bonding networks becoming tightly fixed by steric repulsion between optically active amino acid residues and terminal methyl groups. This result strongly supports the proposal by Shanzer *et al.*[6] In addition, it is revealed that intramolecular hydrogen bonding networks in the benzyl-protected precursor of *R*-TAAE and its iron(III) complex are easily formed due to the existence of an asymmetric site within the hydrogen bonded six-membered ring. These observations suggest that both intramolecular hydrogen bonding networks and optically active amino acid residues operate in concert, which play an important role for the chiral preference of artificial siderophore complex **1**. The bioavailability of **1** was also investigated using *Microbacterium flavescens* which has ferrichrome receptors but lacks the ability to produce siderophores. Interestingly, complex **1** promoted the growth of this mutant. Therefore, the Fe^{III}*R*-TAAE complex, which has structural features that are similar to those of ferrichrome, might be a good functional model compound for the ferrichrome-type siderophore. Detailed investigations are now under way.

This work was supported in part by a Grant-in-Aid for Scientific Research from the Ministry of Education, Science, Sports, and Culture of Japan (H. M.), for which we express our thanks.

Notes and references

‡ *Crystal data*: $C_{21}H_{36}N_7O_9Fe$, M = 586.40, tetragonal, a = 17.237(3), c = 19.432(2) Å, U = 5733(1) Å^3, T = 296 K, space group $P4_12_12$ (no. 92), Z = 8, D_c = 1.349 g cm^{-3}, μ(Cu-Kα) = 46.94 cm^{-1}, F(000) = 2472.0, R = 0.053, R_W = 0.032. A total of 2519 unique reflections (R_{int} = 0.102) were collected on a Rigaku AFC5R diffractometer with graphite monochromated Cu-Kα radiation and a rotating anode generator, of which 1585 reflections with $I > 3\sigma(I_o)$ were used in the structure analysis and refinement using the *teXsan* program system. Absorption correction was applied. The absolute configuration and the space group of the complex were determined by comparison of observed and calculated Bijvoet pair differences, whose details are deposited as supporting information. CCDC 158411. See http://www.rsc.org/suppdata/cc/b1/b100306m/ for crystallographic files in. cif format.

1 J. B. Neilands, *Struct. Bonding*, 1984, **58**, 1.
2 B. F. Matzanke, G. Müller-Matzanke and K. N. Raymond, in *Physical Bioinorganic Chemistry, Vol. 5, Iron Carriers and Iron Proteins*, ed. T. M. Loehr, VCH, New York, 1989, (*a*) pp. 89–102, (*b*) p. 61, (*c*) pp. 59–66, (*d*) pp. 19–22.
3 D. van der Helm, J. R. Baker, D. Eng-Wilmot, L. M. B. Hossain and R. A. Loghry, *J. Am. Chem. Soc.*, 1980, **102**, 4224.
4 (*a*) J. V. McArdle, S. R. Sofen, S. R. Cooper and K. N. Raymond, *Inorg. Chem.*, 1978, **17**, 3075; (*b*) S. S. Isied, G. Kuo and K. N. Raymond, *J. Am. Chem. Soc.*, 1976, **98**, 1763.
5 T. B. Karpishin, T. M. Dewey and K. N. Raymond, *J. Am. Chem. Soc.*, 1993, **115**, 1842.
6 (*a*) Y. Tor, J. Libman, A. Shanzer, C. E. Felder and S. Lifson, *J. Am. Chem. Soc.*, 1992, **114**, 6653; (*b*) Y. Tor, J. Libman, A. Shanzer, C. E. Felder and S. Lifson, *J. Am. Chem. Soc.*, 1992, **114**, 6661; (*c*) J. Libman, Y. Tor and A. Shanzer, *J. Am. Chem. Soc.*, 1987, **109**, 5880.
7 K. Matsumoto, T. Ozawa, K. Jitsukawa, H. Einaga and H. Masuda, *Inorg. Chem.*, 2001, **40**, 190.
8 (*a*) T. Kolasa and A. Chimiak, *Tetrahedron*, 1974, **30**, 3591; (*b*) T. Kolasa and A. Chimiak, *Tetrahedron*, 1977, **33**, 3285.
9 J. B. Dionis, H.-B. Jenny and H. H. Peter, *J. Org. Chem.*, 1989, **54**, 5623.
10 The twist angle is defined by the O(N)–Fe–O(C) angle of a single hydroxamate ligand projected onto the plane perpendicular to the idealized 3-fold axis.

CHEMCOMM Communication
www.rsc.org/chemcomm

Chiral oxovanadium complex catalyzed enantioselective oxidative coupling of 2-naphthols†

Chang-Ying Chu, Der-Ren Hwang, Sheng-Kai Wang and Biing-Jiun Uang*

Department of Chemistry, National Tsing Hua University, Hsinchu, Taiwan 300, Republic of China. E-mail: bjuang@mx.nthu.edu.tw; Fax: +88 6 3 5711082; Tel: +88 6 3 5721224

Received (in Cambridge, UK) 20th February 2001, Accepted 20th April 2001
First published as an Advance Article on the web 15th May 2001

The enantioselective oxidative coupling of 2-naphthols using 2 mol% chiral oxovanadium complex under mild conditions afforded chiral BINOLs in moderate enantioselectivity.

Vanadium plays a vital role in biological systems with its participation in redox processes catalyzed by enzymes such as bromoperoxidase[1] and nitrogenase.[2] The utility of vanadium complexes in oxidation, reduction and Lewis acid promoted reactions is well documented.[3] Except for oxidation of sulfides[4] and epoxidation of allylic alcohols,[5] there are very few vanadium complex catalyzed enantioselective reactions. Recently we reported the aerobic oxidative coupling of 2-naphthols and phenols catalyzed by $VO(acac)_2$.[6] Replacement of acac in this complex by chiral bidentate ligands, such as 3-formylcamphor and 3-heptafluorobutyrylcamphor, did not lead to any enantioselectivity in coupling products. Earlier, Fujita had utilized some chiral tridentate Schiff base ligands containing vanadium complexes in asymmetric oxidation of sulfides with moderate enantioselectivity.[4a]

In the light of these observations, we have studied the oxidative coupling of 2-naphthols using chiral tridentate oxovanadium complexes as a method for the enantioselective synthesis of chiral BINOLs; although enantioselective coupling of naphthols has been earlier reported, Katsuki used a ruthenium complex and Nakajima employed a copper complex as the catalyst in their reactions.[7] Herein, we report chiral oxovanadium complex catalyzed C–C bond formation in aryl compounds with 51% ee and 50–91% isolated yield (Scheme 1).‡

Following the literature procedure,[8] we have synthesized chiral oxovanadium complexes from aldehyde, (*S*)-valine or (*S*)-phenylalanine and vanadyl sulfate, and applied them in our reactions. At first, we examined oxidative coupling of 2-naphthol by using 10 mol% complex **1** as catalyst, molecular oxygen as oxidant and dichloromethane as solvent, but the product could only be isolated in trace amounts (Table 1, entry 1). Earlier Carrano and Tsuchida reported that vanadium(IV) undergoes disproportion to vanadium(III) and vanadium(V) in strong acidic condition.[9] When we added a catalytic amount of trifluoromethanesulfonic acid to the reaction mixture, it led to improved chemical yield but with only 27% ee (Table 1, entry 2). Catalysts **2** to **4** gave similar enantioselectivity in these reactions (Table 1, entries 3–5). Complexes containing bulkier amino acids, such as (*S*)-*tert*-leucine and (*S*)-phenylglycine as ligands, did not produce appreciable enantioselectivity. We

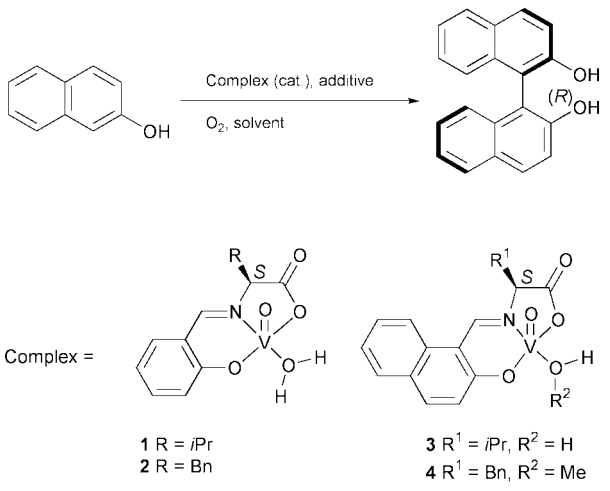

Scheme 1

† Electronic supplementary information available: HPLC analyses. See http://www.rsc.org/suppdata/cc/b1/b101670i/

Table 1 Enantioselective oxidative coupling of 2-naphthol

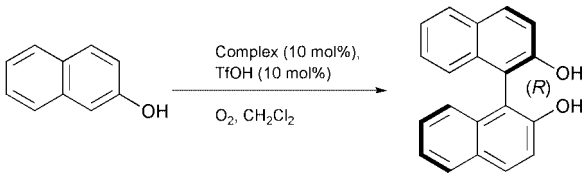

Entry	Complex	Time/h	Yield (%)	Ee (%)[a]
1[b]	**1**	6	trace	—
2	**1**	24	79	27
3	**2**	24	70	23
4	**3**	12	42	26
5	**4**	12	56	27
6[c]	**4**	12	94	23
7[cd]	**4**	12	87	31
8[cde]	**4**	24	80	42

[a] Determined by HPLC with Kromasil 100-5CHI-DMB column (*i*PrOH–hexane = 5:95, 1 mL min^{-1}). [b] TfOH was not added. [c] TMSOTf replaced TfOH. [d] Concentration was 0.5 M. [e] Catalyzed by 2 mol% complex.

Table 2 Promoter effect for enantioselective oxidative coupling of 2-naphthol

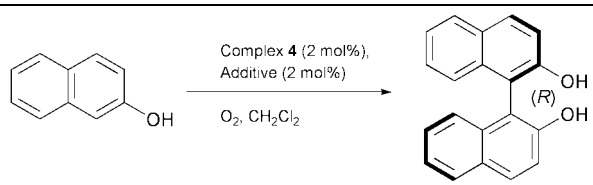

Entry	Additive	Yield (%)	Ee (%)[a]
1	TMSOTf	80	42
2	TFAA	50	43
3	$HClO_4$	64	29
4	TMSCl	73	48
5	TESCl	45	48
6	TBDPSCl	48	49
7	TMSBr	60	48
8	TMSCl + $AgClO_4$	68	31

[a] Determined by HPLC with Kromasil 100-5CHI-DMB column (iPrOH–hexane = 5:95, 1 mL min^{-1}).

 DOI: 10.1039/b101670i

Table 3 Solvent effect for enantioselective oxidative coupling of 2-naphthol

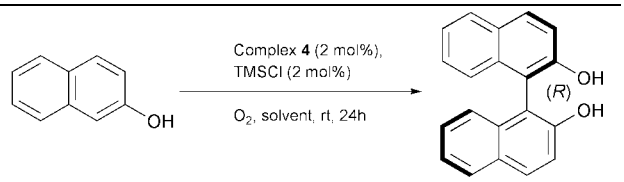

Entry	Solvent	Yield (%)	Ee (%)[a]
1	CH_2Cl_2	73	48
2	$CHCl_3$	82	51
3	$(CH_2Cl)_2$	38	46
4	CCl_4	12	13
5	CH_3CN	46	8
6	THF	24	0

[a] Determined by HPLC with Kromasil 100-5CHI-DMB column (iPrOH–hexane = 5:95, 1 mL min^{-1}).

presumed that the electronic effect of substituents in the aromatic ring could influence catalyzing oxidative coupling, and investigated complexes containing 3,5-di-*tert*-butyl, 3-*tert*-butyl, 5-methoxy and 5-nitro substituents, but no significant enantioselectivity was observed with these complexes. However, we observed a marginal increase in enantioselectivity when the concentration of the substrate was increased from 0.1 to 0.5 M (Table 1, entry 7). An interesting feature was that enantioselectivity increased with decrease in concentration of complexes from 10 to 2 mol%, more so, in the case of complex **4** (Table 1, entry 8), and (*R*)-binaphthol was obtained in 42% ee.

To study the promoter effect, we used various additives. The enantioselectivity was better in TMSCl than in TMSOTf, and the chemical yield was a little lower (Table 2, entry 4). There was no change in enantioselectivity with variation of silyl groups in the additives, but it affected the reaction rate (Table 2, entries 4–6). Polar chlorosolvents such as dichloromethane, chloroform and 1,2-dichloroethane merely improved the enantioselectivity (Table 3).

Table 4 Enantioselective oxidative coupling of 2-naphthol derivatives

Entry	Naphthol	Time/h	Yield (%)	Ee (%)[a]
1	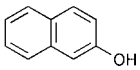	24	82	51
2	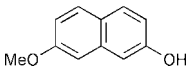	24	91	51
3	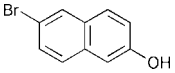	24	50	51
4	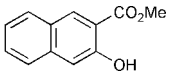	69	trace	—

[a] Determined by HPLC with Kromasil 100-5CHI-DMB column (*i*PrOH–hexane = 5:95, 1 mL min^{-1}).

The results obtained from the enantioselective oxidation of other substituted 2-naphthols catalyzed by complex **4** are summarized in Table 4. No variation in enantioselectivities was observed, but reaction rate was increased with electron donating capacity of the substituent.

In conclusion, oxovanadium complex has been used for the first time[10] in the enantioselective coupling of 2-naphthols. A low concentration requirement of catalyst, mild reaction conditions and high chemical yields render our method attractive.

We are grateful to the National Science Council, Republic of China, for support of this work.

Notes and references

‡ *Representative procedure for enantioselective oxidative coupling of 2-naphthols*: to a stirred solution of complex (0.1 mmol) and TMSCl (13 μL, 0.1 mmol) in chloroform (10 mL) exposed to molecular oxygen at room temperature was added 2-naphthol (5 mmol). After 24 h, the reaction mixture was treated with 6 M HCl (10 mL) and extracted with dichloromethane (3 × 20 mL). The combined organic extracts were dried (Na_2SO_4), and concentrated. The residue was purified by silica gel column chromatography eluting with ethyl acetate–hexane (1:5) to furnish the coupling product.

1 (*a*) H. Vilter, *Phytochemistry*, 1984, **23**, 1387; (*b*) J. M. Arber, E. de Boer, C. D. Garner, S. S. Hasnain and R. Wever, *Biochemistry*, 1989, **28**, 7968.

2 (*a*) B. J. Hales, E. E. Case, J. E. Moringstar, M. F. Dzeda and A. Mautner, *Biochemistry*, 1986, **24**, 7251; (*b*) R. L. Robson, R. R. Eady, T. H. Richardson, R. W. Miller, M. Hawkins and J. R. Postgate, *Nature*, 1986, **322**, 388; (*c*) G. N. George, C. L. Coyle, B. J. Hales and S. P. Cramer, *J. Am. Chem. Soc.*, 1988, **110**, 4057; (*d*) B. J. Hales, A. E. True and B. M. Hoffman, *J. Am. Chem. Soc.*, 1989, **111**, 8519.

3 T. Hirao, *Chem. Rev.*, 1997, **97**, 2707.

4 (*a*) K. Nakajima, K. Kojima, M. Kojima and J. Fujita, *Bull. Chem. Soc. Jpn.*, 1990, **63**, 2620; (*b*) K. Nakajima, M. Kojima, K. Toriumi, K. Saito and J. Fujita, *Bull. Chem. Soc. Jpn.*, 1989, **62**, 760; (*c*) C. Bolm and F. Bienewald, *Angew. Chem., Int. Ed. Engl.*, 1995, **34**, 2640.

5 (*a*) K. B. Sharpless and R. C. Michaelson, *J. Am. Chem. Soc.*, 1977, **99**, 1990; (*b*) D. J. Berrisford, C. Bolm and K. B. Sharpless, *Angew. Chem., Int. Ed. Engl.*, 1995, **34**, 1059; (*c*) C. Bolm, T. K. K. Luong and K. Harms, *Chem Ber./Recl.*, 1997, **130**, 887; (*d*) C. Bolm and T. Kühn, *Synlett*, 2000, 899; (*e*) N. Murase, Y. Hoshino, M. Oishi and H. Yamamoto, *J. Org. Chem.*, 1999, **64**, 338; (*f*) Y. Hoshino and H. Yamamoto, *J. Am. Chem. Soc.*, 2000, **122**, 10 452.

6 D.-R. Hwang, C.-P. Chen and B.-J. Uang, *Chem. Commun.*, 1999, 1207.

7 (*a*) R. Irie, K. Masutani and T. Katsuki, *Synlett*, 2000, 1433; (*b*) M. Nakajima, I. Miyoshi, K. Kanayama and S. Hashimoto, *J. Org. Chem.*, 1999, **64**, 2264.

8 (*a*) L. J. Theriot, G. O. Carlisle and H. J. Hu, *J. Inorg. Nucl. Chem.*, 1969, **31**, 2841; (*b*) J. J. R. Frausto da Silva, R. Wootton and R. D. Gillard, *J. Chem. Soc. A*, 1970, 3369.

9 (*a*) E. Tsuchida, K. Yamamoto, K. Oyaizu, N. Iwasaki and F. C. Anson, *Inorg. Chem.*, 1994, **33**, 1056; (*b*) J. A. Bonadies, W. M. Bulter, L. P. Vincent and C. J. Carrano, *Inorg. Chem.*, 1987, **26**, 1218.

10 Chen and his co-workers have independently done similar work using oxovanadium complexes and published their results concurrently. S.-W. Hon, C.-H. Li, J.-H. Kuo, N. B. Barhate, Y.-H. Liu, Y. Wang and C.-T. Chen, *Org. Lett.*, 2001, **3**, 869.

CHEMCOMM
Communication
www.rsc.org/chemcomm

Evidence for an acid-catalysed reaction subordinated to the occurrence of a previous electron transfer in the incorporation of an electron-rich alkene within NaY zeolite

Isabel Casades,[a] Mercedes Alvaro,[a] Hermenegildo García*[ab] and Mercedes Esplá[a]

[a] *Departamento de Quimica, Universidad Politecnica de Valencia, Apartado 22010, 46071 Valencia, Spain. E-mail: hgarcia@qim.upv.es*
[b] *Instituto de Tecnologia Quimica, Universidad Politecnica de Valencia, Apartado 22010, 46071 Valencia, Spain*

Received (in Cambridge, UK) 6th March 2001, Accepted 9th April 2001
First published as an Advance Article on the web 11th May 2001

The first observation of an acid-catalysed reaction subordinated to the occurrence of an electron transfer upon the incorporation of an electron-rich alkene in NaY zeolite is reported; the key point is the generation in the electron transfer process of suitable hydride donor species that react with the carbocation generated in the acid catalysed mechanism.

It is well documented that acid zeolites can behave either as solid acids or as electron aceptors.[1–8] In the former case the resulting reaction mechanism generally involves carbocations while in the latter case the key reaction intermediates are radical cations. Studies showing the concurrent ocurrence of both type of processes are rare. Herein by using an electron-rich alkene, 1,3,3-trimethyl-2-methyleneindoline **1** (Scheme 1), we provide

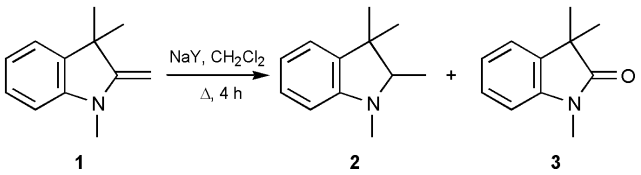

1 **2** **3**

Scheme 1

evidence that: (i) the products of both mechanisms (proton or electron transfer) are different and characteristic of each type of reaction intermediate and (ii) formation of the acid-catalysed product does not occur unless the electron-transfer product is formed previously (subordination).

A highly reactive, electron-rich alkene **1** was selected for the present study.† Upon stirring a dichloromethane solution of this indoline in the presence of thermally dehydrated NaY zeolite at reflux temperature under aerated conditions the progressive disappearance of the starting material, accompanied by the formation of 1,2,3,3-tetramethylindoline **2** (40%) and 1,3,3-trimethyl-2-indolinone **3** (60%) was observed (Scheme 1). This product distribution is not unprecedented and it parallels those found in the reaction of 1,1-diphenylethene over CaY zeolite wherein 1,1-diphenylethane and benzophenone were formed.[9–11]

Addition of a small amount of pyridine (10 mg g^{-1}) totally quenches the reaction and neither of the two products was formed. This can be taken as evidence that the reaction involves the weak acid sites present in commercial batches of NaY. Precedents for acid-catalyzed reactions promoted by NaY have been reported previously for vinylanisole and anethole dimerisation[12] and spectroscopic titration of NaY acid sites has also been reported.[13] We have found that this product distribution is not specific to NaY but that liquid acids such as trifluoroacetic or methanesulfonic acids behave analogously.

It is obvious that the formation of indolinone **3** should involve as reagent either molecular oxygen or water, or both. In an attempt to clarify this point, the reaction of indoline was carried out under argon atmosphere. However, when indoline **1** was refluxed in the presence of thermally activated NaY under Ar atmosphere, not only the formation of indolinone **3** but also the formation of 1,2,3,3-tetramethylindoline **2**, which does not incorporate any oxygen atoms in its molecular formula, is quenched. Clearly, the formation of both products is inhibited by adding a base or in the absence of molecular oxygen.

Raman spectra of indoline **1** adsorbed into NaY zeolite under Ar atmosphere indicates that under conditions in which no products are observed in the liquid phase, indoline **1** is stable upon incorporation within NaY.

Fig. 1 shows the diffuse reflectance UV–VIS spectra of the corresponding NaY sample obtained after incorporation of indoline **1** under argon atmosphere (a) and under aerated conditions (b). In the latter case, the extra band at 440 nm matches the absorption band of indolinone **3** in dichloromethane solution, thus providing spectroscopic evidence that this product is formed rapidly upon incorporation of **1** within NaY in the presence of air.

To disclose the reaction mechanism of formation for both products, indoline **1** was submitted to photochemical oxidation under typical electron transfer conditions. It is known that 1,4-dimethoxybenzene (DMB, E = 1.34 V, *vs.* SCE) in the presence of oxygen is a selective electron transfer photosensitizer that does not generate singlet oxygen.[14] Photosensitized irradiation of indoline **1** (E = 0.76 V, *vs.* SCE) in acetonitrile (0.5 wt% water content) containing DMB gives rise to the formation of indolinone **3** with almost complete selectivity at 98% of indoline conversion (Scheme 2). Thus, based on the known ability of zeolites to promote single electron transfer reactions[15] and on the results of the photoinduced electron transfer that shows that the radical cation of compound **1** leads exclusively to indolinone, we propose that the most reasonable reaction mechanism to explain the formation of indolinone involves the indoline radical cation (Scheme 3).

Concerning the formation of tetramethylindoline **2**, it has been reported that treatment of 1,1-diphenylethylene and benzonorbornadiene with CaY leads to the corresponding saturated 1,1-diphenylethane and benzonorbornane through the

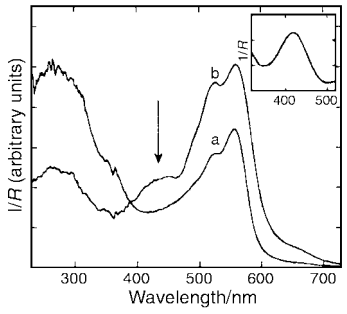

Fig. 1 Diffuse reflectance UV–VIS spectra of indoline **1** adsorbed onto NaY in the presence of air (a) and under Ar atmosphere (b). The insert shows the UV–VIS spectra of a dichloromethane solution of indolinone **2**.

 DOI: 10.1039/b102074i

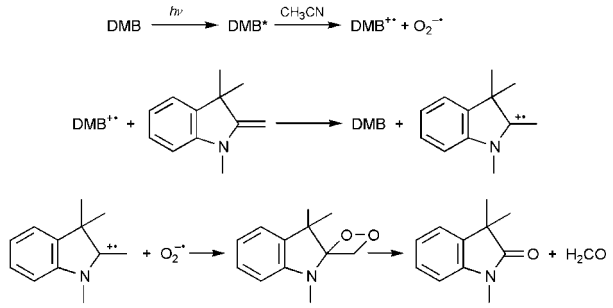

Scheme 2

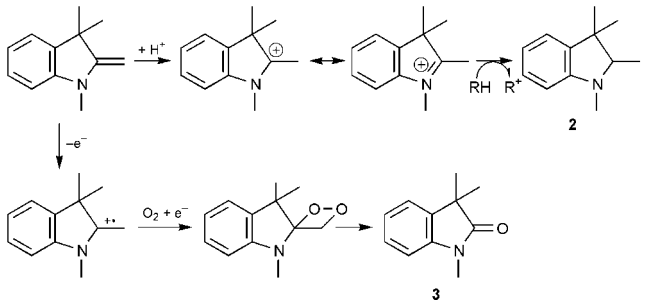

Scheme 3

corresponding radical cation.[16] Other reports have invoked a radical cation intermediate to affect the C=C double bond hydrogenation.[17] However, the fact that the photoinduced DMB electron transfer reaction does not give detectable amounts of compound **2**, seems to rule out this possibility. An alternative explanation for the formation of **2** would be acid-catalyzed protonation to generate a carbocation followed by hydride abstraction. To support this reaction mechanism, a reactive hydride donor such as triphenylmethane (TPM) was added to a solution of indoline **1** in methanosulfonic acid (Scheme 4).

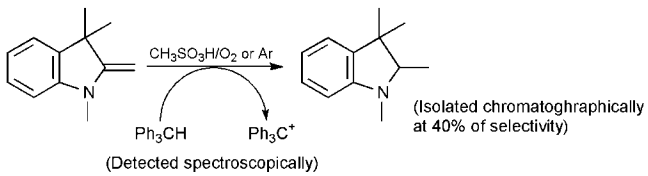

Scheme 4

Under these conditions, both in the presence or absence of oxygen, 1,2,3,3-tetramethylindoline was formed in 40% selectivity at 90% indoline conversion.‡ Concurrently the triphenylmethyl cation characterized by 405 and 425 nm bands in the UV–VIS spectrum of the acid solution was observed.

To further support the mechanism shown in Scheme 4, the NaY zeolite was submitted to deuteration by two consecutive cycles consisting in soaking the NaY solid with D_2O and subsequent drying at 110 °C. The resulting deuterated zeolite was used for the reaction with **1**. The corresponding GC–MS of the reaction mixture showed the presence of 2-deuteromethyl-1,3,3-trimethylindoline at a level of 45% of the total amount of **2** (Scheme 5). This result supports that formation of **2** occurs

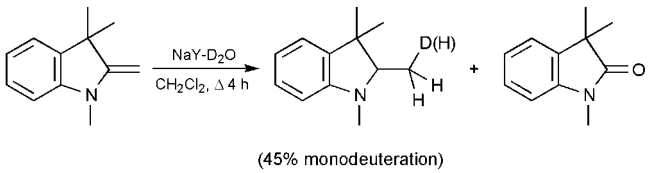

Scheme 5

through proton transfer from the zeolite framework to the 2-methylene substituent in a Markovnikov manner. The incomplete deuteration can be explained by the incomplete deuteration of the zeolite OH or by back H/D exchange.

The absence of oxygen should exclusively inhibit formation of compound **3** the only product containing oxygen. To explain why the absence of oxygen also inhibits formation of **2**, we speculated on the possibility that the hydride donor required in the formation of **2** arises from the formation of **3**. In this context, it should be noted that formation of **2** according to the conditions of Scheme 3 should occur equally well both in the presence or absence of oxygen.

Thus, we suggest that formaldehyde, formic acid or any product derived thereof could act as hydride donors in the formation of **2**. Since these species are formed concommitantly with **3** this would explain why **2** is not formed under conditions in which **3** is inhibited. In this regard, it is well documented that formic acid can be an effective reducing agent and also can act as a hydride donor according to eqn. (1).[18]

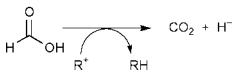

(1)

In summary, incorporation of an electron rich alkene 1,3,3-trimethyl-2-methyleneindoline within the voids of NaY zeolite gives rise to a product distribution characteristic of the concurrent operation of two different reaction mechanisms involving electron transfer and acid catalysis. In the latter case, formation of the corresponding product requires a hydride donor species that arises in the electron transfer pathway. Our report constitutes the first example establishing a connection between the products of these two different mechanisms.

H. G. thanks the Spanish DGICYT for financial support (Project MAT 2000-1678-CO2-01). I. C. also thanks Universidad Politécnica de Valencia for a scholarship.

Notes and references

† Adsorption of indoline (Aldrich) within NaY (P.Q. Industries), was accomplished by heating at reflux temperature under magnetic stirring a suspension of NaY zeolite (1 g) previously dehydrated (500 °C, 5 h) in a solution of indoline **1** (100 mg) in CH_2Cl_2 (25 ml) for 4 h. At the end of the reaction the solid was filtered off, and Soxhlet extracted with CH_2Cl_2. The combined CH_2Cl_2 supernatant and extraction liquor was analysed by GC and GC–MS.

‡ Residual amounts of water interact with the formed cation decreasing the process selectivity.

1 A. Corma, V. Fornés, H. García, V. Martí and M. A. Miranda, *Chem. Mater.*, 1995, **7**, 2136.
2 F. Algarra, A. Corma, H. García and J. Primo, *Appl. Catal. A*, 1995, **128**, 119.
3 F. Algarra, A. Corma, H. García and J. Primo, *Appl. Catal. A*, 1995, **122**, 125.
4 E. Armengol, A. Corma, H. García and J. Primo, *Appl. Catal. A*, 1995, **126**, 391.
5 E. Armengol, M. L. Cano, A. Corma, H. García and M. T. Navarro, *J. Chem. Soc., Chem. Commun.*, 1995, 519.
6 A. Corma, *Stud. Surf. Sci. Catal.*, 1994, **83**, 416.
7 R. B. Powell, E. Hagerman; E. Michael and R. Zoellner, *Inorg. Chem.*, 1995, **7**, 215.
8 F. R. Chen and J. J. Fripiat, *J. Phys. Chem.*, 1992, **96**, 819.
9 K. Pichumani and V. Ramamurthy, *Chem. Commun.*, 1996, 2763.
10 K. Pitchumani, N. Prevost, D. R. Corbin and V. Ramamurthy, *Chem. Commun.*, 1997, 181.
11 K. Pitchumani, D. R. Corbin and V. Ramamurthy, *J. Am. Chem. Soc*, 1998, **118**, 8152.
12 F. L. Cozens, R. Bogdanova, M. Regimbald, H. García, V. Marti and J. C. Scaiano, *J. Phys. Chem. B*, 1997, **101**, 6921.
13 C. Costa, J. M. Lopes, F. Lemos and F. R. Ribeiro, *J. Mol. Catal. A: Chem.*, 1999, **144**, 221.
14 U. T. Bhalerao and M. Sridhar, *Tetrahedron Lett.*, 1993, **34**, 4341.
15 M. Alvaro, H. García, S. García, F. Márquez and J. C. Scaiano, *J. Phys. Chem. B*, 1997, **101**, 3043.
16 H.-M. Ka, C. P. Grey, K. Pitchumani and P. H. Lakshminarasimhan, *J. Phys. Chem. A*, 1998, **102**, 5627.
17 D. D. Tanner and L. Y. Zhang, *J. Am. Chem., Soc.*, 1994, **116**, 6683.
18 M. Asif Musharraf, K. M. Shamuddin and Md. Zobairi Omir, *Tetrahedron Lett.*, 1998, **39**, 8153.

CHEMCOMM
Communication
www.rsc.org/chemcomm

Hydrogen bonding and CH/π interactions for the stabilization of biomimetic zinc complexes: first examples of X-ray characterized alcohol and amide adducts to a tetrahedral dicationic Zn center

Olivier Sénèque,[a] Michel Giorgi[b] and Olivia Reinaud*[a]

[a] *Laboratoire de Chimie et Biochimie Pharmacologiques et Toxicologiques, CNRS UMR 8601, Université René Descartes, 45 rue des Saint-Pères, 75270 Paris cedex 06, France. E-mail: reinaud@biomedicale.univ-paris5.fr*

[b] *Laboratoire de Cristallochimie, CNRS UMR 6517, Centre scientifique Saint-Jérôme, av. Escadrille Normandie-Niemen, 13397 Marseille cedex 20, France*

Received (in Cambridge, UK) 12th March 2001, Accepted 18th April 2001
First published as an Advance Article on the web 11th May 2001

X-Ray analysis of two biomimetic $(N_3ZnL)^{2+}$ complexes with L = ethanol and formamide revealed that hydrogen bonding and CH/π interactions between the guest ligand L and the calix[6]arene host structure play a key role in their stabilization.

Recognition of the importance of zinc enzymes in biological processes is ever increasing. The active site of mononuclear enzymes often displays a pseudo-tetrahedral Zn^{2+} ion coordinated by three amino-acid residues and a labile water molecule. Among them, the recurrent tris(histidine) coordination set (as in Adamalysin II, Atrolysin C, Carbonic Anhydrase)[1] has motivated the design of synthetic analogues based on N_3 ligands. However, tetrahedral dicationic zinc complexes have proved difficult to stabilize. We have recently described a supramolecular system based on a *tert*-butylcalix[6]arene functionalized in alternating positions by three imidazole groups.[2–4] The neutral ligand $X_6Me_3ImMe_3$, which presents three *N*-methyl imidazole donors (ImMe) associated to a cavity that mimics the enzyme pocket, was shown to stabilize four-coordinated zinc species N_3ZnL^{2+} with various neutral molecules L, including amines, alcohols, amides, nitriles and even aldehydes. An amino and a nitrilo complex were characterized crystallographically.[2] We describe here two novel adducts $[Zn(X_6Me_3ImMe_3)L]^{2+}$, one with ethanol (L = EtOH) and the other with formamide (L = NH_2CHO). Their X-ray structures revealed that hydrogen bonding and CH/π interactions between the calix[6]arene host and the guests L play an important role in stabilizing of the complexes. To our knowledge, they provide the first examples of stable four-coordinated Zn dicationic complexes presenting a terminal aliphatic alcohol[5] or amide[6] ligand. Both compounds are strongly relevant to the enzyme/substrate complexes in mononuclear zinc biological systems.

As previously demonstrated by ^{1}H NMR spectroscopy, the water ligand in complex $[Zn(X_6Me_3ImMe_3)(H_2O)](ClO_4)_2$ is easily displaced by alcohols and amides (Scheme 1). We succeeded in growing X-ray quality crystals† of the ethanol adduct $[Zn(X_6Me_3ImMe_3)(EtOH)]^{2+}$ out of an acetone solution of the aqua complex to which 10 molar equivalents of EtOH were added. The molecular structure, displayed in Fig. 1, shows a tetrahedral complex where Zn^{2+} is wrapped by the three imidazole arms of the calixarene-based ligand. The average Zn–

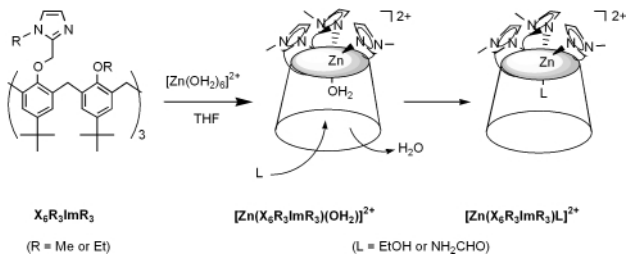

Scheme 1 Synthetic scheme for the calix[6]arene-based biomimetic Zn complexes.

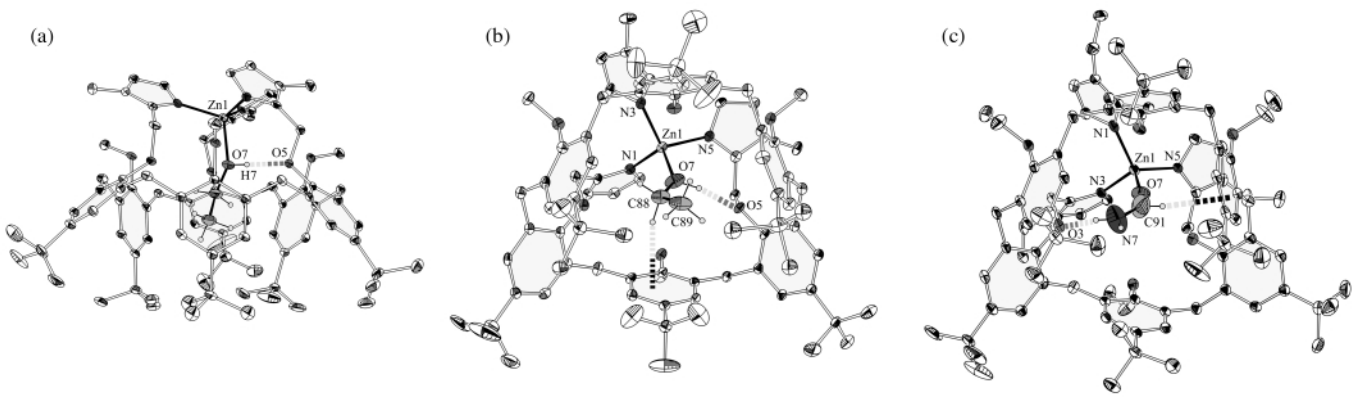

Fig. 1 Crystal structures† of Zn complexes: (a) and (b): $[Zn(X_6Me_3ImMe_3)(EtOH)]^{2+}$, side and top views, respectively. (c): $[Zn(X_6Et_3ImEt_3)(NH_2CHO)]^{2+}$, top view. The hydrogen atoms of the ethanol and formamide ligands could not be located experimentally but their location was calculated and is represented by a plain sphere of arbitrary radius. Other hydrogen atoms and solvents of crystallization are omitted for clarity as well as the perchlorate counter anions. Selected bond lengths (Å) and angles (°): $[Zn(X_6Me_3ImMe_3)(EtOH)](ClO_4)_2$, Zn(1)–N(1) 1.978(5), Zn(1)–N(3) 1.977(5), Zn(1)–N(5) 1.989(5), Zn(1)–O(7) 1.984(5), O(7)–C(88) 1.341(9), N(1)–Zn(1)–O(7) 110.4(2), N(3)–Zn(1)–O(7) 112.0(2), N(5)–Zn(1)–O(7) 99.2(2), N(1)–Zn(1)–N(3) 109.1(2), N(3)–Zn(1)–N(5) 108.0(2), N(1)–Zn(1)–N(5) 117.9(2); $[Zn(X_6Et_3ImEt_3)(NH_2CHO)](ClO_4)_2$, Zn(1)–N(1) 1.972(7), Zn(1)–N(3) 2.000(6), Zn(1)–N(5) 1.981(6), Zn(1)–O(7) 1.897(9), O(7)–C(91) 1.202(11), C(91)–N(7) 1.238(13), N(1)–Zn(1)–O(7) 105.2(3), N(3)–Zn(1)–O(7) 110.7(3), N(5)–Zn(1)–O(7) 107.3(3), N(1)–Zn(1)–N(3) 105.8(2), N(3)–Zn(1)–N(5) 111.1(2), N(1)–Zn(1)–N(5) 116.6(2), Zn(1)–O(7)–C(91) 169.6(10), O(1)–C(91)–N(7) 131.6(8).

 DOI: 10.1039/b102322p

N_{Im} bond length (1.981 Å) is comparable to those of the related propionitrile adduct (1.996 Å) but shorter than in the heptylamine complex (2.007 Å).[2] A bound EtOH molecule is buried deeply inside the calixarene conic cavity. The Zn–O distance [1.984(5) Å] is similar to that of the only other reported four-coordinate Zn–alcohol complex [1.993(3) Å].[5] It is however significantly shorter than those reported for the Zn–alcohol adducts in Liver Alcohol Dehydrogenase (2.0–2.1 Å). This may be attributed to a different overall charge in the coordinated metal center, which is negative in the enzyme.[7] The ethanol OH group points selectively toward one of the OCH_2ImMe units. The corresponding shorter O···O distance (2.86 *vs.* 3.56 and 3.40 Å for the others) indicates the presence of a strong hydrogen bond. Also noteworthy is the position of the ethanol carbon skeleton in the π-basic cavity. The methyl group stands just in front of an aromatic anisole ring with a perpendicular C···Ar distance of 3.67 Å. The methylene group points toward another anisole moiety at a perpendicular C···Ar distance of 3.82 Å. These values are typical of CH/π interactions.[8]

The X-ray structure† of an amide adduct was obtained with a slightly modified ligand, $X_6Et_3ImEt_3$.‡ Single crystals of $[Zn(X_6Et_3ImEt_3)(NH_2CHO)]^{2+}$ were grown by Et_2O diffusion into a benzonitrile solution of the aqua precursor to which 20 molar equivalents of formamide were added. As in the other related structures, the tetrahedral Zn^{2+} ion is coordinated to all three imidazoles with a comparable averaged $Zn–N_{Im}$ bond length (1.984 Å). The amide ligand sits inside the calixarene cavity (Fig. 1) with a short Zn–O distance [1.897(9) Å],[6] which again reflects a highly acidic zinc center. Two additional anchorage points fix the guest molecule in the center of the cavity. On one side, a hydrogen bond hangs the NH_2 group next to one oxygen from the calixarene skeleton [d(N···O) = 3.08 Å and correspondingly, d(NH···O) = 2.29 Å]. In the opposite direction, a CH/π interaction draws the guest CH group in front of one of the aromatic rings of the host with a perpendicular C···Ar distance of 3.60 Å.

The ability of calixarene to undergo a host–guest relationship with organic molecules has already been described in terms of CH/π interaction.[8,9] It has also been recognized that these interactions can help in stabilizing an enzyme–substrate complex.[8,10] In the specific case of Liver Alcohol Dehydrogenase,[7] Phe-93 interacts with sulfoxide-based inhibitors that coordinate the zinc dication.[11,12] The reported distances (3.7–3.8 Å) are very similar to that (3.67 Å) described above for the methyl group of the ethanol ligand. More important however, are the interactions of the calixarene aromatic structure with the CH groups that are directly connected to the O-atom coordinating the metal center (OCH_2– and O=C*H*– for L = EtOH and NH_2CHO, respectively). Indeed, these hydrogen atoms have an exacerbated acidic character that should increase the stabilizing effect of the interactions with π systems. Again, an interesting comparison can be made with the X-ray structure of LADH reporting a tetrahedral Zn center that binds EtOH in close contact with Phe-93.[7] The distance from the ethanol $–CH_2–$ hydrogen atom closest to the center of the aromatic ring is 3.15 Å in the enzyme. For the calixarene-based Zn model complexes, we found 2.92 Å for $–CH_2OH$ (L = EtOH) and 2.70 Å for –C*H*=O (L = NH_2CHO). The distance from the Zn ion to the center of the same phenyl rings is, in each case, 5.45, 5.41, 5.42 Å, respectively. Hence, this can be viewed as a metal ligand aromatic cation/π interaction, as recently suggested in a study concerned precisely with metalloproteins.[10] Finally, hydrogen bond networks have often been observed in enzyme active sites and in particular for the zinc-bound alcohol and Ser-48 in LADH.[13]

In conclusion, we have structurally characterized two novel dicationic tetrahedral Zn complexes that display unusual and remarkable stability. Both the ethanol and the formamide adducts are interesting structural models for the species involved in the catalytic cycle of Zn peptidases or LADH as these enzymes present similar stabilizing interactions. It is worth noting that these new data suggest that a sulfur-rich coordination core as in LADH is not a specific requirement for the stabilization of tetrahedral zinc–alcohol complexes, but might rather be necessary for substrate activation toward hydride transfer. We are currently studying the reactivity of these so-called *Zn funnel complexes*.

Notes and references

† The crystals were measured on a Nonius KappaCCD diffractometer. The structures were solved by direct methods and refined using the program SHELXL97. As usual with this series of compounds, the crystals were very sensitive to desolvation. The hydrogen atoms were added at idealized positions. In the calculations, they were treated as riding atoms and the U_{iso} were free to refine, except for the two hydrogens bonded to the nitrogen of the amide ligand. For these latter, the U_{iso} were fixed at 1.5 × U_{eq} of the nitrogen atom before the last cycles of refinement. *Crystal data* for $[Zn(X_6Me_3ImMe_3)(EtOH)](ClO_4)_2{\cdot}Me_2CO$: $C_{89}H_{120}N_6O_{16}Cl_2Zn$, M_w = 1666.24, triclinic, space group $P1$, a = 13.639(1), b = 16.006(1) c = 22.799(1) Å, α = 88.68(1), β = 78.12(1), γ = 68.24(1)°, V = 4515.8(5) Å^3, Z = 2, D_c = 1.225 g cm^{-3}, μ(Mo-Kα) = 0.396 cm^{-1}, 13013 reflections measured at 173 K, 1039 parameters refined on F^2 using 12869 unique reflections to final indices $R[F^2 > 4\sigma F^2]$ = 0.112, wR = 0.307 [w = $1/[\sigma^2(F_o^2) + (0.2P)^2 + P]$ where P = $(F_o^2 + 2F_c^2)/3$]. One Bu^t and one counter ion oxygen were split on two distinct sites with multiplicities of 0.7 and 0.3 because of static disorders. The final residual Fourier positive and negative peaks were equal to 0.70 and −0.78, respectively.

For $[Zn(X_6Me_3ImMe_3)(NH_2CHO)](ClO_4)_2{\cdot}2PhCN$: $C_{105}H_{133}N_9O_{15}Cl_2Zn$, M_w = 1897.47, monoclinic, space group $P2_1/c$, a = 23.752(1), b = 16.1345(8) c = 27.385(1) Å, β = 96.394(3)°, V = 10429.4(8) Å^3, Z = 4, D_c = 1.208 g cm^{-3}, μ(Mo-Kα) = 3.52 cm^{-1}, 13101 reflections measured at 193 K, 1316 parameters refined on F^2 using 12808 unique reflections to final indices $R[F^2 > 4\sigma F^2]$ = 0.119, wR = 0.278 [w = $1/[\sigma^2(F_o^2) + (0.1116P)^2 + 45.5085P]$ where P = $(F_o^2 + 2F_c^2)/3$]. The final residual Fourier positive and negative peaks were equal to 0.82 and −0.58, respectively.

CCDC 145474 and 161215. See http://www.rsc.org/suppdata/cc/b1/b102322p/ for crystallographic data in .cif or other electronic format.

‡ In ligand $X_6Et_3ImEt_3$, the *O*- and *N*-methyl substituents of $X_6Me_3ImMe_3$ are replaced by ethyl groups. Its synthesis was described in ref 3. The corresponding aqua complex $[Zn(X_6Et_3ImEt_3)(H_2O)](ClO_4)_2$ was obtained following the synthetic procedure described in ref 2.

1 W. N. Lipscomb and N. Sträter, *Chem. Rev.*, 1996, **96**, 2375.
2 O. Sénèque, M.-N. Rager, M. Giorgi and O. Reinaud, *J. Am. Chem. Soc.*, 2000, **122**, 6183.
3 Y. Rondelez, O. Sénèque, M.-N. Rager, A. Duprat and O. Reinaud, *Chem. Eur. J.*, 2000, **6**, 4218.
4 L. Le Clainche, M. Giorgi and O. Reinaud, *Inorg. Chem.*, 2000, **39**, 3436.
5 The first example of a terminal alcohol coordinated to a tetrahedral zinc was recently obtained with a S_3 anionic ligand (Tm). Its stability was ascribed to the sulfur anionic environment. See: C. Kimblin, B. M. Bridgewater, D. G. Churchill and G. Parkin, *Chem. Commun.*, 1999, 2301.
6 X-Ray structures of terminal amido–zinc complexes appear to be rare. Among the tetrahedrally coordinated complexes reported in the Cambridge data bank (all neutral), the shortest Zn–O distance is 1.98 Å for $[ZnBr_2(DMF)_2]$. See: R. A. Edwards, O. P. Gladkikh, M. Nieuwenhuyzen and C. J. Wilkins, *Z. Kristallogr.*, 1999, **214**, 111.
7 Liver Alcohol Dehydrogenase (LADH) is a zinc enzyme that catalyses the reversible dehydrogenation of alcohols to aldehydes *via* hydride transfer with NAD^+. The Zn center is coordinated to two cisteines and one histidine. For X-ray structures with alcohol coordinating Zn, see: H. Li, W. H. Hallows, J. S. Punzi, K. W. Pankiewicz, K. A. Watanabe and B. M. Goldstein, *Biochemistry*, 1994, **33**, 11734.
8 The enthalpy for one unit CH/π interaction is *ca*. 1 kcal mol^{-1}. See: M. Nishio, Y. Umezawa, M. Hirota and Y. Takeuchi, *Tetrahedron*, 1995, **51**, 8865 and references therein.
9 H. Takahashia, S. Tsuboyamaa, Y. Umezawab, K. Hondac and M. Nishio, *Tetrahedron*, 2000, **56**, 6185.
10 For the enzyme superoxide dismutase, the interaction energy between a tryptophan residue and the ligands coordinated to iron was estimated to 10 kcal mol^{-1}. See: S. D. Zaric, D. M. Popovi and E.-W. Knapp, *Chem. Eur. J.*, 2000, **6**, 3935.
11 H. Cho, S. Ramaswamy and B. V. Plapp, *Biochemistry*, 1997, **36**, 382.
12 S. Al-Karadaghi, E. Cedergren-Zeppezauer, S. Hövmoller, K. Petratos, H. Terry and K. S. Wilson, *Acta Crystallogr., Sect. D*, 1994, **50**, 793.
13 S. Ramaswamy, H. Eklund and B. V. Plapp, *Biochemistry*, 1994, **33**, 5230.

CHEMCOMM
Communication
www.rsc.org/chemcomm

Visible light induced ring-opening metathesis polymerisation of cyclooctene

Lionel Delaude, Albert Demonceau and Alfred F. Noels*

Center for Education and Research on Macromolecules (CERM), Institut de Chimie (B6a), Université de Liège, Sart-Tilman par 4000 Liège, Belgium. E-mail: af.noels@ulg.ac.be

Received (in Cambridge, UK) 21st February 2001, Accepted 18th April 2001
First published as an Advance Article on the web 11th May 2001

Under visible light irradiation, ruthenium–arene complexes bearing *N*-heterocyclic carbene ligands with aryl substituents – either preformed or generated *in situ* – are active catalyst precursors for the ROMP of cyclooctene already at room temperature.

Thanks to the development of well-defined ruthenium-based catalyst precursors, ring-opening metathesis polymerisation (ROMP) has become a valuable tool for the preparation of synthetic macromolecules.[1] A major breakthrough was achieved in the mid-nineties by Grubbs and coworkers with the discovery of complex **1**, a very efficient and highly tolerant catalyst precursor for olefin metathesis reactions.[2] At approximately the same time, we reported that the 18-electron complex **2** was also a versatile and efficient promoter for the ROMP of both strained and low-strain olefins when activated by a suitable carbene precursor such as trimethylsilyldiazomethane (TMSD).[3]

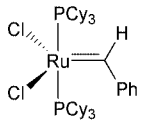

1

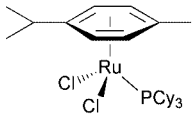

2

Replacement of one of the two phosphine ligands in **1** with more electron-donating *N*-heterocyclic carbene ligands (NHCs) significantly improved its metathesis activity and paved the way for a new generation of ruthenium–alkylidene catalyst precursors.[4] Herein, we present preliminary results obtained for the ROMP of cyclooctene (a typical low-strain cyclic olefin) when a variety of NHCs were substituted for the tricyclohexylphosphine ligand in **2**. Thus, we have prepared complexes **3a–i** and **4** from $[RuCl_2(p\text{-cymene})]_2$ and the corresponding NHCs.[5,6] The free carbene ligands were obtained from the parent imidazole-2(3*H*)-thiones[7] (**3a**,**c**,**e**,**h**) or from imidazol(in)ium chlorides[8] (**3b**,**d**,**f**,**g**, **4**) by reduction with potassium or deprotonation with potassium *tert*-butoxide or hydride, respectively. The dichlorocarbene in **3i** was the adduct of 1,3-dimesitylimidazol-2-ylidene and CCl_4.[9]

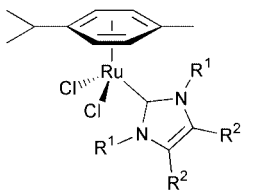

3

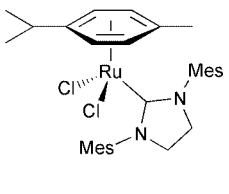

4

3a $R^1 = R^2 = Me$
3b $R^1 = Pr^i$, $R^2 = H$
3c $R^1 = Pr^i$, $R^2 = Me$
3d $R^1 = Cy$, $R^2 = H$
3e $R^1 = Cy$, $R^2 = Me$
3f $R^1 = Dipp$, $R^2 = H$
3g $R^1 = Mes$, $R^2 = H$
3h $R^1 = Mes$, $R^2 = Me$
3i $R^1 = Mes$, $R^2 = Cl$
Cy = cyclohexyl
Dipp = 2,6-diisopropylphenyl
Mes = 2,4,6-trimethylphenyl

Polymerisation of cyclooctene in PhCl for 4 h at 60 °C served as a test reaction for our initial screening. These experimental conditions, complemented by TMSD initiation, were found optimal in our previous studies with **2**.[3] Transposed to the case of ruthenium–NHC catalyst precursors, they led to dichotomous results. Complexes **3a–e** bearing alkyl-substituted imidazol-2-ylidene ligands were devoid of any significant activity for the ROMP of cyclooctene, even in the presence of the TMSD carbene precursor. Monomer conversion stagnated below 16% and no polymer was isolated. Aryl-substituted ligands, on the other hand, afforded much more active catalysts. With **3f** and **3g**, gelation of the reaction mixture occurred within a few minutes and a near quantitative yield of polyoctenamer was obtained after 4 h at 60 °C. When the reaction temperature was lowered to *ca*. 20 °C, this remarkably high activity was maintained. Most interestingly, we found that the polymerisation of cyclooctene with catalysts **3f** and **3g** performed equally well in the absence of TMSD, whereas the addition of a diazo compound was a requisite with complex **2**.[3] The presence of light played a key-role in the nucleophilic carbene-based system and the intervention of a photochemical activation step was evidenced from the results gathered in Table 1.† With exclusion of light, a mere 20% yield of polymer was obtained after 2 h at room temperature. Normal lighting in the laboratory, a combination of daylight and of fluorescent light, was sufficient to raise the conversion to 93% within the same period. More intense visible light sources brought the reaction to completion while ensuring reproducible conditions. Thus, recourse to an ordinary 40 W 'cold white' fluorescent tube or to a 250 W incandescent light bulb standing 10 cm away from the standard Pyrex reaction flasks afforded quantitative yields of polyoctenamer. The differences in the emission spectra of the two light sources did not have any incidence on the polymer microstructure. In both cases, the polyoctenamer obtained was mainly *trans* and had a relatively narrow molecular weight distribution.

To the best of our knowledge, the only precedents of photoinduced ROMP described in the literature involved UV light irradiation. Systems based either on Schrock-type tungsten catalysts or on ruthenium– and osmium–arene complexes similar to **2** were able to polymerise strained cyclic olefins upon exposure to a 200 W Hg lamp, although high molecular weights and broad molecular weight distributions were obtained.[10] It was of note that neon light or strong daylight significantly enhanced the catalytic activity of complex **2** itself or of a

Table 1 Effect of light on the ROMP of cyclooctene using **3g** as a catalyst

Lighting conditions[a]	Monomer conversion[b] (%)	Isolated yield (%)	σ_c[c]	10^{-3} M_n[d]	M_w/M_n[d]
Darkness	22	20	0.36	21	1.53
Normal	93	84	0.27	625	2.00
Neon tube	99	93	0.17	553	1.33
Light bulb	>99	91	0.18	537	1.33

[a] See text for details. [b] Determined by GC. [c] Fraction of *cis* double bonds within the polyoctenamer, determined by ^{13}C NMR. [d] Determined by GPC in THF *vs.* monodisperse polystyrene standards.

 DOI: 10.1039/b101699g

stoichiometric mixture of $[RuCl_2(p\text{-cymene})]_2$ and PCy_3 toward the ring closing metathesis (RCM) of numerous dienes in refluxing CH_2Cl_2.[11] Complexes **3f** and **3g**, on the other hand, displayed the same efficiency in the RCM of diallyl malonate, whether the reaction was carried out in the presence or in the absence of visible light.[6] This is in sharp contrast with our observations for the ROMP of cyclooctene, as we confirmed that complex **2** was completely inactive toward the olefin if the TMSD initiation was replaced by visible light illumination.

The UV–VIS spectra of **2** and **3g** freshly dissolved in PhCl were recorded under the exclusion of air and moisture. The phosphine derivative **2** had an absorption maximum at 369 nm while the carbene compound **3g** displayed two less intense bands centred at *ca.* 350 and 450 nm. The band at 350 nm corresponds to the absorption of the free carbene ligand while the band at 450 nm was more visible when $[RuCl_2(p\text{-cymene})]_2$ and 1,3-dimesitylimidazol-2-ylidene (2 equiv.) were mixed in the UV cell immediately prior to the analysis. Upon exposure to intense visible light for 30 min the band at 450 nm completely disappeared. Hence, we tentatively assign this visible absorption to the *p*-cymene moiety in **3g**. ^{1}H NMR spectroscopy confirmed that free *p*-cymene was released from **3g** when a PhCl-d_5 solution of the complex was irradiated in the presence or in the absence of cyclooctene. A similar arene decoordination had already been reported when **2** was treated with TMSD.[3] In that case concomitant formation of $[Ru]{=}CHSiMe_3$ active species was evidenced, whereas in the present system no propagating carbene was detected by NMR. However, the light-induced decomplexation of the η^6-arene ligand is believed to generate a highly reactive coordinatively unsaturated ruthenium species that triggers the catalytic process, though the exact nature of the active species in solution, as yet, remains elusive.

Next, we synthesised the new complexes **3h**, **3i** and **4** to compare their activities with those of **3f** and **3g**. Thus, the ROMP of cyclooctene initiated by various catalyst precursors was carried out under visible light irradiation and monitored by GC. Fig. 1 depicts the time-course of the polymerisations in PhCl at 20 °C. Compound **3g** remained the best catalyst precursor under the experimental conditions adopted. It slightly outperformed complex **3f** and the Grubbs' catalyst **1** and was a much better ROMP promoter than its saturated imidazolidine analogue **4**. Surprisingly, disubstitution of the 4,5 positions on the heterocyclic imidazole ring by methyl groups (in **3h**) gave a very poor catalyst, while the dichloro derivative **3i** displayed a steady albeit moderate activity, close to that observed with the TMSD-activated complex **2**.

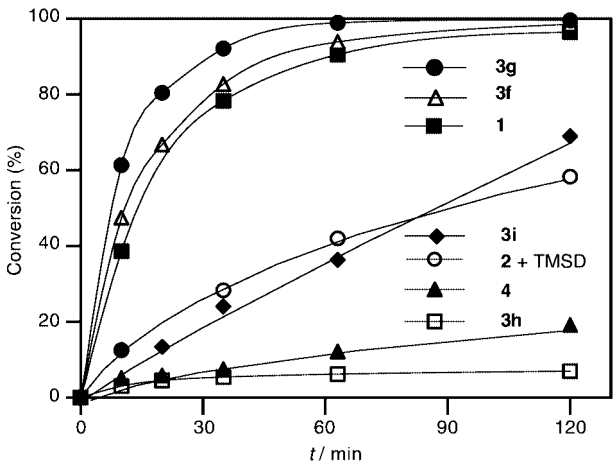

Fig. 1 ROMP of cyclooctene using catalysts **1**, **2**, **3f–i** and **4**. *Conditions*: 0.06 mmol of catalyst in PhCl (5 mL) at 20 °C, neon light irradiation, monomer/catalyst ratio 150. Conversion determined by GC.

Table 2 ROMP of cyclooctene at 60 °C catalysed by complex **3g** preformed or generated *in situ*

Catalyst precursor	Monomer conversion[a] (%)	Isolated yield (%)	σ_c[a]	$10^{-3}\ M_n$[a]	M_w/M_n[a]
5 + **6** + Cs_2CO_3	56	47	0.44	623	3.62
5 + **6** + KOBu^t	99	92	0.20	659	2.02
3g	> 99	84	0.17	269	1.97

[a] See Table 1 for details.

Finally, we examined the replacement of complex **3g** in our reactions by more easily available, commercial precursors. For this purpose, we tested mixtures of $[RuCl_2(p\text{-cymene})]_2$ **5** and 1,3-dimesitylimidazolium chloride **6** (2 equiv.) in the presence of various bases (4 equiv.) *viz*. 2,6-di-*tert*-butyl-4-methylpyridine, Cs_2CO_3, and KOBu^t. With all three bases, cyclooctene conversion did not exceed 10% after 2 h at room temperature, maybe because the ionic components were poorly soluble in PhCl at that temperature. When the polymerisations were carried out at 60 °C, the sterically hindered, non-nucleophilic pyridine did not afford any polymer, but Cs_2CO_3 led to a decent yield of polyoctenamer (Table 2)†. Most gratifyingly, we also noted that complex **3g** generated *in situ* with KOBu^t as a base was almost as effective as the preformed complex, opening the way to new, simple, straightforward polymerisation procedures.

We thank the EUTMR programme (HPRU-2000-10) for financial support.

Notes and references

† *Typical polymerisation procedure*: complex **3g** (3×10^{-5} mol) was dissolved in 5 mL of dry PhCl under Ar. The solution was irradiated by a 40 W 'cold white' fluorescent tube placed 10 cm away from the Pyrex reaction flask. Cyclooctene (7.5×10^{-3} mol) was added *via* a syringe and the reaction mixture was stirred for 2 h at r.t. or at 60 °C. The resulting gel was diluted with $CHCl_3$ (2×10 mL) and slowly poured into 500 mL of MeOH under vigorous stirring. The precipitated polyoctenamer was dried under high vacuum and characterised by NMR and GPC.

1 K. J. Ivin and J. C. Mol, *Olefin Metathesis and Metathesis Polymerization*, Academic Press, New York, 1997.
2 P. Schwab, M. B. France, J. W. Ziller and R. H. Grubbs, *Angew. Chem., Int. Ed. Engl.*, 1995, **34**, 2039; T. M. Trnka and R. H. Grubbs, *Acc. Chem. Res.*, 2001, **34**, 18.
3 A. W. Stumpf, E. Saive, A. Demonceau and A. F. Noels, *Chem. Commun.*, 1995, 1127; A. Demonceau, A. W. Stumpf, E. Saive and A. F. Noels, *Macromolecules*, 1997, **30**, 2127.
4 J. Huang, H.-J. Schanz, E. D. Stevens and S. P. Nolan, *Organometallics*, 1999, **18**, 5375; T. Weskamp, F. J. Kohl, W. Hieringer, D. Gleich and W. A. Herrmann, *Angew. Chem., Int. Ed.*, 1999, **38**, 2416; C. W. Bielawski and R. H. Grubbs, *Angew. Chem., Int. Ed.*, 2000, **39**, 2903.
5 W. A. Herrmann, M. Elison, J. Fischer, C. Köcher and G. R. J. Artus, *Chem. Eur. J.*, 1996, **2**, 772; W. A. Herrmann, C. Köcher, L. J. Goossen and G. R. J. Artus, *Chem. Eur. J.*, 1996, **2**, 1627.
6 L. Jafarpour, J. Huang, E. D. Stevens and S. P. Nolan, *Organometallics*, 1999, **18**, 3760.
7 N. Kuhn and T. Kratz, *Synthesis*, 1993, 561.
8 A. J. Arduengo, III, H. V. R. Dias, R. L. Harlow and M. Kline, *J. Am. Chem. Soc.*, 1992, **114**, 5530; A. J. Arduengo, III, R. Krafczyk, R. Schmutzler, H. A. Craig, J. R. Goerlich, W. J. Marshall and M. Unverzagt, *Tetrahedron*, 1999, **55**, 14523.
9 A. J. Arduengo, III, F. Davidson, H. V. R. Dias, J. R. Goerlich, D. Khasnis, W. J. Marshall and T. K. Prakasha, *J. Am. Chem. Soc.*, 1997, **119**, 12742.
10 P. A. van der Schaaf, A. Hafner and A. Mühlebach, *Angew. Chem., Int. Ed. Engl.*, 1996, **35**, 1845; A. Hafner, A. Mühlebach and P. A. van der Schaaf, *Angew. Chem., Int. Ed. Engl.*, 1997, **36**, 2121.
11 A. Fürstner and L. Ackermann, *Chem. Commun.*, 1999, 95.

CHEMCOMM Communication
www.rsc.org/chemcomm

Mesoporous iron–titania catalyst for cyclohexane oxidation

Nina Perkas,[a] Yanqin Wang,[a] Yuri Koltypin,[a] Aharon Gedanken*[a] and Srinivasan Chandrasekaran[b]

[a] *Department of Chemistry, Bar-Ilan University, Ramat-Gan 52900, Israel. E-mail: gedanken@mail.biu.ac.il*
[b] *Department of Organic Chemistry, Indian Institute of Science, Bangalore 560012, India*

Received (in Cambridge, UK) 25th January 2001, Accepted 19th April 2001
First published as an Advance Article on the web 11th May 2001

This is the first report of using ultrasound radiation for depositing a nanosized catalyst (iron oxide) into the pores of a mesoporous material (titania); the resulting catalyst is used for the oxidation of cyclohexane under mild conditions.

The synthesis of mesoporous materials offers a new possibility for the creation of catalysts that are effective in many technological processes. Their high surface area, large adsorption capacity, and ordered pore structure make them very useful for oil refining, petrochemistry, and organic synthesis.[1] At the same time, mesoporous materials have found many applications as supports for metal oxides, organometallic compounds, and other precursors, achieving high dispersion and functionalization of the active phase.[2] It has been shown that the incorporation of transition metals into the framework of MCM-41 allows the preparation of catalysts which are active in the oxidation of organic compounds.[3] The catalytic activity in the liquid-phase oxidation of cyclohexane with aqueous H_2O_2, exhibited by an iron catalyst incorporated into mesoporous molecular sieves (MCM-41), has been attributed to the formation of heterogenized iron complexes.[4] The yield of target products (cyclohexanol and cyclohexanone) with this catalyst did not exceed 3.5%.

As reported by Suslick *et al.*, the sonochemical method can be used as a tool to prepare nanosized amorphous metals.[5] If ultrasound irradiation is applied in the presence of an oxide support (such as silica, titania, alumina), the initially formed nanoscale clusters can be trapped in the support. Recently, sonication has been further developed to drive the deposition of iron, nickel, and cobalt on the surface of silica and alumina particles.[6] Sonochemistry has also been used for the preparation of mesoporous silica (MCM-41),[7a] mesoporous titania,[7b] and mesoporous yttria–zirconia. The main advantage in using sonochemistry for the synthesis of mesoporous materials is the drastic shortening of the time involved in the fabrication of the products from days to hours. It has been demonstrated that the wall thickness is perhaps also greater when the sonochemical technique is used. This communication is the first report where sonochemistry is employed to deposit amorphous nanoparticles into the pores of a mesoporous material.

The question as to whether or not sonochemistry can also be used for the deposition of a catalyst into the inner pores of mesoporous materials is examined here. Iron oxide was chosen as a testing probe for this purpose, which can be used as a catalyst in the oxidation of alkanes. We have reported recently on the oxidation of cyclohexane using sonochemically prepared nanostructured amorphous iron and cobalt catalysts or an amorphous iron–nickel alloy.[8] In that work, the reaction was carried out under high oxygen pressure (40 atm) at room temperature without a solvent, using isobutyraldehyde as an activator and a catalytic amount of acetic acid. Under these conditions, a high conversion of cyclohexane (*ca.* 40%) was obtained with an almost 80% selectivity to the target products cyclohexanone and cyclohexanol. Later it was found that the active catalyst was the nanostructured, sonochemically prepared transition metal (TM) oxide and not the amorphous TM.[9] In fact, due to the high reactivity of the amorphous materials, it is almost impossible to avoid oxidation of the nanophased TM. We report herein the results of cyclohexane oxidation with an iron oxide catalyst supported over mesoporous titania (MSPT). The preparation of the MSPT and the deposition of the iron oxide into its pores were carried out by a sonochemical method. In our synthesis we have followed the sonochemical preparation of nanophased amorphous Fe_2O_3 described previously.[10] The synthesis was carried out in the presence of mesoporous TiO_2. The activity of this catalyst was tested in the oxidation of cyclohexane under mild conditions.

The mesoporous titanium oxide was synthesized from titanium isopropoxide by ultrasound irradiation, as described elsewhere.[7b] Its surface area, measured by the BET nitrogen adsorption method (Micromeritics Gemini) after removal of the surfactant, reached 850 $m^2\ g^{-1}$ with a pore size of 1.5 nm and a pore volume of 0.53 ml g^{-1}.

The as prepared titania was irradiated by ultrasound with a solution of iron pentacarbonyl in decalin under an atmospheric pressure of air at 0 °C for 3 h.[11] The surface area of the sample was reduced to 570 $m^2\ g^{-1}$, with a pore size of 1.3 nm and a pore volume of 0.23 ml g^{-1}. The reduction in surface area and pore volume is due to the insertion of iron oxide into the mesopores.

The particle size of the titanium oxide, obtained from TEM measurements (microscope JEOL-JEM 100) is of the order of 100–200 nm. The outer surface area is *ca.* 1–2 $m^2\ g^{-1}$ as calculated from the particle size. Coating the outer surface with 5 nm catalyst particles (as estimated from particles found outside the pores) would not lead to the measured reduction in surface area for the titania/iron oxide composite. We, therefore, conclude that the major part of the iron oxide is inserted into the mesopores.

XRD analysis was performed with a Rigaku diffractometer (Model 2028, Cu-Kα radiation). In the as prepared sample, iron oxide was in an amorphous state. After heating under argon at 300 °C for 24 h, it crystallized in the form of magnetite.

Elemental analyses, performed using energy dispersive X-ray (EDX) analysis (Link ISIS Oxford) and atomic adsorption spectroscopy (AAS) (Perkin Elmer 2380 spectrometer) showed a difference in iron content (Table 1), the iron concentration obtained by EDX being higher than in the AAS results. This indicates that part of the iron is located on the surface of the catalyst, since EDX measures the surface concentration of the element, while AAS gives the total quantity. Nevertheless, the difference in concentration between these two analytical methods for the catalysts (prepared by the same method of sonochemical irradiation on mesoporous titania support) is lower than on commercial titania (Degussa P-25) (Table 1). This can occur because of the larger pore volume of mesoporous titania in comparison to that of conventional TiO_2 and thus a deeper impregnation of the active phase in the pores.

The binding energy measured by XPS for the $Fe2P_{3/2}$ and Ti $2P_{3/2}$ did not differ very much for the catalysts supported on

 DOI: 10.1039/b100910a

Table 1 Physicochemical properties of iron oxide catalysts prepared by the sonication method

Catalyst	Fe_2O_3 (mass%)		E_b[a]/eV		Conversion of cyclohexane (%)
	EDX	AAS	Fe $2p_{3/2}$	Ti $2p_{3/2}$	
Fe_2O_3	100	100	710.5 (711.5[a])	—	16.5
Fe_2O_3/TiO_2 (Degussa P-25)	20.3	12.0	710.6	457.6 (458.6,[b] 459.8[c])	21.3
Fe_2O_3/TiO_2 (MSPT)	18.7	14.5	710.9	458.7	25.8

[a] Value for commercial Fe_2O_3. [b] Value for commercial TiO_2. [c] Value for sonicated TiO_2.

titania and sonochemically prepared iron oxide and were close to the values corresponding to conventional Fe_2O_3 and TiO_2 (Table 1).

We have studied the reaction of cyclohexane oxidation with iron oxide supported on mesoporous titania under mild conditions.[12] Table 1 presents the conversion of cyclohexane into oxidation products, using three forms of the catalyst: (a) unsupported nanophased amorphous Fe_2O_3; (b) amorphous Fe_2O_3 deposited on TiO_2 (Degussa P-25), which we have reported on previously[9] and (c) amorphous Fe_2O_3 deposited on TiO_2 (MSPT). Of these the Fe_2O_3/TiO_2 (MSPT) showed the highest activity in cyclohexane oxidation. The main products (selectivity almost 90%) were cyclohexanol and cyclohexanone, in the ratio 1.5:1. GC analysis revealed that in the presence of acetic acid, the activator (isobutyraldehyde) first reacted with oxygen, and the final oxidation product was isobutyric acid. The perisobutyric acid formed *in situ* during this process may react with metal species supported on the carrier to form oxometal complexes. Hydrogen abstraction from cyclohexane by oxometal complexes, followed by the formation of cyclohexanone and cyclohexanol, probably takes place as a result of the same free radical mechanism described earlier.[13]

After the first reaction the liquid phase was separated by centrifugation and the solid catalyst reused under the same conditions.[12] The conversion of a fresh portion of cyclohexane was scarcely changed in comparison with the first cycle. On the basis of these results it is reasonable to conclude that the sonochemically prepared nanosized iron oxide deposited on MSPT is a stable and effective catalyst. It can be used for the oxidation of cyclohexane, other hydrocarbons, and a number of other organic functional groups, which are currently under investigation.

In summary, this work demonstrates that sonochemistry can be used for anchoring nanomaterials in the pores of mesoporous compounds to produce effective catalysts.

Notes and references

1 A. Corma, *Chem. Rev.*, 1997, **97**, 2733; T. J. Barton, L. M. Bull, W. G. Klemperer, D. A. Loy, B. C. McEnaney, M. Misono, P. A. Monson, G. Pez, G. W. Scherer, J. C. Vartuli and O. N. Yaghi, *Chem. Mater.*, 1999, **11**, 2633.

2 I. V. Kozheunikov, A. Sinnema, R. J. J. Jansen, K. Pamin and H. Van Bekkum, *Catal. Lett.*, 1995, **30**, 241; D. Brunel, A. Canvel, F. Fajula and F. Di Renzo, *Stud. Surf. Sci. Catal.*, 1995, **97**, 173.

3 W. A. Carvalho, P. B. Varaldo, M. Wallau and U. Schuchardt, *Zeolites*, 1997, **18**, 408; T. Maschmeyer, F. Rey, G. Sankar and J. M. Thomas, *Nature*, 1995, **378**, 159.

4 W. A. Carvalho, M. Wallau and U. Schuchardt, *J. Mol. Catal. A.: Chem.*, 1999, **144**, 91.

5 K. S. Suslick, S. B. Choe, A. A. Cichowlas and M. S. Grinstaff, *Nature*, 1991, **353**, 414; K. S. Suslick, T. Hyeon, M. Fang and A. A. Cichowlas, *Mater. Sci. Eng. A*, 1995, **204**, 186.

6 S. Ramesh, Y. Koltypin, R. Prozorov and A. Gedanken, *Chem. Mater*, 1997, **9**, 546; S. Ramesh, R. Prozorov and A. Gedanken, *Chem. Mater.*, 1997, **9**, 2996; Z. Zhong, Y. Zhao, Y. Koltypin and A. Gedanken, *J. Mater. Chem.*, 1998, **10**, 2167.

7 (*a*) X. Tang, S. Liu, Y. Wang, W. Huang, E. Sominski, O. Palchik, Yu. Koltypin and A. Gedanken, *Chem. Commun.*, 2000, 2119; (*b*) Y. Wang and A. Gedanken, *Adv. Mater.*, 2000, **12**, 1183.

8 V. Kesavan, P. S. Sivanand, S. Chandersekaran, Y. Koltypin and A. Gedanken, *Angew. Chem., Int. Ed.*, 1999, **38**, 3521.

9 N. Perkas, Y. Koltypin, O. Palchik, A. Gedanken and S. Chandrasekaran, *Appl. Catal. A: Gen.*, 2001, **209**, 125.

10 X. Cao, Y. Koltypin, R. Prozorov, G. Kataby and A. Gedanken, *J. Mater. Chem.*, 1997, **7**, 2447.

11 *Synthesis of mesoporous iron–titania catalyst*: 0.5 g of mesoporous titania prepared by a previously reported method[7b] was added to 80 ml of decalin, and 0.8 ml of iron pentacarbonyl added to the solution (molar ratio of initial substances was 1:1). The mixture was irradiated by ultrasound under an atmospheric pressure of air at 0 °C for 3 h. The product was washed thoroughly with pentane and dried in vacuum.

12 The oxidation of cyclohexane was performed in a thermostated glass reactor using 2 ml (18.5 mmol) of cyclohexane, 2.5 ml (27.75 mmol) of isobutyraldehyde (molar ratio 1.5:1), a catalytic amount of acetic acid (0.06 ml, 1 mmol), and an amount of the catalyst equivalent to 0.015 mmol of iron oxide. The reaction mixture was magnetically stirred at 70 °C and 1 atm of oxygen for 15–17 h. The reaction products were analyzed by GC using the starting alkane as an internal standard. Conversion is defined as the percentage of the starting alkane converted into the products.

13 S. T. Murahashi, Y. Oda and T. Y. Naota, *J. Am. Chem. Soc.*, 1992, **114**, 7913.

CHEMCOMM
Communication
www.rsc.org/chemcomm

The synthesis of peptides using micro reactors†

Paul Watts,[a] Charlotte Wiles,[a] Stephen J. Haswell,*[a] Esteban Pombo-Villar[b] and Peter Styring[c]

[a] *Department of Chemistry, University of Hull, Cottingham Road, Hull, UK HU6 7RX. E-mail: S.J.Haswell@chem.hull.ac.uk*
[b] *Nervous System Research, WSJ-386.07.15, Novartis Pharma Ltd., CH4002, Basel, Switzerland*
[c] *Department of Chemical and Process Engineering, University of Sheffield, Mappin Street, Sheffield, UK S1 3JD*

Received (in Cambridge, UK) 6th March 2001, Accepted 19th April 2001
First published as an Advance Article on the web 15th May 2001

We have demonstrated the first application of multi-step synthesis within a micro reactor and have shown that peptides may be prepared in quantitative yield in a period of 20 min, compared with batch reactions where only moderate yields (40–50%) were obtained in a 24 h period.

During the past ten years, there has been a rapid growth in the development of micro-Total Analytical Systems (μ-TAS)[1–3] which exploit electroosmotic flow (EOF).[4] The development of micro reactor devices for chemical synthesis based on complementary technology is less common. However, recent research has shown that Suzuki[5] and Wittig[6] reactions may be performed using micro reactor systems.[7]

Peptides have been commonly prepared *via* solid supported techniques since its introduction by Merrifield in 1963.[8] Solid phase peptide synthesis is based on the addition of a protected amino acid residue to an insoluble polymeric support. The acid-labile Boc group[9] and base-labile Fmoc group[10] have been commonly used for *N*-protection. After removal of the protecting group the next protected amino acid may be added using either a coupling reagent or a pre-activated amino acid derivative. If this dipeptide is the desired product, it may be cleaved from the polymer support using various reagents, one of the more common methods being treatment with 25–80% HF.[11] If a longer peptide is required additional amino acids can be added by repeating further coupling reactions.

Solid phase peptide synthesis has the disadvantage that a fairly expensive polymer support is required. In addition, extra steps are added to the synthesis as a result of initially linking the amino acid to the support and finally having to remove the peptide from the polymer. In this paper a micro reactor has been used to prepare peptides using solution phase chemistry in an attempt to overcome some of the current problems associated with such syntheses.

The micro reactor devices used in this work were prepared using standard procedures developed at Hull.[12] A schematic of a typical micro reactor produced using such fabrication techniques is shown in the graphical abstract.† Microporous silica frits[13] were placed in the channels to prevent hydrodynamic flow occurring.

In the first instance a one-step reaction was considered in which an *N*-protected β-amino acid was reacted with an *O*-protected β-amino acid, to prepare the protected β-dipeptide. To enable the methodology to be applicable to the synthesis of more complex peptides, the use of orthogonal protecting groups was clearly required. After careful consideration, the base-labile Fmoc protecting group[10] was selected for *N*-protection while the Dmab ester[14] was chosen for protection of the carboxylic acid. Importantly, both protecting groups may be removed under mild conditions, since electroosmotic flow is retarded if the pH of the reaction is outside the range 3–10.

† Electronic supplementary information (ESI) available: schematic of a borosilicate glass micro reactor. See http://www.rsc.org/suppdata/cc/b1/b102125g/

Commercially available Boc-β-alanine **1** was protected as the Dmab ester using an EDCI [1-(3-dimethylaminopropyl)-3-ethylcarbodiimide hydrochloride] and DMAP coupling reaction, to give the ester **2** in 92% yield in a bulk reaction (Scheme 1). Treatment of **2** with trifluoroacetic acid furnished the desired amine **3** in 61% yield, which was subsequently reacted with Fmoc-β-alanine **4** *via* a carbodiimide coupling reaction, to give a synthetic sample of dipeptide **5**.

Having prepared dipeptide **5**, it represented a synthetic target for preparation using the micro reactor. Prior to synthesis, the micro reactor channels were primed with anhydrous DMF to remove any air and moisture from the channels and the microporous silica frits. A standard solution of Fmoc-β-alanine **4** (50 μl, 0.1 M) in anhydrous DMF was added to reservoir A, a solution of EDCI (50 μl, 0.1 M) was placed in reservoir B and a solution of amine **3** (50 μl, 0.1 M) was placed in reservoir C. Anhydrous DMF (40 μl) was placed in reservoir D, which was used to collect the products of the reaction. Platinum electrodes were placed in each of the reservoirs (A, B and C positive, D ground) and an external voltage was applied to the channels inducing electroosmotic flow of the reagents. The reactions were conducted at rt for a period of 20 min, in order to acquire sufficient volume of product to determine the yield of the reaction. Analysis was achieved by high performance liquid chromatography (Jupiter C_{18} 10 μm, 4.6 × 250 mm, obtained from Phenomenex), mobile phase composition: 0.1% TFA in water and 0.1% TFA in acetonitrile, using a gradient system of 30% aqueous to 70% aqueous over 20 min, with a flow rate of 2.5 ml min^{-1} at rt).

When stoichiometric quantities of the reagents were used only *ca*. 10% conversion to peptide **5** was achieved when a voltage of 700 V was applied to the reagents (A, B and C). However, by using two equivalents of EDCI (0.2 M solution) the yield of the reaction was increased to *ca*. 20%. By applying a stopped flow technique (2.5 sec injection length with flow stopped for 10 sec) the yield of the reaction was further increased to 50%. Since the yield of the reaction appeared to greatly depend on the number of equivalents of EDCI used, we wished to further investigate the effect of carbodiimide concentration on the reaction, however we found that EDCI was insoluble in DMF above 0.2 M concentrations. In further experiments DCC was used as the coupling reagent as it was considerably more soluble in DMF. Using 5 eq. of DCC (0.5 M solution in reservoir B) a 93% yield of dipeptide **5** was obtained using the optimised conditions described above.

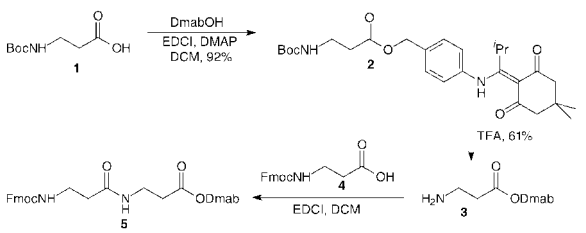

Scheme 1 Synthesis of standard dipeptide derivative.

 DOI: 10.1039/b102125g

Another common method utilised in peptide bond formation involves the reaction of a pre-activated amino acid derivative, such as a pentafluorophenyl ester, with an amine.[15,16] Fmoc-β-alanine **4** was activated as the pentafluorophenyl ester **6** *via* an EDCI coupling reaction (Scheme 2). The pentafluorophenyl ester **6** was stable and could be stored indefinitely in the freezer. The ester **6** was subsequently reacted in bulk with amine **3** to produce dipeptide **5**.

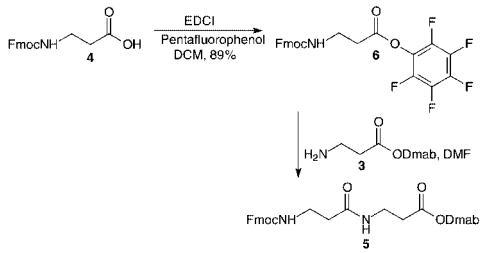

Scheme 2 Preparation and reaction of pentafluorophenyl esters of Fmoc protected amino acids.

Having prepared dipeptide **5** *via* the alternative pre-activated strategy, we wished to investigate if the reaction could be performed in a micro reactor. A standard solution of the pentafluorophenyl ester of Fmoc-β-alanine **6** (50 μl, 0.1 M) in anhydrous DMF was added to reservoir A, a solution of amine **3** (50 μl, 0.1 M) was placed in reservoir B and anhydrous DMF (40 μl) was placed in reservoir D, which was used to collect the products of the reaction. It was found that using continuous flow of both reagents, where the ester **6** was maintained at 700 V and the amine **3** was maintained at 600 V, dipeptide **5** was produced in quantitative yield in just 20 min. This represented a significant increase in yield compared with the traditional batch synthesis where only 40–50% conversions were obtained.

Similarly, the reaction between the pentafluorophenyl ester **7** of Boc-β-alanine and amine **3** was also investigated in the micro reactor (Scheme 3). In this case, when the reagents were mixed under a continuous flow regime, with both reagents maintained at 700 V, a quantitative yield of peptide **8** was observed. Importantly, this result demonstrates that both Boc and Fmoc protecting groups are suitable for use in the preparation of peptides using micro reactors.

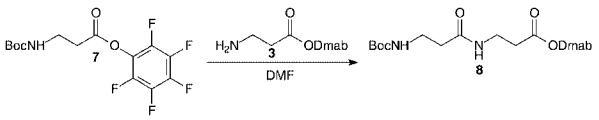

Scheme 3 Reaction of pentafluorophenyl esters of Boc-β-alanine.

Having successfully demonstrated that peptide bonds could be formed in micro reactors using two common methods, we wished to show that we could extend the methodology to the preparation of longer chain peptides. Consequently, we needed to be able to conduct deprotection reactions in the micro reactor and subsequently perform further peptide bond forming reactions. Fmoc-β-alanine **4** was converted into the Dmab ester **9**, in a bulk reaction, using standard conditions (Scheme 4). It was proposed to convert ester **9** into amine **3** by deprotection of the Fmoc group in the micro reactor and subsequently react the amine '*in situ*' with pentafluorophenyl ester **7**, to give the dipeptide **8**. Treatment of **9**, with 10 eq. of piperidine in DMF using the micro reactor, resulted in 60–70% deprotection over a 20 min period, to give amine **3**.[17]

Subsequently, a standard solution of the Dmab ester of Fmoc-β-alanine **9** (50 μl, 0.1 M) in anhydrous DMF was added to reservoir A, a solution of piperidine (50 μl, 1.0 M, 10 eq.) was placed in reservoir B and a solution of pentafluorophenyl ester **7** (50 μl, 0.1 M) was placed in reservoir C, in an attempt to prepare dipeptide **8** using this multi-step approach. Anhydrous DMF (40 μl) was placed in reservoir D, which was used to collect the products of the reaction. The HPLC of the reaction mixture showed that Fmoc deprotection had occurred, however

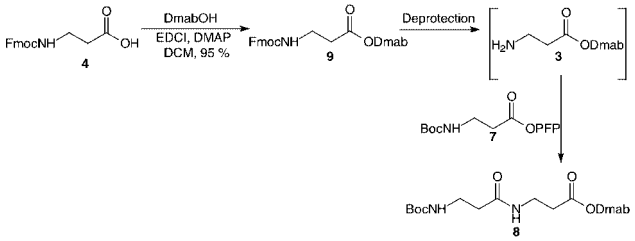

Scheme 4 Multi-step peptide synthesis.

no peptide was evident. It was however found that the excess piperidine used in the reaction was reacting with the pentafluorophenyl ester **7** to give amide **10**.

As a result, an alternative method of Fmoc deprotection was required that would not cause the aforementioned problem. Using the micro reactor, the Dmab ester of Fmoc-β-alanine **9** was reacted with one equivalent of DBU to give the free amine **3** which was then reacted with the pentafluorophenyl ester of Boc-β-alanine **7**, in an attempt to form the dipeptide **8**.

In this case, when the reagents were mixed using continuous flow, with the reagents maintained at 700 V, product **8** was observed in typically 25% yield. By comparing the flows of each reagent at this stage we were able to optimise the reaction. The Dmab ester of Fmoc-β-alanine **9** was maintained at 750 V while reacted with DBU at 800 V. The deprotected amine was then reacted, using continuous flow, with the pentafluorophenyl ester of Boc-β-alanine **7** to give a conversion of 96%, based on the amount of Dmab ester **9** present at the end of the reaction.

Having shown that more complex peptides could be produced by removal of the *N*-protecting group we wished to determine if we could remove the Dmab protecting group using hydrazine. Hence, a solution of the Dmab ester of Fmoc-β-alanine **9** (50 μl, 0.1 M) in anhydrous DMF was added to reservoir A and a solution of hydrazine (50 μl, 0.1 M) was placed in reservoir B. Anhydrous DMF (40 μl) was placed in reservoir D, which was used to collect the products of the reaction. Using continuous flow of both reagents, maintained at 700 V, quantitative deprotection was observed to give carboxylic acid **4**.

We wish to thank Novartis Pharmaceuticals (P. W. and C. W.) for financial support. We are grateful to Dr Tom McCreedy (University of Hull) for help in fabricating the micro reactor devices.

Notes and references

1 S. J. Haswell, *Analyst*, 1997, **112**, 1R.
2 A. Manz, D. J. Harrison, E. Verpoorte and H. M. Widmer, *Adv. Chromatogr.*, 1993, **33**, 1.
3 D. J. Harrison, K. Fluri, K. Seiler, Z. H. Fan, C. S. Effenhauser and A. Manz, *Science*, 1993, **261**, 895.
4 P. D. I. Fletcher, S. J. Haswell and V. N. Paunov, *Analyst*, 1999, **124**, 1273.
5 G. M. Greenway, S. J. Haswell, D. O. Morgan, V. Skelton and P. Styring, *Sensors & Actuators B*, 2000, **63**, 153.
6 V. Skelton, G. M. Greenway, S. J. Haswell, P. Styring, D. O. Morgan, B. Warrington and S. Y. F. Wong, *Analyst*, 2001, **126**, 7.
7 S. J. Haswell, R. J. Middleton, B. O'Sullivan, V. Skelton, P. Watts and P. Styring, *Chem. Commun.*, 2001, 391.
8 R. B. Merrifield, *J. Am. Chem. Soc.*, 1963, **85**, 2149.
9 P. Munster and W. Steglich, *Synthesis*, 1987, 223.
10 B. Penke and J. Rivier, *J. Org. Chem.*, 1987, **52**, 1197.
11 D. B. Whitney, J. P. Tam and R. B. Merrifield, *Tetrahedron*, 1984, **40**, 4237.
12 T. McCreedy, *Anal. Chim. Acta*, 2001, **427**, 39.
13 P. D. Christensen, S. W. P. Johnson, T. McCreedy, V. Skelton and N. G. Wilson, *Anal. Commun.*, 1998, **35**, 341.
14 W. C. Chan, B. W. Bycroft, D. J. Evans and P. D. White, *J. Chem. Soc., Chem. Commun.*, 1995, 2209.
15 L. Kisfaludy and I. Schon, *Synthesis*, 1983, 325.
16 E. Atherton, L. R. Cameron and R. C. Sheppard, *Tetrahedron*, 1988, **44**, 843.
17 L. A. Carpino and G. Y. Han, *J. Org. Chem.*, 1972, **37**, 3404.

CHEMCOMM Communication
www.rsc.org/chemcomm

A comparative study of an MCM-41 anchored quaternary ammonium chloride/$SnCl_4$ catalyst and its silica gel analogue

T. M. Jyothi, M. L. Kaliya, M. Herskowitz and M. V. Landau*

Blechner Center for Industrial Catalysis and Process Development, Dept. of Chemical Engineering, Ben Gurion University of Negev, Beer Sheva-84105, Israel. E-mail: mlandau@bgumail.bgu.ac.il

Received (in Cambridge, UK) 27th February 2001, Accepted 19th April 2001
First published as an Advance Article on the web 15th May 2001

A novel reusable Lewis acid catalyst has been prepared by the heterogenization of a Lewis acid/tetrapropylammonium adduct; anchoring of tin chloride on quaternary ammonium chloride functionalized MCM-41 yielded a catalyst with higher activity compared to the corresponding silica analogue in terms of turnover rates and product yield in the Prins condensation of isobutene and formaldehyde to isoprenol.

The heterogenization of common Lewis acid catalysts is a subject of immense importance in view of achieving clean technology, based on the fact that heterogeneous catalysts are, in principle, best suited for industrial applications, as ideally they can be recycled and reused easily.[1] A direct immobilization of such catalysts on an inorganic support is not often advantageous due to the possible leaching of the supported species during the reaction and also in many cases the activity is considerably less than for the unsupported Lewis acid.[2] To enhance the activity it may be preferable to anchor the metal catalyst to the support through a chemical chain rather than directly bond it to the support surface.

MCM-41 materials which are characterized by highly ordered pore systems with tunable pore sizes, large specific surface area and pore volume, and high density of surface silanols, provide excellent opportunities in inclusion chemistry and catalysis. A large number of functionalized entities including both organic and inorganic ligands has been introduced in the channels to generate novel catalyst materials.[3] Here we report the preparation of a novel Lewis acid catalyst comprising $SnCl_4$ as the active component anchored on a tetraalkylammonium chloride functionalised MCM-41 material. A comparison is made with the corresponding silica gel analogue in the model reaction of isobutene–formaldehyde condensation to 3-methylbut-3-en-1-ol (isoprenol), which is an important synthesis block for industrially valuable terpenes.[4] Lewis acid catalysts such as $SnCl_4$ and $ZnCl_2$ have been employed in the synthesis of isoprenol from isobutene and formaldehyde under mild conditions, however, the yield was low due to the formation of many side products (Scheme 1).[5]

So called ionic liquids or molten salts which can be prepared by the reaction of a tetraalkylammonium halide ($NR_4^+X^-$) and a Lewis acid (MX) are reported to be effective catalysts in Friedel–Crafts reactions and the utility of such catalysts directly

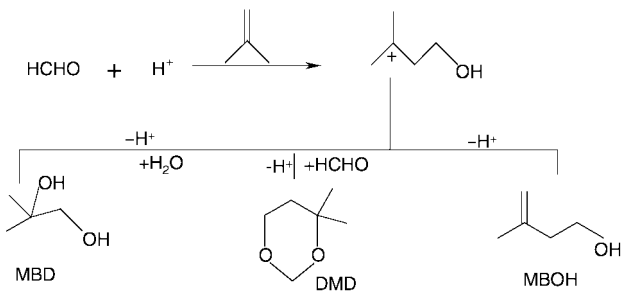

Scheme 1 Prins condensation of isobutene and formaldehyde; IP = 3-methylbut-3-en-1-ol (isoprenol), DMD = 4,4-dimethyl-1,3-dioxane.

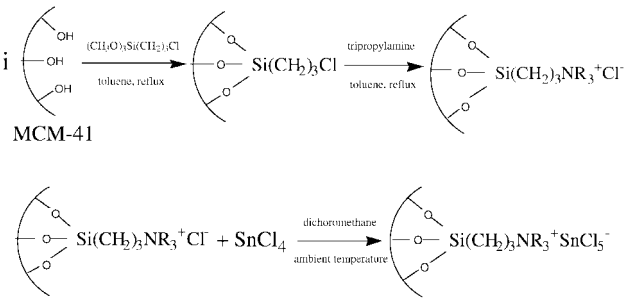

Scheme 2 Preparation of $SnCl_4$ anchored on tetraalkylammonium chloride functionalized MCM-41; TPA = tetrapropylammonium chloride; R = propyl group.

immobilized on inorganic supports has been recently demonstrated by Holderich and coworkers among others.[6] Similarly, we adopted the nucleophilic addition of tetraalkylammonium chloride to tin chloride to obtain penta-coordinated tin anionic species, $[NR_4^+][SnCl_5^-]$.[7] These types of complexes were immobilized on silica gel and MCM-41 supports by a three-step procedure (Scheme 2). Pure silica MCM-41 (pore diameter = 3.7 nm, surface area = 1100 $m^2\ g^{-1}$) was synthesized following a modified procedure involving pH adjustment and salt addition during crystallization to improve the wetting stability.[8] Silica gel (pore diameter r = 6 nm, surface area = 500 $m^2\ g^{-1}$) was purchased from Aldrich. To a suspension of 10 g of dehydrated silica/MCM-41 support in 50 g anhydrous toluene was added 6 g of a toluene solution of trimethoxysilylpropyl chloride. The suspension was refluxed for 6–7 h in an oil bath followed by filtering and washing with excess toluene to remove the excess of reagent. 5 g of chloropropylated silica and 7 g of tripropylamine were further suspended in 30 g of anhydrous toluene and refluxed for 24 h. After the reaction the material was filtered off, washed fully with excess toluene and dried *in vacuo*. Elemental analysis revealed a loading of 0.98 and 2.5 mmol of chloropropyl groups per gram of silica gel and MCM-41 supports, respectively. The amount of chloride ions present on the silica gel and MCM-41 support after the reaction with tripropylamine as determined by titration with standard $AgNO_3$ solution and potassium chromate indicator were found to be 0.50 and 1.20 mmol g^{-1} of support, respectively.

1.04 g of a solution of anhydrous $SnCl_4$ in 10 ml dichloromethane was added dropwise to a suspension of the functionalized silica in 40 ml dichloromethane followed by stirring overnight at ambient temperature. After reaction, the material was exhaustively washed with dichloromethane and dried *in vacuo*. The starting silica gel and MCM-41 before use were dehydrated *in vacuo* at 450 °C. All operations including preparation of the unsupported $SnCl_4$–TPACl complex and its direct reaction with unfunctionalized silica were conducted inside the glove box under dry nitrogen atmosphere in order to prevent any hydrolysis of Sn compounds.

The tin chloride loadings of silica and MCM-41 hybrid catalysts as determined by energy dispersive X-ray analysis (EDAX-JEM-35, JEOL Co., link system AN-1000, Si–Li

 DOI: 10.1039/b101843o

Table 1 Condensation of isobutene and formaldehyde to 3-methylbut-3-en-1-ol (MBOH) over silica based catalysts and catalyst recycling[a]

Entry	Catalyst	$SnCl_4$ loading/mmol (g support)$^{-1}$	Conversion of formaldehyde[b] (%)	MBOH selectivity[c] (%)	MBOH yield[d] (%)
1	$SnCl_4$	—	97.4	54.6	53.0
2	$SnCl_4$–TPACl[e]	—	77.1 (2.68)	89.0	68.7
3	SIL–TPA$^+SnCl_5^-$[f]	0.46	64.1 (2.22)	88.1	56.4
4	MCM–TPA$^+SnCl_5^-$[g]	1.11	76.0 (2.63)	94.0	71.4
5	Recycling 1[h]	1.10	74.3	94.1	69.9
6	Recycling 2	—	74.9	93.5	70.0
7	MCM–TPA$^+SnCl_5^-$[i]	1.11	100	90.1	90.1
8	SIL–TPA–$SnCl_4$[j]	0.32	57.0	79.8	45.5
9	SIL/$SnCl_4$	0.95	77.9	63.2	49.2

[a] 56 g isobutene, 3 g paraformaldehyde, catalyst containing 4 mmol of $SnCl_4$ and 40 g of chloroform solvent were introduced in the reactor and stirred for 2 h at 60 °C. [b] The turnover number (TON) based on the no. of mol of formaldehyde converted per mol of catalyst per s ($\times 10^{-3}$) shown in parentheses. [c] Other products included 4,4-dimethyl-1,3-dioxane and traces of poly-condensation products. [d] Yield was determined by using butan-2-ol as an internal standard. [e] TPACl–$SnCl_4$ complex. [f] TPACl-functionalised silica–$SnCl_4$ complex. [g] TPACl-functionalised MCM-41–$SnCl_4$ complex. [h] Recycling of MCM–TPA$^+SnCl_5^-$ after exhaustive washing with dichloromethane. [i] Reaction continued for 3.5 h. [j] Direct immobilization of complex on silica.

detector, sensitivity > 0.1 wt%) were found to be 0.46 and 1.11 mmol g^{-1}, respectively. The MCM-41 structure remained intact after the catalyst anchoring. The retention of organic groups on the functionalized support after anchoring the $SnCl_4$ was proved by IR spectroscopy. The formation of a complex between tin chloride and tetrapropylammonium chloride in dichloromethane solution was confirmed by ^{119}Sn NMR (external standard). A shift in the NMR signal from −665.0 to −725.2 ppm after the reaction with tetrapropylammonium chloride reflects a change in the coordination number at tin.[7] The tin/chlorine atomic ratio in the anchored catalysts determined by elemental analysis (EDAX): 0.195 for SIL–TPA$^+SnCl_5^-$ and 0.204 for MCM–TPA$^+SnCl_5^-$, was in accordance with such complex formation. The solid state ^{119}Sn MAS NMR study of the $SnCl_4$–tetraalkylammonium adduct anchored on MCM-41 is now in progress in order to obtain more precise definition of the environment around the Sn.

The results of the Prins condensation of isobutene and formaldehyde to isoprenol over different catalysts are summarized in Table 1.†‡ It is clear that complexation of tin chloride with tetrapropylammonium chloride improves the selectivity towards the unsaturated alcohol. Tin chloride alone under anhydrous conditions displayed high activity but the selectivity to MBOH was poor. The tin chloride catalysts immobilized on organic quaternary ammonium functionalized silica/MCM-41 showed highest selectivity towards the unsaturated alcohol, MBOH (88–95%). More interestingly, the MCM-41 based catalyst is far more active than its silica counterpart and outperforms the latter both in terms of isoprenol yield and catalyst turnover. An X-ray fluorescence spectroscopic analysis of the filtrate after the reaction (X-ray spectrometer Phillips PW-1410; sensitivity > 0.5 ppm Sn) revealed that the new catalysts are resistant to leaching under the reaction conditions. Furthermore, when a subsequent reaction was performed with the filtrate after separating the catalyst by adding fresh formaldehyde and isobutene, no formaldehyde conversion was observed. Recycling of the catalyst leads to no appreciable loss in activity. Increasing the reaction time to 3.5 h, increased the MBOH yield to a maximum of 90%. The performance of an $SnCl_4$/silica catalyst, prepared by treating a chloroform solution of tin chloride and silica, in the selective synthesis of MBOH is poor compared to immobilized complexes. Also, a direct immobilization of the complex on silica (Silica/TPA–$SnCl_4$) was not advantageous in terms of MBOH yield.

The present MCM-41 based Lewis acid catalyst system satisfactorily meets the ultimate aims of heterogenization of metal complexes. In short, we have demonstrated the preparation and application of a novel stable, reusable, heterogeneous Lewis acid catalyst, which shows almost the same turnover rate (TON = 2.63×10^{-3} s^{-1}) as that obtained in solution with the homogeneous catalyst (TON = 2.68×10^{-3} s^{-1}). We believe that the accessibility of the active sites for the reactants will be highest in the present case as it is anchored to the support through a organic chain rather than being directly bonded to the support surface. In addition, the regular and well ordered hexagonal array of pores present in the MCM-41 support provides nanosized micro-reactors for the reaction. The better catalytic activity obtained with the MCM-41 supported catalyst compared to the silica supported counterpart indicates a favorable reaction environment inside the well ordered pores of the former where the active sites are grafted through an organic spacer. Another important feature of this catalyst is the higher concentration of active sites per gram of the support compared to the silica support.

T. M. J. is grateful to the Blechner foundation for a post-doctoral fellowship.

Notes and references

† Tetrapropylammonium chloride (4 mmol) was dissolved in 40 g of dry dichloromethane and 1.04 g (4 mmol) of anhydrous tin chloride was added slowly with constant stirring. The mixture was stirred overnight at ambient temperature and the solution was concentrated *in vacuo* to obtain a white crystalline material which was recrystallised from dichloromethane–hexane and stored under moisture free conditions. Analysis: found (calc.) Sn 24.78 (24.61), Cl 36.40 (36.74)%.

‡ The Silica/TPA–$SnCl_4$ catalyst was prepared by adding a chloroform solution of the complex prepared as mentioned above to 4 g of pre-dried silica support suspended in chloroform with constant stirring. The excess solvent was removed after overnight stirring and the material was extracted with chloroform for 12 h in a Soxhlet apparatus. The material was finally dried and kept under moisture free conditions before use.

1 *Chemistry of Waste Minimisation*, ed. J. H. Clark, Chapman and Hall, London, 1995, p. 141.
2 R. S. Drago, S. C. Petrosius and P. B. Kaufman, *J. Mol. Catal.*, 1994, **89**, 317; A. A. Krzywicki and M. Marczewski, *J. Chem. Soc., Faraday Trans. 1*, 1980, 1311; S. J. Barlow, T. W. Bastock, J. H. Clark and S. R. Cullen, *Tetrahedron Lett.*, 1993, **34**, 3339; A. Cornellis, A. Gerstmans, P. Laszlo, A. Mathy and I. Zreba, *Catal. Lett.*, 1990, **6**, 103.
3 D. Brunel, *Microporous Mesoporous Mater.*, 1999, **27**, 329.
4 A. P. Courtot, *J. Chem. Soc.*, 1906, **90**, 788.
5 E. Arundale and L. A. Mikelska, *Chem. Rev.*, 1952, **52**, 505.
6 G. A. Parshall, *J. Am. Chem. Soc.*, 1972, **94**, 8716; P. Wasserscheid and W. Keim, *Angew. Chem., Int. Ed.*, 2000, **39**, 3772; C. DeCastro, E. Sauvage, M. H. Valkenberg and W. F. Holderich, *J. Catal.*, 2000, **196**, 86.
7 S. E. Johnson and C. B. Knobler, *Organometallics*, 1992, **11**, 3684; Kuraray Co. Ltd., *Jpn. Pat.*, H09-262478, 1997.
8 M. V. Landau, S. P. Varkey, M. Herskowitz, O. Regev, S. Pevzner, T. Sen and Z. Luz, *Microporous Mesoporous Mater.*, 1999, **33**, 149.

CHEMCOMM Communication
www.rsc.org/chemcomm

Ambient temperature crystallisation of a lamellar gallium fluorophosphate from the synthesis solution of microporous ULM-5

Carine Livage,[a] Franck Millange,[a] Richard I. Walton,[b] Thierry Loiseau,[a] Nathalie Simon,[a] Dermot O'Hare[c] and Gérard Férey*[a]

[a] *Institut Lavoisier, UMR CNRS 8637, Université de Versailles Saint Quentin-en-Yvelines, 45 Avenue des Etats-Unis, 78035 Versailles Cedex, France. E-mail: ferey@chimie.uvsq.fr*
[b] *School of Chemistry, University of Exeter, Stocker Road, Exeter, Devon, UK EX4 4QD*
[c] *Inorganic Chemistry Laboratory, University of Oxford, South Parks Road, Oxford, UK OX1 3QR*

Received (in Cambridge, UK) 26th March 2001, Accepted 19th April 2001
First published as an Advance Article on the web 15th May 2001

The layered gallium fluorophosphate $Ga_3F_2(OH)_4(H_2PO_4)(HPO_4)_3$ $[H_3N(CH_2)_6NH_3]_2{\cdot}3.5H_2O$ (1) crystallises at room temperature from the supernatant liquid taken during the hydrothermal synthesis of the large-pore material ULM-5; the phase has a topology not previously seen among the Group 13 phosphates.

For almost 20 years a great deal of research has focussed on the synthesis of open-framework phosphates. The work was instigated by Wilson *et al.* who first described aluminium phosphates with zeolite-like structures for potential use in applications such as gas separation, ion-exchange and catalysis.[1] Phosphates of metals from almost every group of the Periodic Table have now been synthesised, usually using the hydrothermal technique ($T \approx 200$ °C).[2] In certain cases these new materials have found use as selective catalysts for organic transformations, further fuelling interest in their properties.[3,4] As well as 3D zeolite-like frameworks, the phosphates exhibit structures of lower dimensionalities, ranging from layered (2D) through chain (1D) to molecular (0D). Understandably, recent research in the area has focussed on determining the reaction mechanism of the formation of phosphates, with the goal of the rational synthesis of a new framework material of pre-designed architecture by application of appropriate synthetic conditions. For example, Taulelle *et al.* have shown by *in situ* NMR the existence of oligomers in the solution[5] whereas Rao *et al.* have, in the past few months, proposed an aufbau principle for the building up of 3D zinc phosphates from lower dimensional structures.[6]

The gallium fluorophosphates represent a large family of open-framework materials that we have been studying.[7] During *in situ* X-ray diffraction studies on their hydrothermal synthesis a number of crystalline transient phases have been observed which appear prior to the crystallisation of the expected product.[8,9] The structural characterisation of these intermediates has been hampered by the fact they are metastable and have never been stabilised under ambient conditions. We have recently begun a study of the isolation of metastable phases from the same reaction mixtures used to the prepare open-framework 3D phases, with the aim of a deeper understanding of the solution chemistry involved in the reactions and of producing possible structural models for the intermediate phases.[10–12]

The novel, layered gallium fluorophosphate **1** was isolated as single crystals from the supernatant liquid remaining after one hour under hydrothermal conditions of the reactant mixture that forms the large-pore gallium fluorophosphate ULM-5.† Structure solution was successfully performed by single-crystal X-ray diffraction and this reveals an unusual topology not previously seen in phosphate chemistry.‡ The phosphate layers have empirical formula $[Ga_3P_4O_{20}F_2H_9]^{4-}$ and are intercalated with charge balancing 1,6-hexanediammonium cations, as well as occluded water molecules [Fig. 1(a)]. Fig. 1(b) shows a view of the structure perpendicular to a single layer, and illustrates how the solid is constructed from corner-sharing $\{H_xPO_4\}$ tetrahedra, and $\{GaO_3(OH)_2F\}$ and $\{GaO_4F_2\}$ octahedra. The $\{GaO_4F_2\}$ units share axial fluorines with two $\{GaO_3(OH)_2F\}$ units to produce a trimer, which is bridged on both sides by four $\{H_xPO_4\}$ tetrahedra. There are three types of $\{H_xPO_4\}$ tetrahedra: the first is shared between three gallium atoms and has a unique terminal P–O bond of 1.575(5) Å corresponding to a P–OH moiety; the second is shared between two gallium atoms and presents two terminal P–O bonds [1.543(5) Å and 1.584(5) Å] while the third is also shared between two gallium atoms but has one longer (1.60 Å) and one shorter P–O bond type (1.49 Å), corresponding to P–OH and P=O moieties.

The secondary building unit (SBU) of the structure can be thought of as a $Ga_3F_2(OH)_2(H_xPO_4)_4$ heptamer, as shown in Fig. 2(a). These are bound by P–O–Ga linkages to produce the porous layer containing ten-ring windows. The lamellar structure of **1** is novel, but parts of the structure bear a striking resemblance to a chain gallium fluorophosphate we have recently isolated at room temperature.[10] The latter phase is constructed from infinite chains of $\{GaO_4F_2\}$ octahedra and

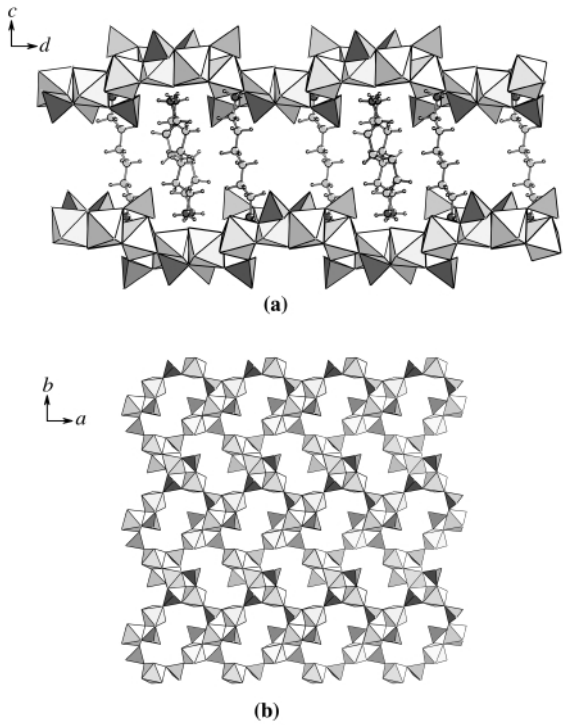

Fig. 1 Polyhedral view of the title compound (a) parallel to the layers, along *a*, showing intercalated 1,6-hexanediammonium cations, and (b) perpendicular to the layers, along *c* (occluded species not shown for clarity). Dark grey polyhedra are phosphorus-centred and pale grey gallium-centred, dark grey circles are N, pale grey circles C, and smaller pale grey circles H.

 DOI: 10.1039/b102753k

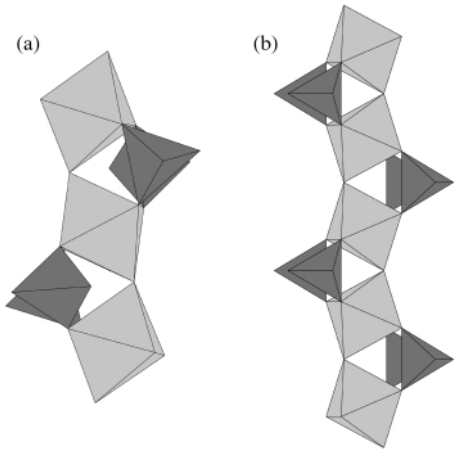

Fig. 2 (a) Polyhedral view of the secondary building unit of the title compound (b) part of the infinite chain of the 1D material Ga(H-PO_4)$_2$F·$H_3N(CH_2)_3NH_3$·$2H_2O$ with the tancoïte-type.[10]

{HPO_4} tetrahedra whose mode of linking is exactly the same as the SBU in the new phase, as illustrated in Fig. 2(b).

We have now isolated phosphates with 1D,[10] 2D (this work) and 3D[12] structures at room temperature, and thus for our system there is no evidence for a particular stability of low-dimensional structures at low temperature. All of these phases have structures not previously seen for the gallium fluorophosphates when hydrothermal synthesis is used and therefore room temperature crystallisation provides a route to novel, open-framework phases. What is particularly noteworthy about the new compound, and the other phases we have now isolated at room temperature, is the existence of gallium in solely octahedral sites, whereas the phases produced under hydrothermal conditions may contain gallium in four-, five- and six-coordinate sites. NMR studies on a related system also showed the transformation of six-coordinate metal centres to a lower coordination number site when hydrothermal conditions are reached.[5] In order to test the generality of this crystallisation model, we are currently surveying phases produced from other gallium fluorophosphate systems under mild conditions.

Notes and references

† The title compound crystallised from the supernatant liquid taken during the synthesis of the gallium fluorophosphate ULM-5.[13] The reaction mixture, 2 GaOOH : 1 P_2O_5 : 1.3 $NH_2(CH_2)_6NH_2$: 1 HF : 80 H_2O (initial pH = 2.5), was sealed in a Teflon-lined, 23 mL autoclave and placed in a furnace preheated at 180 °C for 1 h. After cooling to room temperature, the solid product was recovered by suction filtration and identified by powder X-ray diffraction as a new crystalline phase GaP_2O_7-$(OH_{1-x}F_x)(C_6H_{18}N_2)$·$nH_2O$.[14] The filtrate was retained and allow to stand at room temperature in a closed Teflon vessel. After several months, colourless, rod-shaped crystals of **1** were recovered.

‡ *Crystal data*: for $Ga_3F_2(OH)_4(H_2PO_4)(HPO_4)_3[H_3N(CH_2)_6NH_3]_2$·$3.5H_2O$: M = 999.6, colourless crystals, 0.36 × 0.14 × 0.04 mm, monoclinic, space group $P2_1/c$, a = 10.201(2), b = 14.417(4), c = 23.195(6) Å, β = 95.91(3)°, V = 3393.0(2) Å^3, Z = 4, D_c = 1.957 g cm^{-3}, μ = 2.659 mm^{-1}, index ranges $-12 \leqslant h \leqslant 12$, $-18 \leqslant k \leqslant 10$, $-28 \leqslant l \leqslant 27$, total data 20 065, independent data with $I_o > 2\sigma(I_o)$ 6931. Intensity data were collected at room temperature with a Siemens SMART three-circle diffractometer equipped with a CCD bidimensional detector [λ(Mo-Kα) = 0.71073 Å]. Data reduction was performed with the SAINT software and absorption corrections were applied using the SADABS program.[15] The structure was solved by direct methods and refined by full-matrix, least squares based on F^2 using the SHELXTL software package.[16] All non-hydrogen atoms were refined anisotropically except water molecules. All water molecules were unambiguously located although two of them (Ow3, Ow4) present a disorder with half occupancy of two sites. Hydrogens from the organic molecules were placed in calculated positions and treated as riding (N–H = 0.89 and C–H = 0.97 Å). Number of variables = 395; final $R(F)$ = 0.0562, wR (F^2) = 0.1319, GOF 1.026, minimum and maximum peak in difference electron density map −0.987 and 0.962 e Å^{-3}.

CCDC 161556. See http://www.rsc.org.suppdata/cc/b1/b102753k/ for crystallographic data in .cif or other electronic format.

1 S. T. Wilson, B. M. Lok, C. A. Messina, T. R. Cannan and E. M. Flanigen, *J. Am. Chem. Soc.*, 1982, **104**, 1146.
2 A. K. Cheetham, G. Férey and T. Loiseau, *Angew. Chem., Int. Ed.*, 1999, **38**, 3268.
3 S. I. Zones and M. E. Davis, *Curr. Opin. Solid State Mater. Chem.*, 1996, **1**, 107.
4 J. M. Thomas, R. Raja, G. Sankar and R. G. Bell, *Nature*, 1999, **398**, 227.
5 F. Taulelle, M. Haouas, C. Gerardin, C. Estournes, T. Loiseau and G. Férey, *Colloids Surf., A*, 1999, **158**, 299.
6 C. N. R. Rao, S. Natarajan, A. Choudhury, S. Neeraj and A. A. Ayi, *Acc. Chem. Res.*, 2001, **34**, 80.
7 G. Férey, *J. Fluorine Chem.*, 1995, **72**, 187; G. Férey, *C. R. Acad. Sci., Ser. IIc: Chim.*, 1998, **1**, 1.
8 R. J. Francis, S. O'Brien, A. M. Fogg, P. S. Halasyamani, D. O'Hare, T. Loiseau and G. Férey, *J. Am. Chem. Soc.*, 1999, **121**, 1002.
9 R. I. Walton, T. Loiseau, D. O'Hare and G. Férey, *Chem. Mater.*, 1999, 3201.
10 R. I. Walton, F. Millange, A. L. Bail, T. Loiseau, C. Serre, D. O'Hare and G. Férey, *Chem. Commun.*, 2000, 203.
11 R. I. Walton, F. Millange, D. O'Hare, C. Paulet, T. Loiseau and G. Férey, *Chem. Mater.*, 2000, **12**, 1977.
12 R. I. Walton, F. Millange, T. Loiseau, D. O'Hare and G. Férey, *Angew. Chem., Int. Ed.*, 2000, **39**, 4552.
13 T. Loiseau and G. Férey, *J. Solid State Chem.*, 1994, **111**, 403.
14 F. Millange and C. Livage, unpublished results.
15 G. M. Sheldrick, SADABS: Program for scaling and correction of area detector data, University of Göttingen, Göttingen, Germany, 1996;
16 G. M. Sheldrick, SHELXS97 and SHELXL97, University of Göttingen, Göttingen, Germany, 1997; SHELXTL version 5.10, Software Package for Crystal Structure Determination, Siemens Analytical X-Ray Instruments Inc., Madison, WI, 1994.

CHEMCOMM Communication
www.rsc.org/chemcomm

Highly diastereoselective additions of methoxyallene and acetylenes to chiral α-keto amides†

So Won Youn, Yong Hae Kim,* Jeong-Wook Hwang and Youngkyu Do*

Center for Molecular Design & Synthesis, School of Molecular Science, Department of Chemistry, Korea Advanced Institute of Science and Technology, Taejon, 305-701, Korea. E-mail: kimyh@mail.kaist.ac.kr

Received (in Cambridge, UK) 9th January 2001, Accepted 24th April 2001
First published as an Advance Article on the web 15th May 2001

α-Keto amides bearing (*S*)-indoline chiral auxiliaries reacted with lithiated methoxyallene or lithium acetylides to produce the corresponding dihydrofuranones 7 through formation of the tertiary α-hydroxy allenes, or tertiary α-hydroxy acetylenes, respectively, at −78 °C with high diastereoselectivities (up to > 99% de).

A number of diastereoselective nucleophilic additions of organometallic reagents to α-keto amides[1] bearing appropriate chiral auxiliaries have been reported as useful methods for the synthesis of optically active tertiary α-hydroxy acid derivatives, which are valuable for the asymmetric syntheses of medicinal agents and natural products.[2] Creating a tertiary alcohol center in which the stereochemistry can be controlled by a defined chiral environment in the addition of organometallic reagents to ketones still represents a significant challenge.[3]

Lithiated methoxyallene[4–6] is a promising nucleophile because the products produced by its addition to carbonyl compounds[7–8] can be converted into a variety of interesting compounds such as enones[9] or dihydrofuran derivatives.[10] In particular chiral propargylic alcohols[11] are useful intermediates in the synthesis of natural products.[2,12] Although a number of stereoselective additions of acetylides to aldehydes[11a–c] have been reported, asymmetric addition of acetylides to ketones to produce chiral tertiary alcohols is little known.[11d,e] A highly enantioselective addition of cyclopropanylacetylide to aryltrifluoromethyl ketone as a special substrate has been reported as the first example.[11d,e] However, a general method to prepare chiral tertiary α-hydroxy acetylenes has not yet been reported.

Recently, we reported that chiral α-keto amides derived from (*S*)-indoline-2-carboxylic acid resulted in high stereoselectivity in stereocontrolled additions of organometallics[1b] and allylation.[1c] On the supposition that these chiral α-keto amides might be good chiral auxiliaries, we examined the diastereoselective additions of lithiated methoxyallene **2** and lithium acetylides **3** to various chiral α-keto amides **1**.

The lithiated methoxyallene **2** was generated by treatment of methoxyallene (2.5 eq.) with *n*-BuLi (2.0 eq.) in THF at −78 °C for 30 min.[7b] Lithium acetylide **3** was prepared by addition of *n*-BuLi (1.5 eq.) to a solution of acetylene (1.7 eq.) in THF at 0 °C, followed by cooling to −78 °C after 30 min.[11a] Lithiated methoxyallene or lithium acetylide was reacted with α-keto amides at −78 °C in THF. Since the allene adducts **4** are generally labile[7b,c] so giving low yields (Table 1), the crude product **4** was reacted to obtain **6** without purification. Two equivalents of **2** were added to **1** at −78 °C in THF. The reaction mixture was stirred for 10 min at −78 °C and then quenched with distilled water. Extraction with CH_2Cl_2, drying over $MgSO_4$, and concentration gave crude product **4**, which was treated with a solution of *t*-BuOK (0.5 eq.) in DMSO at 50 °C. The reaction mixture was stirred for 1 h and then quenched with H_2O. Extraction with Et_2O, drying over $MgSO_4$, and concentration gave the crude residue, which was purified by column chromatography on SiO_2 to give dihydrofuran derivatives **6** which were treated with 5% HCl and extracted with diethyl ether and EtOAc at pH 11. The combined organic layers were dried over $MgSO_4$ and concentrated to give dihydrofuranones **7**. The results obtained are summarized in Table 2.

Table 1 Diastereoselective additions of lithiated methoxyallene **2** and lithium acetylides **3** to chiral α-keto amides **1**

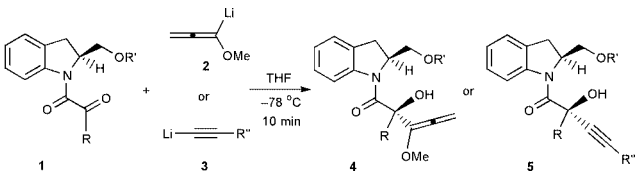

Run	Substrate	R	R′	R″	Product	Yield (%)[a]	dr[b]
1	**1a**	Me	Me	—	**4a**	42	99:1
2	**1b**	Et	Me	—	**4b**	54	94:6
3	**1c**	*n*-Hex	Me	—	**4c**	45	98:2
4	**1d**	Ph	Me	—	**4d**	56	96:4
5	**1e**	Me	$SiMe_2Bu$-*t*	—	**4e**	32	80:20
6	**1f**	Ph	$SiMe_2Bu$-*t*	—	**4f**	33	83:17
7	**1a**	Me	Me	Ph	**5a**	71	98:2
8	**1b**	Et	Me	Ph	**5b**	91	94:6
9	**1d**	Ph	Me	Ph	**5c**	53	95:5
10	**1e**	Me	$SiMe_2Bu$-*t*	Ph	**5d**	62	99:1
11	**1a**	Me	Me	CH_2OMe	**5e**	72	99:1
12	**1a**	Me	Me	*n*-Bu	**5f**	88	99:1
13	**1a**	Me	Me	$SiMe_3$	**5g**[c]	66	> 99:1

[a] Isolated yields. [b] Determined by HPLC (Daicel chiral OD column). [c] R″ = H : $SiMe_3$ was removed.

Table 2 Transformation of crude products **4** to dihydrofuran derivatives **6** and 3(2*H*)-dihydrofuranones **7**

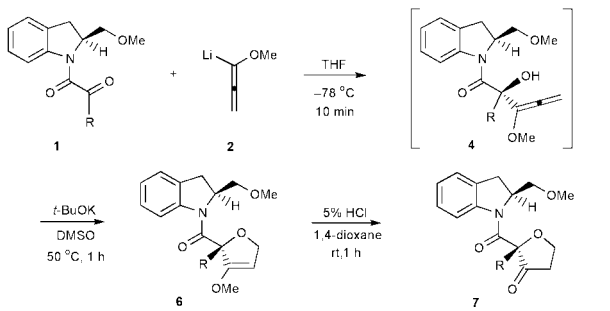

		6		**7**	
Run	R	Yield (%)[a,b]	dr[c]	Yield (%)[a]	dr[c]
1	Me **(1a)**	33 **(6a)**	> 99:1	80 **(7a)**	> 99:1
2	Et **(1b)**	41 **(6b)**	> 99:1	76 **(7b)**	> 99:1
3	*n*-Hex **(1c)**	35 **(6c)**	> 99:1	75 **(7c)**	> 99:1
4	Ph **(1d)**	44 **(6d)**	> 99:1	78 **(7d)**	> 99:1

[a] Isolated yields. [b] Overall yields from **1**. [c] Determined by ^1H NMR.

† Electronic supplementary information (ESI) available: synthesis and spectroscopic data for **4b**, **5g**, **6b** and **7b**. See http://www.rsc.org/suppdata/cc/b1/b100355k/

 DOI: 10.1039/b100355k

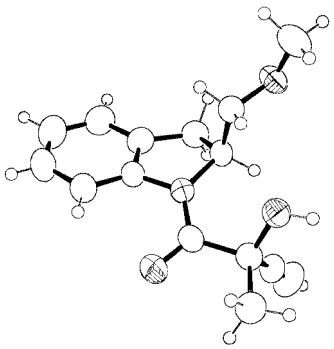

Fig. 1 X-Ray structure of **5g**.

The purified products **4**, **5** and **6** were identified by ^{1}H, ^{13}C NMR,[7b–d] IR and MS. The ratios of diastereomers were determined by HPLC using a chiral OD column. The absolute configuration of **5g** was determined by comparison of the specific rotation of **8** ($[\alpha]_D^{25}$ −40.2°, *c* = 1.7, acetone) with the literature value[13] ($[\alpha]_D^{24}$ −41.0°, c = 10, acetone) and its structure determined by X-ray analysis (Fig. 1).[14] The ratios of diastereomers were unaltered during the process. Compound **8** has been found in plant growth regulators[2e] and highly enantiomeric excess synthesis of **8** has not been reported previously.

Enol ethers of 2,5-dihydrofuran derivatives **6** were readily hydrolyzed by HCl solution (H_2O:1,4-dioxane = 10:1) to provide the corresponding 3(2*H*)-dihydrofuranones **7** in good yields (75–80%), which are interesting intermediates as analogues of muscarone.[15b] Their structural element appears in other biologically active compounds[15] and their transformation to certain deoxy sugar derivatives can be performed. The indoline α-keto amides have a great advantage in terms of cleavage of the amide bond to give chiral products and recover the indoline chiral auxiliary.[1b,c,16] The cleavage of the amide bond of indoline amides is much easier than that of alkyl amides such as proline amides. For instance, the chiral products **5g** or **7b** were readily hydrolyzed with 5% HCl in 1,4-dioxane under reflux for 3 h to give the corresponding 2-hydroxy-2-methylbut-3-ynoic acid **8** or 2-ethyl-3(2*H*)-dihydrofuranone-2-carboxylic acid **9** in 94–98% yields, respectively, as shown in Scheme 1. The chiral auxiliary was recovered in 95–98% yield without loss of optical purity. Earlier work[11d,e] on asymmetric addition of acetylide to a ketone (not a chiral auxiliary) gave one chiral tertiary alcohol from a specific ketone leading to one compound. Our method, however, provides a general methodology to produce chiral tertiary α-hydroxy carboxylic acid acetylenes.

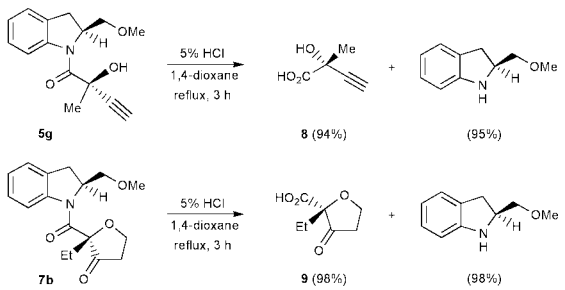

Scheme 1

Conversion of the hydroxyalkylated allenes into the α,β-unsaturated ketones under acidic conditions is also a useful reaction.[9] It is noteworthy that treatment of **4b** with 5% HCl provided enone **10** within 10 min at 25 °C as shown in Scheme 2. The ratio of diastereomers was also unaltered during hydrolysis. The enone moiety may be an interesting precursor for Michael-type additions or cycloadditions.[17]

In summary, it has been demonstrated that the reaction of α-keto amides derived from (*S*)-indoline-2-carboxylic acid with lithiated methoxyallene or lithium acetylide can provide useful

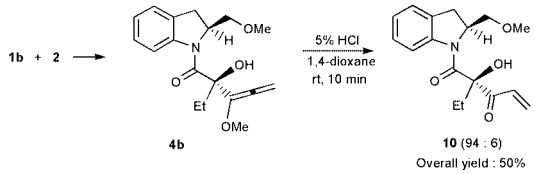

Scheme 2

intermediates, chiral tertiary α-hydroxy acid derivatives with high diastereoselectivities.

Notes and references

1 (*a*) K. Soai and M. Ishizaki, *J. Org. Chem.*, 1986, **51**, 3290; (*b*) Y. H. Kim, I. S. Byun and J. Y. Choi, *Tetrahedron: Asymmetry*, 1995, **6**, 1025; (*c*) Y. H. Kim and S. H. Kim, *Tetrahedron Lett.*, 1995, **36**, 6895; (*d*) C. H. Senanayake, K. Fang, P. Grover, R. P. Bakale, C. P. Vandenbossch and S. A. Wald, *Tetrahedron Lett.*, 1999, **40**, 819, and references therein.

2 (*a*) S. Hanessian, *Total Synthesis of Natural Products: The Chiron Approach*, Pergamon Press, New York, 1983, ch. 2; (*b*) D. W. McPherson and F. F. Knapp, *J. Org. Chem.*, 1996, **61**, 8335; (*c*) Y. Kanda and T. Fukuyama, *J. Am. Chem. Soc.*, 1993, **115**, 8451; (*d*) A. V. R. Rao, J. S. Yadav and M. Valluri, *Tetrahedron Lett.*, 1994, **35**, 3613; (*e*) W. L. White, K. L. Ricciardelli and M. K. Chaguturu, *US Pat.*, 4704161.

3 T. Akiyama, K. Ishikawa and S. Ozaki, *Synlett*, 1994, 275; D. A. Evans, M. C. Kozlowski, S. C. Burgey and D. W. C. MacMillan, *J. Am. Chem. Soc.*, 1997, **119**, 7893; J. L. Wood, B. M. Stoltz, H. J. Dietrich, D. A. Pflum and D. T. Petsch, *J. Am. Chem. Soc.*, 1997, **119**, 9641; P. I. Dosa and G. C. Fu, *J. Am. Chem. Soc.*, 1998, **120**, 445.

4 F. J. Weiberth and S. S. Hall, *J. Org. Chem.*, 1985, **50**, 5308.

5 S. Hoff, L. Brandsma and J. F. Arens, *Recl. Trav. Chim. Pays-Bas*, 1968, **87**, 916.

6 For recent reviews of the chemistry of alkoxyallenes, see: R. Zimmer, *Synthesis*, 1993, 165; P. v. R. Schleyer, C. Lambert and E. U. Würthwein, *J. Org. Chem.*, 1993, **58**, 6377.

7 (*a*) D. Gange and P. Magnus, *J. Am. Chem. Soc.*, 1978, **100**, 7746; (*b*) S. W. Goldstein, L. E. Overman and M. H. Rabinowitz, *J. Org. Chem.*, 1992, **57**, 1179; (*c*) S. Hormuth and H.-U. Reissig, *J. Org. Chem.*, 1994, **59**, 67; (*d*) W. Schade and H.-U. Reissig, *Synlett*, 1999, 632.

8 P. Rochet, J.-M. Vatèle and J. Goré, *Synlett*, 1993, 105; T. Arnold, B. Orschel and H.-U. Reissig, *Angew. Chem., Int. Ed. Engl.*, 1992, **31**, 1033.

9 S. Hoff, L. Brandsma and J. F. Arens, *Recl. Trav. Chim. Pays-Bas*, 1968, **87**, 1179.

10 S. Hoff, L. Brandsma and J. F. Arens, *Recl. Trav. Chim. Pays-Bas*, 1969, **88**, 609.

11 (*a*) T. Mukaiyama and K. Suzuki, *Chem. Lett.*, 1980, 255; (*b*) G. M. R. Tombo, E. Didier and B. Loubinoux, *Synlett*, 1990, 547; (*c*) E. J. Corey and K. A. Cimprich, *J. Am. Chem. Soc.*, 1994, **116**, 3151; (*d*) A. S. Thompson, E. G. Corley, M. F. Huntington and E. J. J. Grabowski, *Tetrahedron Lett.*, 1995, **36**, 8937; (*e*) L. Tan, C. Chen, R. D. Tillyer, E. J. J. Grabowski and P. J. Reider, *Angew. Chem., Int. Ed.*, 1999, **38**, 711; (*f*) D. A. Evans, D. P. Halstead and B. D. Allison, *Tetrahedron Lett.*, 1999, **40**, 4461; (*g*) Z. Li, V. Upadhyay, A. E. DeCamp, L. Di Michele and P. J. Reider, *Synthesis*, 1999, 1453; (*h*) D. E. Frantz, R. Fässler and E. M. Carreira, *J. Am. Chem. Soc.*, 2000, **122**, 1806.

12 K. C. Nicolaou and S. E. Webber, *J. Am. Chem. Soc.*, 1984, **106**, 5734; E. J. Corey, K. Niimura, Y. Konishi, S. Hashimoto and Y. Hamada, *Tetrahedron Lett.*, 1986, **27**, 2199; W. R. Roush and R. J. Sciotti, *J. Am. Chem. Soc.*, 1994, **116**, 6457; D. Vourloumis, K. D. Kim, J. L. Petersen and P. A. Magriotis, *J. Org. Chem.*, 1996, **61**, 4848.

13 D. Dugat, M. Verny and R. Vessière, *Tetrahedron*, 1971, **27**, 1715.

14 *Crystal data* for **5g**: $C_{15}H_{17}NO_3$: M_r = 259.3, orthorhombic, space group $P2_12_12_1$, a = 10.300(2), b = 10.536(2), c = 25.810(6) Å, V = 2800.9(11) Å^3, Z = 8, D_c = 1.230 g cm^{-3}, $F(000)$ = 1104, μ(Mo-Kα) = 0.086 mm^{-1}, R_1 = 0.0333, wR_2 = 0.0404 for 2661 reflections ($F_o > 4\sigma(F_o)$). (Note two independent molecules which have the same configuration are contained in the unit cell of the crystal of **5g**.) The absolute configuration could not be determined (Flack parameter: –0.43 (76)). CCDC 156841. See http://www.rsc.org/suppdata/cc/b1/b100355k/ for crystallographic data in .cif or other electronic format.

15 (*a*) J. E. Semple and M. M. Joullié, *Heterocycles*, 1980, **14**, 1825; (*b*) M. DeAmici, C. Dallanoce, C. DeMicheli, E. Grana, A. Barbieri, H. Ladinsky, G. Schiavi and T. Zonta, *J. Med. Chem.*, 1992, **35**, 1915.

16 S. M. Kim, I. S. Byun and Y. H. Kim, *Angew. Chem., Int. Ed.*, 2000, **39**, 728.

17 For examples: W. Choy, L. A. Reed and S. Masamune, *J. Org. Chem.*, 1983, **48**, 1139.

CHEMCOMM Communication
www.rsc.org/chemcomm

Aqueous solutions of unipositive cadmium; reactions of $(Cd^{I})_2^{2+}$(aq)†

Olga A. Babich* and Edwin S. Gould*

Department of Chemistry, Kent State University, Kent, Ohio 44242, USA. E-mail: obabich@kent.edu

Received (in Irvine, CA, USA) 5th March 2001, Accepted 23rd April 2001
First published as an Advance Article on the web 15th May 2001

Aqueous solutions 10^{-3} mol dm^{-3} in $(Cd^{I})_2$, prepared by treating O_2-free solutions of $Cd(ClO_4)_2$ or $Cd(O_3SCF_3)_2$ with Cd powder at 65 °C, can be handled by conventional methods; the comproportionation constant (Cd^{2+} + Cd ⇌ Cd_2^{2+}) is estimated as 0.018 (24 °C, I = 1.14 M) and the formal oxidation potential as −0.45 V; this atypical state readily reduces I_3^-, $IrCl_6^{2-}$, pyridine complexes of $(NH_3)_5Ru^{III}$, and superoxo derivatives of $(NH_3)_5Co^{III}$.

The atypical oxidation state cadmium(I) has been prepared and identified in the dimeric cation, $(Cd^{I})_2^{2+}$, in aluminium chloride melts by Corbett *et al.*,[2–4] and has been further studied in the crystalline state.[5] Moreover, a highly reactive species, thought to be Cd^{+}(aq), has been generated *via* pulse radiolysis of aqueous Cd^{2+} solutions by several workers.[6–8]

However, we find no reports describing aqueous solutions of unipositive cadmium manipulable by conventional methods. By avoiding halide and other nucleophilic ligands which favor disproportionation of Cd(I), we have generated 10^{-4}–10^{-3} molar solutions of this state, have estimated its redox potential, and have examined several of its reactions.

All preparations and reactions involving Cd(I) were carried out under argon. Typically, cadmium carbonate (0.97 g, G. F. Smith 99.995%)[9] was dissolved in a 5% molar excess of concentrated $HClO_4$ or triflic acid (HTf), diluted to 15 ml, heated to 60–65 °C, treated with 1.90 g of Cd powder (Aldrich 325 mesh) with stirring for 5–10 min, then cooled to 24 °C. Stirring was maintained for 20–30 min. After centrifugation, the Cd(I) content in the supernatant was estimated by reaction with KI_3 (352 nm). At equilibrium (24 °C), 1.7–1.8% of the Cd(II) taken is converted to Cd(I). After separation from Cd metal, it decays slowly ($t_{½}$ = 25 h at 24 °C).

Attempted analogous preparations of Zn^{I} (from Zn metal and $ZnTf_2$) and Mg^{I} (from Mg metal and $MgTf_2$) yielded no soluble reductant.

Concentrations of the reducing ion are very nearly proportional to $[Cd^{II}]$ taken (Fig. 1), thus being consistent with the formulation Cd_2^{2+}, rather than monomeric Cd^{+}. The comproportionation constant [eqn. (1)] corresponds to a $\Delta E°$ value of

$$Cd^{2+} + Cd \rightleftharpoons Cd_2^{2+};\ K = 0.0177 \pm 0.0003\ (24\ °C,\ I = 1.14\ M) \quad (1)$$

−0.10 V, which, in combination with the standard potential for Cd(II,0) (−0.403 V),[10] yields potentials −0.45 V for Cd(II,I) and −0.35 V for Cd(I,0). Dimeric Cd(I) is then a reductant thermodynamically comparable to U(III) ($E°$ −0.52 V).

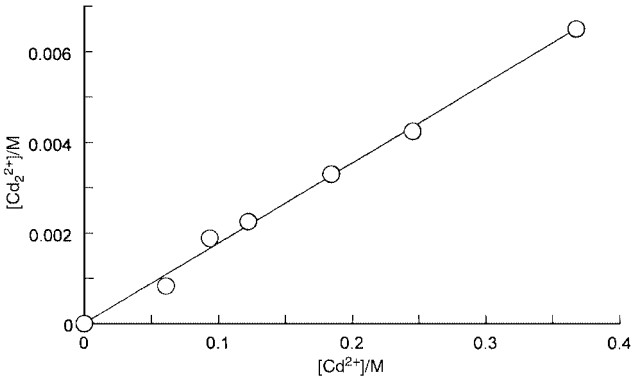

Fig. 1 Variation of concentrations of unipositive cadmium $(Cd_2)^{2+}$ with Cd(II) taken. Reactions with Cd metal powder were initiated at 65 °C and were equilibrated at 24 °C. The slope of the regression line, 0.0177 ± 0.0003, is taken as the equilibrium quotient for the comproportionation reaction: Cd^{2+} + Cd ⇌ Cd_2^{2+}, corresponding to a $\Delta E°$ value −0.10 V.

The sensitivity of Cd(I) to both strong acids and bases limits the number of redox reactions that can be studied. Rate constants for four such reactions are summarized in Table 1. Conversions are first order in both redox partners. Solutions of Cd_2^{2+} do not react perceptibly with $PtCl_6^{2-}$, vitamin B_{12a} (aquacob(III)alamin), quinoxaline, or the *N*-methylphenazonium cation, and its reaction with Cr(VI) in 2-ethyl-2-hydroxybutanoate buffer (pH 3.6) is inconveniently slow.

Reactions with the le$^-$ oxidants, $IrCl_6^{2-}$, Ru(III) and the $[(NH_3)_5Co^{III}]_2$–superoxo cation almost certainly involve an odd-electron species related to monomeric Cd(I). Formation of this from the dimer in a preequilibrium homolysis (Cd_2^{2+} ⇌ 2 Cd^{+}) would be reflected in a half-order dependence on [reductant], contrary to our kinetic picture. Generation of this transient must then require an act of electron transfer to the oxidant. Since it is likely that this transfer precedes breakage of the Cd–Cd bond, we have designated this intermediate as Cd_2^{3+}. We have further chosen this as a reasonable candidate for the necessary follow-up step, although generation and reaction of monomeric Cd^{+} itself cannot be excluded. Kinetic curves obtained with each of these le$^-$ reagents show no irregularity indicative of accumulation or loss of this odd-electron species on the time scale of the principal reaction, pointing to a two-step process, eqns. (2) and (3).

$$Cd_2^{2+} + Ir^{IV} \rightarrow Cd_2^{3+} + Ir^{III}\ \text{(slow, rate-determining)} \quad (2)$$

† Electron Transfer, part 146. For part 145, see ref. 1.

Table 1 Reductions with aqueous cadmium(I), 24 °C[a]

Oxidant	Product	I/M	λ/nm	k/dm^3 mol^{-1} s^{-1}
I_3^{-}[b]	I^-	0.075	352	$(1.00 \pm 0.04) \times 10^5$
$[(4\text{-AcPy})(NH_3)_5Ru]^{3+}$	$[(4\text{-AcPy})(NH_3)_5Ru]^{2+}$	0.030	520	68 ± 3
$[(NH_3)_5Co(O_2)Co(NH_3)_5]^{5+}$	$[(NH_3)_5Co(O_2)Co(NH_3)_5]^{4+}$ [c,d]	0.060	295	$(3.8 \pm 0.1) \times 10^2$
$IrCl_6^{2-}$[c]	$IrCl_6^{3-}$	0.28	489	$(1.41 \pm 0.04) \times 10^3$

[a] $[Cd_2^{2+}] = 2.5 \times 10^{-6}$–$2.6 \times 10^{-4}$ M; $[Cd^{2+}] = 1.5 \times 10^{-4}$–$1.5 \times 10^{-2}$ M; [oxidant] = 5.5×10^{-6}–4.2×10^{-4} M. [b] Solution buffered with 0.025 M *N*-(2-acetamido)-2-aminoethanesulfonic acid (ACES); pH 6.8. [c] Reaction with Cd_2^{2+} in excess. [d] Reduction of $(Co^{III})_2$–superoxo to $(Co^{III})_2$–peroxo cation; pH 5.6.

 DOI: 10.1039/b102041m

$$Cd_2^{3+} + Ir^{IV} \rightarrow 2\ Cd^{2+} + Ir^{III}\ \text{(rapid, kinetically silent)} \quad (3)$$

The relative rates for the two steps imply a much more negative le$^-$ potential for the intermediate Cd_2^{3+} than for Cd_2^{2+}, with the two necessarily totaling 2(−0.45) V. A lower limit for the formal potential of the initiation step (2) can be estimated by applying the simplified Marcus relationship [eqn. (4)][11] to the oxidation by $IrCl_6^{2-}$, for which the outer-sphere rate constant,

$$\log k_{Cd,Ir} = 1/2(\log k_{Cd} + \log k_{Ir} + \Delta E°/0.059) \quad (4)$$

$k_{Cd,Ir}$, is ⩽1400 $M^{-1}\ s^{-1}$ (Table 1). The self-exchange rate, k_{Ir}, for Ir(IV,III) and its standard potential have been documented[12] as $10^{5.4}\ M^{-1}\ s^{-1}$ and 0.87 V, and the self-exchange rate, k_{Cd}, for $(Cd_2)^{3+/2+}$ may be assumed to lie above $10^{-12}\ M^{-1}\ s^{-1}$, the minimum rate recorded for single electron self-exchanges involving simpler aquated metal ions.[11] We then calculate that $\Delta E°$ for the initiation step, eqn. (2), falls below 0.76 V, with $E°$ for $(Cd_2)^{3+/2+}$ thus more positive than +0.11 V, and the formal potential for $(Cd_2)^{3+} \rightarrow 2Cd^{2+}$ therefore more negative than −1.01 V (*vs.* NHE). The wide gap in potentials separating the initial loss of an electron from a main group two-electron metal reducing center and the oxidation of the resulting odd-electron intermediate appears to be a general feature of reagents of this type. The gap in this case (> 1.12 V) lies between that estimated[13] for In(I,II,III) (0.4 V) and that for Tl(I,II,III) (1.92 V).[14]

We are grateful to the National Science Foundation for support of this work, to Dr J. D. Corbett for valuable discussions, to Dr V. Manivannan for preparation of the ruthenium(III) oxidant, and to Mrs Arla McPherson for technical assistance.

Notes and references

1 S. Swavey and E. S. Gould, *Chem. Commun.*, 2000, 2159.
2 J. D. Corbett, W. J. Burkhard and L. F. Druding, *J. Am. Chem. Soc.*, 1961, **83**, 76.
3 J. D. Corbett, *Inorg. Chem.*, 1962, **1**, 700.
4 R. A. Potts, R. D. Barnes and J. D. Corbett, *Inorg. Chem.*, 1968, **7**, 2558.
5 R. Faggiani, R. J. Gillespie and J. E. Vekris, *J. Chem. Soc., Chem. Commun.*, 1986, 517.
6 D. Meyerstein and W. A. Mulac, *J. Phys. Chem.*, 1968, **72**, 784; D. Meyerstein and W. A. Mulac, *J. Phys. Chem.*, 1969, **73**, 1091.
7 G. Navon and D. Meyerstein, *J. Phys. Chem.*, 1970, **74**, 4067.
8 B. H. Ershov, E. Janata and A. Henglein, *J. Phys. Chem.*, 1994, **98**, 7619.
9 Yields of $Cd^{I}(aq)$ are extraordinarily sensitive to the purity of the $CdCO_3$ employed. With less pure (98%) material, concentrations of the reduced species fall to 20–25% those obtained with the purer carbonate.
10 Y. Okinata, in *Standard Potentials in Aqueous Solution*, ed. A. J. Bard, Marcel Dekker, New York, 1985, p. 257.
11 G. Lappin, *Redox Mechanisms in Inorganic Chemistry*, Ellis Horwood, New York, 1994, ch. 2.
12 P. Hurwitz and K. Kustin, *Trans. Faraday Soc.*, 1966, **62**, 427; P. George, I. H. Hanania and G. H. Irvine, *J. Chem. Soc.*, 1957, 3048.
13 A. M. Al-Ajlouni and E. S. Gould, *Res. Chem. Intermed.*, 1998, **6**, 653.
14 H. A. Schwarz, D. Comstock, J. K. Yandell and R. W. Dodson, *J. Phys. Chem.*, 1974, **78**, 488.

CHEMCOMM Communication
www.rsc.org/chemcomm

Calcium oxide and strontium oxide as environmentally benign and highly efficient heterogeneous catalysts for the Tishchenko reaction of furfural

Tsunetake Seki, Kazumasa Akutsu and Hideshi Hattori*

Center for Advanced Research of Energy Technology, Hokkaido University, Kita-13, Nishi-8, Kita-ku, Sapporo 060-8628, Japan. E-mail: hattori@carbon.caret.hokudai.ac.jp

Received (in Cambridge, UK) 13th March 2001, Accepted 24th April 2001
First published as an Advance Article on the web 15th May 2001

CaO and SrO exhibit high activities for the challenging Tishchenko reaction of furfural.

The Tishchenko reaction is dimerization of aldehydes to yield the corresponding esters by the action of aluminium alkoxides.[1–5] For about a century, a number of catalysts for the Tishchenko reaction of various types of aldehydes have been developed to obtain the product esters in high yields. While many aldehydes have been converted to the Tishchenko dimers in good yields, few studies have been successfully carried out on the Tishchenko reaction of furfural. This reaction has been reported to be difficult when carried out using traditional aluminium alkoxides, boric acid or tetracarbonylferrate(−II) as catalysts.[2,6,7] Recently, some homogeneous catalysts such as $(C_5Me_5)_2LaCH(SiMe_3)_2$ and $La[N(SiMe_3)_2]_3$ have been reported to be effective for the Tishchenko reaction of furfural, though these catalysts require a long reaction time to give the product ester in a synthetically satisfactory level of yield.[8,9] In addition, removal of those homogeneous catalysts from the resulting solution causes loss of catalyst and reduction of the product yields. Moreover, in view of environmental concerns, avoidance of use of toxic transition metal catalysts in industrial processes is encouraged. Herein, we report environmentally benign, highly effective heterogeneous catalysts for the Tishchenko reaction of furfural. The general reaction equation is shown in Scheme 1.

Alkaline earth oxides, MgO, CaO, SrO and BaO, were prepared from $Mg(OH)_2$, $Ca(OH)_2$, $SrCO_3$ and $BaCO_3$, respectively, by thermal decomposition at elevated temperatures *in vacuo*. Lanthanum oxide was prepared from $La(OH)_3$ by the same procedure as the alkaline earth oxides, the $La(OH)_3$ being obtained from an aqueous solution of $La(NO_3)_3$ upon hydrolysis with aqueous ammonia, followed by washing with distilled water and drying at 373 K. ZrO_2 and ZnO were prepared from $Zr(OH)_4$ and $Zn(OH)_2$, respectively, by thermal decomposition at elevated temperatures *in vacuo*. γ-Alumina used as a catalyst and as a KOH/alumina-supported catalyst was supplied from the Catalysis Society of Japan (JRC-ALO4). Hydrotalcite (Mg/Al = 2) was synthesized as reported.[10] Alumina-supported KF (KF/alumina) was purchased from Fluka, and its KF content was determined as 8.2 mmol g^{-1} by XRF. Alumina-supported KOH catalyst (KOH/alumina) was prepared by impregnation of γ-alumina (JRC-ALO4) with an aqueous solution of KOH, followed by drying at 373 K in air; the KOH content was 1.2 mmol g^{-1}. The pretreatment temperatures and surface areas of the catalysts examined are listed in Table 1.

Furfural was purchased from Aldrich, and was purified by distillation under a reduced pressure.

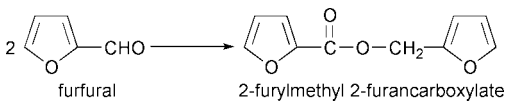

Scheme 1 Tishchenko reaction of furfural.

The reaction was carried out in an H-shaped glass batch reactor. The two branches of the reactor were separated by a breakable seal. A sample of the catalyst precursor was placed in one branch, outgassed at an elevated temperature for 2 h, and sealed. The reactant was stored in the other branch until it was introduced through the breakable seal by distillation into the branch containing the catalyst thermostated at liquid nitrogen temperature. Reaction was initiated by melting the reactant at a reaction temperature followed by stirring. The product was identified by ^{1}H NMR and GC–MS analysis. GC analyses to determine yields of the product ester were carried out using a column of DB-1 (total length: 60 m; diameter: 0.25 mm).

Table 1 shows the activities of solid base catalysts for the Tishchenko reaction of furfural when the reaction was carried out with 100 mg of catalyst using 10 mmol of furfural as reactant. Among the solid base catalysts examined, only CaO and SrO gave the product ester in high yields. When the reaction was carried out at 353 K for 6 h in the presence of 100 mg of SrO, the product ester was obtained in almost quantitative yield. To our knowledge, there have been no reports of catalysts giving the Tishchenko dimer in > 77% yield.[8] Even at a lower reaction temperature of 323 K, the product ester was obtained in a yield of 70% over SrO. In addition to the high activities, the catalytic selectivities of CaO and SrO to 2-furylmethyl 2-furancarboxylate were almost 100%. This clearly emphasizes that CaO and SrO are highly efficient for the Tishchenko reaction of furfural. Although MgO and BaO were reported to

Table 1 Activities of solid base catalysts for the Tishchenko reaction of furfural[a]

Catalyst	Pretreatment temperature/K	Surface area/ m^2 g^{-1}	Yield[b] (%)
MgO	873	267	< 1
CaO	873	48	61
CaO	873	48	78[c]
SrO	1273	12	83
SrO	1273	12	95[c]
SrO	1273	12	70[d]
BaO	1273	2	0
La_2O_3	873	33	0
ZrO_2	873	42	0
ZnO	873	2	0
γ-Alumina	773	173	0
Hydrotalcite (Mg/Al = 2)	673	118	0
Fluka-KF/alumina	673	40	0
1.2 mmol g^{-1}-KOH/alumina	873	160	0

[a] Catalyst weight, 100 mg; furfural, 10 mmol; reaction temp., 353 K; reaction time, 4 h. [b] Yield was determined by the GC analysis of the resulting solution and was calculated by the equation: yield (%) = {[2 × (mol% of 2-furylmethyl 2-furancarboxylate)]/[(mol% of furfural) + 2 × (mol% of 2-furylmethyl 2-furancarboxylate)]} × 100. [c] Reaction time, 6 h. [d] Reaction temp., 323 K; reaction time, 12 h.

 DOI: 10.1039/b102389f

be active for the Tishchenko reaction of other aldehydes such as benzaldehyde and pivalaldehyde,[11,12] they were inactive for the present reaction. Based on a previous study,[11] it is conjectured that both basic (O^{2-}) and acidic (metal cation) sites on alkaline earth oxides participate in the Tishchenko reaction of furfural. The strength of basic sites lies in the order MgO < CaO < SrO < BaO, while that of acidic sites is in the opposite order. Thus, it appears that CaO and SrO having moderate acidic and basic sites in comparison with MgO and BaO are appropriate for the dimerization of furfural.

Other solid base catalysts such as La_2O_3, ZrO_2, ZnO, γ-alumina, hydrotalcite, KF/alumina and KOH/alumina were all inactive for the Tishchenko reaction of furfural. Although KF/alumina has been reported to show high activities for the Tishchenko reaction of benzaldehyde and pivalaldehyde,[12,13] it was not active at all for the Tishchenko reaction of furfural.

This work is supported by a Grant-in aid for Scientific Research of Ministry of Education, Science, Sports, and Culture, Japan.

Notes and references

1 W. Tischtschenko, *Chem. Zentralbl.*, 1906, **77**, **I**, 1309.
2 W. C. Child and H. Adkins, *J. Am. Chem. Soc.*, 1925, **47**, 798.
3 F. J. Villani and F. F. Nord, *J. Am. Chem. Soc.*, 1947, **69**, 2605.
4 L. Lin and A. R. Day, *J. Am. Chem. Soc.*, 1952, **74**, 5133.
5 T. Saegusa and T. Ueshima, *J. Org. Chem.*, 1968, **33**, 3310.
6 P. R. Stapp, *J. Org. Chem.*, 1973, **38**, 1433.
7 M. Yamashita, Y. Watanabe, T-a. Mitsudo and Y. Takegami, *Bull. Chem. Soc. Jpn.*, 1976, **49**, 3597.
8 S. Onozawa, T. Sakakura, M. Tanaka and M. Shiro, *Tetrahedron*, 1996, **52**, 4291.
9 H. Berberich and P. W. Roesky, *Angew. Chem., Int. Ed.*, 1998, **37**, 1569.
10 S. Miyata, T. Kumura, H. Hattori and K. Tanabe, *Nippon Kagaku Zasshi*, 1971, **92**, 514.
11 K. Tanabe and K. Saito, *J. Catal.*, 1974, **35**, 247.
12 H. Kabashima, H. Tsuji, S. Nakata, Y. Tanaka and H. Hattori, *Appl. Catal., A*, 2000, **194–195**, 227.
13 H. Handa, T. Baba, H. Sugisawa and Y. Ono, *J. Mol. Catal.*, 1998, **134**, 171.

CHEMCOMM Communication
www.rsc.org/chemcomm

SERRS detection of PNA and DNA labelled with a specifically designed benzotriazole azo dye†

Duncan Graham,* Rachel Brown and W. Ewen Smith

Department of Pure and Applied Chemistry, University of Strathclyde, 295 Cathedral Street, Glasgow, UK G1 1XL. E-mail: duncan.graham@strath.ac.uk; Fax: (+44) 141 552 0876; Tel: (+44) 141 548 4701

Received (in Cambridge, UK) 8th March 2001, Accepted 27th April 2001
First published as an Advance Article on the web 15th May 2001

PNA and DNA have been detected for the first time with a specifically designed non-fluorescent SERRS active label; this is also the first use of SERRS to detect PNA.

In the post human genome project era a significant effort will centre on the detection of known nucleic acid sequences and variations within those sequences. Currently most methods of achieving this detection rely on the use of specific molecular biological assays and a physical detection technique which selectively identifies a label in a sensitive and discriminatory manner. Fluorescence and radio labelling are the most widely used physical techniques.[1,2] Recently we have reported the detection of labelled oligonucleotides using surface enhanced resonance Raman scattering, SERRS.[3–5] The main benefits of using SERRS rather than fluorescence are the ability to discriminate between labels in a mixture, without separation, at femtomole levels or below and the more extensive, simpler labelling chemistry which can be employed.[4]

To obtain SERRS a dye requires to be adsorbed onto a roughened surface of certain metals of which the most widely used are silver and gold. The dye is required to obtain molecular resonance enhancement and the surface attachment provides enhancement by interaction with the plasmons on the metal surface. The combined enhancement processes provide a Raman signal of equivalent sensitivity to that of fluorescence. The sharp vibrational signals provide much better selectivity and since many dyes which are not fluorophores are effective, the chemistry can be much simpler and more extensive. A very effective metal surface used in this laboratory is that of citrate reduced silver colloid.[6] Aggregating agents such as sodium chloride or acid provide the most effective roughened surface and tune the surface plasmon to match the frequency of the excitation used.[7] In all previous SERRS studies involving DNA we have used commercially available fluorophores as the labels, as fluorescence is quenched in SERRS thus allowing the enhanced light scattering to be observed. Surface adsorption has been by electrostatic attraction of positively charged ammonium groups on the label to negatively charged citrate groups on the surface of the metal colloid used in our studies. In this approach the adsorption is not robust and can be affected by the presence of other agents such as metal chelators and no use is made of the extensive additional chemistry available for use with SERRS methodologies.

Previously we reported the synthesis of benzotriazole monoazo dyes specifically designed to provide SERRS by complexing directly to the silver surface, through the benzotriazole moiety which displaced the citrate surface layer.[8] In this communication we report the synthesis of a derivative of one of the previous dyes which is capable of undergoing solid phase addition to both DNA and PNA to make the oligomers SERRS active. The benefits of using these labels are that they are easy to produce, they give distinctive SERRS signals which are different from the previously used fluorophores, and they bind *via* complexation to the silver surface in a way which produces virtually irreversible binding.

The route followed for synthesis of the dye is shown in Scheme 1. *N*-(1-Naphthyl)ethylenediamine was chosen due to the presence of the primary aliphatic amine. Once an azo linkage has been produced the electron density on the aromatic amine is pulled into the ring system[9] dramatically reducing the reactivity of the amine as a nucleophile. Thus the aliphatic amine provides a reactive functionality to further derivatise the dye once synthesised. Dye synthesis was achieved by a diazonium coupling using 5-aminobenzotriazole to produce the orange dye, *N*-[4-(5′-azobenzotriazolyl)naphthalen-1-yl]ethylenediamine [**1**]. This dye was further functionalised to produce *N*-[2-(4′-(5″-azobenzotriazolyl)naphthalen-1-yl)aminoethyl]-succinamic acid [**2**]. The acidic dye was then capable of addition to amino linked DNA and PNA *via* amide formation on the solid phase.

A DNA oligomer was synthesised by routine solid phase phosphoramidite chemistry[10] and a monomethoxytrityl protected amino link added to the 5′-terminus.[11] Removal of the monomethoxytrityl group and addition of the activated dye produced the 5′-dye labelled DNA on the solid phase. The dye was activated by addition of carbonyl diimidazole to form the active ester. Cleavage and deprotection produced the crude labelled oligonucleotide which was purified by ion exchange HPLC. The coupling efficiency was estimated as > 83% by integration of the peaks from the HPLC.

PNA has a N-terminus which can be used to react in the same way as the amino link in DNA, however two Fmoc protected amino-3,6-dioxaoctanoic acid (AEEA-OH) spacers[12] were

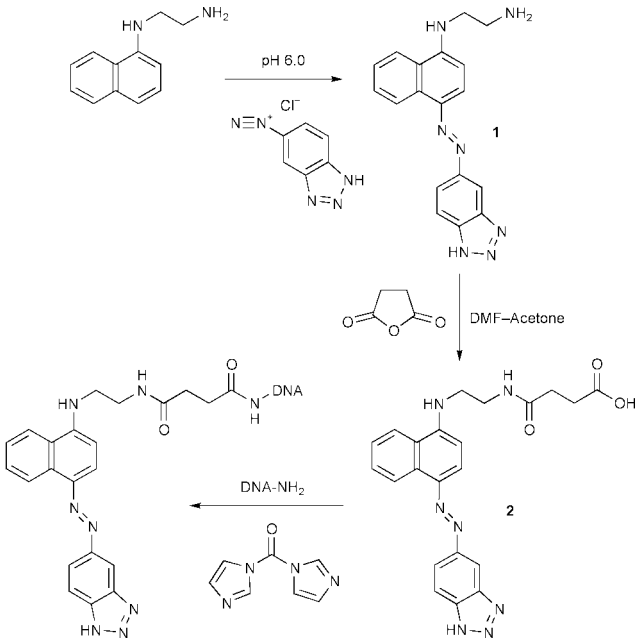

Scheme 1 Synthesis of the benzotriazole label and addition to amino linked DNA.

† Electronic supplementary information (ESI) available: full experimental details. See http://www.rsc.org/suppdata/cc/b1/b102241p/

 DOI: 10.1039/b102241p

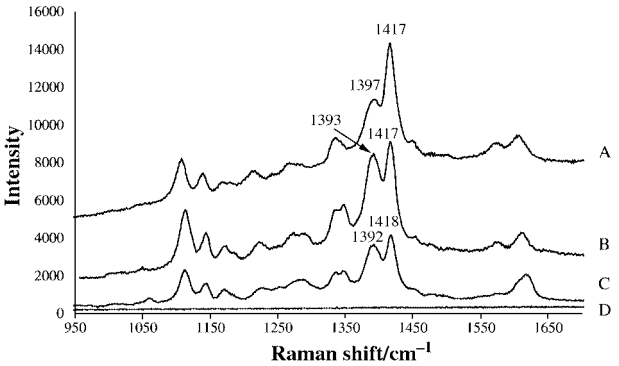

Fig. 1 The SERRS spectra obtained for free dye (A), dye labelled DNA (B), dye labelled PNA (C) and aggregated colloid with no dye (D). The spectra were obtained under different conditions and are scaled to allow comparison.

added to distance the dye from the PNA sequence. An 8mer was synthesised using Fmoc/Bhoc chemistry[12] and the two spacers added to the N-terminus. Removal of the Fmoc protecting group from the terminal spacer allowed addition of the benzotriazole carboxylic acid dye in the same way as for the DNA. Use of the dye as a monomer in the PNA synthesis cycle resulted in a mixture of products and poor coupling due to the unprotected triazole system, hence the use of the carbonyl diimidazole. Deprotection yielded the crude oligomer as a purple solid due to protonation of the azo linkage. Purification by reverse phase HPLC gave the pure dye labelled PNA with an estimated coupling efficiency of ~55% for the dye. The low coupling could be from a number of sources, such as cross-reaction of the unprotected triazole group. However, as only one monomer was being added this yield was acceptable.

The oligomers were then investigated for their ability to produce SERRS using citrate reduced silver colloid. A Renishaw microprobe system was used with 1 mW of 514.5 nm excitation at the sample. The optimum conditions for obtaining SERRS of both benzotriazole labelled oligomers vary. For the DNA oligomer the highest signal intensity was obtained when the phosphate backbone was neutralised by the addition of spermine prior to addition to the silver colloid. Use of an excess of spermine also provides aggregation of the colloid to produce the desired SERRS signals.[4] The spectrum is shown in Fig. 1B. The spectrum is consistent with that of the uncoupled dye (Fig. 1A) and displays the stretches at ~1393 cm^{-1} and 1417 cm^{-1} that are indicative of an azo tautomer.

A citrate assay was used to monitor the release of citrate from the surface after the addition of the benzotriazole dye, to the colloid. This proved that citrate was released from the surface after addition of the benzotriazole dye, but if spermine was added alone to induce aggregation then citrate was not released. This indicates that the benzotriazole is indeed complexing directly with the metal and not by a charge–charge interaction which appears to occur during spermine aggregation. Additionally, SERRS signals can be obtained from the dye labelled oligonucleotide without the use of spermine by using alternative aggregating agents such as phosphate buffer or nitric acid. This is in direct contrast to the oligonucleotides labelled with the fluorophores which in previous studies only produced intense SERRS with spermine. Thus we can conclude that the benzotriazole dye acts as a surface complexing agent and displaces citrate to provide attachment of modified oligonucleotides to a silver surface.

The conditions for obtaining SERRS of the PNA oligomer differ in that the oligomer is dissolved in 0.l% TFA and has a neutral backbone. Thus there is no need for the use of spermine as a charge neutralising agent. Also the TFA acts as an aggregating agent, again negating the need for the addition of spermine as an aggregating agent. The addition of the labelled PNA oligomer to a colloidal suspension produced a strong and distinct SERRS spectrum identical to that obtained for the labelled DNA (Figure 1C). In order to investigate the SERRS of the PNA labelled oligomer, a set of standard aggregating agents was tested with the labelled 8mer and the resulting SERRS recorded (Table 1). The values show that the intensity of the signals for the labelled PNA can be improved by the addition of an aggregating agent. However, if the solution is made basic by the addition of triethylamine then the intensity of the signals decreases, indicating that the PNA provides optimal signal to noise ratios in acidic conditions which are compatible with the conditions used for the standard synthesis of PNA. Spermine still appears to enhance the intensity of the spectrum, as it is an efficient aggregating agent.

Table 1 The intensity of the major peak in the PNA spectrum with different aggregating agents. All spectra were recorded in one scan of ten seconds and at 2×10^{-11} mole equivalents

Species studied	Intensity of peak at 1418 cm^{-1}
Colloid + TFA	No peaks
Colloid + BtDYE PNA + triethylamine	866
Colloid + BtDYE PNA	1074
Colloid + BtDYE PNA + spermine	1269
Colloid + BtDYE PNA + NaCl	2341
Colloid + BtDYE PNA + TFA	4148
Colloid + triethylamine	No peaks

In conclusion, we have synthesised benzotriazole azo dye labelled oligomers specifically designed to give SERRS. This dye is not an effective fluorophore and gives an indication of the additional labelling chemistry available for use with SERRS. The dye has been added to both DNA and PNA and SERRS obtained from both species. This type of label has additional benefits since the covalently attached benzotriazole group gives strong bonding, particularly to silver and copper surfaces, and provides a new and effective DNA–metal bonding chemistry. This is the first time that SERRS has been obtained from PNA and it is clear that it is easier to obtain SERRS from PNA than DNA.‡§

Notes and references

‡ The authors wish to thank the BBSRC for the award of a David Phillips Fellowship to D. G. and Astra Zeneca for funding to R. B.

§ Oligomers synthesised were: DNA 5′-BtDye X GTG CTG CAG GTG TAA ACT TGT ACC AG 3′ (X = amino link) and PNA (N)-BtDye OO ACA TTT GA (C) (O = AEEA spacer).

1 L. J. McBride and M. D. Oneill, *Am. Laboratory*, 1991, **23**, 52 *et seq*.
2 A. Castro and J. G. K. Williams, *Anal. Chem.*, 1997, **69**, 3915.
3 D. Graham, W. E. Smith, A. M. T. Linacre, C. H. Munro, N. D. Watson and P. C. White, *Anal. Chem.*, 1997, **69**, 4703.
4 D. Graham, B. J. Mallinder and W. E. Smith, *Biopolymers (Biospectroscopy)*, 2000, **57**, 85.
5 D. Graham, B. J. Mallinder and W. E. Smith, *Angew. Chem., Int. Ed.*, 2000, **39**, 1061.
6 C. H. Munro, W. E. Smith, M. Garner, J. Clarkson and P. C. White, *Langmuir*, 1995, **11**, 3712.
7 C. Rodger, W. E. Smith, G. Dent and M. Edmondson, *J. Chem. Soc., Dalton Trans.*, 1996, 791.
8 D. Graham, C. McLaughlin, G. McAnally, J. C. Jones, P. C. White and W. E. Smith, *Chem. Comm.*, 1998, 1187.
9 D. Graham, A. R. Kennedy and S. J. Teat, *J. Heterocycl. Chem.*, 2000, **37**, 1555.
10 M. H. Caruthers, *Science*, 1985, **230**, 281.
11 S. L. Beaucage and R. P. Iyer, *Tetrahedron*, 1993, **49**, 1925.
12 R. Castle, I. S. Jensen and M. Egholm, in *Peptide Nucleic Acids: Protocols and Applications*, ed. P. E. Nielsen and M. Egholm, 1999.

CHEMCOMM
Communication
www.rsc.org/chemcomm

Excited state intramolecular proton transfer (ESIPT) in 2-phenylphenol: an example of proton transfer to a carbon of an aromatic ring

Matthew Lukeman and Peter Wan*

Department of Chemistry, Box 3065, University of Victoria, Victoria, British Columbia, Canada V8W 3V6. E-mail: pwan@uvic.ca

Received (in Corvallis, OR, USA) 19th January 2001, Accepted 13th April 2001
First published as an Advance Article on the web 15th May 2001

The title compound undergoes excited state intramolecular proton transfer (ESIPT) from the phenol moiety to the 2′-carbon position of the phenyl ring (not containing the phenol hydroxy group), to generate the corresponding keto isomer (a quinone methide).

Many aromatic organic molecules possessing both acidic and basic functionalities experience simultaneous enhancement of the acidity and basicity of these groups upon electronic excitation. Often this enhancement is sufficient for direct protonation of the basic site by the acidic group through the overall process of excited state intramolecular proton transfer (ESIPT).[1a–c] The basic group is usually an aromatic heterocyclic nitrogen atom or a carbonyl oxygen atom, and the reaction is usually aided by a ground state hydrogen bond with the proton donor.[1a–c] ESIPT is a topic of continued interest for many groups world-wide, as represented by some selected recent papers in this area.[1d–f] All reported examples of ESIPT to oxygen and nitrogen heteroatoms (from OH or NH acids) are reversible, and such 'energy-wasting' reactions have been exploited for use as photostabilizers although other applications have been envisaged due to their inherent photochromic nature.[2] The first example of ESIPT to carbon (from phenol) was reported by Yates and co-workers[3] while studying the photohydration reactions of *o*-hydroxystyrene (**1**) and *o*-hydroxyphenylacetylene [eqn. (1)]. Photolysis of **1** in aqueous

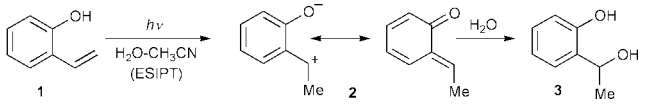

(1)

MeCN gave the hydration product **3** *via* *o*-quinone methide **2**. The primary photochemical step (from S_1) is ESIPT from the phenol to the β-carbon of the alkene moiety. Reverse proton transfer in **2** (from C–H to phenolate oxygen) is highly unfavourable and, instead, the intermediate is trapped completely by water to give **3**.[3,4]

To our knowledge, there are no explicit examples of ESIPT to a carbon atom that is part of an aromatic ring. However, Webb and coworkers[5] have suggested that the geminate recombination process in the ESPT reaction of 1-naphthol could result in protonation at the C-5 and C-8 ring carbons positions, *via* solvent-mediated ESIPT. In addition, reports of the photoprotonation (by aqueous acid) of the ring carbons of a variety of aromatic rings is well-known.[6] What is unknown is whether an explicit ESIPT to an aromatic ring carbon could operate in appropriately designed systems. Such systems would be unique as examples of a new type of ESIPT process. We present results for the photochemical deuterium exchange in 2-phenylphenol (**4**) that is entirely consistent with an explicit ESIPT from the phenol moiety to the ring carbon (position 2′) of the benzene ring not bearing the hydroxy group.

Exhaustive photolysis of **4** in 1 : 1 (v/v) D_2O–MeCN solution (Rayonet RPR-100 photochemical reactor; 254 nm lamps; 10^{-3} M; < 15 °C; argon-purged solutions; 1 h) yielded (after a H_2O-wash) **4** that is deuterated exclusively on the ring not bearing the hydroxy group. ^{1}H NMR (360 MHz) analysis of the sample showed that 70% of the 2′-(*ortho*) positions and 30% of the 4′-(*para*) positions were deuterated (not excluding dideuteration of the 2′-position since there are two such positions). These observations are consistent with an excited state where there is substantial charge transfer from the phenol ring to the benzene ring and would not be unusual based on photochemistry of some hydroxy-substituted biphenyls and biaryls already reported by our group.[6c,7] Similar results were observed for the photolysis of **5**† whereas photolysis of **6**–**8** gave no observable exchange.

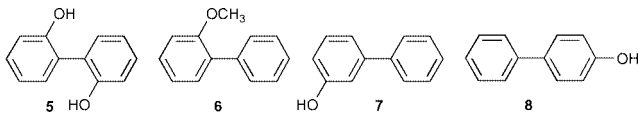

For **4** and **5**, no exchange was observed in solutions that were not photolyzed. Clearly the hydroxy group is necessary for reactivity. The lack of reactivity for **7** and **8** suggest that the exchange observed for **4** and **5** may be due to an explicit ESIPT between the phenol OH and the 2′-position of the other benzene ring.

To investigate the possibility of an ESIPT mechanism for exchange, subsequent photolysis of **4** were carried out in MeCN solutions containing varying concentrations of D_2O and the extent of exchange analyzed by NMR. The results are plotted in Fig. 1. Under the conditions employed for these experiments, exchange at the *para* position was too low to be reliably measured (typically < 10% across the D_2O concentrations used). The plot shows that *ortho* exchange (which is significantly more efficient than exchange at the *para* position) is independent of D_2O concentration above 0.2 M D_2O. At lower concentrations, there is a rapid rise in the efficiency for exchange at the *ortho* position (see inset), reaching a plateau level at about 0.2 M D_2O. These observations strongly suggest that exchange at the *ortho* and *para* positions take place *via* different mechanisms. The rapid rise in yield of *ortho* exchange with increasing D_2O content at low concentrations essentially corresponds with the extent of exchange of the hydroxy proton of **4**; that is, once all of **4** has been deuterated at the hydroxy group (to give **4**-*OD*), the efficiency of photochemical deuteration at the *ortho* position is solvent independent. This is further corroborated by independent photolysis of a crushed crystalline sample of **4**-*OD*, which gave exclusive exchange (about 10%) at the *ortho* position, with no observable exchange at the *para* position. These results are consistent with a mechanism of *ortho* exchange involving ESIPT (Scheme 1). In this mechanism, photolysis of **4**-*OD* results in ESIPT to the 2′-carbon position, to generate the *o*-quinone methide intermediate **9**. Reverse transfer of a proton or water-assisted tautomerization gives **4**-*2′D* (after H_2O wash). A related ESIPT has been reported for compound **10** (and related systems) although in this case, the basic site is a nitrogen of an aromatic heterocyclic ring.[8] What we have shown in this work is that the *ortho* carbon atoms (on a simple

 DOI: 10.1039/b100817j

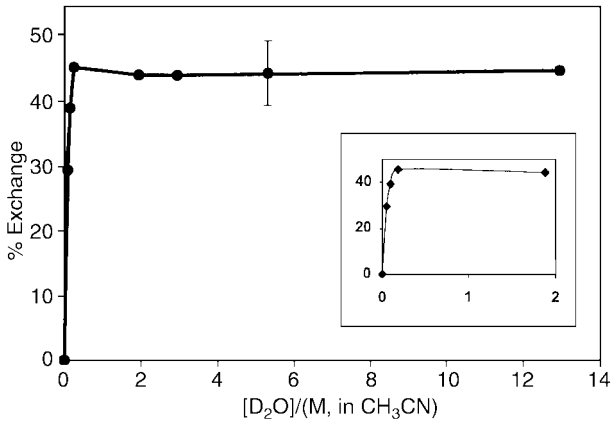

Fig. 1 Plot of % exchange at the *ortho* (2′) position observed for **4** *vs*. D_2O concentration (in MeCN). (Inset: expanded plot at low D_2O concentration).

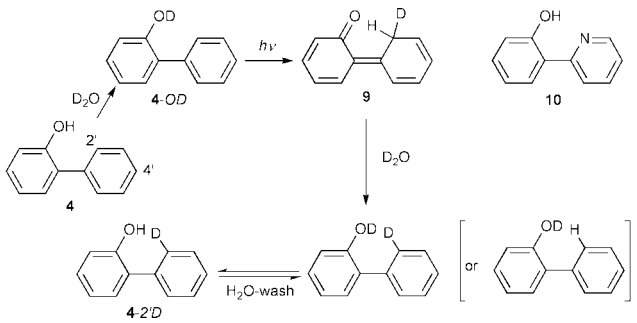

Scheme 1

benzene ring) are sufficiently basic to accept the acidic proton in these systems.‡

The *para* (4′) carbon is too far away from the acidic hydroxy (phenol) proton to be directly protonated intramolecularly. Indeed, its exchange yield is much lower. These results imply that a different mechanism is operative for deuterium incorporation at the *para* position. This is further corroborated by the following experiments. Photolysis of **4** in 1:1 MeOD–MeCN resulted in deuterium incorporation exclusively at the *ortho* position and suggests that only the ESIPT mechanism operates in MeOH–MeCN. Fluorescence emission spectra of **4** in a number of solvents gave additional insights into the mechanism of exchange at the *para* position (Fig. 2). These spectra show that **4** does not undergo excited state dissociation of the phenolic proton in neat MeCN or MeOH whereas 1:1 H_2O–MeCN is sufficiently polar to allow the dissociation, and hence formation of the excited state phenolate ion at 415 nm. That water is generally required for adiabatic deprotonation of phenols is well-known and has been specifically studied for **4** in H_2O–MeOH solutions.[9] These results are consistent with a mechanism of deuterium incorporation at the *para* position involving protonation (at the 4′-carbon) of the excited or ground state phenolate ion, formed *via* deprotonation from S_1 that requires water. This is apparently not an efficient process as the carbon protonation step must compete with fluorescence of the excited state phenolate as well as reprotonation at the oxygen site. This mechanism of deuterium incorporation probably also contributes to the overall exchange observed at the *ortho* position in aqueous solution (the extent of which is unknown at present) although the evidence suggests that ESIPT is the only mode of reaction responsible for exchange in neat organic solvents and in the solid state.

In summary, the results observed are consistent with a new type of ESIPT in which the acidic proton from a phenol is

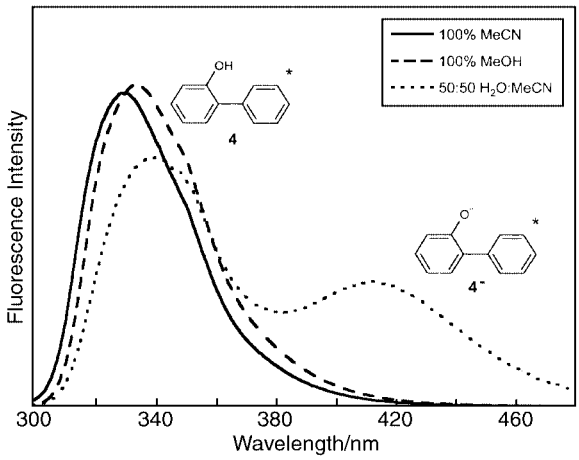

Fig. 2 Fluorescence emission spectra observed for **4** in 1:1 H_2O–MeCN, neat MeCN and neat MeOH (λ_{ex} = 285 nm; τ (neat H_2O) = 0.53 ns;[9] (1:1 H_2O–MeOH) = 1.25 ns;[9] estimated Φ_f (neat MeCN) ≈ 0.1).

directly transferred to a carbon atom of a benzene ring. The transfer is effectively reversible resulting in deuterium incorporation when carried out in D_2O. The dynamics and generality of this new type of ESIPT await further exploration.

We acknowledge the continued support of the Natural Sciences and Engineering Research Council (NSERC) of Canada and the University of Victoria. ML thanks NSERC for a post-graduate scholarship. Dr Y. Shi is acknowledged for preliminary studies.

Notes and references

† In this case, deuteration occurs on both rings since the system is symmetrically substituted.

‡ One would expect the ESIPT efficiency to be substantially lower when nitrogen is replaced by carbon. We have estimated the quantum yield for deuterium incorporation at the *ortho* (2)′-position in 1:1 D_2O–MeCN to be ≈ 0.02.

1 (*a*) S. M. Ormson and R. G. Brown, *Prog. React. Kinet.*, 1994, **19**, 45; (*b*) D. Le Gourrierec, S. M. Ormson and R. G. Brown, *Prog. React. Kin.*, 1994, **19**, 211; (*c*) S. J. Formosinho and L. G. Arnaut, *J. Photochem. Photobiol. A*, 1993, **75**, 21; (*d*) P.-T. Chou, J.-H. Liao, C.-Y. Wei, C.-Y. Yang, W.-S. Yu and Y.-H. Chou, *J. Am. Chem. Soc.*, 2000, **112**, 986; (*e*) A. Kyrychenko, J. Herbich, M. Izydorzak, F. Wu, R. P. Thummel and J. Waluk, *J. Am. Chem. Soc.*, 1999, **112**, 11 179; (*f*) M. C. Rios Rodriguez, J. C. Penedo, R. J. Willemse, M. Mosquera and F. Rodriguez-Prieto, *J. Phys. Chem., A*, 1999, **103**, 7236.

2 (*a*) V. Balzani and F. Scandola, *Supramolecular Photochemistry*, Ellis Horwood, New York, 1991; (*b*) H. Dürr and H. Bouas-Laurent (ed.), *Photochromism: Molecules and Systems*, Elsevier, Amsterdam, 1990.

3 (*a*) M. Isaks, K. Yates and P. Kalanderopoulis, *J. Am. Chem. Soc.*, 1984, **106**, 2728; (*b*) P. Kalanderopoulis and K. Yates, *J. Am. Chem. Soc.*, 1986, **108**, 6290.

4 K. L. Foster, S. Baker, D. W. Brousmiche and P. Wan, *J. Photochem. Photobiol., A*, 1999, **129**, 157.

5 S. P. Webb, L. A. Philips, S. W. Yeh, L. M. Tolbert and J. H. Clark, *J. Am. Chem. Soc.*, 1986, **90**, 5154.

6 (*a*) H. Shizuka, *Acc. Chem. Res.*, 1985, **18**, 141; (*b*) P. Wan and G. Zhang, *Res. Chem. Intermed.*, 1993, **19**, 119; (*c*) Y. Shi and P. Wan, *J. Chem. Soc., Chem. Commun.*, 1995, 1217.

7 (*a*) C.-G. Huang, K. A. Beveridge and P. Wan, *J. Am. Chem. Soc.*, 1991, **113**, 7676; (*b*) Y. Shi and P. Wan, *J. Chem. Soc., Chem. Commun.*, 1997, 273.

8 D. LeGourrierec, V. Kharlanov, R. G. Brown and W. Rettig, *J. Photochem. Photobiol., A*, 1998, **117**, 209.

9 S. G. Schulman, R. W. Townsend and W. R. G. Baeyens, *Anal. Chim. Acta*, 1995, **303**, 25.

CHEMCOMM Communication
www.rsc.org/chemcomm

Improvement in the surface acidity of $Al_2O_3{\cdot}SiO_2$ due to a high Al dispersion

Yasushige Kuroda,* Toshinori Mori and Yuzo Yoshikawa

Department of Chemistry, Faculty of Science, Okayama University, Tsushima, Okayama 700-8530, Japan. E-mail: kuroda@cc.okayama-u.ac.jp

Received (in Cambridge, UK) 17th January 2001, Accepted 26th April 2001
First published as an Advance Article on the web 15th May 2001

Using ethylene glycol derivatives of aluminium isopropoxide and ethyl orthosilicate precursors in the sol–gel process, discrete aluminosilicate nanoparticles were produced that had a strong Brönsted acidity, high surface area and high thermal stability; these properties were ascribed to a high dispersion of the aluminium atoms in the silica matrix.

Acid catalysts have been the subject of considerable fundamental research, since they represent a very relevant family of solid acids that are widely utilized in the chemical and petrochemical industries.[1] In regard to catalysis, pure SiO_2 is of limited use, owing to the absence of active sites in its matrix. The substitution of Si in the SiO_2 matrix by Al, creates a negative charge on the SiO_2 framework with an associated H^+ being bound to a nearby oxygen atom to maintain charge neutrality. This results in the formation of Brönsted acid protons as Al–OH–Si bridges. One factor affecting the Brönsted acidity is the dependency on the bond angle in Si–O–Al,[2,3] while another important factor may be said to result from 'the degree of dispersion of the Al ions'. Taking account of the latter factor, in the multi-component sol–gel processes for the general preparation of aluminosilicates, it is important to control the rate of hydrolysis of the precursors. As the hydrolysis rates of the respective precursors are considerably different in the preparation of aluminosilicates gels composed of different mixtures of the elements will be formed (Al_2O_3 in the SiO_2 matrix), instead of a homogeneous hybrid material. This difficulty can be largely overcome by controlling the hydrolysis rates through the formation of more stable aluminium complexes. Zarur and Ying[4] have recently reported that an ultra-high component dispersion plays a pivotal role in the preparation of catalysts with high reactivity and thermal stability that are needed for a variety of applications. Since solid acidic catalysts are used in various catalytic reactions, it is very important to develop them to have a reproducible and strong surface acidity. In the present work, we aimed to prepare an aluminosilicate acid catalyst containing well-dispersed Al ions, and to then clarify its acidic characteristics.

Discrete nanoparticles of aluminium silicate (denoted $Al_2O_3{\cdot}SiO_2$) having well dispersed Al atoms, were prepared by mixing 0.23 mol of ethyl orthosilicate (TEOS) with aluminium isopropoxide (0.02 mol) to prepare a sample with an Si : Al ratio of 11.5. Ethylene glycol was added to this suspension, and a resultant phase-separated mixture was formed which changed to a white suspension after stirring for 1 h at 35 °C. This suspension was mixed with an aqueous NaOH solution (0.13 mol, 300 cm^3) using a spray gun to form a mist to enable the hydrolysis reaction to proceed slowly and homogeneously. The suspension was kept at 50 °C for 2 d, and then finally aged for a further 2 d at 120 °C. The sample obtained was washed well and dried in air at 35 °C and then finally calcined in an oxygen stream for 10 h at 600 °C. An acidic ZSM-5 zeolite (HZSM-5, Si : Al = 11.9) provided by the Tosoh company, and a silica–alumina sample containing 5 wt% of Al_2O_3 (denoted as SA-5) prepared by a conventional sol–gel method[6] were used as reference samples. The prepared $Al_2O_3{\cdot}SiO_2$ sample had a specific surface area of 711 $m^2\ g^{-1}$, which was larger than that of the SA-5 sample (216 $m^2\ g^{-1}$).

All ^{27}Al and ^1H MAS NMR measurements were carried out in a field of 7 T using a Varian UNITY INOVA 300 spectrometer with a 7-mm diameter zirconia rotor, filled with dry air. Before the ^1H NMR measurements, all samples were evacuated at 450 °C to eliminate any physisorbed water. Tetramethylsilane (TMS) was used as the external reference for the ^1H signals, and all the spectra were calibrated to this reference. ^{27}Al NMR spectra were measured by using a $\pi/20$ pulse and a recycle delay time of 1 s. For Al NMR measurements, all samples were evacuated at 27 °C. The ^{27}Al signals and their chemical shifts were referenced in ppm with respect to an external $Al(H_2O)_6^{3+}$ standard in a 1 M aqueous $Al(NO_3)_3$ solution.

The ^{27}Al MAS NMR spectra for the three samples are shown in Fig. 1. These are potentially very helpful for probing the quantity, coordination and location of aluminium atoms in aluminosilicates, even though the quadrupolar nature of the nucleus does not allow observation of the structurally significant fine structure of the bands. The $Al_2O_3{\cdot}SiO_2$ sample showed an ^{27}Al band centred at 54.6 ppm, in the region corresponding to tetrahedrally coordinated aluminium (Al^{IV}). It is notable that there is virtually no component at 0 ppm, characteristic of an aluminium ion in octahedral coordination (Al^{VI}).[5–7] The spectra of the HZSM-5 and SA-5 samples give a pattern similar to that of $Al_2O_3{\cdot}SiO_2$, with the intensity of the 54.6 ppm band largest for HZSM-5, and smallest for SA-5 among the samples used. The HZSM-5 and SA-5 samples also had a distinctive band at 0 ppm, indicating the presence of six-coordinate aluminium ions. It cannot be emphasized too strongly that this band was not observed in our $Al_2O_3{\cdot}SiO_2$ sample. These NMR results demonstrate that the Al oxide moiety was successfully incorporated into the silica framework by the present preparation method using ethylene glycol.

The resulting spectra from the ^1H MAS NMR measurements are shown in Fig. 2. The ^1H MAS NMR spectrum for HZSM-5 was composed from the sum of the contributions of the following types of OH groups: (i) SiOH at *ca.* 1.8 ppm; and (ii) SiO(H)Al at 4.2 and 6.3 ppm (the latter as a weak shoulder).[8]

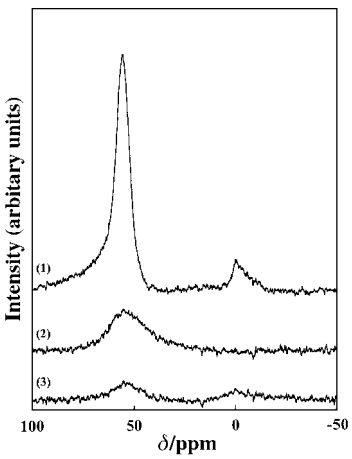

Fig. 1 ^{27}Al MAS NMR spectra for samples evacuated at 27 °C: (1) HZSM-5, (2) $Al_2O_3{\cdot}SiO_2$, (3) SA-5 samples.

 DOI: 10.1039/b100641j

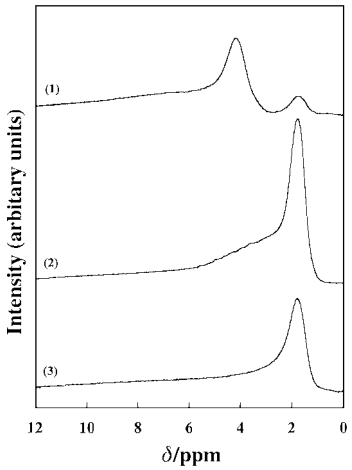

Fig. 2 ^{1}H MAS-NMR spectra for samples evacuated at 450 °C: (1) HZSM-5, (2) $Al_2O_3{\cdot}SiO_2$, (3) SA-5 samples.

Similar to HZSM-5, a distinctive broad feature with a maximum centred around 3.8 ppm was found for the $Al_2O_3{\cdot}SiO_2$ sample, together with the emergence of an intense signal around 1.8 ppm. In contrast to these samples, the broad band was scarcely discernible for the SA-5 sample, and the band at 1.8 ppm was dominant. For the SA-5 sample, a broad band around 2.7 ppm, assigned to an AlOH species, was detected when a deconvolution technique was applied to the observed spectrum.[5,8] As a result, for the $Al_2O_3{\cdot}SiO_2$ sample, the existence of a higher number of strongly acidic Brönsted-acid sites compared to the SA-5 sample is evident, although not so strong in acid strength and in as large a quantity as those observed for the HZSM-5 sample.

It is well known that the adsorption of CO on zeolites gives rise to carbonyl stretching vibration (ν_{CO}) bands at higher wavenumber relative to the free molecule (2143 cm^{-1}), depending on the strength of interaction.[9,10] These bands are expected to be observable through the interaction of CO with Brönsted acid sites, even at room temperature. The procedure used to record the IR spectra *in situ* and the details of the sample cell used have been reported in previous papers.[5,8]

The adsorption of CO on the 450 °C-treated HZSM-5 sample at 22 °C resulted in the development of a distinct ν_{CO} band with a maximum around 2170 cm^{-1}, and its band-maximum shifted to a lower wavenumber of 2168 cm^{-1}, with a distinct shoulder toward the lower wavenumber end (Fig. 3) at a pressure of 26.6 kPa. The spectrum measured at higher pressure was deconvoluted into two components at 2170 and 2165 cm^{-1}. Another feature is the appearance of a band at 2228 cm^{-1}. It should be noted that a similar spectral pattern, except for the 2228 cm^{-1} band, was obtained for the $Al_2O_3{\cdot}SiO_2$ sample, where a strong band was found at 2170 cm^{-1}. As for the SA-5 sample, the two bands discussed for the other samples were scarcely observed, although a strong band could be seen at 2228 cm^{-1}. In addition, the FTIR spectra in the OH vibrational stretch region showed prominent band features with two components for the HZSM-5 sample, one at 3745 cm^{-1}, and the other, a broad band, at around 3620 cm^{-1}. The appearance of the band at 2170 cm^{-1} was accompanied by a shift in the OH band observed at 3620 cm^{-1}, *i.e.* an interaction with the Brönsted acid site, and the 2165 cm^{-1} band was related to an interaction with the silanol group, related to the band at 3745 cm^{-1}.[5,11] For the $Al_2O_3{\cdot}SiO_2$ sample, the IR spectrum showed a discernible shoulder at 3620 cm^{-1} at the foot of a strong band at 3745 cm^{-1}, showing a similar trend to the HZSM-5 system in this regard. On the other hand, the SA-5 sample exhibited a faint shoulder around 3620 cm^{-1}, and a strong band was observed around 3745 cm^{-1}. The strong band around 3745 cm^{-1} scarcely changed even after CO adsorption on the SA-5 sample, coinciding with the absence of a band at around 2170 cm^{-1}. Taking into account the IR and the NMR data, there is no doubt about the existence of the Brönsted acid site in the $Al_2O_3{\cdot}SiO_2$ sample; the $Al_2O_3{\cdot}SiO_2$ sample possesses a larger number of Brönsted acid sites, and a more homogeneous site distribution compared to sample SA-5.

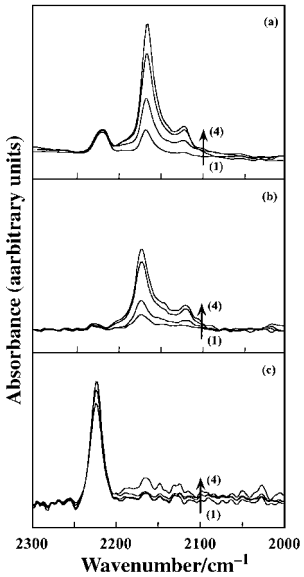

Fig. 3 FTIR spectra of CO adsorbed on the samples: (a) HZSM-5, (b) $Al_2O_3{\cdot}SiO_2$, (c) SA-5. The samples were first evacuated at 450 °C and then equilibrated with increasing pressures of CO gas at 27 °C: (1) 6.65, (2) 13.3, (3) 20.0 and (4) 26.6 kPa.

The distinctive band at 2228 cm^{-1} arising from the adsorbed CO species as observed in the spectra of the HZSM-5 and SA-5 samples is due to the interaction of CO with strong Lewis acid sites through a σ-donor bond.[9,10] It is of note that this band does not appear for the $Al_2O_3{\cdot}SiO_2$ sample, clearly indicating the lack of a Lewis acid centre. This result corresponds well with the NMR data, which shows a lack of octahedral aluminium sites. These data are indicative of the stability of the lattice of the $Al_2O_3{\cdot}SiO_2$ sample.

In conclusion, we have shown that the preparation of an $Al_2O_3{\cdot}SiO_2$ sample utilizing ethylene glycol as a solvent, leads to a sample having a strong Brönsted acid character. The appearance of this strong acidic property is attributable to a high dispersion of aluminium atoms at the atomic level in the SiO_2 lattice, which is more complete than that observed for a sample prepared by the general sol–gel method. Utilizing the present method, we can prepare various hybrid materials that consist of elements which are well dispersed at the atomic level, and expect such highly component-dispersed materials to exhibit many applications in catalysis, adsorption technology and other areas of importance.

Notes and references

1 J. M. Thomas and W. J. Thomas, in *Principles and Practice of Heterogeneous Catalysis*, VCH, Weinheim, 1997.
2 P. J. O'Malley and J. Dwyer, *J. Phys. Chem.*, 1988, **92**, 3005.
3 G. Sastre, V. Fornes and A. Corma, *J. Phys. Chem. B*, 2000, **104**, 4349.
4 A. J. Zarur and J. Y. Ying, *Nature*, 2000, **403**, 65.
5 Y. Kuroda, T. Mori, Y. Yoshikawa, S. Kittaka, R. Kumashiro and M. Nagao, *Phys. Chem. Chem. Phys.*, 1999, **1**, 3807.
6 M. J. Remy, D. Stanica, G. Poncelet, E. J. P. Feijen, P. J. Grobet, J. A. Martens and P. A. Jacobs, *J. Phys. Chem.*, 1996, **100**, 12 440.
7 C. A. Fyfe, J. L. Bretherton and L. Y. Lam, *Chem. Commun.*, 2000, 1575, and references therein.
8 E. Brunner, K. Beck, M. Koch, L. Heeribout and H. G. Karge, *Microporous Mater.*, 1995, **3**, 395.
9 O. Cairon, T. Chevreau and J.-C. Lavalley, *J. Chem. Soc., Faraday Trans.*, 1998, **94**, 3039.
10 A. Zecchina, S. Bordiga, C. Lamberti, G. Spoto, L. Carnelli and C. O. Ane'an, *J. Phys. Chem.*, 1994, **98**, 9577.
11 T. P. Beebe, P. Gelin and J. T. Yates, Jr., *Surf. Sci.*, 1984, **148**, 526.

CHEMCOMM Communication
www.rsc.org/chemcomm

Assembly of a 3D nanoporous framework $[Cu_6(OH)_4(tib)_8]_n^{8+}$ from Cu(II) and the flexible tripodal ligand tib†

Hong-Ke Liu,*[a] Hai-Yan Tan,[a] Ji-Wen Cai,[b] Zhong-Yuan Zhou,[c] Albert S. C. Chan,[c] Sen Liao,[ac] Wen Xiao,[ac] Hua-Xin Zhang,[a] Xiao-Lan Yu[a] and Bei-Sheng Kang*[a]

[a] *School of Chemistry and Chemical Engineering, Zhongshan University, Guangzhou, Guangdong 510275, China. E-mail: hongke_liu@hotmail.com*
[b] *Instrumentation Analysis & Research Center, Zhongshan University, Guangzhou, Guangzhou, Guangdong 510275, China*
[c] *Open Laboratory for Chiral Technology, The Hong Kong Polytechnic University, Hung Hom, Kowloon, Hong Kong SAR, China*

Received (in Cambridge, UK) 8th January 2001, Accepted 19th April 2001
First published as an Advance Article on the web 15th May 2001

The structural characterization of a 3D nanoporous complex $\{[Cu_6(tib)_8(OH)_4](OH)_8\cdot 22H_2O\cdot 4MeOH\}_n$ 1 [tib = 1,3,5-tris-(imidazol-1-ylmethyl)benzene] assembled from the tripodal ligand tib and $Cu(MeCO_2)_2$ shows that π–π interactions resulting from the novel T-shaped conformation of the ligand are the key trigger for the construction of the backbone of a framework with channels of size 12.00 × 18.91 and 10.30 × 13.66 Å.

Employing multidentate organic ligands and metal ions to construct organic–inorganic hybrid materials[1] *via* coordinative metal–ligand bonds has become a major strategy.[1,2] Frameworks with specific topologies such as honeycomb grids and interpenetrating nets have been obtained by assembly of suitable metal ions with rationally designed rigid tripodal ligands such as 1,3,5-trisbenzonitrile (tcb),[3] 1,3,5-tris(4-ethynylbenzonitrile)benzene (teb)[4] and 2,4,6-tris(4-pyridyl)-1,3,5-triazine (tpt).[5–7] For example, tcb gives an extended honeycomb framework[3] by assembly with AgO_3SCF_3, while in the case of tpt, a (12,6) interpenetrating net[6] was obtained by reaction of the ligand with $Ni(NO_3)_2$. Recently, Robson and coworkers[7] reported another honeycomb-like framework[7] obtained by assembly of $Cu(MeCO_2)_2$ with the rigid tripodal ligand tpt.

In order to investigate the relationship between the topology of the assembly and the conformation of the ligand, two flexible tripodal ligands, 1,3,5-tris(imidazol-1-ylmethyl)-2,4,6-trimethylbenzene (titmb)[8,9] and 1,3,5-tris(imidazol-1-ylmethyl)benzene (tib)[10] were employed. Our previous work showed that titmb has two conformations, namely, *cis,cis,cis*-conformation (W-form) and *cis,trans,trans*-conformation (Y-form). An extended honeycomb framework with large cavities[8] was formed with titmb in W-form, whilst a 2D sheet-like framework[9] containing the ligand in both W- and Y-form was obtained from $Cu(dien)^{2+}$ ions and titmb. Most recently, a study also showed that a discrete M_3L_2 cage-like complex was assembled from tib in W-form with zinc(II) acetate.[10]

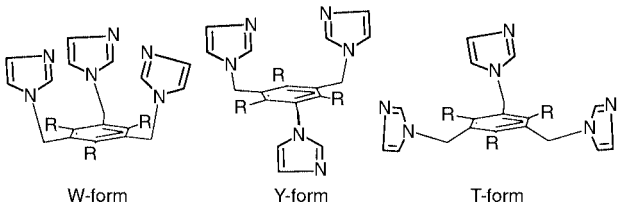

We report herein, to our knowledge, the first example of a 3D nanoporous complex $\{[Cu_6(tib)_8(OH)_4](OH)_8\cdot 22H_2O\cdot 4MeOH\}_n$ assembled from the tripodal ligand tib, in which π–π interactions play important roles in the construction of the backbone of the framework. In addition all the tib ligands are in a novel, unprecedented T-form conformation.

Standing of a blue MeOH–H_2O solution of tib and $Cu(MeCO_2)_2\cdot 2H_2O$ (L : M = 3 : 2) overnight resulted in the formation of blue sheet-like crystals with the formulation $\{[Cu_6(tib)_8(OH)_4](OH)_8\cdot 22H_2O\cdot 4MeOH\}_n$ **1**‡ and the structure was characterized by crystallographic analysis.§ Complex **1** shows no feature for carboxyl antisymmetric (ν_{asym} 1560 cm^{-1}) or symmetric (ν_{sym}, 1416 cm^{-1}) vibrations in the IR spectrum, indicating the absence of acetate anion, in agreement with the elemental analyses and crystallographic results.

There are two types of coordination environments for the copper ions (Fig. 1). Cu1 is coordinated by four N atoms from four tib ligands and one O atom from one OH anion giving a distorted N_4O square-pyramidal geometry, in which the four N atoms form the equatorial plane. By contrast Cu2 is coordinated only by four N atoms from four tib, leading to a distorted N_4 square-planar geometry.

It is interesting that in this complex, all tib ligands are in the T-form, as (Fig. 1). One imidazolyl ring lies outside the phenyl plane, but the centers of the other two imidazolyl rings are in the plane of the phenyl group and situated in a linear manner, to form a capital 'T'. Each tib is ligated to three copper atoms *via* the nitrogen atoms of the three imidazolyl groups. Two adjacent tib ligands adopt a top-to-bottom orientation and are joined together by atoms Cu1 and Cu1a to generate a rhombic Cu_2L_2

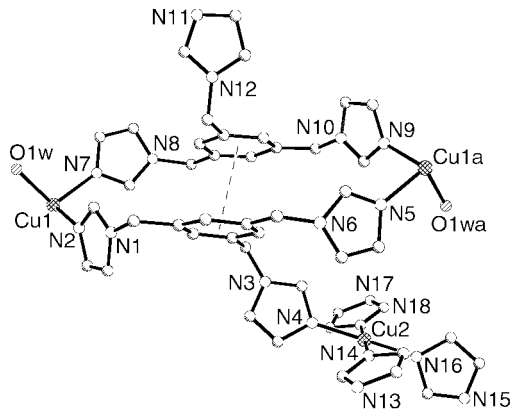

Fig. 1 Coordinative environment of copper atoms in **1** (π–π interactions indicated by dashed lines). Selected atomic distances (Å) and bond angles (°): Cu1–N 1.981(6)–2.006(6), Cu1–O 2.357(8); N–Cu1–N 88.3(2)–91.8(2)/161.1(3)–179.6(3), N–Cu1–O 89.1(3)–101.3(3); Cu2–N 1.991(6), N–Cu2–N 88.2(2)–91.8(2)/180. Cu1–Cu1a 13.76. All hydrogen atoms and solvate molecules are omitted for clarity.

† Electronic supplementary information (ESI) available: part of packing diagram selected to show Cu··O interactions and O··O hydrogen interactions (Fig. 1S). See http://www.rsc.org/suppdata/cc/b1/b100325i/

 DOI: 10.1039/b100325i

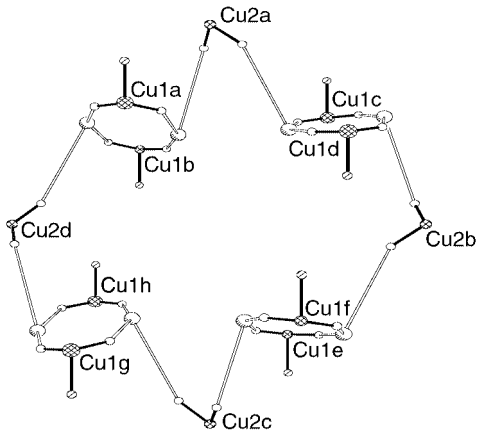

Fig. 2 Schematic drawing of a $Cu_{12}L_8$ macrocyclic ring in the *xz* plane. The large cross-hatched ellipsoids and small hatched ellipsoids represent Cu and O atoms respectively, while the large and small ellipsoids represent phenyl rings and coordinated N atoms, respectively. Heavy lines represent the Cu–N bonds while open lines connect the phenyl rings with coordinated N atoms. All hydrogen atoms and solvate molecules are omitted for clarity.

unit (as shown in Fig. 1), in which strong π–π interactions formed between the two tib ligands, with the two parallel phenyl rings separated by 3.55 Å, and a Cu1···Cu1a distance of 13.76 Å.

Four independent Cu_2L_2 units are joined together by four other Cu atoms, forming an $Cu_{12}L_8$ macrocyclic repeating unit which is composed of $Cu_{12}C_{144}N_{48}$ (as shown in Fig. 2); the total volume of the unit, 23.19 × 18.91 × 13.66 Å, is the same as the cell unit. Repeating the $Cu_{12}L_8$ units in space, a 3D nanoporous framework is then formed (Figs. 3 and 4), in which there are two types of channels with different sizes. Along the *y* axis, a channel with hole dimensions of 12.00 × 18.91 Å, which are defined by the Cu–Cu seperation, is shown in Figs. 2 and 3. However, when viewed along the *z* axis, four Cu_2L_2 units with each two sharing a Cu atom are connected by two other Cu atoms, forming a rectangular Cu_8L_8 unit ($Cu_8C_{144}N_{48}$) opening with dimensions of 10.30 × 13.66 Å (Fig. 4). There are $22H_2O$ and 4MeOH molecules in a complete $Cu_{12}L_8$ repeating unit, all within the channels. Indeed, all the modeled water molecules in this structure are in close contact to either Cu^{2+} ions (*e.g.* Cu1–Ow4 3.097(12) Å, Cu2–Ow2 2.642(10) Å) or the hydrogen atoms of methanol and water molecules (Fig. 1S, see ESI†). The free pore volume of a unit is estimated, using the PLATON program[11] (squeeze), to be 847 Å^3 (15.0% of the total).

The result described here shows that π···π interactions, resulting from the novel T-shaped conformation of the ligand, are the key trigger for the construction of the backbone of the framework. This is the first example determined by X-ray structure analysis showing a 3D nanoporous structure constructed by Cu(II) ions and a flexible tripodal ligand. This work also shows that the topology of assembly is obviously affected by the ligand conformation. The novel T-form of tib is favourable in the formation of π···π interactions between two nearest adjacent ligands. This nanoporous complex may have the ability to selectively enclathrate moderately sized guests. Encapsulation reactions of guest molecules are now under study.

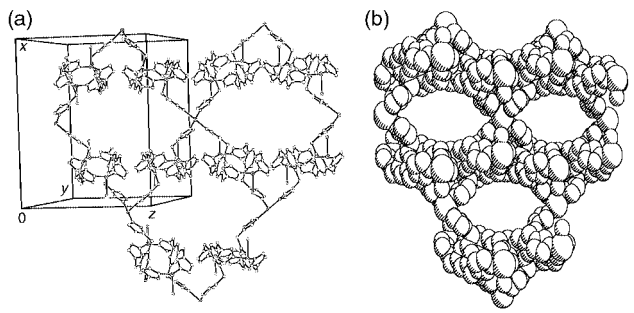

Fig. 3 Structure views of **1** in the *xz* plane, showing the macrocyclic channels. (a) Structure of three channels with cell axes. (b) A space-filling model. All hydrogen atoms and solvate molecules are omitted for clarity.

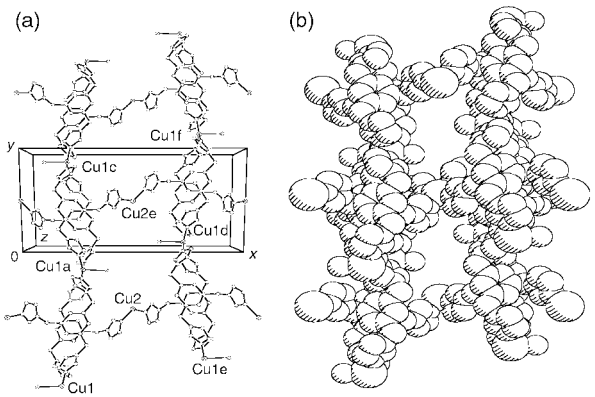

Fig. 4 Structure views of **1** in the *xy* plane, showing the rectangular channels. (a) Structure of two channels with cell axes. (b) A space-filling model. All hydrogen atoms and solvate molecules are omitted for clarity.

We are grateful for funding from the NNSF of China and the postdoctoral fund of Guangdong province and a special fund from the Ministry of Education of China for the vitalization education plan of the 21st century for H.-K. L.

Notes and references

‡ *Experimental:* a solution of tib (48 mg, 0.15 mmol) in methanol (5 ml) was added to an aqueous solution (10 ml) of $Cu(MeCO_2)_2{\cdot}2H_2O$ (22 mg, 0.1 mmol) at room temperature. The mixture was filtered after stirring for *ca.* 1 h to give a blue solution. Standing of this filtrate overnight resulted in the formation of blue sheet-like crystals. Yield 10% (Found: C, 49.52; H, 5.47; N, 18.61%. Calc. for $C_{148}H_{208}N_{48}Cu_6O_{34}$ ($[Cu_6(tib)_8(OH)_4](OH)_8{\cdot}18H_2O{\cdot}4CH_3OH$): C, 49.58; H, 5.84; N, 18.75%. IR(KBr) cm^{-1}, 3411br, 3115s, 3033m, 1638w, 1611w, 1572w, 1522s, 1440m, 1401w, 1345w, 1287w, 1237m, 1100vs, 1030m, 948w, 839w, 742m, 659m, 632w.

§ *Crystal data* for **1**: $C_{148}H_{216}N_{48}Cu_6O_{38}$, M = 3656.92, blue sheet, crystal dimensions 0.15 × 0.11 × 0.04 mm, monoclinic, $P2_1/c$, a = 13.662(2), b = 23.197(4), c = 18.914(4) Å, β = 110.074(3)°, U = 5630.1(17) Å^3, Z = 1, T = 294(2) K, R (wR) = 0.0920 (0.2710) for 9552 reflections with [$I > 2\sigma(I)$]. CCDC 156828. See http://www.rsc.org.suppdata/cc/b1/b100325i/ for crystallographic data in .cif or other electronic format.

1 P. J. Hagrman, D. Hagrman and J. Zubieta, *Angew. Chem., Int. Ed.*, 1999, **38**, 2638.
2 P. J. Langley and J. Hulliger, *Chem. Soc. Rev.*, 1999, **28**, 279.
3 G. B. Gardner, D. Venkataraman, J. S. Moore and S. Lee, *Nature*, 1995, **374**, 792.
4 G. B. Gardner, Y.-H. Kiang, S. Lee, A. Asgaonkar and D. Venkataraman, *J. Am. Chem. Soc.*, 1996, **118**, 6946.
5 S. R. Batten, B. F. Hoskins and R. Robson, *J. Am. Chem. Soc.*, 1995, **117**, 5385; B. F. Abrahams, S. R. Batten, H. Hamit, B. F. Hoskins and R. Robson, *Angew. Chem., Int. Ed. Engl.*, 1996, **35**, 1690.
6 B. F. Abrahams, S. R. Batten, M. J. Grannas, H. Hamit, B. F. Hoskins and R. Robson, *Angew. Chem., Int. Ed.*, 1999, **38**, 1475.
7 S. R. Batten, B. F. Hoskins, B. Moubaraki, K. S. Murray and R. Robson, *Chem. Commun.*, 2000, 1095.
8 H.-K. Liu, W.-Y. Sun, W.-X. Tang, T. Yamamoto and N. Ueyama, *Inorg. Chem.*, 1999, **38**, 6313.
9 H.-K. Liu, W.-Y. Sun, H.-L. Zhu, K.-B. Yu and W.-X. Tang, *Inorg. Chem. Acta*, 1999, **295**,129.
10 H.-K. Liu, W.-Y. Sun, D.-J. Ma, K.-B. Yu and W.-X. Tang, *Chem. Commun.*, 2000, 591.
11 PLATON Program, A. L. Spek, *Acta Crystallogr., Sect. A*, 1990, **46**, C34.

CHEMCOMM
Communication
www.rsc.org/chemcomm

Synthesis and structure of $[Sn_9(Ndmp)_7(HNdmp)_2O_2]$, containing a bidentate double-cubane oxo fragment (H_2Ndmp = 2-amino-4,6-dimethoxypyrimidine

Neil Feeder, Eilís A. Harron, Marta E. G. Mosquera, Anthony D. Woods and Dominic S. Wright*

Chemistry Department, University of Cambridge, Lensfield Road, Cambridge, UK CB2 1EW. E-mail: dsw1000@cus.cam.ac.uk

Received (in Cambridge, UK) 7th February 2001, Accepted 19th April 2001
First published as an Advance Article on the web 15th May 2001

The reaction of $Sn(NMe_2)_2$ with H_2Ndmp (H_2Ndmp = 2-amino-4,6-dimethoxypyrimidine) and H_2O (*ca.* 4:4:1 equivalents, respectively) gives the cage complex $[Sn_9(Ndmp)_7(HNdmp)_2O_2]$ 1, containing an oxo double-cubane fragment $[Sn_7(Ndmp)_6O_2]$ coordinated to a neutral $(HNdmpSn)_2(\mu\text{-}Ndmp)$ unit; 1 is the largest imido Sn(II) complex so far characterised.

The reactions of $Sn(NMe_2)_2$ with aliphatic primary amines (RNH_2) provide an efficient low-temperature route to imido Sn(II) cubanes of the type $[SnNR]_4$.[1] However, we showed recently that the analogous reactions of 2-amino-pyridines and 2-amino-pyrimidines produce mixed-oxidation state complexes of formulae $[Sn_7(NR)_8]$, in which two cubane units are fused *via* a central Sn(IV) atom into double-cubane structures.[2] By illustrating that larger oligomers can be obtained, depending on the nature of the organic substituents present, this discovery provides a new direction in the chemistry of imido Sn(II) compounds (which has previously been dominated by the simple imido cubanes[3–5]). Previous studies by Veith and Lange illustrated that the imido–oxo cubane $[Sn_4(NBu^t)_3O]$,[6] in which formal replacement of Bu^tN group in the cubane $[Sn(NBu^t)]_4$ by isoelectronic O^{2-} has occurred, can be used as an 'ether-like' ligand in the donor–acceptor adduct $[Sn_4(NBu^t)_3O{\cdot}AlMe_3]$.[7] Our interest in this ligand stems from the very high development of negative charge on the O centre, making it a highly effective, sterically demanding donor for high oxidation state metal ions.[8] We show here that the double-cubane framework $[Sn_7(NR)_8]$ provides access to a bidentate homologue of this ligand system, $[Sn_7(NR)_6O_2]$, present within the structure of the cage $[Sn_9(Ndmp)_7(HNdmp)_2O_2]$ (H_2Ndmp = 2-amino-4,6-dimethoxypyrimidine).

Complex **1** was originally obtained fortuitously from the 1:1 reaction of H_2Ndmp with $Sn(NMe_2)_2$ in toluene, in low (15%) yield. Subsequently, it was shown that the 1:1 reaction of rigorously dried H_2Ndmp with $Sn(NMe_2)_2$ gives the expected double-cubane $[Sn_7(Ndmp)_8]$.[2b] These observations suggest that the initial formation of **1** was due to water of crystallisation present in the H_2Ndmp. Complex **1** can be isolated using a variety of stoichiometric ratios of $H_2Ndmp:Sn(NMe_2)_2:H_2O$ (*ca.* 4:4:1, respectively[8]), the cleanest reaction being obtained using the apparently correct mixture of H_2Ndmp (9 equiv.) and H_2O (2 equiv.) with $Sn(NMe_2)_2$ (10 equiv.) (Scheme 1).† Like the formation of the double-cubanes $[Sn_7(NR)_8]$, the production of **1** formally involves disproportionation into Sn(0) and Sn(IV). However, there was no obvious indication of the presence of Sn metal here, so that the exact course of the reaction remains unclear at this stage. Although the ^{119}Sn NMR spectrum of **1** in DMSO at room temperature shows the presence of Sn(II) (a broad resonance at δ −284.8, width *ca.* 210 Hz) and Sn(IV) (at δ +75.4), the low solubility of the complex in other organic solvents (once isolated) precluded variable-temperature studies which may have resolved the two Sn(II) environments.

$$9\ H_2Ndmp + 10\ Sn(NMe_2)_2 \xrightarrow[-Sn(0)]{2H_2O} \underset{1}{[Sn_9(Ndmp)_7(HNdmp)_2O_2]} + 20\ Me_2NH$$

Scheme 1

The low-temperature crystallographic study of **1**‡ shows that it is the cage compound $[Sn_9(Ndmp)_7(HNdmp)_2O_2]$, consisting of a neutral $[Sn_7(Ndmp)_6O_2]$ oxo double-cubane fragment coordinated *via* both O centres to the Sn(II) centres of a $[\{Sn(HNdmp)\}_2(\mu\text{-}Ndmp)]$ fragment (Fig. 1). In addition, there

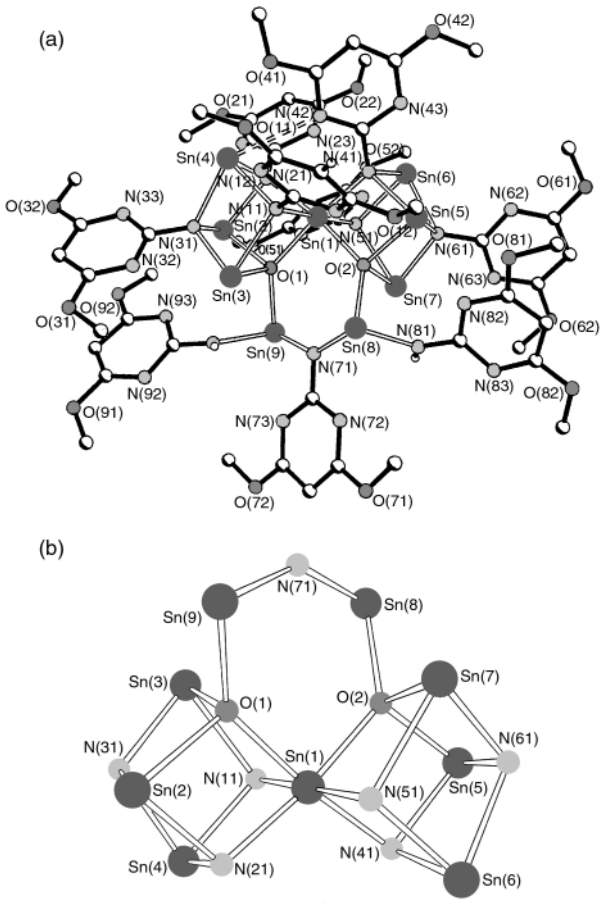

Fig. 1 (a) Molecular structure of **1**. H-atoms and the lattice-solvation by toluene molecules have been omitted for clarity. Selected bond lengths (Å) and angles (°): Sn(1)–O(1) 2.129(5), Sn(1)–O(2) 2.139(4), Sn(1)–N range 2.103(4)–2.139(6), Sn(2,3,5,7)–N range 2.162(6)–2.378(6), Sn(2,3,5,7)–O range 2.238(4)–2.268(4); O(1)–Sn(1)–O(2) 90.2(2), N–Sn(1)–O/N within cubanes range 81.6(2)–82.6(2) [between adjacent 97.3(2)–105.7(2), opposite 171.7(2)–179.3(2)], Sn–O(1,2)–Sn within cubanes 99.9(2)–103.1(2), Sn–N–Sn within cubanes range 96.5(2)–105.2(2), N–Sn–N within cubanes range 76.8(2)–81.8(2), O–Sn–N within cubanes 72.9(2)–76.8(2); Sn(8)–O(2) 2.186(4), Sn(8)–N(81) 2.227(6), Sn(8)–N(71) 2.142(6), Sn(9)–O(1) 2.185(5), Sn(9)–N(91) 2.141(6), Sn(9)–N(71) 2.131(6); Sn(1,2)–O(1,2)–Sn(8,9) mean 133.9, O(1,2)–Sn(8,9)–N(71) mean 88.3, Sn(8)–N(71)–Sn(9) 142.4(3), Sn(2,3,5,7)–O(1,2)–Sn(8,9) range 105.8(2)–110.6(2); (b) The $Sn_9N_7O_2$ 'handbag' core of **1**.

 DOI: 10.1039/b101247i

are three toluene molecules in the lattice. The coordination of the Sn(II) centres by the oxo double-cubane in **1** is similar to the behaviour of $[Sn_4(NBu^t)_3O]$ in its complexes with Al,[7] Li and Fe,[8] and of the $[(Me_3Si)(NBu^t)_2Sn_2O]$ fragment to $SnCl_2$ in $[(Me_3Si)(NBu^t)_2Sn_2O{\cdot}SnCl_2]$.[9] However, apart from $[Sn_4(NBu^t)_3O]$ no other oxo–imido Sn(II) complexes of this type have been structurally characterised. In addition, the structure of **1** (containing a total of nine Sn centres) is the largest Sn imido cage to be structurally characterised.

The Sn–O bond lengths to the central Sn(IV) atom [Sn(1)–O mean 2.13 Å] in **1** are similar to the Sn(IV)–N bonds [Sn(1)–N range 2.103(4)–2.139(6) Å] and to the Sn(II)–O bonds in $[Sn_4(NBu^t)_3O]$ and its metal complexes (*ca.* 2.10–2.17 Å).[9] The Sn(II)–O bonds in **1** are considerably longer than anticipated [Sn(2,3,5,7)–O range 2.238(4)–2.268(4) Å], and are within the range of values observed for the Sn(II)–N bonds [Sn(2,3,5,7)–N 2.162(6)–2.378(6) Å] in **1**. Thus, despite the substitution of two of the imido groups for O centres, the range of bond lengths and angles found in the $[Sn_7(Ndmp)_6O_2]$ oxo double-cubane unit of **1** is broadly similar to that observed in the structurally characterised double-cubanes $[Sn_7(NR)_8]$.[2] The internal Sn–O–Sn angles found in the $[Sn_7(Ndmp)_6O_2]$ unit of **1** [Sn–O(1,2)–Sn range 99.9(2)–103.1(2)°] are similar to those observed $[Sn_4(NBu^t)_3O]$ and its complexes *ca.* 102°].[7,8]

The most obvious difference between the $[Sn_7(NR)_8]$ double-cubanes and the oxo double-cubane core of **1** is found in the geometry of the central Sn(IV) atom. Coordination of the O centres to the [{Sn(HNdmp)}$_2$(μ-Ndmp)] fragment results in the compression of the O(1)–Sn(1)–O(2) angle [90.2(2)°] and in an associated expansion of the N(21)–Sn(1)–N(41) angle [105.7(2)°] [opposite to the Sn(IV)O_2 fragment]. This leads to a departure from the rigid C_2-symmetric geometry found in $[Sn_7(NR)_8]$ (with N–Sn–N angles between the $[Sn_4(NR)_4]$ cubane subunits of *ca.* 99°)[2] to a more irregular octahedral geometry for the central Sn(IV) atom in **1**. The association of the $[Sn_7(Ndmp)_6O_2]$ and [{Sn(HNdmp)}$_2$(μ-Ndmp)] units [O(1,2)–Sn(8,9) mean 2.186 Å] produces an envelope-shaped, six-membered SnO_2Sn_2N ring, in which the plane of the Sn(IV)O_2 unit is inclined to the plane of the Sn(9)N(71)Sn(8) fragment by 31.5°. Structurally characterised Sn(II) complexes containing two-coordinate imido groups are very rare[10–12] and the presence of a 'captured' [{Sn(HNdmp)}$_2$(μ-Ndmp)] unit in **1** is unprecedented in this area. The Sn–(μ-N) bond lengths in this unit [Sn(8)–N(71) 2.142(6), Sn(9)–N(71) 2.131(6) Å] are longer than the Sn–N bonds between the Sn(II) centres and two-coordinate imido-N centres in the closest analogue to **1**, the *nido*-cubane $[\{SnN(C_6H_3OMe\text{-}2\text{-}Me\text{-}6)\}_2Sn(NMe_2)_2]$ [2.106(2) and 2.120(2) Å] (consisting of a 'trapped' $[SnN(C_6H_3OMe\text{-}2\text{-}Me\text{-}6)]_2$ dimer unit coordinated by a $Sn(NMe_2)_2$ monomer).[12] The expansion of the Sn–(μ-N)–Sn angle in the [{Sn(HNdmp)}$_2$(μ-Ndmp)] fragment [142.4(3)°] above that in the $[SnN(C_6H_3OMe\text{-}2\text{-}Me\text{-}6)]_2$ dimer units of the latter [102.4(1)°] is presumably a consequence of the greater ring size in **1**.

In summary, we have illustrated that the double oxo cubane arrangment can be accessed by hydrolysis. This is the next homologue of the monodentate $[Sn_4(NR)_3O]$ ligand, and its synthesis provides a key first step in the expansion of the coordination chemistry of this class of ligands. However, still to be achieved is the synthesis of $[Sn_7(NR)_6O_2]$ in the absence of coordinated Sn(II) fragments, and the investigation of these species as bidentate ligands to a range of metals. The application of **1** as a source of $[Sn_7(Ndmp)_6O_2]$ is under investigation.

We gratefully acknowledge the EPSRC (N. F., E. A. H., A. D. W.) and the EU (Fellowship for M. E. G. M.), The Leverhulme Trust and the British Council (Socrates grant with the University of Oviedo, Spain) for financial support. We also thank Dr J. E. Davies for collecting the X-ray data for **1**.

Notes and references

† *Synthesis* of **1**: a mixture of 2-amino-4,6-dimethoxypyrimidine (0.70 g, 4.5 mmol) and H_2O (18 μdm^{-3}, 1.0 mmol) in toluene (10 ml) was added to a solution of $Sn(NMe_2)_2$[13] (1.04 g, 5.0 mmol) in toluene (20 ml) at −78 °C, and the reaction mixture stirred for 30 min. The mixture was allowed to warm to room temperature and stirred (12 h). A faint white precipitate was then filtered off. The solvent was reduced to *ca.* 10 ml and the light yellow powder formed was dissolved by the addition of further toluene (15 ml). Storage at room temperature gave **1** as a light yellow powder. Crystals can be grown by prolonged storage of dilute solutions at room temperature. Elemental analysis and ^{1}H NMR shows that *ca.* two of the three toluene molecules present in the lattice are removed by placing crystalline or powdered samples of **1** under vacuum (10^{-1} atm, 15 min) during isolation. Yield of powder 0.49 g (40%, based on H_2Ndmp consumed and one toluene in lattice); 215 °C melting with decomp. to brown semi-solid. IR (Nujol, NaCl), ν_{max}/cm^{-1} 3396s (N–H str.), 3303s (N–H str.), other bands at 1491m, 1459vs, 1420m, 1246w, 1214s, 1188s, 1160s, 1119s d, 1065s, 1003w, 935w, 795s. ^{1}H NMR (d_6-DMSO, +25 °C, 400.129 MHz), δ 6.55 (s, 9H, aryl rings), 5.31 (s, 2H, N–H), 3.72 (s, 27H, MeO) [toluene at 7.10 (m, Ph), 2.27 (s, Me), *ca.* one per molecule of **1**]. ^{119}Sn NMR (141.21 MHz, d_6-DMSO, +25 °C, rel. sat. $SnCl_2/D_2O$), δ 75.4 (s), −284.8 (br s). Found (typical of several analyses on different reactions) C 28.8, H 2.9, N 15.5; calc. for **1**·C_6H_5Me, C 28.5, H 2.9, N 14.7%.

‡ *Crystal data* for **1**: $C_{75}H_{89}N_{27}O_{20}Sn_9$, M = 2757.13, monoclinic, space group $P2_1/n$, Z = 4, a = 19.9326(3), b = 16.5364(3), c = 29.3746(4), β = 90.965(9) Å, V = 9680.9(3) Å^3, μ(Mo–Kα) = 2.359 mm^{-1}, T = 180(2) K. Data were collected on a Nonius Kappa CCD diffractometer. Of a total of 53297 reflections collected, 21689 were independent (R_{int} = 0.060). The structure was solved by direct methods and refined by full-matrix least squares on F^2 [with isotropic temperature factors for the light (C,H,O) atoms].[14] Final $R1$ = 0.057 [$I > 2\sigma(I)$] and $wR2$ = 0.159 (all data).

CCDC 159623. See http://www.rsc.org/suppdata/cc/b1/b101247i/ for crystallographic data in .cif or other electronic format.

1 M. A. Beswick, R. E. Allen, M. A. Paver, P. R. Raithby, M.-A. Rennie and D. S. Wright, *J. Chem. Soc., Dalton Trans.*, 1995, 1991.
2 (*a*) F. Benevelli, E. M. Doyle, E. A. Harron, N. Feeder, E. A. Quadrelli, D. Sáez and D. S. Wright, *Angew. Chem.*, 2000, **112**, 1559; F. Benevelli, E. M. Doyle, E. A. Harron, N. Feeder, E. A. Quadrelli, D. Sáez and D. S. Wright, *Angew. Chem., Int. Ed.*, 2000, **39**, 1501; (*b*) F. Benevelli, E. M. Doyle, E. A. Harron, N. Feeder, M. E. G. Mosquera, E. A. Quadrelli, D. Sáez and D. S. Wright, unpublished work.
3 M. Veith and M. Grosser, *Z. Naturforsch., Teil B*, 1982, **37**, 1375; M. Veith and O. Recktenwald, *Z. Naturforsch., Teil B*, 1983, **38**, 1054; M. Veith and G. Schlemmer, *Chem. Ber.*, 1982, **115**, 2141.
4 W. J. Grigsby, T. Hascall, J. J. Ellison, M. M. Olmstead and P. P. Power, *Inorg. Chem.*, 1996, **35**, 3254.
5 H. Chen, R. A. Barlett, H. V. R. Dias, M. M. Olmstead and P. P. Power, *Inorg. Chem.*, 1991, **30**, 3390.
6 M. Veith and W. Frank, *Angew. Chem.*, 1984, **96**, 163; M. Veith and W. Frank, *Angew. Chem., Int. Ed. Engl.*, 1984, **23**, 158; M. Veith and O. Recktenwald, *Z. Naturforsch., Teil B*, 1981, **36**, 944.
7 M. Veith and H. Lange, *Angew. Chem.*, 1980, **92**, 408; M. Veith and H. Lange, *Angew. Chem., Int. Ed. Engl.*, 1980, **19**, 401.
8 This stoichiometry is the same as that used in the preparation of $[Sn_4(NBu^t)_3O]$ from Bu^tNH_2, $Sn(NMe_2)_2$ and H_2O; C. Brown, M. E. G. Mosquera, J. S. Palmer, P. R. Raithby, A. Steiner and D. S. Wright, *J. Chem. Soc., Dalton Trans.*, 2000, 479.
9 M. Veith, *Chem. Ber.*, 1978, **111**, 2536.
10 M. A. Beswick, R. E. Allan, M. A. Paver, P. R. Raithby, A. E. H. Wheatley and D. S. Wright, *Inorg. Chem.*, 1997, **36**, 5202.
11 M. Veith, *Z. Naturforsch., Teil B*, 1980, **35**, 20.
12 A. Bashall, N. Feeder, E. A. Harron, M. McPartlin, M. E. G. Mosquera and D. S. Wright, *J. Chem. Soc., Dalton Trans.*, 2000, 4104.
13 M. M. Olmstead and P. P. Power, *Inorg. Chem.*, 1984, **23**, 413.
14 SHELXTL PC version 5.03, Siemens Analytical Instruments, Madison, WI, 1994.

CHEMCOMM
Communication
www.rsc.org/chemcomm

First observation of a ferromagnetic interaction through an end-to-end azido bridging pathway in a 1D copper(II) system

Tapas Kumar Maji,[a] Partha Sarathi Mukherjee,[a] Golam Mostafa,[b] Talal Mallah,*[c] Joan Cano-Boquera[c] and Nirmalendu Ray Chaudhuri*[a]

[a] *Department of Inorganic Chemistry, Indian Association for the Cultivation of Science, Calcutta–700 032, India. E-mail: icnrc@mahendra.iacs.res.in*
[b] *Department of Physics, Krishnath College, Berhampur–742109, India*
[c] *Laboratoire de Chimie Inorganique, UMR CNRS 8613, Université Paris-Sud, 91405-Orsay, France*

Received (in Cambridge, UK) 15th January 2001, Accepted 5th April 2001
First published as an Advance Article on the web 15th May 2001

A novel one-dimensional copper(II) compound $[Cu(L)(\mu_{1,3}\text{-}N_3)(ClO_4)]_n$ [L = tridentate Schiff base, formed by condensation of pyridine-2-aldehyde and 1-(2-aminoethyl)-piperidine] has been synthesized and structurally characterized; it exhibits ferromagnetic interaction *via* end-to-end azido ($\mu_{1,3}$-N_3) linkages, as rationalised by DFT calculation.

The investigation of magnetic properties of molecule-based magnetic materials (1D, 2D and 3D) has become a fascinating subject in the fields of condensed matter physics, material chemistry as well as inorganic chemistry.[1] Considerable efforts have been directed in preparing and characterizing molecular systems which can exhibit ferromagnetic properties.[2] Bridging ligands play a central role since they transmit the electronic information between the paramagnetic centres; among these the azido ligand has been proved to be efficient. The versatility of the azido ligand lies in its diverse bridging modes that lead to binuclear,[3a] tetranuclear,[3b] cubane-like,[3c] 1D,[3d] 2D[3e] and 3D[3f] compounds. In general, the coordination modes observed for the bridging azido group are end-to-end (μ-1,3) with antiferromagnetic interaction[4] and end-on (μ-1,1) with ferromagnetic interaction.[3a] However, in copper(II) systems where the azido ligand adopts the end-on mode, antiferromagnetic interaction is observed when the bridging M–N–M angle is $> 108°$.[3d] Ribas and coworkers showed, on the basis of theoretical calculations, that there is also a possibility of ferromagnetic interaction between paramagnetic centres when the azido ligand binds in μ-1,3 fashion.[5] Only one compound based on nickel(II) and displaying the end-to-end azido bridging mode exhibiting a ferromagnetic interaction is reported in the literature.[6] To the best of our knowledge, such a magnetic behaviour in 1D copper(II) systems has not been reported to date. Here we report the synthesis and crystal structure of a new one-dimensional (1D) compound, $[Cu(L)(\mu_{1,3}\text{-}N_3)(ClO_4)]_n$ **1**† and the first observation of ferromagnetic interaction through end-to-end azido bridges in copper(II) systems.

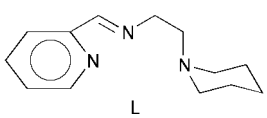

The IR spectrum of **1** shows two very strong bands assigned to the asymmetric stretching vibrations of N_3 [$\nu_{as}(N_3)$] centred at 2073 and 2050 cm^{-1} and the stretching vibrations of C=N bond of Schiff base [ν(C=N)] at 1603 cm^{-1}.

The structure determination‡ reveals that the copper atoms are bridged by azido units in an end-to-end fashion with the occurrence of a 1D polymeric infinite chain along the *a*-axis. A ZORTEP view of the asymmetric unit with the symmetry related fragment is shown in Fig. 1. In the chain each copper atom occupies a pseudo octahedral environment with a CuN_5O chromophore. The three nitrogen atoms (N1, N2 and N3) from the tridentate Schiff base ligand and N4 from the bridging azido ligand form the equatorial plane around Cu1 atom. One nitrogen atom (N6*) from another bridging azido ligand and oxygen atom (O4) of the perchlorate anion are in *trans* axial position around Cu1. The equatorial Cu–N bond distances are in the range [1.936(7)–2.080(6) Å]. The deviation of Cu1 from the mean plane formed by the four equatorial nitrogen atoms is *ca.* 0.076(3) Å while the maximum deviation of any equatorial atom (N2) from the mean plane is 0.032(3) Å. The equatorial least squares planes of the two copper atoms are not parallel and form a dihedral angle of 29.4(7)°. For two adjacent copper(II) atoms within the chain (Cu1 and Cu1*), one nitrogen (N4) of the bridging azido is linked to the equatorial base of Cu1 whereas the other nitrogen (N6) of the same azido is linked in an axial fashion to Cu1*. The torsion angle Cu1–N4–N5–N6–Cu1* is 91.6(8)° while the shortest Cu···Cu separation is 5.773(2) Å within the one-dimensional chain and 8.117(3) Å between two adjacent chains.

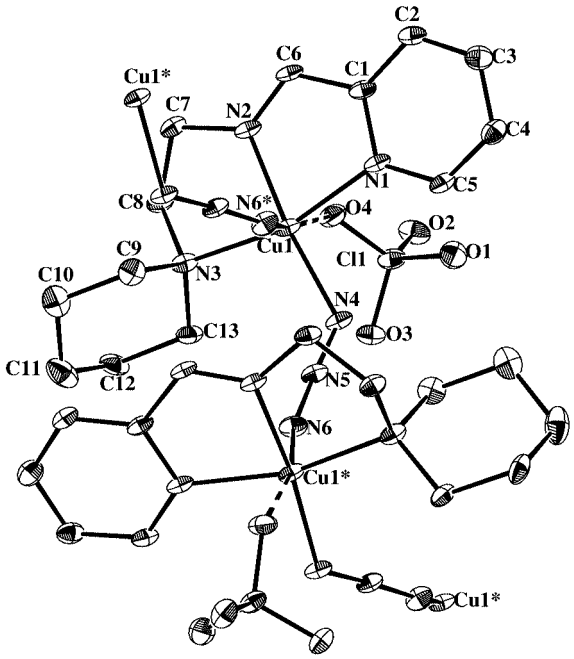

Fig. 1 ZORTEP plot with labelled scheme of $[Cu(L)(\mu_{1,3}\text{-}N_3)(ClO_4)]_n$ **1** (thermal ellipsoids are drawn at 50% probablity). Selected bond lengths (Å) and angles (°): Cu1–N1 2.046(6), Cu1–N2 1.948(6), Cu1–N3 2.080(6), Cu1–N4 1.936(7), Cu1–N6* 2.486(7), Cu1–O4 2.691(7), N4–Cu1-–N6*, 88.0(3), N1–Cu1–N4 94.6(3), N1–Cu1–N3 163.2(2), N1–Cu1–N2 80.1(2), Cu1–N4–N5 125.6(5), N4–N5–N6 177.1(8).

Magnetic studies were performed using a SQUID magnetometer on a crystalline sample in the temperature range 300–2 K in an applied field of 1 kOe. The $\chi_M T = f(T)$ plot (Fig. 2) indicates the occurrence of a ferromagnetic interaction between the Cu(II)

 DOI: 10.1039/b100529o

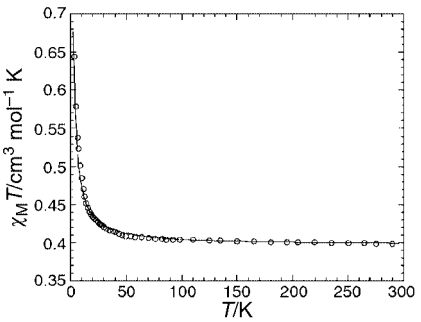

Fig. 2 $\chi_M T$ *vs.* T plot for **1**. The solid line corresponds to the best fit.

ions *via* the end-to-end azido bridge. A fit of the experimental data [where the susceptibility was corrected for TIP (55×10^{-6} cm^3 mol^{-1} per Cu)] was performed using a high-temperature series expansion of the susceptibility;[1a,7] this led to the following parameters: $J = +1.36$ cm^{-1} and $g = 2.06$ with an agreement factor R (defined as $\Sigma[(\chi_M T)_{calc} - (\chi_M T)_{obs}]^2/\Sigma[(\chi_M T)_{obs}]^2$) equal to 10^{-4}. No interchain interaction was included in the fit procedure.

It has already been shown that the different orientations of the equatorial planes (*i.e.* the relative orientations of the $x^2 - y^2$ singly occupied orbitals) of two adjacent Cu atoms are at the origin of the nature and the strength of the magnetic interaction.[8] In order to rationalize the origin of the ferromagnetic interaction, we carried out two types of calculations using the DFT method.[9,12] § The calculation of the exchange parameter within a binuclear unit of the infinite chain leads to a positive J value of +1.6 cm^{-1} indicating that a weak ferromagnetic exchange interaction should be present as observed experimentally. The second calculation was carried out on a mononuclear fragment in order to visualize the magnetic orbital and to try to give a qualitative interpretation of the observed ferromagnetic interaction.[13] It has been found that the magnetic orbital has a contribution from the azido π orbital for the azido nitrogen atom located in the equatorial plane of copper Fig. 3(a)] while a very weak contribution from the σ-like orbital of the azido bridge is found for the nitrogen occupying the axial position as schematized in Fig 3(b). The origin of the ferromagnetic exchange interaction can thus be rationalized as due to the quasi-orthogonality of the magnetic orbitals of the two mononuclear fragments. It is worth noting that the presence of a contribution from the σ orbital of the azido bridge is due to the fact that for a Cu–$\mu_{1,3}$-N3–Cu torsion angle of 91.6(8)° (close to 90°) the Cu–N6–N5 angle [135.7(5)°] is rather large [Fig. 3(b)]. A zero delocalisation should theoretically be observed for a Cu–N6–N5 angle of 90° while it should be maximal for 180°. On the other hand, the fact that the Cu–N4–N5 angle [125.6(5)°] is closer to 90 than to 180° results in a rather large delocalisation of the metal electron density towards the π orbital of the azido bridge. The very weak coupling parameter is mainly due to the unusual axial–equatorial bridging mode of the azido ligand. The consequence is a good π-type delocalisation of the Cu1 electron density towards the bridging azido ligand nitrogen atoms N(4) and N(6), while the apical position of N(6) and the long Cu–N(6) distance results in a rather poor σ-type delocalisation from Cu1*. The overlap density which is mainly localized on N(6) is thus very small leading to a weak exchange coupling parameter.

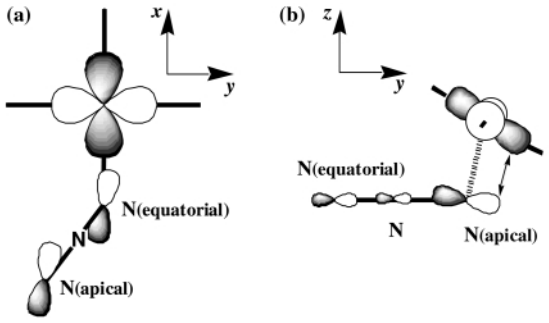

Fig. 3 The magnetic orbital of the copper fragment interacting with (a) the azido nitrogen in the equatorial plane and (b) the azido nitrogen in apical position.

We wish to thank Council of Scientific and Industrial Research, New Delhi for financial support (granted to N. R. C).

Notes and references

† **CAUTION**: perchlorate as well as azide salts should be used in small quantities and handled with care since explosion may occur.

A methanolic solution (5 cm^3) of 1-(2-aminoethyl)piperidine (1 mmol, 0.128 g) was added to a methanolic solution (20 cm^3) of pyridine-2-aldehyde (1 mmol, 0.106 g). The reaction mixture was refluxed for 1 h and evaporated on a water bath until the volume reduced to *ca.* 5 ml to obtain a viscous liquid which was added to the methanolic solution (10 cm^3) of $Cu(ClO_4)_2 \cdot 6H_2O$ (1 mmol, 0.370 g). The resulting reaction mixture was refluxed for 15 min. To it NaN_3 (1 mmol, 0.065 g) dissolved in methanol (5 cm^3) was added and the resulting deep green solution was stirred for 1 h. This was then filtered and the filtrate kept in the open atmosphere. After a few days deep green shiny single crystals suitable for X-ray diffraction were obtained. (Yield 80%). Anal. Found (calc.): C, 36.89 (36.96); H, 4.50 (4.50); N, 19.89 (19.90); Cu, 15.00 (15.05)%.

‡ *Crystal data*: $C_{13}H_{19}ClCuN_6O_4$, M_w = 422.34, monoclinic, space group $P2_1/n$ (no. 14), a = 20.685(4), b = 7.337(2), c = 11.692(2) Å, β = 95.730(10), V = 1765.6(7) Å^3, Z = 4, D_c = 1.589 g cm^{-3}, $F(000)$ = 868, λ(Mo-Kα) = 0.710 70 Å, μ(Mo-Kα) = 1.420 mm^{-1}, crystal size = 0.10 × 0.20 × 0.43 mm, T = 296 K, θ_{max} = 27.5°, total data = 4566, unique data = 4052 (R_{int} 0.028), observed data [$I > 2\sigma(I)$] = 1984, R = 0.0601, wR = 0.0676, S = 1.21. CCDC 156831. See http://www.rsc.org/suppdata/cc/b1/b100529o/ for crystallographic data in .cif or other electronic format.

§ The methodology used to evaluate the coupling exchange constants is described in refs. 9 and 10. Calculations were carried out using the hybrid B3LYP (ref. 11) method as implemented in GAUSSIAN98, with the all-electron double-basis proposed by Ahlrichs, except for the metal atom, where we have used a triple-basis (ref. 12).

1 (*a*) O. Kahn, *Molecular Magnetism*, VCH, Weinheim, 1993; (*b*) D. Gatteschi, O. Kahn, J. S. Miller and F. Palacio, *Magnetic Molecular Materials*, NATO ASI, Kluwer, Dordrecht, 1991.
2 J. Ribas, M. Monfort, C. Diaz, C. Bastos and X. Solans, *Inorg. Chem.*, 1994, **33**, 484; A. Escuer, M. A. S. Goher, F. A. Mautner and R. Vicente, *Inorg. Chem.*, 2000, **39**, 2107.
3 (*a*) S. S. Tandon, L. K. Thompson, M. E. Manuel and J. N. Bridson, *Inorg. Chem.*, 1994, **33**, 5555; (*b*) J. Ribas, M. Monfort, R. Costa and X. Solans, *Inorg. Chem.*, 1993, **32**, 695; (*c*) M. A. Halcrow, J. C. Huffman and G. Christou, *Angew. Chem., Int. Ed. Engl.*, 1995, **35**, 971; (*d*) P. S. Mukherjee, T. K. Maji, G. Mostafa, T. Mallah and N. Ray Chaudhuri, *Inorg. Chem.*, 2000, **39**, 5147; (*e*) M. Monfort, I. Resino, J. Ribas and H. Stoeckli-Evans, *Angew. Chem., Int. Ed.*, 2000, **39**, 191; (*f*) F. A. Mautner, R. Cortes, L. Lezema and T. Roso, *Angew. Chem., Int. Ed. Engl.*, 1996, **35**, 96.
4 J. Ribas, M. Monfort, C. Diaz, C. Bastos, C. Mer and X. Solans, *Inorg. Chem.*, 1995, **34**, 4986.
5 A. Escuer, R. Vicente, J. Ribas, M. S. El Fallah, X. Solans and M. Font-Bardia, *Inorg. Chem.*, 1994, **33**, 1842; J. Ribas, M. Monfort, B. K. Ghosh, R. Cortes, X. Solans and M. Font-Bardia, *Inorg. Chem.*, 1996, **35**, 864.
6 C. S. Hong and Y. Do, *Angew. Chem., Int. Ed.*, 1999, **38**, 193.
7 G. A. Baker, Jr, G. S. Rushbrooke and H. E. Gilbert, *Phys. Rev. A*, 1964, **135**, 1272.
8 M. Julve, M. Verdaguer, A. Gleizes, M. Philoche-Vesailles and O. Kahn, *Inorg. Chem.*, 1984, **23**, 3808; J. Cano, P. Alemany, S. Alvarez, M. Verdaguer and E. Ruiz, *Chem. Eur. J.*, 1998, **4**, 476; F. Fabrizi de Biani, E. Ruiz, J. Cano, J. J. Novoa and S. Alvarez, *Inorg. Chem.*, 2000, **39**, 3221, and references therein.
9 E. Ruiz, P. Alemany, S. Alvarez and J. Cano, *J. Am. Chem. Soc.*, 1997, **119**, 1297.
10 E. Ruiz, J. Cano, S. Alvarez and P. Alemany, *J. Comput. Chem.*, 1999, **20**, 1391.
11 A. D. Becke, *J. Chem. Phys.*, 1993, **98**, 5648.
12 A. Schaefer, H. Horn and R. Ahlrichs, *J. Chem. Phys.*, 1992, **97**, 2571; A. Schaefer, C. Huber and R. Ahlrichs, *J. Chem. Phys.*, 1994, **100**, 5829.
13 O. Kahn, *Molecular Magnetism*, VCH, New York, 1993, p. 145.

CHEMCOMM Communication
www.rsc.org/chemcomm

First selenium-capped carbonyltrichromium complex $[Se_2Cr_3(CO)_{10}]^{2-}$: a novel Cr_3 ring cluster

Minghuey Shieh,*[a] Li-Fang Ho,[a] Li-Fing Jang,[a] Chuen-Her Ueng,[a] Shie-Ming Peng[b] and Yi-Huang Liu[b]

[a] *Department of Chemistry, National Taiwan Normal University, Taipei 116, Taiwan, Republic of China. E-mail: mshieh@scc.ntnu.edu.tw*
[b] *Department of Chemistry, National Taiwan University, Taipei 107, Taiwan, Republic of China*

Received (in Cambridge, UK) 8th February 2001, Accepted 24th April 2001
First published as an Advance Article on the web 15th May 2001

$[Se_2Cr_3(CO)_{10}]^{2-}$, the first selenium-capped trichromium carbonyl cluster, has been prepared and its reaction with $Mo(CO)_6$ studied.

Although numerous carbonylchromium complexes have been reported, they have little tendency to form clusters with Cr–Cr bonds.[1] Up to now, only three homometallic chromium carbonyl clusters with a Cr_3 ring have been structurally characterized.[2–6] The rare Cr–Cr bonds in these clusters are made possible with the stabilizing ligands such as μ_3-S,[4,6] μ_3-PR,[5] and diphosphene,[6] and importantly, with the aid of the existence of the bridging carbonyls in each case.[4–6] Nevertheless, no fully characterized carbonylchromium cluster with Cr–Cr bonds stabilized with heavier main group elements has been known.[7,8] We have prepared the first example of the selenium-capping trichromium carbonyl cluster complex $[Et_4N]_2[Se_2Cr_3(CO)_{10}]$ **1**, in which three Cr–Cr bonds are present and all the carbonyls are terminally coordinated.

Numerous attempts to gain entry to the Se–Cr–CO system using SeO_2 with $Cr(CO)_6$ in basic KOH–MeOH solutions were not successful. However, it was found that use of the highly concentrated NaOH–MeOH solutions followed by cation metathesis with $[Et_4N]Br$ resulted in **1**. Note that the isolation of **1** succeeds only in the NaOH–MeOH solutions but not in the KOH–MeOH solutions due to alkali metal cation effects on the stabilization of the cluster anion. The Mo-substituted dichromium cluster complex $[Et_4N]_2[Se_2Cr_2Mo(CO)_{10}]$ **2** was obtained by treatment of the parent compound **1** with $[Mo(CO)_6]$ in acetone.† The anionic clusters of **1** and **2** represent rare examples of carbonylchromium clusters which possess three and one chromium–chromium bonds, respectively.

The anion of cluster **1** exhibits a trigonal bipyramidal structure with the Cr_3 ring capped above and below by μ_3-Se atoms, in which the Se atom donates four electrons to the Cr_3 ring making it a 48e$^-$ species, in accord with three chromium atoms with three Cr–Cr bonds. The anion possesses two mirror planes: one passing through the Cr_3 ring and the other one lying in the $Cr(1)Se_2$ plane (Fig. 1).‡ The Cr–Cr distances of 2.849(2) and 2.926(3) Å are somewhat longer than predicted from the covalent radius of Cr (1.28 Å).[9] However, they are comparable to Cr–Cr bonds found for $[SCr_3(CO)_{12}\{Cr(CO)_5\}]^{2-}$ (average 2.850 Å),[4] $[(Bu^tP)Cr_3(CO)_{10}(Bu^tPPBu^t)]$ (2.814–2.851 Å),[5] $[SCr_3(CO)_{12}]^{2-}$ (average 2.828 Å),[6] and $[Cr_6Se_8(PEt_3)_6]$ (average 2.81 Å),[10] and are slightly shorter than that in $[\{TeCr(CO)_5\}_2Cr_2(CO)_8]^{2-}$ (3.052 Å).[11] The fairly long Cr–Cr bonds reflect their weakness and may account for the rarity of carbonylchromium clusters. Unlike the previously reported carbonyltrichromium clusters,[4–6] the anion of **1** possesses only terminal carbonyls, with two Cr atoms coordinated with three carbonyls and the unique Cr(1) attached to four carbonyls. Of interest is that the four Cr(1)–C distances [1.832(9)–1.917(9) Å] are somewhat greater than those for Cr(2) [1.816(9)–1.855(7) Å], indicative of weaker Cr–C bonding for the Cr(1) atom with four coordinated carbonyls. The same effect is also observed in the larger Se–Cr(1) distance [2.575(2) Å] compared with the Se–Cr(2) distance [2.387(1) Å].

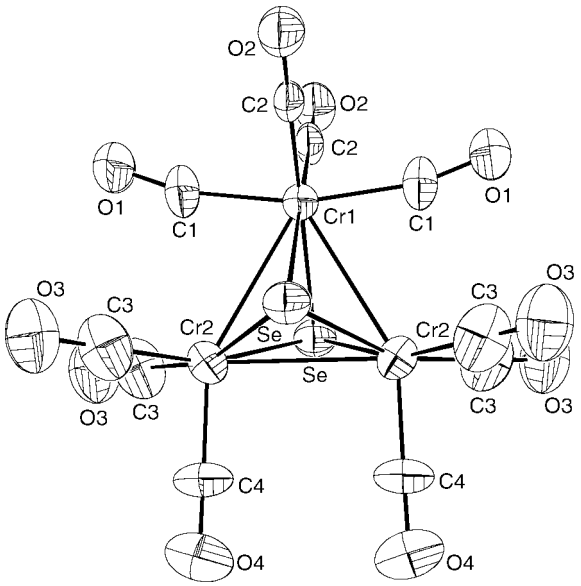

Fig. 1 Crystal structure of the dianion of **1** showing 30% thermal ellipsoids and the atom labelling scheme. Important bond lengths (Å) and angles (°): Se–Cr(1) 2.575(2), Se–Cr(2) 2.387(1), Cr(1)–Cr(2) 2.849(2), Cr(2)–Cr(2a) 2.926(3), Cr(1)–C(1) 1.917(9), Cr(1)–C(2) 1.832(9), Cr(2)–C(3) 1.855(7), Cr(2)–C(4) 1.816(9); Cr(2)–Cr(1)–Cr(2a) 61.81(7), Cr(1)–Cr(2)–Cr(2a) 59.09(3).

Employing a similar methodology to the Se–Mo–CO system failed, and we therefore treated **1** with $[Mo(CO)_6]$ in acetone to see if any carbonylchromium fragment can be replaced by an incoming molybdenum moiety. This was found to be so; the $Cr(CO)_4$ fragment in **1** can be exchanged by $Mo(CO)_4$ to form the mixed-group 6 metal complex **2**, $[Et_4N]_2[Se_2Cr_2Mo(CO)_{10}]$. X-Ray analysis shows that the anion of **2** is structurally similar to that of **1**, with the Cr(1) atom replaced by the Mo(1) atom (Fig. 2).‡ The formulation of **2** was further substantiated by ICP metal analysis. While the Cr–Cr bond of 2.947(2) Å is still long and similar to the Cr–Mo distances (average 2.9512 Å), the average Se–Cr length (2.4157 Å) is significantly shorter than that of the Se–Mo distances (2.6744 Å).

In summary, the first synthesis of a trichromiumcarbonyl cluster anion by the stabilization of the μ_3-Se atoms has been achieved. The ease of replacing one Cr moiety of **1** with the Mo fragment suggests the possibility in making other mixed-metal carbonylchromium clusters which may help elucidate the bonding characteristics of the Cr–Cr and Cr–M bonds. Further investigation is under way.

A research grant (NSC 89-2113-M-003-031 to M. Shieh) from National Science Council of Taiwan is gratefully appreciated.

 DOI: 10.1039/b101283p

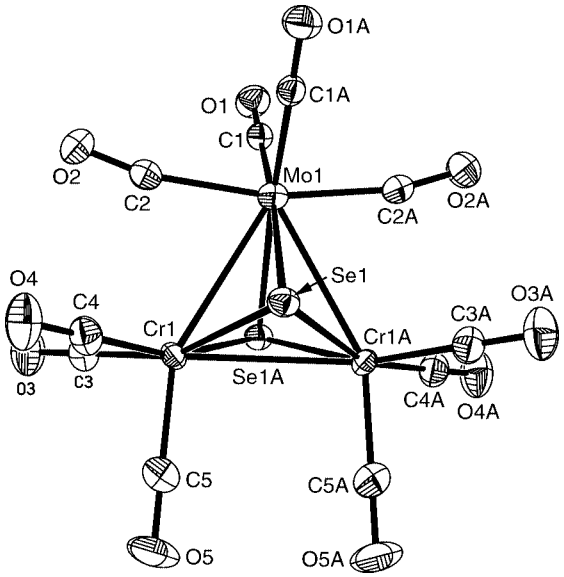

Fig. 2 Crystal structure of the anion of **2** showing 30% thermal ellipsoids and the atom labelling scheme. Important bond lengths (Å) and angles (°): Se(1)–Cr(1A) 2.4123(9), Se(1)–Cr(1) 2.4190(9), Se(1)–Mo(1) 2.6745(7), Se(1A)–Mo(1) 2.6743(7), Mo(1)–Cr(1) 2.9511(9), Mo(1)–Cr(1A) 2.9513(9), Cr(1)–Cr(1A) 2.947(2), Cr(1)–C(3) 1.845(6), Cr(1)–C(4) 1.850(5), Cr(1)–C(5) 1.815(7); Cr(1)–Mo(1)–Cr(1A) 59.92(3), Cr(1A)–Cr(1)–Mo(1) 60.04(2).

Notes and references

† *Synthetic procedure:* All experiemnts were performed under N_2 atomsphere. A mixed solution of MeOH (30 mL) and hexanes (7.5 mL) was added to a mixture of SeO_2 (0.21 g, 1.89 mmol) and $[Cr(CO)_6]$ (0.8 g, 3.64 mmol), and NaOH (3.0 g, 82.5 mmol). The mixed solution was heated to reflux in an oil-bath at 70 °C for 12 h to give a dark-red solution which was filtered and concentrated, and a MeOH solution of $[Et_4N]Br$ (3.0 g, 14.3 mmol) was added dropwise, precipitating the solid. The solid was washed several times with MeOH and CH_2Cl_2. The residue was recrystallized from diethyl ether–MeCN several times to give purplish-red **1** (0.42 g, 0.49 mmol) (52% based on Se). IR (ν_{CO}, MeCN): 1990w, 1914s, 1869m cm^{-1}. Anal. Found for **1**: C, 36.55; H, 4.67; N, 3.31%. Calc.: C, 36.55; H, 4.72; N, 3.28. Compound **1** is soluble in MeCN and acetone, but insoluble in other organic solvents. Crystals suitable for X-ray analysis were grown from CH_2Cl_2–MeCN solution.

Acetone (25 mL) was added to a mixture of **1** (0.23 g, 0.269 mmol) and $[Mo(CO)_6]$ (0.10 g, 0.379 mmol). The mixed solution was stirred at room temperature for 11 days and the color changed from dark-red to brown. The resultant solution was filtered and solvent was removed under vacuum. The residue was washed with CH_2Cl_2, extracted with MeCN, and then recrystallized with CH_2Cl_2–MeCN several times to give purplish-red **2** (0.16 g, 0.178 mmol) (66% based on **1**). IR (ν_{CO}, MeCN): 2068w, 2002m, 1916vs, 1868s, 1827m cm^{-1}. Anal. Found for **2**: C, 35.22; H, 4.56; N, 3.14; Cr, 11.20; Mo, 9.09. Calc.: C, 34.76; H, 4.49; N, 3.12; Cr, 11.57; Mo, 10.68%. Complex **2** is soluble in MeCN and acetone. Crystals suitable for X-ray analysis were grown from diethyl ether–MeCN solution.

‡ *Crystal structure data*: for **1**: $C_{26}H_{40}Cr_3N_2O_{10}Se_2$: M = 854.51, orthorhombic, space group *Cmcm*, Z = 4, a = 8.607(3), b = 24.591(8), c = 15.941(4) Å, V = 3374.0(18) $Å^3$, D_c = 1.682 g cm^{-3}, λ(Mo-Kα = 0.70930 Å, μ = 3.16 mm^{-1}. A total of 1656 unique reflections were collected on a Nonius (CAD-4) diffractometer at 298 K in the 2θ range 2.0–50° using θ–2θ scans, and an absorption correction by azimuthal (ψ) scans was applied. The structure was solved by direct methods and refined both with NRCC-SDP-VAX and SHELXL-97 packages. Both refinements gave the similar results; however, the latter gave the lower R values and smaller esds on distances and angles. Therefore, the results of the SHELXL-97 refinement were used here. The $[Et_4N]^+$ cations are disordered and the H atoms were placed in calculated positions and refined with a riding model. All the other non-hydrogen atoms were refined with anisotropic temperature factors. Full-matrix least squares on F^2 converged to R = 0.1123 (all data), 0.0406 [$I > 2\sigma(I)$]; wR = 0.1142 (all data), 0.1037 [$I > 2\sigma(I)$].

For **2**: $C_{26}H_{40}Cr_2MoN_2O_{10}Se_2$: M = 898.46, orthorhombic, space group *Pnna*, Z = 4, a = 24.8153(3), b = 16.0695(3), c = 8.6204(2) Å, V = 3437.55(11) $Å^3$, D_c = 1.736 g cm^{-3}, λ(Mo-Kα) = 0.71073 Å; CCD SMART diffractometer, and SADABS absorption correction (T_{min} = 0.569, T_{max} = 0.634). A total of 22975 reflections were measured, and 3957 unique reflections ($2\theta < 55°$, R_{int} = 0.0406) were used in the refinement. All the non-hydrogen atoms were refined with anisotropic temperature factors. Full-matrix least squares refinement on F^2 converged to R = 0.0774 (all data), 0.0495 [$I > 2\sigma(I)$]; wR = 0.1697 (all data), 0.1442 [$I > 2\sigma(I)$]. All calculations were performed using SHELXTL packages.

CCDC 159098 and 159099. See http://www.rsc.org/suppdata/cc/b1/b101283p/ for crystallographic data in .cif or other electronic format.

1 F. A. Cotton, G. Wilkinson, C. A. Murillo and M. Bochmann, *Advanced Inorganic Chemistry*, John Wiley & Sons, Inc, Singapore, 6th edn., 1999; D. F. Shriver, H. D. Kaesz and R. D. Adams, *The Chemistry of Metal Cluster Complexes*, VCH, New York, 1990.
2 H. Behrens and W. Haag, *Chem. Ber.*, 1961, **94**, 320.
3 D. J. Darensbourg and D. J. Zalewski, *Organometallics*, 1984, **3**, 1598.
4 M. Hoefler, K.-F. Tebbe, H. Veit and N. E. Weiler, *J. Am. Chem. Soc.*, 1983, **105**, 6338.
5 J. Borm, G. Huttner and L. Zsolnai, *Angew. Chem., Int. Ed. Engl.*, 1985, **24**, 1069.
6 D. J. Darensbourg, D. J. Zalewski, K. M. Sanchez and T. Delord, *Inorg. Chem.*, 1988, **27**, 821.
7 For reviews: W. A. Herrmann, *Angew. Chem., Int. Ed. Engl.*, 1986, **25**, 56; N. A. Compton, R. J. Errington and N. C. Norman, *Adv. Organomet. Chem.*, 1990, **100**, 223; D. Fenske, J. Ohmer, J. Hachgenei and K. Merzweiler, *Angew. Chem., Int. Ed. Engl.*, 1988, **27**, 1277; L. C. Roof and J. W. Kolis, *Chem. Rev.*, 1993, **93**, 1037; K. H. Whitmire, *J. Coord. Chem.*, 1988, **17**, 95; L. Y. Goh, *Coord. Chem. Rev.*, 1999, **185**–**186**, 257.
8 Some E–Cr–CO (E = main group element) complexes with open structures have been published. For recent references: P. Rutsch and G. Huttner, *Angew. Chem., Int. Ed.*, 2000, **39**, 2118; J. J. Cherng, G.-H. Lee, S.-M. Peng, C.-H. Ueng and M. Shieh, *Organometallics*, 2000, **19**, 213.
9 A. F. Wells, *Structural Inorganic Chemistry*, Clarendon, Oxford, 5th edn., 1984; L. Pauling, *The Nature of the Chemical Bond*, Cornell University Press, Ithaca, NY, 3rd edn., 1960.
10 S. Kamiguchi, H. Imoto, T. Saito and T. Chihara, *Inorg. Chem.*, 1998, **37**, 6852.
11 L. C. Roof, W. T. Pennington and J. W. Kolis, *Inorg. Chem.*, 1992, **31**, 2056.

CHEMCOMM Communication
www.rsc.org/chemcomm

Super-microporous aluminosilicate catalysts *via* primary amine templating

E. Bastardo-Gonzalez,[a] Robert Mokaya*[b] and William Jones*[a]

[a] *Department of Chemistry, University of Cambridge, Lensfield Road, Cambridge, UK CB2 1EW*
[b] *School of Chemistry, University of Nottingham, University Park, Nottingham, UK NG7 2RD. E-mail: r.mokaya@nottingham.ac.uk*

Received (in Cambridge, UK) 7th March 2001, Accepted 23rd April 2001
First published as an Advance Article on the web 15th May 2001

Super-microporous aluminosilicate catalysts possessing pores in the range 14–20 Å may be prepared *via* primary amine templating alone or in combination with post-synthesis Al-grafting.

The design and synthesis of materials that have a well defined pore structure similar to that of zeolites, but with larger pores, has been a main research goal in solid acid catalysis over the past decade.[1] Recent advances, which include the synthesis of the M41S family of mesoporous solids,[2] have to some extent achieved this goal. Many other varieties of mesoporous materials with pores of size typically above 25 Å have been prepared.[3] Until recently, much less attention has been paid to the synthesis of materials with pores in the super-microporous (10–20 Å) range. Solid acid materials in this pore size range are important since they bridge the gap between microporous zeolites and mesoporous materials. Bagshaw and Hayman[4] used ω-hydroxy-bolaform surfactants to template the formation of super-microporous silicas. Zhao *et al*.[5] reported the preparation of MCM-41 materials with tailored pore openings in the super-microporous range. Sun *et al*.[6] used adamantanamine while Serranno *et al*.[7] employed cetyltrimethylammonium or dodecyltrimethylammonium ions for the formation of microporous materials. Here we report the primary amine templated synthesis of super-microporous aluminosilicate materials whose pore size can be further tailored *via* post-synthesis grafting of Al. Post-synthesis grafting of extra Al also serves to remarkably improve the acidity and catalytic activity of the materials.

We have previously reported on the preparation of *mesoporous* aluminosilicates (Al-MMS, Al-HMS)[8–10] using the primary amine templating route.[11] Our previous work has shown that the pore size of Al-MMS (Al-HMS) materials is to some extent dependent on the alkyl chain length of the primary amine template with longer amines resulting in larger pores.[12,13] The pore size was also found to be dependent on the Si/Al ratio, *i.e.* the pore size was reduced at low Si/Al ratios.[8–10,12,13] This meant that pore sizes at the lower end of the mesopore range (*ca*. 20 Å) were only obtainable for highly aluminous samples and that pores in the super-microporous range (10–20 Å) could not be achieved even at Si/Al ratios as low as 7.[8–10,12,13] Previous work has also shown that materials prepared at gel Si/Al ratios in the range 80–1 always have higher than expected Si/Al ratios implying relatively low levels of Al incorporation into the solid products.[8–10,12,13] We have now found that it is possible to circumvent the limitation on the lowest pore size obtainable by improving the incorporation of Al. This is achieved by modifying our previous synthesis procedure[10] so as to ensure optimum dissolution of the Al source. Furthermore performing post-synthesis grafting of extra Al can reduce the pore size of the resulting materials further.

The synthesis procedure used[10] was modified as follows: desired quantities of aluminium isopropoxide ($Al(i\text{-}C_3H_7O)_3$) were dispersed in 35 ml of isopropyl alcohol with vigorous mechanical stirring at 70 °C for 15 min in order to dissolve the highest possible amount of the aluminium source. The resulting solution was cooled to room temperature and then added under magnetic stirring to a solution of 0.2 mol tetraethyl orthosilicate (TEOS) in 80 ml of absolute ethanol. The resulting mixture was then heated at 70 °C under vigorous stirring for 4 h to obtain the polymerised Si–O–Al species. After cooling to room temperature (under stirring) the inorganic precursor was added to a clear solution of 0.05 mol dodecylamine (DDA) in a mixture of 80 ml of deionised water and 120 ml of absolute ethanol under slow stirring. The stirring was maintained for 5 min after which the resulting mixture was allowed to age at room temperature for 20 h. The solid product was obtained by filtration, washed with two portions of 100 ml of ethanol, air-dried overnight at room temperature and finally calcined in air at 650 °C for 4 h. This procedure was used to prepare aluminosilicate materials with Si/Al molar ratios of 40 : 1, 20 : 1 and 10 : 1, designated Al-MMSX where X is the synthesis gel Si/Al ratio. Al-grafting was performed on the Al-MMSX samples as follows: 1.28 g of a solution of chlorhydrol ($[Al_2Cl(OH)_5{\cdot}2H_2O]$, 6.4 mol l^{-1} with respect to aluminium) was dissolved in 50 ml of distilled water and stirred at 80 °C for 1 h. 1.0 g of Al-MMSX was added to the solution and the resulting suspension stirred for a further hour at 80 °C. After cooling to room temperature, the solid was filtered off and washed with distilled water until free of Cl^- ions, dried in the oven at 100 °C and finally calcined at 500 °C for 4 h. The resulting Al-grafted materials were designated AlAl-MMSX.

The elemental compositions, *d* spacing and textural properties of the present Al-MMS materials are shown in Table 1 and 2. The bulk Si/Al ratios of the samples indicate that Si and Al are incorporated into the solid framework in proportions closely related to the synthesis gel composition. A significant observation is that Al-MMS40 and Al-MMS10 are Al rich, *i.e.* a greater proportion of Al in the synthesis gel is incorporated into the solid product compared to Si. This is a departure from our previous studies where we always obtained silica rich materials.[8–10,12,13] The modified synthesis procedure used here, in which the dissolution of the Al source is optimised, therefore allows for greater Al incorporation into the solid product. The *d* spacings of the present Al-MMS samples (see Table 2) are in all cases lower (by *ca*. 5%) than those we have previously

Table 1 Elemental composition, acid content and catalytic activity of super-microporous Al-MMS samples

Sample	Si/Al	Acid content/ mmol g^{-1}	Cumene conversion (%)[a] 50 min	150 min
Al-MMS40	39.0	0.36	35	28
AlAl-MMS40	22.8	0.57	53	47
Al-MMS20	22.0	0.56	47	41
AlAl-MMS20	14.9	0.75	59	54
Al-MMS10	9.0	0.73	59	51
AlAl-MMS10	7.4	0.82	67	60

[a] The conversion of cumene was performed in a tubular stainless steel, continuous flow, fixed-bed microreactor system with helium as carrier gas at 300 °C as previously described in ref. 10.

 DOI: 10.1039/b102199k

Table 2 Textural properties of super-microporous Al-MMS samples; values in parenthesis are micropore surface area and volume

Sample	Basal (d_{100}) spacing/Å	Surface area/ $m^2\ g^{-1}$	Pore volume/ $cm^3\ g^{-1}$	Pore size/ Å
Al-MMS40	32.4	1023 (488)	0.45 (0.18)	20.5
AlAl-MMS40	32.0	643 (406)	0.33 (0.17)	17.7
Al-MMS20	31.1	864 (497)	0.38 (0.19)	18.4
AlAl-MMS20	30.2	562 (403)	0.28 (0.17)	16.3
Al-MMS10	30.5	684 (520)	0.31 (0.20)	17.7
AlAl-MMS10	29.8	358 (286)	0.24 (0.18)	14.5

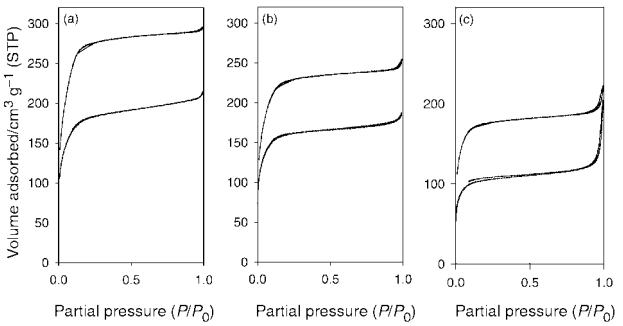

Fig. 1 Nitrogen sorption isotherms of super-microporous primary amine templated aluminosilicates, prepared at gel Si/Al ratios of (a) 40, (b) 20, (c) 10, before (top) and after (bottom) post-synthesis grafting of Al.

observed.[10] It is worth noting that the *d* spacings observed here are generally lower than those normally obtained for M41S type mesoporous materials.[1–3] Powder XRD patterns (not shown), for the present Al-MMS samples are similar to those of comparable mesoporous materials,[10–14] *i.e.* comprising of a single (100) peak at low 2θ values. This is an indication that the present samples are as well ordered as any other primary amine templated mesoporous aluminosilicates.

The clearest indication that the greater Al incorporation attained here results in materials with super-microporous rather than mesoporous character is given by the textural parameters in Table 2. The surface area, pore volume and pore size obtained for the present samples are generally lower than those previously observed for mesoporous Al-MMS (Al-HMS) materials.[10–14] We have previously reported surface areas of 1200, 1195 and 967 $m^2\ g^{-1}$, and pore volumes of 0.65, 0.52 and 0.49 $cm^3\ g^{-1}$ for mesoporous Al-MMS materials prepared (with dodecylamine as template) at gel Si/Al ratios of 40, 20 and 10, respectively.[10] The pore volumes of the present samples are therefore at least 30% lower than those of analogues mesoporous materials.[10] A particular feature of the present Al-MMS samples is that they exhibit a high proportion of micropore surface area and volume as shown in Table 2. The pore size of the materials (obtained using BJH analysis) is, as shown in Table 2, clearly in the super-microporous range. This is illustrated by the N_2 sorption isotherms shown in Fig. 1. The isotherms exhibit high adsorption at low ($P/P_o < 0.2$) partial pressures which is characteristic of super-microporous materials. The isotherms do not exhibit the mesopore filling step (at $P/P_o > 0.2$) normally observed for mesoporous materials.

We have found that performing post-synthesis grafting of Al can increase the microporous character of the Al-MMS samples. The effect of Al-grafting on pore size and porosity is illustrated in Fig. 1; the super-micropore filling step is shifted to lower partial pressures (lower pore size) after grafting. As shown in Table 2, the pore size of AlAl-MMS samples is lower than that of Al-MMS materials by 2–3 Å. This reduction in pore size is accompanied by a decrease in surface area and pore volume, which in turn leads to an increase in the *proportion* of micropore surface area and volume. Indeed sample AlAl-MMS10 is virtually microporous, with a pore size of 14.5 Å and the proportion of micropore surface area and volume is above 75%. It is likely that the Al is grafted into the pore walls thus reducing the pore size. This does not, however, effect the basal spacing (see Table 2). We note that structural ordering (as indicated by powder XRD) is largely unaffected by the grafting process. In addition to tailoring the pore size, Al-grafting also increases the acid content and catalytic activity as shown in Table 1. (The acid content was determined by exposing the samples to cyclohexylamine for 16 h following which they were heated at 100 °C for 4 h to remove physisorbed amine. The samples were then subjected to thermogravimetric analysis and the weight loss between 240 and 420 °C was used to calculate the acid content assuming that each acid site interacts with one base molecule.[9]) The increase in acid content is greatest for AlAl-MMS40 (*ca.* 60%) and lowest for AlAl-MMS10 (*ca.* 12%). The increase in acidity is reflected by the higher cumene cracking[10] activity for the AlAl-MMS samples. Interestingly, the sample (Al-MMS10) with the highest cation exchange capacity (CEC = 42 meq./100 g) takes up less 'extra Al' than Al-MMS40 with a CEC of 12 meq./100 g. (CECs were measured using the Kjeldahl method after NH_4^+ exchange.) This implies that the take up of extra Al is not entirely an ion exchange process. Rather it appears that grafting also occurs on silanol groups as previously described.[15,16] The take up of extra Al is therefore consistent with our previous observation that the concentration of silanols in Al-MMS type materials decreases with Al content.[10] Indeed under similar grafting conditions the pure silica material incorporates at least twice as much Al as the Al-MMS samples.

Primary amine templating of mesostructured aluminosilicates is known to provide solid acid catalysts whose activity is generally higher than that of materials prepared *via* quaternary ammonium ion templating.[10,12,17] Recently, it has also been shown that the wormhole-like structure of primary amine templated aluminosilicates has three-dimensional connectivity.[18] Such connectivity is an important factor with respect to catalytic activity. This report therefore represents the first synthesis of super-microporous aluminosilicates with three-dimensional connectivity. These super-microporous materials combine all the advantages of primary amine templated aluminosilicates, and also offer the potential for size and shape selective catalysis of large substrates, which is not possible for mesoporous materials.

E. B. G. would like to thank CONICIT for the Venezuelan financial support. C.O.T. and O.R.S. scholarships are also acknowledged. R. M. is grateful to the EPSRC for an Advanced Fellowship.

Notes and references

1 A. Corma, *Chem. Rev.*, 1997, **97**, 2373.
2 C. T. Kresge, M. E. Leonowicz, W. J. Roth, J. C. Vartuli and J. S. Beck, *Nature*, 1992, **359**, 710.
3 J. Y. Ying, C. P. Mehnert and M. S. Wong, *Angew. Chem., Int. Ed.*, 1999, **38**, 56.
4 S. A. Bagshaw and A. R. Hayman, *Chem. Commun.*, 2000, 533.
5 X. S. Zhao, G. Q. Lu and X. Hu, *Chem. Commun.*, 1999, 1391.
6 T. Sun, M. S. Wong and J. Y. Ying, *Chem. Commun.*, 2000, 2057.
7 D. P. Serrano, J. Aguado, J. M. Escola and E. Garagorri, *Chem. Commun.*, 2000, 2041.
8 R. Mokaya and W. Jones, *Chem. Commun.*, 1996, 981.
9 R. Mokaya and W. Jones, *Chem. Commun.*, 1996, 983.
10 R. Mokaya and W. Jones, *J. Catal.*, 1997, **172**, 211.
11 P. T. Tanev and T. J. Pinnavaia, *Science*, 1995, **267**, 865.
12 R. Mokaya and W. Jones, *Catal. Lett.*, 1997, **49**, 87.
13 R. Mokaya and W. Jones, *J. Mater. Chem.*, 1998, **8**, 2819.
14 W. Z. Zhang, T. R. Pauly and T. J. Pinnavaia, *Chem. Mater.*, 1997, **9**, 2491.
15 R. Mokaya and W. Jones, *Phys. Chem. Chem. Phys.*, 1999, **1**, 207.
16 R. Mokaya and W. Jones, *J. Mater. Chem.*, 1999, **9**, 555.
17 T. J. Pinnavaia and W. Z. Zhang, *Stud. Surf. Sci. Catal.*, 1998, **117**, 23.
18 J. Lee, S. Yoon, S. M. Oh, C. H. Shin and T. Hyeon, *Adv. Mater.*, 2000, **12**, 359.

CHEMCOMM Communication
www.rsc.org/chemcomm

Catalytic C–O bond cleavage of ethers using group 5 or 6 metal halide/acid chloride systems

Qiaoxia Guo, Taichi Miyaji, Guohua Gao, Ryuichiro Hara and Tamotsu Takahashi*

Catalysis Research Center and Graduate School of Pharmaceutical Science, Hokkaido University and CREST, Science and Technology Corporation (JST), Kita-Ku, Sapporo 060-0811, Japan. E-mail: tamotsu@cat.hokudai.ac.jp

Received (in Cambridge, UK) 24th January 2001, Accepted 19th April 2001
First published as an Advance Article on the web 15th May 2001

Ethers reacted with acid chlorides in the presence of a catalytic amount of $MCl_{5/6}$ (M = Mo, W, Nb or Ta) to give esters in 75–98% yield; a stoichiometric reaction of dioctyl ether with $MoCl_5$ afforded 1-chlorooctane in 93% yield and addition of benzoyl chloride to the resulting mixture gave octyl benzoate in 49% yield.

C–O bond cleavage is a versatile reaction in organic synthesis; in particular, the catalytic cleavage of the C–O bond of ethers is very attractive.[1] There are several examples of catalytic C–O bond cleavage of ethers in the presence of acid chlorides and Lewis acids such as $ZnCl_2$,[2] $FeCl_3$,[3] $SnBr_2$,[4] $CoCl_2$,[5] $AlCl_3$,[6] YCl_3,[7] $LnCl_3$,[8] Al[9] and Zn.[10] As for group 6 metal compounds, low-valent molybdenum compounds such as $Mo(CO)_6$[11] and $ArMo(CO)_3$[12] have been used as catalysts for acylative cleavage of ethers. It is generally believed that these catalytic reactions proceed *via* a cationic mechanism in which the acid chloride reacts with the catalyst first to generate a RCO^+ ion. Addition of an ether gives an oxonium salt ($RCO_2{}^+R'_2$) followed by cleavage of the C–O bond to give an ester. Here, we report a novel catalytic system for acylative cleavage of ethers [eqn. (1)] using group 5 or 6 metal halides and propose a novel catalytic reaction mechanism.

$$R^1OR^2 + R^3COCl \xrightarrow{\text{cat. } MCl_{5/6}} R^3CO_2R^1 \quad (1)$$

M = Mo, W, Nb or Ta

A representative procedure for the catalytic C–O bond cleavage is as follows: All reactions were carried out under nitrogen and metal chlorides were handled under nitrogen. Solvents were dried and distilled. To a mixture of molybdenum(v)chloride (0.1 mmol, 27 mg) and dichloroethane (DCE) (5 ml) was added dibutyl ether (1 mmol, 130 mg) and benzoyl chloride (1 mmol, 141 mg). The reaction mixture was stirred at 80 °C for 3 h. GC analysis of the resulting mixture after hydrolysis showed the formation of butyl benzoate in 95% yield. Purification by column chromatography on silica gel afforded butyl benzoate in 75% isolated yield. The results are summarized in Table 1.

The C–O bond of dibutyl ether was cleaved in the presence of 10 mol% of $MoCl_5$ and *n*-caproyl chlorides at 80 °C for 24 h and the caproic acid *n*-butyl ester was obtained in 96% yield (Run 2). The lower reactivity of aliphatic acid chlorides than that of aromatic acid chlorides has been reported in the case of graphite.[13] In the reaction reported here, there is no significant reactivity difference between the aromatic acid chloride and the aliphatic acid chloride. Dioctyl ether also reacted with benzoyl chloride and *n*-caproyl chloride to give octyl benzoate and *n*-caproyl acid *n*-octyl ester, respectively, in high yield (Runs 3 and 4). It is interesting to note that some unsymmetric ethers showed selective cleavage of the C–O bond. For example, methyl *tert*-butyl ether reacted with benzoyl chloride to give methyl benzoate in 99% yield (Run 5) *i.e.* the Bu^t–O bond in methyl *tert*-butyl ether was selectively cleaved. Allyl propyl ether was also selectively cleaved under the same conditions. The allyl–O bond was cleaved to give caproyl acid propyl ester (Run 6). In contrast, for allyl trimethylsilyl ether, selective cleavage of the Si–O bond was observed (Run 7) and the allyl–O bond was not cleaved. Other group 5 and 6 metal chlorides were also quite active for acylative cleavage of ethers. Dibutyl ether reacted with benzoyl chloride in the presence of 10 mol% of WCl_6 for 24 h to give butyl benzoate in 96% yield (Run 8). When $NbCl_5$ and $TaCl_5$ were used as catalysts, catalytic C–O bond cleavage was also successful and butyl benzoate was obtained in 98 and 96% yield, respectively (Runs 9 and 10).

In order to investigate the reaction mechanism, a stoichiometric reaction of dioctyl ether with molybdenum(v) chloride was carried out at 80 °C. After 3 h, 1-chlorooctane was obtained in 93% yield [eqn. (2)]. To the resulting mixture, benzoyl chloride was added and octyl benzoate was obtained in 49% yield [eqn. (3)].

$$C_8H_{17}OC_8H_{17} + MoCl_5 \xrightarrow[80\ ^\circ C,\ 3\ h]{DCE,} \underset{93\%}{C_8H_{17}Cl} + \underset{\text{reaction mixture}}{[C_8H_{17}OMoCl_n]} \quad (2)$$

$$\underset{\text{reaction mixture}}{[C_8H_{17}OMoCl_n]} \xrightarrow[80\ ^\circ C,\ 3\ h]{PhCOCl} \underset{49\%}{PhCO_2C_8H_{17}} \quad (3)$$

Table 1 Acylative cleavage of ethers with acid chlorides in the presence of $MCl_{5/6}$[a]

Run	Ether	RCOCl	$MCl_{5/6}$	Time/h	Product	Yield[b] (%)
1	Bu_2O	PhCOCl	$MoCl_5$	3	$PhCO_2Bu$	95(75)
2	Bu_2O	$C_5H_{11}COCl$	$MoCl_5$	24	$C_5H_{11}CO_2Bu$	96(78)
3	$C_8H_{17}OC_8H_{17}$	PhCOCl	$MoCl_5$	1	$PhCO_2C_8H_{17}$	88(78)
4	$C_8H_{17}OC_8H_{17}$	$C_5H_{11}COCl$	$MoCl_5$	3	$C_5H_{11}CO_2C_8H_{17}$	94(82)
5	$CH_3OC(CH_3)_3$	PhCOCl	$MoCl_5$	1[c]	$PhCO_2CH_3$	99(76)
6		$C_5H_{11}COCl$	$MoCl_5$	1	$C_5H_{11}CO_2C_3H_7$	98(81)
7	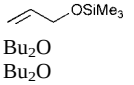	$C_5H_{11}COCl$	$MoCl_5$	3	$C_5H_{11}CO_2CH_2CH{=}CH_2$	75(58)
8	Bu_2O	PhCOCl	WCl_6	3	$PhCO_2Bu$	96
9	Bu_2O	PhCOCl	$NbCl_5$	24	$PhCO_2Bu$	98
10	Bu_2O	PhCOCl	$TaCl_5$	6	$PhCO_2Bu$	96

[a] *Conditions*: $MCl_{5/6}$, 0.1 mmol; ether, 1 mmol; acid chloride, 1 mmol, 80 °C. [b] GC yields: isolated yields in parentheses. [c] 50 °C.

 DOI: 10.1039/b100852h

The results obtained here showed that the ether reacted with $MoCl_5$ first, to form 1-chlorooctane and the $[C_8H_{17}OMoCl_n]$ complex, although this complex was not characterized.† Benzoyl chloride then reacted with the molybdenum complex to give octyl benzoate. A proposed mechanism is shown in Scheme 1. The mechanism proposed here is quite different from the cationic mechanism which has been generally proposed for the catalytic acylative cleavage of the C–O bond of ethers. For example, Alper and Huang[11] and Tsonis[12] used group 6 metal carbonyl or substituted group 6 metal carbonyl complexes to catalyze the acylative cleavage of ethers. In both studies a mechanism was proposed whereby acid chloride reacts with the metal carbonyl to form a RCO^+ ion, followed by the reaction with an ether to produce an oxonium salt which is then cleaved to give the ester.

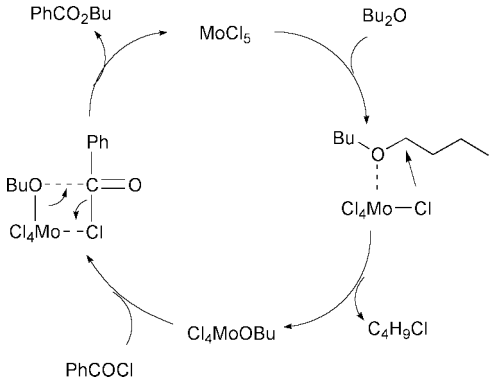

Scheme 1 Proposed reaction mechanism for catalytic acylative cleavage of ethers using $MoCl_5$.

The C–O bond of ethers can be cleaved only by $MoCl_5$ in our system which is similar to stoichiometric C–O bond cleavage of ethers with Lewis acids. The role of the acid chlorides in the reactions reported here does not lead to formation of the oxonium salt but rather provides Cl^- to Cl_4MoOR to regenerate $MoCl_5$ and esters.

Notes and references

† The ^{13}C NMR spectrum of the reaction mixture of Bu_2O and $MoCl_5$ showed the following signals, $\delta_C(CDCl_3, Me_4Si)$: 13.66, 19.56, 29.26, 60.30.

1 M. V. Bhatt and S. U. Kulkarni, *Synthesis*, 1983, 249; R. C. Larock, *Ether cleavage*, in *Comprehensive Organic Transformations*, Wiley-VCH, 2nd edn., 1999.
2 P. Mimero, C. Saluzzo and R. Amouroux, *Tetrahedron Lett.*, 1994, **35**, 1553.
3 B. Ganem and V. R. Small, Jr., *J. Org. Chem.*, 1974, **39**, 3728.
4 T. Oriyama, M. Kimura, M. Oda and G. Koga, *Synlett*, 1993, 437.
5 S. Ahmad and J. Iqbal, *Chem. Lett.*, 1987, 953; J. Iqbal, M. A. Khan and R. R. Srivastava, *Tetrahedron Lett.*, 1988, **29**, 4985; J. Iqbal and R. R. Srivastava, *Tetrahedron*, 1991, **47**, 3155.
6 L. Green, I. Hemeon and R. D. Singer, *Tetrahedron Lett.*, 2000, **41**, 1343.
7 C. Qian, A. Qiu, Y. Huang and W. Chen, *J. Organomet. Chem.*, 1991, **412**, 53.
8 C. Qian, A. Qiu, D. Zhu and X. Yang, *J. Mol. Catal.*, 1994, **87**, 357.
9 F. A. Luzzio and R. A. Bobb, *Tetrahedron*, 1999, **55**, 1851.
10 S. Bhar and B. C. Ranu, *J. Org. Chem.*, 1995, **60**, 745.
11 H. Alper and C.-C. Huang, *J. Org, Chem.*, 1973, **38**, 64.
12 C. P. Tsonis, *J. Mol. Catal.*, 1988, **45**, 145.
13 Y. Suzuki, M. Matsushima and M. Kodomari, *Chem. Lett.*, 1998, 319.

CHEMCOMM
Communication
www.rsc.org/chemcomm

A paramagnetic lamellar polymer with a high semiconductivity

Yingjun Zhao,[a] Maochun Hong,*[a] Yucang Liang,[a] Rong Cao,[a] Wenjie Li,[b] Jiabao Weng[a] and Shaofang Lu[a]

[a] *State Key Laboratory of Structural Chemistry, Fujian Institute of Research on the Structure of Matter, Chinese Academy of Sciences, Fuzhou, Fujian 350002, P. R. China. E-mail: hmc@fjirsm.ac.cn*
[b] *Radio Department, Fuzhou University, Fuzhou, Fujian 350002, P. R. China*

Received (in Cambridge, UK) 13th February 2001, Accepted 17th April 2001
First published as an Advance Article on the web 15th May 2001

The polymer $[Ni_2(C_4N_2H_3S)_4]_n$ with excellent electrical conductivity and ferromagnetic interaction between the nickel(II) centers has been prepared by the hydrothermal reaction of $Ni(O_2CMe)_2$ with pyrimidine-2-thiol in DMF–H_2O; X-ray diffraction shows that the polymer possesses a lamellar structure formed from the conjunction system of pyrimidine rings and Ni(II) centers.

The increasing interest in inorganic–organic hybrid framework assemblies has resulted in a great deal of research effort focused on the development of new functional materials ranging from zeolite-like coordination polymers[1] to multilayered perovskites,[2] which possess various potential applications, such as in electrical conductivity[3] and magnetism.[4,5] For instance, Shimizu *et al.* reported a layered 'inorgano–organic' solid where the inorganic component is composed of sulfonate-bridged silver(I) centers and the organic moiety is a phenyl group.[6a] Monfort *et al.* reported a metamagnetic two-dimensional molecular material prepared from nickel(II) and azide bridging ligand.[6b] In this field, studies have mainly been focused on inorganic–organic hybrid materials containing N-donor ligands, and relatively few efforts have been made to investigate transition metal organosulfur coordination polymers[7,8] although the coordination chemistry of organosulfur compounds has been intensively studied for more than twenty years.[9]

As a result of the tendency of thiolates to bridge metal centers to yield insoluble or sparingly soluble polymers, it is difficult to control the reactions of thiolates with metal ions and obtain single crystals of polymeric metal thiolates suitable for X-diffraction analysis. Our recent researches revealed the reaction of N-donor-containing thiols such as pyridine-2-thiol with silver ions led to soluble complex species, which can be converted into silver–thiolate or silver–thione polymers under appropriate conditions.[10] Considering that pyrimidine-2-thiol can adopt a variety of coordination modes in its coordination chemistry[11] it was deduced that coordination polymers with novel structures may be isolated through the reaction of M(II) transition metal ions with pyrimidine-2-thiol. We have succeeded in the isolation of coordination polymers by the hydrothermal reaction of bivalent transition metal ions and pyrimidine-2-thiol. Here, we demonstrate the formation of a nickel(II)–pyrimidine-2-thiolate polymer $[Ni_2(C_4H_3N_2S)_4]_n$ **1** ($C_4H_3N_2S$ = pyrimidine-2-thiolate), with lamellar structure. In contrast to other Ni(II) compounds and coordination polymers with lamellar structure,[6c] the interesting features of **1** are its paramagnetic and semiconducting properties.

At 90 °C, the hydrothermal reaction of $Ni(O_2CMe)_2$ with pyrimidine-2-thiol in DMF–H_2O (v:v = 1:2) for 48 h and crystallization by slow cooling of the reaction solution to room temperature led to the growth of a large amount of dark-brown, sheet-like crystals of **1**. The crystalline product **1** is very stable even at *ca.* 200 °C in air. Elemental analysis showed the formula of the product was $[Ni(C_4H_3N_2S)_2]$. X-Ray diffraction analysis conformed that **1** is a lamellar polymer built from the $[Ni_2(C_4H_3N_2S)_4]$ dimeric unit† as shown in Fig. 1. This unit develops along the *ab* plane into a honeycomb structure in which the shortest distance between metal centers is 3.774 Å. Therefore, the solid state polymer can be viewed as a two-dimensional lamellar structure composed of $[Ni_2(C_4H_3N_2S)_4]$ dimeric units, wherein the nickel(II) centers are linked by sulfur atoms of thiolate and the pyrimidine ring in the pyrimidine-2-thiolate ligands to form inorganic and organic layers, as shown in Figs. 2 and 3. Each pyrimidine-2-thiolate in **1** acts as a μ_3-bridge to link three nickel atoms through S and N atoms. There are two types of coordination modes for pyrimidine-2-thiolate: one in which pyrimidyl groups of pyrimidine-2-thiolate ligands protrude into the interlayer region [Scheme 1(a)]; and the other in which they act as bridges lying on the layer plane to link Ni(II) centers [Scheme 1(b)]. The interlayer distance is 8.119 Å. Each nickel atom is six-coordinated by three S atoms and three N atoms from three different pyrimidine-2-thiolate ligands in distorted octahedral fashion. The Ni–N bond lengths range between 2.055 and 2.142 Å, while the Ni–S bond lengths range from 2.438 to 2.593 Å. The average S–Ni–N, N–Ni–N and S–Ni–S angles are 85.14,

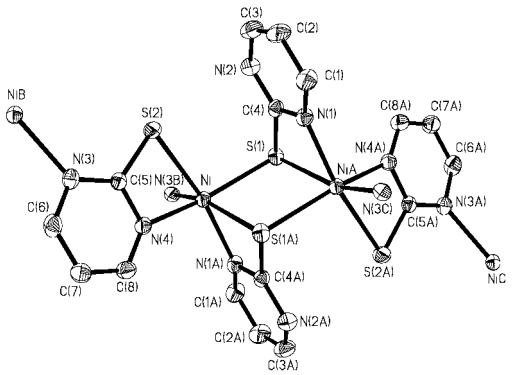

Fig. 1 Structure of the basic unit $[Ni_2(C_4H_3N_2S)_4]$. Selected bond lengths (Å) and angles (°): Ni–N(1A) 2.055(3), Ni–N(4) 2.074(3), Ni–N(3B) 2.142(3), Ni–S(1) 2.4378(10), Ni–S(2) 2.4522(10), Ni–S(1A) 2.5929(10); N(1A)–Ni–N(4) 98.09(12), N(1A)–Ni–N(3B) 93.72(11), N(4)–Ni–N(3B) 101.89(12), N(1A)–Ni–S(1) 91.61(9), N(4)–Ni–S(1) 159.62(8), N(3B)–Ni–S(1) 95.28(8), N(1A)–Ni–S(2) 166.20(9), N(4)–Ni–S(2) 68.52(8), N(3B)–Ni–S(2) 92.46(8), S(1)–Ni–S(2) 100.10(3), N(1A)–Ni–S(1A) 66.76(9), N(4)–Ni–S(1A) 84.59(8), N(3B)–Ni–S(1A) 160.25(8), S(1)–Ni–S(1A) 82.84(4), S(2)–Ni–S(1A) 107.24(3), Ni–S(1)–Ni(A) 97.16(4).

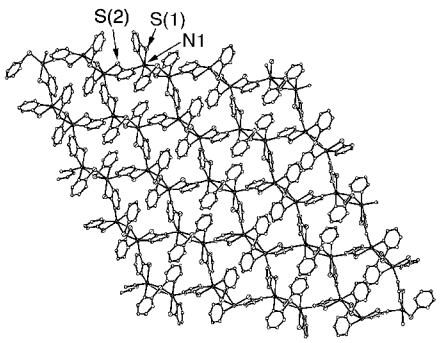

Fig. 2 View of the lamellar structure in **1**.

 DOI: 10.1039/b101422f

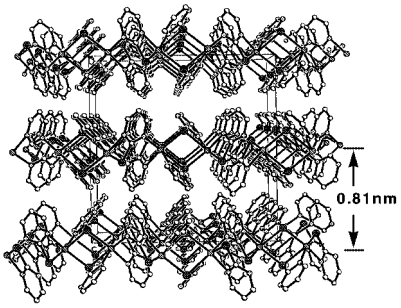

Fig. 3 Structure of **1** showing the interlayer network.

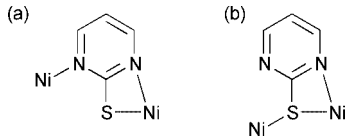

Scheme 1 Coordination modes of pyrimidine-2-thiolate in **1**.

97.90(1) and 96.72°, respectively. All nickel atoms of each layer are nearly coplanar with deviations being within 0.18 Å.

The cryomagnetic behavior of **1** has been studied. $\chi_M T$ and χ_M *vs.* T plots of the temperature-dependent magnetic susceptibility data for **1** are shown in Fig. 4. At room temperature, $\chi_M T$ is 2.60 cm^3 K mol^{-1} per dimer at 299.1 K and increases slightly to a maximum value of 2.78 cm^3 K mol^{-1} at 60 K. It decreases from 60 K and reaches 1.44 cm^3 K mol^{-1} at 7.9 K. The magnetic moments from 300 to 5 °C are slightly smaller than calculated values using the free-ion approximation for Ni(II) with high spin configuration. Least-square fitting using eqn. (1)‡ of all experimental data leads to J, J' and g values of 19.5 cm^{-1}, −7.3 cm^{-1} and 2.103 with the agreement factor $R = 2.0 \times 10^{-4}$. Fitting to this model demonstrates the existence of ferromagnetic interactions between the two nickel(II) centers of the dimer unit and antiferromagnetic interactions both between adjacent dimer units and between adjacent layers. The magnetic behavior for **1** is quite different from a nickel(II)–azide two-dimensional polymer, in which each nickel(II) center are high spin and normally show ferromagnetic interactions.[6b]

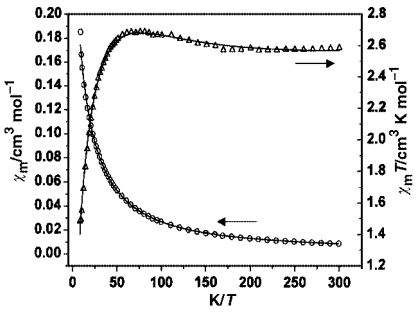

Fig. 4 Temperature–dependent magnetic susceptibility of **1**, (○)χ_m, (△)$\chi_m T$ and (−) the best fit obtained.

According to the literature,[12] the evidence for interaction between metal cations in extended solid structures is provided not only by characteristic uniform structural features but also by their physical properties such as electrical conductivity. The semiconductivity of **1** was therefore studied. Determination of the conductivity of **1** (powder sample from ground crystals) indicates an electrical conductivity of 5.00×10^{-3} S cm^{-1} at 28 °C which increases with temperature (Fig. 5), indicating that **1** is a semiconductor. By examining its structure, the semiconducting property of **1** can be attributed to its characteristic structural feature of the interconnected array of nickel(II) with pyrimidine; the semiconducting property provides evidence for nickel and pyridine ring interactions.

We gratefully acknowledge financial support from the NSF of China and Fujian Provice and Key project from CAS.

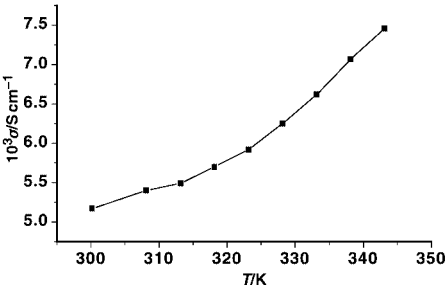

Fig. 5 Temperature dependent electrical conductivity of **1**.

Notes and references

† *Crystal data*: crystal dimensions 0.12 × 0.27 × 0.32 mm, $C_{16}H_{12}N_8S_4Ni_2$, M_r = 562.00, orthorhombic, space group *Pbca*, a = 7.8860(6), b = 15.5844(11), c = 16.2399(12) Å, V = 1995.9(3)Å^3, Z = 4, R (wR) = 0.037 (0.095) for 1402 reflections with $F \geqslant 2.0\sigma(I)$. The intensity data were collected on a Bruker Smart CCD diffractometer with graphite-monochromated Mo-Kα radiation at room temperature. CCDC 159337. See http://www.rsc.org/suppdata/cc/b1/b101422f/ for crystallographic data in .cif or other electronic format.

‡ Magnetic model:

$$\chi_m^{J+J'} = \frac{\chi_m^J}{1 - 2J'\chi_m^J / Ng^{2+}\beta^2} + \text{TIP}$$

$$\chi_M^J = \frac{2N\beta^2 g^2}{kT}\left(\frac{\exp(J/2kT) + 5\exp(3J/2kT)}{1 + 3\exp(J/2kT) + 5\exp(3J/2kT)}\right) + \text{TIP} \qquad (1)$$

Here J is the coupling constant between the two centers of the dimer and J' is the coupling constant both between adjacent dimer units and between adjacent layers; TIP is the temperature-independent paramagnetism.

1 O. M. Yaghi, H. Li, C. Davis, D. Richardson and T. L. Groy, *Acc. Chem. Res.*, 1998, **31**, 374; P. J. Hagrman, D. Hagrman and J. Zubieta, *Angew. Chem., Int. Ed*, 1999, **38**, 2638; O. Philip and J. F. Stoddart, *Angew. Chem., Int. Ed. Engl.*, 1996, **35**, 1154.

2 D. B. Mitzi, *Prog. Inorg. Chem.*, 1999, **48**, 1.

3 D. B. Mitzi, S. Wang, C. A. Field, C. A. Chess and A. M. Guloy, *Science*, 1995, **267**, 1473; S. Wang, D. B. Mitzi, C. A. Field and A. Guloy, *J. Am. Chem. Soc.*, 1995, **117**, 5297.

4 N. Matsumoto, Y. Sunatsuki, H. Miyasaka, Y. Hashimoto, D. Luneau and J.-P. Tuchagues, *Angew. Chem., Int. Ed.*, 1999, **38**, 171; S. Triki, J. S. Pala, M. Decoster, P. Molinié and l. Toupet, *Angew. Chem., Int. Ed.*, 1999, **38**, 113.

5 T. L. Hennigar, D. C. MacQuarrie, P. Losier, R. D. Rogers and M. J. Zaworotko, *Angew. Chem., Int. Ed. Engl.*, 1997, **36**, 972; M. J. Zaworotko, *Chem. Soc. Rew.*, 1994, 283 and references therein.

6 (*a*) G. K. H. Shimizu, G. D. Enright, C. I. Ratcliffe, K. F. Preston, J. L. Reid and J. A. Ripmeester, *Chem. Commun.*, 1999, 1485; (*b*) M. Monfort, I. Resino, J. Ribas and H. Stoecki-Evans, *Angew. Chem., Int. Ed.*, 2000, **39**, 191.

7 K.-W. Kim and M. G. Kanatzides, *J. Am. Chem. Soc.*, 1998, **120**, 8124.

8 Z. Salehi, R. V. Parish and R. Z. Pritchard, *J. Chem. Soc., Dalton Trans.*, 1997, 4241; G. K. H. Shimizu, G. D. Enright, C. Ratcliffe, J. A. Ripmeester and D. D. W. Wayner, *Angew. Chem., Int. Ed.*, 1998, **37**, 1407.

9 I. G. Dance, *Polyhedron*, 1986, **5**, 1037; B. Krebs and G. Henkel, *Angew. Chem., Int. Ed. Engl.*, 1991, **30**, 769; G. K. H. Shimizu, G. D. Enright, C. Ratcliffe, J. A. Ripmeester and D. D. W. Wayner, *Angew. Chem., Int. Ed.*, 1998, **37**, 1407.

10 W. Su, R. Cao, M. Hong, J. Chen and J. Lu, *Chem. Commun.*, 1998, 1389; M. Hong, W. Su, R. Cao, W. Zhang, W.-T. Wong and J. Lu, *Inorg. Chem.*, 1999, **38**, 600; W. Su, M. Hong, J. Weng, R. Cao and S. Lu, *Angew. Chem., Int. Ed.*, 2000, **39**, 2911.

11 M. Gupta, R. E. Cramer, K. Ho, C. Pettersen, S. Mishina, J. Belli and C. M. Jensen, *Inorg. Chem.*, 1995, **34**, 60; J. G. Reynolds, S. C. Sendlinger, A. M. Murray, J. C. Huffman and G. Christou, *Angew. Chem., Int. Ed. Engl.*, 1992, **31**, 1253.

12 C. M. Che, M.-C. Tse, M. C. W. Chan, K.-K. Cheung, D. L. Phillips and K.-H. Leung, *J. Am. Chem. Soc.*, 2000, **122**, 2464; M. Munakata, L. P. Wu and T. Kuroda-Sowa, *Adv. Inorg. Chem.*, 1998, **46**, 173; V. W. W. Yam, K. K. W. Lo, N. K.-M. Fung and C. R. Wang, *Coord. Chem. Rev.*, 1998, **171**, 3.

CHEMCOMM Communication
www.rsc.org/chemcomm

Highly enantioselective asymmetric autocatalysis induced by chiral cobalt complexes due to the topology of the coordination of achiral ligands

Itaru Sato,[a] Kousuke Kadowaki,[a] Yasushi Ohgo,[a] Kenso Soai*[a] and Hiroshi Ogino[b]

[a] *Department of Applied Chemistry, Faculty of Science, Science University of Tokyo, Kagurazaka, Shinjuku-ku, Tokyo, 162-8601, Japan. E-mail: ksoai@ch.kagu.sut.ac.jp*
[b] *Department of Chemistry, Graduate School of Science, Tohoku University, Sendai 980-8578, Japan*

Received (in Cambridge, UK) 7th March 2001, Accepted 25th April 2001
First published as an Advance Article on the web 15th May 2001

Chiral octahedral cobalt complexes, K[Co(edta)]·2H_2O and K[Co(trdta)]·2H_2O, induce enantioselective addition of diisopropylzinc to pyrimidine-5-carbaldehyde, affording the pyrimidyl alkanol with high (85–94%) enantiomeric excesses.

Enantioselective reactions are one of the most important areas in organic chemistry.[1] Chiral transition metal complexes play an important role in asymmetric reactions with most chiral metal complexes being prepared using chiral organic ligands. On the other hand, metal complexes such as the octahedral cobalt complex with achiral ethylenediamine (en) ligands, *i.e.* $[Co(en)_3]^{3+}$ shows chirality due to the topology of coordination of the achiral ligand.[2] A 'chiral-at-metal'[3a] complex with achiral ligands has been used in diastereoselective synthesis,[3b] and a 'chiral-at-metal' complex with chiral ligands has been used in enantioselective synthesis.[4] However, the application of 'chiral-at-metal' complexes with achiral ligands towards enantioselective synthesis has been a difficult problem. It is noteworthy that, as early as 1929, Shibata and Tsuchida[5] reported an enantiomer selective asymmetric oxidation of racemic 3,4-dihydroxyphenylalanine using a chiral cobalt complex $[Co(en)_2NH_3Cl]Br_2$. However, highly enantioselective syntheses using chiral metal complexes (due to the topology of achiral ligands) is a challenge.

One of us (H. O.) previously reported the preparation of chiral octahedral cobalt complexes with ethylenediaminetetraacetate (edta) and trimethylenediaminetetraacetate (trdta), *i.e.* K[Co(edta)]·2H_2O **1**[6a] and K[Co(trdta)]·2H_2O **2**.[6b]

In the course of our continuing study on asymmetric autocatalysis,[7,8] we found that the sense of the enantioselectivity of the addition of diisopropylzinc (*i*-Pr_2Zn) to pyrimidine-5-carbaldehydes is affected by chiral materials[9] such as chiral quartz[9a] and sodium chlorate.[9b]

We report here a highly enantioselective addition of *i*-Pr_2Zn to 2-(*tert*-butylethynyl)pyrimidine-5-carbaldehyde **3** in the presence of chiral metal complex **1** or **2** (Fig. 1). The absolute configurations of the formed pyrimidyl alkanol with high (85–94%) ee's were controlled by the chirality of the octahedral cobalt complexes **1** and **2**.

Experiments were conducted as illustrated in Scheme 1. To a suspension of finely powdered chiral crystals (0.025 mmol) of cobalt complex **1** or **2**, aldehyde **3**[10] (1.05 mmol) and *i*-Pr_2Zn (2.15 mmol)[11] were added portionwise. In the presence of $(+)_{546}$-K[Co(edta)]·2H_2O **1**, (*S*)-alkanol **4** with 91% ee was obtained in 91% yield (Table 1, entry 1). On the other hand, in the presence of $(-)_{546}$-K[Co(edta)]·2H_2O **1**, (*R*)-alkanol **4** with 94% ee was obtained (entry 3). Thus, the absolute configuration of chiral complex **1** determines the absolute configuration of the newly formed pyrimidyl alkanol **4**.

In a typical experiment (Table 1, entry 3), to a toluene suspension (0.1 ml) of $(-)_{546}$-K[Co(edta)]·2H_2O **1** (10.6 mg, 0.025 mmol) and aldehyde **3** (9.4 mg, 0.05 mmol), a toluene solution (1.0 M) of *i*-Pr_2Zn (0.15 mmol) was added over a period of 15 min at 0 °C. After the mixture was stirred for 14 h at 0 °C, toluene (4.8 ml), *i*-Pr_2Zn (0.4 mmol, 1.0 M toluene solution), and a toluene solution (1.5 ml) of aldehyde **3** (37.6 mg, 0.2 mmol) were added successively, and the reaction mixture was stirred for 3.5 h. Then, toluene (14.4 ml), *i*-Pr_2Zn

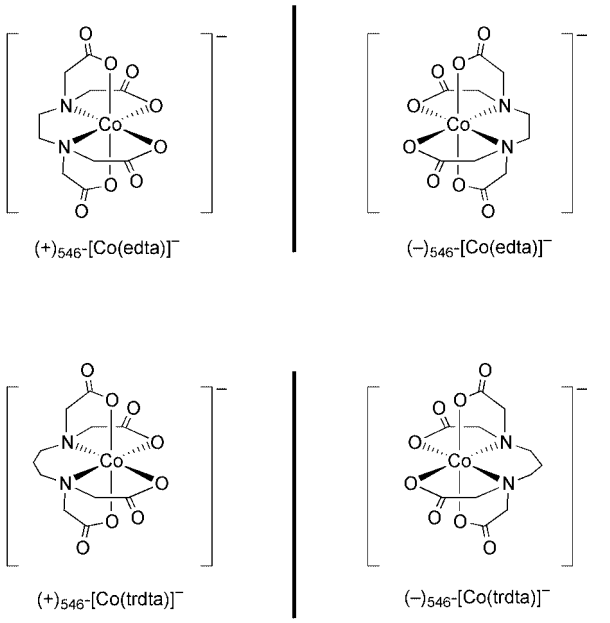

Fig. 1 Chiral structures of ethylenediaminetetraacetatocobaltate(III) and trimethylenediaminetetraacetatocobaltate(III).

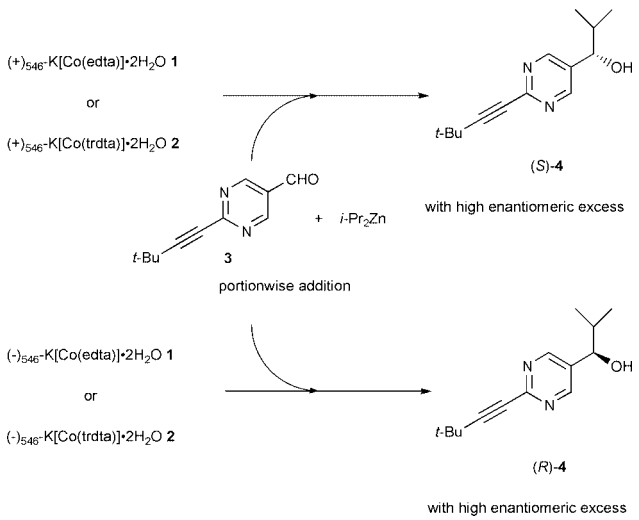

Scheme 1 Highly enantioselective asymmetric autocatalysis in the presense of chiral octahedral cobalt complex **1** and **2**. edta: $(^-O_2CH_2C)_2N(CH_2)_2N(CH_2CO_2^-)_2$; trdta: $(^-O_2CH_2C)_2N(CH_2)_3N(CH_2CO_2^-)_2$.

 DOI: 10.1039/b102143p

(1.6 mmol, 1.0 M toluene solution) and a toluene (4 ml) solution of aldehyde **3** (150.6 mg, 0.8 mmol) were added successively, and the mixture was stirred at 0 °C for an additional 3 h. The reaction was quenched by hydrochloric acid (1 M, 5 ml), and satd. aq. sodium hydrogen carbonate (15 ml) was added. The mixture was filtered using Celite, and the filtrate was extracted with ethyl acetate. The combined organic layers were dried over anhydrous sodium sulfate and evaporated. Purification of the residue by silica gel thin layer chromatography (developing solvent, hexane–ethyl acetate = 2 : 1 v/v) gave (*R*)-pyrimidyl alkanol **4** (244 mg) with 94% ee in an isolated yield of 99%.

Since the cobalt complex **1** is practically insoluble in toluene, enantioselective addition seems to occur at the interface between the crystal of metal complex **1** and the solvent. When $(+)_{546}$-K[Co(trdta)]·2H_2O **2** was used instead of $(+)_{546}$-K[Co(edta)]·2H_2O **1**, the formation of (*S*)-**4** with 85% ee was induced (entry 5), and the reaction using $(-)_{546}$-K[Co(trdta)]·2H_2O (**2**) gave (*R*)-**4** with 88% ee (entry 6).

In summary, enantioselective addition of *i*-Pr_2Zn to pyrimidinecarbaldehyde **4** in the presence of $(+)_{546}$-K[Co(edta)]·2H_2O **1** or $(+)_{546}$-K[Co(trdta)]·2H_2O **2** gave (*S*)-**4** with high ee's, respectively, and the reaction in the presence of $(-)_{546}$-K[Co(edta)]·2H_2O (**1**) or $(-)_{546}$-K[Co(trdta)]·2H_2O **2** afforded (*R*)-**4** with high ee's, respectively. We have clearly demonstrated that the chirality at the cobalt is responsible for the enantioselective addition of *i*-Pr_2Zn.

Table 1 Enantioselective addition of diisopropylzinc to aldehyde **3** in the presence of chiral octahedral cobalt complexes **1** and **2**

		Alkanol **4**[a]		
Entry	Cobalt complex	Yield (%)	Ee (%)	Config.
1	$(+)_{546}$-K[Co(edta)]·2H_2O **1**	91	91	*S*
2		98	89	*S*
3	$(-)_{546}$-K[Co(edta)]·2H_2O **1**	99	94	*R*
4		92	90	*R*
5	$(+)_{546}$-K[Co(trdta)]·2H_2O **2**	90	85	*S*
6	$(-)_{546}$-K[Co(trdta)]·2H_2O **2**	90	88	*R*

[a] Ee was determined by HPLC analysis using a chiral stationary phase (Chiralcel OD).

This work was supported by a Grant-in-Aid for Scientific Research from the Ministry of Education, Science, Sports, and Culture of Japan and by a Daicel Award for Synthetic Organic Chemistry.

Notes and references

1 *Comprehensive Asymmetric Catalysis*, ed. E. R. Jacobsen, A. Pfaltz and H. Yamamoto, Springer, Berlin, 1999; *Catalytic Asymmetric Synthesis*, ed. I. Ojima, John Wiley, New York, 2nd edn., 2000.
2 J.-L. Pierre, *Coord. Chem. Rev.*, 1998, **178**–**180**, 1183.
3 (*a*) C. M. Garner, N. Quiros Méndez, J. J. Kowalczyk, J. M. Fernandez, K. Emerson, R. D. Larsen and J. A. Gladysz, *J. Am. Chem. Soc.*, 1990, **112**, 5146; (*b*) G. B. Richter-Anddo, D. A. Knight, M. A. Dewey, A. M. Arif and J. A. Gladysz, *J. Am. Chem. Soc.*, 1993, **115**, 11863.
4 H. Brunner, *Acc. Chem. Res.*, 1979, **12**, 250; M. Brookhart, D. Timmers, J. R. Tucker, G. D. Williams, G. R. Husk, H. Brunner and B. Hammer, *J. Am. Chem. Soc.*, 1983, **105**, 6721.
5 Y. Shibata and R. Tsuchida, *Bull. Chem. Soc. Jpn.*, 1929, **4**, 142; Y. Shibata, Y. Tanaka and S. Goda, *Bull. Chem. Soc. Jpn.*, 1931, **6**, 210.
6 (*a*) F. P. Dwyer, E. C. Gyarfas and D. P. Mellor, *J. Phys. Chem.*, 1955, **59**, 296; (*b*) H. Ogino, M. Takahashi and N. Tanaka, *Bull. Chem. Soc. Jpn.*, 1970, **43**, 424.
7 Reviews: K. Soai and T. Shibata, *Yuki Gosei Kagaku Kyokaishi (J. Synth. Org. Chem. Jpn.)*, 1997, **54**, 994; C. Bolm, F. Bienewald and A. Seger, *Angew. Chem., Int. Ed. Engl.*, 1996, **35**, 1657; K. Soai, *Enantiomer*, 1999, **4**, 591.
8 K. Soai, T. Shibata and I. Sato, *Acc. Chem. Res.*, 2000, **33**, 382.
9 (*a*) K. Soai, S. Osanai, K. Kadowaki, S. Yonekubo, T. Shibata and I. Sato, *J. Am. Chem. Soc.*, 1999, **121**, 11 235; (*b*) I. Sato, K. Kadowaki and K. Soai, *Angew. Chem., Int. Ed.*, 2000, **39**, 1510; (*c*) T. Shibata, J. Yamamoto, N. Matsumoto, S. Yonekubo, S. Osanai and K. Soai, *J. Am. Chem. Soc.*, 1998, **120**, 12 157; (*d*) S. Tanji, A. Ohno, I. Sato and K. Soai, *Org. Lett.*, 2001, **3**, 287; (*e*) I. Sato, D. Omiya, T. Saito and K. Soai, *J. Am. Chem. Soc.*, 2000, **122**, 11 739; (*f*) I. Sato, R. Yamashima, K. Kadowaki, J. Yamamoto, T. Shibata and K. Soai, *Angew. Chem., Int. Ed.*, 2001, **40**, 1096.
10 T. Shibata, S. Yonekubo and K. Soai, *Angew. Chem., Int. Ed.*, 1999, **38**, 659.
11 Reviews of dialkylzinc addition to aldehydes: K. Soai and S. Niwa, *Chem. Rev.*, 1992, **92**, 833; R. Noyori and M. Kitamura, *Angew. Chem., Int. Ed. Engl.*, 1991, **53**, 138.

CHEMCOMM
Communication
www.rsc.org/chemcomm

A multidentate phosphinoalkoxide ligand as a building block in mixed polylithium aggregates

Alexander Feustel and Gerhard Müller*

Fachbereich Chemie, Universität Konstanz, Universitätsstr. 10, 78464 Konstanz, Germany.
E-mail: gerhard.mueller@chemie.uni-konstanz.de

Received (in Cambridge, UK) 19th December 2000, Accepted 26th April 2001
First published as an Advance Article on the web 15th May 2001

The tris(dimethylphosphinomethyl)-substituted lithium alkoxide [$LiOC(CH_2PMe_2)_3$] acts as a building block in mixed polylithium aggregates, effectively capping triangular Li_3 polyhedral faces; it further reacts with lithium organyls to yield the Y-conjugated, symmetrically tris(dimethylphosphino)-substituted trimethylenemethane dianion.

Chelating phosphinoalkoxides[1] have been used extensively as ligands to transition metals where much of the pertinent interest stems from the fact that many such complexes are effective catalyst precursors in a variety of industrially useful processes.[2,3] In contrast to this, only a few main group metal complexes of phosphinoalkoxides have been described.[3b–d,f,4] The same applies to lanthanide complexes.[5] We are interested in multidentate phosphinoalkoxides which we expect to effectively complex more lithium cations than required for charge neutrality (lithium trap) thereby resulting in mixed multinuclear lithium aggregates which also incorporate additional anions.

The tris(phosphinomethyl)-substituted alcohol **1** was found to be particularly useful in this respect. It was prepared from 1-chloro-2,3-epoxy-2-chloromethylpropane by reaction with 3 equivalents of $LiPMe_2$ (Scheme 1)[6] following the synthesis of the corresponding perphenyl compound.[3c] Compound **1** reacts with excess *n*BuLi (2.5 M solution in hexane)[3c] at −78 °C without additional solvent to form the lithium alkoxide which crystallizes with two equivalents of *n*BuLi as a hexalithium dimer† with crystallographic inversion symmetry (compound **2**; Scheme 1).‡ In the mixed *n*-butyllithium/lithium alkoxide aggregate **2** the six lithium atoms are arranged at the corners of a slightly distorted octahedron (Fig. 1). Two opposite triangular Li_3 faces of the octahedron are capped each by the μ_3-oxygen atoms of one alkoxide ligand. In addition, each of the lithium atoms of these Li_3 faces is coordinated by one of the phosphino groups of the same ligand. Thereby three lithium atoms are held closely together by one of the deprotonated monoanionic ligands **1** in a very compact and effective way. Particular indications of this are the short Li–O bonds and the Li–P bond distances (see Fig. 1).[7] Charge neutrality in dimeric **2** is achieved by four additional *n*-butyl anions which bridge four of the remaining triangular faces of the octahedron. As is often the case for hexameric octahedral compounds with a 1 : 1 stoichiometry of cation to anion, the two unbridged faces of the octahedron are on opposite sides of the polyhedron. It should be noted that solid *n*BuLi itself is an octahedral hexamer.[8] To our knowledge, in addition to [*n*BuLi· Li*O*t*Bu*]$_4$[9] only one other mixed organolithium/lithium alkoxide aggregate has been structurally characterized to date.[10]

Formation and structural details of **2** strongly suggest that [$LiOC(CH_2PMe_2)_3$], formed initially by deprotonation of **1**, has further lithium binding capacity trapping two additional lithium cations. The fragment $[Li_3OC(CH_2PMe_2)_3]^{2+}$ itself seems to be an ideal building block for mixed oligomeric lithium aggregates, in which the lithium atoms are at the vertices of trigonal polyhedral faces.

Proof for this comes from a second, unexpected reaction of **1** with *n*BuLi. In contrast to the synthesis of **2**, which was performed in the absence of solvent (other than the hexane contained in the 2.5 M solution of *n*BuLi), **1** reacts with excess *n*BuLi in toluene alone at room temperature to form the Y-conjugated, symmetrically tris(dimethylphosphino)-substituted trimethylenemethane dianion which, to our knowledge, has not been described before.[11] It crystallizes with the beforementioned fragment $[Li_3OC(CH_2PMe_2)_3]^{2+}$ as counter ion (compound **3**; Scheme 1).† At the center of the molecular structure of **3** (Fig. 2)‡ is an equilateral triangle of lithium atoms which is capped on one side by the deprotonated alcohol **1** in much the same way as in the structure of **2**. The other side of the

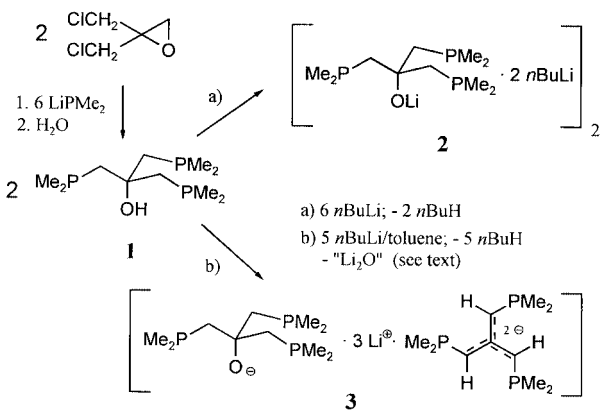

Scheme 1

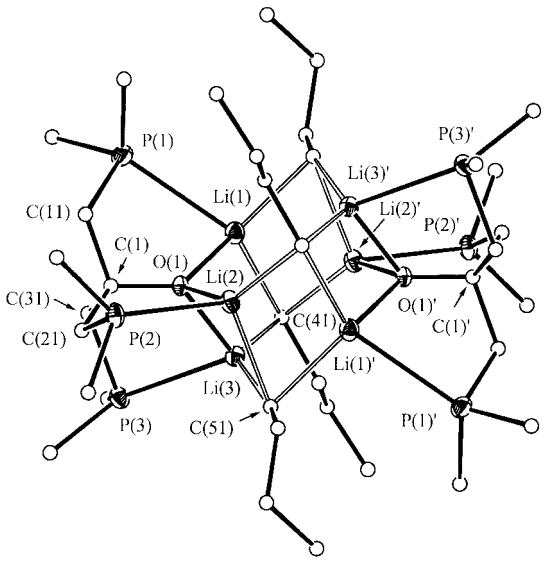

Fig. 1 Molecular structure of **2** in the crystal (ORTEP-III; displacement ellipsoids at the 30% probablility level. For clarity, C atoms are drawn as spheres with arbitray radii, and all H atoms have been omitted. Open bonds serve to highlight the Li–C bonds. Primed atoms are related to those without a prime by a center of inversion). Distances (Å): Li(1)–O(1) 1.904(4), Li(2)–O(1) 1.897(4), Li(3)–O(1) 1.916(4), Li(1)–P(1) 2.755(4), Li(2)–P(2) 2.613(4), Li(3)–P(3) 2.736(4).

 DOI: 10.1039/b010115j

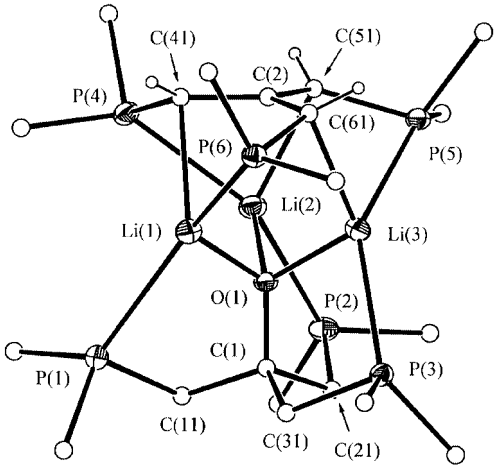

Fig. 2 Molecular structure of **3** in the crystal (ORTEP-III; displacement ellipsoids at the 30% level. For clarity, C atoms are drawn as spheres with arbitray radii; H atoms omitted except those at the methylene C atoms). Distances (Å): Li(1)–O(1) 1.888(4), Li(2)–O(1) 1.877(3), Li(3)–O(1) 1.885(4), Li(1)–P(1) 2.665(4), Li(2)–P(2) 2.696(4), Li(3)–P(3) 2.638(4), Li(1)–P(6) 2.550(3), Li(2)–P(4) 2.592(4), Li(3)–P(5) 2.562(4).

Li_3 triangle is coordinated by the tris(phosphino)-substituted trimethylenemethane dianion. Thereby each lithium atom is coordinated to one of the phosphino groups and a methylene carbanionoid carbon atom of an adjacent arm of the dianion. Each of the lithium atoms are four-coordinate, being bonded to one oxygen, two phosphorus, and one carbon atom. It should be noted that in the only other dilithium trimethylenemethane derivative structurally characterized so far,[12] the lithium atoms are disposed on opposite sides of the trimethylenemethane dianion while in **3** the fragment $[Li_3OC(CH_2PMe_2)_3]^{2+}$ forces the lithium atoms to be located on only one side, in accord with our assumption that $[Li_3OC(CH_2PMe_2)_3]^{2+}$ should be an ideal building block for trigonal polyhedral lithium faces. Both the structural data (Fig. 2) as well as the ^{31}P and particularly the ^{7}Li NMR spectra indicate that the Li atoms in **3** are more tightly bound to the trimethylene dianion rather than to the alkoxide. This follows clearly from the shorter Li–P bonds and the additional Li–C bonds to the dianion while the NMR data indicate that at room temperature the alkoxide is freely rotating around the central C–O axis with respect to the Li_3 triangle (with the dianion being held firmly in place).†

The unexpected formation of the tris(dimethylphosphino)-substituted trimethylenemethane dianion in **3** upon reaction of **1** with excess *n*BuLi involves the formal loss of Li_2O. At present we do not know whether Li_2O is actually formed in the reaction sequence, or whether the O^{2-} anion is part of a larger mixed aggregate.[13] We believe that expulsion of O^{2-} occurs after multiple deprotonation of **1** not only at oxygen but also at one or more of the methylene carbon atoms. The formation of the trimethylenemethane dianion from **1** is then believed to be driven by the reduction of negative charge on the anion by loss of O^{2-} and by the formation of a Y-conjugated π-system.[14]

Notes and references

† *Syntheses*: **2**: to 0.3 g (1.2 mmol) of **1** 2.0 ml (5.0 mmol) of a 2.5 M solution of *n*BuLi in hexane was added at −78 °C. The reaction mixture was warmed to room temperature whereupon a clear solution formed from which immediately small colorless crystals of **2** precipitated. After 30 min the crystals rapidly decomposed to an amorphous solid. The recording of NMR spectra is hampered by the necessity to avoid solvents in the synthesis of **2** (see synthesis of **3**).

3: Toluene (0.75 ml) was added to 110 mg (1.7 mmol) of neat *n*BuLi. Subsequently 140 mg (0.55 mmol) of **1** was added dropwise at room temperature, throughly mixed, and left standing for 2 d. The yield of **3** in solution is *ca.* 70% (^{31}P NMR). Colorless needles formed which proved suitable for X-ray diffraction. Mp 165 °C (decomp.); Anal. $C_{20}H_{45}Li_3OP_6$; calc: C, 47.27; H, 8.92; found: C, 47.02; H, 8.34%. ^{31}P {^{1}H} NMR (162 MHz, toluene-d_8, 25 °C, ext. 85% H_3PO_4): alkoxide: δ −59.5 [br s]; dianion: −64.2 [q (1 : 1 : 1 : 1), $^{1}J_{PLi}$ 58 Hz]; ^{31}P{^{1}H} NMR (toluene-d_8, −80 °C): alkoxide: δ −63.3 [m]; dianion: −64.2 [qd, $^{1}J_{PLi}$ 58, $^{2}J_{PP}$ 19 Hz], $T_C \approx -45$ °C; ^{7}Li {^{1}H} NMR (155 MHz, toluene-d_8, 25 °C, ext. 1 M LiBr in THF-d_8): δ 0.35 [dq, $^{1}J_{LiP}$ 14 Hz, with 3 alkoxide P, $^{1}J_{LiP}$ 58 Hz, with 1 dianion P]; ^{7}Li{^{1}H} NMR (toluene-d_8, −80 °C): δ 0.35 [dd, $^{1}J_{LiP}$ 42 Hz, with 1 alkoxide P, $^{1}J_{LiP}$ 58 Hz, with 1 dianion P], $T_C \approx -20$ °C.

‡ *Crystallography*: single crystals of **2**, grown as described above, were transferred immediately to the diffractometer (Enraf-Nonius CAD4) and examined at −78 °C under strict exclusion of air and moisture in a frozen oil drop (Mo-Kα radiation, λ = 0.71069 Å). *Crystal data* for **2**: $C_{36}H_{84}Li_6O_2P_6$, M = 776.49, monoclinic, space group $C2/c$, a = 21.440(2), b = 17.254(1), c = 14.121(1) Å, β = 103.000(9)°, V = 5089.8(8) Å^3, Z = 4, D_c = 1.013 g cm^{-3}, μ(Mo-Kα) = 2.4 cm^{-1}. 4498 unique reflexions (*hkl* range: ±25, +20, +16) up to $((\sin\theta)/\lambda)_{max.}$ = 0.595 Å^{-1}, *R*/*wR*/*S* = 0.047/0.132/1.04 for 236 refined parameters and all data (non-H atoms anisotropic, H atoms fixed). $\Delta\rho_{fin}$(max./min.) = 0.41/−0.37 e Å^{-3} (SHELXS-97, SHELXL-97).

Single crystals of **3**, grown as described above, were examined at −78 °C in a frozen oil drop. *Crystal data* for **3**: $C_{20}H_{45}Li_3OP_6$, M = 508.20, triclinic, space group $P\bar{1}$, a = 9.087(2), b = 11.851(2), c = 15.175(3) Å, α = 81.323(7), β = 89.812(7), γ = 73.27(2)°, V = 1545.7(5) Å^3, Z = 2, D_c = 1.092 g cm^{-3}, μ(Mo-Kα) = 3.6 cm^{-1}. 5713 unique reflexions (*hkl* range: −10, ±14, ±18) up to $((\sin\theta)/\lambda)_{max.}$ = 0.604 Å^{-1}, *R*/*wR*/*S* = 0.040/0.120/1.04 for 295 refined parameters and all data (non-H atoms anisotropic, methylene H atoms refined freely with isotropic displacement parameters, all others fixed). $\Delta\rho_{fin}$(max./min.) = 0.64/−0.47 e Å^{-3}.

CCDC 155751 and 155752. See http://www.rsc.org/suppdata/cc/b0/b010115j/ for crystallographic data in .cif or other electronic format.

1 J. Holz, M. Quirmbach and A. Börner, *Synthesis*, 1997, 983.
2 W. Keim, *New. J. Chem.*, 1994, **18**, 93; W. Keim, *Angew. Chem.*, 1990, **102**, 251; W. Keim, *Angew. Chem., Int. Ed. Engl.*, 1990, **29**, 235.
3 (*a*) R. Brüll and W. Keim, *J. Chem. Res. (S)*, 1997, 292; (*b*) J. A. van Doorn, H. van der Heijden and A. G. Orpen, *Organometallics*, 1995, **14**, 1278; (*c*) J. A. van Doorn, H. van der Heijden and A. G. Orpen, *Organometallics*, 1994, **13**, 4271; (*d*) M. D. Fryzuk, X. Gao and S. J. Rettig, *Can. J. Chem.*, 1995, **73**, 1175; (*e*) W. Keim and R. P. Schulz, *J. Mol. Catal.*, 1994, **92**, 21; (*f*) P. B. Hitchcock, M. F. Lappert and I. A. MacKinnon, *J. Chem. Soc., Chem. Commun.*, 1993, 1015; (*g*) S. M. Baxter and P. T. Wolczanski, *Organometallics*, 1990, **9**, 2498.
4 T. Koch, S. Blaurock, F. Somoza, Jr. and E. Hey-Hawkins, *Eur. J. Inorg. Chem.*, 2000, 2167; L. M. Engelhardt, J. MacB. Harrowfield, M. F. Lappert, I. A. MacKinnon, B. H. Newton, C. L. Raston, B. W. Skelton and A. H. White, *J. Chem. Soc., Chem. Commun.*, 1986, 846.
5 H. Schumann, E. Palamidis and J. Loebel, *J. Organomet. Chem.*, 1990, **384**, C49; P. B. Hitchcock, M. F. Lappert and I. A. MacKinnon, *J. Chem. Soc., Chem. Commun.*, 1988, 1557.
6 A. Feustel, unpublished work.
7 K. Izod, *Adv. Inorg. Chem.*, 2000, **50**, 33.
8 T. Kottke and D. Stalke, *Angew. Chem.*, 1993, **105**, 619; T. Kottke and D. Stalke, *Angew. Chem., Int. Ed. Engl.*, 1993, **32**, 580.
9 M. Marsch, K. Harms, L. Lochmann and G. Boche, *Angew. Chem.*, 1990, **102**, 334; M. Marsch, K. Harms, L. Lochmann and G. Boche, *Angew. Chem., Int. Ed. Engl.*, 1990, **29**, 308.
10 B. Goldfuss, S. I. Khan and K. N. Houk, *Organometallics*, 1999, **18**, 2927.
11 J. A. van Doorn and H. van der Heijden, *Recl. Trav. Chim. Pays-Bas*, 1990, **109**, 302.
12 D. Wilhelm, H. Dietrich, T. Clark, W. Mahdi, A. J. Kos and P. v. R. Schleyer, *J. Am. Chem. Soc.*, 1984, **106**, 7279; D. Wilhelm, T. Clark, P. v. R. Schleyer, K. Buckl and G. Boche, *Chem. Ber.*, 1983, **116**, 1669.
13 T. Chivers, A. Downard and G. P. A. Yap, *J. Chem. Soc., Dalton Trans.*, 1998, 2603; A. R. Kennedy, R. E. Mulvey and R. B. Rowlings, *J. Am. Chem. Soc.*, 1998, **120**, 7816.
14 J. Klein, *Tetrahedron*, 1983, **39**, 2733, and references therein.

CHEMCOMM
Communication
www.rsc.org/chemcomm

The best structural model of ADH so far: a pyrazolylbis(thioimidazolyl)borate zinc ethanol complex

Jan Seebacher, Mouhai Shu and Heinrich Vahrenkamp*

Institut für Anorganische und Analytische Chemie der Universität Freiburg, Albertstr. 21, D-79104 Freiburg, Germany.

Received (in Cambridge, UK) 8th January 2001, Accepted 17th April 2001
First published as an Advance Article on the web 15th May 2001

The new *N,S,S* ligand $[HB(tim^{o\text{-}An})_2(pz^{Ph,Me})]^-$ (L^1) was combined with zinc perchlorate and ethanol to form the complex $[L^1{\cdot}Zn(ethanol)]ClO_4$ which is the first zinc complex in which the *N,S,S* ligation of zinc and the attachment of ethanol occurring in the active center of horse liver alcoholdehydrogenase (ADH) have been reproduced; the structural details of the $ZnNS_2O$ coordination in the complex and in DMSO-inhibited ADH are in reasonably good agreement.

Both the function and the coordination environment of zinc in horse liver alcoholdehydrogenase, ADH,[1,2] are unusual. Zinc supports, but does not participate in, a redox reaction, *i.e.* the hydride transfer interconverting alcohol and aldehyde; and in the resting enzyme zinc is in an uncharged state, being bound to one histidine and two cysteinate residues. It can be assumed that the latter is the prerequisite for the former, making it possible that in the enzymatic environment the alcohol is bound to zinc as an alkoxide and that its ß-hydrogens are labilized for removal as H^- by NAD^+.

These unusual properties have made it impossible until now to build coordination compounds of zinc which correctly model the coordination environment of the metal[3–5] or which show a reasonable catalytic activity for hydride transfer to NAD^+/NADH systems.[6–8] Most of the *N,S,S* ligands which were designed and used for this purpose have too strong a tendency to form oligonuclear thiolate-bridged zinc complexes, and the fixation of the very labile Zn–OR function in mononuclear zinc alkoxides has required the use of coligands which suppress the desired catalytic activity of zinc. The closest approximations to structural models[9–11] were achieved by Parkin *et al.*[4] and ourselves.[5] Parkin's group prepared tetrahedral L·Zn–X complexes of a new *N,S,S* ligand L. We prepared tetrahedral $(RS)_2Zn(N,O)$ complexes using pyridine-derived alcohols or aldehydes as *N,O* ligands. A realistic functional modelling, *i.e.* by using NAD^+ derivatives as hydride acceptors, has been tried in only a few cases and with little success.[8,12,13]

The work described in this communication was triggered by a report by Reglinski *et al.*,[14] which describes the simple synthesis of tris(thioimidazolyl)borate ligands. In these ligands the thioimidazolyl sulfur donors can be considered 'tame' thiolate donors according to the following resonance formulation:

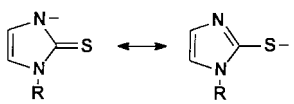

In agreement with this there is no sulfur bridging in metal complexes of thioimidazolylborate ligands and such ligands are quite reliable tetrahedral enforcers.[4,7,14–16] Furthermore, their synthesis allows the incorporation of pyrazolyl functions as mixed pyrazolylthioimidazolylborates with *N,S,S* or *N,N,S* donor sets.[4,15,16] Having realized this, it was a matter of varying the substituents on the pyrazole and thioimidazole groups of a pyrazolylbis(thioimidazolyl)borate[16] (*i.e.* a *N,S,S* ligand) in order to generate an appropriate electronic and geometrical environment for a ligated zinc ion to accommodate an alcoholic substrate in an ADH model complex.

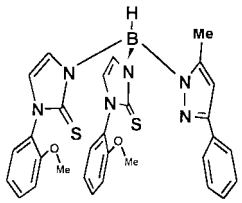

Ligand L^1 was found to fulfil these conditions. Its constituent 1-(*o*-anisyl)-2-thioimidazole† is accessible from 2-methoxyaniline and KSCN by the established procedure.[17] The reaction between two equivalents of the thioimidazole and one equivalent each of 3-phenyl-5-methylpyrazole and KBH_4 in boiling toluene leads to very good yields of $K[L^1]$.† The reaction between $K[L^1]$ and $Zn(ClO_4)_2{\bullet}6H_2O$ in non-dehydrated ethanol produces the raw complex **1** in nearly quantitative yield.‡ Crystals of **1** for the structure determination were obtained by slow evaporation from ethanol.†

$$[HB(tim^{o\text{-}An})_2(pz^{Ph,Me})Zn(C_2H_5OH)]\,ClO_4{\bullet}C_2H_5OH$$

1

Complex **1** fulfils the conditions to be a close structural model of ADH. It bears a tridentate *N,S,S* ligand and an ethanol molecule comprising a $ZnNOS_2$ coordination pattern as in the enzyme and its pentafluorobenzyl alcohol-inhibited derivative.[2] The structure determination§ (see Fig. 1) has shown the complex to be tetrahedral to a good approximation. The alcohol ligand is embedded between the three aromatic substituents of

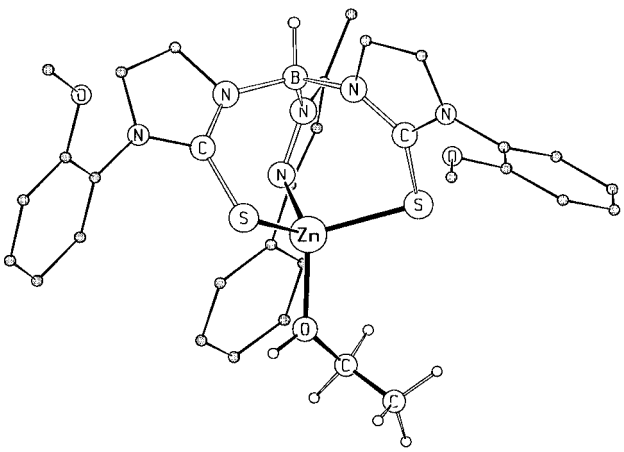

Fig. 1 Molecular structure of the cation of **1**. The OH hydrogen atom, which was not localized crystallographically, was placed on a reasonable position along the hydrogen bond to the attached second ethanol molecule.

 DOI: 10.1039/b100281n

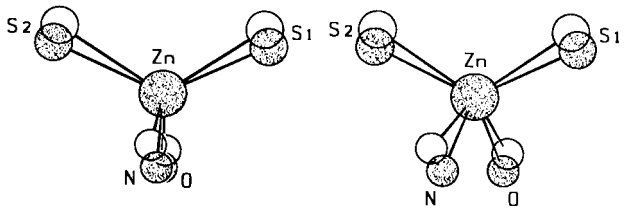

Fig. 2 Superpositions of the $ZnNOS_2$ cores of **1** (open circles) and DMSO-inhibited ADH[2] (filled circles). Left: ZnS_2 in the plane of the drawing, right: rotated by 20° about a vertical axis.

Table 1 Comparison of the $ZnNOS_2$ units in **1** and in DMSO-inhibited ADH[2]

	1	ADH•DMSO
Zn–N/Å	2.012(3)	2.02
Zn–O/Å	1.970(3)	2.13
Zn–S/Å	2.282(1), 2.314(1)	2.19, 2.25
N–Zn–O/°	116.8(1)	94.2
N–Zn–S/°	100.2(1), 111.7(1)	107.4, 113.1
O–Zn–S/°	105.4(1), 109.8(1)	102.5, 103.3
S–Zn–S/°	113.2(1)	129.4

L[1]. It is attached to a second ethanol molecule by a hydrogen bond, sharing this property with Parkin's tris(thioimidazolyl)borate–zinc–CH_3OH•CH_3OH complex.[7] It seems that the electronic 'saturation' of the zinc ion by the soft sulfur donors and the hydrophobicity of the aromatic environment provide the driving force for the preferred attachment of the less polar alcohol ligand, rather than the water or hydroxide ligands which are present in the reaction solution and which become bound to zinc in similar preparations of zinc complexes with tridentate *N,N,N* or *N,N,O* environments.[18]

The bond lengths and bond angles of **1** are very similar to those in Parkin's S_3Zn–CH_3OH complex.[7] Moreover they agree satisfactorily with those in the ADH structure of highest resolution (1.8 Å), *i.e.* that of the DMSO-inhibited enzyme.[2] Fig. 2 and Table 1 give the details for the $ZnNOS_2$ units. Both units can be described as close to tetrahedral, as can be seen in Fig. 2 by the perpendicular arrangements of the SZnS and NZnO planes. Almost all differences in bond lengths and bond angles are within an acceptable range. The major distortions lie in the enzyme's very small N–Zn–O and very large S–Zn–S angles and in the difference between the Zn–O('substrate') bond lengths.

In summary, a new thioimidazolylborate based *N,S,S* ligand has been prepared and used to obtain a zinc complex which binds ethanol on its fourth coordination site. This corresponds to the first step in the catalytic cycle of horse liver alcoholdehydrogenase (ADH), the incorporation of ethanol within the active center which contains *N,S,S* ligated zinc. The resulting complex **1** is the first model complex that reproduces both the *N,S,S* ligation and the alcohol binding.

This work was supported by the Deutsche Forschungsgemeinschaft.

Notes and references

† The new compounds were characterized by elemental analyses. Complex **1** shows the OH absorption in the IR spectrum as a broad band centered at 3150 cm^{-1} which is typical for O–H···O hydrogen bonding. ^1H NMR ($CDCl_3$): δ 1.18 (t, *J* 7.0 Hz, 6H, ethyl-CH_3), 2.50 (s, 3H, pz-CH_3), 3.61 (q, *J* 7.0 Hz, 2H, ethyl-CH_2), 3.62 (q, *J* 7.0 Hz, 2H, ethyl-CH_2), 3.82 (s, 6H, OCH_3), 6.40 (s, 1H, pz-CH), 6.94 (d, *J* 2.1 Hz, 2H, tim-CH), 7.02 (d, *J* 2.1 Hz, 2H, tim-CH), 7.0–7.6 (m, 13H, aromatic).

‡ **Caution**: perchlorate salts of metal–organic compounds should be handled with care and only in small amounts.

§ *Crystal data* for $C_{34}H_{42}BClN_6O_9S_2Zn$: M = 854.5, triclinic, space group $P\bar{1}$ (no. 2), a = 10.962(1), b = 14.131(2), c = 14.834(2) Å, α = 101.011(2), β = 109.568(2), γ = 94.234(2)°, V = 2101.6(4) Å^3, T = 200(2) K, Z = 2, λ(Mo-Kα) = 0.71073 Å, Bruker Smart CCD diffractometer. 19203 reflections were collected and subjected to an empirical absorption correction (SADABS). The final R index for [$I > 2\sigma(I)$] with 5057 reflections was R_1 = 0.061. CCDC 156428. See http://www.rsc.org/suppdata/cc/b1/b100281n/ for crystallographic data in .cif or other electronic format.

1 For the function of ADH, *cf.* H. Eklund, B. Nordström, E. Zeppezauer, G. Söderlund, I. Ohlsson, T. Boiwe, B. O. Söderberg, O. Tapia, C. I. Brändén and A. Akeson, *J. Mol. Biol.*, 1976, **102**, 27.
2 For recent structure determinations of ADH, *cf.* S. Ramaswamy, H. Eklund and B. V. Plapp, *Biochemistry*, 1994, **33**, 5230 ($C_6F_5CH_2OH$ bound to zinc); S. Al-Karadaghi, E. S. Cedergren-Zeppezauer, S. Hövmoller, K. Petratos, H. Terry and K. Wilson, *Acta Crystallogr., Sect. D.*, 1994, **50**, 793 (dimethyl sulfoxide bound to zinc).
3 For references on structural modelling see refs. 4 and 5.
4 C. Kimblin, T. Hascall and G. Parkin, *Inorg. Chem.*, 1997, **36**, 5680.
5 B. Müller, A. Schneider, M. Tesmer and H. Vahrenkamp, *Inorg. Chem.*, 1999, **3**, 1900.
6 For references on functional modelling, see refs. 7 and 8.
7 C. Kimblin, B. M. Bridgewater, D. G. Churchill and G. Parkin, *Chem. Commun.*, 1999, 2301.
8 R. Walz and H. Vahrenkamp, *Inorg. Chim. Acta*, 2001, **314**, 58.
9 *N,S,S* ligands with sulfur in the form of thioether functions, which can form L•Zn–X complexes, have been described by Riordan[10] and Berreau.[11]
10 S. J. Chiou, J. Innocent, C. G. Riordan, K. C. Lam, L. Liable-Sands and A. Rheingold, *Inorg. Chem.*, 2000, **39**, 4347.
11 L. M. Berreau, R. A. Allred, M. M. Makowska-Grzyska and A. Arif, *Chem. Commun.*, 2000, 1423.
12 B. Kaptein, L. Wang-Griffin, G. Barf and R. M. Kellogg, *J. Chem. Soc., Chem. Commun.*, 1987, 1457.
13 A. Shirra and C. J. Suckling, *Tetrahedron Lett.*, 1975, **38**, 3323.
14 M. Garner, J. Reglinski, I. Cassidy, M. D. Spicer and A. R. Kennedy, *Chem. Commun.*, 1996, 1975; J. Reglinski, M. Garner, I. D. Cassidy, P. A. Slavin, M. D. Spicer and D. R. Armstrong, *J. Chem. Soc., Dalton Trans.*, 1999, 2119; J. Reglinski, M. D. Spicer, M. Garner and A. R. Kennedy, *J. Am. Chem. Soc.*, 2000, **121**, 2317.
15 C. Kimblin, B. M. Bridgewater, T. Hascall and G. Parkin, *J. Chem. Soc., Dalton Trans.*, 2000, 1267; C. Kimblin, B. M. Bridgewater, D. G. Churchill, T. Hascall and G. Parkin, *Inorg. Chem.*, 2000, **39**, 4240.
16 R. Walz, M. Tesmer, B. Wu, M. Shu and H. Vahrenkamp, unpublished results.
17 J. Kister and G. Assef, *Can. J. Chem.*, 1979, **57**, 813.
18 H. Vahrenkamp, *Acc. Chem. Res.*, 1999, **32**, 589.

CHEMCOMM
Communication
www.rsc.org/chemcomm

The first luminescent tetranuclear copper(I) μ_4-phosphinidene complex†

Vivian Wing-Wah Yam,* Eddie Chung-Chin Cheng and Nianyong Zhu

Department of Chemistry, The University of Hong Kong, Pokfulam Road, Hong Kong, China. E-mail: wwyam@hku.hk

Received (in Cambridge, UK) 8th February 2001, Accepted 25th April 2001
First published as an Advance Article on the web 15th May 2001

The first luminescent tetranuclear copper(I) phosphinidene complex $[Cu_4(\mu\text{-dppm})_4(\mu_4\text{-PPh})](BF_4)_2$ has been synthesized and isolated; the red-light emitting properties and air-stability of the complex in the solid state may render great potential for this new class of compounds in the future development of semiconducting luminescence materials and applications in LED technology.

The recent growth in interest in the chemistry of transition metal–pnictogenide complexes has been prompted in part by the potential of utilizing such compounds as precursors of binary pnictogenides in the development of electronic and optical materials.[1] With different particle size, the luminescence and optical properties of the transition metal–pnictogenides may vary dramatically due to the quantum size effect.[2] Therefore one of the important aspects in this field is to prepare particles or synthesize model complexes with a controllable and uniform size. In view of this, together with our recent efforts on the syntheses and isolations of a number of polynuclear coinage metal chalcogenide complexes with a d^{10} electronic configuration,[3] we believe that an exploration into the related phosphinidene complexes might give rise to new classes of soluble molecular materials of uniform size, with easily tunable luminescence properties *via* the participation of different ancillary ligands. To the best of our knowledge, phosphinidene complexes of d^{10} transition metals are extremely rare.[4,5] Herein, is described the first report on the isolation, characterization and X-ray crystal structure of a novel red-light emitting tetranuclear copper(I)–phosphinidene complex, $[Cu_4(\mu\text{-dppm})_4(\mu_4\text{-PPh})](BF_4)_2$ **1** [dppm = bis(diphenylphosphino)-methane], which is stable to air in the solid state and highly soluble in common organic solvents. Its photophysical properties have also been investigated.

Reaction of $[Cu_2(\mu\text{-dppm})_2(MeCN)_2](BF_4)_2$[6] with $PhPH_2$ and $Na(acac)\cdot H_2O$ (acac = acetylacetonate) in THF under nitrogen gave an orange precipitate. Recrystallization from dichloromethane–diethyl ether afforded **1** as air-stable orange-red crystals in 80% yield. The formulation of **1** was confirmed by elemental analyses, positive FAB-MS, ^1H and ^{31}P NMR spectroscopy.‡ The solid state structure was established by X-ray crystallography.§

Fig. 1 shows the perspective drawing of the complex cation of **1**. The four copper atoms are almost coplanar and form a rectangular array, with the four bridging dppm ligands arranged in a saddle-like configuration. The Cu–Cu distances range from 2.8225(9) to 3.4451(1) Å, and show no significant $Cu^I\cdots Cu^I$ interactions. The phosphinidenic phosphorus sits at the apex of the distorted square-pyramid and quadruply bridges the four copper atoms, with projection of *ca.* 0.70 Å above the idealized Cu_4 plane. The plane of the phenyl ring on the phosphinidene is perpendicular to the Cu_4 plane and has an orientation that bisects the two longer Cu–Cu edges, Cu1–Cu4 and Cu2–Cu3, so as to minimize the steric hindrance experienced by the phenyl rings on the phosphinidene and the two dppm ligands that were folded upwards. This is also in accordance with the observed elongation of the Cu–Cu long edges and the shortening of the short edges when compared to the isoelectronic but less sterically demanding chalcogenide counterparts, $[Cu_4(\mu\text{-dppm})_4(\mu_4\text{-S})](PF_6)_2$ [3.128(1), 2.869(1) Å] and $[Cu_4(\mu\text{-dppm})_4(\mu_4\text{-Se})](PF_6)_2$ [3.271(4), 2.908(4) Å].[3c,d] The Cu–P(phosphinidene) bond distances of 2.2811(1)–2.3230(1) Å are comparable to other Cu^I–μ_4-PR systems, such as $[Cu_{24}\{P(Me_2(Pr^iMe_2C)Si)\}_{12}]$ [2.226(3) Å] and $[Cu_{18}(PPh)_4(PPh_2)_{10}(PHPh_2)_3]$ [2.272(2)–2.449(2) Å].[4] All the Cu–P(dppm) bond distances are typical of those reported in other copper(I)–dppm systems.[7] It is of note that all Cu–P(dppm) bonds on the same side as the phosphinidene moiety are longer than those on the other side. This is simply a consequence of the steric requirements for the accommodation of the phosphinidene and the dppm ligands on the same side of the Cu_4 rectangle.

The ^1H NMR spectrum of **1** in CD_2Cl_2 at ambient temperature shows four broad methylene proton signals with equivalent integrals, indicative of the absence of a flipping motion for dppm and the rotation of the phosphinidene group. This is different from the situation in $[M_4(\mu\text{-dppm})_4(\mu_4\text{-E})]^{2+}$ (M = Cu, Ag; E = S, Se, Te), where flipping motions of the dppm ligands occurs and only one methylene signal has been observed.[3c–e] The $^{31}P\{^1H\}$ NMR spectrum shows the unresolved phosphinidene P signal at δ −94.97, a much more downfield environment compared to the structurally related AuI–phosphinidene complexes, $[2,4,6\text{-}Bu^t_3C_6H_2P(AuPPh_3)_4](BF_4)_2$ (δ −47.69) and $[2\text{-}MeC_6H_4P(AuPPh_3)_4](BF_4)_2$ (δ −54.6).[5]

The electronic absorption spectrum of **1** in CH_2Cl_2 shows a low-energy absorption band at *ca.* 466 nm (Fig. 2). The electronic absorption spectral data are summarized in Table 1. With reference to previous spectroscopic work on the related metal chalcogenido systems,[3] the low energy absorption band at 466 nm, which is absent in the copper(I) precursor complex, is likely to be originated from the [P(phosphinidene) → Cu]

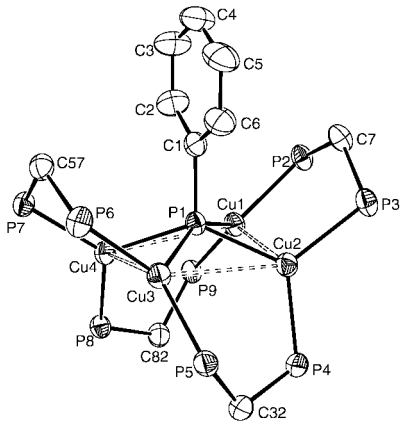

Fig. 1 Perspective view of $[Cu_4(\mu\text{-dppm})_4(\mu_4\text{-PPh})]^{2+}$ with atomic numbering scheme. The phenyl rings of the dppm ligand are omitted for clarity. Thermal ellipsoids are drawn at the 30% probability level.

† Electronic supplementary information (ESI) available: full crystal structure determination details. See http://www.rsc.org/suppdata/cc/b1/b101284n/

 DOI: 10.1039/b101284n

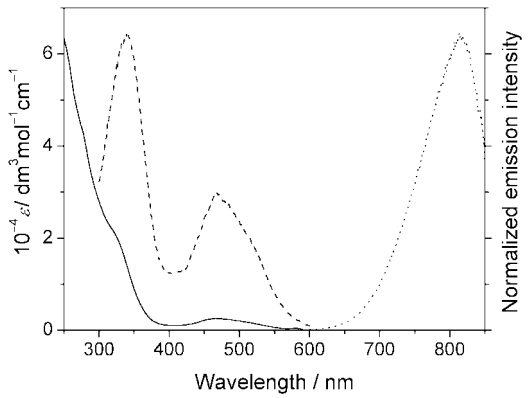

Fig. 2 Electronic absorption (——), emission (-----) and excitation (monitored at 816 nm) (·····)·spectra of **1** in CH_2Cl_2 at 298 K.

Table 1 Photophysical data for **1**

λ_{abs}[a]/nm (ε/dm^3 mol^{-1} cm^{-1})	Medium (T/K)	λ_{em}[c]/nm	τ_o/μs
268 (sh)[b] (49370), 316 sh[b] (23460), 466 (3480)	Solid (298)	718	8.3 ± 0.2
	Solid (77)	754	550 ± 50
	CH_2Cl_2 (298)	816	2.0 ± 0.1
	CH_2Cl_2 (77)	825	330 ± 30

[a] In CH_2Cl_2 at 298 K. [b] The absorption shoulders were determined from the derivatives of the UV–VIS absorption spectra. [c] Corrected for photomultiplier tube response.

ligand-to-metal charge-transfer (LMCT) transition. An assignment of such low-energy bands to intraligand IL (phosphinidene) transitions is unlikely as the related gold(I) phosphinidene complex, $[2\text{-}MeC_6H_4P(AuPPh_3)_4](BF_4)_2$,[5b] is reported to be colourless, indicating the absence of low-energy absorption in this region. The high-energy band at 268 nm is attributed to the intra-ligand transition of dppm.

Excitation of **1** in the solid state and in fluid solutions at $\lambda \approx$ 500 nm results in intense long-lived red luminescence (Table 1). Excitation bands at *ca*. 339 and 469 nm were observed upon monitoring the emission at 816 nm (Fig. 2). The close resemblance of the excitation spectrum to the electronic absorption spectrum is suggestive of an emission origin derived from the [P(phosphinidene) → Cu] LMCT transition. The observed lifetime in the microsecond range indicates the spin-forbidden nature of the emission, that is tentatively assigned to be originated predominantly from the triplet state derived from the [P(phosphinidene) → Cu] LMCT transition that mixed with a metal-centred (d–s/d–p) Cu^I state. Such an assignment is based on the fact that the phosphinidene group, being isoelectronic with and similar to the unsubstituted chalcogenides, is a good σ-donor. The red-shift in the emission energies upon lowering the temperature is supportive of such an assignment as it can readily be rationalized by the shrinking of the Cu_4 skeleton, which lowers the energy of the sσ acceptor orbitals derived from the overlap of the 4s orbitals of copper. Assignment based on similar grounds has been reported on the related systems with d^8–d^8 metal–metal interactions.[8]

The present work demonstrates a facile, high-yield synthesis towards soluble luminescent copper(I) phosphinidene complexes. This may, in one way or the other, open up new avenues to the chemistry of polynuclear copper(I) complexes by utilizing the $[Cu_4(dppm)_4]PR$ unit as the building block for higher nuclearity copper(I) complexes and clusters, through various functionalizations on the organic R group. Examples of polynuclear gold(I) aggregates made by using this approach have been illustrated by Schmidbaur *et al.*[9] The present system may also serve as a potential precursor to advanced luminescent materials for applications in the electro-luminescent technology; the emission colour of which could be readily fine-tuned by employing various R groups that have different electron-donating/withdrawing ability.[10]

V. W.-W. Y. acknowledges financial support from the Research Grants Council and The University of Hong Kong, and the receipt of a Croucher Senior Research Fellowship from the Croucher Foundation. E. C.-C. C. acknowledges the receipt of a postgraduate studentship (1997–99) from The University of Hong Kong and a Croucher Scholarship (1999–2000) from the Croucher Foundation, and N. Z. the receipt of a university postdoctoral fellowship from The University of Hong Kong.

Notes and references

‡ $[Cu_4(\mu\text{-dppm})_4(\mu_4\text{-PPh})](BF_4)_2$ **1**: elemental analyses: calc. for **1**·0.5CH_2Cl_2 (found): C 60.45 (60.66), H 4.48 (4.51)%; positive FAB-MS: *m/z* 1987 $[M - BF_4]^+$, 1602 $[M - dppm - BF_4]^+$, 950 $[M - 2BF_4]^{2+}$; ^{1}H NMR (500 MHz, CD_2Cl_2, 298 K): δ 2.51 (m, 2H, CH_2), 2.87 (m, 2H, CH_2), 3.31 (m, 2H, CH_2), 3.50 (m, 2H, CH_2), 6.30–7.71 (m, 85H, Ph); $^{31}P\{^1H\}$ NMR (202 MHz, CD_2Cl_2, 298 K): δ −10.81 (m, I = 4, dppm), −12.96 (m, I = 4, dppm), −94.97 (m, I = 1, phosphinidene).

§ *Crystal data* for **1**: $C_{106}H_{93}B_2Cu_4F_8P_9$·$2CH_2Cl_2$: M_r = 2243.17, monoclinic, space group *Cc* (no. 9), a = 14.456(2), b = 28.797(3), c = 25.340(3) Å, β = 91.27(2)°, V = 10546(2) Å^3, T = 301 K, Z = 4, D_c = 1.413 g cm^{-3}, μ(Mo-Kα) = 1.094 mm^{-1}, 31947 reflections measured, 17709 unique (R_{int} = 0.0401) which were used in all calculations. The final $R(F^2)$ was 0.0513 [$I > 2\sigma(I)$]. CCDC 154244. See http://www.rsc.org/suppdata/cc/b1/b101284n/ for crystallographic data in .cif or other electronic data format.

1 *Phosphorus 2000: Chemistry, Biochemistry & Technology*, ed. D. E. C. Corbridge, Elsevier, Amsterdam, The Netherlands, 2000.
2 M. Green and P. O'Brien, *Chem. Commun.*, 1999, 2235 and references therein.
3 (*a*) V. W.-W. Yam and K. K.-W. Lo, *Chem. Soc. Rev.*, 1999, 323; (*b*) V. W.-W. Yam and K. K.-W. Lo, *Comments Inorg. Chem.*, 1997, **19**, 209; (*c*) V. W.-W. Yam, W.-K. Lee and T.-F. Lai, *J. Chem. Soc., Chem. Commun.*, 1993, 1571; (*d*) V. W.-W. Yam, K. K.-W. Lo and K.-K. Cheung, *Inorg. Chem.*, 1996, **35**, 3459; (*e*) V. W.-W. Yam, K. K.-W. Lo, C.-R. Wang and K.-K. Cheung, *Inorg. Chem.*, 1996, **35**, 5116.
4 M. Driess, S. Martin, K. Merz, V. Pintchouk, H. Pritzkow, H. Grützmacher and M. Kaupp, *Angew. Chem., Int. Ed. Engl.*, 1997, **36**, 1894; A. Eichhöfer, D. Fenske and W. Holstein, *Angew. Chem., Int. Ed. Engl.*, 1993, **32**, 242.
5 (*a*) E. Zeller, H. Beruda, J. Riede and H. Schmidbaur, *Inorg. Chem.*, 1993, **32**, 3068; (*b*) H. Schmidbaur, E. Zeller, G. Weidenhiller, O. Steigelmann and H. Beruda, *Inorg. Chem.*, 1992, **31**, 2370.
6 J. Díez, M. P. Gamasa, J. Gimeno, A. Tiripicchio and M. T. Camellini, *J. Chem. Soc., Dalton Trans.*, 1987, 1275.
7 N. Brescian, N. Marsich, G. Nardin and L. Randaccio, *Inorg. Chim. Acta*, 1974, **10**, L5; (*b*) D. M. Ho and R. Bau, *Inorg. Chem.*, 1983, **22**, 4079.
8 S.-W. Lai, M. C.-W. Chan, T.-C. Cheung, S.-M. Peng and C.-M. Che, *Inorg. Chem.*, 1999, **38**, 4046.
9 H. Schmidbaur, E. Zeller and J. Ohshita, *Inorg. Chem.*, 1993, **32**, 4524.
10 V. W.-W. Yam, C.-L. Chan. S. W.-K. Choi, K. M.-C. Wong, E. C.-C. Cheng, S.-C. Yu, P.-K. Ng, W.-K. Chan and K.-K. Cheung, *Chem. Commun.*, 2000, 53.

CHEMCOMM
Communication
www.rsc.org/chemcomm

^{1}H-NMR study of the interaction of distamycin A and netropsin with the parallel stranded tetraplex [d(TGGGGT)]$_4$†

Antonio Randazzo, Aldo Galeone and Luciano Mayol*

Dipartimento di Chimica delle Sostanze Naturali, Università degli Studi di Napoli 'Federico II' via D. Montesano 49, I-80131 Napoli, Italy. E-mail: mayoll@unina.it; Fax: +39-081-678552

Received (in Cambridge, UK) 11th January 2001, Accepted 24th April 2001
First published as an Advance Article on the web 15th May 2001

The first ^{1}H-NMR investigation of the reversible interaction of two small minor groove binding molecules with a synthetic tetraplex DNA structure is reported.

Nucleic acids reversibly interact with a broad range of small organic molecules, such as intercalators or minor groove binders, which represent one of the most important lines of drug development and of current chemotherapy against cancer, viral, and some parasitic diseases. Even though these compounds are known to bind to double stranded DNA, several investigations involving the interaction of small ligands with unusual structures of nucleic acids have been reported,[1–3] including multistranded tetraplex forms.[1,4–7] A multitude of proteins have been shown to interact with these structures which, particularly, are implicated in the molecular biology of telomeres.[8–10] A high level of telomerase activity has been associated with cancer cells and may be essential for their immortality. G-quartet DNA[11] inhibits telomerase activity and, therefore, compounds that bind to this arrangement can negatively interfere with telomerase activity. This is the strongest argument in favour of the potential role of G-tetraplexes as a potential target for anticancer drug design. In this frame, we wish to report here the preliminary results from a NMR investigation of the reversible interaction of the minor groove binding agent distamycin A (Dist-A) and the related drug netropsin (Net) with the synthetic tetraplex [d(TGGGGT)]$_4$.

A wide array of G-tetraplex topologies, groove widths, loop conformations, and alternative DNA base associations have been observed to date.[4–7] The structure of the four stranded hexamer [d(TGGGGT)]$_4$ used for the present study has been already characterized by NMR and X-ray crystallography.[12] This tetraplex possesses a four-fold symmetry with all strands parallel to each other, which afford four grooves of identical medium width, and all nucleosides in an anti conformation. The 1D NMR proton spectra (T = 300 K; 500 MHz), recorded at several points during the titration of the tetraplex with Dist-A, are shown in Fig. 1. The first addition of 0.5 mol equiv. of Dist-A to the oligonucleotide caused several notable variations in the spectrum. Particularly, a general change in chemical shift of DNA proton resonances was observed, whereas a new set of broad signals appeared between 6 and 7 ppm which were assigned to the drug protons. An increase of Dist-A concentration up to 2 mol equiv. caused drug resonances to gradually grow in intensity and a progressive drift of DNA signals. Anyhow, during the early stage of the titration, the four strands were magnetically equivalent upon interaction with the drug. Surprisingly, at nearly 2:1 ligand–tetraplex stoichiometry, a further addition of drug caused a complication in the spectrum due to the presence in solution of different species in slow exchange on the chemical shift time scale. In fact, a new set of proton signals could be observed, whose intensities rose with increasing amounts of drug with a concomitant falling off of the original signals, which completely disappeared at a ratio of 4:1 drug–DNA. At this point, in spite of a general broadening of all signals, a single, well-defined species, was plainly observable in solution and any further addition of ligand did not lead to substantial changes. The final NMR spectrum showed that the binding of the ligand to the tetraplex caused the loss of the original four-fold symmetry of the free tetraplex. Particularly, 8 imino proton, 4 methyl and 12 aromatic proton resonances were clearly discernible, thus pointing to a two-fold symmetry for the 4:1 complex.

In order to clarify the binding mode of Dist-A, several NOESY spectra at 300 K (500 MHz) of the final complex were acquired at different mixing times (250, 180, 100, and 50 ms). The whole of the data provided by these experiments allowed us a preliminary conclusion that the tetraplex retained the original

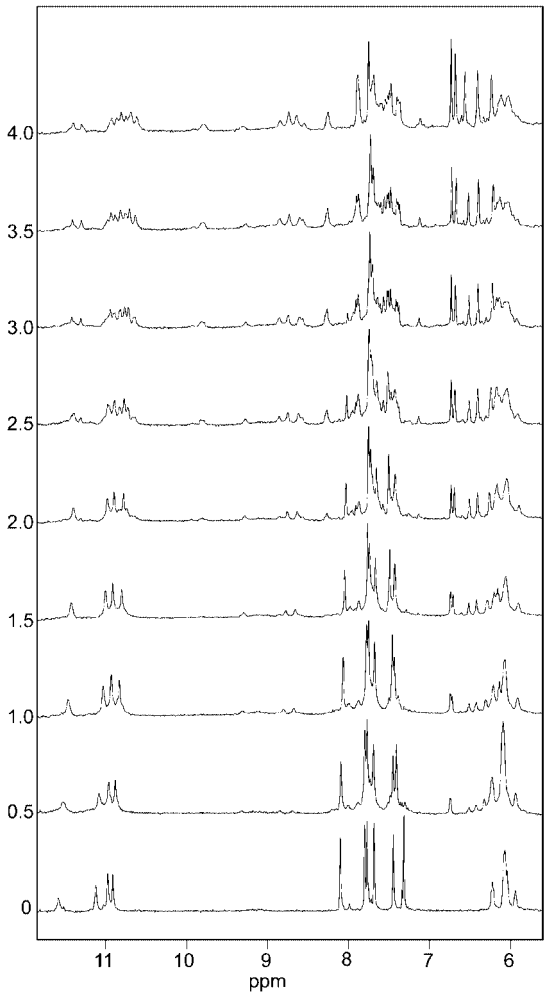

Fig. 1 Titration with Dist-A of 1.4 mM solution of [d(TGGGGT)]$_4$ containing 2 mM phosphate buffer, 0.2 mM EDTA and 70 mM KCl, pH 7.3, in 9:1 H_2O–D_2O at 300 K (500 MHz). ^{1}H NMR spectra were recorded using pulsed-field gradient WATERGATE[15] for H_2O suppression. A time domain deconvolution was used to further reduce the H_2O signal. The drug–DNA mole ratios are shown along the side of the spectra.

† Electronic supplementary information (ESI) available: 2D NOESY and ^{1}H NMR spectra for netropsin/tetraplex and distamycin/tetraplex complexes. See http://www.rsc.org/suppdata/cc/b1/b100460n/

 DOI: 10.1039/b100460n

conformation upon binding of the drug, since all intranucleotide and internucleotide connectivities of the free tetraplex were still visible. However, the evaluation of possible perturbation at the binding sites, such as small changes of the glycosidic bond angle, would require a comprehensive analysis of the NOE buildup rate and a quantitative analysis of internucleotide base to sugar NOE intensities, which have not been carried out at the present. Furthermore, the presence of ligand–ligand contacts between formyl hydrogen (FH) at 7.68 ppm and amidinium protons at 9.75 ppm and among NH1 amide proton at 8.25 ppm, C20 hydrogen at 1.49 ppm and the afore cited hydrogen at 9.75 ppm, indicated that the drug molecules simultaneously bound to the tetraplex two by two, with each term of the dimeric pairs with an antiparallel orientation and in close contact to its partner (as observed with duplex DNA).[13] An alternative explanation, exchange between two orientations of one molecule, so that the ligand–ligand NOEs arise from a combination of transferred NOE and exchange effects, could be ruled out since the NOE contacts were still visible in the NOESY spectra acquired at short mixing time (*i.e.* 50 ms), where spin diffusion phenomenon is dramatically reduced.

NOESY spectra also showed DNA–ligand contacts between imino proton at 11.28 and C20 hydrogen at 1.49 ppm and imino proton at 11.38 and both NH1 amide proton at 8.25 ppm and amidinium protons at 9.75 ppm. Other cross peaks in correspondence with DNA and ligand resonances were present in the NOESY spectra but line broadening and signal overlapping prevented us from unequivocally ascertaining which of them were actually due to ligand–DNA contacts.

It is noteworthy that, throughout the whole titration, a single set of signals was present for Dist-A protons, which only grew in intensity and did not show any significant change in chemical shift values with increasing drug concentration. This observation suggests that, (i), even at low ligand–DNA stoichiometries (*e.g.* 0.5 : 1), simultaneous binding of two Dist-A side by side, in a highly cooperative mode, is dominant; (ii), both in the 2 : 1 and in the 4 : 1 complexes, the bound pair of Dist-A, reorientates itself in a fast process on the NMR time scale, similar to that observed for the binding of Dist-A to duplex DNA structures.[14]

In conclusion, the above preliminary results can be interpreted as follows. Below 2 : 1 ligand–tetraplex stoichiometry, Dist-A, in a dimeric form, binds each groove of the tetraplex to form short-lived complexes on the NMR time scale. Therefore, only one set of signals for the four strands is observed. The fast exchange behavior of the lower complex (2 : 1 Dist-A–tetraplex) could be changed only to an intermediate regime by decreasing the temperature of the system. As the temperature was reduced from 300 to 280 K, there was only a general broadening of the resonances, with peaks belonging to Dist-A broadening more than the other peaks, probably due to the slower reorientation of the Dist-A dimer. At higher drug–DNA ratios, a second Dist-A dimer tightly and specifically binds the tetraplex, to give a 4 : 1 complex, in slow exchange with the 2 : 1 complex, as indicated by the presence of separate proton resonances for the two species. This behavior can be explained assuming that binding of the second drug pair is more favorable than binding of the first one. Finally, the dyad symmetry of the 4 : 1 complex is consistent with a model comprising two Dist-A dimers simultaneously spanning, in fast reorientation, two opposite grooves of the tetraplex, as illustrated in Fig. 2. Notably, a fully saturated complex with all grooves occupied by drug molecules was not observed. Binding of dimer Dist-A may, most likely, expand the binding groove (as observed with duplex DNA),[13] and simultaneously reduce the size of the two adjacent grooves, thus preventing a further interaction with other Dist-A molecules.

Addition of Net to the oligonucleotide (data not shown) caused gradual changes in the chemical shift and a broadening of DNA proton resonances. At a ligand–DNA ratio of 4 : 1 the titration was virtually completed. The four strands were found to be magnetically equivalent throughout the titration, since no splitting of resonances was observed at any stage. This behavior

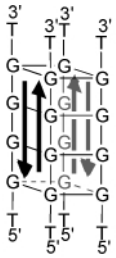

Fig. 2 Pictorial illustration of the proposed binding mode of Dist-A (arrows) to parallel-stranded tetraplex $[d(TGGGGT)]_4$.

could be explained assuming that the ligand is in fast exchange on the NMR time scale with its binding sites on the tetraplex. This fast exchange behavior could not be changed to a slow or intermediate regime by altering the temperature of the system. NOESY experiments at 300 K (500 MHz) performed at different mixing times did not show any long-range ligand–ligand interactions, whereas only a single ligand–DNA contact between H3 proton at 6.43 ppm and aromatic DNA proton at 7.72 could be unambiguously identified. These data can be tentatively explained assuming that electrostatic repulsion between the ends of the doubly charged Net molecules prevents their side-by-side arrangements into the grooves. Thus, in contrast to Dist-A, netropsin complexes the tetraplex with one drug molecule bound per groove. As for Dist-A, a comprehensive analysis of NOESY spectra showed that the structure of the tetraplex remained similar to the original conformation upon binding of netropsin, as indicated by the presence of all the intranucleotide and internucleotide connectivities of the free tetraplex.

The present communication represents the first ^{1}H-NMR investigation of the reversible interaction of groove binding agents with a tetraplex structure of DNA. Detailed structural analysis of the above 4 : 1 distamycin A–DNA complex as well as studies involving other DNA sequences and/or ligands are currently in progress.

This work is supported by Italian M.U.R.S.T. and C.N.R. The authors are grateful to 'Centro Ricerche Interdipartimentale di Analisi Strumentale', C.R.I.A.S., for supplying NMR facilities. Veronica Esposito is acknowledged for her collaboration.

Notes and references

1 R. H. Shafer, *Prog. Nucl. Ac. Res. Mol. Biol.*, 1998, **59**, 55.
2 J. Ren and J. B. Chaires, *Biochemistry*, 1999, **38**, 16 067.
3 Q. Chen, I. D. Kuntz and R. H. Shafer, *Proc. Natl. Acad. Sci. USA*, 1996, **93**, 2635.
4 S. M. Kerwin, *Curr. Pharm. Des.*, 2000, **6**, 441.
5 P. J. Perry and L. R. Kelland, *Expert Opin. Ther. Patents*, 1998, **8**, 1567.
6 P. J. Perry and T. C. Jenkins, *Expert Opin. Invest. Drugs*, 1999, **9**, 1981.
7 T. C. Jenkins, *Curr. Med. Chem.*, 2000, **7**, 99.
8 M. Isalan, S. D. Patel, S. Balasubramanian and Y. Choo, *Biochemistry*, 2001, **40**(3), 830.
9 E. Raymond, J. C. Soria, E. Izbicka, F. Boussin, L. Hurley and D. D. Von Hoff, *Invest. New Drugs*, 2000, **18**(2), 123.
10 G. Sarig, P. Weisman-Shomer and M. Fry, *Biochem. Biophys. Res. Commun.*, 1997, **237**(3), 617.
11 A. M. Zahler, J. R. Williamson, T. R. Cech and D. M. Prescott, *Nature*, 1991, **350**, 718.
12 (*a*) G. Laughlan, A. I. H. Murchie, David G. Norman, M. H. Moore, P. C. E. Moody, D. M. J. Lilley and B. Luisi, *Science*, 1994, **265**, 520; (*b*) F. Aboul-ela, A. I. H. Murchie, D. G. Norman and D. M. J. Lilley, *J. Mol. Biol.*, 1994, **243**, 458; (*c*) K. Phillips, Z. Dauter, A. I. H. Murchie, D. M. J. Lilley and B. Luisi, *J. Mol. Biol.*, 1997, **273**, 171.
13 J. G. Pelton and D. E. Wemmer, *J. Am Chem. Soc.*, 1990, **112**, 1393.
14 R. E. Klevit, D. E. Wemmer and B. R. Reid, *Biochemistry*, 1986, **25**, 3296.
15 M. Piotto, V. Saudek and V. J. Sklenar, *J. Biomol. NMR*, 1992, **2**, 661.

CHEMCOMM
Communication
www.rsc.org/chemcomm

Immobilization of cytochrome c at Au electrodes by association of a pyridine terminated SAM and the heme of cytochrome

Hiromichi Yamamoto, Haiying Liu and David H. Waldeck*

Department of Chemistry, University of Pittsburgh, Pittsburgh, Pennsylvania 15260, USA. E-mail: dave@pitt.edu

Received (in Cambridge, UK) 23rd February 2001, Accepted 23rd April 2001
First published as an Advance Article on the web 9th May 2001

Electrochemical methods are used to demonstrate that cytochrome c can be immobilized on electrodes that are coated with self-assembled monolayers of 4-pyridinyl–CO_2–$(CH_2)_n$–S ($n > 6$) through interaction between the pyridine terminal unit and the heme of the cytochrome.

One avenue toward better sensors and enzyme electrodes is the use of a long tether, whose terminal functionality can selectively bind a biomolecule. Here this strategy is explored with the redox protein cytochrome c. Electron transfer reactions with cytochrome c have been extensively studied, both to clarify its function in biological systems and to provide a canonical example of a redox active protein.[1] Cytochrome c has been immobilized on CO_2H terminated self-assembled monolayers (SAMs) through electrostatic interactions between the carboxylate and the exterior of the protein[2] and by covalent linkage.[3] This work investigates the ligation between the terminal unit of a 4-pyridinyl–CO_2–$(CH_2)_n$–S ($PyCO_2$–C_n, n = 2, 6, 11, 16) SAM and the heme of horse-heart cytochrome c. The data show that immobilization of cytochrome is achieved by the pyridine functionality when the alkane tethers are long enough, n = 6, 11, 16. In addition, the immobilization causes a large negative shift of the formal potential $E^{\circ\prime}$ that does not occur for other immobilization strategies. The data also show that the electron transfer rate for the oxidation is enhanced over that for the reduction; *i.e.* an asymmetry in the rates becomes evident. These data suggest that the pyridine interacts with the iron in the cytrochrome's heme.

The experiments used a three-electrode (Pt auxiliary, Ag/AgCl reference) electrochemical cell with a working electrode that was a Au ball (*ca.* 1 mm diameter) to which the disulfide was self-assembled (see ESI† for details on the construction of the electrode and its characterization). Capacitance measurements were used to assess the quality of the SAM. For the immobilization studies the SAM coated electrodes were incubated in a cytochrome c solution and measurements were made in 25 mM phosphate buffer solution at pH 7. Details on the preparation of the SAM materials are given in the ESI†. For the studies with OH terminated layers and $PyCO_2$–C_2, in which the cyt c is not immobilized, the purified cytochrome c was 30–50 μM in the buffer solution (see ESI† for further details).

Fig. 1 shows cyclic voltammograms for some of the systems that were studied. Fig. 1(a) and (b) show voltammograms for SAMs that have pyridinal functionalities. The solid line curves show the electrode's response after it has been removed from the incubation solution, rinsed, and placed in contact with a buffer/electrolyte solution that does not contain cytochrome c. The data in Fig. 1(a) shows no faradaic response for the buffer solution because cytochrome c does not adsorb onto the surface of $PyCO_2$–C_2, but does show a response when the electrode contacts a solution containing cytochrome c (dashed line). Fig. 1(b) shows that some cytochrome adsorbs on the $PyCO_2$–C_{11} SAM and displays a negative shift in the apparent formal potential. A corresponding experiment using a SAM in which the pyridine nitrogen is blocked with a methyl group shows no faradaic current. Hence the adsorption of cytochrome c requires that the nitrogen atom of the pyridine be accessible to the protein and the alkane chain be long enough. Fig. 1(c) shows voltammograms for HO-terminated films,[4] in contact with cytochrome c solution (dashed line). The solid line voltammogram is the same system with 0.8% pyridine (by volume) added to the solution. Two redox waves (apparent $E^{\circ\prime}$ of −17 and −325 mV) are found upon pyridine addition. The redox wave at −17 mV is assigned to the redox reaction of unmodified cytochrome c and the wave at −325 mV is assigned to the redox reaction of cytochrome c in which pyridine is coordinated to the heme. In this system, a positive potential sweep oxidizes the iron, and complexation with the pyridine occurs (or is strengthened). As the voltage is swept back negative the pyridine is not removed until the iron is reduced at the more negative reduction potential of the pyridine-coordinated moiety. To summarize, these data show that $PyCO_2$–C_{11} SAMs immobilize cytochrome c and cause an $E^{\circ\prime}$ shift that is consistent with an interaction between pyridine and the heme.

Voltammograms were collected as a function of the voltage scan rate for each of the electrodes. For the HO–C_6 and $PyCO_2$–C_2 SAMs with cytochrome in solution, the peak current depended on the square root of the scan rate, indicating that the cytochrome is not immobilized on the electrode surface. For the HO_2C–C_{10} and the $PyCO_2$–C_n (n = 6, 11, 16) SAMs, the peak current was linear with the voltage scan rate, indicating that the

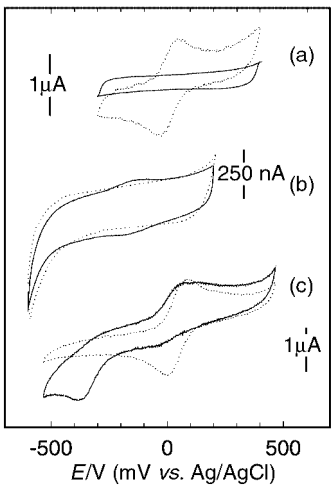

Fig. 1 Cyclic voltammograms are shown for gold electrodes that are coated with (a) 4-pyridinyl–CO_2–$(CH_2)_2$–S, (b) 4-pyridinyl–CO_2–$(CH_2)_{11}$–S, and (c) HO–$(CH_2)_6$–S SAMs. In (a), the solid line shows a voltammogram for an electrode that was incubated in 50 μM cytochrome solution for 30 min and placed in contact with a 25 mM buffer solution, and the dashed line shows the same electrode in contact with a 50 μM cytochrome c buffer solution. In (b) the solid line corresponds to the Py terminated layer after it was incubated in the cytochrome solution and the dashed line corresponds to the background curve. (c) Shows a voltammogram for cytochrome in a buffer solution (dashed line) and a voltammogram for a cytochrome solution containing 0.8% pyridine (solid line).

† Electronic supplementary information (ESI) available: full experimental details. See http://www.rsc.org/suppdata/cc/b1/b101767p/

 DOI: 10.1039/b101767p

Table 1 The apparent formal potential $E^{\circ\prime}$ and the change in peak potential between the high (20 V s^{-1}) and low (0.1 V s^{-1}) scan rates

	$E^{\circ\prime}$/mV[a]	$\Delta E_{p,ox}$/mV	$\Delta E_{p,red}$/mV
$PyCO_2(CH_2)_2S$–	5	—	—
$PyCO_2(CH_2)_6S$–	−159[a] ± 7	0	−11
$PyCO_2(CH_2)_{11}S$–	−152[a] ± 5	0	−21
$PyCO_2(CH_2)_{16}S$–	−147[a]	0	−44
$HO(CH_2)_6S$–	44 ± 2	—	—
$HO_2C(CH_2)_{10}S$–	13 ± 3	32[b]	−24[b]

[a] $E^{\circ\prime} = (E_{p,ox} + E_{p,red})/2$ at 100 mV s^{-1} scan rate and *vs.* the Ag/AgCl reference. [b] Shift in the peak potential upon change in scan rate from 0.6 to 10 V s^{-1}.

cytochrome is immobilized on the surface, as demonstrated by the data in Fig 1. The apparent formal potential, $E^{\circ\prime}$, for the cytochrome immobilized on pyridine are significantly shifted negative of the other systems (see Table 1). For the HO_2C–C_n SAMs, the adsorption is attributed to electrostatic and hydrogen bonding interactions between the lysine groups ($-NH_3^+$) on the cytochrome c periphery and the carboxylic acid group of the SAM.[2] The negative shift of $E^{\circ\prime}$ suggests a different adsorption state for cytochrome on the pyridinyl layers than on the carboxylic acid layers and a significant interaction of the pyridine with the heme. The nitrogen in the pyridinyl moiety of the SAM and the long alkyl chain are both needed for significant adsorption to occur.

Available literature results support the interpretation that the pyridine terminated SAMs coordinate to the heme. Recent Raman and NMR studies show that Met80, which is axially bound to the iron in the heme of cytochrome c, can be displaced by an imidazole or pyridine.[5] The apparent $E^{\circ\prime}$ values in the pyridine containing solution were found to be −17 and −325 mV, which is consistent with the reported result for yeast iso-1-cytochrome c that complexes with imidazole.[6] Thus, the large negative shift of the $E^{\circ\prime}$ (342 mV) by pyridine in solution is caused by the axial ligand exchange from Met80 to pyridine on the heme's iron. The 10–20 mV shift in the $E^{\circ\prime}$ of the unsubstituted cytochrome is consistent with the change in solution dielectric constant caused by 1% pyridine.[7] These observations strongly suggest that the large shift of 150 to 160 mV in the $PyCO_2$–C_n coated electrodes results from association of the pyridine with the heme. Although the potential shift observed on the SAM is about half of the shift found for the free pyridine, such a result is consistent with a reduced ability for optimal coordination when the pyridine is tethered to the SAM. Although a change in the local dielectric constant[7] or local field effects[8] may contribute to the potential shift, they are expected to be smaller than the shift observed here and show a chain length dependence.

The dependence of the voltammogram's peak position on the voltage scan rate can be used to quantify the electron transfer rate constant. For the $PyCO_2$–C_6, $PyCO_2$–C_{11}, and $PyCO_2$–C_{16} SAMs the oxidation waves do not shift with increasing scan rate; *i.e.* the rate remains too fast for the instrument to resolve. In contrast, the reduction peaks shift (see Table 1) and show a dependence on the alkane chain length of the SAM, reflecting the impact of the tunneling barrier thickness[9] on the electron transfer rate. This asymmetry in the transfer rate is consistent with stabilization of the heme by the pyridine. Such an interaction would enhance the oxidation rate and inhibit the reduction rate for which a dependence of the peak position on the voltage scan rate is evident. The increase in the reduction peak's potential shift with scan rate as the alkane chain length increases reflects a slowing of the electron transfer rate because of an increased tunneling barrier width. A more quantitative analysis of the electron transfer kinetics is underway and will be reported elsewhere.

This study shows that cytochrome c can be immobilized on $PyCO_2$–C_nS SAMs with alkane chains of $n > 6$, and the adsorption occurs through association of the pyridine with the cytochrome's heme. This latter conclusion is supported by the large potential shifts, an induced asymmetry in the reduction and oxidation rates, and other literature results. Fig. 2 depicts the mode of binding that is envisioned for this system. In contrast to electrostatic binding with surface functionalities, the pyridine associates directly with the redox center, which should create a better defined geometry between the protein and the electrode. This approach will allow the electron transfer kinetics to be explored without the limitations imposed by an inhomogeneous distribution of protein orientations with respect to the electrode. On a practical level, this strategy of ligating to metal redox centers or binding to a biomolecule's active site promises improved selectivity for the electrochemical detection of biomolecules.

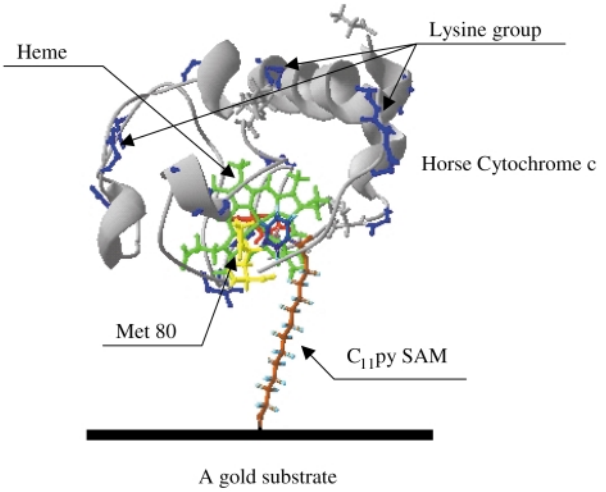

Fig. 2 Illustration of the association of a pyridine tether to the heme of cytochrome c. Also shown are the lysine groups that are present on the protein surface.

We are grateful to Professor J. Shin, A. R. Lajmi, and A. M. Napper for helpful advice. We acknowledge the Department of Energy for partial support of this work. We thank Hach Corporation for loan of the VoltaLab PGZ407 during part of this study.

Notes and references

1 M. Fedurco, *Coord. Chem. Rev.*, 2000, **209**, 263.
2 M. J. Tarlov and E. F. Bowden, *J. Am. Chem. Soc.*, 1991, **113**, 1847; M. Collinson, E. F. Bowden and M. J. Tarlov, *Langmuir*, 1992, **8**, 1247; S. Song, R. A. Clark, E. F. Bowden and M. J. Tarlov, *J. Phys. Chem.*, 1993, **97**, 6564.
3 C. J. McNeil, D. Athey and H. Wo, *Biosens. Bioelectron.*, 1995, **10**, 75.
4 The cytochrome does not adsorb onto these films. See S. Terrettaz, J. Cheng, C. J. Miller and R. D. Guiles, *J. Am. Chem. Soc.*, 1996, **118**, 7857.
5 T. G. Spiro and X. Y. Li, *Resonance Raman Spectra of Heme and Metalloproteins in Biological Applications of Raman spectroscopy*, Wiley, NY, 1988, vol. 3, p. 1; S. Hirota, T. Ogura, I. K. Shingawa, S. Yoshikawa and T. Kitagawa, *J. Phys. Chem.*, 1996, **100**, 15 274; S. R. Yeh and D. L. Rousseau, *J. Biol. Chem.*, 1999, **274**, 17 853; M. Smith and G. Mclendon, *J. Am. Chem. Soc.*, 1981, **103**, 4912; J. C. Ferrer, J. G. Gullemette, R. Bogumil, S. C. Inglis, M. Smith and A. G. Mauk, *J. Am. Chem. Soc.*, 1993, **115**, 7507; G. Liu, Y. Chen and W. Tang, *J. Chem. Soc., Dalton Trans.*, 1997, 795.
6 B. A. Feinberg, X. Liu, M. D. Ryan, A. Schejter, C. Zhang and E. Margoliash, *Biochemistry*, 1998, **37**, 13 091.
7 S. G. Sivakolundu and P. A. Mabrouk, *J. Am. Chem. Soc.*, 2000, **122**, 1513.
8 D. H. Murgida and P. Hildebrandt, *J. Am. Chem. Soc.*, 2001, **123**, ASAP.
9 H. Finklea, *Electroanal. Chem.*, 1996, **19**, 109.

CHEMCOMM Communication
www.rsc.org/chemcomm

Conformational isomerism leads to supramolecular isomerism and nanoscale inclusion in 2D extended framework solids based on *C*-methylcalix[4]resorcinarene

Leonard R. MacGillivray,*[a] Jennifer L. Reid[b] and John A. Ripmeester[b]

[a] *Department of Chemistry, University of Iowa, Iowa City, Iowa 52242, USA. E-mail: len-macgillivray@uiowa.edu*
[b] *Steacie Institute for Molecular Sciences, National Research Council of Canada, Ottawa, Ontario, Canada K1A 0R6*

Received (in Columbia, MO, USA) 14th February 2001, Accepted 25th March 2001
First published as an Advance Article on the web 9th May 2001

Co-crystallization of *C*-methylcalix[4]resorcinarene 1 with 4,4′-bipyridine 2 in the presence of *m*-xylene results in the formation of a 2D brick framework, 3c·2(*m*-xylene), that possesses nanoscale cavities that host four aromatics as guests in which 1 adopts a 'T-shaped' conformation.

With the recognition that strategies for the deliberate design[1] of molecular crystalline solids[2] can lead to new materials with predictable properties realized (*e*.g. inclusion),[3–6] increased efforts have been placed upon understanding and controlling those factors that govern the assembly of molecules and/or ions in the solid state. For the design of extended solids with cavities that accommodate molecules as guests,[7] relatively strong, directional forces (*e.g*. hydrogen bonds) have attracted much attention in this regard owing to the structure-directing abilities of such interactions to be predicted with a reasonable degree of accuracy. Despite successes in exploiting such forces, however, it is, perhaps, surprising to note that nanoscale processes of molecular inclusion,[8] where, for example, multiple copies of a guest occupy a closed cavity in a solid, remain rare. Indeed, the successful engineering of cavities able to accommodate multiple guests can, in principle, provide a route to solids with guests that undergo reaction in the solid state[9] and bear relevance to problems of separations of large molecules.[10]

With this in mind, using a template-based method to molecular self-assembly we report the ability of the components of two supramolecular isomers **3** of composition **1**·2(**2**) (where **1** = *C*-methylcalix[4]resorcinarene, **2** = 4,4′-bipyridine),[11] that define a hydrogen-bonded, wave-like network **3a**[12] and carcer-and-like capsule **3b**,[13] to undergo a structural reorganization in the presence of a suitable aromatic guest to form a two-dimensional (2D) isomer **3c** of the parent components (Scheme 1). The network **3c**·2(*m*-xylene) defines a 2D symmetrical brick framework[14–16] that exhibits closed multi-molecular cavities of nanoscale dimensions, that, owing to the ability of **1** to adopt a 'T-shaped' conformation,[17] accommodate four identical aromatics as guests. Whereas supramolecular isomerism involving ligand conformational isomerism has been observed in inclusion compounds based on coordination polymers,[18] **3c**·2(*m*-xylene) represents, to our knowledge, a novel example of an organic inclusion compound that exhibits supramolecular isomerism involving conformational isomerism by a molecular receptor.†

When **1** (0.020 g) was co-crystallized with 2 equiv. of **2** (0.011 g) from a boiling aliquot of EtOH in the presence of 10 equiv. of *m*-xylene according to eqn. (1), single crystals of

$$\mathbf{1} + 2(\mathbf{2}) + 10(m\text{-xylene}) + \text{EtOH (excess)} \rightarrow \mathbf{3c}\cdot 2(m\text{-xylene}) \quad (1)$$

3c·2(*m*-xylene) suitable for X-ray analysis grew within a period of approximately 4 days. The formulation of **3c**·2(*m*-xylene) was determined by single-crystal X-ray diffraction‡ and ^{1}H NMR spectroscopy.

A space-filling view of the X-ray crystal structure of **3c** is shown in Fig. 1. As in the case of the wave-like framework **3a**·guest (guest = ferrocene, toluene, MeCN)[11,12] and carcer-and-like capsule **3b**·guest (guest = nitrobenzene),[13] four molecules of **2**, each of which serves as a bifunctional hydrogen

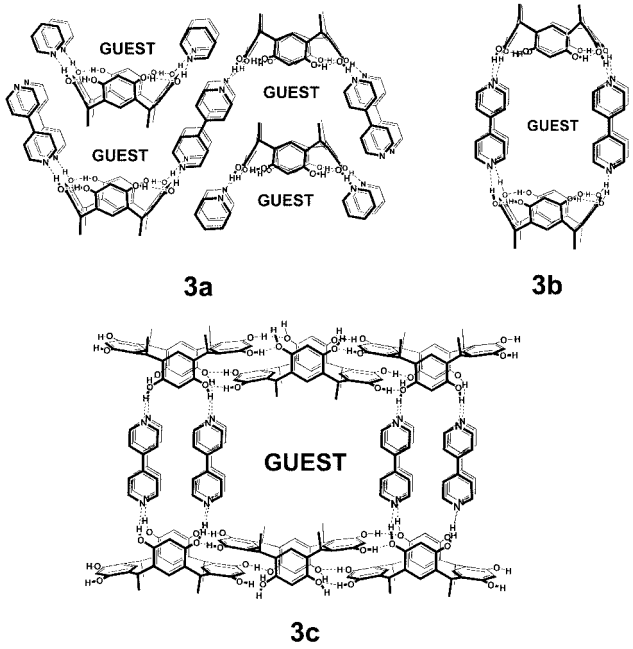

Scheme 1

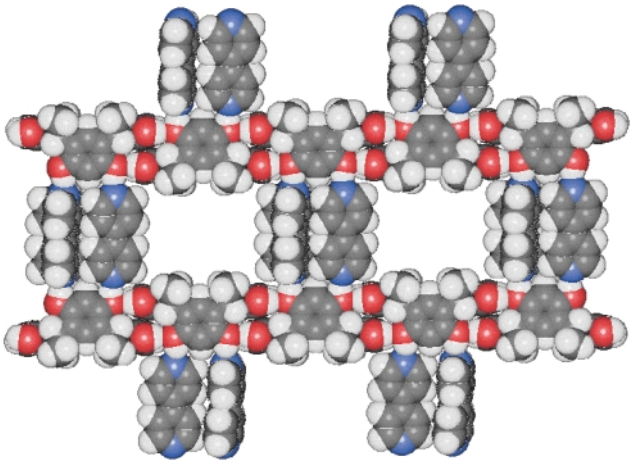

Fig. 1 Space-filling view of the X-ray crystal structure of **3c** (guests have been omitted for clarity). Color scheme: grey = carbon; white = hydrogen; blue = nitrogen; red = oxygen.

 DOI: 10.1039/b102856c

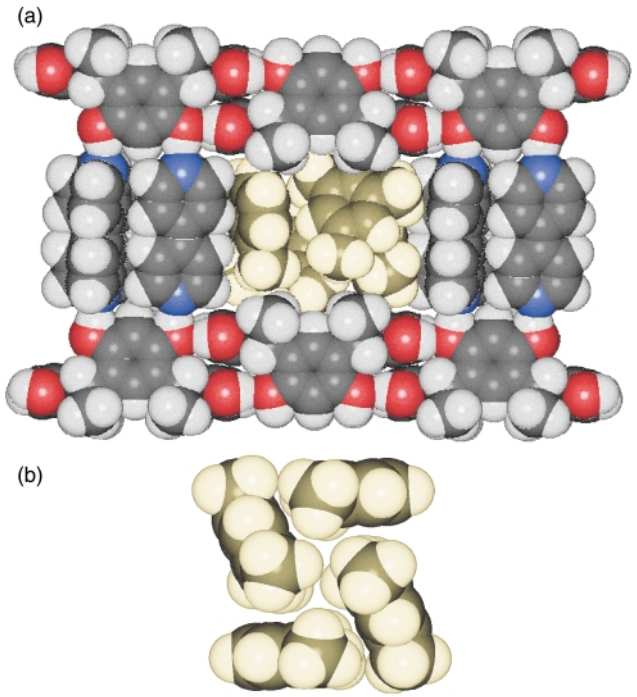

Fig. 2 Space-filling view of the guests of **3c**: (a) a view showing the guests within the brick framework, and (b) a view showing the edge-to-face π–π interactions of the guests. Color scheme: grey–yellow = guest atoms (Note: two *m*-xylene guests lie disordered, each across three sites).

bond acceptor, have assembled with **1** such that the bipyridines participate in four O–H···N hydrogen bonds with two opposite resorcinol units of the macrocycle [O···N separations (Å): O(1)···N(1) 2.770(4), O(2)···N(3) 2.727(4), O(5)···N(4) 2.774(4), O(6)···N(2) 2.725(4)]. Unlike **3a** and **3b**, however, the pyridine units of **3c** interact with **1** such that they participate in edge-to-face, rather than face-to-face, π–π interactions[24] along the upper rim of **1** and the cavity of **1** is closed. The remaining resorcinol units, which are co-planar and lie approximately perpendicular to the resorcinol moieties involved in the O–H···N forces, form four intermolecular O–H···O hydrogen bonds with two neighbouring molecules of **1**, making **1**, in the form of a 'T-shaped' building block,[17] an eight-fold hydrogen bond donor [O···O separations (Å): O(1)···O(4) 2.749(4), O(2)···O(7) 2.754(4), O(3)···O(5) 2.768(4), O(6)···O(8) 2.735(3)]. As a consequence of the assembly process, a 2D layered symmetrical brick framework **3c**, with large, closed rectangular cavities (cavity dimensions *ca*. 14 × 11 × 6 Å) of idealized D_{2h} symmetry, has formed.§

A view depicting the guests of **3c**·2(*m*-xylene) is shown in Fig. 2. Four molecules of *m*-xylene, which lie around a crystallographic center of inversion, are located within each cavity [Fig. 2(*a*)] such that the aromatics assemble by way of edge-to-face π–π interactions [Fig. 2(*b*)].[24] In this arrangement, two guests, which are related by symmetry, are positioned within the cavity such that the aromatic rings of the guests interact with **2** by way of edge-to-face π–π interactions,[23] while the remaining guests, each of which lies equally disordered across three sites, fill the host, in contrast to the ordered guests, such that the aromatics lie approximately parallel to the face of the cavity. Thus, the cavities of **3c**·2(*m*-xylene) have formed by way of template effects involving multiple guests in which the size, shape and electronic properties of an individual guest, presumably, do not favour an assembly process that leads to **3a** or **3b**.[15] Here, the conformational flexibility of **1** has provided access to a cavity, in the form of **3c**, that accommodates four molecules of *m*-xylene in which the O–H···N interactions between **1** and **2** are maintained[11–13] and **1** self-assembles by way of O–H···O forces.[17]

We have revealed the ability of **1**, in a 'T-shaped' conformation,[17] to assemble with **2** in the presence of a suitable guest to form a 2D symmetrical brick framework **3c** that possesses cavities of nanoscale dimensions which host four identical aromatics as guests. With such observations realized, we are currently investigating whether **3c** may be used as a host for multiple guests able to undergo reaction in the solid state.[9] We are also exploring whether molecules may be selected, *a priori*,[15] to induce formation of additional supramolecular isomers, able to accommodate single or multiple guests, based on **3**.¶ These observations should also bear relevance to materials in which derivatives of **1** and **2** are employed for the assembly process.

We are grateful for funding from the Natural Sciences and Engineering Research Council of Canada (graduate scholarship, J. L. R.).

Notes and references

† Molecular receptors typically adopt a number of conformations which make such molecules attractive building blocks for assembly processes leading to supramolecular isomerism by extended frameworks.[19] For an earlier account of **3c** see ref. 20.

‡ *Crystal data* for **3**·2(*m*-xylene): triclinic, space group $P\bar{1}$, a = 12.908(1), b = 13.791(1), c = 16.649(1) Å, α = 93.770(1), β = 102.761(1), γ = 91.189(2)°, U = 2882.3(3) Å^3, D_c = 1.27 g cm^{-3}, Mo-Kα radiation (λ = 0.71070 Å) for Z = 2. Least squares refinement based on 4226 reflections with $I_{net} > 2.0\sigma(I_{net})$ (out of 7512 unique reflections) led to a final value of R = 0.059. Aromatic and hydroxy hydrogen atoms were placed by modelling the moieties as rigid groups with idealised geometry, maximising the sum of the electron density at the calculated hydrogen positions. Structure solution was accomplished using SHELXS-86[21] and refinement was conducted using SHELXL93[22] locally implemented on a pentium-based IBM-compatible computer. Structure refinements and production of the figures were accomplished with the aid of RES2INS.[23]

CCDC 162090. See http://www.rsc.org/suppdata/cc/b1/b102856c/ for crystallographic data in .cif or other electronic format.

§ Adjacent layers lie staggered such that the cavities are closed.

¶ Molecules of similar shape to *m*-xylene may be used to induce formation of **3c** (unpublished results).

1 G. R. Desiraju, *Angew. Chem., Int. Ed. Engl.*, 1995, **34**, 2311.
2 W. Jaunky, M. W. Hosseini, J. M. Planeix, A. D. Cian, N. Kyritsakas and J. Fischer, *Chem. Commun.*, 1999, 2313.
3 K. T. Holman and M. D. Ward, *Angew. Chem., Int. Ed.*, 2000, **39**, 1653.
4 H. Gudbjartson, K. Biradha, K. M. Poirier and M. J. Zaworotko, *J. Am. Chem. Soc.*, 1999, **121**, 2599.
5 K. Endo, T. Ezuhara, M. Koyanagi, H. Masuda and Y. Aoyama, *J. Am. Chem. Soc.*, 1997, **119**, 499.
6 O. M. Yaghi, G. Li and H. Li, *Nature*, 1995, **378**, 703.
7 M. W. Hosseini and A. D. Cian, *Chem. Commun.*, 1998, 727.
8 V. A. Russell and M. D. Ward, *Chem. Mater.*, 1996, **8**, 1654.
9 T. J. Brett, J. M. Alexander, J. L. Clark, C. R. Ross II, G. S. Harbison and J. J. Stezowski, *Chem. Commun.*, 1999, 1275.
10 L. Z. Vilenchik, J. P. Griffith, N. St. Clair, M. A. Navia and A. L. Margolin, *J. Am. Chem. Soc.*, 1998, **120**, 4290.
11 L. R. MacGillivray and J. L. Atwood, *J. Am. Chem. Soc.*, 1997, **119**, 6931.
12 L. R. MacGillivray, H. A. Spinney, J. L. Reid and J. A. Ripmeester, *Chem. Commun.*, 2000, 517.
13 L. R. MacGillivray, P. R. Diamente, J. L. Reid and J. A. Ripmeester, *Chem. Commun.*, 2000, 359.
14 M. Fujita, Y. J. Kwon, O. Sasaki, K. Yamaguchi and K. Ogura, *J. Am. Chem. Soc.*, 1995, **117**, 7287.
15 J. A. Swift, A. M. Pivovar, A. M. Reynolds and M. D. Ward, *J. Am. Chem. Soc.*, 1998, **120**, 5887.
16 H. J. Choi and M. P. Suh, *J. Am. Chem. Soc.*, 1998, **120**, 10622.
17 L. R. MacGillivray and J. L. Atwood, *Supramol. Chem.*, 2000, **11**, 293.
18 T. L. Hennigar, D. C. MacQuarrie, P. Losier, R. D. Rogers and M. J. Zaworotko, *Angew. Chem., Int. Ed. Engl.*, 1997, **36**, 972.
19 J.-M. Lehn, *Struct. Bonding*, 1973, **16**, 1.
20 Y. Zhang, C. D. Kim and P. Coppens, *Chem. Commun.*, 2000, 2299.
21 G. M. Sheldrick, *Acta Crystallogr., Sect. A*, 1990, **46**, 467.
22 G. M. Sheldrick, SHELXL93, University of Göttingen, Germany, 1993.
23 L. J. Barbour, RES2INS, University of Missouri-Columbia, MO, USA, 1997.
24 W. L. Jorgensen and D. L. Severance, *J. Am. Chem. Soc.*, 1990, **112**, 4768.

CHEMCOMM Communication
www.rsc.org/chemcomm

Photochemical generation of acetonitrile oxide *via* the C–N bond cleavage of 3-methyl-2-(4-nitrophenyl)-2*H*-azirine

Hiroshi Inui and Shigeru Murata*

Department of Basic Science, Graduate School of Arts and Sciences, The University of Tokyo, Meguro, Tokyo 153-8902, Japan. E-mail: cmura@mail.ecc.u-tokyo.ac.jp

Received (in Cambridge, UK) 13th March 2001, Accepted 24th April 2001
First published as an Advance Article on the web 15th May 2001

Acetonitrile oxide (2) is produced by the irradiation of the title azirine 1 in the presence of O_2 in fluid solutions and in low-temperature matrices through the capture of the biradical 7 with O_2, which is generated by the photochemical C–N bond cleavage of the azirine ring.

The photochemistry of 2*H*-azirines has aroused wide interest from the mechanistic and synthetic points of view. It has been established that the photolysis of 2*H*-azirines causes the C–C bond cleavage to yield 1,3-dipolar nitrile ylides, the [3 + 2] cycloaddition reactions of which provide a useful method for constructing a variety of five-membered heterocyclic systems.[1] However, in the course of our studies of the reactivities of photolytically-generated intermediates having an electron-withdrawing group,[2] we found that the photodecomposition of the title azirine **1** proceeded by a mechanism drastically different from that reported for 2*H*-azirines so far. In this paper, we report the photochemistry of the azirine **1** in fluid solutions and in low-temperature matrices, where the first example of the selective C–N bond cleavage in the 2*H*-azirine photochemistry, as well as of the photochemical generation of acetonitrile oxide (**2**) through trapping of the intermediate with O_2, is demonstrated.

The new azirine, 3-methyl-2-(4-nitrophenyl)-2*H*-azirine (**1**),[3] was obtained by the reaction of 1-(4-nitrophenyl)propan-2-one trimethylhydrazonium iodide with sodium hydride in dimethyl sulfoxide,[1b,c] and purified by silica gel column chromatography with hexane–chloroform (1 : 1). When a degassed solution of **1** containing 5% (v/v) acrylonitrile in acetonitrile was irradiated with the Pyrex-filtered light of a high-pressure mercury lamp, **1** was recovered nearly quantitatively. In the ^{1}H NMR spectrum of the photoreaction mixture, no signals assigned to the pyrroline, which could be formed by the cycloaddition of the expected nitrile ylide **3** with acrylonitrile, were observed. On the other hand, under conditions identical to those described above, except for the saturation of the solution with O_2, irradiation of **1** afforded 4-nitrobenzaldehyde (**4**, 46%) and 4-nitrobenzoic acid (14%), together with the adduct identified as the isoxazoline **5** (45%). The formation of **5** could be interpreted in terms of the capture of acetonitrile oxide (**2**) generated in the course of the photoreaction of **1** with acrylonitrile. The structure of **5** was confirmed by comparison of spectroscopic data with those of an authentic sample, which was obtained by a chemical generation of **2** by the base-induced reaction of phenylisocyanate with nitroethane in the presence of acrylonitrile.[4,5]

There are no precedents of the photochemical generation of **2** in solution, though it has been reported that photolysis of ozone matrix-isolated in Ar containing acetonitrile at 15 K gave **2** together with hydroxyacetonitrile.[6] We propose that **2** is produced by a fragmentation of the dioxazoline **6**, which is generated by the capture of the biradical **7** with O_2 (Scheme 1). The formation of 4-nitrobenzaldehyde (**4**) in amounts equimolar with the isoxazoline **5** is also explained by this scheme, assuming that the cycloaddition reaction of **2** with acrylonitrile proceeds quantitatively. Thus, the generation of **2**, as well as the failure to obtain the product derived from the nitrile ylide **3**, strongly suggests that the photolysis of **1** causes not the C–C bond but the C–N bond cleavage to produce the biradical **7** as a reactive intermediate.

To gain further evidence of the C–N bond cleavage in the irradiation of **1**, we examined the photochemistry of **1** in an Ar matrix at 10 K. Irradiation (> 300 nm) of **1** matrix-isolated in Ar resulted in a slow decrease in intensities of the IR peaks due to **1** (1537, 1351, and 858 cm^{-1}). Simultaneously, IR peaks appeared at 2046, 1597, and 1340 cm^{-1}, indicating the formation of product having a cumulenic double bond (designated as **A**). In the UV-vis spectrum, upon photolysis of **1** a broad band with a maximum at 341 nm appeared with isosbestic points at 266 and 317 nm. To identify the structure of **A**, we carried out the calculations of vibrational frequencies for the nitrile ylide **3**, which would be a possible candidate for **A**, with the DFT method (B3LYP/6-31G(d)).[7,8] Unfortunately, as shown in Table 1, the vibrational frequencies calculated for **3** are not consistent with those observed for **A** in the following two points: (i) a large deviation of the wavenumber predicted for the C=N$^+$=C$^-$ stretching of **3** from that of the observed cumulenic double bond, and (ii) a lack of the peak predicted to have a relatively large intensity at 1027 cm^{-1} for **3**. However, we have found that the vibrational frequencies calculated for the ketene imine **8** are in excellent agreement with those observed for **A** (Table 1). Therefore, we conclude that the photoproduct of **1** in an Ar matrix at 10 K is not the nitrile ylide **3**, but the

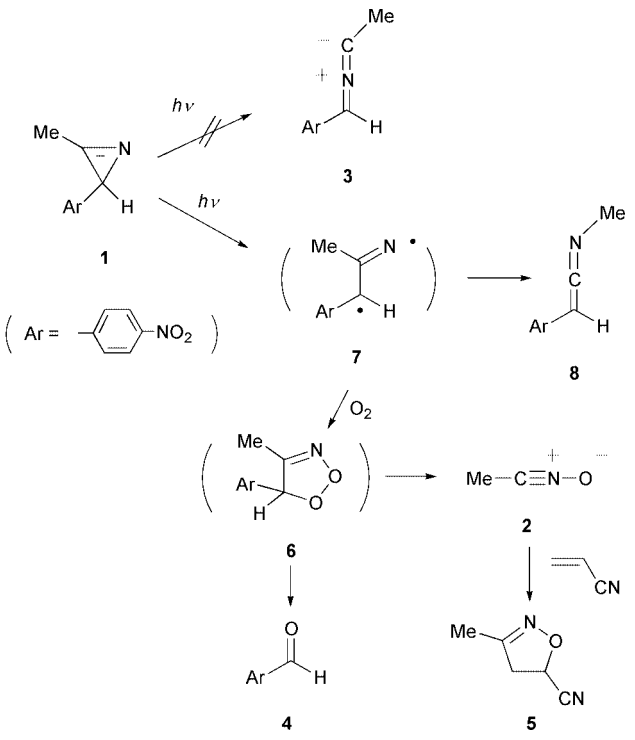

Scheme 1

 DOI: 10.1039/b102384p

Table 1 IR spectroscopic data of the photoproduct **A** generated in Ar at 10 K and of **3** and **8** calculated with the DFT Method

Experimental[a] ν/cm^{-1}	Calculated[b] ν/cm^{-1}		
A	**3**	**8**	Assignment
	2780 (7)	2795 (6)	Me str
2046 s		2024 (100)	C=C=N str
	1946 (81)		C=N$^+$=C$^-$ str
	1585 (11)	1590 (9)	Ar ip, NO_2 unsym
1597 m	1583 (32)	1585 (21)	Ar ip
1539 m	1534 (11)	1539 (10)	Ar ip, NO_2 unsym
	1490 (4)		Ar ip
	1440 (6)	1412 (4)	Me deform
1340 s	1338 (100)	1342 (68)	NO_2 sym
	1329 (8)		Ar ip
1197 w		1180 (5)	CH ip
1111 m	1108 (13)	1106 (12)	ArCH ip
	1027 (47)		Me rock
	856 (7)		ArCH ip
851 w	851 (5)	858 (4)	ArCH op

[a] Measured in Ar at 10 K; s = strong; m = medium; w = weak. [b] Calculated frequencies are scaled by the use of a linear scaling function; See ref. 7. Relative intensities are designated in parentheses. Frequencies with relative intensities greater than 5% were given in the table.

ketene imine **8**. The direct observation of **8** provides a strong piece of evidence in support of the C–N bond cleavage in the photolysis of **1**, because the formation of **8** is rationalized in terms of the Curtius-like rearrangement of the methyl group in the biradical **7** having a vinyl nitrene character.[9]

When **1** was photolyzed (> 300 nm, 10 K) in the Ar matrix doped with a large amount of O_2 (20%), we could observe no IR peaks assigned to **8**. Instead, the irradiation afforded 4-nitrobenzaldehyde (**4**), the structure of which was readily confirmed by comparison of the IR spectrum with that of the authentic sample matrix-isolated in Ar at 10 K, together with a species having IR bands at 2334 and 1315 cm^{-1} (designated as **B**) as primary photoproducts. The species **B** could be identified as acetonitrile oxide (**2**) on the basis of the agreement of the vibrational frequencies with those reported for **2**.[6,10] Isotopic labeling supports this identification of **B**. With use of $^{18}O_2$ (97% doubly labeled), the intense band at 2334 cm^{-1} was slightly shifted (1 cm^{-1}), while a large isotopic shift of 28 cm^{-1} was observed in the band at 1315 cm^{-1}, which is assigned to the N–O stretch. These values are in fair agreement with those reported for the isotopic shifts of the bands assigned to **2**.[6,11] Consequently, the generation of **2** in the photolysis of **1** in the presence of O_2, which is presumed on the basis of the characterization of reaction products in solutions, is unambiguously confirmed by the direct observation using a low-temperature matrix-isolation technique.

It is generally accepted that the photochemical C–C bond cleavage of 2*H*-azirines to produce nitrile ylides proceeds from the excited singlet state having an n–π* character.[1] However, the theoretical calculation using the INDO/S method[12] predicted that the lowest excited singlet state of **1**, S_1, could be roughly described as a local π–π* excitation of its 4-nitrophenyl group. Moreover, it is reasonable to think that a large spin-orbit interaction in the nitro group can accelerate the intersystem-crossing from the S_1 state to the excited triplet state, T_1. Thus, we propose that the selective C–N bond cleavage observed in the photolysis of **1** results from the participation of its T_1 state. This assumption is supported by the DFT calculations on the triplet biradicals which are expected to be formed by the bond cleavage. It was found that the biradical **7** formed by the C–N bond cleavage was more stable by 7.6 kcal mol^{-1} than the triplet biradical formed by the C–C bond cleavage. The triplet biradical **7** can be readily captured by O_2 to afford **6**, while in the absence of O_2, the biradical undergoes the Curtius-like rearrangement to yield **8** from its singlet state which would be accessible from the triplet state.

In conclusion, it is established that on the irradiation of the azirine **1**, the C–N bond is selectively cleaved, in contrast to the C–C bond cleavage of the normal 2*H*-azirines reported so far. On the basis of the calculations, we propose that the selective C–N bond cleavage is due to the participation of the excited triplet state of **1** in the bond cleavage. Moreover, we have demonstrated that acetonitrile oxide (**2**) is produced through the capture of **7** with O_2 followed by the fragmentation, which would provide a convenient method of photochemical generation of **2**.

This work was supported in part by grants from the Ministry of Education, Science, Sports and Culture of Japan (No. 12020214) and from the Core Research for Evolutional Science and Technology (CREST).

Notes and references

1 The photochemistry of 2*H*-azirines has been reviewed: (*a*) A. Padwa, *Acc. Chem. Res.*, 1976, **9**, 371. For recent developments in this field; see, for example: (*b*) A. Padwa, R. J. Rosenthal, W. Dent, P. Filho, N. J. Turro, D. A. Hrovat and I. R. Gould, *J. Org. Chem.*, 1984, **49**, 3174; (*c*) R. L. Barcus, L. M. Hadel, L. J. Johnston, M. S. Platz, T. G. Aavino and J. C. Scaiano, *J. Am. Chem. Soc.*, 1986, **108**, 3928.

2 (*a*) S. Murata, Y. Mori, Y. Satoh, R. Yoshidome and H. Tomioka, *Chem. Lett.*, 1999, 597; (*b*) T. Mizushima, S. Ikeda, S. Murata, K. Ishii and H. Hamaguchi, *Chem. Lett.*, 2000, 1282; see also, (*c*) H. Tomioka, K. Tabayashi and Y. Izawa, *J. Chem. Soc., Chem. Commun.*, 1985, 906; (*d*) T.-Y. Liang and G. B. Schuster, *J. Am. Chem. Soc.*, 1987, **109**, 7803.

3 Light yellow granules: mp 100–102 °C; ^{1}H NMR ($CDCl_3$) δ 2.56 (3H, s), 2.96 (1H, s), 7.19 (2H, d, J = 9.0 Hz), 8.15 (2H, d, J = 9.0 Hz); ^{13}C NMR ($CDCl_3$) δ 12.6, 32.9, 123.5, 126.0, 146.6, 149.1, 163.3; IR (KBr) 1770, 1594, 1516, 1345, 1104, 853, 697 cm^{-1}; UV (MeCN) λ_{max} (log ε) 301 (4.10) nm.

4 (*a*) T. Mukaiyama and T. Hoshino, *J. Am. Chem. Soc.*, 1960, **82**, 5339; (*b*) H. Krawczyk and A. Gryff-Keller, *J. Chem. Res. S*, 1996, 452.

5 A number of experimental and theoretical studies on regiochemistry of 1,3-dipolar cycloaddition of nitrile oxides with dipolarophiles have been reported: A. Rastelli, R. Gandolfi and M. S. Amade, *J. Org. Chem.*, 1998, **63**, 7425, and references therein.

6 Z. Mielke, M. Hawkins and L. Andrews, *J. Phys. Chem.*, 1989, **93**, 558.

7 Calculated vibrational frequencies are scaled by the use of a linear scaling function of 1.009446 − 0.0000306ν, which is determined experimentally by comparison of frequencies calculated by B3LYP/6-31G(d) with those observed for the authentic sample of **1**, **4**, and (4-nitrophenyl)diazomethane matrix-isolated in Ar at 10 K. Using this scaling function, the agreement between calculated and observed frequencies of these three compounds is within ±14 cm^{-1} in the range of 2100 to 750 cm^{-1}.

8 The DFT calculations were carried out by the Gaussian 98 program package.

9 G. Smolinsky and A. P. Pryde, *J. Org. Chem.*, 1968, **33**, 2411.

10 W. G. Isner and G. L. Humphrey, *J. Am. Chem. Soc.*, 1967, **89**, 6442.

11 The vibrational frequencies for **2** (^{16}O), which are calculated with the DFT method (B3LYP/6-31G(d)) and scaled by the use of the function described in ref. 7, are 2319 and 1368 cm^{-1}. The ^{18}O isotopic shifts in these bands are calculated to be 3 and 27 cm^{-1}, respectively, which are in agreement with the experimental values.

12 The INDO/S calculations were carried out by the WinMOPAC program package.

CHEMCOMM Communication
www.rsc.org/chemcomm

Organogel or polymer gel; facilitated gelation of a sugar-based organic gel by the addition of a boronic acid-appended polymer†

Hideki Kobayashi,[a] Masato Amaike,[a] Jong Hwa Jung,[a] Arianna Friggeri,[a] Seiji Shinkai[a] and David N. Reinhoudt*[b]

[a] *Chemotransfiguration Project, Japan Science and Technology Corporation, Aikawa, Kurume, Fukuoka 839-0861, Japan. E-mail: seijitcm@mbox.nc.kyushu-u.ac.jp*
[b] *Chemotransfiguration Project, MESA+ Research Institute, University of Twente, 7500 AE Enschede, The Netherlands*

Received (in Cambridge, UK) 14th March 2001, Accepted 26th April 2001
First published as an Advance Article on the web 15th May 2001

The combination of boronic acid-appended poly(L-lysine) 1 and sugar-based gelator 2 yields a novel organo-polymer gel, consisting of vesicles held together by polymer molecules.

The assembly of certain low-molecular weight compounds (gelators) into complex, three-dimensional networks in which organic solvent molecules are confined, leads to the formation of organic gels.[1] Polymer gels, on the other hand, have three-dimensional structures created by cross-linked covalent bonds.[2] Hence, they are generally more robust than organic gels, however, they lack the characteristic, excellent thermo-reversibility inherent to organogels.[3] Recently, several groups have been able to improve the robustness of hydrogen-bond-based,[3,4] as well as cholesterol-based[5] gels by polymerization of the gelator molecules. Feringa *et. al.*[6] have shown that increased thermostabilization of methacrylate-containing cyclohexane-based gels can be achieved by *in situ* polymerization. In our group, the introduction of multi-point hydrogen bonding sites into cholesterol-based gelators, and the utilization of metal–ligand interactions in sugar-based gelators have resulted in a remarkable stabilization of these gel systems.[7] Moreover, polymerization of a bis(diacetylene)-containing gelator also improves gel stabilization.[3] Thus, combination of polymers with low-molecular weight gelators is a new and interesting concept which can lead to more robust gel systems.

In this paper we show how the gelating capability of cholesterol–saccharide conjugate gelator **2** is facilitated by the addition of boronic acid-appended poly(L-lysine)[8] **1** (Scheme1),

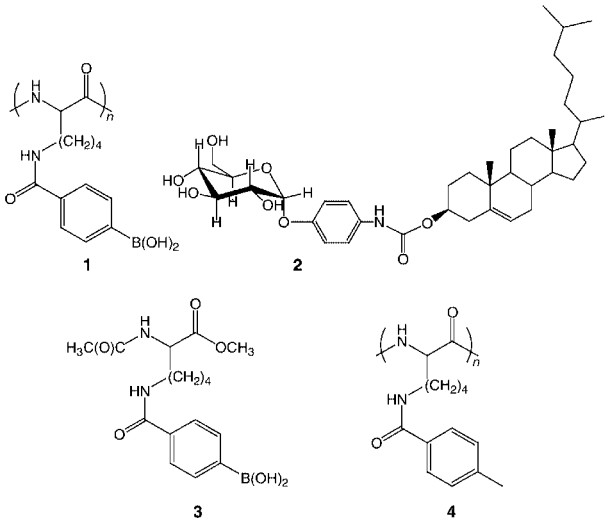

Scheme 1

† Electronic supplementary information (ESI) available: experimental details and synthesis of compounds **3** and **4**. See http://www.rsc.org/suppdata/cc/b1/b102436c/

in a DMSO–H_2O mixture. Moreover, the formation of the gel is shown to be pH-reversible due to the intrinsic properties of the boronic acid–sugar interaction governing the gelation process. Furthermore, transmission electron microscopy (TEM) images[9] of the gel revealed a remarkably novel superstructure consisting of a network of polymer-coated vesicles, held together by boronic acid-appended poly(L-lysine) molecules. This contrasts with most other gels that show structures consisting of fibrous networks. On the basis of TEM and dynamic light scattering (DLS) measurements, a mechanism for gel formation is proposed.

Compounds **1** and **2** were synthesized according to literature procedures[7b,8] and utilized to perform the gel test.[10] To a solution of **2** in DMSO (90 μL) was added a solution of **1** in water (20 μL) at pH 11.5 to favor the boronic acid–sugar interaction.[11] After heating, the system was allowed to cool in order to grow the organogel. This procedure was repeated at several concentrations of **2**, maintaining the concentration of **1** constant (1.8 mmol dm^{-3}), which yielded a maximum T_{gel} of 58 ± 3 °C at a concentration ratio of polymer to gelator of approximately 1:6 (Fig. 1). In good agreement with these results, a maximum T_{gel} of 62 ± 3 °C was observed, at a polymer to gelator ratio of approximately 1:5 by varying the concentration of **1** while maintaining the concentration of **2** constant (10.6 mmol dm^{-3}). Compound **2** has previously been shown to form gels with many solvents.[7b] However, since it did not form a gel in DMSO–H_2O (9:2 v/v) in the absence of **1**, the addition of the latter expands the gelation capabilities of **2** to more polar solvents. To investigate the role of both the poly(L-lysine) chain and the boronic acid moiety in the gelation process, reference compounds **3** and **4** were used respectively (Scheme 1).† Gelation tests carried out with **3** or **4** (1.8 mmol dm^{-3}) and

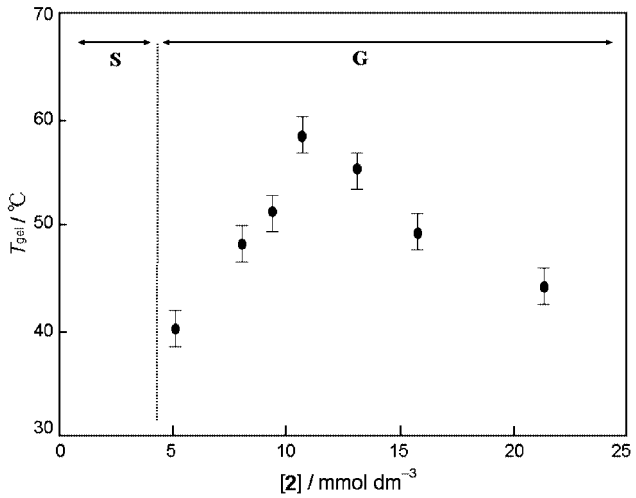

Fig. 1 Concentration dependence of the T_{gel} of **1** (1.8 monomer unit mmol dm^{-3}) upon addition of **2** in DMSO–H_2O (9:2 v/v). S: solution, G: gel.

 DOI: 10.1039/b102436c

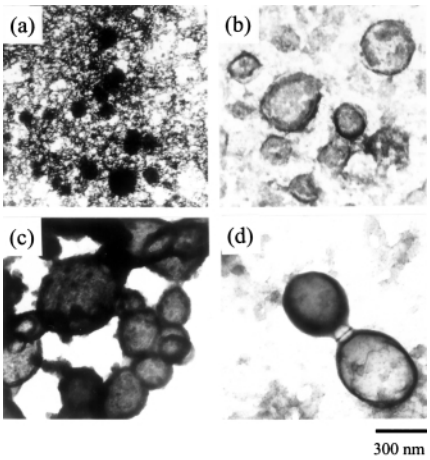

Fig. 2 TEM images of a 10.6 mmol dm^{-3} solution of **2** (a); a solution of **1** (1.8 mmol dm^{-3}) and **2** (2.6 mmol dm^{-3}) (b); a gel of **1** (1.8 mmol dm^{-3}) and **2** (10.6 mmol dm^{-3}) at T_{gel} = 58 ± 3 °C (c); and a gel of **1** (1.8 mmol dm^{-3}) and **2** (15.9 mmol dm^{-3}) at T_{gel} = 44 ± 3 °C (d).

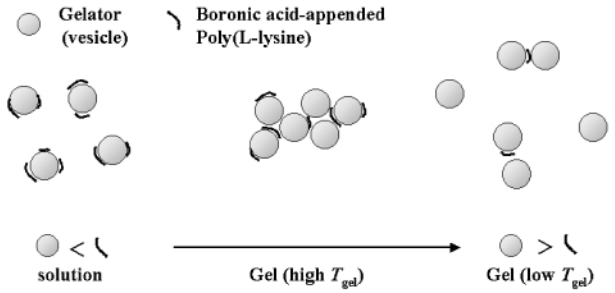

Scheme 2

gelator **2** (0–21 mmol dm^{-3}) did not result in gel formation, indicating that both the poly(L-lysine) chain, and the boronic acid moiety are a prerequisite for gelation to occur. Under alkaline conditions, the boronic acid moiety of **1** can interact with the glucopyranosyl moiety of **2**, forming covalent bonds with the 4,6-diol of the saccharide,[12] thus creating a connection between the polymer (**1**) and the gelator (**2**). Under acidic conditions (pH 5), on the other hand, the addition of **1** to a solution of **2** did not cause gel formation. The gelation behavior of this particular system is obviously pH dependent, since it relies on the boronic acid–saccharide interaction for gel formation.

To shed light on the mechanism of gel formation, TEM was employed (Fig. 2). In sample (a), containing only compound **2** (10.6 mmol dm^{-3}), monodisperse colloidal particles with diameters of approximately 50–100 nm, can be observed.[13] In sample (b), representative of gelator **2** (2.6 mmol dm^{-3}) plus polymer **1** (1.8 mmol dm^{-3}) in the solution state, slightly larger (200–400 nm in diameter), monodisperse vesicles are present. However, in sample (c), representative of the gel state with a high T_{gel} (**1**: 1.8 mmol dm^{-3}, **2**: 10.6 mmol dm^{-3}), no individual structures are present, but only a network of vesicles can be observed. In sample (d), representative of the gel state with a low T_{gel} (**1**: 1.8 mmol dm^{-3}, **2**: 15.9 mmol dm^{-3}), similar features as in sample (b) can be observed. To obtain a more accurate evaluation of the dimensions of the vesicles observed by TEM, DLS measurements were carried out.[14] The average diameters of the features observed in samples (a)–(d) are 121, 302, 2140, and 495 nm, respectively. The high average diameter observed for sample (c) could correspond to either very large vesicles present in solution, or to aggregates of smaller vesicles. In light of the TEM results (see Fig. 2c), the latter is more viable.

From the results presented, a mechanism for gel formation can be proposed (Scheme 2). In the presence of a large excess of **1** with respect to **2**, the gelator can form vesicles which are completely coated by the polymer, giving rise to individual vesicles (Fig. 2b). As a consequence, gel formation is not observed at high concentrations of **1** with respect to **2**. When the concentration of gelator is increased and the ratio of polymer to gelator is approximately 1:6, the number of vesicles increases and the amount of **1** is not sufficient to completely coat all the vesicles (Scheme 2). Therefore, aggregation of the gelator vesicles occurs, giving rise to an extended network of vesicles held together by polymer molecules and thus, the formation of the gel is observed (Fig. 2c). When the concentration of gelator **2** is increased even further, the amount of polymer **1** present in the system is not sufficient anymore for the formation of an extended network of vesicles (Scheme 2). Under these conditions, only dimers can still be observed in the TEM images and T_{gel} decreases.

In contrast to most gel structures that have been reported so far, consisting of fibrous networks running through the gels,[1,15] an assembly of vesicles of gelator **2** held together by polymer **1** is at the basis of this particular gel. Remarkably, the building blocks of this novel gel structure are polymer-coated gelator vesicles, which assemble into a superstructure, the gel, whilst maintaining the identity of vesicles. The gel cannot be defined as a polymer gel since the polymer chain length is far too short (100–200 nm, if fully stretched) to allow cross-linking of polymer chains by vesicles. One can thus regard the gelation as being induced by the 'cross-linking' of vesicles by polymers, but not by the 'cross-linking' of polymers by vesicles. Studies are currently underway to further elucidate the more detailed mechanism of gel formation proposed in this paper and to investigate the possibilities of utilizing poly(L-lysine)-based polymers for the formation of robust gels useful in aqueous systems.

Notes and references

1 P. Terech and R. G. Weiss, *Chem. Rev.*, 1997, **97**, 3133, and references therein.
2 M. Aharoni, in *Synthesis, Characterization, and Theory of Polymeric Networks and Gels*, Plenum, New York, 1992.
3 K. Inoue, Y. Ono, Y. Kanekiyo, S. Kiyonaka, I. Hamachi and S. Shinkai, *Chem. Lett.*, 1999, 225; K. Inoue, Y. Ono, Y. Kanekiyo, K. Hanabusa and S. Shinkai, *Chem. Lett.*, 1999, 429.
4 M. Masuda, T. Hanada, K. Yase and T. Shimizu, *Macromolecules*, 1998, **31**, 9403.
5 N. Tamaoki, S. Shimada, Y. Okada, A. Belaissaoui, G. Kruk, K. Yase and H. Matsuda, *Langmuir*, 2000, **16**, 7545.
6 M. de Loos, J. van Esch, I. Stokroos, R. M. Kellogg and B. L. Feringa, *J. Am. Chem. Soc.*, 1997, **119**, 12 675.
7 (*a*) N. Amanokura, Y. Kanekiyo, S. Shinkai and D. N. Reinhoudt, *J. Chem. Soc., Perkin Trans. 2*, 1999, 1995; M. Amaike, H. Kobayashi and S. Shinkai, *Bull. Chem. Soc. Jpn.*, 2000, **73**, 2553.
8 T. Nagasaki, T. Kimura, S. Arimori and S. Shinkai, *Chem. Lett.*, 1994, 1495.
9 For experimental details of TEM measurements see: J. H. Jung, Y. Ono and S. Shinkai, *Chem. Eur. J.*, 2000, **6**, 4552.
10 To a solution of gelator **2** in DMSO, was added a solution of polymer **1** in H_2O at pH 11.5 (NaOH). The solution containing **1** and **2** was then heated until all components dissolved and allowed to cool slowly to form the gel. Here, T_{gel} is defined as the temperature at which the gel appears.
11 The DMSO–H_2O (9:2 v/v) solution was the only one in which both compounds **1** and **2** dissolve simultaneously.
12 G. Wulff, *Pure Appl. Chem.*, 1982, **545**, 2093; M. Takeuchi, T. Imada and S. Shinkai, *J. Am. Chem. Soc.*, 1996, **118**, 10 658.
13 All TEM samples were shadowed with OsO_4 (2.0 wt% solution in water).
14 Dynamic Light Scattering: diameter and diffusion coefficient measurements were carried out on a Photal Otsuka Electronics VLS-70 super dynamic light scattering spectrophotometer (light source: Ar). Samples for DLS were diluted 10 times with respect to the samples used for gel formation.
15 L. A. Estroff and A. D. Hamilton, *Angew. Chem., Int. Ed.*, 2000, **39**, 3447.

CHEMCOMM Communication
www.rsc.org/chemcomm

Hydrolytic kinetic resolution of mono- and bisepoxides as a key step in the synthesis of insect pheromones†

Sharon Chow and William Kitching*

Department of Chemistry, The University of Queensland, Brisbane, 4072, Australia.
E-mail: kitching@chemistry.uq.edu.au

Received (in Cambridge, UK) 7th March 2001, Accepted 23rd April 2001
First published as an Advance Article on the web 16th May 2001

The synthetic utility of the readily separated epoxides, diols, epoxydiols and tetrols of high enantiomeric excesses, obtained by hydrolytic kinetic resolution (HKR) of functionalised mono- and bisepoxides with (salen)Co(OAc) complexes, is demonstrated by their efficient transformations to important insect pheromones.

Many insect pheromones incorporate a medium to long alkyl chain with some oxygen functionality, often alkyl branching, with a specific or strongly dominating chirality and double bond configuration.[1] These structural features, and the regio- and stereo-regularities associated with nucleophilic opening of terminal epoxides and displacement of sulfonate ester groups, suggest that ready availability of epoxides and 1,2-diols of high enantiomeric excesses (ee's), would expedite acquisition of such pheromones. Most hydrolytic kinetic resolutions (HKR)[2] of terminal epoxides relate to simple epoxides not bearing other functionality.[3] We now demonstrate that structurally more diverse epoxides respond well to the procedures developed by Jacobsen,[2] which utilise (salen)Co(OAc) complexes, such as, (acetato)(aqua)((*R*,*R*)(−)-*N*,*N*′-bis(3,5-di-*tert*-butylsalicylidene)-1,2-cyclohexanediamino)cobalt(III) (**1**).[4]

Our exploratory work was directed towards (*R*)-(−)-10-methyldodecyl acetate **8** and (*R*)-(−)-10-methyltridecan-2-one **12**. The acetate is a pheromone from the smaller tea tortrix moth (*Adoxophyes* species), with the (*R*)-enantiomer slightly more bioactive than the (*S*).[4] (*R*)-(−)-10-Methyltridecan-2-one is the sex pheromone of the southern corn rootworm (*Diabrotica undecimpunctata*).[4] The procedure (Scheme 1) commenced with the benzyl ether of undecen-10-ol, **2**, which was epoxidised to furnish the HKR substrate **3**. This was stirred with 0.5 mole% of (*R*,*R*)-**1** and 0.55 mole eq. H_2O at rt (*ca*. 22 °C) for 20–24 h.[2,4] Chromatography on silica yielded (*R*)-epoxide **4** and (*S*)-diol **5**, with excellent recovery (48 and 46% respectively). Manipulation of the epoxide afforded (*R*)-acetate **8** with $[\alpha]_D^{23}$ −5.40° (*c* 0.97, $CHCl_3$). (Reported for **8**, acquired by longer routes: $[\alpha]_D$ −5.84° ($CHCl_3$)[5] and −5.93° ($CHCl_3$).[6]) Reconstitution of diol **5** afforded the (*S*)-epoxide, which was transformed to the (*S*)-(+)-pheromone, with $[\alpha]_D^{23}$ +5.29° (*c* 1.02, $CHCl_3$).

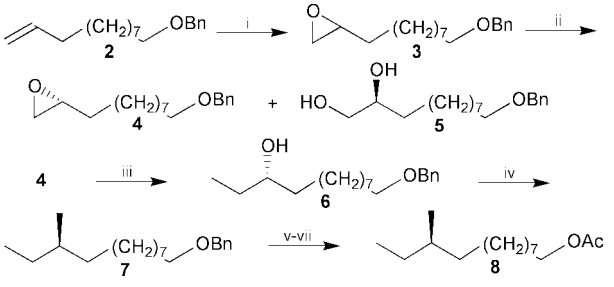

Scheme 1 *Reagents and conditions*: i, *m*-CPBA (78%); ii, 0.5% eq. (*R*,*R*)-**1**, 0.55 eq. H_2O (48% for **4**, 46% for **5**); iii, Me_2CuLi (99%); iv, MsCl, Et_3N then Me_2CuLi (60%); v, O_3, Me_2S (42%); vi, K_2CO_3, MeOH (67%); vii, Ac_2O, Py (100%).

† Electronic supplementary information (ESI) available: references describing previous syntheses of insect pheromones, an illustrative procedure for HKR of a bisepoxide and a comparison between asymmetric dihydroxylation (of an alkene) and HKR (of the corresponding epoxide). See http://www.rsc.org/suppdata/cc/b1/b102181h/

The methyl ketone **12** was obtained by processing epoxide **4** as summarised in Scheme 2. After epoxide opening and mesylate displacement, [2,3]-Wittig rearrangement of **10** afforded terminal alkene **11**, which under Wacker conditions, provided the desired compound **12** ($[\alpha]_D^{23}$ −1.63° (*c* 0.70, $CHCl_3$); reported value, $[\alpha]_D^{24}$ −1.71° ($CHCl_3$)[7]). The less active (*S*)-(+)-ketone could be obtained from the corresponding (*S*)-epoxide, by reconstituting from diol **5**.

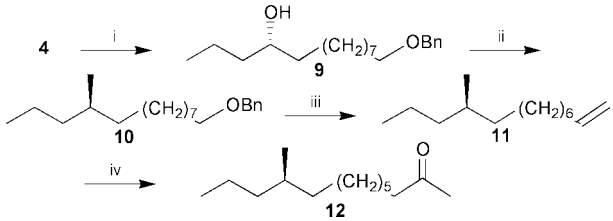

Scheme 2 *Reagents and conditions*: i, EtMgBr, CuI (62%); ii, MsCl, Et_3N then Me_2CuLi (40%); iii, ^{n}BuLi, −78 °C (43%); iv, $PdCl_2$, CuCl, DMF–H_2O, O_2 (90%).

An important component from ant-lions (*Euroleon nostras* and *Grocus bore*) is (*R*)-(−)-(*Z*)undec-6-en-2-ol (nostrenol) **18**,[8] and its synthesis (Scheme 3) begins with chemoselective epoxidation of enyne **13**. HKR of epoxide **14** furnished (*S*)-epoxide **15** of 95% ee (Mosher ester analysis of the alcohol resulting from hydride opening). Ti-mediated stereospecific *Z*-reduction[9] of protected alcohol **17** led to (*R*)-(−)-pheromone **18**, $[\alpha]_D^{23}$ −5.48° (*c* 0.70, $CHCl_3$) (reported value, $[\alpha]_D$ −6.08° (neat).[8]) As before, reconstitution of diol **16** to the (*R*)-epoxide could afford (*S*)-(+)-(*Z*)undec-6-en-2-ol.

Whereas asymmetric dihydroxylation of dienes affords tetrols,[10] successful HKR of bisepoxides would afford three easily separable components, with the predominating epoxydiol facilitating bi-directional and selective functionalisation. The conversions of nona-1,8-diene to (1*R*,7*R*)-1,7-dimethylnonyl propanoate **26** (Scheme 4), the female produced sex pheromone of the western corn rootworm (*Diabrotica virgifera virgifera*),[4]

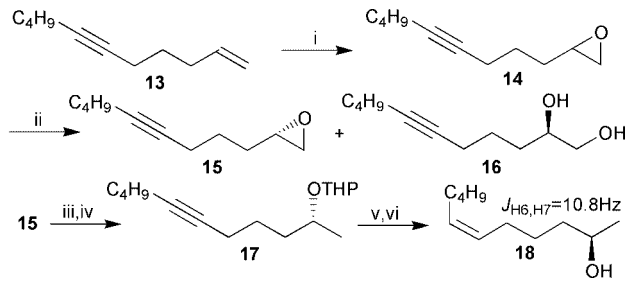

Scheme 3 *Reagents and conditions*: i, *m*-CPBA, CH_2Cl_2; ii, 0.5% eq. (*S*,*S*)-**1**, 0.55 eq. H_2O (43% for **16**); iii, $NaBH_4$, EtOH (73% over 2 steps); iv, DHP, H^+ (84%); v, $Ti(O^iPr)_4$, ^{i}PrMgBr, Et_2O then H_2O; vi, MeOH, H^+ (54% over 2 steps).

 DOI: 10.1039/b102181h

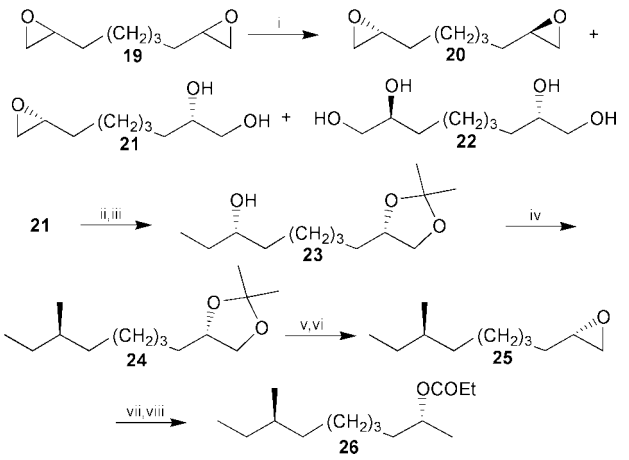

Scheme 4 *Reagents and conditions*: i, 1.0% eq. (*R*,*R*)-**1**, 0.8 eq. H_2O, (24% for **20**, 46% for **21**, 15% for **22**); ii, DMP, H^+ (78%); iii, Me_2CuLi (98%); iv, MsCl, Et_3N then Me_2CuLi (70%); v, MeOH, H^+ (76%); vi, MsCl, Et_3N then K_2CO_3, MeOH (27%); vii, $NaBH_4$, EtOH (92%); viii, $(EtCO)_2O$, Py (79%).

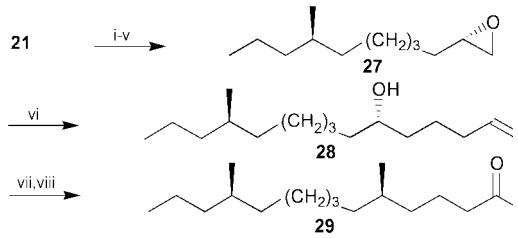

Scheme 5 *Reagents and conditions*: i, DMP, H^+ (82%); ii, EtMgBr, CuI (91%); iii, MsCl, Et_3N then Me_2CuLi (41%); iv, MeOH, H^+ (99%); v, MsCl, Et_3N then K_2CO_3, MeOH (48%); vi, $H_2C{=}CH(CH_2)_2MgBr$, CuI (34%); vii, MsCl, Et_3N then Me_2CuLi (53%); viii, $PdCl_2$, CuCl, DMF–H_2O, O_2 (74%).

and to (6*R*,12*R*)-6,12-dimethylpentadecan-2-one **29**, the female produced pheromone of the banded cucumber beetle (*Diabrotica balteata*)[4] illustrate this. Thus, racemic bisepoxide **19** was exposed to (*R*,*R*)-**1** and 0.8 eq. H_2O to provide (2*R*,8*R*)-bisepoxide **20** (24%), epoxydiol **21** (46%) and tetrol **22** (15%). Manipulation of epoxydiol **21** afforded (1*R*,7*R*)-pheromone **26**, with $[\alpha]_D^{23}$ −7.17° (*c* 0.70, $CHCl_3$) (reported value, $[\alpha]_D$ −7.57° ($CHCl_3$)[11]).

The same epoxydiol, **21**, provided the bioactive (6*R*,12*R*)-6,12-dimethylpentadecan-2-one,[4] **29**, by the procedure summarised in Scheme 5. (For **29**, $[\alpha]_D^{23}$ −0.43° (*c* 0.40, $CHCl_3$); reported value, $[\alpha]_D^{22}$ −0.5° ($CHCl_3$).[12])

HKR of the bisepoxide of dodeca-1,11-diene, **30**, proceeded satisfactorily to afford epoxydiol **32** that has been processed to (2*S*,11*S*)-2,11-diacetoxytridecane **35**, a sex pheromone component of the female pea midge, *Contarinia pisi*, a serious pest of commercial peas.[4,13] (Scheme 6). Similarly, reductive opening

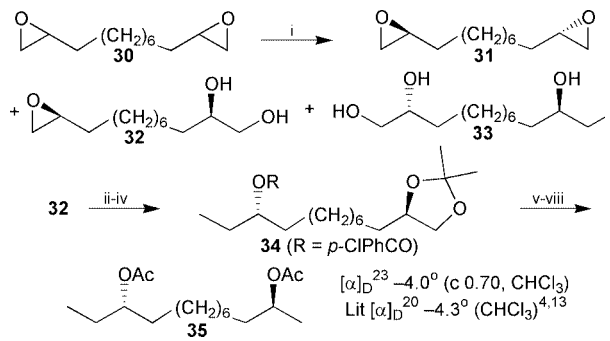

Scheme 6 *Reagents and conditions*: i, 1.0% eq. (*S*,*S*)-**1**, 0.6 eq. H_2O (23% for **31**, 26% for **32**, 12% for **33**); ii, DMP, H^+ (65%); iii, CH_3MgBr, CuI (91%); iv, Ph_3P, *p*-chlorobenzoic acid, DEAD, THF (80%); v, MeOH, H^+ (83%); vi, MsCl, Et_3N then K_2CO_3, MeOH (44%); vii, $LiAlH_4$, Et_2O (79%); viii, Ac_2O, Py (68%).

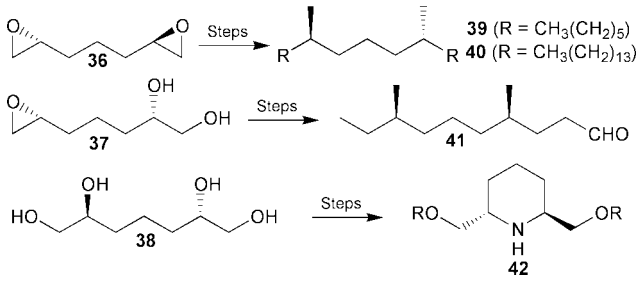

Scheme 7

($NaBH_4$, EtOH, 84%) of the (*R*,*R*)-bisepoxide of tridecan-1,12-diene led to (2*S*,12*S*)-2,12-diacetoxytridecane ($[\alpha]_D^{23}$ +1.77° (*c* 1.21, $CHCl_3$); reported value, $[\alpha]_{578}$ +2.04° ($CHCl_3$)[13]), also from the pea-midge.

The bisepoxide of hepta-1,6-diene with 1.4 mole% (*R*,*R*)-**1** and 1.0 mole eq. H_2O (Scheme 7) afforded bisepoxide **36**, free of its *meso* isomer (NMR), and epoxydiol **37** was stereoisomerically pure. Routes to (4*R*,8*R*)-4,8-dimethyldecanal (Tribolure) **41**, an important pheromone component of several *Tribolure* species including the red flour and confused flour beetles,[4] and C_2 symmetric dimethylalkanes, **39** and **40**, pheromone components of female spring hemlock looper (*Lambdina athasaria*) and female stable flies (*Stomoxys calcitrans*) respectively,[4] have been developed. Tetrol **38** has been converted to C_2 symmetric piperidines **42**.[14]

The above examples considerably widen the scope of the HKR approach. High ee's have resulted, and solvent addition with the longer chain bisepoxides may be beneficial.[3] A full discussion of these and related results will be reported at a later date.

We thank Professor Dr W. Francke for a listing of optical rotations of some compounds described in ref. 13.

Notes and references

1 For a semi-encyclopaedic compilation for the period 1979–1989, see K. Mori, in *The Total Synthesis of Natural Products*, ed. John A. Simon, 1992, vol. 9, John Wiley and Sons Inc., Brisbane, Australia.

2 M. Tokunaga, J. F. Larrow, F. Kakiuchi and E. N. Jacobsen, *Science*, 1997, **277**, 936; M. E. Furrow, S. E. Schaus and E. N. Jacobsen, *J. Org. Chem.*, 1998, **63**, 6776; E. N. Jacobsen, *Acc. Chem. Res.*, 2000, **33**, 421.

3 See, however, Q. Yu, Y. Wu, L.-J. Xia, M.-H. Tang and Y.-L. Wu, *Chem. Commun.*, 1999, 129; Q.-Y. Liu, J.-X. Ji and B.-G. Li, *J. Chem. Soc., Perkin Trans. 1*, 2000, 3519; P. S. Savle, M. J. Lamoreaux, J. F. Berry and R. D. Gandour, *Tetrahedron: Asymmetry*, 1998, **9**, 1843.

4 See the electronic supplementary information. References describing previous syntheses of the insect pheromones, an illustrative procedure for HKR of a bisepoxide and a comparison between asymmetric dihydroxylation (of an alkene) and HKR (of the corresponding epoxide) are provided. New compounds exhibited concordant microanalytical data (C,H), ^1H and ^{13}C NMR spectra and GC-MS data.

5 M. Hjalmarsson and H.-E. Högberg, *Acta Chem. Scand.*, 1985, **B39**, 793.

6 H. C. Brown, R. K. Bakshi and B. Singaram, *J. Am. Chem. Soc.*, 1988, **110**, 1529.

7 P. E. Sonnet, *J. Org. Chem.*, 1982, **47**, 3793.

8 P. Baeckström, G. Bergström, F. Björkling, H.-Z. He, H.-E. Högberg, U. Jacobsson, G.-Q. Lin, J. Löfqvist, T. Norin and A.-B. Wassgren, *J. Chem. Ecol.*, 1989, **15**, 61.

9 N. L. Hungerford and W. Kitching, *J. Chem. Soc., Perkin Trans. 1*, 1998, 1839.

10 Y. Q. Tu, A. Hübener, H. Zhang, C. J. Moore, M. T. Fletcher, P. Hayes, K. Dettner, W. Francke, C. S. P. McErlean and W. Kitching, *Synthesis*, 2000, 1956.

11 K. Mori and H. Watanabe, *Tetrahedron*, 1984, **40**, 299.

12 K. Mori and Y. Igarashi, *Liebigs Ann. Chem.*, 1988, 717.

13 Y. Hillbur, P. Anderson, H. Arn, M. Bengtsson, J. Löfqvist, A. J. Biddle, O. Smitt, H.-E. Högberg, E. Plass, S. Francke and W. Francke, *Naturwissenschaften*, 1999, **86**, 292.

14 H. Takahata, S.-I. Kouno and T. Momose, *Tetrahedron: Asymmetry*, 1995, **6**, 1085.

CHEMCOMM
Communication
www.rsc.org/chemcomm

A kinetically controlled molecular switch based on bistable [2]rotaxane†

Jae Wook Lee, Kyungpil Kim and Kimoon Kim*

National Creative Research Initiative Center for Smart Supramolecules and Department of Chemistry, Division of Molecular and Life Sciences, Pohang University of Science and Technology, San 31 Hyojadong, Pohang 790-784, Republic of Korea. E-mail: kkim@postech.ac.kr; Fax: +82-54-279-8129

Received (in Cambridge, UK) 17th April 2001, Accepted 30th April 2001
First published as an Advance Article on the web 16th May 2001

A bistable [2]rotaxane that behaves as a kinetically controlled molecular switch is synthesized; switching from one state to the other is driven by pH change but the reverse process requires pH change plus thermal activation.

The construction of nanometer-scale devices such as molecular machines and switches from molecular components ('bottom-up' approach) is of much interest in modern science and technology.[1] Mechanically interlocked molecules such as rotaxanes and catenanes have great potential as such molecular devices because the relative positions of their components can be induced to change by external chemical, electrochemical or photochemical stimuli.[2,3] In appropriately designed systems, such mechanical movements occur between two different well-defined states so that they behave as molecular switches that are potentially useful in molecular-scale information storage and processing as well as sensors. In most cases, the molecular switches operate under thermodynamic control. In other words, since such a system is in thermodynamic equilibrium when it responds to a stimulus, it reverts to its initial state upon removal of the stimulus, which means that the new state cannot be 'locked in'.[4] Here we present a novel bistable [2]rotaxane behaving as a kinetically controlled molecular switch—the new state induced by an external stimulus can be 'locked in' after removal of the stimulus.

Cucurbituril (CB[6]),[5] a macrocyclic cage compound forms host–guest complexes with protonated diaminoalkanes (log$K$ = 5.19 at 40 °C for diaminobutane at pH = 1), the stabilities of which, however, depend on pH. Taking advantage of this fact, we[6] and others[7–9] have constructed interlocked species such as rotaxanes, polyrotaxanes, molecular necklaces and molecular switches using CB[6] as a molecular bead. Recently, CB[6] was found to form a stable inclusion complex with 1,6-di(pyridinium)hexane (log$K$ = 4.40 at 25 °C);[10] this complex formation is little affected by the pH of the solution. Taking these inclusion properties of CB[6] into account, we have designed and synthesized a bistable [2]rotaxane (**1**) consisting of CB[6] as a bead, one protonated diaminobutane unit as a station (**A**), two pyridinium groups as linkers, two hexamethylene units as further stations (**B**), and two terminal viologen groups (Scheme 1). [2]Rotaxane **1** is synthesized from the corresponding 'string' and CB[6] by 'slippage'.[11]† The ^{1}H-NMR spectrum of **1** is consistent with the desired [2]rotaxane structure. The signals for the internal CH_2 protons of the protonated diaminobutane unit, which are now located inside CB[6], are up-field-shifted relative to those in the free 'string'. On the other hand, there is no chemical-shift change in the hexamethylene units. These observations are consistent with the structure (state **I**, Scheme 2) in which the CB[6] bead in **1** resides exclusively at station **A**.

Deprotonation of the protonated diaminobutane unit in **1** promotes the movement of CB[6] from station **A** to station **B**.

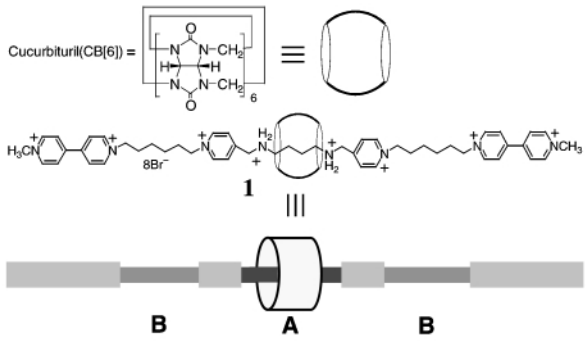

Scheme 1 Bistable [2]rotaxane **1**.

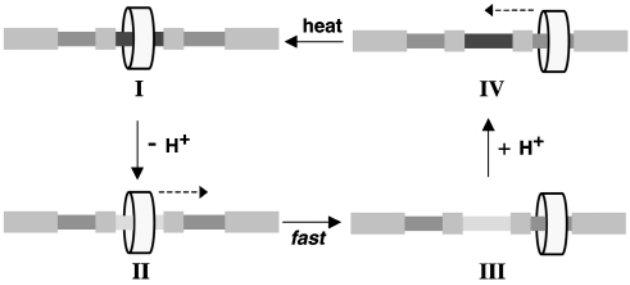

Scheme 2 Switching cycle of bistable [2]rotaxane **1**.

Diisopropylethylamine (DIEA) was found to be an ideal base to drive the switching process because it is strong enough to deprotonate the NH_2^+ while behaving concurrently as an unreactive nucleophile towards the viologen units. Reprotonation can be performed by addition of a suitable acid such as DCl. The pH-controlled switching processes of **1** have been monitored by ^{1}H NMR spectroscopy (Fig. 1).

In a typical experiment, DIEA (2.1 eq.) is added to a solution of **1** (state **I**) in D_2O. The ^{1}H NMR spectrum shows that, upon base addition, deprotonation of the NH_2^+ in station **A** occurs and CB[6] moves from station **A** to station **B**, while leaving the viologen unit intact but the chemical shifts of viologen and pyridinium units are influenced by the CB[6] movement (Fig. 1b). Resonances for $-NH_2^+CH_2(\bullet)CH_2(\blacklozenge)CH_2CH_2NH_2^+-$ protons disappear and new signals, which can be assigned to $-NHCH_2(\bullet)CH_2(\blacklozenge)CH_2CH_2NH-$ protons without CB[6], become visible as a result of the relocation of CB[6]. At the same time, signals for the hexamethylene units (station **B**) split into *two* sets: one set shows dramatic chemical-shift changes (upfield shifts) whereas the other set shows no change.[12] This observation suggests that the CB[6] bead locates at one of the two **B** stations (state **III**, Scheme 2).

Upon addition of DCl (2.2 eq.), the $-NH_2^+CH_2(\bullet)CH_2(\blacklozenge)$ proton signals shift downfield due to protonation of the amine groups, while the signals for the hexamethylene unit remain unchanged, suggesting that the CB[6] bead *does not* shuttle back quickly to station **A** (state **IV**) (Fig. 1c). In fact, the reverse process is very slow at rt: the CB[6] bead shuttles back ~50%

† Electronic supplementary information (ESI) available: synthetic procedure and characterization data of **1** and colour versions of Schemes 1 and 2. See http://www.rsc.org/suppdata/cc/b1/b103380h/

 DOI: 10.1039/b103380h

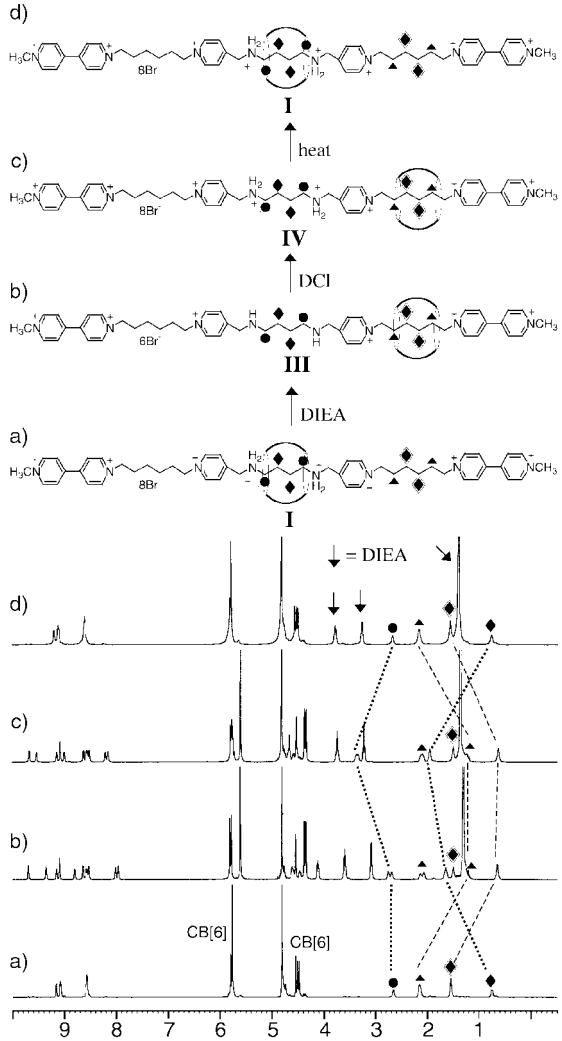

Fig. 1 Comparison of the ^{1}H-NMR spectra (in D_2O at 25 °C) of **1**. (a) **1** (state **I**), (b) after treatment of DIEA (state **III**), (c) after treatment of DCl (state **IV**), and (d) after heating at 80 °C (state **I**); the spectrum was taken after cooling at 25 °C.

to station **A** after two weeks at rt. The extremely slow reverse process at rt indicates that it has a high activation barrier. Indeed, when the same sample is warmed up to 80 °C, the CB[6] bead shuttles back quickly and completely to station **A** (Fig. 1d). The rate of the reverse process is measured to be 7.4×10^{-5} s^{-1} at 60 °C and the activation barrier ($\Delta G^{\ddagger}$) 26 kcal mol^{-1}. Therefore, this novel bistable [2]rotaxane behaves as a kinetically controlled molecular switch in which the kinetically stable new state is maintained at rt after removal of an applied stimulus. The complete cycle of the molecular switch is given in Scheme 2.

In summary, we present a kinetically controlled molecular switch based on [2]rotaxane. The switching of the molecular bead from one site to the other site is driven by pH change, but the reverse process requires pH change plus thermal activation. This novel switching system may thus provide useful insights in designing 'safeguarded' molecular switches.

We gratefully acknowledge Creative Research Initiative Program of the Korean Ministry of Science and Technology for support of this work, Brain Korea 21 Program of Korean Ministry of Education for graduate studentship to Kyungpil Kim, and Professor P. K. Bharadwaj for reading the manuscript.

Notes and references

1 V. Balzani, A. Credi, F. M. Raymo and J. F. Stoddart, *Angew. Chem., Int. Ed.*, 2000, **39**, 3348; M. Gómez-López, J. A. Preece and J. F. Stoddart, *Nanotechnology*, 1996, **7**, 183.

2 Reviews: V. Balzani, M. Gómez-López and J. F. Stoddart, *Acc. Chem. Res.*, 1998, **31**, 405; J.-P. Sauvage, *Acc. Chem. Res.*, 1998, **31**, 611; A. C. Benniston, *Chem. Soc. Rev.*, 1996, **25**, 427.

3 H. Murakami, A. Kawabuchi, K. Kotoo, M. Kinitake and N. Nakashima, *J. Am. Chem. Soc.*, 1997, **119**, 7605; Y. Kawaguchi and A. Harada, *Org. Lett.*, 2000, **2**, 1353; A. S. Lane, A. A. Leigh and A. Murphy, *J. Am. Chem. Soc.*, 1997, **119**, 11 092; A. C. Benniston and A. Harriman, *Angew. Chem., Int. Ed. Engl.*, 1993, **32**, 1459; N. Armaroli, V. Balzani, J.-P. Collin, P. Gavina, J.-P. Sauvage and B. Ventura, *J. Am. Chem. Soc.*, 1999, **121**, 4397; C. P. Collier, G. Mattersteig, E. W. Wong, Y. Luo, K. Beverly, J. Sapaio, F. M. Raymo, J. F. Stoddart and J. R. Heath, *Science*, 2000, **289**, 1172; A. M. Brouwer, C. Frochot, F. G. Gatti, D. A. Leigh, L. Mottier, F. Paolucci, S. Roffia and G. W. H. Wurpel, *Science*, 2001, **291**, 2124.

4 M. D. Ward, *J. Chem. Educ.*, 2001, **78**, 321; M. D. Ward, *Chem. Ind.*, 1997, 640.

5 Review: W. L. Mock, in *Comprehensive Supramolecular Chemistry*, ed. F. Vögtle, Vol. 2, Pergamon, Oxford, 1996, p. 477. New cucurbituril homologues CB[5], CB[7] and CB[8], which are pentameric, heptameric, and octameric species, respectively, have been recently reported: J. Kim, I.-S Jung, S.-Y. Kim, E. Lee, J.-K. Kang, S. Sakamoto, K. Yamaguchi and K. Kim, *J. Am. Chem. Soc.*, 2000, **122**, 540.

6 Y.-M. Jeon, D. Whang, J. Kim and K. Kim, *Chem. Lett.*, 1996, 503; D. Whang, Y.-M. Jeon, J. Heo and K. Kim, *J. Am. Chem. Soc.*, 1996, **118**, 11 333; D. Whang and K. Kim, *J. Am. Chem. Soc.*, 1997, **119**, 451; D. Whang, J. Heo, C.-A. Kim and K. Kim, *Chem. Commun.*, 1997, 2361; D. Whang, K.-M. Park, J. Heo and K. Kim, *J. Am. Chem. Soc.*, 1998, **120**, 4899; S.-G. Roh, K.-M. Park, G.-J. Park, S. Sakamoto, K. Yamaguchi and K. Kim, *Angew. Chem., Int. Ed.*, 1999, **38**, 638; S. I. Jun, J. W. Lee, S. Sakamoto, K. Yamaguchi and K. Kim, *Tetrahedron Lett.*, 2000, **41**, 471; E. Lee, J. Heo and K. Kim, *Angew. Chem., Int. Ed.*, 2000, **39**, 2699; H. Isobe, N. Tomita, J. W. Lee, H.-J. Kim, K. Kim and E. Nakamura, *Angew. Chem., Int. Ed.*, 2000, **39**, 4257; J. W. Lee, Y. H. Ko, S.-H. Park, K. Yamaguchi and K. Kim, *Angew. Chem., Int. Ed.*, 2001, **40**, 746.

7 C. Meschke, H.-J. Buschmann and E. Schollmeyer, *Polymer*, 1999, **40**, 945.

8 D. Tuncel and J. J. G. Steinke, *Chem. Commun.*, 1999, 1509; D. Tuncel and J. J. G. Steinke, *Chem. Commun.*, 2001, 253.

9 W. L. Mock and J. Pierpont, *J. Chem. Soc., Chem. Commun.*, 1990, 1509.

10 H.-J. Buschmann, C. Meschke and E. Schollmeyer, *Anales Quím. Int. Ed.*, 1998, **94**, 241.

11 D. B. Amabilino, P. R. Ashton, M. Belohradsky, F. M. Raymo and J. F. Stoddart, *J. Chem. Soc., Chem. Commun.*, 1995, 747.

12 Upon the movement of CB[6] from station **A** to one of the two **B** stations, the signals for the viologen and pyridinium units also split into two sets due to the disymmetric structure in state **III**. However, the directions of the chemical shift changes are consistent with the idea that the bead is not located *on* the viologen or pyridinium unit but *between* them.

CHEMCOMM
Communication
www.rsc.org/chemcomm

Ambient temperature reversible addition–fragmentation chain transfer polymerisation†

John F. Quinn,[a] Ezio Rizzardo*[b] and Thomas P. Davis*[a]

[a] *Centre for Advanced Macromolecular Design, School of Chemical Engineering and Industrial Chemistry, University of New South Wales, Sydney, New South Wales, Australia. E-mail: t.davis@unsw.edu.au*
[b] *CSIRO Molecular Science, Clayton South, Victoria, Australia, 3169*

Received (in Cambridge, UK) 26th February 2001, Accepted 24th April 2001
First published as an Advance Article on the web 16th May 2001

Reversible addition fragmentation chain transfer was performed at ambient temperature for the first time.

Reversible Addition Fragmentation Chain Transfer Polymerisation (the RAFT process) is a powerful technique for synthesising well-defined polymer architectures with low polydispersity.[1–3] The technique employs a transfer agent of the general formula:

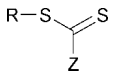

which reacts with growing polymer chains *via* Scheme 1 shown below. Reaction then proceeds with growing polymer chains reacting alternately with the two sulfur atoms in the polymeric RAFT agent. In this system, R must be a good leaving group that is able to re-initiate polymerisation and the Z group strongly influences the stability of the intermediate disulfur macroradical species.[4,5]

In order to synthesise certain novel materials, it is desirable to develop a RAFT agent that can be used at rt and with initiation techniques such as UV or gamma radiation. However, preliminary studies by the authors have shown that at low temperatures (~25 °C), the presence of a common RAFT agent (1-phenylethyl dithiobenzoate, **1**) strongly retards the polymerisation of

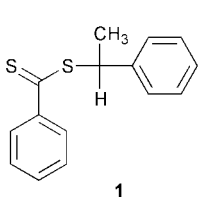

1

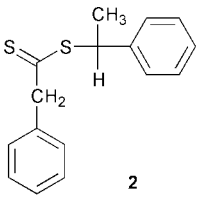

2

alkyl acrylates. This is consistent with previous work from the CSIRO group, which has shown that variation of the Z group from phenyl to methyl reduces retardation in the polymerization of *n*-butyl acrylate at 80 °C.[4] This retardation may be due to either a low rate of fragmentation of the intermediate (lessening the number of propagating radicals), or failure of the phenylethyl group to re-initiate polymerization at these low temperatures. To counter the first problem, a simple variation was made to the Z group of the RAFT agent, in order to give a less stable macroradical intermediate, thereby increasing the rate of fragmentation. In this study, by changing the Z group from a phenyl to a benzyl group, the radical in the RAFT intermediate is changed from being in a disulfur benzylic position to a less stable disulfur alkyl position. This should increase the rate of fragmentation and result in faster establishment of the RAFT equilibrium. Therefore, using such a RAFT agent it could be anticipated to observe living behaviour in the polymerization of alkyl acrylates at lower temperatures, rather than the demonstrated retardation caused by 1-phenylethyl dithiobenzoate. The RAFT agent synthesised for this study was 1-phenylethyl phenyldithioacetate (**2**).‡

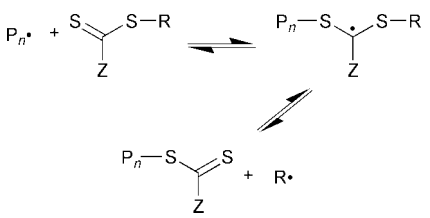

Scheme 1

Methyl acrylate was polymerised in septa capped ampoules in a water bath at rt using AIBN as the initiator and 1-phenylethyl phenyldithioacetate (1-PEPDTA) as the RAFT agent. Given that AIBN has a much longer half-life at 25 °C than it does at 60 °C, a higher than normal concentration was used (36.1×10^{-3} molL^{-1}). A significant exotherm was observed in the control experiments (methyl acrylate, AIBN only), with the resultant runaway reaction causing the monomer to boil and the septa to break in the first ten minutes of the reaction. Conversely, the polymerization of methyl acrylate with added 1-PEPDTA proceeded without autoacceleration *via* pseudo first order kinetics, as shown in Fig. 1.§

Further, use of 1-PEPDTA in polymerisation of methyl acrylate at 25 °C gives low polydispersity poly(methyl acrylate) (M_n = 241,417, PDI = 1.19) that shows living behaviour (*i.e.* the molecular weight increases linearly with conversion). This is demonstrated in Fig. 2.

It should be noted that the molecular weights obtained experimentally adhere closely to those predicted from theory (Fig. 2, unbroken line). The exception to this is the final data point, where the theoretical molecular weight is considerably lower than the experimental one. An explanation for this deviation is the use of Mark Houwink Sakurada coefficients for

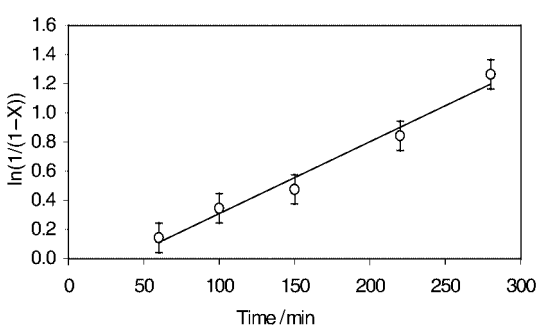

Fig. 1 Pseudo first order rate plot for the bulk polymerisation of methyl acrylate mediated with 1-PEPDTA at 25 °C. Error determined from duplicates.

† Electronic supplementary information (ESI) available: data used for the graphs in Figs. 1 and 2. See http://www.rsc.org/suppdata/cc/b1/b101794m/

 DOI: 10.1039/b101794m

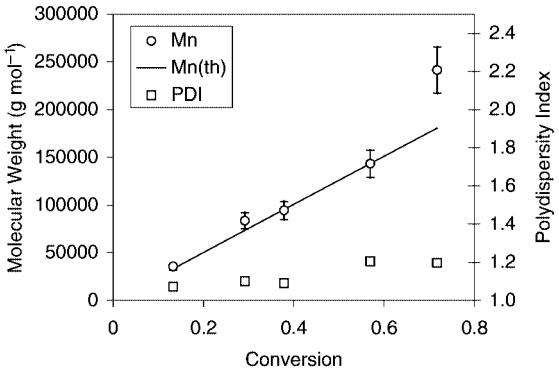

Fig. 2 Evolution of molecular weight and polydispersity index with conversion for 1-PEPDTA mediated polymerisation of methyl acrylate at 25 °C.

polystyrene in the molecular weight determination of the polymer. When analysing a polyacrylate, this would be expected to give an error anywhere between 10 and 100% (with larger error at higher molecular weight), and therefore may account for the observed discrepancy between the actual and theoretical values.

These results demonstrate that by adjusting the structure of the Z group in the RAFT agent living polymerization at rt is possible. The structural adjustment is required to decrease the stability of the intermediate radical, therefore causing the equilibrium (Scheme 1) to shift to increase the concentration of propagating polymer chains. In this study this was achieved by changing the RAFT agent from 1-phenylethyl dithiobenzoate, which gives rise to a disulfur benzylic radical intermediate, to 1-phenylethyl phenyldithioacetate, which yields a less stable disulfur alkyl radical intermediate.

The authors wish to acknowledge the support of the Co-operative Research Centre for Polymers and Dr J. P. A. Heuts and A/Professor R. P. Chaplin for helpful discussions.

Notes and references

‡ *Synthesis*: 1-Phenylethyl phenyldithioacetate was synthesised using the following method. Benzyl chloride (20 g) was added dropwise to a mixture of magnesium turnings (3.75 g) in dry diethyl ether (100 ml). Following the vigorous initial reaction, the solution was refluxed for 3 h to ensure complete reaction. The mixture was then chilled and carbon disulfide (12.0 g) was added dropwise over 30 min, and then the mixture stirred at 0 °C for the following 2 h. The mixture was then poured onto ice-water (300 ml) and the aqueous portion collected following three washes with diethyl ether. A final layer of diethyl ether was added, and the mixture acidified using 30% aqueous HCl. Phenyldithioacetic acid (~7 g) was collected *via* rotary evaporation of the ether. The acid was then reacted with styrene (9.0 g), with a small amount of acid catalyst (toluene-*p*-sulfonic acid) in CCl_4 (10 g). The product was then precipitated in cold methanol and recrystallised from methanol as fine yellow crystals (3.2 g). ^{1}H NMR: δ = 1.7 d 3H, δ = 4.2 s 2H, δ = 5.1 q 1H, δ = 7.3 m 10H. ^{13}C NMR ($CDCl_3$): 20.5, 49.9, 57.9, 127.2, 127.6, 127.7, 128.5, 128.6, 129.1, 136.9, 141.0 and 233.6. IR: Aromatic C–H stretch, 3062, 3028 cm^{-1}; Aliphatic C–H stretch, 2966, 2925 cm^{-1}; Overtone indicative of monosubstituted aromatic 2000–1650 cm^{-1}; Aromatic ring stretch, 1601, 1494, 1453 cm^{-1}; Thiocarbonyl C=S stretch, 1219, 1125, 1028 cm^{-1}; Out of plane aromatic C–H bend 764, 697 cm^{-1}; Weak sulfide C–S stretch, 646, 591 cm^{-1}. Melting point = 35 °C.

§ *Polymerization*: A solution of methyl acrylate with an initial 1-PEPDTA concentration of 3.9×10^{-3} mol L^{-1} and an AIBN concentration of 36.1×10^{-3} mol L^{-1} was prepared. The stock solution was divided into five individual ampoules and deoxygenated by purging with nitrogen for approximately 15 min. The ampoules were then placed in a constant temperature water bath at 25 °C, and an ampoule was removed after 60, 100, 150, 220 and 280 min. The reactions were stopped by cooling the solutions in an ice bath followed by the addition of hydroquinone. The polymer was isolated by evaporating off the residual methyl acrylate, initially in a fume cupboard to remove the bulk of the liquid, and then in a vacuum oven at 25 °C. Final conversions were measured by gravimetry, and the molecular weight distribution measured using gel permeation chromatography. Each experiment was performed in duplicate. Blank solutions, containing only methyl acrylate and AIBN were also prepared and polymerised using the same methods.

1 Y. K. Chong, T. P. T. Le, G. Moad, E. Rizzardo and S. H. Thang, *Macromolecules*, 1999, **32**, 2071.
2 H. De Brouwer, M. A. J. Schellekens, B. Klumpermann, M. J. Monteiro and A. L. German, *J. Pol. Sci. Part A*, 2000, **38**, 19, 3596.
3 E. Rizzardo, J. Chiefari, R. T. A. Mayadunne, G. Moad and S. H. Thang, *'Synthesis of Defined Polymers by Reversible Addition Fragmentation Chain Transfer: The RAFT Process'*, in *ACS Symposium Series 768*, 2000.
4 G. Moad, J. Chiefari, Y. K. Chong, J. Krstina, R. T. A. Mayadunne, A. Postma, E. Rizzardo and S. H. Thang, *Polym Int.*, 2000, **49**, 993.
5 C. Barner-Kowollik, J. F. Quinn, D. R. Morsley and T. P. Davis, *J. Pol. Sci. Part A: Chem.*, 2001, **39**, 1353.

CHEMCOMM
Communication
www.rsc.org/chemcomm

Enhanced chemical reversibility of redox processes in cyanine dye rotaxanes

Jonathan E. H. Buston,[a] Frank Marken[b] and Harry L. Anderson*[a]

[a] *Department of Chemistry, University of Oxford, Dyson Perrins Laboratory, South Parks Road, Oxford, UK OX1 3QY. E-mail: harry.anderson@chem.ox.ac.uk*

[b] *Department of Chemistry, University of Oxford, Physical and Theoretical Chemistry, South Parks Road, Oxford, UK OX1 3QZ. Current address: Department of Chemistry, Loughborough University, Loughborough, Leicestershire, UK LE11 3TU. E-mail: f.marken@lboro.ac.uk*

Received (in Cambridge, UK) 6th March 2001, Accepted 1st May 2001
First published as an Advance Article on the web 16th May 2001

When a cyanine dye is encapsulated inside the cavity of α-cyclodextrin, by rotaxane formation, its one-electron oxidation and reduction become reversible, due to a thousand-fold increase in the kinetic chemical stability of the oxidised and reduced forms of the chromophore.

Encapsulation of redox-active guests inside dendrimers and molecular cages often affects the kinetics and thermodynamics of electron transfer, just as the proteins which wrap round biological redox centres control electron transfer in Nature.[1] Conversely, changes in oxidation state can have a dramatic effect on the strength of host–guest interactions.[2] Stoddart and coworkers have used this phenomenon to create rotaxanes[3] which work as molecular machines;[4] oxidation or reduction of the dumbbell component changes the preferred location of the macrocycle, resulting in translational motion. Here we report a redox-active rotaxane which demonstrates a different effect: the macrocycle acts as a protective sheath, preventing the oxidised and reduced forms of the dumbbell from undergoing further chemistry, making both redox processes reversible, whereas in the absence of the threaded macrocycle, the oxidised and reduced forms of the dumbbell are rapidly destroyed by subsequent irreversible reactions (Scheme 1). Electrochemical devices generally require repeated redox cycling without side reactions, so this encapsulation effect may be widely beneficial.

The rotaxanes studied here consist of a cyanine dye dumbbell threaded through α-cyclodextrin. The two rotaxane isomers **1a** and **1b**, and the analogous free dye **2**, were prepared from julolidine aldehyde **3**[5] and diphenylpyridinium **4**[6] as summarised in Scheme 2. This reaction gives a 28% yield of a 3:2 mixture of **1a** and **1b**. Although this yield is modest, it represents a ten-fold improvement compared with our previous synthesis of cyanine dye rotaxanes[7] from aldehyde **5** and adamantylpyridinium **6**. We have also prepared rotaxanes from

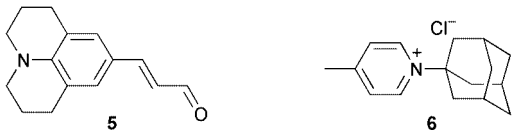

the combinations **3** + **6** and **4** + **5**, but **3** + **4** gives the highest yield. The longer julolidine aldehyde **3** probably forms a stronger complex with α-cyclodextrin, with the carbonyl group protruding further through the macrocycle. The diphenylpyridinium **4** also reacts with this aldehyde at a lower temperature than **6**, which leads to a higher yield of dye, as these dyes gradually degrade under the reaction conditions. The two stereoisomers **1a** and **1b** were separated by chromatography and structurally characterised using 2D NMR techniques. The pattern of NOEs shows that the predominant isomer **1a** has the narrower 6-rim of the cyclodextrin towards the julolidine end of the dye, whereas **1b** has the opposite orientation. These NOE results show that the cyclodextrin is located round the reactive polymethine region of the π-system, in both isomers.

The highly conjugated structure of cyanine dyes results in small HOMO–LUMO gaps, making them easy to oxidise and reduce. The one-electron oxidation and reduction potentials ($E_{1/2}^{Ox}$ and $E_{1/2}^{Red}$) and peak absorption wavelengths (λ_{max}) of rotaxanes **1a** and **1b** and free dye **2**, in DMSO, are compared in Table 1.† The different environment around the chromophore in the rotaxanes slightly shifts the absorption, but there is remarkably little variation in the redox potentials. The inclusion of a redox-active guest inside a cyclodextrin often hinders its electrochemical oxidation or reduction,[1] but this effect is not observed in rotaxanes **1a** and **1b**. However, encapsulation has an amazing effect on the electrochemical reversibility of both redox processes, as seen from the cyclic voltammograms of **1b** and **2**, both at a scan rate of 0.2 V s^{-1}, in Fig. 1. The oxidation and reduction of the free dye **2** are chemically irreversible, as shown by the missing peaks in the reverse sweep and by the appearance of a product signal associated with the reduction process at 0.20 V *vs.* Ag. The cyclic voltammogram of the rotaxane **1b** shows that the oxidation and the reduction are now both fully reversible; both processes are well-defined, diffusion controlled, and remain reversible even when the scan rate is reduced to 0.02 V s^{-1}. Identical behaviour is observed for the other rotaxane isomer **1a**. We have tried increasing the scan rate with the free dye **2** in an attempt to achieve reversible

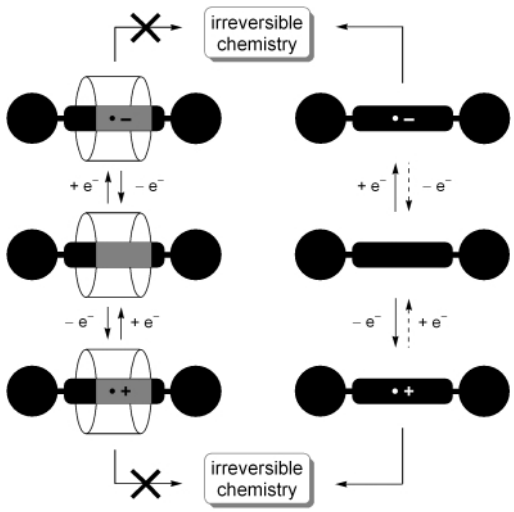

Scheme 1 Rotaxane-encapsulation stabilises the oxidised and reduced forms of the dumbbell, making its electrochemistry reversible.

Table 1 Redox potentials (*vs.* Ag) and λ_{max} for **1a**, **1b** and **2** in DMSO†

Compound	$E_{1/2}^{Ox}$/V	$E_{1/2}^{Red}$/V	λ_{max}/nm
1a	0.75	−0.56	579
1b	0.75	−0.58	590
2	0.74	−0.56	571

 DOI: 10.1039/b102068o

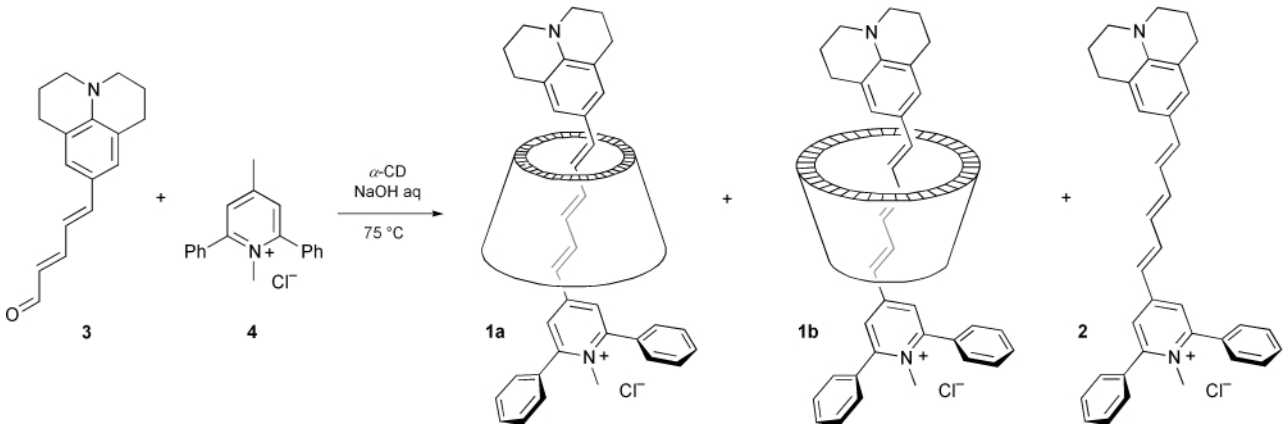

Scheme 2 The cyclodextrin is drawn as a truncated cone with a narrow rim defined by the 6-OH groups and a wide rim defined by the 2,3-OH groups.

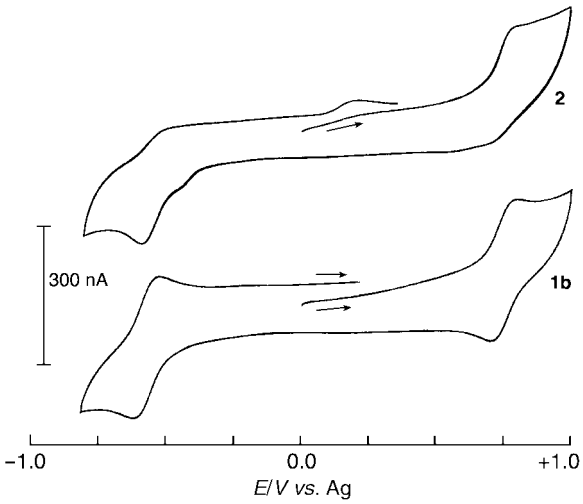

Fig. 1 Cyclic voltammograms for oxidation and reduction of **1b** and **2** DMSO (0.1 M Bu_4NPF_6) with a scan rate of 0.20 V s^{-1}.†

behaviour, and both responses (oxidation and reduction) do indeed become reversible when the scan rate exceeds 20 V s^{-1}. This demonstrates that the shielding effect of the cyclodextrin macrocycle reduces the rate of follow-on reactions of the radical dication and neutral radical forms of the dye by at least three orders of magnitude. The separation between the forward and reverse current peaks (ΔE_p) for both redox processes in both rotaxanes is 78 mV, which is larger than expected for a simple reversible electron transfer process ($\Delta E_p \approx 56$ mV at 298 K). However the peak-to-peak separation does not increase with increasing scan rate, so that there is no evidence that the cyclodextrin retards electron transfer from the electrode surface to the cyanine. These electrochemical measurements were carried out in DMSO (with 0.1 M Bu_4NPF_6) because it is the best solvent for all three compounds. Similar behaviour is also observed in water and in acetonitrile. The rotaxanes **1a** and **1b** are highly soluble in water and give well defined reversible oxidation and reduction signals in this solvent (with 0.1 M KCl electrolyte) whereas the free dye **2** is sparingly soluble in water and exhibits similar irreversible redox processes to those observed in DMSO, complicated by accumulation of material on the electrode surface. In acetonitrile (0.1 M Bu_4NPF_6) the free dye **2** is much more soluble, but its redox processes are still irreversible at 0.2 V s^{-1} scan rate; the rotaxanes are less soluble and tend to adsorb onto the electrode, but both their redox processes remain fully chemically reversible. The electrochemistry of cyanine dyes has been extensively studied because of its relevance to the use of these dyes as photographic silver halide sensitisers.[8] The irreversible oxidation and reduction of **2** is typical for dyes of this type, and fast scan potentiodynamic and AC techniques have been developed to overcome this problem. The irreversiblility of these redox processes is generally attributed to dimerisation of the electrochemically generated radicals, and in a few cases dimeric products have been isolated and characterised.[9]

Previously we have shown that rotaxane formation can enhance the photostability of cyanine dyes. This effect is also observed with these rotaxanes and both compounds fade slower than the free dye **2** when irradiated with visible light in air-saturated aqueous solution (relative rates of fading for **1a**, **1b** and **2** are 0.031 : 0.044 : 1.00 respectively). It is possible that the photo-bleaching of **2** involves photo-induced electron transfer, leading to a direct link between the enhanced photostability and enhanced redox reversibility of these rotaxanes. The mechanisms of these reactions remain to be elucidated but it is significant that rotaxane encapsulation protects the chromophore in both its excited state and in its oxidised and reduced forms. The kinetic stabilisation of the radical dication and neutral radical forms of the dye inside the cyclodextrin cavity is analogous to the stabilisation of radical intermediates by enzymes.[10]

F. M. thanks the Royal Society for a University Research Fellowship and New College, Oxford, for a Stipendiary Lectureship. This work was supported by the EPSRC.

Notes and references

† The redox potential measurements in Table 1 and Fig. 1 were carried out in DMSO (0.1 M Bu_4NPF_6) by cyclic voltammetry using a conventional three-electrode system with a 0.5 mm diameter Pt disc working electrode, a Pt wire counter electrode and a Ag wire pseudo-reference electrode, under argon at 20 °C. The concentration of **1a**, **1b** and **2** was *ca*. 1 mM. The scan rate was 0.20 V s^{-1} in all cases except for the measurements on **2** in Table 1, where a 20 V s^{-1} scan rate was used to achieve reversibility. $E_{1/2}$ values were estimated from the midpoint of the forward and reverse current peak for each redox process, and were calibrated with internal ferrocene ($E_{1/2}^{Ox}$ = 0.78 *vs*. Ag).

1 C. M. Cardona, S. Mendoza and A. E. Kaifer, *Chem. Soc. Rev.*, 2000, **29**, 37; A. E. Kaifer and M. Gómez-Kaifer, *Supramolecular Electrochemistry*, Wiley-VCH, Weinheim, 2000.
2 A. Niemz and V. M. Rotello, *Acc. Chem. Res.*, 1999, **32**, 44.
3 S. A. Nepogodiev and J. F. Stoddart, *Chem. Rev.*, 1998, **98**, 1959.
4 V. Balzani, A. Credi, F. M. Raymo and J. F. Stoddart, *Angew. Chem., Int. Ed.*, 2000, **39**, 3349.
5 A. C. Friedli, E. Yang and S. R. Marder, *Tetrahedron*, 1997, **53**, 2717.
6 J. A. van Allan and G. A. Reynolds, *J. Heterocycl. Chem.*, 1971, **8**, 803.
7 J. E. H. Buston, J. R. Young and H. L. Anderson, *Chem. Commun.*, 2000, 905.
8 J. R. Lenhard and A. D. Cameron, *J. Phys. Chem.*, 1993, **97**, 4916; S. Nomura and S. Okazaki, *Chem. Lett.*, 1990, 2231; T. Tani, K. Ohzeki and K. Seki, *J. Electrochem. Soc.*, 1991, **138**, 1411.
9 R. L. Parton and J. R. Lenhard, *J. Org. Chem.*, 1990, **55**, 49.
10 J. Rétey, *Angew. Chem., Int. Ed. Engl.*, 1990, **29**, 355; J. Stubbe and W. A. van der Donk, *Chem. Rev.*, 1998, **98**, 705.

Typeset and printed by Black Bear Press Limited, Cambridge, England

CHEMCOMM
Feature Article
www.rsc.org/chemcomm

s-Block metal inverse crowns: synthetic and structural synergism in mixed alkali metal–magnesium (or zinc) amide chemistry

Robert E. Mulvey

Department of Pure and Applied Chemistry, University of Strathclyde, Glasgow, UK G1 1XL. E-mail: r.e.mulvey@strath.ac.uk

Received (in Cambridge, UK) 16th February 2001, Accepted 20th March 2001
First published as an Advance Article on the web 20th April 2001

This article focuses on the special chemistry that can take place when certain lithium (or other heavier alkali metal) amides are combined with certain magnesium (or zinc) bisamides. Some of the reaction mixtures studied follow a straightforward path leading to simple heterobimetallic compositions with predictable structures, whereas others take an unexpected turn to behave as powerful oxygen scavengers or as regioselective bases to yield novel products with unpredictable host–guest macrocyclic structures. We refer to these new compounds as 'inverse crown ethers' or 'inverse crowns' because their arrangement of Lewis acidic and Lewis basic sites is opposite to that encountered in conventional crown ether complexes. This developing phenomenon appears to be a direct result of pairing together the two distinct metal types in the same complex, as the chemistry cannot be replicated by complexes containing one or the other metal type on its own.

Introduction

Diagonal neighbours in the periodic table, lithium and magnesium in the form of organolithium (pioneered by Schlenk) and organomagnesium halide (pioneered by Barbier and Grignard) reagents respectively, have both served the synthetic community for nearly one hundred years. Thumb through the pages of any current journal specialising in synthesis and you will almost certainly find several examples of these centenarians at work, performing some or other organic transformation. They are organometallic reagents *par excellence*. Accordingly, the literature on them is vast and ever increasing. Interested readers should consult the following sources[1,2] as a starting point for information. The present article does not deal with organolithium or organomagnesium compounds *per se*, but rather with organolithium–magnesium (and related organosodium–magnesium and organopotassium–magnesium) compounds, *i.e.* heterometallic mutations containing two different s-block metals. In theory, mixing the metal components in this way could promote beneficial synergic effects, and lead to mixed-metal compounds having their own unique chemical profiles distinct from those of the homometallic compounds from which they are derived. This synergism could be manifested in altered reactivities and selectivities as a function of altered activated complexes and intermediates. It could also deliver new chemistry and new structures, not known or not possible for the conventional homometallic compounds. In practice, though as yet only a select few studies have addressed the application of mixed lithium–magnesium compounds in chemistry, several promising observations have already been recorded. Notably, Oshima and coworkers have demonstrated that magnesium-ate complexes '$LiMgR_3$' are more effective than their Grignard counterparts (RMgX) in halogen–magnesium exchange reactions with organic halides for the preparation of aryl- and alkenyl-magnesium reagents, which are subsequently trapped by an assortment of electrophiles.[3] Also, following a systematic study of alkylation reactions of pyridine, Richey and Farkas concluded that 'solutions prepared by mixing solutions of dialkylmagnesium and alkyllithium compounds exhibit behaviour different from that of either organometallic compound alone'.[4] Turning from organic synthesis to coordination chemistry, Karsch and Reisky make the point that the key to the formation of the first magnesium compound with six Mg–P bonds lies in its 'ate formulation $[Li(12\text{-crown-}4)_2]^+[Mg\{(PMe_2)_2C(SiMe_3)\}_3]^-$, *i.e.* a mixed lithium–magnesium system albeit in the form of a solvent (crown ether)—separated ion pair.[5] Combining the two metals together has similarly proved advantageous in areas of polymer chemistry: Hsieh and Wang report that dialkylmagnesium, by itself, is not an active initiator for diene and styrene polymerization, but it participates in polymerization when complexed either with the alkyllithium initiator or with the propagating polymer–lithium molecules;[6] Antkowiak and Hall have patented the use of mixed lithium–magnesium amides based on hexamethyleneimine as anionic initiators for diene polymer and copolymer elastomers.[7] It is pertinent to note that in not one of these molecular/macromolecular applications is the structure of the active lithium–magnesium species known with any certainty. This general lack of knowledge coupled with the potential advantages alluded to earlier have prompted us to follow a programme of research designed to shed light on the fundamental structural consequences of mixing lithium (or another alkali metal) with magnesium (or zinc) in an organoelement environment. Mindful of the need to focus on synthetically useful compounds, we have directed our attention towards amide derivatives. Long-standing favourites of the synthetic chemist and thus commercially available, lithium amide reagents are specialists in the art of selective proton abstraction; recent studies have suggested that magnesium amides may also be useful and exhibit different reactivities/selectivities in this regard.[8] The extensive library of structural data available on these homometallic systems provides a further incentive for concentrating on amide derivatives because if any form of structural synergism were to result from pairing lithium and magnesium in a particular amide environment, then it should be easily recognised. It transpires that

Robert Emmet Mulvey was born in Glasgow in 1959 and educated at Saint Gregory's secondary school. Both of his degrees (B.Sc.-Hons in 1981 and Ph.D. in 1984) were obtained at the University of Strathclyde, the latter achieved under the supervision of the late Dr Ron Snaith. Following two years as a postdoctoral research assistant with Professor Ken Wade at the University of Durham, he returned to Strathclyde in 1986 to take up a Royal Society Research Fellowship. Remaining at Strathclyde in the intervening years, he has held a Personal Professorship there since 1995. Currently the Head of Inorganic Chemistry in the department he was elected to the Fellowship of the Royal Society of Edinburgh (FRSE) in 2001. Past winner of the Meldola Medal and Prize, he is an author of more than 100 research publications in the area of main group metal chemistry.

unique structural arrangements and, linked to this, unique chemistry, can indeed be generated by this heterobimetallic approach, as exemplified by the so-called 'inverse crown ether' complexes and related mixed-metal macrocycles which form the basis of this article. To put the novelty of this new class of compound into context, a brief survey of the contrasting structural types adopted by more mainstream mixed lithium–magnesium compounds is now presented.

'Ordinary' mixed lithium–magnesium compounds

Access to compounds of this type is usually achieved simply by mixing together the component homometallic compounds in the absence or presence of a Lewis base cosolvent [eqn. (1)]. In

$$x\ \mathrm{LiR} + y\ \mathrm{MgR_2} \longrightarrow \begin{cases} (\mathrm{Li}_x\mathrm{Mg}_y\mathrm{R}_z) \\ (\mathrm{Li}_x\mathrm{Mg}_y\mathrm{R}_z{\bullet}\mathrm{L}_n) \quad +n\,\mathrm{L} \end{cases} \qquad (1)$$

homoleptic cases (*i.e.* with only one type of anionic ligand) the product of such mixing need not necessarily be formulated as '$LiMgR_3$', since products with stoichiometries discordant from that employed in the reaction can sometimes prevail. Especially common in this regard is 'Li_2MgR_4'. This phenomenon is a direct consequence of the fact that structural factors dictate the composition (in particular, the Li : Mg ratio) of the mixed-metal product. To elaborate, the building up of their molecular architectures can be formally regarded as a two-stage process, each stage of which involves a distinct type of bonding which may be designated as *anchoring* or *ancillary*.

The foundation/framework of the structure is provided by *anchoring* bonds as they comprise the stronger, more covalent, predominately σ-based Mg–R interactions. Depending mainly on the steric requirements of the surrounding 'R' ligands, this framework is generally either tetrahedral or trigonal planar in disposition. *Ancillary* bonding can be defined as those more ionic interactions, which enable the lithium ions to affix to this framework to give contacted ion pairs. To maximise the number of such electrostatic contacts the lithium atoms will affix μ_2 rather than terminally. Tetrahedral MgR_4 units have six edges, so three diagonally opposed pairs of edges to accommodate pairs of lithium ions, while triangular MgR_3 units have three edges, one of which can accommodate a single lithium ion (Fig. 1): in this way are formed the common Li_2MgR_4 and

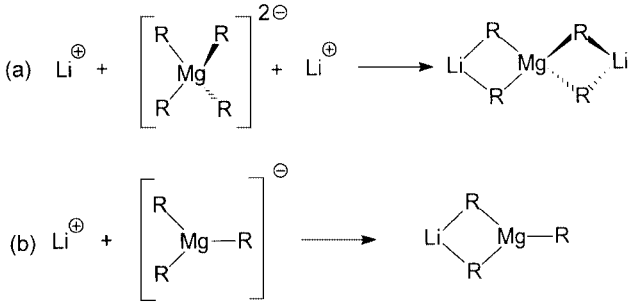

Fig. 1 Building up 2 : 1 and 1 : 1, Li : Mg stoichiometries through tetrahedral (a) and trigonal planar (b) 'anchoring' frameworks, respectively.

$LiMgR_3$ stoichiometries respectively, and charge neutrality is attained. Both of these scenarios can be found within the series of lithium organoC-magnesate structures **1**–**5**[9–12] shown in Scheme 1. An additional point is raised by the structure of **2**:[10] planar 'R' ligands (shown flat here, but in reality would be tilted out of the plane) can rotate to avoid interlocking with each other so creating a sterically relaxed opportunity for two or more Mg atoms to participate in the framework unit (in solvent-free homometallic $[(MgPh_2)_\infty]$[13] this process occurs *ad infinitum* to give a polymeric arrangement). An alternative way to describe the anchoring/ancillary demarcation is to consider that anions will preferentially bind first to magnesium, on account of its

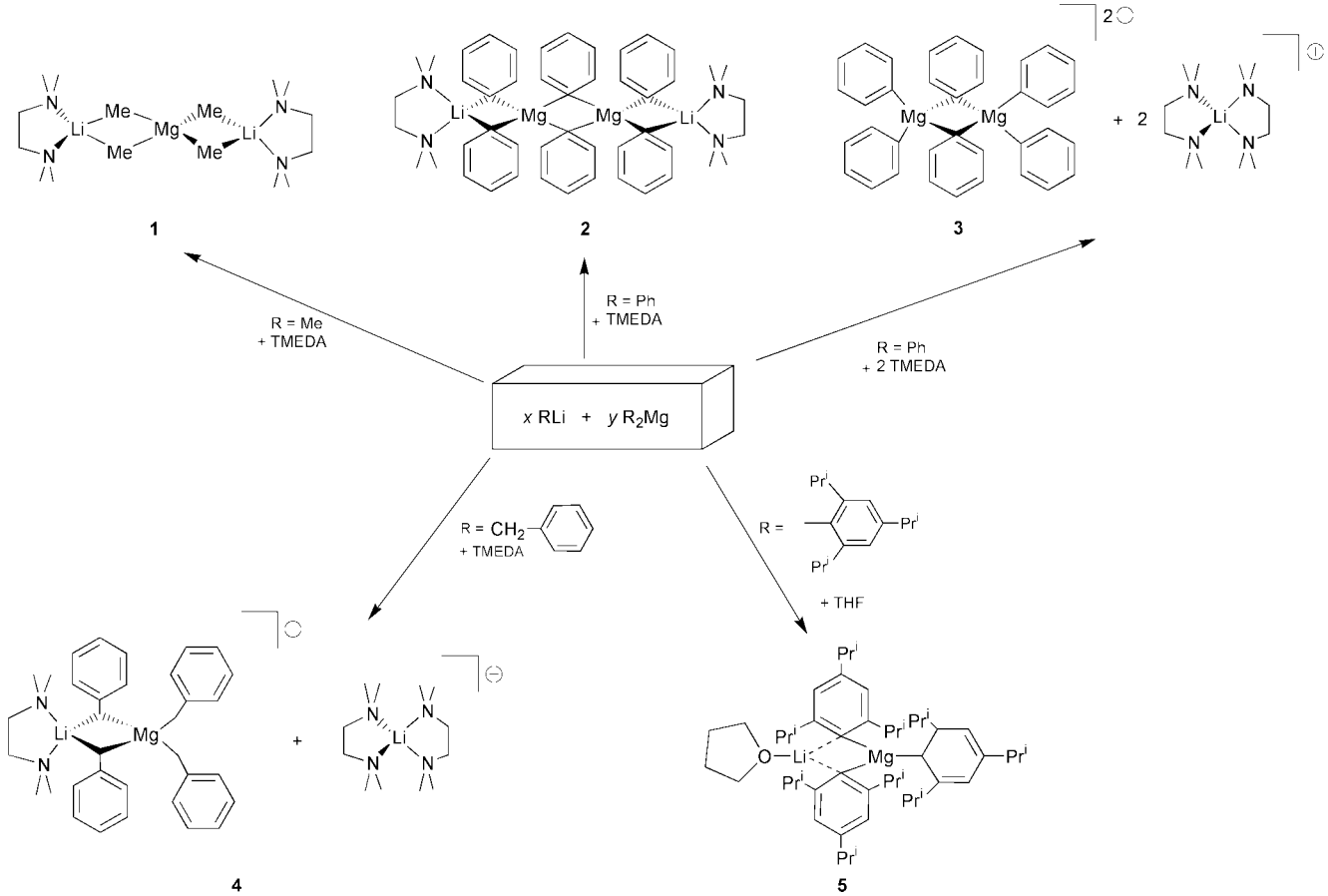

Scheme 1

greater Lewis acidity, until coordinative saturation is reached giving $(MgR_4)^{2-}$ or $(MgR_3)^-$ complex ions. These magnesium-fixed anions can therefore not usually satisfy the coordinative needs of approaching lithium cations within the limitations of a contacted ion pair arrangement and so solvent molecules are required to fill the remaining coordination sites. In certain cases, for example in structure **3**, solvent molecules can completely detach the lithium ions from the primary framework to generate solvent-separated ion pairs.

These basic structural types are not confined to alkyl and aryl ligands, as they also extend to amido systems. A clear example of the delicate balance between the tetrahedral and the trigonal planar frameworks is illustrated in a family of dibenzylamido $[^-N(CH_2Ph)_2]$ systems (Scheme 2).[14,15] Sterically, the optimum number of dibenzylamido ligands to fit around a magnesium atom would appear to be three since homometallic $[\{Mg[N(CH_2Ph)_2]_2\}_2]$ has a trigonal planar magnesium geometry within its dimeric solid-state constitution. However, introducing dibenzylamidolithium into this system induces coordination expansion about magnesium to create an alternative tetrahedral $(MgR_4)^{2-}$ framework made up of four dibenzylamido ligands R, set within a (Li_2MgR_4) formulation. This coordination expansion can be rationalised predominantly in terms of steric and valency effects: with the terminal coordination site on monovalent lithium vacant there is additional space for the benzyl arms of the bridging amido ligands to occupy. In the exclusively-magnesium structure this site is blocked by the presence of a terminally attached dibenzylamido ligand. When pyridine is added to the heterometallic structure a new dative Li–N bond is formed filling the terminal coordination site and forcing the bridging amido ligands closer towards the magnesium atom. This extra steric strain placed on magnesium reduces its ability to tolerate four (tetrahedral) coordination, thus prompting the displacement of one amide ligand (and its Li^+ partner) to leave a more sterically relaxed three-coordinate (trigonal planar) environment. Electronic effects must also be taken into consideration. Pyridine, a good σ donor, will also stabilise the lithium atom electronically. Other monodentate donor solvents such as THF will do likewise in other bulky amide systems, *e.g.* in $[(THF)\cdot LiMg\{N(c\text{-}C_6H_{11})_2\}_3]$.[16] The same basic motif can be found in mixed-anion systems, typified by the alkyl–amido complex $[(py)\cdot LiMg(HMDS)_2(Bu)]$[16] [HMDS = $^-N(SiMe_3)_2$]. Therefore the stabilising role of the solvent ligand in raising the coordination number of the lithium atom to three is an important factor in the conversion of lithium-rich Li_2MgR_4 structures into $LiMgR_3$ alternatives.

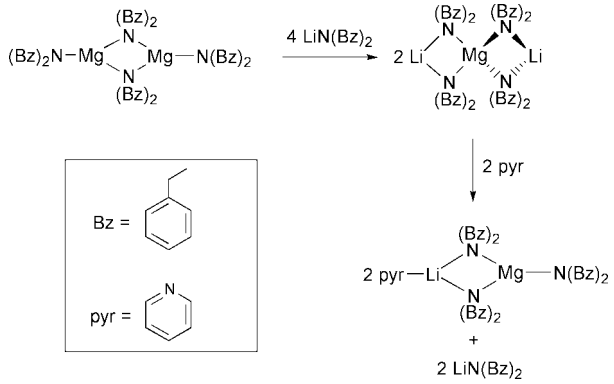

Scheme 2

Pyridine or THF will also stabilise the tris(amide) derived from the sterically demanding hexamethyldisilazane [HMDS(H)]. Interestingly, however, the 1:1, Li:Mg motif remains intact even in the absence of any such solvent molecules.[17] As depicted in Fig. 2, the loss of solvent (N or O donor atom)—lithium dative bonding is balanced by the gain of $H_3C\cdots Li$ interactions (mean length, 2.307 Å) made possible by the bending of the $SiMe_3$ substituents towards the semi-naked lithium atom. Pseudo-agostic interactions of this type are becoming increasingly familiar in structures where alkali metals have low (formal) coordination numbers; here the affinity of the Li atom for the methyl substituent is heightened by the marked polarisation within the $Si^{\delta+}$–$CH_3^{\delta-}$ units, *i.e.* the carbon atoms of the methyl groups carry a substantial negative charge. It is therefore not surprising that, from a standpoint of length, these $H_3C\cdots Li$ interactions can be likened to the electron-deficient C–Li bonds, which formally involve anions, of simple alkyllithiums such as $[(Bu^tLi)_4]$[18] and $[(EtLi)_4]$[19] (mean lengths, 2.246 and 2.25 Å, respectively).

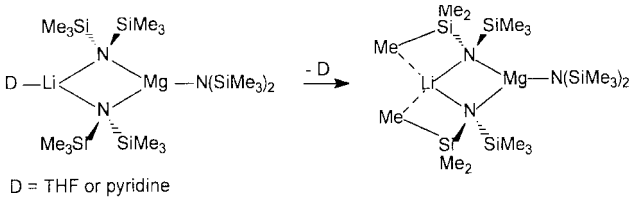

Fig. 2 Additional stabilisation of the Li atom can be achieved through a dative D–Li bond or, in the absence of a donor solvent, through $H_3C\cdots Li$ agostic interactions.

Chelational stabilisation of lithium atoms is possible when the 'R' substituents within bridging amide ligands contain an additional heteroatom, two or three atoms removed from the amido nitrogen atom. The first mixed lithium–magnesium amide $[Li_2Mg\{N(CH_2CH_2NMe_2)CH_2Ph\}_4]$, reported in 1993,[20] exhibits this feature in having five-membered (NCCNLi) chelate rings the tertiary amine nitrogen atoms of which serve to increase the coordination number of the lithium atoms from two to four.

'Extraordinary' mixed alkali metal–magnesium compounds

(i) Inverse crown ether complexes

During our attempts to reprepare the aforementioned solvent-free tris(amide) $[LiMg\{N(SiMe_3)_2\}_3]$ **6** a surprising development came to light. It was found repeatedly that the reaction solutions preferentially crystallised an oxygen-contaminated variant of formula $[Li_2Mg_2\{N(SiMe_3)_2\}_4(O_2)_x(O)_y]$ **7**, despite the fact that an inert-atmosphere protocol was employed throughout the synthetic procedure (or so we had assumed).[17] Reacting the mixtures [eqn. (2)] for 1 h then cooling the

$$BuLi + Bu_2Mg + 3\ HN(SiMe_3)_2 \xrightarrow{\text{trace of } O_2/H_2O} z\ [Li_2Mg_2\{N(SiMe_3)_2\}_4(O_2)_x(O)_y] + z'\ BuH + \text{other products} \quad (2)$$

solutions afforded **7** in typically poor, but reproducible yields of 1–5%: none of the intended (oxygen-free) product **6** precipitated from solution, which perhaps reflects its previously noted high solubility (in arene or hydrocarbon solvents). Since the initial report of **7** we have managed to increase its yield five-fold (best to date, 24%). This improvement came as a direct result of deliberately exposing the reaction mixture to the atmosphere (!) whilst stirring it for four days. Clearly, as small quantities of **7** can be produced even when standard precautions are taken to avoid moisture/oxygen contamination, the mixed lithium–magnesium HMDS system must be an extremely efficient oxygen scavenger. However, the source of the oxygen contamination, whether it be dioxygen or moisture or a combination of both, is yet to be unambiguously established.

The molecular structure of **7** (Fig. 3) reveals a discrete eight-membered ring made up of alternating nitrogen and metal atoms, with the latter atoms themselves alternately lithium and magnesium. Peroxide or oxide ions occupy the core of the ring to render the molecule neutral overall. The peroxide and oxide-

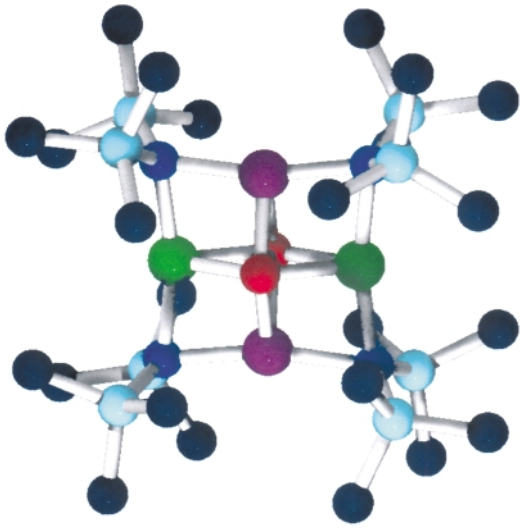

Fig. 3 Molecular structure of $[Li_2Mg_2\{N(SiMe_3)_2\}_4(O_2)_x(O)_y]$ showing peroxide core. Colour code for figures:[39] alkali metal, purple; Mg, green; Zn, yellow; N, dark blue; Si, light blue; C, black; O, red.

based molecules can be differentiated in arene solution by ^{1}H NMR spectroscopic studies. In the conventional host–guest chemistry of crown ether complexes,[21] electron-poor metal cation guests are stabilised by coordination to a series of Lewis basic oxygen centres fixed within a macrocyclic ligand host. Contrast that situation through a representative [12]crown-4 complex with the generalised structure of **7** (Fig. 4) and one can

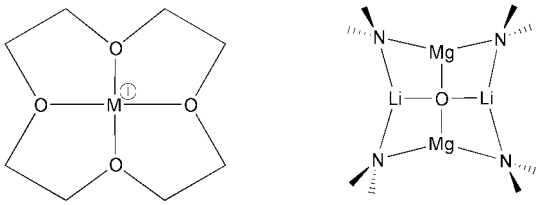

Fig. 4 A representative [12]crown-4 complex *vs*. the generalised structure of **7**.

see at a glance that while both macrocycles offer four built-in binding sites for the entertainment of the core guest the relative positions of metal and oxygen atoms have been interchanged. This topological comparison prompted us to coin the name 'inverse crown ether' complex to describe **7** and its isostructural analogues, even though no ether functionality is actually involved (a referee suggested an alternative name, metal amide chemistry, or 'MAC', crowns: but while this is perhaps more distinctive and certainly more apt given that they were discovered in Scotland, this description could be confused with metallo-crowns which are a known class of compound. In our view, the 'inverse' prefix is also essential to convey the difference with conventional crowns). The idea of a 'crown' made up of metal atoms would certainly sit easily with those people interested in royalty! At this juncture it is germane to mention that a similar description, 'anti-crowns', was introduced a few years prior to our work by Hawthorne and Zheng with regard to a series of [12]mercuracarborand-4 complexes in recognition of their charged-reversed relationship to normal [12]crown-4.[22] Contrary to the situation in the inverse crown systems, oxide or peroxide anions do not feature in anti-crown chemistry presumably because the softer acid Hg atoms prefer to bind softer bases such as Cl^-, Br^-, I^- or *closo*-$B_{10}H_{10}^{2-}$.

On further investigation it soon became apparent that the basic structural motif of **7** was not a unique, one-off oddity, but rather the progenitor of a family of such structures. The synthesis and crystallographic characterisation of **8**[23] (Fig. 5) established that inverse crown ethers could be made using other amide ligands, in this case derived from 2,2,6,6-tetramethyl-

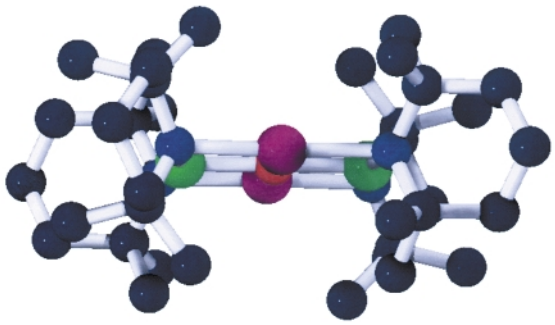

Fig. 5 Molecular structure of $[Li_2Mg_2(TMP)_4(O)]$ viewing the eight-membered ring from the side.

piperidine [TMPH = $HN(Me)_2CCH_2CH_2CH_2C(Me)_2$]. Significantly this cyclic amide ligand is even more sterically demanding about its ligating N head than HMDS, which prompts the thought that extreme steric hindrance may be a prerequisite for the formation of an inverse crown ether. Pre-attached to the metal centres, these bulky ligands may on exposure to the oxygen contaminant, suppress altogether or at least kinetically inhibit the formation of metal oxide salts which would seem more likely products from lattice energy considerations.

More important extensions to the family followed on turning our attention from lithium to the heavier alkali metals. Applying the same synthetic approach but this time using butylsodium or butylpotassium in place of the lithium congener [eqn. (3)],

$$BuM + Bu_2Mg + 3\ HN(SiMe_3)_2 \xrightarrow{\text{trace of } O_2/H_2O} z\ [M_2Mg_2\{N(SiMe_3)_2\}_4(O_2)_x(O)_y] + z'\ BuH + \text{other products} \quad (3)$$

M = Na, K

produced the first sodium–magnesium $[Na_2Mg_2\{N(SiMe_3)_2\}_4(O_2)_x(O)_y]$[23] **9** (Fig. 6) and potassium–magnesium

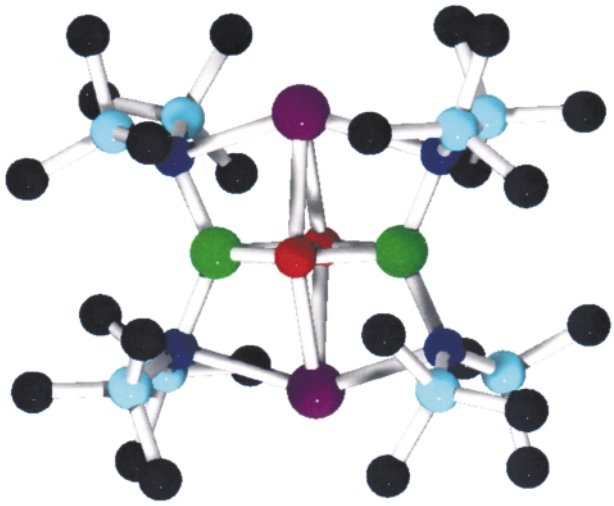

Fig. 6 Molecular structure of $[Na_2Mg_2\{N(SiMe_3)_2\}_4(O_2)_x(O)_y]$.

$[\{K_2Mg_2[N(SiMe_3)_2]_4(O_2)\}_\infty]$[24] **10** (Fig. 7) inverse crown ethers, respectively. Sodium can sometimes mimic the coordinative behaviour of its smaller Group 1 nearest neighbour so the existence of the former category of crown is not that surprising. On the other hand potassium organic derivatives normally exhibit marked structural differences to their lithium counterparts on account of the significantly larger size and softer, more polarisable nature of the K^+ cation; hence the fact that a potassium-based inverse crown ether is readily preparable bears testimony to the stability of these new macrocyclic systems. However there is one major distinction between **10** and **7** for while both have broadly similar molecular structures, in

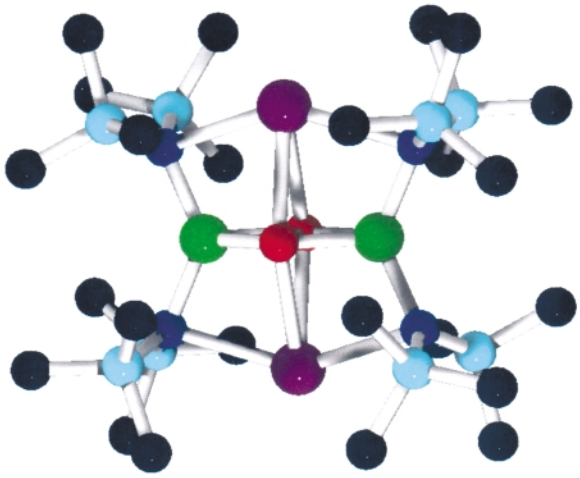

Fig. 7 Double asymmetric unit of $[\{K_2Mg_2[N(SiMe_3)_2]_4(O_2)\}_\infty]$.

the latter it is discrete but in the former it joins up through intermolecular $(Me_2Si)H_3C\cdots K$ interactions to give a linear polymeric arrangement (Fig. 8). Therefore **10** could be

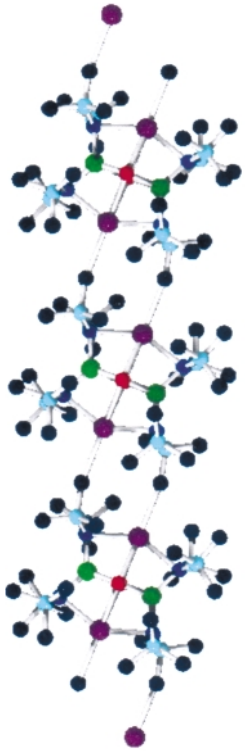

Fig. 8 Extended structure of $[\{K_2Mg_2[N(SiMe_3)_2]_4(O_2)\}_\infty]$.

described as the first supramolecular inverse crown ether structure, but this description exaggerates the distinction because such extended structures are quite common in the wider context of organopotassium chemistry.[25] Certain trends can be discerned from this Li/Na/K series of structures. Most obviously, the pairs of Mg atoms within the dicationic octagonal rings are always displaced towards the centre of the ring as a result of strong Mg–O bonding. The magnitude of this displacement grows in concert with the increasing size of the alkali metal partner in the ring as gauged by the endocyclic N–Mg–N bond angles (mean values 193.3, 218.4 and 227.8° for the Li, Na and K structures respectively). Similarly, the small Li atom in **7** and **8** is pulled towards the centre of the ring through strong Li–O bonding, resulting in endocyclic N–Li–N bond angles greater than 180°. In contrast the Na and K atoms occupy peripheral ring sites with endocyclic N–Na–N and N–K–N bond angles significantly less than 180°, reflecting longer, weaker Na–O/K–O bonding.

Extension to zinc. Having established that it is possible to vary the Group 1 metal in the inverse crown ether octagons, the next logical step was to consider possible replacement of the Group 2 metal, magnesium. The health problems associated with beryllium deterred us from experimenting with the lightest member of Group 2, so instead we turned our attention towards the next nearest neighbour, calcium. Though a significant size differential exists between Mg and Ca (*e.g.* 0.28 Å for ionic radii), that between Li and K is substantially greater (corresponding value, 0.60 Å). This favourable steric comparison, coupled with the knowledge that $[\{Ca[N(SiMe_3)_2]_2\}_2]$[26] is isostructural to the Mg congener, suggested to us that a calcium-based inverse crown would be an easily accessible target. In practice this has not been borne out. Thus far it has proved problematical to obtain any solids from mixtures of $LiN(SiMe_3)_2$ and $Ca[N(SiMe_3)_2]_2$ as they generally remain in solution (in oxygenated arene media) even at subzero temperatures. However on one occasion we did manage to isolate and crystallographically characterise a solid product which transpired to be the calcium analogue of **6**, the tris(amide) $[LiCa\{N(SiMe_3)_2\}_3]$ **11**.[27] This solvent-free system (a THF-solvate was earlier reported by Davies[28]) adopts the same basic motif as **6** but with an additional feature, a double ration of intramolecular agostic interactions $H_3C\cdots Li$ and $H_3C\cdots Ca$, *i.e.* involving both types of metal atom separately. It is still an open question whether or not this extra coordinative stabilisation has a bearing on the failure (hitherto) to observe an inverse crown ether molecule within the mixed lithium–calcium system, but it most certainly contributes to its excellent solubility in organic solvents.

More success in this regard came upon switching our attention to the Group 12 metal zinc. This proved to be a perfect mimic for magnesium in all but one respect: attempts to prepare in donor-free media a lithium–zinc inverse crown ether complex analogous to **7** did not yield any products save unreacted starting material, namely $LiN(SiMe_3)_2$ and $Zn[N(SiMe_3)_2]_2$. This is consistent with the generalisation that reactivity (specifically here, Lewis acidity) diminishes on moving from magnesium to zinc. No such problems were encountered on replacing the lithium amide by its more reactive sodium or potassium congener. Thus the first inverse crown ether complexes of zinc, namely $[Na_2Zn_2\{N(SiMe_3)_2\}_4(O)]$ **12** and $[\{K_2Zn_2[N(SiMe_3)_2]_4(O_2)_x(O)_y\}_\infty]$ **13** were readily prepared by the method outlined in eqn. (4).[29] To obtain the former the

$$\begin{array}{l} ZnCl_2 + 2\ LiN(SiMe_3)_2 \longrightarrow Zn[N(SiMe_3)_2]_2 + 2\ LiCl \\ \qquad\qquad\qquad\qquad\qquad\qquad\qquad\qquad\qquad\qquad \downarrow \text{MN(SiMe}_3)_2,\ \text{trace of } O_2/H_2O \\ \text{other products} + [M_2Zn_2\{N(SiMe_3)_2\}_4(O_2)_x(O)_y] \\ \qquad\qquad\qquad\qquad\qquad\qquad\qquad\qquad\qquad\qquad \text{M = Na, K} \end{array} \qquad (4)$$

solution had to be heated to reflux, whereas to obtain the latter only gentle heating was necessary. This series of reactions therefore follows the classical reactivity trend associated with the alkali metal series (Li < Na < K). Future work will ascertain whether this trend holds for the complete homologous series, *i.e.* will formation of the (thus far hypothetical) Rb and Cs analogues be even more facile than that of K? The structures of **12** and **13** (Figs. 9 and 10, respectively) are isomorphous with each other and with their magnesium-based analogues **9** and **10**. Intermolecular $(Me_2Si)H_3C\cdots K$ contacts give a linear polymeric arrangement in the case of **13**, in the same way as that in **10**. Corresponding bond lengths and bond angles between **12** and **9** and between **13** and **10** show little variation, though the

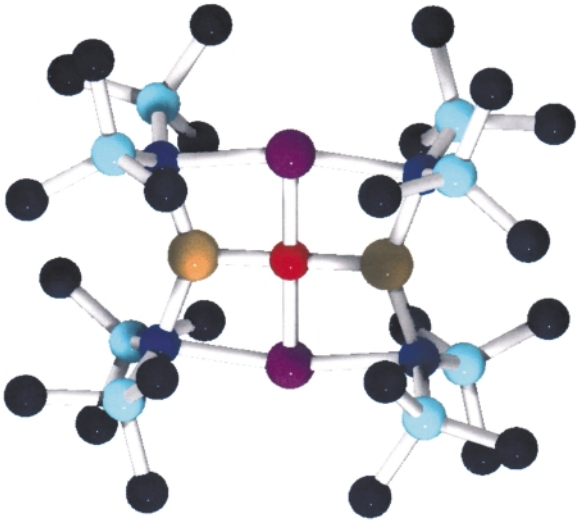

Fig. 9 Molecular structure of $[Na_2Zn_2\{N(SiMe_3)_2\}_4(O)]$.

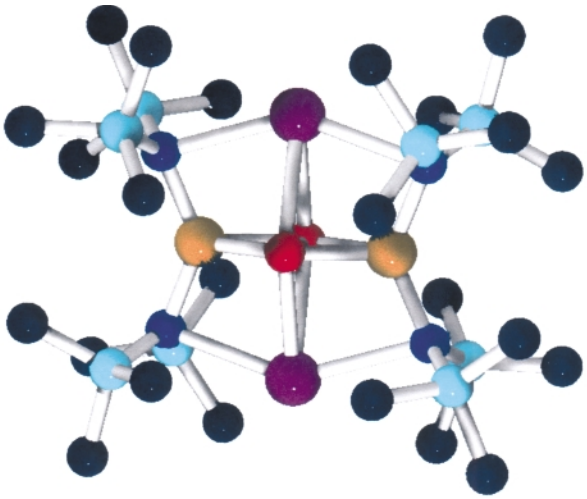

Fig. 10 Double asymmetric unit of $[\{K_2Zn_2[N(SiMe_3)_2]_4(O_2)\}_\infty]$.

Zn–N bonds are systematically 0.07–0.08 Å shorter than the Mg–N bonds.

(ii) Inverse crown complexes

Pioneered by Pederson and first reported in 1967,[30] crown ether compounds and their many offshoots now make up a colossal field within supramolecular chemistry:[31] ring structures in this category come in countless different shapes and sizes, accumulated through the work of over thirty years of intensive research. This knowledge prompted us to pose the question, 'could we extend a stage further the analogy with conventional crown ether chemistry by also synthesising inverse analogues of different ring shapes and ring sizes?' We were pleased to discover that the answer is in the affirmative albeit at this stage to an extremely modest degree. Thus in this section two such types containing twelve or twenty-four ring atoms are discussed. Note that in labelling these larger ring systems 'inverse crown' complexes, as opposed to 'inverse crown ether' complexes, we simply want to draw the distinction that the former type do not contain any oxygen (atoms or anions) at all, though in common with the latter type their Lewis acidic (metal cation)–Lewis basic (heteroatom anion) positions are reversed relative to those in conventional crown ether complexes.

The breakthrough in our quest to prepare a larger inverse crown ring system came unexpectedly when the reaction that previously produced oxo-centred $[Li_2Mg_2(TMP)_4(O)]$ **8**, was repeated but with butylsodium in place of butyllithium as the alkali-metallating source [eqn. (5)]. Remember that in the corresponding HMDS-based system substituting sodium, or

$$BuNa + Bu_2Mg + 3\ HN(Me)_2CCH_2CH_2CH_2C(Me)_2 + arene \rightarrow {}^{1}/_{x}\ [Na_4Mg_2\{N(Me)_2CCH_2CH_2CH_2C(Me)\}_6(arene{-}2H)] + {}^{1}/_{y}\ BuH + other\ products \quad (5)$$

arene = C_6H_5Me, C_6H_6

even potassium, for lithium, does not alter the general nature of the product as all three metals give an inverse crown ether complex. However this time the move to the next heaviest alkali metal induces a dramatic chemical and structural transformation through the formation of the tetrasodium–dimagnesium amide-arenediide $[Na_4Mg_2(TMP)_6\{C_6H_3(CH_3)\}]$ **14**, which is oxygen free.[32] We subsequently prepared a benzene-derived analogue $[Na_4Mg_2(TMP)_6(C_6H_4)]$ **15**, to prove that this novel reaction chemistry is applicable to other arene solvents (toluene was the solvent used in the preparation of **14**). Structural preferences dictate the unusual 4Na : 2Mg stoichiometry of these products, not that used in the original reaction mixtures (*i.e.* 1Na : 1Mg). Yet, perplexingly, attempts to reprepare **14** and **15** using the 'correct' 4Na : 2Mg reaction stoichiometry are hampered by solubility problems. The structures of **14** (Fig. 11) and **15** (not

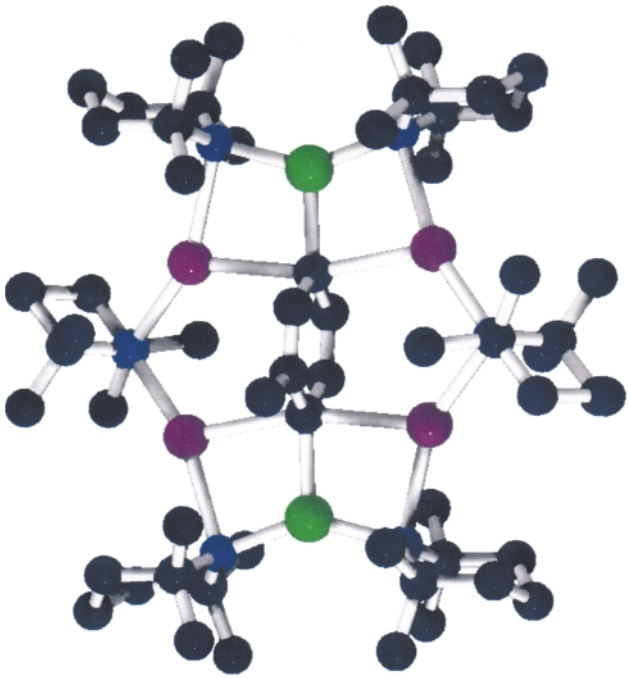

Fig. 11 Molecular structure of $[Na_4Mg_2(TMP)_6(C_6H_3CH_3)]$.

shown) are essentially equivalent. Metal atoms and nitrogen atoms alternate within their $Na_4Mg_2N_6$ ring, which is severely puckered. The encapsulated arene molecules lie approximately orthogonal to the mean plane of this ring, locked into position by a combination of Mg–C σ bonds ('anchoring' bonds—see earlier) and Na–C π bonds ('ancillary' bonds). Of particular interest are the metallation sites of the toluene- and benzene-based dianions (2,5- and 1,4-positions, respectively) which are coincident with the placements of the Mg atoms within the dicationic $Na_4Mg_2N_6$ ring. This signifies that a special type of chemistry beyond the scope of mainstream organometallic reagents is operating here. To elaborate, while toluene can be easily monometallated to generate the resonance-stabilised benzyl carbanion, its dimetallation presents a much more challenging task. Reagents such as butyllithium/TMEDA can pull off more than one hydrogen atom, but only in a random unpredictable way which leads to a complex assortment of incompletely characterised polylithiated species.[33] Contrast this

with the controlled, regioselective dimetallation (dimagnesiation) of toluene facilitating the construction of pure **14**. However, there is another more important distinction: in the case of **14** the CH_3 substituent, which carries the most acidic hydrogen atom (by several pK_a units), remains fully intact (solution ^{1}H NMR studies support the crystal structure determination in this respect), as instead deprotonation occurs exclusively at ring sites. Treating toluene with an appropriate mainstream organometallic base normally leads (ultimately) to benzyl ($PhCH_2^-$) products,[34] since resonance stabilisation reaches a maximum when a hydrogen atom is removed from the CH_3 substituent. Hence it can be reasoned that a special ring template effect is responsible for directing the abnormal metallation chemistry inherent in the synthesis of **14** and for locking the toluene-based dianion in place to prevent any possible tautomerism from taking place which might have generated a thermodynamically more desirable benzyl isomer. The revelation that the weaker carbon acid benzene undergoes an identical double deprotonation during the formation of **15** is also highly significant. This would appear to be direct proof that a powerful synergic effect (the existence of which was speculated upon in the Introduction) is at work here because neither $Mg(TMP)_2$ on its own, nor NaTMP on its own, can metallate benzene (let alone regioselectively dimetallate it!) under the mild conditions used to make **15**. Almost certainly, a single type of structure, the immediate precursor to **14** and **15**, executes both the template effect and the mixed sodium–magnesium synergic effect.

The precise nature of this intermediate structure has not yet been established, but as a working model we tentatively suggest the (hypothetical) $[Na_4Mg_2(TMP)_8]$ molecule depicted in Scheme 3. Made up of authentic features seen in other structures such as mixed-metal Mg–N–Na bridges and tris-amido Mg coordination, this model appears ideally tailored for trapping an arene molecule and bringing about its twofold deprotonation by utilising the terminal amide ligands on the magnesium atoms, the diagonally opposed positions of which are fixed within the constraints of the twelve-membered ring. The byproduct of this process would therefore be the starting amine 2,2,6,6-tetramethylpiperidine. While we are currently investigating the reaction of NaTMP and $Mg(TMP)_2$ in the absence of an arene solvent, it is conceivable that $[Na_4Mg_2(TMP)_8]$ may only have a transient existence (or may not exist at all without arene ligand stabilisation) and thus may not be isolable or easily detected.

The unpredictable nature of this area of heterometallic chemistry was demonstrated again, even more emphatically, when the reaction shown in eqn. (5) was repeated using butylpotassium in place of butylsodium. By analogy with the sodium and potassium inverse crown ether complexes **9** and **10**, it would be logical to expect that the potassium products would adopt the same basic structural motif as that found in **14** and **15**. This time, however, the introduction of the heavier alkali metal effects a spectacular ring expansion in the form of the unprecedented hexapotassium–hexamagnesium twenty-four membered macrocyclic amides $[K_6Mg_6(TMP)_{12}(C_6H_4CH_3)_6]$ **16** and $[K_6Mg_6(TMP)_{12}(C_6H_5)_6]$ **17**.[35] Fig. 12 shows the

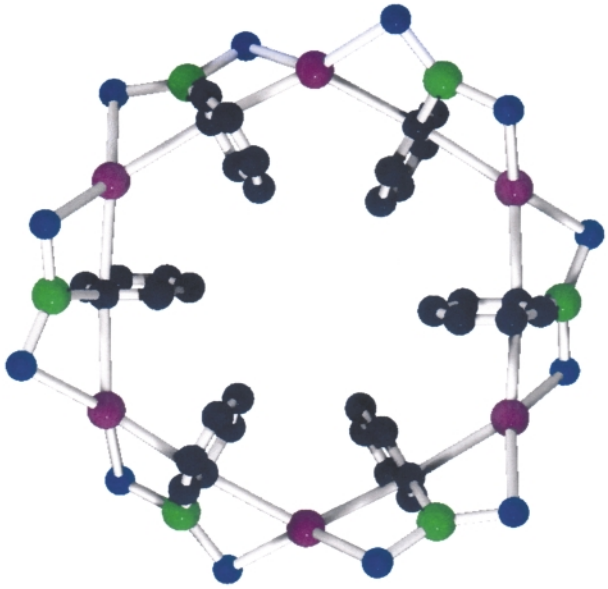

Fig. 12 Molecular structure of $[K_6Mg_6(TMP)_{12}(C_6H_5)_6]$.

structure of **17**, which is representative of both. Here the $[(KNMgN)_6]^{6+}$ ring system acts as a polymetallic host to six singly deprotonated arene anions. Mirroring the situation in **14**, the toluene-derived ligands in **16** have intact Me substituents and hydrogen atoms missing from ring sites, the positions of which are coincident with the placings of the magnesium atoms within the host ring. Thus a ring template effect appears to be operating in this system as well, though in this case the elusive templating molecule must be larger and have more breadth than its sodium counterpart (see Scheme 3) given that only one end of the arene molecule experiences deprotonation, implying that the other end lies distant from a magnesium atom. Following the pattern laid down in the smaller sodium ring systems, the encapsulation of the arene anions is achieved through a combination of anchoring Mg–C σ bonds and ancillary alkali metal–C π bonds but the hapticity of the phenyl rings changes from μ-$\eta^1:\eta^1:\eta^1:\eta^1$ to μ-$\eta^3:\eta^2$ in line with the larger size and coordinative capacity of the potassium atom. The interaction of alkali metal cations with π-systems is becoming an increasingly significant feature in chemistry with implications for biology as discussed in a recent review.[36] It will be interesting to ascertain the structural consequences of introducing rubidium or caesium as the alkali metal in this system: will the transition to a larger ring arrangement (here from one of twelve to one of twenty-four ring atoms) continue or more likely given their propensity for adopting polymeric arrangements, will cyclisation cease and

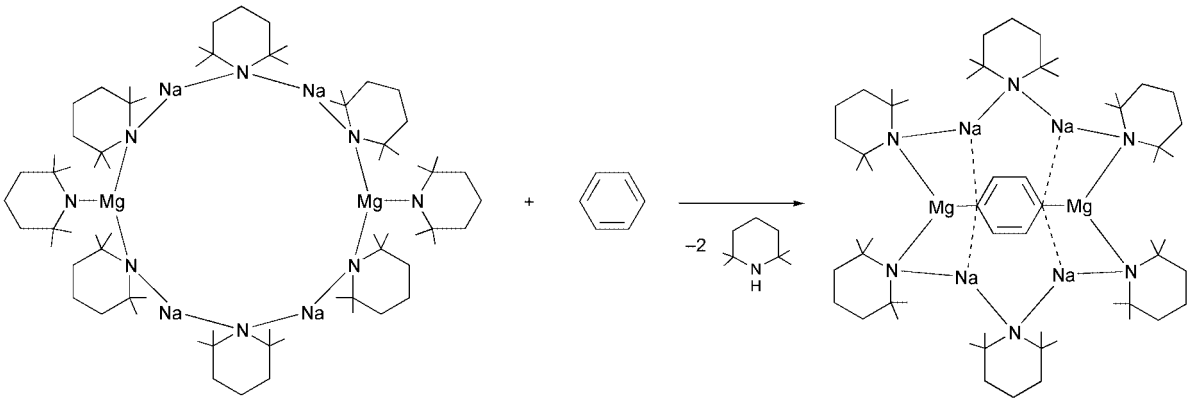

Scheme 3

cede to an infinite chain structure? Studies are in hand to find the answer to this question.

Outlook

Inverse crown ether and inverse crown complexes represent an important new class of s-block compound. The fundamental chemistry controlling their formation is intriguing and complex, and could not have been predicted from previous knowledge of s-block structural chemistry, even through a mountain of such data has been accumulated in recent years. There are clearly still some gaps in our understanding of these existing inverse crown ether complexes and their inverse crown relatives which ongoing research will hopefully soon resolve. Next it will be essential to establish the chemical profiles of this aesthetically attractive collection of ring compounds. For example, will the Mg–C σ bonded systems behave like typical Grignard reagents or will they have a unique chemical character of their own? We are particularly keen to ascertain how far we can extend this new class of compound. Bearing in mind that they are formally composite materials of four distinct component parts (M^+, M^{2+}, R_2N^-, and anion$^-$ or dianion^{2-}), the potential for permutation appears vast. There may even be scope for extending this chemistry beyond the s-block to, for example, the transition metal series in view of the availability therein of M^{2+} cations and the fact that $[LiMn\{N(SiMe_3)_2\}_3]$[37] is essentially isostructural to $[LiMg\{N(SiMe_3)_2\}_3]$. We look forward to continuing this fundamental development work with one eye focussed on how we might usefully apply it in areas such as anion complexation and template synthesis. Artificial organic host molecules for anions are receiving considerable attention at present. Main group metal cations, especially Mg^{2+} and Ca^{2+}, are found in abundance in natural protein receptors where they play decisive roles in binding anionic substrates, in structure enforcement, or in allosteric switching. Yet their use in artificial receptors is not currently well developed. An expanded series of inverse crown type compounds might therefore serve a useful purpose as a database of model structures for learning more about the ways in which metal-based molecules selectively bind anions.[38]

Acknowledgements

I must give special thanks to René Rowlings (for synthetic studies) and Alan Kennedy (for X-ray crystallographic studies) for making the bulk of the discoveries featured in this article. Along the way they have been aided and abetted at Strathclyde by Lorna Barr, Allison Drummond, Glenn Forbes, Jonathan MacLellan, Charlie O'Hara and Phil Rodger, at Newcastle by Bill Clegg and Steve Liddle, and at Melbourne, Australia by Colin Raston and Brett Roberts. I am also indebted to my fellow Strathclyders, David Armstrong and Kenny Henderson for their invaluable advice and significant input to the project, and to Alastair Florence for producing the cover illustration. I must also thank the referees of the manuscript for their helpful, constructive comments. The generous financial support of the EPSRC is also gratefully acknowledged.

Notes and references

1 B. J. Wakefield, *The Chemistry of Organolithium Compounds*, Pergamon, Oxford, 1974; B. J. Wakefield, *Organolithium Methods*, Academic Press, London, 1988; P. G. Williard, *Comprehensive Organic Synthesis*, ed. B. M. Trost, Pergamon Press plc, Oxford, 1991, vol. 1, p. 1; D. S. Wright and M. A. Beswick, *Comprehensive Organometallic Chemistry II*, ed. E. W. Abel, F. G. A. Stone and G. Wilkinson, Elsevier Science Ltd., Oxford, 1995, vol. 1, p. 1.
2 W. E. Lindsell, *Comprehensive Organometallic Chemistry II*, ed. E. W. Abel, F. G. A. Stone and G. Wilkinson, Elsevier Science Ltd., Oxford, 1995, vol. 1, p. 57; B. J. Wakefield, *Organomagnesium Methods in Organic Synthesis*, Academic Press, London, 1995; *Handbook of Grignard Reagents*, ed. G. S. Silverman and P. E. Rakita, Marcel Dekker, New York, 1996; *Grignard Reagents: New Developments*, ed. H. G. Richey Jr., Wiley, Chichester, 2000.
3 K. Kitagawa, A. Inoue, H. Shinokubo and K. Oshima, *Angew. Chem., Int. Ed.*, 2000, **39**, 2481.
4 H. G. Richey, Jr. and J. Farkas, Jr., *Organometallics*, 1990, **9**, 1778.
5 H. H. Karsch and M. Reisky, *Eur. J. Inorg. Chem.*, 1998, 905.
6 H. L. Hsieh and I. W. Wang, *Macromolecules*, 1986, **19**, 299.
7 T. A. Antkowiak and J. E. Hall, *Eur. Pat. Appl.* 0 747 405 A1, 1996.
8 J. F. Allan, K. W. Henderson and A. R. Kennedy, *Chem. Commun.*, 1999, 1325; K. W. Henderson, W. J. Kerr and J. H. Moir, *Chem. Commun.*, 2000, 479; G. Lessène, R. Tripoli, P. Cazeau, C. Biran and M. Bordeau, *Tetrahedron Lett.*, 1999, **40**, 4037.
9 T. Greiser, J. Kopf, D. Thoennes and E. Weiss, *Chem. Ber.*, 1981, **114**, 209.
10 D. Thoennes and E. Weiss, *Chem. Ber.*, 1978, **111**, 3726.
11 B. Schubert and E. Weiss, *Chem. Ber.*, 1984, **117**, 366.
12 K. M. Waggoner and P. P. Power, *Organometallics*, 1992, **11**, 3209.
13 P. R. Markies, G. Schat, O. S. Akkerman, F. Bickelhaupt, W. J. J. Smeets, P. van der Sluis and A. L. Spek, *J. Organomet. Chem.*, 1990, **393**, 315.
14 W. Clegg, K. W. Henderson, R. E. Mulvey and P. A. O'Neill, *J. Chem. Soc., Chem. Commun.*, 1994, 769.
15 W. Clegg, F. J. Craig, K. W. Henderson, A. R. Kennedy, R. E. Mulvey, P. A. O'Neil and D. Reed, *Inorg. Chem.*, 1997, **36**, 6238.
16 G. C. Forbes, A. R. Kennedy, R. E. Mulvey, P. J. A. Rodger and R. B. Rowlings, *J. Chem. Soc., Dalton Trans.*, 2001, DOI: 10.1039/b100052g.
17 A. R. Kennedy, R. E. Mulvey and R. B. Rowlings, *J. Am. Chem. Soc.*, 1998, **120**, 7816.
18 T. Kottke and D. Stalke, *Angew. Chem., Int. Ed. Engl.*, 1993, **32**, 580.
19 H. Dietrich, *Acta Crystallogr.*, 1963, **16**, 681.
20 W. Clegg, K. W. Henderson, R. E. Mulvey and P. A. O'Neil, *J. Chem. Soc., Chem. Commun.*, 1993, 969.
21 G. Gokel, *Crown Ethers and Cryptands*, The Royal Society of Chemistry, Cambridge, 1991; G. Gokel, *Large Ring Molecules*, ed. J. A. Semlyen, John Wiley and Sons Ltd., Chichester, 1996, ch. 7, p. 263.
22 M. F. Hawthorne and Z. Zheng, *Acc. Chem. Res.*, 1997, **30**, 267.
23 A. R. Kennedy, R. E. Mulvey and R. B. Rowlings, *Angew. Chem., Int. Ed.*, 1998, **37**, 3180.
24 A. R. Kennedy, R. E. Mulvey, C. L. Raston, B. A. Roberts and R. B Rowlings, *Chem. Commun.*, 1999, 353.
25 C. Schade and P. v. R. Schleyer, *Adv. Organomet. Chem.*, 1987, **27**, 169.
26 M. Westerhausen and W. Schwarz, *Z. Anorg. Allg. Chem.*, 1991, **604**, 127.
27 A. R. Kennedy, R. E. Mulvey and R. B. Rowlings, unpublished work.
28 R. P. Davies, *Inorg. Chem. Commun.*, 2000, **3**, 13.
29 G. C. Forbes, A. R. Kennedy, R. E. Mulvey, R. B. Rowlings, W. Clegg, S. T. Liddle and C. C. Wilson, *Chem. Commun.*, 2000, 1759.
30 C. J. Pederson, *J. Am. Chem. Soc.*, 1967, **89**, 2495; C. J. Pederson, *J. Am. Chem. Soc.*, 1967, **89**, 7077.
31 For its many subareas, see: *Comprehensive Supramolecular Chemistry*, ed. J. L. Atwood, J. E. D. Davies, D. D. MacNicol and F. Vogtle, Elsevier Science Ltd., Oxford, 1996, vols. 1–11.
32 D. R. Armstrong, A. R. Kennedy, R. E. Mulvey and R. B. Rowlings, *Angew. Chem., Int. Ed.*, 1999, **38**, 131.
33 A. J. Chalk and T. J. Hoogeboom, *J. Organomet. Chem.*, 1968, **11**, 615.
34 D. Hoffman, W. Bauer, F. Hampel, N. J. R. van Eikema Hommes, P. v. R. Schleyer, P. Otto, U. Pieper, D. Stalke, D. S. Wright and R. Snaith, *J. Am. Chem. Soc.*, 1994, **116**, 528.
35 P. C. Andrews, A. R. Kennedy, R. E. Mulvey, C. L. Raston, B. A. Roberts and R. B. Rowlings, *Angew. Chem., Int. Ed.*, 2000, **39**, 1960.
36 G. W. Gokel, S. L. DeWall and E. S. Meadows, *Eur. J. Org. Chem.*, 2000, 2967.
37 B. D. Murray and P. P. Power, *Inorg. Chem.*, 1984, **23**, 4584.
38 Stalke and coworkers are developing other alkali metal molecules based on sulfur ligands which can also bind anions. For a selection of relevant papers, see: R. Fleischer and D. Stalke, *Coord. Chem. Rev.*, 1998, **176**, 431; R. Fleischer, S. Freitag and D. Stalke, *J. Chem. Soc., Dalton Trans.*, 1998, 193; R. Fleischer and D. Stalke, *Chem. Commun.*, 1998, 343.
39 J. W. Lauher, *Chemray: a Molecular Graphics Program*, *J. Mol. Graphics*, 1990, **8**, 34.

CHEMCOMM Communication
www.rsc.org/chemcomm

Concise total syntheses of epothilone A and C based on alkyne metathesis

Alois Fürstner,* Christian Mathes and Karol Grela

Max-Planck-Institut für Kohlenforschung, Kaiser-Wilhelm-Platz 1, D-45470 Mülheim/Ruhr, Germany. E-mail: fuerstner@mpi-muelheim.mpg.de; Fax: ++49 208 306 2994; Tel: ++49 208 306 2342

Received (in Cambridge, UK) 20th February 2001, Accepted 8th May 2001
First published as an Advance Article on the web 25th May 2001

A ring closing alkyne metathesis reaction catalyzed by the molybdenum complex 26 followed by a Lindlar reduction of the resulting cycloalkyne product opens an efficient and stereoselective entry into epothilone A and C.

The discovery that epothilone A (**1**)[1] and congeners share a common mechanism of action with paclitaxel (Taxol®) in triggering programmed cell death (apoptosis) and exert high activity even against paclitaxel-resistant human cancer cell lines *in vitro* has spurred considerable drug development programs worldwide.[2] As a consequence, these compounds became the focal point of many preparative studies aiming at their total synthesis as well as at a synthesis-driven mapping of the structure–activity relationship of these promising natural products.[2,3]

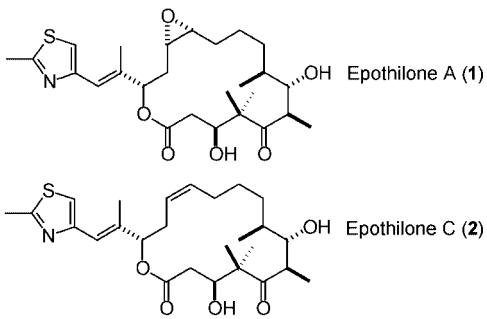

In this context it is remarkable that the first three successful approaches towards **1** were all based on ring closing alkene metathesis (RCM) for the formation of the 16-membered ring. Product **4** thus formed can be selectively epoxidized at the $\Delta^{12,13}$-bond and hence constitutes an excellent precursor for epothilone A.[4–6]

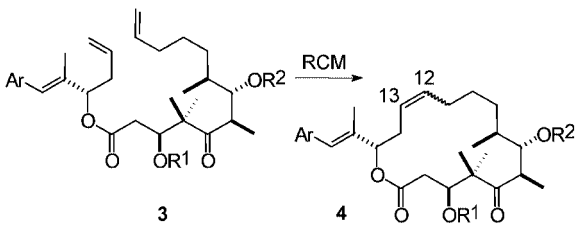

Although these studies were early highlights showing the enormous potential of RCM for advanced organic synthesis,[7] they *invariably suffered from the fact that there was little—if any—selectivity in favor of the required (Z)-alkene* **4** (Table 1). As this serious problem arose only towards the very end of rather laborious sequences and since the isomeric alkenes could not be readily separated at this stage, it is hardly surprising that subsequent total syntheses of **1** were largely based on strategies other than RCM that ensure better control over all structural elements of this target.[8]

Recently, our group was able to show that the ring closing metathesis of *diynes* constitutes a promising alternative that retains all the advantages of metathetic conversions† but allows for the first time the gearing of the stereochemical issue to the cyclization event.[9] If combined with a Lindlar-type reduction, this method opens a *stereoselective entry into (Z)-alkenes* (Scheme 1). We felt that epothilone A constitutes an ideal testing ground for the scope of this emerging new methodology (Scheme 2).[9–11] Described below is the successful reduction of this plan to practice.

Table 1 RCM approaches towards epothilone A and C: formation of (*E*,*Z*)-mixtures (Ar = 2-methyl-4-thiazolyl)

Catalyst[a]	R^1	R^2	Yield	*Z*:*E*	Ref.
[Ru]	TBS	TBS	86%	1.7:1	4*b*
	TBS	TBS	94%	1:1	6*a*
	TBS	H	85%	1.2:1	5*b*
	H	H	65%	1:2	4*b*
[Mo]	TBS	TBS	86%	1:2	4*b*

[a] [Mo] = Mo(=NAr)(=CHCMe$_2$Ph)[OCMe(CF$_3$)$_2$]$_2$; [Ru] = (PCy$_3$)$_2$(Cl)$_2$-Ru=CHPh.

Earlier studies had revealed that the selectivity gained in the formation of the three contiguous stereocenters at C-6, C-7 and C-8 by an aldol reaction strongly depends on the remote functionalization of the enolate partner.[2,3] The best results were reported by Schinzer *et al*. who employed ethyl ketone **11** bearing a conformationally rigid and chelating 1,3-dioxane unit as control element for this purpose.[6] We took recourse to this

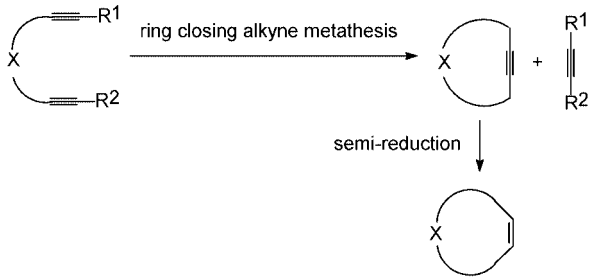

Scheme 1 Stereoselective synthesis of (*Z*)-alkenes by ring closing alkyne metathesis/Lindlar reduction.

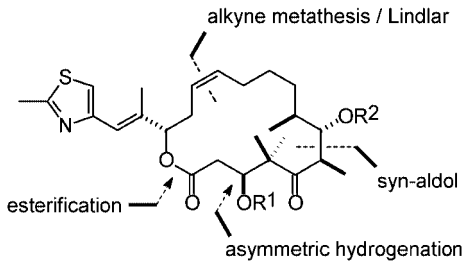

Scheme 2 Retrosynthetic analysis of epothilone C (**2**).

DOI: 10.1039/b101669p

elegant solution, seeking, however, an improved and shorter entry into the required key building block **11**.

Our synthesis starts from commercially available 3-hydroxypropionitrile **5** which reacts with the zinc enolate derived from bromo ester **6** to afford ketoester **7** in 71% yield on a multigram scale (Scheme 3). This Reformatsky-type reaction is best carried out with the assistance of ultrasound.[12] Silylation of **7** with *tert*-butyldiphenylsilyl chloride under standard conditions followed by an asymmetric hydrogenation of **8** catalyzed by [((*S*)-binap)$RuCl_2$](NEt_3) in the presence of Dowex (H-form) to ensure acidic conditions delivers the unprotected diol **9** in high enantiomeric purity (ee = 94%).[13]‡ All attempts to perform the reduction directly with the unprotected substrate **7** resulted in rather poor conversion. Acetalization of **9** followed by reaction of the resulting product **10** with EtMgBr in toluene in the presence of NEt_3 affords compound **11** in excellent overall yield. The presence of the base during the addition of the Grignard reagent to the ester is essential, as it enolizes the ketone primarily formed and thereby avoids the formation of the corresponding tertiary alcohol by addition of a second equivalent of EtMgBr.[14]

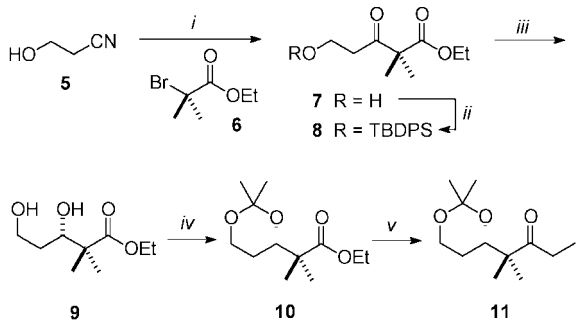

Scheme 3 *Reagents and conditions*: i, Zn, ultrasound, THF; then aq. HCl, 71%; ii, TBDPSCl, imidazole, DMF, 90%; iii, [((*S*)-binap)$RuCl_2$](NEt_3) (6 mol%), H_2 (65 bar), Dowex, EtOH, 80 °C, 71%; iv, 2,2-dimethoxypropane, acetone, camphorsulfonic acid cat., 92%; v, EtMgBr, NEt_3, toluene, 70 °C, 68%.

Having secured an improved access to this key building block, the subsequent aldol reaction was carried out in close analogy to that described by Schinzer *et al.*[6] The required aldehyde component **14** is readily formed as shown in Scheme 4, exploiting the excellent facial guidance exerted by Oppolzer's bornane sultam in the alkylation of substrate **12** (d.r. = 96:4).[15] Reaction of the lithium enolate derived from **11** with compound **14** affords aldol **15** in 70% yield (Scheme 5). The selectivity for the desired *anti*-Cram product was 7:1 (HPLC), which is easily separated from the minor isomer by flash chromatography. Further elaboration of this compound involving deprotection of the acetal, per-silylation of the resulting triol **16**, and regioselective cleavage of the primary TBS-ether in **17** is performed in analogy to literature routes.[5,6] Oxidation of the resulting alcohol **18** with PDC in DMF smoothly affords the desired carboxylic acid **19** ready for esterification with a suitable thiazol fragment.

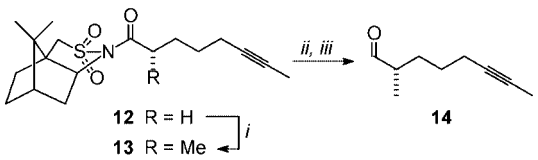

Scheme 4 *Reagents and conditions*: i, n-BuLi, THF–HMPA, MeI, −78 → −60 °C, 94%; ii, $LiAlH_4$, THF, 85%; iii, Pr_4NRuO_4 cat., NMO, CH_2Cl_2, MS 4 Å, 90%.

The preparation of the latter (Scheme 6) starts with an allylation of aldehyde **20** with (+)-Ipc_2B(allyl) as described earlier,[5] followed by silylation of the crude material with TBSCl and imidazole, thus delivering the homoallyl alcohol derivative **21** in 89% yield over both steps in excellent enantiomeric excess

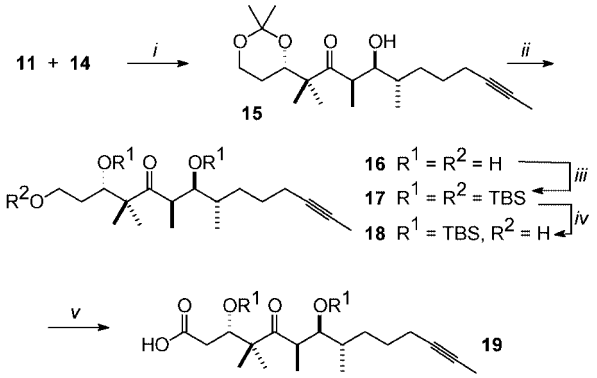

Scheme 5 *Reagents and conditions*: i, LDA, THF, −78 °C, 70%; ii, PPTS, MeOH, 85%; iii, TBSOTf, 2,6-lutidine, 92%; iv, camphorsulfonic acid cat., CH_2Cl_2–MeOH (1:1), 78%; v, PDC, DMF, 83%.

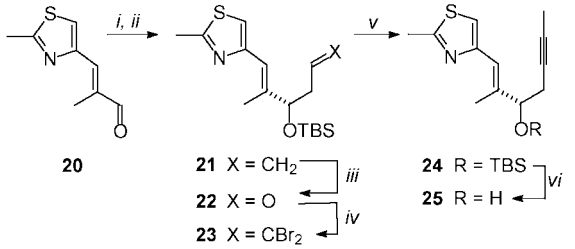

Scheme 6 *Reagents and conditions*: i, (+)-Ipc_2B(allyl); ii, TBSCl, imidazole, DMF, 89% (over both steps); iii, (1) OsO_4 cat., NMO; (2) $Pb(OAc)_4$, 86%; iv, CBr_4, PPh_3, CH_2Cl_2, 68%; v, *n*-BuLi, MeI, THF, 65%; vi, TBAF·$3H_2O$, THF, 74%.

(ee > 97%). Oxidative cleavage of its terminal double bond affords the somewhat unstable aldehyde **22** which is immediately used for a subsequent Corey-Fuchs reaction.[16] Specifically, treatment of **22** with CBr_4 and PPh_3 gives the expected 1,1-dibromo derivative **23**,[2c] which is converted into alkyne **24** by means of *n*-BuLi in THF and trapping of the acetylide anion thus formed with MeI. Desilylation under standard conditions followed by esterification of the resulting alcohol **25** with compound **19** sets the stage for the crucial macrocyclization step. It should also be noted that all attempts to form product **25** from aldehyde **20** by direct asymmetric propargylation were unrewarding in terms of yield and optical purity.

We were pleased to see that diyne **27** is in fact smoothly converted into the 16-membered cycloalkyne **28** in 80% isolated yield on exposure to catalytic amounts of the molybdenum amido complex **26**[17] in toluene–CH_2Cl_2 at 80 °C (Scheme 7). This outcome is particularly noteworthy as it compares well to the results obtained in the conventional RCM approaches (Table 1) in terms of yield and reaction rate. Furthermore, it clearly attests to the mildness and preparative relevance of the method since (i) neither the basic N-atom nor the sulfur group of the thiazole ring interfere with the catalyst, (ii) the labile aldol substructure, the rather electrophilic ketone, as well as the ester- and silyl ether groups are fully preserved, (iii) no racemization of the chiral center α to the carbonyl is encountered, and (iv) the rigorous chemoselectivity of the catalyst is confirmed, which reacts smoothly with alkynes but leaves pre-existing alkene moieties unaffected.§ Therefore, this particular example in concert with the previous applications from our laboratory[9–11] substantiates the notion that alkyne metathesis in general holds great promise for target oriented synthesis.

Lindlar reduction of cycloalkyne **28** followed by cleavage of the silyl ether groups in the resulting (*Z*)-alkene **29** by means of aq. HF in Et_2O–MeCN as the reaction medium delivers epothilone C **2** in 79% yield. Because the selective epoxidation of **29** has already been described by various groups,[2–6] this approach also constitutes a formal total synthesis of epothilone A **1**.

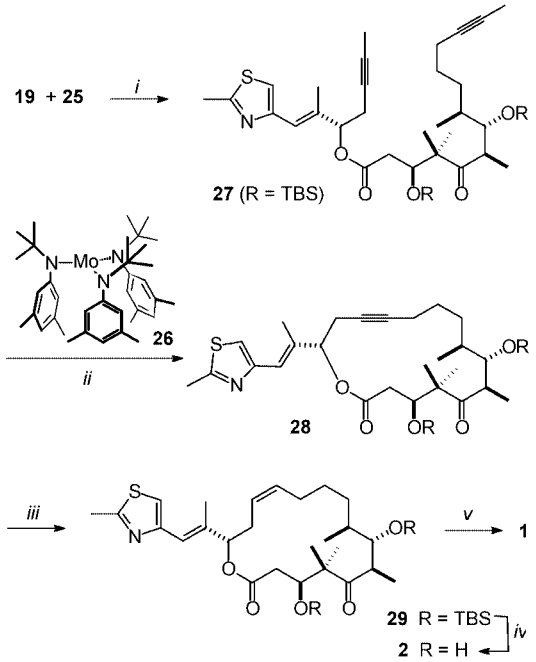

Scheme 7 *Reagents and conditions*: i, DCC, DMAP, CH_2Cl_2, 81%; ii, **26** (10 mol%), toluene–CH_2Cl_2, 80 °C, 8 h, 80%; iii, Lindlar catalyst, quinoline, H_2 (1 atm), CH_2Cl_2, quant.; iv, aq. HF, Et_2O–MeCN, 79%; v, dimethyldioxirane, 70% (ref. 4).

Generous financial support by the Deutsche Forschungsgemeinschaft (Leibniz award to A. F.) and the Fonds der Chemischen Industrie is gratefully acknowledged. K. G. thanks the Alexander-von-Humboldt Foundation for a fellowship.

Notes and references

† For a discussion of the strategic advantages of metathesis in general over more conventional transformations see ref. 18.

‡ The need to perform this reduction under slightly acidic conditions determines the choice of the protecting group for the primary alcohol; the TBDPS group turned out to be optimal, whereas the TBS ether was found to be too unstable.

§ Other available catalysts for alkyne metathesis are (i) $Mo(CO)_6$–*p*-chlorophenol and (ii) alkylidyne complexes such as $(t\text{-}BuO)_3W{\equiv}CCMe_3$. System (i), however, requires very harsh conditions (≥130 °C), whereas the tungsten alkylidyne is sensitive towards basic nitrogen atoms or sulfur(II) groups in the diyne substrate. Therefore they are not appropriate for the cyclization of **27** to **28**. For a more detailed discussion see ref. 11*a*.

1 G. Höfle, N. Bedorf, H. Steinmetz, D. Schomburg, K. Gerth and H. Reichenbach, *Angew. Chem., Int. Ed. Engl.*, 1996, **35**, 1567.
2 Reviews: (*a*) K. C. Nicolaou, F. Roschangar and D. Vourloumis, *Angew. Chem., Int. Ed.*, 1998, **37**, 2014; (*b*) C. R. Harris and S. J. Danishefsky, *J. Org. Chem.*, 1999, **64**, 8434; (*c*) K.-H. Altmann, G. Bold, G. Caravatti, N. End, A. Flörsheimer, V. Guagnano, T. O'Reilly and M. Wartmann, *Chimia*, 2000, **54**, 612; (*d*) J. Mulzer, *Monatsh. Chem.*, 2000, **131**, 205 and lit. cited therein.
3 K. C. Nicolaou, N. P. King and Y. He, *Top. Organomet. Chem.*, 1998, **1**, 73.
4 (*a*) P. Bertinato, E. J. Sorensen, D. Meng and S. J. Danishefsky, *J. Org. Chem.*, 1996, **61**, 8000; (*b*) D. Meng, P. Bertinato, A. Balog, D.-S. Su, T. Kamenecka, E. J. Sorensen and S. J. Danishefsky, *J. Am. Chem. Soc.*, 1997, **119**, 10 073.
5 (*a*) Z. Yang, Y. He, D. Vourloumis, H. Vallberg and K. C. Nicolaou, *Angew. Chem., Int. Ed. Engl.*, 1997, **36**, 166; (*b*) K. C. Nicolaou, Y. He, D. Vourloumis, H. Vallberg, F. Roschangar, F. Sarabia, S. Ninkovic, Z. Yang and J. I. Trujillo, *J. Am. Chem. Soc.*, 1997, **119**, 7960.
6 (*a*) D. Schinzer, A. Limberg, A. Bauer, O. M. Böhm and M. Cordes, *Angew. Chem., Int. Ed. Engl.*, 1997, **36**, 523; (*b*) D. Schinzer, A. Bauer, O. M. Böhm, A. Limberg and M. Cordes, *Chem. Eur. J.*, 1999, **5**, 2483.
7 (*a*) A. Fürstner, *Angew. Chem., Int. Ed.*, 2000, **39**, 3012; (*b*) R. H. Grubbs and S. Chang, *Tetrahedron*, 1998, **54**, 4413.
8 For other total syntheses of **1** see: (*a*) D. Sawada, M. Kanai and M. Shibasaki, *J. Am. Chem. Soc.*, 2000, **122**, 10 521; (*b*) K. C. Nicolaou, S. Ninkovic, F. Sarabia, D. Vourloumis, Y. He, H. Vallberg, M. R. V. Finlay and Z. Yang, *J. Am. Chem. Soc.*, 1997, **119**, 7974; (*c*) A. Balog, D. Meng, T. Kamenecka, P. Bertinato, D.-S. Su, E. J. Sorensen and S. J. Danishefsky, *Angew. Chem., Int. Ed. Engl.*, 1996, **35**, 2801; (*d*) B. Zhu and J. S. Panek, *Org. Lett.*, 2000, **2**, 2575; (*e*) J. W. Bode and E. M. Carreira, *J. Am. Chem. Soc.*, 2001, **123**, 3611.
9 A. Fürstner and G. Seidel, *Angew. Chem., Int. Ed.*, 1998, **37**, 1734.
10 A. Fürstner, C. Mathes and C. W. Lehmann, *J. Am. Chem. Soc.*, 1999, **121**, 9453.
11 Previous applications in total synthesis: (*a*) A. Fürstner, O. Guth, A. Rumbo and G. Seidel, *J. Am. Chem. Soc.*, 1999, **121**, 11 108; (*b*) A. Fürstner, K. Grela, C. Mathes and C. W. Lehmann, *J. Am. Chem. Soc.*, 2000, **122**, 11 799; (*c*) A. Fürstner and K. Grela, *Angew. Chem., Int. Ed.*, 2000, **39**, 1234; (*d*) A. Fürstner and A. Rumbo, *J. Org. Chem.*, 2000, **65**, 2608; (*e*) A. Fürstner, K. Radkowski, J. Grabowski, C. Wirtz and R. Mynott, *J. Org. Chem.*, 2000, **65**, 8758; (*f*) A. Fürstner and T. Dierkes, *Org. Lett.*, 2000, **2**, 2463.
12 (*a*) K. Narkunan and B.-J. Uang, *Synthesis*, 1998, 1713; (*b*) review: A. Fürstner, *Synthesis*, 1989, 571.
13 (*a*) D. F. Taber and L. J. Silverberg, *Tetrahedron Lett.*, 1991, **32**, 4227; (*b*) review: R. Noyori, *Asymmetric Catalysis in Organic Synthesis*, Wiley, New York, 1994.
14 I. Kikkawa and T. Yorifuji, *Synthesis*, 1980, 877.
15 W. Oppolzer, R. Moretti and S. Thomi, *Tetrahedron Lett.*, 1989, **30**, 5603.
16 E. J. Corey and P. L. Fuchs, *Tetrahedron Lett.*, 1972, 3769.
17 For the preparation and inorganic chemistry of complex **26** see: C. C. Cummins, *Chem. Commun.*, 1998, 1777.
18 A. Fürstner, *Synlett*, 1999, 1523.

CHEMCOMM
Communication
www.rsc.org/chemcomm

Synthesis and structure of tetrathiophene with a chiral 1,1′-binaphthyl kink†

Andrzej Rajca,* Hua Wang, Visa Pawitranon, Tom J. Brett and John J. Stezowski

[a] *Department of Chemistry and Center for Materials Research and Analysis, University of Nebraska, Lincoln, NE 68588-0304, USA. E-mail: arajcal@unl.edu*

Received (in Columbia, MO, USA) 14th August 2000, Accepted 10th April 2001
First published as an Advance Article on the web 22nd May 2001

A chiral oligothiophene, possessing in-chain chirality, was prepared and its racemate was characterized by single crystal X-ray crystallography; the in-chain chiral 1,1′-binaphthyl moiety interrupts the π-conjugation and affects the solid state properties of the oligothiophene.

Oligothiophenes are attracting attention as functional materials for (opto)electronic devices.[1,2] Soluble oligothiophenes are especially valuable in applications where reproducible high chemical purity is essential and recently developed solution printing techniques can be utilized, *e.g.* in 'plastic electronics' based upon field effect transistors.[2] The well-defined oligomers are also studied as models for the parent polymers.[3] The crystal structures of a number of oligothiophenes have been reported.[2,4]

The introduction of chirality into the oligo- or polythiophenes is expected to provide an additional engineering tool for these materials, arising not only from intrinsic chirooptical and chiroelectronic properties but also from diastereomeric interactions in the solid state.[5,6] Polythiophenes with various chiral pendant groups and in-chain 1,1′-binaphthyls have been reported.[7,8]

We report on the synthesis and single crystal X-ray structure determination of 6,6′-bis(5-phenyl-2,2′-bithiophen-5′-yl)-2,2′-bis(decyloxy)-1,1′-binaphthyl (**1**), a chiral oligothiophene, possessing in chain chirality.

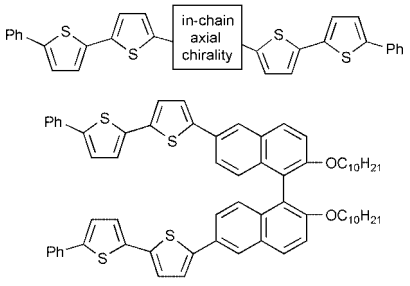

(*R*)-, (*S*)-, and *rac*-**1**

The convergent synthesis of (*R*)-, (*S*)-, and *rac*-**1** is based upon the connection of two achiral modules **2** to the chiral module **4**, which is available in the (*R*)-, (*S*)-, and racemic-forms. 5′-Bromo-5-phenyl-2,2′-bithiophene (**2**) is obtained in two steps: (1) 2,5-dibromothiophene is treated with 1 equiv. of n-BuLi in diethyl ether, followed by oxidation with $CuCl_2$ to give 5,5′-dibromo-2,2′-bithiophene,[9] (2) Suzuki coupling of phenylboronic acid in the presence of an excess of 5,5′-dibromo-2,2′-bithiophene gives **2** in 68% yield.[10,11] 6,6′-Dibromo-2,2′-bis(decyloxy)-1,1′-binaphthyls (**4**) are prepared according to the previously published procedures for analogous bis(dodecyloxy) derivatives by etherification of 6,6′-dibromo-1,1′-binaphthyl-2,2′-diols (**3**) with iododecane in the presence of NaH in DMF.[12] The modules **2** and **4** are linked *via* Negishi coupling providing (*R*)-, (*S*)-, and *rac*-**1** in 59–70% yields (Scheme 1).[13,14] Analogous synthetic procedures were used to obtain the model bithiophene **5**.

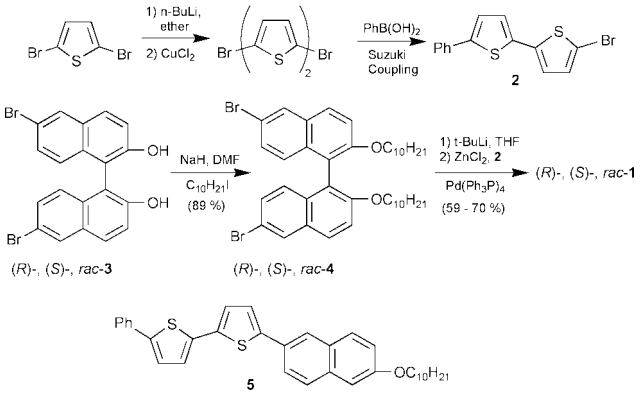

Scheme 1 Synthesis of (*R*)-, (*S*)-, and *rac*-**1**, and the structure of the reference compound **5**.

Orange, block-shaped crystals of *rac*-**1** suitable for X-ray diffraction experiments were grown by slow evaporation of the solvent from a hexane–chloroform solution.[15] The structure displayed by **1** is that of a twisted binaphthyl with the alkoxy chain of one naphthyl unit packing against the naphthyl–thiophene–thiophene–phenyl π-system of the other half of the molecule (Fig. 1). Each of the π-systems is nearly planar, exhibiting small interplanar twist angles.[16] Possible 2-fold symmetry about an axis perpendicular to the C(1)–C(25) binaphthyl linkage is broken by the differing conformations displayed by the alkoxy chains. The difference is a single torsion angle. The conformation about the C(2A)–C(3A) bond is *trans* [C(1A)–C(2A)–C(3A)–C(4A) = −176.2(4)°], whereas the C(2B)–C(3B) conformer is *gauche* [C(1B)–C(2B)–C(3B)–C(4B) = −68.8(5)°]. The remainders of both chains are in all-*trans* conformations. Because of the difference in conformation, the plane containing C(2B–10B) lies parallel to the adjacent π-system, while the C(2A–10A) plane is essentially perpendicular to the adjacent π-system. Both chains lie in close contact with

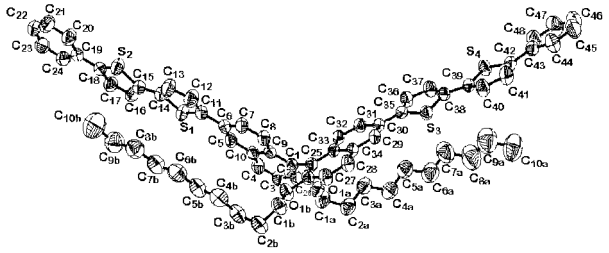

Fig. 1 The conformation for the crystal structure for *rac*-**1**. Ellipsoids are shown at 50% probability.

† Electronic supplementary information (ESI) available: synthesis and characterization data for **1**, **2**, **4**, and **5**; crystal packing plots for *rac*-**1**. See http://www.rsc.org/suppdata/cc/b0/b007355p/

 DOI: 10.1039/b007355p

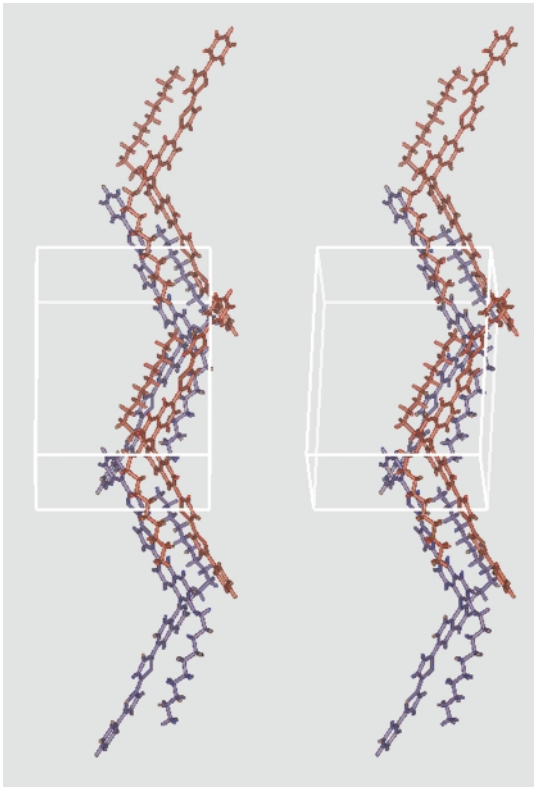

Fig. 2 Crystal packing for *rac*-**1**: stereoview (approximately *bc*-plane) of the tetramer fragment of the zig-zag chain extending along the *c*-axis. The enantiomers are color-coded.

each π-system, with alkyl hydrogens pointing towards the π-systems. We suggest that this interaction influences the conformation of the binaphthyl core. The binaphthyl twist displayed [C(9)–C(1)–C(25)–C(33) = 107.3(3)°] is larger than that observed in binaphthyl (101.4°)[17] and most other 2,2-disubstituted binaphthyls, *e.g.* 2,2′-dihydroxy-1,1′-binaphthyl (92.5°)[18] and 2,2′-bis(bromomethyl)-1,1′-binaphthyl (86.8°).[19]

For the discussion of the crystal packing in *rac*-**1**, the two π-conjugated moieties of **1** may be viewed as a molecular hinge. The phenyl–bithiophene–naphthyl moieties from the mirror image enantiomers form a quasi-one-dimensional zig-zag chain extending along the *c* axis (Fig. 2). Such a chain of molecular hinges is facilitated by the alternating enantiomers. Along the *a* axis, the chains pack side-by-side to form quasi-two-dimensional zig-zag layers, which pack on top of each other in a 'lock-and-key pattern'. The homochiral π–π interactions are negligible as the phenyl–bithiophene–naphthyl moieties form alternating stacks with the alkyl chains.

With bithiophene **5** as a reference, UV-vis spectra of **1** reveal that the nonplanar chiral binaphthyl moiety highly attenuates the π-conjugation.[8] The broad π–π* transitions (λ_{max} = 393 nm) for **1** and **5** are essentially superposable, except for the molar absorptivities, which in **1** are approximately twice those in **5** (log ε_{max} = 4.9 and 4.6). The fingerprint regions of the IR spectra of solid (*R*)- and (*S*)-**1** show small differences compared to the IR spectrum of *rac*-**1**. Also, the melting point of *rac*-**1** is about 40–50 °C higher than those for the (*R*)- and (*S*)-enantiomers, suggesting the presence of a racemic compound.[20] Moreover, the melting point of bithiophene **5** is even higher, about 95 °C above *rac*-**1**. The solubility in chloroform (g mL^{-1}) increases in the following order: (*S*)-**1** (2×10^{-1}) > *rac*-**1** (8×10^{-4}) > **5** (2×10^{-5}), *i.e.* the opposite order to the melting points. These significant differences in solubilites are of importance for the solution processability of oligothiophenes.

In summary, the introduction of chirality into the oligothiophene chain leads to significant differences in solid state properties between stereoisomers and should be an important factor in their solution processability. Further studies on crystal packing and materials properties of chiral molecular hinges in the neutral and doped states are in progress.

This research was supported by the National Science Foundation (CHE-9806954 to A. R. and CHE-9812146 to J. J. S.). We thank Drs Lianhe Yu, Nai Xing Wang, and Jun Li for preparation of synthetic intermediates and conductivity measurements. We thank Dr R. Cerny of the Nebraska Center for Mass Spectrometry for the mass spectral determinations.

Notes and references

1 (*a*) *Handbook of Conducting Molecules and Polymers*, ed. H. S. Nalwa, Wiley, New York, 1997; (*b*) *Conjugated Oligomers, Polymers, and Dendrimers: From Polyacetylene to DNA*, ed. J. L. Bredas, De Boeck Universite, Paris, Bruxelles, 1999.
2 D. Fichou, *Chem. Mater*., 2000, **10**, 571.
3 R. E. Martin and F. Diedrich, *Angew. Chem., Int. Ed.*, 1999, **38**, 1351.
4 (*a*) G. Barbarella, M. Zambianchi, L. Antolini, P. Ostoja, P. Maccagnani, A. Bongini, E. A. Marseglia, E. Tedesco, G. Gigli and R. Cingolani, *J. Am. Chem. Soc*., 1999, **121**, 8920; (*b*) G. Grüner, T. Debaerdemaeker and P. Bäuerle, *Chem. Commun.*, 1999, 1097; (*c*) U. Mitschke, E. M. Osteritz, T. Debaerdemaeker, M. Sokolowski and P. Bäuerle, *Chem. Eur. J.*, 1998, **11**, 2211; (*d*) D. D. Graf, R. G. Duan, J. P. Campbell, L. L. Miller and K. R. Mann, *J. Am. Chem. Soc*., 1997, **119**, 5888; (*e*) P. A. Chaloner, S. R. Gunatunga and P. B. Hitchcock, *J. Chem. Soc., Perkin Trans. 2*, 1997, 1597.
5 Circularly polarized electroluminescence from chiral poly(*p*-phenylenevinylene): E. Peeters, M. P. T. Christiaans, R. A. Janssen, H. F. M. Schoo, H. P. J. M. Dekkers and E. W. Meijer, *J. Am. Chem. Soc*., 1997, **119**, 9909.
6 E. L. Eliel and S. H. Wilen, *Stereochemistry of Organic Compounds*, Wiley, New York, 1994, ch. 13.
7 Selected polythiophenes with chiral pendant groups: M. Lemaire, D. Delabouglise, R. Garreau, A. Guy and J. Roncali, *Chem. Commun.*, 1988, 658; D. Kotkar, V. Joshi and P. K. Ghosh, *Chem. Commun.*, 1988, 917; B. M. W. Langeveld-Voss, R. A. J. Janssen, M. P. T. Christiaans, S. C. J. Meskers, H. P. J. M. Dekkers and E. W. Meijer, *J. Am. Chem. Soc*., 1996, **118**, 4908; J. L. Bredas, D. A. dos Santos, J. Cornil, D. Beljonne and Z. Shuai in ref. 1(*b*), ch. 7.
8 L. Pu, *Chem. Rev*., 1998, **98**, 2405; K. Y. Musick, Q.-S. Hu and L. Pu, *Macromolecules*, 1998, **31**, 2933.
9 5,5′-Dibromo-2,2′-bithiophene: ref 4(*e*) and references therein.
10 Our melting point for 5′-bromo-5-phenyl-2,2′-bithiophene is about 20 °C higher than previously claimed: S. E. Burkart and R. B. Phillips, *PCT Int. Appl.*, 1986, WO 86/05949; *Chem. Abstr.*, 1986, **106**, 98 155.
11 N. Miyaura and A. Suzuki, *Chem. Rev*., 1995, **95**, 2457.
12 (*a*) J. Cuntze, L. Owens, V. Alcazar, P. Seiler and F. Diedrich, *Helv. Chim. Acta*, 1995, **78**, 367; (*b*) 1,1′-binaphthyl-2,2′-diol: non-racemic, Aldrich (ee 99%); racemic, K. Ding, Y. Wang, L. Zhang, Y. Wu and T. Matsuura, *Tetrahedron*, 1996, **52**, 1005.
13 E. Negishi, A. O. King and N. Okukado, *J. Org. Chem.*, 1977, **42**, 1821.
14 The experimental procedures and characterisation data are available as ESI.†
15 *Crystal data* for *rac*-**1**: $C_{68}H_{70}O_2S_4$, M = 1047.48, monoclinic, a = 12.587(1), b = 17.684(1), c = 26.299(1) Å, β = 100.136(1)°, T = 293(3) K, space group $P2_1/c$ (no. 14), Z = 4, MoKα (λ = 0.71073), D_c = 1.207 g cm^{-3}, crystal size 1.0 × 0.4 × 0.1 mm. Structure solved by direct methods and refined by full matrix least squares on F^2. Final refinement statistics: R_1 = 0.0691, wR_2 = 0.1630, and GooF = 1.333 for 4598 reflections with $F_o > 4\sigma(F_o)$. CCDC 163086. See http://www.rsc.org/suppdata/cc/b0/b007355p/ for crystallographic data in .cif or other electronic format.
16 Angles between least-squares planes composed of the following atoms: C(19–24) and S(2)/C(15–18) = 5.4(2)°; S(2)/C(15–18) and S(1)/C(11–14) = 3.6(2)°; S(1)/C(11–14) and C(1–10) = 3.5(2)°; C(25–34) and S(3)/C(35–38) = 5.2(1)°; S(3)/C(35–38) and S(4)/C(39–42) = 7.7(2)°; S(4)/C(39–42) and C(43–48) = 5.8(2)°.
17 The torsional angles (measured analogously to *rac*-**1**) are 101.4° and 69.5° for the enantiomeric and the racemic forms of binaphthyl, respectively: R. B. Kress, E. N. Duesler, M. C. Etter, I. C. Paul and D. Y. Curtin, *J. Am. Chem. Soc*., 1980, **102**, 7709.
18 F. Toda, K. Tanaka, H. Miyamoto, H. Koshima, I. Miyahara and K. Hirotsu, *J. Chem. Soc., Perkin Trans. 2*, 1997, 1877.
19 K. Harata and J. Tanaka, *Bull. Chem. Soc. Jpn.*, 1973, **46**, 2747.
20 J. Jacques, A. Collet and S. H. Wilen, *Enantiomers, Racemates, and Resolutions*, Krieger, Malabar, Florida, 1994, ch. 2.

CHEMCOMM Communication
www.rsc.org/chemcomm

Engineering of porous π-stacked solids using mechanochemistry

Peter J. Nichols,[a] Colin L. Raston*[b] and Jonathan W. Steed*[c]

[a] *School of Chemistry, Monash University, Wellington Road, Clayton, Victoria 3800, Australia*
[b] *University of Leeds, Leeds, UK LS2 9JT*
[c] *Department of Chemistry, King's College London, Strand, London, UK WC2R 2LS. E-mail: jon.steed@kcl.ac.uk*

Received (in Columbia, MO, USA) 2nd April 2001, Accepted 2nd May 2001
First published as an Advance Article on the web 22nd May 2001

Charge-assisted π-stacking interactions result in the formation of large porous arrays formed from the inclusion of metal tris(phenanthroline) cations into *p*-sulfonatocalix[4]arene anions.

A great deal of work in crystal engineering[1–3] has focussed on the manipulation, control or prediction of solid state structure of organic[2,4,5] and organometallic or coordination compounds[6–9] through hydrogen bonding interactions.[10] Lower in energy than many hydrogen bonds, but now reasonably well understood, are π-stacking interactions of the edge-to-face and face-to-face types.[11–13] As early as 1989 Gavezzotti and Desiraju were able to classify the structures of a number of aromatic hydrocarbons based on the ratio of carbon to hydrogen and its effect on their mutual π-stacking interactions.[14] More recently a number of studies have shown that limited π-stacked motifs may be predicted and perhaps conserved over a number of related structures. This is particularly true in cases where there is a significant donor–acceptor or ionic component to the stacking interaction.[15,16] What is most intriguing about π-stacking interactions from a crystal engineering point of view is that such supramolecular 'bonds' represent the interaction of two relatively large surfaces (*cf.* the point-like nature of hydrogen bonds). Thus a well-controlled π-stacked system has the potential to command a very great deal of space within a crystal lattice. In this paper we report the initial successful results of our attempts to engineer extended π-stacked arrays based on charge assisted interactions between *p*-sulfonatocalix[4]arene anions (**1**)[17,18] and metal 1,10-phenanthroline cations.

The molecular cavity in the *p*-sulfonatocalix[4]arene tetra- and pentaanions ($\mathbf{1}^{4-}$ or $\mathbf{1}^{5-}$) is both electron rich and flexible (it is able to alternate between approximate C_{4v} and C_{2v} symmetry while retaining a 'cone' conformation).[17–20] The cleft-shaped C_{2v} conformation is particularly suited to the inclusion of planar aromatic guest species and we reasoned that reaction of Na_5·**1** with transition metal tris(1,10-phenanthroline) dications is likely to result in the formation of a π-stacked motif based on $[M(phen)_3]^{2+} \cap \mathbf{1}^{n-}$ (n = 4–5). This motif should be conserved over a wide variety of structures containing different M and other co-species, particularly solvent molecules (anion **1** is commonly highly hydrated in the solid state[21]). It was found that first row transition metal tris(phen) complexes were extremely readily prepared mechanochemically.[22,23] Simple grinding together of the appropriate stoichiometric ratio of metal salt (halide, nitrate) and phen gave rapid colour changes indicative of the formation of the desired tris(chelate) complexes. Co-complexes with $\mathbf{1}^{n-}$ were similarly prepared by grinding of the resulting mixture with the calixarene. The mixtures were extracted into aqueous solution in order to prepare single crystals suitable for X-ray crystallographic analysis. Thus grinding of $Ni(NO_3)_2 \cdot 6H_2O$ with 1,10-phenanthroline resulted in the formation of a reddish solid over a period of *ca.* two minutes. Subsequent grinding with hydrated Na_5·**1** gave rise to a red-pink, water-insoluble mixture. Similarly, dissolution of the mechanochemically generated $[Ni(phen)_3](NO_3)_2$ in water followed by addition of aqueous Na_5·**1** gave a pink precipitate. This solid was recrystallised from water–acetone (4:1) to give a remarkable crystalline solid of formula $[Ni(phen)_3]_2[\mathbf{1}^{4-}] \cdot n H_2O$ (**2**) (n = *ca.* 28). Under slightly different conditions (small excess of phen) the related $[Na(H_2O)_4(phen)][Ni(phen)_3]_4[\mathbf{1}^{4-}][\mathbf{1}^{5-}] \cdot n H_2O$ (**3**) (n = *ca.* 22) was formed. Complexes **2** and **3** were characterised by X-ray crystallography.† Reaction with a variety of metal phen complexes such as $[Fe(phen)_3]^{2+}$ also gave related products which will be reported separately.

The structure of complex **2** comprises two independent, infinite chains of offset face-to-face π-stacked $[Ni(phen)_3]^{2+}$ cations propagating in the crystal *a* and *b* directions. The strand running along *b* exhibits interplanar separations of 3.356 and 3.546 Å. The former is comparable to the distance of *ca.* 3.35 Å found in graphite and shorter than the 3.48 Å separation for the direct face-to-face overlap observed for $[Cr(C_6H_6)_2] \cdot C_6F_6$.[15] Interplanar separations in the second strand (along *a*) are also short at 3.454 and 3.466 Å and of similar offset to one another, although markedly different to the *b* strand. In the strand running along *b* the independent $[Ni(phen)_3]^{2+}$ cations are included within the cavities of the *p*-sulfonatocalix[4]arene(4−) anion cavities (Fig. 1) with an edge-to-face arrangement, closest $C_{phen} \cdots$calixarene aryl ring centroid distances 3.600 and 3.739 Å. This interaction is facilitated by the C_2 symmetric 'pinched cone' conformation adopted by the calixarene, also noted for water inclusion.[20] The *a* strand also exhibits a herringbone type π-stacking intermediate between the edge-on and face-on modes, with the outside of the calixarenes (*cf.* the 'sandwich herringbone' structure of pyrene[14]). The calixarenes themselves engage in mutual intermolecular face-to-face (sulfonate head to phenolic tail) π-stacking with an interplanar separation of 3.292 Å. This gives the characteristic *p*-sulfonatocalix[4]arene clay-like bilayer packing.[3,21] The overall result is a trapezoidal grid-like arrangement of π-stacked strands leaving void spaces corresponding to large water-filled channels running along the *b* direction, Fig. 2. The intra-channel water is partially ordered, with most oxygen positions located and being modelled as 50% occupancy. This effectively corresponds to the formation of an extremely large hydrophilic portion of the usual bilayer structure and arises from the

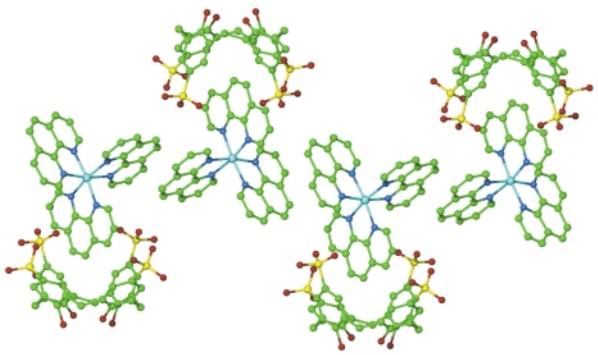

Fig. 1 Infinite π-stacked chain in **2** showing the inclusion of $[Ni(phen)_3]^{2+}$ cations within the cavity of a *p*-sulfonatocalix[4]arene(4−) anion, in a C_{2v} symmetric conformation.

 DOI: 10.1039/b103411c

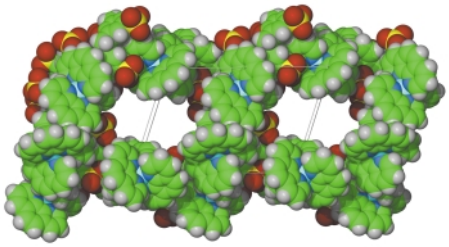

Fig. 2 Crystal packing in **2**. Only one of the two independent $[Ni(phen)_3]^{2+}$ cations is included within the *p*-sulfonatocalix[4]arene(4−) anion (crystal *b* direction). The calixarenes engage in mutual face-to-face π-stacking, while the second chain of $[Ni(phen)_3]^{2+}$ cations runs along the crystallographic *a* axis. The result is large water-filled channels of approximate van der Waals dimensions 7.5 × 10.5 Å.

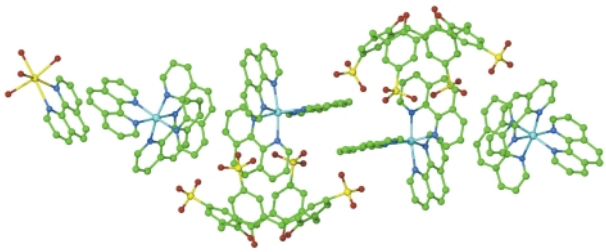

Fig. 3 The $[Na(phen)(H_2O)_4][Ni(phen)_3]_4$[*p*-sulfonatocalix[4]arene-(4−)][*p*-sulfonatocalix[4]arene(5−)] stacked chains in **3**. The two independent $[Ni(phen)_3]^{2+}$ cations both form part of the same chain.

inclusion of the second $[Ni(phen)_3]^{2+}$ cation necessary for charge balance.

The crucial aspect from a crystal engineering perspective is the prediction and conservation of the $[Ni(phen)_3]^{2+}\cap$*p*-sulfonatocalix[4]arene(*n*−) motif with its large, accessible π-surface, resulting in π-stacked chain formation. In this system addition of a small excess of the basic phen is sufficient to deprotonate some of the calixarene anions further to give $[Na(H_2O)_4(phen)][Ni(phen)_3]_4[\mathbf{1}^{4-}][\mathbf{1}^{5-}]\cdot nH_2O$ (**3**). Compound **3** displays an entirely novel packing mode for the much studied *p*-sulfonatocalix[4]arene which is not based on a clay-like bilayer, nor the recently reported spherical or tubular types.[24] Each calixarene is almost entirely surrounded by $[Ni(phen)_3]^{2+}$ cations in order to maximise π-stacking interactions. The core of the structure is again the $[Ni(phen)_3]^{2+}\cap$*p*-sulfonatocalix[4]arene(*n*−) motif and again an infinite 'sandwich herringbone'[14] type π-stacked chain is observed, although it is very different to that found in **2**. In this case the included $[Ni(phen)_3]^{2+}$ cation stacks with a symmetry equivalent of itself on one side and the second independent $[Ni(phen)_3]^{2+}$ unit on the other (interplanar distances *ca*. 3.50 and 3.59 Å). Thus the two independent $[Ni(phen)_3]^{2+}$ cations form part of the same chain, which zig-zags across the unit cell body diagonal. The $[Na(phen)(H_2O)_4]^+$ cation forms the pivot of the chain at which point the face-to-face π-stacking of the $[Ni(phen)_3]^{2+}$ cations gives way to a herringbone type edge-to-face interaction. Thus the full chain exhibits an ···ABCCBABCCB··· arrangement in which A = $[Na(phen)(H_2O)_4]^+$, B = $[Ni(phen)_3]^{2+}$ and C = $[Ni(phen)_3]^{2+}\cap$*p*-sulfonatocalix[4]arene(*n*−), Fig. 3. The water molecules of the $[Na(phen)(H_2O)_4]^+$ cation hydrogen bond to calixarene sulfonato functionalities and one solvent water molecule. The result is again large water filled channels running in the crystallographic *b* direction that are bounded by the interlocking, zig-zag π-stacked chains, Fig. 4. The included water is predominantly ordered with half the oxygen sites being full occupancy and the other half being split across more than one position.

This study has shown that there is a strong solid-state preference for maximising π-stacking interactions and π-surface contact to such an extent that the $[Ni(phen)_3]^{2+}\cap$*p*-sulfonatocalix[4]arene(*n*−) motif is conserved over two very different structures. A further $[Fe(phen)_3]^{2+}$ analogue has also been isolated and will be reported separately. In each case channel structures are a direct and predictable consequence of the very bulky nature of the crystal synthons. Such new porous materials may prove highly interesting in separation/adsorption applications since the intra-channel interactions are very different and distinct from the forces holding the channel framework together.

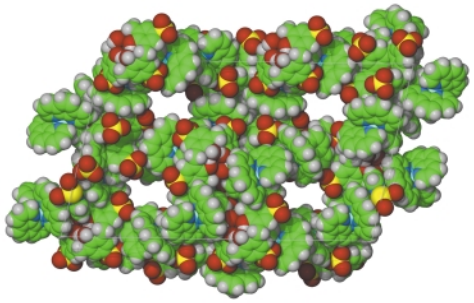

Fig. 4 Water-filled channels in **3**. Approximate channel van der Waals dimensions 4 × 7 Å.

We thank King's College London and Monash University for a travelling scholarship (to J. W. S.).

Notes and references

† *Crystal data* for **2**: $C_{100}H_{140}N_{12}Ni_2O_{50}S_4$, *M* 2555.90, triclinic, space group $P\bar{1}$, *a* = 16.306(3), *b* = 18.802(4), *c* = 23.787(5) Å, α = 104.84(3), β = 104.54(3), γ = 98.56(3)°, *U* = 6644(2) Å^3, D_c = 1.278 Mg m^{-3}, *Z* = 2, μ = 4.32 cm^{-1}, *T* = 123(2) K, reflections measured: 117 913, unique data: 32 533, parameters: 1423, *R*1 [$F^2 > 2\sigma(F^2)$] 0.1322, *wR*2 (all data) 0.4148. For **3**: $C_{106}H_{119.5}N_{13}Na_{0.5}Ni_2O_{39.75}S_4$, *M* 2468.80, monoclinic, space group *C*2/*c*, *a* = 51.7470(8), *b* = 14.8734(3), *c* = 30.5036(6) Å, β = 102.440(6)°, *U* = 22 926.0(7) Å^3, D_c = 1.431 Mg m^{-3}, *Z* = 8, μ = 4.94 cm^{-1}, *T* = 123(2) K, reflections measured: 33 241, unique data: 19 118 (R_{int} = 0.0573), parameters: 1652, *R*1 [$F^2 > 2\sigma(F^2)$] 0.0739, *wR*2 (all data) 0.2263. CCDC 157786 and 157787. See http://www.rsc.org/suppdata/cc/b1/b103411c/ for crystallographic data in .cif or other electronic format.

1 G. R. Desiraju, in *The Crystal as a Supramolecular Entity*, ed. J. M. Lehn, J. Wiley & Sons, Chichester, 1996.
2 G. R. Desiraju, *The Design of Organic Solids*, Elsevier, Amsterdam, 1989.
3 J. W. Steed and J. L. Atwood, *Supramolecular Chemistry: An Introduction*, J. Wiley & Sons, Chichester, 2000.
4 G. R. Desiraju, *Angew. Chem., Int. Ed. Engl.*, 1995, **34**, 2311.
5 A. Gavezzotti and M. Simonetta, *Chem. Rev.*, 1982, **82**, 1.
6 D. Braga, A. Angeloni, L. Maini, A. W. Götz and F. Grepioni, *New J. Chem.*, 1999, **23**, 17.
7 D. Braga, F. Grepioni and G. R. Desiraju, *Chem. Rev.*, 1998, **98**, 1375.
8 D. Braga, L. Maini and F. Grepioni, *Angew. Chem., Int. Ed.*, 1998, **37**, 2240.
9 D. Braga and F. Grepioni, *Acc. Chem. Res.*, 1997, **30**, 81.
10 G. A. Jeffrey, *An Introduction to Hydrogen Bonding*, OUP, Oxford, 1997.
11 H. Adams, K. D. M. Harris, G. A. Hembury, C. A. Hunter, D. Livingstone and J. F. McCabe, *Chem. Commun.*, 1996, 2531.
12 C. A. Hunter and J. K. M. Sanders, *J. Am. Chem. Soc.*, 1990, **112**, 5525.
13 E.-I. Kim, S. Paliwal and C. S. Wilcox, *J. Am. Chem. Soc.*, 1998, **120**, 11 192.
14 G. R. Desiraju and A. Gavezzotti, *J. Chem. Soc., Chem. Commun.*, 1989, 621.
15 C. J. Aspley, C. Boxwell, M. L. Buil, C. L. Higgitt, C. Long and R. N. Perutz, *Chem. Commun.*, 1999, 1027.
16 D. S. Reddy, B. S. Goud, K. Panneerselvam, T. Pilati and G. Desiraju, *J. Chem. Soc., Chem. Commun.*, 1993, 663.
17 C. D. Gutsche, *Calixarenes*, ed. J. F. Stoddart, Royal Society of Chemistry, Cambridge, 1989.
18 C. D. Gutsche, *Calixarenes Revisited*, ed. J. F. Stoddart, Royal Society of Chemistry, Cambridge, 1997.
19 J. Rebek Jr., *Acc. Chem. Res.*, 1999, **32**, 278.
20 J. L. Atwood, F. Hamada, K. D. Robinson, G. W. Orr and R. L. Vincent, *Nature*, 1991, **349**, 683.
21 J. L. Atwood, in *Cation Complexation by Calixarenes*, ed. Y. Inoue and G. Gokel, Marcel Dekker, New York, 1991.
22 J. F. Fernandez-Bertran, *Pure Appl. Chem.*, 1999, **71**, 581.
23 M. Tsuchimoto, G. Hoshina, N. Yoshioka, H. Inoue, K. Nakajima, M. Kamishima, M. Kojima and S. Ohba, *J. Solid State Chem.*, 2000, **153**, 9.
24 G. W. Orr, L. J. Barbour and J. L. Atwood, *Science*, 1999, **285**, 1050.

CHEMCOMM
Communication
www.rsc.org/chemcomm

An unprecedented two-fold interpenetrated heterometallic $4^6 6^4$ network constructed by five-connected copper metal nodes

Long Pan, Nancy Ching, Xiaoying Huang and Jing Li*

Department of Chemistry, Rutgers University, Camden, NJ 08102, USA. E-mail: jingli@crab.rutgers.edu

Received (in Columbia, MO, USA) 3rd March 2001, Accepted 2nd May 2001
First published as an Advance Article on the web 25th May 2001

Hydrothermal reactions making use of dichromate metal anion as a *secondary ligand* yielded a novel three dimensional, bimetallic copper(II)–chromium(VI) network with an unprecedented $4^6 6^4$ topology consisting of Cu(II) ions as five-connected nodes; two such networks, completely identical, interlock to generate a two-fold interpenetrated structure.

Self-assembled inorganic/organic frameworks that mimic prototypical structures have received intense attention in the field of coordination chemistry. Synthetic approaches making use of carefully selected, suitable metal centers as nodes and *exo*-bidentate or multifunctional ligands as connectors have produced numerous fascinating archetypal structures, including diamond (6^6-α),[1] α-Po ($4^{12}6^3$),[2] α-$ThSi_2$ (10^3-b),[3] $SrSi_2$ (10^3-a),[4] PtS (4^28^4),[5] SiO_2 (6^48^2-b),[6] and NbO (6^48^2-a),[7] which have experimentally confirmed the topologies predicted by theory. In certain cases, coordinated systems have generated interesting structures that do not appear to be adopted by simple inorganic compounds, as in the case of the 'dense' net (7^59).[8] These inorganic/organic frameworks often contain large open spaces that may be subject to interpenetration. The interlocking networks may or may not be identical. To date, the highest degree of catenation that has been reported is eleven-fold.[9] All of these extraordinary structures are of fundamental importance in structural design and in the understanding of structure–property correlations. Considering the existing coordination systems, one notes that while numerous monometallic structures have been prepared, there has been little progress concerning the synthesis of heterometallic frameworks. With the premise that metal anion functional groups such as CrO_4^{2-}, MoO_4^{2-}, $Cr_2O_7^{2-}$ and $Mo_2O_7^{2-}$ can form effective M–O–Cr or M–O–Mo bonds,[10] where M is typically a late transition metal, we have successfully applied a synthetic strategy to make use of these metal–anion functional groups as *secondary ligands* in the assembly of heterometallic networks. In this communication, we report a two-fold interpenetrated bimetallic network containing Cu^{2+} metal centers and bridging $Cr_2O_7^{2-}$ metal anions. The structure can be classified as a 4^66^4 topological type built upon pure five-connected nodes,[11] as defined by Wells (Scheme 1).[12] To the best of our knowledge, this structure represents the first example of coordination polymers possessing such a topology.

$Cu(4,4'\text{-bpy})_{1.5}Cr_2O_7{\cdot}H_2O$ **1** was prepared in single-crystal form by the hydrothermal reaction of $Cu(NO_3)_2{\cdot}3H_2O$, 4,4′-bpy, $K_2Cr_2O_7$ and deionized water in the ratio of 1 : 1 : 0.5 : 5555 at 150 °C for 3 days.† A dark-red single crystal suitable for single-crystal X-ray diffraction was isolated.‡ The coordination environment of Cu in **1** is shown in Fig. 1. Each copper metal has a distorted octahedral coordination. The apical positions are occupied by one coordinated water (O8) and one dichromate oxygen ($O6^i$), while the equatorial positions are occupied by three nitrogen atoms (N1, N2 and N3) from different 4,4′-bpy ligands with roughly identical Cu–N bond lengths (2.009–2.033 Å). The remaining equatorial position is occupied by another oxygen (O1) from the second dichromate group. The Cu–O bond distances for the apical oxygen atoms (Cu–$O6^i$ = 2.330 and Cu–O8 = 2.511 Å) are significantly longer than the equatorial Cu–O bond length of 1.972 Å, liable to Jahn–Teller distortion of Cu(II) (d^9). The coordination environments around Cu–O–Cr and the $Cr_2O_7^{2-}$ group are consistent with those reported in a comparable dichromate compound.[13] Each Cu center in the framework acts as a five-connected node by connecting the three pyridine nitrogen atoms from the 4,4′-bpy at the equatorial positions to form a 2D Cu–bpy (6,3) network and by further bonding to the oxygen atoms of the $Cr_2O_7^{2-}$ metal anions to give rise to a unique network with an unprecedented 4^66^4 topology (Fig. 2). The coordination of the Cu(II) in this structure is quite different from those in the two well known Cu–bpy compounds, the six-connected Cu(II) in $Cu(4,4'\text{-bpy})SiF_6$,[14] and the three-connected Cu(I) in $Cu(4,4'\text{-bpy})NO_3{\cdot}1.5H_2O$.[15] As shown in Fig. 2, the single 4^66^4 network of **1** contains large one-dimensional open channels parallel to the *a*-axis. The cross-section of the channel window is *ca.* 11.2 × 22.0 Å. Note that the $Cr_2O_7^{2-}$ anions protrude into the channel, causing a slight distortion of the N2–Cu–N3 bond angle of 170.22(19)°. This results in a narrow 'neck' at the middle of each channel with a shortest O···O distance of *ca.* 4.4

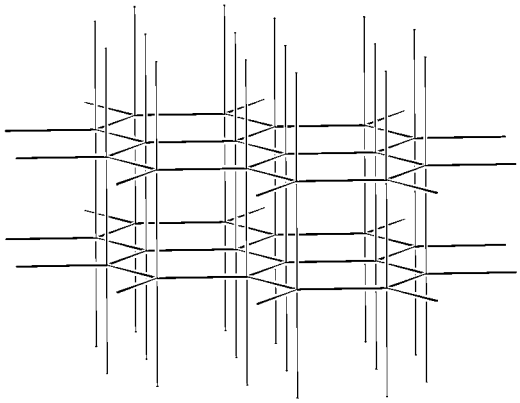

Scheme 1 4^66^4 net.

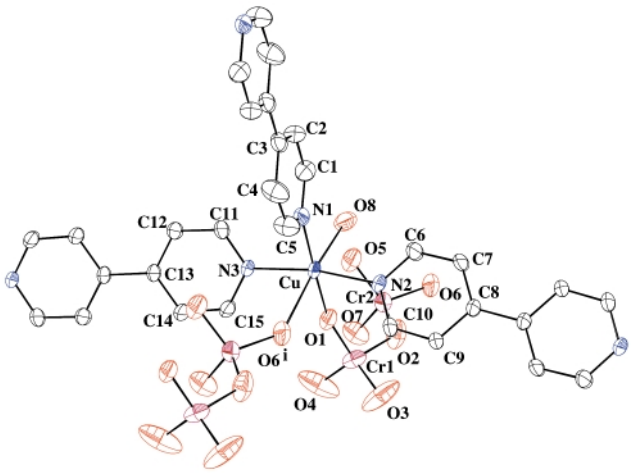

Fig. 1 The coordination environment of Cu in **1** (ORTEP drawing with ellipsoids at 50% probability).

 DOI: 10.1039/b102155a

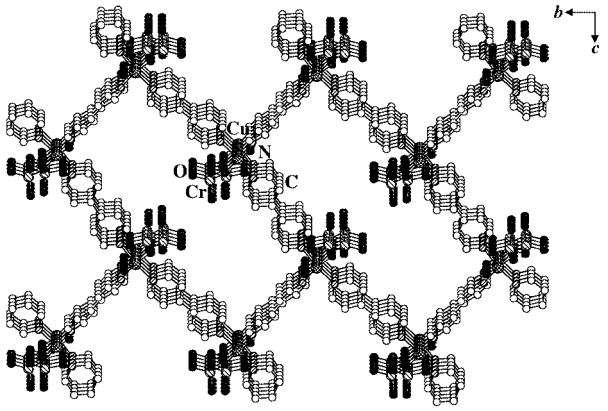

Fig. 2 A view along the crystallographic *a*-axis showing a single $4^6 6^4$ 3D network of **1**. The cross-shaded circles represent Cu atoms; large singly shaded circles are Cr atoms; and small singly shaded, open and solid circles are N, C, and O atoms, respectively.

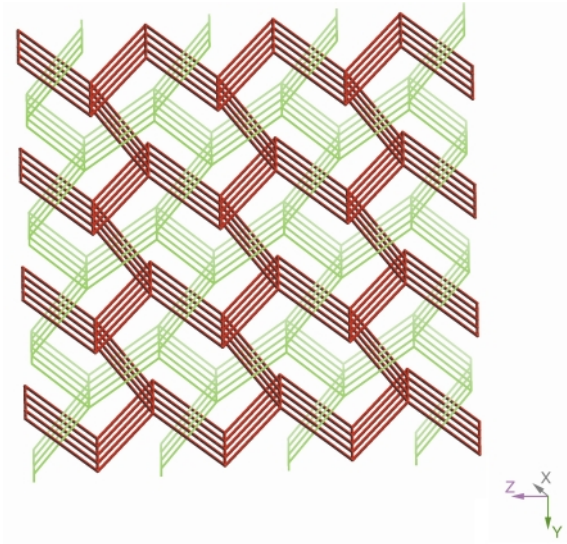

Fig. 3 A view along the *a*-axis showing two identical $4^6 6^4$ nets built upon five-connected copper nodes. These two 3D nets interlock to generate a two-fold interpenetrated structure of **1**.

Å. The two shortest Cu–Cr distances in **1** are 3.543(14) and 5.1629(18) Å, respectively. A two-fold interpenetrating framework is generated by accommodating two identical $4^6 6^4$ networks into the structure (Fig. 3). As clearly illustrated in Fig. 3, pure five-connected copper atoms constitute the nodes of this structure. Note that this $4^6 6^4$ net is topologically analogous to the inorganic network B_2 in AlB_2 (see Scheme 1).[16]

In conclusion, we have shown that the inorganic metal anion $Cr_2O_7^{2-}$ can act as an effective secondary ligand in constructing a bimetallic structure with an unprecedented $4^6 6^4$ topology built upon five-connected Cu^{2+} metal centers. The structure has the same topology as that of the inorganic network B_2 in AlB_2. The design and synthesis of novel bimetallic structures using other metal–anion secondary ligands and metal centers other than Cu(II) are currently under investigation.

We gratefully acknowledge financial support from the National Science Foundation (Grant DMR-9553066).

Notes and references

† *Preparation* of $Cu(4,4'\text{-bpy})_{1.5}Cr_2O_7{\cdot}H_2O$ **1**: hydrothermal reaction of $Cu(NO_3)_2{\cdot}3H_2O$ (0.0242 g, 0.1 mmol), 4,4′-bpy (0.0156 g, 0.1 mmol), $K_2Cr_2O_7$ (0.0143 g, 0.05 mmol) and 10 mL deionized water in the ratio of 1:1:0.5:5555 for 3 days at 150 °C followed by slow cooling to room temperature over an 8 hour period produced block-like dark-red crystals of **1** in about 30% yield and an unidentified brown powder. Reactions which attempted to form a single phase were not successful. When the ratio of $K_2Cr_2O_7$:$Cu(NO_3)_2{\cdot}3H_2O$ was reduced from 0.5:1 to 0.25–0.125:1, only an orange solution resulted. Column-like pink crystals were collected after evaporation of this solution. The structure of these crystal was determined to be $[H_2\text{-}4,4'\text{-bpy}]Cr_2O_7$.[17]

‡ *Crystal data* for **1**: $Cu(4,4'\text{-bpy})_{1.5}Cr_2O_7{\cdot}H_2O$, MW = 531.83, monoclinic, space group $P2_1/c$ (No. 15), a = 8.176(2), b = 14.718(3), c = 15.952(3) Å, Z = 4, V = 1880.4 Å^3, D_c = 1.879 g cm^{-3}, crystal size 0.15 × 0.15 × 0.10 mm, μ(Mo-Kα) = 2.306 mm^{-1}. The intensity data were collected with an Enraf-Nonius CAD4 diffractometer using graphite-monochromated Mo-Kα radiation (λ = 0.71073 Å). 3687 unique reflections of which 2240 with $I > 2\sigma(I)$; $R_1[I > 2\sigma(I)]$ = 0.0538, wR_2 (all data) = 0.0883, GOF = 1.182. The structure was solved by direct methods (SHELXS-86) and refined by full-matrix least-squares methods (SHELXL-97). All non-hydrogen atoms were refined anisotropically. CCDC 159168. See http://www.rsc.org/suppdata/cc/b1/b102155a/ for crystallographic data in .cif or other electronic format.

1 M. J. Zaworotko, *Chem. Soc. Rev.*, 1994, 283.
2 T. Soma, H. Yuge and T. Inwamoto, *Angew. Chem., Int. Ed. Engl.*, 1995, **34**, 1895.
3 G. B. Gardner, D. Venkataraman, J. S. Moore and S. Lee, *Nature*, 1995, **374**, 792.
4 L. Carlucci, G. Ciani, D. M. Proserpio and A. Sironi, *J. Am. Chem. Soc.*, 1995, **117**, 12 861.
5 B. F. Abrahams, B. F. Hoskins, D. M. Michail and R. Robson, *Nature*, 1994, **369**, 727.
6 B. F. Hoskins, R. Robson and N. V. Y. Scarlett, *Angew. Chem., Int. Ed. Engl.*, 1995, **34**, 1203.
7 T. Y. Niu. X. Q. Wang and A. J. Jacobson, *Angew. Chem., Int. Ed.*, 1999, **38**, 1934.
8 L. Carlucci, G. Ciani, P. Macchi and D. M. Proserpio, *Chem. Commun.*, 1998, 1837.
9 D. S. Reddy, T. Dewa, K. Endo and Y. Aoyama, *Angew. Chem., Int. Ed.*, 2000, **39**, 4266.
10 (*a*) L Pan, X.-Y. Huang and J. Li, *Solid State Chemistry of Inorganic Materials III*, 2001, in press; (*b*) P. J. Hagrman, D. Hagrman and J.. Zubieta, *Angew. Chem., Int. Ed.*, 1999, **38**, 2638.
11 S. R. Batten, B. F. Hoskins and R. Robson, *New. J. Chem.*, 1998, **22**, 173.
12 A. F. Wells, *Three-dimensional Nets and Polyhedra*, Wiley, New York, 1977.
13 (*a*) L Pan, N. W. Zhang, X. Zhou, Y. G. Wu, Q. S. Wu and X. L. Jin, *Acta Crystallogr., Sect. C*, 1998, **54**, 1802; (*b*) W. Bensch, N. Seferiadis and H. R. Oswald, *Inorg. Chim. Acta*, 1987, **126**, 113.
14 S.-I. Noro, S. Kitagawa, M. Kondo and K. Seki, *Angew. Chem., Int. Ed.*, 2000, **39**, 2082.
15 O. M. Yaghi and H. Li, *J. Am. Chem. Soc.*, 1995, **117**, 10 401.
16 W. B. Pearson, *The Crystal Chemistry and Physics of Materials and Alloys*, Wiley-Interscience, New York, 1972. Note here the comparison is made solely on the basis of topology without taking into consideration the actual bonding picture.
17 P. Martin-Zarza, P. Gili, F. V. Rodriguez-Romero, C. Ruiz-Perez and X. Solans, 1995, **14**, 2907.

CHEMCOMM
Communication
www.rsc.org/chemcomm

Self-organisation in photoactive fullerene porphyrin based donor–acceptor ensembles†

Dirk M. Guldi,*[a] Chuping Luo,[a] Angela Swartz,[a] Michael Scheloske[b] and Andreas Hirsch*[b]

[a] *Radiation Laboratory, University of Notre Dame, Notre Dame, IN 46556, USA. E-mail: guldi.1@nd.edu; Fax: +1 219 631 7441; Tel: +1 219 631 8068*

[b] *Institut für Organische Chemie, Universität Erlangen-Nürnberg, Henkestr.42, 91054 Erlangen, Germany. E-mail: hirsch@organik.uni-erlangen.de; Fax: +49 9131 85 26864; Tel: +49 9131 85 22537*

Received (in Cambridge, UK) 7th March 2001, Accepted 1st May 2001
First published as an Advance Article on the web 22nd May 2001

Complexation of ZnP-C_{60}-ZnP triads with diazabicyclooctane (DABCO) leads to rigid assemblies that display considerably prolonged charge-separated states.

Control over the separation, specific alignment and composition in donor–acceptor assemblies at a molecular level is a formidable task, especially in artificial reaction centres. Meaningful incentives can be lent from the organisation-principle in the bacterial photosynthetic reaction centre:[1] the different light- and redox-active components are embedded *via* noncovalent interactions into a protein matrix. In principal, biomimetic methodologies, such as hydrogen-bonding, donor–acceptor complexation, electrostatic interactions and π–π stacking, guarantee the control over modulating the composition and, simultaneously, achieving well-defined and rigid architectures, with high directionality and selectivity.[2]

In the present communication we wish to present a simplistic but powerful means to regulate donor–acceptor separations and orientations. Successively, rigid, confined model ensembles are self-assembled, starting from a flexible **ZnP-C_{60}-ZnP** system and DABCO.[3,4] The newly formed tetrads undergo, upon photoexcitation, efficient energy and electron transfer in toluene and *o*-dichlorobenzene solutions, respectively.

We selected for the current investigation the strongly fluorescing zinc tetraphenyl porphyrin (**ZnP**) chromophore as a photo-sensitive marker to monitor the extent of excited state interaction with the adjacent fullerene core. The porphyrinic precursors **1** and **2** were synthesised using a statistical approach,

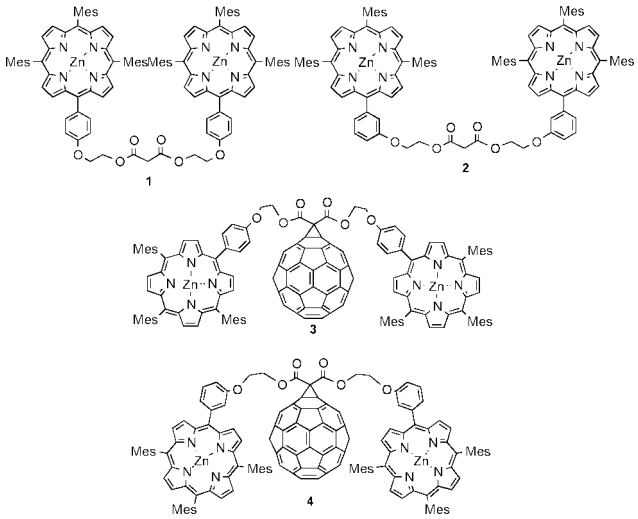

starting with pyrrole and the corresponding benzaldehydes and subsequent reaction with malonyl chloride. In the final step, attachment to C_{60} was achieved *via* modified Bingel-conditions.[4a]

New compounds **1**–**4** were completely characterised (see ESI†). The two different substitutional patterns of the phenyl-linkages (*i.e. para vs. meta*) were chosen to control possible orientations between the fullerene and porphyrin chromophores.

At first the porphyrin's emission in **3** and **4** was recorded in a variety of solvents and compared to that of a **ZnP-ZnP** reference (**1**). Most importantly, the *para*- and *meta*-linked **ZnP-C_{60}-ZnP** systems both gave rise to a fairly strong emission quenching of the ZnP chromophore with fluorescence quantum yields (Φ) on the order of 0.001 (see Table 1). Although the solvent polarity differs quite substantially the emission intensity changed only marginally. For reference the emission quantum yield (Φ) of **3** in toluene and also in *o*-dichlorobenzene is about 0.04.

The anisotropy of the fullerene surface, as it prevails in the well-ordered but alternating assembly of electron rich hexagons with electron deficient pentagons, generally gives rise to marked 'through-space' interactions.[5] Thus, when structurally possible, fullerene-based ensembles adopt conformations in which the fullerene and the donor moieties come in close proximity, from which we hypothesise that the rapid deactivation of the ^{1}*ZnP state in **3** and **4** implies a rate-determining transition to form the electron transfer mediating 'intramolecular exciplex'.

In general a more efficient quenching (~ two-fold) was noted for the *meta*- (**4**) relative to the more electron-rich *para*-linked derivatives (**3**). A possible interpretation for this evidently solvent-independent outcome relates to the different substitution pattern given on the phenyl ring and the subsequent impact that stems from an electronic interaction with the fullerene core.‡ The *meta*-isomer is clearly more susceptible to interactions between the fullerene core and the porphyrin moiety. In line with this purely structural assumption is the observation that a weakly emitting transition around 800 nm was found only for the *meta*-linked **ZnP-C_{60}-ZnP** (**4**) in toluene. This NIR emission originates from a charge transfer state, despite its quantitative cancellation in stronger polar solvents, such as THF, *o*-dichlorobenzene and benzonitrile.

Time-resolved transient absorption spectroscopy was conducted to probe the fate of the photoexcited ZnP chromophore and to inspect the identity of the resulting products. In

Table 1 Photophysical properties of *para*- and *meta*-linked **ZnP-C_{60}-ZnP** (1.3×10^{-5} M) in different solvents

	(τ) ^{1}*ZnP		(ϕ) ^{1}*ZnP $\times 10^3$		(ϕ) $ZnP^{\bullet+}$–$C_{60}^{\bullet-}$	
Solvent	(**3**)	(**4**)	(**3**)	(**4**)	(**3**)	(**4**)
Toluene			1.62	0.83	0.018	0.008
THF	122 ns	70 ns	1.50	0.79	0.02	0.012
o-dichlorobenzene	106 ns	75 ns	1.46	0.81	0.019	0.014
Bzcn	101 ns	58 ns	1.18	0.64	0.016	0.009

† Electronic supplementary information (ESI) available: selected spectroscopic data. See http://www.rsc.org/suppdata/cc/b1/b102141i/

 DOI: 10.1039/b102141i

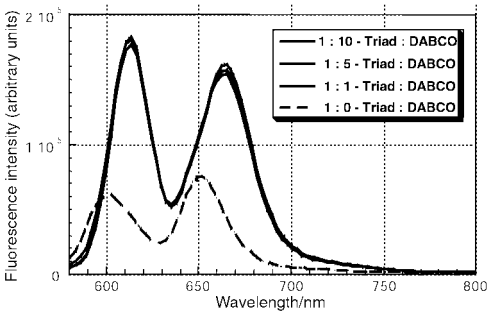

Fig. 1 Emission spectrum of **4** (1.3×10^{-5} M) in *o*-dichlorobenzene (dashed line) and upon addition of various DABCO equivalents (*i.e.*, 1, 5 and 10); excitation wavelength 550 nm.

Table 2 Influence of DABCO on the photophysical properties of *para*- and *meta*-linked **ZnP-C_{60}-ZnP** (1.3×10^{-5} M)

	Solvent	DABCO[a]	(ϕ) ^{1}*ZnP	(τ) $ZnP^{\bullet+}$–$C_{60}^{\bullet-}$	(ϕ) $ZnP^{\bullet+}$–$C_{60}^{\bullet-}$
3	Toluene	0	1.62×10^{-3}	—	0.018
		5	2.50×10^{-3}	—[b]	—[b]
	o-DCB[c]	0	1.46×10^{-3}	290 ns	0.019
		5	2.29×10^{-3}	702 ns	0.082
4	Toluene	0	0.83×10^{-3}	—	0.008
		5	2.14×10^{-3}	—[b]	—[b]
	o-DCB[c]	0	0.81×10^{-3}	150 ns	0.014
		5	2.40×10^{-3}	724 ns	0.086

[a] Equivalents of DABCO. [b] Triplet excited state. [c] *o*-Dichlorobenzene.

particular, the instantaneously formed ZnP singlet–singlet absorption, which is in reference **1** subject to a slow intersystem crossing (2.5 ns) to the triplet excited state, decays rather rapidly (~100 ps) following the completion of the short laser pulse in **3** and **4** (18 ps; 532 nm). Furthermore, this fast deactivation is coupled with a synchronously occurring grow-in of a new transient absorption, which in all solvents revealed a set of VIS and NIR maxima at ~650 and 1030 nm, respectively.[5] These features resemble the spectral fingerprints of the one-electron oxidised ZnP and the one-electron reduced fullerene, respectively. From this we conclude that the resulting $ZnP^{\bullet+}$–$C_{60}^{\bullet-}$ radical pair is formed *via* a photoinduced electron transfer from the ZnP singlet excited state to the electron accepting fullerene. The charge-separated state, formed with moderate quantum yields, decayed on a time scale of a few hundred nanoseconds to regenerate the ground state.

Addition of DABCO to a toluene and *o*-dichlorobenzene solution of triads **3** and **4** led to a strong reactivation of the ZnP emission (Fig. 1 and Table 2). Taking the emission reactivation into account the ZnP in both tetrads disclose nearly the same fluorescence quantum yields. Parallel picosecond experiments, which indicate prolonged ^{1}*ZnP singlet lifetimes (~185 ps) in **5** and **6** compared with **3** (106 ps) and **4** (75 ps), further

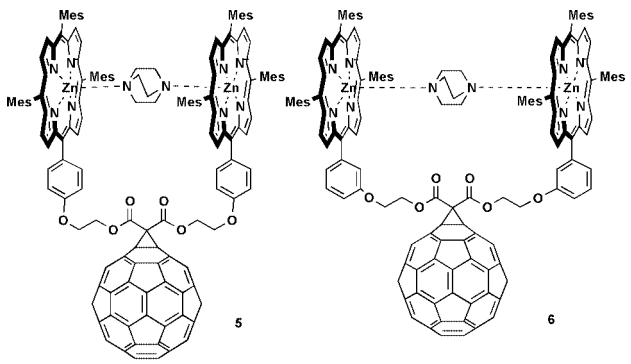

corroborated the emission studies. Both effects can be rationalised in terms that complexation of DABCO to the vacant sites of the two ZnP (*i.e.* dz^2-orbitals)[3] increases the donor–acceptor separation considerably (*i.e.* triad *vs.* tetrad). The bridging motif with the monomeric compounds **5** and **6** was confirmed by molecular modelling using semi-empirical methods. The formation of coordination oligomers can be largely excluded since no dependence of the spectroscopic properties on the DABCO concentration was observed for 1.3×10^{-5} M solutions of **3** and **4**. The amplification of the emission between the triads and corresponding tetrads is less prominent in toluene (ε = 2.38) than in *o*-dichlorobenzene (ε = 9.93). To follow up on this issue, the pathway of ZnP deactivation was examined by revisiting the pico- and nanosecond experiments. In *o*-dichlorobenzene, the typical radical ion fingerprints, formed concurrently with the ^{1}*ZnP decay, unmistakably attest to an electron transfer mechanism.

On the contrary, the absorption features noted upon excitation of a toluene solution are fundamentally different. In fact, new broad absorption maxima at 360 and 720 nm are an exact match of the fullerene triplet features.[5] The above experiments, considered in concert, infer that a rapid intramolecular energy transfer, from the ^{1}*ZnP (2.06 eV) to the energetically lower lying ^{1}*C_{60} (1.79 eV),[5] prevails in toluene with a quantum yield of 0.57. This is then followed by an efficient *intersystem crossing* to generate the triplet excited state (1.50 eV)[5] with a unimolecular rate constant of 7.1×10^8 s^{-1}. The energy transfer pathway in **5** and **6** is in sharp contrast to the excited state behaviour seen for **3** and **4**, disclosing even in toluene the spectral characteristics of the $ZnP^{\bullet+}$-$C_{60}^{\bullet-}$ radical pair.

The forward electron transfer is, however, not the only parameter affected by the increased donor–acceptor separation (*i.e.* triad *vs.* tetrad): in addition, markedly higher quantum yields (Φ) and longer lifetimes (τ) of the $ZnP^{\bullet+}$–$C_{60}^{\bullet-}$ radical pair were noted. Interestingly, the back electron transfer dynamics in **5** and **6** gives rise to approximately the same rate constant of 1.3×10^6 and 1.4×10^6 s^{-1}, respectively, reflecting the nearly equal donor–acceptor separations in these rigid systems.

In conclusion, we have shown by spectroscopic and photochemical means that a simple complexation of DABCO to a series of flexible **ZnP-C_{60}-ZnP** triads, and thereby affording the corresponding tetrads, is a powerful tool to control the design and photophysical properties of rigidly, confined donor–acceptor systems.§

Notes and references

‡ Further support for this difference can be deduced from the ground state absorption spectra, which in the case of the *meta*-substituted isomer reveals a marked red-shift of the *Soret*- and *Q*-band transitions (*e.g.*, in toluene 550 → 552 nm; 588 → 590 nm).

§ This work was supported by the Office of Basic Energy Sciences of the Department of Energy and the Stiftung Volkswagenwerk. This is document NDRL# 4294 from the Notre Dame Radiation Laboratory.

1 J. Deisenhofer, O. Epp, I. Sinning and H. Michel, *J. Mol. Biol.*, 1995, **246**, 429.

2 Leading examples of noncovalent donor–acceptor assemblies (*a*) P. Tecilla, R. P. Dixon, G. Slobodkin, D. S. Alavi, D. H. Waldeck and A. D. Hamilton, *J. Am. Chem. Soc.*, 1990, **112**, 9408; (*b*) P. J. F. de Rege, S. A. Williams and M. J. Therien, *Science*, 1995, **269**, 1409; (*c*) J. P. Kirby, J. A. Roberts and D. G. Nocera, *J. Am. Chem. Soc.*, 1997, **119**, 9230; (*d*) S. L. Springs, D. Gosztola, M. R. Wasielewski, V. Kral, A. Andrievsky and J. L. Sessler, *J. Am. Chem. Soc.*, 1999, **121**, 2281; (*e*) K. Yamada, I. Imahori, E. Yoshizawa, D. Gosztola, M. R. Wasielewski and Y. Sakata, *Chem. Lett.* , 1999, 235; (*f*) M.-J. Blanco, M. C. Jimenez, J.-C. Chambron, V. Heitz, M. Linke and J.-P. Sauvage, *Chem. Soc. Rev.*, 1999, **28**, 293; (*g*) J. L. Sessler, B. Wang, S. L. Springs and C. T. Brown, in *Comprehensive Supramolecular Chemistry*; Y. Murakami (ed.), Pergamon Press Ltd, Oxford, UK, 1996, Vol. 4, pp. 311–335.

3 See for example: (*a*) A. Hunter, M. N. Meah and J. K. M. Sander, *J. Am. Chem. Soc.*, 1990, **112**, 5773; (*b*) P. N. Taylor and H. L. Anderson, *J. Am. Chem. Soc.*, 1999, 121.

4 (*a*) E. Dietel, A. Hirsch, E. Eichhorn, A. Reiker, S. Hackbarth and B. Röder, *Chem. Commun.*, 1998, 1981; (*b*) D. M. Guldi, C. Luo, T. Da Ros, M. Prato, E. Dietel and A. Hirsch, *Chem. Commun.*, 2000, 375; (*c*) D. M. Guldi, C. Luo, M. Prato, E. Dietel and A. Hirsch, *Chem. Commun.*, 2000, 373.

5 D. M. Guldi and M. Prato, *Acc. Chem Res.*, 2000, **33**, 695.

CHEMCOMM
Communication
www.rsc.org/chemcomm

Some mechanistic observations on the borohydride mediated reductive cyclisation of tosylhydrazones

Luis D. Miranda[a] and Samir Z. Zard*[ab]

[a] *Institut de Chimie des Substances Naturelles, CNRS, 91198 Gif-Sur-Yvette, France. E-mail: zard@icns.cnrs-gif.fr*
[b] *Laboratoire de Synthèse Organique associé au CNRS Ecole Polytechnique, 91128 Palaiseau, France*

Received (in Cambridge, UK) 30th January 2001, Accepted 27th March 2001
First published as an Advance Article on the web 22nd May 2001

The previously described, highly stereoselective ring-closure of δ-unsaturated tosylhydrazones upon reduction with borohydride may not be a radical process but rather an ene-type concerted transformation of the intermediate mono-substituted diimide.

Reduction with borohydride of tosylhydrazones derived from ketones may lead to the formation of radical species through loss of molecular nitrogen as shown in Scheme 1.[1] Various other related and important transformations such as the reduction of diazonium salts,[2] the Wolff–Kishner reaction,[3] the Wharton rearrangement,[4] sometimes proceed through a similar radical pathway.

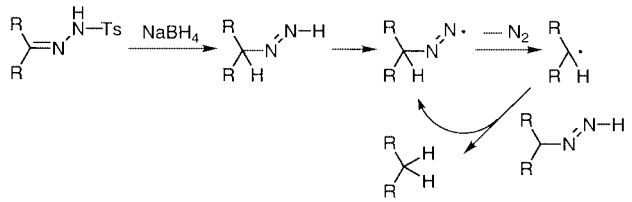

Scheme 1

In a pioneering study in this area, Taber and colleagues[5] described a remarkably diastereoselective cyclisation reaction starting with hydrazone **1** (Scheme 2). This transformation was presumed to involve ring closure of a benzyl type radical **4**, and the unusually high diastereoselectivity (97:3) was ascribed to the non-reversibility of the cyclisation step under these specific conditions. The corresponding tributylstannane mediated ring-closure starting from the imidazole thiocarbamate derivative **2** is much less stereoselective, leading to a 3:7 ratio of the same diastereoisomers **3**, and the possible reversibility of the ring-forming step was invoked as the cause of the erosion in selectivity. While reversible 5-*exo* cyclisations involving benzylic and other stabilised carbon centred radicals are known,[6] it seemed to us that the ring-opening, reverse step, must be too slow in this case to compete with hydrogen atom abstraction from the stannane by the primary radical **5**. In the present study, we adduce evidence indicating that the radical cyclisation is indeed irreversible under the stannane reduction conditions and that the cyclopentane formation in the case of the hydrazone precursor may in fact not be a radical process at all.

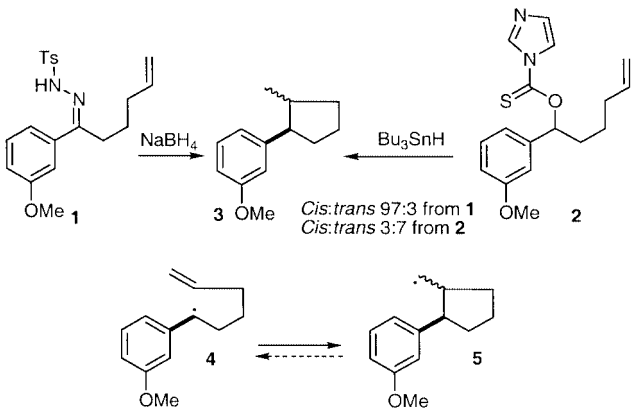

Scheme 2

Our approach hinges on the separate generation of the cyclised radical **5** and showing that this species does *not* undergo ring opening under dilute tributylstannane reduction conditions. This was accomplished by exploiting the properties of the xanthate transfer reaction.[7] In this case, the cyclised product is itself a xanthate and therefore allows the regeneration of the cyclised radical. The requisite starting xanthate **6c** was readily obtained in 66% overall yield by reacting crude bromide **6b**, itself derived from alcohol **6a**, with commercially available potassium *O*-ethyl xanthate. Heating this xanthate with a small amount of lauroyl peroxide in 1,2-dichloroethane (0.1 M) resulted in the smooth formation of cyclopentylmethyl xanthates **7a** and **7b** in a 3:7 ratio and in 78% combined yield (Scheme 3). It is interesting to note that the ratio of the *cis* and *trans* isomers did not change when the reaction was conducted at 1 M concentration. This is a first indication that the cyclisation is not so readily reversible under these conditions.

The two isomers could be separated using preparative thin-layer chromatography, albeit with some difficulty. Reductive dexanthylation of the pure *trans* isomer **7b** using tributylstannane in benzene at 0.001 M concentration gave the corresponding pure *trans* methyl cyclopentanes **3b** in 70% yield. Perhaps more importantly, exposure of an almost pure sample (95:5 *cis*:*trans*) of the thermodynamically less stable *cis* isomer **7a** to the same conditions gave methylcyclopentanes **3a** and **3b** in 85:15 ratio, *i.e. with only a very slight modification of the initial relative stereochemistry*. Clearly, under such highly dilute conditions, a roughly 3:7 mixture of the two diastereoisomers should have been obtained in both cases if the equilibrium between radicals **4** and **5** was fast in comparison to hydrogen atom abstraction from the stannane.

The above findings constitute strong evidence against the operation of a radical mechanism in the transformation of the tosylhydrazone depicted in Scheme 2. The high diastereoselectivity cannot be explained by a kinetically controlled,

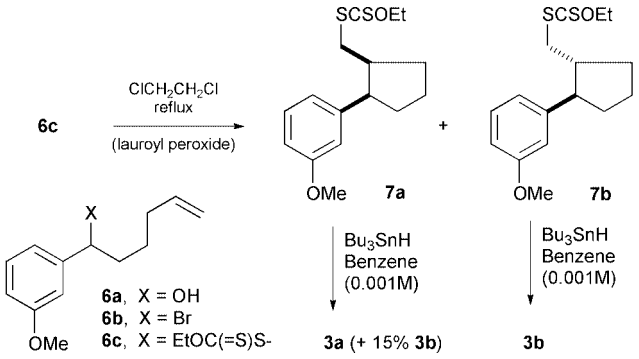

Scheme 3

 DOI: 10.1039/b101053k

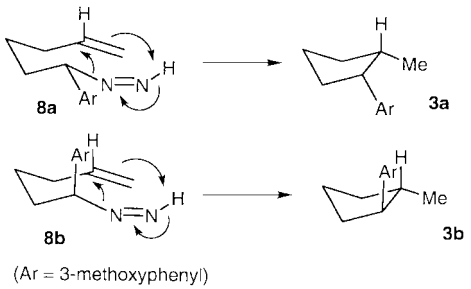

Scheme 4

irreversible radical ring closure. The radical cyclisation in such systems is inherently poorly diastereoselective: a similar 1 : 2.5 *cis* : *trans* ratio was recently reported by Studer,[8] who generated the analogous 1-phenylhex-5-enyl radical by heating the TEMPO derived precursor at 130 °C. Cyclisations involving non-stabilised secondary radicals also take place with a modest preference for the *trans* isomer.[9] The very high *cis*-selectivity observed by Taber and his colleagues in the present case is probably the result of an intramolecular, ene-type pericyclic process, as shown in Scheme 4. Placing the aryl group in the less hindered pseudo-equatorial position leads to the *cis* isomer. Such a concerted mechanism parallels that proposed for reductions with diimide itself,[10] the rigid, highly organised transition state being more consonant with the observed high *cis* selectivity. Thus, depending on the structure, the experimental conditions, and the eventual presence of initiators, monoalkyldimides (monoalkyldiazenes) may react by an ionic, a radical, or a concerted pericyclic-type mechanism. Whatever the exact mechanism operating in the present case, the observations of Taber and co-workers[3,5] will certainly have important consequences for organic synthesis.

Notes and references

1 D. F. Taber, Y. Wang and S. J. Stachel, *Tetrahedron Lett.*, 1993, **34**, 6209; A. G. Myers, M. Movassaghi and B. Zheng, *J. Am. Chem Soc.*, 1997, **119**, 8572; A. G. Myers, M. Movassaghi and B. Zheng, *Tetrahedron Lett.*, 1997, **38**, 6569. For related reactions which may involve radicals, see L. Caglioti, F. Gasparini, D. Misti and G. Palmieri, *Tetrahedron*, 1978, **34**, 135; F. S. Guziec and D. Wei, *Tetrahedron Lett.*, 1992, **33**, 7465; A. J. Bloodworth and D. Korkodilos, *Tetrahedron Lett.*, 1991, **32**, 6953.
2 C. Galli, *Chem. Rev.*, 1988, **88**, 765.
3 D. F. Taber and S. J. Stachel, *Tetrahedron Lett.*, 1992, **33**, 903; D. F. Taber and J. M. Anthony, *Tetrahedron Lett.*, 1980, 2779.
4 G. Stork and P. G. Williard, *J. Am. Chem Soc.*, 1977, **99**, 7067.
5 D. F. Taber, Y. Wang and T. F. Pahutski, Jr., *J. Org. Chem.*, 2000, **65**, 3861.
6 C. Walling and A. Cioffari, *J. Am. Chem. Soc.*, 1972, **94**, 6064. See also: D. P. Curran and C.-T. Chang, *J. Org. Chem.*, 1989, **54**, 3140.
7 S. Z. Zard, *Angew. Chem., Int. Ed. Engl.*, 1997, **36**, 672.
8 A. Studer, *Angew. Chem., Int. Ed. Engl.*, 2000, **39**, 1108.
9 A. L. J. Beckwith and C. H. Schiesser, *Tetrahedron*, 1985, **41**, 3925.
10 D. J. Pasto, in *Comprehensive Organic Synthesis*, B. M. Trost, I. Fleming, eds., Pergamon Press, Oxford, 1991, vol. 8, pp. 471–476.

CHEMCOMM Communication
www.rsc.org/chemcomm

A versatile synthesis of planar chiral ligands

Susan E. Gibson (née Thomas)* and Hasim Ibrahim

Department of Chemistry, King's College London, Strand, London, UK WC2R 2LS. E-mail: susan.gibson@kcl.ac.uk

Received (in Cambridge, UK) 4th April 2001, Accepted 25th April 2001
First published as an Advance Article on the web 22nd May 2001

Introduction of a *p*-Bu^t substituent onto tricarbonylchromium(0) complexes of benzyl ethers facilitates clean and selective *ortho* functionalisation; this reactivity is the basis of a key step in a short and versatile synthesis of enantiomerically pure planar chiral complexes.

The potential of non-racemic chiral (arene)tricarbonylchromium(0) complexes as ligands in asymmetric catalysis has been recognised.[1] As a result, an increase in activity in this area in the last three years has led to the successful application of planar chiral (arene)tricarbonylchromium(0) complexes as catalyst ligands in a diverse range of transformations including rhodium-catalysed hydrogenation of ketones,[2] palladium-catalysed aminations of aryl bromides,[3] palladium-catalysed hydrovinylations of styrene,[4] rhodium-catalysed hydroborations of styrene,[5] palladium-catalysed allylic alkylations,[6] iridium-catalysed hydroaminations[7] and Lewis acid-catalysed Diels–Alder reactions.[8] It is acknowledged, however, that although a variety of different synthetic strategies exists for the preparation of planar chiral (arene)tricarbonylchromium(0) complexes, there is still a need for more general approaches that allow the efficient preparation of a greater number of complexes.[1] We recently demonstrated that tricarbonylchromium(0) complexes of benzyl ethers, **2**, which are readily available from (benzyl alcohol)tricarbonylchromium(0) **1** could be asymmetrically functionalised to give complexes **3** in high yield and ee using chiral base methodology.[9] In view of the current interest in planar chirality and the flexibility and efficiency of our route to **3**, we wanted to convert the central chirality of **3** into complexes with planar chirality, represented by **4**. We report herein how we achieved this goal and in doing so provided the foundations of a novel and versatile route to non-racemic planar chiral (arene)tricarbonylchromium(0) complexes.

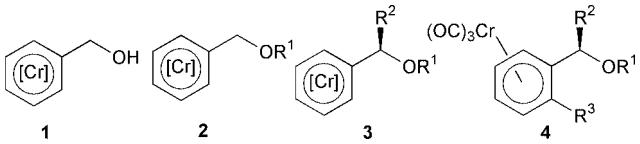

1 **2** **3** **4**

In contrast to the highly selective deprotonation–electrophilic quench chemistry to tricarbonylchromium(0) complexes of derivatives of α-methylbenzylamine,[10–12] deprotonation and subsequent electrophilic quenching of tricarbonylchromium(0) complexes of benzyl ethers is known to be unselective using the bases Bu^{n}Li,[10] Bu^{s}Li[11] and Bu^{t}Li,[11,12] giving rise to mixtures containing *inter alia* products of ring deprotonation and benzylic deprotonation. Our attempts to deprotonate **3a** (R^1 = R^2 = Me) with LiTMP and quench with chlorotrimethylsilane under a wide range of conditions also gave messy mixtures containing *ortho, meta* and *para* silylated products derived from uncontrolled ring deprotonation. Our attention then turned to the novel complex **5**,† synthesised initially in racemic form by thermolysis of the corresponding benzyl ether with hexacarbonylchromium(0) (97%). It was anticipated that the *p*-Bu^t substituent on **5** would direct deprotonation–electrophilic quench to the desired *ortho* positions of the ether. On reaction with LiTMP followed by a chlorotrimethylsilane quench, we were delighted to isolate the *ortho* silylated product **6** in 98% yield (Scheme 1). The ^{1}H NMR spectrum of **6** indicated that

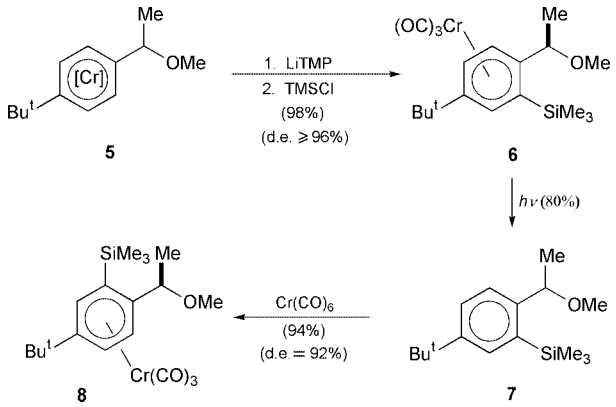

5 **6** **8** **7**

Scheme 1

only one diastereomer had been generated. To confirm that this was the case, the tricarbonylchromium(0) unit was removed from **6** to give **7** which was subsequently heated with hexacarbonylchromium(0) to give a 24:1 mixture of diastereomers **8** and **6**. Re-examination of the ^{1}H NMR spectrum of **6** established the absense of diastereomer **8** and hence the diastereoselectivity for the conversion of **5** to **6** is ≥96%.

In view of the highly selective introduction of a trimethylsilyl group into complex **5**, we decided to investigate the introduction of substituents which would provide useful donor atoms to metals. Deprotonation of **5** with LiTMP followed by addition of benzophenone gave the *ortho*-substituted product **9** in 98% yield (Scheme 2). The relative stereochemistries of the trimethylsilyl isomers **6** and **8** and the hydroxy complex **9** were initially assigned using the model developed for tricarbonylchromium(0) complexes of α-methylbenzylamine derivatives.[10–12] An X-ray crystallographic analysis of **9**[13] revealed that these assignments were correct and that co-ordination of the base to the ether oxygen plays a crucial role in the observed diastereoselectivity. Introduction of a sulfur-containing group was demonstrated on the ethyl ether complex **10**. Reaction of **10** with LiTMP followed by diphenyl disulfide gave complex **11** in 57% yield and ≥96% de (Scheme 3).

Having demonstrated that *ortho* substituents could be introduced into the *p*-Bu^t substituted complexes **5** and **10** in good yield and with high diastereoselectivity, we turned our attention to synthesising complexes of type **4** in enantiomerically pure form. Complex (4-*tert*-butylbenzyl alcohol)tricarbonylchromium(0), **12** [synthesised in 97% yield from the commercially available alcohol and hexacarbonylchromium(0)] was reacted with acidic methanol to give complex **13** in 97% yield (Scheme 4). (It is of note that the *p*-Bu^t substituent not

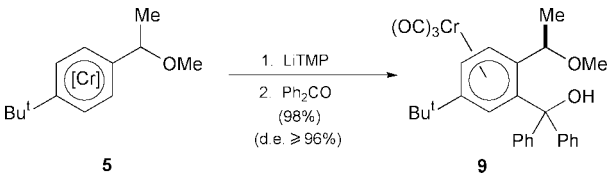

5 **9**

Scheme 2

 DOI: 10.1039/b103058m

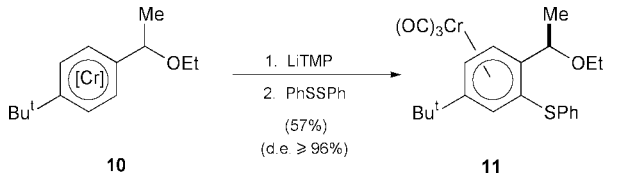

Scheme 3

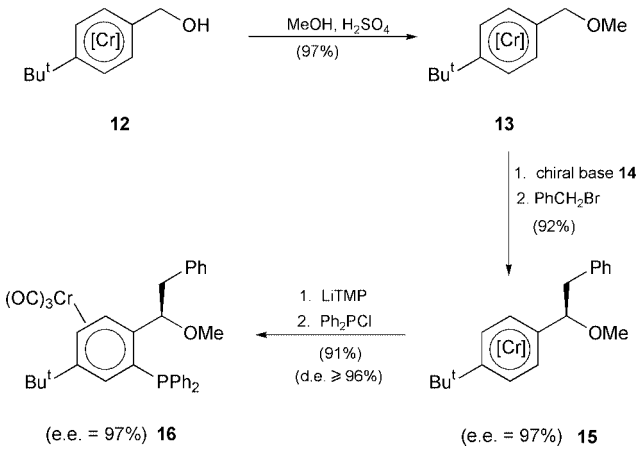

Scheme 4

only gives rise to the excellent selectivity described herein, but it also confers a high degree of stability and crystallinity on its (arene)tricarbonylchromium(0) complexes.) Subsequent treatment of **13** with chiral base **14** followed by benzyl bromide gave complex **15** in 92% yield and 97% ee (as determined by chiral

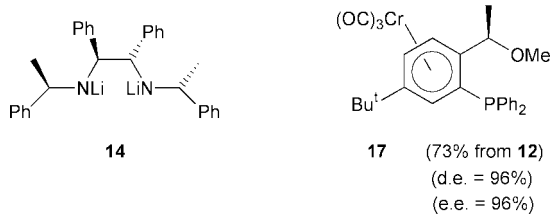

HPLC analysis). The absolute stereochemistry of **15** was assigned as *R* based on results obtained in our previous studies using chiral base **14** and benzyl ether complexes lacking the *p*-Bu^t substitutent.[9] Finally deprotonation of **15** with LiTMP followed by addition of Ph_2PCl gave complex **16** in 91% yield, ⩾96% de and 97% ee. A similar three-step sequence created complex **17** in 96% ee and ⩾96% de in 73% overall yield from complex **12**.

In conclusion, we have demonstrated that the introduction of a *p*-Bu^t substituent onto tricarbonylchromium(0) complexes of benzyl ethers enables them to be cleanly and selectively functionalised at the *ortho*-position for the first time. This new mode of reactivity has enabled us to convert readily-available (4-*tert*-butylbenzyl alcohol)tricarbonylchromium(0), **12**, into enantiomerically pure planar chiral complexes **16** and **17** in three steps. As each step involves the introduction of a new substituent, this sequence constitutes a very versatile synthesis of planar chiral complexes, many of which have potential as ligands in asymmetric synthesis.

The authors thank King's College London for a studentship (H. I.).

Notes and references

† The novel compounds **5**–**13** and **15**–**17** all gave satisfactory spectroscopic (IR, ^{1}H NMR, ^{13}C NMR, ^{31}P NMR and low resolution MS) and microanalytical data.

1 C. Bolm and K. Muniz, *Chem. Soc. Rev.*, 1999, **28**, 51, and references therein.
2 C. Pasquier, S. Naili, L. Pelinski, J. Brocard, A. Mortreux and F. Agbossou, *Tetrahedron: Asymmetry*, 1998, **9**, 193.
3 K. Kamikawa, S. Sugimoto and M. Uemura, *J. Org. Chem.*, 1998, **63**, 8407.
4 U. Englert, R. Haerter, D. Vasen, A. Salzer, E. B. Eggeling and D. Vogt, *Organometallics*, 1999, **18**, 4390.
5 S. U. Son, H.-Y. Jang, J. W. Han, I. S. Lee and Y. K. Chung, *Tetrahedron: Asymmetry*, 1999, **10**, 347.
6 H.-Y. Jang, H. Seo, J. W. Han and Y. K. Chung, *Tetrahedron Lett.*, 2000, **41**, 5083.
7 D. Vasen, A. Salzer, F. Gerhards, H.-J. Gais, R. Stürmer, N. H. Bieler and A. Togni, *Organometallics*, 2000, **19**, 539.
8 G. B. Jones, M. Guzel and S. B. Heaton, *Tetrahedron: Asymmetry*, 2000, **11**, 4303.
9 E. L. M. Cowton, S. E. Gibson, (née Thomas), M. J. Schneider and M. H. Smith, *Chem. Commun.*, 1996, 839.
10 J. Blagg, S. G. Davies, C. L. Goodfellow and K. H. Sutton, *J. Chem. Soc., Perkin Trans. 1*, 1987, 1805.
11 J. A. Heppert, M. E. Thomas-Miller, M. L. Milligan, D. V. Velde and J. Aubé, *Organometallics*, 1988, **7**, 2581.
12 J. A. Heppert, J. Aubé, M. E. Thomas-Miller, M. L. Milligan and F. Takusagawa, *Organometallics*, 1990, **9**, 727.
13 S. E. Gibson (née Thomas), H. Ibrahim and J. W. Steed, unpublished results.

CHEMCOMM
Communication
www.rsc.org/chemcomm

Cyclic dimerization of tetracyanoethylene promoted on linear triplatinum centres leading to novel nitrene-bridged Pt_3 complexes†

Tomoaki Tanase,* Makiko Hamaguchi, Rowshan Ara Begum and Eri Goto

Department of Chemistry, Faculty of Science, Nara Women's University, Kitauoya-higashi-machi, Nara 6308285, Japan. E-mail: tanase@cc.nara-wu.ac.jp

Received (in Cambridge, UK) 2nd February 2001, Accepted 1st May 2001
First published as an Advance Article on the web 22nd May 2001

Reactions of linear triplatinum complexes, *linear*-[Pt_3(μ-dpmp)$_2$(RNC)$_2$](PF$_6$)$_2$ (1), with excess tetracyanoethylene (tcne) afford the novel nitrene-bridged asymmetrical A-frame triplatinum complexes, [Pt_3(μ-dpmp)$_2$(μ-$C_{12}N_8$)(RNC)$_2$](PF$_6$)$_2$ (2a: R = 2,6-xylyl; 2b: R = 2,4,6-mesityl, dpmp = bis(diphenylphosphinomethyl)phenylphosphine), in which two tcne molecules are coupled to form a (heptacyanocyclopent-1-enyl)nitrene moiety.

Studies on organic reactions promoted by multinuclear metal centres are directly implicated in the development of industrial heterogeneous catalysts and could lead to metal–surface mimetic chemistry.[1] Multimetallic systems have the potential to organize different types of reaction processes in synergetic fashion into new homogeneous reactions which are not established by mononuclear metal centres. Recently, we have reported the linearly ordered, side-by-side triplatinum complex, *linear*-[Pt_3(μ-dpmp)$_2$(RNC)$_2$](PF$_6$)$_2$ **1a** (R = xylyl (Xyl)), which reacted with H^+, NO^+, electron-deficient alkynes and *p*-nitrophenyl isocyanide, affording asymmetrical and double A-frame triplatinum clusters through their oxidative insertion into the Pt–Pt single bonds.[2,3] Here, we have examined reactions of **1** (R = Xyl, mesityl (Mes)) with a strongly electron-deficient olefin, tetracyanoethylene (tcne), and have successfully isolated and characterized the novel, nitrene-bridged triplatinum complexes, [Pt_3(μ-dpmp)$_2$(μ-$C_{12}N_8$)(RNC)$_2$](PF$_6$)$_2$, in which two tcne molecules are coupled to form a (heptacyanocyclopent-1-enyl)nitrene moiety.

Complex **1a** readily reacts with excess of tetracyanoethylene (tcne) to afford pale green crystals formulated as [Pt_3(μ-dpmp)$_2$(μ-$C_{12}N_8$)(XylNC)$_2$](PF$_6$)$_2$ **2a** in high yield.‡ Similar reaction of **1b** also gave [Pt_3(μ-dpmp)$_2$(μ-$C_{12}N_8$)(MesNC)$_2$](PF$_6$)$_2$ **2b** in 38% yield. The IR and ^{1}H NMR spectra of **2** indicated the presence of two terminal isocyanide ligands, and the ^{31}P{^{1}H} NMR spectra exhibited three multiplets with ^{195}Pt satellite peaks in a 1 : 1 : 1 ratio. The detailed structure of **2a** was determined by X-ray crystallographic analysis and an ORTEP plot for the complex cation is illustrated in Fig. 1.§ The complex cation involves an asymmetrical triplatinum core supported by two dpmp ligands. The Pt(1)–Pt(2) distance of 2.6446(8) Å corresponds to a Pt–Pt single bond, and the Pt(2)–Pt(3) separation of 3.2150(8) Å is indicative of the absence of a Pt–Pt bond. The two tcne molecules are coupled to form a (heptacyanocyclopent-1-enyl)nitrene moiety which is inserted into one of the Pt–Pt bonds of **1a** (Scheme 1). Structurally characterized nitrene-bridged platinum and palladium complexes are extremely rare[4] in spite of their importance as metal–surface nitrene intermediates in the metal-catalyzed reduction of NO and nitro compounds and, to our knowledge, this is the first example of a trinuclear platinum complex with a nitrene-bridging ligand. The N(11) atom rather asymmetrically bridges Pt(2) and Pt(3) and adopts a planar sp^2 geometry with the sum of the bond angles being 359.9°. The Pt_2N plane is almost co-planar with the [C(11)C(12)] olefin unit and the relatively short N(11)–C(11) bond length indicates that the electron density on the N atom is delocalized through a p_π–p_π interaction between the nitrene and olefin units as shown in Scheme 1. The C(11)–C(12) bond length is longer than that of a usual C–C double bond. A similar tendency was observed in [Ir_2(CO)$_2$(μ-dppm)$_2$(μ-NPh)][5] and [Rh_2(CO)$_2$(dppm)$_2$(μ-N(*p*-$NO_2C_6H_4$))][6] (dppm = bis(diphenylphosphino)methane). The heptacyanocyclopent-1-enyl moiety adopts an envelop conformation with the C(14) atom in the apex site and the C(13), C(14) and C(15) atoms having sp^3 tetrahedral configuration. The present type of tcne cyclic dimerization is very rare; the only related compound reported is *N*-(heptacyanocyclopent-1-enyl)triphenylphosphoranimine which was formed by reaction of tcne with triphenylphosphine.[7]

The cyclic dimerization of tcne did not proceed by the dppm-bridged diplatinum complex, [Pt_2(μ-dppm)$_2$(XylNC)$_2$](PF$_6$)$_2$,[8] although it proceeded rapidly with the triplatinum complex **1a**; the reaction was monitored by electronic absorption spectral change with an isosbestic point at 345 nm. The reaction with excess of tcne (> 10 equiv.) proceeded with a first order dependency on the starting complex **1a** with the pseudo-first order rate constant of 4.0×10^{-3} s^{-1}. Whereas no stable intermediate was observed, the tcne adduct **A** might be formed at the initial step by analogy with the reaction of **1a** with electron-deficient alkynes (Scheme 1).[3] The strong *trans* influence of the Pt–Pt bond may cause the zwitterionic Pt–C bond breaking (**B**), together with the nucleophilic attack of the

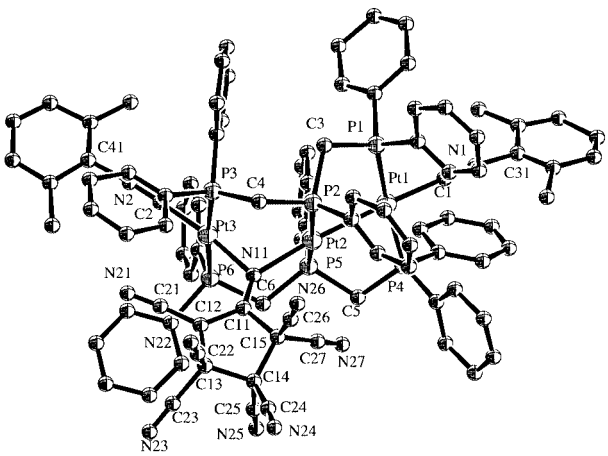

Fig. 1 ORTEP diagram for the complex cation of **2a**. Selected distances (Å) and angles (°): Pt(1)–Pt(2) 2.6446(8), Pt(2)···Pt(3) 3.2150(8), Pt(1)–P(1) 2.312(5), Pt(1)–P(4) 2.328(5), Pt(1)–C(1) 2.01(2), Pt(2)–P(2) 2.263(4), Pt(2)–P(5) 2.277(4), Pt(3)–P(3) 2.341(4), Pt(3)–P(6) 2.349(4), Pt(3)–C(2) 1.90(2), Pt(2)–N(11) 2.18(1), Pt(3)–N(11) 2.05(1), N(11)–C(11) 1.26(2), C(11)–C(12) 1.46(2), C(11)–C(15) 1.54(2), C(12)–C(13) 1.54(3), C(13)–C(14) 1.60(3), C(14)–C(15) 1.57(3); Pt(2)–Pt(1)–C(1) 177.8(6), Pt(1)–Pt(2)–N(11) 175.1(4), N(11)–Pt(3)–C(2) 173.0(6), Pt(2)–N(11)–Pt(3) 98.9(6), Pt(2)–N(11)–C(11) 138(1), Pt(3)–N(11)–C(11) 123(1), N(11)–C(11)–C(12) 129(2), N(11)–C(11)–C(15) 123(2), C(12)–C(11)–C(15) 108(1), C(11)–C(12)–C(13) 110(1), C(11)–C(12)–C(21) 127(2), C(13)–C(12)–C(21) 123(2).

† Electronic supplementary information (ESI) available: further structural and experimental data for **2a**·2(CH$_3$)$_2$CO. See http://www.rsc.org/suppdata/cc/b1/b101805l/

 DOI: 10.1039/b101805l

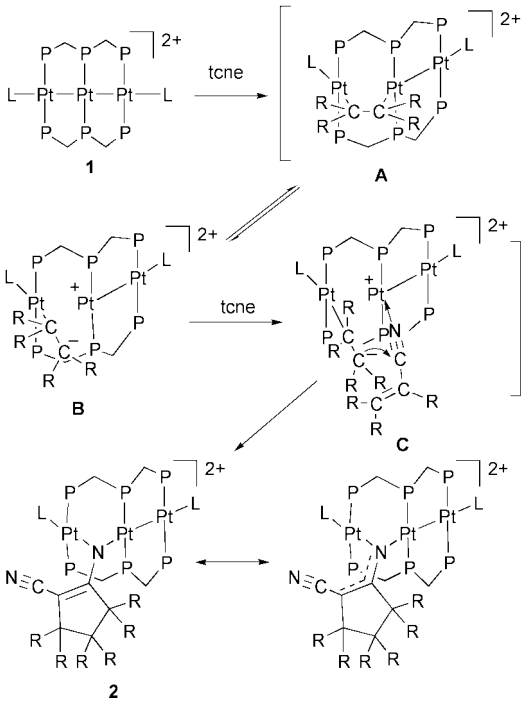

Scheme 1 L = XylNC (**a**), MesNC (**b**); R = CN.

carbanion on the electron-deficient nitrile carbon of the second tcne molecule (**C**) – this was inferred as a key step for the coupling. A detailed study on the reaction mechanism is now in progress.

This work was partly supported by Grants-in-Aid for Scientific Research from the Ministry of Education, Science, Sports, and Culture of Japan.

Notes and references

‡ To 20 mL of dichloromethane solution containing 71 mg of *linear*-[Pt_3(μ-dpmp)$_2$(XylNC)$_2$](PF_6)$_2$ was added 37 mg of tcne (0.29 mmol). The reaction solution was stirred at room temperature for 1 h, and the color of the solution immediately changed from orange to pale green. The solvent was removed under reduced pressure and the residue was washed with benzene and diethyl ether; it was then extracted with 20 mL of dichloromethane. The solution was concentrated to *ca.* 10 mL and was kept in a refrigerator after the addition of a small amount of Et_2O to afford block-shaped pale green crystals of [Pt_3(μ-dpmp)$_2$(μ-$C_{12}N_8$)(XylNC)$_2$](PF_6)$_2$ **2a** in 86% yield. Anal. Calc. for $C_{94}H_{76}N_{10}P_8F_{12}Pt_3$: C, 46.91; H, 3.18; N, 5.82. Found: C, 46.67; H, 3.30; N, 5.54%. IR (Nujol/cm^{-1}): 2189, 2168 (XylN≡C), 1571 (C=C), 840 (PF_6). UV–Vis (CH_2Cl_2): λ_{max}/nm (log ε) 404 (3.22). ^{1}H NMR (C_2Cl_2): δ 1.34, 1.98 (s, *o*-Me, 6H), 2.9–5.5 (m, CH_2, 8H), 6.1–8.8 (m, Ar, 56H). ^{31}P{^{1}H} NMR (CD_2Cl_2): δ −5.7 (m, 1P, $^1J_{PtP}$ 2450 Hz), 0.2 (m, 1P, $^1J_{PtP}$ 2906 Hz), 6.1 (m, 1P, $^1J_{PtP}$ 2556 Hz). Recrystallization of **2a** from a acetone–diethyl ether mixed solvent yielded block-shaped crystals of **2a**·$(CH_3)_2CO$ which were suitable for X-ray crystallography.

A similar procedure using *linear*-[Pt_3(μ-dpmp)$_2$(MesNC)$_2$](PF_6)$_2$ **1b** (62 mg) afforded pale green crystals of [Pt_3(μ-dpmp)$_2$(μ-$C_{12}N_8$)(MesNC)$_2$](PF_6)$_2$·CH_2Cl_2 (**2b**·CH_2Cl_2) in 38% yield. Anal. Calc. for $C_{97}H_{82}N_{10}P_8F_{12}Cl_2Pt_3$: C, 46.24; H, 3.28; N, 5.56. Found: C, 46.48; H, 3.08; N, 5.70%. Complex **1b** was prepared by the reaction of **1a** with MesNC and was characterized by X-ray crystallography, which will be reported elsewhere. IR (Nujol/cm^{-1}): 2186, 2169 (MesN≡C), 1573 (C=C), 838 (PF_6). UV–Vis (in CH_2Cl_2): λ_{max}/nm (log ε) 391 (3.37). ^{1}H NMR (CD_2Cl_2): δ 1.28, 1.90 (s, *o*-Me, 6H), 2.06, 2.20 (s, *p*-Me, 3H), 3.4–5.2 (m, CH_2, 8H), 6.2–8.6 (m, Ar, 54H). ^{31}P{^{1}H} NMR (in CD_2Cl_2): δ −7.3 (m, 1P, $^1J_{PtP}$ 2514 Hz), −1.6 (m, 1P, $^1J_{PtP}$ 2926 Hz), 4.2 (m, 1P, $^1J_{PtP}$ 2571 Hz).

§ *Crystal data* for **2a**·$(CH_3)_2CO$: $C_{97}H_{82}N_{10}OP_8F_{12}Pt_3$, M = 2464.82, T = −118 °C, monoclinic, space group $P2_1/c$, a = 13.872(4), b = 53.155(12), c = 15.130(4) Å, β = 97.90(2)°, V = 11 050(4) Å^3, Z = 4. A pale yellow, block-shaped crystal was fixed on the top of a glass fiber with Paraton N oil. 14381 reflections ($4 < 2\theta < 45°$) were measured on a Rigaku AFC7R diffractometer with graphite monochromated Mo-Kα radiation. The structure was solved by Patterson methods using the program DIRDIF94 and was refined with SHELXL-93 to R_1 = 0.068 for 10081 independent reflections with $I > 2\sigma(I)$ and wR_2 = 0.227 for all data.

CCDC 160684. See http://www.rsc.org/suppdata/cc/b1/b101805l/ for crystallographic data in .cif or other electronic format.

1 R. D. Adams and F. A. Cotton, *Catalysis by Di- and Polynuclear Metal Cluster Complexes*, Wiley, New York, 1998; A. L. Balch, *Homogeneous Catalysis with Metal Phosphine Complexes*, ed. L. H. Pignolet, Plenum Press, New York, 1983, p. 167; J. H. Sinfelt, *Bimetallic Catalysis: Discoveries, Concepts and Applications*, Wiley, New York, 1983; L. Guczi, *Metal Clusters in Catalysis*, ed. B. C. Gates, L. Guczi and H. Knozinger, Elsevier, New York, 1986 and references cited therein.

2 T. Tanase and R. A. Begum, *Organometallics*, 2001, **20**, 106; T. Tanase, M. Hamaguchi, R. A. Begum, S. Yano and Y. Yamamoto, *Chem. Commun.*, 1999, 745; T. Tanase, H. Ukaji, H. Takahata, H. Toda, T. Igoshi and Y. Yamamoto, *Organometallics*, 1998, **17**, 196; T. Tanase, H. Takahata, M. Hasegawa and Y. Yamamoto, *J. Organomet. Chem.*, 1997, **545**/**546**, 531; T. Tanase, H. Toda and Y. Yamamoto, *Inorg. Chem.*, 1997, **36**, 1571; T. Tanase, H. Toda, K. Kobayashi and Y. Yamamoto, *Organometallics*, 1996, **15**, 5272.

3 T. Tanase, H. Ukaji, T. Igoshi and Y. Yamamoto, *Inorg. Chem.*, 1996, **14**, 4114.

4 G. Besenyei, L. Párkányi, I. Foch, L. I. Simándi and A. Kálmán, *Chem. Commun.* 1997, 1143; S. W. Lee and W. C. Trogler, *Inorg. Chem.*, 1990, **29**, 1099; R. Jones, P. K. Kelly, D. J. Williams and J. D. Woollins, *Chem. Commun.*, 1985, 1325; P. F. Kelly, A. M. Z. Slawin, D. J. Williams and J. D. Woollins, *Polyhedron*, 1990, **9**, 1567; R. Meij, D. J. Stufkens, K. Vrieze, A. M. F. Brouwers and A. R. Overbeek, *J. Organomet. Chem.*, 1978, **155**, 123; I. Foch, L. Párkányi, G. Besenyei, L. I. Simándi and A. Kálmán, *J. Chem. Soc., Dalton Trans.*, 1999, 293; W.-H. Leung, J. L. C. Chim and W.-T. Wong, *J. Chem. Soc., Dalton Trans.*, 1997, 3277.

5 C. Ye and P. R. Sharp, *Inorg. Chem.*, 1995, **34**, 55.

6 Y.-W. Ge, F. Peng and P. R. Sharp, *J. Am. Chem. Soc.*, 1990, **112**, 2632.

7 T. Mohan, R. O. Day and R. R. Holmes, *Inorg. Chem.*, 1992, **31**, 2271; P. J. Butterfield, J. C. Tebby and T. J. King, *J. Chem. Soc., Perkin Trans. 1*, 1978, 1237.

8 Y. Yamamoto and H. Yamazaki, *Organometallics*, 1993, **12**, 933.

CHEMCOMM
Communication
www.rsc.org/chemcomm

Complete blocking of Mn^{3+} ion dissolution from a $LiMn_2O_4$ spinel intercalation compound by Co_3O_4 coating

Jaephil Cho,*[a] Tae-Joon Kim,[b] Yong Jeong Kim[b] and Byungwoo Park[b]

[a] *Energy Laboratory, Samsung SDI Co., Ltd, Chonan, Chungchongnam-Do, Korea. E-mail: jpcho@samsung.co.kr*
[b] *School of Materials Science and Engineering, Seoul National University, Seoul, Korea*

Received (in Cambridge, UK) 20th February 2001, Accepted 30th April 2001
First published as an Advance Article on the web 22nd May

Complete elimination of Mn^{3+} dissolution from a $LiMn_2O_4$ spinel compound at 60 °C has been achieved by enclosing each particle with a $LiMn_{2-x}Co_xO_4$ solid-solution thin film having a high Co concentration at the surface.

$LiMn_2O_4$ cathode materials have received much attention due to their environmental friendliness and low cost compared to $LiCoO_2$ and $LiNiO_2$. However, their practical applications as Li-ion cells are hindered by structural instability from acidic HF attack on the spinel particles, as a result of the reaction of the $LiPF_6$ salt with residual water in the cell at elevated temperatures.[1–4] This leads to a disproportionation reaction ($2Mn^{3+} \rightarrow Mn^{4+} + Mn^{2+}$) at the particle surface, resulting in the formation of a defective spinel. The reaction moves progressively inward with increasing exposure to the electrolyte, especially at elevated temperatures. This reduces the intercalation capacity, and therefore should be prevented to ensure long-cycle life for elevated-temperature performance. To reduce such inherent structural degradation, a marginal increase in the overall Mn valence to above +3.5 has been reported.[5–9] However, such methods do not significantly improve the structural stability since a fraction of Mn^{3+} ions still exist in the spinel structure. The most effective way to block Mn dissolution is to completely encapsulate the spinel particles with oxides that are resistant to acidic HF. There have been several attempts to minimize Mn dissolution, but none have blocked the dissolution completely. Such studies even showed a deterioration in cathode-cycle performance compared to unmodified samples or decreased capacity fading during cycling at 55 °C.[10–12]

Here, we report a low-temperature coating method using Co_3O_4, and its effect on the cycling performance at 60 °C in Li/$LiMn_2O_4$ cells. This new approach completely blocks Mn dissolution from the $LiMn_2O_4$ particles.

$LiMn_2O_4$ powder 'bare sample' was prepared by firing a stoichiometric mixture of MnO_2 (EMD) and $LiOH{\cdot}H_2O$ at 750 °C for 20 h. The powder, with an average particle size of 13 μm after sieving, was used for coating and for the electrochemical experiments. To coat each particle with the solution of Co_3O_4, cobalt(III) acetate was first dissolved in methanol, then slowly mixed until it reached the appropriate viscosity. The solution was then mixed with the $LiMn_2O_4$ powder in a mole ratio of 10:1 (Mn:Co). The coated powder was dried at 150 °C for 1 h, and then fired at 400 °C for 8 h in a dry-air atmosphere. The electrochemical cycling experiments were carried out at 60 °C with coin-type cells (size 2016) containing a $LiMn_2O_4$ spinel electrode, a Li metal anode, a microporous polyethylene separator, and an electrolyte consisting of a 1 M $LiPF_6$ solution in a 1:1 EC–DMC mixture (by volume). To fabricate the cathode, the spinel powder was blended with Super-P carbon black (to assist in current collection) and with a polyvinylidene fluoride (PVDF) binder in a mass ratio of 92:4:4.

X-Ray diffraction (XRD) patterns of the bare- and coated-$LiMn_2O_4$ powders were indexed to cubic spinel (*Fd*3*m*). The Co_3O_4-coated sample shows no indication of Co_3O_4 or other phases, except for increased peak broadening compared to the bare sample (Fig. 1). This broadening may be due to the formation of a disordered spinel phase throughout the particle, with decreasing Co concentration inward. Raman spectroscopy of the coated sample clearly showed the presence of a Co_3O_4 phase (peak at 693 cm^{-1}), and electron-probe microanalysis

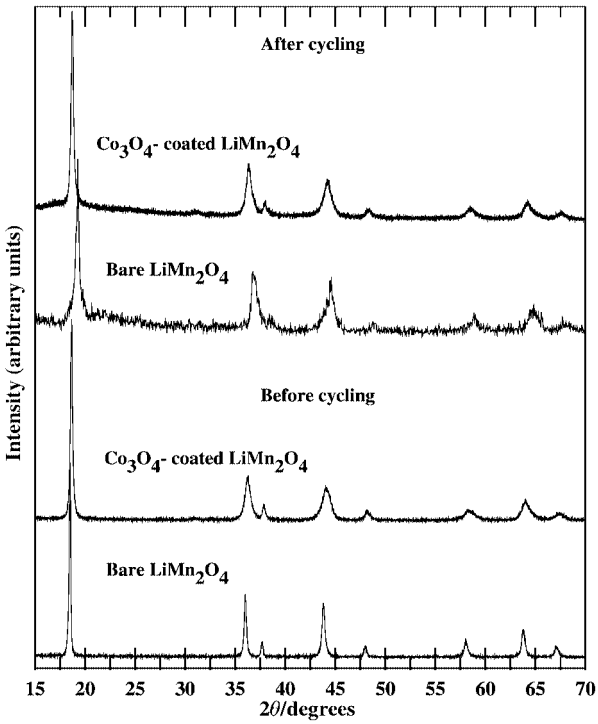

Fig. 1 XRD patterns of bare and Co_3O_4-coated $LiMn_2O_4$ powders before and after cycling.

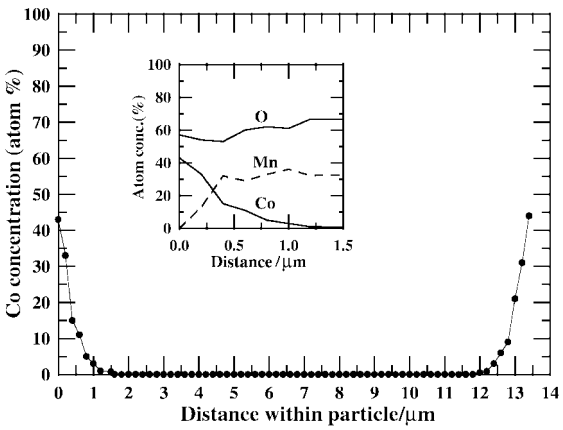

Fig. 2 EPMA of Co concentration across a particle cross-section; the inset corresponds to elemental analysis of the particle within 1.5 μm.

 DOI: 10.1039/b101677f

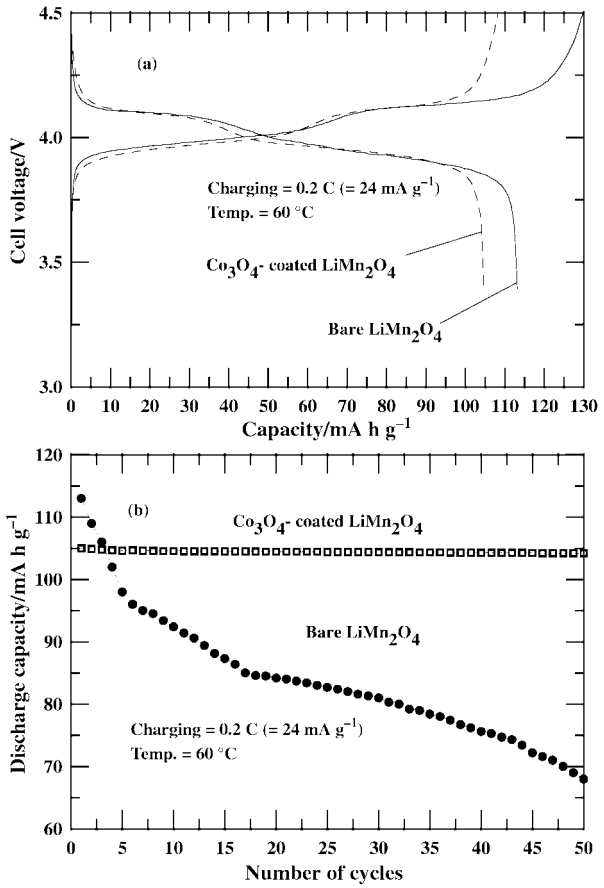

Fig. 3 Plots of (a) voltage profile of bare and Co_3O_4-coated $LiMn_2O_4$ at a charging rate of 0.2 C between 4.5 and 3.4 V, and (b) cycle-life performance of bare and Co_3O_4-coated $LiMn_2O_4$ at a charging rate of 0.2 C between 4.5 and 3.4 V. The coin-type half cells were cycled at 60 °C with a Li-metal anode

(EPMA) of the Co atoms across the particle shows a 43% Co concentration at the surface, as shown in Fig. 2, which is consistent with the Raman data. In addition, Co atoms were mainly distributed within *ca*. 1 μm from the surface, and their concentration sharply decreased further inside the particle. Results indicate the formation of a solid-solution $Li_zMn_{2-x}Co_xO_4$ thin-film phase near the surface by interdiffusion between $LiMn_2O_4$ and Co_3O_4. However, some portion of the unreacted Co_3O_4 resides on the solid solution. It is expected that the coating of each particle with $Li_zMn_{2-x}Co_xO_4$ and Co_3O_4 thin-film coatings, which are resistant to HF attack, can prevent Mn dissolution into the electrolyte.

All spinel compounds with a defective cubic structure have lattice constants smaller than the well-ordered $LiMn_2O_4$ phase, because of the higher concentration of the relatively large Mn^{3+} ion (ionic radii of Mn^{3+} and of Mn^{4+} are, respectively, 0.65 and 0.53 Å).[13] Therefore, from the XRD pattern, all the spinels within the $LiMn_2O_4$–$Li_4Mn_5O_{12}$–λ-MnO_2 tie-line-triangle in the Li–Mn–O phase diagram will have diffraction peaks that lie to higher 2θ values than those of $LiMn_2O_4$. This feature can be seen in the XRD patterns of the spinel electrodes after cycling at 60 °C and after equilibration at 3.4 V for 50 h (Fig. 1). They show a shift in the spinel peaks to higher 2θ values (a = 8.122 ± 0.003 Å), accompanied by peak broadening (the lattice constant of the bare sample before cycling is 8.234 ± 0.005 Å). This shows that the starting $LiMn_2O_4$ spinel becomes defective during cycling at 60 °C. However, the coated sample does not show any peak shift (a = 8.178 ± 0.005 Å) or peak broadening after cycling.

The cycling behavior of bare- and coated-$LiMn_2O_4$ materials was tested in coin-type half-cells using Li metal as the anode between 4.5 and 3.3 V at a rate of 0.2 C (= 24 mA g^{-1}) at 60 °C. Fig. 3 shows the initial voltage profiles of the samples. The discharge capacity of the coated sample was 105 mA h g^{-1}, while that of the bare sample was 113 mA h g^{-1}. The decreased irreversible capacity upon coating, 3 mA h g^{-1} *vs.* 17 mA h g^{-1} in the bare sample, is significant. Furthermore, there is negligible capacity loss in the coated sample over 50 cycles, while that of the bare sample shows a 41% loss. It is believed that surface encapsulation by both Co_3O_4 and $Li_zMn_{2-x}Co_xO_4$ prevents Mn dissolution from HF attack at 60 °C.

Notes and references

1 J. C. Hunter, *J. Solid State Chem.*, 1981, **39**, 142.
2 D. Aurbach and Y. Gofer, *J. Electrochem. Soc.*, 1991, **138**, 3529.
3 A. Blyr, C. Sigala, G. G. Amatucci, D. Guyomard, Y. Chabre and J. M. Tarascon, *J. Electrochem. Soc.*, 1998, **145**, 194.
4 J. Cho, *Solid State Ionics*, 2001, **138**, 267.
5 M. M. Thackeray, *Prog. Solid State Chem.*, 1997, **25**, 1.
6 Y. Toyoguchi, *Eur. Pat. Appl.*, 0390185, 1990.
7 A. Antonini, C. Bellitto, M. Pasquali and G. Pistoia, *J. Electrochem. Soc.*, 1998, **145**, 2726.
8 M. M. Thackeray, A. de Kock, M. H. Rossouw, D. C. Liles, R. Bitthn and D. Hoge, *J. Electrochem. Soc.*, 1992, **139**, 364.
9 Q. Feng, Y. Miyai, H. Kanoh and K. Ooi, *Langmuir*, 1992, **8**, 1862.
10 J. Cho, G. Kim, H. Lim, C. Kim and S. I. Yoo, *Electrochem. Solid State Lett.*, 1999, **2**, 607.
11 G. G. Amatucci, A. Blyr, C. Siagala, P. Alfonse and J. M. Tarascon, *Solid State Ionics*, 1997, **104**, 13.
12 G. G. Amatucci, *US Pat.*, 5759720, 1997.
13 R. D. Shannon, *Acta Crystallogr., Sect. A*, 1976, **32**, 751.

CHEMCOMM Communication
www.rsc.org/chemcomm

The enumeration of structures for γ-alumina based on a defective spinel structure

Graeme W. Watson[a] and David J. Willock*[b]

[a] *Department of Chemistry, Trinity College, Dublin 2, Ireland. E-mail: watsong@tcd.ie*
[b] *Department of Chemistry, Cardiff University, P.O. Box 912, Cardiff, UK, CF10 3TB. E-mail: willockdj@cardiff.ac.uk*

Received (in Cambridge, UK) 27th February 2001, Accepted 20th April 2001
First published as an Advance Article on the web 22nd May 2001

Atomistic potential calculations of the relative energies of γ-alumina structures as a function of tetrahedral Al distribution give an exhaustive list of configurations which is used to estimate thermodynamic probabilities, subsequent relaxations allow the influence of configurational entropy on structure to be assessed.

γ-Alumina finds widespread use as a stable, highly porous medium for the support of active catalysts such as particulate transition metals. The material is formed on dehydration of the hydroxide boehmite and is the stable form of alumina from this route between 750 and 1025 K.[1] The structure is generally regarded as amorphous although it is known that the oxygen anions form an fcc lattice with Al ions occupying both octahedral and tetrahedral sites. The cubic structure resembles a defective spinel in which both tetrahedral and octahedral cation positions are occupied. In the proper spinel structure, $MgAl_2O_4$, Al^{3+} ions appear in half the octahedral holes and Mg^{2+} in 1/8 of the tetrahedral holes. Various experiments have attempted to apportion the Al cations in γ-alumina between the two possible sites. In 1991 X-ray and neutron diffraction were combined to give lattice parameters for the cubic cell.[2] The line widths of specific reflections were used to suggest that the Al tetrahedral sub-lattice is extremely disordered and that the distribution of Al between tetrahedral and octahedral sites was roughly 50 : 50, although the assignment of the occupancy ratio was difficult as no reflections from the octahedral sub-lattice alone are present in the diffraction pattern. More recently, ^{27}Al MAS NMR has been used to show that 70 ± 2% of Al ions occupy octahedral sites.[3] This is close to the proportion that would be expected for a spinel structure in which all octahedral Al are in place and the tetrahedral sites are partially occupied to give 75% of cations in an octahedral environment. Here, we show that this simplified model of the structure allows the calculation of the lattice energy for all possible arrangements of tetrahedral Al in the simplest stoichiometric unit cell using atomistic potentials. Furthermore the structures of the most thermodynamically stable lattices can be geometry optimised to allow thermally averaged structural data such as the lattice constants to be estimated.

Aluminas in general are based around close packed arrangements of O^{2-} anions with Al^{3+} occupying octahedral and/or tetrahedral holes. α-Alumina has the corundum structure with a hexagonal close packed arrangement of anions and exclusively octahedral cations. The α-polymorph has been widely studied using both atomistic potential and periodic quantum chemical approaches. The θ-alumina structure is based on a face centred cubic packing of anions similar to the γ-phase[4] and contains both octahedral and tetrahedral aluminium ions. Based on these two ordered structures new potentials for octahedral and tetrahedral aluminium were fitted using the GULP program[5] starting from the shell model potentials derived for α-alumina by Lewis and Catlow.[6] The full procedure used in fitting and the resulting parameter set will appear at a later date. We note here that the new potentials are able to reproduce the experimental lattice constants of the two phases used in fitting to within 0.15 Å.

A unit cell of overall stiochiometry Al_2O_3 in the spinel form requires a supercell of at least three basic spinel cells ($Al_{64}O_{96}$) which we produce by extension of the *c*-vector. Recently Allan *et al.*[7] have used a sampling technique to consider the configurational entropy for the mixed oxide MnO/MgO and find convergence with supercells containing only 32 atoms; accordingly, we expect this cell to be sufficiently large to avoid artifacts due to cell size affects. In this cell we have 24 possible tetrahedral Al sites to be filled by 16 atoms. The total number of possible distinguishable structures is simply $^{24}C_{16}$ = 735 471. Using an EV5 DEC alpha workstation a single lattice energy calculation for this supercell using GULP takes approximately 1.2 CPU seconds and so the complete set of structures can be assessed in a little over ten days. The amount of data generated would, however, require a considerable amount of computer storage and so to make these calculations feasible we have developed an automated driving program. All that is stored after each of the initial runs is the binary code and the lattice energy. The binary code is formulated so that each tetrahedral site in the structure is assigned a binary digit that is set to 1 for occupancy by Al and 0 for a vacant site. In the current study a 24-bit number uniquely identifies a configuration and is saved as an integer. The program generates all possible configurations simply by counting through all 24-bit integers and generating an input file for those which have 16 bits set to 1. As they are identified the lattice energy is calculated and both input and output files are replaced by the next configuration.

Our procedure gives an exhaustive list of tetrahedral Al occupancies and the corresponding lattice energies for the structure fixed at the standard spinel geometry. The resulting configurations were grouped according to calculated lattice energy and the number of configurations *vs.* lattice energy is shown in Fig. 1. Here we have calculated the lattice energy per mole of Al_2O_3 formula units: the lowest energy configuration was found to be unique together with the number of configuration peaks at around 200 kJ mol^{-1} higher energy where some 55 000 structures have similar energies. Since we store the code for each structure we can easily regenerate a configuration of interest. For example, we find that the lowest energy structures have a uniform distribution of tetrahedral Al atoms whereas the

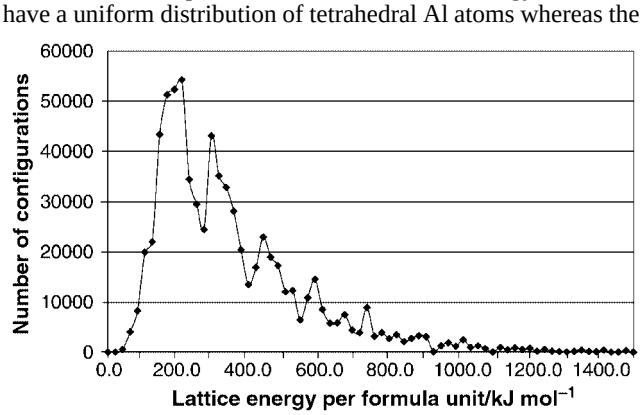

Fig. 1 The number of configurations as a function of calculated lattice energy. Structures are grouped in intervals of 21.1 kJ mol^{-1}.

 DOI: 10.1039/b101877a

highest energy structures have the occupied tetrahedral sites clustered together and one third of the unit cell contains no tetrahedral Al atoms. This calculation also gives us direct access to the partition function for the tetrahedral site distributions allowing the calculation of thermodynamic probabilities. For example, the probability, $P(\Delta E_i)$, of a given lattice energy is:

$$P(\Delta E_i) = \frac{n_i \exp\left(-\frac{\Delta E_i}{RT}\right)}{\Sigma_j n_j \exp\left(-\frac{\Delta E_j}{RT}\right)} \quad (1)$$

where n_i is the number of structures with energy ΔE_i greater than the lowest energy structure. Since γ-alumina is formed from boehmite at elevated temperatures we chose T = 900 K. Even at this high temperature the few low energy structures dominate despite the entropic factor in favour of higher energy states.

In these initial calculations no geometry optimisation was allowed so that all possible structures could be considered. It is well known that structural relaxation can be important in obtaining accurate relative energies using atomistic simulation. In this case the occupation of an Mg^{2+} tetrahedral site by a smaller Al^{3+} cation will cause lattice strain. Despite this we expect the ordering of the structural energies to be a good indication of which are the important structures to consider. Accordingly we carried out relaxations on the most probable of the lattices generated. The list of structures was ordered according to lattice energy and the program adapted to reconstruct them from the list and carry out lattice relaxations using GULP. To determine how far down the list to proceed the thermodynamic probability of each structure was calculated from eqn. (1) (with n_i = 1) using the recorded static lattice energy. Sub-sets of structures were generated by successively decreasing the acceptance probability limit. Geometry optimisations were performed using the same automated procedure as described previously but now the GULP input file was written to perform relaxations at constant pressure, *i.e.* a full relaxation of all atomic co-ordinates and lattice vectors.

Fig. 2 shows the probability distribution of lattice energies at 900 K after relaxations for three sub-sets containing increasing numbers of structures in roughly 50 000 steps. The distribution shows significant differences for the change from 78 137 to 129 205 structures but the addition of a further 50 000 structures results in only minor alterations suggesting that most of the additional structures do not optimise to thermodynamically accessible configurations. There are now two degenerate lowest energy structures. These are found in the smallest list and remain the minima for the longer lists indicating that the initial ordering by structural energy has allowed the minimum energy structure to be identified rapidly. After relaxation the number of

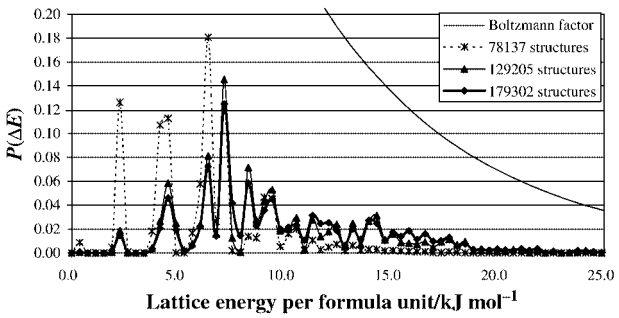

Fig. 2 Probability *vs.* lattice energy from eqn. (1) at 900 K with structural relaxation taken into account for three sub-sets containing 78 137 (crosses, dotted), 129 205 (triangles, thin solid) and 179 302 (diamonds, thick solid) structures. Boltzmann factor shown as a feint line. Structures grouped in 0.38 kJ mol^{-1} intervals.

Table 1 Comparison of calculated and experimental lattice vectors

	Number	*a*/Å	*b*/Å	*c*/Å
Expt. $MgAl_2O$[8]		8.080	8.080	8.080
Expt. γ-alumina[2]		7.911	7.911	7.911
Min. energy structure	1	8.277	8.245	8.203
Thermal average[a]	78 137	8.251	8.251	8.269
	129 205	8.254	8.254	8.271
	179 302	8.254	8.254	8.278

[a] Thermal averages use eqn. (1) with T = 900 K.

structures within a few kJ mol^{-1} of the minimum is much greater than for the simple structural energy calculations and so the entropic effect of tetrahedral ion configurations is much greater. The probability of the lowest energy structures is extremely small and the probability distribution shows a great many structures with configurations up to 20 kJ mol^{-1} above the minimum being significant. The highest peak in $P(\Delta E_i)$ occurs at 7.2 kJ mol^{-1} and represents some 12 200 structural alternatives.

After relaxation the lattice parameters were also recorded for each configuration to allow the lattice vectors, *a*, *b* and *c*, to be calculated as thermodynamic averages of the relaxed structures. Based on the sub-sets of relaxed structures from Fig. 2 we find the lattice parameters given in Table 1 where we also compare the averaged data to experimental results and to one of the minimum energy structures. The other degenerate minimum energy form is identical to that in Table 1 with *a* and *b* interchanged. These minima structures show a distortion away from cubic symmetry. On averaging this is reduced to a small tetragonal distortion of the basic unit cell. The convergence of the cell dimensions with sub-set size is further confirmation that all thermodynamically significant configurations have been taken into account.

Early investigations of γ-alumina reported tetragonal distortions of the unit cell.[9] It appears from these calculations that the observed symmetry comes about from the interplay of many possible configurations of cations. Closer inspection of the listed data shows that the individual microstates occur in pairs with equivalent distortions in the *a* and *b* directions, in the averaging process these are removed to give the experimentally observed cubic structure. In the real crystallites this tendency toward distortion will lead to lattice strain which may contribute to the longer scale defect structure of the material.

This research was funded, in part, through an EPSRC IMI project, a collaboration between chemists, materials scientists and chemical engineers from academia and industry, involving Cardiff, Birmingham, Cambridge and Glasgow Universities with financial support from Synetix, Johnson Matthey, BP-Amoco, Cambridge Reactor Design and Molecular Simulations Inc.

Notes and references

1 K. Wefers and C. Misra, Alcoa Technical Paper No 19, Alcoa Laboratories, Pittsburg, PA, USA, 1987.
2 R.-S. Zhou and R. L. Snyder, *Acta Crystallogr., Sect. B*, 1991, **47**, 617.
3 M.-H. Lee, C.-F. Cheng, V. Heine and J. Klinoski, *Chem. Phys. Lett.*, 1997, **265**, 673.
4 G. Yamaguchi, I. Yasui and W. C. Chui, *Bull. Chem. Soc. Jpn.*, 1970, **43**, 2487.
5 J. D. Gale, *J. Chem. Soc., Faraday Trans.*, 1997, **93**, 629.
6 G. V. Lewis and C. R. A. Catlow, *J. Phys. C: Solid State Phys.*, 1985, **18**, 1149.
7 N. L. Allan, G. D. Barrera, R. M. Fracchia, M. Y. Lavrentiev, M. B. Taylor, I. T. Todorov and J. A. Pruton, *Phys. Rev. B*, 2001, **63**, 094203.
8 R. C. Peterson, G. A. Lager and R. L. Hitterman, *Am. Mineral*, 1991, **76**, 1455.
9 B. C. Lippens and J. H. DeBoer, *Acta Crystallogr.*, 1964, **17**, 1312.

CHEMCOMM
Communication
www.rsc.org/chemcomm

Paper: a cheap yet effective chiral stationary phase for chromatographic resolution of metallo-supramolecular helicates

Michael J. Hannon,*[a] Isabelle Meistermann,[a] Christian J. Isaac,[a] Cedric Blomme,[a] Janice R. Aldrich-Wright[b] and Alison Rodger*[a]

[a] *Department of Chemistry, University of Warwick, Gibbet Hill Road, Coventry, UK CV4 7AL. E-mail: m.j.hannon@warwick.ac.uk; a.rodger@warwick.ac.uk; Fax: (+44) 2476-524112*
[b] *Department of Chemistry, University of Western Sydney, N. S. W. 2560, Australia*

Received (in Cambridge, UK) 1st March 2001, Accepted 1st May 2001
First published as an Advance Article on the web 25th May 2001

Simple paper chromatography using brine as an eluent affords the two enantiomers of metallo-supramolecular triple-helicates. The technique may be scaled up for preparative resolution by using cellulose columns in conventional column chromatography.

We have recently described a facile route for assembly of metallo-supramolecular architectures from inexpensive commercial reagents.[1–3] One of the architectural motifs that we have prepared through this technology is a class of metallo-supramolecular helicates[1] that have a cylindrical architecture of similar dimensions to protein binding units that target the major groove of DNA.[2] Excitingly these synthetic tetracationic units also recognise the major groove of DNA and induce remarkable structural effects, wrapping up double-stranded DNA in an intramolecular fashion.[2] Such structural effects are unprecedented with synthetic DNA binders. Being helical, these supramolecular cylinders exist in two enantiomeric forms and we have been keen to resolve these as we anticipated that the DNA-binding of the two enantiomers might be quite different. There has been considerable recent interest in the resolution of metal complexes, much of which centres around resolution of DNA-binding metal polypyridyl complexes. The main techniques traditionally employed involve the use of chiral anions either to achieve diastereoselective crystallisation or as a component of a chiral chromatographic mobile phase.[4,5] Similar methods have also been applied to some polypyridyl and benzimidazole based metallo-helicates.[4,6]

We have attempted diastereoselective crystallisations of our supramolecular cylinders with a range of chiral anions without success. Chromatographic techniques have proved a little more successful, with some resolution being achieved on SP Sephadex C25 with aqueous disodium (−)-*O*,*O*′-dibenzoyl-(L)-tartrate solution as the mobile phase.[7] The deep purple colour of the bis iron(II) cylinder (arising from an MLCT transition) makes it very easy to follow by eye under chromatographic conditions. Although some resolution is apparent, passing these supramolecular cylinders down Sephadex columns did not lead to the formation of two discrete bands even after multiple cycles. Instead a broad, streaked band was obtained, the front and back of which contained enantio-excesses of the two respective helical isomers. Changing to other chiral anions (*e.g.* sodium *d*-antimonyltartrate, (*S*)-(+)-1,1′-binaphthyl-2,2′-diyl hydrogenphosphate) or to the other enantiomer of the chiral dibenzoyl tartrate anion did not seem to offer further improvement. Frustrated with these conventional chromatographic techniques, we considered whether DNA itself might be used to separate the two enantiomers. To use DNA as a stationary separation phase, we impregnated chromatographic paper with DNA following a previously outlined procedure,[8] and then added a racemic mixture of the di-iron cylinders. Washing the paper with ethanol afforded a solution containing an enantio-excess of one of the isomers (as evidenced by a strong CD spectrum). Solutions containing an excess of the other enantiomer could be obtained by extended washing of the residue with ethanol. Alternatively the DNA-impregnated paper could be used for chromatography using 0.16 M aqueous sodium acetate solution (pH 6.90) as eluent. This led to a spot remaining fixed to the baseline and a spot moving up the plate (associated with some streaking). Washing these two spots off the paper with ethanol gave solutions with opposite CD spectra. However, the solutions obtained from the DNA-impregnated paper technique showed an instability towards hydrolysis (as evidenced by the loss of the MLCT absorption signal over a period of hours), not observed with pure solutions of the compound, indicating that the procedure had introduced some reactive impurities.

Since paper itself is chiral (being essentially a cellulose derived product) we decided to examine whether the chiral fibres in paper might themselves be capable of affording separation. The compound was spotted onto Whatman 3MM CHR chromatography paper, and paper chromatography conducted with brine (aqueous 20 mM NaCl solution) as the eluent. To our surprise and delight the purple product split beautifully into two distinct spots as shown in Fig. 1. Washing the spots from the paper (with saturated aqueous sodium chloride followed by addition of ethanol) afforded solutions with opposite CD spectra (Fig. 2). The UV-Vis absorption and mass spectra of the solutions are identical, confirming that the chromatography is affording two enantiomers and not two otherwise alternate species. The solutions obtained by this method show no evidence of hydrolytic instability. This separation technique has been scaled up to allow preparative separation simply by using commercially available cellulose particles (~20 micron; Aldrich) as the stationary phase in a column and this allows ready resolution of the di-iron and di-nickel triple helical complexes.[9]

A survey of the chiral separation literature (Chirbase) seeking examples of metal complexes being separated on paper or cellulose, revealed that Dwyer and Sargeson[10] had used a

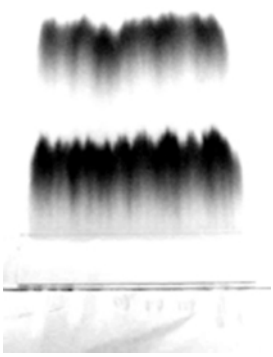

Fig. 1 Photograph of a paper chromatograph of the di-iron triple helical complex on Whatman 3MM CHR paper using 20 mM aqueous NaCl solution as the eluent.

 DOI: 10.1039/b101970h

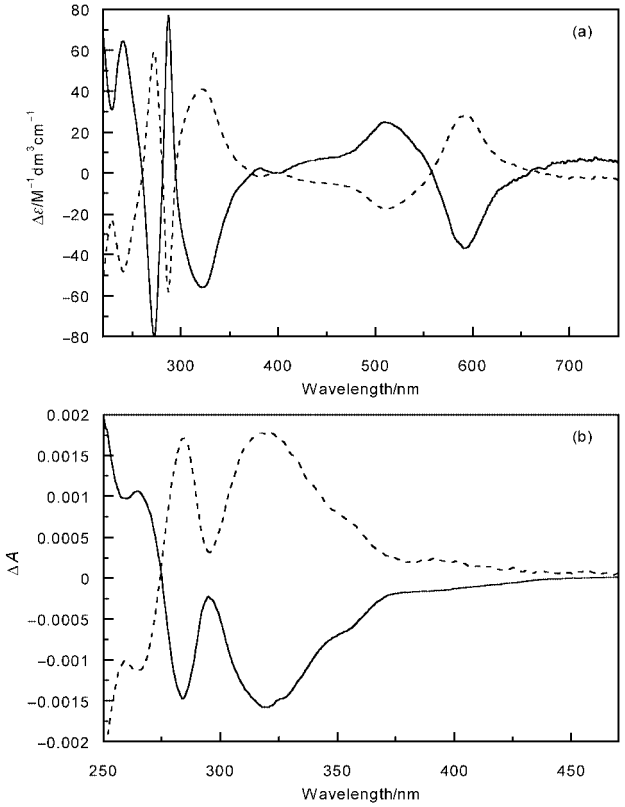

Fig. 2 CD spectra of the two bands eluted from the column for (a) the iron(II) complex ($\Delta\varepsilon$ determined using ε_{545} = 14000; The retention of one compound is significantly greater than the other and so the concentration of the eluted sample is lower for the retained enantiomer) and (b) the nickel(II) complex.

similar technique in 1963 to separate *diastereo*-isomers of cobalt(III) complexes with propane-1,2-diamine ligands but the technique does not subsequently appear to have been widely applied to the separation of enantiomeric metal complexes, although resolution of ruthenium polypyridyls on HPLC columns containing silica modified with cellulose derivatives has recently been described.[11]

We have shown that simple paper chromatography is a powerful method of separating the two enantiomers of our metallo-supramolecular helical cylinders, and that this can be extended to preparative scale resolution using cellulose columns. We are currently investigating the application of this technique to other metal complexes and other metallo-supramolecular architectures, and also investigating the DNA-binding of our resolved cylinders.

We thank the Leverhulme Trust (C.J.I.; F/125/BC), the University of Warwick (I. M.) and the EPSRC lifesciences initiative (GR/M91105) for support and acknowledge the Socrates/Erasmus programme for the exchange visit of C. B. from the University of Lille, France. We acknowledge use of the UK Chemical Database Service at Daresbury.

Notes and references

1 M. J. Hannon, C. L. Painting, J. Hamblin, A. Jackson and W. Errington, *Chem. Commun.*, 1997, 1807.
2 M. J. Hannon, V. Moreno, M. J. Prieto, E. Molderheim, E. Sletten, I. Meistermann, C. J. Isaac, K. J. Sanders and A. Rodger, *Angew. Chem., Int. Ed.*, 2001, **40**, 880.
3 M. J. Hannon, C. L. Painting and N. W. Alcock, *Chem. Commun.*, 1999, 2023; M. J. Hannon, S. Bunce, A. J. Clarke and N. W. Alcock, *Angew. Chem., Int. Ed.*, 1999, **38**, 1277; L. J. Childs, N. W. Alcock and M. J. Hannon, *Angew. Chem., Int. Ed.*, 2001, **40**, 1079.
4 See for example: U. Knof and A. von Zelewsky, *Angew. Chem., Int. Ed.*, 1999, **38**, 303; A. von Zelewsky, *Stereochemistry of Coordination Compounds*, Wiley, Chichester, 1996.
5 See for example: F. R. Keene, *Coord. Chem. Rev.*, 1997, **166**, 121; *Chem. Soc. Rev.*, 1998, **27**, 185.
6 L. J. Charbonniere, G. Bernardinelli, C. Piguet, A. M. Sargeson and A. F. Williams, *J. Chem. Soc., Chem. Commun.*, 1994, 1419; B. Hasenknopf and J.-M. Lehn, *Helv. Chim. Acta*, 1996, **79**, 1643; G. Rapenne, B. T. Patterson, J. P. Sauvage and F. R. Keene, *Chem. Commun.*, 1999, 1853; J. J. Jodry and J. Lacour, *Chem. Eur. J.*, 2000, **6**, 4297.
7 For this approach applied to ruthenium polypyridyl complexes see for example: T. J. Rutherford, P. A. Pellegrini, J. R. Aldrich-Wright, P. C. Junk and F. R. Keene, *Eur. J. Inorg. Chem.*, 1998, 1677.
8 J. R. Aldrich-Wright, I. Greguric, R. S. Vagg, K. Vickery and P. A. Williams, *J. Chromatography, A*, 1995, **718**, 436.
9 Solutions of the iron(II) complex from the column do not show rapid loss of CD signal indicating good stability and long racemisation lifetime (half-life > 3 months at RT).
10 F. P. Dwyer, T. E. MacDermott and A. M. Sargeson, *J. Am. Chem. Soc.*, 1963, **85**, 2913; see also F. Woldbye in *Technique of Inorganic Chemistry, Volume IV* ed. H. B. Jonassen and A. Weissberger, 1965; S. F. Mason *Molecular Optical Activity and the Chiral Discriminations*, Cambridge University Press, Cambridge, 1982.
11 D. Hesek, Y. Inoue, S. R. L. Everitt, H. Ishida, M. Kunieda and M. G. B. Drew, *Chem. Commun.*, 1999, 403. Cellulose-*derivatised* columns are widely used in chiral HPLC and many are commercially available.

CHEMCOMM
Communication
www.rsc.org/chemcomm

Ti–Pt intermetallic compound catalysts more active than Pt for hydrogen dissociation and ethylene hydrogenation

Takayuki Komatsu,* Daigo Satoh and Ayumu Onda

Department of Chemistry, Tokyo Institute of Technology, Meguro-ku, Tokyo 152-8550, Japan. E-mail: komatsu@chem.titech.ac.jp

Received (in Cambridge, UK) 14th March 2001, Accepted 30th April 2001
First published as an Advance Article on the web 25th May 2001

The intermetallic compound, $TiPt_3$, showed much higher catalytic activity than pure Pt catalyst for H_2–D_2 equilibration and ethylene hydrogenation, whereas Ti_3Pt only catalyzed the former reaction with a similar activity to $TiPt_3$.

Intermetallic compounds (IMCs) have unique crystal structures different from those of the component metals. However, the catalytic properties of IMCs have been scarcely studied except for those of so-called hydrogen storage alloys.[1] We have already reported unique catalytic selectivities of some IMCs, such as Co–Ge,[2] Pt–Ge[3,4] and Ni–Sn[5,6] compounds, in hydrogenation and dehydrogenation reactions. For example, Pt_3Ge gives butenes with high selectivity in the hydrogenation of buta-1,3-diene.[3] However, the activity of the above IMCs is always much lower than that of the pure metals, Co, Pt and Ni, because of their very low activity for the dissociation of hydrogen. For example, H_2–D_2 equilibration proceeds on Pt at 298 K, whereas a higher temperature of 523 K is necessary for Pt_3Ge to obtain a similar reaction rate.[3] The low activity of IMC catalysts probably results from their surface structure, that is, the active transition metal atoms are separated by the other element, *e.g.* Ge and Sn, which are almost inert towards the hydrogen dissociation reaction. However, IMCs between two transition metal elements might be expected to be active catalysts for reactions with hydrogen. In this study, we examined the catalytic activity of Ti–Pt IMCs for H_2–D_2 equilibration and the hydrogenation of ethylene and found that they had much higher activity than pure Pt catalyst.

IMC catalysts were prepared by arc melting a mixture of titanium (Soekawa Chemical, 99.9%) and platinum (Tanaka Kikinzoku, 99.95%) under an argon atmosphere. The resultant ingots were crushed in air and filtered into particles with diameters below 25 μm. Powders of pure Ti (Nilaco, 99.98%) and pure Pt (Nilaco, 99.98%) were also filtered into particles with similar diameters. The crystal structure of the IMCs was identified by powder X-ray diffraction (Rigaku, RINT 2400). Single-phase crystals of $TiPt_3$ and Ti_3Pt IMCs were obtained from mixtures with Ti/Pt atomic ratios of 1:3 and 3:1, respectively. The crystallinity of the TiPt IMC obtained from the mixture with Ti:Pt = 1 was not as good as those of $TiPt_3$ and Ti_3Pt. Therefore, we only examined the catalytic properties of $TiPt_3$ and Ti_3Pt as IMC catalysts. H_2–D_2 equilibration was carried out with a glass flow and circulation system connected with a quadrupole mass spectrometer (Spectra International, MICROVISION). Before each reaction, the catalyst was pretreated 'reduced' with flowing hydrogen at a specific temperature for 1 h and evacuated at 298 K for 10 min. A mixture of H_2 (6.6 kPa) and D_2 (6.6 kPa) was then circulated through the catalyst at the reaction temperature of 195 K and the formation of HD was monitored by mass spectrometry. Hydrogenation of ethylene was carried out with the same reaction apparatus. After the same pretreatment of the catalysts, a mixture of ethylene (2.7 kPa) and H_2 (13 kPa) was circulated through the catalyst at the reaction temperature of 251 K. The total pressure was monitored to measure the extent of reaction.

To measure the catalytic activity for the dissociation of hydrogen, the H_2–D_2 equilibration was carried out on $TiPt_3$, Ti_3Pt, Pt and Ti. Fig. 1 shows the fraction of HD in hydrogen as a function of reaction time. On Pt powder catalyst reduced at 573 K, the fraction of HD gradually increased with reaction time. When Pt was reduced at 873 K, the rate of HD formation drastically decreased owing to the agglomeration of the fine powder. It is clear that the surface of the Pt powder is reduced at 573 K and that metallic Pt catalyzed the dissociation of hydrogen at 195 K. On the other hand, Ti powder reduced at 573–1173 K did not catalyze hydrogen dissociation, probably because Ti is not reduced even at 1173 K.

For $TiPt_3$ reduced at 873 K, the rate of HD formation was much higher than that on Pt. SEM images showed that the Pt powder reduced at 573 K consisted of particles with diameters of *ca.* 3–5 μm partially agglomerating to form lumps of 10–25 μm diameter. On the other hand, the reduced $TiPt_3$ consisted of particles with diameters of 10–25 μm. From these observations, the specific surface area of $TiPt_3$ must be lower than that of Pt. Therefore, it is concluded that $TiPt_3$ has higher activity towards hydrogen dissociation than pure Pt. The higher activity of IMC catalysts than their component metals has not previously been reported in the H_2–D_2 equilibration.[2,3,5] The reduction temperature affected the activity of $TiPt_3$ *i.e.* a lower reaction rate was observed when $TiPt_3$ was reduced at 573 or 1173 K. At 573 K, Ti atoms on the surface of $TiPt_3$ would not be reduced completely. XPS measurements would clarify the oxidation state of surface Ti atoms. At 1173 K, $TiPt_3$ particles agglomerated to form large lumps, resulting in lower activity.

The other IMC, Ti_3Pt, reduced at 873 K, also exhibited a higher rate of HD formation than Pt. Its activity was similar to that of $TiPt_3$ reduced at 873 K. It is clear that Ti_3Pt also has a higher activity than Pt towards the dissociation of hydrogen. For Pt–Ge[3] and Ni–Sn[5] IMCs, the activity for the H_2–D_2 equilibration decreases with a decrease in content of Pt and Ni *i.e.* PtGe

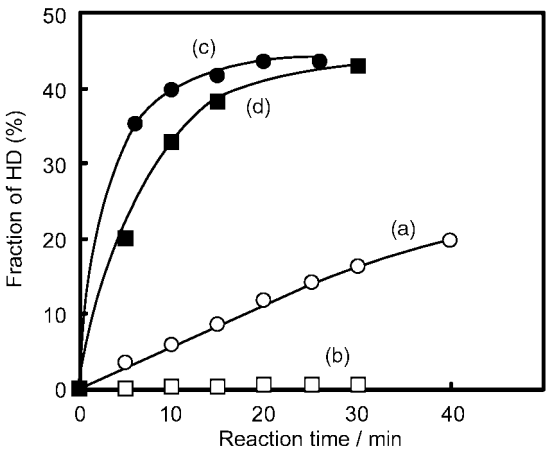

Fig. 1 H_2–D_2 equilibration at 195 K on Pt (a), Ti (b), $TiPt_3$ (c) and Ti_3Pt (d) reduced at 573 K (Pt), 873 K ($TiPt_3$ and Ti_3Pt) and 1173 K (Ti).

 DOI: 10.1039/b102415a

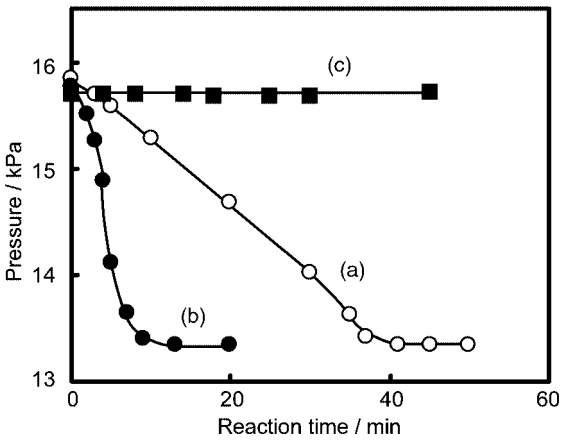

Fig. 2 Hydrogenation of ethylene at 251 K on Pt (a), $TiPt_3$ (b) and Ti_3Pt (c) reduced at 573 K (Pt) and 873 K ($TiPt_3$ and Ti_3Pt).

and Ni_3Sn_4 have much lower activity than Pt_3Ge and Ni_3Sn, respectively. Ge and Sn would retard the activity by reducing the number of adjacent Pt or Ni atoms. The comparable activity of Ti_3Pt to that of $TiPt_3$, which has a nine times larger Pt:Ti atomic ratio, suggests that a pair of Ti and Pt atoms constitutes an active site for the hydrogen dissociation. Reduction of Ti_3Pt at 573 and 1173 K resulted in low activity probably because of the same reasons as for $TiPt_3$.

On the basis of the above it is expected that $TiPt_3$ and Ti_3Pt would have higher activity than Pt for the hydrogenation of ethylene. Fig. 2 shows the change in total pressure with reaction time during the hydrogenation of ethylene at 251 K. On Pt reduced at 573 K, the pressure decreased with reaction time, indicating the consumption of hydrogen to form ethane and reached a steady state after 40 min of reaction. The decrease in pressure (*ca*. 2.5 kPa) suggests the complete conversion of ethylene into ethane. This was confirmed by gas-phase analysis with a gas chromatograph. On $TiPt_3$ reduced at 873 K, the pressure decreased more rapidly than that on Pt and gas-phase analysis revealed that the hydrogenation was complete in 10 min. This indicates that $TiPt_3$ has higher activity than Pt also for the hydrogenation of ethylene, as expected from its higher activity for the dissociation of hydrogen. On the other hand, Ti_3Pt reduced at 873 K did not catalyze the hydrogenation of ethylene at all, though it showed similar activity to $TiPt_3$ for the dissociation of hydrogen. In this case, Ti–Pt pair sites are not able to activate both ethylene and hydrogen.

The higher activity of Ti–Pt IMC catalysts than Pt suggests the possibility of other IMCs consisting of two transition metal elements of being highly active catalysts for hydrogenation and dehydrogenation reactions.

We gratefully thank Professor Takeyama for helping us to prepare the intermetallic compounds.

Notes and references

1 W. E. Wallace, *CHEMTECH*, 1982, **12**, 752.
2 T. Komatsu, M. Fukui and T. Yashima, *Stud. Surf. Sci. Catal.*, 1996, **101**, 1095.
3 T. Komatsu, S. Hyodo and T. Yashima, *J. Phys. Chem. B*, 1997, **101**, 5565.
4 T. Komatsu, M. Mesuda and T. Yashima, *Appl. Catal. A, Gen.*, 2000, **194–195**, 333.
5 A. Onda, T. Komatsu and T. Yashima, *Phys. Chem. Chem. Phys.*, 2000, **2**, 2999.
6 A. Onda, T. Komatsu and T. Yashima, *Chem. Commun.*, 1998, 1507.

CHEMCOMM
Communication
www.rsc.org/chemcomm

Hydrothermal synthesis of a thermally stable porous supramolecular π–π framework: $[\{Co_2(C_{12}H_8N_2)_4(\mu\text{-}C_4O_4)(OH_2)_2\}C_4O_4]\cdot 8H_2O$†

Szu-Fan Lai, Ching-Yuan Cheng and Kuan-Jiuh Lin*

Department of Chemistry, National Chung-Hsing University, Taichung, Institute of Chemistry, Academia Sinica, Taipei, Taiwan. E-mail: kjlin@dragon.nchu.edu.tw

Received (in Cambridge, UK) 25th January 2001, Accepted 23rd March 2001
First published as an Advance Article on the web 25th May 2001

The title compound was synthesized by hydrothermal methods and characterized by single-crystal X-ray diffraction, which reveals an open-framework structure containing dumbbell-shaped windows with hydrophilic and hydrophobic characteristics.

Crystalline porous materials such as aluminosilicates (zeolites), aluminophsphates, pillared clays, and other layers are widely used in catalyst and separation applications.[1,2] Recently, coordination polymers and organic networks sustained by coordinated covalent bonds and directional noncovalent interactions have become a rapidly expanding field. However, a major challenge in the highly porous coordination materials is their fragility. Unlike zeolites, which are held together with rugged covalent bonds, their solid molecules are glued with relatively weak intermolecular forces. To date the number of coordination networks with new structural aspects is increasing,[3–16] but to our knowledge thermally stable network structures sustained by π–π interactions are still rare or lacking.

Using polyfunctional squarates as molecular building blocks, we and other groups have prepared compounds that exist as supramolecular networks in the solid state.[13–15] We have recently focused our attention on introducing noncovalent interactions for constructing new classes of zeolite analogues possessing hydrophilic and hydrophobic void characteristics. In this present work, we report a supramolecular complex, $[\{Co_2(C_{12}H_8N_2)_4(\mu\text{-}C_4O_4)(OH_2)_2\}C_4O_4]\cdot 8H_2O$ **1**, that adopts a neutral open-framework structure with one-dimensional channels containing disordered water molecules.

Hydrothermal reaction of Co_3O_4, squaric acid, and 1,10-phenanthroline (phen) in molar ratios at 1:3:2 at 200 °C for 96 h in water produced crystals of **1**.‡ The X-ray structure analysis of **1** reveals an extended structure composed of the building-block units (Fig. 1).§ The discrete dinuclear cations, two octahedrally coordinated cobalt(II) centers bridged by a squarate ligand, are alternately connected squarate anions *via* hydrogen bonds to form infinite chains, $[\cdots C_4O_4\cdots\{Co(OH_2)_2\text{–}C_4O_4\text{–}Co(OH_2)_2\}\cdots]_n$, incorporating phen ligands (Fig. 2 arrows). The interatomic O···O distances between the ligated waters and the oxygen atoms of squarates are in the range 2.63–2.65 Å indicative of strong hydrogen bonds. The strength of the interionic hydrogen bonds of *ca*. 40–190 kJ mol^{-1} makes for the construction of more robust framework structures.[17] The infinite chains are further held together by the natural tendency of π overlap in phen molecules yielding a planar sheet [Fig. 2(a)]. A significant feature is that the planar sheets are stacked in three dimensions to give 'sinuous' channels with a dimension (phen to phen distances) of nearly 12 × 7 Å, in which free water molecules fill the dumbbell-shaped voids [Fig. 2(b)]. Thermogravimetric analysis (TGA) reveals that the guest water molecules are liberated below 100 °C, a weight loss of 8.73% consistent with the loss of eight water molecules in the

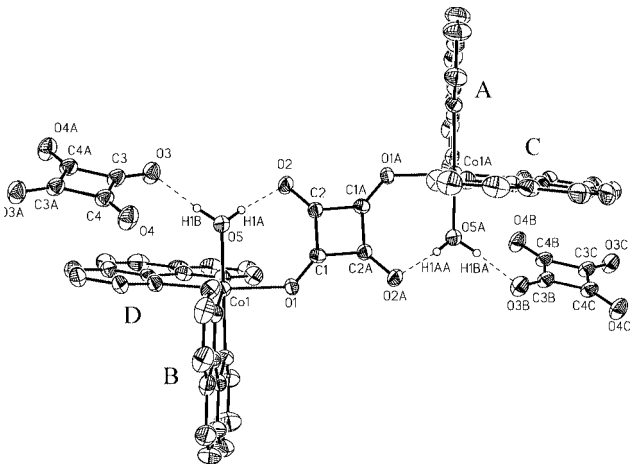

Fig. 1 ORTEP drawing of the building block units relating to the discrete μ-squarate-bridged cobalt(II) cations and squarate anions in **1** with thermal ellipsoids at 50% probability. A and B phen molecules induce the pair of in-planar-sheet π–π interactions while C and D induce the pair of out-of-planar-sheet π–π interactions. Selected bond distances (Å): Co(1)–O(5) 2.076(3), Co(1)–O(1) 2.118(2), C(1)–O(1) 1.256(4), C(2)–O(2) 1.252(4), C(3)–O(3) 1.261(4), C(4)–O(4) 1.257(4), O(5)–O(2) 2.649(3), O(5)–O(3) 2.634(3).

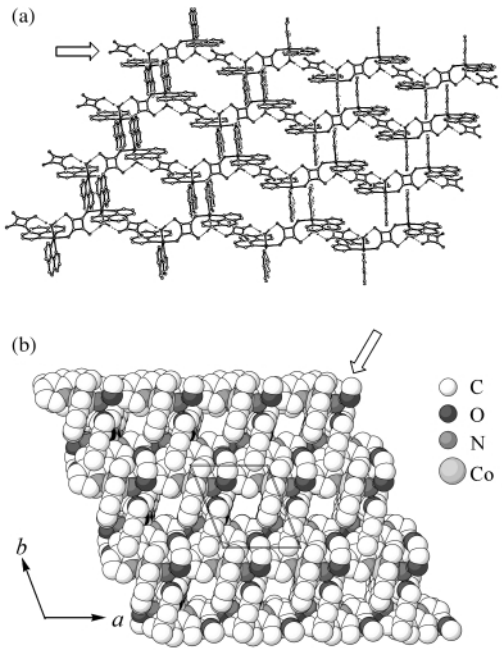

Fig. 2 (a) Ball-and-stick representation of the sheetlike network in **1**, showing the dumbbell-shaped windows (12 × 7 Å) with hydrophilic and hydrophobic characteristics; (b) perspective view of the open-framework structure containing one-dimensional channels along the crystallographic *c* axis. The arrows show the infinite hydrogen-bonding chains. Lattice water molecules are omitted for clarity.

† Electronic supplementary information (ESI) available: TGA curve for **1** and X-ray powder diffraction patterns. See http://www.rsc.org/suppdata/cc/b1/b100921o/

 DOI: 10.1039/b100921o

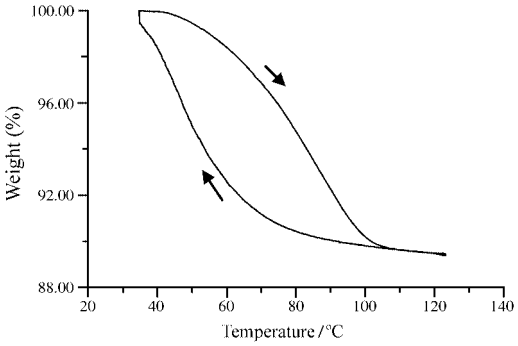

Fig. 3 TGA profile of a reversible N_2 adsorption–desorption cycle on **1**. The sample was initially heated at 120 °C for 0.5 h, cooled to 40 °C, maintained at 40 °C for 0.5 h, and then heated again to 120 °C.

channels. No weight loss was observed the temperature range 100–200 °C. The powder X-ray diffraction pattern of a sample heated to 200 °C for 2 h shows that the positions of the most intense lines remain unchanged relative to the simulated pattern based upon the single-crystal data. In order to examine the porous functionality of **1**, an N_2 adsorption–desorption study was conducted. Fig. 3 reveals a reversible N_2 adsorption–desorption cycle, which was confirmed by TGA with purified N_2 as the purging gas (2 atm). Besides demonstrating that the channel structure is retained throughout this process, this study also indicates that the cooperative π–π interactions are robust enough to sustain such an open space in crystals. Moreover, the most intriguing feature of the dumbbell-shaped windows is the presence of hydrophilic (the pendant C=O groups of squarates protrude into windows) and hydrophobic (phen groups) void characteristics that have a natural affinity for organic molecules. Further experiments to explore whether this nanoporous material can be filled by organic guests are in progress.[18]

This work was supported by the National Science Council of the Republic of China (NSC 89-2113-M-005-021) and the Chinese Petroleum Corporation (NSC 89-CPC-7-005-002).

Notes and references

‡ *Synthesis* of **1**: a mixture of Co_3O_4 (0.1204 g, 0.51 mmol), squaric acid (0.1743 g, 1.53 mmol), phen (0.2018 g, 1.02 mmol), CsOH (0.3 mL, w/w 50%) and H_2O was sealed in a Teflon-lined stainless autoclave (23 mL), heated at 200 °C for four days, and cooled to 80 °C at 6 °C h^{-1}. Needle-shaped orange–yellow crystals of **1** and unidentified black materials were filtered off. Additionally, allowing the deep-orange filtrate to stand at room temperature for one week also gave crystals of **1** (yield: 10%). Elemental analysis (%): calc. C 54.13, N 9.01, H 4.18, O 23.17; found: C 53.20, N 8.52, H 4.17, O 22.72.

§ *Crystal data* for $C_{56}H_{52}Co_2N_8O_{18}$, **1**: M = 1242.92, triclinic, space group $P\bar{1}$, a = 9.918(3), b = 11.292, c = 13.276(4) Å, α = 93.33(2), β = 101.21(3), γ = 110.44(2)°, V = 1353.8(7) Å^3, Z = 1, D_c = 1.525 g cm^{-3}, μ(Mo-Kα, λ = 0.71069 Å) = 6.97 cm^{-1}, $2\theta_{max}$ = 50°. Of the 4982 reflections collected 4757 unique reflections (R_{int} = 0.028) were used in all calculations after Lorentz polarization and empirical absorption corrections; R_1 = 0.041 for 2802 reflections with $I > 2.0\sigma(I)$; $wR_2(F^2)$ 0.121 (all data), GOF = 0.925, residual electron density between −0.32 and 0.35 e Å^{-3}.

CCDC 144421. See http://www.rsc.org/suppdata/cc/b1/b100921o/ for crystallographic data in .cif or other electronic format.

1 M. E. Davis, *Chem. Eur. J.*, 1997, **3**, 1745.
2 J. M. Thomas and W. J. Thomas, *Principles and Practice of Hetergeneous Catalysis*, Weinkeim, VCH, 1996.
3 H. Li, A. Laine, M. O'Keefe and O. M. Yaghi, *Science*, 1999, **283**, 1145.
4 O. M. Yaghi, G. Li and H. Li, *Nature*, 1995, **378**, 703.
5 D. Venkataraman, S. Lee, J. Zhang and J. S. Moore, *Nature*, 1994, **371**, 591.
6 S. S.-Y. Chui, S. M.-F. Lo, J. P. H. Charmant, A. G. Orpen and I. D. Williams, *Science*, 1999, **283**, 1148.
7 G. B. Gardner, D. Venkataraman, J. S. Moore and S. Lee, *Nature*, 1995, **374**, 792.
8 H. Li, M. Eddaoudi, M. O'Keeffe and O. M. Yaghi, *Nature*, 1999, **402**, 276.
9 J. S. Seo, D. Whang, H. Lee, S. I. Jun, J. Oh, Y. J. Jeon and K. A. Kim, *Nature*, 2000, **404**, 982.
10 L. J. Barbour, G. W. Orr and J. L. Atwood, *Nature*, 1998, **393**, 671.
11 P. Brunet, M. Simard and J. D. Wuest, *J. Am. Chem. Soc.*, 1997, **119**, 2737.
12 V. A. Ruswll, C. C. Evans, W. Li and M. D. Ward, *Science*, 1997, **276**, 575.
13 K. J. Lin and K. H. Lii, *Angew. Chem., Int. Ed. Engl.*, 1997, **36**, 2076.
14 S. O. H. Gutschke, M. Molinier, A. K. Powell and P. T. Wood, *Angew. Chem., Int., Ed. Engl.*, 1997, **38**, 991.
15 C. R. Lii, C. C. Wang and Y. Wang, *Acta Crystallogr., Sect. B*, 1996, **118**, 7128.
16 K. J. Lin, *Angew. Chem., Int. Ed. Engl.*, 1999, **38**, 2370.
17 K. J. Lin, M. J. Cheng and Y. Wang, *J. Phys. Chem.*, 1994, **98**, 11 685; C. B. Aakerroy and K. R. Seddon, *Chem. Soc. Rev.*, 1993, 397.
18 This material also reveals thermochromic as well as vaporchromic data that will be published elsewhere.

CHEMCOMM
Communication
www.rsc.org/chemcomm

Construction of 3d–4f heterometallic coordination polymers by simultaneous use of hexacyanometalate building-blocks and exo-bidentate ligands

Stefania Tanase,[a] Marius Andruh,*[a] Achim Müller,*[b] Marc Schmidtmann,[b] Corine Mathonière[c] and Guillaume Rombaut[c]

[a] *University of Bucharest, Faculty of Chemistry, Inorganic Chemistry Laboratory, Str. Dumbrava Rosie nr. 23, 70254-Bucharest, Romania. E-mail: marius.andruh@dnt.ro*
[b] *Fakultät für Chemie der Universität, D-33501 Bielefeld, Germany*
[c] *Laboratoire des Sciences Moléculaires, Institut de Chimie de la Matière Condensée de Bordeaux, 33608 Pessac, France*

Received (in Cambridge, UK) 31st January 2001, Accepted 27th April 2001
First published as an Advance Article on the web 25th May 2001

The reaction of $Pr(NO_3)_3{\cdot}6H_2O$ with 4,4′-bipyridine *N,N′*-dioxide (L) and $K_3[M(CN)_6]$ [M = Fe^{III}, Co^{III}] gives isomorphous heteropolynuclear complexes with formula $[\{(H_2O)_5LPr–NC–M(CN)_5\}(\mu\text{-}L)]{\cdot}0.5L{\cdot}4H_2O$, which exhibit a novel supramolecular architecture created by the interplay of coordinative, hydrogen bonding and π–π stacking interactions.

The design of supramolecular polymetallic architectures with novel topologies of the spin carriers is of current interest in the field of molecular magnetism. A successful strategy leading to heteropolymetallic systems with extended structures consists in self-assembly processes involving anionic building-blocks (templates), which contain a paramagnetic ion, and assembling complex cations with potentially free coordination sites. Terminal cyano groups act as efficient bridging ligands, promoting strong ferro- or antiferro-magnetic interactions between adjacent metal ions.[1] The homoleptic cyanometalates, $[M(CN)_6]^{3-}$ (M = Cr^{III}, Fe^{III}),[2] and, recently, $[Mo^{III}(CN)_7]^{4-}$ and $[W(CN)_8]^{3-}$,[3,4] are among the most employed building-blocks and generate an extremely rich coordination chemistry.

In the past decade, a plethora of cyano-bridged bimetallic systems with interesting architectures and spectacular magnetic and photomagnetic properties have been characterized.[1–4] Most of these systems contain either two different 3d metal ions, or a 3d and a 4d/5d transition metal ion. In contrast, the lanthanide cations have been rarely used as nodes for the construction of cyano-bridged heteropolymetallic coordination networks. The following families of cyano-bridged lanthanide–transition metal complexes, exhibiting extended structures, have been obtained by using homoleptic cyanometalates as templates: (a) $LnM^{III}(CN)_6{\cdot}nH_2O$ (M^{III} = Cr^{III}, Fe^{III}, Co^{III}, Ru^{III}, Ir^{III});[5] (b) $KLnM^{II}(CN)_6{\cdot}nH_2O$ (M^{II} = Fe^{II}, Ru^{II});[6] (c) $Ln_2[M^{II}(CN)_4]_3{\cdot}nH_2O{\cdot}m$DMF ($M^{II}$ = Ni^{II}, Pd^{II}, Pt^{II});[7] (d) one-dimensional chain complexes with the general formula $[LnL_2(H_2O)_m\text{-}Fe^{III}(CN)_6]{\cdot}nH_2O$ (Ln = Gd, L = betaine, m = 3, n = 0;[8] Ln = Sm, L = dimethylacetamide, m = 4, n = 5[9]).

Very recently, Champness and coworkers have characterized interesting 2- and 3-D coordination framework polymers of Er^{III} and Sm^{III}, which have been obtained by using 4,4′-bipyridine *N,N′*-dioxide as a bridging ligand.[10] Surprisingly, in comparison with other divergent ligands (*e.g.* 4,4′-bipyridine), the potentialities of 4,4′-bipyridine *N,N′*-dioxide in the construction of coordination networks and crystal engineering have been little exploited.[11,12]

Aiming to combine the bridging ability of the cyano groups with that of 4,4′-bipyridine *N,N′*-dioxide (L), we have obtained two isomorphous heterometallic compounds, $[\{(H_2O)_5Pr–NC–M(CN)_5\}(\mu\text{-}L)L]{\cdot}0.5L{\cdot}4H_2O$ (M = Fe^{III}, **1**; Co^{III}, **2**), with a novel supramolecular architecture.

The two complexes were obtained by mixing aqueous solutions of $Pr(NO_3)_3$ and $K_3[M(CN)_6]$ (M = Fe, Co) with an ethanolic solution of 4,4′-bipyridine *N,N′*-dioxide.† FTIR spectra show characteristic bands of bridging and terminal cyano groups: 2144, 2065 cm^{-1} (**1**); 2142, 2076 cm^{-1} (**2**).

The crystal structures of **1** and **2** have been solved.‡ Since the cobalt derivative **2**§ is isomorphous with **1**, only the structure of the iron derivative **1** is described here. The supramolecular order at the nanometric scale of $[\{(H_2O)_5LPr–NC–Fe(CN)_5\}(\mu\text{-}L)]{\cdot}0.5L{\cdot}4H_2O$ is created by an interesting interplay of coordinative, hydrogen bonding and π–π stacking interactions. The structure can be described as being formed by $\{(H_2O)_5LPr–NC–Fe(CN)_5\}$ neutral binuclear entities, which are bridged by 4,4′-bipyridine *N,N′*-dioxide, resulting in infinite zigzag chains (Fig. 1). Within the binuclear moieties, the $[Fe(CN)_6]^{3-}$ anion acts as a monodentate ligand, that is, with one CN^- group coordinated to the praseodymium atom [Pr–N 2.636(2) Å]. The Fe–CN–Pr linkage is slightly angular [C–N–Pr 162.87(16)°], with a Fe···Pr distance of 5.664 Å. Three 4,4′-bipyridine *N,N′*-dioxide molecules are directly bonded to one Pr^{III} atom. Two form bridges between the praseodymium atoms, while the third acts as a terminal ligand. The Pr^{III} ion exhibits a coordination number of nine: eight oxygen atoms, arising from five aqua and three L ligands, and one nitrogen atom from the cyano bridge. The Pr–O distances vary between 2.406(1) and 2.518(1) Å. The praseodymium atoms are alternately 'bridged' through intra-chain hydrogen bonds involving uncoordinated 4,4′-bipyridine *N,N′*-dioxide molecules and the aqua ligands (Fig. 1). The distance between the triply 'bridged' praseodymium atoms (13.439 Å) is slightly shorter than that between the simply bridged atoms (13.937 Å).

The terminal organic ligands further extend the structure *via* π–π stacking interactions with identical terminal L ligands from adjacent zigzag chains, resulting in brick wall-like sheets (Fig. 2). The distances associated with the ligand-to-ligand π–π interactions are in the range 3.47–3.51 Å. The perfect face-to-face π-stacked alignment of the peripheral pyridyl *N*-oxide moieties of the terminal ligands is clearly favored by dipole–dipole interactions.[13] The uncoordinated 4,4′-bipyridine *N,N′*-dioxide molecules play a special role in increasing the dimensionality of the supramolecular architecture. Each uncoordinated molecule is simultaneously hydrogen bonded to four aqua ligands, two of these being coordinated to two adjacent praseodymium atoms in a chain, while the other two aqua ligands arise from another chain belonging to a neighboring brick wall sheet (Fig. 3).

The cryomagnetic properties of **1** have been investigated between 2 and 300 K. The value of $\chi_M T$ at room temperature (2.15 $cm^3\ mol^{-1}$ K) roughly corresponds to the expected value for an uncoupled low-spin Fe^{III}(S = ½)–Pr^{III}(J = 4) system.

 DOI: 10.1039/b101070k

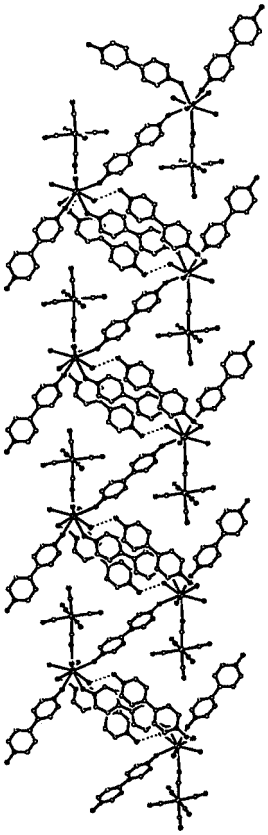

Fig. 1 Perspective view of a zigzag chain, also showing the uncoordinated 4,4′-bipyridine *N,N′*-dioxide molecules, which are hydrogen bonded to the aqua ligands coordinated to two praseodymium atoms. Along a chain, the praseodymium atoms are alternately simply and triply bridged (one genuine bridge and two $OH_2\cdots$4,4′-bipyridine *N,N′*-dioxide$\cdots H_2O$ 'bridges').

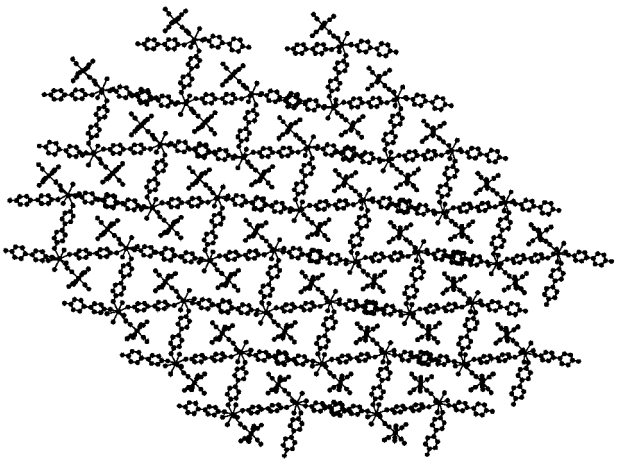

Fig. 2 Packing diagram of compound **1** showing the brick wall-like backbone resulting from π–π stacking interactions between the terminal ligands belonging to different chains. The uncoordinated 4,4′-bipyridine *N,N′*-dioxide molecules, as well as the crystallization water molecules, have been omitted.

The high temperature limit of $\chi_M T$ is calculated using the equation $(\chi_M T)_{HT} = (Ng_{Fe}^2\beta^2/3k)[S_{Fe}(S_{Fe} + 1)] + (Ng_{Pr}^2\beta^2/3k)[J_{Pr}(J_{Pr} + 1)]$, which gives $(\chi_M T)_{HT} = 1.98$ cm^3 mol^{-1} K. The difference between the experimental and calculated values is due to the intervention of the first-order orbital momentum associated with low-spin Fe^{III}. Upon lowering the temperature, $\chi_M T$ decreases continuously reaching 0.40 cm^3 mol^{-1} K at 2 K.

Since both Pr^{III} and low-spin Fe^{III} ions show a temperature dependence for $\chi_M T$,[14] this system is not appropriate for the accurate investigation of the 3d–4f magnetic interaction. However, these complexes open new perspectives to the magnetochemistry of 3d–4f cyano-bridged systems. Further work on similar compounds, especially on those containing Cr^{III} and Gd^{III} ions, both without orbital contributions to the magnetic susceptibility, is in progress and will be presented in subsequent papers.

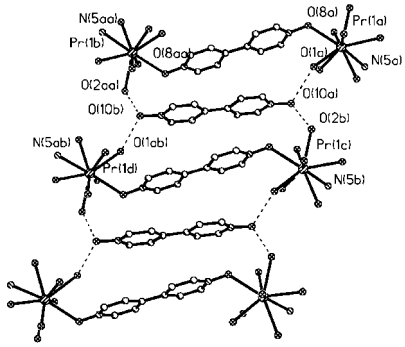

Fig. 3 Hydrogen bond interaction between the uncoordinated 4,4′-bipyridine *N,N′*-dioxide molecule and four aqua ligands arising from two different chains: O(10a)$\cdots$O(1a) 2.832 Å, O(10a)$\cdots$O(2b) 2.739 Å.

This work was supported by the Romanian Council of Scientific Research, CNCSIS, Grants no. 1-D and 30-C.

Notes and references

† *Synthesis*: compounds **1** and **2** were obtained following the same general procedure: to an aqueous solution (20 mL) containing 0.4 mmol $K_3[M(CN)_6]$ and 0.4 mmol $Pr(NO_3)_3\cdot 6H_2O$ was added an ethanolic solution (10 mL) of 4,4′-bipyridine *N,N′*-dioxide (1.4 mmol). Slow evaporation of the resulting mixtures led to orange crystals of **1** and yellowish–green crystals of **2**. Correct elemental chemical analysis.

‡ *X-Ray structure determination*: *crystal data* for **1**: $C_{31}H_{38}FeN_{11}O_{14}Pr$, M = 985.48, triclinic, space group $P\bar{1}$, a = 8.3607(2), b = 15.4388(4), c = 15.4924(4) Å, α = 84.780(1), β = 80.671(1), γ = 85.655(1)°; V = 1961.32 Å^3, Z = 2, D_c = 1.669 g cm^{-3}, μ = 1.677 mm^{-1}, $F(000)$ = 996. Crystals of **1** were measured at 183(2) K on a Bruker AXS SMART diffractometer (Mo-Kα radiation monochromator). A total of 28265 of reflections ($1.33 < \theta < 30.01°$) were collected of which 11383 unique reflections (R_{int} = 0.0182) were used. The structure was solved using the program SHELXS-97 and refined using the program SHELXL-93 to $R1$ = 0.0236, $wR2$ = 0.0637 for 10330 reflections with $I > 2\sigma(I)$ and $R1$ = 0.0282, $wR2$ = 0.0727 (all data). CCDC 158134. See http://www.rsc.org/suppdata/cc/b1/b101070k/ for crystallographic data in CIF or other electronic format.

§ *Crystal data* for **2**: a = 8.375, b = 15.410, c = 15.420 Å, α = 84.88, β = 80.66, γ = 85.63°.

1 See, for example: S. Ferlay, T. Mallah, R. Ouhès, P. Veillet and M. Verdaguer, *Nature*, 1995, **378**, 701; K. R. Dumbar and R. A. Heintz, *Progr. Inorg. Chem.*, 1997, **45**, 283; S. M. Holmes and G. S. Girolami, *J. Am. Chem. Soc.*, 1999, **121**, 5593.

2 M. Ohba and H. Okawa, *Coord. Chem. Rev.*, 2000, **198**, 313 and references therein.

3 See, for example: O. Kahn, J. Larionova and L. Ouahab, *Chem. Commun.*, 1999, 945; A. K. Sra, M. Andruh, O. Kahn, S. Golhen, L. Ouahab and J. V. Yakhmi, *Angew. Chem., Int. Ed.*, 1999, **38**, 2606.

4 Z. J. Zhong, H. Seino, Y. Mizobe, M. Hidai, A. Fujishima, S. Ohkoshi and K. Hashimoto, *J. Am. Chem. Soc.*, 2000, **122**, 2952.

5 See, for example: D. F. Mullica, F. H. Alvarez and E. L. Sappenfield, *J. Solid State Chem.*, 1997, **129**, 12.

6 D. F. Mullica, P. K. Hayward and E. L. Sappenfield, *Inorg. Chim. Acta*, 1996, **253**, 97.

7 B. Du, E. A. Meyers and S. G. Shore, *Inorg. Chem.*, 2000, **39**, 4639 and references therein.

8 B. Yan and Z. D. Chen, *Chem. Lett.*, 2000, 1244.

9 B. Yan, H. D. Wang and Z. D. Chen, *Inorg. Chem. Commun.*, 2000, **3**, 653.

10 D.-L. Long, A. J. Blake, N. R. Champness and M. Schröder, *Chem. Commun.*, 2000, 1369.

11 D.-L. Long, A. J. Blake, N. R. Champness and M. Schröder, *Chem. Commun.*, 2000, 2273.

12 S. Bruda, M. Andruh, H. W. Roesky, Y. Journaux, M. Noltemeyer and E. Rivière, *Inorg. Chem. Commun.*, 2001, **4**, 111.

13 C. Janiak, *J. Chem. Soc., Dalton Trans.*, 2000, 3885.

14 O. Kahn, *Molecular Magnetism*, VCH, New York, 1993.

CHEMCOMM Communication
www.rsc.org/chemcomm

Aldol-type carbon bond formation of ethereal oxonium ylide†

Yuichi Sawada, Takashi Mori and Akira Oku*

Department of Chemistry and Materials Technology, Kyoto Institute of Technology, Matsugasaki, Sakyo-ku, Kyoto 606-8585, Japan. E-mail: oku@ipc.kit.ac.jp

Received (in Cambridge, UK) 8th March 2001, Accepted 2nd May 2001
First published as an Advance Article on the web 25th May 2001

The Rh(2)-catalyzed reaction of 2-(3-diazo-1,1-dimethyl-2-oxopropyl)-2-methyldioxolane (1b) with arylaldehyde in the presence of $(Me)_3SiCl$ and $Ti(i\text{-}PrO)_4$ gave 2-aryl-(hydroxy)methyl-8,8-dimethyl-7-methylene-3,6-dioxocane-1-one (6) and 2-aryl(hydroxy)methyl-4-(2-chloroethoxy)-4,5,5-trimethyl-3-oxacyclopentanone (7); these are the first examples of C–C bond formation of ethereal oxonium ylide *via* enol silyl ether intermediates.

In general, when the ambiphilic character of onium ylides is properly controlled by imparting a relatively long lifetime, consecutive C–C bond formation on the carbanion can be realized as already exemplified widely by phosphonium and sulfonium ylides.[1,2]

However, similar bond formations have not been reported for ethereal oxonium ylides. This is probably because their extremely short lifetime[3] kinetically retards electrophilic attack by ordinary carbon electrophiles. Despite this defect, the [1,*n*]-ambiphilicity of intramolecularly formed bicyclic O-ylide, *e.g.* **8**, will enable the ylide to react with carbon electrophiles under appropriate conditions such as, for example, transforming the ylide to a more stable intermediate which retains the nucleophilic character of the ylide and also the use of a Lewis acid.

As the study model of this reaction, we chose the transition metal-catalyzed reaction of diazo ketones bearing a cyclic acetal ring to be carried out in the presence of a silyl reagent.[4] This is because we recently found evidence that bicyclic oxonium ylide, generated from a diazoketone-substituted cyclic acetal, was transiently transformed by the action of chlorotrimethylsilane (Me_3SiCl) to the corresponding enol silyl ether as evidenced by the chlorosilane-catalyzed ring-expansion reaction (Scheme 1, *route 1*).[5] On this basis, we expected that the intermediate enol ether would react with a carbon electrophile, particularly in the presence of an appropriate acid catalyst, to give a C–C bonded adduct (*route 2*). Considering chlorosilane as the acid-catalyst,[6] we designed a one-pot reaction of diazocarbonyl-substituted cyclic acetals with aldehydes in hope of realizing the aldol-type C–C bond formation in conjunction with a ring-enlargement reaction. In this paper we would like to report the first example of the C–C bond formation of ethereal oxonium ylide.

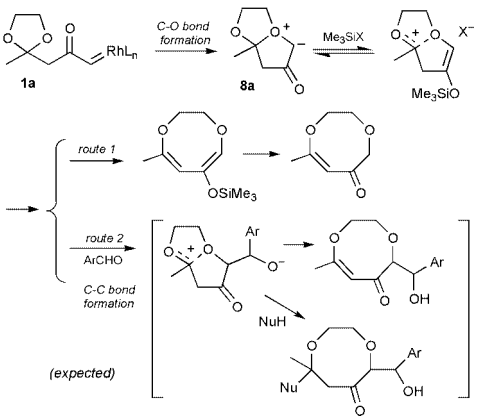

Scheme 1

As the model compounds to be studied, dioxolane-substituted diazoketones **1a** and **1b** were prepared.[4b] First of all, as a standard reaction, Rh(2)-catalyzed reaction of **1a** was performed in the presence of benzaldehyde (3 eq.) but in the absence of chlorosilane reagents. Products obtained were the [1,2]-rearrangement product **2a** and ring-expansion product **3** (Table 1, entry 1), but none of the expected aldol-type products, *e.g.* **6** and **7**. Introducing an electron-withdrawing group to the *para*-position of arylaldehyde was also unsuccessful (entry 2). Thus, the direct reaction of oxonium ylide with aldehyde is much slower than the [1,2]-rearrangement giving **2a** and β-elimination giving **3**. To suppress the rearrangement, Me_3SiCl[7] was added to trap the ylide intermediate and, in fact, remarkably promoted the ring-expansion to give **3** (entry 3).[8] This indicates that Me_3SiCl promotes the β-elimination (ring-expansion) of ylide **8a** whereas it suppresses the [1,2]-rearrangement,[9] when the ylide has enolizable hydrogens at the 4-position of 1-oxonium-6-oxabicylo[3.3.0]octan-3-one (**8a**).

Based on this finding a similar reaction with **1b**, which bears two methyl substituents on the side chain, was examined in expectation of suppressing the enone formation. When benzaldehyde or anisaldehyde was used as the electrophile, the expected C–C bond formation between the ylide and aldehyde did not take place but, instead, ring-expansion product **4** and ring-switching product **5** were obtained (entries 4 and 5). However, with *p*-nitrobenzaldehyde, the expected C–C-bonded products **6d** and **7d** were obtained (entry 6) (Scheme 2). Both were unequivocally formed by the aldol-type reaction between the aldehyde and oxonium ylide **8b** or its enol silyl ethers **10b** and **11b** (Scheme 3). The reaction was highly stereoselective because **6d** and **7d** were formed as a single diastereoisomer.[10] At low temperature (entry 7), although product yields were not improved, ring-expansion product **6d** was suppressed to some

Table 1 Rh(2)-catalyzed reaction of **1** with aldehyde and Me_3SiCl

Entry	Substrate	*Ar*CHO	Lewis acid (mol%)	Products (%)	
1[a]	**1a**	C_6H_5	—	**2a**(15)	**3**(7)
2[a]	**1a**	*p*-$NO_2C_6H_4$	—	**2a**(49)	**3**(35)
3	**1a**	*p*-$NO_2C_6H_4$	—		**3**(91)
4	**1b**	C_6H_5	—	**4**(18)	**5**(14)
5	**1b**	*p*-$MeOC_6H_4$	—	**4**(20)	**5**(14)
6	**1b**	*p*-$NO_2C_6H_4$	—	**6**(54)	**7**(7)
7[b]	**1b**	*p*-$NO_2C_6H_4$	—	**4**(4)	**5**(6)
				6(27)	**7**(8)
8	**1b**	*p*-CNC_6H_4	—	**4**(4)	**5**(6)
				6(38)	**7**(3)
9	**1b**	*p*-$MeOC_6H_4$	$Ti(iPrO)_4$(5)	**6**(25)	**7**(56)
10	**1b**	*p*-$MeOC_6H_4$	$Al(t\text{-}BuO)_3$(5)	**4**(—)	**5**(4)
				6(11)	**7**(17)
11	**1b**	C_6H_5	$Ti(iPrO)_4$(5)	**6**(27)	**7**(32)

[a] Me_3SiCl was not used. In other runs, amount of Me_3SiCl used was 3 mol eq. *vs.* 1. [b] At −40 °C.

† Electronic supplementary information (ESI) available: experimental details, ^1H NMR spectra and ^{13}C NMR spectral data of compounds **1b**, **2b**, **4**–**7**. See http://www.rsc.org/suppdata/cc/b1/b102248m/

 DOI: 10.1039/b102248m

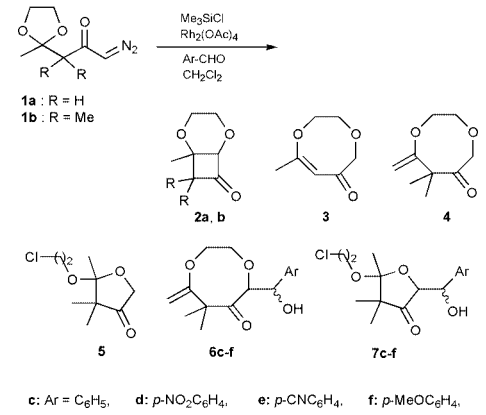

Scheme 2

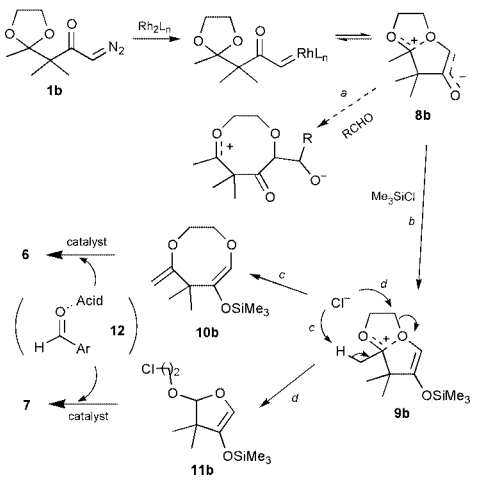

Scheme 3

extent, indicating that the ring-expansion from the bicyclo[3.3.0] system to an eight-membered ring requires a higher activation energy than the S_N2 attack by Cl^- ion (Scheme 3). Similarly, with *p*-cyanobenzaldehyde C–C-bonded products **6e** and **7e** were again obtained (entry 8).

Not only benzaldehydes bearing withdrawing groups but also unsubstituted benzaldehyde and even anisaldehyde afforded similar C–C bonded products provided that an appropriate Lewis acid was used in addition to $Rh_2(OAc)_4$ and Me_3SiCl (entries 9–11). Among several Lewis acids examined, Ti(*i*-OPr)$_4$ was the most appropriate for this reaction. Stereoselectivity of the C–C bond formation in the presence of Lewis acid, however, was not so high as was observed with electron-deficient aldehydes without Lewis acid (*vide supra*). Thus, two isomers were formed for **6f** in which the isomer ratio was *anti*/*syn* = 2.5, whereas for **7f** it was 2.0.

Kanemasa and coworkers recently reported that, in the presence of trimethylsilyl triflate or $ZnCl_2$–Me_3SiCl, ethyl diazoacetate reacts with aldehyde to give a β-keto ester.[11] In the Rh-catalyzed reaction of **1b**, however, a similar diketone was not obtained indicating that **1b** cannot react directly with aldehyde but only *via* oxonium ylide **8b** (Scheme 3).

In Scheme 3, route *a* shows direct nucleophilic attack of ylide **8b** on aldehyde, but that this did not occur is evidenced by the negative results obtained in the absence of Me_3SiCl (Table 1, entries 1 and 2). Route *b* shows an indirect route to the C–C bond formation from **8b** *via* enol silyl ethers **10b** and **11b**. First, oxonium ion intermediate **9b** may be formed from **8b**. Subsequently, conjugate base Cl^- attacks **9b** on either the bridgehead methyl group for abstracting proton (route *c*) or the methylene group of the acetal ring in an S_N2 manner (route *d*), cleaving C–O bonds, to give **10b** or **11b**, respectively. Hydrogen chloride, generated from the proton abstraction process, acts as an acid-catalyst to activate aldehydes and enol silyl ethers as well to undergo the aldol-type C–C bond-forming reaction.[12] This was verified by the finding that addition of Et_3N to the reaction with nitrobenzaldehyde suppressed the formation of **6d** and **7d**. Another possible route to **6** or **7** by the reaction of **4** or **5** with aldehyde was ruled out by the negative result of independent treatment of **4** or **5** with nitrobenzaldehyde in the presence of Me_3SiCl.

In conclusion, the formation of **6** and **7** can be attributed to the aldol-type reaction between aldehyde and enol silyl ethers **10b** and **11b**, both derived from ylide **8b**, in that not only Lewis acids but also Me_3SiCl act as the catalyst. To expand the scope of C–C-bond formation of ethereal oxonium ylides, further study will be needed.

This study was supported by a Grant-in-Aid for Scientific Research on Priority Areas (B) 'Dynamic Control of Stereochemistry', No. 10208203.

Notes and references

1 K. Kondo, I. Tabushi, R. Noyori and S. Fujita, *Carbene, Ylides, Nitrenes and Benzynes*, ed. T. Goto, Hirokawa, Tokyo, 1976; M. P. Doyle and D. C. Forbes, *Chem. Rev.*, 1998, **98**, 911.
2 A. Padwa and S. F. Hornbuckle, *Chem. Rev.*, 1991, **91**, 263; T. Ye and M. A. Mckervey, *Chem. Rev.*, 1994, **94**, 1091; A. Padwa and M. D. Weingarten, *Chem. Rev.*, 1996, **96**, 223.
3 I. Naito, A. Oku, N. Ohtani, Y. Fujiwara and Y. Tanimoto, *J. Chem. Soc., Perkin Trans. 2*, 1996, 725; H. Tomioka, N. Kobayashi, S. Murata and T. Ohtawa, *J. Am. Chem. Soc.*, 1991, **113**, 8771.
4 For the ring-expansion of bicyclic oxonium ylides, see: (*a*) A. Oku, S. Ohki, T. Yoshida and K. Kimura, *Chem. Commun.*, 1996, 1077; (*b*) A. Oku, N. Murai and J. Baird, *J. Org. Chem.*, 1997, **62**, 2123; (*c*) T. Mori, M. Taniguchi, F. Suzuki, H. Doi and A. Oku, *J. Chem. Soc., Perkin Trans. 1*, 1998, 3623.
5 T. Mori and A. Oku, *Chem. Commun.*, 1999, 1339.
6 The Lewis acid character of silyl cation is described in: S. Murata, M. Suzuki and R. Noyori, *J. Am. Chem. Soc.*, 1980, **102**, 3248; H. Sakurai, K. Sasaki and A. Hosomi, *Bull. Chem. Soc. Jpn.*, 1983, **56**, 3195; T. Sato, Y. Wakahara and H. Nozaki, *Tetrahedron Lett.*, 1990, **31**, 1581; K. T. Hollis and B. Bosnich, *J. Am. Chem. Soc.*, 1995, **117**, 4570.
7 Chlorosilanes did not decompose diazoketones **1** under these reaction conditions. They are weaker acids than those reported in: A. B. Smith III and R. K. Dieter, *Tetrahedron*, 1981, **37**, 2407.
8 A catalytic amount of Me_3SiCl was also effectively used.
9 1,2-Rearrangement product **2** might isomerize to ring-expanded product **3** by the catalytic effect of Me_3SiCl. However, this possibility was ruled out by the independent treatment of **2** with Me_3SiCl in the presence of Rh-catalyst.
10 The ^1H NMR coupling constants for the newly composed CH–CH moiety are J = 8.8 and 7.0 Hz for **6d** and **7d**, and also 8.5 and 7.0 Hz for **6e** and **7e**, respectively.
11 S. Kanemasa, T. Kanai, T. Araki and E. Wada, *Tetrahedron Lett.*, 1999, **40**, 5055; S. Kanemasa, T. Araki, T. Kanai and E. Wada, *Tetrahedron Lett.*, 1999, **40**, 5059.
12 R. Mahrwald, *Chem. Rev.*, 1999, **99**, 1095.

CHEMCOMM
Communication
www.rsc.org/chemcomm

Synthesis of an optically active C_3-symmetric cage-like trisamide†

Ruxandra D. Ionescu and Torbjörn Frejd*

Department of Organic Chemistry, Lund University, PO Box 124, 221 00 Lund, Sweden.
E-mail: torbjorn.frejd@orgk1.lu.se

Received (in Cambridge, UK) 6th February 2001, Accepted 27th April 2001
First published as an Advance Article on the web 25th May 2001

The synthesis of the optically active C_3-symmetric cage-like trisamide 2 was easily accomplished by the reaction of 1b with Kemp's triacid; structure elucidation revealed the presence of an array of H-bonds closing the structure as a capsule.

We have for some time been interested in constructing new C_3-symmetric molecules based on amino acid **1**.[1] The tripodal structure of this compound in combination with Kemp's triacid[2] with its unusual triaxial alignment of the carboxylic acid groups,[3] would make possible the synthesis of the cage-like structure **2**. A similar compound **3** was indeed suggested by Kemp and Petrakis in their paper from 1981,[2] but to the best of our knowledge, it has never been synthesised. In this communication, we describe the synthesis of **2**, as shown in Scheme 1.

The protected trisphenylalanine derivative **1a** was synthesised in three steps from commercially available trimesic acid as described previously.[4] Removal of the benzyloxycarbonyl protecting groups by hydrogenation over Pd/C, gave a quantitative yield of **1b**. Slow addition, *via* syringe pump, of a mixture of Kemp's triacid, PyAOP‡ and Hünig's base to **1b** provided **2** in 8–11% yield§ (Scheme 1). This rather low yield was to be expected, as judged from other similar reactions.[5]

Several attempts to improve the yield of the reaction were made by employing different coupling reagents. Replacing PyAOP with the combination EDC–HOBt had no positive effect on the yield and remaining HOBt was difficult to remove from the product during purification. EDC alone failed to provide any product, while HATU gave essentially the same yield as PyAOP. Further, using the PyAOP-procedure as above but increasing the rate of the addition of the coupling reagent or using smaller amounts of the solvent resulted in the formation of more polymeric material, which made purification difficult. Nor did slow addition of the coupling reagent and extending the reaction time (48–72 h), with or without heat, improve the situation; only polymeric material and decomposition of the coupling reagent was indicated by NMR-analysis.

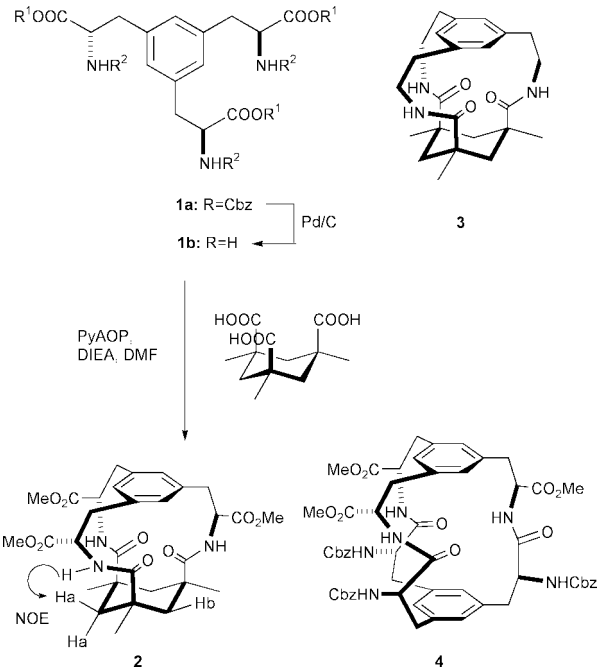

Scheme 1

The free trisamine **1b** could possibly also combine with its corresponding trisacid under amide bond formation. As one of several combinations, one would expect a C_3-symmetric cage-like compound **4** to be formed in which the general structure of **1** served both as the 'top' and the 'bottom' of the cage. Unfortunately, **4** could not be identified in such experiments. Mass spectroscopy revealed only the formation of material with higher molecular weights in the range of oligomers. This outcome was not totally unexpected since the formation of **4** would require a considerable entropy drop of the system. On the other hand, we believe that in the reaction employing Kemp's acid, the preorganisation of its triaxial carboxylic acid groups[3] in the acidic state and also as triester,[2,3c,6] facilitated the formation of the cage.

Since all attempts to grow crystals of **2** useful for X-ray structure determination have hitherto failed, its structure was studied by molecular mechanics computation, NMR- and mass spectroscopy. According to molecular mechanics calculations (MM3),[7] starting from a large number of input structures based on molecular models, the structure of **2** having the cyclohexane ring in the chair conformation had the lowest energy found (Fig. 1). H-bonds between the amide protons of one arm and the carbonyl oxygens of the adjacent arms were clearly seen and the C_3-symmetric character of **2** was indeed reproduced.

It was also evident from the ^{1}H NMR spectrum that **2** was C_3-symmetric, since only one set of signals appeared. As expected, the shift of the various protons had changed as compared to those of **1b**. Thus, the α-proton signal was shifted down-field, from 3.97 ppm in **1b** to 5.25 ppm in **2**, and the multiplicity changed from a double doublet in **1b** to a triple doublet in **2**. This was attributed to the coupling to both the amide protons and the β-protons. In **1b**, no coupling between the α-proton and NH was observed and the signal of the α-proton was a double doublet as a result of its coupling only to the β-protons. For **2**, the N**H**–Hα coupling was clearly seen in the COSY spectrum.† Also the β-proton resonances showed changes in shift and appearance. From being a double doublet at 2.87 ppm, with a coupling constant of 7.2 Hz in **1b**, the corresponding signal in **2** was split into a double doublet at 3.48 ppm and a double doublet

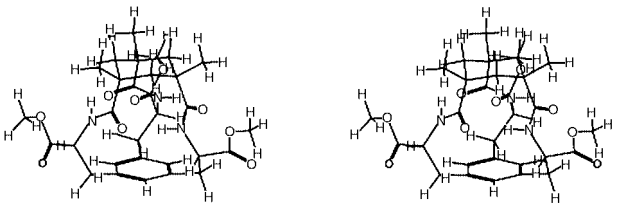

Fig. 1 Stereoview of **2** after steric energy minimization (MM3).[7]

† Electronic supplementary information (ESI) available: spectral data for **1b** and **2**. See http://www.rsc.org/suppdata/cc/b1/b101193f/

 DOI: 10.1039/b101193f

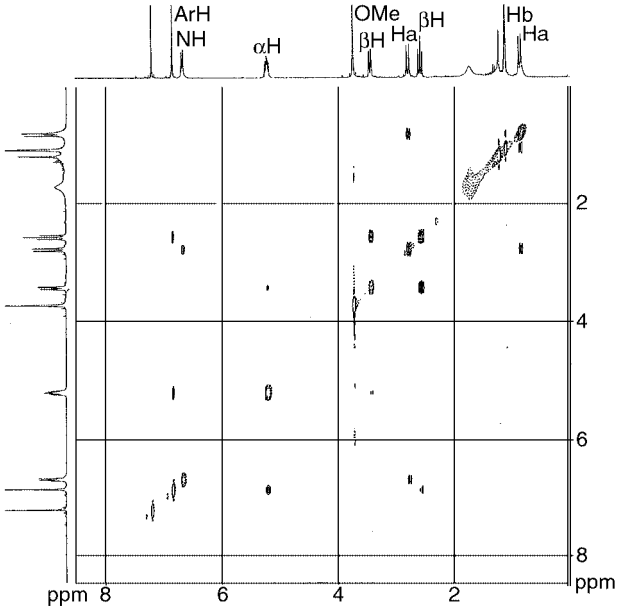

Fig. 2 NOESY spectrum of **2** in $CDCl_3$.

at 2.62 ppm ($J_{\alpha,\beta}$ = 6.9 Hz). One of these protons (at 3.48 ppm) presented a weak NOESY correlation to the α-proton, (Fig. 2). This observation supported the H-bonding in the MM3-model. As seen in Fig. 1, the α- and gauche β-protons are positioned 2.36 Å apart. These protons are located near the extension of the aromatic plane, *i.e.* in the down-field shift region, as can be seen in Fig. 1. The effect was confirmed by ^{1}H NMR. The anti relation between the two β-protons was expressed by the large geminal coupling constant ($J_{\beta-\beta}{}^1$ = 15.7 Hz). The signal originating from the methylene protons in Kemp's acid itself appeared at 2.54 ppm, while the corresponding proton resonance in **2** appeared as two different doublets, one at 2.83 ppm and the other at 0.89 ppm, with a large geminal coupling constant of 15.7 Hz. NOESY experiments revealed that the equatorially positioned protons (the signal at 2.83 ppm) presented a NOE enhancement effect to N**H**CO (Fig. 2). No such effect was observed for the axial protons (0.89 ppm). This observation also supports the H-bonding shown in the MM3-model. As seen in Fig. 1, the NH–Ha distance is only 2.0 Å. The array of NH···O=C hydrogen bonds closes the cage, thus hindering guest molecules to enter. Moreover, the space available inside the cage is probably too small to accommodate a guest particle. This was estimated by MM3[7] energy minimization of an imaginary inclusion complexes between a hydrogen or helium atom and the cage, which resulted in *ca.* 8 kcal mol^{-1} higher energy of both complexes as compared to the empty cage.

The protruding carboxylate groups of **2** may be used as attachment points for various structures *via* ester- or amide bonds. Compound **2** would then serve as a core of dendritic structures. Synthetic work in this direction as well as molecular recognition studies are in progress.

We thank the Swedish Natural Research Council, the Crafoord Foundation and the Royal Physiographic Society in Lund for financial support.

Notes and references

‡ Abbreviations: PyAOP = [7-azabenzotriazol-1-yloxytris(pyrrolidino)-phosphonium hexafluorophosphate]; Hünig's base = *N*,*N*-diisopropyethylamine (DIEA), EDC = 1-[3-(dimethylamino)propyl]-3-ethylcarbodiimide hydrochloride, HOBt = 1-hydroxybenzotriazole hydrate, HATU = *O*-(7-azabenzotriazol-1-yl)-*N*,*N*,*N*′,*N*′-tetramethyluronium hexafluorophosphate.

§ Compounds **1b** and **2** were characterised by ^{1}H and ^{13}C NMR spectroscopy (400 MHz, 298 K) and by mass spectroscopy (FAB). NOESY experiment was used to make individual ^{1}H NMR assignment. Polarimetric measurements were performed at 20 °C.

Preparation of **1b**. Compound **1a**[4] (1.0 g, 1.27 mmol) was dissolved in MeOH (50 mL), Pd/C (50 mg) was added and the mixture was hydrogenated at 1 atm overnight. After removal of the catalyst by filtration through Celite, **1b** was obtained as an amorphous white powder (0.48 g, 99%). mp 207.0–208.8 °C. ν_{max}(KBr)/cm^{-1} 3409.9(NH), 2962.5, 1743.5(CO), 1674.1. ^{1}H NMR (300 MHz, CD_3OD) δ 6.81 (s, 3H), 3.97 (dd, J = 8.5 Hz, 3H), 3.51 (s, 9H), 2.87 (dd, J = 7.2 Hz, 6H). ^{13}C NMR (75 MHz, CD_3OD) δ 171.5, 137.9, 131.9, 55.9, 54.3, 37.8. $[\alpha]_D$ +16.3° (*c* 0.55, MeOH). HRMS (FAB + H$^+$) calculated for $C_{18}H_{27}N_3O_6$ 381.1900. Found 382.1967 [M$^+$ + H].

Preparation of **2**. A solution of Kemp's triacid (0.033 g, 0.13 mmol), PyAOP (0.20 g, 0.38 mmol) and DIEA (65 μL, 0.38 mmol) in DMF (10 mL) was added, *via* a syringe pump, to a solution of **1b** (0.050 g, 0.13 mmol) and DIEA (65 μL, 0.38 mmol) in DMF (90 mL), over 10 h. The reaction mixture was stirred for an additional 12 h at rt. The solvent was then removed under reduced pressure and the residue was dissolved in diethyl ether (20 mL). The organic phase was washed with 1 M HCl (10 × 10 mL) in order to remove remaining PyAOP. The volume of the organic phase was reduced and the crude product was chromatographed (CH_2Cl_2–MeOH 30:1, R_f = 0.5) to give **2** as a semi-solid (7 mg, 8%). ν_{max}(KBr)/cm^{-1} 3379.1(NHCO), 2954.7, 1895.2, 1743.5(CO), 1643.2, 1535.2. ^{1}H NMR (400 MHz, $CDCl_3$) δ 6.91 (s, 3H), 6.73 (d, J = 10.2 Hz, 3H), 5.27 (ddd, $J_{H\alpha-Hb}$ = 6.9 Hz, $J_{H\alpha-NH}$ = 10.2 Hz, 3H), 3.78 (s, 9H), 3.48 (dd, J = 6.9 Hz, 3H), 2.83 (d, J = 15.8 Hz, 3H), 2.62 (dd, J = 7.3 Hz, 3H), 1.15 (s, 9H), 0.89 (d, J = 15.6 Hz, 3H). ^{13}C NMR (100 MHz, $CDCl_3$) δ 176.0, 172.2, 135.3, 129.6, 52.4, 52.2, 43.6, 40.9, 37.2, 35.9. $[\alpha]_D$ −3.4° (*c* 0.35, MeOH). HRMS (FAB + Na$^+$) calculated for $C_{30}H_{39}N_3O_9Na$ 608.2584. Found 608.2588 [M$^+$ + Na].

1 A. Ritzén and T. Frejd, *Chem. Commun.*, 1999, **2**, 207; A. Ritzén and T. Frejd, *Eur. J. Org. Chem.*, 2000, **22**, 3771.
2 D. S. Kemp and K. S. Petrakis, *J. Org. Chem.*, 1981, **46**, 5140.
3 (*a*) J. Rebek Jr., L. Marshall, R. Wolak, K. Parris, M. Killoran, B. Askew, D. Nemeth and N. Islam, *J. Am. Chem. Soc.*, 1985, **107**, 7476; (*b*) F. M. Menger, P. A. Chicklo and M. J. Sherrod, *Tetrahedron Lett.*, 1989, **30**(50), 6943; (*c*) P. Thuéry, M. Neirlich, B. W. Baldwin, Y. Aoki and T. Hirose, *J. Chem. Soc., Perkin Trans. 2*, 1999, 2077.
4 A. Ritzén, B. Basu, A. Wållberg and T. Frejd, *Tetrahedron: Asymmetry*, 1998, **9**, 3491.
5 R. A. Pascal Jr., J. Spergel and D. van Engen, *Tetrahedron Lett.*, 1986, **27**(35), 4099.
6 T. L. Chan, Y. X. Cui, T. C. W. Mak, R. J. Wang and H. N. C. Wong, *J. Crystallogr. Spectrosc. Res.*, 1991, **21**, 297.
7 MacMimic3, InStar Software AB, Ideon Research Park, SE-223 70 Lund, Sweden.

CHEMCOMM
Communication
www.rsc.org/chemcomm

Stereoselective construction of *trans*-1,2-benzooxadecaline frameworks by three-component cascade reactions of an α-phenethyl-β-borylallylsilane with aldehydes†

Michinori Suginome,* Yutaka Ohmori and Yoshihiko Ito*

Department of Synthetic Chemistry and Biological Chemistry, Graduate School of Engineering, Kyoto University, Sakyo-ku, Kyoto 606-8501, Japan. E-mail: suginome@sbchem.kyoto-u.ac.jp

Received (in Cambridge, UK) 20th March 2001, Accepted 3rd May 2001
First published as an Advance Article on the web 25th May 2001

Reactions of α-phenethyl-β-borylallylsilane with aldehydes afforded tricyclic *trans*-1,2-benzooxadecaline frameworks stereoselectively in the presence of Lewis acids *via* sequential incorporation of two different aldehydes followed by cationic cascade cyclization, ending up with intramolecular Friedel–Crafts reaction.

Synthetic reactions in which multiple chemical bonds are created sequentially in a single reaction vessel are highly attractive in terms of efficiency in organic synthesis.[1] In particular, such reactions involving sequential coupling of multiple components have gained increasing attention to achieve high structural diversity which is one of the most important issues in recent synthetic organic chemistry. In our recent report that focused on the alkenylborane synthesis *via* β-borylallylsilanes, we briefly mentioned that reaction of α-phenethyl-β-borylallylsilane **1** with aldehyde afforded tricyclic **2aa** as a sole diastereomer in the presence of TMSOTf [eqn. (1)].[2,3] The reaction may proceed sequentially through allylation of the aldehyde with **1** and acetal formation with the second equiv. of the aldehyde, followed by Prins-type oxonium ion–alkene cyclization, ending up with intramolecular Friedel–Crafts reaction.[4] The remarkable increase in molecular complexity with the high stereoselection prompted us into further investigation. Herein, we report that selective formation of the *trans*-1,2-benzooxadecalines with a wide range of substituents was realized by a sequential reaction of two different aldehydes with **1**. Moreover, formation of related tricyclic frameworks on the basis of the same reaction protocol is also described.

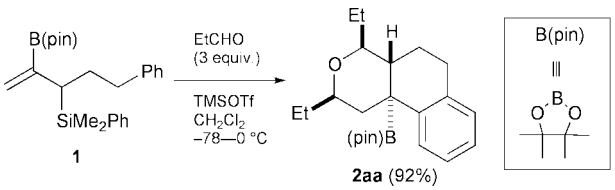

Aiming at the selective, sequential reaction of **1** with aldehydes, we initially tried a stepwise addition of two aldehydes into a solution of **1** in the presence of TMSOTf. Thus, after propionaldehyde (**3a**, 1 equiv.) was completely consumed in the reaction mixture, acetaldehyde (**3b**, 2 equiv.) was subsequently added. Work-up of the reaction mixture, however, gave tricyclic benzooxadecaline derivative **2aa** as a major product, in which two molar equiv. of **3a** were incorporated. Selective synthesis of tricyclic benzooxadecalines, in which two different aldehydes were incorporated in a stepwise manner, was achieved by means of $TiCl_4$ instead of TMSOTf (Scheme 1).[2] In the presence of $TiCl_4$ (1.2 equiv.), aldehyde **3a** (1.0 equiv.) was reacted at −78 °C, to the consumption. Subsequent addition of **3b** (2.0 equiv.) to the reaction mixture at −78 °C, followed by warming the mixture to 0 °C, resulted in the exclusive formation of **2ab** in good yield, which had ethyl and methyl groups selectively at the right positions (Table 1; entry 1). With the optimized reaction conditions, some aliphatic and aromatic aldehydes and acetals as the second electrophile were employed in combination with the first aliphatic aldehydes for the present three component cascade cyclization. When propionaldehyde diethylacetal (**4a**) and isobutyraldehyde (**3c**) were employed as the second electrophiles, the corresponding products were obtained in good yields (entries 2 and 3). However, reaction of pivalaldehyde (**3d**) under the same reaction conditions gave **2ad** only in moderate yield, although the selectivity for the formation of **2ad** was perfect (entry 4). It was found that the yield was much improved by the additional use of TMSOTf in the second step with **3d** (entry 5).‡ A similar but more pronounced effect of the additional use of TMSOTf was found in the reaction of benzaldehyde (**3e**), which hardly

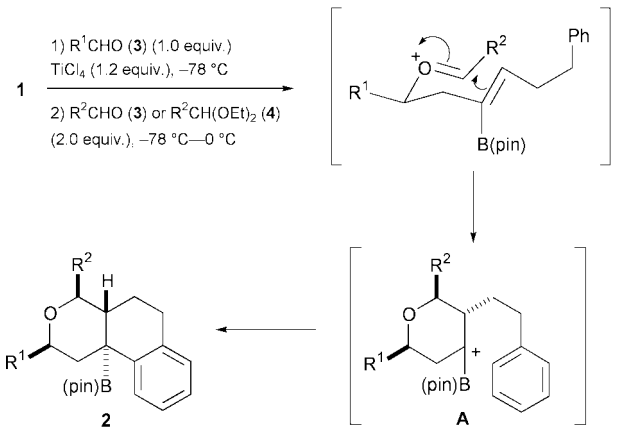

Scheme 1 Three-component cascade reaction of **1** with electrophiles.

Table 1 Stereoselective synthesis of *trans*-1,2-benzooxadecalines **2** *via* sequential reaction of aldehydes (**3**) and diethylacetals (**4**) with **1**

Entry	Aldehyde (R^1)	Aldehyde or acetal (R^2)[a]	Conditions[b]	Product (% yield)[c]
1	**3a** (Et)	**3b** (Me)	A	**2ab** (81)
2	**3a**	**4a** (Et)[d]	A	**2aa** (75)
3	**3a**	**3c** (*i*-Pr)	A	**2ac** (80)
4	**3a**	**3d** (*t*-Bu)	A	**2ad** (47)
5	**3a**	**3d**	B	**2ad** (75)
6	**3a**	**3e** (Ph)	A	**2ae** (trace)
7	**3a**	**3e**	B	**2ae** (85)
8	**3a**	**4f** ((*E*)-PrCH=CH)[d]	B	**2af** (58)
9	**3b** (Me)	**3a**	A	**2ba** (82)
10	**3c** (*i*-Pr)	**3a**	A	**2ca** (33)

[a] Aldehydes were used as the second electrophiles unless otherwise noted. [b] Condition A: (1) R^1CHO (1 equiv.), $TiCl_4$ (1.2 equiv.), −78 °C, (2) R^2CHO or $R^2CH(OEt)_2$ (2 equiv.), −78–0 °C. For condition B, TMSOTf (2 equiv.) was added with the second electrophiles. [c] Isolated yield. [d] The corresponding diethyl acetals were used as the second electrophiles.

† Electronic supplementary information (ESI) available: experimental details and spectral data. See http://www.rsc.org/suppdata/cc/b1/b102613p/

 DOI: 10.1039/b102613p

gave the desired product in the absence of TMSOTf (entries 6 and 7). Although use of (*E*)-2-hexenal as the second electrophile resulted in the formation of a complex mixture of undesired products, the corresponding acetal (**4f**) afforded the tricyclic product **2af** having alkenyl group as R^2 (entry 8). We also examined the variation of the first electrophile. Reaction using **3b** in combination with **3a** gave **2ba** with high selectivity (entry 9). Although we found that use of more sterically demanding **3c** as the first electrophile resulted in much lower yields, only **2ca** without any other tricyclic products were found in the reaction mixture (entry 10). Presumably, **3c** as well as **1** may be consumed completely in the first step by any side reaction, resulting in the highly selective formation of **2ca**.

To evaluate the role of the boryl group in the cyclization, we examined the reactions of the related allylsilanes bearing silyl (**5**) and methyl (**6**) groups at the β-positions.§ Under the same reaction conditions as for the preparation of **2aa** from the β-

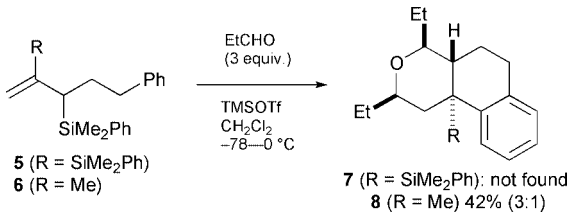

5 (R = $SiMe_2Ph$)
6 (R = Me)

7 (R = $SiMe_2Ph$): not found
8 (R = Me) 42% (3:1)

boryl counterpart **1**, 3 molar equiv. of **3a** were reacted with **5** and **6** in the presence of TMSOTf [eqn. (2)]. While the former (**5**) gave only a complex mixture of products, the methyl derivative afforded tricyclic product **8** along with its diastereomer in a ratio of 3:1 in a total yield of 42%. This result suggests that the sequential reaction with aldehydes giving the tricyclic skeleton is efficiently controlled by the boryl group with respect to yield and stereoselectivity. Presumably, the electronic nature of the β-substituent has the predominant effect on the formation and cyclization of the cationic intermediates, *e.g.*, **A** in Scheme 1.

A related cascade cyclization using 1,1,3,3-tetramethoxypropane with **1** in the presence of $TiCl_4$ afforded boryl-substituted *trans*-1,2-benzodecaline derivative **9** in good yield

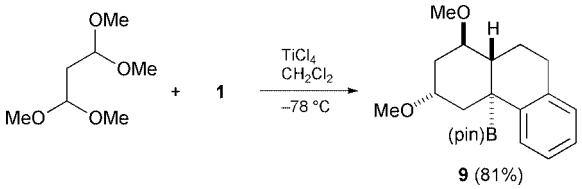

9 (81%)

[eqn. (3)]. Interestingly, the relative stereochemistry of the two methoxy groups was *trans*, indicating the second carbon–oxygen bond activation leading to cyclization may involve chelation of the two methoxy groups onto the titanium metal.

The tricyclic organoboron compounds served as useful synthetic precursors for the corresponding tertiary alcohols bearing the hydroxy groups at the bridgehead carbon atoms (Scheme 2). Thus, treatment of **2aa** with trimethylamine oxide at 160 °C gave the bridgehead alcohol **10** in 85% yield. Further synthetic elaboration was demonstrated by sequential treatment of **2aa** with Li–NH_3 and H_2O_2, which gave the dienyl alcohol **12** *via* isolation of **11**. An attempt at an alternative pathway to **12** *via* Birch reduction of **10** resulted in the reduction of the tertiary, benzylic hydroxy group to give **13** in high yield as a 1:1 mixture of diastereomers, indicating that the boryl group served as a masked hydroxy group in the transformation into **11**.

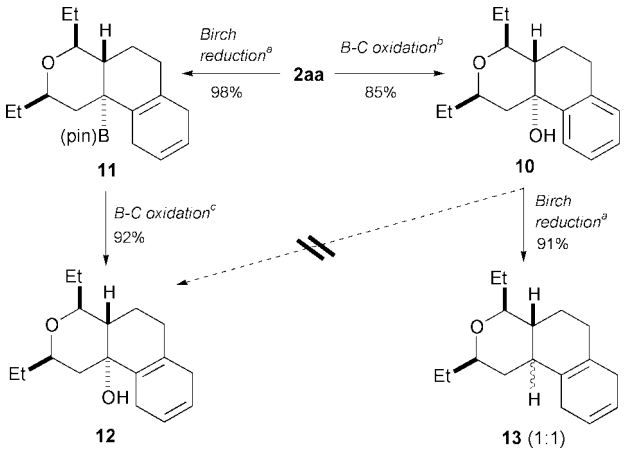

Scheme 2 *Reagents and conditions*: a) Li, liq. NH_3, *t*-BuOH, −33 °C; b) $Me_3NO{\bullet}2H_2O$, diglyme, 160 °C; c) H_2O_2, NaOH aq., THF, 50 °C.

In summary, we report a cascade cyclization giving *trans*-1,2-benzodecaline skeletons *via* sequential reaction of α-phenethyl-β-borylallylsilane **1** with aldehydes. The stereochemical aspects and high structural diversity may deserve further investigation of the present stereoselective cyclization. Furthermore, the boryl group incorporation at the bridgehead tertiary carbon atom as a hydroxy equivalent may open up new possibilities for the synthesis of polycyclic bridgehead alcohols *via* cationic cyclization.

Notes and references

‡ A general procedure (A) for the three component cascade reaction of **1** with electrophiles. To a mixture of **1** (50 mg, 0.12 mmol) and **3** (0.12 mmol) in CH_2Cl_2 (0.12 mL) was added a CH_2Cl_2 solution of $TiCl_4$ (2.0 M, 74 × 10^{-3} mL, 0.15 mmol) at −78 °C, and the mixture was stirred at −78 °C for 2 h. To this was added **3** or **4** (0.25 mmol) at −78 °C, and the mixture was stirred at 0 °C for 3 h. Aqueous $NaHCO_3$ (sat.) was added to the mixture. Extraction with AcOEt followed by silica gel column chromatography afforded **2**. For procedure B, the addition of the second electrophile (**3** or **4**) was followed by the addition of TMSOTf (45 × 10^{-3} mL, 0.25 mmol) at −78 °C.

§ The requisite β-silylallylsilane **5** and β-methylallylsilane **6** were prepared by palladium-catalyzed bis-silylation of 5-phenylpenta-1,2-diene[5] and Suzuki-Miyaura cross-coupling of **1** with iodomethane,[6] respectively.

1 For reviews on domino, cascade, and tandem reactions, see: L. F. Tietze, *Chem. Rev.*, 1996, **96**, 115; S. E. Denmark and A. Thorarensen, *Chem. Rev.*, 1996, **96**, 137; J. D. Winker, *Chem. Rev.*, 1996, **96**, 167; I. Ryu, N. Sonoda and D. P. Curran, *Chem. Rev.*, 1996, **96**, 177; P. J. Parsons, C. S. Penkett and A. J. Shell, *Chem. Rev.*, 1996, **96**, 195; K. K. Wang, *Chem. Rev.*, 1996, **96**, 207; A. Padwa and M. D. Weingarten, *Chem. Rev.*, 1996, **96**, 271.

2 M. Suginome, Y. Ohmori and Y. Ito, *J. Am. Chem. Soc.*, 2001, **123**, 4601.

3 For the synthesis of β-borylallylsilanes by palladium-catalyzed silaboration of allenes, see: M. Suginome, Y. Ohmori and Y. Ito, *Synlett*, 1999, 1567; S.-y. Onozawa, Y. Hatanaka and M. Tanaka, *Chem. Commun.*, 1999, 1863; M. Suginome, Y. Ohmori and Y. Ito, *J. Organomet. Chem.*, 2000, **611**, 403.

4 For the related cyclizations of allylsilanes with aldehydes giving 4-halotertahydropyrans, see: L. Coppi, A. Ricci and M. Taddei, *J. Org. Chem.*, 1988, **53**, 913; Z. Y. Wei, D. Wang, J. S. Li and T. H. Chan, *J. Org. Chem.*, 1989, **54**, 5768.

5 H. Watanabe, M. Saito, N. Sutou, K. Kishimoto, J. Inose and Y. Nagai, *J. Organomet. Chem.*, 1982, **225**, 343.

6 N. Miyaura and A. Suzuki, *Chem. Rev.*, 1995, **95**, 2457.

CHEMCOMM
Communication
www.rsc.org/chemcomm

Observation of some pore wall ordering in mesoporous silica

Robert Mokaya

School of Chemistry, University of Nottingham, University Park, Nottingham, UK NG7 2RD.
E-mail: r.mokaya@nottingham.ac.uk

Received (in Cambridge, UK) 26th February 2001, Accepted 18th April 2001
First published as an Advance Article on the web 25th May 2001

Increasing the time allowed for hydrothermal crystallisation during high temperature (150 °C) synthesis of MCM-41 appears to result in some ordering (nanocrystallites) within the pore walls which is accompanied by increase in pore wall thickness, pore size, silica condensation and the formation of elongated or rod-like particles.

The synthesis of organised inorganic materials is currently the subject of a great deal of research effort in materials science. Since the discovery of the M41S family of mesoporous silicas, prepared *via* a mechanism in which supramolecular assemblies of surfactant micelles act as templates for the organisation of inorganic silicate precursors,[1,2] the use of surfactant species to direct the organisation of mesoporous silica has been achieved over a wide range of synthesis conditions.[3] Recent advances indicate that mesoporous silica materials with a wide range of properties may be prepared by careful control of the synthesis conditions.[4–7] However, despite their excellent structural ordering and well defined pore size distribution, mesoporous silicas possess a largely amorphous inorganic framework; their pore walls are amorphous and in many ways exhibit properties similar to those of amorphous silica. The preparation of mesoporous silicas with semi-crystalline or crystalline walls, similar to those of zeolites, is desirable with respect to their stability and use as heterogeneous catalysts or ion exchangers.[8] Although the preparation of surfactant-templated mesoporous oxides (*e.g.* titania, zirconia) with semi-crystalline walls has been recently achieved,[9,10] there are no reports on mesoporous silica with any degree of pore wall ordering. This report describes some pore wall ordering observed in mesoporous silica materials which suggests the presence of nanocrystallites within the pore walls. The pore wall ordering, observed during the course of our work on high temperature (> 150 °C) synthesis of MCM-41, may provide some insights into the preparation of MCM-41 materials with crystallographically ordered pore walls. Materials with pore wall ordering (nanocrystallites) were obtained by extending the crystallisation time in an otherwise normal MCM-41 synthesis procedure under basic conditions. The emergence of pore wall order (*i.e.* nanocrystallites within the pore walls) was accompanied by an increase in the unit cell parameter and the formation of thick and highly condensed silica pore walls along with morphological transformation from the usual spherical shaped particles to elongated or rod-like particles. The apparent pore wall ordering was observed using transmission electron microscopy (TEM) and selected area electron diffraction (SAED).

The nanocrystallite containing MCM-41 materials were prepared using a normal procedure which was modified by increasing the time allowed for hydrothermal crystallisation from 48 to 96 h as follows; tetramethylammonium hydroxide (TMAOH) and cetyltrimethyammonium bromide (CTAB) were dissolved in distilled water by stirring at 35 °C to give a clear solution. The silica source, fumed silica (Sigma), was then added to the template solution under stirring for 1 h. After further stirring for 1 h to allow the silica to be fully dispersed, the resulting synthesis gel of molar composition SiO_2 : 0.25 CTAB : 0.2 TMAOH : 40 H_2O was left to age for 20 h at room temperature following which the gel was transferred to a Teflon-lined autoclave and heated at 150 °C for 96 h. The solid product was obtained by filtration, washed with distilled water, dried in air at room temperature and calcined in air at 550 °C for 8 h to obtain the final material designated as MCM-41(96).[11,12] We note that careful control of the crystallisation temperature was essential for obtaining nanocrystallite-containing MCM-41. In particular temperatures significantly lower than 150 °C resulted in materials with lower unit cell parameters, thinner pore walls and no evidence of pore ordering or nanocrystallites.

Fig. 1 shows typical TEM micrographs obtained for MCM-41(96). The particle morphology is consistent with the elongated or rod-like particles previously observed for this type of material.[12] We have previously reported that the morphology of materials (such as MCM-41(96)), which are prepared for extended crystallisation periods, differs from the normal spherical shaped particle morphology observed for MCM-41, and that they are mainly made up of elongated rod-like spheres.[12] Similar rod-like MCM-41 particles have also been previously obtained *via* a two-step synthesis procedure involving post-synthesis restructuring.[13] Fig. 2 shows representative TEMs with the corresponding SAED patterns. First we note that from the TEMs in Fig. 2, it is possible to observe the pore channels which run along the particle axis. Secondly, the SAEDs are unusual for MCM-41 in that they show several diffuse diffraction rings which is an indication that the MCM-41(96) particles exhibit some local ordering. A likely explana-

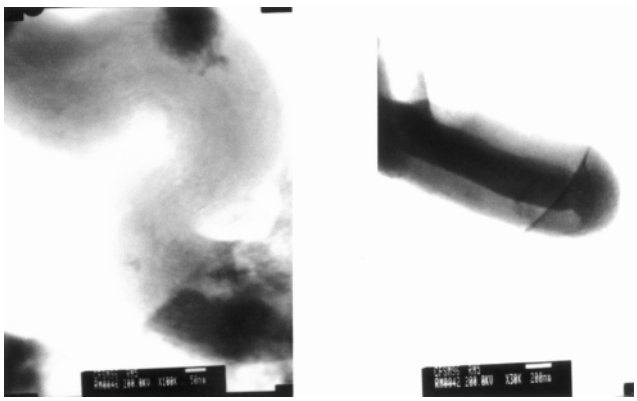

Fig. 1 Representative TEM micrographs of MCM-41(96).

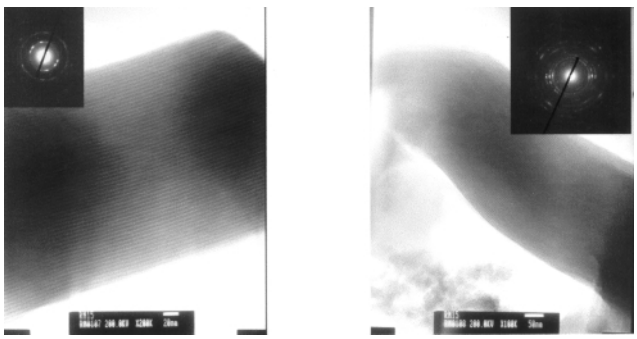

Fig. 2 Representative TEM micrographs and corresponding SAED patterns for MCM-41(96).

 DOI: 10.1039/b101812o

tion for the diffraction rings is that the pore walls of MCM-41(96) possess some crystalline character, perhaps in the form of nanocrystallites which occur within the pore walls.[9] We have previously shown that the pore wall thickness of materials similar to the MCM-41(96) sample reported here is much higher than that of conventional MCM-41.[11] The pore walls of such materials are up to twice as thick as those of conventional MCM-41 (crystallised at 150 °C for 48 rather than 96 h).[11] Indeed the pore walls of MCM-41(96) type materials are amongst the thickest we have encountered for any MCM-41 material. It is therefore possible that nanocrystallites can nucleate within the thick pore walls of MCM-41(96) thus resulting in semi-crystalline pore walls and the pore ordering observed in Fig. 2. Mesoporous metal oxides possessing thick pore walls and semi-crystalline frameworks have previously been reported.[9] The presence of thick pore walls was considered as being important in the nucleation and growth of nanocrystallites within the mesoporous metal oxide frameworks.[9]

The typical surface area and pore volume of MCM-41(96) materials was in the range 650–700 $m^2\ g^{-1}$ and 0.70–0.8 $cm^3\ g^{-1}$, respectively. These values are rather lower than those of conventional MCM-41 presumably due to the thicker pore walls. The thick pore walls also, in part, account for the large unit cell size observed (typically 70 Å). The pore size is however not compromised by the thick pore walls and is indeed much larger than that in conventional MCM-41.[11,12] The powder X-ray diffraction (XRD) pattern for a typical MCM-41(96) sample is shown in Fig. 3. The XRD pattern is typical of a relatively well ordered material and shows an intense basal (100) diffraction peak and some higher order peaks. The 100 peak is shifted to lower 2θ values (compared to conventional MCM-41) indicating an expansion in the lattice parameter. We note that although we did not observe any clearly defined high angle peaks in the powder XRD patterns of MCM-41(96), the amorphous silica 'halo' peak usually present in MCM-41 materials was virtually absent. Typical N_2 sorption isotherms (not shown) for MCM-41(96) materials exhibit a well developed step in the relative pressure (P/P_o) range 0.45–0.6 characteristic of capillary condensation (filling) into uniform mesopores.[11,12,14] The isotherms also exhibit some (triangle shaped) hysteresis which is characteristic of MCM-41 materials with pores larger than 40 Å.[14] It is worth noting that the thick walls of MCM-41(96) are accompanied by greater silica condensation. ^{29}Si MAS NMR spectra of as-synthesised (surfactant containing) MCM-41(96) indicated that the pore walls are primarily made up of fully condensed Q^4 silica units with a small contribution from incompletely cross-linked Q^3 units.[11,12] Q^4/Q^3 ratios in the range 4.0 to 5.0 and typically *ca.* 4.5 were obtained for MCM-41(96) materials compared to a ratio of 1.4 for conventional MCM-41. As expected the Q^4/Q^3 ratio was even higher for the calcined MCM-41(96) samples that were used for TEM analysis. It is worth noting that the thick, highly condensed pore walls and the implied presence of nanocrystallites is consistent with the improved thermal and hydrothermal stability previously observed for MCM-41(96) materials.[11]

We have considered other possible explanations for the origin of the diffraction rings observed in Fig. 2. A possible explanation is that the diffraction rings arise from multi-particles or particle aggregates. Although we do not rule out this possibility, we were however unable to obtain diffuse diffraction rings from multi-particles of several other MCM-41 materials that were prepared under different conditions; the diffraction rings were a feature of MCM-41(96) materials. It appears therefore, that mesoporous MCM-41 silica with semi-crystalline pore walls may be prepared by increasing the time allowed for hydrothermal crystallisation, in an otherwise normal MCM-41 synthesis procedure under basic conditions. In the present case it is likely that extending the crystallisation time allows for more extensive diffusion of additional silicate units and surfactant species into the growing surfactant/silica mesophase. Additional silicate units increase the wall thickness and extent of silica condensation while additional surfactant species increase the volume and density of the surfactant (micellar) phase thus increasing the pore size. The increased silicate accretion may favour the nucleation and growth of nanocrystallites. The findings reported here suggest that crystallisation temperature and time are likely to be important factors in attempts to prepare mesoporous silicas with semi-crystalline or crystalline pore walls.

The author is grateful to the EPSRC for an Advanced Fellowship and the Royal Society for an equipment grant.

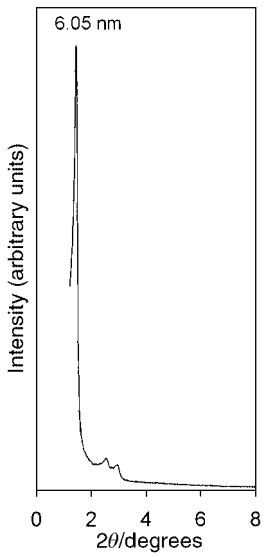

Fig. 3 Powder XRD patterns of MCM-41(96).

Notes and references

1 C. T. Kresge, M. E. Leonowicz, W. J. Roth, J. C. Vartuli and J. S. Beck, *Nature*, 1992, **359**, 710.
2 J. S. Beck, J. C. Vartuli, W. J. Roth, M. E. Leonowicz, C. T. Kresge, K. D. Schmitt, C. T.-U. Chu, D. H. Olsen, E. W. Sheppard, S. B. McCullen and J. L. Schlenker, *J. Am. Chem. Soc.*, 1992, **114**, 10 834.
3 J. Y. Ying, C. P. Mehnert and M. S. Wong, *Angew. Chem., Int. Ed.*, 1999, **38**, 56.
4 H.-P. Lin and C.-H. Mou, *Science*, 1996, **273**, 765.
5 H. Yang, N. Coombs and G. A. Ozin, *Nature*, 1997, **386**, 692.
6 H.-P. Lin, S.-B. Liu, C.-Y. Mou and C.-Y. Tang, *Chem Commun.*, 1999, 583.
7 P. Schmidt-Winkel, P. Yang, D. I. Margolese, B. F. Chmelka and G. D. Stucky, *Adv. Mater.*, 1999, **11**, 303.
8 A. Corma, *Chem. Rev.*, 1997, **97**, 2373.
9 P. Yang, D. Zhao, D. I. Margolese, B. F. Chmelka and G. D. Stucky, *Chem. Mater.*, 1999, **10**, 2813.
10 Y. Yue and Z. Gao, *Chem. Commun.*, 2000, 1755.
11 R. Mokaya, *J. Phys. Chem. B*, 1999, **103**, 10 204.
12 R. Mokaya, *Microporous Mesoporous Mater.*, 2001, **44-5**, 119.
13 M. Grun, K. Unger, A. Matsumoto and K. Tsutumi, *Microporous Mesoporous. Mater.*, 1999, **27**, 207.
14 M. Kruk, M. Jaroniec and A. Sayari, *Langmuir*, 1997, **13**, 6267.

CHEMCOMM Communication
www.rsc.org/chemcomm

A concise route to (−)-morphine

Hiroshi Nagata, Norio Miyazawa and Kunio Ogasawara*

Pharmaceutical Institute, Tohoku University, Aobayama, Sendai 980-8578, Japan.
E-mail: konol@mail.cc.tohoku.ac.jp; Fax: +81 22-217-6845; Tel: +81 22-217-6846

Received (in Cambridge, UK) 20th February 2001, Accepted 3rd May 2001
First published as an Advance Article on the web 25th May 2001

A concise enantio- and diastereocontrolled route to (−)-morphine has been developed starting from a bicyclo[3.2.1]octenone chiral building block through an acid-catalyzed tandem retro-aldol-oxonium ion-mediated hydrophenanthrene formation reaction as the key step.

The total synthesis of (−)-morphine **1**, the main alkaloid of the opium poppy, has been a challenging target for organic chemists for many decades.[1,2] Although a number of successful syntheses have been developed to date since the first accomplishment by Gates[3] in 1952, only a few could produce the alkaloid in an enantio- and diastereocontrolled manner. We report here a concise diastereocontrolled synthesis of the key intermediate[4] dihydrocodeinone ethylene ketal (−)-**2** of (−)-morphine **1** and the related opium alkaloids starting from the bicyclo[3.2.1]octenone chiral building block[5] (−)-**3** by employing a tandem retro-aldol cleavage and oxonium ion-mediated cyclization[6] as the key step (Scheme 1).

Enantiopure enone **3**, $[\alpha]_D^{26}$ −438.6 (*c* 1.6, $CHCl_3$)], was reacted with 3-lithioveratrole generated *in situ* by reaction of veratrole with butyllithium,[7] to give diastereoselectively tertiary alcohol† **4**, mp 82–84 °C, $[\alpha]_D^{26}$ −151.6 (*c* 1.5, $CHCl_3$)], which on oxidation with pyridinium chlorochromate (PCC) afforded β-aryl-enone **5**, $[\alpha]_D^{26}$ +173.5 (*c* 3.0, $CHCl_3$)], in 81% yield. Construction of the dihydrobenzofuran moiety of the target molecule was carried out at this point by employing the procedure developed by Mulzer and coworkers[4] in their synthesis of **1**. Thus, reaction of **5** with vinylmagnesium chloride in THF containing HMPA in the presence of copper(I) bromide and trimethylsilyl chloride furnished silyl enol ether **6** in 75% yield by concurrent diastereoselective 1,4-addition and *O*-silylation. Exposure of **6** to *N*-bromosuccinimide (NBS) gave α-bromoketone **7** in excellent yield as an inseparable mixture of two epimers (5:1). When the mixture was refluxed in DMF,[4e] intramolecular etherification took place to give rise to dihydrobenzofuran **8**, mp 80–82 °C, $[\alpha]_D^{23}$ −109.7 (*c* 0.5, $CHCl_3$)], in 81% yield as a single diastereomer. Since terminal hydroxylation of the vinyl functionality of **8** under hydroboration–oxidation conditions[8] brought about formation of a mixture by concomitant reduction of the carbonyl functionality in the molecule, the ketone was first protected under mild conditions[9] using 1,2-bis(trimethylsiloxy)ethane in the presence of trimethylsilyl triflate. Under these conditions, **8** furnished hydroxyketal **9** in 71% yield with concurrent removal of the MOM-protecting group. Primary hydroxylation carried out at this stage under standard hydroboration–oxidation conditions[8] afforded diol **10** whose primary hydroxy functionality was selectively acylated with pivaloyl chloride to give hydroxypivalate **11**, the substrate of the key acid-catalyzed hydrophenanthrene formation reaction, in 72% yield. Overall yield of **11** from (−)-**3** was 22% in eight steps (Scheme 2).

Conversion of **11** into the key hydrophenanthrene intermediate **16** could be accomplished in one step just by refluxing with ethylene glycol in benzene with removal of generating water. Thus, **11**, on reflux with ethylene glycol in benzene using a Dean–Stark apparatus in the presence of a catalytic amount of toluene-*p*-sulfonic acid,[2c] furnished the hydrophenanthrene **16**,

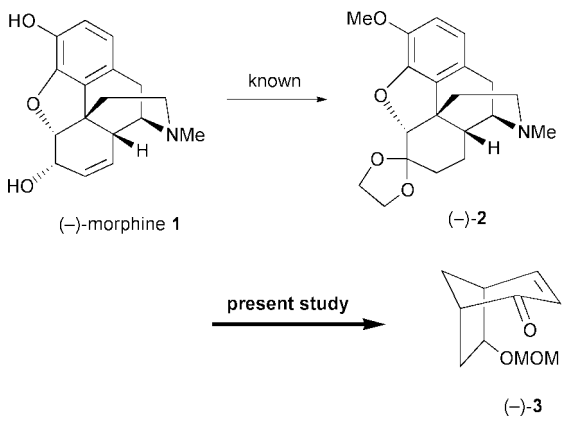

Scheme 1

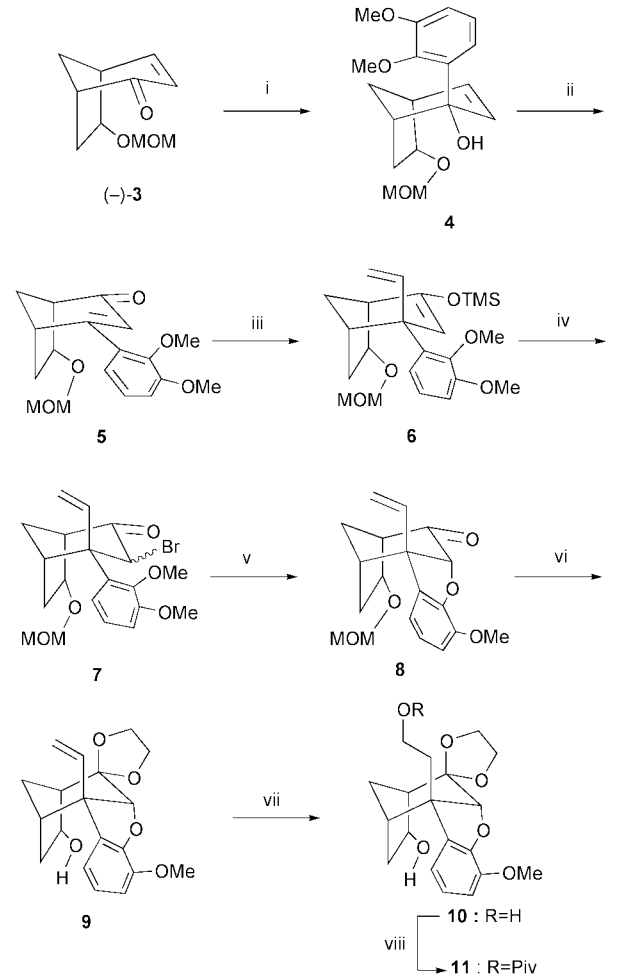

Scheme 2 *Reagents and conditions*: i) 3-Li-veratrole, THF, −78 °C. ii) PCC, CH_2Cl_2 (81% in 2 steps). iii) vinyl-MgCl, CuBr-Me_2S, TMS-Cl, HMPA, THF (75%). iv) NBS, CH_2Cl_2, rt (99%). v) DMF, reflux, 30 min (82%). vi) $(CH_2OTMS)_2$, TfOTMS(cat.), CH_2Cl_2 (71%). vii) BH_3-Me_2S then 30% H_2O_2, NaOH (72%). viii) Piv-Cl, pyridine (87%).

 DOI: 10.1039/b101668g

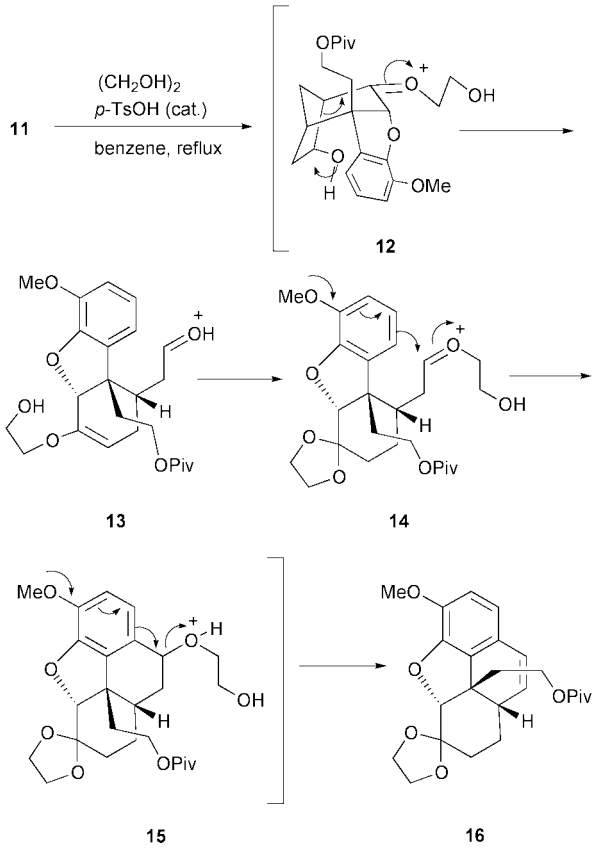

Scheme 3

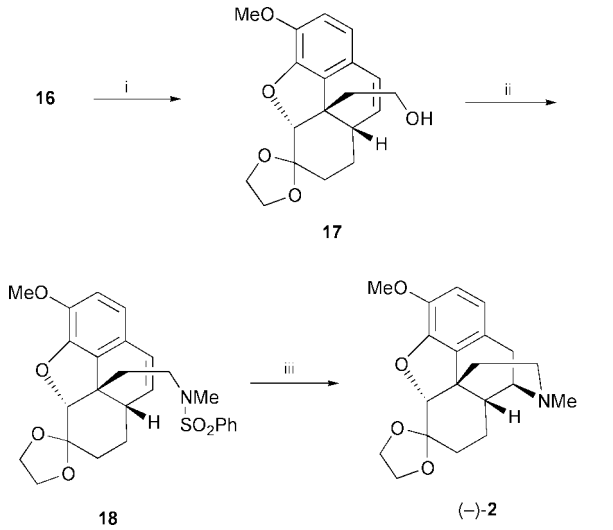

Scheme 4 *Reagents and conditions*: i) $LiAlH_4$, THF, rt (100%). ii) $PhSO_2NHMe$, 1,1′-(azodicarbonyl)dipiperidine, Bu_3P, THF (78%). iii) Li, NH_3, *t*-BuOH, THF (70%).

$[\alpha]_D^{25}$ +20.6 (*c* 0.7, $CHCl_3$), in 50% yield as a single product after 15 h. The reaction may be explained by initial formation of oxonium ion **12** which underwent retro-aldol cleavage leading to another oxonium ion **14** *via* protonated aldehyde **13** after reaction with an ethylene glycol in the reaction medium.[2c] The reaction proceeded further under the conditions to bring about cyclization to give hydrophenanthrene **16** through a transient **15**. Although we did not examine this point extensively, the addition of ethylene glycol seemed to be essential to accelerate this cyclization reaction[2c] (Scheme 3).

Transformation of **16** into the penultimate intermediate **18** of the target molecule (−)-**2** could be carried out in a straightforward manner. The pivaloyl group from **16** was first removed by reduction and the resulting primary alcohol **17**, mp 92–94 °C, $[\alpha]_D^{28}$ +31.4 (*c* 0.7, $CHCl_3$), was then transformed into the tertiary sulfonamide **18** by employing the modified Mitsunobu reaction.[4,10] Thus, the reaction of **17** with *N*-methylbenzenesulfonamide in the presence of 1,1′-(azodicarbonyl)dipiperidine[10] and tributylphosphine gave **18**, mp 113–115 °C, $[\alpha]_D^{26}$ −28.5 (*c* 0.1, $CHCl_3$)]{ref. [4d]: mp 115–117 °C, $[\alpha]_D^{20}$ −24.1 (*c* 1.0, $CHCl_3$)}, in 78% yield, whose spectroscopic data were identical with those reported.[4d] Since this compound has been transformed into (−)-morphine **1** and the related opium alkaloids *via* the key intermediate **(**−)-2,[4] the present synthesis constitutes a formal synthesis at this point. Actually, our product (−)-**18** furnished the key morphinan (−)-**2**, mp 170–172 °C, $[\alpha]_D^{27}$ −167.1 (*c* 0.1, $CHCl_3$)]{ref.[4d]: mp 173–175 °C, $[\alpha]_D^{20}$ −173.3 (*c* 1.0, $CHCl_3$)}, in 70% yield on treatment with lithium in liquid ammonia containing *tert*-butanol.[4d,11] Overall yield of (−)-**2** from **11** was 27% in four steps, thus, 6% in twelve steps from the chiral building block (−)-**3** (Scheme 4).

The present methodology for the synthesis of the key intermediate of (−)-morphine may be utilized widely not only for the construction of the alkaloids having a *cis*-fused tetrahydrophenanthrene framework but also for the synthesis of the *trans*-fused congeners as the bicyclo[3.2.1]octenone chiral building block allows diastereocontrolled construction of the pivotal stereogenic center owing to its inherent convex-face selectivity.

Notes and references

† Satisfactory analytical (combustion and/or high resolution mass) and spectral (IR, 1H NMR, and MS) data were obtained for new compounds.

1 For pertinent reviews, see: T. Hudlicky, G. Butora, S. P. Fearnley, A. G. Gum and M. R. Stabile, *Studies in Natural Products Chemistry*, Atta-ur-Rahman ed., Elsevier, Amsterdam, 1996, Vol. 18, pp. 43–154; B. H. Novak, T. Hudlicky, J. W. Reed, J. Mulzer and D. Trauner, *Curr. Org. Chem.*, 2000, **4**, 343; K. W. Bentley, *Nat. Prod. Rep.*, 2000, **17**, 247 and previous reports.

2 For the synthesis of morphine alkaloids after ref. 1, see: (*a*) J. D. White and P. Hrncier, *J. Org. Chem.*, 1999, **64**, 7271; (*b*) J. D. White, P. Hrncier and F. Stappenbeck, *J. Org. Chem.*, 1999, **64**, 7871; (*c*) O. Yamada and K. Ogasawara, *Org. Lett.*, 2000, **2**, 2785.

3 M. Gates and G. Tschudi, *J. Am Chem. Soc.*, 1952, **72**, 1109.

4 (*a*) J. Mulzer, G. Durner and D. Trauner, *Angew. Chem., Int. Ed. Engl.*,1996, **35**, 2836; (*b*) J. Mulzer, J. W. Bats, B. List, T. Opatz and D. Trauner, *Synlett*, 1997, 441; (*c*) D. Trauner, S. Porth, T. Opatz, J. W. Bats, G. Giester and J. Mulzer, *Synthesis*, 1998, 653; (*d*) D. Trauner, J. W. Bats, A. Werner and J. Mulzer, *J. Org. Chem.*, 1998, **63**, 5908; (*e*) J. Mulzer and D. Trauner, *Chirality*, 1999, **11**, 475.

5 H. Nagata, M. Kawamura and K. Ogasawara, *Synthesis*, 2000, 1825; H. Nagata, N. Miyazawa and K. Ogasawara, *Synthesis*, 2000, 2013.

6 H. Nagata, N. Miyazawa and K. Ogasawara, *Org. Lett.*, 2001, in press.

7 E. D. Bergmann, P. Pappo and D. Ginsburg, *J. Chem. Soc.*, 1950, 1369.

8 C. F. Lane, *J. Org. Chem.*, 1974, **39**, 1437.

9 T. Tsunoda, M. Suzuki and R. Noyori, *Tetrahedron Lett.*,198, **21**, 1357.

10 T. Tsunoda, Y. Yamamiya and S. Ito, *Tetrahedron Lett.*, 1993, **34**, 1639.

11 K. A. Parker and D. Fokas, *J. Am. Chem. Soc.*, 1992, **114**, 9688.

CHEMCOMM Communication
www.rsc.org/chemcomm

Enzyme-coated micro-crystals: a 1-step method for high activity biocatalyst preparation

Michaela Kreiner,[a] Barry D. Moore,[b] and Marie Claire Parker*[a]

[a] *Department of Chemistry, University of Glasgow, Joseph Black Building, Glasgow, UK G12 8QQ. E-mail: mariec@chem.gla.ac.uk*
[b] *Department of Pure and Applied Chemistry, University of Strathclyde, Glasgow, UK G1 1XL*

Received (in Cambridge, UK) 19th January 2001, Accepted 4th May 2001
First published as an Advance Article on the web 25th May 2001

A rapid, inexpensive method for producing water-soluble enzyme-coated micro-crystals which exhibit dramatically enhanced catalytic activity and stability in non-aqueous media and can be re-dissolved easily in aqueous solution is described.

Enzymes can frequently show poor activity in organic media when compared to their respective activities in aqueous solution.[1] It has been well documented that lyophilisation (a frequent choice of enzyme preparation for storage and use in organic media) causes pronounced structural perturbation for most proteins, including one of the enzymes in this study, subtilisin Carlsberg (SC).[2,3] To overcome these problems, many strategies aimed at optimising enzyme activity, such as a range of immobilisation methods and manipulation of the micro-environment have been studied. Amongst others, the mode of enzyme preparation,[4–6] co-lyophilisation with lyoprotectants[7] and salts,[8,9] imprinting with substrates and substrate analogues,[10] additives[11] and cross-linked protein crystals[12] have been explored. Here we demonstrate how enzyme preparations of high activity can be rapidly and economically produced using a novel process[13] resulting in the formation of protein-coated micro-crystals (PCMCs).

The procedure for the preparation of PCMCs is summarised in Fig. 1. An aqueous protein solution is mixed with a concentrated solution of an excipient, such as a salt (*e.g.* K_2SO_4), a sugar or an amino acid. A primary requirement is that the excipient (the crystal-forming component) should show high solubility in water and negligible solubility in the precipitating water-miscible organic solvent. This combined aqueous mixture is then added dropwise with rapid mixing to a water miscible solvent (*e.g.* 1-PrOH), whereupon the protein and excipient instantly co-precipitate. The structure of the co-precipitate (SC loading in SC–K_2SO_4 = 8 wt%) typically consists of micron-sized crystals with protein molecules located at their surface. A major advantage is that during the process the organic solvent dehydrates the enzymes by a mechanism that minimises denaturation and appears to leave the majority of enzyme molecules in an active conformation. In addition a fine-particle (0.1–5 μm) suspension is formed so that the protein-coated crystals are homogeneously dispersed in the organic solvent. We have found that routine transferral of this suspension either by pipette or an automated liquid-handling system is very straightforward. This therefore means that enzyme-coated micro-crystals are ideally suited for use in biocatalyst screening programmes. For use in organic solvents, the enzyme-coated micro-crystals can be dried *in situ* to form a fine powder, or the precipitating solvent can be decanted off and replaced by a different solvent. Alternatively for aqueous applications, the enzyme-coated micro-crystals can be rapidly re-dissolved into aqueous solution.†

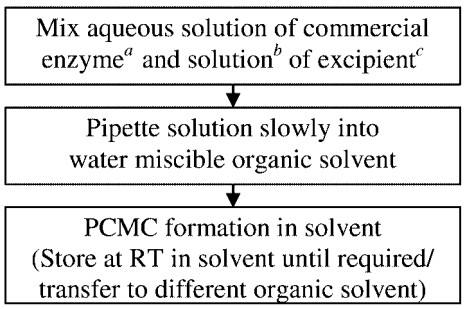

Fig. 1 Procedure for preparation of protein-coated micro-crystals.[a] At pH optimum, both pure and impure preparations can be used. [b] At or near saturation. [c] Component of crystal immobilisation matrix consists of either a salt, an amino acid or a sugar.

Table 1 shows a comparison of the catalytic activity of SC either as a lyophilised powder or after formation of the SC-coated K_2SO_4 micro-crystals (SC-K_2SO_4)‡ in different solvents. The transesterification reaction of *N*-AcTyrOEt using 1-PrOH was monitored in acetonitrile (AcCN–1% H_2O v/v). Significantly, the catalytic rate for all PCMC preparations was over three orders of magnitude higher than that typically found using a lyophilised preparation.[5] Among the solvents tested (Table 1), propan-1-ol and ethanol were found to be the most effective, whereas with SC polar aprotic solvents gave lower activity, but nevertheless markedly increased the activity compared to lyophilised preparations. We found that the water content of the organic solvent used for precipitation is quite flexible (0–20% H_2O v/v). Only at water contents greater than 20% is the activity significantly reduced.

Transmission electron microscopy (TEM) showed that co-precipitates formed in organic solvent were crystalline, resulting in rectangular crystals as shown in Fig. 2 for SC–K_2SO_4 produced in 1-PrOH. Tapping-mode atomic force microscopy (TM-AFM) imaging (data not shown) shows that the protein molecules are located in a fairly uniform layer on the surface of the crystal, where they are easily accessible to the substrate. Interestingly K_2SO_4 crystals formed in the absence of protein are larger. This too indicates that enzyme molecules, located at

Table 1 Effect of preparation method on the transesterification performance in AcCN–1% H_2O (v/v) of PCMC-SC

Enzyme form	Precipitating solvent	Relative rate[a]
Freeze-dried[b]	—	0.1
PCMC	1-PrOH–1% H_2O	97
PCMC	1-PrOH–7% H_2O	90
PCMC	1-PrOH–25% H_2O	79
PCMC	EtOH[c]	100
PCMC	AcCN[c]	45
PCMC	Acetone[c]	52
PCMC	THF[c]	76
PCMC, after storage (14 months, RT)	1-PrOH [c]	86

[a] Relative rate (100 = 29% conversion measured after 3 h). Reaction conditions: 10 mM *N*-acetyl-L-tyrosine ethyl ester, 1 M 1-PrOH, 0.47 mg SC in 3 ml of AcCN–1% H_2O (v/v), T = 25 °C and shaken at 200 rpm. [b] Freeze-dried (10 mM Tris-buffer, pH = 7.8). [c] Containing 1% (v/v) water. Samples were analysed by HPLC.¶

 DOI: 10.1039/b100722j

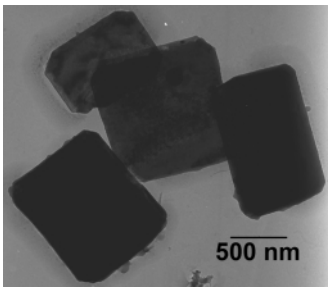

Fig. 2 Transmission electron microscopy (TEM)‖ image of K_2SO_4 crystals co-precipitated with SC using 1-PrOH–1% H_2O as precipitating solvent.

the crystal surface, limit crystal growth by acting like a 'poison'.

There are two ways the PCMCs can be stored, as a dry powder or *in situ* as a suspension in 1-PrOH. Historically, drying to a powder has been the preferred route for storage of enzyme and protein powders, but we find a loss of (up to 40%) catalytic activity as a result of air-drying, which can be regained by coating in surfactant (PPG 2025 or Span 80). Alternatively, when stored directly in the precipitating solvent, remarkably a suspension of PCMC-subtilisin can be stored for 14 months at RT with negligible loss in activity (see Table 1).

In order to assess the generality of this novel method we extended our study to lipases employing the kinetic resolution of (±)-1-phenylethanol as a model reaction. We chose as a starting point a lipase screening kit consisting of a set of 10 lipases which are available in lyophilised form and are of varying purity. Initially we screened the lipases in the set for high enantioselectivity E[14] (E > 200) in a model reaction: the conversion of (*R*,*S*)-phenylethanol to (*R*)-phenyl ethyl acetate using vinyl acetate as acyl donor. The activities of these lipases either *as received* or after precipitation to form the enzyme-coated micro-crystals are shown in Fig. 3. Remarkably, the catalytic activity is enhanced significantly for most of the enzyme-coated lipases§ when compared to the *as received* preparations. For PCMC-*Pseudomonas* sp. lipase and PCMC-using lipase B from *Candida antarctica* (CALB) the reaction is complete in 0.5 and 2 h, respectively. PCMC-*Pseudomonas* sp. lipase was found to be 200-fold more active than the *as received* preparation. Coated micro-crystals of CALB and lipase from *M. miehei* showed a 5 and 15-fold increase in catalytic activity, respectively. No change in the enantiomeric ratio (E > 200 in all cases) was observed. A 60-fold increase in the activity of K_2SO_4–CALA (E = 1) was observed. However, one enzyme system K_2SO_4–*Alcaligenes sp.* showed no improvement.

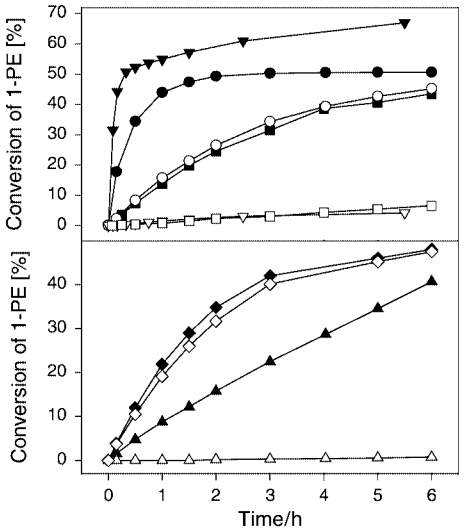

Fig. 3 Comparison in catalytic activity of lipase-coated micro-crystals and the *as received* preparations for the kinetic resolution of (±)-1-phenyl-ethanol (1-PE). PCMCs were made using K_2SO_4 as support and 1-PrOH–1% H_2O as precipitating solvent. (▼) PCMC-*Pseudomonas* sp. lipase; (▽) lipase from *Pseudomonas* sp.; (●) PCMC-CALB; (○) CALB; (■) PCMC-*Mucor miehei* lipase; (□) lipase from *Mucor miehei* lipase; (◆) PCMC-*Alcaligenes* sp. lipase; (◇) *Alcaligenes* sp. lipase; (▲) PCMC-CALA; (△) CALA. Reaction conditions: dry *tert*-butyl methyl ether (2.5 ml), lipase** (2.5 mg, except for CALA: 5 mg), 1-PE (0.1 M), vinyl acetate (0.3 M), T = 30 °C and shaken at 200 rpm. Samples were analysed by HPLC.††

The preparation of enzyme-coated micro-crystals for routine biocatalysis in organic media is fast, cheap, and requires only standard laboratory equipment. Suspensions of highly active PCMCs show significantly improved ease of handling/dispensing and storage in liquids compared to their lyophilised counterparts. This suggests that the methodology may find widespread application as a generic method for the production of biocatalysts with predictable morphology and handling capacity in automated screening applications.

We would like to thank Dr David McComb and Mr Jim Gallagher for the use of EM facilities at the University of Glasgow. The work was supported by the BBSRC, a David Phillips Research Fellowship (MCP) and funding for MK. We would also like to thank Mr Andreas Elmecker for image processing.

Notes and references

† Specific activity of subtilisin Carlsberg, *Candida antarctica* lipase B and *Mucor miehei* lipase is fully retained upon re-dissolution into aqueous solution. Other enzymes used were not investigated in this regard.

‡ Subtilisin Carlsberg, Type VIII (Sigma, UK) (4 mg) was dissolved in 100 μl of Tris buffer (10 mM, pH 7.8). To this, 300 μl of a saturated solution of excipient was added. This combined solution was then added drop-wise to a shaking vial (150 rpm) containing 6 ml of the organic solvent.

§ PCMC-lipases: *Candida antarctica* lipases L-2, and L-5, *Pseudomonas* sp. lipase L-6, *Mucor miehei* lipase L-9, *Alcaligenes* sp. lipase L-10 (Roche Diagnostics, Germany). Procedure as for SC except: 2.5 mg of L-2, L-6, L-9, L-10; 5 mg of L-5 dissolved in 62 μl of phosphate buffer (50 mM, pH 7.0) and 188 μl of a saturated solution of K_2SO_4 was then added. Addition to 3.75 ml of 1-PrOH–1% H_2O as described above. The PCMCs were washed with dry *tert*-butyl methyl ether to remove 1-PrOH.

¶ WATERS 2690 HPLC (Waters, UK) equipped with a Spherisorb S5 ODS2 column (4.6 × 250 mm) (Waters, UK). λ_{max} = 280 nm.

‖ Air-dried PCMCs were examined using a Jeol JEM 1200 EX transmission electron microscope (JEOL, Tokyo, Japan).

** Weight of *as received* powders is the same as weight of powder used for formation of PCMCs. Protein loading not determined.

†† HPLC (as above) using a Chiracel OD column (250 × 4.6 mm) (Daicel, Japan). λ_{max} = 210 nm.

1 M. Klibanov, *Trends Biotechnol.*, 1997. **15**, 97.
2 K. Griebenow and A. M. Klibanov, *Biotechnol. Bioeng.*, 1997, **53**, 351.
3 K. Griebenow and A. M. Klibanov, *Proc. Natl. Acad. Sci. U.S.A.*, 1995, **92**, 10969.
4 H. Noritomi, O. Almarsson, G. L. Barletta and A. M. Klibanov, *Biotechnol. Bioeng.*, 1996, **51**, 95.
5 J. Partridge, P. J. Halling and B. D. Moore, *Chem. Commun.*, 1998, **7**, 841.
6 T. Ke and A. M. Klibanov, *Biotechnol. Bioeng.*, 1998, **57**, 746.
7 K. Dabulis and A. M. Klibanov, *Biotechnol. Bioeng.*, 1993, **41**, 566.
8 Y. L. Khmelnitzky, S. H. Welch, D. S. Clark and J. S. Dordick, *J. Am. Chem. Soc.*, 1994, **116**, 2647.
9 M. T. Ru, J. S. Dordick, J. A. Reimer and D. S. Clark, *Biotechnol. Bioeng.*, 1999, **63**, 233.
10 J. O. Rich and J. S. Dordick, *J. Am. Chem. Soc.*, 1997, **119**, 3245.
11 F. Theil, *Tetrahedron*, 2000, **56**, 2905.
12 J. J. Lalonde, C. Govardhan, C. Khalaf, A. G. Martinez, K. Visuri and A. Margolin. *J. Am. Chem. Soc.* , 1995, **117**, 6845.
13 UK Patent disclosed: WO 00/69877, *Rapid dehydration of proteins*, M. C. Parker, B. D. Moore, P. J. Halling and J. Partridge.
14 C-S. Chen, Y. Fujimoto, G. Girdaukas and C. J. Sih, *J. Am. Chem. Soc.*, 1982, **104**, 7294.

CHEMCOMM
Communication
www.rsc.org/chemcomm

Formation of a single-stranded silver(I) helical-coordination polymer containing π-stacked planar chiral N_4S_2 ligands

Paula L. Caradoc-Davies and Lyall R. Hanton*

Department of Chemistry, University of Otago, PO Box 56, Dunedin, New Zealand.
E-mail: lhanton@alkali.otago.ac.nz

Received (in Cambridge, UK) 27th February 2001, Accepted 2nd March 2001
First published as an Advance Article on the web 25th May 2001

***In-situ* planar chirality was induced in an achiral ligand by intramolecular π-stacking interactions upon complexation with silver(I) and crystallisation, to give a single-stranded helix with a nanoscale pitch which assembled into a three-dimensional network.**

The utilisation of chirality in coordination-polymer chemistry is best exemplified by helicity. However, the factors controlling the formation of coordination helices are still not well understood despite the considerable attention this area has received.[1] When achiral ligands are employed to form helices they usually give racemates[2] although there are a few exceptions where spontaneous resolution upon crystallisation (conglomerate crystallisation) occurs.[1b,3] When chiral ligands are employed they can be used as either enantiopure ligands or racemic mixtures. Enantiopure ligands often lead to the stereoselective synthesis of helices[4] whereas racemic mixtures of ligands are less predictable.[5] Typically, helical architectures have been constructed using simple heterocycles[1a,c,2b,6] or flexible oligopyridines.[2c,4a,7] The use of thioether-heterocyclic ligands in this context has been less well studied.[1b] Recently we observed[8] that an acyclic thioether-oligopyridine ligand, 2,6-bis(2′-pyridylmethylsulfanylmethyl)pyridine, upon interaction with Ag(I) folded, through strong intraligand π-stacking interactions, in such a way as to exhibit planar chirality. Our strategy was to develop this flexible ligand for polymer formation by retaining most of its features but replacing the central pyridine ring with a 2,3-substituted pyrazine linker. In terms of investigating helix self-assembly, this achiral ligand system has properties in common with chiral ligands derived from racemic mixtures for it may develop planar chirality *in situ* through complexation and conformational folding upon crystallisation. Recently, planar-chiral elements have been incorporated into cyclophanes and used to influence the self-assembly of supramolecular arrays.[9]

The new ditopic ligand **L** (Fig. 1) was prepared in moderate yield (67%) by the base coupling of 2,3-bis(chloromethyl)pyrazine[10] and 6-methyl-2-(sulfanylmethyl)pyridine.[11]† Reaction of **L** with $AgClO_4$ in a 1:2 molar ratio in MeCN gave a pale-yellow solution which was partially reduced in volume and then treated with diethyl ether to give a white precipitate in 85% yield. Microanalysis of the complex was consistent with a 1:2 ligand:metal ratio.‡ The complex was moderately soluble in MeCN but not appreciably soluble in other common organic solvents. Electrospray mass spectrometry under normal operating conditions in MeCN showed only one peak at *m/z* 489.0 with an appropriate isotopic pattern for the 1:1 $[Ag(\mathbf{L})]^+$ ion. ^{1}H and ^{13}C NMR spectra were consistent with a symmetrical structure for the complex. Variable temperature ^{1}H NMR spectra measured in CD_3CN showed no significant changes other than broadening of peaks down to the temperature limit of the solvent. The symmetrical nature of the ^{1}H NMR spectra implied that the solution species was either symmetric and static, or more likely, asymmetric and undergoing dynamic processes. X-Ray crystal structure analysis§ of the complex revealed a one-dimensional single-stranded helix consisting of repeating $[Ag_2(\mathbf{L})](ClO_4)_2$ units (Fig. 2). The complex underwent conglomerate crystallisation and the crystal chosen for X-ray analysis belonged to the enantiomorphic space group $P6_522$. As is necessary for this space group only the *M* enantiomer of the helix is observed in the crystal. Since **L** was achiral when reacted with Ag(I), the bulk sample should contain equal amounts of both types of enantiomorphic crystals. The helix runs along the 6_5 screw axis with an exceptionally long pitch of 52.48(2) Å, equal to the length of the *c* axis (Fig. 3).[3a,4a] The pitch is long despite the compact nature of the 'three-layer' π-stacked ligand. The intraligand π-stacking distances determined from atom···atom contacts between rings range from

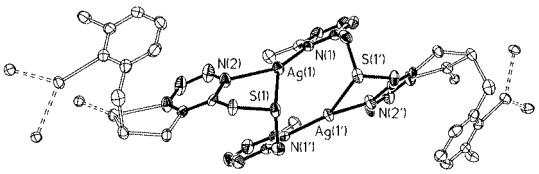

Fig. 2 Fragment of the helix showing the folding of the ligand. The coordination geometry and π stacking about the silver ions are highlighted in black, and dashed bonds indicate the continuation of the polymer (50% probability ellipsoids). Selected bond lengths (Å) and angles (°): Ag(1)–N(1) 2.234(5), Ag(1)–N(2) 2.374(5), Ag(1)–S(1) 2.588(2); N(1)–Ag(1)–N(2) 134.6(2), N(1)–Ag(1)–S(1) 144.9(1), N(2)–Ag(1)–S(1) 77.1(1).

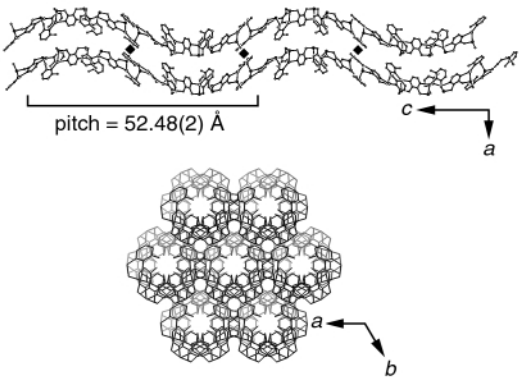

Fig. 3 Views of the helix with H atoms and ClO_4^- anions omitted. (Top) view of two adjacent strands of the helix. The π–stacking interaction between the helices is indicated by diamonds ◆. (Bottom) view down the crystallographic *c*–axis showing the three–dimensional homochiral assembly.

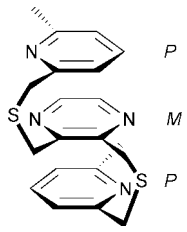

Fig. 1 Ligand **L** folded as the enantiomer found in the crystal structure of $\{[Ag_2(\mathbf{L})](ClO_4)_2\}_\infty$ showing *P,M,P* planar chirality.

 DOI: 10.1039/b101875m

3.30–4.41 Å, with symmetry-related pyridine rings tilted at 22.2° to the central pyrazine ring. The 'three-layer' stack causes the two sets of ligand donors, $N_{pyridine}SN_{pyrazine}$, to be arranged in opposite directions which is ideal for the linking of metal centres in polymer formation. The 'three-layer' π-stacking also confers planar chirality on the ligands, with the same *P*,*M*,*P* enantiomer being observed throughout the helix (Fig. 1).[12] CPK models indicate that it is not possible to build the diastereomerically-related *P* helix with this *P*,*M*,*P* enantiomer of the ligand but that the enantiomerically-related *P* helix can be built with the *M*,*P*,*M* enantiomer. Each Ag(I) atom adopts a distorted trigonal planar arrangement, which links symmetry-related ligands by $N_{pyrazine}$,S chelation from one ligand and $N'_{pyridine}$ donation from the other. Thus each ligand binds to four Ag(I) ions. In the repeating units the distance between the Ag(I) ions is 3.116(1) Å, which lies within the range (2.86–3.22 Å) for similar systems.[8,13] The trigonal planes in the repeating unit are tilted at 68.2° with respect to each other. In addition, the trigonal planes across the pyrazine are tilted by a further 16.3°. The combined tilting of these planes across the 'three-layered' π-stacked ligands generates the shallow helical twist and hence is responsible for the long pitch of the helix. Previously, we found that the related ligand bis(2-pyridylmethyl)sulfide formed a dimeric side-by-side complex with silver(I).[8] That discrete complex was almost identical to the section of the helix highlighted in black in Fig. 2 and indicates that this dimeric arrangement is particularly favourable for ligands of this type in the presence of silver(I).

The helices are close packed (Fig. 3) in such a way that each pyridine ring is involved in an intermolecular π-stacking interaction with a pyridine ring on an adjacent helix (atom···atom contacts between rings range from 3.63 to 3.74 Å). Between any two adjacent helices there are two such interactions per turn of helix. These interactions help to generate a tightly packed three-dimensional network with no solvent accessible volume (Fig. 3). This is further evidenced by the relatively short Ag···Ag distance [8.210(2) Å] between adjacent helices. These intermolecular interactions are probably responsible for the packing together of homochiral helices on crystallisation and the resulting conglomerate crystallisation.

We have shown that an achiral ligand predisposed to intramolecular π-stacking can generate *in-situ* planar chirality on coordination to silver(I) and the formation of a coordination polymer. In addition, this property results in the formation of a single-stranded helix and the packing of homochiral helices. This work points to a complementary approach to that of using racemic mixtures of ligands as a means of investigating the effect of chirality in molecular recognition processes in coordination-polymer chemistry. Currently we are actively pursuing the use of *in-situ* chirality in the formation of supramolecular architectures.

We thank Professor Ward T. Robinson and Dr Jan Wikaira (University of Canterbury) for X-ray data collection, Associate Professor Bill Henderson (University of Waikato) for electrospray MS data and the University of Otago for financial support.

Notes and references

† *Synthesis* of 2,3-bis(6′-methyl-2′-pyridylmethylsulfanylmethyl)pyrazine **L**: 6-methyl-2-(sulfanylmethyl)pyridine (4.4 g, 0.031 mol) was added to degassed MeOH (250 ml) containing 0.72 g (0.031 mol) Na metal and was stirred for 1 h. 2,3-Bis(chloromethyl)pyrazine (2.8 g, 0.016 mol) was dissolved in degassed CH_2Cl_2, added to the above solution, refluxed for 4 h, and stirred overnight. The resulting solution was reduced to give a brown residue which was dissolved in CH_2Cl_2 (100 ml), washed with H_2O (2 × 100 ml), dried ($MgSO_4$) and reduced to give a golden oil. Yield: 4.0 g (67%). NMR: δ_H(500 MHz, $CDCl_3$) 8.32 (s, 2H), 7.49 (t, 2H, ^3J 7.5 Hz), 7.16 (d, 2H, ^3J 7.5 Hz), 6.99 (d, 2H, ^3J 7.5 Hz), 3.96 (s, 4H), 3.78 (s, 4H), 2.52 (s, 6H). Anal. Calc. for $C_{20}H_{22}N_4S_2{\cdot}H_2O$: C, 59.97; H, 6.04; N, 13.99; S, 16.01. Found: C, 59.69; H, 6.03; N, 14.10; S, 16.03%.

‡ *Synthesis* of $[Ag_2(\mathbf{L})](ClO_4)_2$: $AgClO_4$ (54 mg, 0.26 mmol) was dissolved in degassed MeCN and added *via* cannula to **L** (50 mg, 0.14 mmol) dissolved in degassed MeCN and allowed to stir for 1 h. The lemon solution was reduced in volume to 2 ml, diethyl ether was added and the resulting white precipitate was filtered off and dried *in vacuo*. Yield: 89 mg (85%). NMR: δ_H(300 MHz; CD_3CN) 8.03 (s, 2H), 7.82 (t, 2H, ^3J 7.5 Hz), 7.39 (d, 2H, ^3J 7.5 Hz), 7.29 (d, 2H, ^3J 7.5 Hz), 4.30 (s, 4H), 4.13 (s, 4H), 2.51 (s, 6H). Anal. Calc. for $C_{20}H_{22}N_4S_2Ag_2Cl_2O_8$: C, 30.13; H, 2.78; N, 7.03; S, 8.04. Found: C, 30.33; H, 2.76; N, 6.99; S, 7.88%; Colourless crystals were grown from the slow evaporation of an acetonitrile solution of the complex.

§ *Crystal data* for $\{[Ag_2(\mathbf{L})](ClO_4)_2\}_\infty$: $C_{20}H_{22}Ag_2Cl_2N_4O_8S_2$, M = 797.18, hexagonal, $P6_522$ (no. 179), a = 9.182(2), c = 52.48(2) Å, U = 3832(2) Å^3, T = 163(2) K, Z = 6, μ(Mo-Kα) = 1.961 mm^{-1}, 49 638 reflections measured, 2623 independent reflections (R_{int} = 0.0455) , [2553, $I \geqslant 2\sigma(I)$], R_1 = 0.0420, 0.0434 (all data), wR_2 = 0.0887, 0.0893 (all data).

CCDC 150985. See http://www.rsc.org/suppdata/cc/b1/b101875m/ for crystallographic data in .cif or other electronic format.

1 (*a*) A. J. Blake, N. R. Champness, P. A. Cooke and J. E. B. Nicolson, *Chem. Commun.*, 2000, 665; (*b*) M. Hong, W. Su, R. Cao, M. Fujita and J. Lu, *Chem. Eur. J.*, 2000, **6**, 427; (*c*) T. Ezuhara, K. Endo and Y. Aoyama, *J. Am. Chem. Soc.*, 1999, **121**, 3279; (d) M. Munakata, L. P. Wu and T. Kuroda-Sowa, *Adv. Inorg. Chem.*, 1999, **46**, 173.

2 (*a*) M. Munakata, G. L. Ning, Y. Suenaga, K. Sugimoto, T. Kuroda-Sowa and M. Maekawa, *Chem. Commun.*, 1999, 1545; (*b*) M.-L. Tong, X.-M. Chen, B.-H. Ye and S. W. Ng, *Inorg. Chem.*, 1998, **37**, 5278; (*c*) O. J. Gelling, F. van Bolhuis and B. L. Feringa, *J. Chem. Soc., Chem. Commun.*, 1991, 917.

3 (*a*) M. A. Withersby, A. J. Blake, N. R. Champness, P. Hubberstey, W. S. Li and M. Schröder, *Angew. Chem., Int. Ed. Engl.*, 1997, **36**, 2327; (*b*) K. Biradha, C. Seward and M. J. Zaworotko, *Angew. Chem., Int. Ed.*, 1999, **38**, 492; (*c*) A. Erxleben, *Inorg. Chem.*, 2001, **40**, 412.

4 (*a*) O. Mamula, A. von Zelewsky, T. Bark and G. Bernardinelli, *Angew. Chem., Int. Ed.*, 1999, **38**, 2945; (*b*) B. Wu, W.-J. Zhang, S.-Y. Yu and X.-T. Wu, *J. Chem. Soc., Dalton Trans.*, 1997, 1795.

5 M. A. Masood, E. J. Enemark and T. D. P. Stack, *Angew. Chem., Int. Ed.*, 1998, **37**, 928; T. Kawamoto, B. S. Hammes, B. Haggerty, G. P. A. Yap, A. L. Rheingold and A. S. Borovik, *J. Am. Chem. Soc.*, 1996, **118**, 285; T. Suzuki, H. Kotsuki, K. Isobe, N. Moriya, Y. Nakagawa and M. Ochi, *Inorg. Chem.*, 1995, **34**, 530.

6 L. Carlucci, G. Ciani, D. M. Proserpio and A. Sironi, *Inorg. Chem.*, 1998, **37**, 5941.

7 P. K. Bowyer, K. A. Porter, A. D. Rae, A. C. Willis and S. B. Wild, *Chem. Commun.*, 1998, 1153; L. Carlucci, G. Ciani, D. W. van Gudenberg and D. M. Proserpio, *Inorg. Chem.*, 1997, **36**, 3812.

8 P. L. Caradoc-Davies, L. R. Hanton and K. Lee, *Chem. Commun.*, 2000, 783.

9 P. R. Ashton, S. E. Boyd, S. Menzer, D. Pasini, F. M. Raymo, N. Spencer, J. F. Stoddart, A. J. P. White, D. J. Williams and P. G. Wyatt, *Chem. Eur. J.*, 1998, **4**, 299.

10 G. R. Newkome, G. E. Kiefer, Y.-J. Xia and V. K. Gupta, *Synthesis*, 1984, 676.

11 L. R. Hanton and K. Lee, *Inorg. Chem.*, 1999, **38**, 1634.

12 E. L. Eliel, S. H. Wilen and L. N. Mander, *Stereochemistry of Organic Compounds*, Wiley-Interscience, New York, 1994, pp. 1119–1190.

13 S.-M. Kuang, Z.-Z. Zhang, Q.-G. Wang and T. C. W. Mak, *J. Chem. Soc., Dalton Trans.*, 1998, 2927; C. M. Hartshorn and P. J. Steel, *Inorg. Chem.*, 1996, **35**, 6902; A. Bilyk, M. M. Harding, P. Turner and T. W. Hambley, *J. Chem. Soc., Dalton Trans.*, 1995, 2549; R. J. Anderson and P. J. Steel, *Acta Crystallogr., Sect. C*, 1998, **54**, 223.

CHEMCOMM
Communication
www.rsc.org/chemcomm

A Ru–carbene complex with a metallacycle involving a 1,8-naphthylidine framework

Takashi Tomon,[ab] Dai Ooyama,[c] Tohru Wada,[ab] Kazushi Shiren[b] and Koji Tanaka*[ab]

[a] *Department of Structural Molecular Science, Graduate University for Advanced Studies, 38 Nishigonaka, Myodaiji, Okazaki, Aichi 444-8585, Japan*
[b] *Institute for Molecular Science and CREST, Japan Science and Technology Corporation (JST), 38 Nishigonaka, Myodaiji, Okazaki, Aichi 444-8585, Japan*
[c] *Faculty of Education, Fukushima University, Kanayagawa, Fukushima 960-1296, Japan*

Received (in Cambridge, UK) 30th January 2001, Accepted 2nd May 2001
First published as an Advance Article on the web 25th May 2001

The reaction of $[Ru(bpy)_2(napy\text{-}\kappa^2N,N')](PF_6)_2$ [1]$(PF_6)_2$ (napy = 1,8-naphthyridine) with propiolic acid yielded a Ru–carbene complex with a five-membered metallacycle involving a 1,8-naphthylidine framework.

Reactions of transition metal complexes with terminal alkynes have been utilized to prepare vinylidene complexes,[1] which are characterized by the electrophilicity of the α carbon. In fact, vinylidene–metal complexes are converted to alkoxy–alkyl carbene complexes by reaction with alcohols.[2] We have reported that the non-bonded nitrogen of napy-κ*N* of $[Ru(bpy)_2(napy\text{-}\kappa N)(CO)]^{2+}$ attacks the carbonyl carbon to form a five-membered metallacycle upon one-electron reduction of the napy moiety (napy = 1,8-naphthyridine).[3] Moreover, $[Ru(bpy)_2(napy\text{-}\kappa^2N,N')]^{2+}$ exists in equilibrium with $[Ru(bpy)_2(napy\text{-}\kappa N)(solvent)]^{2+}$ in polar solutions.[4] Thus $[Ru(bpy)_2(napy\text{-}\kappa^2N,N')]^{2+}$ readily forms a 1:1 adduct with various substrates upon opening of the chelate ring. The reaction of $[Ru(bpy)_2(napy\text{-}\kappa^2N,N')](PF_6)_2$ [1]$(PF_6)_2$ with propiolic acid in alcohol was conducted to elucidate whether the non-bonded nitrogen of napy or alcohol attacks the α carbon of the vinylidene moiety. Here we report the isolation of a Ru–carbene complex with a metallacycle **2a**$^{2+}$ (eqn. 1), and the reversible conversion between **2a**$^{2+}$ and the vinyl complex **3**$^{+}$ upon acid–base treatment.

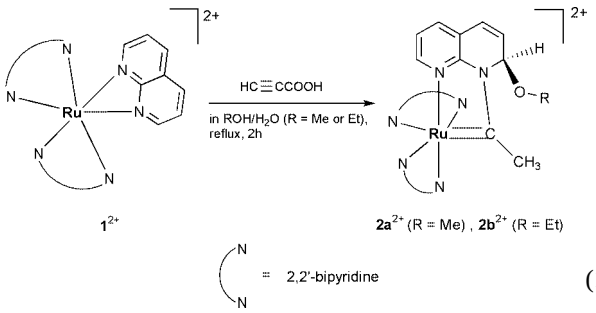

(1)

A CH_3OH/H_2O (3:2 v/v) solution containing [**1**]$(PF_6)_2$ (60 mg, 72 μmol) and HCCC(O)OH (7 mg, 100 μmol) was refluxed for 2 h, and [**2a**]$(PF_6)_2$ was obtained from the solution (eqn. 1). Recrystallization of the crude product from CH_3CN/CH_3OH (4:1 v/v) gave single crystals of [**2a**]$(PF_6)_2 \cdot CH_3CN$ in 64% yield.† The similar reaction between [**1**]$(SbF_6)_2$ and HCCC(O)OH in C_2H_5OH/H_2O (4:1 v/v) under similar reaction conditions afforded [**2b**]$(SbF_6)_2$ in 56% yield (eqn. 1).†

The molecular structure of **2a**$^{2+}$ determined by X-ray diffraction analysis is shown in Fig. 1.[5] The ruthenium atom of **2a**$^{2+}$ has octahedral geometry with four nitrogen atoms of two bpy ligands, one nitrogen from napy and one carbon of the CCH_3 group. The characteristic features of **2a**$^{2+}$ are the C–N bond formation between the CCH_3 group and one nitrogen of napy, and the attachment of the CH_3O group to the 2-position of the napy moiety. The resultant five-membered metallacycle consisting of Ru, N(1), C(11), N(2), and C(2) atoms in an almost planar structure, and the sum of the bond angles around the five-membered ring is almost 360°. Despite the attachment of CH_3O to the 2-positon of the napy moiety, the resultant ligand still maintains the planar structure in **2a**$^{2+}$. As a result, the napy moiety and the five-membered metallacycle are co-planar. The Ru–N(4) (2.156(9) Å) bond *trans* to Ru–C(2) is substantially longer than the other Ru–N bonds of **2a**$^{2+}$ (2.03(1)–2.08(1) Å), suggesting a strong *trans* effect of the carbene ligand. The Ru–C(2) bond distance (1.93(1) Å) is in the expected range of hexa-coordinated ruthenium carbene bonds (1.941–1.98 Å),[6] and the bond length is longer than those expected for penta-coordinated ruthenium carbene complexes (1.810–1.861 Å).[7] The ^{13}C NMR spectrum of **2a**$^{2+}$ also showed the α-carbon signal of the Ru–CCH_3 group at δ 293 as a singlet, similar to most Ru carbene complexes.[2,6a–c,7e,f]

The complex [**2a**]$(PF_6)_2$ was stable in $CH_3OH/(CH_3)_2CO$ and $H_2O/(CH_3)_2CO$. On the other hand, the methyl signals of the CH_3O and the Ru–CCH_3 groups of **2a**$^{2+}$ (δ 2.95 and 2.85, respectively) gradually weakened with time in the ^1H NMR spectrum in $(CD_3)CO/CD_3OD$ (1:1 v/v). The Ru–CCH_3 signal vanished in 30 min at ambient tenperature, and the CH_3O one disappeared after 12 h at 65 °C. At the same time, the methyl signal of free methanol appeared at δ 3.33. Moreover, **2a**$^{2+}$ was

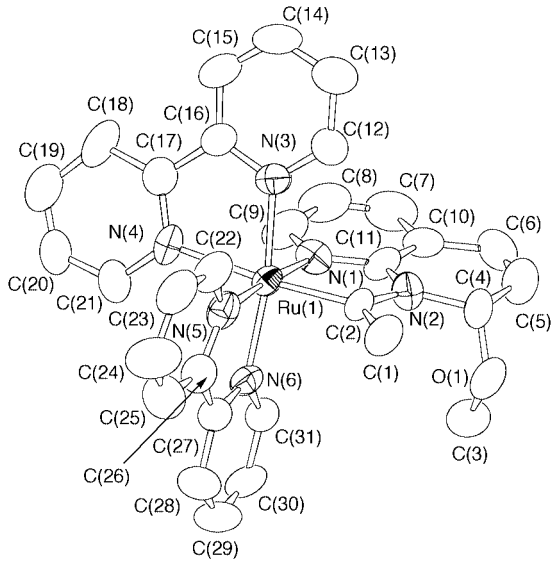

Fig. 1 An ORTEP view of complex **2a**$^{2+}$. Selected intramolecualr distances (Å): Ru(1)–N(1), 2.03(1); Ru(1)–N(3), 2.061(9); Ru(1)–N(4), 2.156(9); Ru(1)–N(5), 2.08(1); Ru(1)–N(6), 2.052(9); Ru(1)–C(2), 1.93(1); C(1)–C(2), 1.53(2); C(2)–N(2), 1.41(1); C(4)–O(1), 1.40(2); C(3)–O(1), 1.40(2). Selected bond angles (degrees): N(1)–Ru(1)–C(2), 79.8(5); Ru(1)–C(2)–C(1), 127.1(9); Ru(1)–C(2)–N(2), 116.3(8); C(1)–C(2)–N(2), 117(1); C(2)–N(2)–C(4), 123(1); C(2)–N(2)–C(11), 114(1); C(4)–N(2)–C(11), 122(1); N(2)–C(4)–O(1), 112(1); N(2)–C(4)–C(5), 112(1); C(5)–C(4)–O(1), 111(1).

 DOI: 10.1039/b101045j

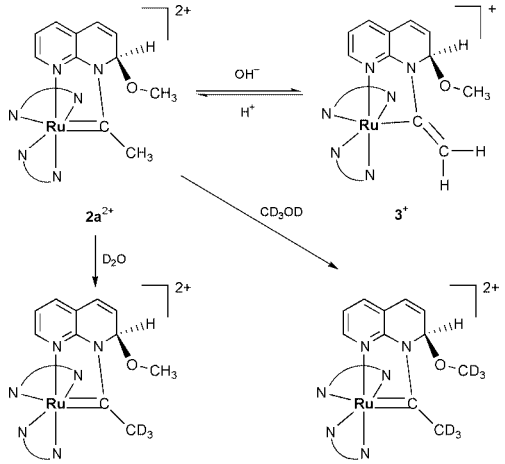

Scheme 1

converted to **2b**$^{2+}$ in $C_2H_5OH/(CH_3)_2CO$ for 1 week at room temperature. Thus, the Ru–CCH_3 and CH_3O groups of **2a**$^{2+}$ underwent H/D exchange and substitution, respectively, by CD_3OD (Scheme 1). The rate of the H/D exchange was faster than substitution by CD_3OD, and the H/D exchange reaction was greatly enhanced in D_2O, since the Ru–CCH_3 signal (δ 2.78) disappeared after 5 min in the ^{1}H NMR spectrum of **2a**$^{2+}$ in $(CD_3)_2CO/D_2O$ (10 : 1 v/v). On the other hand, treatment of [**2a**]$(PF_6)_2$ with an equiv. amount of aqueous NaOH in CD_2Cl_2 caused the appearance of new signals at δ 4.96 and 2.99, and δ 92.5 in the ^{1}H NMR and ^{13}C NMR spectra, respectively, and the proton and carbon signals of the Ru–CCH_3 group of **2a**$^{2+}$ completely disappeared. The addition of 1 equiv. of HPF_6 to the solution regenerated the ^{1}H NMR and ^{13}C NMR spectra of **2a**$^{2+}$. Such complete recovery of **2a**$^{2+}$ in the cycle of the acid–base treatments without producing CH_3OH is indicative of the reversible conversion between the carbene complex **2a**$^{2+}$ and the vinyl complex **3**$^+$ without opening the five-membered metallacycle (Scheme 1).

The carbene complex **2a**$^{2+}$ is probably formed *via* a Ru–vinylidene intermediate formed by the reaction of **1**$^{2+}$ with HCCC(O)OH, though it is not clear whether the decarboxylation takes place before or after the formation of the Ru–vinylidene framework. Although vinylidene complexes react with alcohols to produce a variety of alkoxy–alkyl carbene complexes, the α-carbon of the carbene moiety of **2a**$^{2+}$ linked exclusively with the non-bonded nitrogen of napy in MeOH. Such novel N–C bond formation must be assisted by the attachment of the CH_3O^- group at the 2-position of the napy ligand, since intra-molecular attack of the non-bonded nitrogen of napy to the carbonyl carbon of $[Ru(bpy)_2(napy\text{-}\kappa N)(CO)]^{2+}$ is initiated by the ligand localized one-electron reduction.

Notes and references

† *Spectroscopic data* for [**2a**]$(PF_6)_2\cdot CH_3CN$: ^{1}H NMR (500 MHz, CD_3CN): δ 8.52–6.33 (m, 22H, aromatic H), 2.84 (s, 3H, OCH_3), 2.68 (s, 3H, CCH_3). ^{13}C NMR (270 MHz, CD_3CN): δ 293.6 (Ru=CCH$_3$), 157.5–119.0 (aromatic C), 82.8 (OCH_3), 50.2 (Ru=CCH_3). IR (KBr): 2252, 1659, 1605 cm^{-1}. ESI-MS: m/z = 301 (M^{2+}). Anal. Calcd. for $C_{33}H_{31}N_7OF_{12}P_2Ru$: C, 42.50; H, 3.35; N,10.51. Found: C, 42.31; H, 3.37; N, 10.39%. [**2b**]$(SbF_6)_2$: ^{1}H NMR (500 MHz, CD_3CN): δ 8.50–6.45 (m, 22H, aromatic H), 3.76 and 3.59 (q, 2H, OCH_2CH_3), 2.69 (s, 3H, CCH_3), 1.28 (t, 3H, OCH_2CH_3). ^{13}C NMR (270 MHz, CD_3CN): δ 294.7 (Ru=CCH$_3$), 157.3–121.1 (aromatic C), 81.8 (OCH_2CH_3), 61.8 (Ru=CCH_3), 15.4 (OCH_2CH_3). IR (KBr): 1653, 1605 cm^{-1}. ESI-MS: m/z = 308 (M^{2+}). Anal. Calcd. for $C_{32}H_{30}N_6OF_{12}Sb_2Ru$: C, 35.35; H, 2.78; N, 7.73. Found: C, 35.15; H, 2.90; N, 7.45%. [**3**](PF_6): ^{1}H NMR (500 MHz, CD_2Cl_2): δ 9.12–5.84 (m, 22H, aromatic H), 4.96 and 2.99 (s, 2H, C=CH_2), 2.54 (s, 3H, OCH_3). ^{13}C NMR (270 MHz, CD_2Cl_2): δ 184.6 (C=CH$_2$), 157.2–114.6 (aromatic C), 92.5 (C=CH_2), 79.9 (OCH_3). ESI-MS: m/z = 601 (M^+).

Crystal data for [**2a**]$(PF_6)_2\cdot CH_3CN$: $C_{33}H_{31}F_{12}N_7OP_2Ru$, M = 932.65, orthorhombic, space group $Pna2_1$ (no. 33), a = 12.495(2), b = 19.134(4), c = 15.602(3) Å, V = 3729(1) Å^3, T = 296 K, Z = 4, D_c = 1.661 g cm^{-3}, μ(Mo-Kα) = 6.06 cm^{-1}, 4889 reflections measured, 4778 unique reflections, 2566 observed reflections [$I > 3.00\sigma(I)$]. Final R = 0.051 and Rw = 0.071. CCDC reference number 157684. See http://www.rsc.org/suppdata/cc/b1/b101045j/ for crystallographic data in .CIF or other electronic format.

1 M. C. Puerta and P. Valerga, *Coord. Chem. Rev.*, 1999, **193–195**, 977.
2 M. P. Gamasa, J. Gimeno, B. M. Martín-Vaca, J. Borge, S. García-Granda and E. Perez-Carreño, *Organometallics*, 1994, **13**, 4045.
3 H. Nakajima and K. Tanaka, *Chem. Lett.*, 1995, 891.
4 H. Nakajima, H. Nagao and K. Tanaka, *J. Chem. Soc., Dalton Trans.*, 1996, 1405.
5 Disorder was found for one of two PF_6^- ions in the crystal structure of [**2a**]$(PF_6)_2\cdot CH_3CN$.
6 (*a*) V. W. W. Yam, B. W. K. Chu and K. K. Cheung, *Chem. Commun.*, 1998, 2261; (*b*) J. Yang, J. Yin, K. A. Abboud and W. M. Jones, *Organometallics*, 1994, **13**, 971; (*c*) D. Pilette, K. Ouzzine, H. L. Bozec and P. H. Dixneuf, *Organometallics*, 1992, **11**, 809; (*d*) L. M. Boyd, G. R. Clark and W. R. Roper, *J. Organomet. Chem.*, 1990, **397**, 209; (*e*) G. J. Irvine, C. E. F. Rickard, W. R. Roper and L. J. Wright, *J. Organomet. Chem.*, 1990, **387**, C5.
7 (*a*) L. Jafarpour, E. D. Stevens and S. P. Nolan, *J. Organomet. Chem.*, 2000, **606**, 49; (*b*) P. A. Schaaf, R. Kolly, H. J. Kirner, F. Rime, A. Mühlebach and A. Hafner, *J. Organomet. Chem.*, 2000, **606**, 65; (*c*) P. Hofmann, M. A. O. Volland, S. M. Hansen, F. Eisenträger, J. H. Gross and K. Stengel, *J. Organomet. Chem.*, 2000, **606**, 88; (*d*) S. Chang, L. Jones II, C. Wang, L. M. Henling and R. H. Grubbs, *Organometallics*, 1998, **17**, 3460; (*e*) P. Schwab, R. H. Grubbs and J. W. Ziller, *J. Am. Chem. Soc.*, 1996, **118**, 100; (*f*) Z. Wu, S. T. Nguyen, R. H. Grubbs and J. W. Ziller, *J. Am. Chem. Soc.*, 1995, **117**, 5503.

CHEMCOMM Communication
www.rsc.org/chemcomm

Ruthenium(II)-catalyzed [2 + 2 + 2] cycloaddition of 1,6-diynes with electron-deficient nitriles†

Yoshihiko Yamamoto, Satoshi Okuda and Kenji Itoh*

Department of Molecular Design and Engineering, Graduate School of Engineering, Nagoya University, Chikusa, Nagoya 464-8603, Japan. E-mail: Itohk@apchem.nagoya-u.ac.jp

Received (in Cambridge, UK) 20th March 2001, Accepted 3rd May 2001
First published as an Advance Article on the web 25th May 2001

Ru(II)-catalyzed cycloaddition of 1,6-diynes with electron-deficient nitriles gave the desired bicyclic pyridines in moderate to high yields.

Transition-metal-catalyzed [2 + 2 + 2] cyclocotrimerization of two alkyne molecules and a nitrile has been recognized as a straightforward protocol providing substituted pyridines.[1,2] Although the selective cyclocotrimerization of two different alkynes and a nitrile was achieved using stoichiometric cobalt[1] or zirconium reagents,[3] the catalytic controls of both the chemo- and regiochemistries have remained as a crucial problem. In this context, the intermolecular coupling between an α,ω-diyne and a nitrile was first pioneered by Vollhardt *et al*. in their work on the catalytic reactions of $CpCo(CO)_2$,[4,5] and subsequently this strategy has been successfully applied for the synthesis of Vitamin B_6.[6] Electron-deficient nitriles, however, have been reported to be hardly involved in such a useful pyridine annulation. Ethyl cyanoformate and pentafluorobenzonitrile gave the desired pyridines only in poor yields, lower than 10%. In sharp contrast, we found that a ruthenium(II) complex, Cp*Ru(cod)Cl (Cp* = pentamethylcyclopentadienyl **1**), effectively catalyses the cycloaddition of 1,6-diynes and nitriles activated by an electron-withdrawing group (Scheme 1), although the same Ru(II) complex failed to promote the reaction with simple nitriles such as acetonitrile or benzonitrile.[7]

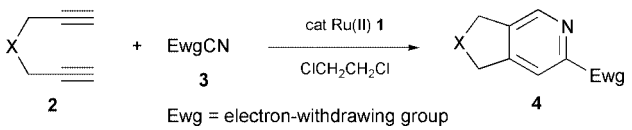

Scheme 1

Typically, to a solution of dimethyl dipropargylmalonate (**2a**)‡ in 1,2-dichloroethane was added a solution of the catalyst **1** and ethyl cyanoformate (**3a**) (0.02 and 1.5 equiv. to **2a**, respectively) in 1,2-dichloroethane at rt. The solution was stirred for 30 min at 60 °C to give the desired pyridine **4a** in 83% yield (Table 1, entry 1). The side reaction of **2a** leading to arene byproducts was completely suppressed. In the same manner, benzoyl cyanide (**3b**) gave the corresponding pyridine **4b** as a sole product in high yield (entry 2). On the other hand, acetyl cyanide (**3c**) and tosyl cyanide (**3d**) required higher catalyst loading (10 mol%) and temperature (80 °C). The former selectively gave the desired pyridine **4c** in 90% yield (entry 3), although the concomitant formation of the dimer **5a** was observed in the reaction of **3d** (entry 4). In addition to acyl and sulfonyl cyanides, polyhaloalkylcyanides could be used for the

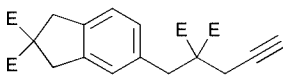

5a E = CO_2Me

† Electronic supplementary information (ESI) available: experimental procedures and analytical data for compounds **4**, **7** and **8**. See http://www.rsc.org/suppdata/cc/b1/b102588k/

Table 1 Cp*Ru(cod)Cl-catalyzed cycloaddition of 1,6-diynes **2a–c** with electron-deficient nitriles **3a–f**[a]

Entry	X	Ewg	Catalyst/ mol %	*T*/°C	*t*/h	Yield[b]
1	$C(CO_2Me)_2$	CO_2Et	2	60	0.5	**4a**, 83%
2	$C(CO_2Me)_2$	COPh	2	60	0.5	**4b**, 84%
3	$C(CO_2Me)_2$	COMe	10	80	1	**4c**, 90%
4	$C(CO_2Me)_2$	Ts	10	80	24	**4d**, 31%
5	$C(CO_2Me)_2$	CCl_3	10	60	24	**4e**, 44%
6	$C(CO_2Me)_2$	C_6F_5	5	60	1	**4f**, 67%
7	NTs	CO_2Et	2	60	0.5	**4g**, 75%
8	O	CO_2Et	2	60	2	**4h**, 49%

[a] All reactions were carried out with a nitrile (1.5 equiv.) in 1,2-dichloroethane under Ar. [b] Isolated yields.

present ruthenium-catalyzed pyridine annulation. In the presence of 10 mol% **1**, trichloroacetonitrile (**3g**) and pentafluorobenzonitrile (**3f**) were reacted with **2a** at 60 °C to afford pyridines **4e** and **4f** in 44 and 67% yields, respectively (entries 5 and 6). By employing *N*,*N*-dipropargyl tosylamide (**2b**) and dipropargyl ether (**2c**) as diyne components, 3-pyrroline- and 2,5-dihydrofuran-fused pyridines **4g** and **4h** were obtained in 75 and 49% yields, respectively (entries 7 and 8).

In order to establish the regiochemistry of the Ru(II)-catalyzed pyridine annulation, unsymmetrical 1,6-diynes **6a–c** were subjected to cycloaddition with **3a**, leading to 2,3,4,6-substituted isomers **7** and/or 2,3,4,5-substituted isomers **8** (Scheme 2). As a result, one of these isomers was predominantly obtained, depending on the nature of the alkyne substituents. In the presence of 5 mol% **1**, a octa-1,6-diyne **6a** (R = Me) reacted with **3a** at 60 °C for 2 h to afford a 88 : 12 mixture of **7a** and **8a** in 78% yield. The presence of an alkyl-substituent at the terminal position of the diyne decreased the reactivity. Similarly, the cycloaddition between a phenyl-substituted diyne **6b** (R = Ph) and **3a** was carried out using the 20 mol% catalyst at 60 °C. In this case, **7b** was isolated as a sole pyridine isomer in 50% yield. In contrast, the reaction of an ester **6c** and **3a** proceeded at rt and, unexpectedly, a 2,3-dialkoxycarbonyl isomer **8c** was obtained as a major product along with a minor isomer **7c** in 78% total yield. Therefore, the electron-

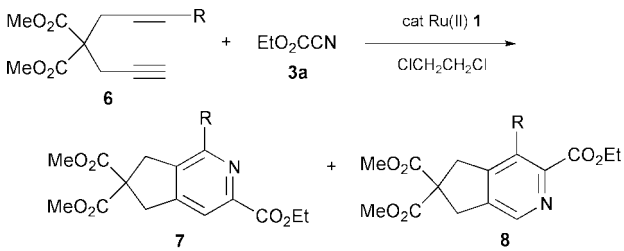

R = Me: 5 mol%, 60 °C, 2 h; 78% (**7a** : **8a** = 88 : 12)
R = Ph: 20 mol%, 60 °C, 6 h; 50% (**7b** : **8b** = 100 : 0)
R = CO_2Me: 5 mol%, r.t., 1 h; 78% (**7c** : **8c** = 13 : 87)

Scheme 2

 DOI: 10.1039/b102588k

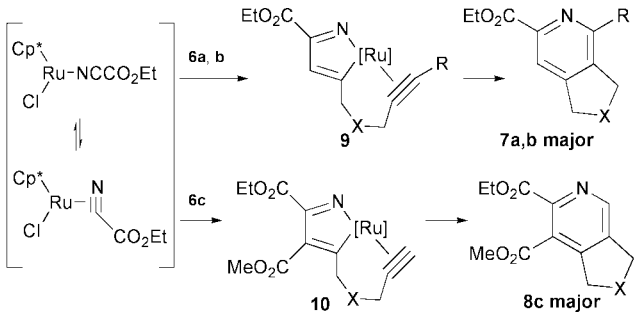

Scheme 3

withdrawing ester group in **6c** reversed both the reactivity and the regioselectivity.

The origin of the observed regiochemistry and the difference in reactivity can be reasonably explained by the following mechanism (Scheme 3). The substituent on a nitrile component plays a critical role in the present protocol: electron-deficient nitriles having a carbonyl, sulfonyl, or polyhaloalkyl substituent gave rise to the desired pyridine product, although acetonitrile and benzonitrile gave little of the corresponding cycloadduct. This is probably because the electron-withdrawing group lowers the antibonding orbital level of the C–N triple bond to facilitate the oxidative cyclization involving the nitrile. In this situation, the catalytic cycle starts from the oxidative cyclization of a nitrile **3** and one alkyne terminus of a diyne **6** on the ruthenium center to form an azaruthenacyclopentadiene intermediate **9** or **10**. The regiochemistry of the product is determined in this stage. In the case of the alkyl- or aryl-substituted diynes **6a** and **6b**, the sterically less hindered terminal alkyne moiety can be favorably involved in the oxidative cyclization to form the intermediate **9**. The subsequent intramolecular alkyne insertion and reductive elimination steps afford the final pyridine product **7** as a major isomer. On the other hand, the diyne monoester **6c** forms predominantly the intermediate **10** because the oxidative cyclization occurs at the electron-deficient alkyne terminus due to its effective accommodation of the d-electron from the ruthenium center. As a result of the efficient formation of **10**, the cycloaddition of **6c** proceeded smoothly even at rt and gave **8c** as a major product.

We gratefully acknowledge financial support (10132222, 11119223, and 12450360) from the Ministry of Education, Science, Sports, and Culture, Japan.

Notes and references

‡ The IUPAC name for propargyl is prop-2-ynyl.

1 Y. Wakatsuki and H. Yamazaki, *J. Chem. Soc., Chem. Commun.*, 1973, 280; Y. Wakatsuki and H. Yamazaki, *J. Chem. Soc., Dalton. Trans.*, 1978, 1278.

2 For review, see: H. Bönnemen, *Angew. Chem., Int. Ed. Engl.*, 1985, **24**, 248; K. P. C. Vollhardt, *Angew. Chem., Int. Ed. Engl.*, 1984, **23**, 539; B. Grotjahn, in *Comprehensive Organometallic Chemistry II*, ed. L. S. Hegedus, E. W. Abel, F. G. A. Stone and G. Wilkinson, Pergamon, Oxford, 1995, vol. 12, pp. 741–770.

3 T. Takahashi, F.-Y. Tsai and M. Kotora, *J. Am. Chem. Soc.*, 2000, **122**, 4994.

4 A. Naiman and K. P. C. Vollhardt, *Angew. Chem., Int. Ed. Engl.*, 1977, **16**, 708.

5 For other examples of the cycloaddition between α,ω-diynes and nitriles, see: Z. Zhou, L. P. Battaglia, G. P. Chiusoli, M. Costa, M. Nardelli, C. Pelizzi and G. Predieri, *J. Organomet. Chem.*, 1991, **417**, 51; G. P. Chiusoli, L. Pallini and G. Terenghi, *Transition Met. Chem.*, 1983, **8**, 250; L. P. Battaglia, D. Delledonne, M. Nardelli, G. Predieri, G. P. Chiusoli, M. Costa and C. Pelizzi, *J. Organomet. Chem.*, 1989, **363**, 209; G. Vitulli, S. Bertozzi, R. Lazzaroni and P. Salvadori, *J. Organomet. Chem.*, 1986, **307**, C35: G. Vitulli, S. Bertozzi, M. Vignali, R. Lazzaroni and P. Salvadori, *J. Organomet. Chem.*, 1987, **326**, C33.

6 C. A. Parnell and K. P. C. Vollhardt, *Tetrahedron*, 1985, **41**, 5791; R. E. Geiger, M. Lalonde, H. Stoller and K. Schleich, *Helv. Chim. Acta*, 1984, **67**, 1274.

7 For Cp*Ru(cod)Cl-catalyzed cycloadditions of 1,6-diynes, see: Y. Yamamoto, R. Ogawa and K. Itoh, *Chem. Commun.*, 2000, 549; Y. Yamamoto, H. Kitahara, R. Ogawa, H. Kawaguchi, K. Tatsumi and K. Itoh, *J. Am. Chem. Soc.*, 2000, **122**, 4310.

CHEMCOMM
Communication
www.rsc.org/chemcomm

Templated SAMs for metal ion recognition

Barbara Colonna and Luis Echegoyen*

Department of Chemistry and Center for Supramolecular Science, University of Miami, Coral Gables, Florida 33124, USA. E-mail: echegoyen@miami.edu

Received (in Columbia, MO, USA) 29th January 2001, Accepted 17th April 2001
First published as an Advance Article on the web 25th May 2001

Self assembled monolayers of a polyether derivative selectively detect potassium cations when templated in their presence.

Self-assembled monolayers (SAMs) that incorporate receptor molecules can act as molecular recognition interfaces and thus as selective sensors for specific analytes.[1–3] Binding sites can also be formed within the SAMs during their preparation, if they are grown in the presence of appropriate analytes that template the aggregation processes.[4] This process could also be described as molecular imprinting, although this term is usually reserved for polymer systems, where binding of functionalized monomers by a template molecule is followed by polymerization and template removal.[4–6] Well-defined cavities with selective binding properties are thus formed in the polymeric backbone which are able to recognize analytes that are similar or identical to the template.

The first preliminary report involving imprinted SAMs was published by Sagiv[7] in 1979, but the concept went largely unexplored for a long time until recently, when the strategy was employed to generate binding sites for organic substrates at the surface of modified electrodes.[8–11] It seems as if more examples are appearing more frequently, probably due to the simplicity of the approach which largely relies on the principle of self-assembly and requires minimal synthetic effort. Perhaps surprisingly and to the best of our knowledge, no examples of SAM formation involving metal ions as templates have been reported to date. In this communication, we report the preparation and the electrochemical investigation of potassium-templated SAMs on gold which selectively detect K^+ but not Na^+.

Receptor **1** was designed to bind metal cations in the polyether loop, which was purposely fused to the aromatic ring

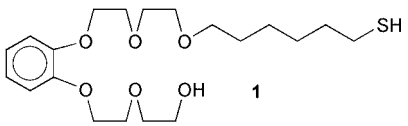

1

for rigidity, but allowed to retain enough flexibility for intra- as well as inter-molecular templating upon self-assembly on the gold surface. The thiol group provides the anchoring point to the gold substrate. The polymethylene spacer separating the polyether recognition site and the anchoring group should facilitate the formation of the monolayers by van der Waals forces. The compound was synthesized in three steps. Reaction of catechol with 2-chloroethoxyethanol afforded a diol **2**, which was monoalkylated with a small excess of 1,6-dibromohexane. Finally, the resulting bromide **3** was converted into **1** by treatment with thiourea followed by basic hydrolysis.†

SAMs **A** and **B** were prepared by immersing glass-sealed gold bead electrodes for 24 h in an EtOH solution of **1** (1 mM) (**A**) or an EtOH–H_2O (1 : 1) solution of **1** (1 mM) and KCl (0.1 M) (**B**). The electrodes were then rinsed with H_2O, EtOH and CH_2Cl_2 and dried under a stream of Ar. Impedance measurements were performed using an aqueous solution of Et_4NCl (0.1 M) and $[Ru(NH_3)_6]Cl_3$ (1 mM), a SAM modified gold bead as the working electrode, a coiled platinum counter electrode and a Ag/AgCl reference electrode. Experiments were conducted at the formal redox potential of the $[Ru(NH_3)_6]^{3+/2+}$ couple with a frequency ranging from 100 kHz to 0.1 Hz. The spectra were analyzed by the 'EquivalentCircuit'[12] software package. Binding of cations to the receptor moiety of a non-electroactive SAM can be monitored by impedance spectroscopy using the positively charged redox couple $[Ru(NH_3)_6]^{3+/2+}$ as a probe.[13] An increase in the charge transfer resistance (R_{ct}) is observed upon complexation of the metal cations,[13,17] and is due to electrostatic repulsion between the cation and the positively charged ruthenium redox couple. These changes were used to monitor the recognition of alkali metal cations by monolayers of **1**.

The charge transfer resistances (R_{ct}) of the SAMs **A** and **B** were measured in the presence of increasing concentrations of KCl. For **A** [Fig. 1(a)], R_{ct} is 1.35 kΩ cm^2 immediately after preparing the SAM and in the absence of KCl. Upon KCl additions, R_{ct} increases slightly until it reaches a limiting value of 2.14 kΩ cm^2 at a salt concentration of 100 mM. Thus, the effect of salt addition is reasonably small. For **B** [Fig. 1(b)], R_{ct} is 2.20 kΩ cm^2 in the absence of KCl but upon addition of this salt the resistance increases dramatically and reaches a value of

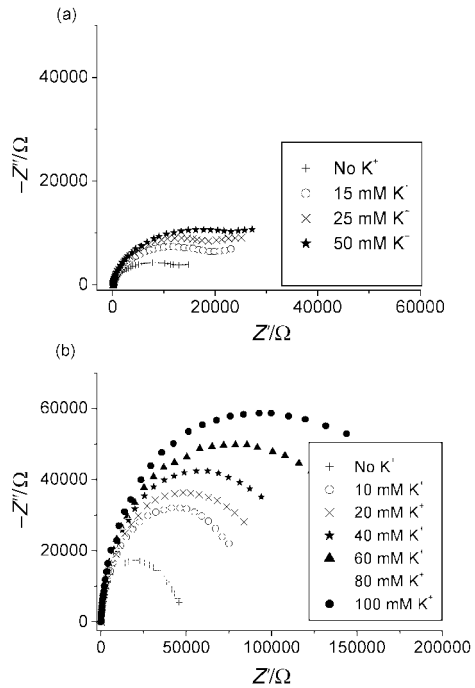

Fig. 1 (a) Nyquist electrochemical impedance spectroscopy plot of the monolayer of **1** grown in the absence of KCl (**A**), and exposed to different K^+ concentrations. Experiments were conducted in H_2O, using Et_4NCl (0.1 M) as supporting electrolyte and $[Ru(NH_3)_6]Cl_3$ (1 mM) as redox probe at E = −0.165 V and the frequency range 100 kHz–0.1 Hz. (b) Nyquist electrochemical impedance spectroscopy plot of the monolayer of **1** grown in the presence of 0.1 M KCl (**B**), and exposed to different K^+ concentrations. Experiments were conducted in H_2O, using Et_4NCl (0.1 M) as supporting electrolyte and $[Ru(NH_3)_6]Cl_3$ (1 mM) as redox probe at E = −0.165 V in the frequency range 100 kHz–0.1 Hz.

 DOI: 10.1039/b102144n

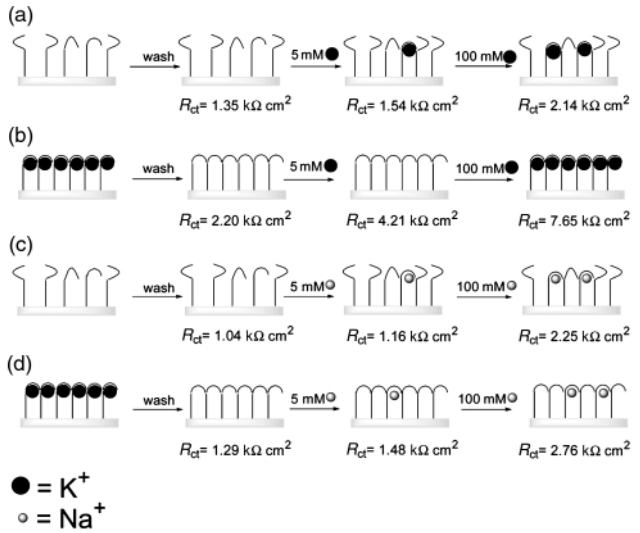

Fig. 2 Cartoon representation of the binding of metal cations by SAM of **1** grown: (a) in the absence of KCl (**A**), K^+ titration; (b) in the presence of 0.1 M KCl (**B**), K^+ titration; (c) in the absence of KCl (**A**), Na^+ titration; (d) in the presence of 0.1 M KCl (**B**), Na^+ titration.

7.65 kΩ cm^2 at a salt concentration of 100 mM. The area coverage for monolayers **A** ($\phi_A = 1.96 \times 10^{-9}$ mol cm^{-2}) and **B** ($\phi_B = 2.43 \times 10^{-9}$ mol cm^{-2}) were determined by reductive desorption in a 0.5 M KOH solution,[18] and are in accordance with the relative R_{ct} values of **A** and **B**. The association constants (K) for potassium binding by **A** and **B** were determined by fitting the experimental R_{ct} values and concentrations of KCl using a Langmuir isotherm.[13] The value of K was found to be 124 ± 20 M^{-1} for **A** and 353 ± 30 M^{-1} for **B**). The difference between these two values demonstrates that the templated monolayer **B** has a higher binding affinity for potassium cations than **A**. In the case of **B**, the self-assembly of **1** on gold is assisted by the cations which induce the formation of optimal binding domains [Fig. 2(b)]. The resulting pre-organized recognition sites favor cation recognition at the interface. The template effect is also reflected in the response to changes in cation concentration. The addition of 5 mM KCl produces a small change in the R_{ct} of **A** but a large increase in the R_{ct} of **B** [Fig. 2(a) and (b)].

The ability of **A** and **B** to recognize sodium cations was also tested. In both instances, however, small changes in the R_{ct} values were observed [Fig. 2(c) and (d)] upon addition of NaCl, suggesting that recognition of Na^+ ions by the monolayer of **1** is very modest. Interestingly, the R_{ct} of the templated monolayer **B** is only 2.76 kΩ cm^2 in the presence of 100 mM NaCl. This monolayer has instead a R_{ct} of 7.65 kΩ cm^2 in the presence of 100 mM KCl. The different behavior indicates that **B** has a pronounced selectivity for potassium cations.

Summarizing, we have demonstrated for the first time that binding sites for potassium cations can be imprinted into SAMs when the monolayer is assembled on gold in the presence of this metal cation. The resulting modified gold electrodes detect potassium cations in water with good selectivity over sodium cations. This approach to chemical sensors is simple and efficient and can be easily extended to the realization of SAMs for the recognition of analytes other than potassium cations.

This work was supported by the National Science Foundation, grant CHE-9816503.

Notes and references

† *Experimental conditions*: Preparation of 2-(2-{2-[2-(2-hydroxyethoxy)-ethoxy]phenoxy}ethoxy)ethanol **2**: a mixture of catechol (5.5 g, 50 mmol) and K_2CO_3 (35 g, 250 mmol) in anhydrous MeCN, was heated for 30 min under a stream of Ar. 2-Chloroethoxyethanol (14.9 g, 120 mmol) was added and reflux was maintained for 40 h. The suspension was then filtered and the solids washed with CH_2Cl_2 (150 mL). The combined organic phases were evaporated under reduced pressure and the residue was re-dissolved in CH_2Cl_2 (150 mL) and washed with water (3 × 50 mL). Purification by column chromatography [SiO_2, CH_2Cl_2–EtOAc (1:1) to EtOAc–EtOH (9:1)] afforded **2** in 44% yield.

Preparation of 2-[2-(2-{2-[2-(6-bromohexyloxy)ethoxy]ethoxy}phenoxy)ethoxy]ethanol **3**: a mixture of **2** (0.9 g, 3.15 mmol) and NaH (60% in mineral oil) (0.36 g, 9 mmol) in anhydrous THF (200 mL) was stirred at room temperature under a stream of Ar. After 30 min 1,6-dibromohexane (4.76 g, 19.5 mmol) was added and the mixture was left stirring for 16 h. After addition of MeOH the solvent was evaporated under reduced pressure. The residue was dissolved in CH_2Cl_2 (200 mL) and washed with H_2O (3 × 100 mL). Purification by column chromatography [SiO_2, hexane–EtOAc (1:1)] afforded **3** in 76% yield.

Preparation of 2-[2-(2-{2-[2-(6-mercaptohexyloxy)ethoxy]ethoxy}-phenoxy)ethoxy]ethanol **1**: a solution of 2 (1.2 g, 2.7 mmol) and thiourea (0.813 g, 10.7 mmol) in EtOH (80 mL) was left refluxing under a stream of Ar for 16 h. The solvent was evaporated under reduced pressure and the residue suspended in an aqueous solution of KOH (60 mL, 0.84 g, 15 mmol), and stirred for 2 h. The reaction mixture was acidified with HCl and CH_2Cl_2 (150 mL) was added. Washing with H_2O (3 × 100 mL) and purification by column chromatography afforded **1** in 33% yield. $\delta_H(CDCl_3)$ 1.28–1.39 (5H, m), 1.54–1.63 (4H, m), 2.48 (2H, t, *J* 7.3 Hz), 3.45 (2H, t, *J* 6.7 Hz), 3.59 (2H, t, *J* 5.2 Hz), 3.64–3.76 (6H, m), 4.12–4.20 (4H, m), 6.88–6.90 (4H, m); *m/z* (FAB+): 402 (M^+,70%), 403 (M^+ + 1, 100%).

1 S. Flink, F. C. J. M van Veggel and D. N. Reinhoudt, *Adv. Mater.*, 2000, **12**, 1315.
2 R. M. Crooks and A. J. Ricco, *Acc. Chem. Res.*, 1998, **31**, 219.
3 A. E. Kaifer, *Isr. J. Chem.*, 1996, **36**, 389.
4 K. Haupt and K. Mosbach, *Chem. Rev.*, 2000, **100**, 2495.
5 H. Asanuma, T. Hishiya and M. Komiyama, *Adv. Mater.*, 2000, **12**, 1019.
6 G. Wulff, *Angew. Chem., Int. Ed. Engl.*, 1995, **34**, 1812.
7 J. Sagiv, *Isr. J. Chem.*, 1979, **18**, 346.
8 V. M. Mirsky, T. Hirsch, S. Piletsky and O. S. Wolfbeis, *Angew. Chem., Int. Ed.*, 1999, **38**, 1108.
9 M. Lahav, E. Katz, A. Doron, F. Patolsky and I. Willner, *J. Am. Chem. Soc.*, 1999, **121**, 862.
10 O. Chailapakul, R. M. Crooks, C. B. Ross, L. Sun and J. Schoer, *Interfacial Design and Chemical Sensing*, ed. T. E. Mallouk and D. J. Harrison, ACS Symp. ser. 561, Washington, DC, 1994.
11 S. A. Piletsky, E. V. Piletskaya, T. A. Sergeyava, T. L. Panasyuk and A. V. El'skaya, *Sens. Actuators B*, 1999, **60**, 216.
12 B. A. Boukamp, Equivalent Circuit version 4.55, University of Twente, Department of Chemical Technology, Enschede, The Netherlands, 1996.
13 S. Flink, B. A. Boukamp, A. van der Berg, F. G. J. M. van Veggel and D. N. Reinhoudt, *J. Am. Chem. Soc.*, 1998, **120**, 4652.
14 S. Flink, F. G. J. M. van Veggel and D. N. Reinhoudt, *J. Phys. Chem. B*, 1999, **103**, 6515.
15 K. Bandyopadhyay, H. Liu, S.-G. Liu and L. Echegoyen, *Chem. Commun.*, 2000, 141.
16 K. Bandyopadhyay, H. Liu, S.-G. Liu and L. Echegoyen, *Chem. Eur. J.*, 2000, **6**, 1176.
17 K. Bandyopadhyay, H. Liu, S.-G. Liu and L. Echegoyen, *Langmuir*, 2000, **16**, 2706.
18 Y. Wang and A. E. Kaifer, *J. Phys. Chem. B*, 1998, **102**, 9922.

CHEMCOMM
Communication
www.rsc.org/chemcomm

Short syntheses of enantiopure calystegine B_2, B_3, and B_4

Philip R. Skaanderup and Robert Madsen*

Department of Chemistry, Building 201, Technical University of Denmark, DK-2800 Lyngby, Denmark. E-mail: rm@kemi.dtu.dk

Received (in Corvallis, OR, USA) 12th March 2001, Accepted 26th April 2001
First published as an Advance Article on the web 31st May 2001

Calystegine B_2, B_3, and B_4 have been prepared in 5 steps from the benzyl protected methyl 6-iodoglycopyranosides of glucose, galactose and mannose, respectively, by using a zinc-mediated domino reaction followed by ring-closing olefin metathesis as the key steps.

Many polyhydroxylated alkaloids are important glycosidase inhibitors due to their structural resemblance to sugars.[1] A special class of these alkaloids is the calystegines which consist of a polyhydroxy-nortropane ring system.[2] Up to date, 14 different calystegines have been isolated from various plant species. Their structures have been elucidated mainly by NMR spectroscopy and they have been divided into four different classes: A, B, C and N. The absolute configuration, however, is known only for calystegine B_2 (**1**) and the configuration of all the remaining calystegines is presumed to be analogous to that of **1** based on biosynthetic considerations.[2] So far, only calystegine A_3 and B_2 have been prepared by chemical synthesis.[3]

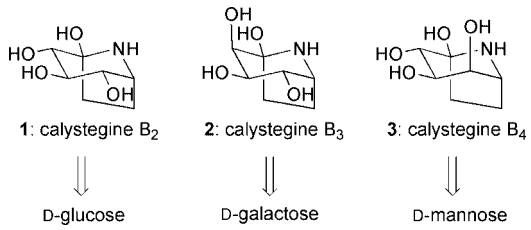

We have recently introduced a zinc-mediated domino reaction followed by ring-closing olefin metathesis for synthesis of polyhydroxylated carbocycles from sugars.[4,5] The domino reaction allows for the stereocontrolled introduction of an amino group and is then well suited for preparing the seven-membered carbocycle in the calystegines. Herein, we exploit these reactions for short syntheses of calystegine B_2, B_3 (**2**) and B_4 (**3**) starting from glucose, galactose and mannose, respectively.[6] Calystegine B_2 and B_4 are potent inhibitors of β-glucosidase and trehalase.[7]

The starting material for all three syntheses is the corresponding benzyl protected methyl 6-deoxy-6-iodo-α-D-glycopyranoside (Scheme 1). Sonicating a mixture of glucopyranoside **4** and excess zinc dust in dry THF caused a reductive fragmentation to generate the 5,6-unsaturated aldehyde[8] which was trapped *in situ* as the corresponding benzyl imine. Slow addition of allyl bromide to the mixture led to allylation of the imine to give a 5:1 mixture of amino dienes. The major diastereomer **5**[3a] was isolated in 71% yield and the stereochemistry verified after completing the synthesis of **1**. Cbz-protection of the amino group gave **6**† which was metathesised into cycloheptene **7** with the saturated *N*-heterocyclic carbene catalyst $(PCy_3)(C_3H_4N_2mes_2)Cl_2Ru{=}CHPh$.[4,9,10] The double bond in **7** is slightly polarized and can be hydroborated[11] followed by oxidation[12] in

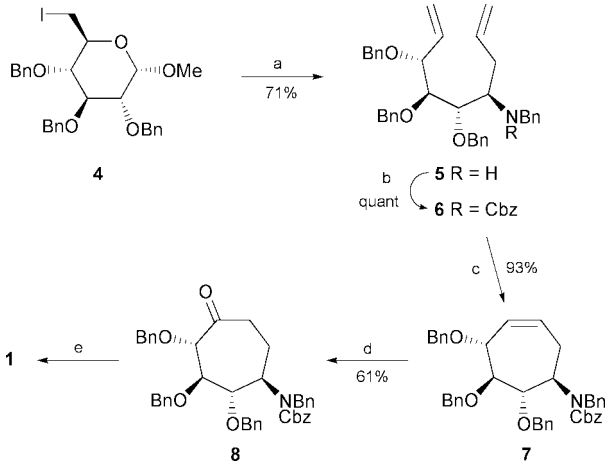

Scheme 1 *Reagents and conditions*: (a) Zn, $BnNH_2$, $CH_2{=}CHCH_2Br$, THF, sonication, 40 °C; (b) CbzCl, $KHCO_3$, EtOAc, H_2O; (c) 2% $(PCy_3)(C_3H_4N_2mes_2)Cl_2Ru{=}CHPh$, CH_2Cl_2, rt; (d) BH_3·THF, THF, −50 → 0 °C, then NaOH, H_2O_2, 0 °C, then Dess-Martin periodinane, CH_2Cl_2, rt; (e) H_2, Pd/C.

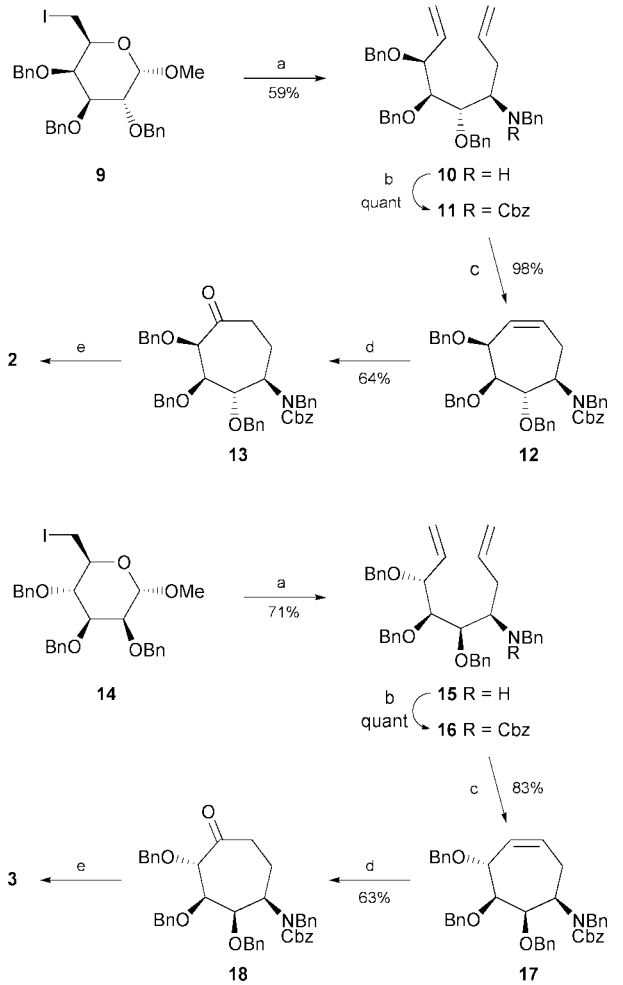

Scheme 2 *Reagents and conditions*: (a) Zn, $BnNH_2$, $CH_2{=}CHCH_2Br$, THF, sonication, 40 °C; (b) CbzCl, $KHCO_3$, EtOAc, H_2O; (c) 2% $(PCy_3)(C_3H_4N_2mes_2)Cl_2Ru{=}CHPh$, CH_2Cl_2, rt; (d) BH_3·THF, THF, −50→ 0 °C, then NaOH, H_2O_2, 0 °C, then Dess-Martin periodinane, CH_2Cl_2, rt; (e) H_2, Pd/C.

 DOI: 10.1039/b102353p

a one pot procedure to give a 3:1 mixture of ketones. Major ketone isomer **8** was isolated in 61% yield and hydrogenated to give calystegine B_2 ($[\alpha]_D^{20}$ +23.8 (*c* 0.31, H_2O)). NMR data and optical rotation were in accordance with those reported for the natural product.[13]

The same sequence was then applied to the synthesis of calystegine B_3 and B_4 (Scheme 2). Subjecting galactose-derived iodoglycoside **9** to the domino reaction gave a 2:1 mixture of amino dienes. Major diastereomer **10**‡ was isolated in 59% yield and then converted into cycloheptene **12**. Hydroboration and oxidation gave a 3:1 mixture of ketones and the major isomer **13** was isolated in 64% yield. Hydrogenation then furnished calystegine B_3 ($[\alpha]_D^{20}$ +75.6 (*c* 0.55, H_2O)) with NMR data and optical rotation in accordance with the data for the natural compound.[13] Subjecting mannose-derived iodoglycoside **14** to the domino reaction gave a 8:1 mixture of amino dienes and the major diastereomer **15**§ was isolated in 71% yield. The stereochemical outcome in these allylations is noteworthy. In all three cases the major product is the (*R*)-benzylamine which is the correct stereochemistry for the calystegines. The major product **15** from mannose is consistent with predictions from the Felkin-Anh model while the major isomers from glucose and galactose are not. This, however, does correspond with our previous experience on zinc-mediated alkylations of glucose and mannose substrates.[4a] Finally, amine **15** was converted into cycloheptene **17** which was hydroborated and oxidised to give a 3:1 ratio of ketones. The major isomer **18** was isolated in 63% yield and deprotected to give calystegine B_4 ($[\alpha]_D^{20}$ −46.4 (*c* 0.18, H_2O)). NMR data and optical rotation were similar to those reported for the natural product.[7]

In conclusion, a general strategy for preparation of the calystegines has been devised. Calystegine B_3 and B_4 have been prepared for the first time and their absolute configuration confirmed. These syntheses should hold great promise for making the calystegines and their analogues more readily available for biological investigations.

We thank the Danish Natural Science Research Council for financial support.

Notes and references

† All Cbz-protected compounds showed mixtures of rotamers by NMR.

‡ Spectral data for **10**: δ_H ($CDCl_3$) 7.35–7.22 (m, 20H), 5.98 (ddd, 1H, *J* 17.9, 10.0, 8.5), 5.65 (m, 1H), 5.31 (bd, 1H, *J* 10.0), 5.15 (bd, 1H, *J* 17.5), 5.00 (m, 2H), 4.92 (d, 1H, *J* 11.1), 4.84 (d, 1H, *J* 11.1), 4.72 (d, 1H, *J* 11.1), 4.56 (d, 1H, *J* 12.8), 4.53 (d, 1H, *J* 12.4), 4.29 (d, 1H, *J* 11.9), 4.18 (bs, 1H), 3.90 (d, 1H, *J* 13.2), 3.83 (dd, 1H, *J* 7.8, 3.2), 3.67 (d, 1H, *J* 13.2), 3.56 (bs, 1H), 2.66 (bs, 1H), 2.45 (m, 1H), 2.29 (m, 1H); δ_C ($CDCl_3$) 140.5, 139.1, 139.0, 138.7, 135.8, 135.1, 128.2–126.6 (20C), 118.9, 116.7, 82.6, 81.5, 80.1, 74.7, 74.5, 69.7, 56.7, 50.7, 34.5.

§ Spectral data for **15**: δ_H ($CDCl_3$) 7.43–7.25 (m, 20H), 6.00 (ddd, 1H, *J* 17.7, 10.4, 8.1), 5.79 (m, 1H), 5.39 (bd, 1H, *J* 17.5), 5.34 (bd, 1H, *J* 10.4), 5.10 (bd, 1H, *J* 17.9), 5.09 (bd, 1H, *J* 9.8), 4.83 (d, 1H, *J* 11.5), 4.75 (d, 2H, *J* 11.5), 4.71 (d, 1H, *J* 11.9), 4.58 (d, 1H, *J* 11.1), 4.44 (d, 1H, *J* 11.9), 4.29 (m, 1H), 3.89 (m, 1H), 3.83 (d, 1H, *J* 12.8), 3.82 (m, 1H), 3.77 (d, 1H, *J* 12.8), 3.08 (dt, 1H, *J* 8.0, 3.9), 2.51 (m, 1H), 2.36 (m, 1H); δ_C ($CDCl_3$) 140.6, 138.8, 138.6, 138.5, 136.4, 136.2, 128.8–125.9 (20C), 118.1, 117.0, 82.3, 81.1, 79.4, 74.4, 73.1, 70.4, 57.1, 51.7, 34.6.

1 *Iminosugars as Glycosidase Inhibitors*, ed. A. E. Stütz, Wiley-VCH, Weinheim, 1999.
2 N. Asano, R. J. Nash, R. J. Molyneux and G. W. J. Fleet, *Tetrahedron: Asymmetry*, 2000, **11**, 1645; A. A. Watson, D. R. Davies, N. Asano, B. Winchester, A. Kato, R. J. Molyneux, B. L. Stegelmeier and R. J. Nash, in *ACS Symposium Series*, vol. 745, ed. A. T. Tu and W. Gaffield, ACS, Washington, DC, 2000, p. 129.
3 (*a*) F.-D. Boyer and I. Hanna, *Tetrahedron Lett.*, 2001, **42**, 1275; (*b*) T. Faitg, J. Soulié, J.-Y. Lallemand and L. Ricard, *Tetrahedron: Asymmetry*, 1999, **10**, 2165; (*c*) C. R. Johnson and S. J. Bis, *J. Org. Chem.*, 1995, **60**, 615; (*d*) F.-D. Boyer and J.-Y. Lallemand, *Tetrahedron*, 1994, **50**, 10443; (*e*) O. Duclos, M. Mondange, A. Duréault and J. C. Depezay, *Tetrahedron Lett.*, 1992, **33**, 8061.
4 (*a*) L. Hyldtoft and R. Madsen, *J. Am. Chem. Soc.*, 2000, **122**, 8444; (*b*) L. Hyldtoft, C. S. Poulsen and R. Madsen, *Chem. Commun.*, 1999, 2101.
5 For application to seven- and eight-membered rings, see: I. Hanna and L. Ricard, *Org. Lett.*, 2000, **2**, 2651.
6 Recently, the method in ref. 4 was used for a very similar synthesis of **1** (see ref. 3a) which has prompted us to publish our results now.
7 N. Asano, A. Kato, H. Kiza, K. Matsui, A. A. Watson and R. J. Nash, *Carbohydr. Res.*, 1996, **293**, 195.
8 B. Bernet and A. Vasella, *Helv. Chim. Acta*, 1979, **62**, 1990.
9 M. Scholl, S. Ding, C. W. Lee and R. H. Grubbs, *Org. Lett.*, 1999, **1**, 953.
10 For a recent review on olefin metathesis in carbohydrate chemistry, see: M. Jørgensen, P. Hadwiger, R. Madsen, A. E. Stütz and T. M. Wrodnigg, *Curr. Org. Chem.*, 2000, **4**, 565.
11 W. Wang, Y. Zhang, M. Sollogoub and P. Sinaÿ, *Angew. Chem., Int. Ed.*, 2000, **39**, 2466.
12 D. B. Dess and J. C. Martin, *J. Am. Chem. Soc.*, 1991, **113**, 7277.
13 N. Asano, A. Kato, K. Oseki, H. Kizu and K. Matsui, *Eur. J. Biochem.*, 1995, **229**, 369.

CHEMCOMM Communication
www.rsc.org/chemcomm

Calculation of reaction rate constants for hydrogen–deuterium exchange reactions of methane catalysed by acid zeolites

Ann M. Vos,[a] Frank De Proft,[b] Robert A. Schoonheydt*[a] and Paul Geerlings[b]

[a] *Centre for Surface Chemistry and Catalysis, Katholieke Universiteit Leuven, Kasteelpark Arenberg 23, 3001 Leuven, Belgium. E-mail: robert.schoonheydt@agr.kuleuven.ac.be*
[b] *Eenheid Algemene Chemie, Vrije Universiteit Brussel, Pleinlaan 2, 1050 Brussels, Belgium. E-mail: pgeerlin@vub.ac.be*

Received (in Cambridge, UK) 8th March 2001, Accepted 3rd May 2001
First published as an Advance Article on the web 31st May 2001

Hydrogen–deuterium exchange between methane and an acid zeolite is a model reaction (refs. 1–6) for which experimental rate constants and activation energies can be compared with theoretical values, obtained with Eyring's transition state theory (ref. 7).

Obtaining rate constants for zeolite catalysed reactions, is neither experimentally nor theoretically straightforward. Experimentally, the apparent reaction rates are influenced by the adsorption behaviour of the molecules.[8,9] Intrinsic reaction parameters can only be obtained by fitting the reaction rate data to a model. Another problem is the uncertainty about the exact number of acid sites in a zeolite, due to the existence of extra-framework Al and lattice defects. The accuracy of theoretically calculated rate constants depends strongly on the model used to represent the zeolite. Usually a fully relaxed cluster,[3,4] which can only model the local environment of the acid site, is employed. Thus adsorption, and structural, long range effects cannot be accounted for in model cluster calculations.

The aim of the present paper is to check the validity of calculated rate constants. Therefore we compared them with reliable experimental values.[6] The kinetics of hydrogen–deuterium exchange between methane and deuterated acid FAU- and MFI-type zeolites have been determined in a circulation batch reactor with on-line mass spectrometric product analysis, in the temperature range 450–550 °C. The apparent activation energy was in the range 122–150 kJ mol^{-1} and a kinetic isotope effect ($k_{OH/CD}/k_{OD/CH}$, see Fig. 1) of *ca.* 1.7 was found for MFI catalysts. This was explained by suggesting that the O–D/O–H bond dissociation is the rate determining step or that the mechanism is not concerted.

Rate constants can be calculated when all the steps involved in the reaction are characterised. The reactants, transition states, and products are localised with cluster type calculations as used successfully before.[10] During the geometry optimisation we look for a local minimum for reactants, and products and for a first-order saddle point for transition states. The cluster we used consists of three T-atoms (one Al and two Si) and was allowed to relax completely during the optimisations. The DFT calculations used the B3LYP functional[11] and a 6-31G* basis set. They were done with Gaussian98.[12]

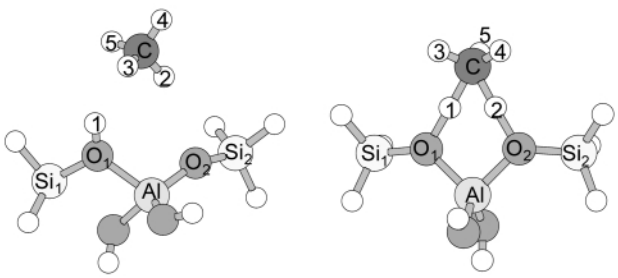

Fig. 1 Geometry of (a) CH_4 adsorbed on acid site of zeolite, (b) transition state, with the labelling of the atoms as in Table 1. For $k_{OH/CD}$: 1 = H, 2–5 = D and for $k_{OD/CH}$: 1 = D, 2–5 = H.

We found a symmetrical transition state with the exchanging hydrogens in the middle between the methane carbon and the cluster oxygen, as can be seen in Fig. 1. The interatomic distances are given in Table 1 along with the values obtained in previous studies using another level of calculations.[1,3,4]

The reaction rate constants are evaluated by using the canonical transition state theory of Eyring, Evans and Polanyi.[7] The general expression for the reaction rate constant k_r is:

$$k_r = \frac{k_B T}{h} \cdot \frac{Q^{\ddagger}}{\prod_i Q_i} \cdot e^{-\frac{E_{bar}}{k_B T}} \quad (1)$$

where k_B and h are respectively Boltzman's and Planck's constants, T is the temperature. E_{bar} is the activation barrier of the reaction. It is the energy difference between energies of reactants and transition-state and contains the zero point energy corrections. Q_i and $Q^{\ddagger}$ represent the partition function of reactants and transition-state (the index i running over all reactants). For the evaluation of eqn. (1) we use molecular partition functions.[7] With the assumption that rotational (r), vibrational (v) and electronic (e) movements are independent of each other, the molecular partition function Q is given by $Q=Q_tQ_rQ_vQ_e$, Q_t being the translational partition function.

For the H–D exchange reaction of methane, the reaction rate constant per acid proton becomes:

$$k_r = (N_A V)\left(\frac{k_B T}{h}\right) \cdot \frac{\left(Q_v^{\ddagger} Q_r Q_t\right)_{TS}}{\left(Q_v Q_r Q_t\right)_{CH_4}\left(Q_v Q_r Q_t\right)_{HZ}} \cdot e^{-\frac{E_{bar}}{k_B T}} \quad (2)$$

N_A is Avogadro's number and V is the volume of one mol under the considered P and T. It appears because of the use of concentrations in the rate laws.

Numerical values for the rigid rotor, harmonic oscillator partition functions are obtained after a frequency calculation by Gaussian98.[12,13] Eqn. (2) was used to calculate the rate constants for a temperature ranging from 300 to 800 K. An Arrhenius-plot gives an apparent activation energy of 157.0 kJ mol^{-1}, in close agreement with the experimental value.[6]

A comparison between the experimentally measured values of the exchange rate and the theoretically calculated ones can be found in Fig. 2. The rate constant depends on both the zeolite structure type and the Al content of the zeolite. Since our cluster contains two Si and one Al the Si/Al ratio is two. The calculated reaction rate constant $k_{OH/CD}$ of 1.97×10^{-7} s^{-1} agrees well with the experimentally obtained values at low Si/Al ratio.[6]

On deuteration, the reaction rate will decrease. In Table 1 rate constants for reaction of non-deuterated/deuterated zeolite (indicated with subscript OH or OD, respectively) with non-deuterated/deuterated methane (indicated subscript with CH or CD, respectively) are given. Deuteration of one of the exchanging atoms has a larger impact than deuteration of the non-exchanging atoms of methane: $k_{OH/CH}/k_{OD/CH} \approx k_{OH/CD}/$

 DOI: 10.1039/b102249k

Table 1 Selected geometrical and energetical parameters, with **ADS** = adsorption of CH_4 on cluster, **TS** = transition state, E_{bar} = E(TS) − E(cluster) − $E(CH_4)$ including ZPE

	ADS	**TS**	**ADS**	**TS**	**ADS**	**TS**	**ADS**	**TS**
Method	B3LYP/6-31G*		MP2/6-31++G** // HF/6-31G*		HF/6-31G**		PB86/DZPV	
Cluster	$AlSi_2O_4H_9$		AlO_2H_5		$AlSi_2O_4H_9$		$AlSi_2O_4H_9$	
Reference	This work		1		3		4	
Distances/Å AlO_1	1.901	1.836	—	1.860	1.942	1.801	—	1.883
AlO_2	1.720	1.836	—	1.860	1.706	1.801	—	1.883
O_1H_1	0.970	1.330	—	1.156	0.949	1.399	—	1.332
CH_1	2.477	1.332	—	1.496	—	1.282	—	1.356
E_{bar}/kJ mol^{-1}	159.71		166.94		—		—	
Imaginary frequency/cm^{-1}	−1745.64		−2095		−1423.38		−1389.4	
$k_{OH/CH}$/s^{-1}	3.36×10^{-7} [a]		—		—		3.38×10^{-6} [b]	
$k_{OH/CD}$/s^{-1}	1.97×10^{-7} [a]		—		—		—	
$k_{OD/CH}$/s^{-1}	1.92×10^{-7} [a]		—		—		—	
$k_{OD/CD}$/s^{-1}	1.09×10^{-7} [a]		—		—		—	

[a] At 750 K. [b] At 673 K.

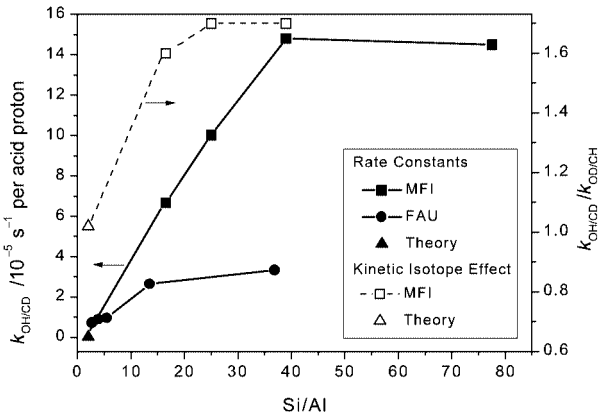

Fig. 2 Solid line and symbols: rate constants, $k_{OH/CD}$, at 700 K in function of Al-content. Dashed line and open symbols: kinetic isotope effect, $k_{OH/CD}$/$k_{OD/CH}$, at 700 K. Experimental values are taken from ref. 6.

$k_{OD/CD} \approx 1.7$ whereas $k_{OH/CD}/k_{OD/CH} = 1.02$. This is a consequence of the symmetrical transition state.

The experimental values for the kinetic isotope effect, $k_{OH/CD}/k_{OD/CH}$, are larger than the theoretical values (see Fig. 2). Unfortunately there are not enough experimental data to extrapolate to lower Si/Al ratios to validate the theoretical prediction.

It is promising to see that present day quantum chemical techniques allow the evaluation of rate constants of a simple zeolite catalysed reaction as they are yielding a lower limit for high alumina zeolites. Feasible differences between theory and experiment can be explained in several ways: (1) the cluster is only an approximation to a real zeolite lattice and does not include structural and long range effects; (2) different Si/Al ratio compared to real zeolites; (3) uncertainty on the obtained frequencies. We will use our method of calculation of rate constants for more complex reactions, *e.g.* acid zeolite catalysed methylation of toluene to form xylene[14] to check its validity.

Notes and references

1 E. M. Evleth, E. Kassab and L. R. Sierra, *J. Phys. Chem.*, 1994, **98**, 1421.
2 G. J. Kramer, R. A. van Santen, C. A. Emeïs and A. K. Nowak, *Nature*, 1993, **363**, 529.
3 R. A. van Santen and G. J. Kramer, *J. Am. Chem. Soc.*, 1995, **117**, 1766.
4 S. R. Blaszkowski, A. P. J. Jansen, M. A. C. Nascimento and R. A. van Santen, *J. Phys. Chem.*, 1994, **98**, 12 938.
5 G. O. A. Janssens, H. Toufar, B. G. Baekelandt, W. J. Mortier and R. A. Schoonheydt, *J. Phys. Chem.*, 1996, **100**, 14 443.
6 B. Schoofs, J. A. Martens, P. A. Jacobs and R. A. Schoonheydt, *J. Catal.*, 1999, **183**, 355.
7 S. Glasstone, *Physical Chemistry*, D. Van Nostrand Company, Inc, Toronto, Canada, 1946.
8 J. F. Denayer, G. V. Baron, W. Souverijns, J. A. Martens and P. A. Jacobs, *Ind. Eng. Chem. Res.*, 1997, **36**, 3242.
9 J. F. Denayer, G. V. Baron, G. Vanbutsele, P. A. Jacobs and J. A. Martens, *J. Catal.*, 2000, **190**, 469.
10 R. A. van Santen and G. J. Kramer, *Chem. Rev.*, 1995, **95**, 637.
11 A. D. Becke, *J. Chem. Phys.*, 1993, **98**, 5648.
12 M. J. Frisch, G. W. Trucks, H. B. Schlegel, M. A. Scuseria, M. A. Robb, J. R. Cheeseman, V. G. Zakrzewski, J. A. Montgomery, R. E. Stratmann, J. C. Burant, S. Dapprich, J. M. Millam, A. D. Daniels, K. N. Kudin, M. C. Strain, O. Farkas, J. Tomasi, V. Barone, M. Cossi, R. Cammi, B. Mennucci, C. Pomelli, C. Adamo, S. Clifford, J. Ochterski, G. A. Petersson, P. Y. Ayala, Q. Cui, K. Morokuma, D. K. Malick, D. K. Rabuck, K. Raghavachari, J. B. Foresman, J. Cioslowski, J. V. Ortiz, B. B. Stefanov, G. Liu, A. Liashenko, P. Piskorz, I. Komaromi, R. Gomperts, R. L. Martin, D. J. Fox, T. Keith, M. A. Al-Laham, C. Y. Peng, A. Nanayakkara, C. Gonzalez, M. Challacombe, P. M. W. Gill, B. G. Johnson, W. Chen, M. W. Wong, J. L. Andress, M. Head-Gordon, E. S. Replogle and J. A. Pople, Gaussian 98 (revision A.7), Gaussian, Inc, Pittsburg, PA, 1998.
13 A. P. Scott and L. Radom, *J. Phys. Chem.*, 1996, **100**, 16 502.
14 A. M. Vos, K. H. L. Nulens, F. De Proft, R. A. Schoonheydt and P. Geerlings, submitted.

CHEMCOMM
Communication
www.rsc.org/chemcomm

The first full-sandwich potassacarborane and a novel 'carbons-adjacent' $R_2C_2B_{10}H_{11}^-$ monoanion

Guofu Zi, Hung-Wing Li and Zuowei Xie*

Department of Chemistry, The Chinese University of Hong Kong, Shatin, New Territories, Hong Kong, China

Received (in Cambridge, UK) 7th March 2001, Accepted 2nd May 2001
First published as an Advance Article on the web 31st May 2001

By taking advantage of a cage carbon-linked *o*-carborane, the full-sandwich potassacarborane and a novel carborane monoanion have been prepared and structurally characterized for the first time, in which the cage carbon atom adjacency of the precursor is maintained.

It has been well documented that *o*-$R_2C_2B_{10}H_{10}$ (R = H, alkyl, aryl) can be readily reduced by alkali metals to form the [*nido*-$R_2C_2B_{10}H_{10}]^{2-}$ dianion in which the cage carbon atoms are in *meta* positions.[1] The cage C–C bond is completely broken during this two-electron reductive process.[1] The structures of its alkali metal salts have recently been reported.[2] These salts are very useful versatile synthons for the production of numerous metallacarboranes of s-, p-, d-, and f-block elements.[1] Protonation of [*nido*-$R_2C_2B_{10}H_{10}]^{2-}$ affords two isomers, the kinetic one **A** and the thermodynamic product **B**, as shown in Scheme 1.[3] Isomer **B** is more stable than **A** by 6.7 kcal mol^{-1} according to the computational results.[4] We have found that the two cage carbon atoms remain adjacent in *ortho* positions during the two-electron reductive process if they are linked by a short bridge, which leads to the isolation and structural characterization of the first full-sandwich potassacarborane and the novel isomer of the $[R_2C_2B_{10}H_{11}]^-$ monoanion. These new findings are reported in this communication.

Treatment of μ-1,2-[*o*-$C_6H_4(CH_2)_2$]-1,2-$C_2B_{10}H_{10}$[5] with excess finely cut potassium metal in THF at room temperature gives, after recrystallization from a THF/CH_3CN solution of 18-crown-6, the first full-sandwich potassacarborane [*closo-exo*-{μ-1,2-[*o*-$C_6H_4(CH_2)_2$]-1,2-$C_2B_{10}H_{10}$}$_2K_3$(18-crown-6)$_2$][(18-crown-6)K$(CH_3CN)_2$] (**1**) as yellow crystals in 74% yield.† **1** is extremely air- and moisture-sensitive but remains stable for months at room temperature under an inert atmosphere. Protonation of **1** generates a novel carborane monoanion [{μ-1,2-[*o*-$C_6H_4(CH_2)_2$]-1,2-$C_2B_{10}H_{11}$}K(18-crown-6)]$_n$ (**2**) as colorless crystals.† These transformations are summarized in Scheme 2. Both **1** and **2** have been fully characterized by various spectroscopic, elemental and X-ray analyses.

The ^{1}H NMR spectra show that methylene protons on the carborane cage in both **1** and **2** are non-equivalent in solution, and support the ratios of 1.5 18-crown-6 and one acetonitrile molecule per carboranyl ligand for **1**, and one 18-crown-6 molecule per ligand for **2**, respectively. The ^{13}C NMR spectra are consistent with the results derived from their ^{1}H NMR spectra. The ^{11}B NMR spectra exhibit 2:2:1:2:1:1:1 and 1:4:3:1:1 splitting patterns for **1** and **2**, respectively. Their solid-state IR spectra display both a characteristic doublet centered around 2450 cm^{-1} and a shoulder at about 2360 cm^{-1} attributable to a K–H–B stretching mode.[6]

An X-ray analysis‡ reveals that **1** is a centrosymmetric molecule consisting of well-separated, alternating layers of discrete cations [(18-crown-6)K$(CH_3CN)_2]^+$ and complex anions [*closo-exo*-{μ-1,2-[*o*-$C_6H_4(CH_2)_2$]-1,2-$C_2B_{10}H_{10}$}$_2K_3$(18-crown-6)$_2]^-$. In the anion, the K2 atom sits at an inversion center and bonds to two *nido*-carboranyl ligands in a η^6 fashion to form a fully sandwiched metallacarborane, shown in Fig. 1. It is interesting to note that the cage carbon atom adjacency of the precursor is maintained in the product due to the presence of the short bridge between the two cage carbon atoms. The six atoms of the hexagonal C_2B_4 bonding face are coplanar compared with the staggered arrangement of the two carbon atoms of the hexagonal face in the 'carbons-apart' dianionic species [*nido*-$R_2C_2B_{10}H_{10}]^{2-}$.[3] The average K2–cage atom distance of 3.064(4) Å is close to the corresponding value of 3.174(2) Å observed in [*closo-exo*-{$(C_6H_5CH_2)_2C_2B_{10}H_{10}$}$K_2(THF)_2(O_2C_4H_8)_{0.5}]_n$.[2]

In contrast to **1**, **2** adopts a polymeric structure in which the carboranyl and potassium ions serve as alternating bridging groups to give a zigzag carborane–K–carborane–K chain that is maintained in one-dimension throughout the lattice (Fig. 2). The

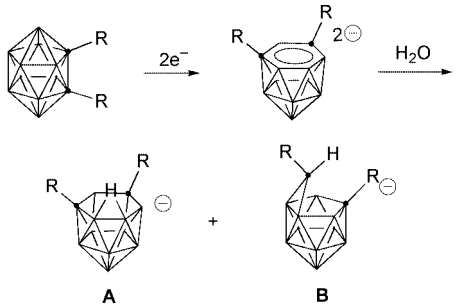

Scheme 1

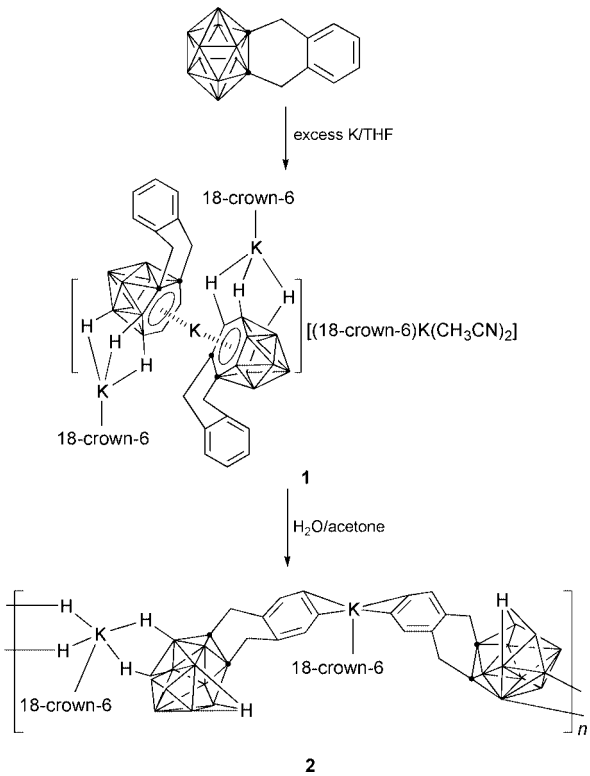

Scheme 2

 DOI: 10.1039/b102131c

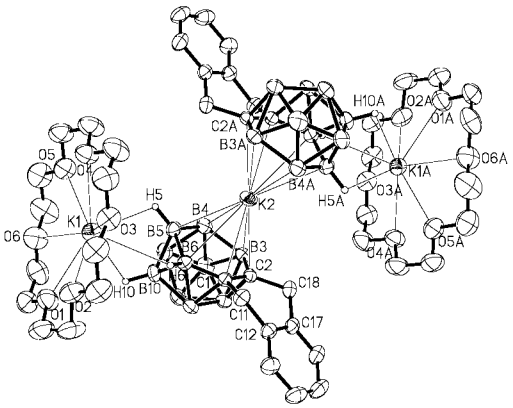

Fig. 1 ORTEP illustration of [*closo-exo*-{μ-1,2-[*o*-$C_6H_4(CH_2)_2$]-1,2-$C_2B_{10}H_{10}$}$_2$$K_3$(18-crown-6)$_2$]$^-$ in **1** with thermal ellipsoids drawn at the 35% probability level.

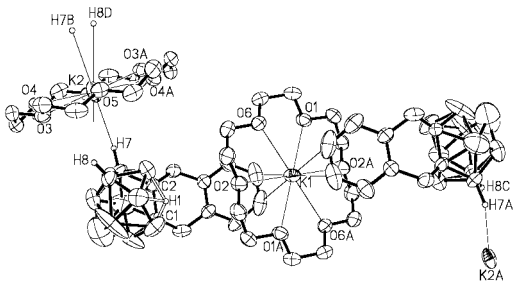

Fig. 2 ORTEP illustrations of **2** showing a portion of the infinite polymeric chain (thermal ellipsoids drawn at the 35% probability level).

most significant part of this structure is the arrangement of the cage atoms: 5-coordinate carbon and boron (C1, C2 and B11), 6-coordinate boron (B3–B5, B7, B8, B10 and B12), and 7-coordinate boron (B9 and B6), shown in Fig. 3. There are two pentagonal belts, one (B6B7B8B9B10) is capped by two boron atoms (B11 and B12) and the other (C1C2B3B4B5) is partially capped by one μ_3-H atom. This is a brand new isomer of the $[R_2C_2B_{10}H_{11}]^-$ monoanion which has never been observed before. Since **2** is prepared in a hot acetone solution, it is reasonable to suggest that **2** is the thermodynamic ('stable') product, which is also supported by ^{11}B NMR data. It is very obvious that the presence of a short bridge plays a significant role in the generation of the novel carborane monoanion in **2**.

In summary, the 'carbons-adjacent' carborane dianion and monoanion of the C_2B_{10} system can be readily produced by introducing a short bridge between two cage carbon atoms of an *o*-carborane. This study implies that these anions may exhibit a different chemistry from the corresponding 'carbons-apart' species.

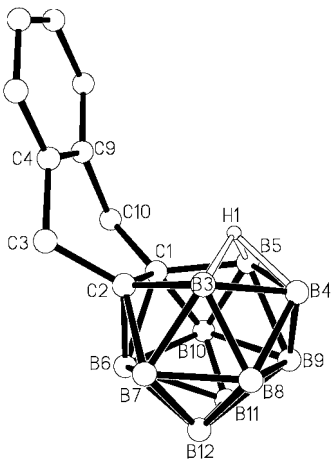

Fig. 3 Closer view of [μ-1,2-{*o*-$C_6H_4(CH_2)_2$}-1,2-$C_2B_{10}H_{11}$]$^-$ in **2**.

We thank the Research Grants Council of the Hong Kong Special Administration Region (Project No. CUHK 4267/00P) for financial support.

Notes and references

† *Preparation of* **1**: To a THF (25 mL) solution of μ-1,2-[*o*-$C_6H_4(CH_2)_2$]-1,2-$C_2B_{10}H_{10}$ (0.246 g, 1.00 mmol) was added finely cut K metal (0.25 g, 6.39 mmol), and the mixture was stirred at room temperature for a week. After removal of excess K, the clear orange solution was concentrated to about 10 mL to which was added a CH_3CN solution (10 mL) of 18-crown-6 (0.53 g, 2.00 mmol). **1** was isolated as yellow crystals after this solution stood at room temperature for a week (0.56 g, 74%). ^{1}H NMR (pyridine-d_5): δ 7.22 (m, 2H, aryl H), 7.10 (m, 2H, aryl H), 4.29 (d, J = 15.0 Hz, 2H, $C_6H_4(CH_2)_2$), 4.15 (d, J = 15.0 Hz, 2H, $C_6H_4(CH_2)_2$), 3.47 (s, 36H, $C_{12}H_{24}O_6$), 1.87 (s, 3H, CH_3CN); ^{13}C NMR (pyridine-d_5): δ 141.28, 125.99, 124.73 ($C_6H_4(CH_2)_2$), 117.60 (CH_3CN), 69.54 ($C_{12}H_{24}O_6$), 48.54 ($C_6H_4(CH_2)_2$), 0.35 (CH_3CN), the cage carbon atoms were not observed; ^{11}B NMR (pyridine-d_5): δ 3.23 (2B), −3.25 (2B), −5.83 (1B), −11.59 (2B), −18.06 (1B), −22.28 (1B), −24.16 (1B); IR (KBr, cm^{-1}): ν_{BH} 2456 (vs), 2398 (s), 2351 (s). Anal. Calc. for $C_{60}H_{114}B_{20}K_4N_2O_{18}$: C, 47.28; H, 7.54; N, 1.84. Found: C, 46.92; H, 7.53; N, 1.94%.

2: To a THF (25 mL) solution of **1** (0.38 g, 0.25 mmol) was added degassed H_2O (2 mL), and the mixture was stirred at room temperature for 0.5 h. After removal of the solvent, the residue was extracted with hot acetone (2 ×10 mL). The clear colorless solution was concentrated to about 4 mL. **2** was isolated as colorless crystals after this solution stood at room temperature for a week (0.24 g, 87%). ^{1}H NMR ($CDCl_3$): δ 7.10–6.96 (m, 4H, aryl H), 3.92 (d, J = 9.0 Hz, 1H, $C_6H_4(CH_2)_2$), 3.68 (d, J = 9.0 Hz, 1H, $C_6H_4(CH_2)_2$), 3.60 (s, 24H, $C_{12}H_{24}O_6$), 3.24 (d, J = 15.0 Hz, 1H, $C_6H_4(CH_2)_2$), 2.95 (d, J = 15.0 Hz, 1H, $C_6H_4(CH_2)_2$), 1.70 (s, 1H, μ-*H*); ^{13}C NMR ($CDCl_3$): δ 138.62, 127.02, 125.55 ($C_6H_4(CH_2)_2$), 48.66, 39.16 ($C_6H_4(CH_2)_2$), 70.09 ($C_{12}H_{24}O_6$), the cage carbon atoms were not observed; ^{11}B NMR ($CDCl_3$): δ −8.78 (1B), −13.06 (4B), −22.39 (3B), −37.01 (1B), −39.73 (1B); IR (KBr, cm^{-1}): ν_{BH} 2525 (vs), 2460 (s), 2379 (m). Anal. Calc. for $C_{22}H_{43}B_{10}KO_6$: C, 47.97; H, 7.87. Found: C, 47.82; H, 8.05%.

‡ *Crystal data*: for **1**: $C_{60}H_{114}B_{20}K_4N_2O_{18}$, M = 1524.13, triclinic, space group $P\bar{1}$, a = 11.645(1), b = 12.209(1), c = 16.194(1) Å, α = 97.77(1), β = 103.46(1), γ = 104.23(1)°, V = 2124.7(2) Å^3, D_c = 1.191 g cm^{-3}, Z = 1, $2\theta_{max}$ = 50°, μ(Mo-Kα) = 0.269 mm^{-1}, 11 476 reflections used, 7439 unique, R_1 = 0.060 ($I > 2.0\sigma(I)$), wR_2 = 0.158 on F^2.

For **2**: $C_{22}H_{43}B_{10}KO_6$, M = 550.76, monoclinic, space group $P2_1/n$, a = 8.953(1), b = 18.667(2), c = 18.642(2) Å, β = 101.12(1)°, V = 3056.9(6) Å^3, D_c = 1.197 g cm^{-3}, Z = 4, $2\theta_{max}$ = 50°, μ(Mo-Kα) = 0.208 mm^{-1}, 14 719 reflections used, 4787 unique, R_1 = 0.063 ($I > 2.0\sigma(I)$), wR_2 = 0.171 on F^2.

Data were collected at 293 K on a Bruker SMART 1000 CCD diffractometer using Mo-Kα radiation. An empirical absorption correction was applied using the SADABS program.[7] All structures were solved by direct methods and subsequent Fourier difference techniques and refined anisotropically for all non-hydrogen atoms by full-matrix least squares calculations on F^2 using the SHELXTL program package.[8] CCDC reference numbers 160868 and 160869. See http://www.rsc.org/suppdata/cc/b1/b102131c/ for crystallographic data in CIF or other electronic format.

1 A. K. Saxena, J. A. Maguire and N. S. Hosmane, *Chem. Rev.*, 1997, **97**, 2421; R. N. Grimes, in *Comprehensive Organometallic Chemistry II*, ed. E. W. Abel, F. G. A. Stone and G. Wilkinson, Pergamon Press, Oxford, U.K., 1995, vol. 1, p. 373; A. K. Saxena and N. S. Hosmane, *Chem. Rev.*, 1993, **93**, 1081.
2 K. Chui, H.-W. Li and Z. Xie, *Organometallics*, 2000, **19**, 5447.
3 T. G. Getman, C. B. Knobler and M. F. Hawthorne, *Inorg. Chem.*, 1990, **29**, 158; E. I. Tolpin and W. N. Lipscomb, *Inorg. Chem.*, 1973, **12**, 2257; M. R. Churchill and B. G. DeBoer, *Inorg. Chem.*, 1973, **12**, 2674.
4 M. L. McKee, M. Bühl and P. v. R. Schleyer, *Inorg. Chem.*, 1993, **32**, 1712.
5 G. Zi, H.-W. Li and Z. Xie, unpublished results; D. S. Matteson and R. A. Davis, *Inorg. Chem.*, 1974, **13**, 859.
6 Z. Xie, S. Wang, Z.-Y. Zhou and T. C. W. Mak, *Organometallics*, 1999, **18**, 1641; Z. Xie, S. Wang, Q. Yang and T. C. W. Mak, *Organometallics*, 1999, **18**, 2420; S. Wang, Q. Yang, T. C. W. Mak and Z. Xie, *Organometallics*, 1999, **18**, 1578; S. Wang, Q. Yang, T. C. W. Mak and Z. Xie, *Organometallics*, 2000, **19**, 334; K. Chui, Q. Yang, T. C. W. Mak, W.-H. Lam, Z. Lin and Z. Xie, *J. Am. Chem. Soc.*, 2000, **122**, 5758.
7 G. M. Sheldrick, SADABS: program for empirical absorption correction of area detector data, University of Göttingen, Germany, 1996.
8 G. M. Sheldrick, SHELXTL 5.10 for Windows NT: structure determination software programs, Bruker Analytical X-ray systems, Inc., Madison, Wisconsin, USA, 1997.

CHEMCOMM Communication
www.rsc.org/chemcomm

Tailored palladium containing silica spheres

Lubomira Tosheva and Johan Sterte*

Division of Chemical Technology, Luleå University of Technology, S-971 87 Luleå, Sweden. E-mail: jost@km.luth.se

Received (in Cambridge, UK) 2nd March 2001, Accepted 4th May 2001
First published as an Advance Article on the web 31st May 2001

Palladium containing silica spheres are tailored by a multi-step procedure consisting of: (i) preparation of ion exchange resin–silica composites, (ii) Pd ion exchange, and (iii) calcination.

Controlled preparation of porous materials is of great technological interest for areas such as heterogeneous catalysis and molecular sieving.[1,2] Advanced porous structures *e.g.* metallic macrostructures, have attracted special attention due to their unique properties. By colloidal crystal templating porous gold flakes have been produced with the size of the pores corresponding to the size of the latex micospheres used as templates.[3] A number of macroporous, free-standing metal films have been prepared employing colloidal silica crystals as pore-size determining templates.[4] Silica sol has been used as a nanoglue to synthesise composite aerogels containing different guest components *e.g.* Pt and Au.[5] Recently, we reported a method for the preparation of silica-based macrostructures using anion exchange resins as templates.[6,7] This method involves treatment of resin beads with silica solutions followed by calcination. The resin bead templates determine the final shape of the macrostructures whereas the combustion of the resin provides the materials with high and controlled porosity. Here, we report the synthesis of palladium containing silica spheres prepared by resin templating. The procedure is based on the fact that the resin–silica composites obtained after the ion exchange of silica species retain a high anion exchange capacity facilitating introduction of negatively charged ions such as $PdCl_4^{2-}$ in a second step. Upon calcination the resin bead templates are removed and the palladium is obtained in an oxide form.

Macroporous strongly basic Dowex MSA-1 resin beads (mesh size 20–50, chloride form) were used as received from Sigma. In a typical synthesis batch, 30 g of resin were mixed with 150 g of sodium water glass solution (21.4 wt% SiO_2, 6.7 wt% Na_2O, Akzo Nobel) in a polyethylene reactor. The synthesis mixture was treated in an oil bath preheated to 100 °C under reflux until the initially floating resin particles sank, after 4 h. The resin–silica composites obtained were separated by decanting, rinsed repeatedly with distilled water and dried at 105 °C. Palladium was subsequently introduced into the composites by ion exchange using a solution of 0.01 M palladium chloride ($PdCl_2$, Aldrich) dissolved in 1 M hydrochloric acid. Composites and palladium solutions were mixed in different weight ratios (*e.g.* 1 g composite mixed with 5, 10 or 20 g of Pd solution and the corresponding samples were designated as Pd5, Pd10 and Pd20) in a beaker and placed on a shaker overnight. After this procedure the initially brownish color of the Pd solutions turned colorless. The Pd–resin–silica composites were decanted, rinsed repeatedly with distilled water and dried at 105 °C. Finally, the composites were calcined at 600 °C for 5 h after heating to this temperature at a rate of 1 °C min^{-1}.

Visually the Pd materials obtained after the removal of the ion exchanger consisted of solid and hard brownish spheres. The color intensity was increased with an increase in the palladium solution to composite weight ratio used. A SEM image representative for those spheres is shown in Fig. 1(a). The shape of the particles was identical to the shape of the initial ion exchange resin beads but the spheres shrunk upon calcination. A similar result was obtained for the silica spheres obtained after calcining the resin–silica composites and correspondingly the shrinkage observed was not related to the insertion of palladium into the composites. The Pd spheres were built up by fine particles with a size of < 100 nm which is comparable to the pore size of macroporous resins.[8] The primary particles of the Pd silica spheres were similar to those of calcined resin–silica composites and no conclusions about the palladium dispersion can be drawn by the SEM investigation.

Pd silica spheres were ground into a powder and X-ray diffraction patterns were recorded in order to identify the form of palladium obtained after the calcination. During the grinding no white material was observed suggesting that the palladium was distributed within the spheres. Fig. 1(b) shows the XRD pattern of the Pd20 sample. Two phases may be seen in this pattern: an amorphous one, emanating from the amorphous silica phase, and a crystalline one, corresponding to the presence of palladium oxide in the spheres.[9] The XRD patterns of the Pd10 and Pd5 samples were similar to that shown in Fig. 1(b) but with lower peak intensities related to the decreased Pd loading. No additional peaks due to the presence of other

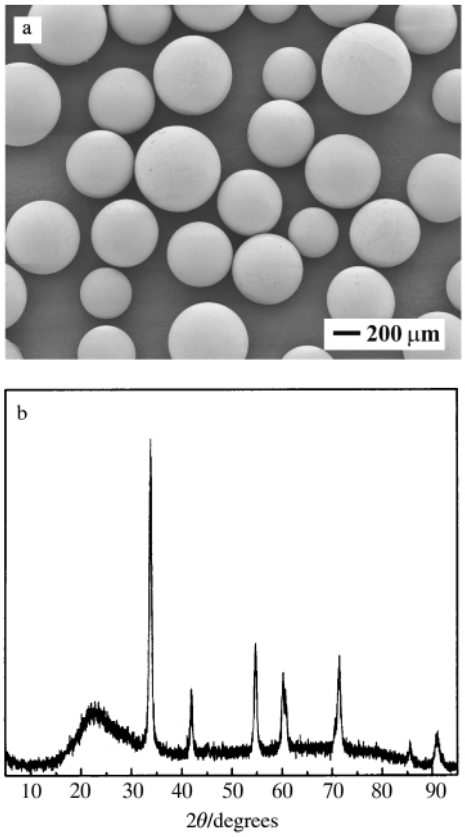

Fig. 1 A representative SEM image of the Pd containing silica spheres (a) and XRD pattern of the Pd20 sample (b). SEM was performed on a Philips XL scanning electron microscope equipped with a LaB_6 emission source. XRD patterns were collected at room temperature with a Cu-Kα X-ray source using a Siemens D5000 instrument.

 DOI: 10.1039/b102012a

Table 1 BET surface areas, total pore volumes, yield, Pd loading and Pd uptake for the spheres prepared

Spheres	BET surface/ area/$m^2\ g^{-1}$	Total pore volume[a]/$cm^3\ g^{-1}$	Yield (wt%)	Pd loading/(wt%)	Pd uptake[b](%)
Silica	93	0.26	38.39	—	—
Pd5	840	0.64	38.84	1.37	99.8
Pd10	1043	0.75	38.05	2.80	99.3
Pd20	1203	0.88	38.08	5.59	97.9

[a] Calculated by converting the volume adsorbed at a relative pressure of 0.995 to the volume of the liquid adsorbate. [b] Calculated from the Pd concentration in the initial Pd solution and in the solution after the ion exchange as determined by atomic absorption spectrometry.

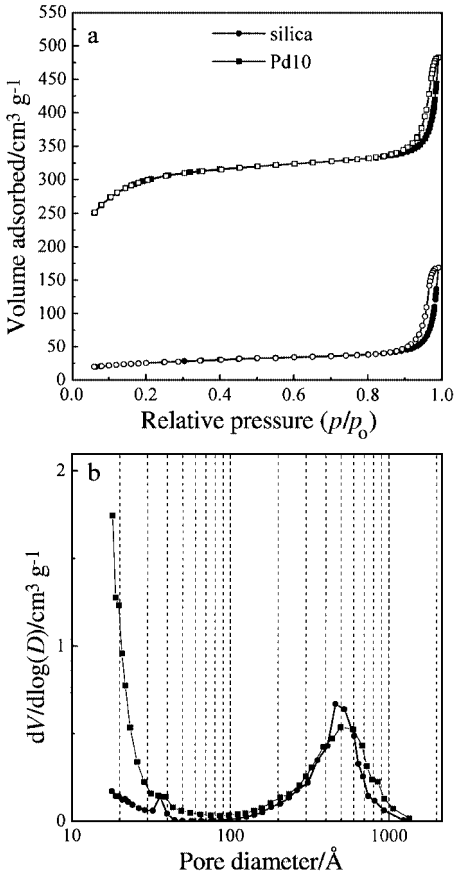

Fig. 2. Nitrogen adsorption isotherms at 77 K for calcined silica and Pd10 spheres; solid symbols, adsorption; open symbols, desorption (a) and the corresponding pore size distributions (b). The pore size distributions were calculated from the desorption branch of the nitrogen isotherm by the BJH method. The data was collected with a Micromeritics 2010 Gas Adsorption Analyser after the materials were degassed at 300 °C for 12 h.

palladium phases were detected in the XRD patterns of the Pd containing spheres prepared.

Fig. 2(a) shows nitrogen adsorption isotherms for calcined silica and Pd10 spheres. The isotherm for the calcined silica spheres was of type IV which is typical for mesoporous materials.[10] Langmuir type isotherms typical of microporous materials, with identical, nearly horizontal, adsorption and desorption branches, were obtained for the Pd containing spheres. Some mesopores were also present in these spheres as seen from the distinct hysteresis loop at high relative pressures. From the pore-size distributions presented in Fig. 2(b) is seen that the amount of mesopores (imposed by the removal of the ion exchange resin) is approximately the same for the two samples, whereas the amount of micropores is increased for the Pd containing spheres. The surface area values, calculated with the BET equation as well as the total pore volumes are listed in Table 1. Judging from these values and the pore-size distributions one can conclude that: (i) the insertion of palladium into the resin–silica composites leads to substantially larger BET surface areas of the calcined samples; (ii) the increase in the surface area is related to the amount of palladium present within the spheres; and (iii) the increase in the surface areas may be related to an increase in the micropore volume of the calcined materials. These results are surprising and further investigations are needed in order to explain the rather dramatic changes observed.

Finally, the yield, the amount of solid material obtained per gram of composite, was determined from the weight difference between dried composites at 150 °C and calcined spheres (Table 1). From the yield and from the similar hardness of the silica and the Pd silica spheres one may conclude that there was no substantial silica leakage from the resin–silica composites during the Pd ion exchange. Based on the yields, the Pd loading was calculated and listed in Table 1. Considering the Pd uptake data (also included in Table 1) one may conclude that the ion exchange of Pd into the resin–silica composites was almost complete.

The results presented show that hard and solid silica spheres containing a controllable amount of palladium can be prepared using macroporous ion exchange resins as templates. Owing to the high surface areas and large pore volumes, these materials are interesting for catalytic applications. Currently our efforts are directed to further characterise the palladium in the silica spheres and results will be presented in a subsequent publication. The procedure may also be used for the preparation of silica spheres containing other active catalytic phases.

We thank the Swedish Research Council for Engineering Sciences (TFR) for partial financial support of this work.

Notes and references

1 N. K. Raman, M. T. Anderson and C. J. Brinker, *Chem. Mater.*, 1996, **8**, 1682.
2 T. J. Barton, L. M. Bull, W. G. Klemperer, D. A. Loy, B. McEnaney, M. Misono, P. A. Monson, G. Pez, G. W. Scherer, J. C. Vartuli and O. M. Yaghi, *Chem. Mater.*, 1999, **11**, 2633.
3 O. D. Velev, P. M. Tessier, A. M. Lenhoff and E. W. Kaler, *Nature*, 1999, **401**, 548.
4 P. Jiang, J. Cizeron, J. F. Bertone and V. L. Colvin, *J. Am. Chem. Soc.*, 1999, **121**, 7957.
5 C. A. Morris, M. L. Anderson, R. M. Stround, C. I. Merzbacher and D. R. Rolison, *Science*, 1999, **284**, 622.
6 L. Tosheva, V. Valtchev and J. Sterte, *Microporous Mesoporous Mater.*, 2000, **35**–**36**, 621.
7 L. Tosheva, V. Valtchev and J. Sterte, *J. Mater. Chem.*, 2000, **10**, 2330.
8 C. E. Harland, in *Ion Exchange: Theory and Practice*, The Royal Society of Chemistry, Cambridge, 1994, p. 46.
9 PDF file 6-515, PDF-2 Database Sets 1-45, ICDD, 1995.
10 S. J. Gregg and K. S. W. Sing, in *Adsorption, Surface Area and Porosity*, Academic Press, New York, 1982.

CHEMCOMM Communication
www.rsc.org/chemcomm

Controlling the formation of discrete complexes or a 1-D directional coordination network by the binding ability of anions†

Abdelaziz Jouaiti, Valérie Jullien, Mir Wais Hosseini* Jean-Marc Planeix and André De Cian

Laboratoire de Chimie de Coordination Organique, Université Louis Pasteur, F-67000 Strasbourg, France. E-mail: hosseini@chimie.u-strasbg.fr

Received (in Cambridge, UK) 5th March 2001, Accepted 8th May 2001
First published as an Advance Article on the web 31st May 2001

Based on the coordination ability of ClO_4^-, BF_4^- and Cl^- anions, a switch from discrete octahedral Co(II) complexes to a directional 1-D network was demonstrated using organic tectons based on a pyridine unit as a monodentate coordination site and a terpyridine moiety as a tridentate coordination pole; whereas with non-coordinating anions discrete mononuclear complexes were obtained, for Cl^- anion a 1-D coordination network was obtained in the presence of $CoCl_2$ under self-assembly conditions; the X-ray study on a single crystal revealed the centrosymmetric packing of the 1-D networks.

The self-assembly process based on the use of metals and organic ligands is a powerful strategy allowing generation of polynuclear assemblies displaying a variety of finite architectures.[1] The same strategy is also currently used to prepare coordination networks which are infinite assemblies possessing translational symmetry.[2]

Let us focus on 1-D coordination networks obtained by a single translation of an assembling core defined by the coordination of the metal to the organic tecton. Although many examples of 1-D networks using metals with linear coordination geometrics and bis-monodentate tectons have been prepared, for metals adopting other coordination geometries such as square planar, tetrahedral or octahedral only a rather small number of investigations have been reported. The majority of coordination networks reported so far are based on 4,4′-bipyridine,[3] however, few examples based on bis-bidentate[4,5] or tetrakis-monodentate[6,7] ligands have been also reported. Finally, only a few structurally characterised networks based on bis-tridentate tectons have been published.[8–10]

For coordination networks based on metal cations and anionic organic tectons bearing the same but opposite charges, the charge compensation criteria is fulfilled. In this case, the design of the network may be based on the match between the coordination features of the metal and the organic tecton. However, when charge neutrality is not achieved by the two partners, the presence of a third component is required thus leading to a three-component system. For a combination of neutral tectons and metal cations, based on the binding ability of the anion, two possibilities may be considered. Non-coordinating anions would mainly play a charge compensating role without interfering directly with the metal centres, whereas coordinating anions form direct bonds with the metal cation. In the latter case, one may take advantage of this requirement to control the coordination sphere around the metal cation. For example, for metal centres adopting O_h geometry, the use of bulky and coordinating anions such as Cl^- would lead to the occupation of the two axial positions thus leaving the square planar base for construction of coordination networks.[11]

Here we report the design and synthesis of a tecton **1** and, depending on the coordinative nature of the anion (Cl^-, ClO_4^-), the formation of either a discrete complex **4** or a 1-D directional network **5** using Co(II) complexes.

Ligand **1** (Scheme 1) is based on a combination of a pyridine (py) and terpyridine (terpy) units. The junction between the mono- and tri-dentate units was achieved using an ethynyl spacer. The latter was chosen because it should minimise possible steric effects affecting the packing of 1-D networks in the solid state and should allow electronic communication between the py and terpy sites.[12] An example of a py directly connected to a terpy has been reported by Constable *et al.*[13]

For Co(II) cations adopting O_h geometry, in the case of non-coordinating anions such as ClO_4^-, all six available coordination positions may be occupied by two terpy moieties belonging to two molecules of **1** acting as ligands thus leading to a discrete complex **4** (Scheme 1). However, in the presence of coordinating anions such as Cl^-, the two anions would occupy the two axial positions leaving four coordination sites located at the square planar plane of the octahedron. Then **1** may act as a tecton by connecting the metal centres into a 1-D network such as **5**. Indeed, the four available coordination positions may be occupied by a terpy moiety belonging to one tecton **1** and by the py unit belonging to another tecton **1**, leading by a single translation of an assembling core defined as [py–$CoCl_2$–terpy], to a 1-D network. Moreover, owing to the unsymmetrical nature of **1**, a directional 1-D network should be obtained. The latter point is of interest for directional physical properties if one could avoid centrosymmetric packing of directional 1-D networks.

The starting material for the synthesis of **1** was **2**[14] which was prepared according to published procedures.[14] The synthesis of **1** was achieved by coupling **2** with **3**[15] in the presence of $Pd(OAc)_2$ and Ph_3P in Et_3N under reflux for 48 h. Pure ligand **1** was obtained as a white powder in 98% yield after chromatography (Al_2O_3, hexane–diethyl ether 6:4).

Upon slow diffusion at room temp. of a MeOH solution containing $Co(ClO_4)_2{\cdot}6H_2O$ (4 mg) into a $CHCl_3$ solution of **1** (5 mg), orange crystals were obtained after *ca.* 4 h. An X-ray study‡ on a single-crystal showed the presence of **4** with the following relevant features: the crystal (monoclinic) was

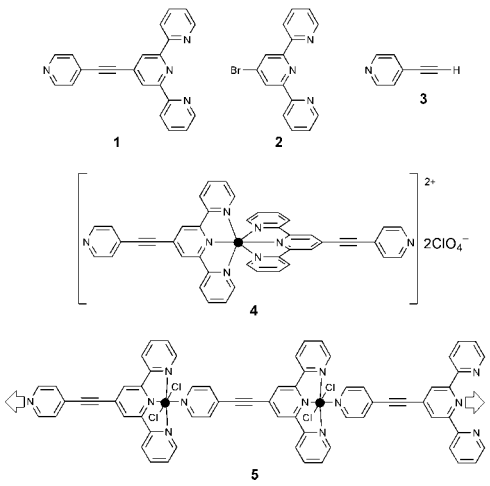

Scheme 1

† Dedicated to François Mathey on the occasion of his 60th birthday.

 DOI: 10.1039/b102042k

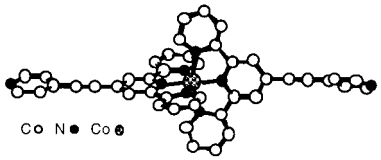

Fig. 1 X-Ray crystal structure of the mononuclear Co complex **4**. ClO_4^- anions, H atoms and solvent molecules are omitted for clarity. For distances and angles see text.

composed of **1**, Co^{2+}, $2ClO_4^-$ and $2CHCl_3$. For the cationic complex **4** comprised of one cation and two ligands **1**, the metal adopts a distorted O_h geometry with all six coordination positions occupied by 6 N atoms belonging to two terpy units. Whereas the two N–Co distance are 1.88 and 1.92 Å in the case of both central py units, the other N–Co distances are between 2.00 and 2.14 Å. For nitrogen atoms in *cis* disposition the N–Co–N angle varies from 78.5 to 103.0°, whereas for those in *trans* configuration, the N–Co–N angle varies from 156.9 to 178.4° (Fig. 1). No specific interactions between **4** and ClO_4^- anions are observed. Interestingly, the same observations were made for an analogous ligand (in which the terpy unit was connected by the same ethynyl spacer to the py moiety at the position 3) upon treatment with $Co(BF_4)_2{\cdot}6H_2O$ (synthesis and X-ray data not reported here).

Upon slow diffusion at room temp. of a MeOH solution containing $CoCl_2{\cdot}6H_2O$ (6 mg) in to a CH_2Cl_2 solution of **1** (6 mg,), purple crystals were obtained after *ca*. 24 h. An X-ray study‡ revealed the presence of the 1-D network **5**. The crystal (monoclinic) was composed of **1**, Co^{2+}, $2Cl^-$ and 1 CH_2Cl_2. As expected for the coordinating Cl^- anion, a directional 1-D neutral network based on the interconnection of $CoCl_2$ units by **1** is observed. The assembling core is a distorted octahedral Co(II) complex for which the coordination sphere is composed of two Cl^- and four N atoms. The two Cl^- anions occupy the two axial positions with a Co–Cl distance of *ca* 2.463 Å and Cl–Co–Cl angle of 179.5°. The square base of the octahedron is composed of one py belonging to **1** and one terpy unit belonging to next tecton **1** with Co–N distances of 2.131 Å for the py unit and 2.048 Å for the central py of the terpy moiety. The other two Co-N distances are *ca*. 2.162 Å. Whereas the Cl–Co–N angle varies from 88.6 to 91.3°, the N–Co–N angle varies between *ca*. 76.7 and 103.3°. The N–Co–N angle between the py and the central py unit of the terpy moiety is 180.0°. The py and the terpy units are not coplanar but are tilted by *ca* 112 ° (Fig. 2).

Owing to the unsymmetrical nature of **1**, the 1-D network is directional by nature. In principle, a directional 1-D network may either be packed in centrosymmetric or non-centrosymmetric modes in the crystalline phase. In the example reported here, the directional networks are positioned in a parallel fashion but oriented in opposite directions, thus leading to an overall non-directional system (Fig. 2). This centrosymmetric packing may be due to cancellation of dipolar moments.

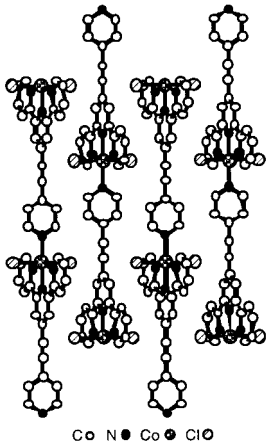

Fig. 2 A portion of the X-Ray crystal structure of the directional 1-D network **5** showing the packing of consecutive networks in 'head-to-tail' fashion. H atoms and solvent molecules are omitted for clarity. For distances and angles see text.

In conclusion, using a neutral tecton such as **1** and Co(II), depending on the its coordination ability, the role of the auxiliary anions in directing either the formation of discrete complexes or a 1-D network was demonstrated. Indeed, unsymmetrical ligand **1** based on two different coordination poles and non-coordinating anions such as ClO_4^- lead to the formation of a discrete Co(II) octahedral complex **4**, whereas, for a coordinating anion such as Cl^-, the self-assembly of $CoCl_2$ and **1** leads to the formation of a neutral and directional 1-D network **5** in the solid state. The directional 1-D networks are packed parallel to each other with opposite orientation. Since the discrete complex **4** possesses two non-coordinating pyridine units, it may act as an exo-ligand and thus may be used as a metallatecton[16] for generating heteronuclear coordination networks. This aspect is under current investigation.

Notes and references

‡ *Crystal data*: **4**: (orange, 173 K), $C_{44}H_{28}CoN_8{\cdot}2CHCl_3{\cdot}2ClO_4$, M = 1165.36, monoclinic, space group $P2/c$, a = 8.8059(2), b = 34.3527(7), c = 16.8241(4) Å, β = 104.779(5), U = 4921.0(2) Å^3, Z = 4, D_c = 1.57 g cm^{-3}, μ(Mo-Kα) = 0.845 mm^{-1}, 3744 data with $I > 3\sigma(I)$, R = 0.077, R_w = 0.087. **5**: (purple, 173 K), $C_{22}H_{14}Cl_2CoN_4{\cdot}CH_2Cl_2$, M = 549.16, monoclinic, space group $P2/n$, a = 8.7151(7), b = 13.792(1), c = 10.2996(5) Å, β = 112.095(5), U = 1147.1(1) Å^3, Z = 2, D_c = 1.59 g cm^{-3}, μ(Mo-Kα) = 1.234 mm^{-1}, 1295 data with $I > 3\sigma(I)$, R = 0.063, R_w = 0.074. Data were collected on a Nonius Kappa CCD and structural determination was achieved using the Nonius OpenMolenN package.[18]

CCDC 163354 and 163355. See http://www.rsc.org/suppdata/cc/b1/b102042k/ for crystallographic data in CIF or other electronic format.

1 G. F. Swegers and T. J. Malefetse, *Chem. Rev.*, 2000, **100**, 3483.
2 R. Robson, in *Comprehensive Supramolecular Chemistry*, ed. J. L. Atwood, J. E. D. Davies, D. D. Macnicol and F. Vögtle, vol. 6 (ed. D. D. Macnicol, F. Toda and R. Bishop), Pergamon, New York, 1996, p. 733; S. R. Batten and R. Robson, *Angew. Chem., Int. Ed.*, 1998, **37**, 1460.
3 M. Fujita, in *Comprehensive Supramolecular Chemistry*, vol. 9 (ed. J. P. Sauvage and M. W. Hosseini), Pergamon, New York, 1996, p. 253; O. M. Yaghi, H. Li, C. Davis, D. Richardson and T. L. Groy, *Acc. Chem. Res.*, 1998, **31**, 474; T. L. Hennigar, D. C. MacQuarrie, P. Losier, R. D. Rogers and M. J. Zaworotko, *Angew. Chem., Int. Ed. Engl.*, 1997, **36**, 972; J. Blake, N. R. Champness, S. S. M. Chung, W-S. Li and M. Schröder, *Chem. Commun.*, 1997, 1675; M. A. Withersby, A. J. Blake, N. R. Champness, P. Hubberstey, W-S. Li and M. Schröder, *Chem. Commun.*, 1997, 2327.
4 U. Velten and M. Rehahn, *Chem. Commun.*, 1996, 2639
5 C. Kaes, M. W. Hosseini, C. E. F. Rickard, B. W. Skelton and A. White, *Angew. Chem., Int. Ed.*, 1998, **37**, 920.
6 G. Mislin, E. Graf, M. W. Hosseini, A. De Cian, N. Kyritsakas and J. Fischer, *Chem. Commun.*, 1998, 2545.
7 C. Klein, E. Graf, M. W. Hosseini, A. De Cian and J. Fischer, *Chem. Commun.*, 2000, 239; C. Klein, E. Graf, M. W. Hosseini, A. De Cian and J. Fischer, *New J. Chem.*, 2001, **25**, 207.
8 E. C. Constable and A. M. W. Cargill Thompson, *J. Chem. Soc., Dalton Trans.*, 1992, 3467; E. C. Constable, A. J. Edwards, D. Philips and P. R. Raithby, *Supramol. Chem.*, 1995, **5**, 93.
9 S. J. Loeb and G. K. H. Shimizu, *Chem. Commun.*, 1993, 1395; M. Ferigo, P. Bonhôte, W. Marty and H. Stoeckli-Evans, *J. Chem. Soc., Dalton Trans.*, 1994, 1549; A. Neels, B. Mathez Neels and H. Stoeckli-Evans, *Inorg. Chem.*, 1997, **36**, 3402.
10 M. Loï, E. Graf, M. W. Hosseini, A. De Cian and J. Fischer, *Chem. Commun*, 1999, 603; M. Loï, M. W. Hosseini, A. Jouaiti, A. De Cian and J. Fischer, *Eur. J. Inorg. Chem.*, 1999, 1981.
11 A. Jouaiti, M. W. Hosseini and A. De Cian, *Chem. Commun.*, 2000, 1863.
12 R. Ziessel, *Synthesis*, 1999, 1839.
13 E. C. Constable and A. M. W. Cargill Thomson, *J. Chem. Soc., Dalton Trans*, 1992, 2947.
14 E. C. Constable and M. D. Ward, *J. Chem. Soc., Dalton Trans.*, 1990, 1405; B. Whittle, S. R. Batten, J. C. Jeffrey, L. H. Rees and M. D. Ward, *J. Chem. Soc., Dalton Trans.*, 1996, 4249.
15 L. Della Ciana and A. Haim, *J. Heterocycl. Chem.*, 1984, **21**, 607.
16 H. Akdas, E. Graf, M. W. Hosseini, A. De Cian and J. McB. Harrowfield, *Chem. Commun.*, 2000, 2219.
17 OpenMolenN, Interactive Structure Solution, Nonius B. V., Delft, The Netherlands, 1997.

CHEMCOMM Communication
www.rsc.org/chemcomm

A simple route to organic–inorganic hybrid materials containing Eu^{3+} complexes

Robert J. P. Corriu,* Frank Embert, Yannick Guari, Ahmad Mehdi and Catherine Reyé

Laboratoire de Chimie Moleculaire et Organisation du Solide, UMR 5637 CNRS, Université de Montpellier II, Sciences et Techniques du Languedoc, Place E. Bataillon, F-34095 Montpellier Cedex 5, France. E-mail: reye@crit.univ-montp2.fr

Received (in Cambridge, UK) 22nd March 2001, Accepted 4th May 2001
First published as an Advance Article on the web 31st May 2001

Direct complexation of europium nitrate into HMS materials containing phosphine oxide groups covalently linked to a silica matrix is accomplished and is shown to work much better than into the corresponding materials prepared in the absence of surfactant.

The study of luminescent materials has been the subject of extensive research in the past decade.[1–3] Of particular interest are rare-earth-ion-based systems which can give rise to a variety of optical applications such as fiber amplifiers and solid-state lasers.[4,5] The sol–gel approach is an attractive means of synthesising these materials since it allows both the control of the devices and a great diversity of chemical composition.[6] Numerous studies have been carried out on nanocomposite hybrid materials prepared by incorporating Eu^{3+} or Tb^{3+} complexes into sol–gel matrices.[7–9] With a view to avoiding the inhomogeneous dispersion of rare-earth complexes within the silica matrix, we have recently studied the hydrolytic polycondensation of isolated europium complexes with phosphine oxides bearing one hydrolysable $Si(OR)_3$ group.[10] We have shown that the Eu^{3+} are well encapsulated within the resulting nanostructured hybrid materials which present highly luminescent properties. We now report a very simple and original route to Eu^{3+} containing hybrid materials. This method consists of the direct incorporation of europium salts into a hybrid organic–inorganic material containing phosphine oxide groups covalently linked to the silica matrix and able to complex Eu^{3+}.[11] This rare-earth ion was selected as a representative rare-earth ion because of its unique fluorescence properties.[12] We show that ordered HMS materials containing phosphine oxide groups prepared by using the direct synthetic approach[13] are much more convenient for the complexation of Eu^{3+} than the corresponding materials prepared in the absence of surfactant. The luminescence behaviour of the materials was considered.

The hybrid materials $\mathbf{A}_n$ (Scheme 1) were obtained by co-hydrolysis and polycondensation of a mixture of $Ph_2P(CH_2)_3Si(OMe)_3$[14] and of n equiv. of $Si(OEt)_4$ (n = 4, 7, 9, 12, 14, 19 and 35) in the presence of *n*-hexadecylamine as template (route A). The corresponding materials $\mathbf{B}_n$ (route B) were prepared in the absence of template but in the presence of 1% TBAF as catalyst [n in index for materials $\mathbf{A}_n$ and $\mathbf{B}_n$ corresponds to the number n of equiv. of $Si(OEt)_4$]. The xerogels were prepared according to published procedures.[15] Treatment of the materials $\mathbf{A}_n$ and $\mathbf{B}_n$ with a large excess of an aqueous H_2O_2 solution for 12 h at 30 °C afforded the solids $\mathbf{A}_n$**[O]** and $\mathbf{B}_n$**[O]**, respectively (Scheme 1).[16] After washing and drying, the solid-state ^{31}P NMR spectroscopy of the resulting white solids revealed the complete formation of P=O centres. Some relevant physical properties of these materials are given in Table 1. The BET surface areas of both materials were determined by the N_2 adsorption–desorption isotherm measurements. The materials $\mathbf{A}_n$**[O]** (n = 4–35) exhibit type IV isotherms, characteristic for mesoporous materials while the materials $\mathbf{B}_n$**[O]** display type II isotherms, indicative of macroporosity. The XRD patterns of the materials $\mathbf{A}_n$**[O]** exhibit an intense diffraction peak corresponding to the d_{100} spacing (Table 1). and in some cases (for $n \geqslant 19$) a much less intense peak corresponding to d_{110} and d_{200} spacings indicating a hexagonal mesostructure. In contrast, the XRD patterns of the solids $\mathbf{B}_n$**[O]** display no peak. Both types of solids were subsequently treated with an excess of an ethanol solution of $Eu(NO_3)_3{\cdot}6H_2O$ (2 equiv. of Eu^{3+} per P=O) heated under reflux for 14 h. The resulting solids **EuA**$_n$**[O]** and **EuB**$_n$**[O]** were copiously washed with acetonitrile to eliminate the non-complexed salt until no traces of $Eu(NO_3)_3$ were detected in the filtrate. After drying, the extent of the complexation reaction within both types of materials was first determined by solid-state ^{31}P NMR spectroscopy. For $n \leqslant 14$, the ^{31}P NMR spectra of the materials exhibit two signals (Table 2), one was attributed to the free P=O groups (33.1–37.4 ppm) and the other which was shifted upfield (−107.1 to −112.0 ppm), to P=O groups coordinated to Eu^{3+}. The percentage of complexed P=O sites was calculated by integration of the signals and the results are reported in Table 2 and in Fig. 1. When $n > 14$, the solid state ^{31}P NMR spectra of both materials display only one signal attributed to the starting phosphine oxide. Elemental analyses for Eu, P, N (and in some cases Si) were carried out, and the percentages of complexed Eu^{3+} were then calculated considering that one Eu^{3+} coordinates three P=O groups (Table 2).[17] This method of calculation afforded percentages of complexed Eu^{3+} in good agreement with the percentages calculated by ^{31}P NMR spectroscopy. This strongly suggests that the uptake of one Eu^{3+} requires three P=O groups within the materials.

Thus, direct incorporation of $Eu(NO_3)_3{\cdot}6H_2O$ within both types of materials is possible for $7 \leqslant n \leqslant 14$. The uptake of Eu^{3+} depends highly on the type of the materials (prepared in the presence or in the absence of surfactant) and on the dilution of the organic moiety into silica (Fig. 1), the higher percentage of

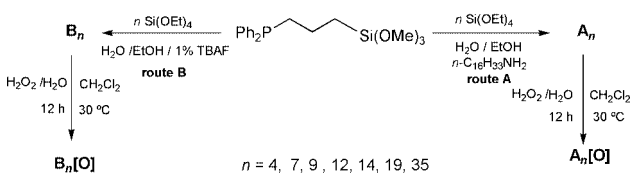

Scheme 1 $\mathbf{A}_n$**[O]** and $\mathbf{B}_n$**[O]** corresponds to materials $Ph_2PO(CH_2)_3SiO_{1,5}/nSiO_2$ prepared in the presence and in the absence of surfactant, respectively.

Table 1 Physicochemical properties of $\mathbf{A}_n$**[O]** materials containing phosphine oxide moieties

Sample	^{31}P NMR[a] (HPDEC MAS)	d_{100} lattice spacing/Å	D_p/Å	S_{BET}/m^2 g^{-1}	Total pore volume/ cm^3 g^{-1}
$\mathbf{A_7}$**[O]**	32.9	37	30	515	0.28
$\mathbf{A_9}$**[O]**	35.0	39.7	35	1000	0.30
$\mathbf{A_{12}}$**[O]**	33.9	38.1	35	680	0.35
$\mathbf{A_{14}}$**[O]**	33.0	40.8	37	750	0.47
$\mathbf{A_{19}}$**[O]**	34.3	40.5	34	1110	0.77
$\mathbf{A_{35}}$**[O]**	33.2	40.8	36	1025	0.92

[a] δ/ppm.

 DOI: 10.1039/b102681j

Table 2 Percentage of complexed P=O groups calculated from ^{31}P NMR spectroscopy and percentage of Eu^{3+} calculated from elemental analyses for materials **EuA$_n$[O]** and **EuB$_n$[O]**

Sample	^{31}P NMR chemical shifts. Complexed P=O[a] (%)	Found formula[b] [Eu^{3+},[c] (%)]
EuA$_7$[O]	−107.1 (62)	$Eu_{0.18}N_{0.53}P_{1.00}$ (55)
EuA$_9$[O]	−110.3 (76)	$Eu_{0.27}N_{0.82}P_{1.00}$ (82)
EuA$_{14}$[O]	−108.5 (15)	$Eu_{0.06}N_{0.17}P_{1.00}Si_{12.30}$ (17)
EuA$_{19}$[O]	(0)	$Eu_{<0.02}N_{<0.22}P_{1.00}$ (< 8)
EuB$_7$[O]	−109.8 (18)	$Eu_{0.07}N_{0.19}P_{1.00}$ $Si_{7.96}$ (21)
EuB$_9$[O]	−112.0 (16)	$Eu_{0.06}N_{0.15}P_{1.00}$ (18)
EuB$_{12}$[O]	−110.0 (10)	$Eu_{0.04}N_{0.11}P_{1.00}$ (12)
EuB$_{19}$[O]	(0)	$Eu_{<0.03}N_{<0.22}P_{1.00}$ (< 9)

[a] From ^{31}P NMR spectroscopy. [b] From elemental analyses. [c] Calculated by using the theoretical formula $Eu_{0.33}NP$.

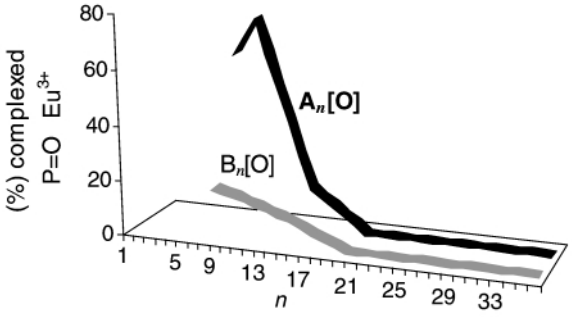

Fig. 1 Percentage of complexed P=O–Eu^{3+} groups (calculated from solid-state ^{31}P NMR spectroscopy) within **A$_n$[O]** and **B$_n$[O]** materials as a function of the 'dilution' n.

complexation (about 80%) being obtained for the material **A$_9$[O]**. Furthermore, it is remarkable to observe (Fig. 1) that, for a given 'dilution' of phosphine oxide moieties into silica, in particular for n = 7 and 9, the amount of incorporated Eu^{3+} is always low for the materials prepared in the absence of surfactant. This great difference between the properties of materials **A$_n$[O]** and **B$_n$[O]** towards the complexation of Eu^{3+}, shows that the ordered mesoporous hybrid materials **A$_9$[O]** and **A$_7$[O]** in which the P=O are located within the pores[18] are suitable for the complexation of Eu^{3+}, while the materials **B$_n$[O]** (n = 7 and 9) in which the distribution of P=O groups is uncontrolled, are not. This suggests that the complexation of Eu^{3+} requires not only three P=O groups in close proximity to each other but in a favourable geometry. It is worth noting that the complexation of Eu^{3+} is optimum but incomplete (80%) for **A$_9$[O]**. For n < 9, the P=O groups are certainly in close proximity to each other but nevertheless they do not allow an optimum complexation of Eu^{3+} probably for steric reasons. That illustrates how restrained is the complexation of Eu^{3+} within the materials. For the dilutions n > 14, there is neither complexation for the ordered materials **A$_n$[O]** nor for **B$_n$[O]**. The distances between the P=O groups are then likely much too large to allow the complexation.

The emission spectra of both types of materials were measured at 2 K under laser excitation at 325 nm. Fig. 2 displays the emission spectra of materials **EuA$_9$[O]** and **EuB$_7$[O]** as examples. The line emission of materials incorporating Eu^{3+} ions were assigned to the transition from the $^5D_0$ level to the ^7F_i levels (i = 0, 1, 2, 3, 4).[19] The strongest transition, $^5D_0 \rightarrow {}^7F_2$ occurs at 618 nm and is the characteristic 'europium red'

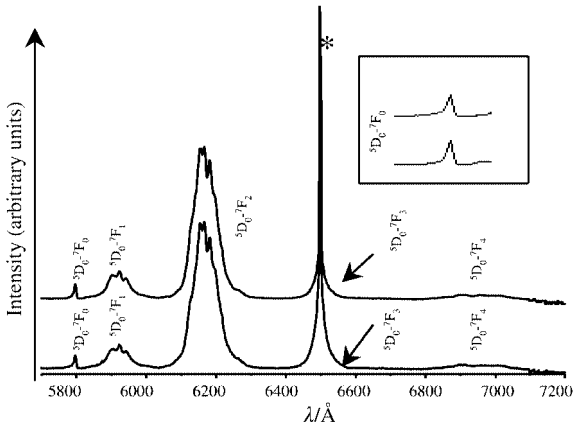

Fig. 2 Emission spectra of **EuA$_9$[O]** (upper) and **EuB$_7$[O]** (lower) recorded under laser excitation at 325 nm at 2 K. * Corresponds to 2nd order-scattered laser beam. The insert shows the $^5D_0 \rightarrow {}^7F_0$ emission.

luminescence. We observed a decrease of the red colour as the percentage of Eu^{3+} decreases. It is of note that the emission spectra are very similar for both types of materials. Of special interest is the $^5D_0 \rightarrow {}^7F_0$ emission which exhibits in both cases only one line indicating a unique chemical environment around the Eu^{3+} ions.[19] Thus, when the complexation of Eu^{3+} is possible within the materials **A$_n$[O]** or **B$_n$[O]**, the local environment around Eu^{3+} is the same whatever the route for the preparation of hybrid materials (route A or B).

In summary, we describe for the first time, a very simple method for the complexation of Eu^{3+} within hybrid materials. We show that the ordered HMS materials containing phosphine oxide groups within the pores are mostly convenient for the complexation of Eu^{3+} which requires three P=O centres.

Notes and references

1 J. D. Mackensie, ed., *SPIE Proc. Ser.*, 1994, 2288.
2 D. M. Burland, R. D. Miller and C. A. Walsh, *Chem. Rev.*, 1994, **94**, 31.
3 L. L. Beecroft and C. K. Ober, *Chem. Mater.*, 1997, **9**, 1302.
4 M. J. Weber, *J. Non-Cryst. Solids*, 1990, **123**, 208.
5 L. C. Klein, *Annu. Rev. Mater. Sci.*, 1993, **23**, 437.
6 C. J. Brinker and G. W. Scherer, *Sol–Gel Science*, Academic Press, Boston, MA, 1990.
7 B. Yan, H. Zhang, S. Wang and J. Ni, *Mater. Chem. Phys.*, 1997, **51**, 92.
8 B. Yan, H. Zhang, S. Wang and J. Ni, *J. Photochem. Photobiol. A: Chem.*, 1998, **112**, 231.
9 H. Li, S. Inoue, K. Machida and G. Adachi, *Chem. Mater.*, 1999, **11**, 3171.
10 R. J. P. Corriu, F. Embert, A. Mehdi and C. Reyé, *Chem. Mater.*, submitted.
11 D. R. Cousins and F. A. Hart, *J. Nucl. Chem.*, 1967, **29**, 1745.
12 J.-C. G. Bunsli and G. R. Choppin, *Lanthanide Probes in Life, Chemical, and Earth Sciences*, Elsevier, New York, 1989.
13 D. J. Macquarie, D. B. Jackson, J. E. G. Mdoe and J. H. Clark, *New J. Chem.*, 1999, **23**, 529.
14 M. Capka, *Synth. React. Inorg. Met. Org. Chem.*, 1977, **7**, 347.
15 R. J. P. Corriu, A. Mehdi and C. Reyé, *C. R. Acad. Sci. Paris, Ser. IIc*, 1999, 35.
16 J. P. Bezombes, C. Chuit, R. J. P. Corriu and C. Reyé, *J. Mater. Chem.*, 1999, **9**, 1727.
17 G. Valle, G. Casotto, P. L. Zanonato and B. Zarli, *Polyhedron*, 1986, **5**, 2093.
18 R. J. P. Corriu, C. Hoarau, A. Mehdi and C. Reyé, *Chem. Commun.*, 2000, 71.
19 F. Richardson, *Chem. Rev.*, 1982, **82**, 541.

CHEMCOMM Communication
www.rsc.org/chemcomm

Syntheses and structures of the first examples of zinc compounds with bridging fluorine and hydrogen atoms

Haijun Hao, Chunming Cui, Herbert W. Roesky,* Guangcai Bai, Hans-Georg Schmidt and Mathias Noltemeyer

Institut für Anorganische Chemie der Universität Göttingen, Tammannstrasse 4, 37077 Göttingen, Germany. E-mail: hroesky@gwdg.de

Received (in Cambridge, UK) 9th March 2001, Accepted 3rd May 2001
First published as an Advance Article on the web 31st May 2001

The first examples of zinc compounds with bridging fluorine and hydrogen atoms [{HC(CMeNAr)$_2$}Zn(μ-X)]$_2$ (Ar = 2,6-Me$_2$C$_6$H$_3$, X = F, 8; X = H, 9) have been synthesised and structurally characterised.

Recent reports have shown increasing interest in the utilisation of zinc hydride complexes as reducing reagents[1] and as precursors for various transformations.[2] Generally, zinc hydride complexes are synthesised from ZnH_2.[3] However, the impurity, thermal mobility and the inertness of ZnH_2 compared to its group 13 analogues often resulted in impure products.[4,5] In addition, hydrogen is believed to play a bridging role between two zinc atoms in many zinc hydride complexes as presumed in ZnH_2, resulting in polymeric or oligomeric species that are difficult to crystallise and characterise.[5] Therefore, zinc hydride complexes are less well known and have been less thoroughly investigated than the group 13 analogues and other zinc reagents. Before this work started, only three zinc hydride complexes had been structurally characterised, namely [Me$_2$N(CH$_2$)$_2$N(Me)ZnH]$_2$ **1**,[6] [{η^3-HB(3-RC$_3$N$_2$H$_2$)$_3$}ZnH] (R = Bu^t) **2**[2] and [(Me$_3$PN)ZnH]$_4$·4THF **3**.[7] In these three compounds, all hydrogen atoms are terminally arranged. The bridging role of hydrogen atoms in zinc hydride complexes remains crystallographically unveiled. Kläui *et al.*[8] had successfully synthesised [{η^3-HB(3-R-5-MeC$_3$N$_2$H$_2$)$_3$}ZnH] (R = *p*-Tol) **4** from the metathesis reaction of Et$_3$SiH with the first structurally characterised zinc fluoride compound [{η^3-HB(3-R-5-MeC$_3$N$_2$H$_2$)$_3$}ZnF] (R = *p*-Tol) **5**.[8] However, Kläui's fluorination method is not applicable for most of the other zinc precursors due to their moisture sensitivity.

Recently, we trapped 'molecular' ZnF_2 and MeZnF by using organotitanium fluorides as matrices to yield [(Cp*TiF$_3$)$_8$(ZnF$_2$)$_3$] **6** and [(Cp*TiF$_3$)$_4$(MeZnF)$_2$] **7**, respectively.[9] Compound **7** is an intermediate for the formation of **6**, the methyl groups in **7** can be easily exchanged by Me$_3$SnF to afford **6**. This implies that zinc fluorides can be made by fluorination of the corresponding alkyl derivatives with Me$_3$SnF[10] if suitable supporting ligands are chosen. Herein, we describe the preparation and structural characterisation of [{HC(CMeNAr)$_2$}Zn(μ-X)]$_2$ (Ar = 2,6-Me$_2$C$_6$H$_3$, X = F, **8**; X = H, **9**).

The reaction of [{HC(CMeNAr)$_2$}ZnR] (R = Me, Et)[11] with 1 equiv. of Me$_3$SnF in toluene at 100 °C for 8 h resulted in the disappearance of solid Me$_3$SnF. After removal of all volatiles *in vacuo*, the residue was recrystallised from hot toluene affording **8** as colourless crystals suitable for X-ray single crystal determination in high yield (80%). EI-MS shows the molecular ion peak of the dimeric **8**, in agreement with the structure established by X-ray analysis. Having observed several cases of the same bridging fashion of fluorine and hydrogen,[12] we inferred that the corresponding hydride should similarly contain bridging hydrogen atoms with a composition of [{HC(CMeNAr)$_2$}Zn(μ-H)]$_2$ **9**. The electron deficient three-centre–two-electron intermolecular Zn–H–Zn bonds are more favoured in **9** due to the bulky substituents at N of the diketiminato ligand that prevent the condensation through N atoms as seen in **1** and **3**. Consequently, we treated **8** with an excess amount of Et$_3$SiH (5–10 equiv.) in benzene under refluxing conditions for 16 h. After the removal of all volatiles, the residue was recrystallised from hot benzene resulting in colourless crystals of **9** in high yield (75%). The dimeric nature of the compounds is indicated by EI-MS and confirmed by X-ray crystallography. Unlike **1** and **2,** compound **9** cannot be obtained from the reaction of ZnH_2 with [ArN=C(Me)CH=C(Me)NHAr]. However, upon treatment of **9** with Me$_3$SnF in benzene under reflux for 6 h, compound **9** can be readily converted back to **8** (Scheme 1). Satisfactory microanalyses of **8** and **9** have been obtained.† The ^{1}H NMR spectrum reveals a singlet for the bridging hydrogens of **9** (δ 4.59), while the ^{19}F NMR of compound **1** shows a singlet for μ-F at δ −61.6.

The structures of **8** and **9** have been determined by X-ray single crystal analysis and are shown in Figs. 1 and 2, respectively.‡ Both molecular structures are dimeric with an inversion centre in the centroid of the four-membered Zn$_2$X$_2$ (X = F, H) ring. The two zinc atoms in **8** and **9** are bridged by fluorine and hydrogen atoms, respectively, forming the three-centre–four electron Zn–F–Zn and the three-centre–two-electron Zn–H–Zn bonds.

The average Zn–N bond length in **8** (1.955 Å) is quite close to that in **9** (1.967 Å), but the six-membered ring in **9** formed by Zn and the ligand backbone is essentially planar (mean deviation 0.0149 Å). There is a C_2 axis passing through C(2), Zn(1), Zn(1A) and C(2A) atoms in **9**. However, in compound **8**, the ligand backbone is slightly folded. The (μ-F)–Zn bond lengths in **8** [F(1)–Zn(1) 2.0034(11), F(1)–Zn(1A) 1.9473(12), av. 1.975 Å] are close to the sum of the covalent radii, and *ca.* 0.126 Å longer than the terminal F–Zn bond length found in **5** [1.849(4) Å]; they are also comparable to those in **6** and **7**. The (μ-H)–Zn bond lengths (1.766 Å) from the refinement of X-ray diffraction data are slightly shorter than those in the ionic MeZnBH$_4$ (av. 1.82 Å).[13] The distances are longer than the terminal H–Zn bond lengths found in **1** (1.62 Å) and **3** (1.50 Å), respectively.

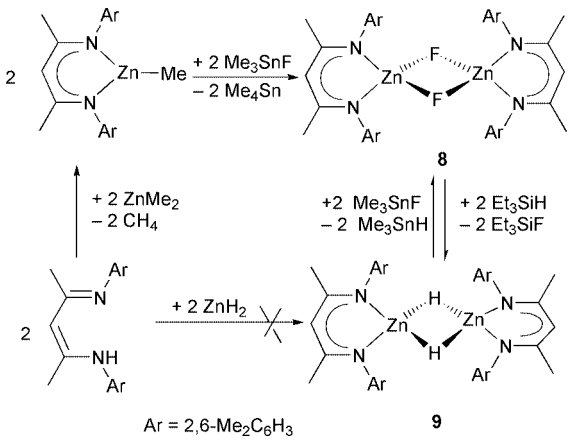

Scheme 1

 DOI: 10.1039/b102275j

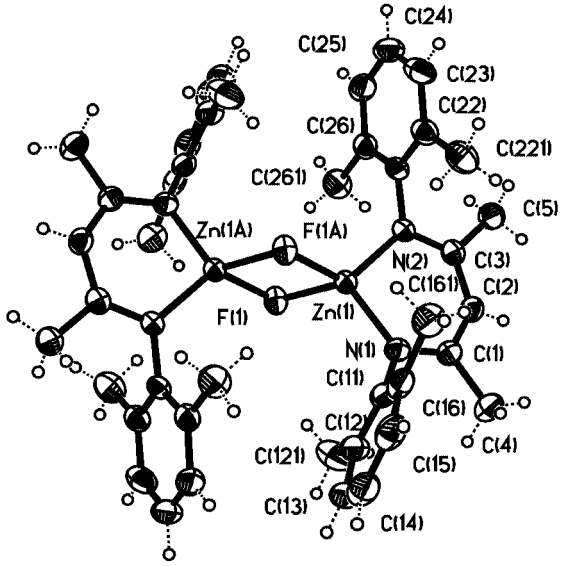

Fig. 1 The molecular structure of **8** in the crystal (with 50% probability elllipsoids). Selected bond lengths (Å) and angles (°): Zn(1)–N(2) 1.951(2), Zn(1)–N(1) 1.9588(14), Zn(1)–F(1) 2.0034(11), Zn(1)–Zn(1A) 2.9754(6), F(1)–Zn(1A) 1.9473(12), F(1A)–Zn(1)–F(1) 82.28(5), Zn(1A)–F(1)–Zn(1) 97.72(5).

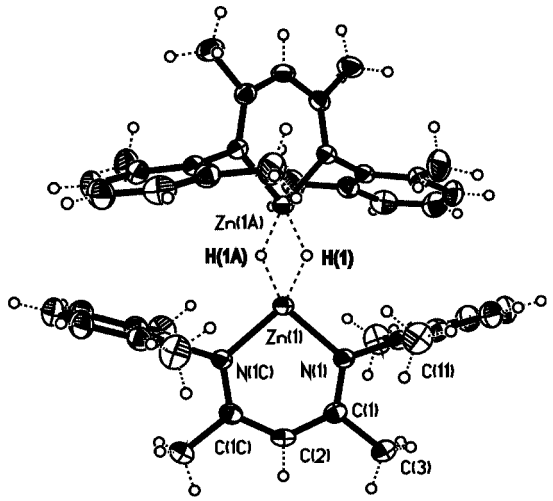

Fig. 2 The molecular structure of **9** in the crystal (with 50% probability ellipsoids). Lattice solvents are omitted. Selected bond lengths or distances (Å) and angles (°): Zn(1)–H(1) 1.766, Zn(1)–N(1) 1.9672(17), Zn(1)–N(1A) 1.9673(17), Zn(1)–Zn(1A) 2.4513(9), Zn(1)–H(1)–Zn(1A) 87.9, H(1)–Zn(1)–H(1A) 92.1.

The shorter (μ-H)–Zn distance compared to the (μ-F)–Zn bond length correlates well with a smaller Zn(1)–H(1)–Zn(1A) angle (87.9°) and a wider Zn(1)–F(1)–Zn(1A) angle (97.72°). Consequently, a wider H(1)–Zn(1)–H(1A) angle (92.1°) results compared to the F(1)–Zn(1)–F(1A) angle (82.28°), which leads to a significantly shorter Zn–Zn distance [2.4513(9) Å] in **9** (by 0.522 Å) than that in **8** [2.9754(6) Å]. This short Zn–Zn distance is in the range of the sum of the covalent radii (2.50 Å), but a Zn–Zn interaction is unlikely.

In summary, we have developed an efficient route to zinc fluorides that are key precursors for the corresponding hydrides. We have also established the first examples of zinc compounds with bridging fluorine and bridging hydrogen atoms. Further studies with **2** are in progress.

This work was supported by the Deutsche Forschungsgemeinschaft and the Fonds der Chemischen Industrie.

Notes and references

† For **8**: mp 278–281 °C. EI-MS: *m/z* (%) 778 (M^+, 100). ^{1}H NMR (C_6D_6, 200.131 MHz): δ 6.80–6.95 (m, 12 H, Ar *H*), 4.68 (s, 2H, γ-CH), 1.99 (s, 24 H, Ar–*Me*), 1.35 (s, 12 H, β-CMe). ^{19}F NMR (C_6D_6, 188.28 MHz): δ −61.62. Anal. Calc. (found) for $C_{42}H_{50}F_2N_4Zn_2$: C, 64.70 (64.76); H, 6.46 (6.49); N, 7.19 (7.16)%.

For **9**: mp 215–217 °C. EI-MS: *m/z* 743 [M − H]$^+$. ^{1}H NMR (C_6D_6, 200.131 MHz): δ 6.92 (s, 12 H, Ar H), 4.82 (s, 2 H, γ-CH), 4.59 [s, 2 H, Zn–(μ-H)], 2.03 (s, 24 H, Ar–*Me*), 1.44 (s, 12 H, β-CMe). Anal. Calc. (Found) for $C_{48}H_{58}N_4Zn_2$ (incl. one molecule C_6H_6): C, 70.16 (69.97); H, 7.11 (7.03); N, 6.82 (7.15)%.

‡ *Crystallography*: the data were collected on a Stoe-Siemens four-circle diffractometer by using Mo-Kα (λ = 0.71073 Å) radiation. The structures were solved by direct methods (SHELXS-97) and refined against F^2 using SHELXL-97.[14] All non-hydrogen atoms were refined anisotropically. All hydrogen atoms were included in the refinement in geometrically ideal positions.

Crystal data for **8**: $C_{42}H_{50}F_2N_4Zn_2$, M = 779.60, monoclinic, space group $P2_1/n$, a = 13.02.6(2), b = 8.8051(12), c = 17.309(2) Å, β = 105.240(11)°, U = 1915.5 Å^3, Z = 2, D_c = 1.352 g cm^{-3}, $F(000)$ = 2514, T = 203(2) K, μ(Mo-Kα) = 1.296 mm^{-1}, 7.02 ⩽ 2θ ⩽ 50.04°, 6762 reflections measured, 3381 unique (R_{int} = 0.0650) were used in all calculations. $R1$ = 0.0273 [$I > 2\sigma(I)$] and $wR2$ = 0.0723 (all data); max./min. residual electron density: 0.380 / −0.233 e Å^{-3}. CCDC 155083.

For **9**: $C_{48}H_{58}N_4Zn_2$ (incl. one molecule benzene), M = 821.72 orthorhombic, space group *Fddd*, a = 1.6941(5), b = 2.0576(3), c = 2.4918(4) Å, U = 8686(3) Å^3, Z = 8, D_c = 1.257 g cm^{-3}, $F(000)$ = 3472, T = 200(2) K, μ(Mo-Kα) = 1.141 mm^{-1}, 7.04 ⩽ 2θ ⩽ 50.06°; 3065 reflections measured, 1915 unique (R_{int} = 0.0279) which were used in all calculations. $R1$ = 0.0309 [$I > 2\sigma(I)$] and $wR2$ = 0.0831 (all data); max./min. residual electron density: 0.286 / −0.579 e Å^{-3}. CCDC 155084.

See http://www.rsc.org/suppdata/cc/b1/b102275j/ for crystallographic data in CIF or other electronic format.

1 N. A. Bell and A. L. Kassyk, *J. Organomet. Chem.*, 1988, **345**, 245; Y. Gao, K. Harada, T. Hata, H. Urabe and F. Sato, *J. Org. Chem.*, 1995, **60**, 290; N. A. Bell and A. L. Kassyk, *Inorg. Chim. Acta*, 1996, **250**, 345.

2 R. Han, I. B. Gorrell, A. G. Looney and G. Parkin, *J. Chem. Soc., Chem. Commun.*, 1991, 717; A. Looney, R. Han, I. B. Gorrell, M. Cornebise, K. Yoon, G. Parkin and A. L. Rheingold, *Organometallics*, 1995, **14**, 274.

3 E. C. Ashby and A. B. Goel, *J. Organomet. Chem.*, 1977, **139**, C89; E. C. Ashby and A. B. Goel, *Inorg. Chem.*, 1981, **20**, 1096.

4 T. L. Neils and J. M. Burlitch, *Inorg. Chem.*, 1989, **28**, 1607.

5 A. J. de Koning, J. Boersma and G. J. M. van der Kerk, *J. Organomet. Chem.*, 1980, **186**, 159.

6 N. A. Bell, P. T. Moseley, H. M. M. Shearer and C. B. Spencer, *J. Chem. Soc., Chem. Commun.*, 1980, 359.

7 M. Krieger, B. Neumüller and K. Dehnicke, *Z. Anorg. Allg. Chem.*, 1998, **624**, 1563.

8 W. Kläui, U. Schilde and M. Schmidt, *Inorg. Chem.*, 1997, **36**, 1598.

9 P. Yu, P. Müller, H. W. Roesky, M. Noltemeyer, A. Demsar and I. Usón, *Angew. Chem.*, 1999, **111**, 3518; P. Yu, P. Müller, H. W. Roesky, M. Noltemeyer, A. Demsar and I. Usón, *Angew. Chem., Int. Ed.*, 1999, **38**, 3319.

10 E. F. Murphy, R. Murugavel and H. W. Roesky, *Chem. Rev.*, 1997, **97**, 3425.

11 M. Cheng, E. B. Lobkovsky and G. W. Coates, *J. Am. Chem. Soc.*, 1998, **120**, 11018.

12 See, for example: P. Yu, E. F. Murphy, H. W. Roesky, P. Lubini, H.-G. Schmidt and M. Noltemeyer, *Organometallics*, 1997, **16**, 313; C. Cui, H. W. Roesky, M. Noltemeyer, M. F. Lappert, H.-G. Schmidt and H. Hao, *Organometallics*, 1999, **18**, 2257; C. Cui, H. W. Roesky, M. Noltemeyer and H.-G. Schmidt, *Organometallics*, 1999, **18**, 5123.

13 S. Aldridge, A. J. Blake, A. J. Downs, S. Parsons and C. R. Pulham, *J. Chem. Soc., Dalton Trans.*, 1996, 853.

14 G. M. Sheldrick, SHELXL-97, Program for Crystal Structure Solution and Refinement, University of Göttingen, Germany, 1997.

CHEMCOMM Communication
www.rsc.org/chemcomm

Theoretical study of triple bonds to germanium: relative stabilities of germanitriles and germaimines

Chin-Hung Lai,[a] Ming-Der Su*[b] and San-Yan Chu*[a]

[a] *Department of Chemistry, National Tsing Hua University, Hsinchu 30043, Taiwan, R.O.C.*
[b] *School of Chemistry, Kaohsiung Medical University, Kaohsiung 80708, Taiwan, R.O.C.*
E-mail: ggs@chu1.chem.nthu.edu.tw

Received (in Cambridge, UK) 14th February 2001, Accepted 18th April 2001
First published as an Advance Article on the web 31st May 2001

Both B3LYP and CCSD(T) computational results suggest that fluorine substitution can dramatically stabilize FGe≡N, with respect to Ge=NF, both from a kinetic and from a thermodynamic viewpoint.

The chemistry of unsaturated organometallic compounds with multiple bonds between a group 14 atom and a heteroatom has assumed increasing importance during the last two decades, as shown by the large number of reviews[1] dealing with both experimental and theoretical aspects. In organogermanium chemistry, several very interesting new compounds with pπ–pπ bonds between the heteroatoms have been reported: Ge=C,[2] Ge=O,[3] Ge=S,[4] Ge=Ge[5] and Ge=N.[6] Of these species, the germaimines, compounds with a Ge=N double bond, have been studied extensively both experimentally[7] and theoretically.[8] Although there have been a great number of reports concerning the chemical and physical properties of these stable species, stable compounds with a Ge≡N triple bond (*i.e.* germanitriles) are still unknown. Naturally, the steric protection of the linear grouping of atoms in the triple bond system is much less possible than for a double bond system so that prospective syntheses are very problematical. Indeed, it has already been proposed that compounds of triply bonded germanium are the next frontier.[9,10]

These novel germanitriles raise a number of intriguing questions regarding their structures, energies, physical properties, and stabilities. Experimental difficulties have so far frustrated attempts to answer these questions. Nevertheless, this information can be obtained by the application of reliable computational methods. Thus, in this work we use carefully calibrated density functional theory (DFT) and high level *ab initio* computations to predict systems where XGe≡N is more stable than the isomeric Ge=NX, and where relatively large barriers separate the two isomers, hoping to stimulate experimental testing of these theoretical predictions.

To the best of our knowledge, no quantum chemical calculations for such compounds have yet been carried out, let alone a systematic theoretical study of substituent effects on the stabilities of germanitrile species. In view of the interest in isolating compounds containing a Ge≡N triple bond, we consider the possibility of stabilizing this moiety with various substituents. At present, we report a theoretical study concerning the effect of various substituents X (X = H, Li, BeH, BH_2, CH_3, SiH_3, NH_2, PH_2, OH, SH, F and Cl) on the relative stability of XGe≡N and Ge=NX isomers, as well as on the transition states connecting them.

Three regions on the potential energy surfaces are considered in this work: XGe≡N (germanitriles), the transition states, and Ge=NX (germaimines); see eqn. (1) in Table 1. The geometries and energetics of the stationary points on the potential energy surface of eqn. (1) have been calculated using non-localized DFT in conjunction with the 6-311++G(d,p) basis set, which is denoted as B3LYP/6-311++G(d,p).[11] All the stationary points have been positively identified as equilibrium structures (number of imaginary frequencies N_{imag} = 0) or transition states (N_{imag} = 1). Single-point energies were also calculated at CCSD(T)(frozen)/6-311++G(3df,3pd)//B3LYP/6-311++G(d,p) (hereafter designated CCSD(T)), to improve the treatment of electron correlation. Unless otherwise noted, relative energies given in the text are those determined at CCSD(T) and include vibrational zero-point energy (ΔZPE) corrections determined at B3LYP/6-311++G(d,p).[12]

The results of our theoretical study of unimolecular reaction [eqn. (1)] are summarized in the schematic reaction profiles in Scheme 1. Selected geometrical parameters of XGe≡N, Ge=NX, and the transition state for the reaction are collected in Table 1. Several intriguing results from Scheme 1 and Table 1 are as follows.

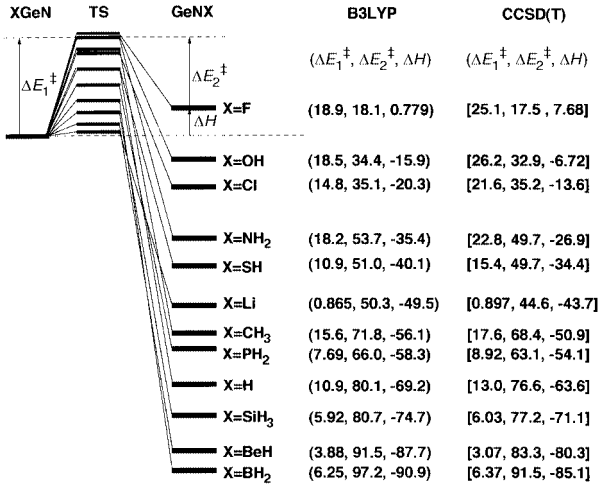

Scheme 1

First, as one can see in Scheme 1, the calculated energy difference between XGe≡N and Ge=NX, Δ*H*, is strongly dependent on the substituent X. Namely, for most substituents (*i.e.* X = H, Li, BeH, BH_2, CH_3, SiH_3, NH_2, PH_2, OH, SH and Cl), germaimines, Ge=NX, are more stable than the isomeric germanitriles, XGe≡N, by −6.7 to −85 kcal mol^{-1} at the B3LYP and CCSD(T) levels of theory. Additionally, it is apparent in Scheme 1 that electronegative substituents can reduce the energy difference between XGe≡N and GeN=X. Furthermore, Δ*H* is positive only for X = F. That is to say, FGe≡N is more stable than the corresponding Ge=NF by 7.7 kcal mol^{-1} at the same level of theory. It is therefore predicted that the more electronegative the substituent, the more stable the germanitrile (XGe≡N).

Secondly, it is found that the energy difference (Δ*H*) between XGeN and GeNX increases as the X element moves from left to right across both the first-row (from B to F) and second-row (from Si to Cl) in the periodic table. For instance, Δ*H* increases in the order (in kcal mol^{-1}) : BH_2 (−85) < CH_3 (−51) < NH_2 (−27) < OH (−6.7) < F (+7.7) and SiH_3 (−71) < PH_2 (−54) < SH (−34) < Cl (−14). In addition, there is a reduction in Δ*H* energies between the first- and second-row X substituents. That is, CH_3 > SiH_3, NH_2 > PH_2, OH > SH, and F > Cl. The

 DOI: 10.1039/b101459p

Table 1 Geometrical parameters of structures for eqn. (1) at the B3LYP/6-311++G(d,p) level of theory (distances in Å, angles in degrees)

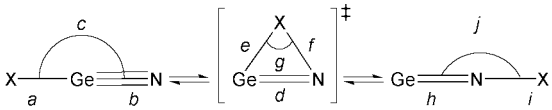

(1)

X	*a*	*b*	*c*	*d*	*e*	*f*	*g*	*h*	*i*	*j*
H	1.522	1.638	180.0	1.714	1.573	2.313	47.79	1.657	1.006	180.0
Li	2.415	1.660	180.0	1.666	2.414	3.755	18.90	1.677	1.748	180.0
BeH	2.160	1.649	180.0	1.672	2.177	3.246	27.99	1.677	1.499	180.0
BH_2	2.021	1.651	180.0	1.690	2.066	2.830	36.33	1.682	1.398	179.9
CH_3	1.959	1.642	180.0	1.715	2.089	2.696	39.51	1.663	1.423	179.9
SiH_3	2.400	1.646	180.0	1.686	2.443	3.289	29.81	1.671	1.723	180.0
NH_2	1.822	1.646	173.8	1.755	1.938	2.626	41.93	1.675	1.356	174.6
PH_2	2.342	1.647	172.3	1.703	2.414	3.163	32.15	1.675	1.694	171.1
OH	1.773	1.649	173.9	1.792	1.865	2.519	45.28	1.673	1.354	169.1
SH	2.221	1.648	176.5	1.736	2.298	2.967	35.72	1.679	1.657	171.9
F	1.748	1.651	180.0	1.834	1.827	2.413	48.88	1.670	1.346	180.0
Cl	2.145	1.649	180.0	1.770	2.241	2.867	38.13	1.673	1.660	180.0

reason for these trends can easily be understood in terms of the X–Ge *vs*. X–N bond energies. Generally speaking, elements which are more electronegative than Ge increase the XGe≡N *vs*. XN=Ge energy differences (relative to X = H), while more electronegative elements decrease them. For example, ΔH is positive for X = F, where a very strong F–Ge bond and a very weak F–N bond[13] can overturn the large (*ca*. 64 kcal mol^{-1}) intrinsic preference of HN=Ge over HGe≡N.

Thirdly, as we can see in Scheme 1, electronegative substitution not only reduces the energy gap (ΔH) between XGe≡N and Ge=NX, but it also raises the barrier ($\Delta E_1^{\ddagger}$) to the XGe≡N → Ge=NX isomerization, thus increasing the kinetic stability of the germanitrile molecules. For instance, our CCSD(T) calculations suggest that the barrier for the isomerization of XGe≡N to Ge=NX decreases in the order (in kcal mol^{-1}): X = OH (26) > X = F (25) > X = NH_2 (23) > X = Cl (22) > X = CH_3 (18) > X = SH (15) > X = H (13) > X = PH_2 (8.9) > X = BH_2 (6.4) ≈ X = SiH_3 (6.0) > X = BeH (3.1) > X = Li (0.90). Likewise, the barrier height ($\Delta E_2^{\ddagger}$) for the reverse reaction (from Ge=NX to XGe≡N) is also dependent on the electronegativity of substituents X. That is to say, the more electronegative the substituent, the smaller the activation barrier from Ge=NX to XGe≡N. For example, our CCSD(T) results indicate that the trend in activation energy ($\Delta E_2^{\ddagger}$; in kcal mol^{-1}) mirrors the trend in electronegativity of the substituent: X = F (18) < X = OH (33) < X = Cl (35) < X = Li (45) < X = NH_2 (50) ≈ X = SH (50) < X = PH_2 (63) < X = CH_3 (68) < X = H (77) ≈ X = SiH_3 (77) < X = BeH (83) < X = BH_2 (91). Taken together, our theoretical findings suggest that fluorine is a particularly appealing possibility because of the strength of the Ge–F bond.

In summary, from our survey of the unimolecular isomerization of XGe≡N → Ge=NX reactions, the present computational results predict that germanitrile XGe≡N itself lies at the minimum of the potential energy surface, and can be strongly stabilized in both a kinetic and thermodynamic sense with a proper choice of substituents. In particular, based on the DFT and CCSD(T) results, we confidently predict that FGe≡N should be stable with respect to the products of unimolecular isomerization and should be the most likely of the species to be detected experimentally.

We encourage experimentalists to carry out further experiments to confirm our predictions.

We are grateful to the National Center for High-Performance Computing of Taiwan for generous amounts of computing time. We also thank the National Science Council of Taiwan for their financial support.

Notes and references

1 For recent reviews, see: (*a*) G. Raabe and J. Michl, in *The Chemistry of Organic Silicon Compounds*, ed. S. Patai and Z. Rappoport., John Wiley, New York, 1989, ch. 17, p. 1015; (*b*) J. Barrau, J. Esoudié and J. Satgé, *Chem. Rev.*, 1990, **90**, 283; (*c*) R. S. Grev, *Adv. Organomet. Chem.*, 1991, **33**, 125; (*d*) J. Esoudié, C. Couret, H. Ranaivonjatovo and J. Satgé, *Coord. Chem. Rev.*, 1994, **130**, 427; (*e*) R. Okazaki and R. West, *Adv. Organomet. Chem.*, 1996, **39**, 31; (*f*) K. W. Klinkhamme, *Angew. Chem., Int. Ed. Engl.*, 1997, **36**, 2320; (*g*) J. Barrau and G. Rina, *Coord. Chem. Rev.*, 1998, **178**, 593; (*h*) P. P. Power, *J. Chem. Soc., Dalton Trans.*, 1998, 2939; (*i*) N. Tokitoh, T. N. Matsumoto and R. Okazaki, *Bull. Chem. Soc. Jpn.*, 1999, **72**, 1665; (*j*) G. H. Robinson, *Acc. Chem. Res.*, 1999, **32**, 773; (*k*) P. P. Power, *Chem. Rev.*, 1999, **99**, 3463; (*l*) W. J. Leigh, *Pure Appl. Chem.*, 1999, **71**, 453; (*m*) N. Tokitoh, *Pure Appl. Chem.*, 1999, **71**, 495; (*n*) R. Okazaki and N. Tokitoh, *Acc. Chem. Res.*, 2000, **33**, 625.

2 J. Escudié, C. Couret and H. Ramaivonjatovo, *Coord. Chem. Rev.*, 1998, **178**, 565 and references therein; J. Satgé, *Adv. Organomet. Chem.*, 1982, **21**, 241.

3 (*a*) M. Rivière-Baudet, J. Satgé and F. El-Baz, *J. Chem. Soc., Chem. Commun.*, 1995, 1687; (*b*) T. Tsumuraya and W. Ando, *Chem. Lett.*, 1989, 1043; (*c*) C. Glidewell, D. Lloyd, K. W. Lumbard and J. S. McKechnie, *Tetrahedron Lett.*, 1987, **28**, 343; (*d*) A. Meller, G. Ossig, W. Maringgele, D. Stalke, R. Herbst-Irmer, S. Freitag and G. M. Sheldrick, *J. Chem. Soc., Chem. Commun.*, 1991, 1123; (*e*) H. G. Ang and F. K. Lee, *J. Chem. Soc., Chem. Commun.*, 1989, 310.

4 P. G. Harrison, in *Comprehensive Coordination Chemistry*, ed. G. Wilkinson, R. D. Gillard and J. A. McCleverty, Pergamon, New York, 1987, vol. 3, ch. 26; J. Satgé, *Pure Appl. Chem.*, 1984, **56**, 137; T. Tsumuraya, S. A. Batcheller and S. Masamune, *Angew. Chem., Int. Ed. Engl.*, 1991, **30**, 902; J. Satgé, *J. Organomet. Chem*.., 1990, **400**, 121; R. Okazaki, N. Tokitoh, A. Ishii, N. Ishii, Y. Matsuhashi, T. Matsumoto and H. Suzuki, *Phosphorus, Sulfur Silicon Relat. Elem.*, 1992, **67**, 49.

5 N. Wiberg, *J. Organomet. Chem.*, 1984, **273**, 141; P. B. Hitchcock, M. F. Lappert, J. J. Miles and A. Thorne, *J. Chem. Soc., Chem. Commun.*, 1984, 480; J. T. Snow, S. Murakami, S. Masamune and D. J. Williams, *Tetrahedron Lett.*, 1984, **25**, 419; W.-C. Chen, M.-D. Su and S.-Y. Chu, *Organometallics*, 2001, **20**, 564 and references therein.

6 N. C. Norman, *Polyhedron*, 1993, **12**, 2431; W. Kutzelnigg, *Angew. Chem., Int. Ed. Engl.*, 1984, **23**, 272; L. E. Guselñikov and N. S. Nametkin, *Chem. Rev.*, 1979, **79**, 529.

7 The germaimines were first characterized indirectly using various trapping reagents [see ref. 3(*a*)]. Only in the last ten years have sufficiently stable germaimines been stabilized to allow their analysis in the solid state, solution, and in the gas phase [see refs. 3(*b*)–(*e*)].

8 G. Trinquier, J.-C. Barthelat and J. Satgé, *J. Am. Chem. Soc.*, 1982, **104**, 5931.

9 See ref. 1(*h*) and 3(*a*); P. Jutzi, *Angew. Chem., Int. Ed.*, 2000, **39**, 3797.

10 For XSiN study see: Y. Apeloig and K. Albrecht, *J. Am. Chem. Soc.*, 1995, **117**, 7263 and references therein.

11 A. D. Becke, *J. Chem. Phys.*, 1993, **98**, 5648; C. Lee, W. Yang and R. G. Parr, *Phys. Rev. B*, 1988, **37**, 785.

12 M. J. Frisch, *et al*. Gaussian 94, Gaussian, Inc., Pittsburgh, PA, 1995.

13 Bond dissociation energetics (kcal mol^{-1}): Ge–F 116, N–F 82.0, Ge–Cl ≈ 103, N–Cl 79.8 ± 2.29, Ge–O 158 ± 3.01, N–O 151 ± 0.031, Ge–S 132 ± 0.598, N-S 111 ± 5.02, Ge–C 110 ± 5.02, N–C 180 ± 2.39, Ge–Si 71.9 ± 5.02, N–Si 112 ± 3.59. See: D. R. Lide and H. P. R. Frederikse, *CRC Handbook of Chemistry and Physics*, CRC Press, New York, 1998, pp. 9–51.

CHEMCOMM Communication
www.rsc.org/chemcomm

Ionic liquids as powerful media in scandium triflate catalysed Diels–Alder reactions: significant rate acceleration, selectivity improvement and easy recycling of catalyst

Choong Eui Song,*[a] Woo Ho Shim,[b] Eun Joo Roh,[a] Sang-gi Lee[a] and Jung Hoon Choi*[b]

[a] *Life Sciences Division, Korea Institute of Science and Technology, PO Box 131, Cheongryang, Seoul, 130-650, Korea. E-mail: s1673@kist.re.kr*
[b] *Department of Chemistry, Hanyang University, Seoul, 133-791, Korea*

Received (in Cambridge, UK) 2nd February 2001, Accepted 8th May 2001
First published as an Advance Article on the web 31st May 2001

Ionic liquids act as powerful media (or additives) in scandium triflate catalysed Diels–Alder reactions not only for facilitating of catalyst recovery but also for accelerating reaction rate and improving selectivity.

Scandium triflate catalysed C–C bond formation reactions, pioneered by Kobayashi, have recently been received considerable attention due to their broad synthetic utility.[1] However, there are limitations to performing these catalytic reactions on a large scale due to their low turnover numbers (TONs are usually < 10–20). To explore the possibility of repetitive use of catalyst, several polymer- or dendrimer-bound scandium catalysts have very recently been employed.[2] However, most supported scandium catalysts require complicated synthetic manipulations and, moreover, their catalytic activity still remains far from satisfactory. Recently, a new approach has been adopted for catalyst separation and recycling in a few types of catalytic reaction involving the use of room-temperature ionic liquids,[3] *i.e.* a salt mixture with a melting point below ambient. Air- and moisture-stable room-temperature ionic liquids consisting of 1,3-dialkylimidazolium cations and their counter anions, in particular, have attracted growing interest in the last few years. In these solvents, catalysts having polar or ionic character can be immobilised without additional structural modification and thus the ionic solutions containing the catalyst can be easily separated from reagents and products.

Herein, we report that ionic liquids [bmim][X] **1a–c** ([bmim]$^+$ = 1-butyl-3-methylimidazolium cation; **1a**: X = PF_6; **1b**: X = SbF_6; **1c**: X = OTf)[4] act as powerful media (or additives) in scandium triflate catalysed Diels–Alder reactions[5] not only for facilitating of catalyst recovery but also for accelerating reaction rate and improving selectivity.

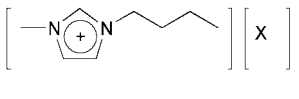

[bmim][X] **1a-c**
a: X = PF_6
b: X = SbF_6
c: X = OTf

In a preliminary study, 1,4-naphthoquinone dissolved in [bmim][PF_6] **1a** was treated with 3.0 equiv. of 1,3-dimethylbutadiene in the presence of 10 mol% of $Sc(OTf)_3$, the amount used usually in conventional organic solvents.[6] Surprisingly, under such conditions, the reaction proceeded in seconds with sudden generation of heat and color change of the reaction mixture to dark brown. This observation may suggest that the reaction using 10 mol% of catalyst was too fast to control. Therefore, we reduced the amount of catalyst gradually to 0.2 mol%, for which the reaction was completed smoothly within 2 h at room temperature whereas the same reaction in CD_2Cl_2 is extremely sluggish (compare Table 1, entries 5 and 1). Even use of only 0.1 mol% of $Sc(OTf)_3$ catalyst in ionic liquid **1a** was sufficient to complete the reaction. It was found that the catalytic activity was not much affected by the counter ions of ionic liquids **1a–c** employed in this work (Table 1, entries 5–7). Moreover, very interestingly, the use of only 1 equiv. of the ionic liquid **1a** as an additive in CH_2Cl_2 solvent gave a satisfactory rate acceleration effect (entry 4, Table 1). A kinetic study clearly illustrates the remarkable difference in reaction rate in ionic liquid **1a** and in CH_2Cl_2 (Fig. 1).

Table 1 $Sc(OTf)_3$ catalyzed Diels–Alder reactions[a]

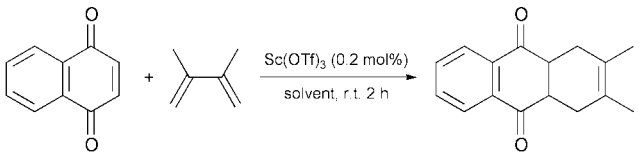

Entry	Solvent	Yield(%)[b]
1	CD_2Cl_2	22
2	**1a** (0.1 equiv.) + CD_2Cl_2	46
3	**1a** (0.5 equiv.) + CD_2Cl_2	85
4	**1a** (1 equiv.) + CD_2Cl_2	> 99
5	**1a**	> 99
6	**1b**	> 99
7	**1c**	> 99

[a] *Reaction conditions*: 3 mmol of 2,3-dimethylbuta-1,3-diene, 1 mmol of 1,4-naphthoquinone, 0.2 mol% of $Sc(OTf)_3$, 1 mL of solvent, 20 °C, 2 h. [b] Estimated by ^{1}H NMR spectroscopy.

We next examined Diels–Alder reactions of other substrates in the presence of 0.2 mol% of $Sc(OTf)_3$ at 20 °C. As shown in Table 2, in all cases the reactions proceeded with increased reaction rate and were complete within 4 h. Similar rate acceleration effects have been observed in Diels–Alder reactions using water or $LiClO_4$ in diethyl ether as reaction medium.[7] It should be also noted here that the rate acceleration effect of ionic liquids have been observed by us in other catalytic reactions, *e.g.*, (salen)Mn catalysed asymmetric epox-

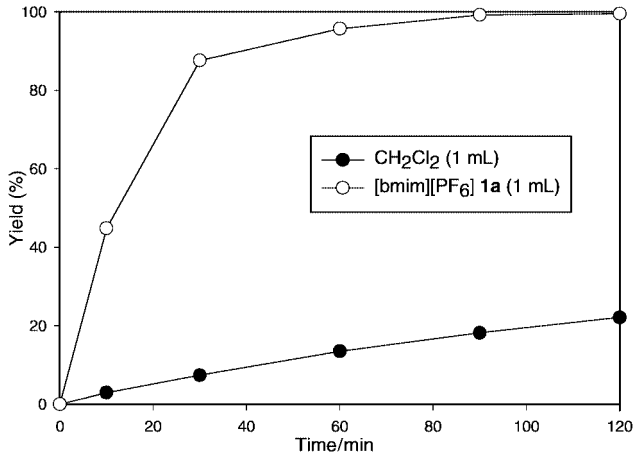

Fig. 1 Kinetic studies in the reaction of 1,4-naphthoquinone (1 mmol) with 2,3-dimethylbuta-1,3-diene (3 mmol) in the presence of 0.2 mol% of $Sc(OTf)_3$ at 20 °C.

 DOI: 10.1039/b101140p

Table 2 $Sc(OTf)_3$ catalyzed Diels–Alder reactions in ionic liquid **1a**[a]

Entry	Dienophile	Diene	Product	*Endo*:*exo*[b]	Yield (%)[c]
1	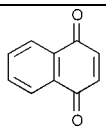		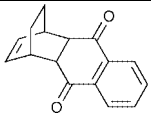	> 99:1 (94:6)	94
2			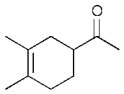	—	88
3			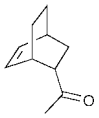	> 99:1 (95:5)	96
4	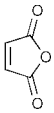		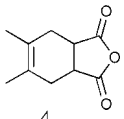	—	80
5	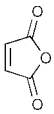		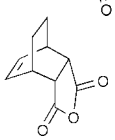	> 99:1	84
6	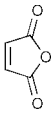		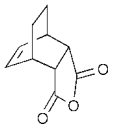	> 99:1	71

[a] *Reaction conditions*: 3 mmol of diene, 1 mmol of dienophile, 0.2 mol% of $Sc(OTf)_3$, 1 mL of **1a**, 20 °C, 4 h. [b] *Endo*/*exo* selectivities were estimated by ^{1}H NMR spectroscopy; *endo*/*exo* selectivity obtained in CH_2Cl_2 shown in parentheses; see ref. 6. [c] Isolated yield.

idation of olefins,[8] $Sc(OTf)_3$ catalysed Friedel–Crafts alkylation of arenes,[9] and $Sc(OTf)_3$ catalysed Friedel–Crafts alkenylation of arenes.[10] Another exciting point of the use of ionic liquids is the improvement of the *endo*/*exo* selectivity in the studied reactions. In ionic liquid **1a**, reaction proceeded with *endo* selectively (*endo*:*exo* = > 99:1, Table 2, entries 1, 3, 5 and 6). This compares to 94:6 (entry 1) in CH_2Cl_2.[6]

Finally, upon completion of the reaction, the ionic liquid phase containing **1c** and $Sc(OTf)_3$ was almost quantitatively recovered by simple extraction of product with Et_2O. The recovered ionic liquid phase containing the catalyst was reused several times without any loss of activity even after the eleventh use (Table 3).

In conclusion, we have demonstrated that ionic liquids act as powerful media (or additives) not only for facilitating catalyst recycling but also for accelerating reaction rate and selectivity enhancement in scandium triflate catalysed Diels–Alder reactions. Therefore, this novel immobilisation methodology involving the use of ionic liquids can be expected to have great

Table 3 Recovery and reuse of the ionic liquid phase containing $Sc(OTf)_3$[a]

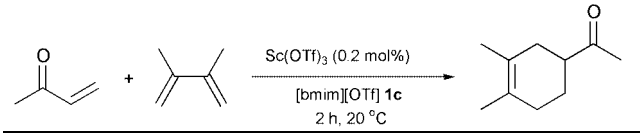

Run	1	2	3	4	5	6	7	8	9	10	11
Yield (%)[b]	94	86	81	88	86	85	83	87	89	91	90

[a] *Reaction conditions*: 3 mmol of 2,3-dimethylbuta-1,3-diene, 1 mmol of methyl vinyl ketone, 0.2 mol% of $Sc(OTf)_3$, 1 mL of **1c**, 20 °C, 2 h. [b] Isolated yield.

potential ability to solve the intrinsic problems (decrease of catalytic activity and selectivity, and complicated structural modification of catalysts) of the conventional immobilisation methodology of homogeneous catalysts. Further applications of this methodology to other catalytic reactions are under investigations in our laboratory.

This research was supported by a grant from the Ministry of Science and Technology in Korea.

Notes and references

1 For a review, see: S. Kobayashi, *Synlett*, 1994, 689.
2 K. Manabe, Y. Mori, T. Wakabayashi, S. Nagayama and S. Kobayashi, *J. Am. Chem. Soc.*, 2000, **122**, 7202; M. T. Reetz and D. Giebel, *Angew. Chem., Int. Ed.*, 2000, **39**, 2498; S. Nagayama and S. Kobayashi, *Angew. Chem., Int. Ed.*, 2000, **39**, 567; S. Kobayashi and S. Nagayama, *J. Am. Chem. Soc.*, 1998, **120**, 2985; S. Kobayashi and S. Nagayama, *J. Am. Chem. Soc.*, 1996, **118**, 8977; S. Kobayashi and S. Nagayama, *J. Org. Chem.*, 1996, **61**, 2256.
3 P. Wasserscheid and W. Keim, *Angew. Chem., Int. Ed.*, 2000, **39**, 3772; T. Welton, *Chem. Rev.*, 1999, **99**, 2071 and references therein.
4 Ionic liquids **1a**–**c** were prepared according to the reported procedures; P. A. Z. Suarez, J. E. L. Dullius, S. Einloft, R. F. de Souza and J. Dupont, *Polyhedron*, 1996, **15**, 1217; P. Bonhôte, A.-P. Dias, N. Papageorgiou, K. Kalyanasundaram and M. Grätzel, *Inorg. Chem.*, 1996, **35**, 1168.
5 Diels–Alder reactions in ionic liquids have been recently carried out without any catalysts; M. J. Earle, P. B. McCormac and K. R. Seddon, *Green Chem.*, 1999, **1**, 23; C. W. Lee, *Tetrahedron Lett.*, 1999, **40**, 2461; T. Fischer, A. Sethi, T. Welton and J. Woolf, *Tetrahedron Lett.*, 1999, **40**, 793; J. Howarth, K. Hanlon, D. Fayne and P. McCormac, *Tetrahedron Lett.*, 1997, **38**, 3097; F. Zufigar and T. Kitazume, *Green Chem.*, 2000, **2**, 137.
6 S. Kobayashi, I. Hachiya, M. Araki and H. Ishitani, *Tetrahedron Lett.*, 1993, **34**, 3755.
7 P. A. Grieco, *Aldrichim. Acta*, 1991, **24**, 59.
8 C. E. Song and E. J. Roh, *Chem. Commun.*, 2000, 837.
9 C. E. Song, W. H. Shim, E. J. Roh and J. H. Choi, *Chem. Commun.*, 2000, 1695.
10 (*a*) Our unpublished results: Friedel–Crafts alkenylation of benzene with phenylacetylene was complete within 12 h at 20 °C in the presence of 10 mol% of $Sc(OTf)_3$ in the SbF_6 salt **1b**, whereas the same reaction without the ionic liquid **1b** did not occur at all. To obtain similar conversion without an ionic liquid, much more severe reaction conditions are needed (170 h at 85 °C);[10b] (*b*) T. Tsuchimoto, T. Maeda, E. Shirakawa and Y. Kawakami, *Chem. Commun.*, 2000, 1573.

CHEMCOMM Communication
www.rsc.org/chemcomm

A novel, zeolite-encapsulated μ_3-oxo Co/Mn cluster catalyst for oxidation of *para*-xylene to terephthalic acid

Suhas A. Chavan, D. Srinivas and Paul Ratnasamy*

National Chemical Laboratory, Pune 411 008, India. E-mail: prs@ems.ncl.nes.in

Received (in Cambridge, UK) 2nd March 2001, Accepted 10th May 2001
First published as an Advance Article on the web 31st May 2001

Trinuclear, μ_3-oxo mixed metal acetato complexes, $[CoMn_2(\mu_3\text{-}O)(MeCO_2)_6(py)_3]$ (py = pyridine) encapsulated in zeolite HY, exhibit high catalytic efficiency in the selective aerial oxidation of *para*-xylene to terephthalic acid; interestingly, the formation of 4-carboxybenzaldehyde, the worrisome impurity in the conventional process, is suppressed significantly over these solid catalysts.

Terephthalic acid, one of the largest volume commodity chemicals, is commercially manufactured by dioxygen oxidation of *para*-xylene using cobalt and manganese salts, at 473–500 K, in acetic acid ($MeCO_2H$) solvent and bromide ion as promoter.[1,2] High yields and selectivity for terephthalic acid are obtained. Replacement of the homogeneous catalyst with a solid catalyst is a desirable alternative which will eliminate toxic metal ions from the waste effluents in the process. One such method of preparing solid, heterogeneous catalysts is encapsulation of active metal complexes inside the pores of zeolites or zeolitic materials.[3–5] We had reported earlier the presence of reactive μ_3-oxo Co/Mn mixed cluster complexes in homogeneous reaction medium.[6] In this communication we report, for the first time, the encapsulation of these complexes, $[CoMn_2(\mu_3\text{-}O)(MeCO_2)_6(py)_3]^n$ (n = +1 or 0) inside the cages of zeolite HY [hereafter referred to as $CoMn_2$(O)-Y]. The hydrothermal stability and catalytic activity of these solid cluster catalysts in the *heterogeneous* dioxygen oxidation of *para*-xylene are also reported. It is found that these heterogeneous catalysts were highly active and selective for the oxidation of *para*-xylene to terephthalic acid. A comparative study indicates that the zeolite-Y-encapsulated *heteronuclear*, cluster complex, $CoMn_2$(O)-Y is more efficient than the corresponding *homonuclear* cobalt and manganese cluster complexes, $[Co_3(\mu_3\text{-}O)(MeCO_2)_6(py)_3]$ and $[Mn_3(\mu_3\text{-}O)(MeCO_2)_6(py)_3]$, respectively, in HY [hereafter referred to as Co_3(O)-Y and Mn_3(O)-Y, respectively].

Co(II), Mn(II) and mixed Co(II)/Mn(II) exchanged HY zeolites were prepared by the ion exchange method, wherein zeolite HY was contacted with aqueous solutions of $Co(MeCO_2)_2{\cdot}4H_2O$ and $Mn(MeCO_2)_2{\cdot}4H_2O$ in requisite proportions at 338 K with stirring for 4 h. The ion-exchanged zeolites (Co-Y, Mn-Y, Co,Mn-Y) were washed with distilled water several times and dried at 373 K. In a typical preparation of the encapsulated metal cluster complex, the corresponding ion exchanged zeolite Y sample (1.5 g) was suspended in 15 ml glacial $MeCO_2H$. To this slurry was added pyridine (3 ml), NaBr (0.5 g), aq. H_2O_2 (50%, 10 ml) and distilled water (5 ml). The mixture was stirred, while bubbling air through the solution, for 2 h at 298 K. The solid product [Co_3(O)-Y, pink; Mn_3(O)-Y, pale brown; $CoMn_2$(O)-Y, purple] was filtered off, washed with glacial $MeCO_2H$ and dried under vacuum. 'Neat' cluster complexes of the composition $[Co_3(\mu_3\text{-}O)(MeCO_2)_6(py)_3]ClO_4$ [referred to as Co_3(O)], $[Mn_3(\mu_3\text{-}O)(MeCO_2)_6(py)_3]ClO_4$ [referred to as Mn_3(O)] and $[CoMn_2(\mu_3\text{-}O)(MeCO_2)_6(py)_3]$ [referred to as $CoMn_2$(O)] were prepared, for comparative studies, by known procedures.[7–9] The formation and purity of the complexes was confirmed by elemental analysis, FT-IR, UV–VIS and EPR spectroscopies.

The FT-IR spectra of the encapsulated complexes showed characteristic bands corresponding to acetate groups at *ca.* 2924, 1624, 1458, 1340, 1221, 680 and 623 cm^{-1}. The FT-IR bands due to pyridine were observed at around 1545, 1489 and 790 cm^{-1}. A shift in the position of the bands due to encapsulation was observed. Representative FT-IR spectra of encapsulated clusters, Mn_3(O)-Y and $CoMn_2$(O)-Y, are shown in Fig. 1. The 'neat' cluster complexes in $MeCO_2H$–H_2O–NaBr medium showed a characteristic band of ligand origin and a charge transfer band (O $\rightarrow$ Mn/Co) in the UV–VIS spectra, the positions of which were sensitive to the metal ions [Co_3(O): 250, 355 nm; Mn_3(O): 254, 320 nm and $CoMn_2$(O): 254, 345 nm). The encapsulated clusters in zeolite-Y exhibited a marked shift in the band positions (Fig. 2). The diffuse reflectance UV-VIS spectra (Fig. 2) are dominated by the band of ligand origin; the weak charge transfer band could be seen only in Co_3(O)-Y.

EPR spectra provided evidence for the formation and stability of cluster complexes in zeolite-Y. Mn_3(O) and Co_3(O) complexes showed a broad EPR signal at g = 2.008 (peak-to peak line width = 500 G) and 2.259 (peak-to-peak linewidth of 1050 G), respectively. The intensity of these signals decreased with temperature to 77 K corresponding to an antiferromagnetic behaviour of the complexes. For Co_3(O), the signal arises from the low lying excited states while Co_2Mn(O) was EPR silent. Mn_3(O) in frozen solutions of 38 ml HOAc–5.6 ml H_2O–86.5 mg NaBr [Fig. 3(a)] at 82 K, showed an EPR signal with partially resolved Mn hyperfine features. These hyperfine features could not be seen in the solid complexes due to intermolecular interactions. Encapsulated Mn_3(O) clusters showed EPR signals (g = 2.012) similar to that of frozen solutions [see Fig. 3(a) and (b)] and indicate the formation and isolation of cluster molecules in zeolite-Y. $CoMn_2$(O)-Y exhibited signals at g = 2.026. Co_3(O)-Y showed a broad signal

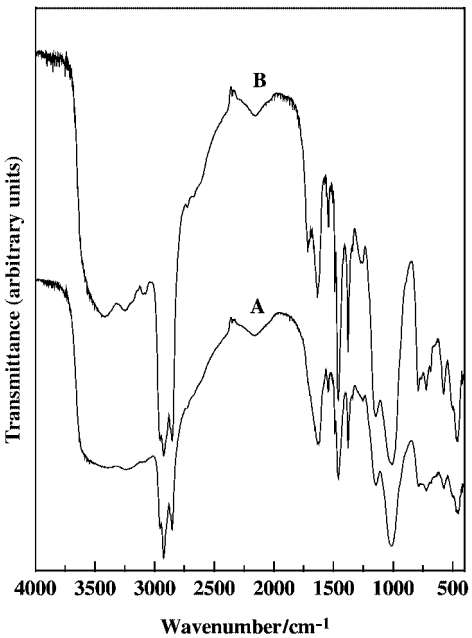

Fig. 1 FT-IR spectra (Nujol mull) of cluster complexes Mn_3(O) (A) and $CoMn_2$(O) (B) encapsulated in zeolite HY.

 DOI: 10.1039/b102016c

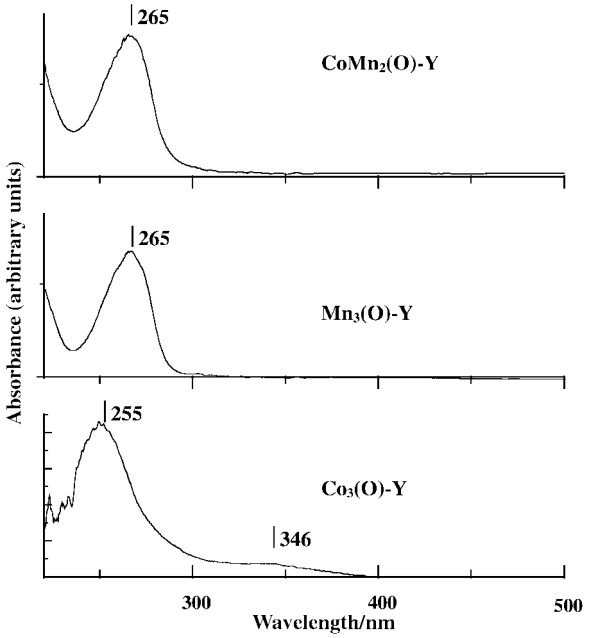

Fig. 2 Diffuse reflectance UV-VIS spectra of solid encapsulated clusters.

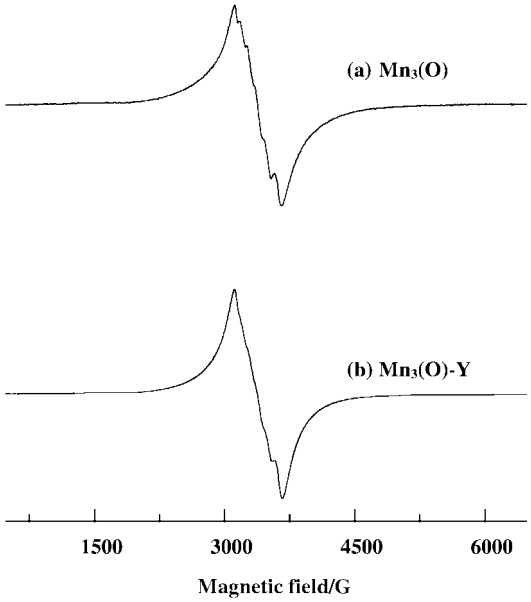

Fig. 3 X-band EPR spectra of $Mn_3(O)$ in 38 ml HOAc–5.6 ml H_2O–86.5 mg NaBr at 82 K (a) and $Mn_3(O)$-Y (b) at 298 K.

at g = 2.220 at 298 K which disappeared on lowering the temperature below 120 K.

The encapsulated cluster catalysts are highly active in the dioxygen oxidation of *para*-xylene at 550 psig (air) and 473 K (Table 1). The oxidation products (identified by GC and GC-MS) are *para*-tolyl alcohol (A), *para*-tolualdehyde (B), *para*-toluic acid (C), 4-carboxybenzaldeyde (D) and terephthalic acid (E). Small amounts of benzoic acid (F) were also observed. Among the 'neat' complexes, the mixed metal cluster complex, $CoMn_2(O)$ exhibited high catalytic activity similar to that of the conventional catalyst system[6] [$3Co(MeCO_2)_2$ + $1Mn(MeCO_2)_2$] with 100% *para*-xylene conversion and > 97% selectivity for terephthalic acid. The solid, heterogenized catalyst, $CoMn_2(O)$-Y, at 100% conversion of *para*-xylene, was even more selective (99.4% selectivity for terephthalic acid; only 0.01% of 4-carboxybenzaldehyde, a worrisome impurity in the conventional process which imparts colour to the terephthalic acid product and whose concentration must be reduced at great cost by post-oxidation processes) than the 'neat' cluster and conventional homogeneous catalysts. A longer reaction time (4 h) was required for complete conversion of *para*-xylene (Table 1). The 'neat' and conventional catalysts required only 2 h. This is probably due to diffusional limitations in the zeolite catalysts. The solid catalysts were separated by simple filtration from the terephthalic acid by converting the latter into a water-soluble sodium salt. The separated catalyst has similar activity (on recycling) and spectroscopic characteristics as that of the fresh catalyst indicating the preservation of its structural integrity and reusability. The EPR spectra of the catalysts, at 82 K, before and after the reaction were almost the same confirming the stability of these complexes under the reaction conditions. Leaching of metal ions (Co and Mn) into solution at the end of the oxidation reaction [550 psig (air), 473 K and 4 h] was investigated by AAS and EPR spectroscopies. While AAS did not reveal any leaching of metal ions, EPR spectral measurements revealed trace amounts of Mn ions (*ca*. 0.5% of the metal in the zeolite; about 50 ppm of Mn in solution) leached into the reaction solution which is too low to account for the catalytic activity. Catalytic runs with this trace amount of metal ions in solution exhibited low *para*-xylene conversions (25 wt%) with *para*-tolyl alcohol (A) and *para*-tolyl aldehyde (B) as products; terepthalic acid was not detected.

Our studies also revealed that mixed metal *heteronuclear* catalysts [$CoMn_2(O)$] are more active than the *homonuclear* catalysts [$Mn_3(O)$ and $Co_3(O)$]. To our knowledge this is the first example of a solid catalyst for the oxidation of *para*-xylene to terephthalic acid with catalytic efficiencies comparable, if not superior to that of state-of-art homogeneous catalysts.

Table 1 Catalytic activity of μ_3-oxo metal cluster complexes in selective oxidation of *para*-xylene[a]

Catalyst	Time/ h	Conv. (wt%)	Product distribution (wt%)[c] A	B	C	D	E	F
$Co_3(O)$	2	73.1	0.7	32.4	20.4	28.9	16.6	1.0
$Mn_3(O)$	2	77.0	—	35.8	8.6	1.6	53.8	0.2
$CoMn_2(O)$	2	100	—	—	1.8	0.4	97.8	—
$Co_3(O)$-Y	4	69.9	—	28.4	49.5	7.7	12.7	1.7
$Mn_3(O)$-Y	4	99.9	—	—	20.1	0.7	79.2	—
$CoMn_2(O)$-Y	4	100	—	—	0.6	0.01	99.4	—
$Co(MeCO_2)_2{\cdot}4H_2O$ + $Mn(MeCO_2)_2{\cdot}4H_2O$ (3 : 1)[b]	2	100	—	—	0.7	1.4	97.9	—

[a] *Reaction conditions*: medium *para*-xylene (2 ml)–NaBr (86.5 mg)–H_2O (5.6 ml)–$MeCO_2H$ (38 ml); weight of 'neat' cluster catalyst = 34.2 mg; weight of encapsulated cluster catalyst = 299.5 mg; pressure = 550 psig; reaction temperature = 473 K; oxidant = air. [b] Conventional catalyst system [$Co(MeCO_2)_2{\cdot}4H_2O$ = 107 mg; $Mn(MeCO_2)_2{\cdot}4H_2O$ = 35.7 mg] . [c] A = *para*-tolyl alcohol, B = *para*-tolualdehyde, C = *para*-toluic acid, D = 4-carboxybenzaldehyde, E = terephthalic acid, F = benzoic acid.

Notes and references

1 W. Partenheimer, *Catal. Today*, 1995, **23**, 69; A. K. Suresh, M. M. Sharma and T. Sridhar, *Ind. Eng. Chem. Res.*, 2000, **39**, 3958; *The Activation of Dioxygen and Homogeneous Catalytic Oxidation*, ed. D. H. R. Barton, A. E. Martell and D. T. Sawyer, Plenum Press, New York, 1993.

2 *US. Pat.*, 2833816, 1958; *PCT Int. Appl.*, WO 9,931,038 A1 (24 June 1999).

3 M. J. Sabater, A. Corma, A. Domenech, V. Fornés and H. Garcia, *Chem. Commun.*, 1997, 1285.

4 G. J. Hutchings, *Chem. Commun.*, 1999, 301.

5 P. Piaggio, P. McMorn, C. Langham, D. Bethell, P. C. Bulman-Page, F. E. Hancock and G. J. Hutchings, *New J. Chem.*, 1998, 1167.

6 S. A. Chavan, S. B. Halligudi, D. Srinivas and P. Ratnasamy, *J. Mol. Catal. A: Chem.*, 2000, **161**, 49.

7 C. E. Sumner Jr. and G. R. Steinmetz, *Inorg. Chem.*, 1989, **23**, 4290.

8 J. B. Vincent, H.-R. Chang, K. Folting, J. C. Huffman, G. Christou and D. N. Hendrickson, *J. Am. Chem. Soc.*, 1987, **109**, 5704.

9 R. D. Cannon, U. A. Jayassooriya, L. Montri, A. K. Saad, E. Karu, S. K. Bollen, W. R. Sanderson, A. K. Powell and A. B. Blake, *J. Chem. Soc., Dalton Trans.*, 1993, 2005.

CHEMCOMM
Communication
www.rsc.org/chemcomm

Synthesis of a 2D polymeric cluster $\{[NEt_4][Mo_2O_2S_6Cu_6I_3(4,4'\text{-bipy})_5]\cdot MeOH\cdot H_2O\}_n$ with a significant improvement of optical limiting effect†

Qian-Feng Zhang,[ab] Yunying Niu,[a] Wa-Hung Leung,*[b] Yinglin Song,[c] Ian D. Williams[b] and Xinquan Xin*[a]

[a] *Coordination Chemistry Institute and Department of Chemistry, Nanjing University, Nanjing 210093, P.R. China. E-mail: xxin@netra.nju.edu.cn*
[b] *Department of Chemistry, The Hong Kong University of Science and Technology, Clear Water Bay, Kowloon, Hong Kong, P.R. China. E-mail: chleung@ust.hk*
[c] *Department of Physics, Harbin Institute of Technology, Harbin 150001, P.R. China*

Received (in Cambridge, UK) 28th February 2001, Accepted 3rd May 2001
First published as an Advance Article on the web 31st May 2001

The self-assembly reaction of the monomeric nest-shaped cluster $[NEt_4]_2[MoOS_3Cu_3I_3]$ 1 or twin nest-shaped cluster $[NEt_4]_4[Mo_2O_2S_6Cu_6I_6]$ 2 with the bridging ligand 4,4′-bipyridine (4,4′-bipy) gave a 2D polymeric cluster $\{[NEt_4][Mo_2O_2S_6Cu_6I_3(4,4'\text{-bipy})_5]\cdot MeOH\cdot H_2O\}_n$ 3, which exhibits a significant improvement of optical limiting effect in its nonlinear optical properties relative to 1 or 2.

Thiometallic clusters continue to attract great interest not only because of their unusual catalytic activities in biological and industrial processes[1] but also their intriguing optical and electrical properties.[2] Among these physical properties, there is an interest in their optical limiting effect for potential application in protecting optical sensors from laser beams of high intensity. The design and synthesis of new materials with large optical limiting capability represents an active field in modern chemistry, physics, and material science.[3] Results from previous studies suggest that structural, geometrical and constitutional alternations of these clusters can give rise to variations in nonlinear optical properties (NLO).[4] Thus, the relative contributions of different NLO mechanisms change with the types of clusters, which is expected to explore a switching for NLO properties of inorganic clusters. In particular, polymeric aggregation of thiometallic clusters could result in enhancement of the optical limiting effect (OL).[5] However, it is suspected that the polymeric structures in the solid state could dissociate in solution due to the weak bridging interaction of labile anions. We herein report a significant improvement in OL effect by converting a monomeric thiometallic cluster to an inorganic–organic polymeric hybrid material, which shows a low tendency to dissociate in solution using 4,4′-bipyridine (4,4′-bipy), a versatile linker, for the synthesis of open chain polymers and supramolecular cyclophanes.

It was reported that when $[NEt_4]_2[MoOS_3Cu_3I_3]$ **1** was treated with an excess of NEt_4I in CH_2Cl_2, dimerisation occurred affording a twin nest-shaped cluster $[NEt_4]_4[Mo_2O_2S_6Cu_6I_6]$ **2**.[6] The iodide anion in clusters **1** and **2** can be substituted by pyridine (py) to give a neutral cluster $[MoOS_3Cu_3I(py)_5]$.[6,7] Based on this finding, reaction of **1** or **2** with an excess of 4,4′-bipy in DMF–MeCN resulted in the formation of an air-stable, two-dimensional (2D) polymeric cluster with two different nest-shaped cluster subunits, $\{[NEt_4][Mo_2O_2S_6Cu_6I_3(4,4'\text{-bipy})_5]\cdot MeOH\cdot H_2O\}_n$ **3**.‡ Polymeric cluster **3** shows good stability in the solid state as well as in solution.

A single-crystal X-ray diffraction study of **3** reveals an infinite 2D coordination network that crystallizes in a triclinic system with space group *P*1.§ The polymeric cluster has no center of symmetry. This feature has an important influence on the optical properties of cluster compounds. The structure of **3** consists of an open 2D anionic network with distorted hexagonal chair cavities, $[NEt_4]^+$ counter ions and lattice solvent molecules. As shown in Fig. 1, some of the iodine atoms in clusters **1** and **2** were substituted by 4,4′-bipy ligands, with the remaining iodine atoms terminally coordinating to copper atoms. Apart from one non-bridged 4,4′-bipy ligand, the other 4,4′-bipy ligands form nearly linear bridges between Cu atoms of neighboring nest-shaped $[MoOS_3Cu_3]$ cores. Interestingly, the configuration of polymeric anions can be viewed as two zigzag chains, which are propagated by cell translations along the *a* and *b* axes (Fig. 2). The edges of one chain formed by $[Cu_2(\mu\text{-}S)(\mu\text{-}4,4'\text{-bipy})]_2$ double bridges and a $[Cu_2(\mu\text{-}4,4'\text{-}$

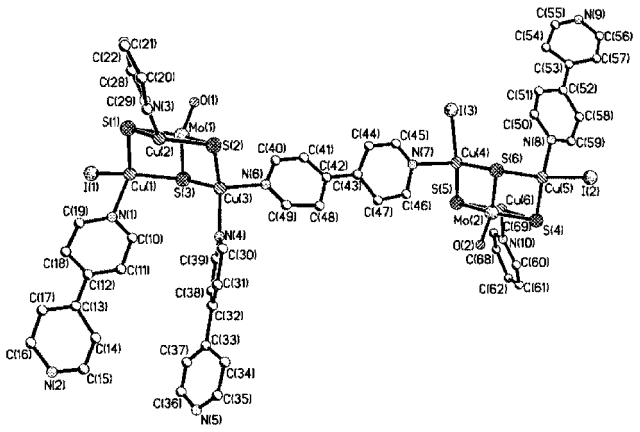

Fig. 1 Structure of the anion in **3** with the atom-numbering scheme. Hydrogen atoms are omitted for clarity.

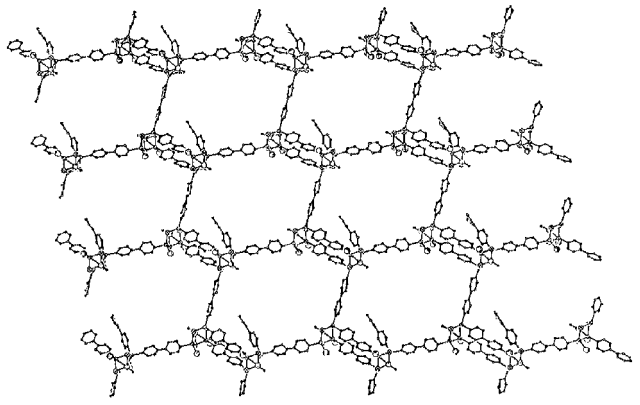

Fig. 2 Perspective view along the *c* axis of the 2D network in $[Mo_2O_2S_6Cu_6I_3(4,4'\text{-bipy})_5]^-{}_\infty$, showing the cavities.

† Electronic supplementary information (ESI) available: preparation, crystal structure details and nonlinear optical measurements for **3**. See http://www.rsc.org/suppdata/cc/b1/b101929p/

 DOI: 10.1039/b101929p

bipy)] single bridge are alternately perpendicular to each other by turning points of 4,4′-bipy shared copper atoms, while another chain is extended *via* [Cu(μ-S)Cu] moieties. Two zigzag chains share the same $[Cu_2(\mu\text{-}S)(\mu\text{-}4,4'\text{-bipy})]_2$ double bridges, the intersections of which are nest-shaped $[MoOS_3Cu_3]$ cluster cores. Another important structural feature of the cluster anion is the cross extending of two zigzag chains that creates very large chair-shaped inner cavities (*ca*. 21.67 × 21.74 Å). These dimensions are much larger than those in other reported 2D network complexes with 4,4′-bipy bridges.[8] The average distance between adjacent Mo atoms is 14.84 Å in the inner cavity. The coordination at the Mo centers remains nearly tetrahedral: the angles range from 107.77(19) to 113.5(6)°. The angles around Cu atoms range from 95.9(6) to 122.0(5)°, suggesting that the coordination geometry of the Cu atoms is highly distorted tetrahedral. This, together with the observation of 4,4′-bipy with non-planar pyridine rings bridging many Cu centers with elongation of the Mo–Cu bond lengths relative to **1** and **2**, is necessary for building up a 2D network polymeric cluster **3** with very large cavities. To our best knowledge, polymer **3** features the first example of a heterometallic cluster polymer with thiometalates and 4,4′-bipy bridges.

The NLO properties of polymeric cluster **3** were investigated. The nonlinear refractive negative n_2-values of nest-shaped Mo/Cu/S clusters indicate strong self-defocusing performances.[6,7,9] Our motivation to study clusters of this structural mode originates from the fact that the combination of the self-defocusing and nonlinear absorption makes the cluster a competent candidate for optical limiting application.[10] Furthermore, an obvious improvement of optical limiting capability is found when the monomeric nest-shaped clusters are assembled to lead to twin nest-shaped clusters, probably due to skeletal extension of the metal nuclei.[4] Accordingly, it is speculated that the clusters **1** and **2** in polymeric forms such as **3** may also possess large optical limiting effects.

With reference to the similar measurement conditions for clusters **1** and **2**, *z*-scan theory was employed to obtain the NLO parameters for **3**.[11] The peak fluence for a *z* scan is *ca*. 1 J cm^{-2} for a *z* scan over 1 ns. The α_2 and n_2 values extracted from 7 ns experimental data are 2.6×10^{-5} m W^{-1} M^{-1} and -4.2×10^{-12} m^2 W^{-1} M^{-1}, respectively. The nonlinear absorptivity is comparable to those of $[W_2S_8Ag_4(AsPh_3)_4]$[12] and $[MoS_4Cu_6I_4(py)_4]_n$,[5] but, is obviously superior to those of **1**[9] and **2**.[6] The nonlinear refractive self-defocusing behavior is also stronger in **3** than in **1**[9] and **2**.[6] Of note is the optical limiting results for **3** at a relatively low concentration of 1.2×10^{-4} mol L^{-1} in DMF solution (Fig. 3). The transmittance is normalized to its linear transmittance at low incident fluence. The thresholds (fluence at which transmittance drops to half its linear value) of the sample are 0.4 and 0.7 J cm^{-2}, respectively, when irradiated by 0.5 and 10 Hz repetition-rate laser pulses. These values are much lower than those of 10 and 2 J cm^{-2} for **1**[9] and **2**,[6] respectively, indicating that the optical limiting performance for polymeric cluster **3** was efficiently improved compared with that of the monomer and twin nest-shaped clusters **1** and **2**. Also, polymeric cluster **3** shows good photostability during the optical determinations. Important evidence for this is that the sample still retained good optical limiting behaviour while the fluence of the 10 Hz laser pulses is passed through the solution sample.[13] Further support arises from the fact that the sample remained effective three months after its preparation.

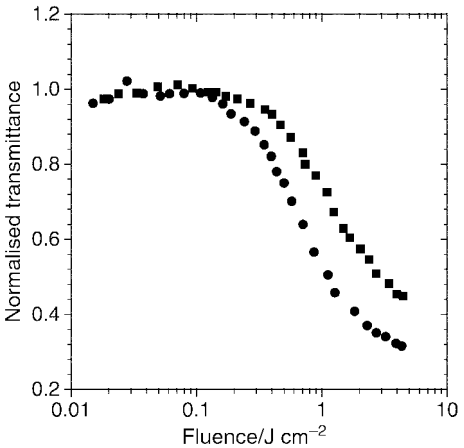

Fig. 3 Optical limiting response of **3** obtained for 7 ns, 532 nm laser pulses with various pulse intervals: 0.5 Hz (●) and 10 Hz (■). The solution was loaded in a 1 mm cell with a linear transmittance of 72%.

This research was supported by the Ministry of Education of China and the Hong Kong University of Science and Technology.

Notes and references

‡ *Characterization* of **3**: FTIR (KBr, cm^{-1}): ν(O–H) 3438br, ν(Mo–O) 951s, ν(Mo–μ-S) 459m, ν(Mo–μ_3-S) 434m. ^{1}H NMR (DMSO-d_6): δ 1.10 (CH_3 in NEt_4), 2.92 (CH_2 in NEt_4), 7.64 (d, H in py), 8.72 (d, H in py). ^{95}Mo NMR (DMSO-d_6): δ 663, 687. Found: C, 32.84; H, 2.92; N, 7.26. Calc. for $C_{58}H_{60}N_{11}O_2I_3S_6Cu_6Mo_2{\cdot}CH_3OH{\cdot}H_2O$: C, 33.12; H, 3.11; N, 7.20%.

§ *Crystallographic data* for **3**: $C_{59}H_{66}N_{11}O_4I_3S_6Cu_6Mo_2$, M = 2139.41, triclinic, space group $P\bar{1}$, a = 11.03290(10), b = 11.8242(2), c = 15.3874(2) Å, α = 72.2980(10), β = 81.4440(10), γ = 84.8620(10)°, V = 1888.94(4) Å^3, Z = 1, T = 293(2) K, D_c = 1.881 g cm^{-3}, μ(Mo-Kα) = 3.416 mm^{-1}, 13 699 reflections measured, 10 605 unique (R_{int} = 0.0598) which were used in the calculations. The final $R1$ = 0.0646 and $wR2$ = 0.1531 for 6228 reflections with $I > 2.0\sigma(I)$ and 795 variable parameters.

CCDC 158546. See http://www.rsc.org/suppdata/cc/b1/b101929p/ for crystallographic data in CIF or other electronic format.

1 D. Coucouvanis, *Acc. Chem. Res.*, 1991, **24**, 1; R. H. Holm, *Adv. Inorg. Chem.*, 1992, **38**, 1; J. B. Howard and D. J. Low, *Chem. Rev.*, 1996, **96**, 2965.

2 S. Shi, W. Ji., S. H. Tang, J. P. Lang and X. Q. Xin, *J. Am. Chem. Soc.*, 1994, **116**, 3615; T. Xia, A. D. K. Mansour, D. J. Hagan, A. A. Said, E. W. Van Stryland and S. Shi, *J. Opt. Soc. Am. B*, 1998, **15**, 1497.

3 T. S. Ahmadi, Z. L. Wang, T. C. Green, A. Henglein and M. A. El-Sayed, *Science*, 1996, **272**, 1924; J. W. Perry, K. Mandour, I. Y. S. Lee, X. L. Wu, P. V. Bedworth, C. T. Chen, D. Ng, S. R. Marder, P. Miles, T. Wada, M. Tian and H. Sasabe, *Science*, 1996, **273**, 1533.

4 Z. R. Chen, H. W. Hou, X. Q. Xin, K. B. Yu and S. Shi, *J. Phys. Chem.*, 1995, **99**, 8717; S. Shi, Z. Lin, Y. Mo and X. Q. Xin, *J. Phys. Chem.*, 1996, **100**, 10 695.

5 J. P. Lang, K. Tatsumi, K. Kawaguchi, J. M. Lu, P. Ge, W. Ji and S. Shi, *Inorg. Chem.*, 1996, **35**, 7924; H. W. Hou, Y. T. Fan, C. X. Du, Y. Zhu, W. L. Wang, X. Q. Xin, M. K. M. Low, W. Ji and H. G. Ang, *Chem. Commun.*, 1999, 647; C. Zhang, Y. L. Song, Y. Xu, H.-K. Fun, G. Y. Fang, Y. X. Wang and X. Q. Xin, *J. Chem. Soc., Dalton Trans.*, 2000, 2823.

6 H. W. Hou, D. L. Long, X. Q. Xin, X. Y. Huang, B. S. Kang, P. Ge, W. Ji and S. Shi, *Inorg. Chem.*, 1996, **35**, 5363.

7 P. Ge, S. H. Tang, W. Ji, S. Shi, H. W. Hou, D. L. Long, X. Q. Xin, S. F. Lu and Q. J. Wu, *J. Phys. Chem. B*, 1997, **101**, 27.

8 Recent examples: Q. M. Wang, X. T. Wu, W. J. Zhang, T. L. Sheng, P. Lin and J. M. Li, *Inorg. Chem.*, 1999, **38**, 2223; H. Gudbjartson, K. Biradha, K. M. Poirier and M. J. Zaworotko, *J. Am. Chem. Soc.*, 1999, **121**, 2599; Z. Shi, S. H. Feng, S. Gao, L. R. Zhang, G. Y. Yang and J. Hua, *Angew. Chem., Int. Ed.*, 2000, **39**, 2325; S. M. F. Lo, S. S. Y. Chui, L. Y. Shek, Z. Lin, X. X. Zhang, G. H. Wen and I. D. Williams, *J. Am. Chem. Soc.*, 2000, **122**, 6293.

9 H. W. Hou, Y. R. Ye, X. Q. Xin, J. Liu, M. Q. Chen and S. Shi, *Chem. Mater.*, 1995, **7**, 472; S. Shi, W. Ji, W. Xie, T. C. Chong, H. C. Zeng, J. P. Lang and X. Q. Xin, *Mater. Chem. Phys.*, 1995, **39**, 298.

10 See, for example: M. J. Soileau, ed., *Proc. Soc. Photo-Opt. Instrum. Eng.*, 1989, 1105; S. Link and M. A. El-Sayed, *J. Phys. Chem. B*, 1999, **103**, 8410.

11 M. Sheik-Bahae, A. A. Said, T. M. Wei, D. J. Hagan and E. W. Van Stryland, *IEEE J. Quantum Electron.*, 1990, **26**, 760.

12 G. Sakane, T. Shibahara, H. W. Hou, X. Q. Xin and S. Shi, *Inorg. Chem.*, 1995, **34**, 5363.

13 I. C. Khoo, M. V. Wood, B. D. Guenther, M. Shih and P. H. Chen, *J. Opt. Soc. Am. B*, 1998, **15**, 1533.

CHEMCOMM Communication
www.rsc.org/chemcomm

Reactions of coordinated geminal dichromium reagents with aldehydes: stereoselective formation of (*Z*)-2-chloroalk-2-en-1-ols†‡

Kazuhiko Takai,* Ryo Kokumai and Takahumi Nobunaka

Department of Applied Chemistry, Faculty of Engineering, Okayama University, Tsushima, Okayama 700-8530, Japan. E-mail: ktakai@cc.okayama-u.ac.jp

Received (in Cambridge, UK) 13th March 2001, Accepted 8th May 2001
First published as an Advance Article on the web 31st May 2001

Treatment of a carbonate ester of 2,2,2-trichloroethanol derivative with $CrCl_2$–DMF in THF gives a β-carbonate-coordinated geminal dichromium species, which adds to an aldehyde and eliminates an acyloxychromium group to afford a (*Z*)-2-chloroalk-2-en-1-ol stereoselectively.

Intramolecular coordination of a hetero atom to a metal center often fixes the molecular conformation,[1] and thus carbon–carbon bond formation proceeds in a stereoselective manner. We disclose here that the effect is observed in geminal dichromium species, and that a stereoselective coupling between a geminal trichloroalkane having an adjacent acyloxy group and an aldehyde leading to a (*Z*)-2-chloroalk-2-en-1-ol proceeds with chromium(II) chloride. Chromium(II) reduces geminal dihaloalkanes, such as 1,1-diiodoalkanes,[2a] iodoform,[2b] $Me_3SiCHBr_2$,[2c] and $Bu_3SnCHBr_2$,[2d] to give geminal dichromium species, which add to aldehydes to afford Wittig-type olefins with high *E*-selectivity. However, such Wittig-type olefinations do not proceed in the trichloroalkane **1e**, and a new double bond is formed between the carbons bearing halogen and the acyloxy group [eqn. (1)].

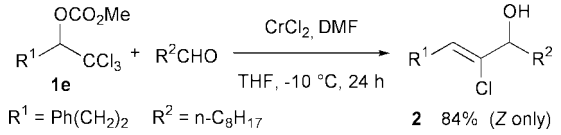

In 1986, Steckhan reported the reduction of 1-phenyl-2,2,2-trichloroethanol with $CrCl_2$ in aqueous DMF to obtain (*Z*)-2-chlorostyrene in 44% yield, along with 2,2-dichlorostyrene in 10% yield.[3] Although the yield of 2-chlorostyrene was moderate, the observed *Z*-selectivity was quite high. The stereoselectivity was explained by 1) fixation of the conformation by intramolecular coordination of the β-hydroxy group to chromium(III) of the monochromium species **3**, and 2) selective reduction of a chlorine atom at the less hindered side leading to geminal dichromium species **4** (Scheme 1). Because the reduction was performed in the presence of proton sources, *i.e.*, aqueous conditions and the hydroxy group of the starting trichloride, the procedure could not be applied for carbon–carbon formation. Thus, we first examined the effects of solvents using a hydroxy-protected 2,2,2-trichloroethanol **1a** [Table 1, R^1 = $Ph(CH_2)_2$, R = Ac].

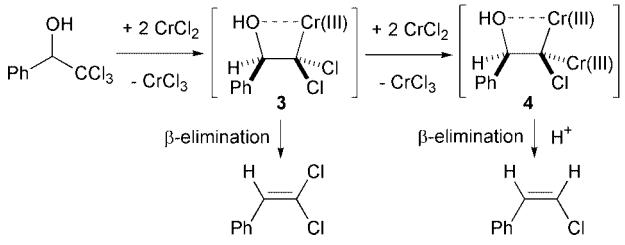

Scheme 1

† Electronic supplementary information (ESI) available: experimental procedure. See http://www.rsc.org/suppdata/cc/b1/b102387j/

‡ Dedicated to Professor Jean F. Normant on the occasion of his 65th birthday.

Table 1 Reactions of 2,2,2-trichloroalkanol derivatives and nonanal with chromium(II)[a]

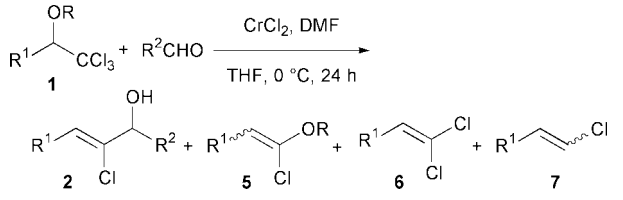

		Yield (%)[b]				Recov. (%)	
Run	R	**2**	**5**	**6**	**7**	Aldehyde	**1**
1	Ac (**a**)	62	29	< 5	< 5	15	7
2		30[c]	2	35	16	33	0
3		27[d]	52	0	0	56	32
4	COPh (**b**)	61	23	7	2	15	13
5	$CO(C_5H_4N)$ (**c**)[e]	< 5	0	89	0	94	0
6	Ms (**d**)	0	0	96	0	91	0
7	CO_2Me (**e**)	77	8	19	6	8	13
8	Me_3Si (**f**)	60	0	< 5	< 5	< 5	44

[a] R^1 = $Ph(CH_2)_2$, R^2 = n-C_8H_{17}; Reaction was conducted on a 1.0 mmol scale. Two mmol of trichloride **1**, 8 mmol of $CrCl_2$, 8 mmol of DMF were used per mmole of nonanal. [b] Isolated yields. [c] The reaction was conducted in DMF solvent. [d] The reaction was conducted without addition of DMF. [e] $CO(C_5H_4N)$ = pyridine-2-carbonyl.

Treatment of **1a** in the presence of nonanal with $CrCl_2$ in DMF at 0 °C for 24 h gave the desired coupling product **2** in 30% yield along with **6** and **7** in 35% and 16% yields, respectively (Table 1 run 2).[4] A *Z*-isomer was obtained exclusively as expected.[5] Although the yield could not be improved in THF solvent (run 3), pre-treatment of 1 equiv. of $CrCl_2$ with DMF before addition of the trichloride **1a** and nonanal accelerated the reaction, and the yield was improved to 62% (run 1).[2a] Benzoate **1b** gave almost the same yield with **2**. However, reactions with the pyridine-2-carbonyloxy compound **1c** and mesylate **1d** produced the 1,1-dichloroalkene **6** as a main product, and most of the aldehyde was recovered. Among the protecting groups examined, a carbonate gave the best result (run 7).

There are three possible reaction pathways which have different timings of the elimination steps of acyloxychromium (Scheme 2). In Path A, acyloxychromium is smoothly eliminated when one of the chlorine atoms is reduced, and 1,1-dichloroalkene **10** is produced as an intermediate. Then, the chlorine atom at the less hindered *trans* position of **10** is selectively reduced to give **11**, which adds to an aldehyde. In Path B, acyloxychromium is eliminated after the second reduction to the geminal dichromium species **9**.[2,6] The elimination gives the alkenylchromium **11** directly, and addition to an aldehyde proceeds. The third Path C also includes the acyloxy-coordinated geminal dichromium species **9**, and addition to an aldehyde at a non-coordinated chromium of **9** occurs before elimination of acyloxychromium.

The hydroxy-protecting groups with oxygen act as leaving groups in the reaction sequence.[7] Trichlorides **1c** and **1d**, which

 DOI: 10.1039/b102387j

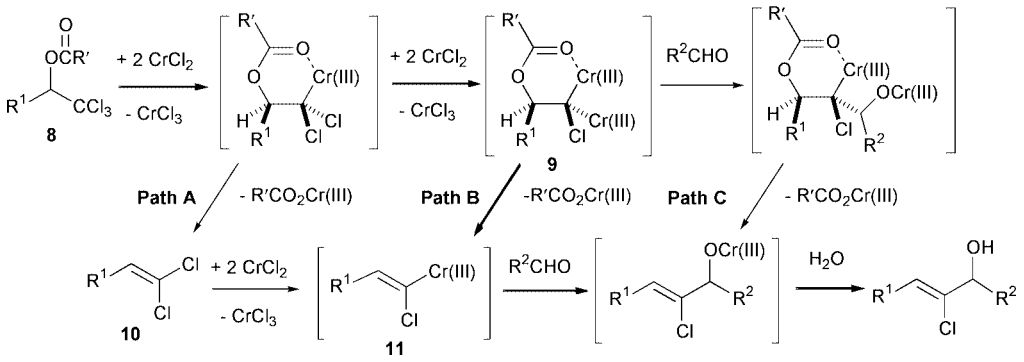

Scheme 2 Possible reaction pathways for the coupling reaction.

have good leaving groups, afforded **6** as a major product, and only a small amount of the 1,1-dichloroalkene **6** was produced when the adduct **2** was obtained in high yield. In addition, treatment of a mixture of 1,1-dichloroalkene **12** and nonanal with $CrCl_2$–DMF in THF at 0 °C for 24 h produced the adduct **2** in only 4% yield, and most of **12** (75%) was recovered unchanged [eqn. (2)].[8] These results suggest that this addition

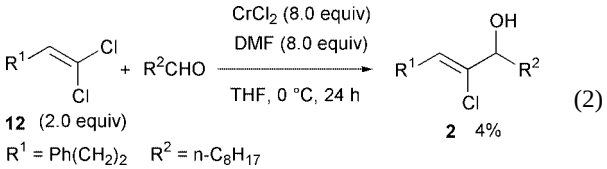

(2)

reaction does not proceed through the 1,1-dichloroalkene **10** (Path A) but through the geminal dichromium species **9**.

During the reactions of **1a**, **1b** and **1e** with nonanal, the Wittig-type olefination[2a] leading to 1-phenyl-4-chlorotridec-4-en-3-ol derivatives was not observed. This suggests that the coupling reaction does not proceed *via* Path C either, leaving Path B as the only possible reaction pathway.

The results of the coupling reactions between carbonates of 2,2,2-trichloroethanols and aldehydes are shown in Table 2.[9]

Table 2 (*Z*)-Selective coupling of 2,2,2-trihaloalkyl carbonates and aldehydes with chromium(II)[a]

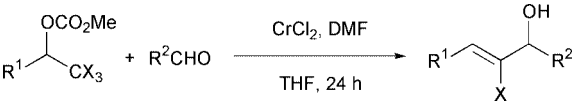

Run	R^1	R^2	X	Temp/°C	Yield (%)[b]
1	$Ph(CH_2)_2$	n-C_8H_{17}	Cl	−10	84
2				0	77
3				25	52[c]
4			Br	−10	X = Br 16[d] X = Cl 31[d]
5		c-C_6H_{11}	Cl	−10	69
6		Ph	Cl	−10	71
7		(*E*)-PrCH=CH	Cl	−10	46
8	c-C_6H_{11}	n-C_8H_{17}	Cl	−10	68
9	Ph	n-C_8H_{17}	Cl	−10	63

[a] Reaction was conducted on a 1.0 mmol scale. Two mmol of trihalides, 8 mmol of $CrCl_2$, and 8 mmol of DMF were used per mmole of an aldehyde. [b] Isolated yields. Isomer ratios were determined by isolation, GLPC, and/or NMR. [c] 0.8 mmol of $CrCl_2$, 9 mmol of manganese, and 9 mmol of Me_3SiCl were employed per mmole of nonanal. [d] *Z*-Isomers were obtained exclusively.

2-Chloroalk-2-en-1-ols having a *Z*-configuration were produced selectively in all cases. To reduce the amount of chromium salt used in the reaction, we attempted a catalytic reaction using manganese as a reductant of chromium(III).[10] The reaction proceeded at 25 °C, however, the yield decreased to 52% (run 3). When 2,2,2-tribromoethanol derivative was used as the trihalide, the corresponding bromo and chloro compounds were obtained (run 4).[2b,11,12]

This work was supported by a Grant-in-Aid from the Ministry of Education, Culture, Sports, Science and Technology of Japan.

Notes and references

1 (*a*) For geminal dimetallic species, see: I. Marek and J. F. Normant, *Chem., Rev.*, 1996, **96**, 3241; J. F. K. Müler, *Eur. J. Inorg. Chem.*, 2000, 789; (*b*) J. M. Concellón, P. L. Bernad and J. A. Pérez-Andrés, *Angew. Chem., Int. Ed.*, 1999, **38**, 2384; (*c*) R. W. Hoffmann, M. Bewersdorf, K. Ditrich, M. Krüger and R. Stürmer, *Angew. Chem., Int. Ed. Engl.*, 1988, **27**, 1176.

2 (*a*) T. Okazoe, K. Takai and K. Utimoto, *J. Am. Chem. Soc.*, 1987, **109**, 951; (*b*) K. Takai, K. Nitta and K. Utimoto, *J. Am. Chem. Soc.*, 1986, **108**, 7408; D. A. Evans and W. C. Black, *J. Am. Chem. Soc.*, 1993, **115**, 4497; (*c*) K. Takai, Y. Kataoka, T. Okazoe and K. Utimoto, *Tetrahedron Lett.*, 1987, **28**, 1443; (*d*) D. M. Hodgson, *Tetrahedron Lett.*, 1992, **33**, 5603; D. M. Hodgson, A. M. Foley and P. J. Lovell, *Tetrahedron Lett.*, 1998, **39**, 6419.

3 R. Wolf and E. Steckhan, *J. Chem. Soc., Perkin Trans. 1*, 1986, 733.

4 The reaction in DMA gave almost the same yield in DMF. However, the reduction of the trichloride **1a** did not occur in ether, DME or acetonitrile.

5 An authentic sample was prepared according to the following literature; S.-i. Narita, A. Takahashi, H. Sato, T. Aoki, S.-i Yamada and M. Shibasaki, *Tetrahedron Lett.*, 1992, **33**, 4041.

6 C. E. Castro and W. C. Kray, Jr., *J. Am. Chem. Soc.*, 1966, **88**, 4447; D. Dodd and M. D. Johnson, *J. Chem. Soc. (A)*, 1968, 34.

7 (*a*) J. K. Kochi, D. M. Singleton and L. J. Andrews, *Tetrahedron*, 1968, **24**, 3503; (*b*) H. Cohen, D. Meyerstein, A. J. Shusterman and M. Weiss, *J. Am. Chem. Soc.*, 1984, **106**, 1876.

8 The reaction with a nickel-doped (5 mol%) $CrCl_2$, which is effective for the coupling reactions between alkenyl halides and aldehydes, did not proceed; the reactant dichloride **12** was recovered in 96% yield. See: K. Takai, M. Tagashira, T. Kuroda, K. Oshima, K. Utimoto and H. Nozaki, *J. Am. Chem. Soc.*, 1986, **108**, 6048; H. Jin, J.-i. Uenishi, W. J. Christ and Y. Kishi, *J. Am. Chem. Soc.*, 1986, **108**, 5644.

9 Reactions using the corresponding benzoates gave about 5–10% less yields of the same products.

10 A. Fürstner and N. Shi, *J. Am. Chem. Soc.*, 1996 **118**, 12349.

11 For an example of the utilization of a 2-bromoalk-2-en-1-ol, see: W.-M. Dai and A. Wu, *Tetrahedron Lett.*, 2001, **42**, 81.

12 For the synthesis of (*Z*)-alkenyl bromides, see: B. M. Trost and A. B. Pinkerton, *Angew. Chem., Int. Ed.*, 2000, **39**, 360.

CHEMCOMM
Communication
www.rsc.org/chemcomm

Can a fluorous biphase solvent system improve a polymer immobilized heterogeneous hydrogenation catalyst?

Shannon L. Vinson and Michel R. Gagné*

Department of Chemistry, University of North Carolina at Chapel Hill, Chapel Hill, NC 27599-3290, USA. E-mail: mgagne@unc.edu

Received (in Corvallis, OR, USA) 29th January 2001, Accepted 23rd April 2001
First published as an Advance Article on the web 31st May 2001

When diphosphine rhodium(I) hydrogenation catalysts are incorporated into organic polymers that contain a permanent pore structure, they can be utilized in fluorous biphase solvent systems, where reaction rates increase with the fluorous content of the solvent.

The application of a fluorous biphase system (FBS) to separate products from a catalyst was both an intellectual and technical achievement in catalysis research.[1] At its heart, the FBS relies on the reversible temperature dependent miscibility of perfluorinated and nonfluorinated liquids,[2] and the solvent preferences of organic products, substrates, and catalysts that contain ligands with perfluorinated substituents. This reversible temperature dependent miscibility provides the means to separate a catalyst from its product, and as such it has been applied in a number of catalyzed reactions.[2] These methods are characterized by high turnover numbers and relatively low catalyst leaching. Moreover, fluorous solvents show gas solubilities modestly higher than typical organic solvents,[2b] a property that could lead to higher reaction rates, in for example, olefin hydrogenation and hydroformylation.

We recently reported an olefin hydrogenation catalyst that was copolymerized into the matrix of a highly cross-linked macroporous (permanent pore structure) polymer.[3] The advantage of this solid support is that it does not require polymer swelling for access to its internal volume, and should thus be compatible with any solvent system. These heterogenized catalysts have already demonstrated easy separation and efficient recyclability in polar, nonpolar, and protic organic solvents, however, they can be less active than their solution-based analogues.[4,5] The combination of higher gas solubility coupled with the ease of adapting an existing heterogeneous catalyst for use in fluorous solvents[6] (*i.e.* no synthetic modifications) suggested that the combination be examined.

For testing purposes, a cationic diphosphine hydrogenation catalyst (2 mol%) was copolymerized into an ethylene dimethacrylate-based polymer (98%) as shown in Scheme 1. These materials contain ~100 μmol Rh g^{-1} dry polymer and ~400 m^2 g^{-1} surface areas (N_2 BET).[3,7]

To compare the activity and longevity of $\mathbf{P_{Rh}}$ in a FBS and a typical organic solvent, we carried out a series of catalyst recycling experiments under conditions where substrate conversion was incomplete, enabling run-to-run and solvent-to-solvent comparisons. Longer reaction times always provided 100% conversion to product. We examined a relatively simple hydrogenation substrate, methyl-*trans*-cinnamate **1** (Scheme 2), toluene for our organic phase, and the benchmark 1:1 perfluoromethylcyclohexane (PFMC)–toluene for our FBS.[8] In the PFMC–toluene mixture the polymer floats at the interface, while it sinks in toluene. Once monophasic (~103 °C when [**1**] = 0.2 M),[9] the polymer in the FBS floats to the surface until cooling and phase separation.[10].

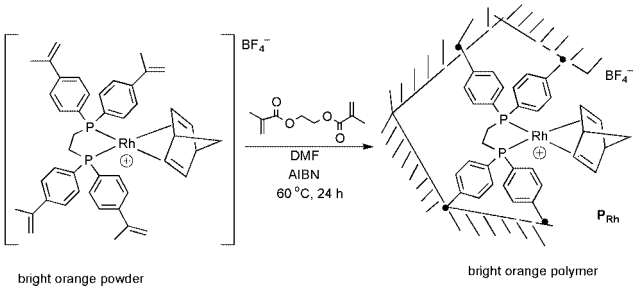

Scheme 1

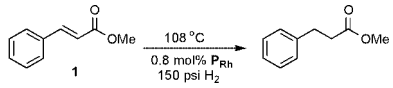

Scheme 2

The plot in Fig. 1 charts the evolution of $\mathbf{P_{Rh}}$ activity in the hydrogenation of **1** in FBS and toluene. Each reactor was run side by side, and percentage conversions were determined after 1 h by GC after careful venting. Once an aliquot was obtained for analysis, the vessels were re-introduced into the glove box and the product/substrate removed from the catalysts. For the FBS, the organic phase was removed with a pipette and the fluorous layer washed 3 times with additional toluene (this results in some PFMC loss, *vide infra*). In the toluene case, the solution was decanted and the polymer similarly washed with toluene. Additional substrate/toluene was added under the inert atmospheric conditions, and in the fluorous case additional PFMC was added every 2–3 runs to a total volume of 2 mL.

It is evident from the graph that the FBS yields a slightly more active catalyst than in toluene alone, and although the rate is reproducibly higher in the FBS, the absolute rate difference may not be significant as batch to batch variability exists (±20%).[11] Over the 15 runs, the catalysts completed ~1400 and ~800 turnovers in the FBS and toluene, respectively. Combining the filtrate solutions for the 15 runs and analyzing for Rh

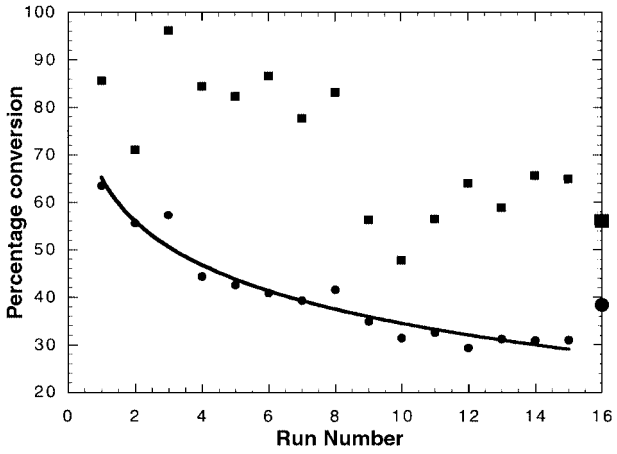

Fig. 1 Catalyst recycling for the hydrogenation of **1**. FBS (■)—1:1 $CF_3C_6F_{11}$–toluene, 0.79 mol% $\mathbf{P_{Rh}}$; toluene (●)—0.76 mol% $\mathbf{P_{Rh}}$. 108 °C,150 psi H_2, 1 h. For run # 16, both samples were run under identical FBS conditions.

 DOI: 10.1039/b101203g

(ICP), indicated that only minor catalyst leaching (~1%) occurred in both systems.

To determine if the toluene catalyst's activity was inherently lower, or if it had slightly less Rh than the FBS,[11] a 16th run was carried out in the 1:1 PFMC–toluene biphase. A 10% increase in conversion (Fig. 1) indicates that under the reaction conditions, the FBS does increase the absolute product output and thus the rate difference cannot be solely ascribed to a difference in the polymer's Rh content. Although we don't know unequivocally the reason(s) for loss of activity in the two solvents, we suspect that it comes from catalyst deactivation during the recycling process, as both systems routinely reach 10,000 turnovers in side-by-side experiments, although complete conversion was always achieved 2–3× more quickly in the FBS.[12]

It is also apparent from Fig. 1 that the run-to-run throughput of the catalyst in the FBS is not as reproducible as in toluene. Based on the mechanics of this recycle experiment, we suspected that the variability might be due to changes in the PFMC–toluene ratio. In practice, PFMC losses occurred during product extraction and washing (3×) of each run as it is slightly soluble in toluene, and the aliquots were removed at or near the reaction temperature leading to some evaporative loss (bp ~77 °C). Since the reactivity spikes coincided with the addition of fluorous solvent (every 2–3 runs, to 4 mL), we hypothesized that higher fluorous–organic solvent ratios might be responsible for the enhanced reactivity.

This hypothesis was tested by a series of control experiments varying the ratio of PFMC–toluene (1:3, 2:2, 3:1 and 4:0; 4 mL total volume). To eliminate batch-to-batch variability effects we measured the effect of fluorous composition in a series of recycle experiments where the same catalyst was used for each solvent ratio. Moreover, the experiments were conducted from least to most reactive to ensure that catalyst decomposition would not be misinterpreted as a decrease in activity.

The plot in Fig. 2 clearly shows that the 1 h conversion increases with increasing fluorous content, suggesting that the 'noise' in Fig. 1 is actually due to small changes in the volume fraction of PFMC in the FBS. This trend is unusual as homogeneous catalysts typically become *less reactive* as the fluorous content of the solvent increases.[13] Several possibilities are *a priori* possible: (1) changes in H_2 diffusion rates under mass transport limited conditions. The possibility that H_2 diffusion from gas to solution is slower than catalysis, and sensitive to fluorous content has been eliminated by showing that under similar homogeneous conditions, a doubling and tripling of the soluble catalyst, [(dppe)Rh(nbd)$^+$ B(Ar$_f$)$_4^-$] leads to a doubling and tripling of product turnover.[14] Thus, H_2 diffusion through the meniscus occurs faster than does catalysis.[15] (2) Increasing substrate concentration in the polymer phase with increasing fluorous content (a fluorophobic effect). For example, model experiments show that 80 mg of blank EDMA polymer will lower the [decane] in PFMC from 75 to 50 mM. To compensate for the decrease, the [decane] in the polymer phase must be ~600 mM. A similar effect leading to higher local substrate concentration in the catalyst containing polymer phase could lead to the observed rate accelerations. Experiments to assess the probability that these or other effects are responsible for this unusual rate acceleration are underway.

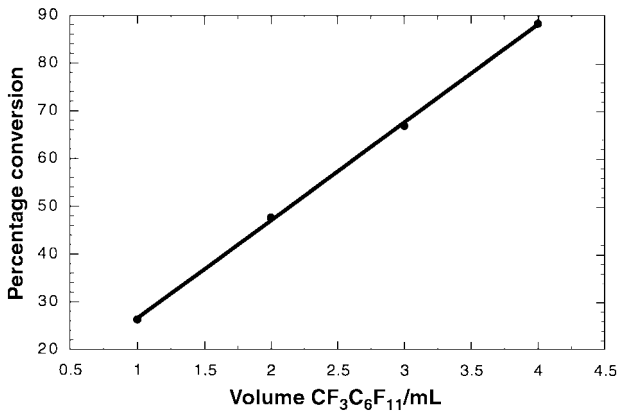

Fig. 2 Hydrogenation of **1** at different $CF_3C_6F_{11}$–toluene ratios (4 mL total volume, 0.76 mol% $\mathbf{P_{Rh}}$, 106 °C, 150 psi H_2, 1 h).

Although the polymer catalyst $\mathbf{P_{Rh}}$ does not suffer from the problem of catalyst/product separation of typical solution catalysts, the FBS does engender some useful and interesting properties to these immobilized catalysts. Chief among these is an increase in activity that directly correlates with the fluorous content of the solvent. The ease of utilizing a catalyst designed for use in organic solvents to operate in fluorous solvents is also noteworthy.

This research was partially supported by the Kenan Center for the Utilization of Carbon Dioxide in Manufacturing, NSF (CHE-0075717), the Petroleum Research Fund, and Union Carbide. M. R. G is a Camille Dreyfus Teacher Scholar (2000).

Notes and references

1 (*a*) I. T. Horváth, G. Kiss, R. A. Cook, J. E. Bond, P. A. Stevens, J. Rábai and E. J. Mozeleski, *J. Am. Chem. Soc.*, 1998, **120**, 3133; (*b*) I. T. Horváth and J. Rábai, *Science*, 1994, **266**, 72; (*c*) I. T. Horváth and J. Rábai, U.S. Patent 5,463,082, 1995; (*d*) M. Vogt, Dissertation, Technische Hochschule Aachen, 26 August 1991.

2 For reviews see: (*a*) E. G. Hope and A. M. Stuart, *J. Fluorine Chem.*, 1999, **100**, 75; (*b*) L. P. Barthel-Rosa and J. A. Gladysz, *Coord. Chem. Rev.*, 1999, **190**–**192**, 587; (*c*) R. H. Fish, *Chem. Eur. J.*, 1999, **5**, 1677; (*d*) I. T. Horváth, *Acc. Chem. Res.*, 1998, **31**, 641; (*e*) E. de Wolf, G. van Koten and B. J. Deelman, *Chem. Soc. Rev.*, 1999, **28**, 37.

3 R. A. Taylor, B. P. Santora and M. R. Gagné, *Org. Lett.*, 2000, **2**, 1781.

4 B. P. Santora, P. S. White and M. R. Gagné, *Organometallics*, 1999, **18**, 2557; B. P. Santora, A. O. Larsen and M. R. Gagné, *Organometallics*, 1998, **17**, 3138; K. Nozaki, Y. Itoi, F. Shibahara, E. Shirakawa, T. Ohta, H. Takaya and T. Hiyama, *J. Am. Chem. Soc.*, 1998, **120**, 4051; K. Nozaki, F. Shibahara, Y. Itoi, E. Shirakawa, T. Ohta, H. Takaya and T. Hiyama, *Bull. Chem. Soc. Jpn.*, 1999, **72**, 1911.

5 The polymer's interior pores are essentially unstirred therefore access to the catalyst sites is controlled by passive diffusion processes.

6 For an alternative approach using fluorous soluble polymeric ligands, see: W. Chen, L. Xu and J. Xiao, *Chem. Commun.*, 2000, **10**, 830; D. E. Bergbreiter, J. G. Franchina and B. L. Case, *Org. Lett.*, 2000, **2**, 393

7 B. P. Santora, M. R. Gagné, K. G. Moloy and N. S. Radu, *Macromolecules*, 2001, **34**, 658.

8 In a typical run ~80 mg of polymer (~100 μmol Rh g^{-1}) and 150 mg of **1** were used along with 4.0 mL of toluene or 2.0 mL toluene and 2.0 mL PFMC. The Fischer–Porter vessel was emmersed into a pre-equilibrated oil bath, and when monophasic, the vessel was charged and vented 3× with 150 psi H_2 and charged to the final pressure.

9 The consolute temperate rises above 108 °C when concentrations of **1** are greater than 1 M.

10 The polymer sinks in the 25% v/v fluorous solution, while it floats to the surface for the 50, 75 and 100% PFMC experiments.

11 Analysis of different physical sections of the polymer monolith by AA indicates that Rh is *not* evenly distributed in the matrix (±20%). Crushing and mixing macroscopically homogenizes the Rh, however, this makes the reported recycling experiments more cumbersome, and was avoided.

12 In a typical high turnover experiment ~5 mg of polymer (0.01 mol%) and 800 mg of **1** were subjected to the same conditions listed in ref. 8. To minimize evaporative loss of solvent, aliquots to measure reaction progress were taken approximately every 24 h. After 40 h the toluene typically completes ~2300 turnovers, while the FBS completes ~9000; both systems do eventually show complete conversion.

13 D. Rutherford, J. J. J. Julliette, C. Rocaboy, I. T. Horváth and J. A. Gladysz, *Catal. Today*, 1998, **42**, 381; B. Richter, A. L. Spek, G. van Koten and B. Deelman, *J. Am. Chem. Soc.*, 2000, **122**, 3945.

14 These experiments were carried out with 25, 50 and 66% fluorous content (0.5, 1.0 and 1.5 mol% catalyst). Differences in activity as a function of fluorous content varied less than 10%, with absolute rates being similar to polymer rates.

15 At this time we cannot rule out the possibility that H_2 diffusion *from solution to polymer* is sensitive to fluorous content.

CHEMCOMM Communication
www.rsc.org/chemcomm

Diphosphites as a promising new class of ligands in Pd-catalysed asymmetric allylic alkylation

Montserrat Diéguez,*[a] Susanna Jansat,[b] Montserrat Gomez,*[b] Aurora Ruiz,[a] Guillermo Muller[a] and Carmen Claver[a]

[a] *Departament de Química Física i Inorgànica, Universitat Rovira i Virgili, Pl. Imperial Taraco 1, 43005 Tarragona, Spain. E-mail: dieguez@quimica.urv.es*
[b] *Departament de Química Inorgànica, Universitat de Barcelona, Martí i Franquès, 1-11, E-08028 Barcelona, Spain. E-mail: montserrat.gomez@qi.ub.es*

Received (in Cambridge, UK) 16th February 2001, Accepted 3rd May 2001
First published as an Advance Article on the web 31st May 2001

A series of diphosphite ligands, derived from readily available D-(+)-glucose, have been used for the first time in the palladium-catalysed allylic alkylation reaction with high enantioselectivity (ee up to 95%) and activity in standard conditions.

One of the main objectives in modern synthetic organic chemistry is the catalytic enantioselective formation of C–C bonds.[1] In this respect, Pd-catalysed allylic alkylation is a powerful and highly versatile procedure. In recent years, the asymmetric version of this reaction has been reported with various C_2- and C_1-symmetric bidentate chiral ligands providing excellent enantiomeric excesses.[2] However, one drawback of using these ligands is that they are often synthesised from expensive chiral sources and in tedious synthetic steps. Therefore it is important to develop new chiral ligands derived from readily available simple starting materials and to show their applicability in C–C bond formation. In this context, carbohydrates, which have been widely used in organic synthesis as inexpensive starting materials or as chiral auxiliaries,[3] have only recently shown their huge potential as a source of highly effective chiral ligands.[4]

In this context, we have recently described the synthesis of a new class of furanoside diphosphite ligands (Scheme 1), prepared in a few steps from readily available D-(+)-glucose, and their successful use in the rhodium catalysed asymmetric hydroformylation of vinyl arenes (ee values up to 91%).[5]

The advantage of these ligands is that their modular nature allows a facile systematic variation in the configuration of the stereocenters (C-3, C-5) at the ligand bridge and in the biphenyl substituents, allowing the optimum configuration for maximum stereoselectivity to be determined. In this paper we report on the use of this new class of sugar diphosphite ligands in enantioselective Pd-catalysed allylic alkylation. We also examined the effect of the configuration of the stereogenic centers C-3 and C-5 since this was expected to be important for the catalytic reaction because of the proximity of these centers to the metal. The influence of the substituents on the biphenyl moieties was also studied. Although the combination of mixed phosphite–oxazoline,[6] phosphite–thioether[7] functionalities and phosphite–phosphine[8] ligands has already been successfully used in Pd-catalysed allylic alkylation, to the best of our knowledge this is the first example of diphosphite ligands being applied to this type of reaction.

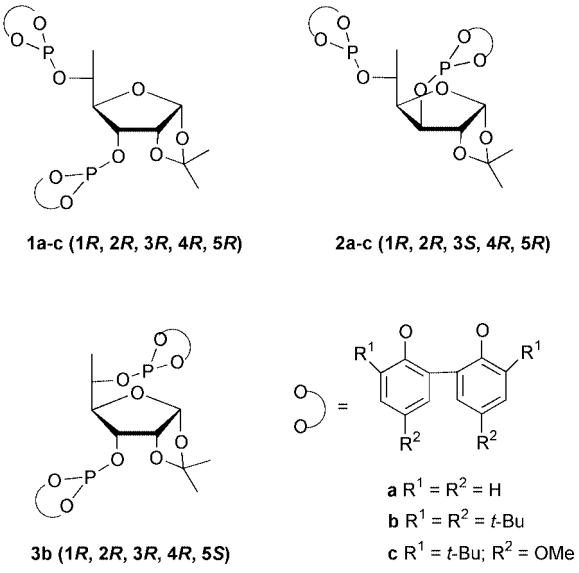

Scheme 1

For initial evaluation of the new ligands we chose the palladium(0)-catalysed addition of dimethyl malonate to *rac*-1,3-diphenyl-3-acetoxyprop-1-ene (**4**) [eqn. (1)] because this

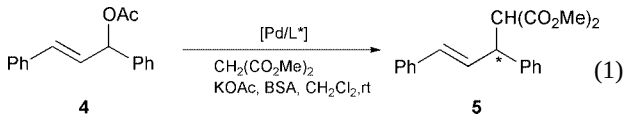

4 **5** (1)

reaction has been carried out with a wide variety of ligands carrying different donor groups, enabling direct comparison of the efficacy of different ligand systems. In addition, many successful ligands developed for this reaction have been found to have broader applicability in other related reactions.[2]

Asymmetric allylic substitution of **4** was carried out with the palladium complex generated *in situ* by mixing the corresponding chiral ligand and $[Pd(\eta^3\text{-}C_3H_5)Cl]_2$, under basic Trost conditions.[9] Results are given in Table 1.

Table 1 Palladium-catalysed asymmetric allylic alkylation with chiral ligands **1**–**3**[a]

Entry	L*	Time/min	% Conv.[b]	% ee[c]
1	**1a**	1440	50	2 (*R*)
2	**1b**	15	100	64 (*R*)
3	**1c**	19	100	45 (*R*)
4	**2c**	35	60	9 (*S*)
5	**2b**	5	100	84 (*S*)
6	**2c**	10	100	95 (*S*)
7	**3b**	3600	100	52 (*S*)
8	**6**	71	100	61 (*S*)
9	**7**	65	100	59 (*S*)
10[d]	**8**	1440	100	61 (*S*)

[a] Reaction conditions: 1 mmol of substrate, 3 mmol of dimethyl malonate, 3 mmol of *N*,*O*-bis(trimethylsilyl)acetamide (BSA), 1 mol% of $[Pd(\eta^3\text{-}C_3H_5)Cl]_2$, 2.5 mol% of L* and 2 mol % of KOAc, in 4 cm^3 of CH_2Cl_2 at room temperature. [b] Conversion percentage based on the substrate determined by ^{1}H NMR spectroscopy. [c] Enantiomeric excesses determined by HPLC on a Chiralcel-OD column. Absolute configuration, in parentheses, determined by optical rotation.[10] [d] Data from reference 11.

 DOI: 10.1039/b101567m

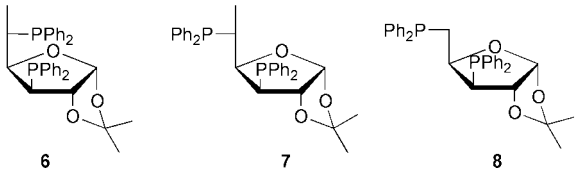

6 7 8

Scheme 2

The reaction at room temperature using ligand **1a** with two unsubstituted biphenol moieties provided (*R*)-**5** with an ee value of only 2% (entry 1). The presence of bulky *tert*-butyl groups in the *ortho*-positions of the biphenyl moiety (ligands **1b** and **1c**) had a positive effect on the enantioselectivity (ee values up to 64%, entries 2 and 3). Furthermore, the presence of *tert*-butyl groups also had an extremely positive effect on the activity (entry 1 *vs.* entries 2 and 3).

The use of ligands **2a**–**c**, in which the configuration of carbon atom C-3 is opposite to those of ligands **1a**–**c** (Scheme 1), produced improved enantioselectivities and activities (entries 1–3 *vs.* entries 4–6). Thus, ligand **2b** showed not only higher asymmetric induction (84%) but also very high catalytic activity (5 minutes for total conversion of substrate, entry 5). Such remarkably high activity, which can be explained by the large π-acceptor ability of the diphospite ligands, contrasts with the low activity reported for other homo-donor ligands.[2,4k,12] The enantioselectivity was increased to 95% (*S*)-**5** when ligand **2c**, with methoxy groups instead of *tert*-butyl groups in the *para* positions of the biphenyl moieties, was used (entry 5 *vs*. entry 6).

The use of ligand **3b**, which resulted from changing the configuration of C-5 from (*R*) to (*S*) in ligands **1**, leads to lower activity and slightly lower enantioselectivity than the catalytic system Pd/**1** (entry 2 *vs.* entry 7). Moreover, comparison of entries 2, 5 and 7 clearly shows that the enantiomeric excesses are strongly dependent on the absolute configuration of the carbon C-3 stereocenter of the carbohydrate backbone. The best enantioselectivities were obtained using ligands **2b** and **2c** with (*S*) configuration at C-3. The presence of methoxy groups in the biphenyl moieties significantly improved the enantioselectivity (ee up to 95%).

Note that these diphosphite ligands showed higher enantioselectivity and reaction rates than their corresponding diphosphines **6** and **7**[13] (entries 8 and 9) and the *xylo*-furanoside diphosphine **8**[11] analogue (entry 10) under the same reaction conditions (Scheme 2). The similar enantioselectivities obtained with ligands **6** and **7** confirms that the configuration of C-5 has no relevant influence on the enantiodiscrimination as observed for the diphosphite ligands.

In summary, we have described the first application of diphosphite ligands in asymmetric allylic alkylation reactions. These ligands can be prepared in a few steps from commercial D-(+)-glucose as an inexpensive natural chiral source. The combination of high enantioselectivities (ee up to 95%) and high activities in simple unoptimized reactions and the low cost of the ligands makes these catalyst systems very attractive for further research. These results also open up a new class of ligands for enantioselective Pd-catalysed allylic alkylation, which will be of great practical interest. For example, phosphites are less sensitive to oxidation than phosphines. Moreover, because of the modular construction of diphosphites, structural diversity is easy to achieve, so enantioselectivity can be maximised for each new substrate as required. Studies of this kind, as well as mechanistic studies, are currently under way.

We thank the Spanish Ministerio de Educación y Cultura and the Generalitat de Catalunya (CIRIT) for their financial support (PB97-0407-C05-01 and 04).

Notes and references

1 J. Tsuji, *Palladium Reagents and Catalysis, Innovations in Organic Synthesis*, Wiley, New York, 1995.
2 For an overview see: (*a*) B. M. Trost and D. L. Van Vranken, *Chem. Rev.*, 1996, **96**, 395; (*b*) A. Pfaltz and M. Lautens, *Allylic substitution reactions in Comprehensive Asymmetric Catalysis*, ed. E. N. Jacobsen, A. Pfaltz and H. Yamamoto, Springer, Heidelberg, 1999, vol. 2, ch. 24.
3 (*a*) J. S. Penne, in *Chiral Auxiliaries and Ligands in Asymmetric Synthesis*, John Wiley & Sons, New York, 1995; (*b*) S. Hanessian, in *Total Synthesis of Natural Products: The 'Chiron' Approach*, Pergamon Press, London, 1983, vol. 3; (*c*) D. Steinborn and H. Junicke, *Chem. Rev.*, 2000, **100**, 4283.
4 For some recent applications see: (*a*) M. Beller, J. G. E. Kraute and A. Zapf, *Angew. Chem., Int. Ed. Engl.*, 1997, **36**, 772; (*b*) M. Reetz and S. R. Waldvogel, *Angew. Chem., Int. Ed. Engl.*, 1997, **36**, 865; (*c*) K. Boog-Wick, P. S. Pregosin and G. Trabesinger, *Organometallics*, 1998, **17**, 3254; (*d*) K. Yonehara, T. Hashizume, K. Mori, K. Ohe and S. Uemura, *J. Org. Chem.*, 1999, **64**, 9374; (*e*) T. V. RajanBabu, B. Radetich, K. K. You, T. A. Ayers, A. L. Casalnuovo and J. C. Calabrese, *J. Org. Chem.*, 1999, **64**, 3429 and references cited therein; (*f*) O. Pàmies, M. Diéguez, G. Net, A. Ruiz and C. Claver, *Organometallics*, 2000, **19**, 1488; (*g*) O. Pàmies, G. Net, A. Ruiz and C. Claver, *Eur. J. Inorg. Chem.*, 2000, 2011; (*h*) O. Pàmies, M. Diéguez, G. Net, A. Ruiz and C. Claver, *Chem. Commun.*, 2000, 2383; (*i*) W. Li, Z. Zhang, D. Xiao and X. Zhang, *J. Org. Chem.*, 2000, **65**, 3489; (*j*) O. Pàmies, M. Diéguez, G. Net, A. Ruiz and C. Claver, *Tetrahedron: Asymmetry*, 2000, **11**, 4377; (*k*) Y.-Y. Yan and T. V. RajanBabu, *Org. Lett.*, 2000, **2**, 199.
5 (*a*) M. Diéguez, O. Pàmies, A. Ruiz, S. Castillón and C. Claver, *Chem. Commun.*, 2000, 1607; (*b*) M. Diéguez, O. Pàmies, A. Ruiz, S. Castillón and C. Claver, *Chem. Eur. J.*, in press.
6 R. Prétôt and A. Pfaltz, *Angew. Chem., Int. Ed.*, 1998, **37**, 323.
7 K. Selvakumar, M. Valentini, P. S. Pregosin and A. Albinati, *Organometallics*, 1999, **18**, 4591.
8 S. Deerenberg, H. S. Schrekker, G. P. F. Van Strijdonck, P. C. J. Kamer, P. W. N. M. van Leeuwen and K. Goubitz, *J. Org. Chem.*, 2000, **65**, 4810.
9 The standard Pd-catalysed enantioselective allylic alkylation procedure is described in: B. M. Trost and D. J. Murphy, *Organometallics*, 1985, **4**, 1143.
10 U. Leutenegger, G. Umbricht, C. Fahrni, P. V. Matt and A. Pfaltz, *Tetrahedron*, 1992, **48**, 2143.
11 O. Pàmies, A. Ruiz, G. Net, C. Claver, H. Kalchhauser and M. Widhalm, *Monatsh. Chem.*, 2000, **131**, 1173.
12 A. K. Ghosh, P. Mathivanan and J. Cappiello, *Tetrahedron: Asymmetry*, 1998, **9**, 1.
13 For comparative purposes diphosphine ligands **6** and **7** were tested in the Pd-catalysed enantioselective allylic alkylation under the same reaction conditions (see footnotes in Table 1). Ligands **6** and **7** differ in the configuration of carbon C-5, being (*S*) and (*R*), respectively. Their synthesis can be found in: M. Diéguez, O. Pàmies, A. Ruiz, S. Castillón and C. Claver, *Tetrahedron: Asymmetry*, 2000, **11**, 4701.

CHEMCOMM
Communication
www.rsc.org/chemcomm

Optical thermometer based on the stability of a phosphorescent 6-bromo-2-naphthol/α-cyclodextrin$_2$ ternary complex

R. Elizabeth Brewster, Matthew J. Kidd and Merlyn D. Schuh*

Department of Chemistry, POB 1719, Davidson College, Davidson, NC 28036, USA. E-mail: meschuh@davidson.edu

Received (in Columbia, MO, USA) 6th March 2001, Accepted 24th April 2001
First published as an Advance Article on the web 31st May 2001

The phosphorescence lifetime of a water-soluble ternary complex of 6-bromo-2-naphthol and α-cyclodextrin has been found to decrease by more than two orders of magnitude over a 58 °C temperature range, which makes this molecular system well suited for use as the first optical thermometer based solely on phosphorescence lifetimes.

A ternary molecular complex consisting of two molecules of α-cyclodextrin (CD) and one molecule of 6-bromo-2-naphthol (BN) emits readily detectable BN phosphorescence in aqueous solutions containing molecular oxygen, an efficient triplet-state quencher.[1] It is believed that the triplet-state BN molecule is protected from quenching by being encapsulated in the hydrophobic core of the CD molecules, which are assumed to make contact with each other concentrically along the rim of the larger opening of the toroidal CD molecule. The phosphorescence lifetime of the BN/CD$_2$ complex is reported herein to have a very high temperature sensitivity and to be useful as the first reported aqueous optical molecular thermometer based only on phosphorescence lifetimes.

There has been increasing interest in the use of molecular luminescence to make remote temperature measurements by passing the luminescence signal from the sensor material through an optical fiber[2] or by incorporating the luminescent probe molecule directly into the site at which the temperature is to be measured.[3] Most of these optical thermometers make use of fluorescence and have been designed around temperature-dependent excited state lifetimes,[2–10] shifts in fluorescence or absorption spectra,[11–14] changes in fluorescence intensity,[3,10,15] or black-body radiation spectra.[16]

One of the highest sensitivities for an optical thermometer was reported for the delayed fluorescence of acridine yellow dissolved in a rigid saccharide glass.[10] In this sensor material the sensitivity is ultimately determined by the triplet-state lifetime. Over the reported temperature range, the lifetime of delayed fluorescence and the ratio (intensity of delayed fluorescence)/(intensity of phosphorescence), I_{df}/I_p, changed only about four-fold, and the average percentage relative sensitivities to temperature of the delayed fluorescence lifetime and the I_{df}/I_p ratio were reported to be 2.0% and 4.5%, respectively.[10]

The following is a brief description of our instrumentation and experimental procedure. Excitation pulses (FWHM of 6–7 ns and typical energy of 1–10 mJ) at 280 nm or 345 nm were produced as the frequency-doubled output of a Quanta Ray Nd/YAG-pumped dye laser. Phosphorescence was focused into a 0.25 m Jarrell Ash spectrometer and detected at 525 nm, the wavelength for maximum phosphorescence intensity. The spectrometer was operated with a spectral resolution of approximately 40 nm. The photomultiplier was gated off electronically for 2 μs to coincide with the occurrence of the large scattered light signal. For each lifetime measurement, 500–1000 oscilloscope traces were averaged so that a drop of phosphorescence intensity of up to three orders of magnitude could be analyzed. Sample temperature was maintained within ±0.1 °C by using a circulating constant-temperature bath. All solutions contained CD and BN concentrations of 0.01 M and 9.4×10^{-5} M, respectively.

Phosphorescence signals were fitted by non-linear least squares regression and generally were found to be single exponential for at least the first two to three orders of magnitude decay in signal. The only exception was at the highest temperature, 59.7 °C, where the phosphorescence intensity was reduced sufficiently to prevent reliable curve-fitting beyond the initial drop of 1.5 orders of magnitude. The residuals for single-exponential fits were random, and correlation coefficients were usually greater than 0.998. The standard deviation for all measured phosphorescence lifetimes, τ, was less than 0.5%. Within experimental uncertainty, τ values were the same when either 280 nm or 345 nm was used as the excitation wavelength.

The value of $1/\tau$ increases dramatically from 800 s^{-1} to 133 000 s^{-1} over the temperature range 1.6–59.7 °C, and the good fit of the Arrhenius equation to the data is seen in Fig. 1. The slight leveling of the plot at the lowest temperature is not unexpected in view of the approach of the reciprocal phosphorescence lifetime to a limiting value, which for 1-bromonaphthalene in glass is 71 s^{-1} at 77 K.[17] Nevertheless, if all data are included, the Arrhenius activation energy, E_a, of 69 ± 2 kJ mol^{-1} for Fig. 1 is 2.4 times larger than the activation energy of 28.3 kJ mol^{-1} for the delayed fluorescence lifetime of acridine yellow.[10] For a plot of $1/\tau$ *vs.* temperature (K) the relative sensitivity is defined as the slope divided by the value of $1/\tau$ and is expressed as E_a/RT^2. The percentage relative sensitivity ranges from 11% at 1.6 °C to 7.5% at 59.7 °C. The large sensitivity reported herein is, to our knowledge, the largest value reported for an optical thermometer, and the small standard deviations associated with the values of τ reveal that temperature differences smaller than 0.1 °C can be measured.

Since BN phosphorescence is detectable only from the ternary complex in aerated solutions, the following mechanism, which has been used for similar phosphorescent complexes,[18,19] is reasonable.

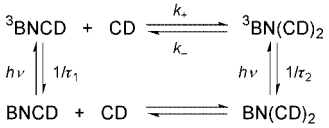

Use of the steady state approximation in solving the associated rate equations shows that the phosphorescence should decay with a single exponential lifetime, τ, expressed in eqn. (1).

$$(1/\tau - 1/\tau_2)^{-1} = \frac{k_+[\mathrm{CD}]}{k_-/\tau_1} + \frac{1}{k_-} \quad (1)$$

Values of τ were measured for [CD] in the range 0.008–010 M at 24 °C and 50 °C. The value of τ_2 is independent of [^{3}BN(CD)$_2$] and was varied until a plot of the left-hand side of eqn. (1) *vs.* [CD] was linear and had the largest correlation coefficient. The value of k_- was determined from the intercept. The percentage increase was found to be larger for k_- than for $1/\tau_2$ as the temperature was increased from 24 °C to 50 °C and showed the cause for the large value of E_a to be dissociation of the ternary complex.[20] Excellent support for this conclusion

 DOI: 10.1039/b102156g

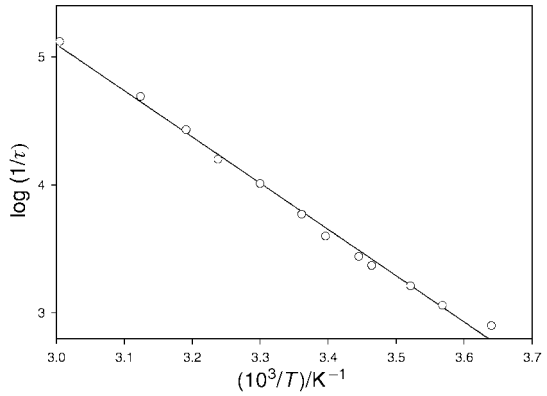

Fig. 1 Arrhenius plot of the reciprocal phosphorescence lifetime, $1/\tau$ for the $BN(CD)_2$ complex.

comes from recent theoretical and experimental studies of the ternary complex of triplet state naphthalene with two α-cyclodextrin molecules.[21] The optimized, low-energy theoretical structure of the complex shows that naphthalene is longitudinally encapsulated between the CD molecules, the secondary cyclodextrin hydroxylic rims face each other, and hydrogen bonds between the hydroxylic groups stabilize the complex. Triplet–triplet absorption was used experimentally to measure an activation energy of 66.5 kJ mol^{-1} associated with oxygen quenching of encapsulated triplet state naphthalene. The similarity of the activation energies reported herein and in reference 21 shows that the shortening of τ with increasing temperature depends little on the structural difference between BN and naphthalene. Since quenching by oxygen occurs upon complete or partial dissociation of the complex, the activation energy arises primarily from the breaking of several hydrogen bonds between the cyclodextrin rings.

BN does not have good long-term stability by itself in aqueous solution, and a sample kept in the dark for seven months developed a light brownish tint. However, CD acts as a good stabilizer, and a sample of the $BN(CD)_2$ complex stored for seven months in the dark developed no tint, and no change in the UV/visible spectrum was detected. Although prolonged use of a solution containing BN and CD at room temperature produced no change in phosphorescence signal, prolonged use at 60 °C caused the phosphorescence intensity to decrease by a few percent.

In summary, the first optical thermometer based only on phosphorescence lifetimes is reported, which has the following important advantages. 1) It has perhaps the highest sensitivity reported for an optical thermometer. 2) Adequate phosphorescence can be produced by using a range of excitation wavelengths, notably between 280–345 nm. The laser-induced phosphorescence intensities of the $BN(CD)_2$ complex and 6-bromo-2-naphthyl sulfate (BNS) in deaerated solution are similar.[22] Since similar phosphorescence intensity of BNS is produced by both laser and broad bandpass-filtered, 7 J flashlamp excitation, it should also be possible to produce adequate phosphorescence from the $BN(CD)_2$ complex using a simple, relatively inexpensive flashlamp excitation source. 3) The instrumentation required to produce and detect long-lived phosphorescence is relatively low in cost. 4) The water solubility of the molecular complex should make it useful as a direct probe of temperature in physiological samples and solutions. 5) Over most of the operational temperature range, the phosphorescence lifetime changes in accordance with the Arrhenius equation which permits a direct correlation to be drawn between τ and temperature without additional calibration. The limitations of the $BN(CD)_2$ optical thermometer are its relatively limited operational temperature range and its slow degradation at prolonged high temperatures. However, the small amounts of BN and CD required as samples in a functional thermometer are inexpensive and can be replaced as necessary.

Notes and references

1 S. Hamai, *J. Chem. Soc., Chem. Commun.*, 1994, 2243.
2 Model 790 Technical Data Sheet, Luxtron Corp., Santa Clara, CA, 1993.
3 C. F. Chapman, Y. Liu, G. J. Sonek and B. J. Tromberg, *Photochem. Photobiol.*, 1995, **62**, 416.
4 K. T. V. Grattan and A. W. Palmer, *Rev. Sci. Instrum.*, 1985, **56**, 1784.
5 Z. Zhiyi and A. W. Palmer, *Rev. Sci. Instrum.*, 1991, **62**, 1735.
6 F. Anghel, C. Lliescu, K. T. V. Grattan, A. W. Palmer and Z. Y. Zhang, *Rev. Sci. Instrum.*, 1995, **66**, 2611.
7 R. R. Sholes and J. G. Small, *Rev. Sci. Instrum.*, 1980, **51**, 882.
8 K. T. V. Grattan and A. W. Palmer, *Sens. Actuators*, 1987, **12**, 375.
9 N. Sabbatani, M. Guardigli, I. Manet, F. Bolletta and R. Ziessel, *Inorg. Chem.*, 1994, **33**, 955.
10 J. C. Fister III, D. Rank and J. M. Harris, *Anal. Chem.*, 1995, **67**, 4269.
11 K. T. V. Grattan, R. K. Selli and A. W. Palmer, *Rev. Sci. Instrum.*, 1987, **58**, 1231.
12 A. Seilmer, P. O. J. Scherer and W. Kaiser, *Chem. Phys. Lett.*, 1984, **105**, 140.
13 K. F. Schrum, A. M. Williams, S. A. Haerther and D. Ben-Amotz, *Anal. Chem.*, 1994, **66**, 2788.
14 K. T. V. Grattan, R. K. Selli and A. W. Palmer, *Rev. Sci. Instrum.*, 1986, **57**, 1175.
15 M. Engeser, L. Fabbrizzi, M. Licchelli and D. Sacchi, *Chem. Commun.*, 1999, 1191.
16 Z. Zhiyi and A. W. Palmer, *Rev. Sci. Instrum.*, 1992, **63**, 3177.
17 S. P. McGlynn, R. Sunseri and N. Christodouleas, *J. Chem. Phys.*, 1962, **37**, 1818.
18 N. J. Turro, J. D. Bolt, Y. Kuroda and I. Tabushi, *Photochem. Photobiol.*, 1982, **35**, 69.
19 T. C. Barros, K. Stefaniak, J. F. Holzwarth and C. Bohne, *J. Phys. Chem. A*, 1998, **102**, 5639.
20 R. E. Brewster and M. D. Schuh, unpublished work.
21 G. Grabner, K. Rechthaler, B. Mayer and G. Köhler, *J. Phys. Chem. A*, 2000, **104**, 1365.
22 S. W. Bayles, S. Beckham, P. R. Leidig, A. Montrem, M. L. Taylor, T. M. Wright, Y. Wu and M. D. Schuh, *Photochem. Photobiol.*, 1991, **54**, 175.

CHEMCOMM
Communication
www.rsc.org/chemcomm

Imine chloroboration: reaction of boron trichloride with a bulky diazadiene gives not a diazaborolium salt, but a 2,4,5 trichloro-1,3,2-diazaborolidine†

Francis S. Mair,* Robert Manning, Robin G. Pritchard and John E. Warren

Department of Chemistry, UMIST, PO Box 88, Manchester, UK M60 1QD.
E-mail: frank.mair@umist.ac.uk

Received (in Cambridge, UK) 19th February 2001, Accepted 3rd May 2001
First published as an Advance Article on the web 31st May 2001

Reaction of *N,N′*-bis(2,6-diisopropylphenyl)-1,4-diazadiene with BCl_3 in hexane gave the crystalline product of double chloroboration, *N,N′*-bis(2,6-diisopropylphenyl)2,4,5-trichloro-1,3,2-diazaborolidine, which was characterised by single crystal X-ray diffraction, microanalysis and multinuclear NMR spectroscopy.

Hydroboration has become one of the principal vehicles of functional group interconversion. Additions of B–H across all manner of unsaturated bonds, including C=O and C=N, are extremely well documented.[1] Haloboranes, conversely, are best known as Lewis acids and ether cleavage agents, where the mode of reactivity is insertion into a single bond,[2] as opposed to addition across a multiple bond. Addition of a haloborane reagent across a multiple bond, 'haloboration', is less widely studied; though isolated reports of such reactivity began in the mid-20th century, covering alkynes, aldehydes and isocyanates,[3] only recently through the work of Suzuki and coworkers has the synthetic utility of the reaction type been systematically probed, concentrating on the bromoboration of alkynes.[4] Chloroboration of alkenes has also been recently identified as the mechanism for the living cationic polymerisation of isobutene.[5] During the attempted synthesis of a very bulky diazaborolium salt, it was discovered that the compound produced was the product of a double B–Cl addition across two aldimine C=N bonds, the first case, to our knowledge, of imine haloboration. In our attempts to explore novel metal boryl chemistry, it became necessary to prepare extremely bulky diazaborolium salts. These species have been known for some time to be available *via* the addition of boron halides to diazadiene ligands.[6] Interest in the area has recently been revived,[7] spurred by the isolation of stable carbenes by Arduengo *et al.*[8] However, during all of these syntheses, which were in most cases directed at further reduction of the putative diazaborolium halides to produce 6π pseudoaromatic diazaborole compounds, no diffraction data were collected on the diazaborolium compounds.

Reaction† of $(2,6\text{-}Pr^i_2C_6H_3NCH)_2$ with BCl_3 in hexane produced an orange powder, **1a**. This was isolated by filtration and from the filtrate, diffraction quality crystals of **1b** were grown. Both the orange powder **1a** and the crystals **1b** showed the same microanalysis, corresponding to the 1 : 1 product, and had identical NMR spectra in $CDCl_3$. The spectra appeared consistent with the expected diazaborolium formulation $[(2,6\text{-}Pr^i_2C_6H_3NCH)_2BCl_2]^+Cl^-$, save for the fact that the 'diazaborolium' ring CH protons resonated at 6.9 ppm, slightly upfield of where they are normally found (8–9 ppm)[6,7] in the ^1H NMR spectrum, and the ^{11}B NMR signal was slightly shifted from its expected position, and much broader than expected for a pseudo-tetrahedral boron site. More puzzling was the observance of two distinct isopropyl methine resonances. This was indicative not only of extremely slowed aryl ring rotation, but also of a lack of an approximate plane of symmetry in the molecule in any conformation.

The reason for the spectral anomalies became clear upon solution of the X-ray diffraction data:‡ The crystalline compound is not an ionic salt **1a**, but the neutral diazaborolidine molecule **1b** (see Fig. 1 and Scheme 1), the result of a double chloroboration of the diazadiene. Only a single chloride remains

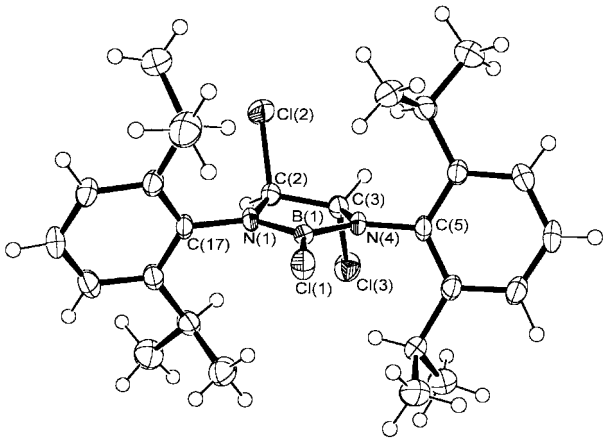

Fig. 1 Crystal and molecular structure of **1b**. Selected bond lengths (Å) and angles (°): B(1)–N(1) 1.403(3), B(1)–N(4) 1.416, B(1)–Cl(1) 1.743(3), N(1)–C(2) 1.413(3), N(1)–C(17) 1.445(3), N(4)–C(3) 1.417(3), N(4)–C(5) 1.433(3), Cl(3)–C(3) 1.841(3), Cl(2)–C(2) 1.840(3), C(2)–C(3) 1.528(3); N(1)–B(1)–N(4) 109.4(2), N(1)–B(1)–Cl(1) 125.5(2), N(4)–B(1)–Cl(1) 125.1(2), B(1)–N(1)–C(2) 109.10(19), B(1)–N(1)–C(17) 128.9(2), C(2)–N(1)–C(17) 121.98(19), B(1)–N(4)–C(3) 108.82(19), B(1)–N(4)–C(5) 129.4(2), C(3)–N(4)–C(5) 121.78(19), N(1)–C(2)–C(3) 105.45(19), N(1)–C(2)–Cl(2) 112.93(17), C(3)–C(2)–Cl(2) 107.26(16), N(4)–C(3)–C(2) 105.05(19), N(4)–C(3)–Cl(3) 112.85(17), C(2)–C(3)–Cl(3) 107.51(17).

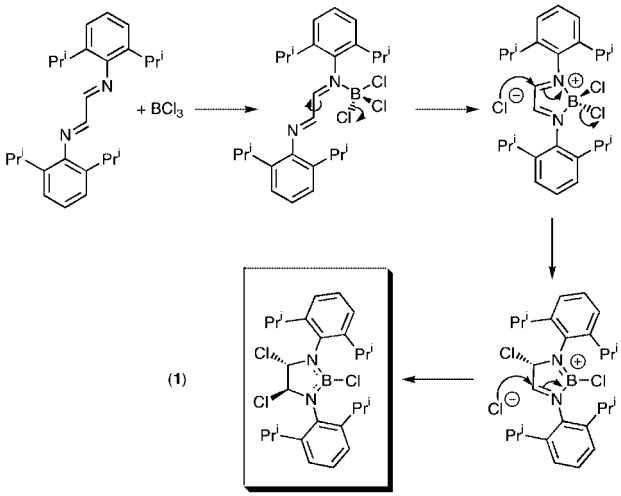

Scheme 1

† Electronic supplementary information (ESI) available: Experimental details and characterisation data for **1**. See http://www.rsc.org/suppdata/cc/b1/b101580j/

 DOI: 10.1039/b101580j

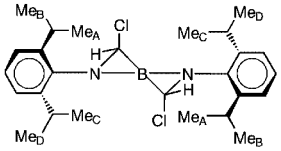

Scheme 2

bound to boron, completing the trigonal-planar geometry around that atom. The other two chlorides have added to the carbons of the diazadiene fragment, in an *anti* configuration, generating two chiral centres. Structurally **1b** bears close similarities with previously reported diazaborolidines of which there are two characterised by single-crystal X-ray diffraction [$(MeNCH_2)_2BMe$ and $(EtNCH_2)_2BMe$],[9] and one by gas-phase electron diffraction [$(MeNCH_2)_2BCl$].[10] All exhibit a puckered ring with slight pyramidalization at nitrogen, and one methylene group lying above, and one below, the mean ring plane. However, in **1b**, each nitrogen is rigorously planar, due to the bulky aromatic substituent. These aryl rings are slightly skewed from orthogonality (+14.4 and −14.3°) with the diazaborolidine ring by repulsions from the chlorides. This generates a C_2-symmetric environment about the boron (Scheme 2).

The IR spectrum of **1a** showed an absorption in the region 1580–1590 cm^{-1} indicative of a boron-coordinated imine,[6,7] whereas that of the crystals **1b** contained no such band. Furthermore, **1a** and **1b** were established to be different materials by powder X-ray diffraction. This identified **1a** as the expected diazaborolium salt, even though NMR spectroscopy in $CDCl_3$ showed it to be identical to **1b**. This leads to the conclusion that conversion of the initially formed diazaborolium salt to **1b** is completed in that solvent. The alternative possibility that in $CDCl_3$ the chlorides in **1b** dissociate from the carbons is excluded by the observation of distinct signals for the isopropyl methine resonances, directly ascribable to the reduction in symmetry generated by the addition of the chlorides above and below the diazaborolium ring plane (Scheme 1). Similar behaviour was observed in CD_3CN.

The fact that **1b** is indistinguishable by elemental analysis from the diazaborolium formulation, and the previous lack of diffraction data, offered the possibility that this unexpected reactivity had been missed in previous literature, but careful re-examination of published data showed that the diazaborolium formulation was amply supported by conductivity, IR and ^1H and ^{11}B NMR data.[6,7] The chloroboration reaction is therefore exclusive to **1**. Since previously reported examples include close analogues of **1**, including one case[7] which is identical save for the substitution of methyl groups in the aryl 2- and 6-positions for the isopropyl groups in **1**, the key to the reactivity appears to lie in the increased bulk. It may be that the boron atom cannot sustain four-coordination in the presence of the two diisopropylphenyl groups. In hexane solvent, the nucleophilicity of chloride, once ejected from the coordination sphere of the boron atom, would be high. Allying this to the fact that boron halides in their role as Lewis acids are often employed in order to encourage attack by nucleophiles at *ipso* carbon atoms, including such roles for imine additions[11] leads to a tentative mechanism such as that shown in Scheme 1. That the reaction proceeds to completion in the more polar solvents deuterochloroform and deuteroacetonitrile, more facilitative of ionization, further supports a description of the reactivity as a double 1,3-nucleophilic rearrangement.

A structural factor of particular note is the pronounced shortening in the diazaborolidine ring C–N bonds, which at a mean distance of 1.415(3) Å lie closer to the distances found in the pseudo-aromatic diazaboroles (mean of known values to date: 1.404 Å)[7,9] than to the more normal single bond values found in other known diazaborolidines (mean 1.459 Å).[9,10] The C–Cl distances in **1b** are conversely rather long at 1.84 Å, but are comparable to those in $(CHCl_2)_3N$ obtained by chlorination of triformamide;[12] the C–N and C–Cl distances in that case were 1.418(2) and 1.800(1) Å, respectively. It is a very rare situation because chloroamides are normally assumed to adopt an ionic

Scheme 3

form, *i.e.* the equilibrium shown in Scheme 3 lies to the left.[13] The analogy between this long-known behaviour and the newly discovered diazaborolium/diazaborolidine dichotomy is a strong one. In both cases, the molecular form would appear to retain a significant contribution from the ionic form in the ground-state equilibrium structure, as evidenced by the short C–N and long C–Cl bonds and rigorously planar nitrogen.[12] This type of behaviour has previously been termed single-bond–no-bond resonance.[14] No such behaviour is apparent in the much more common quaternary ammonium α-chloro-organonitrogen species.[14]

An important distinction between the two cases discussed[12,13] above is that there is only one chloride on each carbon in **1**; as an isolable synthon for a mono-α-chloro secondary amine, **1** is unique. We intend to pursue this analogy in parallel with the reduction chemistry of the current system to access highly hindered diazaboroles. It is also apposite to reflect that the use of extreme steric bulk does not always merely pacify chemical reactivity, but in certain circumstances can engender new and unexpected directions of that reactivity.

We thank the EPSRC and Creators Ltd for a Total Technology studentship, the Nuffield Foundation for an Undergraduate Research Bursary, and the Royal Society for an equipment grant.

Notes and references

‡ *Crystal data* for **1b**: $C_{26}H_{36}BCl_3N_2$, M = 493.73, triclinic, space group $P\bar{1}$, a = 8.323(4), b = 9.8086(3), c = 17.35350(10) Å, α = 93.246(3), β = 90.208(2), γ = 115.0350(10)°, U = 1281.0(6) $Å^3$, Z = 2, D_c = 1.246 Mg m^{-3}, μ = 0.375 mm^{-1} (Mo-Kα, λ = 0.71073 Å), $F(000)$ = 524, T = 203 K. Nonius MACH 3 diffractometer, crystal size 0.4 × 0.3 × 0.3 mm, θ_{max} = 24.97°, 4812 reflections measured, 4475 unique. Final wR_2 = $[\Sigma w(F_o^2 - F_c^2)^2/\Sigma(wF_o^2)^2]^{1/2}$ = 0.1257 for all data, conventional R = 0.0445 for 3324 observed reflections. CCDC 160079. See http://www.rsc.org/suppdata/cc/b1/b101580j/ for crystallographic data in CIF or other electronic format.

1 H. C. Brown, *Hydroboration*, Benjamin, New York, 1962.
2 Y. Guindon, C. Yoakim and H. C. Morton, *Tetrahedron Lett.*, 1983, **24**, 2969; Y. Guindon, M. Therien, Y. Girard and C. Yoakim, *J. Org. Chem.*, 1987, **52**, 1680 and references therein. See also, J. March, *Advanced Organic Chemistry*, Wiley Interscience, New York, 4th edn., 1992, pp. 433–434.
3 M. F. Lappert, *Angew. Chem.*, 1960, **72**, 36; M. F. Lappert and B. Prokai, *J. Chem. Soc.*, 1963, 4223.
4 A. Suzuki, *Rev. Heteroat. Chem.*, 1997, **17**, 271, and references therein.
5 L. Balogh, L. F. Wang and R. Faust, *Macromolecules*,1994, **27**, 3453.
6 L. Weber and G. Schmid, *Angew. Chem., Int. Ed. Engl.*, 1974, **13**, 467; G. Schmid and J. Schulze, *Chem. Ber.*, 1977, **110**, 2744.
7 L. Weber, E. Dobbert, H.-G. Stammler, B. Neumann, R. Boese and D. Bläser, *Chem. Ber.*, 1997, **130**, 705; L. Weber, E. Dobbert, R. Boese, M. T. Kirchner and D. Bläser, *Eur. J. Inorg. Chem.*, 1998, 1145; L. Weber, M. Schnieder, R. Boese and D. Bläser, *J. Chem. Soc., Dalton Trans.*, 2001, 378.
8 A. J. Arduengo III, R. L. Harlow and M. Kline, *J. Am. Chem. Soc.*, 1991, **113**, 361.
9 G. Schmid, M. Polk and R. Boese, *Inorg. Chem.*, 1990, **29**, 4421.
10 H. M. Seip, R. Seip and K. Niedenzu, *J. Mol. Struct.*, 1973, **17**, 361.
11 H. Yamada, T. Kawate, A. Nishida and M. Nakagawa, *J. Org. Chem.*, 1999, **64**, 8821.
12 E. Allenstein, W. Schwarz and E. Schrempf, *Z. Anorg. Allg. Chem.*, 1987, **546**, 107.
13 H. Eilingsfeld, M. Seefelder and H. Weidinger, *Angew. Chem.*, 1960, **72**, 836.
14 E. Anders, A. Opitz, K. Wermann, B. Wiedel, M. Walther, W. Imhof and H. Görls, *J. Org. Chem.*, 1999, **64**, 3113; Ch. Lambert and P. v. R. Schleyer, *Houben-Weil Carbanionen-Polare Organometall-Verbindungen*, Georg Thieme Verlag, Stuttgart, 1993, p. 1–98.

CHEMCOMM Communication
www.rsc.org/chemcomm

Chiral discrimination with a fluorescent boron–dipyrromethene dye

Gerhard Beer,[a] Knut Rurack*[b] and Jörg Daub*[a]

[a] *Institut für Organische Chemie der Universität Regensburg, Universitätsstraße 31, D-93040 Regensburg, Germany. E-mail: joerg.daub@chemie.uni-regensburg.de*
[b] *Bundesanstalt für Materialforschung und -prüfung (BAM), Dept. I.3902, Richard-Willstätter-Straße 11, D-12489 Berlin, Germany. E-mail: knut.rurack@bam.de*

Received (in Cambridge, UK) 13th March 2001, Accepted 1st May 2001
First published as an Advance Article on the web 22nd May 2001

The optically active binaphthalene boron–dipyrromethene (BDP) conjugate 1 shows chiral discrimination towards the enantiomers of 1-phenylethylamine by distinguishable quenching rates of the BDP fluorescence.

The chiral discrimination between enantiomers during molecular recognition processes[1] is of great importance in many fields of pharmaceutical chemistry, bio- and food technology.[2] For instance, the knowledge of the stereochemical structure of a potential drug is essential for rational and successful drug design as potency, selectivity and bioavailability can differ markedly for enantiomers of a chiral compound.[3] Solution-based sensor systems can be an important aid in these development processes,[4] since they allow the study of the processes of drug–receptor interactions. A functionalization with chromogenic[5] or fluorescent[6] reporter molecules facilitates the application of spectrophotometric and fluorometric analytical techniques that offer many advantages for highly sensitive chiral recognition. The use of steady-state and time-resolved fluorometry especially can improve rapid and quantitative analysis and is well-suited for high-throughput screening.[7] In our approach towards efficient enantioselective fluorescent sensor molecules, we relied on the versatile[8,9] and, when equipped with an appropriate receptor, efficiently chemically switchable[9] boron–dipyrromethene (BDP) fluorophore and designed the enantiomerically pure BDP conjugate **1**. 1,1′-bi-2-naphthol, known to selectively recognize optically active amines or amino acids,[5d,10] was chosen by us as the chiral receptor unit. In this communication, we report on the ability of **1** to differentiate between (*R*)- and (*S*)-1-phenylethylamine by specific modulation of its fluorescence signal at wavelengths > 500 nm.

The optically active *R*-enantiomers of **1** and the reference

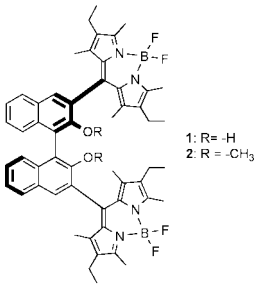

compound **2** were obtained from enantiomerically pure 1,1′-binaphthalene carbaldehydes[11a,b] and 2,4-dimethyl-3-ethylpyrrole by literature procedures.[11c,d]

In agreement with earlier studies on a phenol-appended BDP dye,[9a] deprotonation of the hydroxy groups of **1** leads to a strong decrease of the fluorescence (Φ_f^1 = 0.62), most probably involving a photoinduced electron transfer-like quenching mechanism. Fig. 1 shows this 'switching OFF' of the BDP emission at 542 nm for a microtitration of **1** with diisopropylethylamine in acetonitrile.† Whereas the emission band position does not change during the titration, the BDP $S_1 \leftarrow S_0$ absorption band shifts slightly to the blue (from 523 to 521 nm). For **2**, where the hydroxy groups are exchanged with methoxy groups, no spectral shifts occurred in either, absorption (526 nm) or emission (542 nm, Φ_f^2 = 0.80), and only at comparatively high amine concentrations (*ca.* $> 10^{-2}$ M) was a slight reduction in fluorescence observed. To get better insight into the nature of the quenching process(es) involved, time-resolved fluorescence titrations were carried out. In the case of purely static quenching, *i.e.* when a non-fluorescent ground-state complex is formed, the fluorescence lifetime remains constant (τ_f = const.) and only the amplitude is gradually decreased during the titration ($a \neq$ const.). When dynamic quenching occurs, the number of emitting molecules is not changed (a = const.) but the lifetime is reduced ($\tau_f \neq$ const.) with increasing quencher concentration as a result of an increase in collisional frequency of an excited fluorophore with a quencher. Time-resolved quenching experiments with diisopropylethylamine revealed single exponential decays for both dyes. However, whereas for **2** the amplitude of the 6.17 ns component does not change, in the case of **1** an increase in base concentration leads to a concomitant decrease of the amplitude of the 5.15 ns decay species. At high amine concentrations, a slight but gradual decrease of the fluorescence lifetime is found for **1** and **2**, with an unchanged amplitude in the case of **2**. These results, along with the spectrophotometric changes, suggest that the reaction of diisopropylethylamine with **1** leads to the formation of an entirely non-fluorescent, deprotonated species of **1**, *i.e.* static quenching occurs, the respective K_S being determined to 1.1×10^4 M^{-1}.‡ Moreover, at high concentrations, base-induced dynamic quenching seems to be responsible for a reduction in fluorescence decay time for both, the sensor molecule as well as the reference compound. Reprotonation by TFA restored the initial fluorescence intensity.

These findings, along with our recent investigations on the transfer of chiral information from the optically active 1,1′-binaphthalene skeleton to the appended BDP-chromophores,[12] encouraged us to test the ability of **1** for chiral discrimination of optically active bases, (*R*)-(+)- and (*S*)-(–)-1-phenylethylamine (*R*-/*S*-PEA). In analogy to the results reported in the preceding

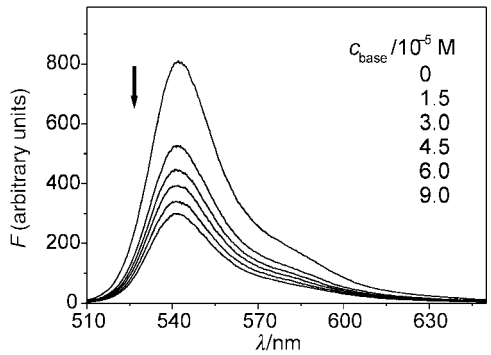

Fig. 1 Decrease in BDP fluorescence upon addition of diisopropylethylamine to a 5×10^{-6} M solution of **1** in acetonitrile; excitation at 490 nm.

 DOI: 10.1039/b102376b

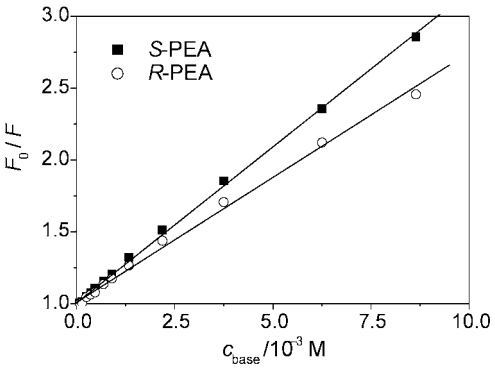

Fig. 2 Plots for the quenching of **1** with *S*-PEA and *R*-PEA in acetonitrile ($c_1 = 5 \times 10^{-6}$ M, excitation/emission at 490/540 nm, $r = 0.999/0.998$ for *S*-PEA/*R*-PEA).

paragraph, an interaction between a chiral quencher and the 1,1′-binaphthalene receptor unit should be detectable by specific changes of the BDP fluorescence signal. Upon addition of *R*- and *S*-PEA respectively, a decrease of the intensity of the fluorescence band was observed (Fig. 2), the emission maximum remaining virtually unchanged. The hypsochromic shifts in absorption (to 518 and 519 nm for *R*-PEA/**1** and *S*-PEA/**1**) are twice as large as those measured for the achiral bases. In addition, the molar absorptivities increase, the presence of *R*-PEA resulting in a stronger effect. The fluorescence lifetimes of **1** are unaffected by *R*- and *S*-PEA, and only at amine concentrations $>10^{-2}$ M does the excess of base lead to bimolecular, diffusion-controlled quenching. Analogous studies of **2** revealed that the fluorescence signal shows no comparable response upon addition of PEA, except for the dynamic quenching. This indicates that the hydroxy groups are essential for an interaction between the chiral analytes and the binaphthalene BDP conjugate, entailing specific modulations of the spectroscopic signal. Enantiomer-specific changes in the absorption spectra of 1,1′-binaphthol–amine associates have been reported before[13] and have been attributed to the formation of differently structured diastereomeric complexes,[13,14] most probably involving (more or less) strongly hydrogen-bound ground-state complexes (R–OH$\cdots$NR$_3$) or ion pairs of RO$^-\cdots$HNR$_3^+$-type. In the case of **1**, such differences in binding of *R*- and *S*-PEA can also result in a structural reorientation of the BDP chromophores. A better verification of the nature of the sensor molecule–analyte interaction/complex formation was not possible with the methods employed here, because several BDP-localized transitions which are centered in the region of the binaphthyl absorption hampered a closer inspection of the spectroscopic changes taking place directly at the binding/reaction site.[13]

In order to examine the efficiency of the quenching process for *R*- and *S*-PEA, the experimental data were analysed according to the equation for static quenching.‡ Fig. 2 shows the corresponding plots for the quenching of **1** with *R*- and *S*-PEA. The different slopes clearly indicate the suitability of **1** as a chirally discriminating sensor for optically active amines. The steeper slope for quenching with *S*-PEA, based on a higher $K_S = 226$ M^{-1} for *S*-PEA–**1** as compared to $K_S = 161$ M^{-1} for *R*-PEA–**1**, suggests that association of the *S*-enantiomer and **1** is more efficient. The ratio of $K_S(R–S)/K_S(R–R) = 1.40$ is comparatively high for amine complexes of a simple binaphthol receptor unit in acetonitrile[10*f*,*g*,13] and clearly stresses the potential of **1** as an enantioselective sensor molecule.

In conclusion, we have shown that the combination of the chiral recognition features of a substituted 1,1′-binaphthalene unit with the favourable spectroscopic properties of the BDP chromophore presents a promising approach towards 'ON'–'OFF' signaling of chiral analytes, advantageous both in spectral region and time domain.

Notes and references

† For the equipment used and general experimental procedures including fluorescence quantum yield determination, see ref. 9*b*. All quantum yields and lifetime data were obtained at 295 K, the uncertainties of the quenching constants are $< \pm 4\%$ ($n = 4$).

‡ If fluorescence quenching is caused by static as well as dynamic interactions of sensor and analyte molecules, the single quenching constants can in principle be separated by considering time-resolved emission data (for details, see J. R. Lakowicz, *Principles of Fluorescence Spectroscopy*, Plenum, New York, 1983, p. 260). In the case of **1**, dynamic quenching was only observed at very high concentrations of the corresponding bases. The quenching of the BDP fluorescence was nearly complete at much lower base concentrations due to static interactions, *i.e.* deprotonation (for diisopropylethylamine) or association (for the chiral amines) reactions. Therefore, the static quenching constants K_S reported here could readily be determined according to $F_0/F = 1 + K_S c_Q$, where F_0 is the fluorescence yield in the absence of quencher Q, F is the respective parameter in the presence of Q, c_Q is the concentration of the quencher and K_S is the association constant, in a concentration range where no reduction in fluorescence lifetime was observed. In all of these cases, plots of F_0/F *vs.* c_Q were strictly linear with correlation coefficients $r > 0.99$.

1 T. H. Webb and C. S. Wilcox, *Chem. Soc. Rev.*, 1993, **22**, 383.
2 R. Marchelli, A. Dossena and G. Palla, *Trends Food Sci. Technol.*, 1996, **7**, 113; S. C. Stinson, *Chem. Eng. News*, 1998, **76**, (**38**), 83.
3 R. J. Crossley, *Chirality and the Biological Activity of Drugs*, CRC Press, Boca Raton, FL, 1995; M. Eichelbaum and A. S. Gross, *Adv. Drug Res.*, 1996, **28**, 1.
4 R. Hovius, P. Vallotton, T. Wohland and H. Vogel, *Trends Pharmacol. Sci.*, 2000, **21**, 266; D. L. Taylor, E. S. Woo and K. A. Giuliano, *Curr. Opin. Biotechnol.*, 2001, **12**, 75.
5 (*a*) F. Vögtle and P. Knops, *Angew. Chem., Int. Ed. Engl.*, 1991, **30**, 958; (*b*) T. Nishi, A. Ikeda, T. Matsuda and S. Shinkai, *J. Chem. Soc., Chem. Commun.*, 1991, 339; (*c*) Y. Kubo, S. Maeda, S. Tokita and M. Kubo, *Nature*, 1996, **382**, 522; (*d*) Y. Kubo, *Synlett*, 1999, 161.
6 T. Grady, S. J. Harris, M. R. Smyth, D. Diamond and P. Hailey, *Anal. Chem.*, 1996, **68**, 3775; L. Prodi, F. Bolletta, M. Montalti, N. Zaccheroni, P. Huszthy, E. Samu and B. Vermes, *New J. Chem.*, 2000, **24**, 781; C. V. Kumar, A. Buranaprapuk and H. C. Sze, *Chem. Commun.*, 2001, 297.
7 I. Hemmilä and S. Webb, *Drug Discovery Today*, 1997, **2**, 373; G. A. Korbel, G. Lalic and M. D. Shair, *J. Am. Chem. Soc.*, 2001, **123**, 361.
8 J. Karolin, L. B.-Å. Johansson, L. Strandberg and T. Ny, *J. Am. Chem. Soc.*, 1994, **116**, 7801.
9 (*a*) T. Gareis, C. Huber, O. S. Wolfbeis and J. Daub, *Chem. Commun.*, 1997, 1717; (*b*) M. Kollmannsberger, K. Rurack, U. Resch-Genger and J. Daub, *J. Phys. Chem. A*, 1998, **102**, 10211; (*c*) K. Rurack, M. Kollmannsberger, U. Resch-Genger and J. Daub, *J. Am. Chem. Soc.*, 2000, **122**, 968; (*d*) K. Rurack, M. Kollmannsberger and J. Daub, *Angew. Chem., Int. Ed.*, 2001, **40**, 385.
10 P. Qian, M. Matsuda and T. Miyashita, *J. Am. Chem. Soc.*, 1993, **115**, 5624; T. D. James, K. R. A. S. Sandanayake and S. Shinkai, *Nature*, 1995, **374**, 345; K. S. Parker, A. Townshend and S. J. Bale, *Anal. Commun.*, 1996, **33**, 265; M. Asakawa, C. L. Brown, D. Pasini, J. F. Stoddart and P. G. Wyatt, *J. Org. Chem.*, 1996, **61**, 7234; X. X. Zhang, J. S. Bradshaw and R. M. Izatt, *Chem. Rev.*, 1997, **97**, 3313; D. Wang, T.-J. Liu, W.-C. Zhang, W. T. Slaven IV and C.-J. Li, *Chem. Commun.*, 1998, 1747; V. J. Pugh, Q.-S. Hu and L. Pu, *Angew. Chem., Int. Ed.*, 2000, **39**, 3638; A. Bähr, B. Felber, K. Schneider and F. Diederich, *Helv. Chim. Acta*, 2000, **83**, 1346.
11 (*a*) H. Brunner and J. Goldbrunner, *Chem. Ber.*, 1989, **122**, 2005; (*b*) H. T. Stock and R. M. Kellog, *J. Org. Chem.*, 1996, **61**, 3093; (*c*) R. W. Wagner and J. S. Lindsey, *Pure Appl. Chem.*, 1996, **68**, 1373; (*d*) M. Kollmannsberger, T. Gareis, S. Heinl, J. Breu and J. Daub, *Angew. Chem., Int. Ed. Engl.*, 1997, **36**, 1333.
12 G. Beer, C. Niederalt, S. Grimme and J. Daub, *Angew. Chem., Int. Ed.*, 2000, **112**, 3252.
13 W. Iwanek and J. Mattey, *J. Photochem. Photobiol. A Chem.*, 1992, **76**, 209.
14 V. R. Meyer and M. Rais, *Chirality*, 1989, **1**, 167.

Typeset and printed by Black Bear Press Limited, Cambridge, England

CHEMCOMM
Feature Article
www.rsc.org/chemcomm

Unique acid catalysis of heteropoly compounds (heteropolyoxometalates) in the solid state

Makoto Misono

Department of Environmental Chemical Engineering, Kogakuin University, 1-24-2 Nishi-Shinjuku, Shinjuku-ku, Tokyo 163 8677, Japan. E-mail: misono@cc.kogakuin.ac.jp

Received (in Cambridge, UK) 20th March 2001, Accepted 11th May 2001
First published as an Advance Article on the web

Fundamental and superior characteristics of heteropoly compounds (heteropolyoxometalates) in the solid state that make them suitable for catalyst design at the atomic/molecular levels are described, together with important principles required for the understanding and design of solid heteropoly catalysts. First, the molecular nature of heteropolyanions (metal oxide clusters), which can be preserved in the solid state, enables control of the acid and redox properties over a wide range. Second, the presence of hierarchical structures (primary, secondary and tertiary structures) can lead to three catalysis modes—surface-type, pseudoliquid (or bulk-type I) and bulk-type II. Precise control of pore size is possible through the understanding of the microstructure, which results in unique shape selectivity observed for various reactions. Heteropoly compounds are green catalysts functioning in a variety of reaction fields and efficient bifunctional catalysts when combined with other components. The elucidation of catalytic processes is also possible at the atomic/molecular level due to their molecular nature. The positions and dynamic nature of protons as well as organic reaction intermediates in the pseudoliquid phase can be clarified by spectroscopic techniques. Various reactions promoted by solid heteropoly catalysts are collected from recent publications to illustrate the usefulness of the above ideas and of heteropoly catalysts themselves.

1 Catalyst design at the atomic/molecular level

1.1 Importance and feasibility

Efficient catalysts are key materials in chemical technologies which supply useful substances to society and assist maintaining the environment as healthy as possible: in short, catalysts represent a key technology for a sustainable society. Although recent progress has been remarkable for homogeneous and biochemical catalysts, in particular the latter, heterogeneous (solid) catalysts are still of substantial importance in catalytic technology, and have several advantages. Therefore development of these is centred to solving global and local problems.

It is much more difficult to design heterogeneous catalysts than to interpret reactions over model solid catalysts. Hence, the development of practical (or commercial) catalysts still mostly relies on trial-and-error approaches, assisted by phenomenological knowledge on existing commercial catalysts and sophisticated knowledge on simple model catalysts. The design of practical catalysts at the atomic or molecular level has long been pursued,[1,2] since precisely designed multifunctional catalysts are obviously desirable. However, catalyst design at this level is still a distant goal in many instances.

1.2 Our approach

We have endeavored in the last two decades to establish the methodology of catalyst design by studying crystalline mixed oxides. In addition to their crystallinity, our criteria to choose catalyst materials are; (i) wide variation of composition whilst retaining the basic crystal structure and (ii) catalytic performance near the level required for practical application. Such materials include heteropoly compounds, perovskite-type mixed oxides and zeolites whose structures can be well defined at least for the solid bulk phases. Differences between the surface and solid bulk phase appear to be much smaller for these metal oxides than for metallic catalysts. This is particularly true for heteropoly compounds if the preparation and characterization of catalysts are carefully carried out. Here, the term 'heteropoly compounds' (abbreviated as HPAs) will be used for heteropolyoxometalates which include heteropolyacids and their derivatives. Heteropolyacids are hydrogen forms of heteropolyanions produced by the condensation of more than two kinds of oxoanions. Typical heteropolyanions are shown in Fig. 1. Using heteropoly compounds we attempted to establish the following relationships at the atomic/molecular levels as shown in Scheme 1.

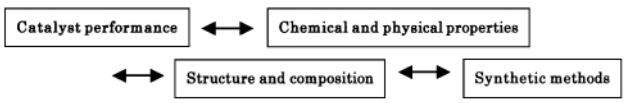

Scheme 1

This article reports important progress to establish the basis for catalysts design since the publication of special issue of *Chemical Reviews* on polyoxometalates in 1998.[3] It will attempt to show that heteropoly compounds have various attractive and important characteristics in terms of catalysis and are promising materials for catalyst design at the atomic/molecular level.

Makoto Misono received his Bachelor, Master, and Doctor's degree in Engineering from the University of Tokyo and started his academic career in 1966 at the University of Tokyo, where he became a full professor in 1983. He spent two years in the USA for his postdoctorate (1967–1969; at the University of California, Santa Barbara, and Mellon Institute, Pittsburgh). He has been studying heterogeneous catalysis mainly of mixed oxides for 40 years and gave a plenary lecture at the 10th International Congress on Catalysis, Budapest, in 1992 on the subject of molecular catalyst design of solid heteropoly compounds. Since his retirement from the University of Tokyo with the Emeritus professorship in 1999, he has been a professor at Kogakuin University, a private technical university located in the center of Tokyo. He is a former president of Catalysis Society and a vice president of Chemical Society of Japan. He was elected a member of Science Council of Japan in 2000. He is now more involved in various activities related to the environment and chemistry such as green/sustainable chemistry and clean fuel-exhaust of automobiles.

DOI: 10.1039/b102573m

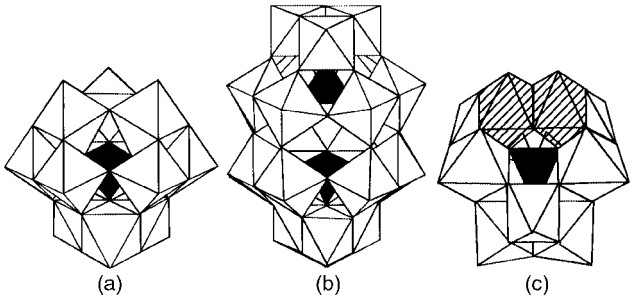

Fig. 1 Examples of heteropolyanions: (a) Keggin-type polyanion *e.g.* α-$PW_{12}O_{40}^{3-}$, (b) Dawson-type polyanion *e.g.* $P_2W_{18}O_{62}^{6-}$; (c) disubstituted polyanion *e.g.* γ-$SiW_{10}Fe_2O_{40}^{10-}$.

Catalysts based on heteropoly compounds are hereafter denoted heteropoly (or HPA) catalysts. Earlier books and review articles may be referred to regarding the basic chemistry[4] and general catalysis[5] of HPAs. HPA catalysts have already been applied to several large-scale commercial processes.[6]

2 Basic concepts unique for solid HPA catalysts

In my view, the following concepts are essential to understand and design HPA catalysts, in addition to the knowledge generally required to understand heterogeneous catalysis of the ordinary mixed oxides.

2.1 Primary, secondary and tertiary structures

At an early stage of our study it was recognized that the hierarchical structure of solid HPAs was important for the understanding of the heterogeneous HPA catalysis, and we denoted the substructures as primary, secondary and tertiary.[7] This may appear a very simple idea, but enormously helped the progress of our research. Fig. 2 shows a simplified illustration of such hierarchical structures. The primary structure is the structure of heteropolyanion itself *i.e.* the metal oxide cluster molecule and details the molecular nature of solid HPA catalyst. Fig. 2 shows the most ubiquitous form which has the Keggin structure. The secondary structure is the three-dimensional (usually regular) arrangement consisting of polyanions, counter cations and additional molecules. The secondary structure is flexible to different extents depending on the counter cation and the structure of the polyanion, and is the basis of bulk-type catalysis of solid HPA catalysts (see below). The tertiary structure represents the manner in which the secondary structure assembles into solid particles and relates to properties such as particle size, surface area, and pore structure,[8] and plays an important role in heterogeneous catalysis. Without understanding this hierarchical structure, one can neither understand solid HPA catalysts properly nor take advantage of their molecular nature, and the idea of bulk-type catalysis described below would not have evolved.

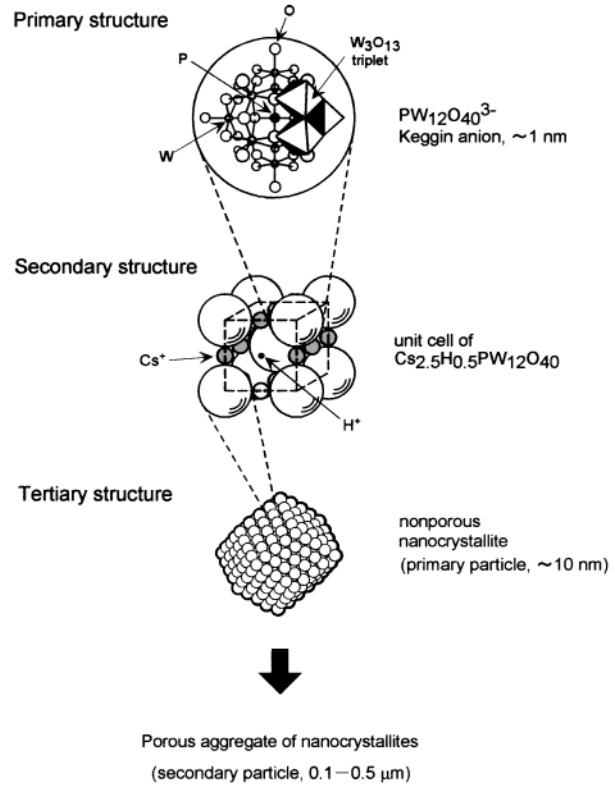

Fig. 2 Primary, secondary and tertiary structures; hierarchical structure of heteropoly compounds (HPAs) in the solid state.

2.2 Three types of catalysis

We have demonstrated that there are three totally different modes of catalysis for solid HPAs (Fig. 3). Surface-type catalysis (a) is ordinary heterogeneous catalysis which takes place on the solid surface (two-dimensional reaction field on outer surface and pore wall). Modes (b) and (c) represent bulk-type catalysis where the reaction fields are three-dimensional in contrast to the surface-type catalysis. When the diffusion of reactant molecules in the solid (diffusion in the lattice rather than pores) is faster than the reaction, the solid bulk forms a pseudo-liquid phase in which catalytic reaction can proceed [Fig. 3(b)]. In this instance, reactant molecules in the gas or liquid phase penetrate in between the polyanions (primary structure), sometimes expanding the distance between the polyanions, and react inside the bulk solid. The products come out to the surface and are released to the gas or liquid phase. Pseudoliquid catalysis, proposed in 1979, was not favourably accepted initially, since it appeared very unusual for heterogeneous mixed oxide catalysts. Now, however, such catalysis is more firmly established.[5a–c] In the pseudoliquid phase such catalysts appear as solids but behave like liquids (solvent). As the active sites in the solid bulk *e.g.* protons, take part in catalysis, very high catalytic activities are often observed in the bulk phase. Phase transitions accompanied by an abrupt change in catalytic performance are also observed.[5a]

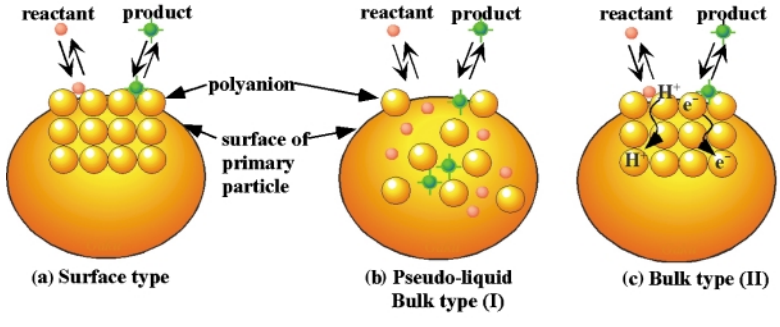

Fig. 3 Three types of catalysis for solid heteropoly compounds: (a) surface type; (b) pseudoliquid: bulk type (I), (c) bulk type (II).

The second bulk-type catalysis [bulk-type (II), Fig. 3(c)] is found for oxidation catalysis at high temperature when the diffusion of redox carriers (protons and electrons in this case) is rapid in the solid bulk, and the whole bulk participates in the reduction–oxidation cycle.[9] It should be noted that, as the contribution towards catalysis of the solid bulk varies with the relative rate of diffusion to that of reaction, intermediate cases between surface and bulk catalysis arise. Solid HPAs containing cations of low ionic radii to charge ratio (H^+, Na^+, Cu^{2+}, *etc.*) readily absorb small polar molecules and tend to exhibit pseudoliquid behaviour and are soluble in water. Cs and NH_4 salts (scarcely soluble in water, due to low solvation energy) usually show only surface-type catalysis.

The importance of this idea may be clearly understood by the following examples. Fig. 4(a) plots the relative activity and number of strong acid sites *vs.* the extent of neutralization (or the Na content) for acidic Na salts of $H_3PW_{12}O_{40}$.[10] Hereafter, $H_3PW_{12}O_{40}$, one of the most widely used HPA catalysts is abbreviated as HPW unless stated otherwise. The reactions are of bulk type (I) and the acidity is related to the number of protons in the entire bulk. It is evident in Fig. 4(a) that the rates of bulk-type reactions and the bulk acidity decrease monotonically with the Na content, thus showing good parallelism between catalytic activity and acidity. This also demonstrates that the acid catalysts can be designed by control of their acidity in this manner. In contrast, no monotonical change is found for several reactions catalyzed by acidic Cs salts, $Cs_xH_{3-x}PW_{12}O_{40}$ (denoted CsX), as shown in Fig. 4(b).[5a,b,11] These reactions are of surface type, as revealed by plots of the rates *vs.* the *surface acidity* (number of protons on the surface). The surface area sharply rises from 1–2 $m^2\ g^{-1}$ for Cs1 and Cs2 to *ca.* 150 $m^2\ g^{-1}$ for Cs3. The mechanism of the increase in surface area is interpreted in a later section of the article. As is obvious in Fig. 4(c), a good correlation is obtained.[12] Another important point to be noted is that the specific activity of CsX [catalytic activity per surface proton, the slope in Fig. 4(c)] is much higher than known solid acids such as zeolites and silica–alumina. This fact demonstrates the high performance of HPA catalysts.

Bulk-type catalysis (II) is also an essential concept required to understand and design HPA catalysts.[13] This has been found to be relevant for oxidation reactions at high temperatures. If the rates of *bulk-type oxidation* (*e.g.* oxidative dehydrogenation) are plotted against the surface redox property, very poor correlations are found, but the rates exhibit good correlations with *bulk* redox property. In contrast, the rate of *surface-type* oxidation correlates very well with the *surface redox property*. This is very similar to the acid catalysis shown in Fig. 4. Without knowing this fact, the development of practical oxidation catalysts would be very difficult.

2.3 Merits of HPA catalysts

The advantages of hetreopoly compounds for heterogeneous catalysts are summarized in Table 1.[5] There are several large-scale industrial processes utilizing HPA catalysts as oxidation and acid catalysts both in the solid state and in solution.[5a,b,6] Most are environmentally friendly, so that HPA catalysts are regarded as promising green (or sustainable) catalysts.[14,15]

Table 1 Merits of solid heteropoly catalysts for catalyst design at the atomic/molecular level

1	Systematic variation of acid and redox properties are possible for catalyst design.
2	Molecular nature of solid heteropoly compounds originating from heteropolyanion molecules enables precise design of catalysts and molecular description of catalytic processes
3	A variety of reaction fields are available for catalytic systems.
4	The unique basicity of polyanions

3 Novel aspects of pseudoliquid catalysis

3.1 Variety of reaction fields

Pseudoliquid behavior [bulk-type (I) catalysis] has also been found for liquid–solid heterogeneous systems. For example, the relative catalytic activities of HPW and Cs2.5 dramatically change with the polarity of reacting molecules;[5b] HPW > Cs2.5 for pinacol rearrangement (pseudoliquid catalysis) and HPW < < Cs2.5 for alkylation of aromatics (surface-type catalysis). HPW shows high activities for the reactions in the solid bulk (pseudoliquid), since protons inside the solid can be utilized, while Cs2.5 having a large quantity of protons on the surface (see below) is active for surface-type reactions. Bulk type (II) catalysis has not yet been observed probably because the reaction temperatures are low. The various reaction fields containing a liquid phase are illustrated in Fig. 5.

The catalysis of solid HPAs in the liquid phase has been well documented.[16] For example, three reactions differing in polarity of reactants were compared using several alkali- and alkaline-earth salts of HPW. It was shown that the decomposition of cyclohexyl acetate is catalyzed on the solid surface (surface-type), and that pinacol rearrangement proceeds in the pseudo-liquid phase. On the other hand, esterification of benzoic acid and butan-1-ol is mainly catalyzed by HPA dissolved in solution, although most of HPA remains in the solid state. The order of catalytic activity, therefore, is very different between the reactions. This again demonstrates the importance of distinguishing surface- and bulk-type catalysis for the catalyst

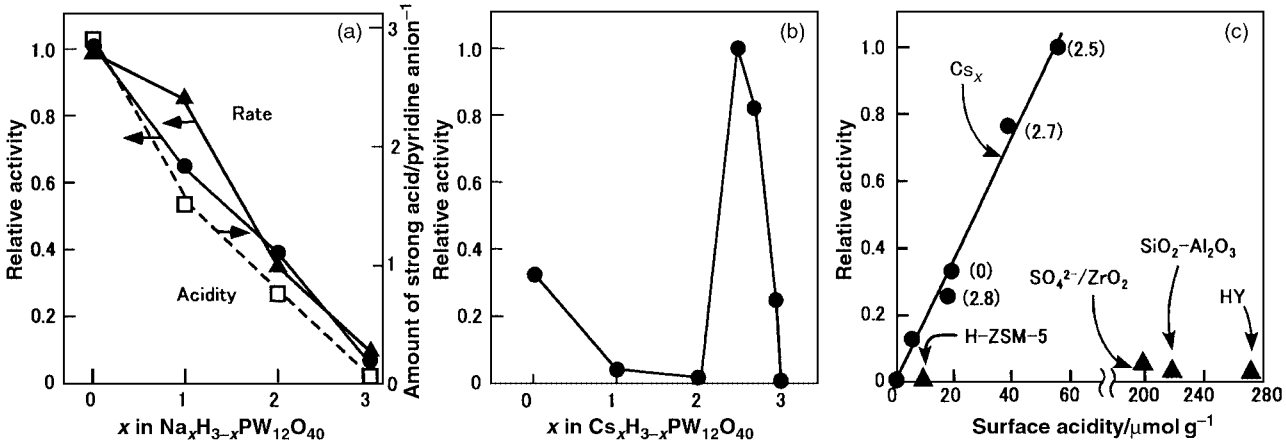

Fig. 4 Importance of differentiating surface- and bulk-type catalysis. (a) Bulk-type (I) (pseudoliquid) catalysis and bulk acidity of Na salts of $H_3PW_{12}O_{40}$ (HPW): (▲) conversion of methanol, (●) dehydration of propan-2-ol, and (□) bulk acidity measured by strongly held pyridine. (b) Rates of alkylation of 1,3,5-trimethylbenzene by cyclohexene catalyzed by Cs salts of HPW (surface-type catalysis). (c) Rates of alkylation over Cs salts [data from Fig. 4(b)] are plotted *vs.* the surface acidity, together with the same plots for several other solid acids.

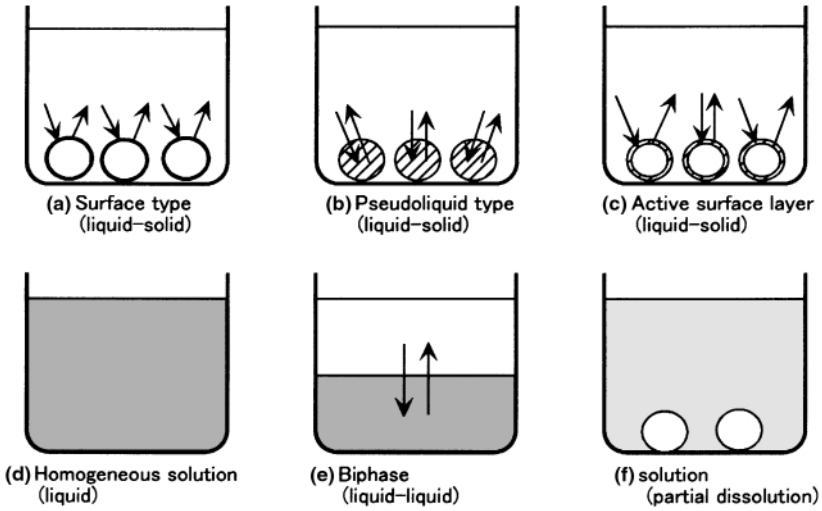

Fig. 5 Various reaction fields of HPA catalysis in reaction systems containing a liquid phase.

design of HPAs. Fig. 5(a) and (d) correspond to the ordinary heterogeneous catalysis (liquid–solid) and homogeneous (solution) catalysis, respectively. Phase-transfer catalysis for liquid–liquid biphase systems [Fig. 5(e)] is well known and there are at least two large-scale commercial processes using HPA catalysts.[6,14] Catalysis by solid HPAs for solid state reactions[17] and in a new phase formed on the surface layer[14] [Fig. 5(c)] are new. In the latter, protons introduced on the surface layer of Cs3 create a new active phase similar to a 'pseudoliquid' (Fig. 6).

Among other recent interesting observations is the unique relationship between the shape of the primary structure, the resulting secondary structures, and the remarkable influence on the catalytic activity.[18] The thermodynamically favored synthesis of methyl *tert*-butyl ether (MTBE) from isobutylene and methanol proceeds at low temperature (323 K) on Dawson-type hetropolyacids ($H_6P_2W_{18}O_{62}$ and $H_6P_2Mo_{18}O_{62}$) rapidly and selectively. In contrast, the reaction is very slow over Keggin-type heteropolyacids, in spite of the higher acid strength and comparable acid content. We found that Dawson-type heteropolyacids are amorphous under the reaction conditions due to the ellipsidal shape of the polyanion, whereas Keggin-type polyanions having spherical shape are crystalline (bcc structure). Owing to this difference the former forms active pseudoliquids, while the latter are much less active (Table 2). As for MTBE synthesis catalyzed by $H_4SiW_{12}O_{40}$, Bielanski's group has made an extensive study and proposed a hypothesis that the reaction takes place on the surface to which methanol and protons are supplied from the pseudoliquid phase.[19]

3.2 Protons, water and organic molecules in pseudoliquids

To understand and design pseudoliquid catalysts at the molecular level, information about the acidic protons, such as their location, mobility and donating ability (acid strength), is indispensable. Information about the interactions between acidic protons and small basic molecules such as water and alcohols provides useful knowledge about pseudoliquid catalysis, since water is often contained in the working state and plays an important role. Furthermore, the states and dynamics of protons in the solid are interesting subjects of solid-state chemistry. In our early studies we observed protons in HPW using MAS NMR, then directly detected (by a combination of NMR and IR) the reaction intermediates of ethanol dehydration in the pseudoliquid phase, and disclosed the dynamic behavior of methanol.[5b,6]

While IR is usually a powerful tool to study solid catalysts the IR spectra of OH bands of heteropolyacids are ambiguous. For highly hydrated HPW, the OH stretching and bending modes of water and protonated water are detectable, but for more dehydrated states they do not show any clear IR bands in contrast to silica or zeolite catalysts.

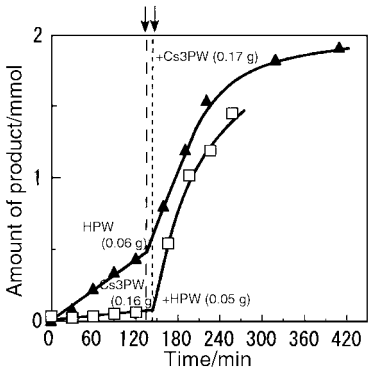

Fig. 6 Catalysis in a novel phase formed on the surface layer of a solid HPA for a liquid–solid reaction system. Hydrolysis of bistrimethylol propane monoformal in water at 348 K. The reaction rate rises sharply when the second component is added after a certain reaction time (indicated by arrows). The rates after the addition are much higher than the sum of the rates of each component, indicating the formation of an active layer on the surface of Cs3.

Table 2 Unique relationships between shape of polyanion (primary structure), secondary structure and catalytic activity

Primary structure[a] (shape)	Secondary structure at the working state	Catalytic activity for MTBE synthesis at 323 K
Dawson (ellipse) $H_6P_2W_{18}O_{62}$ $H_6P_2Mo_{18}O_{62}$	Amorphous	Very high
Keggin (spherical) $H_3PW_{12}O_{40}$ $H_4SiW_{12}O_{40}$	Crystalline (bcc)	Very low

[a] See Fig. 1.

Recently, reliable IR spectra of HPW·$n$$H_2O$ with different degrees of hydration have been reported independently by us[20b] and Zecchina's group.[21] Fig. 7 shows our results where the water contents are quantified (reliable at least for n = 0 and 6). Very broad bands ranging from 3500 to 1200 cm^{-1} are evident. For n = 6 (hexahydrate) for which the structure has been established,[5] an extremely broad band is observed which we assigned to $H_5O_2^+$ ($H_2O\cdots H^+\cdots OH_2$) present in the hexahydrate. A broad band having a peak at about 3200 cm^{-1} was observed for dehydrated sample (n = 0–0.5), which was

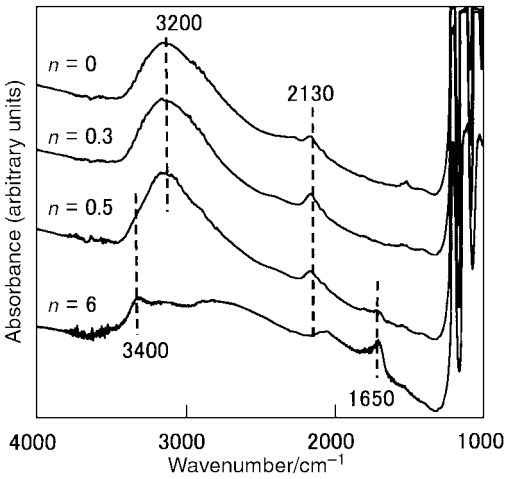

Fig. 7 IR spectra of $H_3PW_{12}O_{40}{\cdot}nH_2O$ with a variety of hydration states ($0 < n < 6$).

assigned to isolated acidic protons bonded to peripheral oxygens of the polyanion. These bands seem to exist in the IR spectra reported in earlier studies, but their presence and significance have not been well recognized.

Zecchina's group reported high quality IR spectra and provided valuable discussion of the IR bands.[21] The extremely broad band observed for the hexahydrate is reasonably interpreted by the nearly flat potential of a proton in a hydrogen bond. However, they possibly underestimated the water content of some samples (see below) and therefore their assignment of the IR bands is probably partially incorrect. The evacuation of hydrated HPW at 300–340 K leads to the hexahydrate which is fairly stable.[5a–c] Usually a higher temperature (as high as *ca.* 350 K) is necessary for further dehydration. Therefore, the sample of Zecchina's group which was obtained upon evacuation at room temperature for 3 min has probably $n > 6$, whereas the sample obtained by evacuation for 150 min is most likely the hexahydrate.

The states and dynamics of protons and water in HPW have been clarified by an extensive study using solid-state ^1H, ^{31}P and ^{17}O MAS NMR.[22] For example, the P NMR spectra of $HPW{\cdot}nH_2O$ (n = 0–6) which was prepared from the hexahydrate by evacuation at 373–423 K are shown in Fig. 8. H NMR spectra measured at 298 and 173 K showed a very broad peak for $n = 6$ due to the dipole–dipole interaction in $H_5O_2^+$, and a sharp peak for the other samples. The following important conclusions can be deduced from the NMR data.

(a) Acidic protons are present in three forms; (i) proton attached to polyanions, (ii) H_3O^+ (hydronium ion monomer) or H_2O strongly interacting with acidic protons, and (iii) $H_5O_2^+$ (hydronium ion dimer). H_3O^+ and $H_5O_2^+$ weakly interact with polyanions by hydrogen bonding. Acidic protons in the anhydrous sample attach to the polyanion leading to a significant chemical shift in the ^{31}P NMR spectrum. The probable bonding states are schematically illustrated in Fig. 9.

On the basis of IR studies, Zecchina's group concluded that for intermediate hydration states ($0 < n < 3$), the acidic proton does not form H_3O^+ but rather O–H···OH_2 .[21] However, the close resemblance in the chemical shifts of the P NMR spectra (*e.g.* $n = 2.1$ measured at 173 K, Fig. 8) and of CsX[8,25] suggests the formation of H_3O^+; acidic protons interact very weakly with polyanions. The remainder of the acidic protons remain directly bonded to the polyanions. It should also be noted that the acid strength of HPW is greater than that of zeolites (see below, Table 3).

(b) The broad peak observed at 298 K (n = 0 .5–4) splits into several peaks at 173 K (Fig. 8, $n = 0.5$, 2.1 and 4.0). This means that the rate of proton migration (exchange) is slow at 173 K and at 298 K is of the order of 200 Hz which is much faster than the rate of ordinary catalytic reactions. This study also indicated

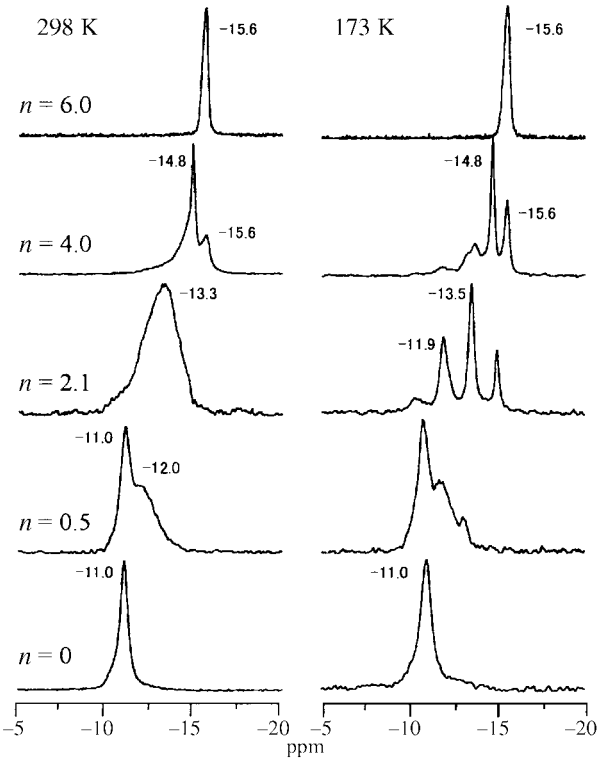

Fig. 8 ^{31}P NMR spectra of $H_3PW_{12}O_{40}{\cdot}nH_2O$ with a variety of hydration states ($0 < n < 6$) measured at 298 and 173 K.

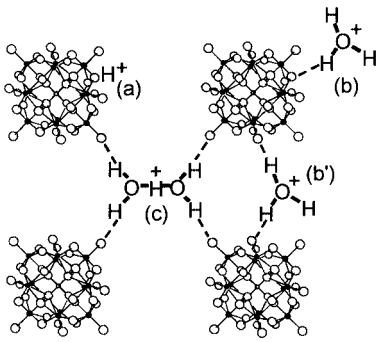

Fig. 9 Models proposed for the states of acidic protons and water in solid $H_3PW_{12}O_{40}{\cdot}nH_2O$ ($0 < n < 6$); two possible positions are shown for H_3O^+.

Table 3 Acid strengths of various solid acids

Solid acid	Initial heat of NH_3 sorption/kJ mol^{-1}	Approximate peak temperature of NH_3 desorption/K
$H_3PW_{12}O_{40}$	195	850
$Cs_{0.5}H_{2.5}PW_{12}O_{40}$	170	830
SO_4/ZrO_2	165 (190)[a]	1000 (as N_2)
HZSM-5 (Si/Al = 13)	150	670
SiO_2-Al_2O_3	145	600

[a] Value in parentheses refers to the very initial value.

that water in the lattice enhances the mobility of protons. The high mobility of protons may facilitate protonation in acid catalysis.

(c) The relative intensities of the split peaks follow a binominal distribution, indicating a uniform (random) distribution of protons and water in the solid.

(d) In the anhydrous state ($n = 0$), there is one type of acidic proton species attached to the polyanion at least on the NMR time scale. This is consistent with our IR data. We observed an apparently single broad band for the dehydrated sample (n = 0).

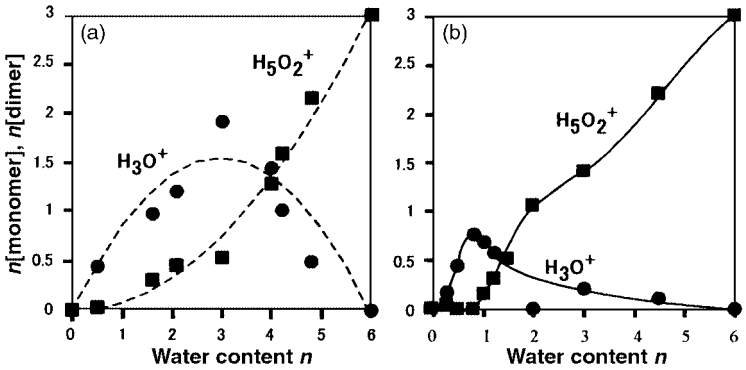

Fig. 10 Amounts of H_3O^+ (monomer) and $H_5O_2^+$ (dimer) per polyanion in $H_3PW_{12}O_{40}{\cdot}nH_2O$ ($0 < n < 6$). (a) Samples prepared by evacuation of the hexahydrate at 373–423 K. Dashed lines were calculated by assuming that water molecules are randomly removed from the hexahydrate. (b) Samples prepared by rehydration of anhydrous $H_3PW_{12}O_{40}$ at room temperature.

(e) The concentrations of the three proton species in $HPW{\cdot}nH_2O$ (n = 0–6) change with the extent of dehydration as shown in Fig. 10(a). The trends are in agreement with those calculated by assuming random removal of water.

In contrast, $HPW{\cdot}nH_2O$ prepared by the addition of water to an anhydrous sample at room temperature is quite different [Fig. 10(b)]. The main reason for the difference may be the lower temperature of preparation for which the diffusion of water is slow. Rehydration leads mainly to $H_5O_2^+$ instead of H_3O^+ at $n > 2$. Careful preparations are always necessary to obtain HPA samples having uniform composition. In particular, special caution must be taken to avoid rehydration, since anhydrous HPAs are very sensitive to moisture (even from water adsorbed on walls of apparatus).

3.3 Acidity

The acid strength of HPAs vary in a wide range depending on the polyanion structure and its constitutuent elements (both hetero and addenda atoms), as well as on the extent of hydration and reduction. Most results indicate that HPW after dehydration, the strongest HPA known so far, is a much stronger solid acid than zeolites including ZSM-5, and is close to that of superacids.[5,23] Indeed some believe HPW to be a superacid[24] while others claim that its acidity is comparable with zeolites.[21] The counter cation is also an important factor. Table 3 summarizes the acid strength as monitored by ammonia sorption (adsorption and absorption) and desorption for several solid acids,[23,25] and Fig. 11 shows the results of calorimetric measurements of NH_3 sorption on Cs2.5 and HPW at 423 K. Caution in interpretation of the results may be necessary for HPW which tends to exhibit pseudoliquid behaviour. Ammonia is absorbed into the bulk and forms ammonium salts, so that the lattice energy of the salts should be considered in calculating the heat of sorption.

Quantum chemical studies with higher levels of approximation on a full Keggin unit have recently been attempted. The stronger acidity of HPW than $H_3PMo_{12}O_{40}$ (HPMo) is indicated by density functional theory (DFT).[26] In early calculations, the position of protonation was inferred to be at bridging oxygen atoms.[27] Recently the same conclusion was deduced by a DFT calculation applied to a full Keggin unit including geometrical optimization.[28] Our ^{17}O MAS NMR and IR data are in agreement with this conclusion.[20b,22]

There are at least five different mechanisms for the evolution of acidity of solid HPA salts[5a] and hence the acidic properties are complicated unless the structures are carefully scrutinized. NMR studies revealed that protons of a novel nature are formed by the reduction of Ag and Pd salts of HPW.[29] Protons are reversibly formed by the reduction of $Ag_3PW_{12}O_{40}$ and are much more catalytically active than the protons in HPW for several reactions in the presence of H_2. ^1H NMR spectroscopy showed that protons in the former are more mobile than those of the latter. The influence of the mobility of protons on catalytic performance is an interesting topic. Similar behaviour is observed for Ag zeolites and can be formulated by reactions (1)–(3).[29c]

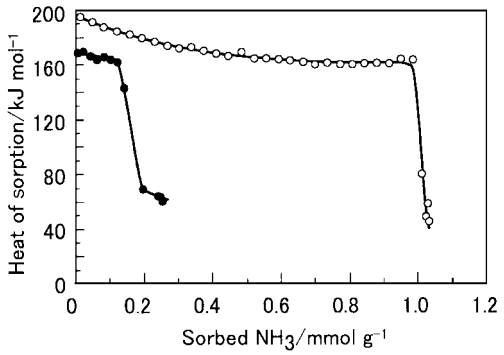

Fig. 11 Differential heats of NH_3 sorption measured at 423 K: (○) $H_3PW_{12}O_{40}$, (●) $Cs_{2.5}H_{0.5}PW_{12}O_{40}$.

$$2Ag^+ + H_2 \rightarrow 2Ag^0 + 2H^+ \quad (1)$$

$$2Ag^0 + Ag^+ \rightarrow Ag_3^+ \quad (2)$$

$$Ag_3^+ + H_2 \rightarrow Ag_3H + H^+ \quad (3)$$

4 Recent topics in surface-catalysis of Cs and NH_4 salts of HPW

4.1 Microstructure

The microstructure, or the tertiary structure (particle size, surface area, pore distribution, *etc.*) of insoluble acidic Cs and NH_4 salts of HPW is of great interest since Cs2.5 showed extremely high catalytic activities for various reactions in the liquid phase as a strong solid acid.[5a–c] The activity is often more than ten times greater than that of zeolites and more than three times that of the parent HPW. Activity much higher than that of HPW was also reported for Cs2.4 prepared in a slightly different manner.[30] Furthermore, the size of the micropores of Cs2.5 is nearly uniform, can be controlled at the sub nm level and leads to remarkable shape selective catalysis.[23,31] Acidic NH_4 salts are also active and for benzoylation $(NH_4)_4HPW_{12}O_{40}$ was more acive than Cs2.5.[32] Ag and Tl salts seem to have similar microstructures.[33]

The main reason for the high activity of Cs2.5 is its high surface acidity *i.e.* the large number of strongly acidic protons on the surface.[5a–c] The number of surface sites is about half of the total number of protons contained in the solid owing to its high surface area (*ca.* 150 $m^2\ g^{-1}$). Cs2.5 is a strong acid being only slightly weaker than the parent HPW (Table 3). Other

reasons for the high activity are moderate hydrophobicity of the surface, a bimodal pore distribution and acid–base bifunctionality (see below). All of these factors are interesting and important for heterogeneous catalysis.

Extensive and detailed studies using ^{31}P NMR, XRD, electron diffraction, AFM and SEM, adsorption of N_2, Ar, *etc*, as well as quantitative chemical analysis, have recently been carried out to clarify the microstructures of the acidic Cs and NH_4 salts.[25] Those measurements were applied comprehensively to the preparation processes *i.e.* solutions, precipitates and resulting solids obtained after drying and heat treatment, and provided a consistent view about the microstructures of Cs2.5 and other CsX salts. Their formation processes thus deduced are schematically illustrated in Fig. 12.

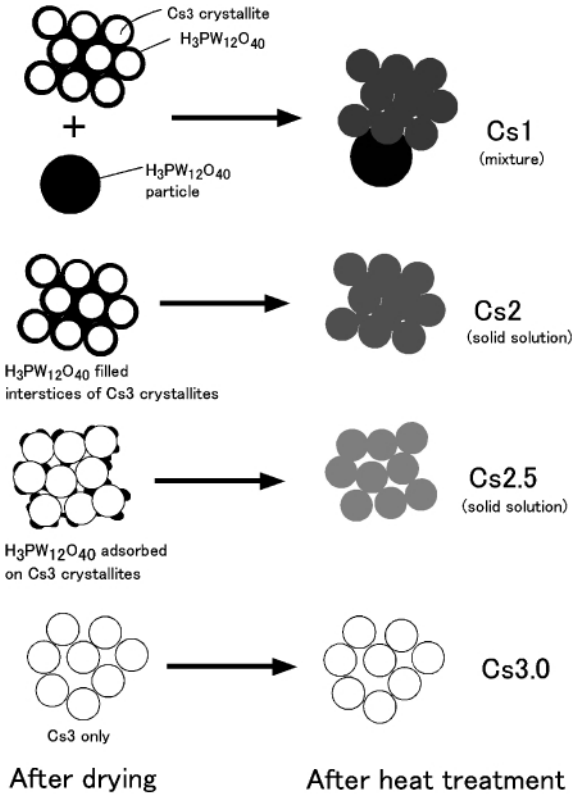

Fig. 12 Schematic illustration of the formation processes of acidic Cs salts: Left; after drying, right; after heat treatment.

Upon titration of an aqueous solution of HPW with a Cs_2CO_3 aqueous solution at 298 K, very fine precipitates of Cs3 (nanoparticles of *ca*. 10 nm in diameter) are formed, to which HPW is partly adsorbed with the remaining HPW present in the solution. As the titration proceeds, the amount of HPW in solution decreases, forming Cs3 precipitates. At the stoichiometry of Cs2 (Cs_2CO_3 added: HPW = 1 : 1), the precipitates are fine particles (also *ca*. 10 nm in diameter) of Cs3, the surface of which are covered by nearly a monolayer of HPW. Their surface area is very low (1 $m^2\,g^{-1}$), since the fine particles stick together densely after drying. This model is supported by the fact that the particle size estimated from XRD linewidths is *ca*. 10 nm, while that estimated from the BET surface area is 500 –1000 nm.

When Cs_2CO_3 is added beyond a stoichiometry of X = 2, the surface area increases sharply, since most of HPW precipitates as Cs3 and the amount of HPW remaining in solution or adsorbed on precipitates diminishes rapidly. Hence, micropores start to develop which would have been absent if the remaining HPW had densely connected the nanoparticles. ^{31}P NMR (which can differentiate between polyanions containing 0, 1, 2 or 3 protons) demonstrated that thermal treatment at 373–473 K leads to a nearly uniform solid solution of $Cs_3PW_{12}O_{40}$ (Cs3) and $H_3PW_{12}O_{40}$ (HPW) *via* diffusion of protons and Cs^+ ions, the lattice constant changing accordingly. This process has been unambiguously confirmed by the formation of the identical solid solutions when Cs3, impregnated by various amounts of HPW, is treated at 473 K, as shown by the P NMR spectroscopy (Fig. 13).

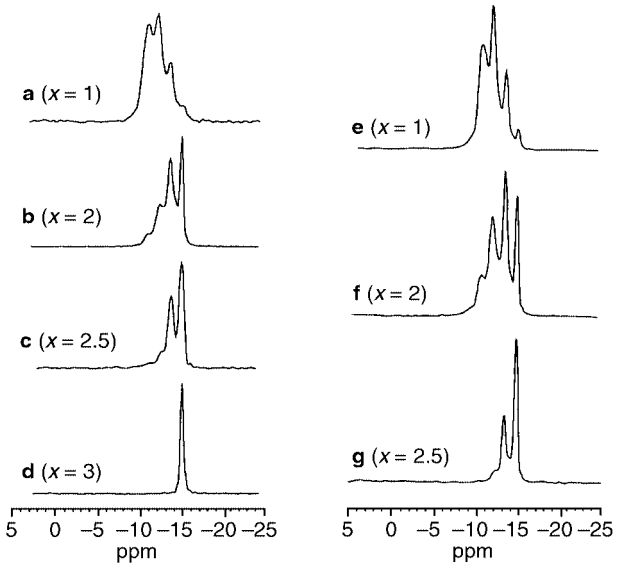

Fig. 13 Comparison of the ^{31}P NMR spectra of $Cs_xH_{3-x}PW_{12}O_{40}$ (CsX) [(a)–(d)] with Cs salts having the same compositions (CsX, X = 1, 2, 2.5) prepared by impregnation of $Cs_3PW_{12}O_{40}$ (Cs3) by HPW [(e)–(g)]. All samples were thermally treated at 473 K.

Cs2.5 has a bimodal pore size distribution; micropores ranging from 0.5 to 1.0 nm (peak at 0.65 nm and mostly > 0.75 nm) and mesopores (peak at 4–5 nm).[30,34] It is deduced that the micropores arise from spaces between nanocrystallites (10–20 nm) in loose and random aggregates and mesopores arise from spaces between the nanocrystallites and between aggregates of size *ca*. 100–500 nm (see Fig. 2). The micropores account for about 70% of the total surface area of Cs2.5 [see below, Fig. 15(d)]. Misfits in the connection of nanocrystallites have recently been suggested as the origin of small micropores (see below).[35] Another possible origin of micropores are polyanion vacancies as proposed for $Cs_4PMo_{11}VO_{40}$.[36] However, no firm and detailed conclusion has been obtained for the origin of the micropores which have a rather sharp size distribution.

A surprising finding of the microstructure is the epitaxial assembly of Cs and NH_4 salts, which was discovered unexpectedly [Fig. 14 and Fig. 15].[37,38] When the Cs salts are

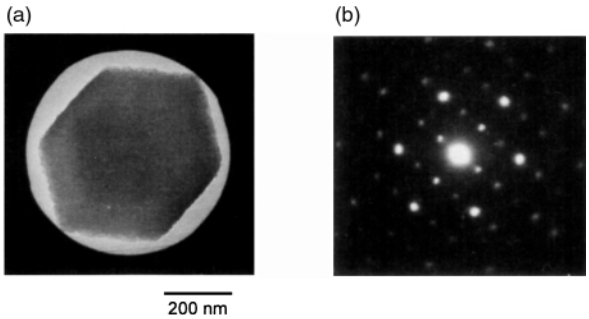

Fig. 14 Electron diffraction pattern of $(NH_4)_3PW_{12}O_{40}$ prepared by titration at 368 K using NH_4HCO_3: (a) the area in which the diffraction pattern was taken and (b) diffraction pattern.

prepared at a temperature as high as 370 K, the initially formed nanocrystallites (*ca*. 10 nm) assemble together with the identical orientation of crystal planes, leaving micropores between the nanoparticles [Fig. 15(b)], in contrast to Cs2.5

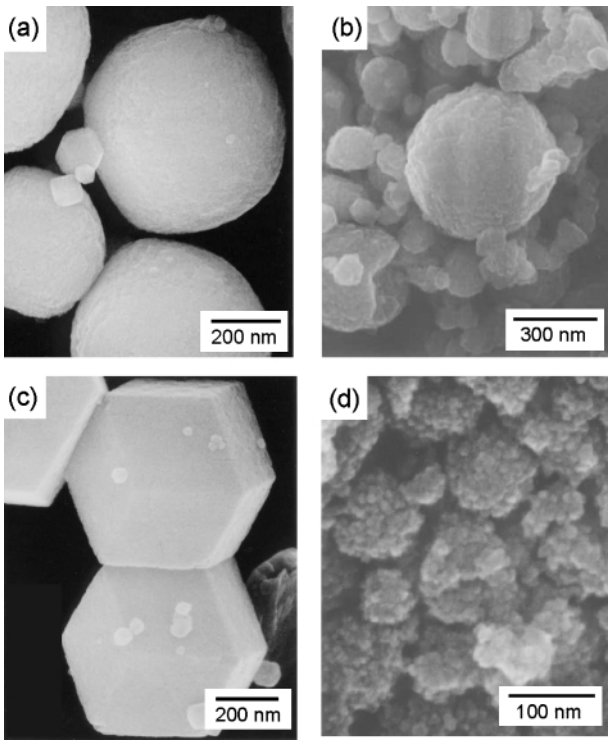

Fig. 15 SEM images of (a) $(NH_4)_3PW_{12}O_{40}$ prepared by titration at 273 K, (b) $Cs_3PW_{12}O_{40}$ (Cs3) prepared by titration at 368 K, (c) $(NH_4)_3PW_{12}O_{40}$ prepared by titration at 368 K and (d) $Cs_3PW_{12}O_{40}$ (Cs3) prepared by titration at 298 K. Cs2.5 is similar to Cs3 in appearance.

prepared at room temperature [Fig. 15(d)]. This is most remarkable when a stoichiometric NH_4 salt is prepared by means of homogeneous precipitation using urea decomposition.[34] The initially formed particles are spherical and slightly oriented aggregates [resembling the NH_4 salt formed by titration at low temperature shown in Fig. 15(a)], that are comprised of nanocrystallites of size *ca*. 10 nm with micropores (*ca*. 0.6 nm) in the spaces between the nanocrystallites, and mesopores (2–10 nm) between the loosely bound nanocrystallites and/or between the aggregates (100–1000 nm). The particles then gradually turn into large 'crystalline' microporous aggregates (400–1000 nm) having regular dodecahedral shape and few mesopores [similar to but larger than the particles shown in Fig. 15(c)]. The particle size estimated by XRD linewidth measurements (> 260 nm) is much greater than the size calculated from the surface area (10–20 nm), indicating that epitaxial connections occur between nanocrystallites. AFM and SEM images confirm that aggregates consist of fine particles of size *ca.* 10 nm. Electron diffraction (ED) shows regular discrete spots indicating crystallinity (Fig. 14). All of these observations indicate that the dodecahedral particles are 'crystalline' aggregates of nanoparticles and are porous. A monodispersed particle size (*ca*. 1000 nm) can be obtained by controlling the precipitation procedure (Fig. 16).[39] Spherical aggregates shown in Fig. 15(a) and (b) also give discrete ED patterns.

4.2 Shape selectivity

Remarkable shape selectivity has been reported for several acid-catalyzed reactions over Cs salts using molecules having different sizes. While Cs2.5 is active for most reactions, Cs2.1 and Cs2.2 only catalyzed reactions of small molecules.[5a,b,23] Shape selective catalysis has also recently been found for oxidation and hydrogenation reactions. Okuhara and coworkers confirmed that Cs2.1 has only micropores of size *ca.* 0.45 nm (in contrast to Cs2.5 for which both micropores of > 0.75 nm and mesopores of *ca*. 5 nm are present), and demonstrated shape selective catalysis, on the basis of the comparison of the catalytic activities of Pt-Cs2.1, Pt-Cs2.5 and Pt-SiO_2, for (i) oxidation of methane, carbon monoxide and benzene, and (ii) hydrogenation of ethylene and cyclohexene.[40] Shape selectivity in the products was found for the reaction of *n*-butane.[41] The large-pore Pt-Cs2.5 was very selective for the isomerization to isobutylene (94%), while cracked products (C_1–C_3) markedly increased with a decrease in the size of micropore (only 48% isobutene formed for Pt-Cs2.1) attributed to slow diffusion of the branched alkane in small micropores. Okuhara and coworkers proposed that small spaces formed by misfits in the connection of nanocrystallites are the origin of the small micropores of Cs2.1 (0.45 nm),[34] as illustrated in Fig. 17.

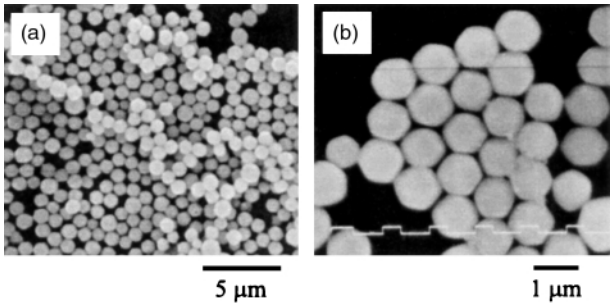

Fig. 16 SEM images of monodispersed $(NH_4)_3PW_{12}O_{40}$ prepared by titration at 368 K.

4.3 Surface acidity of $Cs_xH_{3-x}PW_{12}O_{40}$, CsX

The unusual change with X of the catalytic activity of CsX is reasonably interpreted by the surface acidity [Fig. 4(c)]. Here, the surface acidity is estimated by multiplying the number of polyanions on the surface (calculated from the surface area and the size of polyanion) and the number of protons per polyanion on the surface (from the proton content of the solid, or the chemical formula). Recently, the surface acidity, or the number of protons, on the surface of CsX (X = 2–3), has directly been measured by an IR study of CO adsorption at 110 K (Fig. 18).[20a] CO adsorbed on Cs2.5, for example, exhibits three bands; a band at 2165 cm^{-1} attributable to CO adsorbed on acidic proton sites, at 2154 cm^{-1} to CO on Cs^+ ion, and at 2139 cm^{-1} to physisorbed CO [Fig. 18(d)]. For comparison, the IR spectra of Cs3 is also shown, where both the 2165 cm^{-1} band and a broad band in the OH stretching region are absent [Fig. 18(b)].

As expected, the intensity of the first band (2165 cm^{-1}, CO on proton site) changed in parallel with the catalytic activity as shown in Fig. 19.[20a] In this way, the surface acidity estimated previously as described above has been confirmed by the direct measurement of the surface proton sites. None of the IR bands of adsorbed CO were detected for CsX (X = 0–2). Even if the very low surface areas of these Cs salts (X = 0–2) are taken into account, the IR bands would have been detected at least for HPW (4–5 $m^2\ g^{-1}$). The reason for the absence of the IR bands for HPW is not clear.

4.4 Hydrophobicity: water-tolerant solid acid catalysts

It has been shown in an earlier study that the surface of organic salts of HPW exhibit hydrophobicity.[42] Recently, the hydrophobicity was semi-quantitativley evaluated for Cs2.5 and Cs3 by comparison of water and benzene adsorption.[43] The hydrophobicity thus evaluated is in the order of HZSM-5 (high silica) > silica ≈ Cs3 > Cs2.5 ≈ HZSM-5 (low silica) > silica–alumina > alumina (ZSM-5 and silica were pretreated at 673 K, silica–alumina and alumina at 573 K, and Cs2.5 and C3 at 473 K). This indicates that Cs2.5 is moderately hydrophobic similarly to low-silica HZSM-5. As expected from this fact, it was demonstrated that Cs2.5 was very active as a water-tolerant solid acid catalyst.[44,45] The relative activity of water-tolerant solid acids varies with the nature of the reaction. Cs2.5 is usually much more active for the hydrolysis of esters than other inorganic solid acids, but less active than acidic organic resins.

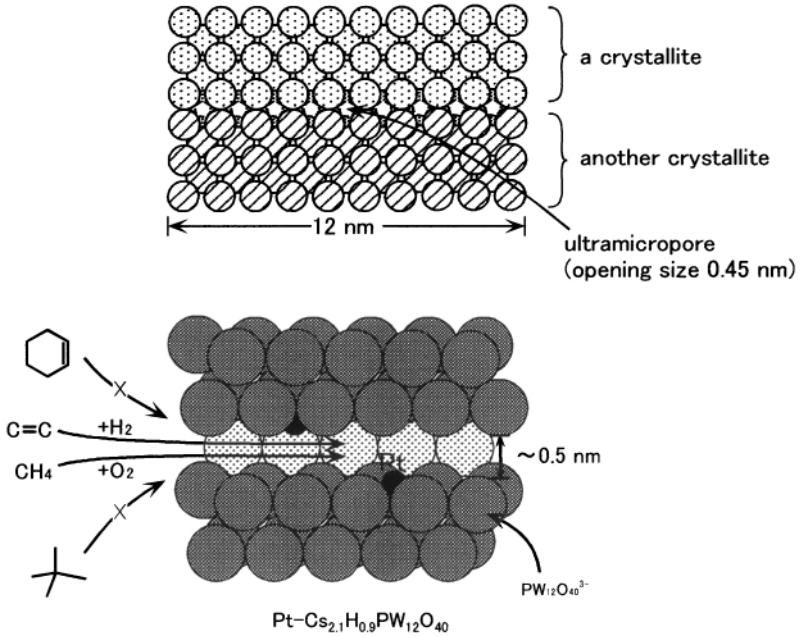

Fig. 17 A model of small micropores formed by misfits of two naoncrystallites of Pt–$Cs_{2.1}H_{0.9}PW_{12}O_{40}$.

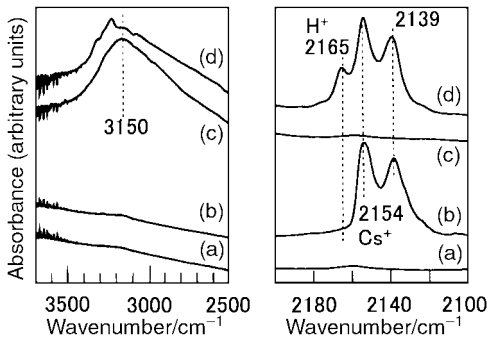

Fig. 18 IR spectra of CO adsorbed on HPAs measured at 100 K. (a) Before and (b) after adsorption of CO on $Cs_3PW_{12}O_{40}$ (Cs3); (c) before and (d) after adsorption of CO on $Cs_{2.5}H_{0.5}PW_{12}O_{40}$.

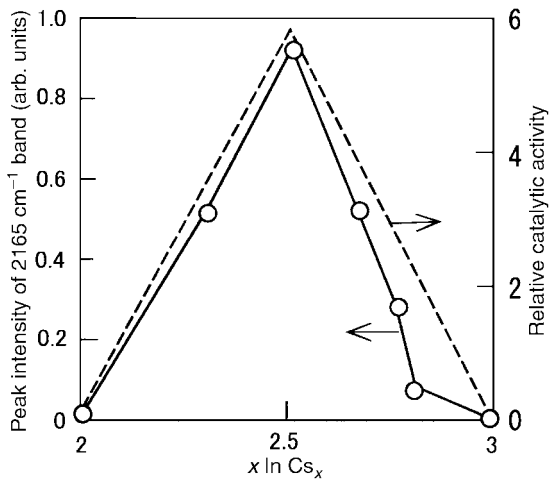

Fig. 19 Changes of the peak intensity of the 2165 cm^{-1} band (CO adsorbed on proton sites) and the catalytic activity of $Cs_xH_{3-x}PW_{12}O_{40}$ (CsX) as a function of X for the rate of alkylation of 1,3,5-trimethylbenzene by cyclohexene at 353 K.

However, for the reaction of a nitrile and an alcohol in an excess of water, Cs2.5 was the most active as shown in Table 4.[45]

5 Efficient catalysts developed based on HPA

Table 5 lists recent examples of catalytic reactions using solid HPA. Earlier examples may be found in ref. 5(*b*).

Table 4 Comparison of catalytic activities of various solid acids for the reaction of acrylnitrile and *N*-adamantanol to form *N*-adamantylacrylamide (NAA) in the presence of an excess of water.[a] Results in the absence of water shown in parentheses

Catalyst	Yield[b](%)	Selectivity[c](%)	TON[d]
$Cs_{2.5}H_{0.5}PW_{12}O_{40}$	84 (97)	92 (93)	36 (42)
HY zeolite	8 (79)	82 (89)	2 (0.2)
Amberlyst 15	68 (100)	82 (81)	1 (1)
Nafion-H	77 (97)	84 (92)	6 (8)
Nafion-SiO_2	40 (97)	94 (93)	22 (61)

[a] *Reaction conditions*; catalyst: 0.2 g, acrylnitrile: 60 mmol, 1-adamantanol: 1.3 mmol, 373 K, 6 h. [b] % Yield; 100 × (NAA formed)/(*N*-adamantanol added). [c] % Selectivity; 100 × (NAA formed)/(NAA formed + acrylamide formed). [d] TON (turnover number); mol NAA formed/mol acid sites in catalyst.

5.1 Bifunctional catalysts

HPAs show acidity as well as unique basicity; these properties as well as their oxidizing ability can be controlled over a wide range which is of use in catalyst design. The co-existence of these properties can be utilized to prepare bifunctional and multifunctional catalysts. It has been shown that the oxidation of methacrolein to methacrylic acid proceeds in two steps; the first step is acid-catalyzed esterification to form an intermediate and the second step the oxidation of the intermediate which is rate-determining. Hence this reaction can be catalyzed in a synergistic manner utilizing acidity and oxidizing ability.[7] It is interesting to note that these two properties compete in the case of oxidation of isobutyric acid to methacrylic acid, with acidity accelerating side-reactions (Scheme 2).

The much higher activity of Cs2.5 than conventional solid acids can not be explained by acidic properties alone [Fig. 3(c)], so that acid–base bifunctional catalysis was suggested for Cs2.5.[5b]

Efficient catalytic reactions can be realized by the combination of HPA catalysts with noble metals. One-stage oxidation of ethylene to acetic acid has been commercialized (10000 ton yr^{-1}) by combining a Keggin-type HPA catalyst and Pd.[46] Here, the addition of Se or Te to Pd is essential to suppress the complete oxidation to CO_2. The overall reaction [eqn. (6)] is suggested to proceed in two steps [eqn. (4) and (5)], a Wacker-type mechanism (*via* acetaldehyde) being excluded. Control of acidity and tertiary structure was important for catalyst

Table 5 Acid-catalyzed reactions with solid heteropoly compounds[a]

Reaction	Catalyst	Reference
$RCO_2H + R'OH \rightarrow RCO_2R'$	$H_3PW_{12}O_{40}$, $H_4SiW_{12}O_{40}$/MCM-41	59
Alkylation of alkylphenol by isobutylene (shape selective)	$H_3PW_{12}O_{40}$/MCM-41	53*b*
Trioxane + phenol	Silica-included $H_3PW_{12}O_{40}$	60
Isobutane + n-butenes $\rightarrow$ C_8 alkylates	$H_3PW_{12}O_{40}$/MCM-41	61
	$K_{2.6}H_{0.4}PW_{12}O_{40}$ (supercritical)	62
Diels–Alder reaction of quinone	$H_3PW_{12}O_{40}$	63
Acylation of xylene	$Cs_2HPW_{12}O_{40}$	53*a*
Adamantylamide synthesis	$Cs_{2.5}H_{0.5}PW_{12}O_{40}$	45
Hydration of dimethylbutene	$Cs_{2.5}H_{0.5}PW_{12}O_{40}$	44*a*
n-C_n $\rightarrow$ iso-C_n	$(NH_4,Cs,H)_3PW_{12}O_{40}$ Pt-$Cs_{2.5}H_{0.5}PW_{12}O_{40}$	64
Oxidation of ethylene to acetic acid *via* ethanol	Pd(Te)-$SiW_{12}O_{40}$ (commercialized)	46
Ethyl acetate from acetic acid	HPA (commercialized)	
Michael addition	$H_3PW_{12}O_{40}$ (pseudoliquid)	16*a*
$EtC(CH_2OH)_2CH_2OCH_2OCH_2C(CH_2OH)_2Et + H_2O \rightarrow 2EtC(CH_2OH)_2CH_2OH + HCHO$	$H_3PW_{12}O_{40}$, *etc*. (a new phase?)	14

[a] These reactions are mostly taken from a list produced by Professor T. Okuhara.

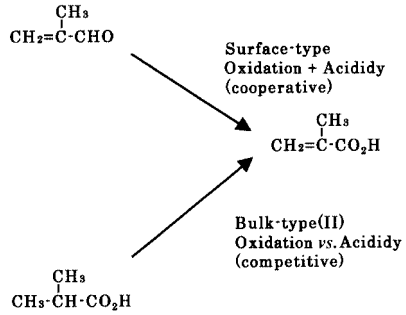

Scheme 2

development. (The photo on the cover is the plant used for this process developed by Showa Danko, Co., Ltd.)

$C_2H_4 + H_2O \rightarrow EtOH$ (acid catalysis) (4)

$EtOH + O_2 \rightarrow MeCO_2H + H_2O$ (oxidation) (5)

$C_2H_4 + O_2 \rightarrow MeCO_2H$ [overall reaction] (6)

The combination of Pd or Pt with Cs2.5 creates active and selective catalysts for the isomerization of *n*-alkanes (C_4–C_7).[47] Deactivation and cracking which are significantly observed over Cs2.5 alone are dramatically diminished by the addition of noble metals in the presence of H_2. Without acidity, the activity is very low. Interestingly, acidity completely prevents the hydrogenolysis of alkanes catalyzed by noble metals. A mechanism essentially based on a classical bifunctional catalysis has been proposed; acid catalyzed isomerization + dehydrogenation–hydrogenation. Recently, a mechanistic study using ^{13}C labeled *n*-butane[48] has revealed that the selective isomerization to isobutane over Pt dispersed on Cs2.5 mostly takes place by a monomolecular mechanism, while the reaction proceeds less selectively *via* a bimolecular mechanism in the case of Cs2.5 alone (Scheme 3). At higher reaction temperatures, the

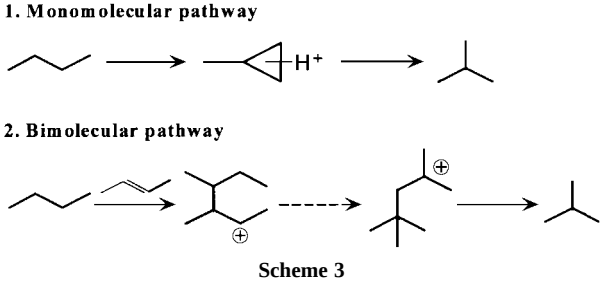

Scheme 3

contribution of the bimolecular mechanism increases also for Pt-Cs2.5. Kozhevnikov and coworkers reported that HPW combined with Pd produces only soft coke in the oligomerization of propene and the removal of coke by combustion takes place at a much lower temperature than in the case of HPW alone which forms both soft and hard cokes.[49]

5.2 Supported HPA catalysts

Hydrogen forms (or free acids) of HPAs usually have low surface areas. On the other hand, very active Cs2.5 having a large surface area tends to become a milky suspension during liquid-phase reactions, which makes it difficult to separate the catalyst after the reaction is finished. To solve these problems, many attempts have been made to disperse and fix HPA catalysts on various supports, where the stability of the HPA and firm fixation are the key issues. Support materials such as silica, carbon, and organic resins have been applied with varying levels of success, with new supporting materials and methods being actively pursued. Although the structure and composition of supported HPAs are sometimes uncertain, high catalytic activities are often observed and separation made easier.

Izumi *et al*, prepared HPW and Cs2.5 included in a silica matrix by an *in situ* sol–gel method. Recently, shape selectivity was observed for alkylation of phenol by formaldehyde owing to the micropores of a silica matrix.[50] Supported HPAs prepared by this method have been applied as photocatalysts.[51] Soled *et al*. reported an *in situ* preparation of Cs2.5 inside silica particles.[52] Cs-containing silica is added to an aqueous solution of HPA. As the HPA solution diffuses into pores of silica, a Cs salt starts to precipitate at a certain level of concentration, resulting in an egg-yolk type impregnation. Large-pore zeolites like MCM-41[53] and layered clays[54] have been applied as supports of HPA. HPAs loaded in layered double hydroxide were active for epoxidation and showed shape selectivity.[54] *In situ* synthesis of HPAs in the supercage of Y-zeolite is an interesting method for the preparation of supported HPA catalysts.[55] For metal oxide supports, interactions between the surface and the HPA often degrade the polyanion structure. On basic solids such as MgO and Al_2O_3, the Keggin structure readily decomposes, as expected from instability of HPAs in aqueous solution at high pH. Even on the surface of silica, which has only weak interactions with HPAs, these tend to decompose to smaller clusters. In most cases the decomposition is significant at a low loading level whereas the starting polyanion structure is predominant when the loading level is high. Supporting on or imbedding in organic polymers has also been attempted. Recent examples include polyazamethines,[56*a*] polyaniline,[56*b*] and polyphenylene oxide.[56*c*] As expected from

the moderate stabilities of organic ammonium and oxonium salts, the HPA structures appear to remain mostly intact. In addition, chemical interactions between the polymer and HPA sometimes modify the catalytic performance in a desirable manner.

6 Future

Notable progress has been achieved recently in heterogeneous acid catalytic reactions of HPAs. Full utilization of the pseudo-liquid phase and further development of bifunctional and shape-selective catalysis will be interesting targets for the future. Specifically organized secondary and tertiary structures that are synthesized by using novel cations and polyanions may open up new areas of catalysis. If the structure, composition and stability of polyanions are properly controlled on supports, solid HPA catalysts will find much wider practical applications. The development of regeneration methods for deactivated HPA catalysts is another important subject for practical applications. As for catalysis in solution, unconventional reaction fields such as multi-phase catalysis are promising. From the viewpoint of fundamental study of HPA catalysis, the basicity of the surface of the heteropolyanion (or unique complexation character) together with its role in catalysis is of interest and understanding of the catalytic reaction at the molecular/atomic level is expected to be accomplished in the near future.

More progress is anticipated for oxidation catalysis of HPAs although oxidation catalysis lies outside the scope of the present article. The design of primary structures (structure and composition) has been successful for oxidation in solution and may be extended to heterogeneous catalysis, if HPAs are stabilized or reaction systems chosen carefully. Examples include diiron and dimanganese substsituted Keggin anions as shown in Fig. 1(c)[57] which efficiently catalyze selective oxidation of alkanes, although enhancement of reaction rate is still desirable. A variety of polyanion structures and compositions (new and known) as well as recent progress in novel synthetic methods promises the development of efficient catalysts based on HPAs. For example, an exotic HPA synthesized by Newmann and Dahan is efficient in selective oxidation.[58] Owing to various advantages, HPAs are hoped to play important roles as green catalysts in chemical syntheses in a sustainable manner.

Acknowledgements

Useful discussions with Profs. T. Okuhara, K. Inumaru, and N. Mizuno, Drs. G. Koyano and T. Ito, and Ms. S. Uchida are gratefully acknowledged. Thanks is given to Showa Denko Co. Ltd. for permitting the use of the photo of the Plant (cover).

Notes and references

1 J. M. Thomas, *Angew. Chem., Int. Ed.*, 1988, **27**, 1673.
2 M. Misono, *Stud. Surf. Sci. Catal.*, 1990, **54**, 13.
3 C. L. Hill, ed., *Chem. Rev.*, 1998, **98** (1).
4 See, for example: G. A. Tsigdinos, *Top. Curr. Chem.*, 1978, **76**, 1; M. T. Pope, *Heteropoly and Isopoly Oxometalates*, Springer-Verlag, Berlin, 1983.
5 See, for example: (*a*) M. Misono, *Catal. Rev.-Sci. Eng.*, 1987, **29**, 269; M. Misono, 1988, **30**, 339; (*b*) T. Okuhara, N. Mizuno and M. Misono, *Adv. Catal.*, 1996, **41**, 113; (*c*) N. Mizuno and M. Misono, *Chem. Rev.*, 1998, **98**, 199; (*d*) I. V. Kozhevnikov and K. I. Matveev, *Appl. Catal.*, 1983, **5**, 135; (*e*) I. V. Kozhevnikov, *Chem. Rev.*, 1998, **98**, 171; (*f*) Y. Izumi, K. Urabe and A. Onaka, *Zeolite, Clay, and Heteropoly acids in Organic Reactions*, Kodansha, Tokyo, VCH, Weinheim, 1992; (*g*) Y. Ono, in *Perspectives on Catalysis*, ed. J. M. Thomas and K. I. Zamaraev, Blackwell, London, 1992, p. 341; (*h*) A. Corma, *Chem. Rev.*, 1995, **95**, 559.
6 M. Misono and N. Nojiri, *Appl. Catal.*, 1990, **64**, 1; N. Nojiri and M. Misono, *Appl. Catal.*, 1993, **93**, 103.
7 M. Misono, K. Sakata, Y. Yoneda and W. Y. Lee, *Proc. 7th Int. Congr. Catal., Tokyo*, 1980, p. 1047.
8 M. Misono, *Proc. 10th Int. Congr. Catal., Budapest*, 1992, p. 69, Elsevier, Amsterdam/Akademiai Kiado, Budapest, 1993.
9 T. Komaya and M. Misono, *Chem. Lett.*, 1983, 1177; N. Mizuno, T. Watanabe and M. Misono, *J. Phys. Chem.*, 1990, **94**, 890.
10 T. Okuhara, A. Kasai, N. Hayakawa, Y. Yoneda and M. Misono, *J. Catal.*, 1983, **83**, 121.
11 S. Tatematsu, T. Hibi, T. Okuhara and M. Misono, *Chem. Lett.*, 1980, 865.
12 T. Okuhara, T. Nishimura, H. Watanabe, K. Na and M. Misono, in *Acid-Base Catalysis II*, Kodansha, Tokyo/Elsevier, Amsterdam, 1994, p 419.
13 M. Misono, N. Mizuno, H. Mori, K. Y. Lee and J. Jiao, *Stud. Surf. Sci. Catal.*, 1991, **67**, 87.
14 M. Misono, I. Ono, G. Koyano and A. Aoshima, *Pure Appl. Chem.*, 2000, **72**, 1305.
15 M. Misono, *C. R. Acad. Sci. Paris, Ser. IIc, Chim.*, 2000, **3**, 471.
16 (*a*) T. Kengaku, Y. Matsumoto, K. Na and M. Misono, *J. Mol. Catal.*, 1998, **134**, 237; (*b*) G. Koyano, K. Ueno and M. Misono, *Appl. Catal. A: Gen.*, 1999, **181**, 267.
17 Y. Toyoshi, T. Nakato and T. Okuhara, *Bull. Chem Soc. Jpn.*, 1998, **71**, 2817.
18 (*a*) S. Shikata and M. Misono, *Chem. Commun.*, 1998, 1293; (*b*) S. Shikata, T. Okuhara and M. Misono, *J. Mol. Catal. A: Chem.*, 1995, **100**, 49.
19 A. Malecka, J. Pozniczek, A. Micek-Ilnicka and A. Bielanski, *J. Mol. Catal. A: Chem.*, 1999, **138**, 67.
20 (*a*) T. Saito, G. Koyanao and M. Misono, *Chem. Lett.*, 1998, 1075; (*b*) G. Koyano, T. Saito, M. Hashimoto and M. Misono, *Stud. Surf. Sci. Catal.*, 2000, **130**, 3077.
21 C. Peze, S. Bordiga and A. Zecchina, *Langmuir*, 2000, **16**, 8139.
22 S. Uchida, K. Inumaru and M. Misono, *J. Phys. Chem. B*, 2000, **104**, 8108.
23 T. Okuhara, T. Nishimura and M. Misono, *Stud. Surf. Sci. Catal.*, 1996, **101**, 559.
24 R. S. Drago, J. A. Dias and T. O. Maier, *J. Am. Chem. Soc.*, 1997, **119**, 7702.
25 T. Okuhara, H. Watanabe, T. Nishimura, K. Inumaru and M. Misono, *Chem. Mater.*, 2000, **12**, 2230.
26 B. B. Bardin, S. V. Bordaweker, M. Neurock and R. J. Davis, *J. Phys. Chem. B*, 1998, **102**, 10817.
27 J. B. Moffat, *J. Mol. Catal.*, 1984, **26**, 385; H. Taketa, S. Katsuki, K. Eguchi, T. Seiyama and N. Yamazoe, *J. Phys. Chem.*, 1986, **90**, 2959.
28 T. T. Ali-Saad, A. A. El-Smahy, R. M. Gabr, R. V. Belosludov, S. Takami, M. Kubo, A. Miyamoto and M. Misono, *87th Symp. Catal. Soc. Jpn.*, April, 2001.
29 (*a*) T. Baba and Y. Ono, *Appl. Catal.*, 1999, **181**, 227; (*b*) T. Baba, Y. Hasada, M. Nomura, Y. Ohono and Y. Ono, *J. Mol. Catal.*, 1996, **114**, 247; (*c*) T. Baba, N. Komatsu, H. Sawada, Y. Yamada, T. Takahashi, H. Sugisawa and Y. Ono, *Langmuir*, 1999, **15**, 7894.
30 M. Guisnet, Ph. Bichon, N. S. Gnep and N. Essayem, *Top. Catal.*, 2000, **11/12**, 247.
31 T. Okuhara and T. Nakato, *Catal. Surv. Jpn.*, 1998, **2**, 31.
32 Y. Izumi, M. Ogawa and K. Urabe, *Appl. Catal.*, 1995, **132**, 127.
33 A. Parent and J. B. Moffat, *J. Catal.*, 1998, **177**, 335.
34 T. Ito, K. Inumaru and M. Misono, *Chem. Mater.*, 2001, **13**, 824.
35 T. Yamada, Y. Yoshinaga and T. Okuhara, *Bull. Chem. Soc. Jpn.*, 1998, **71**, 2727.
36 S. Berndt, D. Herein, F. Zemlin, E. Beckmann, G. Weinberg, J. Schutze, G. Metsl and R. Schlogl, *Ber. Bunsen-Ges. Phys. Chem.*, 1998, **102**, 763.
37 K. Inumaru, H. Nakajima, T. Ito and M. Misono, *Chem. Lett.*, 1996, 559; T. Oto, I. K. Song and M. Misono, *Chem. Lett.*, 1997, 727.
38 T. Ito, K. Inumaru and M. Misono, *J. Phys. Chem. B*, 1997, **101**, 9958.
39 T. Ito, K. Inumaru and M. Misono, *Chem. Lett.*, 2000, 830.
40 Y. Yoshinaga, K. Seki, T. Nakato and T. Okuhara, *Angew. Chem., Int. Ed. Engl.*, 1997, **36**, 2833; T. Okuhara, T. Yamada, K. Seki, K. Johkan and T. Nakato, *Microporous Mesoporous Mater.*, 1998, **21**, 637.
41 T. Okuhara, R. Watanabe and Y. Yoshinaga, *ACS Symp. Ser.*, 2000, **758**, 369.
42 N. Mizuno, K. Inumaru and M. Misono, *Hyoumen Kagakkaishi*, 1989, **10**, 21.
43 T. Yamada and T. Okuhara, *Langmuir*, 2000, **16**, 2321.
44 (*a*) T. Okuhara, M. Kimura and T. Nakato, *Chem. Lett.*, 1997, 839; (*b*) T. Nakato, M. Kimura, S. Nakata and T. Okuhara, *Langmuir*, 1998, **14**, 319.
45 T. Okuhara, X. Chen and H. Matsuda, *Appl. Catal. A: Gen.*, 2000, **200**, 109.

46 K. Sano, H. Uchida and S. Wakabayashi, *Catal. Surv. Jpn.*, 1999, **3**, 55.
47 K. Na, T. Okuhara and M. Misono, 1997, **170**, 96; K. Na, T. Okuhara and M. Misono, *J. Mol. Catal.*, 1997, **115**, 499; Y. Liu, G. Koyano and M. Misono, *Top. Catal.*, 2000, **11**/**12**, 239.
48 T. Suzuki and T. Okuhara, *Chem. Lett.*, 2000, 470; T. Sazuki and T. Okuhara, *Catal. Lett.*, in press.
49 M. R. H. Siddiqui, S. Holmes, H. He, W. Smith, E. N. Coker and I. V. Kozhevnikov, *Catal. Lett.*, 2000, **66**, 53.
50 Y. Izumi, M. Ono, M. Ogawa and K. Urabe, *Chem. Lett.*, 1993, 825; Y. Izumi, K. Hisano and T. Hida, *Appl. Catal. A: Gen.*, 1999, **181**, 277.
51 Y. Guo, Y. Wang, C. Hu, Y. Wang and E. Wang, *Chem. Mater.*, 2000, **12**, 3501.
52 S. Soled, S. Miseo, G. McVicker, W. E. Gates, A. Gutierrez and J. Paes, *Catal. Today*, 1997, **36**, 441.
53 (*a*) C. De. Castro, J. Primo and A. Corma, *J. Mol. Catal. A: Chem.*, 1998, **134**, 215; (*b*) I. V. Kozhevnikov, A. Sinnema, R. J. J. Jansen, K. Pamin and H. van Bekkum, *Catal. Lett.*, 1995, **30**, 241.
54 (*a*) Y. Watanabe, K. Yamamoto and T. Tatsumi, *J. Mol. Catal. A: Gen.*, 1999, **145**, 281; (*b*) T. Tatsumi, K. Yamamoto, H. Tajima and H. Tominaga, *Chem. Lett.*, 1992, 816.
55 B. Sulikowski, J. Haber, A. Kubacka, K. Pamin, Z. Olejniczak and J. Ptaszynski, *Catal. Lett.*, 1996, **39**, 27; S. Mukai, T. Masuda, I. Ogino and K. Hashimoto, *Appl. Catal. A: Gen.*, 1997, **165**, 219.
56 (*a*) W. Turek, E. S. Pormarzanska, A. Pron and J. Haber, *J. Catal.*, 2000, **189**, 297; (*b*) A. Bielanski, R. Dziembaj and A. Malecka, *J. Catal.*, 1999, **185**, 363; (*c*) S. L. Lim, Y. H. Kim, G. I. Park, W. Y. Lee, I. K. Song and H. K. Youn, *Catal. Lett.*, 1999, **60**, 199.
57 N. Mizuno, C. Nozaki, I. Kiyoto and M. Misono, *J. Am. Chem. Soc.*, 1998, **120**, 9267.
58 R. Neumann and M. Dahan, *Nature*, 1997, **388**, 353.
59 M. J. Verhoef, P. J. Kooyman, J. A. Peters and H. van Bekkum, *Microporous Mesoporous Mater.*, 1999, **27**, 365.
60 Y. Izumi, K. Hisano and T. Hida, *Appl. Catal A: Gen.*, 1999, **181**, 277.
61 T. Blasco, A. Corma, A. Martinez and P. Martinez-Escolano, *J. Catal.*, 1998, **177**, 306.
62 P. Y. Gayraud, I. H. Stewart, S. B. Deroune-Abd Hamid, N. Essayem, E. G. Derouane and J. C. Vedrine, *Catal. Today*, 2000, **63**, 223.
63 G. Meuzelaar, L. Maat, R. Sheldon and I. V. Kozhevnikov, *Catal. Lett.*, 1997, **45**, 249.
64 A. Corma, A. Martinez and C. Martinez, *J. Catal.*, 1996, **164**, 422; N. Essayem, S. Keiger, G. Coudurier and J. C. Vedrine, *Stud, Surf. Sci. Catal.*, 1996, **101**, 591; B. B. Bardin and R. Davis, *Top. Catal.*, 1998, **6**, 77; K. Na, T. Okuhara and M. Misono, *J. Catal.*, 1997, **170**, 96; Y. Liu, K. Na and M. Misono, *J. Mol. Catal. A: Chem.*, 1999, **141**, 145; Y. Liu, G. Koyano and M. Misono, *Top. Catal.*, 2000, **11**/**12**, 239; C. Travers, N. Essayem, M. Delage and S. Quelen, *Catal. Today*, 2000, **65**, 355.

CHEMCOMM
Communication
www.rsc.org/chemcomm

Rhodium bis-phosphine catalysts on mesoporous silica supports: new highly efficient catalysts for the hydrogenation of alkenes†‡

Cathleen M. Crudden,* Daryl Allen, Michael D. Mikoluk and Jian Sun

Department of Chemistry, University of New Brunswick, Fredericton, New Brunswick, P.O. Box 45222, Canada, E3B 6E2. E-mail: Cruddenc@unb.ca

Received (in Corvallis, OR, USA) 9th March 2001, Accepted 27th April 2001
First published as an Advance Article on the web 7th June 2001

A bidentate rhodium phosphine complex anchored onto a mesoporous molecular sieve was shown to be an active catalyst for the hydrogenation of alkenes, with the activity dependent on the method of grafting, and in general, exceeding that of related homogeneous catalysts.

Remarkable developments in homogeneous catalysis have taken place over the past two decades.[1] Unfortunately, the recovery of the precious metals and expensive ligands from the reaction medium is often not feasible. For this reason, there have been many approaches to 'heterogenizing' homogeneous catalysts by attaching well defined molecular species to polymeric supports.[2] Despite the development of some very effective supported systems,[3] a general strategy for mimicking solution phase behaviour is yet to be developed. Reactions on supports are generally slower and less predictable than their solution counterparts, commonly requiring excesses of reagents, higher temperatures and longer reaction times.[4]

The discovery of mesoporous molecular sieves has provided new possibilities in catalysis.[5] These mesoporous materials have unique structures characterized by high surface areas, large pores, and high long-range order; properties that make them ideal catalyst supports. MCM-41-type silicates have been used as supports for a variety of metals and metal complexes.[6] Recently, Shyu *et al.* described a supported analogue of Wilkinson's catalyst, prepared by treating MCM-41 with $(EtO)_3Si$-$(CH_2)_3$-PPh_2 and then $RhCl(PPh_3)_3$.[7] Our approach to the preparation of a Rh complex supported on a mesoporous molecular sieve involves the use of a bidentate phosphine in order to minimize leaching, and a cationic complex to prevent dimerization through chloride bridges[8] (Fig. 1). The catalysts thus obtained are highly active for the hydrogenation of olefins, even more than the corresponding homogeneous complexes. The magnitude of the activity and the nature of the grafted species is strongly dependent on the method of grafting. To the best of our knowledge, this is the first report of a bidentate rhodium phosphine complex grafted onto a mesoporous molecular sieve.

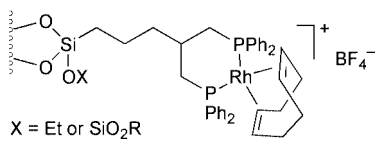

Fig. 1 Supported Rh catalyst.

Catalyst **1** is prepared as shown in Scheme 1.[9] Alkylation of diethyl malonate with allyl bromide (89% yield) and reduction of the ester groups with $LiAlH_4$ (69% yield) provides diol **2**. Treatment of **2** with PPh_3 in CCl_4 followed by hydrosilylation of the pendant olefin using H_2PtCl_6 yields **3**. The phosphine substituents were introduced using Ph_2PLi, and protected prior to isolation. Compound **4** was purified by flash chromatography and then deprotected with morpholine. Treatment with $[Rh(COD)(THF)_2]^+BF_4^-$§ generated the homogeneous Rh complex **1**. This was spectroscopically characterized and then grafted onto the surface of a molecular sieve (SBA-15-type)[5] at 25, 110 and 165 °C (method A). Grafting was also carried out in the presence of an inert spacer, $EtSi(OEt)_3$ (method B).[10] The resulting catalysts were characterized by MAS NMR, TEM, and nitrogen adsorption.

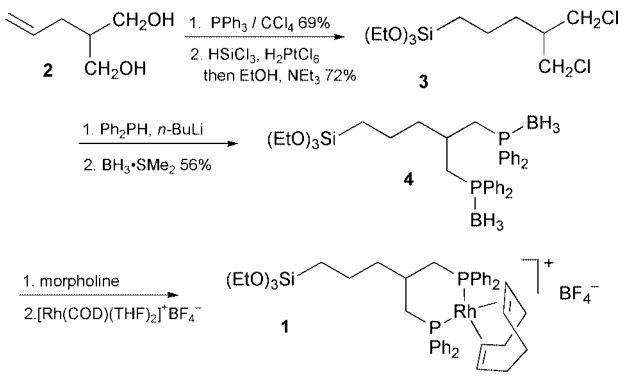

Scheme 1 Synthesis of Rh catalyst **1**.

^{31}P MAS NMR analysis of these materials revealed that as the grafting temperature was increased, the resonance at 14 ppm which corresponded to the homogeneous complex **1** (Fig. 2A) decreased while a new peak at 35 ppm, attributable to a P(V) species, appeared.[11] When the complex was grafted in refluxing mesitylene, the resulting material (**1-mps-165A**) was composed entirely of the P(V) species (Fig. 2B). Grafting in the presence of an inert spacer (method B) proved to be optimal (Fig. 2B).

The various Rh complexes were examined for their ability to catalyze the hydrogenation of isosafrole (**5**), Table 1.¶ With the exception of **1-mps-25A**, all the mesoporous catalysts tested are *more active than the corresponding homogeneous catalysts* (entries 1, 2).

Catalyst **1-mps-25B**, prepared in the presence of $EtSi(OEt)_3$, has the highest activity (3300 turnovers h^{-1}, entry 6). These results are consistent with the results of Shyu,[7] who found that their MCM-41-modified catalyst was *ca.* 3× more active than Wilkinson's catalyst. Since **1-mps-25B** also had the lowest loading on support, the increased activity may be due to site isolation.[12] The least active catalyst of those examined, **1-mps-25A**, also has the highest Rh loading of 2.0%, consistent with this postulate. Studies are currently underway to measure the proximity of the Rh complexes on support.[12] Simple mixing of $[Rh(COD)_2]^+BF_4^-$ with the mesoporous support in the absence of any phosphine also led to an active hydrogenation catalyst (entry 7). The presence of an intermediate heteropoly acid species to aid in adsorption was not found to be necessary in this case.[13]

Retention of Rh on the surface was also a function of the grafting method. Supported systems with lower loadings of Rh were found to be more prone to leaching as determined by ICP-

† Electronic supplementary information (ESI) available: NMR data. See http://www.rsc.org/suppdata/cc/b1/b102355c/

‡ Presented in part: 80th Canadian Society for Chemistry conference, Whistler, B.C., June, 1998.

 DOI: 10.1039/b102355c

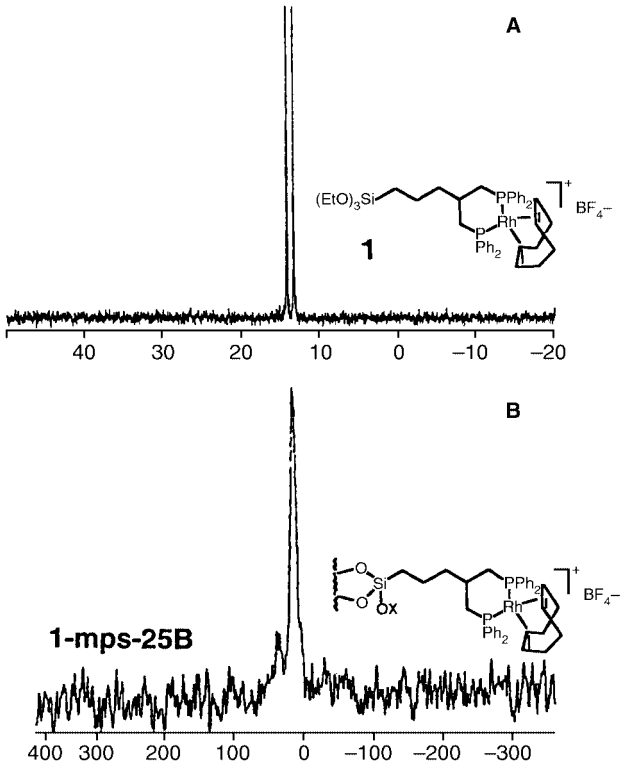

Fig. 2 ^{31}P NMR of homogeneous (**A**) supported (**B**) Rh complexes.

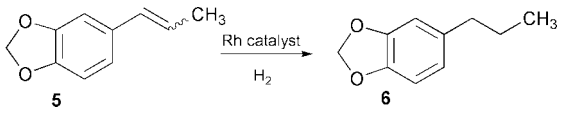

Table 1 Hydrogenation of **5**[a]

Entry	Catalyst[b]	Loading on support[c]	Turnover Frequency[d]
1	**Rh$^+$/DPPP**	n.a.	350
2	**1**	n.a.	750
3	**1-mps-110A**	1.4%	> 1600
4	**1-mps-25A**	2.0%	200
5	**1-mps-165A**	1.4%	1030
6	**1-mps-25B**	0.34%	3300
7	**Rh$^+$/mps**	3.3%	2300

[a] All reactions were carried out at rt, 750 psi of H_2, $[substrate]_{init}$ = 0.06 M in dry, deoxygenated, distilled THF. Reaction times were between 30 and 90 min. Solutions were prepared in a glove box under argon. [b] mps = mesoporous silicate. [c] Wt%, determined by ICP MS analysis. [d] Turnovers per hour.

MS analysis of the reaction mixture after filtration through a nylon filter. Catalyst **1-mps-25B** (0.3% Rh by weight) lost a significant amount of Rh after the first use (21–36%) and less (*ca.* 5%) in subsequent runs. Catalyst **1-mps-110A** (1.4% Rh by weight) was much more robust, and lost only 2–3% Rh during the first run.

In conclusion, we have demonstrated that rhodium complexes heterogenized on mesoporous molecular sieves are highly active catalysts for the hydrogenation of olefins. With one exception (**1-mps-25A**), the supported complexes are all more active than the corresponding homogeneous catalysts.

Dr Robert Young and Merck & Company are thanked for their generous support of this research, along with the Natural Sciences and Engineering Research Council of Canada (NSERC) and the Canada Foundation for Innovation (CFI). Michael Lumsden of Dalhousie University is thanked for the MAS NMR data. Professor Stephen Bergens is thanked for helpful discussions and an anonymous reviewer is thanked for very valuable suggestions.

Notes and references

§ Prepared by treatment of $[Rh(COD)Cl]_2$ in THF with $AgBF_4$ and filtration of the resulting solution through Celite-545 (not acid washed).
¶ Isosafrole was purified by column chromatography, distillation, deoxygenated with three freeze, pump, thaw cycles, and purified immediately prior to use by passage through a short plug of dry alumina. The catalyst was found to be extremely sensitive to trace amounts of oxygen and deactivates with time, even when stored in a glove box.

1 R. Noyori, *Asymmetric Catalysis in Organic Synthesis*, John Wiley & Sons, Inc., New York, 1994; I. Ojima, *Catalytic Asymmetric Synthesis*, VCH Publishers, New York, 1993.
2 D. C. Bailey and S. H. Langer, *Chem. Rev.*, 1981, **81**, 109; C. U. Pittman, Jr., in *Comprehensive Organometallic Chemistry*, ed. G. Wilkinson, Pergamon, Oxford, 1982, Vol. 8, 553; S. C. Bourque, H. Alper, L. E. Manzer and P. Arya, *J. Am. Chem. Soc.*, 2000, **122**, 956.
3 C. Bianchini, D. G. Burnaby, J. Evans, P. Frediani, A. Meli, W. Oberhauser, R. Psaro, L. Sordelli and F. Vizza, *J. Am. Chem. Soc.*, 1999, **121**, 5961; H.-B. Yu, Q.-S. G. Hu and L. Pu, *Tetrahedron Lett.*, 2000, **41**, 1681; H. Gao and R. J. Angelici, *J. Mol. Catal.*, 1999, **149**, 63; K. Nozaki, Y. Itoi, F. Shibahara, E. Shirakawa, T. Ohta, H. Takaya and T. Hiyama, *J. Am. Chem. Soc.*, 1998, **120**, 4051; A. Corma, M. Iglesias, C. del Pino and F. Sanchez, *J. Chem. Soc., Chem. Commun.*, 1991, 1253; S. Itsuno, K. Kamahori, K. Watanabe, T. Koizumi and K. Ito, *Tetrahedron: Asymmetry*, 1994, **5**, 523; H. Brunner and J. C. Bailar, Jr., *Inorg. Chem.*, 1973, **12**, 1465; B. M. Trost and E. Keinan, *J. Am. Chem. Soc.*, 1978, **100**, 7779; J. Collman, L. Hegedus, M. Cokke, J. Norton, G. Dolcetti and D. Marquardt, *J. Am. Chem. Soc.*, 1972, **94**, 1789.
4 D. J. Gravert and K. D. Janda, *Chem. Rev.*, 1997, **97**, 489 and references cited therein; R. H. Grubbs and L. C. Kroll, *J. Am. Chem. Soc.*, 1971, **93**, 3062.
5 C. T. Kresge, M. E. Leonowicz, W. J. Roth, J. C. Vartuli and J. S. Beck, *Nature*, 1992, **359**, 710; D. Zhao, Q. Huo, J. Feng, B. F. Chmelka and G. D. Stucky, *J. Am. Chem. Soc.*, 1998, **120**, 6024.
6 P. Sutra and D. Brunel, *Chem. Commun.*, 1996, 2485; Y. V. S. Rao, D. E. De Vos, T. Bein and P. A. Jacobs, *Chem. Commun.*, 1997, 355; C.-J. Liu, S.-G. Li, W.-Q. Pang and C.-M. Che, *Chem. Commun.*, 1997, 65; T. Maschmeyer, R. D. Oldroyd, G. Dankar, J. M. Thomas, I. J. Shannon, J. A. Klepetko, A. F. Masters, J. K. Beattie and C. R. A. Catlow, *Angew. Chem., Int. Ed. Engl.*, 1997, **36**, 1639; B. F. G. Johnson, S. A. Raynor, D. S. Shephard, T. Maschmeyer, J. M. Thomas, G. Sankar, S. Bromley, R. Oldroyd, L. Gladden and M. D. Mantle, *Chem. Commun.*, 1999, 1167; L. Zhang, T. Sun and J. Y. Ying, *Chem. Commun.*, 1999, 1103; K. Kageyama, J.-I. Tamazawa and T. Aida, *Science*, 1999, **285**, 2113; For an excellent review of catalytic applications in general see: J. Y. Ying, C. P. Mehnert and M. S. Wong, *Angew. Chem., Int. Ed. Engl.*, 1999, **38**, 56.
7 S.-G. Shyu, S.-W. Cheng and D.-L. Tzou, *Chem. Commun.*, 1999, 2337.
8 J. A. Osborn, F. H. Jardine, J. F. Young and G. Wilkinson, *J. Chem. Soc. A*, 1966, 1711.
9 E. Lindner, A. Enderle and A. Baumann, *J. Organomet. Chem.*, 1998, **555**, 247.
10 N. Bellocq, S. Abramson, M. Lasperas, D. Brunel and P. Moreau, *Tetrahedron: Asymmetry*, 1999, **10**, 3229.
11 L. Bemi, H. C. Clark, J. A. Davies, C. A. Fyfe and R. E. Wasylishen, *J. Am. Chem. Soc.*, 1982, **104**, 438; K. D. Behringer and J. Blumel, *Inorg. Chem.*, 1996, **35**, 1814.
12 J. P. Collman, J. A. Belmont and J. I. Brauman, *J. Am. Chem. Soc.*, 1983, **105**, 7288.
13 R. Augustine, S. Tanielyan, S. Anderson and H. Yang, *Chem. Commun.*, 1999, 1257; M. Burk, A. Gerlach and D. Semmeril, *J. Org. Chem.*, 2000, **65**, 8933.

CHEMCOMM
Communication
www.rsc.org/chemcomm

Preparation of a novel β-CD–dimanganese complex with covalently bound photosensitizer†

Nicole Van Hoof,[a] Tia E. Keyes,*[a] Robert J. Forster,[b] Andrea McNally[a] and Noel R. Russell*[a]

[a] *School of Chemistry, Dublin Institute of Technology, Kevin St., Dublin 8, Ireland. E-mail: tia.keyes@dit.ie*
[b] *School of Chemical Sciences, Dublin City University, Glasnevin, Dublin 9, Ireland*

Received (in Cambridge, UK) 17th April 2001, Accepted 3rd May 2001
First published as an Advance Article on the web 7th June 2001

The synthesis and structure of a novel donor–acceptor complex comprised of a photosensitising ruthenium polypyridyl moiety covalently linked to a β-cyclodextrin unit bearing a hydroxy-bridged manganese(III) dimer 1 is described; the dimanganese complex undergoes a photoinduced electron transfer and may represent an attractive model system for elucidating aspects of photosystem II.

The current interest in novel donor–acceptor systems capable of photoinduced charge separation is driven by applications such as biomimetic chemistry, charge storage devices and nanoelectronic components. Recently, a number of elegant systems have been developed,[1] employing flash-quench methods and sacrificial quenchers to mimic part of the photoinitiated processes leading to oxidation of water in photosystem II.[2] We aimed on the other hand to develop a system incorporating a dimanganese site, in which the excited state energy of the sensitiser was sufficient to drive the electron transfer without the need for sacrificial reagents.

In the approach outlined here we have developed a $Ru(bpy)_2$ sensitiser linked *via* a β-cyclodextrin bridge to a hydroxo bridged Mn(III) dimer (Scheme 1). This is the first report in which the donor and acceptor moieties are external to cyclodextrin which acts as the mediating bridge in the D–A system.

By employing the highly rigid CD bridge, the inter-site separation and relative orientation of the reactants is thought to be consistent with those estimated for photosytem II. Moreover, this system mimics an important feature of PSII in that up to 10 water molecules are included in the cyclodextrin. In the photosystem, water oxidation is thought to be thermodynamically promoted by association of water with the Mn sites.

Our synthetic strategy is outlined in Scheme 1. The chelating β-cyclodextrin phenanthroline ligand, was prepared by refluxing 5-amino-1,10-phenanthroline, NH_2phen,[3] with 6^A-deoxy-6^A-*O*-*p*-toluenesulfonyl-β-cyclodextrin[4] in NMP for 5 h, the product was purified *via* recrystallization and purity confirmed by ^{1}H NMR (ESI†). This ligand was then coordinated to $Ru(bpy)_2$, by reaction with *cis*-$Ru(bpy)_2Cl_2$. The progress of the reaction was monitored by cation exchange HPLC and **2** was purified by column chromatography, on neutral alumina with acetonitrile–methanol (1 : 2 v/v), and isolated as a dichloride salt prior to coordination of the dimanganese centre.

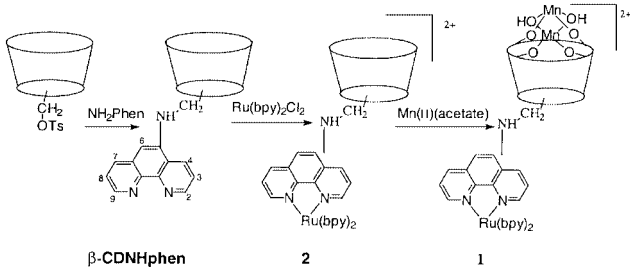

Scheme 1

The ability of β-CD to coordinate metals such as Zn(II), Cu(II), Co(II) and Mn(III) has been known for some time, the metals are proposed to bind as hydroxo bridged dimers to the CD *via* the secondary hydroxyls, O-2 and O-3 of adjacent pyranose rings.[5–7] Mn was shown previously to coordinate effectively to β-CD *via* oxidative addition, on stirring of $Mn(OAc)_2$ and β-CD in an ethanol–DMF mixture containing 0.2 mol dm^{-3} NaOH under an inert atmosphere. Following this procedure, as outlined by Nair and Dismukes,[6] **2** was employed in place of β-CD and the formation of a high yield (*ca.* 60%), of the dimanganese bound complex was observed. The reaction was followed by TLC as **1** was found to be unstable in the aqueous solution employed for HPLC. This complex is soluble but unstable in water decomposing to **2** within minutes. It is stable over weeks in DMF and DMSO. At pH > 9.5 the complex was observed to be stable in water for up to 30 min.

Purity and structural confirmation for ligands and complexes were obtained through cation exchange HPLC, one- and two-dimensional ^{1}H NMR (ESI†), elemental analysis (ESI†) and magnetic susceptibility studies.

The ^{1}H NMR spectrum of **2** reveals well-resolved signals between 6 and 10 ppm, integrating for the 23 protons associated with the $Ru(bpy)_2(NH_2phen)$ unit and a complex pattern of signals associated with the β-CD are observed between 3 and 5 ppm. The paramagnetic dimanganese centre causes significant broadening of the ^{1}H NMR spectrum for **1**. However bands associated with the $Ru(bpy)_2$ unit remained sharp because of their distance from the paramagnetic Mn(III) centres.

Coordination of the bridged Mn(III) sites to the cyclodextrin moiety is accompanied by the appearance or enhancement of prominent features in the FTIR spectrum between 1700 and 1200 cm^{-1} (ESI†). Such bands, ascribed to alterations in included water on coordination of the metal sites, and to the OH bridging groups are analogous to those described previously in the simple Mn_2CD complex and for other OH bridged metallocyclodextrins,[8,9] Their presence is consistent with coordination of the manganese site to the secondary 2- and 3-hydroxy sites on the β-CD.[9–11]

The effective magnetic moment of complex **1** was found to be 3.46 μ_B per Mn at 296 K which is lower than the anticipated value of 4.9 μ_B for the spin-only value for the high-spin d^4 electronic configuration of Mn(III), calculated on the basis that no magnetic interactions are occurring between the metal ions.[12] This value is however, consistent with that reported for Mn_2CD by Nair and Dismukes[6] for a weakly antiferromagnetically coupled OH bridged dimanganese(III) moiety, the (III) oxidation state of which was confirmed to be EPR silent.[13]

Exhaustive experiments were performed on **1** and **2** using positive and negative ion ES and FAB MS techniques. No identifiable molecular ions were observable for either complex, however, the results obtained from ES and FAB positive ion

† Electronic supplementary information (ESI) available: FTIR, NMR, UV–VIS, elemental analysis and CV data. See http://www.rsc.org/suppdata/cc/b1/b103363h/

 DOI: 10.1039/b103363h

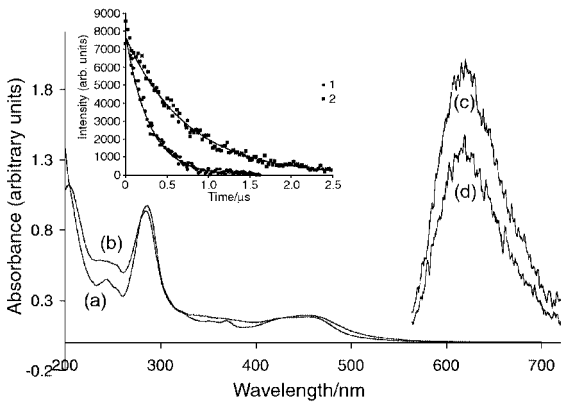

Fig. 1 Absorption of (a) **2** and (b) **1** and normalised emission spectra of (c) **1** and (d) **2** at room temperature in DMF, inset, emission decays of **1** and **2** at room temp. in DMF monitored at 620 nm and excited at 355 nm.

experiments showed the presence of many CD containing ions and also species such as $[Ru(bpy)_2(NHphen\beta\text{-}CD)Cl]^+$ (*m/z* 890) and $[Ru(bpy)_2(NHphen)]^+$ (*m/z* 608) were identified for both **1** and **2**. Although many of the spectra were far too weak to identify ions associated with the $Mn_2(OH)_2$ bridging system in **1** they do support the general structure of the ruthenium coordinated cyclodextrin species. The absorption and emission spectra of **1** and **2** are shown in Fig. 1, the main features in the visible region for both complexes are associated with Ru(II) to bpy charge transfer transitions, 450 nm for **1** ($\log \varepsilon = 4.15$) and 453 ($\log \varepsilon = 4.52$) for **2**. The strong similarity between the UV–VIS spectra of **1** and **2** is anticipated on the basis that the simple Mn_2CD shows a very weak transition at 480 nm, ($\log \varepsilon = 0.9$), which would be expected to have little impact on the strong CT transitions in the visible region. Significantly, no new features are present which would indicate ground state interactions across the molecule or that the manganese oxidation state is altered by comparison with Mn_2CD.

The formal potentials for the $Ru^{2+/3+}$ redox reaction are essentially indistinguishable in **1** and **2** (at 1.06 and 1.09 V *vs.* SCE respectively). Consistent with the spectroscopic data, this conformity suggests that there is little ground state interaction between the Ru and Mn sites. The Mn sites of **1** can be oxidised and reduced within an accessible potential window, with reduction appearing as a single electron step at −1.08 V and oxidation occurring as a single electron step at 1.41 V *vs.* Ag/AgCl. The electrochemical behaviour of Mn is scan rate dependent, under slower scan rate conditions, both $Mn^{2+/3+}$ and $Mn^{3+/4+}$ couples are irreversible. This is thought to be due to decomposition of the complex on formation of Mn(II) and Mn(IV). At faster scan rates (>1000 V s^{-1}) these redox processes become chemically reversible. Thus, while the oxidised state is not indefinitely stable thermodynamically, its lifetime is at least 40 μs.

This observation is important for photoinduced electron transfer and indicates that the Mn(IV) state will be stable if the time constant for back electron transfer is less than a few microseconds.

1 and **2** both emit at cryogenic and room temp. Although emission intensities and lifetimes at 77 K are comparable for **1** and **2**, at room temp. the luminescence of **1** is significantly reduced by binding of the manganese centre, as shown in Fig. 1. This behaviour is reflected by the luminescence quantum yield, where ϕ_{em} of **2**, 0.012, is reduced by 50% to 0.006 for **1** and also in the emission lifetime data (Fig. 1, inset), where the lifetime of **2** is reduced from 820 to 220 ns on coordination of the Mn_2 site. Calculation of the radiative and non-radiative rate constants for **1** and **2** reveals that the primary source of this decrease is a reduction in k_{nr} for **1**.

Assuming electron transfer is the source of quenching in **1,** we have used eqn. (1), where $\tau_{complex}$ is the emission lifetime of

$$k_{et} = (1/\tau_{complex}) - (1/\tau_{model}) \quad (1)$$

1 and τ_{model} the emission lifetime of a suitable structurally analogous model complex, in this case complex **2**, to estimate the electron transfer rate k_{et}, as 2×10^6 s^{-1}. Consistent with the rather large distance and weak electronic coupling that would be anticipated between the donor and acceptor sites, this electron transfer rate constant is low. This result is entirely consistent with the ground-state spectroscopic and electrochemical data presented earlier. It is important to consider whether a photoinduced electron transfer is likely to involve oxidation or reduction of the Ru^{3+}* centre. An insight into this process can be obtained by combining the ground state spectroscopic and electrochemical data.[14] This analysis reveals that the driving force for manganese oxidation is *ca.* −1.94 eV while the manganese reduction is thermodynamically uphill by *ca.* 0.04 eV. Therefore, it appears that the PET will involve electron transfer from the Mn(III) centre to Ru^{3+}* leading to the formation of Ru^{2+}. We are currently undertaking flash photolysis studies on **1** in order to confirm the photoinduced process is electron transfer and to investigate the issue of subsequent ground state electron transfer reactions.

In conclusion, we present here the synthesis of a novel β-CD bridged D–A complex in which a hydroxy-bridged dinuclear Mn site appears to behave as a donor in an excited state electron transfer. Beyond creating a novel supermolecule with potential biomimetic properties, this work represents a new approach to developing donor–acceptor systems in which interactions can be modulated by simple alterations in the synthetic procedure. For example, a number of alternative metals may be coordinated to the CD in an analogous manner to the manganese described here. Furthermore, the synthetic strategy employed here preserves access to CD cavity by guests such as phenols, quinones and even ferrocene. These guests are likely to allow us direct control over the strength of electronic coupling between donor and acceptor without having to synthetically functionalize the materials.

We thank Dr Mary McNamara, DIT, for useful discussions and Mr M. Burke, DCU for NMR. T. E. K. and R. J. F. acknowledge Johnson Matthey for a generous loan of ruthenium trichloride under the Loans Scheme. The DIT scholarship programme and Higher Education Authority are gratefully acknowledged for supporting this work.

Notes and references

1 L. Sun, H. Berglund, R. Daydov, T. Norrby, L. Hammarström, P. Korrall, A. Börje, C. Philouze, K. Berg, A. Tran, M. Andersson, G. Stenhagen, J. Måtensson, M. Almgren, S. Styring and B. Åkermark, *J. Am. Chem. Soc.*, 1997, **119**, 6996; D. Burdinski, K. Wieghardt and S. Steenken, *J. Am. Chem. Soc.*, 2000, **121**, 10 781; D. Burdinski, E. Bothe and K. Wieghardt, *Inorg. Chem.*, 2000, **39**, 105.
2 J. Limburg, V. A. Szalai and G. W. Brudvig, *J. Chem. Soc., Dalton Trans.*, 1999, 1353, and references therein.
3 NH_2phen was prepared by reducing NO_2phen under H_2S gas.
4 J. Defaye, A. Gadelle, A. Guiller, R. Darcy and T. O'Sullivan, *Carbohydr. Res.*, 1989, **192**, 251.
5 R. Fuchs, N. Habermann and P. Klufers, *Angew. Chem., Int. Ed.*, 1993, **32**, 853.
6 B. U. Nair and G. C. Dismukes, *J. Am. Chem. Soc.*, 1983, **105**, 124.
7 N. R. Russell and M. McNamara, *J. Incl. Phenom. Mol. Recognit. Chem.*, 1989, **7**, 455; M. McNamara, Ph.D. Thesis, University College Dublin, Dublin 1991.
8 D. M. Adams and P. J. Lock, *J. Chem. Soc., A*, 1971, 2801.
9 M. McNamara and N. R. Russell, *J. Incl. Phenom Mol. Recognit. Chem.*, 1991, **10**, 485.
10 J. F. Stoddart and R. Zarzycki, *Recl. Trav. Chim. Pays-Bas*, 1988, **29**, 2103.
11 P. K. Bose and P. L. Polavarapu, *Carbohydr. Res.*, 2000, **323**, 63.
12 μ_{eff}, was determined on a Sherwood Scientific, magnetic susceptibility balance, spin only values were calculated according to $\mu_{Mn} = 2[S_{Mn}(S_{Mn}+1)]^{1/2}$.
13 Results to be published.
14 The free energy was estimated from the Rehm–Weller expression; ΔG (eV) $= [E(D^{\cdot+}/D) - E(A/A^{\cdot-})] - E_{0-0}$ where $E(D^{\cdot+}/D)$ and $E(A/A^{\cdot-})$ are the oxidation and reduction potentials of donor and acceptor sites respectively and E_{0-0} is the zero–zero spectroscopic energy calculated from the 77 K emission spectrum.

CHEMCOMM Communication
www.rsc.org/chemcomm

Carbene transposition involving double dehydrogenation of an sp^3 carbon†

Joseph N. Coalter III, John C. Huffman and Kenneth G. Caulton*

Department of Chemistry and Molecular Structure Center, Indiana University, Bloomington, IN 47405-7102, USA. E-mail: caulton@indiana.edu

Received (in Cambridge, UK) 14th March 2001, Accepted 3rd May 2001
First published as an Advance Article on the web 7th June 2001

***Two* benzylic hydrogens of 2,6-$Me_2C_6H_3O^-$ coordinated to $RuCl(PCy_3)_2(CHPh)^+$ are transferred to the benzylidene ligand, liberating toluene to form a new carbene which is covalently linked to the aryloxide ligand.**

Replacement of the chloride ligand in the olefin metathesis catalyst $RuCl_2(CHR)LL'$ (L, L′ = tertiary phosphines or other neutral donors) by other pseudohalides has been actively studied, but no clear trends or dramatic improvements in reactivity have yet to emerge.[1] Two groups[2,3] have recently reported replacement of both chlorides by alkoxides on the benzylidene complex, with the result [eqn. (1)] that some

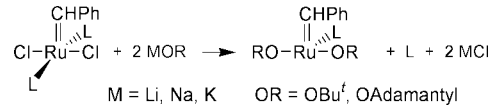

(1)

combination of steric and electronic (*e.g.* π-donor) effects causes loss of one PCy_3 to give a four-coordinate species with an apparent 14-valence electron count. This species is attractive because it has an empty orbital *cis* to the carbene ligand, a feature lacking in isolable $RuCl_2(CHR)L_2$. Fluoroalkoxide analogs have also been synthesized,[2] but phenoxides behave very differently[3] [eqn. (2)], proceeding further to a benzylidyne

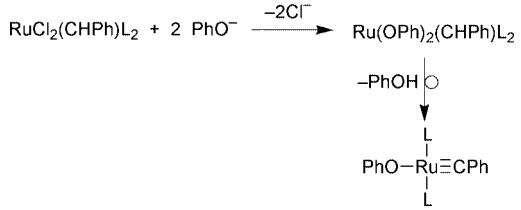

(2)

product by liberation of phenol. We now report the wholly distinct consequence of increasing the steric bulk of the phenoxide

Reaction of $RuCl_2(CHPh)(PCy_3)_2$ with $NaOC_6H_3Me_2$-2,6·THF (NaOAr·THF: 1 equiv) in THF proceeds rapidly to a benzylidene complex with only one coordinated phosphine and *one* coordinated aryloxide (a second equivalent of NaOAr·THF does not replace a second Cl^-) [**A**, eqn. (3)]. This product is

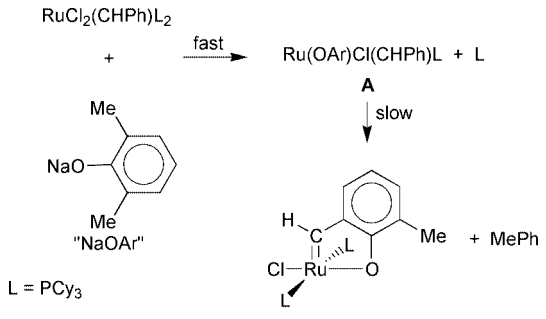

(3)

† Electronic supplementary information (ESI) available: synthetic and spectroscopic data. Crystallographic data and selected bond lengths and angle for **B**. See http://www.rsc.org/suppdata/cc/b1/b102422c/

proven to have only one phosphine by the carbene proton doublet structure (16.8 ppm), as well as by the observation of free phosphine (by ^{31}P NMR). This product then evolves more slowly by transfer of two hydrogens from one *ortho*-methyl group of the aryloxide to the benzylidene carbon [**B**, eqn. (3)]. After purification on an alumina column, the product **B** clearly shows the following ^1H NMR signals: *one* aryl methyl signal, of intensity three, only *three* aryl ring chemical shifts, each of unit intensity, and a Ru=C*H*R singlet at 16.4 ppm (unit intensity). Curiously, this carbene proton signal of **B** shows no resolved multiplet structure, although unresolved broadening is evident. The formation of toluene is also observed, as is the *disappearance* of free PCy_3, in the conversion of **A** to **B**. The $^{13}C\{^1H\}$ NMR supports this assignment, showing six aromatic signals, one Ar*C*H_3 signal (16.1 ppm), diastereotopic *C*H_2 ring carbons for the PCy_3 ligands, and a broad signal at 277.7 ppm for Ru=*C*.

A crystal structure determination of **B** (Fig. 1)‡ confirms this remarkable transformation. The coordination geometry at Ru is the traditional square-pyramidal, but one anionic ligand is now covalently linked to the carbene ligand. As shown in **C**

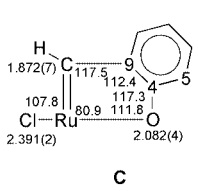

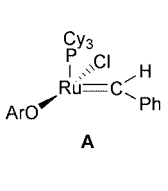

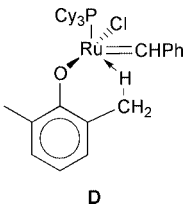

(distances in Å, angles in degrees), this unusual carbene/aryloxide ligand forms a planar five-membered chelate ring without substantial angular distortion at the carbene carbon. The

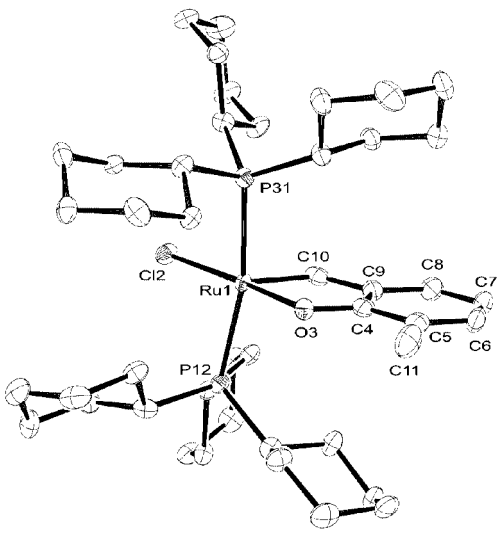

Fig. 1 ORTEP drawing of the nonhydrogen atoms of **B**. Selected distances (Å): Ru–C(10) 1.872(7), Ru–O(3) 2.082(4), Ru–Cl(2) 2.3910(17), Ru–P(12) 2.3947(19), Ru–P(31) 2.4005(19).

 DOI: 10.1039/b102422c

five-membered ring interior angles sum to 539.9° (540° if planar), and the angles that suffer the greatest compression are that at aryloxide oxygen (111.8° is small for M–O–Aryl) and at Ru (compare C=Ru–O of 80.9° to C=Ru–Cl of 107.8°). There are no agostic interactions between the cyclohexyl hydrogens and the open coordination site *trans* to the carbene (shortest Ru–C 3.3 Å).

The accumulated empirical evidence[1] shows that the magnitude of the $^3J_{PH}$ value is dependent on the dihedral angle P–Ru=C–H, and thus the orientation of the carbene plane with respect to the P–Ru line can be estimated. In intermediate **A**, $^3J_{PH}$ is large enough to be readily resolved (6 Hz), consistent with calculation and experiment, which give a dihedral angle of *ca.* 0°. In **B**, where no $^3J_{PH}$ is resolved, the carbene hydrogen has a dihedral angle of 90°, consistent with earlier reports that $^3J_{PH}$ in this conformation is near zero.[1]

Numerous recent developments in olefin metathesis chemistry have been directed to appending a good leaving group to reduce the L : Ru ratio in the molecule to 1 : 1, or to attach the molecule to a polymer to facilitate separation of catalyst from product.[4] What the present report offers is the potential for more permanent (*i.e.* anion-tethered) attachment of the *initial* carbene to the molecule, which contrasts to attachment *via* a pendant neutral donor (olefin[5] or ether[6]).

The *mechanism* of the double hydrogen transfer that converts a methyl to a carbene in eqn. (3) is not yet established. However, the precedent[7] that 14-electron Ru^{II} recruits agostic interactions from sterically accessible C–H hydrogens makes **D** a likely starting point on this transformation. The driving *force* for this reaction appears to be steric in origin, since only *one* ArO^- replaces chloride in the initial step of eqn. (3) and since the sterically expelled phosphine recoordinates when the bulky aryloxide and the benzylidene ligands are combined compactly into a single ligand incorporating both RO^- and carbene functionalities. Toluene elimination also provides an entropic assist worth *ca.* 8 kcal mol^{-1} at 300 K.[8] The different behavior shown by tertiary alkoxides or phenoxide and by 2,6-dimethylphenoxide is certainly due to the reactivity of benzylic hydrogens.

This work was supported by the donors of the Petroleum Research Fund, administered by the American Chemical Society.

Notes and references

‡ *Crystal data* for $C_{47}H_{80}ClOP_2Ru$ **B**: M = 859.62, triclinic, space group $P\bar{1}$, brown/green crystals, a = 12.5352(16), b = 13.7485(18), c = 14.4562(20) Å, α = 73.591(4), β = 69.803(4), γ = 78.316(4)°, V = 2227.6(8) $Å^3$, Z = 2, T = −161 °C, D_C = 1.282 g cm^{-3}, μ = 5.17 cm^{-1}, $F(000)$ = 922. The final conventional R factor was 0.0503 for 6249 data and 465 parameters, $R_w(F)$ = 0.0440 and GOF = 1.21. CCDC 161342. See http://www.rsc.org/suppdata/cc/b1/b102422c/ for crystallographic data in CIF or other electronic format.

1 T. M. Trnka and R. H. Grubbs, *Acc. Chem. Res.*, 2001, **34**, 18.
2 M. S. Sanford, L. M. Heling, M. W. Day and R. H. Grubbs, *Angew. Chem., Int. Ed.*, 2000, **39**, 3451.
3 J. N. Coalter, III, J. C. Bollinger, O. Eisenstein and K. G. Caulton, *New J. Chem.*, 2000, **24**, 925.
4 Q. Yao, *Angew. Chem., Int. Ed.*, 2000, **39**, 3896.
5 J. A. Tallarico and P. J. Bonitatebus and M. L. Snapper, *J. Am. Chem. Soc.*, 1997, **119**, 7157.
6 J. S. Kingsbury, J. P. A. Harrity, P. J. Bonitatebus and A. H. Hoveyda, *J. Am. Chem. Soc.*, 1999, **121**, 791.
7 D. Huang, K. Folting and K. G. Caulton, *J. Am. Chem. Soc.*, 1999, **121**, 10 318.
8 M. E. Minas da Piedade and J. A. M. Simoes, *J. Organomet. Chem.*, 1996, **518**, 167.

CHEMCOMM
Communication
www.rsc.org/chemcomm

Light harvesting and energy transfer in a ruthenium–coumarin-2 copolymer†

Xavier Schultze, Jason Serin, Alex Adronov and Jean M. J. Fréchet*

University of California, Berkeley, CA 94720-1460, USA. E-mail: frechet@cchem.berkeley.edu; Fax: +1(510) 643-3079; Tel: +1(510) 643-3077

Received (in Cambridge, UK) 26th April 2001, Accepted 15th May 2001
First published as an Advance Article on the web 7th June 2001

Copolymers containing Ru(bpy)$_3$ and coumarin-2 chromophores prepared using both grafting and copolymerization approaches exhibit Förster-type energy-transfer efficiencies ranging from 70% to above 98%.

Molecular assemblies capable of harvesting light and transforming the absorbed energy have attracted great interest in recent years because of their applicability in such domains as light emitting diodes, fluorescent labeling of biological molecules, and photonic devices.[1] We have recently described several dendritic systems containing light-harvesting dyes at the periphery that efficiently absorb and channel light to a different dye at the focal point by a Förster-type mechanism.[2] Although these systems exhibit extremely high energy-transfer efficiencies, the demanding multi-step synthesis required for their preparation may limit their use to speciality applications. To circumvent this limitation, we have explored analogous light-harvesting linear polymers in which the donor–acceptor ratios were optimized by mimicking the dendrimer models and found that their antenna properties,[3] although less impressive than those of the corresponding dendrimers, are nevertheless very good.

Ruthenium-containing macromolecules are attracting widespread interest due to their photochemical and electrochemical properties.[4,5] We now report our results concerning the synthesis and characterization of a linear Ru(bpy)$_3$–coumarin-2 copolymer (**1**) that exhibits the energy transfer efficiency generally observed with light harvesting dendrimers,[5] without requiring the multi-step synthesis involved in the design of these molecules. Two strategies were used (Scheme 1): (i) grafting the ruthenium complex **2** on a bipyridine–coumarin-2 functionalized copolymer (**3**), and (ii) copolymerization of a ruthenium functionalized monomer (**4**) with a coumarin-2 functionalized monomer (**5**). The first route enabled us to obtain a copolymer that exhibits an energy transfer efficiency of 70% between the coumarin-2 and the Ru(bpy)$_3$ units. More interestingly, the copolymerization route afforded a better performing copolymer that displays quantitative energy transfer efficiency.

The styrene functionalized coumarin-2 monomer (**5**) was synthesized by coupling coumarin-2 with vinyl benzyl chloride as described elsewhere.[3] The 4-vinyl-4′-methylbipyridine monomer (**6**) was obtained using a modified literature procedure.[6] Copolymerization of these two monomers using a 3 to 1 feed ratio (mol fraction of **5** = 0.75) was carried out at 90 °C with AIBN as the initiator in a minimum amount of dichlorobenzene. The polymer was precipitated twice into Et_2O to remove the unreacted monomers. Molecular weights ranging from 5000 to 15 000 Daltons were obtained along with a polydispersity of 1.6, typical of AIBN initiated polymerizations. Elemental analysis of copolymer **3** showed that the resulting polymer was composed of *ca.* 25% of the bipyridine monomer and 75% of the coumarin-2 monomer, as expected from the feed ratio.

To perform grafting of the ruthenium complex, we used the method reported by Fraser and co-workers.[7] Two equiv. of dichloride **2** were refluxed in MeOH in the presence of an excess of $AgPF_6$ for 12 h and the solution was then added to a suspension of copolymer **3** in dimethoxyethane. After 48 h at reflux, the reaction mixture was filtered, concentrated, redissolved in dichloromethane and extensively washed with water to remove any unreacted ruthenium complex. A dark red polymer was obtained after precipitation in Et_2O.

The UV spectra of the polymer before and after the grafting reaction with ruthenium complex **2** are given in Fig. 1. The starting polymer displays two strong absorption bands at 290 and 350 nm, which are characteristic of the coumarin-2 and the bipyridine units. After reaction with the ruthenium complex a new absorption band was observed at 465 nm, which indicates successful grafting of the ruthenium bis(bipyridine) onto the

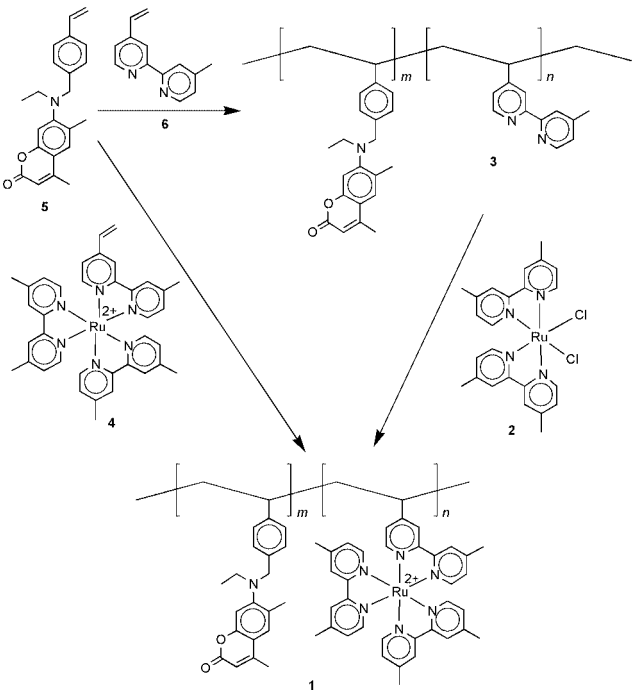

Scheme 1

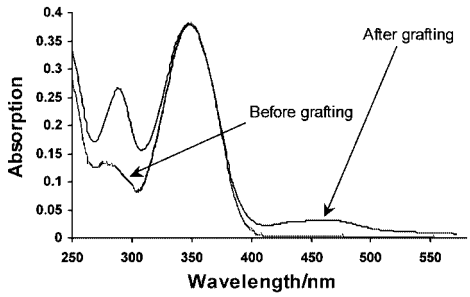

Fig. 1 Normalized UV-Vis spectra of copolymer **3** before and after grafting.

† Electronic supplementary information (ESI) available: experimental details. See http://www.rsc.org/suppdata/cc/b1/b103792g/

 DOI: 10.1039/b103792g

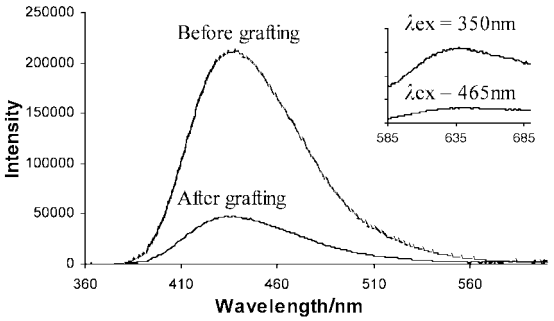

Fig. 2 Fluorescence spectrum of copolymer **3**, in the region of coumarin-2 emission, before and after grafting. Inset shows the spectrum of the same copolymer in the region where the $Ru(bpy)_3$ acceptor complex emits.

polymer. The absorption band at 290 nm is further increased due to the two additional bipyridine ligands introduced by the reaction. Fluorescence resonance energy transfer studies were carried out to determine the efficiency of energy transfer from the coumarin-2 chromophore to the ruthenium complex. The efficiency was calculated by comparing the coumarin-2 emission in the starting polymer **3** (a donor model compound) to the emission of this dye in the polymer obtained after grafting of ruthenium (Fig. 2). Based on the quenching of this emission, an energy transfer efficiency of 70% was determined for the grafted copolymer. Additionally, a 5-fold increase of the ruthenium emission was observed upon excitation of the coumarin-2 units (λ_{ex} = 350 nm) over excitation of the ruthenium complex directly (λ_{ex} = 465 nm), this type of amplification is the direct result of energy transfer (Fig. 2, inset).

Although the grafting route enabled us to obtain a polymer displaying good energy transfer characteristics, the functionalization of the polymer, estimated from the relative UV-Vis absorbance of the coumarin-2 and $Ru(bpy)_3$ units, was not quantitative (*ca.* 30%) and some insoluble material was also formed, decreasing the polymer yield. Therefore the copolymerization of monomers **4** and **5** was studied. The ruthenium-containing monomer **4** was prepared using a modified literature procedure.[8] Polymerization of the monomers was then performed at 90 °C with AIBN in DMF (mol fraction of **5** = 0.75). The resulting polymer was purified by precipitation in Et_2O and extensive washing with MeOH. The UV-visible spectrum of the polymer showed that incorporation of the ruthenium monomer **4** was as expected from the feed ratio, *ca.* 25%, with the remainder of the polymer repeat units consisting of the coumarin-containing monomer **5,** therefore the copolymerization route is much more effective for the introduction of the $Ru(bpy)_3$ complex than the grafting reaction.

The absorption spectrum of the copolymer (Fig. 3) is similar to that of the material obtained by the grafting route except that it displays stronger bipyridine and ruthenium metal to ligand charge transfer bands at 290 and 465 nm. Excitation of this polymer at 350 nm results in an emission spectrum (Fig. 4) that is totally quenched at 440 nm (the coumarin emission), indicating that quantitative energy transfer between the coumarin-2 and the $Ru(bpy)_3$ units occurs in this copolymer. Furthermore, the intensity of the ruthenium emission at 630 nm is increased by a factor of 2.7 when the polymer is illuminated at 350 nm *vs.* 465 nm. This increase is lower than that observed for the grafted copolymer, again indicating that, as a result of incomplete grafting, a higher concentration of donors relative to acceptors was present in that case.

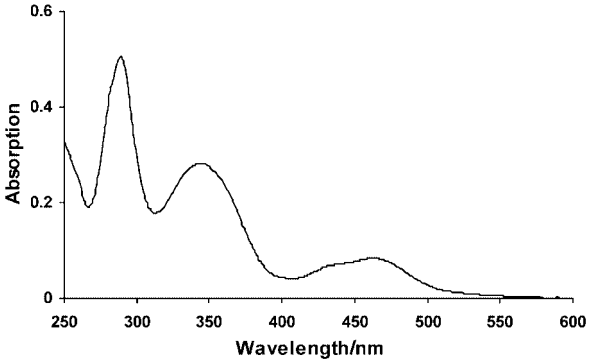

Fig. 3 UV spectrum of polymer **1**, obtained by the copolymerization route.

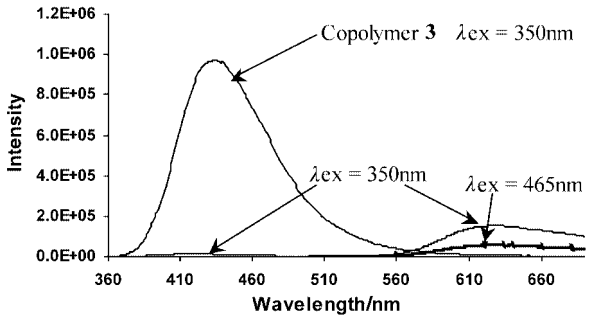

Fig. 4 Fluorescence spectrum of polymer **1**, obtained by the copolymerization route.

In conclusion, readily accessible linear copolymers containing coumarin-2 and $Ru(bpy)_3$ units can provide quantitative energy transfer from the coumarin-2 units to the ruthenium centers. This finding opens interesting perspectives in the field of solar energy conversion.[9] The application of such a system to photovoltaic devices is currently under investigation.

Financial support of this research by the AFOSR (F-49620-01) and the U. S. Department of Energy (# DE-AC03-76SF00098). Fellowship support from the Eastman Kodak Company is also gratefully acknowledged (A. A).

Notes and references

1 A. Adronov and J. M. J. Fréchet, *Chem. Commun.*, 2000, 1701.
2 A. Adronov, S. L. Gilat, J. M. J. Fréchet, K. Ohta, F. V. R. Neuwahl and G. R. Fleming, *J. Am. Chem. Soc.*, 2000, **122**, 1175; S. L. Gilat, A. Adronov and J. M. J. Fréchet, *Angew. Chem., Int. Ed.*, 1999, **38**, 1422; A. Adronov, P. R. L. Malenfant and J. M. J. Fréchet, *Chem. Mater.*, 2000, **12**, 1463.
3 A. Adronov, D. R. Robello and J. M. J. Fréchet, *J. Polym. Sci. A*, 2001, **39**, 1366.
4 Q. Wang and L. Yu, *J. Am. Chem. Soc.*, 2000, **122**, 11806; P. M. Ennis, J. M. Kelly and C. M. O'Connel, *J. Chem. Soc., Dalton Trans.*, 1986, 2485; E. A. Seddon and K. R. Seddon, in *The Chemistry of Ruthenium*, ed. R. J. H. Clark, Elsevier, 1984, ch. 15 p. 1173; M. Devenney, L. A. Worl, S. Gould, A. Guadalupe, B. P. Sullivan, J. V. Caspar, R. L. Leasure, J. R. Gardner and T. J. Meyer, *J. Phys. Chem. A*, 1997, **101**, 4535.
5 X. Zhou, D. S. Tyson and F. N. Castellano, *Angew. Chem., Int. Ed.*, 2000, **39**(23), 4301.
6 M. Wörner, G. Greiner and H. Rau, *J. Phys. Chem.*, 1995, **99**, 14161.
7 X. Wu and C. L. Fraser, *Macromol.*, 2000, **33**, 4053.
8 P. K. Ghosh and T. G. Spiro, *J. Am. Chem. Soc.*, 1980, **102**, 5543.
9 A. Hagfeldt and M. Grätzel, *Chem. Rev.*, 1995, **95**, 49.

CHEMCOMM
Communication
www.rsc.org/chemcomm

Design of histidine-Zn^{2+} binding sites within a β-hairpin peptide: enhancement of β-sheet stability through metal complexation

Geoffrey Platt,[a] Chun-Wa Chung[b] and Mark S. Searle*[a]

[a] *School of Chemistry, University of Nottingham, University Park, Nottingham, UK NG7 2RD. E-mail: Mark.Searle@nottingham.ac.uk*

[b] *Glaxo-SmithKline, Medicines Research Centre, Stevenage, Hertfordshire, UK*

Received (in Cambridge, UK) 18th January 2001, Accepted 9th May 2001
First published as an Advance Article on the web 8th June 2001

We describe the design and characterisation of two simple 'metalloproteins' based on Zn^{2+} co-ordination sites involving histidine residues close to the N- and C-termini of two β-hairpin peptides (His_2-β, KHYTVSINGKKITVHI and His_3-β, HKHYTV-SINGKKITVHI); we show by NMR and circular dichroism spectroscopy that Zn^{2+} complexation co-operatively enhances the stability of these partially pre-organised β-sheet peptides.

Metals play a pivotal structural and catalytic role in numerous protein and enzyme scaffolds.[1] Metal complexation stabilises some of the smallest structural motifs known (zinc finger domains),[2] while changes in metal co-ordination shell and ligand lability are central to catalytic turnover in enzymatic processes.[3–5] Previously, metal binding sites have been designed into proteins and short peptides, through the incorporation of both natural and non-natural amino acids, to study the effects on protein stability and peptide secondary structure.[6–9] While effects on structural enhancement of α-helical peptides have been described,[7] the extension of these principles to the templating of β-sheet structures[10] for subsequent use as novel molecular architectures for molecular recognition or catalysis, has been rather limited. Previously, the His_3-Zn^{2+} co-ordination site within carbonic anhydrase, which employs residues within β-sheet and β-turn,[11] has been used successfully to design a zinc binding site on one face of an octapeptide incorporating a type II (Pro-^{D}Ser) turn.[9] Here, we investigate by NMR and CD spectroscopy the effect of zinc co-ordination on the stability of β-sheet secondary structure in a partially pre-organised β-hairpin peptide. We show that engineering a metal binding site between the termini of two β-strands, resulting in both His_2-Zn^{2+} and His_3-Zn^{2+} co-ordination shells, co-operatively enhances β-sheet secondary structure in a β-hairpin system.

In previous studies, we have described the folding of a model 16-residue β-hairpin system (KKYTVSINGKKITVSI) that is ~50% populated in aqueous solution.[12] We have replaced a Lys-Ser cross-strand pair in the β-hairpin sequence (underlined) with a His-His pair to facilitate cross-strand metal binding initially through a His_2-Zn^{2+} co-ordination site (peptide **His_2**-β; residues Lys2 to Ile17 in Fig. 1(a)). In a second peptide, we have extended the N-terminal sequence by an additional overhanging His residue to generate a potential His_3-Zn^{2+} co-ordination site (peptide **His_3**-β). We envisaged that the greater conformational flexibility of the terminal His (which is not part of the β-sheet), should greatly facilitate Zn^{2+} co-ordination, with the final tetrahedral site occupied by either the C-terminal carboxylate group or a solvent molecule [Fig. 1(b)] in an analogous fashion to the carbonic anhydrase catalytic site.

NMR analysis of Hα chemical shift deviations from random coil values[13] provides a useful handle on the extent of folding prior to metal complexation, showing that the two β-hairpins (**His_2**-β and **His_3**-β) are similarly populated in aqueous solution at pH 7.0 and that the additional N-terminal His residue has little effect on β-hairpin folding. A number of cross-strand Hα↔Hα NOEs, in particular between Ser 7↔Lys12 and Thr5↔Thr14, together with long range NH↔NH (Val6↔Ile13) and NH↔Hα NOEs (Ser7↔Ile13) establish that the peptides fold with the proposed strand alignment shown in Fig. 1(a), with stabilising interactions between side chains consistent with this fold (for example Tyr4↔Val15). The similarity of the Hα shifts for His3 and His16 precludes the observation of an Hα↔Hα NOE between these residues, but Hα chemical shift perturbations are consistent with cross-strand interactions close to the N- and C-termini. Calculation of His pK_a values from pH titration analysis of His Hε chemical shifts, shows them to fall in the range 5.73 to 6.36 suggesting that metal complexation will be optimum around pH 7 where all imidazole rings are unprotonated. The pH-dependent stability profile determined from changes in CD ellipticity and Hα chemical shifts shows that the population of folded hairpin decreases below pH 5.5, consistent primarily with the formation of a $HisH^+$-$HisH^+$ pair between opposing β-strands that has a significant destabilising effect on β-hairpin structure. The difference in Hα chemical shift deviations from random coil values at pH 3.5 and 7.2 are shown in Fig. 2 for **His_2**-β. Interestingly, all shifts are perturbed at low pH suggesting that an electrostatic repulsion between $HisH^+$ residues (His3 and His16) close to the N- and C-termini, as well as protonation of the C-terminal carboxylate group, has a co-operative destabilising effect on the hairpin that is sensed by all residues, including those in the distant NG turn sequence. Similar effects are observed for both peptides **His_2**-β and **His_3**-β. Thus, the data indicate that at pH 7 the two peptides are already populating a partially pre-organised β-hairpin conformation.[12]

The uncomplexed peptide shows a very weak band at 216 nm in the CD spectrum due to β-sheet and β-turn conformation in equilibrium with random coil, the latter resulting in a strong negative ellipticity at 200 nm (Fig. 3).[14] CD data are also shown

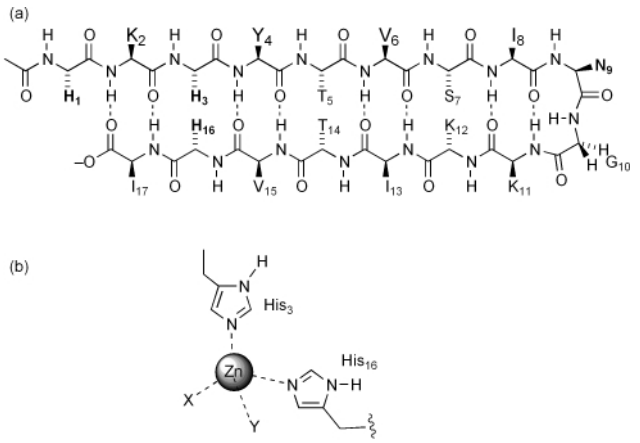

Fig. 1 (a) Schematic representation of peptide **His_3**-β (1–17) showing the peptide main chain alignment; residues are identified using the single letter amino acid code. **His_2**-β (2–17) lacks the N-terminal His (Lys2-*N*-acetylated), the same numbering scheme is used for each peptide; (b) proposed zinc co-ordination site; for **His_3**-β X = His1, Y = H_2O or the C-terminal carboxylate group of Ile17, for **His_2**-β X = H_2O, Y = H_2O or CO_2^-.

 DOI: 10.1039/b100702p

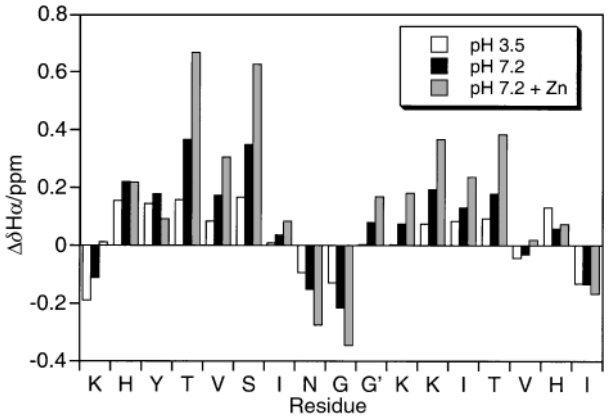

Fig. 2 Deviations of Hα chemical shifts from random coil values ($\Delta\delta$Hα, ppm) for **His$_2$**-β in water at pH 3.5 and 7.2 (298 K), and in aqueous solution (pH 7.2) and 1 equiv. of $ZnCl_2$. All $\Delta\delta$Hα values were determined after full assignment of NOESY and TOCSY data collected at 500 MHz.

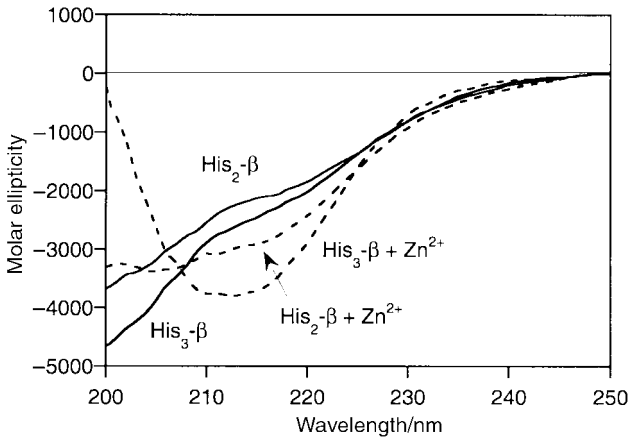

Fig. 3 Far UV-CD spectra of **His$_2$**-β and **His$_3$**-β in aqueous solution (pH 7.2) in the absence of zinc and in the presence of 10 equiv. of $ZnCl_2$. All spectra were recorded on an Aviv 62DS spectrophotometer at 293 K, as previously described.[12]

for the two peptides in the presence of excess $ZnCl_2$ at pH 7.0. In both cases the negative ellipticity at 216 nm becomes more pronounced, however, the effect is greatest for **His$_3$**-β, with the ellipticity also approaching zero at 200 nm. The data imply that Zn^{2+} chelation with **His$_3$**-β induces a greater degree of β-sheet secondary structure.

Significant perturbations to Hα chemical shifts are also consistent with further induction of β-sheet secondary structure by metal binding. In particular, Thr5 and Ser7 are shifted further downfield by > 0.2 ppm ($\Delta\delta$Hα values of 0.67 and 0.63 ppm, respectively for **His$_2$**-β; see Fig. 2); secondly, His Hε resonances are seen to broaden considerably, consistent with metal complexation. The effects of zinc titration on the folding of peptide **His$_3$**-β are equally pronounced but more significant at low concentrations of the metal ion. The Gly residue in the turn sequence has previously proved to be a good indicator of the extent of folding, since the two Hα resonances experience a large difference in chemical shift in the folded state due to the anisotropic effects of neighbouring carbonyl groups.[15] In this case the Gly residue in the turn is well removed from the direct effects of zinc binding. In the presence of Zn^{2+} the Gly Hα splitting for **His$_3$**-β is much larger than for the free peptide (300 *versus* 141 Hz), indicating that chelation of zinc by residues close to the peptide N- and C-termini co-operatively stabilises β-sheet secondary structure along the full length of the hairpin. **His$_2$**-β achieves the same magnitude of Gly Hα splitting but only at much higher metal ion concentrations (>10 equiv.). Using the quantitative methods previously described to estimate hairpin stability from the Gly Hα splitting,[15] we conclude that zinc binding enhances the stability of each hairpin by up to 3 kJ mol^{-1} at 298 K, reflecting the net balance between favourable electrostatic interactions with the metal and opposing entropic effects of organising the peptide backbone and His side chains. Although we cannot state unambiguously that all three His residues of **His$_3$**-β are simultaneously involved in complexation, the observed differences between the two peptides suggest that the overhanging His residues plays some role (dynamic or otherwise) in metal complexation.

In native proteins where Zn^{2+} is used solely in a structural capacity, His_3-Zn^{2+} is less common in the stabilisation of β-sheet structure than alternative His_2-Cys_2 or His-Cys_3 motifs. A recent report of a redesigned zinc-finger motif has shown that His_4-Zn^{2+} co-ordination can be accommodated with two His residues located in the β-sheet,[16] although structural analysis suggests that the short β-hairpin component (only three residues per strand) is distorted by the tetrahedral co-ordination geometry around the Zn^{2+} ion. Here we have used a significantly larger element of β-sheet secondary structure than previously reported with the metal co-ordination site incorporated close to the N- and C-termini to minimise distortions. Our preliminary data from NMR and CD indicate that the integrity of the β-sheet is enhanced although tetrahedral co-ordination around zinc must produce some local distortion.

We thank the EPSRC and Glaxo-SmithKline for financial support through a CASE collaboration, and John Keyte in the School of Biomedical Sciences for peptide synthesis. We are grateful to S. R. Griffiths-Jones and M. Jourdan for helpful discussions.

Notes and references

1 T. V. O'Halloran, *Science*, 1993, **261**, 715; J. C. Rutherford, J. S. Cavet and N. J. Robinson, *J. Biol. Chem.*, 1999, **274**, 25 827; M. A. Carrion, W. A. Link, F. Ledo, B. Mellstrom and J. R. Naranjo, *Nature*, 1999, **398**, 80.
2 A. Klug and D. Rhodes, *Trends Biochem. Sci.*, 1987, **12**, 464; J. M. Berg and Y. Shi, *Science*, 1996, **271**, 1081.
3 B. L. Vallee and R. J. P. Williams, *Proc. Natl. Acad. Sci. USA*, 1968, **59**, 498.
4 R. J. P. Williams, *Polyhedron*, 1987, **6**, 61.
5 G. Parkin, *Chem. Commun.*, 2000, 1971.
6 F. Ruan, Y. Chen and P. B. Hopkins, *J. Am. Chem. Soc.*, 1990, **112**, 9403.
7 T. Handel and W. F. Degrado, *J. Am. Chem. Soc.*, 1990, **112**, 6710; A. Pessi, E. Bianchi, A. Crameri, S. Venturini, A. Tramontano and M. Sollazzo, *Nature*, 1993, **362**, 367; T. M. Handel, S. A. Williams and W. F. DeGrado, *Science*, 1993, **261**, 879.
8 B. A. Krizek, D. L. Merkle and J. M. Berg, *Inorg. Chem.*, 1993, **32**, 937.
9 B. Imperiali and T. M. Kapoor, *Tetrahedron*, 1993, **49**, 3501.
10 R. P. Cheng, S. L. Fisher and B. Imperiali, *J. Am. Chem. Soc.*, 1996, **118**, 11349.
11 J. E. Coleman, *Curr. Opin. Struct. Biol.*, 1998, **2**, 222.
12 A. J. Maynard, G. J. Sharman and M. S. Searle, *J. Am. Chem. Soc.*, 1998, **120**, 1996; S. R. Griffiths-Jones, A. J. Maynard and M. S. Searle, *J. Mol. Biol.*, 1999, **292**, 1051.
13 D. S. Wishart, B. D. Sykes and F. M. Richards, *Biochemistry*, 1992, **31**, 1647.
14 W. C. Johnson, *Ann. Rev. Biophys. Biophys. Chem.*, 1988, **17**, 145.
15 M. S. Searle, S. R. Griffiths-Jones and H. Skinner-Smith, *J. Am. Chem. Soc.*, 1999, **121**, 11615.
16 Y. Hori, K. Suzuki, Y. Okuno, M. Nagaoka, S. Futaki and Y. Sugiura, *J. Am. Chem. Soc.*, 2001, in press.

CHEMCOMM Communication
www.rsc.org/chemcomm

Novel smart ligand for immobilizing a highly efficient Rh-catalyst

Jin-Kyu Lee,* Tae-Jong Yoon and Young Keun Chung

School of Chemistry and Center for Molecular Catalysis, Seoul National University, Seoul 151-747, Korea. E-mail: jinklee@snu.ac.kr

Received (in Cambridge, UK) 15th February 2001, Accepted 11th May 2001
First published as an Advance Article on the web 8th June 2001

Novel highly efficient Rh-based catalysts with a good regioselectivity in olefin hydroformylation have been prepared by deliberately choosing 11-mercaptoundecanoic acid as a ligating molecule to $[Rh(cod)Cl]_2$ (cod = cyclooctadiene) and a simple recovery process for their recycling was investigated.

Catalyst recovery processes are becoming more important, especially when expensive and toxic heavy metal complexes are employed. Owing to these economic and environmental factors, many attempts have been made to recover homogenous catalysts and recycle them. The homogeneous catalysts are usually recovered by thermal operations such as distillation, which normally leads to thermal stress on the catalyst and seldom yields quantitative recovery. Since the separation of catalyst from products is much simpler in two-phase (or biphasic) systems incorporating a water-soluble catalyst,[1–3] water-soluble organometallic compounds have been studied for many years. They are normally prepared by incorporating highly polar functional groups such as sulfonate salt[4,5] carboxylate salt,[1] amino,[6] or hydroxide[7] into the ligands. Recently, Rh-based catalysts have attracted much attention due to their high activity and selectivity, and some attempts to immobilize these expensive catalysts have also been reported.[6,8–13] In this communication, we will introduce a simple synthetic method of preparing novel water-soluble Rh-based hydroformylation catalysts and discuss their unique solubility and reactivity, which make catalyst recycling much simpler.

$[Rh(\mu\text{-}S(CH_2)_{10}CO_2Na)(cod)]_2$ **1** was prepared in 89% yield as a yellow–orange solid by treating $[Rh(\mu\text{-}Cl)(cod)]_2$ with 11-mercaptoundecanoic acid disodium salt† (Scheme 1). Complex **1** is a very stable solid in air and soluble in water, slightly soluble in MeOH, and insoluble in most organic solvents. This complex shows a very sensitive change of solubility in water when pH values are varied, compared to other known water-soluble organometallic compounds that usually contain sulfonate groups and show no pH-dependent solubility.[4,5] When an aqueous solution of **1** was treated with acid to pH < 4, $[Rh(\mu\text{-}S(CH_2)_{10}CO_2H)(cod)]_2$ **2** was quickly precipitated as a yellow–orange powder from the aqueous solution, this powder being very soluble in polar organic solvents such as THF. Complex **2** can also be quantitatively converted back into **1** by treating with a base such as NaOH aqueous solution. These interconversions between **1** and **2** can be repeated several times without any significant degradation of the complexes (Scheme 1).

The catalytic activity of both **1** and **2** for the hydroformylation of arylolefins was checked, and the large differences in their solubility (depending on the pH) were used to recover the catalyst after the reaction.‡ The water-soluble Rh catalyst **1**, in general, showed a high catalytic activity with the exception of α-methylstyrene (Table 1, entry 1), probably due to its steric bulkiness preventing the effective binding of the disubstituted styrene onto the Rh catalysts. Although the hydroformylation of aromatic olefins showed very good regioselectivity, the electron donating or withdrawing substituents on styrene (Table 1, entries 2–6) did not give rise to any further enhancement of selectivity. Unlike other reported hydroformylation catalysts,[1] compound **1** showed a very high degree of catalytic activity even towards long alkyl olefins such as oct-1-ene, undec-1-ene, and dodec-1-ene (Table 2). It is expected that the long alkyl chains in 11-mercaptoundecanoic acid themselves behave like a surfactant to enhance the solubility of the long aliphatic olefins in the aqueous catalyst phase. The low regioselectivity resulting from the hydroformylation of aliphatic terminal olefins suggests that regioselectivity is related not only to steric but also to electronic factors. After the reaction, the products were easily separated by extraction with Et_2O and the aqueous layer containing catalyst **1** could be reused without any further treatment. Reaction results from the consecutive usage (five times) of aqueous

Table 1 Hydroformylation results of substituted styrenes by employing water-soluble catalyst **1**

Entry	Olefin	*b*/*l*[a]	Conversion yield (%)[b]
1	α-Methylstyrene		~3
2	4-Bromostyrene	87/13	100
3	4-Chlorostyrene	88/12	100
4	Styrene	91/9	100
5	4-Methylstyrene	97/3	100
6	4-Vinylanisole	92/8	100

[a] Structural ratios of aldehyde products were measured by ^{1}H NMR spectroscopy (*b*: 9.62 ppm, *l*: 9.78 ppm); *b* stands for a branch form (*e.g.* acetophenone) and *l* for linear form (*e.g.* phenylacetaldehyde). [b] Determined by ^{1}H NMR spectroscopy.

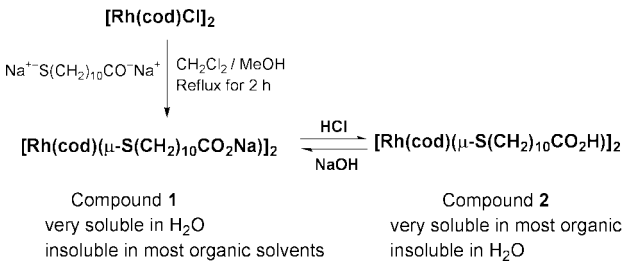

Scheme 1 Synthesis of novel sulfur bridged [Rh] catalysts.

 DOI: 10.1039/b101506k

Table 2 Hydroformylation results of long alkyl olefins by catalyst **1**

Entry	Olefin	*b/l*	Conversion yield (%)
1	Oct-1-ene	50/50	100
2	Undec-1-ene	48/52	100
3	Dodec-1-ene	78/22	92

Catalytic reaction and analysis process was as for Table 1.

solutions containing catalyst **1** did not indicate any differences in catalytic activity. Further detailed study on the long-term stability of catalyst **1** is under investigation.

When organic-soluble compound **2** was used as a catalyst, the reactions were carried out in homogeneous THF solution. All the reaction results were the same as for the case of catalyst **1**, thereby confirming the high catalytic activity of the new Rh-based catalysts in either a homogeneous or a heterogeneous system. However, the recovery process of catalyst **2** from THF solution was different. It was isolated by treating with NaOH solution to precipitate as **1**, followed by filtering off and dissolving it in water. It was then treated with HCl solution again to precipitate as compound **2**, then filtered off and dried for recycling. Recycled catalyst **2** showed the same activity, but there was always a small amount of weight loss during the filtration and drying procedures. From the practical point of view of recycling, therefore, it is much easier and simpler to use compound **1** in a biphasic (water/organic bilayer) system.

We are quite certain that the present catalyst should exhibit a high degree of regioselectivity toward various olefins. Further experiments to obtain a detailed mechanistic understanding and the application of these novel Rh-catalysts to other types of catalytic reactions such as hydrosilylation and stereoselective hydrogenation reactions, are currently under investigation.

This work was supported by the Korean Science and Engineering Foundation through the Center for Molecular Catalysis at Seoul National University. We are grateful to Dr J. W. Han for his kind technical assistance. T. J. Yoon is also grateful to the BK21 fellowship.

Notes and references

† A mixed solution of NaOH (3 M, 3.06 ml) and $HS(CH_2)_{10}CO_2H$ (1.00 g, 4.58 mmol) in 10 ml of THF was stirred at room temperature for 30 min to precipitate the salt $Na^+{-}S(CH_2)_{10}CO_2{-}Na^+$. The precipitate was filtered off, and then washed with THF in order to eliminate excess NaOH. 0.53 g (2.00 mmol) of dried $Na^+{-}S(CH_2)_{10}CO_2{-}$ Na^+ salt was added to a stirred solution of $[Rh(\mu\text{-}Cl)(cod)]_2$ (0.49 g, 1.00 mmol) in dried MeOH (10 ml). The mixed solution was refluxed with vigorous stirring for 30 min. Solvent was evaporation to dryness, and the residual solid was rinsed with cold CH_2Cl_2 (3×10 ml) and crystallized from H_2O–THF mixed solvent. Solid crystals were filtered off and vacuum dried to give 0.80 g of pure complex **1** (89% yield). ^{1}H NMR (300 MHz, D_2O): δ 2.18 and 2.3 (br, total 8H, cod –C*H*$_2$–), 4.3 (br, 4H, cod =C*H*–), 2.19 (t, 2H, $-O_2CCH_2$–), 1.27 (m, 12H, internal –C*H*$_2$–), 2.53 (t, 2H, –SC*H*$_2$–), 1.51(m, 4H, $–SCH_2CH_2–$ and $–O_2CCH_2CH_2–$). Anal. Found: C, 50.66; H, 7.16; S, 7.12%. Calc. for $C_{38}H_{64}O_4S_2Na_2Rh_2$: C, 50.69; H, 7.12%; S, 7.12%. MS (FAB, negative): 901 (M^+).

‡ Neat substituted styrenes (2.5 mmol) over 5.0 mL of the aqueous solution of catalyst **1** (1.3×10^{-3} M) were hydroformylated with pressurized H_2/CO (500 psi, 2:1 ratio of H_2:CO) gas mixtures in a stainless steel autoclave reactor at 55 °C for 22 h. Structural ratios of aldehyde products were measured by ^{1}H NMR spectroscopy. (*b*: 9.62 ppm, *l*: 9.78 ppm)

1 A. N. Ajjou and H. Alper, *J. Am. Chem. Soc.*, 1998, **120**, 1466.
2 Y. M. Chung, K. K. Kang, W. S. Ahn and P. K. Lim, *J. Mol. Catal. A: Chem.*, 1999, **137**, 23.
3 J. H. Chen and H. Alper, *J. Am. Chem. Soc.*, 1997, **119**, 893.
4 W. A. Herrmann, C. W. Kohlpaintner, R. B. Manestsberger, H. Bahrmann and H. Kottmann, *J. Mol. Catal. A: Chem.*, 1995, **97**, 65.
5 T. Hayashi and M. Ishigedani, *J. Am. Chem. Soc.*, 2000, **122**, 976.
6 J. Balué and J. C. Bayón, *J. Mol. Catal. A: Chem.*, 1999, **137**, 193.
7 S. U. Son, J. W. Han and Y. K. Chung, *J. Mol. Catal. A: Chem.*, 1998, **135**, 35.
8 L. Huang, Y. Xu, G. Piao, A. Liu and W. Zhang, *Catal. Lett.*, 1994, **23**, 87.
9 M. Sawamura, R. Kuwano and Y. Ito, *J. Am. Chem. Soc.*, 1995, **117**, 9602.
10 J. Holz, D. Heller, R. Strumer and A. Borner, *Tetrahedron Lett.*, 1999, **40**, 7059.
11 T. Sento, S. Shimazu, N. Khikuni and T. Vematsu, *J. Mol. Catal. A: Chem.*, 1999, **137**, 263.
12 T. Malmström, H. Weigl and C. Andersson, *Organometallics*, 1995, **14**, 2593.
13 Z. Freixa, E. Martin, S. Gladiali and J. C. Bayón, *Appl. Organomet. Chem.*, 2000, **14**, 57.

CHEMCOMM Communication
www.rsc.org/chemcomm

A biomimetic synthesis of (−)-$N_{(a)}$-methylervitsine

M.-Lluïsa Bennasar,*[a] Ester Zulaica,[a] Yolanda Alonso,[a] Ignasi Mata,[b] Elies Molins[b] and Joan Bosch[a]

[a] *Laboratory of Organic Chemistry, Faculty of Pharmacy, University of Barcelona, Barcelona 08028, Spain. E-mail: bennasar@farmacia.far.ub.es*
[b] *Institut de Ciència de Materials (CSIC), Campus UAB, 080193-Cerdanyola, Spain*

Received (in Cambridge, UK) 2nd March 2001, Accepted 15th May 2001
First published as an Advance Article on the web 8th June 2001

A straightforward, biomimetic synthesis of (−)-$N_{(a)}$-methylervitsine involving the nucleophilic addition of the enolate derived from 2-acetylindole 1 to chiral, non-racemic pyridinium salt 2, followed by (Me_2N^+=CH_2) I^- induced cyclization of the resultant 1,4-dihydropyridine, with subsequent elaboration of the exocyclic 16-methylene and 20*E*-ethylidene substituents, is reported.

Biomimetic syntheses of natural products reproduce the key steps of their biosynthesis through processes similar to those believed to be occurring in nature.[1] The conjugate iminium cation **A** has been postulated as the key biogenetic intermediate *en route* to ervitsine, a rare 2-acylindole alkaloid isolated from *Pandaca boiteaui*,[2] with a particular skeleton in which the tryptamine carbon atoms C_5–C_6 are in a rearranged situation forming the unusual C_7–C_5–C_{16}–C_6 bond array.[3] Consequently, this bridged alkaloid incorporates a seven membered C ring and a piperidine moiety bearing two different (16-methylene and 20*E*-ethylidene) exocyclic double bonds (Scheme 1).

We report here a biomimetic synthesis of (−)-$N_{(a)}$-methylervitsine *via* the dihydropyridinium cation **B**, which can be envisaged as a synthetic equivalent of the key biogenetic intermediate **A**. This cation incorporates a latent exocyclic methylene group (the dimethylaminomethyl substituent), and *a priori* should be accessible by nucleophilic addition of a 2-acetylindole enolate to the 4-position of a 3-acyl-*N*-alkylpyridinium salt, followed by electrophile (Me_2N^+=CH_2)-induced cyclization of the resulting 1,4-dihydropyridine. The acyl substituent X* would act as a chiral auxiliary, thus allowing the stereoselective generation of the stereocentre at the pyridine 4-position (corresponding to C-15 in ervitsine), and it would then be stereoselectively converted into the exocyclic *E*-ethylidene substituent of the alkaloid. In this approach, taking into account the bridgehead character of C-5 and C-15, the configuration of the latter determines that of the former after the biomimetic cyclization.

The stereoselective synthesis of chiral non-racemic 1,4-dihydropyridines[4] has been previously achieved by diastereoface-selective addition of suitable organometallic reagents to *N*-acylpyridinium salts carrying chiral auxiliaries, usually at the 3-position of the pyridine ring: oxazoline,[5] aminal,[6] [(η^5-C_5H_5)Fe(CO)(PPh_3)],[7] and amides derived from (*S*)-thiazolidine-2-thiones and (*S*)-oxazolidinones.[8]

In our case, we decided to study the addition of the enolate derived from 2-acetylindole **1** to *N*-methylpyridinium salt **2**, a nicotinic amide derived from (*S*)-*O*-methylprolinol (Scheme 2). The addition of indole-containing enolates to *N*-alkylpyridinium salts bearing an electron-withdrawing group at the 3-position has extensively been used in our laboratory as the initial step of a general scheme for the synthesis of indole alkaloids in the racemic series.[9] However, there are few examples of the use of this methodology for the enantioselective synthesis of alkaloids, and they deal with chiral enolates instead of chiral pyridinium salts.[10]

As can be observed in Table 1, acid induced cyclization of the initially formed dihydropyridine **3** gave a 3:1 diastereomeric mixture of tetracycles **4a** and **4b** (entry 1), whereas PhSeCl (entry 2) or (Me_2N^+=CH_2) I^- (entry 3) induced cyclization afforded 2:1 diastereomeric mixtures of the C-16 substituted tetracycles **5** or **6**, respectively, in which the 15-H β isomers (**a** series) predominated (see below for the determination of the absolute stereochemistry).

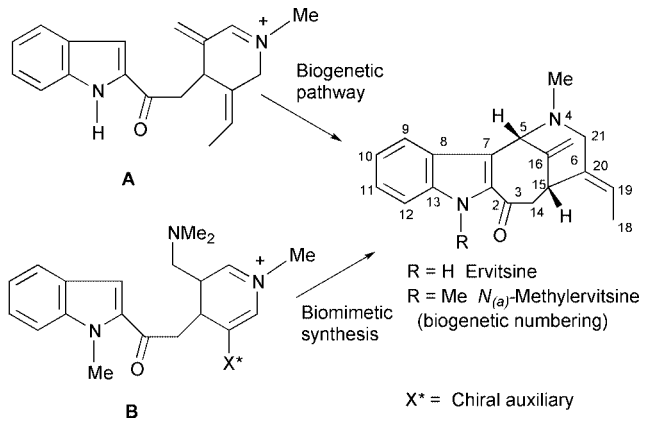

Scheme 1

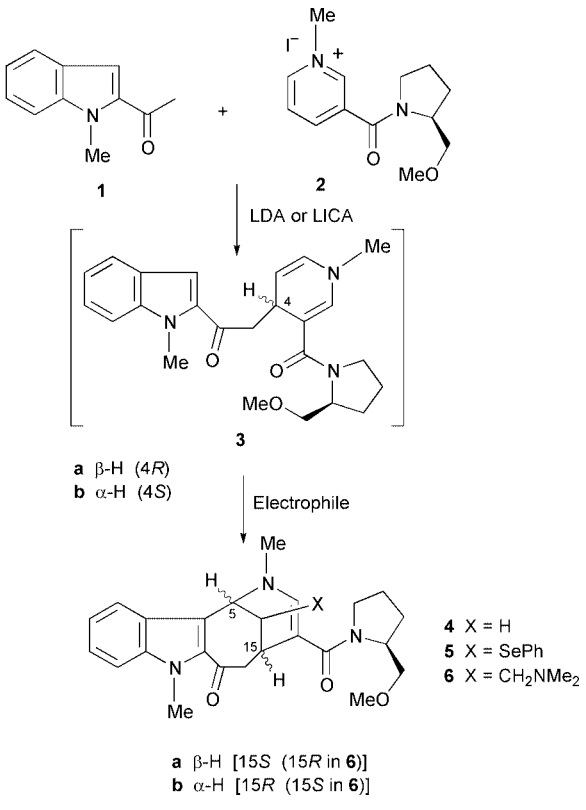

Scheme 2

 DOI: 10.1039/b102010m

Table 1 Reactions of the enolate derived from **1** with pyridinium iodide **2**[a]

Entry	Electrophile[b]	Product (yield, %)[c]	Diastereomer ratio (a:b)
1	HCl/C_6H_6	**4** (25)	74:26[d]
2	ClSePh	**5** (40)	2:1[e]
3	$CH_2{=}NMe_2\ I^-$	**6** (40)	68:32[d]

[a] Generation of the enolate with LDA (LICA in entry 3) at −78 °C for 30 min, then interaction with **2** at −30 °C for 1.5 h. [b] Addition at −30 °C to the reaction mixture, then rt for 2 h. [c] Isolated yield of chromatographically pure diastereomeric mixtures. [d] Calculated by HPLC. [e] Approximate ratio calculated by ^{1}H-NMR.

In this way, the tetracyclic ring system of ervitsine has been assembled in a straightforward manner, in a one-pot process involving the formation of three carbon–carbon bonds (C_{14}–C_{15}, C_6–C_{16} and C_5–C_7). This clearly indicates that the interaction of 1,4-dihydropyridine **3** with $(Me_2N^+{=}CH_2)\ I^-$ generates the key biomimetic intermediate **B**, which undergoes the crucial biomimetic cyclization.

The formation of tetracycles **4a**–**6a** as the major products implies that the lithium enolate of **1** preferentially approaches the *Re* face of pyridinium ring **2**, probably after the initial complexation of the lithium cation to both the carbonyl oxygen and the methoxy group of the auxiliary.

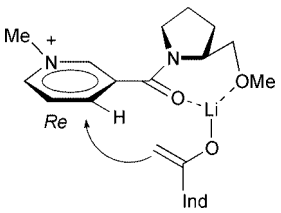

The diastereomeric mixture of tetracycles **6a**,**b** was converted into the corresponding 16-methylene derivatives by Cope elimination *via* the respective *N*-oxides in 45% overall yield (Scheme 3). At this point both diastereomers were efficiently separated by crystallization (ether–acetone–hexanes). The absolute configuration of the major diastereomer **7**,[11] coincident with that of natural (−)-ervitsine, was unambiguously determined by X-ray crystallography.[12] Removal of the chiral auxiliary from **7** required the previous chemoselective reduction of the 2-acylindole carbonyl group with lithium borohydride to give alcohol **8** (80%), which was converted into the acetyl derivative **9** by reaction with methyllithium (54%). Finally, after regeneration of the 2-acylindole carbonyl group with MnO_2 (quantitative), the stereoselective elaboration of the 20*E*-ethylidene substituent was accomplished by treatment of **10** with trimethyloxonium tetrafluoroborate followed by controlled sodium borohydride reduction (25%).[13] The ee (> 99%) of the resulting (−)-$N_{(a)}$-methylervitsine (**11**), $[\alpha]_D$ −60.5 (*c* 0.1, $CHCl_3$), was determined by chiral HPLC using racemic $N_{(a)}$-methylervitsine as reference. Finally the NMR spectra of **11** matched those of the racemic material.[9e]

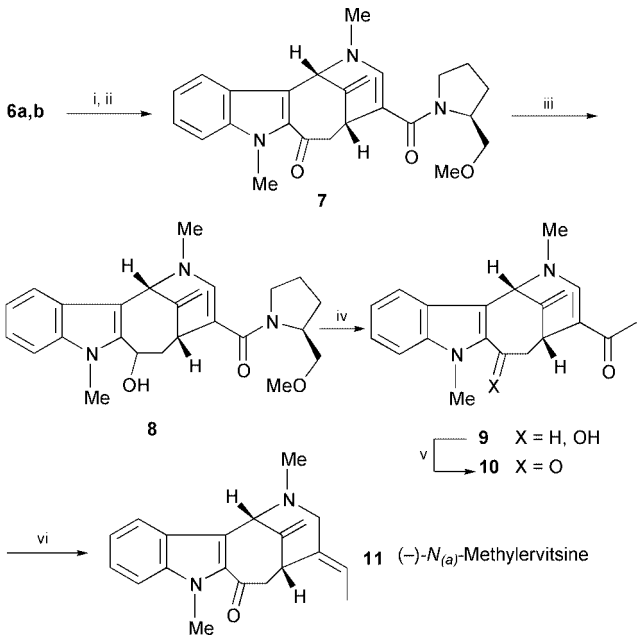

Scheme 3 Synthesis of (−)-$N_{(a)}$-methylervitsine. *Reagents and conditions*: i, 70% *m*-CPBA, CH_2Cl_2, −10 °C, 2 h; ii, toluene, reflux, 1 h, 45%, then separation of diastereomers; iii, $LiBH_4$, THF, rt, overnight, 80%; iv, MeLi, THF, 0 °C, 4 h, 54%; v, MnO_2, CH_2Cl_2, rt, 2 d, quantitative; vi, $Me_3O{\cdot}BF_4$, CH_2Cl_2, rt, 2 h, then $NaBH_4$, MeOH, 0 °C, 1 h, 25%.

Financial support from the 'Ministerio de Ciencia y Tecnología', Spain (project BQU2000-0785) is gratefully acknowledged. Thanks are also due to the 'Comissionat per a Universitats i Recerca' (Generalitat de Catalunya) for Grant 1999SGR00079. One of us (Y. A.) also thanks the 'Ministerio de Educación, Cultura y Deporte' for a Grant.

Notes and references

1 U. Scholz and E. Winterfeldt, *Nat. Prod. Rep.*, 2000, **17**, 349.
2 M. Andriantsiferana, R. Besselièvre, C. Riche and H.-P. Husson, *Tetrahedron Lett.*, 1977, 2587.
3 (*a*) J. A. Joule, *The Monoterpenoid Indole Alkaloids*, ed. J. E. Saxton, in *The Chemistry of Heterocyclic Compounds*, ed. A. Weissberger and E. C. Taylor, Wiley, New York, 1983, vol. 25, part 4, pp. 232–239; (*b*) M. Alvarez and J. A. Joule, *Monoterpenoid Indole Alkaloids*, ed. J. E. Saxton, in *The Chemistry of Heterocyclic Compounds*, ed. E. C. Taylor, Wiley, Chichester, 1994, vol. 25, supplement to part 4, pp. 234–236.
4 For the synthesis of chiral non-racemic 1,2-dihydropyridines, see: (*a*) D. L. Comins and S. P. Joseph, in *Advances in Nitrogen Heterocycles*, ed. C. J. Moody, JAI Press, London, 1996, vol 2, pp. 251–294; For more recent work see: (*b*) D. L. Comins, D. H. LaMunyon and X. Chen, *J. Org. Chem.*, 1997, **62**, 8182; (*c*) D. L. Comins, A. H. Libby, R. S. Al-awar and C. J. Foti, *J. Org. Chem.*, 1999, **64**, 2184; (*d*) D. L. Comins, Y.-M. Zhang and S. P. Joseph, *Org. Lett.*, 1999, **1**, 657; (*e*) D. L. Comins and A. L. Williams, *Tetrahedron Lett.*, 2000, **41**, 2839; (*f*) J. T. Kuethe and D. L. Comins, *Org. Lett.*, 2000, **2**, 855; see also: (*g*) Y. Génisson, C. Marazano and B. C. Das, *J. Org. Chem.*, 1993, **58**, 2052.
5 (*a*) A. I. Meyers, N. R. Natale, D. G. Wettlaufer, S. Rafii and J. Clardy, *Tetrahedron Lett.*, 1981, **22**, 5123; (*b*) A. I. Meyers and N. R. Natale, *Heterocycles*, 1982, **18**, 13; (*c*) A. I. Meyers and T. Oppenlaender, *J. Chem. Soc., Chem. Commun.*, 1986, 920; (*d*) A. I. Meyers and T. Oppenlaender, *J. Am. Chem. Soc.*, 1986, **108**, 1989.
6 (*a*) P. Mangeney, R. Gosmini, S. Raussou, M. Commerçon and A. Alexakis, *J. Org. Chem.*, 1994, **59**, 1877; (*b*) S. Raussou, R. Gosmini, P. Mangeney, A. Alexakis and M. Commerçon, *Tetrahedron Lett.*, 1994, **35**, 5433; See also: (*c*) F. Rezgui, P. Mangeney and A. Alexakis, *Tetrahedron Lett.*, 1999, **40**, 6241.
7 (*a*) S. G. Davies, R. T. Skerlj and M. Whittaker, *Tetrahedron Lett.*, 1990, **31**, 3213; (*b*) R. P. Beckett, V. A. Burgess, S. G. Davies and M. Whittaker, *Tetrahedron Lett.*, 1993, **34**, 3617.
8 S. Yamada and M. Ichikawa, *Tetrahedron Lett.*, 1999, **40**, 4231.
9 (*a*) For a review, see: J. Bosch and M.-L. Bennasar, *Synlett*, 1995, 587. For more recent work, see: (*b*) M.-L. Bennasar, J.-M. Jiménez, B. Vidal, B. A. Sufi and J. Bosch, *J. Org. Chem.*, 1999, **64**, 9605; (*c*) M.-L. Bennasar, E. Zulaica, A. Ramírez and J. Bosch, *Tetrahedron*, 1999, **55**, 3117; (*d*) M.-L. Bennasar, B. Vidal, R. Kumar, A. Lázaro and J. Bosch, *Eur. J. Org. Chem.*, 2000, 3919. For the synthesis of ervitsine in the racemic form, see: (*e*) M.-L. Bennasar, B. Vidal and J. Bosch, *J. Org. Chem.*, 1997, **62**, 3597.
10 R. Amann, K. Arnold, D. Spitzner, Z. Majer and G. Snatzke, *Liebigs Ann.*, 1996, 349.
11 All new compounds were fully characterized by spectroscopic analysis (NMR) and gave satisfactory HRMS and/or combustion data.
12 Crystal data for $C_{25}H_{29}N_3O_3$ (**7**) at 293(2) K: M = 419.51, monoclinic, space group $P2_1$, a = 10.418(1), b = 8.826(1), c = 12.670(2) Å, β = 106.91(1)°, U = 1114.6(2) Å^3, Z = 2, μ(Mo-Kα) = 0.083 mm^{-1}, 3961 reflections collected, 3565 independent reflections (R_{int} = 0.0175). The final $R1$ and $wR2$ were 0.0374 [$I > 2\sigma(I)$] and 0.1120 (all data), respectively. CCDC 162511. See http://www.rsc.org/suppdata/cc/b1/b102010m/ for crystallographic data in .cif format.
13 E. Wenkert, Y. D. Vankar and J. S. Yadav, *J. Am. Chem Soc.*, 1980, **102**, 7971.

CHEMCOMM
Communication
www.rsc.org/chemcomm

Extended scope of *in situ* iodotrimethylsilane mediated selective reduction of benzylic alcohols

Gary A. Cain* and Edward R. Holler

Chemical and Physical Sciences, DuPont Pharmaceuticals Company, P.O. Box 80336, Experimental Station E336/109, Wilmington, DE 19880-0336, USA. E-mail: gary.a.cain@dupontpharma.com

Received (in Corvallis, OR, USA) 14th March 2001, Accepted 7th May 2001
First published as an Advance Article on the web 25th May 2001

Iodotrimethylsilane, generated *in situ* from chlorotrimethylsilane and sodium iodide in acetonitrile, selectively reduces moderately electron deficient benzylic alcohols to the analogous toluenes; other reduction sensitive functional groups such as ketone, aldehyde, nitrile, and nitro are unaffected.

The use of iodotrimethylsilane (TMSI), generated *in situ* from $ClSiMe_3$ (TMSCl) and NaI in dry CH_3CN, is known to be a useful reagent for the reduction of secondary benzylic alcohols.[1–3] Although infrequently utilized, this reagent provides high yields of the deoxygenated toluene products, particularly for electron rich aromatic systems. The near exclusive use of these conditions for electron rich substrates may be associated with the proposed intermediacy of a benzylic stabilized carbocation at the reduction site. We now report that *in situ* TMSI reductions can be extended to moderately electron deficient benzylic alcohols, and that these conditions are selective in the presence of other reduction sensitive functional groups.

Our interest in the area began when we required a preparation of 3-(4-fluorobenzyl)pyridine. Being a previously unknown compound, we envisaged that it should be accessible *via* a Grignard reaction to form the benzylic alcohol, followed by selective benzylic –OH reduction in the presence of the potentially reduced pyridine ring (Scheme 1). In practice, the Grignard reaction, using commercially available 4-fluorophenylmagnesium bromide **1** and 3-formylpyridine **2** in Et_2O at 0 °C, readily provided the benzylic alcohol **3** in 74% yield after flash chromatography. At this stage of our work we followed the *in situ* TMSI benzylic alcohol reduction conditions from the first pertinent literature paper we could locate.[3] This reference used 6 eq. each of TMSCl and NaI with acetonitrile as solvent at 0 °C for 5 min. Under these conditions, however, we did not observe any reduction product. Eventually we found that upon heating the reaction to 55 °C (the boiling point of TMSCl) overnight we obtained a near quantitative yield of the desired reduction product **4** after standard workup (see Table 1, Ex. 1).

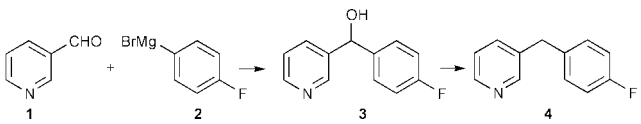

Scheme 1

Upon subsequently conducting a more thorough literature search, we were surprised to find that the defluoro analog of our above example was reported[4] to provide a 0% yield under attempted TMSI reduction. Because this particular paper was mainly concerned with electron rich systems, which proceeded quickly at low temperature, these workers may not have attempted the higher temperature and longer time that we had found necessary. Indeed, when we attempted the reduction of 1-(3-pyridyl)phenylmethanol at 55 °C (Ex. 2), we found that the reduction did proceed, although quite slowly. After 5 days the reduction was observed to be 67% complete by proton NMR.

Having thus established that electron poor 3-pyridyl benzylic alcohols were successful substrates for the *in situ* TMSI reduction, we then explored several other electron deficient examples to begin to understand the scope of the reaction. These results are summarized in the Table 1, Examples 1–8.

It is apparent from these results that moderately electron deficient diarylmethanols are good substrates for this reduction. Comparison of Ex. 3–5 illustrates that increasingly electron deficient systems, as by the sequential introduction of more fluorines onto the rings, led to much slower reactions and poorer yields. The reaction of the 2-pyridyl analog (Ex. 6), with the electron deficient node directly adjacent to the reaction center, failed completely. Strongly electron deficient 4-nitrophenyl

Table 1 *In situ* TMSI reduction of electron deficient benzylic alcohols

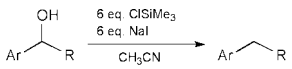

Ex. #	Ar	R	Time	Temp/°C	Yield (%)[a]
1	3-Pyridyl	4-F-Ph	18 h	55	99
2	3-Pyridyl	Ph	5 d	55	26[b] (67)
3	4-F-Ph	4-F-Ph	4 h	rt	98
4	3,4,5-Tri-F-Ph	3,4,5-Tri-F-Ph	6 d	55	12[b] (74)
5	F_5-Ph	F_5-Ph	7 d	55	0
6	2-Pyridyl	Ph	5 d	55	0
7	4-NO_2-Ph	Me	6 d	55	0
8	4-NO_2-Ph	Ph	24 h	55	38
9	4-F-Ph	4-CN-Ph	3 h	rt	96
10	4-Ac-Ph	4-Ac-Ph	15 min	rt	100
11	4-F-Ph	4-CHO-Ph	18 h	rt	58
12	4-Ac-Ph	Me	18 h	rt	99

[a] Yields are for isolated and fully characterized pure products. Yields in parentheses are estimated amounts in the crude product ^{1}H NMR. [b] Additional product was present in mixed chromatography fractions.

 DOI: 10.1039/b102495g

groups provide poor substrates, giving a low yield for the doubly aromatic analog Ex. 8, and failing to react for monobenzylic analog Ex. 7.

With this success for the *in situ* TMSI reduction of moderately electron poor benzylic alcohols, we then sought to take advantage of these conditions for selective reductions. Aldehydes, ketones, and nitriles are examples of mild electron withdrawing aromatic substituents which are widely found in the chemical literature. For substrates containing any of these three functional groups, reductive cleavage of a benzylic –OH under more standard conditions,[5] such as catalytic hydrogenation,[6] could be problematic. In fact, a literature search for benzylic alcohol reduction in the presence of an aldehyde or ketone failed to identify any direct methods. As shown in Examples 9–12, we have applied the *in situ* TMSI method to a series of these sensitive molecules. In all cases, the benzylic –OH was reductively cleaved to provide the toluene product and leave the –CN, –Ac, and –CHO groups intact. These conditions, therefore, appear to be suitable for more widespread use.

Notes and references

1 T. Sakai, K. Miyata, M. Utaka and A. Takeda, *Tetrahedron Lett.*, 1987, **28**, 3817.
2 T. Sakai, K. Miyata, S. Tsuboi, A. Takeda, M. Utaka and S. Torii, *Bull. Chem. Soc. Jpn.*, 1989, **62**, 3537.
3 P. J. Perry, V. H. Pavlidis and I. G. C. Coutts, *Synth. Commun.*, 1996, **26**, 101.
4 E. J. Stoner, D. A. Cothron, M. K. Balmer and B. A. Roden, *Tetrahedron*, 1995, **51**, 11043.
5 M. Hudlicky, *Reductions in Organic Synthesis*, American Chemical Society, Washington, D.C., 1996, pp. 107–108.
6 H. O. House, *Modern Synthetic Reactions, 2nd Ed.*, Benjamin Cummings, Reading, Massachusetts, 1972, ch. 1.

CHEMCOMM
Communication
www.rsc.org/chemcomm

A self-assembled novel octanuclear Cu(II) 'pin-wheel' cluster exhibiting ferromagnetic coupling

Zhiqiang Xu, Laurence K. Thompson* and David O. Miller

Department of Chemistry, Memorial University of Newfoundland, St. John's, NFLD, Canada A1B 3X7. E-mail: lthomp@morgan.ucs.mun.ca

Received (in Cambridge, UK) 1st March 2001, Accepted 14th May 2001
First published as an Advance Article on the web 5th June 2001

The heptadentate, 'tritopic' ligand 2poapH_2 reacts with $Cu(NO_3)_2$ in the presence of $Gd(NO_3)_3$ to give a novel, self-assembled, ferromagnetically coupled, alkoxide bridged octanuclear Cu(II) cluster in the shape of a pin-wheel, with a central $Cu_4[\mu\text{-}O_4]$ core, and isolated Curie-like $[Gd(NO_3)_4(H_2O)_2]^-$ anions.

Self-assembly reactions with polytopic ligands have led to a number of novel polynuclear cluster complexes, and with the ligand coordination pockets held in a linear array 2D grid structures are produced with tetranuclear,[1–4] hexanuclear,[5] nonanuclear,[6–9] and hexadecanuclear[10] examples. Interest in such systems stems from their ability to produce high nuclearity metallic clusters with pre-determined geometrical arrangements of closely spaced metal centres. With appropriate bridging groups arranged strategically in the ligand backbone magnetic coupling between the metal ions can occur. Examples of alkoxide bridged nonanuclear grids show antiferromagnetic coupling ($M_9(\mu\text{-}O)_{12}$; M = Mn(II), Co(II), Ni(II)), while with copper(II) ferromagnetic exchange prevails due to strict magnetic orbital orthogonality *via* the μ-O bridges.

In an attempt to generate a mixed lanthanide/copper complex of the ligand 2poapH_2 (Scheme 1), with the possibility of enhanced ferromagnetic exchange, $Gd(NO_3)_3$ and $Cu(NO_3)_2$ were reacted with the ligand sequentially.† The resulting green complex, $[Cu_8(2poap)_4(CH_3OH)_4(CH_3CN)_4][Gd(NO_3)_4(H_2O)_2]_2(NO_3)_6\cdot 1.3Cu(NO_3)_2\cdot(H_2O)_{10}$ (**1**),‡ has been shown to contain both copper and gadolinium, but the main fragment consists of a self-assembled octanuclear $Cu(II)_8$ cation accompanied by two isolated $[Gd(NO_3)_4(H_2O)_2]^-$ anions, and a fourth component which has been identified crystallographically as a $Cu(NO_3)_2$ based fragment trapped in the lattice. Fig. 1 shows the octanuclear cation with four opposed ligands in parallel pairs bound *via* terminal coordination pockets to a central square 2 × 2 core of four octahedral Cu(II) centres, which are bridged by alkoxide oxygen atoms, in an arrangement common to other $[M_4(\mu\text{-}O)_4]$ square grids[4] with the ditopic ligand poapH (M = Mn(II), Co(II), Ni(II), Cu(II), Zn(II)). The other ends of the four ligands radiate from the core to create a pin-wheel structure with the external coppers connected to the core by alkoxide bridges. The external tridentate ligand pockets fill only three copper coordination sites, and other sites at these square pyramidal copper centres are occupied by solvent molecules (CH_3OH, CH_3CN from solvent used to produce crystals). The core structure showing the alkoxide bridging connections is illustrated in Fig. 2. Cu–O–Cu angles overall fall in the range 139.0–142.0°. Cu–Cu distances within the core fall in the range

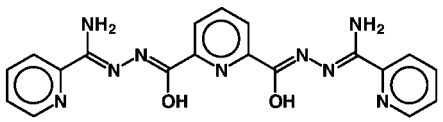

2poapH2

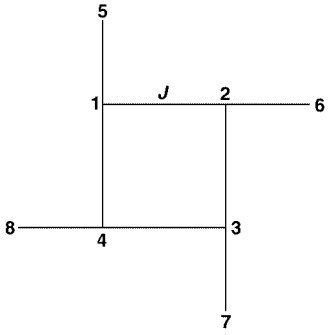

Scheme 1

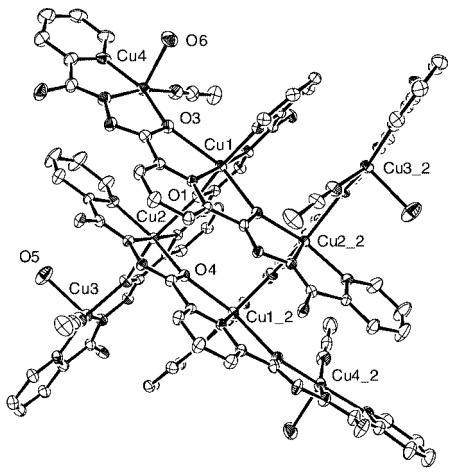

Fig. 1 Structural representation of the cation $[Cu_8(2poap)_4(CH_3OH)_4(CH_3CN)_4]$ in (**1**) (40% probability thermal ellipsoids). Cu(1)–O(4)' 2.307(4), Cu(1)–O(1) 2.020(4), Cu(2)–O(1) 2.283(4), Cu(2)–O(4) 2.030(4), Cu(3)–O(2) 1.969(5), Cu(3)–O(5) 2.215(6), Cu(2)–O(2) 2.340(4), Cu(1)–O(3) 2.404(5), Cu(4)–O(3) 1.983(5), Cu(4)–O(6) 2.224(6), Cu(1)–Cu(2) 4.082(2), Cu(2)–Cu(1)' 4.038(2), Cu(2)–Cu(3) 4.038(2), Cu(1)–Cu(4) 4.151(2), Cu(3)–Cu(3)' 12.805(2), Cu(4)–Cu(4)' 12.676(2) Å; Cu–O–Cu 139.0–142.0°.

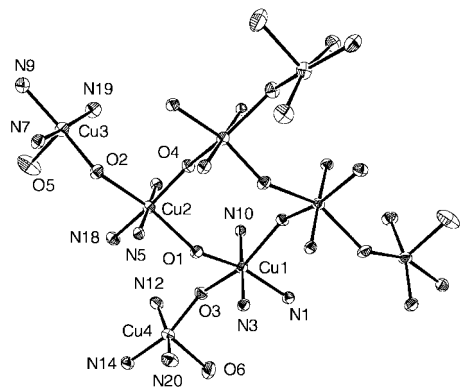

Fig. 2 Structural representation of the octanuclear core in **1**.

 DOI: 10.1039/b101966j

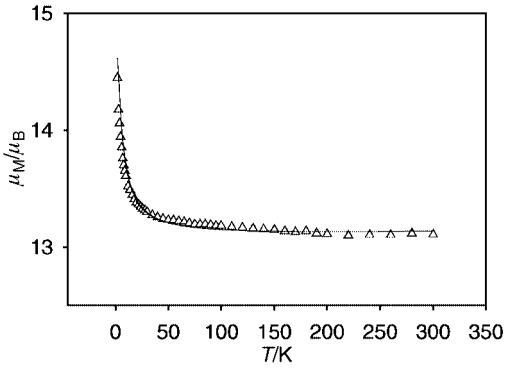

Fig. 3 Magnetic properties of **1** plotted as μ_{mol} *vs.* temperature. The solid line is the best fit of the data to eqn. (1) (see text for fitting parameters).

4.03–4.09 Å, and in the range 4.03–4.15 Å outside. The diagonal external Cu–Cu distances exceed 12.6 Å. The coppers within the core are six-coordinate, with elongated tetragonal stereochemistry. The long contacts involve all the ring oxygen bridging atoms and all *trans* related oxygens (*e.g.* Cu(2)–O(1) 2.283(4) Å; Cu(2)–O(2) 2.340(5) Å). The external square pyramidal coppers have short contacts to the oxygen bridges (Cu(3)–O(2) 1.969(5) Å, Cu(4)–O(3) 1.983(5) Å), and long axial contacts to the weakly bound methanol molecules (Cu(3)–O(5) 2.215(6) Å, Cu(4)–O(6) 2.224(6) Å). This leads to a unique arrangement of the copper atoms, in which all the oxygen bridging connections involve strict metal magnetic orbital ($d_{x^2-y^2}$) orthogonality, resulting in unique ferromagnetic properties (*vide infra*). A related, antiferromagnetically coupled complex $[Cu_8(dpd-2H)_4(\mu\text{-}O_2CMe)_4\{pyOH\}_4](ClO_4)_4$ (**2**) (dpd−2H = dianion from the *gem*-diol $(py)_2(OH)_2$; pyOH = 2-hydroxypyridine), reported recently has a $Cu_4(\mu\text{-}O)_4$ core and four pendant copper centres linked by carboxylate bridges.[11]

Fig. 3 shows the profile of molar magnetic moment *vs.* temperature for **1**, with a moment rising slightly from 13.1 μ_B at 300 K to 13.3 μ_B at about 25 K, followed by a sharp rise to a maximum value of 14.5 μ_B at 2 K.§ Given the fact that the isolated Gd(III) and Cu(II) centres should behave as Curie components the overall magnetic behaviour of **1** indicates the presence of a ferromagnetically coupled cluster. The magnetic data were fitted to an isotropic exchange expression based on a spin Hamiltonian [eqn. (1); Scheme 1],

$$H = -J(S_1S_2 + S_2S_3 + S_3S_4 + S_1S_4 + S_1S_5 + S_2S_6 + S_3S_7 + S_4S_8) \quad (1)$$

reflecting equivalent exchange interactions (J) between adjacent copper(II) centres. The total spin states, and their energies, were calculated using the normal spin vector coupling method,[12] and substituted into the van Vleck equation in the usual way. Curie components corresponding to 2 Gd(III) ions and 1.3 Cu(II) ions identified in the X-ray structure were included. An excellent data fit was obtained using a non-linear regression procedure, and the solid line in Fig. 3 was calculated for g_{av} = 2.113(2), J = 5.0(2) cm^{-1}, TIP = 0.000500 emu mol^{-1}, θ = −0.10 K (R = 1.0%) (θ is a Weiss-like corrective term, TIP = temperature independent paramagnetism). The positive J confirms the intramolecular ferromagnetic behaviour, with a value comparable to related 2 × 2 and 3 × 3 grid systems,[4,8,9] and illustrates another example in which there appears to be a spontaneous tendency for the closely spaced magnetic planes to tilt away from each other in the alkoxide bridged cluster. Magnetization *vs.* field data at 2 K showed incomplete saturation at 5 T, with a value of 24.8 $N\beta$ at 5 T. This is consistent with the sum of the ferromagnetically coupled Cu_8 cluster, and the Curie-like Gd(III) and Cu(II) centers.

The novel ferromagnetically coupled Cu_8 pinwheel cluster forms in a mixed metal self-assembly reaction. Gd(III) is assumed to influence the cluster self assembly, possibly by a pre-coordination step at one end of a ligand, prior to formation of the central square core, followed by displacement of the Gd(III) by Cu(II) ions. Similar reactions are being studied with other first row transition metals.

This research was supported by NSERC (Natural Sciences and Engineering Research Council of Canada). We thank Dr. R. McDonald, University of Alberta, for X-ray crystallographic data.

Notes and references

† $2poapH_2$ was synthesized by a published procedure.[7] $2poapH_2$ (0.40 g, 1.0 mmol) was added to a warm methanol solution (25 mL) of $Gd(NO_3)_3\cdot 6H_2O$ (0.23 g, 0.5 mmol) and the mixture stirred for several minutes until the ligand dissolved, forming a clear yellowish solution. CH_3CN (20 mL) was added and the solution refluxed, and a warm solution of $Cu(NO_3)_2\cdot 3H_2O$ (0.75 g, 3.1 mmol) in methanol (10 mL) added slowly. A brownish powder formed initially, which then dissolved forming a clear deep green solution. Well formed dark green crystals, suitable for X-ray analysis, were produced from the filtered solution after several days (yield 85%). Found (vacuum dried sample): C, 25.87; H, 2.56; N, 19.53. Calc. for $(C_{19}H_{15}N_9O_2)_4\text{-}Cu_8Gd_2(CH_3CN)_4(CH_3OH)_4](NO_3)_{14}\cdot 14H_2O\cdot 1.3Cu(NO_3)_2$: C, 25.87; H, 2.86; N, 19.41. ν_{max}/cm^{-1} (Nujol) 3436 (H_2O), 3343, 3172 (NH), 1665 (C=N) and 1026 (py). λ_{max}/nm (Nujol) 700. $\mu_{(RT)}$ = 13.1 μ_B (mol).

‡ *Crystal data* for $[Cu_8(2poap)_4(CH_3OH)_4(CH_3CN)_4][Gd(NO_3)_4\text{-}(H_2O)_2]_2(NO_3)_6\cdot 1.3Cu(NO_3)_2\cdot(H_2O)_{10}$ (**1**): $C_{44}H_{52.5}N_{27.3}O_{31.65}Cu_{4.65}Gd$ **1**; M = 1922.9, monoclinic, space group $C2/c$ (no. 15), a = 26.647(1), b = 18.1576(9), c = 30.423(2) Å, β = 90.282(1)°, U = 14720(1) Å^3, Z = 8, D_c = 1.735 g cm^{-3}, T = 193(1) K, μ(Mo-Kα) = 23.12 cm^{-1}. 954 parameters were refined with 10976 unique reflections ($I > 2.0\sigma(I)$) to give $R1$ = 0.057, $wR2$ = 0.178 (15062 independent reflections, R_{int} = 0.041) (Bruker P4/CCD with graphite-monochromatized Mo-Kα X-radiation, and a rotating anode generator). Hydrogen atoms were introduced in calculated positions with isotropic thermal parameters set 20% greater than bonding partners and were not refined. A total of six hydrogens from the gadolinium waters and the methanol molecules were omitted from the model. One methyl group from a bound methanol was fixed for the final round of refinement. CCDC reference number 160557. See http://www.rsc.org/suppdata/cc/b1/b101966j/ for crystallographic data in CIF or other electronic format.

§ SQUID magnetometer (Quantum Design MPMS5S) with fields of 0.1–5 T. Diamagnetic corrections for the sample holder and the sample were applied.

1 M.-T. Youinou, N. Rahmouni, J. Fischer and J. A. Osborn, *Angew. Chem., Int., Ed. Engl.*, 1992, **31**, 733.
2 G. S. Hannan, D. Volkmer, U. S. Schubert, J-M. Lehn, G. Baum and D. Fenske, *Angew. Chem., Int. Ed. Engl.*, 1997, **36**, 1842.
3 P. J. van Koningsbruggen, E. Müller, J. G. Haasnoot and J. Reedijk, *Inorg. Chim. Acta*, 1993, **208**, 37.
4 C. J. Matthews, K. Avery, Z. Xu, L. K. Thompson, L. Zhao, D. O. Miller, K. Biradha, K. Poirier, M. J. Zaworotko, C. Wilson, A. E. Goeta and J. A. K. Howard, *Inorg. Chem.*, 1999, **38**, 5266.
5 P. N. W. Baxter, J.-M. Lehn, B. O. Kneisel and D. Fenske, *Angew. Chem., Int. Ed. Engl.*, 1997, **36**, 1978.
6 P. N. W. Baxter, J.-M. Lehn, J. Fischer and M.-T. Youinou, *Angew. Chem., Int. Ed. Engl.*, 1994, **33**, 2284.
7 L. Zhao, C. J. Matthews, L. K. Thompson and S. L. Heath, *Chem. Commun.*, 2000, 265.
8 L. Zhao, Z. Xu, L. K. Thompson, S. L. Heath, D. O. Miller and M. Ohba, *Angew. Chem., Int. Ed. Engl.*, 2000, **39**, 3114.
9 O. Waldmann, R. Koch, S. Schromm, P. Müller, L. Zhao and L. K. Thompson, *Chem. Phys. Lett.*, 2000, **332**, 73.
10 A. M. Garcia, F. J. Romero-Salguero, D. M. Bassani, J.-M. Lehn, G. Baum and D. Fenske, *Chem. Eur. J.*, 1999, **5**, 1803.
11 M.-L Tong, K. H. Lee, Y.-X. Tong, X.-M. Chen and T. C. W. Mak, *Inorg. Chem.*, 2000, **39**, 4666.
12 K. Kambe, *J. Phys. Soc. Jpn.*, 1950, **5**, 48.

CHEMCOMM
Communication
www.rsc.org/chemcomm

Chiral modification of platinum catalysts by cinchonidine adsorption studied by *in situ* ATR-IR spectroscopy

Davide Ferri, Thomas Bürgi and Alfons Baiker*

Laboratory of Technical Chemistry, Swiss Federal Institute of Technology, ETH-Zentrum, CH-8092 Zurich, Switzerland. E-mail: baiker@tech.chem.ethz.ch

Received (in Cambridge, UK) 29th March 2001, Accepted 18th May 2001
First published as an Advance Article on the web 8th June 2001

Adsorption of cinchonidine on a platinum model catalyst studied by *in situ* ATR-IR spectroscopy revealed that the adsorption mode depends on surface coverage and is affected by concomitant adsorption and fragmentation of solvent molecules.

Heterogeneous asymmetric hydrogenation on chirally modified catalysts is a promising route for producing chiral molecules with high optical purity from prochiral reactants. At present, tartaric acid modified Ni catalysts[1,2] and cinchona modified Pt based catalysts[3–5] are the most successful systems for the hydrogenation of β-keto esters and α-keto esters, respectively. With respect to the latter, the adsorption mode of cinchonidine (CD) is a critical factor, and still a matter of debate. Direct spectroscopic information is available only from earlier XPS and LEED[6] and recent NEXAFS[7] studies of the adsorption of 10,11-dihydrocinchonidine on Pt(111) under UHV conditions. At 298 K the quinoline ring was found to lie almost parallel to the metal surface, whereas a tilting angle of *ca.* 60° was found at 323 K. However, these studies fail to describe the adsorption under reaction conditions, *i.e.* in the presence of both the solvent and H_2. With the present work we aim at closing this gap by studying the adsorption of CD using attenuated total reflection IR spectroscopy (ATR-IRS)[8] close to reaction conditions. For this purpose we have developed a model system based on a Pt/Al_2O_3 coated Ge internal reflection element.[9] In the following it will be shown that the presence of a solvent acting as a competing adsorbate is a crucial factor for modifier adsorption. Adsorption of CD on Pt/Al_2O_3 turns out to be complex. Several adsorption modes of CD can be distinguished, depending on coverage and time similar to recent findings for the Ni–tartrate system.[10]

ATR spectra of cinchonidine (CD) adsorbed from H_2-saturated CH_2Cl_2 solvent on Pt/Al_2O_3 are shown in Fig. 1.† Before recording the ATR spectra the Pt/Al_2O_3 film was treated with hydrogen saturated CH_2Cl_2 which results in a cleaning of the Pt.[9] After this the background spectrum was recorded. Upon admitting a H_2-saturated solution of CD to the sample positive and negative signals were immediately observed in the ATR spectra. The positive signals arise from molecules, which are added to, negative signals from molecules, which are removed from the interface, with respect to the reference spectrum. We assign the positive signals to adsorbed CD, whereas the negative signals are due to simultaneous removal of adsorbed solvent decomposition products as well as the displacement of solvent from near the interface, as detailed below. The spectra exhibit distinct concentration [compare Fig. 1(a) and (c)] and time dependence [Fig. 1 (b) and (e)] and are clearly different from the solution spectrum as a consequence of the interaction of CD with the Pt/Al_2O_3. By contacting quinoline (Q, not shown) with Pt/Al_2O_3, the same concentration and time behaviour of the corresponding vibrational bands was observed, indicating that the interaction of CD with the surface is dominated by the quinoline moiety. The change of the relative intensity of the vibrational bands with concentration and time and the appearance of new bands with respect to the solution spectrum can arise due to (i) a chemical reaction of CD or (ii) a change in adsorption geometry. Feasible chemical reactions of the quinoline moiety under the applied conditions are hydrogenation and α-H abstraction. As concerns hydrogenation, several possible hydrogenation products (1,2,3,4- and 5,6,7,8-tetrahydroquinoline and decahydroquinoline) were adsorbed from CH_2Cl_2 on the Pt/Al_2O_3 film. Although for most of them adsorption could be observed, none of them exhibited the vibrational bands shown in Fig. 1 and hence we exclude adsorbed hydrogenation products as the origin of the bands in Fig. 1. To our knowledge no analysis of the vibrational spectrum of quinoline (intact and/or after α-H abstraction) on Pt has been reported so far. On the other hand for the chemically related pyridine on Pt detailed analysis exists.[11] Intact pyridine and pyridine after α-H abstraction can clearly be distinguished. After adsorption of pyridine from hydrogen-saturated CH_2Cl_2 we predominantly observed the bands which have been associated with intact pyridine in a tilted orientation and bound *via* the N-atom.[11] Although α-H abstraction is feasible, we conclude that it is not a dominant process under the applied conditions. On the other hand the absence of the signal at 1635 cm^{-1} corresponding to ν(C=C) of the vinyl moiety indicates that CD is hydrogenated at this site.

Based on the above mentioned results we conclude that the observed positive bands are mainly associated with chemically intact CD and that the changes in relative intensity of the bands in Fig. 1 are associated with changes in adsorption geometry. At

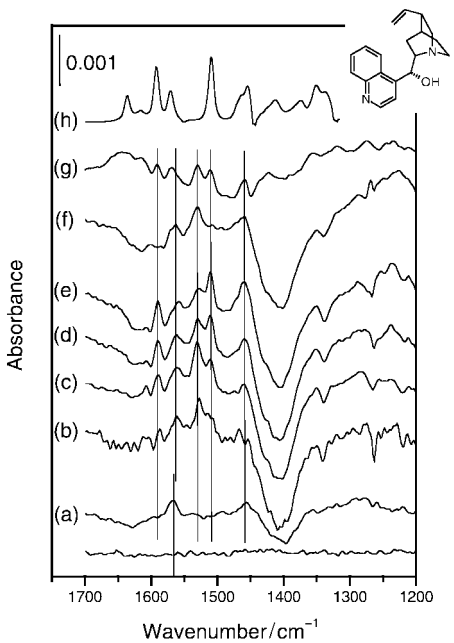

Fig. 1 ATR-IR spectra of cinchonidine adsorption on Pt/Al_2O_3 at 283 K from (a) 10^{-7} mol l^{-1} and (b)–(e) 10^{-3} mol l^{-1} solution in CH_2Cl_2 (recorded after 2, 3, 42 and 122 min, respectively), (f) followed by neat solvent flow; (g) from a 10^{-4} mol l^{-1} solution in cyclohexane at 293 K; (h) scaled (1:80) transmission spectrum of cinchonidine in CH_2Cl_2.

 DOI: 10.1039/b102884g

least three different adsorption geometries of CD (in the following termed 'species') can be distinguished by analysing the spectral region between 1500 and 1650 cm^{-1}, associated with the quinoline ring vibrations. A first species associated with only one band in this region at 1567 cm^{-1} predominates at 10^{-7}–10^{-6} mol l^{-1} [Fig. 1(a)]. At higher solution concentration, signals at 1610, 1590, 1567, 1530, 1511 and 1460 cm^{-1} are observed, having relative intensities changing with adsorption time. A slight red-shift is observed for the signal at around 1570 cm^{-1} upon increasing the concentration above 10^{-6} mol l^{-1} together with the appearance of the signal at 1530 cm^{-1}. The features at 1530 and 1567 cm^{-1} dominate the spectrum: (i) when slowly increasing the concentration of CD from 10^{-7} to 10^{-5} mol l^{-1}, (ii) at the very first stages of adsorption when flowing higher concentration ($> 10^{-5}$ mol l^{-1}) of CD [Fig. 1(b)], and (iii) when flowing neat solvent after saturating the sample [Fig. 1(f)]. They are attributed to a second species that is therefore strongly adsorbed. A third species is associated with strong bands at 1511 and 1590 cm^{-1} with a spectrum resembling that of CD in solution [Fig. 1(h)]. This species appears only at later stages of adsorption and at high concentration [Fig. 1(c)–(e)] and disappears when flowing neat solvent. This species is therefore only weakly bound, which is in line with the fact that its spectrum very much resembles the (unperturbed) solution spectrum. Interestingly, the intensity of the bands associated with the second and third species are anticorrelated, which is best seen by comparing the signals at 1511 and 1530 cm^{-1} in Fig. 1(b)–(e). Such behaviour is consistent with mutually interconverting species, the driving force for this process being the solution concentration. The signal at 1460 cm^{-1} observed for all three species is associated with the quinuclidine moiety of CD as the adsorption of quinuclidine (QD) on Pt/Al_2O_3 clearly indicated (not shown).

Knowledge of the direction of the dynamic dipole moment of a selection of vibrations (from *ab initio* calculations) combined with the metal surface selection rule[12] allows information to be gained about the local adsorbate orientation. Fig. 2 shows that the vibration at 1509 cm^{-1} in the solution spectrum is polarised roughly along the long axis of the quinoline moiety, whereas the mode at 1570 cm^{-1} is polarised perpendicular to it.

In line with the calculated polarisation of the bands, the following interpretation of the spectra can be given: the species associated with only one strong signal at 1567 cm^{-1} has the long axis of the quinoline moiety nearly parallel to the surface with a degree of tilting of the short axis, probably induced by the quinoline-N and the O–H group. For the second species the appearance of a second band at 1530 cm^{-1} indicates a change in orientation. We tentatively assign the band at 1530 cm^{-1} to the 1509 cm^{-1} band in solution, which is blue-shifted due to an interaction with the surface. A similar blue-shift of the corresponding bands was observed for pyridine on Pt adsorbed through the N atom in a tilted orientation.[11,13] The pyridine spectrum recorded in the presence of H_2 and CH_2Cl_2 shows bands with A_1 and B_1 symmetry,[11] indicating that none of the molecular axes are oriented parallel to the surface. Hence, the observed blue-shift of the 1530 cm^{-1} band, in analogy with adsorbed pyridine under our conditions, and the calculated polarisation of the 1530 cm^{-1} band are consistent with the interpretation that for the second species the long axis of the quinoline moiety is no longer parallel to the surface. The weakly bound third species does not show significant orientation preferences.

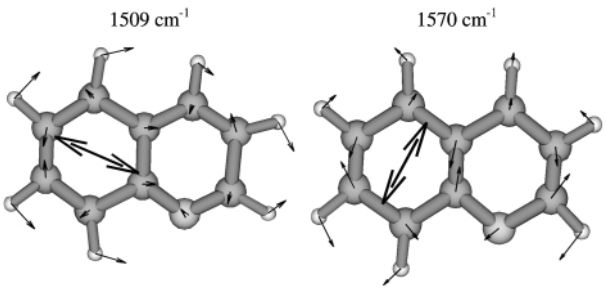

Fig. 2 Schematic of two of the vibrational modes of quinoline used to identify adsorption orientation. Arrows indicate atomic displacement vectors and the direction of the dynamic dipole moment, respectively. The corresponding experimental IR frequencies for cinchonidine in CH_2Cl_2 are also given.

As a general trend the quinoline moiety of CD is tilted more with increasing solution concentration and coverage. This is consistent with an increase of the average thickness of the adsorbate layer (defined as the distance between the Pt/adsorbate and the adsorbate/solution interfaces) and thus the displacement of solvent from very near the interface. This effect is directly observed in the ATR spectra. The negative peak at 1260 cm^{-1} corresponds to the strongest solvent vibration. Upon adsorption of CD (increasing the thickness of the adsorbate layer) this peak becomes negative, since, with respect to the reference spectrum, less solvent is probed by the electromagnetic field. The other negative signals at around 1635, 1400, 1338 and 1120 cm^{-1} (not shown) are associated with removal of water, CH_x and ethylidyne (CCH_3), respectively, from the adsorbate layer. CH_x fragments (1400 cm^{-1}) are formed from CH_2Cl_2 decomposition.[14] Upon admission of a solution of CH_2Cl_2 in cyclohexane on the Pt/Al_2O_3 sample the band was also observed supporting this view. Ethylidyne (1338, 1120 cm^{-1}) is likely formed by recombination of CH_x fragments, which is supported by the observed evolution of ethene on Pt/Al_2O_3 in contact with CH_2Cl_2.[14] CD adsorption from cyclohexane solvent afforded the same positive signals associated with CD, but not the negative signals associated to CH_x fragments and ethylidyne [Fig. 1(g)].

The ATR spectra clearly show that the adsorption mode of CD is coverage dependent and that CD competes with solvent decomposition products for adsorption sites. This observation adds an important new facet to the interpretation of the 'solvent effect' in enantioselective hydrogenation over cinchona-modified platinum.

We gratefully acknowledge the financial support of the Swiss Federal Institute of Technology (ETH), the Swiss National Science Foundation and CSCS Manno.

Notes and references

† *In situ* experiments were carried out with a home-made stainless steel flow through cell by recording spectra at 283 K and co-adding 200 scans at 4 cm^{-1} resolution with a Bruker IFS/66 spectrometer equipped with a liquid-N_2-cooled MCT detector. Adsorption was carried out from H_2-saturated millimolar solutions in CH_2Cl_2 solvent (if not otherwise specified) after cleaning of the metal surface with H_2-saturated solvent. ATR spectra are presented in absorbance units with the last spectrum recorded during H_2-cleaning serving as reference. Pt/Al_2O_3 model films were prepared as described elsewhere.[9] Density functional theory (B3PW91 / cc-pvtz) was used to calculate frequencies and determine the dynamic dipole moment of each vibration.

1 Y. Izumi, *Adv. Catal.*, 1983, **32**, 215.
2 G. Webb and P. B. Wells, *Catal. Today*, 1992, **12**, 319.
3 Y. Orito, S. Imai and S. Niwa, *J. Chem. Soc. Jpn.*, 1979, 1118.
4 K. E. Simons, P. A. Meheux, S. P. Griffiths, I. M. Sutherlands, P. Johnston, P. B. Wells, A. F. Carley, M. K. Rajumon, M. W. Roberts and A. Ibbotson, *Recl. Trav. Chim. Pays Bas*, 1994, **113**, 465.
5 A. Baiker, *J. Mol. Catal. A: Chem.*, 1997, **115**, 473.
6 A. F. Carley, M. K. Rajumon, M. W. Roberts and P. B. Wells, *J. Chem. Soc., Faraday Trans.*, 1995, **91**, 2167.
7 T. Evans, A. P. Woodhead, A. Gutiérrez-Sosa, G. Thornton, T. J. Hall, A. A. Davis, N. A. Young, P. B. Wells, R. J. Oldman, O. Plashkevych, O. Vahtras, H. Ågren and V. Carravetta, *Surf. Sci.*, 1999, **436**, L691.
8 N. J. Harrick, in *Internal reflection spectroscopy*, Interscience Publishers, New York, 1967.
9 D. Ferri, T. Bürgi and A. Baiker, *J. Phys. Chem. B*, 2001, **105**, 3187.
10 M. Ortega-Lorenzo, S. Haq, T. Bertrams, P. Murray, R. Raval and C. J. Baddeley, *J. Phys. Chem. B*, 1999, **103**, 10661.
11 S. Haq and D. A. King, *J. Phys. Chem. B*, 1996, **100**, 16957.
12 R. G. Greenler, *J. Chem. Phys.*, 1966, **44**, 310.
13 V. H. Grassian and E. L. Muetterties, *J. Phys. Chem.*, 1986, **90**, 5900.
14 E. Toukoniity, P. Mäki-Arvela, A. N. Villela, A. K. Neyestanaki, T. Salmi, R. Leino, R. Sjöholm, E. Laine, J. Väyrynen, T. Ollonqvist and P. J. Kooyman, *Catal. Today*, 2000, **60**, 175.

CHEMCOMM Communication
www.rsc.org/chemcomm

Condensation of acetonitrile into *N*-acetimidoylacetamidine promoted by a dinuclear nickel(II) complex†‡

Sergey V. Kryatov,[a] Alexander Y. Nazarenko,*[b] Millicent B. Smith[a] and Elena V. Rybak-Akimova*[a]

[a] *Department of Chemistry, Tufts University, Medford, Massachusetts 02155, USA. E-mail: erybakak@emerald.tufts.edu*
[b] *Department of Chemistry, State University of New York, College at Buffalo, Buffalo, New York 14222-1095, USA. E-mail: nazareay@buffalostate.edu*

Received (in Irvine, CA, USA) 27th February 2001, Accepted 15th May 2001
First published as an Advance Article on the web 8th June 2001

Acetonitrile reacts with a dinuclear nickel(II) complex $[Ni_2(\mu\text{-}OH)_2(tpa)_2](ClO_4)_2$ [tpa = tris-(2-pyridylmethyl)-amine] in solution forming a novel square-planar nickel(II) complex $Ni\{HN{=}C(Me){-}N{=}C(Me){-}NH\}_2$.

Acetonitrile is one of the common solvents that is widely used to study processes in solution. With most 3d-transition metal ions acetonitrile behaves as a relatively weak monodentate ligand, providing inorganic chemists with a perfect media for numerous reactions.[1] However, transition metal complexes are well known to catalyze and promote the reactions of nitriles, *e.g.* their reduction, redox coupling, hydrolysis, and addition of nucleophiles.[2,3] In some cases nitrile, R–C≡N, adds to a ligand (L^- or LH) yielding a new composite ligand (L–C(R)=N^- or L–C(R)=NH) within the coordination sphere of a metal ion.[2,4] Here we report the first case of a reaction, in which acetonitrile undergoes self-condensation into an efficient bidentate ligand (*N*-acetimidoylacetamidine) under the action of a metal complex, $[Ni_2(\mu\text{-}OH)_2(tpa)_2](ClO_4)_2$ **1**.

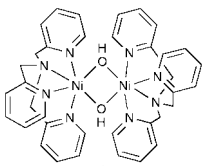

1

Metal complexes with the tripodal tetramine ligand tpa and its homologs have been widely used in metalloenzyme modeling.[5,6] In particular, complex **1** was found to be a good catalyst for transesterification and carbon dioxide hydration.[7,8]

We prepared complex **1** by a simplified, one-pot procedure adapted from the original method proposed by Ito and Takita.[7] Its identity was established by elemental analysis, mass spectrometry, and UV–VIS spectroscopy.§ Solid **1** gives a blue solution in acetonitrile. When stored in a tightly sealed container at room temperature, this solution very slowly (within months) turns dark-purple and precipitates an orange–yellow crystalline material. If the acetonitrile solution of **1** is kept at 75 °C, the transformation is completed in 2 days. Recrystallization from acetonitrile and drying under vacuum gives pure diamagnetic complex **2** with the formula $Ni(C_4H_8N_3)_2$.¶

A single crystal X-ray diffraction study of solvated complex **2**·$2H_2O$ revealed that tpa and hydroxide ligands around Ni(II) ions are lost and substituted by a new unexpected ligand, *N*-acetimidoylacetamidine (Fig. 1).‖ Each Ni(II) ion is coordinated by two bidentate *N*-acetimidoylacetamidinate anions, forming the mononuclear molecular complex **2**. A molecule of **2** contains two six-membered flat metallocycles (deviation of atoms from the mean plane < 0.02 Å, and < 0.05 Å, if methyl groups are taken into account). The Ni–N bond lengths (1.85 Å) are similar to other Ni(II) square planar low-spin complexes with imine nitrogen donor atoms.[1] In the crystal lattice of **2**·$2H_2O$, individual molecules of **2** are connected *via* hydrogen bonding with water molecules (Fig. 1; Table S1†).

A mass spectrometry study showed that *N*-acetimidoylacetamidine originated from the solvent (acetonitrile). The crude reaction solution after heating complex **1** in acetonitrile shows signals at *m/z* 255, 291, 347, 407 and 447, which can be ascribed to the molecular ions of $\mathbf{2}^+$, $[tpaH]^+$, $[Ni(tpa)]^+$, $[Ni(tpa)(MeCO_2)]^+$ and $[Ni(tpa)(ClO_4)]^+$, respectively, according to their positions and the relative intensities of isotope satellites. When the reaction is carried out with CD_3CN instead of regular acetonitrile, the peaks of $\mathbf{2}^+$ and $[Ni(tpa)(MeCO_2)]^+$ are shifted 12 and 3 daltons up, respectively. Therefore, the source of the four methyl groups in the molecule of **2** is acetonitrile. There is a concomitant formation of acetate from acetonitrile. The tpa ligand remains intact in the course of the reaction and is partially released in the free form. The stoichiometry of the overall transformation can be tentatively expressed by eqn. (1)

$$2[Ni_2(OH)_2(tpa)_2]^{2+} + 6MeCN \rightarrow Ni(C_4H_8N_3)_2 + 2Ni(tpa)(MeCO_2)^+ + Ni(tpa)^{2+} + tpa \quad (1)$$

The role of **1** as a nickel complex promoting the acetonitrile transformation is specific. In separate experiments under similar conditions, no reaction with acetonitrile was observed, if complex **1** was substituted by $NiX_2{\cdot}6H_2O$ (X = Cl, ClO_4, NO_3), $Ni(MeCO_2)_2{\cdot}4H_2O$, $Ni(ClO_4)_2{\cdot}6H_2O$ + py (1:4), or $Ni(ClO_4)_2{\cdot}6H_2O$ + tpa (1:1).

There are only scarce reports of metal complexes with protonated *N*-acetimidoylacetamidine ligand

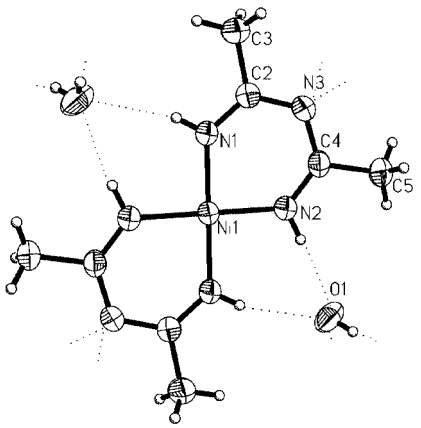

Fig. 1 ORTEP drawing of **2**·$2H_2O$. Selected bond lengths (Å) and angles (°): Ni–N2 1.850(2), Ni–N1 1.851(2), N1–C2 1.296(3); C2–N3 1.360(3), N3–C4 1.353(3); C4–N2 1.296(3), N1–Ni–N2 89.31(8).

† Electronic supplementary information (ESI) available: Table S1: hydrogen bonds in the crystal structure of complex **2**·$2H_2O$. See http://www.rsc.org/suppdata/cc/b1/b101893k/

‡ Dedicated to Professor Konstantin B. Yatsimirskii on the occasion of his 85th birthday.

 DOI: 10.1039/b101893k

[HN{C(Me)=NH}$_2$, HL]. Two copper(II) complexes ($CuCl_2$·*n*HL, *n* = 1, 2) have been prepared, but not characterized in detail.[9] The only compound characterized by X-ray diffraction is a protonated form of complex **2**, namely green **2**·1.5HCl·3H_2O, formed upon self-condensation of acetamidine [MeC(=NH)NH_2] and $NiCl_2$·6H_2O in methanolic solution.[10] The structures of both complexes with square-planar Ni(II) centers are very similar. The C–N bond lengths in **2** are more uniform than in the protonated complex in agreement with more 'aromatic' character of the chelate metallocycle. Complex **2** seems to be the first molecular *N*-acetimidoylacetamidinate metal complex prepared to date. This is in contrast to the chemistry of metal acetylacetonates, which have been extensively studied and found numerous practical applications.[1] *N*-Acetimidoylacetamidinate is isoelectronic with acetonylacetonate, but has a significantly stronger ligand field. As a result, **2** and **2**·2H_2O have low-spin square-planar Ni(II) ions, while [Ni_3(acac)$_6$] and [Ni(acac)$_2$(H_2O)$_2$] are high-spin pseudo-octahedral Ni(II) complexes with bridging acac ligands and coordinated water molecules, respectively.[1,11]

Based upon known literature precedence, we can propose a sequence of events resulting in the overall transformation of acetonitrile into the acetimidoylacetamidinate complex and acetate (Scheme 1).

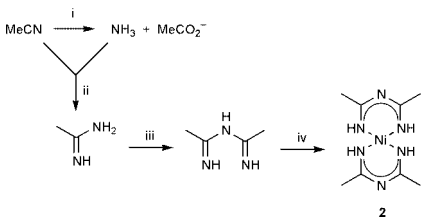

Scheme 1 Tentative mechanism of formation of complex **2** from acetonitrile and complex **1** (see text for the explanation of steps).

(i) Acetonitrile reacts with the hydroxide ligands of complex **1** or with trace water forming acetamide and, subsequently, acetate and ammonia. Catalytic activity of transition metal complexes in the hydrolysis of nitriles is well documented.[2] On the other hand, complex **1** is known to be a potent catalyst of transesterification.[8]

(ii) Acetonitrile and NH_3 yield acetamidine. This reaction is also known to be catalyzed by metal ions.[12]

(iii) *N*-Acetimidoylacetamidine is formed upon condensation of an acetamidine molecule with acetonitrile, acetamide, or another acetamidine molecule. Templated condensation of acetamidine in the presence of $NiCl_2$·6H_2O in methanolic solution to form **2**·1.5HCl·3H_2O has been reported.[10]

(iv) *N*-Acetimidoylacetamidine, which is isoelectronic with acetylacetone, but apparently has a much stronger ligand field, can act as a good new ligand for Ni(II). The net result of the reaction is the total displacement of the old ligands in complex **1**, including the tetradentate tpa, and the formation of a new complex Ni{HN=C(Me)–N=C(Me)–NH}$_2$ **2**.

Some other precedence for the reaction exists. Coupling of alkyl nitriles into 3,5-dialkyl-1,2,4-triazoles promoted by a dicopper complex has been reported.[3] Oligomerization of CF_3CN and CCl_3CN in the presence of transition metal complexes leads to the formation of the corresponding halogenated *N*-acetimidoylacetamidines, but acetonitrile is unreactive under the same conditions.[13,14] To the best of our knowledge, the transformation of a non-halogenated nitrile into an *N*-imidoylamidine promoted by a metal complex has not been observed before.

The behavior of dinickel(II) complex **1** can be contrasted to its diiron(III) analog, [Fe_2(μ-O)(tpa)$_2$(OH)(H_2O)]$^{3+}$, which reacts with MeCN to form a complex with a bridging acetamide ligand [Fe_2(μ-O){μ-OC(Me)NH}(tpa)$_2$]$^{3+}$.[5] In that case, the transformation of acetonitrile stops on acetamide, probably because the amidate [Fe_2^{III}(μ-O)(μ-OC(R)NH)(tpa)$_2$]$^{3+}$ complexes are coordinatively saturated and stable towards hydrolysis or dissociation.[15] In an additional experiment we found that complex **1** does not bind acetamide in solution as its diferric analog does.

In conclusion, we have demonstrated that a dinuclear hydroxo-bridged nickel(II) complex promotes self-condensation of acetonitrile into *N*-acetimidoylacetamidine, which acts as an efficient acetylacetone-like bidentate ligand, displacing the old ligands around Ni(II) and forming a new molecular homoleptic bis(*N*-acetimidoylacetamidinate)nickel(II) complex. This reaction shows that possible side-reactions should always be considered in studies involving metal complexes and acetonitrile.

Notes and references

§ *Synthesis* of **1**. Ni(ClO_4)$_2$·6H_2O (0.366 g, 1 mmol) and tpa (0.29 g, 1 mmol) were dissolved in 10 ml of water on stirring. To the resulting purple solution was added 1 ml of 1 M NaOH solution. The light-blue precipitate of crude complex **1** was left overnight for ripening, filtered off, washed with ice water, and dried under vacuum. Its recrystallization from acetonitrile–diethyl ether under N_2 gave pure **1** as dark-blue crystals. Yield: 0.37 g (80%). Calc. for $C_{36}H_{38}Cl_2N_8Ni_2O_{10}$: C, 46.44; H, 4.11; N, 12.04. Found: C, 46.47; H, 3.98; N, 11.92%; (ESMS+, MeCN): *m/z* 833 ([Ni_2(OH)$_2$(tpa)$_2$-(ClO_4)]$^+$, 5%), 447 ([Ni(tpa)(ClO_4)]$^+$, 95%), 383 ([Ni(tpa)(H_2O)(OH)]$^+$, 100%); UV–VIS: λ_{max}/nm (ε/M^{-1} cm^{-1} per Ni_2): MeOH: 589 (28), 795 (sh) (18), 980 (46); MeCN: 588 (40), 790 (sh) (12), 980 (34).

¶ *Synthesis and properties* of **2**: complex **1** (0.37 g; 0.4 mmol) and 3.7 ml of acetonitrile are placed into a vial, tightly closed, and heated for 2 days at 75 °C. The resulting dark-purple solution is cooled forming orange–yellow crystalline material (**2**·2H_2O as suggested by a single crystal X-ray diffraction study).‖ Its recrystallization from hot acetonitrile and drying under vacuum gives pure complex **2**. Yield: 0.031 g (15% based on Ni). Calc. for $C_8H_{16}N_6Ni$: C, 37.69; H, 6.33; N, 32.96. Found: C, 37.58; H, 6.39; N, 32.81%; ESMS (MeCN): *m/z* +255 (**2**H^+, 100%); −253 (**2** − H, 100%); NMR (25°C, D_6-DMSO): ^{1}H, δ 6.20 (s, 4H, NH), 1.795 (s, 12H, Me); ^{13}C, δ 164.5, 26.2; UV–VIS (DMSO): λ_{max}/nm (ε/mM^{-1} cm^{-1}): 290 (sh) (3.0), 321 (1.9), 336 (1.7), 465 (0.040); FT-IR (KBr): ν/cm^{-1}: 3280 (νNH), 2960 (ν_{as}Me), 2850 (ν_sMe), 1580 (ν_{as}CN), 1470, 1420, 1378, 1190, 946, 665, 516.

‖ *Crystal data* for **2**·2H_2O: $C_8H_{20}N_6NiO_2$, M_w = 291.01, orthorhombic, space group *Pbca* (no. 61), *a* = 13.040(3), *b* = 14.150(3), *c* = 7.4400(10) Å, *V* = 1372.8(5) Å^3, *Z* = 4, μ(Mo-Kα) = 1.415, *T* = 293(2) K, 1823 reflections measured, ψ-scan absorption correction, $R_1[I > 2\sigma(I)]$ = 0.032, wR_2 = 0.098 for all reflections. The structure was solved by direct methods using SHELXS-97 and refined with all data by full-matrix least squares on F^2 using SHELXL-97. All non-hydrogen atoms were refined anisotropically and hydrogen atoms were refined as isotropic. CCDC 162662. See http://www.rsc.org/suppdata/cc/b1/b101893k/ for crystallographic data in CIF or other electronic format.

1 *Comprehensive Coordination Chemistry*, ed. G. Wilkinson, R. D. Gillard and J. A. McCleverty, Pergamon, Oxford, 1987.
2 R. A. Michelin, M. Mozzon and R. Bertani, *Coord. Chem. Rev.*, 1996, **147**, 299.
3 M. G. B. Drew, P. C. Yates, J. Trocha-Grimshaw, K. P. McKillop and S. M. Nelson, *J. Chem. Soc., Chem. Commun.*, 1985, 262.
4 V. V. Pavlishchuk, S. V. Kolotilov, A. W. Addison, M. J. Prushan, R. J. Butcher and L. K. Thompson, *Inorg. Chem.*, 1999, **38**, 1759; J. L. Schneider, V. G. Young, Jr. and W. B. Tolman, *Inorg. Chem.*, 2001, **40**, 165.
5 E. C. Wilkinson, Y. Dong and L. Que, Jr., *J. Am. Chem. Soc.*, 1994, **116**, 8394; A. Hazell, K. B. Jensen, C. J. McKenzie and H. Toftlund, *Inorg. Chem.*, 1994, **33**, 3127.
6 L. Que, Jr., *J. Chem. Soc., Dalton Trans.*, 1997, 3933.
7 M. Ito and Y. Takita, *Chem. Lett.*, 1996, 929.
8 M. Ito, K. Sakai, T. Tsubomura and Y. Takita, *Bull. Chem. Soc. Jpn.*, 1999, **72**, 239; M. Ito, H. Kawano, T. Takeuchi and Y. Takita, *Chem. Lett.*, 2000, 372.
9 O. Keijiro and I. Eiichi, *Jpn. Pat.*, 48003811, 1973.
10 R. Norrestam, *Acta Crystallogr., Sect. C*, 1984, **40**, 955.
11 H. Montgomery and E. C. Lingafelter, *Acta Crystallogr.*, 1964, **17**, 1481.
12 N. C. Stephenson, *J. Inorg. Nucl. Chem.*, 1962, **24**, 801; J. H. Forsberg, V. T. Spaziano, T. M. Balasubramanian, G. K. Liu, S. A. Kinsley, C. A. Duckworth, J. J. Poteruca, P. S. Brown and J. L. Miller, *J. Org. Chem.*, 1987, **52**, 1017.
13 V. Robinson, G. E. Taylor, P. Woodward, M. I. Bruce and R. C. Wallis, *J. Chem. Soc., Dalton Trans.*, 1981, 1169.
14 K. Suematsu, *Chem. Pharm. Bull.*, 1984, **32**, 291.
15 S. V. Kryatov, A. Y. Nazarenko, P. D. Robinson and E. V. Rybak-Akimova, *Chem. Commun.*, 2000, 921.

CHEMCOMM
Communication
www.rsc.org/chemcomm

A novel, organic-additive-free synthesis of nanometer-sized NaX crystals

Bi-Zeng Zhan,[a] Mary Anne White,*[a] Katherine N. Robertson,[a] T. Stanley Cameron[a] and Michael Gharghouri[b]

[a] *Department of Chemistry, Dalhousie University, Halifax, Nova Scotia B3H 4J3, Canada. E-mail: Mary.Anne.White@DAL.ca*
[b] *Department of Mining and Metallurgical Engineering, Dalhousie University, Halifax, Nova Scotia B3J 2X4, Canada*

Received (in Cambridge, UK) 26th March 2001, Accepted 11th May 2001
First published as an Advance Article on the web 8th June 2001

Ultra-fine NaX zeolite crystals of dimensions *ca*. 20–100 nm have been synthesized with a novel, efficient, organic-additive-free hydrothermal approach.

The synthesis of nanometer-sized zeolites has received much attention recently owing to their utility in fundamental studies of zeolite crystal growth, in the preparation of ultra-thin zeolite films and nano-composites, and as supports for catalytic and photochemical reactions.[1–10] Reduction of the particle size from the micrometer to the nanometer scale can improve the mass- and heat-transfer in catalytic and sorption processes, thereby enhancing their catalytic selectivity and reducing coke formation in some petroleum reactions.[11] Furthermore, zeolite nano-crystals can be used to fabricate ordered porous structures.[12] Zeolite nano-crystals are usually synthesized *via* hydrothermal procedures using clear aluminosilicate solutions, most commonly in the presence of organic additives as templates. Nano-crystalline faujasite (FAU) zeolites have been synthesized using tetramethylammonium (TMA) as a template.[1–3,6] However, the conditions have to be critically controlled in order to get pure FAU crystals, as TMA is also a template for growth of zeolite A; furthermore, removal of the templates can lead to an irreversible aggregation of nano-crystals into larger solid particles.[13] Moreover, organic additive template routes are not suited for nano-scale synthesis, whereas the 'build-the-bottle-around-the-ship' method (or one-step approach) can directly synthesize the zeolite host matrix around guest molecules, as very pure and homogeneous nano-composites.[14,15] We are interested in developing novel organic-additive-free routes to ultra-fine FAU zeolites. These materials could have very different physical properties from microcrystalline zeolites, and could provide insights into nucleation and crystal growth during the hydrothermal process. Here we report an efficient, organic-additive-free synthesis of NaX zeolite with particle sizes in the range 20–100 nm.

The hydrothermal synthesis was conducted in a shaker with a temperature controller. Aluminosilicate gel was prepared by mixing freshly prepared aluminate and silicate solutions together in the molar ratio 5.5 Na_2O : 1.0 Al_2O_3 : 4.0 SiO_2 : 190 H_2O. Typically, an aluminosilicate gel containing 5.34 g NaOH, 2.42 g $NaAlO_2$, 3.43 g SiO_2 and 50.0 g H_2O was used. $NaAlO_2$ was freshly prepared from $Al(OH)_3$ and NaOH. SM-30 colloidal silica (Aldrich), silica fume (Sigma), and TEOS (tetraethyl orthosilicate, Aldrich) were chosen as the silicate sources, with no significant difference observed in the final particle size-distribution. For TEOS, the hydrolysis was controlled at 0 °C in order to obtain nanometer-sized aluminosilicate gel. Hydrothermal crystallization was conducted at 60 °C for 2–4 days in a shaker with a rotation rate of 250 rpm. The powder product, henceforth referred to as NaX-*nano*, was recovered *via* centrifugation, washed with DI water until pH < 8, and then dried at room temperature for 24 h. In a control experiment, larger particle sizes of FAU zeolite, here denoted NaX-μ, were synthesized with exactly the same aluminosilicate gel composition, but the hydrothermal crystallization was performed at 90 °C for 2 days with no shaking.

Powder X-ray diffraction (XRD) diagrams of as-synthesized zeolite samples and commercial micron-sized FAU zeolite (from Aldrich) are shown in Fig. 1. The XRD patterns of the two synthesized samples and the commercial FAU powder match very well, demonstrating that our approach can indeed be used to synthesize pure FAU crystals. The XRD peaks for the NaX-μ sample are almost the same as for the commercial sample, in both intensity and width. However, the diffraction lines of the NaX-*nano* sample are significantly less intense and much broader, indicating that the crystals are much smaller. From the diffraction peaks (2θ) at 6° [111], 16° [331], and 27° [642] and Scherrer's equation, we calculate an average crystal dimension of 23 ± 4 nm.[2,16] XRD patterns taken after different hydrothermal synthesis periods reveal that NaX-*nano* is more than 95% crystalline after two days of shaking at 60 °C. Longer crystallization times might slightly increase the particle size. The Si/Al ratio was found to be 1.25 ± 0.05 for NaX-*nano* (by X-ray fluorescence) and 1.3 ± 0.1 for NaX-μ (from ^{29}Si solid state NMR). These values fall in the Si/Al range of 1–1.5 for NaX zeolites. Therefore, both synthesized samples are NaX. The as-synthesized samples have slightly lower 2θ values than the commercial sample, as would be expected for reduced Si/Al ratios.

Uncoated NaX-*nano* and NaX-μ samples were imaged with a Hitachi S-4700 cold-field emission scanning electron microscope (SEM) operated at 1 kV. A typical micrograph of NaX-*nano* (Fig. 2) clearly shows that most particle sizes of NaX-*nano* are in the range 20–100 nm. This is one of the smallest faujasite particle sizes reported.[1–4,6] This size distribution is consistent with the results calculated from the XRD patterns, proving that our method does indeed successfully synthesize ultra-fine NaX

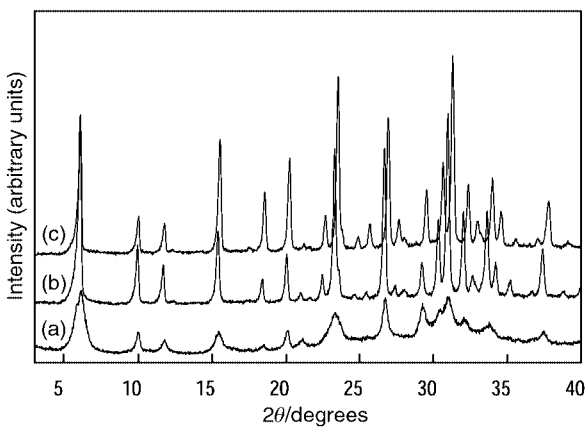

Fig. 1 XRD powder patterns for (a) NaX-*nano*, (b) NaX-μ and (c) a commercial NaX sample (Aldrich). The XRD data were recorded on a Rigaku Miniflex System using Cu-Kα radiation, 30 kV, 15 mA with a scanning speed of 1° (2θ) min^{-1}, T = 20 °C.

 DOI: 10.1039/b102733f

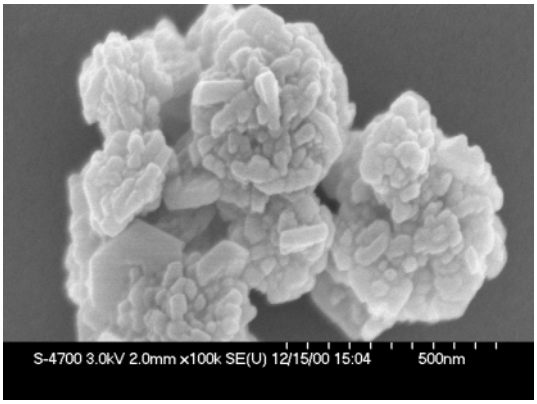

Fig. 2 SEM images of NaX-*nano* (HITACHI S-4700 cold-field emission SEM, 1 kV).

crystals without the assistance of any organic additives. The micrographs of NaX-μ show the particles to be in the micron range (*ca*. 0.8 μm). The significant decrease in particle size from NaX-μ to NaX-*nano* indicates that lower crystallization temperatures and strong shaking conditions, which would together accelerate the nucleation process and lower the crystal growth rates, are key factors in controlling the size of zeolite crystals obtained. By controlling the crystallization temperature, shaking time and silicate source (and its particle size), we successfully synthesized several NaX zeolite samples with average particle sizes ranging from 20 nm to 1 μm.

Both NaX-*nano* and NaX-μ were further characterized by FT-IR and ^{29}Si solid-state NMR. In the FT-IR spectra, three features were noted. First, a symmetric stretching band at 744 cm^{-1} was observed in NaX-*nano*,[17,18] with a corresponding peak at 750 cm^{-1} in the NaX-μ sample. Secondly, the double-ring vibration at 566 cm^{-1}, characteristic of faujasite zeolites, appears as two bands at 608 and 566 cm^{-1} in NaX-*nano*. Thirdly, a new broad band at 860 cm^{-1} was observed in the ultra-fine sample, and it can reasonably be assigned to the silanol (Si–OH) bending mode associated with the Q^3 silicon species (Si connected to three O that have connections to Si or Al),[17] detected with ^{29}Si solid-state NMR. The existence of an abundance of silanol groups in NaX-*nano* is attributed to the large total particle surface area, associated with the reduction to the ultra-fine particle size. From a simple calculation assuming cubic particles, one would expect about 12% Q^3 from the external surface in an NaX zeolite with a 50 nm particle size. Q^3 species could also be formed at internal defects. It was reported that about 20% of Si was in the silanol form in an 18–100 nm particle-size silicalite-1 zeolite studied by solid-state NMR.[5] With both single-pulse and cross-polarization ^{29}Si solid-state NMR techniques, we found all four Q^3 bands and five Q^4 bands in the NaX-*nano* sample. To our knowledge, this is the first time that Q^3 bands have been observed in a nanometer-sized NaX sample. This finding agrees well with the observation of silanol bending modes in the vibrational spectroscopy experiment. On the other hand, only the five Q^4 bands, located at −84.8, −89.5, −94.2, −99.3 and −103 ppm, were detected in the larger-particle NaX-μ sample, as expected.

In conclusion, a novel organic-additive-free approach has been developed to synthesize nanometer-sized faujasite NaX. The XRD pattern of the as-synthesized NaX-*nano* sample matches very well with the commercial micron-sized FAU, but it is broader and less intense. The average crystal size of 23 nm calculated from XRD is in accord with SEM images. The crystal size depends critically on the synthetic conditions, *e.g.* temperature and shaking. In comparison with the micron-sized zeolite, ultra-fine NaX shows a broad silanol vibration peak at 860 cm^{-1}, associated with the Q^3 silicon detected in ^{29}Si solid-state NMR.

We thank N. Burford, M. Lumsden (Atlantic Region Magnetic Resonance Centre) and R. L. White for assistance. This work was financially supported by the Natural Sciences and Engineering Research Council and the Killam Trusts (the latter for a postdoctoral research fellowship to B. Z. Z. and research professorship to M. A. W.).

Notes and references

1 B. J. Schoeman, J. Sterte and J.-E. Otterstedt, *Zeolites*, 1994, **14**, 110.
2 N. B. Castagnola and P. K. Dutta, *J. Phys. Chem. B*, 1998, **102**, 1696.
3 G. Zhu, S. Qiu, J. Yu, Y. Sakamoto, F. Xiao, R. Xu and O. Terasaki, *Chem. Mater.*, 1998, **10**, 1483.
4 Wang Bo and Ma Hongzhu, *Microporous Mesoporous Mater.*, 1998, **25**, 131.
5 R. Ravishankar, C. Kirschhock, B. J. Schoeman, P. Vanoppen, P. J. Grobet, S. Storck, W. F. Maier, J. A. Martens, F. C. De Schryver and P. A. Jacobs, *J. Phys. Chem. B*, 1998, **102**, 2633.
6 S. Mintova and V. Valtchev, *Stud. Surf. Sci. Catal.*, 1999, **125**, 141.
7 C. Madsen and C. J. H. Jacobsen, *Chem. Commun.*, 1999, 673.
8 S. Mintova, N. H. Olson, V. Valtchev and T. Bein, *Science*, 1999, **283**, 958.
9 M. Xu, M. Cheng and X. Bao, *Chem. Commun.*, 2000, 1873.
10 M. Lassinantti, J. Hedlund and J. Sterte, *Microporous Mesoporous Mater.*, 2000, **38**, 25.
11 *Method of Analysis for Fluid Cracking Catalysts*, Grace and Co., Division Chemicals, Baltimore, MD, 1980.
12 L. Huang, Z. Wang, J. Sun, L. Miao, Q. Li, Y. Yan and D. Zhao, *J. Am. Chem. Soc.*, 2000, **122**, 3530.
13 H. Wang, Z. Wang and Y. Yan, *Chem. Commun.*, 2000, 2333.
14 B.-Z. Zhan and X.-Y. Li, *Chem. Commun.*, 1998, 349.
15 C. O. Oriakhi, *J. Chem. Educ.*, 2000, **77**, 1138.
16 B. D. Cullity, *Elements of X-Ray Diffraction*, Addison-Wesley, Reading, MA, 1978.
17 R. Szostak, *Molecular Sieves: Principles of Synthesis and Identification*, Van Nostrand Reinhold, NY, 1989.
18 J. E. D. Davis and H. Förster, *Vibrational Spectroscopy*, in *Comprehensive Supramolecular Chemistry, Vol. 8: Physical Methods in Supramolecular Chemistry*, ed. J. E. D. Davies and J. A. Ripmeester, Elsevier Science Ltd., Oxford, 1996, pp. 33–119.

CHEMCOMM Communication
www.rsc.org/chemcomm

A novel synthesis route to rare earth polyborates†

Peichao Lu,[a] Yingxia Wang,[a] Jianhua Lin*[a] and Liping You[b]

[a] *State Key Laboratory for Rare Earth Materials Chemistry and Applications, College of Chemistry and Molecular Engineering, Peking University, Beijing 100871, P. R. China. E-mail: jhlin@chem.pku.edu.cn*

[b] *Laboratory of Electron Microscopy, Department of Physics, Peking University, Beijing 100871, P. R. China*

Received (in Cambridge, UK) 5th March 2001, Accepted 14th May 2001
First published as an Advance Article on the web 30th May 2001

The proposed two-step preparation route for rare earth polyborates, *i.e.* dehydration of boric acid in the presence of rare earth oxide at low temperature followed by careful annealing at 700 °C, led to, for the gadolinium case, a new gadolinium pentaborate (GdB_5O_9) that can not be prepared by conventional high-temperature reaction.

The structural chemistry of borates is characterized by a variety of discrete and condensed BO_3 and BO_4 groups;[1] as a general rule, the tendency to form polyborates is increased by decreasing cation valence.[2] This promotes stability and a wide variety of polyborate structures with 1+ and 2+ valence cations have been produced. The rare earth borates, on the other hand, usually consist of isolated borate anions (BO_3 or BO_4) or low polymerized borate groups; thus, in the Ln_2O_3–B_2O_3 (Ln = rare earth) system[3] only three compounds, oxyborate,[4,5] orthoborate[6] and metaborate,[7] have been identified; the more borate-rich phases remain unknown. Recently, we found that, in the flux of boric acid, hydrated rare earth polyborates are formed by the reaction of boric acid and rare earth oxides at low temperature. Subsequent annealing of the hydrated polyborates yields anhydrous rare earth polyborates. We describe herein our exploratory syntheses in this area.

The synthesis of hydrated gadolinium polyborate was carried out in a sealed Teflon autoclave at 260 °C for 5 days, starting from H_3BO_3 and Gd_2O_3 in a 20 : 1 ratio. The product **1**, isolated by dissolving the excess boric acid in water, consists of colorless well-crystallized polycrystals. Chemical analysis (ICP) reveals that the approximate atomic ratio Gd : B is about 1 : 6.2, and the IR spectrum indicates the presence of both BO_3 and BO_4 groups in this compound. Fig. 1a shows the X-ray diffraction pattern of **1**. Structural analysis using X-ray powder diffraction techniques[8] established that the product **1** is a hydrated gadolinium polyborate with the composition $H_3GdB_6O_{12}$; it crystallizes with a rhombohedral structure in the space group *R*3*c* with lattice constants a = 8.4076(2) and c = 20.7427(5) Å. The synthesis reaction is:

$$12H_3BO_3 + Gd_2O_3 \xrightarrow{260\ ^{\circ}C} 2H_3GdB_6O_{12} + 15H_2O \quad (1)$$

$H_3GdB_6O_{12}$ is stable at low temperature and decomposes at high temperature. X-Ray powder diffraction studies carried out at high temperatures indicate that the decomposition of $H_3GdB_6O_{12}$ occurs at about 650 °C; it transforms to an amorphous form between 650 °C and 700 °C. During the decomposition, significant weight loss (6.04 wt%) was observed *via* TGA. Therefore, the decomposition reaction is essentially the dehydration of $H_3GdB_6O_{12}$. Careful annealing at 700 °C for 5 days resulted in another new phase (**2**) as shown in Fig. 1b.

The structural study by X-ray powder techniques established that **2** is a rare earth pentaborate GdB_5O_9. It crystallizes in a body centered tetragonal cell (a = 8.2439(4), c = 33.6671(2) Å) in the space group $I4_1/acd$.[9] The basic borate fragments in GdB_5O_9 are B_4O_9 and BO_3 units. The B_4O_9 is a common structure unit in many borates. For example, isolated and 1D chains of B_4O_9 are present in borax ($Na_2[B_4O_5(OH)_4]\cdot 8H_2O$) and $Na_2[B_4O_6(OH)_3]$ respectively.[1] In the structure of GdB_5O_9, the B_4O_9 units form 1D chains by sharing the oxygen atoms of the BO_4 groups (Fig. 2); the 3D-polyborate framework is composed of 1D chains linked by additional BO_3 groups. Fig. 3 shows an overview of the structure of GdB_5O_9, where the triangles and tetrahedra represent BO_3 and BO_4 groups respectively. The decomposition reaction of $H_3GdB_6O_{12}$ is then expressed as:

$$2H_3GdB_6O_{12} \xrightarrow{650-700\ ^{\circ}C} 2GdB_5O_9 + 3H_2O + B_2O_3 \quad (2)$$

The expected weight loss from eqn. (2) is 6.473 wt%, which agrees reasonably well with that observed in the TGA study (6.04 wt%). Moreover, GdB_5O_9 is not stable at higher temperatures; further annealing at 900 °C yielded gadolinium metaborate and another unknown phase. Therefore, this compound cannot be synthesized by conventional high temperature solid state reaction.

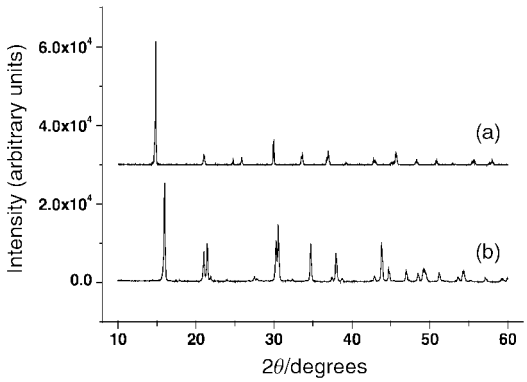

Fig. 1 X-Ray powder diffraction patterns (a) of the hydrated gadolinium polyborate $H_3GdB_6O_{12}$ (**1**) and (b) of the anhydrous gadolinium polyborate GdB_5O_9 (**2**) after annealing at 700 °C for 5 days.

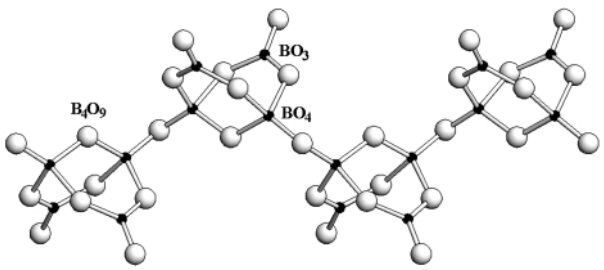

Fig. 2 One-dimensional chain formed by B_4O_9 groups in the structure of GdB_5O_9.

† Electronic supplementary information (ESI) available: crystallographic, TGA/DTA, IR and XRD profile fits for $H_3GdB_6O_{12}$ and GdB_5O_9. See http://www.rsc.org/suppdata/cc/b1/b102045p/

 DOI: 10.1039/b102045p

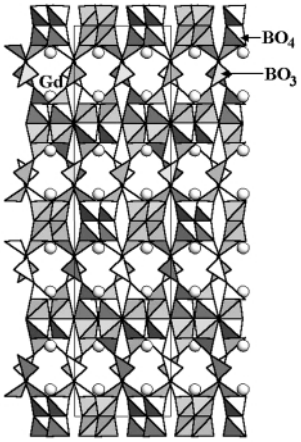

Fig. 3 A projection of the crystal structure of GdB_5O_9 (**2**); triangles and tetrahedra represent BO_3 and BO_4 groups.

In summary, although polyborate is an important resource for functional materials, such as nonlinear optical and luminescent materials, our knowledge of rare earth polyborates was limited due to the instability of these phases at high temperatures. In this communication, we have demonstrated that careful dehydration of a hydrated rare earth polyborate may lead to the anhydrous rare earth polyborate. We believe that the proposed preparative strategy will be very useful in exploiting new polyborate materials for rare earth systems.

We are grateful for the financial support from NSFC (29731010), Rhodia Rare Earth Co. and State Key Basic Research Program of China.

Notes and references

1 A. F. Wells, *Structural Inorganic Chemistry*, Oxford University Press, 5th edn., 1984, p. 1045.
2 N. I. Leonyuk, *J. Cryst. Growth*, 1997, **174**, 301.
3 E. M. Levin, C. R. Robbins and J. L. Warring, *J. Am. Ceram. Soc.*, 1961, **44**, 87.
4 J. H. Lin, M. Z. Su, K. Wurst and E. Schweda, *J. Solid State Chem.*, 1996, **126**, 287.
5 J. H. Lin, S. Zhou, L. W. Yang, G. Q. Yao, M. Z. Su and L. P. You, *J. Solid State Chem.*, 1997, **134**, 158.
6 M. Ren, J. H. Lin, Y. Dong and M. Z. Su, *Chem. Mater.*, 1999, **11**, 1576.
7 G. K. Abdullaev, Kh. S. Mamedov and G. G. Dzhafarov, *Sov. Phys. Crystallogr.*, 1975, **20**, 161.
8 The X-ray powder diffraction pattern was collected for $H_3GdB_6O_{12}$ (**1**) on a Rigaku D/max-2000 diffractometer and indexed by using TEROR90.[10] $H_3GdB_6O_{12}$ crystallizes in a rhombohedral system with lattice constants a = 8.4076(2) and c = 20.7427(5) Å. The systematic absences of reflections indicated that the space group is either $R3c$ or $R\bar{3}$. Optimal estimates of the individual reflection intensities were extracted by a profile-fitting method using the EXTRA program.[11] The gadolinium positions in the structure were obtained by direct methods (Sirpow92[12]). The Rietveld refinement (GSAS)[13] and subsequent difference Fourier analysis identified the oxygen and boron positions. During the structure determination, both space groups $R3c$ and $R\bar{3}$were used, but only $R3c$ led to a chemically reasonable solution. The final refinement using the X-ray diffraction data in the range of 20–120° yielded R_p = 0.089 and R_{wp} = 0.115. The structure analysis was not able to locate the hydrogen atoms; the hydrogen component in **1** was estimated by charge balance of the compound, as well as the weight loss in TGA analysis.
9 The lattice constants of GdB_5O_9 (**2**) were established by using TREOR90.[10] **2** crystallizes in the tetragonal space group $I4_1/acd$ with lattice constants a = 8.2380(1), c = 33.6372(6) Å. Similar to **1**, the gadolinium positions were located by direct methods (Sirpow92[12]); subsequent Rietveld refinement and different Fourier analysis revealed the oxygen and boron positions. The final refinement yielded R_p = 0.069 and R_{wp} = 0.098.
10 D. Cheng, *J. Appl. Crystallogr.*, 1999, **32**, 838.
11 A. Altomare, M. C. Burla, G. Cascarana, C. Glacovazzo, A. Guagliardi, A. G. G. Moliterni and G. Polidiori, *J. Appl. Crystallogr.*, 1995, **28**, 842.
12 A. Altomare, G. Cascarana, C. Glacovazzo and A. Guagliardi, *Sirpow User's Manual*, Inst. Di Ric. Per lo Sviluppo di Metodologie Cristllografiche, CNR.
13 A. C. Larson and R. B. von Dreele, *Report LAUR 86-748*, Los Alamos National Laboratory, 1985.

CHEMCOMM
Communication
www.rsc.org/chemcomm

Crystal chemistry and phase composition of the MoVTeNbO catalysts for the ammoxidation of propane

M. Aouine,[a] J. L. Dubois[b] and J. M. M. Millet*[a]

[a] *Institute de Recherches sur la catalyse, CNRS, Conventionné à l'Université Claude-Bernard, Lyon I, 2 avenue Albert Einstein, 69626 Villeurbanne Cedex, France. E-mail: millet@catalyse.univ-lyon1.fr*
[b] *Elf Atochem S.A. Centre de Recherches et développement de l'Est, B.P. 61005-57501 Saint-Avold Cedex, France*

Received (in Cambridge, UK) 1st May 2001, Accepted 16th May 2001
First published as an Advance Article on the web 8th June 2001

Unit cell parameters and space group symmetry have been determined for the two main phases of the MoVTeNbO catalysts; models of their structures are proposed based on electron micrographes, EDX data and comparison with other crystal structures.

New processes of production of acrylonitrile by ammoxidation of propane will be implemented on the industrial scale in the coming years.[1] Two catalytic systems, AlVSbWO and MoV-TeNbO have been shown to be effective and will most likely be used. The former has been extensively described in the literature whereas the latter has mostly been covered in the patent literature.[1–4]

The presence in the MoVTeNbO catalyst of two major phases, denoted M1 and M2, has been shown to be key to obtain high yields.[5] Very little is known about these phases whose presence has been verified almost exclusively employing X-ray diffraction. The role of these phases remains under debate mainly because none of these phases have been synthesised and studied independently.

We have synthesised a MoVTeNbO catalyst using a method described in the literature[5] and characterised it by electron microscopy and X-ray diffraction. The catalyst was prepared from an aqueous slurry comprising Mo, V, Te and Nb in the ratios Mo:V:Te:Nb = 1:0.33:0.22:0.11, ratios most frequently reported in patent examples. The slurry was evaporated to dryness at 423 K and successively calcined at 573 K under air and 873 K under nitrogen for 2 h.

Powder X-ray diffraction patterns were obtained using a Siemens D5005 diffractometer and Cu-Kα radiation. They were recorded with 0.02° (2θ) steps over the angular range 3–88° with 16 s counting time per step. High-resolution electron microscopy was performed with a JEM 2010 (C_s = 0.5 mm). The accelerating voltage was 200 kV with a LaB_6 emission current, a point resolution of 0.195 nm and a useful limit of information of 0.14 nm. The instrument was equipped with an EDS LINK-ISIS (spatial resolution: 1 nm). An EDX study was conducted using a probe size of 25 nm to analyse isolated grains of the phases and avoid simultaneous analysis of grains of the two phases. Standard deviations were evaluated for atomic ratios from at least 20 analyses.

The X-ray diffraction pattern of the synthesised catalyst showed the sets of peaks reported in the literature for the two phases,[1] the more intense corresponding to the M2 phase. The electron diffraction spectra of the two phases have been indexed (Figs. 1 and 2). The M1 phase crystallises in the hexagonal system with possible space groups *P*6*mm*, *P*$\bar{6}$*m*2, *P*622 or *P*6/*mmm* while phase M2 crystallises in the orthorhombic system. Extinction conditions observed for the latter are only compatible with the space group $P2_12_12$. The data obtained by electron microscopy made it possible to index the X-ray diffraction powder pattern of the phase mixture and to refine the cell parameters of the phases. The cell parameters of the M1 and M2 phases are, respectively, a = 2.61(2), c = 0.403(1) nm and a = 2.1207(8)(3), b = 2.6831(1) and c = 0.8047(4) nm.

The structure of M1 is isomorphous to that of the phase $Sb_{0.4}MoO_{3.1}$ reported by Parmentier *et al.*[6] and corresponds to a hexagonal tungsten bronze structure.[7] Although the structure is only partial; it can be schematized as shown in Fig. 3. Tellurium occupies the sites in the channels formed by the MO_6

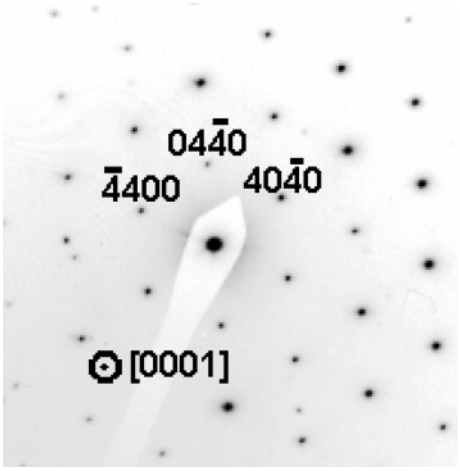

Fig. 1 Indexed electron diffraction pattern of the phase M1.

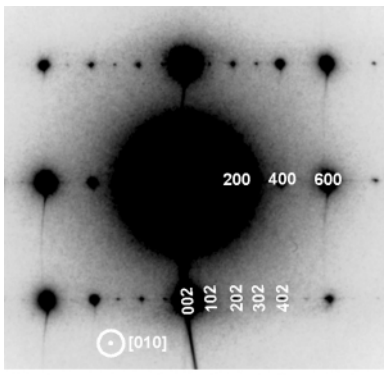

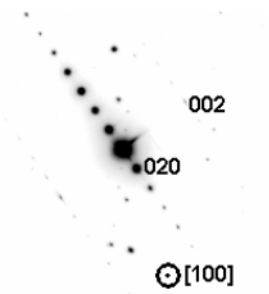

Fig. 2 Indexed electron diffraction patterns of the phase M2.

 DOI: 10.1039/b103895h

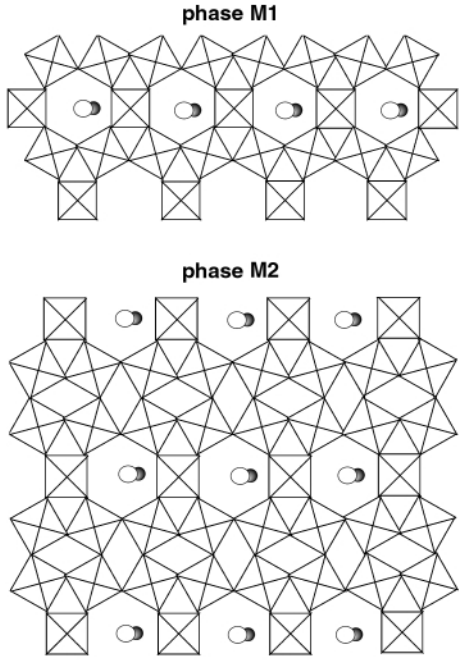

Fig. 3 Representation of the structures of the phases M1 and M2 along the *c* axis.

octahedra (M = Mo, V, Nb). In the case of the antimony bronze, it was proposed that Sb partially occupies the M sites which was not possible with Te, due to steric hindrance. Consequently the stoichiometry of the M1 phase should correspond to $Te_{0.33}MO_3$. Such stoichiometry is in accord with that calculated from EDX analyses (Table 1).

Table 1 EDX analyses of the two phases; standard deviations are given in parentheses

Phase	Te/Mo	V/Mo	Nb/Mo	Te/(Mo + V + Nb)	(Te + Nb)/(Mo + V)
M1	0.32(2)	0.30(2)	0.07(1)	0.23(4)	
M2	0.11(2)	0.23(2)	0.14(5)	0.08(4)	0.20(4)

The structure of M2 shows similarities with those of $TeMo_5O_{16}$ and $Sb_2Mo_{10}O_{31}$ (Table 2) and should present the atomic arrangement of $TeMo_5O_{16}$ (Fig. 3). A lattice image of the phase M2 taken with the incident beam parallel to the *b* axis shows an array of intense fringes having a separation of 1.04 nm (*i.e.* half of the *a* parameter) with in between streaks forming two less intense lines (Fig. 4). These fringes can respectively be attributed to the planes containing tellurium and molybdenum cations and molybdenum cations, as they appear in the structure model of $TeMo_5O_{16}$. The *a* parameters of the two phases (M2 and $TeMo_5O_{16}$) are quite similar, the *c* parameter of the former corresponds to twice that of the latter and the *b* parameter is *ca*. four times larger. These features could be related to a more

Table 2 Comparison of the unit cell parameters of the phase M2, $Sb_2Mo_{10}O_{31}$ and $TeMo_5O_{16}$

Phase	*a*/nm	*b*/nm	*c*/nm	Space group	Ref.
M2	2.1207(3)	2.6831(1)	0.8047(4)	$P2_12_12$	This study
$Sb_2Mo_{10}O_{31}$	2.023(1)	0.809(1)	0.717(1)	*Pma*2	8
$TeMo_5O_{16}$	2.0010(1)	0.72254(4)	0.40650(2)	*Pma*/2	9

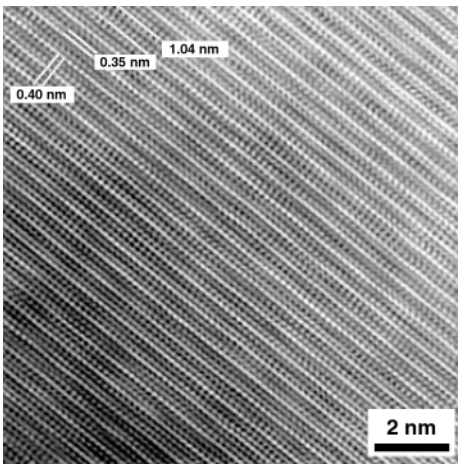

Fig. 4 High-resolution transmission electron imaging of the phase M2.

complex chemical composition of the M2 phase. Such a complex chemical composition should result from both the high degree of substitution of the molybdenum cations by the smaller vanadium cations and a possible ordering of the M cations on the sites. These features may also be due to the possible intergrowth of M2 and M1 structures as proposed earlier for $TeMo_5O_{16}$.[10] The stoichiometry of the phase M2 should correspond to $Te_{0.2}MO_{3.2}$ (with M = Mo, V and Nb). The stoichiometry calculated from EDX data with 0.08 Te per M cation does not agree well with this stoichiometry. It may be possible that niobium, which is in a larger amount in this phase, partially occupies the hexagonal window sites. The sub-stoichiometry in oxygen observed in the case of antimony is due to the absence of infinite chains $[Te–O]_\infty$ in the [001] direction caused by a different orientation of the free electron pairs. This limits to three instead of four the number of oxygens neighboring the Sb cation. The presence of infinite chains could be an important parameter in the formation of this structure and explain the difficulties encountered when preparing the same catalysts with antimony in place of tellurium.

From the data generated from this study, the structures of the two phases can be described on the basis of two closely related stacking models. These models are built up from simple or double sheets of MO_6 (M = Mo, V, Nb) separated by rows of hexagonal windows occupied by tellurium cations (Fig. 3). These structures correspond to the same general formula $Te[MO_3]_{2n+1}$ with $n = 1$ for M1 and $n = 2$ for M2. This feature should explain why the two phases are systematically formed concomitantly.

Notes and references

1 M. Hatano and K. Kayou, *Eur. Pat.*, 318 295, 1988.
2 T. Ushikubo, K. Oshima, A. Kayo, T. Umezawa, K. Kiyono and I. Sawaki, *Eur. Pat.*, 529 853, 1992.
3 T. Ushikubo, K. Oshima, A. Kayou, T. Umezawa, K. Kiyono, I. Sawaki and H. Nakamura, *US Pat.*, US5472925; 1995.
4 H. Hinago and S. Komada, *Ger. Pat.*, DE19835247 A1, 1998.
5 T. Ushikubo, K. Oshima, A. Kayou and M. Hatano, *Stud. Surf. Sci. Catal.*, 1997, **112**, 473.
6 M. Parmentier, C. Gleitzer and R. J. D. Tilley, *J. Solid State Chem.*, 1980, **31**, 305.
7 A. Magneli, *Acta Chem. Scand.*, 1953, **7**, 315.
8 M. Parmentier, C. Gleitzer, A. Courtois and J. Protas, *Acta Crystallogr., Sect. B*, 1963, **35**, 1979.
9 P. Forestier and M. Gereaud, *C.R. Acad. Sci. Paris Ser. II*, 1991, **312**, 1141.
10 S. Vallar and M. Goreaud, *J. Solid State Chem.*, 1997, **129**, 303.

CHEMCOMM
Communication
www.rsc.org/chemcomm

A [2]catenane quantitatively assembled *via* copper(I) and palladium(II) coordination

Christiane Dietrich-Buchecker,*[a] Neri Geum,[b] Akiko Hori,[c] Makoto Fujita,*[cd] Shigeru Sakamoto,[e] Kentaro Yamaguchi[e] and Jean-Pierre Sauvage*[a]

[a] *Laboratoire de Chimie Organo-Minérale, UMR 7513 du CNRS, Université Louis Pasteur, Faculté de Chimie, 4, rue Blaise Pascal, 67070 Strasbourg Cedex, France. E-mail: sauvage@chimie.u-strasbg.fr*
[b] *Dankook University, 8 Hannam-dong, Yongsan-ku, Seoul 140-714, Korea*
[c] *Department of Applied Chemistry, Graduate School of Engineering, Nagoya University, Chikusaku, Nagoya 464-8603, Japan*
[d] *CREST, Japan Science and Technology Corporation (JST)*
[e] *Chemical Analysis Center, Chiba University, Yayoicho, Inageku, Chiba, 263-8522, Japan*

Received (in Cambridge, UK) 13th March 2001, Accepted 4th May 2001
First published as an Advance Article on the web 13th June 2001

A [2]catenane consisting of 41-membered interlocking rings is formed quantitatively, following a two metal based [Cu(I) and Pd(II)] strategy; the compound is obtained as the thermodynamic product.

Catenanes are experiencing a spectacular revival in relation to topology as well as switches, machines and motors at the molecular level.[1–4] Copper(I) has been extensively used as templating metal centre, allowing the preparation of simple to complex interlocking or knotted topologies.[5] The use of coordination bonds to construct interlocking rings has been recently proposed.[6,7] It is especially attractive when the metal-to-ligand bond is labile and the catenane is obtained as the thermodynamically most stable product, thus leading to quantitative yields of the desired species. In this respect, palladium(II) has turned out to be particularly well adapted.[6]

By combining copper(I) and palladium(II) in the same assembly, it has been possible to make a doubly-interlocking molecule, *i.e.* a 4-crossing [2]catenane.[8] This unexpected structure was obtained because the organic ligand used was too short to afford a ring incorporating a single palladium(II) atom.

We would now like to report that, by utilising a sufficiently large bridging ligand, quantitative formation of a [2]catenane was observed. The strategy is depicted in Scheme 1.

According to CPK models, ligand **1** is perfectly adapted to the strategy of Scheme 1. **1** is relatively rigid, and, in particular, the distance between the two oxygen atoms of **1** is more or less fixed and does not depend on rotation about C–C bonds (O···O ~16 Å). After coordination of $enPd^{2+}$ (en = 1,2-diaminoethane) two interlocking 41-membered rings are obtained. The size of the palladium(II) containing cycles is such that the final [2]catenane should not be strained, even if one considers that solubilizing groups (C_6H_{13}) have been attached at the back of the phen units.

The real reactions are represented in Fig. 1. Ligand **1** was obtained by a double Ullmann coupling reaction[9] between 4,7-di-*n*-hexyl-2,9-bis[4-(4-hydroxyphenyl)phenyl]-1,10-phenanthroline[10] and 4-(4-bromophenyl)pyridine.[11] The latter reaction was performed in refluxing toluene in the presence of Cs_2CO_3 and excess $Cu(CH_3CN)_4{\cdot}PF_6$ over 3 days. After demetallation of the crude reaction mixture with KCN and purification by chromatography over silica gel, **1** was obtained in 10% yield as a pale yellow glass. It could be fully characterized by ^1H NMR and mass spectroscopy.

The reaction of **1** (0.010 mmol) and $Cu(CH_3CN)_4{\cdot}PF_6$ (0.005 mmol) in MeCN–DMF (1:1) solution (1 ml), immediately afforded **2**, which is the precursor to catenane **3**. To this solution, $enPd(NO_3)_2$ (0.010 mmol) was added and the reaction was stirred for 1 h at rt. In solution, **3** was obtained quantitatively. It was isolated in 85% yield as a red micro-

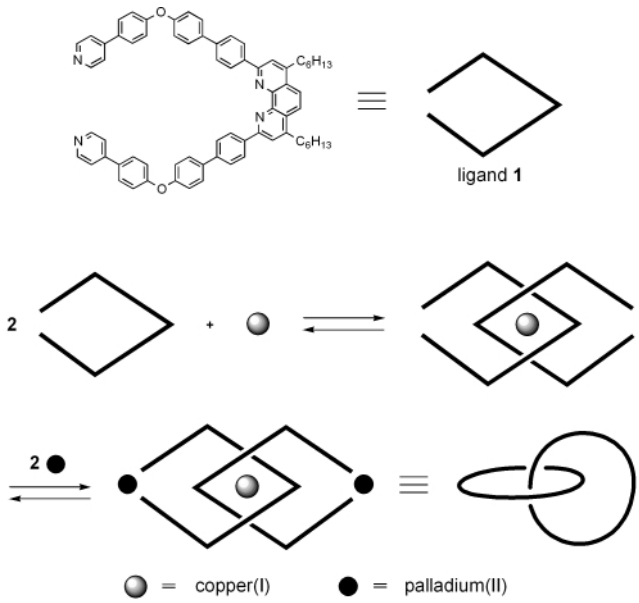

Scheme 1 Ligand **1** can be regarded as an open lozenge. The 1,10-phenanthroline (phen) site reacts with copper(I) to afford an entwined complex. Cyclisation is carried out by completing the two interlocking lozenges, the 'clipping' metal being palladium(II).

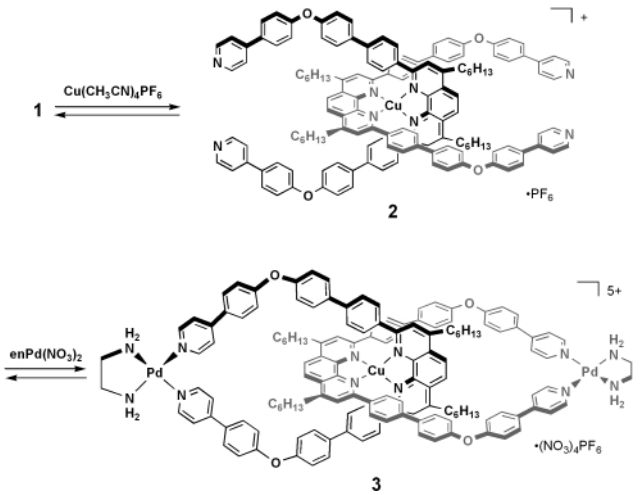

Fig. 1 Quantitative formation of catenane **3** in two steps from **1**, by successive addition of Cu(I) and Pd(II).

 DOI: 10.1039/b102373j

crystalline solid by addition of diethyl ether. **2** and **3** are formed as thermodynamic products since copper(I) complexes and, especially palladium(II) compounds are substitutionally labile.

The formation of **2** and **3** as single products was confirmed by both ^{1}H NMR and CSI-MS (Cold Electro Spray Ionization Mass Spectroscopy).[12] The ^{1}H NMR spectrum of **2** in CD_3CN–DMF-d_7 solution showed the expected signals for the aromatic protons, in accordance with the symmetric structure of **2**, except for the protons borne by the two pyridine nuclei which are probably too broad to lead to clear signals. CSI-MS of **2** in MeCN–DMF solution showed a prominent peak at *m/z* 2046, $[M\text{-}(PF_6)]^+$.

The ^{1}H NMR spectrum of **3** in CD_3CN–DMF-d_7 is also in agreement with its structure. The chemical shifts of the peaks are slightly different from those of **2**. Not surprisingly, the pyridinic protons α to the Pd(II)-coordinated N atoms appear at low field (δ = 9.67). CSI-MS of **3** in CH_3CN–DMF solution at 20 mM concentration showed predominant peaks for $[M\text{-}(PF_6)\text{-}(NO_3)_n]^{(n+1)+}\cdot(dmf)_m$: *e.g. m/z* 548, $[M\text{-}(PF_6)\text{-}(NO_3)_4]^{5+}\cdot(dmf)_5$; 646, $[M\text{-}(PF_6)\text{-}(NO_3)_3]^{4+}\cdot(dmf)_2$; 834, $[M\text{-}(PF_6)\text{-}(NO_3)_2]^{3+}$. Interestingly, **3** is obtained quantitatively, regardless of the concentration of **2** and $enPd(NO_3)_2$. This is in contrast with other previous examples for which catenane dissociation to simple rings was observed at low concentration.[13] In MeCN–DMF, **3** does not dissociate over the concentration range investigated (0.005 to 20 mM). This particularly high stability suggests that no dissociation takes place during the MS measurements. It is probably due to the excellent fit of the ligand to coordination of Pd(II) and especially to the appropriate length of the 4 sides of the constitutive 'lozenges' of **3**.

The results presented in this work together with those discussed in reference 8 (synthesis of a 4-crossing [2]catenane) highlight the utmost importance of the nature of the ligands used in directed syntheses involving both copper(I) and palladium(II) coordination. The balance between the structural parameters (length, angles, flexibility, steric hindrance) of the ligands and stereoelectronic requirements of both metals clearly appears highly crucial and narrow, therefore dictating irrevocably the very nature of the molecular assembly generated by means of such methodology.

We thank the CNRS for its financial support.

Notes and references

1 J.-P. Sauvage, C. Dietrich-Buchecker and G. Rapenne, in *Molecular Catenanes, Rotaxanes and Knots*, ed. J.-P. Sauvage and C. Dietrich-Buchecker, Wiley-VCH, Weinheim, 1999.
2 V. Balzani, A. Credi, F. M. Raymo and J. F. Stoddart, *Angew. Chem., Int. Ed.*, 2000, **39**, 3348.
3 J.-P. Sauvage, *Acc. Chem. Res.*, 1998, **31**, 611.
4 C. P. Collier, G. Mattersteig, E. W. Wong, Y. Luo, K. Beverly, J. Sampaio, F. M. Raymo, J. F. Stoddart and J. R. Heath, *Science*, 2000, **289**, 1172.
5 *Comprehensive Supramolecular Chemistry*, ed. J. L. Atwood, J. E. D. Davies, D. D. MacNicol, F. Vögtle, J.-M. Lehn, J.-P. Sauvage and M. W. Hosseini, vol. 9, *Templating, self-assembly and self-organization*, 1996.
6 M. Fujita, *Acc. Chem. Res.*, 1999, **32**, 5.
7 D. J. Cárdenas, P. Gaviña and J.-P. Sauvage, *Chem. Commun.*, 1996, 1915.
8 F. Ibukuro, M. Fujita, K. Yamaguchi and J.-P. Sauvage, *J. Am. Chem. Soc.*, 1999, **121**, 11 014.
9 A. V. Kalinin, J. F. Bower, P. Riebel and V. Snieckus, *J. Org. Chem.*, 1999, **64**, 2986.
10 J.-M. Kern, J.-P. Sauvage, J.-L. Weidmann, N. Armaroli, L. Flamigni, P. Ceroni and V. Balzani, *Inorg. Chem.*, 1997, **36**, 5329.
11 M. Fujita, H. Oka and K. Ogura, *Tetrahedron Lett.*, 1995, **36**, 5247.
12 S. Sakamoto, M. Fujita, K. Kim and K. Yamaguchi, *Tetrahedron*, 2000, **56**, 955.
13 M. Fujita, F. Ibukuro, H. Hagihara and K. Ogura, *Nature*, 1994, **367**, 720.

CHEMCOMM
Communication
www.rsc.org/chemcomm

Unique structural isomerism involving tetrazole and amide/azide derivatives of gallium

Ned J. Hardman and Philip P. Power*

Department of Chemistry, University of California, Davis, One Shields Avenue, Davis, CA, 95616, USA. E-mail: pppower@ucdavis.edu

Received (in Irvine, CA, USA) 1st January 2001, Accepted 3rd May 2001
First published as an Advance Article on the web 13th June 2001

The reaction between {HC(MeCDippN)$_2$}Ga: (Dipp = C$_6$H$_3$Pr$^i_2$-2,6) and N$_3$SiMe$_3$ afforded the tetrazole {HC(MeCDippN)$_2$}GaN(SiMe$_3$)NNN(SiMe$_3$) 1 and its amide/azide isomer {HC(MeCDippN)$_2$}Ga(N$_3$)N(SiMe$_3$)$_2$ 2 whose stabilities are due to the unique steric properties of the [HC(MeCDippN)$_2$]$^-$ ligand.

Recent investigations of derivatives of the sterically encumbered β-diketiminate ligand [HC(MeCDippN)$_2$]$^-$ (Dipp = C$_6$H$_3$Pr$^i_2$-2,6) have shown that it can stabilize a wide variety of species with unusual coordination numbers and bonding throughout the Periodic Table.[1] In particular, its use in connection with low-valent heavier group 13 elements has resulted in the isolation of the monomeric, two-coordinate M(I) species {HC(MeCDippN)$_2$}M: (M = Al[2] or Ga[3]) which contain a stereochemically active lone pair of electrons at the metals. Previous work on less hindered, weakly associated M(I) species such as Cp*M (Cp* = C$_5$Me$_5$; M = Al[4] or Ga[5]) has shown that they can react with azides to give dimeric imides such as Cp*AlN(AlCp*$_2$)Al{N(SiMe$_3$)$_2$}N{Al(Cp*)N(SiMe$_3$)$_2$}[6] or {Cp*GaN(C$_6$H$_3$Me$_2$-2,6)}$_2$[7] under elimination of N$_2$. We reasoned that the more crowded Ga(I) species {HC(MeCDippN)$_2$}Ga: might react with the simple azide N$_3$SiMe$_3$ to afford a monomeric imide {HC(MeCDippN)$_2$}Ga=NSiMe$_3$ which could have a GaN multiple bond. We now report that, although unassociated products were obtained from this reaction, neither of these involved a terminal gallium imide moiety. Instead, the isomers **1** and **2**, involving the reaction of 2 equivalents of N$_3$SiMe$_3$ with {HC(MeCDippN)$_2$}Ga:, were isolated and characterized.

The reaction of {HC(MeCDippN)$_2$}Ga: with N$_3$SiMe$_3$ afforded the products **1** and **2** in accordance with Scheme 1.† It is probable that the species {HC(MeCDippN)$_2$}GaNSiMe$_3$ is generated initally, and this is prevented from dimerizing to give [{HC(MeCDippN)$_2$}GaNSiMe$_3$]$_2$ for steric reasons. Instead, {HC(MeCDippN)$_2$}GaNSiMe$_3$ reacts with a further equivalent of N$_3$SiMe$_3$ to give the tetrazole **1**‡ and the amide/azide product **2**. Solution ^{1}H NMR spectroscopy of the reaction mixture shows that both **1** and **2** as well as unreacted {HC(MeCDippN)$_2$}Ga: and N$_3$SiMe$_3$ are detectable after stirring for 30 min at *ca*. 25 °C. Heating at *ca*. 75 °C results in a *ca.* 1:3 ratio of **1** and **2** which can be isolated in 73% overall yield. Both **1** and **2** were obtained as colorless crystals. However, the solubility of the tetrazole **1** is considerably less than that of **2**, so that the products can be separated quite easily by crystallization. The compound **1** is thermally robust having a melting point > 200 °C. It decomposes at *ca.* 235 °C to a red solid with N$_2$ elimination. Compound **2** melts at a lower temperature (161–163 °C) and also decomposes at *ca*. 230 °C to give a red solid and N$_2$ evolution.§

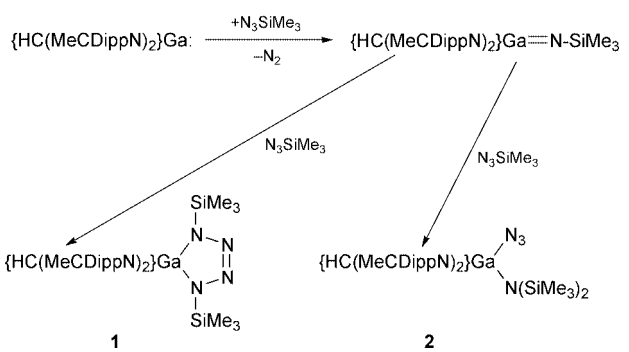

Scheme 1 Reactions of {HC(MeCDippN)$_2$}Ga: (Dipp = C$_6$H$_3$Pr$^i_2$-2,6) with N$_3$SiMe$_3$ to give **1** or **2**.

Compounds **1** and **2** were characterized by ^{1}H and ^{13}C NMR spectroscopy, by C,H,N analysis and by X-ray crystallography.¶ The structure of the tetrazole **1** (Fig. 1) features GaN$_4$ and GaN$_2$C$_3$ rings that are fused at gallium. The metal has distorted tetrahedral geometry and the Ga–N bonds [av. 1.947(2) Å] to the β-diketiminate nitrogens N(1) and N(2) are significantly longer than the average distance of 1.875(16) Å to the tetrazole nitrogens. The longer pair of Ga–N distances is consistent with equal components of normal and dative character in these bonds.[8] These Ga–N bond lengths also resemble those observed in other Ga(III) β-ketiminate species.[9] The shorter Ga–N distances involving the tetrazole nitrogens are in agreement with known values for bonding between four-coordinate gallium and terminal amide groups.[10] The gallium tetrazole ring is essentially planar, and the N(4)–N(5) distance of 1.265(3) Å is consistent with NN double bonding. In contrast, the gallium β-diketiminate ring is folded along the N(1)···N(2) axis such that Ga(I) lies *ca.* 0.34 Å from the averaged N$_2$C$_3$ plane. This structural feature is common to many bulky β-diketiminate derivatives.[1] The folding of the ring results in different magnetic environments for the two SiMe$_3$ groups (as well as slightly different bond lengths for Ga–N(3) and Ga–N(6)) which is manifested in different ^{1}H NMR chemical shifts for the SiMe$_3$ resonances.

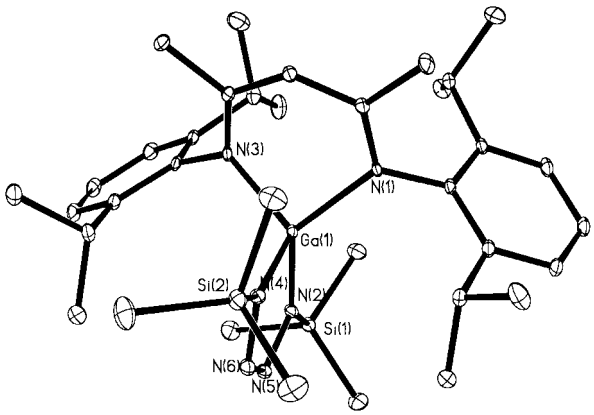

Fig. 1 Thermal ellipsoid (30%) plot of **1** with H atoms not shown. Selected bond distances (Å) and angles (°): Ga(1)–N(1) 1.945(2), Ga(1)–N(2) 1.949(2), Ga(1)–N(3) 1.858(2), Ga(1)–N(6) 1.891(2), N(3)–N(4) 1.402(3), N(4)–N(5) 1.265(3), N(5)–N(6) 1.406(2), Si(1)–N(3) 1.737(2), Si(2)–N(6) 1.750(2); N(1)–Ga(1)–N(2) 95.40(8), N(3)–Ga(1)–N(6) 85.74(7), N(1)–Ga(1)–N(6) 117.49(8), N(2)–Ga(1)–N(6) 115.64(8), N(1)–Ga(1)–N(3) 126.41(8), N(2)–Ga(1)–N(3) 118.11(8).

 DOI: 10.1039/b100466m

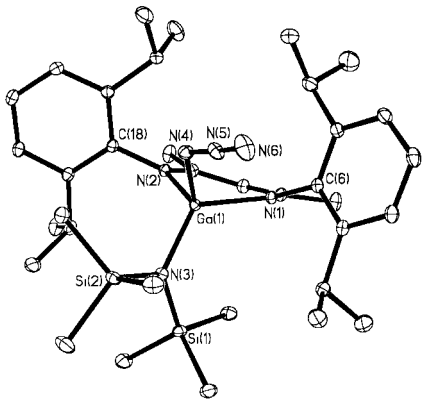

Fig. 2 Thermal ellipsoid (30%) plot of **2** with H atoms not shown. Selected bond distances (Å) and angles (°): Ga(1)–N(1) 1.946(1), Ga(1)–N(2) 1.958(1), Ga(1)–N(3) 1.884(1), Ga(1)–N(4) 1.918(1), Si(1)–N(3) 1.746(1), Si(2)–N(3) 1.751(1); N(1)–Ga(1)–N(2) 98.28(5), N(3)–Ga(1)–N(4) 111.82(6), N(1)–Ga(1)–N(3) 122.45(5), N(2)–Ga(1)–N(3) 113.23(5), Ga(1)–N(3)–Si(1) 123.39(7), Ga(1)–N(3)–Si(2) 115.32(7).

The structure of amide/azide compound **2** (Fig. 2) also features gallium bound to four nitrogens in a distorted tetrahedral fashion. The Ga–N(β-diketiminate) bonds [av. 1.952(7) Å] have very similar lengths to the corresponding bonds in **1**. The β-diketiminate ring is folded along the N(1)···N(2) axis such that Ga(I) lies *ca.* 0.21 Å from the averaged N_2C_3 plane. The Ga–N($SiMe_3$)$_2$ bond length [1.884(1) Å] is close to the 1.872(2) Å reported for {Cp*{(Me_3-Si)$_2$N}Ga(μ-N_3)}$_2$.[7] The Ga–N(azide) bond length, 1.918(3) Å, is essentially the same as the 1.921(4) Å observed in a bulky aryl-substituted bis(azide) of gallium.[11] Within the N_3 moiety, the N–N distances are similar to those previously observed in gallium azides.[12] Like **1**, compound **2** displays two different resonances for the $SiMe_3$ peaks—probably due to restricted rotation of the amide moiety around the Ga–N bond as a result of steric effects. Rotational barriers as high as 18.6 kcal mol^{-1} have been observed for group 13 metal–nitrogen bonds in sterically congested systems.[13] Variable temperature ^{1}H NMR studies of **1** or **2** in toluene did not result in the collapse of the $SiMe_3$ signals to a single resonance.

The isolation of tetrazole–amide/azide isomers appears to be unique.‖[14] Their stability can be rationalized on the basis of the size of the [HC(MeCDippN)$_2$]$^-$ ligand which prevents dimerization of the intermediate {HC(MeCDippN)$_2$}GaNSiMe_3, but allows reaction with a further equivalent of the less hindered N_3SiMe_3. Owing to the multipolar nature of the NNNSi array, this reaction proceeds by two distinct pathways to afford **1** and **2**.

We thank the National Science Foundation for Financial Support.

Notes and references

† All manipulations were carried out under anaerobic and anhydrous conditions. A toluene solution (50 mL) of N_3SiMe_3 (0.38 mL, 2.9 mmol) was added dropwise to a rapidly stirred solution of {HC(MeCNDipp)$_2$}Ga: (0.66 g, 1.41 mmol) in toluene (20 mL), with cooling in an ice-bath. The solution was allowed to rise to room temperature and was then heated to *ca*. 75 °C for 1 h. The solution was concentrated to *ca*. 20 mL and cooled for 24 h in a *ca*. 4 °C refrigerator to afford colorless crystals of the product **1** (0.18 g, 19%). Anal. Calc. (found) for $C_{35}H_{59}N_6GaSi_2$: C, 60.94 (61.11), H, 8.62 (8.81), N, 12.25 (12.01)%. Mp 217–220 °C. ^{1}H NMR (300 MHz, C_6D_6) δ 7.06–7.04 (m, 6H, aromatic H of Ar group), 4.89 (s, 1H, methine CH), 3.30 (sept, $^3J_{HH}$ = 6.6 Hz, 2H, C*H*Me), 3.20 (sept, $^3J_{HH}$ 6.6 Hz, 2H, C*H*Me), 1.50 (s, 6H, CMe), 1.32 (d, $^3J_{HH}$ 6.6 Hz, 6H, CH*Me*$_2$), 1.14 (d, $^3J_{HH}$ 6.6 Hz, 6H, CH*Me*$_2$), 1.08 (d, $^3J_{HH}$ 6.6 Hz, 6H, CH*Me*$_2$), 1.06 (d, $^3J_{HH}$ 6.6 Hz, 6H, CH*Me*$_2$), 0.54–0.12 [s, 9H, Si(CH_3)$_3$]: ^{13}C{^{1}H} (75 MHz, C_6D_6) δ 172.81 (CN), 145.48 (*C*Me) 142.76, 140.50 (*o*-C on C_6H_3), 127.54 (*p*-C on C_6H_3), 125.52, 124.26 (*m*-C on C_6H_3), 99.94 (γ-C), 29.10, (*C*HMe$_2$), 28.92 (CH*Me*$_2$), 25.30, 25.25 (CH*Me*$_2$) 24.37 (C*Me*) 1.93, 0.99 [Si(*C*H_3)$_3$]. The isomeric product **2** was obtained by decanting the supernatant liquid from **1** and cooling in a *ca*. −20 °C freezer for 48 h to afford colorless crystals of **2** (0.52 g, 54%). Mp 161–163 °C. ^{1}H NMR (300 MHz C_6D_6) δ 7.15 (s, 6H, aromatic H or Ar groups), 4.83 (s, 1H, methine CH), 3.60 (sept, $^3J_{HH}$ 6.6 Hz, 2H, C*H*Me), 3.29 (sept, $^3J_{HH}$ 6.6 Hz, 2H, C*H*Me), 1.48 (d, $^3J_{HH}$ 6.6 Hz, 6H, CH*Me*$_2$), 1.44 (d, $^3J_{HH}$ 6.6 Hz, 6H, CH*Me*$_2$), 1.40 (s, 6H, CMe), 1.16 (d, $^3J_{HH}$ 6.6 Hz, 6H, CH*Me*$_2$), 1.11 (d, $^3J_{HH}$ 6.6 Hz, 6H, CH*Me*$_2$), 0.23, 0.41 [s, 9H, Si(CH_3)$_3$]: ^{13}C{^{1}H} (75 MHz, C_6D_6) δ 171.39 (CN), 145.11 (*C*Me) 144.25, 141.01 (*o*-C on C_6H_3), 128.08 (*p*-C on C_6H_3), 125.58, 124.92 (*m*-C on C_6H_3), 100.32 (γ-C), 29.09, 28.45 (*C*HMe$_2$), 25.93, 25.58 (CH*Me*$_2$), 25.25 (C*Me*), 25.09, 24.82 (CH*Me*$_2$), 5.90, 5.78 [Si(*C*H_3)$_3$].

‡ Professor H. W. Roesky has informed us that a similar reaction involving {HC(MeCDippN)$_2$}Al: and N_3SiMe_3 affords the aluminium analog of **1**. The contrasting behavior of the gallium system, with its preference for the amide/azide over the tetrazole product, is another illustration of the differences between aluminium and gallium chemistry.

§ Attempts at thermal interconversion of **1** and **2** have so far been unsuccessful.

¶ *Crystal data* for **1** and **2** at 90 K with Mo-Kα radiation (λ = 0.71073 Å): **1**: $C_{35}H_{59}GaN_6Si_2$, M = 689.78, colorless parallelepiped, monoclinic, space group $P2_1/n$, a = 12.3462(4), b = 21.9781(7), c = 14.0957(4) Å, β = 91.064(1)°, Z = 4, D_c = 1.198 g cm^{-3}, μ = 0.813 mm^{-1}, $R1$ = 0.0454 for 4934 [$I > 2\sigma(I)$] data.

2: $C_{35}H_{59}Ga_2N_6Si_2$, M = 689.78, colorless parallelepiped, orthorhombic, space group *Pbcn*, a = 20.1655(8), b = 17.8134(7), c = 21.546(9) Å, Z = 8, D_c = 1.200 g cm^{-3}, μ = 0.815 mm^{-1}, $R1$ = 0.0354 for 9374 [$I > 2\sigma(I)$] data. CCDC 156697 and 156698. See http://www.rsc.org/suppdata/cc/b1/b100466m/ for crystallographic data in .cif or other electronic format.

‖ Non-isomeric amide/azide and tetrazole derivatives of germanium have been obtained by reaction of Ge(II) species with azides that have different substituents. See ref. 14.

1 For example: J. Feldman, S. J. McLain, A. Parthasarathy, W. J. Marshall, J. C. Calabrese and S. D. Arthur, *Organometallics*, 1997, **16**, 1514; M. F. Lappert and D.-S. Liu, *J. Organomet. Chem.*, 1995, **500**, 203; B. Qian, D. L. Ward and M. R. Smith, *Organometallics*, 1998, **17**, 3070; V. C. Gibson, P. J. Maddox, C. Newton, C. Redshaw, G. A. Solar, A. J. P. White and D. J. Williams, *Chem. Commun.*, 1998, 651; P. H. M. Budzelaar, R. de Gelder and A. W. Gal, *Organometallics*, 1998, **17**, 4121; W.-K. Kim, M. J. Fevola, L. M. Liable-Sands, A. L. Rheingold and K. H. Theopold, *Organometallics*, 1998, **17**, 4541; M. Chen, E. B. Lobkovsky and G. W. Coates, *J. Am. Chem. Soc.*, 1998, **120**, 11 018; L. W. M. Lee, W. E. Piers, M. R. J. Elsegood, W. Clegg and M. Parvez, *Organometallics*, 1999, **18**, 2947; B. Qian, W. J. Scanlon, M. R. Smith, III and D. H. Motry, *Organometallics*, 1999, **18**, 1693; C. E. Radzewich, I. A. Guzei and R. F. Jordan, *J. Am. Chem. Soc.*, 1999, **121**, 8673; B. Qian, S. W. Bach and M. R. Smith, *Polyhedron*, 1999, **18**, 2405; P. L. Holland and W. B. Tolman, *J. Am. Chem. Soc.*, 1999, **121**, 7270; P. L. Holland and W. B. Tolman, *J. Am. Chem. Soc.*, 2000, **122**, 6331; C. Cui, H. W. Roesky, H. Hao, H.-G. Schmidt and M. Noltemeyer, *Angew. Chem., Int. Ed.*, 2000, **39**, 1815.

2 C. Cui, H. W. Roesky, H.-G. Schmidt, M. Noltemeyer, H. Hao and F. Cimpoesu, *Angew. Chem., Int. Ed.*, 2000, **39**, 4274.

3 N. J. Hardman, B. E. Eichler and P. P. Power, *Chem. Commun.*, 2000, 1911.

4 C. Dohmeier, C. Robl, M. Tacke and H. Schnöckel, *Angew. Chem., Int. Ed. Engl.*, 1991, **30**, 564.

5 D. Loos and H. Schnöckel, *J. Organomet. Chem.*, 1993, **463**, 37.

6 S. Schulz, L. Häming, R. Herbst-Imer, H. W. Roesky and G. M. Sheldrick, *Angew. Chem., Int. Ed. Engl.*, 1994, **33**, 969.

7 P. Jutzi, B. Neumann, G. Reumann and H.-G. Stammler, *Organometallics*, 1999, **18**, 2037.

8 A. Haaland, in *Coordination Chemistry of Aluminum*, ed. G. H. Robinson, VCH, New York, 1993.

9 M. Stender, B. E. Eichler, N. J. Hardman, P. P. Power, P. Prüst, M. Noltemeyer and H. W. Roesky, *Inorg. Chem.*, in press.

10 K. M. Waggoner, M. M. Olmstead and P. P. Power, *Polyhedron*, 1990, **9**, 257.

11 A. H. Cowley, F. P. Gabbaï, F. Olbrich, S. Corbelin and R. J. Lagow, *J. Organomet. Chem.*, 1995, **487**, C5.

12 C. J. Carmalt, A. H. Cowley, R. D. Culp and R. A. Jones, *Chem. Commun.*, 1996, 1453.

13 R. J. Wehmschulte and P. P. Power, *Inorg. Chem.*, 1998, **37**, 2106.

14 J. Pfeiffer, W. Maringgelle, M. Noltemeyer and A. Meller, *Chem. Ber.*, 1989, **122**, 245.

CHEMCOMM Communication
www.rsc.org/chemcomm

Ionic liquids: polar, but weakly coordinating solvents for the first biphasic oligomerisation of ethene to higher α-olefins with cationic Ni complexes

Peter Wasserscheid,*[a] Charles M. Gordon,*[b] Claus Hilgers,[a] Mark J. Muldoon[b] and Ian R. Dunkin[b]

[a] *Institut für Technische Chemie und Makromolekulare Chemie der RWTH Aachen, Worringer Weg 1, 52074 Aachen, Germany. E-mail: wasserscheidp@itmc.rwth-aachen.de*
[b] *Department of Pure and Applied Chemistry, University of Strathclyde, 295 Cathedral Street, Glasgow, Scotland, UK G1 1XL. E-mail: c.m.gordon@strath.ac.uk*

Received (in Cambridge, UK) 13th February 2001, Accepted 9th May 2001
First published as an Advance Article on the web 13th June 2001

Ethylene oligomerisation in ionic liquids gives predominately alk-1-ene products with better reactivity and selectivity than in conventional solvents; turnover frequencies are correlated with polarity data obtained using solvatochromic dyes.

Ionic liquids are salts/salt mixtures with melting points below ambient temperature. The first use of ionic liquids in homogeneous catalysis was reported in 1990 for dimerisation[1] and polymerisation[2] reactions. Since then, a rapidly growing number of transition metal catalysed reactions have been described in various ionic liquids (for general reviews see ref. 3). Several papers describing the oligomerisation of ethylene and higher olefins in ionic liquids have been published.[1,4] However, all work described to date has used chloroaluminate ionic liquids, giving a high degree of isomerisation, and the formation of mainly internal olefins. For example, 9% of but-1-ene, but 91% of but-2-enes are obtained in the C_4-fraction from the reaction of ethylene with $[Ni(MeCN)_6][BF_4]_2$ in chloroaluminate ionic liquid at room temperature.[4c]

Higher α-olefins (HAOs) represent an important group of industrial chemicals. Depending on chain length, they are used as intermediates for plastics, plasticizers, lubricants and surfactants. HAOs can be obtained from ethylene *via* oligomerisation processes, such as those practised by BP Amoco (alkylaluminium catalyst) and Shell (SHOP, neutral nickel/phosphine catalyst). The latter is a biphasic process, the catalyst being dissolved in butane-1,4-diol, and the products forming a second layer easily removed by phase separation.

Besides the neutral nickel/phosphine compounds used in SHOP, cationic Ni complexes have attracted some attention as highly active catalysts for ethylene oligomerisation.[5] The positive charge means that they usually possess a more electrophilic Ni centre, often resulting in higher oligomerisation activity. To our knowledge, no example of biphasic ethylene oligomerisation to HAOs with cationic Ni complexes could be realised to date owing to the lack of a suitable solvent for the catalyst.

Here, we report the use of ionic liquids **1a**–**d** as catalyst solvents in the biphasic oligomerisation of ethylene to higher α-olefins using the cationic Ni catalyst **2**.[5a] Ionic liquids **1a**–**d** were synthesised by reacting the appropriate chloride salt[6] with HPF_6, following a method described by Fuller *et al.*,[7] or purchased from Solvent Innovation GmbH, Cologne, Germany.[8] It was important that the liquids were completely free of water and chloride ions for **2** to exhibit good activity. The catalytic experiments were carried out under a constant pressure of ethylene in a 150 ml autoclave specially designed for biphasic ethylene oligomerisation (four paddles, stirrer with special gas inlet, baffles).

Catalyst **2** is found to be highly active in ionic liquid **1a**, selectively forming HAOs *via* a biphasic reaction (Table 1, entry 1). The products separated as a clear and colorless organic layer from the ionic catalyst solution after reaction (catalyst leaching being < 0.1% (detection limit)), with high selectivity for linear alk-1-enes. Previously, internal isomers have been the major components in reactions of this type.[4] The ionic catalyst solution was recyclable with little change in selectivity, although with somewhat lower activity (Table 1, entries 2 and 3). Since catalyst **2** is very sensitive to traces of water, the deactivation may be assigned to the practical problem of quantitative transfer back into the autoclave under completely inert conditions. In contrast, almost no ethylene conversion was observed in butane-1,4-diol, presumably due to catalyst deactivation (Table 1, entry 4). Butane-1,4-diol was chosen since this solvent is used successfully in biphasic reactions with neutral Ni complexes (*e.g.* SHOP). Following these observations, we decided to investigate the polarity and coordination properties of **1a** in comparison to butane-1,4-diol.

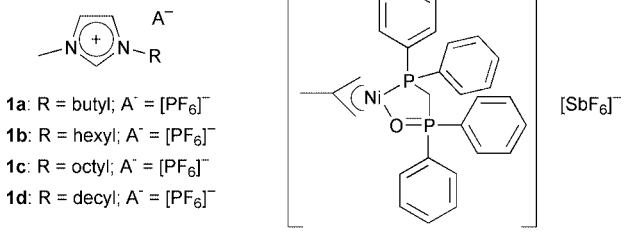

1a: R = butyl; A⁻ = $[PF_6]^-$
1b: R = hexyl; A⁻ = $[PF_6]^-$
1c: R = octyl; A⁻ = $[PF_6]^-$
1d: R = decyl; A⁻ = $[PF_6]^-$

2

Solvatochromic dyes have been widely used to help quantify solute–solvent interactions.[9] Many different scales exist, but most probe only particular interactions of a given solvent. Defining the 'polarity' of ionic liquids is made difficult by the wide range of interactions possible within systems like **1a**. The

Table 1 Comparison of ethylene oligomerisation in different solvents

Entry	Solvent (cycle)	TOF[a]/ h^{-1}	$L(C_6)$[b] (%)	$S(\alpha)$[c] (%)	Oligomer distribution[d]	C_n (max)[e]
1	**1a**	12712	95	93	0.16	14
2	**1a** (2)	9889	94	92	0.16	14
3	**1a** (3)	7952	93	91	0.16	14
4	Butane-1,4-diol	< 10	—	—	—	—
5	CH_2Cl_2	1852	95	88	0.48	18
6	**1b**	5527	91	89	0.18	14
7	**1c**	2885	92	90	0.22	14
8	**1d**	2058	96	94	0.24	16

Conditions: T = 25 °C; t = 2 h; p(ethylene) = 50 bar; 0.05 mmol **2**; 20 ml heptane, 10 ml ionic liquid (entries 1–3, 6–8); 20 ml organic solvent (entries 4, 5). [a] TOF = turnover frequency; mol feedstock converted per mol catalyst. [b] $L(C_6)$ = linear hexene selectivity in C_6-fraction of product. [c] Hex-1-ene selectivity in the linear hexene fraction of the product. [d] Schultz–Flory distribution calculated from α = mol C_{10}/mol C_8. [e] C_n (max) = maximum chain length of detected products.

 DOI: 10.1039/b101400p

few studies reported to date suggest that ionic liquids are low dielectric materials,[10] whose apparent 'polarity' depends on the probe molecule employed.[11]

One of the most widely quoted scales of solvent polarity is the E_T scale, based on the position of the charge transfer band of betaine dyes such as **3**.[9] This molecule displays an extremely large wavelength shift in its charge-transfer band between non-polar solvents (λ_{max} = 810 nm for Ph_2O) and polar solvents (λ_{max} = 453 nm for H_2O). The position of the CT band is most strongly influenced by specific interactions with the highly basic phenoxide oxygen atom.[12] When **3** is dissolved in **1a** (*ca.* 1 mM), which had been dried under vacuum at 70 °C for several hours, λ_{max} = 547 nm [$E_T(30)$ = 52.3 kcal mol^{-1}],† approximately the same as that obtained for butane-1,4-diol [$E_T(30)$ = 53.5 kcal mol^{-1}]. Karl–Fischer titration measurements indicated a water content of *ca.* 6.0×10^{-3} M in the dried **1a**. It was found that extended drying and different concentrations of **3** resulted in no further change in the value of $E_T(30)$. Clearly the residual water may have some influence on the recorded value of $E_T(30)$, given the similar concentrations of probe molecule and water, but it is likely that removal of all traces of water will be impossible in any synthetic applications. By way of contrast, for undried [bmim][PF_6] (water content *ca.* 0.15 M), λ_{max} = 541 nm [$E_T(30)$ = 52.9 kcal mol^{-1}]. With regard to this polarity scale, **1a** can be regarded as behaving similarly to alcohols, possibly as a result of specific interactions between the hydrogen atoms on the imidazolium ring and the phenoxide oxygen. Thus, these results give no explanation for the difference in ethylene oligomerisation activity between **1a** and butane-1,4-diol.

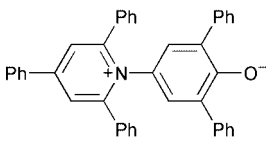

3

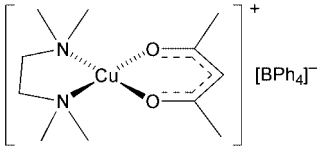

4

Since catalyst activity is most likely to be affected by the solvent basicity, we decided to probe this parameter using **4**, a complex whose d–d absorption band shifts to longer wavelengths as the degree of solvent coordination at the copper atom increases. A relationship has been reported between λ_{max} and the Gutmann donor number of the solvent, allowing **4** to be used as a measure of solvent and anionic basicity.[13]

When **4** is dissolved in dried **1a** ([**4**] = 10–50 mM), λ_{max} = 516.5 nm, while λ_{max} = 598.0 nm for butane-1,4-diol indicating much stronger coordination of the latter to the Cu(II) centre. The same probe in undried **1a** (water content *ca.* 0.15 M) gave a λ_{max} value of 535 nm, suggesting that the presence of water has a more significant effect than is the case for probe **3**. Thus, we conclude that the beneficial properties of **1a** with regard to the ethylene oligomerisation with catalyst **2** can be explained, at least in part, by a unique combination of high polarity and low coordination power displayed by this ionic liquid.

Our data suggested that the coordination strength of **1a** is only slightly higher than that of CH_2Cl_2. Consequently, we applied this solvent to the ethylene oligomerisation reaction with catalyst **2**. In CH_2Cl_2, the reaction is monophasic, thus preventing simple product recovery by phase separation (Table 1, entry 5). More importantly, a comparison with entry 1 reveals a much higher activity of **2** in the ionic liquid. Bearing in mind the similar λ_{max} values, this result seems to be somewhat surprising at first.

Therefore, a comparison of **1a** with other [PF_6]$^-$-based ionic liquids **1b**–**d** was carried out. As expected, measurements with **3** reveal a slight decrease in polarity on increasing alkyl chain length at the imidazolium cation [λ_{max} = 557 nm, $E_T(30)$ = 51.3 kcal mol^{-1} for dried **1c**]. In contrast, **4** displays effectively identical λ_{max}-values for the series **1a**–**d** (λ_{max} = 516.5 nm for dried **1c**), indicating that the strength of interaction at the metal centre is purely anion dependent. All ethylene oligomerisation experiments with catalyst **2** in **1b**–**d** showed enhanced activity compared to the reaction in CH_2Cl_2, but decreasing activity was observed with increasing alkyl chain length at the imidazolium cation. We suggest that weak coordination of the solvent to **2** is a prerequisite for catalytic activity, but is clearly not the only factor to explain the special usefulness of **1a** in this reaction. The greater reactivity may be explained by inhibition of the cationic Ni catalyst **2** by the oligomers formed. This would explain why the oligomerisation activity is reduced by both a monophasic reaction (*e.g.* CH_2Cl_2) and increasing solubility of the products in the catalyst solvent (*e.g.* **1b**–**d**).

Remarkably, the oligomer distribution also shows a strong solvent dependence. The lower α-value of the Schulz–Flory distribution shows that the yield of low molecular weight HAOs is much higher for biphasic reactions in **1a**–**d** than for the reaction in CH_2Cl_2. This observation may be explained by the lower ethylene solubility (25 °C/50 bar) in *e.g.* **1a** (0.110 g ethylene/g **1a**) and **1c** (0.183 g ethylene/g **1c)** compared with CH_2Cl_2 (0.651 g ethylene/g CH_2Cl_2).[14] Since the rate of insertion (k_{ins}) is dependent on the ethylene concentration, while the rate of elimination (k_{elim}) is not, a solvent with lower ethylene solubility shifts the ratio k_{ins}/k_{elim} to lower values since it decreases the relative ethylene concentration at the catalyst.

In conclusion, we believe that our results are of general importance, since many cationic transition metal complexes are excellent catalysts, but are often poorly soluble in non-polar solvents, thus requiring a compromise between the solvation and coordination properties of a solvent. Our investigations clearly show that hexafluorophosphate ionic liquids are very interesting solvents for these applications. We propose to pursue these investigations, and will report our findings in due course.

P. W. and C. H. thank Professor Wilhelm Keim for his continuous interest in this research and many inspiring discussions, and C. M. G. thanks the Royal Society of Edinburgh for funding, and the EPSRC (Grant no. GR/M56852) for a research studentship.

Notes and references

† Molar transition energy $E_T(30)$/kcal mol^{-1} = 28591/(λ_{max}/nm).

1 Y. Chauvin, B. Gilbert and I. Guibard, *J. Chem. Soc., Chem. Commun.*, 1990, 1715.
2 R. T. Carlin and J. Wilkes, *J. Mol. Catal.*, 1990, **63**, 125.
3 P. Wasserscheid and W. Keim, *Angew. Chem., Int. Ed.*, 2000, **39**, 3772; T. Welton, *Chem. Rev.*, 1999, **99**, 2071; K. R. Seddon, *J. Chem. Technol. Biotechnol.*, 1997, **68**, 351.
4 (*a*) B. Ellis, W. Keim and P. Wasserscheid, *Chem. Commun.*, 1999, 337; (*b*) Y. Chauvin, H. Oliver and S. Einloft, *Ind. Eng. Chem.*, 1995, **34**, 1149; (*c*) S. Einloft, F. K. Dietrich, R. F. de Souza and J. Dupont, *Polyhedron*, 1996, **19**, 3257.
5 (*a*) I. Brassat, U. Englert, W. Keim, D. P. Keitel, S. Killat, G. P. Suranna and R. Wang, *Inorg. Chim. Acta*, 1998, **280**, 150; (*b*) J. R. Ascenso, M. A. A. F. De C. T. Carrando, A. R. Dias, P. T. Gomes, M. F. M. Piadade, C. C. Romao, A. Revillon and I. Tkatschenko, *Polyhedron*, 1989, **8**, 2449; (*c*) J.-P. Gehrke, R. Taube, E. Balbolov and K. Kurtev, *J. Organomet. Chem.*, 1986, **304**, C4.
6 J. S. Wilkes, J. A. Levisky, R. A. Wilson and C. L. Hussey, *Inorg. Chem.*, 1982, **21**, 1263.
7 J. Fuller, R. T. Carlin, H. C. de Long and D. Haworth, *J. Chem. Soc., Chem. Commun.*, 1994, 299.
8 http://www.solvent-innovation.de
9 C. Reichardt, *Chem. Rev.*, 1994, **94**, 2319.
10 P. Bonhôte, A.-P. Dias, N. Papageorgiou, K. Kalyanasundaram and M. Grätzel, *Inorg. Chem.*, 1996, **35**, 1168.
11 A. J. Carmichael and K. R. Seddon, *J. Phys. Org. Chem.*, 2000, **13**, 591; S. N. V. K. Aki, J. F. Brennecke and A. Samanta, *Chem. Commun.*, 2001, 413; M. J. Muldoon, C. M. Gordon and I. R. Dunkin, *J. Chem. Soc., Perkin Trans. 2*, 1994, 433.
12 R. W. Taft and M. J. Kamlet, *J. Am. Chem. Soc.*, 1976, **98**, 2886.
13 R. W. Soukup and K. Sone, *Bull. Chem. Soc. Jpn.*, 1987, **60**, 2286; W. Linert, R. F. Jameson and A. Taha, *J. Chem. Soc., Dalton Trans.*, 1993, 3181.
14 Ethylene solubilities under reaction conditions were determined according to S. Mecking, L. K. Johnson, L. Wang and M. Brookhardt, *J. Am. Chem. Soc.*, 1998, **120**, 888.

CHEMCOMM
Communication
www.rsc.org/chemcomm

Selective anion sensing based on a dual-chromophore approach†

Dong Hoon Lee,[a] Ho Yong Lee,[a] Kwan Hee Lee[a] and Jong-In Hong*[ab]

[a] *School of Chemistry and Molecular Engineering, Seoul National University, Seoul 151-742, South Korea. E-mail: jihong@plaza.snu.ac.kr*

[b] *Center for Molecular Design and Synthesis, KAIST, Taejon 305-701, Korea*

Received (in Cambridge, UK) 7th March 2001, Accepted 22nd May 2001
First published as an Advance Article on the web 14th June 2001

A new anion sensor 1 with an azophenol and *p*-nitrophenyl moieties as chromophores allows for easy colorimetric differentiation of F^-, $H_2PO_4^-$ and AcO^- with similar basicity.

Currently, the development of receptors for biologically important anions is emerging as a research area of great importance.[1] One of the more attractive approaches in this field involves the construction of chemosensors.[2–4] This kind of system is generally composed of two parts. One is the anion-binding part employing various combinations of pyrroles, guanidiniums, Lewis acids, amides and urea/thioureas.[1–5] The other is the chromophore which turns binding-induced changes into optical signals.[2–4] These two parts are either covalently attached[4] or intermolecularly linked.[2a,b,3] Previously, we presented a new chromogenic azophenol–thiourea based anion sensor which allows for the colorimetric detection of F^-, $H_2PO_4^-$ and AcO^-.[6] However, this system is not able to discriminate between $H_2PO_4^-$, AcO^- and F^-.

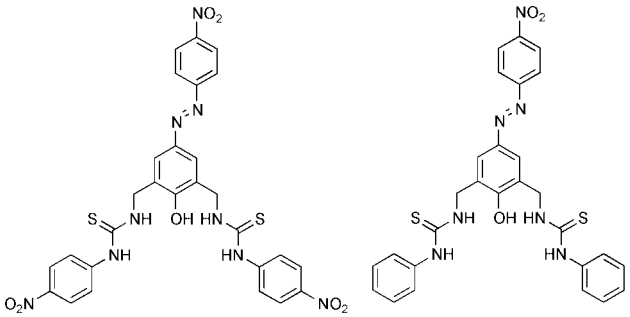

1 **2**

We now present a dual-chromophore anion sensor **1** with *p*-nitrophenylazophenol[1a,7] and *p*-nitrophenylthiourea moieties as two different chromophores.[8] The anion recognition *via* hydrogen-bonding interactions can be easily monitored by anion-complexation induced changes in UV-vis absorption spectra and with the naked eye.

Synthesis of sensors **1** and **2** is described in the ESI†,[6,7,9a] **1** and **2** contain four thiourea NH groups as hydrogen-bonding donors for anions[9b] and one azophenol OH group as both an additional binding site and a color-monitoring unit.[6] In the case of **1**, the introduction of a *p*-nitrophenyl group to the thiourea moiety as another chromophore enables color differentiation of anions in a cooperative manner, along with an azophenol group upon anion binding. This approach brings together changes in λ_{max} of two chromophores to render colorimetric detection of anions more effective than with only one chromophore.

It turns out that the UV-vis absorption band of **1** in chloroform undergoes a red shift as a phosphate anion is bound. In the absence of anions, the spectrum of **1** is characterized by the presence of one absorption maximum at 339 nm. Upon addition of increasing amounts of $H_2PO_4^-$, the peak at 339 nm decreases while the new peaks gradually move to longer wavelengths finally reaching maximum values at 374 nm (due to a *p*-nitrophenyl group) and 538 nm (due to an azophenol group) (Fig. S1a). Complexation with a series of anions results in similar red shift tendencies. Clear isosbestic points are observed, which demonstrates the existence of two states of a 1:1 complex. As can be expected from the UV-vis data, color change occurs through addition of anions to the solution of **1**. Upon the addition of $H_2PO_4^-$, the color of the solution changes from light yellow to violet. The color change terminates after the addition of 40 equiv. of $H_2PO_4^-$. However, in the case of HSO_4^-, Cl^- and Br^-, no detectable color changes are observed upon excess addition of anions to the solution of **1**.

The qualitative changes explained above are reflected in the quantitative data in the UV-vis absorption experiment. In these chromophores, electronic excitation generally occurs through a charge transfer from the donor oxygen of the azophenol and donor nitrogen of the thiourea to the acceptor substituent ($-NO_2$) of each chromophore. Upon the complex formation of **1** with an anion, the excited state would be more strongly stabilized by anion binding, resulting in a bathochromic shift in λ_{max}.[8] The color discrimination comes from different λ_{max} values in each complex and the relative contribution of the two chromophores (Fig. 1).

The degree of a red shift for **1** was determined to be $H_2PO_4^- \gg AcO^- \approx F^- > Br^- \approx Cl^- > HSO_4^- \approx I^-$. The maximum red-shift value (λ_{max} = 538 nm) for $H_2PO_4^-$ can be understood on the basis of the guest basicity and structure of the complex. According to the basicity of anions,[9b,10] $H_2PO_4^-$, F^- and AcO^- give stronger complexes and thus show noticeable color changes compared to other anions. $H_2PO_4^-$ with four oxygens affects both chromophores *via* multitopic hydrogen bonds to give rise to a pronounced color change, while F^- and AcO^- have a relatively weaker effect on the *p*-nitrophenyl group with respect to inducing color changes. This enables color discrimination between $H_2PO_4^-$, F^- and AcO^-. In the case of sensor **2** with only an azophenol group as the chromophore, λ_{max} values upon complexation with $H_2PO_4^-$, F^- and AcO^- are similar

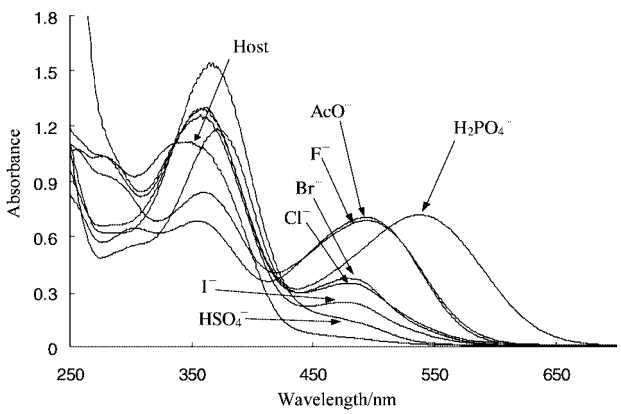

Fig. 1 UV-vis changes of **1** operated in $CHCl_3$ (5.0×10^{-5} M) after the addition of 40 equiv. of anions.

† Electronic supplementary information (ESI) available: experimental details for **1** and **2**, Figs. S1 and S2. See http://www.rsc.org/suppdata/cc/b1/b102187g/

 DOI: 10.1039/b102187g

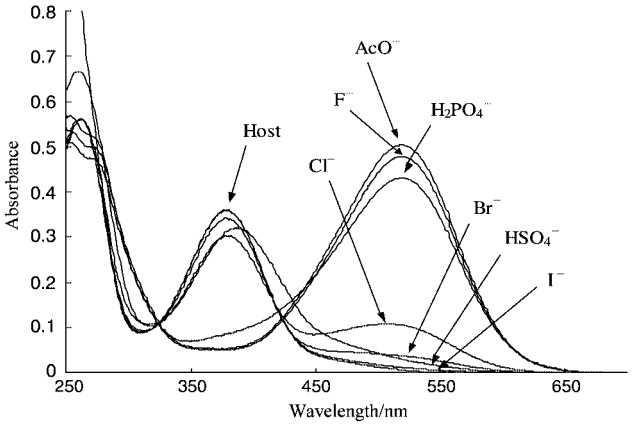

Fig. 2 UV-vis changes of **2** operated in $CHCl_3$ (1.5×10^{-5} M) after the addition of 40 equiv. of anions.

(Fig. S1b and Fig. 2) and thus the color differentiation between $H_2PO_4^-$, F^- and AcO^- is not feasible. This means that the cooperativity of dual-chromophores enables color discrimination of anions $H_2PO_4^-$, F^- and AcO^- with similiar basicity. Considering that an azophenol on its own does not exhibit color changes through addition of anions except for F^-,[11] this result indicates that the introduction of *p*-nitrophenylthiourea groups as an anion-binding site increases the electronic interaction between **1** and the anion, and furthermore results in color discrimination between $H_2PO_4^-$, F^- and AcO^-.

In summary, we have developed a new anion sensor **1** with azophenol and *p*-nitrophenyl moieties as two chromophores. This dual-chromophore system allows for colorimetric differentiation of $H_2PO_4^-$, F^- and AcO^- with similar basicity.

Financial support from the KRF (Grant No. KRF-99-042-D00073) is gratefully acknowledged. We thank the Ministry of Education (BK 21 program) for a postdoctoral fellowship awarded to K. H. L., and predoctoral fellowships awarded to H. Y. L. and D. H. L.

Notes and references

1 (*a*) *Comprehensive Supramolecular Chemistry*, Chair ed. J.-M. Lehn, ed. J. L. Atwood, J. E. D. Davies, D. D. MacNicol and F. Vögtle, Pergamon, Oxford, 1996, Vol. 1; (*b*) *Chemosensors of Ion and Molecular Recognition*, ed. J.-P. Desvergne and A. W. Czarnik, Kluwer, Dordrecht, 1997, Vol. 492; (*c*) F. P. Schmidtchen and M. Berger, *Chem. Rev.*, 1997, **97**, 1609.
2 (*a*) K. Niikura and E. V. Anslyn, *J. Am. Chem. Soc.*, 1998, **120**, 8533; (*b*) A. Metzger and E. V. Anslyn, *Angew. Chem., Int. Ed.*, 1998, **37**, 649; (*c*) Y. Kubo, S. Maeda, S. Tokita and M. Kubo, *Nature*, 1996, **382**, 522.
3 (*a*) J. J. Lavigene and E. V. Anslyn, *Angew. Chem., Int. Ed.*, 1999, **38**, 3666; (*b*) P. A. Gale, L. J. Twyman, C. I. Handlin and J. L. Sessler, *Chem. Commun.*, 1999, 1851.
4 (*a*) C. B. Black, B. Andrioletti, A. C. Try, C. Ruiperez and J. L. Sessler, *J. Am. Chem. Soc.*, 1999, **121**, 10 438; (*b*) H. Miyaji, W. Sato and J. L. Sessler, *Angew. Chem., Int. Ed.*, 2000, **39**, 1777; (*c*) P. Anzenbacher, K. Jursíková and J. L. Sessler, *J. Am. Chem. Soc.*, 2000, **122**, 9350.
5 For reviews, see (*a*) *Supramolecular Chemistry of Anions*, ed. A. Binachi, K. Bowman-James and E. Garcia- Espana, Wiley-VCH, New York, 1997; (*b*) *Supramolecular Chemistry, Concepts and Perspectives*, ed. J. M. Lehn, Wiley-VCH, Weinheim, 1995.
6 D. H. Lee, K. H. Lee and J.-I. Hong, *Org. Lett.*, 2001, **3**, 5.
7 A. Tsuge, T. Moriguchi, S. Mataka and M. Tachiro, *J. Chem. Soc., Perkin Trans. 1*, 1993, 2211.
8 S. Nishizawa, R. Kato, T. Hayashita and N. Teramae, *Anal. Sci.*, 1998, **14**, 595.
9 (*a*) M.-S. Muche and M. W. Göbel, *Angew. Chem., Int. Ed. Engl.*, 1996, **35**, 2126; (*b*) S. Nishizawa, P. Bühlmann, M. Iwao and Y. Umezawa, *Tetrahedron Lett.*, 1995, **36**, 6483.
10 T. R. Kelly and M. H. Kim, *J. Am. Chem. Soc.*, 1994, **116**, 7072.
11 K. H. Lee and J.-I. Hong, *Tetrahedron Lett.*, submitted.

CHEMCOMM Communication
www.rsc.org/chemcomm

Non-uniform rate for platination of guanine-N7 located in short DNA oligomers†

Åse Sykfont,[a] Anna Ericson[a] and Sofi K. C. Elmroth*[a]

[a] *Inorganic Chemistry 1, Chemical Center, Lund University, P.O. Box 124, SE-221 00 Lund, Sweden. E-mail: sofi.elmroth@inorg.lu.se; Fax: 46 46 222 44 39; Tel: 46 46 222 8106*

Received (in Cambridge, UK) 5th April 2001, Accepted 18th May 2001
First published as an Advance Article on the web 13th June 2001

The rate for adduct formation between *cis*-[Pt(NH$_3$)(c-NH$_2$C$_6$H$_{11}$)Cl(OH$_2$)]$^+$ and guanine-N7 in d(T$_n$GT$_{16-n}$) decreases gradually from the maximum rate found for platination of the middle position towards both the 3′ and 5′ ends.

Short DNA and RNA fragments are currently of great scientific interest. Modified DNA fragments have emerged as promising candidates for the treatment of both cancers and viral infections.[1] In addition, increasing knowledge about the nature of the interactions between metal ions or naturally occurring proteins and the surface of ribonucleic acids *in vivo* allows for detailed models system studies under well defined conditions *in vitro*.[2] The use of oligonucleotides, rather than extended ribonucleic acids for such studies is, however, likely to change the magnitude of the electrostatic interactions between the oligonucleotide surface and approaching charged or dipolar species.[3–8] A goal for current work in our laboratory is to increase the understanding of how the reduced electrostatic interactions of such model systems influence the overall adduct formation process with charged anticancer active metal complexes. We here present a study that allows for a unique comparison of the kinetic influence from the DNA environment during metalation of the non-charged guanine-N7, G-N7, with that of the previously studied charged phosphorothioate group, p(S).[9,10] The obtained reaction profile reveals a less pronounced kinetic influence from the surrounding DNA, which suggests the distance from the phosphodiester backbone as a parameter of influence on the adduct formation process.

The present study has been designed to obtain detailed information concerning the magnitude of the kinetic influence from the DNA environment as a function of position of G-N7 within a given size DNA fragment. The reaction between *cis*-[Pt(NH$_3$)(c-NH$_2$C$_6$H$_{11}$)Cl(OH$_2$)]$^+$ **1** and a single-stranded 17-mer poly(dT) oligonucleotide with one guanine base at variable position was used as a model system; d(T$_n$GT$_{16-n}$), *n* = 0, 2, 4, 6, 8, 10, 12, 14, and 16. The platinum complex is considered to be the active metabolite of the orally adiministered anticancer active compound *cis*,*trans*,*cis*-[Pt(NH$_3$)(c-NH$_2$C$_6$H$_{11}$)(OC(O)CH$_3$)$_2$Cl$_2$] (JM216).[11–13] Like cisplatin, it preferentially forms intrastrand adducts between adjacent G-N7, but exhibits a reduced preference for formation of the mutagenic AG-lesion.[14,15] Determination of the rate constants for the adduct formation reactions with deoxyguanosine 5′-phosphate, d(pG), was included to illustrate the kinetic influence from the surrounding polymer. A low concentration salt buffer with [cation] = 1.0 mM was used to obtain maximum kinetic resolution between the different positions along the oligonucleotide. The kinetics were studied under pseudo-first-order conditions with a 40-fold excess of **1**. Samples were taken from the thermostated reaction mixture (pH 4.1 ± 0.1, 298 K) at different time intervals, and were analyzed by use of HPLC as described previously.[16] Observed pseudo-first-order rate constants, k_{obs}, were derived by a fit of a single-exponential function to the time dependent decrease or increase of peak areas corresponding to unplatinated and platinated oligomer respectively. During reactions with the oligomers, the concentrations of **1** and DNA were kept constant. The pseudo-first-order rate constants can thus be directly compared and used as a measure of the kinetic influence from surrounding DNA.

The observed rate constants were found to vary significantly with the location of the common G-N7 nucleophile along the oligomer d(T$_n$GT$_{16-n}$), see Fig. 1. The shape of the reaction profile shows that platination is kinetically favoured when the G-N7 site is located in the central part of the oligomer with a maximum for platination of d(T$_8$GT$_8$) with k_{obs} = 6.46 ± 0.04 s^{-1}. The platination rate decreases gradually in both the 5′- and 3′-directions, reaching a similar value at both ends, *viz.* k_{obs} = 1.9 ± 0.5 and 2.48 ± 0.13 s^{-1}, respectively. The observed reactivity of the mononucleotide d(pG) with k_{obs} = 0.27 ± 0.04 s^{-1} is *ca.* one order of magnitude slower compared with platination of the oligomers despite the larger Pt(II)-concentration used (C_{Pt} = 3.2 × 10^{-4} M).

The observed increased reactivity of purine N7 in the DNA environment, compared with the reactivity of its corresponding monomeric form,[17,18] agrees qualitatively well with previous observations made for reactions with the charged p(S)-group.[9,10,19,20] However, the present study shows clearly that the influence from the DNA environment is significantly reduced for reaction with the non-charged G-N7 when the gradient between the concentration of bulk cations and those accumulated on the DNA is increased.[3–8] For example, the second-order rate constant for adduct formation with the d(T$_8$GT$_8$) oligomer is *ca.* 50 times larger compared with that observed for the d(pG) monomer, whereas the reactivity of d(T$_8$p(S)T$_8$) exceeds that of d(Tp(S)T) with a factor of *ca.* 200 at comparable salt concentration.[10] The effect is further

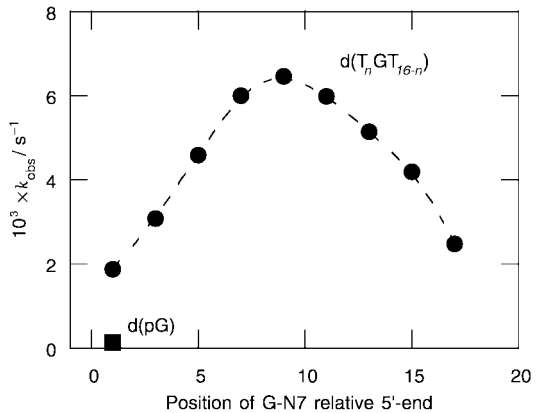

Fig. 1 Observed pseudo-first-order rate constants as a function of G-N7 position with respect to the 5′-end for reaction of **1** with d(pG), and d(T$_n$GT$_{16-n}$); *n* = 0, 2, 4, 6, 8, 10, 12, and 16, *T* = 25 °C, [cation] = 1.0 mM. For reactions with oligonucleotides: C_{Pt} = 1.6 × 10^{-4} M, [DNA] = 4.0 × 10^{-6} M, for reactions with d(pG): C_{Pt} = 3.2 × 10^{-4} M, [DNA] = 3.3 × 10^{-5} M.

† Electronic supplementary information (ESI) available: observed pseudo-first-order and apparent second-order rate constants for platination of G-N7 located in short DNA oligomers. See http://www.rsc.org/suppdata/cc/b1/b103087f/

 DOI: 10.1039/b103087f

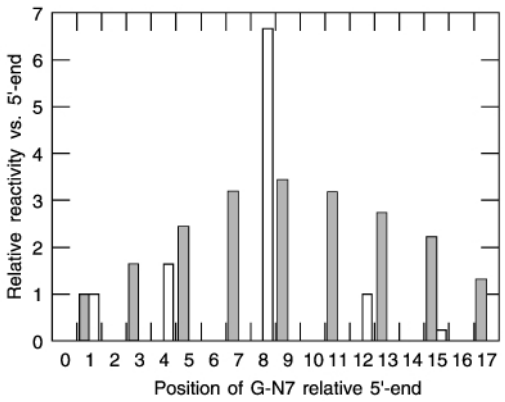

Fig. 2 Relative reactivity for adduct formation of **1** with G-N7 (hatched bars) and p(S) (open bars)[10] as a function of distance from the 5′-end of $d(T_nGT_{16-n})$ and $d(T_np(S)T_{16-n})$.

illustrated by a comparison of the reaction profiles obtained for $d(T_nGT_{16-n})$ and $d(T_np(S)T_{16-n})$, see Fig. 2. The figure reveals a similar overall tendency for a gradual increase of the reactivity towards the middle of the oligomer. Normalization of the reactivity with respect to the rate obtained for the 5′-end positions shows however that the relative change is less pronounced for formation of the platinated G-N7 moiety.

In mechanistic terms, these observations have several implications. First of all, the DNA promoted reactivity is in line with the previously suggested reaction mechanism where an electrostatically driven preequilibrium between the charged metal complex and the oligonucleotide contributes to increase the rate of adduct formation with reactive groups located on the oligomer.[9,10,19,20] Second, the gradual increase of k_{obs} towards the middle of the oligomer rules out a strict sequence dependent influence on the observed reactivity. The common platination environment of the type 5′-T_4GT_4-3′ should be large enough to provide a constant local structural and electrostatic environment around G-N7 in the centrally located positions, *i.e.* $d(T_nGT_{16-n})$; n = 4, 6, 8, 10, and 12 in the absence of other effects. Rather, the similar shape of the reaction profiles speaks in favour of a reaction model where the tendency for preaccumulation varies along the oligomer, in a fashion similar to the one calculated for short double-stranded DNA oligomers.[3,4] The less pronounced influence from such effect in the present investigation, compared with adduct formation with p(S), suggests further that the local concentration of preaccumulated cations decreases with increasing distance from the phosphodiester backbone.‡ To our knowledge, this is the first experimental investigation giving information about the corresponding variation in reactivity for a bimolecular reaction between an external, cationic metal reagent and reactive groups located on the DNA surface.

In summary, the present results support a reaction model where a varying local concentration of preassociated cationic platinum complexes significantly influences the observed reactivity during adduct formation with non-charged groups located on the DNA surface. The lower sensitivity of G-N7, compared with phosphorothioate reactions, can be explained by the larger distance between the electrostatically preferred interaction sites along the phosphodiester backbone and G-N7.[21] These results should be of importance for synthetic strategies and for a fundamental understanding of reaction mechanisms *in vivo* involving interactions between charged species and reactive groups located on small ribonucleic acid fragments or their charged antisense mimics.

Financial support from the Swedish Cancer Society (grant 3308-B00-07XCC, S.K.C.E.) is gratefully acknowledged.

Notes and references

‡ The increased reactivity in the DNA environment can be accounted for by assuming a reaction mechanism where preaccumulation of **1** on the DNA surface contributes to the adduct formation rate by electrostatic condensation and resulting increased local concentration of **1** in the vicinity of G-N7.[10,16,20]

1 For a recent review see: G. Romano, P. Mitcheli, C. Pacilio and A. Giordano, *Stem Cells*, 2000, **18**, 19.
2 Of particular interest for Pt(II) anticancer activity: P. M. Takahara, A. C. Rosenzweig, C. A. Frederick and S. J. Lippard, *Nature*, 1995, **377**, 649; U.-M. Ohndorf, M. A. Rould, Q. He, C. O. Pabo and S. J. Lippard, *Nature*, 1999, **399**, 708.
3 M. C. Olmsted, C. F. Anderson and M. T. Record, Jr., *Proc. Natl. Acad. Sci. U.S.A.*, 1989, **86**, 7766.
4 M. O. Fenley, G. S. Manning and W. K. Olson, *Biopolymers*, 1990, **30**, 1191.
5 M. C. Olmsted, J. P. Bond, C. F. Anderson and M. T. Record, Jr., *Biophys. J.*, 1995, **68**, 634.
6 V. M. Stein, J. P. Bond, M. W. Capp, C. F. Anderson and M. T. Record, Jr., *Biophys. J.*, 1995, **68**, 1063.
7 W. Zhang, J. P. Bond, C. F. Anderson, T. M. Lohman and M. T. Record, Jr., *Proc. Natl. Acad. Sci. U.S.A.*, 1996, **93**, 2511.
8 W. Zhang, H. Ni, M. W. Capp, C. F. Anderson, T. M. Lohman and M. T. Record, Jr., *Biophys. J.*, 1999, **76**, 1008.
9 J. Kjellström and S. K. C. Elmroth, *Chem. Commun.*, 1997, 1701.
10 J. Kjellström and S. K. C. Elmroth, *Inorg. Chem.*, 1999, **38**, 6193.
11 L. R. Kelland, B. A. Murrer, G. Abel, C. M. Giandomenico, P. Mistry and K. R. Harrap, *Cancer Res.*, 1992, **52**, 822.
12 G. K. Poon, F. I. Raynaud, P. Mistry, D. E. Odell, L. R. Kelland, K. R. Harrap, C. F. J. Barnard and B. A. Murrer, *J. Chromatogr. A*, 1995, **712**, 61.
13 L. K. Kelland, *Expert Opin. Invest. Drugs*, 2000, **9**, 1373.
14 J. F. Hartwig and S. J. Lippard, *J. Am. Chem. Soc.*, 1992, **114**, 5646.
15 K. J. Yarema, J. M. Wilson, S. J. Lippard and J. M. Essigmann, *J. Mol. Biol.*, 1994, **236**, 1034.
16 M. Meroueh, J. Kjellström, K. S. M. Mårtensson, S. K. C. Elmroth and C. S. Chow, *Inorg. Chim. Acta*, 2000, **297**, 145.
17 J. Arpalahti and B. Lippert, *Inorg. Chem.*, 1990, **29**, 104.
18 J. Arpalahti, M. Mikola and S. Mauristo, *Inorg. Chem.*, 1993, **32**, 3327.
19 S. K. C. Elmroth and S. J. Lippard, *J. Am. Chem. Soc.*, 1994, **116**, 3633.
20 S. K. C. Elmroth and S. J. Lippard, *Inorg. Chem.*, 1995, **34**, 5234.
21 J. M. Martínez, S. K. C. Elmroth and L. Kloo, *manuscript in preparation.*

CHEMCOMM
Communication
www.rsc.org/chemcomm

Enantiospecificity of sterol–lipid interactions: first evidence that the absolute configuration of cholesterol affects the physical properties of cholesterol–sphingomyelin membranes

S. Lalitha,[a] A. Sampath Kumar,[a] Keith J. Stine[b] and Douglas F. Covey*[a]

[a] *Division of Bioorganic Chemistry, Department of Molecular Biology and Pharmacology, Washington University School of Medicine, 660 South Euclid Avenue, St. Louis, Missouri, 63110, USA. E-mail: dcovey@molecool.wustl.edu*

[b] *Department of Chemistry and Center for Molecular Electronics, University of Missouri–St. Louis, St. Louis, Missouri, 63121, USA. E-mail: kstine@jinx.umsl.edu*

Received (in Columbia, MO, USA) 4th May 2001, Accepted 11th May 2001
First published as an Advance Article on the web 13th June 2001

Results from monolayer studies using the enantiomers of cholesterol (*nat*- and *ent*-cholesterol) and egg yolk sphingomyelin show for the first time that enantiospecific interactions between sterols and lipids can affect the physical properties of membranes.

Because the sterols and lipids of cellular membranes occur in enantiomerically pure form, it is possible that the physical properties of the membranes could, in part, be dependent on enantiospecific sterol–lipid interactions. This possibility has seldom been addressed because the unnatural enantiomers of sterols and lipids are not readily available. Nevertheless, in the few studies that have been performed, where interactions of the enantiomers of dipalmitoylphosphatidylcholine, (or its close structural analogues) with natural cholesterol (*nat*-cholesterol)

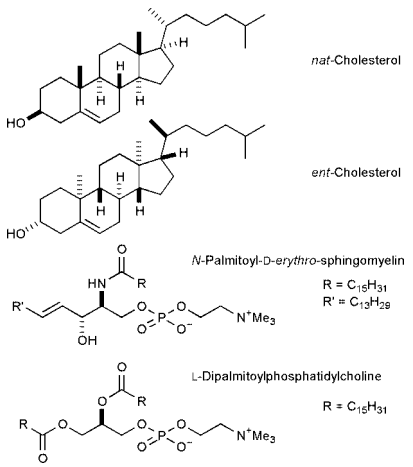

were investigated, no enantioselective sterol–lipid interactions were detected.[1] Thus, it is perhaps not surprising that enantiospecific sterol–lipid interactions are widely believed to be too weak to influence the physical properties of membranes. Here, we show that this view is unwarranted for certain sterol–lipid interactions. Specifically, we show that enantiospecific interactions between cholesterol and egg yolk sphingomyelin (SPM) influence the physical properties of cholesterol–sphingomyelin monolayers at the air–water interface in a Langmuir–Blodgett trough.

The *ent*-cholesterol was prepared by us as described previously.[2] Enantioselectivity for the interactions of either *nat*- or *ent*-cholesterol with egg yolk sphingomyelin was investigated by examining the well known condensing effect of cholesterol on the packing of monolayers of cellular membrane lipids on a water surface in a Langmuir–Blodgett trough.[3] At low surface pressures, the rigid steroid acts as a template to orient the lipid hydrocarbon chains into fully extended conformations thereby allowing the lipid to occupy less area on the water surface than it would occupy if the steroid were not present. Thus, enantioselectively for the sterol–lipid interactions is detected as a difference in the plots of surface pressure (Π) *vs.* mean molecular area (mmA) during the compression of mixed monolayers containing the same mol% of either cholesterol enantiomer cospread on the surface with SPM.

In data not shown, the Π–mmA compression isotherms of the cholesterol enantiomers and SPM were recorded. The compression isotherms of the cholesterol enantiomers are identical. A gaseous to liquid ordered phase transition ($\Pi \geqslant 0.5$ mN m^{-1}) occurs at mmA ≈ 42 Å^2 molecule^{-1} and the film collapses when $\Pi \approx 49$ mN m^{-1} and mmA ≈ 36 Å^2 molecule^{-1}. In the absence of cholesterol, SPM monolayers compressed on a water subphase undergo a gaseous to liquid ordered phase transition ($\Pi \geqslant 0.5$ mN m^{-1}) at mmA ≈ 82 Å^2 molecule^{-1}. At collapse, the SPM monolayers have $\Pi \approx 55$ mN m^{-1} and mmA ≈ 35 Å^2 molecule^{-1}. These experimental parameters are in agreement with published values for the compression isotherms of similar cholesterol or SPM films.[4]

Results for the Π–mmA compression isotherms of monolayer films containing 30 mol% of either *nat*- or *ent*-cholesterol and 70 mol% SPM are shown in Fig. 1. Differences in mmA values at all Π are observed and are highly significant ($P < 0.00001$).[5] The *ent*-cholesterol has a greater condensing effect on SPM than *nat*-cholesterol.

In experiments not shown, mixed cholesterol–SPM films containing 10–50 mol% of either cholesterol enantiomer were compressed. Enantioselectivity during compression was observed when the mol% of the steroid was varied in 10 mol% increments between 20 and 40 mol%. Enantioselectivity was greatest at 30 mol% sterol and was not observed at either 10 or

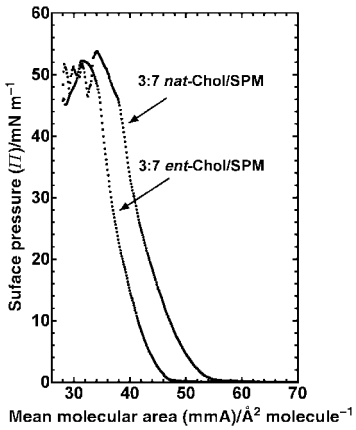

Fig. 1 Pressure–area isotherms for 3:7 mixtures of each cholesterol enantiomer with egg yolk sphingomyelin.

 DOI: 10.1039/b104081m

50 mol% sterol. Also in experiments not shown, mixed cholesterol–DPPC (natural L-dipalmitoylphosphatidylcholine) films containing 10–60 mol% of either cholesterol enantiomer were compressed. These DPPC experiments provide a chirality crosscheck on the earlier reported studies that used DPPC enantiomers. In agreement with the earlier cited studies, we found no enantioselectivity using cholesterol enantiomers and natural DPPC.

The appearance of the 30 mol% *nat*- and *ent*-cholesterol–SPM films during compression was examined using Brewster angle microscopy.[6] Fig. 2 shows micrographs of the films at similar degrees of compression. The SPM film containing *ent*-cholesterol exhibits a greater fraction of the gas (dark) phase than the corresponding SPM film containing *nat*-cholesterol. At this stage of compression the *nat*-cholesterol, but not the *ent*-cholesterol, containing film has undergone the gaseous-to-liquid condensed phase transition (refer to Fig. 1). Thus, the films are visually different at similar degrees of compression. Additionally, there are two phases evident for the *nat*-cholesterol containing film, but three phases present for the *ent*-cholesterol containing film. This difference in the number of phases present also occurs when the films are more expanded and neither film has undergone a phase transition. Further compression of either film after the phase transition has occurred gives uniform films with a similar bright appearance. Although further experiments are needed to characterise the identity of the third phase present in the *ent*-cholesterol containing film, the presence of this additional phase emphasised that the differences between the Π–mmA isotherms of the cholesterol enantiomer–SPM films are not experimental artefacts.

Thus, we confirm that the physical properties of cholesterol–DPPC containing membranes are not measurably influenced by enantiospecific interactions between the sterol and the lipid. In contrast, we report that enantiospecific interactions between cholesterol and SPM do affect the physical properties of these membranes. It is likely that the varying degrees of enantioselectivity observed for DPPC and SPM in their interactions with cholesterol are explained by differences in the hydrogen bonding between the cholesterol hydroxyl group and the polar head groups of the two lipids.

The only chiral center in DPPC is the central carbon in the glycerol backbone of the lipid. Thus, unless the carbonyl oxygen in the ester group attached to this carbon is directly involved in a hydrogen bonding interaction with the hydroxy group attached to the C-3 chiral center in cholesterol, there is little opportunity for the molecules to interact in an enantioselective manner. However, evidence suggests that the DPPC ester carbonyl group and the cholesterol hydroxyl group do not hydrogen bond to each other, but instead hydrogen bond to intervening water molecules.[7,8] Hence, it may not be surprising that cholesterol–DPPC packing interactions are not measurably enantioselective.

The D-*erythro*-sphingosine base of SPM has two chiral centers and a double bond proximate to the zwitterionic choline head group. Additionally, since the polar head group of SPM contains both hydrogen bond donor and acceptor groups it is possible for hydrogen bonding to organise SPM into aggregates in a way that is not possible for DPPC. If hydrogen bonding to cholesterol alters these intermolecular SPM–SPM hydrogen bonding interactions, it seems reasonable that cholesterol could do this in an enantiospecific manner. Further experiments will be needed to investigate this possibility. Nevertheless, the hypothesis seems consistent with published views regarding the idea that intermolecular hydrogen bonding between cholesterol and SPM has important biophysical and biochemical consequences.[8]

This study provides the first evidence that enantioselective interactions between sterols and lipids can affect the physical properties of membranes. In a larger context, *ent*-cholesterol may prove to be a useful reagent for studying cellular cholesterol homeostasis and the role that cholesterol–SPM raft formation plays in the functioning and trafficking of proteins involved in cell-signalling pathways.[9] We have previously used *ent*-cholesterol to demonstrate that the absolute configuration of cholesterol has an effect on the transport of daunomycin by the multidrug resistance transporter P-glycoprotein (Pgp) in human HepG2 and Chinese hamster ovary (CHO) cells.[10] Additional studies to further define the effect that the absolute configuration of cholesterol has on the physical properties of cell membrane lipids and studies of *ent*-cholesterol binding to proteins are in progress.

We thank the NIH for grant GM 47969 that supported this work.

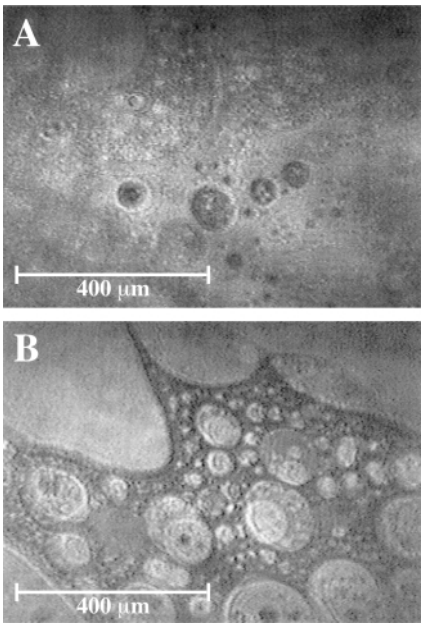

Fig. 2 Brewster angle microscopy of monolayer films. A: *nat*-cholesterol–SPM (3:7); mmA, 50 Å^2 molecule^{-1}; B: *ent*-cholesterol–SPM; mmA, 52 Å^2 molecule^{-1}.

Notes and references

1 K. Agarwal, A. Bali and C. M. Gupta, *Biochim. Biophys. Acta*, 1986, **856**, 36; K. Agarwal, A. Bali and C. M. Gupta, *Biochim. Biophys. Acta*, 1986, **883**, 468; W. Guyer and K. Bloch, *Chem. Phys. Lipids*, 1983, **33**, 313; E. M. Arnett and J. M. Gold, *J. Am. Chem. Soc.*, 1982, **104**, 636; D. Ghosh, R. L. Lyman and J. Tinoco, *Chem. Phys. Lipids*, 1971, **7**, 173; A. Hermetter and F. Paltauf, *Chem. Phys. Lipids*, 1982, **31**, 283.

2 A. S. Kumar and D. F. Covey, *Tetrahedron Lett.*, 1999, **40**, 823.

3 A KSV Minitrough Langmuir–Blodgett instrument was used. Films were spread in $HCCl_3$ and compressed at 24 °C on a pure water subphase.

4 D. Ghosh and J. Tinoco, *Biochim. Biophys. Acta*, 1972, **266**, 41; F. Müller-Landau and D. A. Cadenhead, *Chem. Phys. Lipids*, 1979, **25**, 315; J. P. Slotte, *Biochim. Biophys. Acta*, 1992, **1123**, 326; J. M. Smaby, H. L. Brockman and R. E. Brown, *Biochemistry*, 1994, **33**, 9135; T. G. Anderson and H. M. McConnell, *J. Phys. Chem.*, 2000, **104**, 9918.

5 Student's t test, two tailed, two-sample unequal variance, $n = 6$.

6 A commercial BAM 1 plus instrument with an XY translation stage was used. For details see: K. J. Stine, A. R. Leventhal, D. P. Parazak and J. Y.-J. Uang, *Enantiomer*, 1996, **1**, 41.

7 R. Bittman, *Subcell. Biochem.*, 1997, **28**, 145.

8 R. E. Brown, *J. Cell Sci.*, 1998, **111**, 1.

9 D. A. Brown and E. London, *J. Biol. Chem.*, 2000, **275**, 17221; F. Schroeder, J. R. Jefferson, A. B. Kier, J. Knittel, T. J. Scallen, W. G. Wood and I. Hapala, *Proc. Soc. Exp. Biol. Med.*, 1991, **196**, 235; C. J. Fielding and P. E. Fielding, *J. Lipid Res.*, 1997, **38**, 1503; P. L. Yeagle, *Cholesterol in Membrane Models*, CRC Press, Boca Raton, FL, 1993, p. 1; M. S. Brown and J. L. Goldstein, *Proc. Natl. Acad. Sci. USA*, 1999, **96**, 11 041; Y. Lange and T. L. Steck, *Trends Cell Biol.*, 1996, 205.

10 G. D. Luker, C. M. Pica, A. S. Kumar, D. F. Covey and D. Piwnica-Worms, *Biochemistry*, 2000, **39**, 7651.

CHEMCOMM Communication
www.rsc.org/chemcomm

The water-soluble β-cyclodextrin–[60]fullerene complex

C. N. Murthy and K. E. Geckeler*

Laboratory of Applied Macromolecular Chemistry, Department of Materials Science and Engineering, Kwangju Institute of Science and Technology, 1 Oryong-dong, Buk-gu, Kwangju 500-712, South Korea. E-mail: keg@kjist.ac.kr

Received (in Cambridge, UK) 7th March 2001, Accepted 21st May 2001
First published as an Advance Article on the web 13th June 2001

A stable inclusion complex of β-cyclodextrin with [60]fullerene is reported for the first time, synthesized by using a novel synthetic procedure; radical scavenging studies of the water-soluble complex indicate that it has potential for a number of medical applications.

The supramolecular chemistry of cyclodextrins (CD) in aqueous solution is a topic of commercial interest with a variety of biomedical applications.[1] Nonpolar drug molecules have been solubilized in water by making their inclusion complexes with cyclodextrins. Among the cyclodextrins, the β-cyclodextrin is the cheapest commercially available, being about four times cheaper than γ-cyclodextrin. [60]Fullerene is a nonpolar molecule and much of the research on the inclusion complexes of cyclodextrins and [60]fullerene has centered on γ-cyclodextrins,[2a–c] as recent research has shown the biological activity of water-soluble [60]fullerene derivatives such as its DNA-cleaving ability and anti-HIV activity.[3] There are only a few reports on inclusion complexation of [60]fullerene.[2] The procedures described are based on heterogeneous reaction media and all have reported that only γ-cyclodextrin forms an inclusion complex (2:1) and β-cyclodextrin or α-cyclodextrin do not form complexes. The reason given is the comparable size of the [60]fullerene and the cavity diameter of the γ-cyclodextrin molecule and that the C_{60} molecule does not intrude deeply into the γ-cyclodextrin cavity. In fact, these reports describe the experimental failure to prepare the inclusion complex of β-cyclodextrin with [60]fullerene.[2b,c]

There are only a few reports on the inclusion complexation of [60]fullerene by CD derivatives.[2d,e] However, when studying the data in detail and conducting molecular modeling studies, it becomes evident that the dimensions of the cyclodextrins do principally not rule out the formation of an inclusion complex between β-cyclodextrin and [60]fullerene. The larger cavity diameter of β-cyclodextrin is 780 pm and the outer rim diameter is 1530 pm on the polar side of the molecule as compared to 950 pm and 1690 pm, respectively, for the γ-cyclodextrin. Thus the cavity diameters are much smaller than the van der Waals diameter of [60]fullerene (~1000 pm). On the other hand, based on crystallographic studies it has been reported that the β-cyclodextrin cavity is suitable for spherically shaped guests such as adamantane derivatives[4] or naphthalene,[5] and the space enclosed by the head-to-head dimer is ~2.5 times wider than the cavity of the single molecule.[6] Consequently, the reason for the unsuccessful attempts to form inclusion complexes of β-cyclodextrin and [60]fullerene is not only the size but seems to also depend on the reaction conditions. Due to the lower cost of β-CD and its widespread applications, there are also considerably more data available on toxicity and other pharmacological studies. Here we report a novel method for a water-soluble, stable β-cyclodextrin–[60]fullerene inclusion complex.

The synthesis of the CD–C_{60} inclusion complex (Scheme 1) was achieved in a mixed organic solvent system containing DMF and toluene (typically 50–90% DMF, v:v), where both the β-cyclodextrin and [60]fullerene formed a homogeneous reaction medium. The inclusion of the fullerene into the CD cavity was monitored over a period of two weeks by UV-Vis spectroscopy (Fig. 1). The CD–C_{60} complex was isolated by removing the organic solvents, and subsequent addition of distilled water, to yield a light yellow aqueous solution. The complex was purified in aqueous solution by membrane filtration using a polymer membrane with a molar mass cut-off of 2 kg mol^{-1} (Yield: 60%, solubility in water: 4 g L^{-1}).[7] The FTIR spectra of the inclusion complex showed the typical band at 527 cm^{-1} assigned to [60]fullerene. The UV-Vis spectrum showed the absorption at 342 nm and the peak broadening beyond 350 nm. Further corroboration for the formation of the inclusion complex was obtained by ^1H and ^{13}C NMR spectroscopy. The complex showed a slight shift in the resonances of the C^3 carbon of the CD unit, but no shift in the resonance of the C^5, indicating that the fullerene does not intrude into the cavity completely. This is supported by the energy minimization calculations (Fig. 2). These studies also showed that the visible and accessible fullerene surface in the complex is increased by a factor of ~8 compared to the γ-cyclodextrin complex, which is very important with respect to biological applications. Under these conditions, in contrast, the α-cyclodextrin did not form an inclusion complex.

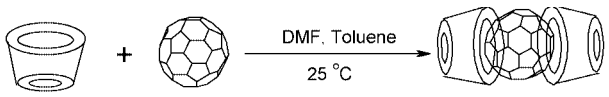

Scheme 1 Synthesis of the β-cyclodextrin–[60]fullerene inclusion complex.

Generally, β-cyclodextrin can form a 2:1, 1:1, or 1:2 complex with a guest and the theoretical calculated mass content of β-cyclodextrin in the complex for these three types would be 75.9, 61.2, and 44.1%, respectively. Thermogravimetric analysis of the complex formed showed that the total mass loss of the cyclodextrin at 325 °C was 72.5%. This result clearly indicates that this inclusion complex is of the 2:1 type.

It is known that the two main driving forces for inclusion complexation are the repulsive forces between the included water molecules and the apolar cyclodextrin cavity on the one

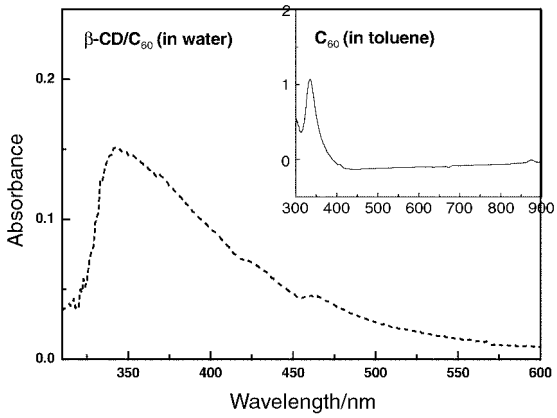

Fig. 1 UV-Vis spectra of C_{60} (in toluene) and the β-cyclodextrin–C_{60} inclusion complex (in water).

 DOI: 10.1039/b102142g

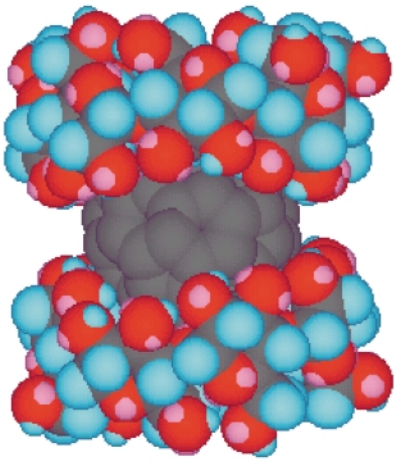

Fig. 2 Energy-minimized molecular model of the β-cyclodextrin–C_{60} inclusion complex (2:1).

hand, and between the apolar [60]fullerene and the bulk water on the other. However, the second factor is not relevant in the dry state and thus the product isolated from the solution could be just a fine dispersion of β-cyclodextrin and [60]fullerene. The X-ray diffraction pattern of the freeze-dried inclusion complex (Fig. 3), however, shows that the product isolated has neither the typical 2θ values of CD nor those of [60]fullerene. It can be seen that the complex has a different structure to the parent β-cyclodextrin (2θ = 9, 12.5, 19.6, 23.0, 27.0, 34.8°) and C_{60}[8] (2θ = 11.0, 17.5, 21.7°), with the total suppression of the crystalline

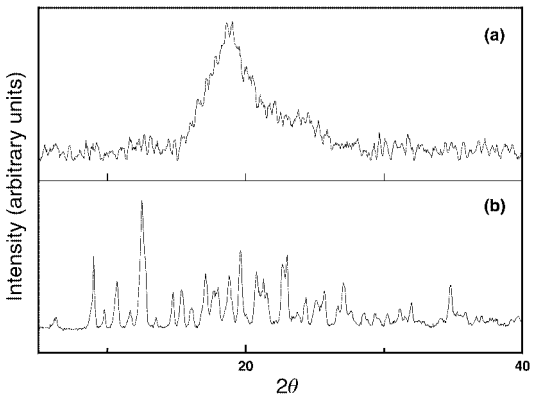

Fig. 3 X-ray diffractograms of (a) the inclusion complex of C_{60} with β-cyclodextrin and (b) the pristine β-cyclodextrin.

structure of β-CD. This is in accord with similar observations for the γ-CD complex.[2b]

Water-soluble fullerene compounds have potential biomedical applications and previous attempts involved its functionalization[9] with a significant modification of the fullerene molecule, which could lead to toxicity problems. The approach adopted here overcomes such problems, as at present only the parent β-CD has been cleared for human consumption. Radical scavenging studies were carried out using a screening test with the stable free radical, 2,2-diphenyl-1-picrylhydrazyl (DPPH), developed in our laboratory.[10] There was a visual bleaching of the purple color of the DPPH solution with time, which was monitored by UV-Vis spectroscopy showing a gradual shift and decrease in the absorbance of the 517 nm peak of the DPPH solution. This shows that the [60]fullerene in the complex with β-cyclodextrin retains its radical scavenging activity in the aqueous solution.

Financial support from the Ministry of Education for the 'Brain Korea 21' project is gratefully acknowledged.

Notes and references

1 *Comprehensive Supramolecular Chemistry*, Vol. 3, *Cyclodextrins*, ex. ed. J. L. Atwood, J. E. D. Davies, D. D. MacNicol and F. Vogtle, vol. ed. J. Szejtli and T. Osa, Elsevier, New York, 1996.
2 (*a*) T. Andersson, K. Nilsson, M. Sundahl, G. Westman and O. Wennerstrom, *J. Chem. Soc., Chem. Commun.*, 1992, 604; (*b*) K. I. Priyadarsini, H. Mohan, A. K. Tyagi and J. P. Mittal, *J. Phys. Chem.*, 1994, **98**, 4756; (*c*) K. Kanazawa, H. Nakanishi, Y. Ishizuka, T. Nakamura and M. Matsumoto, *Fullerene Science and Technology*, 1994, **2**, 189; (*d*) D. D. Zhang, J. W. Chen, Y. Yang, R. F. Chai and X. L. Shen, *J. Incl. Phenom.*, 1993, **16**, 245; (*e*) F. Diederich and M. Gomez-Lopez, *Chem. Soc. Rev.*, 1999, **28**, 263.
3 R. Sijbesma, G. Srdanov, F. Wudl, J. A. Castoro, C. Wilkins, S. H. Friedman, D. L. DeCamp and G. L. Kenjon, *J. Am. Chem. Soc.*, 1993, **115**, 6510; S. H. Friedman, D. L. DeCamp, R. Sijbesma, G. Srdanov, F. Wudl and G. L. Kenyon, *J. Am. Chem. Soc.*, 1993, **115**, 6506.
4 J. A. Hamilton and M. N. Sabesan, *Acta Crystallogr., Sect. B*, 1982, **38**, 3063.
5 M. Czugler, E. Eckle and J. J. Stezowski, *J. Chem. Soc., Chem. Commun.*, 1981, 1291; K. Harata, *J. Chem. Soc., Chem. Commun.*, 1993, 546.
6 K. H. Jogun, E. Eckle and K. Bartels, *Nature*, 1978, **274**, 617.
7 K. E. Geckeler, in *Bioanalytical and Biochemical Laboratory Methods*, ed. K. E. Geckeler and H. Eckstein, Vieweg, Wiesbaden, Germany, 1998, ch. 1.6.
8 T. Pradeep. K. K. Singh, A. P. S. Sinha and D. E. Morris, *J. Chem. Soc., Chem. Commun.*, 1992, 1747.
9 M. Brettreich and A. Hirsch, *Tetrahedron Lett.*, 1998, **39**, 2731; T. Da Ros, M. Prato, F. Novello, M. Maggini and E. Banfi, *J. Org. Chem.*, 1996, **61**, 9070; L. Y. Chiang, J. B. Bhonsle, L. Wang, S. F. Shu, T. M. Chang and J. R. Hwu, *Tetrahedron*, 1996, **52**, 4963; S. Samal and K. E. Geckeler, *Chem. Commun.*, 2000, **13**, 1101.
10 K. E. Geckeler and S. Samal, *Full. Sci. Technol.*, 2001, **9**, 17.

CHEMCOMM
Communication
www.rsc.org/chemcomm

The first application of Selectfluor™ in electrophilic fluorination of amines: a new route to $-NF_2$, –NHF, and >NF compounds

Rajendra P. Singh and Jean'ne M. Shreeve*

Department of Chemistry, University of Idaho, Moscow, ID 83844-2343, USA.
E-mail: jshreeve@uidaho.edu; Fax: +1 208-885-9146

Received (in Cambridge, UK) 21st February 2001, Accepted 18th May 2001
First published as an Advance Article on the web 13th June 2001

Reactions of primary amines, RNH_2 [R = $(CH_3)_3C$–, $(CH_3)_2CH$–, $CH_3(CH_2)_2$–, $(CH_3)_2CHCH_2$–, $CH_3(CH_2)_3$–] and secondary amines, R_2NH [(R = CH_3CH_2–, $CH_3(CH_2)_2$–, $(CH_3)_2CHCH_2$–], with Selectfluor™ in acetonitrile or DMF or DMA result in formation of the corresponding RNF_2, RNHF, and R_2NF in high yields.

The synthesis and reactivity of compounds that contain the nitrogen–fluorine bond have been studied extensively.[1–7] Many methods have been developed to prepare *N*-fluoroamines and *N*,*N*-difluoroamines by using either elemental fluorine or other fluorine-transfer reagents which often gave poor yields of the final products and required extreme precautions. In 1960, Frazer reported the formation of RNF_2 (R = CH_3, C_2H_5) in moderate yields from photolysis of RI + N_2F_4 through Pyrex.[8] Thermolysis of mixtures of alkanes and N_2F_4 at 300 °C resulted in mono and disubstituted difluoroamino compounds.[9] However, with the advent of modern day electrophilic fluorinating reagents, such as CF_3OF, XeF_2, ClO_3F and $CsSO_4F$, as well as fluorine itself, it has been possible to prepare a variety of >NF or −NHF compounds.[9–11] A decade ago we reported the effective synthesis of acyclic secondary and cyclic fluoroamines, in addition to *N*-nitrosoamines, by using trifluoroamine oxide (NF_3O) as the fluorinating agent at < 0 °C.[12]

The application of Selectfluor™ for the electrophilic fluorination of primary and secondary amines provides a powerful straightforward one step route to $-NF_2$ and >NF compounds and, for the first time, the opportunity to prepare –NHF compounds *via* control of reaction stoichiometry. Since the discovery of this reagent, considerable success in the electrophilic fluorination of organic molecules, especially in the formation of C–F bonds, has been realized but the mechanism of the fluorine-transfer step has remained minimally understood.[13-15]

Initially, *tert*-butylamine (3 mmol) was reacted with Selectfluor™ (6.2 mmol) at 0 °C in acetonitrile for 6 h. Analysis of the reaction mixture with GCMS showed complete consumption of the *tert*-butylamine. Separation of *tert*-butyldifluoroamine from acetonitrile was not very clean due to the small difference between the boiling points of the solvent and the product. *tert*-Butyldifluoroamine was characterized spectroscopically in acetonitrile solution. The above reaction was also found to be equally successful when DMF or DMA was used as solvent and was completed within an hour. These solvents were found to be suitable due to their high boiling points which made the separation of the products from the solvent relatively straightforward. In some cases, the formation of $(CH_3)_2NCOF$[16] (≤ 5%) was observed as a byproduct when DMF was used as a solvent. By using similar reaction conditions,† the other primary amines, RNH_2 [R = $(CH_3)_2CH$–, $CH_3(CH_2)_2$–, $(CH_3)_2CHCH_2$–, $CH_3(CH_2)_3$–], were converted in DMA solution into the corresponding difluoroamines in good yields (Scheme 1, Table 1). An attempt to prepare *tert*-butyl fluoroamine [$(CH_3)_3CNHF$] by the slow addition of a DMF solution of *tert*-butylamine (3 mmol) into a stirred suspension of Selectfluor™ (3 mmol) solution in DMF resulted in the formation of a mixture of difluoro and fluoroamine in a 9:1 ratio. However, when the addition of the reagents was reversed, *tert*-butylfluoroamine was formed as the sole product (Scheme 1, Table 1).

Several secondary amines, R_2NH [(R = CH_3CH_2–, $CH_3(CH)_2$–, $(CH_3)_2CHCH_2$–], were reacted at 0 °C to 25 °C with 1.2 equiv. of Selectfluor™ in DMA‡ for 2 h. Separation of

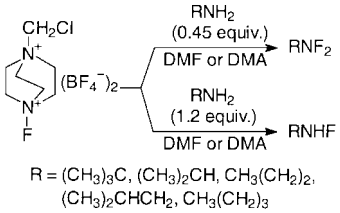

Scheme 1

Table 1 Electrophilic fluorination of amines with Selectfluor™[a]

Entry	Substrates	Products[b]	Conversion (%)	Yield (%)[c] (pure)	^{19}F NMR (δ in ppm)
1	$(CH_3)_3CNH_2$	$(CH_3)_3CNF_2$	100	80	28.6
2	$(CH_3)_3CNH_2$	$(CH_3)_3CNHF$[d]	100	85	−120.3
3	$(CH_3)_2CHNH_2$	$(CH_3)_2CNF_2$	100	78	39.0
4	$(CH_3)_2CHNH_2$	$(CH_3)_2CHNHF$[d]	100	82	−131.7
5	$CH_3(CH_2)_2NH_2$	$CH_3(CH_2)_2NF_2$	100	75	55.0
6	$CH_3(CH_2)_2NH_2$	$CH_3(CH_2)_2NHF$[d]	100	63	−117.3
7	$(CH_3)_2CHCH_2NH_2$	$(CH_3)_2CHCH_2NF_2$	100	74	33.0
8	$(CH_3)_2CHCH_2NH_2$	$(CH_3)_2CHCH_2NHF$[d]	100	66	−140.9
9	$CH_3(CH_2)_3NH_2$	$CH_3(CH_2)_3NF_2$	100	72	54.8
10	$CH_3(CH_2)_3NH_2$	$CH_3(CH_2)_3NHF$[d]	100	80	−116.6
11	$(CH_3CH_2)_2NH$	$(CH_3CH_2)_2NF$	100	65	−53.0
12	$(CH_3CH_2CH_2)_2NH$	$(CH_3CH_2CH_2)_2NF$	100	76	−50.3
13	$[(CH_3)_2CHCH_2]_2NH$	$[(CH_3)_2CHCH_2]_2NF$	100	73	−46.5

[a] All the reactions were carried out in *N*,*N*-dimethylacetamide (DMA). [b] All the products were characterized by spectroscopic analysis and known compounds were identified by comparing with the spectroscopic data reported in the literature. [c] The yields in entries No. 1–4 were identical when either DMF or DMA was used as solvent. [d] New compounds.

 DOI: 10.1039/b101689j

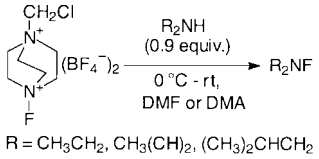

Scheme 2

the product by low temperature trap-to-trap distillation gave the corresponding *N*-fluoroamines, R_2NF [(R = CH_3CH_2–, $CH_3(CH)_2$–, $(CH_3)_2CHCH_2$–] in good isolated yields (Scheme 2).

The present report describes a powerful and simple method for the preparation of *N*-difluoro and *N*-fluoro compounds (high energy molecules) with some advantages in comparision with some other routes. The stability of these volatile liquids is variable. While all are stable in solution in Pyrex glass containers for several days at 25 °C, various degrees of decomposition occur over time. For example, $(CH_3)_3CNF_2$ was found to be stable in a sealed tube for at least three months under refrigeration, while $CH_3CH_2CH_2CH_2NHF$ decomposed fully after an equal time in Pyrex at 25 °C. A sample of $(CH_3)_3CNHF$ refrigerated in a vial for several months showed no decomposition based on NMR spectral measurements. However, R_2NF compounds are reported to be unstable in Pyrex glass for extended periods.[12]

We are grateful to Dr Robert G. Syvret (Air Products and Chemical, Inc.) for generous gifts of Selectfluor™ reagent. This work was supported by the National Science Foundation (Grant No. CHE – 9720365) and the Office of Naval Research (Award No. N00014-00-1-0721). *Warning*: While no problems arose during these syntheses, adqeuate precautions should be employed since fluoroamines and difluoroamines can be unpredictably shock and thermally unstable.

Notes and references

† To a solution of 3 mmol (1.06 g) of Selectfluor™ in 3.5 mL of DMF or DMA, 1.35 mmol of primary amine or 2.7 mmol of secondary amine in 1.5 mL of DMF or DMA was added dropwise at 0 °C. After 0.5 h stirring, the reaction mixture was stirred for an additional 1.5 h at 25 °C. In general, trap-to-trap distillation under vacuum allowed the separation of the solvent (trap at −20 °C) from the product which may be stopped in a trap at −78 °C or may pass through a trap at −78 °C and stop in a trap at −100 °C. **$(CH_3)_3CNF_2$**:[9] IR (gas phase): 2991 vs, 2944 s, 1485 s, 1375 vs, 1253 m, 1222 m, 980 vs, 880 vs, 587 m cm^{-1}; δ_H (200 MHz, CD_3CN): 1.24 (t, 9H, $J_{H\text{-}F}$ = 1.6 Hz); δ_F (188 MHz, CD_3CN): 28.7 broad singlet; δ_C (50 MHz, CD_3CN): 22.8, 70.6 (t, J = 6.8 Hz); MS (EI) *m/e* (species intensity): 110 (M + H, 1), 94 ($M^+ - CH_3$, 5), 57 ($(CH_3)_3C^+$, 85), 41 (CH_3CN^+, 100). **$(CH_3)_2CHCH_2]_2NF$**:[12] (trapped at −78 °C, passing −40 °C) IR (gas phase): 2986 vs, 2897 vs, 2808 s, 1472 s, 1390 s, 1371 s, 1290 w, 1243 w, 1142 s, 1111 m, 930 w, 833 m cm^{-1}; δ_F (188 MHz, CD_3CN): 0.98 (d, 12H, J = 21 Hz), 2.1 (m, 2H), 2.88 (dd, 4H, $J_{H\text{-}F}$ = 40.8 Hz); δ_F (200 MHz, CD_3CN): −46.5 q ($J_{F\text{-}H}$ = 40.0 Hz); MS (EI) *m/e* (species intensity): 147 (M^+, 6), 127 ($M^+ - HF$, 1), 104 ($M^+ - (CH_3)_2CH$, 63), 57 ($(CH_3)_2CHCH_2^+$, 100).

‡ To a stirred solution of primary amine (3.2 mmol in 2 mL of DMF or DMA), a Selectfluor™ solution (3 mmol in 3 mL of DMF or DMA) was added dropwise at 0 °C. After 0.5 h stirring, the reaction mixture was stirred at 25 °C for an additional 0.5 h. Solvent was retained in a trap at −20 °C and the product was isolated from a trap maintained at −78 °C. **$(CH_3)_3CNHF$**: δ_H (200 MHz, CD_3CN): 1.06 (d, 9H, $J_{H\text{-}F}$ = 2.2 Hz), 8.70 (br d, $J_{H\text{-}F}$ = 45 Hz); δ_F (188 MHz, CD_3CN): −131.7 (broad doublet, $J_{H\text{-}F}$ = 45 Hz); δ_C (50 MHz, CD_3CN): 25.2, 59.0 (d, J = 10.7 Hz); MS (EI) *m/e* (species intensity): 92 (M + H, 1), 76 ($M^+ - CH_3$, 100), 57 ($(CH_3)_3C^+$, 40), 41 (CH_3CN^+, 92). **$(CH_3)_2CHNHF$**: 2977 vs, 2895 s, 1466 s, 1379 s, 1006s, 937m, 868 vs; δ_H (200 MHz, CD_3CN): 1.20 (br dd, 6H), 3.41 (d sept, $J_{CH3\text{-}H}$ = 6.2 Hz, $J_{CH\text{-}F}$ = 37.5 Hz), 8.44 (br d, $J_{H\text{-}F}$ = 46.5 Hz); δ_F (188 MHz, CD_3CN): −120.3 (dd sept, $J_{NH\text{-}F}$ = 46.0 Hz, $J_{CH3\text{-}F}$ = 1.3 Hz); δ_C (50 MHz, CD_3CN): 23.0, 24.18, 41.28; MS (EI) *m/e* (species intensity): 77 (M^+, 3), 63 ($M^+ - CH_3$, 71), 62 ($M^+ - (CH_3 + H)$, 100), 42 ($(CH_3)_2C^+$, 81).

1 H. J. Emeléus, J. M. Shreeve and R. D. Verma, *Adv. Inorg. Chem.*, 1989, **33**, 139, and references therein.
2 A. L. Logothetis, *J. Org. Chem.*, 1966, **31**, 3686.
3 A. L. Logothetis and G. N. Sausen, *J. Org. Chem.*, 1966, **31**, 3689.
4 C. J. Hoffman and R. A. Neville, *Chem. Rev.*, 1963, **62**, 1.
5 H. M. Marsden and J. M. Shreeve, *Inorg. Chem.*, 1987, **26**, 169, and references therein.
6 E. O. John and J. M. Shreeve, *Inorg. Chem.*, 1988, **27**, 3100.
7 E. O. John, R. D. Willett, B. Scott, R. L. Kirchmeier and J. M. Shreeve, *Inorg. Chem.*, 1989, **28**, 893.
8 J. W. Frazer, *J. Inorg. Nucl. Chem.*, 1960, **16**, 63.
9 R. L. Petry and S. F. Read, Jr., *U.S. Patent*, 1967, 3,350, 453.
10 A. A. Gakh, S. V. Romaniko, B. I. Ugak and A. A. Fainzilberg, *Tetrahedron*, 1991, **47**, 7447.
11 M. A. Tius, *Tetrahedron*, 1995, **51**, 6605.
12 O. D. Gupta, R. L. Kirchmeier and J. M. Shreeve, *J. Am. Chem. Soc.*, 1990, **112**, 2383.
13 R. E. Banks, *J. Fluorine Chem.*, 1998, **87**, 1, and references therein.
14 G. S. Lal, G. P. Pez and R. G. Syvret, *Chem. Rev.*, 1996, **96**, 1737.
15 G. G. Furin, *Introduction of Fluorine by N–F Compounds*, ed. B. Baasner, H. Hagemann and J. C. Tatlow, in *Methods of Organic Chemistry (Houben-Weyl) Organo-Fluorine Compounds*, Georg Thieme Verlag, New York, 1999, 432.
16 Characterization data: IR (gas phase): 2975 vs, 2877 vs, 1738 s $\nu_{C=O}$, 1475 s, 1440 s, 1205 s, 927 s, 927 s, 786 vs cm^{-1}; NMR: δ_H (200 MHz, CD_3CN): 2.92 (d, 6H, $J_{H\text{-}F}$ = 36.5 Hz); δ_F (188 MHz, CD_3CN): −24.49 (sept, 1F, $J_{H\text{-}F}$ = 36.5 Hz); δ_C (50 MHz, CD_3CN): 55.7, 112.7. MS (EI) *m/e* (species intensity): 91 (M^+, 1), 76 ($M^+ - CH_3$, 2), 48 (COF^+ + 1, 100), 44 (CH_3CN^+, 3).

CHEMCOMM
Communication
www.rsc.org/chemcomm

Interlinked molecular squares with [Cu(2,2′-bipy)]$^{2+}$ corners generating a three-dimensional network of unprecedented topological type

Lucia Carlucci,[a] Gianfranco Ciani,*[b] Davide M. Proserpio[b] and Silvia Rizzato[b]

[a] *Dipartimento di Biologia Strutturale e Funzionale, Università dell'Insubria, Via J. H. Dunant 3, 21100 Varese, Italy*
[b] *Dipartimento di Chimica Strutturale e Stereochimica Inorganica and Centro CNR, Via G. Venezian 21, 20133 Milano, Italy. E-mail: davide@csmtbo.mi.cnr.it*

Received (in Cambridge, UK) 25th April 2001, Accepted 24th May 2001
First published as an Advance Article on the web 13th June 2001

A noteworthy three-dimensional framework, obtained by reacting the preformed molecular corner [Cu(2,2′-bipy)]$^{2+}$ (with BF_4^- counter ions) and 1,2-bis(4-pyridyl)ethane (bpetha) in the presence of chlorides, contains molecular square units [Cu(2,2′-bipy)(bpetha)]$_4$ that are linked *via* chloride bridges into a triconnected architecture of unprecedented topology.

In the rational development of new strategies for the crystal engineering of coordination networks[1] and of supramolecular architectures[2] the use of preformed metal-based units has assumed an increasing relevance in recent times. Molecular corners containing transition metals with programmed coordination angles can been employed for the self-assembly of frameworks and, especially, of macromolecular polygons and polyhedral cages,[3] of potential utility for molecular recognition. In particular, *cis*-protected Pd^{II} and Pt^{II} units have been widely employed for the building of molecular squares.[3,4] We are currently studying the use of a different corner unit, namely [Cu(2,2′-bipy)]$^{2+}$ **1** (2,2′-bipy = 2,2′-bipyridyl), that contains two *cis*-equatorial and, possibly, also two axial free coordination sites, and is produced from the parent complex [Cu(2,2′-bipy)Cl_2] by removing the chlorides with different AgX salts of poorly coordinating anions (X = triflate, tetrafluoroborate or nitrate). These [(**1**)X_2] species have already been reacted with a variety of bidentate spacer ligands, mainly affording one-dimensional zigzag polymeric chains.[5] Monochloride species [(**1**)Cl]X, obtained by removing only one half of the chloride content from the parent complex, were also employed, and, interestingly, the reaction of [(**1**)Cl](BF_4) with 1,2-bis(4-pyridyl)ethane (bpetha) has produced the novel polymeric species [{(**1**)(bpetha)}$_2$Cl(BF_4)](BF_4)$_2$·8.5H_2O **2**, containing molecular square units joined by bridging chloride ions into an extended array. We describe here this three-dimensional network, containing large interstitial cavities and exhibiting a topology unprecedented within coordination networks. We report also on a strictly related species, compound **3**, obtained using 1,2-bis(4-pyridyl)ethene (bpethe) as spacer, that, in spite of the similarity of the ligands, shows a completely different frame. Compound **2** is obtained in high yield in a two step process. In the first step the parent [Cu(2,2′-bipy)Cl_2] was treated with $AgBF_4$ in a 2:3 molar ratio in EtOH under stirring for 2 h. The solution was then filtered and layered on a solution of bpetha in CH_2Cl_2 (molar ratio Cu:bpetha from 1:1 to 1:3). After a few days beautiful blue crystals of **2** were obtained. Compound **3**, [{(**1**)(bpethe)}$_2$Cl](BF_4)$_3$·2.5H_2O·CH_2Cl_2, was obtained in the same way, using in the second step the bpethe ligand in CH_2Cl_2 solution. Both species have been characterized by single crystal X-ray analysis.†

The crystal structure of **2** consists of [(**1**)(bpetha)]$_4$ square units interconnected *via* chloride bridges into a three-dimensional non-interpenetrated network. The squares are comprised of [Cu(2,2′-bipy)]$^{2+}$ corners and bpetha edges, with a Cu···Cu separation of 13.23 Å (Fig. 1, top); they are moderately folded about their diagonal axes by *ca.* 27° (Fig. 1, bottom). Similar previously reported macrocyclic motifs, containing Pt^{II} or Pd^{II} corners, are all individual molecules, held together essentially by van der Waals interactions.[4] The peculiar structural feature of **2**, on the other hand, consists in that these square units are organized in an extended architecture sustained by slightly bent chloride bridges [Cu···Cu 5.12 Å, Cu–Cl 2.582(2) Å, Cu–Cl–Cu 164.3(2)°]. Each square is bound to four similar motifs, two

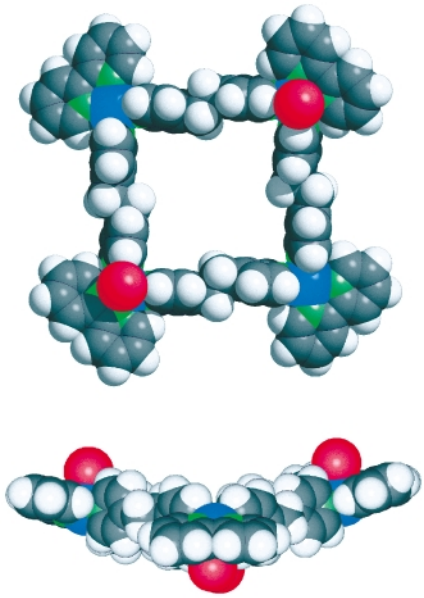

Fig. 1 Two views of the molecular squares in compound **2**.

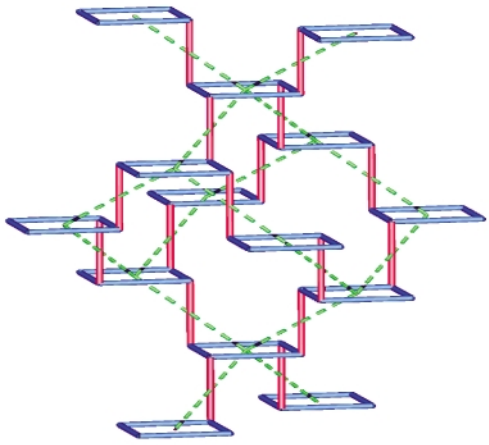

Fig. 2 A schematic view of the three-dimensional network in **2**, with the chloride bridges in red. The broken lines show the underlying diamondoid net, obtained by connecting the baricentres of the squares.

 DOI: 10.1039/b103736f

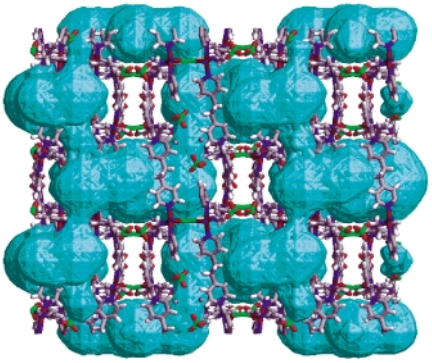

Fig. 3 The overall packing in **2** (down *a*, horizontal *c*) showing the surface of the large interconnected cavities.

above and two below the molecular plane, in an alternate fashion. The Cu^{II} coordination geometry is octahedral, with four equatorial Cu–N(pyridyl) bonds [in the range 2.00(1)–2.04(1) Å], one axial Cu–Cl bond and one axial weak interaction with a BF_4^- anion [Cu–F 2.79(1) Å].

The topology of this uninodal triconnected three-dimensional frame (Fig. 2) is $4{\cdot}14^2$, a relatively simple topological type already considered by Wells in his enumeration,[6] but completely new within coordination polymer chemistry. Interestingly, the baricentres of the squares define a diamondoid network (see Fig. 2), so that the net of **2** can be defined, according to O'Keeffe,[7] as an '*augmented diamond*' net.

The network contains large voids (38% of the cell volume),[8] with connected chambers (Fig. 3) that are filled by water molecules. Samples of **2** start to lose the solvated water at room temperature and TGA analyses show that all the water content (*ca.* 13% weight loss) is completely removed on heating up to *ca.* 120 °C, without demolition of the array (as confirmed by X-ray powder diffraction). Decomposition starts at *ca.* 180 °C, leading to copper metal above *ca.* 400 °C. The desolvated network, however, seems stable as such for an extended period and appears unable to regain solvated molecules to a significant extent even after immersion in different solvents (*e.g.* water, ethanol, isopropyl alcohol, toluene, CCl_4) for some days.

The structure of compound **3**, obtained under reaction conditions quite similar to those leading to **2** but using the bpethe ligand, consists of zigzag polymeric chains all running

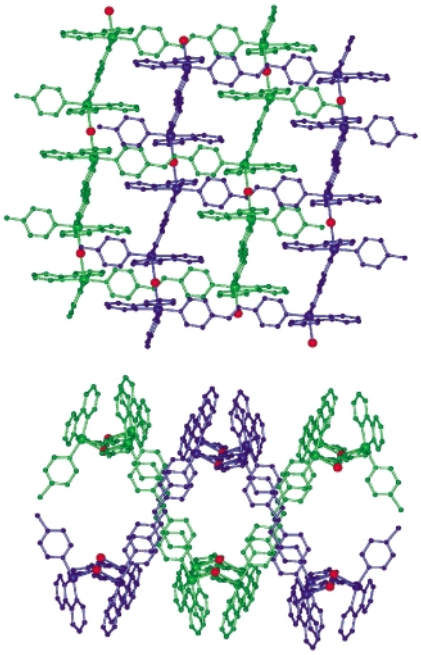

Fig. 4 A side view of the double-layer of **3** (top), showing the highly undulated shape of the sheets, and a view approximately down *b* showing the two-fold interpenetration (bottom). The Cl^- ions are in red.

along the [3 0 1] direction (Cu···Cu contacts of 13.31 Å av.) connected by chloride bridges [Cu–Cl 2.511(1) Å, Cu–Cl–Cu 139.5(1)°] into two-dimensional sheets of six-membered rings (6^3 topology). The Cu^{II} coordination is of the square pyramidal type, with the axial Cu–Cl interaction and four equatorial Cu–N(pyridyl) bonds [in the range 2.012(5)–2.025(5) Å]. The layers are highly undulated, with crankshaft-like sections (Fig. 4, top) and exhibit two-fold parallel interpenetration (Fig. 4, bottom). Moreover, these double-layers are superimposed with high interdigitation involving the nearest neighbours. Again, the array contains large channels along [1 0 0] (28% of the cell volume), located inside the double-layers.

Such different structures for **2** and **3**, in the presence of similar framework stoichiometries, are difficult to rationalize. The higher rigidity of the bpethe ligand and the presence of solvated CH_2Cl_2 molecules in **3** can play some role. While the *ideal* elimination of the chloride ions from **3** leaves polymeric zigzag chains, similar to those recently reported,[5] in the case of **2** this process should result in isolated molecular motifs. However, attempts to disentangle the squares of **2** by dissolution were made impossible by its poor solubility in all common solvents.

Notes and references

† *Crystal data*: for **2**: $C_{44}H_{57}B_3ClCu_2F_{12}N_8O_{8.50}$, M = 1256.94, tetragonal, space group $I\bar{4}2d$ (no. 122), a = 21.479(2), c = 29.303(3) Å, U = 13519(2) Å^3, T = 223 K, Z = 8, μ(Mo-Kα) = 0.749 mm^{-1}, 25456 reflections measured, 5073 unique (R_{int} = 0.071) which were used in all calculations. The final agreement index $R1$ was 0.0982 for 2933 independent significant [$I > 2\sigma(I)$] absorption corrected data. All but one of the solvated water molecule were refined with partial occupancy.

For **3**: $C_{45}H_{43}B_3Cl_3Cu_2F_{12}N_8O_{2.50}$, M = 1229.73, monoclinic, space group $C2/c$ (no. 15), a = 11.457(5), b = 40.814(17), c = 14.502(6) Å, β = 111.42(1)°, U = 6313(5) Å^3, T = 293 K, Z = 4, μ(Mo-Kα) = 0.875 mm^{-1}, 14189 reflections measured, 4937 unique (R_{int} = 0.054) which were used in all calculations. The final agreement index $R1$ was 0.0851 for 3240 independent significant [$I > 2\sigma(I)$] absorption corrected data. All the solvated water molecules were refined with half occupancy and suitable disordered models were applied to both anions.

CCDC 164240–164241. See http://www.rsc.org/suppdata/cc/b1/b103736f/ for crystallographic data in CIF or other electronic format.

1 R. Robson, B. F. Abrahams, S. R. Batten, R. W. Gable, B. F. Hoskins and J. Liu, in *Supramolecular Architecture*, ACS, Washington DC, 1992, ch. 19; M. J. Zaworotko, *Chem. Soc. Rev.*, 1994, 283; O. M. Yaghi, H. Li, C. Davis, D. Richardson and T. L. Groy, *Acc. Chem. Res.*, 1998, **31**, 474; M. Munakata, L. P. Wu and T. Kuroda-Sowa, *Adv. Inorg. Chem.*, 1999, **46**, 173; P. J. Hagrman, D. Hagrman and J. Zubieta, *Angew. Chem., Int. Ed.*, 1999, **38**, 2638; A. J. Blake, N. R. Champness, P. Hubberstey, W. S. Li, M. A. Withersby and M. Schröder, *Coord. Chem. Rev.*, 1999, **183**, 117.

2 *Comprehensive Supramolecular Chemistry*, ed. J.-M. Lehn, Pergamon Press, Oxford, 1995.

3 S. Leininger, B. Olenyuk and P. J. Stang, *Chem. Rev.*, 2000, **100**, 853; M. Fujita, *Acc. Chem. Res.*, 1999, **32**, 53; M. Fujita, K. Umemoto, M. Yoshizawa, N. Fujita, T. Kusukawa and K. Biradha, *Chem. Commun.*, 2001, 509.

4 M. Fujita, J. Yazaki and K. Ogura, *J. Am. Chem. Soc.*, 1990, **112**, 5645; M. Fujita and K. Ogura, *Coord. Chem. Rev.*, 1996, **148**, 249; M. Fujita, O. Sasaki, T. Mitsuhashi, T. Fujita, J. Yazaki, K. Yamaguchi and K. Ogura, *Chem. Commun.*, 1996, 1535; S. B. Lee, S. Hwang, D. S. Chung, H. Yun and J.-I. Hong, *Tetrahedron Lett.*, 1998, **39**, 873.

5 L. Carlucci, G. Ciani, A. Gramaccioli, D. M. Proserpio and S. Rizzato, *CrystEngComm*, 2000, **29**.

6 A. F. Wells, *Three-dimensional Nets and Polyhedra*, J. Wiley & Sons, New York, 1977, p. 80.

7 Complete symbol is $4{\cdot}14_{12}{\cdot}14_{12}$ see: M. O'Keeffe and B. G. Hyde, *Crystal Structures I. Patterns and Symmetry*, Mineralogical Society of America, Washington, DC, 1996; M. O'Keeffe, M. Eddaoudi, H. Li, T. Reineke and O. M. Yaghi, *J. Solid State Chem.*, 2000, **152**, 3.

8 An analysis of the holes was performed with the PLATON program: A. L. Speck, PLATON, A Multipurpose Crystallographic Tool, Utrecht University, 1999. The graphic representation of the surfaces of the cavities was obtained with SURFNET: R. A. Laskowski, *J. Mol. Graph.*, 1995, **13**, 323.

CHEMCOMM
Communication
www.rsc.org/chemcomm

Iridium(III) complexes of the new tridentate bis(8-quinolyl)silyl ('NSiN') ligand†

Mark Stradiotto, Kyle L. Fujdala and T. Don Tilley*

Department of Chemistry, University of California at Berkeley, Berkeley, California 94720-1460, USA. E-mail: tdtilley@socrates.berkeley.edu

Received (in Columbia, MO, USA) 22nd March 2001, Accepted 16th May 2001
First published as an Advance Article on the web 13th June 2001

Bis(8-quinolyl)methylsilane reacts cleanly with $[Ir(coe)_2Cl]_2$ (coe = cyclooctene) to give a complex containing an NSiN tridentate ligand, [Ir(NSiN)(coe)(H)(Cl)]; preliminary reactivity studies indicate that the (NSiN)Ir fragment is chemically robust.

Multidentate ligands have featured prominently in the recent development of new transition metal chemistry. Such ligands provide stability to a metal complex, and offer diverse possibilities for the manipulation of steric and electronic properties in controlling reactivity at the metal center. Notwithstanding the significant advances in transition metal–silicon chemistry over the past several years,[1,2] multidentate ligands containing silicon as part of the chelate architecture have received little attention. The incorporation of silicon into such structures may offer certain advantages, given (for example) the high strength of metal–silicon bonds and the strong *trans*-effect for silicon ligands.[1,3] Stobart and coworkers[4] have synthesized a number of metal complexes supported by a PSiP ligand framework; tridentate connectivity is attained in these systems *via* oxidative addition of an Si–H functionality. This general strategy should provide synthetic routes to various silicon-containing multidentate ligands.

With the goal of developing reactive metal fragments supported by new tridentate ancillary ligands, we identified nitrogen-based NSiN chelates as potential synthetic targets. A tridentate system based on the bis(8-quinolyl)silyl framework appeared particularly attractive, since the resulting five-membered metallacyclic rings are expected to stabilize a complex towards reductive elimination of the silyl unit, while providing a rather rigid ligand binding arrangement. Support for the viability of such a ligation strategy comes from the work of Watts and coworkers,[5] who have prepared Rh(III) and Ir(III) complexes of the bidentate (8-quinolyl)dimethylsilyl ligand. In this contribution, synthesis of the tridentate ligand precursor bis(8-quinolyl)methylsilane **1** and Ir(III) complexes supported by this NSiN fragment are reported.

Addition of 0.5 equivalents of methyldichlorosilane to 8-lithioquinoline in THF, followed by purification, provided **1** as pale yellow crystals in moderate yield.†‡ The characterization of **1** is based on IR and NMR spectroscopic data. Notably, the C_S symmetry of this compound results in observation of only one set of quinoline ^1H and ^{13}C NMR resonances.

Treatment of **1** with 0.5 equivalents of $[Ir(coe)_2Cl]_2$ in CH_2Cl_2 resulted in rapid liberation of cyclooctene (coe) and near quantitative formation (by NMR spectroscopy) of the new coordination complex **2** as a *single* diastereomer (Scheme 1). Vapor diffusion of diethyl ether into the reaction mixture permitted isolation of **2** as analytically pure, yellow crystals in 87% yield. As expected, two sets of NMR resonances are observed for the quinoline groups of compound **2**. Evidence for the presence of the hydride ligand in **2** was obtained from IR (2172 cm^{-1}) and ^1H NMR (−15.6 ppm) spectroscopic data.

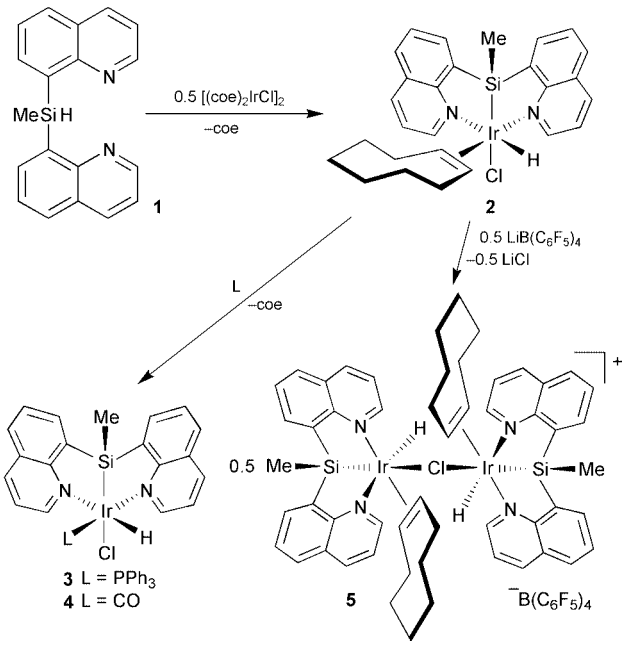

Scheme 1

The crystallographically determined structure of compound **2** is shown in Fig. 1.†‡ The non-equivalence of the quinoline groups noted in the ^1H and ^{13}C NMR spectra is consistent with the observed facial binding mode of the NSiN fragment. Constraints imposed by this ligand give rise to an Ir(III) center which is distorted considerably from ideal octahedral geometry. The chelate ligand 'bite' angles [N–Ir–N 87.5(3), N–Ir–Si 83.2(3) and 83.2(2)°] are all significantly compressed, underscoring the 'pinned-back' nature of the NSiN chelating framework. Geometric distortions are also observed at the silicon center. For example, the C(Me)–Si–Ir angle [131.2(4)°] is expanded well beyond the normal tetrahedral value. The Ir–Si distance [2.275(3) Å] in **2** can be compared to those in *fac*-tris[(8-quinolyl)dimethylsilyl]iridium (av. 2.30 Å),[5] and falls within the previously observed range (2.235–2.454 Å) for such

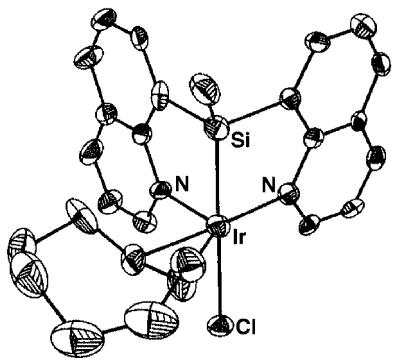

Fig. 1 Crystallographically determined structure of **2**, depicted with 50% thermal ellipsoids; all hydrogen atoms have been omitted for clarity.

† Electronic supplementary information (ESI) available: synthetic and crystallographic details for **1**–**5**. See http://www.rsc.org/suppdata/cc/b1/b102821a/

 DOI: 10.1039/b102821a

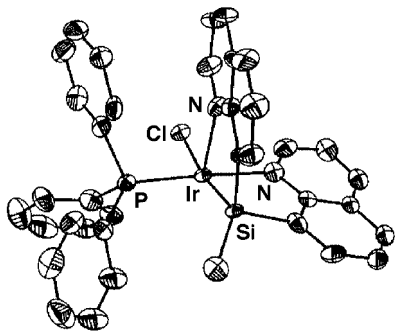

Fig. 2 Crystallographically determined structure of **3**, depicted with 50% thermal ellipsoids; all hydrogen atoms have been omitted for clarity.

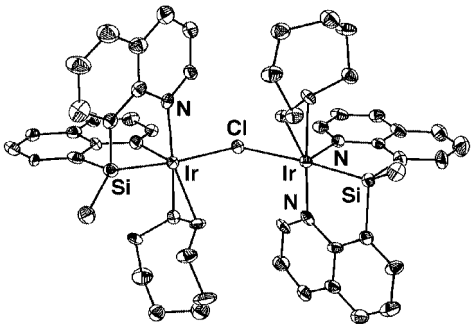

Fig. 3 Crystallographically determined structure of **5**, depicted with 50% thermal ellipsoids; the anion, solvates and all hydrogen atoms have been omitted for clarity. Only one component of the disordered coe fragment is shown.

bonds.[2] In contrast, the *trans*-labilizing nature[1–3] of the silyl group is manifested in a long Ir–Cl bond [2.572(3) Å].[6] The *trans*-influence of the hydride ligand is also indicated by elongation of an Ir–N bond [2.191(9) Å], relative to the other Ir–N bond [2.120(8) Å] in this complex.[7]

Preliminary reactivity studies reveal that the NSiN moiety is a robust ancillary ligand. Treatment of **2** with either PPh_3 or CO resulted in substitution of the coe ligand, yielding compounds **3** and **4**, respectively. Compound **3** gives rise to a singlet (17.0 ppm) in the $^{31}P\{^1H\}$ NMR spectrum and a phosphorus-coupled doublet (−19.1 ppm) in the hydride region of the ^1H NMR spectrum. The solid-state structure of compound **3** (Fig. 2) confirmed that the conversion of **2** to **3** occurs with retention of configuration at the Ir(III) center. In general, the geometric features associated with **3** parallel those described for **2** (*vide supra*). However, the Ir–P distance in **3** [2.234(3) Å] is noteworthy, since it appears to be contracted relative to Ir–P bonds found in related Ir(III) compounds (2.264–2.381 Å).[4,6,7] The coordination of a terminal carbonyl ligand to the Ir(III) center in **4** was confirmed by observation of a strong IR absorption attributed to this fragment (2010 cm^{-1}) and by the presence of a resonance at 169.9 ppm in the ^{13}C NMR spectrum. In contrast to the aforementioned transformations, no reaction was observed when a degassed CD_2Cl_2 solution of **2** was exposed to an atmosphere of H_2—even after prolonged heating (72 h at 90 °C). Collectively, these observations indicate that the Ir–Si linkage in **2** is relatively stable toward reductive elimination of Si–H.

In an attempt to prepare a cationic NSiN complex of iridium, CH_2Cl_2 was added to an equimolar mixture of **2** and $LiB(C_6F_5)_4{\cdot}2.5Et_2O$. Surprisingly, the major product obtained from this reaction was not that resulting from simple anion exchange, but rather the dinuclear complex **5**, which formally results from *in situ* trapping of the anticipated cationic species by an additional molecule of **2**. Complex **5** is formed exclusively as the racemic (C_2-symmetric) diastereomer, as confirmed by X-ray crystallography (Fig. 3).†‡ The overall connectivity pattern in **5** mirrors that found in **2**, with the exception that both of the Ir–Cl distances in the former [2.638(2) and 2.645(2) Å] are significantly longer than the Ir–Cl distance in the latter. Subsequently, compound **5** was prepared in 93% yield *via* treatment of **2** with 0.5 equiv. of the lithium borate. However, slow addition of **2** to an equiv. of $LiB(C_6F_5)_4{\cdot}2.5Et_2O$ under more dilute conditions led to clean formation (by NMR spectroscopy) of a new product, which we assume to be the desired mononuclear complex. Attempts are currently underway to isolate this species in pure form.

In conclusion, Ir(III) complexes containing the new bis(8-quinolyl)methylsilyl ligand have been prepared as single diastereomers in excellent yield. The diastereoselectivity associated with the clean formation of **2** and its derivatives indicates that the NSiN chelating ligand may have a directing effect on transformations at the Ir(III) center.[4] The synthesis and reactivity of various metal complexes supported by NSiN hybrid ligands will be the subject of future reports.

Acknowledgment is made to the National Science Foundation for their generous support of this work. M. S. thanks the Natural Sciences and Engineering Research Council of Canada for financial support in the form of an NSERC Postdoctoral Fellowship.

Notes and references

‡ CCDC 164004–164006. See http://www.rsc.org/suppdata/cc/b1/b102821a/ for crystallographic data in CIF or other electronic format.

1 M. S. Eisen, *The Chemistry of Organic Silicon Compounds*, ed. Z. Rappoport and Y. Apeloig, Wiley, New York, 1998, vol. 2, ch. 35, p. 2037; T. D. Tilley, *The Silicon–Heteroatom Bond*, ed. S. Patai and Z. Rappoport, Wiley, New York, 1991, ch. 9, 10, pp. 245, 309; T. D. Tilley, *The Chemistry of Organic Silicon Compounds*, ed. S. Patai and Z. Rappoport, Wiley, New York, 1989, ch. 24, p. 1415.
2 J. Y. Corey and J. Braddock-Wilking, *Chem. Rev.*, 1999, **99**, 175.
3 M. Aizenberg and D. Milstein, *J. Am. Chem. Soc.*, 1995, **117**, 6456.
4 G. W. Bushnell, M. A. Casado and S. R. Stobart, *Organometallics*, 2001, **20**, 601, and references therein; R. D. Brost, G. C. Bruce, F. L. Joslin and S. R. Stobart, *Organometallics*, 1997, **16**, 5669; R. A. Gossage, G. D. McLennan and S. R. Stobart, *Inorg. Chem.*, 1996, **35**, 1729; M. J. Auburn, R. D. Holmes-Smith, S. R. Stobart, P. K. Bakshi and T. S. Cameron, *Organometallics*, 1996, **15**, 3032; M. J. Auburn and S. R. Stobart, *Inorg. Chem.*, 1985, **24**, 318.
5 P. I. Djurovich, A. L. Safir, N. L. Keder and R. J. Watts, *Inorg. Chem.*, 1992, **31**, 3195; P. I. Djurovich, A. Safir, N. Keder and R. J. Watts, *Coord. Chem. Rev.*, 1991, **111**, 201.
6 G. B. Robertson and P. A. Tucker, *J. Am. Chem. Soc.*, 1982, **104**, 317.
7 F. Neve, M. Ghedini, A. Tiripicchio and F. Ugozzoli, *Inorg. Chem.*, 1989, **28**, 3084; R. H. Crabtree, E. M. Holt, M. Lavin and S. M. Morehouse, *Inorg. Chem.*, 1985, **24**, 1986; F. R. Hartley, *Chem. Soc. Rev.*, 1973, **2**, 163.

CHEMCOMM Communication
www.rsc.org/chemcomm

Evaluation of a sparteine-like diamine for asymmetric synthesis

Justin R. Harrison,[a] Peter O'Brien,*[a] David W. Porter[a] and Neil M. Smith[b]

[a] *Department of Chemistry, University of York, Heslington, York, UK YO10 5DD. E-mail: paob1@york.ac.uk*
[b] *GlaxoSmithKline, New Frontiers Science Park (North), Third Avenue, Harlow, Essex, UK CM19 5AW*

Received (in Cambridge, UK) 10th April 2001, Accepted 21st May 2001
First published as an Advance Article on the web 13th June 2001

Evaluation of a sparteine-like diamine indicates that only the ABC rings of sparteine are required for high enantioselectivity in the lithiation–substitution of *N*-Boc pyrrolidine.

Sparteine **1** is a naturally occurring alkaloid extracted from plants such as Scotch Broom. It is commercially available and has been widely used as a chiral diamine ligand in asymmetric synthesis over the last 30 years.[1] For example, asymmetric lithiation–electrophilic quench using the combination of sparteine and alkyllithiums on a wide range of substrates occurs routinely with > 90% enantioselectivity. The groups of Hoppe[2] and Beak[3] have led the way with pioneering contributions in the applications of sparteine in synthesis. More recently, Hoppe *et al.*[4] and Wiberg and Bailey[5] have carried out theoretical calculations of transition state energies aimed at elucidating how sparteine exerts such high levels of enantiodifferentiation.

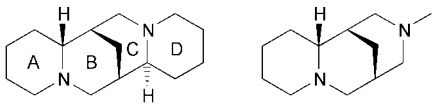

One of the main limitations of using sparteine in synthesis is that it is only commercially available in one enantiomeric form. Attempts to find other chiral diamine ligands capable of matching the enantioselectivity of sparteine have been moderately successful.[6,7] With the long term aim of developing a ligand that will function as the enantiomer of sparteine, we have investigated whether diamine **2**, which lacks the D-ring of sparteine as well as one of the chiral centres, mimicks sparteine sufficiently to give high enantioselectivity. Structural comparisons of diamines **1** and **2** complexed to lithium together with a recent calculated transition state for reaction[5] suggested that the D-ring of sparteine was not a key element in the enantiodiscriminating process. In this communication, we provide experimental evidence in support of this conjecture.

Although racemic diamine **2** is a known compound[8] and has found recent application in the functionalisation of terminal epoxides,[9] there have been no reports on the preparation of enantiomerically enriched diamines like **2**. An approach from amino acids investigated in our laboratory[10] was unsuccessful due to unavoidable racemisation in one of the steps. Thus, we resorted to resolution as a means of preparing non-racemic diamine **2** as outlined in Scheme 1.

Racemic diamine **2** was prepared using a published route:[8] double Mannich reaction of ketone **3** gave a single diastereoisomer of **4** (58% yield) which was converted into the required diamine **2** (68% yield) using Wolff–Kishner reduction. Unfortunately, we were unable to develop a resolution protocol for racemic **2** using commercial chiral acids (*e.g.* tartaric acid and derivatives, malic acid and camphorsulfonic acid). However, we had more success with resolution by inclusion complex formation using a method previously described by Toda *et al.*[11] Toda had discovered that it was possible to use naturally ocurring sparteine **1** to resolve racemic acetylinic alcohols such as **5**. Since diamine **2** is structurally similar to sparteine, we speculated that enantiomerically pure **5** could be used for resolution.

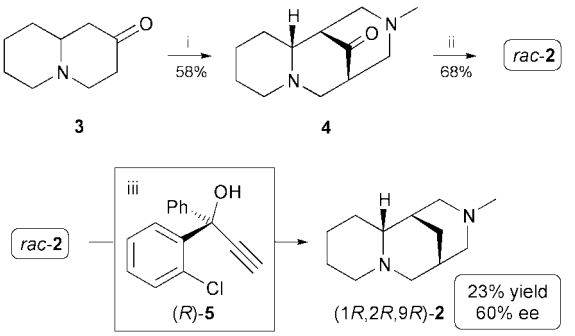

Scheme 1 *Reagents and conditions*: i, $MeNH_2$, $(CH_2O)_n$, AcOH, MeOH, reflux, 16 h; ii, N_2H_4, H_2O, KOH, diethylene glycol, reflux, 2 h; iii, acetone, evaporation over 64 h.†

Thus, Toda's method was employed to synthesise alcohol (*R*)-**5** of 98% ee (by chiral HPLC on an Astec Cyclobond I 2000-RSP column) and it was used in turn to partially resolve diamine **2**. In this way, we obtained a 23% yield of enantiomerically enriched diamine **2**† ($[\alpha]_D$ −15.7 (*c* 0.5 in EtOH); ~60% ee by chiral shift NMR). This resolution was reproducible in the 50–60% ee range and after repeating it a few times, we obtained a sufficient quantity of diamine **2** of ~55% ee. Since alcohol (*R*)-**5** had been obtained *via* crystal formation with sparteine **1**, it seemed likely that resolved diamine **2** (isolated *via* crystal formation with (*R*)-**5**) would have the same *absolute* stereochemistry as the ABC rings of sparteine.

With diamine **2** of ~55% ee in hand, we elected to directly compare it with sparteine **1** using lithiation of *N*-Boc pyrrolidine **6** and subsequent trapping with Me_3SiCl.[6,12] The results are presented in Table 1. Using sparteine **1**, we obtained a 73% isolated yield of silylated pyrrolidine (*S*)-**7** of 95% ee (by chiral GC). Under the same conditions, use of diamine **2** of ~55% ee gave an unoptimised 41% yield of silylated pyrrolidine (*S*)-**7** of 53% ee (by chiral GC).‡ The sense of asymmetric induction was

Table 1 Lithiation–substitution of *N*-Boc pyrrolidine using diamines **1** and **2**

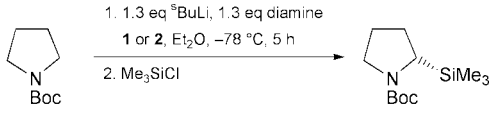

Diamine	Yield of (*S*)-**7** (%)[a]	ee (%)[b]
Sparteine **1**	73	95
(1*R*,2*R*,9*R*)-**2** (~55% ee)	41	53

[a] Isolated yield after column chromatography; [b] Enantiomeric excess determinined by chiral GC on a Chiraldex G-PN 20 m × 0.25 mm id (γ-cyclodextrin, propionyl derivative in the 3-position) column.

 DOI: 10.1039/b103220h

the same in both reactions indicating that resolved diamine **2** does indeed possess the same absolute stereochemistry as the ABC rings of sparteine. More importantly, however, the results presented in Table 1 provide the first experimental evidence that only the ABC rings of sparteine **1** are required for high enantioselectivity in the lithiation of *N*-Boc pyrrolidine **6**.

In summary, our results indicate that diamine **2** exhibits essentially the same level of enantioselectivity as sparteine **1** in the lithiation of *N*-Boc pyrrolidine **6**. Thus, we conclude that the sparteine D-ring is superfluous and is not a prerequisite for high enantioselectivity.

We thank the EPSRC and GlaxoSmithKline for the award of an Industrial CASE award (to D. W. P.), The Leverhulme Trust for the award of a fellowship (to J. R. H.) and Dr D. B. Matthews for chiral HPLC and GC analyses.

Notes and references

† *Resolution of diamine rac*-**2**: A solution of freshly distilled diamine *rac*-**2**[8] (742 mg, 3.8 mmol) in acetone (3 cm^3) was added dropwise to a solution of alcohol (*R*)-**5** (929 mg, 3.8 mmol; 98% ee by chiral HPLC on an Astec Cyclobond I 2000-RSP column) in acetone (3 cm^3) at rt. The solvent was allowed to evaporate slowly by standing at rt for 64 h and pale yellow crystals formed. Petrol (5 cm^3) was added and the crystals were collected by filtration and washed well with petrol (3 × 5 cm^3). The crystals were dissolved in Et_2O (15 cm^3) and 2 M $HCl_{(aq)}$ (10 cm^3), the layers were separated and the organic layer was extracted with 2 M $HCl_{(aq)}$ (2 × 10 cm^3). Then, 20% $NaOH_{(aq)}$ was added to the combined aqueous layers until pH 9 and the solution was extracted with Et_2O (3 × 10 cm^3), dried (K_2CO_3) and evaporated under reduced pressure to give diamine (1*R*,2*R*,9*R*)-**2** (171 mg, 23%; ~60% ee by ^1H NMR spectroscopy in the presence of (*R*)-2,2,2-trifluoro-1-(9-anthryl)ethanol) as a colourless oil, $[\alpha]_D$ −15.7 (*c* 0.5 in EtOH). Treatment of the petrol washings in the same way as described above for the crystals gave diamine (1*S*,2*S*,9*S*)-**2** (503 mg, 68%; ~30% ee by ^1H NMR spectroscopy in the presence of (*R*)-2,2,2-trifluoro-1-(9-anthryl)ethanol) as a colourless oil, $[\alpha]_D$ +6.1 (*c* 0.6 in EtOH).

‡ In theory, silylated pyrrolidine (*S*)-**7** of >55% ee could have been generated if a non-linear effect was occurring. Our results clearly indicate the absence of a non-linear effect and are in line with the calculated transition state for reaction[5] which invokes deprotonation by a monomeric complex.

1 For a review, see: D. Hoppe and T. Hense, *Angew. Chem., Int. Ed. Engl.*, 1997, **36**, 2282.
2 For recent developments, see: A. Deiters, R. Frölich and D. Hoppe, *Angew. Chem., Int. Ed.*, 2000, **39**, 2105.
3 For recent developments, see: T. A. Johnson, M. D. Curtis and P. Beak, *J. Am. Chem. Soc.*, 2001, **123**, 1004.
4 E.-U. Würthwein, K. Behrens and D. Hoppe, *Chem. Eur. J.*, 1999, **5**, 3459.
5 K. B. Wiberg and W. F. Bailey, *Angew. Chem., Int. Ed.*, 2000, **39**, 2127; K. B. Wiberg and W. F. Bailey, *Tetrahedron Lett.*, 2000, **41**, 9365.
6 D. J. Gallagher, S. Wu, N. A. Nikolic and P. Beak, *J. Org. Chem.*, 1995, **60**, 8148.
7 X. Li, L. B. Schenkel and M. C. Kozlowski, *Org. Lett.*, 2000, **2**, 875.
8 P. Scheiber and P. Nemes, *Liebigs Ann. Chem.*, 1994, 1033.
9 D. M. Hodgson and S. L. M. Norsikian, *Org. Lett.*, 2001, **3**, 461.
10 J. R. Harrison, P. O'Brien, D. W. Porter and N. M. Smith, *J. Chem. Soc., Perkin Trans. 1*, 1999, 3623.
11 F. Toda, K. Tanaka, H. Ueda and T. Oshima, *Chem. Commun.*, 1983, 743.
12 P. Beak, S. T. Kerrick, S. Wu and J. Chu, *J. Am. Chem. Soc.*, 1994, **116**, 3231.

CHEMCOMM Communication
www.rsc.org/chemcomm

Structure and magnetism of the first cyano-bridged hetero-one-dimensional Gd^{III}–Cr^{III} complexes

Albert Figuerola,[a] Carmen Diaz,[a] Mohamed S. El Fallah,[a] Joan Ribas,*[a] Miguel Maestro[b] and José Mahía[b]

[a] *Departament de Química Inorgànica, Universitat de Barcelona, Diagonal, 647, 08028-Barcelona, Spain. E-mail: joan.ribas@qi.ub.es*
[b] *Servicios Xerais de Apoio á Investigación, Facultade de Ciencias, Universidade da Coruña, E-15071 A Coruña, Spain*

Received (in Cambridge, UK) 26th March 2001, Accepted 15th May 2001
First published as an Advance Article on the web 13th June 2001

A reaction between $Gd(NO_3)_3{\cdot}6H_2O$, $K_3[Cr(CN)_6]$ and dmf or bpy has allowed the synthesis of two new ferrimagnetic Gd^{III}–Cr^{III} chains which are the first low-dimensional 4f–Cr^{III} systems; magnetic susceptibilty data indicate antiferromagnetic coupling between Gd^{III} and Cr^{III}.

The association of 3d–4f ions in cyanide-bridged low dimensional arrays is original and may open new perspectives for the use of the optical properties of rare earth ions included in magnetic molecular media.[1,2] In general, little is known about the nature of the exchange interactions of rare earth ions either with one another or with other magnetic groups. Until recently few simple compounds containing magnetically coupled f-block ions were available. Most of them are Gd^{III}–Cu^{II} or Gd^{III}–radical organic systems.[3,4] Among those with cyanide bridges, several tri-dimensional polycyano metallates(III) (Fe, Co, Cr) with 4f ions[5] and two heteropolynuclear Ln^{III}–Fe^{III} compounds have been reported.[6] Some heterometallic one-dimensional arrays containing cyanide-bridged lanthanide(III) and diamagnetic $[M(CN)_4]^{2-}$ (M = Ni, Pd, Pt) have also been described.[7] In contrast, to the best of our knowledge, discrete or low-dimensional derivatives of $[Cr(CN)_6]^{3-}$ with 4f ions have not been reported. This communication is devoted to the preparation,† characterization including structural determination, and magnetic properties of the two first one-dimensional derivatives from $[Cr(CN)_6]^{3-}$ and Gd^{III}: *cis*-$[Cr(CN)_4(\mu\text{-}CN)_2Gd(H_2O)_2(dmf)_4]_n{\cdot}nH_2O$ **1** and *trans*-$[Cr(CN)_4(\mu\text{-}CN)_2Gd(H_2O)_4(bpy)]_n{\cdot}4nH_2O{\cdot}1.5n$bpy **2**. Fig. 1 shows the X-ray crystal structure of **1**.‡ The crystallographic analysis of **1** revealed that its crystal structure is a one-dimensional (1D) chain polymer. The chain shows an alternation of Gd^{III} and Cr^{III} units linked by cyanide bridges in *cis* geometry with respect to Cr^{III}. The coordination sphere around gadolinium comprises four oxygen atoms of dimethylformamide (dmf) ligands, two oxygen atoms of two water molecules and two nitrogen atoms of the cyanide bridges. The eight-coordinate gadolinium atom lies in a distorted dodecahedral environment. The Gd–Cr intramolecular distance is 5.65 Å and the Gd–Cr–Gd angle is 98.432° indicating the *cis*-geometry. As shown in Fig. 1, the chains are aligned in the *x*-direction where two neighboring chains are linked by water molecules, giving a slipped packing.

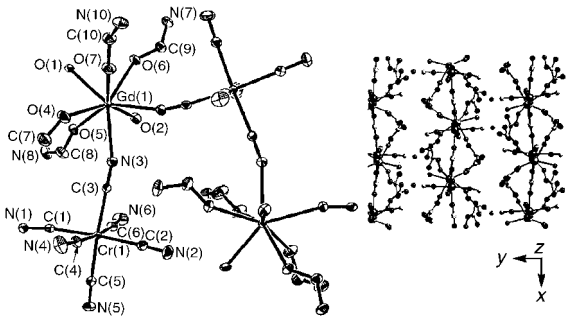

Fig. 1 Left: Crystal structure of *cis*-$[Cr(CN)_4(\mu\text{-}CN)_2Gd(H_2O)_2(dmf)_4]_n{\cdot}nH_2O$. Selected bond lengths [Å] and angles [°], hydrogen atoms and the methyl groups of the dmf ligands are omitted for clarity: Gd(1)–O(1) 2.3552(17), Gd(1)–O(2) 2.4026(17), Gd(1)–O(4) 2.3768(18), Gd(1)–O(5) 2.3617(17), Gd(1)–O(6) 2.3805(16), Gd(1)–O(7) 2.3946(18), Gd(1)–N(1′) 2.521(2), Gd(1)–N(3) 2.517(2), Cr(1)–C(1) 2.092(2), Cr(1)–C(2) 2.065(2), Cr(1)–C(3) 2.084(2), Cr(1)–C(4) 2.074(2), Cr(1)–C(5) 2.069(2), Cr(1)–C(6) 2.069(2), C(1)–N(1) 1.152(3), Cr(1)–C(1)–N(1) 170.6(2), C(1)–N(1)–Gd(1) 163.58(18), O(1)–Gd(1)–O(5) 71.84(6), O(1)–Gd(1)–O(4) 79.69(7), O(5)–Gd(1)–O(4) 79.89(7), O(1)–Gd(1)–O(6) 73.35(6), O(1)–Gd(1)–O(7) 81.93(7), O(4)–Gd(1)–O(7) 70.77(7), N(1′)–Gd(1)–N(3) 74.80(6). Right: Arrangement in the crystal.

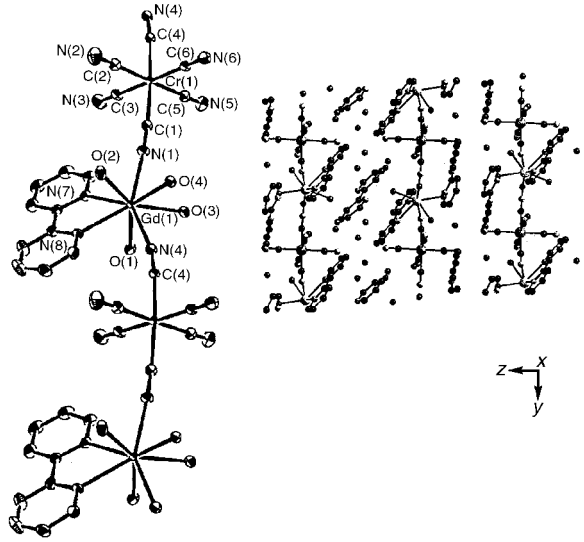

Fig. 2 Left: Crystal structure of *trans*-$[Cr(CN)_4(\mu\text{-}CN)_2Gd(H_2O)_4(bpy)]_n{\cdot}4nH_2O{\cdot}1.5n$bpy. Selected bond lengths [Å] and angles [°], hydrogen atoms are omitted for clarity: Gd(1)–O(1) 2.392(2), Gd(1)–O(2) 2.348(2), Gd(1)–O(3) 2.417(2), Gd(1)–O(4) 2.393(2), Gd(1)–N(1) 2.479(3), Gd(1)–N(7) 2.537(3), Gd(1)–N(8) 2.569(2), Cr(1)–C(1) 2.074(3), Cr(1)–C(2) 2.068(3), Cr(1)–C(3) 2.062(3), Cr(1)–C(4) 2.072(3), Cr(1)–C(5) 2.076(3), Cr(1)–C(6) 2.080(3), C(1)–N(1) 1.151(4), C(1)–N(1)–Gd(1) 176.0(3), Cr(1)–C(1)–N(1) 174.8(3), O(2)–Gd(1)–O(4) 73.76(8), O(1)–Gd(1)–O(3) 70.21(8), O(1)–Gd(1)–N(4) 77.75(8), O(4)–Gd(1)–N(4) 72.66(8), O(3)–Gd(1)–N(4) 81.42(8), O(2)–Gd(1)–N(1) 80.20(9), O(4)–Gd(1)–N(1) 74.64(8), N(1)–Gd(1)–N(4) 145.06(9). Right: Arrangement in the crystal.

Fig. 2 shows the X-ray crystal structure of **2**.‡ The crystallographic analysis of **2** revealed that its crystal structure is a one-dimensional (1D) chain polymer. The chain shows an alternation of Gd^{III} and Cr^{III} units linked by cyanide bridges in *trans* geometry with respect to Cr^{III}. The coordination sphere around gadolinium comprises two nitrogen atoms of the 2,2′-bipyridine (bpy) ligand, four oxygen atoms of four water molecules and two nitrogen atoms of the cyanide bridges. The eight-coordinate gadolinium atom lies in a distorted dodecahe-

 DOI: 10.1039/b102739p

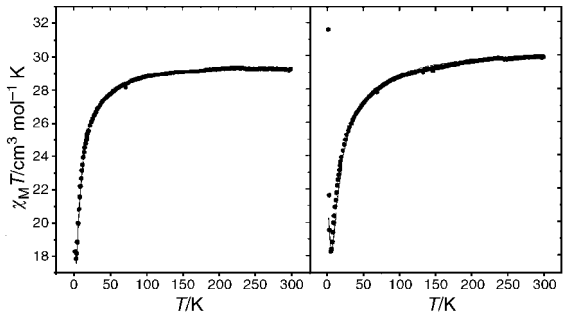

Fig. 3 Left: Temperature dependence of $\chi_M T$ for **1**. The solid line represents the best-fit curve (see text for parameters). Right: Temperature dependence of $\chi_M T$ for **2**. The solid line represents the best-fit curve (see text for parameters).

dral environment. The Gd–Cr intramolecular distance is 5.59 Å and the Gd–Cr–Gd angle is 159.28° indicating the *trans*-geometry. As shown in Fig. 2 the chains are aligned in the *y*-direction. Between two neighboring chains are water molecules and two different bpy crystallization molecules. One of them is not planar showing a dihedral angle between the two pyridine planes of 20° and the other is planar but the same dihedral angle is 180°.

The susceptibility measurements for complexes **1** and **2** are shown in Fig. 3 as $\chi_M T$ *vs.* T respectively. There is no mathematical expression for fitting a one-dimensional system with alternated $S = 7/2$ and 3/2. To fit the experimental data we have assumed a ring of six atoms (three Gd^{III} and three Cr^{III}) (Fig. 4), which should describe the behavior of the infinite chain when J is small. The fit of experimental data was performed according to the following Hamiltonian:

$$H = -J(S_1S_2 + S_2S_3 + S_3S_4 + S_4S_5 + S_5S_6 + S_6S_1)$$

where J corresponds to the coupling through the cyanide bridges. The free parameters were J and g (average). The fit made by the irreducible tensor operator formalism (ITO) using the CLUMAG program[8] gave the following results: $J = -0.52$ cm^{-1}, $g = 2.01$ and $R = 2.07 \times 10^{-5}$ for complex **1** (Fig. 3) and $J = -1.06$ cm^{-1}, $g = 2.05$ and $R = 2.137 \times 10^{-4}$ for complex **2** (Fig. 3). Both complexes show a weak antiferromagnetic interaction between Cr^{III} and Gd^{III} ions to give a ferrimagnetic chain. For complex **2**, the two values of $\chi_M T$ at low temperatures are not fitted because in our model the limit of $\chi_M T$ is that corresponding to three Gd^{III} + three Cr^{III} ($\chi_M T = 21$ cm^3 mol^{-1} K; $S_T = 6$). In the actual structure (one-dimensional complex) $\chi_M T$ tends to infinity, as shown in Fig. 4.

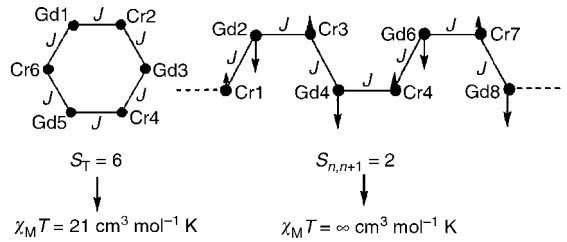

Fig. 4 Left: Scheme of a ring of six atoms used in the fit made by the ITO formalism. Right: Scheme of the spin topology assuming antiferromagnetic coupling.

A simulation of $\chi_M T$ *vs.* T for the ring of six atoms was calculated using the same method as that described above. The g value was fixed as 2.00. The value of J was simulated between 0 cm^{-1} and -2 cm^{-1}. As expected, with these small J values, the variation of $\chi_M T$ *vs.* T is observed only at low temperatures. The theoretical $\chi_M T$ *vs.* T curves are shown in Fig. 5. When the J coupling is more negative the minimum of $\chi_M T$ is shifted to a higher temperature.

This work was supported by the Spanish Dirección General de Investigación Científica y Técnica (project BQU2000-0791).

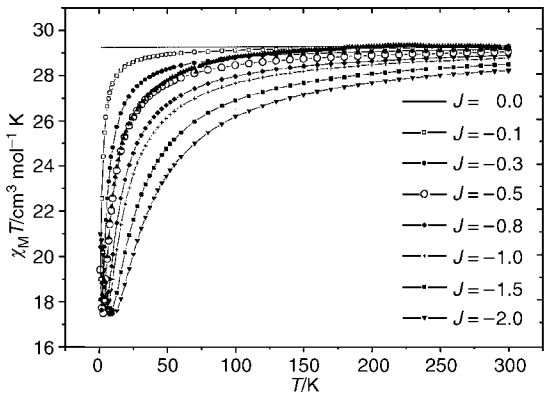

Fig. 5 Theoretical curves obtained by the CLUMAG program for different J values; g was maintained constant and equal to 2.00.

Notes and references

† *Experimental*: Compound **1** was obtained by adding a solution of $K_3[Cr(CN)_6]$ (0.43 g, 1.33 mmol) in water (15 mL) to a solution of $Gd(NO_3)_3{\cdot}6H_2O$ (0.60 g, 1.33 mmol) in dimethylformamide (10 mL). The solution was left undisturbed and well-formed yellow crystals were obtained after several days (yield 63%). Anal. Calc. for $C_{18}H_{34}CrGdN_{10}O_7$: C, 30.37; H, 4.81; N, 19.68. Found: C, 30.14; H, 4.99; N, 19.50%. Compound **2** was obtained by adding a solution of $K_3[Cr(CN)_6]$ (0.713 g, 2.2 mmol) in water (50 mL) to a solution of $Gd(NO_3)_3{\cdot}6H_2O$ (1.00 g, 2.2 mmol) in water (50 mL). To this mixture, an ethanolic solution (10 mL) of 2,2′-bipyridine (1.03 g, 6.6 mmol) was added. The solution was left undisturbed and well-formed yellow crystals were obtained after several days (yield 60%). Anal. Calc. for $C_{31}H_{36}CrGdN_{11}O_8$: C, 41.37; H, 4.03; N, 17.12. Found: C, 41.15; H, 3.97; N, 17.30%.

‡ *Crystal data* for **1**: $C_{18}H_{34}CrGdN_{10}O_7$, $M = 711.80$, monoclinic, space group $P2_1/n$, $a = 13.159(1)$, $b = 12.878(1)$, $c = 18.978(1)$ Å, $\beta = 109.835(1)°$, $V = 3025.3(1)$ Å^3, $Z = 4$, $D_c = 1.563$ g cm^{-3}, $\mu = 2.582$ mm^{-1}, $T = 173.2$ K, Bruker SMART CCD, Mo-Kα radiation ($\lambda = 0.71073$ Å), 20152 reflections measured, 7471 unique ($R_{int} = 0.0321$) which were used in all calculations. The final $wR(F^2) = 0.0678$ (all data). 342 variables. For **2**: $C_{31}H_{36}CrGdN_{11}O_8$, $M = 899.96$, triclinic, space group $P\bar{1}$, $a = 9.815(1)$, $b = 10.773(1)$, $c = 19.704(1)$ Å, $\alpha = 83.549(1)$, $\beta = 83.775(1)$, $\gamma = 65.092(1)°$, $V = 1873.3(1)$ Å^3, $Z = 2$, $D_c = 1.595$ g cm^{-3}, $\mu = 2.107$ mm^{-1} , $T = 173.2$ K, Bruker SMART CCD, Mo-Kα radiation ($\lambda = 0.71073$ Å), 12920 reflections measured, 8824 unique ($R_{int} = 0.0308$) which were used in all calculations. $wR(F^2) = 0.0810$ (all data), 488 variables. The structures were solved using the Bruker SHELXTL-PC software by direct methods and refined by full-matrix least-squares methods and non-hydrogen atoms refined anisotropically.

CCDC reference numbers 150442 and 150443. See http://www.rsc.org/suppdata/cc/b1/b102739p/ for crystallographic data in CIF or other electronic format.

1 G. F. de Sá, O. P. Malta, C. de Mello Donegá, A. M. Simas, R. L. Longo, P. A. Santacruz and E. F. da Silva Jr., *Coord. Chem. Rev.*, 2000, **196**, 165 and references therein.
2 M. Andruh, I. Ramade, E. Codjovi, O. Guillou, O. Kahn and J. C. Trombe, *J. Am. Chem. Soc.*, 1993, **115**, 1822; M. L. Kahn, C. Mathonière and O. Kahn, *Inorg. Chem.*, 1999, **38**, 3692; J. P. Costes, F. Dahan, A. Dupuis and J. P. Laurent, *Inorg. Chem.*, 2000, **39**, 169.
3 A. Benin, C. Benelli, A. Canneschi, R. L. Carlin, A. Dei and D. Gatteschi, *J. Am. Chem. Soc.*, 1985, **107**, 812; A. Blake, P. E. Milne and R. E. P. Winpenny, *Angew. Chem., Int. Ed. Engl.*, 1991, **30**, 1139; Y. Liang, R. Cao, W. Su, M. Hong and W. Zhang, *Angew. Chem., Int. Ed.*, 2000, **39**, 3304.
4 O. Guillou, O. Kahn, R. L. Oushoorn, K. Boubekeur and P. Batail, *Angew. Chem., Int. Ed. Engl.*, 1992, **31**, 626; J. P. Sutter, M. L. Kahn, S. Golhen, L. Ouahab and O. Kahn, *Chem. Eur. J*, 1998, **4**, 571; A. Canneschi, A. Dei, D. Gatteschi, L. Sorace and K. Vostrikova, *Angew. Chem., Int. Ed.*, 2000, **39**, 246.
5 F. Huliger, M. Landolt and H. Vetsch, *J. Solid State Chem.*, 1976, **18**, 307; F. Huliger, M. Landolt and H. Vetsch, *J. Solid State Chem.*, 1976, **18**, 283.
6 S. Gao, B. Ma, Z. Wang, T. Yi, C. Liao, C. Yan and G. Xu, *Mol. Cryst. Liq. Cryst.*, 1999, **335**, 201; B.-Q. Ma, S. Gao, G. Su and G.-X. Xu, *Angew. Chem., Int. Ed.*, 2001, **40**, 434.
7 D. W. Knoeppel, J. Liu, E. A. Meyers and S. G. Shore, *Inorg. Chem.*, 1998, **37**, 4828.
8 D. Gatteschi and L. Pardi, *Gazz. Chim. Ital.*, 1993, **123**, 231.

CHEMCOMM
Communication
www.rsc.org/chemcomm

A new binuclear ruthenium complex with an annelated C_7 bridge *via* an unprecedented [2 + 2] coupling reaction†

Stéphane Rigaut,*[a] Luc Le Pichon,[a] Jean-Claude Daran,[b] Daniel Touchard*[a] and Pierre H. Dixneuf[a]

[a] *Institut de Chimie de Rennes, UMR 6509 CNRS-Université de Rennes: Organométalliques et Catalyse, Campus de Beaulieu 35042 Rennes, France. E-mail: daniel.touchard@univ-rennes1.fr*
[b] *Laboratoire de Chimie de Coordination, 205 Route de Narbonne, 31042 Toulouse Cedex, France*

Received (in Cambridge, UK) 12th April 2001, Accepted 22nd May 2001
First published as an Advance Article on the web 14th June 2001

Treatment of $[Cl(dppe)_2Ru–C\equiv C–C\equiv C–SiMe_3]$ with $[Fe(C_5H_5)_2]PF_6$ leads to an unprecedented metal-assisted [2 + 2] coupling reaction on $C^{\gamma}\equiv C^{\delta}$ bonds to obtain $[Cl(dppe)_2Ru–C\equiv C–\overline{C=CHC(CH_2)}=C=C=Ru(dppe)_2Cl]PF_6$ with the charge highly delocalized over seven carbon atoms and including a cyclobutenyl bridge; the crystal structure was solved.

Polynuclear transition metal complexes with unsaturated carbon rich bridges retain much attention,[1,2] for their potential to scale down electronic components *i.e.* to form molecular wires and other nanoelectronic devices.[2] The literature is now extensive for complexes with an even number of conjugated carbon atoms spanning two metal fragments of various structures[1,2] such as $L_nMC_xML_n$ or $L_nM(CH)_xML_n$. By contrast, the synthesis of bimetallic compounds with odd carbon chains has not been extensively explored considering the variety of fragments available. Only few bridges with one, three or five unsaturated carbons capped with two metal moieties have been reported.[3–5] Current extension of the chemistry of vinylidene $[M=C=CR^1R^2]$ and acetylide $[M–C\equiv C–R]$ complexes to obtain new bridges *via* [2 + 2] cycloaddition led to a class of complexes $[M–\overline{C=CR–C(CR^2R^3)}=M]^+$ including rigid cyclic four-membered bridges with a delocalised C_3 path between metals.[4,5] Interestingly, when the reaction was applied to allenylidene[4c] $[M=C=C=CR^1R^2]$ or diyne[4d] $[M–C\equiv C–C\equiv C–R]$ complexes, the resulting ring bears an exocyclic double or triple bond, respectively, with a similar C_3 conjugated path. The formation of these carbon ligands is highly regioselective and the product of addition with the most activated $C^{\alpha}–C^{\beta}$ bond is always obtained. We now report an unprecedented radical-promoted [2 + 2] coupling reaction occurring on the $C^{\gamma}\equiv C^{\delta}$ bonds of a 1,3-diynyl metal derivative to lead to a novel type of metal complex $[M–C\equiv C–C=CHC(CH_2)=C=CM]^+$ including a carbon-rich annelated C_8H_3 bridge with seven conjugated carbons between remote metals.

Previous studies[6] on ruthenium allenylidenes $[Cl(dppe)_2Ru=C=CR^1R^2]$ and acetylides $[Cl(dppe)_2Ru–C\equiv C–R]$ (dppe = 1,2-diphenylphosphinoethane) showed that the bulky ruthenium $[RuCl(dppe)_2]^+$ moiety prevents C^{α} from nucleophilic attack while promoting reactions on C^{γ}. The $C^{\alpha}\equiv C^{\beta}$ bond in diyne complexes such as $[Cl(dppe)_2Ru–C\equiv C–C\equiv C–SiMe_3]$ is sterically protected by the dppe groups and [2 + 2] cycloaddition using this type of complex is likely to occur on the $C^{\gamma}\equiv C^{\delta}$ triple bond. The pale yellow diynyl ruthenium complex *trans*-$[Cl(dppe)_2Ru–C\equiv C–C\equiv C–SiMe_3]$ **2** was obtained (63%) *via* substitution of one chloride of *cis*-$[RuCl_2(dppe)_2]$ **1** with a slight excess (1.5 equiv.) of lithium acetylide in THF (Scheme 1). The *trans* structure was evidenced by ^{31}P NMR spectroscopy showing a singlet at δ 49.09 for the four phosphorus atoms. Upon treatment of complex **2** with half an equivalent of ferrocenium hexafluorophosphate as oxidant a metal-assisted C–C forming reaction took place and dark purple crystals of **3** were isolated after several crystallisations in moderate yield (45%). This compound was fully characterised by NMR, IR, UV–VIS and HR-MS (ESI†). ^{31}P analysis of **3** shows only one singlet at δ 45.2 indicating that (i) the two metal sites are equivalent and (ii) the four phosphorus are also equivalent on each metal centre with the Cl atom and the bridge in a *trans* position. ^{13}C NMR analysis shows only five different signals for the unsaturated bridges linking the two rutheniums. The Ru–C(1) resonance at δ 247.7 (quint, $^2J_{pc}$ 14 Hz) is downfield compared to that of an alkynyl (δ 105.5 for $[Cl(dppe)_2Ru–C\equiv C–CPh_2H]$)[6b] and upfield from that of an allenylidene complex (δ 308.6 for $[Cl(dppe)_2Ru=C=C=CPh_2]$).[6c] The same phenomenon is observed for the C(2) (δ 166.0) and C(3) (δ 147.1) resonances. The ^1H spectrum shows two characteristic resonances for the C_4 ring at δ 2.07 (s, 2H) and δ 5.11 (s, 1H). These NMR studies are consistent with a highly delocalized structure giving a formal half positive charge on each ruthenium as sketched on Scheme 1. The FTIR spectrum shows an intense absorption band at 1909 cm^{-1} indicative of the cumulenylidene character of the system.[6a,c]

X-Ray-structural analysis[7] (Fig. 1) verifies that the complex is formed with two identical bulky ruthenium fragments $[RuCl(dppe)_2]^+$ connected by a C_8H_3 ligand. The Cl atoms adopt a *trans* position with respect to the bridge and the Cl(1)–Ru(1)–bridge–Ru′(1)–Cl(1)′ arrangement is linear. The four-membered ring is planar so giving maximum orbital overlap across the bridge. Owing to the inversion centre which relates the two parts of the complex, the four-membered ring is symmetric. Moreover as the two distances, C(3)–C(4) 1.457(5) Å and C(3)–C(4′) 1.459(5) Å, are identical within experimental error, the four C–C bond lengths are identical within the ring.[7b]

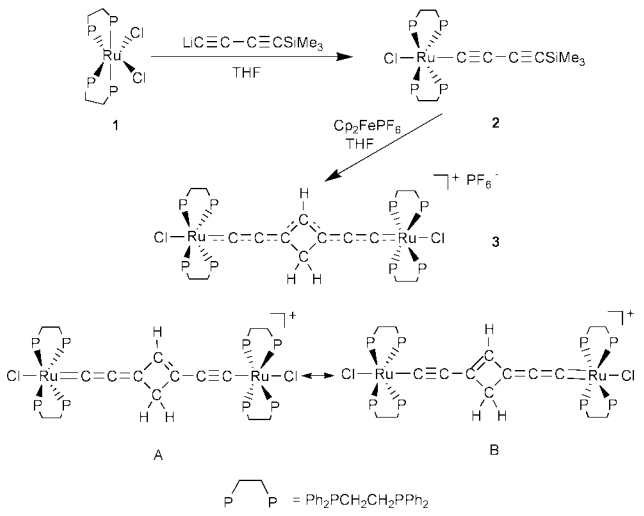

Scheme 1

† Electronic supplementary material (ESI) available: selected spectroscopic data. See http://www.rsc.org/suppdata/cc/b1/b103301h/

 DOI: 10.1039/b103301h

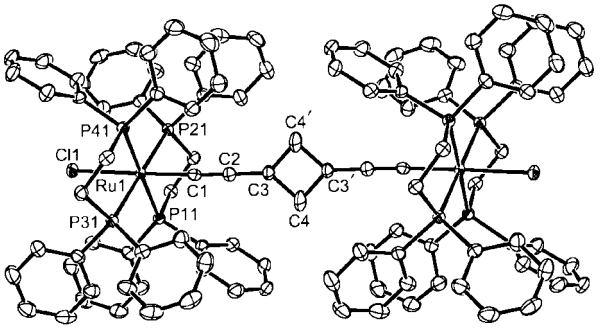

Fig. 1 Molecular structure of **3** (ORTEP view). Ellipsoids represent 50% probability level. Selected distances (Å) and angles (°): Ru(1)–C(1) 1.933(3), C(1)–C(2) 1.225(4), C(2)–C(3) 1.372(4), C(3)–C(4) 1.457(5), C(3)–C(4′) 1.459(5); C(1)–Ru(1)–Cl(1) 178.49(9), C(2)–C(1)–Ru(1) 174.4(2), C(1)–C(2)–C(3) 178.3(3), C(2)–C(3)–C(4) 134.2(3), C(3)–C(4)–C(3′) 88.3(3).

In order to account for the inversion centre, we should consider the occurrence of a fully delocalised system with a disorder between CH and CH_2. Indeed, Ru–C(1) (1.933 Å), C(2)–C(3) (1.372 Å) bonds are found to be shorter than the single bonds in an acetylenic system such as $[Cl(dppe)_2Ru–C{\equiv}C–C_6H_4NO_2)]$[8] (1.986 and 1.442 Å) and longer than the double bonds in an allenylidene system $[Cl(dppm)_2Ru{=}C{=}C{=}C(C_{14}H_{10})]PF_6$[6d] (1.852 and 1.393 Å). On the other hand the C(1)–C(2) bond length (1.225 Å) is intermediate between the values found in these mononuclear systems (1.206 and 1.255 Å, respectively) demonstrating a bond order between one and two for Ru(1)–C(1), C(1)–C(2), C(2)–C(3) bonds indicative of a hybrid structure.

The UV–VIS spectrum of the complex recorded in CH_2Cl_2 exhibits a strong charge transfer band (λ_{max} = 633 nm) with a high absorption coefficient (ε = 141 000 mol^{-1} L cm^{-1}) (ESI†). For comparison, the allenylidene compound $[ClRu(dppe)_2(=C=C=CPh_2)]PF_6$ shows a MLCT band at λ_{max} = 505 nm, ε = 18 000 mol^{-1} L cm^{-1}. The charge transfer is considerably more intense in the bimetallic compound and this can be best rationalized by the two canonical forms A and B. It is of note that **3** shows a stronger absorption than the related 'V' shaped compound $[CpRu(PPh_3)_2{=}C{=}C{=}CH–C{\equiv}C–Ru(PPh_3)_2Cp]BF_4$ (λ_{max} = 600 nm, ε = 72 000 mol^{-1} L cm^{-1}) which exhibits the same type of conjugation between the two remote metals.[3d,9] This is certainly due to the better planarity and rigidity of **3** and subsequent stronger conjugation. Cyclic voltammetry (CV) was used to investigate the electrochemical behaviour of **3** (CH_2Cl_2, $Bu^n_4NPF_6$ 0.1 M 200 mV s^{-1}). The binuclear compound undergoes a well defined one-electron reversible oxidation ($E°$ = 0.42 V *vs*. ferrocene) and an irreversible second oxidation at higher potential (E_{pa} = 0.91 *vs*. ferrocene). It also shows a one-electron reversible reduction ($E°$ = −1.48 V *vs*. ferrocene). The oxidation processes can be attributed to the successive oxidation of the two ruthenium centres[3d,6c,e] due to substantial electronic interaction between the metallic centres.[2] The reduction process can be attributed to the reduction of the C_8H_3 ligand.[3e,6b,e] Indeed, carrying out the reduction of complex **3** with cobaltocene[10] in a THF solution in a capped EPR tube allows the direct observation of the radical species **3**· which generates an intense and persistent feature at 293 K. A signal without detectable hyperfine structure is located in a characteristic region for organic radicals with g = 2.009. The electrochemical behaviour of **3** is in accord with that found for the related 'V' shaped compound $[CpRu(PPh_3)_2{=}C{=}C{=}CH–C{\equiv}C–Ru(PPh_3)_2Cp]BF_4$.[3d]

In summary, we have developed an easy method to prepare a bimetallic complex containing a novel C_8H_3 bridge with new interesting spectroscopic and structural properties. The unprecedented regioselectivity of the addition is explained by the steric hindrance of the bulky diphosphines with only the $C^{\gamma}{\equiv}C^{\delta}$ bond being reactive.[6] Despite the unfavourable potential, the reaction is likely initiated by an electron transfer between ferrocenium and **2** ($E°$ = 0.130 V *vs*. ferrocene) generating an electrophilic organometallic radical. The latter would be able to couple with another molecule of acetylide **2**. This mechanism (and the driving force) remains unverified but we anticipate that the resulting radical incorporates hydrogen atoms from the medium.[11]

We thank the CNRS and the Université de Rennes 1 for support, Drs P. Guenot and O. Maury for helpful discussion and M. Krueger (Erasmus student) for help.

Notes and references

1 For examples, see: R. Dembinski, T. Bartik, B. Bartik, M. Jaeger and J. A. Gladysz, *J. Am. Chem. Soc.*, 2000, **122**, 810; J. Gil-Rubio, M. Laubender and H. Werner, *Organometallics*, 2000, **19**, 1365; C. Hartbaum, Z. Mauz, G. Roth, K. Weissenbach and H. Fischer, *Organometallics*, 1999, **18**, 2619; K. T. Wong, J.-M. Lehn, S.-M. Peng and G.-H. Lee, *Chem. Commun.*, 2000, 2259.

2 F. Paul and C. Lapinte, *Coord. Chem. Rev.*, 1998, **178**–**180**, 431; B. Hong and J. V. Ortega, *Angew. Chem., Int. Ed.*, 1998, **37**, 15; A. M. McDonagh, M. G. Humphrey, M. Samoc, B. Luther-Davies, S. Houbrechts, T. Wada, H. Sasabe and A. Persoons, *J. Am. Chem. Soc.*, 1999, **121**, 1405.

3 (*a*) T. Bartik, W. Weng, J. A. Ramsden, S. Szafert, S. B. Falloon, A. M. Arif and J. A. Gladysz, *J. Am. Chem. Soc.*, 1998, **120**, 11 071; (*b*) R. Dembinski, S. Szafert, P. Haquette, T. Lis and J. A. Gladysz, *Organometallics*, 1996, **18**, 5438; (*c*) G. Jia, H. P. Xia, W. F. Wu and W. S. Ng, *Organometallics*, 1997, **16**, 1; (*d*) H. P. Xia, W. S. Ng, J. S. Ye, X. Y. Li, W. T. Wong, Z. Lin, C. Yang and G. Jia, *Organometallics*, 1999, **18**, 4552.

4 (*a*) T. Bartik, M. T. Johnson, A. M. Arif and J. A. Gladysz, *Organometallics*, 1995, **14**, 889; (*b*) H. Fischer, F. Leroux, G. Roth and R. Stumpf, *Organometallics*, 1996, **15**, 13 723; (*c*) H. Fischer, F. Leroux, R. Stumpf and G. Roth, *Chem. Ber.*, 1996, **129**, 1475; (*d*) F. Leroux, R. Stumph and H. Fischer, *Eur. J. Inorg. Chem.*, 1998, 1225.

5 N. E. Kolobova, T. V. Ozantseva, Y. T. Struchkov, A. S. Batsanoy and V. I. Bakhmutov, *J. Organomet. Chem.*, 1985, **292**, 247; N. Y. Kolokova, V. V. Skripkin, G. G. Alexandrov and Y. T. Struchkov, *J. Organomet. Chem.*, 1979, **169**, 293; W. Weng; J. R. Berenguer, J. Fornies, E. Lalind, F. Martinez, L. Sanchez and B. Serrano, *Organometallics*, 1998, **17**, 1640; R. M. Bullock, *J. Am. Chem. Soc.*, 1987, **109**, 8087.

6 (*a*) D. Touchard and P. H. Dixneuf, *Coord. Chem. Rev.*, 1998, **178**–**180**, 409; (*b*) S. Rigaut, O. Maury, D. Touchard and P. H. Dixneuf, *Chem. Commun.*, 2001, 373; (*c*) D. Touchard, P. Haquette, A. Daridor, A. Romero and P. H. Dixneuf, *Organometallics*, 1998, **17**, 3844; (*d*) N. Pirio, D. Touchard and P. H. Dixneuf, *Chem. Commun.*, 1991, 980; (*e*) R. F. Winter, *Eur. J. Inorg. Chem.*, 1999, 2121.

7 (*a*) *Crystal data* for **3**: $C_{112}H_{99}Cl_2F_6P_9Ru_2$, M = 2110.68, triclinic, space group $P\bar{1}$, a = 9.7811(10), b = 12.1069(14), c = 20.503(2) Å, α = 95.204(13), β = 98.910(12), γ = 101.264(13)°, U = 2334.0(4) Å^3, Z = 1, D_c = 1.500 Mg m^{-3}, Mo-Kα (λ = 0.71073), μ = 0.599 mm^{-1}, F(000) = 1079, Stoe IPDS diffractometer, T = 180(2) K, crystal size 0.24 × 0.16 × 0.08 mm, θ_{max} 24.20°, data/restraints/parameters ratio 6976/336/592, R = 0.0303, wR_2 = 0.0723 [5466 reflections with $F > 4\sigma(F_0)$], wR_2 = 0.0766 (all data), S = 0.958. CCDC 162902. See http://www.rsc.org/suppdata/cc/b1/b103301h/ for crystallographic data in CIF or other electronic format. (*b*) No H atoms could be located in the vicinity of C(4) which presents a thermal ellipsoid elongated perpendicular to the ring plane. Attempts to define a disorder model showing the possible occurrence of a C=C bond in the cycle failed.

8 M. Younus, N. J. Long, P. R. Raithby, J. Lewis, N. A. Page, A. J. P. White, D. J. Williams, M. C. B. Colbert, A. J. Hodge, M. S. Khan and D. G. Parker, *J. Organomet. Chem.*, 1999, **578**, 198.

9 The absorptions of the respective mononuclear allenylidenes present similar values of ε, see M. Tamm, T. Jentzsch and W. Werncke, *Organometallics*, 1997, **16**, 1424.

10 The potential of **3** is 150 mV negative to that of $[CoCp_2]$ (−1.33 V *vs*. ferrocene). However, the values are close enough to observe a slight displacement of the equilibrium and to detect the reduced species **3**· using EPR spectroscopy. See N. G. Connelly and W. E. Geiger, *Chem. Rev.*, 1996, **96**, 877.

11 It is likely that **2** is oxidized and further desilylation would lead to a radical species of type $Ru^{\cdot+}–C{\equiv}C–C{\equiv}CH \leftrightarrow Ru^{+}{=}C{=}C{=}C{=}CH^{\cdot}$ that can react with **2** [0.5 equiv. of oxidant is necessary, [2 + 2] coupling reaction]. The resulting cyclic radical would be desilylated and incorporate hydrogen atoms from the medium. It is of note that treatment of **2** with $CuCl_2$ or $FeCl_3$ also leads to **3** and that protonation of **2** with an acid (HBF_4) does not lead to **3** *via* a butatrienylidene intermediate.

CHEMCOMM
Communication
www.rsc.org/chemcomm

Preparation of carbonyltungsten(0) complexes of 2-chloro-3,3-diphenyl-1-(2,4,6-tri-*tert*-butylphenyl)-1,3-diphosphapropene

Shigekazu Ito and Masaaki Yoshifuji*

Department of Chemistry, Graduate School of Science, Tohoku University, Aoba, Sendai 980-8578, Japan. E-mail: yoshifj@mail.cc.tohoku.ac.jp

Received (in Cambridge, UK) 27th March 2001, Accepted 10th May 2001
First published as an Advance Article on the web 13th June 2001

(*Z*)-2-Chloro-3,3-diphenyl-1-(2,4,6-tri-*tert*-butylphenyl)-1,3-diphosphapropene was prepared from chlorodiphenylphosphine and 1-chloro-2-(2,4,6-tri-*tert*-butylphenyl)-2-phosphaethenyllithium and used for metal complex formation as a ligand to provide carbonyltungsten(0) complexes.

The 1,3-diphosphapropene system is an attractive ligand system for metal complex formation because two different types of phosphorus atoms are included within the system; *i.e.* a low-coordinated $\lambda^3\sigma^2$-phosphorus atom[1,2] and a common $\lambda^3\sigma^3$-phosphorus atom. However, research on coordination of the 1,3-diphosphapropene derivatives toward transition metals has been limited, whereas several metal complexes of η^3-1,3-diphosphaallyl ligands have been reported so far.[3,4] Indeed, the only reported example concerns the X-ray structural analysis of an iron(0) complex of 1,3-diphosphapropene prepared through an intramolecular cyclization of a bulky 1,3-diphosphaallene by ourselves.[5] There have been no reports on X-ray structural analysis of transition metal complexes of 1,3-diphosphapropene itself. Furthermore, the catalytic abilities of transition metal complexes of low-coordinated phosphorus compounds are of current interest,[6–10] and thus detailed study of the coordination chemistry of the 1,3-diphosphapropene system is crucial. Here we report the preparation and X-ray structural determination of carbonyltungsten complexes of a 1,3-diphosphapropene derivative kinetically stabilized by the 2,4,6-tri-*tert*-butylphenyl group (Mes*) including a selective coordination reaction of either the monodentate or chelate form.

A kinetically stabilized (*Z*)-1-chloro-2-(2,4,6-tri-*tert*-butylphenyl)-2-phosphaethenyllithium (*Z*-**1**) was prepared from 2,2-dichloro-1-(2,4,6-tri-*tert*-butylphenyl)-1-phosphaethene and butyllithium, and was allowed to react with chlorodiphenylphosphine (Scheme 1)[11] to afford the corresponding 2-chloro-1,3-diphosphapropene (*Z*-**2**) in good yield (78%) after silica-gel column chromatographic purification (hexane–toluene, v/v = 5/1). Compound *Z*-**2** was characterized spectroscopically.† In the ^{31}P NMR spectrum, a peak due to the P=C phosphorus atom appeared at low field (δ_P 302.4) with a large $^2J_{PP}$ value (277 Hz), suggesting an *E*-configuration. Similarly, starting from *E*-**1** and chlorodiphenylphosphine,[11a] an attempt was made to prepare *E*-**2**. Although NMR signals due to *E*-**2** were observed in the reaction mixture (δ_P 325.1, 3.0, $^2J_{PP}$ 15 Hz), *E*-**2** was isomerized to *Z*-**2** after the usual work-up procedure, probably due to large repulsion between the Mes* group and the Ph_2P group.

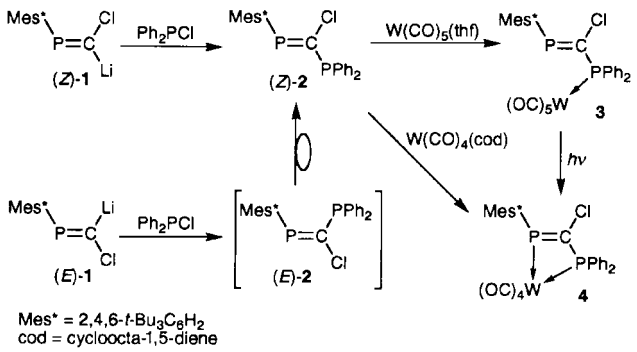

Scheme 1

Next we investigated the coordination property of *Z*-**2** towards tungsten(0). Initially, *Z*-**2** was allowed to react with an equivalent amount of $W(CO)_5$(thf) for 6 h at room temperature to afford the corresponding pentacarbonyltungsten(0) complex **3** in 39% yield as yellow prisms after recrystallisation from hexane (Scheme 1).‡ The coordination on tungsten seemed to occur at the Ph_2P phosphorus atom as suggested by a satellite signal due to the tungsten atom in the ^{31}P NMR spectrum of **3**. The reason for this type of coordination might be explicable taking the stronger basicity of the Ph_2P group into account,[12] while Bertrand and coworkers reported an NMR study to suggest the coordination at the low-coordinated $\lambda^3\sigma^2$-phosphorus atom in a 1,3-diphosphapropene system.[4] In the ^{13}C NMR spectrum, the chemical shift of the P=C carbon atom is similar to that for *Z*-**2**, but the two $^1J_{PC}$ values are quite different (79 and 4 Hz) indicating low electronic interaction between the PPh_2 group and the P=C carbon atom. The structure of **3** was unambiguously determined by X-ray crystallography and Fig. 1 displays an ORTEP drawing.§ The P2–W distance is 2.540(1) Å, which is similar to that for $W(CO)_5(PPh_3)$ [2.545(1) Å].[13] The P1–C(1) distance is 1.675(4) Å, which is a normal value for the P=C bond.[1] The P1, P2, C1, Cl, W atoms are almost coplanar and the tungsten atom is located on the same side of lone pairs of the P1 atom with a P1···W distance of 3.97 Å. Complex **3** did not react with an excess amount of $W(CO)_5$(thf) to afford the bis-tungsten complex, probably due to steric congestion around the P=C phosphorus atom.[4]

The structure of **3** indicates that *Z*-**2** is a good chelating ligand, and therefore we tried to prepare a chelate complex of *Z*-**2** by use of $W(CO)_4$(cod) (cod = cycloocta-1,5-diene) at room

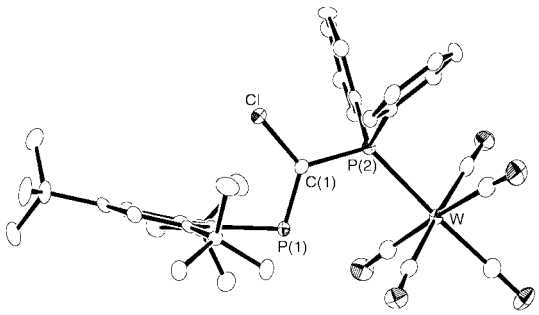

Fig. 1 An ORTEP drawing of **3** with 50% probability ellipsoids. Hydrogen atoms are omitted for clarity. Bond lengths (Å) and angles (°): W–P(2) 2.540(1), C(1)–Cl 1.740(4), P(1)–C(1) 1.675(4), P(1)–C_{ipso}(Mes*) 1.840(4), C(1)–P(2) 1.829(4), P(2)–C_{ipso}(Ph) 1.828(4), P(2)–C_{ipso}(Ph′) 1.835(4); C(1)–P(1)–C_{ipso}(Mes*) 103.1(2), W–P(2)–C(1) 119.3(1), W–P(2)–C_{ipso}(Ph) 110.6(1), W–P(2)–C_{ipso}(Ph′) 116.5(1), C(1)–P(2)–C_{ipso}(Ph) 104.6(2), C(1)–P(2)–C_{ipso}(Ph′) 99.8(2), C_{ipso}(Ph)–P(2)–C_{ipso}(Ph′) 104.3(2), Cl–C(1)–P(1) 124.9(2), Cl–C(1)–P(2) 115.4(2), P(1)–C(1)–P(2) 119.2(2).

 DOI: 10.1039/b102810n

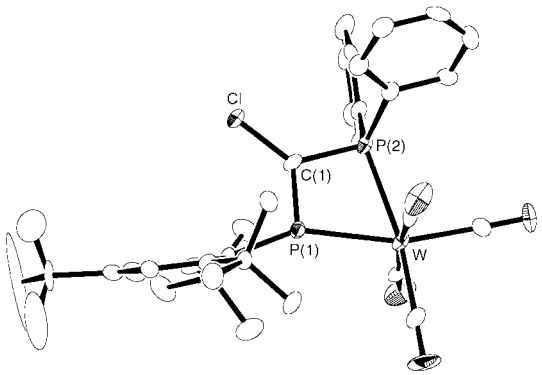

Fig. 2 An ORTEP drawing of **4** with 50% probability ellipsoids. Hydrogen atoms are omitted for clarity. Bond lengths (Å) and angles (°): W–P(1) 2.489(3), W–P(2) 2.526(3), C(1)–Cl 1.73(1), P(1)–C(1) 1.651(10), P(1)–C_{ipso}(Mes*) 1.82(1), C(1)–P(2) 1.82(1), P(2)–C_{ipso}(Ph) 1.83(1), P(2)–C_{ipso}(Ph′) 1.81(1), C(1)–P(1)–C_{ipso}(Mes*) 108.6(5), P(1)–W–P(2) 65.1(1), W–P(2)–C(1) 93.5(3), W–P(1)–C(1) 99.4(4), W–P(1)–C_{ipso}(Mes*) 152.0(3), W–P(2)–C_{ipso}(Ph) 115.6(4), W–P(2)–C_{ipso}(Ph′) 127.6(4), C(1)–P(2)–C_{ipso}(Ph) 109.7(5), C(1)–P(2)–C_{ipso}(Ph′) 104.5(5), C_{ipso}(Ph)–P(2)–C_{ipso}(Ph′) 103.9(5), Cl–C(1)–P(1) 131.2(6), Cl–C(1)–P2 126.8(6), P(1)–C(1)–P(2) 101.8(5).

temperature. After 12 h, **4** was obtained in 19% yield as red crystals together with 63% recovery of *Z*-**2**, after purification by gel permeation chromatographic separation (Scheme 1).‡ A trace amount of **4** was also obtained by the reaction of *Z*-**2** and $W(CO)_5$(thf). In the ^{31}P NMR spectrum of **4**, a peak due to the P=C phosphorus atom is observed at a higher field than that for *Z*-**2**, and both of the two phosphorus atoms show satellite peaks due to the presence of the tungsten atom. Moreover, the coupling constant between the P=C phosphorus and the tungsten (213 Hz) is reasonable for a complex with an end-on coordinating mode.[14] On the other hand, Appel and coworkers reported a side-on coordination with Fe(0) on the P=C moiety in the 1,3-diphosphapropene system.[3] In the ^{13}C NMR spectrum of **4**, a peak due to the P=C carbon atom has a higher chemical shift than that for *Z*-**2**, and the two $^1J_{PC}$ values are small (23 and 9 Hz). Two different chemical shifts were observed for CO_{eq} carbons together with two different $^2J_{PC}$ values, probably due to the coordination by two different types of phosphorus atoms. The structure of **4** was unambiguously determined by X-ray crystallography and Fig. 2 depicts an ORTEP drawing.§ The P=C phosphorus atom coordinates in the end-on mode which leads to a large $^1J_{PW}$ value in the NMR spectrum. The P1–W distance [2.489(3) Å] is shorter than the P2–W distance [2.526(3) Å], and the P1–C(1) distance [1.651(10)] is normal for the P=C bond. The P1–W–P2 angle is small with a value of 65.1(1)°. The P1–C(1)–P2 and C(1)–P2–W angles, 93.5(3) and 101.8(5)°, respectively, are smaller than the corresponding angles for **3**.

Chelate complex **4** was also derived by photo-irradiation of **3**. A THF solution of **3** was irradiated with a medium-pressure mercury lamp at 5 °C for 16 h in an NMR tube to afford **4** almost quantitatively. No *E*/*Z* isomerization of **3** was observed probably due to the steric hindrance between the Mes* and Ph_2P moieties.[15]

Compound **2** contains a chlorine atom at the sp^2-carbon atom which can potentially be substituted. We are now attempting to prepare various types of 1,3-diphosphapropenes from **2**, as well as metal complexes of the type **3** and **4**.

This work was supported in part by a Grant-in-Aid for Scientific Research (No. 12042208) from the Ministry of Education, Science, Sports and Culture, Japan.

Notes and references

† *NMR data* for **2**: ^{1}H NMR (200 MHz, $CDCl_3$) δ 7.4–7.5 (4H, arom.), 7.3–7.4 (8H, arom.) 1.41 (18H, *o*-Bu^t), 1.31 (9H, *p*-Bu^t); ^{13}C{^{1}H} NMR (50 MHz, $CDCl_3$) δ 169.0 (dd, $^1J_{PC}$ 72, $^1J_{PC}$ 54 Hz, P=C), 153.2 (d, $^2J_{PC}$ 2 Hz, *o*-Mes*), 150.8 (*p*-Mes*), 136.2 (dd, $^1J_{PC}$ 62, $^3J_{PC}$ 27 Hz, *ipso*-Mes*), 135.8 (dd, $^1J_{PC}$ 16, $^3J_{PC}$ 11 Hz, *ipso*-Ph), 133.6 (d, $^2J_{PC}$ 20 Hz, *o*-Ph), 128.8 (*p*-Ph), 122.0 (*m*-Mes*), 37.8 (d, $^3J_{PC}$ 1 Hz, *o*-CMe_3), 35.1 (*p*-CMe_3), 32.9 (d, $^4J_{PC}$ 7 Hz, *o*-CMe_3), 31.4 (*p*-CMe_3); ^{31}P{^{1}H} NMR (81 MHz, $CDCl_3$) δ 302.4 (P=C), 13.4 (PPh_2), $^2J_{PP}$ 277 Hz.

‡ *Spectroscopic data*: for **3**: yellow prisms (hexane), mp 196–198 °C (decomp.); ^{1}H NMR (200 MHz, $CDCl_3$) δ 7.6–7.7 (4H, arom.), 7.4–7.5 (6H, arom.), 7.36 (2H, d, $^4J_{PH}$ 2 Hz, *m*-Mes*), 1.35 (18H, *o*-Bu^t), 1.29 (9H, *p*-Bu^t); ^{13}C{^{1}H} NMR (50 MHz, $CDCl_3$) δ 199.3 (d, $^2J_{PC}$ 23 Hz, CO_{ax}), 197.0 (dd, $^2J_{PC}$ 7, $^2J_{PC}$ 7 Hz, CO_{eq}), 163.5 (dd, $^1J_{PC}$ 79, $^1J_{PC}$ 4 Hz, P=C), 153.3 (d, $^2J_{PC}$ 3 Hz, *o*-Mes*), 151.3 (*p*-Mes*), 135.1 (dd, $^1J_{PC}$ 61, $^3J_{PC}$ 18 Hz, *ipso*-Mes*), 134.5 (dd, $^1J_{PC}$ 44, $^3J_{PC}$ 10 Hz, *ipso*-Ph), 132.7 (d, $^2J_{PC}$ 12 Hz, *o*-Ph), 130.2 (d, $^4J_{PC}$ 2 Hz, *p*-Ph), 128.6 (d, $^3J_{PC}$ 10 Hz, *m*-Ph), 122.3 (*m*-Mes*), 37.5 (*o*-CMe_3), 35.0 (*p*-CMe_3), 32.6 (d, $^4J_{PC}$ 7 Hz, *o*-CMe_3), 31.2 (*p*-CMe_3); ^{31}P{^{1}H} NMR (81 MHz, $CDCl_3$) δ 328.0 (P=C), $^1J_{PW}$ 187 Hz, 34.2 (PPh_2), $^2J_{PP}$ 187 Hz; IR (KBr) ν 2071, 1988, 1936, 1919 cm^{-1}, FAB-MS *m*/*z* 804 (M^+ − CO; 53%), 692 (M^+ −5CO; 79%), 275 (Mes*P$^+$ − 1; 100%). Anal. Calc. for $C_{36}H_{39}ClO_5P_2W$: C, 51.91; H, 4.72; Cl, 4.26. Found: C, 51.92; H, 4.78; Cl, 4.30%. For **4**: red prisms (hexane), mp 220–222 °C (decomp.); ^{1}H NMR (200 MHz, $CDCl_3$) δ 7.6–7.7 (4H, arom.), 7.4–7.5 (8H, arom.), 1.61 (18H, *o*-Bu^t), 1.34 (9H, *p*-Bu^t); ^{13}C{^{1}H} NMR (50 MHz, $CDCl_3$) δ 208.4 (dd, $^2J_{PC}$ 36, $^2J_{PC}$ 6 Hz, CO_{eq}), 207.7 (dd, $^2J_{PC}$ 25, $^2J_{PC}$ 12 Hz, CO_{eq}), 203.2 (dd, $^2J_{PC}$ 10, $^2J_{PC}$ 7 Hz, CO_{ax}), 156.4 (dd, $^1J_{PC}$ 23, $^1J_{PC}$ 9 Hz, P=C), 155.6 (d, $^2J_{PC}$ 2 Hz, *o*-Mes*), 153.6 (d, $^4J_{PC}$ 2 Hz, *p*-Mes*), 132.5 (d, $^2J_{PC}$ 14 Hz, *o*-Ph), 131.5 (dd, $^1J_{PC}$ 38, $^3J_{PC}$ 16 Hz, *ipso*-Ph), 130.9 (d, $^4J_{PC}$ 2 Hz, *p*-Ph), 130.8 (d, $^3J_{PC}$ 11 Hz, *m*-Ph), 125.7 (dd, $^1J_{PC}$ 26, $^3J_{PC}$ 26 Hz, *ipso*-Mes*), 122.5 (d, $^3J_{PC}$ 6 Hz, *m*-Mes*), 38.3 (d, $^3J_{PC}$ 1 Hz, *o*-CMe_3), 35.3 (d, $^5J_{PC}$ 1 Hz, *p*-CMe_3), 33.2 (d, $^4J_{PC}$ 3 Hz, *o*-CMe_3), 31.0 (*p*-CMe_3); ^{31}P{^{1}H} NMR (81 MHz, $CDCl_3$) δ 263.7 (P=C), $^1J_{PW}$ 213 Hz, 19.1 (PPh_2), $^1J_{PW}$ 202 Hz, $^2J_{PP}$ 116 Hz; IR (KBr) ν 2019, 1923, 1903, 1890 cm^{-1}, FAB MS *m*/*z* 804 (M^+; 59%), 692 (M^+ − 4CO; 96%), 275 (Mes*P$^+$ − 1; 90%), 154 (PhPCCl$^+$ − 1; 100%). Anal. Calc. for $C_{35}H_{39}ClO_4P_2W$: C, 52.23; H, 4.88; Cl, 4.40. Found: C, 52.50; H, 4.95; Cl, 4.52%.

§ *Crystal data*: for **3**: $C_{36}H_{39}ClO_5P_2W$, M = 832.95, monoclinic, $P2_1/c$ (no. 14), a = 10.062(5), b = 25.244(3), c = 13.845(2) Å, β = 93.920(3)°, V = 3508(1) Å^3, Z = 4, D_c = 1.577 g cm^{-3}, μ = 3.504 mm^{-1}, T = 120(1) K, $2\theta_{max}$ = 50.1°, 5861 total reflections, 5487 observed reflections [$I > 1\sigma(I)$], $R1$ = 0.031, R_w = 0.073, S = 0.96 for 562 parameters, CCDC 159934.

For **4**: $C_{35}H_{39}ClO_4P_2W$, M = 804.94, orthorhombic, $P2_12_12_1$ (no. 19), a = 16.687(2), b = 21.984(3), c = 9.310(3) Å, V = 3415(1) Å^3, Z = 4, D_c = 1.565 g cm^{-1}, μ = 3.594 mm^{-1}, T = 125(1) K, $2\theta_{max}$ = 50.1°, 3318 total reflections, 3132 observed reflections [$I > 2\sigma(I)$], $R1$ = 0.049, R_w = 0.110, S = 1.27 for 389 parameters, CCDC 159933.

See http://www.rsc.org/suppdata/cc/b1/b102810n/ for crystallographic data in CIF or other electronic format.

1 M. Regitz and O. J. Scherer, *Multiple Bonds and Low Coordination in Phosphorus Chemistry*, Georg Thieme Verlag, Stuttgart, 1990; K. B. Dillon, F. Mathey and J. F. Nixon, *Phosphorus: The Carbon Copy*, John Wiley & Sons, Chichester, 1998.

2 M. Yoshifuji, I. Shima, N. Inamoto, K. Hirotsu and T. Higuchi, *J. Am. Chem. Soc.*, 1981, **103**, 4587; M. Yoshifuji, I. Shima, N. Inamoto, K. Hirotsu and T. Higuchi, *J. Am. Chem. Soc.*, 1982, **104**, 6167.

3 R. Appel and W. Schuhn, *J. Organomet. Chem.*, 1987, **329**, 179.

4 D. Bourissou, Y. Canac, M.-I. Collado, A. Baceiredo and G. Bertrand, *Chem. Commun.*, 1997, 2399; D. Bourissou, Y. Canac, H. Gornitzka, C. J. Marsden, A. Baceiredo and G. Bertrand, *Eur. J. Inorg. Chem.*, 1999, 1479.

5 C. A. Akpan, P. B. Hitchcock, J. F. Nixon, M. Yoshifuji, T. Niitsu and N. Inamoto, *J. Organomet. Chem.*, 1988, **338**, C35.

6 W. Keim, R. Appel, S. Gruppe and F. Knoch, *Angew. Chem., Int. Ed. Engl.*, 1987, **26**, 1012.

7 K. Toyota, K. Masaki, T. Abe and M. Yoshifuji, *Chem. Lett.*, 1995, 221.

8 B. Breit, *J. Mol. Catal. A*, 1999, **143**, 143.

9 R. Shintani, M. M.-C. Lo and G. C. Fu, *Org. Lett.*, 2000, **2**, 3695.

10 S. Ikeda, F. Ohhata, M. Miyoshi, R. Tanaka, T. Minami, F. Ozawa and M. Yoshifuji, *Angew. Chem., Int. Ed.*, 2000, **39**, 4512.

11 (*a*) M. Yoshifuji, S. Ito, K. Toyota and M. Yasunami, *Bull. Chem. Soc. Jpn.*, 1995, **68**, 1206; (*b*) M. van der Sluis, F. Bickelhaupt, N. Neldman, H. Kooijman, A. L. Spek, W. Eisfeld and M. Regitz, *Chem. Ber.*, 1995, **128**, 465.

12 T. C. Klebach, R. Lourens and F. Bickelhaupt, *J. Organomet. Chem.*, 1981, **210**, 211.

13 M. J. Aroney, I. E. Buys, M. S. Davies and T. W. Hambley, *J. Chem. Soc., Dalton Trans.*, 1994, 2827.

14 M. Yoshifuji, *Bull. Chem. Soc. Jpn.*, 1997, **70**, 2881.

15 M. Yoshifuji, K. Toyota and N. Inamoto, *Tetrahedron Lett.*, 1985, **26**, 1727.

CHEMCOMM Communication
www.rsc.org/chemcomm

The first polymer with a fluorosilicate backbone and a non-polar shell

Rudolf Pietschnig* and Klaus Merz

Lehrstuhl für Anorganische Chemie I, Ruhr-Universität Bochum, Universitätsstraße 150, 44780 Bochum, Germany. E-mail: rudolf.pietschnig@ruhr-uni-bochum.de

Received (in Cambridge, UK) 28th March 2001, Accepted 22nd May 2001
First published as an Advance Article on the web 14th June 2001

A novel type of linear inorganic–organic hybridic polymer is presented in which terphenyl ligands are covering the inorganic backbone, providing it with a non-polar coating.

Over recent years coordination polymers have attracted considerable interest.[1] Besides their properties and potential application,[2] controlling the self organisation of the monomeric units to build one or higher dimensional frameworks has been a major achievement in this fascinating research area.[3] Most of these inorganic–organic hybrid materials are constructed from metal cations connected by organic ligands, forming a hybrid inorganic–organic backbone.[4] There are also examples of coordination polymers with a completely inorganic backbone showing a wealth of different coordination modes.[5]

Several examples of crystal structures of organo-tetrafluorosilicates are known to date.[6–8] In all of these structures the anions show no direct interaction with more than one counter-cation. Organofluorosilicates with a potassium counter-cation are usually destabilized due to potassium–fluorine interactions. These interactions can be minimised by complexation of the cation with 18-crown-6[7] or completely removed with [2,2,2]-cryptand.[8]

Earlier we reported[9] a globular-terphenyl substituted fluorosilicate in which both tetra- and penta-fluoro silicate units are interconnected in a network built together by the counter-cation interaction. Herein we report the first inorganic fluorosilicate based coordination polymer enveloped by a non-polar organic shell, starting from a multidentate ligand site offering steric control. In order to investigate the balance between electrophilicity and steric protection of the silicon centre in such compounds, we allowed 2,6-dimesitylphenyl trifluorosilane **1** to react with an excess of KF. We exclusively observed the formation of the terphenyl tetrafluorosilicate **2** (Scheme 1) and the product adopts a one dimensional polymeric structure in the solid state (see Fig. 1). To our knowledge this is the first

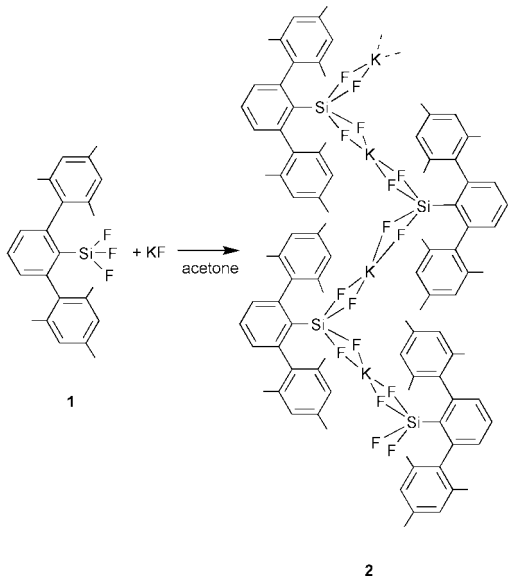

Scheme 1 Synthesis of **2**.

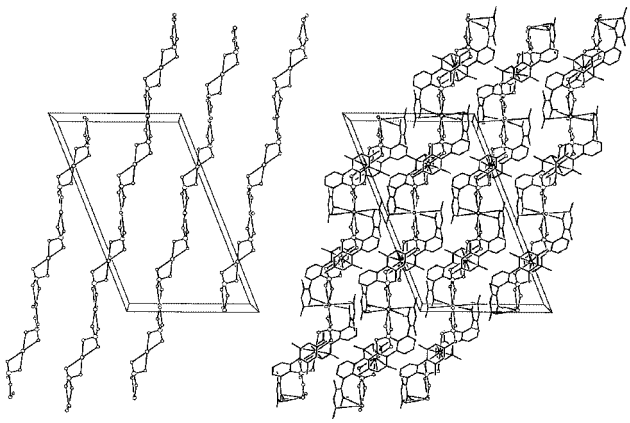

Fig. 1 Inorganic backbone of **2** with (right) and without (left) ligand shell.

structurally characterised potassium organo–tetrafluorosilicate polymer. The interaction of the counter ions leads to association forming a K–F–Si–F–K type of a linear coordination polymer.

Under stoichiometric conditions 2,6-dimesitylphenyl tetrafluorosilicate **2** can be readily synthesised† from the corresponding trifluorosilane **1** and KF. It is a one dimensional coordination polymer the structure of which has been established by X-ray diffraction analysis (see Fig. 2).‡ Polymer **2** is built by organo-tetrafluorosilicate units each of which acts as a bidentate ligand towards two potassium ions. The potassium cations are surrounded by fluorine atoms forming a square planar coordination environment. The axial positions above and below the potassium are occupied by the mesityl substituent of the organic ligand. Additionally one molecule of acetone is present in the coordination sphere of every second potassium ion.

The inorganic backbone consists of four membered SiF_2K rings which are spiro connected at the silicon and the potassium centres. The zig-zag arrangement of the inorganic backbone is shielded by the organic terphenyl ligands attached to each silicon atom. The bulky aryl ligands prevent extensive coordination of solvent to the potassium centres, which instead interact with the π-systems of the mesityl rings of the terphenyl system. This interaction of the cation with the organic shell

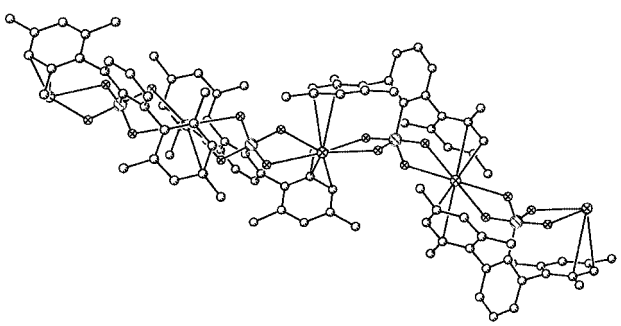

Fig. 2 Detail of the structure of **2**.

 DOI: 10.1039/b102853g

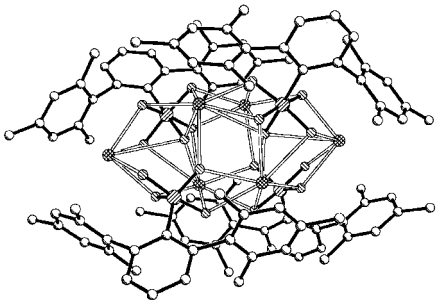

Fig. 3 Crystal structure of **3**.[9]

seems to be crucial for the stability of the polymer, and despite some effort we have not been able to observe similar structures with smaller alkali metal ions.

These findings are in good accordance with previous observations that, due to their preference for increased coordination numbers, the larger alkali metal cations have a tendency to participate in the formation of higher aggregates than smaller alkali metal cations,[10] even though the cation π-system stabilisation energies are smaller for potassium than those observed for lithium.[11,12] The K–C distances in **2** (3.1–3.5 Å) fall in the normal range of such interactions.[6]

The linear polymer **2** is somewhat related to a structural isomer **3** which however shows no polymeric structure but does start a fluorosilicate network in which a globular inorganic core is covered by a shell of organic terphenyl ligands (see Fig. 3).[9] This globular adduct is formed under different kinetic conditions than **2**. The chain **2** forms when both starting materials, dimesitylphenyl trifluorosilane and potassium fluoride, are present in equal concentration in the reaction mixture. In contrast the formation of the globular system **3** is characterised by a large excess of the bulky trifluorosilane in the presence of a small concentration of potassium fluoride. The latter is continuously formed in the course of a slow reductive process.[9] This illustrates how delicately the reaction parameters control the resulting architecture of the polymer. Starting with identical components and controlling reaction conditions globular **3** or linear arrangement **2** can be obtained.

The structure of **2** is not retained in solution as indicated by NMR studies. In acetone solution the coordination polymer dissociates into two species as indicated by ^{19}F-NMR. The main signal at −113.3 ppm is sharp and shows ^{29}Si satellites (214 Hz), while a minor signal at –127.3 ppm is relatively broad ($\nu_{1/2}$ = 30 Hz) probably due to chemical exchange. Simple ^{29}Si-NMR experiments are hampered by the fact that the expected fluorosilicates show their resonance in the same region as the broad resonance of the glass peak of the NMR tube. Moreover the Si–H coupling constants and the number of protons that are close enough to be used for INEPT or DEPT experiments are to small for this purpose. However, with ^{1}H{^{29}Si}-2D-HMQC experiments we have been able to observe ^{29}Si spectra and to assign the data to the respective dissociation products. The predominant species shows a ^{29}Si signal at −123 ppm ($^{1}J_{SiF}$ = 214 Hz) and can be assigned to the monomeric $Mes_2C_6H_3SiF_4^-$ ion. For comparison $PhSiF_4^-$ shows a ^{29}Si resonance at −126 ppm. The ^{29}Si resonance of the other dissociation product appears at −59 ppm (J_{SiF} = 249 Hz), but due to the low signal intensity the multiplet cannot be unambiguously assigned. It should be mentioned that the dissociation process in solution is reversible and the linear polymer **2** forms again on evaporation of the solvent.

For similar reasons as in solution the presence of proton and fluorine nuclei and their dipolar interaction with the silicon nucleus interferes with conventional CP-MAS NMR techniques. More sophisticated experiments with observation of ^{29}Si with simultaneous decoupling of ^{19}F and ^{1}H are in progress. Due to the complexity of these experiments, their results will be reported in context with monomeric organofluorosilanes elsewhere in the future.

We thank PD Dr. Dietrich Gudat (University of Bonn) for recording the HMQC NMR spectra and Prof. Matthias Drieß for intellectual and financial support. Funding for R. P. by the Fonds der Chemischen Industrie (Liebig-fellowship) is gratefully acknowledged.

Notes and references

† Synthesis of **2**: $Mes_2C_6H_3SiF_3$[9] (0.80 g, 2 mmol) is dissolved in acetone (10 mL) and potassium fluoride (0.12 g, 2 mmol) is added to this solution at room temperature. The mixture is heated to reflux giving a clear solution. After cooling to room temperature the solvent is slowly evaporated and **2** is obtained as colourless crystals which can be separated by filtration (0.76 g, 82.6%). Elemental analysis calc. (%) for $C_{51}H_{56}F_8K_2OSi_2$: C: 63.06, H: 5.81; found: C: 63.29, H: 5.54. ^{19}F-NMR (acetone-d_6): −113.3 ppm, ^{29}Si-NMR (acetone-d_6): −123 ppm ($^{1}J_{SiF}$ = 214 Hz).

‡ *Crystal data* for **2**: Formula = $C_{51}H_{56}F_8K_2OSi_2$, M = 971.34, monoclinic, space group $C2/c$; a = 27.63(2) Å; b = 11.432(12) Å; c = 17.03(2) Å; β = 111.50(4)°; V = 5005(10) Å^3; Z = 8; D_c = 1.289 Mg m^{-3}; λ = 0.71073 Å; reflections collected/unique 12806/4429; $R1$ = 0.0556, $wR2$ = 0.1121.

CCDC reference number 164463. See http://www.rsc.org/suppdata/cc/b1/b102853g/ for crystallographic data in CIF or other electronic format.

1 A. J. Blake, N. R. Champness, P. Hubberstey, W.-S. Li, M. A. Withersby and M. Schröder, *Coord. Chem. Rev.*, 1999, **183**, 117; A. Clearfield, *Prog. Inorg. Chem.*, 1998, **47**, 371; R. P. Kingsborough and T. M. Swager, *Prog. Inorg. Chem.*, 1999, **48**, 123; J. P. Sauvage, *Transition Metals in Supramolecular Chemistry*, Wiley, Chichester, 1999; C. Janiak, *Angew. Chem., Int. Ed. Engl.*, 1997, **36**, 1431.

2 O. M. Yaghi, G. li and H. Li, *Nature*, 1995, **378**, 703; D. B. Mitzi, S. Wang, C. A. Field, C. A. Chess and A. M. Guloy, *Science*, 1995, **267**, 1473; J. S. Miller and A. J. Epstein, *Chem. Commun.*, 1998, 1319.

3 T. L. Hennigar, D. C. MacQuarrie, P. Losier, R. D. Rogers and M. J. Zaworotko, *Angew. Chem., Int. Ed. Engl.*, 1997, **36**, 972; M. J. Zaworotko, *Chem. Soc. Rev.*, 1994, 283.

4 J. P. Sauvage, J.-P. Collin, J.-C. Chambron, S. Guillerez, C. Coudret, V. Balzani, F. Barigelletti, L. De Cola and L. Flamigni, *Chem. Rev.*, 1994, **94**, 993; V. Balzani, A. Juris, M. Venturi, S. Campagna and S. Serroni, *Chem. Rev.*, 1996, **96**, 759.

5 W. S. Sheldrick and I. M. Müller, *Coord. Chem. Rev.*, 1998, **182**, 125.

6 R. R. Holmes, *Chem. Rev.*, 1996, **96**, 927; C. Chuit, R. J. P. Corriu, C. Reye and J. C. Young, *Chem. Rev.*, 1993, **93**, 1371.

7 S. E Johnson, R. O. Day and R. R. Holmes, *Inorg. Chem.*, 1989, **28**, 3182; C. Brelière, F. H. Carré, R. J. P. Corriu, W. E. Douglas, M. Poirier, G. Royo and M. Wong Chi Man, *Organometallics*, 1992, **11**, 1586; K. Tamao, T. Hayashi, Y. Ito and M. Shiro, *Organometallics*, 1992, **11**, 2099.

8 S. Yamaguchi, S. Akiyama and K. Tamao, *Organometallics*, 1999, **18**, 2851.

9 R. Pietschnig, D. R. Powell and R. West, *Organometallics*, 2000, **19**, 2724.

10 C. Schade and P. R. Schleyer, *Adv. Organomet. Chem.*, 1987, **27**, 169.

11 R. H. Staley and J. L. Beauchamp, *J. Am. Chem. Soc.*, 1975, **97**, 5920.

12 J. Sunner, K. Nishizawa and P. Kebarle, *J. Phys, Chem.*, 1981, **85**, 181.

CHEMCOMM
Communication
www.rsc.org/chemcomm

Novel, covalently bonded hybrid materials of europium (terbium) complexes with silica

H. R. Li, J. Lin,* H. J. Zhang,* H. C. Li, L. S. Fu and Q. G. Meng

Key Lab of Rare Earth Chemistry and Physics, Changchun Institute of Applied Chemistry, Chinese Academy of Sciences, Changchun 130022, P. R. China. E-mail: jlin@ns.ciac.jl.cn. E-mail: hongjie@ns.ciac.jl.cn

Received (in Cambridge, UK) 7th March 2001, Accepted 14th May 2001
First published as an Advance Article on the web 6th June 2001

New kinds of hybrid materials containing covalently bonded Eu^{3+} (Tb^{3+}) bipyridine complexes in a silica network have been prepared and their luminescence properties reported.

The sol–gel method has been proven to be a suitable approach for the preparation of hybrid materials. One advantage of this method is its low processing temperature, allowing the incorporation of organic moieties that cannot withstand high temperatures into the networks.[1,2] Unfortunately, there are significant drawbacks in using these systems, which include inhomogeneous distribution of both components, leaching of dopants and limitations on the concentrations of dopants used. Covalent grafting of ligands on to the backbone of networks *via* Si–C bonds can greatly overcome the above-mentioned shortcomings.[3,4]

Herein, we present a new compound (denoted as bipyridine–Si) for sol–gelcontaining bipyridine, which plays a double role, *i.e.* as a ligand for lanthanide ions and as a sol–gel precursor. The hybrid luminescent materials were prepared using bipyridine–Si as one of the precursors, which reacted with the tetraethoxysilane (TEOS) by hydrolysis and condensation in the presence of lanthanide ions (see Scheme 1).

The IR spectra for 2,2′-bipyridine-4,4′-dicarboxylic acid (**I**), bipyridine–Si (**II**) and the hybrid material doped with Eu^{3+} (**III**) are shown in Fig. 1(A, B, C), respectively.‡ The absorption band at 1713 cm^{-1} in Fig. 1A corresponds to the asymmetric carbonyl stretch of carboxylic acid. This band is replaced by bands at 1653 and 1638 cm^{-1} due to the absorption of amide groups (CONH) in Fig. 1B and Fig. 1C, respectively, indicating that (3-aminopropyl)triethoxysilane (APS) has been successfully grafted on to 2,2′-bipyridine. Further evidence for this is the presence of the stretching ν(NH, 3379 cm^{-1}) and bending δ(NH, 1542 cm^{-1}) vibration modes, together with the stretching vibration of Si–O at 1094 cm^{-1} and the bending vibration of Si–O at 462 cm^{-1} (from APS) in Fig. 1B. The addition of Eu^{3+}, TEOS and water to bipyridine–Si (**II**) is also responsible for changes in the IR spectra (*cf.* Fig. 1C and Fig. 1B) due to hydrolysis/condensation of TEOS and bipyridine–Si (**II**) together with formation of a complex between Eu^{3+} and bipyridine–Si (**II**). The ν(Si–C) vibration located at 1198 cm^{-1} is still observed in the IR spectra of hybrid materials (Fig. 1C), which is consistent with the fact that no (Si–C) bond cleavage occurs during hydrolysis/condensation reactions. Furthermore, in Fig. 1C the broad absorption band at 1087 cm^{-1}, ν(Si–O–Si), indicates the formation of siloxane bonds.

The excitation spectrum monitored using the Eu^{3+} $^5D_0$–$^7F_2$ transition at 614 nm is dominated by a broad band centered at 336 nm, which is the characteristic absorption of the ligands due to their efficient $\pi \rightarrow \pi^*$ transition. This indicates that an energy transfer occurs from the ligands to the central Eu^{3+}. Upon excitation at the ligands (336 nm), only the emission lines of Eu^{3+} $^5D_0$–^7F_J (J = 0,1,2,3,4) were observed with the hypersensitive transition $^5D_0$–$^7F_2$ (614 nm) as the most prominent group; no emission from the ligands was detected, suggesting that the energy transfer from the ligands to Eu^{3+} is efficient in the hybrid sample. However, when the excitation is at 396 nm (*i.e.* at the $^7F_0$–$^5L_6$ absorption band of Eu^{3+}), the obtained emission spectrum contains not only the emission of Eu^{3+}, but also a broad emission band in the blue region with a maximum at 458 nm. Apparently, the red emission of Eu^{3+} produced in

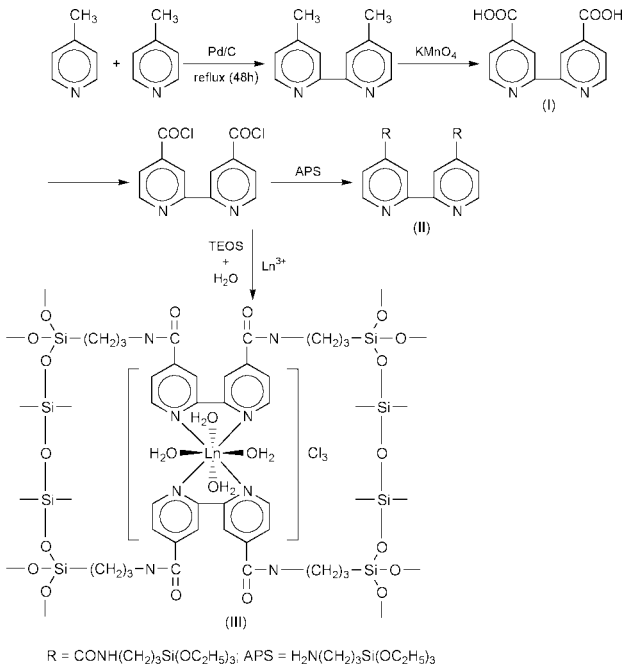

Scheme 1 Synthesis procedure of bipyridine–Si and the predicted structure of hybrid materials.

† Electronic supplementary information (ESI) available: Excitation (A) and emission (B, C) spectra of hybrid materials in Scheme 1 (Ln = Eu). See http://www.rsc.org/suppdata/cc/b1/b102160p/

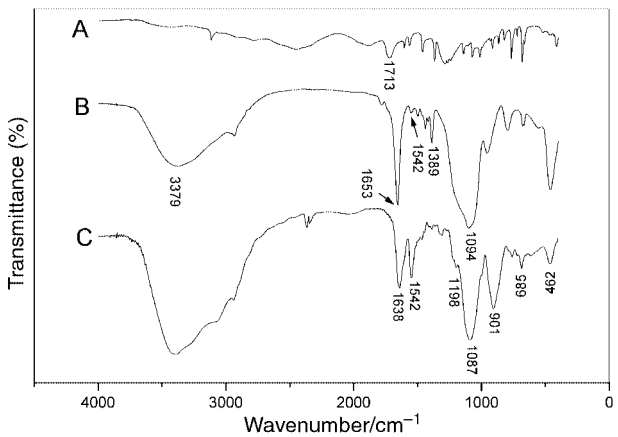

Fig. 1 IR spectra for 2,2′-bipyridine-4,4′-dicarboxylic acid (A), bipyridine–Si (B) and hybrid materials doped with Eu^{3+} (C).

 DOI: 10.1039/b102160p

this case results from direct excitation into Eu^{3+}. Here it is interesting from the appearance of the broad blue band, which can have no other cause than the excitation of the complex. Because the ligands can by no means be excited at 396 nm, it is obvious that the blue emission originates from an intracomplex due to metal-to-ligand energy transfer, possibly by charge transfer. A similar situation has been reported for Eu^{3+} in bipyridine and PEG200 by Bekiari and Lianos.[5] It can be concluded that both the red and blue emissions originate mainly from an intracomplex energy transfer process because the Eu^{3+} ion does not absorb at 336 nm and the ligand does not absorb at 396 nm, further pointing out the formation of a complex between Eu^{3+} and the ligands in bipyridine–Si.

The decay curve of the hybrid material with Eu^{3+} was singly exponential, confirming that the chemical environment of Eu^{3+} is uniform in the hybrid material, from which the luminescence lifetime was determined to be 123.6 μs. This value is much shorter than that of Eu^{3+} in inorganic solid host lattices (generally in the millisecond range),[6] indicating an important quenching by the OH groups (from the coordinated H_2O) or silanol (Si–OH) groups in the hybrid materials (see Scheme 1).

Very similar results were obtained when the Eu^{3+} was replaced by Tb^{3+} in the hybrid materials, *i.e.* the excitation spectrum was identical to that of Eu^{3+}, and the emission consisted of $^5D_4$–^7F_J (J = 3,4,5,6) transitions of Tb^{3+}, with the $^5D_4$–$^7F_5$ (543 nm) green emission as the most prominent group.

In conclusion, modification of 2,2′-bipyridine with APS results in the formation of a hybrid compound, which can act as both the ligand of lanthanide ions and as a sol–gel precursor.

This work is supported by '973' – National key project for Fundamental Research of Rare Earth Functional Materials, the Nation Natural Science Key Foundation of China (No. 29731010, 29971030), National Noble Youth Sciences Foundation of China (No. 29225102) and 'Beiren Jihua' of Chinese Academy of Sciences. We gratefully thank S. B. Wang and Y. N. Yu for the luminescence and lifetime measurements.

Notes and references

‡ *Experimental*: Compound **I** was prepared according to the literature procedure.[7] Anal. Calc. for $C_{12}H_8N_2O_4$: C, 59.10; H, 3.30; N, 11.50. Found: C, 59.12; H, 2.14; N, 11.52%. Compound **II** was synthesized according to the literature procedure.[3] Hybrid materials **III** were prepared as follows: bipyridine–Si was dissolved in 4 mL ethanol; TEOS and H_2O (pH 2) were added to it in the molar ratio 1 : 4 : 16 (bipyridine–Si : TEOS : H_2O) with stirring. $EuCl_3$ (or $TbCl_3$) was added to the resulting mixture with the molar ratio of bipyridine–Si : Eu^{3+} (or Tb^{3+}) of 2 : 1. The mixture was agitated magnetically to achieve a single phase and then transferred into cuvettes. A thermal curing was performed at 40 °C and was continued for three weeks until the sample solidified.

1 P. Tien and L. K. Chau, *Chem. Mater.*, 1999, **11**, 2141.
2 L. L. Hench and J. K. West, *Chem. Rev.*, 1990, **90**, 33.
3 A. C. Franville, D. Zambon and R. Mahiou, *Chem. Mater.*, 2000, **12**, 428.
4 D. W. Deng, S. C. Jiang, Y. F. Men, X. L. Ji and B. Z. Jiang, *Adv. Mater.*, 2000, **12**, 646.
5 V. Bekiari and P. Lianos, *Adv. Mater.*, 1998, **10**, 1455.
6 M. Buijs, A. Meijerink and G. Blasse, *J. Lumin.*, 1987, **37**, 9.
7 G. Sprintschnik, H. W. Sprintschnik, P. P. Kirsch and D. G. Whitten, *J. Am. Chem. Soc.*, 1977, **99**, 4947.

CHEMCOMM Communication
www.rsc.org/chemcomm

The hetero-Diels–Alder addition of sulfur dioxide: structure of the first crystalline sultine. Quantum calculations on the conformations of 6-fluoro-3,6-dihydro-1,2-oxathiine 2-oxides†

Elena Roversi,[a] Rosario Scopelliti,[a] Euro Solari,[a] Raphaël Estoppey,[a] Pierre Vogel,*[a] Pedro Braña,[b] Bibiana Menéndez[b] and José Ángel Sordo*[b]

[a] *Section de chimie de l'Université de Lausanne, BCH, CH 1015 Lausanne-Dorigny, Switzerland. E-mail: pierre.vogel@ico.unil.ch; Fax: (+41) 21 692 3955*
[b] *Laboratorio de Química Computacional, Departamento de Química Física y Analítica, Universidad de Oviedo, Oviedo, Spain*

Received (in Cambridge, UK) 5th April 2001, Accepted 18th May 2001
First published as an Advance Article on the web 14th June 2001

The hetero-Diels–Alder addition of sulfur dioxide to (*E*)- and (*Z*)-4-(fluoromethylidene)-3-methylene-2,3-dihydronaphthalene follows the *endo* Alder rule. The first example of a crystalline sultine has been obtained. In agreement with high level quantum calculations, (1*SR*,3*SR*)-1-fluoro-1,4,5,6-tetrahydronaphtho[2,1-*d*][1,2]oxathiine 3-oxide adopts a sofa conformation in its ground state.

At low temperature and in the presence of a catalyst, simple alkyl-substituted 1,3-dienes add reversibly to SO_2 *via* hetero-Diels–Alder additions to generate the corresponding 3,6-dihydro-1,2-oxathiine 2-oxides (sultines).[1] They are unstable above −50 °C and undergo fast cycloreversion liberating the starting 1,3-dienes and SO_2 that can undergo the expected chelotropic additions at higher temperature. Until now sultines have been characterised in solution by their NMR data only.[1,2] Because of their instability, none of them have been isolated and better characterised. We report here the successful crystallisation of a fluorosultine and its structure determination by X-ray radiocrystallography. Whereas cyclohexene adopts a *pseudo*-chair conformation in its ground-state that interconverts through sofa transition structures, 6-fluoro-3,6-dihydro-1,2-oxathiine 2-oxides seem to prefer sofa conformation in their ground state with the intra-ring oxygen atom lying in the plane of the four carbon centres. We demonstrate also that the hetero-Diels–Alder addition of SO_2 obeys the *endo* Alder rule.[3]

The fluorodienes (*E*)-**3** and (*Z*)-**3** were derived from **1**[4] as shown in Scheme 1.[5] SO_2 added to (*Z*)-**3** at −80 °C (2 h) giving sultine **4**. When allowed to stand at −40 °C it isomerised into **5**. Above −30 °C, **5** was decomposed, no trace of the corresponding sulfolene could be detected! Diene (*E*)-**3** was less reactive than (*Z*)-**3**. It reacted with SO_2 at −40 °C (15 h) giving sultine **5** that could be crystallised at −50 °C and analysed by X-ray radiocrystallography at −100 °C (Fig. 1), thus establishing its structure unambiguously. That of the *cis*-sultine **4** was deduced from its NMR data and by its isomerization into the more stable *trans*-isomer **5**.[6]

Compound **5** represents the first example of a crystalline sultine.[7] The most striking observation is that it adopts a nearly sofa conformation in the crystalline state. This may not be the unique conformation available in solution as suggested by the ^{1}H NMR spectrum. Assuming validity of the relation $^5J_{H,H} = (5\ \text{Hz})\ (\sin\theta)^2(\sin\theta')^2$ for the coupling constants between the homoallylic proton pairs[8] at C-2 and C-5, a larger value should be measured for ^5J(H-2,H$_t$-5) than for ^5J(H-2,H$_c$-5) since H$_t$ makes a greater angle with the C-2, 1, 6, 5 plane than H$_c$ (see Fig. 1). However, one finds similar values ^5J(H-2,H$_c$-5) < 0.2 Hz, ^5J (H-2,H$_t$-5) = 0.8 Hz and ^5J(F-2,H$_t$-5) = ^5J(H-2,H$_c$-3) = 6.2 Hz suggesting that **5** exists as an equilibrium of several conformers in solution.

We have explored using high-level quantum calculations the potential energy surface (PES) of the Diels–Alder additions of SO_2 to (*E*)- and (*Z*)-1-fluorobutadiene (Figs. 2 and 3). The relative energies were computed using G3 theory[9] with the ΔE(2df,p) contribution estimated at the MP2 level (while the

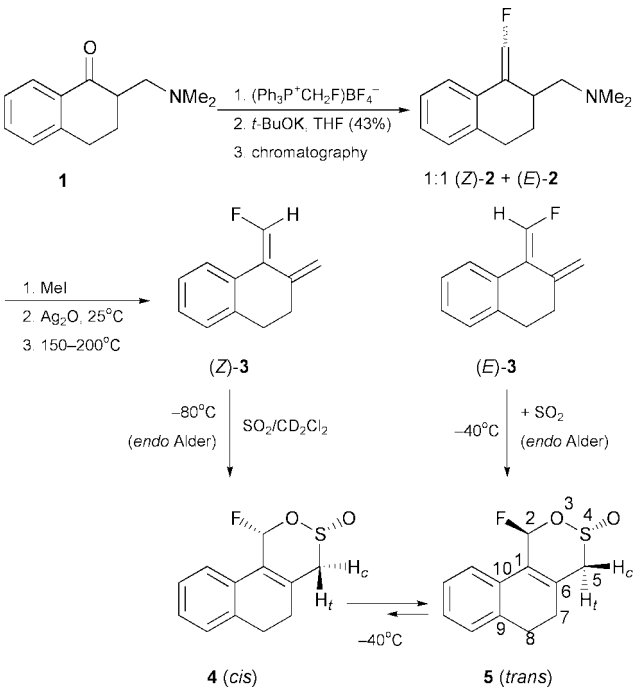

Scheme 1 Synthesis of fluorosultines.

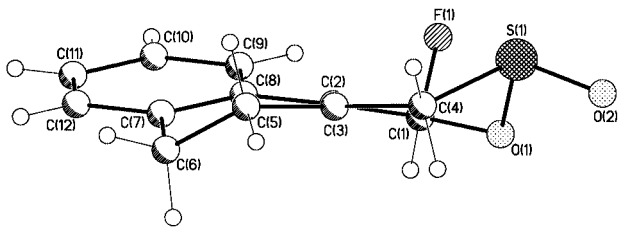

Fig. 1 ORTEP representation of **5** showing the nearly sofa conformation of this 6-fluorosultine. For reasons of commodity atom numbering does not follow IUPAC recommendations. Selected bond lengths (Å), bond angles (°) and torsion angles (°): S1–O2 1.475(2), S1–O1 1.6840(19), S1–C4 1.796(3), O1–C1 1.413(3), C1–F1 1.414(3), O2–S1–O1 102.91(11), O2–S1–C4 106.94(13), O1–S1–C4 93.57(11), O1–C1–F1 106.6, O2–S1–O1–C1 179.11(18), C1–C2–C3–C4 10.4(4).

† Electronic supplementary information (ESI) available: synthetic procedures, data for (*E*)-**3**, (*Z*)-**3**, **4** and **5**. Crystal and molecular structures of **5**, tables of calculated data and representations of calculated minima and transition structures. See http://www.rsc.org/suppdata/cc/b1/b103096p/

 DOI: 10.1039/b103096p

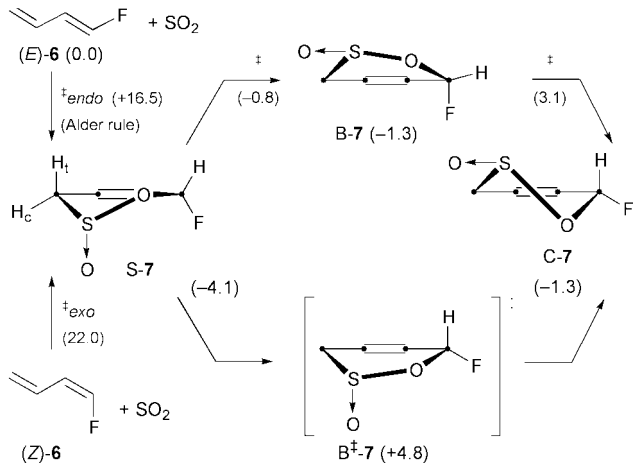

Fig. 2 G3 calculated energies for the hetero-Diels–Alder additions of SO_2 to **6** giving sultine **7** (*cis*). Values (kcal mol^{-1}) given relative to cycloaddends.

CPU times on a NEC SX-4 supercomputer were affected by a factor near 10, a difference of only 0.3 kcal mol^{-1} was found when computing this term for (*S*)-**7** at the MP4 level). The spin-orbit term was not included because of the lack of data for sultines, the zero-point energy was computed from MP2/6-31G(d) harmonic frequencies scaled by a factor of 0.96, and the frozen-core approximation was employed to carry out the geometry optimizations (see ESI†). Both dienes (*E*)-**6** and (*Z*)-**6** prefer the *endo* mode (Alder rule)[3] of addition and (*Z*)-**6** is less reactive than (*E*)-**6**, in agreement with our results with dienes (*Z*)-**3** and (*E*)-**3**, respectively. The calculations predict that *cis*-fluorosultine **7** prefers a sofa conformation S-**7** with *pseudo* axial S=O (Fig. 2). The interconversions of S-**7** and of the pseudo-chair conformer C-**7** can follow two paths. That with the lowest energy barrier involves equilibrium with a boat conformer B-**7**. In the case of the *trans*-fluorosultine **8** (Fig. 3) a sofa S-**8** with *pseudo*-equatorial S=O bond (corresponds to the X-ray structure of **5**) and a 'flattened' *pseudo*-chair conformer C-**8** of similar stabilities are found in agreement with our NMR data for **5**. A boat conformer B-**8** is only 1 kcal mol^{-1} above S-**8** and C-**8** and is reached with an energy barrier of 1.2 kcal mol^{-1}. Alternatively, interconversion S-**8** = C-**8** can operate through a boat transition structure B‡-**8** with an energy barrier of 4.3 kcal mol^{-1} only, suggesting that **8** is more flexible than **7**. If such a flexibility difference should prevail in the cases of **4** and **5**, it could contribute to make **5** more stable than **4**.

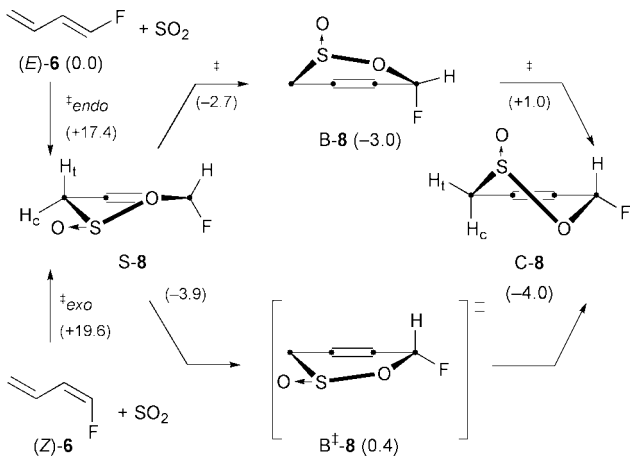

Fig. 3 G3 calculated energies for the hetero-Diels–Alder additions of SO_2 to **6** giving sultine **8** (*trans*). Values (kcal mol^{-1}) given relative to cycloaddends.

We have proposed that sultines are intermediates in our new carbon–carbon forming reaction between electron-rich dienes and enoxysilanes.[10] These species raise fundamental questions concerning their reactivity[11] and, as shown here, about their structure.

This work was supported by the Swiss National Science Foundation, the Centro Svizzero di Calcolo Scientifico (Manno), and by DGES (Madrid) under project PP97-0399-C03.03.

Notes and references

1 B. Deguin and P. Vogel, *J. Am. Chem. Soc.*, 1992, **114**, 9210; B. Deguin and P. Vogel, *Tetrahedron Lett.*, 1993, **34**, 6269; T. Fernández, J. A. Sordo, F. Monnat, B. Deguin and P. Vogel, *J. Am. Chem. Soc.*, 1998, **120**, 13 276.

2 T. Fernández, D. Suárez, J. A. Sordo, E. Roversi, A. Estrella de Castro, K. Schenk and P. Vogel, *J. Org. Chem.*, 1998, **63**, 9490; E. Roversi, F. Monnat, K. Schenk, P. Vogel, P. Braña and J. A. Sordo, *Chem. Eur. J.*, 2000, **6**, 1858.

3 K. Alder and G. Stein, *Angew. Chem.*, 1937, **50**, 510; J. Sauer and R. Sustmann, *Angew. Chem., Int. Ed. Engl.*, 1980, **19**, 779; R. Gleiter and M. C. Böhm, *Pure Appl. Chem.*, 1983, **55**, 237.

4 D. S. Black and L. M. Johnstone, *Aust. J. Chem.*, 1984, **37**, 117.

5 D. Burton and D. Wiemers, *J. Fluorine Chem.*, 1985, 85.

6 Selected data of **4**: ^{1}H NMR (400 MHz, CD_2Cl_2–SO_2–$CFCl_3$, 203 K): δ = 7.25 (m, 4H), 6.37 (dddd, ^2J(H,F) = 52.0 Hz, ^5J(H-2,H$_t$-5) = 1.55 Hz, ^5J(H-2,H$_t$-7) = 1.50 Hz, ^5J(H-2,H$_c$-7) = 1.45 Hz, H-2), 3.89 (ddddd, ^2J = 17.7 Hz, ^5J(H,F) = 7.6 Hz, ^4J(H$_t$-5,H$_t$-7) ≅ ^4J(H$_t$-5,H$_c$-7) ≅ ^5J(H$_t$-5,H-2) = 1.5 Hz, H$_t$-5), 3.40 (br dd, ^2J = 17.7, ^5J(H,F) = 6.3 Hz, H$_c$-5), 2.91 (m, 2H), 2.50 (m, 2H) (H$_c$ ≙ *cis*, H$_t$ ≙ *trans* with respect to F). Selected data of **5**: ^{1}H NMR (400 MHz, CD_2Cl_2–SO_2–$CFCl_3$, 233 K): δ = 7.28 (m, 4H), 6.65 (br d, ^2J(H,F) = 53.0 Hz, H-2), 3.82 (dd, ^2J = 16.3 Hz, ^5J(H,F) = 6.2 Hz, ^5J(H-2,H$_c$-5) < 0.2 Hz, H$_c$-5), 3.63 (ddd, ^2J = 16.3 Hz, ^5J(H,F) = 5.6 Hz, ^5J(H-2,H$_t$-5) = 0.8 Hz, H$_t$-5), 2.91, 2.47 (2m, 4H).

7 $C_{12}H_{11}FO_2S$ (238.27), monoclinic, *a* = 7.8271(9) Å, α = 90°, *b* = 13.982(2) Å, *β* = 106.577(12)°, *c* = 10.1237(15) Å, *γ* = 90°; *V* 1061.9(3) Å^3, 143(2) K, *P*2(1)/*n*, *Z* = 4, *μ* = 0.299 mm^{-1}, 1795 independent reflexion [*R*(int) = 0.0459], reflexion collected: 5521, final *R* indices (all data): *R*1 = 0.0572, *wR*2 = 0.1293. CCDC 157490. See http://www.rsc.org/suppdata/cc/b1/b103096p/

8 M. Barfield and S. Sternhell, *J. Am. Chem. Soc.*, 1972, **94**, 1905; J. Kowalewski, *Prog. Nucl. Magn. Reson. Spectrosc.*, 1978, **11**, 1.

9 L. A. Curtiss, K. Raghavachari, P. C. Redfern, V. Rassolov and J. A. Pople, *J. Chem. Phys.*, 1998, **109**, 7764.

10 J.-M. Roulet, G. Puhr and P. Vogel, *Tetrahedron Lett.*, 1997, **38**, 6201; V. Narkevitch, K. Schenk and P. Vogel, *Angew. Chem., Int. Ed. Engl.*, 2000, **39**, 1806.

11 S. Megevand, J. Moore, K. Schenk and P. Vogel, *Tetrahedron Lett.*, 2001, **42**, 673.

CHEMCOMM Communication
www.rsc.org/chemcomm

Electrochemical and luminescent properties of poly(fluorene) derivatives for optoelectronic applications

Ana Charas,[a,b] Jorge Morgado,*[a] José M. G. Martinho,[a] Luís Alcácer[a] and Franco Cacialli[c]

[a] *Instituto Superior Técnico, Av. Rovisco Pais, P-1049-001 Lisboa, Portugal. E-mail: jmorgado@gcsi.ist.utl.pt*
[b] *Instituto Tecnológico e Nuclear, P-2686-953 Sacavém, Portugal*
[c] *Department of Physics and Astronomy, University College London, Gower Street, London, UK WC1E 6BT*

Received (in Cambridge, UK) 10th April 2001, Accepted 25th May 2001
First published as an Advance Article on the web 14th June 2001

We report the synthesis of novel alternating copolymers of the kind A-*alt*-B, where A is a dialkylfluorene unit and B is an aromatic moiety unit which is varied in order to change the position of the frontier energy levels; in particular we find that the B unit thiophene *S*,*S*-dioxide is particularly effective at increasing the polymer electron affinity and ionisation potential.

Poly(9,9-dialkylfluorene)s and derivatives are attracting significant interest in the context of polymer-based optoelectronic devices and in particular for the fabrication of efficient and long-lived light-emitting diodes.[1] Both colour tunability and control of the position of the frontier energy levels (electron affinity, EA, and ionisation potential, IP) are important in order to extend the applicability of this class of polymers, with a view to fabrication of full-colour displays and also to optimisation of charge injection from environmentally stable electrodes. From the synthetic point of view, a successful strategy to achieve this goal is the preparation of copolymers combining the fluorene moiety with other electroactive ones, in an alternating coupling pattern (A-*alt*-B). For example, a moiety of interest is the thiophene *S*,*S*-dioxide, which has been shown to produce an effective increase of EA in oligothiophenes.[2,3]

Here, we report the synthesis and the electrochemical and optical properties of a variety of well-defined A-*alt*-B copolymers, where A is a 9,9-bis(2′-ethylhexyl)fluorene unit and B is either a thiophene unit, a thiophene derivative, an oligothiophene or an oligothienylenevinylene (Scheme 1).

We synthesised the copolymers *via* palladium-catalysed Suzuki coupling[4] from the appropriate dibrominated and boron ester monomers, with a polymerisation yield in the range of 47–58%. The choice of the bulkier 2-ethylhexylfluorene solubilizing substituents, at variance with the more commonly used dioctyl or dihexyl linear chains, is aimed at reducing interchain interactions and ordering. The detrimental role of the interchain excited states on the luminescent polymer properties has been widely reported, in particular for polyfluorenes.[5,6] The polymerisation was carried out in a refluxing tetrahydrofuran–aqueous potassium carbonate solution (2 M) containing $Pd(PPh_3)_4$ as catalyst, for several days, in the dark and under N_2. Copolymers were then purified by dissolution in the minimum amount of $CHCl_3$ and by addition of the filtered solution to a non-solvent (methanol). This process was repeated at least three times, after which the copolymers were dried under vacuum. Monomers and polymers were characterised by standard spectroscopic techniques and elemental analysis. Details of the synthesis and structural characterisation will be reported in a future publication. The molecular weight of the polymers was determined by gel permeation chromatography of their THF solutions, relative to polystyrene standards. The obtained values (Table 1) are typical of the Suzuki type polymerisation reaction.

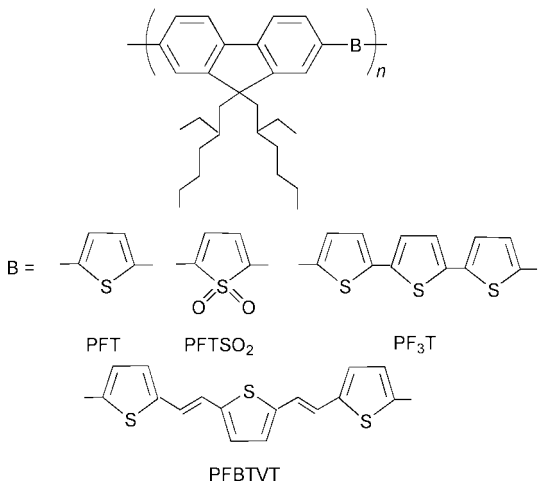

Scheme 1 Molecular structure of the synthesised copolymers.

We investigated the electrochemical behaviour of the copolymer films by cyclic voltammetry. The ionisation potential (IP) and electron affinity (EA) were estimated from the oxidation and reduction onset potentials determined against a saturated calomel electrode (calibrated against ferrocene, Fc/Fc^+ 0.41 V), considering that the energy level of Fc/Fc^+ is 4.8 eV below the vacuum level.[7] These values are summarised in Table 1. On going from PFT to the copolymers with longer B segments (PF3T and PFBTVT), we observe a decrease of IP whereas EA remains nearly constant. The most significant alteration of these two parameters occurs when the sulfur atom of PFT is functionalised to SO_2; namely, a significant increase of both IP and EA is observed in going from PFT to PFTSO2. The stabilisation of the frontier levels upon such functionalisation was previously reported for oligothiophenes,[2] though, for those systems, the increase of EA was larger than the increase of IP.

The UV-vis absorption of the copolymer films is also dependent on the B unit (Fig. 1). The copolymers'optical gap values, E_g, estimated from the onset of the UV-vis absorption spectra, are given in Table 1. E_g decreases on going from PFT

Table 1 Number-average molecular weight (M_n), polydispersity (M_w/M_n), ionisation potential (IP), electron affinity (EA), optical gap (E_g) and fluorescence quantum yields (Φ_{FL}) determined in solution and in solid films of the investigated copolymers

Polymer	M_n	M_w/M_n	IP[a]/ eV	EA[a]/ eV	E_g/ eV	Φ_{FL} Soln.	Φ_{FL} Film
PFT	14100	3.4	5.49	2.84	2.5	0.51	0.032
PFTSO2	8700	3.1	5.62	2.94	2.2	0.16	0.008
PF3T	2800	1.5	5.39	2.81	2.3	0.37	0.081
PFBTVT	5300	3.5	5.24	2.89	2.2	0.11	0.005

[a] CV in MeCN–NBu_4BF_4 (0.2 M) at 50 mV s^{-1}.

 DOI: 10.1039/b103179c

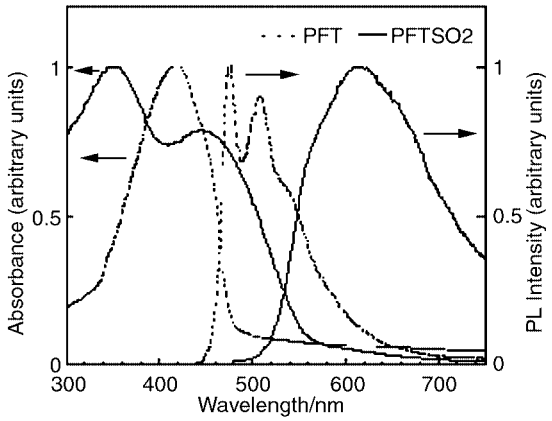

Fig. 1 Normalised UV-vis absorption and photoluminescence (PL) spectra of PFT (λ_{exc} = 408 nm) and PFTSO2 (λ_{exc} = 445 nm) thin films deposited on spectrosil.

to the copolymers with longer conjugated B units, PF3T and PFBTVT, indicating an increase of the conjugation length, despite the decrease of the molecular weight. A similar decrease of E_g is observed upon S to SO_2 functionalisation, showing that such chemical modification of the thiophene unit has a comparable effect to the increase of the number of thiophene rings in the B unit. Furthermore, two distinct bands are observed in the PFTSO2 absorption spectra while a single one is observed for PFT (Fig. 1). Correspondingly, a red-shift of the photoluminescence, PL, spectra is also observed on going from PFT to the other copolymers. Namely, while PFT fluorescence occurs in the green region (λ_{max} = 476 nm), PFTSO2 emits in the orange region of the visible spectrum (λ_{max} = 604 nm). Fluorescence quantum yields (Φ_{FL}) of these polymers were determined both for chloroform solutions and films. Solution Φ_{FL} were calculated by the relative method,[8] by comparing the corrected areas of the fluorescence spectra of a standard and of the sample. As reference substances, we used quinine sulfate in 0.1 M H_2SO_4 (Φ_{FL} = 0.546[9]) and rhodamine 101 in ethanol (Φ_{FL} = 0.89[10]). Solid state Φ_{FL} was determined following the procedure of de Mello *et al.*,[11] using an integrating sphere, upon excitation with the blue line (442 nm) of a He–Cd laser. As shown in Table 1, PFT has the highest solution Φ_{FL}, whereas PF3T shows the highest solid state efficiency. All polymers show a strong reduction of efficiency on going from solution to the solid state, which is indicative of the quenching effects associated to the interchain interactions. We further note that the fluorescence efficiency of PFTSO2 is lower than that of PFT, both in solution and solid state, indicating a detrimental effect of the *S*,*S*-dioxide functionalisation of the thiophene unit.

Φ_{FL} for PFT in solution, 0.51, is comparable to the value of 0.49 reported by Ranger and Leclerc[12] for a similar alternating copolymer combining 9,9-dioctylfluorene and an unsubstituted thiophene unit, prepared by Suzuki coupling. They reported also a decrease of Φ_{FL} to 0.30 when two thiophene rings are used instead of one. Interestingly, we find a higher value of 0.37 for PF3T (which has three thiophene rings), though this value is lower than that of PFT.

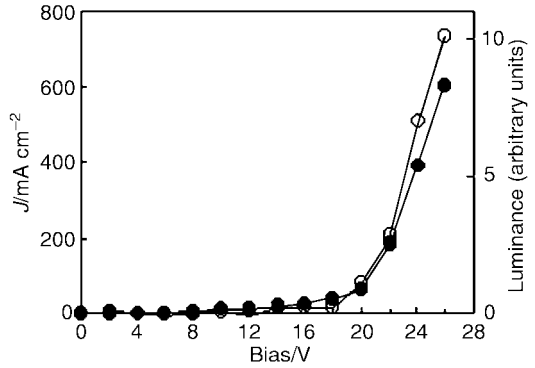

Fig. 2 Current density (J) (-●-) and luminance (-○-), as a function of the applied voltage (V) for an ITO/PEDOT(40 nm)/PFTSO2 (100 nm)/Ca device. The active area of the device is *ca*. 0.02 cm^2.

We fabricated light-emitting diodes using the copolymers shown in Scheme 1 as electroluminescent materials, with Ca cathodes and indium–tin oxide, ITO, or ITO/PEDOT:PSS anodes (where PEDOT:PSS is polyethylenedioxythiophene, doped with polystyrene sulfonic acid) and we found that the electroluminescence spectra are similar to the fluorescence spectra. Fig. 2 shows current density (J) and luminance (L) as a function of the applied voltage (V) for an ITO/PEDOT:PSS/PFTSO2/Ca device. Light-emission starts at about 14 V, and typical external electroluminescence efficiencies of these PFTSO2-based devices are on the order of 10^{-3}%.

In summary, we synthesised well defined alternating copolymers combining fluorene and thiophene-based moieties whose colour emission and position of frontier levels can be tuned upon structural modifications in the thiophene-based aromatic block.

We thank Fundação para a Ciência e a Tecnologia (Project N^0 PRAXIS/3/3.1/MMA/1792/95 and PhD grant to Ana Charas) and The British Council/CRUP (Project N. B-20/00) for financial support. FC is a Royal Society Research Fellow.

Notes and references

1 J. S. Kim, R. H. Friend and F. Cacialli, *Appl. Phys. Lett.*, 1999, **74**, 3084.
2 G. Barbarella, O. Pudova, C. Arbizzani, M. Mastragostino and A. Bongini, *J. Org. Chem.*, 1998, **63**, 1742.
3 G. Barbarella, L. Favaretto, G. Sotgiu, M. Zambianchi, L. Antolini, O. Pudova and A. Bongini, *J. Org. Chem.*, 1998, **63**, 5497.
4 T. Ishiyama, M. Murata and N. Miyaura, *J. Org. Chem.*, 1995, **60**, 7508.
5 D. D. C. Bradley, M. Grell, X. Long, H. Mellor and A. Grice, *SPIE Proc.*, 1997, **3145**, 254.
6 J. Lee, G. Klaerner and R. D. Miller, *Synth. Met.*, 1999, **101**, 126.
7 J. Pommerehne, H. Vestweber, W. Guss, R. F. Mahrt, H. Bässler, M. Porsh and J. Daub, *Adv. Mater.*, 1995, **7**, 551.
8 J. N. Demas and G. A. Crosby, *J. Phys. Chem.*, 1971, **75**, 991.
9 W. H. Melhuish, *J. Phys. Chem.*, 1961, **65**, 229.
10 E. J. N. Pereira, M. N. Berberan-Santos, A. Fedorov, M. Vincent, J. Gallay and J. M. G. Martinho, *J. Chem. Phys.*, 1999, **110**, 1600.
11 J. C. de Mello, H. F. Wittmann and R. H. Friend, *Adv. Mater.*, 1997, **9**, 230.
12 M. Ranger and M. Leclerc, *Can. J. Chem.*, 1998, **76**, 1571.

CHEMCOMM Communication
www.rsc.org/chemcomm

$Zr(OtBu)_4$-catalysed synthesis of acetone aldol adducts and domino aldol-Tishchenko reactions with diacetone alcohol as enol equivalent†

Christoph Schneider* and Markus Hansch

Institut für Organische Chemie der Georg-August-Universität Göttingen, Tammannstr. 2, D-37077 Göttingen, Germany. E-mail: cschnei1@gwdg.de; Fax: (+ 49)551-399660

Received (in Cambridge, UK) 2nd April 2001, Accepted 16th May 2001
First published as an Advance Article on the web 14th June 2001

$Zr(OtBu)_4$ was found to be a potent catalyst for the synthesis of acetone aldol adducts with diacetone alcohol as enol equivalent and for domino aldol-Tishchenko reaction giving rise to 1,3-*anti*-diol monoesters with excellent diastereoselectivity.

Catalytic aldol reactions are currently being intensely investigated. Most processes that have been developed share as a general feature the formation of a silyl enolate in a preceding synthetic operation which in a separate step is then treated with the aldehyde under Lewis acid[1] or Lewis base[2] catalysis. Only very recently few methods for direct, catalytic aldol reactions have been reported.[3] Typically these catalysts exhibit Brønsted base as well as Lewis acid activity to form the metal enolate *in situ* and activate the aldehyde, respectively.

Recently, pharmaceutical chemists aiming at modifying the chemical structure of the immunosuppressant rapamycin reported that the homogeneous stereochemistry of the aldol moiety of the natural product was lost under the action of excess $Ti(OiPr)_4$.[4] They proposed a facile retro-aldol aldolisation process to account for this observation and pointed to the possible use of aldol products as enolate precursors. Inspired by this report we reasoned that a ketone aldol adduct should be an even better source for the *in situ* generation of a metal enolate through a retro-aldol mechanism and selected diacetone alcohol (**1**) as a promising substrate for a direct and catalytic aldol synthesis.[5]

We report here that $Zr(OtBu)_4$ catalyses the synthesis of aldol products from aromatic and α,β-unsaturated aldehydes **2** and diacetone alcohol (**1**) to give rise to the acetone aldol products **3** in typically good yields. Moreover, with most aliphatic aldehydes a rapid $Zr(OtBu)_4$-catalysed Tishchenko reduction of the β-hydroxyketones immediately succeeds the aldol reaction to yield the 1,3-*anti*-diol monoesters **4**/**5**.

In the first step various metal alkoxides (10 mol%) were tested for their catalytic activity in the reaction of benzaldehyde and diacetone alcohol in THF at −20 °C (Table 1). NaO*t*Bu and KO*t*Bu apparently catalysed the reaction but yielded mainly the dehydrated aldol condensation product (entries 1, 2). $Ti(OiPr)_4$ and $Ti(OtBu)_4$ required elevated temperatures for product formation and gave mixtures of **3a** and the condensation product in moderate yields (entries 3, 4). Whereas $Zr(OiPr)_4$ also exhibited poor catalytic activity, $Zr(OtBu)_4$[6] turned out to be the catalyst of choice furnishing the desired aldol adduct **3a** in 80% yield with only traces of the condensation product being formed (entry 6). $La(OtBu)_3$ yielded mainly the direct aldol adduct of diacetone alcohol and benzaldehyde as one might have expected in light of the results reported by Shibasaki (entry 7).[3]

We then subjected a range of aromatic and conjugated aldehydes to the reaction with diacetone alcohol (2 eq.) and $Zr(OtBu)_4$ (10 mol%) in THF at −20 °C which gave rise to the corresponding aldol adducts **3a**–**f** in moderate to very good yields (Table 2).[7] Not unexpectedly, electron-deficient aromatic aldehydes appear to be slightly more reactive than electron-rich ones (entries 2, 3). As byproduct in 5–10% yield we occasionally isolated 1,3-*anti*-diol monoesters comprising two molecules of aldehyde and one acetone fragment which were apparently formed in a $Zr(OtBu)_4$-catalysed Tishchenko reduction[8] of the initially formed β-hydroxy ketones with the aldehyde as hydride source.

This domino aldol-Tishchenko process[9,10] was found to be the dominant reaction pathway in the case of most aliphatic aldehydes (Table 3). Straight chain as well as α-branched aliphatic aldehydes gave the 1,3-*anti*-diol monoesters **4**/**5a**–**e** in good yields upon reaction with diacetone alcohol (1 eq.) and $Zr(OtBu)_4$ (10 mol%) whereas the initial aldol adducts were isolated in < 5% yield. Lowering the amount of aldehyde equivalents resulted in a decrease in yield but did not increase the proportion of the aldol adducts, indicating that the Tishchenko reduction proceeded much faster than the formation of the aldol adducts. Only pivalaldehyde as a sterically very hindered aliphatic aldehyde yielded mainly the initial aldol

Table 1 Metal alkoxide-catalysed synthesis of acetone aldol adduct **3a**

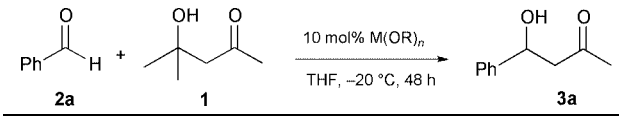

2a **1** **3a**

Entry	Metal alkoxide	Yield of **3a** [%][a]
1	NaO*t*Bu	23 (35)
2	KO*t*Bu	17 (49)
3	$Ti(OiPr)_4$[b]	20 (16)
4	$Ti(OtBu)_4$[b]	35 (28)
5	$Zr(OiPr)_4$	14 (0)
6	$Zr(OtBu)_4$	80 (2)
7	$La(OtBu)_3$	15[c]

[a] Yield of dehydrated aldol condensation product in brackets. [b] This reaction was run at rt. [c] In addition the 'direct' aldol product was formed in 46% yield.

Table 2 $Zr(OtBu)_4$-catalysed synthesis of acetone aldol adducts **3**

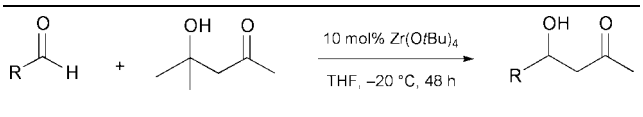

2 **1** **3**

Entry	RCHO	Aldol **3**	Yield [%][a]
1	Ph	**3a**	80
2	4-NO_2-Ph	**3b**	85
3	4-MeO-Ph	**3c**	68
4	1-naphthyl	**3d**	86
5	2-naphthyl	**3e**	71
6	PhCH=CH	**3f**	60
7	*t*Bu	**3g**	60

[a] 5–10% of the corresponding aldol Tishchenko products were formed additionally.

† Dedicated to Professor David A. Evans on the occasion of his 60th birthday.

 DOI: 10.1039/b102941j

Table 3 $Zr(OtBu)_4$-catalysed domino aldol-Tishchenko reactions

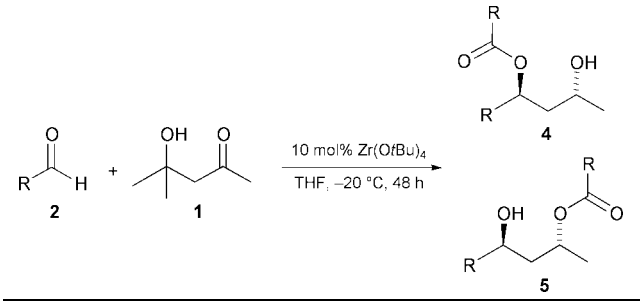

Entry	RCHO	4/5	Yield [%][a]
1	C_2H_5	**4/5a** (3:1)	75
2	nC_6H_{13}	**4/5b** (2:1)	89
3	$PhCH_2CH_2$	**4/5c** (1:1)	75
4	iC_3H_7	**4/5d** (9:1)	85
5	cC_6H_{11}	**4/5e** (22:1)	70

[a] Combined yield of both regioisomers; the initial aldol products were formed in < 5% yield.

adduct **3g** in 60% yield along with 6% of the aldol Tishchenko product (Table 2, entry 7).

The initial Tishchenko products **4** suffered partial acyl migration to give rise to mixtures of regioisomeric 1,3-*anti*-diol monoesters which were, however, converted to a single 1,3-*anti*-diol upon hydrolysis with KOH in methanol. ^{13}C NMR analysis of the corresponding acetonides confirmed their *anti*-stereochemistry.[11] The degree of acyl migration was dependent on the steric bulk of the acyl group with straight-chain acyl groups being more readily transferred than α-branched acyl groups. The exclusive (> 97:3 by NMR) formation of the 1,3-*anti*-diol monoesters may be explained through intramolecular hydride delivery of a chelated Zr-hemiacetal alkoxide in transition structure **A** which has been previously put forth for transition metal-catalysed Tishchenko reductions (Fig. 1).[8]

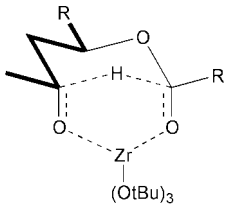

A

Fig. 1

In an additional experiment we treated aldol adduct **6** with propionaldehyde under the typical reaction conditions and obtained the Tishchenko product **7** in 62% yield (15:1-mixture of regioisomers) with no formation of a crossover product being observed (Scheme 1). This result suggests that the Tishchenko reduction proceeded faster than a possible retro-aldol aldolisation process.

At present, we can only speculate about the exact mechanism of the reported aldol synthesis. Although it is very likely that the reaction proceeds stepwise *via* a retro-aldol aldolisation pathway and *in situ* generation of a zirconium enolate, we can not rule out a concerted mechanism analogous to a Meerwein–Ponndorf–Verley reduction.[12] Attempts to detect the presumed zirconium enolate spectroscopically have failed so far which, however, may be due to the very low concentration of the enolate that reacts with the aldehyde as soon as it is formed.

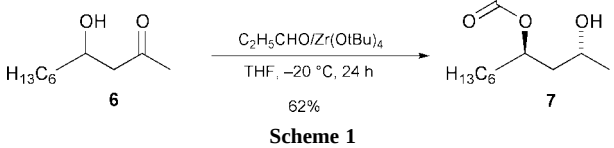

Scheme 1

In conclusion, we have demonstrated that $Zr(OtBu)_4$ is an effective catalyst for the synthesis of acetone aldol adducts using diacetone alcohol as an enol equivalent. With most aliphatic aldehydes $Zr(OtBu)_4$ exhibits a dual activity as an aldol and Tishchenko catalyst. Further studies are aimed at understanding the exact reaction mechanism and expanding the scope of the reaction.

Financial support of this work by the Fonds der Chemischen Industrie is gratefully acknowledged. We thank Professor Tietze for his support.

Notes and references

1 For excellent reviews see: E. M. Carreira, in *Comprehensive Asymmetric Catalysis*, eds. E. N. Jacobsen, A. Pfaltz and H. Yamamoto, Springer, Heidelberg, 1999, vol. **3**, p. 998; H. Gröger, E. M. Vogel and M. Shibasaki, *Chem. Eur. J.*, 1998, **4**, 1137; S. G. Nelson, *Tetrahedron: Asymmetry*, 1998, **9**, 357.

2 S. E. Denmark and R. A. Stavenger, *Acc. Chem. Res.*, 2000, **33**, 432 and ref. cited; S. Matsukawa, N. Okano and T. Imamoto, *Tetrahedron Lett.*, 2000, **41**, 103.

3 N. Yoshikawa, Y. M. A. Yamada, J. Das, H. Sasai and M. Shibasaki, *J. Am. Chem. Soc.*, 1999, **121**, 4168; B. List, R. A. Lerner and C. F. Barbas, *J. Am. Chem. Soc.*, 2000, **122**, 2395; B. M. Trost and H. Ito, *J. Am. Chem. Soc.*, 2000, **122**, 12003; N. Yoshikawa, N. Kumagai, S. Matsunaga, G. Moll, T. Ohshima, T. Suzuki and M. Shibasaki, *J. Am. Chem. Soc.*, 2001, **123**, 2466.

4 W. Yang, C. A. Digits, M. Hatada, S. Narula, L. W. Rozamus, C. M. Huestis, J. Wong, D. Dalgarno and D. A. Holt, *Org. Lett.*, 1999, **1**, 2033.

5 While this work was in progress Nevalainen *et al.* reported a Al-catalysed aldol synthesis based on the same concept, see: I. Simpura and V. Nevalainen, *Angew. Chem., Int. Ed.*, 2000, **39**, 3422.

6 H. Sasai, Y. Kirio and M. Shibasaki, *J. Org. Chem.*, 1990, **55**, 5306.

7 Typical experimental procedure for the aldol synthesis: in a dry flask under nitrogen 0.10 ml (1.00 mmol) freshly distilled benzaldehyde and 0.25 ml (2.00 mmol) of diacetone alcohol were dissolved in 1 ml THF and cooled to −20 °C. At that temperature 39 μl (0.10 mmol) $Zr(OtBu)_4$ were added with a syringe and the reaction mixture remained at −20 °C for 48 h. The reaction was quenched with pH 7 buffer, the product was extracted twice with ether and the organic extracts were dried with $MgSO_4$. Flash chromatography over silica gel with ether–pentane 1:2 furnished 132 mg (80%) of aldol adduct **3a** as a colourless oil along with 18 mg (7%) of the corresponding Tishchenko product. All products gave satisfactory analytical and spectroscopic data.

8 For metal-catalysed Tishchenko reductions of β-hydroxy ketones see: D. A. Evans and A. H. Hoveyda, *J. Am. Chem. Soc.*, 1990, **112**, 6447; T. Ooi, T. Miura, K. Takaya and K. Maruoka, *Tetrahedron Lett.*, 1999, **40**, 7696.

9 For other stoichiometric aldol Tishchenko reactions see: E. R. Burckhardt, R. G. Bergman and C. H. Heatchcock, *Organometallics*, 1990, **9**, 30; D. P. Curran and R. L. Wolin, *Synlett*, 1991, 317; A. Baramee, N. Chaichit, P. Intawee, C. Thebtaranonth and Y. Thebtaranonth, *J. Chem. Soc., Chem. Commun.*, 1991, 1016; Y. Horiuchi, M. Taniguchi, K. Oshima and K. Utimoto, *Tetrahedron Lett.*, 1995, **36**, 5353; P. M. Bodnar, J. T. Shaw and K. A. Woerpel, *J. Org. Chem.*, 1997, **62**, 5674; F. Abu-Hasanayn and A. Streitwieser, *J. Org. Chem.*, 1998, **63**, 2954.

10 For other catalytic aldol Tishchenko reactions see: R. Mahrwald and B. Costisella, *Synthesis*, 1996, 1087; L. Lu, H. Y. Chang and J. M. Fang, *J. Org. Chem.*, 1999, **64**, 843; C. M. Mascarenhas. M. O. Duffey, S. Y. Liu and J. P. Morken, *Org. Lett.*, 1999, **1**, 1427; C. Delas and C. Moise, *Synthesis*, 2000, 251; C. Mascarenhas, S. P. Miller, P. S. White and J. P. Morken, *Angew. Chem., Int. Ed.*, 2001, **40**, 601.

11 S. D. Rychnovsky, B. N. Rogers and T. I. Richardson, *Acc. Chem. Res.*, 1998, **31**, 9.

12 Maruoka *et al.* have reported Meerwein–Ponndorf–Verley alkynylations and cyanations of aldehydes, see: T. Ooi, T. Miura and K. Maruoka, *J. Am. Chem. Soc.*, 1998, **120**, 10790; T. Ooi, K. Takaya, T. Miura and K. Maruoka, *Synlett*, 2000, 69; T. Ooi, K. Takaya, T. Miura, H. Ichikawa and K. Maruoka, *Synlett*, 2000, 1133.

CHEMCOMM
Communication
www.rsc.org/chemcomm

Palladium-catalysed asymmetric allylic alkylation in the presence of a chiral 'light fluorous' phosphine ligand

Marco Cavazzini,[a] Gianluca Pozzi,*[a] Silvio Quici,[a] David Maillard[b] and Denis Sinou*[b]

[a] *Centro CNR Sintesi e Stereochimica di Speciali Sistemi Organici, via Golgi 19, 20133 Milano, Italy. E-mail: gianluca.pozzi@unimi.it; Fax: +39 02 2663354; Tel: +39 02 2663354*

[b] *Laboratoire de Synthèse Asymétrique, UMR UCBL/CNRS 5622, Université Claude Bernard Lyon 1, 43, boulevard du 11 novembre 1918, 69622 Villeurbanne, France. E-mail: sinou@univ-lyon1.fr; Fax: +33 04 72448160; Tel: +33 04 72446263*

Received (in Cambridge, UK) 4th April 2001, Accepted 23rd May 2001
First published as an Advance Article on the web 14th June 2001

The easily accessible, enantiopure (*R*)-(+)-2-diarylphosphino-2′-alkoxy-1,1′-binaphthyl 1 bearing three fluorous ponytails is an efficient ligand in the palladium-catalysed asymmetric allylic substitution of 1,3-diphenylprop-2-enyl acetate affording chiral products of up to 87% ee.

The advantages brought about by the use of CO_2 (supercritical or compressed) or fluorinated solvents in catalytic reactions are well-documented.[1,2] These novel reaction media offer the possibility of cleaner technology for the chemical industry, and might also promote reactions that are not attainable in common organic solvents, along with selectivity improvements related to the unique solvation environment.[3] In both cases, good solubility of the catalyst in the peculiar reaction medium is a major requirement. To reach this goal, several ligands featuring long-chain perfluoroalkyl substituents ('fluorous ligands') have been synthesized,[4] including a few examples of chiral compounds.[5] Indeed, the presence of long-chain perfluoroalkyl substituents increases the affinity of an organometallic compound both for CO_2 and perfluorocarbons. In the latter case, an increasing body of literature data indicates that only a fluorine content of at least 60% can ensure the very high partition coefficients required for the application of the original fluorous biphase strategy.[6] In order to circumvent this limitation, new fluorous techniques have been recently proposed, based on the recovery of fluorinated molecules by liquid–liquid or solid–phase extraction.[7] This makes 'minimally' or 'light' fluorous reagents and catalysts (*i.e.* compounds with a fluorine content below 60%) potentially useful for small-scale and discovery-oriented research.[8]

As phosphorous-based ligands are extensively used in catalytic reactions, many efforts have been devoted to the synthesis of their fluorous analogues.[1,9] However, such enantiopure compounds are not easily available yet.[10] Here we describe the simple synthesis of a fluorous chiral phosphine, namely (*R*)-(+)-2-{bis[4-(1*H*,1*H*-perfluorooctyloxy)phenyl]phosphino}-2′-(1*H*,1*H*-perfluorooctyloxy)-1,1′-binaphthyl (*R*)-(+)-**1**, a new member of this restricted family of compounds.†

Palladium-catalysed coupling of bis(aryl) phosphonic acids with commercially available (*R*)- or (*S*)-1,1′-bi-2-naphthol bis(trifluoromethanesulfonate) provides an easy access to optically pure 2-(diphenylphosphino)-2′-alkoxy-1,1′-binaphthyls.[11] Leitner and Franciò took advantage of this versatile reaction in the synthesis of a chiral phosphine/phosphite ligand bearing two $-(CH_2)_2C_6F_{13}$ ponytails, structurally similar to (*R*,*S*)-BINAPHOS.[10] The introduction of the perfluoroalkyl substituents required the use of a properly functionalised bis(aryl) phosphonic acid at an early stage of the synthesis. In order to increase the flexibility of this approach, we decided to postpone the introduction of perfluorinated residues. This allows the insertion of the required perfluoroalkyl chains onto a preformed ligand structure, thus increasing the number of possible locations. The synthesis of enantiopure (*R*)-(+)-**1** is outlined in Scheme 1.

Bis(4-methoxyphenyl)phosphonic acid **3**, obtained from the corresponding *para*-substituted aryl bromide **2** according to a literature procedure,[12] allowed the easy monophosphinylation of the commercially available (*R*)-(−)-1,1′-bi(2-naphthol) bis(trifluoromethanesulfonate) (*R*)-(−)-**4**. This reaction was carried out in the presence of equimolar amounts of $Pd(OAc)_2$ and 1,4-bis(diphenylphosphino)butane (dppb) in DMSO at 100 °C. Cleavage of the methoxy group of the phosphinyl derivative (*R*)-(+)-**5** with BBr_3 in CH_2Cl_2 afforded the dihydroxy derivative (*R*)-(+)-**6** in 99% yield, after recrystallisation from diethyl ether. Subsequent hydrolysis of the remaining triflate group with aqueous sodium hydroxide in a methanol–dioxane mixture led to (*R*)-(+)-2-[bis(4-hydroxyphenyl)phosphinyl]-2′-hydroxy-1,1′-binaphthyl (*R*)-(+)-**7** in 91% yield. Three fluorous ponytails were then introduced by reaction of the free hydroxy groups of (*R*)-(+)-**7** with 1*H*,1*H*-perfluorooctan-1-ol perfluorobutanesulfonate **8** in DMF, in the presence of caesium carbonate.[13] Phosphine oxide (*R*)-(+)-**9** was obtained in 70% yield after simple flash chromatography (eluent Et_2O). Finally, reduction with Cl_3SiH in boiling toluene afforded pure (*R*)-(+)-**1** in 90% yield.

The partition coefficients for (*R*)-(+)-**1** between *n*-perfluorooctane and three organic solvents (CH_2Cl_2, toluene and

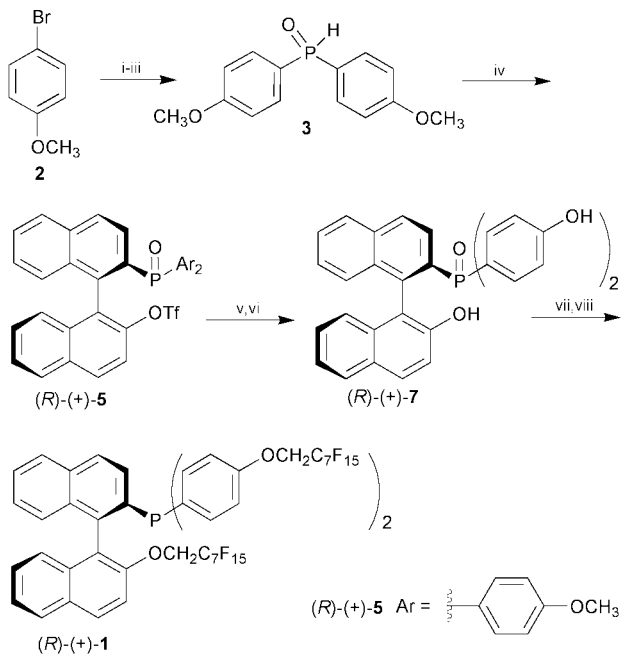

Scheme 1 *Reagents and conditions*: i, Mg, THF, reflux; ii, $ClP(NEt_2)_2$, −20 °C; iii, aqueous 36% HCl, −10 °C; iv, (*R*)-(−)-**4**, $Pd(OAc)_2$, dppb, diisopropylethylamine, DMSO, 100 °C; v, BBr_3, CH_2Cl_2, 0 °C; vi, NaOH, MeOH, dioxane, rt; vii, $C_7F_{15}CH_2OSO_2C_4F_9$ **8**, Cs_2CO_3, 100 °C; viii, Cl_3SiH, toluene, 110 °C.

 DOI: 10.1039/b103074b

Scheme 2 *Reagents and conditions*: Nucleophile (see Table 1), 2 eq.; BSA, 2 eq.; KOAc, 0.1 eq.; $[Pd(\eta^3\text{-}C_3H_5)Cl]_2$, 2 mol%; (*R*)-(+)-**1**, 8 mol%.

CH_3OH) were found to be 0.20, 0.23 and 7.42, respectively. As expected, the new ligand shows a certain affinity for organic solvents, due to the relatively low fluorine content of (*R*)-(+)-**1** (52.4%) and to its aromatic backbone. This mixed behaviour makes (*R*)-(+)-**1** an ideal candidate for the application of 'light fluorous' techniques. Palladium complexes of enantiopure 2-(diphenylphosphino)-2′-alkoxy-1,1′-binaphthyls (MOPs) catalyse several asymmetric transformations.[11] A number of applications of related fluorous compounds could be thus envisaged. It was previously shown that palladium(0)-catalysed allylic substitution reactions can be conveniently performed under fluorous biphase conditions, in the presence of a 'light fluorous' triarylphosphine with a fluorine content of 57%.[14] On the other hand, chiral MOPs have been recently used for the asymmetric allylic alkylation of 1,3-diphenylprop-2-enyl acetate **10** in standard solvents (Scheme 2).[15] We decided therefore to investigate the potentiality of this new fluorous MOP (*R*)-(+)-**1** as a ligand in the same reaction. The results obtained are summarized in Table 1.‡

Table 1 Asymmetric allylic alkylation of 1,3-diphenylprop-2-enyl acetate in benzotrifluoride

Entry	Nucleophile	*T*/°C	*t*/h	Yield[a] (%)	Ee[a] (%)	Conf.[b]
1	$CH_2(CO_2Me)_2$	25	36	99	81	*R*
2[c]	$CH_2(CO_2Me)_2$	25	25	88	87	*R*
3[cd]	$CH_2(CO_2Me)_2$	0	48	95	99	*R*
4	$CH_2(COCH_3)_2$	25	1	100	85	*R*
5	$MeCH(CO_2Me)_2$	25	48	7	76	*S*
6	$MeCH(CO_2Me)_2$	50	48	69	44	*S*
7	$AcNHCH(CO_2Et)_2$	50	25	67	85	*S*

[a] Determined by HPLC analysis (column Chiralpak AD 0.46 × 25 cm). [b] Determined by comparison with an authentic sample. [c] Reaction run in toluene. [d] See ref. 15.

The reaction of **10** with dimethyl malonate using MOP (*R*)-(+)-**1** (8 mol%) and $[Pd(C_3H_5)Cl]_2$ (2 mol%) in the presence of bis(trimethylsilyl)acetamide (BSA, 2 eq.) and potassium acetate (10.1 eq.) in benzotrifluoride (a standard solvent for 'light fluorous' compounds) proceeded quantitatively at rt to give, after 36 h, the corresponding alkylated product in 99% yield with 81% ee (Table 1, entry 1). This value is quite close to the value obtained using toluene as the solvent (Table 1, entry 2). It is to be noticed that non-perfluorinated MOP gave the alkylated product in 95% yield and 99% ee using toluene as the solvent (Table 1, entry 3).

Next we investigated the asymmetric reaction with other carbon nucleophiles. Reaction of **10** with acetylacetone gave the product nearly quantitatively after 1 h with 85% ee (Table 1, entry 4). Substituted dimethyl malonate gave lower chemical yields. Dimethyl methylmalonate gave the alkylated product with 69% yield and 44% ee at 50 °C (Table 1, entry 6), although 76% ee was obtained at rt, but in 7% yield (Table 1, entry 5). Diethyl acetamidomalonate gave also the expected alkylated compound in 67% yield with 85% ee (Table 1, entry 7).

When toluene was used as a solvent, the simple extraction of the reaction mixture with *n*-perfluorooctane (2 × 5 ml) allowed the complete removal of the fluorous ligand and of the corresponding palladium complexes, as shown by the absence of phosphine resonances in the ^{1}H-NMR of the crude product. As pointed out by Curran, this ease of separation together with the possible use of standard reaction conditions could be helpful in discovery-oriented synthesis and parallel synthesis.[8] However, a drawback of this 'light fluorous' approach is the absence of catalytic activity of the recovered fluorous palladium complex. We are currently investigating this problem, which seems to be due to the separation procedure followed. Indeed, recyclability of a 'light fluorous' phosphine used in the same reaction under classical fluorous biphase conditions was feasible.[14]

We thank the Programme Galilée 1999 no. 99023 for financial support.

Notes and references

† ^{1}H-NMR (300 MHz, $CDCl_3$): 4.16 (dt, *J* = 24.6 Hz, 12.6 Hz, 2H), 4.48 (dt, *J* = 13.1 Hz, 13.1 Hz, 4H), 6.72 (d, *J* = 8.4 Hz, 2H), 6.86–6.92 (m, 3H), 7.03 (dd, *J* = 7.1 Hz, 8.5 Hz, 2H), 7.06–7.12 (m, 1H), 7.17–7.35 (m, 6H), 7.41 (dd, *J* = 3.0 Hz, 8.5 Hz, 1H), 7.44–7.50 (m, 1H), 7.86–7.91 (m, 3H), 8.01 (d, *J* = 9.1 Hz, 1H); ^{13}C-NMR (75.4 MHz, $CDCl_3$): 65.5 (t, *J* = 27 Hz), 66.7 (t, *J* = 27 Hz), 105–120 (m, C_7F_{15}), 124.9–131.4, 133.4–136.4, 140.7, 141.1, 153.0, 158.0, 158.2; ^{31}P-NMR (122 MHz, $CDCl_3$): −15.5; mp = 49 °C, $[\alpha]^{20}_D$ = +23.1 (*c* 0.3, $CHCl_3$). Anal. Calcd. for $C_{56}H_{26}F_{45}O_3P$: C, 41.17; H, 1.61; P, 1.90. Found: C, 40.56; H, 1.53; P, 2.19%.

‡ Reactions were run under nitrogen in Schlenk glassware. $[Pd(C_3H_5)Cl]_2$ and the ligand (*R*)-(+)-**1** was dissolved in 2 ml of solvent. After stirring for 40 min at rt, a solution of **10** in 2 ml of solvent was added. After 20 min, the resulting solution was transferred into a reactor previously charged with BSA, KOAc and the nucleophile dissolved in 4 ml of solvent. The reaction mixture was stirred at the desired temperature for the time indicated in Table 1.

1 *Chemical Synthesis in Supercritical Fluids*, ed. P. G. Jessop and W. Leitner, Wiley-VCH, New York, 1999.
2 I. T. Horvàth and J. Ràbai, *Science*, 1994, **266**, 72; I. T. Horváth, *Acc. Chem. Res.*, 1998, **31**, 641.
3 R. S. Oakes, A. A. Clifford, K. D. Bartle, M. T. Pett and C. M Rayner, *Chem. Commun.*, 1999, 247.
4 E. G. Hope and A. M. Stuart, *J. Fluorine Chem.*, 1999, **100**, 75 and references cited therein.
5 M. Cavazzini, A. Manfredi, F. Montanari, S. Quici and G. Pozzi, *Chem. Commun.*, 2000, 2171 and references cited therein.
6 C. Rocaboy, D. Rutherford, B. L. Bennet and J. A. Gladysz, *J. Phys. Org. Chem.*, 2000, **13**, 596.
7 D. P. Curran, *Angew. Chem., Int. Ed.*, 1998, **37**, 1175; D. Crich, X. Hao and M. Lucas, *Tetrahedron*, 1999, **55**, 14261.
8 Q. Zhang, Z. Luo and D. P. Curran, *J. Org. Chem.*, 2000, **65**, 8866.
9 B. Richter, A. L. Spek, G. van Koten and B.-J. Deelman, *J. Am. Chem. Soc.*, 2000, **122**, 3945 and references cited therein.
10 A. Klose and J. A. Gladysz, *Tetrahedron Asymmetry*, 1999, **10**, 2665; G. Franciò and W. Leitner, *Chem. Commun.*, 1999, 1663; S. Kainz, A. Brinkmann, W. Leitner and A. Pfaltz, *J. Am. Chem. Soc.*, 1999, **121**, 6421.
11 T. Hayashi, *J. Organomet. Chem.*, 1999, **576**, 195 and references cited therein.
12 F. G. Mann and E. J. Chaplin, *J. Chem. Soc.*, 1937, 527.
13 D. Sinou, G. Pozzi, E. G. Hope and A. M. Stuart, *Tetrahedron Lett.*, 1999, **40**, 849.
14 R. Kling, D. Sinou, G. Pozzi, A. Choplin, F. Quignard, S. Busch, S. Kainz, D. Koch and W. Leitner, *Tetrahedron Lett.*, 1998, **39**, 9439.
15 K. Fuji, H. Ohnishi, S. Moriyama, K. Tanaka, T. Kawabata and K. Tsubaki, *Synlett*, 2000, 351.

CHEMCOMM
Communication
www.rsc.org/chemcomm

A dense coordination polymer bearing an extensive and highly intricate hydrogen bonding array†

Timothy J. Prior and Matthew J. Rosseinsky*

Department of Chemistry, Robert Robinson Laboratories, University of Liverpool, UK L69 7ZD. E-mail: m.j.rosseinsky@liv.ac.uk

Received (in Cambridge, UK) 27th March 2001, Accepted 21st May 2001
First published as an Advance Article on the web 14th June 2001

Linking of hydrogen bonded sheets by coordination polymer chains produces a three-dimensional solid derived from two distinct structural components.

Enhanced design strategies for the synthesis of extended molecular solids are of considerable current interest.[1] Existing methods focus on single supramolecular synthons and give rise to solids whose structures are dominated by one specific interaction. Here we describe the use of two molecular tectons, with both coordinative and hydrogen bonding[2] abilities, to construct a phase in which there are two distinct extended structural units.

There are two principal methods for the construction of extended molecular solids: hydrogen bonding or coordinative metal–ligand interactions. The construction of organic hosts from hydrogen bonding moieties has been widely studied.[3] This approach potentially offers excellent control over the construction of materials through the manipulation of the hydrogen bonding interactions. Although hydrogen bonding architectures containing metal ions exist, those exhibiting true coordination polymer units are rare,[4] being limited to frameworks in which the coordination polymer is the primary structural element, subsequently linked by hydrogen bonds. For example several 4,4′-bipyridyl frameworks display this formulation: metal–bipyridyl chains or layers are held together by secondary bipy···water or bipy···nitrate hydrogen bonds.[5]

The tectons selected in this work are trimesic acid (1,3,5-benzenetricarboxylic acid, H_3btc) and 1,4-diaminobenzene (1,4-DAB). Trimesic acid has attracted considerable interest as a host for inclusion compounds, co-crystallising with a wide variety of species.[6] 1,4-DAB is known to act as a rigid spacer between transition metal dimers,[7] although it has not previously been observed linking discrete metal cations. Reaction of these molecular components with Ni^{2+} under hydrothermal conditions‡ affords a dense metal–organic solid, N3DAB, with both coordination polymer and hydrogen bonded structural features.

Analysis of single crystal X-ray diffraction data§ collected using synchrotron radiation shows that N3DAB displays the first example of infinite hydrogen bonded sheets linked by coordination polymer chains (Fig. 1).

The structure is based on nickel centres octahedrally coordinated by three types of ligand, in an '*all trans*' geometry (Fig. 2) allowing the formation of the two distinct sub-arrays: *trans* 1,4-DAB units form coordination polymer chains while *trans* $btcH_2$ units form hydrogen bonded sheets and are locked into the conformation allowing the formation of this infinite sheet by hydrogen bonding to water ligands (Fig. 3). In other systems where two *trans* btc units coordinate to the same metal centre, interligand hydrogen bonding of this type is very important in determining the geometry about the metal and hence the orientation of the btc units. In N3DAB this interaction is clearly also important as shown by the extreme rotation about the C7–C8 bond (ring-carboxylate): the torsion angle defined by C6, C7, C8 and O5 is 156.2°. In the absence of this hydrogen bond the angle would be expected to be very near 180°. The $btcH_2$ units joined to the Ni(1,4-DAB) chain display an unusual mode of coordination, being deprotonated at only one acid functionality. It is the dense and co-operative net of hydrogen bonding interactions which prevents the expected complete deprotonation of the H_3btc under the basic synthetic conditions used.

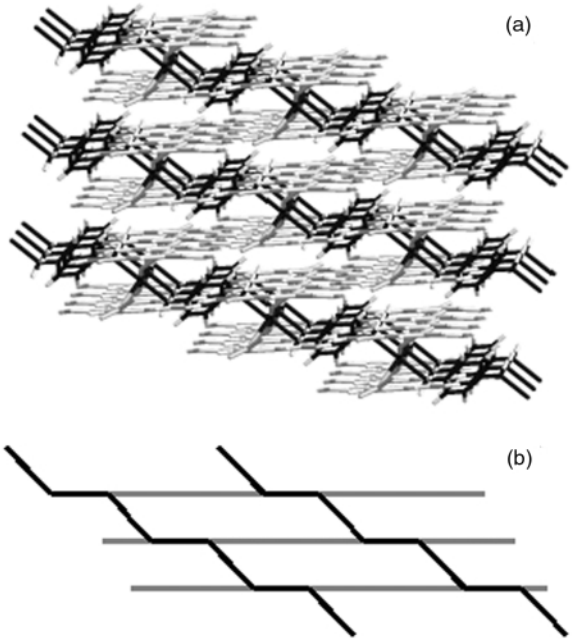

Fig. 1 (a) Infinite 2-D hydrogen bonded decks (grey) linked by 1-D coordination polymer chains (black). (b) Schematic illustration of the two infinite motifs in the structure of N3DAB.

The coordination polymer chains have stoichiometry Ni(1,4-DAB) and run parallel to the crystallographic *b* axis. The Ni–N–C angle is very close to 120° which gives the chain the zigzag arrangement shown in Fig. 2. These chains are decorated with pairs of $btcH_2$ at every nickel centre.

The hydrogen bonded sheets are composed of chains made up from Z-shaped links as shown in Fig. 4. These chains are knit

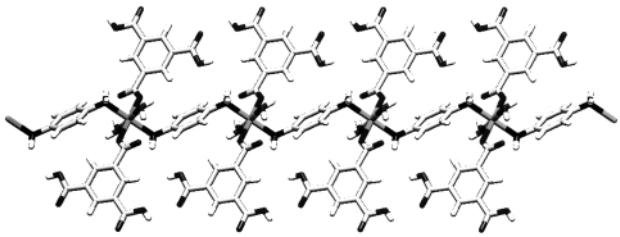

Fig. 2 A single Ni(1,4-DAB) zigzag coordination polymer chain decorated at every nickel with two $btcH_2$ units. Each $btcH_2$ forms part of an infinite hydrogen bonded layer (see Fig. 4).

† Electronic supplementary information (ESI) available: tables of crystallographic data. Full analysis of hydrogen bonding networks. Thermogravimetric data. See http://www.rsc.org/suppdata/cc/b1/b102809j/

 DOI: 10.1039/b102809j

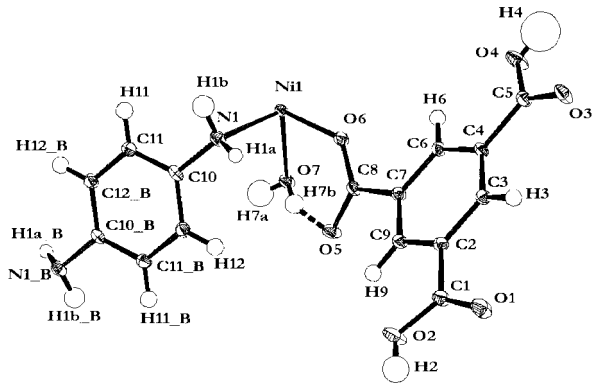

Fig. 3 ORTEP plot of the asymmetric unit of N3DAB. Atoms are shown as 50% thermal ellipsoids. Ni1 lies on the inversion centre. Note the hydrogen bond between O7 and O5 (2.70 Å). Symmetry equivalent atoms appended _B are generated by the symmetry operator $1 - x, - y, 1 - z$.

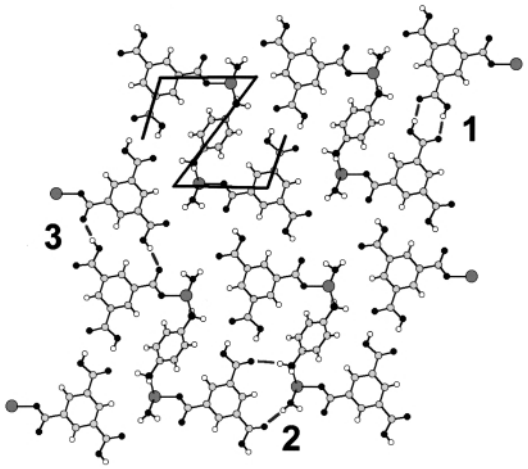

Fig. 4 Part of one of the infinite hydrogen bonded decks composed of Z-shaped links. One such link is highlighted. The three hydrogen bonds responsible for the formation of the infinite sheet are labelled 1, 2 and 3.

together into infinite sheets by further hydrogen bonds. However additional hydrogen bonding networks exist throughout the entire structure and are not constrained to run within the layers, reinforcing the remarkable extent of hydrogen bonding within the structure. Full analysis of the hydrogen bonding is given in the electronic supplementary information (ESI).† The highly electron-rich hydrogen bonded decks lie parallel to each other and their mean separation, 3.324(2) Å (a/2), is sufficiently close to suggest that the $btcH_2$ rings engage in π-stacking.

The unusual mode of coordination of 1,4-DAB offers potential for the formation of a wide range of coordination polymer networks. The coupling of the 1-D chains with different equatorial ligands offers the prospect of novel, potentially porous frameworks. The combination of coordination polymer chains with species known to form extended hydrogen bonded networks opens up a new avenue for synthesis of supramolecular hosts. This two-component approach to synthesis is attractive because of the control which may be exerted through the tectons present.

We thank Dr S. J. Teat for his expert assistance on DL Station 9.8 and the UK EPSRC for a studentship to T. J. P. and support through GR/N 08537.

Notes and references

‡ Very dark purple crystals of N3DAB were grown under hydrothermal conditions. Reagents were purchased from the Aldrich Chemical Company and used without further purification: 0.176 g (0.605 mmol) $Ni(NO_3)_2{\cdot}6H_2O$, 0.2543 g (1.21 mmol) H_3btc, 0.1966 g (1.82 mmol) 1,4-diaminobenzene and 12 ml water were loaded into a 23 cm^3 Teflon-lined stainless-steel reactor which was then sealed. The reactor was heated in an autoclave for 16 h at 150 °C and then cooled to room temperature at a rate of 0.5 °C min^{-1}. Yield 74% (based on Ni). This synthesis affords phase pure N3DAB as demonstrated by the full indexing of powder diffraction patterns given in the ESI† (81 peaks) and chemical analysis (Calc.: C, 46.40; H, 3.58; N, 4.52; Ni, 9.45. Found: C, 46.41; H, 3.58; N, 4.55; Ni, 9.38%).

§ Single-crystal X-ray diffraction data were collected on a Bruker AXS SMART CCD area-detector diffractometer at Station 9.8 of the CLRC Daresbury Laboratory Synchrotron Radiation Source, UK. A dark purple platelet with dimensions 160 × 80 × 60 μm was covered in a thin film of perfluoropolyether oil and mounted on the tip of a two-stage glass fibre. The crystal was cooled to 123 K in an Oxford Instruments nitrogen gas cryostream. Synchrotron radiation of wavelength 0.6941 Å was employed (the wavelength is determined by measurement of unit cell parameters of a known structure). A sphere of data in reciprocal space was collected in three series of ω-rotation exposure frames each with different crystal orientation φ angles: each 1 s exposure employs a 0.15° rotation in ω. Reflection data were integrated using Bruker software.[8] Semiempirical corrections were applied to account for absorption and beam decay.[9] The structure was solved using direct methods in SHELXS-86.[10] Subsequent difference Fourier methods to locate all other atoms and full-matrix least-squares refinement on F^2 was carried out with SHELXL-97.[11] N3DAB, Ni(1,4-DAB)$(btcH_2)_2(H_2O)_2$, crystallises in the centrosymmetric space group $P\bar{1}$ (no. 2). The nickel atom lies in a pseudo-octahedral environment on the inversion centre.

Crystal data: a = 6.6480(18), b = 8.550(2), c = 11.124(3) Å, α = 70.280(6), β = 79.594(6), γ = 76.093(6)°, V = 574.43 Å^3, Z = 2, μ = 0.932 mm^{-1}. Using a single detector position, 5650 intensities were recorded, producing 2987 unique data (θ_{max} 29.38°). R_{int} = 0.0103. Conventional R [$I > 2\sigma(I)$, all data] 0.0462 (0.0526), $wR2$ 0.1256 (0.1279). GOF on F^2 1.135 (1.136). CCDC 162906. See http://www.rsc.org/suppdata/cc/b1/b102809j/ for crystallographic data in CIF or other electronic format.

1 T. J. Barton, L. M. Bull, W. G. Klemperer, D. A. Loy, B. McEnaney, M. Misono, P. A. Monson, G. Pez, G. W. Scherer, J. C. Vartuli and O. M. Yaghi, *Chem. Mater.*, 1999, **11**, 2633; G. F. Swiegers and T. J. Malefetse, *Chem. Rev.*, 2000, **100**, 3483; A. K. Cheetham, G. Ferey and T. Loiseau, *Angew. Chem., Int. Ed.*, 1999, **38**, 3269.

2 C. B. Aakeröy, A. M. Beatty and K. R. Lorimer, *J. Chem. Soc., Dalton Trans.*, 2000, 3869.

3 G. R. Desiraju, *Chem. Commun.*, 1997, 1475; A. Anthony, G. R. Desiraju, R. K. R. Jetti, S. S. Kuduva, N. N. L. Madhavi, A. Nangia, R. Thaimattam and V. R. Thalladi, *Mater. Res. Bull.*, 1998, 1; A. J. Blake, N. R. Champness, P. Hubberstey, W. S. Li, M. A. Withersby and M. Schröder, *Coord. Chem. Rev.*, 1999, **183**, 117; C. B. Aakeröy and A. S. Borovik, *Coord. Chem. Rev.*, 1999, **183**, 1.

4 A. D. Burrows, D. M. P. Mingos, A. J. P. White and D. J. Williams, *Chem. Commun.*, 1996, 97; S. R. Breeze and S. N. Wang, *Inorg. Chem.*, 1993, **32**, 5981.

5 L. Carlucci, G. Ciani, D. M. Proserpio and A. Sironi, *J. Chem. Soc., Dalton Trans.*, 1997, 1801; C. J. Kepert and M. J. Rosseinsky, *Chem. Commun.*, 1999, 375; M. X. Li, G. Y. Xie, Y. D. Gu, J. Chen and P. J. Zheng, *Polyhedron*, 1995, **14**, 1235; M. Kondo, T. Yoshitomi, K. Seki, H. Matsuzaka and S. Kitagawa, *Angew. Chem., Int. Ed. Engl.*, 1997, **36**, 1725; Y. B. Dong, M. D. Smith, R. C. Layland and H. C. zur Loye, *J. Chem. Soc., Dalton Trans.*, 2000, 775.

6 F. H. Herbstein, *Top. Curr. Chem.*, 1987, **140**, 107; K. Biradha, D. Dennis, V. A. MacKinnon, C. V. K. Sharma and M. J. Zaworotko, *J. Am. Chem. Soc.*, 1998, **120**, 11 894; R. E. Melendez and M. J. Zaworotko, *Supramol. Chem.*, 1997, **8**, 157; G. Ferguson, C. Glidewell, G. D. McManus and P. R. Meehan, *Acta Crystallogr., Sect. C*, 1998, **54**, 418.

7 I. M. Müller, T. Röttgers and W. S. Sheldrick, *Chem. Commun.*, 1998, 823.

8 Bruker AXS Inc., Madison, WI, SMART (control) and SAINT (integration) software, version 4, 1994.

9 G. M. Sheldrick, SADABS, Universität Göttingen, 1997.

10 G. M. Sheldrick, SHELXS-86, Universität Göttingen, 1986.

11 G. M. Sheldrick, SHELXL-97: program for the refinement of crystal structures, Universität Göttingen, 1997.

CHEMCOMM
Communication
www.rsc.org/chemcomm

Unusual molybdenum mediated C–N bond activation†

Thomas M. Cameron, Khalil A. Abboud and James M. Boncella*

Department of Chemistry and Center for Catalysis, University of Florida, Gainesville, FL 32611-7200, USA. E-mail: boncella@chem.ufl.edu

Received (in Irvine, CA, USA) 27th February 2001, Accepted 24th May 2001
First published as an Advance Article on the web 14th June 2001

The compounds [Mo(NPh)(η²-olefin){*o*-(Me$_3$SiN)$_2$C$_6$H$_4$}] (olefin = propene 1a or isobutene 1b) react with excess pyridine affording the Mo(IV) bis-pyridine complex, [Mo(NPh)(Py)$_2${*o*-(Me$_3$SiN)$_2$C$_6$H$_4$}] 2 which when heated to 90 °C in toluene undergoes a C–N bond cleavage reaction and is converted to 3, a bimetallic molybdenum species; the crystal structures of both 2 and 3 are reported.

Reactions providing a straightforward example of C–N single bond activation, a most desirable transformation, are rare.[1] The metal-mediated rupture of C–N bonds is for the most part limited to those of strained amines[2] or amidines.[3] Activation of non-activated substrates such as aniline[4] and the ring opening of pyridine[5] has been observed with highly reactive, trivalent, Group 5 metal complexes. A slight variation on this theme involves the recently reported C–N bond cleavage reactivity of a Nb(II) cluster upon ligand replacement by anionic amides.[6] An observation related to this reaction type, made in 1985 by Chisholm *et al.*,[7] involved the isolation of a carbide/imide cluster that may have arisen *via* degradation of an amide ligand. We have recently been able to isolate a bimetallic molybdenum complex **3** arising by C–N activation of the *o*-(Me$_3$SiN)$_2$C$_6$H$_4$ ligand in the bis-pyridine complex [Mo(NPh)(Py)$_2${*o*-(Me$_3$SiN)$_2$C$_6$H$_4$}] **2** (Scheme 1). We herein report the synthesis and solid-state structures of **2** and **3** providing a rare example of C–N activation.

Addition of an excess of pyridine to a stirring pentane solution of **1a** or **1b** resulted in the precipitation of **2** as a purple solid that was isolated by filtration in high yield (Scheme 1).† The room temperature ^{1}H NMR spectrum of **2** displays a significant broadening of the pyridine protons in the 2 and 6 positions. At low temperature (−55 °C) two distinct resonances are observed in the ^{1}H NMR spectrum for these *ortho* protons: one for the two *ortho* protons *syn* to the imido group and the second for two *ortho* protons *anti* to the imido functionality. These observations are consistent with slow rotation of the pyridine rings about the Mo–N bond on the NMR time scale at −55 °C.

An X-ray structural analysis was carried out on a single crystal of **2** grown at room temperature by layering a saturated toluene solution of **2** with pentane. Selected bond lengths and angles are listed in the legend to Fig. 1.‡ The solid-state structure reveals a square pyramidal geometry about the Mo atom, with the imido ligand in the apical position. The Mo–N(4) and Mo–N(5) bond lengths are consistent with a Mo(IV)–Py Lewis acid–base interaction. A space-filling model of **2**, derived from the X-ray study, reveals a sterically congested area around the pyridine ligands due to the presence of the Me$_3$Si groups.[8] It is this steric crowding of the pyridine ligands by the Me$_3$Si groups that hinders their rotation.

The structure of the *o*-(Me$_3$SiN)$_2$C$_6$H$_4$ ligand in **2** differs significantly from that observed in square pyramidal M(VI) complexes containing both NPh imido and *o*-(Me$_3$SiN)$_2$C$_6$H$_4$ ligands. In **2** the C$_6$H$_4$ ring, the N atoms, and the metal center are nearly co-planar. In the related M(VI) complexes the ligand is folded along the N–N vector. This folding has been attributed to π-donation from the NSiMe$_3$ lone pairs to the d$_{xy}$ orbital of the d^0 M(VI) metal center.[9,10] In **2** such π-donation is unfavorable since it would involve a filled–filled interaction between the ligand and the d^2 metal center. The flattened conformation of the *o*-(Me$_3$SiN)$_2$C$_6$H$_4$ ligand in **2** places the SiMe$_3$ groups in the

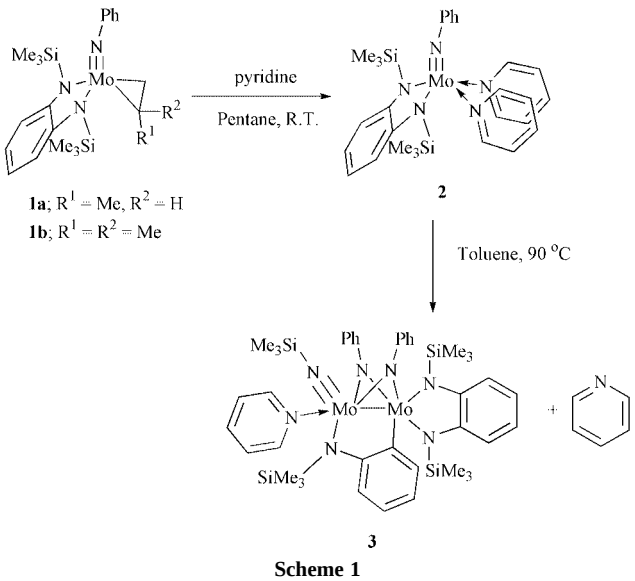

Scheme 1

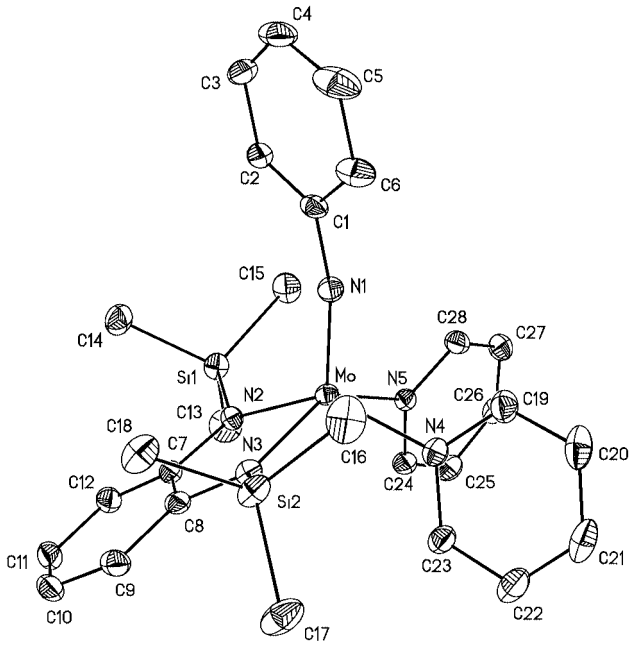

Fig. 1 Thermal ellipsoid plot of **2** (50% probability thermal ellipsoids). Selected bond lengths (Å) and angles (°): Mo–N(1) 1.7476(14), Mo–N(2) 2.0779(16), Mo–N(3) 2.0637(16), Mo–N(4) 2.1247(16), Mo–N(5) 2.1460(16); C(1)–N(1)–Mo 166.35(13).

† Electronic supplementary information (ESI) available: characterisation of complexes **2** and **3**, ^{1}H NMR spectra of **1**–**3** and space-filling diagram of **2**. See http://www.rsc.org/suppdata/cc/b1/b101894i/

 DOI: 10.1039/b101894i

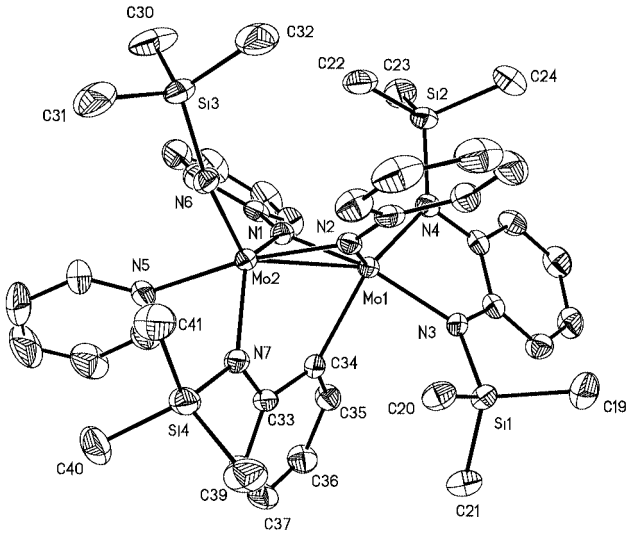

Fig. 2 Molecular structure of **3** (50% probability thermal ellipsoids). The solvating dichloromethane molecules have been omitted for clarity. Selected bond lengths (Å) and angles (°): Mo(1)–Mo(2) 2.5669(4), Mo(1)–C(34) 2.179(3), Mo(2)–N(7) 2.047(2), Mo(2)–N(6) 1.745(2), Mo(2)–N(5) 2.285(3); Mo(1)–N(1)–Mo(2) 80.74(9), Mo(1)–N(2)–Mo(2) 81.48(9).

basal plane of the molecule resulting in steric congestion between the Py and $SiMe_3$ groups which causes the hindered rotation of the Py ligands.

Monomeric **2** is stable at room temperature under an inert atmosphere for extended periods of time. However, when heated to 90 °C in toluene, **2** converts cleanly to the bimetallic compound **3** (Scheme 1) in > 90% yield over the course of 2 h.‡ This air-sensitive, diamagnetic compound is stable in solution for extended periods of time at 90 °C.

A single crystal of **3** was grown from a pentane–dichloromethane solution at −30 °C. Compound **3** crystallizes with two molecules of dichloromethane. An X-ray diffraction study shows that **3** contains two Mo atoms bridged by two phenyl imido groups as well as a $Me_3SiNC_6H_4$ ligand (Fig. 2).§ This unusual $Me_3SiNC_6H_4$ group is apparently formed by cleavage of one $NSiMe_3$ group from an *o*-$(Me_3SiN)_2C_6H_4$ ligand. The $NSiMe_3$ group that was cleaved remains as an additional terminal imido ligand on one of the Mo atoms. The formal oxidation state at each metal center is best described as Mo(V). The Mo(1)–Mo(2) distance of 2.5669(4) Å, although short for a Mo–Mo single bond, indicates the existence of a metal–metal bond, and accounts for the observed diamagnetism of **3**.[11] Four upfield resonances, assigned to the four inequivalent Me_3Si groups, are observed in the ^{1}H NMR spectrum of **3** and this is consistent with the structure as determined by X-ray crystallography.

The unusual C–N bond cleavage reaction that is observed during the pyrolysis of **2** is presumably driven by the formation of the Mo–N triple bond and demonstrates the reactivity of the Mo(IV) moiety towards oxidation. Further reactivity studies of **2** and **3** are currently in progress.

We thank the National Science foundation (CHE 9523279) for funding of this work. K. A. A. thanks the NSF and the University of Florida for funding X-ray equipment purchases.

Notes and references

‡ All reactions and manipulations were carried out using standard Schlenk techniques or in a dry-box under a nitrogen atmosphere. Complexes **1a** and **1b** were synthesized according to published procedures.[12] A representative synthesis of **2**: to a green pentane solution of freshly generated **1b** (1.07 g, 2.18 mmol) was added an excess of pyridine (0.51 g, 6.54 mmol). Upon addition of pyridine, **2** precipitated from solution and was isolated by filtration in 90% yield.

Synthesis of **3**: a toluene solution of **2** (0.200 g, 0.336 mmol) was heated to 90 °C in a sealed ampoule for 2 h. Concentration of the reaction mixture under reduced pressure afforded **3** as a black solid in 92% yield.

§ *Crystal data*: for **2**: $C_{28}H_{37}MoN_5Si_2$, M = 595.75, a = 15.5947(8), b = 10.3170(5), c = 18.4572(9) Å, V = 2969.6 Å^3, orthorhombic, space group $Pna2_1$, Z = 4, μ(Mo-Kα) = 0.547 mm^{-1}, T = 173(2) K, final $R1$ = 0.0218, $wR2$ = 0.0517, GOF (on F^2) = 0.994.

For **3**: $C_{41}H_{59}Mo_2N_7Si_4{\cdot}2CH_2Cl_2$, M = 1124.04, a = 14.4655(8), b = 23.572(1), c = 15.9891(9) Å, β = 104.390(1)°, V = 5280.8(5) Å^3, monoclinic, space group $P2_1/n$, Z = 4, μ(Mo-Kα) = 0.805 mm^{-1}, T = 173(2) K, final $R1$ = 0.0384, $wR2$ = 0.0824, GOF (on F^2) = 0.994.

The structures were solved by direct methods in SHELXTL5,[13] and refined using full-matrix least squares. The non-H atoms were treated anisotropically, whereas the hydrogen atoms were calculated in ideal positions and were riding on their respective carbon atoms. The asymmetric unit of **3** consists of the complex and two dichloromethane molecules, one of which is disordered and refined in three parts. Their site occupation factors were dependently refined until the final cycle of refinement after which they were fixed at 0.50, 0.35 and 0.15, respectively.

CCDC 159480 and 159481. See http://www.rsc.org/suppdata/cc/b1/b101894i/ for crystallographic data in CIF or other electronic format.

1 CX (X = N, O) multiple bond cleavage reactions are more common. See: K. A. Hall and J. M. Mayer, *J. Am. Chem. Soc.*, 1992, **114**, 10 402; F.-M. Su, J. C. Bryan, S. Jang and J. M. Mayer, *Polyhedron*, 1989, **8**, 1261; R. L. Miller, P. T. Wolczanski and A. L. Rheingold, *J. Am. Chem. Soc.*, 1993, **115**, 10 422; K. E. Meyer, P. J. Walsh and R. G. Bergman, *J. Am. Chem. Soc.*, 1995, **117**, 974; R. R. Schrock, M. L. Listemann and L. G. Sturgeoff, *J. Am. Chem. Soc.*, 1982, **104**, 4291.

2 G. Proulx and R. G. Bergman, *J. Am. Chem. Soc.*, 1994, **116**, 7953; L. M. Atagi, D. E. Over, D. R. McAlister and J. M. Mayer, *J. Am. Chem. Soc.*, 1991, **113**, 870; C. C. Cummins, R. R. Schrock and W. M. Davis, *Inorg. Chem.*, 1994, **33**, 1448.

3 F. A. Cotton, J. H. Matonic, C. A. Murillo and X. Wang, *Bull. Soc. Chim. Fr.*, 1996, **133**, 711; F. A. Cotton, L. M. Daniels, C. A. Murillo and X. Wang, *Inorg. Chem.*, 1997, **36**, 896; J. R. Agadorn and J. Arnold, *Organometallics*, 1994, **13**, 4670.

4 J. B. Bonanno, T. P. Henry, D. R. Neithamer, P. T. Wolczanski and E. B. Lobkovski, *J. Am. Chem. Soc.*, 1996, **118**, 5132.

5 T. S. Kleckley, J. L. Bennet, P. T. Wolczanski and E. B. Lobkowski, *J. Am. Chem. Soc.*, 1997, **119**, 247; S. D. Gray, K. J. Weller, M. A. Bruck, P. M. Briggs and D. E. Wigley, *J. Am. Chem. Soc.*, 1995, **117**, 10 678.

6 M. Tayebani, S. Gambarotta and G. P. A. Yap, *Angew. Chem., Int. Ed.*, 1998, **37**, 3002; M. Tayebani, S. Gambarotta and G. P. A. Yap, *Organometallics*, 1998, **17**, 3639; M. Tayebani, K. Feghali, S. Gambarotta and C. Bensimon, *Organometallics*, 1997, **16**, 5084.

7 M. H. Chisholm, K. Folting, J. C. Huffman, J. Leonelli, N. S. Marchant, C. A. Smith and C. E. Taylor, *J. Am. Chem. Soc.*, 1985, **107**, 3722.

8 See electronic supplementary information (ESI†).

9 A. Galindo, A. Ienco and C. Mealli, *New J. Chem.*, 2000, **2**, 73.

10 S. Wang, K. A. Abboud and J. M. Boncella, *J. Am. Chem. Soc.*, 1997, **119**, 11 990.

11 R. D. Adams, D. M. Collins and F. A. Cotton, *Inorg. Chem.*, 1974, **13**, 1086; R. J. Klingler, W. Butler and M. D. Curtis, *J. Am. Chem. Soc.*, 1975, **97**, 3535.

12 T. M. Cameron, C. G. Ortiz, I. Ghiviriga, K. A. Abboud and J. M. Boncella, *Organometallics*, 2001, **20**, 2032; we have reported the synthesis of **1b** previously, T. M. Cameron, C. G. Ortiz, K. A. Abboud, J. M. Boncella, R. T. Baker and B. L. Scott, *Chem. Commun.*, 2000, 573.

13 SHELXTL/NT Version 5.10, Bruker Analytical X-ray Instruments, Inc., Madison, WI, 53719, 1997.

CHEMCOMM
Communication
www.rsc.org/chemcomm

New insight on the photoreactivity of the phototoxic anti-cancer flutamide: photochemical pathways selectively locked and unlocked by structural changes upon drug compartmentalization in phospholipid bilayer vesicles

Salvatore Sortino,*[a] Giancarlo Marconi[b] and Giuseppe Condorelli[a]

[a] *Dipartimento di Scienze Chimiche, Università di Catania, Viale Andrea Doria 8 I-95125 Catania, Italy. E-mail: ssortino@mbox.unict.it*

[b] *Istituto di Fotochimica e Radiazioni d'Alta Energia, Area della Ricerca, Via Pietro Gobetti 101, 40129 Bologna, Italy*

Received (in Cambridge, UK) 13th March 2001, Accepted 29th May 2001
First published as an Advance Article on the web 14th June 2001

It is shown that structural changes of the phototoxic anti-cancer drug flutamide after its compartmentalization in unilamellar phospholipid bilayer vesicles lead to a highly selective modification of the photochemical outcome, locking the main photodegradation pathways observed in homogeneous media and unlocking a new and more efficient photoreactive channel.

Photochemical investigation of phototoxic drugs in organized assemblies mimicking biological systems is becoming an extremely active area of research in the wide arena of supramolecular photochemistry. Indeed, despite the knowledge of the drug photochemical behavior in homogeneous media is a first step for the understanding of molecular basis of the drug-photoinduced disorders, photoreactivity and phototoxicity are often not directly correlated to each other. The main reasons for these incongruities lie in the fact that real life photoprocesses occur at surfaces, interfaces and in multiphase heterogeneous systems. As a consequence it appears evident that a stepwise approach consisting of the investigation of the drug photobehavior in biologically mimicking systems of increasing complexity, represents an adequate strategy for a more appropriate correlation between phototoxicity and photochemical behavior. Furthermore, from a strictly photochemical point of view, studies concerning the drug photoreactivity in micromedia with particular polarity features in the presence of specific interaction and/or steric constraints provide a useful tool for the understanding of the factors influencing the molecular reactivity in order to control it.

Flutamide (FM), 2-methyl-*N*-[4-nitro-3-(trifluoromethyl)-phenyl]propanamide, is a non-steroidal anti-androgen drug that blocks androgen receptor sites and it is widely used in advanced prostate cancer.[1] Recent reports have shown the capability of FM to induce phototoxic and photoallergic effects in patients after drug treatment.[2,3]

Our recent study performed by using UVA light excitation and dilute FM solutions[4] has shown that the photoreactivity of the drug in homogeneous solvents is almost exclusively characterized by a nitro-to-nitrite photorearrangement leading to the phenol derivative **1** as the main stable photoproduct (path **a** Scheme 1). It has been pointed out that the twisted geometry of the nitro group with respect to the aromatic plane plays a key role in triggering such a photoprocess. Indeed, such 'out of plane' geometry makes the p orbital of the oxygen atom have a constructive overlap with the adjacent p orbital of the aromatic ring in the ground state (see Scheme 1). This kind of molecular conformation determines a lowest excited state triplet state characterized by a low biradical character and, as a consequence, by a considerable inefficiency towards hydrogen abstraction (H-abstraction) even in hydrogen donating solvents[4] contrary to what is commonly observed for nitroaromatic compounds in which the nitro group is conjugated with the aromatic plane.[5,6]

In this study, the photoreactivity of FM (5×10^{-5} M) in unilamellar phospholipid bilayer vesicles (liposomes)[7] of L-α-phosphatidylcholine (10^{-3} M) was analyzed. Such organized systems are smectic mesophases of phospholipids with water interspaced among them and characterized by both high aggregation and occupancy number.[8,9] The general observation was that the self-incorporation of FM into the vesicles leads to a highly selective modification of the photochemical outcome. In fact, the chromatographic analysis† performed after 325 nm

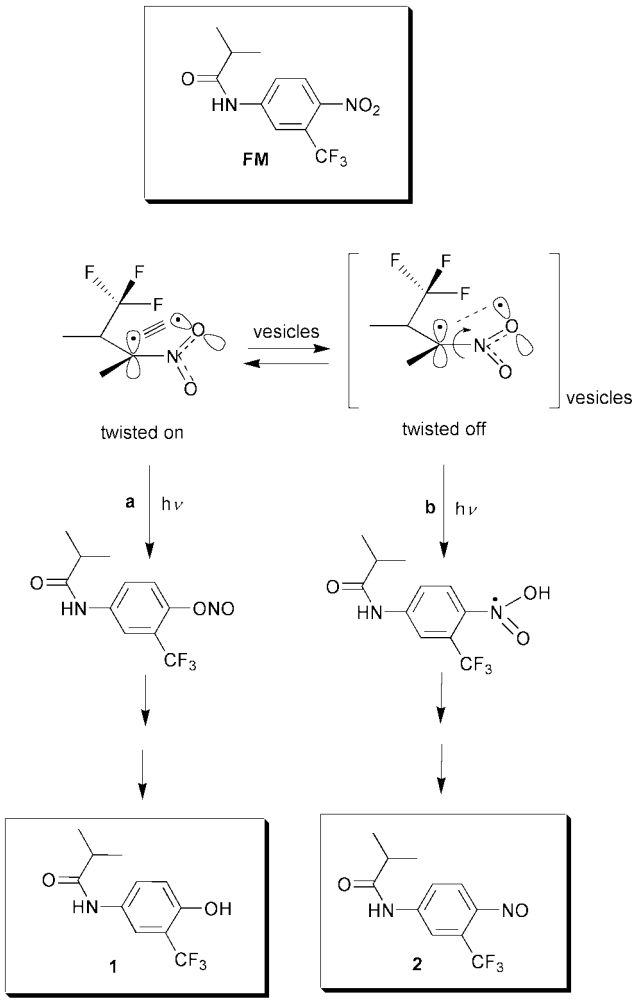

Scheme 1

 DOI: 10.1039/b102359b

irradiation revealed the total absence of **1** being consistent with the dramatic inhibition of the nitro-to-nitrite photorearrangement. On the contrary, the nitroso derivative **2** originated by an unexpected H-abstraction photoprocess was noticed as the sole stable photoproduct (path **b** Scheme 1). Furthermore, the photodegradation quantum yield of FM increased *ca*. 30-fold if compared to aqueous solution ($\Phi_{water} \approx 3 \times 10^{-3}$).[4]

The present scenario cannot be roughly rationalized on the basis of either the presence of the abstractable hydrogen atoms of the bilayer or on its low polarity. Actually, as outlined earlier, the irradiation of FM performed in solvents characterized by good hydrogen donating properties and polarity similar to the vesicles, interior did not activate the photonitroreductive pathway.[4]

We believe that a plausible explanation to account for the inhibition of **1** and the photogeneration of **2** may be consistent with structural changes of FM occurring upon its compartmentalization in the bilayer. In this regard, a less perpendicular geometry of the nitro group with respect to the aromatic ring, more likely caused by steric constrains and specific weak interactions (*i.e.* H-bond involving the CF_3 and/or NO_2) with the close packed lipids, would account well for the obtained results. Such changes in the perpendicularity of the nitro group would lead in fact to a less extended overlap of the p atomic orbital of oxygen with the adjacent orbital of the aromatic ring (see Scheme 1) with consequent loss of the twisted conformation. As well-documented in the literature,[10,11] such a conformation is a prerequisite for the nitro-to-nitrite photorearrangement responsible for the formation of **1**. The consequence of the loss of the twisted conformation is in turn reflected in the logical increase of the biradical character of the n,π* triplet and the consequent high ability of this latter in abstracting hydrogen in the presence of a suitable H-donor. Under these conditions, an intra-vesicles H-abstraction photoprocess involving the nitro group and the hydrogen atoms of the lipid chains might be activated, thus giving rise to the formation of **2** according to the very well known mechanistic pathways (path **b** Scheme 1).[5,6] Our hypothesis is supported well by spectroscopic data combined with theoretical calculations. In fact, from the calculated values of the dipole moments of the ground and first π,π* state, responsible for the first large absorption band (Delta μ about 10 Debyes), one would expect a blue shift of this band going from water to a less polar solvent, such as methanol and isopropyl alcohol (Fig. 1). *Vice versa*, in the vesicles (Fig. 1), where the relative permittivity is similar to that of isopropyl alcohol[9] and where in principle a blue shift should occur, one observes a marked red shift of this band (about 15 nm), consistent with a larger conjugated system which can only occur through a planarization of the NO_2 group.

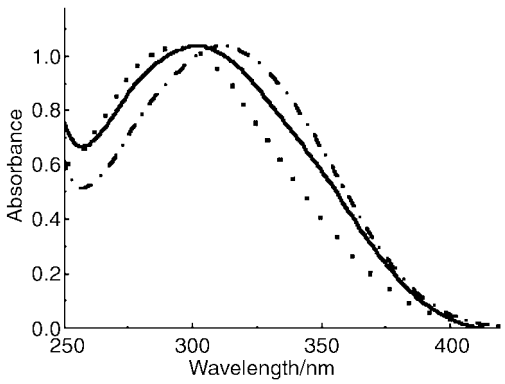

Fig. 1 Normalized absorption spectra of FM in (—) water, (···) isopropyl alcohol and (-·-·-) vesicles.

We believe that these preliminary results may be of chemical, biological and industrial relevance. From a strict chemical point of view, they represent a significant case of photochemical reactions selectively locked and unlocked by conformational changes of the molecular geometry upon substrate confinement in an organized system. From a biological point of view, given the potential of the bilayer in providing an useful model to mimic the biological membranes and by considering that the photogeneration of **2** is mediated by radical pathways[5,6] the obtained results represent a good step forward in understanding the origin of the phototoxic effects displayed by FM. Actually, the compartmentalization of the drug in particular biological sites in the presence of steric constraints and specific interactions, could lead to a relevant increase in the photoproduction of reactive radical species as a consequence of the photogeneration of a new product. Finally, from an industrial point of view, by taking into account the efforts that the scientific community has been making in the development of suitable carrier systems able to increase the FM solubility,[12] our study suggests that in light of the high photolability of the FM–liposome adduct if compared with the free molecule the use of liposome-based drug/carrier systems may not be the right approach to the aforementioned goal.

Financial support from MURST "cofinanziamento di programmi di ricerca di rilevante interesse nazionale" (Progetto: Meccanismi di Processi Fotoindotti in Sistemi Organizzati) and from Istituto Superiore di Sanità (Progetto: Proprietà Chimico-Fisiche dei Medicamenti e loro Sicurezza d'Uso) are gratefully acknowledged.

Notes and references

† The analysis of the reaction mixture was performed by HPLC-MS on a LiChroCart RP-18 column (5 μm packing, 4 × 250 mm Hewlett Packard) eluting with a linear gradient of CH_3CN in 0.01 M phosphate buffer (pH 7) from 0 to 75% in 25 min. Both retention time and integrated area for the non-irradiated FM were the same either in the absence or in the presence of vesicles, suggesting that no complex existed during the elution. Full spectroscopic data concerning the characterization of **2** are available in ref. 4.

1 D. K. Ornstein, *Urology*, 1998, **48**, 901 and references therein.
2 R. Yokote, Y. Tokura, N. Igarashi, O. Ishikawa and Y. Miyachi, *Eur. J. Dermatol.*, 1998, **8**, 427.
3 J. Vilaplana, C. Romaguera, A. Azon and M. Lecha, *Contact Dermatitis*, 1998, **38**, 68.
4 S. Sortino, S. Giuffrida, G. De Guidi, R. Chillemi, S. Petralia, G. Marconi, G. Condorelli and S. Sciuto, *Photochem. Photobiol.*, 2001, **73**, 6.
5 J. A. Barltropp and N. J. Bunce, *J. Chem Soc.*, 1968, 1467.
6 A. Gilbert and J. E. Baggott, *Essentials of Molecular Photochemistry*, Blackwell Scientific Publications, Oxford, 1991, pp. 436–442.
7 Liposomes were prepared by solvent injection method: J. M. H. Kremer, M. W. J. v. d. Esker, C. Pathmamanoharan and P. H. Wiersema, *Biochemistry*, 1977, **16**, 3932.
8 J. H. Fendler, *J. Phys. Chem.*, 1980, **84**, 1485.
9 S. L. Neal and M. M. Villegas, *Anal. Chem.*, 1985, **67**, 2659.
10 K. Hamanoue, M. Amano, M. Kimoto, Y. Kajiwara, T. Nakayama and H. Teranishi, *J. Am. Chem. Soc.*, 1984, **106**, 5993.
11 D. Dopp, in *Handbook of Organic Photochemistry and Photobiology*, ed. W. M. Horspool and P. S. Song, CRC Boca Raton, New York, 1995, pp. 1019–1062.
12 M. A. Adel, A. S. Geneidi, R. Ali Shoukri and I. Saad, *Pharmazie*, 1997, **52**, 373.

Typeset and printed by Black Bear Press Limited, Cambridge, England

CHEMCOMM
Feature Article
www.rsc.org/chemcomm

Dendrimers at surfaces and interfaces: chemistry and applications

David C. Tully and Jean M. J. Fréchet*

Department of Chemistry, University of California, Berkeley, CA 94720-1460, USA. E-mail: frechet@cchem.berkeley.edu, dtully@gnf.org

Received (in Cambridge, UK) 16th May 2001, Accepted 31st May 2001
First published as an Advance Article on the web 27th June 2001

The highly compact and globular shape, as well as the uniform size and plurifunctionality of dendrimers make them ideal molecular building blocks for a wide range of interfacial materials involving self-assembled monolayers, Langmuir films, multilayers, and other surface-confined assemblies. Moreover, the study of the behavior of dendrimers at surfaces and interfaces provides unique insight into their chemical and physical properties. Dendritic macromolecules play an increasingly important role in the materials and surface sciences, where applications utilizing polymer thin films can benefit from their distinctive chemical and physical properties. Recent investigations have highlighted the use of dendrimers as functional surfaces and as interfacial materials for applications in membranes, adhesion, microelectronics or in chemical and biological sensing.

Introduction

Dendrimers constitute a unique class of polymers that are distinguished from all other synthetic macromolecules by their globular shape resulting from their perfectly branched architecture and their monodisperse nature.[1–3] The size, molecular weight, and chemical functionality of dendrimers can be easily controlled through the synthetic methods used for their preparation both by divergent[4] and by convergent[5] methods. With both of these approaches, a branch point is inserted in the dendritic structure at each monomer unit leading to a well-defined macromolecule with a 'degree of branching'[6] (DB) of 100%. This highly branched dendritic architecture causes the molecules to adopt three-dimensional globular conformations to minimize their free energy, with an immediate effect on macromolecular properties. In addition, the chemical composition of the chain-ends of the dendrimers has a determining effect on many of their physical properties such as solubility, glass transition temperature, or intrinsic viscosity. Finally, free energy considerations[2] dictate that the compositional contrast—match or mismatch—between the chain ends and the building blocks of a dendrimer will largely determine whether the chain-ends are mostly peripheral or distributed through their volume.

Over the past 16 years a wide range of 'designer' dendrimers[3] have been developed and synthesized, and their chemical and physical properties as well as their solution behaviors have been studied and well characterized.[3,7] In contrast, it is only recently that interest in the study and use of novel dendrimers for applications at surfaces and interfaces has grown.[7–9] As a result of their compact globular shape and easily controlled size and functionality, dendrimers constitute ideal molecular building blocks for a wide range of surface-related applications. Langmuir monolayers formed from amphiphilic dendrimers have recently been utilized by several research groups in order to probe behaviors such as shape, compressibility, and the localization of end-groups. Moreover, by studying their behavior at the air–water interface, one can gain further understanding of the relationship between physical properties and dendrimer generation. Similarly, the study of self-assembled monolayers of dendrimers on solid substrates has enhanced our understanding of the novel properties that are only accessible through surface confinement. Examples of applications of monolayers and other ultra-thin films assembled from tailor-made dendritic macromolecules have recently begun to appear in mission-oriented research such as functional materials for sensors or for microelectronics. Finally, the globular shape and multifunctional periphery of dendrimers makes them well suited for the construction of multilayer nanocomposite materials. These novel materials have recently been utilized to fabricate chemical and biological sensor devices as well as membranes responsive to external stimuli. The main goal of this article is to highlight the recent activity in both the study and the applications of dendrimers at surfaces and interfaces.

David Tully was born New York in 1973 and grew up in Wisconsin. He graduated cum laude with a B.S. in Chemistry from the University of Minnesota in 1996, where he did his undergraduate thesis research with Professor Larry L. Miller. He recently completed his PhD in Chemistry at the University of California, Berkeley, under the direction of Professor Jean M. J. Fréchet. He currently holds a position as a staff scientist at the Genomics Institute of the Novartis Research Foundation in San Diego, California.

Jean M. J. Fréchet obtained his first degree at the Institut de Chimie et Physique Industrielles (now CPE) in Lyon, France, and PhD degrees from the College of Environmental Sciences and Forestry and Syracuse University. Following academic appointments at the University of Ottawa (1973–1986) and Cornell University (1987–1996), he joined the Department of Chemistry at the University of California in Berkeley where he also heads the polymer program at the Lawrence Berkeley National Laboratory. J. Fréchet received both the American Chemical Society awards in Polymer Chemistry and in Applied Polymer Science; in 2000 he was elected a Fellow of the American Academy of Arts and Sciences, a member of the National Academy of Engineering, and a member of the National Academy of Science.

Dendrimers at the air–water interface

Initial studies of dendrimers at the air–water interface were carried out by Saville *et al.*[8] using convergent Fréchet-type poly(benzyl ether)† dendrons with a hydrophilic alcohol moiety at the focal point and hydrophobic benzyl groups at their periphery. Langmuir films were prepared from a homologous series of dendrons ranging from Generation 2 ([G-2]-OH) through Generation 6 ([G-6]-OH). As expected, surface pres-

† The IUPAC name for poly(benzyl ether) is poly(oxymethylphenylene).

DOI: 10.1039/b104290b

sure *versus* molecular area (*Π–A*) isotherms for this series showed that the higher molecular weight dendrons better resist collapse as the pressure is increased. Within the same series, only the lower molecular weight dendrons, [G-2]-OH through to [G-4]-OH, exhibit surfactant-like behavior while the much larger [G-5]-OH and [G-6]-OH dendrons no longer behave as surfactants. This suggests that the focal point of the larger dendrons is sterically shielded within the interior of the molecule, and, as a result, is inaccessible for association with the water surface, in agreement with the results of solvatochromic studies on comparable dendrons with a dye at their focal point.[10]

Neutron reflectivity studies carried out on Langmuir films prepared from analogous [G-4]-OH dendrons with chain-ends deuterated for additional contrast, support a monolayer structure as shown in Fig. 1. The peripheral benzyl groups are located on the outside of the molecule and away from the water interface, while the alcohol at the focal point is associated with the surface of the water. Further evidence from these neutron reflectivity experiments indicates that the [G-4]-OH Langmuir monolayer collapses easily into a stable bilayer. The bottom layer of dendrons, which afforded full surface coverage at all compressions, contained approximately 25% water. Meanwhile, the top layer, which varied in the extent of coverage from 50 to 100%, contained little or no water. This suggests that the bottom dendrimer layer acts as a hydrophobic barrier and prevents water from penetrating this layer. Furthermore, at low compressions, the [G-4]-OH dendrons within the Langmuir film assumed a spherical shape. However, at higher compressions, the dendrons in the lower layer adopted an elliptical shape with a 2:1 aspect ratio as depicted in Fig. 2. This phenomenon will be discussed in further detail below.

Hawker, White, and co-workers also explored the effect of peripheral group chemistry on the surface activity of dendrimers at the air–water interface.[11] For this study, poly(benzyl ether) dendrons were again synthesized with a single alcohol at the focal point but also included either nitrile or methyl ester functional groups at their periphery. The Langmuir film structure of these dendrimers was also analyzed by neutron specular reflectivity and *Π–A* isotherm measurements. It was found that functionalization of the periphery of the dendrons with polar nitrile and ester functionalities leads to monolayers

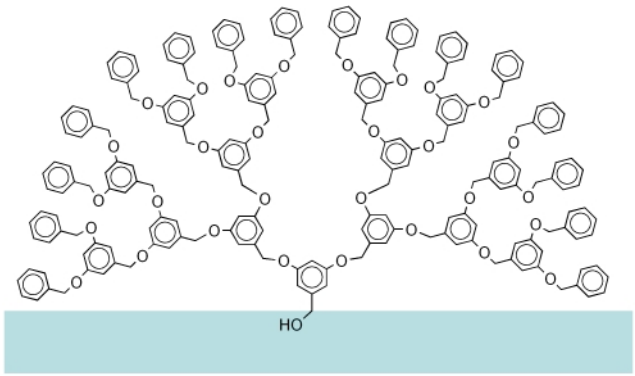

Fig. 1 Idealized structure of [G-4]-OH at the air–water interface.

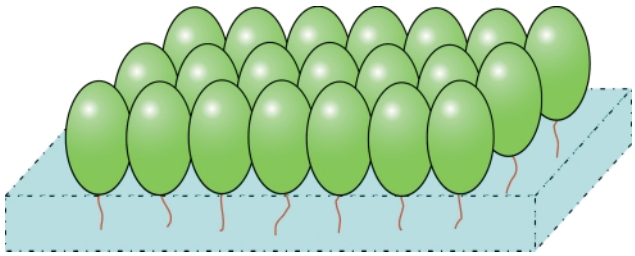

Fig. 2 Poly(benzyl ether) dendrons assume a prolate shape at the air–water interface.

with a structure very different from that of the unfunctionalized, hydrophobic dendrons used in the previous study. In this case the dendrons formed thinner films in which the presence of polar, more hydrophilic nitrile and methyl ester groups increased the affinity of the molecule for the water surface leading to more spreading as the molecules flattened across the interface. In addition, the formation of a bilayer film was not observed as the more polar dendrons tended to move into the water sub-phase under high compression, rather than form bilayers.

A more systematic study was recently carried out by Hawker, Frank and co-workers, in which the researchers examined the Langmuir monolayer structure of a series of dendrimers by changing chemistry at the focal point.[12] Again, Fréchet-type poly(benzyl ether) monodendrons functionalized with benzyl ether groups at the periphery were used for this study. However, this time the chemistry at the focal point of the molecules was adjusted by incorporating oligo(ethylene glycol) chains of varying length. In particular, [G-3] and [G-4] dendrons with mono- through to hexakis-(ethylene glycol) chains at the focal point were used for this study (Fig. 3). Studies of the *Π–A* isotherms for the series of [G-3] dendrons led to the conclusion that the hydrophilic oligo(ethylene glycol) chains extended into the water sub-phase thereby increasing the stability of the monolayer. It was also found that the stability of the monolayers increased with the length of the oligo(ethylene glycol) chain. A similar relationship between monolayer stability and the chain length of the hydrophilic oligo(ethylene glycol) focal point was also observed for the series of [G-4] monodendrons. However, the study concluded that the stability trends for the dendrimer monolayers depended on the relative sizes between the hydrophobic dendron and the hydrophilic focal point chain, as opposed to the absolute size of the oligo(ethylene glycol) unit. The larger [G-4] dendrons produced more stable films, presumably due to the amplified dispersive interactions amongst larger neighboring hydrophobic moieties, which apparently result in a stronger attraction of the hydrophilic focal point for the water sub-phase in the larger dendrons. Previous studies on monolayers consisting of linear fatty acids have also found that monolayer stability was increased by increasing the length of the alkyl chains as a result of the increased attraction between chains.[13]

The comprehensive study by Hawker and co-workers[12] also provided additional insight into the molecular shape of monodendrons assembled into a Langmuir monolayer. The molecular area was measured as a function of molecular weight for the [G-3] through to [G-5] poly(benzyl ether) dendrons, each possessing a hexakis(ethylene glycol) chain at the focal point. A linear relationship was observed for the molecular area as a function of molecular weight [Fig. 4(A)]. However, this measured trend is much smaller than the analogous relationship

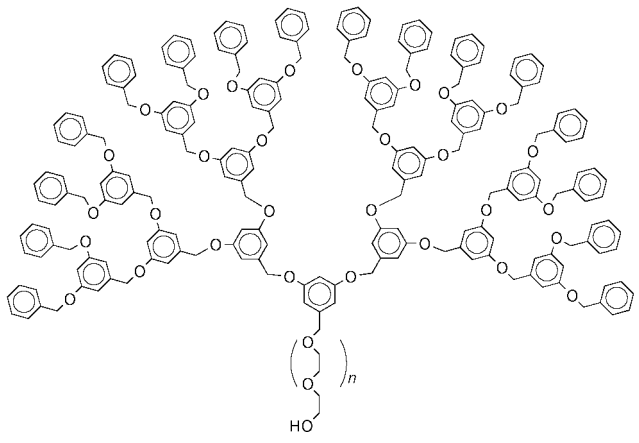

Fig. 3 Hydrophobic poly(benzyl ether) dendron functionalized with a hydrophilic oligo(ethylene glycol) focal point.

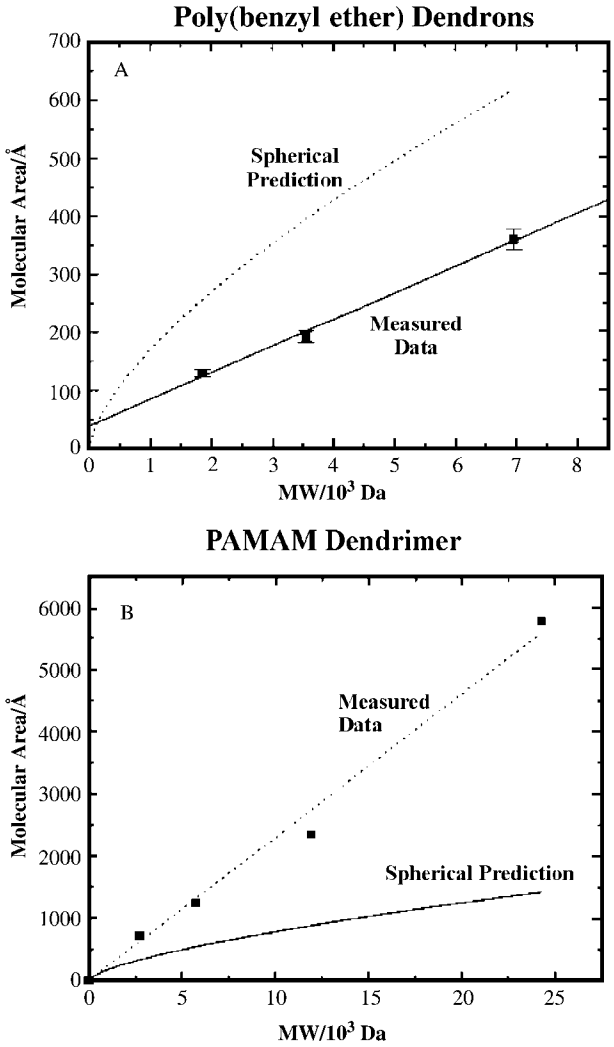

Fig. 4 A. Molecular area (in Å²) of poly(benzyl ether) dendrons as a function of molecular weight. B. Molecular area (in Å²) of PAMAM dendrimers as a function of molecular weight.

predicted for dendrons assuming a spherical shape. Hence, Hawker and co-workers concluded that the monodendrons assumed an ellipsoidal shape at the air–water interface (Fig. 2), in agreement with the conclusions drawn in the earlier studies by Saville *et al.*[8] that involved the same dendrons but with only a single hydroxy group at the focal point. Overall, these studies confirm that once a certain size is reached, poly(benzyl ether) dendrons possess and maintain an overall globular shape than can range from spherical to ovoid depending on the circumstances of their environment. As expected from simple structural considerations, it is only the largest structures or those with considerable steric requirements that can be expected to possess significant rigidity.

Percec and co-workers have used X-ray reflectivity and *Π–A* isotherm measurements to gain additional insight into the molecular structure of a series of functionalized poly(benzyl ether) monodendrons at the air–water interface.[14] In this study, the dendrons' periphery were functionalized with hydrophobic dodecyl chains, while the focal points were substituted with crown ether moieties or oligo(ethylene glycol) units. Their data provide additional evidence that the dendrimer Langmuir monolayers possess a structure consisting of a hydrophilic focal point at or beneath the water surface, and a high density region above the surface consisting of the dendritic block and the peripheral alkyl chains extending upwards from the surface.

The interfacial properties of PEG–poly(benzyl ether) linear-dendritic hybrid block copolymers were also recently examined.[15] Narrow polydispersity poly(ethylene glycol) chains with varying molecular weights were attached to the focal point of [G-2] poly(benzyl ether) dendrons to afford water-soluble hybrid block copolymers. These dendritic-PEG hybrids were then used to modify the surface properties of various polymeric substrates, which were then characterized by water contact angles on polymeric substrates submerged in oil. Treatment of hydrophobic poly(ethylene terephthalate) (PET) surfaces with a dilute aqueous solution of dendritic-PEG copolymer resulted in a marked decrease in the hydrophobicity of the PET surface. This is most likely due to the physisorption of the hydrophobic dendritic block to the lipophilic PET surface, while the hydrophilic PEG chain is extended into the aqueous phase. In contrast, modification of more polar regenerated cellulose resulted in a competitive adsorption between the dendritic head block and the PEG tail also leading to an overall increase in the hydrophilicity of the cellulose surface. These studies have significant implications in the context of stain-proofing fabrics and surface modification in general. They also demonstrate the promising utility of dendrons as modifiers for linear polymer chains as the relatively small dendritic block can impart significant functionality onto the end group of the linear polymer.

Tomalia and co-workers initially examined the behavior at the air–water interface of a series of poly(amido amine) (PAMAM) dendrimers that had been functionalized at the periphery with hydrophobic alkyl chains of varying length.[16] As part of this study, the researchers conducted a series of surface pressure *versus* molecular area isotherm measurements. It was found that the length of the hydrophobic end-group, when varied from hexyl to dodecyl, did not significantly influence the molecular area of the dendrimer at the collapse point in the isotherm. Tomalia and co-workers speculated that the lower generation dendrimers might adopt a conformation in which the hydrophilic dendrimer interior associates with the water surface, while the hydrophobic endgroups either extend upwards and away from the water surface or interdigitate with neighboring molecules. They also proposed a second model in which the dendrimers behaved like hydrophobic spheroids floating on the water surface, in order to account for the observation that the length of the alkyl chains at the periphery did not significantly affect the molecular areas even for the higher generation [G-4] and [G-5] dendrimers.

Shortly after Tomalia's initial account[16] Meijer and co-workers reported on a comprehensive study involving a series of poly(propyleneimine) dendrimers, [G-1] through to [G-5], that were functionalized with a wide variety of different hydrophobic end groups *via* acylation of the peripheral primary amines (Fig. 6).[17] Similar to PAMAM dendrimers, poly(propyleneimine) dendrimers possess a relatively hydrophilic interior due to the presence of a large number of aliphatic tertiary amines. When functionalized at the periphery with either palmitoyl chains (**A**) or long *n*-alkyl chains (**C**) containing an azobenzene chromophore, the amphiphilic dendrimers form stable monolayers, as was shown in a series of *Π–A* isotherms. In addition, the molecular areas of the macromolecules increased linearly with molecular weight, and matched the values that could be calculated for monolayers comprised of palmitoyl chains or alkyloxy–azobenzene chain surfactants alone. Meijer and co-workers concluded that the behavior of these amphiphilic dendrimers could be explained by one model only: namely that the flexible dendrimers assume a flattened conformation in which the hydrophilic dendrimer interior maximizes its association with the water surface, while the hydrophobic end groups are forced upwards and away from the water surface (Fig. 5). Further proof was obtained upon examination of a monolayer that was formed with dendrimer **C** and then transferred to a glass substrate. UV-Vis absorption spectroscopy revealed that the absorption maximum was blue shifted, suggesting the formation of H-type aggregates.[18] This evidence further supports the conclusion by Meijer and co-

workers that the hydrophobic chains adopt a conformation involving a parallel-packed array oriented perpendicular to the water surface.

Although the molecular areas of the series of *n*-alkane-functionalized PAMAM dendrimers at the air–water interface was previously measured and reported by Tomalia and co-workers,[16] the authors did not specifically explore the fundamental relationship between area and molecular weight. Following Meijer's instructive study on poly(propyleneimine) dendrimers,[17] Hawker and co-workers re-examined Tomalia's data concerning the series of epoxy-alkane functionalized dendrimers.[12] They also showed that the molecular area increased linearly with molecular weight (Fig. 4B) in agreement with the data collected earlier for poly(benzyl ether) dendrons.[8,12] However, in contrast to the behavior of the more hydrophobic Fréchet-type dendrons, the measured molecular area for the PAMAM dendrimers was found to be much larger than expected for a spherical model. It appears that the PAMAM dendrimers also assume a flattened, or oblate, conformation when assembled into a Langmuir monolayer (Fig. 5), in a manner similar to the poly(propyleneimine) dendrimers, discovered by Meijer and co-workers.[17] Upon consideration of the chemistry of the three types of dendrimers, these models describing the molecular shapes of dendrimers at the air–water interface can easily be reconciled. Both the PAMAM and poly(propyleneimine) dendrimers possess a polar, hydrophilic interior, resulting from the presence of a large number of amides and tertiary amines. As a result, they minimize their free-energy by association of their polar interior with the water surface, leading to somewhat flattened macromolecules that occupy a larger area than a sphere of comparable volume. Similarly, the hydrophobic chain-ends of the alkyl-modified PAMAM and poly(propyleneimine) dendrimers minimize their free-energy by extending upwards, away from the water surface. Such reasoning, based on simple energy minimization concepts, also explains the initial observation of Tomalia and co-workers that the molecular area of the PAMAM dendrimers does not change upon varying the length of the hydrophobic chain ends from hexyl to dodecyl groups.

In contrast, when poly(propyleneimine) dendrimers were functionalized with bulky adamantyl groups (dendrimer **B**), a different behavior was observed altogether.[17] These dendrimers did not behave like amphiphilic molecules at the air–water interface, but rather formed multi-layers. In addition, the molecular area of these molecules demonstrated a non-linear dependence on molecular weight. As a result, Meijer and co-workers concluded that dendrimer **B** adopts a shape persistent spherical conformation due to the significant steric constraints resulting from the incorporation of bulky peripheral adamantyl groups.

A fifth generation poly(propyleneimine) dendrimer was then randomly substituted with equimolar ratios of palmitoyl chains and azobenzene groups (dendrimer **[G-5]D**).[19] Not surprisingly, this dendrimer also formed stable monolayers with a cylindrical molecular structure similar to that of monolayers formed from the dendrimer series **A** and **C** (Fig. 6). However, while the dendrimers functionalized with 100% azobenzene units (**C**)

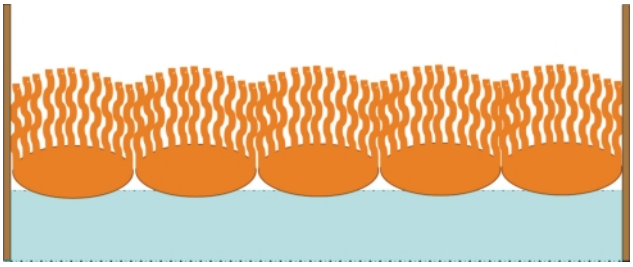

Fig. 5 Peripherally functionalized poly(propyleneimine) and PAMAM dendrimers assume an oblate shape at the air–water interface.

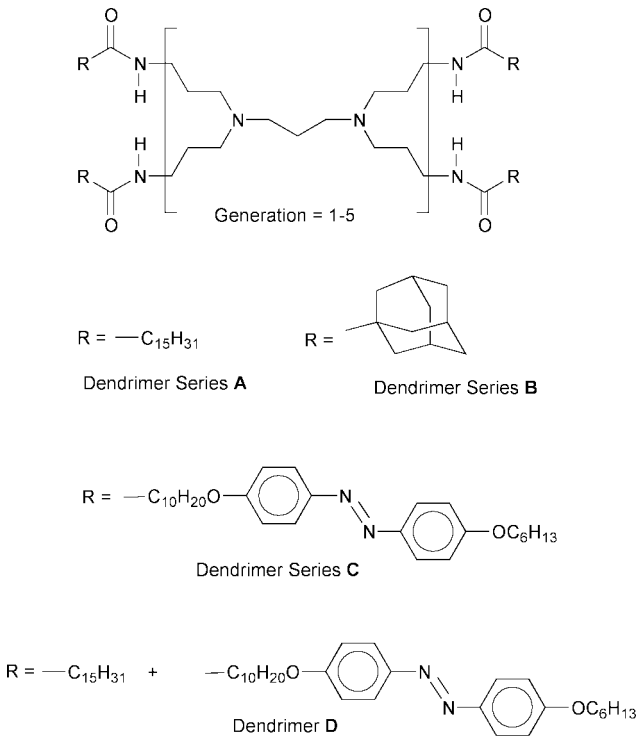

Fig. 6 Functionalized poly(propyleneimine) dendrimers.

exhibited a blue-shifted absorption maximum, indicating favorable π–π stacking among neighboring azobenzene moieties, dendrimer **[G-5]D** did not exhibit this behavior. Presumably the π-stacking of azobenzene groups is prevented by their dilution and solvation by the palmitoyl chains within the monolayer. As a result, reversible photo-switching is enabled for dendrimer **D** with the observation of changes in surface area at constant pressure when the monolayer was alternately irradiated with UV and IR.[19]

McGrath and co-workers have also developed photoresponsive Langmuir monolayers made from functionalized Fréchet-type poly(benzyl ether) dendrons.[20] In this case, the [G-1] through to [G-3] monodendrons were functionalized at their peripheries using *n*-decyl chains while their focal point consisted of an azobenzene unit. Each of the dendrons exhibited amphiphilic behavior and assembled into stable monolayers at the air–water interface. Upon UV irradiation of the [G-1] and [G-2] monolayers, a 10–20% increase in the cross-sectional molecular area A_0, was observed, which was attributed to the photo-switching of the azobenzene moiety from the *trans* to the *cis* isomer. With the monolayers prepared from the larger [G-3] dendrimer, illumination only afforded a minor change in A_0, suggesting that any change occurring within the azobenzene moiety is too small to have a significant effect on the large [G-3] dendron that surrounds it.

Dendrimers have also recently been employed as amphiphilic frameworks for the fabrication of derivatized C_{60} fullerene Langmuir monolayers. Hydrophobic C_{60} does not normally form stable monolayers at the air–water interface, and previous attempts have only led to the formation of ill-defined aggregates. However, in a collaborative effort involving the research groups of Stoddart, Diederich, Echegoyen, and Leblanc, an example of a stable Langmuir monolayer of a fullerene derivative was demonstrated.[21] This was accomplished by attaching C_{60} to hydrophilic glycodendrimer derivatives to afford fullerene–glycodendron conjugates **1** and **2** (Fig. 7). The stable Langmuir monolayers formed by C_{60}-glycodendrons **1** and **2** demonstrated reversible monolayer formation upon successive compression and expansion cycles. The researchers also succeeded in transferring the ordered monolayers onto a quartz substrate and concluded that the bulky

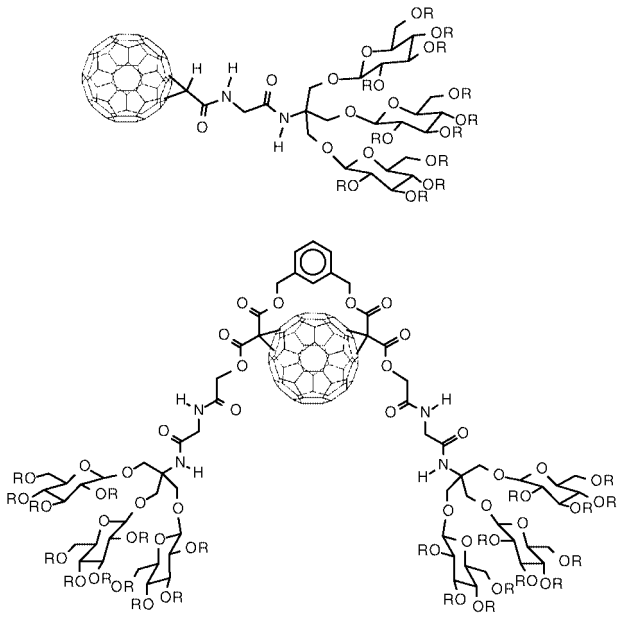

Fig. 7 Fullerene–glycodendron conjugates **1** (upper) and **2** (lower).

dendritic units were responsible for preventing aggregation of the fullerenes, thereby enabling the formation of stable monolayers.

Using an alternative approach, Nierengarten and co-workers functionalized the periphery of polyester dendrons with C_{60} units in order to promote stable monolayer formation at the air–water interface.[22] Upon successive compression and decompression cycles, reversible formation of Langmuir monolayers was observed. The researchers also succeeded in forming stable Langmuir–Blodgett films by transferring the fullerene functionalized dendrimer monolayers onto hydrophobic substrates.

Dendrimer self-assembled monolayers

Self-assembled monolayers (SAMs) of small organic molecules on metal and semiconductor surfaces constitute an area of widespread research.[23] Two systems that have undergone extensive study are alkanethiols on gold and alkylsiloxanes on hydroxylated silicon surfaces. A wide range of different surface chemistries has been employed in applications ranging from lithographic imaging[24–28] and chemical sensing[29] to corrosion passivation[30] and adhesion promotion or inhibition.[31]

The first example of covalent attachment of PAMAM dendrimers to a solid surface was reported by Crooks and co-workers nearly 5 years ago.[32] This was accomplished by forming amide bonds between the peripheral amino-groups of the PAMAM dendrimer and the carboxylic acid groups of a self-assembled monolayer (SAM) of mercaptoundecanoic acid on gold. This, and subsequent research by Crooks and co-workers[33,34] focusing on the development of dendrimer based films as surface-confined chemical sensor arrays has been the subject of a recent review,[29] and will therefore not be covered in detail in this article.

The chemical and physical properties of amine-terminated PAMAM dendrimers adsorbed to gold(111) surfaces have been thoroughly examined by Crooks and co-workers using a variety of analytical techniques.[35–37] When the gold substrate is immersed in a solution of PAMAM dendrimer in ethanol, a stable monolayer is formed presumably due to chemisorption of the terminal amines to the gold surface. PAMAM dendrimer monolayers prepared in this manner were found to be much more stable than monolayers of primary *n*-alkylamine on gold. The polydentate binding interactions between the amine groups of the dendrimer and the gold surface is thought to be responsible for the better stabilization of the dendritic monolayer. The surface-bound conformations of the dendrimers monolayers were also characterized by AFM.[36,37] Monolayer heights for the [G-8] dendrimers were measured to be only approximately 60% of their hydrodynamic diameter, again presumably due to the favorable interactions of the many peripheral amine groups with the gold surface. When the surface is subsequently treated with hexadecanethiol the heights of adsorbed dendrimer monolayers increase although their density on the surface decreases (Fig. 8). The change in height is presumably due to a distortion in the dendrimer shape from a flattened conformation to an upright, prolate shape, or possibly even an agglomeration of dendrimers as the surface amine interactions are replaced by those from a competing hexadecanethiolate monolayer.

Crooks and co-workers also functionalized the periphery of PAMAM dendrimers with varying amounts of thiol groups, and, as expected, these dendrimers formed stable monolayers on gold.[38] X-Ray photoelectron spectroscopy (XPS) suggests that fully thiolated dendrimers are bound to the gold surface utilizing only *ca.* 30% of their terminal thiol groups. Other dendrimers prepared by random functionalization of approximately 20% of their peripheral functionalities with thiol groups form monolayers in which nearly all the peripheral thiol functionalities are bound to the gold surface. This finding attests to the flexibility of the poly(amido amine) dendrimer framework, since randomly distributed peripheral thiols are able to become localized on the same side of the molecule in order to minimize their free energy through interaction with the gold surface.

Self-assembled monolayers of dendrimers on gold were also investigated by Gorman and co-workers,[39] who functionalized the focal point of poly(ether) dendrons with a thiol group. The dendrons, based on the 4,4-bis(4′-hydroxyphenyl)pentanol monomer unit previously developed by our group,[40] were protected at the periphery with hydrophobic benzyl ether groups and then functionalized at the focal point with a benzenethiol moiety (Fig. 9).[41] Self-assembled monolayers were prepared by

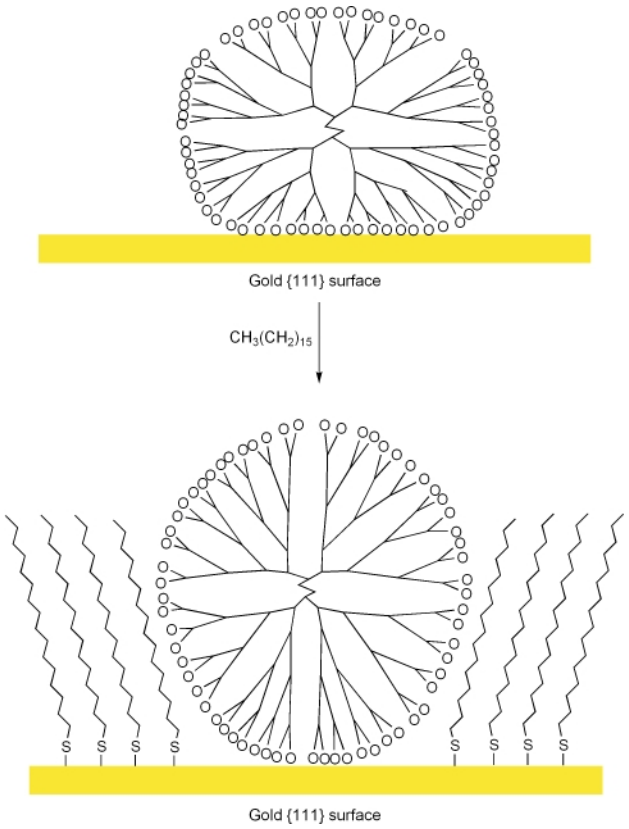

Fig. 8 PAMAM dendrimers adsorbed to gold change shape from oblate to prolate upon co-adsorption of hexadecanethiol.

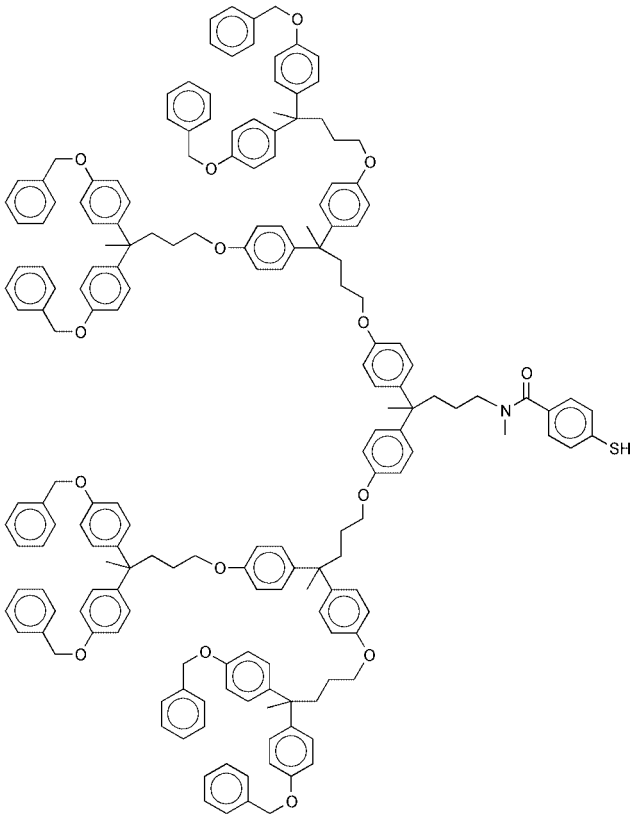

Fig. 9 Poly(ether) dendron with thiol-functionalized focal point.

immersing the polycrystalline gold substrate into a solution of the dendritic thiol. Analysis of the SAM structure by XPS verified that the dendrons were covalently bound to the gold substrate as the aryl thiolate, which is not unexpected considering the relatively flexible nature of the specific dendritic scaffold used. The extent of surface coverage for [G-1] and [G-2] dendrons analyzed by optical ellipsometry was close to 100%. Ellipsometric data for the SAMs formed from [G-3] dendrons showed thinner than expected film thicknesses, indicating either incomplete surface coverage or flattening of the macromolecules. In addition, the relative permeabilities of the dendrimer SAMs were determined using capacitance and redox probe measurements. The capacitance measurements showed that the dendrimer monolayers were more permeable to F^- and Cl^- anions than *n*-alkanethiolate SAMs of comparable thicknesses. This result is not unexpected given the disordered structure of a dendritic SAM in comparison to the ordered quasi-crystalline packing of *n*-alkanethiolate SAMs.

In our own laboratories, we have investigated the preparation of ultra-thin dendrimer films and self-assembled monolayers on silicon surfaces for their possible use as resist materials for scanning probe nanolithography.[42,43] In earlier studies, the scanning probe microscope (SPM) had been used as a direct-write-and-read tool for the lithographic patterning of passivated surfaces with several different chemistries, including self-assembled monolayers on gold[44–46] or silicon,[47–49] and thin polymer films.[50–52]

We first designed modified poly(benzyl ether) dendrimers covalently tethered to a silicon substrate that could serve as passivation resists in scanning probe lithography.[42] The concept of using dendrimers as lithographic resist materials stems from the consideration of their uniform size (several nm in diameter) and globular shape, which might serve as the ideal macromolecular template for a pixel-based approach to lithographic imaging. Specifically, an arrayed monolayer of dendrimers on a surface could act as a resist material for scanning probe lithography by protecting or passivating the surface against a wet etching process. Therefore, we prepared a series of sterically congested, hydrophobic dendrons that could protect the surface of a silicon wafer from an aqueous fluoride etchant. Fréchet-type poly(benzyl ether) dendrons, protected at the periphery with either benzyl ether or *tert*-butyldiphenylsilyl ether groups, were functionalized at the focal point with a covalent tether, consisting of a long alkyl chain derivatized with a terminal chlorosilane coupling agent (Fig. 10). Covalently bound self-assembled monolayers were prepared under anhydrous conditions using these reactive dendrons, and the dendrimer films were characterized by standard analytical techniques.

In addition to covalently bound dendrimer SAMs we have also investigated the synthesis and preparation of ionically bound dendrimer films by an acid/base self-assembly process.[43] In this instance, the poly(benzyl ether) dendrons we designed had a tethered carboxylic acid moiety at their focal point (Fig. 10). A monolayer of dendrons could then be assembled onto an aminated silicon wafer surface prepared by pre-treatment of the clean silicon surface with (3-aminopropyl)triethoxysilane.

We then examined the ability of both types of dendrimer SAMs to serve as etch resists for scanning probe lithography. In the process of scanning probe lithography, the conductive tip of the scanning probe microscope acts as the exposure source (Fig. 11). After the tip is brought into contact with the monolayer surface, a voltage is applied between the tip and the substrate, normally a doped Si(100) wafer. When the process is performed in air, any organic monolayer within the proximity of the intense electric field created between the tip and the substrate undergoes oxidative decomposition. At even higher field strengths, the underlying silicon wafer may also be oxidized, resulting in the formation of raised oxide relief features on the substrate. This occurs as a result of the volume expansion of the silicon wafer due to the incorporation of oxygen into the silicon crystalline lattice. Finally, the latent image in the monolayer can be transferred into the underlying substrate using a selective etch process.

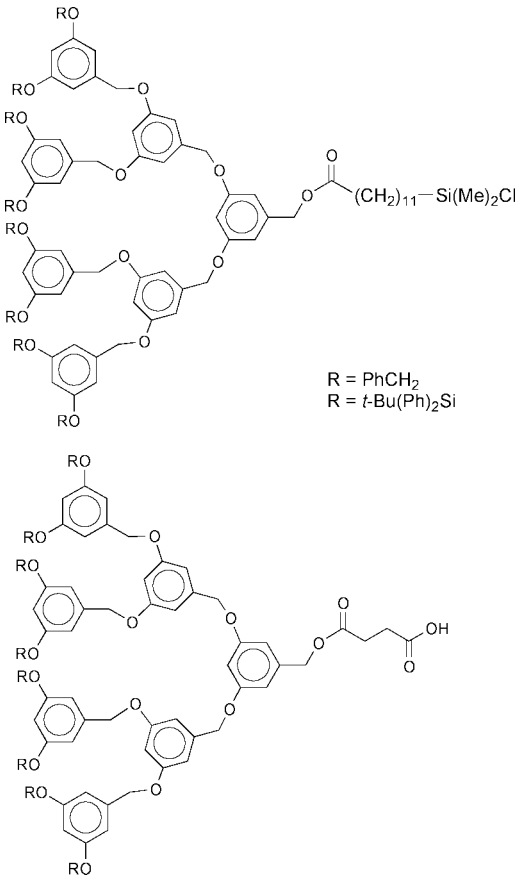

Fig. 10 Poly(benzyl ether) dendrons for covalent and ionic assembly.

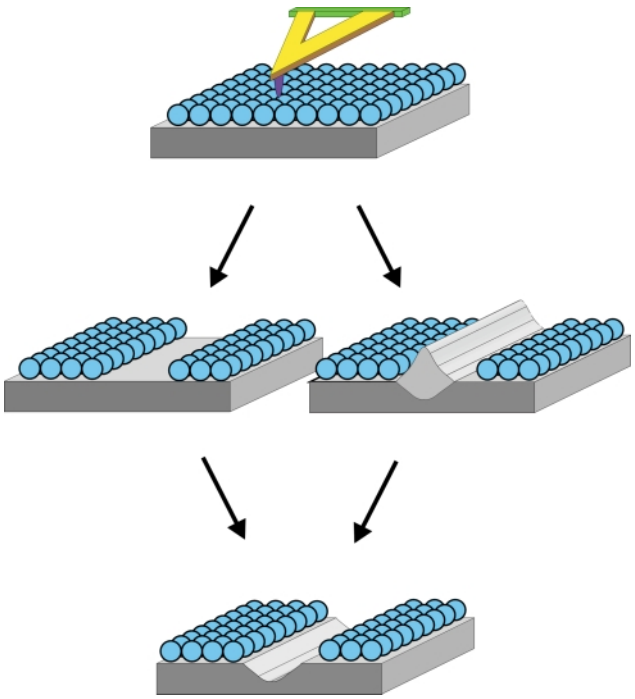

Fig. 11 Schematic representation of field enhanced oxidation: dendrimer self-assembled monolayer (top); oxidative degradation of dendrimer monolayer at low field intensity (center left); oxidation of silicon substrate at high field intensity (center right); aqueous HF transfers pattern into positive tone image in silicon wafer (bottom).

Our experiments have demonstrated that dendrimer monolayers can indeed serve as effective passivation resists for scanning probe lithography. Although these experiments were performed without optimization of either the instrumental or the processing parameters, we were able to successfully create latent patterns on the surface that had feature sizes of *ca.* 35 nm. Furthermore, the dendrimer monolayers efficiently resisted the aqueous fluoride etching process, as evidenced from the lack of any line broadening or pitting in the unexposed regions of the film during the wet etching process. While the dimensions of imaged features far exceed the size of individual dendrimer molecules, it is clear that with optimization of the tip and of the processing conditions could lead to images with sizes in the range of 5–15 nm. Practical implementation would of course also require multiplexing of a very large number of tips.

Other interesting examples of applications involving dendritic SAMs include the use of biomolecule functionalized dendrimer monolayers for the development of affinity biosensors. Kim and co-workers have developed an electrochemical biosensor device that is capable of detecting the avidin–biotin interaction by monitoring the redox properties of free glucose oxidase in a glucose containing electrolyte solution using cyclic voltammetry. Self-assembled monolayers of amine-terminated PAMAM dendrimers were prepared on gold electrodes and the periphery was randomly functionalized with both ferrocenyl groups and biotin analogues.[53,54] In the absence of avidin, an electrochemical signal is generated by the enzymatic activity of glucose oxidase. As the concentration of avidin in the electrolyte solution is increased, the electrochemical signal is decreased due to steric blockage by the avidin adlayer formed on the modified electrode. Finally, the biosensor device can be regenerated by treating it with a solution of excess biotin, which results in desorption of avidin from the biotinylated dendrimer surface.

Multilayer dendrimer films

The earliest known study involving the assembly of dendrimers onto solid surfaces was based on the formation of dendrimer-composite multilayers. Regen and Watanabe[55] first demonstrated this concept by using PAMAM dendrimers to construct multilayers using a method involving coordination chemistry to prepare the thin films. An oxidized silicon surface was treated with (3-aminopropyl)triethoxysilane, followed by adsorption of K_2PtCl_4 from solution to the aminated surface. Next, PAMAM dendrimers, terminated on the periphery with primary amines, were adsorbed to the Pt^{2+} activated surface. This process could be repeated many times over to build up a multilayer of dendrimers with thicknesses of *ca.* 100 nm.

Other examples of PAMAM dendrimer multilayer formation include the formation of dendrimer-polyanhydride composite films on a variety of substrates. Bergbreiter and co-workers developed a multistep process that involves the sequential deposition of orthogonally reactive functional polymers to prepare the composite films that constitute the basis for a variety of ultrathin membrane materials.[56] An amino-functionalized surface is first prepared by treating glass or oxidized silicon with (3-aminopropyl)triethoxysilane. The aminated surface is then treated with a solution of poly[maleic anhydride-*co*-(methyl vinyl ether)] (Gantrez™) that reacts with the surface amines through amide bond formation with the maleic anhydride monomer units. Next, treatment of this modified surface with a solution of amine terminated PAMAM dendrimer results in the grafting of dendrimer molecules onto the surface *via* reaction of the amines with any previously unreacted anhydrides remaining in the first layer of Gantrez. Further sequential deposition of Gantrez and PAMAM dendrimer results in an alternating layer-by-layer build-up of the two polymers. Deposition of the grafted polymers was verified by optical ellipsometry, which demonstrated a linear increase of thickness with each stage of deposition.

These Gantrez–PAMAM composite thin films were shown to function as pH-responsive permeable membranes, as confirmed by a variety of electrochemical experiments.[57,58] The internal chemical composition of the composite films is thought to be homogeneous, and the incorporation of poly(amine) segments and poly(carboxylic acid) segments results in an amphoteric copolymer film. Composite films were coated onto a gold electrode, and cyclic voltammetry was used to monitor the permeability of the films towards cations and anions at different pH. In acidic solution (pH = 3.0), the dendrimer–Gantrez composite films were permeable to anions, such as $Fe(CN)_6^{3-}$, and impermeable to cations, such as $Ru(NH_3)_6^{3+}$. Conversely, in an alkaline solution (pH = 11.0) the films are impermeable to anions and permeable to cations. Furthermore, at neutral pH, the composite films allowed both cations and anions to diffuse through to the electrode. Finally, thermally annealing the dendrimer–Gantrez composite films at 120 °C, for 2 h led to further crosslinking, and resulted in the formation of a new film that was highly impermeable to ionic species over the entire pH range studied.[58] This simple approach to highly-crosslinked, polyfunctional films is quite versatile, and one could easily conceive of variations on this theme that could easily be adapted to other applications. Furthermore, the chemically robust nature and impermeability of the annealed films demonstrates their potential for use as coating materials for the prevention of corrosion.

A recent report from Crooks and co-workers details the use of this sequential deposition technique in conjunction with microcontact printing[24,25] to fabricate patterned PAMAM–Gantrez composite multilayer films.[59] This was accomplished by initial formation of a patterned monolayer of *n*-hexadecanethiol on a gold-coated silicon wafer using a prefabricated poly(dimethylsiloxane) (PDMS) stamp. Next, the substrate was treated with a solution of amine-terminated [G-4] PAMAM dendrimer. A monolayer of this poly(amine) dendrimer was preferentially adsorbed only onto the regions of the gold surface that are not passivated with the *n*-hexadecanethiolate monolayer. Finally, the substrate is treated with a solution

of Gantrez, resulting in the selective deposition of the anhydride containing copolymer only onto the patterned dendrimer regions. This sequential layer-by-layer deposition is repeated in a fashion analogous to the method previously described[56] to build up patterned PAMAM–Gantrez composite films. This method provides a convenient approach to patterned ultrathin organic films for applications in which durable, polyfunctional films are required, such as the patterning of biological molecules or cells.

An alternative method for dendrimer multilayer formation was later developed by Tsukruk and coworkers,[60,61] which hinges on the technique of electrostatic self-assembly developed by Decher.[62] The motivation for this work was said to be related to the development of modified tribological surfaces for boundary lubrication, however no specific applications were reported. Although electrostatic self-assembly is a simple and versatile method for the deposition of polymer multilayers, the resulting films are not as chemically robust as those developed by Bergbreiter and co-workers due to the absence of any covalent bonds among the adjoining layers. Once again, PAMAM dendrimers functionalized with either primary amines or carboxylic acids at their periphery were used for this study. Deposition of an initial layer of amine-terminated dendrimers was performed at pH < 3 to promote adsorption of the positively charged ammonium salts to the anionic silicon surface. A layer of carboxylic acid terminated PAMAM dendrimer was then deposited at pH > 6, a value that favors assembly of the anionic carboxylate salts onto the positively charged ammonium salt layer. Alternating sequential deposition of oppositely charged dendrimers led to a multilayer dendrimer–salt composite film. Thickness measurements of the initial dendrimer layer and subsequent multilayers were performed using atomic force microscopy (AFM). The data showed that the thicknesses of the initial dendrimer monolayers were much smaller than the previously measured hydrodynamic diameters of the PAMAM dendrimers.[2] Furthermore, the thickness of the composite multilayers was also much less than expected for superposed layers of spherical macromolecules. This indicates again that the charged PAMAM dendrimers assume a highly compressed or flattened conformation when arranged on the surface. However, it is also likely that incomplete surface coverage contributes to the lower than expected thickness measurements that were obtained.

Tomalia and co-workers have also used the electrostatic deposition technique to form gold-dendrimer nanocomposite films.[63,64] A layer of cationic poly[dimethyl(diallyl)ammonium chloride] was first deposited onto a negatively charged substrate, followed by the deposition of anionic poly(sodium styrene-4-sulfonate). The bilayer modified substrate was then treated with a solution of positively charged PAMAM dendrimer–gold nanoparticle nanocomposite, which uniformly assembles onto the surface. The authors contend that such materials may be useful for catalysis or optoelectronic applications in which ultrathin nanocomposite films are required, however this concept has yet to be realized.

Dendrimers have also recently been employed as polyfunctional templates for the surface immobilization of biological macromolecules. Anzai and co-workers have recently demonstrated that alternating sequential deposition could be utilized to prepare dendrimer–protein composite multilayer films.[65] This was accomplished by first depositing a layer of fluorescein isothiocyanate-labeled avidin (FITC-avidin) onto a hydrophobic gold or quartz surface. Next, the substrate was treated with a solution of biotin-labeled PAMAM dendrimer, which then assembled onto the surface *via* the well-known avidin–biotin complexation. The sequential deposition process could be repeated to build up dendrimer–avidin composite multilayer films. Although these materials have no distinctive utility by themselves, their preparation constitutes a convenient generalized approach toward functional polymer–biomolecule thin film materials that could potentially incorporate other useful functionalities.

Another example of dendrimer–protein composite multilayers was recently reported by Kim and Yoon.[66] This involves the deposition of an initial layer of periodate treated glucose oxidase (GOx) onto an aminated gold surface *via* the formation of Schiff bases between the aldehyde groups of oxidized GOx with the primary amines on the surface. In the next step, the substrate was treated with a solution of amine-terminated PAMAM dendrimer, which then reacts with any remaining GOx aldehydes also *via* imine formation to covalently bind the dendrimer molecules to the surface. Reductive amination of the Schiff bases was then employed to ensure against dendrimer desorption. Cyclic voltammetry was then used to probe the extent of active enzyme immobilized within the dendrimer–GOx multilayers. It was found that the electrocatalytic response of the electrode was significantly enhanced with respect to multilayer growth, suggesting that sensitivity is tunable by controlling the thickness of the multilayer films. Finally, the film stability with time was investigated, and it was found that over 80% of the initial electrode response was maintained after 20 days.

Solvent cast dendrimer films

There has been considerable interest in the properties and potential applications of dendrimer films prepared by drop- and spin-casting from solution onto solid substrates. A number of groups have focused on investigating the physical properties of dendrimers on solid surfaces using AFM. Sheiko and co-workers first examined the properties of hydrophobic carbosilane dendrimers deposited onto mica and pyrolytic graphite surfaces.[67] The wetting behavior was investigated by spin-casting dilute solutions of the dendrimer onto chemically different surfaces. AFM was then used to analyze the microscopic contact angles of the sub-micron sized droplets of dendrimers formed on the surface. It was found that the hydrophobic dendrimers did not interact specifically with the substrate and the molecules were observed to aggregate into large clusters that behaved like fluid droplets. When the periphery of the carbosilane dendrimers was functionalized with hydroxy groups, the resulting dendrimer possessed an amphiphilic structure with a hydrophobic interior and a hydrophilic periphery, hence leading to a reorganization of the films due to a preferential adsorption of the peripheral hydroxy groups onto the polar mica surface.[68]

Mülhaupt and co-workers used AFM to investigate the film formation of carbosilane dendrimers functionalized at the periphery with mesogenic cholesteryl groups.[69] Films of the mesogen-substituted dendrimers were prepared by drop-casting solutions of varying concentrations onto mica surfaces, followed by evaporation of the solvent. Analysis using AFM showed the formation of both monolayers and multilayers, depending on the initial concentration of the casting solution. Annealing of the lower generation dendrimers led to a reorientation of the molecules on the surface, presumably as a result of the reorganization of the mesogenic peripheral units.

De Schryver and co-workers have also used AFM to probe the physical properties of poly(phenylene) dendrimers.[70] By spin-casting from very dilute solution, poly(phenylene) dendrimers were deposited onto mica surfaces as well separated, individually resolved molecules. Using non-contact mode AFM, the researchers were able to obtain measurements of the dendrimer heights, which were in agreement with the sizes calculated using molecular dynamics simulations. In addition, the adhesion and stiffness properties of individual dendrimer molecules were measured using a pulsed force mode AFM. In comparison with the mica substrate, poly(phenylene) dendrimers and their aggregates exhibited low adhesion and high stiffness, which is not unexpected given the chemical composi-

tion of the hydrophobic, rigid molecular architecture of the poly(phenylene) dendrimer.

Klein and co-workers have used a surface force balance to measure surface interactions and friction in dendrimers adsorbed between mica surfaces. Their first report concerned low surface energy hydrophobic poly(propyleneimine) dendrimers that were functionalized at the periphery with *N*-Boc-phenylalanine.[71] Both shear and frictional forces were measured between two sliding surfaces treated with an adsorbed ultra-thin film of dendrimers. The compressibility of the dendrimer spheres was found to decrease as the molecules were progressively compressed. Furthermore, the researchers concluded that the behavior of these hydrophobic dendrimers was intermediate between that of a solid and a flexible polymer, as they did not exhibit stick–slip sliding. In the following study, Klein and co-workers examined the behavior of a high surface energy, or polar dendrimers under the same conditions.[71] For this comparative study, carbosilane dendrimers terminated with peripheral alcohol groups were used for the surface force balance measurements. In this case, the hydrophilic carbosilane dendrimer behaved more like a rigid sphere. Upon shearing, the molecules underwent relaxation of stored stress. In addition, these dendrimers exhibit stick–slip behavior similar to frozen monolayers of confined liquids.

We have recently investigated the interfacial properties of alkyl chain-modified dendrimers as surface primers for bonding polyolefin substrates. In this study, the end groups of poly(propyleneimine) dendrimers were functionalized with long-alkyl chain aldehydes *via* imine formation followed by reductive amination.[72] A thin film of the alkyl-modified dendrimer was then used as a primer layer for the adhesive joining of a variety of different polyolefin surfaces. Initial studies made use of cyanoacrylate adhesives that are normally incapable of bonding polyolefin surfaces. Block-shear testing of the adhesive strength revealed that in most cases failure could be attributed to substrate rather than adhesive failure, thereby demonstrating that the dendrimer films functioned as highly effective primers for ethyl cyanoacrylate bonding of poly(ethylene) and poly(propylene) substrates.

Recently, there have been a growing number of reports concerning the use of dendrimer-based thin films in a variety of microelectronics-related applications. Dendrimers in the condensed phase display many physical properties that differ significantly from their linear counterparts. We have been interested in exploring some of the unique properties of dendrimers for the development of new materials for applications in microelectronics. While our group has long been active in the areas of photolithography[73] and resist materials,[74] we have recently initiated a study of the various parameters that control resist material performance as a function of polymer architecture. The current state of the art resist materials incorporating chemical amplification[74] are all based on linear polymers as the matrix resin. The use of dendrimers as resist materials for 'next-generation lithography' may prove advantageous when the desired feature sizes approach macromolecular dimensions. In contrast to linear polymers, dendritic polymers are relatively free of chain entanglement. This may have important implications in designing resist materials for ultra-high resolution imaging, where parameters such as line-edge roughness, acid diffusion, and dissolution rates begin to have a serious impact on resist performance.

We have recently reported the first dendrimer-based chemically amplified resist.[75,76] Fréchet-type poly(benzyl ether) dendrimers with Boc (Fig. 12) or *tert*-butyl ester groups at their periphery were synthesized *via* a modification of the convergent route. Resist films were prepared by spin-casting a dendrimer-solution containing a catalytic amount of photo-acid generator (typically a triaryl sulfonium salt) onto a silicon wafer. These dendrimer films, normally several hundred nm thick, exhibited high sensitivity to both deep ultra-violet (DUV) and electron

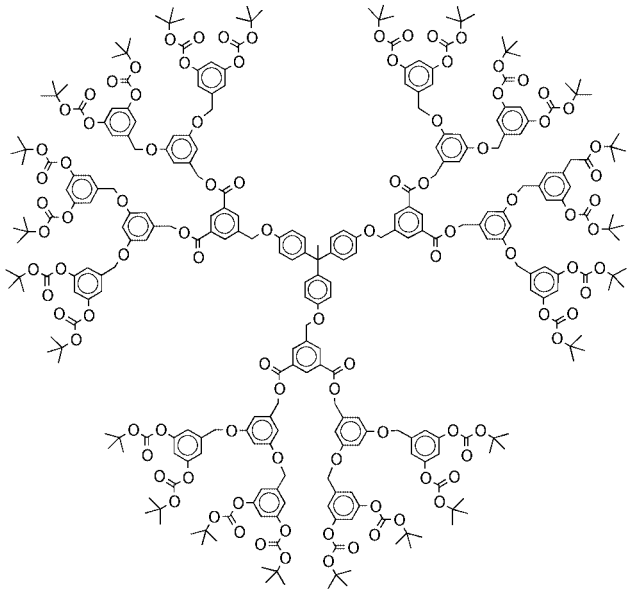

Fig. 12 Boc terminated [G-3] dendrimer.

beam radiation (E-beam). Since we are primarily interested in the performance of dendritic polymers for imaging feature sizes below 100 nm and there is a serious lack of imaging tools capable of such performance, we focused on electron-beam lithography and explored the performance of our dendrimer films as E-beam resists. As expected, these chemically amplified dendrimer resists displayed a high sensitivity to E-beam radiation while allowing image development in either the positive or the negative tone (Fig. 13). The scanning electron micrograph of Fig. 14 shows an example of a line pattern fabricated in a film cast from Boc terminated poly(benzyl ether) dendrimer. Even without optimization of the lithographic

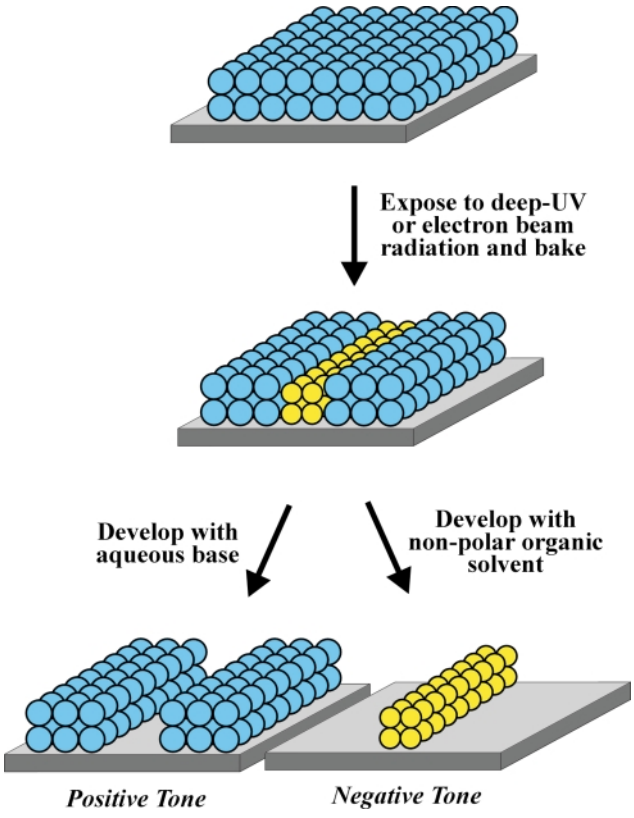

Fig. 13 UV or E-Beam exposure, followed by a bake step removes Boc protecting groups creating a latent, or chemical, image in the film. The dual tone resist can be developed with either aqueous base to afford positive tone images, or with anisole, to produce negative tone images.

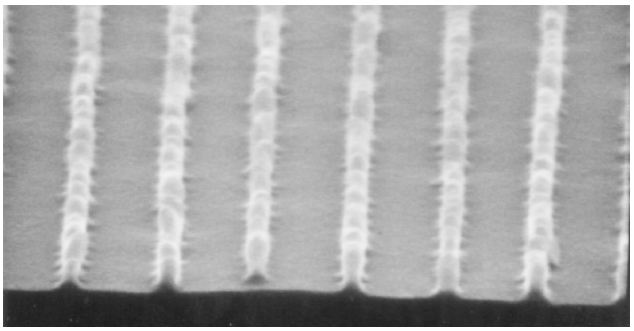

Fig. 14 SEM of negative tone images generated in Boc dendrimer resist. Linewidths: 50 nm; line heights: 100 nm; dose: 15 μC cm^{-2}.

processing parameters, feature sizes below 50 nm could consistently be printed. We are currently involved in the development of several new designs for dendritic polymers that may contribute to vastly enhanced lithographic resist performance. However there are undoubtedly serious limitations in the actual utility of dendrimers as commercial resist materials due to the obvious synthetic difficulty and expense of a multistep convergent dendrimer synthesis. As a result, the performance of a variety of related dendritic structures including hyperbranched polymers as chemically amplified resist materials is also under investigation.[77]

Functional dendritic polymers have also recently been used as templating agents to prepare nanoporous thin films for use as dielectric insulators. Therefore, Hedrick and co-workers have prepared highly branched copolymers by the ring opening polymerization of ε-caprolactone from dendritic initiators.[78,79] Composite films were made by spin-casting a solution of the dendritic polymer and a poly(silsesquioxane) precursor onto a silicon wafer. When the film is thermally annealed at 250 °C, a crosslinked organic–inorganic nanocomposite material is formed. Upon further heating to over 400 °C, the dendritic organic component of the film thermally decomposes into volatile byproducts, leaving behind a closed-cell nanoporous silicate foam. Since a significant proportion of the volume of this new material is occupied by air with a relative permittivity $k \cong 1.0$, an overall bulk relative permittivity below 2.0 is observed, making these materials promising candidates for high-end microelectronic applications where low-*k* dielectric materials are urgently needed. The commercial exploitation of this approach is now well under way.

Other recent applications that make use of dendrimer-based thin film materials include sensor devices that detect volatile organic compounds (VOCs). One such sensor device, developed by Miller and co-workers, detects VOCs on the basis of electrical conductivity changes in a dendrimer-based thin film.[80,81] The periphery of poly(amide) dendrimers was functionalized with oligothiophene derivatives, which function as the charge carriers. Thin films were prepared by first casting the neutral dendrimers from solution, followed by an oxidative doping with iodine vapor. The doped films were stable in air and exhibited true electronic conductivity ($\sigma = 10^{-3}$ S cm^{-1}). Upon exposure to organic vapors, the conductivity of the films was increased by as much as three orders of magnitude. Importantly, the conductivity response was fully reversible, and the magnitude of the response varied uniquely with the identity of the vapor.

The surface chemistry and interfacial properties of related classes of dendritic macromolecules,[2] such as hyperbranched polymers,[82–84] dendritic-linear hybrid block copolymers,[85] and dendronized or dendron-jacketed linear polymers,[86,87] have also recently become an area of growing interest, although they are beyond the scope of this brief review focusing specifically on dendrimers. Finally, the design and application of dendrimers and dendrimer-based films for opto-electronic applications such as light harvesting and light emitting diodes have been the focus of a recent review,[88] and therefore will not be discussed in this article.

Conclusions and outlook

The past several years have seen a considerable growth in the use of dendrimers at surfaces and interfaces. This results from the realization that the unique dendritic architecture of dendrimers can translate into unusual chemical and physical properties. While the demanding methods used for the preparation of dendrimers currently negate their use as commodity materials, it is clear that they are well suited for practical application at surfaces and interfaces where small amounts of materials only are needed. Early work with self-assembled dendrimer monolayers in applications such as resists for scanning probe lithography, affinity biosensors, and chemosensor devices have already demonstrated some of the capabilities of dendrimers. Such findings, coupled to others related to the rheological properties of dendrimers,[89] their ability to encapsulate[90] or harvest and concentrate energy[88] will no doubt continue to fuel interest in numerous 'designer' dendrimers for applications in nanotechnology. Another area of growth for dendrimers will involve their use at biological interfaces as their shape and surface functionality make them ideally suited for accessing, recognizing, coating or penetrating cell membranes. The outlook for continued activity in this field is strong, and many new discoveries and developments in chemistry, materials science, and biology involving dendrimers at surfaces and interfaces can be anticipated.

Acknowledgements

We thank the National Science Foundation (DMR-9816166), Semiconductor Research Corporation (SRC contract 96-LC-460), the Defense Advanced Research Projects Agency (DARPA grant MDA972-97-1-0010), and the AFOSR and ARO-MURI programs for their generous support of our research.

Notes and references

1 D. A. Tomalia, A. M. Naylor and W. A. Goddard III, *Angew. Chem., Int. Ed. Engl.*, 1990, **29**, 138.
2 J. M. J. Fréchet, *Science*, 1994, **263**, 1710.
3 G. R. Newkome, C. N. Moorefield and F. Vögtle, *Dendritic Molecules: Concepts, Syntheses, Perspectives*, VCH, Weinheim, Germany, 1996.
4 D. A. Tomalia, H. Baker, J. Dewald, J. M. Hall, G. Kallos, R. Martin and J. Ryder, *Polym. J.*, 1985, **17**, 117; G. R. Newkome, Z. Yao, G. R. Baker and V. K. Gupta, *J. Org. Chem.*, 1985, **50**, 2003.
5 C. J. Hawker and J. M. J. Fréchet, *J. Am. Chem. Soc.*, 1990, **112**, 7638; S. Grayson and J. M. J. Fréchet, *Chem. Rev.*, 2001, in the press.
6 C. J. Hawker, R. Lee and J. M. J. Fréchet, *J. Am. Chem. Soc.*, 1991, **113**, 4583.
7 A. W. Bosman, H. M. Janssen and E. W. Meijer, *Chem. Rev.*, 1999, **99**, 1665.
8 P. M. Saville, J. W. White, C. J. Hawker, K. L. Wooley and J. M. J. Fréchet, *J. Phys. Chem.*, 1993, **97**, 293; P. M. Saville, P. A. Reynolds, J. W. White, C. J. Hawker, J. M. J. Fréchet, K. L. Wooley, J. Penfold and J. R. P. Webster, *J. Phys. Chem.*, 1995, **99**, 8283.
9 V. V. Tsukruk, *Adv. Mater.*, 1998, **10**, 253.
10 C. J. Hawker, K. L. Wooley and J. M. J. Fréchet, *J. Am. Chem. Soc.*, 1993, **115**, 4375.
11 G. F. Kirton, A. S. Brown, C. J. Hawker, P. A. Reynolds and J. W. White, *Physica B*, 1998, **248**, 184.
12 J. P. Kampf, C. W. Frank, E. E. Malmström and C. J. Hawker, *Langmuir*, 1999, **15**, 227.
13 M. C. Petty, *Langmuir-Blodgett Films: An Introduction*, Cambridge University Press, Cambridge, 1996.
14 W. J. Pao, M. R. Stetzer, P. A. Heiney, W. D. Cho and V. J. Percec, *Phys. Chem. B*, 2001, **105**, 2170.
15 J. M. J. Fréchet, I. Gitsov, T. Monteil, S. Rochat, J. F. Sassi, C. Vergelati and D. Yu, *Chem. Mater.*, 1999, **11**, 1267.
16 Y. Sayed-Sweet, D. M. Hedstrand, R. Spinder and D. A. Tomalia, *J. Mater. Chem.*, 1997, **7**, 1199.

17 A. P. H. J. Schenning, C. Elissen-Roman, J. W. Weener, M. W. P. L. Baars, S. J. van der Gaast and E. W. Meijer, *J. Am. Chem. Soc.*, 1998, **120**, 8199.
18 M. Shimorura and T. Kunitake, *Chem. Lett.*, 1981, 1001.
19 J. W. Weener and E. W. Meijer, *Adv. Mater.*, 2000, **12**, 741.
20 A. Sidorenko, C. Houphouet-Boigny, O. Villavicencio, M. Hashemzadeh, D. V. McGrath and V. V. Tsukruk, *Langmuir*, 2000, **16**, 10 569.
21 F. Cardullo, F. Diederich, L. Echegoyen, T. Habicher, N. Jayaraman, R. M. Leblanc, J. F. Stoddart and S. Wang, *Langmuir*, 1998, **14**, 1955.
22 D. Felder, J. L. Gallani, D. Guillon, B. Heinrich, J. F. Nicoud and J. F. Nierengarten, *Angew. Chem., Int. Ed.*, 2000, **39**, 201.
23 A. Ulman, *Chem. Rev.*, 1996, **96**, 1533.
24 Y. Xia, J. A. Rogers, K. E. Paul and G. M. Whitesides, *Chem. Rev.*, 1999, **99**, 1823.
25 Y. Xia and G. M. Whitesides, *Angew. Chem., Int. Ed.*, 1998, **37**, 550.
26 J. K. Schoer and R. M. Crooks, *Langmuir*, 1997, **13**, 2323.
27 M. Husemann, M. Morrison, D. Benoit, K. J. Frommer, C. M. Mate, W. D. Hinsberg, J. L. Hedrick and C. J. Hawker, *J. Am. Chem. Soc.*, 2000, **122**, 1844.
28 R. Maoz, S. R. Cohen and J. Sagiv, *Adv. Mater.*, 1999, **11**, 55.
29 R. M. Crooks and A. J. Ricco, *Acc. Chem. Res.*, 1998, **31**, 219.
30 R. M. Crooks and F. P. Zamborini, *Langmuir*, 1997, **13**, 122.
31 R. G. Chapman, E. Ostuni, S. Takayama, R. E. Holmlin, L. Yan and G. M. Whitesides, *J. Am. Chem. Soc.*, 2000, **122**, 8303.
32 M. Wells and R. M. Crooks, *J. Am. Chem. Soc.*, 1996, **118**, 3988.
33 M. Q. Zhao, H. Tokuhisa and R. M. Crooks, *Angew. Chem., Int. Ed. Engl.*, 1997, **36**, 2596.
34 H. Tokuhisa and R. M. Crooks, *Langmuir*, 1997, **13**, 5608.
35 H. Tokuhisa, M. Zhao, L. A. Baker, V. T. Phan, D. L. Dermody, M. E. Garcia, R. F. Peez, R. M. Crooks and T. M. Mayer, *J. Am. Chem. Soc.*, 1998, **120**, 4492.
36 A. Hierlemann, J. K. Campbell, L. A. Baker, R. M. Crooks and A. J. Ricco, *J. Am. Chem. Soc.*, 1998, **120**, 5323.
37 W. M. Lackowski, J. K. Campbell, G. Edwards, V. Chechik and R. M Crooks, *Langmuir*, 1999, **15**, 7632.
38 V. Chechik and R. M. Crooks, *Langmuir*, 1999, **15**, 6364.
39 C. B. Gorman, R. L. Miller, K. Y. Chen, A. R. Bishop, R. T. Haasch and R. G. Nuzzo, *Langmuir*, 1998, **14**, 3312.
40 K. L. Wooley, C. J. Hawker and J. M. J. Fréchet, *J. Am. Chem. Soc.*, 1991, **113**, 4252.
41 K. Y. Chen and C. B. Gorman, *J. Org. Chem.*, 1996, **61**, 9229.
42 D. C. Tully, K. Wilder, J. M. J. Fréchet, A. R. Trimble and C. F. Quate, *Adv. Mater.*, 1999, **11**, 314.
43 D. C. Tully, A. R. Trimble, J. M. J. Fréchet, K. Wilder and C. F. Quate, *Chem. Mater.*, 1999, **11**, 2892.
44 L. Stockman, G. Neuttiens, C. Van Haesendonck and Y. Bruynseraede, *Appl. Phys. Lett.*, 1993, **62**, 2935.
45 M. J. Lercel, G. F. Redinbo, H. G. Craighead, C. W. Sheen and D. L. Allara, *Appl. Phys. Lett.*, 1994, **65**, 974.
46 J. K. Schoer and R. M. Crooks, *Langmuir*, 1997, **13**, 2323.
47 H. C. Day, D. R. Allee, R. George and V. A. Burrows, *Appl. Phys. Lett.*, 1993, **62**, 1629.
48 C. R. K. Marrian, F. K. Perkins, S. L. Brandow, T. S. Koloski, E. A. Dobisz and J. M. Calvert, *Appl. Phys. Lett.*, 1994, **64**, 390.
49 H. Sugimura and N. Nakagiri, *J. Am. Chem. Soc.*, 1997, **119**, 9226.
50 T. R. Albrecht, M. M. Dovek, C. A. Lang, P. Grütter, C. F. Quate, S. W. J. Kuan, C. W. Frank and R. F. W. Pease, *J. Appl. Phys.*, 1988, **64**, 1178.
51 K. Wilder, H. T. Soh, A. Atalar and C. F. Quate, *J. Vac. Sci. Technol., B*, 1997, **15**, 1811.
52 K. Wilder, C. F. Quate, B. Singh and D. F. Kyser, *J. Vac. Sci. Technol., B*, 1998, **16**, 3864.
53 H. C. Yoon, M. Y. Hong and H. S. Kim, *Anal. Biochem.*, 2000, **282**, 121.
54 H. C. Yoon, M. Y. Hong and H. S. Kim, *Langmuir*, 2001, **17**, 1234.
55 S. L. Regen and S. Watanabe, *J. Am. Chem. Soc.*, 1994, **116**, 8855.
56 Y. Liu, M. L. Bruening, D. E. Bergbreiter and R. M. Crooks, *Angew. Chem., Int. Ed. Engl.*, 1997, **36**, 2114.
57 Y. Liu, M. Zhao, D. E. Bergbreiter and R. M. Crooks, *J. Am. Chem. Soc.*, 1997, **119**, 8720.
58 M. Zhao, Y. Liu, R. M. Crooks and D. E. Bergbreiter, *J. Am. Chem. Soc.*, 1999, **121**, 923.
59 P. Ghosh, W. M. Lackowski and R. M. Crooks, *Macromolecules*, 2001, **34**, 2131.
60 V. V. Tsukruk, F. Rinderspacher and V. N. Bliznyuk, *Langmuir*, 1997, **13**, 2171.
61 V. N. Blitznyuk, F. Rinderspacher and V. V. Tsukruk, *Polymer*, 1998, **39**, 5249.
62 G. Decher, *Science*, 1997, **277**, 1232.
63 J. A. He, R. Valluzzi, K. Yang, T. Dolukhanyan, C. Sung, J. Kumar, S. K. Tripathy, L. Samuelson, L. Balogh and D. A. Tomalia, *Chem. Mater.*, 1999, **11**, 3268.
64 The subject of dendrimer-encapsulated nanoparticles has been recently reviewed: R. M. Crooks, B. I. Lemon, L. Sun, L. K. Yeung and M. Zhao, *Top. Curr. Chem.*, 2001, **212**, 81; R. M. Crooks, M. Zhao, L. Sun, V. Chechik and L. K. Yeung, *Acc. Chem. Res.*, 2001, **34**, 181.
65 J. Anzai, Y. Kobayashi, N. Nakamura, M. Nishimura and T. Hoshi, *Langmuir*, 1999, **15**, 221.
66 H. C. Yoon and H. S. Kim, *Anal. Chem.*, 2000, **72**, 922.
67 S. S. Sheiko, G. Eckert, G. Ignateva, A. M. Muzafarov, J. Pickermann, H. J. Rader and M. Moller, *Macromol. Rapid Commun.*, 1996, **17**, 283.
68 S. S. Sheiko, A. M. Muzafarov, R. G. Winkler, E. V. Getmanova, G. Eckert and P. Reineker, *Langmuir*, 1997, **13**, 4172.
69 M. C. Coen, K. Lorenz, J. Kressler, H. Frey and R. Mülhaupt, *Macromolecules*, 1996, **29**, 8069.
70 H. Zhang, P. C. M. Grim, P. Foubert, T. Vosch, P. Vanoppen, U. M. Wiesler, A. J. Berresheim, K. Müllen and F. C. De Schryver, *Langmuir*, 2000, **16**, 9009; H. Zhang, P. C. M. Grim, T. Vosch, U. M. Wiesler, A. J. Berresheim, K. Müllen and F. C. De Schryver, *Langmuir*, 2000, **16**, 9294.
71 X. Zhang, M. Wilhelm, J. Klein, M. Pfaadt and E. W. Meijer, *Langmuir*, 2000, **16**, 3884; X. Zhang, J. Klein, S. S. Sheiko and A. M. Musafarov, *Langmuir*, 2000, **16**, 3893.
72 M. Liu and J. M. J. Fréchet, *Polym. Bull.*, 1999, **43**, 379; US Patent Pending WO 99.15580 PCT/US98/19783.
73 For recent reviews on lithography and photoresists, see for example: G. M. Wallraff and W. D. Hinsberg, *Chem. Rev.*, 1999, **99**, 1801; E. Reichmanis, O. Nalamasu and F. M. Houlihan, *Acc. Chem. Res.*, 1999, **23**, 659.
74 S. A. MacDonald, C. G. Willson and J. M. J. Fréchet, *Acc. Chem. Res.*, 1994, **27**, 151.
75 D. C. Tully, A. R. Trimble and J. M. J. Fréchet, *Adv. Mater.*, 2000, **12**, 1118.
76 D. C. Tully, A. R. Trimble and J. M. J. Fréchet, *Poly. Prep.*, 2000, **41**, 142.
77 A. R. Trimble, D. C. Tully, J. M. J. Fréchet, D. R. Medeiros and M. Angelopolous, *Poly. Prep.*, 2000, **41**, 325.
78 J. L. Hedrick, R. D. Miller, C. J. Hawker, K. R. Carter, W. Volksen, D. Y. Yoon and M. Trollsås, *Adv. Mater.*, 1998, **10**, 1049.
79 C. V. Nguyen, K. R. Carter, C. J. Hawker, J. L. Hedrick, R. L. Jaffe, R. D. Miller, J. F. Remenar, H. W. Rhee, P. M. Rice, M. F. Toney, M. Trollsås and D. Y. Yoon, *Chem. Mater.*, 1999, **11**, 3080.
80 L. L. Miller, Y. Kunugi, A. Canavesi, S. Rigaut, C. N. Moorefield and G. R. Newkome, *Chem. Mater.*, 1998, **10**, 1751.
81 L. L. Miller, J. S. Bankers, A. J. Schmidt and D. C. Boyd, *J. Phys. Org. Chem.*, 2000, **13**, 808.
82 B. Voit, *J. Polym. Sci. Part A: Polym. Chem.*, 2000, **38**, 2505.
83 M. E. Mackay, G. Carmenzini, B. B. Sauer and W. Kampert, *Langmuir*, 2001, **17**, 1708.
84 D. E. Bergbreiter and G. Tao, *J. Polym. Sci., Part A: Polym. Chem.*, 2000, **38**, 3944.
85 V. Percec, C. H. Ahn, W. D. Cho, A. M. Jamieson, J. Kim, T. Leman, M. Schmidt, M. Gerle, M. Möller, S. A. Prokhorova, S. S. Sheiko, S. Z. D. Cheng, A. Zhang, G. Ungar and D. J. P. Yeardley, *J. Am. Chem. Soc.*, 1998, **120**, 8619.
86 W. Stocker, B. Karakaya, B. L. Schürman, J. P. Rabe and A. D. Schlüter, *J. Am. Chem. Soc.*, 1998, **120**, 7691.
87 S. A. Prokhorova, S. S. Sheiko, C. H. Ahn, V. Percec and M. Möller, *Macromolecules*, 1999, **32**, 2653.
88 A. Adronov and J. M. J. Fréchet, *Chem. Commun.*, 2000, 1701.
89 P. J. Farrington, C. J. Hawker, J. M. J. Fréchet and M. E. Mackay, *Macromolecules*, 1998, **31**, 5043; C. J. Hawker, P. J. Farrington, M. E. Mackay, K. L. Wooley and J. M. J. Fréchet, *J. Am. Chem. Soc.*, 1995, **117**, 4409; T. H. Mourey, S. R. Turner, M. Rubinstein, J. M. J. Fréchet, C. J. Hawker and K. L. Wooley, *Macromolecules*, 1992, **25**, 2401.
90 S. Hecht and J. M. J. Fréchet, *Angew. Chem., Int. Ed*, 2001, **40**, 74.

CHEMCOMM Communication
www.rsc.org/chemcomm

Catalytic enantioselective addition of aromatic amines to enones: synthesis of optically active β-amino acid derivatives

Wei Zhuang, Rita G. Hazell and Karl Anker Jørgensen*

Center for Metal Catalysed Reactions, Department of Chemistry, Aarhus University, DK-8000 Aarhus C, Denmark. E-mail: kaj@kemi.aau.dk

Received (in Cambridge, UK) 12th April 2001, Accepted 18th May 2001
First published as an Advance Article on the web 14th June 2001

A catalytic enantioselective addition of aromatic amines to enones has been developed; the potential of the reaction is shown for aromatic amines reacting with alkyl oxazolidinones in good yield and with moderate to excellent enantiomeric excess, and the transformation of the products to β-amino acid amides.

Optically active β-amino acids are important molecules[1] which show biological activity in their free from, or as present in many different types of molecules, *e.g.* peptides and depsipeptides.[2a] Furthermore, β-amino acid derivatives can easily be converted into important molecules such as β-lactams.[2b]

Optically active β-amino acids are traditionally prepared by a diastereoselective approach,[1b,3] while only very few methods are available for the direct formation of these compounds by the addition of nitrogen compounds to α,β-unsaturated carbonyl compounds catalysed by chiral Lewis acids as the catalysts.[4] In these investigations *O*-benzylhydroxylamine, hydrazoic acid or imines were used as the nitrogen source in the presence of different chiral Lewis acids.

In the following we will present the first enantioselective addition of secondary aromatic amines **1** to alkyl oxazolidinones **2** catalyzed by chiral Lewis acids [eqn. (1)].[5] This reaction gives the Michael adduct **3**, which leads to a simple synthetic approach of optically active β-amino acids.

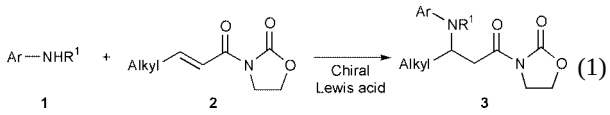

1 2 3 (1)

The reaction of *N*-methylaniline **1a** with 3-[(*E*)-2-butenoyl]-1,3-oxazolidin-2-one **2a** proceeds well in the presence of chiral Lewis acids. The results for the use of DBFOX-Ph[6] (*R*)-**4** and *t*-Bu-BOX[7] (*S*)-**5** as ligands in combination with different Lewis acids are presented in Table 1.

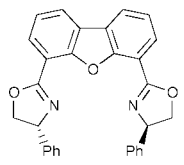

(*R*)-**4**

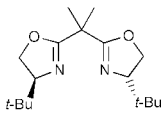

(*S*)-**5**

The reaction of **1a** with **2a** proceeds with high conversion and **3a** is obtained in up to 90% ee using (*R*)-**4**-Ni$(ClO_4)_2 \cdot 6H_2O$ (5 mol%) as the catalyst (Table 1, entries 1,2).† The solvent effect is notable for the reaction as only 19% conversion is found in THF (entry 3), while much higher conversion is obtained in CH_2Cl_2 (entries 1,2). Other metal salts can also be used in combination with (*R*)-**4** as the chiral ligand with various degree of success (entries 4,5). Surprisingly, the *t*-Bu-BOX (*S*)-**5** ligand in combination with copper salts, which has been found to be an excellent chiral catalyst for reactions of *e.g.* **2**,[7a,c] gave no conversion in the present reaction (entry 6), while the corresponding *t*-Bu-BOX-Zn$(OTf)_2$ catalyst gave moderate conversion and low enantioselectivity (entry 7).

A selection of aromatic amines **1a–f** has been reacted with the oxazolidinones **2a–c** in the presence of (*R*)-**4**-Ni$(ClO_4)_2 \cdot 6H_2O$ (5 mol %) as the catalyst [eqn. (2)] and the results are shown in Table 2.

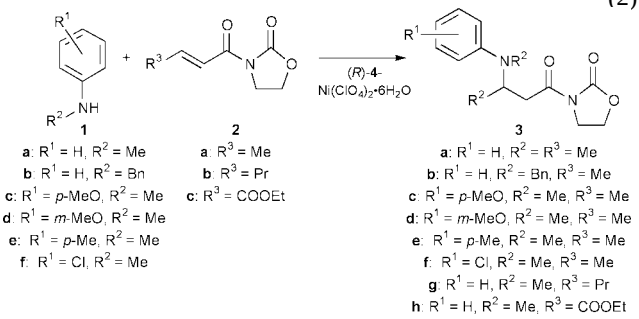

(2)

The N-substituent is important for the conversion as an exchange of *N*-methyl to *N*-benzyl gives a significant reduction in yield and enantioselectivity (Table 2, entries 1,2). The reaction of *N*-methylanilines, having electron-donating substituents (**1c–e**) with **2a** proceeds in high yield and with up to 89% ee (entries 3–5). It should be noted that applying Ni$(ClO_4)_2 \cdot 6H_2O$ (5 mol%) and varying the equivalents of (*R*)-**4** from 2 to 0.6 relative to the Lewis acid does not alter the yield

Table 1 Screening of chiral ligands, Lewis acids and reaction conditions for the reaction of *N*-methylaniline **1a** with 3-[(*E*)-2-butenoyl]-1,3-oxazolidin-2-one **2a** at room temperature

Entry	Catalyst	Loading (%)	Solvent	Conv.[a] (%)	Ee[b] (%)
1	(*R*)-**4**-Ni$(ClO_4)_2 \cdot 6H_2O$	10	CH_2Cl_2	76	88
2	(*R*)-**4**-Ni$(ClO_4)_2 \cdot 6H_2O$	5	CH_2Cl_2	62	90
3	(*R*)-**4**-Ni$(ClO_4)_2 \cdot 6H_2O$	5	THF	19	84
4	(*R*)-**4**-Mg$(ClO_4)_2 \cdot 6H_2O$	5	CH_2Cl_2	63	39
5	(*R*)-**4**-Zn$(ClO_4)_2 \cdot 6H_2O$	5	CH_2Cl_2	15	64
6	(*S*)-**5**-Cu$(OTf)_2$	10	CH_2Cl_2	—	—
7	(*S*)-**5**-Zn$(OTf)_2$	10	CH_2Cl_2	50	14

[a] Determined by 1H-NMR spectroscopy. [b] Determined by chiral HPLC.

Table 2 Reaction of aromatic amines **1a–f** with the oxazolidonones **2a–c** in the presence of (*R*)-**4**-Ni$(ClO_4)_2 \cdot 6H_2O$ (5 mol%) as the catalyst in CH_2Cl_2 at room temperature

Entry	Amine	Oxazolidinone	Yield[a] %	Ee[b] %
1	**1a**	**2a**	**3a**–62	90
2	**1b**	**2a**	**3b**–6	34
3	**1c**	**2a**	**3c**–75	76
4	**1d**	**2a**	**3d**–73	89
5	**1e**	**2a**	**3**–87	48
6	**1f**	**2a**	**3f**–23	96
7	**1a**	**2b**	**3g**–25	95
8	**1a**	**2c**	**3h**–93	0

[a] Isolated yield after column chromatography. [b] Determined by chiral HPLC.

 DOI: 10.1039/b103334b

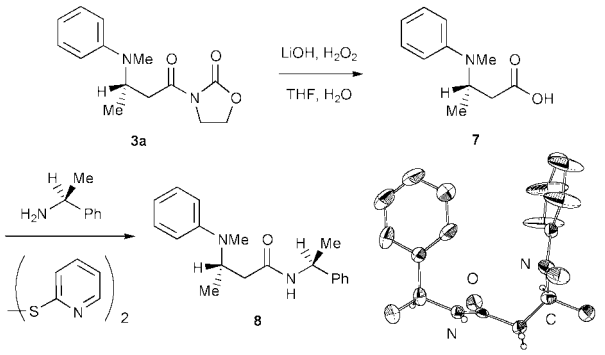

Scheme 1

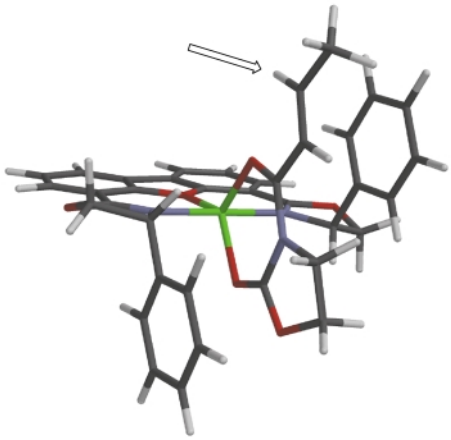

Fig. 1 Proposed intermediate for the catalytic enantioselective addition of secondary aromatic amines to enones catalyzed by (*R*)-DBFOX-Ph-Ni(II).

and enantioselectivity of the reaction of **1c** with **2a**. The reaction of *N*-methyl-*p*-chloroaniline **1f** with **2a** proceeds also with an excellent enantioselectivity, 96% ee of **3f**, however the yield at rt was moderate (entry 6); increasing the reaction temperature to 40 °C improves the yield to 53% and a reduction in enantioselectivity to 60% ee. The reaction of **1a** with **2b** proceeds with an excellent enantioselectivity, 95% ee of **3g** being obtained at rt (entry 7). The yield of **3g** was improved to 52% by performing the reaction in dichloroethane at 60 °C where 69% ee was obtained.

An important aspect of the present chemistry is that the products can be converted easily into various types of β-amino acid ester derivatives. The N-protecting group such as the *p*-methoxyphenyl group can be removed by standard chemistry.[8] In the following we will show that the oxazolidinone in **3** can be removed and exchanged with *e.g.* a chiral amine, which has been used to assign the absolute configuration of the product (Scheme 1). The adduct **3a** was first hydrolyzed with LiOH–H_2O_2 in a THF–H_2O solution giving the carboxylic acid **7**. Condensation with (*S*)-phenylethylamine gave the crystalline diastereomer **8**. The stereochemistry of **8** was assigned by X-ray analysis to be (*S*,*S*) (Scheme 1), *i.e.* the absolute configuration of the stereocenter formed in the addition reaction is (*S*).‡

Based on the absolute configuration of **8** we have proposed the intermediate in Fig. 1. The intermediate has a trigonal bipyrimidal coordination[6] at the metal center with the DBFOX-Ph (*R*)-**4** ligand occupying three sites and the oxazolidinone the remaining two. This intermediate has the β-*Si* face of the alkene shielded by the phenyl substituent of the chiral ligand, while the β-*Re* face is available for approach of the secondary aromatic amine leading to the addition adduct having an absolute configuration consistent with the experimental results.

In summary, a new catalytic enantioselective addition reaction of secondary aromatic amines to enones has been developed. This reaction proceeds in good yields and with moderate to excellent enantioselectivity in the presence of a chiral nickel complex. It was demonstrated that one of the products could be converted into an optically active amide which was used for the assignment of the absolute configuration of the addition adduct. Based on the absolute configuration, a chiral trigonal bipyrimidal nickel complex was proposed as the intermediate.

We are indebted to The Danish National Research Foundation for financial support.

Notes and references

† *Representative experimental procedure*: to a flame dried Schlenk tube was added $Ni(ClO_4)_2 \cdot 6H_2O$ (4.6 mg, 0.0125 mmol) and (*R*)-**4** (6.4 mg, 1.1 eq.). The mixture was dried under vacuum for 1 h and freshly distilled anhydrous CH_2CI_2 (1.0 ml) was added and the solution was stirred for 0.5 h. Subsequently, **2a** (38.8 mg, 0.25 mmol) and **1a** (135 μl, 1.25 mmol) were added and reacted for 40 h. The product **3a** was obtained by FC (50% Et_2O in pentane) as a pale yellow oil in 62% yield with 90% ee detected by HPLC using a Daicel Chiralpak AS column (hexane : *i*-PrOH 95 : 5; t_r(min) = 18.9 min, t_r(major) = 21.6 min.), $[\alpha]^{rt}D = -19.2°$ (c = 14.1 mg ml^{-1} in $CHCl_3$); ^{1}H NMR ($CDCl_3$) δ 7.23 (m, 2H; Ar), 6.85 (d, J = 9.2 Hz, 2H; Ar), 6.71 (td, J = 7.2, 0.8 Hz, 1H; Ar), 4.66 (m, 1H; NHC*H*CH_3), 4.24 (m, 2H; $OCOCH_2$), 3.86 (ddd, J = 16.4, 10.8, 7.2 Hz, 1H; NCH_2), 3.70 (ddd, J = 16.0, 10.8, 7.2 Hz, 1H, NCH_2), 3.27 (dd, J = 15.2, 8.4 Hz, 1H; $CHCH_2$), 3.08 (dd, J = 15.2, 6.0 Hz, 1H; $CHCH_2$), 2.76 (s, 3H; $CHCH_3$), 1.25 (d, J = 6.8 Hz, 3H; $CHCH_3$); ^{13}C NMR δ 171.8, 153.8, 150.4, 129.3, 117.5, 114.3, 62.3, 51.9, 42.7, 39.7, 30.6, 18.2; HRMS [M$^+$] Calcd $C_{14}H_{18}N_2O_3$, 262.1317; found 262.1315.

‡ *Crystallographic data* for **8**: $C_{19}H_{24}N_2O$; MW: 296.42; hexagonal, space group *P*65, a = 10.329(1), b = 10.329(1), c = 28.108(4) Å, V = 2597(1) Å^3, Z = 6. 5067 independent reflections measured at 120 K on a Siemens SMART CCD diffractometer. Mo-Kα. 1824 reflections with $I > 3\sigma(I)$ and 199 variables yields R = 0.049, R_w = 0.052. CCDC 1626611. See http://www.rsc.org/suppdata/cc/b1/b103334b/ for crystallographic data in .cif or other format.

1 See *e.g.*: (*a*) *Enantioselective Synthesis of* β-*Amino Acids*, ed. E. Juaristi, Wiley-VCH, New York, 1997; (*b*) G. Cardillo and C. Tomasini, *Chem. Soc. Rev.*, 1996, 117.

2 For review: (*a*) C. N. C. Drey, in *Chemistry and Biochemistry of the Amino Acids*, ed. G. C. Barrett, Chapman and Hall, London, 1985, p. 25; (*b*) *The Organic Chemistry of* β-*Lactams*, ed. G. I. Georg, VCH Publishers, New York, 1993.

3 See *e.g.*: (*a*) E. Juaristi, D. Quintana and J. Escalante, *Aldrichim. Acta*, 1994, **27**, 3; (*b*) P. Lakshmipathi and A. V. R. Rao, *Tetrahedron Lett.*, 1997, **38**, 2551; (*c*) P. Chalard, R. Remuson, Y. Gelas-Mialhe, J. Gramain and I. Canet, *Tetrahedron Lett.*, 1999, **40**, 1661; (*d*) S. G. Davies, A. J. Edwards and A. A. S. Walters, *Recl. Trav. Chim. Pays-Bas*, 1995, **114**, 115; (*e*) A. Volonterio, P. Bravo and M. Zanda, *Org. Lett.*, 2000, **2**, 1827.

4 See *e.g.*: (*a*) J. K. Myers and E. N. Jacobsen, *J. Am. Chem. Soc.*, 1999, **121**, 8959; (*b*) N. P. Sibi, J. J. Shay, M. Liu and C. P. Jasperse, *J. Am. Chem. Soc.*, 1998, **120**, 6615; (*c*) L. Falborg and K. A. Jørgensen, *J. Chem. Soc., Perkin Trans. 1*, 1996, 2823; (*d*) S. Kobayashi, H. Ishitani and M. Ueno, *J. Am. Chem. Soc.*, 1998, **120**, 431.

5 This reaction was found during our investigations of catalytic enantioselective Friedel–Crafts alkylation reactions: (*a*) K. B. Jensen, J. Thorhauge, R. G. Hazell and K. A. Jørgensen, *Angew. Chem., Int. Ed.*, 2001, **40**, 160; (*b*) W. Zhuang, T. Hansen and K. A. Jørgensen, *Chem. Commun.*, 2001, 347.

6 (*a*) S. Kanemasa, Y. Oderaotoshi, S. Sakaguchi, H. Yamamoto, H. Tanaka, E. Wada and D. P. Curran, *J. Am. Chem. Soc.*, 1998, **120**, 3074; (*b*) S. Kanemasa, Y. Oderaotoshi and E. Wada, *J. Am. Chem. Soc.*, 1999, **121**, 8675.

7 (*a*) J. S. Johnson and D. A. Evans, *Acc. Chem. Res.*, 2000, **33**, 325; (*b*) K. A. Jørgensen, M. Johannsen, S. Yao, H. Audrain and J. Thorhauge, *Acc. Chem. Res.*, 1999, **32**, 605; (*c*) A. K. Ghosh, P. Mathivanan and L. Cappiello, *Tetrahedron: Asymmetry*, 1998, **9**, 1.

8 S. Yao, S. Saaby, R. G. Hazell and K. A. Jørgensen, *Chem. Eur. J.*, 2000, **6**, 2435.

CHEMCOMM Communication
www.rsc.org/chemcomm

Double stranded interwound infinite linear silver coordination network†

Bruno Schmaltz, Abdelaziz Jouaiti, Mir Wais Hosseini* and André De Cian

Laboratoire de Chimie de Coordination Organique, Université Louis Pasteur, F-67000 Strasbourg, France. E-mail: hosseini@chimie:u-strasbg.fr

Received (in Cambridge, UK) 27th April 2001, Accepted 4th June 2001
First published as an Advance Article on the web 27th June 2001

Upon self-assembly of a bismonodentate ligand based on two pyridine units interconnected at the *para* position by a hexaethylene glycol fragment using ester junctions and Ag^+ cation, a double stranded interwound infinite linear network was obtained in the crystalline phase; the formation of this unprecedented architecture is a result of the loop type conformation of the connector segment which forms a pseudo-crown ether. The loop surounds the metal cation which is linearly coordinated to two pyridines belonging to consecutive units, thus forming the 1-D network.

The design of molecular networks, in particular in the crystalline phase, can be based on concepts developed in the context of molecular tectonics.[1a] The latter concerns the self-assembly of molecular tectons[1b] or building blocks with programmed information into their structure about the energy of inter- and intra-molecular interactions. For metallo-organic coordination networks[2,3] which are generated upon self-assembly[4] of metal cations with organic ligands and in some cases the anion[5] as tectons, the design principle lies in the match between the requirements of different partners. Under self-assembly conditions, discrete metallo-organic complexes are generated from endo-ligands in the presence of cations. In contrast, the formation of coordination networks, based on translational symmetry of assembling cores, requires the use of exo-ligands *i.e.* organic ligands for which the coordination sites are oriented in a divergent fashion.

When using flexible fragments connecting two coordination poles (composed of one or several coordination sites), depending on the conformation of the spacer, in the presence of metal cations one may expect the formation of either discrete complexes (metallamacrocycle) by an obturation process or infinite coordination networks by iteration (Fig. 1).

Pursuing our efforts to understand the basic principles governing the formation of coordination networks,[6] the above mentioned competition between the formation of discrete and infinite coordination networks was investigated by designing the bis-monodentate ligand **1**. The design of the latter was based on two coordinating pyridine units interconnected by the hexaethyleneglycol moiety using ester junctions. The two coordination sites were connected at the 4 position of the pyridine ring. The latter was chosen as a monodentate coordination site because of its frequent use in the design of coordination networks.[7] Concerning the flexible spacer, this may either be an innocent segment such as a polymethylene chain or a functionalised fragment. Owing to its well known ability to interact with cations, the hexaethylene glycol unit appeared to be the most attractive fragment since it may play both structural and recognition roles.

Here we report the first example in the crystalline phase of an intertwound double stranded linear coordination network based on the self assembly of ligand **1** and Ag^+ cations.

The rather straightforward synthesis of **1** (slightly yellowish oil) was achieved in THF under argon by condensing, in the presence of Et_3N, the commercially available isonicotinoyl chloride **2** with hexaethyleneglycol **3** in 86% yield (Scheme 1).

Depending on the conformation of the polyethylene glycol chain and rotations around the C(O)O bond, compound **1** (Scheme 1) may either behave as an endo-ligand with a convergent orientation of both pyridines or as an exo-ligand for which the two monodentate coordination sites are oriented in a divergent fashion. Thus, in the presence of metal cations adopting a linear coordination geometry, whereas for the first case a metallamacrocycle would be expected, for the divergent orientation an infinite coordination network should be obtained (Fig. 1).

The best suited cation appeared to be Ag^+ due to its extended coordination flexibility, in particular its ability to adopt a linear coordination geometry.

Upon slow diffusion at room temp. of a EtOH solution containing $AgClO_4$ into a PhCl solution of **1**, stable colourless crystals were obtained overnight. X-Ray diffraction‡ on a single-crystal revealed the following relevant features: the crystal (monoclinic system, space group *C*2/*c*) was only composed of **1**, Ag^+ cations and ClO_4^- anions. No solvent molecules were present in the crystal. The combination of **1** and Ag^+ leads to the formation of an infinite polycationic linear coordination network. The latter is obtained by translation of an assembling core composed of a silver cation bridging two consecutive organic tectons. No specific interactions between the polycationic network and the ClO_4^- anions are observed. In a first approximation, the metal cation adopts a linear

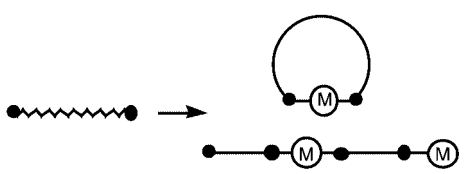

Fig. 1 Schematic representation of the competition between the formation of a metallamacrocycle and an infinite coordination polymer when a bismonodentate ligand is used in conjunction with a metal cation adopting a linear coordination geometry.

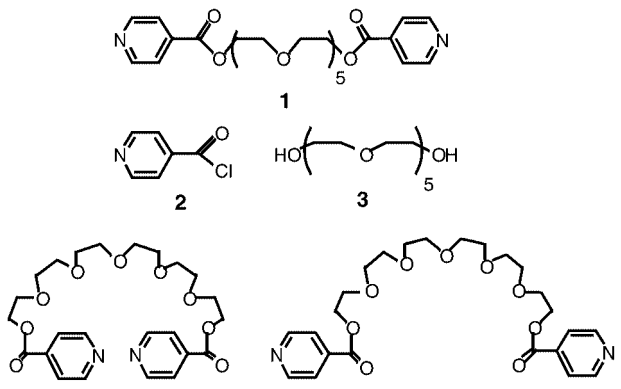

Scheme 1

† Dedicated to G. Ourisson on the occasion of his 75 birthday.

 DOI: 10.1039/b103824a

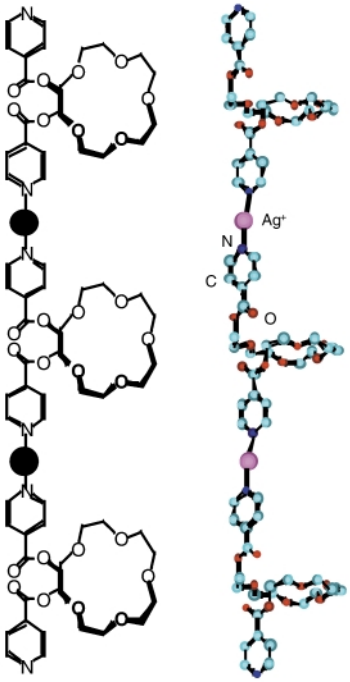

Fig. 2 Schematic (left) and a portion of the X-ray structure (right) of the cationic 1-D network obtained upon self-assembly of ligand **1** and Ag^+. H atoms and anion molecules are omitted for clarity.

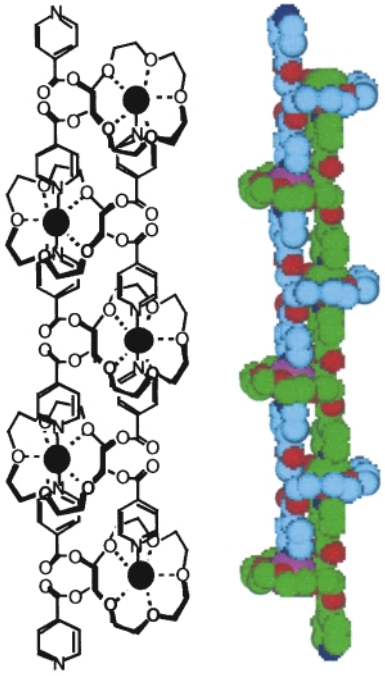

Fig. 3 Schematic (left) and a portion of the X-ray structure (right) of the double stranded cationic interwound 1-D network obtained due to interactions between Ag^+ cations and hexaethylenglycol units adopting a pseudo crown ether type conformation. H atoms and anions molecules are omitted for clarity.

coordination geometry with an N–Ag–N angle of 173.6°. Due to the unsymmetrical environment of the Ag^+ cation, the two N–Ag distances of 2.154 and 2.169 Å are slightly different. The ligand **1** adopts an interesting and particular conformation. The two pyridine units are almost parallel and co-planar but are oriented in opposite directions, thus allowing the formation of the network. Because of the *gauche* conformation of all six OCH_2CH_2O units, the hexaethylene glycol fragment adopts an almost circular conformation which closely resembles crown ether type units (Fig. 2). Furthermore, all pseudo-crown ether moieties adopt the same orientation and are located on the same side of the 1-D network. Of the six OCH_2CH_2O units, only one is disordered.

What was not predicted but is particularly interesting is that two adjacent linear networks are interwoven, leading thus to a double stranded interwound infinite linear network (Fig. 3). The driving force for the formation of such an architecture seems to be the loop type disposition of the polyethylene glycol units leading to interactions between silver cations belonging to one strand and selected ether oxygen atoms of the other strand. Taking into account these interactions, the coordination sphere around the cation may be described as comprising two nitrogen and five oxygen atoms. Among the five O atoms interacting with the cation, there are two rather short Ag–O distances of *ca*. 2.70 and 2.74 Å, one Ag–O distance in the medium range (3.05 Å) and two rather long Ag–O distances of *ca*. 3.26 and 3.44 Å. From this perspective, the assembling core may be regarded as a Ag^+ cation interacting strongly with two pyridine units belonging to one strand and weakly with five O atoms belonging to the other strand. Another curious feature is the orientation of loops within the double stranded interwound network: whereas for one strand all the loops adopt the same type of turn, for example left, for the other strand the opposite turn (right) is observed.

In conclusion, using the neutral acyclic tecton **1** based on two pyridines interconnected by the hexaethylene glycol through two ester junctions and Ag^+ cation, an unusual architecture consisting of a double stranded interwound infinite linear network was obtained unexpectedly in the crystalline phase. This observation opens the way to the design of other systems for which the nature of the coordination site, the connecting segment as well as the metal cation may be varied. Work along these lines is in progress.

Notes and references

‡ *Crystal data* for **1**·$AgClO_4$: $C_{24}H_{32}AgN_2O_9{\cdot}ClO_4$, colourless, M = 699.85, monoclinic, space group $C2/c$, a = 34.290(4), b = 10.902(2), c = 19.323(4) Å, β = 114.855(5)°, U = 6554(1) Å^3, Z = 8, D_c = 1.42 g cm^{-3}, λ(Mo-Kα) = 0.71073 Å, μ (Mo-Kα) = 0.756 mm^{-1}, 2352 data with $I > 3\sigma(I)$, R = 0.077, R_w = 0.115; Data were collected on a Nonius Kappa CCD and structural determination was achieved using the Nonius OpenMolenN package.[8] CCDC reference number 163024. See http://www.rsc.org/suppdata/cc/b103824a/ for crystallographic data in CIF or other electonic format.

1 (*a*) S. Mann, *Nature*, 1993, **365**, 499; (*b*) M. Simard, D. Su and J. D. Wuest, *J. Am. Chem. Soc.*, 1991, **113**, 4696.

2 S. R. Batten and R. Robson, *Angew. Chem., Int. Ed.*, 1998, **37**, 1460.

3 M. W. Hosseini, in *NATO ASI Series; Series C*, ed. D. Braga, F. Grepiono and G. Orpen, Kluwer, Dordrecht, Netherlands, 1999, vol. 538, p. 181.

4 J. S. Lindsey, *New J. Chem.*, 1991, **15**, 153; O. M. Yaghi, H. Li, C. Davis, D. Richardson and T. L. Groy, *Acc. Chem. Res.*, 1998, **31**, 474; F. Swegers and T. J. Malefetse, *Chem. Rev.*, 2000, **100**, 3483; M. Fujita, K. Umemoto, M. Yoshizawa, N. Fujita, T. Kusukawa and K. Biradha, *Chem. Commun.*, 2001, 509.

5 A. Jouaiti, V. Jullien, M. W. Hosseini, J.-M. Planeix and A. De Cian, *Chem. Commun.*, 2001, 1114.

6 C. Kaes, M. W. Hosseini, C. E. F. Rickard, B. W. Skelton and A. White, *Angew. Chem., Int. Ed.*, 1998, **37**, 920; G. Mislin, E. Graf, M. W. Hosseini, A. De Cian, N. Kyritsakas and J. Fischer, *Chem. Commun.*, 1998, 2545; M. Loï, M. W. Hosseini, A. Jouaiti, A. De Cian and J. Fischer, *Eur. J. Inorg. Chem.*, 1999, 1981; M. Loï, E. Graf, M. W. Hosseini, A. De Cian and J. Fischer, *Chem. Commun.*, 1999, 603; C. Klein, E. Graf, M. W. Hosseini, A. De Cian and J. Fischer, *Chem. Commun.*, 2000, 239; H. Akdas, E. Graf, M. W. Hosseini, A. De Cian and J. McB. Harrowfield, *Chem. Commun.*, 2000, 2219; A. Jouaiti, M. W. Hosseini and A. De Cian, *Chem. Commun.*, 2000, 1863; C. Klein, E. Graf, M. W. Hosseini, A. De Cian and J. Fischer, *New J. Chem*, 2001, **25**, 207.

7 T. L. Hennigar, D. C. MacQuarrie, P. Losier, R. D. Rogers and M. J. Zaworotko, *Angew. Chem., Int. Ed. Engl.*, 1997, **36**, 972; J. Blake, N. R. Champness, S. S. M. Chung, W-S. Li and M. Schröder, *Chem. Commun.*, 1997, 1675; M. A. Withersby, A. J. Blake, N. R. Champness, P. Hubberstey, W-S. Li and M. Schröder, *Chem. Commun.*, 1997, 2327, L. Carlucci, G. Ciani and D. M. Proserpio, *Chem. Commun.*, 1999, 449, S. Sailaja and M. V. Rajasekharan, *Inorg. Chem.*, 2000, **39**, 4586.

8 OpenMolenN, Interactive Structure Solution, Nonius B. V., Delft, The Netherlands, 1997.

CHEMCOMM
Communication
www.rsc.org/chemcomm

Synthesis and application of dimeric *Cinchona* alkaloid phase-transfer catalysts: α,α′-bis[*O*(9)-allylcinchonidinium]-*o*, *m*, or *p*-xylene dibromide†

Sang-sup Jew,* Byeong-Seon Jeong, Mi-Sook Yoo, Hoon Huh and Hyeung-geun Park*

College of Pharmacy, Seoul National University, Seoul 151-742, Korea. E-mail: ssjew@plaza.snu.ac.kr

Received (in Cambridge, UK) 20th March 2001, Accepted 18th May 2001
First published as an Advance Article on the web 20th June 2001

A dimeric *Cinchona* alkaloid ammonium salt, α,α′-bis[*O*(9)-allylcinchonidinium]-*m*-xylene dibromide 4, has been developed as a new efficient phase-transfer catalyst; the catalytic enantioselective alkylation of *N*-(diphenylmethylene)glycine *tert*-butyl ester using 4 provided 7 in a high enantiomeric excess (90–99% ee).

Although phase-transfer catalytic reactions have been widely applied in organic synthesis,[1,2] asymmetric synthetic reactions using chiral phase-transfer catalysts have not been extensively studied as compared to general asymmetric synthetic reactions, such as asymmetric dihydroxylation,[3] asymmetric catalytic reduction,[2] and so on. Since the pioneering work of O'Donnell *et al*. (**1a**),[4] the enantioselective alkylation of a prochiral protected glycine derivative, using *Cinchona* alkaloid ammonium salts, has become a very attractive method for the preparation of both natural and unnatural α-amino acids. Especially, the Lygo[5] and Corey[6] groups independently reported the excellent phase-transfer catalysts, *N*-9-anthracenylmethylcinchonidinium chloride (**2a**) and *O*(9)-allyl-*N*-9-anthracenylmethylcinchonidinium bromide (**2b**), respectively, by replacing the phenyl group of **1** with the bulkier anthracenyl moiety. Recently, the Maruoka group developed very efficient non-*Cinchona* catalysts, the C_2-symmetric chiral quaternary ammonium salts prepared from (*S*)-binaphthol.[7]

In connection with the development of Sharpless asymmetric dihydroxylation, the discovery of ligands with two independent *Cinchona* alkaloid units attached to heterocyclic spacers led to considerable increases in both the enantioselectivity and the scope of the substrate.[3] This dimerization effect prompted us to develop dimeric *Cinchona* alkaloid ammonium salts for enantioselective phase-transfer catalytic reactions. In this communication, we report the preparation of new dimeric catalysts, α,α′-bis[*O*(9)-allylcinchonidinium]-*o*, *m*, or *p*-xylene dibromides **3**–**5**, and their application to the catalytic enantioselective alkylation of *N*-(diphenylmethylene)glycine *tert*-butyl ester **6** under mild phase-transfer conditions (Fig. 1).

Compounds **3**–**5** were prepared in two steps from cinchonidine and α,α′-dibromo-*o*, *m*, or *p*-xylene, respectively. Cinchonidine and α,α′-dibromo-*o*-, *m*-, or *p*-xylene were stirred at 100 °C in EtOH–DMF–$CHCl_3$ (v/v = 2.5:3:1)[8] for 6 h followed by *O*(9)-allylation with allyl bromide and 50% aq. KOH, to give the corresponding dimeric *Cinchona* alkaloid catalysts **3**–**5** in 90–92 % overall yields. The enantioselective efficiency of the prepared catalysts was evaluated by enantioselective phase-transfer alkylation using 5 mol% of catalysts **3**–**5** along with **6**, benzyl bromide, and 50% aq. KOH in toluene–$CHCl_3$[4f,9] (v/v = 7:3) at 0 °C or −20 °C for 2–6 h. Surprisingly, the *meta*-dimeric catalyst **4**‡ showed the highest enantioselectivity (*S*-form, 90% ee at 0 °C; 95% ee at −20 °C) among the three dimeric catalysts **3**–**5** (Table 1). The order of enantioselectivity of the three catalysts along with the monomer catalyst **1b** was as follows: *meta*-dimer (**4**) > *para*-dimer (**5**) ≅ monomer (**1b**) ≫ *ortho*-dimer (**3**). The precise mechanism for the high enantioselectivity of **4** is not clear, but it is thought to be similar to the reported mechanism of **2**.[6a] There are two possible conformations, **4a** and **4b**, as shown in Fig. 2. The **4a** conformer seems to be preferred, because of the steric hindrance between the quinoline and *O*-allyl moieties and the *Cinchona* unit (CD^+) in **4b**. In addition, the dramatic increase in the

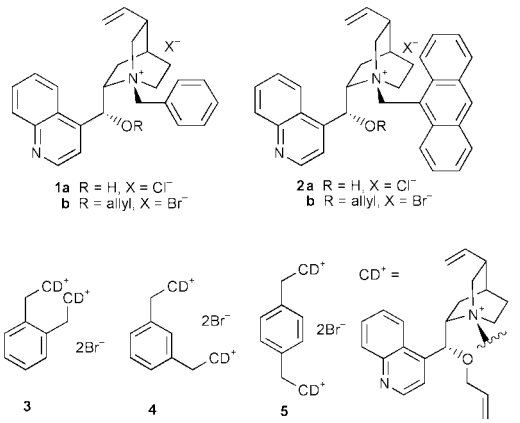

Fig. 1

Table 1 Enantioselective catalytic phase-transfer alkylation

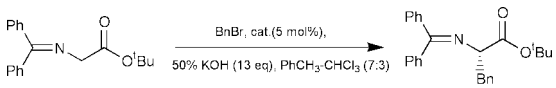

6 → 7g

Entry	Catalyst	Temp./°C	Time/h	% yield[a]	% ee[b] (Config.)[c]
1	**1b**	0	2	92	75 (*S*)
2	**1b**	−20	5	94	81 (*S*)
3	**3**	0	3	90	31 (*S*)
4	**3**	−20	6	88	35 (*S*)
5	**4**	0	2	91	90 (*S*)
6	**4**	−20	5	94	95 (*S*)
7	**5**	0	4	92	80 (*S*)
8	**5**	−20	6	92	86 (*S*)

[a] Isolated yield of purified material. [b] Enantiopurity was determined by HPLC analysis using a chiral column (DAICEL Chiralcel OD). [c] Absolute configuration was determined by comparison of the HPLC retention time with the authentic samples independently synthesized by the reported procedure.[4–7]

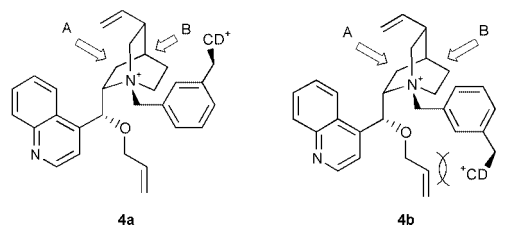

Fig. 2

† Electronic supplementary information (ESI) available: experimental details. See http://www.rsc.org/suppdata/cc/b1/b102584h/

 DOI: 10.1039/b102584h

Table 2 Enantioselective catalytic phase-transfer alkylation

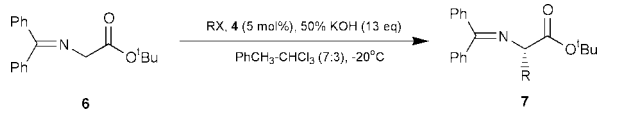

6 7

Entry	RX	Time/h	% Yield[a]	% ee[b] Config.[c]
a	CH_3I	3	72	90 (*S*)
b	CH_3CH_2I	10	50	92 (*S*)
c	$CH_3(CH_2)_4CH_2I$	5	64	99 (*S*)
d		4	86	94 (*S*)
e		4	88	97 (*S*)
f	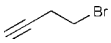	3	92	90 (*S*)
g	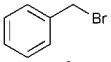	5	94	95 (*S*)
h	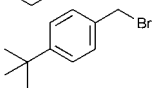	5	87	95 (*S*)
i	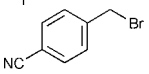	8	75	96 (*S*)
j	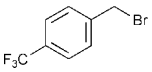	6	98	95 (*S*)
k	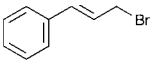	8	90	90 (*S*)
l	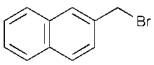	5	96	90 (*S*)

[a] Isolated yield of purified material. [b] Enantiopurity was determined by HPLC analysis of the alkylated imine **7** using a chiral column (DAICEL Chiralcel OD) with hexane–propan-2-ol (500/2 for **7a**, **7b**, **7g**, **7h**, **7j**, **7k**, **7l**; 500/1 for **7c**, **7d**, **7e**, **7f**; 500/5 for **7i**) as solvent. [c] Absolute configuration was determined by comparison of the HPLC retention time with the authentic samples independently synthesized by the reported procedure.[4–7]

enantioselectivity from **1b** to **4** implies that the *Cinchona* unit (CD^+) is located near the B site. Consequently, as the direction B is sterically hindered by the counter *Cinchona* unit in **4**, the *E*-enolate of **6** forms an ion-pair with **4** from the less hindered direction A. We expect that as the *re*-face of the enolate can be effectively blocked by the formation of the ion-pair, the alkyl halide can approach only the *si*-face of *E*-enolate, to give the *S*-form. The lack of a difference in the enantioselectivity between the *para*-dimer **5** and the monomer **1b** implies that the *Cinchona* units of the *para*-dimer **5** do not sterically affect each other. In the case of the *ortho*-dimer **3**, the severe steric repulsion between the two *Cinchona* units may lead to a less efficient conformation for enantioselectivity. Generally, the lower temperature (−20 °C) yielded higher enantioselectivity (Table 1). Catalyst **4** was chosen for the further investigation of the enantioselective phase-transfer alkylation with various alkyl halides. Table 2 indicates the results obtained for the alkylation of **6** with various alkyl halides, using catalyst **4** under the same reaction conditions as in Table 1, except for the temperature (−20 °C). The very high enantioselectivities (90–99% ee) shown in Table 2 indicate that catalyst **4** is a very efficient enantioselective phase-transfer catalyst for the synthesis of natural and unnatural α-amino acids.

In conclusion, we prepared the dimeric *Cinchona* alkaloid ammonium salt catalysts **3**–**5** to enhance catalytic efficiency by the dimerization effect. Among the dimeric catalysts, the *meta*-isomer (**4**) showed the highest catalytic activity (90–99% ee) in the alkylation of **6**. The high catalytic efficiency, the easy preparation, and the lower preparation cost relative to **2a,b** could make **4** a practical catalyst in industrial synthetic processes for natural and unnatural chiral α-amino acids. Applications to other various types of phase-transfer catalytic reactions using **4** are currently being investigated.

This work was supported by grants from Aminogen Co., Korea, *via* the Research Center of New Drug Development of Seoul National University and the Research Institute of Pharmaceutical Sciences in the College of Pharmacy of Seoul National University.

Notes and references

‡ All new compounds gave satisfactory analytical and spectral data.

Selected data for **4**: mp 181 °C (decomp.); $[\alpha]^{25}_D$ −156 (*c* 0.320, $CHCl_3$); IR (KBr) 3437, 2922 cm^{-1}; δ_H (400 MHz, DMSO-d_6) 9.03 (d, *J* = 4.4 Hz, 2 H), 8.35 (d, *J* = 8.3 Hz, 2 H), 8.15 (d, *J* = 9.0 Hz, 3 H), 7.97 (d, *J* = 7.5 Hz, 2 H), 7.90–7.86 (m, 2 H), 7.81–7.76 (m, 3 H), 7.72 (d, *J* = 4.4 Hz, 2 H), 6.53 (s, 2 H), 6.22–6.16 (m, 2 H), 5.78–5.70 (m, 2 H), 5.49 (d, *J* = 17.2 Hz, 2 H), 5.37–5.28 (m, 4 H), 5.20–5.14 (m, 4 H), 4.99 (d, *J* = 10.5 Hz, 2 H), 4.46 (dd, *J* = 12.5, 5.3 Hz, 2 H), 4.06–4.03 (m, 6 H), 3.82–3.76 (m, 2 H), 3.69–3.64 (m, 2 H), 3.51–3.40 (m, 2 H), 2.84–2.75 (m, 2 H), 2.34–2.26 (m, 2 H), 2.15–2.00 (m, 4 H), 1.92–1.81 (m, 2 H), 1.51–1.42 (m, 2 H); δ_C (100 MHz, DMSO-d_6) 150.6, 148.4, 141.7, 139.3, 138.3, 135.9, 134.6, 130.3, 130.0, 129.9, 128.8, 127.9, 125.4, 124.1, 120.0, 118.0, 116.9, 72.3, 69.7, 68.2, 63.4, 59.3, 51.2, 37.2, 26.3, 24.5, 21.2; MS (ESI): 772 $[M]^{2+}$; HRMS (ESI) calcd for $[C_{52}H_{60}N_4O_2]^{2+}$: 772.4716, found: 772.4739.

Representative procedure for enantioselective catalytic alkylation of **6** *under phase-transfer conditions (benzylation)*: to a mixture of *N*-(diphenylmethylene)glycine *tert*-butyl ester **6** (50 mg, 0.17 mmol) and chiral catalyst **4** (8 mg, 0.0085 mmol) in toluene–$CHCl_3$ (v/v = 7:3, 0.75 mL) was added benzyl bromide (0.1 mL, 0.85 mmol). The reaction mixture was then cooled (−20 °C), 50% aq. KOH (0.25 mL) was added, and the reaction mixture was stirred at −20 °C until the starting material had been consumed (5 h). The suspension was diluted with ether (20 mL), washed with water (2 × 5 mL), dried over $MgSO_4$, filtered and concentrated *in vacuo*. Purification of the residue by flash column chromatography on silica gel (hexane:EtOAc = 50:1) afforded the desired product **7g** (61 mg, 94% yield) as a colorless oil. The enantioselectivity was determined by chiral HPLC analysis (DAICEL Chiralcel OD, hexane:propan-2-ol = 500:2.5, flow rate = 1.0 ml min^{-1}, 23 °C, λ = 254 nm; retention times *R* (minor) 12.2 min, *S* (major) 22.5 min, 95% ee). The absolute configuration was determined by comparison of the HPLC retention time with the authentic sample synthesized by the reported procedure.[4–7]

1 (*a*) E. V. Dehmlow and S. S. Dehmlow, *Phase Transfer Catalysis*, 3rd edn., VCH, Weinheim, 1993 and references therein; (*b*) A. Nelson, *Angew. Chem., Int. Ed.*, 1999, **38**, 1583.

2 I. Ojima, *Catalytic Asymmetric Synthesis*, 2nd edn., Wiley-VCH, New York, 2000 and references therein.

3 H. C. Kolb, M. S. VanNieuwenhze and K. B. Sharpless, *Chem. Rev.*, 1994, **94**, 2483 and references therein.

4 (*a*) M. J. O'Donnell, W. D. Benett and S. Wu, *J. Am. Chem. Soc.*, 1989, **111**, 2353; (*b*) K. B. Lipkowitz, M. W. Cavanaugh, B. Baker and M. J. O'Donnell, *J. Org. Chem.*, 1991, **56**, 5181; (*c*) M. J. O'Donnell and S. Wu, *Tetrahedron: Asymmetry*, 1992, **3**, 591; (*d*) M. J. O'Donnell, S. Wu and J. C. Huffman, *Tetrahedron*, 1994, **50**, 4507; (*e*) M. J. O'Donnell, S. Wu, I. Esikova and A. Mi, U.S. Patent 5 554 753, September 10, 1996; (*f*) M. J. O'Donnell, I. A. Esikova, A. Mi, D. F. Shullenberger and S. Wu, in *Phase-Transfer Catalysis*, ed. M. E. Halpern, ACS Symposium Series 659, American Chemical Society, Washington, DC, 1997, ch. 10; (*g*) M. J. O'Donnell, F. Delgado and R. Pottorf, *Tetrahedron*, 1999, **55**, 6347.

5 (*a*) B. Lygo and P. G. Wainwright, *Tetrahedron Lett.*, 1997, **38**, 8595; (*b*) B. Lygo, J. Crosby and J. A. Peterson, *Tetrahedron Lett.*, 1999, **40**, 1385; (*c*) B. Lygo, *Tetrahedron Lett.*, 1999, **40**, 1389; (*d*) B. Lygo, J. Crosby and J. A. Peterson, *Tetrahedron Lett.*, 1999, **40**, 8671; (*e*) B. Lygo, J. Crosby, T. R. Lowdon and P. G. Wainwright, *Tetrahedron*, 2001, **57**, 2391; (*f*) B. Lygo, J. Crosby, T. R. Lowdon, J. A. Peterson and P. G. Wainwright, *Tetrahedron*, 2001, **57**, 2403.

6 (*a*) E. J. Corey, F. Xu and M. C. Noe, *J. Am. Chem. Soc.*, 1997, **119**, 12414; (*b*) E. J. Corey, M. C. Noe and F. Xu, *Tetrahedron Lett.*, 1998, **39**, 5347; (*c*) E. J. Corey, Y. Bo and J. Busch-Peterson, *J. Am. Chem. Soc.*, 1998, **120**, 13000.

7 (*a*) T. Ooi, M. Kameda and K. Maruoka, *J. Am. Chem. Soc.*, 1999, **121**, 6519; (*b*) T. Ooi, M. Takeuchi, M. Kameda and K. Maruoka, *J. Am. Chem. Soc.*, 2000, **122**, 5228.

8 N. Baba, J. Oda and M. Kawaguchi, *Agric. Biol. Chem.*, 1986, **50**, 3113.

9 The optimal solvent condition was determined by benzylation of **6** at −20 °C using **4**. Toluene–$CHCl_3$ (v/v, 7:3) gave the highest enantioselectivity (95% ee) compared to toluene (87% ee), CH_2Cl_2 (85% ee), $CHCl_3$ (90% ee), and toluene–CH_2Cl_2 (v/v, 7:3, 93% ee).

CHEMCOMM
Communication
www.rsc.org/chemcomm

First intramolecular trapping and structural proof of the key intermediate in the formation of indolizine photochromics†

Yongsheng Tan,[a] Saleh A. Ahmed,[a] H. Dürr,*[a] V. Huch[a] and A. Abdel-Wahab[b]

[a] *FB 11.2, Organische Chemie, Universität des Saarlandes, 66041 Saarbrücken, Germany*
[b] *Department of Chemistry, Assiut University, Assiut, Egypt*

Received (in Cambridge, UK) 30th January 2001, Accepted 22nd May 2001
First published as an Advance Article on the web 20th June 2001

The reaction of substituted spirocyclopropenes 1 with 1-(3,5-dinitrophenyl)-3,4-dihydroisoquinoline 2 in dry ether solution afforded not only the expected THI 4 by 1,5-electrocyclization but also novel fluorenespiroazanorcaradienes 5 which is the first intramolecularly trapped product of the key intermediate in the formation of indolizine photochromics.

The reaction of the easily accessible spirocyclopropenes **1** with isoquinolines **2** has been shown to be an extremely powerful tool to prepare new photochromic dihydroindolizines (DHI), tetrahydroindolizines (THI) and pyrrolopyrrolizidines.[1–4] A vast number of tailormade molecules having interesting properties for applications such as ophthalmic lenses,[5] molecular switches,[6] dental material[7] and potential application in information recording and data storage and holography[8] has been published. We have shown recently that the reaction of 1-styryl-3,4-dihydroisoquinolines with spirocyclopropenes **1** is controlled by substituents to afford a pericyclic reaction to either THI's **4** or azepine derivatives **6**.[9] This reaction is governed by the substituents in the fluorene part and can form in a periselective way THI's **4** or azepines **6**. These results incited us to introduce strongly electron attracting groups (NO_2) which might stabilize the first intermediate in this reaction or even allow isolation of the product directly derived from this—until now—unproved intermediate. In this paper we describe the isolation of fluorenespiroazanorcaradienes **5** the trapped key intermediate in the indolizine formation and their X-ray structure, and also new THIs **4**.

Analogues of **2** with an unsubstituted 2-phenyl-ring, or with halogen or one nitro-group in the ring led only to ring-closed THIs when reacted with spirocyclopropenes **1** (see Table 1). The reaction of spirocyclopropenes **1** with dinitrosubstituted **2** in diethyl ether at rt after 5 d not only afforded the ring-closed THI **4** but a novel product, the azanorcaradiene **5**. Both products were isolated using column chromatography on silica gel (eluent CH_2Cl_2 and CH_2Cl_2–MeOH), their structures were determined *via* elemental analysis, ^{1}H-NMR, ^{13}C-NMR, IR-spectra and X-ray analysis (see ESI†).The general mechanism for the reaction of **2** with **1** is shown in Scheme 1. The reaction of **1** with **2** can proceed in three possible ways. The carbon atoms 2″ and 6″ in the 5′-phenyl ring of intermediate **A** are positively polarised because of the influence of two strong electron withdrawing nitro-groups in *ortho*- and *para*-positions. In the first case (path **a**), after nucleophilic addition of **2** on the double-bond of **1** starting from the intermediate cyclopropylcarbanion **A** by 1,6-electrocyclization through attack of the negative C2′ on the positive C2″ and finally by rearrangement results in **5** which must be regarded as the product of the intramolecularly trapped intermediate **A**. This is the first direct proof of intermediate **A** postulated in the mechanism of indolizine formation. In the second case (path **b**), the intermediate **A** rearranges to the betaine **3** through a cyclopropylallylanion rearrangment, which yields THI **4** through 1,5-electrocyclization. In the third possible case (path **c**), the betaine **3** may form through 1,7-electrocyclization to produce the 7-membered compound **6′**, a reaction not observed here.

Besides spectral data, the structure of products was confirmed by X-ray analysis for the fluorenespiroazanorcaradiene dye **5b** (Fig. S1†) and tetrahydroindolizine **4f** (Fig. S2†).

The green to green-blue dyes **5** have two absorption bands in the visible. The UV–Vis data and color are shown in Table 2.

The novel azanorcaradienes **5** possess acidochromic or halochromic properties, for example the ethanol solution of **5a** has a green color (459 and 655 nm); the color changed at once from green to deep violet (548 nm) after adding a few drops of aqueous sodium hydroxide. This process is reversible with hydrochloric acid many times without decreasing the absorption intensity. It is suggested that the acidochromism of dye **5** giving the anion **5′** (proton abstracted at 4′a position) is due to dissociation of the **4′**a-H atom and the reversible reprotonation

† Electronic supplementary information (ESI) available: Figs. S1 and S2. See http://www.rsc.org/suppdata/cc/b1/b101044l/

Table 1 The physical data of newly prepared tetrahydroindolizines **4a–g** and betaines **3a–d**

4	R	E	λ_{max}/nm $t_{½}$/s of betaine	Mp/°C	Yield (%)	^{1}H-NMR ($CDCl_3$) δ in ppm 5′-CH_2	6′-CH_2	^{13}C-NMR ($CDCl_3$) δ in ppm 5′-C	6′-C
4a	H	CO_2Me	500, 700 1.57	262–264	47.5	3.58(m, 1H) 3.81(m, 1H)	2.71(dt, 1H) 3.18(m, 1H)	41.00	29.24
4b	H	CO_2Et	500, 700 1.0	253–255	46.2	3.59(m, 1H) 3.84(m, 1H)	2.71(dt, 1H) 3.19(m, 1H)	40.79	29.14
4c	Br	CO_2Me	500, 750 0.579	305–307	50.4	3.58(m, 1H) 3.85(m, 1H)	2.77(dt, 1H) 3.22(m, 1H)	41.02	29.20
4d	Cl	CO_2Et	500, 750 0.418	258–260	48.7	3.58(m, 1H) 3.87(m, 1H)	2.75(dt, 1H) 3.23(m, 1H)	40.83	29.17
4e	H	CO_2iPr	480, 725 0.417	232–234	24.3	3.59(m, 1H) 3.75(m, 1H)	2.65(m, 1H) 3.13(m, 1H)	40.49	29.58
4f	H	CO_2tBu	500, 725 0.213	200–202	21.5	3.54(m, 1H) 3.90(m, 1H)	2.64(m, 1H) 3.21(m, 1H)	40.55	29.14
4g	H	$CO_2C_6H_{11}$	500, 725 0.278	168–170	18.5	3.49(m, 1H) 3.89(m, 1H)	2.61(m, 1H) 3.20(m, 1H)	40.42	29.14

 DOI: 10.1039/b101044l

Table 2 Analytical and spectral data of fluorenespiroazanorcaradiene dyes **5a–g**

5	R	E	mp/°C	Yield (%)	^{1}H-NMR ($CDCl_3$) δ in ppm 4′a-H	8′-CH_2	9′-CH_2	^{13}C-NMR ($CDCl_3$) δ in ppm 4′a-C	8′-C	9′-C	λ_{max}/ nm	Color of dye
5a	H	CO_2Me	218-220	33	5.27 (s, 1H)	3.47(d,1H) 3.66(td,1H)	2.77(d,1H) 3.20(td,1H)	35.92	47.13	27.4 3	453 656	Green
5b	H	CO_2Et	212–214	40	5.24(s, 1H)	3.47(d,1H) 3.66(td,1H)	2.77(d,1H) 3.27(td,1H)	35.98	47.16	27.4 1	457 659	Green
5c	Br	CO_2Me	227–229	30	5.04(s, 1H)	3.44(d,1H) 3.61(td,1H)	2.82(d,1H) 3.20(td,1H)	36.10	47.02	27.4 6	446 639	Green–blue
5d	Cl	CO_2Et	213–215	35	5.03(s, 1H)	3.41(td,1H) 3.62(td,1H)	2.81(td,1H) 3.26(td,1H)	36.28	46.95	27.5 8	448 646	Green–blue
5e	H	CO_2Pr^i	215–217	17	5.02(s, 1H)	3.40(m,1H) 3.60(m,1H)	2.71(m,1H) 3.23(m,1H)	35.8	46.92	27.4 5	458 663	Green
5f	H	CO_2Bu^t	181-183	13	5.12(s, 1H)	3.43(m,1H) 3.64(m,1H)	2.84(m,1H) 3.25(m,1H)	35.9	46.87	27.6	454 660	Green
5g	H	$CO_2C_6H_{11}$	171–173	11	5.08(s, 1H)	3.40(m,1H) 3.62(m,1H)	2.81(m,1H) 3.20(m,1H)	36.3	46.81	28.0	453 659	Green

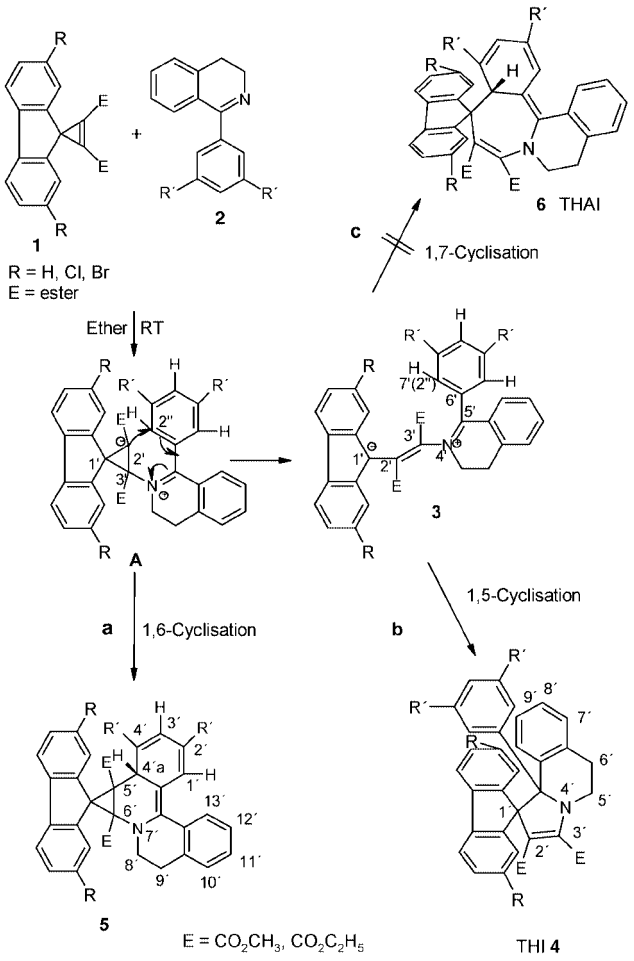

Scheme 1

of the resulting carbanion. This has been proved also by ^{1}H-NMR measurements.

Compound **5a** in CD_3CN shows a singlet for 4′a-H at 5.38 and 1′-H at 8.06 ppm as well as a doublet for 3′-H at 8.27 ppm. The addition of NaOD–D_2O changed the green color to violet, 4′a-H disappeared completely and 3′-H is shifted to 4.74 ppm (s) and 1′-H to 7.59 ppm. The original spectrum appears again after addition of DCl. Thus it is clear that the colored species **5′** is the anion where a proton has been abstracted from the 4′a-position. In summary, the intramolecular trapping of intermediate **A** to afford fluorenespiroazanorcaradienes **5** is the first proof for the mechanism of the cyclopropane anion intermediate postulated[1–4] after nucleophilic attack of **2** to the double bond of **1**. The cyclopropyl anion is intramolecularly trapped to give cyclopropane derivatives **5**. The THI **4** are formed *via* the betaine **3** to its precursor the cyclopropylanion **A**.

Financial support from the Deutsche Forschungsgemeinschaft and the Volkswagen Stiftung is gratefully acknowledged.

Notes and references

1 H. Dürr and G. Hauck, *Angew. Chem.*, 1979, **912**, 1010.
2 H. Dürr and H. Bouas-Laurent, *Photochromism—Molecules and Systems*, Elsevier, Amsterdam, 1990
3 H. Dürr and G. Hauck, DOS 2906193, 1980.
4 H. Dürr, *Photochromism of Dihydroindolizines and Related Systems*, in *Organic photochromic and Thermochromic Compounds*, ed. J. C. Crano and R. J. Gugliemetti, Plenum Press, New York, 1998, pp. 223–266.
5 C. B. McArdle, in *Applied Photochromic Polymer Systems*, Blackie and Son Ltd., Glasgow, 1992.
6 (*a*) F. Rustemeyer, J. L. Pozzo, H. Dürr and H. Bouas-Laurent, *J. Mater. Chem.*, 1999, **9**, 2245; (*b*) C. Weber, F. Rustemeyer and H. Dürr, *Adv. Mater.*, 1998, **10**(16), 1348.
7 P. Burtscher, H. Dürr, V. Rheinberger and U. Salz, *Ger. Pat.*, DE 195 20 016.0, 1995.
8 H. Dürr, *J. Information Recording*, in press.
9 H. Dürr, Y. Tan, T. Hartmann, P. Valat and J. Kossanyi, *J. Org. Chem.*, 2001, **66**, 1130.

CHEMCOMM
Communication
www.rsc.org/chemcomm

A new reaction of cyclohexanone enolate with nitroarenes

Nikolai Moskalev and Mieczysław Mąkosza*

Institute of Organic Chemistry, Polish Academy of Sciences, ul. Kasprzaka 44, 01-224 Warszawa 42, POB 58, Poland. E-mail: icho-s@icho.edu.pl; Fax: +48 22 6326681

Received (in Cambridge, UK) 19th February 2001, Accepted 15th May 2001
First published as an Advance Article on the web 20th June 2001

Reaction of cyclohexanone enolate with some nitroarenes carried out at 60–80 °C proceeds *via* addition to the nitro group followed by a series of transformations giving *o*-hydroxydiarylamines.

Carbanions react with nitroarenes mainly *via* addition to electron-deficient rings, in positions *ortho*- or *para*- to the nitro group giving anionic σ adducts. Addition at positions occupied by nucleofugal substituents X give σ^x adducts rapidly converted into products of S_NAr reaction.[1] Faster and reversible addition at positions occupied by hydrogen produces σ^H adducts,[2,3] which can be converted into products of nucleophilic substitution of hydrogen on a few pathways such as oxidation,[4] vicarious nucleophilic substitution VNS,[5] formation of nitroso compounds[6] *etc*. Direct intermolecular addition of stabilized carbanions to the nitro group is almost unknown, although there are numerous examples of such addition proceeding as intramolecular processes resulting in the formation of heterocyclic systems.[7,8] Addition of indan-1-one enolate to the nitro group of *o*-nitrobenzaldehyde appears to be assisted by initial addition to the carbonyl group, thus being in fact an intramolecular process.[9] Of particular interest in this respect is the observation reported by Scorrano[10] and subsequently by one of us[11] that methyl aryl ketones react with some nitroarenes giving 1,2-diaroyl-1-arylaminoethylenes. The reaction proceeds apparently *via* direct addition of the enolates to the nitro group, although redox process and nitrosoarene intermediates are suggested by Scorrano.[10]

In this communication we report that treatment of some nitroarenes **1a**–**d** with cyclohexanone **2a** and 2- and 3-methylcyclohexanones **2b**,**c** in presence of base results in the formation of substituted *o*-hydroxydiarylamines **3a**–**f** in reasonable yields. Since these anilines are sensitive to oxidation, particularly in basic media, some problems were encountered in isolation and purification, and thus the reaction mixtures were treated with MeI to produce stable *o*-methoxydiarylamines **4a**–**f**, which were then readily isolated and purified.† Some results are collected in Table 1.

The reaction proceeds apparently *via* direct addition of the enolate to the nitro group in nitroarenes and is undoubtedly related to reported earlier formation of 1,2-diaroyl-1-arylaminoethylenes.[10,11] The speculative mechanistic pathway of these complicated processes, which bifurcate at the stage of further transformation of the nitrone intermediate **5**, is shown in Scheme 1.

Direct addition of the enolate to the nitro group produces the anionic adduct converted into nitrone **5**. Nitrone **5a** derived from cyclohexanone undergoes 1,3-proton shift leading to the hydroxylamine derivative, followed by 1,4-dehydration giving the imino ketone which tautomerizes in basic media to form the aromatic system of *o*-hydroxyaniline **3**. In the similar reaction of acetophenone there is no possibility for such proton shift and 1,4-dehydration in the linear nitrone intermediate **5b**, so addition of the second enolate molecule to the nitrone takes place to produce hydroxylamine **6** which upon dehydration and tautomerisation gives the final diaroylethylenes **7**.

The main problem to be clarified is the reason for the observed dichotomy of the reaction course of enolates with nitroarenes. At low temperature, enolates generated by treatment of ketones with base or activation of silyl enol ethers with F^- anions add at the *ortho*- or *para*-position of halonitrobenzenes.[12] Subsequent oxidation of the σ^H adducts leads to nitrobenzylic ketones—products of the oxidative substitution of hydrogen. On the other hand, as has been shown in previous papers[10,11] and in this report, at higher temperature the same enolates add to the nitro group of nitroarenes. Since it is not reasonable to assume that changing the temperature changes the mode of the initial step, one can suppose that also in the latter reaction reversible addition to the ring is a fast initial process. At low temperature the σ^H adducts produced are long lived species and are oxidized, whereas at high temperature the concentration of the σ^H adducts becomes so low that the bimolecular oxidation process does not occur and the reaction proceeds *via* addition of the enolate to the nitro group.

The possibility that the reaction, in analogy to other processes,[13,14] proceeds *via* nitrosoarenes, was excluded by experiments in which *p*-nitroso-*N*,*N*-dimethylaniline subjected to the reaction with cyclohexanone under the identical conditions gave mainly *p*,*p*-bis(*N*,*N*-dimethylamino)azoxybenzene in a fast process, whereas slow introduction of this nitrosoarene to the reaction mixture of *p*-nitrodimethylaniline and cyclohexanone did not improve the yield of the *o*-hydroxydiarylamine, being rapidly converted into the azoxycompound. Direct

Table 1 Reaction of nitrobenzenes **1** with cyclohexanones **2**

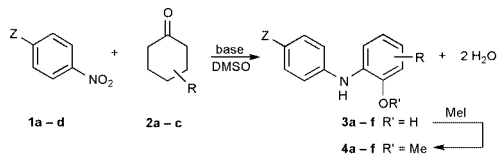

Z	R	Conditions	Time/h	Product yield (%)[a]
1a, H	**2a**, H	KF/Al_2O_3, 80 °C	1	**4a**, 15
1b, MeO	**2a**, H	KF/Al_2O_3, 80 °C	2	**4b**, 30
1c, Me_2N	**2a**, H	KOH, 60 °C	3	**4c**, 50
1d, Et_2N	**2a**, H	KOH, 80 °C	1	**4d**, 60
1d, Et_2N	**2b**, 2-Me	KOH, 80 °C	3	**4e**, 63
1d, Et_2N	**2c**, 3-Me	KOH, 80 °C	1	**4f**, 57

[a] Isolated products.

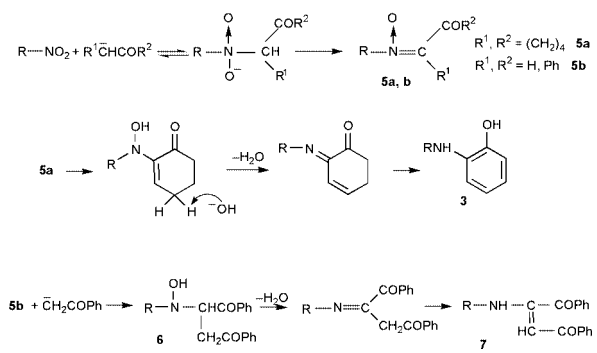

Scheme 1 The reaction pathways of nitroarenes R = Ar with enolates of cyclohexanone R′, $R^2 = (CH_2)_4$ and acetophenone R′ = H, R^2 = Ph.

 DOI: 10.1039/b101612l

intermolecular addition of carbanions to the NO_2 group is a common process when it is connected with oxygen used as a preparative method for nitration of enolates with alkyl nitrates.[15] Such reaction can occur with nitroalkanes provided they are not C–H acids. Thus we found that when *tert*-nitrobutane was allowed to react with cyclohexanone in the presence of KOH in DMSO at 80 °C, *N*-*tert*-butyl-2-hydroxyaniline **3g** was isolated in moderate yield 12%.‡

It is worth stressing that the presented reaction is a useful one-pot alternative to only a few methods designed for the synthesis of diarylamines containing electron-donating substituents in both rings.[16,17]

This work was supported by the State Committee for Scientific Research, grant Nr. PBZ 6.01.

Notes and references

† Typical procedure: to a stirred solution of **1** (5 mmol) and **2** (5–15 mmol) in DMSO (10 ml) under argon, powdered KOH (30 mmol) or KF/Al_2O_3 was added in one portion. The mixture was treated as shown in Table 1, cooled to rt and MeI (10 mmol) was added. After stirring for 5 min the mixture was poured into aq. NH_4Cl, the product was extracted with EtOAc and chromatographed on silica gel (hexane–toluene 1 : 3). **3a**: mp 68–70 °C, lit. 71 °C.[18] **4a**: bp 158–162 °C/5 mm, lit. 151–156 °C/5 mm.[19] **4b**: mp 69–70 °C, lit. 71–72 °C.[16] *Selected spectral data for compounds not reported earlier:* **4c**: mp 44–45 °C; ^{1}H NMR (200 MHz, $CDCl_3$, TMS); δ = 2.92 (s, 6 H, $N(CH_3)_2$), 3.89 (s, 3 H, OCH_3), 5.90 (br s, 1 H, NH), 6.74 (d, J = 9 Hz, 2 H, arom H), 6.80–7.01 (m, 4 H, arom H), 7.10 (d, J = 9 Hz, 2 H, arom H); **4d**: oil; ^{1}H NMR ($CDCl_3$): δ = 1.15 (t, J = 7 Hz, 6 H, $(CH_3)_2$), 3.32 (q, J = 7 Hz, 4 H, $N(CH_2)_2$), 3.89 (s, 3 H, OCH_3), 5.88 (br s, 1 H, NH) 6.68 (d, J = 9 Hz, 2 H, arom H), 6.70–6.98 (m, 4 H, arom H), 7.07 (d, J = 9 Hz, 2 H, arom H); **4e**: mp 59–60 °C; ^{1}H NMR ($CDCl_3$): δ = 1.15 (t, J = 7 Hz, 6 H, $(CH_3)_2$), 2.30 (s, 3 H, CH_3), 3.32 (q, J = 7 Hz, 4 H, $N(CH_2)_2$), 3.78 (s, 3 H, OCH_3), 5.87 (br s, 1 H, NH), 6.58 (m, 1 H, arom H), 6.68 (d, J = 9 Hz, 2 H, arom H), 6.83 (m, 2H, arom H), 7.07 (d, J = 9 Hz, 2 H, arom H); **4f**: mp 80–82 °C, ^{1}H NMR ($CDCl_3$); δ = 1.14 (t, J = 7 Hz, 6 H, $(CH_3)_2$), 2.28 (s, 3 H, CH_3), 3.30 (q, J = 7 Hz, 4 H, $(CH_2)_2$), 3.86 (s, 3 H, OCH_3), 5.70 br s, 1 H, NH), 6.60 (m, 2 H, arom H), 6.68 (d, J = 9 Hz, 2 H, arom H), 6.87 (d, J = 8 Hz, 1 H), 7.05 (d, J = 9 Hz, 2 H, arom H).

‡ **3g**: mp 76–77 °C; ^{1}H NMR ($CDCl_3$): δ = 1.2 (s. 9 H, *tert*-C_4H_9), 4.40 (br s, 2 H, NH, OH) 6.60–7.10 (m, 4 H, arom H).

1 J. Miller, *Aromatic Nucleophilic Substitution*, Elsevier, Amsterdam, 1968; F. Terrier, *Nucleophilic Aromatic Displacement*, VCH Publishers Inc., New York, 1991.
2 M. Mąkosza, *Russ. Chem. Bull.*, 1996, **45**, 491.
3 O. N. Chupakhin, V. N. Charushin, H. C. van der Plas, *Nucleophilic Aromatic Substitution of Hydrogen*, Academic Press, San Diego, 1994.
4 M. Mąkosza and K. Staliński, *Polish J. Chem.*, 1999, **73**, 151.
5 M. Mąkosza and J. Winiarski, *Acc. Chem. Res.*, 1987, **20**, 282; M. Makosza and K. Wojciechowski, *Liebigs Ann./Recueil*, 1997, 1805.
6 W. Danikiewicz and M. Mąkosza, *J. Org. Chem.*, 1991, **56**, 1283.
7 P. N. Preston and G. Tennant, *Chem. Rev.*, 1972, **72**, 627.
8 Z. Wróbel and M. Mąkosza, *Tetrahedron Lett.*, 1997, **53**, 5501; M. Mąkosza and A. Tyrała, *Acta Chem. Scand.*, 1992, **46**, 689.
9 A. Hassner and D. R. Fitchmun, *Tetrahedron Lett.*, 1966, 1991.
10 C. Paradisi, M. Prato, U. Quintily and G. Scorrano, *J. Org. Chem.*, 1981, **46**, 5156; M. Prato, U. Quintily and G. Scorrano, *J. Chem. Soc., Perkin Trans. 2*, 1986, 1419.
11 N. V. Moskalev and M. I. Tartynova, *Mendeleev Commun.*, 1996, 72; N. V. Moskalev and M. I. Tartynova, *Russ. Chem. Bull.*, 1998, **46**, 1603.
12 M. Hamana, G. Iwasaki and S. Saeki, *Heterocycles*, 1982, **17**, 177; T. V. RajanBabu, A. S. Reddy and T. Fukunaga, *J. Am. Chem. Soc.*, 1985, **107**, 5473.
13 P. Erlich and F. Sachs, *Ber.*, 1899, **32**, 2341.
14 M. Bosco, R. Dalpozzo, G. Bartoli, G. Palmieri and M. Petrini, *J. Chem. Soc., Perkin Trans. 2*, 1991, 657; G. Bartoli, M. Bosco, R. Dalpozzo, G. Palmieri and E. Marcantoni, *J. Chem. Soc., Perkin Trans. 1*, 1991, 2757.
15 N. Kornblum, *Org. React.*, 1962, **12**, 120; H. Feuer and P. M. Pivawer, *J. Org. Chem.*, 1966, **31**, 3152.
16 I. G. C. Coutts and M. Hamblin, *J. Chem. Soc., Perkin Trans. 1*, 1975, **23**, 2445.
17 D. H. R. Barton, M. X. Donney, J. P. Finet and B. J. Quiry, *J. Chem. Soc., Perkin Trans. 1*, 1991, 2095.
18 D. B. Denny and D. Z. Denny, *J. Am. Chem. Soc.*, 1960, **82**, 1389.
19 K. Plat, V. Jesina, V. Dusek and C. Vrba, *Ceskoslov. Farm.*, 1959, **8**, 569.

CHEMCOMM
Communication
www.rsc.org/chemcomm

Cystine-based cyclic oligoureas: a new class of hydrogen-bonding electroneutral anion receptors†

Darshan Ranganathan* and C. Lakshmi

Discovery Laboratory, Indian Institute of Chemical Technology, Hyderabad-500 007, India. E-mail: ranganathan@iict.ap.nic.in; Fax: 040-7173757/7173387

Received (in Cambridge, UK) 23rd March 2001, Accepted 21st May 2001
First published as an Advance Article on the web 20th June 2001

Cystine-based symmetrical cyclic oligoureas, synthesized in a one-pot reaction from L-cystine dimethyl ester and triphosgene, are demonstrated to act as versatile neutral receptors for both inorganic and organic anions operating exclusively through hydrogen bonds; ^{1}H NMR studies have shown that while the cyclic triurea prefers to complex with spherical (halides) and trigonal planar (nitrate) anions, the higher oligomer tetraurea can trap the tetragonal planar squarate dianion with modest efficiency.

Rational design of artificial receptors for anion complexation is an area of intense current interest[1] that has relevance to biology, industry and environment. Considering the intense activity and the vast literature that has accumulated over the past two decades in the field of supramolecular chemistry and the development of preorganization concepts in molecular recognition, it was surprising to find only a handful of designs for cyclic anion receptors and barring few exceptions of neutral cyclic anion hosts,[2] most of these interestingly, centred around the use of protonated macro mono or polycyclic amines.[3] Thus, whereas in Nature it is the neutral anion-binding proteins regulating the transport of anions largely through hydrogen bonds,[4] the synthetic designs of positively charged anion receptors operated mainly through coloumbic interactions. The idea of using amino acid-based macrocycles with multiple hydrogen-bonding pockets, uniformly distributed in the cyclic backbone, appeared an exciting possibility to create neutral receptors that would not only be close to natural systems but may also show high selectivity in multifunctional anion complexation.

In this communication, we provide the first illustration[5] of such a concept and report on the design, synthesis and anion recognition of L-cystine-based cyclic oligourea receptors wherein the multiple urea groups are held as part of the ring framework in a cyclic arrangement. Among the hydrogen bonding groups, the urea unit was particularly favoured because of its double hydrogen bond donor capacity. Choice of cystine unit was based on the consideration that apart from being a neutral amino acid, the presence of S–S linkage in its framework and its 1,ω-diamine nature would facilitate the ring closure to cyclicureas.

For the construction of homocyclic oligomers of cystine ureas, the synthetic strategy envisaged one-step condensation of L-cystine diOMe with triphosgene, a commercially available precursor of phosgene (Scheme 1). The reaction carried out under high dilution conditions afforded a mixture of two products with similar TLC behaviour, which were separated by chromatography on silica gel with dichloromethane–methanol (98 : 2) as eluent. The products **1** and **2** were isolated in yields of 37 and 15% respectively, and were fully characterized by spectroscopic and analytical data.[6] The ES-MS and FAB-MS results (ESI†) confirmed the cyclic trimeric and tetrameric nature of macrocycles **1** and **2** respectively. A noteworthy feature in the cyclization reaction of cystine dimethyl ester with triphosgene was the formation of 27-membered 3 + 3 macrocycle **1** as the major product (37%), followed by 15% of the 36-membered higher oligomer **2**, the 4 + 4 cyclization product. The near complete absence of 9- and 18-membered macrocycles that could arise from 1 + 1 and 2 + 2 cyclization reaction is in agreement with our earlier observations[7] with cystine-containing macrocycles where the most preferred ring size in cyclooligomerization was found to be 26-membered. Our recent finding[8] that 18-membered cyclic bisurea was the only product in the cyclooligomerization reaction of cystamine with triphosgene also supports the notion that the asymmetric cystine unit has more stringent steric demands with respect to the ring size.

The highly symmetrical structure of macrocycles **1** and **2** laced with multiple units of hydrogen-bonding urea functions, positioned equidistant from each other and all converging towards the centre of the cavity, appeared particularly suited for the molecular recognition of anionic substrates with spherical shapes. We also expected these receptors to bind polyoxyanions

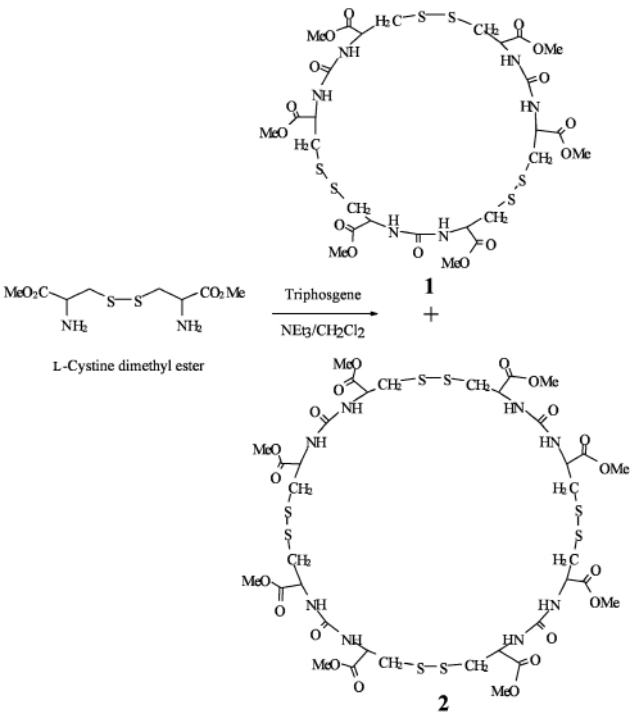

Scheme 1 One step condensation of triphosgene and cystine dimethyl ester to give cyclic oligoureas **1** and **2**.

† Electronic supplementary information (ESI) available: ^{1}H NMR of **1** (Fig. S1), **2** (Fig. S2); ROESY NMR of **1** (Fig. S3), **2** (Fig. S4); ES-MS of **1** (Fig. S5), **2** (Fig. S6), FAB-MS of **1** (Fig. S7); NMR titration of **2** with squarate TBA salt (Fig. S8); ^{1}H NMR of **1** in $CDCl_3$ (host alone) (Fig. S9), **1** with Cl^- in 1 : 1 molar ratio (Fig. S10), **1** with Br^- in 1 : 1 molar ratio (Fig. S11), **1** with NO_3^- in 1 : 1 molar ratio (Fig. S12), **2** in $CDCl_3$ (host alone) (Fig. S13), **2** with squarate dianion in 1 : 1 molar ratio (Fig. S14). See http://www.rsc.org/suppdata/cc/b1/b102720b/

 DOI: 10.1039/b102720b

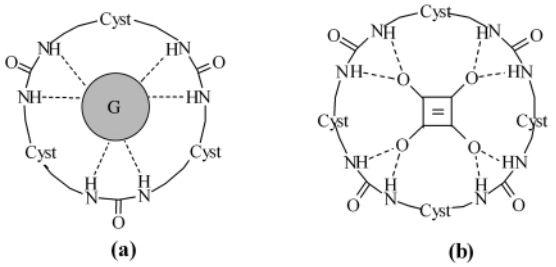

Fig. 1 (a) Proposed hexahydrogen-bonded complex of **1** with Cl^-/Br^- or nitrate anion; G = $Cl^-/Br^-/NO_3^-$; Cyst = L-cystine unit. (b) Proposed octahydrogen-bonded complex of **2** with squarate dianion.

provided their electronic and geometric features are compatible with each other.

Binding studies with halide anions (as tetrabutylammonium (TBA) salts) using ^{1}H NMR, showed that while cyclic triurea **1** showed modest affinity for chloride and bromide ions and no affinity for iodide ion, the macrocyclic tetraurea **2** was unable to bind any of the halide anions. Interestingly, the host **1**, only sparingly soluble in $CDCl_3$, was found to rapidly go into solution upon the addition of chloride or bromide TBA salt, indicating effective host–guest recognition. There was considerable downfield shift ($\sim$0.5–0.8 ppm) of NH protons in **1** suggesting their involvement in hydrogen bonding with the anion. Using NMR titration method,[9] the association constants (K_a) for **1** with chloride and bromide TBA salts were measured as 2.05×10^3 and 2.01×10^2 M^{-1} respectively. The triurea **1** with three-fold symmetry in its structure also suggested a possible complexation with trigonal anionic guests. Thus, while trimesic acid anion was found to be too big for the cavity of **1** to show any detectable NH shift, the trigonal planar geometry of nitrate anion seemed to have a complementary fit with **1** showing appreciable binding in $CDCl_3$ ($K_a = 5.2 \times 10^2$ M^{-1}). In conformity with the above notion, the cyclic tetraurea **2** was demonstrated to act as an excellent host for the squarate dianion $[SQ]^{2-}$, a truly delocalized planar tetraoxyanion[10] with four-fold symmetry. Using NMR titration, the association constant for **2** with squarate TBA salt in $CDCl_3$ was measured as 3.21×10^3 M^{-1}. The significant downfield shift ($\Delta\delta \sim 1.5$) observed for the urea NH protons of **2** is indicative of highly effective hydrogen bonding. The almost 100-fold selectivity of macrocyclic triurea **1** for planar, 3-fold symmetric nitrate anion and of cyclic tetraurea **2** for planar four-fold symmetric squarate tetraoxyanion guest was shown by complete absence of any anion induced shifts in the ^{1}H NMR of **1** and **2** in $CDCl_3$ even with excess molar proportions of the guest substrates. The proposed tris-bidentate or hexahydrogen-bonded structure for complex of **1** with Cl^-/Br^- or NO_3^- [Fig. 1(a)] and octahydrogen-bonded structure for the complex of **2** with $[SQ]^{2-}$ [Fig. 1(b)] is supported by the maximum NH shift at a mole ratio of 1:1 (ESI†).

The cystine-based macrocyclic oligoureas described here represent a new class of electroneutral anion receptors that operate exclusively through hydrogen bonds. The multiple hydrogen-bonding sites distributed symmetrically all over the ring make these macrocycles especially suited for molecular recognition of spherical and polyfunctional anions. Their remarkable affinity for planar polyoxyanions and selectivity according to size complementarity combined with extremely simple synthesis from commercially available materials should open up new challenges in this area. Additionally, the receptor modification through the COOH handles on the cystine unit should provide attractive hosts for membrane anion transport. Studies in this direction are in progress.

We thank Professor S. Ranganathan for valuable discussions. Financial support from DST, New Delhi is gratefully acknowledged. D. R. is also an honorary faculty member of Jawaharlal Nehru Centre for Advanced Scientific Research.

Notes and references

1 J. Scheerder, J. F. J. Engbersen and D. N. Reinhoudt, *Recl. Trav. Chim. Pays Bas.*, 1996, **115**, 307; F. P. Schmidtchen and M. Berger, *Chem. Rev.*, 1997, **97**, 1609; J.-M. Lehn, *Supramolecular Chemistry: Concepts and Perspectives*, VCH, Weinheim, Germany, 1995; J. L. Atwood, K. T. Holman and J. W. Steed, *Chem. Commun.*, 1996, 1401; P. D. Beer, *Chem. Commun.*, 1996, 689; B. Dietrich, *Pure Appl. Chem.*, 1993, **65**, 1457; M. M. G. Antonisse and D. N. Reinhoudt, *Chem. Commun.*, 1998, 443.

2 A. M. Kelly-Rowley, V. M. Lynch and E. V. Anslyn, *J. Am. Chem. Soc.*, 1995, **117**, 3438; P. A. Gale, J. L. Sessler, V. Kral and V. Lynch, *J. Am. Chem. Soc.*, 1996, **118**, 5140.

3 E. Kimura, A. Sakonaka, T. Yatsunami and M. Kodama, *J. Am. Chem. Soc.*, 1981, **103**, 3041; M. W. Hosseini and J.-M. Lehn, *J. Am. Chem. Soc.*, 1982, **104**, 3525; M. W. Hosseini and J.-M. Lehn, *Helv. Chim. Acta*, 1998, **71**, 749.

4 J. J. He and F. A. Quiocho, *Science*, 1991, **251**, 1479; Z. F. Kanyo and D. W. Christianson, *J. Biol. Chem.*, 1991, **266**, 4246; H. Luecke and F. A. Quiocho, *Nature*, 1990, **347**, 402.

5 Although open chain urea-based hosts have been used for complexation of oxyanions (T. R. Kelly and M. H. Kim, *J. Am. Chem. Soc.*, 1994, **116**, 7072; E. Fan, S. A. Van Arman, S. Kincaid and A. D. Hamilton, *J. Am. Chem. Soc.*, 1993, **115**, 369; C. Raposo, M. Almaraz, M. Martin, V. Weinrich, M. L. Mussons, V. Alcasar, M. C. Caballero and J. R. Moran, *Chem. Lett.*, 1995, 759; K. S. Jeong, J. W. Park and Y. L. Cho, *Tetrahedron Lett.*, 1996, **37**, 2795; P. Buhlmann, S. Nishizawa, K. P. Xiao and Y. Umezawa, *Tetrahedron*, 1997, **53**, 1647. To the best of our knowledge with the sole exception of one recent reference. B. H. M. Snellink-Ruël, M. M. G. Antonisse, J. F. J. Engbersen, P. Timmerman and D. N. Reinhoudt, *Eur. J. Org. Chem.*, 2000, 165 wherein phenylene-bridged macrocyclic tetraureas have been shown to bind $H_2PO_4^-$ with complete selectivity over Cl^- in DMSO solvent, there are no reports in literature on the use of cyclic oligoureas wherein the urea units form part of the ring backbone as anion receptors. However, urea-appended cyclic hosts for spherical halide anions R. C. Jagessar, M. Shang, W. R. Scheidt and D. H. Burns, *J. Am. Chem. Soc.*, 1998, **120**, 11684; J. Scheerder, M. Fochi, J. F. J. Engbersen and D. N. Reinhoudt, *J. Org. Chem.*, 1994, **59**, 7815 have been reported.

6 Selected data: **1**: Yield 37%; mp 202–203 °C; IR (KBr) 3376, 2956, 1736, 1634, 1565 cm^{-1}; ^{1}H NMR (500 MHz, DMSO-d_6) δ 3.11 (m, 12H), 3.63 (s,18H), 4.42 (m, 6H), 6.81 (d, J = 7.5 Hz, 6H); FAB-MS *m/z*: (%) 905 (10) $[M + Na^+]$, 883 (45) $[M + H]^+$; ES-MS *m/z*: (%) 905 (100) $[M + Na^+]$, 883 (80) $[M + H]^+$. **2**: Yield 15%; mp 204–206 °C; IR (KBr) 3360, 2960, 1741, 1636, 1563 cm^{-1}; ^{1}H NMR (500 MHz, DMSO-d_6) δ 3.07 (m, 16H), 3.66 (s, 24H), 4.44 (m, 8H), 6.77 (d, J = 8.0 Hz, 8H); ES-MS *m/z*: (%) 1199 (100) $[M + Na^+]$.

7 D. Ranganathan, V. Haridas and I. L. Karle, *J. Am. Chem. Soc.*, 1998 **120**, 2695; D. Ranganathan, V. Haridas, K. P. Madhusudanan, R. Roy, R. Nagaraj, G. B. John and M. B. Sukhaswami, *Angew. Chem., Int. Ed. Engl.*, 1996, **35**, 1105; D. Ranganathan, V. Haridas, R. Nagaraj and I. L. Karle, *J. Org. Chem.*, 2000, **65**, 4415.

8 D. Ranganathan and C. Lakshmi, unpublished results.

9 The association constant (K_a) was obtained by using the following equation: $K_{assoc} = \alpha/[(1 - \alpha)([G] - \alpha[H])$, where $\alpha = (\delta - \delta_0)/(\delta_{max} - \delta_0)$, δ_0 is the initial chemical shift (host alone), δ is the chemical shift at each titration point, and δ_{max} is the chemical shift when the receptor is entirely bound. [*G*] and [*H*] are the concentrations of guest and host, respectively, at each titration point. (T. R. Kelly and M. H. Kim, *J. Am. Chem. Soc.*, 1994, **116**, 7072 and references therein).

10 I. L. Karle, D. Ranganathan and V. Haridas, *J. Am. Chem. Soc.*, 1996, **118**, 7128.

CHEMCOMM Communication
www.rsc.org/chemcomm

Biosynthesis of the di-*meta*-hydroxyphenylglycine constituent of the vancomycin-group antibiotic chloroeremomycin

Alan M. Sandercock, Elizabeth H. Charles, Wendy Scaife, Peter N. Kirkpatrick, Simon W. O'Brien, Eduardo A. Papageorgiou, Jonathan B. Spencer* and Dudley H. Williams*

Cambridge Centre for Molecular Recognition, University Chemical Laboratories, Lensfield Road, Cambridge, UK CB2 1EW. E-mail: dhw1@cam.ac.uk; Fax: +44 1223 336913; Tel: +44 1223 336368

Received (in Cambridge, UK) 24th April 2001, Accepted 29th May 2001
First published as an Advance Article on the web 20th June 2001

The biosynthetic pathway to the L-di-*meta*-hydroxyphenylglycine (DHPG) constituent of chloroeremomycin (A82846B), has been investigated by a combination of feeding experiments with ^{13}C-labelled substrates, and expression and assay of HpgT from the chloroeremomycin biosynthetic cluster.

The rising incidence of resistance to vancomycin and teicoplanin[1,2]—currently the antibiotics of last resort for treating many nosocomial infections—necessitates the development of new therapeutic agents. An understanding of the mode of action of vancomycin group antibiotics[3] and the emerging resistance mechanisms[4,5] should facilitate rational design of new antibiotics capable of defeating vancomycin resistant bacteria. Some of our recent research on the vancomycin group of antibiotics has focussed on the biosynthesis of chloroeremomycin **1** (Fig. 1), also known as A82846B and LY264826, which differs from vancomycin in only its appended sugars. A gene cluster from *Amycolatopsis orientalis* A82846 for the biosynthesis of **1** has been sequenced.[6] Protein homologies have suggested roles for many of the putative enzymes encoded therein, and a number of these roles have now been confirmed experimentally.[7–11]

The heptapeptide core of chloroeremomycin contains several unusual amino acids, including four residues with D-stereochemistry at the alpha carbon, and five with non-proteinogenic side chains. Here we report two intermediates and the role of one enzyme, HpgT (*p*-hydroxyphenylglycine transaminase), in the biosynthetic pathway (Scheme 1) leading to L-di-*meta*-hydroxyphenylglycine (L-DHPG) **2**, found as the *C*-terminal residue of **1**. DHPG has previously been shown to be derived from four units of acetate,[12] but the subsequent biosynthetic steps have hitherto been uncertain.

We synthesised two possible precursors to DHPG, di-*meta*-hydroxyphenylacetic acid **3** and (±)-di-*meta*-hydroxymandelic acid **4** (Scheme 1), with ^{13}C-labelled carboxylate groups. These were characterized by NMR and mass spectroscopy; [1-^{13}C]-**3** δ_H (500 MHz, D_2O) 3.44 (2H, d, J^{13}_{CH} = 12 Hz), 6.21 (1H, s), 6.30 (2H, s): δ_C (100 MHz, D_2O, proton decoupled) 41.40 (d, $J^{13}_C{}^{13}_C$ = 54.2), 102.37, 109.56, 137.98, 157.88, 177.48 (^{13}C enriched): *m*/*z* (EI+) [M$^{+\cdot}$] = 169.0454, calculated for $^{12}C_7{}^{13}C_1{}^1H_8{}^{16}O_4$ = 169.0456; [1-^{13}C]-**4** δ_H (500 MHz, DMSO-d_6) 4.74 (1H, d, J^{13}_{CH} = 4.6 Hz), 6.02 (1H, br), 6.23 (2H, br), 9.13 (br): δ_C (125 MHz, DMSO-d_6, proton decoupled) 72.51 (d, $J^{13}_C{}^{13}_C$ = 58 Hz), 101.73, 104.84, 142.25, 158.17, 174.06 (^{13}C enriched): *m*/*z* (EI+) [M$^{+\cdot}$] = 185.0414, calculated for $^{12}C_7{}^{13}C_1{}^1H_8{}^{16}O_5$ = 185.0405. (Details of the syntheses will be published separately.) If incorporated by the producing strain, both should lead to isotopic enrichment at the carbonyl group of L-DHPG. To investigate the uptake of labelled substrates by *A. orientalis* A82846.2 (NRRL 18100), the strain was inoculated into CSM[13] (50 ml) and incubated at 30 °C/250 rpm for 3 days. A 2.5 ml aliquot of this culture was inoculated into FermB medium (50 ml) and incubated at 30 °C/250 rpm for 110 h. Labelled substrates were fed aseptically, in 4 × 5 mg portions, at either 36, 40, 44 and 48 h (for **3**) or 34, 38, 42 and 44 h (for **4**) after inoculation. Cells were removed by centrifugation, and the antibiotics purified from the filtered supernatant by affinity chromatography on sepharose-D-Ala-D-Ala (prepared from Activated CH-Sepharose 4B), desalted by reverse-phase HPLC and lyophilised. Typically, 5–10 mg of purified antibiotic was recovered. The ^{13}C NMR spectra of isolated chloroeremomycin showed enrichment of a peak at 172.1 ppm. The corresponding HMBC spectra, for **1** produced both from **3** and from **4**, showed a cross-peak to a proton at 4.42 ppm, identified as the C_α proton of DHPG, x_7 (see Fig. 1), confirming the identity of the enriched carbon as CX_7. No other cross peaks due to **1** were observed in these spectra. All spectra were run in DMSO-d_6 as **1** does not dimerise in DMSO, thus simplifying the spectra considerably. The natural abundance ^{13}C resonances were too weak to be seen in any of the spectra. Thus **3** and **4** are incorporated in the biosynthesis of DHPG.

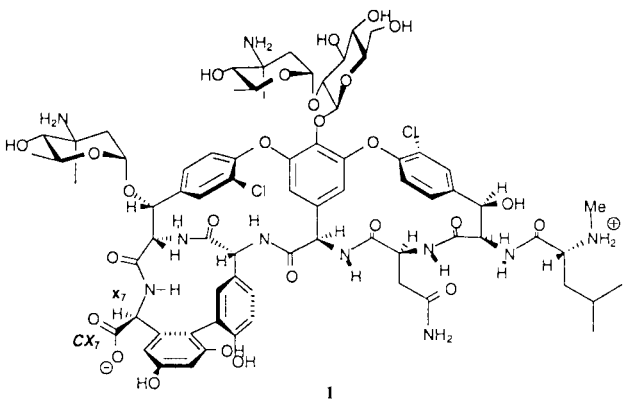

Fig. 1 The structure of chloroeremomycin **1**, showing the carbonyl position of DHPG, CX_7, and the adjacent C_α proton, x_7.

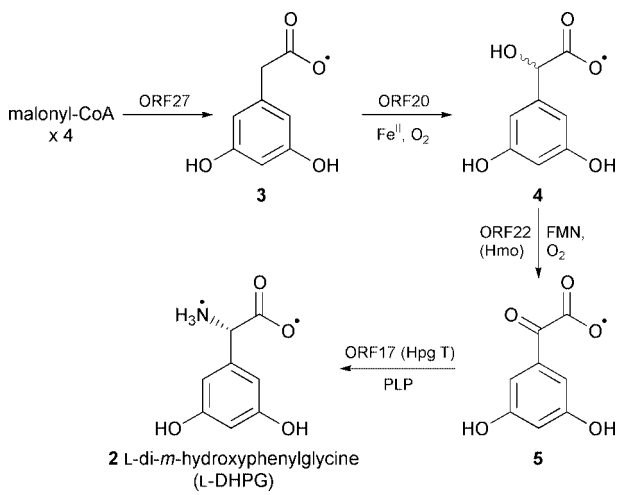

Scheme 1 Proposed biosynthetic pathway to L-DHPG.

 DOI: 10.1039/b103668h

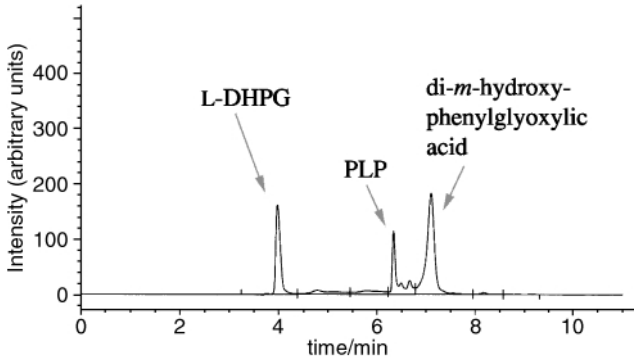

Fig. 2 HPLC trace (monitored at 254 nm) showing the HpgT-catalysed formation of di-*meta*-hydroxyphenylglyoxylic acid **5** from L-DHPG **2**.

To investigate the role of HpgT in the formation of DHPG, *hpgT* from the chloroeremomycin gene cluster was PCR amplified and cloned into the expression vector pET28a(+) (Novagen) as an *N*-terminal His_6-tagged protein. The resulting recombinant plasmid was used to transform the expression host *E. coli* BL21(DE3) (Novagen), and the cells grown for 16 h at 16 °C in 2 × YT medium, following induction by isopropyl β-D-thiogalactoside (IPTG, 1 mM). HpgT was purified using Novagen His-Bind Quick 900 cartridges, and then transferred to Tris-HCl (50 mM, pH 7.5) using Millipore™ centrifugal filters. The purified protein was visualised as a single band by SDS-PAGE, and the relative molecular mass determined by electrospray ionisation (ESI) mass spectrometry to be 49.80 kDa (predicted = 49.808 kDa).

The HpgT catalysed interconversion of **5** (Scheme 1) and L-DHPG was assayed as follows: HpgT (100 μg) was incubated with L-DHPG (1 mM), α-ketoglutarate (2 mM) and pyridoxal phosphate (PLP, 100 μM) in Tris-HCl (300 μl) for 1 h at 30 °C, after which time HPLC analysis showed a new, strongly absorbing peak (Fig. 2). ESI mass spectrometric analysis identified this peak as di-*meta*-hydroxyphenylglyoxylic acid ($[M + H]^+$ = 183.0, calculated for $C_8H_7O_5^+$ = 183.14). These results indicate that, in addition to its previously documented role in *p*-hydroxyphenylglycine biosynthesis,[11] HpgT is responsible for the transamination from **5** to L-DHPG, **2**.

Since another enzyme from the cluster, Hmo, has been shown to oxidise **4** to **5**,[14] the results given here identify the biosynthetic steps and intermediates from di-*meta*-hydroxyphenylacetate to L-DHPG in *A. orientalis* (Scheme 1) except the required benzylic hydroxylation (**3** to **4**). We have shown that ORF27 (a chalcone synthase homologue) produces di-*meta*-hydroxyphenylacetate from malonyl-CoA[15] and propose ORF20 (which shows homology to the P450 family of heme-binding proteins) from the chloroeremomycin biosynthetic cluster as a candidate for the benzylic hydroxylation; experiments are underway to investigate these proposals.

We thank the BBSRC (A. M. S., W. S.), the EPSRC (P. N. K., E. H. C.) and Eli Lilly (S. W. O'B.) for funding. P. Solenberg (Eli Lilly, Indianapolis) is thanked for donating *A. orientalis* A82846.2 and for advice on optimal conditions for antibiotic production. L-DHPG was kindly donated by Professor D. Evans (Harvard University).

Notes and references

1 V. Krcmery and A. Sefton, *Int. J. Antimicrob. Agents*, 2000, **14**, 99.
2 Y. Cetinkaya, P. Falk and C. G. Mayhall, *Clin. Microbiol. Rev.*, 2000, **13**, 686.
3 D. H. Williams and B. Bardsley, *Angew. Chem., Int. Ed.*, 1999, **38**, 1172.
4 M. Arthur, P. Reynolds and P. Courvalin, *Trends Microbiol.*, 1996, **4**, 401
5 H. Hanaki, H. Labischinski, Y. Inaba, N. Kondo, H. Murakami and K. Hiramatsu, *J. Antimicrob. Chemother.*, 1998, **42**, 315
6 A. M. A. v. Wageningen, P. N. Kirkpatrick, D. H. Williams, B. R. Harris, J. K. Kershaw, N. J. Lennard, M. Jones, S. J. M. Jones and P. J. Solenberg, *Chem. Biol.*, 1998, **5**, 155.
7 D. P. O'Brien, P. N. Kirkpatrick, S. W. O'Brien, T. Staroske, T. I. Richardson, D. A. Evans, A. Hopkinson, J. B. Spencer and D. H. Williams, *Chem. Commun.*, 2000, 103.
8 P. N. Kirkpatrick, W. Scaife, T. M. Hallis, H.-W. Liu, J. B. Spencer and D. H. Williams, *Chem. Commun.*, 2000, 1565.
9 O. W. Choroba, D. H. Williams and J. B. Spencer, *J. Am. Chem. Soc.*, 2000, **122**, 5389.
10 H. Chen, M. G. Thomas, B. K. Hubbard, H. C. Losey, C. T. Walsh and M. D. Burkart, *Proc. Natl. Acad. Sci. USA*, 2000, **97**, 11 942.
11 B. K. Hubbard, M. G. Thomas and C. T. Walsh, *Chem. Biol.*, 2000, **7**, 931.
12 S. J. Hammond, M. P. Williamson, D. H. Williams, L. D. Boeck and G. G. Marconi, *J. Chem. Soc., Chem. Commun.*, 1982, 344.
13 T. J. Hosted and R. H. Baltz, *Microbiology*, 1996, **142**, 2803.
14 T. L. Li, O. W. Choroba, E. H. Charles, A. M. Sandercock, D. H. Williams and J. B. Spencer, manuscript in preparation.
15 T. L. Li, O. W. Choroba, D. H. Williams and J. B. Spencer, manuscript in preparation.

CHEMCOMM
Communication
www.rsc.org/chemcomm

Counter anion dependent symmetry of Cu^{II}–4-amino-1,2,4-triazole polymeric chains

Krzysztof Drabent* and Zbigniew Ciunik

Faculty of Chemistry, University of Wroclaw, 14 F. Joliot-Curie Str., 50-383 Wroclaw, Poland. E-mail: drab@wchuwr.chem.uni.wroc.pl

Received (in Cambridge, UK) 28th February 2001, Accepted 30th May 2001
First published as an Advance Article on the web 20th June 2001

The symmetry changes and length of the symmetry independent part of $[Cu(amtrz)_3]_n^{2+}$ (amtrz = 4-amino-1,2,4-triazole) polymeric chains driven by different anions in crystals with BF_4^- (1), BF_4^-/SiF_6^{2-} (2) and SiF_6^{2-} (3) have been studied by single crystal X-ray method.

A variety of coordination compounds with *N*4-substituted 1,2,4-triazoles as a ligand coordinating to first-row transition metal ions have been reported.[1] The interesting magnetic properties of iron(II) and copper(II) compounds with 1,2,4-triazole ligands have been extensively investigated and polynuclear iron(II) 1,2,4-triazole compounds have been found to show spin-crossover behaviour.[2] These ground electronic state related properties depend strongly both on the nature of *N*4-substituent of the ligand[3,4] and non-coordinating anion molecule.[5–7] So far no single crystals suitable for X-ray diffraction were obtained for these iron(II) complexes, however structural information deduced from EXAFS (X-ray absorption fine structure) spectroscopy at the iron K edge indicates the presence of linear chains. On the other hand more detailed analysis of these results leads to ambiguous conclusions. For example, the dependence between the Fe–N bond distances and the size of anions suggested by Erenburg *et al*.[7] were not confirmed by Kojima *et al*.[6] It has been assumed that the copper(II) polymers are isostructural with their iron(II) analogues. Crystallographic studies of copper(II) polymeric chains in different anion environments might reveal the nature of cation–anion interactions. However, only two structures of $[Cu(4\text{-R-trz})_3]A_2$ type crystals have been presented (both with $A = ClO_4^-$ anions).[8,9] The number of data is limited because single crystals of 1-D polymeric metal(II) 1,2,4-triazoles are generally difficult to obtain due to rapid precipitation of the compounds formed.[4]

Because knowledge of the spatial structure of these polymers seems to be necessary to understand the nature of anion–cation interactions we looked for a useful procedure for growing single crystals of copper(II) analogues. Reaction between amtrz in hot MeCN (0.1 mmol in 10 mL) and an aqueous solution of an appropriate copper salt (0.03 mmol, 2 mL) gave a blue amorphous precipitate. The precipitate was filtered off, washed with 5 mL of MeCN and *immediately*[10] dissolved (at least partially) in water giving a light blue solution. After a few weeks $\{[Cu(amtrz)_3](BF_4)_2\cdot H_2O$ **1** and $[Cu(amtrz)_3](BF_4)(SiF_6)_{0.5}\cdot 2H_2O$ **2**$\}$ or days $\{[Cu(amtrz)_3](SiF_6)\cdot 8/3H_2O$ **3**$\}$ well shaped crystals appeared. To obtain **1** the reaction must be carried on in a polyethylene vessel because when glassware is used the mixed anion salt **2** is obtained. It is of note that the synthesis of **2** is reproducible when Pyrex glassware is used. On the other hand, decomposition due to loss of non-coordinated water molecules is observed for compound **3.**† The molecular structures of **1**–**3** were elucidated by X-ray crystallography.‡

The crystals under investigation are composed of linear coordination polymers $[Cu(amtrz)_3]_\infty$ with BF_4 (**1**), BF_4/SiF_6 (**2**) and SiF_6 (**3**) counter ions placed between them as well as different number of water molecules (1, 2 and 8/3, respectively). The μ-N^1,N^2-1,2,4-triazoles act as bidentate ligands bridging copper(II) ions *via* their nitrogen atoms (Fig. 1). The Cu–Cu distances are 3.922 Å in **1**, 3.877 and 3.886 Å in **2**, and 3.855, 3.886 and 3.904 Å in **3**. These values suggest a lack of relation between metal–metal distances and size of counter ion in the crystals. Such a relation was previously postulated for iron(II) triazole complexes on the basis of EXAFS studies.[6]

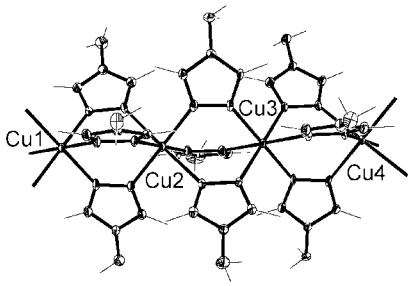

Fig. 1 View of the 1-D coordination polymer in **3**. The anions and water solvate molecules have been omitted for clarity.

In **1**–**3** all copper(II) ions have a distorted (4 + 2), axially elongated octahedral environment (Fig. 2). There are two distinguishable orientations of octahedra along the polymeric chain resulting in alternate *ababa*… order, whereas less regular *abcbab*… order is found for [Cu(4-hydroxyethyl-1,2,4-triazole)$_3$]$(ClO_4)_2\cdot 3H_2O$.[8] In contrast to **1**–**3**, the latter pattern results from intramolecular hydrogen bonds between neighbouring ligands. The above illustrates very well the distribution of elongation of Cu–N bonds due to the Jahn–Teller effect but this distribution is independent of the size of the counter ions in the crystals. In investigating relations between architectures of the chains and size or charge of counter anions we, however, have found a different interesting phenomenon, neither observed nor even postulated for metal–triazole 1-D polymeric complexes.

The *ababa*... order in **1**–**3** does not reflect the distribution of local symmetry of copper(II) ions. In the present structures copper atoms in the crystals occupy inversion centres ($\bar{1}$) or both

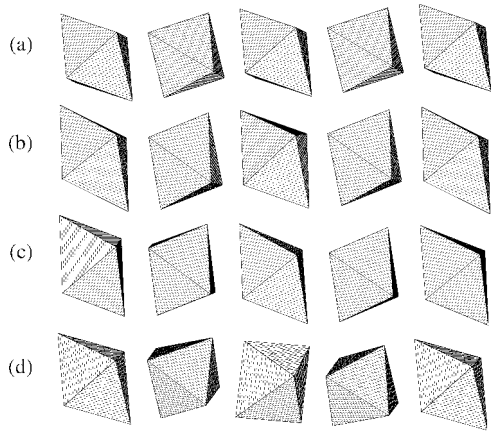

Fig. 2 The orientation of CuN_6 coordination octahedra in polymers of **1** (a), **2** (b) and **3** (c). (d) Shows the orientation detected by Garcia *et al.* for [Cu(4-hydroxyethyl-1,2,4-triazole)$_3$]$(ClO_4)_2\cdot 3H_2O$.[8]

 DOI: 10.1039/b101936h

inversion centres and general (1) positions. In **1** all copper atoms are located at inversion centres and the sequence of point symmetries in the chain is $\bar{1},\bar{1},\bar{1},\bar{1}$, *etc.* whereas in **2** consecutive copper(II) ions form the sequence $\bar{1},1,\bar{1},1,\bar{1}$, *etc.*, and in **3** the observed sequence can be described as $\bar{1},1,1,\bar{1},1,1,\bar{1}$, *etc.* Moreover, the symmetry independent parts of the chains have different lengths. The shortest unit, {Cu(amtrz)$_3$Cu}, is observed with BF_4 ions in crystals of **1**, the longest one, {Cu(amtrz)$_3$Cu(amtrz)$_3$Cu(amtrz)$_3$Cu} with SiF_6 ions for **3**, whereas for the anionic BF_4/SiF_6 mixed salt **2**, an intermediate {Cu(amtrz)$_3$Cu(amtrz)$_3$Cu} unit was observed. The different size of non-coordinated anions should also be reflected in the packing of the crystals. Analysis of crystal packing in **1**–**3** showed that counter ions link polymeric chains *via* N–H···F hydrogen bonds and determine the distances between them. Each polymeric chain is surrounded by four chains in **1** and by six chains in **2** and **3**. Perpendicular distances between neighbouring chains are 10.4 and 10.6 Å in **1**, 10.3, 11.3 and 13.3 Å in **2**, and 10.5, 11.4 and 12.3 Å in **3**. The data calculated for mixed anion crystal **2** clearly show that not only do the larger counter ions determine the distances but that the distances are dependent also on the spatial distribution of all anions and water molecules around the rigid polymeric chains and on the parallel displacement of the chains. Detailed analysis of this distribution shows that the symmetry of polymeric chain is dependent on type of counter ions, though this dependence is very complicated. This relation is a function of several factors, namely number of water molecules, charge of counter ions, hydrogen bond systems *etc*. which directly influence the crystal packing as well as the structure of the polymeric chain.

In summary, we conclude that the symmetry and length of independent units of $[Cu(amtrz)_3]_n^{2+}$ polymeric chains is dependent on the type of counter ions present in the crystals. In view of published results of EXAFS studies on similarities between structures of copper(II) and iron(II) complexes with 1,2,4-triazoles[8] the counter ion dependent symmetry of polymeric chains in the latter seems to be a crucial factor in spin-crossover phenomena.

Notes and references

† Anal. for **1**. Calc.: C, 14.20; H, 2.78; N, 33.14. Found: C, 14.15; H, 2.80; N, 33.20. For **2**. Calc.: C, 14.14; H, 3.17; N, 33.01. Found: C, 14.25; H, 2.93; N, 33.32. For **3**. Calc.: C, 15.16; H, 2.97; N, 35.37. Found: C, 15.00; H, 3.00; N, 35.52%. Analysis for **3** corresponds to one water molecule in the formula (see text for discussion).

‡ *Crystal data*: **1**: $C_6H_{14}B_2F_8N_{12}OCu$, M = 507.45, triclinic, space group $P\bar{1}$ (no. 2), a = 7.8433(15), b = 10.5221(14), c = 10.8374(12) Å, α = 76.796(10), β = 77.881(12), γ = 80.354(13)°, V = 844.6(2) Å^3, T = 100 K, Z = 2, μ(Mo-Kα) = 1.409 mm^{-1}, 12363 reflections measured, 4633 unique (R_{int} = 0.0379) which were used in all calculations. The final $wR(F^2)$ was 0.1158 (all data).

2: $C_{12}H_{32}B_2F_{14}N_{24}O_4SiCu_2$, M = 1019.41, triclinic, space group $P\bar{1}$ (no. 2), a = 10.285(2), b = 11.727(2), c = 15.521(3) Å, α = 104.99(3), β = 91.45(3), γ = 103.49(3)°, V = 1751.1(6) Å^3, T = 100 K, Z = 2, μ(Mo-Kα) = 1.389 mm^{-1}, 12688 reflections measured, 8014 unique (R_{int} = 0.0321) which were used in all calculations. The final $wR(F^2)$ was 0.1742 (all data).

3: $C_{18}H_{52}F_{18}N_{36}O_8Si_3Cu_3$, M = 1517.85, triclinic, space group $P\bar{1}$ (no. 2), a = 12.417(2), b = 13.150(3), c = 18.030(4) Å, α = 73.63(3), β = 72.64(3), γ = 70.28(3)°, V = 2590.8(9) Å^3, T = 100 K, Z = 2, μ(Mo-Kα) = 1.436 mm^{-1}, the crystal was mounted in inert oil and transferred to the cold gas stream of the diffractometer, 18608 reflections measured, 11646 unique (R_{int} = 0.0455) which were used in all calculations. The final $wR(F^2)$ was 0.1742 (all data).

CCDC reference numbers 164098–164100. See http://www.rsc.org/suppdata/cc/b1/b101936h/ for crystallographic data in CIF or other electronic format.

1 J. G. Haasnoot, *Coord. Chem. Rev.*, 2000, **200**–**202**, 131.
2 L. G. Lavrenova and S. V. Larionov, *Koord. Khim.*, 1998, **24**, 403; P. Gütlich, A. Hauser and H. Spiering, *Angew. Chem., Int. Ed. Engl.*, 1994, **33**, 2024 and references therein.
3 Y. Garcia, V. Ksenofontov, G. Levchenko and P. Gütlich, *J. Mater. Chem.*, 2000, **10**, 2274.
4 O. Raubeau, J. M. A. Gomez, E. Balskus, J. J. A. Kolnaar, J. G. Haasnoot and J. Reedijk, *New J. Chem.*, 2001, **25**, 144; Y. Garcia, P. J. van Koningsbruggen, R. Lapouyade, L. Rabardel, O. Kahn, M. Wieczorek, R. Bronisz, Z. Ciunik and M. F. Rudolf, *C. R. Acad.Sci. Paris, Ser. IIc*, 1998, 523.
5 P. J. van Koningsbruggen, Y. Garcia, E. Codjovi, R. Lapouyade, O. Kahn, L. Fournes and L. Rabardel, *J. Mater. Chem.*, 1997, **7**, 2069.
6 N. Kojima, Y. Muraka, T. Komatsu and T. Yokoyama, *Synth. Met.*, 1999, **103**, 2154.
7 S. B. Erenburg, N. V. Bausk, L. G. Lavrenova, V. A. Varnek and L. N. Mazalov, *Solid State Ionics*, 1997, **101**–**103**, 571.
8 Y. Garcia, P. J. van Koningsbruggen, G. Bravic, P. Guionneau, D. Chasseau, G. L. Cascarano, J. Moscovici, K. Lambert, A. Michalowicz and O. Kahn, *Inorg. Chem.*, 1997, **36**, 6357.
9 V. P. Sinditskii, V. I. Sokol, A. E. Fogelzang, M. D. Dutov, V. V. Serushkin, M. A. Porai-Koshits and B. S. Svetlov, *Zh. Neorg. Khim.*, 1987, **32**, 1950.
10 The compounds become insoluble after desiccation.

CHEMCOMM Communication
www.rsc.org/chemcomm

A novel methodology towards deep desulfurization of light oil effected by sulfimides formation

Yasuhiro Shiraishi, Tomoko Naito, Takayuki Hirai* and Isao Komasawa

Department of Chemical Science and Engineering, Graduate School of Engineering Science, and Research Center for Solar Energy Chemistry, Osaka University, Toyonaka 560-8531, Japan. E-mail: hirai@cheng.es.osaka-u.ac.jp

Received (in Cambridge, UK) 4th April 2001, Accepted 23rd May 2001
First published as an Advance Article on the web 20th June 2001

A novel desulfurization process for light oil, based on *N*-tosylsulfimide formation by the reaction of sulfur compounds with chloramine T (sodium *N*-chlorotoluene-*p*-sulfonamide), has enabled deep desulfurization at ambient temperature.

Much attention has been focused on the deep desulfurization of light oil, since the sulfur oxy-acids (SOx) contained in diesel exhaust gas cause air pollution and acid rain. The sulfur level in diesel fuels is limited presently to 0.05 wt%, both in Japan and Europe. The current technology of hydrodesulfurization (HDS) can desulfurize aliphatic and acyclic sulfur-containing compounds quite adequately, when adopted on the industrial scale. The above process however is limited, when treating dibenzothiophene (DBT), especially DBTs having alkyl substituents on their 4 and/or 6-position.[1] Thus, the production of light oil, of very low level sulfur, inevitably requires severe high energy conditions and specially active catalysts. In the development of any alternative energy-efficient desulfurization process, a radical approach, which is not limited to conventional HDS technology, is required.

Various kinds of sulfur-containing compounds have been reported to react with chloramine T, in hydrogen-donating solvents such as alcohol and water, to give rise at ambient temperature to crystalline powders of the corresponding *N*-tosylsulfimides.[2–5] These sulfimides are highly polarized and are insoluble in nonpolar hydrocarbon solvents. Thus, such a synthetic method, if applied to the desulfurization of nonpolar light oil, might thus be able to remove the DBTs specifically from the light oil under moderate conditions.

In order to test the feasibility of this idea, a *n*-tetradecane solution (50 ml) containing DBT (11 mmol l^{-1}), corresponding to a sulfur content of 0.05 wt%, was used as a model light oil. An alcohol solution (10 ml), to which a required amount of chloramine T trihydrate was dissolved, was then added to the above tetradecane solution at 323 K. In this procedure, the removal efficiency for DBT from tetradecane, following 3 h of reaction, was however only 5%, as shown in Table 1 (entry 1). As reported[6] and shown in Scheme 1, the sulfimide **5** is formed *via* the chlorination of the sulfur atom for **3** by the free-state chloramine T **2**, produced by the hydrolysis of **1**. The rate of the chlorination is therefore accelerated with decreasing pH of the solution, owing to the acceleration of the hydrolysis of **1**. The desulfurization of DBT, when a small amount of AcOH was added into the reaction mixture, was accelerated significantly (entry 2). The addition of the AcOH improves the desulfurization when used with MeOH, but is ineffective when used with the other solvents such as EtOH and *i*-PrOH (entries 3 and 4). This is because the hydrogen-donation ability of the latter two solvents is lower than that of MeOH. The desulfurization of DBT was also accelerated with increasing the concentrations of chloramine T and AcOH (entries 5–7). Both MeOH and chloramine T are insoluble in the nonpolar tetradecane, such that the resulting tetradecane is recovered easily using a separation funnel. When an equal volume of water to that of MeOH was added into the resulting MeOH solution, the *N*-tosylsulfimide of the DBT precipitated on the bottom of the flask, thus suggesting that the sulfimide formed is removed successively into the MeOH solution during the reaction.

Table 1 Desulfurization yield of DBT from tetradecane following the reaction with chloramine T under differing conditions[a]

Entry	Alcohol	AcOH/ml	Chloramine T/mmol	Desulfurization (%)
1	MeOH	–	1.1	5.0
2	MeOH	1	1.1	70.6
3	EtOH	1	1.1	1.5
4	*i*-PrOH	1	1.1	6.7
5	MeOH	1	5.5	98.5
6	MeOH	1	2.75	95.2
7	MeOH	2	1.1	> 99.9

[a] Temperature: 323 K, time: 3 h, tetradecane volume: 50 ml, alcohol volume: 10 ml, initial DBT content in tetradecane: 11 mmol l^{-1} (0.55 mmol).

The above procedure was then tested for the desulfurization of methyl-substituted DBTs, which are key compounds in the HDS technology.[1] In the present process, as shown in Fig. 1, the desulfurization rates for 4-methyl- and 4,6-dimethyl-DBT from tetradecane were higher than that of nonsubstituted DBT. This tendency differs completely from that obtained by the HDS method.[1] As shown in Scheme 1, the rate-determining step for the present reaction is the chlorination of the nucleophilic sulfur atom for the DBT **3** by **2**. Semiempirical MO calculation[7] showed that the electron density on the sulfur atom for DBTs lies in the order 4,6-dimethyl (5.7597) > 4-methyl (5.7586) > DBT (5.7577), which agrees well with the actual desulfurization reactivity (Fig. 1). The result suggests that the rate of the chlorination depends on the electron density (nucleophilicity) on the sulfur atom for DBTs, and as a result, methyl-substituted

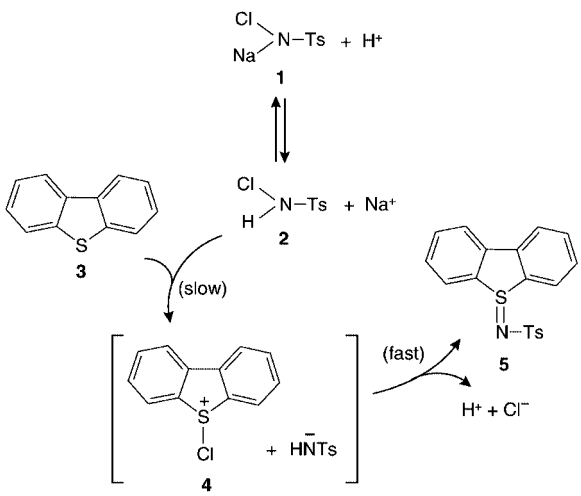

Scheme 1 Formation of DBT sulfimide by chloramine T.

 DOI: 10.1039/b103061m

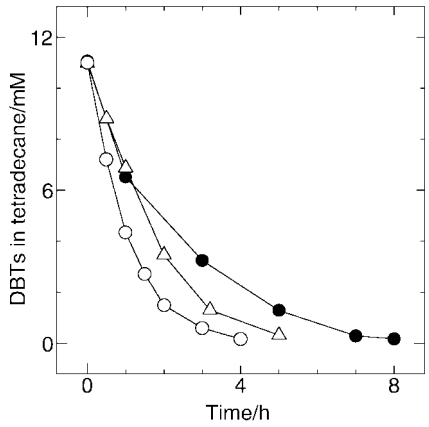

Fig. 1 Time-course variation in the concentration of (●) DBT, (△) 4-methyl-DBT and (○) 4,6-dimethyl-DBT in tetradecane. Temperature: 323 K, tetradecane volume: 50 ml, MeOH volume: 10 ml, AcOH volume: 1 ml, initial DBTs content in tetradecane: 11 mmol l^{-1} (0.55 mmol).

DBTs, having high electron density are desulfurized more easily than the nonsubstituted DBT.

The above process was then applied to the desulfurization of actual light oil containing *ca.* 0.19 wt% sulfur (2.47 mmol), which is just below the previous regulatory value that used to apply in Japan (0.2 wt%). The MeOH solution (50 ml) containing various amount of chloramine T was then added to the light oil (50 ml) in the presence of 2 ml AcOH, and was stirred at 323 K. Upon addition of water to the resulting MeOH solution, a yellow–white solid precipitate adhered to the bottom of the flask. As shown in Fig. 2b, the IR spectrum for the precipitate demonstrated two intense absorption bands at 1180 and 1300 cm^{-1} owing to the sulfonyl group and also a small band at 980 cm^{-1} owing to the S–N bond for the sulfimides. The spectrum is similar to that for *N*-tosylsulfimide of DBT (Fig. 2a), thus indicating that the sulfimides, formed during the reaction, are removed successfully from the light oil into the MeOH solution. As shown in Table 2, the sulfur content of the light oil decreased with increasing the chloramine T concentration. However, the deep desulfurization (0.05 wt%) was hardly achieved, even in the presence of 10-fold molar excess of chloramine T based on the initial sulfur concentration of the feed light oil (entry 3). The desulfurization yields obtained are significantly smaller than those expected from the data for the model light oil, as shown in Fig. 1.

The actual light oil contains a large amount of DBTs, with several types of hydrophobic alkyl substituents on the molecule,

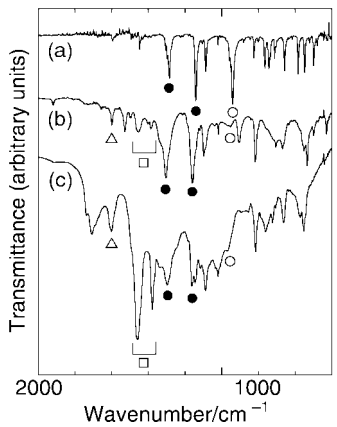

Fig. 2 IR spectra for (a) *N*-tosylsulfimide of DBT, (b) precipitate obtained by the addition of water to the MeOH solution following the reaction of light oil with chloramine T, and (c) adsorbed material obtained by the addition of silica gel to the light oil following the reaction with chloramine T. (○) S–N bond, (●) sulfonyl group, (□) aliphatic hydrogen (C–H) and (△) aromatic hydrogen (C–H).

Table 2 Variations in the sulfur content of light oil following (a) reaction with chloramine T and (b) subsequent addition of adsorbents[a]

	(a)		(b)	
Entry	Chloramine T/mmol	Sulfur content/wt%	Adsorbent/g ml^{-1}-oil	Sulfur content/wt%
1	4.65	0.099	—	—
2	11.6	0.079	0.2 (Al_2O_3)	0.054
			0.2 (SiO_2)	0.050
			0.3 (SiO_2)	0.048
3	23.3	0.066	—	—

[a] Temperature: 323 K, time: 10 h, light oil volume: 50 ml, MeOH volume: 50 ml, AcOH volume: 2 mL, initial sulfur content of light oil: 0.190 wt% (2.47 mmol).

and the polarity of the DBTs is decreased with increasing the carbon number of the substituents.[8] The low desulfurization efficiency of the light oil is thus probably because the low polarity sulfimides of DBTs having large carbon number of substituents, formed by the reaction with chloramine T, are not removed into the MeOH solution but remain in the resulting light oil. Since the sulfimides have a higher polarity as compared to the other constituents of the light oil, they might be removed by the addition of solid adsorbents, such as aluminum oxide and silica gel. As shown in Table 2 (entry 2b), the sulfur concentration of light oil was actually decreased by the addition of the adsorbents, with the deep desulfurization (0.05 wt%) being achieved successfully. As shown in Fig. 2c, the adsorbed materials showed absorption bands owing to the sulfonyl group and the S–N bond for sulfimides as also found for the spectrum of the precipitate (Fig. 2b). The spectrum for the adsorbed material also showed a larger absorption band at 1620 cm^{-1}, owing to the alkyl group, as compared to that obtained for the precipitate, indicating that the sulfimides of the DBTs, having a large carbon number of alkyl substituents, are adsorbed successfully.

The present study describes a novel desulfurization process for light oil, based on the removal of *N*-tosylsulfimides produced by the reaction of sulfur compounds with chloramine T. The deep desulfurization was achieved successfully at ambient temperature. The refractory DBTs in the current HDS process are desulfurized easily by the present process, thus showing that the present process is both energy-saving and effective as a new deep desulfurization process for light oil. The sulfimides have been reported to have antimicrobial, diuretic and hypotensive properties on tumor growth and activity as antidepressants and stimulants of the central nervous system.[5] It may thus be interesting to use the recovered sulfimides from the desulfurization process, as novel materials for medicinal supplies.

The authors are grateful for financial support by Grant-in-Aid for Scientific Research (No. 12555215) from the Ministry of Education, Science, Sports and Culture, Japan.

Notes and references

1 M. Houalla, D. H. Broderick, A. V. Sapre, N. K. Nag, V. H. J. De Beer, B. C. Gates and H. Kwart, *J. Catal.*, 1980, **61**, 523.
2 B. H. Nicolet and J. Willard, *Science*, 1921, **53**, 217.
3 F. G. Mann and W. J. Pope, *J. Chem. Soc.*, 1922, **121**, 1052.
4 T. L. Gilchrist and C. J. Moody, *Chem. Rev.*, 1977, **77**, 409.
5 B. M. Tros and L. S. Melvin, Jr., *Sulfur Ylides*, Academic Press, New York, 1975.
6 K. Tsujihara, N. Furukawa, K. Oae and S. Oae, *Bull. Chem. Soc. Jpn.*, 1969, **42**, 2631.
7 The theoretical calculations of the electron density on sulfur atom for DBTs were performed with the PM3 semiempirical method within the WinMOPAC ver 2.0 software (Fujitsu, Inc).
8 Y. Shiraishi, Y. Taki, T. Hirai and I. Komasawa, *Ind. Eng. Chem. Res.*, 2001, **40**, 1213.

CHEMCOMM
Communication
www.rsc.org/chemcomm

Unexpected results of enyne metathesis using a ruthenium complex containing an *N*-heterocyclic carbene ligand

Tsuyoshi Kitamura, Yoshihiro Sato and Miwako Mori*

Graduate School of Pharmaceutical Sciences, Hokkaido University, Sapporo 060-0812, Japan

Received (in Cambridge, UK) 14th February 2001, Accepted 24th May 2001
First published as an Advance Article on the web 20th June 2001

Metathesis of enyne having 1,1-substituted alkene, carried out with the new generation of a ruthenium carbene complex containing an *N*-heterocyclic carbene ligand, gave five- and six-membered cyclic compounds in high yield.

In recent synthetic organic chemistry, transition metals play an important role and enable bond cleavage of multiple bonds, such as a double bond or triple bond. A metathesis reaction[1] using a metal carbene complex is quite interesting because multiple bonds are cleaved and, at the same time, a multiple bond is formed. Enyne metathesis[2,3] is particularly attractive, since the double bond of enyne is cleaved and the alkylidene part of the alkene migrates to the alkyne carbon to give a cyclized compound. However, in this reaction, the substituents on the alkyne or the alkene are important. It has been shown that the reaction rate of an enyne having a terminal alkyne is slow because the generated diene moiety coordinates to the ruthenium carbene complex.[3*a*] On the other hand, the effect of the substituent on the alkene is also important. In the case of an enyne having a mono- or 1,2-disubstituted alkene, the metathesis reaction proceeded smoothly and the desired product was obtained.[3*a*]

However, when enyne **2b** (R^3 = Me) having 1,1-disubstituted alkene was treated in a similar manner, no cyclized product was obtained and the starting material was recovered (Scheme 1). This means that ruthenium carbene complex **i** formed by the reaction of the alkyne part of enyne and **1a**[4*a*] does not react intramolecularly with a 1,1-disubstituted alkene. Recently, a new generation of ruthenium carbene complexes containing *N*-heterocyclic carbene ligands was reported.[4*b*,*c*] The reactivity of these complexes is greater than that of **1a**, and the metathesis of an olefin having a 1,1-disubstituted alkene proceeded smoothly using **1b** or **1c** to give a cyclized product having tri- or tetra-substituted olefin. Thus, we decided to use the novel ruthenium carbene complex **1b** or **1c** for enyne metathesis.†

When a toluene solution of enyne **2c** was warmed in the presence of 5 mol% of **1b** at 80 °C for 5 h, two metathesis products, **3c** and **4c**, were obtained in 85% yields along with compound **5c** in 5% yield (Scheme 2). Compounds **3c** and **4c** were obtained as a mixture of two inseparable isomers, and they could be isolated by iterative chromatography on silica gel. Compound **3c** has a five-membered ring, which is usually formed by the reaction of enyne having a mono-substituted alkene and **1a**.[3*a*] On the other hand, the ^{1}H NMR spectrum of **4c** is similar to that of **3c**, and other spectral data such as ^{13}C NMR, HMQC, HMBC and mass spectra supported this structure. This compound should be produced by C–C bond formation between the disubstituted alkene carbon (C7) and the outside alkyne carbon (C2), and the methylene carbon of the alkene migrates to the inside alkyne carbon (C3).

Compound **5c** is formed by reductive elimination from ruthenacyclobutane **III** as shown in Scheme 2. When ruthenium carbene complex **1c** was used for this reaction, the same compounds **3c** and **4c** were each obtained in 32% yield, along with a small amount of **5c**. This indicates that the six-membered ring **4c** was formed from 1,6-ene-yne using ruthenium carbene complex **1b** or **1c**.

A possible reaction course is shown in Scheme 3. It is thought that there are two pathways in the reaction of the alkyne part of the enyne with the methylidene ruthenium carbene complex.[5] If the reaction proceeds through path A, ruthenium carbene complex **II** would be formed.

Intramolecular [2 + 2]cycloaddition affords **III**. Thus, a smaller ring-sized product is formed (five-membered ring). However, when ruthenium metal of the carbene complex bonds to the outside carbon of alkyne, ruthenacycle **IV** would be formed and would be converted into ruthenium carbene complex **V** by ring opening. Then the ruthenium carbene complex reacts intramolecularly with the alkene part to give ruthenacyclobutane **VI**, which affords a six-membered ring compound.[6]

Various enynes were treated with **1b** in a similar manner, and the results are shown in Table 1. In all cases, enyne metathesis

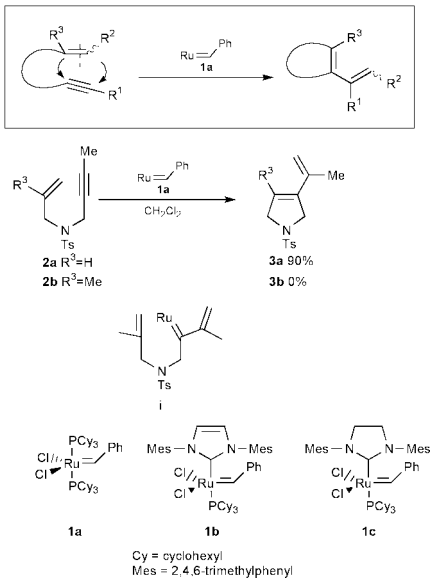

Scheme 1 Ruthenium-catalyzed intramolecular enyne metathesis.

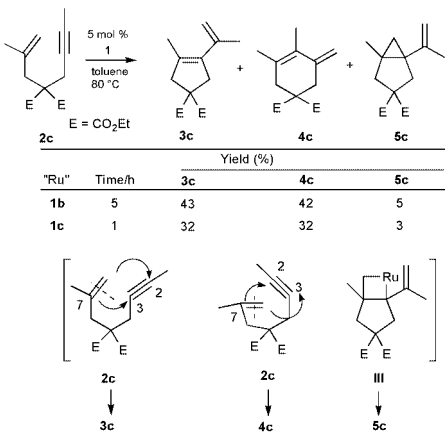

Scheme 2 Reaction of **2c** with ruthenium catalyst **1**.

 DOI: 10.1039/b101453f

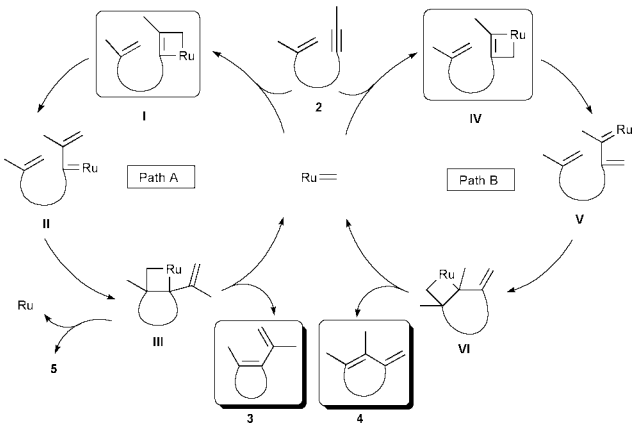

Scheme 3 Two possible reaction pathways for enyne metathesis.

products **3** and **4** were obtained as an inseparable mixture of two isomers. In some cases, we could isolate each pure compound after iterative of flash column chromatography on silica gel. In each case, a small amount of **5** was produced. Although all spectral data supported the structures of compounds **4**, the structure of a derivative of **4b** was further confirmed by X-ray crystallographic analysis.[7]

Table 1 Enyne metathesis using **1b**[a]

Run	Substrate	Conditions	Products, yield[b]	
1	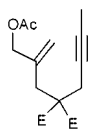 **2d**	80 °C 6 h E = CO_2Me	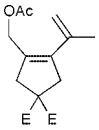 **3d** 50%	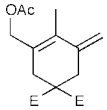 **4d** 39%
2	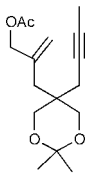 **2e**	80 °C 15 h	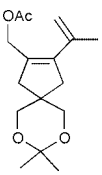 **3e** 47%	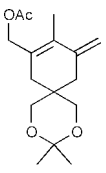 **4e** 27%
3	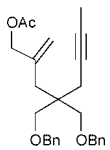 **2f**	80 °C 24 h	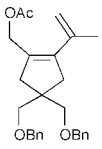 **3f** 50%	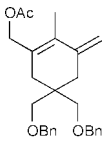 **4f** 42%
4	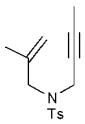 **2b**	80 °C 6 h	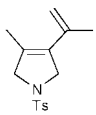 **3b** 34%	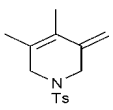 **4b** 30%
5	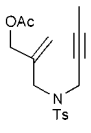 **2g**[c]	50 °C 3 h	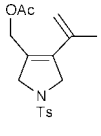 **3g** 41%	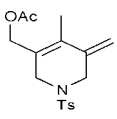 **4g** 30%
6	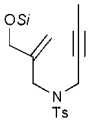 **2h**[c]	50 °C 24 h *Si* = TBDMS	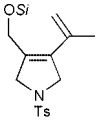 **3h** 29%	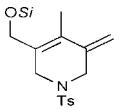 **4h** 17%

[a] All reactions were carried out using **1b** (5 mol%) in toluene. [b] All yields were calculated from ^{1}H NMR spectra after isolation as a mixture of two isomers. [c] 10 mol% of **1b** was used.

Although the reason why the reaction of enyne **2a** with **1a** gave only **3a**,[3a] but enyne **2b** reacts with **1b** or **1c** gave **3b** and **4b** is not clear, the results are quite interesting.

Further studies of enyne metathesis using **1b** or **1c** are in progress.

Notes and references

† *Typical procedure for the metathesis reaction* of **2d.** To a solution of **2d** (34.2 mg, 115 μmol) in toluene (3.8 ml, 0.03 M) was added **1b** (4.9 mg, 5.8 μmol, 5 mol%), and the solution was heated at 80 °C for 6 h. After the solvent was removed, the residue was purified three times by flash column chromatography on silica gel (C_6H_{12}–C_6H_6–AcOEt 8:1:2) to yield **3d** (17.1 mg, 58 μmol, 50%), and **4d** (13.3 mg, 46 μmol, 39%) as colorless oils, respectively.

Selected spectral data for **3d** *and* **4d**. *3-Acetoxymethyl-4-isopropenyl-cyclopent-3-ene-1,1-dicarboxylic acid dimethyl ester (***3d***). ν*/(neat) 1740, 1636, 1603, 1230 cm^{-1}; δ_H(270 MHz, $CDCl_3$) 1.86 (s, 3 H), 2.06 (s, 3 H), 3.15 (s, 2 H), 3.18 (m, 2 H), 3.75 (s, 6 H), 4.73 (s, 2 H), 4.81 (s, 1 H), 5.02 (s, 1 H); δ_C(67.8 MHz, $CDCl_3$) 20.9 (CH_3), 21.9 (CH_3), 42.7 (CH_2), 43.5 (CH_2), 52.9 ($CH_3 \times 2$), 57.0 (C), 60.8 (CH_2), 116.0 (CH_2), 129.3 (C), 139.2 (C), 139.8 (C), 170.9 (C), 172.3 (C × 2); LRMS *m/z* 296 (M^+), 236, 204, 191, 177, 145, 131, 117; HRMS calcd for $C_{15}H_{20}O_6$ (M^+) 296.1260, found 296.1251. *3-Acetoxymethyl-4-methyl-5-methylenecyclohex-3-ene-1,1-dicarboxylic acid dimethyl ester* (**4d**). *ν*/(neat) 1738, 1640, 1610, 1230 cm^{-1}; δ_H(270 MHz, $CDCl_3$) 1.85 (s, 3 H), 2.08 (s, 3 H), 2.73 (s, 2 H), 2.88 (s, 2 H), 3.70 (s, 6 H), 4.71 (s, 2 H), 4.99 (s, 1 H), 5.13 (s, 1 H); δ_H(67.8 MHz, $CDCl_3$) 13.7 (CH_3), 20.9 (CH_3), 34.2 (CH_2), 37.2 (CH_2), 52.7 ($CH_3 \times 2$), 53.8 (C), 64.6 (CH_2), 112.8 (CH_2), 127.9 (C), 131.1 (C), 140.6 (C), 171.0 (C), 171.1 (C × 2); LRMS *m/z* 296 (M^+), 254, 236, 223, 204, 177, 163, 117; HRMS calcd for $C_{15}H_{20}O_6$ (M^+) 296.1260, found 296.1258.

1 For recent reviews on metathesis, see R. H. Grubbs and S. J. Miller, *Acc. Chem. Res.*, 1995, **28**, 446; M. Schuster and S. Blechert, *Angew. Chem., Int. Ed. Engl.*, 1997, **36**, 2036; H.-G. Schmalz, *Angew. Chem., Int. Ed. Engl.*, 1995, **34**, 1833; A. Fürstner, *Topics in Organometallic Chemistry, Vol. 1*, Springer-Verlag, Berlin, Heidelberg, 1998; R. H. Grubbs and S. Chang, *Tetrahedron*, 1998, **54**, 4413; S. K. Armstrong, *J. Chem. Soc., Perkin Trans. 1*, 1998, 371; A. J. Phillips and A. D. Abell, *Aldrichimica Acta*, 1999, **32**, 75; A. Fürstner, *Angew. Chem., Int. Ed.*, 2000, **39**, 3013.

2 For a review on enyne metathesis, see M. Mori, *Top. Organomet. Chem.*, 1998, **1**, 133; for recent applications, see; R. T. Hoye, S. M. Donaldoson and T. Vos, *Org. Lett.*, 1999, **1**, 277; A. G. M. Barrett, S. P. D. Baugh, D. C. Braddock, K. Flack, V. C. Gibson, M. R. Giles, E. L. Marshall, P. A. Procopiou, A. J. P. White and D. J. Williams, *J. Org. Chem.*, 1998, **63**, 7893; J. Renaud, C.-D. Graf and L. Oberer, *Angew. Chem., Int. Ed.*, 2000, **39**, 310; A. Fürstner, H. Szillat and F. Stelzer, *J. Am. Chem. Soc.*, 2000, **122**, 6785; R. Stragies, U. Voigtmann and S. Blechert, *Tetrahedron Lett.*, 2000, **41**, 5465; D. Bentz and S. Laschat, *Synthesis*, 2000, 1766.

3 (*a*) A. Kinoshita and M. Mori, *Synlett*, 1994, 1020; (*b*) A. Kinoshita and M. Mori, *J. Org. Chem.*, 1996, **61**, 8356; (*c*) A. Kinoshita and M. Mori, *Heterocycles*, 1997, **46**, 287; (*d*) M. Mori, N. Sakakibara and A. Kinoshita, *J. Org. Chem.*, 1998, **63**, 6082; (*e*) A. Kinoshita, N. Sakakibara and M. Mori, *J. Am. Chem. Soc.*, 1997, **119**, 12 388; (*f*) A. Kinoshita, N. Sakakibara and M. Mori, *Tetrahedron*, 1999, **55**, 8155; (*g*) M. Mori, T. Kitamura, N. Sakakibara and Y. Sato, *Org. Lett.*, 2000, **2**, 543.

4 For **1a**, see (*a*) P. Schwab, M. B. France, J. W. Ziller and R. H. Grubbs, *Angew. Chem., Int. Ed. Engl.*, 1995, **34**, 2039; for **1b** see (*b*) T. Weskamp, W. C. Schattenmann, M. Spiegler and W. A. Herrmann, *Angew. Chem., Int. Ed.*, 1998, **37**, 2490; (*c*) J. Huang, E. D. Stevens, S. P. Nolan and J. L. Peterson, *J. Am. Chem. Soc.*, 1999, **121**, 2674; (*d*) M. Scholl, T. M. Trnka, J. P. Morgan and R. H. Grubbs, *Tetrahedron Lett.*, 1999, **40**, 2247; for **1c** see (*e*) M. Scholl, S. Ding, C. W. Lee and R. H. Grubbs, *Org. Lett.*, 1999, **1**, 953.

5 If this reaction proceeds by the reaction of the methylene carbene complex and the olefin part of the enyne, a similar reaction pathway is described.

6 In the synthesis of an eight-membered ring compound using ruthenium catalyst **1a**, we considered the same possibility, but no other products were observed. See ref. 3*g*.

7 Treatment of compound **4d** with K_2CO_3 in MeOH followed by Dess–Martin oxidation (D. B. Dess and J. C. Martin, *J. Org. Chem.*, 1983, **48**, 4156) afforded an aldehyde, which was converted into 2,4-dinitrophenylhydrazone, whose X-ray crystallography shows that a six-membered ring is formed. CCDC 161214. See http://www.rsc.org/suppdata/cc/b1/b101453f/ for crystallographic data in CIF or other format.

CHEMCOMM Communication
www.rsc.org/chemcomm

Optimum conformational flexibility of subtilisin to maximize the enantioselectivity for subtilisin-catalysed transesterification in an organic solvent with an addition of dimethyl sulfoxide

Keiichi Watanabe,[a] Takashi Yoshida[b] and Shin-ichi Ueji*[ab]

[a] *The Graduate School of Science and Technology, Kobe University, Nada, Kobe 657-8501, Japan*
[b] *Division of Natural Environment and Bioorganic Chemistry, Faculty of Human Development and Sciences, Kobe University, Nada, Kobe 657-8501, Japan. E-mail: ueji@kobe-u.ac.jp; Fax: +81-78-803-7761*

Received (in Cambridge, UK) 8th February 2001, Accepted 21st May 2001
First published as an Advance Article on the web 20th June 2001

For subtilisin-catalysed transesterification of the racemic esters in *i*-octane containing dimethyl sulfoxide as an additive, the relationship between the enantioselectivity and the conformational flexibility of subtilisin estimated from the ESR spectroscopic study provides the first experimental evidence that the enzyme has the optimum flexibility to produce the maximal enantioselectivity toward the given substrates.

The ability of enzymes to discriminate between enantiomers has been applied to the optical resolution of racemates in organic syntheses.[1] Among the strategies to improve the enzyme's enantioselectivity, organic chemists and enzymologists often employ various additives for enzyme-catalysed reactions in organic solvents,[2] because of their simplicity of use. Although the variation of the enzyme's flexibility caused by an additive, such as a small amount of water in organic solvents, is anticipated to control its enantioselectivity,[3] definite information is lacking as to the relationship between the enzyme's flexibility and its enantioselectivity for enzyme-catalysed reactions. According to research done so far, the only reported observation is that the effect on enantioselectivity by the variation of organic solvents is related to the enzyme's flexibility, estimated from time-resolved fluorescence anisotropic study.[4]

In this communication, for subtilisin-catalysed transesterification in *i*-octane, we wish to report the mechanism of enantioselectivity enhancement caused by addition of dimethyl sulfoxide on the basis of the relationship between the initial rates for each enantiomer of the substrates used here and the conformational flexibility of subtilisin estimated from ESR spectroscopic study. Furthermore, the relationship established reveals that the optimum conformational flexibility of subtilisin gives the maximal enantioselectivity.

For subtilisin-catalysed transesterification of ethyl (*R*)- or (*S*)-2-(4-ethylphenoxy)propionate **1** with *n*-butyl alcohol in *i*-octane, we investigated the behaviour of the initial rates for each enantiomer of **1** caused by addition of a small amount of various additives such as water or polar organic solvents (Scheme 1), because this method of enantioselectivity improvement by additives is the simplest one. In a typical subtilisin-catalysed transesterification, the substrate **1** (0.025 mmol) and *n*-butyl alcohol (0.15 mmol) were added to dry *i*-octane (2 ml) containing the additives (0–0.60 vol%), followed by ultrasonic dispersion, and then addition of subtilisin (10 mg).† The reaction mixture was shaken (170 strokes min^{-1}) at 37 °C.

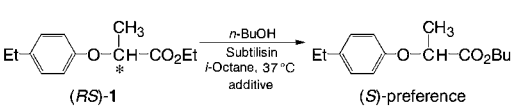

(*RS*)-**1** (*S*)-preference

Scheme 1 Subtilisin-catalysed transesterification of ethyl 2-(4-ethylphenoxy)propionate **1** with *n*-butyl alcohol in *i*-octane.

The effects of the additives (0.45 vol%) on the initial rates as a measure of the enzymatic activity for subtilisin-catalysed transesterification of **1** in *i*-octane were investigated. When a small amount of DMSO (0.45 vol%) was added to the reaction medium, the initial rate for the correctly binding *S* enantiomer was found to be dramatically enhanced (V_S = 20 nmol h^{-1} mg^{-1}), as compared with those for the addition of other general additives such as water (V_S = 0.21 nmol h^{-1} mol^{-1}) or polar organic solvents (DMF, THF, acetone and acetonitrile), although the reaction for no additive conditions did not proceed at all. The effect of DMSO on the enantioselectivity enhancement was also observed for subtilisin-catalysed hydrolysis of **1** in aqueous buffer containing DMSO.[5]

In order to elucidate the optimum amount of added DMSO, the initial rates for each enantiomer of **1** for subtilisin-catalysed transesterification in *i*-octane were determined for a range of added DMSO (0–0.60 vol%). As is seen in Table 1, the initial rate for the correctly binding *S* enantiomer was dramatically enhanced by DMSO added to the reaction medium, as compared with that for the incorrectly binding *R* enantiomer. In particular, upon the addition of 0.45 vol% of DMSO, subtilisin displayed the largest initial rate for the *S* enantiomer, thus resulting in the maximal enantioselectivity (V_S/V_R = 9.6). A serious decrease in the enzymatic activity, however, was produced by addition of an excess amount of DMSO (0.60 vol%). This is probably because the increased flexibility of subtilisin caused by the excess addition of DMSO does not contribute to accommodating the substrate **1** into the subtilisin's binding site, thus leading to the decrease of the enzymatic activity accompanying the loss of the enantioselectivity. This assumption is also supported by the discussion below on the basis of the results obtained from the ESR spectroscopic study.

Furthermore, in order to investigate the DMSO effect on the other substrate, methyl mandelate **2** was submitted to the model reaction. For subtilisin-catalysed transesterification in *i*-octane, subtilisin preferentially catalysed the *R* enantiomer of **2**. The maximal enantioselectivity (V_R/V_S = 7.0) with an increase of

Table 1 Effects of DMSO on the enantioselectivity (V_S/V_R) and the initial rates for each enantiomer of ethyl 2-(4-ethylphenoxy)propionate **1** for subtilisin-catalysed transesterification in *i*-octane

	Initial rate (10^{-1} nmol h^{-1} mg^{-1})		
Amount (vol%)	V_S	V_R	V_S/V_R
0	0	0	—
0.150	0	0	—
0.300	17	9.9	1.7
0.375	105	26	4.0
0.450	201	21	9.6
0.500	65	19	3.4
0.600	14	10	1.4

 DOI: 10.1039/b101269j

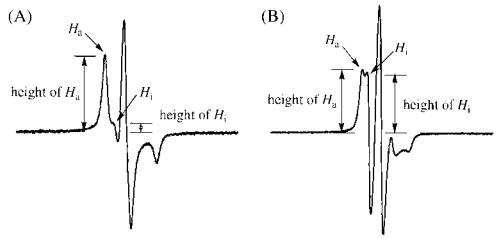

Fig. 1 Typical ESR spectrum of the spin-labeled subtilisin in *i*-octane; (A) no additive condition, (B) 0.45 vol% DMSO.

the enzymatic activity was produced by addition of 0.375 vol% of DMSO. Therefore, our approach using DMSO as the additive was found to be valid for the improvement of the enantioselectivity for subtilisin-catalysed reaction in an organic solvent, although there is the difference in the optimum amount of DMSO between **1** and **2** to obtain the maximal enantioselectivity.

The remarkable enhancement of the enantioselectivity observed is anticipated to be strongly affected by the change of the subtilisin's conformational flexibility caused by addition of DMSO. This view promoted us to investigate the relationship between the initial rates of each enantiomer of **1** and **2**, and the subtilisin's conformational flexibility estimated from ESR spectroscopy. The ESR measurement was carried out under the same conditions as that for the subtilisin-catalyzed transesterification of **1** and **2**, using a spin-labeled subtilisin with 1-oxy-2,2,6,6,-tetramethyl-4-piperidinyl ethoxyphosphorofluoridate prepared by the known method.[6] The spin-labeled subtilisin was indicated by MALDI-TOF MS, in which a fragment (27543) was found which almost corresponded to the sequence of subtilisin (27287) plus the weight of a spin-label (282) less the weight of F (19) and H (1). The spin-labeled subtilisin showed a decrease of enzymatic activity for our model reaction, due to the inhibition by the spin label attached to the active site serine. Fig. 1 shows a typical ESR spectrum, in which two parts of the spectrum are arbitrarily labeled H_a and H_i, respectively. The degree of the subtilisin's conformational flexibility can be monitored roughly by the change in the ratio of the peak height of H_i to $(H_a + H_i)$,[7] because each peak of H_a and H_i represents the anisotropy and the isotropy of the subtilisin's spin-label, respectively.[8] Thus, the increase of the $H_i/(H_a + H_i)$ value reflects that the subtilisin's conformation becomes more flexible. Fig. 2 shows the variation of the $H_i/(H_a + H_i)$ value estimated from the ESR spectra in *i*-octane as a function of the amount of DMSO, in which the increased amount of DMSO in *i*-octane is found to increase the conformational flexibility of subtilisin. In addition, under other additive conditions that give poor enantioselectivity and low enzymatic activity, the ESR signal showed the characteristics of a conformationally rigid enzyme ($H_i/(H_a + H_i)$ = 0.10–0.27).

The plots of the initial rates for each enantiomer of **1** for subtilisin-catalysed transesterification in *i*-octane containing a small amount of DMSO as a function of the $H_i/(H_a + H_i)$ value

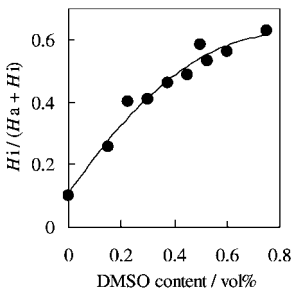

Fig. 2 The variation of the $H_i/(H_a + H_i)$ value estimated from the ESR spectra in *i*-octane as a function of the amount of DMSO.

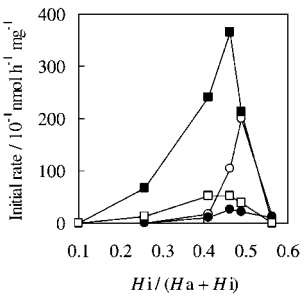

Fig. 3 The relationship between the $H_i/(H_a + H_i)$ value and the initial rates for subtilisin-catalysed transesterifications of **1** and **2** in *i*-octane, ●: **1**-(*R*), ○: **1**-(*S*), ■: **2**-(*R*), □: **2**-(*S*).

are depicted in Fig. 3. The initial rate for the correctly binding *S* enantiomer was significantly enhanced by an increase of the $H_i/(H_a + H_i)$ value. On the other hand, for the incorrectly binding *R* enantiomer, the initial rate is almost unchanged, in spite of the increase of the $H_i/(H_a + H_i)$ value. For subtilisin-catalysed transesterification, the variation of the subtilisin's conformational flexibility caused by addition of DMSO is found to be ascribed to the acceleration of the initial rate for the correctly binding *S* enantiomer, as compared with that for the incorrectly binding *R* enantiomer. Thus, the larger value of the ratio of the initial rates, arising from the marked difference in the flexibility effect on the initial rates for each enantiomer, is significantly responsible for the enhancement of the subtilisin's enantioselectivity.

A serious drop in the initial rates, however, was produced by a small increase of the $H_i/(H_a + H_i)$ value from the optimum flexibility to produce the largest initial rate (Fig. 3). This result is explained by assuming that the subtilisin's flexibility caused by the excess addition of DMSO does not induce the stable association between the substrate **1** and the subtilisin's binding site. Thus, subtilisin is found to display the optimum flexibility to produce the maximal enantioselectivity and the enzymatic activity toward the substrates used here. Furthermore, as is seen in Fig. 3, the change of the substrate from **1** to **2** shows the difference in the optimum flexibility to maximize the enantioselectivity [$(H_i/(H_a + H_i)$ for the largest V_S/V_R value of **1**] > [$H_i/(H_a + H_i)$ for the largest V_R/V_S of **2**], which suggests that the optimum conformational flexibility is responsible for the substrate's structure. Our first observation offers an important insight into the mechanism of the enantioselectivity enhancement for the enzyme-catalysed reactions under the various reaction conditions.

Notes and references

† Because the presence of water is important in the activity of enzymes in non-polar solvents, *i*-octane, *n*-butyl alcohol, and additives used here were dried over Molecular Sieves 4 Å. For our model reactions, however, the enzymatic activity was insensitive to the addition of water (0–0.9 vol%) into *i*-octane.

1 G. Carrea and S. Riva, *Angew. Chem., Int. Ed.*, 2000, **39**, 2226; T. Sugai, *Curr. Org. Chem.*, 1999, **3**, 373; S. M. Roberts, *J. Chem. Soc., Perkin Trans. 1*, 1999, 1; H. Stecher and K. Faber, *Synthesis*, 1999, 1.
2 F. Theil, *Tetrahedron*, 2000, **56**, 2905.
3 T. Okamoto and S. Ueji, *Chem. Commun.*, 1999, 939; K. Kawashiro, H. Sugahara, S. Sugiyama and H. Hayashi, *Biotechnol. Lett.*, 1995, **17**, 1161; H. Kitaguchi, I. Itoh and M. Ono, *Chem. Lett.*, 1990, 1203.
4 J. Broos, A. J. W. G. Visser, J. F. J. Engbersen, W. Verboom, A. Hoek and D. N. Reinhoudt, *J. Am. Chem. Soc.*, 1995, **117**, 12657.
5 K. Watanabe and S. Ueji, *Biotechnol. Lett.*, 2000, **22**, 599.
6 J. D. Morrisett and C. A. Broomfield, *J. Biol. Chem.*, 1972, **247**, 7224.
7 L. J. Berliner, *Biochemistry*, 1972, **11**, 2921.
8 P. P. Wangikar, P. C. Michels, D. S. Clark and J. S. Dordick, *J. Am. Chem. Soc.*, 1997, **119**, 70; R. Affleck, Z.-F. Xu, V. Suzawa, K. Focht, D. S. Clark and J. S. Dordick, *Proc. Natl. Acad. Sci. U.S.A.*, 1992, **89**, 1100.

CHEMCOMM
Communication
www.rsc.org/chemcomm

Biomimetic alkane hydroxylation by cobalt(III) porphyrin complex and *m*-chloroperbenzoic acid†

Wonwoo Nam,*[a] Inwoo Kim,[a] Youngmee Kim[a] and Cheal Kim*[b]

[a] *Department of Chemistry and Division of Molecular Life Sciences (BK 21), Ewha Womans University, Seoul 120-750, Korea. E-mail: wwnam@mm.ewha.ac.kr*

[b] *Department of Fine Chemistry, Seoul National University of Technology, Seoul 139-743, Korea*

Received (in Cambridge, UK) 3rd May 2001, Accepted 25th May 2001
First published as an Advance Article on the web 20th June 2001

The catalytic hydroxylation of alkanes by an electron-deficient cobalt(III) porphyrin complex and *m*-chloroperbenzoic acid yielded alcohols as major products with a high k_H/k_D value, > 99% retention of stereochemistry, and a high regioselectivity; a high-valent cobalt–oxo porphyrin complex was suggested as a reactive hydroxylating intermediate.

Cytochrome P-450 enzymes are capable of catalyzing a variety of oxidation reactions, including the most energetically difficult hydroxylation of unactivated C–H bonds of alkanes.[1] Since selective oxygenations of hydrocarbons under mild conditions are of importance in both synthetic chemistry and industrial processes, biomimetic hydroxylation reactions with synthetic metalloporphyrins have been intensively studied over the past two decades.[2] It has been shown that metalloporphyrins containing iron, manganese, and ruthenium ions, especially with electron-deficient porphyrin ligands, are efficient catalysts for the hydroxylation of alkanes by various oxidants.[2,3] However, cobalt porphyrin complexes have been rarely used as catalysts in alkane hydroxylation reactions, since the reactions of cobalt complexes with hydroperoxides often proceed *via* free-radical type of oxidation reactions.[4] In the present study, we report for the first time that an electron-deficient cobalt(III) porphyrin complex catalyzes the hydroxylation of alkanes by *m*-chloroperbenzoic acid (*m*-CPBA) *via* a non-radical type of oxidation reaction.

† Electronic supplementary information (ESI) available: Fig. S1. See http://www.rsc.org/suppdata/cc/b1/b103986p/

The catalytic hydroxylation of alkanes by Co(TPFPP)(CF_3SO_3) [**1**, TPFPP = *meso*-tetrakis(pentafluorophenyl)porphinato dianion] and *m*-CPBA was carried in a solvent mixture of CH_3CN and CH_2Cl_2 at rt.‡ The results in Table 1 show that alcohols were yielded as major products with high alcohol to ketone ratios under mild reaction conditions, indicating that *m*-CPBA is a competent terminal oxidant for the alkane hydroxylations by the cobalt porphyrin complex.§¶‖ The kinetic isotope effect (KIE) for the cyclohexanol formation by **1** and *m*-CPBA was determined to be 8 ± 1 by carrying out intermolecular competitive hydroxylation with cyclohexane and cyclohexane-d_{12} (Table 1, entry 5).[5,6]

The stereochemistry of the alkane hydroxylations by **1** and *m*-CPBA was investigated with *cis*- and *trans*-1,2-dimethylcyclohexane. The alkane hydroxylations were highly stereospecific with > 99% retention; no formation of isomerized alcohol products (*e.g.* the formation of *trans*-1,2-dimethylcyclohexanol in the hydroxylation of *cis*-1,2-dimethylcyclohexane was observed (Table 1, entries 2 and 3). Interestingly, only small amounts of secondary alcohol products such as 2,3- and 3,4-dimethylcyclohexanol were formed in these reactions, and these results are different from those of the hydroxylations of *cis*- and *trans*-1,2-dimethylcyclohexane by iron complexes of porphyrin and non-porphyrin ligands.[6] In the latter reactions, moderate to high amounts of secondary alcohol products were yielded. In a competitive hydroxylation of *cis*- and *trans*-1,2-dimethylcyclohexane, the former was found to react 2.9 times faster than the latter (Table 1, entry 6). The alkane hydroxylation by **1** and *m*-CPBA was also found to be highly

Table 1 Hydroxylation of alkanes by **1** and *m*-CPBA[a]

Entry	Substrate	Products	Yields (%)[b,c]
A. Hydroxylation of alkanes			
1	Cyclohexane	Cyclohexanol	39 ± 4
		Cyclohexanone	8 ± 2
2	*cis*-1,2-Dimethylcyclohexane	*cis*-1,2-Dimethylcyclohexanol	65 ± 5
		trans-1,2-Dimethylcyclohexanol	< 1
		2,3- and 3,4-Dimethylcyclohexanol[d]	5 ± 1
3	*trans*-1,2-Dimethylcyclohexane	*cis*-1,2-Dimethylcyclohexanol	0
		trans-1,2-Dimethylcyclohexanol	43 ± 4
		2,3- and 3,4-Dimethylcyclohexanol[d]	8 ± 2
4	Adamantane[e]	Adamantan-1-ol	53 ± 3
		Adamantan-2-ol	9 ± 2
		Adamantan-2-one	> 1
B. Competitive hydroxylation of alkanes[f]			
5	Cyclohexane	Cyclohexanol	32 ± 3
	+		
	Cyclohexane-d_{12}	Cyclohexanol-d_{12}	4 ± 1
6	*cis*-1,2-Dimethylcyclohexane	*cis*-1,2-Dimethylcyclohexanol	41 ± 3
	+		
	trans-1,2-Dimethylcyclohexane	*trans*-1,2-Dimethylcyclohexanol	14 ± 1

[a] See footnote ‡ for detailed reaction procedures. Since the hydroxylation reactions were not affected by molecular oxygen, all the reactions were performed in air. [b] All reactions were run at least triplicate, and the yields reported represent the average of these reactions. [c] Based on the amount of *m*-CPBA added. [d] The yield of 3,4-dimethylcyclohexanol was determined with commercially available 2,3-dimethylcyclohexanol, with an assumption that the response factors for these alcohols are identical. [e] Reaction was run with 0.2 mmol of adamantane in CH_2Cl_2 (0.5 mL) due to the low solubility of adamantane. [f] Equal amounts of competing substrates (1 mmol each) were used.

 DOI: 10.1039/b103986p

regioselective, in which a high degree of selectivity for tertiary C–H bond over secondary C–H bond was observed in the hydroxylation of adamantane (Table 1, entry 4). The ratio of 3°/2° oxygenated products was ~18 after statistical correction; such a high 3°/2° ratio was usually observed in iron and manganese porphyrin-catalyzed hydroxylation of adamantane.[7]

The results presented above demonstrate unambiguously that the alkane hydroxylations by **1** and *m*-CPBA occur *via radical-free* oxidation reactions:[6] (1) the fact that alcohols were the major products with high alcohol to ketone ratios and the ratios of alcohol to ketone products were not affected by the presence of O_2, (2) a high KIE value for the formation of cyclohexanol, and (3) a complete retention of stereochemistry in the hydroxylations of *cis*- and *trans*-alkanes. Then, what is the nature of a hydroxylating intermediate? Is a high-valent cobalt–oxo porphyrin complex involved as a reactive species? Since isotopically labeled water ($H_2{}^{18}O$) experiments are a useful mechanistic probe to test the involvement of high-valent metal oxo intermediates in metal-mediated oxygen atom transfer reactions,[8] the hydroxylation of cyclohexane by **1** and *m*-CPBA was conducted in the presence of a small amount of $H_2{}^{18}O$ [eqn. (1)].** As the results show in Table 2 (entries 1 and 2), some of

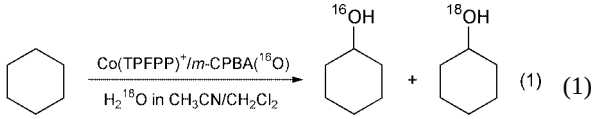

(1) (1)

the oxygen in the cyclohexanol product came from $H_2{}^{18}O$ and the percentage of ^{18}O in the alcohol product was dependent on the amount of $H_2{}^{18}O$ present in the reaction media. These results imply that a reactive hydroxylating intermediate generated in the reaction of **1** and *m*-CPBA exchanges its oxygen with labeled water prior to the oxygen atom transfer from the intermediate to cyclohexane.[8,9] For comparison, the ^{18}O-labeled water experiment was carried out with an iron porphyrin complex, Fe(TPFPP)(CF_3SO_3), under the identical reaction conditions, since we have shown previously that an oxoiron(IV) porphyrin cation radical complex was generated as a reactive hydroxylating intermediate in the hydroxylation of alkanes by Fe(TPFPP)(CF_3SO_3) and *m*-CPBA.[10] The degree of ^{18}O-incorporation in the Fe(TPFPP)(CF_3SO_3) reaction was about two times greater than that in the Co(TPFPP)(CF_3SO_3) reaction (Table 2, entries 3 and 4). Since the observation of ^{18}O-incorporation from $H_2{}^{18}O$ into oxygenated products is indirect evidence for the involvement of high-valent metal oxo intermediates in metal-catalyzed oxygenation reactions,[8–10] we suggest that a high-valent cobalt–oxo porphyrin complex participates as a reactive species in the cobalt porphyrin-catalyzed hydroxylation of alkanes by *m*-CPBA.

In conclusion, we have shown for the first time that an electron-deficient cobalt(III) porphyrin complex catalyzes the hydroxylation of alkanes by *m*-CPBA *via* a non-radical type of oxidation reactions. We suggest that a high-valent cobalt–oxo porphyrin complex is generated as a reactive hydroxylating intermediate in the reaction of the cobalt porphyrin complex and *m*-CPBA. Future studies will focus on attempts to understand the exact nature of the reactive intermediate.

This work was supported by the Korea Research Foundation (KRF-99-042-D00068).

Table 2 Percentages of ^{18}O incorporated from $H_2{}^{18}O$ into cyclohexanol product[a]

Entry	Catalyst	Amount (μL) of $H_2{}^{18}O$ present in reaction soln.	Cyclohexanol	
			^{18}O (%)	Yield (%)[b]
1	Co(TPFPP)(CF_3SO_3)	5	5 ± 1	18 ± 2
2		10	10 ± 1	17 ± 3
3	Fe(TPFPP)(CF_3SO_3)	5	11 ± 2	51 ± 4
4		10	18 ± 2	53 ± 4

[a] See footnote ** for detailed reaction procedures. All reactions were run at least triplicate, and the data reported represent the average of these reactions. [b] Based on the amount of *m*-CPBA added.

Notes and references

‡ Reaction conditions: *m*-CPBA (5×10^{-3} mmol, diluted in 20 μL of CH_3CN) was added to a reaction solution containing **1** (1×10^{-3} mmol) and substrate (1 mmol) in a solvent mixture (0.5 mL) of CH_3CN and CH_2Cl_2 (1:1) at rt. After the reaction mixture was stirred for 1 h, the reaction solution was directly analyzed by a Hewlett-Packard 5890 II Plus gas chromatograph with a FID detector and 30 m capillary column (Hewlett-Packard HP-1 or HP-5). Product yields were determined by comparison of peak area with that of decane or dodecane standard.

§ By following the time course of the hydroxylation of cyclohexane by **1** with 5 eq. of *m*-CPBA, we found that the alkane hydroxylation by **1** and *m*-CPBA takes place slowly, and the formation of cyclohexanol lasted for 1 h (data not shown).

¶ A control reaction carried out in the absence of the cobalt porphyrin catalyst did not show the formation of cyclohexanol and cyclohexanone products. Also, other cobalt porphyrin complexes such as Co(TMP)(CF_3SO_3) [TMP = *meso*-tetramesitylporphinato dianion] yielded only small amounts of cyclohexanol (~8%) and cyclohexanone (~2%). All cobalt(III) porphyrin complexes were obtained from Mid-Century and used without further purification.

‖ The catalytic activity of the cobalt porphyrin complex was examined by adding 50 eq. of *m*-CPBA (10 aliquots of 5 eq. of *m*-CPBA each at 1 h time intervals) into a reaction solution containing **1** (1×10^{-3} mmol) and *cis*-1,2-dimethylcyclohexane (1 mmol). Total reaction time was 10 h (see footnote ‡ for detailed experimental procedures). The yield of *cis*-1,2-dimethylcyclohexanol was 40% based on *m*-CPBA added, equivalent to 20 turnovers (see Fig. S1 for a plot of eq. of *m*-CPBA added *vs.* turnover number). By comparing UV-vis spectra of **1** taken before and after the reaction, we found that about 20% of the cobalt porphyrin catalyst was degraded.

** ^{18}O-labeled water experiments were performed under the identical reaction conditions described in footnote ‡ except that $H_2{}^{18}O$ (5 μL, 95% ^{18}O enriched), cyclohexane (0.5 mmol), and 15 eq. of *m*-CPBA (3 aliquots of 5 eq. of *m*-CPBA each at 1 h time intervals) were used. The ^{16}O and ^{18}O compositions in cyclohexanol were determined by the relative abundances of mass peaks at m/z = 57 for ^{16}O and 59 for ^{18}O (HP 5989B mass spectrometer). A control experiment showed that cyclohexanol does not exchange its oxygen with water under the experimental conditions.

1 M. Newcomb and P. H. Toy, *Acc. Chem. Res.*, 2000, **33**, 449; A. E. Shilov and A. A. Shteinman, *Acc. Chem. Res.*, 1999, **32**, 763; M. Sono, M. P. Roach, E. D. Coulter and J. H. Dawson, *Chem. Rev.*, 1996, **96**, 2841.

2 F. Montanari and L. Casella, *Metalloporphyrins Catalyzed Oxidations*, Kluwer Academic Publishers, Dordrecht, 1994; R. A. Sheldon, *Metalloporphyrins in Catalytic Oxidations*, Marcel Dekker, Inc., New York, 1994; B. Meunier, *Chem. Rev.*, 1992, **92**, 1411.

3 J. L. McLain, J. Lee and J. T. Groves, in *Biomimetic Oxidations Catalyzed by Transition Metal Complexes*, ed. B. Meunier, Imperial College Press, London, 2000, pp. 91–169.

4 F. A. Chavez and P. K. Mascharak, *Acc. Chem. Res.*, 2000, **33**, 539; R. A. Sheldon and J. K. Kochi, *Metal Catalyzed Oxidations of Organic Compounds*, Academic Press, New York, 1981; D. Mansuy, J.-F. Bartoli and M. Momenteau, *Tetrahedron Lett.*, 1982, **23**, 2781; M. A. Brook and J. R. Lindsay Smith, *J. Chem. Soc., Perkin Trans. 2*, 1985, 1049.

5 F. Ogliaro, M. Filatov and S. Shaik, *Eur. J. Inorg. Chem.*, 2000, 2455; J. I. Manchester, J. P. Dinnocenzo, L. A. Higgins and J. P. Jones, *J. Am. Chem. Soc.*, 1997, **119**, 5069.

6 W. Nam, Y. M. Goh, Y. J. Lee, M. H. Lim and C. Kim, *Inorg. Chem.*, 1999, **38**, 3238; C. Kim, K. Chen, J. Kim and L. Que, Jr., *J. Am. Chem. Soc.*, 1997, **119**, 5964.

7 E. Baciocchi, T. Boschi, C. Galli, A. Lapi and P. Tagliatesta, *Tetrahedron*, 1997, **53**, 4497; A. Sorokin, A. Robert and B. Meunier, *J. Am. Chem. Soc.*, 1993, **115**, 7293; J. T. Groves and T. E. Nemo, *J. Am. Chem. Soc.*, 1983, **105**, 6243.

8 K. Chen and L. Que, Jr., *Chem. Commun.*, 1999, 1375; J. Bernadou and B. Meunier, *Chem. Commun.*, 1998, 2167; K. A. Lee and W. Nam, *J. Am. Chem. Soc.*, 1997, **119**, 1916.

9 Y. M. Goh and W. Nam, *Inorg. Chem.*, 1999, **38**, 914.

10 W. Nam, M. H. Lim, S. K. Moon and C. Kim, *J. Am. Chem. Soc.*, 2000, **122**, 10805.

CHEMCOMM
Communication
www.rsc.org/chemcomm

DNA-driven self-assembly of gold nanorods

Erik Dujardin,[a] Long-Bao Hsin,[b] C. R. Chris Wang[b] and Stephen Mann*[a]

[a] *School of Chemistry, University of Bristol, Bristol, UK BS8 1TS. E-mail: s.mann@bristol.ac.uk*
[b] *Department of Chemistry, National Chung Cheng University, Min-Hsiung, Chia-Yi 621, Taiwan, Republic of China. E-mail: checrw@ccunix.edu.tw*

Received (in Cambridge, UK) 12th March 2001, Accepted 25th May 2001
First published as an Advance Article on the web 20th June 2001

Specific organization of gold nanorods into anisotropic 3D-aggregates is obtained by DNA hybridisation.

Symmetry breaking and the associated introduction of anisotropy in nanoparticle systems have been a major challenge for chemists and physicists working on nano-materials in recent years. Two distinct approaches have been explored. First, lower symmetries can be obtained by assembling spherical particles in anisotropic environments. Mixtures of different types of particles,[1] microcontact printing,[2] 1D arrays of particles along biolipid tubules[3] or in block copolymers[4] are some examples of this approach. The synthesis of anisotropic nanoparticles constitutes a second strategy. A wide variety of materials has recently been made available in the shapes of elongated rods[5–8] or more complex morphologies.[9] The anisotropy of these building blocks can be transferred to superstructures even by isotropic interactions such as hydrophobicity.[7,10] Although these interactions are efficient in producing large architectures, they are neither specific or selective, thus preventing a rational design of the self-assemblies. In this report, we show how the selective and reversible DNA-driven assembly of nanoparticles can be applied to gold nanorods.

The formation of networks of spherical gold nanoparticles crosslinked by well-defined oligonucleotide duplexes has been recently demonstrated.[11–13] In this approach, two non-complementary strands of DNA are immobilised on the surface of two batches of 13-nm particles. Upon mixing the two populations, no recognition occurs but adding a third strand half complementary to each of the grafted sequences induces hybridisation, which drives the self-assembly.[11,12] Not only is this method selective enough to allow the detection of a single base mismatch in the oligonucleotide sequence,[12] but the self-organisation is also reversible as the DNA duplex can be dissociated by heating.[13] By transferring this technique to non-spherical nanoparticles, we define a method to organise anisotropic materials that may exhibit orientation-dependant physical properties.

Gold nanorods used in this work were prepared by the electrochemical conversion of a gold anodic material into particles in an electrolytic co-surfactant system as described elsewhere.[5] The surfactants were hexadecyltrimethylammonium bromide (CTABr, Sigma, 99%) and tetradodecylammonium bromide (TDABr, Fluka, 98%). After synthesis, the colloidal suspensions were repeatedly centrifuged and washed with deionised water to remove excess surfactant. The concentration of nanorods was then adjusted to an optical density of *ca.* 0.5 at 800 nm in 5-mm lightpath UV cells. The average aspect ratio of the rods was 4.7 (*ca.* 10 nm in diameter and 50 nm in length) as inferred from transmission electron microscopy (TEM) images as well as from the position of the longitudinal plasmon band (850 nm).[5]

Two oligonucleotide systems were examined and all sequences were purchased from Oswell DNA Service, Southampton, UK. The first one, which is shown in the insert of Fig. 2, was identical to the complementary three-strand system reported by Mirkin and coworkers.[12] The second system was composed of two directly complementary strands of thiolated oligonucleotides. The sequence of this duplex is shown in Fig. 3.

Functionalisation of the nanorod surface was performed according to the reported method.[12] Briefly, the thiol group of the DNA strands was activated by treatment in 0.1 M of dithiothreitol (DTT, Aldrich, 99%) at pH 8.4 and room temperature for 1 h. The solutions were then purified through a desalting column (NAP-5, Sephadex G-25 Medium). The different thiolated oligonucleotides were then left to react at room temperature with the nanorod solutions for up to 72 h. Typical final concentrations were *ca.* 5×10^8 nanorods per mL (*i.e.* 1 pM) and 1 nM of DNA. After incubation, the suspensions were centrifuged at 5000 rpm for 20 min, decanted and redispersed in double distilled water to the same concentration.

For hybridisation experiments, identical volumes of equimolar suspensions of functionalised nanorods were mixed in a 5-mm lightpath UV cell at room temperature. Aggregation was monitored by recording UV–VIS spectra as a function of time on a Lambda 11 Perkin-Elmer spectrophotometer. For the complementary two-strand system, duplexation occurred immediately upon mixing the complementary nanorods suspensions. For the three-strand system, aggregation was initiated by adding the free, non-thiolated oligonucleotide, the final concentration of which was typically 10 nM.

As hybridisation progressed, the colour of the suspension changed from red to purple and macroscopic precipitation was observed after 24 h. The nature of the organisation of the nanorods in the purple suspensions was elucidated by TEM. In contrast to as-synthesised or DNA-covered but non-duplexed nanorod suspensions, which showed totally random aggregates when examined under the same conditions, numerous organised aggregates, often several micrometers in size, were observed for the hybridised suspensions. The samples were composed of 3-D bundles of hundreds of nanorods aligned in parallel stacks (Fig. 1). Both alternate and superimposed vertical stacking of the rods could be seen. The inter-particle distance was about

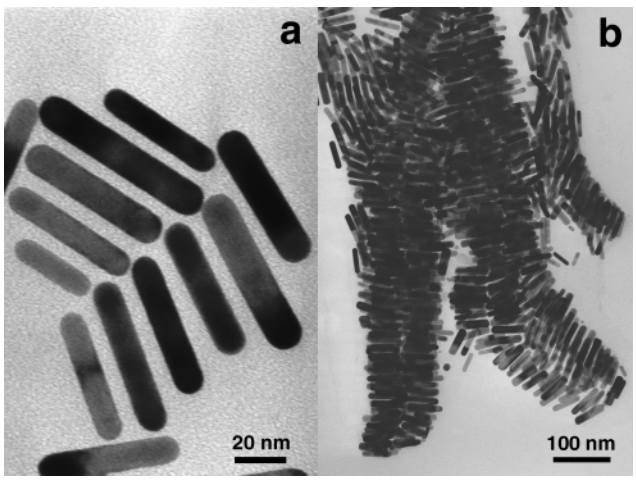

Fig. 1 Transmission electron micrographs of bundles of DNA-linked gold nanorods. Topological characteristics of the three-strand (a) or two-strand (b) DNA linking systems were similar.

 DOI: 10.1039/b102319p

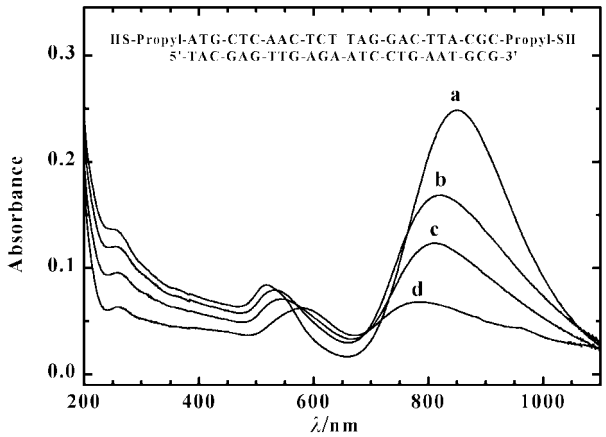

Fig. 2 UV–VIS spectra of a suspension of non-complementary DNA-functionalised nanorods. (a) 0 s, (b) 10 min, (c) 1 h, (d) 2 h after duplex initiation arising from the addition of the third complementary strand. Sequences of the three oligonucleotides are shown in the insert.

6 nm (Fig. 1a), which is longer that an interdigitated CTA bilayer (*ca*. 3 nm)[14] but commensurate with the length of a 24-base pair helix with two propyl spacers (6.5–9.0 nm). This is consistent with an aggregation process resulting from DNA duplex formation rather than from hydrophobic interactions between the CTA alkane chains.

Fig. 2 shows a typical series of spectra taken at various times after the addition of the third complementary oligonucleotide in the three-strand system. The colour change, which the nanorods share with the DNA-driven assembly of isotropic particle suspensions, was confirmed by the decrease in intensity and the red-shift of the transverse plasmon band (520 nm).[12,15] The UV–VIS spectra also showed a longitudinal band at 850 nm that decreased markedly in intensity and was blue-shifted with aggregation. A shoulder peak at 260 nm confirmed the presence of the nucleotides. Moreover, the intensity of this peak was reduced with time, consistent with the onset of base-pairing.[13] In the two-strand system, the decrease in intensity of the three bands upon hybridisation was also observed (Fig. 3, solid and dotted lines). However, the plasmon bands undergo almost no wavelength shift.

Further evidence that the aggregation was driven by DNA duplex formation was given by 'melting' analysis. This consists in dissociating the duplex by heating the sample above a temperature, which, in the case of the three-strand system, is 53 °C.[12] For this purpose, the purple suspensions were heated up to 70 °C by a thermostated bath and UV–VIS spectra were recorded at regular intervals. Hence, upon heating the duplexed suspension of the two-strand system, the intensities of the three bands were essentially recovered at 60 °C (Fig. 3, dashed curve), indicating reversible duplex formation between the complementary nanorod surfaces. Surprisingly, no change in the spectrum of the duplexed three-strand system could be observed and the suspension stayed irreversibly self-assembled.

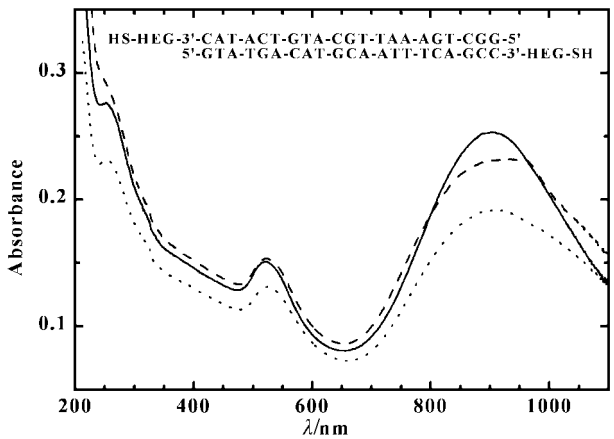

Fig. 3 UV–VIS spectra of the two-strand nanorod system before (—) and after (···) duplexation at 25 °C. The dashed curve was obtained after melting the DNA above 60 °C. The mismatch at higher wavelengths between the initial and denatured spectra is attributed to imperfect background compensation at high temperature. The sequences of the two strands are shown in the insert; HEG = hexaethyleneglycol.

Although further experiments are needed to explain this irreversibility, it is probable that the aspect ratio of the rods and/or the residual CTA molecules on the gold surface play a role. Indeed, whereas the base pairing is certainly the driving force of the self-assembly in both systems, a 12-base oligonucleotide with a propyl spacer (three-strand system) would barely emerge from a residual CTA bilayer. Once the aggregates are formed by duplexation, a multilayered CTA structure could rearrange between neighbouring rods and hydrophobic interactions could then become dominant. Upon heating for the 'melting' experiments, increases in the hydrophobic forces by dehydration of the alkane chains as well as electrostatic interactions between the $-NMe_3^+$ headgroups and the now unpaired DNA strands would reinforce this multilayered structure making rod aggregation irreversible. By contrast, the 21-base HEG-coupled oligonucleotides used in the two-strand system are sufficiently long to extend well beyond a residual CTA bilayer. Thus, in this case, the surfactant layers are not close enough to rearrange and the base pairing is therefore reversible. In addition, as no free DNA strand is released upon 'melting', the multilayered CTA structure would not be stabilised by electrostatic interactions.

In conclusion, this report has shown that large scale uniaxial organisation of metallic nanorods can be tailored by using the specific DNA duplex formation. Beyond DNA, antigen/antibody or protein/substrate bindings can be envisioned to obtain similar programmable assembly of anisotropic building blocks.[16] Systematic organisation of nanorods made of different materials is a straightforward development of this approach that should lead to anisotropic nanomaterials with more complex properties.

We thank Dr C. Murphy, C. Johnson and Dr W. Shenton for valuable discussions and the European Union for a Marie Curie Individual Fellowship (HPMF-CT-1999-00254) to E. D.

Notes and references

1 C. J. Kiely, J. Fink, J. G. Zheng, M. Brust, D. Bethell and D. J. Schiffrin, *Adv. Mater.*, 2000, **12**, 640.
2 P. C. Hidber, W. Helbig, E. Kim and G. M. Whitesides, *Langmuir*, 1996, **12**, 1375.
3 S. L. Burkett and S. Mann, *Chem. Commun.*, 1996, 321.
4 R. W. Zehner and L. R. Sita, *Langmuir*, 1999, **15**, 6139.
5 Y. Y. Yu, S. S. Chang, C. L. Lee and C. R. C. Wang, *J. Phys. Chem. B*, 1997, **101**, 6661; S. S. Chang, C. W. Shih, C. D. Chen, W. C. Lai and C. R. C. Wang, *Langmuir*, 1999, **15**, 701.
6 B. A. Korgel and D. Fitzmaurice, *Adv. Mater.*, 1998, **10**, 661.
7 M. Li, H. Schnablegger and S. Mann, *Nature*, 1999, **402**, 393.
8 X. Peng, L. Manna, W. Yang, J. Wickham, E. Scher, A. Kadavanich and A. P. Alivisatos, *Nature*, 2000, **404**, 59.
9 L. Manna, E. C. Scher and A. P. Alivisatos, *J. Am. Chem. Soc.*, 2000, **122**, 12700.
10 B. Nikoobakht, Z. L. Wang and M. A. El-Sayed, *J. Phys. Chem. B*, 2000, **104**, 8635.
11 C. A. Mirkin, R. L. Letsinger, R. C. Mucic and J. J. Storhoff, *Nature*, 1996, **382**, 607; A. P. Alivisatos, K. Johnson, X. Peng, T. E. Wilson, C. J. Loweth, M. Bruchez and P. G. Schultz, *Nature*, 1996, **382**, 609.
12 J. J. Storhoff, R. Elghanian, R. C. Mucic, C. A. Mirkin and R. L. Letsinger, *J. Am. Chem. Soc.*, 1998, **120**, 1959.
13 C. A. Mirkin, *Inorg. Chem.*, 2000, **39**, 2258 and references therein.
14 M. W. Rutland and J. L. Parker, *Langmuir*, 1994, **10**, 1110.
15 A. A. Lazarides and G. C. Schatz, *J. Phys. Chem. B*, 2000, **104**, 460.
16 S. Mann, W. Shenton, M. Li, S. Connolly and D. Fitzmaurice, *Adv. Mater.*, 2000, **12**, 147.

CHEMCOMM Communication
www.rsc.org/chemcomm

A facile and new type of route to the redox-active rigid-rod complex $[\{Mn(dmpe)_2(C{\equiv}CH)\}_2(\mu\text{-}C_4)][PF_6]$ *via* Mn–C_2· radical coupling†

Francisco J. Fernández, Olivier Blacque, Montserrat Alfonso and Heinz Berke*

Anorganisch-Chemisches Institut der Universität Zürich, Winterthurerstrasse 190, CH-8057 Zürich, Switzerland. E-mail: hberke@aci.unizh.ch

Received (in Cambridge, UK) 14th March 2001, Accepted 29th May 2001
First published as an Advance Article on the web 21st June 2001

The binuclear rigid-rod complex $[\{Mn(dmpe)_2(C{\equiv}CH)\}_2(\mu\text{-}C_4)][PF_6]$ was spontaneously obtained from the reaction of $[Mn(dmpe)_2(C{\equiv}CSiMe_3)_2][PF_6]$ with one equivalent of TBAF.

Di- and oligo-nuclear organometallic complexes, in which two neighboring metal centers are connected by a C_x chain, have recently attracted great interest due to their potential in NLO applications[1] and the possibility to use them as precursors for molecular wires.[2] During the last decade several organometallic research groups therefore focused on the development of facile synthetic routes to ML_n–C_x–ML_n rigid-rod transition metal complexes.[3–7] Studies of the electrochemical properties of these species have demonstrated that for $x = 4$ there is strong metal–metal interaction across the carbon chain. This confers great stability to the corresponding mixed-valent species, as indicated by the value of the comproportionation constant (K_c) which lies in the range of 10^8–10^{12}. This metal–metal interaction decreases with the length of the chain (C_x) and is very small for complexes with values of $x \geqslant 20$.[6a] With regard to the design of new molecular wires particularly great interest arose in new synthetic accesses to short-chain bridged species and polarizable end groups.

We have recently reported the syntheses and characterization of $[\{Mn(dmpe)_2I\}_2(\mu\text{-}C_4)]^{n+}$ ($n = 0, 1, 2$) complexes by the reaction of (MeCp)(dmpe)MnI with 0.5 Me_3Sn–C_4–$SnMe_3$ and dmpe.[7] In order to extend the scope of available versatile routes we initiated reactivity studies on $[Mn(dmpe)_2(C{\equiv}CSiMe_3)_2]^n$ ($n = -1, 0, +1$) complexes.[8] As silyl protected acetylide derivatives they were expected to allow deprotection and recovery of the quite reactive parent acetylide species.

Indeed, the reaction of $[Mn(dmpe)_2(C{\equiv}CSiMe_3)_2]^+$ **1**$^+$ with one equivalent of NBu_4F (TBAF) containing 5% H_2O[9] led to the deprotected species $[Mn(dmpe)_2(C{\equiv}CH)_2]^+$ **2a**$^+$ and subsequent deprotonation of this species produced under the reaction conditions a $[(HC{\equiv}C)Mn(dmpe)_2(C{\equiv}C)]$ intermediate **2b** (Scheme 1).‡ Spontaneous dimerization of **2b** generated $[\{Mn(dmpe)_2(C{\equiv}CH)\}_2(\mu\text{-}C_4)]$ **3** and subsequently the mixed-valent compound $[\{Mn(dmpe)_2(C{\equiv}CH)\}_2(\mu\text{-}C_4)]^+$ **3**$^+$. DFT calculations[10]† performed on the hydrogen substituted model $Mn(dHpe)_2(C{\equiv}CH)(C{\equiv}C)$ simulating **2b** revealed that, of the two possible states, triplet and singlet, the triplet state of **2b(A)** with two unpaired electrons is more stable than the singlet state **2b(B)** by *ca.* 90 kJ mol^{-1}. Furthermore, the computed spin densities of +1.45α and +0.61α, at the manganese atom and at the terminal carbon atom, respectively, clearly indicate that the electronic structure of **2b** is well described by the resonance formula **2b(A)**. The relative stability and therefore longevity of the Mn^{II} free radical apparently supports the C–C coupling process to produce the neutral dinuclear Mn^{II}–Mn^{II} species **3**. Under the given redox conditions, *i.e.* in the presence of the mildly oxidizing **2a**$^+$, **3** is converted to **3**$^+$ with additional formation of the corresponding $Mn(dmpe)_2(C{\equiv}CH)_2$ **2a** which is not stable and decomposes.[8] Indeed, the THF soluble fraction of the reaction contains a mixture of **3** and other not specifically identified Mn^{II} and Mn^{I} complexes.[8]

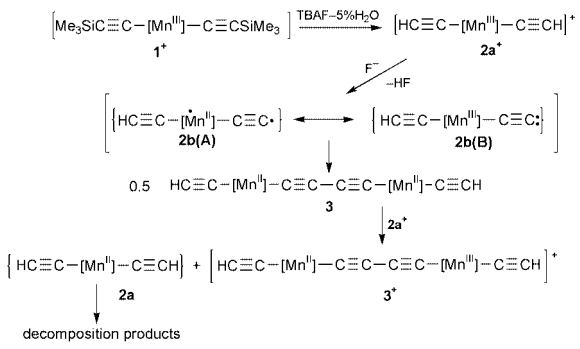

Scheme 1 [Mn] = $Mn(dmpe)_2$.

Based on **1**$^+$, the new dinuclear mixed-valent complex **3**$^+$ was obtained in about 65% yield, which is almost the ideal yield based on the stoichiometry of Scheme 1. This reaction involving acid–base chemistry in conjunction with the versatile redox properties of the Mn center thus furnishes a new and a facile method to obtain M–C_4–M complexes starting from easily accessible M–C_2SiR_3 units. Mechanistically it appears that there is some relationship of these conversions to the coupling of terminal acetylides with Cu^{II} reagents.[6] However, the intramolecular fashion, along which the redox chemistry of Scheme 1 proceeds, is quite unique. In addition, species **3**$^+$ possesses two reactive terminal acetylenic moieties, which might be utilized in further organometallic substitution processes of the H terminus. Compound **3**$^+$ has been characterized as a violet solid, soluble only in polar and ionizing solvents such as CH_2Cl_2. The ^{1}H NMR spectrum of **3**$^+$ (20 °C, CD_2Cl_2) shows four broad signals for the dmpe protons at δ −0.28, −4.58, −6.49 and −6.65, and a resonance at δ −46.40 due to the C≡CH proton. The paramagnetism is indicated by the broadness of the resonances and more quantitatively confirmed by the contact shift induced Curie–Weiss behavior of **3**$^+$ in the temperature range from −80 to 20 °C. The fact that only one set of resonances was observed for the protons of the dmpe ligands is taken as a strong hint for electron delocalization with both manganese ends equivalent on the NMR time scale (10^{-6} s). In the solid state, **3**$^+$ has a magnetic moment of 2.53 μ_B at 290 K that drops to 1.95 μ_B at 100 K demonstrating strong intramolecular antiferromagnetic interaction comparable to that observed for $[\{Mn(dmpe)_2I\}_2(\mu\text{-}C_4)][BF_4]$.[7]

Cyclic voltammetry (CV) of complex **3**$^+$ in acetonitrile solution displays two fully reversible waves ($\Delta E_p = 0.070$ V and $i_{pa}/i_{pc} \approx 1$ for scan rates of 0.100–0.500 V s^{-1} at 20 °C, *vs.* Fc/Fc^+) at $E_{1/2} = -0.89$ V and $E_{1/2} = -1.46$ V corresponding to the Mn^{III}–Mn^{III} (**3**$^{2+}$)/Mn^{III}–Mn^{II} (**3**$^+$) and Mn^{III}–Mn^{II} (**3**$^+$)/Mn^{II}–Mn^{II} (**3**) redox couples. The difference of these values of $\Delta E_{1/2}$ (= 0.576 V) establishes a comproportionation constant of 7.5×10^9 [$K_c = \exp(F\Delta E_{1/2}/RT)$].[11] Another somewhat irreversible redox couple was identified at $E_{1/2} = -2.29$ V attributed to the Mn^{II}–Mn^{II}/Mn^{II}–Mn^{I} reduction. In accord with this CV behavior the monocation **3**$^+$ could

† Electronic supplementary information (ESI) available: detailed DFT calculation outputs. See http://www.rsc.org/suppdata/cc/b1/b102396a/

 DOI: 10.1039/b102396a

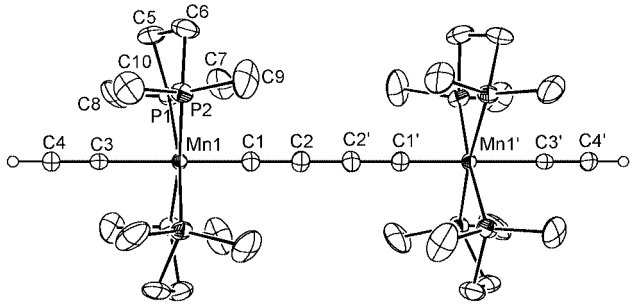

Fig. 1 Molecular structure of $\mathbf{3}^{+}[PF_6]^{-}$. Selected bond lengths (Å) and angles (°): Mn1–C1 1.818(4), Mn1–C3 2.026(5), C1–C2 1.285(6), C2–C2′ 1.307(9), C3–C4 1.189(6); Mn1–C1–C2 180.0(4); the $[PF_6]^{-}$ anion is omitted.

chemically be reduced to the dark-green paramagnetic complex **3** using $Cp(C_6Me_6)Fe$ and oxidized with $[Cp_2Fe][PF_6]$ to give the dark-brown diamagnetic $[\{Mn(dmpe)_2(C{\equiv}CH)\}_2(\mu\text{-}C_4)]^{2+}$ species $\mathbf{3}^{2+}$. Both processes can be fully reversed with $[Cp_2Fe]^{+}$ and Cp_2Co, respectively [eqn. (1)]. Complexes **3** and $\mathbf{3}^{2+}$ were isolated and fully characterized.

$$3 \underset{Cp(C_6Me_6)Fe}{\overset{[Cp_2Fe]^{+}}{\rightleftharpoons}} 3^{+} \underset{Cp_2Co}{\overset{[Cp_2Fe]^{+}}{\rightleftharpoons}} 3^{2+} \qquad (1)$$

The highly symmetric structure of $\mathbf{3}^{+}$ was determined by single-crystal X-ray diffraction (Fig. 1),§ which indeed revealed two equivalent manganese centers adopting pseudo-octahedral geometry. The C1–C2 and C2–C2′ bond lengths show only little alteration and compare very well to those obtained for the related species $[\{Mn(dmpe)_2I\}_2(\mu\text{-}C_4)]^n$ [n = 0, 1.26(2)–1.33(3) Å; n = 1, 1.275(3)–1.313(5) Å and n = 2, 1.289(5)–1.295(5) Å].[7] The C_4 linear chain is thus best described by a cumulenic resonance structure.

Support from the Swiss National Science Fundation and the Fonds of the University of Zürich are gratefully acknowledged. We also thank Dr A. Shengelaya, Institute of Experimental Physics of the University of Zürich, for the magnetic studies of $\mathbf{3}^{+}$.

Notes and references

‡ All operations were performed using standard Schlenck or Glove-box techniches. ^{1}H NMR data for $\mathbf{2a}^{+}$ prepared *in situ* (CD_2Cl_2, 300 MHz, −10 °C), δ −33.0 (br, 8H, PCH_2), −44.0 (br, 24H, PCH_3).

Synthesis of $\mathbf{3}^{+}$ $[PF_6]^{-}$: A 1 M solution of TBAF (0.15 mL) was added to a CH_2Cl_2 solution (15 mL) of $\mathbf{1}^{+}$ (0.1 g, 0.15 mmol). After 1.5 h the dark-green solution was concentrated *in vacuo* to 3 mL. Addition of Et_2O precipitated $\mathbf{3}^{+}[PF_6]^{-}$, which was dried *in vacuo*. Yield 0.046 g, (65%). Anal. Calc. for $C_{32}H_{66}F_6Mn_2P_9$: C, 40.31; H, 6.98. Found: C, 40.01; H, 6.80. ^{1}H NMR (CD_2Cl_2, 300 MHz, 20 °C): δ −0.29 (br, 8H, PCH_2), −4.60 (br, 24H, PCH_3), −6.55 (br, 24H, PCH_2), −6.71 (br, 24H, PCH_3), −46.39 (br, 2H, ≡CH). ^{31}P NMR (121.471 MHz, CD_2Cl_2, 20 °C, 85% H_3PO_4 ext.): δ −145.62 (sept., $^1J_{PF}$ 717.9 Hz, PF_6^{-}).^{19}F NMR (CD_2Cl_2, 282.324 MHz, 20 °C, $C_6H_5CF_3$ ext.): δ −75.09 (d, 717.9 Hz, PF_6^{-}). IR (CH_2Cl_2, 20 °C): 2140s 1819w (C_4 unit), 1960m cm^{-1} [ν(C≡CH)].

Synthesis of $\mathbf{3}^{2+}[PF_6]^{-}_2$: $[Cp_2Fe][PF_6]$ (0.017 g, 0.052 mmol) was added to a CH_2Cl_2 solution (10 mL) of $\mathbf{3}^{+}$ (0.050 g, 0.052 mmol). After 3 h the solution was concentrated *in vacuo* to 3 mL. Addition of Et_2O precipitated $\mathbf{3}^{2+}[PF_6]^{-}_2$, which was dried *in vacuo*. Yield 0.051 g, (90%). Anal. Calc. for $C_{32}H_{66}F_{12}Mn_2P_{10}$: C, 34.99; H, 6.06. Found: C, 34.86; H, 6.06. ^{1}H NMR (CD_2Cl_2, 300 MHz, 20 °C): δ 1.93 (br, 8H, PCH_2), 1.83 (br, 24H, PCH_2), 1.38 (br, 24H, PCH_3), 1.27 (br, 24H, PCH_3), −2.30 (br, 2H, ≡CH). ^{31}P NMR (121.471 MHz, CD_2Cl_2, 20 °C, 85% H_3PO_4 ext.): δ −145.44 (sept, $^1J_{PF}$ 719 Hz, PF_6^{-}). ^{19}F NMR (CD_2Cl_2, 282.324 MHz, 20 °C, $C_6H_5CF_3$ ext.): δ −74.02 (d, 719 Hz, PF_6^{-}). IR (KBr, 20 °C): 1929 cm^{-1} [ν(C≡C)], 2025, 1915, 1920 cm^{-1} [ν(C≡C)$_2$].

Synthesis of **3**: $Cp(C_6Me_6)Fe$ (0.017 g, 0.053 mmol) dissolved in toluene (5 mL) was added to a THF suspension (5 mL of $\mathbf{3}^{+}[PF_6]^{-}$ (0.050 g, 0.052 mmol). After 2 h the solution was filtered and the solvent removed to give **3**. Yield 0.038 g, (90%). Anal. Calc. for $C_{32}H_{66}Mn_2P_8$: C, 47.54; H, 8.23. Found: C, 47.62; H, 8.53. ^{1}H NMR (C_6D_6, 300 MHz, 40 °C): δ −9.47 (br, 8H, PCH_2), −14.89 (br, 32H, PMe_3 + PCH_2), −18.78 (br, 24H, PCH_3), −149.44 (br, 2H, ≡CH). IR: no ν(C≡C) are observed.

§ *Crystal data* for $\mathbf{3}^{+}[PF_6]^{-}$: $C_{32}H_{66}F_6Mn_2P_9$, M = 953.46, dark red block, 0.30 × 0.24 × 0.15 mm, tetragonal, space group $I\bar{4}c2$, a = b = 16.1403(9), c = 18.141(1) Å, V = 4725.9(5) Å^3, Z = 4, D_c = 1.340 Mg m^{-3}, μ = 0.884 mm^{-1}. Data were collected on a STOE IPDS diffractometer [graphite monochromatised Mo-Kα, λ = 0.71073 Å, T = 183(2) K]. 22664 reflections collected, 2924 unique (R_{int} = 0.0202). Refinement converged to R_1 = 0.0303, wR_2 = 0.0732 [$I > 2\sigma(I)$] and R_1 = 0.0529, wR_2 = 0.0777 (all data). CCDC reference number 161685. See http://www.rsc.org/suppdata/cc/b1/b102396a/ for crystallographic data in CIF or other electronic format.

1 M. D. Ward, *Chem. Soc. Rev.*, 1995, 121; I. R. Whittall, A. M. McDonagh, M. G. Humphrey and M. Samoc, *Adv. Organomet. Chem.*, 1998, **42**, 291; I. R. Whittall, A. M. McDonagh, M. G. Humphrey and M. Samoc, *Adv. Organomet. Chem.*, 1998, **43**, 349.

2 G. Frapper and M. Kertesz, *Inorg. Chem.*, 1993, **32**, 732; D. Osella, L. Milone, C. Nervi and M. Ravera, *Eur. J. Inorg. Chem.*, 1998, 1473; F. Paul and C. Lapinte, *Coord. Chem. Rev.*, 1998, **178**–**180**, 431.

3 H. Lang, *Angew. Chem.*, 1994, **106**, 569; H. Lang, *Angew. Chem., Int. Ed. Engl.*, 1994, **33**, 547; U. Bunz, *Angew. Chem.*, 1996, **108**, 1047; U. Bunz, *Angew. Chem., Int. Ed. Engl.*, 1996, **35**, 969; M. I. Bruce, *Coord. Chem. Rev.*, 1997, **166**, 91.

4 Homobimetallic species: M. Guillemot, L. Toupet and C. Lapinte, *Organometallics*, 1998, **17**, 1928; F. Coat, M.-A. Guillevic, L. Toupet, F. Paul and C. Lapinte, *Organometallics*, 1997, **16**, 5988; M. Akita, M.-C. Chung, A. Sakurai, S. Sugimoto, M. Terada, M. Tanaka and Y. Moro-oka, *Organometallics*, 1997, **16**, 4882; V. W.-W. Yam, V. C.-Y. Lau and K.-K. Cheung, *Organometallics*, 1996, **15**, 1740; M. I. Bruce, P. J. Low, K. Costuas, J.-F. Halet, S. P. Best and G. A. Heath., *J. Am. Chem. Soc.*, 2000, **122**, 1949; T. Rappert, O. Nurnberg and H. Werner, *Organometallics*, 1993, **12**, 1359; J. Gil-Rubio, M. Laubender and H. Werner, *Organometallics*, 2000, **19**, 1365; M. Brady, W. Weng, Y. Zhou, J. W. Seyler, A. J. Amoroso, A. M. Arif, M. Böhme, G. Frenking and J. A. Gladysz, *J. Am. Chem. Soc.*, 1997, **119**, 775; T. Ren, G. Zou and J. C. Alvarez, *Chem. Commun.*, 2000, 1197.

5 Heterobimetallic species: W. Weng, T. Bartik, M. Brady, B. Bartik, J. A. Ramsden, A. M. Arif and J. A. Gladysz, *J. Am. Chem. Soc.*, 1995, **117**, 11 922; P. Frédéric, W. E. Meyer, L. Toupet, H. Jiao, J. A. Gladysz and C. Lapinte, *J. Am. Chem. Soc.*, 2000, **122**, 9405; M. I. Bruce, B. G. Ellis, B. W. Skelton and A. H. White, *J. Organomet. Chem.*, 2000, **607**, 137.

6 Complexes with long chains: (*a*) R. Dembinski, T. Bartik, B. Bartik, M. Jaeger and J. A. Gladysz, *J. Am. Chem. Soc.*, 2000, **122**, 810; (*b*) M. I. Bruce, B. D. Kelly, B. W. Skelton and A. H. White, *J. Organomet. Chem.*, 2000, **604**, 150; (*c*) T. Bartik, B. Bartik, M. Brady, R. Dembinski and J. A. Gladysz, *Angew. Chem.*, 1996, **108**, 467; T. Bartik, B. Bartik, M. Brady, R. Dembinski and J. A. Gladysz, *Angew. Chem., Int. Ed.*, 1996, **35**, 414; (*d*) F. Coat and C. Lapinte, *Organometallics*, 1996, **15**, 477.

7 S. Kheradmandan, K. Heinze, H. Schmalle and H. Berke, *Angew. Chem.*, 1999, **111**, 2412; S. Kheradmandan, K. Heinze, H. Schmalle and H. Berke, *Angew. Chem., Int. Ed.*, 1999, **38**, 2270.

8 F. J. Fernández, M. Alfonso, H. W. Schmalle and H. Berke, *Organometallics*, in press; V. V. Krivykh, I. L. Eremenko, D. Veghini, I. A. Petrunenko, D. L. Pountney, D. Unseld and H. Berke, *J. Organomet. Chem.*, 1996, **511**, 111; D. Unseld, V. V. Krivykh, K. Heinze, F. Wild, G. Artus, H. W. Schmalle and H. Berke, *Organometallics*, 1999, **18**, 1525; D. Unseld, PhD Thesis University of Zürich, 1999.

9 Only catalytic amounts of TBAF are required to induce deprotection of the metal–C≡CSiMe$_3$ units. For example: R. Dembinski, T. Lis, S. Szafer, C. L. Mayne, T. Bartik and J. A. Gladysz, *J. Organomet. Chem.*, 1999, **578**, 229.

10 The DFT calculations reported in this paper were performed using the Amsterdam Density Functional program package ADF, release 2000.01. The detailed DFT calculation outputs are available as ESI.†

11 C. Creutz, *Prog. Inorg. Chem.*, 1983, **30**, 1.

CHEMCOMM
Communication
www.rsc.org/chemcomm

Base catalysed phosphate diester hydrolysis

Nicholas H. Williams* and Paul Wyman

Department of Chemistry, Sheffield University, Sheffield, UK S3 7HF.
E-mail: N.H.Williams@Sheffield.ac.uk; Fax: 0114 2738673; Tel: 0114 2229469

Received (in Cambridge, UK) 12th April 2001, Accepted 22nd May 2001
First published as an Advance Article on the web 21st June 2001

The rate of attack of hydroxide on dialkyl phosphate diesters is far slower than previously estimated, allowing us to estimate the stability of the diester link in DNA and showing that ethylene phosphate is 10^{11} fold more reactive towards attack by hydroxide than an acyclic diester (1000 fold more than previously estimated).

Nature has selected phosphate diesters to hold together the genetic code. This linkage needs to be very stable to keep the sequence of bases intact, but is also the site at which DNA is hydrolysed in the course of its repair and destruction by nucleases.[1] To be able to understand the efficiency of the enzymes (and ribozymes) which catalyse hydrolysis, it is important to quantify the background reactivity. This information will also define the catalytic efficiency which must be achieved by artificial catalysts before they can be used as useful substitutes for natural nucleases. As this is not the most reactive site of DNA,[2] direct measurement of the hydrolysis reaction at phosphorus is not possible and so the hydrolysis of simpler phosphate diesters has to be studied. Here we report the rate of hydroxide catalysed hydrolysis of phosphate diesters with poor leaving groups, revealing that the phosphate diesters in DNA are far more resistant to hydrolysis than has been previously estimated.

The hydrolysis of phosphate diesters with alkoxy leaving groups is extremely slow in the absence of efficient catalysts. Westheimer[3] reported the rate of hydroxide attack on dimethyl phosphate at high temperatures, but Bunton *et al.*[4] used isotopically labeled solvent to show that the majority of the reaction occurs by C–O cleavage (pathway A, Scheme 1a), giving the same products but showing that the attack at phosphorus (pathway B, Scheme 1a) must be slower still. This was confirmed by Westheimer and Haake,[5] and modifying the original rate data to allow for competing attack at carbon gives 6.8×10^{-12} M^{-1} s^{-1} as the best estimate for DNA reactivity with hydroxide at 25 °C.[6] Recently, Wolfenden and Radzicka re-examined the hydrolysis of dimethyl phosphate, and by extrapolating kinetic data from high temperatures arrived at an estimate of 130 000 years as the half life for DNA at pH 6.8 and 25 °C.[7] More detailed study revealed that only pathway A was occurring, and so only an upper limit for the biologically relevant hydrolysis reaction can be derived from these data.[8] These later data also showed that hydrolysis of monomethyl phosphate proceeds only by P–O cleavage and is rapid enough to occur to a similar extent as solvent incorporation under the conditions of the original labeling studies. This could account for the reported isotope labeling results, without involving any P–O cleavage in the initial reaction of dimethyl phosphate. We decided to try and establish the reactivity of dialkyl phosphodiesters to hydrolysis by studying **1** (Scheme 1b) which has a leaving group pK_a comparable to that in DNA.

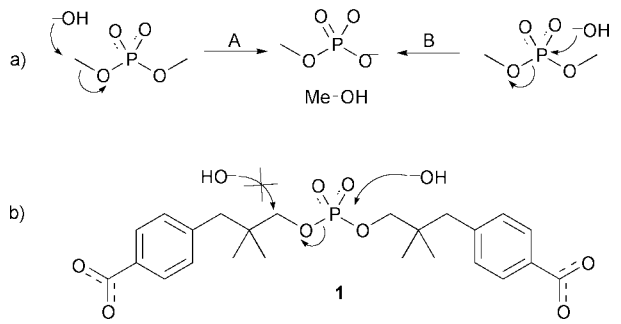

Scheme 1 (*a*) Pathways for hydrolysis of dimethyl phosphate. (*b*) Compound **1** has pathway A selectively hindered.

Compound **1**† uses the neopentyl effect to prevent attack at carbon without hindering attack at the phosphorus. The steric effect of an alkyl group can significantly retard substitution rates when it is branched α or β to a reaction centre, but the impact of branching at the γ position is minimal.[9] Indeed, the hydrolysis of alkyl 4-nitrophenyl phosphate is only slowed ~2 fold when the alkyl group is changed from methyl to neopentyl.[10] To facilitate analysis by HPLC, we appended aromatic rings, which required the addition of carboxylate groups for solubility in aqueous solution. These anionic groups are distant to the reacting diester, so in a polar, protic solvent such as water, we expect no electrostatic impact on its reactivity; initial studies (using ^{1}H NMR) confirmed that dineopentyl phosphate had the same reactivity as **1**. To study the hydrolysis of **1**, we sealed 0.5 ml aliquots of a 10 mM solution of the diester (with 4-methylbenzoic acid as an internal reference) in 1 M KOH in stainless steel reaction vessels with a PTFE liner and graphite gasket. These were kept at constant temperature by being immersed in a circulating oil bath and removed for analysis at various times.

We investigated the site of reaction by using 94% ^{18}O labeled water. Stopping the reaction after ~50% reaction at 240 °C and analysing the solution by LC-MS revealed that the carboxylate oxygens of **1** and the product alcohol were isotopically labeled at solvent levels, but that the alcohol OH was still at natural abundance—and so the biologically relevant hydrolysis of a phosphate diester mimicking the DNA link is being observed.

Over the range 160–260 °C, we could observe the disappearance of the diester and corresponding appearance of the alcohol product by HPLC analysis of aliquots removed at various time intervals (Fig. 1).‡ Under these conditions, the monoester intermediate does not accumulate to any significant extent. Maintaining the ionic strength at 1 M with KCl, we also measured the rates at 0.33 M KOH, and observed a 3 fold decrease in rate, showing that in 1 M base, the reaction is catalysed by hydroxide.§

In Fig. 2, we plot this data as the log of the second order rate constant for the hydroxide attack against 1/*T* which shows the expected linear relationship. The activation enthalpy is 129 ± 4 kJ mol^{-1} and the activation entropy is −102 ± 9 J mol^{-1} K^{-1}, consistent with a bimolecular reaction and very similar to the entropy of activation (−117 ± 7 J mol^{-1} K^{-1}) measured for the hydroxide catalysed hydrolysis of methyl 4-nitrophenyl phosphate.[11] Extrapolating this data to 25 °C predicts a second order rate constant for attack of hydroxide at the phosphate diester of $10^{-15 \pm 0.5}$ M^{-1} s^{-1}. (*i.e.* half life at pH 14 is ~20 million years!).

If base catalysis is the dominant reaction at pH 7,[12] then the rate of hydrolysis of dialkyl diesters at neutral pH and ambient temperature would be ~10^{-22} s^{-1}. This means that *staphyloccocal nuclease*, which has a turnover number of 95 s^{-1},[13] is

 DOI: 10.1039/b103317b

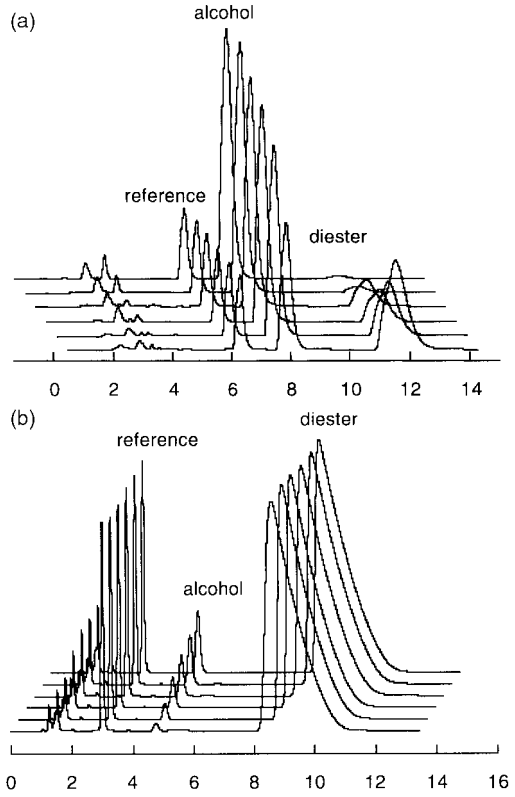

Fig. 1 HPLC traces for the hydrolysis of **1** in 1 M KOH. Upper traces at 240 °C (250 mm column); lower traces at 180 °C (150 mm column). Detection is at 236 nm and retention times are in minutes.

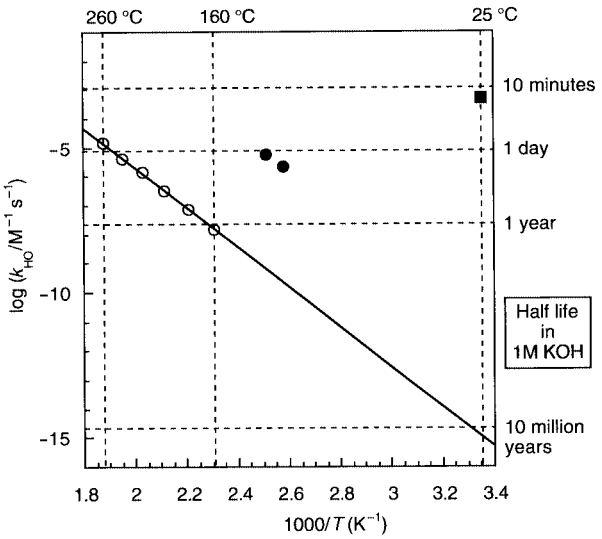

Fig. 2 Arrhenius plot of the second order rate constant for the hydrolysis of **1** (open circles) by hydroxide. The filled circles are the second order rate constant for hydroxide attack on dimethyl phosphate at 125 and 115 °C, and the filled squares for attack on ethylene phosphate at 25 °C.[5]

accelerating the rate of reaction (of the bound diester) by some 23 orders of magnitude. This data also means that the enhanced reactivity of ethylene phosphate is significantly greater than previously estimated. Constraining the ester groups in a 5 membered ring raises the rate constant for attack by hydroxide to 5×10^{-4} M^{-1} s^{-1} at 25 °C.[3] Our data shows that this represents about 10^{11} fold rate enhancement compared to the acyclic compound, 1000 fold more than previously estimated[5] suggesting that rationalisations of this observation will require further study.

Finally, the previously reported rates of reaction of dimethyl phosphate with hydroxide[3] are about 10 000 fold faster than predicted by extrapolating our data (Fig. 2), and so are unlikely to have any significant contribution from pathway B. Approximating the steric effect of the 5′ position of DNA to an isobutyl substituent (which retards S_N2 attack at carbon by an oxyanion in a protic solvent by about 100 fold compared to a methyl substituent[9a]) means that DNA hydrolysis through hydroxide attack at this carbon may be faster than attack at phosphorus. Apparently, biological catalysts have evolved to accelerate attack at phosphorus, rather than the lower energy reaction in solution which would be more energetically efficient.

In conclusion, we have measured the rate of hydroxide attack at the phosphorus of a dialkyl phosphate diester, and found it to be far slower than previously estimated. Consequently, nucleases are considerably more proficient than previously appreciated and the target for making useful artificial nucleases is even more challenging than has previously been appreciated. To be able to artificially manipulate DNA in the same way, catalysts will have to be developed which provide a rate acceleration of about 18 orders of magnitude to reduce the half life to useful levels.

We thank Professor R. Wolfenden for helpful discussion in the course of this work, S. Thorpe for obtaining LC-MS data, the Royal Society and Nuffield Foundation for financial support, and the EPSRC for a studentship to P. W.

Notes and references

† Diester **1**: δ_H (250 MHz, D_2O) 0.85 (12H, s, CH_3), 2.60 (4H, s, CH_2Ar), 3.45 (4H, d, *J* 4.1, CH_2O), 7.25 (4H, d, *J* 8.2, ArH), 7.75 (4H, d, *J* 8.2, ArH); δ_P (101 MHz, D_2O) 1.69; MS(ES$^-$), 477 (M − H$^+$); **1**·0.5H_2O Anal. Calcd. for $C_{24}H_{32}O_{8.5}P$: C, 59.13; H, 6.62. Found: C, 59.26; H, 6.80. Alcohol: δ_H (250 MHz, $CDCl_3$) 0.80 (6H, s, CH_3), 2.60 (2H, s, CH_2Ar), 3.30 (2H, s, CH_2O), 7.25 (2H, d, *J* 9.4, ArH), 7.80 (2H, d, *J* 9.4, ArH); MS(EI$^+$) Calcd. for $C_{12}H_{16}O_3$: 208.109945. Found: 208.110790.

‡ HPLC analysis: 10 μl of each aliquot was injected onto a Luna RP C-18 5 μm column (either 4.6 × 150 mm or 4.6 × 250 mm) and eluted isocratically with 60% 20 mM sodium phosphate buffer (pH 7), 40% methanol, and monitored at 236 nm. The integrated peaks were normalised against the internal reference and observed rate constants obtained either from a first order fit or by initial rate analysis.

§ The observed pseudo-first order rate constants are: in 1 M KOH, 260 °C, 1.5×10^{-5} s^{-1}; 240 °C, 4.0×10^{-6} s^{-1}; 220 °C, 1.3×10^{-6} s^{-1}; 200 °C, 3.6×10^{-7} s^{-1}; 180 °C, 7.2×10^{-8} s^{-1}; 160 °C, 1.8×10^{-8} s^{-1}. In 0.33 M KOH, 260 °C, 3.9×10^{-6} s^{-1}; 240 °C, 1.2×10^{-6} s^{-1}; 200 °C, 8.4×10^{-8} s^{-1}. These data were averaged to obtain the second order rate constants plotted in Fig. 2.

1 F. H. Westheimer, *Science*, 1987, **235**, 1173.
2 T. Lindahl, *Nature*, 1993, **362**, 709.
3 J. Kumamoto, J. R. Cox, Jr. and F. H. Westheimer, *J. Am. Chem. Soc.*,1956, **78**, 4858.
4 C. A. Bunton, M. M. Mhala, K. G. Oldham and C. A. Vernon, *J. Chem. Soc.*, 1960, 3293.
5 P. C. Haake and F. H. Westheimer, *J. Am. Chem. Soc.*, 1961, **83**, 1102.
6 J. P. Guthrie, *J. Am. Chem. Soc.*, 1977, **99**, 3991.
7 A. Radzicka and R. Wolfenden, *Science*, 1995, **267**, 90.
8 R. Wolfenden, C. Ridgeway and G. Young, *J. Am. Chem. Soc.*, 1998, **120**, 833.
9 (*a*) M. Charton, *J. Am. Chem. Soc.*, 1975, **97**, 3694; (*b*) M. Charton and B. I. Charton, *J. Org. Chem.*, 1978, **43**, 2383.
10 A. C. Hengge and W. W. Cleland, *J. Org. Chem.*, 1991, **56**, 1972.
11 N. H. Williams, W. Cheung and J. Chin, *J. Am. Chem. Soc.*, 1998, **120**, 8079.
12 For diaryl phosphate hydrolysis the pH rate profile between 2 and 10 is made up solely of acid and base terms for leaving groups with pK_a > 8; at pH 7 base catalysis dominates (A. J. Kirby and M. Younas, *J. Chem. Soc. B*, 1970, 510). For intramolecular transesterification in RNA dimers with alkoxy leaving groups, base catalysis also dominates at pH 7 (P. Järvinen, M. Oivanen and H. Lönnberg, *J. Org. Chem.*, 1991, **56**, 5396). Interestingly, extrapolating the pH independent reaction observed for good leaving groups to a leaving group pK_a of 15 predicts a spontaneous reaction of ~10^{-21} s^{-1}, in rather good agreement with our extrapolation for a base catalysed reaction.
13 E. H. Serpersu, D. Shortle and A. S. Mildvan, *Biochemistry*, 1986, **25**, 68.

CHEMCOMM
Communication
www.rsc.org/chemcomm

Chiral 2,6-lutidinyl-biscarbene complexes of palladium†

Arran A. D. Tulloch,[a] Andreas A. Danopoulos,*[a] Graham J. Tizzard,[a] Simon J. Coles,[a] Michael B. Hursthouse,[a] Robyn S. Hay-Motherwell[b] and William B. Motherwell[b]

[a] *Department of Chemistry, University of Southampton, Highfield, Southampton, UK SO17 1BJ. E-mail: ad1@soton.ac.uk*
[b] *Christopher Ingold Laboratories, University College London, 20 Gordon Str., London, UK WC1H 0AJ*

Received (in Cambridge, UK) 12th April 2001, Accepted 29th May 2001
First published as an Advance Article on the web 21st June 2001

Chiral complexes of palladium, 1, with the new tridentate 'pincer' ligand 2,6-lutidinyl-biscarbene (C^N^C), have been prepared; in the solid state they exhibit helical C_2 symmetrical structures which are persistent in solution at least up to 80 °C; the chiral nature of 1 has been established by NMR methods using Pirkle's acid as a chiral discriminating agent; racemic mixtures of 1 are highly active catalysts in Heck coupling reactions.

The use of *N*-heterocyclic carbene transition metal complexes in catalysis is an area of intense current research activity.[1] This has been stimulated by a number of attractive ligand characteristics, including electronic similarity to the alkyl phosphines,[2] formation of strong and inert metal–ligand bonds and ease of electronic and steric tuning. Compared with the electronically similar phosphine ligands, carbenes appear not to dissociate easily from the metal centre and are less prone to metal assisted decomposition leading to catalyst deactivation. Considerable effort has also been directed to the development of new chiral ligands due to the growing importance of transition metal catalysed asymmetric synthesis.[3] Diphosphines, especially those with C_2 symmetry, have proven to be especially useful, resulting in good enantioselective control of the catalytic reactions, although the potential of chiral auxilliary ligands which bind to the metal through nitrogen and carbon atoms is now being evaluated.[4] In sharp contrast, chiral carbene complexes are very rare and have only recently attracted interest, with current examples of ligands including (i) chiral imidazolin-2-ylidenes and imidazol-2-ylidenes [stereogenic centre(s) on the alkyl substituents of the rings],[5] (ii) chiral imidazolin-2-ylidenes (stereogenic centres integrated in the imidazoline ring),[6] (iii) *N*-functionalised imidazol-2-ylidenes and precursors thereof (stereogenic centres on the functional group)[7] and (iv) binaphthyl bridged dicarbenes (stereogenic axis of the binaphthyl framework).[8] Herein we communicate our results on the isolation and full characterisation of the first racemic carbene complexes of palladium as a result of two carbene moieties being linked by a lutidine backbone, together with a preliminary study of their catalytic activity.

As a logical extension of our own work and that of McGuiness and Cavell on the use of pyridine- and picoline-functionalised carbene complexes of palladium[9] we decided to explore the use of tridentate 'pincer' architectures bearing carbene ligands. Toward this end the complexes [(C^N^C)PdCl]X [C^N^C = α,α′-bis-(3-arylimidazol-2-ylidene)-2,6-picoline, **1a**: Ar = 2,6-$Pr^i_2C_6H_3$, **1b**: Ar = mes (2,4,6-$Me_3C_6H_2$); X = Cl^-, $AgCl_2^-$] were prepared by interaction of the analogous silver complexes[10] with (COD)$PdCl_2$ in dichloromethane.

Complexes **1a**, **b** are air stable, colourless high-melting solids (ESI).† The structure of **1a** was determined by X-ray crystallography, and the cationic component is shown in Fig 1.‡ The 'pincer' ligand is coordinated to the square planar palladium centre with the carbene ends disposed *trans* to each other and the lutidine nitrogen *trans* to the chloride. The observed geometrical parameters are similar to those previously reported for analogous complexes.[9] However, as a direct result of the combination of the puckering of the two six-membered chelate rings and the bulk of the aromatic substituents around the carbene moieties a beautiful helical structure is generated with a C_2 proper axis coinciding with the N–Pd–Cl vector. The conformation of the cation is best described by the orientation of the ligand ring systems with respect to each other and to the palladium square plane. Thus, the lutidine ring forms a dihedral angle of 40.04(10)° with the square plane, the N1 and N5 carbene rings form dihedral angles of 42.50(13) and −39.70(11)°, respectively, with the square plane and the carbene rings form dihedrals of 81.93(17) and –79.85(14)°, respectively, with the C1 and C26 Ar moieties. As a consequence of the centrosymmetric nature of the space group ($P2_1/c$), the second enantiomer is generated through the inversion centre leading to a racemic mixture in the crystal lattice.

It is interesting that 'pincer' complexes [(CNC)PdCl]X [CNC = 2,6-bis(3-arylimidazol-2-ylidene)pyridine; **2a**: Ar = 2,6-$Pr^i_2C_6H_3$, **2b**: Ar = mes; X = Cl^-, $AgCl_2^-$] have also been obtained following similar synthetic methods (ESI).† The structure of **2a** was also determined by X-ray crystallography and is shown in Fig.2.‡ The coordination sphere of the metal is

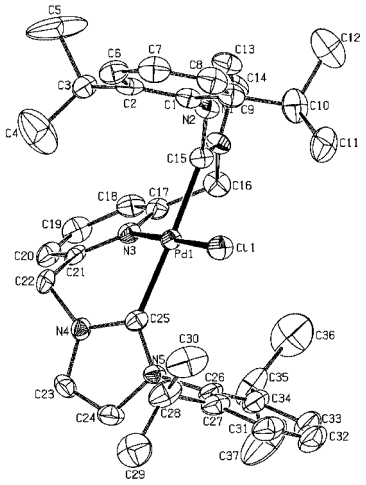

Fig. 1 Molecular structure of the cation in **1a** (view along the N–Pd–Cl vector). Selected bond lengths (Å) and angles (°): Pd1–C15 2.025(4), Pd1–C25 2.029(4), Pd1–N3 2.074(3); N3–Pd1–C15 87.41(14), N3–Pd1–C25 87.67(14).

† Electronic supplementary information (ESI) available: spectroscopic data for **1a**, **1b**, **2a** and **2b**; Table S1: representative results of the Heck reaction. See http://www.rsc.org/suppdata/cc/b1/b103330c/

 DOI: 10.1039/b103330c

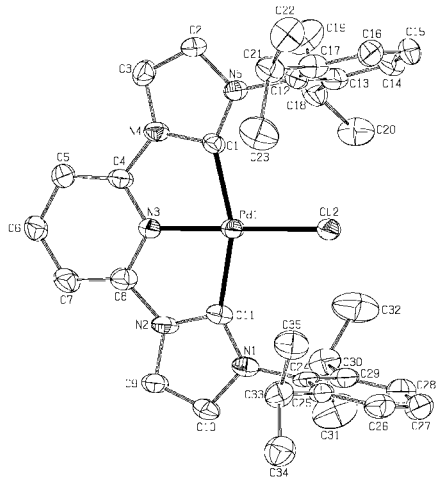

Fig. 2 Molecular structure of the cation in **2a**. Selected bond lengths (Å) and angles (°): Pd1–N3 1.977(16), Pd1–C13 2.02(2), Pd1–C21 2.03(2); N3–Pd1–C13 79.1(8), N3–Pd1–C21 79.0(8).

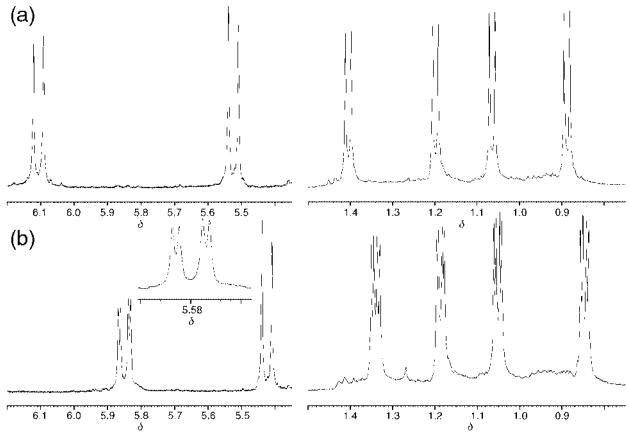

Fig. 3 The isopropyl methyl- and bridging methylene-regions of the ^{1}H NMR spectrum of **1a** before (a) and after (b) the addition of Pirkle's acid.

similar to **1a**. However, the whole molecule is virtually planar, with the Ar groups twisted 76.68(11) and 89.63(22)° out of the plane for rings C12 and C24, respectively. All other geometrical data are very similar to **1a**. It is instructive to view the generation of **1** by desymmetrisation of **2** through a twist deformation around the C_2 axis. The direction of the twist determines the chirality generated. A compound related to **2a** with methyl substituted carbene functionalities has also recently been reported.[11]

The structures of **1a** and **2a** observed in the solid state are persistent in solution. The ^{1}H NMR (CD_2Cl_2) spectrum of **1a** (ESI†) shows four anisochronous doublets which can be assigned to the isopropyl methyl protons. Furthermore, the methylene-bridge protons appear as an AB pattern in the range δ5.5–6.3 [Fig. 3(a)]. In order to demonstrate the chiral nature of **1a** in solution Pirkle's acid. [TFAE, *S*-(+)-2,2,2-trifluoro-1-(9-anthryl)ethanol] was used as a chiral discriminating agent.[12] The isopropyl methyl groups and the bridging methylene regions of the spectrum obtained after addition of 3.4 equivalents of TFAE in CD_2Cl_2 solution of **1a** are shown in Fig 3(b). The doubling of the four anisochronous doublets and one of the doublets due to the methylene linkers originates from the strong interaction of the chiral discriminating agent with one of the two enantiomers of **1a** (degree of non-equivalence $\Delta\delta$ *ca.* 0.2 ppm). The conformation of **1a** is rigid at least up to 80 °C as evidenced by variable temperature ^{1}H NMR spectroscopy (C_6D_5Cl). This supports the contention that a high activation barrier exists for enantiomer interconversion, thus leading to the realistic possibility of resolving the racemic mixture by chemical or chromatographic means.

In contrast to **1a,** the spectrum of the planar **2a** contains only two diastereotopic isopropyl methyl protons and remains also unchanged over the temperature range studied.

Preliminary data show that **1** and **2** are active catalysts in Heck coupling reactions (Table S1, ESI†).[9] The catalysts show excellent long term stability at high temperatures. Furthermore, the activity is sensitive to the steric congestion at the reactive site (**1b** is more active than **1a**). It is interesting that aryl chlorides can also be used as substrates. The mechanism and the nature of the active species in these reactions is far from clear. Heck reaction catalysed by 'pincer' phosphine ligated palladium complexes have been reported.[13]

Isolation of the enantiomerically pure complexes and extension of this methodology to other transition metals and their catalytic reactions are currently under way.

We thank Dr J. E. Anderson for a helpful discussion, and acknowledge Mr S. Winston, Mr J. Gonzalez-Outeirino and Mrs J. M. Street for assistance in solving the structure of **1a** and VT NMR spectroscopy, respectively.

Notes and references

‡ *Crystal data*: for **1a**: crystals were obtained by layering a CH_2Cl_2 solution of **1a** with light petroleum (bp = 40–60 °C); $C_{40}H_{45}AgCl_9N_5Pd$, M = 1129.13, monoclinic, space group $P2_1/c$, a = 11.559(2), b = 42.043(8), c = 10.631(2) Å, β = 112.51(3)°, U = 4772.6(16) Å^3, T = 150(2) K, Z = 4, μ(Mo-Kα) = 1.325 mm^{-1}, 28393 reflections collected, 10436 unique reflections, R_{int} = 0.0867), Final R indices: wR_2 = 0.1185 and R_1 = 0.0514 [$F^2 > 2\sigma(F^2)$] and 0.1340 and 0.0897 for all data.

For **2a**: crystals were obtained by layering a CH_2Cl_2 solution of **2a** with light petroleum (bp = 40–60 °C), $C_{36}H_{41}Cl_{4.5}N_5Pd$, M = 809.66, triclinic, space group $P\bar{1}$, a = 8.4782(4), b = 11.8790(6), c = 20.8146(11) Å, α = 75.077(3), β = 83.364(3), γ = 71.322°, U = 1917.65 (17) Å^3, T = 150(2) K, Z = 2, μ(Mo-Kα) = 0.829 mm^{-1}, 14147 reflections collected, 6524 unique reflections, R_{int} = 0.0839), Final R indices: wR_2 = 0.2213 and R_1 = 0.0838 [$F^2 > 2\sigma(F^2)$] and 0.2562 and 0.1316 for all data.

The refinement of both structures was hampered by severe disorder of dichloromethane solvent molecules, and, not unrelated, limited quality data from poor crystals, especially for compound **2a**. At the present stage, the modelling of the disorder is not complete, but the definition of the cation is reliable in each case, with reasonable positional esds and good displacement parameters for all component atoms. CCDC reference numbers 162457 and 162458.

See http://www.rsc.org/suppdata/cc/b1/b103330c/ for crystallographic data in CIF or other electronic format.

1 For recent reviews see: D. Bourisou, O. Guerret, F. P. Gabbai and G. Bertrand, *Chem. Rev.*, 2000, **100**, 39; W. A. Herrmann and C. Kocher, *Angew. Chem., Int. Ed. Engl.*, 1997, **36**, 2162.
2 J. C. Green, R. G. Scurr, P. L. Arnold and F. G. N. Cloke, *Chem. Commun.*, 1997, 1963.
3 *Catalytic Asymmetric Synthesis*, ed. I. Ojima, Wiley-VCH, 2nd edn., 2000.
4 F. Fache, E. Schulz, M. L. Tommasino and M. Lemaire, *Chem. Rev.*, 2000, **100**, 2159; A. H. Hoveida and J. P. Moren, in *Metallocenes*, ed. A. Togni and R. L. Halterman, Wiley-VCH, Weinheim, 1998.
5 A. W. Coleman, P. B. Hitchcock, M. F. Lappert, R. K. Maskell and J. H. Muller, *J. Organomet. Chem.*, 1985, **296**, 173; W. A. Herrmann, L. J. Goosen, C. Koecher and G. R. J. Artus, *Angew. Chem., Int. Ed. Engl.*, 1996, **35**, 2805.
6 M. Scholl, S. Ding, C. W. Lee and R. H. Grubbs, *Org. Lett.*, 1999, **1**, 953.
7 W. A. Herrmann, L. J. Goosen and M. Spiegler, *Organometallics*, 1998, **17**, 2162.
8 D. S. Clyne, J. Jin, E. Genest, J. C. Gallucci and T. V. RajanBabu, *Org. Lett.*, 2000, **2**, 1125.
9 A. A. D. Tulloch, A. A. Danopoulos, R. P. Tooze, S. M. Cafferkey S. Kleinhenz and M. B. Hursthouse, *Chem. Commun.*, 2000, 1247; D. S. McGuiness and K. J. Cavell, *Organometallics*, 2000, **19**, 741.
10 A. A. D. Tulloch, A. A. Danopoulos, S. Winston, S. Kleinhenz and G. Eastham, *J. Chem. Soc., Dalton Trans.*, 2000, 4499.
11 E. Peris, J. A. Loch, J. Mata and R. H. Crabtree, *Chem. Commun.*, 2001, 201.
12 W. H. Pirkle and M. S. Hoekstra, *J. Am. Chem. Soc.*, 1976, **98**, 1832.
13 M. Ohff, A. Ohff, M. E. van der Boom and D. Milstein, *J. Am. Chem. Soc.*, 1997, **119**, 11 687.

CHEMCOMM
Communication
www.rsc.org/chemcomm

Equilibrium between neutral hexacoordinate silicon complexes and ionic pentacoordinate siliconium salts through fast dissociation–recombination of the Si–Cl bond

Vijeyakumar Kingston, Boris Gostevskii, Inna Kalikhman* and Daniel Kost*

Department of Chemistry, Ben-Gurion University, Beer-Sheva 84105, Israel.
E-mail: kostd@bgumail.bgu.ac.il

Received (in Cambridge, UK) 14th March 2001, Accepted 25th May 2001
First published as an Advance Article on the web 21st June 2001

Equilibrium between neutral hexacoordinate silicon complexes and ionic siliconium chlorides, which is highly temperature, solvent, counterion, ligand and substituent dependent, was observed by low temperature ^{29}Si NMR and confirmed by crystal analysis.

Numerous well established neutral octahedral silicon complexes[1] are now shown to undergo unusual ionic (Si–Cl) dissociation in suitable solvents upon cooling, and consist of equilibrium mixtures with pentacoordinate siliconium chlorides. The only reported similar equilibria are between neutral pentacoordinate and ionic tetra-[2] or pentacoordinate complexes.[3,4] This appears to be the first report of a dissociation–recombination of the Si–Cl bond in hexacoordinate silicon compounds. Substantial temperature, solvent, substituent and counterion effects on the neutral-hexacoordinate/ionic-pentacoordinate population ratio are found.

We have recently reported the unexpected spontaneous formation of ionic pentacoordinate siliconium complexes (**1**), stabilized by two O→Si dative bonds,[5] where neutral hexacoordinate complexes were expected, based on the chemistry of the isomeric N→Si analogs (**2**) (Scheme 1).[1]

In search for dissociation of **2**, to form siliconium complexes analogous to **1**, the ^{29}Si NMR spectra of **2a** in CD_2Cl_2 were measured at low temperature. Line broadening over a large temperature range was observed, followed by the emergence of two signals, at −73.0 and −135.6 ppm, below 200 K, assigned to **5a** and **2a**, respectively (Fig. 1).† Thus, a reversible equilibrium reaction between neutral hexacoordinate complexes (**2a**–**d**) to ionic pentacoordinate complexes (**5a**–**d**) is demonstrated (Scheme 2).

The equilibrium constant K = [**5a**]/[**2a**] changes quite dramatically with temperature, as is shown by the ^{29}Si NMR spectra below 190 K, when *both* signals are narrow (Table 1, Fig. 1). K values above the coalescence temperature were assessed by the temperature dependence of the weighted-average ^{29}Si chemical shift, and are listed in Table 1. Interestingly, the K values cross over from $K < 1$ to $K > 1$ upon a decrease in temperature, *i.e.* at higher temperatures **2a** is predominant, and at lower temperatures **5a** predominates. The K values obtained directly and from the weighted averages (below and above T_c) were used to calculate $\Delta H°$ and $\Delta S°$ (Table 1).

A similar measurement of the temperature dependence of δ^{29}Si of **2b** showed, likewise, line broadening and splitting of the signal, at the slow exchange limit temperature (180 K), to two signals characteristic of hexa- and pentacoordinate silicon complexes (Table 1). However, in sharp contrast with **2a**, the population ratio K = [**5b**]/[**2b**] is barely temperature dependent over the range 180–300 K. It follows that by changing the remote substituent (R) alone, a vast change in equilibrium constant and in its temperature dependence is generated.

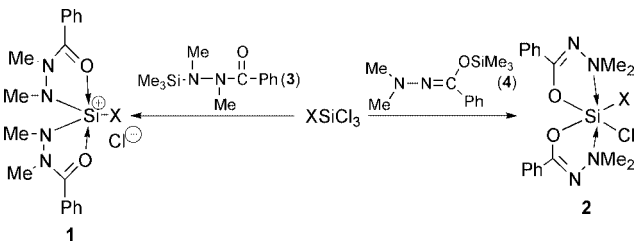

Scheme 1

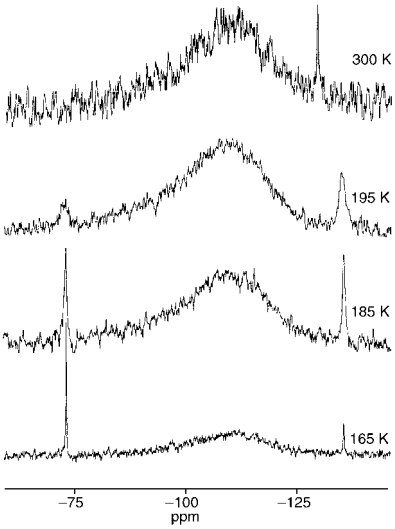

Fig. 1 ^{29}Si NMR spectra (99.325 MHz) of **2a**⇄**5a** in CD_2Cl_2 solution at various temperatures.

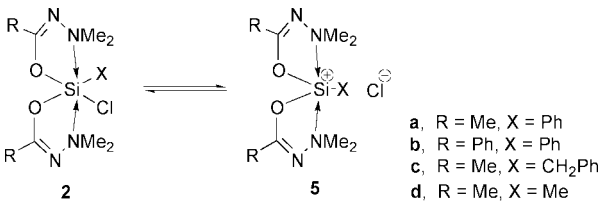

Scheme 2

An even more dramatic manifestation of this effect is found in the equilibrium K = [**5c**]/[**2c**]: K changes from 1 : 25 at 300 K to 30 : 1 at 165 K, *i.e.* from an essentially all hexacoordinate to an essentially all pentacoordinate species (Table 1).

In **2d** the exchange rate is too fast to permit full splitting of the broad signal and evaluation of K down to 165 K. However, the huge temperature dependence of K is evident by the continuous change in δ^{29}Si, from −123.9 at 300 K, to −66.5(br) at 165 K. Like in **2c**, this change indicates an essentially complete turnover from a hexacoordinate to a pentacoordinate complex upon cooling.

The wide temperature ranges over which line broadening took place in the equilibria **2**⇄**5** provided approximate barrier heights, which are summarized in Table 1 It appears that while the equilibrium constant and its temperature dependence are

 DOI: 10.1039/b102427m

Table 1 ^{29}Si Chemical shifts and thermodynamic and activation parameters for the mixtures **2**⇌**5** in CD_2Cl_2 solution at selected temperatures

Comp.	^{29}Si Chemical shift (ppm)			Equilibrium constant K = [**5**]/[**2**]			$\Delta H°^b$/ kcal mol^{-1}	$\Delta S°^b$/cal mol^{-1} K^{-1}	T_c (±5)/K^a	ΔG_{T_c}* (± 0.5)^a/ kcal mol^{-1}
	300 K	253 K	165 K	300 K	180 K	165 K				
2a⇌**5a**	−131.3	−128.9	−73.0; −135.6	0.08	1.38	4.00	−2.8	−15.0	215	8.4
2b⇌**5b**	−133.7	−132.8	−73.2; −137.0	0.05	0.13		−0.8	−8.6	215	8.4
2c⇌**5c**	−125.4	−118.1	−66.0^c	0.04		30.0	−3.9	−17.5	195	7.5
2d⇌**5d**	−123.9	−120.7	−66.5 br^d						170	6.5

^{a} The large chemical shift difference causes line broadening over a large temperature range, preventing accurate barrier determination. ^{b} Obtained from plots of ln$K$ *vs.* T^{-1}. $R > 0.99$. ^{c} At this temperature only the major component can be observed. ^{d} Barrier too low to permit resolution of the components.

affected primarily by the remote substituent R, the exchange rate constants strongly depend on the ligand X.

The remarkable counter-intuitive temperature dependence of the equilibria (*i.e.* dissociation upon cooling) may result from increased solvent organization around the ions. Alternatively, the N→Si coordination may strengthen upon cooling, in agreement with some observations in pentacoordinate complexes,[1e,2a,b] driving the chloro ligand away as a chloride anion.

Solvent and counterion effects shift the equilibrium: when the apolar toluene-d_8 was used as solvent instead of CD_2Cl_2, the equilibrium shifted toward the hexacoordinate side and only **2** could be observed.‡ When the chloro ligand in **2** was replaced by triflate (OTf), using trimethylsilyl triflate (TMSOTf),[3,4,6] only the pentacoordinate **6a**–**d** were observed (Scheme 3).

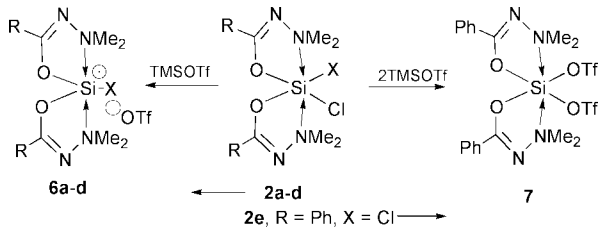

Scheme 3

The crystal structure of **6a** (Fig. 2a) features a well separated triflate anion and a distorted trigonal bipyramid geometry, confirming the assigned pentacoordinate siliconium complex structure.§

The pentacoordination of **6** in solution is confirmed by the large downfield changes in ^{29}Si chemical shifts (**6a**, −73.2; **6b**, −72.3; **6c**, −65.3 and **6d**, −61.7 ppm) relative to the parent hexacoordinate **2**. Moreover, these shifts correspond almost exactly to those found for **5a**–**d** at 165 K (Table 1), also confirming the structural assignments of the latter.

A notable exception from the behaviour of **2a**–**d** was found in the low temperature ^{29}Si NMR spectra of **2e** (Scheme 3). Temperature independent ^{29}Si chemical shift, and the absence of exchange phenomena upon cooling, indicated that in this case no ionization took place. Even replacement of the Cl ligands by OTf, which drove the **2**⇌**5** equilibrium completely to the ionic side in **2a**–**d**, failed for **2e** and resulted in the covalent **7**, which was characterized by its crystal structure (Fig. 2b).§ This different behaviour of **2e** relative to **2a**–**d** may be accounted for by the greater electron withdrawing power of the chloro ligand, causing a greater electron defficency at silicon and hence stabilizing the hexacoordinate relative to the pentacoordinate complex.

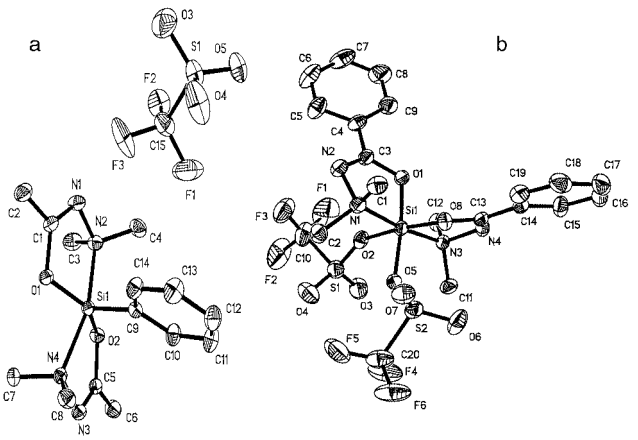

Fig. 2 Crystal structures of **6a** (a) and **7** (b) at 50% probability level. Hydrogen atoms have been omitted for clarity.

We thank Dr Arkady Ellern for the crystallographic analyses. Financial support from the Israel Science Foundation and the German Israeli Foundation (GIF) is gratefully acknowledged.

Notes and references

† These chemical shifts are highly characteristic, respectively, of penta- and hexacoordination in silicon chelates.[1e] The ^{1}H and ^{13}C NMR spectra featured only line broadening, but no splitting.

‡ The use of toluene-d_8 as solvent prevented earlier detection of the dissociation reported here.[1b]

§ *Crystal data* for **6a**: $C_{15}H_{23}F_3N_4O_5SSi$, M = 456.52, triclinic, space group $P\bar{1}$, a = 8.4678(15), b = 11.032(2), c = 11.517(2) Å, V = 1033.7(3) Å^3, Z = 2, μ(Mo-Kα) = 0.118 mm^{-1}, 12650 reflections measured, 5128 unique (R_{int} = 0.0241) which were all used in calculations. Final $R1$ = 0.0365 and wR_2 = 0.1016 (all data). For **7**: $C_{20}H_{22}F_6N_4O_8S_2Si$, M = 652.63, monoclinic, space group $P2_1/n$, a = 16.466(5), b = 8.193(3), c = 20.861(7) Å, V = 2748.3(15) Å^3, Z = 4, μ(Mo-Kα) = 0.330 mm^{-1}, 26602 reflections measured, 3920 unique (R_{int} = 0.0500) which were all used in calculations. Final R_1 = 0.0506 and wR_2 = 0.1258 (all data). Data were measured at 173(2) K on a Bruker SMART CCD 1000 diffractometer [λ(Mo-Kα) = 0.711069 Å, graphite monochromator, a scan width of 0.3° in ω and exposure time of 10 s frame^{-1}, detector–crystal distance = 4.95 cm]. Bruker SHELX software was used. CCDC 157088 (**6a**) and 157089 (**7**). See http://www.rsc.org/suppdata/cc/b1/b102427m/ for crystallographic data in CIF or other electronic format.

1 (*a*) A. O. Mozzhukhin, M. Yu. Antipin, Yu. T. Struchkov, B. A. Gostevskii, I. D. Kalikhman, V. A. Pestunovich and M. G. Voronkov, *Metalloorg. Khim.*, 1992, **5**, 658; *Chem. Abstr.*, 1992, **117**, 234095w; (*b*) D. Kost, I. Kalikhman and M. Raban, *J. Am. Chem. Soc.*, 1995, **117**, 11 512; (*c*) I. Kalikhman, S. Krivonos, D. Stalke, T. Kottke and D. Kost, *Organometallics*, 1997, **16**, 3255; (*d*) D. Kost, I. Kalikhman, S. Krivonos, D. Stalke and T. Kottke, *J. Am. Chem. Soc.*, 1998, **120**, 4209; (*e*) D. Kost and I. Kalikhman, in *The Chemistry of Organic Silicon Comounds, Vol 2*, ed. Z. Rappoport and Y. Apeloig, Wiley, Chichester, 1998, pp. 1339–1445.

2 (*a*) D. Kummer, S. C. Chaudhry, J. Seifert, B. Deppisch and G. Mattern, *J. Organomet. Chem.*, 1990, **382**, 345; (*b*) D. Kummer and S. H. Abdel Halim, *Z. Anorg. Allg. Chem.*, 1996, **622**, 57; (*c*) A. R. Bassindale and M. Borbaruah, *J. Chem. Soc., Chem. Commun.*, 1991, 1499.

3 (*a*) M. Chauhan, C. Chuit, R. J. P. Corriu and C. Reyé, *Tetrahedron Lett.*, 1996, **37**, 845; (*b*) M. Chauhan, C. Chuit, R. J. P. Corriu, A. Mehdi and C. Reyé, *Organometallics*, 1996, **15**, 4326.

4 (*a*) J. Belzner, D. Schär, B. O. Kneisel and R. Herbst-Irmer, *Organometallics*, 1995, **14**, 1840; (*b*) D. Schär and J. Belzner, in *Organosilicon Chemistry III*, ed. N. Auner and J. Weis, VCH, Weinheim, 1997, p. 429.

5 I. Kalikhman, S. Krivonos, L. Lameyer, D. Stalke and D. Kost, *Organometallics*, 2001, **20**, 1053.

6 U.-H. Berlekamp, P. Jutzi, A. Mix, B. Neumann, H.-G. Stammler and W. W. Schoeller, *Angew. Chem., Int. Ed.*, 1999, **38**, 2048.

CHEMCOMM Communication
www.rsc.org/chemcomm

Chemically amplified soft lithography of a low band gap polymer

Jianfei Yu and Steven Holdcroft*

Department of Chemistry, Simon Fraser University, Burnaby, BC, V5A 1S6, Canada. E-mail: holdcrof@sfu.ca

Received (in Cambridge, UK) 5th April 2001, Accepted 25th May 2001
First published as an Advance Article on the web 21st June 2001

A solid state, acid-catalyzed reaction leading to chemically amplified soft lithography is demonstrated with a low band gap conjugated polymer; poly({3-[11-(tetrahydropyran-2-yloxy)undecyl]thiophene-2,5-diyl}-3,4-ethylenedioxythiophene-2,5-diyl).

π-Conjugated polymers are promising materials with which to fabricate organic microelectronic and optoelectronic devices.[1–4] Due to their increasing complexity there is a growing need to deposit multi-layers of conjugated polymers in a spatially controlled fashion. Previous reports describing photolithography of conjugated polymers have been based on photocrosslinking, photoinduced doping/dedoping, photochemical structural transformation,[5] and chemically amplification.[6] Inexpensive soft photolithographic techniques[7] including microcontact printing, lift-up and micromolding have also been investigated, as have ink-jet[8] and screen printing.[9]

In this communication, a novel method for patterning conjugated polymer films is described. This technique, we term chemically amplified soft lithography, is demonstrated with a novel regioregular conjugated polymer; poly({3-[11-(tetrahydropyran-2-yloxy)undecyl]thiophene-2,5-diyl}-3,4-ethylenedioxythiophene-2,5-diyl) (**I**). 3,4-Ethylenedioxythiophene-based polymers are receiving considerable attention due to their low band-gap, high conductivity, stability and high transmittance contrast ratio between its reduced and oxidized states.[10]

Monomer {3-[11-(tetrahydropyran-2-yloxy)undecyl]thiophenediyl}-3,4-ethylenedioxythiophene and the analogous polymer, **I**, were synthesized according to Scheme 1.† Films of polymer **I** are deep purple in color exhibiting a λ_{max} of 570 nm and a band-gap of ~1.67 eV (740 nm). These values are comparable to that of poly(3,4-ethylenedioxythiophenediyl) (PEDOT).[11]

The presence of the tetrahydropyranyloxy alkyl side chain imparts solubility and reactivity.[12] Similarly to that reported for poly{3-[2-(tetrahydropyran-2-yloxy)ethyl]thiophenediyl} (PTHPET),[13] **I** undergoes a solid state acid-catalyzed reaction depicted Scheme 2. In the absence of acid, thermogravimetric analysis (TGA) (Fig. 1) shows that **I** is stable up to ~230 °C but undergoes an 18% loss in mass between 230 and 270 °C. The observed weight loss is consistent with theoretical value of 17.6% corresponding to cleavage and volatilization of the tetrahydropyranyl moiety as dihydropyran. In the presence of 5% camphorsulfonic acid (mol% based on the thienyl unit) TGA (Fig. 1) indicates that elimination of THP occurs at a much lower temperature. 5 mol% acid is responsible for complete deprotection and thus provides evidence that the reaction is acid catalyzed, *i.e.*, chemically amplified. DSC indicated that the onset of the reaction decreased from ~230 to 85 °C in the presence of acid. Reaction of the polymer was confirmed by FTIR, which showed the emergence of a broad peak at ~3400 cm^{-1} attributed to the formation of ω-hydroxy groups, and a decrease in signals at ~2900 cm^{-1} corresponding to loss of THP-methylene.

In a novel variation of chemically amplified photolithography and soft lithographic techniques, **I** was pattered by spatial deposition of acid onto the surface of a neat film (90 nm thick), followed by heating and development. In this process, shown schematically in Fig. 2, an 'acidic ink' comprising 0.01 M camphorsulfonic acid in THF–hexane was transferred to the

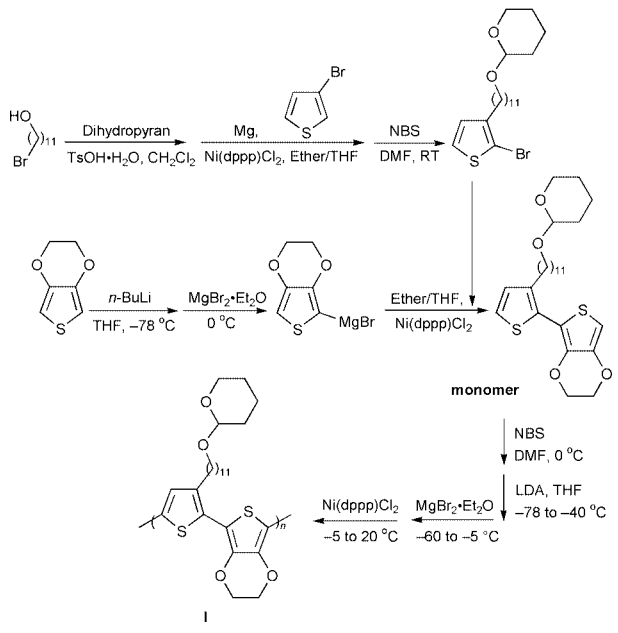

Scheme 1 Synthetic scheme for monomer and polymer.

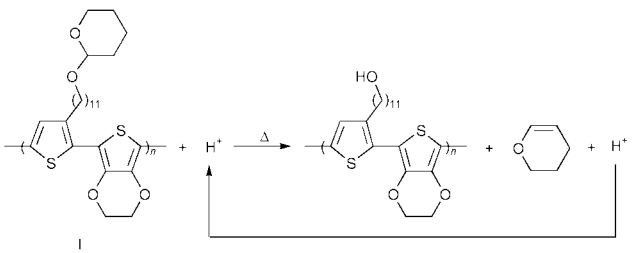

Scheme 2 Acid-catalyzed elimination of dihydropyran from **I**.

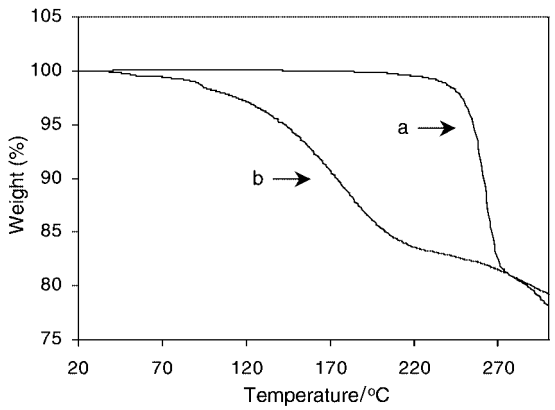

Fig. 1 TGA thermograms of **I**: (a) in the absence of acid and (b) in the presence of 5 mol% camphorsulfonic acid.

 DOI: 10.1039/b103128g

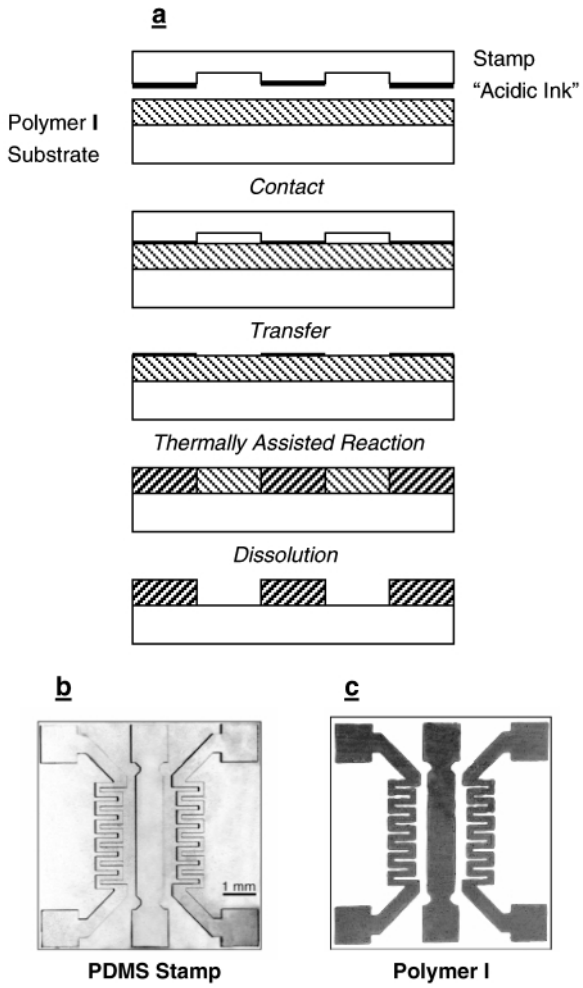

Fig. 2 (a) Scheme depicting chemically amplified soft lithographic process. Micrographs of (b) PDMS stamp and (c) conjugated polymer patterns of **I**.

top of the film by way of a custom-made polydimethylsiloxane (PDMS) rubber stamp. Heating to 130 °C for just 10 s caused elimination of THP in the regions where acid was deposited. No reaction was observed to occur prior to heating as judged by FTIR analysis. The regions reacted were rendered insoluble by virtue of the residual hydroxy group and the overall change in polarity.[6] A positive image of the stamp was obtained by developing the film in solvent (Fig. 2).

Using UV-vis and FTIR spectroscopic analysis, it was found that 2.1 μg cm^{-2} acid was typically transferred to the surface of film using the stamping procedure. The molar ratio of acid to thienyl rings is calculated to be 1 : 4 for a 90 nm thick film. The reaction is thus catalytic in acid and chemically amplified. FTIR of the imaged polymer film indicted a loss of THP and formation of –OH as described previously. UV-vis spectra of the polymeric patterns were similar to **I** indicating that the conjugated polymer backbone is left intact. Furthermore, redox doping of the film with oxidants such as $FeCl_3$ resulted in a color change from deep purple to transparent pale gray and an increase in transmittance from 46 to 91% at 570 nm (for a 50 nm thick film) indicating its potential suitability for patterned electrochromic devices. The conductivity of the doped form is 12 S cm^{-1}, on a par with poly(3-alkylthiophenediyl).

In summary, chemically amplified soft lithography is a non-photolithographic method that circumvents photochemical damage. Films are formed prior to patterning, which may allow for further control of film thickness, morphology, and adhesion over other deposition methods. Furthermore, since the patterned polymer is rendered insoluble, it is possible to deposit multiple layers of similar or dissimilar conjugated polymers. Evaluation of patterned films in field effect transistors, light emitting devices, and electrochromic devices is in progress.

We thank the Natural Sciences and Engineering Research Council of Canada for financial support and Ms Ewa Czyzewska and Mr Bill Woods for their help in the fabrication of the PDMS stamp. We also thank Bayer Corp. for the gift of 3,4-ethylenedioxythiophene (EDOT) monomer.

Notes and references

† *Analytical and spectroscopic data* of monomer {3-[11-(tetrahydropyran-2-yloxy)undecyl]thiophenediyl}-3,4-ethylenedioxythiophene and the analogous polymer **I**. Monomer: ^{1}H NMR: 7.23 (d, J = 5.2 Hz, 1H), 6.92 (d, J = 5.2 Hz, 1H), 6.36 (s, 1H), 4.57 (m, 1H), 4.24 (m, 4H), 3.92–3.82 (m, 1H), 3.73 (m, 1H), 3.54–3.44 (m, 1H), 3.38 (m, 1H), 2.67 (t, J = 7.9 Hz, 2H), 1.83–1.21 (m, 24H). Elemental analysis: Calcd. for $C_{26}H_{38}S_2O_4$: C 65.21, H 8.00. Found: C 64.97, H 7.92. Polymer **I**: ^{1}H NMR: 7.05 (s), 4.56 (s), 4.38–4.32 (m), 3.92–3.35 (m), 2.73 (s), 1.83–1.27 (m). Mw = 4000 g mol^{-1}. Elemental analysis: Calcd. for $H(C_{26}H_{36}S_2O_4)_nBr$: C 63.97, H 7.46. Found: C 65.15, H 7.42.

1 H. Sirringhaus, N. Tessler and R. H. Friend, *Science*, 1998, **280**, 1741.
2 Z. Bao, A. Dodabalapur and A. J. Lovinger, *Appl. Phys. Lett.*, 1996, **69**, 4108.
3 A. R. Brown, D. M. Deleeuw, E. E. Havinga and A. Pomp, *Synth. Met.*, 1994, **68**, 65.
4 J. H. Burroughes, D. D. C Bradley, A. R. Brown, R. N. Marks, K. MacKay, R. H. Friend, P. L. Burns and A. B. Holmes, *Nature*, 1990, **347**, 539.
5 S. Holdcroft, in *Handbook of Organic Conductive Molecules and Polymers*, ed. H. S. Nalwa, vol. 4, John Wiley & Sons, Chichester, 1997.
6 J. Yu, M. Abley, C. Yang and S. Holdcroft, *Chem. Commun.*, 1998, 1503.
7 W. S. Beh, I. T. Kim, D. in, Y. Xia and G. M. Whitesides, *Adv. Mater.*, 1999, **11**, 1038.
8 T. R. Hebner and J. C. Sturm, *Appl. Phys. Lett.*, 1998, **73**, 1775.
9 Z. Bao, Y. Feng, A. Dodabalapur and A. Lovinger, *Chem. Mater.*, 1997, **9**, 1299.
10 L. Groenendaal, F. Jonas, D. Freitag, H. Pielartzik and J. R. Reynolds, *Adv. Mater.*, 2000, **12**, 481.
11 A. Kumar and J. R. Reynolds, *Macromolecules*, 1996, **29**, 7629.
12 K. A. Murray, S. C. Moratti, D. R. Baigent, N. C. Greenham, K. Pichler, A. B. Holmes and R. H. Friend, *Synth. Met.*, 1995, **69**, 395.
13 J. Yu and S. Holdcroft, *Macromolecules*, 2000, **33**, 5073.

CHEMCOMM Communication
www.rsc.org/chemcomm

Synthesis of polyesteramides by a new palladium catalyzed carbonylation–polycondensation reaction

Shrikant M. Kulkarni, Ashutosh A. Kelkar and Raghunath V. Chaudhari*

Homogeneous Catalysis Division, National Chemical Laboratory, Pune – 411008 India. E-mail: rvc@ems.ncl.res.in

Received (in Cambridge, UK) 18th April 2001, Accepted 30th May 2001
First published as an Advance Article on the web 21st June 2001

Alternating polyesteramides are prepared by palladium catalyzed carbonylation–polycondensation reactions of aromatic diiodides and aminohydroxy compounds in the presence of an organic base.

Palladium catalyzed carbonylation–polycondensation reactions are emerging as a new versatile synthetic tool for the preparation of a number of high performance polymers such as polyamides, polyesters, polyimides, polybenzoxazoles, poly(acylhydrazides) *etc.*[1–5] The most rewarding feature of these catalytic reactions is that they allow direct use of carbon monoxide, which is one of the cheapest and most easily available monomers. Conventionally, most of the above polymers are prepared by condensation reactions employing aromatic diacids or their suitable derivatives. One of the major problems associated with conventional condensation reactions is that they use corrosive and moisture sensitive acid chlorides as raw materials. Also, such condensation methods are suitable only if the appropriate diacid is easily available. However, difficulty arises if diacids with less common substitution patterns are required. Thus, it is highly desirable to have a simple alternative synthetic procedure for the synthesis of these polymers which do not require the presence of acid functionalities on the monomer. Palladium catalyzed carbonylation–polycondensation is certainly a promising reaction, at least on the laboratory scale for the preparation of such macromolecules.

We are currently exploring the synthetic utility of transition metal catalyzed carbonylation reactions in the preparation of functional polymers. Here, we report for the first time, on the synthesis of novel alternating polyesteramides by palladium catalyzed carbonylation–polycondensation reactions of aromatic diiodides with aminohydroxy compounds. Polyesteramides contain both ester and amide functions and thus are hybrid structures of polyesters and polyamides. These polymers are of interest because of their good heat resistance and gas barrier properties.[6] Polyesteramides containing mesogenic biphenylene units would be of particular interest because of their liquid crystalline properties. Until now these polymers have been prepared by condensation of diacids or their derivatives with aminohydroxy compounds. The carbonylation route proposed here eliminates the need for diacid derivatives and provides a cleaner synthetic route.

The reaction of aromatic diiodides and aminohydroxy compounds in the presence of carbon monoxide, a catalytic amount of palladium complex and a base leads to carbonylation–polycondensation polymerization to give polyesteramides (Scheme 1).† The carbonylation reactions were carried out under comparatively mild conditions (120 °C and 45 psi of CO pressure) and a variety of polyesteramide derivatives were prepared using this approach. The results are presented in Table 1. Experiments using fully aromatic substrates (Table 1, entries 1 and 5) gave products which were insoluble in common solvents while those obtained from flexible units were soluble in *N*-methylpyrrolidone (NMP). A typical molecular weight of the THF soluble fraction of polyesteramide (Table 1, entry 2) as determined from GPC analysis was 5000 (polystyrene standard). All polymers exhibited distinct and characteristic IR frequencies corresponding to ester carbonyl (around 1720 cm^{-1}) and amide carbonyl functional groups (around 3340 and 1640 cm^{-1}). Thermogravimetric analysis (TGA) indicated that all polymers were stable in air up to at least 350 °C. A typical proton NMR spectrum of the polyesteramide (Table 1, entry 2) shown in Fig. 1 is in accordance with the earlier literature report on similar polymers.[7] The spectrum indicates the absence of any ether or amine linkages, at least in detectable amounts, (arising because of competing *N* and/or *O*-arylation reactions) and confirms the structural homogeneity of the polyesteramide produced by the catalytic carbonylation route.

It was observed that no polyesteramide could be formed in the absence of a base. The organic base employed served as a scavanger for the HI released during the reaction course. Sterically hindered tertiary amines like 1,8-diazabicyclo-[5.4.0]undec-7-ene (DBU) were particularly effective.

The effect of solvent on the carbonylation–polycondensation was investigated and results are presented in Table 2. It was observed that the highest yield (85%) of polyesteramide was obtained in chlorobenzene as solvent while no polymer was obtained in dichloromethane. Similarly, highest inherent viscosity (0.25 dL g^{-1}) of the polyesteramide was obtained in chlorobenzene solvent.

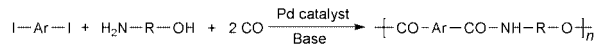

Scheme 1 Polyesteramide synthesis by carbonylation–polycondensation.

Table 1 Synthesis and properties of polyesteramides[a]

Entry	Diiodide	Aminohydroxy compound	Yield[b] (%)	$[\eta]_{inh}$[c]/dL g^{-1}	T_{10}[d]/°C	IR (ν/cm^{-1})
1	4,4′-Diiodobiphenyl	4-Aminophenol	95	—[e]	410	3354, 1727, 1653, 1531, 1266, 1194
2	4,4′-Diiodobiphenyl	3-Aminopropan-1-ol	85	0.25	320	3350, 1712, 1638, 1542, 1278, 1111
3	4,4′-Diiodobiphenyl	3-Aminobenzyl alcohol	40	0.20	385	3371, 1714, 1648, 1541, 1274, 1111
4	4,4′-Diiodobiphenyl	Ethanolamine	35	0.18	331	3321, 1718, 1639, 1541, 1273, 1108
5	1,4-Diiodobenzene	4-Aminophenol	90	—[e]	430	3351, 1729, 1653, 1509, 1268, 1196
6	1,4-Diiodobenzene	3-Aminobenzyl alcohol	25	0.17	392	3436, 1716, 1645, 1542, 1370, 1107

[a] *Reaction conditions*: diiodide: 5 mmol; aminohydroxy compound: 5 mmol; $PdCl_2$: 0.011 mmol; triphenylphosphine: 0.044 mmol; DBU: 10 mmol; chlorobenzene: 25 mL, CO pressure: 45 psi; temperature: 120 °C; agitation: 900 rpm; reaction time: 1 h. [b] Isolated yields. [c] $[\eta]_{inh}$ (intrinsic viscosity) measured at a concentration of 0.5 g dL^{-1} in NMP at 30 °C. [d] 10% weight-loss temperature (T_{10}) in air determined by TGA. [e] Insoluble in NMP.

 DOI: 10.1039/b103438n

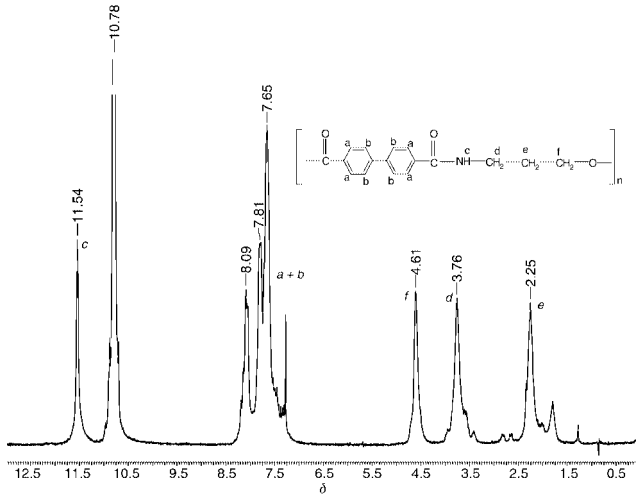

Fig. 1 Proton NMR spectra (200 MHz, trifluoroacetic acid–chloroform-d_1, 20:80) of the polyesteramide prepared by the carbonylation route (Table 1, entry 2).

The effect of temperature on polymer yield and viscosity was also investigated using chlorobenzene as a solvent and the results are given in Fig. 2. There was no significant change in the polymer yield as a function of temperature but the viscosity of the resulting polymer was influenced by the reaction temperature. The viscosity was highest at 120 °C and decreased above or below this temperature.

It is well known that Pd(0) complexes can oxidatively add aryl iodide even in the absence of added phosphine ligand because of the high reactivity of iodo derivatives.[8] However, we preferred adding phosphine ligand during these studies for efficient separation and recycling of the catalyst. The polymers were insoluble in chlorobenzene and therefore could be separated by simple filtration or decantation. The filtrate containing the soluble Pd–phosphine complex was then recycled with fresh reactants. We found that even after four recycles, there was no appreciable loss in the catalytic activity, yield and the inherent viscosity of the resulting polymer.

It was also noted that the dibromoaromatics were less effecive in these reactions and the resulting polymers were obtained in lower yields and with lower viscosities than those obtained with the corresponding diiodoaromatics.

In conclusion, we have successfully demonstrated the application of palladium catalyzed carbonylation–polycondensation reaction for the preparation of polyesteramides. Our studies indicate that a variety of polyesteramides can be prepared efficiently by this method. This approach has three important advantages. First, it eliminates the need for corrosive, moisture-sensitive acid chlorides. Second, literature reports indicate the possibility of preparing a wide variety of diiodoaromatic substrates with high regioselectivity.[9] Third, the catalyst and iodine recyclability is good. The iodide formed during the reaction can be reoxidized to iodine and used in the subsequent iodination to prepare the diiodoaromatics.[1] The only serious problem at present seems to be the fairly low degree of polymerization. We are currently exploring this reaction in more detail to optimize reaction conditions to obtain higher molecular weight polyesteramides.

S. M. K. thanks the Council of Scientific and Industrial Research, New Delhi, India for the award of a Senior Research Fellowship for this work.

Table 2 The effect of solvent on polymerization[a]

Entry	Solvent	Yield (%)	$[\eta]_{inh}$/dL g^{-1}
7	Chlorobenzene	85	0.25
8	*N*-Methylpyrollidone	20	0.11
9	*N*,*N*-Dimethylformamide	60	0.17
10	*N*,*N*-Dimethylacetamide	62	0.16
11	Toluene	43	0.15
12	Dichloromethane	0	—

[a] *Reaction conditions*: 4,4′-diiodobiphenyl: 5 mmol; 3-aminopropan-1-ol: 5 mmol; $PdCl_2$: 0.011 mmol; triphenylphosphine: 0.044 mmol; DBU: 10 mmol; solvent: 25 mL, CO pressure: 45 psi; temperature: 120 °C; agitation: 900 rpm; reaction time: 1 h.

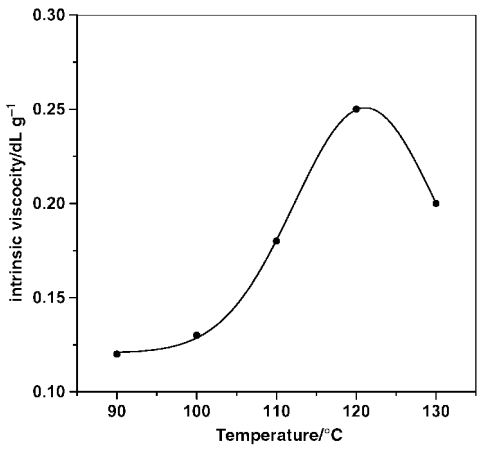

Fig. 2 Effect of temperature on intrinsic viscosity.

Notes and references

† *Experimental procedure*: polymerization reactions were carried out in a 50 mL capacity autoclave. The contents were charged into the reactor and flushed twice with nitrogen to ensure removal of air. The autoclave was then heated to the desired temperature. After the temperature had equilibrated at a set point, CO was introduced at the desired level. During the course of the reaction the CO pressure in the reactor was maintained constant by adding more CO as it was consumed. After completion of the reaction, the reactor was cooled and the excess CO vented. The polymers separated either as solids or viscous oils. The solution containing the catalyst was separated either by filtration or decantation accordingly. The crude polymer was dissolved in NMP and precipitated by methanol, filtered off and dried *in vacuo*.

1 R. J. Perry, *CHEMTECH*, 1994, **2**, 18.
2 Y. Kubota, K. Takeuchi, T. Hanoka and Y. Sugi, *Bull. Chem. Soc. Jpn.*, 1994, **67**, 563.
3 R. J. Perry, S. E. Tunney and B. D. Wilson, *Macromolecules*, 1996, **29**, 1014; R. J. Perry, B. D. Wilson, S. R. Turner and R. W. Belving, *Macromolecules*, 1995, **28**, 3509; R. J. Perry and S. R. Turner, *Makromol. Symp.*, 1991, **54/55**, 159.
4 R. J. Perry and B. D. Wilson, *Macromolecules*, 1994, **27**, 40.
5 M. Yoneyama, M. Kakimoto and Y. Imai, *Macromolecules*, 1989, **22**, 4152.
6 R. B. Barbee and L. A. Minnick, *US Pat.*, 4855397, 1989 (*Chem. Abstr.*, 1989, **112**, 78234).
7 P. J. M. Serrano, B. A. Van de Werff and R. J. Gaymans, *Polymer*, 1998, **39**, 83.
8 A. Schoenberg, I. Bartoletti and R. F. Heck, *J. Org. Chem.*, 1974, **39**, 3318.
9 M. Rule, D. W. Lane, T. H. Larkins and G. C. Tustin, *US Pat.*, 4746758, 1988; M. Rule, D. W. Lane, T. H. Larkins and G. C. Tustin, *US Pat.*, 4792641, 1988; M. Rule, D. W. Lane, T. H. Larkins and G. C. Tustin, *US Pat.*, 4792642, 1988.

CHEMCOMM
Communication
www.rsc.org/chemcomm

Liquid crystalline non-covalent supermolecules of a styrylstilbazole ligand

Jean-François Eckert, Urszula Maciejczuk, Daniel Guillon and Jean-François Nierengarten*

Institut de Physique et Chimie des Matériaux de Strasbourg, Groupe des Matériaux Organiques, Université Louis Pasteur et CNRS, 23 rue du Loess, 67037 Strasbourg Cedex, France. E-mail: niereng@ipcms.u-strasbg.fr; Fax: +33 388 10 72 46; Tel: +33 388 10 71 63

Received (in Cambridge, UK) 26th February 2001, Accepted 1st June 2001
First published as an Advance Article on the web 21st June 2001

Dimerization of a new styrylstilbazole ligand through non-covalent interactions leads to polycatenar calamitic supramolecular structures with liquid crystalline properties.

The organization of a molecular assembly into a liquid crystalline phase requires a microphase separation resulting from the amphipathic character of two chemically incompatible parts in the molecules, in general a rigid core and paraffinic chains. The self-assembly of building blocks through non-covalent bonds is also able to generate such a structural segregation, thus allowing molecular units without intrinsic mesomorphic properties to form supramolecules presenting liquid crystalline properties.[1–7] The most widely used interactions to obtain self-assembled structures with mesomorphic properties are coordination to a metal center[2–4] (metallomesogens) or hydrogen bonds.[5–7] The use of weaker interactions such as van der Waals or hydrophobic forces have been probed to a much lesser degree.[8] Here we report on the synthesis of a calamitic polycatenar non-mesogenic pyridine containing ligand, and the preparation of supramolecular mesogens by using coordination to a metal and ionic bonds, but also van der Waals forces.

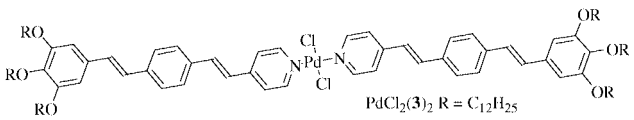

$PdCl_2(\mathbf{3})_2$ R = $C_{12}H_{25}$

The synthesis of **3** is depicted in Scheme 1. Treatment of benzaldimine **1**[7] with 4-iodotoluene under Siegrist conditions gave iodostilbene *E*-**2**. Subsequent Heck coupling of *E*-**2** with 4-vinylpyridine with $Pd(OAc)_2$ as catalyst in Et_3N–toluene in presence of tri-*o*-tolylphosphine (POT) gave **3** in 80% yield. All of the spectroscopic studies and elemental analyses were consistent with the proposed molecular structures.† In particular, coupling constants of *ca*. 16.5 Hz for the two AB systems corresponding to the two sets of vinylic protons in the ^{1}H-NMR spectrum confirmed the *E* stereochemistry of both double bonds in **3**. The electronic absorption and emission of styrylstilbazole

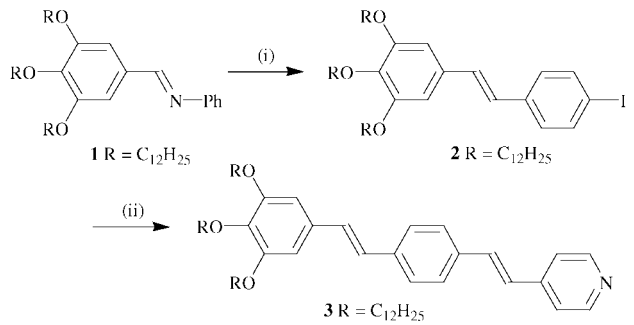

1 R = $C_{12}H_{25}$ **2** R = $C_{12}H_{25}$ **3** R = $C_{12}H_{25}$

Scheme 1 *Reagents and conditions:* i, 4-iodotoluene, *t*-BuOK, DMF, 80 °C, 1 h (50%); ii, 4-vinylpyridine, $Pd(OAc)_2$, POT, Et_3N–toluene, 90 °C, 12 h (80%).

3 are reported in Fig. 1. Compound **3** exhibits a strong absorption (λ_{max} = 367 nm). Interestingly, addition of increasing amounts of TFA to a solution of **3** causes dramatic changes in the absorption spectrum, the peak being completely shifted at *ca*. 10 equivalents of acid added. Isosbestic points are maintained at 313 and 388 nm indicating that a single chemical process occurs, *i.e.* protonation of the pyridine ring. The initially pale yellow solution becomes orange–yellow at the end of titration. The addition of acid also leads to changes in the emission properties (λ_{exc} = 313 nm, isosbestic point). The strong blue luminescence of the ligand (λ_{max} = 501 nm) progressively disappears and a very weak red-shifted emission (λ_{max} = 615 nm) corresponding to the luminescence of protonated **3** is detected at the end of the titration (Fig. 1). Addition of a base (DBU) restores the initial absorption and luminescence properties. Therefore ligand **3** also presents characteristic features that make it an interesting building block for the preparation of new molecular switches.[9]

The observation of **3** under optical microscopy does not reveal any liquid crystalline properties and only shows a melting point at 83 °C. It is well known that metal complexes of polycatenar stilbazole derivatives show mesomorphic properties.[3,4] Ligand **3** is also a suitable building block for the preparation of related metallomesogens. The *trans*-Pd(II) complex of **3** has been prepared according to the procedure developed by Bruce and co-workers.[3] Treatment of **3** with $PdCl_2(CH_3CN)_2$ in a mixture of CH_2Cl_2–CH_3CN 1 : 1 afforded $PdCl_2(\mathbf{3})_2$ in 95% yield.‡

Observation of this Pd(II) complex under a polarizing microscope reveals typical textures of a columnar mesophase from 165 to 234 °C. Differential scanning calorimetry (DSC) analyses and X-ray diffraction patterns recorded for $PdCl_2(\mathbf{3})_2$ at different temperatures were in full agreement with these observations. Indeed, the X-ray pattern is characterized in the small angle region by two sharp reflections in the ratio 1 : $\sqrt{3}$, corresponding to a two-dimensional hexagonal lattice. The

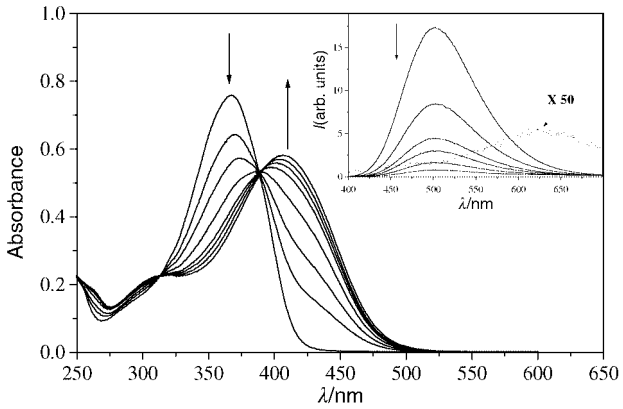

Fig. 1 Absorption and (inset) fluorescence (λ_{exc} = 313 nm, isosb. point) spectra of CH_2Cl_2 solutions of ligand **3** containing 0, 0.5, 1, 2, 4, 6, 10, 100 equiv. of TFA (the emission spectrum recorded after addition of 100 eq. of TFA is multiplied by a factor of 50).

 DOI: 10.1039/b103563k

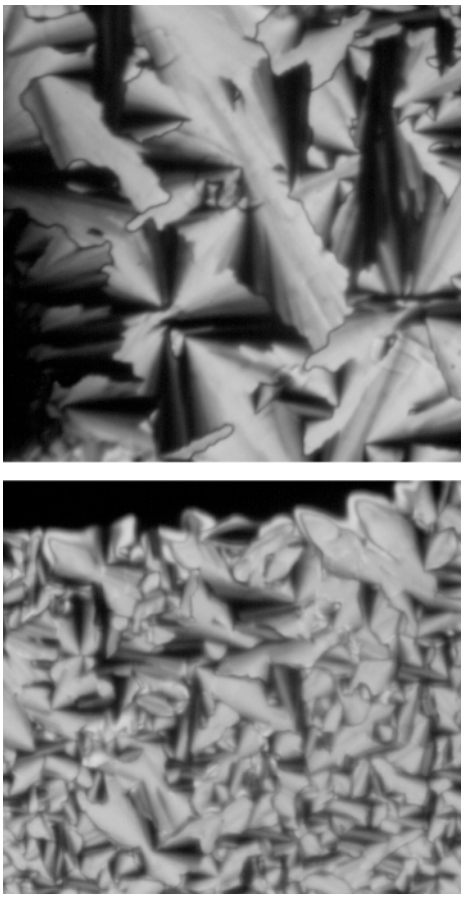

Fig. 2 Top: optical texture observed with a polarizing microscope at 150 °C for the complex prepared from **3** and perfluorosuberic acid. Bottom: optical texture observed with a polarizing microscope at 120 °C for the complex prepared from **3** and TFA.

dimerization of **3** *via* coordination to a metal center is therefore able to produce a polycatenar calamitic supramolecule with liquid crystalline properties.

It has been shown that H-bonding can be used to assemble pyridine derivatives with carboxylic acids to produce linear structures that exhibit liquid crystalline behavior.[5] The treatment of styrylstilbazole **3** with various dicarboxylic acids (oxalic acid, α,ω aliphatic dicarboxylic acids of different lengths and terephthalic acid) was therefore attempted in order to obtain supramolecular derivatives with an appropriate shape to produce columnar mesophases. Unfortunately, homogeneous samples could not be obtained and macrophase separation was observed in all the cases. The interactions (if any) of **3** with these dicarboxylic acid derivatives seem to be too weak to allow the preparation of the desired supramolecular assemblies. This observation prompted us to use a more acidic derivative able to protonate styrylstilbazole **3** in order to produce a stable adduct thanks to the resulting ionic interactions. Slow evaporation of a CH_2Cl_2 solution of **3** and perfluorosuberic acid [HO_2C-$(CF_2)_6CO_2H$; 0.5 equiv.] afforded an orange crystalline solid. The orange color and the presence of a strong band at 1623 cm^{-1} in the IR spectrum (neat) are in good agreement with the formation of a carboxylate salt.

Observation of the resulting complex under a polarizing microscope reveals an optical texture characteristic of a columnar mesophase from 124 to 170 °C (Fig. 2). The dicarboxylic acid and **3** seem therefore able to form a supramolecular dimer stabilized by electrostatic forces with the appropriate polycatenar calamitic shape to produce a columnar liquid crystalline phase.

The treatment of **3** with TFA (1 equiv.) under similar conditions also leads to an orange crystalline solid and the development of typical columnar texture was observed from 70 to 143 °C for the resulting compound (Fig. 2). In addition to the electrostatic interactions among **3** and TFA, it seems that fluorophilic interactions allow the dimerization of the resulting **3** TFA species and, thus are able to direct their self-organization into a columnar liquid crystalline phase. It is worth noting that salts prepared from **3** and inorganic acids such as HCl do not exhibit any mesomorphic properties. The latter observation shows that protonation of **3** alone is not sufficient to produce liquid crystalline derivatives. Thus the fluorophilic interactions must play an important role.

The mesomorphic properties of the complexes obtained from **3** and perfluorosuberic acid or TFA have been studied by DSC and X-ray diffraction. The hexagonal lattice parameters deduced from the X-ray patterns (50 Å at 140 °C for the adduct with perfluorosuberic acid and 48 Å at 140 °C for the adduct with TFA) are similar to that found for the complex $PdCl_2(\mathbf{3})_2$ (45 Å at 160 °C). This observation strongly suggests an effective dimerization of **3** through non-covalent interactions as discussed above.

Treatment of **3** with a palladium salt, perfluorosuberic acid or TFA afforded discrete assemblies with new properties. Effectively, **3** itself does not show any mesomorphic properties, but its dimerization through self-assembling by coordination, ionic or fluorophilic interactions leads to discrete supramolecular structures with liquid crystalline properties.

We thank B. Heinrich for his help with the X-ray measurements and L. Oswald for technical assistance.

Notes and references

† *Selected spectroscopic data* for **3**: Yellow crystals (mp 83 °C). UV-Vis (CH_2Cl_2): 367 (40000). δ_H (200 MHz, $CDCl_3$): 8.58 (d, *J* 6, 2 H), 7.53 (s, 4 H), 7.37 (d, *J* 6, 2 H), 7.12 (AB, *J* 16.5, 2 H), 7.02 (AB, *J* 16.5, 2 H), 6.73 (s, 2 H), 4.03 (t, *J* 6.5, 4 H), 4.00 (t, *J* 6.5, 2 H), 1.80–1.70 (m, 6 H), 1.50–1.20 (m, 54 H), 0.90 (t, *J* 6.5, 9 H). Anal. calc. for $C_{57}H_{89}NO_3$: C 81.86, H 10.73, N 1.67; found: C 81.58, H: 10.75, H 1.66%.

‡ *Selected spectroscopic data* for $PdCl_2(\mathbf{3})_2$: Yellow crystals. UV-Vis (CH_2Cl_2): 392 (118000). δ_H (200 MHz, $CDCl_3$): 8.70 (d, *J* 7, 4 H), 7.56 (s, 8 H), 7.42 (d, *J* 7, 4 H), 7.41 (d, *J* 16.5 Hz, 2 H), 7.08 (d, *J* 16.5, 2 H), 7.06 (AB, *J* 16, 4 H), 6.74 (s, 4 H), 4.01 (t, *J* 6.5 Hz, 8 H), 3.98 (t, *J* 6.5, 4 H), 1.80–1.70 (m, 12 H), 1.50–1.20 (m, 108 H), 0.90 (t, *J* 6.5, 18 H). Anal. calc. for $C_{114}H_{178}N_2O_6PdCl_2$: C 74.01, H 9.70, N 1.51; found: C 73.61, H: 9.52, H 1.55%.

1 J.-M. Lehn, *Supramolecular chemistry-concepts and perspectives*, VCH, Weinheim, 1995.
2 C. Tschierske, *Angew. Chem., Int. Ed.*, 2000, **39**, 2454 and references cited therein.
3 B. Donnio and D. W. Bruce, *J. Chem. Soc., Dalton Trans.*, 1997, 2745; D. J. Price, K. Willis, T. Richardson, G. Ungar and D. W. Bruce, *J. Mater. Chem.*, 1997, **7**, 883.
4 D. W. Bruce, *Acc. Chem. Res.*, 2000, **33**, 831.
5 T. Kato, *Handbook of Liquid Crystals*, D. Demus, J. Goodby, G. W. Gray, H.-W. Spiess and V. Vill, eds, Wiley: VCH, Weinheim, 1998, Vol. 2B, pp. 969–979.
6 M. Suarez, J.-M. Lehn, S. C. Zimmerman, A. Skoulios and B. Heinrich, *J. Am. Chem. Soc.*, 1998, **120**, 9526; A. El-ghayoury, E. Peeters, A. P. H. J. Schenning and E. W. Meijer, *Chem. Commun.*, 2000, 1969; A. P. H. J. Schenning, P. Jonkheijm, E. Peeters and E. W. Meijer, *J. Am. Chem. Soc.*, 2001, **123**, 409.
7 J.-F. Eckert, J.-F. Nicoud, D. Guillon and J.-F. Nierengarten, *Tetrahedron Lett.*, 2000, **41**, 6411.
8 D. Felder, B. Heinrich, D. Guillon, J.-F. Nicoud and J.-F. Nierengarten, *Chem. Eur. J.*, 2000, **6**, 3501; J. L. M. van Nunen, B. F. B. Folmer and R. J. M. Nolte, *J. Am. Chem. Soc.*, 1997, **119**, 283.
9 N. Armaroli, J.-F. Eckert and J.-F. Nierengarten, *Chem. Commun.*, 2000, 2105.

CHEMCOMM
Communication
www.rsc.org/chemcomm

Polymers and rings in gold(I) diphosphine complexes: linking gold rings through aurophilic interactions

Marie-Claude Brandys and Richard J. Puddephatt*

Department of Chemistry, University of Western Ontario, London, Canada, N6A 5B7. E-mail: pudd@uwo.ca

Received (in Columbia, MO, USA) 3rd April 2001, Accepted 24th April 2001
First published as an Advance Article on the web 21st June 2001

Gold(I) complex cations of empirical formula $Au[Ph_2P(CH_2)_nPPh_2]^+$ crystallize as rings $[Au_2\{Ph_2P(CH_2)_nPPh_2\}_2]^{2+}$ when n = 3 or 5 but as a polymer $[\{Au[Ph_2P(CH_2)_nPPh_2]\}_x]^{x+}$ when n = 4. In favorable cases, the ring complexes can be connected through aurophilic bonding by addition of $[Au(CN)_2]^-$, and crystals contain pentagold units when n = 3 or polymeric pleated chains when n = 5.

In the context of the rapidly developing field of coordination polymers,[1] and of gold(I) diphosphine complexes that may have interesting photophysical and biological properties,[2] this article reports two new one-dimensional polymers containing gold(I) diphosphine units, one being the first polymer containing linear gold(I) centres with only diphosphine ligands and the other the first to contain gold rings stitched together by using aurophilic attractions.[1,3] The factors that are important in giving self-assembly of polymeric structures are elucidated.

The complexes of empirical formula $AuX[Ph_2P(CH_2)_nPPh_2]$ have been suggested to exist as ring complexes $[Au_2\{\mu\text{-}Ph_2P(CH_2)_nPPh_2\}_2]^{2+}(X^-)_2$,[4] though more complex structures may be formed in cases when the anion X^- is also a ligand to give a higher coordination number than two at gold(I).[1,4] However, it is now shown that the derivatives with X = CF_3CO_2, prepared as in Scheme 1, exist as rings **1** when n = 1, 2, 3 or 5 but as a unique polymeric chain complex **2** when n = 4.

The ring complexes **1** give sharp singlet resonances in the ^{31}P NMR spectra while **2** gives several overlapping and broader resonances.† The complexes were isolated as the trifluoroacetate salts, and complexes **1c** and **2** were characterized by X-ray structure determination (Fig. 1).‡

Why does complex **2** have a structure that is different from the others? The answer is not obvious but can be analyzed in terms of two effects. First, when n = 1 or 2, the ring structure is favored because transannular Au···Au attractions are possible[1–4] and this effect is dominant in these cases. Second, there is a relative preference for the *anti*, rather than *syn*, orientation of the two PPh_2 groups, and hence formation of chains rather than rings, when n is an even integer.[1] Only when n = 4 does the preference for the *anti* conformation prevail and lead to the novel polymeric structure of **2** (Fig. 1). The NMR data suggest, but do not prove, that the solid state structures are maintained in solution.

Can the rings **1** (Scheme 1) be linked to form polymers? The complexes **1** were reacted with potassium dicyanoaurate in the expectation that both ionic and aurophilic attractions between the cationic and anionic gold(I) centres in **1** and $[Au(CN)_2]^-$ would promote association. In solution, these reactions lead to mixtures containing the original ions and the neutral diphosphine gold(I) cyanide complexes **3** (Scheme 2) as established by NMR [^1H, ^{13}C on ^{13}CN enriched samples, ^{31}P; complexes **3** are readily identified by the large coupling $^2J(PC)$].† Crystallization from these solutions gave **3** when n = 1 or 2, but the linked ring complex **4** when n = 3 and the novel polymer **5** when n = 5 (Scheme 2). Both **4** and **5** crystallized as the dicyanoaurate salts and so also contain free $[Au(CN)_2]^-$ anions.‡

The structures of **4** and **5** are shown in Fig. 2. In complex **4** two rings are connected by an $[Au(CN)_2]^-$ ion through aurophilic interactions to give the unit $[\{Au_2(\mu\text{-}Ph_2PCH_2CH_2CH_2PPh_2)_2\}_2\{Au(CN)_2\}]^{3+}$, with only one of the two AuP_2^+ centres of each ring involved in Au···Au bonding. However, in complex **5** all the AuP_2^+ centres are involved in

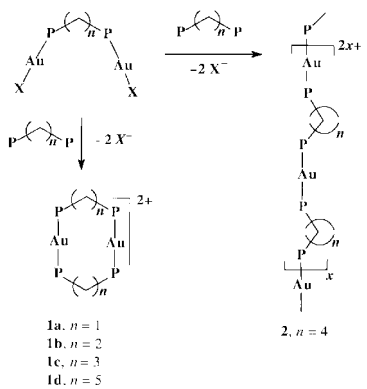

Scheme 1 P = PPh_2.

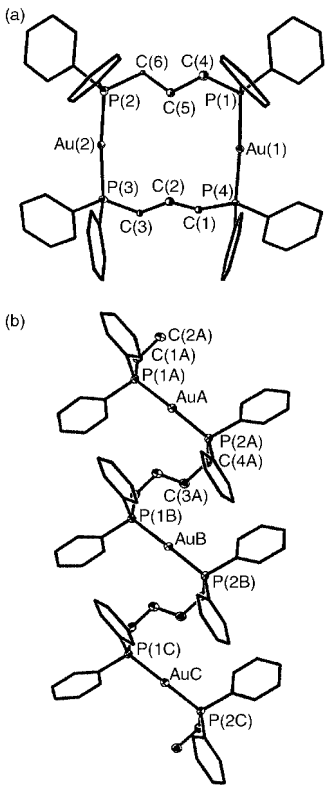

Fig. 1 Structures of the cationic units in (a) the ring complex **1c** and (b) the polymeric complex **2**. For clarity, thermal ellipsoids are not shown for phenyl carbon atoms.

 DOI: 10.1039/b103020p

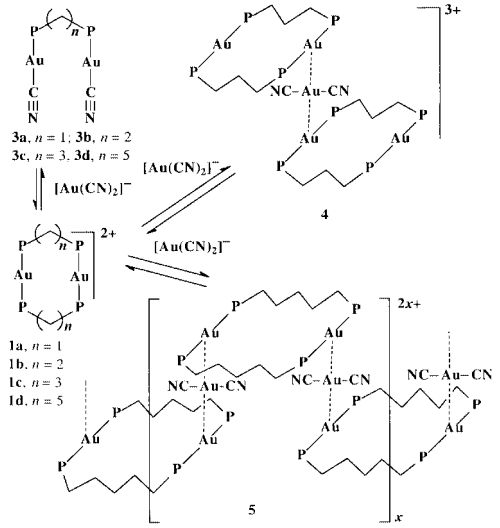

Scheme 2 P = PPh_2.

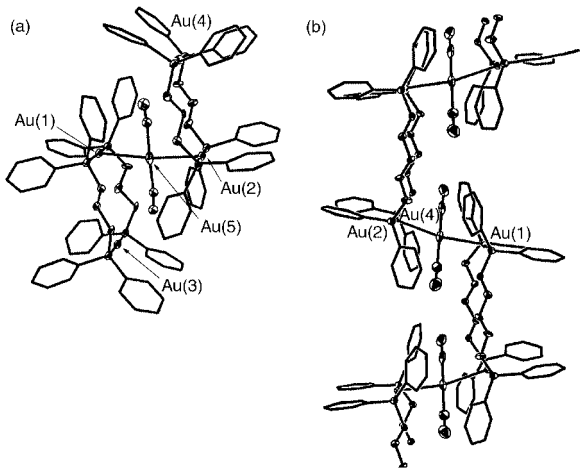

Fig. 2 Structures of the linked ring complex cations in (a) complex **4** and (b) complex **5**. The parameters corresponding to aurophilic attractions are: for complex **4**, Au(1)–Au(5) 3.059(3) Å, Au(2)–Au(5) 3.034(3) Å; Au(1)–Au(5)–Au(2) 172.1(1)°. For complex **5**, Au(1)–Au(4) 2.9906(8), Au(2)–Au(4) 3.0665(8) Å, Au(1)–Au(4)–Au(2) 165.26(3)°.

Au···Au bonding and so the pleated-chain polymeric structure $[\{Au_2[\mu\text{-}Ph_2P(CH_2)_5PPh_2]_2\}_2\{Au(CN)_2\}_2]_x^{2x+}$ results. By inspection of Fig. 2, it is immediately clear that the structure observed for **5** would not be possible for **4** because the transannular Au···Au distance is too short to allow both gold atoms to be linked to approximately collinear $[Au(CN)_2]^-$ units. Phenyl–phenyl repulsions prevent bridging in other ways to link units of **1a**, **1b** or **1c**.

The complexes **4**, **2** and **5**, as the dicyanoaurate salts, give rather similar solid state emission spectra, with maxima at 419, 414 and 411 nm, respectively. This indicates that the extended structures present in **2** (n = 4) and **5** (n = 5) do not greatly affect the photophysical properties of the complexes, when compared to the more limited association in **4**.

The ability to control the self-assembly of extended structures is becoming increasingly important. This article shows how conformational differences in simple, commonly used diphosphine ligands can be used to control whether ring or polymeric structures will be formed in gold(I) complexes and, for the ring compounds, how the distance between phosphorus donors is critical in determining if the rings can be linked to give extended structures.

We thank the NSERC (Canada) for financial support and for a scholarship to M.-C. B. and R. J. P. thanks the Government of Canada for a Canada Research Chair. We thank Dr M. C. Jennings for X-ray data collection.

Notes and references

† *Selected data*: for **1** and **2**: $\delta(^{31}P)$ in CD_3OD: **1a**, 38.3; **1b**, 41.1; **1c**, 44.3; **1d**, 45.6; **2**, 44.7. For **3a**: $\delta(^{13}CN)$ 155.7; $\delta(^{31}P)$ 34.9. For **3b**: $\delta(^{13}CN)$ 155.9 [J(PC) 132 Hz]; $\delta(^{31}P)$ 33.5. For **3c**: $\delta(^{13}CN)$ 157.2 [J(PC) 123 Hz]; $\delta(^{31}P)$ 31.9. For **3d**: $\delta(^{13}CN)$ 157.7 [J(PC) 124 Hz]; $\delta(^{31}P)$ 35.8.

Complexes were prepared in methanol solution, NMR data were obtained in CD_2Cl_2/CD_3OD solution, and crystals were grown by slow diffusion of pentane into these solutions.

‡ *Crystal data*: for **1c**·$2CH_2Cl_2$: $C_{60}H_{56}Au_2Cl_4F_6O_4P_4$, M = 1586.61, orthorhombic, space group $Pna2_1$, a = 22.7641(8), b = 13.3249(3), c = 19.5994(8) Å, V = 5945.1(3) Å^3, Z = 4, $R1$ = 0.0739 and $wR2$ = 0.1787 for 12645 reflections with $I > 2\sigma(I)$ at 150 K.

For **2**: $C_{30}H_{28}AuF_3O_2P_2$, M = 736.43, monoclinic, space group Pc, a = 6.7570(1), b = 11.7756(3), c = 20.3694(5) Å, β = 93.629(1)°, V = 1617.50(6) Å^3, Z = 2, $R1$ = 0.0752 and $wR2$ = 0.2057 for 8807 reflections with $I > 2\sigma(I)$ at 300 K.

For **3a**: $C_{27}H_{22}Au_2N_2P_2$, M = 830.34, monoclinic, space group $C2/c$, a = 22.039(1), b = 7.4488(3), c = 18.3838(6) Å, β = 122.193(2)°, V = 2554.0(2) Å^3, Z = 4, $R1$ = 0.0364 and $wR2$ = 0.0883 for 3723 reflections with $I > 2\sigma(I)$ at 200 K.

For **3b**: $C_{28}H_{24}Au_2N_2P_2$, M = 844.36, monoclinic, space group $P2_1/n$, a = 12.597(1), b = 11.4020(9), c = 19.258(1) Å, β = 108.34(6)°, V = 2625.5(4) Å^3, Z = 4, $R1$ = 0.0641 and $wR2$ = 0.1676 for 4262 reflections with $I > 2\sigma(I)$ at 298 K.

For **4**: $C_{58}H_{52}Au_4N_4P_4$, M = 1716.78, monoclinic, space group $P2_1/n$, a = 26.860(1), b = 17.425(1), c = 28.026(1) Å, β = 96.439(4)°, V = 13034(1) Å^3, Z = 10, $R1$ = 0.1357 and $wR2$ = 0.3699 for 15165 reflections with $I > 2\sigma(I)$ at 200 K.

For **5**: $C_{62}H_{60}Au_4N_4P_4$, M = 1772.89, monoclinic, space group $P2_1/c$, a = 13.7149(3), b = 25.056(1), c = 19.4449(8) Å, β = 97.46(2)°, V = 6625.5(4) Å^3, Z = 5, $R1$ = 0.0561 and $wR2$ = 0.1633 for 13231 reflections with $I > 2\sigma(I)$ at 296 K.

CCDC 164205–164210. See http://www.rsc.org/suppdata/cc/b1/b103020p/ for crystallographic data in CIF or other electronic format.

1 *Gold: Progress in Chemistry, Biochemistry and Technology*, ed. H. Schmidbaur, Wiley, New York, 1999; M. C. Brandys, M. C. Jennings and R. J. Puddephatt, *J. Chem. Soc., Dalton Trans.*, 2000, 4601; R. J. Puddephatt, *Chem. Commun.*, 1998, 1055; W. E. Van Zyl, R. J. Staples and J. P. Fackler Jr., *Inorg. Chem. Commun.*, 1998, **1**, 51; D. Perrault, M. Drouin, A. Michel and P. D. Harvey, *Inorg. Chem.*, 1991, **30**, 2.

2 L. Hao, R. J. Lachicotte, H. J. Gysling and R. Eisenberg, *Inorg. Chem.*, 1999, **38**, 4616; V. W. W. Yam and K. K. W. Lo, *Chem. Soc. Rev.*, 1999, **28**, 323; B. C. Tzeng, K. K. Cheung and C. M. Che, *Chem. Commun.*, 1996, 1689; S. J. Berners-Price, L. A. Colqhoun, P. C. Healey, K. A. Byriel and J. V. Hanna, *J. Chem. Soc., Dalton Trans.*, 1992, 3357.

3 S. S. Pathameni and G. R. Desiraju, *J. Chem. Soc., Dalton Trans.*, 1993, 319; P. M. Van Calcar, M. M. Olmstead and A. L. Balch, *Inorg. Chem.*, 1997, **36**, 5231; M. J. Irwin, G. Jia, N. C. Payne and R. J. Puddephatt, *Organometallics.*, 1996, **15**, 51; M. J. Irwin, L. M. Muir, K. W. Muir and R. J. Puddephatt, *Chem. Commun.*, 1997, 219.

4 A. Burini, R. Galassi, B. R. Pietroni and G. Rafaini, *J. Organomet. Chem.*, 1996, **519**, 161; S. Al-Baker, W. E. Hill and C. A. McAuliffe, *J. Chem. Soc., Dalton Trans.*, 1985, 2655; W. P. Schaeffer, R. E. Marsh, T. M. McCleskey and H. B. Gray, *Acta Crystallogr., Sect. C*, 1991, **47**, 2553; D. Perrault, M. Drouin, A. Michel, V. M. Miskowski, W. P. Schaefer and P. D. Harvey, *Inorg. Chem.*, 1992, **31**, 695; M. C. Gimeno and A. Laguna, *Chem. Rev.*, 1997, 511; A. Bayler, A. Schier and H. Schmidbaur, *Inorg. Chem.*, 1998, **37**, 4353; H.-R. C. Jaw, M. M. Savas, R. D. Rogers and W. R. Mason, *Inorg. Chem.*, 1989, **28**, 1028; A. Houlton, D. M. P. Mingos, D. M. Murphy, D. J. Williams, L. T. Phang and T. S. A. Hor, *J. Chem. Soc., Dalton Trans.*, 1993, 3629; M. N. I. Khan, C. King, D. D. Heinrich, J. P. Fackler Jr. and L. C. Porter, *Inorg. Chem.*, 1989, **28**, 2150.

CHEMCOMM Communication
www.rsc.org/chemcomm

Molecularly imprinted ionically permeable membrane for uranyl ion

Anael Kimaro,[a] Lisa A. Kelly[a] and George M. Murray*[b]

[a] *Department of Chemistry and Biochemistry, University of Maryland, Baltimore County, Baltimore, MD, USA*
[b] *Johns Hopkins University Applied Physics Laboratory, Laurel, MD, USA. E-mail: george.murray@jhuapl.edu*

Received (in Cambridge, UK) 4th April 2001, Accepted 4th June 2001
First published as an Advance Article on the web 27th June 2001

A polymeric membrane for the separation of specific metal ions can be designed by the application of the molecular imprinting technique.

The transport of metal ions through membranes has been studied as a means of separation, concentration and recovery of both valued and toxic metal ions.[1–5] These efforts are driven by environmental concerns and dwindling natural resources. The development of efficient and selective metal ion transporting systems for use in such operations is of great interest. Two types of membranes are predominant in membrane transport systems: supported liquid membranes and polymeric membranes. The convenience and high flux characteristics of supported liquid membranes have made popular these types of membranes.[5–7] However, the low stability, strength and finite solubility of the active agent used in liquid supported membranes limit their practical application. Polymeric membranes have the physical and chemical stability for practical applications, but are often hampered by low transport flux. In many applications, selectivity is the most important function. The most selective membrane will have a specific transporting or penetrating path, pore or matrix through which only the desired substrate is able to pass. Specific receptor sites in polymeric membranes can be introduced by the molecular imprinting technique.[8]

Molecular imprinting is a process for making selective recognition sites in synthetic polymers. The process employs a target molecule as the template. The template is surrounded by molecular compliments that possess polymerisable functionalities. The template complex is typically copolymerised with a matrix monomer and a cross-linking monomer in the presence of a suitable solvent. The cross-linking monomers add rigidity to the finished polymer and the solvent provides site accessibility. Removal of the template molecules leaves behind cavities that exhibit enhanced affinity for rebinding the target molecule. Previously, using vinylbenzoic acid and vinylsalicyladoxime, we used the molecular imprinting technique to prepare ion exchange resins that are selective for the sequestration of uranyl ions.[9] Recently, Saunders *et al.* reported an imprinted polymer extractant based on chloroacetic acid.[10] However, the utility of a permeable membrane for the selective transport of metal ions has remained relatively unexplored. In this communication, we report our initial results and observations concerning the transport of uranyl ions through an imprinted polymer membrane. The molecular imprinting technique has been exploited in preparing membranes with molecular recognition sites for low weight organic molecules, as reported in a recent review.[11] Mathew-Krotz and Shea[12] reported imprinted polymer membranes for the selective transport of targeted neutral (organic) molecules with fluxes up to 0.5 nmol cm^{-2} h^{-1}. The highest selectivity factor was 3.4 for adenosine *vs*. guanosine with 9-ethyladenine imprinted membrane.

The polymeric membranes were synthesized with ingredients for both selective binding and improved permeability. The selective binding site was prepared by using uranyl ion imprinting. Permeability was addressed using a polyester that associates with the metal ions. The length of the alkyl chain in the diol that was used to make the polyester controlled the spacing of association sites. The polyester was removed from the membrane by the same acid treatment used to remove the uranyl ion. Removal was detected by GC-MS of the membrane acid-wash solutions. The polyester is intended to create channels, directing ion migration to the imprinted sites, thus increasing flux but maintaining selectivity. The addition of polyester to the formula had two significant results: the amount of swelling of the membrane in aqueous solutions was dramatically increased, and in the absence of the polyester there was no detectable migration of ions.

Membranes were prepared using uranyl vinylbenzoate, $UO_2(VBA)_2$, as the ion imprinting complex. Styrene was used as the matrix monomer and divinylbenzene was used as the cross-linking monomer. Membrane synthesis was carried out in a screw-top vial by dissolving the uranyl vinylbenzoate complex (20–150 mg) in 400 μL of 2-methoxyethanol. Nitrophenyl octyl ether (NPOE) as a plasticizer and 22 mg of a polyester, prepared from diglycolic acid and 1,6-hexanediol, was added to the polymerisation mixture. After deaeration with dry nitrogen, 20 mg of a free radical initiator, 2,2′-azobisisobutyronitrile (AIBN) were added. The vial was sealed and placed in a sonicator at 60 °C. The solution was sonicated until viscous and then poured into a Teflon mold. The resultant sample was kept in a sealed container and placed in an oven at 60 °C for 18 h to complete the polymerisation. The thickness of the resulting membranes was approximately 100 microns. Table 1 summarizes the composition of membranes A, Q and R. A reference membrane imprinted with Ni^{2+} was prepared in the same manner as membrane Q. The metal templates and the polyester were removed using a 0.1 M acetic acid solution followed by a 5% nitric acid solution. Metal ions were removed using acid until the entire template was recovered. The membrane was then washed with deionised water until the acid was removed.

Transport studies were carried out in a U-shaped tube consisting of two detachable parts. The membrane, with an exposed cross-sectional area of 0.613 cm^2, was placed between the two halves of the tube. The halves were held together with a screw-actuated clamp that compresses an o-ring seal to tightly secure the connection. Experiments were performed under quiescent conditions and also by stirring the solutions. The time-dependence of uranyl ion transport in quiescent solution is

Table 1 The composition of the membrane in wt% of the total components in the original mixture

Reagent	Membrane A	Membrane Q	Membrane R
$UO_2(VBA)_2$[a]	6.7	1.5	1.5
Divinylbenzene	2.0	14.5	24.5
Polyester	1.8	1.8	1.8
AIBN	0.9	1.6	1.6
NPOE	4.6	8.3	8.3
Styrene	84.0	72.3	62.3

[a] $UO_2(VBA)_2$ was dissolved in 0.4 ml of 2-methoxyethanol in each case.

 DOI: 10.1039/b103077a

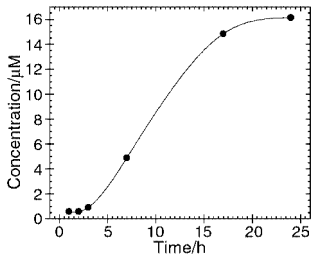

Fig. 1 Transport of uranyl ions across the membrane with time.

given in Fig. 1. The concentration of uranium in the receiving phase was determined by ICP-MS. An experiment performed while stirring the solutions (both the source and the receiving solution) showed that higher fluxes could be obtained by convection. After 24 h of stirring, 25% of UO_2^{2+} in the source solution containing 42 μM UO_2^{2+} was transported through the membrane, compared to 6.5% when the solution was unstirred.

The selectivity of the membrane was evaluated by carrying out competitive transport experiments. A solution containing 0.2 mM of UO_2^{2+}, Ni^{2+}, Cd^{2+}, Cu^{2+} and Zn^{2+} was used as a source solution. After 22 h, a portion of the receiving solution was analysed by ICP-MS to determine the amount of each ion that was transported across the membrane. Fluxes of the competing ions were found to be very small (Table 2). UO_2^{2+} was transported at higher rate, with a selectivity factor (α) ranging from 114 to 152. The selectivity factor is defined as the ratio of the molar concentration of uranyl ion to the molar concentration of the competing metal ions measured in the receiving solution.

Table 2 Transport of uranyl ion through the membrane in the presence of competitors; selectivity

Metal ion	Amount diffused/μM	Flux/nmol cm^{-2} h^{-1}
UO_2^{2+}	11.8 ± 0.1	2.74
Ni^{2+}	0.104 ± 0.002	0.024
Cd^{2+}	0.086 ± 0.001	0.019
Zn^{2+}	0.076 ± 0.001	0.018
Cu^{2+}	none detected	

Membrane A, composition: 6.7 wt% complex, 2 wt% cross-linker.

The origin of selective transport can be attributed to the selective binding of uranyl ion to imprinted sites along channels that span the membrane. The reference membrane prepared by imprinting with nickel showed little permeation of uranyl ions, but higher permeation of some of the competing metal ions. The transport fluxes of UO_2^{2+}, Cu^{2+} and Co^{2+} through the reference membrane were 0.015 ± 0.002, 0.142 ± 0.003 and 0.045 ± 0.001 nmol cm^{-2} h^{-1} respectively. No Ni^{2+} or Zn^{2+} was detected in the effluent, suggesting that the conditions for membrane preparation may need to be established on a case by case basis. The results do show that the Ni^{2+} ion imprinted membrane does not have sites selective for uranyl ions. The selective transport observed in the uranyl ion imprinted membrane arises from a process that involves preferential and reversible complexation for uranyl ion. Metal ion transport across the membrane requires a counter flow of cations in the reverse direction to maintain electroneutrality. A surplus of protons was maintained in the receiving solution by the addition of acid. A scanning electron micrograph of the membrane shows that the surface of the membrane has pores in the micron and submicron range (Fig. 2). Micrographs of the inside of the membranes show an open porous structure. Energy dispersive X-ray emission spectra of the pore area show larger amounts of uranium in the pores relative to the surrounding area, suggesting that the pores are involved in metal ion transport.

The effects of the imprinting conditions on the membrane performance were investigated by preparing membranes with different degrees of cross-linking. Each membrane's performance towards uranyl ion was examined. Using source solutions that contained a range of UO_2^{2+} concentrations from 0.25 to 0.42 mM, the transport fluxes were measured and compared. These results are shown in Table 3.

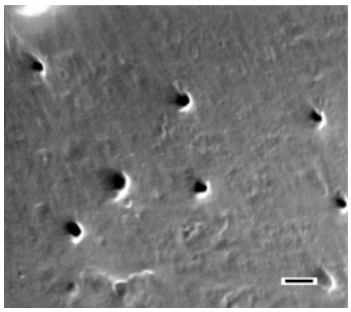

Fig. 2 Scanning electron micrograph of the membrane (bar = 1 μm).

Table 3 Effects of cross-linker and concentration of the source solution on the transport flux

	Flux/nmol cm^{-2} h^{-1}	
UO_2^{2+} (source)/mM	Membrane Q[a]	Membrane R[b]
0.25	0.83 ± 0.03	0.34 ± 0.02
0.34	0.96 ± 0.04	0.68 ± 0.02
0.42	1.21 ± 0.02	0.91 ± 0.03

[a] 1.5 wt% complex, 14.5 wt% cross-linker. [b] 1.5 wt% complex, 24.5 wt% cross-linker.

The membrane with a lower degree of cross linking (Q) exhibited higher fluxes than the membrane with a higher degree of cross-linking (R). The selectivity of the two membranes was verified by the competitive transport test described above. The results show that the membrane with the higher flux also exhibits higher selectivity (α_{Cd} for Q = 56 and for R = 10). Repeated uses of the membranes did not show a loss of selectivity. This result is in agreement with previous work on Pb^{2+} imprinted ion-exchange resins.[13]

In conclusion, the present study demonstrates that a polymeric membrane can be designed for the separation of a specific metal ion from a mixed metal ion solution. The selectivity imparted by the imprinting technique is high.

This work was supported by the US Department of Energy through grant number DE-FG07-97ER14823.

Notes and references

1 F. Guyon, N. Parthasarathy and J. Buffle, *Anal. Chem.*, 1999, **71**, 819.
2 J. P. Shukla, A. Kumar and R. K. Singh, *Radiochim. Acta*, 1992, **57**, 185.
3 T. Nonaka and M. Kawamoto, *J. Membr. Sci.*, 1995, **101**, 135.
4 S. Shinkai, Y. Shiramana, H. Satoh and O. Manabe, *J. Chem. Soc., Perkin Trans. 2*, 1989, 1167.
5 E. G. Reichen-Buitenhuis, H. C. Visser, F. De Jong and D. N. Reinhoudt, *J. Am. Chem. Soc.*, 1995, **117**, 3913.
6 T. M. Fyles, V. A. Malik-Diemer, C. A. McGavin and D. M. Whitfield, *Can. J. Chem.*, 1982, **60**, 2259.
7 L. A. Fredrick, T. M. Fyles and N. P. Guprasad, *Can. J. Chem.*, 1981, **59**, 1724.
8 G. Wulff, *Angew. Chem., Int. Ed. Engl.*, 1995, **34**, 1812.
9 G. M. Murray and O. M. Uy, *Report to the Environmental Management Science Program, Project ID Number 59977*, June 1998.
10 G. D. Saunders, S. P. Foxon, P. H. Walton, M. J. Joyce and S. N. Port, *Chem. Commun.*, 2000, 273
11 S. A. Piletsky, T. L. Panasyuk, E. V. Piletskaya, I. A. Nicholls and M. Ulbricht, *J. Membr. Sci.*, 1999, **157**, 263.
12 J. Mathew-Krotz and K. J. Shea, *J. Am. Chem. Soc.*, 1996, **118**, 8154.
13 X. Zeng and G. M. Murray, *Sep. Sci. Technol.*, 1996, **31**, 24.

CHEMCOMM
Communication
www.rsc.org/chemcomm

Mixed-valence, tetranuclear cobalt(III, IV) complexes: preparation and properties of $[Co_4O_4(O_2CR)_2(bpy)_4]^{3+}$ salts

Katerina Dimitrou,[a] Angelica D. Brown,[a] Thomas E. Concolino,[b] Arnold L. Rheingold[b] and George Christou*[a]

[a] *Department of Chemistry, Indiana University, Bloomington, IN 47405, USA. E-mail: christou@indiana.edu*
[b] *Department of Chemistry, University of Delaware, Newark, DE 19716, USA*

Received (in Cambridge, UK) 2nd March 2001, Accepted 1st June 2001
First published as an Advance Article on the web 27th June 2001

Cyclic voltammetric examination of $[Co_4O_4(O_2CR)_2(bpy)_4](ClO_4)_2$ cubane complexes 1 (R = various; bpy = 2,2′-bipyridine) in MeCN reveals a one-electron reversible oxidation in the range 0.68–0.86 V *vs.* ferrocene; the one-electron oxidized clusters can be obtained in analytical purity by either controlled potential electrolysis to give $[Co_4O_4(O_2CR)_2(bpy)_4](ClO_4)_3$ 2 or oxidation with $(NH_4)_2Ce(NO_3)_6$ to give $[Co_4O_4(O_2CR)_2(bpy)_4][Ce(NO_3)_6]$ 3.

The ability of hard oxide (O^{2-}) ions to stabilize unusually high metal oxidation states has long been recognized in such textbook species as MnO_4^- and CrO_4^{2-}. More recently, some interesting new examples have been identified in which bridging O^{2-} ions stabilize rare oxidation states of Fe and Cu in non-mononuclear chemistry: apart from their intrinsic importance, such species offer insights into the mode of action of certain metalloenzymes. Thus, the $Fe^{III}Fe^{IV}$ oxidation level, thought to correspond to species X of ribonucleotide reductase,[1,2] has been obtained in oxide-bridged Fe_2 complexes,[2,3] whereas a $2Fe^{IV}$ species is believed to be species Q of methane monooxygenase.[1] Similarly, the $[Cu_2(\mu\text{-}O)_2]^{2+}$ core ($2Cu^{III}$) has been structurally characterized,[4,5] as well as a related species containing the $[Cu_3(\mu_3\text{-}O)_2]^{3+}$ core ($2Cu^{II}$, Cu^{III}).[6] Such species offer valuable insights into Cu-mediated O_2-activation biochemistry. We have now discovered that the cubane $[Co_4(\mu_3\text{-}O_4)_4]^{4+}$ core containing $4Co^{III}$ can be oxidized to a $3Co^{III}$, Co^{IV} form, and we describe the preparation and characterization of several such novel species.

As reported previously,[7] the D_{2d} symmetry complex $[Co_4O_4(O_2CR)_2(bpy)_4](ClO_4)_2$ **1** (R = Me; bpy = 2,2′-bipyridyl) can be prepared by deprotonating $[Co_2(OH)_2(O_2CMe)_3(bpy)_2](ClO_4)$ with Li_2O_2 in DMSO. A series of $[Co_4O_4(O_2CR)_2(bpy)_4](ClO_4)_2$ **1** complexes has now been prepared by ligand substitution with RCO_2H in refluxing MeCN, and electrochemical examination of these $[Co_4O_4]^{4+}$ complexes by cyclic voltammetry (CV) reveals irreversible reductions at $\leqslant -1.4$ V *vs.* ferrocene and a reversible one-electron oxidation at *ca.* 0.7 V *vs.* ferrocene. The CV scan for the R = $C_6H_4NO_2$-4 complex is shown in Fig. 1, and the oxidation potentials as a function of R group are listed in Table 1. The peak separations are comparable with that of the ferrocene/ferrocenium couple used as an internal reference (Fig. 1). Controlled potential coulometry at 0.90 V *vs.* ferrocene for the R = C_6H_4Me-4 and C_6H_4OMe-4 species gave 0.9–1.0 e^-/Co_4 transferred, confirming a one-electron oxidation process. The CV are thus consistent with oxidation to $[Co_4O_4(O_2CR)_2(bpy)_4]^{3+}$, which would contain $3Co^{III}$,Co^{IV} if the oxidation were metal-based. Metal/bpy complexes can often exhibit bpy-based reversible reductions but not oxidations.[8]

Analytically-pure oxidized clusters† were prepared in bulk by two methods: (i) controlled potential electrolysis in MeCN or MeCN–CH_2Cl_2 containing 0.4 M $LiClO_4$ at 0.90–1.00 V *vs.* ferrocene, which caused precipitation of $[Co_4O_4(O_2CR)_2(bpy)_4](ClO_4)_3$ **2** in $\geqslant$ 85% yield as microcrystalline powders; and (ii) oxidation with $(NH_4)_2Ce(NO_3)_6$ in MeCN, which caused precipitation of sparingly soluble microcrystalline $[Co_4O_4(O_2CR)_2(bpy)_4][Ce(NO_3)_6]$ **3**.‡ Complexes **2** can be recrystallized from MeCN–Et_2O. EPR spectra at 5 and 75–100 K of the R = C_6H_4Me-4 and C_6H_4OMe-4 derivatives as powders (**3**) or MeCN–toluene (1 : 1) glasses (**2**) show a broad (*ca.* 800 G) signal at g = 2.20 with no resolved hyperfine, consistent with a S = ½ species and a Co-based oxidation. Solid-state magnetic susceptibility studies at room temperature on the same two derivatives of **2** gave $\mu_{eff} \approx 2.2\ \mu_B$, consistent with one unpaired electron. ^{1}H NMR spectra show paramagnetically shifted and broadened signals for **2**, again consistent with S = ½ oxidized clusters whereas complexes **1** are diamagnetic. Comparison of the spectra for **1** and **2** (R = C_6H_4Me-4), for example, show that only four bpy and three carboxylate signals are observed and that the bpy signals are much more shifted on oxidation than the carboxylate signals,

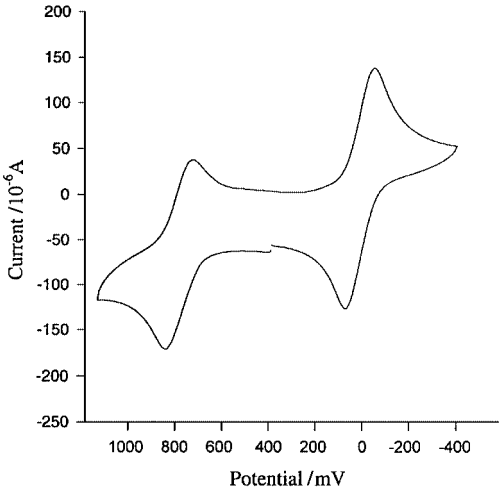

Fig. 1 Cyclic voltammogram at a glassy carbon electrode of **1**; R = $C_6H_4NO_2$-4 (1 mM) in MeCN containing 0.1 M $NBu^n_4PF_6$ and ferrocene as an internal standard ($E_{½}$ = 0.00 V).

Table 1 Cyclic voltammetric data for the oxidation of $[Co_4O_4(O_2CR)_2(bpy)_2](ClO_4)_2$ **1** complexes in MeCN[ab]

R	$E_{½}$[c]/V	R	$E_{½}$[c]/V
Me	0.69	C_6H_4OMe-4	0.68
CH=CHMe	0.70	$C_6H_3(OMe)_2$-2,4	0.68
Ph	0.70	C_6H_4Cl-4	0.72
C_6H_4Me-4	0.70	$C_6H_4NO_2$-4	0.77
C_6H_4Et-4	0.69	C_6F_5	0.86
$C_6H_4Bu^t$-4	0.67		

[a] In volts *vs.* the ferrocene/ferrocenium couple as an internal standard; ±0.01 V. [b] Glassy carbon working, Pt wire auxiliary, and SCE reference electrodes; 0.1 M $NBu^n_4PF_6$ supporting electrolyte. [c] $E_{½}$ is the midpoint of the forward (anodic) and reverse (cathodic) peak potentials.

 DOI: 10.1039/b102008k

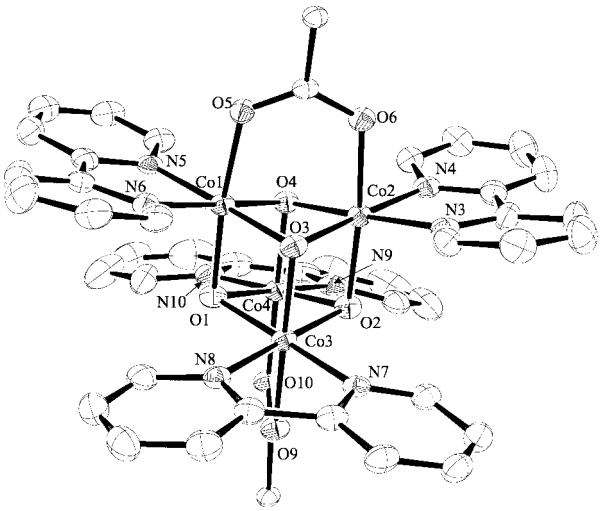

Fig. 2 ORTEP plot of the cation of **2** (R = $C_6H_4NO_2$-4) at the 40% probability level; for clarity, only the *ipso*-C atom of the carboxylate group is shown. Selected distances (Å): Co(1)···Co(2) 2.641(1), Co(1)···Co(3) 2.872(1), Co(1)···Co(4) 2.874(1), Co(2)···Co(3) 2.855(1), Co(2)···Co(4) 2.861(1), Co(3)···Co(4) 2.662(1), Co(1)–O(1) 1.903(4), Co(1)–O(3) 1.882(4), Co(1)–O(4) 1.876(3), Co(2)–O(2) 1.900(4), Co(2)–O(3) 1.877(4), Co(2)–O(4) 1.871(4), Co(3)–O(1) 1.902(4), Co(3)–O(2) 1.878(4), Co(3)–O(3) 1.886(4), Co(4)–O(1) 1.894(4), Co(4)–O(2) 1.882(4), Co(4)–O(4) 1.899(4).

consistent with greater spin delocalization onto the former groups. On the ^{1}H NMR timescale, therefore, the oxidized clusters retain D_{2d} symmetry, which is consistent with electronic delocalization, or detrapping that is fast on the ^{1}H NMR timescale.

The crystal structure‡ of complex **2** (R = $C_6H_4NO_2$-4) was obtained at –100 °C. The cation (Fig. 2) has no crystallographic symmetry, but has virtual D_{2d} symmetry. There is a $[Co_4O_4]$ cubane with a bpy at each Co and a RCO_2^- group bridging two opposite faces; the virtual S_4 axis passes through the latter. Three independent ClO_4^- groups confirm the 3+ charge of the cation. Examination of the bond distances shows that the four Co ions are all equivalent, indicating electronic delocalization and a $Co^{3.25+}$ oxidation state description, even in the solid state at −100 °C. The anisotropic thermal parameters of core Co and O atoms do not appear abnormally large, arguing against a static disorder of a trapped-valence $3Co^{III},Co^{IV}$ system. Protonation of a core O^{2-} ion (and a resulting $4Co^{III}$ description) is ruled out by the absence of Co–O bond lengthening as seen previously[9] in the genuinely protonated species $[Co_4O_3(OH)(O_2CR)_2(bpy)_4]^{3+}$ and $[Co_4O_2(OH)_2(O_2CR)_2(bpy)_4]^{4+}$. Comparison of the structure of **2** (R = $C_6H_4NO_2$-4) with that of **1** (R = C_6H_4Me-4) indicates no significant difference: the largest variation is in the Co–O (carboxylate) distances (average 1.942 Å for **2** *vs*. 1.955 Å for **1**) but these and all the other Co–X distances are statistically the same within the 3σ criterion.

The combined results indicate that the diamagnetic $[Co_4O_4]^{4+}$ core can be oxidized to a paramagnetic (S = ½) $[Co_4O_4]^{5+}$ core that is electronically delocalized, as might be expected for mixed-valence, low-spin Co^{III} (t_{2g}^6), Co^{IV} (t_{2g}^5) species. Cobalt(IV) is still a rare oxidation state, and isolated, well characterized examples that are stable at room temperature are few and all mononuclear,[10] but the combined results above establish that stable $[Co_4O_4]^{5+}$ clusters can be accessed which formally contain $3Co^{III}$, Co^{IV}. Such species could prove useful as a new family of strong oxidizing agents soluble in organic solvents, particularly since their oxidizing strength can be tuned by appropriate choice of organic ligands.

This work was supported by the National Science Foundation.

Notes and references

† The complexes analysed satisfactorily. Calc. (found) for $[Co_4O_4(O_2CC_6H_4Me\text{-}4)_2(bpy)_4](ClO_4)_3\cdot H_2O$: C, 44.51 (44.31); H, 3.20 (3.34); N, 7.42 (7.44); Cl, 7.04 (7.59). $[Co_4O_4(O_2CC_6H_4OMe\text{-}4)_2(bpy)_4](ClO_4)_3\cdot 3/2CH_2Cl_2$: C, 41.79 (41.78); H, 2.99 (3.15); N, 6.78 (6.93); Cl, 12.87 (12.18). $[Co_4O_4(O_2CC_6H_4Me\text{-}4)_2(bpy)_2][Ce(NO_3)_6]\cdot 2H_2O$: C, 38.59 (38.34); H, 2.89 (2.69); N, 11.25 (11.26). $[Co_4O_4(O_2CC_6H_4OMe\text{-}4)_2(bpy)_4][Ce(NO_3)_6]\cdot MeCN\cdot 2H_2O$: C, 39.19 (38.95); H, 2.96 (2.92); N, 12.19 (12.15). Electronic spectra in MeCN for the R = C_6H_4Me-4 complexes: **1**; 556 (sh), 414 (10800), 293 (65800). **2**; 520 (sh), 332 (sh), 314 (sh), 302 (47100).

‡ *Crystal data* for $[Co_4O_4(O_2CC_6H_4NO_2\text{-}4)_2(bpy)_4](ClO_4)_3\cdot MeCN\cdot 3H_2O$: $C_{56}H_{49}Cl_3Co_4N_{11}O_{27}$, M = 1650.16, triclinic, $P\bar{1}$, a = 11.6330(2), b = 14.1304(2), c = 20.7165(2) Å, α = 91.8195(6), β = 95.8450(8), γ = 110.1203(4)°, V = 3172.78(4) Å^3, Z = 2, D_c = 1.727 g cm^{-3}, λ = 0.71073 Å, T = −100 °C, $4 < 2\theta < 50°$, $R(R_w)$ = 0.0846 (0.2279) for refinement on F^2 using all 10537 unique reflections. The structure was solved and refined using SHELXTL-97. All non-hydrogen atoms were refined anisotropically. Three independent ClO_4^- ions were located, each at 100% occupancy. Hydrogen atoms were included as fixed atom contributors. No disorder problems were encountered.

CCDC reference number 161550. See http://www.rsc.org/suppdata/b1/b102008k/ for crystallographic data in CIF or other electronic format.

1 B. J. Wallar and J. D. Lipscomb, *Chem. Rev.*, 1996, **96**, 2625 and references therein.
2 H. Zheng, S. J. Yoo, E. Munck and L. Que, Jr., *J. Am. Chem. Soc.*, 2000, **122**, 3789 and references therein.
3 H.-F. Hsu, Y. Dong, L. Shu, V. G. Young, Jr. and L. Que, Jr., *J. Am. Chem. Soc.*, 1999, **121**, 5230.
4 J. A. Halfen, S. Mahapatra, E. C. Wilkinson, S. Kaderli, V. G. Young, Jr., L. Que, Jr., A. D. Zuberbühler and W. B. Tolman, *Science*, 1996, **271**, 1397; W. B. Tolman, *Acc. Chem. Res.*, 1997, **30**, 227; S. Mahapatra, V. G. Young, S. Kaderli, A. D. Zuberbühler and W. B. Tolman, *Angew. Chem., Int. Ed. Engl.*, 1997, **36**, 130.
5 V. Mahadevan, Z. Hou, A. P. Cole, D. E. Root, T. K. Lal, E. I. Solomon and T. D. P. Stack, *J. Am. Chem. Soc.*, 1997, **119**, 11 996.
6 A. P. Cole, D. E. Root, P. Mukherjee, E. I. Solomon and T. D. P. Stack, *Science*, 1996, **273**, 1848; D. E. Root, M. J. Henson, T. Machonkin, P. Mukherjee, T. D. P. Stack and E. I. Solomon, *J. Am. Chem. Soc.*, 1998, **120**, 4982.
7 K. Dimitrou, K. Folting, W. E. Streib and G. Christou, *J. Am. Chem. Soc.*, 1993, **115**, 6432.
8 C. A. Crawford, J. H. Matonic, J. C. Huffman, K. Folting, K. R. Dunbar and G. Christou, *Inorg. Chem.*, 1997, **36**, 2361; P. S. Braterman, J.-I. Song, F. M. Wimmer, S. Wimmer, W. Kaim, A. Klein and R. D. Peacock, *Inorg. Chem.*, 1992, **31**, 5084, and references therein.
9 K. Dimitrou, A. D. Brown, K. Folting and G. Christou, *Inorg. Chem.*, 1999, **38**, 1834.
10 F. C. Anson, T. J. Collins, R. J. Coots, S. L. Gipson and T. G. Richmond, *J. Am. Chem. Soc.*, 1984, **106**, 5037; E. K. Byrne and K. H. Theopold, *J. Am. Chem. Soc.*, 1987, **109**, 1282; J. W. Quail and G. A. Rivett, *Can. J. Chem.*, 1972, **50**, 2447; M. Koikawa, M. Gotoh, H. Okawa, S. Kida and T. Kohzuma, *J. Chem. Soc., Dalton Trans.*, 1989, 1613; J.-P. Barbier, B. M. Ondo and R. P. Hugel, *J. Chem. Soc., Dalton Trans.*, 1985, 597; Y. Yamamoto, E. Toyota and H. Konno, *Bull. Chem. Soc. Jpn.*, 1991, **64**, 1398.

CHEMCOMM Communication
www.rsc.org/chemcomm

Synthesis and structural characterisation of a boralumoxane capable of activating a zirconocene ethene polymerisation catalyst†‡

Bodo Richter, Auke Meetsma, Bart Hessen* and Jan H. Teuben

Dutch Polymer Institute/Centre for Catalytic Olefin Polymerisation, Stratingh Institute of Chemistry and Chemical Engineering, University of Groningen, Nijenborgh 4, 9747 AG Groningen, The Netherlands. E-mail: hessen@chem.rug.nl

Received (in Cambridge, UK) 24th April 2001, Accepted 1st June 2001
First published as an Advance Article on the web 27th June 2001

The reaction of Bu^t_3Al with $ArB(OH)_2$ (Ar = 2,6-diisopropylphenyl) leads, *via* the intermediate $[Bu^t_2Al(O)BAr(OH)]_2$ 1, to the crystallographically characterised boralumoxane $Al(Bu^t_2Al)(Bu^tAl)_2(O_2BAr)_4$ 3 which is able to activate Cp_2ZrMe_2 to effect catalytic ethene polymerisation.

The discovery of methylalumoxane (MAO) and its use as a cocatalyst for zirconocene-based olefin polymerisation catalysts[1] has spurred an explosive development of 'single-site' olefin polymerisation catalysts.[2] Despite its widespread use as a cocatalyst for these systems, the actual nature of MAO and the species responsible for its activating ability has still not been unequivocally established. Work by Barron and coworkers on *tert*-butylalumoxane model systems,[3] and various theoretical studies[4] have shown that this property is likely to stem from oligomeric $(MeAlO)_n$ clusters containing four-coordinate Al, that exhibit 'latent' Lewis acidity through ring-opening of strained Al_2O_2 four-membered rings. In several patents it was shown that boronic acids $RB(OH)_2$, boronic esters or boroxines $(RBO)_3$ can act as promotors, enhancing the activating properties of MAO.[5] Boralumoxane materials obtained from reactions of aluminium alkyls with boronic acids or boroxines have been shown to be active as cocatalysts in olefin polymerisation, but these are generally poorly defined species.[6] Very recently, reactions of borinic acids R_2BOH with aluminium trialkyls have yielded some well-defined complexes, but there have been no reports of their properties as cocatalysts.[7] Here we describe the synthesis and structural characterisation of the first well-defined boralumoxane with overall composition $[(RAlO)(R'BO)]_n$, and show that this species is capable of activating zirconocene dimethyl to effect catalytic ethene polymerisation.

In studying the reactivity between trialkylaluminium compounds and boronic acids $RB(OH)_2$ we have focused on Al and B compounds bearing sterically demanding ligands, in order to enhance the possibility of obtaining well-defined species. The reaction of $AlBu^t_3$ with an equimolar amount of the arylboronic acid $ArB(OH)_2$ (Ar = 2,6-diisopropylphenyl) in *n*-pentane solvent at 0 °C initially yielded the species $[Bu^t_2Al(O)BAr(OH)]_2$ **1**, obtained as an analytically pure solid in 83% yield (Scheme 1). The presence of isolated hydroxy groups was established by IR spectroscopy (ν_{OH} 3591 cm^{-1}) and ^1H NMR (OH δ 4.73).[8] It proved difficult to obtain **1** as single crystals suitable for X-ray structure determination. Its formulation as a dimer was supported by its reaction with Bu^nLi followed by the crystallisation of the Li salt $[Bu^t_2Al(O)BAr(OLi)]_2$ **2**, obtained as a benzene solvate. A structure determination§ of **2**·$2C_6H_6$ (Fig. 1) revealed an eight-membered $Al_2B_2O_4$ ring core. Two oxygen atoms on opposite positions on the ring bear Li atoms, that are further stabilised by the proximity of benzene molecules present in the crystal lattice (Li–$C_{benzene}$ distances range over 2.80–3.05 Å). The Al–O–B angle around the unsubstituted oxygen atom O(1) is relatively obtuse, 168.3(2)°, compared to the Al–O(2)–B angle of 128.1(1)°, and the Al(1)–O(1) distance of 1.744(2) Å is clearly shorter than Al(1)–O(2) of 1.821(2) Å. Based on this structure it seems reasonable to formulate **1** as the cyclic species $[Bu^t_2Al(\mu\text{-}O)BAr(\mu\text{-}OH)]_2$.

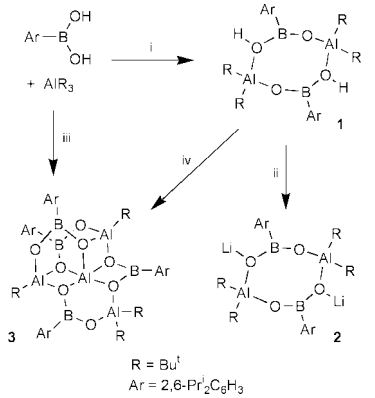

Scheme 1 *Reagents and conditions*: i, *n*-pentane, 0 °C, 1 h; ii, Bu^nLi, 20 °C, benzene; iii, toluene, 50 °C, recryst. from benzene; iv, hexane, reflux, 2 h.

Allowing a highly concentrated (0.38 M) solution of **1** in benzene-d_6 to stand at ambient temperature and monitoring the sample by ^1H NMR spectroscopy showed that isobutane is evolved gradually, and that various (as yet unidentified) transient species are formed. Eventually, all resonances attributable to hydroxy groups disappear, and a colourless crystalline compound is deposited. This product **3** could be obtained on a preparative scale (Scheme 1), either from **1** by refluxing in hexane for 2 h (48% isolated yield), or from a mixture of

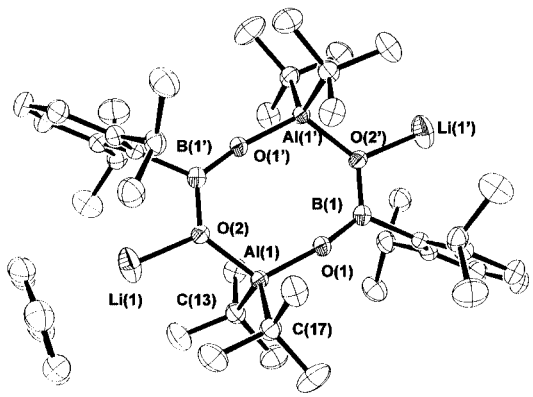

Fig. 1 Molecular structure of **2** (hydrogen atoms omitted for clarity). Selected interatomic distances (Å) and angles (°): Al(1)–O(1) 1.744(2), Al(1)–O(2) 1.821(2), Al(1)–C(13) 1.998(3), Al(1)–C(17) 2.003(2), B(1)–O(1) 1.319(3), B(1)–O(2) 1.380(3), O(2)–Li(1) 1.841(5); O(1)–Al(1)–O(2) 116.20(8), C(13)–Al(1)–C(17) 119.6(1), O(1)–B(1)–O(2) 123.7(2), Al(1)–O(1)–B(1) 168.3(2), Al(1)–O(2)-B(1′) 128.1(1).

† Electronic supplementary information (ESI) available: experimental, spectroscopic and polymerisation details. See http://www.rsc.org/suppdata/cc/b1/b103670j/

‡ Netherlands Institute for Catalysis Research (NIOK) publication no. RUG 01-4-03.

 DOI: 10.1039/b103670j

$ArB(OH)_2$ and Bu^t_3Al by warming in toluene at 50 °C followed by crystallization from benzene (79% isolated yield of its benzene solvate). Compound **3** was identified, by a crystal structure determination of its benzene solvate,§ as $Al(Bu^t_2Al)(Bu^tAl)_2(O_2BAr)_4$ (Fig. 2). The overall composition of the compound corresponds to a tetramer of 'Bu^{t}AlOBArO', but it is clear that the remaining *tert*-butyl groups are not evenly distributed over the four Al atoms. The central Al atom bears no alkyl substituent, and is bound to five oxygen atoms. The other three Al atoms are four-coordinate, and all B-atoms are three-coordinate. The structure of **3** may be described as consisting of three six- and three four-membered Al/B–O rings that share the central Al atom. One of the most notable features in the structure is that there are two edge-sharing four-membered rings, containing Al(1)O(2/7)Al(3) and Al(1)O(1/2)B(1), respectively. This arrangement is highly strained, as seen *e.g.* from the angles O(2)–Al(3)–O(7) 83.03(6)°, O(2)–Al(1)–O(7) 81.48(6)° and O(1)–Al(1)–O(2) 71.90(6)°, and may result in 'latent' Lewis acidic behaviour. The longest Al–O distances to four-coordinate Al in the structure are Al(2)–O(1), 1.940(1) Å, a bond to the relatively electron-rich Bu^t_2Al-group, and Al(3)–O(7), 1.890(2) Å, a bond to the Bu^{t}Al group in the edge-sharing four-membered ring assembly. In solution, the structure of **3** appears to be highly fluxional, showing at ambient temperature only two resonances for the Bu^t groups in the ^{1}H NMR spectrum. This fluxionality is likely to be due to rapid decomplexation/complexation of O(1) and O(6) to the central Al(1) atom. This results in an average C_2-symmetry of the complex, with the C_2 axis passing through Al(1) and bisecting the O(7)–Al(1)–O(4) angle.

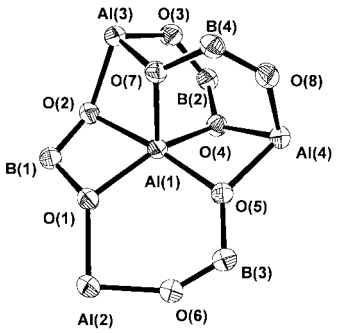

Fig. 2 Molecular structure of **3** (carbon and hydrogen atoms omitted for clarity; each B atom bears one 2,6-diisopropylphenyl group, Al(2) bears two Bu^t groups, Al(3) and Al(4) one Bu^t group each). Selected interatomic distances (Å) and angles (°): Al(1)–O(1) 1.869(1), Al(1)–O(2) 1.924(1), Al(1)–O(4) 1.867(1), Al(1)–O(5) 1.823(1), Al(1)–O(7) 1.851(1), Al(2)–O(1) 1.940(1), Al(2)–O(6) 1.761(2), Al(3)–O(2) 1.827(1), Al(3)–O(3) 1.747(2), Al(3)–O(7) 1.890(2), Al(4)–O(4) 1.873(1), Al(4)–O(5) 1.856(1), Al(4)–O(8) 1.759(1); O(1)–Al(1)–O(2) 71.86(6), O(1)–Al(1)–O(5) 104.00(7), O(4)–Al(1)–O(5) 81.54(6), O(2)–Al(1)–O(4) 97.24(6), O(2)–Al(1)–O(7) 81.48(6), O(1)–B(1)–O(2) 105.8(2), O(1)–Al(2)–O(6) 94.56(7), O(2)–Al(3)–O(7) 83.03(6).

Compounds **1** and **3** were each combined with an equimolar amount of the zirconocene dialkyl Cp_2ZrMe_2 **4** in toluene solvent and exposed to ethene (5 bar), in order to determine whether these species can act as activators for single-site olefin polymerisation catalysts. The combination of **1** and **4** (in an Al : Zr ratio of 2 : 1) did not result in ethene polymerisation activity. In contrast, the combination of **3** and **4** (in an Al : Zr ratio of 4 : 1) readily polymerised ethene to polyethene (M_w = 16600, M_w/M_n = 1.9) with a productivity of 2.59 kg mol^{-1} h^{-1} bar^{-1} (toluene, 5 bar ethene, 23 °C, 30 min run time).

In conclusion, we have shown that the reaction of the boronic acid $ArB(OH)_2$ (Ar = 2,6-diisopropylphenyl) with Bu^t_3Al results in stepwise formation of a well-defined boralumoxane species, $Al(Bu^t_2Al)(Bu^tAl)_2(O_2BAr)_4$ **3**, that is able to act as an activator for zirconocene alkyl olefin polymerisation catalysts. Although **3** contains structural units similar to those in the alumoxanes $[Bu^tAlO]_n$ obtained by Barron and coworkers[3] (six- and four-membered $[(Al/B)O]_n$ rings), it is topologically quite different from these due to three-coordinate B acting as structural element (compared to four-coordinate Al in the alumoxanes). It has in common with these species the presence of edge-sharing four-membered rings, and it is therefore possible that its activating properties are also due to the 'latent' Lewis acidic behaviour of these moieties, as proposed by Barron for the alumoxanes. Further research into the structural and reactivity features of these and related boralumoxanes is expected to shed more light on the nature and activating behaviour of alumoxane-based activators.

Notes and references

§ *Crystallographic data*: for **2**·2C$_6$H$_6$: $(C_{20}H_{35}AlBLiO_2)_2$·2C$_6$H$_6$, M = 860.64, monoclinic, space group $P2_1/n$, a = 11.773(1), b = 14.868(1), c = 15.097(2) Å, β = 90.863(6)°, U = 2642.3(5) Å^3, T = 180 K, Z = 2, D_c = 1.082 g cm^{-3}, μ = 0.95 cm^{-1}, Enraf-Nonius CAD4-F diffractometer, λ(Mo-Kα) = 0.71073 Å, 6058 unique reflections, final residuals $wR(F^2)$ = 0.1207, $R(F)$ = 0.0571 for 3501 reflections with $F_o \geqslant 4\sigma(F_o)$ and 444 parameters.

For **3**·2.5C$_6$H$_6$: $C_{64}H_{104}Al_4B_4O_8$·2.5C$_6$H$_6$, M = 1344.96, triclinic, space group $P\bar{1}$, a = 14.0027(5), b = 14.2483(5), c = 22.7478(9) Å, α = 79.888(1), β = 86.886(1), γ = 65.389(1)°, U = 4061.2(3) Å^3, T = 200 K, Z = 2, D_c = 1.100 g cm^{-3}, μ = 1.08 cm^{-1}, Bruker SMART APEX CCD diffractometer, λ(Mo-Kα) = 0.71073 Å, 20435 unique reflections, final residuals $wR(F^2)$ = 0.1689, $R(F)$ = 0.0582 for 13923 reflections with $F_o \geqslant 4\sigma(F_o)$ and 912 parameters. CCDC reference numbers 163150 and 163151. See http://www.rsc.org/suppdata/cc/b1/b103670j/ for crystallographic data in CIF or other electronic format.

1 W. Kaminsky, *J. Chem. Soc., Dalton Trans.*, 1998, 1413 and references therein.

2 H. H. Brintzinger, D. Fischer, R. Mülhaupt, B. Rieger and R. M. Waymouth, *Angew. Chem., Int. Ed. Engl.*, 1995, **34**, 1143; A. L. McKnight and R. M. Waymouth, *Chem. Rev.*, 1998, **98**, 2587; G. J. P. Britovsek, V. C. Gibson and D. F. Wass, *Angew. Chem., Int. Ed.*, 1999, **38**, 428 and references therein.

3 R. M. Mason, J. M. Smith, S. G. Bott and A. R. Barron, *J. Am. Chem. Soc.*, 1993, **115**, 4971; C. J. Harlan, M. R. Mason and A. R. Barron, *Organometallics*, 1994, **13**, 2957; C. C. Landry, C. J. Harlan, S. G. Bott and A. R. Barron, *Angew. Chem., Int. Ed. Engl.*, 1995, **34**, 1201; C. J. Harlan, S. G. Bott and A. R. Barron, *J. Am. Chem. Soc.*, 1995, **117**, 6465; M. Watanabi, C. N. McMahon, C. J. Harlan and A. R. Barron, *Organometallics*, 2001, **20**, 460.

4 T. Yamasaki, *Catal. Today*, 1995, **23**, 425; L. Boiteau, I. Demachy and F. Volatron, *Chem. Eur. J.*, 1997, **3**, 1860; M. Ystenes, J. L. Eilertsen, J. Liu, M. Ott, E. Rytter and J. A. Støvneng, *J. Polym. Sci. A*, 2000, **38**, 3106; E. Zurek, T. K. Woo, T. K. Firman and T. Ziegler, *Inorg. Chem.*, 2001, **40**, 361.

5 H. C. Welborn, *World Pat.*, WO9201005, 1992; F. Langhauser, M. Lux, R. Mülhaupt and D. Fischer, *World Pat.*, WO9316116, 1992; M. O. Kristen and D. Fischer, *World Pat.*, WO9840418, 1998.

6 R. L. Geerts, T. G. Hill and S. E. Kufeld, *US Pat.*, 5411925, 1995; R. L. Geerts and T. G. Hill, *US Pat.*, 5414180, 1995; R. L. Geerts, *US Pat.*, 5480840, 1996; T. Sugano and T. Takahama, *US Pat.*, 5449650, 1995; H. Bohnen, *World Pat.*, WO9906414, 1999.

7 R. Anulewicz-Ostrowska, S. Lulinsky and J. Serwatowsky, *Inorg. Chem.*, 1999, **38**, 3796; R. Anulewicz-Ostrowska, S. Lulinsky, J. Serwatowsky and K. Suwinska, *Inorg. Chem.*, 2000, **39**, 5763; V. C. Gibson, S. Mastroianni, A. J. P. White and D. J. Williams, *Inorg. Chem.*, 2001, **5**, 826.

8 NMR data for **1**: ^{1}H NMR (500 MHz, C$_6$D$_6$, 298 K) δ 7.22 (t, $^3J_{HH}$ 7.5 Hz, 1 H, *p*-H), 7.05 (d, $^3J_{HH}$ 7.5 Hz, 2 H, *m*-H), 4.73 (s, 1 H, OH), 3.24 (sept, $^3J_{HH}$ 7.0 Hz, 2 H, C*H*Me$_2$), 1.38 (br, 6 H, CH*Me*$_2$), 1.28 (br, 6 H, CH*Me*$_2$), 1.11 (s, 18 H, CMe$_3$). ^{13}C{^{1}H} NMR (75 MHz, C$_6$D$_6$, 298 K) δ 151.2 (*o*-ArC), 130.6 (*p*-ArCH), 123.3 (*m*-ArCH), 35.8 (*C*HMe$_2$), 30.0 (*CMe*$_3$), 26.8 (br, CH*Me*$_2$) 25.0 (br, CH*Me*$_2$). ^{11}B NMR (160 MHz, C$_6$D$_6$, 298 K) δ 21.5 ($W_{1/2}$ = 1495 Hz). ^{27}Al NMR (130 MHz, C$_6$D$_6$, 298 K) δ 128.6 ($W_{1/2}$ = 18.9 kHz).

9 NMR data for **3**: ^{1}H NMR (500 MHz, toluene-d$_8$, 298 K) δ 7.26 (t, $^3J_{HH}$ 8.0 Hz, 2 H, *p*-H), 7.13 (m, 6 H, *p*- and *m*-H), 7.02 (d, 4 H, *m*-H), 3.31 (sept, $^3J_{HH}$ 6.5 Hz, 2 H, C*H*Me$_2$), 3.27 (sept, $^3J_{HH}$ 6.5 Hz, 2 H, C*H*Me$_2$), 3.23 (br, 4 H, C*H*Me$_2$), 1.49 (br, 12 H, CH*Me*$_2$), 1.40 (br, 24 H, CH*Me*$_2$), 1.33 (br, 12 H, CH*Me*$_2$), 1.16 (s, 18 H, CMe$_3$), 0.56 (s, 18 H, CMe$_3$). ^{13}C NMR (75 MHz, toluene-d$_8$, 298 K) δ 153.4 (*o*-ArC), 153.0 (*o*-ArC), 131.4 (*p*-ArCH), 130.9 (*p*-ArCH), 123.1 (*m*-ArCH), 123.0 (*m*-ArCH), 36.2 (br, *C*HMe$_2$), 35.9 (*C*HMe$_2$), 35.8 (*C*HMe$_2$), 30.5 (C*Me*$_3$), 29.3 (CH*Me*$_3$), 26.4 (br, CH*Me*$_2$), 25.7 (CH*Me*$_2$). ^{11}B NMR (160 MHz, toluene-d$_8$, 298 K) δ 31.9 ($W_{1/2}$ = 2957 Hz). ^{27}Al NMR (130 MHz, toluene-d$_8$, 353 K) δ 123.3 ($W_{1/2}$ = 34.5 kHz), 50.3 ($W_{1/2}$ = 3550 Hz).

CHEMCOMM
Communication
www.rsc.org/chemcomm

The X-ray crystal structure of *N*,*S*-bis[(4′-chloro-2,2′:6′,2″-terpyridine)platinum(II)]-2-mercaptoimidazole tris-hexafluorophosphate and tris[(2,2′:6′,2″-terpyridine)platinum(II)]sulfonium tetra-perchlorate†

Gordon Lowe,*[a] Steven A. Ross,[a] Michael Probert[b] and Andrew Cowley[b]

[a] *The Dyson Perrins Laboratory, Department of Chemistry, Oxford University, South Parks Road, Oxford, UK OX1 3QY. E-mail: gordon.lowe@chem.ox.ac.uk*
[b] *Chemical Crystallography, Department of Chemistry, Oxford University, 9 Parks Road, Oxford, UK OX1 3PD*

Received (in Cambridge, UK) 24th April 2001, Accepted 1st June 2001
First published as an Advance Article on the web 27th June 2001

Intramolecular stacking of the (4′-chloro-2,2′:6′,2″-terpyridine)platinum(II) moieties occurs in *N*,*S*-bis[(4′-chloro-2,2′:6′,2″-terpyridine)platinum(II)]-2-mercaptoimidazole tris-hexafluorophosphate; *N*,*S*-bis[(2,2′:6′,2″-terpyridine)-platinum(II)]thioacetimine trinitrate is slowly transformed in aqueous solution to the molecular propeller-like tris-[(2,2′:6′,2″-terpyridine)platinum(II)]sulfonium ion.

We have recently shown that (2,2′:6′,2″-terpyridine)platinum(II) complexes are cytotoxic to human ovarian carcinoma and that bis[(2,2′:6′,2″-terpyridine)platinum(II)] complexes with short and rigid linkers are particularly effective.[1] This study has been extended to (2,2′:6′,2″-terpyridine)platinum(II) thiolate complexes.[2] Since intercalation into DNA of such molecules may contribute to their antitumour activity we investigated the crystal structure of *N*,*S*-bis[(4′-chloro-2,2′:6′,2″-terpyridine)platinum(II)]-2-mercaptoimidazole tris-hexafluorophosphate **1** in order to determine whether the two (4′-chloro-2,2′:6′,2″-terpyridine)platinum(II) moieties were stacked. If they are, this might be expected to preclude intercalation into DNA.

As seen in Fig. 1 the two (4′-chloro-2,2′:6′,2″-terpyridine)platinum(II) moieties stack virtually parallel to each other, the platinum–platinum distance being 3.2903 Å.‡ The crystals were obtained from water. This stacking of the (4′-chloro-2,2′:6′,2″-terpyridine)platinum(II) moieties in **1**, is maintained in solution,[3] and should preclude it from intercalating into DNA. This supports the conclusion reported recently that DNA is not the principal target for the antitumour activity of these complexes.[2]

The bis-complex **2**, which was characterised spectroscopically (ESI)† is expected to adopt a similar conformation to **1**. However, unlike **1** and its analogue *N*,*S*-bis[(2,2′:6′,2″-terpyridine)platinum(II)]-2-mercaptoimidazole ion (which were stable), it was observed that on storing the bis-complex **2** in aqueous solution over a period of weeks, decomposition occurred ($t_{1/2}$ = 10.5 days at 20 °C) releasing acetamide and a new complex[4] which was shown by electrospray mass spectrometry to have *m*/*z* = 444 (M^{2+} with isotope distribution for two Pt atoms) consistent with the complex **3** (Scheme 1). The thioacetimine moiety in **2** would be activated by the 2,2′:6′,2″-terpyridine platinum(II) complexes and the tetrahedral intermediate formed from **2** by the nucleophilic attack of water would be expected to collapse to **3** and acetamide. The X-ray

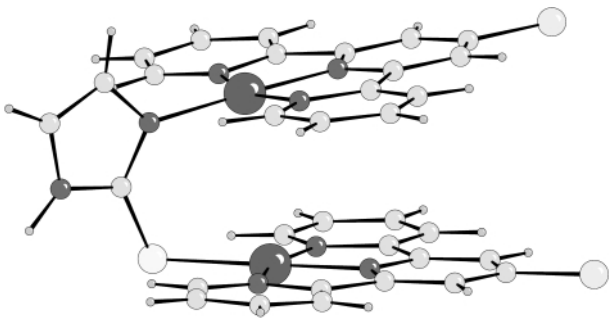

Fig. 1 The X-ray crystal structure of *N*,*S*-bis[(4′-chloro-2,2′:6′,2″-terpyridine)platinum(II)]-2-mercaptoimidazole tris-hexafluorophosphate **1**, showing the stacked (4′-chloro-2,2′:6′,2″-terpyridine)platinum(II) complexes with a Pt–Pt distance of 3.2903 Å and an interplanar angle of 7.5(5)°. The bond lengths to 2-mercaptoimidazole are Pt–S [2.312(4) Å] and Pt–N [2.021(4) Å]. The counter ions and solvent of crystallization are excluded for clarity.

† Electronic supplementary information (ESI) available: spectroscopic data for **1** and **2**. See http://www.rsc.org/suppdata/cc/b1/b103637h/

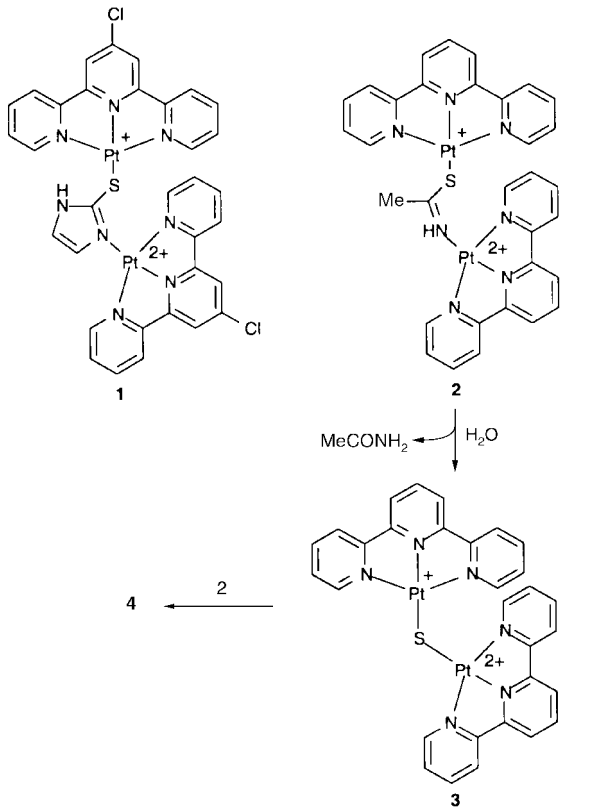

Scheme 1

 DOI: 10.1039/b103637h

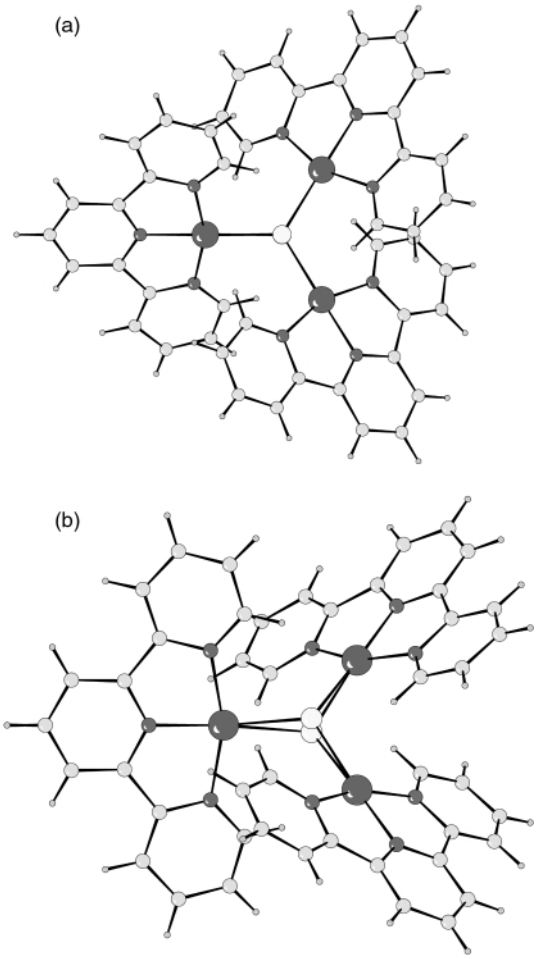

Fig. 2 The X-ray crystal structure of tris[(2,2′:6′,2″-terpyridine)platinum(II)]sulfonium tetra-perchlorate **4**: (a) down the three-fold axis and (b) at an angle to the three-fold axis showing molecules with the same propeller helicity with the sulfur atom above or below the reference plane of the three Pt atoms. The Pt–S bond lengths are 2.32 ± 0.01 Å and the tilt of the three (2,2′:6′,2″-terpyridine)platinum(II) planes is 40 ± 1° to the reference plane of the three Pt atoms. The counter ions and solvent of crystallization are excluded for clarity.

crystal structure of the product [Fig. 2(a)] is clearly not **3**. This tris[(2,2′:6′,2″-terpyridine)platinum(II)]sulfonium salt **4**‡ could be formed from **3** by sulfur abstracting (2,2′:6′,2″-terpyridineplatinum(II) from **2**. Tris[(2,2′:6′,2″-terpyridine)platinum(II)]sulfonium ion **4** would be expected to readily fragment to **3** in the mass spectrometer. Although aliphatic thioethers (*e.g.* methionine)[5] and dimethyl sulfoxide[6] will not ligate to 2,2′:6′,2″-terpyridine)platinum(II) because of the steric hindrance with the 6,6″ hydrogens, the planar nature of the substituents at sulfur in **3** and the longer S–Pt bond compared with the S–C bond make it possible to form **4**.

The X-ray crystal structure shows that the three (2,2′:6′,2″-terpyridine)platinum(II) moieties generate propeller-like helicity which can be right- or left-handed. Sulfur is at the apex of a shallow pyramid, with the S atom 0.354 Å above or below the reference plane formed by the three Pt atoms which are at the apices of an equilateral triangle (Fig. 2). It is not however a stereogenic centre. The three N′–Pt–S bond angles are 172° to accommodate the pyramidalization at sulfur. Thus flipping the molecule through 180° leaves the molecular helicity unchanged but with the sulfur atom on the opposite side of the reference plane formed by the three Pt atoms. Thus each enantiomer (left or right-handed molecular propeller) has crystallised in two orientations in the crystal lattice with equal probability leading to the two positions observed for the sulfur atom [Fig. 2(b)]. The tilt of the (2,2′:6′,2″-terpyridine)platinum(II) moieties from the reference plane of the Pt atoms is 40 ± 1° for each 'blade' of the propeller. Thus the flanking pyridine rings of each (terpyridine)platinum(II) moiety that are on the same side of the reference plane as the sulfur atom are in a different molecular environment from the flanking pyridine rings on the side opposite the sulfur atom. Consequently all ^{1}H resonances of the terpyridines in the NMR spectrum have different chemical shifts and are not resolved.

Propeller-like molecules have been extensively investigated.[7] Because of the necessity for the correlated rotation of the (2,2′:6′,2″-terpyridine)platinum(II) moieties, the tris-[(2,2′:6′,2″-terpyridine)platinum(II)]sulfonium ion forms stable left- and right-handed propeller-like molecules.

We gratefully acknowledge EPSRC/BBSRC support for this work.

Notes and references

‡ Crystal structure determinations: complex **1**: *Crystal data*: $C_{33}H_{23}Cl_2F_{18}N_8O_2P_3Pt_2S$, M = 1491.63, triclinic, space group $P\bar{1}$, a = 11.9306(1), b = 14.3873(2), c = 15.3729(2) Å, α = 97.1106(5), β = 112.5601(5), γ = 109.7985(5)°, U = 2192.8 Å^3, T = 190 K, Z = 2, μ(Mo-Kα) = 6.773 mm^{-1}, 33327 reflections measured, 8930 unique (R_{int} = 0.032), 7689 observed with $I > 3\sigma(I)$ which were used in all calculations. The final $wR(F)$ was 0.0375 for observed data.

Complex **4**: *Crystal data*: $C_{57}H_{57}Cl_4N_9O_{20}Pt_3S$, M = 973.63, monoclinic, space group $C12/c1$, a = 15.2505(3), b = 24.4126(5), c = 17.3087(3) Å, β = 90.0327(15), U = 6444.1 Å^3, T = 190 K, Z = 4, μ(Mo-Kα) = 6.776 mm^{-1}, 20122 reflections measured, 6940 unique (R_{int} = 0.031), 6004 observed with $I > 3\sigma(I)$ which were used in all calculations. The final $wR(F)$ was 0.0306 for observed data. Owing to the volatility of the solvate the crystal was mounted in a Lindemann tube.

CCDC reference numbers 162979 and 162980. See http://www.rsc.org/suppdata/cc/b1/b103637h/ for crystallographic data in CIF or other electronic format.

1 G. Lowe, A. S. Droz, T. Vilaivan, G. W. Weaver, J. J. Park, J. M. Pratt, L. Tweedale and L. R. Kelland, *J. Med. Chem.*, 1999, **42**, 3167.
2 K. Becker, C. Herold-Mende, J. J. Park, G. Lowe and R. H. Schirmer, *J. Med. Chem.*, 2001, **44**, in press.
3 The UV–VIS spectrum of **1** in aqueous solution (determined by Dr R. Quarrell) shows absorption bands at λ_{max}/nm (ε/dm^3 mol^{-1} cm^{-1}) 205 (100600), 243 (69050), 273 (52500), 300–360 (charge transfer) and 477 (3260). The broad band at 477 nm is characteristic of stacking of the (4-chloro-2,2′:6′,2″-terpyridine)platinum(II) moieties, see: H.-K. Yip, C.-M. Che, Z.-Y. Zhou and T. C. W. Mak, *J. Chem. Soc., Chem. Commun.*, 1992, 1369; G. Lowe and T. Vilaivan, *J. Chem. Soc., Perkin Trans. 1*, 1996, 1499.
4 Complex **2** (50 mg) was dissolved in water (2 mL) to which was added excess sodium perchlorate, followed by acetone (2 mL). The solution was allowed to evaporate slowly over 3 weeks which gave **4** as red crystals (*ca.* 20 mg).
5 E. M. A. Ratilla, H. M. Brothers and N. M. Kostic, *J. Am. Chem. Soc.*, 1987, **109**, 4592; S. L. Pinnow, H. M. Brothers II and N. M. Kostic, *Croat. Chem. Acta*, 1991, **64**, 519.
6 C. A. Carr, J. M. Richards, S. A. Ross and G. Lowe, *J. Chem. Res. (S)*, 2000, 566.
7 K. Mislow, *Acc. Chem. Res.*, 1976, **9**, 26; E. L. Eliel and S. H. Wilen, *Stereochemistry of Organic Compounds*, John Wiley & Sons, Inc., 1994, 1156.

CHEMCOMM Communication
www.rsc.org/chemcomm

Synthesis of planar chiral tricarbonylcyclopentadienylmanganese complexes using a $Mn(CO)_3^+$ transfer reaction†

Seung Uk Son,[a] Kang Hyun Park,[a] Seung Jung Lee,[a] Young Keun Chung*[a] and Dwight A. Sweigart*[b]

[a] *School of Chemistry and Center for Molecular Catalysis, Seoul National University, Seoul 151-747, Korea. E-mail: ykchung@plaza.snu.ac*
[b] *Department of Chemistry, Brown University, Providence, RI 02912, USA*

Received (in Cambridge, UK) 22nd March 2001, Accepted 30th May 2001
First published as an Advance Article on the web 27th June 2001

Planar chiral ligand transfer reactions can be carried out by the reaction of [(naphthalene)$Mn(CO)_3$]BF_4 with planar chiral ferrocene derivatives.

Ligand transfer from one metal to another is a useful reaction when the complex cannot be easily prepared by conventional methods and is popular in organometallic chemistry.[1] Among these, cyclopentadienyl transfer reactions may be of synthetic interest,[2,3] in particular if cheap substrates such as commercially available ferrocene derivatives can be used as starting materials. However, there have been no reports of ligand transfer reactions from ferrocene derivatives to a manganese moiety to prepare cyclopentadienyl manganese complexes. Such complexes have many notable features such as high thermal stability, lack of substantial air or water sensitivity, kinetic inertness toward substitution reactions, and stereochemical robustness. These characteristics will be useful properties when manganese complexes are used as auxiliaries in other reactions.

Herein we report the synthesis of planar chiral cyclopentadienyltricarbonylmanganese complexes from the reaction of planar chiral ferrocenes with [(η^6-naphthalene)$Mn(CO)_3$]BF_4[4] and their application in asymmetric reactions. Planar chiral chelates of $CpMn(CO)_3$ derivatives are quite rare and hence their use in asymmetric reactions has not been developed. There has been a report[5] of enantioselective allylic substitution of cyclic substrates by catalysis with palladium complexes of *P*,*N*-chelate ligands attached to a $CpMn(CO)_3$ unit.

Refluxing equimolar amounts of a planar chiral ferrocene derivative **1a** and [(η^6-naphthalene)$Mn(CO)_3$]BF_4 in the presence of 4 Å molecular sieves in CH_2Cl_2, followed by standard work-up procedures, led to a 46% yield of the air-stable, planar chiral tricarbonylcyclopentadienylmanganese complex **2a** [eqn. (1)].‡

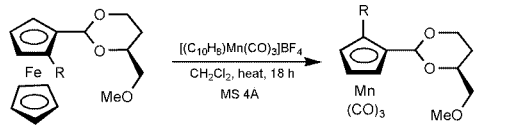

(1)

1a-c

2a R = Me
2b R = $SiMe_3$
2c R = $SiMe_2(CH{=}CH_2)$

As far as we are aware, this is the first use of a ligand transfer reaction in the synthesis of a planar chiral tricarbonylcyclopentadienylmanganese complex. Interestingly, formation of $CpMn(CO)_3$ was not observed in the reaction products. Birch *et al.*[6] first tested the idea of chirality transfer in the reaction between a chiral donor complex and an unsymmetrical diene ligand. Since then, there have been many reports on the synthesis of chiral organometallic compounds.[7] However, there have been no known reactions on the synthesis of tricarbonylcyclopentadienylmanganese derivatives. Surprisingly, during the transfer reaction, a *complete inversion* of the absolute configuration occurred [eqn. (1)]. This suggests that a bimetallic species [Cp–Fe–Cp–$Mn(CO)_3$]$^+$ **A**, in which one of the Cp rings

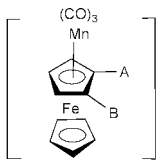

A

is coordinated to both metals, occurs as an intermediate in this reaction especially given the recent isolation and characterization of bimetallic complexes [Cp*–M–Cp*–$Mn(CO)_3$]$^+$ (M = Fe, Ru, Os).[8] In the same way, compounds **2b**,**c** were synthesized from the corresponding mixed ferrocenes **1b**,**c**. According to the study of Herberich *et al.*,[9] the migrating Cp is always the unsubstituted ligand. They explained this observation based upon on the electronic structural differences between Cp^- and Cp^{*-}. However, in our case, the substituted cyclopentadienyl ligand always migrated.

Acid hydrolysis of **2a** yielded the known compound **3** [eqn. (2)];[10] according to the ^1H NMR spectrum of **2a** and the optical rotation of **3**, compound **3** is optically pure.

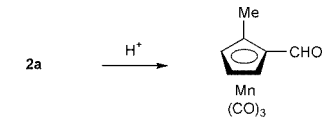

(2)

3

We investigated whether the triol group in **2** could be used as a directing group in the functionalization of the cyclopentadienyl ring. Deprotonation of **2a** by Bu^{t}Li followed by the addition of PPh_2Cl yielded **4** in 67% yield [eqn. (3)].

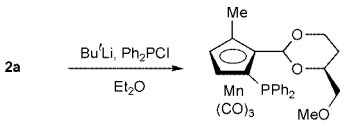

(3)

4

The structure of **4** was confirmed by an X-ray crystal structure determination (Fig. 1).[11] Thus, the diphenylphosphino group was successfully introduced with the aid of the triol group.

We next investigated the use of the ligand transfer reaction in the synthesis of *P*,*N*-ligands and studied palladium-catalyzed asymmetric allylic alkylation. The use of ligands derived from (arene)$Cr(CO)_3$ as a chiral chelating ligand is quite popular.[12] However, the use of $CpMn(CO)_3$ as a chiral chelating ligand is quite rare.[5]

† Electronic supplementary information (ESI) available: characterization of **2b**, **2c**, **4**, **6**, **7**, **8** and **9**, and a typical procedure for Pd-catalyzed allylic alkylation. See http://www.rsc.org/suppdata/cc/b1/b102693n/

 DOI: 10.1039/b102693n

The planar chiral *P*,*N*-ligands **9** were synthesized from **5** [eqn. (4)].

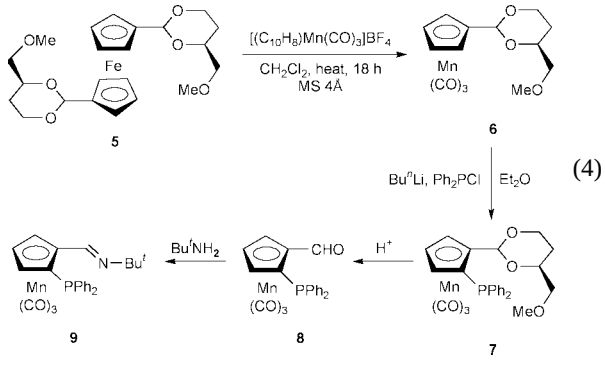

(4)

Ligand transfer reaction of **5** afforded **6** in 74% yield. Deprotonation of **6** followed by the addition of PPh_2Cl and subsequent reaction with acid gave **8** in 75% yield. The condensation reaction of **8** with *tert*-butyl amine gave a *P*,*N*-ligand **9a** in 96% yield. The de of **7** prepared from **6** was 75%. However, after recrystallization, the de of **7** was > 99.5%.

The palladium-catalyzed asymmetric allylic alkylation of *rac*-1,3-diphenylprop-2-en-1-yl acetate with dimethyl malonate was successfully carried out [eqn. (5)].

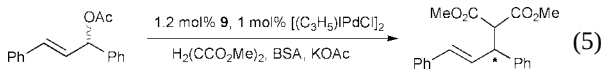

(5)

Reaction of *rac*-1,3-diphenylprop-2-en-1-yl acetate with dimethyl malonate in the presence of 1 mol% Pd catalyst at 15 °C for 4 h gave the allylic alkylation product methyl-2-carbomethoxy-3,5-diphenylpent-4-enolate in high yields and high ee values (95% yield and 89% ee in CH_2Cl_2; 96% yield and 92% ee in DMSO). Lowering the reaction temperature to −20 °C in CH_2Cl_2 led to an increase of the ee value to 94% with a 74% yield.

In conclusion, we have conducted the first demonstration that a planar chiral ligand transfer reaction can be carried out by the reaction of $[(naphthalene)Mn(CO)_3]BF_4$ with planar chiral ferrocene derivatives and we have shown that the *P*,*N*-ligand prepared in this study can be employed in palladium-catalyzed asymmetric allylic alkylation.

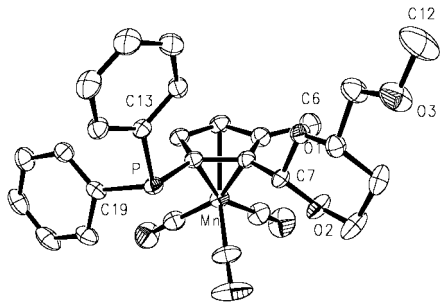

Fig. 1 X-Ray structure of **4**.

Notes and references

‡ Compounds $(\eta^6\text{-}C_{10}H_8)Mn(CO)_3]BF_4$, **1** and **5** were synthesized as previously described.[4a,13,14]

Synthesis of **2a**: a Schlenk flask containing 0.50 g of molecular sieves was flame-dried. After the flask was cooled to r.t., **1a** (0.35 g, 1.06 mmol), $[(\eta^6\text{-}C_{10}H_8)Mn(CO)_3]BF_4$ (0.40 g, 1.13 mmol), and 15 mL of CH_2Cl_2 were added to the flask. The resulting solution was heated at reflux for 18 h. After the solution was cooled to r.t., the solution was filtered over a pad of Celite. The filtrate was evaporated to dryness and chromatographed on a silica gel column eluting with hexane and diethyl ether (10 : 1 v/v). Removal of the solvent gave **2a** (oil, 46%, 0.17 g). IR ν(CO) 2012, 1920 cm^{-1}; δ_H(300 MHz, d_6-benzene, TMS) 5.21 (br s, 1 H), 5.03 (br s, 1 H), 4.15 (br s, 1 H), 4.07 (dd, 3.7, 11.0 Hz, 1 H), 3.85 (m, 1 H), 3.60 (m, 2 H), 3.56 (m, 1 H), 3.55 (s, 3 H), 2.05 (s. 3 H), 1.87 (m, 1 H), 1.26 (d, 13.0 Hz, 1 H); δ_C(75 MHz, d_6-benzene) 225.7, 102.8, 99.5, 96.4, 82.6, 81.1, 79.8, 76.1, 75.3, 66.6, 59.1, 28.0, 12.1; HRMS calc. for $C_{15}H_{16}MnO_6$: *m*/*z* 349.0484; obs: 349.0483. $[\alpha]_D^{21} = -36$ (*c* 0.42 in CH_2Cl_2).

1 A. Z. Rubezhov and S. P. Gubin, *Adv. Organomet. Chem.*, 1972, **10**, 347; A. Efraty, *J. Organomet. Chem.*, 1973, **57**, 1; P. E. Garrou, *Adv. Organomet. Chem.*, 1984, **23**, 95.

2 S. Top, C. Lescop, J.-S. Lehm and G. Jaouen, *J. Organomet. Chem.*, 2000, **593**–**594**, 167; R. L. Halterman, *Chem. Rev.*, 1992, **92**, 965.

3 T. W. Spradau and J. A. Katzenellenbogen, *Organometallics*, 1998, **17**, 2009; M. Wenzel, *J. Labelled Compd. Radiopharm.*, 1992, **31**, 641.

4 (*a*) S. Sun, L. K. Yeung, D. A. Sweigart, T.-Y. Lee, S. S. Lee, Y. K. Chung, S. R. Switzer and R. D. Pike, *Organometallics*, 1995, **14**, 2613; (*b*) J. E. Kim, J. S. U. Son, S. S. Lee and Y. K. Chung, *Inorg. Chim. Acta*, 1998, **281**, 229; (*c*) I. S. Lee, H. M. Seo and Y. K. Chung, *Organometallics*, 1999, **18**, 1091.

5 S. Kudis and G. Helmchen, *Angew. Chem., Int. Ed.*, 1998, **37**, 3047.

6 A. J. Birch, W. D. Raverty and G. R. Stephenson, *Tetraheron Lett.*, 1980, 197.

7 V. I. Sokolov, *Chirality and Optical Activity of Organometallics Compounds*, Gordon and Breach, New York, 1990; A. Togni, *Metallocenes*, ed. A. Togni and R. L. Halterman, Wiley-VCH: Weinheim, Germany, 1998, vol. 2.

8 E. J. Watson, K. L. Virkaitis, H. Li, A. J. Nowak, J. S. D'Acchioli, K. Yu, G. B. Carpenter, Y. K. Chung and D. A. Sweigart, *Chem. Commun.*, 2001, 457.

9 G. E. Herberich, U. Englert, F. Marken and P. Hofmann, *Organometallics*, 1993, **12**, 4039.

10 N. M. Loim, M. A. Kondratenkp and V. I. Sokolov, *J. Org. Chem.*, 1994, **59**, 7485; Y. Yamazaki, *J. Chromatogr.*, 1991, **542**, 129.

11 *Crystal data*: for **4**: monoclinic, space group $P2_1$; a = 8.0816(7), b = 15.0390(4), c = 10.9049(9) Å, β = 90.422(3)°, V = 1325.34(16) Å^3, Z = 2, D_c = 1.334 Mg m^{-3}; $-10 < h < 10$, $-17 < k < 17$, $-14 < l < 13$, $R1$ = 0.0379, $wR2$ = 0.10791. For **7**: orthorhombic, space group $P2_12_12_1$; a = 7.6659(2), b = 17.7774(8), c = 18.6479(10) Å; V = 2541.33(19) Å^3, Z = 4; D_c = 1.355 Mg m^{-3}; $-9 < h < 9$, $-23 < k < 22$, $-24 < l < 24$; $R1$ = 0.0526, $wR2$ = 0.1398. CCDC reference numbers 157495 and 157496. See http://www.rsc.org/suppdata/cc/b1/b102693n/ for crystallographic data in CIF or other electronic format.

12 M. Uemura, R. Miyake and Y. Hayashi, *J. Chem. Soc., Chem. Commun.*, 1991, 1696; S. B. Heaton and G. B. Jones, *Tetrahedron Lett.*, 1993, **33**, 1693; Y. Hayashi, H. Sakai, N. Kaneta and M. Uemura, *J. Organomet. Chem.*, 1995, **503**, 143; H.-Y. Jang, H. Seo, J. W. Han and Y. K. Chung, *Tetrahedron Lett.*, 2000, **41**, 5083; C. Bolm and K. Muniz, *Chem. Soc. Rev.*, 1999, **28**, 51.

13 O. Riant, O. Samuel, T. Flessner, S. Tandien and H. Kagan, *J. Org. Chem.*, 1997, **62**, 6733.

14 G. Hftime, J.-C. Daran, E. Manoury and G. G. A. Balavoine, *J. Organomet. Chem.*, 1998, **565**, 115.

CHEMCOMM
Communication
www.rsc.org/chemcomm

Unusual binding mode of the biimidazolate bridging ligand in two novel heteropolynuclear complexes with an M_2Ag_2 [M = Ru(II) or Os(II)] core†

Partha Majumdar,[a] Kunal K. Kamar,[a] Alfonso Castiñeiras[b] and Sreebrata Goswami*[a]

[a] *Department of Inorganic Chemistry, Indian Association for the Cultivation of Science, Calcutta 700 032, India. E-mail: icsg@mahendra.iacs.res.in*
[b] *Departamento de Quimica Inorganica, Facultade de Farmacia, Universidade de Santiago de Compostela, 15706 Santiago de Compostela, Spain*

Received (in Cambridge, UK) 4th January 2001, Accepted 4th June 2001
First published as an Advance Article on the web 27th June 2001

Two novel examples of heteronuclear tetrametallic M_2Ag_2 (M = Ru, Os) complexes are described which show strong argentophilic interactions.

The coordination ability of 2,2′-biimidazole is varied and interesting.[1] As a bidentate chelate it can bind as a neutral molecule H_2Biim, the monoanion $[HBiim]^-$ or the dianion $[Biim]^{2-}$. In addition, the mono- and the di-anions also can act as bridging ligands leading to the synthesis of di- and polynuclear complexes. Such polynuclear ruthenium complexes of 2,2′-biimidazolate and its derivatives[2] have received much attention in recent years. Usually the biimidazolate dianion coordinates as a bis-chelating tetradentate ligand (type I). The ligand can also behave as a tetradentate bridge attached to three metal centers (type II). However, the latter coordination mode of bridging $[Biim]^{2-}$ is very limited. As far as we are aware, the rhodium complex, $Rh_4(CO)_8(Biim)_2$ is the only structurally authenticated compound[3] which belongs to this category.

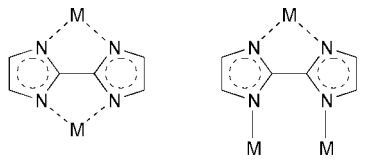

I II

This communication deals with the isolation and characterisation of two novel heterometallic tetranuclear compounds with Ru_2Ag_2 and Os_2Ag_2 cores where the bridging $[Biim]^{2-}$ attaches to three metal atoms (type II).

In a recent publication[4] we have shown that in the presence of a strong π-acid co-ligand 2-(phenylazo)pyridine (pap), the complexes $[M(pap)_2(BiimH_2)]^{2+}$ (M = Ru, Os), exhibit relatively low pK_a values (pK_a: M = Ru, 4.2 and 8.0; M = Os, 3.8 and 6.5). The neutral conjugate bases, $[M(pap)_2(Biim)]$, behave as potential chelating ligands and react with appropriate metal complexes to yield di- and tri-metallic complexes.[4,5] In an attempt to prepare heteropolymetallic M–Ag complexes, methanolic solutions of $[M(pap)_2(BiimH_2)]^{2+}$ were reacted with ammoniacal silver nitrate (Tollen's reagent) in 1:1 molar proportion. It was anticipated that the alkalinity of the Tollen's reagent would be strong enough for the dissociation of biimidazole protons from the above ruthenium/osmium building units. The reaction mixture became blue–violet in an hour. Upon crystallisation of the crude product from acetonitrile–water (1:1), dark crystals of the tetrameric cationic M_2Ag_2 compounds were obtained as their perchlorate salts in high yields (*ca.* 80%) [eqn. (1), M = Ru, Os].

$$[M(pap)_2(BiimH_2)]^{2+} + 2[Ag(NH_3)_2]^+ \longrightarrow [\{M(pap)_2(Biim)\}_2Ag_2]^{2+} \quad (1)$$

The mass spectra of M_2Ag_2 compounds fully corroborate with their formulations. For example, the weak peak at 1514 in the ESIMS spectrum of $[\{Ru(pap)_2(Biim)\}_2Ag_2](ClO_4)_2$ is assigned to $[M_c - X]$, where M_c and X represent the molecule and ClO_4, respectively. The experimental isotopic distributions for the above molecular ions corresponded with the simulated patterns. Representative ESIMS spectra (Fig. S1–S4) are deposited as electronic supplementary information.†

Final authentication of these unusual M_2Ag_2 species, however, were made by X-ray crystallographic characterization‡ of the representative Ru_2Ag_2 compound. The complex cation consists of two approximately octahedral $[Ru(pap)_2(Biim)]$ units which are linked by two silver atoms in a head-to-tail fashion. The asymmetric unit consists of half of the molecule. The other half of the molecule is related by the crystallographic two-fold axis passing through the two silver atoms. The local geometry around each silver atom is nearly linear (N–Ag–N *ca.* 179°). The Ag–Ag distance is 2.8899(19) Å, which is similar to that observed[6] in metallic silver (2.89 Å). An ORTEP plot of $[\{Ru(pap)_2(Biim)\}_2Ag_2]^{2+}$ is shown in Fig. 1. In the solid state the cations are arranged in chains with water molecules present between alternate layers. The small Ag–Ag separation in the compound indicates the presence of argentophilic interactions between the two Ag(I) ($4d^{10}$) ions. The present M_2Ag_2 compounds clearly demonstrate the unique feature of $[M(pap)_2(Biim)]$ as building units, *viz.* their ability to encapsulate two Ag(I) such that these come in proximity giving rise to metallophilic interactions.[7] Heterometallic compounds with

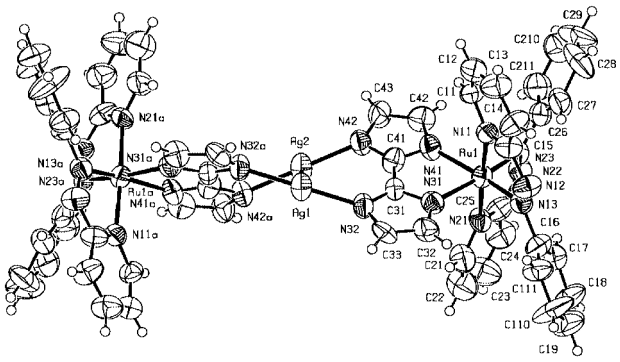

Fig. 1 An ORTEP plot and atom numbering scheme of $[\{Ru(pap)_2(Biim)\}_2Ag_2]^{2+}$ in $[\{Ru(pap)_2(Biim)\}_2Ag_2](ClO_4)_2 \cdot H_2O$. Selected bond distances (Å) and angles (°): Ag(1)–Ag(2) 2.8899(19), C(41)–N(41) 1.329(14), C(41)–N(42) 1.349(14), Ru(1)–N(41) 2.093(10), Ru(1)–N(11) 2.042(9), Ru(1)–N(13) 1.980(9), Ag(1)–N(32) 2.081(10); N(32)–Ag(1)–N(32a) 179.3(5), N(41)–C(41)–C(31) 115.0(11), N(42)–C(41)–C(31) 131.2(11).

† Electronic supplementary information (ESI) available: details of crystal structure solution and refinement: Fig. S1–S4: representative ESIMS spectra. See http://www.rsc.org/suppdata/cc/b1/b100171j/

 DOI: 10.1039/b100171j

such small Ag–Ag separations[8] are unprecedented in the literature. Attractive interactions between formally closed shell (d^{10}) metal centres containing coinage monovalent metals have been known predominantly for gold.[9] In comparison, argentophilic compounds are rare and the M_2Ag_2 compounds, described here are the first examples of heterometallic Ru–Ag and Os–Ag compounds which show metallophilic interactions. In the recent past, however, there have been a few reports[10] on tetranuclear Ru_2Ag_2 compounds in which the Ag–Ag separations are large.

To look for the reason for this mode of binding in the Ru–Ag compound, we compared the separations between the coordinated nitrogen atoms of the biimidazolate ring in the present Ru–Ag heterometallic compound with those in the symmetrical cationic compound,[4] $[\{Ru(bpy)_2\}_2(Biim)]^{2+}$. The separation between the coordinating N(31) and N(41) in $[\{Ru(pap)_2(Biim)\}_2Ag_2]^{2+}$ is 2.622 Å and that between N(32) and N(42) is 3.222 Å. The first pair of nitrogens are attached to the $Ru(pap)_2^{2+}$ moiety as a chelate whereas the other two are coordinated linearly to two Ag(I). This effect is also reflected in the uneven C–N lengths and bond angles in the biimidazolate rings. For example, the bond lengths C(41)–N(41) [1.329(14) Å] and C(31)–N(31) [1.350(13) Å] are shorter than C(41)–N(42) [1.349(14) Å] and C(31)–N(32) [1.371(13) Å], respectively. Moreover, the bond angles N(41)–C(41)–C(31) [115.0(11)°] and N(31)–C(31)–C(41) [117.3(10)°] are narrower than the corresponding angles N(42)–C(41)–C(31) [131.2(11)°] and N(32)–C(31)–C(41) [130.7(11)°]. This wider separation between N(32) and N(42) undoubtedly favours monodentate type II coordination of the $[Ru(pap)_2(Biim)]$ bridging unit over chelate type I coordination. Interestingly, in the symmetrical compound $[\{Ru(bpy)_2\}_2(Biim)]^{2+}$, the reference C–N bond distances, the respective angles and the separation between the coordinated N atoms are very similar.[4]§ In the M–Ag compounds, one half of the bridging biimidazolate is coordinated to M(II) which are known to participate in dπ–pπ interactions very effectively[11] and the other half is attached to two Ag(I) which is known to be a σ-acceptor. The presence of $[M(pap)_2]^{2+}$ moiety together with a preferential affinity of the Ag(I) for a linear coordination[12] are believed to be the two important factors for the trinuclear coordination of the $[Biim]^{2-}$ anion in $[M(pap)_2(Biim)]$.

Finally, we note here that the ESIMS spectral measurements together with experimental results on the reactions of $[M(pap)_2(Biim)]$ with Cu^{2+} indicate a similar binding mode of $[Biim]^{2-}$ resulting in the formation of heteropolymetallic compounds with M_4Cu_2 cores. However, X-ray structural authentication of the products, which are in progress, are essential to make further conclusions. These will be reported in due course.

Financial support received from the Department of Science and Technology, New Delhi is acknowledged.

Notes and references

‡ The M_2Ag_2 compounds appear to be crystalline but, in general, were not suitable for X-ray study. Fortunately, after several trials X-ray quality crystals of $[\{Ru(pap)_2(Biim)\}_2Ag_2](ClO_4)_2\cdot H_2O$ could be formed. Crystals of this compound were found to be weak scatterers and thus the quality of the structure is not very high. However, the structural analysis of the reference Ru_2Ag_2 compound suffices to establish the identity and gross features of the system. Further details of the diffraction experiment are provided as ESI.†

Crystal data: $[\{Ru(pap)_2(Biim)\}_2Ag_2](ClO_4)_2\cdot H_2O$: $C_{56}H_{46}N_{20}O_9Cl_2Ag_2Ru_2$, M = 1631.91, orthorhombic, space group *Pnna* (No. 52), a = 34.037(5), b = 19.467(4), c = 10.0362(12) Å, Z = 4, D_c = 1.630 Mg m^{-3}, crystal dimensions 0.25 × 0.15 × 0.15 mm. Intensity data were collected on an Enraf Nonius CAD4 automatic diffractometer using Cu-Kα radiation (λ = 1.54184 Å) and the ω-scan technique, and corrected for Lorentz and polarisation effects.[13] The number of reflections measured was 7708, of which 6955 were unique and were used for refinement. A semi-empirical absorption correction (ψ-scans) was made.[14] The structure was solved by Patterson and Fourier methods[15] and refined on F^2 by a full-matrix least-squares procedure using anisotropic displacement parameters.[16] All hydrogen atoms were located in their calculated positions (C–H 0.93 Å) and were refined using a riding model. The hydrogen atoms of one water molecule, O(1), were not located. The final R indices [$I > 2(\sigma)I$] was 0.078 while $wR2$ for all data was 0.2514. CCDC reference number 156515. See http://www.rsc.org/suppdata/cc/b1/b100171j/ for crystallographic data in CIF or other electronic format.

§ Reference C–N bond distances[4] (Å): 1.322(10), 1.327(10), 1.327(10), 1.322(10); reference N–C–C bond angles (°) : 121.5(7), 121.7(7), 121.7(7), 121.5(7). Separation between the two pairs of coordinating N, N are identical: 2.811 Å.

1 R. Usón, J. Gimeno, J. Forniés and F. Martínez, *Inorg. Chim. Acta*, 1981, **173**, 50; S. W. Kaiser, R. B. Saillant, W. M. Butler and P. G. Rasmussen, *Inorg. Chem.*, 1976, **11**, 2681.

2 D. P. Rillema, R. Sahai, P. Matthews, A. K. Edwards, R. J. Shaver and L. Morgan, *Inorg. Chem.*, 1990, **29**, 167; M. Haga, M. Md. Ali, S. Koseki, K. Fujimoto, A. Yoshimura, K. Nozaki, T. Ohno, K. Nakajima and D. J. Stufkens, *Inorg. Chem.*, 1996, **35**, 3335; M. Haga, M. Md. Ali, H. Maegawa, K. Nozaki, A. Yoshimura and T. Ohno, *Coord. Chem. Rev.*, 1994, **132**, 99; M. Haga, M. Md. Ali and R. Arakawa, *Angew. Chem., Int. Ed. Engl.*, 1996, **35**, 76; E. V. Dose and L. J. Wilson, *Inorg. Chem.*, 1978, **17**, 2660.

3 S. W. Kaiser, R. B. Saillant, W. M. Butler and P. G. Rasmussen, *Inorg. Chem.*, 1976, **11**, 2688.

4 P. Majumdar, S. M. Peng and S. Goswami, *J. Chem. Soc., Dalton Trans.*, 1998, 1569.

5 P. Majumdar, S. M. Peng and S. Goswami, *Polyhedron*, 1999, **18**, 2543.

6 *International Tables for X-ray Crystallography*, Kynoch Press, Birmingham, UK, 1962, vol. 3.

7 P. Pyykkö, *Chem. Rev.*, 1997, **97**, 597; F. A. Cotton, X. Feng, M. Matusz and R. Poli, *J. Am. Chem. Soc.*, 1998, **110**, 7077; U. Siemeling, U. Vorfeld, B. Neumann and H. G. Stammler, *Chem. Commun.*, 1997, 1723; K. Singh, J. R. Long and P. Stavropoulos, *J. Am. Chem. Soc.*, 1997, **119**, 2942.

8 I. P. Y. Shek, W. Y. Wong and T. C. Lau, *New J. Chem.*, 2000, **24**, 733.

9 H. Shan and P. R. Sharp, *Angew. Chem., Int. Ed. Engl.*, 1996, **35**, 635; B. Ahrens, P. G. Jones and A. K. Fischer, *Eur. J. Inorg. Chem.*, 1999, 1103; A. Grohmann, *Angew. Chem., Int. Ed. Engl.*, 1995, **34**, 2107.

10 G. Fries, B. Weberndörfer, K. Ilg and H. Werner, *Eur. J. Inorg. Chem.*, 2000, 1651; I. De los Rios, M. J. Tenorio, M. C. Puerta and P. Valerga, *Organometallics*, 1998, **17**, 3356.

11 R. E. Shepherd and H. Taube, *Inorg. Chem.*, 1973, **12**, 1392; T. Hasegawa, T. C. Lau, H. Taube and W. P. Schaefer, *Inorg. Chem.*, 1991, **30**, 2921; G. Wilkinson, R. D. Gillard and J. A. McCleverty, *Comprehensive Coordination Chemistry*, Pergamon Press, Oxford, 1987, vol. 4, p. 519.

12 F. A. Cotton, G. Wilkinson, C. A. Murillo and M. Bochmann, *Advanced Inorganic Chemistry*, John Wiley & Sons, Inc., 6th edn., p. 1087.

13 M. Kretschmar, GENHKL Program for the reduction of CAD4 Diffractometer data, University of Tübingen, Germany, 1997.

14 A. C. T. North, D. C. Phillips and F. S. Mathews, *Acta Crystallogr., Sect. A*, 1968, **24**, 351.

15 G. M. Sheldrick, *Acta Crystallogr., Sect. A*, 1990, **46**, 467.

16 G. M. Sheldrick, SHELXL-97. Program for the Refinement of crystal Structures, University of Göttingen, Germany, 1997.

CHEMCOMM
Communication
www.rsc.org/chemcomm

Formation and ethene substrate reactions of iridium(II) porphyrin metal-centered dπ radicals

Huili Zhai, Andrew Bunn and Bradford Wayland*

Department of Chemistry, University of Pennsylvania, Philadelphia, PA 19104-6323, USA. E-mail: wayland@a.chem.upenn.edu

Received (in Cambridge, UK) 16th May 2001, Accepted 1st June 2001
First published as an Advance Article on the web 27th June 2001

Monomeric iridium(II) porphyrin complexes of tetrakis-(2,4,6-trialkylphenyl)porphyrin ligands that are generated by photolysis of the Ir–Me derivatives are found to have the $d_{xy}^2\ d_{z^2}^2\ d_{xz,yz}^3$ ground electron configuration which differs from the $d_{xy}^2\ d_{xz,yz}^4\ d_{z^2}^1$ configuration observed for the Co(II) and Rh(II) analogs; reactions of these Ir(II) species with ethene reflect both the metallo-radical reactivity and the varying steric demands for the series of porphyrin ligands.

Monomeric iridium(II) complexes[1] are unusual because of the dominant characteristic for these d^7 species to form diamagnetic Ir^{II}–Ir^{II} bonded dimers.[2] All of the currently reported iridium(II) porphyrin complexes are diamagnetic dimers,[3,4] and the range of thermodynamically favorable substrate reactions is limited by the dimer homolytic dissociation energy. This article reports on the generation of iridium(II) complexes with sterically demanding porphyrin ligands along with studies relevant to the electronic structure and ethene substrate reactions.

Tetramesitylporphyrin (TMP) and derivatives where the mesityl methyl groups in TMP are replaced by ethyl (TTEPP) and isopropyl (TTiPP) provide a series of ligands that require interporphyrin distances too large to support metal–metal bonding.[5,6] Photolysis ($\lambda > 350$ nm) of (octaethylporphyrinato)iridium methyl [(OEP)Ir–Me) gives selective Ir–Me bond homolysis and near quantitative formation of the Ir^{II}–Ir^{II} bonded dimer $\{[(OEP)Ir]_2\}$.[4] Photolysis of (por)Ir-CH_3 (por = TMP, TTEPP, TTiPP) provides an approach to generate iridium(II) porphyrin derivatives that are sterically unable to dimerize by Ir^{II}–Ir^{II} bonding [(eqn. (1)].

$$\text{(por)Ir–Me} \xrightarrow[\lambda > 350\ \text{nm}]{h\nu} \text{(por)Ir}^{II} + \cdot\text{Me} \qquad (1)$$

Photolysis of (por)Ir–Me complexes in C_6D_6 results in the direct observation of $(TTiPP)Ir^{II}$ **1** and $(TTEPP)Ir^{II}$ **2**† and evidence for the formation of $(TMP)Ir^{II}$ **3** through the characteristic reaction with ethene to form (TMP)Ir–CH_2CH_2–Ir(TMP)[eqn. (2)].†

$$2(TMP)Ir^{II} + CH_2{=}CH_2 \rightarrow (TMP)Ir{-}CH_2CH_2{-}Ir(TMP) \qquad (2)$$

The paramagnetism of $(TTiPP)Ir^{II}$ **1** produces shifts and broadening for all of the ^{1}H NMR resonances in **1**† and the high field position for the pyrrole hydrogens [δ_1 (pyr) −20.9 (296 K)] is particularly significant (Fig. 1). The ground electron configuration for both Co(II) and Rh(II) porphyrin complexes is known to be $d_{xy}^2\ d_{xz,yz}^4\ d_{z^2}^1$[7] and downfield pyrrole ^{1}H NMR shifts[8] are observed for these metalloporphyrins which is opposite in sign to that for $(TTiPP)Ir^{II}$ **1**. Upfield pyrrole porphyrin contact shifts are associated with spin density in the porphyrin π orbitals.[9] Low spin (d^5) Fe(III) porphyrin complexes such as $[(TPP)Fe(Im)_2]Cl$ (Im = imidazole)[10] have the $d_{xy}^2\ d_{xz,yz}^3$ ground configuration and upfield pyrrole ^{1}H NMR shift positions comparable to that for **1**.[10] The pyrrole proton contact shifts for **1** clearly indicate that $(TTiPP)Ir^{II}$ has a $d_{xy}^2\ d_{z^2}^2\ d_{xz,yz}^3$ electron configuration which contrasts with the $d_{xy}^2\ d_{xz,yz}^4\ d_{z^2}^1$ configuration observed for the d^7 metalloporphyin complexes of cobalt(II) and rhodium(II).

Plots of the porphyrin pyrrole shifts *vs.* T^{-1} for $(TTiPP)Ir^{II}$ and $(TTiPP)Rh^{II}$ are shown in Fig. 2. Linear dependence of the

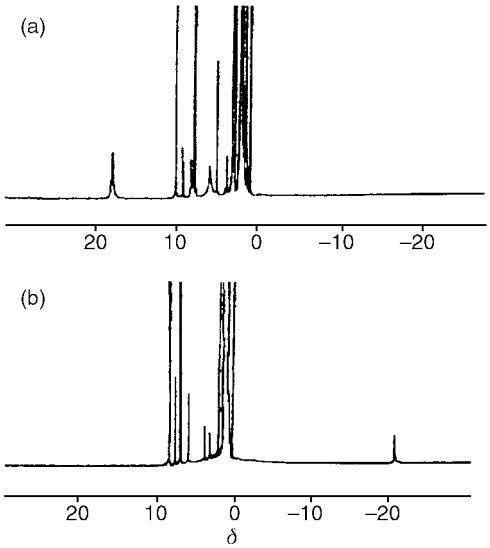

Fig. 1 ^{1}H NMR spectra illustrating the pyrrole resonance (296 K): (a) $(TTiPP)Rh^{II}$, δ_{pyr} +17.5; (b) $(TTiPP)Ir^{II}$, δ_{pyr} −20.9.

paramagnetic shift with T^{-1} for $(TTiPP)Rh^{II}$ is indicative of simple Curie paramagnetic behavior associated with a single contributing state, but curvature of the plot for $(TTiPP)Ir^{II}$ suggests that several states are thermally populated. The deviation from linearity in the shift *vs.* T^{-1} as the temperature is lowered is in the direction of larger upfield contact shift which clearly indicates that the ground configuration has an unpaired electron in the dπ ($d_{xz,yz}$) orbitals. Repeated attempts to determine EPR parameters for $(TTiPP)Ir^{II}$ in toluene glass (20–100 K) did not result in an observed EPR spectrum. The presence of one or more excited states with energy close to that of the ground state may hamper observation of EPR spectra by producing rapid electron spin relaxation.

Differences in steric demands of $(TMP)Ir^{II}$, $(TTEPP)Ir^{II}$ and $(TTiPP)Ir^{II}$ are clearly manifested by the different products that

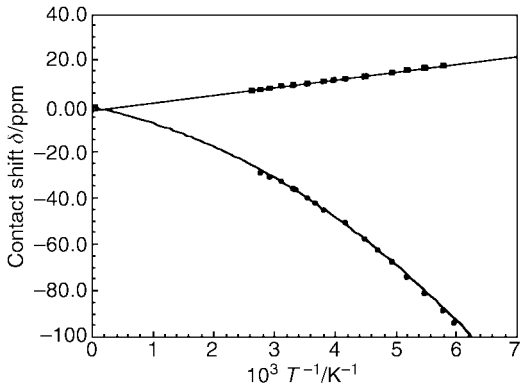

Fig. 2 Plots of the pyrrole ^{1}H NMR contact shifts in toluene-d_8 *vs.* T^{-1} [$(TTiPP)Rh^{II}$ (■); $(TTiPP)Ir^{II}$ (●)].

 DOI: 10.1039/b104301n

result from reactions with ethene. Reaction of (TTEPP)Ir^{II} with ethene produces a four-carbon bridged complex (TTEPP)Ir–CH_2CH_2–CH_2CH_2–Ir(TTEP) [eqn. (3)] without any evidence for the two-carbon ethylene bridged species observed for (TMP)Ir^{II} [(TMP)Ir–CH_2CH_2–Ir(TMP)] [eqn. (1)].

$$2(\text{TTEPP})\text{Ir}^{II} + 2\ CH_2{=}CH_2 \rightarrow (\text{TTEPP})\text{Ir}{-}CH_2CH_2{-}CH_2CH_2{-}\text{Ir}(\text{TTEPP}) \quad (3)$$

The increased steric demands of (TTEPP)Ir compared to (TMP)Ir inhibits formation of the two-carbon bridged complex and an ethene coupling process occurs to yield a four-carbon bridged complex that relieves the steric congestion. The reactions of (TMP)Ir^{II} and (TTEPP)Ir^{II} with ethene to form two- and four-carbon bridged complexes directly parallel reactions of the rhodium(II) derivatives.[6] Further increase in the ligand steric requirements to those of (TTiPP)Ir^{II} inhibits formation of even a four-carbon bridged species which is also a property observed for the rhodium(II) derivative.[6] When a toluene solution of (TTiPP)Ir^{II} is exposed to ethene the porphyrin NMR spectrum disappears, new electronic absorption maxima appear at 444 and 730 nm and an intense EPR signal is observed [$< g >$ = 1.987(290 K); $g_{\|}$ = 1.96, $g_{\perp}$ = 1.998(90 K)]. These spectroscopic changes are indicative of a donor induced intramolecular electron transfer from the Ir^{II} center to the porphyrin ligand π^* which forms an iridium(III) porphyrin anion radical species.[11,12] This behavior differs from (TTiPP)-Rh^{II} which reacts with ethene to form a 1 : 1 complex where the unpaired electron is in a metal centered d_{z^2} molecular orbital.[6] (TTiPP)Rh^{II} requires an excess of a strong donor like pyridine in order to elevate the d_{z^2} above the porphyrin π^* to produce an intramolecular electron transfer.[7] A higher energy position for the iridium d orbitals and or stronger iridium–substrate binding compared to that of rhodium(II) and cobalt(II) is inferred by these results.

Generation of monomeric iridium(II) porphyrins permits study of the fundamental electronic structure of Ir(II) and by removing the thermodynamic restrictions from Ir^{II}–Ir^{II} bonding provides an opportunity to evaluate the full range of Ir(II) substrate reactions.

This research was supported by the Department of Energy Division of Chemical Sciences, Office of Science through grant DE-FG02-86ER-13615.

Notes and references

† The synthesis of iridium complexes of TMP, TTEPP and TTiPP follows the general procedures described by Ogoshi for the synthesis of (OEP)Ir complexes: (por)Ir^{II} (por = TMP, TTEPP, TTiPP) is generated by photolysis of (por)Ir–Me in benzene in a Rayonet photoreactor equipped with RPR-350 nm lamps.

Selected spectroscopic data: (TTiPP)Ir^{II}: $\delta_H(C_6D_6$; 294 K): 8.14 (8H, br s, *m*-H), 5.88 [8H, br, *o*-C*H*$(CH_3)_2$], 3.79 [4H, sept, *p*-C*H*$(CH_3)_2$], 2.08 (24H, br, *p*-CH(C*H*$_3)_2$], 1.73 [48H, br, *o*-CH(C*H*$_3)_2$], −20.89 (8H, br, pyrrole H).

(TTEPP)Ir^{II}: $\delta_H(C_6D_6$; 294 K): 7.62 (8H, br s, *m*-H), 4.08 (16H, br, *o*-C*H*$_2$CH$_3$), 3.23 (8H, br, *p*-C*H*$_2$CH$_3$), 1.83 (12H, br, *p*-CH$_2$C*H*$_3$), 1.61 (24H, br, *o*-CH$_2$C*H*$_3$), −21.46 (8H, br, pyrrole H).

Reaction of (TMP)Ir with ethene in benzene solution produces (TMP)Ir–CH_2CH_2–Ir(TMP), which is identified by ^{1}H NMR spectroscopy by the δ −7.85 resonance characteristic of the –CH_2CH_2– bridge.[6]

Reaction of (TTEPP)Ir with ethene in benzene solution produces (TTEPP)Ir–$CH_2CH_2CH_2CH_2$–Ir(TTEPP). The ^{1}H NMR spectrum displays two high field resonances centered at δ −5.87 and −6.42 that are characteristic of the four-carbon bridge.[6]

1 M. Kubota, M. Chan and K. Mann, *Inorg. Chem.*, 1987, **26**, 3261.
2 P. G. Rasmussen, J. Anderson, O. H. Bailey, M. Tamres and J. Bayon, *J. Am. Chem. Soc.*, 1985, **107**, 279.
3 K. Chan and Y. Leung, *Inorg. Chem.*, 1994, **33**, 3184.
4 K. Del Rossi and B. B. Wayland, *J. Chem. Soc., Chem. Commun.*, 1986, 1653.
5 J. P. Collman, H. T. Fish, P. S. Wagenknecht, D. A. Tyvoll, L. Chang, T. A. Eberspacher, J. Brauman, J. W. Bacon and L. H. Pignolet, *Inorg. Chem.*, 1996, **35**, 6746.
6 A. Bunn and B. B. Wayland, *J. Am. Chem. Soc.*, 1992, **114**, 6917.
7 B. B. Wayland, A. Sherry and A. Bunn, *J. Am. Chem. Soc.*, 1993, **115**, 7675.
8 B. B. Wayland, A. Sherry, G. Poszmik and A. Bunn, *J. Am. Chem. Soc.*, 1992, **114**, 1673.
9 J. Satterlee and G. La Mar, *J. Am. Chem. Soc.*, 1976, **98**, 2804.
10 G. La Mar and F. Walker, *J. Am. Chem. Soc.*, 1973, **95**, 1782.
11 J. Cornillon, J. Anderson, C. Swistak and K. Kadish, *J. Am. Chem. Soc.*, 1986, **108**, 7633.
12 K. Kadish, D. Sazou, G. Maiya, B. Han, Y. Liu, A. Saoiabi, M. Ferhat and R. Guilard, *Inorg. Chem.*, 1988, **27**, 2745.

CHEMCOMM
Communication
www.rsc.org/chemcomm

Observation of a stable *cis*-diphosphine solvate rhodium dihydride derived from PHANEPHOS

Hanjo Heinrich,[a] Ralf Giernoth,[b] Joachim Bargon*[a] and John M. Brown*[b]

[a] *Institute of Physical and Theoretical Chemistry, University of Bonn, Wegelerstr. 12, D-53115 Bonn, Germany. E-mail: bargon@uni-bonn.de*
[b] *Dyson Perrins Laboratory, South Parks Road, Oxford, UK OX1 3QY. E-mail: bjm@ermine.ox.ac.uk*

Received (in Cambridge, UK) 12th March 2001, Accepted 24th May 2001
First published as an Advance Article on the web 27th June 2001

The methanol solvate rhodium(PHANEPHOS) forms a stable dihydride which has been characterised in solution by NMR as a pair of equilibrating diastereomers.

Early experiments designed to elicit the mechanism of asymmetric homogeneous hydrogenation provided a contrast between chelate diphosphine and bisphosphine rhodium complexes. The solvate **1a** showed no tendency to react with

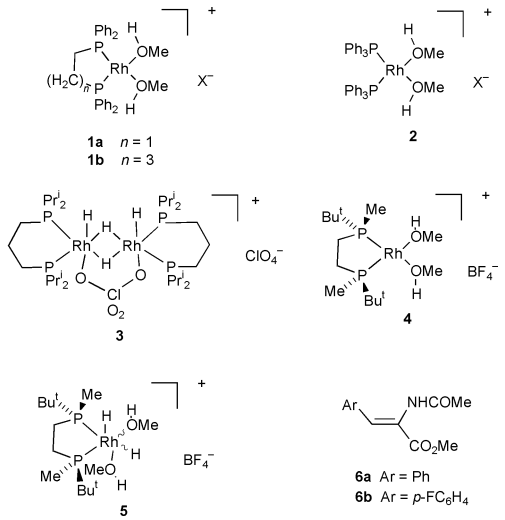

ambient hydrogen, whilst the solvate **2** formed a characterised dihydride;[1] the difference was attributed to a requirement for *trans*-diphosphine geometry in the stable solvate with H correspondingly *trans* to solvent oxygen. This observation has generally been sustained until recently. Aside from reversible *ortho–para* dihydrogen equilibration by complexes **1a** and **1b**,[2] and the likely mediation of a *cis*-dihydride in the formation of the dimeric species **3**,[3] no further progress had been made prior to the work of Gridnev, Imamoto and coworkers.[4] They demonstrated that the corresponding solvate **4** from a simple P-chiral alkylphosphine ligand formed significant quantities of the *cis*-dihydride **5** (20% at −95 °C and ambient pressure), with two diastereomers formed in a ratio of 10:1.[5] Further, this intermediate reacted with the catalytic substrate **6a** to form a Rh alkylhydride,[6] which then underwent reductive elimination at −50 °C to give the hydrogenated product. Taken together with labelling studies, the results are compatible with path **A** in Scheme 1, in contrast to the more generally accepted sequence **B**.[7]

We recently demonstrated the presence of an agostic dihydride intermediate **7** in the hydrogenation cycle of compound **6a** by [PHANEPHOS]Rh$^+$, employing *para*-enriched hydrogen and the precursor complex **8** (or the NBD analogue) to identify the transient at −10 to −30 °C by ^{1}H NMR.[8] When hydrogenation is complete and the substrate exhausted a second species can be observed, however. By carrying out the hydrogenation of the catalyst precursor in the absence of

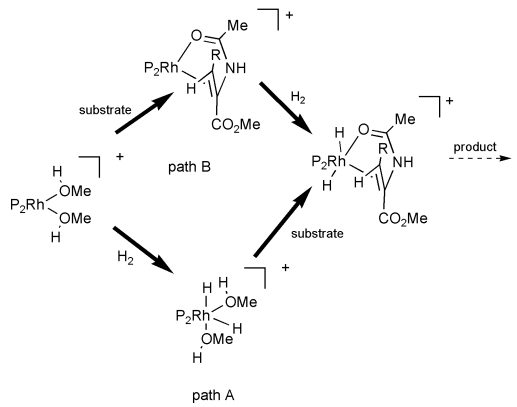

Scheme 1 The possible paths for addition of dihydrogen to a dehydroamino ester; path **A**: H_2 addition prior to substrate (dihydride route). Path **B**: substrate addition prior to H_2 addition (unsaturate route).

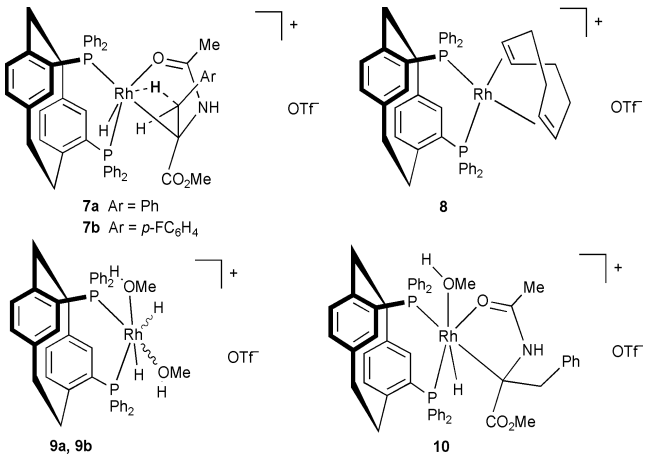

substrate the same intermediate is seen, optimally at −40 °C. The δ and J values are entirely consistent with a *cis*-dihydride structure **9**, with one hydride *trans* to phosphorus (δ *ca.* −11) and one *trans* to one of the two solvent oxygens (δ *ca.* −20). Both the intensity and persistence of the signals indicate that it is a relatively robust species. There are two diastereomers **9a** and **9b** in 2:1 ratio, and their NMR spectra have been fully assigned using PHIP++ [Fig. 1(a)].[9] The chemical shifts are very different from the previous case[4] where the observed major diastereomer resonates at δ −7.7 and −23.0.

When hydrogenation is carried out under conventional NMR conditions at −80 °C, the same dihydride **9** may be observed, along with small amounts of other Rh hydride resonances not seen in the PHIP spectrum. It is stable up to −40 °C [Fig. 1(b)], and a rough estimate based on integration of the high-field ^{1}H NMR signals against the CH_2-region of the ligand indicates that 45% of species **9** is formed at equilibrium, making it more accessible than the previously observed case,[4,5] and to higher

 DOI: 10.1039/b102316k

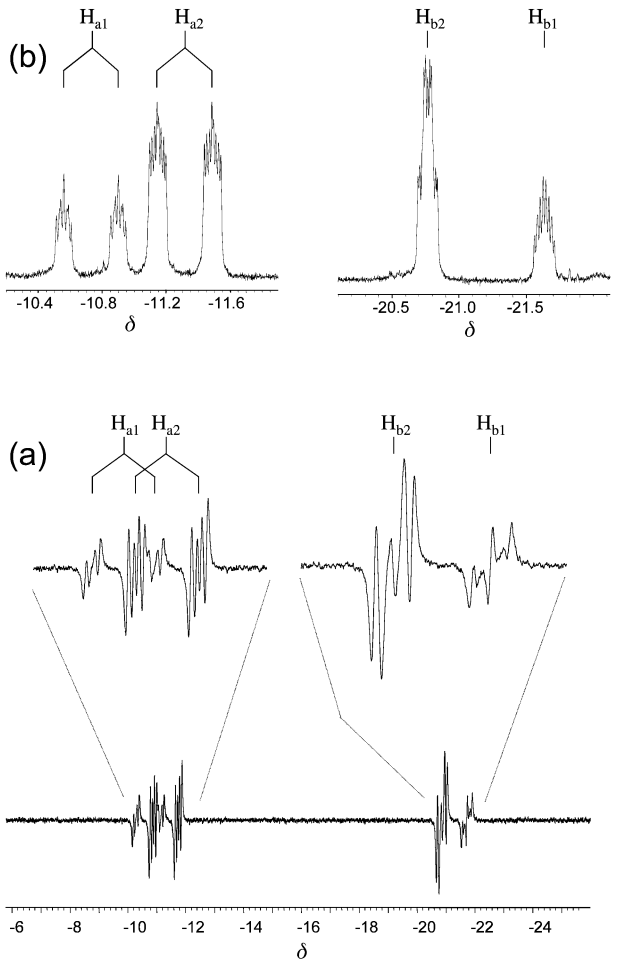

Fig. 1 (a) The PHIP ^{1}H NMR spectrum (CD_3OD, 200 MHz) of dihydrides **9a** and **9b** taken after parahydrogen (98% enriched) passage through a solution of complex **8** in CD_3OD at −40 °C. Minor diastereomer: δ −10.87 (J_{HP} 170, 24, J_{HRh} 14, J_{HH} −9.0 Hz), −21.77, (J_{HP} 32, 12, J_{HRh} 21 Hz); major diastereomer : δ −11.46 (J_{HP} 171, 28, J_{HRh} 15.5, 15, J_{HH} −7.5 Hz), −20.91, (J_{HP} 29, 16, J_{HRh} 22.5 Hz). (b) The ^{1}H NMR spectrum (CD_3OD, 500 MHz) of dihydrides **9a** and **9b** formed in the hydrogenation of complex **8** at −80 °C, taken at −40 °C, with comparable J and δ values.

temperatures. This may be attributed to the high level of electron donation ensuing from the [2.2]paracyclophane backbone,[10] together with the large bite angle of PHANEPHOS,[11] which will favour the dihydride at equilibrium. The two diastereomers are in equilibrium by an unselective mechanism, as indicated by a selective homodecoupling experiment.[12]

When the solution containing complex **9** is held at −80 °C and a solution of compound **6a** in MeOH added, rapid formation of the agostic dihydride **7a** occurs. The signals at δ −2 and −19 are broad at that temperature, and at −70 °C they decay over time without formation of any further observable intermediates. The absence of a 'classical' alkylhydride **10** indicates that **7a** is the only accessible intermediate on the hydrogenation pathway. Further, it must be formed directly from an assumed dihydride precursor rather than by reinsertion of rhodium into the β-CH of **10** after formation of the latter, since the latter pathway would vitiate the earlier PHIP experiment by uncoupling the H–H spins.

In the earlier publication of Gridnev, Imamoto and coworkers,[4] it was suggested that path **A** could be a viable alternative to the accepted reaction mechanism of path **B** (Scheme 1). We

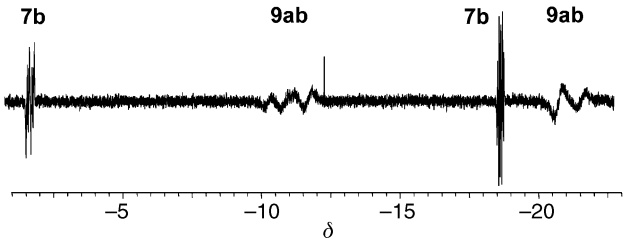

Fig. 2 The PHIP ^{1}H NMR spectrum of the hydrogenation of reactant **6b** in CD_3OD in the presence of Rh complex **8** at −27 °C, after 40 5 s pulses of parahydrogen (98%). Spectra taken earlier in the sequence after 16 pulses show only traces of complex **9**.

observed that when the PHIP experiment was carried out with **6b** as substrate at the lower temperature of −27 °C, the solvate dihydride **9a**, **b** could be observed in significant amount, but only late in the reaction sequence when the substrate concentration was depleted (Fig. 2). This opens up the possibility that path **A** may contribute to catalytic turnover in the PHANEPHOS case. Earlier INEPT experiments demonstrated that the agostic intermediate **7a** is in reversible equilibrium with the solvate complex and substrate.[7] This makes the discrimination between the two pathways quite subtle. Given that both species **7** and **9** are observed in the same experiment under turnover conditions, the result is accessible in principle and a challenge for further work.

We thank Philip Pye and Kai Rossen (Merck, Rahway) for a generous gift of PHANEPHOS, and Johnson-Matthey for the loan of $RhCl_3$. R. G. thanks BASF AG and Studienstiftung des Deutschen Volkes for a Fellowship. JMB is very pleased to acknowledge an unrestricted grant from Merck, Inc. H. H. and J. B. thank the Deutsche Forschungsgemeinschaft for financial support.

Notes and references

1 J. Halpern, D. P. Riley, A. S. C. Chan and J. J. Pluth, *J. Am. Chem. Soc.*, 1977, **99**, 8055; D. A. Slack, I. Greveling and M. C. Baird, *Inorg. Chem.*, 1979, **18**, 3125
2 J. M. Brown, L. R. Canning, A. J. Downs and A. M. Forster, *J. Organomet. Chem.*, 1983, **255**, 103.
3 K. Tani, T. Yamagata, Y. Tatsuno, T. Saito, Y. Yamagata and N. Yasuoka, *J. Chem. Soc., Chem. Commun.*, 1986, 494.
4 I. D. Gridnev, N. Higashi, K. Asakura and T. Imamoto, *J. Am. Chem. Soc.*, 2000, **122**, 7183.
5 A stable Rh solvate dihydride has been observed recently: I. D. Gridnev, N. Higashi and T. Imamoto, *Organometallics*, 2001, submitted; we thank Dr Gridnev for a useful exchange of information.
6 I. D. Gridnev, N. Higashi and T. Imamoto, *J. Am. Chem. Soc.*, 2000, **122**, 10486; J. A. Ramsden, T. Claridge and J. M. Brown, *J. Chem. Soc., Chem. Commun.*, 1995, 2469; J. M. Brown and P. A. Chaloner, *J. Chem. Soc., Chem. Commun.*, 1980, 344; A. S. C. Chan and J. Halpern, *J. Am. Chem. Soc.*, 1980, **102**, 838.
7 S. Feldgus and C. R. Landis, *J. Am. Chem. Soc.*, 2000, **122**, 12714.
8 R. Giernoth, H. Heinrich, N. J. Adams, R. J. Deeth, J. Bargon and J. M. Brown, *J. Am. Chem. Soc.*, 2000, **122**, 12381.
9 Simulations were conducted with the help of the program PHIP++ written by T. Greve (PhD thesis 1996, University of Bonn, Institute of Physical and Theoretical Chemistry).
10 D. J. Cram and J. M. Cram, *Acc. Chem. Res.*, 1971, **4**, 204; Z. Yang, B. Kovac, E. Heilbronner, S. Eltamany and H. Hopf, *Helv. Chim. Acta*, 1981, **64**, 1991.
11 P. W. Dyer, P. J. Dyson,S. L. James, C. M. Martin and P. Suman, *Organometallics*, 1998, **17**, 4344; PPdP = 103.7° in the $PdCl_2$ complex.
12 Selective irradiation at the site of H_{b2} demonstrates concurrent loss of 50% intensity at H_{a1}, H_{a2} and H_{b1} without selectivity. We thank Dr Tim Claridge for help with this experiment.

CHEMCOMM Communication
www.rsc.org/chemcomm

A novel self-indicative vesicle based on a iron(II) complex

Paula Garcia,[a] João Marques,[a] Eulália Pereira,*[a] Paula Gameiro,[a] Roberto Salema[b] and Baltazar de Castro[a]

[a] *CEQUP/Faculdade de Ciências do Porto, Rua do Campo Alegre, 687, 4169-007 Porto, Portugal. E-mail: efpereir@fc.up.pt*
[b] *Instituto Botânico – Faculdade de Ciências do Porto, Rua do Campo Alegre, 1191, 4160-007 Porto, Portugal*

Received (in Cambridge, UK) 15th January 2001, Accepted 5th June 2001
First published as an Advance Article on the web 27th June 2001

An iron(II) complex with a lipophilic derivative of 2,2′-bipyridine was synthesized and found to aggregate in aqueous solution, yielding vesicles with a mean diameter of 1000 nm; preliminary cyclic voltammetry experiments show that the complex forms redox-active films at the electrode surface.

The design of new amphiphilic molecules incorporating transition metal complexes is a recent topic of interest due to their potential use in catalysis,[1] medicine[2] and materials science.[3] Self-assembling amphiphilic systems containing metal ions are particularly promising since they combine the special solvation and interfacial behaviour of organised media with the rich chemical reactivity of transition metal complexes. Several applications may be envisaged for this type of molecules, such as the development of environmentally friendly catalysts, medical applications such as carriers of diagnostic metals and metal-complex drugs with specific targeting ability, and as models for biological membrane processes. Nevertheless, the special characteristics imparted by metal ions in organised media are much more poorly understood.[4]

In this work we have synthesised and studied the complex *cis*-bis(4,4′-dinonyl-2,2′-bipyridine)dicyanoiron(II) **1**. Complexes of the type $[FeL_2(CN)_2]$, where L is a bidentate diimmine

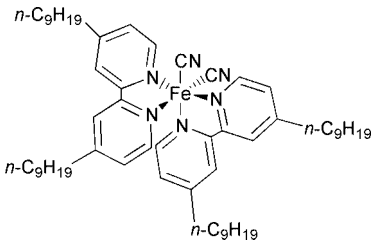

ligand, have been extensively used as inorganic solvatochromic probes of solvent polarity. In the course of a systematic study on the solvatochromic behaviour of complexes of this type with different hydrolipophilic balance[5] we have prepared complex **1**, using a published procedure with minor modifications.[6] Synthesis of 4,4′-dinonyl-2,2′-bipyridine was performed by reaction of 4,4′-dimethyl-2,2′-bipyridine with lithium diisopropylamide, followed by condensation with 1-bromooctane.[7] The desired complex was obtained by reaction of $(NH_4)_2Fe(SO_4)_2{\cdot}5H_2O$ with three-fold the stoichiometric amount of the ligand, followed by addition of an excess of KCN; purification by chromatography afforded the pure complex.† Its solvatochromic behaviour was studied in a large range of solvents with different properties, from methanol to *n*-pentane. The results obtained are indicative that the solvatochromic sensitivity of **1** is similar to that of the related complex *cis*-$[Fe(bpy)_2(CN)_2]$, which is, however, insoluble in low-polarity solvents. Thus, the introduction of two nonyl chains in the diimmine ligand results in a complex that may act as a solvent polarity probe in lipophilic systems.

In order to evaluate possible preferential solvation effects we have studied the solvatochromic behaviour of complex **1** in water–methanol, water–acetone and water–acetonitrile. The solvatochromic behaviour in water–methanol mixtures is very different from that observed in the two other mixed solvents (Fig. 1). Addition of water to a methanol solution of **1** results in a small but regular decrease of λ_{max}, and thus indicates the absence of preferential solvation. On the contrary, the addition of small amounts of water to acetone or acetonitrile solutions results in a sharp decrease in band maxima, typical of a strong preferential solvation by water.

In the three mixed solvents studied at water content of 33, 40 and 50% (v:v) in methanol, acetone and acetonitrile, respectively, an abrupt increase in λ_{max} is observed with a perceptible colour change from red to deep blue (typical of a very lipophilic environment) accompanied by the appearance of turbidity. Light-scattering of these solutions shows that they contain aggregates with a mean hydrodynamic diameter of *ca.* 1000 nm.‡ Since light-scattering studies and the morphology of the aggregates may depend on the presence of small quantities of organic solvent, we have repeated the analysis using several reported methods for the preparation of lipid aggregates in aqueous solutions,[8]§ and the results were similar. The size of the aggregates was confirmed by electron microscopy (Fig. 2). Several grids were observed and in all of them a regular and relatively homogeneous population of round aggregates were observed with most of them with diameters varying between 870 and 1020 nm.¶

The type of aggregate formed was identified by a well established method,[8b,9] with 4(5)-carboxyfluorescein as a fluorescent probe, that is highly hydrophilic and auto-quenches at high concentrations. Aggregates were prepared in an aqueous 1 M solution of 5(6)-carboxyfluorescein, and separated from unincorporated probe by passing through a Sephadex G-50 column. Elution profiles showed clearly two fluorescent bands, one corresponding to the free aqueous probe and the other to the solution containing the aggregated complex (confirmed by UV–VIS spectroscopy). Addition of TRITON-X to the fraction

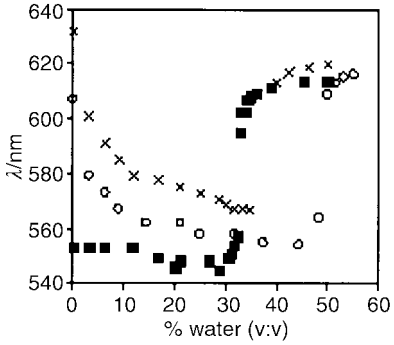

Fig. 1 Variation of λ_{max} of the LMCT band of complex **1** with water content in mixed solvents methanol–water (■), acetone–water (×) and acetonitrile–water (○).

 DOI: 10.1039/b100504i

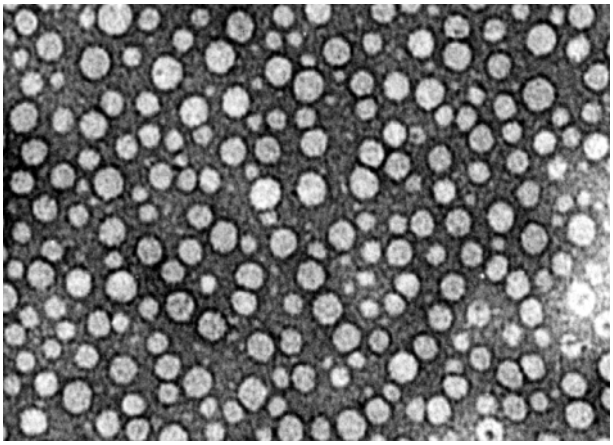

Fig. 2 Negative stain transmission electron micrograph of vesicles at magnification 3000×.

containing the aggregates causes their disruption and an 100-fold increase in fluorescence intensity is observed. This result clearly shows that complex **1** aggregates by forming vesicles—double layer spherical aggregates containing an inner aqueous core.

Preliminary studies of the redox behaviour of this complex in the monomeric and aggregated forms were performed by cyclic voltammetry. Solutions of **1** in acetonitrile show one reversible redox process ($E_{1/2}$ = 0.39 V *vs*. Ag/AgCl,1 M NaCl), a value that is significantly lower than that of $[Fe(bpy)_2(CN)_2]$ obtained in the same conditions ($E_{1/2}$ = 0.49 V *vs*. Ag/AgCl,1 M NaCl), which shows that the introduction of the alkyl chains results in a stabilization of the +3 oxidation state for Fe. Addition of water up to a concentrations of 55% (v/v) does not affect the voltammograms of $[Fe(bpy)_2(CN)_2]$, but for the more lipophilic complex the redox process gradually changes toward more positive potential ($E_{1/2}$ = 0.50 V for 55% H_2O–MeCN). In water rich solvents, where formation of vesicles in solution is observed, immersion of a platinum or vitreous carbon electrode in the solution for 5 min leads to the formation of a redox active film with $E_{1/2}$ = 0.60 V.

The results obtained in this work show that complex **1** is a new metallo-surfactant that readily forms vesicles in water-rich media and with solvatochromic properties that make aggregation self-indicated. This aggregation behaviour provides a simple way to localize metal-ion reactivity in organized media, and the preliminary studies performed by CV show that aggregation, although affecting the redox potential of the iron center, does not inhibit its redox behaviour. Complex **1** is thus a promising compound to test possible synergetic effects of conjugating redox reactivity and the special solvation effects of organized systems, *e.g*. in redox catalysis of lipophilic compounds in water-rich media.

Notes and references

† Chromatography in silica gel 60 (Merck, 230–400 mesh) using acetone and methanol as eluents. δ_H(200 MHz, $CDCl_3$): 0.83–0.90 (m, 12 H, 4 × $-CH_3$); 1.24–1.37 (m, 56 H, 4 × $-(CH_2)_7CH_3$); 2.61 (t, *J* 7.9 Hz, 4 H, 2 × $Ar-CH_2$); 2.77 (t, *J* 7.9 Hz, 4 H, 2 × $Ar-CH_2$); 6.88 (d, *J* 5.8 Hz, 2 H, 2 × 4-Ar-H); 7.12 (d, *J* 5.7 Hz, 2 H, 2 × 3-Ar-H); 7.22 (t, *J* 5.6 Hz, 2 H, 2 × 4′-Ar-H); 7.80 (s, 4 H, 2 × 6,6′-Ar-H); 9.81 (d, *J* 5.6 Hz, 2 H, 2 × 3′-Ar-H). MS (10 keV, FAB$^+$): *m*/*z*: 925 (3) (M^+); 899 (37) [M^+ − CN]; 873 (23) [M^+ − $(CN)_2$].

‡ Dynamic light-scattering was used to determine the diameter of the aggregates, using a Malvern Instrument ZetaSizer 5000, with a 5 mV He–Ne laser operating at 633 nm. Measurements were performed at a scattering angle of 90° at a temperature of 25 °C. All the measurements were performed 2 and 24 h after preparation of the samples. Correlation analysis was performed using CONTIN software from Malvern Instruments.

§ One of the methods more commonly used was the following: 0.1 ml of a methanol solution of the complex (2.0×10^{-4} M) was injected with a Hamilton air-tight syringe into 10 ml of an aqueous solution at 60 °C, under Ar bubbling. After injection the solution was maintained at the same temperature for 5 min with Ar bubbling for complete organic solvent elimination.

¶ A drop of the solution was placed onto 400 mesh copper grids coated with Parlodion (nitrocellulose) film stabilised with vacuum evaporated carbon. After 30 s the excess fluid was drained off with filter paper and a drop of the negative stain added. After 1 min the remainder of the 2% aqueous solution of phototungstic acid with the pH adjusted to 7.2 with 0.1 M NaOH was removed with filter paper and the grid immediately placed in the electron microscope.

1 See, for example: M. S. Goedheijt. B. E. Hanson, J. N. H. Reek, P. C. J. Kamer and P. W. N. M. Leeuwen, *J. Am. Chem. Soc.*, 2000, **122**, 1650; F. Mancin, P. Tecilla and U. Tonellato, *Langmuir*, 2000, **16**, 227; P. Scrimin, S. Caruso, N. Paggiarin and P. Tecilla, *Langmuir*, 2000, **16**, 203; F. Hampl, F. Liska, F. Mancin, P. Tecilla and U. Tonellato, *Langmuir*, 1999, **15**, 205; R. Jairam, P. G Potvin and S. Balsky, *J. Chem. Soc., Perkin Trans. 2*, 1999, 2363; F. Bertoncin, F. Mancin, P. Scrimin, P. Tecilla and U. Tonellato, *Langmuir*, 1998, **14**, 975; S. Bhatttacharya, K. Snehalatha and S. K. George, *J. Org. Chem.*, 1998, **63**, 27.

2 See, for example: N. Nishiyama, M. Yokoyama, T. Aoyagi, T. Okano, Y. Sakurai and K. Kataoka, *Langmuir*, 1999, **15**, 377; G. Ghirlanda, P. Scrimin, P. Tecilla and A. Toffoletti, *Langmuir*, 1998, **14**, 1646; X. Zhia, R. Zhuo, Z. Lu and W. Liu, *Polyhedron*, 1997, **16**, 2755.

3 See, for example: M. Kimura, T. Muto, H. Takimoto, K. Wada, K. Ohta, K. Hanabusa, H. Shirai and N. Kobayashi, *Langmuir*, 2000, **16**, 2078; J. F. Létard, O. Nguyen, H. Soyer, C. Mingotaud, P. Delhaès and O. Kahn, *Inorg. Chem.*, 1999, **38**, 3020.

4 E. C. Constable, W. Meyer, C. Nardin and S. Mundwiler, *Chem. Commun.*, 1999, 1483; N. A. J. M. Sommerdijk, K. J. Booy, A. M. A. Pistorius, M. C. Feiters, R. J. M. Nolte and B. Zwanenburg, *Langmuir*, 1999, **15**, 7008; M. D. Everaars, A. T. M. Marcelis and E. J. R. Sudhölter, *Eur. J. Org. Chem.*, 1999, 627; J. H. van Esch, A. L. H. Stols and R. J. M. Nolte, *J. Chem. Soc., Chem. Commun.*, 1990, 1659; X . Wang, Y. Shen, Y. Pan and Y. Linag, *Langmuir*, 2000, **16**, 7358; P. Ghosh, T. K. Khan and P. K. Bharadwaj, *Chem. Commun.*, 1996, 189; I. A. Fallis, P. C. Griffiths, D. E. Hibbs, M. B. Hursthouse and A. L. Winnington, *Chem. Commun.*, 1998, 665.

5 P. Gameiro, A. Maia, E. Pereira, B. de Castro and J. Burgess, *Transition Met. Chem.*, 2000, **25**, 283.

6 A. A. Schilt, *J. Am. Chem. Soc.*, 1960, **82**, 3000.

7 D. K. Ellison and R. T. Iwamoto, *Tetrahedron Lett.*, 1983, **24**, 31.

8 (*a*) I. M. Cuccovia, A. Sesso, E. B. Abuin, P. F. Okino, P. G. Tavares, J. F. S. Campos, F. H. Florenzano and H. Chaimovich, *J. Mol. Liq.*, 1997, **72**, 323; (*b*) R. R. C. New, in *Liposomes–A practical approach*, ed. R. R. C. New, Oxford University, Oxford, 1990.

9 Y. Sumida, A. Masuyama, H. Maekawa, M. Tasaku, T. Kida, Y. Nakatsuji, I. Ikeda and M. Nojima, *Chem. Commun.*, 1998, 2385.

CHEMCOMM Communication
www.rsc.org/chemcomm

Hydrogen bonds between polyphenol (p-$HOC_6H_4O)_6W$ and bipyridines: (4,4′-bipy·$HOC_6H_4O)_6W$ and 3-D networks $[\{4,4'\text{-}(NC_5H_4)_2(CH_2CH_2)\}_n\{(HOC_6H_4O)_6W\}]_\infty$ (n = 2, 3)

Thomas P. Vaid, Orson L. Sydora, Richard E. Douthwaite, Peter T. Wolczanski* and Emil B. Lobkovsky

Cornell University, Baker Laboratory, Department of Chemistry and Chemical Biology, Ithaca, New York 14853, USA. E-mail: ptw2@cornell.edu

Received (in Irvine, CA, USA) 16th January 2001, Accepted 24th May 2001
First published as an Advance Article on the web 27th June 2001

Polyphenol (p-$HOC_6H_4O)_6W$ is stable with respect to condensation, and formed (4,4′-bipy·$HOC_6H_4O)_6W$ and the 3-D networks $[\{4,4'\text{-}(NC_5H_4)_2(CH_2CH_2)\}_n\{(HOC_6H_4O)_6W\}]_\infty$ (n = 2, 3), when treated with 4,4′-bipy and 1,2-di-4-pyridylethane, respectively.

The construction of coordination networks[1] and dendrimeric materials[2,3] often utilizes a polyfunctionalized molecular core from which branches may emanate. While such organic cores exhibit various functionalities, inorganic equivalents are less structurally diverse, and most metals can be considered as Lewis acidic nodes amidst an organic framework. Creating functionality pendant to a metal can be a difficult problem,[4] especially for early transition metals, which are intolerant to many groups. For example, modeling studies indicated that (4-HO-2,6-$C_6R_2H_2O)_4M$ (M = Ti, Zr) would be effectively blocked from self-condensations *via* appropriately sized substituents R, yet trace 4-HO-2,6-$C_6R_2H_2OH$ and rapid alkoxide exchange chemistry hampered all efforts at isolating such species, and oligomeric materials were obtained.

In contrast, $(PhO)_6W$[5] is known to be stable in basic media, and is only susceptible to acid catalyzed phenoxide exchange at elevated temperatures.[6] The innate stability of hexaphenoxidetungsten complexes suggested a route to a polyhydroxylated inorganic core, namely (p-$HOC_6H_4O)_6W$.

As Scheme 1 illustrates, treatment of $W(OMe)_6$, prepared from $W(OMe)_4Cl_2$, MeOH and NEt_3,[7] with p-$HOC_6H_4OCH_2Ph$ in toluene for 24 h at 213 °C in a bomb reactor yielded the polybenzyl ether, (p-$PhCH_2OC_6H_4O)_6W$ **1** (91%).† Deprotection was effected *via* hydrogenation (H_2 (1 atm), Pd/C) in ethanol–toluene, and dark red (p-$HOC_6H_4O)_6W$·2THF·C_6H_6 (**2**·2THF·C_6H_6) was crystallized in 60% yield from THF–benzene.† An intricate, three-dimensional hydrogen-bonding network[8] is observed for **2**·2THF·C_6H_6.‡ Fig. 1. reveals rings of $(p\text{-}OH)_4$ that comprise one connectivity, another loop that alternately involves two p-OH and two phenoxide oxygens, and a single p-OH···THF hydrogen bond. The WO···HO hydrogen bond renders the W–O2 bond long (1.934(4) Å) in contrast to the 1.889(14) Å average distance of the normal tungsten aryloxide bonds.[9] The W–O–C angles range from 136.8(4) to 148.0(4)° to accommodate the network, and little distortion from octahedral coordination is observed in the WO_6 core ($\angle OWO_{cis}$ = 90.0(21)°$_{av}$; $\angle OWO_{trans}$ = 176.7(24)°$_{av}$).

Attempts to generate a hydrogen-bonded network[8] from (p-$HOC_6H_4O)_6W$ **2** and 4,4′-bipyridine failed when efforts to control stoichiometry continually led to the hexa-4,4′-bipyridine derivative (4,4′-bipy·$HOC_6H_4O)_6W$ **3** (Scheme 1, Fig. 2).‡ Hexabasic **3** has a regular core ($\angle OWO_{cis}$ = 90.0(7)°$_{av}$; $\angle OWO_{trans}$ = 178.8(2)°$_{av}$; d(W–O) = 1.901(10) Å$_{av}$; $\angle WOC$ = 137.8(16)°$_{av}$), and packs in hexagonal columns due to face-to-face π-stacking interactions of the bipyridines.[10]

Concern that 4,4′-bipy was rendered an ineffective linker due to the weaker basicity of the second nitrogen upon formation of the initial hydrogen-bond, or its conformational rigidity, prompted a change to 1,2-di-4-pyridylethane. When combined with (p-$HOC_6H_4O)_6W$·2THF·C_6H_6 **2**, two materials of stoichiometry $[\{4,4'\text{-}(NC_5H_4)_2(CH_2CH_2)\}_2\{(HOC_6H_4O)_6W\}]_\infty$ **4** and $[\{4,4'\text{-}(NC_5H_4)_2(CH_2CH_2)\}_3\{(HOC_6H_4O)_6W\}\cdot THF]_\infty$ (**5**·THF) were isolated in *ca.* 1:3 ratio (Scheme 1). Fig. 3(a) reveals the OH···N, N···HO bonds of **4** as a zigzag chain-link motif, while Fig. 3(b) shows how additional phenols interact with the OH groups of these units to form a box.‡ Similar H-bonds connect the boxes and a redundant network interpenetrates to form an overall doubly interpenetrating 3-D network.[1] Again the tungsten core is regular ($\angle OWO_{cis}$ =

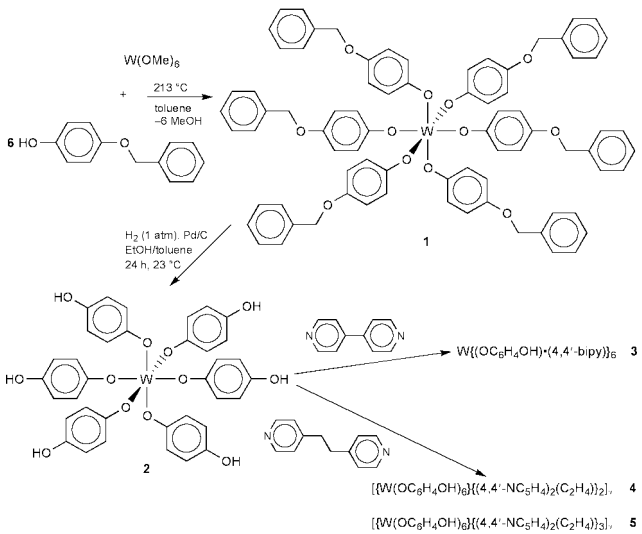

Scheme 1

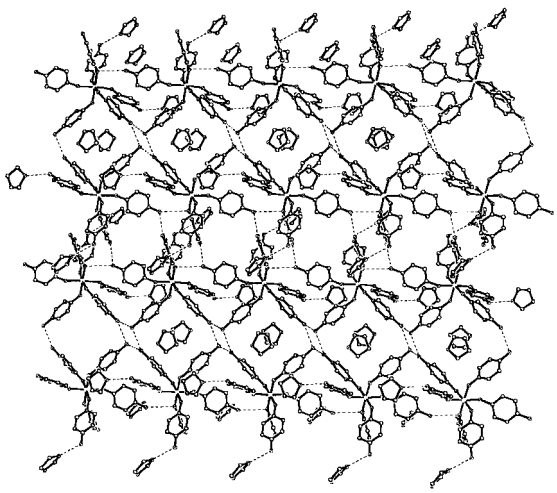

Fig. 1 A sheet of three-dimensional (p-$HOC_6H_4O)_6W$·2THF·C_6H_6 (**2**·2THF·C_6H_6) showing the different H-bonding connectivities.

 DOI: 10.1039/b100561h

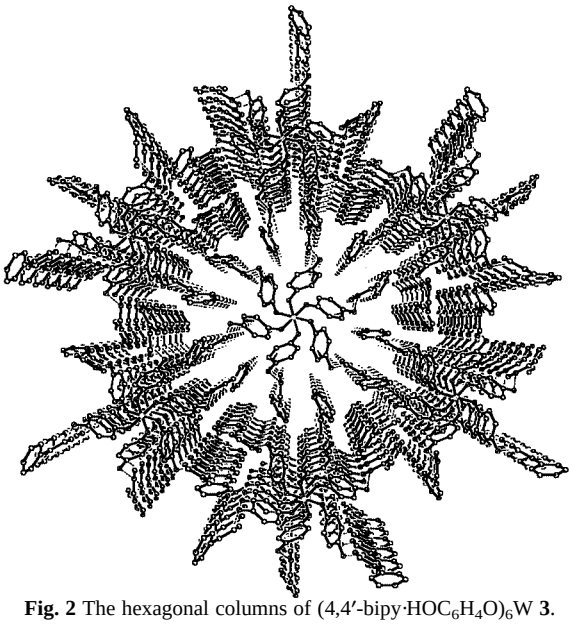

Fig. 2 The hexagonal columns of (4,4′-bipy·$HOC_6H_4O)_6W$ **3**.

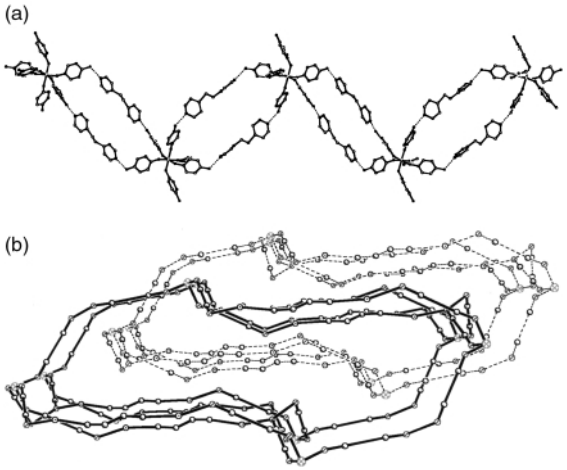

Fig. 3 (a) The zigzag OH···N, N···HO connectivity of [{4,4′-$(NC_5H_4)_2(CH_2CH_2)$}$_2${$(HOC_6H_4O)_6W$}]$_\infty$ **4**. (b) Additional phenolic H-bonds generate the doubly interpenetrating three-dimensional boxes of **4** (W = ⊗, O = ∅, N = ☉, *p*-C and ethane carbons (○)).

90.0(18)°$_{av}$; ∠OWO$_{trans}$ = 178.4(8)°$_{av}$; *d*(W–O) = 1.88(2) Å$_{av}$), but substantial variation in ∠WOC (143.6(54)°$_{av}$) is observed to reflect the constraints of the network.

Fig. 4(a) illustrates the connectivity of [{4,4′-$(NC_5H_4)_2(CH_2CH_2)$}$_3${$(HOC_6H_4O)_6W$}·THF]$_\infty$ (**5**·THF), whose tungsten centers are linked *via* OH···N, N···HO bonds to form an irregular box. The familiar octahedral core of the $(HOC_6H_4O)_6W$ group is evident (∠OWO$_{cis}$ = 90.0(25)°$_{av}$; ∠OWO$_{trans}$ = 177.6(17)°$_{av}$; *d*(W–O) = 1.86(5) Å$_{av}$), yet the W–O–C angles vary greatly (135.7(18)° to 169.4(19)°) to accommodate geometric features of the three-dimensional network. The box described above is voluminous, hence the structure triply interpenetrates[1] [Fig. 4(b)].

In summary, hexaphenol (*p*-$HOC_6H_4O)_6W$ **2** does not self-condense into μ-OC_6H_4O oligomers and can be utilized to form hydrogen-bonded complexes and networks.

Financial support from the National Science Foundation (CHE-9816134), the Cornell High Energy Synchrotron Source (CHESS), the Cornell Center for Materials Research (DMR-9632275), and The English-Speaking Union, for a Lindemann Trust Fellowship (RED), is gratefully acknowledged.

Notes and references

† *Selected analytical data*: **1** (acetone-d_6), δ_H 5.04 (2 H, s, CH_2), 6.87 (4 H, br s, OCHCHO), 7.4 (5 H, m, C_6H_5); δ_C 70.88 (CH_2), 115.77 (*m*-C_a), 121.96

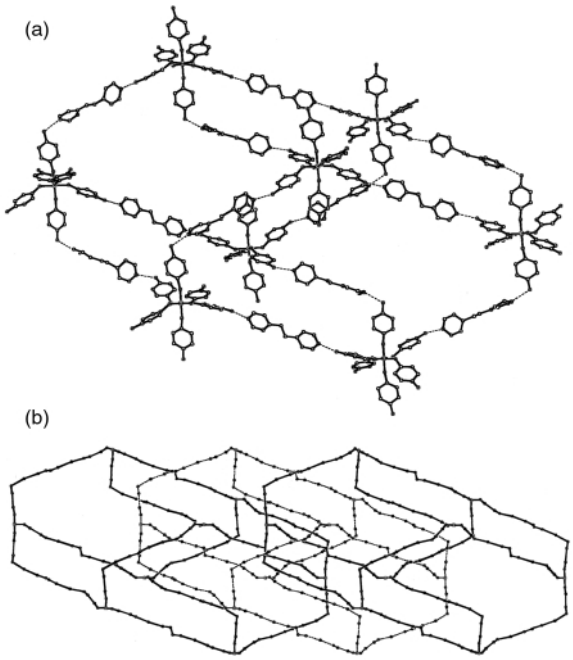

Fig. 4 (a) The OH···N, N···HO connectivity generating the irregular three-dimensional box of [{4,4′-$(NC_5H_4)_2(CH_2CH_2)$}$_3${$(HOC_6H_4O)_6W$}·THF]$_\infty$ **5**. (b) Triple interpenetration of the boxes W = ⊗, O = ∅, N = ☉, *p*-C and ethane carbons (○)).

(*o*-C_a), 128.48, 129.32 (*o*-C_b, *m*-C_b), 128.66 (*p*-C_b), 138.45 (*ipso*-C_b), 155.87, 157.13 (*ipso*-C_a, *p*-C_a). **2** (acetone-d_6), δ_H 6.72 (4 H, m, CH), 8.14 (1 H, s, OH); δ_C 115.82, 115.91 (*m*-C), 121.99 (*o*-C), 154.09, 154.19 (*p*-C), 156.39 (*ipso*-C), doubled resonances caused by OC_6H_4OD.

‡ *Crystal data*: **2**·2THF·C_6H_6: $C_{50}H_{52}O_{14}W$, *M* = 1060.77, triclinic, space group $P\bar{1}$, *a* = 10.3360(10), *b* = 11.8990(10), *c* = 21.761(3) Å, α = 97.120(10), β = 102.200(10), γ = 108.510(10)°, *U* = 2427.3(5) Å^3, *T* = 293(2) K, *Z* = 2, μ(Mo-Kα) = 2.444 mm^{-1}, 6303 (R_{int} = 0.0272) independent reflections, $R_1(2\sigma)$ = 0.0326. **3**: $C_{96}H_{78}N_{12}O_{12}W_5$, *M* = 1775.56, hexagonal, space group *R*3, *a* = 27.1402(1), *c* = 9.7013(1) Å, *U* = 6188.52(7) Å^3, *T* = 173(2) K, *Z* = 6, μ(Mo-Kα) = 1.473 mm^{-1}, 4778 (R_{int} = 0.0420) independent reflections, $R_1(2\sigma)$ = 0.0325. **4**: $C_{60}H_{54}N_4O_{12}W$, *M* = 1206.92, triclinic, space group $P\bar{1}$, *a* = 9.5723(3), *b* = 11.2623(4), *c* = 26.9897(9) Å, α = 86.9380(10), β = 83.5980(10), γ = 88.5040(10)°, *U* = 2886.79(17) Å^3, *T* = 296(2) K, *Z* = 2, μ(Mo-Kα) = 2.064 mm^{-1}, 9721 (R_{int} = 0.0502) independent reflections, $R_1(2\sigma)$ = 0.0740. **5**·THF: $C_{76}H_{74}N_6O_{13}W$, monoclinic, space group $P2_1/c$, *a* = 25.132(3), *b* = 11.6991(18), *c* = 25.988(4), β = 104.724(3)°, *U* = 7389.9(19) Å^3, *T* = 295(2) K, *Z* = 4, 3445 (R_{int} = 0.0731) independent reflections, $R_1(2\sigma)$ = 0.1002.

CCDC reference numbers 156504–156507. See http://www.rsc.org/suppdata/cc/b1/b100561h/ for crystallographic data in CIF or other electronic format.

1 S. R. Batten and R. Robson, *Angew. Chem., Int. Ed.*, 1998, **37**, 1460; M. O'Keeffe, M. Eddaoudi, H. Li, T. Reineke and O. M. Yaghi, *J. Solid State Chem.*, 2000, **152**, 3.
2 M. A. Hearshaw and J. R. Moss, *Chem. Commun.*, 1999, 1.
3 V. Percec, W.-D. Cho, M. Möller, S. A. Prokhorova, G. Ungar and D. J. P. Yeardly, *J. Am. Chem. Soc.*, 2000, **122**, 4249.
4 J. J. S. Lamba and C. L. Fraser, *J. Am. Chem. Soc.*, 1997, **119**, 1801.
5 von H. Funk and W. Baumann, *Z. Anorg. Chem.*, 1937, **231**, 264.
6 P. I. Mortimer and M. I. Strong, *Aust. J. Chem.*, 1965, **18**, 1579.
7 L. B. Handy, K. G. Sharp and F. E. Brinckman, *Inorg. Chem.*, 1972, **11**, 523.
8 For some recent hydrogen-bonding networks featuring inorganic cores, see: J. C. MacDonald, P. C. Dorrestein, M. M. Pilley, M. M. Foote, J. L. Lundburg, R. W. Henning, A. J. Schultz and J. L. Manson, *J. Am. Chem. Soc.*, 2000, **122**, 11 692; C. B. Aakeroy, A. M. Beatty and K. R. Lorimer, *J. Chem. Soc., Dalton Trans.*, 2000, 3869; C. V. K. Sharma and R. D. Rogers, *Chem. Commun.*, 1999, 83.
9 M. L. Listemann, J. C. Dewan and R. R. Schrock, *J. Am. Chem. Soc.*, 1985, **107**, 7207; M. A. Lockwood, P. E. Fanwick, O. Eisenstein and I. P. Rothwell, *J. Am. Chem. Soc.*, 1996, **118**, 2762.
10 S. Mecozzi, A. P. West and D. Dougherty, *Proc. Natl. Acad. Sci. USA*, 1996, **93**, 10 566; G. Klebe and F. Diederich, *Philos. Trans. R. Soc. London A*, 1993, **345**, 37; G. E. Bacon, N. A. Curry and S. A. Wilson, *Proc. R. Soc. London A*, 1964, **279**, 98.

CHEMCOMM Communication
www.rsc.org/chemcomm

Liquid crystal effect on neutral-carrier-type ion-sensing membranes

Keiichi Kimura,*[a] Yoshikazu Kawai,[a] Setsuko Yajima[a] and Yoshiaki Sakurai[b]

[a] *Department of Applied Chemistry, Faculty of Systems Engineering, Wakayama University, Sakae-dani 930, Wakayama 640-8510, Japan. E-mail: kimura@sys.wakayama-u.ac.jp*
[b] *Department of Technology, Research Institute of Osaka Prefecture, Ayumino 2-Chome 7-1, Izumi, Osaka 594-1157, Japan*

Received (in Cambridge, UK) 24th April 2001, Accepted 6th June 2001
First published as an Advance Article on the web 27th June 2001

Liquid crystallinity of membrane solvent and neutral carriers for potentiometric ion sensors affects the orientation of neutral carrier molecules in the ion-sensing membranes, thus bringing about significant changes in the ion selectivity for the membrane electrodes.

Neutral-carrier-type ion-sensing membranes are very attractive for potentiometric ion sensors such as ion-selective electrodes (ISEs) and ion-sensitive field-effect transistors.[1] The ion selectivities are governed not only by the original selectivity of neutral carriers themselves but also by the kind of plasticizers, because their ion-exchange equilibrium resembles that for liquid–liquid extraction.[2,3] We became very much interested in how the orientation of neutral carrier and solvent molecules affects their ion exchange in the membrane interface. The ion sensor property might be controlled by the orientation of the membrane components. Since liquid crystals possess some molecular orientation as well as mobility, they may be a useful material for PVC-based ion-sensing membranes.[4] We have therefore attempted to use a liquid-crystalline membrane solvent and a neutral carrier as the membrane components for ISEs, expecting some improvement of ion sensor property. Here we report a remarkable liquid crystal effect of membrane solvent and neutral carrier on the resulting membrane electrodes.

In order to elucidate the 'pure' liquid crystal effect on the ion sensor property, we decided to use bulk liquid-crystalline membranes, not PVC-dispersed liquid-crystalline membranes. Bulk membranes consisting of 5.0 wt% neutral carrier, 1.3 wt% potassium tetrakis(*p*-chlorophenylborate) (KTpClPB), and 93.7 wt% solvent were incorporated into the plastic tip of an adjustable pipette (Quality Science Plastics, Q-110) for the neutral carrier-type ion-sensors. For the membrane solvent we employed liquid-crystalline compound, 4-cyano-4′-hexylbiphenyl **1** (K-18, Merck) (Scheme 1), as well as 2-nitrophenyl octyl ether (NPOE) for comparison. The neutral carriers were a liquid-crystalline neutral carrier **2**[5] and [bis(benzo-15-crown-5)-4-methyl] pimelate [bis(benzo-15-crown-5)]. The electrochemical cell for the emf measurements was Ag | AgCl | 1×10^{-3} mol dm^{-3} KCl | ion-sensing membrane | sample solution || 1 mol dm^{-3} CH_3CO_2Li || 3 mol dm^{-3} KCl | AgCl | Ag. The selectivity coefficients of K^+ with respect to Na^+ were determined by a mixed solution method, that is, the fixed interference method (FIM) at the Na^+ background concentration of 1×10^{-2} or 3×10^{-1} mol dm^{-3}.

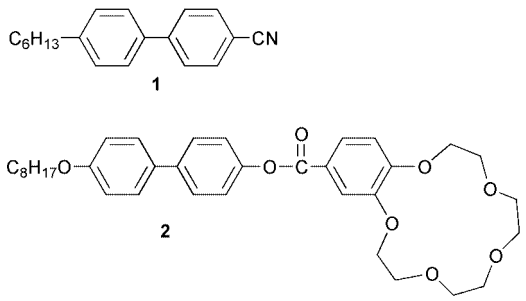

Scheme 1 Liquid-crystalline solvent (**1**) and neutral carrier (**2**) employed here.

Potassium ion-selective electrodes based on the liquid-crystalline membrane containing liquid-crystalline neutral carrier **2** as well as KTpClPB responded to K^+ activity changes with a Nernstian or near-Nernstian slope in the activity range of 3×10^{-6} to 1×10^{-1} mol dm^{-3} at 25 °C. This was the case for the corresponding liquid membrane systems containing NPOE instead of **1**. There was not any significant difference in the sensitivity at the three measuring temperatures of 19, 25, and 35 °C. The potential response was as fast as that for conventional plasticized-PVC membrane electrodes with t_{90} of several seconds.

The selectivity for K^+ over Na^+ (selectivity coefficient of K^+ with respect to Na^+, $k^{Pot}_{K,Na}$) was measured in the liquid-crystalline membrane systems at the three different temperatures (Fig. 1). It should be noted that the selectivity coefficients depend significantly on the measuring temperatures in the membrane systems containing neutral carrier **2**. On the other hand, little significant change in the selectivity with temperature was observed in the membrane system with bis(benzo-15-crown-5) and without any neutral carrier. The selectivity coefficients of K^+ with respect to Na^+ measured at temperatures of 19 and 25 °C are much smaller than those at 35 °C in the membrane systems containing **2**.

The phase transition temperatures for the above-mentioned membrane systems were followed by differential scanning calorimeter, and are summarized in Table 1. The liquid-crystalline compound **1**, by itself, has a transition from crystal to nematic phase (K–N) at 15.3 °C and from nematic to isotropic phase (N–I) at 29.2 °C. The addition of a small amount of neutral carrier and/or KTpClPB altered the transition temperature to some extent, as anticipated. The drastic temperature dependence of the ion selectivities as shown in Fig. 1 indicates that the higher selectivity for K^+ over Na^+ is attained in the nematic state in the neutral-carrier-type liquid-crystalline membranes of **2**. This means that the highly oriented nematic phase enhances the K^+ selectivity of the 15-crown-5 derivatives over Na^+, as compared with the corresponding isotropic liquid phase. The selectivity coefficients for the membrane system of

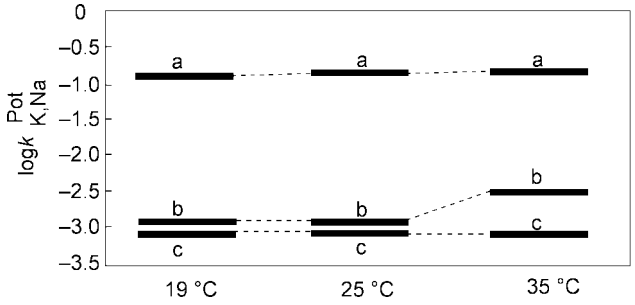

Fig. 1 Temperature dependence of selectivity coefficient for K^+ with respect to Na^+ in the ion-sensing membranes: (a) **1**/KTpClPB (without neutral carrier), (b) **2**/**1**/KTpClPB, and (c) bis(benzo-15-crown-5)/**1**/KTpClPB.

 DOI: 10.1039/b103638f

Table 1 Phase transition temperatures measured by differential scanning calorimetry (°C)

Membrane system	K–N (Crystal-nematic)	N–I (Nematic-isotropic)
1	15.3	29.2
1/KTpClPB	15.2	23.3
2/**1**/KTpClPB	15.3	32.5
Bis(b15C5)[a]/**1**/KTpClPB	15.7	31.1

[a] Bis(b15C5): bis(benzo-15-crown-5) or [bis(benzo-15-crown-5)-4-methyl] pimelate

2/**1**/KTpClPB at 19 and 25 °C are quite comparable to those for the corresponding membrane system containing a bis(benzo-15-crown-5) derivative, bis[(benzo-15-crown-5)-4-methyl] pimelate, instead of **2**. It is well-known that bis(benzo-15-crown-5) derivatives display excellent K^+ selectivity over Na^+ by cooperative action of two adjacent crown ether rings.[6,7] This implies that the highly oriented phase in the membrane urges the monocyclic neutral carriers to aggregate to each other, which in turn allows the neutral carriers to behave as if they were bis(crown ether) neutral carriers.

Even when the bis(benzo-15-crown-5) derivative was employed for the neutral carrier of the liquid-crystalline membrane (**1**/KTpClPB), the K^+ selectivity over Na^+ hardly depended on the temperature over the range from 19 to 35 °C. Also, no significant temperature dependence on the K^+ selectivity over Na^+ was found when NPOE, a well-known plasticizer for PVC-based ion-sensing membranes, was applied as the membrane solvent instead of the liquid- crystalline solvent **1**. This confirms that the enhanced K^+ selectivity over Na^+ for the liquid-crystalline membrane system is quite specific to the highly oriented state of neutral carrier in the membrane.

Thus, the present results suggest that the ordered orientation of neutral carrier molecules in ion-sensing membranes modifies their ion-sensor selectivities to a great extent. The orientation control of neutral carriers not only by temperature but also other external stimuli, such as electric field and light, would switch their membrane ion selectivity. Further study is now under way.

Notes and references

1 P. Bühlmann, E. Pretsch and E. Bakker, *Chem. Rev.*, 1998, **98**, 1593.
2 S. Cinani, G. Eisenman and G. Szabo, *J. Membr. Biol.*, 1969, **1**, 1.
3 D. Ammann, *Ion-Selective Microelectrodes—Principles, Design and Applications*, Springer-Verlag, Berlin, 1986.
4 J. Shah, J. W. Brown, E. M. Buckley-Dhoot and A. J. Bandara, *J. Mater. Chem.*, 2000, **10**, 2627.
5 H. Tokuhisa, M. Yokoyama and K. Kimura, *J. Mater. Chem.*, 1988, **8**, 889.
6 M. Bourgoin, K. H. Wong, J. Y. Hui and J. Smid, *J. Am. Chem. Soc.*, 1975, **97**, 3462.
7 K. Kimura, T. Maeda, H. Tamura and T. Shono, *J. Electroanal. Chem. Interfacial Electrochem.*, 1979, **95**, 91.

CHEMCOMM Communication
www.rsc.org/chemcomm

Synthetic equivalents of alkynyl and propargyl radicals

Peter Boutillier and Samir Z. Zard*

Laboratoire de Synthèse Organique associé au CNRS Ecole Polytechnique, 91128 Palaiseau, France. E-mail: zard@poly.polytechnique.fr

Received (in Cambridge, UK) 23rd February 2001, Accepted 4th June 2001
First published as an Advance Article on the web 27th June 2001

Radicals derived from β-ketoesters can, depending on the position of the unpaired electron, represent synthetic equivalents to the high energy and elusive alkynyl radicals or to the stabilised and relatively unreactive propargyl radicals by application of the xanthate transfer reaction followed by nitrosative cleavage of the corresponding isoxazolinones.

Retrosynthetic disconnections of acetylenic targets and intermediates almost never encompass the possibility of using synthons equivalent to propargyl or alkynyl radicals. Synthetic plans rely mostly on the corresponding hypothetical anionic or cationic species and on organometallic coupling or methathesis reactions.[1] Propargylic radicals are stabilised species and are relatively unreactive: although they do undergo ring-closure to non-activated olefins, *intermolecular* additions require activated olefins for success.[2] Alkynyl radicals, in contrast, are highly energetic species, accessible only with great difficulty[3] and, as far as we know, have very rarely been used in synthesis. One notable example is the photochemical generation of phenylethynyl radical from phenyliodoacetylene and its capture by aromatic compounds.[4] The instability of alkynyl radicals is reflected in the strength of the corresponding C–H bond, estimated to be around 130 kcal mol^{-1}, nearly 20 kcal mol^{-1} higher than that of an alkene C–H bond.[3] In view of the central role played by acetylenes in organic chemistry, it seemed worthwhile developing a route which would be an overall synthetic equivalent to either alkynyl or propargyl radicals.

Our approach is based on combining two reactions we have developed in recent times: the nitrous acid mediated cleavage of isoxazolinones[5] with the intermolecular radical addition of xanthates.[6] As shown in the top sequence in Scheme 1, addition of a radical located in position 2 of a β-ketoester and derived from the corresponding xanthate **1** to olefin **2** gives an adduct **3**, where a new C–C bond has been formed in an intermolecular manner. Reductive removal of the xanthate, formation of the isoxazolinone **5** (only one tautomeric form is drawn),[7] and cleavage with nitrous acid finally provides the desired alkyne **6**. This compound corresponds formally to the addition of the inaccessible alkynyl radical **7** to the starting olefin **2**. If the initial radical is located at position 4 of the β-ketoester (*i.e.* starting with xanthate **8**), the overall sequence leading to acetylene **10** is equivalent to the addition of a propargyl radical **11** to the olefin. This approach, involving an electron attracting α-acetonyl radical, complements the use of the propargyl radical itself which, as was stated above, has a rather nucleophilic character and therefore requires an olefin activated by an electrophilic group as partner.

The examples collected in Table 1 give an idea of the scope of the sequence corresponding to the overall addition of an alkynyl radical. Both the radical addition and the nitrosative cleavage occur under mild conditions and are tolerant of various functional groups commonly encountered in organic synthesis. In the case of the isoxazoline **5e** derived from *N*-tosylallylamine **2e** (entry 5), *N*-nitrosation occurred to give **6′e** (**6**, R′ = $-CH_2N(NO)Ts$) in 46% yield, in addition to the 'normal' alkyne **6e**, itself formed in 20% yield. The *N*-nitroso group in **6′e** could be removed by warming with triethylamine in aqueous THF, thus bringing the overall yield of alkyne **6e** to 47%.[8]

For convenience, the xanthate group in the adduct was reductively removed either by treatment with a stoichiometric quantity of lauroyl peroxide in isopropanol (yields with an asterisk in Table 1)[9] or, more conventionally, with tributylstannane; its presence, however, allows the insertion of another radical transformation, namely cyclisation onto an aromatic ring.[10] This is illustrated by the synthesis of the 3-alkynyl indoline pictured in Scheme 2. Thus, addition of xanthate **1c** to *N*-allyl-*N*-mesyl-*p*-bromoaniline **2e** gave the expected adduct **12** in a reasonable yield (43%, along with 28% of recovered xanthate). Exposure of this adduct to stoichiometric amounts of lauroyl peroxide (added portion-wise over several hours) in refluxing 1,2-dichloroethane resulted in ring-closure to indoline **13** (86%). Finally, conversion into the corresponding isox-

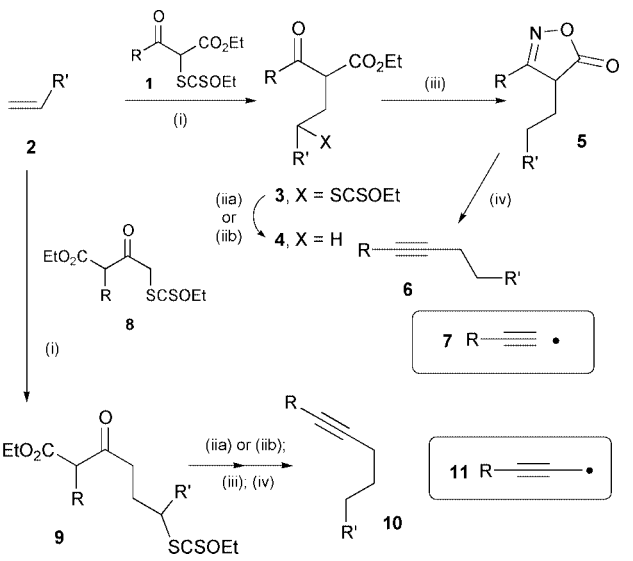

Scheme 1 *Reagents and conditions*: (i) lauroyl peroxide (5–20 mol%), 1,2-dichloroethane, reflux; (iia) lauroyl peroxide (100–110%), isopropanol, reflux; (iib) Bu_3SnH (AIBN), cyclohexane, reflux; (iii) $NH_2OH{\cdot}HCl$, AcONa, EtOH, reflux; (iv) $NaNO_2$, $FeSO_4$, AcOH, H_2O, RT.

Table 1 Yield (%) of compounds **3**–**6** (Piv = pivalate)

R	1	R′	2	3	4	5	6
Ph	**1a**	$-CH_2SiMe_3$	**2a**	**3a** (86)	**4a** (75)	**5a** (80)	**6a** (76)
Ph	**1a**	$-CH_2PO(OEt)_2$	**2b**	**3b** (78)	**4b** (85)	**5b** (74)	**6b** (80)
c-C_3H_5-	**1b**	$-(CH_2)_9OPiv$	**2c**	**3c** (74)	**4c** (75)*	**5c** (83)	**6c** (75)
c-C_3H_5-	**1b**	$-CH_2PO(OEt)_2$	**2b**	**3d** (68)	**4d** (84)*	**5d** (90)	**6d** (67)
c-C_3H_5-	**1b**	$-CH_2NHTs$	**2d**	**3e** (65)	**4e** (92)	**5e** (89)	**6e** (20)
Me	**1c**	$-(CH_2)_9OPiv$	**2c**	**3f** (75)	**4f** (72)*	**5f** (81)	**6f** (60)

 DOI: 10.1039/b101751i

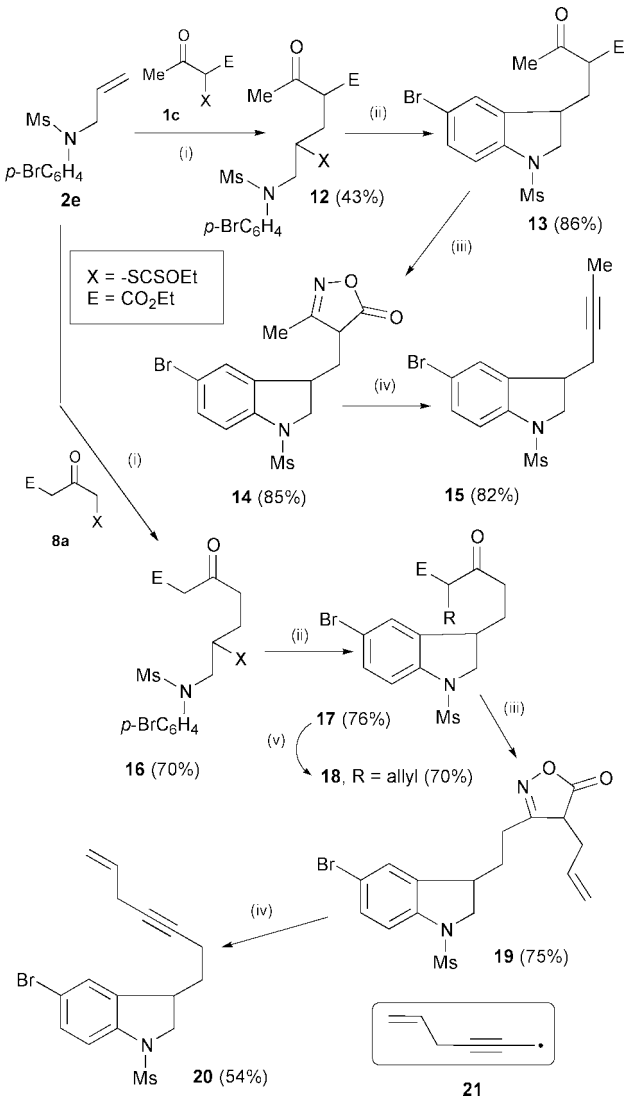

Scheme 2 *Reagents and conditions*: (i) lauroyl peroxide (5–30 mol%), 1,2-dichloroethane, reflux; (ii) lauroyl peroxide (100–110%), 1,2-dichloroethane, reflux; (iii) $NH_2OH.HCl$, AcONa, EtOH, reflux; (iv) $NaNO_2$, $FeSO_4$, AcOH, H_2O, RT; (v) allyl bromide, K_2CO_3, acetone, reflux.

azolinone and nitrosation furnished the desired alkyne **15** in 70% yield for the two steps.

A similar sequence can be used to illustrate the case of a propargyl radical equivalent. As shown in the bottom part of Scheme 2, radical addition of xanthate **8a** to the same olefin **2e** and similar ring closure provided indoline **17** in 42% overall yield. Allylation of the ketoester with allyl bromide, formation of the isoxazolinone, and nitrosative cleavage gave compound **20** containing the delicate, skipped enyne motif. This sequence corresponds to effecting the addition of stabilised and unreactive propargylic radical **21** to the unactivated olefin present in **2e**. Incidentally, the elaboration of a β-ketoester in the 4-position under neutral conditions *via* xanthate **8a** is worth underlining. Usually, it is necessary to resort to the highly basic di-anion[10] or to the bis-silylenol ether under Lewis acid catalysis[11] in order to functionalise position 4 without affecting the much more acidic position 2 of the ketoester.

In summary, the present approach complements existing methods by allowing the rapid assembly of a variety of otherwise inaccessible alkynes. It also brings a practical solution to the longstanding problem of finding synthetically useful and tame surrogates for the unavailable and unruly alkynyl radicals.

Notes and references

1 D. A. Ben-Efraim, in *The Chemistry of the Carbon–Carbon Triple Bond*, ed. S. Patai, John Wiley & Sons, Chichester, 1978, chap. 18, pp. 755–812; V. Jäger, in *Methoden Org. Chem. (Houben-Weyl)*, Georg Thieme Verlag, Stuttgart, 1977; Vol. 5/2a; L. Brandsma, *Preparative Acetylenic Chemistry*, Elsevier Science, New York, 1992; *Modern Acetylene Chemistry*, ed. P. J. Stang and F. Diederich, Wiley-VCH, Weinheim, 1995.

2 M.-P. Denieul, B. Quiclet-Sire and S. Z. Zard, *Tetrahedron Lett.*, 1996, **37**, 5495.

3 K. M. Erwin, S. Gronert, S. E. Barlow, M. K. Gilles, A. G. Harrison, V. M. Bierbaum, C. H. DuPuy, W. C. Lineberger and G. B. Ellison, *J. Am. Chem. Soc.*, 1990, **112**, 5750; M. S. Robinson, M. L. Polek, V. M. Bierbaum, C. H. DuPuy and W. C. Lineberger, *J. Am. Chem Soc.*, 1995, **117**, 6766.

4 G. Martelli, P. Spagnolo and M. Tiecco, *J. Chem. Soc. (B)*, 1970, 1413.

5 J. Boivin, L. Elkaim, P. G. Ferro and S. Z. Zard, *Tetrahedron Lett.*, 1991, **32**, 5321; J. Boivin, S. Huppé and S. Z. Zard, *Tetrahedron Lett.*, 1995, **36**, 5737; J. Boivin, S. Huppé and S. Z. Zard, *Tetrahedron Lett.*, 1996, **37**, 8735.

6 S. Z. Zard, *Angew. Chem., Int. Ed. Engl.*, 1997, **36**, 672.

7 A. R. Katritzky, P. Barczynski, D. L. Osterkamp and T. I. Yousaf, *J. Org. Chem.*, 1986, **51**, 4037.

8 L. Garcia-Rio, E. Iglesias, J. Ramos Leis, M. Elena Peita and A. Rios, *J. Chem. Soc., Perkin Trans. 2*, 1993, 29; L. Garcia-Rio, J. Ramos Leis, J. A. Moreira and F. Norberto, *J. Chem. Soc., Perkin Trans. 2*, 1998, 1613; L. Garcia-Rio, J. Ramos Leis, J. A. Moreira and F. Norberto, *J. Org. Chem.*, 2001, **66**, 381.

9 A. Liard, B. Quiclet-Sire and S. Z. Zard, *Tetrahedron Lett.*, 1996, **37**, 5877.

10 A. Liard, B. Quiclet-Sire, R. N. Saicic and S. Z. Zard, *Tetrahedron Lett.*, 1997, **38**, 1759; N. Cholleton and S. Z. Zard, *Tetrahedron Lett.*, 1998, **39**, 7295; T.-M. Ly, B. Quiclet-Sire, B. Sortais and S. Z. Zard, *Tetrahedron Lett.*, 1999, **40**, 2533.

11 S. N. Huckin and L. Weiler, *J. Am. Chem Soc.*, 1974, **96**, 1082.

12 T.-H. Chan and P. Brownbridge, *J. Chem. Soc., Chem. Commun.*, 1979, 578; H. Hagiwara, K. Kimura and H. Uda, *J. Chem. Soc., Perkin Trans. 1*, 1992, 693.

CHEMCOMM Communication
www.rsc.org/chemcomm

Toluene-*p*-sulfonyl-mediated radical cyclization of bis(allenes) utilizing *p*-TsBr and *p*-TsSePh

Suk-Ku Kang,*[a] Young-Hwan Ha,[a] Doo-Hwan Kim,[a] Yoongho Lim[b] and Jihyun Jung[b]

[a] *Department of Chemistry and BK-21 School of Molecular Science, Sungkyunkwan University, Suwon 440-746, Korea. E-mail: skkang@chem.skku.ac.kr; Fax: 82-31-290-7079; Tel: 82-31-290-7064*
[b] *Department of Applied Biology and Chemistry, Konkuk University, Seoul 143-701, Korea*

Received (in Cambridge, UK) 27th February 2001, Accepted 30th May 2001
First published as an Advance Article on the web 28th June 2001

The regio- and stereoselective toluene-*p*-sulfonyl-mediated radical cyclization of bis(allenes) with *p*-TsBr and *p*-TsSePh was carried out in the presence of a catalytic amount of AIBN to afford the *trans*-fused five-membered ring containing vinyl sulfones and bromide or selenide functionalities.

Recently the use of radical cyclization for carbon–carbon bond forming reactions has become widespread in organic chemistry[1] for the construction of carbocyclic and heterocyclic natural products.[2] The majority of commonly employed methods utilize tributyltin hydride to induce homolysis of an organic halide or alcohol derivative in forming the reactive carbon radical species. An alternative approach is to use the addition of a free-radical to two carbon–carbon double bonds, one double bond and one triple bond, or two triple bonds, which has the advantage of incorporating some useful additional functional groups into the cyclized products. The utility of this type of method using dienes,[3,4] enynes,[3a,5] and diynes[5e,6] with sulfonyl halides, thiols, sulfonyl selenides, and tin hydrides *etc*. has been demonstrated. However the radical reaction of allenic derivatives has received little attention,[7,8] because the addition reaction to allenes will be complicated in terms of chemo-, regio-, and stereoselectivity. To the best of our knowledge the radical induced cyclization of bis(allenes) is not known and we reasoned that the radical cyclization addition reaction of bis(allenes) is appealing because useful functionality is introduced in one simple step in which new carbon–carbon bond formation occurs stereoselectively coupled with two unsaturated appendages with distinguished reactivity.[9] The resulting cyclic compounds would be particularly useful to allow further synthetic transformations. Here we report the diastereoselective tosyl-mediated radical cyclization[10] of bis(allenes) **1** with *p*-tosyl bromide[11] and TsSePh[12] in the presence of a catalytic amount of AIBN to afford the *trans*-fused cyclopentane compounds **3**,† in which vinyl sulfones and vinyl bromides, or selenophenyl functionalities are introduced (Scheme 1).

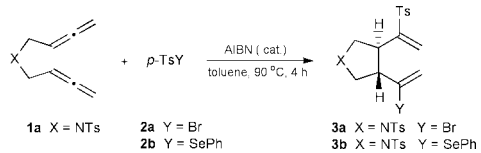

Scheme 1

Our initial work began with TsCl and benzoyl peroxide (BPO).[3b] However, it turned out to be unpromising. The reaction of **1a**[9] with TsI and AIBN in a sealed tube gave the cyclized products **4a** and **4b**‡ as a separable mixture in a low (22%) yield in the ratio of *cis* and *trans* (8:3). With sulfonyl iodides the chain transfer step seems to be too fast to allow efficient stereoselective cyclization (Scheme 2).

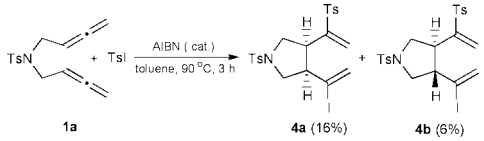

Scheme 2

Although with *p*-TsBr and AIBN simple heating did not give the clean product, by the use of a pressure tube (30 mL) capped

Table 1 Radical cyclization of bis(allenes) with TsBr and TsSePh in the presence of AIBN

Entry[a]	Bis(allenes)	TsX	Product	Isolated yield (%)
1	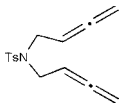 **1a**	TsBr **2a**	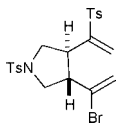 **3a**	73
2	**1a**	TsSePh **2b**	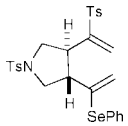 **3b**	59
3	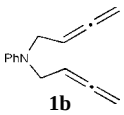 **1b**	**2a**	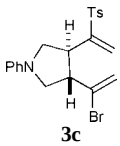 **3c**	48
4	**1b**	**2b**	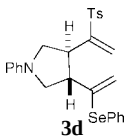 **3d**	65
5	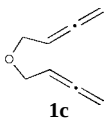 **1c**	**2a**	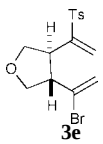 **3e**	64
6	**1c**	**2b**	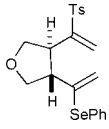 **3f**	55
7	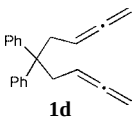 **1d**	**2a**	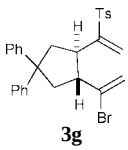 **3g**	63

[a] All reactions were carried out at 90 °C for 4 h with AIBN (20 mol%) in toluene.

 DOI: 10.1039/b101870l

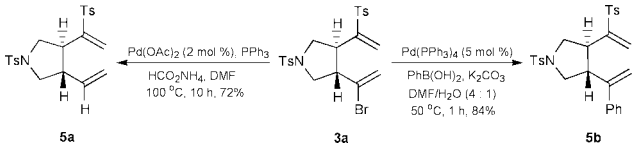

Scheme 3

with a teflon screw§ the reaction of **1a** with TsBr (1.1 equiv.) and AIBN (0.2 equiv.) in toluene at 90 °C for 4 h afforded the *trans*-fused cyclized product **3a** as the sole product in 73% isolated yield (entry 1 in Table 1).¶ The *trans* stereochemistry of the cyclized product **3a** was confirmed by the coupling constant (J = 9.6 Hz) for the protons (δ 2.97 and 2.87 ppm) at the ring junction in COSY experiments and 2D-NOESY experiments of the two protons at ring juncture and two *ortho* protons of the *p*-tosyl group in ^{1}H NMR.[13] It is presumed that the addition of tosyl radical to the central carbon atom of the allene moiety gives the allylic radical intermediates in the propagation step followed by cyclization with the other tethered allene moiety in a *trans* fashion stereoselectively to give the energetically more favorable and more stable *trans* product **3a** (entry 1 in Table 1). More clearly the *trans* stereochemistry of **3a** was determined by X-ray crystallography.

The cyclized product **3a** was transformed to the compounds **5a** and **5b** by the palladium-catalyzed reductive hydrogenolysis and Suzuki coupling reaction, respectively (Scheme 3).

Using *p*-TsSePh[12] as the radical source[14] in a pressure tube with AIBN in toluene, the *trans* cyclized selenide **3b** was obtained as the only isolated product in 59% yield (entry 2 in Table 1). The *trans* stereochemistry of **3b** was confirmed by X-ray crystallography.

We have applied this radical cyclization to the other bis(allenes) **1b**, **1c**, and **1d**, summarized in Table 1. The *N*-phenyl-substituted bis(allene) **1b** was treated with TsBr and TsSePh to give the cyclized products **3c** and **3d** in 48 and 65% yields, respectively (entries 3 and 4). For the bis(allenyl) ether **1c** the radical cyclization with **2a** and **2b** gave oxacycles **3e** and **3f** in 64 and 55% yields, respectively (entries 5 and 6). The *trans* stereochemistry of **3f** was determined by the coupling constant (J = 8.8 Hz) for the protons (δ 3.10 and 3.20 ppm) at the ring junction in COSY experiments. The diphenyl-substituted bis(allene) **1d** was smoothly cyclized to furnish vinyl bromide **3g** in 63% yield (entry 7).

In conclusion, *p*-tosyl-mediated radical cyclization of bis(allenes) with *p*-TsBr and *p*-TsSePh was accomplished stereoselectively in the presence of a catalytic amount of AIBN to afford the *trans* cyclized rings containing vinyl sulfone and vinyl bromide or vinyl phenylselenide.

The authors wish to acknowledge financial support by KOSEF-CMDS (Center for Molecular Design and Synthesis).

Notes and references

† A solution containing *p*-TsBr **2a** (94 mg, 0.40 mmol), bis(allene) **1a** (100 mg, 0.36 mmol) and AIBN (0.20 equiv.) in 4.0 mL of toluene was degassed and heated in a pressure tube at 90 °C for 4 h and toluene was evaporated *in vacuo*. The crude product was separated by column chromatography (hexanes–ethyl acetate = 2 : 1). Spectral data for (**3a**), yield: 135 mg, 73%; white solid; TLC, SiO_2, R_f 0.31 (2 : 1 hexane–EtOAc); mp 158 °C; IR (neat) ν = 3061, 2925, 1596, 1338, 1171, 1012, 812 cm^{-1}; ^{1}H NMR (500 MHz, $CDCl_3$): δ = 2.45 (s, 3H), 2.48 (s, 3H), 2.87 (ddd, 1H, J = 7.8, 8.9, 9.6 Hz), 2.97 (ddd, 1H, J = 8.0, 8.9, 9.6 Hz), 3.04 (dd, 1H, J = 8.9, 10.5 Hz), 3.18 (dd, 1H, J = 8.9, 10.4 Hz), 3.61 (dd, 1H, J = 8.0, 10.4 Hz), 3.65 (dd, 1H, J = 7.8, 10.5 Hz), 5.33 (d, 1H, J = 2.2 Hz), 5.46 (d, 1H, J = 2.2 Hz), 5.77 (d, 1H, J = 1.4 Hz), 6.46 (d, 1H, J = 1.4 Hz), 7.31 (d, 2H, J = 8.1 Hz), 7.37 (d, 2H, J = 8.0 Hz), 7.64 (d, 2H, J = 8.1 Hz), 7.70 (d, 2H, J = 8.0 Hz); ^{13}C NMR (125 MHz, $CDCl_3$): δ = 22.3, 22.4, 43.0, 52.0, 53.2, 54.4, 121.2, 125.0, 128.4, 129.2, 130.5, 130.6, 130.7, 134.1, 135.6, 144.6, 145.5, 149.7; HRMS for $C_{22}H_{24}BrNO_4S_2$; calcd: 509.0330; found: 509.0343.

Spectral data for (**3b**), yield: 59%; white solid; TLC, SiO_2, R_f 0.21 (3 : 1 hexane–EtOAc); mp 100–102 °C; IR (neat) ν = 3058, 2954, 1598, 1347, 1311, 1163, 814 cm^{-1}; ^{1}H NMR (500 MHz, $CDCl_3$): δ = 2.44 (s, 3H), 2.48 (s, 3H), 2.91 (m, 3H), 3.08 (m, 1H), 3.62 (m, 2H), 5.01 (d, 1H, J = 0.9 Hz), 5.23 (d, 1H, J = 0.9 Hz), 5.57 (d, 1H, J = 1.5 Hz), 6.38 (d, 1H, J = 1.5 Hz), 7.26–7.35 (m, 9H), 7.65 (m, 4H); ^{13}C NMR (125 MHz, $CDCl_3$): δ = 21.6, 21.7, 42.2, 50.9, 52.6, 54.1, 120.0, 123.8, 127.6, 128.1, 128.4, 128.6, 129.5, 129.8, 130.0, 133.6, 134.5, 135.1, 138.7, 143.8, 145.1, 149.5; HRMS for $C_{28}H_{29}NO_4S_2Se$; calcd: 587.0703; found: 587.0715.

‡ The *trans* configuration was deduced by the coupling constant of the two protons (J = 9.8 Hz) (δ 2.72 and 2.55 ppm) at the ring junction.

§ The pressure tube (made of borosilicate glass) was purchased from Aldrich Chem. Co., Inc. (Catalog Number Z18,109-9 type B).

¶ However when the same reaction was conducted with *p*-TsBr at threefold higher concentration for a shorter reaction time (1 h), we could isolate the *trans* product **3a**, the kinetic *cis* product and the monoadduct in the ratio 5 : 1 : 0.6 in 34% total yield and there remained 46% of the starting material.

1 B. Giese, in *Radicals in Organic Synthesis, Formation of Carbon–Carbon Bonds*, Pergamon Press, Oxford, 1986; D. P. Curran, *Synthesis*, 1988, 417; D. P. Curran, *Synthesis*, 1988, 489; D. J. Hart, *Science*, 1984, **223**, 883; W. P. Neuman, *Synthesis*, 1987, 665; M. Ramaiah, *Tetrahedron*, 1987, **43**, 3541.

2 C. P. Jasperse, D. P. Curran and T. L. Fevig, *Chem. Rev.*, 1991, **91**, 1237.

3 Cyclizations using *p*-TsCl, *p*-TsBr, and *p*-TsSePh: (*a*) J. E. Brumwell, N. K. Simpkins and N. K. Terrett, *Tetrahedron Lett.*, 1993, **34**, 1219; (*b*) with *p*-TsCl and BPO: C.-P. Chuang and T. H. Ngoi, *Tetrahedron Lett.*, 1989, **30**, 6369; (*c*) A. C. Serra, C. M. M. Da Silva Correa and M. L. C. Do Vale, *Tetrahedron*, 1991, **47**, 9463; (*d*) R. Nouguier, C. Lesueur, E. De Riggi, M. P. Bertrand and A. Virgili, *Tetrahedron Lett.*, 1990, **31**, 3541; (*e*) I. De Riggi, S. Gastaldi, J.-M. Surzur, M. P. Bertrand and A. Virgili, *J. Org. Chem.*, 1992, **57**, 6118.

4 The light-induced addition of tosyl bromide to some 1,6-dienes led to a mixture of *cis*- and *trans*-carbocycles and heterocycles was known by Bertrand and Silva Correa. See: I. De. Riggi, J.-M. Surzur and M. P. Bertrand, *Tetrahedron*, 1988, **23**, 7119; A. C. Serra, C. M. M. Da Silva Correa, M. A. M. S. A. Vieira and M. A. Gomes, *Tetrahedron*, 1990, **46**, 3061.

5 Cyclizations using R_3SnH: (*a*) G. Stork, Jr. and R. Mook, *J. Am. Chem. Soc.*, 1987, **109**, 2829; (*b*) K. Nozaki, K. Oshima and K. Utimoto, *J. Am. Chem. Soc.*, 1987, **109**, 2547; (*c*) cyclizations using thiols: Y. Ichinose, K. Wakamatsu, K. Nozaki, J.-L. Birbaum, K. Oshima and K. Utimoto, *Chem. Lett.*, 1987, 1647; (*d*) C. A. Broka and D. E. C. Reichert, *Tetrahedron Lett.*, 1987, **28**, 1503; (*e*) A. Padwa, H. Nimmesgern and G. S. K. Wong, *J. Org. Chem.*, 1985, **50**, 5620.

6 Cyclizations using R_3SnH: D. Crich and S. M. Fortt, *Tetrahedron Lett.*, 1987, **28**, 2895; cyclizations using *p*-TsBr: S. Caddick, C. L. Shering and S. N. Wadman, *Chem. Commun.*, 1997, 171.

7 Truce *et al.*, reported light-initiated addition of sulfonyl iodides to allenes. See: W. E. Truce, D. L. Heuring and G. C. Wolf, *J. Org. Chem.*, 1974, **39**, 238.

8 Hatem *et al.*, reported only one example of the allylallene **6**, to give the cyclized compounds **6**, and **7**, and **8**, in a ratio which is conditioned by the R substituent steric hindrance. See: F. E. Gueddari, J. R. Grimaldi and J. M. Hatem, *Tetrahedron Lett.*, 1995, **36**, 6685.

9 We have studied the palladium-catalyzed carbocyclization of bis(allenes). S.-K. Kang, T.-G. Baik, A. Kulak, Y.-H. Ha, Y. Lim and J. Park, *J. Am. Chem. Soc.*, 2000, **122**, 11 529.

10 For review on the sulfonyl radical, see: M. P. Bertrand, *Org. Prep. Proced. Int.*, 1994, **26**, 257.

11 A. C. Poshkus, J. E. Herweh and F. A. Magnotta, *J. Org. Chem.*, 1963, 2766.

12 T. G. Back, S. Collins and M. V. Krishna, *Can. J. Chem.*, 1987, **65**, 38.

13 Recently, Denmark *et al.*, reported the stereostructural assignment of *trans*-3, 4-disubstituted-*N*-(*p*-tolylsulfonyl)pyrrolidines by analysis of their ^{1}H NMR coupling constants. See: S. E. Denmark and L. R. Marin, *J. Org. Chem.*, 1993, **58**, 3857.

14 Light induced addition of TsSePh to allenes is known. See: Y.-H. Kang and J. L. Kice, *Tetrahedron Lett.*, 1982, **23**, 5373.

CHEMCOMM
Communication
www.rsc.org/chemcomm

Ring-opening of lactides and related cyclic monomers by triaryltin(IV) alkoxides and amides†

Malcolm H. Chisholm* and Ewan E. Delbridge

Department of Chemistry, The Ohio State University, 100 W 18th Avenue, Columbus Ohio, 43210-1185, USA. E-mail: chisholm@chemistry.ohio-state.edu

Received (in Cambridge, UK) 29th March 2001, Accepted 5th June 2001
First published as an Advance Article on the web 27th June 2001

Ar_3SnX, where Ar = *p*-MeC_6H_4, *p*-$CF_3C_6H_4$ or Ph and X = OBu^t or NMe_2, are catalyst precursors for the ring-opening of lactides in benzene at 80 °C and the rate of ring-opening of lactides and a variety of related cyclic monomers is influenced by Ar and X such the chemistry of the ring-opening event and the initially formed product may be examined.

The ring-opening polymerization of lactides (L, D, *rac* and *meso*) by well-defined coordination complexes is a topic of current interest since polylactides (PLAs) have numerous applications ranging from bulk packing materials[1] to drug delivery reagents,[2] artificial sutures[2,3] and scaffolds[4] for tissue engineering. There have been some exciting recent reports documenting stereoselective polymerization of *rac*- and *meso*-lactides to give heterotactic, isotactic and syndiotactic PLAs.[5] Much remains to be learned at this time, however, since very little is known about the details of factors controlling the rate of ring-opening, the stereoselectivity of this event and the deleterious side reactions of both intra- and inter-chain transfer and transesterification reactions, which can lead to loss of control of stereochemistry and molecular weight of PLAs. For example, the β-diiminate complex $[(BDI)Zn(OPr^i)]_2$ shown in **A** is reported to give >90% heterotactic PLA from *rac*-lactide

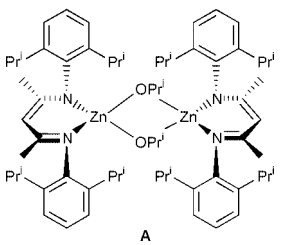

A

at 25 °C in CH_2Cl_2[5c] whereas the related magnesium complex gives atactic polymer under similar conditions with rapid transesterification.[6]

The stereocontrol in the polymerization of *rac*-lactide by $[(BDI)Zn(OPr^i)]_2$ has been attributed to end-group control which is fostered by the bulky BDI ligand, yet even bulkier ligands such as pyrazolylborate LMOR complexes [L = $(3\text{-}Bu^tpz)_3BH$, M = Mg and Zn] show little stereoselectivity.[7] We reasoned that much might be learned from studies of the kinetics of reactions employing Ar_3SnOR catalyst precursors since, unlike trispyrazolylborate ligands or other tridentate ligands, reversible bond breaking is not likely for the Sn–C and Sn–O bonds under mild conditions. Moreover the influence of electronic and steric factors can be examined by the use of *para*- and *meta*-substituents on the aryl ligands. We report here on initial findings from studies involving Ar_3SnX precursors, where Ar = *p*-MeC_6H_4, *p*-$CF_3C_6H_4$ or Ph and X = OBu^t or NMe_2.

† Electronic supplementary information (ESI) available: additional experimental data. See http://www.rsc.org/suppdata/cc/b1/b102896k/

The compounds Ar_3SnX were prepared from either metathetic reactions involving the respective Ar_3SnCl compound and $LiNMe_2$ or by an alcoholysis reaction involving Ar_3SnNMe_2 and Bu^tOH in hydrocarbons.‡ The compounds are white, hydrocarbon-soluble, microcrystalline materials with the exception of $(p\text{-}MeC_6H_4)_3SnNMe_2$ which is a colorless oil. These compounds were characterized by ^1H, $^{13}C\{H\}$ and ^{119}Sn NMR spectroscopy (and for Ar = *p*-$CF_3C_6H_4$ by ^{19}F) together with mass spectrometry, IR spectroscopy and elemental analysis. These compounds were found to be kinetically inert at 80 °C in benzene, conditions under which ring-opening polymerization (ROP) of lactides was subsequently studied.

In a typical polymerization reaction 50 equivalents of lactide was allowed to react with the Ar_3SnX compound in C_6D_6 at 80 °C (or in some instances at 52, 67 and 70 °C) and the reaction was monitored with time by NMR spectroscopy. Reactions were quite slow requiring *ca.* 3 days to approach 90% conversion. From the plots of $-\ln(A/A_0)$ *vs.* time (where A = concentration of lactide) we can estimate the rates of consumption of lactide to be $k_{obs} = 2.8(1) \times 10^{-6}$ and $2.0(1) \times 10^{-6}$ s^{-1} for X = NMe_2 and Ar = *p*-$CF_3C_6H_4$ and Ph, respectively. In reactions between Ph_3SnOBu^t and L-lactide, we can also obtain a reasonable estimate of the rate of the initial ring-opening event, $k_{ro} = 2.8(1) \times 10^{-6}$ s^{-1} which is faster than the rate of propagation $k_{prop} = 1.4(1) \times 10^{-6}$ s^{-1}. From studies of the rates of polymerization reactions with temperature we have obtained estimates of the enthalpy and entropy of activation for the ring-opening event for Ar = Ph and X = NMe_2 at a [lactide]:[catalyst] ratio of 50 to 1: $\Delta H^{\ddagger} = 12(1)$ kcal mol^{-1} and $\Delta S^{\ddagger} = -51(5)$ cal K^{-1} mol^{-1}. The rather large entropy of activation is consistent with a bimolecular reaction with a highly ordered transition state. However, the role of solvation has not been examined. It is noteworthy that these polymerization reactions are slower than those recently reported for a tin(II) catalyst system employing $(BDI)SnOPr^i$[8] as an initiator and also that whereas the latter shows a preference for heterotactic, *rmr* and *mrm*, tetrads in the polymerization of *rac*-lactide, no such preference is found in reactions employing Ar_3SnX precursors. The rate of polymerization is probably influenced by the relative polarity of the Sn–OR bond which is greater for Sn(II) than Sn(IV) but, given the relative size of Sn(II) *vs.* Sn(IV) (0.69 Å),[9] the stereoselectivity attributed to end-group control involving the SnOC*HMeC(O)OC*HMeC(O)OP unit of the growing polymer chain must arise from the pocket created by the two 2,6-diisopropylphenyl ligands in the (BDI)M(OR) catalyst systems.

Although the Ar_3SnX precursors are kinetically inert at 80 °C in benzene-d_6 for several days and the system that is initially active in the polymerization can be reasonably represented by $Ar_3Sn(OP)$, where OP represents the growing polymer chain, with the onset of polymerization, Ar_4Sn compounds are formed (as identified by ^1H, ^{13}C and ^{119}Sn NMR as well as electrospray mass spectrometry). Ar_4Sn compounds are inactive and the systems that are believed to be catalytically active are $Ar_{3-n}Sn(OP)_n$, where n = 1 or 2. The formation of Ar_4Sn clearly implicates the facility of chain transfer and, in addition, from studies of molecular weight distributions with time, we

 DOI: 10.1039/b102896k

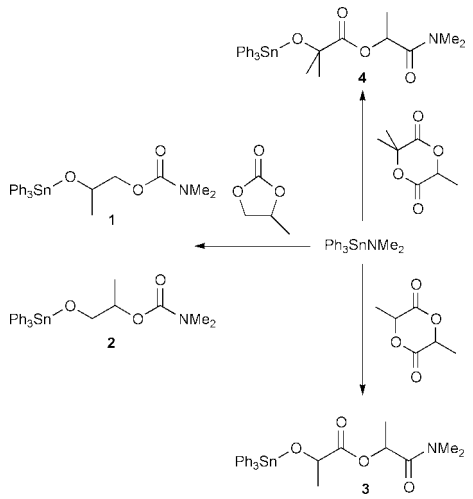

Scheme 1

observe extensive transesterification. Thus, even the seemingly simple and kinetically slow system for the ROP of lactides employing Ar_3SnX precursors has proved to be complicated.

One important point to emerge from these studies is the rate of ring-opening of lactide and related monomers occurs much more rapidly when X = NMe_2 than for X = OBu^t. Thus, *at room temperature*, Ph_3SnNMe_2 in benzene ring-opens the cyclic oxygenates shown in Scheme 1. The regiochemistry of the ring-opening event can be reliably determined from NMR studies.‡ The Sn–O^{13}C carbon shows coupling to ^{119}Sn and the amide methyl protons appear as two singlets due to the restricted rotation about the C–NMe_2 bond. Notable here is the ring-opening of propylene carbonate (PC) to give **1** and **2** (Scheme 1) a required step in the ring-opening decarbonation polymerization of PC by tin catalysts at higher temperatures.[10]

The ring-openings shown in Scheme 1 convert an Sn–NMe_2 group to an Sn–OR group and at 25 °C no further insertion/ring-opening occurs. The compounds are, however, not indefinitely persistent in solution. The compound $Ph_3SnOCHMeC(O)OCHMeCONMe_2$ **3** which we can represent as $Ph_3Sn[OCHMeC(O)]_2NMe_2$ is labile to transesterification reactions as represented by eqn. (1).

$$Ph_3Sn[OCHMeC(O)]_2NMe_2 \rightarrow Ph_3Sn[OCHMeC(O)]NMe_2 + Ph_3Sn[OCHMeC(O)]_nNMe_2\ (n \geqslant 3) \quad (1)$$

Reaction (1) is also accompanied by chain transfer and phenyl migration yielding Ph_4Sn. The compound $Ph_3Sn[OCMe_2C(O)OCHMeC(O)NMe_2]$ **4** is less labile to transesterification of the type shown in eqn. (1), presumably because of the bulky *gem*-dimethyl group, but still enters into chain/aryl group transfer. However, **4** does react with $Ph_3Sn(OBu^t)$ to give $Ph_3SnOCHMeC(O)NMe_2$ and $Ph_3Sn[OCMe_2C(O)OBu^t]$, products of transesterification. $Ph_3SnOCHMeC(O)NMe_2$ is formed from the reaction between Ph_3SnNMe_2 and lactide (2 : 1 ratio) in benzene as the major kinetic product in eqn. (2).

$$Ph_3Sn[OCHMeC(O)OCHMeC(O)NMe_2] + Ph_3SnNMe_2 \rightarrow 2Ph_3Sn[OCHMeC(O)NMe_2] \quad (2)$$

Reactions employing $Ph_2Sn(NMe_2)_2$ and lactide (1 : 1 ratio) yield $Ph_2Sn[OCHMeC(O)NMe_2]_2$ by consecutive ring-opening of lactide followed by intramolecular attack on the chain, eqn. (3).

$$Ph_2Sn(NMe_2)[OCHMeC(O)OCHMeC(O)NMe_2] \rightarrow Ph_2Sn[OCHMeC(O)NMe_2]_2 \quad (3)$$

In conclusion, these initial studies reveal that this seemingly most simple system for ring-opening polymerization of lactide is complicated by mischievous side-reactions. Insight into the latter, namely ligand exchange and transesterification and the ring-opening event can be gleaned from studies of model reactions such as those shown in reactions (1), (2) and (3).

We thank the Department of Energy, Office of Basic Science, Chemistry Division for financial support.

Notes and references

‡ *General considerations*: the synthesis of R_3SnNMe_2 and $Ph_2Sn(NMe_2)_2$ complexes was based on the reported synthesis[11] of Ph_3SnNMe_2 and $Ph_2Sn(NMe_2)_2$. See ESI for additional spectroscopic data.†

$SnPh_3[OCHMeC(O)OCHMeC(O)NMe_2]$: δ_H(400 MHz, C_6D_6): 0.99 [d, CH*Me*C(O)NMe_2, 3H], 1.53 (d, SnOCH*Me*, 3H), 2.11 (s, NMe_2, 3H), 2.47 (s, NMe_2, 3H), 4.75 (q, SnOC*H*Me, 1H), 4.83 [q, C*H*MeC(O)NMe_2, 1H], 7.16 (m, *m*- and *p*-H, 9H), 7.80 (dd, *o*-H, 6H, J_{HH} 7.9, 1.5 Hz, $^{119/117}$Sn satellites J_{SnH} ^{117}Sn 64, ^{119}Sn 49 Hz).

$SnPh_2[OCHMeC(O)NMe_2]_2$: δ_H(400 MHz, C_6D_6): 1.43 (d, SnOCH*Me*, 6H), 1.87 (s, NMe_2, 6H), 2.26 (s, NMe_2, 6H), 4.87 (q, SnOC*H*Me, 2H), 7.21 (t, *p*-H, 2H), 7.35 (t, *m*-H, 4H), 8.37 (dd, *o*-H, 4H, J_{HH} 7.6, 1.2 Hz, $^{119/117}$Sn satellites J_{SnH} ^{117}Sn 75, ^{119}Sn 59 Hz).

$SnPh_3[OCMe_2C(O)OCHMeC(O)NMe_2]$: δ_H(500 MHz, C_6D_6): 1.06 (d, CH*Me*C$ONMe_2$, 3H), 1.56 (s, SnOC*Me*$_2$, 3H), 1.65 (s, SnOC*Me*$_2$, 3H), 2.12 (s, NMe_2, 3H), 2.47 (s, NMe_2, 3H), 4.87 [q, C*H*MeCO)NMe_2, 1H], 7.17 (m, *p*-H, 3H), 7.23 (m, *m*-H, 6H), 7.87 (dd, *o*-H, 6H, J_{HH} 8.2, 1.3 Hz, $^{119/117}$Sn satellites J_{SnH} ^{117}Sn 64, ^{119}Sn 48 Hz).

Polymerization reactions: standard solutions of the appropriate R_3SnX complex (0.027 M) and L- or *rac*-lactide (0.338 M) were prepared in C_6D_6 and stored in a dry-box. Aliquots (100, 50, 25 and 12.5 μL for 25 : 1, 50 : 1, 100 : 1 and 200 : 1, respectively) of R_3SnX solutions were transferred along with an aliquot (200 μL) of either L- or *rac*-lactide to a J. Young® NMR tube. The total volume was made up to 800 μL with C_6D_6 to ensure a constant lactide concentration (0.084 M). Rates of polymerization were determined from ^{1}H NMR data where the sum of the area of monomer and polymer peaks (CH and CH_3) was assumed to be 100% and rates of disappearance of monomer were calculated by the subtraction of the integral of the polymer peaks from the integral of the monomer peaks and dividing by the concentration of monomer at t = 0. The natural log of this ratio was then plotted against time with a straight line being indicative of pseudo-first order kinetics. The gradient of this plot was used to determine values of k_{obs}.

1 Ecochem is a polylactide based packaging material developed by DuPont ConAgra.
2 Leupron Depot is a product of Takeda Chemical Industries, Ltd., Japan for drug delivery purposes; *Taehan Hwakakhoe Chi*, 1990, **34**, 203; *Chem. Abstr.*, 1990, **113**, 98014g.
3 E. E. Schmitt and R. A. Polistina, *US Pat.*, 3463158, 1969; E. J. Frazza and E. E. Schmitt, *J. Biomed. Mater. Res. Symp.*, 1971, **1**, 43; Dexon and Vicry are products of Davis & Geek Corporation., Wayne, NJ, and Ethicon, Inc., Somerville, NJ, respectively; J. P. Pennings, H. Dijkstra and A. J. Pennings, *Polymer*, 1993, **34**, 942.
4 J. A. Hubbell and R. Langer, *Chem. Eng. News*, 1995, March 13, 42; R. Langer and J. P. Vacanti, *Science*, 1993, **260**, 920.
5 T. M. Ovitt and G. W. Coates, *J. Am. Chem. Soc.*, 1999, **121**, 4072; C. P. Radano, G. L. Baker and M. R. Smith, *J. Am. Chem. Soc.*, 2000, **122**, 1552; M. Cheng, A. B. Attygalle, E. B. Lobkovsky and G. W. Coates, *J. Am. Chem. Soc.*, 1999, **121**, 11 845.
6 M. H. Chisholm, J. C. Huffman and K. Phomphrai, *J. Chem. Soc., Dalton Trans.*, 2001, 222.
7 M. H. Chisholm, N. W. Eilerts, J. C. Huffman, S. S Iyer, M. Pacold and K. Phomphrai, *J. Am. Chem. Soc.*, 2000, **122**, 11 845.
8 A. P. Dove, V. C. Gibson, E. L. Marshall, A. J. P. White and D. J. Williams, *Chem. Commun.*, 2001, 283.
9 R. D. Shannon, *Acta Crystallogr., Sect. A*, 1976, **32**, 751.
10 R. F. Storey and D. C. Hoffman, *Macromolecules*, 1992, **25**, 5369; L. Vogdanis, B. Martens, H. Uchtmann, F. Hensel and W. Hetiz, *Makromol. Chem.*, 1990, **191**, 465.
11 K. Jones and M. F. Lappert, *J. Chem. Soc. A*, 1965, 1944.

CHEMCOMM
Communication
www.rsc.org/chemcomm

An organometallic polyrotaxane and a new type of polyrotaxane architecture

Christopher S. A. Fraser, Michael C. Jennings and Richard J. Puddephatt*

Department of Chemistry, University of Western Ontario, London, Canada, N6A 5B7. E-mail: pudd@uwo.ca

Received (in Cambridge, UK) 3rd May 2001, Accepted 5th June 2001
First published as an Advance Article on the web 28th June 2001

A new architecture, comprising two interpenetrating chains of rings, has been discovered in the first organometallic polyrotaxane; the synthesis combines the techniques of organometallic chemistry, coordination chemistry and self-assembly through hydrogen bonding.

Functional polymers having novel architectures are of great current interest and polyrotaxanes are viewed as particularly significant. Admirable synthetic strategies have been developed to polymers with the rotaxanes on the main chain or side chain,[1–5] (**A** and **B** in Chart 1), and potential applications

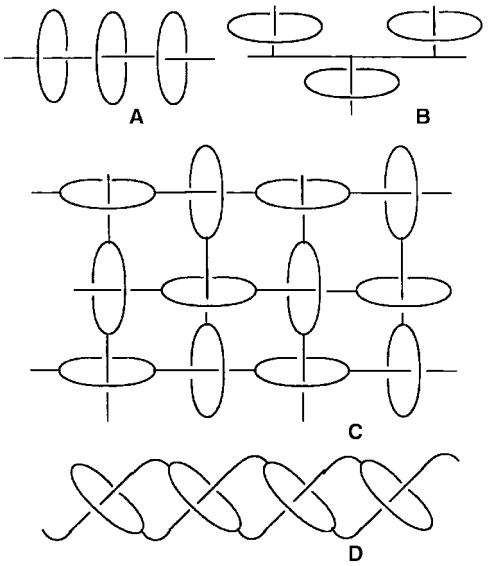

Chart 1 Polyrotoxanes.

ranging from drug delivery vehicles[6] to sensor devices[7–9] have been identified. If polymeric chains also contain ring components, then interpenetration can occur and this has been demonstrated in a two-dimensional sheet polyrotaxane (**C** in Chart 1).[10] This paper describes a new polyrotaxane architecture in which a related form of interpenetration occurs to give a one-dimensional polyrotaxane of type **D** (Chart 1). The synthesis involves introduction of a hydrogen-bonding group by oxidative addition (organometallic chemistry), assembly of three of these units at a tridentate templating ligand (coordination chemistry) and then formation of the polyrotaxane product by self-assembly through the hydrogen-bonding substituents. The combination of these interdisciplinary methods has great potential for forming new functional materials but has very rarely been used in the past.[11,12]

The reaction of $[PtMe_2(Bu_2bipy)]$, **1**, (Bu_2bipy = 4,4′-di-*tert*-butyl-2,2′-bipyridine)[11] with α-bromo-4-toluic acid gave the complex $[PtBrMe_2(Bu_2bipy)(CH_2C_6H_4CO_2H)]$, **2**, containing a carboxylic acid functional group designed to take part in intermolecular hydrogen bonding (Scheme 1). Three of these organoplatinum(IV) units were assembled at a tridentate ligand by substitution of bromide ligands by the pyridyl donors of *sec*-tris(4-pyridyl)triazine, Py_3T, which is known to give interesting structures in coordination chemistry.[13] The bromide abstraction step in the synthesis was effected by use of $AgPF_6$, to give the product $[\{(HO_2CC_6H_4CH_2)(Bu_2bipy)Me_2Pt\}_3\{(\beta\text{-}NC_5H_4)_3(C_3N_3)\}]^{3+}$, **3**, as the hexafluorophosphate salt. In the successful crystallization, 0.5 equiv. of HPF_6 and five acetone molecules were incorporated for each complex $\mathbf{3}[PF_6]_3$.[14]

The ions **3** self-assemble into chains of rings in the following way: the two carboxylic acid groups labelled **R** in Scheme 1 hydrogen bond to the group of a neighbouring molecule to form 56-membered rings and the group labelled **C** hydrogen bonds to the equivalent carboxylic acid group of a second neighbouring molecule to make a chain. Part of the one-dimensional polymer, comprised of rings connected by chains, that results from this self-assembly is illustrated in Fig. 1. Most remarkably, two of these polymeric units interpenetrate, with each ring section of one polymer penetrated by the chain section of the other, to form a new type of polyrotaxane (**D**, Chart 1) as illustrated in Fig. 2.

The infrared spectrum of **3** as a Nujol mull contains peaks due to ν(O–H) in the range 2545–2672 cm^{-1}, and the O···O distances between the hydrogen-bonded carboxylic acid groups in **3** are in the range 2.6–2.7 Å, Fig. 1, indicating the presence

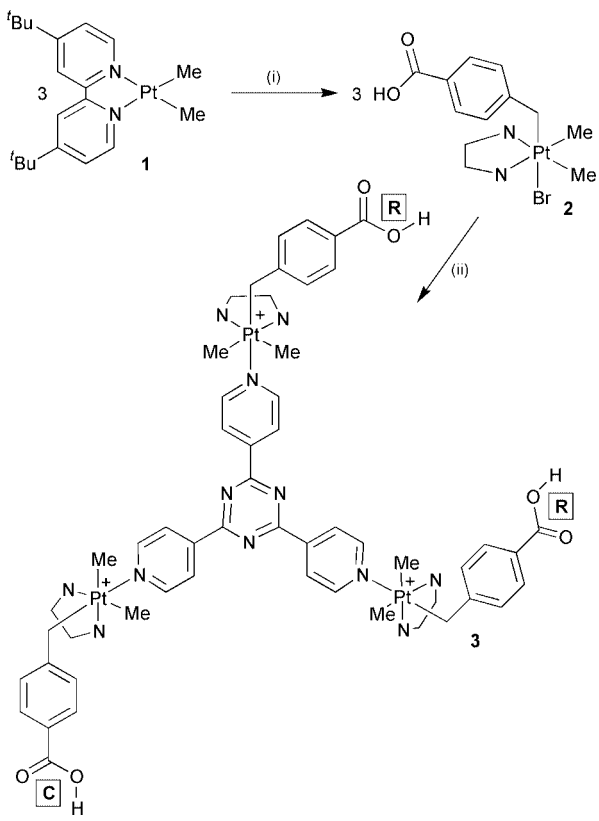

Scheme 1 NN = Bu_2bipy. *Reagents*: (i) 3 $BrCH_2C_6H_4CO_2H$; (ii) 3 Ag^+, $C_3N_3(C_5H_4N)_3$, −AgBr.

 DOI: 10.1039/b103967a

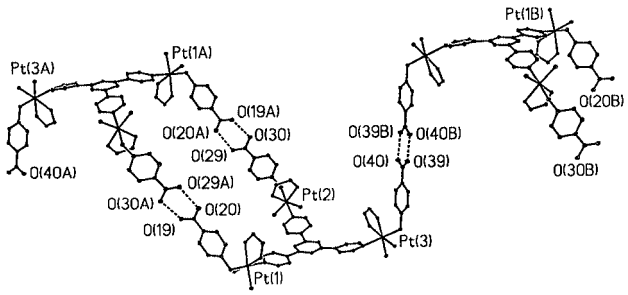

Fig. 1 The structure of complex **3**. The hydrogen bonding to give chains [O(39)···O(40B) = 2.60 Å] of rings [O(20)···O(29A) = 2.64 Å, O(19)···O(30A) = 2.70 Å] is illustrated for a central molecule and its two neighbours. Only the NCCN atoms of the Bu_2bipy ligands are shown for clarity.

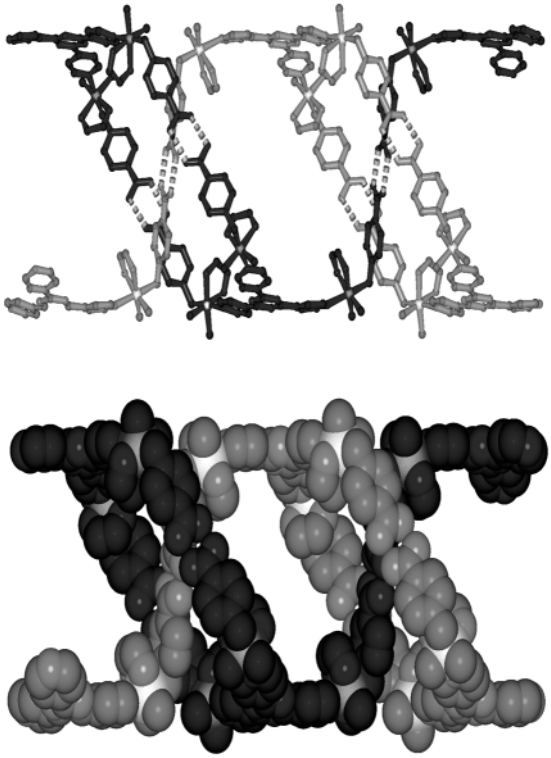

Fig. 2 A section of the polyrotaxane structure formed by two interpenetrating polymer units; only the central NCCN atoms of the Bu_2bipy ligands are shown for clarity. Above, ball and stick and, below, space filling representations.

of strong hydrogen bonds.[15] Are these hydrogen bonds maintained in solution? In acetone-d_6 solution, the ^{1}H NMR spectrum of **3** contains two methylplatinum resonances and two *tert*-butyl resonances in an approximately 2 : 1 intensity ratio, that are tentatively assigned to organoplatinum units within rings and chains respectively, suggesting that at least fragments of the structure are maintained in solution.

Complex **3** appears to be the first organometallic polyrotaxane and it has a unique structure of type **D** (Chart 1). Its formation involves three easy steps, using organometallic chemistry to introduce the hydrogen bonding group, coordination chemistry to assemble three hydrogen bonding groups around a central bridging ligand, and then the final self-assembly of the polyrotaxane through hydrogen bonding. Similar procedures have the potential to lead to many new and interesting forms of molecular architecture.

We thank the NSERC (Canada) for financial support and R. J. P. thanks the Government of Canada for a Canada Research Chair.

Notes and references

1 (*a*) H. W. Gibson, M. C. Bheda and P. T. Engen, *Prog. Polym. Sci.*, 1994, **19**, 843; (*b*) H. W. Gibson, L. Hamilton and N. Yamaguchi, *Polym. Adv. Technol.*, 2000, **11**, 791.

2 (*a*) J.-M. Kern, J.-P. Sauvage, G. Bidan, M. Billon and B. Divisia-Blohorn, *Adv. Mater.*, 1996, **8**, 580; (*b*) P.-L. Vidal, B. Divisia-Blohorn, G. Bidan, J.-M. Kern, J.-P. Sauvage and J.-L. Hazemann, *Inorg. Chem.*, 1999, **38**, 4203.

3 (*a*) D. B. Amabilino and J. F. Stoddart, *Chem. Rev.*, 1995, **95**, 2725; (*b*) S. A. Nepogodiev and J. F. Stoddart, *Chem. Rev.*, 1998, **98**, 1959.

4 (*a*) A. Harada, J. Li and M. Kamachi, *Nature*, 1993, **364**, 516; (*b*) T. Hoshino, M. Miyauchi, Y. Kawaguchi, H. Yamaguchi and A. Harada, *J. Am. Chem. Soc.*, 2000, **122**, 9876.

5 (*a*) D. Whang and K. Kim, *J. Am. Chem. Soc.*, 1997, **119**, 451; (*b*) E. Lee, J. Kim, J. Heo, D. Whang and K. Kim, *Angew. Chem., Int. Ed.*, 2001, **40**, 398; (*c*) J. W. Lee, Y. H. Ko, S.-H. Park, K. Yamaguchi and K. Kim, *Angew. Chem., Int. Ed.*, 2001, **40**, 746.

6 T. Ooya, K. Arizono and N. Yui, *Polym. Adv. Technol.*, 2000, **11**, 642.

7 E. Ishow, A. Creda, V. Balzani, F. Spadola and L. Mandolini, *Chem. Eur. J.*, 1999, **5**, 984.

8 (*a*) H. Murakami, A. Kawabuchi, K. Kotoo, M. Kunitake and N. Nakashima, *J. Am. Chem. Soc.*, 1997, **119**, 7605; (*b*) P. R. Ashton, R. Ballardini, V. Balzani, E. C. Constable, A. Credi, O. Kocian, S. J. Langford, J. A. Preece, L. Prodi, E. R. Schofield, N. Spencer, J. F. Stoddart and S. Wenger, *Chem. Eur. J.*, 1998, **4**, 2413; (*c*) M. Tamura and A. Ueno, *Bull. Chem. Soc. Jpn.*, 2000, **73**, 147; (*d*) S. I. Jun, J. W. Lee, S. Sakamoto, K. Yamaguchi and K. Kim, *Tetrahedron Lett.*, 2000, **41**, 471.

9 H. Fujita, T. Ooya and N. Yui, *Macromolecules*, 1999, **32**, 2534.

10 B. F. Hoskins, R. Robson and D. A. Slizys, *J. Am. Chem. Soc.*, 1997, **119**, 2952.

11 (*a*) C. S. A. Fraser, H. A. Jenkins, M. C. Jennings and R. J. Puddephatt, *Organometallics*, 2000, **19**, 1635; (*b*) S. Achar, J. D. Scott, J. J. Vittal and R. J. Puddephatt, *Organometallics*, 1993, **12**, 4592.

12 N. C. Gianneschi, E. R. T. Tiekink and L. M. Rendina, *J. Am. Chem. Soc.*, 2000, **122**, 8474.

13 (*a*) H. L. Anderson, S. Anderson and J. K. M. Sanders, *J. Chem. Soc., Perkin Trans. 1*, 1995, 2231; (*b*) B. F. Abrahams, S. R. Batten, H. Hamit, B. F. Hoskins and R. Robson, *Chem. Commun.*, 1996, 1313; (*c*) B. F. Abrahams, S. R. Batten, M. J. Grannas, H. Hamit, B. F. Hoskins and R. Robson, *Angew. Chem., Int. Ed.*, 1999, **38**, 1475; (*d*) M. Fujita, K. Umemoto, M. Yoshizawa, N. Fujita, T. Kusukawa and K. Biradha, *Chem. Commun.*, 2001, 509.

14 *Crystal data* for complex **3**$[PF_6]_3$·0.5H$[PF_6]$·5Me_2CO: $C_{117}H_{153.50}F_{21}N_{12}O_{11}P_{3.50}Pt_3$, M = 2996.68, triclinic, space group $P\bar{1}$, a = 18.9270(4), b = 19.1763(4), c = 21.8457(5) Å, α = 103.335(1), β = 97.786(1), γ = 118.221(1)°, V = 6515.6(2) Å^3, Z = 2, D_c = 1.527 Mg m^{-3}, T = 200 K, μ = 3.344 mm^{-1}, no. of reflections 63523, R_1 [$I > 2\sigma(I)$] = 0.0506, wR_2 = 0.1318. Partial (disordered) protonation of N(72) of the triazine is thought to occur; the proton was tentatively located in this position and appears to participate in H-bonding. CCDC reference number 164614. See http://www.rsc.org/suppdata/cc/b1/b103967a/ for crystallographic data in CIF or other electronic format. NMR in acetone-d_6: (^{1}H) = 1.38, 1.40 [s, 54H, Bu]; 1.44, 1.48 [s, 18H, ^2J(PtH) = 66, 71 Hz, PtMe]; 3.09, 3.11 [s, 6H, ^2J(PtH) = 92, 93 Hz, $PtCH_2$]. IR (Nujol mull): ν(CO) = 1613, 1701 cm^{-1}; ν(OH) = 2547, 2672 cm^{-1}.

15 (*a*) J. B. Lambert, H. F. Shurvell, D. Lightner and R. G. Cooks, *Structural Spectroscopy*, Prentice-Hall, Englewood Cliffs, NJ, 1998; (*b*) G. R. Desiraju and T. Steiner, *The Weak Hydrogen Bond*, Oxford Science, Oxford, UK, 1999; (*c*) G. A. Jeffrey, *An Introduction to Hydrogen Bonding*, Oxford University Press, Oxford, UK, 1997.

CHEMCOMM
Communication
www.rsc.org/chemcomm

β-Cyclodextrin dimers as potential tumor pretargeting agents†‡

W. Barry Edwards,[a] David E. Reichert,[a] D. André d'Avignon[b] and Michael J. Welch*[a]

[a] *Mallinckrodt Institute of Radiology, Washington University School of Medicine, 510 South Kingshighway Boulevard, St. Louis, MO 63110, USA. E-mail: welchm@mir.wustl.edu*
[b] *Department of Chemistry, Washington University, St. Louis, MO 63110, USA*

Received (in Columbia, MO, USA) 27th March 2001, Accepted 1st June 2001
First published as an Advance Article on the web 27th June 2001

A β-cyclodextrin dimer binds a di-*tert*-butylbenzyl–Cu–cyclen with high affinity, demonstrating potential as a receptor/ligand system for tumor pretargeting with monoclonal antibodies.

Monoclonal antibodies (Mabs) have advantages for the delivery of a radioisotope (or toxin) to tumor sites due to their high affinity and specificity for their antigen.[1,2] However, the results of radioimmunotherapy of solid tumors have been disappointing because radiolabeled Mabs targeted to cell surface antigens impart a high radiation dose to normal organs causing toxicity.[3] In part, this is due to the long circulating times for Mabs.

Successful imaging or therapy with radiolabeled Mabs depends not only on the concentration of the Mab at the targeted site but on clearance rates from normal tissues relative to that from the tumor. Imaging studies in humans have shown that maximum concentrations of Mabs at the tumor site are attainable within 24 h, but several more days are required before the concentration of the radiolabeled Mab in the circulation decreases to levels low enough for successful imaging to take place.[4] Pretargeting techniques seek to maintain high accumulation of the radionuclide at the target site while minimizing non-target tissue toxicity (see reviews[1,2]). One current approach at pretargeting utilizes a Mab conjugated to a receptor with a high affinity for a ligand bearing the radionuclide. The most often utilized receptor/ligand system is avidin (or streptavidin/biotin).[5] After the Mab-receptor conjugate has localized at the tumor site, a low molecular weight radiolabeled ligand, one that is rapidly excreted *via* the kidneys, is administered to visualize the tumor. To be effective, the ligand must be rapidly excreted from the body to provide the desired high tumor accumulation with relatively low non-target accumulation.

An alternative receptor for tumor pretargeting could be a β-cyclodextrin dimer. Breslow *et al.* studied a series of β-cyclodextrin dimers and achieved some of the highest affinities reported to date.[6,7] While the best match between a guest molecule and single cyclodextrin subunit will provide affinities on the order of 10^{-4} M, cyclodextrin dimers can increase affinities to 10^{-8} to 10^{-10} M.[8] With affinities of this magnitude, β-cyclodextrin dimers could serve as receptors for tumor pretargeting. A potential strategy for pretargeting is the development of a radiometal-binding macrocycle containing pendant hydrophobic groups with the appropriate geometry for inclusion into the cavity of the cyclodextrins. Ultimately, the β-cyclodextrin dimer would be concentrated at the tumor site by conjugation *via* a covalent bond to a Mab. Radiometals such Cu-64 [$t_{1/2}$ = 12.7 h; $E_{\beta max}$ = 0.653 MeV (17.4%); $E_{\beta max}$ = 0.573 MeV (40%)] and Cu-67 [$t_{1/2}$ = 62 h; $E_{\beta max}$ = 0.392 MeV (56%)] have been used previously in imaging[9] and therapy[10,11] of tumors. To demonstrate the feasibility of this new approach, Cu–BBC (Scheme 1) and a β-cyclodextrin dimer (Scheme 2) were synthesized and affinities determined in an equilibrium binding assay. A fluorescent dye, BNS, was synthesized as previously described.[12]

Breslow *et al.* reported binding affinities for a β-cyclodextrin dimer with a single linkage in the low nanomolar region for substrates bearing two *tert*-butylphenyl substituents.[6] Therefore, a β-cyclodextrin dimer with a single linkage, was synthesized to serve as a host for a copper chelate-complex bearing two *tert*-butylphenyl substituents. The dimer **1** was prepared from commercially available tosyl-β-cyclodextrin and 2,6-naphthalene dithiol[13] (Scheme 2). The cyclodextrin dimer was purified by HILIC then by silica-gel chromatography.[14] Analysis by ^{1}H, ^{13}C, HMQC, COSY NMR and MALDI-MS confirmed the dimeric structure of the cyclodextrin.

Cyclen was chosen as the chelator because of its high stability (log K_f = 24.6) for copper(II).[15] Based on synthetic methodology for selectively protecting the 1 and 7 nitrogens of tetraazamacrocycles,[16] alkylation of the nitrogens with commercially available *tert*-butylbenzyl bromide appeared to be the most expedient way of introducing a pair of hydrophobic substituents onto the chosen chelator (Scheme 1). Molecular modeling showed that a distance of *ca.* 16 Å is attainable between the two tertiary carbons of the *tert*-butyl groups and between the midpoints of the β-cyclodextrin subunits of dimer **1** when the faces containing the primary hydroxyl groups are opposed to each other.[17]

Equimolar amounts of copper(II) acetate and BBC resulted in the quantitative formation of Cu–BBC. While Cu–BBC and BBC co-eluted on a C-18 column, a diphenyl column resolved a co-injected mixture of the two. Analysis of the reaction

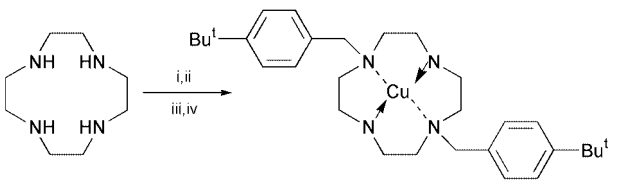

Scheme 1 *Reagents and conditions*: i, pH 2.5, water, chloroethylformate; ii, *tert*-butylbenzyl bromide, DMF; iii, hydrazine, ethylene glycol, KOH; iv, copper(II) acetate, aq. NH_4O_2CMe, pH 6.4.

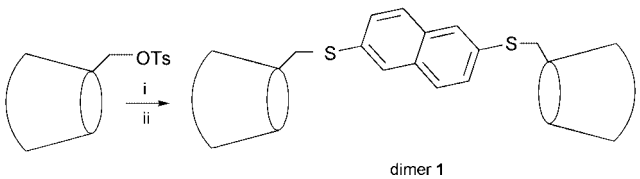

Scheme 2 *Reagents and conditions*: i, KI, DMF, 85 °C; ii, 2,6-naphthalenedithiol, NH_4HCO_3, DMF, 85 °C.

† Electronic supplementary information (ESI) available: experimental section. See http://www.rsc.org/suppdata/cc/b1/b102814f/

‡ Abbreviations: Mabs, monoclonal antibodies; HILIC, hydrophilic interaction chromatography; HMQC, heteronuclear multiple quantam coherence; COSY, H–H correlated spectroscopy; MALDI-MS, matrix assisted laser desorption-ionization mass spectrometry; K_f, formation constant; BBC, 1,7-(4-*tert*-butylphenylmethyl)cyclen; Cu–BBC, copper-1,7-(4-*tert*-butylphenylmethyl)cyclen; ES-MS, electrospray mass spectrometry; HPLC, high pressure liquid chromatography; BNS, 6-(4-*tert*-butylphenylamino)naphthalene-2-sulfonic acid; K_D, equilibrium dissociation constant; K_i, the concentration of the competing ligand that will bind to half the binding sites at equilibrium; IC_{50}, concentration of competitive ligand that inhibits half of the binding of a ligand; Cheng–Prusoff equation, $K_i = IC_{50}(1 + [ligand]/K_{D,ligand})^{-1}$

 DOI: 10.1039/b102814f

Table 1 Affinities of BNS and Cu–BBC for β-cyclodextrin and dimer **1**

Guest	Host	Calculated affinities	95% CI
BNS	β-Cyclodextrin	K_{D1} = 14 μM	10–18 μM
		K_{D2} = 1.6 mM	0.6–2.6 mM
BNS	Dimer **1**	K_D = 388 nM	112–664 nM
Cu–BBC[a]	Dimer **1**	K_i = 18 nM	12–28 nM
		IC_{50} = 120 nM	76–189 nM

[a] BNS was included. Cu–BBC was a competitive ligand with varying concentration.

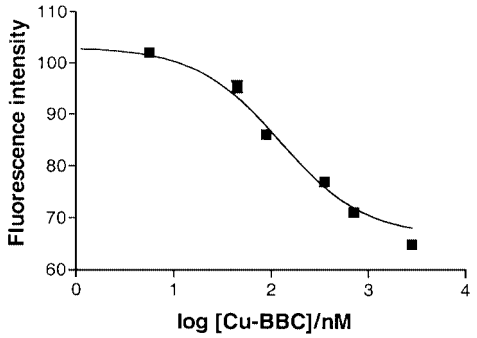

Fig. 1 Heterologous competitive binding assay between Cu–BBC and BNS for dimer **1**.

mixture on the diphenyl column showed that BBC accounted for < 1% of the total peak area observed (λ = 215 nm, Cu–BBC and BBCs strongest absorbance). Analysis by ES-MS confirmed that the component observed by HPLC was Cu–BBC.

Affinity constants for β-cyclodextrin dimers and their substrates are often ascertained by fluorescence spectroscopy§ since saturation binding will be attained at concentrations too low to utilize NMR and UV spectroscopy. Therefore a fluorescent dye, BNS, was synthesized. BNS fluoresces weakly in water, but its inclusion into a hydrophobic environment, such as that of the cavity of β-cyclodextrin, enhances its fluorescence. This dye has been used extensively in the characterization of other β-cyclodextrin dimers (see review[8]). Curve fitting with commercially available software will then yield the affinity of dye. After the affinity of dye for its host has been quantified, a heterologous competitive binding assay between the dye and another guest can provide the affinity of the guest. These approaches were taken to evaluate the affinity of BNS and Cu–BBC for dimer 1 (Table 1).

BNS exhibited an enhancement of fluorescence in aqueous solution when interacting with the β-cyclodextrin subunits. The interaction was characteristic of a receptor–ligand (host–guest) complex because of its saturable and reversible nature. The observed affinity of BNS agrees with the previously determined value of K_D = 20 μM.[12] Previous affinities of BNS observed for β-cyclodextrin dimers with a single linkage have ranged from *ca.* 3 μM to 100 nM.[18,19] The increase in affinity of BNS is consistent with previously observed increases when two β-cyclodextrin subunits are linked face to face.

Because the fluorescence of Cu–BBC is unaffected by the presence of dimer **1**, its affinity must be determined by competition with BNS. The log-dose dependent displacement of BNS from dimer **1** with Cu–BBC indicates that both Cu–BBC and BNS have formed a complex with dimer **1** (Fig. 1). By substituting the value of the IC_{50} of Cu–BBC and the K_D of BNS into the Cheng–Prussof equation, the K_i of Cu–BBC is obtained.[20] This remarkably strong affinity bodes well for the success of dimer **1** and Cu–BBC as a receptor/ligand system for tumor pretargeting.

In conclusion, a β-cyclodextrin dimer with a naphthalene linker, dimer **1**, was synthesized for evaluation as the receptor in a new approach to tumor pretargeting. Dimer **1** showed a higher affinity for a fluorescent dye, BNS, than did β-cyclodextrin. BBC, a derivative of cyclen, was synthesized and Cu–BBC was prepared. Cu–BBC was strongly bound to dimer **1** (K_i = 18 nM relative to BNS). With affinities in the low nanomolar region, Cu-64–BBC and dimer **1** could serve as a receptor/ligand system for tumor pretargeting.

This work was supported by the United States Department of Energy (DE-FG02-87ER60512).

Notes and references

§ *Determination of affinity constants*: Utilizing GraphPad Prism® software (GraphPad Software Inc., San Diego, CA), the data were fit by non-linear regression to: $F = (F_{max})[BNS]/(K_D + [BNS])$ where F is the observed fluorescence intensity generated from incorporation of BNS into the hydrophobic interior of β-cyclodextrin (corrected for background fluorescence from unincorporated BNS or dimer **1**) to determine values for K_D.[21,22] To determine the IC_{50} value, the data were fit by non-linear regression to: $F_{obs} = T + (T - B)/1 + 10 \exp(\log[Cu–BBC] - \log IC_{50})$, where T and B are the top and bottom plateaus of the fitted curve and F_{obs} is the observed fluorescence.[21,22] To calculate K_i for Cu–BBC, the value obtained for the K_D of BNS and Cheng–Prussof equation were utilized.[20–22] The data were fit to both one or two binding sites in all experiments and the results for two binding sites are reported when $P < 0.05$. The error is represented in terms of 95% confidence interval (95% CI).

1 D. A. Goodwin and C. F. Meares, *Cancer Biother. Radiopharm.*, 1999, **14**, 145.
2 J. Barbet, F. Kraeber-Bodere, J. Vuillez; E. Gautherot, E. Rouvier and J. Chatal, *Cancer Biother. Radiopharm.*, 1999, **14**, 153.
3 R. B. Wilder, G. L. DeNardo and S. J. DeNardo, *J. Clin. Oncol.*, 1996, **14**, 1383.
4 D. A. Goodwin, *J. Nucl. Med.*, 1995, **36**, 876.
5 D. B. Axworthy, P. L. Beaumier, B. J. Bottino, S. Goshorn, R. W. Mallet, K. M. Stone, F. M. Su, L. F. Theodore, E. K. Yau and J. M. Reno, *Tumor Targeting*, 1996, **2**, 156.
6 R. Breslow, N. Greenspoon, T. Guo and R. Zarzycki, *J. Am. Chem. Soc.*, 1989, **111**, 8296.
7 R. Breslow and S. Chung, *J. Am. Chem. Soc.*, 1990, **112**, 9659.
8 R. Breslow, S. Halfon and B. Zhang, *Tetrahedron*, 1995, **51**, 377.
9 C. J. Anderson, L. A. Jones, L. A. Bass, E. L. Sherman, D. W. McCarthy, P. D. Cutler, M. V. Lanahan, M. E. Cristel, J. S. Lewis and S. W. Schwarz, *J. Nucl. Med.*, 1998, **39**, 194.
10 C. J. Anderson, F. Dehdashti, P. D. Cutler, S. W. Schwarz, R. Laforest, L. R. Bass, J. S. Lewis and D. W. McCarthy, *J. Nucl. Med.*, 2001, **42**, 213.
11 G. R. Mirick, R. T. O'Donnell, S. J. DeNardo, S. Shen, C. F. Meares and G. L. DeNardo, *Nucl. Med. Biol.*, 1999, **26**, 841.
12 S. Chung, Ph.D. Thesis, Columbia University, 1991.
13 V. N. Lisitsyn, L. S. Kukalenko and A. M. Tsatkis, *Zh. Org. Khim.*, 1985, **21**, 161.
14 A. J. Alpert, *J. Chromatogr.*, 1990, **499**, 177.
15 R. M. Smith and A. E. Martell, *Crictical Stability Constants*, Plenum, New York, 1989.
16 Z. Kovacs and A. D. Sherry, *J. Chem. Soc., Chem. Commun.*, 1995, 185.
17 CambridgeSoft Corporation, CS Chem3D Std, 4.0, Cambridge MA, 1997.
18 R. Breslow and B. Zhang, *J. Am. Chem. Soc.*, 1996, **118**, 8495.
19 R. C. Petter, C. T. Sikorski and D. H. Waldeck, *J. Am. Chem. Soc.*, 1991, **113**, 2325.
20 Y. Cheng and W. H. Prusoff, *Biochem. Pharmacol.*, 1973, **22**, 3099.
21 L. E. Limbird, *Cell Surface Receptors: A short course on theory and methods*, Kluwer Academic Publishers, Hingham, 1986.
22 H. J. Molutsky, *Analyzing Data with GraphPad Prism*, GraphPad Software Inc., San Diego, 1999.

CHEMCOMM
Communication
www.rsc.org/chemcomm

Nonenzymatic kinetic resolution of β-amino alcohols: chiral BINAP mediated S_N2 displacement of hydroxy groups by halogens through formation of an aziridinium ion intermediate

Govindasamy Sekar and Hisao Nishiyama*

School of Materials Science, Toyohashi University of Technology, Tempaku-cho, Toyohashi, Aichi 441-8580, Japan. E-mail: hnishi@tutms.tut.ac.jp

Received (in Cambridge, UK) 15th March 2001, Accepted 6th June 2001
First published as an Advance Article on the web 27th June 2001

A series of optically active cyclic *trans*-β-amino alcohols were obtained (up to 97% ee) from nonenzymatic kinetic resolution of corresponding racemic amino alcohols using commercially available (*S*)-BINAP and NCS by halogenation of hydroxy groups through formation of a *meso*-aziridinium ion intermediate.

Enantiopure β-amino alcohols are an important class of organic compounds that have found much use in asymmetric synthesis[1] and medicinal chemistry,[2] and can be produced by reduction of optically active α-amino acids.[3] Kinetic resolution of β-amino alcohols through enzyme-catalysed acylation or deacylation is also one of the most efficient methods for the synthesis of chiral β-amino alcohols.[4] Nonenzymatic kinetic resolution (NKR) is the alternative for the enzymatic process, which is considered to be a challenging issue in organic synthesis.[5,6] Very recently, we reported the NKR of secondary alcohols by S_N2 displacement of the hydroxy groups by halogens using chiral BINAP (**1**).[7] In

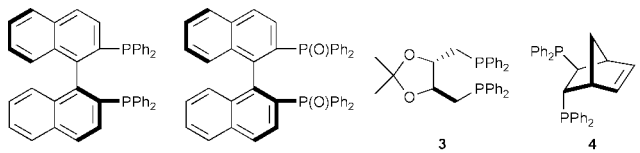

1 **2** **3** **4**

this communication, we report highly enantioselective NKR of racemic *trans*-β-amino alcohols by halogenation of the hydroxy groups through an aziridinium ion intermediate.

First, we have chosen racemic *trans*-2-(*N*-methyl-*N*-phenylamino)cyclohexanol, (±)-*trans*-**5**, as a model substrate, which was subjected to kinetic resolution with NCS (1 equiv. compared to (±)-*trans*-**5**) and (*S*)-BINAP (0.5 equiv.) in CH_2Cl_2 at room temperature [eqn. (1)]. The reaction was found

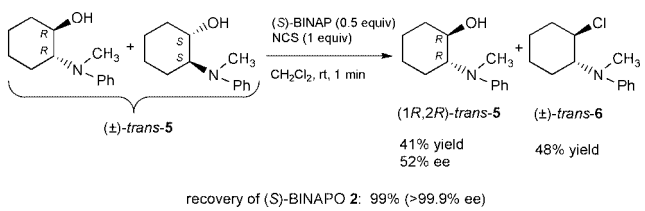

(1)

to be extremely fast with moderate selectivity. After 1 min, 41% of optically active amino alcohol (1*R*,2*R*)-*trans*-**5**[8] (52% ee) and 48% of racemic *trans*-β-amino chloride (±)-*trans*-**6** were isolated. BINAP was recovered as BINAP dioxide **2** in quantitative yield without any racemization (> 99.9% ee),[9] which can be reused after reduction.[10] In this reaction, the hydroxy group of the (1*S*,2*S*)-enantiomer of the racemic amino alcohol was selectively replaced by chloride ion through double S_N2 reactions (intramolecular S_N2 displacement of hydroxy group by amine followed by intermolecular S_N2 attack by chloride ion) to produce racemic *trans*-β-amino chloride **6**.

In order to improve the enantioselectivity of the kinetic resolution, the reaction was carried out in a wide range of solvents and the effect of other commercially available C_2-symmetric diphospine ligands were also examined (Table 1). Comparatively the reaction was very much faster and higher enantiomeric excess was obtained for recovered (1*R*,2*R*)-*trans*-**5** when the reaction was carried out in polar solvents than in non-polar solvents. THF turned out to be the solvent of choice among the solvents examined as it provided (1*R*,2*R*)-*trans*-**5** in 87% ee (entry 5). When the NKR was carried out with other commercially available C_2-symmetric diphospine ligands such as (+)-DIOP **3** and (+)-Norphos **4** the ee of (1*S*,2*S*)-*trans*-**5** dropped to 52 and 40%, respectively (entries 8 and 9). Lowering the reaction temperature to −10 °C–rt slightly improved the ee to 89% but longer reaction times discouraged us from doing the reaction at that temperature (entry 10). Surprisingly, the ee of (1*R*,2*R*)-*trans*-**5** dropped to 82% when the reaction was carried out at −74 °C–rt (entry 11). We next studied the effect of other halogenating agents such as *N*,*N*-dichlorocarbamic acid ethyl ester, NBS, *N*-bromosuccinimide, and *N*-bromoacetamide for the kinetic resolution of (±)-*trans*-**5** with (*S*)-BINAP in THF at room temperature. Although all the reactions proceeded smoothly to give corresponding products, a very poor ee was obtained for recovered (1*R*,2*R*)-*trans*-**5** (5–12%).

Using the optimized conditions, a series of racemic cyclic *trans*-β-amino alcohols[11] were resolved and the results are summarized in Table 2. When the kinetic resolution was allowed for 60–70% conversion, excellent enantiomeric excess was obtained for all the six- and seven-membered cyclic β-

Table 1 Effect of solvents, temperature and various diphosphine ligands in NKR of (±)-*trans*-**5**

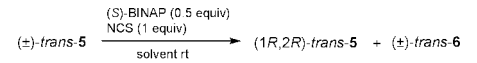

Entry	Diphosphine	Solvent	Time	Yield of **6** (%)[a]	Recovery of **5** (%)[a]	Ee of recovered **5** (%)[b]
1	**1**	Hexane	1 day	11	68	7
2	**1**	Benzene	30 min	47	43	38
3	**1**	Toluene	5 h	25	49	19
4	**1**	Ether	1 day	36	49	5
5	**1**	THF	20 min	61	27	87
6	**1**	CH_2Cl_2	1 min	48	41	52
7	**1**	CH_3CN	1 min	57	39	55
8	**3**	THF	3.5 h	54	29	52[c]
9	**4**	THF	4 h	63	27	40[c]
10[d]	**1**	THF	10 h	60	31	89
11[e]	**1**	THF	10 h	60	33	82

[a] Isolated yield. [b] Determined by HPLC analysis using Chiralcel OD column. [c] (1*S*,2*S*)-*trans*-**5** was the major enantiomer. [d] Reaction temperature was −10 °C–rt. [e] Reaction temperature was −74 °C–rt.

 DOI: 10.1039/b102460b

Table 2 NKR of variety of cyclic β-amino alcohols with (*S*)-BINAP and NCS[a]

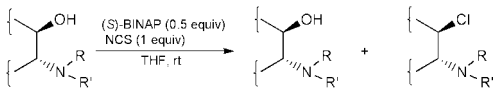

Entry	β-Amino alcohol	Time	Recovery of β-amino alcohol (%)[b]	Ee of recovered β-amino alcohol (%)[c]
1	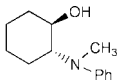	20 min	27	87
2	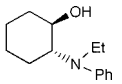	30 min	29	80
3	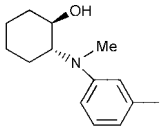	20 min	27	94
4	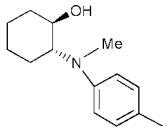	25 min	26	89
5	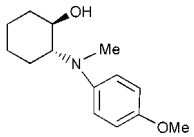	25 min	26	97
6	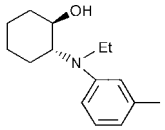	2 h	33	73
7	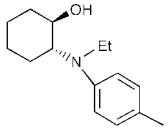	30 min	38	72
8	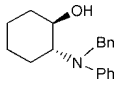	2 h	33	76
9[d]	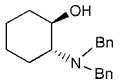	25 min	38	72
10	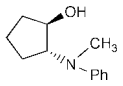	15 min	25	59
11	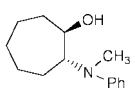	10 min	35	86

[a] To a mixture of (*S*)-BINAP (0.125 mmol) and NCS (0.25 mmol) was added β-amino alcohol (0.25 mmol) in THF (2 mL) at room temperature. The white turbid reaction mixture turning to a colorless or slightly brown homogeneous solution shows the completion of the reaction. In all the reactions (±)-*trans*-β-amino chlorides were obtained in 42–69% isolated yield. [b] Isolated yield (the theoretical maximum yield in a kinetic resolution is 50%). [c] Determined by HPLC using chiral columns. [d] 2 equiv. of NCS were used.

tertiary amino alcohols (72–97% ee, 25–38% yield). Moderate enantiomeric excess was obtained for the five-membered β-amino alcohol (59% ee, entry 10). When the reaction was carried out with an acyclic amino alcohol such as racemic 1-(*N*-methyl-*N*-phenylamino)octadecan-2-ol, the (+)-amino alcohol was recovered in 34% yield with poor ee (15%).[12]

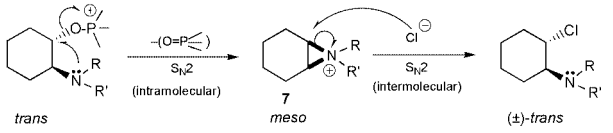

Scheme 1

Although at this moment the mechanism of the present reaction is not very clear, we assume that the reaction proceeds through an ionic phosphonium alkoxide intermediate (quaternary phosphonium salt) in which the amino group attacks the alkoxide by an intramolecular S_N2 reaction (neighboring group participation) to provide *meso*-aziridinium ion **7**. This is followed by an intermolecular S_N2 attack of *meso*-aziridinum ion **7** by chloride ion to provide racemic *trans*-β-amino chloride and dioxide **2** (Scheme 1). This phenomenon was supported as the dioxide **2** was recovered after the reaction and the product β-amino chloride was racemic with *trans* stereochemistry rather than optically active with *cis* stereochemistry. Formation of optically active β-amino chloride from the kinetic resolution of acyclic amino alcohol confirms the formation of an aziridinum ion intermediate. However, detailed mechanistic studies are under progress.

In conclusion, we have demonstrated highly enantioselective nonenzymatic kinetic resolution of racemic *trans*-β-amino alcohols using commercially available chiral BINAP and NCS. When the reaction was allowed for 60–70% conversion, excellent enantiomeric excess was obtained for all cyclic β-tertiary amino alcohols (up to 97% ee).

Notes and references

1 *Catalytic Asymmetric Synthesis 2nd edn.*, ed. I. Ojima, Wiley-VCH, NewYork, 2000; *Comprehensive Asymmetric Catalysis I-III*, ed. E. N. Jacobsen, A. Pfaltz and H. Yamamoto, Springer-Verlag, Berlin, 1999.

2 C. I. Fincham, M. Higginbottom, D. R. Hill, D. C. Horwell, J. C. O'Toole, G. S. Ratcliffe, D. C. Rees and E. Roberts, *J. Med. Chem.*, 1992, **35**, 1472; C. Auvin-Guette, S. Rebuffat, Y. Prigent and B. Bodo, *J. Am. Chem. Soc.*, 1992, **114**, 2170.

3 For a recent method for reduction of α-amino acids to β-amino alcohols, see: M. J. McKennon, A. I. Meyers, K. Drauz and M. Schwarm, *J. Org. Chem.*, 1993, **58**, 3568 and references cited therein.

4 G. Sekar, R. M. Kamble and V. K. Singh, *Tetrahedron: Asymmetry*, 1999, **10**, 3663 and references cited therein.

5 Nonenzymatic kinetic resolution of β-tertiary amino alcohols by enantioselective *N*-oxide formation using a stoichiometric chiral complex (1.2 equiv. of titanium tartrate complex was used) and *tert*-butyl hydroperoxide, see: S. Miyano, L. D.-L. Lu, S. M. Viti and K. B. Sharpless, *J. Org. Chem.*, 1985, **50**, 4350.

6 For a recent review on NKR of alcohols using chiral or achiral acylating agents, see: A. C. Spivey, A. Maddaford and A. J. Redgrave, *Org. Prep. Proced. Int.*, 2000, **32**, 331 and references cited therein.

7 G. Sekar and H. Nishiyama, *J. Am. Chem. Soc.*, 2001, **123**, 3603.

8 Absolute configuration was determined by the comparison of the sign of its optical rotation with that in literature. H. Yamashita, *Bull. Chem. Soc. Jpn.*, 1988, **61**, 1213; H. Yamashita, *Chem. Lett.*, 1987, 525.

9 The ee of **2** was determined by HPLC analysis with a Chiralpak AD column (hexane–propan-2-ol = 75:25).

10 For the deoxygenation of chiral BINAP dioxide **2** to BINAP without loss of enantiomeric excess, see: H. Takaya, S. Akutagawa and R. Noyori, *Org. Synth.*, 1988, **67**, 20.

11 For the synthesis (±)-β-amino alcohols see: G. Sekar and V. K. Singh, *J. Org. Chem.*, 1999, **64**, 287; M. Chini, P. Critti and F. Macchia, *J. Org. Chem.*, 1991, **56**, 5939; J. Iqbal and A. Pandey, *Tetrahedron Lett.*, 1990, **31**, 575.

12 The product β-amino chloride was a mixture of two products (86.5:13.5) due to the attack of chloride ion on terminal and internal carbon atoms of the aziridinum ion intermediate. The ee of the major isomer (terminal-attacked product) was 16% which was determined by HPLC using a Chiralcel OD column (hexane–propan-2-ol = 1000:6).

CHEMCOMM
Communication
www.rsc.org/chemcomm

Regioselective formation of highly functionalised heterofullerenes: pentamalonates of $RC_{59}N$ involving an octahedral addition pattern

Frank Hauke and Andreas Hirsch*

Institut für Organische Chemie, Henkestrasse 42, D-91054 Erlangen, Germany.
E-mail: hirsch@organik.uni-erlangen.de; Fax: +49 9131 85 26864; Tel: +49 9131 85 22537

Received (in Cambridge, UK) 10th April 2001, Accepted 4th June 2001
First published as an Advance Article on the web 27th June 2001

The treatment of monomeric azafullerene derivatives $RC_{59}N$ with an excess of diethyl bromomalonate in the presence of DBU and dimethylanthracene leads to the regioselective formation of azafullerene pentamalonates with an octahedral C_s symmetrical addition pattern.

The organic chemistry of the parent azafullerene $C_{59}N$ in the form of its dimer **1**[1] has been so far restricted to the synthesis of monoadducts $RC_{59}N$. In these azafullerene derivatives the addend R is always bound to the cluster C-atom which forms a [6,6]-bond to the heteroatom.[2–5] We have shown recently, that monomeric derivatives $RC_{59}N$ such as **2** and **3** are easily

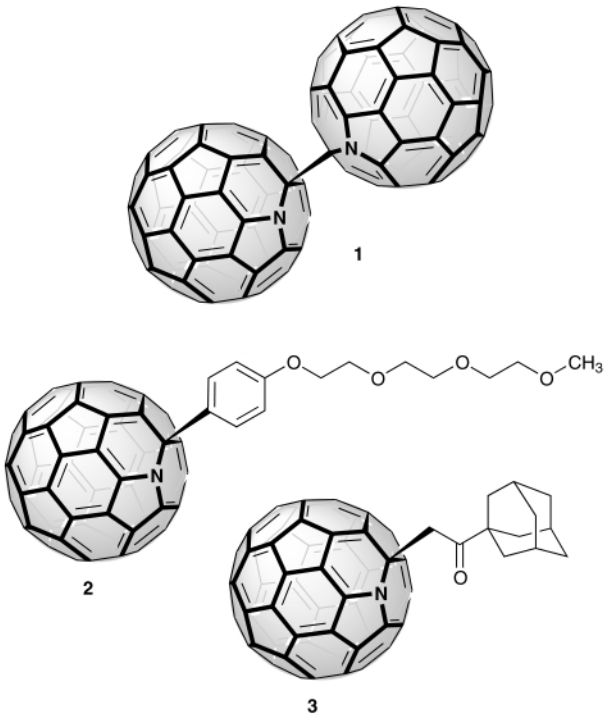

available by treatment of the dimer **1** with electron rich aromatics or enolizable carbonyl compounds in the presence of oxygen and *p*-TsOH.[3–5] The only example of a multiple adduct of $C_{59}N$ is the tetrachloride $Cl_4ArC_{59}N$ containing a pyrrole moiety within the fullerene cage.[6]

Here we report on the first multiple functionalisation of $C_{59}N$ with organic addends. As a model reaction the template mediated generation of oligomalonates, which we developed for the highly regioselective functionalisation of octahedral sites within C_{60} has been chosen.[7] This approach allows us to synthesize pentakisadducts of $RC_{59}N$ containing a C_s symmetrical addition pattern and a cage π-electron system consisting of eight isolated benzenoid rings.

After stirring a solution of the monoadduct **2** and a fivefold excess of dimethylanthracene (DMA) in 1,2-dichlorobenzene (ODCB) for 3 h, a tenfold excess of DBU and diethyl bromomalonate was added (Scheme 1). After stirring this reaction mixture for 2 days a colour change of the olive green solution into orange was observed.

After purification by HPLC using a Buckyclutcher column and toluene–ethyl acetate (8:2) as eluent, the pentamalonate **4** was obtained in 20% yield. The other regioisomeric multi-adducts could not be separated by chromatographic methods.

The complete structural characterisation of **4** was carried out by ^{1}H NMR, ^{13}C NMR, UV-Vis and FT-IR spectroscopy as well as by mass spectrometry.† The ^{1}H NMR spectrum shows two doublets for the aromatic AB spin system at δ 7.95 and 7.00. The methyl group of the polyether side chain resonates as a singlet at δ = 3.31. The signals for the methylene groups of the polyether side chain are found in the region between δ = 4.25–3.45. The four different methylene groups of the malonate function resonate as a broad multiplet at δ = 4.2 and the signals for the four different methyl groups of the malonate function can be found as a broad multiplet at δ = 1.25. The determination of the symmetry was unambiguously carried out by ^{13}C NMR spectroscopy. The ^{13}C NMR spectrum of **4** (Fig. 1) shows five signals for the ten carbonyl groups at δ = 164 with one signal showing double intensity. For a C_s symmetrical pentamalonate six signals are expected. In the sp^2 region between δ = 115–160 28 signals are found, four of which belong to the aromatic addend. The remaining 24 signals are due to the sp^2 C-atoms of the C_s symmetrical fullerene cage. The most striking evidence for a C_s symmetrical adduct can be found in the region between δ = 42–48 where four signals appear, one having double intensity. These are the signals of the methano C-atoms of the malonate bridges. Three of those C-atoms are located on the mirror plane of the molecule giving rise to three

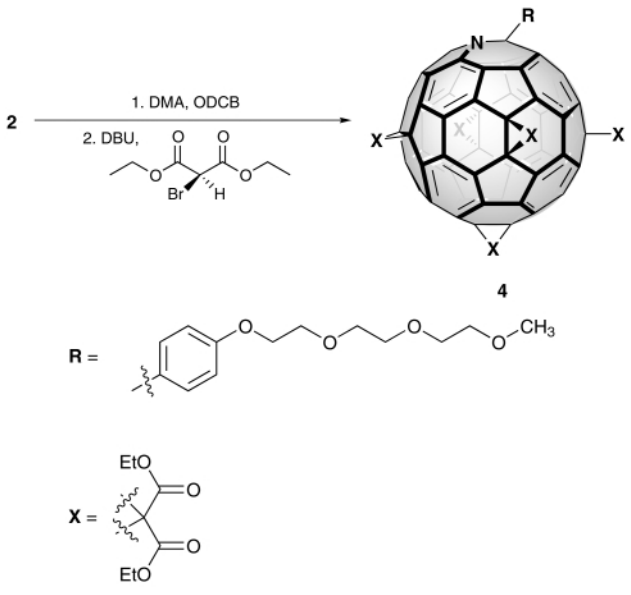

Scheme 1

 DOI: 10.1039/b103169b

well resolved signals. The other two methano C-atoms in equatorial positions are chemically equivalent due to the C_s plane, causing the appearance of just one signal with double intensity. The C-atoms of the methylene groups give rise to just one signal at δ = 62.81 and one signal at δ = 45.37. The methyl groups of the malonate addends resonate at δ = 14.04. The signals of the six different fullerene sp^3 C-atoms and the sp^3 C-cage atom which is adjacent to the N-atom appear as seven different signals in the region between δ = 62.81–77.88. The UV-Vis spectrum of the orange pentakisadduct **4** is completely different from those of monomeric derivatives $RC_{59}N$.[2–5] The characteristic fullerene absorption at λ_{max} = 320 nm has disappeared. Similarly to hexakisadducts of C_{60} containing a T_h-symmetrical addition pattern[7] the most intensive absorption is shifted to λ_{max} = 281 nm.

The reaction of the adamantyl derivative **3** applying the same reaction conditions afforded compound **5**. The structural characterisation of this azafullerene derivative was carried out by ^{1}H NMR, ^{13}C NMR, UV-Vis and FT-IR spectroscopy. In the ^{13}C NMR spectrum no symmetry can be detected; *e.g.* each of the five methano C-atoms gives an individual signal in the region between δ = 42–48. The FAB-MS clearly shows a peak for M^+ at *m/z* 1769. This peak displays the characteristic Br isotope pattern. In the ^{1}H NMR spectrum the methine proton resonates at δ = 5.6, which is characteristic for an α-bromo ketone. Again the resonances for the methylene protons of the malonate addends can be found in the region between δ = 4.1–4.5 forming a broad multiplet. The individual protons for the adamantyl group resonate in the region between δ = 1.2–2.0 and the methyl groups of the malonate addends can be found as a broad multiplet at δ = 1.3. Significantly, the UV-Vis spectrum of **5** is similar to that of **4**, indicating that the same addition patterns are involved. Obviously, the five-fold cyclopropanation of **3** in octahedral positions is accompanied by bromination of the methylene group of the ketone addend. As a consequence, a chiral center is introduced, which causes symmetry lowering to C_1. The facile formation of **5** clearly demonstrates that the α-methylene protons of azafullerenated ketones such as **3** are very acidic. Their deprotonation with DBU used as base generates an intermediate enolate which is able to attack diethyl bromomalonate to efficiently form an α-brominated ketone.

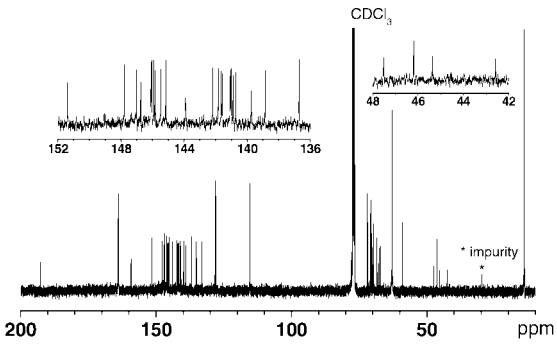

Fig. 1 100 MHz ^{13}C NMR spectrum of **4**.

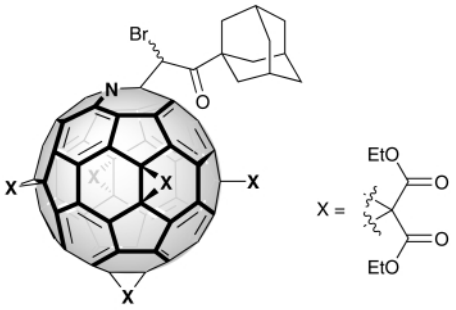

5

We thank the Deutsche Forschungsgemeinschaft DFG and the Graduiertenkolleg 'Homogener und heterogener Elektronentransfer' for financial support.

Notes and references

† Selected data for compound **4**: ν(KBr)/cm^{-1} 2979, 2932, 2904, 2872, 1744, 1608, 1509, 1464, 1459, 1391, 1368, 1252, 1221, 1178, 1095, 1021, 857, 710, 667 and 532; $\lambda_{max}(CH_2Cl_2)$/nm 265, 281, 514; ^{13}C NMR δ (100 MHz, $CDCl_3$) 163.96 (C=O, 2C), 163.81 (C=O, 4C), 163.78 (C=O, 2C), 163.73 (C=O, 1C), 163.70 (C=O, 1C), 159.19 (Ar–C–O, 1C), 151.41, 147.80, 147.04, 146.76, 146.11, 146.08, 145.93, 145.85, 145.49,145.17, 143.92, 142.19, 141.85, 141.66, 141.59, 141.09, 141.04, 140.92, 140.72, 139.75, 138.87, 136.73, 135.23, 134.83, 132.97, 127.96 (Ar–C, 2C), 115.21 (Ar–C, 2C), 77.88, 71.93, 70.87, 70.67, 70.58, 70.44, 70.14, 69.91, 69.68, 68.50, 68.29, 67.64, 67.07, 62.81 (–OCH_2CH_3, 8C), 62.71 (–OCH_2CH_3, 2C), 59.03 (–OCH_3, 1C), 47.52 (1C), 46.20 (2C), 45.37 (1C), 42.59 (1C), 14.04 (–CH_3, 10C); ^{1}H NMR δ (400 MHz, $CDCl_3$) 7.95 (d, 2H, ^3J = 8.8 Hz, Ar–H), 7.00 (d, 2H, ^3J = 8.8 Hz, Ar–H), 4.24 (br m, 24 H, –O*C*H_2CH$_3$ + 2 × –O*C*H_2CH$_2$), 3.84 (m, 2H, –O*C*H_2CH$_2$), 3.70 (m, 2H, –O*C*H_2CH$_2$), 3.64 (m, 2H, –O*C*H_2CH$_2$), 3.61 (m, 2H, –O*C*H_2CH$_2$), 3.49 (m, 2H, –O*C*H_2CH$_2$), 3.31 (s, 3H, −OCH_3), 1.25 (br m, 30 H, –CH_3); *m/z* (FAB) 1752 (M^+ + H), 1707 (M^+ + H – OEt), 1595 (M^+ – $C(CO_2Et)_2$ + 2H), 722 ($C_{59}N$). Selected data for compound **5**: ν(KBr)/cm^{-1} 2981, 2930, 2907, 2852, 1746, 1635, 1451, 1447, 1392, 1368, 1263, 1221, 1094, 1072, 1022, 858, 711, 669, 539, 528 and 511; $\lambda_{max}(CH_2Cl_2)$/nm 268, 285, 312, 501; ^{13}C NMR δ (100 MHz, $CDCl_3$) 207.01 (C=O, 1C), 163.60–163.90 (C=O, 10C), 152.41, 152.11, 147.51, 147.28, 147.26, 147.20, 146.81, 146.63, 146.58, 146.49, 145.98, 145.93, 145.89, 145.76 (2C), 145.70, 145.61, 145.55, 145.13, 145.08, 143.88, 143.85, 143.64, 142.79, 142.32, 142.27, 141.97, 141.86, 141.61, 141.58, 141.15, 141.08, 140.78 (2C), 140.66 (2C), 139.85, 139.83, 138.36, 138.24, 137.87, 137.77, 137.01, 136.99, 135.36, 135.27, 133.60, 133.13, 77.70 (1C), 70.39, 70.30, 69.88, 69.80, 68.42, 68.29, 67.16, 67.12, 62.82–62.71 (–OCH_2CH_3, 10C), 62.67 (–CHBr–, 1C) 48.17, 47.89, 47.55, 46.07, 45.36, 42.65, 38.40, 36.22, 27.78, 14.13–13.86 (–CH_3, 10C); ^{1}H NMR δ (400 MHz, $CDCl_3$) 5.62 (s, 1H), 4.36–4.19 (br m, 24 H, –O*C*H_2CH$_3$), 2.02 ('d', 6 H), 1.89 ('d', 3H), 1.72 (dd, 6H), 1.33–1.19 (br m, 30 H, –CH_3); *m/z* (FAB) 1767 and 1769 (M^+), 1722 and 1724 (M^+ − OCH_2CH_3), 1689 (M^+ − Br), 1513, 722 ($C_{59}N$).

1 J. C. Hummelen, B. Knight, J. Pavlovich, R. González and F. Wudl, *Science*, 1995, **269**, 1554.
2 C. Bellavia-Lund, R. González, J. C. Hummelen, R. G. Hicks, A. Sastre and F. Wudl, *J. Am. Chem. Soc.*, 1997, **119**, 2946.
3 B. Nuber and A. Hirsch, *Chem. Commun.*, 1998, 406.
4 F. Hauke and A. Hirsch, *Chem. Commun.*, 1999, 2199.
5 F. Hauke and A. Hirsch, *Tetrahedron*, 2001, **57**, 3697
6 U. Reuther and A. Hirsch, *Chem. Commun.*, 1998, 1401.
7 A. Hirsch and O. Vostrowsky, *Eur. J. Org. Chem.*, 2001, 829.

CHEMCOMM
Communication
www.rsc.org/chemcomm

Design of boron bis-oxazolinate (B-BOXate) complexes: a new class of stable organometallic catalysts

Marco Bandini, Pier Giorgio Cozzi,* Magda Monari, Rossana Perciaccante, Simona Selva and Achille Umani-Ronchi*

Dipartimento Chimico 'G. Ciamician', Università di Bologna, Via Selmi 2, 40126 Bologna, Italy. E-mail: pgcozzi@ciam.unibo.it; umani@ciam.unibo.it; Fax: +39-51-2099515; Tel: +39-51-2099509

Received (in Cambridge, UK) 20th April 2001, Accepted 4th June 2001
First published as an Advance Article on the web 27th June 2001

A new class of remarkably stable B-BOXate complexes has been synthesised, isolated and employed as chiral catalysts for asymmetric reduction of variously substituted prochiral ketones.

Enantioselective catalytic processes have emerged as among the most powerful of methodologies for the preparation of enantiomerically enriched compounds.[1] Of all the catalytic asymmetric procedures, the use of metal complexes bearing chiral ligands is receiving a great deal of attention from the chemical community.[2] In the class of the 'privileged ligands' reported in literature, chiral bis-oxazoline (BOX) ligations have been demonstrated to be effective motifs in many stereocontrolled reactions.[3] Normally, bis-oxazoline metal complexes are designed to behave as chiral Lewis acids, and free coordination sites are available for the incoming electrophile. Our attention was addressed towards the design of stable and coordinatively saturated BOX complexes where simultaneous binding of electrophiles and nucleophiles is possible.[4] With this in mind our interest was drawn to the preparation of coordinatively saturated boron bis-oxazolinate complexes. We discovered that the achiral BOX[5] **1** reacted smoothly with catecholborane (CATBH) in CH_2Cl_2 affording, after removal of the solvent, the boron bis-oxazolinate adduct **3** (B-BOXate) as a white solid stable to moisture in 85% yield.† The ^{1}H NMR, ^{13}C NMR and ^{11}B NMR spectroscopy investigations supported the formation of a single symmetric complex derived from the reaction between the CATBH and the BOX **1** (Scheme 1). To the best of our knowledge, B-BOXate complexes have not been reported until now. As a matter of fact, although the BOX ligands are easily deprotonated, only a few cases of BOXate–metal complexes have been described.[6] Diagnostic signals for **3** are the singlet for the proton bridge at δ = 4.45 ppm, the ^{13}C signal at δ = 57.8 ppm for the methine carbon of the ligand and the ^{11}B signal at δ = 8.87 ppm typical for a tetrahedral coordination of the boron atom.[7] These findings were also confirmed by an X-ray crystallographic analysis of **3**.‡ The structure reported in Fig. 1 shows that the BOX and the catechol motifs lie in two perpendicular planes, whereas the boron atom adopts a tetrahedral coordination slightly deviating from the idealised geometry as a consequence of the ring constraints. The molecule would conform to an idealised C_{2v} symmetry, but

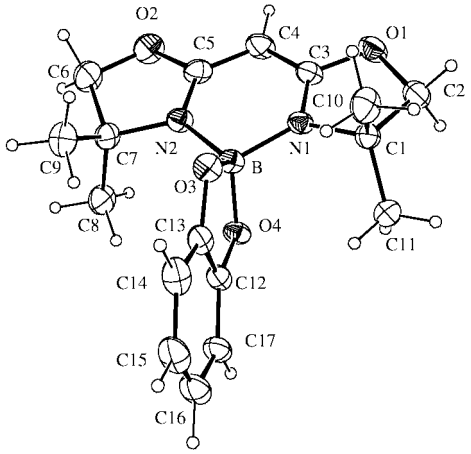

Fig. 1 An ORTEP plot of the molecular structure of **3**. Thermal ellipsoids are drawn at the 30% probability level. Selected bond lengths (Å) and angles (°): B–N(1) 1.541(2), B–N(2) 1.548(2), B–O(3) 1.479(2), B–O(4) 1.481(2), N(1)–C(1) 1.494(2), N(1)–C(3) 1.316(2), N(2)–C(5) 1.319(2), N(2)–C(7) 1.493(2), C(3)–C(4) 1.375(2), C(4)–C(5) 1.370(2); O(3)–B–O(4) 104.5(1), N(1)–B–N(2) 105.8(1), O(3)–B–N(1) 111.8(1), O(4)–B–N(1) 111.3(1), O(3)–B–N(2) 111.6(1), O(4)–B-N(2) 111.9(1). Dihedral angle between plane N(1)–B–N(2) and O(3)–B–O(4) is 89.69(8).

C(2) and C(6) atoms lie out the plane of their oxazoline rings [±0.223(5) Å] therefore the actual idealised symmetry is only C_2.

Employing chiral BOX ligands, the corresponding B-BOXate complexes can be isolated as stable solids. For instance, starting from the 2,2′-methylenebis[(4*R*,5*S*)-4,5-diphenyl-2-oxazoline] **2** and CATBH following the synthetic protocol employed for **3** the chiral B-BOXate **4** is isolated (diagnostic signals for **4** are as follows: ^{1}H NMR δ = 5.03 ppm and ^{13}C NMR δ = 57.8 ppm). In the course of our studies on the enantioselective reduction of prochiral ketones in the presence of M-BOX complexes,[6a,8] we found that the complex **3** was able to catalyse effectively the reduction of acetophenone with CATBH yielding the corresponding 1-phenylethanol in 86% yield after 18 h (Scheme 2). The use of **4** in catalytic amount (8 mol%) gave the desired (*R*)-1-phenylethanol (**6a**) in 80% yield and 44% enantiomeric excess. With the aim of searching for the optimal reaction protocol we screened, in the asymmetric

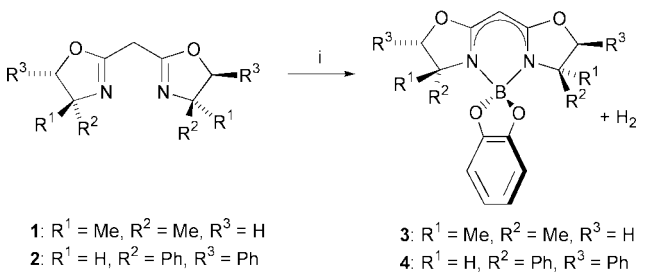

1: R^1 = Me, R^2 = Me, R^3 = H
2: R^1 = H, R^2 = Ph, R^3 = Ph

3: R^1 = Me, R^2 = Me, R^3 = H
4: R^1 = H, R^2 = Ph, R^3 = Ph

Scheme 1 *Reagents and conditions*: (i) BOX (1 eq.), CATBH (1.5 eq.), CH_2Cl_2, rt, 4 h.

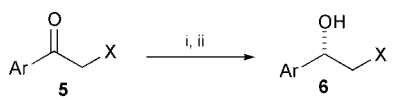

5 **6**

a: Ar = Ph, X = H;
b: Ar = Ph, X = Et;
c: Ar = Ph, X = Cl;
d: Ar = Ph, X = Br;
e: Ar = α-Naphthyl, X = H

Scheme 2 *Reagents and conditions*: (i) **5** (1 eq.), B-BOX (8 mol%), CATBH (2 eq.), CH_2Cl_2, 0 °C. (ii) NaOH (2 M).

 DOI: 10.1039/b103571c

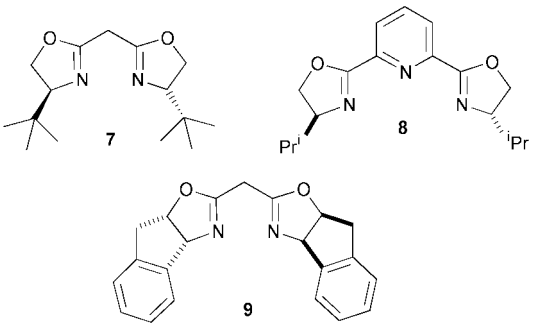

Fig. 2 BOX ligands.

reduction, other chiral C_2 bis-oxazoline ligands (BOX **7**–**9**, Fig. 2) preparing the catalytic precursors *in situ*, in order to simplify the procedure.[9]

The best result was obtained using 8 mol% of the BOX **9** that furnished the enantioenriched alcohol in 76% ee (Table 1, entry 4),§ while the use of non-enolizable BOXs such as the PyBOX **8**, significantly decreased the enantioselectivity (ee = 18%, entry 3). Moreover, the catalytic protocol can be successfully applied in the reduction of branched aromatic ketones and α-halo ketones[10] (Table 1, entries 5–8). Although the mechanism of the present reduction is still unclear, a cooperative action in which ketones and CATBH simultaneously bind to the chiral catalyst (chemzyme) could be invoked. In summary, the design of a new class of B-BOXate complexes and their use in the catalytic asymmetric reduction of ketones is presented. The fine-tuning of the stereo-electronical features (both the bis-oxazoline and the catechol motifs can be opportunely matched), makes these systems promising catalysts for a variety of stereocontrolled organic transformations.

Table 1 Enantioselective reduction of ketones in the presence of boron BOX complexes as catalysts

Entry[a]	BOX	Ketone	Yield (%)[b]	Ee (%)[c]	Config.[d]
1	**2**	**5a**	80	67	*S*
2	**7**	**5a**	40	30	*S*
3	**8**	**5a**	52	18	*S*
4	**9**	**5a**	78	76	*R*
5	**9**	**5b**	65	76	*R*
6	**9**	**5c**	85	84	*S*
7	**9**	**5d**	56[e]	86	*S*
8	**9**	**5e**	78	72	*R*

[a] The reactions were carried out as described in the note §. [b] Isolated yields after flash chromatography. [c] Evaluated by chiral GC analysis with a chiral cyclodextrin Megadex-5 column. [d] The absolute configuration was assigned by comparison of the $[\alpha]_D$ value reported in the literature (see: ref. 6*a*, 8). [e] The corresponding epoxide was isolated in 24% yield (ee = 86%) as a by-product of the reaction.

Acknowledgements are made to C.N.R. and M.U.R.S.T. (Progetto Nazionale 'Stereoselezione in Sintesi Organica: Metodologie ed Applicazioni') and Bologna University (funds for selected research topics) for the financial support of these researches. Dr Rossana Perciaccante thanks C.I.N.M.P.I.S. for a research grant. Dr Chris Senanayake (Sepracor INC.) is acknowledged for the generous gift of chiral (1*R*,2*S*)-*cis*-1-amino-2-indanol.

Notes and references

† *Synthesis of the B-BOXate* **3***:* A 25 mL round-bottom flask containing a stirring bar was charged with dry CH_2Cl_2 (4 mL), BOX **1** (105 mg, 0.5 mmol) and CATBH (80 μL, 0.75 mmol) at 0 °C. The resulting solution was stirred 4 h, then the solvent was evaporated under reduced pressure. The crude white product obtained was washed with dry Et_2O (5 mL), collected by filtration and dried under vacuum. Yield = 85%. δ_H ($CDCl_3$, 300 MHz) 6.71 (m, 4H), 4.46 (s, 1H), 4.10 (s, 4H), 1.30 (s, 12H); δ_C ($CDCl_3$, 50 MHz) 150.7, 119.1, 109.3, 109.0, 81.7, 62.8, 57.8, 26.3; δ_B (Ref. $BF_3{\cdot}OEt_2$): 8.87; diagnostic chemical shifts for **1** and CATBH: δ_H (**1**) 3.95 (s, 4H), 3.29 (s, 2H), 1.26 (s, 12H); δ_C (**3**) 160.2, 79.5, 67.3, 28.6, 28.2; δ_B (CATBH) 29.92 (d, $J_{B\text{-}H}$ = 554.1 Hz).

‡ *Crystal data* for **3**: $C_{17}H_{21}O_4BN_2$, M = 328.17, triclinic, a = 8.9871(3), b = 9.4340(4), c = 11.1411(4) Å, α = 67.378(2), β = 75.067(2), γ = 77.487(2)°, U = 835.12(5) Å^3, T = 293 K, space group $P\bar{1}$ (No. 2), Z = 2, μ(Mo-Kα) = 0.092 mm^{-1}, 11678 reflections measured by Bruker AXS SMART 2000 diffractometer with a CCD detector, 4866 unique (R_{int} = 0.0293) which were used in all calculations. Final $R1(F)$ = 0.0455 [$I > 2\sigma(I)$] and $wR2(F^2)$ = 0.1260 (all data). Software contained in the SHELXTL (5.1) library (G. M. Sheldrick, Bruker AXS, Madison, WI). CCDC 163357. See http://www.rsc.org/suppdata/cc/b1/b103571c/ for crystallographic files in .cif format.

§ *Catalytic reduction reaction*: To a stirring solution of **9** (13.2 mg, 0.04 mmol) in dry CH_2Cl_2 (2 mL) at 0 °C was added CATBH (100 μL, 1 mmol). The clear mixture was stirred for 2–3 h at the same temperature then acetophenone (58 μL, 0.5 mmol) was added by syringe. The reaction was kept without stirring for 48–72 h at 0 °C, quenched with NaOH (2 mL, 2 M) and then stirred for 10 min. After the usual workup (Et_2O, Na_2SO_4) the crude product was purified by flash chromatography (cyclohexane–Et_2O 85 : 15) to afford the (*R*)-(+)-phenylethanol as a pale yellow oil in 78% yield and 76% ee (Chiral GC analysis, Megadex-5 column).

1 B. M. Trost, *Angew. Chem., Int. Ed. Engl.*, 1995, **34**, 259.
2 (*a*) A. Pfaltz, E. N. Jacobsen, H. Yamamoto, ed., in *Comprehensive Asymmetric Catalysis*, Springer, Berlin, 1999; (*b*) I. Ojima, ed., in *Catalytic Asymmetric Synthesis*, Wiley, VCH, New York, 2nd edn., 2000.
3 For a recent and comprehensive review see: A. K. Ghosh, P. Mathivanan and J. Cappiello, *Tetrahedron: Asymmetry*, 1998, **9**, 1.
4 Chiral oxazaborolidines are known to act as chemzyme systems in which nucleophile and electrophile are bound in proximity affording a synergic catalytic action see: E. J. Corey and C. J. Helal, *Angew. Chem., Int. Ed.*, 1998, **37**, 1986.
5 For the synthesis of **1** see ref. 2.
6 (*a*) Ti-BOXate: M. Bandini, P. G. Cozzi, L. Negro and A. Umani-Ronchi, *Chem. Commun.*, 1999, 39; (*b*) Zn-BOXate: M. Nakamura, A. Hirai and M. Sogi, *J. Am. Chem. Soc.*, 1998, **120**, 546; R. P. Singh, *Bull. Soc. Chim. Fr.*, 1997, **134**, 765; (*c*) Mg-BOXate: V. Schulze and R. W. Hoffmann, *Chem. Eur. J.*, 1999, **5**, 337; (*d*) Yb/Ln-BOXate: H. W. Görlitzer, M. Spiegler and R. Anwander, *J. Chem. Soc., Dalton Trans.*, 1999, 4287; (*e*) Cu-BOXate: D. Müller, G. Umbricht, B. Weber and A. Pfaltz, *Helv. Chim. Acta*, 1991, **74**, 1; R. Schumacher, F. Dammast and H. U. Reißig, *Chem. Eur. J.*, 1997, **3**, 614; (*f*) Rh-BOXate: J. M. Brown, P. J. Guiry, D. W. Price, M. B. Hursthouse and K. Karalulov, *Tetrahedron: Asymmetry*, 1994, **5**, 561.
7 For a recent elegant study concerning trigonal and tetrahedral structure of chiral boron complexes see: K. Ishihara, H. Kurihara, M. Matsumoto and H. Yamamoto, *J. Am. Chem. Soc.*, 1998, **120**, 6920.
8 M. Bandini, P. G. Cozzi, M. de Angelis and A. Umani-Ronchi, *Tetrahedron Lett.*, 2000, **41**, 1601.
9 Other boron reducing agents were tested in the asymmetric reduction (*i.e.* $BH_3{\cdot}S(Me)_2$, $BH_3{\cdot}$2,6-lutidine and $BH_3{\cdot}$4-phenylmorpholine). However the enantiomeric excesses were significantly lower.
10 Aliphatic carbonyl substrates afforded the secondary alcohol in low chemical and optical yields (2-methylheptan-3-one: yield = 31%, ee = 26%).

Typeset and printed by Black Bear Press Limited, Cambridge, England

CHEMCOMM
Feature Article
www.rsc.org/chemcomm

The formyl C–H···O hydrogen bond as a critical factor in enantioselective Lewis-acid catalyzed reactions of aldehydes

E. J. Corey* and Thomas W. Lee

Department of Chemistry and Chemical Biology, Harvard University, Cambridge, MA 02138, USA. E-mail: corey@chemistry.harvard.edu

Received (in Cambridge, UK) 1st June 2001, Accepted 18th June 2001
First published as an Advance Article on the web 11th July 2001

X-Ray crystallographic studies have provided experimental evidence for the existence of intramolecular formyl C–H hydrogen bonds to oxygen or fluorine ligands in complexes of aldehydes and boron Lewis acids. This type of hydrogen bond can be regarded as 'induced' or 'cooperative' in the sense that its strength can be expected to increase as the bonding between the formyl oxygen and the Lewis acid becomes stronger. Coplanarity of the formyl group and the metal–X subunit to which it is bound in a five-membered ring effectively restricts rotation about the donor–acceptor bond between the formyl oxygen and the metal center of the Lewis acid, thus creating an additional organizing element in these complexes. This organizing element provides a simple and logical basis for understanding the mechanistic basis for enantioselectivity in many reactions of achiral aldehydes which are catalyzed by chiral Lewis acids. These reactions include aldol, allylation and ene addition to the formyl C=O group and Diels–Alder reactions of α,β-unsaturated aldehydes with 1,3-dienes. The idea of the induced formyl C–H hydrogen bond can serve as a guide in the design of new enantioselective catalysts as well as a mechanistic principle for understanding preferred transition state assemblies.

Introduction

One important aspect of research on enantioselective catalysis is the study of the detailed mechanistic basis of enantioselectivity in terms of transition-state structure. A clear understanding of the origin of enantioselection is crucial to the rational development of new synthetic methodology and to the successful application and/or extension of enantioselective reactions. Indeed, highly enantioselective catalytic reactions provide an unparalleled opportunity to discern the fine details of transition-state structure for many key synthetic processes.

Recent X-ray crystallographic studies[1] have provided evidence for a new kind of hydrogen bond in complexes of Lewis acids with the formyl group, exemplified generally by structures **1** and **2** (Fig. 1). The X-ray crystal structures of boron trifluoride

Fig. 1 Examples of formyl C–H···F and C–H···O hydrogen bonds.

complexes with benzaldehyde, methacrolein, 2,3-methylenedioxybenzaldehyde and dimethylformamide (DMF) show a preference for conformer **1** in which the formyl group and one of the B–F bonds are coplanar (eclipsed).[1] The H···F distances of 2.35–2.36 Å in these complexes are within the sum of the van der Waals radii of 2.67 Å (H = 1.20 Å and F = 1.47 Å).[2] Formyl C–H···O hydrogen bonding is indicated by the X-ray structures of [catecholborane·$(DMF)_2$]$^+Br^-$ (**3**) and [2-(*N*,*N*-dimethylamino)phenoxyboron·$(DMF)_2$]$^+I^-$ (**4**) (Fig. 2); the H···O distances of 2.41–2.59 Å in these complexes are well below the sum of the van der Waals radii of 2.72 Å (H = 1.20 Å and O = 1.52 Å).

Although the formyl proton of an uncomplexed substrate normally lacks the electrophilicity (*i.e.* acidity or positive charge) required for hydrogen bonding, coordination to a Lewis acid greatly enhances the positive charge at the formyl hydrogen while increasing the electron density at the oxygen or fluorine atoms attached to boron. Thus, the observed formyl hydrogen bonds shown in **1** and **2** (Fig. 1) are logical from an electronic structural point of view and in agreement with molecular orbital calculations.[3] There may also be a contribution from an anomeric effect in which electrons from the non-complexed lone pair on aldehyde oxygen delocalize into the σ* orbital of the eclipsed B–F or B–O bond (n → σ*). The authors of one study[3a] attributed a value of 6 kJ mol^{-1} to the anomeric effect and 9 kJ mol^{-1} to the formyl hydrogen bond.[4]

A recent publication[5] from this laboratory has provided the first discussion of the role of formyl hydrogen bonding in determining transition-state geometry in chiral Lewis acid-catalyzed reactions of aldehydes.[6] For instance, the highly enantioselective Diels–Alder reactions of 1,3-dienes with 2-bromoacrolein under the control of two very effective boron catalysts[7,8] can be explained in terms of the transition-state assembly shown in **5** or **6**, which contains a key formyl hydrogen bond as an organizing factor (Fig. 3). The *N*-

Elias J. Corey, born in 1928 in Methuen, 30 miles north of Boston, studied chemistry from 1945–1950 at the Massachusetts Institute of Technology, where he gained his doctorate for work on synthetic penicillins under the supervision of John C. Sheehan. In January 1951 he joined the University of Illinois at Urbana-Champaign as an Instructor in Chemistry and was promoted in 1956 to full Professor. Since 1959 he has been at Harvard University. For as long as he can remember he has enjoyed study, adventure and discovery.

Thomas W. Lee was born in 1973 in Hong Kong, and obtained his bachelor's degree in chemistry in 1995 at the Massachusetts Institute of Technology where he also worked for three years in the laboratory of Rick L. Danheiser as an undergraduate research assistant. He then joined the PhD program at Harvard University under the direction of E. J. Corey to study novel catalytic enantioselective Diels–Alder reactions and their applications in natural product synthesis. He received the PhD degree in chemistry in June 2001.

DOI: 10.1039/b104800g

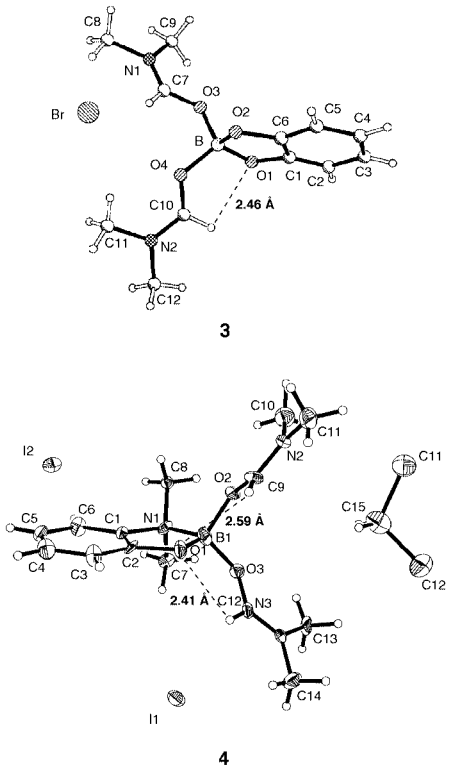

Fig. 2 X-Ray structures of [catecholborane·$(DMF)_2$]$^+Br^-$ (**3**) and [2-(*N*,*N*-dimethylamino)phenoxyboron·$(DMF)_2$]$^+I^-$ (**4**) showing formyl C–H···O hydrogen bonds.

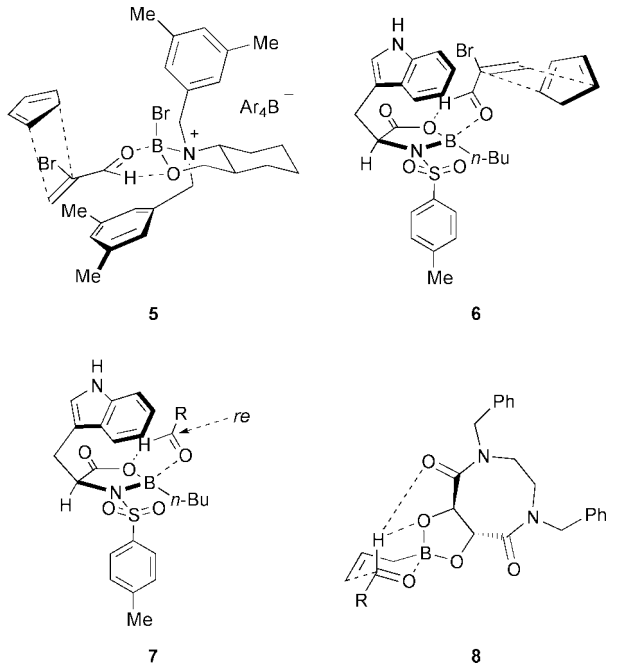

Fig. 3 Formyl hydrogen bond as an organizing element in enantioselective reactions.

tosyltryptophan-derived oxazaborolidine structure which appears in assembly **6** can also function very effectively to direct catalytic Mukaiyama aldol reactions.[9] The *re* face selectivity of these carbonyl additions can be predicted using the same line of analysis (see **7**). In addition, the Roush enantioselective allylboration of aldehydes,[10] a stoichiometric reaction for which there was no satisfactory explanation previously, can be understood in terms of a preference for the doubly hydrogen bonded structure **8**. It should be noted that the formyl hydrogen bond is only one of several structural elements contributing to the high enantioselectivities observed in these reactions.[7–10]

Pathways for enantioselective reactions of aldehydes involving formyl C–H···O hydrogen bonding

This section describes the application of the formyl hydrogen bond as an organizing stereochemical element to the understanding of a number of catalytic reactions involving aldehydes and chiral Lewis acids (*e.g.* Diels–Alder, aldol, ene reaction, hydrocyanation, allylation and alkylation) which have recently been developed and for which there has been no clear mechanistic rationale.

It has been pointed out[5] that the absolute stereochemical course of aldol reactions which are promoted by Yamamoto's chiral acyloxyborane (CAB) catalyst can be explained readily by formyl hydrogen bonding to *two* oxygens of the chiral ligand. The favored mode of binding of the (*R*,*R*)-tartrate-derived CAB catalyst with benzaldehyde as ligand is shown in **9** of Fig. 4.[11] The combination of the double (bifurcated) hydrogen bond and the π-attractive interaction of the bound formyl group with the neighboring substituted aromatic ring defines a unique structure which involves strong screening of the *si* face of the aldehyde formyl group. On the basis of a preference for this structure for the complex, it is expected that an enol silyl ether would attack benzaldehyde at the *re* face of the formyl carbon to form the (*R*)-Mukaiyama aldol product, as has been observed experimentally.[12] This simple explanation of the absolute stereochemical course of the CAB-catalyzed Mukaiyama aldol reaction can also be applied to CAB-catalyzed allylations of aldehydes[12d,e] and Diels–Alder reactions of α,β-enals.[13]

Formyl hydrogen bonding also seems to be a significant factor in determining the stereochemical course of reactions of aldehydes which are mediated by chiral complexes of Ti(IV). Keck and coworkers have described allylation[14] and aldol[15] reactions catalyzed by a 2 : 1 complex derived from (*R*)-1,1′-bi-2-naphthol ((*R*)-BINOL) and Ti(O*i*-Pr)$_4$. The catalytic species in these reactions is probably the bis-BINOL titanate ester, $BINOL_2Ti$. In the case of catalytic allylation of an aldehyde with allyltri-*n*-butyltin, the latter reagent probably allylates Ti(IV) while the Bu_3Sn group attaches to one of the BINOL oxygens and causes dissociation of that oxygen from Ti. Coordination of benzaldehyde to this species with formation of the trigonal bipyramidal, hydrogen bonded structure **10** (Fig. 4) should be preferred since this arrangement uniquely satisfies three conditions: (1) minimize non-bonded steric repulsion, (2) allow formation of a stereoelectronically and entropically favorable formyl hydrogen bond to one of the oxygens of the bidentate BINOL ligand, and (3) place the allyl group in the basal position and the formyl oxygen in the apical position, ideal for the allylation reaction. Structure **10** leads to the observed absolute configuration of the homoallylic alcohol adduct ((*R*) from (*R*)-BINOL; (*S*) from (*S*)-BINOL).[14] It should be noted that interchanging allyl and benzaldehyde ligands in **10** places the aldehyde in a basal site which does not allow formation of a good formyl hydrogen bond to oxygen.[16]

For the Keck catalytic aldol process using $BINOL_2Ti$, an aldehyde and $H_2C{=}C(St\text{-}Bu)OSiMe_3$ as nucleophile, a structure analogous to **10** with $H_2C{=}C(St\text{-}Bu)O$ replacing allyl leads unambiguously to the observed absolute configuration of the predominant Mukaiyama aldol adduct.[15,17]

A Ti-based system related to that of Keck for the catalytic enantioselective Mukaiyama acetate aldol reaction of aldehydes with $H_2C{=}C(OMe)OSiMe_3$ using a catalyst derived from Ti(O*i*-Pr)$_4$, a Schiff base of 2-amino-2′-hydroxy-1,1′-binaphthyl and 3-bromo-5-*tert*-butylsalicylaldehyde, and 3,5-di-*tert*-butylsalicylic acid has been described by Carreira.[18] The Schiff base probably serves as a tridentate ligand with a coplanar arrangement of the two phenolic oxygens and the imine nitrogen, while

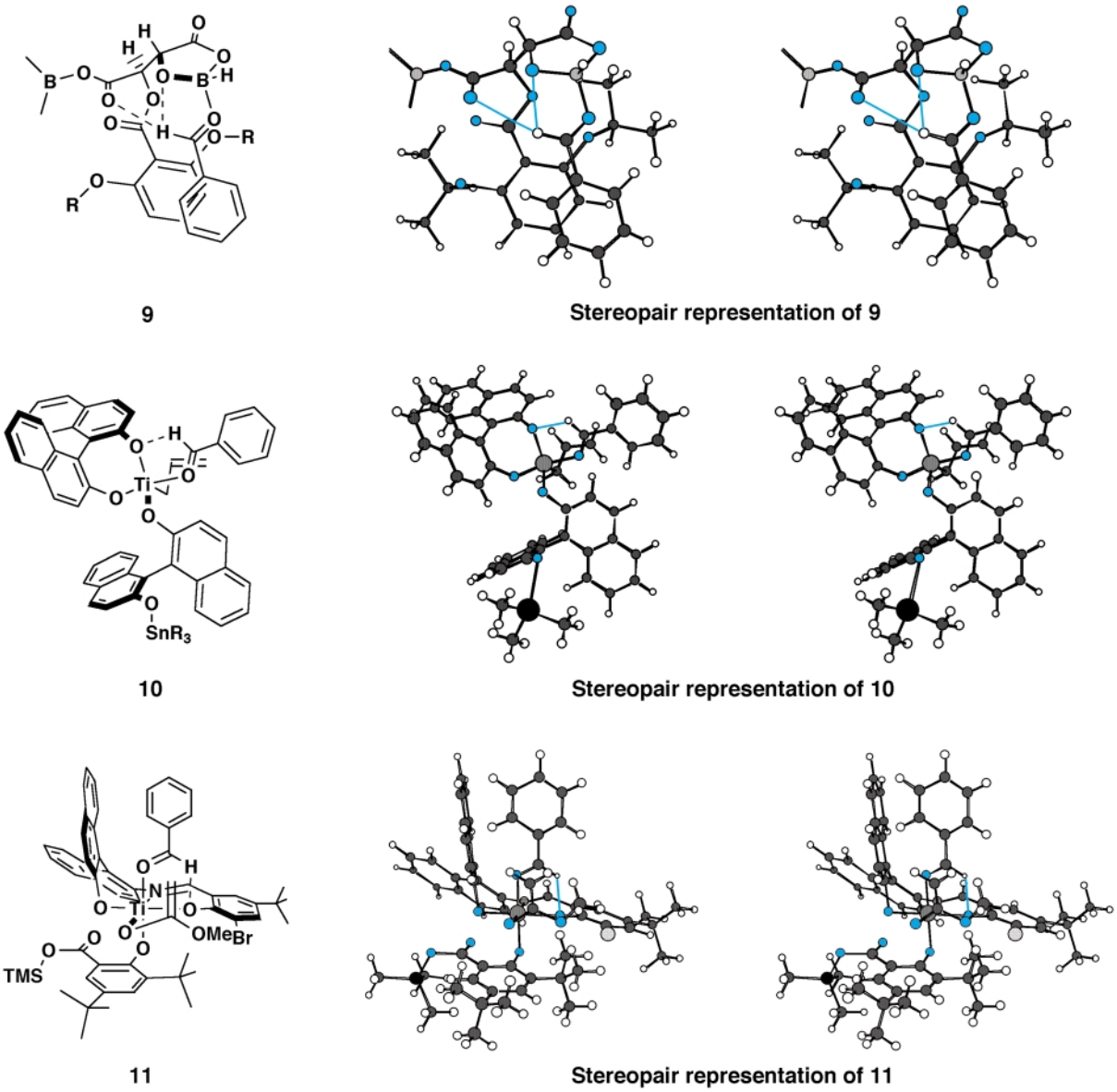

Fig. 4 Transition-state structures of Yamamoto's CAB aldol (**9**), Keck allylation (**10**) and Carreira aldol reaction (**11**). (Blue circles represent oxygen atoms and blue lines represent hydrogen bonds).

the salicylic acid acts as a bidentate ligand which is capable of accepting a trimethylsilyl group at the carboxy oxygen by reaction with $H_2C{=}C(OMe)OSiMe_3$. The reactive complex in the aldol-forming step is thus likely to have the following ligands coordinated octahedrally to Ti(IV): (1) the tridentate Schiff base, (2) an aryloxy group, (3) the aldehyde, and (4) the enol of methyl acetate. Clearly, the aldehyde and enolate ligands must be *cis* to one another in the octahedral arrangement in order to react. Although there are two possible arrangements of the complex which satisfy this condition, only that which is shown in **11** (Fig. 4) permits formyl C–H···O hydrogen bonding while minimizing steric repulsion involving the bulky 2,4-di-*tert*-butyl-6-trimethylsilyloxycarbonylphenoxide ligand. Structure **11** unambiguously leads to the observed enantiomeric aldol product.[18] The use of the formyl C–H···O hydrogen bond concept simplifies the analysis of the absolute stereochemical course of the Carreira aldol and, simultaneously provides a simple explanation of the effectiveness of the *bulky* substituted salicylic acid ligand.

Yamamoto has prepared a catalyst (Brønsted acid-assisted chiral Lewis acid, BLA) for enantioselective reactions of α,β-enals from trimethyl borate and (*R*)-3,3′-bis(2-hydroxyphenyl)-2,2′-dihydroxy-1,1′-binaphthyl.[19] Although a possible transition state was proposed for this process which involved s-*trans*-complexed α,β-enal, the corresponding structure with the s-*cis*-complexed α,β-enal seems equally plausible, even though it would lead to the enantiomer of the observed product in each case. Probably for this reason, the s-*cis*-α,β-enal transition state was ignored. If the condition of formyl C–H···O hydrogen bonding is imposed on the Yamamoto BLA system, a unique explanation of the absolute stereochemical result emerges, as shown in **12** (Fig. 5) for the (*R*)-catalyst. A favorable hydrogen bond is only possible to the terminal aryloxy oxygen as is shown in Fig. 5. In **12** the α,β-enal is coordinated to boron in the s-*cis* form. Addition of the diene to the unobstructed *si* face of the α,β-enal (*i.e.* top face of **12** as viewed) then leads to the observed Diels–Alder adduct. This mode of addition minimizes steric repulsion involving the α-substituent of the α,β-enal and the cofacial neighboring π-aromatic ring in the transition state. This steric compression factor[8a] in the transition state clearly favors reaction *via* the s-*cis*-α,β-enal in this system.

Recently, Yamamoto has described another (*R*)-BINOL-based BLA Diels–Alder system (**13** in Fig. 5) which produces adducts of opposite absolute configuration in comparison with (*R*)-BINOL-based **12**.[20] A simple explanation for this difference is provided by the formyl hydrogen bonded transition structure shown in **13**, which contains the s-*cis*-complexed α,β-

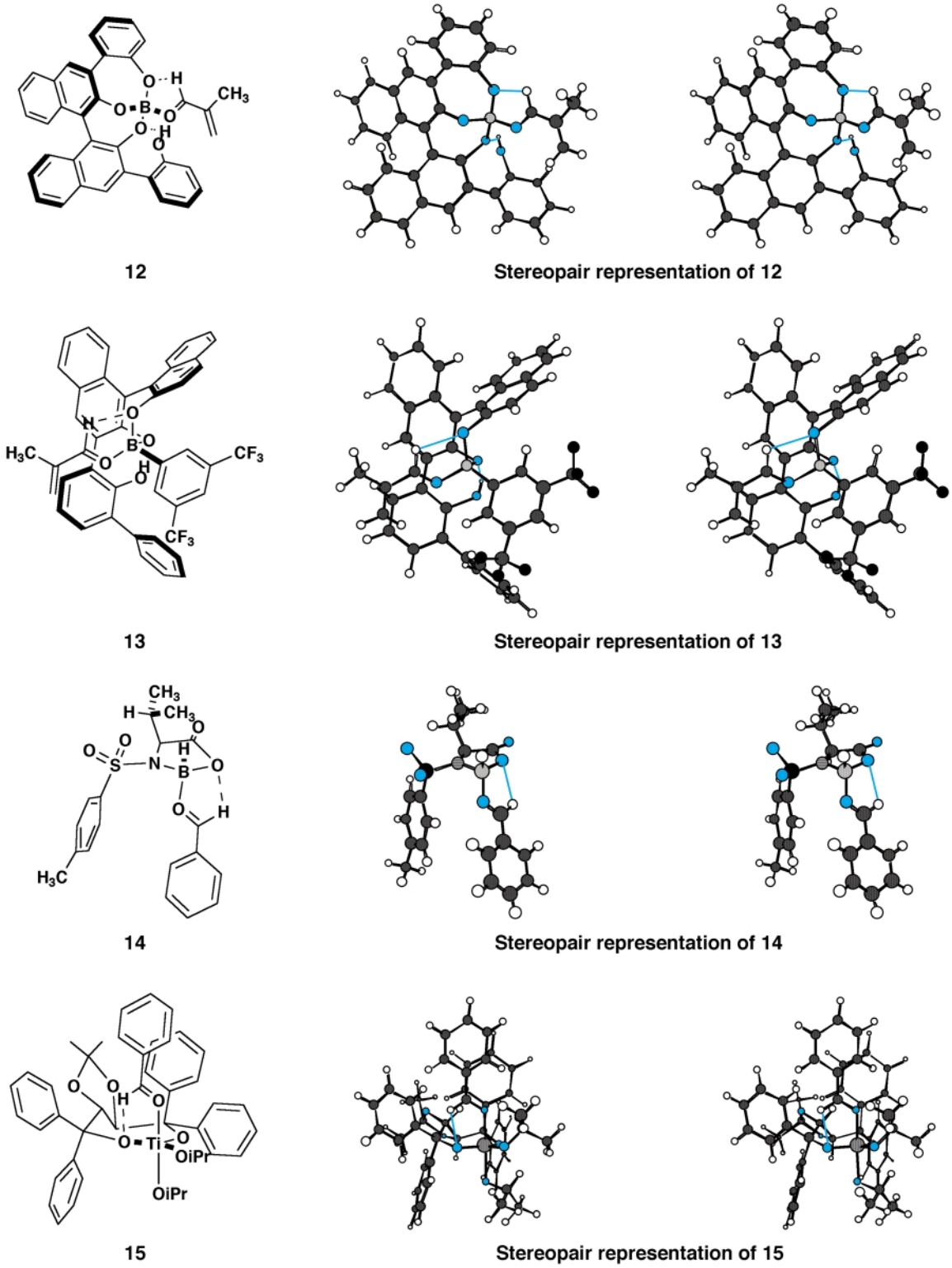

Fig. 5 Favored binding modes of Yamamoto's BLA catalysts (**12** and **13**), Kiyooka's oxazaborolidine catalyst (**14**) and Ti–TADDOL catalyst (**15**) with aldehyde substrates. (Blue circles represent oxygen atoms and blue lines represent hydrogen bonds.)

enal for the reasons described for **12**. Structure **13** is optimal with regard to favorable stereoelectronics for the hydrogen bond and conformation of the coordinated ligand.

Kiyooka and coworkers[21] have studied enantioselective Mukaiyama aldol reactions of aldehydes with various silyl enol ethers using an *N*-arylsulfonylvaline-derived oxazaborolidine catalyst. Structure **14** (Fig. 5) illustrates the proposed transition-state assembly in which the isopropyl and arylsulfonyl appendages are disposed *trans* to one another about the oxazaborolidine ring and in the sterically most stable arrangement. The aldehyde can coordinate to the face of boron *trans* to isopropyl, thereby minimizing steric repulsion and providing for the necessary hydrogen bonding between the formyl hydrogen and the oxazaborolidine oxygen. Preferential attack of the nucleophilic enol ether at the *si* face of the formyl group (corresponding to the front face in **14**) is predicted, in agreement with the experimental findings.[21] Kiyooka *et al.*[21a] have proposed a transition state which is the same as **14** with respect to the Lewis acid moiety, but which differs with regard to the absence of a formyl C–H···O hydrogen bond and the rotational orientation of the complexed aldehyde about the B–O bond (arbitrarily assumed by them).[22]

Seebach, Narasaka and coworkers have pioneered the use of titanium alkoxide catalysts containing a chiral tartrate-derived tetraaryl-1,3-dioxolane-4,5-diyldimethanol (TADDOL) bidentate ligand as a promoter of reactions of aldehydes with diethylzinc[23] and trimethylsilyl cyanide.[24] The transition-state assembly shown in **15** possesses the following features: (1) the pentacoordinate Ti has trigonal bipyramidal geometry with the TADDOL ligand bound to basal positions, both to minimize angle strain and to allow access to the Lewis acidic Ti by the aldehyde; (2) coordination of the aldehyde to Ti occurs through one of the two symmetry equivalent apical bonds (apical binding of the aldehyde is favored because it is the least basic ligand[25] and because it allows formyl C–H···O hydrogen bonding); (3) the orientation of the complexed aldehyde is fixed by a stereoelectronically favorable formyl C–H···O hydrogen bond and avoidance of steric repulsion with the axial phenyl group; (4) attack on the formyl group by the nucleophile EtZnX occurs at the more open *si* face of the formyl carbon, leading to the observed predominant product. The hydrocyanation of the benzaldehyde could also proceed *via* **15** with attack of cyanide ion on the *si* face of the formyl carbon, again in accord with experiment.[23,24] These models for the TADDOL-catalyzed ethylation and hydrocyanation of aldehydes are consistent with the less specific scheme proposed by Seebach and coworkers,[23] which does not contain the key formyl C–H···O hydrogen bond but which assumes a similar orientation of the complexed aldehyde. It should be pointed out that in the event that the aldehyde was coordinated to Ti in a basal position (unlikely because it is the most electronegative ligand[25]) the formyl C–H···O hydrogen bond would not be possible and little or no enantioselectivity would result.

Oguni and coworkers have introduced a chiral reagent which is derived from the reaction of titanium tetraisopropoxide with the Schiff base of 3,5-di-*tert*-butylsalicylaldehyde and (*S*)-valinol for the catalyzed reaction of aldehydes with diketene (aldol)[26] or trimethylsilyl cyanide.[27] The mechanistic basis for enantioselectivity in these cases has been unclear. Our analysis of the Oguni enantioselective diketene aldol reaction of aldehydes has led unequivocally to the favored transition-state assembly **16** which is shown in Fig. 6. In this structure there is octahedral hexacoordination to titanium with the three donor groups of the ligand coplanar with the metal, and the five-membered chelate ring is puckered to allow an equatorial[28] isopropyl group. Axial coordination of the aldehyde, so as to allow the best formyl C–H···O hydrogen bond, occurs at the top face of Ti in **16** (hydrogen bond to the axial lone pair on O). The enolate ligand is coordinated *cis* to the aldehyde to allow carbonyl addition *via* a six-membered chair transition state; the remaining isopropoxy ligand is *trans* to the coordinated aldehyde. In the model shown in **16** attack by the enolate occurs at the *si* face of the aldehyde to produce the (*S*)-aldol enantiomer, the observed product.[26] Switching the aldehyde and enolate ligands of **16** to the arrangement shown in **17**, does not allow good formyl C–H···O hydrogen bonding because each of the two lone pairs on the valinol oxygen of the tridentate chiral ligand is poorly positioned to interact with the formyl hydrogen.

Hydrocyanation of aldehydes using the (*S*)-Oguni catalyst, which also occurs by attack at the *si* face of the coordinated aldehyde, can be explained by a transition-state structure similar to **16** except for an isopropoxy replacing the enolate ligand. Rearward (*si* face) attack by CN^- then occurs on the rigidly held formyl group to give the observed (*R*)-cyanohydrin derivative.[27]

Kagan and coworkers have reported a Diels–Alder catalyst system derived from (*S*)-1,1-diphenyl-1,2-dihydroxypropane and $EtAlCl_2$ (1 : 1).[29] A linear relationship was demonstrated for $\ln R_e$ *vs.* $1/T$ where R_e is the ratio of enantiomeric products (*R*/*S*) and *T* is the Kelvin temperature, and values were obtained for $\Delta\Delta G^{\ddagger}$ (−0.74 kcal mol^{-1}), $\Delta\Delta H^{\ddagger}$ (−2.46 kcal mol^{-1}) and $-T\Delta\Delta S^{\ddagger}$ (+1.73 kcal mol^{-1}). The enthalpic barrier is lower for formation of the predominating enantiomer, but this is partly counterbalanced entropically due to the more ordered transition state for the major pathway. The most likely structure for the effective catalyst is the dioxaluminolidine **18** shown in Fig. 7. Steric repulsion between the adjacent phenyl and methyl substituents fixes the conformation of the five-membered dioxaluminolidine ring and thus orients one of the four oxygen lone pairs suitably for hydrogen bonding. This complex also minimizes steric repulsion between the aldehyde and the phenyl or methyl substituent and allows for a favorable π,π-attractive interaction between the positive formyl carbon and the neighboring phenyl group (spacing *ca.* 3.5 Å). The s-*trans* arrangement of the complexed dienophile can be expected to lead to a lower energy transition state than the s-*cis* form, because in the former there will be less repulsion between the α-methyl substituent of the dienophile and the phenyl of the catalyst in the transition state. As shown in **18**, the α-methyl group remains clear of the neighboring phenyl group as C(α) goes from sp^2 to sp^3 hybridization. Diene addition to the *si* face of **18** leads to the observed[29] predominating enantiomer. The high degree of organization in the transition state corresponding

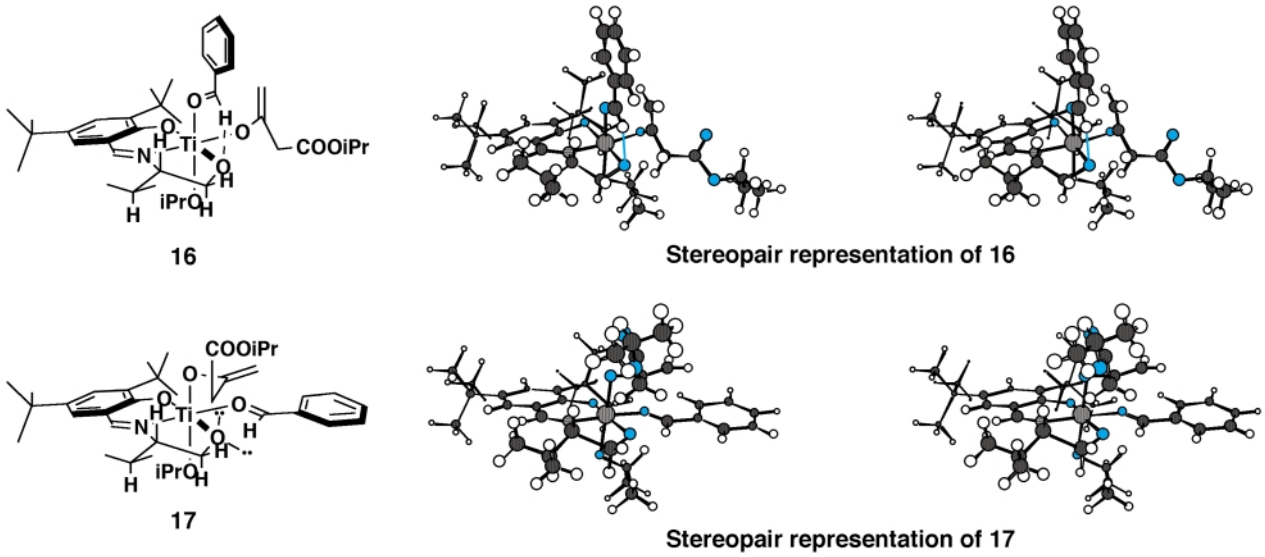

Fig. 6 Favored (**16**) and disfavored (**17**) transition-state assemblies of Oguni diketene aldol reaction. (Blue circles represent oxygen atoms and blue lines represent hydrogen bonds.)

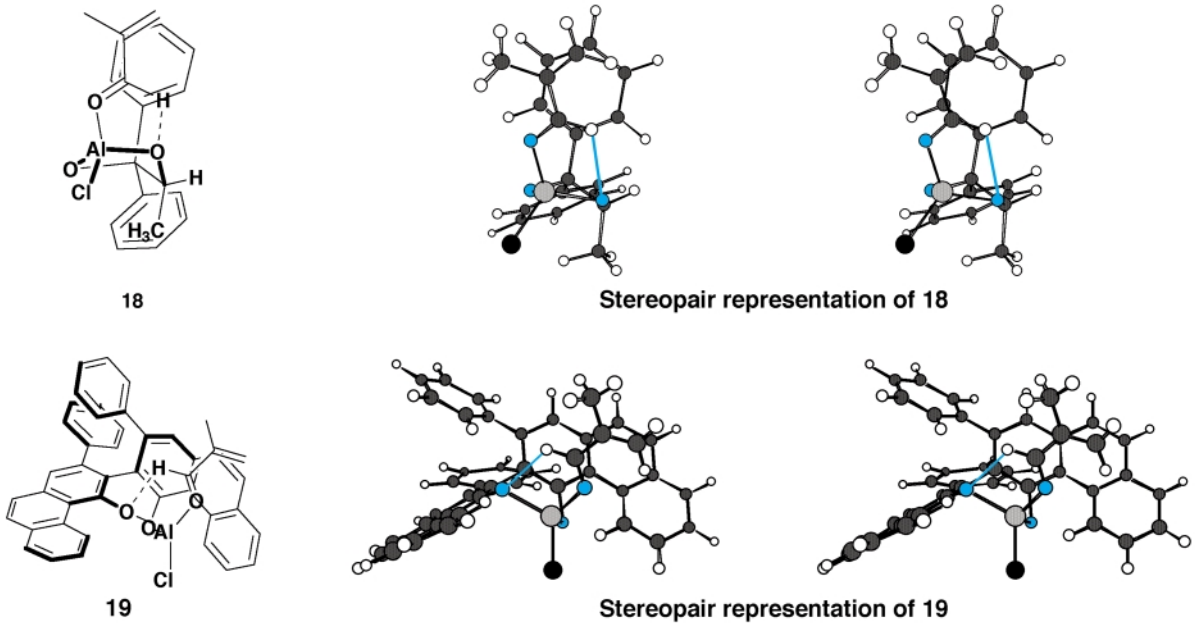

Fig. 7 Favored binding mode of Kagan's dioxaluminolidine catalyst (**18**) and Wulff's Al–VAPOL catalyst (**19**) with α-methacrolein. (Blue circles represent oxygen atoms and blue lines represent hydrogen bonds.)

to **18** is consistent with the observed greater loss of entropy for the pathway leading to the major enantiomer.[29]

A highly enantioselective Diels–Alder reaction using a catalyst derived from diethylaluminum chloride and a substituted 2,2′-bi-1-phenanthrol (vaulted biphenanthrol, VAPOL) has been described by Wulff.[30] No transition-state structure was proposed, and indeed it is difficult to understand the absolute stereochemical course of this reaction without the organizing influence of a formyl C–H···O hydrogen bond. A favorable hydrogen bond is only possible in the arrangement depicted in **19** (Fig. 7). The addition of cyclopentadiene to the accessible *si* (front) face of the coordinated s-*cis*-2-methylacrolein leads to the correct absolute configuration of the observed major enantiomer.[30] In this case the α-methyl substituent of the dienophile is clear of the neighboring π-aromatic group in the s-*cis* but not in the s-*trans* rotamer, leading to faster reaction *via* the s-*cis* form.

One of the most interesting findings in the field of catalytic enantioselective synthesis is the development by the Mikami group of a family of enantioselective ene reactions between unusually electrophilic (*e.g.* glyoxylic) aldehydes and a series of terminal olefins under the influence of chiral Lewis acids, especially BINOL–TiX_2 (derived from 1,1′-bi-2-naphthol and $TiCl_2$(O*i*-Pr)$_2$ and 4 Å molecular sieves).[31,32] Numerous examples of the ene reaction have been described by Mikami which proceed with excellent enantioselectivity, as illustrated by the example shown in eqn. (1).[33]

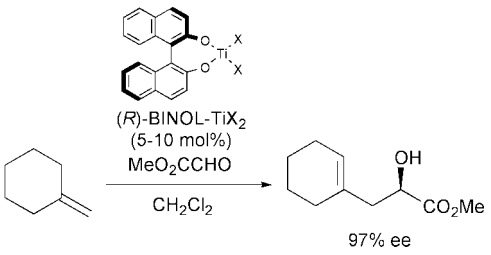

(1)

In addition to the high facial selectivity of this process with regard to the aldehyde component, remarkable selectivity for the olefinic component with regard to π-facial attack and C–H cleavage has been observed, as shown in eqn. (2).[34] The detailed

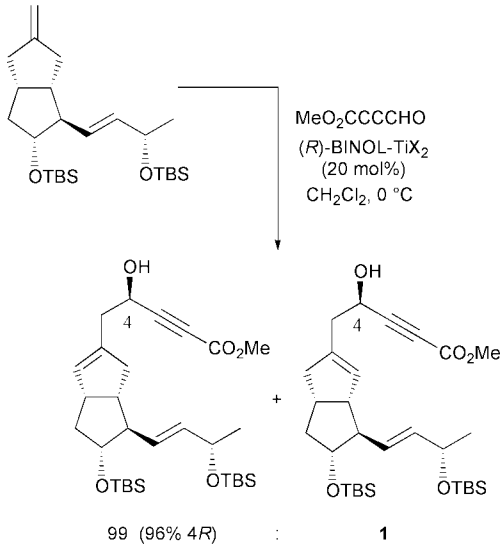

(2)

mechanistic basis for such high stereoselectivity has remained obscure, although a chair-like six-membered pericyclic transition state has been proposed for the $SnCl_4$-catalyzed diastereoselective reaction of glyoxylate esters and olefins, with the glyoxylate substrate chelated to the metal through the 1,2-dicarbonyl subunit.[31e,35]

A transition-state structure has been derived for the Mikami ene reaction by use of the following logical steps. (1) The aldehyde is activated by complexation with the chiral catalyst (*R*)-BINOL–TiX_2 *via* the formyl lone electron pair which is *syn* to the formyl hydrogen to form a pentacoordinate Ti structure. The comparable behavior of glyoxylic esters (eqn. (1)) and 3-methoxycarbonylpropynal (eqn. (2)) in the Mikami ene reaction argues against bidentate coordination of both carbonyl groups of glyoxylic esters since bidentate coordination is clearly not possible with the latter. (2) The resulting complex prefers trigonal bipyramidal geometry with the apical substituents being the coordinated aldehyde and one of the chlorines. This arrangement follows from the preference for the two most electronegative (*i.e.* weakest) ligands to be in the apical

positions for d^0 pentacoordinated structures such as Ti(IV) complexes.[25] (3) Formyl CH···O hydrogen bonding occurs to the stereoelectronically most favorable oxygen lone pair of the BINOL ligand to generate structure **20** (Fig. 8). In this structure,

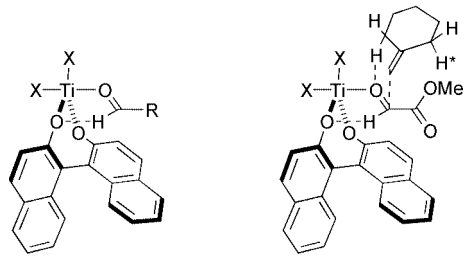

20 **21**

Fig. 8 Mechanistic rationale for the Mikami ene reactions.

the top (*re*) face of the formyl group is much more accessible to a nucleophile than the bottom (*si*) face since the latter is strongly shielded by the nearby naphthol subunit. Formyl C–H···O hydrogen bonding to the other BINOL oxygen is stereoelectronically and sterically disfavored (strong steric repulsion exists between the formyl group and the proximate naphthol ring). (4) The transition-state structure for the ene reaction is likely to involve some degree of proton transfer from the scissile allylic C–H to the formyl oxygen as the new C–C bond is being formed and the olefinic substrate is gaining positive charge β to the scissile C–H. Structure **21** exemplifies that type of transition-state structure for the reaction described in eqn. (1). It also predicts the absolute configuration of the Mikami ene product as shown in eqn. (1) and, as well, preferential cleavage of the allylic C–H shown rather than C–H* of **21**. Cleavage of C–H* is obviously unfavorable because it necessitates strong steric repulsion (clash) between the cyclohexane ring and the nearby basal chlorine ligand.

The favored transition-state structure **22** (Fig. 9) for the ene reaction described in eqn. (2) can be derived in the same way with the additional proviso that the face of the olefinic component which binds to the aldehyde is that on the convex side of the bicyclo[3.3.0]octyl ring pair. Structure **22** predicts the stereochemistry and structure of the product shown in eqn. (2).[36] The corresponding transition-state structure for forming the position isomeric olefin in the Mikami ene reaction is depicted in **23**. It is clearly very unfavorable because of a serious steric clash between the basal chlorine substituent and the proximate five-membered ring.

Mikami and coworkers have also applied the BINOL–$TiCl_2$ catalyzed ene reaction to the desymmetrization of a symmetrical diolefinic substrate as shown in eqn. (3).[37] Outstanding enantio-

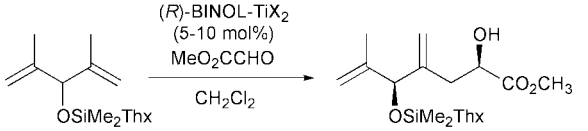

(3)

>99% ee, >99% de

and diastereoselectivity were observed (> 99% ee and > 99% de). Our analysis leads to the proposed transition-state structure **24** (Fig. 10) as most favorable. In this structure the approach of the complexed aldehyde to the olefin occurs so as to minimize steric repulsion, with the bulky $SiMe_2Thx$ (Thx = thexyl, 1,1,2-trimethylpropyl) substituent remote and the small H* in proximity to the attacking electrophile, as indicated. An analogous transition state for reaction at the diastereotopic double bond is less stable than **24** for steric reasons. Transition-state structure **24** leads to the overall stereochemistry shown in eqn. (3).

Ene reactions such as those described herein are calculated to be exothermic by *ca.* 20 kcal mol^{-1}.[38] The reaction of the Lewis acid coordinated aldehyde will be much more exothermic—possibly 30 kcal mol^{-1}. Therefore, the transition state for the

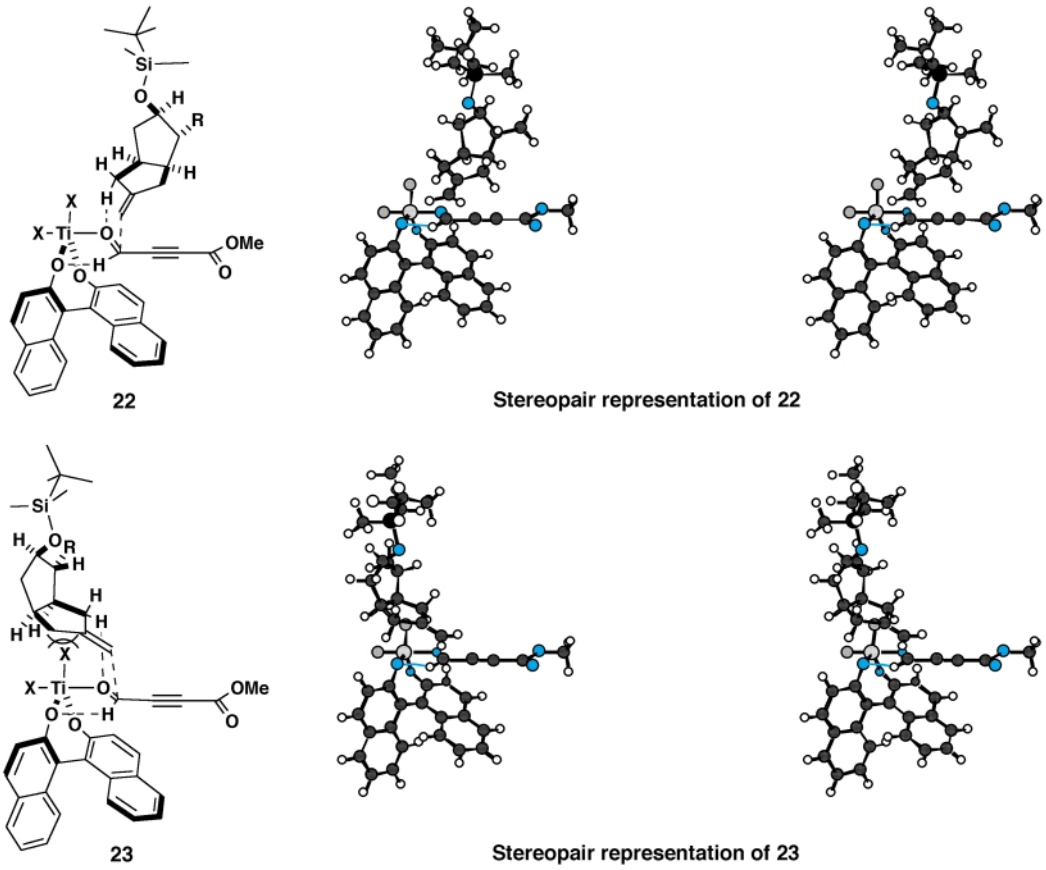

Fig. 9 Mechanistic rationale for the Mikami ene reaction shown in eqn. (2). (Blue circles represent oxygen atoms and blue lines represent hydrogen bonds.)

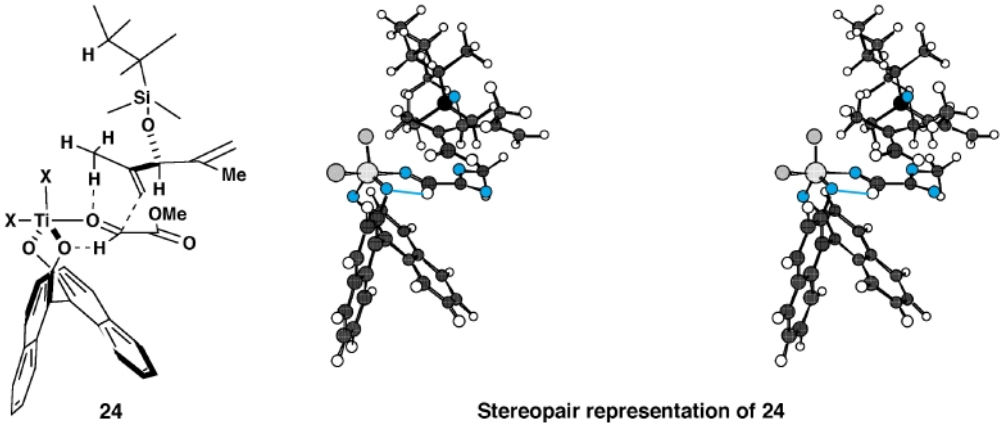

Fig. 10 Mechanistic rationale for the Mikami ene reaction shown in eqn. (3). (Blue circles represent oxygen atoms and blue lines represent hydrogen bonds.)

reaction of an unhindered olefin and a Lewis acid–aldehyde complex should be early, *i.e.* 'starting-material like', and the organizing structural elements in the complex are likely to be preserved in the transition state. Because highly organized, activated and sterically favored reactant complexes can lead to products *via* early transition states, the type of analysis presented herein should be valid since structural factors such as steric repulsions which disfavor alternative complexes also disfavor the corresponding transition states.

(*R*)- and (*S*)-BINOL–TiX_2 catalysts have also been utilized successfully to promote enantioselective Mukaiyama aldol, allylic silane mediated allylation and hetero-Diels–Alder reactions of glyoxylic esters.[39] The absolute stereochemical course of these reactions can be readily explained by the same considerations which are outlined herein for the Mikami ene reaction.

Conclusion

The understanding of the catalytic enantioselective reactions discussed in this appendix would be very difficult without some restriction of rotation of the bond between the catalytic Lewis acidic metal and the carbonyl group of the aldehyde. In each of approximately thirty known enantioselective reactions of aldehydes under chiral Lewis acid catalysis, the rational use of the formyl C–H···O hydrogen bond and strongly precedented structural principles has led to a transition-state assembly which predicts the observed absolute configuration of the predominating enantiomer. The success of the formyl C–H···O hydrogen bond idea in clarifying and unifying such a large and varied body of reactions, together with supporting evidence from X-ray crystallographic studies of formyl-Lewis acid complexes add credence to its validity. We believe that this formyl C–H···O hydrogen bonding concept will be useful in future catalyst design.

Acknowledgements

We are grateful to the National Science Foundation and Boehringer Ingelheim Co. for graduate fellowships to T. W. L. and to Jeff Rohde for his contributions to this project.

Notes and references

1 (*a*) M. T. Reetz, M. Hullmann, W. Massa, S. Berger, P. Rademacher and P. Heymanns, *J. Am. Chem. Soc.*, 1986, **108**, 2405; (*b*) E. J. Corey, T.-P. Loh, S. Sarshar and M. D. Azimioara, *Tetrahedron Lett.*, 1992, **33**, 6945; (*c*) E. J. Corey, J. J. Rohde, A. Fischer and M. D. Azimioara, *Tetrahedron Lett.*, 1997, **38**, 33. For other variants of this formyl hydrogen bonding interaction, see: (*d*) E. P. Kündig, C. M. Saudan and G. Bernardinelli, *Angew. Chem., Int. Ed.*, 1999, **38**, 1220; (*e*) D. J. Parks, W. E. Piers, M. Parvez, R. Atencio and M. J. Zaworotko, *Organometallics*, 1998, **17**, 1369.

2 These van der Waals radii were taken from the compilation of A. Bondi, *J. Phys. Chem.*, 1964, **68**, 441.

3 For theoretical calculations, see: (*a*) M. D. Mackey and J. M. Goodman, *Chem. Commun.*, 1997, 2383; (*b*) B. W. Gung and M. A. Wolf, *J. Org. Chem.*, 1992, **57**, 1370; (*c*) B. W. Gung, *Tetrahedron Lett.*, 1991, **32**, 2867; (*d*) J. M. Goodman, *Tetrahedron Lett.*, 1992, **33**, 7219; (*e*) L. Salvatella, A. Mokrane, A. Cartier and M. F. Ruiz-Lopez, *J. Org. Chem.*, 1998, **63**, 4664; (*f*) N. Bernardi, A. Bottoni, S. Casolari and E. Tagliavini, *J. Org. Chem.*, 2000, **65**, 4783.

4 Preliminary experimental results from the Singleton group have shown an inverse isotope effect of 0.826(7) for the formyl proton in the boron trifluoride-catalyzed Diels–Alder reaction of isoprene with crotonaldehyde which is 'indicative of a strong interaction of the formyl hydrogen and fluoride at the transition state.' See S. R. Merrigan, M. P. Meyer and D. A. Singleton, *Book of Abstracts*, 215th ACS National Meeting, Dallas, March 29–April 2, 1998, ORGN-216. Recent discussion revealed that this work is still ongoing.

5 E. J. Corey and J. J. Rohde, *Tetrahedron Lett.*, 1997, **38**, 37.

6 For other references on this topic, see: (*a*) E. J. Corey, D. Barnes-Seeman and T. W. Lee, *Tetrahedron Lett.*, 1997, **38**, 1699; (*b*) E. J. Corey, D. Barnes-Seeman and T. W. Lee, *Tetrahedron Lett.*, 1997, **38**, 4351; (*c*) E. J. Corey, D. Barnes-Seeman, T. W. Lee and S. N. Goodman, *Tetrahedron Lett.*, 1997, **38**, 6513.

7 Y. Hayashi, J. J. Rohde and E. J. Corey, *J. Am. Chem. Soc.*, 1996, **118**, 5502.

8 (*a*) E. J. Corey, T.-P. Loh, T. D. Roper, M. D. Azimioara and M. C. Noe, *J. Am. Chem. Soc.*, 1992, **114**, 8290; (*b*) E. J. Corey and T.-P. Loh, *J. Am. Chem. Soc.*, 1991, **113**, 8966.

9 (*a*) E. J. Corey, C. L. Cywin and T. D. Roper, *Tetrahedron Lett.*, 1992, **33**, 6907; (*b*) K. Ishihara, S. Kondo and H. Yamamoto, *J. Org. Chem.*, 2000, **65**, 9125.

10 W. R. Roush and L. Banfi, *J. Am. Chem. Soc.*, 1988, **110**, 3979.

11 The stereopair formulas used in this appendix were generated by CSC Chem3D Pro® using standard bond distances and angles.

12 (*a*) K. Furuta, T. Maruyama and H. Yamamoto, *Synlett*, 1991, 439; (*b*) K. Furuta, T. Maruyama and H. Yamamoto, *J. Am. Chem. Soc.*, 1991, **113**, 1041; (*c*) K. Ishihara, T. Maruyama, M. Mouri, Q. Gao, K. Furuta and H. Yamamoto, *Bull. Chem. Soc. Jpn.*, 1993, **66**, 3483; (*d*) K. Furuta, M. Mouri and H. Yamamoto, *Synlett*, 1991, 561; (*e*) J. A. Marshall and M. R. Palovich, *J. Org. Chem.*, 1998, **63**, 4381.

13 (*a*) K. Furuta, S. Shimizu, Y. Miwa and H. Yamamoto, *J. Org. Chem.*, 1989, **54**, 1481; (*b*) K. Furuta, Y. Miwa, K. Iwanaga and H. Yamamoto, *J. Am. Chem. Soc.*, 1988, **110**, 6254; (*c*) Q. Gao, T. Maruyama, M. Mouri and H. Yamamoto, *J. Org. Chem.*, 1992, **57**, 1951.

14 (*a*) G. E. Keck, K. H. Tarbet and L. S. Geraci, *J. Am. Chem. Soc.*, 1993, **115**, 8467; (*b*) G. E. Keck, D. Krishnamurthy and M. C. Grier, *J. Org. Chem.*, 1993, **58**, 6543; (*c*) G. E. Keck and L. S. Geraci, *Tetrahedron Lett.*, 1993, **34**, 7827.

15 (*a*) G. E. Keck and D. Krishnamurthy, *J. Am. Chem. Soc.*, 1995, **117**, 2363; (*b*) G. E. Keck, X.-Y. Li and D. Krishnamurthy, *J. Org. Chem.*, 1995, **60**, 5998.

16 Carbonyl allylation from a Ti complex in which both allyl and aldehyde ligands occupy basal sites can be expected to be relatively unfavorable since the 120° bond angle places the atoms which are required to bond at an improbably large distance (*ca.* 4.5 Å).

17 A product-forming complex analogous to **10** explains the absolute stereochemical course of catalytic reactions analogous to those of Keck

including: (*a*) Tagliavini aldehyde allylation with BINOL–$Zr(OiPr)_4$; P. Bedeschi, S. Casolari, A. L. Costa, E. Tagliavini and A. Umani-Ronchi, *Tetrahedron Lett.*, 1995, **36**, 7897; (*b*) aldehyde allylation with BINOL–TiF_4–CH_3CN according to D. R. Gauthier Jr. and E. M. Carreira, *Angew. Chem., Int. Ed. Engl.*, 1996, **35**, 2363; (*c*) Mikami aldehyde aldol with BINOL–$TiCl_4$; (*d*) K. Mikami and S. Matsukawa, *J. Am. Chem. Soc.*, 1994, **116**, 4077 (Cl replaces monodentate aryloxy).

18 (*a*) E. M. Carreira, R. A. Singer and W. Lee, *J. Am. Chem. Soc.*, 1994, **116**, 8837; (*b*) R. A. Singer and E. M. Carreira, *J. Am. Chem. Soc.*, 1995, **117**, 12 360.

19 K. Ishihara and H. Yamamoto, *J. Am. Chem. Soc.*, 1994, **116**, 1561.

20 K. Ishihara, H. Kurihara and H. Yamamoto, *J. Am. Chem. Soc.*, 1996, **118**, 3049.

21 (*a*) S.-i. Kiyooka, Y. Kaneko and K.-i. Kume, *Tetrahedron Lett.*, 1992, **34**, 4927; (*b*) S.-i. Kiyooka and M. A. Hena, *Tetrahedron: Asymmetry*, 1996, **7**, 2181; (*c*) S.-i. Kiyooka, Y. Kaneko, M. Komura, H. Matsuo and M. Nakano, *J. Org. Chem.*, 1991, **56**, 2276.

22 An analysis similar to that shown for **14** can be used to explain the results of Masamune *et al.* for enantioselective aldol reactions of related oxazaborolidine catalysts. See: (*a*) E. R. Parmee, O. Tempkin, S. Masamune and A. Abiko, *J. Am. Chem. Soc.*, 1991, **113**, 9365; (*b*) E. R. Parmee, Y. Hong, O. Tempkin and S. Masamune, *Tetrahedron Lett.*, 1992, **33**, 1729.

23 (*a*) Y. N. Ito, X. Ariza, A. K. Beck, A. Boháč, C. Ganter, R. E. Gawley, F. N. M. Kühnle, J. Tuleja, Y. M. Wang and D. Seebach, *Helv. Chim. Acta*, 1994, **77**, 2071; (*b*) D. Seebach, A. K. Beck and A. Heckel, *Angew. Chem., Int. Ed.*, 2001, **40**, 93.

24 H. Minamikawa, S. Hayakawa, T. Yamada, N. Iwasawa and K. Narasaka, *Bull. Chem. Soc. Jpn.*, 1988, **61**, 4379.

25 (*a*) A. R. Rossi and R. Hoffmann, *Inorg. Chem.*, 1975, **14**, 365; (*b*) C. Mahadevan, M. Seshasayee and A. S. Kothiwal, *Cryst. Struct. Commun.*, 1982, **11**, 1725.

26 (*a*) M. Hayashi, K. Tanaka and N. Oguni, *Tetrahedron: Asymmetry*, 1995, **36**, 1833; (*b*) M. Hayashi, H. Kaneda and N. Oguni, *Tetrahedron: Asymmetry*, 1995, **6**, 2511; (*c*) M. Hayashi, T. Inoue and N. Oguni, *J. Chem. Soc., Chem. Commun.*, 1994, 341.

27 M. Hayashi, Y. Miyamoto, T. Inoue and N. Oguni, *J. Org. Chem.*, 1993, **58**, 1515.

28 E. J. Corey and J. C. Bailar Jr., *J. Am. Chem. Soc.*, 1959, **81**, 2620.

29 F. Rebiere, O. Riant and H. B. Kagan, *Tetrahedron: Asymmetry*, 1990, **1**, 199.

30 J. Bao, W. D. Wulff and A. L. Rheingold, *J. Am. Chem. Soc.*, 1993, **115**, 3814.

31 For reviews see: (*a*) K. Mikami, *Pure Appl. Chem.*, 1996, **68**, 639; (*b*) K. Mikami, *Advances in Asymmetric Synthesis*, ed. A. Hassner, JAI Press, Greenwich, Connecticut, 1995, vol. 1, pp. 1–44; (*c*) K. Mikami, M. Terada and T. Nakai, *Advances in Catalytic Processes*, ed. M. P. Doyle, JAI Press, Greenwich, Connecticut, 1995, vol. 1, pp. 123–149; (*d*) K. Mikami, M. Terada, S. Narisawa and T. Nakai, *Synlett*, 1992, 255; (*e*) K. Mikami and M. Shimizu, *Chem. Rev.*, 1992, **92**, 1021.

32 The exact structure of the effective Mikami catalyst is unclear. Since the presence of water in the 4 Å molecular sieves seems to increase catalyst effectiveness (with regard to rate and yield, but not necessarily with regard to enantioselectivity), the actual catalytic species could be BINOL–$TiCl_2$, BINOL–TiCl(OH), or BINOL–Ti(μ-O,μ-O)Ti–BINOL. In the following discussion, these catalysts are referred to generically as BINOL–TiX_2. See M. Terada, Y. Matsumoto, Y. Nakamura and K. Mikami, *Chem. Commun.*, 1997, 281.

33 (*a*) K. Mikami, M. Terada, S. Narisawa and T. Nakai, *Org. Synth.*, 1993, **71**, 14; (*b*) K. Mikami, M. Terada and T. Nakai, *J. Am. Chem. Soc.*, 1990, **112**, 3949.

34 K. Mikami, A. Yoshida and Y. Matsumoto, *Tetrahedron Lett.*, 1996, **37**, 8515.

35 K. Mikami, T.-P. Loh and T. Nakai, *Tetrahedron Lett.*, 1988, **29**, 6305.

36 In contrast, a transition-state model in which the scissile allylic C–H proton is transferred to an oxygen of the BINOL ligand leads to the *disfavored* product of eqn. (2) in which the double bond is in the 6,7-position.

37 K. Mikami, S. Narisawa, M. Shimizu and M. Terada, *J. Am. Chem. Soc.*, 1992, **114**, 6566.

38 Standard bond energy calculation: (C–OH = 92) + (O–H = 112) + (C–C = 84) − (RCH=O = 170) − (C–H = 98) = 20 kcal mol^{-1}.

39 (*a*) K. Mikami and S. Matsukawa, *J. Am. Chem. Soc.*, 1993, **115**, 7039; (*b*) K. Mikami and S. Matsukawa, *Tetrahedron Lett.*, 1994, **35**, 3133; (*c*) S. Aoki, K. Mikami, M. Terada and T. Nakai, *Tetrahedron*, 1993, **49**, 1783; (*d*) M. Terada, K. Mikami and T. Nakai, *Tetrahedron Lett.*, 1991, **32**, 935.

CHEMCOMM
Communication
www.rsc.org/chemcomm

Stereoselective formation of a trinuclear hexa-stranded helicate-type zinc(II) complex

Markus Albrecht,*[a] Karen Witt,[a] Herbert Röttele[a] and Roland Fröhlich[b]

[a] *Institut für Organische Chemie der Universität, Richard-Willstätter-Allee, D-76131 Karlsruhe, Germany. E-mail: albrecht@ochhades.chemie.uni-karlsruhe.de*
[b] *Organisch-Chemisches Institut der Universität, Corrensstraße 40, D-48149 Münster, Germany*

Received (in Cambridge, UK) 5th April 2001, Accepted 21st June 2001
First published as an Advance Article on the web 11th July 2001

8-Hydroxyquinoline derivatives HL[1] with urea moieties in the 7-position form hexa-stranded trinuclear coordination compounds with a helicate-type arrangement of the ligands; the chiral ligand HL[2] stereoselectively produces *P*-[$Zn_3(L^2)_6$].

Supramolecular architectures and molecular machines can be formed from simple components by self-assembly, which is controlled by the programming ('molecular recognition') which is encoded in the molecular building-blocks.[1] In this respect the control of stereo- and regio-chemistry during the self-assembly process is essential for the formation of specific, well-defined aggregates.[2]

Helicates are chiral di- or oligo-nuclear coordination compounds which are formed in self-assembly processes. One or more linear oligodonor ligand-strands wrap around the metal centers and thus possess a helical twist (left-handed *vs.* right-handed). Single-, double-, or triple-stranded helicates are obtained depending on the preferred coordination chemistry of the metal ions and on the kind of the ligands.[3] Only a few examples of analogous quadruple-stranded complexes are known.[4]

To our knowledge helicates with more than four ligand strands are not known although some complexes were described in which six ligands wrap around a metaloxo-cluster containing eight metal ions (M = Zn^{2+}, Cd^{2+}, Mn^{2+}) and two bridging μ_3-O^{2-} ligands.[5]

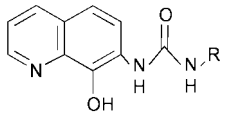

R = *n*-C_8H_{17}: HL^1
R = (*S*)-CH(Me)Ph: HL^2

The urea-substituted 8-hydroxyquinoline derivatives H**L** can be formed by reaction of 7-amino-8-hydroxyquinoline[6] with the *n*-octyl- or (*S*)-1-phenylethylisocyanate. Reaction of H**L** with zinc(II) acetate in methanol leads to zinc complexes which exhibit a metal/ligand ratio of 1:2. ^{1}H NMR spectroscopy (in $CDCl_3$) shows only one distinct set of signals for the coordinated ligand (Fig. 1) which possesses significant differences to those observed for the free ligand. For the zinc complex of $\mathbf{L}^1$ two signals are observed for the methylene unit which is attached to the urea-NH at δ 2.42 and 1.69 indicating diastereotopic behavior and thus a chiral environment. The remarkable high field shift of the protons in the 2- and 3-position of the alkyl chain [δ = 0.05 and 0.33 with $\Delta\delta$(ligand − complex) = 3.04 and 1.07] should be due to a close contact to the aromatic system of the hydroxyquinoline ligand. Indeed cross-peaks of alkyl signals with protons of the hydroxyquinoline can be observed by NOESY or ROESY NMR spectroscopy.

The complex of the chiral ligand $\mathbf{L}^2$ shows similar NMR spectroscopic features (Fig. 1) and a high optical rotation

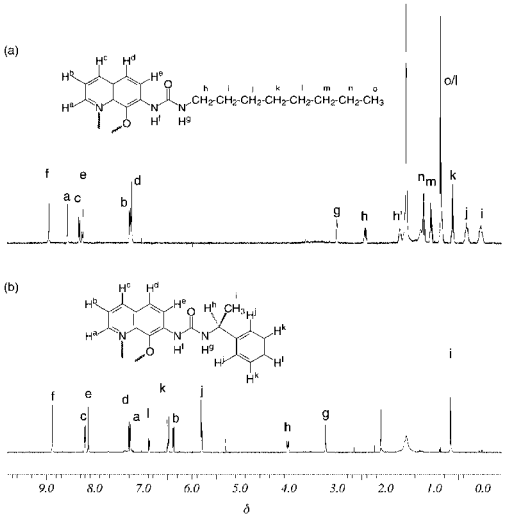

Fig. 1 ^{1}H NMR spectra of [$Zn_3(\mathbf{L}^1)_6$] (a) and *P*-[$Zn_3(\mathbf{L}^2)_6$] (b) in $CDCl_3$.

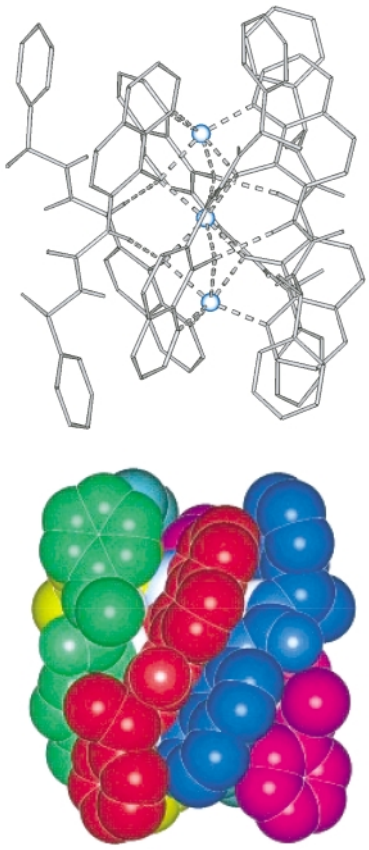

Fig. 2 Representations of the structure of *P*-[$Zn_3(\mathbf{L}^2)_6$] as found in the solid state, showing the helical arrangement of the six ligands around the three metal centers.

 DOI: 10.1039/b103090f

{$[\alpha]_D$ = −1762 (dioxane, c = 0.1); *cf.* **L²**: $[\alpha]_D$ = +27,6 (dioxane, c = 0.5)} which indicates a helical arrangement of the ligands in the complex.[7] The ^{1}H and ^{13}C NMR spectra reveal that this complex is formed in a highly stereoselective fashion; only one stereoisomer is present. The enantiomeric trinuclear zinc(II) complex of the corresponding (*R*)-configurated ligand leads to $[\alpha]_D$ = +1815 (dioxane, c = 0.1).

For the zinc(II) complex of the chiral ligand **L²** we obtained X-ray quality crystals from dioxane and the structural analysis shows that a trinuclear helicate-type complex $[Zn_3(\mathbf{L^2})_6]$ is formed.† Three zinc atoms are arranged linearly with the central atom possessing a separation of 2.884(3) and 2.879(3) Å to the two terminal ones. Six ligands are coordinating in a helical fashion to the metal centers with an alternating 'up' or 'down' orientation of the urea moieties (Figs. 2 and 3). Due to the chiral (*S*)-phenylethyl substituent *P*-helicity is induced at the hexa-stranded helix. This substituent at the urea is located close to the hydroxyquinoline units of a neighboring strand and thus leads to the anisotropic shifts found in the NMR spectra.

The complex $[Zn_3(\mathbf{L^2})_6]$ is made up from two terminal tris(8-hydroxyquinolinato) zinc complex units in which the chelating ligands are orientated *cis* to each other.[8] The three oxygen-donor atoms of each complex unit are located at facial positions and are able to bridge to the central zinc(II) ion (distances: O–$Zn_{terminal}$ 2.137–2.130 Å, O–$Zn_{central}$ 2.055–2.131 Å).[9,10] The trinuclear complex additionally is stabilized by interstrand hydrogen-bonding interactions between the aryl-NH protons and the quinolinato oxygen atoms. Thus, the oxygen-donors possess a tetracoordinated environment, bridging two metal centers and binding to one carbon and one hydrogen atom.

To summarise, we have presented the self-assembly of the first trinuclear hexa-stranded helicate-type complexes $[Zn_3(\mathbf{L})_6]$ from a total of nine components (six ligands and three metals). Alternatively, the compounds can be described as hexahelices made up from two interlocking triple-helical complexes '$[Zn(\mathbf{L})_3]^-$' connected by a zinc(II) ion and six hydrogen bonds. The unusual structure in the solid state is proven by an X-ray structure analysis of the chiral complex *P*-$[Zn_3(\mathbf{L^2})_6]$. NMR spectroscopy indicates that the same structure is present in solution and that the chiral complex *P*-$[Zn_3(\mathbf{L^2})_6]$ is formed highly stereoselective.

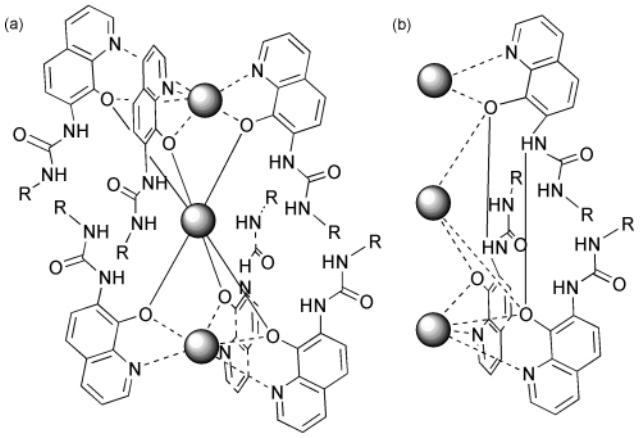

Fig. 3 Schematic representation of the structure of the complexes $[Zn_3(\mathbf{L})_6]$ (a), and the intramolecular interstrand hydrogen bonding (b).

This work was supported by the Deutsche Forschungsgemeinschaft and the Fonds der Chemischen Industrie.

Notes and references

† *Crystal data* for $C_{108}H_{96}N_{18}O_{12}Zn_3 \cdot 3C_4H_8O_2$, M = 384.38, monoclinic, space group $P2_1$ (No. 4), a = 14.729(1), b = 18.049(1), c = 21.493(1) Å, β = 108.50(1)°, V = 5418.5(5) Å^3, D_c = 1.409 g cm^{-3}, μ = 7.37 cm^{-1}, Z = 2, λ = 0.71073 Å, T = 198 K, 13203 reflections collected (±h, ±k, ±l), [(sinθ)/λ] = 0.54 Å^{-1}, 13203 independent and 8392 observed reflections [$I \geq 2\,\sigma(I)$], 1276 refined parameters, R = 0.097, wR^2 = 0.182, Flack parameter 0.07(2). CCDC reference number 157218. See http://www.rsc.org/suppdata/cc/b1/b103090f/ for crystallographic data in CIF or other electronic format.

1 J.-M. Lehn, *Supramolecular Chemistry*, VCH, Weinheim, 1995; D. Philp and J. F. Stoddart, *Angew. Chem.*, 1996, **108**, 1243; D. Philp and J. F. Stoddart, *Angew. Chem., Int. Ed. Engl.*, 1996, **35**, 1154.

2 M. Albrecht, *J. Inclusion Phenom. Macrocycl. Chem.*, 2000, **36**, 127; M. Albrecht, *Chem. Eur. J.*, 2000, **6**, 3485.

3 C. Piguet, G. Bernardinelli and G. Hopfgartner, *Chem. Rev.*, 1997, **97**, 2005; M. Albrecht, *Chem. Soc. Rev.*, 1998, **27**, 281.

4 D. A. McMorran and P. J. Steel, *Angew. Chem.*, 1998, **110**, 3495; D. A. McMorran and P. J. Steel, *Angew. Chem., Int. Ed.*, 1998, **37**, 3295; A. F. Cotton, L. M. Daniels, G. T. Jordan and C. A. Murillo, *J. Am. Chem. Soc.*, 1997, **119**, 10377; P. N. W. Baxter, J.-M. Lehn, G. Baum and D. Fenske, *Chem. Eur. J.*, 2000, **6**, 4510.

5 R. W. Saalfrank, N. Löw, S. Trummer, G. M. Sheldrick, M. Teichert and D. Stalke, *Eur. J. Inorg. Chem.*, 1998, 559.

6 M. Albrecht, K. Witt, E. Wegelius and K. Rissanen, *Tetrahedron*, 2000, **56**, 591.

7 W. Zarges, J. Hall, J.-M. Lehn and C. Bolm, *Helv. Chim. Acta*, 1991, **74**, 1843; E. J. Enemark and T. D. P. Stack, *Angew. Chem.*, 1995, **107**, 1082; E. J. Enemark and T. D. P. Stack, *Angew. Chem., Int. Ed. Engl.*, 1995, **34**, 996; M. Albrecht, *Synlett*, 1996, 565; E. C. Constable, T. Kulke, M. Neuburger and M. Zehnder, *Chem. Commun.*, 1997, 489; O. Mamula, A. Von Zelewsky and G. Bernardinelli, *Angew. Chem.*, 1998, **110**, 302; O. Mamula, A. Von Zelewsky and G. Bernardinelli, *Angew. Chem., Int. Ed.*, 1998, **37**, 290; R. M. Yeh, M. Ziegler, D. W. Johnson, A. J. Terpin and K. N. Raymond, *Inorg. Chem.*, 2001, **40**, 2216.

8 See for comparison: Y. Kai, M. Morita and N. Yasuoka, *Bull. Chem. Soc. Jpn.*, 1985, **58**, 1631.

9 M. Tesmer, B. Müller and H. Vahrenkamp, *Chem. Commun.*, 1997, 721; T. C. Higgs, K. Spartalian, C. J. O'Connor, B. F. Matzanke and C. J. Carrano, *Inorg. Chem.*, 1998, **37**, 2263.

10 For a related heterotrinuclear complex, see: A. K. Das, A. Rueda, L. R. Falvello, S.-M. Peng and S. Bhattacharya, *Inorg. Chem.*, 1999, **38**, 4365.

CHEMCOMM Communication
www.rsc.org/chemcomm

Nanocomposite of CdS particles in polymer rods fabricated by a novel hydrothermal polymerization and simultaneous sulfidation technique

Jing-hui Zeng,[ab] Jian Yang,[a] Yu Zhu,[a] Yuan-fang Liu,[a] Yi-tai Qian*[ab] and Hua-gui Zheng[b]

[a] *Department of Chemistry, USTC, Hefei, Anhui, 230026, P. R. China. E-mail: ytqian@ustc.edu.cn*
[b] *Structural Research Laboratory, USTC, Hefei, Anhui, 230026, P. R. China*

Received (in Cambridge, UK) 17th January 2001, Accepted 12th June 2001
First published as an Advance Article on the web 4th July 2001

A hydrothermal polymerization and simultaneous sulfidation (HPSS) process and the mechanism for the fabrication of one-dimensional (1-D) nanocomposites of well dispersed CdS nanoparticles self-assembled in the polymer nanorods is presented.

Low dimensional, especially 1-D arrays of metal and semiconductor nanoparticles, owing to their potential applications in optical and electronic sensors,[1,2] nanoscale electronics,[2,3] and catalysis,[4] are receiving extensive attention. The synthesis and characterization of such materials, especially of inorganic–polymer nanocomposites has aroused much research interest.[5–7]

Many methods have been applied to prepare semiconductor–polymer nanocomposites with different sizes and/or morphologies. Meissner *et al.*[8] first reported a system involving dispersed semiconductor/polymer arrangements by physically embedding monograin CdS particles of *ca.* 40 μm diameter in a thin, nonconducting polyurethane membrane and various photoprocesses were examined. Marinakos *et al.* synthesized interconnected arrays of Au/polypyrrole colloids of 1-D morphology using Al_2O_3 membranes as the template.[9] However, few reports have appeared regarding the synthesis of coupled 1-D nanoparticle systems. Notable exceptions are 1-D strands of iron oxide particles used for navigation by magnetotactic bacteria,[10] self-organized 1-D CdS chains observed by Chemseddine *et al.*,[11] and dithiol-linked CdSe dimers and DNA-linked Au trimers synthesized by Alivisatos *et al.* [12]

Polymers have advantages over other templates due to the maintenance of the superstructures of the monomers during the polymerization. Thus, a series of inorganic–polymer composites with different sizes and morphologies can be synthesized.[13] Here we report a novel hydrothermal polymerization and simultaneous sulfidation (HPSS) process to fabricate 1-D CdS nanoparticle/poly(vinyl acetate) (PVAc) nanorod composites. This method is based on the mechanism that the polymerization of organic monomers and the formation of the CdS nanoparticles simultaneously take place in aqueous solution. The CdS nanoparticles were well dispersed in the PVAc nanorods to form 1-D composites.

In a typical experiment, 0.005 mol thioacetamide (taa) was added to 50 ml 2×10^{-2} mol l^{-1} $CdCl_2 \cdot 2.5H_2O$ aqueous solution in a Teflon lined autoclave of 60 ml capacity. Then 0.4 ml vinyl acetate (VAc) was added to the above solution. 0.008 g of 2,2′-azobisisobutyronitrile (AIBN) as initiator was then added. The autoclave was maintained at 80 °C for 12 h then allowed to cool to room temperature. The products were filtered off and washed with distilled water and absolute ethanol, dried in a vacuum at 60 °C, and collected for further characterization.

Powder X-ray diffraction (XRD) patterns for the products were collected on a Japan Rigaku D/max-γA diffractometer equipped with graphite-monochromatized high-intensity Cu-Kα radiation (λ = 1.51478 Å) at a scanning rate of 0.02° s^{-1} in the 2θ range 10–70°. IR spectra were measured on a Bruker Vector-22 FT-IR spectrometer from 4000 to 400 cm^{-1} at room temperature. Samples were ground with KBr and pressed into pellets. UV–VIS absorption spectra were recorded on a Shimadzu UV-2100 spectrophotometer scanning from 700 to 300 nm at room temperature with ethanol as the reference. TEM images were taken on a Hitachi H-800 transmission electron microscope, using an accelerating voltage of 200 kV. The samples were dispersed in absolute ethanol ultrasonically, then the suspension was dropped onto copper grids coated with amorphous carbon film.

A representative XRD pattern is shown in Fig. 1. All the diffraction peaks can be indexed to the wurtzite structure CdS with cell constants a_0 = 4.136, c_0 = 6.713 Å. The values are close to those in the JCPDS card (card No. 41-1049). Applying the Scherrer equation, the average crystallite size was estimated to be 10 nm. Although there is no apparent broad peak corresponding to the polymer matrix in the XRD pattern, which may be due to the low content of PVAc in the final product and the low crystallinity of PVAc, the existence of PVAc was fully verified by FT-IR spectroscopy. The presence of PVAc in the 1-D nanocomposite was also detected in TEM micrographs.

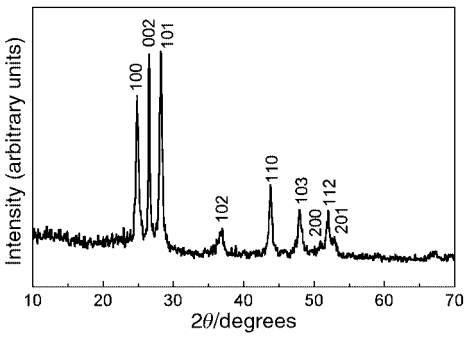

Fig. 1 XRD pattern of a CdS nanoparticle/PVAc nanorod composite fabricated by the HPSS technique at 80 °C for 12 h.

A representative FT-IR spectrum of a sample is illustrated in Fig. 2. The peak at 1739.4 cm^{-1} ($\upsilon_{C=O}$), and characteristic peaks at 1239.9, 1020.9 cm^{-1} (υ_{C-O}), and 1375.7 cm^{-1} (δ_{CH_3}) corresponding to PVAc are clearly seen. The IR spectrum is similar to the standard IR spectrum curve of PVAc (Sprouse collection of IR, card No. 187–189) and distinctly different from that of the VAc monomer (Standard IR Grating Spectra,

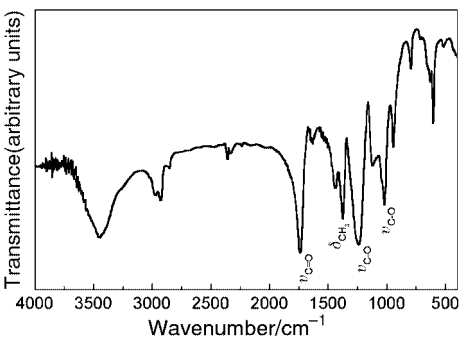

Fig. 2 FT-IR spectrum of the CdS/PVAc composite.

 DOI: 10.1039/b100632k

card No. 8112), which indicates the successful polymerization of VAc and confirms the existence of PVAc in the final product.

Fig. 3 shows a typical TEM micrograph of nanorods in the CdS/PVAc composite. The image shows that the nanorods are *ca.* 75 nm in width and several hundred nm in length. The average crystalline size for the CdS particles in the polymer nanorods is *ca.* 13 nm, well consistent with that calculated by the Scherrer equation from half-widths of the diffraction peaks. Because polymers show low contrast in TEM micrographs, light areas in the spaces among the CdS nanoparticles suggest the existence of PVAc in the composite.

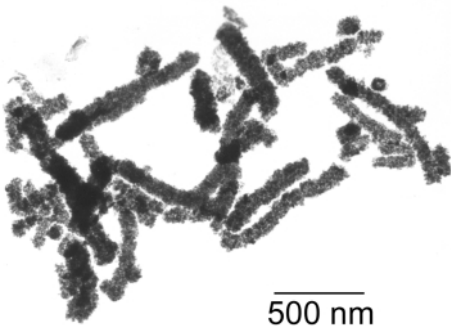

Fig. 3 TEM micrograph of the CdS/PVAc nanocomposite.

According to a typical UV–VIS spectrum, the wavelength of the maximum absorption peak, λ_{max}, for the CdS nanoparticles in the CdS/PVAc nanorod composite is at *ca.* 478 nm, which is blue shifted relative to that for bulk CdS, 515 nm.[14] This can be explained as due to a size confined effect as a result of the tiny dimensions of the nanoparticles in the CdS/PVAc composite.

It is well known that the radical initiator AIBN decomposes at 45–65 °C, according to eqn. (1).

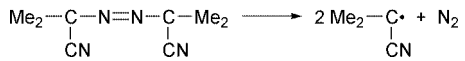

(1)

The produced radicals initiate the polymerization of VAc. Accompanying the polymerization, CdS nanoparticles are also simultaneously formed by the hydrolysis of taa as described in eqns. (2) and (3).

(2)

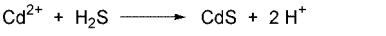

(3)

The formation of VAc emulsions, the subsequent maintenance of the superstructure by polymerization, the simultaneous sulfidation of Cd^{2+}, and the sticking of polymer spheres explain the self-assembly of the 1-D CdS nanoparticles/PVAc nanorod composites. In 1962, a spherical morphology of PVAc was reported by Napper, *et al.* when the monomer, VAc, was polymerized thermally.[15] Computer simulations of the development of rodlike semiconductor–polymer hybrids from hybrid spheres was reported by Stoll and Buffle.[16] In the present HPSS process, VAc emulsions are formed in aqueous solution.[17] At the same time, Cd^{2+} cations originally coordinated to carboxyl groups in the monomer react with released S^{2-} to form CdS clusters. With increasing reaction time, VAc emulsions are polymerized into PVAc spheres. Owing to their glutinosity the PVAc spheres stick together to form polymer nanorods. The increasing viscosity of these polymer nanorods inhibit growth of the CdS nanoparticles. This mechanism is further suggested by the fact that spherical CdS/PVAc nanocomposites are observed in samples reacted for only short reaction times.

In summary, a hydrothermal polymerization and simultaneous sulfidation (HPSS) process to prepare CdS nanoparticle/poly(vinyl acetate) nanorod composites has been presented. CdS nanoparticles of *ca.* 10 nm were self-assembled and well dispersed in the nanorods of PVAc to form 1-D nanocomposites. The experiments indicated that the 1-D morphology was favored by agglomeration of several PVAc spheres. The polymerization of VAc turns the VAc emulsions into polymer spheres and prevented further growth of CdS nanoparticles. The present HPSS technique may provide a new route to prepare other 1-D metal sulfide semiconductor–polymer hybrid nanocomposites.

This work was supported by the Nation Science Foundation of China. Kun-song Chen, Xian-ming Liu, and Wan-qun Zhang are gratefully thanked for their help on the IR, TEM and XRD measurements.

Notes and references

1 C. A. Mirkin, R. L. Letsinger, R. C. Mucic and J. J. Storhoff, *Nature*, 1996, **382**, 607.
2 D. L. Feldheim and C. D. Keating, *Chem. Soc. Rev.*, 1998, **27**, 1.
3 K. Mullen, E. Ben-Jacob, R. C. Jaklevic and Z. Schuss, *Phys. Rev. B*, 1988, **37**, 98.
4 H. Feilchenfeld, G. Chumanov and T. M. Cotton, *J. Phys. Chem.*, 1996, **100**, 4937.
5 E. Shouji and D. A. Buttry, *Langmuir*, 1999, **15**, 669.
6 J. D. Holmes, P. A. Bhargava, B. A. Korgel and K. P. Johnston, *Langmuir*, 1999, **15**, 6613.
7 M. P. Pileni, *Catal. Today*, 2000, **58**, 151.
8 D. Meissner, R. Memming and B. Kastening, *Chem. Phys. Lett.*, 1983, **96**, 34.
9 S. M. Marinakos, L. C. Brousseau III, A. Jones and D. L Feldheim, *Chem. Mater.*, 1998, **10**, 1214.
10 S. Mann, *J. Chem. Soc., Delton Trans.*, 1993, 1.
11 A. Chemseddine, H. Jungblut and S. Boulmaaz, *J. Phys. Chem.*, 1998, **100**, 12 546.
12 A. P. Alivisatos, K. P. Johnsson, X. Peng, T. E. Wilson, C. J. Loweth, M. P. Bruchez and P. G. Schultz, Jr., *Nature*, 1996, **382**, 609.
13 Y. Xie, Z. P. Qiao, M. Chen, X. M. Liu and Y. T. Qian, *Adv. Mater.*, 1999, **11**, 1512.
14 Y. M. Gao, P. Wu, J. Baglio, K. M. Dwight and A. Wold, *Mater. Res. Bull.*, 1989, **24**, 1215.
15 D. H. Napper and A. G. Parts, *J. Polym. Sci.*, 1962, **61**, 113.
16 S. Stoll and J. Buffle, *J. Colloid Interface Sci.*, 1996, **180**, 548.
17 G. Odian, *Priciples of Polymerization*, John Wiley & Sons, New York, 2nd edn., 1981.

CHEMCOMM
Communication
www.rsc.org/chemcomm

Strong evidence for stereoselective 1,3-additions of transient nitrilium phosphane-ylide complexes: synthesis of the first 1-aza-3-phosphabuta-1,3-diene complexes†

Rainer Streubel,* Udo Schiemann, Nils Hoffmann and Peter G. Jones

Institut für Anorganische und Analytische Chemie der Technischen Universität Braunschweig, Postfach 3329, D-38023, Braunschweig, Germany, E-mail: r.streubel@tu-bs.de

Received (in Cambridge, UK) 8th March 2001, Accepted 6th June 2001
First published as an Advance Article on the web 4th July 2001

Synthesis of the first 1-aza-3-phosphabuta-1,3-diene complexes was achieved by heating solutions of 2*H*-azaphosphirene tungsten complexes, 1-piperidinonitrile and [bis(trimethylsilyl)methylene]chlorophosphane; X-ray structure analysis of one new complex revealed a *cisoid* position of the chlorine atom and the phosphaalkene unit at the C,N,P-core of the trapped nitrilium phosphane-ylide complex and a distorted heterobutadiene π-system.

[3+2] cycloaddition reactions of *P*-chlorophosphaalkenes[1] **I** with nitrilium betaines **II** such as nitrile ylides[2] and sulfides[3] are very useful in phosphorus heterocycle synthesis, especially if an elimination of chlorotrimethylsilane occurs subsequently (**III** → **IV**), thus yielding aromatic heterocycles **IV** (Scheme 1). Recently, we reported trapping reactions of nitrilium phosphane-ylide complexes with alkynes,[4] nitriles[5] and phosphaalkynes[6] giving five-membered phosphorus heterocycle complexes. If phenylacetylene was used as trapping reagent and solvent we obtained a product mixture that consisted of a 1*H*-phosphirene and a 2*H*-1,2-azaphosphole complex and two acyclic compounds, which, at least formally, resulted from two differently orientated 1,3-addition reactions of the C–H bond of phenylacetylene to the 1,3-dipole system of a transient nitrilium phosphane-ylide complex.[7] Because of this complicated situation, we were not sure about the mechanism and/or the concertedness of these 1,3-addition reactions.

Here we report the synthesis of the first 1-aza-3-phosphabuta-1,3-diene complexes using our thermal three-component methodology: 2*H*-azaphosphirene complexes, 1-piperidinonitrile and a *P*-chlorophosphaalkene. The products were obtained in pure form by column chromatography and fully characterized by various means; one complex was characterized additionally by an X-ray diffraction study.

Heating toluene solutions of the 2*H*-azaphosphirene tungsten complexes **1a**[8] and **1b**[9] with 1-piperidinonitrile and [bis-(trimethylsilyl)methylene]chlorophosphane[10] (**3**) for 2 h afforded selectively the 1-aza-3-phosphabuta-1,3-diene complexes **5a,b** as trapping products of the transiently formed nitrilium phosphane-ylide complexes **2a,b** (Scheme 2). Complexes **5a**,**b** were confirmed by elemental analyses, NMR spectroscopy and mass spectrometry.‡ Only traces (< 5%) of other phosphorus-containing products were observed by ^{31}P NMR spectroscopy displaying resonances at δ 106.2 and 337.4 (reaction of **1a**) and at δ 104.1 and 349.9 (reaction of **1b**); complexes **4a**,**b** could not be detected. It is remarkable that the attack at the P–Cl σ-bond is preferred to that at the π-system of the *P*-chlorophosphaalkene, which might be caused by strong steric repulsion between the substituents of the carbon centre of the P=C unit and those of the phosphorus centre of the 1,3-dipole in the transition state of the cycloaddition reaction; if this interpretation of the reaction course is correct this example would be unprecedented in nitrilium betaine chemistry.

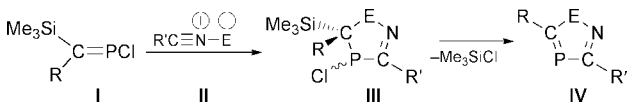

Scheme 1 Phosphaalkenes **I**, nitrilium betaines **II** and phosphorus heterocycles **III**, **IV** (**I–IV**: R, R′ = organic substituents; E = CR_2 or S).

† This work is dedicated to Professor Henning Hopf on the occasion of his 60th birthday.

The ^{31}P NMR spectra of complexes **5a**,**b** showed resonances at low field (**5a**: δ 339.5, $|^3J(PP)|$ 15.5 Hz; **5b**: δ 342.3, $|^3J(PP)|$ 8.0 Hz), which can be assigned to the phosphaalkene nuclei, and those at higher field (**5a**: δ 111.8, $|^3J(PP)|$ 15.5, $|^1J(PW)|$ 284.7 Hz; **5b**: δ 112.9, $|^3J(PP)|$ 8.0 Hz, $|^1J(PW)|$ 305.1 Hz) to the *N*-bonded phosphorus nuclei. With respect to the resonances of the low-coordinated phosphorus centres, the ^{31}P NMR data of **5a**,**b** are quite different from those found for non-coordinated 1-aza-3-phosphabuta-1,3-dienes, which have been synthesized using trimethylsilyl shift reactions, and which show resonances in the range δ 0–100.[11,12] These differences are probably associated with the different substituents at the P=C carbon atoms, which, in our case, represent acceptor groups and in the other cases donor groups. The structure of the complexes **5a**,**b** were unambiguously confirmed by the ^{13}C{^{1}H} NMR spectra, which displayed resonances of the C=N and C=P carbon atoms with two phosphorus–carbon couplings each, whereby the greater magnitude values establish the direct bonding of one phosphorus centre to two different sp^2-carbon centres. The molecular structure of complex **5a** (Fig. 1), as established for the solid state by X-ray crystallography,§ shows a significantly distorted heterobutadiene π-system [N(1)–C(6)–P(2)–C(7) −106.6°] with bond lengths typical of localized double bond systems

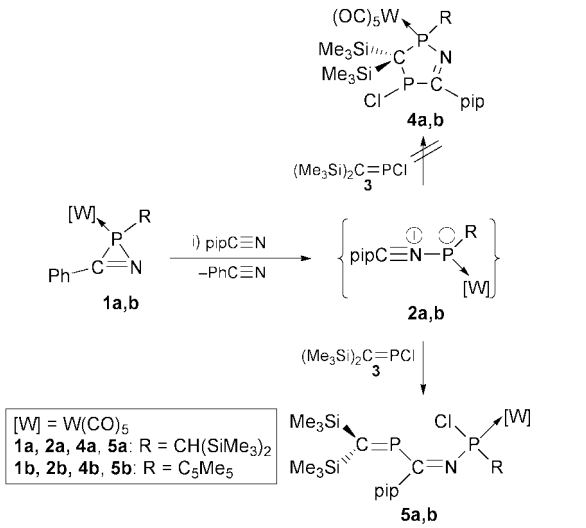

Scheme 2 *Reagents and conditions*: 615 mg of complex **1a** or 534 mg of complex **1b**, 100 μL 1-piperidinonitrile, 449 mg phosphaalkene **2**, 2.5 mL toluene, 75 °C, 2 h; column chromatograpy (Al_2O_3, −20 °C, *n*-hexane); **5a**: yellow solid, yield: 44%, mp 128 °C (decomp.); **5b**: yellow solid, yield: 34%, mp 118 °C (decomp.).

 DOI: 10.1039/b102250b

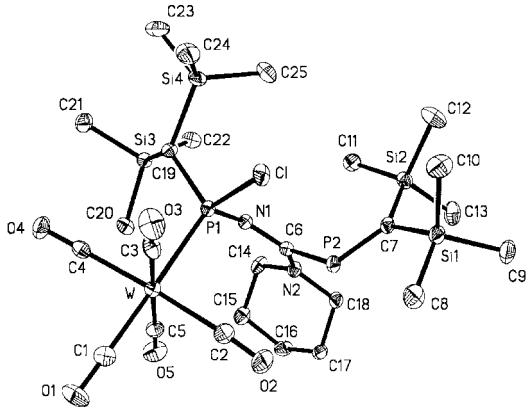

Fig. 1 Molecular structure of **5a** in the crystal (ellipsoids represent 30% probability levels; hydrogen atoms are omitted for clarity). Selected bond lengths (Å) and angles (°): W–C(1) 1.999(6), W–P(1) 2.5332(13), P(1)–N(1) 1.626(4), P(1)–C(19) 1.820(4), N(1)–C(6) 1.303(5), P(2)–C(6) 1.880(5), N(2)–C(6) 1.333(6), P(2)–C(7) 1.669(5); C(1)–W–P(1) 178.43(15), W–P(1)–C(19) 116.35(16), P(1)–N(1)–C(6) 134.4(3), N(1)–C(6)–P(2) 119.2(3), C(6)–P(2)–C(7) 110.7(2).

[N1–C6 1.303(5) and P2–C7 1.669(5) Å]. The P(2)–C(6) distance 1.880(5) Å represents a P–C single bond (average value: 1.885).[13] The coordination environment of the P1 atom is tetrahedral with a P1–Cl distance of 2.143(1) Å and a P1–W distance of 2.5323(16) Å. Furthermore, the structure confirmed the *cisoid* position of the chlorine atom and the phosphaalkene unit at the C,N,P-core of the trapped nitrilium phosphane-ylide complex and thereby strengthened the assumption of a concerted 1,3-addition process that is responsible for the product formation.

Currently we are investigating the role of sterically less bulky P-substituents of transient nitrilium phosphane-ylide complexes (*cf.* ref. 4*c*), in three-component reactions on the reaction course.

We are grateful to the Deutsche Forschungsgemeinschaft and the Fonds der Chemischen Industrie for financial support.

Notes and references

‡ Satisfactory elemental analysis were obtained for complexes **5a**,**b**. NMR data were recorded in $CDCl_3$ solutions (295 K) at 50.3 MHz (^{13}C) and 81.0 MHz (^{31}P), using TMS and 85% H_3PO_4 as standard references; *J*/Hz. *Selected spectroscopic data* for **5a**,**b**: **5a**: $^{13}C\{^1H\}$ NMR: δ 1.2 [d, ^3J(PC) 2.6, CSi(*C*H$_3$)$_3$], 1.5 [d, ^3J(PC) 13.0, CSi(*C*H$_3$)$_3$], 3.4 [d, ^3J(PC) 2.7, CHSi(*C*H$_3$)$_3$], 4.1 [d, ^3J(PC) 2.6, CHSi(*C*H$_3$)$_3$], 24.4 (s, NCH$_2$CH$_2$*C*H$_2$), 25.2 (s, NCH$_2$*C*H$_2$CH$_2$), 26.0 (s, NCH$_2$*C*H$_2$CH$_2$), 40.8 [d, ^3J(PC) 8.5, *C*H(SiCH$_3$)$_2$], 45.9 (s, N*C*H$_2$CH$_2$CH$_2$), 50.6 [d, ^3J(PC) 4.5, N*C*H$_2$CH$_2$CH$_2$], 175.9 [dd, ^1J(PC) 101.1, ^2J(PC) 7.1, C=N], 199.0 [d, ^2J(PC) 8.2, ^5J(PC) 2.9, ^1J(WC) 127.0, *cis*-CO], 200.3 [d, ^1J(PC) 85.9, C=P], 201.1 [d, ^2J(PC) 33.0, *trans*-CO]. MS (pos.-CI; NH_3, ^{184}W) *m/z* (%): 851 (2) [M+H]$^+$. **5b**: $^{13}C\{^1H\}$ NMR: δ 1.0–2.3 [m, br, CSi(*C*H$_3$)$_3$], 11.9–14.1 [C$_5$(*C*H$_3$)$_4$], 22.7 [d, ^3J(PC) 36.4, C$_5$(*C*H$_3$)], 24.6 (s, NCH$_2$CH$_2$*C*H$_2$), 25.0 (s, NCH$_2$*C*H$_2$CH$_2$), 25.8 (s, NCH$_2$*C*H$_2$CH$_2$), 46.3 [d, ^3J(PC) 1.9, N*C*H$_2$CH$_2$CH$_2$], 50.4 [d, ^3J(PC) 4.8, N*C*H$_2$CH$_2$CH$_2$], 67.8 [d, ^1J(PC) 16.2, C$_5$(CH$_3$)$_5$-*C*1], 136.9 [d, ^2J(PC) 5.2, C$_5$(CH$_3$)$_5$-*C*2/5], 137.3 [d, ^2J(PC) 8.2, C$_5$(CH$_3$)$_5$-*C*2/5], 141.9 [d, ^3J(PC) 6.4, C$_5$(CH$_3$)$_5$-*C*3/4], 142.2 [d, ^3J(PC) 5.8, C$_5$(CH$_3$)$_5$-*C*3/4], 174.7 [dd, ^1J(PC) 101.4, ^2J(PC) 8.0, *C*=N], 197.0 [dd, ^2J(PC) 8.4, ^5J(PC) 2.4, ^1J(WC) 126.9, *cis*-CO], 199.5 [d, ^2J(PC) 34.7, *trans*-CO], 199.9 [d, ^1J(PC) 84.9, C=P]. MS (pos.-CI; NH_3, ^{184}W) *m/z* (%): 825 (4) [M+H]$^+$.

§ *Crystal structure determination* of **5a**: *Crystal data*: $C_{25}H_{46}ClN_2O_5P_2Si_4W$; monoclinic, space group $P2_1/c$, a = 10.854(2), b = 11.864(2), c = 29.372(4) Å, β = 94.16(2)°, U = 3772.3 Å^3, Z = 4, μ = 3.4 mm^{-1}, T = −130 °C. *Data collection*: a colourless crystal *ca.* 0.4 × 0.3 × 0.3 mm was used to record 9019 intensities on a Stoe STADI-4 diffractometer (Mo-Kα radiation, $2\theta_{max}$ = 50°); 6639 reflections were independent (R_{int} = 0.025). An absorption correction based on ψ-scans was applied, with transmissions 0.72–0.80. *Structure refinement*: the structure was solved by the heavy-atom method and refined anisotropically on F^2 (program SHELXL-97, G. M. Sheldrick, Univ. of Göttingen) to *wR*2 0.072, *R*1 0.033 for 373 parameters and 59 restraints; S = 1.05, max. $\Delta\rho$ 1.2 e Å^{-3}. The hydrogen atoms were included using a riding model or rigid methyl groups.

CCDC 161074. See http://www.rsc.org/suppdata/cc/b1/b102250b/ for crystallographic data in CIF or other electronic format.

1 R. Appel, in *Multiple Bonds and Low Coordination in Phosphorus Chemistry*, ed. M. Regitz and O. J. Scherer, Thieme, Stuttgart, 1990, p. 155.
2 G. Märkl and S. Pflaum, *Tetrahedron Lett.*, 1988, **29**, 785.
3 M. Regitz and P. Binger, *Angew. Chem., Int. Ed. Engl.*, 1988, **27**, 1484.
4 (*a*) R. Streubel, H. Wilkens, A. Ostrowski, C. Neumann, F. Ruthe and P. G. Jones, *Angew. Chem., Int. Ed. Engl.*, 1997, **36**, 1492; (*b*) R. Streubel, U. Schiemann, N. Hoffmann, Y. Schiemann, P. G. Jones and D. Gudat, *Organometallics*, 2000, **19**, 475; (*c*) R. Streubel, U. Schiemann, P. G. Jones, N. H. Tran Huy and F. Mathey, *Angew. Chem., Int. Ed.*, 2000, **39**, 3686.
5 H. Wilkens, F. Ruthe, P. G. Jones and R. Streubel, *Chem. Eur. J.*, 1998, **4**, 1542.
6 G. N. Cloke, P. B. Hitchcock, U. Schiemann, R. Streubel, J. F. Nixon and D. J. Wilson, *Chem. Commun.*, 2000, 1659.
7 H. Wilkens, A. Ostrowski, J. Jeske, F. Ruthe, P. G. Jones and R. Streubel, *Organometallics*, 1999, **18**, 5627.
8 R. Streubel, A. Ostrowski, S. Priemer, U. Rohde, J. Jeske and P. G. Jones, *Eur. J. Inorg. Chem.*, 1998, 257.
9 R. Streubel, U. Rohde, J. Jeske, F. Ruthe and P. G. Jones, *Eur. J. Inorg. Chem.*, 1998, 2005.
10 R. Appel and A. Westerhaus, *Tetrahedron Lett.*, 1981, **22**, 2159.
11 K. Issleib, H. Schmidt and C. Wirkner, *Synth. React. Inorg. Met.-Org. Chem.*, 1981, **11**, 279.
12 L. N. Markovskii, V. D. Romanenko and T. V. Pidvarko, *Zh. Obshch. Khim.*, 1984, **53**, 1672.
13 F. H. Allen, O. Kennard, D. G. Watson, L. Brammer, A. G. Orpen and R. Taylor, *J. Chem. Soc., Perkin Trans. 2*, 1987, S1.

CHEMCOMM
Communication
www.rsc.org/chemcomm

Route towards diselenadiazafulvalenes

Zdenko Časar,[a] Patricia Bénard-Rocherullé,[b] Alenka Majcen-Le Maréchal[c] and Dominique Lorcy*[a]

[a] *Synthèse et Electrosynthèse Organiques, UMR CNRS 6510, Université de Rennes 1 35042, Rennes cedex, France. E-mail: Dominique.Lorcy@univ-rennes1.fr*
[b] *Chimie du solide et inorganique moléculaire, UMR CNRS 6511, Université de Rennes 1 35042, Rennes cedex, France*
[c] *University of Maribor, Smetanova 17 2000, Maribor, Slovenija*

Received (in Cambridge, UK) 23rd February 2001, Accepted 1st June 2001
First published as an Advance Article on the web 27th June 2001

The first diselenadiazafulvalene has been chemically synthesised and electrochemically characterised, it presents similar air sensitiveness to its sulfur analogue and affords a spiroamide derivative upon oxidation as confirmed by its crystal structure.

Among the numerous π-donor molecules described in the literature as precursors of organic materials various heterocyclic derivatives have been studied, mainly conjugated frameworks including sulfur atoms, such as tetrathiafulvalene (TTF).[1] Several modifications of the TTF skeleton have been performed, for example replacement of two sulfur atoms by nitrogen atoms has led to dithiadiazafulvalene (DTDAF) derivatives which have recently attracted attention owing to their high electron donating properties.[2] DTDAFs present the disadvantage of being air-sensitive in the neutral form but they can be trapped *in situ* by organic or inorganic acceptors and form molecular materials.[3] As the physical properties of organic materials are close-knit to molecular assembly, it was thus of interest to replace the sulfur atoms by selenium atoms, in order to increase the interactions between the donor cores. Otherwise diselenadiazafulvalene (DSeDAF) should exhibit properties close to DTDAF. Herein, we report the synthesis and the electrochemical behaviour of the first DSeDAF, namely benzo-DSeDAF, starting from selenazole moieties.

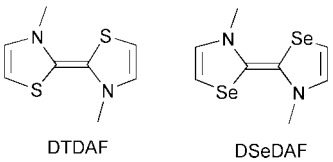

Compared to the chemistry carried out on 1,3-thiazole ring systems, 1,3-selenazole derivatives have been scarcely studied recently. Indeed, and as pointed out by Bogert *et al.*, selenazole derivatives are rather more difficult to prepare and less stable than their sulfur analogues.[4] Our approach for the synthesis of the 1,3-selenazole core consists of the preparation of bis(*o*-nitrophenyldiselenide) **1** starting from *o*-nitroaniline.[5]

We improved the chemical pathway to prepare benzo-1,3-selenazole-2(3*H*)-thione **2** by reaction of bis(*o*-nitrophenyldiselenide) **1** with sodium hydrosulfide in basic medium followed by the addition of carbon disulfide as described in Scheme 1.[6] Alkylation of **2** in the presence of base and methyl iodide led to 2-methylthiobenzo-1,3-selenazole **3**.[7] Preparation of the sulfur analog of **4**, the 3-alkylbenzo-1,3-thiazole-2(3*H*)-thione by rearrangement of 2-alkylthiobenzo-1,3-thiazole in the presence of a catalytic amount of iodine has been described.[8] Thus, we investigated the possibility of forming 3-methylbenzo-1,3-selenazole-2(3*H*)-thione **4** using the same strategy starting from **3**. Heating a mixture of **3** with iodine at 200–220 °C gave **4** in 67% yield (Scheme 1). Selenazole-2(3*H*)-thione **4** does not undergo intermolecular coupling by treatment with tertiary phosphorus derivatives. Therefore, we converted **4**,

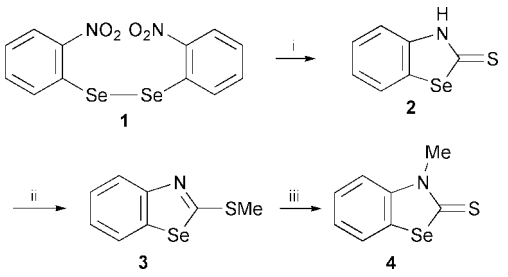

Scheme 1 *Reagents and conditions*: i, NaSH, NaOH, CS_2, H_2O, reflux, 90%; ii, MeI, NEt_3, CH_2Cl_2, rt, 93%; iii, I_2, 200–220°C, 67%.

in the presence of boron trifluoride diethyl etherate and triethyl orthoformate into 2-alkylthiobenzo-1,3-selenazolium salts **5**, following literature precedent for thiazole derivatives.[2] Another method for the preparation of this salt **5** utilises the alkylation of **3** with methyl iodide (Scheme 2).

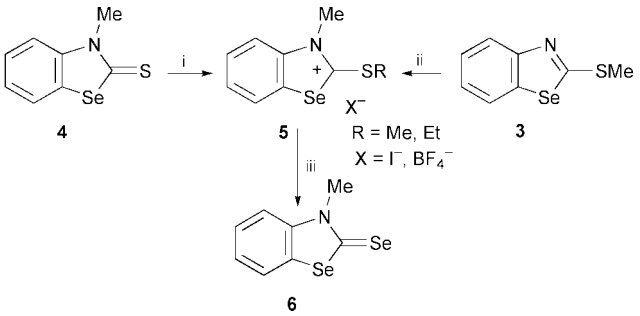

Scheme 2 *Reagents and conditions*: $BF_3{\cdot}Et_2O$, $CH(OEt)_3$, $CHCl_3$, reflux, 97%; ii, MeI, reflux, 81%; iii,NaHSe, EtOH, rt, 95%.

Then, we treated 2-alkylthiobenzo-1,3-selenazolium salts **5** with sodium hydrogen selenide and we isolated the 3-methylbenzo-1,3-selenazole-2(3*H*)-selone **6**.† Coupling of **6** in the presence of triethyl phosphite in refluxing toluene under an inert atmosphere afforded DSeDAF **7**. Formation of this novel π-donor molecule can be observed by the important change of colour of the medium, due to the formation of a conjugated framework (Scheme 3).

Presence of electroactive species can be confirmed by cyclic voltammetry directly on the medium where the donor was formed.[9] Therefore after the chemical coupling of **6** in the presence of triethyl phosphite we added, under inert atmosphere, a degassed solution of tetrabutylammonium hexafluorophosphate in CH_2Cl_2 and we performed electrochemical investigations. Two reversible monoelectronic waves are observed at low potentials on the cyclic voltammogram and are associated with the redox behaviour of the DSeDAF formed in the medium. They correspond respectively to the formation of the radical cation and dication of **7** (E_{pa1} = −0.07 V and E_{pa2} = +0.09 V *vs* SCE) and indicate an extremely good donor character of benzo-DSeDAF. These oxidation potentials are

 DOI: 10.1039/b101757h

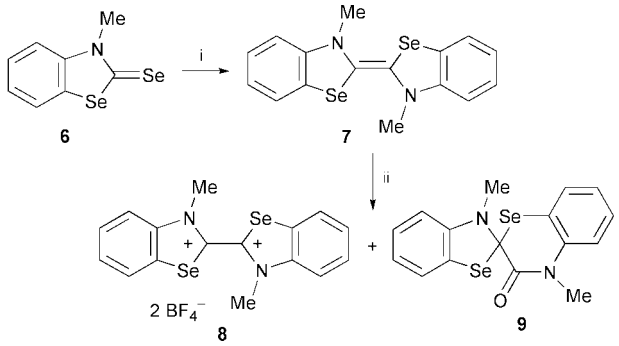

Scheme 3 *Reagents and conditions*: i, $P(OEt)_3$, toluene, reflux; ii, $AgBF_4$, THF, rt.

slightly higher than the one observed for the benzo-DTDAF[10] also obtained *in situ* following the same experimental procedure (E_{pa1} = −0.15 V and E_{pa2} = +0.05 V *vs* SCE). In order to prepare the dicationic salt of benzo-DSeDAF, chemical oxidation was performed by adding a solution of $AgBF_4$ in the medium where **7** was formed. The first dicationic, benzo-DSeDAF **8**, was obtained as its BF_4 salt together with a minor amount of a neutral compound (Scheme 3). ^{1}H NMR data and X-ray crystal structure determination of the latter proved this compound to be the spiroamide **9**.‡ As shown Fig. 1, the 4-methylbenzo-2*H*-1,4-selenazin-3(4*H*)-one ring is folded along the Se2–C4 vector, where the angle between the planes formed by Se2, C3, C7, N2, C4 and Se2, C1, C4 is 122.3 (2)° and N2 lies 0.200(3)Å from the first plane. The benzoselenazole system is not planar owing to a slight fold along the Se1–N1 vector leading to a torsion angle of 155.3(3) ° between the two planes formed by Se1, C2, C6, N1 and Se1, C1, N1, respectively.

The behavior of **7** is closely related to what was observed with its sulfur analogue the benzo-DTDAF. Indeed, in the presence of air benzo-DTDAF is easily oxidised and converted into the spiro amide derivative or further into a ten-membered ring compound.[11–13]

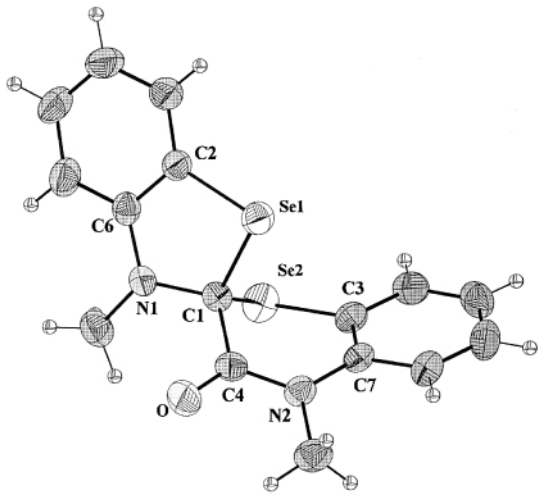

Fig. 1 Molecular structure of spiroamide **9** (50% displacement ellipsoids).

In summary, a novel heterocyclic donor has been synthesised, namely the benzo-DSeDAF, opening a route to a new family of π-donor molecules. This derivative exhibits similar redox behaviour and air-sensitivity to its sulfur analogue. Work is currently in progress in order to trap this derivative with appropriate acceptors and to analyse the potentialities of this new type of donor.

We thank Thierry Roisnel for performing the X-ray diffraction data collection.

Notes and references

† Selected data for **6** (which was prepared in a scale up to 1.2 g): yellow crystals, mp 100 °C; $\delta_H(CDCl_3)$ 3.97 (s, 3H), 7.28–7.69 (m, 4H); Elemental analysis: calcd.for $C_8H_7NSe_2$: C, 34.93; H, 2.57; N, 5.09. Found: C, 35.08; H, 2.55; N, 4.72%; for **8**: colorless powder, $\delta_H(CD_3CN)$ 4.12 (s, 6H), 7.78–8.55 (m, 8H); for **9**: colorless crystals, mp 193 °C; $\delta_H(CDCl_3)$ 3.07 (s, 3H), 3.47 (s, 3H), 6.51–6.63 (m, 1H), 6.70–6.83 (m, 1H), 6.95–7.41 (m, 6H).

‡ Crystal data for compound **9** $C_{16}H_{14}N_2OSe_2$, M = 408.21, monoclinic, space group $P2_1/c$, a = 5.883(5), b = 15.922(5), c = 16.188(5) Å, β = 98.954(5)°, U = 1497.8(14) Å^3, Z = 4, T = 293(2) K, μ(Mo-Kα) = 4.94 mm^{-1}, D_c = 1.810 g cm^{-3}, 19344 reflections measured, of which 4370 independent (R_{int} = 0.0911) R_f = 0.054 [2906 data, $I > 2\sigma(I)$], $wR(F^2)$ = 0.148. The largest residual density peak (1.45 e Å^{-3}) is located close to the Se2 atom (0.94 Å). CCDC 164964. See http://www.rsc.org/suppdata/cc/b1/b101757h/ for electronic files in .cif or other format.

1 G. Schukat and E. Fanghänel, *Sulfur Rep.*, 1996, **18**, 1.
2 G. V. Tormos, M. G. Bakker, P. Wang, M. V. Lakshmikantham, M. P. Cava and R. M. Metzger, *J. Am. Chem. Soc.*, 1995, **117**, 8528.
3 (*a*) N. Bellec, D. Lorcy, A. Robert, R. Carlier, A. Tallec, C. Rimbaud, L. Ouahab, R. Clerac and P. Delhaes, *Adv. Mater.*, 1997, **9**, 1052; (*b*) N. Bellec, D. Lorcy, K. Boubekeur, R. Carlier, A. Tallec, Sz. Los, W. Pukacki, M. Trybula, L. Piekara-Sady and A. Robert, *Chem. Mater.*, 1999, **11**, 3147.
4 (*a*) M. T. Bogert and A. Stull, *J. Am. Chem. Soc.*, 1927, **49**, 2011; (*b*) R. D. Larsen, in *Comprehensive Heterocyclic Chemistry II*, ed. A. R. Katritzky, C. W. Rees, E. F. V. Scriven, Elsevier, Oxford, 1996, vol. 3.08, pp. 493–510.
5 H. Bauer, *Ber.*, 1913, **46**, 92.
6 C. Hasan and R. F. Hunter, *J. Chem. Soc.*, 1935, 1762.
7 S. Hünig and H. Balli, *Liebigs Ann. Chem.*, 1957, **609**, 160.
8 A. F. Halasa and G. E. P. Smith, *J. Org. Chem.*, 1971, **36**, 636.
9 N. Bellec, D. Guérin, D. Lorcy, A. Robert, R. Carlier and A. Tallec, *Acta Chem. Scand.*, 1999, **53**, 861.
10 S. Hünig, H. Schlaf and G. Kießlich, *Tetrahedron Lett.*, 1969, **27**, 2271.
11 (*a*) A. Takamizawa, K. Hirai and Y. Hamashima, *Chem. Pharm. Bull.*, 1969, **17**, 1462; (*b*) K. Akiba, T. Kawamura, M. Ochiumi and N. Inamoto, *Bull. Chem. Soc. Jpn.*, 1976, **49**, 1913.
12 (*a*) H. W. Wanzlick, H. J. Kleiner, I. Lasch, H. U. Füldner and H. Steinmaus, *Liebigs Ann. Chem.*, 1967, **708**, 155; (*b*) J. E. Baldwin and J. A. Walker, *J. Am. Chem. Soc.*, 1974, **96**, 596; (*c*) T. Koizumi, N. Bashir, A. R. Kennedy and J. Murphy, *J. Chem. Soc., Perkin Trans. 1*, 1999, 3637.
13 (*a*) M. Nojima, G. Nagao, N. Kakeya, M. Takagi and N. Tokura, *J. Chem. Soc., Chem. Commun.*, 1976, 486; (*b*) T. Itoh, K. Nagata, M. Okada, K. Yamaguchi and A. Ohsawa, *Tetrahedron Lett.*, 1992, **33**, 6983.

CHEMCOMM Communication
www.rsc.org/chemcomm

Detection of difference in acidity between arrayed carboxy groups and the groups dissolved in solution by reductive desorption of a self-assembled monolayer of carboxy-terminated thiols†

Hirokazu Munakata and Susumu Kuwabata*

Department of Materials Chemistry, Graduate School of Engineering, Osaka University, 2-1 Yamada-oka, Suita, Osaka 565-0871, Japan. E-mail: kuwabata@chem.eng.osaka-u.ac.jp

Received (in Cambridge, UK) 2nd March 2001, Accepted 6th June 2001
First published as an Advance Article on the web 4th July 2001

The pK_a value of arrayed carboxy groups and that of groups dissolved in solution can easily be determined by electrochemical desorption of a self-assembled monolayer of carboxy-terminated thiols in aqueous solutions.

Monolayers composed of closely packed organic species are of great interest as models of biomembranes. In particular, monolayers containing acidic and basic groups are useful for understanding roles of those species in various functions of cell membranes, such as cell fusion, enzymatic catalysis, and ion transfers. One of the well-known specific properties of closely arrayed groups is that acidities of groups like carboxy and amino are different from their original values. Such behaviour has been first found by potentiometric titration of micellar solutions of various surfactants.[1] A self-assembled monolayer (SAM) of alkanethiols adsorbed on a gold surface provides another monolayer system. Ease of preparation of the organized monolayer with high reproducibility and high stability of the resulting monolayer facilitate investigation of the properties of monolayers.[2] If alkanethiols substituted by functional groups at ω-positions are used, one can prepare a surface in which the functional groups are closely arrayed. In this case also, determination of acidity of the arrayed groups is currently attracting great attention. To detect properties of the delicate monolayer surfaces special techniques must be adopted, paying deliberate attention to such matters as measurements of contact angles of water drops on the thiol-SAM,[3] the double layer interaction measurements using the atomic force microscope,[4] double layer capacitance measurements by AC impedance spectroscopy,[5] and quartz crystal microbalance measurements.[6] In some cases, the help of difficult theory and calculations is needed to determine the desired parameters. We would like to show herein that electrochemical desorption reaction of a thiol-SAM measured by conventional voltammetry becomes a useful method to evaluate acidity, *i.e.* pK_a, of the groups substituted to the terminals of alkanethiols. This method allows direct determination of not only pK_a value of the arrayed groups but also that of the groups dissolved in solution simultaneously from the obtained titration curve. In this paper, a typical method is introduced by showing the results obtained for a SAM of 3-mercaptopropionic acid (MPA) formed on a gold substrate.

The gold substrate used in this study was an Au-coated mica having a quasi (111) surface [Au(111)], which was prepared by vacuum evaporation of Au.[7] The mica sheet was heated at 300 °C for at least 2 h prior to evaporation and heating was maintained during deposition and post-annealing for 1 h. Formation of a MPA-SAM on the Au(111) electrode was conducted by immersion of the electrode in an ethanolic solution containing 1 mmol dm^{-3} MPA for 1 h. The resulting electrode is denoted here as MPA/Au(111). Reductive desorption experiments were carried out in 0.1 mol dm^{-3} phosphate buffer solutions prepared by using Milli-Q gradient A10 water (ρ > 18.2 MΩ cm). The electrolysis cell was a one-compartment cell having Ag/AgCl in KCl-saturated aqueous solution and a Pt foil electrode as reference and counter electrodes, respectively. The MPA/Au(111) electrode was placed at the bottom hole of the cell with a Teflon-coated O-ring, giving an effective surface area of 0.4 cm^2.[7]

Fig. 1 shows linear sweep voltammograms of the MPA/Au (111) electrodes taken at 200 mV s^{-1} in buffer solutions having pH 3.57, 5.98, 7.04, 8.04, 8.85, and 9.97. The cathodic waves representing reductive desorption of MPA-SAM appeared and their peak potentials were negatively shifted with increasing pH of the electrolyte solution. In general, the reductive desorption of an alkanethiol-SAM was made by using highly alkaline solutions.[8] In those cases, the reaction can be formulated as Au–S–R + e$^-$ → Au + $^-$S–R where R denotes an alkyl group. However, since pH values of the solutions chosen in this study were smaller than pK_a of thiol group in MPA, which is 11,[9] the group must be protonated when MPA is dissolved in the solutions. As a result, the desorption reaction can be given by eqn. (1).

$$\text{Au–S–R} + e^- + H^+ \rightarrow \text{Au} + \text{HS–R} \quad (1)$$

This equation including one proton and one electron predicts negative shifts of the reaction potential with an increase in pH of the electrolyte solution. The integration of each current peak shown in Fig. 1 gave a charge density of 71 (± 4) × 10^{-6} C cm^{-2}, allowing an estimate of the amount of adsorbed MPA to be 0.74 (± 4) × 10^{-9} mol cm^{-2}. The obtained values were close to the coverage (0.77 × 10^{-9} mol cm^{-2}) expected for a ($\sqrt{3} \times \sqrt{3}$)R30° overlayer structure of alkanethiols on a Au(111) surface.[8]

Plots of cathodic peak potentials as a function of pH of the electrolyte solution gave the relationship shown in Fig. 2. Since the obtained graph has two distinct bending points at pH = 4.3 and 7.5, the pH regions of pH < 4.3, 4.3 < pH < 7.5, and 7.5

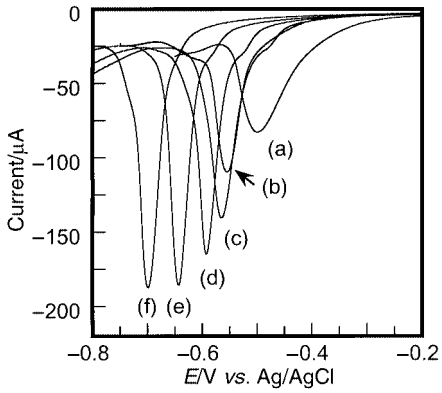

Fig. 1 Linear sweep voltammograms of MPA/Au(111) electrodes taken at 200 mV s^{-1} in 0.1 mol dm^{-3} phosphate buffer having pH of (a) 3.57, (b) 5.98, (c) 7.04, (d) 8.04, (e) 8.85, and (f) 9.97.

† Electronic supplementary information (ESI) available: titration curves from linear sweep voltammograms. See http://www.rsc.org/suppdata/cc/b1/b102601c/

 DOI: 10.1039/b102601c

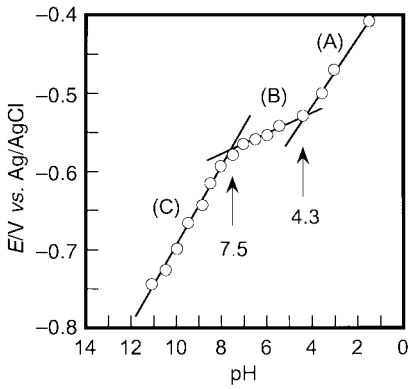

Fig. 2 Plots of peak potentials of cathodic waves due to reductive desorption of MPA as a function of pH of the electrolyte solution.

< pH are denoted here as the regions (A), (B), and (C), respectively. At the regions (A) and (C), linear relations were observed and the same slope of −50 mV per pH unit was estimated. If the eqn. (1) occurs, the experimentally obtained slope was a little smaller than the value (−59 mV per pH unit) expected from the Nernst equation. In the case of the reductive desorption of the thiol-SAM, protons in the electrolyte solution need to penetrate through the closely packed alkyl chains of the thiols in the initial stage. It is then suggested that some time is required for the pH around the sulfate groups to become the same as that of the solution bulk. Such kinetic factors seem to be the cause of differences between the experimentally obtained slope and the theoretical one.

The finding that one of the bending points appeared at pH = 4.3 coincident with the pK_a value of carboxy group of MPA,[9] allowed us to regard R in eqn. (1) as $(CH_2)_2$–COOH and $(CH_2)_2$–COO^- at the regions (A) and (C), respectively. However, a small pH dependence of −10 mV per pH unit was observed at the region (B). As mentioned in the introductory remarks, closely arrayed carboxy groups possess pK_a values that differ from the original. In the case of the MPA-SAM on Au(111) electrode, values ranging from 5.8 to 8 were evaluated by atomic force microscopy,[4] AC impedance,[5] and quartz crystal microbalance measurements.[6] If such a phenomenon is considered, one can imagine that there is a pH region where carboxylic acid groups in MPA-SAM are protonated but deprotonated in the solution. By combining this idea with the reductive desorption reaction given by eqn. (1), the reaction given in eqn. (2) is appropriate at that pH region.

$$Au–S–(CH_2)_2–COOH + e^- \rightarrow Au + HS–(CH_2)_2–COO^- \quad (2)$$

The deprotonation of the carboxy group and protonation of the generated thiolate take place simultaneously, resulting in the exclusion of protons from the reaction. The reaction having lower pH dependence observed at the region (B) is attributable to the reaction given by eqn. (2) and pH = 7.5 where another bending point appeared can be regarded as the pK_a value of the carboxy groups in MPA-SAM. Nevertheless a pH dependence of −10 mV per pH unit was observed at this region, but this might be also due to the kinetic factors mentioned above.

The desorption experiments were made at 10, 50, and 200 mV s^{-1}. The peak potential was positively shifted with a decrease in the sweep rate because of abatement of potential drop in the monolayer, as already shown in our previous paper.[10] Interestingly, however, the titration curves obtained from the voltammograms taken at different sweep rates (see Fig. S1) exhibited bending points at the same pH within experimental errors of ± 0.1, indicating that the above-mentioned kinetic factors did not affect pK_a values estimated by this method. The investigations aiming to elucidate the kinetic factors and applicability of the method developed in this study are underway.

We thank Dr Araki Masuyama for stimulating discussions. This research was supported by CREST of JST (Japan Science and Technology Corporation) and by the Millennium Project (No. 12310) from the Ministry of Education, Culture, Sports, Science and Technology, Japan.

Notes and references

1 F. Van Voorst Vader, *Trans. Faraday Soc.*, 1961, **57**, 2263; F. Van Voorst Vader, *Trans. Faraday Soc.*, 1963, **59**, 1225; F. Tokiwa and K. Ohki, *J. Phys. Chem.*, 1967, **71**, 1824.
2 For review, see A. Ulman, *An Introduction to Ultrathin Organic Films: From Langmuir-Blodgett to Self-Assembly*, Academic Press, Boston, 1991; H. O. Finklea, in *Electroanalytical Chemistry*, ed. A. J. Bard and I. Rubinstein, Marcel Dekker, New York, 1996, vol. 19, p. 109; A. Ulman, *Chem. Rev.*, 1996, **96**, 1533.
3 S. R. Holmes-Farley, R. H. Reamey, T. J. McCarthy, J. Deutch and G. M. Whitesides, *Langmuir*, 1985, **1**, 725; C. D. Bain and G. M. Whitesides, *Langmuir*, 1989, **5**, 1370; T. R. Lee, R. I. Carey, H. A. Biebuyck and G. M. Whitesides, *Langmuir*, 1994, **10**, 741; R. C. Chatelier, C. J. Drummond, D. Y. C. Chan, Z. R. Vasic, T. R. Gengenbach and H. J. Griesser, *Langmuir*, 1995, **11**, 4122.
4 K. Hu and A. J. Bard, *Langmuir*, 1997, **13**, 5114.
5 M. A. Bryant and R. M. Crooks, *Langmuir*, 1993, **9**, 385; K. Aoki and T. Kakiuchi, *J. Electroanal. Chem.*, 1999, **478**, 101; T. Kakiuchi, M. Iida, S. Imabayashi and K. Niki, *Langmuir*, 2000, **16**, 5397.
6 J. Wang, L. M. Frostman and M. D. Ward, *J. Phys. Chem.*, 1992, **96**, 5224; K. Shimazu, T. Teranishi, K. Sugihara and K. Uosaki, *Chem. Lett.*, 1998, 669; K. Sugihara, T. Teranishi, K. Shimazu and K. Uosaki, *Electrochemistry*, 1999, **67**, 1172; K. Sugihara, K. Shimazu and K. Uosaki, *Langmuir*, 2000, **16**, 7101.
7 D. Oyamatsu, M. Nishizawa, S. Kuwabata and H. Yoneyama, *Langmuir*, 1998, **14**, 3298; D. Oyamatsu, S. Kuwabata and H. Yoneyama, *J. Electroanal. Chem.*, 1999, **473**, 59.
8 C. A. Widrig, C. Chung and M. D. Porter, *J. Electroanal. Chem.*, 1991, **310**, 335; M. M. Walczak, D. D. Popenoe, R. S. Deinhammer, B. D. Lamp, C. Chung and M. D. Porter, *Langmuir*, 1991, **7**, 2687; S. Imabayashi, M. Iida, D. Hobara, Z. Q. Feng, K. Niki and T. Kakiuchi, *J. Electroanal. Chem.*, 1997, **428**, 33; S. Imabayashi, N. Gon, T. Sasaki, D. Hobara and T. Kakiuchi, *Langmuir*, 1998, **14**, 2348.
9 W. P. Jencks and J. Regenstein, in *Handbook of Biochemistry and Molecular Biology*, ed. G. D. Fasman, CRC Press, Cleveland, 1976, vol. 3, p. 305.
10 H. Munakata, S. Kuwabata, Y. Ohko and H. Yoneyama, *J. Electroanal. Chem.*, 2001, **496**, 29.

CHEMCOMM
Communication
www.rsc.org/chemcomm

Diastereoselective intramolecular Diels–Alder reactions of masked *o*-benzoquinones: a short entry to highly functionalized tricyclic [*m*.2.2.0] ring systems

Yua-Kuang Chen, Rama Krishna Peddinti and Chun-Chen Liao*

Department of Chemistry, National Tsing Hua University, Hsinchu, Taiwan 300. E-mail: ccliao@mx.nthu.edu.tw; Fax: +886-3-5728123

Received (in Cambridge, UK) 18th April 2001, Accepted 12th June 2001
First published as an Advance Article on the web 4th July 2001

Masked *o*-benzoquinones bearing a chiral center in the carbon-tether with a terminal olefin underwent diastereoselective intramolecular Diels–Alder reactions resulting in highly functionalized tricyclic ring systems.

The intramolecular Diels–Alder (IMDA) reaction is a powerful tool for the rapid construction of highly substituted polycyclic carbon skeletons.[1] Milder reaction conditions and superior reactivity and selectivities are often experienced as a result of the entropy factor in IMDA reactions in comparison to bimolecular Diels–Alder reactions. Recently, we have reported the IMDA reactions of masked *o*-benzoquinones (MOBs)[2] and masked *p*-benzoquinones (MPBs)[3] producing functionalized ring systems. Herein, we report our preliminary results regarding the diastereoselective IMDA reactions of MOBs bearing a chiral centre in the carbon-tether with a terminal olefin leading to highly functionalized tricyclic ring systems.

Masked *o*-benzoquinones,[4] a highly reactive class of 6,6-dialkoxycyclohexa-2,4-dienones, can be easily generated *in situ* by the oxidation of the corresponding 2-methoxyphenols with hypervalent iodine reagents in MeOH. The *in situ* generated MOBs undergo facile Diels–Alder reactions with a wide variety of dienophiles.[5] When the oxidation was carried out in the presence of an alkenol, MOBs undergo IMDA reactions *via* a tandem oxidative acetalization process.[2] It was envisioned that if MOBs bearing a chiral center in the alkenyl-tether undergo intramolecular cycloaddition, easy access to highly substituted tricyclic ring systems that are precursors for several linear and angular tricyclic skeletons (Scheme 1), could be achieved.

The substrates required for this strategy were prepared from benzaldehydes **1**, **2** and **3**. The Grignard reaction of **1** and **2** with alkenylmagnesium reagents of varying chain length afforded 2-methoxyphenols **4a**–**9a**, having a chiral center in the alkenyl-tether, in 80–92% yield. The oxidation of **4a** in MeOH to the corresponding MOB **4b** *via* the slow addition of diacetoxyiodobenzene (DAIB) at room temperature (Method A) did not give satisfactory results. However, the slow addition of DAIB to a methanolic solution of **4a** (n = 1) at reflux temperature (Method B) afforded IMDA adducts **4c** and **4d** of five-membered ring annulation *via* transiently generated **4b**, in 51 and 6% chemical yield, respectively, resulting from *endo*-addition, in addition to 17% of a mixture of dimers (Scheme 2, Table 1).† Similar results were obtained when the chain length was increased by one carbon (n = 2) (entry 2). However, when the reaction conditions were extended to **6a** (n = 3), only a mixture of dimers of MOB **6b** were obtained. To prevent the dimerization,[6,7] we have examined the reaction of 4-bromophenols **7a** and **8a** with DAIB in MeOH at room temperature, which furnished the single diastereomers **7c** and **8c** resulting from IMDA reaction of MOBs **7b** and **8b** in very good yields (entries 4 and 5). The reaction of bromophenol **9a** (n = 3) proceeded slowly and afforded only 4% of the seven-membered ring annulated cycloadduct **9c** in 12 h.

To ascertain whether the protection of the hydroxy function at the tetrahedral carbon of **4a**–**9a** has influenced the stereochemical outcome of the reaction, we have prepared their *tert*-butyldimethylsilyl derivatives **10a**–**15a** and evaluated the IMDA reaction of MOBs **10b**–**15b** (Scheme 2). Gratifyingly, the 2-methoxyphenols **10a**, **11a** and **13a**–**15a** furnished a single diastereomer in each case with an improved chemical yield. The reaction of phenol **12a** at either room temperature or reflux temperature failed to produce the cycloadduct. These results are summarized in Table 1.

Given the success in the IMDA reactions of *in situ* generated MOBs, it seemed to us that a related process could be used for the more stable MOBs to synthesize the tricyclic ring skeletons. To test this proposition, phenols **16a**–**18a** were synthesized from **3**. From our previous work, it was found that MOBs bearing substituents at C-5 are quite stable and could be isolated.[7] Likewise, **16a**–**18a** were oxidized with DAIB in MeOH to the MOBs **16b**–**18b** in excellent to quantitative yields (Scheme 3). Interestingly, the IMDA reaction of **16b** (n = 1) proceeded in toluene at reflux temperature to furnish the *endo*-diastereomeric adducts **16c**,**d** in 38 and 15%, respectively, in addition to 19% of *exo*-isomer **16e**. Nevertheless, the **17b** reacted intramolecularly in THF at reflux temperature to afford six-membered ring annulated adducts **17c** and **17d** in 93 and 4% yield, respectively, with complete *endo*-selectivity, albeit with longer reaction time. Similarly, **18b** (n = 3) when heated at reflux in mesitylene for 24 h, produced IMDA adducts **18c** and **18d** in rather poor yields. The MOB **19b** formed from TBS protected phenol **19a**, upon reflux in toluene produced quantitatively *endo*-**19c** and *exo*-**19e** in 3:2 ratio. In contrast, a single

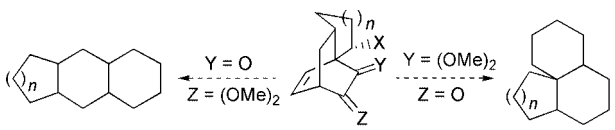

Scheme 1

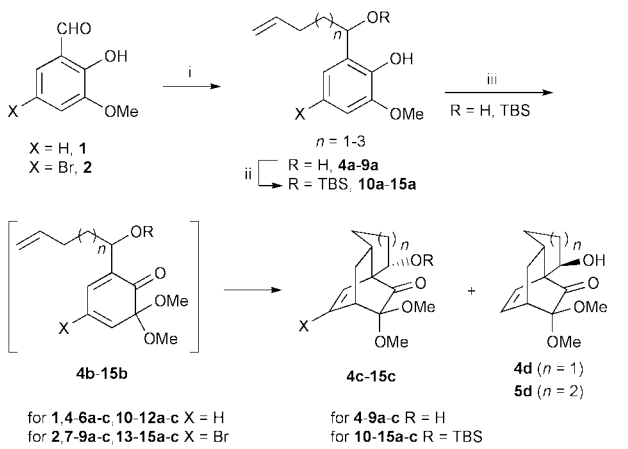

Scheme 2 *Reagents and conditions*: (i) $CH_2CH(CH_2)_{n+1}$ MgBr, THF, rt (80–92%); (ii) TBSOTf, 2,6-lutidine, CH_2Cl_2, −10 °C (89–100%); (iii) DAIB, MeOH (Methods A and B).

 DOI: 10.1039/b103440p

Table 1 IMDA reactions of MOBs **4b**–**21b** generated from phenols **4a**–**21a**

Entry	Phenol	Method/ time[a]	MOB	Time[b]	DA adduct(s) (Yield %)[c]
1	**4a** (X = H, R = H, *n* = 1)	B/2 h	**4b**	0.5 h	**4c** (51), **4d** (6)
2	**5a** (X = H, R = H, *n* = 2)	B/2 h	**5b**	0.5 h	**5c** (46), **5d** (2)
3	**6a** (X = H, R = H, *n* = 3)	B/2 h	**6b**	0.5 h	**6c** —
4	**7a** (X = Br, R = H, *n* = 1)	A/1.5 h	**7b**	3.5 h	**7c** (80)
5	**8a** (X = Br, R = H, *n* = 2)	A/1 h	**8b**	1 h	**8c** (71)
6	**9a** (X = Br, R = H, *n* = 3)	A/2 h	**9b**	12 h	**9c** (4)
7	**10a** (X = H, R = TBS, *n* = 1)	B/1.5 h	**10b**	1 h	**10c** (53)
8	**11a** (X = H, R = TBS, *n* = 2)	B/2 h	**11b**	0.5 h	**11c** (73)
9	**12a** (X = H, R = TBS, *n* = 3)	B/2 h	**12b**	0.5 h	**12c** —
10	**13a** (X = Br, R = TBS, *n* = 1)	A/1 h	**13b**	1.5 h	**13c** (90)
11	**14a** (X = Br, R = TBS, *n* = 2)	A/1 h	**14b**	2 h	**14c** (95)
12	**15a** (X = Br, R = TBS, *n* = 3)	B/2 h	**15b**	1 h	**15c** (15)
13	**16a** (R = H, *n* = 1)	C	**16b**	7.5 h	**16c** (38), **16d** (15), **16e** (19)
14	**17a** (R = H, *n* = 2)	C	**17b**	6 d	**17c** (93), **17d** (4)
15	**18a** (R = H, *n* = 3)	C	**18b**	24 h	**18c** (12), **18d** (3)
16	**19a** (R = TBS, *n* = 1)	C	**19b**	4 h	**19c** (60), **19e** (40)
17	**20a** (R = TBS, *n* = 2)	C	**20b**	20 h	**20c** (98)
18	**21a** (R = TBS, *n* = 3)	C	**21b**	18 h	**21c** (10)

[a] Time during which DAIB was added. DAIB in MeOH was added to the phenol in MeOH at either rt (Method A) or reflux temperature (Method B). In Method C, MOB was isolated and the IMDA reaction was carried out at reflux temperature in a solvent (toluene for entries 13, 16 and 17; THF for entry 14; and mesitylene for entries 15 and 18). [b] The reaction time after the addition of DAIB in entries 1–12. [c] Yields are of pure and isolated adducts.

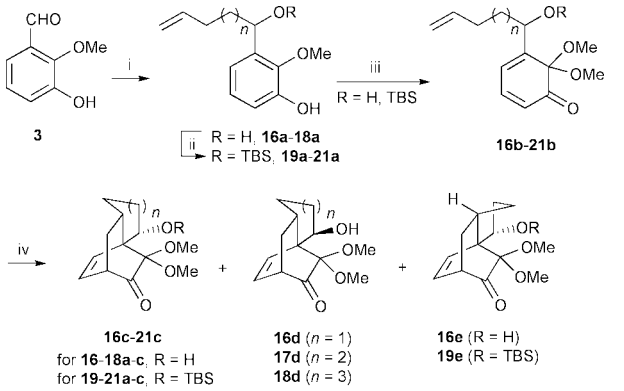

Scheme 3 *Reagents and conditions*: (i) $CH_2CH(CH_2)_{n+1}$ MgBr, THF, rt (71–77%); (ii) TBSOTf, 2,6-lutidine, CH_2Cl_2, −10 °C (89–99%); (iii) DAIB, MeOH, rt; (iv) solvent, reflux (Method C).

endo-diastereomer **20c** was produced in near quantitative yield from MOB **20b** (Scheme 3, Table 1).

The stereoselectivity of the cycloadduct of each successful case is completely analogous to the first example (entry 1), with the major, or sole, diastereomer arising from an approach in which all three rings adopt conformations of *endo*-mode with α-OH or α-OTBS in the transition state. The stereochemistries of **5c′** (3,5-dinitrobenzoate of **5c**), **7c**, **16c** and **16e′** (3,5-dinitrobenzoate of **16e**) were confirmed from their X-ray structures‡ and that of the other adducts were confirmed by chemical correlation and/or by comparing ^{1}H NMR data.

The IMDA reactions of the MOBs with 4-Br substitution proceeded in a highly diastereoselective manner leading to a single *endo*-, α-OR isomer. With one exception (**19b**), all the MOBs having OTBS functionality at the chiral center provided a single diastereomer (*endo*-, α-OTBS). The reduced reactivity of IMDA reactions with increased tether length as reflected in seven-membered ring annulations (*n* = 3) has been previously recorded.[8] However, the yields of these reactions (*n* = 3) were partially improved (**6c**: 28; **9c**: 25; **15c**: 59%) by the pyrolysis of the crude mixture which contains dimers, obtained after oxidation in mesitylene.

In summary, we have demonstrated here that masked *o*-benzoquinones bearing a chiral center in the carbon-tether underwent IMDA reactions to provide densely substituted tricyclic ring systems. Transformation of these adducts to linear and angular tricyclic skeletons, and the asymmetric version of the present protocol are under active investigation.

Financial support from the National Science Council (NSC) of the Republic of China is sincerely acknowledged. We thank Mr G.-H. Lee of NTU and Mrs F.-L. Liao of NTHU for X-ray diffraction studies. R. K. P. thanks NSC for a postdoctoral fellowship.

Notes and references

† All the new compounds were charaterized by IR, ^{1}H (400 MHz), and ^{13}C NMR (100 MHz), DEPT, and low and high resolution MS analyses.

‡ *Crystal data for* ***5c′***: $C_{21}H_{22}N_2O_9$, *M* = 446.41, triclinic, *a* = 6.3649(3), *b* = 9.8499(4), *c* = 17.6830(7) Å, *α* = 82.19, *β* = 85.9730(10), *γ* = 72.0600(10)°, *V* = 1044.45(8) Å^3, *T* = 293(2) K, space group *P*1, *Z* = 2, *μ*(Mo-Kα) = 0.112 mm^{-1}. 10153 reflections collected, independent reflections 4527 (R_{int} = 0.0384), final *R* indices [$I > 2\sigma(I)$] *R*1 = 0.0523, *wR*2 = 0.1102. CCDC 160765. See http://www.rsc.org/suppdata/cc/b1/b103440p/

Crystal data for ***7c***: $C_{13}H_{17}BrO_4$, *M* = 317.18, triclinic, *a* = 7.9569(2), *b* = 12.4857(4), *c* = 14.1058(3) Å, *α* = 82.922(1), *β* = 83.764(1), *γ* = 77.597(1)°, *V* = 1353.35(6) Å^3, *T* = 295(2) K, space group *P*1, *Z* = 4, *μ*(Mo-Kα) = 3.041 mm^{-1}. 13761 reflections collected, independent reflections 5460 (R_{int} = 0.0324), final *R* indices [$I > 2\sigma(I)$] *R*1 = 0.0488, *wR*2 = 0.1096. CCDC 160763.

Crystal data for ***16c***: $C_{13}H_{18}O_4$, *M* = 238.27, monoclinic, *a* = 6.7251(2), *b* = 24.8959(4), *c* = 7.5943(3) Å, *α* = 90, *β* = 109.260(2), *γ* = 90°, *V* = 1200.33(6) Å^3, *T* = 295(2) K, space group *Cc*, *Z* = 4, *μ*(Mo-Kα) = 0.097 mm^{-1}. 3372 reflections collected, independent reflections 2080 (R_{int} = 0.0187), final *R* indices [$I > 2\sigma(I)$] *R*1 = 0.0412, *wR*2 = 0.1070. CCDC 160762.

Crystal data for ***16e′***: $C_{20}H_{20}N_2O_9$, *M* = 432.38, monoclinic, *a* = 20.8010(1), *b* = 12.5757(2), *c* = 15.9854(2) Å, *α* = 90, *β* = 112.123(1), *γ* = 90°, *V* = 3873.72(8) Å^3, *T* = 295(2) K, space group $P2_1/c$, *Z* = 8, *μ*(Mo-Kα) = 0.119 mm^{-1}. 18200 reflections collected, independent reflections 7835 (R_{int} = 0.0254), final *R* indices [$I > 2\sigma(I)$] *R*1 = 0.0502, *wR*2 = 0.1174. CCDC 160764.

1 For recent reviews see: W. R. Roush, in *Comprehensive Organic Synthesis*, Vol. 5, ed. B. M. Trost and I. Fleming, Pergamon, New York, 1991, pp. 513–550; D. Craig, in *Stereoselective Synthesis*, ed. G. Helmchen, R. W. Hoffmann, J. Mulzer and E. Schaumann, Thieme, Stuttgardt, 1996, Vol. E21c, pp. 2872–2904.
2 P.-Y. Hsiu and C.-C. Liao, *Chem. Commun.*, 1997, 1085; C.-S. Chu, T.-H. Lee, P. D. Rao, L.-D. Song and C.-C. Liao, *J. Org. Chem.*, 1999, **64**, 4111.
3 Y.-F. Tsai, R. K. Peddinti and C.-C. Liao, *Chem. Commun.*, 2000, 475.
4 S. Quideau and L. Pouysegu, *Org. Prep. Proced. Int.*, 1999, **31**, 617.
5 S.-Y. Gao, S. Ko, Y.-L. Lin, R. K. Peddinti and C.-C. Liao, *Tetrahedron*, 2001, **57**, 297 and references therein.
6 C.-H. Lai, Y.-L. Shen and C.-C. Liao, *Synlett*, 1997, 1351.
7 C.-F. Yen, R. K. Peddinti and C.-C. Liao, *Org. Lett.*, 2000, **2**, 2909.
8 For reactions of tethered 1,2,4-triazines see: J.-H. Li and J. K. Snyder, *J. Org. Chem.*, 1993, **58**, 516 and references therein.

CHEMCOMM
Communication
www.rsc.org/chemcomm

Organic template-directed crystallization of the complex fluoride NH_4MnF_3 with perovskite structure

Lehui Lu, Haishui Wang, Hongjie Zhang* and Shiquan Xi*

Laboratory of Rare Earth Chemistry and Physics, Changchun Institute of Applied Chemistry, Chinese Academy of Sciences, Changchun 130022, China. E-mail: xisq@public.cc.jl.cn

Received (in Cambridge, UK) 21st March 2001, Accepted 14th June 2001
First published as an Advance Article on the web 5th July 2001

(100)-oriented NH_4MnF_3 perovskite with different morphologies have been obtained *in situ via* an organic template; experimental results can be rationalized in terms of electrostatic interactions and lattice matching between the organic template and the ions undergoing nucleation.

Recently, complex fluorides with perovskite structure have been extensively studied because of their interesting structures and particular physical properties such as magnetic, piezoelectric characteristics and photoluminescence behavior.[1–4] However, traditional preparation methods, to a great degree, have limited such studies on their properties since many exploitable properties are often related to the structure, size, morphology and orientation of inorganic materials. Such conventional preparation methods often fail to generate consistent results with respect to the control over the structure, size, morphology and orientation. Thus it is important to develop new synthetic strategies. A recent advance in this field involves the use of organic templates (Langmuir or SAM monolayers) for orientation nucleation of inorganic crystals.[5–7] One of the advantages of this method is that the crystal structure, size, morphology and orientation can be readily controlled *via* selection of the template and experimental conditions at room temperature. In this communication, the behenic acid (BA) monolayer template-directed room-temperature crystallization of NH_4MnF_3 is studied.

The experimental procedure was similar to that described elsewhere.[6] Throughout the experiment, the temperature was maintained at room temperature. Briefly, subphases **1** and **2** were prepared by mixing NH_4F (A.R.) and $Mn(NO_3)_2$ (A.R.) solutions. The concentrations of F^- ions in subphases **1** and **2** were 0.71 and 1.065 mol L^{-1} and that of Mn^{2+} ions were 0.355 and 0.533 mol L^{-1}, respectively. The monolayer template was prepared by spreading a measured quality of behenic acid (1 mg mL^{-1} in chloroform) over the surface of the subphase. After the evaporation of chloroform, the monolayer was compressed to the targeted pressure (28 mN m^{-1}) and the crystals formed under the monolayer transferred onto glass or wafer silicon substrates *via* a down stroke for further characterization. The aging time between the spreading and transferring was 55 and 45 min for subphases **1** and **2**, respectively. Crystals grown in the absence of monolayer were collected on a glass substrate placed at the bottom of the trough allowing a collection time of 5 h. The experiment of controlled crystallization under the BA monolayer was performed using a KSV 5000 instrument (Finland). The morphology of crystals formed under the monolayer were examined by scanning electron microscopy (SEM; JXA-840). The crystal faces of the samples were measured by X-ray diffraction (XRD; D/max2000, Rigaku, Cu-Kα). Elemental analysis of the samples was performed by energy dispersive X-ray analysis (EDXA).

In the absence of the monolayer, the majority of crystals were located at the bottom of the trough as a result of sedimentation. The crystals are obviously irregular in shape and the corresponding XRD pattern of crystals showed several groups of diffraction peaks roughly consistent with the reflections of cubic NH_4MnF_3 [Fig. 1A(a)] indicative of poor crystal quality.

In the presence of the monolayer, crystallization exclusively occurred at the monolayer–solution interface. Fig. 1B shows the typical morphology of crystals grown under the BA monolayer template over subphase **1**. As is evident from Fig. 1B, the crystals formed under the BA monolayer exhibit a square morphology and have a rather homogeneous size distribution with an average grain size of 6 μm. The corresponding XRD pattern of the crystals shows two sharp and strong diffraction lines at 2θ 20.90 and 42.56° [Fig. 1A(b)]. These diffraction lines correspond to the (100) and (200) reflections for cubic NH_4MnF_3 with perovskite structure indicating that the crystals are (100)-oriented. The high quality and uniformity of the crystals is evidenced by the sharp and strong (*n*00) reflections. Moreover, by comparison with the XRD pattern of the standard sample, we find that the crystals formed under the monolayer template are pure and no other impurity peaks were present. Interestingly, changing the concentration of the supersaturated solution has a marked effect on the morphology of crystal growns under the BA monolayer. For subphase solution **2**, the crystals grown under the BA monolayer exhibit a needle-like morphology (Fig. 2B) while in the XRD pattern (Fig. 2A), two sharp and strong diffraction lines together with a weak line appear at 2θ 20.90, 42.56 and 66.00°, which are assigned to the (100), (200), and (300) reflections, respectively, of cubic NH_4MnF_3 with perovskite structure.

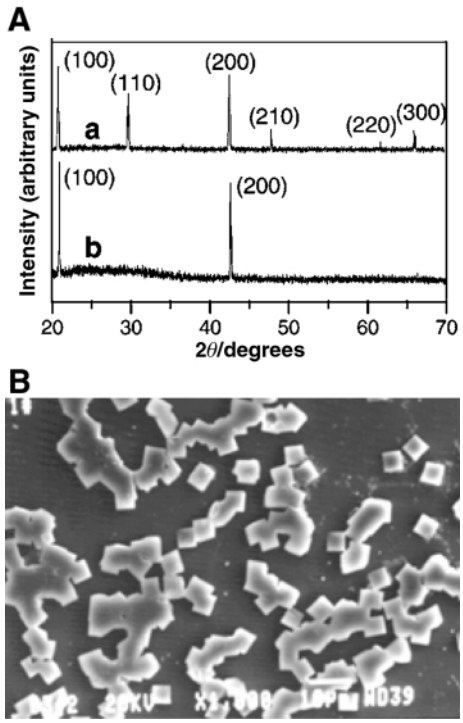

Fig. 1 (A) (a): XRD pattern of NH_4MnF_3 crystals collected at the bottom of the trough. (b): XRD pattern of NH_4MnF_3 crystals grown under the monolayer template from subphase **1**. (B) SEM image of NH_4MnF_3 crystals grown under the monolayer template from subphase **1**.

 DOI: 10.1039/b102642a

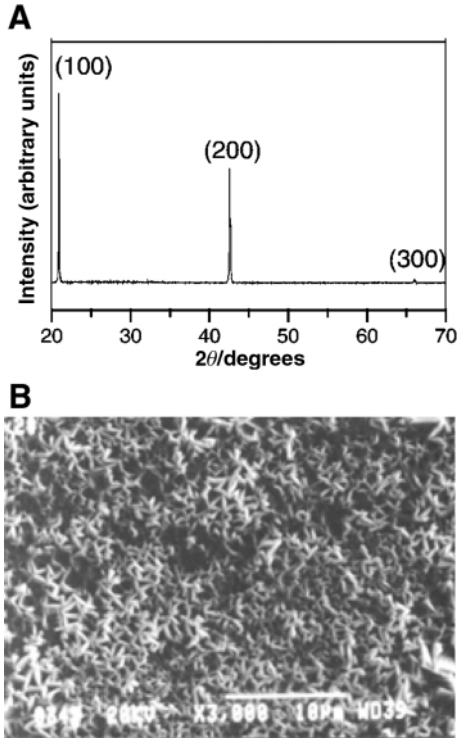

Fig. 2 (A) XRD pattern and (B) SEM image of NH_4MnF_3 crystals grown under the monolayer template from subphase **2**.

In addition, elemental analysis of crystals grown *via* the monolayer template was performed by EDXA. The EDXA patterns showed the presence of N, F, Mn, O and C peaks, which also further confirmed the XRD result. The C and O peaks originate from the BA monolayer indicating that the NH_4MnF_3 crystals are attached to the monolayer.

What aspects of the (100) face of NH_4MnF_3 crystal could be simulated by the interactions between the monolayer template and the crystal? According to an AFM study[8] on the compressed BA monolayer over the solution containing Mn^{2+} ions, the BA monolayer adopts rectangular packing with unit cell dimensions of 0.46 × 0.87 nm. We can compare the structure of the BA monolayer with the two-dimensional packing of Mn atoms in different crystal faces of cubic NH_4MnF_3 by simulation techniques. It is found that the superimposition of a rectangular lattice of the monolayer template on the (100) face of the NH_4MnF_3 crystal provides a good lattice matching. A comparison of the Mn–Mn distance (0.424 nm) along the (010) direction in the (100) crystal face with the monolayer lattice ***a*** (0.46 nm) reveals a misfit of 8%. Moreover, the interatomic Mn–Mn distance (0.424 nm) in the (001) direction of the (100) crystal face is approximately 0.5 times the monolayer lattice ***b*** (0.87 nm) with a misfit of only 2% (Fig. 3). However, such lattice matching does not exist with other crystal faces of NH_4MnF_3. Thus the rectangular packing arrangement of the monolayer generates a template similar to the (100) face of NH_4MnF_3 crystal which directs crystallization of NH_4MnF_3 along the (100) face.

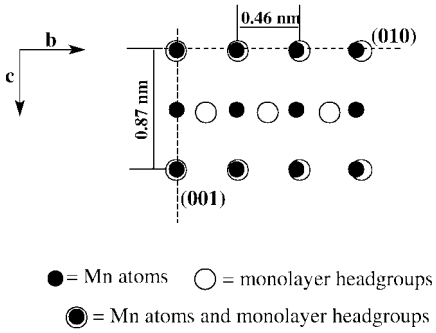

Fig. 3 Schematic two-dimensional representation of the proposed overlap between the monolayer template and Mn atoms in the (100) face of NH_4MnF_3 crystals.

The dependence of crystal morphology on the concentration of supersaturated solution can be explained as follows. A previous study[9] showed that the concentration/ionic strength of the reagents and the extent of nuclei–ion binding influence the structure and the morphology of the crystals grown under the monolayer. In the present study, the variation of the concentration of supersaturated solution results in a change of ionic strength and the extent of nuclei–ion binding, *i.e.* the Stern and boundary layers under the monolayer by electrostatic interactions. As a result, NH_4MnF_3 crystals with different morphologies were obtained under the BA monolayer.

A more detailed mechanism will be investigated further.

In summary, (100)-oriented NH_4MnF_3 perovskite crystals with different morphologies were prepared *via* a monolayer template at room temperature. The solution conditions, the electrostatic interactions and lattice matching between the organic template and ions undergoing nucleation are important factors for control over the morphology, size, and orientation of crystals. Compared with traditional methods, the organic template technique appears advantageous in terms of lower synthesis temperature, high purity, and providing controllable morphology and orientation of crystals.

This work was supported by the National Natural Science Foundation of China.

Notes and references

1 M. A. Laguna, M. L. Sanjuan, V. M. Orera, J. Rubin, E. Palacios, M. C. Pique, J. Bartolome and J. F. Berar, *J Phys: Condens. Matter*., 1993, **5**, 283.
2 C. Zhao, S. Feng, R. Xu, C. Shi and J. Ni, *Chem. Commun.*, 1997, 945.
3 O. Pilla, P. T. C. Freire and V. Lemos, *Phys. Rev. B.*, 1997, **52**, 177.
4 M. Eibschutz, *Phys. Lett. A*, 1969, 409.
5 A. L. Litvin, S. Valiyaveettil, D. L. Kaplan and S. Mann, *Adv. Mater.*, 1997, **9**, 124.
6 L. Lu, H. Cui, W. Li, H. Zhang and S. Xi, *Chem. Mater.*, 2001, **13**, 325.
7 H. Q. Shi, W. B. Tsai and B. D. Ratner, *Nature*, 1999, **96**, 9933.
8 R. Wiswanathan, J. A. Zasadzinski and D. K. Schwartz, *Science*, 1993, **261**, 449.
9 S. Mann, D. D. Archibald, J. M. Didymus, T. Douglas, B. R. Heywood, F. C. Meldrum and N. J. Reeves, *Science*, 1993, **261**, 1286.

CHEMCOMM Communication
www.rsc.org/chemcomm

Oriented growth of thin films of titanium oxyfluoride at the interface of an air/water monolayer

Isamu Moriguchi,* Kouhei Sonoda, Kengo Matsuo, Shuichi Kagawa and Yasutake Teraoka*

Department of Applied Chemistry, Faculty of Engineering, Nagasaki University, 1-14 Bunkyo-machi, Nagasaki 852-8521, Japan. E-mail: yasu@net.nagasaki-u.ac.jp

Received (in Cambridge, UK) 15th February 2001, Accepted 15th June 2001
First published as an Advance Article on the web 5th July 2001

When a monolayer of dioctadecyldimethylammonium bromide is formed on the surface of mixed aqueous solutions of $(NH_4)_2TiF_6$ and H_3BO_3 with a B/Ti molar ratio below 1.5, oriented crystallites of NH_4TiOF_3 are produced and grown at the hydrophilic interface of the monolayer to yield a self-supporting thin film within a few days.

In recent years, soft solution chemistry has attracted a great deal of attention from the viewpoint of low energy-consuming material processing and morphological control of inorganic materials. In this area, crystalline metal oxides have been synthesized in the liquid phase *via* ligand-exchange (hydrolysis) equilibrium reactions of the corresponding metal fluorides at an ambient temperature.[1,2] For example, the overall reaction (1) for TiO_2 synthesis consists of three equilibrium reactions (2)–(4),[3–5] in which H_3BO_3 acts as an F^- scavenger and forces the equilibrium to shift to the product side. By this liquid-phase deposition (LPD) method, TiO_2 crystalline films are successfully prepared on a substrate at room temperature.[2]

$$[TiF_6]^{2-} + 3/2\ H_3BO_3 + 2H^+ \rightleftharpoons TiO_2 + 3/2\ HBF_4 + 5/2\ H_2O \quad (1)$$

$$[TiF_6]^{2-} + n\ H_2O \rightleftharpoons [TiF_{6-n}(OH)_n]^{2-} + n\ HF \quad (2)$$

$$H_3BO_3 + 4\ HF \rightleftharpoons HBF_4 + 3\ H_2O \quad (3)$$

$$[Ti(OH)_6]^{2-} + 2\ H^+ = TiO_2 + 4\ H_2O \quad (4)$$

So far, we have been investigating inorganic synthesis using (multi)layered organic films as reaction fields and templates.[6–10] On the other hand, Langmuir monolayers have been successfully employed to direct the growth of oriented arrays of inorganic salts and metal sulfides.[11–13] These results motivated the present study to combine the LPD reactions and an air/water monolayer as a template. As reported below, self-supporting thin films of NH_4TiOF_3, which acts as a stable intermediate in LPD synthesis of TiO_2, were produced at the interface of the air/water monolayer, and were dominated by (00*l*) oriented crystallites. The conversion of NH_4TiOF_3 into TiO_2 while retaining the orientation was also suggested.

The LPD solution used for the subphase was a mixed aqueous solution of ammonium hexafluorotitanium [$(NH_4)_2TiF_6$, 0.1 mol dm^{-3}] and boric acid (H_3BO_3, 0.1–0.3 mol dm^{-3}). An air/water monolayer of dioctadecyldimethylammonium bromide (DODMABr) was formed at 298 K on the surface of the LPD solution by spreading a 100 μl portion of a toluene–ethanol solution (9:1, v/v) of DODMABr (*ca.* 1 mg cm^{-3}). After evaporating the spreading solvent for 20 min, two-dimensional compression was performed by using a computer-controlled film balance (USI system Co. Ltd., FSD 110). The DODMA monolayer on pure water showed an expanded surface pressure-area (π–*A*) isotherm characteristic of a liquid phase. On the LPD solution, on the other hand, the monolayer exhibited a condensed π–*A* isotherm, suggesting that the cationic DODMA monolayer interacts with inorganic ionic species such as TiF_6^{2-} and borate ions.[14] The monolayer-assisted crystal growth was performed at a constant π value of 20 mN m^{-1}, which is in the middle of solidus region of the π–*A* isotherms. The monolayer of octadecyl alcohol (ODA) was formed in the same manner using a toluene solution of ODA, but the π–*A* isotherms were almost the same on either pure water or the LPD solution, indicating no interaction between the neutral monolayer and the ionic species. The products were characterized by X-ray diffraction (XRD, Rigaku LINT-2200), scanning electron microscopy (SEM; HITACHI Co. Ltd., S-2250N) and transmission electron microscopy (TEM; JEOL, JEM-2010 UHR) equipped with an energy dispersive X-ray spectrometer (EDX, Oxford Link ISIS).

In the $(NH_4)_2TiF_6/H_3BO_3$ LPD solutions, a white precipitate was produced at room temperature within a few days, and the main products were different below and above the stoichiometry of the overall reaction (1) (B/Ti = 1.5). At B/Ti ⩾ 1.5, the main product was anatase-type TiO_2 [Fig. 1(b)], in agreement with a previous report.[2] The main product at 1 ⩽ B/Ti < 1.5 was NH_4TiOF_3 [Fig. 1(a)],[15] with the oxyfluoride convertable into anatase TiO_2 either by treatment with aqueous H_3BO_3 or by air-calcination at 873 K for 1 h [Fig. 1(c)]. These results indicate that NH_4TiOF_3 is a stable intermediate in the LPD synthesis of TiO_2.

On the surface of LPD solution with B/Ti = 1, no product was formed in the absence of the DODMA monolayer, but pale violet-colored transparent films were formed within a few days in the presence of the monolayer. The floating films thus formed were transferred onto quartz substrates by scooping up or by horizontal dipping. SEM observation showed that the thickness of the film after 3 days was *ca.* 0.5 μm [Fig. 2(a)]; thickness at the sub-micron level was also suggested by the interference UV–VIS absorption spectrum. It is seen that the surface of the film at the air or monolayer side was smooth while that of the solution or crystal-growth side was rough and that morphology

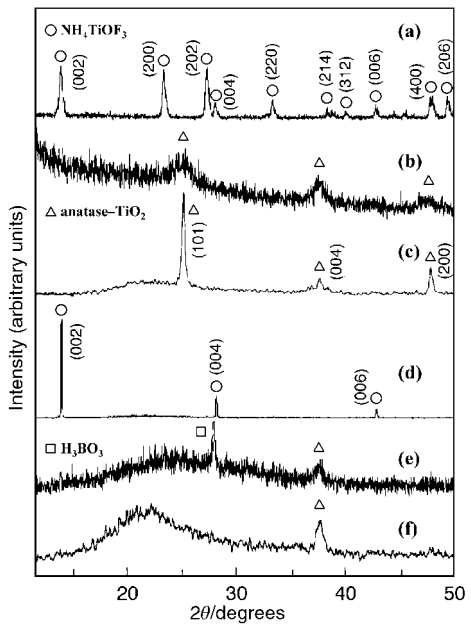

Fig. 1 XRD patterns of (a), (b) precipitates in the LPD solutions, (d), (e) thin films deposited at the surface of the DODMA monolayer after 3 days, and (c), (f) air-calcined precipitates of (a) and (d) at 873 K for 1 h. The solution compositions were B/Ti = 1 [(a), (d)] and B/Ti = 2 [(b), (e)].

 DOI: 10.1039/b101488i

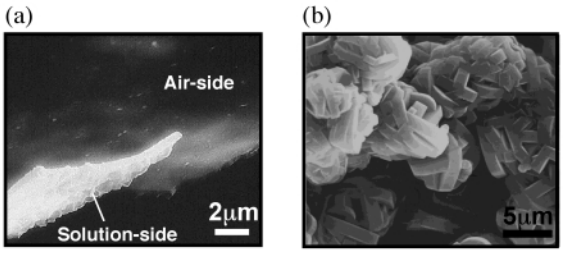

Fig. 2 SEM images of (a) NH_4TiOF_3 film deposited at the surface of DODMA monolayer and (b) NH_4TiOF_3 precipitate in the LPD solution. Solution composition: B/Ti = 1, deposition time: 3 days.

of the film was totally different from that of the precipitate [Fig. 2(b)]. XRD results on the quartz-supported films [Fig. 1(c)] showed that the crystalline product on the surface of solution (B/Ti = 1) was NH_4TiOF_3 *i.e.* the same as the precipitate from the same LPD solution but the NH_4TiOF_3 films was preferentially oriented with the (00*l*) crystal planes parallel to the solution surface.

In the presence of neutral octadecyl alcohol (ODA) monolayer, no crystalline product was observed on the solution surface, consistent with the suggestion from the π–*A* isotherm measurement that the ODA monolayer scarcely interacts with the ionic species. The result implies that electrostatic interaction between the cationic monolayer and inorganic species is indispensable to form stable and oriented NH_4TiOF_3 films. The importance of the electrostatic interaction was also confirmed by monitoring the deposition of NH_4TiOF_3 from the LPD solution (B/Ti = 1, pH = 4.5) with a QCM microbalance (Sogo Pharmaceutical Co., SF-105A). Here, three types of quartz resonators (AT cut, 9 MHz) with different Au electrodes (area: 0.34 cm^2) were used; bare, derivartized with mercaptoethylsulfonate (MES, anionic surface) and 2-amino-1-ethanethiol (AET, cationic at pH = 4.5). The amount of deposition of NH_4TiOF_3 was almost the same on the bare and anionic MES electrodes, while the amount on the cationic AET surface was much larger than those on the other two electrodes at the same immersion time; for example, deposited amounts on AET and bare electrodes were 300 ng and 50 ng after 2 h and 1100 ng and 200 ng after 6 h, respectively.

The initial stage of precipitate and film formation was studied by TEM and EDX. Products in solution and on the surface were mounted on TEM micro-grids covered with a carbon ultrathin film (Oken Shouji Co. Ltd) by dropping the solution and scooping up, respectively. In the LPD solution with B/Ti = 1, discoid crystallites, *ca.* 400 nm diameter by 150 nm thickness, on average, were observed 1 h after the preparation of the solution. The atomic composition of the crystallites measured by EDX was close to that for NH_4TiOF_3 (Ti:O:F = 1:1.2:2.8). With increasing time, the crystallites grew, aggregated and eventually precipitated as irregularly shaped particles [Fig. 2(b)]. On the surface of the LPD solution (B/Ti = 1) with the DODMA monolayer, discoid crystallites of NH_4TiOF_3 with nearly the same size as in the solution were present after 1 h the majority being oriented with the circular plane parallel to the monolayer surface [Fig. 3(a)]: smaller crystallites with diameter below 50 nm were also observed. Electron diffraction [Fig. 3(c)] showed each discoid crystallite was a single crystal with the circular plane corresponding to the (00*l*) or *ab* plane of tetragonal NH_4TiOF_3. The amount and size of the crystallites increased at the monolayer surface with increasing time and a continuous thin film composed of nanoparticulates was eventually produced after 12 h [Fig. 3(b)]. With further time, the thickness of the film increased to, for example, 0.45 μm after 3 days and 0.64 μm after 5 days as estimated from the UV–VIS interference. The results clearly indicate that the oriented deposition of NH_4TiOF_3 discoids is a crucial step in the monolayer-assisted formation of oriented NH_4TiOF_3 films. It is also reasonable to propose that in the initial stage the discoid crystallites deposited at the monolayer surface with the *ab* plane preferentially parallel to the surface and act as seeds for the subsequent crystal growth.

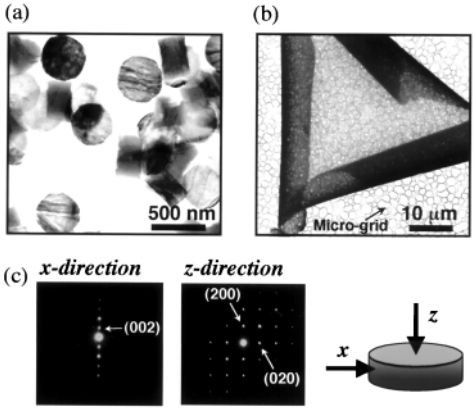

Fig. 3 TEM images of NH_4TiOF_3 crystallites deposited at a DODMA monolayer surface after (a) 1 h and (b) 12 h after the preparation of the monolayer. (c) Electron diffraction patterns of the crystallites of (a). Arrows indicate the direction of electron beam.

Monolayer-assisted LPD synthesis was also investigated for a B-rich LPD solution (B/Ti = 2), from which non-oriented anatase TiO_2 was precipitated [Fig. 1(b)]. The formation of the oriented NH_4TiOF_3 crystallites was observed by TEM electron diffraction measurements in the early stage up to 6 h. After 3 days, however, a weak XRD peak corresponding to the (004) peak of anatase TiO_2 was observed [Fig. 1(e)]. The absence of (101) and (200) peaks which are stronger than the (004) in non-oriented powder anatase indicates the presence of (00*l*) oriented crystallites in the film. In addition, when the (00*l*) oriented NH_4TiOF_3 film prepared from the B/Ti = 1 LPD solution was air-calcined at 873 K for 1 h, only the (004) XRD line of anatase TiO_2 was observed [Fig. 1(f)]: the broad peak around 2θ = 20–25° is due to the quartz substrate. These results suggest the possibility of synthesizing oriented TiO_2 films directly by the monolayer-assisted LPD method on a B rich solution or indirectly by heat-treatment of an oriented NH_4TiOF_3 film. Detailed investigation is in progress with respect to the conversion of NH_4TiOF_3 to TiO_2 with retention of orientation as well as the mechanism of the deposition and growth of oriented crystallites at the monolayer surface.

This work was financially supported by The Sumitomo Foundation in Japan. The study made use of instruments in the Center for Instruments Analysis (XRD, TEM) of Nagasaki University.

Notes and references

1 H. Nagayama, H. Honda and H. Kawahara, *J. Electrochem. Soc.*, 1988, **359**, 2013.
2 S. Deki, Y. Aoi, O. Hiroi and A. Kajinami, *Chem. Lett.*, 1996, **6**, 433.
3 S. Deki, Y. Aoi, Y. Asaoka, S. Kajinami and M. Mizuhata, *J. Mater. Chem.*, 1997, **7**, 733.
4 R. H. Schmitt, E. L. Glove and R. D. Grown, *J. Am. Chem. Soc.*, 1960, **82**, 5292.
5 C. A. Wamser, *J. Am. Chem. Soc.*, 1951, **73**, 409.
6 I. Moriguchi, I. Tanaka, Y. Teraoka and S. Kagawa, *J. Chem. Soc., Chem. Commun.*, 1991, 1401.
7 I. Moriguchi, K. Hosoi, H. Nagaoka, I. Tanaka, Y. Teraoka and S. Kagawa, *J. Chem. Soc., Faraday Trans.*, 1994, **90**, 349.
8 I. Moriguchi, H. Maeda, Y. Teraoka and S. Kagawa, *J. Am. Chem. Soc.*, 1995, **117**, 1139.
9 I. Moriguchi, Y. Tsujigo, Y. Teraoka and S. Kagawa, *Adv. Mater.*, 1999, **11**, 997.
10 I. Moriguchi, Y. Tsujigo, Y. Teraoka and S. Kagawa, *J. Phys. Chem. B*, 2000, **104**, 8101.
11 B. R. Heywood and S. Mann, *J. Am. Chem. Soc.*, 1992, **114**, 4681.
12 J. H. Fendler and F. C. Meldrum, *Adv. Mater.*, 1995, **7**, 607.
13 J. Yang and J. H. Fendler, *J. Phys. Chem.*, 1995, **99**, 5505.
14 I. Moriguchi, N. Fujiyoshi, R. Sakamoto, Y. Teraoka and S. Kagawa, *Colloids Surf. A*, 1997, **126**, 159.
15 The XRD pattern of NH_4TiOF_3 has been reported in JCPD 33-82 in the absence of crystallographic data. X-Ray and electron diffraction results in this study tentatively suggest a tetragonal unit cell with a = 0.7573(3) nm and c = 1.2647(6) nm.

CHEMCOMM
Communication
www.rsc.org/chemcomm

A three component fully interlocked 3-D network: crystal structure and magnetic properties†

Partha Sarathi Mukherjee,[a] Sudipta Dalai,[a] Golam Mostafa,[b] Ennio Zangrando,[c] Tian-Huey Lu,[b] Guillaume Rogez,[d] Talal Mallah*[d] and Nirmalendu Ray Chaudhuri*[a]

[a] *Department of Inorganic Chemistry, Indian Association for the Cultivation of Science, Calcutta-700032, India. E-mail: icnrc@mahendra.iacs.res.in*
[b] *Department of Physics, National Tsing Hua University, Hsinchu 300, R.O.C.*
[c] *Dipartimento di Scienze Chimiche, University of Trieste, 34127, Italy*
[d] *Laboratoire de Chimie Inorganique, UMR CNRS 8613, Universit de paris-Sud, 91405 Orsay, France. E-mail: mallah@icmo.u-psud.fr*

Received (in Cambridge, UK) 6th March 2001, Accepted 12th June 2001
First published as an Advance Article on the web 5th July 2001

A one-pot reaction of three different components [Cu(II), fumarate dianion and piperazine] leads to the self assembly of a magnetic molecular fully interlocked 3D structure with (4,4) nets formed by equal 2D sheets.

One of the challenges in modern inorganic chemistry is the design of molecular extended systems possessing original architectures and predictable physical properties. Such novel molecular assemblies include networks mimicking zeolites or possessing magnetic metallic ions.[1,2] One of the intriguing assemblages encountered is that consisting of interlocked structures like catenanes where interlacing rings may be achieved by a rational synthetic approach.[3] A few systems with interpenetrated two-dimensional networks are known and during the last decade three examples of molecular systems containing paramagnetic ions with fully interlocked structures have been reported.[4,5]

We report, here, a new molecular magnetic system with a fully interlocked three-dimensional structure of general formula $[Cu(fum)(ppz)(H_2O)_2]$ (fum = fumarate dianion and ppz = piperazine) obtained from a one-pot synthesis of three different components *i.e.* Cu(II), piperazine and fumarate, using an unusual crystallization process. To the best of our knowledge, this is the first molecular interlocked system where the 2D sheets are assembled from two different types of organic bridges.

Reaction of $CuCl_2$, Na_2fum, and piperazine in H_2O–MeOH results in the formation of a sky blue insoluble solid. Deep blue single crystals were obtained by slow evaporation of an ammoniacal solution of the solid,‡ and the structure was determined by single crystal X-ray diffraction.§ As shown in Figs. 1 and 2, the present compound is a 3D polymeric, interpenetrating network consisting of equivalent 2D sheets, of composition $[Cu(fum)(ppz)(H_2O)_2]_n$ with a (4,4) topology, where copper ions provide the 4-connecting nodes bridging through ppz and fum ligands. In the structure Cu^{II} ions, ppz and fum ligands are situated at crystallographic centres of symmetry. The sides of the parallelogram forming the grid are provided by the ppz molecules in the direction of the crystallographic *c* axis (6.947 Å), the others are part of zigzag Cu–fum chains running parallel to the diagonal of plane *ab* (length of 8.960 Å). The coordinating dicarboxylate oxygen atoms are those in *anti* position with respect to the adjacent H atom of the ligand. The metals within a sheet are all coplanar in an essentially square planar environment, since two water molecules at pseudo-axial positions are at 3.058(6) Å, too far apart to attest an octahedral geometry around copper. The (4,4) nets are inclined interpenetrated to form an interlocked 3D structure. This is the highest dimensionality found for fum bridged Cu^{II} complexes since all previous such complexes are dimeric or 1D chains.[2] Along the line of intersection of any particular pair of interpenetrating sheets each $Cu(fum)_2(ppz)_2$ window encircles a Cu–fumarate–Cu entity of the other sheet, in such a way to allow the formation of weak hydrogen bonds [3.035(4) Å] between unligated oxygen O(2) and ppz nitrogen

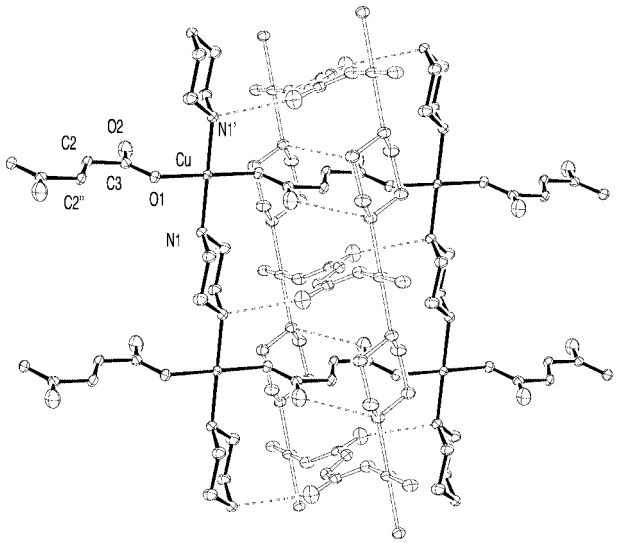

Fig. 1 Perspective view of two interpenetrated sheets (represented by open and filled bonds) showing the N(1)–H···O(2) hydrogen bonds (dashed lines). Selected bond lengths (Å), angles and torsion angles (°): Cu–O(1) 1.968(2), Cu–N(1) 2.047(3); O(1)–Cu-O(1′) 180.00(1), O(1)–Cu–N(1′) 93.05(9), O(1)–Cu–N(1) 86.95(9), N(1′)–Cu–N(1) 180.00(2), C(2)–C(3)–O(1)–Cu, −172.2(2), C(2″)–C(2)–C(3)–O(1) −8.3(5)°.

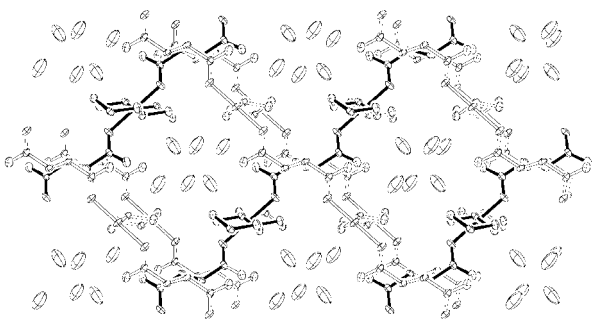

Fig. 2 View of the crystal structure of $[Cu(fum)(ppz)(H_2O)_2]_n$ down the crystallographic *c* axis, showing the channels hosting the water molecules.

† Electronic supplementary information (ESI) available: magnetic results and further crystallographic details (atomic coordinates, bond distances and angles and hydrogen bonds). See http://www.rsc.org/suppdata/cc/b1/b102072m/

 DOI: 10.1039/b102072m

N(1). The dicarboxylate bridging ligands lie at a repeat distance of half the crystallographic axis *c*, suggesting π contacts among these groups (the closest C–C separation is 3.492 Å). When viewed along the *c* axis the structure is seen to contain 168 Å^3 channels filled with water of crystallization (Fig. 2). The crystallographically independent water molecule, located at 2.761(5) Å from O(2), is rather disordered and is weakly hydrogen bonded also to two close symmetry related units [2.95(1) and 3.02(1) Å]. This crystal structure which displays an inclined interpenetration of two (4,4) nets is unique and unprecedented. To the best of our knowledge, only one structure with this type of interpenetration has been reported to date where the sheets are different, formed by a 2D layer and 1D chains, the latter connected through H-bonds.[6] Thermogravimetric analysis reveals a weight loss at 155 °C corresponding to the loss of two water molecules per formula unit [calc. 12.0; obs. 11.8%].

The magnetic behaviour of the complex was investigated using a SQUID magnetometer in the temperature region 280–3 K within an applied magnetic field of 50 kOe. The $\chi_M = f(T)$ plot (Fig. 3) is consistent with the presence of an antiferromagnetic interactions between the Cu^{II} ions within the compound. It has already been reported that through-bond coupling leads to important magnetic interaction in Cu^{II}–piperazine–Cu^{II} entities while the interaction through fumarate is very small since through-bond coupling is negligible.[7] The susceptibility data were thus fitted by the theoretical law for an antiferromagnetic $S = 1/2$ regular infinite chain. The least square fit leads to the following parameters: $J = -15.3$ cm^{-1}, $g = 2.04$, $\rho = 0.011$, TIP $= 60 \times 10^{-6}$ and an agreement factor $R = 2.4 \times 10^{-4}$. The quality of the fit may be improved by introducing an intermolecular interaction parameter *zj* that takes into account the interaction between the magnetic chains in the framework of the molecular field approximation.[8] The inset of Fig. 3 shows that a better fit of the maximum can then be obtained with the following parameters: $J = -14.7$ cm^{-1}, $g = 2.04$, $\rho = 0.013$, $zj = -4.2$ cm^{-1}, TIP $= 60 \times 10^{-6}$ and an agreement factor of 6.5×10^{-6}. Since each piperazine bridged chain is surrounded by two other chains within the 2D layers, *z* is equal to 2 (we have neglected the interaction through H-bonds) which leads to an exchange coupling parameter of -2 cm^{-1} between the Cu^{II} ions through fumarate. DFT calculations is underway in order to rationalize in a more quantitative way the amplitude of the magnetic interaction between the two different bridges.

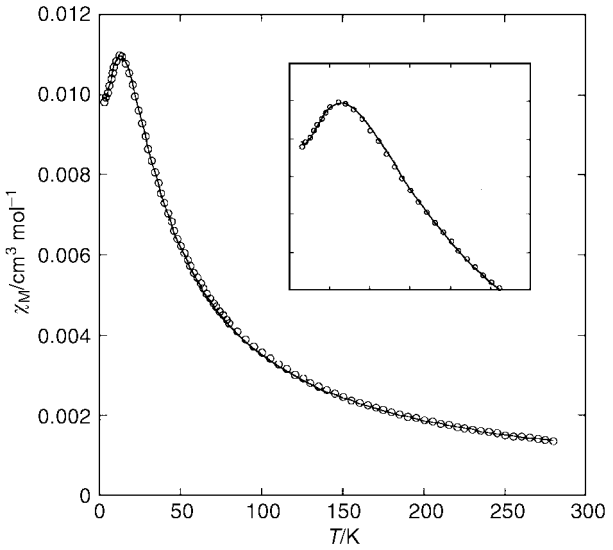

Fig. 3 Molar magnetic susceptibility *vs.* temperature plot for [Cu(fum)ppz$(H_2O)_2]_n$. Solid lines shows the best fit obtained considering the interchain magnetic interaction in addition to intrachain interaction.

We thank the Council of Scientific and Industrial Research, New Delhi for financial support (granted to N. R. C).

Notes and references

‡ A 5 mL aqueous solution of $CuCl_2 \cdot 2H_2O$ (1 mmol, 0.1705 g) was mixed with an aqueous solution (10 mL) containing Na_2fum (1 mmol, 0.1600 g) and piperazine (1 mmol, 0.0860 g). A sky blue solid, insoluble in common organic solvents separated out immediately. It was filtered off, washed with water and dissolved in a minimum amount of ammonia (14 M). Suitable blue single crystals for X-ray diffraction were obtained by slow evaporation of the ammoniacal solution of the solid in a refrigerator.

§ *Crystal data*: $C_8H_{16}CuN_2O_6$, $M = 299.77$, monoclinic, space group *C*2/*c*, $a = 12.785(8)$, $b = 12.556(8)$, $c = 6.947(5)$ Å, $\beta = 99.69(1)°$, $U = 1099.3(12)$ Å^3, $F(000) = 620$, $Z = 4$, $D_c = 1.811$ g cm^{-3}, μ(Mo-Kα) = 2.007 mm^{-1}. Intensity data collected on an Enraf-Nonius CAD-4 single crystal diffractometer employing the ω–2θ scan method; absorption correction was applied. The structure was refined using a full matrix refinement procedure (SHELXL97), with anisotropic thermal parameters assigned to all non-hydrogen atoms. All hydrogen atoms were observed in the difference map; those of fumarate and piperazine molecules were constrained at geometrical estimates, while coordinates of hydrogen atoms of water molecule were refined. At convergence $R1 = 0.0428$, $wR2 = 0.1081$ for 1292 unique reflections and 86 parameters, [3358 reflections collected, $R_{int} = 0.0701$, 1216 with $I > 2\sigma(I)$].

CCDC reference number 160683. See http://www.rsc.org/suppdata/cc/b1/b102072m/ for crystallographic data in CIF or other electronic format.

1 O. M. Yaghi and G. Li, *Angew. Chem., Int. Ed. Engl.*, 1995, **34**, 207; F. B. Hoskins and R. Robson, *J. Am. Chem. Soc.*, 1990, **112**, 1546; S. R. Batten, B. F. Hoskins and R. Robson, *Angew. Chem., Int. Ed. Engl.*, 1995, **34**, 820.

2 *Magnetic Molecular Materials*, ed. D. Gatteschi, O. Kahn, J. S. Miller and F. Palacio, NATO ASI Series E198, Kluwer Academic Publishers, Dordrecht, 1991; C. E. Xanthopoulos, M. P. Sigalas, G. A. Katsoulos, C. A. Tsipis, A. Terzis and A. Hountas, *Inorg. Chim. Acta*, 1993, **153**, 214; T. Mallah, S. Thiébaut, M. Verdaguer and P. Veillet, *Science*, 1993, **262**, 1554; M. Ohba, N. Maruono, H. Okawa, T. Enoki and J.-M. Latour, *J. Am. Chem. Soc.*, 1994, **116**, 11 566; W. R. Entley and G. S. Girolami, *Science*, 1995, **268**, 397; S. Descurtins, H. W. Schmalle, R. Pellaux, P. Scheuwly and A. Hause, *Inorg. Chem.*, 1996, **35**, 1451; M. S. El Fallah, E. Rentshler, A. Caneschi, R. Sessoli and D. Gatteschi, *Angew. Chem., Int. Ed. Engl.*, 1996, **35**, 1947; N. Re, R. Crescenzi, C. Floriani, H. Miyasaka and N. Matsumoto, *Inorg. Chem.*, 1998, **37**, 2717; E. Colacio, J. M. Dominguez-Vera, M. Ghazi, R. Kivekés, F. Lloret, J. M. Moreno and H. Stoeckli-Evans, *Chem. Commun.*, 1999, 987; S. Han, J. L. Manson, J. Kim and J. S. Miller, *Inorg. Chem.*, 2000, **39**, 4182, P. S. Mukherjee, T. K. Maji, G. Mostafa, T. Mallah and N. R. Chaudhuri, *Inorg. Chem.*, 2000, **39**, 5147; H.-Z. Kou, S. Gao., B.-Q. Ma and D.-Z. Liao, *Chem. Commun.*, 2000, 1309; P. Jensen, D. J. Price, S. R. Batten, B. Moubaraki and K. Murray, *Chem. Eur. J.*, 2000, **6**, 3186; J. L. Manson, Q. Huang, J. W. Lynn, H. Koo, M. Whangbo, R. Bateman, T. Otsuka, N. Wada, D. N. Argyriou and J. S. Miller, *J. Am. Chem. Soc.*, 2001, **123**, 162; E. Coronado, J. R. Galán-Mascarós, C. J. Gómez-García and J. M. Martínez-Agudo, *Inorg. Chem.*, 2001, **40**, 113; P. S. Mukherjee, T. K. Maji, G. Mostafa, J. Ribas, M. S. El Fallah and N. R. Chaudhuri, *Inorg. Chem.*, 2001, **40**, 928; A. Marvilliers, S. Parsons, E. Rivière, J.-P. Audière, M. Kurmo and T. Mallah, *Eur. J. Inorg. Chem.*, 2001, in press.

3 G. Shill, *Catenanes, Rotoxanes and Knots*, Academic Press, New York, 1971; J. P. Sauvage, *Acc. Chem. Res.*, 1990, **23**, 319.

4 J. Konnert and D. Britton, *Inorg. Chem.*, 1966, **7**, 1193; R. W. Gable, B. F. Hoskins and R. Robson, *Chem. Commun.*, 1990, 1667; S. R. Batten and R. Robson, *Angew. Chem., Int. Ed.*, 1998, **37**, 1460.

5 H. O. Stumpf, L. Ouahab, Y. Pei, D. Grandjean and O. Kahn, *Science*, 1993, **261**, 447; J. A. Real, E. Andrés, M. C. Muñoz, M. Julve, T. Granier, A. Bousseksou and F. Varret, *Science*, 1995, **268**, 265; N. Moliner, C. Muñoz, S. Létard, X. Solans, N. Menéndez, A. Goujon, F. Varret and J. A. Real, *Inorg. Chem.*, 2000, **39**, 5390.

6 T. Soma and T. Iwamoto, *Acta. Crystallogr., Sect. C*, 1996, **52**, 1200.

7 B. Chiari, O. Piovesana, T. Tarantelli and P. F. Zanazzi, *Inorg. Chem.*, 1984, **23**, 2542; R. Hoffmann, *Acc. Chem. Res.*, 1970, **1**, 1; J. C. Colin, T. Mallah, Y. Journaux, F. Lloret, M. Julve and C. Bois, *Inorg. Chem.*, 1996, **246**, 249.

8 O. Kahn, *Molecular Magnetism*, VCH, Weinheim, 1993.

CHEMCOMM Communication
www.rsc.org/chemcomm

Synthesis and structure of *N*-heterocyclic carbene complexes of uranyl dichloride

Warren J. Oldham, Jr.,*[a] Susan M. Oldham,[a] Brian L. Scott,[b] Kent D. Abney,[b] Wayne H. Smith[a] and David A. Costa*[a]

[a] *Nuclear Materials and Technology Division, Los Alamos National Laboratory, MS J514, Los Alamos, New Mexico 87545, USA. E-mail: woldham@lanl.gov; dcosta@lanl.gov*
[b] *Chemistry Division, Los Alamos National Laboratory, MS J514, Los Alamos, New Mexico 87545, USA*

Received (in Irvine, CA, USA) 21st March 2001, Accepted 13th June 2001
First published as an Advance Article on the web 5th July 2001

Treatment of $UO_2Cl_2(thf)_3$ in THF with two equivalents of 1,3-dimesitylimidazole-2-ylidene (IMes) or 1,3-dimesityl-4,5-dichloroimidazole-2-ylidene ($IMesCl_2$) yields novel monomeric uranyl *N*-heterocyclic carbene complexes, representing the first examples of actinyl carbon bonds.

The coordination chemistry of *N*-heterocyclic carbenes (NHC) is a topic of much current interest, motivated in part by promising applications in homogeneous catalysis[1] and materials science.[2] NHC complexes have also been identified as principal species formed upon dissolution of certain metal salts in *N*,*N*′-dialkylimidazolium-based room-temperature ionic liquids (RTILs).[3] We have recently initiated a general program to characterise the basic coordination chemistry and electrochemical properties of lanthanide and actinide ions dissolved in RTILs with the goal of developing advanced, environmentally responsible, nuclear processing and purification strategies. In support of this effort, the reaction chemistry of isolable and easily handled NHC ligands with lanthanide[4] and actinide complexes is of interest. Given the central role of actinyl ions (*e.g.* MO_2^{2+}, M = U, Np, Pu) in nuclear chemistry,[5] we report here the synthesis and structural characterisation of uranyldichloride complexes stabilised by sterically demanding NHC ligands. Well characterised 1,3-dimesitylimidazole-2-ylidene ligands were chosen in this study in order to favour highly crystalline reaction products, amenable to detailed structural characterisation.

Addition of a THF solution containing two equivalents of IMes[6] or $IMesCl_2$[7] to a bright yellow solution of $UO_2Cl_2(thf)_3$[8] in THF rapidly gives a bleached yellow solution from which pale yellow powders separate that correctly analyse for $UO_2Cl_2L_2$ [L = IMes **1**, $IMesCl_2$ **2**, see eqn. (1)].† The isolated

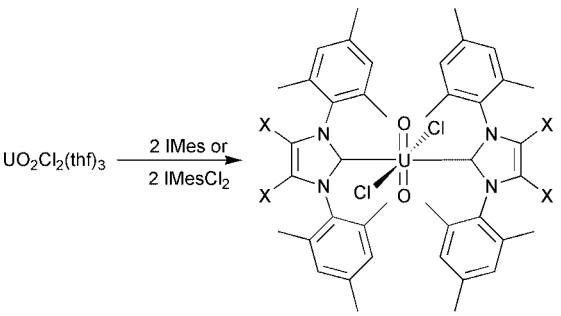

(1)

powders are insoluble in aliphatic hydrocarbons, slightly to moderately soluble in THF and toluene, and readily decompose in CH_2Cl_2.

Crystals suitable for X-ray structural analysis could be obtained for **1** as the THF solvate, by carefully layering a cold solution of $UO_2Cl_2(thf)_3$ in THF with a second solution of IMes, followed by slow diffusion over several days at –30 °C. For **2**, simply cooling a saturated THF solution at –30 °C overnight gave well formed single crystals.‡ Thermal ellipsoid representations of **1** and **2** are shown in Fig. 1. For both complexes the uranium(VI) metal atom lies at the centre of a nearly perfect octahedron. The uranyl U–O bond lengths of 1.761(4) and 1.739(3) Å (**1** and **2**, respectively) are within the range previously observed in $UO_2Cl_2L_2$ complexes.[9–12] The significantly shorter U–O bond length observed for **2** is consistent with $IMesCl_2$ being a weaker σ-donor ligand compared to IMes, which is also reflected in UO_2 vibrational data (*vide infra*). The

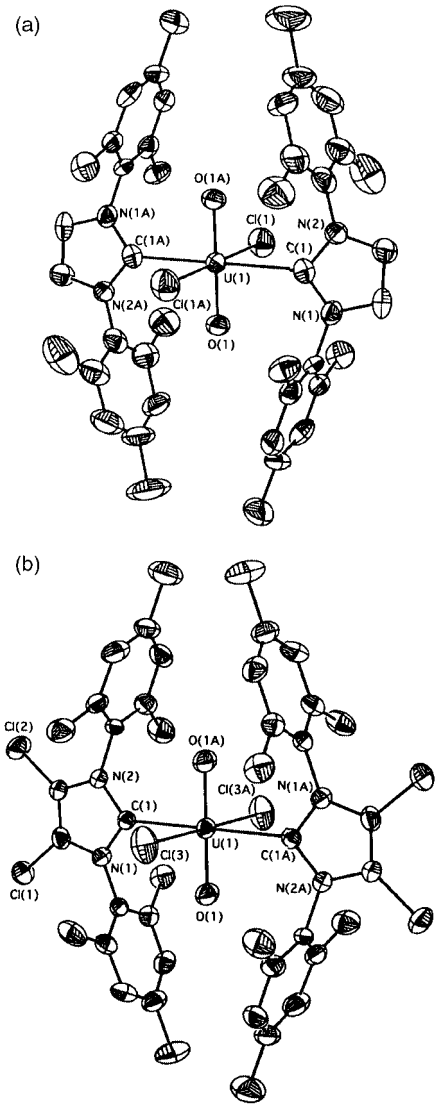

Fig. 1 Thermal ellipsoid representation of (a) **1** and (b) **2** shown at the 50% probability level. THF solvent of crystallisation and hydrogen atoms have been omitted for clarity.

 DOI: 10.1039/b102649f

U–Cl bond lengths also fall within the normal range. The uranium–carbene bond lengths are considerably lengthened at 2.626(7) and 2.609(4) Å (**1** and **2**, respectively) compared to the U–L bond lengths in $UO_2Cl_2L_2$ complexes [L = $OPPh_3$,[9] $OC(CHCHPh)_2$,[10] $OP(NMe_2)_3$,[11] or $OC(NMe_2)_2$[12]], which are observed between 2.27 and 2.30 Å. The electron-withdrawing 4,5-dichloro substituents of $IMesCl_2$ are expected to reduce the bonding radius of the carbene lone pair, which is reflected in the relative U–C bond lengths of **1** and **2** [2.626(7) and 2.609(4) Å, respectively]. The imidazol-2-ylidene rings lie nearly coplanar, twisted along the C(1)–U(1)–C(1A) axis by *ca.* 6° (**1**) and 8° (**2**). The plane defined by N(1)–C(1)–N(2) eclipses the O–U–O axis [torsion angles: *ca.* 11° (**1**) and 4° (**2**)], thereby minimising steric interaction between the mesityl substituents and the chloride ligands. Instead, the mesityl groups form a basket around the uranyl oxo ligands in which the closest non-bonded oxygen contacts are *ca.* 3.1–3.2 Å to the *ipso*-mesityl carbons.

A measure of the relative donor strength of the NHC ligands in $UO_2Cl_2L_2$ complexes can be estimated using vibrational spectroscopy. Within an isostructural series of uranyl complexes, the frequency of the symmetric (ν_1) and asymmetric (ν_3) UO_2 stretch is inversely proportional to the donor strength of the equatorial ligands which lie orthogonal to the $[UO_2]^{2+}$ moiety.[13] For **1** and **2**, the highest intensity peak in the IR spectra (Nujol), assigned to the asymmetric UO_2 stretch is observed at 938 and 942 cm^{-1}, respectively. These values are among the highest reported for $UO_2Cl_2L_2$ complexes,[14] suggesting correspondingly weak electron donation from the NHC ligands. A slightly higher frequency ν_3 observed for **2** is consistent with the electron withdrawing effect of the 4,5-dichloro substituted imidazol-2-ylidene ligand. It should be pointed out that the weak donor ability of NHC ligands in these uranyl complexes is in marked contrast to their exceptionally strong donor strength observed in low valent transition metal complexes.[15] The isolation of uranyl complexes stabilised by soft σ-donor ligands like NHCs is without precedent. Prior to this report, actinyl complexes have been exclusively stabilised by hard donor ligands (*e.g.* halide, oxygen and nitrogen ligation). In fact, even tertiary phosphine complexes are unknown in the actinyl series. A useful comparison can be made to a related tungsten complex, $WO_2Cl_2L_2$ (L = 1,3-dimethylimidazol-2-ylidene),[16] which further demonstrates the suitability of NHCs as competent stabilising ligands for hard, Lewis acidic metal complexes.

The synthetic and structural results reported in this work suggest that related actinide NHC complexes might reasonably be formed in RTIL solutions. Through control of the effective pH of these media, the concentration of free NHCs could be reversibly adjusted to allow manipulation of the coordination sphere of dissolved metal ions. Novel separations technology based on the imidazolium-RTIL/NHC interconversion is currently under development. Extension of this synthetic and structural investigation to transuranium actinyl complexes and to low valent actinides is being actively pursued.

We thank Dr David L. Clark of the Glenn T. Seaborg Institute for Transactinide Science for providing financial support of this work. Los Alamos National Laboratory is operated by the University of California for the U.S. Department of Energy.

Notes and references

† *Preparation* of $UO_2Cl_2(IMes)_2$ **1**: to a solution of $[UO_2Cl_2(thf)_2]_2$ (100 mg, 0.103 mmol) dissolved in THF (4 mL) was added a second THF solution (4 mL) of IMes (125 mg, 0.415 mmol). The resulting yellow suspension was stirred for 15 min, diluted with hexanes (5 mL), then filtered off and washed with hexanes (2 × 2 mL). Yield 145 mg (74%). ^{1}H NMR (300 MHz, toluene-d_8): δ 2.08 (s, 6H, *p*-CH_3), 2.26 (s, 12H, *o*-CH_3), 6.26 (s, 2H, 4,5-imidazole-CH), 6.49 (s, 4H, 3,5-mesityl-CH). IR (Nujul): ν (cm^{-1}) 1304 (w), 1273 (m), 1229 (m), 1160 (w), 1100 (m), 1064 (w), 1033 (w), 962 (w), 938 (vs), 920 (s), 847 (m), 749 (m), 722 (m). Anal. Calc. for $C_{42}H_{48}Cl_2N_4O_2U$: C, 53.11; H, 5.09; N, 5.90. Found: C, 53.62; H, 5.76; N, 5.71%.

Preparation of $UO_2Cl_2(IMesCl_2)_2$ **2**: a similar procedure as that described for **1** was followed. Yield 62%. ^{1}H NMR (300 MHz, toluene-d_8): δ 2.02 (s, 6H, *p*-CH_3), 2.25 (s, 12H, *o*-CH_3), 6.47 (s, 4H, 3,5-mesityl-CH). IR (Nujul): ν/cm^{-1} 1304 (w), 1273 (m), 1195 (w), 1180 (w), 1149 (w), 1131 (m), 1076 (w), 1036 (w), 984 (w), 942 (vs), 851 (m), 733 (w), 722 (w). Anal. Calc. for $C_{42}H_{44}Cl_6N_4O_2U$: C, 46.34; H, 4.07; N, 5.15. Found: C, 47.23; H, 4.56; N, 4.63%.

‡ *Crystal data*: for **1**·6THF: $C_{66}H_{96}Cl_2N_4O_8U$, M = 1382.40, a = 29.330(1), c = 18.879(1) Å, V = 14065(1) Å^3, trigonal, space group $R\bar{3}$, Z = 9, T = 203 K, $R1(I > 2\sigma)$ = 0.0656, and $wR2(I > 2\sigma)$ = 0.1311.

For **2**·THF: $C_{50}H_{60}Cl_6N_4O_4U$, a = 10.1563(5), b = 17.3511(8), c = 13.6466(6) Å, β = 95.162(1)°, V = 2480.2(2) Å^3, monoclinic, space group $P2_1/n$, Z = 2, T = 203 K, $R1(I > 2\sigma)$ = 0.0456, and $wR2(I > 2\sigma)$ = 0.0855.

The reflection data for both structures were collected on a Bruker P4/CCD using a combination of ϕ and ω scans. The structures were solved using standard direct methods techniques (SHELXS-97),[17] and refined using full-matrix least squares based on F^2 (SHELXL-97).[17] Hydrogen atom positions were idealized, and all non-hydrogen atoms were refined anisotropically. Disordered lattice THF molecules in both structures were eliminated from the refinement using PLATON/SQUEEZE.[18] CCDC reference numbers 160347 and 160348 for **1** and **2**, respectively. See http://www.rsc.org/suppdata/cc/b1/b102649f/ for crystallographic data in CIF or other electronic format.

1 A. J. Arduengo III, *Acc. Chem. Res.*, 1999, **32**, 913; W. A. Herrmann and C. Köcher, *Angew. Chem., Int. Ed. Engl.*, 1997, **36**, 2162; T. Weskamp, V. P. W. Böhm and W. A. Herrmann, *J. Organomet. Chem.*, 2000, **600**, 12.
2 R. Faust and B. Göbelt, *Chem. Commun.*, 2000, 919.
3 L. Xu, W. Chen and J. Xiao, *Organometallics*, 2000, **19**, 1123; M. Hasan, I. V. Kozhevnikov, M. R. H. Siddiqui, A. Steiner and N. Winterton, *J. Chem. Res. (S)*, 2000, 392; M. Hasan, I. V. Kozhevnikov, M. R. H. Siddiqui, C. Femoni, A. Steiner and N. Winterton, *Inorg. Chem.*, 2001, **40**, 795.
4 W. A. Herrmann, F. C. Munck, G. R. J. Artus, O. Runte and R. Anwander, *Organometallics*, 1997, **16**, 682.
5 F. Weigel, in *The Chemistry of the Actinide Elements*, ed. J. J. Katz, G. T. Seaborg and L. R. Morss, Chapman and Hall, New York, 2nd edn., 1986, pp. 169–442.
6 A. J. Arduengo, III, H. V. R. Dias, R. L. Harlow and M. Kline, *J. Am. Chem. Soc.*, 1992, **114**, 5530.
7 A. J. Arduengo III, F. Davidson, H. V. R. Dias, J. R. Goerlich, D. Khasnis, W. J. Marshall and T. K. Prakasha, *J. Am. Chem. Soc.*, 1997, **119**, 12 742.
8 M. P. Wilkerson, C. J. Burns, R. T. Paine and B. L. Scott, *Inorg. Chem.*, 1999, **38**, 4156.
9 G. Bombieri, E. Forsellini, J. P. Day and W. I. Azeez, *J. Chem. Soc., Dalton Trans.*, 1978, 677; S. B. Akona, J. Fawcett, J. H. Holloway and D. R. Russell, *Acta Crystallogr. Sect. C*, 1991, **47**, 45.
10 N. W. Alcock, P. de Meester and T. J. Kemp, *J. Chem. Soc., Perkin 2*, 1979, 921.
11 J. C. Russell, M. P. du Plessis, L. R. Nassimbeni, J. G. H. du Preez and B. J. Gellatly, *Acta Crystallogr., Sect. B*, 1977, **33**, 2062; P. R. Julien, N. Rodier and P. Khodadad, *Acta Crystallogr., Sect. B*, 1977, **33**, 2411.
12 L. A. Jacobs, C. P. J. van Vuuren and P. H. van Rooyen, *S. Afr. J. Chem.*, 1986, **39**, 174.
13 R. G. Denning, in *Gmelin Handbuch der Anorganischen Chemie Suppl. Ser. Uranium*, 1986, vol. A6, pp. 31–79; A. A. Zazhogin, H. D. Lutz and A. I. Komyak, *J. Mol. Struct.*, 1999, **482–483**, 189.
14 L. V. Kobets and D. S. Umreiko, *Zh. Prikl. Spektrosk. (Engl. Transl)*, 1986, **44**, 643.
15 J. Huang, H.-J. Schanz, E. D. Stevens and S. P. Nolan, *Organometallics*, 1999, **18**, 2370; T. Weskamp, F. J. Kohl, W. Hieringer, D. Gleich and W. A. Herrmann, *Angew. Chem., Int. Ed.*, 1999, **38**, 2416.
16 W. A. Herrmann, G. M. Lobmaier and M. Elison, *J. Organomet. Chem.*, 1996, **520**, 231.
17 SHELXTL/NT Version 5.1, Bruker AXS, Inc., Madison, WI 53719, USA.
18 A. L. Spek, *Acta Crystallogr., Sect. A*, 1990, **46**, C34.

CHEMCOMM Communication
www.rsc.org/chemcomm

Manganese(III) acetate mediated radical reactions in the presence of an ionic liquid

Gregory Bar, Andrew F. Parsons* and C. Barry Thomas

Department of Chemistry, University of York, Heslington, York, UK YO10 5DD. E-mail: afp2@york.ac.uk

Received (in Cambridge, UK) 19th April 2001, Accepted 13th June 2001
First published as an Advance Article on the web 5th July 2001

A new, mild and practical method for conducting manganese(III)-mediated radical reactions, which lead to the formation of carbon–carbon bonds, has been developed using the ionic liquid 1-butyl-3-methylimidazolium tetrafluoroborate ([bmim][BF_4]).

Manganese(III) acetate is known to oxidise a variety of carbonyl compounds, including β-diketones and β-keto esters, to form radicals.[1] These α-carbonyl radicals can undergo cyclisation or intermolecular addition reactions to form radical adducts, which may be oxidised by a second equivalent of manganese(III) acetate. The resultant cations can undergo nucleophilic attack or β-deprotonation reactions leading, for example, to acetates or alkenes. These carbon–carbon bond forming reactions are synthetically attractive because manganese(III) acetate is inexpensive and, in contrast to related tributyltin hydride reactions, this oxidative method of radical generation leads to functionalised products.

One significant drawback to the use of manganese(III) acetate, however, is the harsh reaction conditions. As manganese(III) acetate has poor solubility in organic solvents, acetic acid is invariably used and this severely limits the range of substrates which can be employed, especially as many reactions require heating (often to ⩾70 °C). An additional drawback to the use of acetic acid involves the separation and recovery of the manganese acetate at the end of the reaction. The standard workup procedure involves addition of large quantities of water and/or aqueous sodium hydrogen carbonate to remove the acetic acid and so large-scale reactions would generate considerable amounts of aqueous waste. With a view to establishing milder reaction conditions, as well as facilitating the recovery of the manganese acetate, we have investigated the novel use of an ionic liquid in manganese(III)-mediated radical reactions.

Ionic liquids have recently been found to be excellent, environmentally benign solvents for a variety of reactions.[2] These liquids offer an attractive alternative to conventional organic solvents because, for example, they are easy to recycle and are non-volatile. Of particular note are air and moisture stable imidazolium ionic liquids, which have been used as solvents for a variety of transition metal catalysed reactions (*e.g.* oxidation,[3] allylation,[4] living radical polymerisation[5] and hydrogenation[6]). This suggested that ionic liquids such as 1-butyl-3-methylimidazolium tetrafluoroborate ([bmim][BF_4]), which is miscible with polar solvents (*e.g.* methanol, dichloromethane) but immiscible with less polar solvents (*e.g.* ethyl acetate, diethyl ether, toluene), could be compatible with manganese(III)-mediated radical reactions.

Although our initial manganese(III) acetate reactions in neat [bmim][BF_4] were low yielding, we found that cyclised products could be isolated in good yield when 1,3-dicarbonyl compounds and alkenes were reacted in a mixed [bmim][BF_4]–dichloromethane solvent system (Scheme 1). Thus, reaction of cyclohexane-1,3-dione (1 equiv.), α-methylstyrene (5 equiv.) and manganese(III) acetate (2.1 equiv.) in a 1:4 mixture of [bmim][BF_4]–dichloromethane produced tetrahydrofuranone **1** in 50% yield after column chromatography.†‡ Similar yields of **1** were obtained when using different ratios of starting materials

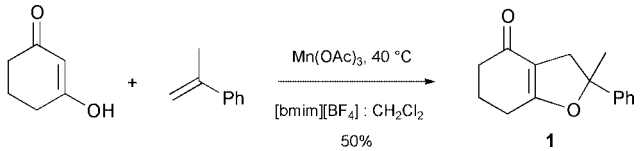

Scheme 1

and different amounts of the ionic liquid and dichloromethane. This showed that only small amounts of the ionic liquid are required for the reaction to proceed. For example, when a 1:19 mixture of [bmim][BF_4]–dichloromethane was used, **1** was isolated in 45% yield. The reaction could also be carried out using [bmim][BF_4] in the presence of alternative solvents to dichloromethane, including methanol, acetone or acetonitrile and **1** was isolated in 27–58% yield. Even solvents that are immiscible with [bmim][BF_4] can be employed. For instance, when the reaction was carried out in a 1:19 mixture of [bmim][BF_4]–ethyl acetate, **1** was isolated in 30% yield. It should also be noted that cerium(IV) ammonium nitrate (CAN), another efficient one-electron oxidant, can be used in place of manganese(III) acetate and when [bmim][BF_4]–dichloromethane was used as the solvent with this reagent, tetrahydrofuranone **1** was isolated in an excellent 82% yield. This is an interesting result because CAN, like manganese(III) acetate, has only limited solubility in organic solvents and so CAN oxidations are usually carried out in aqueous acetonitrile.

Related manganese(III)-mediated reactions can also be carried out using acyclic 1,3-dicarbonyl precursors (Scheme 2). Hence, β-keto esters can be reacted with electron-rich alkenes in the presence of 2.0 equiv. of manganese(III) acetate to give dihydrofurans **2a**–**d**. These types of reactions do not require a nitrogen atmosphere. For example, **2c** was isolated in 46 and 50% yield from reactions carried out in the presence or absence of a nitrogen atmosphere, respectively.

The yields of **1** and **2a**–**d** are similar or higher than those reported for related manganese(III) acetate/acetic acid reactions or alternative cyclisation methods.[7] This was also apparent using quinolone precursors when reaction of **3** (1 equiv.) with oct-1-ene (10 equiv.) in a mixed [bmim][BF_4]–chloroform

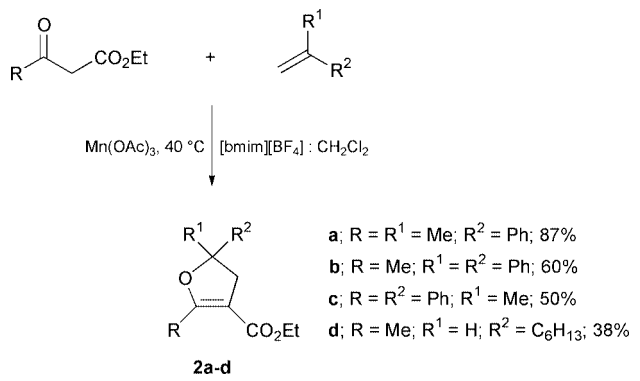

Scheme 2

 DOI: 10.1039/b103544b

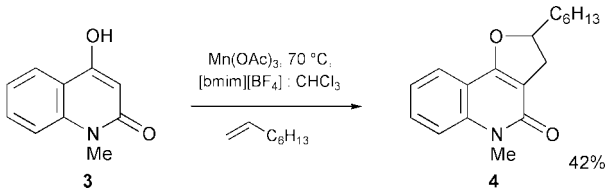

Scheme 3

solvent system produced the dihydrofuroquinolone **4** in 42% yield (Scheme 3).§ This can be compared to the corresponding manganese(III) acetate/acetic reaction at 60 °C, which required ultrasonic irradiation (because of the poor solubility of **3** in acetic acid) to give quinolone **4** in 50% yield.[8] A similar manganese(III)-mediated reaction using quinoline-2,4-diol (1 equiv.) and α-methylstyrene (5 equiv.) in [bmim][BF_4]–dichloromethane gave a 1:1 mixture of the angular and linear tricycles **5** and **6**, respectively, in a combined 78% yield.

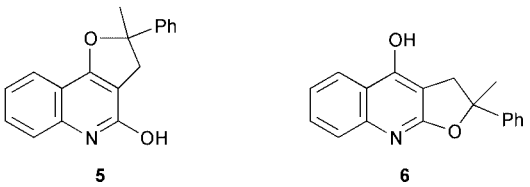

This work has shown, for the first time, that manganese(III)-mediated radical reactions can be carried out in alternative solvents to acetic acid in the presence of the ionic liquid [bmim][BF_4]. The ability to carry out manganese(III) reactions in a variety of solvents, under much milder reaction conditions than when using acetic acid, should extend the range of precursors which can be employed in these types of reactions. For example, we have shown that the *tert*-butyl ester **7** can be reacted with α-methylstyrene in [bmim][BF_4]–dichloromethane to give **8** in 43% yield (Scheme 4). The same reaction at 50 °C in acetic acid afforded **8** in a much lower yield of 25%, presumably because of the harsher (acidic) reaction conditions.

At the end of the reaction, the manganese acetate can be easily recovered (on precipitation) by addition of further organic solvent to the reaction mixture. After filtration, the manganese acetate was reacted with potassium permanganate to re-oxidise the manganese(II) back to manganese(III).[9] The manganese(III) acetate can therefore easily be recycled although this does depend on the nature of ionic liquid. For example, when the related ionic liquid [bmim][PF_6] was used, complete removal of the manganese byproducts was problematic. The ionic liquid [bmim][BF_4], which is believed to act as a co-

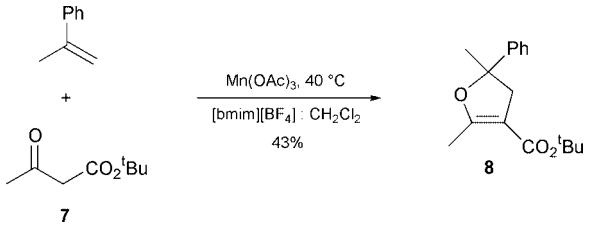

Scheme 4

solvent in these reactions,¶ can also be recovered on workup (in ⩾95% yield) and we have shown that this can be reused without any detriment to the product yields. For example, dihydrofuran **2c** was isolated in similar yields (*ca*. 50%) when using freshly prepared ionic liquid or ionic liquid recovered from other reactions. This work offers the potential for carrying out a variety of metal-mediated radical reactions in ionic liquids and this is currently under investigation.

We thank BP Amoco Chemicals, the EU (under the ERASMUS scheme) and The University of York for funding.

Notes and references

† To a solution of [bmim][BF_4][10] (2 cm^3) and dichloromethane (8 cm^3) containing cyclohexane-1,3-dione (0.10 g, 0.89 mmol) and α-methylstyrene (0.53 g, 2.63 mmol, 5 equiv.) was added manganese(III) acetate dihydrate (0.50 g, 1.88 mmol, 2.1 equiv.) under an atmosphere of nitrogen. The reaction mixture was then heated overnight until the solution changed from brown to yellow. Dichloromethane (40 cm^3) was then added and manganese(II) acetate was removed by filtration. The filtrate was then washed with water (4 × 10 cm^3) to remove the ionic liquid from the organic phase. (The ionic liquid can be recovered by extracting the aqueous phase with dichloromethane). The organic phase was then dried ($MgSO_4$), evaporated and purified using column chromatography (silica) to give 2-methyl-2-phenyl-3,5,6,7-tetrahydro-2*H*-benzofuran-4-one **1** (0.10 g, 50%) as an oil.

‡ All spectral data were in accord with the structures assigned. *Selected data* for **1**: δ_H(300 MHz, $CDCl_3$) 7.30–7.15 (5H, m, aromatics), 2.98 and 2.89 (2H, dt, *J* 14.5, 1.9, CH_2CPh), 2.45–2.40 (2H, m, CH_2), 2.29–2.23 (2H, m, CH_2), 2.02–1.91 (2H, m, CH_2), 1.62 (3H, s, CH_3); δ_C(75 MHz, $CDCl_3$) 196.0 (C=O), 176.4 (O–*C*=C), 146.0 (PhC^1), 128.9, 127.9, 124.6 (PhC$^{2–6}$), 113.0 (*C*=C–O), 93.0 (OCPh), 41.0 (PhCCH_2), 36.8 (*C*H_2C=O), 30.2 (CH_3), 24.5, 22.1 (*C*H_2CH_2CH_2).

§ When the reaction was carried out in dichloromethane in the absence of the ionic liquid, quinolone **4** was not formed even after heating in an ultrasonic bath (300 W, 30–40 kHz) for 24 h.

¶ Addition of the ionic liquid presumably increases the polarity of the medium and similar reactions can be carried out using dichloromethane in the presence of $Et_4N^+{}^-$OTs. Reaction of cyclohexane-1,3-dione with α-methylstyrene in a 0.1 M solution of $Et_4N^+{}^-$OTs in dichloromethane also gave tetrahydrofuranone **1** in 50% yield.

1 B. B. Snider, *Chem. Rev.*, 1996, **96**, 339; T. Linker, *J. Prakt. Chem.*, 1997, **339**, 488; G. G. Melikyan, *Aldrichim. Acta*, 1998, **31**, 50; A. F. Parsons, *An Introduction to Free Radical Chemistry*, Blackwell Science, Oxford, 2000.
2 T. Welton, *Chem. Rev.*, 1999, **99**, 2071; P. Wasserscheid and W. Keim, *Angew. Chem., Int. Ed.*, 2000, **39**, 3773.
3 C. E. Song and E. J. Roh, *Chem. Commun.*, 2000, 837; J. Howarth, *Tetrahedron Lett.*, 2000, **41**, 6627.
4 W. Chen, L. Xu, C. Chatterton and J. Xiao, *Chem. Commun.*, 1999, 1247.
5 A. J. Carmichael, D. M. Haddleton, S. A. F. Bon and K. R. Seddon, *Chem. Commun.*, 2000, 1237.
6 R. A. Brown, P. Pollet, E. McKoon, C. A. Eckert, C. L. Liotta and P. G. Jessop, *J. Am. Chem. Soc.*, 2001, **123**, 1254.
7 F. Z. Yang, M. K. Trost and W. E. Fristad, *Tetrahedron Lett.*, 1987, **28**, 1493; E. I. Heiba and R. M. Dessau, *J. Org. Chem.*, 1974, **39**, 3456; T. Hirao, T. Fujii, S-i. Miyata and Y. Ohshiro, *J. Org. Chem.*, 1991, **56**, 2264; A. Asouti and L. P. Hadjiarapoglou, *Tetrahedron Lett.*, 1998, **39**, 9073.
8 G. Bar, A. F. Parsons and C. B. Thomas, *Tetrahedron Lett.*, 2000, **41**, 7751.
9 G. Midgley and C. B. Thomas, *J. Chem. Soc., Perkin Trans. 2*, 1984, 1537.
10 J. D. Holbrey and K. R. Seddon, *J. Chem. Soc., Dalton Trans.*, 1999, 2133.

CHEMCOMM Communication
www.rsc.org/chemcomm

Nitration of alkanes with nitric acid catalyzed by *N*-hydroxyphthalimide

Shinji Isozaki, Yoshiki Nishiwaki, Satoshi Sakaguchi and Yasutaka Ishii*

Department of Applied Chemistry, Faculty of Engineering and High Technology Research Center, Kansai University, Suita, Osaka 564-8680, Japan. E-mail: ishii@ipcku.kansai-u.ac.jp

Received (in Cambridge, UK) 13th March 2001, Accepted 11th June 2001
First published as an Advance Article on the web 5th July 2001

Catalytic nitration of alkanes with nitric acid was first successfully achieved by the use of *N*-hydroxyphthalimide (NHPI) under mild conditions; the key to the present nitration was found to be the *in situ* generation of NO_2 and phthalimide *N*-oxyl radical by the reaction of NHPI with nitric acid.

Nitration of saturated hydrocarbons using nitric acid is usually carried out at fairly high temperature (250–400 °C) because of difficulty in generating NO_2 from HNO_3.[1] The nitration under such severe conditions resulted in not only the homolysis of C–H bonds but also the cleavage of the C–C bonds of hydrocarbons. As a consequence, the reaction is messy and often difficult to control, and exhibits poor product selectivity. To carry out the nitration selectively, *in situ* generations of alkyl radicals from alkanes and NO_2 from HNO_3 must be achieved under mild conditions. Recently, we have developed a novel catalytic method for the nitration of aliphatic hydrocarbons with NO_2 using NHPI as the catalyst under mild conditions.[2] We now find that alkanes can be nitrated with nitric acid through the *in situ* generation of NO_2 and alkyl radicals by the use of NHPI as a catalyst under mild conditions.

The nitration of adamantane (**1**) was chosen as a model reaction and carried out in the presence of nitric acid and a catalytic amount of NHPI in trifluorotoluene, affording 1-nitroadamantane (**2**) (64%) and 1,3-dinitroadamantane (**3**) (3%) along with oxygenated products, adamantan-1-ol (**4**) (9%) and adamantan-2-one (**5**) (5%) [eqn. (1), Table 1 entry 1]. In a previous paper, we showed that the nitration of **1** with NO_2 as a nitrating reagent affords **2** in 66% yield.[2] The nitration of **1** with HNO_3 which is easier to handle than NO_2 was found to be almost same as that with NO_2.

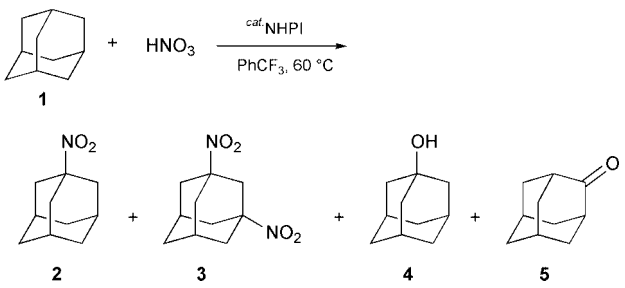

(1)

Table 1 shows the catalytic nitration of **1** with nitric acid by the NHPI under several reaction conditions.† Among the solvents examined, trifluorotoluene and acetic acid were found to be good solvents. Acetonitrile and ethyl acetate considerably retarded the nitration (entries 3 and 4). No reaction took place in the absence of NHPI (entry 5). The present nitration under air afforded oxygenated products, **4** and **5**, rather than nitro compounds (entry 6).

Upon treatment of NHPI with nitric acid at 60 °C, we found the evolution of brown gas attributed to NO_2. This finding suggests that the nitric acid reacts easily with the NHPI to generate NO_2 in the reaction system [eqn. (2)]. Importantly, nitric acid was easily converted into NO_2 in the presence of

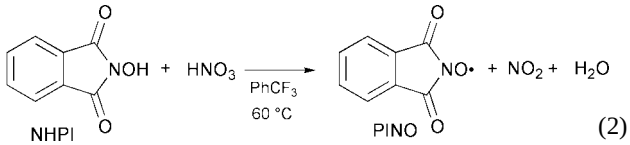

(2)

NHPI under relatively mild conditions, although it is known that the nitration of alkane with HNO_3 must be carried out at high temperature because of the difficulty in decomposing HNO_3 to NO_2.[1c] From EPR measurements, it was found that the phthalimide *N*-oxyl radical (PINO) was formed with the evolution of NO_2 by the reaction of the NHPI with nitric acid.‡ NHPI is known to be easily oxidized with $Pb(OAc)_4$ to the PINO.[3] In the present reaction, nitric acid serves as a good oxidizing agent of the NHPI to form the PINO and NO_2 [eqn. (2)].

In order to obtain further insight into the present nitration, **1** was allowed to react with nitric acid in the presence of copper in place of NHPI, since it is known that nitric acid reacts with copper metal, generating NO_2 according to eqn. (3).[4] However,

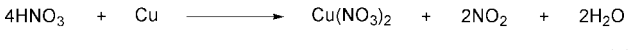

(3)

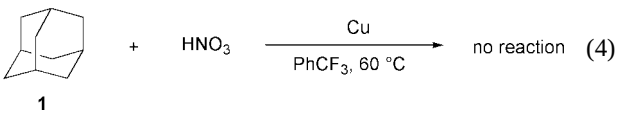

(4)

no nitration took place, although the generation of NO_2 was observed [eqn. (4)].

Table 2 summarizes the representative results for the nitration of various saturated hydrocarbons and their derivatives with nitric acid under the influence of the NHPI in trifluorotoluene at 60 °C for 15 h.

1,3-Dimethyladamantane (**6**) reacted with nitric acid under these conditions to give 1-nitro-3,5-dimethyladamantane (**7**) in 67% selectivity at 77% conversion (entry 1). When the NHPI used was increased from 0.1 mmol to 0.2 mmol, **7** was obtained in higher conversion and selectivity (entry 2). The nitration

Table 1 Nitration of adamantane (**1**) with HNO_3 by NHPI under various conditions[a]

			Select. (%)			
Entry	Solvent	Conv. (%)	**2**	**3**	**4**	**5**
1	$PhCF_3$	87	64	3	9	5
2	AcOH	93	62	n.d.	6	4
3	CH_3CN	55	38	n.d.	9	4
4	AcOEt	34	24	n.d.	21	3
5[b]	AcOH	> 2	n.d.	n.d.	n.d.	n.d.
6[c]	$PhCF_3$	40	n.d.	n.d.	33	13

[a] **1** (1 mmol) was reacted with HNO_3 (1.5 mmol) in the presence of NHPI (0.1 mmol) at 60 °C for 15 h. [b] In the absence of NHPI. [c] Under air.

 DOI: 10.1039/b102374h

Table 2 Nitration of various substrates with HNO_3 by NHPI[a]

Entry	Substrate	Conv. (%)	Product	Select. (%)
1	 **6**	77	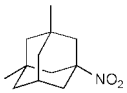 **7**	67
2[b]	**6**	89	**7**	81
3[c]	**6**	50	**7**	95[d]
4	 **8**	89 (74)	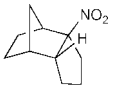 **9**	57 (47)
5		75	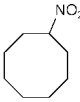	56[e]
6[f]		—		32[dg]
7[f]		—	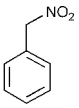	60[dh]
8	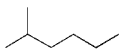	80	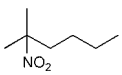	65
9		59	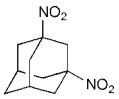	61
10		73	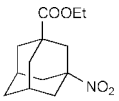	79
11		32	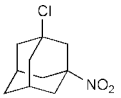	91

[a] Reaction is shown in text. Parentheses show the conversion and selectivity in the nitration using NO_2 instead of HNO_3. [b] NHPI (0.2 mmol) was used. [c] Substrate (3.0 mmol) was used. [d] Based on HNO_3 used. [e] Dinitrocyclooctane (14%) and cyclooctanone (10%) were obtained. [f] Substrate (5 mL) was used. [g] Adipic acid (5%) was obtained. [h] Benzyl alcohol (21%) and benzaldehyde (19%) were obtained.

using excess **6** with respect to nitric acid resulted in **7** in excellent yield (95%). The nitration of *endo*-tricyclo-[5.2.1.$0^{2,6}$]decane (**8**) occurred selectively at the fused tertiary C–H bond to give the corresponding nitro compound **9** (57%). On the other hand, the nitration of **8** with NO_2 instead of HNO_3 resulted in **9** in low yield (47% selectivity, 74% conversion). Consequently, **8** was found to be nitrated with HNO_3 in higher selectivity. Cyclooctane was also nitrated to form nitrocyclooctane (56%) and a regioisomeric mixture of dinitrocyclooctane (14%) as well as a small amount of cyclooctanone (10%) at 75% conversion. Cyclohexane was difficult to nitrate selectively because of the formation of adipic acid (5%).[5] Aliphatic hydrocarbon like 2-methylhexane was nitrated at the tertiary position to lead to 2-methyl-2-nitrohexane in relatively good selectivity. Several substituted adamantanes were subjected to the nitration under these reacion conditions. Thus, 1-chloroadamantane, 1-nitroadamantane, and ethyl 1-adamantanecarboxylate were nitrated to the corresponding nitro compounds in fair to good selectivities (entries 9–11).

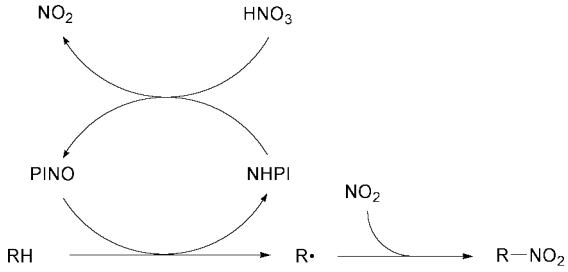

Scheme 1 A possible nitration path of alkanes with nitric acid by NHPI.

On the basis of these results, a possible reaction path for the present catalytic nitration of alkanes with nitric acid by the NHPI is shown in Scheme 1.

The nitration is initiated by the *in situ* generation of PINO and NO_2 from NHPI and nitric acid, respectively. The resulting PINO abstracts the hydrogen atom from alkanes to give NHPI and alkyl radicals which are readily trapped by NO_2 to form nitroalkanes.

In conclusion, the present alkane nitration with nitric acid provides a facile method for the preparation of nitroalkanes, by the use of cheap and easily available nitric acid compared with NO_2.

This work was partially supported by the Research for the Future program, JSPS and DAICEL Chemical Industries, Ltd.

Notes and references

† *A typical reaction was carried out as follows:* economic grade concentrated nitric acid (60% over) was used without any treatment. The reaction was carried out as follows: to a two necked flask was added adamantane (**1**) (1 mmol), NHPI (0.1 mmol) and nitric acid (1.5 mmol) in trifluorotoluene (3 mL), and the mixture was reacted under argon at 60 °C for 15 h. After evaporation of the solvent under reduced pressure, the reaction mixture was extracted with diisopropyl ether and the extracts were washed with aq. $NaHCO_3$. After separation of the organic phase, the mixture was subjected to silica gel chromatograph, giving 1-nitroadamantane (**2**) (57%), 1,3-dinitroadamantane (**3**) (3%) together with oxygenated products, adamantan-1-ol (**4**) (8%) and adamantan-2-one (**5**) (4%) (Table 1, entry 1).

‡ Electron paramagnetic resonance (EPR) measurements were carried out under selected conditions. To a two necked flask was added NHPI (0.1 mmol) and nitric acid (1.5 mmol) in trifluorotoluene (10 mL), and the mixture was reacted under argon at 60 °C for 1 h. The EPR spectrum attributed to PINO was clearly observed as a triplet signal based on hyperfine splitting (hfs) by the nitrogen atom (g = 2.0074, a_N = 0.46 mT). The g-value and hfs constant observed for PINO were consistent with those (g = 2.0073, a_N = 0.423 mT) reported by Mackor *et al.*[3b]

1 (*a*) F. L. Albright, *Chem. Eng.*, 1966, **73**, 149, and references therein; (*b*) G. B. Bachman, *J. Org. Chem.*, 1952, **17**, 906; (*c*) L. F. Albright, in *Kirk-Othmer Encyclopedia of Chemical Technology*, Vol 17, eds. J. I. Kroschwite and M. Howe-Grant, Wiley, New York, 1995, 68; (*d*) H. B. Hass, E. B. Hodge and B. M. Vanderbilt, *Ind. Eng. Chem.*, 1936, 339.

2 S. Sakaguchi, Y. Nishiwaki, T. Kitamura and Y. Ishii, *Angew. Chem. Int. Ed.*, 2001, **40**, 222.

3 (*a*) A. Calder, A. R. Forrester and R. H. Thomson, *J. Chem. Soc. (C)*, 1969, 567; (*b*) A. Mackor, A. J. Wajar and J. de Boer, *Tetrahedron*, 1968, **24**, 1623.

4 R. Lee and F. L. Albright, *Ind. Eng. Chem. Proc. Des. Dev.*, 1965, **4**, 441.

5 V. Anantharaj, J. Bhonsle, T. Canteenwala and L. W. Chiang, *J. Chem. Soc., Perkin Trans. 1*, 1999, 31.

CHEMCOMM Communication
www.rsc.org/chemcomm

A new MFI-type zeolite containing uniform supermicropores: synthesis by structural transformation of CTA^+-MCM-41 and application in SCR of NO_x

Xiaoyin Chen and S. Kawi*

Department of Chemical and Environmental Engineering, National University of Singapore, 10 Kent Ridge Crescent, Singapore 119260, Republic of Singapore. E-mail: chekawis@nus.edu.sg

Received (in Cambridge, UK) 12th April 2001, Accepted 12th June 2001
First published as an Advance Article on the web 5th July 2001

A new MFI-type zeolite containing uniform 17 Å supermicropores has been successfully synthesized through structural transformation of CTA^+-MCM-41 and shows better activity for SCR of NO_x than conventional ZSM-5 under lean burn conditions.

The discovery of ordered mesoporous materials, due to their tailor-made pore sizes from 20 to 100 Å, has inaugurated potential pathways to selective catalysis and separation of large molecules.[1,2] Unfortunately, the hydrolysis of the amorphous silica framework and collapse of mesostructures under hydrothermal conditions or even at room atmosphere prevent practical applications of these surfactant-templated silicates.[3,4] Microporous zeolites are widely used as catalysts and sorbents due to their crystalline structure.[5] However, micropores restrict the diffusion rates of reactant and products,[6] hence limiting the activity of zeolite catalysts for certain reactions. Therefore, an attempt to synthesize or fabricate new porous crystalline materials having the advantages of both microporous and ordered macroporous structures is of interest recently for potential industrial applications.[7]

The difference between the synthesis of amorphous mesoporous and crystalline microporous materials lies primarily in the use of templates with different alkyl-chain quaternary ammoniumions. Long-chain quaternary ammoniumions ($\geqslant C_{12}$) form regular arrays of micelles to cast amorphous frameworks of mesostructures;[1] however, short-chain ones (C_1–C_4) template the formation of crystalline microporous zeolites.[8] Detailed investigation by different alkyltrimethylammonium surfactants $C_nH_{2n+1}NMe_3Br$ (n = 6, 8, 10, 12, 14, 16) showed that the shortest chain length (n = 6) gave predominantly MFI-type materials, while longer chains (n = 14, 16) produced mesoporous MCM-41 or amorphous materials.[9] Only mixed phases of MFI/MCM-41 were obtained using a mixed template consisting of C_6- and C_{14}-trimethylammonium ions.[10] Crystalline microporous structures can be formed in the presence of CTA^+ only.[11,12] Recently a two-step crystallization process was introduced into the amorphous framework of mesoporous materials to form MCM-41/ZSM5 composites, where mesoporous MCM-41 was first formed by CTA^+ and the amorphous framework of MCM-41 was then crystallized with TPA^+.[13] However, no literature has ever reported the formation of a crystalline composite containing both micropores and supermicropores (D_p = 15 and 20 Å) by using CTA^+ as the only template. This approach is of importance both for the investigation of the templating role of the surfactant and for the synthesis of a new shape-selective catalysts as supermicropores bridge the gap between micropores and mesopores. Here we report, for the first time, the transformation of the CTA^+–MCM-41 mesostructure into a hydrothermally stable MFI-type composite containing additional uniform supermicropores of 17 Å.

The new MFI-type material was synthesized according to the reported hydrothermal procedure.[12] However, in this work, the starting gel of sodium silicate was not acidified and a final molar composition of SiO_2: x Al_2O_3: y CTAB: z H_2O (x = 0–0.03, y = 0.05–0.5, z = 60–120) was used. After stirring for 60 min at room temperature, the white and viscous surfactant-silicate mixture was transferred to a Teflon-lined autoclave and then heated at 170 °C for different times. The resulting solids were recovered by filtration, thoroughly washed with distilled water and then dried at 100 °C overnight. The products were finally calcined at 550 °C in air for 10 h. For a comparison, conventional ZSM-5 material was synthesized using TPAOH according to the literature procedure.[14]

When SiO_2: y CTA^+: 120 H_2O was treated at 170 °C for 144 h, XRD and FTIR spectra showed that the products are of typical MFI structure. Fig. 1 shows different morphologies of products obtained under different crystallization times, which correspond to hexagonal MCM-41, lamellar phase and MFI structure in XRD patterns, respectively. Fig. 2 shows XRD patterns of the resulting products with varying crystallization times. For the sample formed under 6 h, the XRD pattern of the resulting CTA^+–silica composite clearly shows the hexagonal mesoporous structure of MCM-41. However, the calcined MCM-41 mesostructure completely collapsed when the calcined sample was kept in air at room temperature for two months or treated in boiling water for only 24 h, as shown in Fig. 3(a). For the sample formed under 12 h of crystallization, the hexagonal MCM-41 is transformed to a typical lamellar structure characterized by XRD and N_2 adsorption/desorption

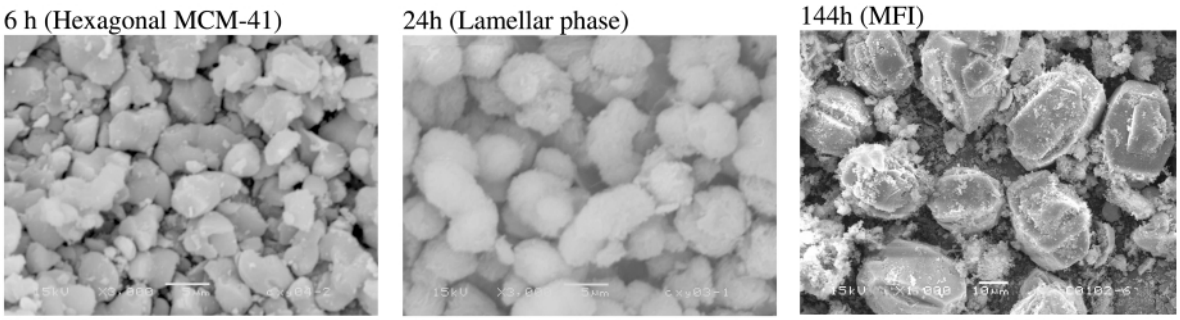

Fig. 1 SEM images of products obtained after crystallization times of 6, 24 and 144 h. SEM was performed on a JEOL JSM-5600LV scanning electron microscope operating at 15 kV.

 DOI: 10.1039/b103327c

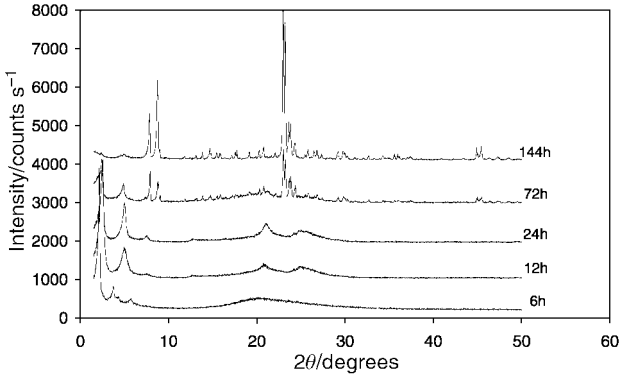

Fig. 2 XRD patterns of as-synthesized products obtained after different crystallization times.

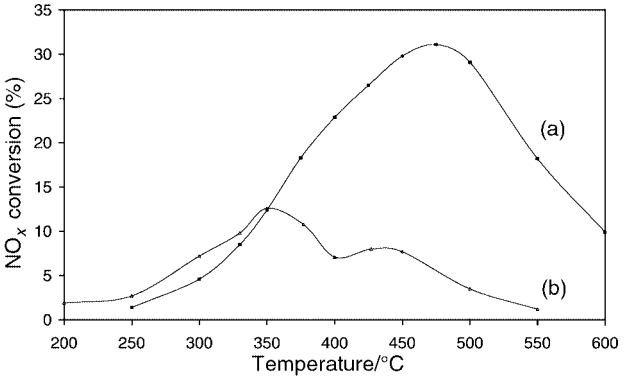

Fig. 4 Comparison of SCR of NO_x over new Co/MFI (a) and conventional Co/ZSM-5 (b). SCR of NO_x was carried out using a continuous flow reactor operating under 1 atm. *Reaction conditions*: 1000 ppm of NO, 1000 ppm of C_3H_8, 5% of O_2 (in He) and SV of 30 000 h^{-1}.

isotherms.[12] Once this product was calcined at 550 °C, all the XRD peaks disappeared and its N_2 adsorption/desorption isotherms remain unchanged after being kept in air at room temperature for two months, as shown in Fig. 3(b). After increasing the crystallization time to 72 h, XRD patterns show that both lamellar phase and MFI structure are present in the resulting product. After further crystallization for 144 h, XRD patterns corresponding to the MFI structure only are observed.

The ratios CTA^+/Si, Si/H_2O and Si/Al are found to be crucial factors influencing the structural transformation of the resulting material. The optimal values of y for successful synthesis of the new MFI materials is 0.1–0.4. Too low a value for CTA^+/Si results in the formation of a mixture containing MFI materials and cristobalite. However, amorphous silica was easily formed at $CTA^+/Si \geqslant 0.5$. Using $y = 0.2$, the new MFI possesses BET surface area and pore volumes of micropores of 409 $m^2\ g^{-1}$ and 0.172 ml g^{-1}, respectively, higher than those for a sample formed from TPA^+ (358 $m^2\ g^{-1}$ and 0.160 ml g^{-1}). Furthermore, N_2 isotherms of the new MFI-type material display capillary condensation characteristics. A H1-type hysteresis loop is clearly observed at $P/P_0 < 0.2$ [Fig. 3(c)], which corresponds to a narrow pore size distribution with a diameter of 17 Å. This pore size is much lower than that of CTA^+-templated MCM-41.[1]

CTA^+-templated MCM-41 readily becomes amorphous when subjected to refluxing in water for short periods of time (24 h).[3,4] In order to eliminate the possibility that the new material contains a mixture of MFI and MCM-41 as those reported elsewhere,[10] hydrothermal treatment was performed on the calcined sample in boiling water for 1 to 30 days. Fig. 3(d) and 3(e) show the N_2 isotherms for these samples, respectively. The hysteresis loops for samples treated in boiling water are similar to that of the untreated one. The pore size distribution of the sample treated in boiling water for 30 days, as shown in Fig. 3 (inset), is still maintained at 17 Å. Furthermore, its BET surface area, morphology and framework structure (which were characterized by SEM, XRD and FTIR) also remain unchanged.

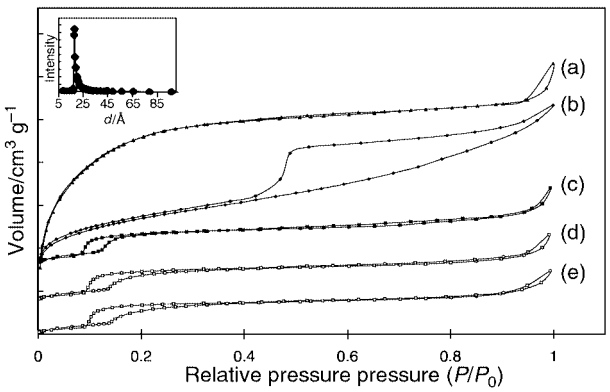

Fig. 3 N_2 adsorption/desorption isotherms of hexagonal MCM-41 (a), lamellar phase (b) and new MFI (c) after being kept in air at room temperature for 2 months prior to N_2 adsorption measurements. N_2 adsorption/desorption isotherms of the new MFI after being kept in boiling water for 10 days (d) and 30 days (e), and its BJH pore size distribution (Å) after 30 days in boiling water (inset).

Small crystals of Co/ZSM-5 were reportedly more active than larger ones for selective catalytic reduction (SCR) of NO_x by propane, showing the influence of mass transfer diffusion on the activities of the catalyst.[15] In this work, we used a new aluminium-containing MFI (Si/Al = 40) with a pore size of 17 Å, which was successfully synthesized using the above method, to investigate the effect of pore size of a catalyst on the conversion of NO_x by propane under lean burn conditions. 1.2 wt% cobalt-supported catalysts were prepared from the new MFI and conventional ZSM-5 by solid-state ion exchange with cobalt nitrate solution. Fig. 4 compares the conversion curves of NO_x on these two catalysts. It is obvious that the NO_x conversion over the new Co/MFI catalyst is much higher than that over conventional Co/ZSM-5 catalyst. The presence of uniform supermicropores of 17 Å in the new MFI catalyst is believed to be helpful for the mass transfer of reactants and reaction products across the pores, hence increasing the activity of the catalyst as diffusion control in microporous channels generally predominates in shape-selective catalysts such as MFI zeolite.[6]

Notes and references

1 J. S. Beck, J. C. Vartuli, W. J. Roth, M. E. Leonowicz, C. T. Kresge, K. D. Schmitt, C. T.-W. Chu, D. H. Olson, E. W. Sheppard, S. B. McCullen, J. B. Higgins and J. L. Schlenker, *J. Am. Chem. Soc.*, 1992, **114**, 10 834.
2 A. Corma, *Chem. Rev.*, 1997, **97**, 2373 and references therein.
3 J. M. Kim and R. Ryoo, *Bull. Korean Chem. Soc.*, 1996, **17**, 66.
4 R. Mokaya, *J. Phys. Chem. B*, 2000, **104**, 8279.
5 *Catalysis and Zeolites: Fundamentals and Applications*, ed. J. Weitkamp and L. Puppe, Springer, New York, 1999.
6 J. Karger, *Diffusion in Zeolites and Other Microporous Solids*, ed. J. Karger and D. M. Ruthven, Wiley, New York, 1992.
7 L. Huang, Z. Wang, J. Sun, L. Miao, Q. Li, Y. Yan and D. Zhao, *J. Am. Chem. Soc.*, 2000, **122**, 3530.
8 M. E. Davis and R. F. Lobo, *Chem. Mater.*, 1992, **4**, 756.
9 J. S. Beck, J. C. Vartuli, G. J. Kennedy, C. T. Kresge, W. J. Roth and S. E. Schramm, *Chem. Mater.*, 1994, **6**, 1816.
10 A. Karlsson, M. Stocker and R. Schmidt, *Microporous Mesoporous Mater.*, 1999, **27**, 181.
11 R. B. Borade and A. Clearfield, *Zeolites*, 1994, **14**, 458.
12 X. Chen, L. Huang and Q. Li, *J. Phys. Chem. B*, 1997, **101**, 8460.
13 L. Huang, W. Guo, P. Deng, Z. Xue and Q. Li, *J. Phys. Chem. B*, 2000, **104**, 2817.
14 R. A. Kensington and G. R. Landolt, *US Pat.*, 1972, 3702886.
15 T. Tabata and H. Ohtsuka, *Catal. Lett.*, 1997, **48**, 203.

CHEMCOMM Communication
www.rsc.org/chemcomm

Oxidation of propene by molecular oxygen over Ti-modified silicalite catalysts

Kazuhisa Murata* and Yoshimichi Kiyozumi

Research Institute for Green Technology, National Institute of Advanced Industrial Science and Technology (AIST), AIST Tsukuba Central 5, 1-1-1, Higashi, Tsukuba, Ibaraki 305-8565, Japan. E-mail: kazu-murata@aist.go.jp

Received (in Cambridge, UK) 27th February 2001, Accepted 13th June 2001
First published as an Advance Article on the web 5th July 2001

Ti-modified high silica zeolite with an Si/Al ratio of 1900 was found to be effective for the oxidation of propene to oxygenates such as propene oxide, in the presence of molecular oxygen at 573 K.

Propylene oxide is an important industrial intermediate which has traditionally been produced by the epoxidation of propene with organic hydroperoxides. In this proress, organic alcohols are stoichiometrically produced as by-products. Recently, titanium silicate-1 (TS-1) zeolite has been shown to be active for the reaction with H_2O_2.[1] This process is still liquid phase whereas the gas phase is more favorable due to product separation. Concerning the gas phase, Haruta and coworkers[2] and Moulijn *et al.*[3] have published work relating to epoxidation with propene/O_2/H_2 over Au dispersed on TS-1 and other Ti-containing supports. In these cases, selectivity to propene oxide is high ($>90\%$), but propene conversion is $<5\%$ and a large amount of H_2 is consumed to form H_2O. Direct propene oxidation by molecular oxygen without H_2 into propene oxide would be of value. The possibility to form propene oxide (PO), in particular, was shown, using $AgNO_3$ or KNO_3 supported on TS-1 and K_2CO_3 or KCl on the same matrix with a PO yield of 0.02%.[4] ARCO Chemical Technology has recently reported improved propene oxide yield in the presence of ethyl chloride.[5] In these cases without gaseous co-reactant such as hydrogen, acidic compounds such as nitrates and chlorides on the catalyst surface could be important for propene activation. In the course of our research program on direct oxidation of propene without any co-reactant, we have reported that titanium sulfate-modified amorphous zirconia was effective for this reaction,[6] although the propene conversion was below 6% and the PO yield only *ca.* 0.5%. Thus, in order to improve propene oxide yield, we tried the use of zeolite families as catalyst supports. In the present study, we report titanium-modified high silica zeolites with different ratios of Si/Al which are effective for the propene oxidation by O_2 without any co-reactant.

High silica zeolite (denoted silicalite) with Si/Al ratio of 3000 was prepared from $Si(OEt)_4$ and tetraethylammonium hydroxide by a hydrothermal method followed by calcination in a air flow at 823 K for 5 h. The other high silica zeolites (denoted HSZ) employed were provided by TOSO Co. Ltd. [HSZ(68),† HSZ(190)† and HSZ(1900)†]. Titanium-modified HSZ samples containing 7.5 wt% Ti[Ti/HSZ(68)] were prepared by the impregnation method.‡ All chemicals were purchased from Wako Pure Chemicals Co.. The amounts of adsorption of ammonia or CO_2 were estimated by using a Thermal Analysis System 001 instrument (MAC SCIENCE Co.).§

The catalytic reaction was performed under atmospheric pressure at temperatures between 473 and 673 K. A tubular fixed-bed reactor (OD = 1.25 cm, length = 60 cm) was filled with 1.0 g of catalyst powder and quartz sand (2.0 g). A pretreatment was done prior to each reaction at 673 K under air flow (25 ml min^{-1}) for 2 h. The reactant feeds were C_3H_6 (7.5 ml min^{-1}) and air (17.5 ml min^{-1}). Hydrocarbons and oxygenated compounds were detected by TCD and FID gas chromatography, the former with Porapack Q (1 m) at 673 K, the latter with 20 wt% FFAP on Chromosorb W (3 m) at 373 K. Products in the gas phase was analyzed by another TCD equipped with a Porapak Q column (3 m) and molecular sieve 5 Å column (3 m) kept at 343 K. The reaction products were also confirmed by mass spectrometry. In order to check the initial activities of catalysts, GC analyses were started 15 min after reaching the reaction temperature. The products were propene oxide (PO), acetaldehyde (AA), C_1–C_8 hydrocarbons (HC), CO and CO_2 (CO_x) and small amounts of other oxygenates [propanal, acetone, formaldehyde, alcohols (MeOH, EtOH, Pr^iOH)] were also detected.

The catalytic performances at 573 K are summarized in Table 1. No product was formed through the reactor in the absence of catalyst. Both Ti/SiO_2 (run 1) and Ti/TiO_2 (run 2) exhibited low propene conversion and only hydrocarbons (HC) and CO_x were produced. For the HSZ family we found that the catalyst

Table 1 Results of the oxidation of propene by molecular oxygen 573 K[a]

Run		Conv. propene (%)	PO yield (%)	Selectivity (%)[d]									
				PO	PA	AA	HA	AL	AC	Alc	HC	CO_x	Residue[e]
1	7.5% Ti/SiO_2	3.76	0	0	0	0	0	0	0	0	72.7	24.7	2.6
2	7.5% Ti/TiO_2	2.11	0	0	0	0	0	0	0	0	47.0	52.9	0.1
3	7.5% Ti/HSZ(68)[b]	97.8	3.11	3.18	5.85	6.25	0	0	0	5.39	44.5	5.12	35.6
4	7.5% Ti/HSZ(190)[b]	95.5	8.90	9.32	9.85	20.0	0	28.3	0	0	31.4	1.13	9.85
5	7.5% Ti/HSZ(1900)[b]	47.7	17.3	36.3	0	29.6	2.64	0.66	0	2.87	27.8	0	0.13
6	7.5% Ti/silicalite(3000)[b]	1.89	Trace	Trace	0	0	0	0	0	0	100	0	0
7	15% Ti/HSZ(1900)[b]	78.2	20.4	26.1	0	23.6	2.92	0	0	2.60	43.9	0.74	0.14
8	15% Ti/HSZ(1900)[bc]	9.03	3.69	40.9	0	23.5	0.12	0	0	0	35.3	0	0
9	HSZ(1900)[b]	83.2	6.60	7.93	0	11.3	1.73	3.43	0.30	5.32	69.1	0.53	0
10	7.5% Ti/HSZ(1900)[be]	37.3	8.81	23.6	0	16.2	0.06	0	0	0	59.7	0.44	0

[a] *Reaction conditions*: see text. [b] Number in parentheses is the Si/Al ratio for the catalyst support employed. [c] Reaction carried out at 523 K. [d] Products propene oxide (PO), acetaldehyde (AA), formaldehye (HA), acrolein (AL), acetone (AC), alcohol [Alc, (MeOH + EtOH + Pr^iOH)], hydrocarbons [HC, (C_1 + C_2 + C_3 + C_4 + C_5 + C_6 + C_7 + C_8)], CO and CO_2 (CO_x). [e] Residue estimated using the equation 100 − sum of all detectable products. Calcination of the catalyst carried out at 173 K.

 DOI: 10.1039/b101857o

Table 2 Quantitative estimation of acid and base sites on Ti-modified HSZ catalysts by NH_3- or CO_2-TPD[a]

Sample	Base sites[b]			Acid sites[b]		
	x Within 673 K CO_2(g)/Cat(g)	*y* Within 440 K CO_2(g)/Cat(g)	*y*/*x*[c] (%)	*x* Within 673 K NH_3(g)/Cat(g)	*y* Within 440 K NH_3(g)/Cat(g)	*y*/*x*[c] (%)
7.5% Ti/silicalite(3000)	0.0104	0.0080	76.9	0.0129	0.00956	74.1
7.5% Ti/HSZ(1900)	0.0187	0.0143	76.6	0.0495	0.042	85.3
7.5% Ti/HSZ(68)	0.0196	0.0147	75.0	0.0339	0.0233	68.7

[a] Thermogravimetric analysis conducted in argon in the range 300–673 K. [b] The acid or base sites were estimated by the amounts of NH_3 or CO_2 desorbed within each prescribed temperature. [c] These values, calculated [100 (*y*/*x*)] can be regarded as the percentage of *weak* base or acid sites.

performances were strongly dependent on the Si/Al ratio of the supports. For 7.5% Ti/HSZ(68) (run 3), propene conversion was very high (97.8%) and some oxygenates were produced with CO_x and a substantial amount of residue, but the PO yield was only 3.11%. The 7.5% Ti/HSZ(190) (run 4) also showed high propene conversion of 95.5% and both CO_x and the amount of residue were decreased, while the selectivities to oxygenates were increased. In this case the PO yield was 8.90%.

On the other hand, the conversion of propene on 7.5% Ti/HSZ(1900) was approximately half the propene conversion of 7.5% Ti/HSZ(190), while selectivities to CO_x and residue (0.13%) were dramatically lower than for 7.5% Ti/HSZ(190). For 7.5% Ti/HSZ(1900) (run 5) the selectivity to PO was found to be 36.3% and major by-products were acetaldehyde (AA) and hydrocarbons (HC). As a result, the PO yield (17.3%) on 7.5% Ti/HSZ(1900) was twice that of 7.5% Ti/HSZ(190). 7.5% Ti/silicalite (3000) (run 6), on the other hand, showed much lower propene conversion (1.89%) than 7.5% Ti/HSZ(1900). Therefore, it is indicated that titanium-modified HSZ with an Si/Al ratio of 1900 not only has a moderate ability to activate propene using molecular oxygen, but also properties suitable for predominant formation of oxygenates (in particular, PO) over hydrocarbons (HC).

The 15% Ti/HSZ(1900) catalyst (run 7) exhibited higher propene conversion (78.2%) than 7.5% Ti/HSZ(1900), although the PO selectivity was slightly decreased, while HC selectivity was increased. In this case, the PO yield was 20.4%, > 10 times those previously reported under O_2/H_2 conditions[2,3] and, at least, > 3 times recently reported for Ag-containing catalyst[4,5] or photocatalyst[7] systems. At 523 K, the PO selectivity on 15% Ti/HSZ(1900) was as high as 40.9%, while the propene conversion was 9.03% (run 8). HSZ(1900) alone (run 9) showed higher propene conversion and HC selectivity than 7.5% Ti/HSZ(1900), while less selectivity to oxygenates was observed. This indicated that surface properties for oxygenate formation were improved by Ti modification.¶

The mechanism of oxidation of propene over Ti/HSZ catalysts is not clear. However, catalyst performances are dependent on Si/Al ratio of the HSZ supports (Table 1) and, therefore, it seems likely that surface acid–base properties are responsible for the catalyst behavior, in particular, propene conversion and residue yield. In fact, as shown in Table 2, where NH_3- or CO_2-TPD was conducted by using thermogravimetric methods, 7.5% Ti/silicalite(3000) catalyst exhibited weaker adsorption for NH_3 as well as CO_2 than the other two catalysts; This is in good accordance with much lower propene conversion of this catalyst relative to the other catalysts (Table 1, runs 3, 5 and 6).

NH_3 adsorption on 7.5% Ti/HSZ(1900) catalyst was slightly larger than that on 7.5% Ti/HSZ(68), while the amount of CO_2 adsorbed was similar (Table 2). However, as much as 85.3% of NH_3 adsorbed on 7.5% Ti/HSZ(1900) was found to be desorbed below 440 K (Table 2, *y*/*x* ratio and Fig. 1), whereas the ratio of NH_3 desorption below 440 K on 7.5% Ti/HSZ(68) was only 68.7%; These findings indicated that the ratio of strong to weak acid sites on 7.5% Ti/HSZ(1900) is smaller than that on 7.5% Ti/HSZ(68). This could be consistent with the fact that the 7.5% Ti/HSZ(1900) catalyst showed lower propene conversion and smaller amounts of residue product than those for 7.5% Ti/HSZ(68) (Table 2, runs 3 and 5). The calcination of

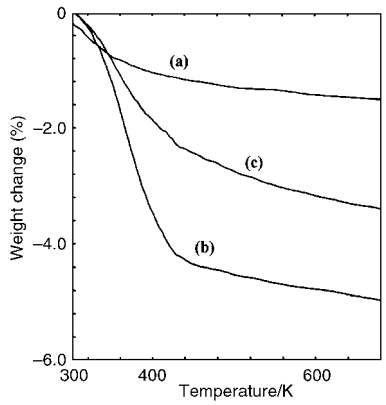

Fig. 1 NH_3-TPD data for (a) 7.5% Ti/silicalite(3000), (b) 7.5% Ti/HSZ(1900) and (c) 7.5% Ti/HSZ(68).

7.5% Ti/HSZ(1900) at 1073 K, higher by 100 K than the standard calcination temperature (973 K), would result in a decrease in weak acid sites, while strong acid sites might still be retained. As a result, propene conversion was decreased to 37.3% and selectivity to hydrocarbon formation (HC) was raised to 59.7% (Table 1, run 10).

In summary, Ti-modified HSZ(1900) was found to catalyse the oxidation of propene to oxygenates, such as propene oxide, by molecular oxygen at 573 K. The catalyst performances are affected by the Si/Al ratio of the HSZ supports as well as the presence of titanium. Cooperation between moderate acid properties of HSZ(1900) and titanium favors oxygenate formation. It is expected that fine control of acid properties of these supports and titanium content well enhance the catalyst performances for propene oxide formation.

Notes and references

† These zeolites are of H-ZSM-5 type where the number in parentheses is the Si/Al ratio.

‡ The calcined HSZ was evacuated at 673 K for 3 h in order to eliminate a small amount of water. Then, the HSZ was impregnated with $Ti(OPr^i)_4$ in Pr^iOH, followed by addition of H_2O (25 g) leading to precipitation of titanium oxide. The sample was then dried at 373 K for 10 h and finally calcined at 973 K for 3 h.

§ The sample was evacuated at 673 K for 2 h then, after cooling to 373 K, ammonia adsorption on to the surface was allowed to occur to saturation. Evacuation was then applied for 1 h at the same temperature followed by thermal gravimetric (TG) analysis. CO_2 adsorption was carried out at 300 K.

¶ The TS-1 catalyst contains 1.68 wt% Ti and an Si/Al ratio of 46,[1] in contrast to 7.5% Ti and Si/Al ratio of 1900 for 7.5% Ti/HSZ(1900). TS-1 is thus less effective for selective PO formation than 7.5% Ti/HSZ(1900) catalyst under propene/O_2.

1 L. Y. Chen, G. K. Chuah and S. Jaenicke, *J. Mol. Catal. A: Chemical*, 1998, **132**, 281; M. G. Clerici, G. Bellussi and U. Romano, *J. Catal.*, 1991, **129**, 159.

2 T. Hayashi, K. Tanaka and M. Haruta, *Am Chem. Soc., Div. Pet. Chem.*, 1996, **41**, 71.

3 T. A. Nijhuis, B. J. Huizinga, M. Makkee and J. A. Moulijn, *Ind. Eng. Chem. Res.*, 1999, **38**, 884.

4 S. Yagi and K. Sugita, *Jap. Pat.*, JP 09-291084 A2, 1997.

5 A. P. Kahn, *US Pat.*, US 1997-903127, 30 July 1997.

6 C. Murata, K. E. Bere, T. Hayakawa, S. Hamakawa, K. Suzuki and K. Matano, *React. Kinet. Catal. Lett.*, 2001, **72**, 57.

7 A. Yoshida, C. Murata and T. Hattori, *Chem. Commun.*, 1999, 1551.

CHEMCOMM
Communication
www.rsc.org/chemcomm

Enantioselective binding of dipeptides using acyclic receptors†

Enrique Botana,[a] Sandrine Ongeri,[a] Rosa Arienzo,[b] Mariangela Demarcus,[b] Jeremy G. Frey,[b] Umberto Piarulli,[c] Donatella Potenza,[a] Cesare Gennari*[a] and Jeremy D. Kilburn*[b]

[a] *Dipartimento di Chimica Organica e Industriale, Università di Milano, Centro CNR per lo Studio delle Sostanze Organiche Naturali, via G. Venezian 21, I-20133 Milano, Italy. E-mail: cesare.gennari@unimi.it; Fax: +39 02 2663079*

[b] *Department of Chemistry, University of Southampton, Highfield, Southampton, UK SO17 1BJ. E-mail: jdk1@soton.ac.uk; Fax: +44 23 80596905*

[c] *Dipartimento di Scienze Mat. Fis. e Chimiche, Università dell'Insubria, via Valleggio 11, I-22100 Como, Italy*

Received (in Cambridge, UK) 13th March 2001, Accepted 6th June 2001
First published as an Advance Article on the web 5th July 2001

Novel receptors featuring a 2,6-diamidopyridine 'head' group and bearing sulfonamidopeptide sidearms have been prepared on the solid-phase; one receptor showed high selectivity for *N*-Cbz-D-Ala-D-AlaOH over its enantiomer *N*-Cbz-L-Ala-L-AlaOH, but absolute binding constants were relatively weak, which can be understood in terms of receptors which have to unfold, breaking intramolecular hydrogen bonds, in order to accommodate the guests.

While several macrocyclic hosts have been prepared and shown to bind amino acids or peptide fragments with excellent selectivity,[1] during the last decade a different class of receptors for peptides called 'tweezer receptors' or 'two-armed' receptors have been developed.[2,3] Many of these systems bind substrates, and particularly peptides, with selectivities which are in many ways surprising, given the apparent flexibility of such acyclic receptor structures.

Whereas in many such 'two-armed' receptor systems the head group plays only a limited role in the binding of the guest, the group in Southampton have recently developed receptors utilising a diamidopyridine as the head group which can specifically bind to carboxylic acid functionality, and such receptors, with peptidic arms, have proven to be selective receptors for peptides with a carboxylic acid terminus.[3] In this paper we report studies on novel 'two-armed' receptors consisting of a 2,6-diamidopyridine head group bearing sulfonamidopeptide sidearms,[4] one of which, in particular, shows high binding selectivity for the dipeptide *N*-Cbz-D-Ala-D-AlaOH (Cbz = benzyloxycarbonyl) over its enantiomer *N*-Cbz-L-Ala-L-AlaOH. In contrast to the CONH moiety of peptides, which provides both a strong hydrogen-bond donor and acceptor, the SO_2NH moiety of sulfonamidopeptides provides a very strong donor NH, but the SO_2 group is only a weak acceptor.[5,6]

The synthesis of the novel receptors was accomplished on the solid phase starting from *N*-Fmoc-Gly Wang resin **1** (loading 0.88 mmol g^{-1}) (Scheme 1). After deprotection of the amino-group, diamidopyridine derivative **2**[3] was coupled using a 20% excess of resin, and the unreacted amino groups on the resin were capped with acetylimidazole. Deprotection of the Fmoc groups and coupling with the L-valine-derived β-*N*-Fmoc-amino sulfonyl chloride using DMAP as catalyst and dimethylketene methyl trimethylsilyl acetal (MTDA) as HCl scavenger,[5,7] gave a resin bound disulfonamide. Cleavage of Fmoc protection, followed by acetylation gave the desired disulfonamide derivative, which was cleaved from the resin by a direct basic methanolysis or by acidic TFA–H_2O cleavage followed by esterification to give receptor **4**. Alternatively the resin bound sulfonamide could be deprotected and subjected to a further coupling with the L-valine-derived β-*N*-Fmoc-amino sulfonyl chloride, followed by deprotection, acetylation and cleavage to give receptor **5**.

Binding studies with receptors **4** and **5** were carried out with a series of substrates in deuteriochloroform, using a standard NMR titration experiment.[8] Titration of **4** with simple amino acid derivatives such as *N*-Cbz-L-AlaOH or *N*-Boc-L-AlaOH gave modest binding constants (K_{ass} = 207 and 119 M^{-1} respectively) and little apparent enantioselectivity (*N*-Cbz-L-AlaOH: K_{ass} = 207 M^{-1}, *N*-Cbz-D-AlaOH: K_{ass} = 270 M^{-1}, Table 1). Binding of all three amino acid substrates led to significant downfield shifts of the amidopyridine NH[1] (≥0.5 ppm).[9] Binding of dipeptide guests gave slightly higher binding constants, and titration of **4** with, for example, *N*-Cbz-L-

† Electronic supplementary information (ESI) available: details of temperature dependence experiments, NMR binding studies and chemical shift data. See http://www.rsc.org/suppdata/cc/b1/b102383g/

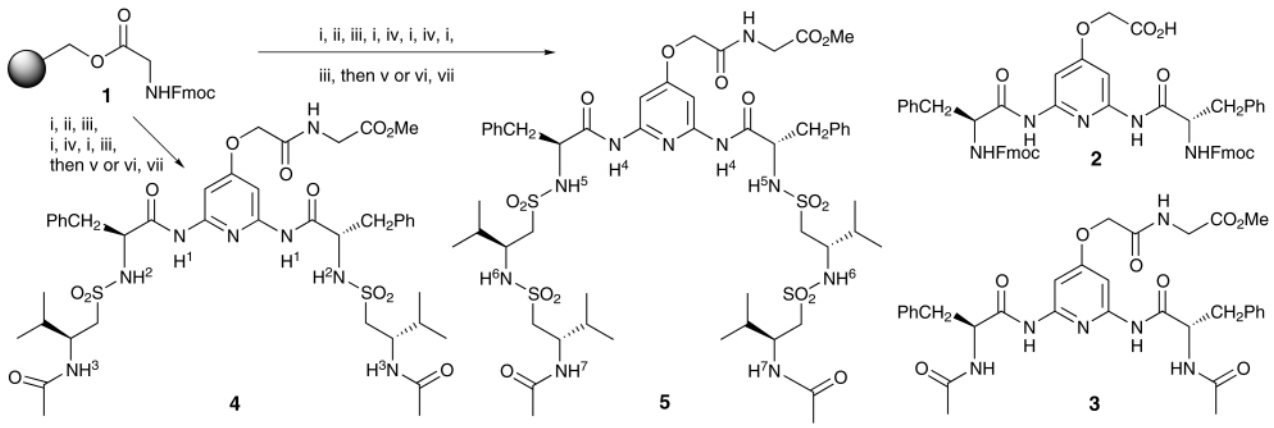

Scheme 1 *Reagents and conditions*: (i) piperidine (20% in DMF); (ii) **2**, DIC, HOBT, DMAP, DCM; (iii) AcIm, DCM; (iv) $FmocNHCH(CHMe_2)CH_2SO_2Cl$, DMAP, MTDA, DCM, two cycles; (v) Et_3N, MeOH, DMF; (vi) TFA, H_2O; (vii) EDC, DMAP, MeOH, THF.

 DOI: 10.1039/b102383g

Ala-L-AlaOH gave a binding constant of 245 M^{-1} and led to downfield shifts of both the amidopyridine and sulfonamide NH's (NH^1: $\Delta\delta$ = 0.25 ppm, NH^2: $\Delta\delta$ = 0.30 ppm) and an upfield shift of acetamide NH^3 ($\Delta\delta$ = 0.12 ppm). Binding of dipeptides was also associated with downfield shifts for both the amide and carbamate NH signals of the guest ($\Delta\delta$ = 0.10–0.35 ppm). Titration with *N*-Cbz-D-Ala-D-AlaOH led to little change to the amidopyridine NH^1 ($\Delta\delta \leqslant 0.03$ ppm), but analysis of the downfield shift of sulfonamide NH^2 ($\Delta\delta$ = 0.28 ppm) and the upfield shift of acetamide NH^3 ($\Delta\delta$ = 0.19 ppm) gave a binding constant of 242 M^{-1} indicating that **4** also shows little enantioselectivity for dipeptides (K_{ass} for *N*-Cbz-L-Ala-L-AlaOH = 245 M^{-1}, Table 1). Thus receptor **4** does appear to bind dipeptides and simple amino acid derivatives, but the absolute binding constants are rather low in comparison to other diamidopyridine based receptors, and the shifts of the various NH signals on binding are also rather small in comparison to those seen in other related receptor systems.[1b,10,11] We therefore studied receptor **5**, reasoning that with additional binding functionality in the longer sidearms it might show increased affinity for peptide guests. In practice, receptor **5** initially gave absolute binding constants somewhat lower than **4** (Table 1) and again only small shifts were observed for the various NH signals on addition of guest. However, binding of the *N*-Cbz-Ala-AlaOH dipeptide enantiomers showed marked selectivity. Titration of **5** with *N*-Cbz-L-Ala-L-AlaOH gave a binding constant of 107 M^{-1} and led to a downfield shift of 0.3 ppm for the amidopyridine NH^4 but only small changes to the sulfonamide and acetamide NH's (NH^5, NH^6, NH^7, $\Delta\delta \leqslant 0.07$ ppm). In contrast, titration of **5** with *N*-Cbz-D-Ala-D-AlaOH gave a binding constant of 2404 M^{-1} with a particularly large downfield shift for the sulfonamide NH^6 ($\Delta\delta$ = 0.72 ppm) but an upfield shift for sulfonamide NH^5 ($\Delta\delta$ = 0.38 ppm) and even a small upfield shift for the amidopyridine NH^4 ($\Delta\delta$ = 0.05 ppm)! Binding of *N*-Cbz-D-Ala-D-AlaOH was also accompanied by significant shifts of several CH signals of the host (up to 0.37 ppm) and significant shifts for the guest NH protons ($\Delta\delta \approx 0.5$ ppm).[9]

The small shifts on binding for the NH signals, and generally low absolute binding constants, for receptors **4** and **5**, can be rationalised by considering the unbound conformation of the receptors, which were investigated in detail by NMR.

In the ^{1}H-NMR spectra of **4** and **5** in $CDCl_3$ peaks are rather broad, indicating slow conformational equilibria at room temperature (on the NMR time scale). The NH protons, for both **4** and **5** display a very small concentration dependence in $CDCl_3$ indicating that the receptors do not aggregate in the concentration range considered (0.5–20 mM). At a concentration of 8.5 mM in $CDCl_3$ the signals of the amidopyridine NH protons appear at unexpectedly low field [$NH^1$1(**4**): 9.41, NH^4(**5**): 9.32 ppm compared to standard values[1b,11] 8.0–8.5 ppm], and the sulfonamide NH protons are also strongly deshielded [NH^2(**4**): 6.32, NH^5(**5**): 5.78, NH^6(**5**): 6.32 ppm compared to their standard values[5] 4.50–4.74 ppm], while the acetamide protons, NH^3(**4**) and NH^7(**5**), are closer to their normal chemical shifts (6.2 compared to 6.0–6.2 ppm). In comparison, the spectrum of the control compound **3** (Scheme 1) in $CDCl_3$ is perfectly resolved, and the amidopyridine NH signal is found at 8.83 ppm (for a concentration of 8.5 mM), whereas the acetamide NH proton is found at 6.56 ppm. This suggests that receptors **4** and **5** collapse to give folded structures stabilised by intramolecular hydrogen bonds. Such a conclusion is supported by NOESY and ROESY experiments, which revealed a large number of NOE contacts consistent with a folded structure.

Thus binding of substrates by **4** or **5** involves a degree of unfolding of the receptor, and breaking of intramolecular hydrogen bonds (with an associated energetic cost), to allow interaction with the guest, resulting in rather low binding constants and only small overall changes to the signals for the hydrogen bonding NH protons. In particular, the only significant change in the NMR for **5**, on binding of *N*-Cbz-L-Ala-L-AlaOH, is a downfield shift of the amidopyridyl NH^4, indicating breaking of an intramolecular hydrogen bond to this NH and binding with the carboxylic acid of the guest. In contrast, the binding of *N*-Cbz-D-Ala-D-AlaOH by **5** leads to significant shifts of several CH as well as NH signals throughout the spectrum (although there is little overall shift to the amidopyridine NH^4) suggesting a much more dramatic conformational change for the receptor on binding this guest[12] and that binding of this guest is sufficiently strong to overcome the penalty of unfolding the receptor. In any event such high enantioselectivity, > 20 : 1 (effectively discriminating between methyl groups and hydrogen atoms), has rarely been observed in synthetic receptors,[1,10] and is particularly noteworthy in such a structurally simple acyclic receptor, which appears to lack much, if any, preorganisation for binding.

Table 1 Binding constants[a] (K_{ass}) for the 1 : 1 complexes[b] formed between receptors **4** and **5** and various amino acid and dipeptide derivatives, in $CDCl_3$ at 25 °C

	K_{ass}[a]/M^{-1}	
Substrate	**4**	**5**
N-Cbz-L-AlaOH	207	32
N-Boc-L-AlaOH	119	—[c]
N-Cbz-D-AlaOH	270	—[c]
N-Cbz-L-Ala-L-AlaOH	245	107
N-Boc-L-Ala-L-AlaOH	361	—[c]
N-Cbz-D-Ala-D-AlaOH	242	2404[d]

[a] Calculated from the chemical shifts of various ^{1}H signals of **4** and **5**. Unless otherwise stated errors for K_{ass} estimated as < 10%.[8] [b] 1 : 1 stoichiometry was confirmed by Scatchard analysis.[13] [c] Experiment not performed. [d] Error was estimated as < 5%, using data from five different ^{1}H signals.

We thank the Commission of the European Union (TMR Network grant 'Enantioselective separations' ERB FMRX-CT-98-0233) for financial support and postgraduate and postdoctoral fellowships (E. B., M. D. and S. O.).

Notes and references

1 For a recent review on peptide receptors, see: (*a*) M. W. Peczuh and A. D. Hamilton, *Chem. Rev.*, 2000, **100**, 2479. See also: (*b*) P. D. Henley, C. P. Waymark, I. Gillies and J. D. Kilburn, *J. Chem. Soc., Perkin Trans. 1*, 2000, 1021, and references therein.
2 For original work on tweezer receptors, see: C.-W. Chen and H. W. Whitlock, Jr., *J. Am. Chem. Soc.*, 1978, **100**, 4921.
3 T. Braxmeier, M. Demarcus, T. Fessmann, S. McAteer and J. D. Kilburn, *Chem. Eur. J.*, 2001, **7**, 1889, and references therein.
4 For earlier use of sulfonamidopeptides in tweezer-like receptors, see: D. W. P. M. Löwik, M. D. Weingarten, M. Broekema, A. J. Brouwer, W. C. Still and R. M. J. Liskamp, *Angew. Chem., Int. Ed.*, 1998, **37**, 1846; C. Gennari, H. P. Nestler, B. Salom and W. C. Still, *Angew. Chem., Int. Ed. Engl.*, 1995, **34**, 1765.
5 C. Gennari, M. Gude, D. Potenza and U. Piarulli, *Chem. Eur. J.*, 1998, **4**, 1924.
6 B. Salom, D. Potenza, C. Gennari, C. Longari, E. Fioravanzo, O. Carugo and N. Sardone, *Chem. Eur. J.*, 1996, **2**, 644.
7 M. Gude, U. Piarulli, D. Potenza, B. Salom and C. Gennari, *Tetrahedron Lett.*, 1996, **37**, 8589.
8 Data was analysed using a modified version of the algorithm described by C. A. Hunter and used in his software NMRTit HG (A. P. Bisson, C. A. Hunter, J. C. Morales and K. Young, *Chem. Eur. J.*, 1998, **4**, 845), to allow simultaneous evaluation of data from several signals in the NMR of the host. For full details see the electronic supplementary information.
9 Chemical shifts given for individual protons during titration experiments are those observed at the end of the titration (after addition of 10 equiv. of guest) and are therefore less than the chemical shifts that would be reached on saturation.
10 P. D. Henley and J. D. Kilburn, *Chem. Commun.*, 1999, 1335.
11 J. Dowden, P. D. Edwards, S. S. Flack and J. D. Kilburn, *Chem. Eur. J.*, 1999, **5**, 79, and references therein.
12 Intermolecular NOE experiments on the 1 : 1 complex formed between *N*-Cbz-D-Ala-D-AlaOH and **7** were inconclusive, due to the limited solubility of *N*-Cbz-D-Ala-D-AlaOH.
13 R. E. Lenkinski and J. Reuben, *J. Am. Chem. Soc.*, 1976, **98**, 3089.

CHEMCOMM Communication
www.rsc.org/chemcomm

Hydroformylation of 1-hexene with rhodium in non-aqueous ionic liquids : how to design the solvent and the ligand to the reaction

Frédéric Favre, Hélène Olivier-Bourbigou,* Dominique Commereuc and Lucien Saussine

Institut Français du pétrole, 1-4 Avenue de Bois-Préau, 92852 Rueil-Malmaison, France. E-mail: helene.olivier-bourbigou@ifp.fr

Received (in Cambridge, UK) 10th May 2001, Accepted 7th June 2001
First published as an Advance Article on the web 6th July 2001

A wide range of ionic liquids based on imidazolium and pyrrolidinium cations and weakly coordinating anions proved to be efficient solvents for the biphasic rhodium catalyzed hydroformylation of 1-hexene; the reaction rate and regioselectivity, and the retention of the rhodium can be optimized by fitting the nature of the anions and cations of the ionic liquid and the modified phosphite or phosphine ligands.

Ionic liquids are good solvents for transition-metal complexes in many homogeneously catalyzed reactions, *e.g.* olefin hydrogenation, hydroformylation, oligomerization and Pd mediated carbon–carbon coupling reactions.[1] In many cases the reaction products are very weakly soluble in the ionic phase so that the catalyst can be separated by simple decantation and recycled. The aqueous two-phase catalysis concept, which has been already applied industrially for propene hydroformylation,[2] can then be extended to substrates and ligands that are poorly soluble or non stable in water. Higher olefin Rh-hydroformylation has been performed using different 1-butyl-3-methylimidazolium room-temperature liquid salts as solvents, in the presence of phosphine ligands. The main difficulty is to immobilize the rhodium catalyst in the ionic liquid phase while maintaining its activity and selectivity. A solution is to modify the neutral phosphine ligands with ionic groups.[3] Thanks to their chemical and physical versatility,[4] ionic liquids can be specially designed to fit with the ligand and the operating conditions that provide the best performances in catalysis.

In this communication, for the first time we report the effect of the nature of the cations and anions of the ionic liquids on the Rh-catalyzed hydroformylation of 1-hexene. We also provide our preliminary study on the performances of different phosphorus ligand–ionic liquid systems.

We have prepared a wide range of ionic liquids by varying the nature of the cation *e.g.* 1,3-dialkylimidazolium, 1,2,3-trialkylimidazolium and *N*,*N*-dialkylpyrrolidinium and the nature of the anion *e.g.* BF_4^-, PF_6^-, $CF_3CO_2^-$, $CF_3SO_3^-$ (OTf^-) and $N(CF_3SO_2)_2^-$ (NTf_2^-). The BF_4^-, NTf_2^- and PF_6^- ionic liquids were prepared by anion exchange starting from imidazolium or pyrrolidinium chloride. The $CF_3SO_3^-$ and $CF_3CO_2^-$ salts were prepared by direct methylation of 1-alkylimidazole or 1-alkylpyrrolidine with the corresponding methyl esters.[5] We have measured the solubility of 1-hexene in these ionic liquids (Fig. 1). For a given anion, *e.g.* $CF_3CO_2^-$, the solubility of 1-hexene increases upon increasing the length of the alkyl chain of the 1,3-dialkylimidazolium *e.g.* 1-butyl-3-methylimidazolium (BMI^+) *vs.* 1-hexyl-3-methylimidazolium (HMI^+). Methylation of the C(2) atom of the imidazolium ring tends to decrease the solubility of 1-hexene *e.g.* 1-butyl-2,3-dimethylimidazolium $BDMI^+NTf_2^-$ *vs.* $BMI^+NTf_2^-$. No significant differences are observed by changing the 1-butyl-3-methylimidazolium cation for *N*,*N*-butylmethylpyrrolidinium (BMP^+). For a same cation, *e.g.* BMI^+, the solubility of 1-hexene increases as follows: $BF_4^- < PF_6^- < OTf^- < CF_3CO_2^- < NTf_2^-$.

In a first series of experiments, we performed 1-hexene hydroformylation using these different ionic liquids as solvents for the $Rh(CO)_2(acac)$ precursor associated with the sodium salt of monosulfonated triphenylphosphine (TPPMS) (Fig. 1). The results reveal that there is a correlation between the reaction rates (TOF min^{-1}) and the solubility of 1-hexene in ionic

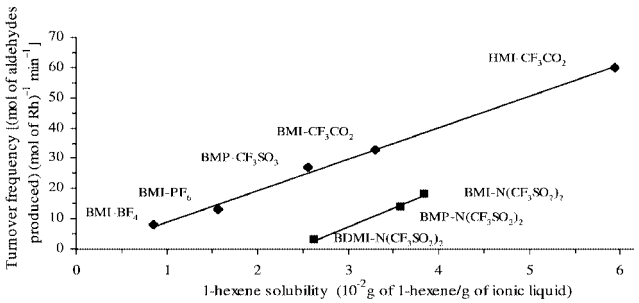

Fig. 1 Turnover frequency as a function of 1-hexene solubility in the ionic liquids. *Reaction conditions*: $Rh(CO)_2(acac)$ 0.075 mmol, 1-hexene/Rh = 800, TPPMS/Rh = 4 , heptane was used as internal standard, CO/H_2 (molar ratio) = 1, $P(CO/H_2)$ = 2 MPa, T = 80 °C, TOF determined at 25% conversion of 1-hexene.

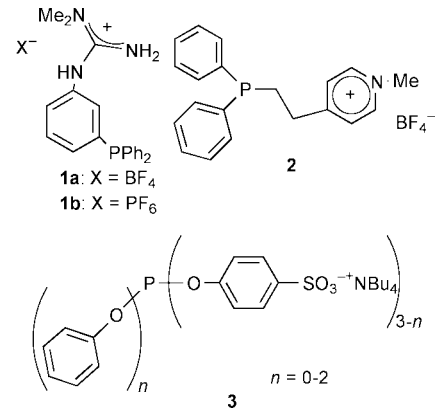

Scheme 1

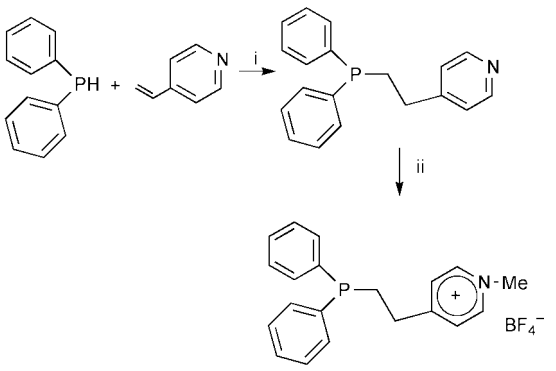

Scheme 2 Synthesis of ligand **2**. *Reagents and conditions*: i, $KOBu^t$, reflux for 3 h in THF; ii, $Me_3O^+BF_4^+$ in CH_2Cl_2, −78 °C.

 DOI: 10.1039/b104155j

Table 1 Hydroformylation with different ligand–ionic liquid systems[a]

Entry	Ligand L	L/Rh	Ionic liquid	Reaction time/min	Conversion[b] (%)	Aldehydes[c] (mol %)	n/i[d]	TOF[e]/min^{-1}
1	**1a**	10	$BMI^+BF_4^-$	180	77	74	3.7	3
2	**1b**	7		210	83	78	4	3
3	**2**	4		180	87	96	2.6	4
4	**3**	9.5	$BMI^+PF_6^-$	180	96	88	12.6	4
5[f]	**3**			240	85	89	11.2	2
6[g]	**3**			330	42	88	11.7	1

[a] *Reaction conditions*: $Rh(CO)_2(acac)$ 0.075 mmol, 1-hexene/Rh = 800, CO/H_2 (molar ratio) = 1 ; $P(CO/H_2)$ = 2 MPa, T = 80 °C, heptane (internal standard) = 2 mL, 1-hexene = 7.5 mL, ionic liquid = 4 mL. [b] Conversion = [(initial 1-hexene) − (1-hexene after reaction)]/(initial 1-hexene). [c] The other products are 2- and 3-hexenes. [d] Linear to branched aldehyde ratio. [e] Mol of aldehydes per mol Rh per minute at 25% conversion. [f] Recycling of 4. [g] Recycling of 5.

liquids. In all cases, the selectivity in aldehydes is > 97%, the remainder being isomerized hexenes. Surprisingly, in the NTf_2^- based ionic liquids, lower TOF are obtained despite the relatively good solubility of 1-hexene in these media. As suggested by the determination of ionic liquid relative polarity,[6] the NTf_2^- based salts could be more coordinating than the PF_6^- salts. In all cases, the n/i ratio is not affected by the nature of the solvent.

In a second series of experiments, we have synthesized the monosubstituted guanidinium triphenylphosphine ligands **1a** and **1b**,[7] and the pyridinium diphenylethylphosphine ligand **2** (Scheme 1). Ligand **2** was prepared in two steps according to Scheme 2. Ligands **1a** and **1b** show good solubility in the ionic liquid $BMI^+BF_4^-$. They give good selectivities towards the linear aldehydes. Similar catalytic performances were obtained by using **1a** or **1b** (Table 1, entries 1 and 2). However, the retention of the Rh in the $BMI^+BF_4^-$ phase was more efficient with **1a** (the Rh content in the organic phase was lower than the detection limit according to ICP analysis for **1a**, while the level was 0.8% of the initial Rh for **1b**). Ligand **2** (entry 3) presents higher reaction rates and higher selectivity towards aldehydes than **1a** and **1b**. However, the leaching of the Rh in the organic phase was found to be higher for **2** (2% of the initial Rh).

Phosphites and bisphosphites are well known ligands for Rh-hydroformylation to afford higher reaction rates.[8] Because of their instability toward hydrolysis, examples of their use in aqueous two-phase hydroformylations are rare.[9] Ionic liquids offer suitable alternative solvents. We describe here the first use of phosphite based ligands for the biphasic hydroformylation of 1-hexene in ionic liquids. Ligand **3**, a mixture of tetrabutylammonium salt of the mono- di- and tri-sulfonated triphenylphosphites, has been prepared by transesterification of triphenylphosphite with the tetrabutylammonium salt of *p*-hydroxyphenylsulfonic acid.[9] In the reaction with the ligand **3**, using $BMI^+PF_6^-$ as the solvent, good catalytic activity is observed (entry 4). The selectivity for the linear aldehyde is much higher than the selectivity obtained with phosphine ligands (enties 1–3). The use of the modified phosphite **3** limits the loss of the Rh in the organic phase (leaching is 2% of the initial Rh used). At the end of the run, the organic phase is decanted and separated from the ionic liquid which is reused (entry 5 and 6). Despite a loss of activity which could be ascribed to a partial degradation of the Rh active catalyst during the separation, the n/i ratio remains high after two recyclings.

In conclusion, it is shown that thanks to the great versatility of ionic liquids, it is possible to optimize Rh-hydroformylation performances by adjusting the nature of the anions and cations present in the solvent and the nature of the ligands. Phosphite ligands, which are unstable in an aqueous two-phase system, can be used. The problem of Rh leaching can be minimized by the modification of phosphorus ligands with cationic (guanidinium or pyridinium) or anionic (sufonate) groups. By adjusting the ligand and the ions of the solvent, excellent Rh retention has been achieved.

Notes and references

1 For a review see: H. Olivier, in *Aqueous-Phase Organometallic Catalysis*, ed. B. Cornils and W.A. Herrmann, Wiley-VCH, Weinheim, 1998, p. 553. T. Welton, *Chem. Rev.*, 1999, **99**, 2071; P. Wasserscheid and W. Keim, *Angew. Chem., Int. Ed.*, 2000, **39**, 3772; J. Dupont, C. S. Consorti and J. Spencer, *J. Braz. Chem.*, 2000, **11**, 337; J. D. Holbrey and K. R. Seddon, *Clean Prod. Processes*, 1999, **1**, 223.

2 E. G. Kuntz, *Fr. Pat.*, 2314910, 1975 (to Rhône-Poulenc); B. Cornils and E. Wiebus, *CHEMTECH*, 1995, **25**listlistr, 33.

3 Y. Chauvin, L. Mussmann and H. Olivier, *Angew. Chem., Int. Ed.*, 1995, **34**, 2698; C. C. Brasse, U. Englert, A. Salzer, H. Waffenschmidt and P. Wasserscheid, *Organometallics*, 2000, **19**, 3818; P. Wasserscheid, H. Waffenschmidt, P. Machnitzki, K. W. Kottsieper and O. Stelzer, *Chem. Commun.*, 2001, 451.

4 A. J. Carmichael, C. Hardacre, J. D. Holbrey, K. R. Seddon and M. Nieuwenhuyzen, *Electrochem. Soc. Proceedings, Molten Salts XII*, ed. P. C. Trulove, H. C. De Long, G. R. Stafford and S. Deki, The Electrochemical Society, Pennington, NJ, 2000, vol. 91-41, p. 209.

5 P. Bonhôte, A. Dias, N. Papageorgiou, K. Kalyanasundaram and M. Grätzel, *Inorg. Chem.*, 1996, **35**, 1168.

6 A. J. Carmichael and K. Seddon, *J. Phys. Org. Chem.*, 2000, **13**, 591.

7 A. Hessler, O. Stelzer, H. Dibowski, K. Worm and F. P. Schmidtchen, *J. Org. Chem.*, 1997, **62**, 2362; P. Machnitzki, M. Tepper, K. Wenz, O. Stelzer and E. Herdtweck, *J. Organomet. Chem.*, 2000, **602**, 158.

8 P. C. J. Kamer, J. N. H. Reek and P. W. N. M. van Leeuwen, in *Rhodium Catalyzed Hydroformylation*, ed. P.W.N.M. van Leeuwen and C. Claver, Kluwer Academic Publishers, Netherlands, 2000, p. 35.

9 B. Fell, G. Papadogianakis, W. Konkol, J. Weber and H. Bahrmann, *J. Prakt. Chem.*, 1993, **335**, 75.

CHEMCOMM
Communication
www.rsc.org/chemcomm

In situ stopped-flow (SF) MAS NMR spectroscopy: a novel NMR technique applied for the study of aniline methylation on a solid base catalyst

Wei Wang,[a] Michael Seiler,[a] Irina I. Ivanova,[b] Jens Weitkamp[a] and Michael Hunger*[a]

[a] *Institute of Chemical Technology, University of Stuttgart, D-75500 Stuttgart, Germany. E-mail: michael.hunger@po.uni-stuttgart.de*
[b] *Department of Chemistry, Moscow State University, Leninskie Gory, 119899 Moscow, Russia*

Received (in Cambridge, UK) 10th May 2001, Accepted 15th June 2001
First published as an Advance Article on the web 5th July 2001

By the novel *in situ* stopped-flow MAS NMR technique allowing the observation of adsorbates on a solid catalyst after stopping the continuous reactant flow, *N*-methyleneaniline was identified as an intermediate in the formation of *N*-methylaniline by methylation of aniline with methanol on a basic CsOH/Cs,Na-Y zeolite.

In the past decade, *in situ* MAS NMR spectroscopy has been developed as a powerful tool for investigating heterogeneously catalyzed reactions.[1] Since 1995, a number of new *in situ* MAS NMR techniques have been developed allowing the study of reactions under continuous flow conditions.[2] With these techniques, a direct NMR investigation of the formation and transformation of surface compounds under steady-state conditions and a simultaneous gas chromatographic analysis of the reaction products are possible. In the present communication we report on the application of a new *in situ* stopped-flow (SF) MAS NMR experiment which is suitable to determine intermediates of heterogeneously catalyzed reactions. With this method, an intermediate involved in aniline methylation on basic zeolite CsOH/Cs,Na-Y under flow conditions was determined for the first time.

The zeolite CsOH/Cs,Na-Y used as catalyst in the present work had an n_{Si}/n_{Al} ratio of 2.6 and was prepared as described elsewhere.[3] After the sodium/caesium exchange (sodium exchange degree of 70%), zeolite Cs,Na-Y was impregnated with an aqueous solution of caesium hydroxide such as to arrive at a loading of 14 CsOH per unit cell. Subsequently, the material was calcined for 12 h at 723 K. The NMR experiments were performed on a Bruker MSL 400 spectrometer at a resonance frequency of 100.4 MHz, with direct excitation ($\pi/2$ pulse), a repetition time of 5 s and *ca*. 500 scans per spectrum. For the *in situ* measurements, the equipment described in ref. 2(*f*) and a modified 7 mm high-temperature Doty MAS NMR probe were used. The protocol of the 'stopped-flow' experiment is shown in Fig. 1. After filling the calcined catalyst into the MAS rotor and transferring the rotor into the spectrometer, the temperature was raised to 473, 498 and 523 K while the carrier gas (nitrogen) loaded with the reactants was flowing. In all experiments, a methanol (^{13}C-enriched) flow according to a modified residence time of W/F = 40 g h mol^{-1} (m_{cat} = 250 mg, $\dot{n}_{me}$ = 6.25 mmol h^{-1}) was used. The molar ratio of the methanol–aniline (natural ^{13}C-abundance) mixture was 4:1. After recording the ^{13}C MAS NMR spectra under steady-state conditions at reaction temperatures of 473, 498 and 523 K, the reactant flow was stopped, and the further conversion of the adsorbate compounds was observed, without purging the catalyst (see Fig. 1).

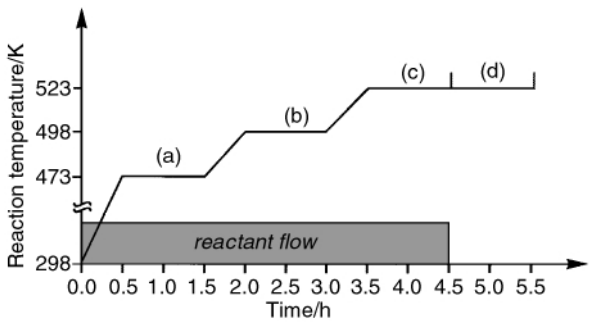

Fig. 1 Protocol of the *in situ* SF MAS NMR experiment consisting of periods (a) to (c) for the study of heterogeneously catalyzed reactions under steady-state conditions at different temperatures and a period (d), in which the consecutive conversion of previously formed compounds can be investigated.

Methanol was applied as methylating agent, and the conversion of this reactant alone on zeolite CsOH/Cs,Na-Y was investigated in the first experiments. Fig. 2(a)–(c), left, show the *in situ* ^{13}C MAS NMR spectra obtained at reaction temperatures of 473–523 K under steady-state conditions. The signal at 49 ppm is due to adsorbed methanol molecules. With increasing reaction temperature, a second signal appears at 166 ppm which is caused by surface formate species.[4] In an earlier work on methylation of toluene on a basic zeolite CsOH/Cs,Na-X it was shown that surface formate species occurring at 166 ppm are consumed by the reaction which indicates that these species can act as methylating agents.[4c] The ^{13}C MAS NMR spectrum recorded immediately after stopping the methanol flow at 523 K shows a significant decrease of the methanol signal at 49 ppm and only a weak decrease of surface formate species at 166 ppm [Fig. 2(d), left]. This indicates that the surface formate species are quite stable at 523 K.

Fig. 2(a)–(c), right, show the ^{13}C MAS NMR spectra recorded during conversion of the methanol–aniline mixture on zeolite CsOH/Cs,Na-Y at reaction temperatures of 473–523 K. While the spectrum obtained at 473 K consists only of a single signal due to methanol molecules at 49 ppm, in the spectrum obtained at 498 K additional signals occur at 29 and 157 ppm. The signal at 29 ppm is due to the reaction product *N*-methylaniline.[5] The signal at 157 ppm can be assigned to *N*-methyleneaniline, based on work by Kamachi and coworkers who observed a signal at *ca*. 155 ppm in the ^{13}C NMR spectrum of *N*-methyleneaniline in THF-d_8.[6] Further increase of the reaction temperature to 523 K leads to the formation of surface formate species at 166 ppm and a strong increase of the signal at 29 ppm due to the reaction product *N*-methylaniline.

To find out whether the *N*-methyleneaniline species at 157 ppm is an intermediate in the formation of *N*-methylaniline on zeolite CsOH/Cs,Na-Y, a stopped-flow experiment was performed: the reactant flow was suddenly stopped, and a spectrum was recorded while keeping the temperature at 523 K. In the spectrum obtained [Fig. 2(d), right], the signal at 166 ppm remained constant. On the other hand, the signals of methanol at 49 ppm and of *N*-methyleneaniline at 157 ppm disappeared completely, while the signal of the reaction product *N*-methylaniline at 29 ppm gained significantly in intensity. Hence, not only methanol, but also the *N*-methyleneaniline species are consumed by the formation of *N*-methylaniline. This finding indicates that the *N*-methyleneaniline species occurring

 DOI: 10.1039/b104115k

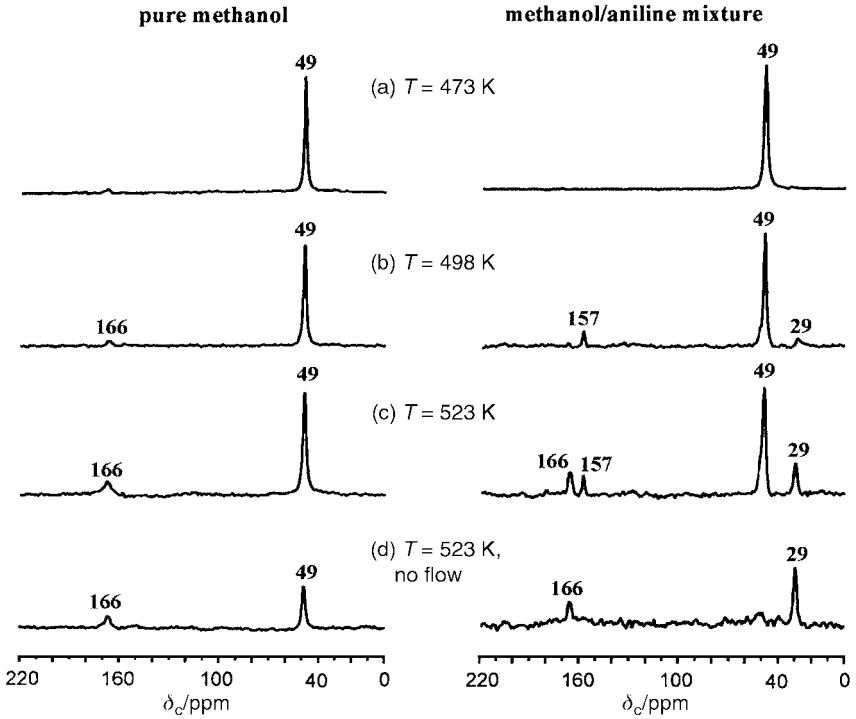

Fig. 2 *In situ* ^{13}C MAS NMR spectra obtained during the conversion of pure methanol (left) and a methanol–aniline mixture (right) on zeolite CsOH/Cs,Na-Y under flow conditions (W/F = 40 g h mol^{-1}) at reaction temperatures of 473 (a), 498 (b) and 523 K (c) and after stopping the reactant flow at 523 K (d).

at 157 ppm acts as an intermediate in the methylation of aniline.

The detection of *N*-methyleneaniline as an intermediate species can be accounted for by a mechanistic pathway which includes dehydrogenation of methanol to formaldehyde, [eqn. (1)], condensation of aniline with formaldehyde leading to *N*-methyleneaniline [eqn. (2)] and hydrogenation of *N*-methyleneaniline to *N*-methylaniline by H_2 produced during the methanol dehydrogenation [eqn. (3)]:

$$^{13}CH_3OH\ (49\ ppm) \rightarrow H^{13}CHO + H_2 \quad (1)$$

$$C_6H_5NH_2 + H^{13}CHO \rightarrow C_6H_5N{=}^{13}CH_2\ (157\ ppm) + H_2O \quad (2)$$

$$C_6H_5N{=}^{13}CH_2\ (157\ ppm) + H_2 \rightarrow C_6H_5NH^{13}CH_3\ (29\ ppm) \quad (3)$$

Based on the results of the present study we cannot decide whether the formate species observed at 166 ppm, or formaldehyde directly formed by conversion of methanol, acts as the methylating agent in the first reaction step. Our previous results demonstrated that the formation of formate species and aniline alkylation are parallel, *i.e.*, competing reactions on basic zeolites and that formate species most probably do not participate in the alkylation.[8] The fact that we did not observe formaldehyde species in the *in situ* MAS NMR experiments is due to its high reactivity on basic zeolites and, consequently, can be explained by a higher rate of reaction (2) compared to reaction (3).

It should be mentioned that the mechanism proposed for aniline alkylation in the present study is consistent with those suggested previously for side-chain alkylation of toluene on basic zeolites.[4b,7] Furthermore, it is also in line with the mechanism proposed on the basis of a recent *in situ* MAS NMR spectroscopic study of aniline methylation performed under batch conditions.[8] However, a direct proof for the role of *N*-methyleneaniline as an intermediate is now possible for the first time by applying the novel *in situ* SF MAS NMR method. It is obvious that this new NMR technique is an extremely useful tool in heterogeneous catalysis and possesses high potential for elucidating the mechanisms of a broad variety of reactions.

We gratefully acknowledge financial support by Volkswagen-Stiftung, Deutsche Forschungsgemeinschaft, Max-Buchner-Forschungsstiftung and Fonds der Chemischen Industrie.

Notes and references

1 For reviews, see: J. Klinowski, *Chem. Rev.*, 1991, **91**, 1459; M. W. Anderson, *Top. Catal.*, 1996, **3**, 195; J. F. Haw, J. B. Nicholas, T. Xu, L. W. Beck and D. B. Ferguson, *Acc. Chem. Res.*, 1996, **29**, 259; E. G. Derouane, H. He, S. B. Derouane-Abd Hamid and I. I. Ivanova, *Catal. Lett.*, 1999, **58**, 1; I. I. Ivanova, *Colloids Surf.*, 1999, **158**, 189; M. Hunger and J. Weitkamp, *Angew. Chem., Int. Ed.*, 2001, in press.

2 (*a*) M. Hunger and T. Horvath, *J. Chem. Soc., Chem. Commun.*, 1995, 1423; (*b*) P. W. Goguen and J. F. Haw, *J. Catal.*, 1996, **161**, 870; (*c*) M. Hunger and T. Horvath, *J. Catal.*, 1997, **167**, 187; (*d*) P. K. Isbester, A. Zalusky, D. H. Lewis, M. C. Douskey, M. J. Pomije, K. R. Mann and E. J. Munson, *Catal. Today*, 1999, **49**, 363; (*e*) C. Keeler, J. Xiong, H. Lock, S. Dec, T. Tao and G. E. Maciel, *Catal. Today*, 1999, **49**, 377; (*f*) M. Hunger, M. Seiler and T. Horvath, *Catal. Lett.*, 1999, **57**, 199; (*g*) H. Mori, H. Kono, M. Terano, A. Nosov and V. A. Zakharov, *Macromol. Rapid Commun.*, 1999, **20**, 536.

3 U. Schenk, M. Hunger and J. Weitkamp, *Magn. Reson. Chem.*, 1999, **37**, S75.

4 (*a*) N. D. Lazo, D. K. Murray, M. L. Kieke and J. F. Haw, *J. Am. Chem. Soc.*, 1992, **114**, 8552; (*b*) A. Philippou and M. W. Anderson, *J. Am. Chem. Soc.*, 1994, **116**, 5774; (*c*) M. Hunger, U. Schenk, M. Seiler and J. Weitkamp, *J. Mol. Catal. A: Chemical*, 2000, **156**, 153.

5 E. Breitmaier and W. Voelter, *Carbon-13 NMR Spectroscopy*, VCH, Weinheim, 1990, p. 257.

6 A. Hashidzume, A. Kajiwara, A. Harada and M. Kamachi, *Macromolecules*, 1998, **31**, 535.

7 H. Itoh, A. Miyamoto and Y. Murakami, *J. Catal.*, 1980, **64**, 284.

8 I. I. Ivanova, E. B. Pomakhina, A. I. Rebrov, Yu. G. Kolyagin, M. Hunger and J. Weitkamp, *Proc. 13th International Zeolite Conference, Montpellier, France*, 2001, in press.

CHEMCOMM
Communication
www.rsc.org/chemcomm

Hierarchical zeolite structures with designed shape by gel-casting of colloidal nanocrystal suspensions†

Huanting Wang, Limin Huang, Zhengbao Wang, Anupam Mitra and Yushan Yan*

Department of Chemical and Environmental Engineering, University of California, Riverside, CA 92521, USA. E-mail: yushan.yan@ucr.edu

Received (in Cambridge, UK) 15th May 2001, Accepted 18th June 2001
First published as an Advance Article on the web 5th July 2001

Hierarchical zeolite structures with designed shapes were fabricated by a ceramic processing method—gel-casting of colloidal nanocrytal suspensions.

There is considerable interest in porous zeolite and zeolite-type materials with designed shapes.[1–4] Hierarchical porous structures with different levels of porosity can significantly aid the diffusion of guest species through the inorganic network of pores and channels to improve their performance. Nanometer-sized zeolite particles have been used as building blocks to construct hierarchical porous structures such as films, spheres and fibers *via* templated self-assembly.[2–4] Very recently, a bulk-material dissolution technique has been developed for the preparation of various shaped MFI structures including tubes and fibers.[5] The shaped zeolite structures can faithfully reproduce the shapes of the starting bulk material. However, the conversion process is extremely slow (*e.g.* 1–2 months) and the final structure is usually a composite of the starting material and the zeolite with non-uniform microstructure.

Ceramic forming techniques such as pressing, extrusion, tape casting, dip (slip)-casting, and gel-casting are powerful for shaping inorganic materials due to their simplicity and versatility. In particular, gel-casting is a method for fabrication of complex-shaped ceramic bodies from ceramic particle suspensions by means of *in situ* polymerization, where a macromolecular network is created to hold the ceramic particles together before sintering.[6,7] Zeolite nanocrystals such as silicalite, ZSM-5, TS-1, Beta, A and FAU have been synthesized from precursor solutions,[9–13] and can be readily handled in colloidal systems. In this communication, we report the first demonstration of fabrication of shaped hierarchical zeolite structures with well-controlled microstructures using a ceramic forming technique—gel-casting. As an example, the gel-casting of colloidal silicalite nanocrystal suspensions was used to prepare hierarchical tubular silicalite structures (HTSSs).

Silicalite nanocrystals were hydrothermally synthesized using a clear synthesis solution.[4,14]‡ The silicalite nanocrystals with diameter *ca*. 50 nm and with narrow particle size distribution were re-dispersed in water with a solid loading of 30–40 wt%. Water soluble organic monomer acrylamide, crosslinker *N*,*N*′-methylenebisacrylamide, and initiator ammonium persulfate $(NH_4)_2S_2O_8$ were added to the colloidal silicalite suspension.‡ The gel-casting of the resulting colloidal suspension was carried out in a home-made mold. The fabrication process of HTSSs is illustrated in Fig. 1. Since the suspension with monomer, crosslinker, and initiator has low viscosity and good fluidity, it can be readily transferred into the mold. The suspension-filled mold was hand-shaken for a few minutes to release air bubbles inside the suspension. Once the temperature was increased to 50 °C, the monomers in the suspension were quickly polymerized and crosslinked free-radically into an elastic hydrogel.[6,7] A highly crosslinked polyacrylamide hydrogel obtained is expected to be compatible to silicalite nanocrystals whose surface silanol groups interact

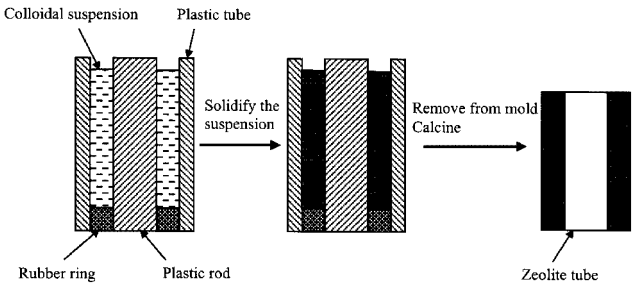

Fig. 1 Schematic representation of the gel-casting forming process for a hierarchical tubular silicalite structure (HTSS). The colloidal suspension consists of zeolite silicalite nanocrystals and organic monomer (AM), crosslinker (MBAM), and initiator $(NH_4)_2S_2O_8$.

favorably with $-NH_2$ groups. The solidified suspension (a gelcast) was mechanically strong and was easily removed from the mold. The tubular gelcast was dried under ambient laboratory conditions for 2–3 days, and was then further dried at 100 °C overnight. A linear shrinkage of 4.0–4.5% of the gelcast was observed during the drying process. After drying, the tubular gelcast was sintered under air at a heating rate of 1 °C min^{-1} up to 500 °C, and kept at that temperature for 8 h to burn off the organic polymer and the structure-directing agent (tetrapropylammonium hydroxide),[14] and to sinter together the silicalite nanocrystals through condensation crosslinking of surface silanol groups of nanocrystals.[4,14] The sintering leads to a linear shrinkage of $< 0.5\%$. In order to examine the thermal stability of the HTSSs, another sample was sintered at 1000 °C for 2 h with the same heating rate.

Fig. 2 shows a photograph, SEM micrographs and XRD pattern of an HTSS. SEM images show uniformly distributed

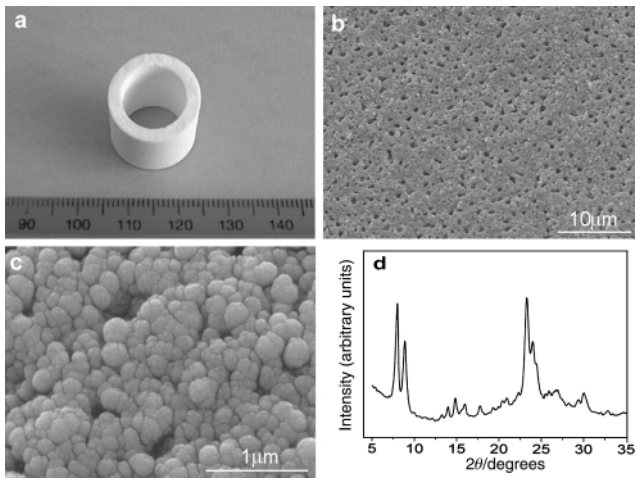

Fig. 2 Photograph, SEM images and XRD pattern of a hierarchical tubular silicalite structure (HTSS) sintered at 1000 °C for 2 h. (a) A photograph (taken with a digital camera), (b) microstructure at low magnification under SEM, and (c) microstructure at high magnification under SEM, (d) XRD pattern.

† Electronic supplementary information (ESI) available: nickel doping procedure. S-Fig. 1: pore size distributions. S-Fig. 2: nickel and silicon mapping images. see http://www.rsc.org/suppdata/cc/b1/b104275k/

 DOI: 10.1039/b104275k

submicrometer-sized pores in the HTSS at low magnification, and a hierarchical morphology of densely packed silicalite nanocrystals at high magnification. The submicrometer-sized pores were formed by packing of nanocrystal agglomerates during gel-casting. Small nanocrystals tend to agglomerate to minimize surface energy when the nanocrystal loading is high (30–40 wt%). This is confirmed by SEM observation that shows that there are already micrometer-sized pores in the dried gel-cast. The XRD pattern of the sample sintered at 1000 °C for 2 h matches the pure silicalite structure. This suggests that the HTSS sintered at 1000 °C retains the silicalite structure.

N_2 adsorption–desorption measurements were used to determine the mesopore and micropore structures of HTSSs. N_2 adsorption–desorption isotherms of samples sintered under different conditions are shown in Fig. 3. The adsorption steps at low relative pressures signify the filling of silicalite micropores, and the hysteresis loops at higher relative pressures are the consequence of N_2 filling the textural mesopores, and clearly the sample has a bimodal pore size distribution (see S-Fig. 1, ESI).† The pore size distribution is narrow in both the micropore and mesopore range. The sintering temperature has an influence on the pore structure of the HTSS. When the sintering temperature is increased from 500 to 1000 °C, the micropore volume and mesopore volume slightly decrease from 0.16 to 0.12 $cm^3\ g^{-1}$, and from 0.35 to 0.33 $cm^3\ g^{-1}$, respectively. The corresponding Brunaer–Emmett–Teller (BET) surface area drops from 516 to 423 $m^2\ g^{-1}$. The maximum pore size in the micropore range of HTSSs is 5.5 Å, which is characteristic of silicalite. The average mesopore size varies from 16.7 to 13.1 nm, which are similar to that of hierarchical materials self-assembled by pure silicalite nanocrystals.[4]

The HTSSs have three-level porosities including macropores (submicrometer), mesopores (16–13 nm) and micropores (0.55 nm). Based on a measured HTSS density of 0.85 g cm^{-3} and assuming a dense silica density of 2.3 g cm^{-3}, the total pore volume is estimated to be 0.74 $cm^3\ g^{-1}$. From the micropore and mesopore volumes obtained from nitrogen adorption–desorption isotherms, the macropore volume is calculated to be 0.29 and 0.23 $cm^3\ g^{-1}$ for HTSSs sintered at 500 and 1000 °C, respectively.

Gel-casting processing also offers an effective way to add functionalities to HTSSs by doping with other components.[7] Unlike commonly used impregnation methods, the dopant can be introduced easily into the colloidal suspension system so that the dopant concentration can be precisely controlled. The uniformity of dopant distribution also will be significantly improved. Here the doping of nickel is used as an example to illustrate that dopant can be easily incorporated. Ni-based catalysts are useful for various catalytic processes such as alkylation, methanation, hydrogenation of aromatic compounds and methane reforming. Elemental mapping images (S-Fig. 2)† clearly show Ni is uniformly distributed in the silicalite matrix.

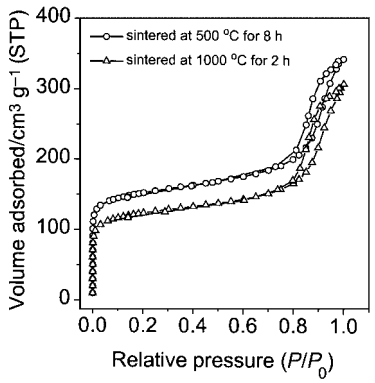

Fig. 3 Nitrogen adsorption–desorption isotherms of hierarchical tubular silicalite structures (HTSSs) sintered under different conditions.

We have demonstrated that hierarchical zeolite structures with designed shape can be readily obtained from colloidal zeolite nanocrystal suspensions simply by applying ceramic gel-casting processing. The hierarchical (macro-, meso- and micro-porous) zeolite structure can be readily functionalized by incorporation of a functional component, or by chemical grafting of organic functional groups. Zoned zeolite structures[15] with designed shapes can also be generated by adding a secondary growth step[8] to our gel-casting process. Our process should also allow the fabrication of shaped structures with mixed zeolites by using suspensions of two or more types of zeolite nanocrystals. It is believed that the strategy described here is promising for the preparation of various functional zeolite-based structures with designed shapes, in catalysis, separation membranes, and microelectronics, and work in these areas are in progress.

This work was supported in part by UC-SMART, Honeywell International, US-EPA, UC-TSR&TP, UC-EI and CE-CERT.

Notes and references

‡ Aqueous colloidal suspensions of silicalite nanocrystals were synthesized as follows.[4,14] A clear synthesis solution was prepared by dropwise adding tetrapropylammonium hydroxide solution (TPAOH, SACHEM) into tetraethyl orthosilicate (TEOS, Aldrich) with strong agitation followed by 1–3 days of aging at 30 °C under stirring. The final solution has a molar composition 1 TPAOH : 2.8 SiO_2 : 11.2 EtOH : 40 H_2O. Crystallization was carried out at 80 °C for 3 days with a constant stirring at 250 rpm. A stable aqueous suspension of silicalite nanocrystals was obtained by repeated cycles of centrifugation at 15 000 rpm, decanting, and ultrasonic redispersion in pure water until the pH of the suspension was < 8. The solid loading of the suspension is 30–40 wt% for gel-casting. Water soluble organic monomer acrylamide, CH_2=$CHCONH_2$ (AM, Aldrich), crosslinker *N*,*N*′-methylenebisacrylamide, CH_2=$CHCONH_2)_2CH_2$ (MBAM, Aldrich), and initiator ammonium persulfate, $(NH_4)_2S_2O_8$ Aldrich) were added under stirring into the silicalite colloidal suspension. Final composition (weight ratio) : 5–10 AM : (0.05–0.1) MBAM : (0.01–0.025) $(NH_4)_2S_2O_8$: 90–95 silicalite solid. After the monomer, the crosslinker, and the initiator were dissolved, the whole suspension was ultrasonicated for 5–10 min to ensure good homogeneity.

Nitrogen adsorption–desorption measurements were carried out at −196 °C on a Micromeritics ASAP 2010 instrument. HTSS samples were crushed and ground for X-ray diffraction analysis (Siemens D-500 diffractometer using Cu-Kα radiation). SEM imaging and elemental mapping were conducted with a scanning electron microscope (SEM, Philips XL30-FEG at 20 kV) equipped with an EDAX detector.

1 S. Oliver, A. Kuperman, N. Coombs, A. Lough and G. A. Ozin, *Nature*, 1995, **378**, 47.
2 X. D. Wang, W. L. Yang, Y. Tang, Y. J. Wang, S. K. Fu and Z. Gao, *Chem. Commun.*, 2000, 2161.
3 B. J. Zhang, S. A. Davis, N. H. Mendelson and S. Mann, *Chem. Commun.*, 2000, 781; K. H. Rhodes, S. A. Davis, F. Caruso, B. J. Zhang and S. Mann, *Chem. Mater.*, 2000, **12**, 2832.
4 L. M. Huang, Z. B. Wang, J. Y. Sun, L. Miao, Q. Z. Li, Y. Yan and D. Y. Zhao, *J. Am. Chem. Soc.*, 2000, **122**, 3530.
5 S. Shimizu and H. Hamada, *Adv. Mater.*, 2000, **12**, 1332.
6 C. Young, O. O. Omatete, M. A. Janney and P. A. Menchhofer, *J. Am. Ceram. Soc.*, 1991, **74**, 612.
7 H. T. Wang, X. Q. Liu, H. Zheng, W. J. Zheng and G. Y. Meng, *Ceram. Int.*, 1999, **25**, 177.
8 L. C. Boudreau, J. A. Kuck and M. Tsapatsis, *J. Membr. Sci.*, 1999, **152**, 41.
9 E. Persson, B. J. Schoeman and J. Otterstedt, *Zeolites*, 1994, **14**, 557.
10 S. Mintova, N. H. Olson, V. Valtchev and T. Bein, *Science*, 1999, **283**, 958.
11 G. Zhu, S. Qiu, J. Yu, Y. Sakamoto, F. Xiao, R. Xu and O. Terasaki, *Chem. Mater.*, 1998, **10**, 1483.
12 M. A. Comblor, A. Corma, A. Mifsud, J. Perez-Pariente and S. Valencia, *Stud. Surf. Sci. Catal.*, 1997, **105**, 341.
13 N. B. Castagnola and P. K. Dutta, *J. Phys. Chem. B*, 1998, **102**, 1696.
14 H. T. Wang, Z. B. Wang and Y. Yan, *Chem. Commun.*, 2000, 2333.
15 Q. H. Li, J. Hedlund, D. Creaser and J. Sterte, *Chem. Commun.*, 2001, 527.

CHEMCOMM
Communication
www.rsc.org/chemcomm

A catalytic synthesis and structural characterization of a new [84]fullerene isomer

Nikos Tagmatarchis,[a] Kozue Okada,[a] Tetsuo Tomiyama,[a] Takuya Yoshida,[b] Yuji Kobayashi[b] and Hisanori Shinohara*[a]

[a] *Department of Chemistry, Nagoya University, Nagoya 464-8602, Japan. E-mail: nori@nano.chem.nagoya-u.ac.jp*
[b] *Department of Pharmacology, Osaka University, Osaka 565-0871, Japan*

Received (in Cambridge, UK) 24th April 2001, Accepted 8th June 2001
First published as an Advance Article on the web 5th July 2001

The synthesis, separation and isolation of a new [84]fullerene isomer from arc-burned soot of dysprosium-doped graphite composite rods is reported; high-resolution ^{13}C NMR and electronic absorption UV-VIS-NIR spectroscopy were used to characterize this material, which was found to possess C_2 molecular symmetry; the successful synthesis of the new [84-C_2]fullerene isomer can be ascribed to a catalytic role played by the doped Dy metal atoms in the composite rods.

[84]Fullerene, C_{84}, has been solvent extracted in macroscopic quantities since the early stages of fullerene research.[1] It is the third most abundant fullerene having 24 structural isomers that obey the so-called isolated pentagon rule (IPR).[2] Taylor *et al.* reported ^{13}C NMR measurements on a partially separated [84]fullerene mixture.[3] However, to date only nine of these isomeric materials have been isolated and structurally characterized by high resolution ^{13}C NMR spectroscopy. Two of them, abundantly produced, possess D_2(IV) and D_{2d}(II) molecular symmetry,[4] while the other five minor isomers having C_s(a), C_s(b), C_2, D_2(II) and D_{2d}(I) symmetries[5] and a mixture of D_{3d}/D_{6h}[6] have already been isolated and structurally characterized.

One important aspect on the production and isolation of the above minor [84]fullerene isomers is that some of them have been produced only from metal-doped/graphite composite rods and not from pure graphite rods. This means that such isomers can be produced by catalytic effects of the doped metal atoms. For example, the D_{3d}/D_{6h} isomers have been identified in the arc burned soot of gadolinium doped composite rods[6] while they were absent in the arc burned soot of calcium doped composite rods.[5] In the latter, only the C_s(a), C_s(b), C_2, D_2(II) and D_{2d}(I) symmetrical [84]fullerenes were found, in different yields compared to Gd-doped soot, together with the most abundant D_2(IV) and D_{2d}(II) isomers. These findings led us to consider the possibility that the doped metal atoms play a significant role not only in the relative production yield of these isomers but also in the nature of the isomer that is formed.

In this communication, we report the production of a new isomer of [84]fullerene, C_{84}, by using arc burning of dysprosium-doped composite rods. Briefly, soot containing various dysprosium metallofullerenes[7] was produced by the direct current arc discharge method of Dy_2O_3–graphite composite rods (12.5 × 12.5 × 300 mm, 0.8 wt%, Toyo Tanso Co.). The dysprosium composite rods were heat treated at a high temperature of 1600 °C. The soot produced was collected under totally anaerobic conditions to avoid any degradation from air during the collection procedure. It was then soxhlet extracted first by carbon disulfide and then by pyridine. The separation of [84]fullerene isomers was achieved by multi-stage high-performance liquid chromatography (LC-908-C60, Japan Analytical Industry) using a Buckyprep (20 × 250 mm, nakalai tesque) and a 5PYE (20 × 250 mm, nakalai tesque) columns.[4–7] The purity of the newly synthesized material (> 99.9%) was confirmed by both positive and negative laser-desorption time-of-flight (LD-TOF) mass spectrometry. The UV-VIS-NIR spectrum was recorded between 400 and 2000 nm in carbon disulfide solutions by using a Shimadzu UV-3101PC spectrophotometer. Finally, the high resolution ^{13}C NMR measurements were performed on a Varian Inova-600 spectrometer at 600 MHz (CS_2 solution, $Cr(acac)_3$ relaxant, acetone-d_6 lock at 25 °C).

In the first HPLC stage, the fraction that contains the [84]fullerene isomeric mixture was separated from the empty [76], [78] and [86]fullerenes as well as from the endohedral metallofullerenes Dy@C_{82} and Dy_2@C_{84} by using a Buckyprep column (15 ml min^{-1} flow rate, toluene eluent).[7] In the second stage, the fraction, which was identified by LD-TOF mass spectrometry as empty [84]fullerenes, was re-injected into a 5PYE column (15ml min^{-1} flow rate, toluene eluent) and a recycling HPLC was performed. After recycling for 90 min, the mixture of the two most abundant [84]fullerene isomers with D_2(IV) and D_{2d}(II) symmetry was separated from a mixture of various minor [84]fullerene isomers. In the last HPLC stage, the fraction that contained the mixture of the minor isomers was re-injected into a 5PYE column (15 ml min^{-1} flow rate, toluene eluent) for the final separation. Four different compounds were identified after recycling for more than 3 h, all of which corresponded to [84]fullerene isomers. The purity of the isolated material was more than 99.9% as determined by both negative and positive laser desorption time-of-flight mass spectrometry.

Three of the four isomeric [84]fullerenes described above (hereafter referred as I, III and IV in order of increasing retention time) showed identical UV-Vis-NIR absorption spectra with those of the known minor [84]fullerene isomers with molecular symmetries C_2, C_s(b) and C_s(a), respectively,[5] albeit in different yields. However, the material corresponding

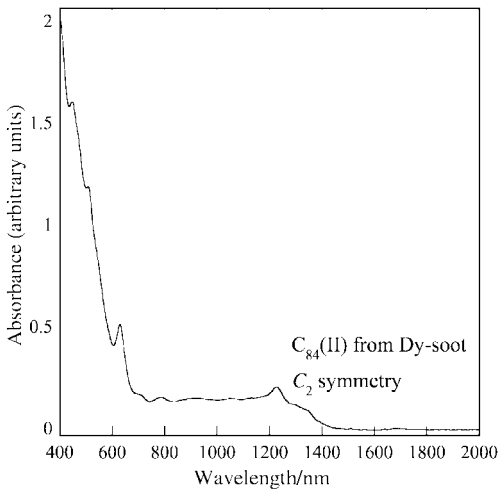

Fig. 1 Electronic absorption UV-VIS-NIR spectrum of the C_{84}(II) minor isomer, with C_2 molecular symmetry in carbon disulfide solution.

 DOI: 10.1039/b103679n

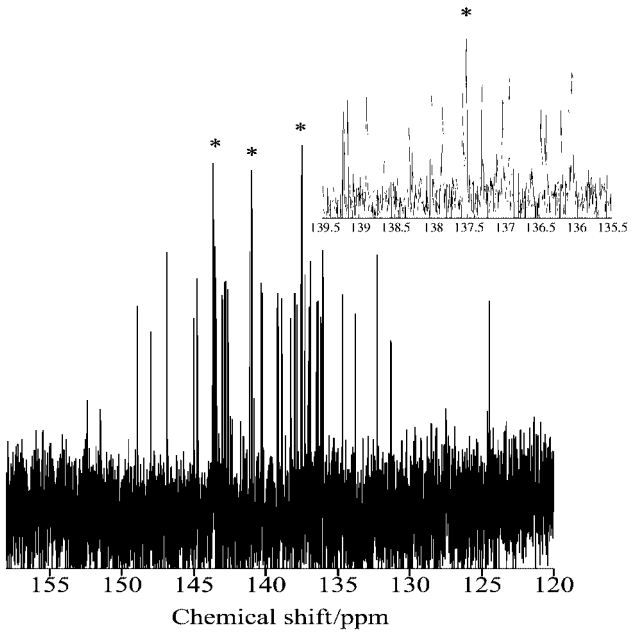

Fig. 2 High-resolution ^{13}C NMR spectrum [600 MHz, CS_2 solution, $Cr(acac)_3$ as relaxant and acetone-d_6 for the internal lock] of the purified minor isomer of C_{84}(II) with C_2 molecular symmetry. The chemical shifts for the forty-two lines are at δ: 148.93, 148.00, 146.87, 145.01, 144.77, 144.72, 143.66 (double line), 143.55, 143.48, 143.03, 142.98, 142.86, 142.76, 142.63, 141.12, 140.99 (double line), 140.32, 140.25, 139.21, 139.14, 138.88, 138.30, 138.00, 137.84, 137.56, 137.50 (double line), 137.29, 137.00, 136.91, 136.47, 136.42, 136.19, 136.09, 136.04, 134.67, 133.80, 132.28, 131.31 and 124.47 ppm. The * corresponds to two signals which are overlapped with each other. Inset is an expanded region between 139.5–135.5 ppm for clarity.

to the second fraction on the 5PYE column, C_{84}(II), showed an entirely different absorption profile from those of the previously isolated [84]fullerene isomers.

Fig. 1 shows the UV-VIS-NIR electronic absorption spectrum of [84]fullerene (II) in carbon disulfide solution. There are characteristic absorptions at 444, 506, 631, 715, 782, 1231 nm and a broad profile from 830 to 1400 nm with the onset around 1500 nm. From all isomeric [84]fullerenes, this particular isomer has the lowest energy onset. Since the onset of a UV-VIS-NIR electronic absorption spectrum corresponds to the lowest electronic transitions, this is a good measure for the HOMO–LUMO energy gap of fullerenes. Because of the red shift of the absorption onset relative to the other [84]fullerene isomers, the HOMO–LUMO band gap of [84]fullerene (II) should be smaller than that of the rest materials.

Fig. 2 shows the high resolution ^{13}C NMR spectrum of the newly synthesized and isolated [84]fullerene (II) in carbon disulfide solution with chromium tris(acetylacetonate) as relaxant and acetone-d_6 as internal lock after accumulating more than 120,000 scans. The spectrum consists of forty-two equal intensity lines which are spread over a wide range of the chemical shift from 125 to 150 ppm. The current isolated [84]fullerene isomer is thus unambiguously assigned to possess C_2 molecular symmetry. Rotation of 180 degrees around the symmetry axis generates 42 equivalent carbon atoms. There are six structural isomers of [84]fullerene with C_2 symmetry that satisfy the isolated pentagon rule.[2] Two-dimensional high resolution ^{13}C NMR spectroscopy could reveal which one, out of the six possible isomers, is the present [84-C_2]fullerene, in the future.

Theoretical calculations on the relative stability of isomeric [84]fullerenes have shown a relatively good agreement between the theoretical stability order and the observed abundance of the isomers.[8] These calculations predict that the most stable isomers after D_2(IV) and D_{2d}(II) are those with C_2(IV), C_s(V), D_{3d} and D_{6h} molecular symmetries. We have found, however, that under similar experimental conditions employing different metal-doped composite rods not only the produced amounts of minor isomers of [84]fullerenes are different but more importantly different isomers are formed. This implies a catalytic effect for the doped-metal in the early stage of the growth of these isomers. Although progress in this research area is rapid, there are still lots of questions opened concerning the growth mechanism of fullerenes and metallofullerenes.[9] The current finding that the doped metal atoms play a crucial role in producing a new [84]fullerene isomer strongly suggests the presence of interplay between an encapsulation and a catalytic role of the doped metal atoms in the early stage of fullerene growth.

N. T. thanks the Japan Society for the Promotion of Science (JSPS) for a Post Doctoral Fellowship for Foreigner Researchers. H. S. thanks JSPS for the Future Program on New Carbon Nano-Materials.

Notes and references

1 H. Ajie, M. M. Alvarez, S. J. Anz, R. D. Beck, F. Diederich, F. Fostiropoulos, D. R. Huffman, W. Kraetschmer, Y. Rubin, K. E. Schrivens, D. Sensharma and R. L. Whetten, *J. Phys. Chem.*, 1990, **94**, 8630.
2 P. W. Fowler and D. E. Manolopoulos, *An Atlas of Fullerenes*, Clarendon, Oxford, 1995, pp. 73–80.
3 A. G. Avent, D. Dubois, A. Penicaud and R. Taylor, *J. Chem. Soc., Perkin Trans. 2*, 1997, 1907.
4 T. J. S. Dennis, T. Kai, T. Tomiyama and H. Shinohara, *Chem. Commun.*, 1998, 619.
5 T. J. S. Dennis, T. Kai, K. Asato, T. Tomiyama, H. Shinohara, T. Yoshida, Y. Kobayashi, H. Ishiwatari, Y. Miyake, K. Kikuchi and Y. Achiba, *J. Phys. Chem. A*, 1999, **103**, 8747.
6 N. Tagmatarchis, A. G. Avent, K. Prassides, T. J. S. Dennis and H. Shinohara, *Chem. Commun.*, 1999, 1023.
7 N. Tagmatarchis and H. Shinohara, *Chem. Mater.*, 2000, **12**, 3222.
8 B. L. Zhang, C. Z. Wang and K. M. Ho, *J. Chem. Phys.*, 1992, **96**, 7183.
9 H. Shinohara, *Rep. Prog. Phys.*, 2000, **63**, 843.

CHEMCOMM
Communication
www.rsc.org/chemcomm

1D porous framework of copper(II) showing a novel coordination mode of $Ni(CN)_4^{2-}$†

Tapas Kumar Maji,[a] Partha Sarathi Mukherjee,[a] Golam Mostafa,[b] Ennio Zangrando[c] and Nirmalendu Ray Chaudhuri*[a]

[a] *Department of Inorganic Chemistry, Indian Association for the Cultivation of Science, Jadavpur, Calcutta-700 032, India. E-mail: icnrc@mahendra.iacs.res.in*
[b] *Department of Physics, Krishnath College, Berhampur-742109, India*
[c] *Dipartimento di Scienze Chimiche, University of Trieste, 34127, Trieste, Italy*

Received (in Cambridge, UK) 27th April 2001, Accepted 13th June 2001
First published as an Advance Article on the web 5th July 2001

A novel porous framework $[\{Cu_2(medpt)_2Ni(CN)_4\}(ClO_4)_2\cdot 2.5H_2O]_n$ 1, [medpt = bis(3-aminopropyl)methylamine] is prepared where all the CN groups of $Ni(CN)_4^{2-}$ are involved in bridging; this material retains single crystallinity upon removal of water guest molecules and the dehydrated species 2 selectively binds organic molecules.

The design and synthesis of microporous inorganic materials mimicking zeolites finds widespread application in heterogeneous catalysis, adsorption, ion exchange processes, selective binding of guest molecules *etc.*[1] Self assembly is the most efficient approach towards elaboration and construction of such types of molecular systems. Currently, a successful example of this process is the construction of cyano bridged complexes[2] in which the cyanometallate anion [*e.g.* $Ag(CN)_2^-$, $Cu(CN)_3^{2-}$, $Ni(CN)_4^{2-}$, $M(CN)_6^{3-}$ (M = Cr(III), Fe(III) *etc.*)] behaves as the bridging moiety to build a multidimensional structure with a second coordination centre and the resulting complexes demonstrate unique properties. Usually the second coordination centres are transition metal ions since $\sigma \rightarrow \pi$ back-bonding stabilizes the resulting complex. The rigidity and stability of such frameworks allow for shape and size selective inclusion of organic solvents, water molecules, aromatic amines,[3] *etc*. to fill up the void space so stabilizing the crystal structure.

The reaction of $Cu(medpt)(H_2O)_2(ClO_4)_2$ [medpt = bis(3-aminopropyl)methyl amine] and $K_2Ni(CN)_4\cdot 2H_2O$ in aqueous medium leads to the formation of deep blue plates of $Cu_2(medpt)_2Ni(CN)_4(ClO_4)_2\cdot 2.5H_2O$ **1**.‡ The IR spectrum of compound **1** shows one sharp ν_{CN} band at 2150 cm^{-1} which is at a higher wavenumber than that of the free $Ni(CN)_4^{2-}$ unit (ν_{CN} band at 2128 cm^{-1}), indicating that all the CN groups act as bridging ligands with the copper(II) centre. Although one discrete square cyano-bridged compound[2c] has been reported, to our knowledge, 1D square compounds where all the cyano groups are involved in bridging have not yet been reported in the literature.

The structure determination§ of **1** discloses a 1D square type open microporous material, consisting of infinite chains elongated in the direction of the crystallographic *b* axis (Fig. 1). In the polymer there are intra-chain H-bonds [2.94(1) Å] between amino nitrogens [N(1), N(1″)] and the bridging water molecule O(3w), the latter interacting also with O(2w) at 2.79(2) Å. A third crystallization water molecule O(1w) connects through hydrogen bonds the amino nitrogens N(3) of adjacent chains, in a diamond shape pattern. These inter-chain interactions of 2.913(9) and 3.021(9) Å, illustrated in Figs. 1 and 2, give rise to a 2-D structure. The water molecules, all at half occupancy, are guests in the crystalline channels and, from a topological point of view, have the ability to leave the host lattice. The dehydration process, detected by thermogravimetric analysis, occurs but leads to no deterioration of crystallinity, indicating that the structure can be envisaged as an inclusion compound and that removal of the H-bond network does not lead to destruction of the structure. A similar behaviour was described for the structure $[Ni(en)_2Ni(CN)_4]\cdot 2.5H_2O$,[4a] where the role of the water molecules was interpreted using a molecular mechanics investigation. Other examples, with phenol and aniline as guest molecules accommodated among $[M(en)_2Ni(CN)_4]_n$ chains (M = Ni, Cu, Zn or Cd), were reported by Iwamoto *et al.*[4b]

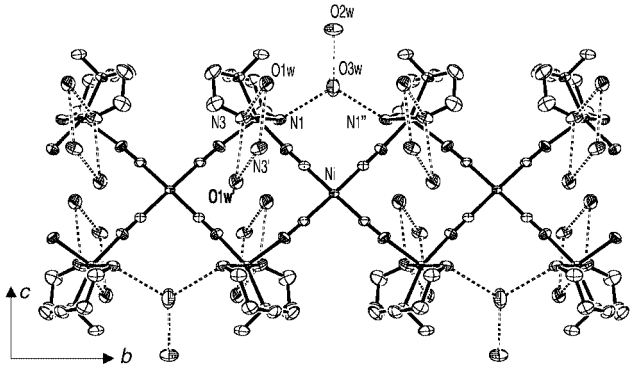

Fig. 1 ORTEP drawing of the polymeric structure of **1**, extending in the direction of crystallographic *b* axis, with guest water molecules (dotted lines indicate H-bonds; ClO_4^- anions omitted for clarity).

The copper presents a square pyramidal coordination where the medpt ligand donors and a cyanide nitrogen occupy the basal plane, the metal being slightly displaced by 0.27 Å from the N4 mean plane towards the apical position occupied by a cyanide ligand of a different $Ni(CN)_4^{2-}$ anion. The latter Cu–N bond distance is significantly longer [2.186(4) Å] with respect to those in the basal plane [2.000(4)–2.072(3) Å]. The $Ni(CN)_4^{2-}$ anion, with the metal located on a symmetry plane, coordinates four adjacent copper ions. The cyanide groups show different geometries, being linear coordinated in the basal plane

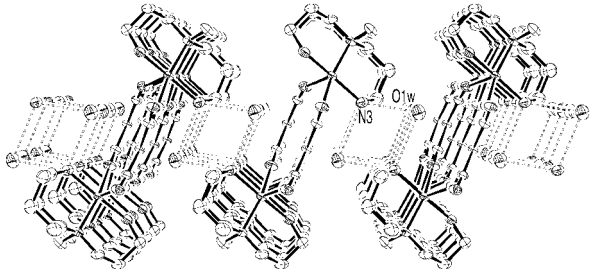

Fig. 2 Packing diagram down the *b* axis showing the diamond pattern of H-bonds linked the –Ni–Cu_2– polymeric chains.

† Electronic supplementary information (ESI) available: Fig. 4: ORTEP view of **2**. Fig. 5: view of **2** down the crystallographic *b* axis. Fig. 6: TG-DTA curves of **1**, **1a** and **1b**. Fig. 7: view of **1** showing the water filled channels. See http://www.rsc.org/suppdata/cc/b1/b103823k/

 DOI: 10.1039/b103823k

of copper, but significantly bent at the apical position of the pyramidal Cu environment [Cu–N≡C bond angles of 176.0(4) and 155.3(3)°, respectively].

Thermogravimetric analysis of a crystalline sample showed a weight loss of 5.5% at 70 °C, corresponding to the loss of the guest water occupying the channels. The remaining compound was heated to 180 °C without any additional weight decrease, indicating a robust open Cu–Ni framework. Examination of the single crystals with an optical microscope at 100 °C showed that they retained their morphology and crystallinity upon loss of the water molecules.

The X-ray structural determination of a dehydrated single crystal of **2**§ sealed in a glass capillary reveals a 1D open microporous framework and confirms the $[\{Cu_2(medpt)_2Ni(CN)_4\}(ClO_4)_2]_n$ formulation. Besides a contraction in cell volume, the space group changes from $P2_1/m$ to $P2_1/c$, which requires the loss of the crystallographic symmetry plane in which nickel atoms, as well as water molecules Ow2 and Ow3, were located (Fig. 1). The polymer backbone of Ni atoms is now almost collinear, and the angle and distance between the consecutive metals are 169.12(4)° and 7.109(2) Å, respectively, *cf.* the zigzag Ni arrangement in the hydrated species **1** where the corresponding values are 156.95(3)° and 7.460(3) Å. In addition, the conformation of the Cu(medpt) moiety appears to change slightly, and a noteworthy modification related to the dehydration process is the change in distance between nitrogens N1··N1″ (5.37 Å), which for the corresponding atoms involved in H-bonding with bridging water molecules in **1**, is 4.81 Å (Fig. 1).

To examine the inclusion chemistry of this material, the synthesised microcrystalline solid was heated at 100 °C for 30 min, in order to remove the guest molecules. It is worth noting that upon reintroducing water into the pores over a period of 1 h, the XRD pattern¶ of the resulting solid is simultaneously regenerated with the peak positions and their intensities being fully coincident to those observed for the original solid, serving as evidence to the reversibility of the inclusion process (Fig. 3).

It is also interesting that the evacuated solid selectively binds MeOH (**1a**) and MeCN (**1b**)‖ in the pores among the number of organic solvents tested (ethanol, benzene, carbontetrachloride, chloroform, dichloromethane *etc*). In DMF and DMSO, the morphology of the complex breaks down. The XRD patterns of these two solids containing guest MeOH or MeCN molecules show diffraction peaks which are sharp but with slightly different positions and line widths compared to the original species containing water as guest molecules. IR spectra also corroborate the retention of morphology with MeOH or MeCN as guest molecules. Thermogravimetric analyses of **1a** and **1b** show weight losses at 130 and 170 °C, respectively, that can be attributed to the loss of *ca.* two methanol and two acetonitrile molecules per formula unit, respectively. It is also important to note that the reversibility of the inclusion process found for water guest molecules is also observed for **1a** but not **1b** for which removal of the two acetonitrile molecules per formula unit leads to instantaneous decomposition.

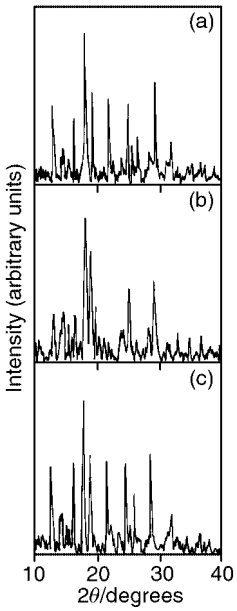

Fig. 3 The XRD patterns of (a) as-synthesized material, $[\{Cu_2(medpt)_2Ni(CN)_4\}(ClO_4)_2\cdot 2.5H_2O]_n$ **1**; (b) dehydrated solid, $[\{Cu_2(medpt)_2Ni(CN)_4\}(ClO_4)_2]_n$ **2** and (c) regenerated solid, resulting from the reintroduction of water molecules into the channels of the dehydrated solid.

Notes and references

‡ *Experimental procedure and selected data*: bis(3-aminopropyl)methylamine) (medpt) (2 mmol, 0.290 g) was added dropwise to an aqueous solution (10 cm³) of $Cu(ClO_4)_2\cdot 6H_2O$ (2 mmol, 0.741 g) with constant stirring. $K_2[Ni(CN)_4]\cdot 2H_2O$ (1 mmol, 0.276 g) dissolved in water (5 cm³) was poured to the resulting blue solution and instantaneous deep blue precipitation occurred. The reaction mixture was stirred for 30 min and then filtered. After a few days suitable shining deep blue single crystals of **1** were obtained from the filtrate. IR: ν(N–H): 3200–3400; ν(CN): 2150; $\nu(ClO_4)$: 1098–984 cm^{-1}.

§ *Crystal data*: for **1**: $C_{18}H_{43}Cu_2NiCl_2N_{10}O_{10.5}$, M = 824.31, monoclinic, space group $P2_1/m$, a = 7.806(2), b = 14.619(7), c = 15.069(5) Å, β = 97.41(2)°, V = 1705.3(11) Å^3, Z = 2, D_c = 1.605 g cm^{-3}, μ(Cu-Kα) = 4.075 mm^{-1}, 3247 unique reflections, $R1$ (F_o) = 0.0559 for 2960 reflections with $I > 2\sigma(I)$, $wR2$ (F_o^2) = 0.1672.

For **2**: $C_{18}H_{38}Cu_2NiCl_2N_{10}O_8$, M = 779.27, monoclinic, space group $P2_1/c$, a = 14.410(6), b = 14.154(4), c = 16.014(5) Å, β = 91.86(2)°, V = 3264.5(19) Å^3, Z = 4, D_c = 1.586 g cm^{-3}, μ(Mo-Kα) = 2.080 mm^{-1}, 5018 unique reflections, $R1$ (F_o) = 0.0690 for 3110 reflections with $I > 2\sigma(I)$, $wR2$ (F_o^2) = 0.1983.

The structure determination was affected by the low crystallinity ($2\theta_{max}$ = 48°), leading to geometrical data of poor accuracy, with disordered perchlorate anions being observed.

CCDC reference numbers 154468 and 163231. See http://www.rsc.org/suppdata/cc/b1/b103823k/ for crystallographic data in CIF or other electronic format.

¶ X-Ray powder diffraction data were collected using Seifert XRD-3000P instrument, where the source of X-rays was Cu-Kα radiation.

‖ For the preparation of complexes **1a** and **1b**, the parent species **1** in a micro-conical flask was heated to 100 °C for 30 min and cooled to ambient temperature whilst keeping it in a fused $CaCl_2$-vacuum desiccator. Dry methanol (**1a**)/acetonitrile (**1b**) was then added in excess and the sample kept in the desiccator for a day.

1 O. M. Yaghi, G. Li and H. Li, *Nature*, 1995, **378**, 703; P. J. Hagrman, D. Hagrman and J. Zubieta, *Angew. Chem., Int. Ed.*, 1999, **38**, 2638; H. Li, M. Eddaoudi, M. O'Keeffe and O. M. Yaghi, *Nature*, 1999, **402**, 276; C. J. Kepert and M. J. Rosseinsky, *Chem. Commun.*, 1999, 375; T. Niu and A. J. Jacobson, *Inorg. Chem.*, 1999, **38**, 5346; H. Gudbjartson, K. Biradha, K. M. Poirer and M. J. Zaworotko, *J. Am. Chem. Soc.*, 1999, **121**, 2599; D. M. L Goodgame, D. A. Grachvogel and D. J. Willams, *Angew Chem., Int. Ed.*, 1999, **3**, 641; L. R. MacGillivray, R. H. Groenman and J. L. Atwood, *J. Am. Chem. Soc.*, 1998, **120**, 2676.

2 (*a*) G. A. Bowmaker, B. J. Kennedy and J. C. Reid, *Inorg. Chem.*, 1998, **37**, 3968; (*b*) M. Ohba, N. Usuki, N. Fukita and H. Okawa, *Angew. Chem., Int. Ed.*, 1999, **38**, 1795; (*c*) L. R. Falvello and M. Tomas, *Chem. Commun.*, 1999, 273; (*d*) D. J. Chesnut and J. Zubieta, *Chem. Commun.*, 1998, 1707; (*e*) T. Iwamoto, T. Nakano, M. Morita, T. Miyoshi and Y. Sasaki, *Inorg. Chim. Acta*, 1968, **2**, 313; (*f*) D. G. Fu, J. Chen, X. S. Tan, L. J. Jiang, S. W. Zhang, P. J. Zheng and W. X. Tang, *Inorg. Chem.*, 1997, **36**, 220; (*g*) P. S. Mukherjee, T. K. Maji, T. Mallah, E. Zangrando, L. Randaccio and N. Ray Chaudhuri, *Inorg. Chim. Acta*, 2001, **315**, 249.

3 T. Iwamoto, *Supramolecular Chemistry in Cyanometallate Systems*, in *Comprehensive Supramolecular Chemistry*, ed. D. D. MacNicol, F. Toda and R. Bishop, Pergamon, Oxford, 1996, vol. 6, ch. 19; I. Muga, J. M. Gutierrez-Zorrila, A. Luque, P. Roman and F. Lloret, *Inorg. Chem.*, 1997, **36**, 743.

4 (*a*) J. Cernak, J. Chomic, P. Domiano, O. Ori and G. D. Andreetti, *Acta Crystallogr., Sect. C*, 1990, **46**, 2103; (*b*) H. Yuge and T. Iwamoto, *J. Chem. Soc., Dalton Trans.*, 1994, 1237.

CHEMCOMM
Communication
www.rsc.org/chemcomm

Synthesis and characterization of the heteroaromatic MF_6^- (M = As, Sb) salts of the 1,2,4-trithiolanylium dication $[PhCSSC(Ph)S]^{2+}$†

T. Stanley Cameron,[a] Andreas Decken,[b] Min Fang[b] and Jack Passmore*[b]

[a] *Department of Chemistry, Dalhousie University, Halifax, Nova Scotia, Canada B3H 4J3*
[b] *Department of Chemistry, University of New Brunswick, Fredericton, New Brunswick, Canada E3B 6E2*

Received (in Cambridge, UK) 2nd January 2001, Accepted 3rd May 2001
First published as an Advance Article on the web 5th July 2001

$PhCSSC(Ph)S(MF_6)_2$ (M = As, Sb), (X-ray crystal structure, FT Raman, ^1H, ^{13}C NMR and theoretical calculations) containing the first example of a dicationic 6π five-membered C–S heterocycle and sulfur were formed on disproportionation of $PhCSSS(MF_6)$ in liquid SO_2 solution.

We previously prepared **3** in low yield, containing the first structurally characterized example of the $RCSSS^+$ ring.[1] In an

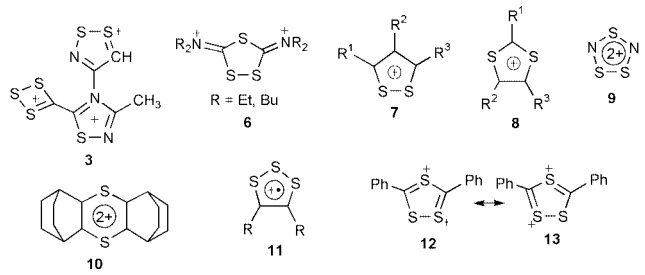

attempt to prepare a simple derivative of this ring system in good yield we reacted the previously reported[2] $PhCS_3Cl$ with $AgSbF_6$ and to our surprise obtained $PhCSSC(Ph)S(SbF_6)_2$ **2**$(SbF_6)_2$. On further investigation we obtained $PhCSSS(SbF_6)_2$ **1**SbF_6 and found that it disproportionates in SO_2 solution to give **2**$(SbF_6)_2$ and elemental sulfur. **2** is the first example of a dicationic 6π five-membered C–S heterocycle. RCS_3Cl (R = Ph, *p*-$MeOC_6H_4$, 1-naphthyl) are known.[2] Therefore the synthesis of $RCSSC(R)S(MF_6)_2$ is likely general, although it may require an R group onto which some of the +2 positive charge on the C_2S_3 ring can be delocalized. There are many examples of five- and six-membered C–S containing heteroaromatic rings,[3,4] however the only aromatic dication previously reported is **10**. Related analogues of **2** are **6** (R = Et, Bu), in which the $C_2S_3^{2+}$ ring is non-planar and charges are largely localized on the exocyclic N atoms as drawn.[5] The other C–S containing 6π five-membered cyclic heterocylcles are thiophene, 1,2-dithiolium **7**, and 1,3-dithiolium **8**.[3] **2** is isolobal to $SNSSN^{2+}$ **9** in $(SNSSN)^{2+}(MF_6^-)_2$ (M = As, Sb).[6] However unlike the $S_3N_2^{2+}$ ring, which dissociates to SNS^+ and SN^+, **2** retains its identity in SO_2 solution. The isomeric 1,2,4-trithiolanylium dication $RCSSSCR^{2+}$ has not been reported, although the 7π 1,2,3-trithiolynium monocation radical **11** is known.[7]

2$(SbF_6)_2$ was first prepared by adding the soluble product (0.586 g, 1.697 mmol) of the $PhCS_2H/SCl_2$ reaction to $AgSbF_6$ (1.331 g, 3.874 mmol) in liquid SO_2.‡ The mixture was stirred for 2 h in bulb 1 of a two-bulb Pyrex glass vessel incorporating a medium sintered-glass frit (see ref. 8). A solution over a precipitate was obtained in bulb 2 by repeatedly extracting the soluble material into bulb 2 leaving the insolubles (including AgCl) in bulb 1. The solvent in bulb 2 was then condensed back to bulb 1. About 2 ml SO_2 was condensed back (three times) onto the precipitate (in bulb 2) and the obtained solution containing the most soluble components (*e.g.* unreacted $AgSbF_6$ and other impurities) filtered to bulb 1. **2**$(SbF_6)_2$ was recovered with a trace of S_8 (Raman) from bulb 2 as an orange solid (0.446 g, 0.600 mmol, 35% yield). Single crystals of **2**$(SbF_6)_2$§ were grown from SO_2 solution. This implies the presence of $[PhCSSC(Ph)S]Cl_2$ as a main component of the soluble product of the $PhCSSH/SCl_2$ reaction. Crystals of **2**$(AsF_6)_2$ were obtained similarly by using $AgAsF_6$. An ORTEP diagram of **2** in **2**$(SbF_6)_2$ (−60 °C) is shown in Fig. 1. The observed and calculated (MPW1PW91/3-21G*)¶ bond distances and angles are in reasonable agreement. The structure of **2** in **2**$(AsF_6)_2$ (−100 °C)§ is similar. The FT Raman spectrum of **2**$(SbF_6)_2$ in the 50–800 cm^{-1} region is shown in Fig. 2 (full Raman spectra of **2**$(SbF_6)_2$ is shown in S-Fig. 1†). The observed and calculated Raman frequencies and ^{13}C, ^1H chemical shifts are in good agreement (Fig. 2, Table 1 and S-Table 1†).

The precipitate in the $PhCSSH/SCl_2$ reaction was found to be $PhCS_3Cl$.‖ $PhCS_3Cl$ (0.570 g, 2.59 mmol) was reacted with $AgSbF_6$ (0.953 g, 2.79 mmol) in liquid SO_2 (9.1 g) to give **1**SbF_6 (0.492 g, 1.17 mmol, 45% yield). The procedure was the same as described above except that the reaction time was < 30 min and light was excluded. The initial failure to obtain **1**SbF_6 is because the soluble rather than the insoluble product of the $PhCSSH/SCl_2$ reaction was reacted with $AgSbF_6$. ^1H (Fig. 3) and ^{13}C NMR spectra of **1**SbF_6 in liquid SO_2 were studied as a function of time. Observed and calculated chemical shifts of **1** are in good agreement and are given in Table 1 (Similar ^1H NMR spectra found for **1**AsF_6).** Peaks due to **1** decreased over time with the appearance of those of **2** and precipitation of

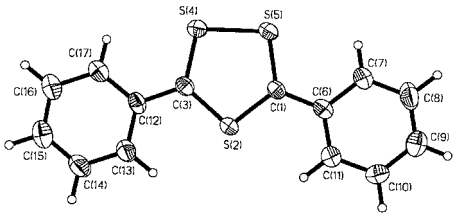

Fig. 1 ORTEP of **2** in **2**$(SbF_6)_2$ (−60 °C) drawn at the 50% probability level. Selected bond lengths (Å), bond angles (°); and calculated results (MPW1PW91/3-21G*) are given in parentheses and in bold: C(3)–C(12) 1.424(10) (**1.418**), C(12)–C(17) 1.397(12) (**1.427**), C(12)–C(13) 1.392(11) (**1.426**), C(13)–C(14) 1.351(12) (**1.378**), C(17)–C(16) 1.365(12) (**1.378**), C(16)–C(15) 1.363(14) (**1.403**), C(15)–C(14) 1.359(14) (**1.404**), C(3)–S(4) 1.680(8) (**1.710**), S(4)–S(5) 2.024(3) (**2.062**), S(5)–C(1) 1.683(7) (**1.710**), C(1)–S(2) 1.699(7) (**1.729**), C(1)–C(6) 1.412(10) (**1.418**); C(3)–S(2)–C(1) 100.8(4) (**100.7**), S(2)–C(3)–S(4) 119.4(4) (**119.2**), C(3)–S(4)–S(5) 100.4(3) (**99.8**), S(4)–S(5)–C(1) 99.8(3) (**99.8**), S(5)–C(1)–S(2) 119.5(4) (**119.2**), C(12)–C(3)–S(4) 121.8(6) (**120.1**), C(12)–C(3)–S(2) 118.8(6) (**120.6**).

† Electronic supplementary information (ESI) available: S-Table 1: FT-Raman data for **2**$(MF_6)_2$ (M = As, Sb). S-Table 2: calculated/observed bond distances and angles for **2**. S-Table 3: FT-Raman data for **1**MF_6 (M = As, Sb). S-Fig. 1: FT-Raman spectrum of **2**$(SbF_6)_2$ in the 50–4000 cm^{-1} region. S-Fig. 2: calculated Pauling bond orders of **2** in **2**$(SbF_6)_2$. S-Fig. 3: FT-Raman spectrum of **1**SbF_6 in the 50–800 cm^{-1} region. See http://www.rsc.org/suppdata/cc/b1/b100001m/

 DOI: 10.1039/b100001m

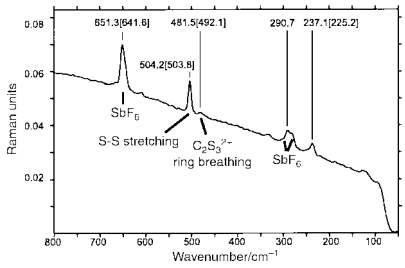

Fig. 2 FT-Raman spectrum of **2**$(SbF_6)_2$ in the 50–800 cm^{-1} region. Data in square brackets are the calculated frequencies (MPW1PW91/3-21G*).

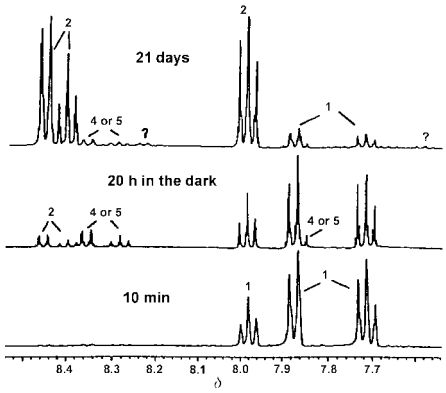

Fig. 3 *In situ* ^1H NMR study of **1**SbF_6 in liquid SO_2.

S_8 (Raman) and an intermediate we propose could be either **4** or **5** (see Scheme 1), the mechanism of which warrants further study. Light was found to facilitate this process.

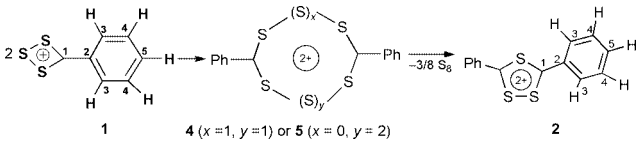

Scheme 1 Proposed mechanisms for the rearrangement of **1** to **2** in liquid SO_2.

The phenyl and C_2S_3 ring of **2** are planar [Σ angles for C_2S_3 rings: 539.9° (25 °C), 540.1° (−60 °C) in **2**$(SbF_6)_2$, 540.0° in **2**$(AsF_6)_2$ (−100 °C)]. The benzyl rings and the dication ring are nearly coplanar in **2**$(MF_6)_2$ (M = Sb, As) with $Ph_1/\overline{CSCSS}^{2+}$, $Ph_2/\overline{CSCSS}^{2+}$ and Ph_1/Ph_2 torsion angles of 3.4° (12.6°), 7.0° (168.3°) and 3.8° (176.7°) respectively in **2**$(SbF_6)_2$ (25 °C) and **2**$(AsF_6)_2$ (−100 °C) (angles in parentheses). This implies the π electrons and charges are delocalized over the three rings, supported by the short Ph–C bond distance†† and the significant F–H and F–S contacts. The sum of the Pauling bond orders (BOs)‡‡ for the C_2S_3 ring is 6.8–6.9 in both salts (S-Fig. 2†) and the π bonding mostly in the C–S region, *cf.* **12** and **13**. The S–S bond distance of 2.024(3) [in **2**$(SbF_6)_2$, −60 °C] and 2.032(3) [in **2**$(AsF_6)_2$ (−100 °C)] implies the BO is slightly greater than 1 (*cf.* S–S distance: 2.05 Å in S_8 and 2.08 Å in C–SS–C containing compounds with C–S–S–C dihedral angle of 0°[10]). Consistently, the S–S stretching frequency at 504 cm^{-1} (see Fig. 2) is greater than that of S_8 (473 cm^{-1}).

Table 1 Observed[a] [in **1**SbF_6 and **2**$(SbF_6)_2$] and calculated[b] (in parentheses) ^1H and ^{13}C NMR chemical shifts of **1** and **2**

δ_H	C1-H	C2-H	C3-H	C4-H	C5-H
1	—	—	7.87 d (7.88)	7.71 t (7.91)	7.98 t (8.44)
2	—	—	8.44 d (8.28)	7.98 t (8.37)	8.39 t (9.14)
δ_C	C1	C2	C3	C4	C5
1	204.9 (213.7)	133.8 (135.2)	123.6 (125.6)	130.7 (135.6)	139.5 (153.3)
2	216.4 (218.8)	131.0 (135.0)	133.2 (140.0)	134.4 (140.9)	148.2 (167.6)

[a] Chemical shifts were obtained at room temperature in liquid SO_2, using TMS in liquid SO_2 as external standard. [b] Isotropic NMR shielding tensors were calculated at the MPW1PW91/6-311G(2DF)//MPW1PW91/3-21G* level and referenced against calculated TMS values; d = doublet, t = triplet.

We thank Dr. Larry Calhoun (UNB) for his assistance with NMR experiments, and NSERC for an operating grant (J. P.) and the Province of New Brunswick for a Women's Doctoral Fellowship (M. F.).

Notes and references

‡ Filtration of the $PhCS_2H/SCl_2$ reaction mixture about 10 min after initial $PhCS_2H$ addition, followed by immediate removal of solvent *in vacuo*, gave the soluble product as a mixture of yellow powder and some red sticky material. (Campaine *et al.*[2] obtained red sticky oil as the soluble product, as they did not immediately remove the solvent.) The product was reacted with $AgSbF_6$ according to: $[PhCSSC(Ph)S]Cl_2 + 2\ AgSbF_6 \rightarrow$ **2**$(SbF_6)_2 + 2$ AgCl and assuming it was all $[PhCSSC(Ph)S]Cl_2$.

§ *Crystal data*: for **2**$(SbF_6)_2$ (room temp.): $C_{14}H_{10}S_3F_{12}Sb_2$, M = 745.89, monoclinic, space group $P2_1/n$ (no. 14), a = 9.359(5), b = 15.148(2), c = 15.762(2) Å, β = 104.56(2)°, U = 2162.8(9) Å^3, Z = 4, D_c = 2.291 g cm^{-3}, T = 296.0 K, $F(000)$ = 1408.00, μ(Mo-Kα) = 28.85 cm^{-1}. 6923 reflections measured, 6564 independent reflections, $R(R_w)$ = 0.051 (0.202), $R = \Sigma||F_o| - |F_c||/\Sigma|F_o|$, $R_w = [\Sigma w(|F_o| - |F_c|)^2/\Sigma wF_o^2]^{1/2}$.

For **2**$(SbF_6)_2$ (−60 °C): $C_{14}H_{10}S_3F_{12}Sb_2$, M = 745.89, monoclinic, space group $P2_1/n$ (no. 14), a = 9.345(4), b = 15.005(5), c = 15.745(4) Å, β = 104.71(3)°, U = 2135(1) Å^3, Z = 4, D_c = 2.320 g cm^{-3}, T = 213 K, $F(000)$ = 1408.00, μ(Mo-Kα) = 29.22 cm^{-1}. 6683 reflections measured, 6334 independent reflections, $R1$ ($wR2$) = 0.0391 (0.1487).

For **2**$(AsF_6)_2$ (−100 °C): $C_{14}H_{10}S_3F_{12}As_2$, M = 652.24, monoclinic, space group $P2_1/c$ (no. 14), a = 9.1371(9), b = 14.850(2), c = 15.427(2) Å, β = 107.747(7)°, U = 1993.6(4) Å^3, Z = 4, D_c = 2.173 g cm^{-3}, T = 173(1) K, $F(000)$ = 1264.00, μ (Mo-Kα) = 37.77 cm^{-1}. 5041 reflections measured, 5041 independent reflections, R (R_w) = 0.076 (0.214). CCDC 156699–15670. See http://www.rsc.org/suppdata/cc/b1/b100001m/ for crystallographic data in CIF or other electronic format.

¶ GAUSSIAN 98W, Revision A. 3, Gaussian, Inc., Pittsburgh PA, 1998.

‖ $PhCS_3Cl$ was prepared by a modification of the reported method.[2] The molar ratio of $PhCSSH:SCl_2$ was changed from 1:2 to 1:1 and the solvent from diethyl ether-CCl_4 to diethyl ether. The melting point (90–93 °C) and Raman spectrum are identical to the product obtained following the procedure of Campaine *et al.*.[2]

** **1**(SbF_6) was characterized also by Raman and elemental analysis [found (calc): C, 19.63 (19.90); H, 1.26 (1.20); S, 24.65 (22.80); Sb, 29.39 (28.90), F, 28.63 (27.10)%]. The observed and calculated (MPW1PW91/3-21G*) Raman frequencies are in good agreement (S-Fig. 3, S-Table 3†). A preliminary X-ray crystal structure confirms the atom connectivity [a = 6.899(3), b = 6.905(2), c = 14.651(4) Å, α = 88.78(1), β = 88.44(1), γ = 60.34(1)°].

†† The average Ph–C bond distance is 1.41(1) Å in **2**$(SbF_6)_2$ and 1.44(1) Å in **2**$(AsF_6)_2$, which are slightly shorter than a C_{sp^2}–C_{sp^2} single bond distance (1.48 Å).

‡‡ The Pauling bond order is given by $D_b = D_1 - 0.71 \log b$ where D_b is the observed bond distance and D_1 is the single bond distance [D_1(S–S) 2.05; D_1(C–S) 1.81, D_1(C_{sp^2}–C_{sp^2}) 1.48 Å]; see ref. 9.

1 T. S. Cameron, A. Decken, M. Fang, S. Parsons, J. Passmore and D. J. Wood, *Chem. Commun.*, 1999, 1801.
2 E. Campaine, M. Pragnell and F. Haaf, *J. Heterocycl. Chem.*, 1968, **5**, 141.
3 R. D. Hamilton and E. Campaigne, in *Special Topics in Heterocyclic Chemistry*, ed. A. Weissberger and E. C. Taylor, John Wiley & Sons, New York, 1977, p. 271.
4 R. T. Oakley, *Prog. Inorg. Chem.*, 1988, **36**, 299.
5 J. Willemse, J. A. Cras and P. J. H. A. M. van de Leemput, *J. Inorg. Nucl. Chem. Lett.*, 1976, **12**, 255.
6 W. V. F. Brooks, T. S. Cameron, S. Parsons, J. Passmore and M. J. Schriver, *Inorg. Chem.*, 1994, **33**, 6230.
7 T. S. Cameron, R. C. Haddon, S. M. Mattar, S. Parsons, J. Passmore and A. P. Ramirez, *J. Chem. Soc., Dalton Trans.*, 1992, 1563 and references therein.
8 M. P. Murchie, R. Kapoor, J. Passmore and G. Schatte, *Inorg. Synth.*, 1997, **31**, 115.
9 L. Pauling, *The Nature of the Chemical Bond*, 3rd edn., Cornell University Press, Ithaca, NY, 1960.
10 K. L. McCormack, P. R. Mallinson, B. C. Webster and D. S. Yufit, *J. Chem. Soc., Faraday Trans.*, 1996, **92**, 1709.

CHEMCOMM Communication
www.rsc.org/chemcomm

A push–pull 4a,4b-dihydrophenanthrene†

Frederick D. Lewis,*[a] Todd L. Kurth[a] and Rajdeep S. Kalgutkar[ab]

[a] *Department of Chemistry, Northwestern University, 2145 Sheridan Road, Evanston, IL 60208 USA. E-mail: lewis@chem.northwestern.edu*
[b] *Science Research Center, 3M Company, St. Paul, MN 55144, USA*

Received (in Corvallis, OR) 17th May 2001, Accepted 12th June 2001
First published as an Advance Article on the web 6th July 2001

Irradiation of (*Z*)-3-cyano-3′-aminostilbene in the absence of oxygen yields a push–pull substituted dihydrophenanthrene with substantial quinoidal character as evidenced by the pronounced solvent dependence of its absorption spectrum.

The photocyclization of diarylethenes is among the most extensively studied of photochromic reactions.[1–5] The prototype for this reaction is the photocyclization of the colorless (*Z*)-stilbene **Ia** to the yellow 4a,4b-dihydrophenanthrene **IIa**, which is rapidly converted to phenanthrene in the presence of oxygen (Scheme 1). In the absence of oxygen **IIa** undergoes ring opening to reform **Ia** both thermally and photochemically. Lack of thermal stability and sensitivity to oxygen has limited the utility of stilbene photocyclization in photochromic applications. The search for photochromic molecules which are thermally stable even in the presence of oxygen has led to the development of diarylethenes with heterocyclic aryl groups.[5,6] The presence of an electron donating group on one heterocycle and an electron accepting group on the other has provided photochromic systems that absorb throughout the visible and into the infrared. Curiously, the photochemical generation of push–pull stabilized 4a,4b-dihydrophenanthrenes has not been investigated.

The effects of single electron donating or accepting substituents on the quantum yield for phenanthrene formation (Φ_p) from (*Z*)-stilbenes in the presence of oxygen was investigated by Güsten and co-workers.[7,8] They report higher values of Φ_p for 3-cyanostilbene **Ib** and 3-aminostilbene **Ic** (0.012 and 0.28, respectively) than for their 4-substituted isomers. Irradiation of either **Ib** or **Ic** in the presence of oxidizing agents results in the formation of both 2- and 4-substituted phenanthrenes (**III** and **IV**), in a *ca*. 3.5 : 1 ratio. Muszkat *et al.*[9] have investigated the anaerobic irradiation of several monosubstituted (*Z*)-stilbenes and report a higher quantum yield for formation of dihydrophenanthrene **IIb** from **Ib** (0.012) than for its 4-substituted isomer. The photochemistry of a large number of push–pull 4,4′-disubstituted stilbenes including 4-cyano-4′-aminostilbene has also been investigated.[10–13] These stilbenes undergo reversible *trans–cis* photoisomerization. However, to our knowledge there have been no reports of their photocyclization. As part of our study of the photochemical behavior of aminostilbenes,[14–17] we have investigated the anaerobic irradiation of **Ic**, its *N*,*N*-dimethylamino analog **Id**, and (*Z*)-3-amino-3′-cyanostilbene **Ie**.

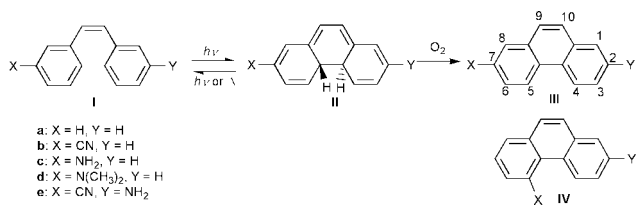

Scheme 1

Irradiation of the (*Z*)-3-aminostilbenes **Ic**, **Id**, and **Ie** in freeze–pump–thaw degassed cyclohexane (C_6H_{12}) or acetonitrile (CH_3CN) solution promptly followed by acquisition of the absorption spectrum results in the observation of a broad absorption band at long wavelengths.[18] The deconvoluted absorption spectra of **IIc**, **IId**, and **IIe** in acetonitrile solution are shown in Fig. 1. These spectra are obtained by means of singular value decomposition (SVD)-self modeling from a matrix of absorption spectra obtained at different conversions (see: supplementary information). This procedure also establishes the presence of one major dihydrophenanthrene product along with the (*Z*)- and (*E*)-stilbenes in each case. The major products are assigned structures **IIc**–**IIe** on the basis of formation of the corresponding 2-aminophenanthrenes **IIIc**–**IIIe** as the major products obtained from the irradiation of aerated solutions. In the case of **Ie** irradiation of an aerated solution results in the formation of **IIIe** and **IVe** in a 4.3 : 1 ratio, but no detectable 4-amino-7-cyano isomer.[19] The absence of evidence for the presence of 4-aminodihydrophenanthrene products under anaerobic conditions may reflect more rapid thermal ring opening of the 4-amino-substituted dihydrophenanthrenes.

The absorption band of **IIc** (Fig. 1) is rapidly bleached by visible light but is stable in the dark for a period of several days in CH_3CN solution and undergoes repeated formation and bleaching without degradation. This permits acquisition of the ^{1}H NMR spectrum of **IIc** as a mixture with **Ic**.[20] Salient features of the spectrum include singlets at 3.23 and 3.27 ppm assigned to the 4a,4b protons and unresolved multiplets between 5–7 ppm assigned to the vinyl protons.[3] Optimum conversions of **Ic** to **IIc** are obtained using monochromatic 276 nm irradiation as observed for conversion of **Ia** to **IIa** by Muszkat and Fischer.[21] The absorption bands of **IId** and **IIe** bleach rapidly in the dark and thus no attempt was made to obtain their NMR spectra.

Absorption spectral data for the (*Z*)-stilbenes **Ia**–**Ic**, and **Ie** in C_6H_{12} and CH_3CN are summarized in Table 1. The presence of 3-amino substituents in **Ic** and **Ie** results in a large red-shift in their absorption bands compared to that of **Ia**. Similar red-shifts are observed for the *trans* isomers of **Ic** and **Id** and are attributed

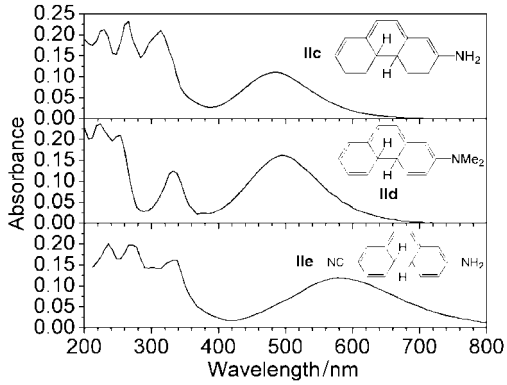

Fig. 1 Deconvoluted absorption spectra of the aminodihydrophenanthrenes **IIc**, **IId**, and **IIe** in acetonitrile solution.

† Electronic supplementary information (ESI) available: electronic absorption spectral matrices for the irradiated aminostilbenes and SVD analyses (6 figures). See http://www.rsc.org/suppdata/cc/b1/b104510p/

 DOI: 10.1039/b104510p

Table 1 Absorption spectral data and calculated dipole moments for (*Z*)-stilbenes and dihydrophenanthrenes

Compd.	λ_{max}/nm (C_6H_{12})	λ_{max}/nm (CH_3CN)	μ_g/D[a]	μ_e^{FC}/D[b]
Ia	276	276		
Ib[c]	277			
Ic[d]	315	320		
Ie	317	328		
IIa[e]	450	450	0.7	0.7
IIb[e]	467			
IIc[d]	470	482	2.4	11.4
IId	482	494	2.1	11.7
IIe	530	578	7.2	16.0

[a] Calculated ground state dipole moment. [b] Dipole moment of the Franck–Condon singlet state calculated using eqn. (2). [c] Data from ref. 8. [d] Data from ref. 17. [e] Data from ref. 3.

to splitting of the long-wavelength band which results from configuration interaction.[15,16] Much smaller shifts are observed for the 3-cyano substituents in **Ib** (*vs.* **Ia**) and **Ie** (*vs.* **Ic**).[9] Also reported in Table 1 are the absorption maxima for the dihydrophenanthrenes **IIa**–**IIe**. The substituent-induced red-shifts are larger than those observed for the corresponding (*Z*)-stilbenes and similar shifts are observed for the 3-amino and 3-cyano substituents in **IIb** and **IIc**. The shift for **IId** is larger than that for **IIc**, as previously observed for (*E*)-3-dimethylamino- *vs.* 3-aminostilbenes.[16] The aminodihydrophenanthrenes **IIc** and **IId** display large solvent-induced red-shifts in CH_3CN *vs.* C_6H_{12} solution and an exceptionally large red-shift is observed for **IIe** (1600 cm^{-1}). This shift is nearly as large as that reported for **IIf**, the ring-closed form of the more elaborate diarylethene **If** (eqn. (1), $\Delta\nu \approx 2000$ cm^{-1} in DMSO *vs.* hexane).[6]

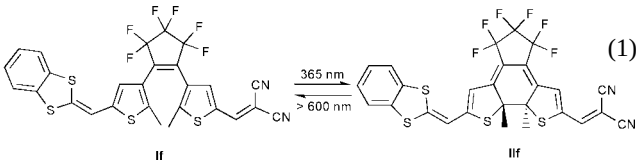

(1)

If **IIf**

The solvent-induced red-shift for the absorption maximum **IIe** is exceptionally large for an uncharged molecule, indicative of both a large ground state dipole moment and a change in the dipole moment upon electronic excitation. Ground state dipole moments calculated using the INDO/S-SCF-CI (ZINDO) algorithm[22] for **IIa** and **IIc**–**IIe** are reported in Table 1. The values calculated for **IIc** and **IId** are larger than that for (*E*)-4-dimethylaminostilbene (μ_g = 1.8 D) and the value calculated for **IIe** is larger than that for (*E*)-4-dimethylamino-4′-cyanostilbene (μ_g = 6.6 D).[16] The dipole moment of the Franck–Condon excited state (μ_e^{FC}) may be estimated by using the Lippert equation [eqn. (2)]

$$\bar{\nu}_a = -\frac{2\mu_g(\mu_e - \mu_g)}{4\pi\varepsilon_0 hca^3}\Delta f;\ \Delta f = \frac{\varepsilon - 1}{2\varepsilon + 1} - \frac{n^2 - 1}{2n^2 + 1} \qquad (2)$$

where $\bar{\nu}_a$ is the absorption maximum, h is Planck's constant, ε_0 is the vacuum permittivity, c is the speed of light, a is the radius of the solvent cavity, ε is the relative permittivity, and n is the solvent refractive index.[23] Calculated values of μ_e^{FC} for **IIc** and **IId** (Table 1) are larger than that for (*E*)-4-dimethylaminostilbene (μ_e^{FC} = 7.7 D)[16] and the calculated value for **IIe** is much larger than that for (*E*)-4-dimethylamino-4′-cyanostilbene (μ_e^{FC} = 9.0 D).[12]

The relatively large ground and excited state dipole moments of the aminodihydrophenanthrenes **IIc**–**IIe** reflect the important contributions of quinoidal resonance structures to both the ground and excited states [eqn. (3)]. These values are larger than

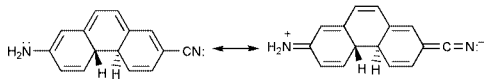

(3)

those for the corresponding 4- or 4,4′-substituted (*E*)-stilbenes, even though the distance between the donor and acceptor substituents is smaller for the dihydrophenanthrenes. Thus the extent of charge separation must be significantly larger for the dihydrophenanthrenes. Photocyclization of push–pull 4,4′-substituted stilbenes would result in the formation of 3,3′-substituted dihydrophenanthrenes for which quinoidal resonance is not possible. This may explain the absence of reports of photocyclization of these stilbenes. In addition to providing the first example of a simple push–pull stabilized dihydrophenanthrene, these results provide a design principle which may prove useful in the development of new photochromic systems. While the dihydrophenanthrene **IIe** reacts with oxygen, its stability in the absence of oxygen, ease of synthesis and compact molecular structure may provide advantages for **Ie** when compared to more complex photochromic molecules such as **If**.[5,6]

Funding for this project was provided by NSF grants CHE-9734941 and CHE-0100596. We thank Dr Wilfried Weigel for providing a sample of **Id**.

Notes and references

1 J. Saltiel and J. L. Charlton, in *Rearrangements in Ground and Excited States*, ed. P. de Mayo, Academic Press, New York, 1980.
2 J. Saltiel and Y.-P. Sun, in *Photochromism, Molecules and Systems*, ed. H. Durr and H. Bouas-Laurent, Elsevier, Amsterdam, 1990.
3 K. A. Muszkat, *Top. Curr. Chem.*, 1980, **88**, 89.
4 F. B. Mallory and C. W. Mallory, in *Organic Reactions*, John Wiley and Sons, Inc., New York, 1984.
5 M. Irie, *Chem. Rev.*, 2000, **100**, 1685.
6 S. L. Gilat, S. H. Kawai and J.-M. Lehn, *Chem. Eur. J.*, 1995, **1**, 275.
7 H. Güsten and L. Klasinc, *Tetrahedron*, 1968, **24**, 5499.
8 H. Jungmann, H. Güsten and D. Schulte-Frohlinde, *Chem. Ber.*, 1968, **101**, 2690.
9 K. A. Muszkat, H. Kessel and S. Sharafi-Ozeri, *Israel J. Chem.*, 1977, **10**, 765.
10 J.-F. Letard, R. Lapouyade and W. Rettig, *J. Am. Chem. Soc.*, 1993, **115**, 2441.
11 J.-F. Letard, R. Lapouyade and W. Rettig, *Chem. Phys. Lett.*, 1994, **222**, 209.
12 V. Il'ichev, W. Kuehnle and K. A. Zachariasse, *Chem. Phys.*, 1996, **211**, 441.
13 Y. V. Il'ichev and K. A. Zachariasse, *Ber. Bunsenges. Phys. Chem.*, 1997, **101**, 625.
14 F. D. Lewis and J.-S. Yang, *J. Am. Chem. Soc.*, 1997, **119**, 3834.
15 F. D. Lewis, R. S. Kalgutkar and J.-S. Yang, *J. Am. Chem. Soc.*, 1999, **121**, 12045.
16 F. D. Lewis and W. Weigel, *J. Phys. Chem. A*, 2000, **104**, 8146.
17 F. D. Lewis and R. S. Kalgutkar, *J. Phys. Chem. A*, 2001, **105**, 285.
18 Typical experiments used 50 μM–5 mM solutions that were degassed by five freeze–pump–thaw cycles at < 0.1 mTorr followed by flame sealing of the cuvet. Irradiation was carried out in a Rayonet RPR-100 photochemical reactor fitted with RPR-3000A bulbs. All UV–Vis spectra were promptly acquired on a Hewlett-Packard HP8452A diode array spectrometer.
19 ^{1}H NMR of **IIIe** (500 MHz, $CDCl_3$) δ: 7.08 (d, 2.3 Hz), 7.11 (dd, 8.8, 2.3 Hz), 7.63 (2H, s), 7.74 (dd, 8.6, 1.6 Hz), 8.14 (d, 1.6 Hz), 8.46 (d, 8.6), 8.56 (d, 8.8). **IVe**: 7.08 (d, 2.5 Hz), 7.12 (dd, 8.5, 2.5 Hz), 7.49 (dd, 7.1, 7.6 Hz), 7.61 (2H, s), 7.98 (dd, 7.1, 1.7 Hz), 8.01 (dd, 7.6, 1.7 Hz), 9.59 (d, 8.5 Hz).
20 ^{1}H NMR of **IIc** (300 MHz, CD_3CN) δ: 3.23 (s), 3.27 (s), 5.38 (s), 5.67 (m), 5.77 (m), 5.98 (m), 6.25 (m). Signals of **IIc** downfield from 6.5 ppm were unresolved from those of the *cis* and *trans* isomers of **Ic**.
21 K. A. Muszkat and E. Fischer, *J. Chem. Soc.*, 1967, 662.
22 Cache Release 3.5 reference, Oxford Molecular Group, Inc., Campbell, CA 95008. (800) 876-9994. http://www.oxmol.com.
23 E. Z. Lippert, *Z. Naturforsch., Teil A*, 1955, **10**, 541.

CHEMCOMM
Communication
www.rsc.org/chemcomm

In situ formation of gold nanoparticles within functionalised ordered mesoporous silica *via* an organometallic 'chimie douce' approach†

Yannick Guari,[a] Chloé Thieuleux,[a] Ahmad Mehdi,[a] Catherine Reyé,[a] Robert J. P. Corriu,*[a] Silvia Gomez-Gallardo,[b] Karine Philippot,[b] Bruno Chaudret*[b] and Roger Dutartre[c]

[a] *Laboratoire de Chimie Moléculaire et Organisation du Solide, UMR 5637 CNRS, Université de Montpellier II, Sciences et techniques du Languedoc, Place E. Bataillon, F-34095 Montpellier Cédex 5, France. E-mail: reye@crit.univ-montp2.fr*

[b] *Laboratoire de Chimie de Coordination du CNRS, 205, route de Narbonne, F-31077 Toulouse Cédex 04, France. E-mail: chaudret@lcc-toulouse.fr*

[c] *Laboratoire des Agrégats Moléculaires et des Matériaux Inorganiques, UMR 5072 CNRS, Université de Montpellier II, Sciences et techniques du Languedoc, Place E. Bataillon, F-34095 Montpellier Cédex 5, France*

Received (in Cambridge, UK) 20th March 2001, Accepted 5th June 2001
First published as an Advance Article on the web 6th July 2001

Functionalized SBA-15 type materials containing mercaptopropyl groups have been used for controlling the growth of gold(0) nanoparticles from $HAuCl_4$ or AuCl(THT) which were chemically complexed within the channels prior to mild chemical reduction.

Metal particles in the nanosize range represent a transition between the molecular and solid states and are therefore of great interest due to their unique properties attributed to quantum confinement or surface effects.[1] Thus, selective synthesis of such nanomaterials with well-defined size[2] and their dispersion in an insulator like SiO_2 is a significant challenge.[3] One approach to obtain such materials consists of using the regular channels of hexagonal mesoporous silica[4] as matrices either for the inclusion of already prepared metal particles[5] or for controlling the growth of metal particles. Such matrices should give rise to composite materials organised at the nano- and the mesoscopic length scales. Thus, the ordered mesoporous silica MCM-41,[6–10] MCM-48,[11] and FSM-16[12] materials have been used as matrices for the growth of mono-[7–12] or bimetallic[6] transition metal nanoparticles. The general procedure was to generate the nanoparticles by calcination of the metallic precursor onto the support. The final nanoparticle size is controlled by the pore size but depends also on the calcination temperature. Furthermore, outer pores growth of nanoparticles is a major frequently encountered drawback of the impregnation/calcination method. This problem has been circumvented by suspending the previously impregnated material in deionised water in order to allow complete migration of the metal salt within the pores[9] or by adding the metal salt during the preparation of the material.[10] Here, we describe a new methodology based on the chemical control of the growth of nanoparticles from organometallic precursors previously reported.[13] The precursor is chemically complexed within the channels of functionalised mesoporous silica[14] and the metal nanoparticles growth is achieved by mild chemical reduction which makes the final particle size only dependent of the pore size on the matrix used.

Materials $HS(CH_2)_3SiO_{1.5}/xSiO_2$ **1** (with $\mathbf{1_a}$: x = 9, $\mathbf{1_b}$: x = 19) were elaborated by the co-condensation route of 3-mercaptopropyltrimethoxysilane (MPTMS) with tetraethoxysilane (TEOS) in the presence of Pluronic 123 [$PEO_{20}PPO_{70}PEO_{20}$ with PEO = poly(ethylene oxide) and PPO = poly(propylene oxide)] as structure directing agent in acidic media.[15] After extraction of the surfactant by using a Soxhlet apparatus, the materials were vacuum dried at 120 °C.

^{29}Si MAS NMR spectroscopy showed resonances for siloxane (Q^n) and organosiloxane (T^n) centres with a predominance of T^3 compared to T^2 or T^1 centres indicative of extensive condensation of the organic moiety in the wall structure. The solid state ^{13}C CP MAS NMR spectra show signals at δ 27 (C1, C2) in addition to a slightly shifted downfield CH_2–(Si) (C3) signal at δ 11 for the $-(CH_2)_3SH$ moiety. This confirms the presence of mercaptopropyl groups anchored to the pore walls. Furthermore, IR spectra of $\mathbf{1_a}$ (x = 9) display a characteristic S–H stretching vibration of low intensity at 2575 cm^{-1}. High values for the BET surface areas were obtained (Table S1†). The BJH pore size distribution was calculated from adsorption and desorption branches (53/46 Å for $\mathbf{1_a}$ and 71/61 Å for $\mathbf{1_b}$). These values show a significant decrease with increasing the content of thiol groups on the channel surface (Table S1†). The low angle X-ray diffraction (XRD) patterns of the materials show the (100) reflection while higher order (110) and (200) reflections were not well observed.[15]

Anchoring of gold within materials **1** was performed by using two gold precursors with a similar strategy (Scheme 1). The protocols used were based on procedures affording gold(0) nanoparticles in solution.[16] Path A: hydrogenotetrachloroaur-

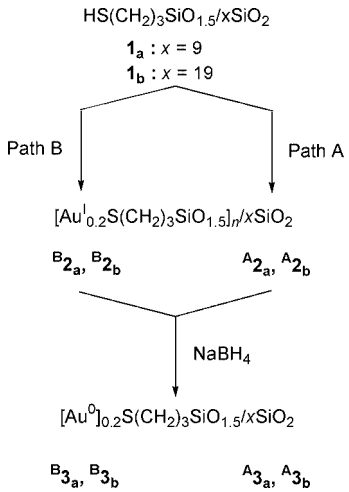

Scheme 1 Preparation of the gold(0) nanoparticle-containing materials. *Reagents and conditions*: path A: i, $HAuCl_4{\cdot}3H_2O$; ii, $HOC(CO_2Na)(CH_2CO_2Na)_2$. Path B: i, AuCl(THT); ii, Na(acac); H_2O.

† Electronic supplementary information (ESI) available: Table S1: Physical properties of ordered mesoporous materials. Fig. S1: Nitrogen adsorption/desorption isotherms of $\mathbf{1_b}$, $^{B}\mathbf{2_b}$ and $^{B}\mathbf{3_b}$ and pore size distributions. Fig. S2: Low angle XRD patterns of $\mathbf{1_b}$, $^{B}\mathbf{2_b}$ and $^{B}\mathbf{3_b}$ Fig. S3: UV–VIS spectrum of $^{B}\mathbf{3_b}$. Fig. S4: High angle XRD pattern of $^{A}\mathbf{3_a}$. Fig. S5: TEM image of $^{A}\mathbf{3_a}$. Fig. S6 TEM image of $^{B}\mathbf{3_b}$. See http://www.rsc.org/suppdata/cc/b1/b102575a/

 DOI: 10.1039/b102575a

ate(III) hydrate ($HAuCl_4 \cdot 3H_2O$) was added to a suspension of the material in water heated under reflux and allowed to stir until the yellowish solution colour was transferred onto the solid. Then, sodium citrate [$HOC(CO_2Na)(CH_2CO_2Na)_2$] was added. This is the well known Turkevitch method which affords in solution particles of mean size centred near 12 nm. Using this procedure it will therefore be easy to discriminate between nanoparticle growth inside or outside the channels of the mesoporous material previously prepared. Path B: chloro-(thiophene)gold(I) [AuCl(THT)] was added at 60 °C to a suspension of the material in THF followed by addition of sodium acetylacetonate hydrate [Na(acac)·H_2O]. This procedure is expected to be milder and to lead to a more homogeneous system.

The presence of gold in the expected quantities for the resulting materials **2** was established by elemental analysis. The decrease in BET surface area as well as the decrease in pore volume are consistent with pore filling (Table S1†).

In all cases, it was observed for the X-ray diffractograms that when comparing the results on empty materials **1** and composite materials **2**, the intensity of the reflections was reduced in the latter case. This provides a confirmation of the pore filling of the host material, which reduces the scattering contrast between the pores and the walls of the materials.[17] For materials **2**, absence of plasmon band absorbances in the UV–VIS spectra or of diffraction peaks in the X-ray diffractograms (their presence being characteristics of gold(0) nanoparticles-containing materials) were observed. TEM images show weakly contrasted particles with diameter sizes less than 1.5 nm. These particles, the size of which is not dependent on the host material pore size, were attributed to formation of $(–Au^{I}SR–)_n$ polymers.[18] Therefore, the colourless solids **2** obtained at this stage were treated with an ethanolic sodium borohydride ($NaBH_4$) solution at 60 °C. This mild reduction afforded, after 12 h, purple solids **3** for which further decrease in BET surface area and pore volume was observed (Table S1†). Materials **3** exhibit intense plasmon band absorbance at 520 nm indicative of gold(0) nanoparticles. XRD patterns of materials **3** for the high angle region (2θ = 20–70) show broad reflections characteristic of gold(0) nanoparticles. TEM studies clearly show a narrow gold(0) nanoparticle distribution size for materials **3** whatever the pathway followed (A or B) (Fig. S5 and S6†). It is also clear that in both cases the growth of the particles occurs within the channels of the silica matrix since the size of the particles is quite small (centred near 2.5 and 4.5 nm). The size distribution was found to be more narrow *via* path B ($^{B}\mathbf{3_b}$) than *via* path A ($^{A}\mathbf{3_b}$) in agreement with the milder conditions needed for the reduction of the gold(I) precursor. In all cases, a good correlation was demonstrated between the pore size values derived from BET and the gold nanoparticles diameter size observed on TEM micrographs when taking into account experimental uncertainties (Fig. 1).

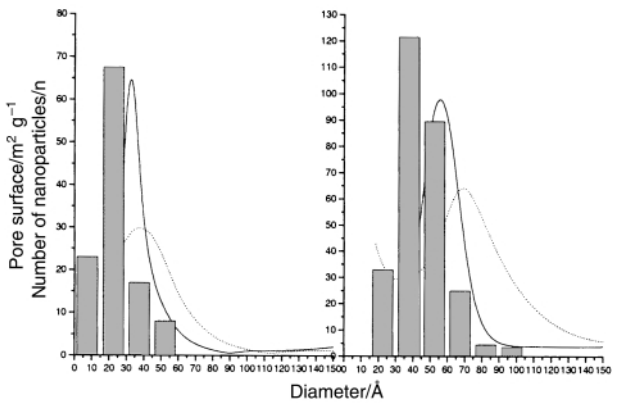

Fig. 1 Correlation between the pore diameter (solid/dotted lines for adsorption/desorption data from N_2 studies) and the gold(0) nanoparticle size (columns) for: left $^{A}\mathbf{3_a}$, right $^{B}\mathbf{3_b}$.

In conclusion, two main results are reported in this communication:

(i) The growth of gold nanoparticles can be achieved selectively within the pores of a mesoporous silica previously functionalized with thiol substituents. The nanoparticle growth follows a two step procedure implying first the anchoring of the gold precusors and secondly a chemical reduction.

(ii) This procedure allows a strict control of the size of the particles, which in each experiment, remain smaller than the pore size determined by BET and which furthermore adopt a narrow size distribution. Further work is in progress to explore the scope and limitations of this process.

The authors thank the CNRS and the Université de Montpellier II for financial support. C. T. thanks Air Liquide for a grant. S. G. G. thanks EU, TMR network CLUPOS for a grant.

Notes and references

1 A. P. Alivisatos, *Science*, 1996, **271**, 933; J. Shi, S. Gider, D. Babcock and D. D. Awschalom, *Science*, 1996, **271**, 937.
2 *Clusters and Colloids, from Theory to Applications*, ed. G. Schmid, VCH, Weinheim, 1994.
3 F. Tian and K. J. Klabunde, *New J. Chem.*, 1998, 1275.
4 C. T. Kresge, M. E. Leonowicz, W. J. Roth, J. C. Vartuli and J. S. Beck, *Nature*, 1992, **359**, 710; J. S. Beck, J. C. Vartuli, W. J. Roth, M. E. Leonowicz, C. T. Kresge, K. D. Schmitt, C. T.-W. Chu, D. H. Olsen, E. W. Sheppard, S. B. McCullen, J. B. Higgins and J. L. Schlenker, *J. Am. Chem. Soc.*, 1992, **114**, 10834.
5 D. S. Shephard, T. Maschmeyer, B. F. G. Johnson, J. M. Thomas, G. Sankar, D. Oskaya, W. Zhou, R. D. Oldroyd and R. G. Bell, *Angew. Chem., Int. Ed. Engl.*, 1997, **36**, 2242; D. S. Shephard, T. Maschmeyer, G. Sankar, J. M. Thomas, D. Ozkaya, B. F. G. Johnson, R. Raja, R. D. Olkroyd and R. G. Bell, *Chem. Eur. J.*, 1998, **4**, 1214; R. Raja, G. Sankar, S. Hermans, D. S. Shephard, S. Bromley, J. M. Thomas and B. F. G. Johnson, *Chem. Commun.*, 1999, 1571.
6 D. Ozkaya, W. Zhou, J. M. Thomas, P. Midgley, V. J. Keast and S. Hermans, *Catal. Lett.*, 1999, **60**, 113; F. Schweyer, P. Braunstein, C. Estournès, J. Guille, H. Kessler, H.-L. Paillaud and J. Rosé, *Chem. Commun.*, 2000, 1271.
7 Z. Y. Yuan, S. Q. Liu, T. H. Chen, J. Z. Wang and H. X. Li, *Chem. Commun.*, 1995, 973; Y. Plyuto, J.-M. Berquier, C. Jacquiod and C. Ricolleau, *Chem. Commun.*, 1999, 1653.
8 P. Mukherjee, C. R. Patra, R. Kumar and M. Sastry, *Phys. Chem. Commun.*, 2001, 5.
9 T. Abe, Y. Tachibana, T. Uematsu and M. Iwamoto, *J. Chem. Soc., Chem. Commun.*, 1995, 1617; M. Iwamoto, T. Abe and Y. Tachibana, *J. Mol. Catal. A: Chem.*, 2000, **155**, 143.
10 R. S. Mulukutla, K. Asakura, S. Namba and Y. Iwasawa, *Chem. Commun.*, 1998, 1425.
11 M. Fröba, R. Köhn, G. Bouffaud, O. Richard and G. van Tendeloo, *Chem. Mater.*, 1999, **11**, 2858.
12 A. Fukuoka, M. Osada, T. Shido, S. Inagaki, Y. Fukushima and M. Ichikawa, *Inorg. Chim. Acta.*, 1999, **294**, 281.
13 F. Dassenoy, K. Philippot, T. Ould Ely, C. Amiens, P. Lecante, E. Snoeck, A. Mosset, M.-J. Casanove and B. Chaudret, *New J. Chem.*, 1998, 703; O. Vidoni, K. Philippot, C. Amiens, B. Chaudret, O. Balmes, J. O. Malm, J. O. Bovin, F. Senocq and M.-J. Casanove, *Angew. Chem., Int. Ed.*, 1999, **38**, 3736; C. Pan, F. Dassenoy, M.-J. Casanove, K. Philippot, C. Amiens, P. Lecante, A. Mosset and B. Chaudret, *J. Phys. Chem. B*, 1999, **103**, 10 098; S. Gomez, K. Philippot, V. Collière, B. Chaudret, F. Senocq and P. Lecante, *Chem. Commun.*, 2000, 1945; K. Soulantica, A. Maisonnat, M.-C. Fromen, M.-J. Casanove, P. Lecante and B. Chaudret, *Angew. Chem., Int. Ed.*, 2001, **40**, 448.
14 R. J. P. Corriu, C. Hoarau, A. Mehdi and C. Reyé, *Chem. Commun.*, 2000, 71; R. J. P. Corriu, A. Mehdi and C. Reyé, *C.R. Acad. Sci. Paris, Sér. IIc*, 1999, 35; R. J. P. Corriu, Y. Guari, A. Mehdi, C. Reyé and C. Thieuleux, *Chem. Commun.*, 2001, 763.
15 D. Margolese, J. A. Melero, S. C. Christiansen, B. F. Chmelka and G. D. Stucky, *Chem. Mater.*, 2000, **12**, 2448.
16 J. Turkevitch, P. C. Stevenson and J. Hillier, *Discuss. Faraday Soc.*, 1951, **73**, 55.
17 B. Marler, U. Oberhageman, S. Vortmann and H. Gies, *Microporous Mater.*, 1996, **6**, 375.
18 A. C. Templeton, W. P. Wuelfing and R. W. Murray, *Acc. Chem. Res.*, 2000, **33**, 27.

CHEMCOMM
Communication
www.rsc.org/chemcomm

The effect of *N*-methylation on the chemical reactivity of binuclear Ni amine-thiophenolate complexes†

Berthold Kersting* and Gunther Steinfeld

Institut für Anorganische und Analytische Chemie, Universität Freiburg, Albertstr. 21, D-79104 Freiburg, Germany. E-mail: kerstber@sun2.ruf.uni-freiburg.de

Received (in Cambridge, UK) 4th April 2001, Accepted 20th June 2001
First published as an Advance Article on the web 6th July 2001

Macrocyclic amine thiophenolate ligands are shown to form face-sharing bioctahedral nickel complexes with a central $N_3Ni(\mu\text{-}SR)_2(\mu\text{-}Cl)NiN_3$ core structure. The bridging halide ion can be readily replaced when all six nitrogen atoms are tertiary amine donors.

Thiolate complexes of first row transition metals are generally labile and it is therefore difficult to control their chemical reactivity. This is true in particular for binuclear species.[1,2] For systematic investigations, complexes of macrocyclic thiophenolate ligands seem to be ideal, because of their greater thermodynamic stability and proper positioning of free coordination sites for substrate binding. However, traditional routes developed for the corresponding phenolate macrocycles[3] fail for the synthesis of sensitive thiophenolates. This situation has changed greatly in the last few years due to the work by the groups of Brooker,[4] McKee[5] and Schröder[6] who have used (*S*)-(2,6-diformyl-4-methylphenyl)dimethylthiocarbamate as thiophenolate precursor in metal templated Schiff-base condensation reactions with α,ω-diamines. The resulting thiophenolate macrocycles bear additional imine, secondary amine, and even hydroxy groups in the linking side arms. However, it has not been possible to access derivatives with tertiary amine functions. We describe here the syntheses, X-ray crystal structures and properties of binuclear Ni complexes of such ligands.

Macrocycle **2** was obtained by a [2 + 1] condensation reaction between tetraaldehyde **1**[7] and bis(aminoethyl)amine in an ethanol–dichloromethane mixed solvent system using medium-dilution conditions followed by reduction with $NaBH_4$ (Scheme 1). The yields of the new bicyclic amine-thioether are excellent (> 90%). An attractive feature of **2** compared to unprotected thiolate ligands is that its secondary amines are readily alkylated without affecting the masked thiolate functions. Thus, reductive methylation of **2** with formaldehyde and formic acid under Eschweiler–Clarke conditions gave the permethylated derivative **3** in nearly quantitative yield. Compound **3** displays only twelve resonances in its ^{13}C NMR spectrum ruling out the possibility that it exists as a mixture of conformationally stable isomers. Both the unmethylated and the permethylated thioether could be converted to the corresponding thiophenols H_2L^H and H_2L^{Me} by using sodium in liquid ammonia as reducing agent.

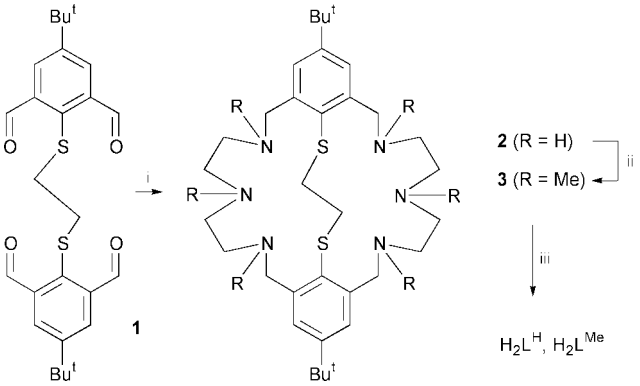

Scheme 1 *Reagents and conditions*: i, $NH(CH_2CH_2NH_2)_2$, CH_2Cl_2–EtOH (high-dilution); ii, CH_2O, HCO_2H, reflux; iii, Na, NH_3, −70 °C.

The reaction of $NiCl_2{\cdot}6H_2O$ with $H_2L^H{\cdot}6HCl$ in methanol using NEt_3 as base (2 : 1 : 8 molar ratio) was found to produce the

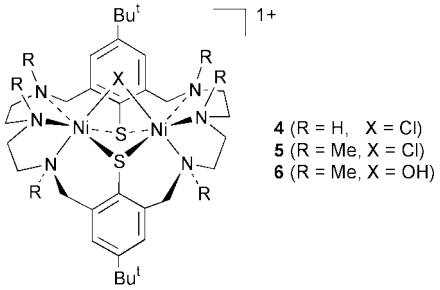

green, air-stable complex $[(L^H)Ni^{II}_2(\mu\text{-}Cl)]^{1+}$ **4**. The cation was isolated as the perchlorate salt **4**·ClO_4 in 80% yield. Crystallographic characterization of **4**·ClO_4,‡ using crystals obtained by recrystallization from methanol, confirmed the structure of **4** to consist of a confacial bioctahedral species (Fig. 1). The coligand is found in a bridging position. In the context of coordinatively unsaturated Ni thiolate complexes, the presence of a bridging halide ligand in **4** is without precedent. Most binuclear

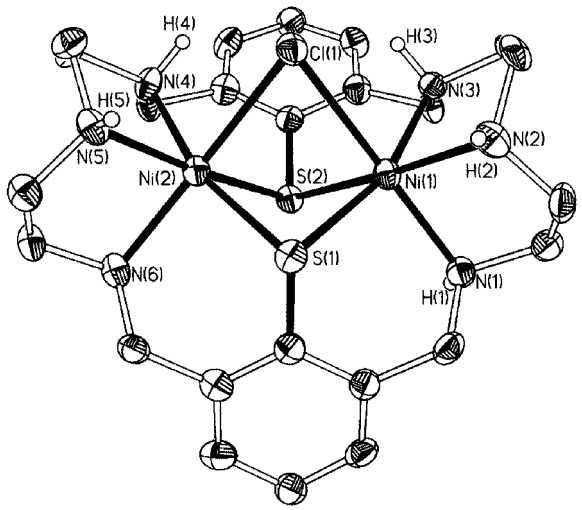

Fig. 1 Structure of the μ-Cl complex **4** with thermal ellipsoids drawn at the 50% probability level. *tert*-Butyl groups and hydrogen atoms are omitted for clarity. Selected bond lengths. Values in square brackets represent bond lengths for **5**. (Å): Ni(1)–Cl(1) 2.639(2) [2.433(2)], Ni(1)–S(1) 2.418(2) [2.471(2)], Ni(1)–S(2) 2.419(2) [2.405(2)], Ni(1)–N(1) 2.078(6) [2.352(5)], Ni(1)–N(2) 2.103(7) [2.173(5)], Ni(1)–N(3) 2.085(6) [2.181(5)], Ni(2)–Cl(1) 2.602(2) [2.450(2)], Ni(2)–S(1) 2.423(2) [2.498(2)], Ni(2)–S(2) 2.405(2) [2.423(2)], Ni(2)–N(4) 2.099(7) [2.171(5)], Ni(2)–N(5) 2.141(7) [2.175(6)], Ni(2)–N(6) 2.134(7) [2.380(6)]; Ni···Ni 3.098(2) [3.184(2)].

† Electronic supplementary information (ESI) available: Characterization data for all new compounds. ORTEP plots for complexes **5** and **6**. See http://www.rsc.org/suppdata/cc/b1/b103050g/

 DOI: 10.1039/b103050g

complexes feature a dithiolate bridged Ni(μ-SR)$_2$Ni core structure.[4–6] However, all attempts to replace the halide substituent in **4** have failed so far.

On these grounds, we synthesized the complex [(L^{Me})Ni$^{II}_2$(μ-Cl)]$^{1+}$ **5** by using reaction conditions similar to those described above for **4**. It was isolated as the yellow microcrystalline perchlorate salt **5**·ClO$_4$ in 85% yield. Electronic absorption spectroscopy (ESI†) and X-ray crystal structure determination‡ provided new insights into the coordination chemistry of the permethylated amine-thiolate ligand H$_2$L^{Me}. Two bands assigned as ν_1 ($^3A_{2g} \rightarrow {}^3T_{2g}$, splitting due to lower symmetry) are observed at 920 and 1002 nm in the UV–VIS spectrum of **5**·ClO$_4$. Compared to **4** (894 and 941 nm) these bands are shifted to lower energies indicative of a significantly weaker ligand field strength of H$_2$L^{Me}. The crystal structure determination of **5**·BPh$_4$‡ revealed the structure of the μ-chloro complex **5** to be very similar to **4**. The structure of **5** may be simply derived from that of **4** by replacing the six NH hydrogen atoms by methyl groups. The conversion of secondary into tertiary amines results in an increase of the average Ni–N bond length by 0.139 Å, which in turn results in a decrease of the average Ni–Cl distance by 0.178 Å. Similar effects have also been observed for nickel complexes of other azamacrocycles and their methylated derivatives.[8]

Preliminary binding studies demonstrate that utilization of the permethylated ligand H$_2$L^{Me} in place of H$_2$L^H drastically alters the ease of substitution of the bridging halide substituent, presumably because of the more hydrophobic microenvironment about the μ-Cl function in **5**. Thus, while the latter reacts with NBu$^n_4$OH in acetonitrile to produce the μ-OH complex **6**, complex **4** was found to be unreactive. Even the addition of a halide scavenger such as Pb^{II}(ClO$_4$)$_2$ did not lead to substitution of the Cl$^-$ ion.

A crystallographic analysis of **6**·BPh$_4$‡ revealed **6** to be isostructural with **5**. The OH group replaces the μ-Cl ligand, demonstrating that the substitution reaction takes place without gross structural changes of the parent complex. The average Ni–O bond length at 2.10 Å is typical for hydroxide-bridged dinickel centers.[9] The Ni–N and Ni–S bond lengths are similar to those in **5**, however, the separation of the Ni atoms has decreased to 3.037(3) Å. It is also worth mentioning that the OH unit [ν(OH) = 3543 cm^{-1}] is not involved in hydrogen bonding interactions.

Cyclic voltammetry experiments have shown that **4**·ClO$_4$ undergoes two one-electron oxidations at $E^1_{1/2}$ = +0.27 V [≡ $E_{1/2}$(Ni^{III}Ni^{II}/Ni^{II}Ni^{II}), ΔE_p = 91 mV] and at $E^2_{1/2}$ = 1.05 V [≡ $E_{1/2}$(Ni^{III}Ni^{III}/Ni^{III}Ni^{II}), irrev.] *vs.* SCE. The cyclic voltammogram of **5**·ClO$_4$ is very similar, but this complex is oxidized at more positive potentials at $E^1_{1/2}$ = +0.43 V (85 mV) and at $E^2_{1/2}$ = +1.37 V (irrev.) *vs.* SCE. The first oxidation of complex **6**·BPh$_4$, on the other hand, occurs at less positive potentials [$E^1_{1/2}$ = +0.26 V (94 mV); the value for $E^2_{1/2}$ could not be determined due to oxidation of the BPh$_4^-$ anion; a ClO$_4^-$ salt of **6** could not be obtained in a pure form]. The shifts of the redox potentials can be explained by the different coordination environments about the Ni ions. Tertiary amine donors exert weaker ligand fields than secondary amine functions. Complex **5** is thus more difficult to oxidize than **4**. The OH ligand in **6**, on the other hand, exerts a stronger ligand field than the halide ion in **5** and the former complex is thus more easily oxidized. Remarkably, all Ni^{III}Ni^{III} species are not stable on the timescale of a cyclic voltammetry experiment. This is in marked contrast to the behavior of coordinatively saturated Ni amine-thiolate complexes,[10] which can be reversibly oxidized to Ni^{III}Ni^{III} species. It is assumed that the different electrochemical properties are due to redox transformations of the bridging coligand or decomposition reactions of the Ni^{III} species.

In summary, the macrocyclic amine-thiolate ligand H$_2$L^H gives rise to an unprecedented type of coordinatively unsaturated amine-thiolate complex. The use of H$_2$L^{Me} in place of H$_2$L^H facilitates rapid substitution reactions at the bridging position, which encourages further exploration of the chemical reactivity of complex **5** and its derivatives.

This research was supported by the Deutsche Forschungsgemeinschaft. We thank Professor Dr H. Vahrenkamp for his generous support of this work.

Notes and references

‡ *Crystal data* for **4**·ClO$_4$·MeOH: $C_{33}H_{56}Cl_2N_6Ni_2O_5S_2$, M_r = 869.28, orthorhombic, space group *Iba*2 (no. 45), T = 293(2) K, μ(Mo-Kα) = 0.22 mm^{-1}, a = 23.941(5), b = 26.974(5), c = 12.477(2) Å, V = 8058(3) Å^3, Z = 8. 25074 measured reflections, 8935 were unique (R_{int} = 0.1201), R_1, wR_2 = 0.0587, 0.1289 [$I > 2\sigma(I)$]. For **5**·BPh$_4$·MeOH: $C_{63}H_{88}BClN_6Ni_2OS_2$, M_r = 1173.19, triclinic, space group $P\bar{1}$ (no. 2), T = 180(2) K, μ(Mo-Kα) = 0.754 mm^{-1}, a = 14.668(3), b = 20.140(4), c = 22.960(5) Å, α = 87.65(3), β = 80.96(3), γ = 69.39(3)°, V = 6269.0(22) Å^3, Z = 4. 55881 measured reflections, 28884 were unique (R_{int} = 0.0557), R_1, wR_2 = 0.0674, 0.1933 [$I > 2\sigma(I)$]. For **6**·BPh$_4$·MeOH: $C_{63}H_{89}BN_6Ni_2O_2S_2$, M_r = 1154.75, triclinic, space group $P\bar{1}$ (no. 2), T = 180(2) K, μ(Mo-Kα) = 0.672 mm^{-1}, a = 13.734(3, b = 14.093(3) Å, c = 18.094(4) Å, α = 103.24(3)°, β = 97.42(3), γ = 98.09(3)°, V = 3327.5(13) Å^3, Z = 2. 30866 measured reflections, 15786 were unique (R_{int} = 0.0959), R_1, wR_2 = 0.0893, 0.2381 [$I > 2\sigma(I)$]. The structures were determined by direct methods in SHELXS-86, refinements were carried out with SHELXL-93.[11]

CCDC reference numbers 162721–162723. See http://www.rsc.org/suppdata/cc/b1/b103050g/ for crystallographic data in CIF or other electronic format.

1 A. J. Atkins, D. Black, A. J. Blake, A. Marin-Becerra, S. Parsons, L. Ruiz-Ramirez and M. Schröder, *Chem. Commun.*, 1996, 457.
2 B. Krebs and G. Henkel, *Angew. Chem., Int. Ed. Engl.*, 1991, **30**, 769; B. Krebs and G. Henkel, *Angew. Chem.*, 1991, **103**, 785; M. A. Halcrow and G. Christou, *Chem. Rev.*, 1994, **94**, 2421.
3 H. Okawa, H. Furutachi and D. E. Fenton, *Coord. Chem. Rev.*, 1998, **174**, 51.
4 S. Brooker, P. D. Croucher and F. M. Roxburgh, *J. Chem. Soc., Dalton Trans.*, 1996, 3031; S. Brooker and P. D. Croucher, *Chem. Commun.*, 1997, 459; S. Brooker and T. C. Davidson, *Chem. Commun.*, 1997, 2007; S. Brooker, P. D. Croucher, T. C. Davidson, G. S. Dunbar, A. J. McQuillan and G. B. Jameson, *Chem. Commun.*, 1998, 2131.
5 A. Christensen, H. S. Jensen, V. McKee, C. J. McKenzie and M. Munch, *Inorg. Chem.*, 1997, **36**, 6080; P. E. Kruger and V. McKee, *Chem. Commun.*, 1997, 1341.
6 A. J. Atkins, A. J. Blake and M. Schröder, *J. Chem. Soc., Chem. Commun.*, 1993, 1662; N. D. J. Branscombe, A. J. Blake, A. Marin-Becerra, W.-S. Li, S. Parsons, L. Ruiz-Ramirez and M. Schröder, *Chem. Commun.*, 1996, 2573.
7 B. Kersting, G. Steinfeld, T. Fritz and J. Hausmann, *Eur. J. Inorg. Chem.*, 1999, 2167.
8 E. K. Barefield, G. M. Freeman and D. G. Van Derveer, *Inorg. Chem.*, 1986, **25**, 552; P. Chaudhuri and K. Wieghardt, *Prog. Inorg. Chem.*, 1987, **35**, 329.
9 D. Volkmer, B. Hommerich, K. Griesar, W. Haase and B. Krebs, *Inorg. Chem.*, 1996, **35**, 3792.
10 B. Kersting, D. Siebert, D. Volkmer, M. J. Kolm and C. Janiak, *Inorg. Chem.*, 1999, **38**, 3871; B. Kersting and D. Siebert, *Inorg. Chem.*, 1998, **37**, 3820; G. Steinfeld and B. Kersting, *Chem. Commun.*, 2000, 205.
11 G. M. Sheldrick, *Acta Crystallogr., Sect. A.*, 1990, **46**, 467; G. M. Sheldrick, SHELXL-93, Program for the Refinement of Crystal Structures, University of Göttingen, 1993.

CHEMCOMM Communication
www.rsc.org/chemcomm

Development of acidic sites in WO_x/ZrO_2

Thomas Onfroy, Guillaume Clet and Marwan Houalla*

Laboratoire de Catalyse et Spectrochimie (UMR CNRS 6506), ISMRA-Université de Caen, 6 Bd. du Maréchal Juin, 14050 Caen (cedex), France. E-mail: marwan.houalla@ismra.fr

Received (in Cambridge, UK) 28th March 2001, Accepted 20th June 2001
First published as an Advance Article on the web 6th July 2001

Evidence is shown of the appearance of Brønsted acidic sites in WO_x/ZrO_2 at a given W loading and of a direct correlation between the abundance of 'strong' Brønsted acidic sites in these catalysts and propan-2-ol decomposition activity.

It is well established that addition of W onto zirconia induces the formation of acid sites. With suitable preparation methods solid acid catalysts can be obtained which can isomerise *n*-hexane.[1] However, the genesis of acidity and the actual nature of the acid sites have not been fully investigated. Previous work with WO_x/ZrO_2 obtained by the incipient wetness impregnation method, indicated that a threshold of W loading was required for any activity for propan-2-ol decomposition to develop.[2] Similar behaviour was already reported for solids obtained by impregnation of zirconium hydroxide, for different reactions such as *o*-xylene[3] and *n*-pentane[4,5] isomerisation. It was proposed,[2] but not verified, that the origin of this behaviour is due to the formation of different types of acid sites at a given W loading. Furthermore, the simultaneous presence of polymeric surface WO_x and bulk WO_3 in active catalysts complicated any attempt to elucidate the nature of the active sites.

In the present work, a series of WO_x/ZrO_2 catalysts was prepared by the equilibrium adsorption method.[6] This procedure was shown to prevent WO_3 formation. A direct correlation between the surface structure and the catalytic activity for propan-2-ol decomposition is reported.

Tungsten surface species were monitored by Raman spectroscopy. The number, the strength and the type of acidity were characterised by IR spectroscopy. Propan-2-ol decomposition was used as a probe reaction to assay the acidity of the solids.

Catalysts were prepared by adsorption of W from aqueous solutions of ammonium metatungstate on zirconia (ZrO_2).[6] The support was prepared by hydrolysis of zirconium *n*-propoxide [$Zr(OPr)_4$, 70% in *n*-propanol; Aldrich]. The precipitate thus obtained was washed free of propanol, dried and calcined at 823 K in air for 24 h.[7] The original zirconia had a BET surface area of 43 $m^2\ g^{-1}$. A series of WO_x/ZrO_2 catalysts was prepared by suspending a known amount of ZrO_2 in a large volume of aqueous ammonium metatungstate solution [$(NH_4)_6H_2W_{12}O_{40}$, Aldrich] at a given pH. The samples were filtered off, dried and calcined at 773 K in air for 24 h. Solids with various W loadings ranging from 1.1 to 4.6 wt% W were obtained by modifying either the pH of the adsorption solution (adsorption time = 96 h) or the adsorption time (at pH = 12). No significant surface area loss was observed on W deposition.

Raman spectra were recorded with a Nicolet FT-Raman spectrometer attachment for a Nicolet Nexus FTIR spectrometer between 100 and 1100 cm^{-1} (resolution: 8 cm^{-1}). The samples were analysed in powder form and under ambient conditions without any pre-treatment. The technique was used to monitor the structure of the support (monoclinic; tetragonal), WO_3 formation and the evolution of surface W species.

IR spectra were recorded with a Nicolet 710 FT-IR spectrometer (resolution: 4 cm^{-1}). Samples were pressed into discs (*ca.* 20 mg; 2 cm^2) and activated alternatively in vacuum and O_2 at 723 K. Acidic properties (type and abundance) of the samples were characterised by two basic probe molecules (CO and 2,6-dimethylpyridine). CO was introduced at room temperature by doses (from 2.6 to 664 μmol g^{-1}) up to an equilibrium pressure of 133 Pa. 2,6-dimethylpyridine (lutidine) was introduced at room temp. ($P_{equilibrium}$ = 133 Pa) followed by thermodesorption from 373 to 573 K.

The catalytic conversion of propan-2-ol was measured in a fixed bed flow reactor. A mass of 100 mg of sample was pretreated at 723 K in N_2 for 2 h. The reaction was carried out at atmospheric pressure with 120 ml min^{-1} N_2 as carrier gas ($P_{propan\text{-}2\text{-}ol}$ = 1.23 kPa) at 413 K. Reactants and products were analysed with an on line Gas Chromatograph (HP 5890 Serie II) equipped with a capillary column (CP WAX 52 CB) and an FID detector. Catalytic study was conducted in non diffusional conditions, with conversions typically below 10%. Neither an induction period nor deactivation were observed during the analysis time (2 h). The rate of propene formation was calculated from eqn. (1), assuming a first order reaction for propan-2-ol:

$$r = -\frac{F_0}{W}\ln\left(\frac{100 - C}{100}\right) \quad (1)$$

where r is the rate of propene formation (mol h^{-1} g^{-1}), F_0 is the propan-2-ol molar flux (mol h^{-1}) and C is the % conversion to propene.

Raman spectra of WO_x/ZrO_2 catalysts and the zirconia support showed intense peaks between 100 and 700 cm^{-1} characteristic of the monoclinic phase of zirconia.[8] No Raman peaks which can be ascribed to bulk WO_3 were detected.[9] A band at 935 cm^{-1} attributed to the W surface phase appears on W deposition and increases in intensity with W loading. A shift in the position of this band to higher wavenumbers is observed with W content in accordance with previous results.[10] This is indicative of monomeric to polymeric transformation of W species.

The IR spectra of tungstated zirconias show significant dehydroxylation which increases with W loading. This indicates that W deposition occurs *via* replacement of the hydroxyl groups.

The presence of Lewis acid sites was monitored by FTIR and CO adsorption. The amount of CO required to saturate the sites decreased on W addition but it remained the same for all the tungstated solids.

The adsorption of lutidine at room temp. followed by evacuation at 423 K evidenced the presence of Brønsted acidic sites on the surface of WO_x/ZrO_2 catalysts. This is illustrated in Fig. 1(a) by the appearance of a doublet at 1645 and 1628 cm^{-1} attributed to lutidinium species and the subsequent increase of its intensity with increasing W loading. The peaks at 1610 and 1580 cm^{-1} are attributed to Lewis acid sites. After desorption of lutidine at 423 K, Brønsted acid sites were still observed for a W loading of 1 atom nm^{-2}. However, following desorption at 523 K only the Brønsted acid sites of solids containing more than 1.4 atom W nm^{-2} were sufficiently strong to retain the probe molecule on the surface [Fig. 1(b)]. These results are comparable to those reported by Wachs[11] concerning the appearance of Brønsted acidity on molybdenum, vanadium and niobium oxide supported on alumina.

The catalysts were tested for the reaction of propan-2-ol decomposition. Only two products, propene and diisopropyl ether were observed. For all catalysts, the selectivity to propene was high (≥ 85%) and increased with temperature as expected

 DOI: 10.1039/b102867g

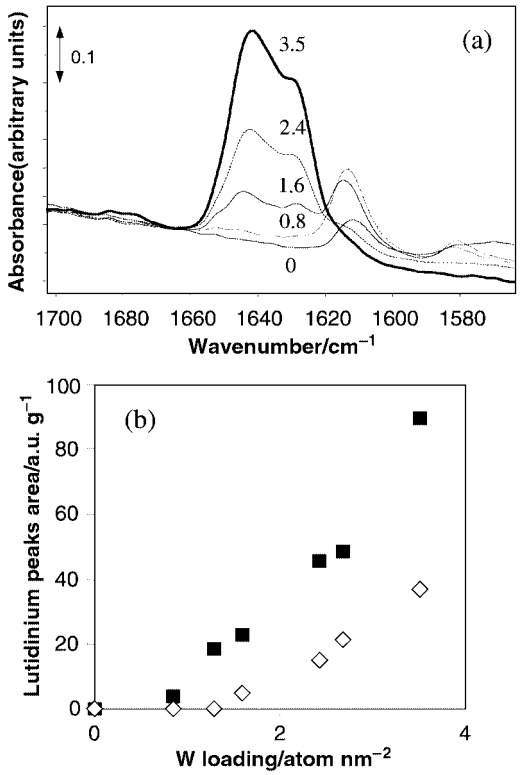

Fig. 1 Evolution of the lutidinium band. (a) IR spectra of lutidine evacuated at 423 K. (b) Evolution of the area of the band (1620–1660) after desorption of lutidine at 423 K (■) and 523 K (◇). [Numbers in (a) refer to the W loading in W atom nm^{-2}].

from thermodynamics. These results are consistent with acid catalysis.[7] In Fig. 2 the rate of propene formation was plotted *vs.* W content. The results show a very low rate up to 1.4 atom W nm^{-2}, followed by a steep increase for higher loadings. Similar behaviour was observed for measurements performed with different flows and temperatures. Fig. 2 compares the evolution of catalytic activity with that of the intensity of lutidinium band. Note that the onset of catalytic activity coincides with the appearance of 'strong' Brønsted sites. In addition, the evolution of the rate of decomposition parallels that of the abundance of Brønsted acid sites. The decomposition of propan-2-ol appears, thus, directly related to the presence and abundance of 'strong' Brønsted acid sites. Note that in the present study Brønsted acid sites are formed *prior* to any reductive treatment. This is in variance with previous studies[12] where strong Brønsted acid sites were reportedly formed on reduction of WO_x clusters in H_2 or by the reactant mixture. The appearance and the evolution of the abundance of the Brønsted sites on our catalysts suggest that

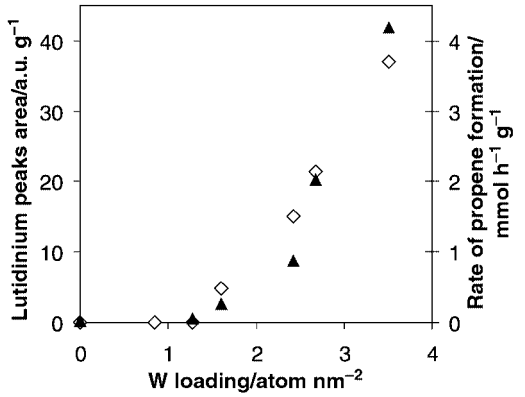

Fig. 2 Correlation between propene formation rate (▲) and abundance of "strong" Brönsted sites as evidenced by lutidinium peaks area after desorption at 523 K (◇).

a minimum degree of polymeric WO_x units may be necessary for the formation of acidic sites. A similar behaviour was observed for WO_x/Al_2O_3 catalysts and was attributed to an enhanced stabilisation of the proton by delocalisation among adjacent W atoms.[13,14] This interpretation is consistent with the observed lack of activity for low loading catalysts where W is reportedly present in a monomeric form. These results highlight the importance of extended W coverage for the development of Brønsted acid sites on supported catalysts.

Notes and references

1 M. Hino and K. Arata, *J. Chem. Soc., Chem. Commun.*, 1987, 1259.
2 N. Vaidyanathan, Ph. D. Thesis, University of Pittsburgh, 1998.
3 D. G. Barton, S. L. Soled, G. D. Meitzner, G. A. Fuentes and E. Iglesia, *J. Catal.*, 1999, **181**, 57.
4 J. G. Santiesteban, J. C. Vartuli, S. Han, R. D. Bastian and S. D. Chang, *J. Catal.*, 1997, **168**, 431.
5 M. Scheithauer, T.-K. Cheung, R. E. Jentoft, R. K. Grasselli, B. C. Gates and H. Knözinger, *J. Catal.*, 1998, **180**, 1.
6 D. Gazzoli, M. Valigi, R. Dragone, A. Marucci and G. Mattei, *J. Phys. Chem. B*, 1997, **101**, 11129.
7 C. Lahousse, F. Maugé, J. Bachelier and J. C. Lavalley, *J. Chem. Soc., Faraday Trans.*, 1995, **91**, 2907.
8 B. K. Kim, J. W. Hahn and K. R Han, *J. Mater. Sci. Lett.*, 1997, **16**, 669.
9 B. Zhao, X. Xu, J. Gao, Q. Fu and Y. Tang, *J. Raman Spectrosc.*, 1996, **27**, 549.
10 M. A. Vuurman, I. E. Wachs and A. M. Hirt, *J. Phys. Chem.*, 1991, **95**, 9928.
11 I. E. Wachs, *Catal. Today*, 1996, **27**, 437.
12 S. Kuba, P. Concepción Heydorn, R. K. Grasselli, B. C. Gates, M. Che and H. Knözinger, *Phys. Chem. Chem. Phys.*, 2001, **3**, 146.
13 S. L. Soled, G. B. McVicker, L. L. Murrell, L. G. Sherman, N. C. Dispenziere, S. L. Hsu and D. Waldman, *J. Catal.*, 1988, **111**, 286.
14 D. G. Barton, S. L. Soled and E. Iglesia, *Top. Catal.*, 1998, **6**, 87.

CHEMCOMM
Communication
www.rsc.org/chemcomm

Synthesis and structure of an unprecedented high-symmetry $[Fe_4S_4Cl_4]$ cubane-type unit in supramolecular $[K_4(FeCl_4)(C_{12}H_{24}O_6)_4][Fe_4S_4Cl_4]$†

Johannes B. Willems and Martin Köckerling*

Institut für Synthesechemie, Fachbereich 6, Gerhard-Mercator-Universität, Lotharstr. 1, D-47057 Duisburg, Germany. E-mail: hi356ko@uni-duisburg.de

Received (in Cambridge, UK) 30th April 2001, Accepted 18th June 2001
First published as an Advance Article on the web 6th July 2001

The reduction of SCN^- ions with iron containing zirconium chloride clusters in the presence of 18-crown-6 gives crystals of $[K_4(FeCl_4)(C_{12}H_{24}O_6)_4][Fe_4S_4Cl_4]$ which contain $[Fe_4S_4Cl_4]$ cubane-type clusters with full T_d symmetry, as well as supramolecular $[K_4(FeCl_4)(C_{12}H_{24}O_6)_4]$ complex cations.

The chemistry of iron–sulfur clusters has attracted much scientific interest due to the occurrence of such structural units in biological systems like ferrodoxines, high potential iron proteins, nitrogenases, and others.[1–5] For the class of cubane-type $[Fe_4S_4]$ clusters which are believed to be involved in biological electron transfer processes, synthetic investigations have revealed a large number of compounds with the general formula $[Fe_4E_4X_4]^{n-}$ with E = S, Se or Te; X = SR (R = organic group), SH, OR, NO, Cl, Br, I; $n = -1, -2,$ or -3.[1,2,6] They all contain cubane-type iron–sulfur cores which can be described as a tetrahedron of iron atoms, superimposed by a larger tetrahedron of chalcogen (E) atoms such that the E atoms are triply bridging the faces of the Fe tetrahedron. The tetrahedral coordination environment of each Fe atom is completed by an additional ligand X, bonded at each exo position of the Fe tetrahedron. The symmetry of the metal–chalcogen core of all the so far characterised molecular examples deviates significantly from the ideal T_d case. The core is usually compressed or elongated in one direction leaving an overall D_{2d} symmetry. This observation holds so far for all structurally characterised cubane-type iron–sulfur clusters, including those with $[Fe_4S_4Cl_4]^{2-}$ cores. The latter have been described with $[Et_4N]^+$, $[Pr^n{}_4N]^+$, $[Fe^{II}(MeCN)_2(POMe)_3]^{2+}$ and $[Ph_4P]^+$ counter cations.[10,13–15] This deviation from ideal symmetry has been discussed in terms of crystal packing and Jahn–Teller type electronic effects.[7,8]

Here we present the synthesis and structure of $[K_4(FeCl_4)(C_{12}H_{24}O_6)_4][Fe_4S_4Cl_4]$ **1** which contains the $[Fe_4S_4Cl_4]^{2-}$ cluster **2** of T_d symmetry as well as the uncommon $[K_4(FeCl_4)(C_{12}H_{24}O_6)_4]^{2+}$ complex cation **3**. **1** was an unexpected product from the reaction of $K[(Zr_6Fe)Cl_{15}]$[9] with KSCN in MeCN, to which 18-crown-6 (1,4,7,10,13,16-hexaoxacyclooctadecane) was added. In a typical synthesis, 20 mg (0.017 mmol) $K[(Zr_6Fe)Cl_{15}]$, 10 mg (0.102 mmol) KSCN, and 31 mg (0.12 mmol) 18-crown-6 were dissolved in 5 ml thoroughly dried acetonitrile. The initially dark blue solution loses its colour within *ca.* 3 h. Diisopropyl ether was slowly added by diffusion and after 4 weeks **1** was isolated as a black, crystalline material (yield 3.1 mg; 76% with respect to the cluster starting material). Apparently, the Zr-cluster becomes oxidised in solution, thereby releasing Fe cations, whereas the SCN^- ions are reduced, leaving S^{2-} ions. In a further reaction step the $[Fe_4S_4Cl_4]^{2-}$ cluster anions are formed. The structure of **1** was determined by single-crystal X-ray crystallography.‡

Within crystals of **1** the three symmetry independent atoms of the $[Fe_4S_4Cl_4]^{2-}$ cubane-type complex anion are located on 16e Wyckoff-sites (*x*,*x*,*x*) of the cubic space group *F*23 nearby the 4d site such that with the symmetry elements present, molecular units with full T_d symmetry are formed, even though the point symmetry of the 4d site does not imply full T_d symmetry (23 instead of $\bar{4}$ symmetry). This is shown by the equivalence of all the twelve Fe–S bonds [with a length of 2.294(2) Å] and Fe–Fe–Fe angles of exactly 60°. An ORTEP plot of the structure of **2** is shown in Fig. 1. The Fe–S, Fe–Cl, and Fe–Fe distances compare well with the average values of the $[Fe_4S_4Cl_4]^{2-}$ clusters in other compounds with different cations.[10] Because of the equivalence of all the Fe atoms in **2** the charge is delocalized completely with a net charge of +2.5 on each metal atom.

In crystals of **1** the central iron atom of the $[K_4(FeCl_4)(C_{12}H_{24}O_6)_4]^{2+}$ complex cation is located on the 4c Wyckoff site of the space group *F*23. Similar to the cluster anion on the 4d site the supramolecular entity also shows full T_d symmetry. The molecular structure of **3** is shown in Fig. 2. Compound **3** is composed of a central $[FeCl_4]^{2-}$ tetrahedron (with perfect tetrahedral Cl–Fe–Cl angles of 109.5°) and Fe–Cl distances of 2.260(4) Å. Above each triangular face of the tetrahedron a potassium cation is located which is encapsulated within a 18-crown-6 molecule. Comparable supramolecular complex cations are found so far only in a series of thallium compounds with the general formula $[A_4(MX_4)(C_{12}H_{24}O_6)_4][TlX_4]_2$ with A

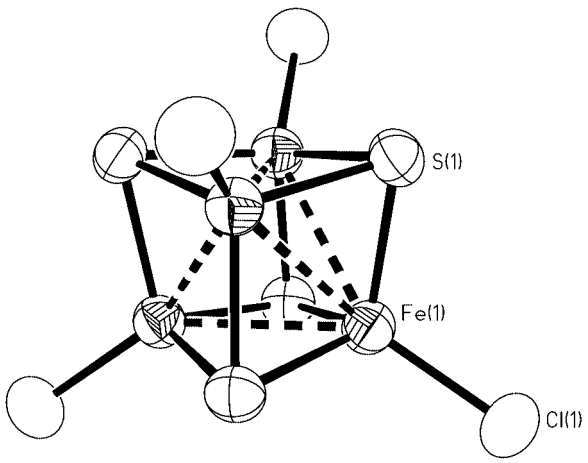

Fig. 1 Molecular structure of the $[Fe_4S_4Cl_4]^{2-}$ cluster anion **2** in crystals of **1** showing the atom labelling scheme (50% thermal probability ellipsoids). Important atom distances (Å): Fe(1)–S(1) 2.294(2), Fe(1)–Cl(1) 2.222(3), Fe(1)–Fe(1) 2.790(2); angles (°): Fe(1)–Fe(1)–Fe(1) 60, Fe(1)–S(1)–Fe(1) 74.92(8), Fe(1)–Fe(1)–Cl(1) 144.7, S(1)–Fe(1)–S(1) 103.25(6), S(1)–Fe(1)–Cl(1) 115.14(5).

† Electronic supplementary information (ESI) available: Fig. S1: packing diagram of the molecular units in crystals of **1**. Fig. S2: structure of the supramolecular cation **3** in crystals of **1**. See http://www.rsc.org/suppdata/cc/b1/b103871k/

 DOI: 10.1039/b103871k

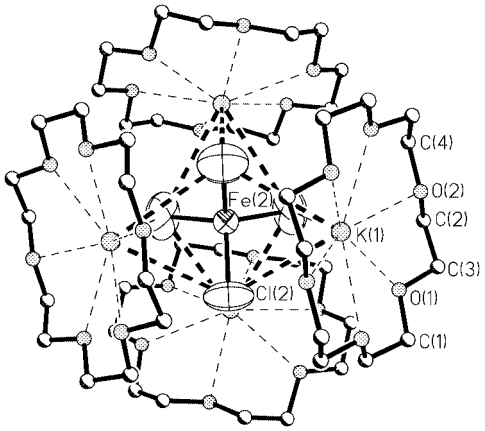

Fig. 2 Structure of the supramolecular $[K_4(FeCl_4)(C_{12}H_{24}O_6)_4]^{2+}$ complex cation **3** in crystals of **1** with atom labelling scheme (50% thermal probability ellipsoids for the central $FeCl_4$ moiety), without hydrogen atoms. Important atom distances (Å): Fe(2)–Cl(2) 2.260(4), Fe(2)–K(1) 3.777(3), Cl(2)–K(1) 3.699(3), average distances (Å): K(1)–O 2.890, C–O 1.44, C–C 1.41; angles (°): Cl(2)–Fe(2)–Cl(2) 109.5, Cl(2)–K(1)–Cl(2) 59.8(1).

= Tl, K, Rb, Ba, NH_4; M = Cu, Mn, Zn; and X = Cl, Br which all crystallise in the same cubic space group $F23$.[11,12]

The recognition of a molecular $[Fe_4S_4Cl_4]^{2-}$ cubane-type cluster with full T_d symmetry, as reported here demonstrates clearly that intramolecular electronic Jahn–Teller type effects are not responsible for the symmetry reduction as observed in many other examples of compounds with such clusters. Rather the lattice symmetry which is, besides other factors, also affected by the local symmetry of the counter cation determines the cluster symmetry.

Financial support from the Gerhard-Mercator-University Duisburg, from the Deutsche Forschungsgemeinschaft (DFG), and from the Fonds der Chemischen Industrie (FCI) is gratefully acknowledged. We thank M. Wickleder (University of Köln) for collecting X-ray data, and G. Henkel (University of Duisburg) for his support.

Notes and references

‡ *Crystal data*: $[K_4(FeCl_4)(C_{12}H_{24}O_6)_4][Fe_4S_4Cl_4]$: M = 1904.74, cubic, a = 21.241(2) Å, U = 9583(4) Å^3, T = 293(2) K, space group $F23$ (no. 196), Z = 4, μ(Mo-Kα) = 1.277 mm^{-1}, 23259 reflections collected, 1973 unique (R_{int} = 0.093) which were used in all calculations, two constraints, $R1(F)$ = 0.0645, $wR2(F^2)$ = 0.1750.

All thermal ellipsoids of the atoms of the 18-crown-6 molecules are elongated tangentially to the three-fold axis which cuts through the enclosed K cation, indicating that these almost flat molecules have some rotational freedom within the crystals. A thermal ellipsoid plot of the $[K_4(FeCl_4)(C_{12}H_{24}O_6)_4]$ cation in crystals of $[K_4(FeCl_4)(C_{12}H_{24}O_6)_4][Fe_4S_4Cl_4]$ is given as ESI.†

CCDC reference number 162244. See http://www.rsc.org/suppdata/cc/b1/b103871k/ for crystallographic data in CIF or other electronic format.

1 B. Krebs and G. Henkel, *Angew. Chem.*, 1991, **103**, 785; B. Krebs and G. Henkel, *Angew. Chem., Int. Ed. Engl.*, 1991, **30**, 769, and references therein.
2 R. Cammack, *Inorg. Chem.*, 1992, **38**, 281.
3 G. J. Leigh, in *The Chemistry of Iron*, ed. J. Silver, Chapman and Hall, London, 1992.
4 D. J. Evans, R. A. Henderson and B. E. Smith, in *Bioinorganic Catalysis*, ed. J. Reedijk and E. Bouwman, Marcel Dekker, New York, 2nd edn., 1999.
5 T. O'Sullivan and M. M. Millar, *J. Am. Chem. Soc.*, 1985, **107**, 4096.
6 S. Harris, *Polyhedron*, 1989, **8**, 2843.
7 M.-J. Carney, G. C. Papaefthymiou, R. B. Frankel and R. H. Holm, *Inorg. Chem.*, 1989, **28**, 1497, and references therein.
8 C. Y. Yang, K. H. Johnson, R. H. Holm and J. G. Norman, Jr., *J. Am. Chem. Soc.*, 1975, **97**, 6596.
9 R. P. Ziebarth and J. D. Corbett, *J. Am. Chem. Soc.*, 1987, **109**, 4844.
10 M. A. Bobrik, K. O. Hodgen and R. H. Holm, *Inorg. Chem.*, 1977, **16**, 1851, and references therein.
11 N. S. Fender, F. R. Fronczek, V. John, I. A. Kahwa and G. L. McPherson, *Inorg. Chem.*, 1997, **36**, 5539, and references therein.
12 N. S. Fender, S. S. Finegan, D. Miller, M. Mitchel, I. A. Kahwa and F. R. Fronczek, *Inorg. Chem.*, 1994, **33**, 4002, and references therein.
13 B. M. Segal, H. R. Hoveyda and R. H. Holm, *Inorg. Chem.*, 1998, **37**, 3440.
14 M. Kawano, C. Hoshino, K. Sakai and K. Matsumoto, *Anal. Sci.*, 1991, **7**, 829.
15 A. Müller, N. H. Schladerbeck, E. Krickemeyer, H. Bögge, K. Schmitz, E. Bill and A. X. Trautwein, *Z. Anorg. Allg. Chem.*, 1989, **570**, 7.

CHEMCOMM
Communication
www.rsc.org/chemcomm

Photochemical behavior of 2,5-di-*tert*-butyl-3*H*-azepine: unexpected formation of a dicyclopenta[*b,e*]pyridine derivative and a *cis,cis*-cyclodeca-1,6-diene derivative

Kyosuke Satake,*[a] Shizuka Takami,[b] Yuko Tawada[a] and Masaru Kimura[b]

[a] *Department of Chemistry, Faculty of Science, Okayama University, Tsushima-Naka 3-1-1, Okayama 700-8530, Japan. E-mail: satake@cc.okayama-u.ac.jp*
[b] *Institute for Fundamental Research of Organic Chemistry (IFOC), Kyushu University, Hakozaki 6-10-1, Higashi-ku, Fukuoka 812-8581, Japan*

Received (in Cambridge, UK) 7th February 2001, Accepted 11th June 2001
First published as an Advance Article on the web 2nd July 2001

Hitherto unknown photochemical behavior of 3*H*-azepine giving cyclopent[*c*]azete and a (4π + 4π) photodimer is reported on the basis of an unexpected formation of a tricyclic dicyclopenta[*b,e*]pyridine derivative and a ten-membered-ring dicarbaldehyde by irradiation of 2,5-di-*tert*-butyl-3*H*-azepine in hexane.

Photochemistry of cycloheptatriene (CHT) derivatives has been extensively examined, whereas those of 3*H*-azepines have rarely been explored in spite of having a similar profile in both molecular and electronic structure to each other. Generally, irradiation of CHT derivatives has resulted in the formation of bicyclic compounds *via* intramolecular 4π photochemical electrocyclic reaction[1] and/or isomerized CHT *via* photochemically allowed [1,7] hydrogen shift.[2] Under gas-phase conditions, a ring contraction reaction leading to toluene derivatives was also observed.[3] A few photochemical researches have examined 3*H*-azepine with an electron donating group (–OR or $–NR_2$) at the 2 position. The reaction was rationalized by the formation of a cyclobuta[*b*]pyrrole derivative *via* ring closure between the 4 and 7 positions, exclusively.[4] Although 3*H*-azepine without any substituents has been found to be a labile substance[5] an electron donating group, imino ether or amidine conjugation, has been found to stabilize it.

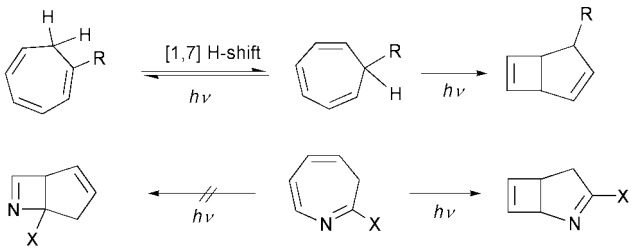

We have reported the synthesis of dialkyl 3*H*-azepines, the stability of which was sufficient for treatment under atmospheric conditions when substituents were *tert*-butyl groups.[6] Since the stability of our 3*H*-azepines is not owing to conjugative stabilization, but steric protection by the bulky substituents, the behavior upon photoirradiation can be expected to be different from those reported. We wish to report the hitherto unknown photochemical behavior of 2,5-di-*tert*-butyl-3*H*-azepine **1**.

A solution of **1** (112 mg, 0.55 mmol) in hexane (100 ml) was irradiated using a high-pressure mercury lamp (100 W) with pyrex filter for 3 h at rt. Chromatography on silica gel of the resulting mixture gave 1,4a,7-tri-*tert*-butyl-3-pivaloyl-3,3a,4,4a,5,7a,8,8a-octahydrodicyclopenta[*b,e*]pyridin-8-ol **2** (63 mg, 61%) as colorless needles and 5,10-diamino-2,5,7,10-tetra-*tert*-butylcyclodeca-2,7-diene-1,6-dicarbaldehyde **3** (5 mg, 5%) as a yellow oil along with recovered 3*H*-azepine **1** (11 mg, 10%).[7] Fortunately, the structure of crystalline product **2** was determined by X-ray structural analysis (Fig. 1).[8] The obtained structure is considered to be an indirect product from the starting material because the molecule contains oxygen atoms which strongly suggests that it comes from a kind of dimer of **1**. The other product, **3**, showed a negative ion peak at *m*/*z* 445 (M − H, 7%) in the FAB MS spectrum. The mass number observed is compatible with two moles of **1** and two moles of water, therefore the precursor for **3** is also considered to arise from the dimer of **1**. The ^1H and ^{13}C NMR spectra of **3** suggest a symmetrical structure having formyl groups owing to δ_H 9.55 (d, J = 5.4 Hz) and δ_C 205.6 (d). The IR absorption bands at 3399 and 1707 cm^{-1} are attributable to amino and formyl groups, respectively. Therefore, the structure of **3** is considered to be a *cis,cis*-cyclodeca-1,6-diene skeleton formed from the hydrolysis of the imine moiety of the (4π + 4π) dimer **5**. According to the conformational analysis for *cis,cis*-cyclodeca-1,6-diene based on molecular mechanics, a chair form has been found to be the most stable form.[9] When the conformation of the ring maintains a chair form, the stereochemistry of **3** is determined to be as illustrated in Scheme 1 owing to both W-letter coupling, J = 2.1 Hz, between an *ipso*-proton of a formyl group and a methylene proton at δ_H 2.28 and molecular symmetry suggested by NMR spectra.

To obtain more detailed information about the reaction, we observed the *in situ* ^1H NMR spectrum during irradiation of **1** in cyclohexane-d_{12} under similar conditions. A gradual inverse relationship varying in time was observed between the peaks of 3*H*-azepine **1** and the peaks of **3** and a new compound **4**. No peaks corresponding to **2** were found during the irradiation. This means **3** formed quickly from (4π + 4π) photodimer **5** by hydrolysis with a trace of water in the solvent, but **2** formed

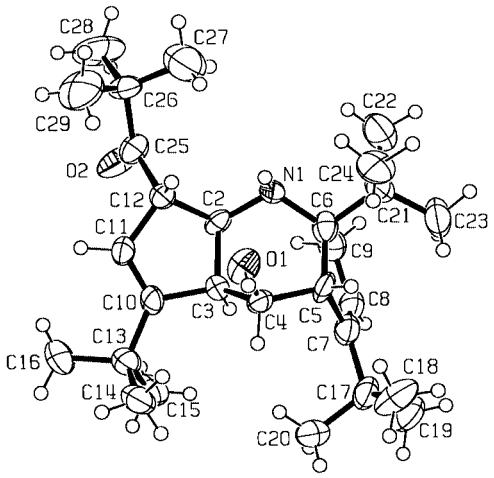

Fig. 1 Ortep drawing of structure **2**.

 DOI: 10.1039/b101225h

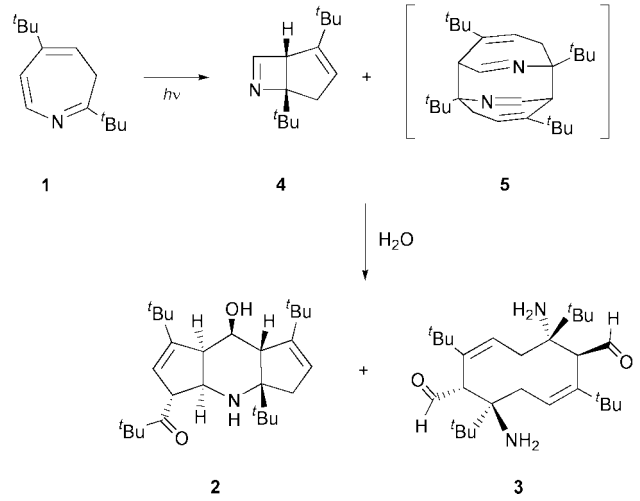

Scheme 1

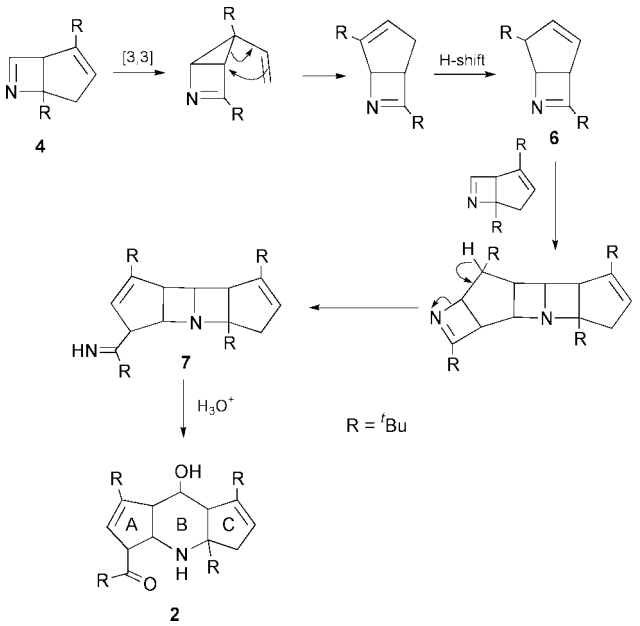

Scheme 2

during chromatographic work from the initially formed photoproduct **4**. Attempts to isolate compound **4** were unsuccessful, however, GCMS showed *m*/*z* 205 (M^+, 0.4%) which is the same mass number as **1**. ^{1}H NMR data for **4** was obtained by the subtraction of known peak sets of **1**, **2** and **3** from the spectrum of a reaction mixture. The structure of **4** is estimated as 3,5a-di-*tert*-butyl-5,5a-dihydro-2a*H*-cyclopent[*c*]azete because of the doublet signal at δ_H 8.16 which is attributable to a –CH = N– moiety.

A possible route to **2** is illustrated in Scheme 2. The structure of the C-ring and a half of the B-ring of **2** are already in photoisomer **4** itself, but the pivaloyl group on the A-ring is not in the structure **4**. To access compound **2**, it is necessary to consider a formal ($2\pi + 2\pi$) addition between **4** and **6** which arises from **4** through the following sequence, [3,3] sigmatropic rearrangement, vinylcyclopropane rearrangement and finally 1,3-prototropy. Appropriate ring opening with participation of water on the adduct **7** leads to dicyclopenta[*b*,*e*]pyridine **2**.

We report here a new photochemical intramolecular ring closure at the 2 and 6 positions of 3*H*-azepine and ($4\pi + 4\pi$) photodimerization, although the yield of ($4\pi + 4\pi$) dimerization is relatively low compared to that of 4π electrocyclic reaction. An investigation is underway to clarify the photochemical behavior of 3*H*-azepine.

We are grateful to Professor S. Kashino of Okayama University for his helpful advice for X-ray structural analysis. We thank the SC-NMR Laboratory of Okayama University for ^{1}H and ^{13}C NMR measurements.

Notes and references

1 For a review see O. L. Chapman, *Adv. Photochem.*, 1963, **1**, 323; G. W. Borden, O. L. Chapman, R. Swindell and T. Tezuka, *J. Am. Chem. Soc.*, 1967, **89**, 2979; W. G. Dauben and R. L. Cargill, *Tetrahedron.*, 1961, **12**, 186.

2 T. Tezuka, M. Kimura, A. Sato and T. Mukai, *Bull. Chem. Soc. Jpn.*, 1970, **43**, 1120; A. P. ter Boorg and H. Kloosterziel, *Rec. Trav. Chim.*, 1965, **84**, 241.

3 R. Srinivasan, *J. Am. Chem. Soc.*, 1962, **84**, 3432.

4 R. A. Odum and B. Schmall, *J. Chem. Soc., Chem. Commun.*, 1969, 1209.

5 E. Vogel, H.-J. Altenbach, J.-M. Drossard, H. Schmickler and H. Stegelmeier, *Angew. Chem., Int. Ed. Engl.*, 1980, **19**, 1016.

6 K. Satake, R. Okuda, M. Hashimoto, Y. Fujiwara, H. Okamoto, M. Kimura and S. Morosawa, *J. Chem. Soc., Perkin Trans. 1*, 1994, 1753.

7 Physical data for **2**: colorless needles, mp 178–179 °C; ^{1}H NMR (270 MHz, $CDCl_3$) δ 5.49 (br s, 1H), 5.31 (br s, 1H), 4.34 (br s, 1H), 4.04 (dd, J = 6.8 and 5.4 Hz, 1H), 3.9 (m, 1H), 3.5 (br, 1H), 3.07 (br s, 1H), 2.90 (br d, J = 6.8 Hz, 1H), 2.65 (br d, J = 17.6 Hz, 1H), 2.5 (br, 1H), 2.21 (dd, J = 17.6 and 2.4 Hz, 1H), 1.18 (s, 9H), 1.14 (s, 9H), 1.12 (s, 9H), 0.89 (s, 9H); ^{13}C NMR (50 MHz, $CDCl_3$) δ 217.9 (s), 155.1 (s), 151.5 (s), 126.1 (d), 122.4 (d), 70.0 (d), 68.3 (s), 61.0 (d), 57.6 (d), 52.7 (d), 45.3 (d), 44.5 (t), 37.4 (s), 34.6 (s, 2C), 33.3 (s), 31.1 (q), 30.2 (q), 25.8 (q), 24.5 (q); IR (KBr) 3476, 2960, 2872, 1694 cm^{-1}; MS (FAB) *m*/*z* 430 (M^+, 100%), 372 (48), 57 (19); UV-Vis λ_{max} (EtOH) 204 (log ε 3.87) nm; HRMS (FAB) calcd for $C_{28}H_{48}NO_2$ 430.3685, found 430.3654; anal. calcd for $C_{28}H_{47}NO_2$: C, 78.27; H, 11.03; N, 3.26. Found: C, 78.16; H, 11.00; N, 3.24%. Physical data for **3**: yellow oil; ^{1}H NMR (300 MHz, $CDCl_3$) δ 9.55 (d, J = 5.4 Hz, 2H), 5.68 (ddd, J = 2.8 and 2.7 and 0.9 Hz, 2H), 3.35 (ddd, J = 5.4 and 2.1 and 0.9 Hz, 2H), 2.72 (dd, J = 17.1 and 2.7 Hz, 2H), 2.28 (ddd, J = 17.1 and 2.8 and 2.1 Hz, 2H), 1.50 (br, 4H), 1.03 (s, 18H), 0.88 (s, 18H); ^{13}C NMR (67 MHz, $CDCl_3$) δ 205.6 (d), 150.0 (s), 126.5 (d), 70.1 (s), 63.1 (d), 43.9 (t), 38.7 (s), 33.5 (s), 29.7 (q), 24.3 (q); IR (neat) 3399, 2966, 2872, 1707, 1436, 1365 cm^{-1}; UV-Vis λ_{max} (hexane) 246 sh (log ε 3.35), 293 (3.37) nm; HRMS (FAB) calcd for $C_{28}H_{49}N_2O_2$ 445.3794, found 445.3768. ^{1}H NMR data for **4** (300 MHz, cyclohexane-d_{12}): δ 8.16 (br d, 1H), 5.35 (t, J = 2.4 Hz, 1H), 3.64 (dd, J = 3.6 and 1.5 Hz, 1H), 2.53 (dd, J = 18 and 2.4 Hz, 1H), 2.22 (ddd, J = 18 and 2.4 and 1.5 Hz, 1H), 1.05 (s, 9H), 0.92 (s, 9H).

8 Crystal data for **2**: $C_{28}H_{47}NO_2$, M = 429.68, orthorhombic, a = 11.400(2), b = 21.835(6), c = 10.935(5) Å, V = 2721.9(12) Å^3, T = 298 K, space group $P2_12_12_1$, Z = 4, μ(Mo-K$_\alpha$) = 0.060 mm^{-1}, 2693 unique ($2\theta_{max}$ = 50°, R_{int} = 0.050) reflections were used in refinement. The final $wR(F)$ was 0.178 for the unique reflections and $R(F)$ was 0.089 for 1468 reflections larger than $2\sigma(I)$. The reflections in the high 2θ range were weak probably because of the large thermal displacements of the four *tert*-butyl groups in the molecule. Relatively large final $wR(F)$ and $R(F)$ may be caused by this fact. The absolute configuration has not been determined. CCDC 158826. See http://www.rsc.org/suppdata/cc/b1/b101225h/ for crystallographic data in .cif or other electronic format.

9 N. L. Allinger, M. T. Tribble and J. T. Spraguue, *J. Org. Chem.*, 1972, **37**, 2423.

CHEMCOMM Communication
www.rsc.org/chemcomm

A practical catalytic Wittig-type reaction

Zheng-Zheng Huang, Song Ye, Wei Xia and Yong Tang*

Laboratory of Organometallic Chemistry, Shanghai Institute of Organic Chemistry, 354 Fenglin Lu, Shanghai 200032, China. E-mail: tangy@pub.sioc.ac.cn

Received (in Cambridge, UK) 9th May 2001, Accepted 12th June 2001
First published as an Advance Article on the web 9th July 2001

Soluble PEG-supported telluride 2 was synthesized and found to be an effective catalyst for the catalytic Wittig-type reaction to give a variety of α,β-unsaturated esters in high yields with excellent *E*-stereoselectivity in the presence of sodium bisulfite as well as triphenyl phosphite.

In the past decades, highly efficient catalysis has become one of the most important frontiers in exploratory organic synthetic research.[1] Although the ylide reaction is one of the most useful approaches in both constructing C–C double bonds[2] and forming small ring compounds,[3] surprisingly, relatively few catalytic ylide reactions, in particular Wittig-type reactions, were reported in literature.[4] The first example of catalytic Wittig-type reactions appeared in 1989, in which Huang *et al.* found tributylarsine could be used as the catalyst in the presence of triphenyl phosphite.[5] Later on, they described the catalytic ylide olefination, epoxidation, and cyclopropanation reactions mediated by *n*-butyl telluride or isobutyl telluride.[6] Dai *et al.* also reported the first catalytic ylide aziridination and provided a facile way to the synthesis of vinyl-type aziridines.[7] Aggarwal *et al.* realized excellent catalytic asymmetric ylide epoxidation, cyclopropanation and aziridination reactions by a carbene approach.[8] In this process, the ylide was formed directly from phenyldiazomethane in the presence of a catalytic amount of both chiral sulfide and rhodium acetate. In all of the reactions described above, however, the amount of catalyst used was 20 mol%. Reduction of the catalyst means low yield even if the reaction time was prolonged.[9] Needless to say, these processes need to be improved before it can be considered as a useful synthetic tool. In our continuing studies on the application of ylides in organic synthesis,[10] we focused on the economy of ylide reactions. In this paper, we wish to report a highly effective Wittig-type olefination catalyzed by the soluble poly(ethyleneglycol) (PEG)-supported telluride **2** (PEG–Te–Bu).[11]

When *p*-chlorobenzaldehyde was mixed with ethyl bromoacetate in the presence of triphenyl phosphite and 1 mol% of compound **2** in toluene at 80 °C, we found that the Wittig-type reaction product was afforded in 88% yield with excellent stereoselectivity.† This meant that the catalytic efficiency of this reaction was improved greatly compared with other catalytic ylide reactions reported to date. By optimizing the reaction conditions, the desired olefin could be obtained in quantitative yield when 2 mol% of telluride **2** was used. To determine the generality of this reaction, a variety of structurally different aldehydes were employed. Some results are summarized in Table 1 (entries 1, 3, 5, 7, 9, 11, 13, 15 and 17). From Table 1, both aliphatic and aromatic aldehydes worked well with high stereoselectivity in reasonable yields.

To make this reaction more practical, we tried to use inorganic reducing reagents instead of triphenyl phosphite and found excellent results were achieved when sodium bisulfite

Table 1 Olefination of aldehydes catalyzed by PEG-supported telluride

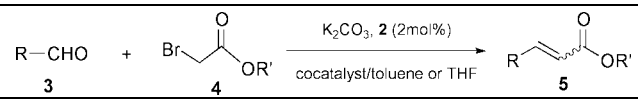

Entry	Aldehyde	R′	*t*/h	Cocatalyst	Yield (%)[a]	*E*/*Z*[b]
1	*p*-$CH_3OC_6H_4CHO$[c]	Et	43	$P(OPh)_3$	94	> 99:1
2		Bu^t	43	$NaHSO_3$	87	> 99:1
3	*p*-$CH_3C_6H_4CHO$	Et	23	$P(OPh)_3$	93	90:10
4		Bu^t	24	$NaHSO_3$	96	94:6
5	*trans*-$C_6H_4CH=CHCHO$[c]	Et	48	$P(OPh)_3$	74	> 99:1
6		Bu^t	23	$NaHSO_3$	88	> 99:1
7	C_6H_5CHO	Et	18	$P(OPh)_3$	98	> 99:1
8		Bu^t	11	$NaHSO_3$	92	> 99:1
9	*p*-ClC_6H_4CHO	Et	7	$P(OPh)_3$	98	> 99:1
10		Bu^t	48	$NaHSO_3$	93	> 99:1
11	*p*-$CF_3C_6H_4CHO$	Et	12	$P(OPh)_3$	74	> 99:1
12	*p*-$NO_2C_6H_4CHO$	Bu^t	11	$NaHSO_3$	77	> 99:1
13	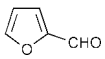	Et	12	$P(OPh)_3$	96	> 99:1
14		Bu^t	11	$NaHSO_3$	88	> 99:1
15	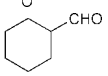	Et	48	$P(OPh)_3$	70	> 99:1
16		Bu^t	48	$NaHSO_3$	76	> 99:1
17	*n*-$C_9H_{19}CHO$	Et	48	$P(OPh)_3$	74	86:14
18		Bu^t	72	$NaHSO_3$	84	95:5
19	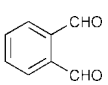	Bu^t	24	$NaHSO_3$	74	> 99:1
20[d]	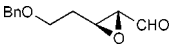	Bu^t	48	$NaHSO_3$	69	> 99:1

[a] Isolated yields. [b] The ratio of *E*:*Z* isomers was determined by ^1H NMR. [c] 5 mol% catalyst used. [d] The aldehyde used in this reaction was the crude product by Swern oxidation of 2,3-epoxy-5-benzyloxypentan-1-ol. The yield refers to the total yields of oxidation reaction and Wittig-type reaction based on 2,3-epoxy-5-benzyloxypentan-1-ol.

 DOI: 10.1039/b104100m

was used as the cocatalyst. Both aromatic aldehydes and aliphatic aldehydes could react with *tert*-butyl bromoacetate to afford the corresponding products in high yields with high stereoselectivity (enties 2, 4, 6, 8, 10, 12, 14, 16 and 18) in the presence of sodium bisulfite. It was noteworthy that phthalaldehyde could react with bromoacetate under these conditions and both aldehyde groups could be olefinated in high yield (entry 19 in Table 1). γ,δ-Epoxy-α,β-unsaturated ester, a useful building block, could also be synthesized by the current method in moderate yield with excellent stereoselectivity (entry 20 in Table 1).

This modification simplified the purification greatly and realized a phosphorus-free catalytic reaction. One could get the product just by filtering off the solid inorganic compounds and precipitating the catalyst after the reaction was completed.

Further study showed that α,β-unsaturated esters can be mass-produced under these reaction conditions and the catalyst could be recovered in quantity but lost its activity partially through multiple cycles. 2-Furaldehyde (10.85 mmol) was reacted with *tert*-butyl bromoacetate in the presence of sodium bisulfite and the desired product was obtained in 90% yield when 2 mol% of PEG-telluride was used. The catalyst was recovered in 100% yield by filtering off the solid of the reaction mixture, followed by addition of ether and collection of the precipitate. The recovered catalyst could be used in the second run but only 69% yield was obtained probably due to the decomposition of PEG-telluride during the catalytic olefination.[12]

Despite the advantages of easy separation and purification of products, the uses of polymer-supported catalysts suffered from lowered catalytic activity and stereoselectivity due to the restriction of polymer matrix that resulted in limited mobility and the accessibility of the active site. The PEG-telluride for catalytic ylide olefination reported here represents a novel, highly efficient polymer-supported catalyst that shows higher catalytic activity as compared to the free corresponding catalysts. Thus, we have developed an effective catalytic ylide olefination, which involves a simple procedure, mild reaction conditions, the use of catalytic PEG-telluride, and in particular, the use of sodium bisulfite as cocatalyst. The high catalytic efficiency, together with the ability to easily purify the product, demonstrates our method to be practical for the synthesis of α,β-unsaturated esters. The extension of our method to other olefination, epoxidation, cyclopropanation and aziridinations is in progress in our laboratory.

This research was supported by 'Hundred Scientist Program' from Chinese Academy of Sciences and State Key Project of Basic Research (PROJECT 973, No.2000 48007).

Notes and references

† Typical procedure for the synthesis of α,β-unsaturated esters. A, $P(OPh)_3$ as the cocatalyst: a mixture of catalyst **2** (0.0680 g, 2 mol%), ethyl bromoacetate (0.06 mL, 0.5 mmol), $P(OPh)_3$ (0.36 mL, 1.4 mmol) in toluene (3.0 mL) was stirred at 80 °C for 10 min and then K_2CO_3 (0.1796 g, 1.3 mmol) was added. The resulting suspension was stirred for 1 min, followed by addition of a mixture of aldehyde (1.0 mmol) and ethyl bromoacetate (0. 1 mL, 0.90 mmol) in toluene (1.0 mL) in portions in 3.5 h. After the reaction was completed (monitored by TLC), the mixture was filtered rapidly through a glass funnel with a thin layer of silica gel and washed with ethyl acetate. The filtrate was concentrated and the residue was purified by flash column chromatography to afford the desired product.

B, $NaHSO_3$ as the cocatalyst: a mixture of catalyst **2** (0.0680 g, 2 mol%), *tert*-butyl bromoacetate (0.06 mL, 0.4 mmol), $NaHSO_3$ (0.1664 g, 1.6 mmol) and in THF (3.0 mL) was refluxed for 10 min and then H_2O (0.04 mL) was added. The resulting mixture was stirred for 10 min, followed by addition of K_2CO_3 (0.2760 g, 2.0 mmol). After being stirred for 1 min, to this suspension was added a mixture of aldehyde (1.0 mmol), *tert*-butyl bromoacetate (0.12 mL, 0.8 mmol) and water (0.03 mL) in THF (1.0 mL) in portions in 3.5 h. The reaction was quenched by anhydrous $MgSO_4$ after the reaction was complete (monitored by TLC). The resulting mixture was filtered rapidly through a glass funnel with a thin layer of silica gel and washed with ethyl acetate. The combined filtrate was concentrated and the residue was purified by flash column chromatography to afford the desired product.

1 S. D. Burke and R. L. Danheiser, *Oxidizing and Reducing Agents*, in *Handbook of Reagents for Organic Synthesis*, Vol. 2, ed. L. A. Paquette, John Wiley & Son, New York, 1999; I. Ojima, *Asymmetric Synthesis*, VCH, New York, 1993; M. Santelli and J.-M. Pons, *Lewis Acid and Selectivity in Organic Synthesis*, CRC Press, Florida, 1995.

2 O. I. Kolodiazhnyi, *Phosphorus Ylides: Chemistry and Application in Organic Synthesis*, Wiley-VCH, New York, 1999; B. E. Maryanoff and A. B. Reitz, *Chem. Rev.*, 1989, **89**, 863, and references therein.

3 A. Solladié-Cavallo and A. Diep-Vohuule, *J. Org. Chem.*, 1995, **60**, 3494; Y.-G. Zhou, A.-H. Li, X.-L Hou and L.-X. Dai, *Chem. Commun.*, 1996, 1353; J. D. His and M. Koreeda, *J. Org. Chem.*, 1989, **54**, 3229; J. B. Ousset, C. Mioskowski and G. Solladié, *Synth. Commun.*, 1983, **13**, 1193; H. J. Bestman and F. Seng, *Angew. Chem.*, 1962, **74**, 154; E. J. Corey and M. Chaykovsky, *J. Am. Chem. Soc.*, 1965, **87**, 1353; C. R. Johnson, *Acc. Chem. Res.*, 1973, **6**, 341; F. Toda and N. Imai, *J. Chem. Soc., Perkin Trans. 1*, 1994, 2673; Y. Shen and Q. Liao, *Synthesis*, 1988, 321; J. L. G. Ruano, I. Fernandez and C. Hamdouchi, *Tetrahedron Lett.*, 1995, **36**, 295; A.-H. Li, L-X. Dai and X.-L. Hou, *Chem. Commun.*, 1996, 491; A.-H. Li, L.-X. Dai, X.-L. Hou and M.-B. Chen, *J. Org. Chem.*, 1996, **61**, 4641.

4 A.-H. Li, L.-X. Dai and V. K. Aggarwal, *Chem. Rev.*, 1997, **97**, 2341.

5 L. Shi, W. Wang, Y. Wang and Y.-Z. Huang, *J. Org. Chem.*, 1989, **54**, 2028.

6 Y.-Z. Huang, L.-L. Shi, S.-W. Li and X.-Q. Wen, *J. Chem. Soc., Perkin Trans. 1*, 1989, 2397; Z.-L. Zhou, L.-L. Shi and Y.-Z. Huang, *Tetrahedron Lett.*, 1990, **31**, 7657; Y.-Z. Huang, Y. Tang, Z.-L. Zhou, W. Xia and L.-P. Shi, *J. Chem. Soc., Perkin Trans. 1*, 1994, 893.

7 A.-H. Li, L.-X. Dai and X.-L. Hou, *J. Chem. Soc., Perkin Trans. 1*, 1996, **9**, 867.

8 V. K. Aggarwal, J. G. Ford, A. Thompson, R. V. Jones and H. M. C. H. Standen, *J. Am. Chem. Soc.*, 1996, **118**, 7004; V. K. Aggarwal, *Synlett*, 1998, 329.

9 S.-W. Li, *PhD Thesis*, 1990, Shanghai Institute of Organic Chemistry.

10 Y.-Z. Huang, Y. Tang, Z.-L. Zhou and J.-L. Huang, *J. Chem. Soc., Chem. Commun.*, 1993, 7; Y.-Z. Huang, Y. Tang, Z.-L. Zhou, W. Xia and L.-P. Shi, *J. Chem. Soc., Perkin, Trans. 1*, 1994, 893; Y. Tang, Y.-Z. Huang, L.-X. Dai, Z.-F. Chi and L.-P. Shi, *J. Org. Chem.*, 1996, **61**, 5762; Y. Tang, Y.-Z. Huang, L.-X. Dai, J. Sun and W. Xia, *J. Org. Chem.*, 1997, **62**, 954; Y. Tang, Z.-F. Chi, Y.-Z. Huang, L.-X. Dai and Y.-H. Yu, *Tetrahedron*, 1996, **52**, 8747; Y.-Z. Huang, Y. Tang and Z.-L. Zhou, *Tetrahedron*, 1998, **53**, 1667; S. Ye, L. Yuan, Z.-Z. Huang, Y. Tang and L.-X. Dai, *J. Org. Chem.*, 2000, **65**, 6257.

11 PEG-supported telluride **2** was prepared readily from PEG 4,000 (MW Av. 3,000) in two steps by the sequential tosylation of PEG and the substitution of tosylate **1** with lithium butyltelluride in high yield as shown in the following scheme.

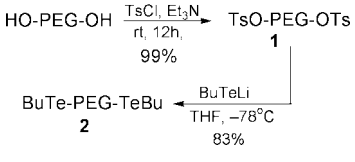

12 M. D. Detty, *J. Org. Chem.*, 1980, **45**, 560; H. D. K. Drew, *J. Chem. Soc.*, 1929, 560.

CHEMCOMM
Communication
www.rsc.org/chemcomm

Antibody-catalyzed activation of a model tripartate prodrug by a tandem hydrolysis–1,6-elimination reaction†

A. Nicole Dinaut and Scott D. Taylor*

Department of Chemistry, University of Waterloo, 200 University Avenue West, Waterloo, Ontario, Canada, N2L 3G1. E-mail: s5taylor@sciborg.uwaterloo.ca

Received (in Corvallis, OR, USA) 26th April 2001, Accepted 7th June 2001
First published as an Advance Article on the web 11th July 2001

Activation of a model tripartate prodrug was achieved by abzyme-catalyzed hydrolysis of an *N*-methylcarbamate moiety followed by a spontaneous 1,6-elimination reaction.

Researchers have long been searching for ways of delivering drugs specifically to cancer cells. One such tactic is known as antibody-directed enzyme prodrug therapy (ADEPT).[1] In this approach, an enzyme–antibody conjugate is used to target an enzyme to the surface of tumour cells. An inactive prodrug is administered which is converted into the drug only by the tumour-bound enzyme. This results in a high concentration of the drug in the vicinity of the cancer cell while minimizing its presence at healthy cells. One of the key requirements for a clinically useful ADEPT system is the absence of an equivalent endogenous enzyme in humans. Consequently, the enzyme component has commonly been of non-human origin. However, the immunogenicity of the non-human enzymes has severely limited the clinical potential of ADEPT. To overcome this problem, researchers have suggested replacing the enzyme component with a catalytic antibody (antibody-directed abzyme prodrug therapy—ADAPT).[2a–d] Abzymes can be designed to act upon substrates that are not readily acted upon by human enzymes. In addition, antibodies can be humanized thus reducing the serious problem of immunogenicity.[3]

A number of abzymes have been developed that convert prodrugs into drugs.[2a–d] In most instances, the transition state analogues (TSA's) to which these abzymes were raised contained the drug or a structural analogue of the drug.[2a–c] Such abzymes were designed to activate bipartate prodrugs in which the moiety acted upon by the abzyme (known as the specifier[4]) is directly attached to the drug. An alternative to using bipartate prodrugs is to use tripartate prodrugs. In tripartate prodrugs, the specifier is separated from the drug by a linker. After cleavage of the specifier from the linker, the linker–drug product is designed to spontaneously fragment to release the drug. An example of a tripartate prodrug system is outlined in Scheme 1. Here, specific hydrolysis of the moiety separating the specifier and linker in **1** releases unstable intermediate **2** which undergoes a spontaneous 1,6-elimination reaction to release the drug. This prodrug design was first described by Katzenellenbogen and coworkers.[4] Prodrugs based upon this general design have been used extensively in ADEPT and for other applications.

Several years ago, we suggested that abzymes that are designed to activate tripartate prodrugs might be more versatile for ADAPT than those that act upon bipartate prodrugs.[5] If an abzyme could be designed to recognize only the specifier and linker of a tripartate prodrug, then a single abzyme could be used to activate a variety of different prodrugs.[5] This would be advantageous both in terms of economy and for dealing with tumours that have developed resistance to a certain drug. We reasoned that this could be accomplished by raising antibodies

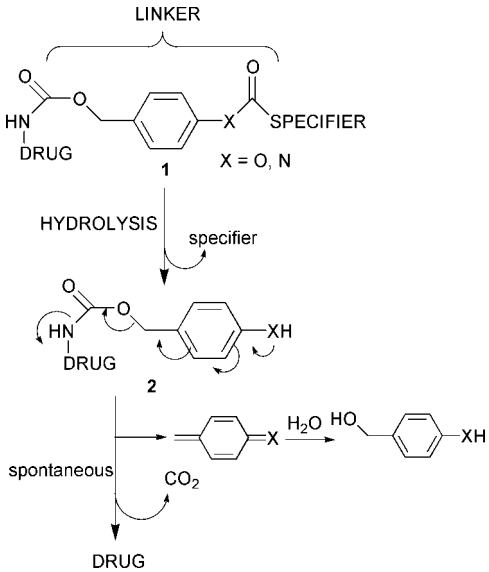

Scheme 1

to TSA's in which the drug was *not* incorporated into the TSA.[5] Instead, the carrier protein (necessary for antibody production) could be attached to a position on the TSA that is equivalent to the point of attachment of the drug to the prodrug. Since abzymes are usually insensitive to changes in the region of the substrate that corresponds to the part of the TSA that is attached to the carrier protein,[6] then abzymes raised to such TSA's might be capable of acting as generic activators of tripartate prodrugs.

To test this approach we constructed the model tripartate prodrug **3**† (Scheme 2). In this system, drug release is triggered by abzyme-catalyzed hydrolysis of the *N*-methylcarbamate moiety to release *p*-nitrophenol (PNP, the specifier), CO_2 and intermediate **4**. Intermediate **4** then undergoes the spontaneous 1,6-elimination reaction to produce the amino acid L-tryptophan (Trp) as the model 'drug'.[7] Abzymes were raised to TSA-hapten **6**,[8] which mimics the rate-determining transition state for the hydrolysis of the *N*-methylcarbamate moiety in **3**. We recently reported that an antibody raised to **6**, called ST51, is capable of catalyzing the hydrolysis of *N*-methylcarbamate **7**.[8] Since the carrier protein in **6** was attached to a position on the TSA that corresponds to the point of attachment of tryptophan to **3**, we reasoned that ST51 should be capable of activating model prodrug **3**.

Model prodrug **3** was examined as a substrate for ST51 by removing aliquots from solutions containing ST51 (5 μM) and varying amounts of **3**, in buffer at pH 9.0 (100 mM bicine, 100 mM NaCl, 5% DMSO, 25 °C), at various time intervals, and then examining the aliquots for production of both PNP and Trp by HPLC. Under these conditions, we were unable to detect any PNP or Trp in the absence of ST51 after 40 hours. However, in the presence of ST51, both of these products were readily detectable. The antibody-catalyzed reaction obeys saturation

† Electronic supplementary information (ESI) available: the synthesis and characterization of **3**, and **9**–**11**, and experimental details for kinetic studies and Lineweaver–Burk plots. See http://www.rsc.org/suppdata/cc/b1/b103971g/

 DOI: 10.1039/b10371g

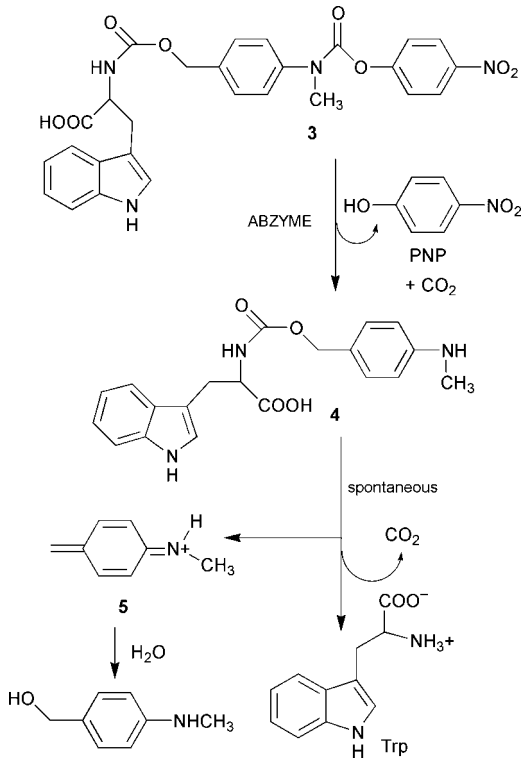

Scheme 2

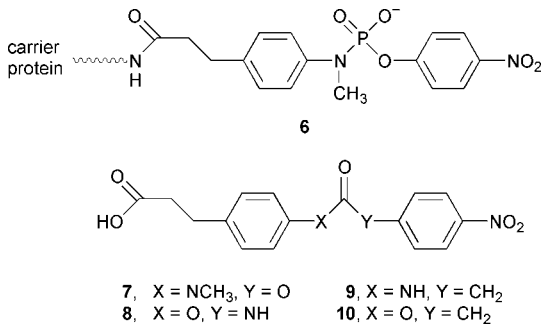

kinetics, and approximately equimolar quantities of PNP and Trp were detected for the duration of the time the reactions were monitored. When following the production of PNP, ST51 exhibited a k_{cat} = 0.075 h^{-1} and a K_m = 137 μM. Similar values were obtained from data following the production of Trp. We also found that ST51 was unable to catalyze the hydrolysis of Z-Trp. Taken together, these results indicate that the production of Trp is not a result of hydrolysis of the *N*-H carbamate moiety, but rather initial hydrolysis of the *N*-methylcarbamate followed by the spontaneous fragmentation reaction and that the abzyme-catalyzed step is slow compared to the fragmentation reaction. We also found that ST51 was capable of catalyzing the activation of **3** with multiple turnover. This indicates that **5**, which is produced as an intermediate during the reaction, does not inactivate the abzyme after a single turnover by reacting with crucial residues in the active site.

Assuming that the spontaneous rate of hydrolysis of the *N*-methylcarbamate moiety in **3** is similar to that of **7** ($t_{\frac{1}{2}}$ = 5.7 years in 100 mM bicine, 100 mM NaCl, 5% DMSO, pH 9.0) then the rate enhancement (k_{cat}/k_{uncat}) with **3** is about 5000-fold. This is only slightly less than the rate enhancement found for ST51 using substrate **7** (6500-fold).[8] It is also important to note that **3** and **7** exhibit similar K_m values (266 μM for **7** and 137 μM for **3**). These results indicate that the 'drug' portion of the prodrug is not an important recognition site for the antibody-catalyzed reaction and this is consistent with our hapten design.

In summary, we have reported the first example of antibody-catalyzed activation of a model tripartate prodrug of type **1** by a tandem hydrolysis–1,6-elimination reaction.[9] We have demonstrated that it is possible to obtain an abzyme that can activate a tripartate system without incorporating the 'drug' into the TSA by attaching the carrier protein to a position on the TSA that corresponded to the point of attachment of the 'drug' to the tripartate prodrug. Although ST51 can catalyze the hydrolysis of *N*-methylcarbamates at physiological pH, the rate of the reaction is too slow for an accurate kinetic analysis and effective prodrug activation. It has been estimated that for ADEPT systems, a k_{cat} value of about 1.0 s^{-1} is required.[2c] Nevertheless, the approach outlined here should be readily applicable to tripartate prodrugs of type **1** bearing moieties that are more amenable to antibody–catalyzed hydrolysis, under physiological conditions, than *N*-methylcarbamates, which are highly challenging substrates for antibody catalysis.[8] An *N*-H carbamate linkage between the specifier and linker, of the type recently exploited by Blackburn and coworkers for abzyme catalysis,[2c] should be very suitable to the approach reported here.[11] However, tripartate prodrugs of type **1** bearing such a moiety cannot be used as substrates for ST51 since ST51 will not hydrolyze *N*-H carbamate **8**, amide **9**, or even ester **10**. Studies to elucidate the mechanism of ST51 are in progress and we are continuing our work to develop abzymes that can trigger tripartate prodrugs of type **1** under physiological conditions.

We thank the Canadian Institutes of Health Research (CHIR) for financial support of this work. We would also like to thank Katherine Majewska and Parham Daneshvar for assistance in synthesizing compounds **8**–**10**.

Notes and references

1 For recent reviews see: K. N. Syrigos and A. A. Epenetos, *Anticancer Res.*, 1999, **19**, 605; W. A. Denny and W. R. Wilson, *J. Pharm. Pharmacol.*, 1998, **50**, 387.

2 (*a*) H. Miyashita, Y. Karaki, M. Kikuchi and I. Fujii, *Proc. Natl. Acad. Sci, USA*, 1993, **90**, 5337; (*b*) D. A. Campbell, B. Gong, L. M. Kochersperger, S. Yonkovich, M. A. Gallop and P. G. Schultz, *J. Am. Chem. Soc.*, 1994, **116**, 2165; (*c*) P. Wentworth, A. Datta, D. Blakey, T. Boyle, L. J. Partridge and G. M. Blackburn, *Proc. Natl. Acad. Sci USA*, 1996, **93**, 799; (*d*) D. Shabat, C. Rader, B. List, R. A. Lerner and C. F. Barbas III, *Proc. Natl. Acad. Sci. USA*, 1999, **96**, 6925.

3 G. Winter and C. Milstein, *Nature*, 1991, **349**, 293.

4 P. L. Carl, P. K. Chakavarty and J. A. Katzenellenbogen, *J. Med. Chem.*, 1981, **24**, 479.

5 S. D. Taylor, M. J. Chen, A. N. Dinaut and R. A. Batey, *Tetrahedron*, 1998, **54**, 4223.

6 L. J. Liotta, P. A. Benkovic, G. P. Miller and S. J. Benkovic, *J. Am. Chem. Soc.*, 1993, **115**, 350; F. Tanaka, K. Kinoshita, R. Tanimura and I. Fujii, *J. Am. Chem. Soc.*, 1996, **118**, 2332.

7 Since the primary objective of these studies was to determine if ST51 could trigger the tripartate system, it was not necessary to use an actual drug to make the model 'prodrug'. Indeed, for these studies any amine-bearing molecule would have sufficed for the 'drug' so long as it (1) had no resemblance to the specifier (PNP) portion of the prodrug, (2) was relatively easy to detect and quantitate, (3) had a charged moiety that would enhance the solubility of the prodrug and, (4) was readily available and allowed for economic and facile synthesis of the model prodrug. Tryptophan was chosen since it satisfied all of these requirements.

8 A. N. Dinaut, M.-J. Chen, A. Marks, R. A. Batey and S. D. Taylor, *Chem. Commun.*, 2000, 385.

9 While our work was in progress, Shabat *et al*. reported abzyme-catalyzed activation of tripartate prodrugs by a tandem retro-aldol–retro-Michael reaction (see ref. 2*d*). Although the abzyme was not originally designed to act as a prodrug activator (see also ref. 10), generic tripartate prodrug activation was achievable because of the broad substrate specificity of the abzyme.

10 J. Wagner, R. A. Lerner and C. F. Barbas, *Science*, 1995, **270**, 1797.

11 For tripartate prodrugs of type **1** based upon *N*-H carbamates of the kind examined by Blackburn and coworkers (see ref. 2*c*), the specifier would be an amino acid and atom X in Scheme 1 would be oxygen and so the self-immolative intermediate **2**, would be a phenol derivative. Phenols also undergo the spontaneous 1,6-elimination reaction. For a recent example of this see: I. Niculescu-Duvaz, D. Niculescu-Duvaz, F. Friedlos, R. Spooner, J. Martin, R. Marais and C. J. Springer, *J. Med. Chem.*, 1999, **42**, 2485.

CHEMCOMM Communication
www.rsc.org/chemcomm

Unexpected reactivity of two-coordinate palladium–carbene complexes; synthetic and catalytic implications†

Lisa R. Titcomb,[a] Stephen Caddick,*[a] F. Geoffrey N. Cloke,*[a] D. James Wilson[a] and Darren McKerrecher[b]

[a] *The Chemistry Laboratory, C.P.E.S., University of Sussex, Falmer, Brighton, UK BN1 9QJ. E-mail: f.g.cloke@sussex.ac.uk*
[b] *AstraZeneca Pharmaceuticals, Mereside, Macclesfield, Cheshire, UK SK10 4TF*

Received (in Cambridge, UK) 16th May 2001, Accepted 21st June 2001
First published as an Advance Article on the web 11th July 2001

Ligand exchange reactions reveal unexpected lability of the carbene ligands in two coordinate palladium(0) *N*-heterocyclic carbene complexes; the latter are found to be very effective catalysts for amination of aryl chlorides.

In recent years it has become clear that *N*-heterocyclic carbenes can offer an interesting alternative class of ligand to the ubiquitous phosphines, especially for catalytic applications.[1] The extraordinary advantage that this class of ligand has afforded to metathesis catalysts is a testament to the potential of metal complexes derived from these ligands for organic synthesis.[2] Palladium catalysed protocols utilising imidazolium salts have also been shown to offer a significant advantage for a range of synthetically valuable coupling processes.[3] These salts can be precursors to heterocyclic carbenes and the *in situ* generation of metal–carbene complexes has been suggested as a key step in such reactions. However, although there are a number of reports describing structures of four-coordinate metal(II) carbene species[4] there is relatively little structural, mechanistic or theoretical work pertaining to the two-coordinate palladium(0) carbene species which might be expected to be generated under many of the reaction conditions.[5] It is important to establish whether such isolated complexes are indeed able to effectively mediate coupling reactions; this approach would also facilitate mechanistic studies essential for further developments. Herrmann and coworkers have recently reported the use of pre-formed two-coordinate palladium(0) carbene complexes for Suzuki reactions and noted significant differences in activity between the pre-formed complexes and those assumed to be generated *in situ*.[6] We have embarked upon a programme of work, which has been directed toward the synthesis and characterisation of a range of two-coordinate palladium(0) carbene complexes[7] and examination of their reactivity. Here we describe the synthesis and reactivity of two-coordinate palladium carbene complexes shown in Fig. 1.

We have previously prepared complex **1**, initially using metal vapour synthesis and more recently *via* a solution phase method,

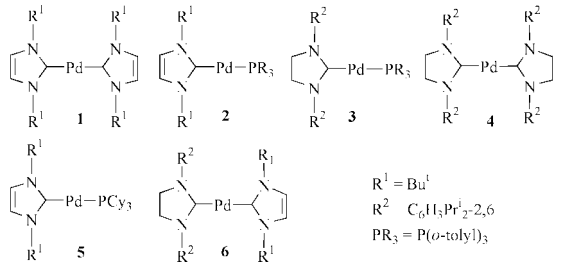

Fig. 1 Two-coordinate palladium carbene complexes.

† Electronic supplementary information (ESI) available: details of experimental procedures and characterisation data for complexes **2**–**6**, ligand substitution reactions and general procedure for coupling reactions. See http://www.rsc.org/suppdata/cc/b1/b104297c/

and we reported that **1** can be used to mediate a Sonogashira and an amination reaction.[8] However we found procedures using **1** to be less general than protocols already available and so from a preparative sense this was disappointing. Seminal work by Hartwig and coworkers suggested that a key aspect of pre-catalyst design would be the presence of a ligand which could dissociate to generate a mono(carbene)palladium species which, if consistent with other catalytic systems, could then undergo oxidative addition.[9,10] Moreover given the precedents in both palladium and ruthenium catalysis, we also decided to explore saturated *N*-heterocyclic carbenes as ligands since these would offer improved donor capabilities and render catalytic species more active.[11] For these reasons we have prepared the new, two-coordinate palladium complexes **2**, **3** and **4** and evaluated their ability to promote the amination of *p*-chlorotoluene under catalytic conditions.[12]

Displacement of both phosphine ligands in [Pd{P(*o*-tolyl)$_3$}$_2$] by *N*-heterocyclic carbenes has been previously employed to prepare the corresponding [Pd(carbene)$_2$] complexes;[6] however, careful control of stoichiometry enabled the synthesis of the mixed carbene–phosphine complex **2** in good yield.

Contrary to our expectation we found that attempted amination of 4-chlorotoluene with morpholine using **2** led to a disappointing yield of 56% for the coupling which compared poorly to the yield obtained with the bis-carbene complex **1** (95%). We decided to examine two further pre-catalysts **3** and **4**, both of which incorporate the saturated heterocyclic carbene as ligand. The mixed catalyst **3** was prepared in very good yield, again by phosphine displacement from [Pd{P(*o*-tolyl)$_3$}$_2$]; however bis-carbene **4** could be more readily prepared using our alternative route employing sodium dimethyl malonate.[8]

We examined the ability of these complexes to promote amination reactions of 4-chlorotoluene and both catalysts gave excellent yields of isolated products shown in Scheme 1 for the amination of 4-chlorotoluene using primary, secondary and aryl-amines. Isolated yields were generally in excess of 95% using either catalyst and the reactions were generally complete within 1 h at 100 °C. Reactions utilising hexylamine required an

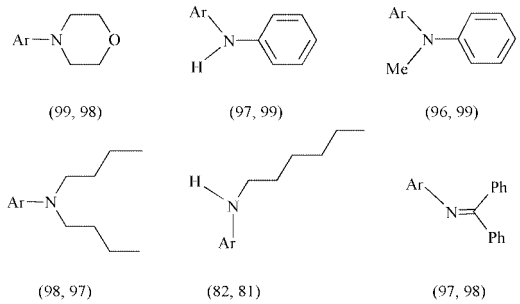

Scheme 1 Products prepared from 4-chlorotoluene using **3** and **4**.‡ Numbers in parentheses refer to isolated percentage yields from reactions employing catalysts (**3**, **4**); Ar = C_6H_4Me-4.

 DOI: 10.1039/b104297c

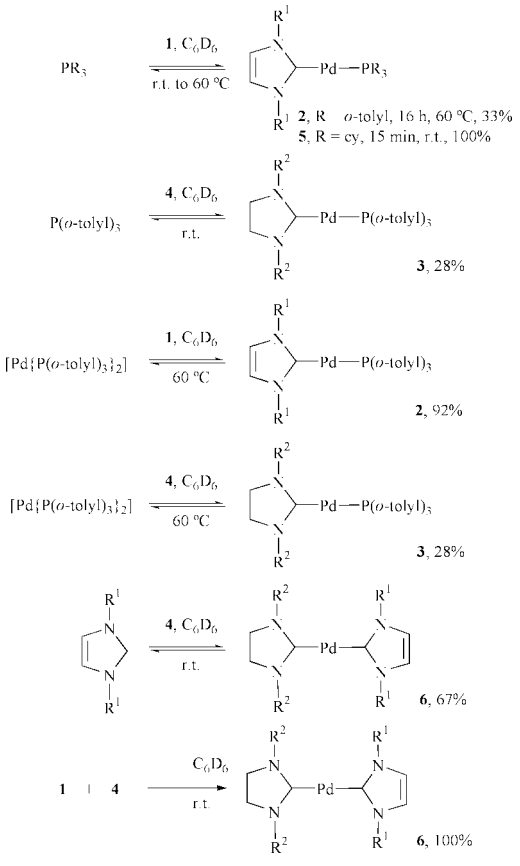

Scheme 2 R^1 = Bu^t; R^2 = $C_6H_3Pr^i_2$-2,6.

excess of amine (4 equivalents), and proceeded in slightly lower yield. In general the overall yields indicate that these are extremely good catalysts for amination, however in contrast to reported *in situ* methods, we were unable to promote these reactions at room temperature.[9]

The ability of the sterically encumbered catalysts **1** and **4** to undergo facile oxidative addition required for these amination reactions is surprising, as is the similarity in catalytic behaviour between **3** and **4**. Given the currently accepted view that metal *N*-heterocyclic carbene bonds are relatively strong compared to metal phosphine bonds,[1c] we had expected that the mixed species **3** would offer a superior class of pre-catalyst, as phosphine dissociation to generate a mono-carbene palladium species, followed by oxidative addition,[10,13] should be more facile than the required carbene dissociation in **4**. However the efficient behaviour of **4** as a pre-catalyst led us to conclude that carbene dissociation from palladium may be more facile than generally envisioned and this is borne out by further experimentation (Scheme 2).

Treatment of **1** with P(*o*-tolyl)$_3$ at 60 °C for 16 h resulted in a 33% conversion to the mixed carbene–phosphine **2**; prolonged heating had no effect on the product ratio. Similar behaviour was also observed in reaction of **1** with PCy_3, to give **5**, although in this case the reaction proceeded to 100% completion in < 15 min at room temperature, and in the reaction of **4** with P(*o*-tolyl)$_3$, which gave the mixed complex **3** (28%). Ligand redistribution reactions between **1** and [Pd{P(*o*-tolyl)$_3$}$_2$] and between **4** and [Pd{P(*o*-tolyl)$_3$}$_2$] were also found to occur to give **2** and **3** (92% and 28%, respectively). Finally we found that treatment of complex **4** with free unsaturated carbene gave the mixed bis-carbene complex **6** (67%); the latter could also be obtained quantitatively by ligand redistribution between **1** and **4** at room temperature. These experiments demonstrate that ligand substitution at palladium between phosphine and carbene is fairly general and that the metal carbene bond may be more labile than previously thought. This would explain the ability of complexes **1** and **4** to mediate amination and Sonagashira reactions and could be consistent with a mechanism requiring ligand dissociation prior to oxidative addition in the latter,[14] although associative pathways for the ligand exchange reactions in Scheme 2 cannot be ruled out at this stage.

In conclusion we have shown that two-coordinate palladium bis-carbene and mixed carbene–phosphine complexes will efficiently promote amination of aryl halides and demonstrated an unexpected lability of the palladium–carbene bond. These findings may be important in the design of new palladium–carbene catalysts for organic synthesis.

We are grateful to AstraZeneca and EPSRC for support of this project. We are grateful to Dr Abdul Sada for his contribution.

Notes and references

‡ *General procedure*: KOBu^t (1.18 mmol) and complex **3** or **4** (0.016 mmol) were weighed into an ampoule (fitted with a Youngs tap) in a glove-box. Dioxane (10 ml) was added and then 4-chlorotoluene (0.79 mmol) and amine (0.95 mmol) added and the mixture heated at 100 °C. The reaction was allowed to cool to room temperature, the solvent removed and the resulting mixture loaded directly onto a silica-gel plug and eluted using ethyl acetate in hexane (20%). The solvent was evaporated and the product was determined to be > 95% pure by spectroscopic and analytical methods.

1 For reviews: (*a*) D. Bourissou, O. Guerret, P. Gabbai and G. Bertrand, *Chem. Rev.*, 2000, **100**, 39; (*b*) A. J. Arduengo, *Acc. Chem. Res.*, 1999, **32**, 913; (*c*) M. Regitz, *Angew. Chem.*, 1996, **35**, 725.
2 For reviews: L. Jafarpour and S. P. Nolan, *Adv. Org. Chem.*, 2001, **46**, 181; T. Weskamp, V. P. W. Bohm and W. A. Herrmann, *J. Organomet. Chem.*, 2000, **600**, 12; T. M. Trnka and R. H. Grubbs, *Acc. Chem. Res.*, 2001, **34**, 18.
3 For recent examples: A. Furstner and A. Leitner, *Synlett*, 2001, 290; G. A. Grasa and S. P. Nolan, *Org. Lett.*, 2001, **3**, 119; H. M. Lee and S. P. Nolan, *Org. Lett.*, 2000, **2**, 2053; J. Huang, G. Grasa and S. P. Nolan, *Org. Lett.*, 1999, **1**, 1307.
4 For recent examples: D. J. Nielsen, K. J. Cavell, B. W. Skelton and A. H. White, *Organometallics*, 2001, **20**, 995; D. S. McGuinness, K. J. Cavell and B. F. Yates, *Chem. Commun.*, 2001, 355; T. Weskamp, V. P. W. Bohm and W. A. Herrmann, *J. Organomet. Chem.*, 1999, **585**, 348; A. A. D. Tulloch, A. A. Danopoulos, R. P. Tooze, S. M. Cafferkey, S. Kleinhenz and M. B. Hursthouse, *Chem. Commun.*, 2000, 1247; E. Peris, J. A. Loch and R. H. Crabtree, *Chem. Commun.*, 2001, 201.
5 J. C. Green, J. G. Scurr, P. L. Arnold and F. G. N. Cloke, *Chem. Commun.*, 1997, 1963.
6 V. P. W. Bohm, C. W. K. Gstottmayr, T. Weskamp and W. A. Herrmann, *J. Organomet. Chem.*, 2000, **595**, 186.
7 P. L. Arnold, F. G. N. Cloke, T. Geldbach and P. B. Hitchcock, *Organometallics*, 1999, **18**, 3228.
8 S. Caddick, F. G. N. Cloke, G. K. B. Clentsmith, P. B. Hitchcock, D. McKerrecher, L. R. Titcomb and M. R. V. Williams, *J. Organomet. Chem.*, 2001, **617**, 635.
9 S. R. Stauffer, S. Lee, J. P. Stambuli, S. I. Hauck and J. F. Hartwig, *Org. Lett.*, 2000, **2**, 1423.
10 L. M. Alcaraz-Roman, J. F. Hartwig, A. L. Rheingold, L. M. Liable-Sands and I. A. Guzei, *J. Am. Chem. Soc.*, 2000, **122**, 4618.
11 J. Huang, E. D. Stevens and S. P. Nolan, *J. Am. Chem. Soc.*, 1999, **121**, 2674; J. Huang, H. J. Shanz, E. D. Stevens and S. P. Nolan, *Organometallics*, 1999, **18**, 2370.
12 For examples: J. F. Hartwig, in *Modern Amination Methods*, ed. A. Ricci, Wiley-VCH, Weinheim, 2000; B. H. Yang and S. L. Buchwald, *J. Organomet. Chem.*, 1999, **576**, 125; J. F. Hartwig, *Angew. Chem., Int Ed.*, 1998, **37**, 2047.
13 For a discussion of oxidative addition see: C. Amatore and F. Pfluger, *Organometallics*, 1990, **9**, 2276; C. Amatore, A. Jutand and A. Suarez, *J. Am. Chem. Soc.*, 1993, **115**, 9531.
14 J. F. Hartwig and F. Paul, *J. Am. Chem. Soc.*, 1995, **117**, 5373; M. S. Sanford, M. Ulman and R. H. Grubbs, *J. Am. Chem. Soc.*, 2001, **123**, 749.

CHEMCOMM Communication
www.rsc.org/chemcomm

Se,Se′-Diphenyl carbonodiselenoate: preparation and characterization of its molecular structure and thermal reactivity

Jason T. Lowe,[a] A. Chandrasekaran,[b] Roberta O. Day*[b] and William Rosen*[a]

[a] *Department of Chemistry, University of Rhode Island, Kingston Rhode Island 02881, USA. E-mail: wrosen@chm.uri.com*
[b] *Department of Chemistry, University of Massachusetts, Amherst, MA 01003-9336, USA. E-mail: rday@chemserv.chem.umass.edu*

Received (in Corvallis, OR, USA) 10th April 2001, Accepted 6th June 2001
First published as an Advance Article on the web 3rd July 2001

Reaction of dipotassium nitroacetate with benzeneselenenyl bromide produces the title compound as a thermally unstable product, which has been characterized by X-ray crystallography.

Dipotassium nitroacetate, **1**, was first synthesized by Steinkopf[1] in 1909. Since that time the yield and simplicity of preparation of **1** has been improved a number of times.[2] The reported utility of employing this easily prepared dianionic organic salt in reaction with electrophilic reagents has been somewhat limited however. Reaction with electrophilic reagents such as the halogens,[3] the strong mineral acids,[4] and several transition metal salts[5] have been noted but our preliminary attempts to directly react **1** with organo-electrophilic reagents proved frustrating.† One exception, we discovered, was the direct reaction of benzeneselenenyl bromide with **1** in methanol,‡ which produced CO_2 and diphenyl diselenide, **2**, along with two other organic products, **3** and **4**. This communication thus reports our characterization of one of these three organic products, **3**, and additionally elaborates upon its easy thermolytic conversion to produce **2**. (The chemical characterization of **4** is still under investigation.§)

Addition of **1** to an ice-cold solution of benzeneselenenyl bromide in methanol resulted in three TLC separable organic compounds after effervescence of CO_2 had subsided. Separation of the three organic compounds using silica gel chromatography could be achieved by elution with hexane–methylene chloride mixtures. The initial band off the column was easily identified as **2**. The compounds **3** and **4** were then eluted in sequence, with both compounds decomposing to **2** if strict cooling conditions were not maintained (see Scheme 1). Compound **3** could be crystallized by slow evaporation of the elution solvent at 0 °C to deliver X-ray quality crystals. Initial observations on crystals of **3** indicated that yellow crystals of **2** began to grow from the colorless crystals if **3** was allowed to sit at room temperature or above for any extended period of time. (Storage in the refrigerator was mandatory.)

Spectral analysis of compound **3** yielded the following important information: (1) the solution IR spectrum (CCl_4) exhibited a carbonyl stretch at 1711 cm^{-1} in addition to bands similar to those exhibited by **2**. Attempts to obtain the IR spectrum of **3** as a KBr pellet resulted in a spectrum identical to that of **2**. (2) The ^{1}H-NMR spectrum of a solution ($CDCl_3$) of **3** exhibited phenyl resonance lines only. (3) The ^{13}C-NMR spectrum ($CDCl_3$) of **3** exhibited a carbonyl resonance at δ = 182.7 in addition to four resonance lines in the aromatic region. (4) The ^{77}Se-NMR spectrum ($CDCl_3$) of **3** exhibited a single resonance line at δ = 749 relative to dimethyl selenide.[6] (5) The

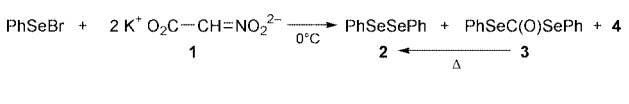

BnSeC(O)SeBn **5** PhOC(O)OPh **6** PhSC(O)SPh **7**

Scheme 1

CI/MS spectrum of **3** exhibited a molecular ion centered at 343 amu with appropriate isotopic satellite peaks for a compound having two selenium atoms in its molecular structure. Major fragment peaks were observed at 312, 237 and 159 amu as well as the base peak at 78 amu. The EI/MS spectrum was identical to that of **2**. (Carbonodithioates fragment in a similar manner in the EI/MS.[7]) (6) The UV-VIS spectrum of **3** exhibited no absorbance above 300 nm in contrast to **2** which has a characteristic thermochromic[8] band at 337 nm (log ε = 3.1). While this spectral information was indicative that **3** had a molecular structure that contained two phenyl selenium moieties, in addition to a carbonyl group, we were uncertain whether our compound was similar to *Se,Se′*-dibenzyl carbonodiselenoate (**5**) prepared by Devillanova *et al.*[9] (Reported spectral information available for **5** consisted only of an IR band at 1680 cm^{-1} which was attributed to a carbonyl band.) Consequently we determined the X-ray crystal structure for **3** which confirmed our suspicions that we had isolated *Se,Se′*-diphenyl carbonodiselenoate as a rather unstable molecular entity. We hoped that the reasons for the instability of **3** might then become apparent.

A perspective view of the molecular structure obtained for **3** is shown in Fig. 1. (We had to collect the data at 173 K because of the instability of **3** in the X-ray beam.¶) The space group was found to be *C*2/*c* with a twofold axis passing through the carbonyl function.‖ The unit cell contained four molecules of **3**. The bond lengths for the phenyl selenium moieties were found to be almost identical[10] to those of **2** including the Se–C_{ipso} bond length = 191.5(3) pm. The bond angles around the carbonyl function of **3** are somewhat different from those of diphenyl carbonate (**6**);[11] for **3** Se–C(O)–Se is 110.2(2)°, Se–C = O is 124.9(1)°, and C(O)–Se–C_{ipso} is 97.1(1)° while for **6** O–C(O)–O is 104.6°, O–C = O is ~127.5° and C(O)–O–C_{ipso} is ~118.5°. The bond lengths around the carbonyl function of **3** appeared to be normal, and similar to those of **6** when comparable: for **3** Se–C(O) is 193.5(2) pm, and C = O is 118.5(5) pm while for **6** C = O is 119.1 pm.

There are several interesting interactions within **3**. That exhibited between the two intramolecular selenium atoms is one of them. These two selenium atoms are separated by a distance of 319 pm which is well within the sum of two Van der Waals radii for selenium (~400 pm). Whether there is a partial

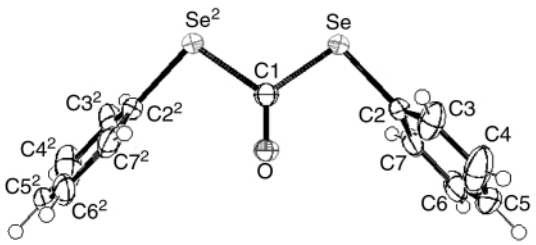

Fig. 1 ORTEP representation of **3** with the *b* axis being the 2-fold axis and roughly in the plane of the page. Atoms with the same label, but superscripted 2, are related by a crystallographic 2-fold axis.

 DOI: 10.1039/b103499p

intramolecular bond between the two selenium atoms of **3**, implying some hypervalency,[12] is not immediately obvious. Secondly, while the overall molecular structure for **3** is similar to that exhibited by **6**, the comparative bond angles around the carbonyl function are different implying that any interaction between selenium atoms in **3** is very different from those manifested by the oxygen atoms in **6**. It was therefore of interest to determine the thermodynamic activation parameters associated with the thermal conversion of **3** to yield **2**.

Dilute solutions of **3** could be quantitatively converted to **2** while monitoring changes in the visible spectrum at 350 nm. (A clean isosbestic point was observed at ~300 nm.) Compound **3**, which is colorless, smoothly and completely converted to yellow **2** in ethylene glycol solvent within 2 h at 60 °C and ½ h at 90 °C. The first order (or pseudo-first order) kinetics were linear over the entire temperature range studied, after taking into account the thermochromic properties of **2**.[8] The thermodynamic activation values of E_a = +65.8 kJ mol^{-1} and ΔS_a = −227 J deg^{-1} could be derived using the method of Arrhenius. The low activation energy for the thermolysis reaction thus indicated that the process of forming the 229 pm bond in **2** may be partially on the way to completion within the molecular structure of **3** itself. Consequently the preliminary conclusion that there may be a partial Se–Se bond in **3** seems plausible. (See footnotes ** and †† which were added in proof.)

The negative entropy of activation generated during the thermolysis reaction of **3**, where one molecule fragments to two molecular products, may imply that the associated disorder in the overall reaction can be offset, to some extent, by some factors of orderliness in the activated complex. The first factor implied is that the solvent (ethylene glycol) could be involved in creating more order during the thermolysis process. This possibility is buttressed by our observation that thermolysis of **3** in hydrocarbon solvent requires higher temperatures and is thus slower than in $HOCH_2CH_2OH$.** A second factor implicated is that a shorter than usual movement of the phenyl selenium substituents, during the extrusion of CO, may be inherent in **3**. As the crystal structure‖ of **3** shows the angle between the phenyl selenium groups is compressed in comparison to a normal sp^2 hybridized situation around a carbonyl group. (It has to be noted here that the compression of the analogous angle in **6** is even greater.[11]) And a third possible factor is the proposed hypervalent interaction between the selenium atoms of **3**. This proposal bolsters a hypothetical mechanistic process where the thermolytic transition state structure is a loosely organized diselenacyclopropanone ring structure. Consequently contrasting the thermal lability of **3** with the thermal stability of **6** suggests that these factors may not be available during analogous bond formation processes associated with the parent chalcogen.†† Comparing the molecular structures of *Se*,*Se*′-diphenyl carbonodiselenoate, **3**, and *S*,*S*′-diphenyl carbonodithioate (**7**) to that of diphenyl carbonate,[11] **6**, should prove interesting.‡‡

We (ROD and AC) would like to thank NSF (CHE-9974648) and the University of Massachusetts for funds to purchase the Nonius KappaCCD diffractometer. JTL and WR would like to thank the URI Foundation for partial support to fund this research and to Michael Callahan for recording the CI/MS for us.

Notes and references

† For example: reaction of **1** with simple alkyl halides in methanol (or other solvents) produced no identifiable materials other than the starting compounds.

‡ *Preparation of* **3**: 1.0 g of benzeneselenenyl bromide was dissolved in 15 ml of cold (0 °C) methanol and placed in a round bottom flask containing a stir bar. Solid, freshly prepared **1**, 0.77 g, was added in a controlled manner so that effervescence did not become too vigorous. Monitoring of progress was done by TLC over the duration of the ~1 h reaction. During the course of the reaction the color changed from dark red to a light yellow. Rotary evaporation of the resultant mixture was done under vacuum at approximately 0 °C after adding some silica gel. The product, adsorbed onto silica gel, was then mixed with 70:30 hexane–CH_2Cl_2 and added to the top of a chromatography column. Elution was commenced and the fractions were monitored using TLC. The organic products were eluted from the column in sequence (numerically). The fractions containing **3** were combined and allowed to evaporate in the cold until clear colorless crystals had formed. % Yield of **3** = 19%; mp = 48–50 °C.

§ The molecular characterization of **4** has proven difficult since it more readily decomposes to **2** than even **3**. We believe **4** may be either a hydrate or hemihydrate of **3**, since **4** exhibits CI/MS data with ion peaks centered around major masses, having two and four selenium atoms respectively, at 359 and 699 amu.

¶ The compound **3** decomposed in the X-ray beam within 5 min at rt.

‖ *X-Ray study of* **3**: Data was collected on a Nonius KappaCCD diffractometer. Satisfactory crystal stability was obtained by mounting the crystal inside of a sealed, thin walled glass capillary and by collecting the data at 173(2) K. *Crystal data for* **3**: $C_{13}H_{10}OSe_2$, *FW* = 340.13, monoclinic space group *C*2/*c*, *a* = 2140.38(5), *b* = 523.60(2), *c* = 1291.76(4) pm, β = 119.960(2)°, *V* = 1.25423(7) × 10^9 pm^3, *Z* = 4, *D*calc = 1.801 g cm^{-3}, μ = 5.871 mm^{-1}. Intensities were obtained for 2055 reflections ($2\theta_{max}$ = 50.1°) of which 1104 were unique. Refinement on F^2 was based on all of the data. The final agreement factors for the 941 unique reflections with $I > 2\sigma_I$ are *R* = 0.0262 and *Rw* = 0.0595. CCDC 163698.

** As pointed out by referee K this observation '…strongly argues for a polar transition state…' that is '…hydrogen bonded resulting in increasing order in the transition state.' We agree with this comment and note that a diselenacyclopropanone molecular entity would most likely be polar and H-bonded in ethylene glycol.

†† This same referee K has stated: '…the factors that the authors ascribe to the thermal lability of **3** are said to be not available for thermally stable **6**. A more obvious difference for this differing reactivity is that the thermodynamic driving force is substantially different *i.e.* a C(O)–O bond is stronger than a C(O)–Se bond and an O–O bond is much weaker than an Se–Se bond.' We again agree and we wish to thank this referee for these cogent ideas lending further support to our diselenacyclopropanone transition state proposal.

‡‡ Thermolytic studies of carbonodithioate esters have been referenced[13] to **7** but the molecular structure of **7** has not been determined as far as we are aware.

1 W. Steinkopf, *Chem. Ber.*, 1909, **42**, 3925.
2 S. Koto, M. Koyama and S. Zen, *Org. Synth.*, 1988, **Coll. Vol. V**, 797.
3 W. Steinkopf and M. Kuhnel, *Chem. Ber.*, 1942, **75B**, 1323.
4 H. Feuer, H. B. Hass and K. S. Warren, *J. Am. Chem. Soc.*, 1949, **71**, 3078.
5 D. J. Sutor, F. J. Llewellyn and H. S. Maslen, *Acta Crystallogr.*, 1954, **7**, 145.
6 H. C. E. MacFarland and W. MacFarland, *Multinuclear NMR*, ed. J. Mason, Plenum, New York, 1987, p. 417.
7 C. Djerassi, P. Brown and J. B. Thompson, *J. Am. Chem. Soc.*, 1966, **88**, 4049.
8 H. Kunkely, A. Vogler and J. K. Nagle, *Inorg. Chem.*, 1995, **34**, 4511.
9 F. A. Devillanova, G. Verani and L. Henriksen, *Tetrahedron*, 1980, **36**, 1451.
10 R. Marsh, *Acta Crystallogr.*, 1952, **5**, 458.
11 J. A. King, Jr. and G. L. Bryant, Jr., *Acta Crystallogr., Sect. C.*, 1993, **49**, 550.
12 N. Furukawa and S. Sato, *Chemistry of Hypervalent Compounds*, ed. K. Akiba, Wiley-VCH, New York, 1999, p. 241.
13 E. Marianucci, F. Pilati and C. Berti, *Polym. Degrad. Stab.*, 1986, **16**, 297.

CHEMCOMM Communication
www.rsc.org/chemcomm

One-step assembling reaction to the pentacyclic acetal of pinnatoxins

Jun Ishihara, Shingo Tojo, Akio Kamikawa and Akio Murai*

Division of Chemistry, Graduate School of Science, Hokkaido University, Sapporo 060-0810, Japan. E-mail: amurai@sci.hokudai.ac.jp; Fax: +81-11-706-2714; Tel: +81-11-706-2714

Received (in Cambridge, UK) 9th May 2001, Accepted 13th June 2001
First published as an Advance Article on the web 11th July 2001

Treatment of acyclic tetraketone 8 with HF·py in MeCN afforded the pentacyclic system 1 in pinnatoxins with a high selectivity in good yield.

The intramolecular acetal functionalities widely appear as subunits of many biologically active natural products, including polyether ionophores, and the construction of these acetal systems represents a synthetic challenge.[1,2] The favored conformation of the spiroacetal is predictable on the basis of stabilizing anomeric and *exo*-anomeric effects that direct C–O bonds to axial positions on the respective rings.[3] Pinnatoxins, which were isolated from *Pinna muricata* by Uemura, included the unique dispiroacetal and bicycloacetal moieties in their skeletons.[4] Recently, Kishi and co-workers accomplished the total synthesis of pinnatoxin A, and the absolute stereochemistry was determined at the same time.[5,6] Independently, we reported an efficient formation of the trioxadispiroacetal moieties,[7] and also the construction of the BCDEF ring system of pinnatoxins, however acetal formation of the BCDEF ring system was rather problematic as an undesired acetal was generated as a major product.[8] On our way to the syntheses, it was found that both of the BCD-fragment and the EF-fragment could be constructed under the same conditions. These results suggested the possibility of a one-step formation of two intramolecular acetals, which would allow fewer steps and seemed to be more attractive. Herein, we describe a one-step assembling reaction to the pentacyclic system of pinnatoxin A, **1**† (Fig. 1).

In our initial efforts, tetra-TBS‡ compound **2** was selected as a precursor for the cyclization in the unnatural enantiomeric form (Scheme 1). Various conditions were examined, however, none of the acidic conditions provided compound ***ent*-1**. Upon terminating the reaction after 1 hour, it seemed that the TBS groups at C-29 and 30 positions still remained intact, while the BCD-ring moiety might be gradually formed. At longer reaction time, the cyclic products were overreacted to afford a complex mixture, including β-eliminated and retro-aldol compounds. These results suggested that the formation of the EF-ring should precede the cyclization of the BCD-ring, which implied the faster hydrolysis of the protective groups at C-29 and 30 than the others. Therefore, 29,30-di-TES compound, which would be more detachable than di-TBS, was directed at the next stage.

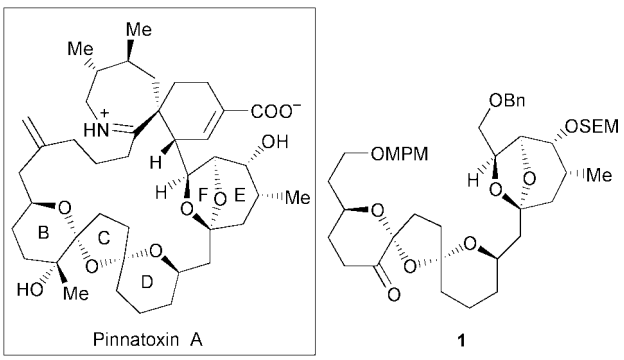

Fig. 1

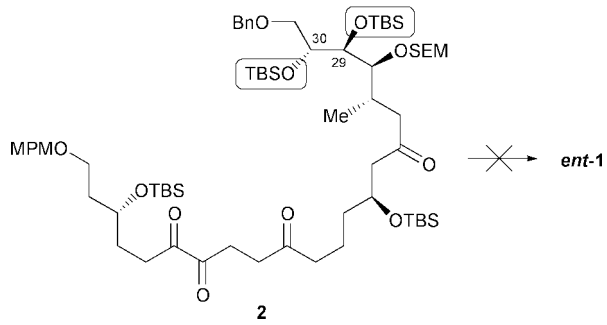

Scheme 1

Prior to one-step assembling reaction, stepwise acetalization was elucidated, which involves the construction of the BCD-ring after formation of diacetal moiety (Scheme 2). The acetalization reaction of **3**[9] was performed with HF·py in MeCN at 23 °C for 4 h to afford the desired compound **1** in 90% yield as a sole component of the pentacyclic compounds in spite of the possibility of eight products.[10] According to our previous results, the acetal formation of BCD-ring would be controlled by the thermodynamic effect,[11] which is based on the anomeric effect enhanced by the presence of an α-ketone.[12]

Since formation of the BCD-ring acetal proceeded independently of the EF-ring, the one-step assembling reaction to the pentacyclic system seemed to be realized. Reaction of **4** and **5**, followed by oxidation and desulfurization,[13] gave a coupled ketone in 84% yield in 4 steps (Scheme 3). The MMTr‡ group was detached with PPTS in MeOH and CH_2Cl_2 to the alcohol in 86% yield,[14] which was subsequently oxidized to aldehyde **7** in 99% yield. Analogous reaction of the sulfone **6** and **7** proceeded moderately to furnish another coupled ketone in 60% yield in 3 steps, which was converted to tetraketone **8** by ruthenium oxidation in 77%. Now the precursor for cyclization was obtained in our hands. When **8** was exposed to HF·py in MeCN at 24 °C for 7.5 h, the desired pentacyclic acetal compound **1** was produced as a single pentacyclic isomer in 71% yield, which was accompanied by a mixture of by-products lacking the pentacyclic system. The incompletely cyclized by-products were convertible to **1** under the same conditions. Eventually, the desired **1** was provided in an 83% combined yield from **8**. On the other hand, in the case of THF as a solvent, the reaction afforded the pentacyclic compound as a mixture of three isomers (**9**:**10**:**1** = 2:1:1) in 83% yield (Scheme 4). When this

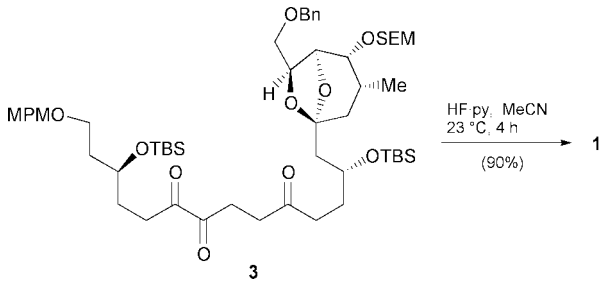

Scheme 2

 DOI: 10.1039/b104200a

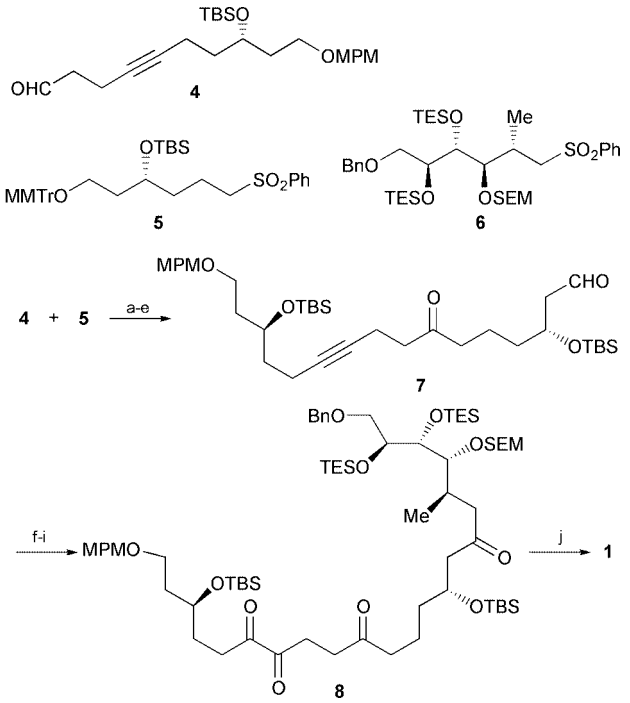

Scheme 3 (a) **5**, BuLi, THF, −78 °C, 30 min, then **4**, −78 °C, 30 min; (b) Swern oxidation; (c) (i) SmI_2, MeOH, THF, 0 °C, 30 min, (ii) Al(Hg), THF–H_2O (10:1), 23 °C, 16 h (84% in 4 steps); (d) PPTS (cat.), MeOH–CH_2Cl_2 (1:50), 21 °C, 10.5 h (88%); (e) DMPI,‡ $NaHCO_3$, CH_2Cl_2, 23 °C, 20 h (99%); (f) **6**, BuLi, Et_2O, −78 °C, 30 min, then **7**, −78 °C, 15 min; (g) DMPI, $NaHCO_3$, CH_2Cl_2, 23 °C, 11.5 h; (h) SmI_2, MeOH, THF, 0 °C, 30 min (60% in 3 steps); (i) $RuO_2·H_2O$, $NaIO_4$, CCl_4–MeCN–pH 7 buffer (1:1:1.5), 23 °C, 195 min (77%); (j) HF·py, MeCN, 24 °C, 7.5 h (83% after one recycle).

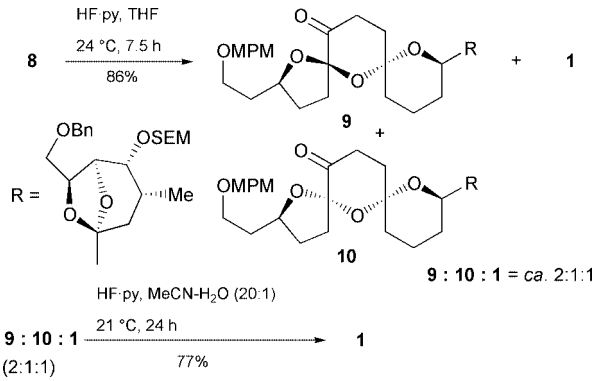

Scheme 4

mixture of **9**, **10**, and **1** was treated with HF·py in MeCN–H_2O (20:1) at 21 °C for 24 h, **1** was generated in 77% yield. The exclusive formation of **1** seems to be reasonable judging from the results of MM2* calculation using MacroModel 6.5 for the relative energies of the compounds, which suggested that the potential energy of **1** would be > 3.5 kcal mol^{-1} lower than any others. In addition, the axial preference of the C–O bond of the cyclic acetal would be enhanced by the presence of an α-ketone due to the cyclic stereoelectronic effect of π-electron donation. The acetalization in THF proceeded under the kinetic control, while the thermodynamic effect played an important role in the case of MeCN. The difference between the selectivities in MeCN and THF were induced by the solvation effect, which appeared in the glycosidation, involving the intermediacy of the acetonitrilium ion.[15] Thus, the one-step assembling reaction of the tetraketone to the complicated acetal was achieved to provide selectively the pentacyclic compound in an excellent yield. Further synthetic study is now under way in our laboratory.

This study was supported by a Grant-in-Aid for Scientific Research from the Ministry of Education, Science, Sports, and Culture, Japan (11780410, J. I.).

Notes and references

† **1**: colorless oil. $[\alpha]_D^{22}$ +19.7 (*c* 0.14, $CHCl_3$); ^{1}H-NMR (C_6D_6, 400 MHz) δ 7.32 (2H, d, *J* 8.5 Hz), 7.25–7.06 (5H, m), 6.85 (2H, d, *J* 8.5), 4.79 (1H, d, *J* 6.8), 4.68 (1H, dd, *J* 1.3, 4.6), 4.65 (1H, d, *J* 6.8), 4.51–4.43 (2H, m), 4.43 (1H, d, *J* 11.2), 4.43–4.32 (3H, m), 4.23 (1H, d, *J* 12.2), 3.85 (1H, dd, *J* 6.6, 10.0 Hz), 3.82 (1H, dd, *J* 8.3, 8.7), 3.69 (1H, dd, *J* 8.3, 8.7), 3.67–3.58 (3H, m), 3.57 (1H, dd, *J* 1.3, 3.4), 3.30 (3H, s), 2.83 (1H, ddd, *J* 2.4, 8.8, 12.2), 2.62 (1H, ddd, *J* 7.4, 12.7, 14.6), 2.37–2.28 (1H, m), 2.32 (1H, dd, *J* 6.8, 14.2), 2.25–2.13 (3H, m), 2.08–1.96 (4H, m), 1.94–1.83 (1H, m), 1.79-1.65 (3H, m), 1.63–1.53 (2H, m), 1.46–1.17 (4H, m), 1.13 (3H, d, *J* 6.8), 0.98 (2H, t, *J* 8.5), and −0.01 (9H, s); ^{13}C-NMR (C_6D_6, 100 MHz) δ 201.5, 159.7, 138.7, 131.4, 129.4, 128.6, 127.9, 114.1, 108.9, 108.7, 108.5, 94.8, 78.3, 77.8, 73.8, 73.5, 73.0, 70.0, 68.5, 68.1, 67.2, 65.4, 54.9, 45.6, 40.1, 38.6, 35.9, 35.2, 34.0, 33.0, 32.5, 31.3, 30.3, 29.5, 20.6, 18.4, and 17.0; IR (neat), ν_{max} 2926, 2855, 1733, 1612, 1514, 1454, 1367, 1303, 1249, 1099, 1036, 984, 952, 861, 836, 749, and 698 cm^{-1}; FD-HR-MS: found: 796.4228, calcd. for $C_{44}H_{64}O_{11}Si$ (M^+): 796.4218.

‡ SEM = 2,2-(trimethylsilyl)ethoxymethyl. TBS = *tert*-butyldimethylsilyl. MMTr = 4-methoxyphenyldiphenylmethyl. DMPI = Dess-Martin periodinane {IUPAC name: 1,1,1-tris(acetyloxy)-1,1-dihydro-1,2-benziodoxol-3(1*H*)-one}. MPM = 4-methoxybenzyl.

1 For reviews on spiroketal synthesis see: A. F. Kluge, *Heterocycles*, 1986, **24**, 1699; T. L. B. Boivin, *Tetrahedron*, 1987, **43**, 3309; F. Perron and K. F. Albizati, *Chem. Rev.*, 1989, **89**, 1617; V. Vaillancourt, N. E. Pratt, F. Perron and K. F. Albizati, *Total Synth. Nat. Prod.*, 1992, **8**, 533; M. A. Brimble and F. A. Far, *Tetrahedron*, 1999, **55**, 7661.

2 F. Perron and K. F. Albizati, *J. Org. Chem.*, 1989, **54**, 2047; M. A. Brimble and G. M. Williams, *Tetrahedron Lett.*, 1990, **31**, 3043; M. A. Brimble and G. A. Williams, *J. Org. Chem.*, 1992, **57**, 5818; K. Horita, S. Nagato, Y. Oikawa and O. Yonemitsu, *Tetrahedron Lett.*, 1987, **28**, 3253; D. R. Williams, P. A. Jass and R. D. Gaston, *Tetrahedron Lett.*, 1993, **34**, 3231; G. J. McGarvey and M. W. Stepanian, *Tetrahedron Lett.*, 1996, **37**, 5461; G. J. McGarvey, M. W. Stepanian, A. R. Bressette and J. F. Ellena, *Tetrahedron Lett.*, 1996, **37**, 5465.

3 P. Delongchamps, *Stereoelectronic Effects in Organic Chemistry*, Pergamon Press, Oxford, pp. 4–53, 1983.

4 D. Uemura, T. Chou, T. Haino, A. Nagatsu, S. Fukuzawa, S. Z. Zeng and H. S. Chen, *J. Am. Chem. Soc.*, 1995, **117**, 1155; T. Chou, O. Kamo and D. Uemura, *Tetrahedron Lett.*, 1996, **37**, 4023; T. Chou, T. Haino, M. Kuramoto and D. Uemura, *Tetrahedron Lett.*, 1996, **37**, 4027.

5 J. A. McCauley, K. Nagasawa, P. A. Lander, S. G. Mischke, M. A. Semones and Y. Kishi, *J. Am. Chem. Soc.*, 1998, **120**, 7647.

6 For synthetic studies see: T. Noda, A. Ishiwata, S. Uemura, S. Sakamoto and M. Hirama, *Synlett*, 1998, 298; B. D. Suthers, M. F. Jacobs and W. Kiching, *Tetrahedron Lett.*, 1998, **39**, 2621; A. Ishiwata, S. Sakamoto, T. Noda and M. Hirama, *Synlett*, 1999, 692; A. Nitta, A. Ishikawa, T. Noda and M. Hirama, *Synlett*, 1999, 695.

7 T. Sugimoto, J. Ishihara and A. Murai, *Tetrahedron Lett.*, 1997, **38**, 7379.

8 T. Sugimoto, J. Ishihara and A. Murai, *Synlett*, 1999, 541.

9 A. Kamikawa, J. Ishihara and A. Murai, unpublished results.

10 The structure of **1** was determined by NMR spectroscopy (^{1}H-,^{13}C-NMR, DQFCOSY, HMQC, HMBC, and NOESY spectra).

11 J. Ishihara, T. Sugimoto and A. Murai, *Synlett*, 1998, 603.

12 A. J. Kirby, *The Anomeric Effect and Related Stereoelectronic Effects at Oxygen*, Springer-Verlag, Berlin, Heidelberg, New York, pp. 20–23, 1983.

13 G. A. Molander, *Chem. Rev.*, 1992, **92**, 29.

14 R. W. Armstrong, J.-M. Beau, S. H. Cheon, W. J. Christ, H. Fujioka, W.-H. Ham, L. D. Hawkins, H. Jin, S. H. Kang, Y. Kishi, M. J. Martinelli, W. W. McWhorter, M. Mizuno, M. Nakata, A. E. Stutz, F. X. Talamas, M. Taniguchi, J. A. Tino, K. Ueda, J. Uenishi, J. B. White and M. Yonaga, *J. Am. Chem. Soc.*, 1989, **111**, 7525.

15 P. Sinay and J. R. Pougny, *Tetrahedron Lett.*, 1976, 4073; R. R. Schmidt and J. Michel, *Carbohydr. Chem.*, 1985, **4**, 141; R. U. Lemieux and R. M. Ratcliffe, *Can. J. Chem.*, 1979, **57**, 1244.

CHEMCOMM
Communication
www.rsc.org/chemcomm

Different positions of the formally isolobal moieties H^+ and $(AuPPh_3)^+$ in *N*-(5-methoxyquinolyl-8)-2,4,6-trinitroaniline and its auration product

Lyudmila G. Kuz'mina,*[a] Alexander A. Bagatur'yants,[b] Andrei V. Churakov[a] and Judith A. K. Howard[c]

[a] *Institute of General and Inorganic Chemistry, Russian Acad. Sci., Leninskii pr. 31, Moscow, 119991 Russia. E-mail: kuzmina@igic.ras.ru*
[b] *Center of Photochemistry, Russian Acad. Sci., Novator Str. 7a, Moscow, 117421 Russia. E-mail: sasha@photonics.ru*
[c] *Department of Chemistry, University of Durham, South Road, Durham, UK DH1 3LE. E-mail: j.a.k.howard@durham.ac.uk*

Received (in Cambridge, UK) 2nd April 2001, Accepted 20th June 2001
First published as an Advance Article on the web 11th July 2001

It has been shown by an X-ray crystallographic analysis of *N*-(triphenylphosphinegold)-*N*-(5-methoxyquinolyl-8)-2,4,6-trinitroaniline 1 and quantum chemical calculations on *N*-(5-methoxyquinolyl-8)-2,4,6-trinitroaniline 2 that H^+ and $(AuPPh_3)^+$ sub-units in 1 and 2 occupy different positions at the amine and quinoline nitrogen atoms, respectively.

This paper is part of our systematic investigations into the structural chemistry of gold(I) compounds. It is well known that the singly charged heavy-metal complex cation AuL^+ (L = neutral ligand) is isolobal with the cation HgR^+ (R = acido ligand). Both these metals commonly form 14-electron linear complexes QAuL or QHgR (Q = organic ligand). In real structures, the strict collinearity of metal bonds can be disturbed because of weak interactions (secondary bonds) of the metal with a heteroatom (X) involved in Q.[1] Commonly, the HgR^+ moiety behaves like a proton. Structures of chemically related organic and organomercury compounds display high similarity and secondary bonds M···X formed by Hg in QHgR are analogous to hydrogen bonds H···X in the corresponding organic compounds QH.[2] In accordance with isolobal analogy, it could be expected that the AuL^+ moiety also behaves like a proton; that is, in QAuL compounds, it forms a covalent bond with the same atom as the proton in QH compounds.

To explore the limits of the analogy between the corresponding isolobal particles AuL^+, HgR^+ and H^+, we subjected compound **2** to auration and investigated the structures of compounds **1** and **2** (Scheme 1.)

The X-ray structure of complex **1** and selected geometric parameters are shown in Fig. 1. The gold atom of the $AuPPh_3$ moiety forms a chemical bond with the quinoline nitrogen N(2) in **1**. The Au(1) atom adopts a T-shaped coordination. Two covalent bonds Au(1)–N(2) and Au(1)–P(1) are of normal length [2.121(8) and 2.231(3) Å, respectively].[3–6] The Au(1)···N(1) distance [2.621(9) Å] corresponds to a secondary bond. A similar distance [2.627(9) Å] was found in (8-Squ)$AuPPh_3$ (8-Squ = 8-mercaptoquinolinate) for the Au···N(quinoline) secondary bond.[6] The N(2)–Au(1)–P(1) bond angle is equal to 168.4(2)° with the Au(1)–P(1) bond bent away from N(1). In contrast to $AuPPh_3^+$ in **1**, the proton in *N*-substituted 2,4,6-trinitroanilines is always located at the amino nitrogen atom. According to the CSD,[2] the N(amino)–C(Ar) bond length varies within 1.33–1.37 Å, the C(*ipso*)–C(*ortho*) bond lengths range within 1.41–1.45 Å, and the other C–C bonds in the aniline Ph ring lie within 1.37–1.39 Å. Thus, the bonds C(*ipso*)–C(*ortho*) are longer than the others in the ring and no bond length alternation is observed within the C(*ortho*)···C(*para*) fragment. The C(*ortho*)–C(*ipso*)–C(*ortho*) angle varies within 112–115°.

The formation of the Au–N covalent bond with the quinoline rather than amine nitrogen atom is the most interesting property of molecule **1**. This fact means that the formal zwitterionic bond structure is characteristic of this molecule. As a result, a

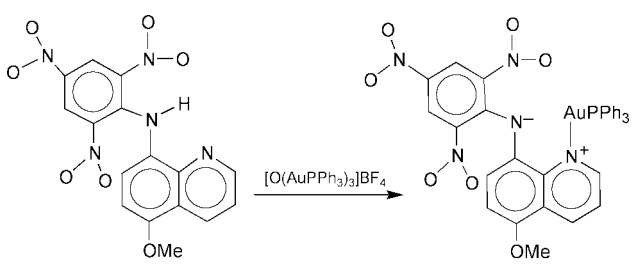

2 **1**

Scheme 1

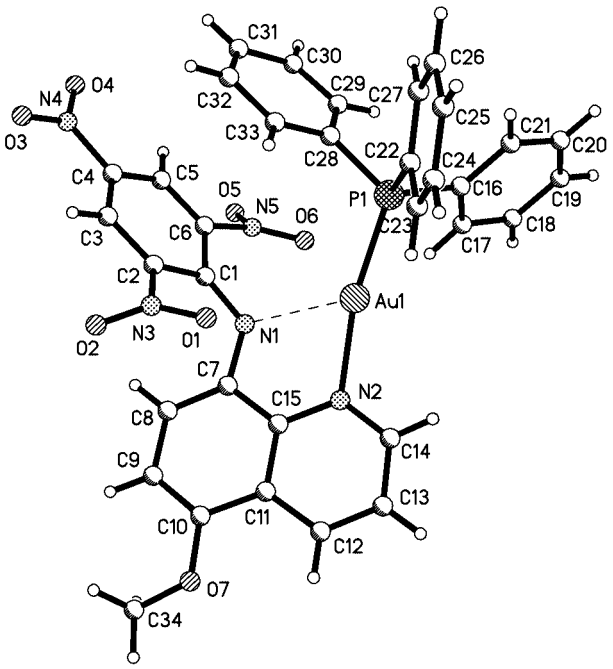

Fig. 1 Molecular structure of **1**. Bond lengths (Å) and bond angles (°) are: Au(1)–P(1) 2.231(3), Au(1)–N(2) 2.121(8), N(2)–Au(1)–P(1) 168.4(2), Au(1)···N(1) 2.621(9), N(1)–Au(1)–N(2) 71.6(3), N(1)–Au(1)–P(1) 120.0(2), N(1)–C(1) 1.30(1), C(1)–C(2) 1.47(1), C(1)–C(6) 1.47(1), C(2)–C(3) 1.36(1), C(6)–C(5) 1.35(1), C(3)–C(4) 1.38(1), C(4)–C(5) 1.39(1), N(1)–C(7) 1.44(1), C(1)–N(1)–C(7) 120.5(8), N(2)–C(15) 1.36(1), N(2)–C(14) 1.33(1), C(14)–N(2)–C(15) 121.4(8).

 DOI: 10.1039/b102938j

significant redistribution of bond lengths in the trinitroaniline moiety should be observed for molecule **1**. Actually, in **1**, the N(1)–C(1) bond 1.30(1) Å is shorter, both the C(1)–C(2) and C(1)–C(6) bonds 1.47(1) Å are longer, and the C(2)–C(1)–C(6) angle is more strongly reduced [109.5(8)°] than the analogous parameters in *N*-substituted 2,4,6-trinitroanilines. A pronounced alternation of bond lengths corresponding to the *para*-quinoid structure of the aniline sub-unit is observed; the C(2)–C(3) and C(5)–C(6) bonds [1.36(1) and 1.35(1) Å] are systematically shorter than the C(3)–C(4) and C(4)–C(5) bonds [1.38(1) and 1.39(1) Å]. Apparently, because of the contribution of the *para*-quinoid structure to the total molecular structure of **1**, the colour of this compound is deeper (black) than those of *N*-aryl-2,4,6-trinitroanilines (tones of red).†

The structure of **1** also contrasts with that of *N*-(5-methoxyquinolyl-8)-2,4,6-trinitroaniline **2**. To provide an insight into subtle geometric changes in the molecular skeleton caused by substituting the proton for the $AuPPh_3$ moiety, *ab initio* quantum chemical calculations were performed for **2**.

Geometry optimisation[7] resulted in the structure shown in Fig. 2. Molecule **2** exists in the same neutral form as all substituted trinitroanilines.

The distribution of bond lengths in **2** agrees well with that observed for *N*-(naphthyl)-2,4,6-trinitroaniline **3**.[8] However, the general conformation of **2** differs significantly from that found for **3**. For instance, dihedral angles between the C(1)–N(1)–C(7) fragment and C(1)···C(6) and C(7)···C(15) rings are 27.3 and 12.3° in **2**, whereas these angles are of 17.4 and 49.8°, respectively, in **3**. The N–H group in **2** forms a bifurcated hydrogen bond with the quinoline nitrogen (H···N 2.104 Å) and one of the oxygen atoms of one *ortho*-nitro group (H···O 1.862 Å). Therefore, the geometry of **2** is somewhat flattened compared to that of **3**, where the N–H group forms only one hydrogen bond with the oxygen of the *ortho*-nitro group. This particular *ortho*-nitro group is twisted from the C(1)···C(6) plane by only 16.8°, whereas another *ortho*-nitro group is twisted by 52.0°. In **2**, these values are equal to 5.3 and 38.0°.

In **1**, the C(1)–N(1)–C(7)/C(1)···C(6) dihedral angle is also rather small (27.0°). The flattened conformation at the formally double N(1)–C(1) bond is a result of a compromise between two effects. One of these is conjugation between the formally double N(1)–C(1) bond and the C(1)···C(6) benzene ring while the other is steric interaction between two ring systems. There is no weak interaction between Au(1) and the nearest *ortho*-nitro group N(5)–O(5)–O(6). Because of steric interactions both *ortho*-NO_2 groups are strongly twisted from the C(1)···C(6) plane by 43.4 and 38.1°.

On the other hand, the C(1)–N(1)–C(7)–C(8) torsion angle in **1** is 41.7° (*cf.* 49.8° in **3**), indicating that there is no significant conjugation between the amine nitrogen lone pair and the quinoline moiety. The coordination of Au(1) with the aminoquinoline moiety causes only minor changes in the geometry of the quinoline fragment. Only the endocyclic angle at N(2) increases to 121.4(8)° *vs.* 117.0° in aminoquinolines and 117.7° in **2**. Such an increase in this angle is typical for *N*-protonated pyridines (CSD).

We wish to thank The Royal Society, the RFBR for financial support (projects No. 99-03-33180 and 01-03-32474) and the EPSRC for a Senior Research Fellowship (J. A. K. H.).

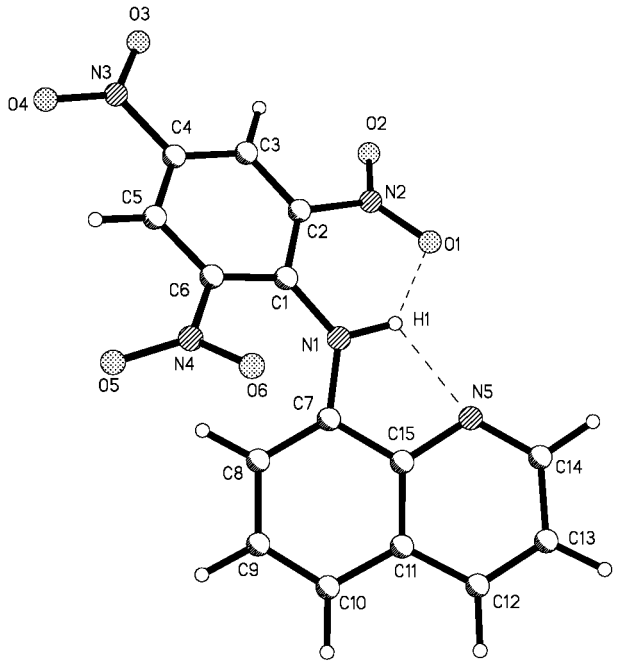

Fig. 2 Structure of **2** on the basis of *ab initio* quantum chemical calculation (MP2). Bond lengths (Å) and bond angles (°): N(1)–C(1) 1.374, C(1)–C(2) 1.426, C(1)–C(6) 1.436, C(2)–C(3) 1.390, C(6)–C(5) 1.388, C(3)–C(4), 1.388, C(4)–C(5) 1.388, N(1)–C(7) 1.405, C(1)–N(1)–C(7) 131.0, N(2)–C(15) 1.386, N(2)–C(14) 1.347, C(14)–N(2)–C(15) 117.7.

Notes and references

† *Crystal data* for **1**: $C_{34}H_{25}AuN_5O_7P$, M = 843.53, triclinic, space group $P\bar{1}$, a = 7.5814(2), b = 13.0849(4), c = 16.6256(4) Å, α = 74.433(1), β = 77.980(1), γ = 82.332(1)°, V = 1548.68(7) Å^3, Z = 2, D_c = 1.809 g cm^{-3}, μ(Mo-Kα) = 4.861 mm^{-1}. A black needle-like crystal was covered with perfluoropolyether oil and mounted on a Bruker SMART-CCD diffractometer (ω scan, 0.3° frame, 15 s per frame, 150 K). A total of 10117 reflections were collected in the θ range 1.29–26.00° using Mo-Kα radiation (λ = 0.71073 Å). Of these, 6080 were considered unique (R_{int} = 0.0689). A semi-empirical absorption correction was applied (min. and max. transmissions are 0.74362 and 0.97352). The structure was solved by direct methods and refined by full-matrix least squares based on F^2 for all data using SHELXL software. All non-hydrogen atoms were refined with anisotropic displacement parameters. H atoms were placed geometrically at the calculated positions and refined with the riding model. Final R_1 = 0.0662 (5616 observed reflections) and R_1 = 0.0989 (all data), number of variables is 435, GOF = 1.127, $\Delta\rho_{min,max}$ = −1.455 and 1.757 e Å^{-3}.

CCDC reference number 162720. See http://www.rsc.org/suppdata/cc/b102938j/ for crystallographic data in CIF or other electronic format.

1 L. G. Kuz'mina, *Russ. J. Coord. Chem.*, 1999, **25**, 599.
2 F. H. Allen and O. Kennard, *Chem. Des. Autom. News*, 1993, **8**, 1.
3 A. V. Churakov, L. G. Kuz'mina and J. A. K. Howard, *Acta Crystallogr., Sect. C*, 1998, **54**, 212.
4 A. V. Churakov, L. G. Kuz'mina, J. A. K. Howard and K. I. Grandberg, *Acta Crystallogr., Sect. C*, 1998, **54**, 54.
5 L. G. Kuz'mina, A. A. Bagatur'yants, J. A. K. Howard, K. I. Grandberg, A. V. Karchava, E. S. Shubina, L. N. Saitkulova and E. V. Bakhmutova, *J. Organomet. Chem.*, 1998, **575**, 39.
6 L. G. Kuz'mina, N. V. Dvortsova, O. Yu. Burtseva, M. A. Porai-Koshits, E. I. Smyslova and K. I. Grandberg, *Metalloorg. Khim.*, 1990, **3**, 364.
7 The calculations were carried out using the MP2 method with the 3-21G* basis sets. Full geometry optimisation was performed starting from two initial geometries. In the first the quinoline fragment was considered as coplanar to the amino group and the N(2)–O(1)–O(2) nitro group was twisted by 60° from this plane. In the second this nitro group was considered as coplanar to the amino group, whereas the quinoline fragment was twisted by 60° from this plane. Both calculations converged to the same flattened geometry.
8 G. V. Gridunova, V. N. Petrov, Yu. T. Struchkov, I. G. Il'ina and O. V. Mikhalev, *Kristallografiya.*, 1990, **35**, 59.

CHEMCOMM
Communication
www.rsc.org/chemcomm

[Ru(η⁶-*p*-cymene)Cl$_2$(pta)] (pta = 1,3,5-triaza-7-phosphatricyclo-[3.3.1.1]decane): a water soluble compound that exhibits pH dependent DNA binding providing selectivity for diseased cells

Claire S. Allardyce, Paul J. Dyson,* David J. Ellis and Sarah L. Heath

Department of Chemistry, The University of York, Heslington, York, UK YO10 5DD. E-mail: pjd14@york.ac.uk

Received (in Cambridge, UK) 4th May 2001, Accepted 20th June 2001
First published as an Advance Article on the web 11th July 2001

The water soluble complex [Ru(η⁶-*p*-cymene)Cl$_2$(pta)] (pta = 1,3,5-triaza-7-phosphatricyclo[3.3.1.1]decane), exhibits pH dependent DNA damage; the pH at which damage is greatest correlates well to the pH environment of cancer cells.

Current inorganic drugs such as cisplatin are successfully used in the treatment of many cancers, including testicular, ovarian, oropharyngeal, bronchogenic, cervical and bladder carcinomas, lymphoma, osteosarcoma, melanoma and neuroblastoma.[1] However there are problems associated with their use including general toxicity (leading to side effects) and drug resistance. The general toxicity of cisplatin has been reduced by the development of special drug-dosing protocols,[2] but the need for further improvements remains. In contrast, the ruthenium based anticancer drug, recently launched in the clinic ImH[*trans*-RuCl$_4$(DMSO)Im] (NAMI-A), shows a remarkably low general toxicity.[3] Since ruthenium complexes have been shown to specifically accumulate in tumour cells,[4] the reduced general toxicity of NAMI-A compared to platinum drugs could be due to ruthenium selectivity. In this paper we describe a new ruthenium compound that exhibits pH dependent DNA damage, which could show increased selectivity towards cancer cells and reduce toxic side effects in healthy cells.

The reaction of [Ru(η⁶-*p*-cymene)Cl$_2$]$_2$ with two equivalents of 1,3,5-triaza-7-phosphatricyclo[3.3.1.1]decane, pta,[5] under reflux in methanol, for 24 h affords [Ru(η⁶-*p*-cymene)Cl$_2$(pta)] **1** in high yield.[6] Characterisation of **1** was achieved using mass spectrometry and NMR spectroscopy.[7]

The molecular structure of **1** (Fig. 1) has been determined by single crystal X-ray diffraction [8] and contains two independent molecules in the asymmetric unit. The C$_6$-ring is coordinated to the ruthenium(II) centre with an average Ru–C bond length of 2.20 and 2.21 Å in each molecule. Two chlorine ligands (mean Ru–Cl 2.42 Å and 2.43 Å in each molecule) and the pta group [Ru–P 2.296(2) and 2.298(3) Å in each molecule] make up the rest of the coordination sphere. All parameters are in keeping with previously determined structures related to **1**, which vary in the nature of the arene and phosphine ligands.[9]

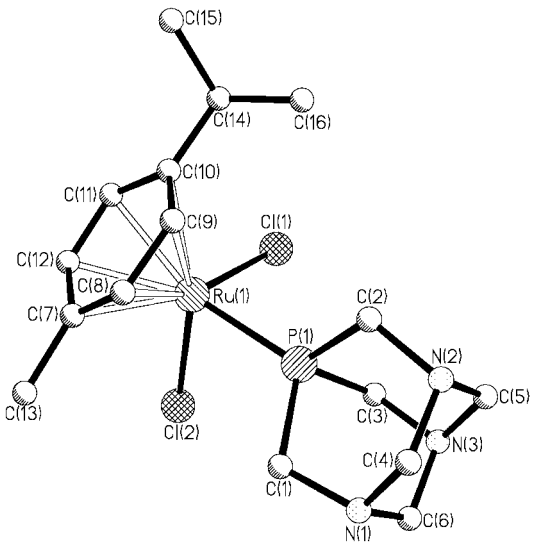

Fig. 1 The molecular structure of one of the independent molecules of **1**.

The presence of the pta ligand provides **1** with versatile soluble properties. For example, **1** and **1** + H$^+$ are soluble in water and polar organic solvents such as $CHCl_3$, CH_2Cl_2 and $(CH_3)_2CO$. Protonation of the pta ligand influences the solubility properties, with the deprotonated species having a higher solubility in organic solvents. The pK_a of **1** was estimated as 6.5 by monitoring the change in absorbance at 455 nm. We recognised that the pH dependant solubility of phosphaamine ligands like pta could also be exploited in biological systems, with the possibility of providing clinical uses. At physiological pH the predominant species carries no charge and hence can diffuse through lipid membranes and move freely into and within cells. In some diseased tissues the pH is reduced due to the associated changes in metabolism and in this environment the pta ligand is protonated, trapping **1** in the cell. In addition, we have shown that the protonated species induces DNA damage more readily than unprotonated **1** (see below).

The DNA substrate used in agarose gel electrophoresis[10] is 95% supercoiled (SC) and 5% open circular (OC), and their positions can be distinguished on the gel (Fig. 2). The results show that when DNA is incubated with **1** at pH 7.5 or above, the DNA migrates similarly to the DNA substrate. These results are in accordance with independent studies using a ruthenium(II)–arene compound, with a DMSO ligand in place of the pta in **1**, that did not detect an interaction with DNA.[11] However, at pH 7.0, the SC form of DNA incubated with **1** is slightly retarded compared to the substrate DNA and the retardation is progressively increased as the pH is reduced. At all pH values the position of OC DNA in the gel remains the same, indicating that the pH dependent retardation of SC DNA by **1** is not due to charge neutralisation.

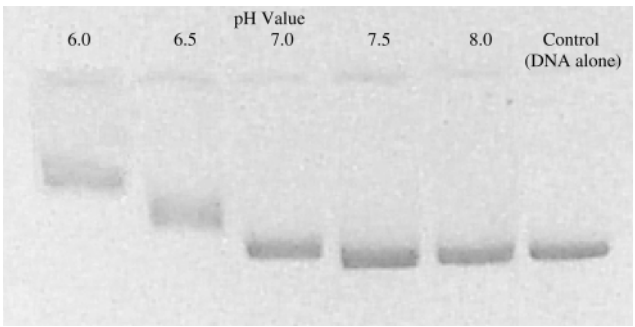

Fig. 2 Comparison of DNA damage induced by **1** incubated at different pH values; visualised by electrophoretic DNA migration in an agarose gel.

 DOI: 10.1039/b104021a

The pH range over which **1** retards DNA migration closely matches the pK_a of the pta ligand, and as DNA is negatively charged, it would be expected that the interaction between these two species would be promoted if they each carried opposite charges. The importance of this result is that DNA binding is not favoured at physiological pH. Many diseased cells have a reduced pH, due to metabolic changes in part associated with the accelerated cell division.[12] Thus, **1** would have a higher affinity for DNA in diseased cells, compared to healthy cells, providing a means of selectivity.

Further studies are currently in progress to delineate the way in which **1** with interacts with DNA. We are also comparing the effect that the type of arene ligand has on DNA and the results obtained from these studies will be reported in due course.

We would like to thank to thank The Royal Society for a University Research Fellowship (P. J. D. and S. L. H.) and The University of York for financial support (D. J. E).

Notes and references

1 J. Reedijk, *Chem. Commun.*, 1996, 801; E. Wong and C. M. Giandomenico, *Chem. Rev.*, 1999, **99**, 2451 and references therein.

2 J. Reedijk, *Chem. Rev.*, 1999, **99**, 2499 and references therein.

3 R. Gagliardi, G. Sava, S. Pacor, G. Mestroni and E. Alessio, *Clin. Exp. Metastasis.*, 1994, **12**, 93.

4 S. C. Srivastava, P. Richard, G. E. Meinken, S. M. Larson and Z. Grunbaum, in *Radiopharmaceuticals–Structure–Activity relationships*, ed. R. P. Spencer, Grune & Stratton Inc., New York, 1981, pp. 207–223.

5 *Synthesis* of pta: D. J. Daigle, A. B. Pepperman Jr. and S. L. Vail, *J. Heterocycl. Chem.*, 1974, **17**, 407.

6 *Synthesis* of Ru(η^6-*p*-cymene)Cl_2(pta) **1**: a methanolic solution of [Ru(η^6-*p*-cymene)Cl_2]$_2$ (200 mg, 0.33 mmol) and pta (1,3,5-triaza-7-phosphatricyclo[3.3.1.1]decane), 103 mg, 0.66 mmol) was refluxed for 24 h. The solution was allowed to cool to room temperature and filtered. Removal of the solvent affords a red microcrystalline product Ru(η^6-*p*-cymene)Cl_2(pta) **1** (281 mg, 92%).

7 *Spectroscopic data* for **1**: Positive ion electrospray mass spectrum (H_2O): 486 (rel. int. 13) [Ru(η^6-*p*-cymene)Cl_2(pta) + Na]$^+$ (calc. 486.358), 464 (rel. int. 4) [Ru(η^6-*p*-cymene)Cl_2(pta) + H]$^+$ (calc. 464.376), 428 (rel. int. 100) [Ru(η^6-*p*-cymene)Cl(pta)]$^+$ (calc. 427.918). ^{31}P NMR ($CDCl_3$) δ −36.63 (s). ^{1}H NMR ($CDCl_3$) δ 5.46 (q, *J* 19.73 Hz, 4 *p*-cymeme), 4.53 (s, 6 NCH_2N), 4.32 (s, 6 PCH_2N), 2.78 (septet, *J* 41.37 Hz, CH), 2.08 (s, 3 CH_3), 1.22 (d, *J* 6.93 Hz, 6 CH_3). Anal. Found: (calc.) C, 41.14 (41.47); H, 5.66 (5.66)%.

8 Structural details of **1**: single crystals of **1**·CH_2Cl_2 suitable for crystallography were grown from a dichloromethane–hexane solution at 4 °C. Data were collected on a Bruker SMART-CCD equipped with an Oxford Cryostreams low temperature device. *Crystal data* for **1:** [$RuCl_2(PC_6H_{12}N_3)(C_{10}H_{14})$]·$CH_2Cl_2$, red needle of dimensions 0.38 × 0.12 × 0.10, M = 548.26, orthorhombic, space group *Pna*21, Z = 8, a = 13.2180 (11), b = 15.8201(13), c = 20.8468(18), U = 4354.3(6) Å^3, D_c = 1.673 g cm^{-3}, T = 150(2) K, F(000) = 2224, Mo-Kα radiation (λ = 0.71073), μ = 1.292 mm^{-1}, reflections measured in the range 1.62 ≤ θ ≤ 23.32°, 5356 unique (R_{int} = 0.0744). The structure was solved by direct methods and refined by full-matrix least squares on F^2 [SHELXTL NT (G. M. Sheldrick, SHELXL97, an integrated system for solving and refining crystal structures from diffraction data, University of Göttingen, Germany, 1997)] to $R1$ = 0.0476, $wR2$ = 0.1255, S = 1.060, for 4825 reflections with $F > 4\sigma(F)$ and 476 refined parameters with allowance for the thermal anisotropy of all non-hydrogen atoms. A semi-empirical absorption correction was applied based on symmetry equivalent and repeated reflections (minimum and maximum transmission coefficients 0.657 and 0.928). Minimum and maximum final electron density −1.089 and 1.607 e Å^{-3}. The largest residual electron density peak 1.61 e$^-$ lies close to a dichloromethane of crystallisation and no sensible crystallographic or chemical model for this peak could be found. CCDC reference number 161466. See http://www.rsc.org/suppdata/cc/b1/b104021a/ for crystallographic data in CIF or other electronic format.

9 E. A. V. Ebsworh, R. O. Gould, R. A. Mayo and M. Walkinshaw, *J. Chem. Soc., Dalton Trans.*, 1987, 2831; W. Keim, P. Kraneburg, G. Dahmen, G. Deckers, U. Englert, K. Linn, T. P. Spaniol, G. Raabe and C. Krüger, *Organometallics*, 1994, **13**, 3085; M. R. J. Elsegood and D. A. Tocher, *Polyhedron*, 1995, **14**, 3147; I. Moldes, E. de la Encarnación, J. Ros, Á. Alvarez-Larena and J. F. Piniella, *J. Organomet. Chem.*, 1998, **566**, 165.

10 In this assay 2.5 mM **1** in 10 mM phosphate buffer, pH 5.5–8.0 in 0.5 step increments, was incubated for 4 h with 0.05 mg ml^{-1} pBR322 DNA. The DNA damage was assessed by comparing the electrophoretic migration of the species in a 1% agarose gel, prepared in TAE buffer [40 mM tris(hydroxymethyl)aminomethane acetate and 1 mM EDTA] with similar migrations of the control incubations: control 1 tested the activity of **1** under similar assay conditions known to result in DNA retardation (as above but with no phosphate buffer) and control 2 was DNA under the same conditions without **1**. From each assay, 8 μl were mixed with 1 μl dye (0.025 mg bromophenol blue, 1 ml glycerol and 1 ml distilled water) and pipetted into wells on the horizontal gel. A potential difference of 30 mV was applied over the gel for 4 h and the bands visualised by staining with ethidium bromide. The effect of pH alone on DNA was assessed by performing a similar experiment in the absence of **1**.

11 Y. N. A. Gopal, D. Jayaraju and A. K. Kondapi, *Biochemistry*, 1999, **38**, 4382.

12 For example, see: G. R. Martin and R. K. Jain, *Cancer Res.*, 1994, **54**, 5670.

CHEMCOMM Communication
www.rsc.org/chemcomm

Crystal structure of a polycyano–polycadmate host clathrate including a charge-transfer complex of methylviologen dication and mesitylene as a guest

Hirofumi Yoshikawa,[a] Shin-ichi Nishikiori,*[a] Kinga Suwinska,[b] Roman Luboradzki[b] and Janusz Lipkowski[b]

[a] *Department of Basic Science, Graduate School of Arts and Sciences, The University of Tokyo, Komaba 3-8-1, Meguro, Tokyo 153-8902, Japan. E-mail: cnskor@mail.ecc.u-tokyo.ac.jp*
[b] *Institute of Physical Chemistry, Polish Academy of Sciences, Kasprzaka 44/52, 01224, Warsaw, Poland*

Received (in Cambridge, UK) 6th March 2001, Accepted 12th June 2001
First published as an Advance Article on the web 4th July 2001

The crystal structure of a methylviologen dication (MV^{2+})–mesitylene clathrate, one of a newly synthesized polycyano–polycadmate host clathrates, including a charge-transfer complex of MV^{2+} and an aromatic molecule, has been revealed by X-ray diffraction.

As a trial to develop functional materials using a polycyano–polycadmate host, we previously synthesized a series of polycyano–polycadmate host clathrates including a methyl viologen dication (MV^{2+} = 1,1′-dimethyl-4,4′-bipyridinium ion) as a guest.[1] MV^{2+} is widely used in the fields of photochemistry, electrochemistry, *etc*. owing to its strong electron accepting nature.[2,3] MV^{2+} is easily reduced to become a monopositive cation radical $MV^{\cdot+}$ whose color is blue, and forms a charge-transfer (CT) complex with a donor. Although some of our previous clathrates showed a color change from colorless to blue on UV irradiation, the formation of a CT complex in the clathrates was not confirmed clearly.[1] In this study we have newly synthesized nine polycyano–polycadmate host clathrates including a CT complex of MV^{2+} and an aromatic molecule, and have determined one crystal structure.

The polycyano–polycadmate host is a Cd cyano complex of chemical formula $[Cd_x(CN)_y]^{2x-y}$. The cyano group links two Cd atoms to from a framework host structure. Two typical structure types of the host are known.[4] One is a zeolite-like structure, which has a 3-D framework host while the other is a clay-like structure, which is a layered structure of 2-D Cd cyano complexes. Another important feature of the host complex is that it is anionic. Therefore, the polycyano–polycadmate host clathrate has a cationic guest that neutralizes the negative charge of the host, and a neutral guest that is an ordinary neutral organic molecule. Depending on the combination of the cationic guest and the neutral guest, the formation of a wide variation of clathrates is possible.[5] In this study, we attempted to form a CT complex of MV^{2+} (a cationic guest) and a donor (a neutral guest) in a polycyano–polycadmate host.

The synthetic procedure was as follows: into water (50 cm^3), $K_2Cd(CN)_4$ (5 mmol, 1.47 g), $CdCl_2{\cdot}2.5H_2O$ (5 mmol, 1.14 g) and methylviologen dichloride (2 mmol, 0.50 g) were dissolved. After the solution was filtered, a neutral guest solution was poured onto the filtrate. Various aromatic compounds were tried as neutral guests diluted 1–50 times with *n*-propylbenzene and the mixture left at 277 K. After several days, colored clathrates were obtained in a crystalline or a powdered state. The presence of a polycyano–polycadmate host, MV^{2+} and a neutral guest was confirmed by IR spectroscopy. The new clathrates and their absorption maximum wavelengths as determined from UV–VIS diffuse reflectance spectra are listed in Table 1.

Among the clathrates, the crystal structure of the MV^{2+}–mesitylene clathrate **1** was determined by single crystal X-ray diffraction.[6] The host Cd complex of **1**, $[Cd_3(CN)_6Cl_2]^{2-}$, contains two chloride ions together with cyano groups. Each cyano group bridges Cd atoms to form a 3-D framework structure, and each chloride ion coordinates to each Cd atom [Fig. 1(a)]. The host structure of **1** can be classified as a zeolite-like structure, but its framework structure is new. Although the host is a 3-D framework, the cavity formed within has a 1-D channel-like structure running along the *b* axis of the crystal. Each chloride ligand protrudes from the wall of the channel cavity into the inside of the cavity.

One MV^{2+} and one mesitylene molecule are stacked to form a CT complex as shown in Fig. 1(b). The twist angle of the two rings of MV^{2+} is 0°. The molecular plane of MV^{2+} is almost parallel to that of the mesitylene molecule. The center of the aromatic ring of the mesitylene molecule is directed toward one of the N atoms of MV^{2+}. This overlapping arrangement of MV^{2+} and the donor is typical for a π donor.[2,7] The interspacing between MV^{2+} and the mesitylene molecule of 3.30(1) Å[8] is apparently shorter than van der Waals contact of stacked aromatic rings. The diffuse reflectance spectrum of **1** and absorption spectrum of an acetonitrile solution of $MV(PF_6)_2$ and mesitylene are shown in Fig. 2. The CT absorption band of **1** was red-shifted compared with that of the solution. It is considered that the short interspacing contributes to the red-shift. The CT complex lies in the channel cavity, and is related to neighboring CT complexes by a two-fold screw axis parallel to the *b* axis. The molecular planes of MV^{2+} and the mesitylene molecule are parallel to the two-fold screw axis, so that the CT complexes are not stacked mutually. The two chloride ligands are located near the reverse side of the MV^{2+} molecular plane that is in contact with the mesitylene molecule. The distances between MV^{2+} and the chloride ligands are 3.256(5) Å for Cl(1) and 3.841(6) Å for Cl(2^{I}).[9] This structural situation may suggest the existence of an interaction between MV^{2+} and the host Cd complex through the chloride ligands. The CT interaction between MV^{2+} and chloride ion in solution and in the solid state has been established,[10] and the existence of a host–acceptor(MV^{2+})–donor triad interaction was recently shown for a zeolite including an MV^{2+} CT complex.[11]

For *n*-propylbenzene, 1,2,3-trimethylbenzene, 1,2,4-trimethylbenzene, 1,2,4,5-tetramethylbenzene, pentamethylbenzene, hexamethylbenzene, naphthalene or anthracene as neutral guests, no clathrates was obtained. Considering their ionization

Table 1 Polycyano–polycadmate host clathrates including a MV^{2+}-donor CT complex

Neutral guest(donor)	Color	λ_{max}/nm
Ethylbenzene	Slightly yellow	400
Mesitylene	Yellow	420
Anisole	Orange	446
Phenol	Yellow	411
o-Cresol	Orange	424
m-Cresol	Yellow	406
p-Cresol	Orange	424
Aniline	Red	443
Pyrrole	Yellow	432

λ_{max} = wavelength at the maximum of diffuse reflectance spectrum.

 DOI: 10.1039/b102076p

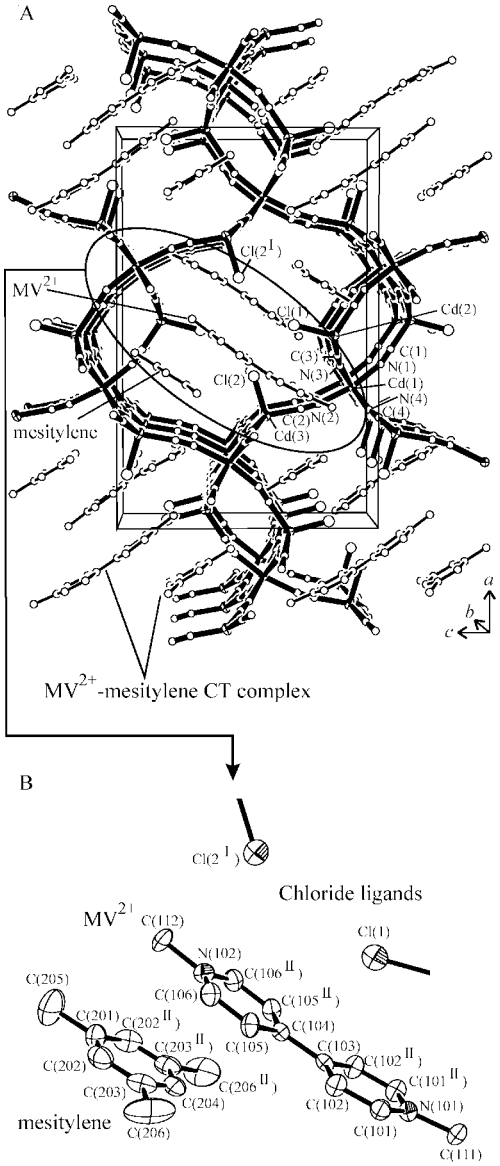

Fig. 1 (A) A perspective view of $[MV^{2+}][Cd_3(CN)_6Cl_2^{2-}]\cdot C_6H_3(CH_3)_3$ **1** along the *b* axis. (B) Crystal structure around the MV^{2+}–mesitylene CT complex of **1**. Selected interatomic distances (Å): Cl(1)···C(103) 3.37(1), Cl(1)···C(104) 3.51(1), Cl(2^{I})···N(102) 3.79(1) (I = $-x + 1$, $y - 1/2$, $-z + 1$), Cl(2^{I})···C(112) 3.77(1), N(102)···C(201) 3.84(1), N(102)···C(202) 3.78(1), N(102)···C(203) 3.59(1), N(102)···C(204) 3.47(2).

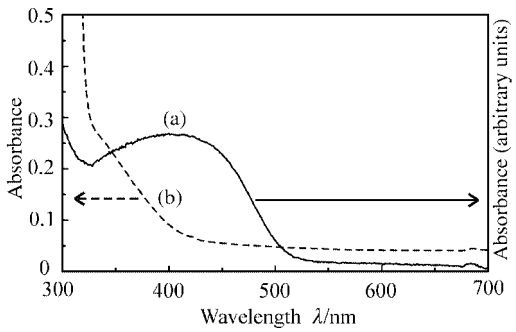

Fig. 2 Diffuse reflectance spectrum of **1** (a) and absorption spectrum of a $MV(PF_6)_2$ (0.03 M) and mesitylene (0.03 M) acetonitrile solution (b).

potentials relative to that for mesitylene, the formation of complexes might be expected for some of them. However, they are less symmetrical or larger than mesitylene. As such, crystal packing and a limitation of inclusion ability of the polycyano–polycadmate host are considered. The cavity that the host must prepare for a CT complex with MV^{2+} and a neutral guest is very large. In our preparative experiments, mesitylene is the most symmetrical and largest clathrate forming molecule (Table 1).

In summary, it has been revealed that the polycyano–polycadmate host acts as a host for a MV^{2+} CT complex, and the presence of an interaction between MV^{2+} and the host is suggested. Considering the structural variety of the polycyano–polycadmate host clathrate,[4,5] it is expected that the host structure of the new clathrates depends on the neutral guest. Structure determinations of the other clathrates are now in progress. At the same time, the preparation of single crystalline samples suitable for spectroscopic experiments are in progress. Although intensive studies of MV^{2+} CT complexes confined in a solid state matrix have been carried out,[11,12] there have been few examples in which crystal structures have been clarified. Structural and spectroscopic data obtained from single crystals are useful for developing studies in this field. In this regard our clathrates have an advantage.

Notes and references

1 H. Yoshikawa and S. Nishikiori, *Chem. Lett.*, 2000, 142.

2 P. M. S. Monk, *The Viologens: Physicochemical Properties, Synthesis and Applications of the Salts of 4,4′-Bipyridine*, John Wiley & Sons, New York, 1998.

3 C. L. Bird, *Chem. Soc. Rev.*, 1981, **10**, 49; W. Sliwa, B. Bachowska and N. Zelichowicz, *Heterocycles*, 1991, **32**, 2241; K. B. Yoon, *Chem. Rev.*, 1993, **93**, 321 and references therein.

4 T. Kitazawa, S. Nishikiori, R. Kuroda and T. Iwamoto, *Chem. Lett.*, 1988, 459; T. Kitazawa, S. Nishikiori, R. Kuroda and T. Iwamoto, *Chem. Lett.*, 1988, 1729; T. Kitazawa, S. Nishikiori and T. Iwamoto, *J. Chem. Soc., Dalton Trans.*, 1994, 3695; T. Kitazawa, S. Nishikiori and T. Iwamoto, *Mater. Sci. Forum*, 1992, **91**–**93**, 257.

5 B. F. Hoskins and R. Robson, *J. Am. Chem. Soc.*, 1990, **112**, 1546; B. F. Abraham, B. F. Hoskins, J. Lui and R. Robson, *J. Am. Chem. Soc.*, 1991, **113**, 3045; T. Iwamoto, in *Comprehensive Supramolecular Chemistry*, ed. D. D. MacNicol, F. Toda and R. Bishop, Oxford, 1996, vol. 6, ch. 19, pp. 643–690; T. Iwamoto, *J. Inclusion Phenom. Mol. Recognit. Chem.*, 1996, **24**, 61; T. Iwamoto, S. Nishikiori, T. Kitazawa and H. Yuge, *J. Chem. Soc., Dalton Trans.*, 1997, 4127 and references therein.

6 *Crystal data* for $[MV^{2+}][Cd_3(CN)_6Cl_2^{2-}]\cdot C_6H_3(CH_3)_3$ **1**: $C_{27}H_{26}N_8Cl_2Cd_3$, M = 870.7, orthorhombic, space group *Pnma* (no. 62), a = 23.7905(7), b = 8.8535(2), c = 15.5522(4) Å, U = 3275.8(2) Å^3, T = 293 K, Z = 4, μ(Mo-Kα) = 21.08 cm^{-1}, 21797 reflections measured, 3952 unique, $R(F)$ = 0.0564 and $R_w(F^2)$ = 0.1133 for 2739 used reflections with $I > 3\sigma(I)$. CCDC reference number 160670. See http://www.rsc.org/suppdata/cc/b1/b102076p/ for crystallographic data in CIF or other electronic format.

7 C. K. Prout and J. D. Wright, *Angew. Chim., Int. Ed. Engl.*, 1968, **7**, 659.

8 The distance between the least squares mean plane of MV^{2+} [C(101), C(101^{II}), C(102), C(102^{II}), C(103), C(104), C(105), C(105^{II}), C(106), C(106^{II}), N(101), N(102), II = x, $-y + 1/2$, z] and the center of the aromatic ring of the mesitylene molecule.

9 The distance between the least squares mean plane of MV^{2+} and the chloride ligand [Cl(1) or Cl(2^{I}), I = $-x + 1$, $y - 1/2$, $-z + 1$].

10 J. H. Russell and S. C. Wallwork, *Acta Crystallogr., Sect. B*, 1972, **28**, 1527; S. G. Bertolotti, J. J. Cosa, H. E. Gsponer and C. M. Previtail, *Can. J. Chem.*, 1987, **65**, 2425; P. M. S. Monk and N. M. Hodgkinson, *Electrochim. Acta*, 1998, **43**, 245.

11 Y. S. Park, S. Y. Um and K. B. Yoon, *J. Am. Chem. Soc.*, 1999, **121**, 3193; S. Hashimoto, *Tetrahedron*, 2000, **56**, 6957.

12 K. B. Yoon and J. K. Kochi, *J. Am. Chem. Soc.*, 1988, **110**, 6586; K. B. Yoon and J. K. Kochi, *J. Am. Chem. Soc.*, 1989, **111**, 1128; K. B. Yoon and J. K. Kochi, *J. Phys. Chem.*, 1991, **95**, 3780; K. B. Yoon, T. J. Huh, D. R. Corbin and J. K. Kochi, *J. Phys. Chem.*, 1993, **97**, 6492; B. Xiang and L. Kevan, *J. Phys. Chem.*, 1994, **98**, 5120; K. B. Yoon, T. J. Huh and J. K. Kochi, *J. Phys. Chem.*, 1995, **99**, 7042; Y. Mao, N. E. Breen and J. K. Thomas, *J. Phys. Chem.*, 1995, **99**, 9909; K. B. Yoon, Y. S. Park and J. K. Kochi, *J. Am. Chem. Soc.*, 1996, **118**, 12 710.

CHEMCOMM
Communication
www.rsc.org/chemcomm

TEMPO: a novel chameleonic ligand for s-block metal amide chemistry†

Glenn C. Forbes, Alan R. Kennedy, Robert E. Mulvey* and Philip J. A. Rodger

Department of Pure and Applied Chemistry, University of Strathclyde, Glasgow, UK G1 1XL. E-mail: R.E.Mulvey@strath.ac.uk

Received (in Cambridge, UK) 5th June 2001, Accepted 22nd June 2001
First published as an Advance Article on the web 12th July 2001

The first structurally characterised examples of the nitroxide TEMPO acting as a ligand towards Li, Na or Mg are described, through a series of hexamethyldisilazide complexes which reveals a remarkable breadth of variety in structure and in the mode of ligation.

TEMPO (2,2,6,6-tetramethyl-1-piperidinyloxy) is a molecule which attracts a phenomenal level of interest. A stable nitroxide free radical, it is utilised within a remarkably diverse assortment of areas. A key ingredient in the development of 'living' free radical polymerisations,[1] it is employed also as a spin label in the study of biological systems.[2] Often the reagent of choice for effecting the mild and selective oxidation of primary and secondary alcohols,[3] TEMPO also finds utility as a radical trapping agent.[4] It is also well established as a Lewis base in d-block coordination chemistry,[5] with crystal structures known where it binds to Co, Cu, Mn, Mo or Pd atoms. Surprisingly, however, the s-block group of metals has hitherto been a virgin territory for TEMPO in this regard.[6] Here this situation is redressed with the disclosure of the first reported TEMPO complexes of Li, Na, Mg or Zn. This series establishes that TEMPO is a versatile new ligand for these electropositive metal atoms, offering more flexibility in its modes of ligation and electronic structures than the conventional O-based donor molecules usually encountered in s-block chemistry.

To minimise the number of variables that could influence structure, the study was confined to 1,1,1,3,3,3-hexamethyldisilazide [HMDS, $(Me_3Si)_2N^-$] derivatives and reactions were carried out in the same bulk solvent (hexane). Hence the predominant discriminating factor in the structures obtained would be the particular metal cation/TEMPO combination/s used. Furthermore since this was explicitly a structural study, product yields were not optimised as the immediate aim was to perfect crystals of a quality suitable for X-ray crystallographic study. As revealed in Scheme 1, five crystalline products **1**–**5** were successfully obtained using this approach. This scheme also lists the components of each reaction mixture studied. The details of the synthesis of **3** serve to illustrate the similar methodology used for each new complex: under argon gas in a Schlenk tube, a 1:1 mixture of crystalline LiHMDS and TEMPO was dissolved in hexane and stirred at ambient temperature for one day, from which orange crystals of [{Li(μ-HMDS)·TEMPO}$_2$] **2** were isolated; these crystals were then mixed with an equimolar amount of crystalline $Mg(HMDS)_2$ and redissolved in warm hexane solution which, when surrounded by a hot water Dewar flask and left to cool slowly to ambient temperature, deposited orange–yellow crystals of [{Li_2(μ-HMDS)(μ-TEMPO)·2TEMPO}$^+${$Mg(HMDS)_3$}$^-$] **3**.

X-Ray crystallographic studies have been carried out on all five new complexes. ChemWin representations of their structures are shown in Scheme 1.‡ The structures of the aforementioned **2** and its sodium analogue [{Na(μ-HMDS)·TEMPO}$_2$] **4** warrant only a brief mention here as they belong to a familiar structural type. Filling the terminal coordination site on the alkali metal atom within a planar, dimeric $(MN)_2$ ring, TEMPO is acting here as an orthodox neutral, monodentate O donor molecule in the mould of THF (*cf.* the structure of [{Li(μ-HMDS)·THF}$_2$][7]). The third homometallic structure [{Mg(HMDS)(μ-TEMPO$^-$)}$_2$] **1** (Fig. 1) is also a dimer, but it is as remarkable and unpredictable as the first

† Electronic supplementary information (ESI) available: experimental, synthesis and characterisation data. See http://www.rsc.org/suppdata/cc/b1/b104937m/

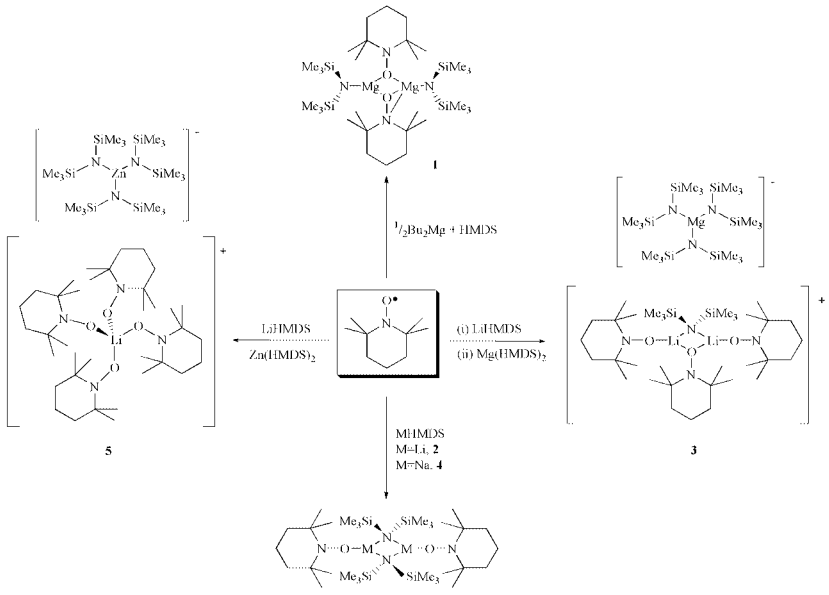

Scheme 1

 DOI: 10.1039/b104937m

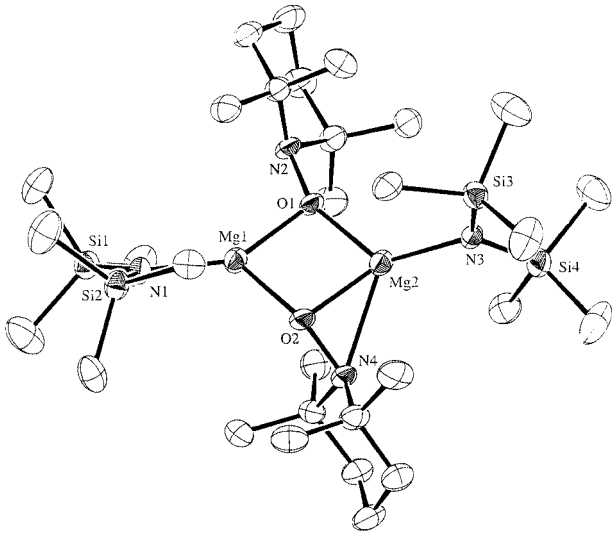

Fig. 1 Molecular structure of **1** without hydrogen atoms. Key dimensions (Å and °): Mg1–O1 1.944(3), Mg1–O2 1.946(3), Mg2-O1 1.967(3), Mg2–O2 1.979(3), Mg1–N1 1.952(3), Mg2–N3 1.965(3), Mg2–N4 2.395(3), O1–Mg1–O2 84.28(10), O1–Mg2-O2 82.80(10), Mg1–O1–Mg2 96.69(11), Mg1–O2–Mg2 96.22(11).

two structures are unremarkable and predictable. First, the positions of its ligands are mutually reversed relative to those in **2** and **4**, with HMDS occupying a terminal site and TEMPO occupying a bridging site. Second, there are two distinct types of TEMPO ligation: one involves a μ_2-O bonding mode through O(1), while the other involves a combination of μ_2-O bonding and η^2-O/N chelation through O(2)/N(4). Third, whereas in **2** and **4** the TEMPO ligands are neutral, free radicals, in **1** they must both be monoanionic (*i.e.*, reduced with respect to normal free TEMPO) to balance the charge of the $[Mg(HMDS)]_2^{2+}$ fragment: thus **1** contains a heteroleptic (anionic) ligand set. Several Lewis base complexes of this Mg bis(amide) have been structurally characterised,[8] but none in which the donor molecule bridges a pair of Mg atoms. TEMPO has therefore changed its ligating role here to be more like that of an anionic O donor such as the aldolate ligand in $[\{Mg(HMDS)[\mu\text{-}OC(Me)Bu^tCH_2C(Bu^t)=O]\}_2]$.[9] Furthermore, there also appears to be no precedent in the library of d-block metal TEMPO complexes for the nitroxide functioning as a μ_2-O donor ligand in either its neutral or anionic form, though the η^2-O/N chelating mode has been observed previously.[5] The dimensions of **1** show that the N–O and Mg–O bond lengths are insensitive to the TEMPO ligating mode with values of 1.461(3) and 1.471(3) Å for the former, and of 1.955 (mean) and 1.979(3) Å for the latter, for the monodentate O and didentate O/N types, respectively. There is significantly more discrimination between these bridging anionic ligands and the terminal radical type found in **2** and **4** in both N–O bond lengths (mean values: in **2**, 1.279 Å; in **4**, 1.275 Å) and the geometry of the N atom {sum of bond angles (mean): in **1**, 333.5° [discounting those involving Mg(2)]; in **2**, 357.9°; in **4**, 356.4°}. This ability of the N atom to oscillate between a highly pyramidal and a planar geometry is one important factor in TEMPO's coordinative flexibility. Yet another variation is revealed in the first heterometallic structure, **3**. Here, TEMPO acts simultaneously as a bridging and terminal ligand within an unusual dinuclear asymmetrical cation $[\{Li_2(\mu\text{-}HMDS)(\mu\text{-}TEMPO)\cdot 2TEMPO\}^+]$ (Fig. 2). Its Li–O bond lengths [(mean): bridging, 1.969 Å; terminal, 1.816 Å] are in accord with the different coordination numbers involved, but again the N–O bond lengths [bridging, 1.301(3) Å; (mean) terminal, 1.284 Å] appear rather insensitive to such differences. However, the N(5) atom of the bridging TEMPO ligand adopts a near-planar geometry (sum of bond angles, 357.8°) in contrast to the highly pyramidalised geometries of its bridging counterparts in **1**: hence the major discriminating factor is the electronic nature of the N–O unit (*i.e.*, free radical or anionic). The other half of the discrete ion pair structure of **3**, $[\{Mg(HMDS)_3\}^-]$, is

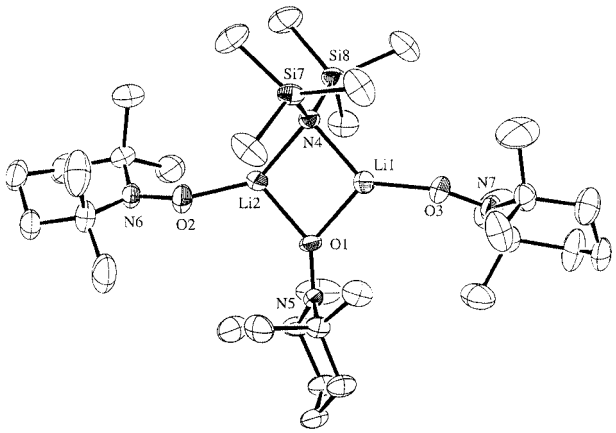

Fig. 2 The cationic moiety of **3** without hydrogen atoms. Key dimensions (Å and °): Li1–O1 1.982(6), Li1–O3 1.812(6), Li2–O1 1.957(6), Li2–O2 1.821(6), Li1–N4 1.993(6), Li2–N4 1.951(6), Li1–O1–Li2 83.0(2), Li1–N4–Li2 82.8(2), O1–Li1–N4 96.0(3), N4–Li2-O1 98.2(3).

also special. Examples are known where this metallate species is tethered to Li as in $[pyr\cdot Li(\mu\text{-}HMDS)_2Mg(HMDS)]$,[10] but this discrete arrangement is unprecedented. This comparison highlights the effectiveness of TEMPO relative to even strong donors such as pyridine. A more emphatic demonstration of this point is provided by the final structure, $[(Li\cdot 4TEMPO)^+\{Zn(HMDS)_3\}^-]$ **5**. Substituting Zn for Mg takes place with retention of the trigonal planar anionic moiety, but surprisingly the cationic moiety changes to a simple mononuclear arrangement with Li tetrahedrally surrounded by TEMPO radicals. Here the four TEMPO ligands co-operate to sequester a Li^+ cation and separate it from the anionic moiety.

In conclusion, using a single amido system as a case study, TEMPO has been established as a promising versatile new ligand for the s-block metals.

We thank the University of Strathclyde (Faculty Studentship to P. J. A. R.) and the EPSRC (grant award no. GR/M78113) for financial support, and Dr P. A. G. Cormack for helpful discussions.

Notes and references

‡ CCDC reference numbers 160882–160886. See http://www.rsc.org/suppdata/cc/b1/b104937m/ for crystallographic data in CIF or other electronic format.

1 E. E. Malmström and C. J. Hawker, *Macromol. Chem. Phys.*, 1998, **199**, 923.
2 S. S. Eaton and G. R. Eaton, *Coord. Chem. Rev.*, 1978, **26**, 207.
3 A. E. J. de Nooy, A. C. Besemer and H. v. Bekkum, *Synthesis*, 1996, 1153.
4 L. M. Lawrence and G. M. Whitesides, *J. Am. Chem. Soc.*, 1980, **102**, 2493.
5 For pertinent examples see: M. H. Dickman and R. J. Doedens, *Inorg. Chem.*, 1982, **21**, 682; J. Laugier, J.-M. Latour, A. Caneschi and P. Rey, *Inorg. Chem.*, 1991, **30**, 4474.
6 There is one structure known containing sodium and derived from 4-carboxy-TEMPO, though this is formally a carboxylate salt with a CO_2Na function. See: A. Misiolek, R. Huang, B. Kahr and J. E. Jackson, *Chem. Commun.*, 1996, 2119.
7 L. M. Engelhardt, B. S. Jolly, P. C. Junk, C. L. Raston, B. W. Skelton and A. H. White, *Aust. J. Chem.*, 1986, **39**, 1337; H. Mack, G. Frenzen, M. Bendikov and M. S. Eisen, *J. Organomet. Chem.*, 1997, **549**, 39.
8 For example, see: D. C. Bradley, M. B. Hursthouse, A. A. Ibrahim, A. M. Abdul, R. Motevalli, R. Moseler, H. Powell, J. D. Runnacles and A. C. Sullivan, *Polyhedron*, 1990, **9**, 2459.
9 J. F. Allan, K. W. Henderson and A. R. Kennedy, *Chem. Commun.*, 1999, 1325.
10 G. C. Forbes, A. R. Kennedy, R. E. Mulvey, P. J. A. Rodger and R. B. Rowlings, *J. Chem. Soc., Dalton Trans.*, 2001, 1477.

CHEMCOMM
Communication
www.rsc.org/chemcomm

Carbon dioxide thermal system: an effective method for the reduction of carbon dioxide

Q. Chen*[ab] and Y. Qian[c]

[a] *Structure Research Laboratory, University of Science & Technology of China (USTC), Hefei 230026, P.R. China. E-mail: cqw@ustc.edu.cn*
[b] *Department of Materials & Engineering, USTC, Hefei 230026, P.R. China*
[c] *Department of Chemistry, USTC, Hefei 230026, P.R. China*

Received (in Cambridge, UK) 4th January 2001, Accepted 19th June 2001
First published as an Advance Article on the web 12th July 2001

When carbon dioxide is in the supercritical state and reduced by Fe_3O_4, multicarbon bearing hydrocarbon molecules such as phenol (rather than CO or formate usually formed in electrochemical or photochemical techniques) can be obtained, the reduction yield is improved remarkably and the transformation yield for CO_2 to phenol can reach 7.6%.

The reduction of carbon dioxide has been extensively studied using electrochemical[1,2] and photochemical[3–5] reactions in light of the problems of global warming and depletion of fossil fuels.[6–8] Results obtained are still not satisfactory as to useful valuable reaction products and reaction rates need to be further improved. In addition the detailed reduction mechanism could not be established in most cases. At present, much interest has focused on the use of 14-membered transition-metal microcycles in CO_2 electrochemical reduction,[9–12] however, the catalysis efficiency for these transition-metal complexes is poor and the catalyst is rapidly destroyed by hydrogenation and/or carboxylation of the microcycles.[13] On the other hand, although research to optimise the reaction products is active, multicarbon containing hydrocarbon molecules such as products containing benzene rings have never been obtained. CO is often the main reduction product while formate may also be formed depending on the reaction condition.[9,14] Photochemical CO_2 reduction has been carried out in a catalytic system using $Ru(bpy)_3^{2+}$ as the sensitizer, cobalt or nickel macrocycles as the electron relay catalysts, and ascorbate as the sacrificial reductive quencher.[3,4] These systems, however, also produce CO. Furthermore, the rate of CO_2 reduction is limited by the low mass transfer of CO_2 both in electrochemical and photochemical techniques. Hence, the conversion of CO_2 to useful products by a simple effective method is clearly an interesting and important topic in CO_2 chemistry. Here we report that, when CO_2 is in the supercritical state and reduced with Fe_3O_4 powder, it can be transformed to phenol and diphenyl ether. In some cases, we can obtain ethanol, acetaldehyde and acetic acid. This novel reduction method could allow studies of continuous reduction systems for practical industrial applications.

An autoclave (flexible Au/Ti) capable of heating the system up to 400 °C was used. A sufficient amount of solid CO_2, freshly made from high purity CO_2 gas (99+%), was placed in an autoclave to ensure that the CO_2 is in a supercritical state at high temperatures. An appropriate amount of Fe_3O_4 (chemical purity reagent) and a small amount of water obtained from the Milli-Q water purification system were placed into the autoclave (50 ml), which was heated to 100–350 °C for 1–3 h and then rapidly cooled to room temperature naturally. The vapor phase was sampled and analyzed by GC–MS, (Shimadzu, GC-MS-QP-1100EX) to detect hydrocarbons. An appropriate amount of water was placed into the autoclave, then the product was collected, and filtered. After filtration, the filtrate was analyzed by GC–MS and quantified by gas chromatography (GC), while solid products were examined by X-ray diffraction (XRD). A gas chromatograph with a flame ionization detector (GC/FID) (Ohkura, GC-202 with Porapak R column packing) was used to determine the content of the hydrocarbon molecules formed.

A typical reaction used 8.0 g CO_2, 22 g Fe_3O_4 and 0.5 ml H_2O, in which CO_2 was in excess for the oxidation of Fe^{2+} in Fe_3O_4, to ensure a high pressure in the system when it was heated to appropriate temperatures. It was found that the degree of transformation in carbon dioxide reduction increases with increasing temperature and time, and reaches a maximum value after 2.5 h treatment, then remains nearly constant. The total yield of ethanol and acetic acid was around 4.2% (mol ratio) when the reaction was carried out at 200 °C for 2.5 h and was decreased with an increase of temperature and the amount of H_2O included. However, temperatures higher than 300 °C yielded aromatic compounds with phenol and diphenyl ether being the main products with ethanol, acetic acid and acetaldehyde also present. Fig. 1(a) depicts the mass spectrum of standard phenol while that of phenol formed in the experiment

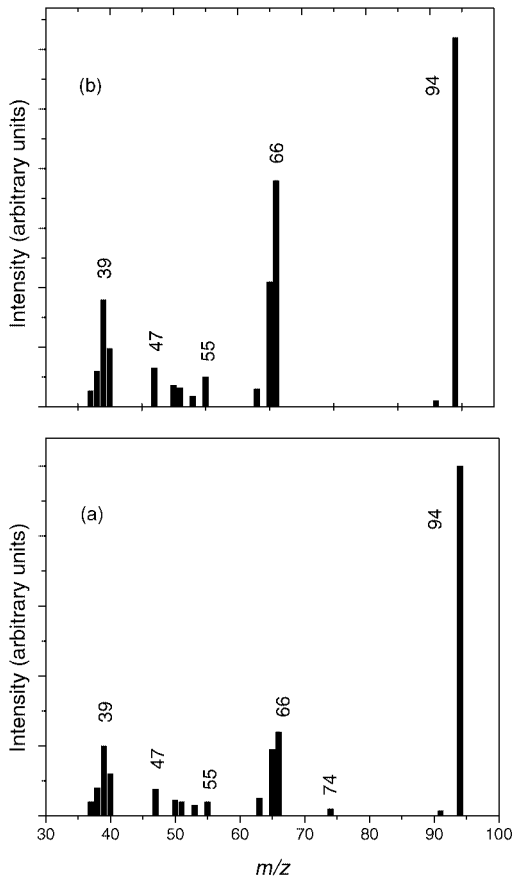

Fig. 1 Mass spectrum of phenol: (a) standard sample, (b) phenol formed *via* CO_2 reduction.

 DOI: 10.1039/b100183n

is shown in Fig. 1(b). The peak at *m*/*z* 94 in Fig. 1 is assigned to the molecular ion, $C_6H_6O^+$. Almost all of the corresponding peaks in Fig. 1(a) and (b) appear at the same positions, indicating that phenol formed in the reaction. On the basis of this result, the formation of diphenyl ether in the present system can be rationalized in terms of phenol production in the carbon dioxide thermal reduction system. Crystals of phenol can be obtained by slowly heating the aqueous filtrate. A scanning electron microscope image of the sample shows the sample consists of typical grains with size 0.2 × 0.3 mm (not shown). The total yield of phenol was nearly 7.6%. The GC–MS spectrum (not shown) shows no detectable organic compounds in the starting CO_2 gas ruling out contamination in the starting material. GC analysis showed ethane, propane and isobutane, were the main products in the vapor phase, while no CO in the vapor phase or formic acid in aqueous solution was detected (the main products in electrochemical and photochemical reduction techniques). These results indicate that the mechanism of the reduction in our reaction is different from that for an electrochemical reduction process. Carbon dioxide is a low-energy molecule, with the standard potential of the $CO/CO_2^{\cdot -}$ couple in an aprotic solvent such as *N*,*N*′-dimethylformamide (DMF) containing a non ion-pairing counter cation (NEt_4^+), being as negative as −2.2 V *vs.* SCE.[13] The potential for the Fe^{3+}/Fe^{2+} redox couple is not as negative as that for the CO_2 reduction to $CO_2^{\cdot}$ anion radical. Hence reduction most probably occurs on the surface of Fe_3O_4 particles, and a surface-mediated process may be involved. The XRD pattern of the solid product shows the coexistence of Fe_2O_3 and Fe_3O_4. This is possibly due to the surface layer of Fe_3O_4 being oxidized by carbon dioxide. Furthermore, hydrocarbon molecules containing more than one carbon atom are the products, suggesting that the mechanism of this reaction could involve multielectron reductive coupling of a pair of or several carbonyls to produce an intermediate bound to the surface of the solid Fe_3O_4 particles (at Fe^{II} sites). The presence of a small amount of water is required in this reaction system as this is the source of hydrogen. Too much water, however, is unfavorable for the reduction of carbon dioxide. It has also been found that the transformation ratio increases with a decrease of Fe_3O_4 particle size, which suggests the Fe_3O_4 surface area seems to have an influence on the reaction. All these results suggest that adsorption, formation of intermediates and hydrolysis processes are involved in the reaction. More work should be carried out to establish the reduction mechanism more fully.

It is known that the rate of CO_2 reduction is limited by the low mass transfer of CO_2 both in electrochemical and photochemical techniques. Under supercritical conditions, the polarity of CO_2 can be changed by controlling its density, the dielectric constant of CO_2 ranging from 1 to 1.6.[15] The increased polarity in a high pressure system is favorable for CO_2 absorption on the surface of Fe_3O_4 particles, and may accelerate the electron transfer from Fe^{II} ions to an intermediate due to the changed adsorption energy level in the energy gap of Fe_3O_4 semiconductor. Further details about the mechanism will be discussed later. The most significant feature is that the reductant used for CO_2 reduction is easily obtained and this reaction can be performed in a continuous autoclave, which could lead to practical applications.

In conclusion, we have reported, for the first time, the reduction of carbon dioxide in the supercritical state. Valuable products such as ethanol, acetaldehyde, acetic acid and, especially, phenol can be obtained. The maximum transformation ratio for CO_2 to phenol was found to be as high as 7.6% at temperatures > 300 °C. The reduction is suggested to occur on the surface of the Fe_3O_4 particles and to occur *via* a multielectron reductive coupling of a pair of or several carbonyls to produce an intermediate. This might open a route for industrial reduction of CO_2, which previously was only viable *via* an electrochemical technique.

Notes and references

1 J. L. Roberts and D. T. Sawyer, *J. Electroanal. Chem.*, 1965, **9**, 1.
2 P. G. Russel, N. Novac, S. Srinivasan and M. Sterrinberg, *J. Electrochem. Soc.*, 1977, **124**, 1329.
3 J. L. Grant, K. Goswami, L. O. Spreer, J. W. Otvos and M. Calvin, *J. Chem. Soc., Dalton Trans.*, 1987, 2105.
4 C. A. Craig, L. O. Spreer, J. W. Otvos and M. Calvin, *J. Phys. Chem.*, 1990, **94**, 7957.
5 G. M. Brown, B. S. Brunschwing, C. Creutz, J. F. Endicott and N. Sutin, *J. Am. Chem. Soc.*, 1979, **101**, 1298.
6 T. Inone, A. Fujishima, S. Konishi and K. Honda, *Nature*, 1979, **277**, 637.
7 P. G. Jessop, T. Ikariya and R. Nayori, *Nature*, 1994, **368**, 231.
8 K. R. Thampi, J. Kiwi and M. Gratzel, *Nature*, 1987, **327**, 506.
9 B. Fisher and R. Eisenberg, *J. Am. Chem. Soc.*, 1980, **102**, 7361.
10 G. B. Balazs and F. C. Anson, *J. Electroanal. Chem.*, 1992, **322**, 325.
11 M. H. Schmidt, G. M. Miskelly and N. S. Lewis, *J. Am. Chem. Soc.*, 1990, **112**, 3420.
12 C. A. Kelly, Q. G. Mulazzani, M. Venturi, E. L. Blinn and M. A. Rodgers, *J. Am. Chem. Soc.*, 1995, **117**, 4911.
13 I. Bhugun, D. Lexa and J.-M. Saveant, *J. Phys. Chem.*, 1996, **100**, 19 981.
14 T. Ogata, S. Yanagida, B. S. Brunschwig and E. Fujita, *J. Am. Chem. Soc.*, 1995, **117**, 6708.
15 B. D. Drake and R. L. Smith, Jr., *J. Supercrit. Fluids*, 1990, **3**, 162.

CHEMCOMM Communication
www.rsc.org/chemcomm

Hydrocarbon reaction pathway in selective NO reduction over a bifunctional SnO_2/Al_2O_3 catalyst

Jong-H Lee, Alex Yezerets, Mayfair C. Kung* and Harold H. Kung*

Department of Chemical Engineering, Northwestern University, Evanston, IL 60208-3120, USA. E-mail: m-kung@northwestern.edu; hkung@northwestern.edu

Received (in Cambridge, UK) 25th May 2001, Accepted 20th June 2001
First published as an Advance Article on the web 12th July 2001

Propene reduction of NO on SnO_2/γ-Al_2O_3 proceeds *via* the formation of acrolein and acetaldehyde, and the latter reduces NO_x to N_2 over Al_2O_3.

Catalytic reduction of nitric oxide (NO) from the exhaust of a lean-burn engine, which contains only a very low concentration (500 ppm level) of NO_x but much higher concentrations of oxygen (5–10%) and water (10–15%), has been a great challenge. Zeolite-supported catalysts are among the most promising known using a hydrocarbon reductant, but they lack the necessary durability because of hydrothermal degradation.[1] Alumina-based catalysts are more hydrothermally stable. Recently, they have shown promising activities for this reaction (*e.g.* refs. 2 and 3), especially under conditions of higher temperatures and partial pressures of oxygen that are suitable for treating heavy duty diesel engine or lean-burn gasoline engine exhausts. Nonetheless, higher activities are still very desirable for a practical catalyst, as well as a broader temperature window.

Understanding the reaction mechanism could facilitate improvement of these catalytic systems. On zeolite-based catalysts, a commonly observed first step of the reaction is the oxidation of NO to NO_2, which is a strong oxidant that activates the hydrocarbon.[4–7] However, the steps beyond that are not known. Various surface intermediates have been detected, and their involvement in the reaction implicated, such as organic nitro compounds,[8,9] isocyanate and nitrile,[10–12] and oxime,[13] but the steps leading to their formation and further reaction remain mostly speculative. As for alumina-supported catalysts, it is known that alumina itself is active for hydrocarbon reduction of NO,[14] and especially for NO_2,[2] but relatively inactive for NO oxidation to NO_2.[15] Various surface species are detected by IR spectroscopy in the reduction reaction, including nitrate, isocyanate, nitrile or cyanide.[16–18]

We have recently discovered that SnO_2/γ-Al_2O_3 is a bifunctional catalyst.[3,19,20] Using a standard reaction feed mixture of 0.1% propene, 0.1% NO, 10% H_2O and 15% O_2, it was found that a mixture of SnO_2/SiO_2 and γ-Al_2O_3 was as effective in reducing NO_x as an active SnO_2/γ-Al_2O_3 catalyst, while SnO_2/SiO_2 was completely unable to produce N_2.[20] In addition, the mixture of SnO_2/SiO_2 and γ-Al_2O_3 was only effective if SnO_2/SiO_2 was positioned upstream of Al_2O_3 and not *vice versa*. Since the NO_2 concentration at the exit of a reactor containing SnO_2/SiO_2 was the same as the background level within experimental uncertainty. Thus oxidizing NO to NO_2 is not the function of SnO_2. Therefore, this system provides a new opportunity to elucidate the hydrocarbon reaction pathway, which is the subject of this report.

When 0.1 g of SnO_2/SiO_2 was placed in a separate reactor upstream of 0.1 g γ-Al_2O_3, it was found that no N_2 was detected at the exit of the SnO_2/SiO_2 reactor, even when the propene conversion was 40%. Instead, a significant concentration of acrolein (C_3H_4O, *ca.* 120 ppm) and some acetaldehyde (CH_3CHO, *ca.* 40 ppm) were detected. Thus, the function of SnO_2 was selective oxidation of propene, primarily to acrolein. Removing NO from the reaction feed did not change the yield of acrolein. Thus, this selective oxidation step utilizes molecular oxygen as the oxidant.

Isotope labeling provides additional information. When 0.1% ^{13}C-prop-2-ene (99% purity) was used as the reductant, and the reaction feed mixture was passed over SnO_2/SiO_2, only 2-^{13}C-labeled acrolein was detected. This was similar to the results obtained using a Bi–Mo–O catalyst. Thus, the oxidation reaction proceeds *via* a symmetric π-allyl intermediate commonly observed in selective oxidation of propene [eqn. (1)].

$$CH_2{=}C^*H{-}CH_3 \xrightarrow[SnO_2]{O_2} CH_2{-}C^*H{-}CH_2 \xrightarrow[SnO_2]{O_2} CH_2{=}C^*H{-}CHO \quad (1)$$

The selective oxidation product acrolein is transported to γ-Al_2O_3 where its subsequent reaction resulted in the formation of N_2. This reaction was studied by using acrolein as the reductant at a concentration of 160–170 ppm instead of 0.1% propene. The concentrations of various products formed at 475 °C as a function of residence time are shown in Fig. 1. Sometimes, small amounts (< 10 ppm) of HCN could be detected. HCHO (not shown) was also formed but was difficult to quantify because of the high concentration of water used. The data showed that acrolein was rapidly converted to acetaldehyde over γ-Al_2O_3. Interestingly, this reaction was not accompanied by the production of N_2. Further reaction of acetaldehyde was much slower, and N_2 was produced.

This reaction sequence is substantiated by the experiment using acetaldehyde as the reductant instead of acrolein. CO, CO_2 and N_2 were formed, and their concentrations increased with increasing residence time. A large CO to CO_2 ratio was observed, similar to that shown in Fig. 1. Sometimes, trace amounts of HCN were detected.

When 2-^{13}C-labeled acrolein was passed over γ-Al_2O_3 at short residence time, the acetaldehyde in the product consisted of 85% $^{13}CH_3CHO$. Thus, the formation of acetaldehyde from acrolein is by cleavage of the C=C bond. Water is important for this cleavage reaction and the evolution of acetaldehyde from Al_2O_3. When NO reduction by acrolein on γ-Al_2O_3 was repeated but without water in the feed stream, no acetaldehyde was detected in the product. In addition, the N_2 yield dropped to *ca.* 60% of the yield with water. Since at 475 °C, it is unlikely that desorption of acetaldehyde requires displacement by water, the data suggest that the formation of acetaldehyde involves hydrolysis of a surface intermediate.

The following reaction [eqn. (2)] explains the formation of acetaldehyde that is consistent with the observations. It is the

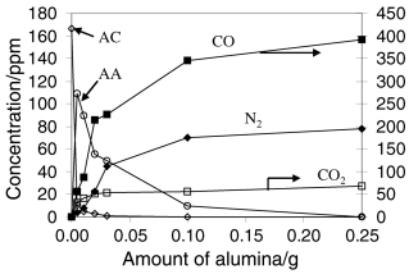

Fig. 1 Product distribution as a function of residence time for the NO_x reduction reaction over γ-Al_2O_3 using *ca.* 160 ppm acrolein. The residence time was changed by using different amounts of γ-Al_2O_3. AA: acetaldehyde, AC: acrolein.

 DOI: 10.1039/b104630f

reverse of an aldol condensation reaction. We postulate that a bridging Al–O–Al is the catalytic site.

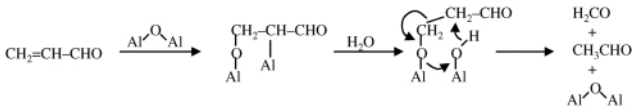

(2)

Thus, the primary hydrocarbon pathway in NO_x reduction for this catalyst system can be summarized in Fig. 2. The interesting features of this mechanism are the role of SnO_2 in the selective oxidation of propene using molecular O_2 and the role of γ-Al_2O_3 in N_2 formation. The reaction of acetaldehyde on alumina probably leads to the formation of surface nitrocompounds, nitrile or cyanide, isocyanate, and eventually N_2. The reactions of nitromethane have been studied over Cu-ZSM-5[9] and Al_2O_3.[16] Over Al_2O_3, nitromethane reacts to form isocyanate, carbamite, and eventually NH_3, the latter then reacts with NO to form N_2. It is quite possible that these steps apply to the system here.

In separate experiments, the reaction of acetaldehyde with O_2 on 0.1 g Al_2O_3 was compared with reaction with NO or NO_2 with and without O_2 under otherwise standard conditions. It was found that the reaction of acetaldehyde with NO alone was slow. Less than 40% of the acetaldehyde was converted. The reaction with a mixture of NO and O_2 was substantially faster and about the same as with only O_2. This is consistent with the low activity for NO oxidation to NO_2 on Al_2O_3.[15] The reaction of acetaldehyde with NO_2 or NO_2 + O_2 was the fastest, such that all the acetaldehyde was consumed. Thus, the initial step in the subsequent reaction of acetaldehyde under our reaction conditions does not involve adsorbed NO_x species. Instead, a possible pathway is its oxidation by oxygen to form adsorbed acetate, which has been observed by others.[21] The acetate decarboxylates in the presence of NO to form nitromethane.

In order to confirm the absence of a significant parallel reaction pathway for acrolein on γ-Al_2O_3, the N_2 production efficiencies of acrolein and acetaldehyde were compared. The results are shown in Fig. 3 for various NO_x/reductant ratios in the feed. Over a wide range of these ratios, the number of N_2 molecules produced for every reductant molecule consumed was independent of the reductant. Thus, the conversion of acrolein to acetaldehyde must be quantitative, and this step does not produce N_2. The N_2 production efficiencies for these two reductants approached the limit of unity, that is, one reductant molecule consumed per N_2 produced, consistent with the reaction mechanism in Fig. 2. Furthermore, the N_2 production efficiencies were higher using NO_2 than NO at low NO_x/reductant ratios.

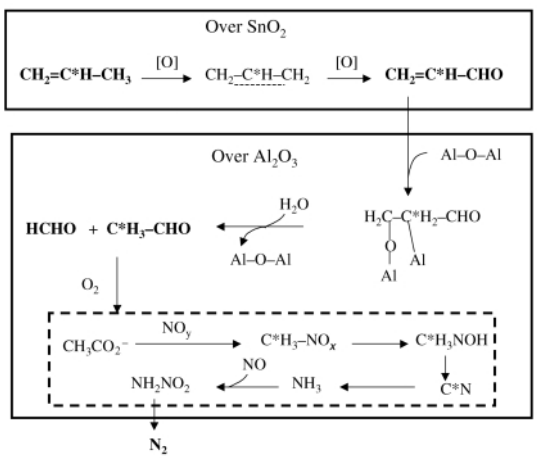

Fig. 2 Proposed mechanism for propene reduction of NO over SnO_2/γ-Al_2O_3. Reactions occurring over the SnO_2 or γ-Al_2O_3 are enclosed by solid lines, and reactions enclosed by dashed lines are formulated using literature information. Compounds in bold letters denote detected gaseous products and the remainder are surface intermediates. C* denotes labeled positions.

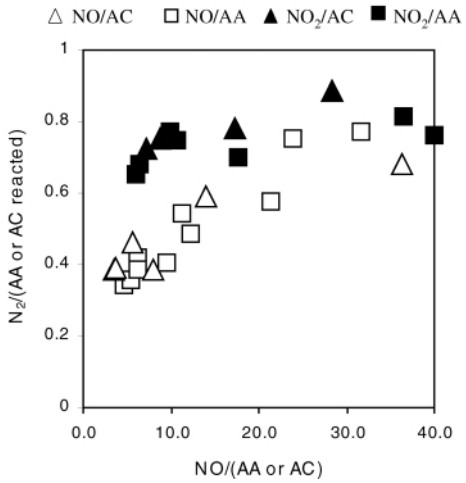

Fig. 3 N_2 formation efficiency, defined as number of molecules of nitrogen formed per acetaldehyde (AA) or acrolein (AC) molecule reacted, as a function of NO_x/reductant ratio in the feed. The NO_x/reductant ratio was changed by varying the concentration of NO (open symbols) or NO_2 (filled symbols) from 703 to 5921 ppm, and the concentration of the organic from 27 to 282 ppm. Standard concentrations of O_2 and H_2O were used, and the total flow rate was 200 ml min^{-1} with 0.1 g of Al_2O_3. The temperature was between 475 and 525 °C to obtain high conversions of the organic.

In summary, we have elucidated a substantial portion of the reaction pathway of the hydrocarbon for propene reduction of NO over SnO_2/γ-Al_2O_3. The slow step of this reaction has been identified to be the reaction of acetaldehyde on alumina. This information can be used to improve the catalytic activities for N_2 formation.

We acknowledge support of this research by the EMSI program of the NSF and the US Department of Energy Office of Science (CHE-9810378) at the Northwestern University Institute of Environmental Catalysis.

Notes and references

1 J. Y. Yan, G.-D. Lei, W. M. H. Sachtler and H. H. Kung, *J. Catal.*, 1996, **161**, 43.
2 K. A. Bethke and H. H. Kung, *J. Catal.*, 1997, **172**, 93.
3 M. C. Kung, P. W. Park, D.-W. Kim and H. H. Kung, *J. Catal.*, 1999, **181**, 1.
4 M. Misono, *CATTECH*, 1998, **4**, 183.
5 E. Kikuchi and K. Yogo, *Catal. Today*, 1994, **22**, 73.
6 Y. Li and J. N. Armor, *J. Catal.*, 1994, **145**, 1.
7 J.-Y. Yan, H. H. Kung, W. M. H. Sachtler and M. C. Kung, *J. Catal.*, 1998, **175**, 294.
8 H. Yasuda, C. Yokoyama and M. Misono, *ACS Symp. Ser.*, 1995, **587**, 110.
9 N. W. Cant, A. D. Cowan, I. O. Y. Liu and A. Satsuma, *Catal. Today*, 1999, **54**, 473.
10 C. Li, K. A. Bethke, H. H. Kung and M. C. Kung, *J. Chem. Soc., Chem. Commun.*, 1995, 813,
11 A. W. Aylor, L. J. Lobree, J. A. Reimer and A. T. Bell, *Stud. Surf. Sci. Catal.*, 1996, **101**, 661.
12 F. Radtke, R. A. Koeppel, E. G. Minardi and A. Baiker, *J. Catal.*, 1997, **167**, 127.
13 B. J. Adelman, T. Beutel, G.-D. Lei and W. M. H. Sachtler, *Catal. Lett.*, 1996, **37**, 125.
14 H. Hamada, *Catal. Today*, 1994, **22**, 21.
15 F. C. Meunier, J. P. Breen and J. R. H. Ross, *Chem. Commun.*, 1999, 259.
16 V. Zuzaniuk, F. C. Meunier and J. R. H. Ross, *Chem. Commun.*, 1999, 815.
17 T. Maunula, J. Ahola and H. Hamada, *Appl. Catal. B. Environmental*, 2000, **26**, 173.
18 S. Kameoka, Y. Ukisu and T. Miyadera, *Phys. Chem. Chem. Phys.*, 2000, **2**, 367.
19 P. W. Park, H. H. Kung, D.-W. Kim and M. C. Kung, *J. Catal.*, 1999, **184**, 440.
20 A. Yezerets, Y. Zheng, P. W. Park, M. C. Kung and H. H. Kung, *Stud. Surf. Sci. Catal.*, 2000, **130**, 629.
21 K. Shimizu, H. Kawabata, A. Satsuma and T. Hattori, *J. Phys. Chem. B*, 1999, **103**, 5240.

CHEMCOMM
Communication
www.rsc.org/chemcomm

Solvent incorporation during *N*-iodosaccharin mediated glycosylation: facile synthesis of acetal linked disaccharides†

M. Aloui and A. J. Fairbanks*

Dyson Perrins Laboratory, Oxford University, South Parks Road, Oxford, UK OX1 3QY. E-mail: antony.fairbanks@chem.ox.ac.uk; Fax: +44 1865 275 674

Received (in Cambridge, UK) 14th May 2001, Accepted 15th June 2001
First published as an Advance Article on the web 12th July 2001

Solvent incorporation between glycosyl donor and acceptor occurs during glycosylation reactions initiated by *N*-iodosaccharin (NISac) performed in acetone and cyclohexanone solvents to stereoselectively produce acetal linked α-glycosides.

Considerable work has been performed to understand the role of solvent during the glycosylation process[1,2] However the situation is complicated by the identity of anomeric leaving group, the activator and the protecting groups on the donor. Therefore although there are several general 'guiding principles' as to how the choice of solvent may affect the stereochemical outcome of glycosylation for donors with non-participating OH-2 protecting groups, there is still requirement for further mechanistic insight into each particular glycosylation reaction.

One of the best-established examples of solvent participation during the glycosylation process is the preferential formation of β-glycoside products observed when using acetonitrile as solvent.[3] This β stereoselectivity has been ascribed to trapping of the glycosyl cation formed during the glycosylation reaction by solvent to produce an intermediate α-nitrilium ion, which then undergoes S_N2 type glycosylation, resulting in preferential formation of the β-product.[4] The isolation of α-nitrilium trapped species has provided substantial supporting evidence for this hypothesis.[5] Reported herein are investigations into glycosylation reactions performed in ketone solvents, in which solvent incorporation invariably occurs to produce good yields of mixed acetal linked α-glycosides and α-disaccharides, in an entirely stereoselective manner.

We recently reported the use of *N*-iodosaccharin (NISac) **1** for the activation of thiophenyl glycosides under mild conditions.[6] During the course of these studies it became clear that reduced yields of disaccharide products were obtained by saccharin trapping of the glycosyl cation, which is probably produced during the glycosylation reaction. In an attempt to promote *O*-glycosylation, and in particular increase yields of disaccharide products, studies turned to the use of more polar solvents. Use of acetonitrile as solvent[7] resulted in an increase in the yield of disaccharides, but saccharin trapping was still observed. For this reason acetone was also investigated as the solvent for glycosylation. Although acetone has frequently been employed as an organic co-solvent for enzyme catalysed glycosylation, it has not been particularly widely used for chemical glycosylation reactions.[8]

Glycosylation of perbenzylated thioglycoside **2** was undertaken with methanol as glycosyl acceptor in acetone with *N*-iodosaccharin (NISac, **1**) as activator. Quite surprisingly none of the desired methyl glycoside was observed, and the sole reaction product was identified as the pure α-glycoside **3** (Scheme 1). Moreover, **3** was produced entirely as the α-anomer. Formation of **3** can be explained by initial formation of the α-acetonium ion **4**, by solvent participation in a manner

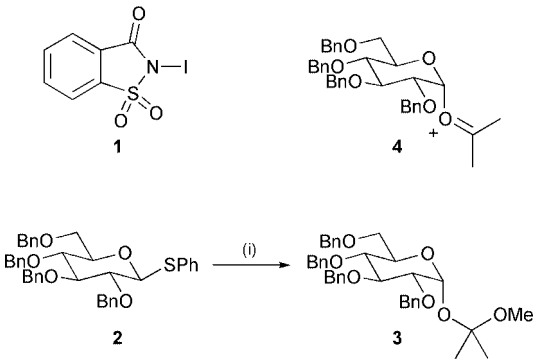

Scheme 1 *Reagents and conditions*: (i) NISac **1**, MeOH (3 equiv.), acetone, −78 to 0 °C, 2.5 h, 76%.

analogous to glycosylation in acetonitrile. Nucleophilic attack on **4** by methanol then yields the mixed acetal. To the best of our knowledge solvent participation by acetone during a glycosylation reaction has only been observed on two previous occasions.[9,10] Investigations then turned to the use of carbohydrates as glycosyl acceptors to investigate if solvent trapping would occur to produce disaccharides linked as mixed acetals. Reaction of thioglycoside **2** with diacetonide galactose **5**, in acetone with NISac activation, produced acetal-linked disaccharide **6** in an excellent 84%, as the pure α-anomer (Scheme 2).‡§ Carbohydrates with secondary hydroxy groups also produced good yields of acetal-linked products. Thus reaction of donor **2** with the *manno* acceptor **7** produced the mixed acetal linked disaccharide **8**, as the pure α-anomer, in 78% yield.

Investigation then turned to the use of other solvents to determine the potential generality of the process. Initial attempted reaction of **2** with methanol and NISac as activator in butanal as an aldehyde solvent produced a complex mixture of products and no appreciable amount of acetal glycoside. However with cyclohexanone as solvent again good yields of pure α-glycoside products were isolated. Thus reaction of donor **2** with methanol in cyclohexanone initiated by NISac produced a good yield of the α-mixed acetal **9** (Scheme 3). Carbohydrate acceptors also reacted well; diacetonide galactose **5** produced the acetal linked α-disaccharide **10** in 73% yield.

In summary we have demonstrated that NISac[11] activation of thioglycosides in ketone solvents[12] leads exclusively to the formation of α-mixed acetal products, in which a solvent molecule is incorporated between the anomeric centre of the glycosyl donor and the hydroxy group of the glycosyl acceptor. Formation of these mixed acetal products probably occurs by trapping of an incipient α-acetonium ion **4** by the glycosyl acceptor, and provides substantial evidence for the intermediacy of such species during glycosylation reactions performed in acetone as solvent. Furthermore this synthetic route to pure α-acetal glycosides, which have been proposed as potential anti-cancer prodrugs, compares favourably with the other published routes.[13,14]

Further investigations into the generality of this novel glycosylation reaction, and its development for the synthesis of

† Electronic supplementary information (ESI) available: spectral data for compounds **3**, **6** and **8**–**10**. See http://www.rsc.org/suppdata/cc/b1/b104196g/

 DOI: 10.1039/b104196g

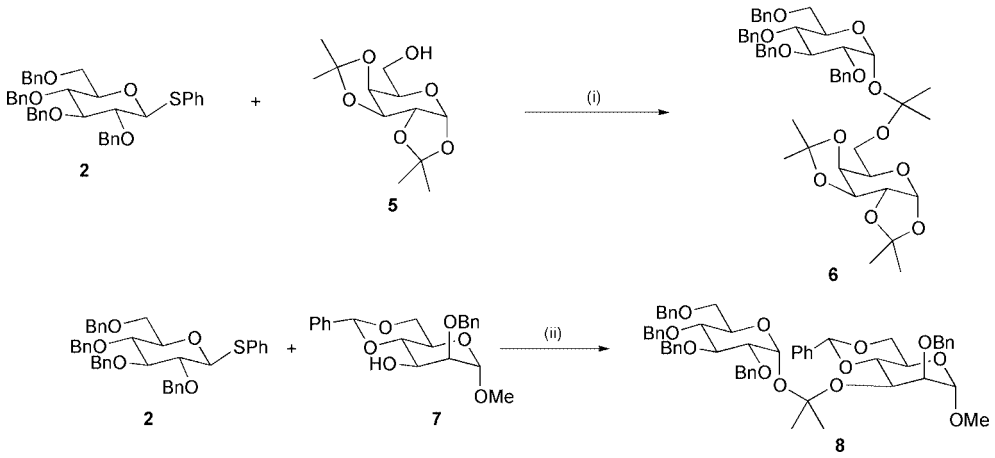

Scheme 2 *Reagents and conditions*: (i) NISac **1**, acetone, −78 to 0 °C, 2.5 h, 84%; (ii) NISac **1**, acetone, −78 to 0 °C, 3 h, 78%.

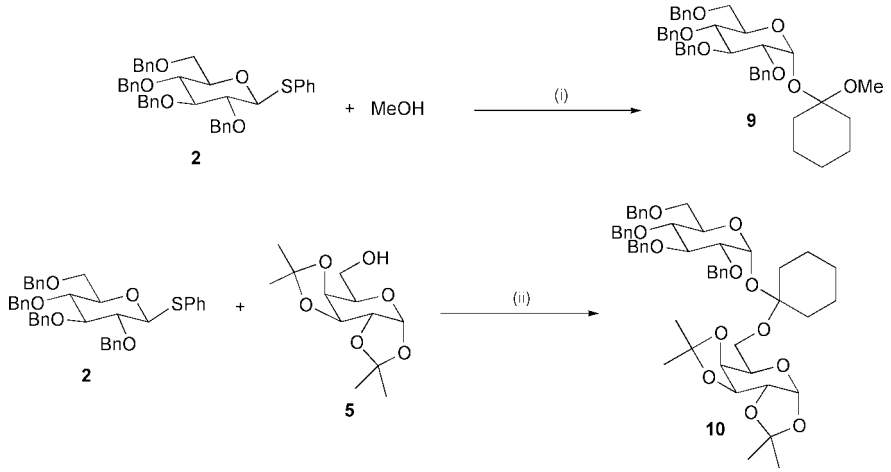

Scheme 3 *Reagents and conditions*: (i) NISac **1**, acetone, −78 to 0 °C, 2.5 h, 84%; (ii) NISac **1**, cyclohexanone, −40 to 5 °C, 3 h, 62%; (ii) NISac **1**, cyclohexanone, −40 to 0 °C, 2 h, 73%.

glycomimetics are currently in progress and will be reported in due course. We gratefully acknowledge financial support from the Leverhulme Trust (postdoctoral fellowship to M. A.), and also the use of the Chemical Database Service (CDS) at Daresbury, UK, and the EPSRC National Mass Spectrometry Service at Swansea.

Notes and references

‡ Typical experimental procedure: a mixture of the perbenzylated phenyl thioglucoside **2** (0.091 g, 0.14 mmol), diacetonide galactose **5** (0.056g, 0.21 mmol) and molecular sieves 4 Å (0.2 g) were stirred in dry acetone (3 ml) under an atmosphere of argon at −78 °C. *N*-Iodosaccharin **1** (0.066 g, 0.021 mmol) was then added rapidly. The reaction mixture was then stirred with warming to 0 °C until TLC (R_f 0.44, ethyl acetate–petroleum ether, 1:3) indicated complete consumption of the thioglycoside (*ca*. 2.5 hours). Triethylamine (1 ml) was added and stirring was continued for a further 15 minutes at 0 °C. The reaction mixture was then diluted with dichloromethane (30 ml) and then filtered through Celite®. The filtrate was then washed with 10% aqueous sodium thiosulfate (10 ml), saturated aqueous sodium bicarbonate (10 ml) and water (10 ml). The organic extracts were then dried (anhydrous sodium sulfate), filtered, and the solvent removed *in vacuo*. The residue was then purified by flash column chromatography (ethyl acetate–petroleum ether, 1:4) to give the acetal-linked disaccharide **6** (0.102 g, 84 %), as a colourless oil.

§ All new compounds possess NMR and high-resolution mass spectral data consistent with their structures.

1 G. Wulff and G. Röhle, *Angew. Chem., Int. Ed. Engl.*, 1974, **13**, 157.
2 S. Hashimoto, M. Hayashi and R. Noyori, *Tetrahedron Lett.*, 1984, **25**, 1379; A. Demchenko, T. Stauch and G. J. Boons, *Synlett*, 1997, 818.
3 R. R. Schmidt, M. Behrendt and A. Toepfer, *Synlett*, 1990, 694; J-R. Pougny and P. Sinaÿ, *Tetrahedron Lett.*, 1976, **17**, 4073.
4 A. J. Ratcliffe and B. Fraser-Reid, *J. Chem. Soc., Perkin Trans. 1*, 1990, 747.
5 L. G. Nair, B. Fraser-Reid and A. N. Szardenings, *Org. Lett.*, 2001, **3**, 317 and references cited therein.
6 M. Aloui and A. J. Fairbanks, *Synlett*, 2001, 797.
7 Interestingly no nitrilium trapped species were observed during any NISac mediated glycosylations in acetonitrile.
8 For some glycosylation reactions performed in acetone see: F. J. Kronzer and C. Schuerch, *Carbohydr. Res.*, 1974, **34**, 71; F. J. Kronzer and C. Schuerch, *Carbohydr. Res.*, 1974, **34**, 79.
9 L. Somsák, L. Kovács, V. Gyóllai and E. Ösz, *Chem. Commun.*, 1999, 591.
10 S. Koto, S. Inada, T. Narita, N. Morishima and S. Zen, *Bull. Chem. Soc. Jpn.*, 1982, **55**, 3665.
11 *N*-Iodosuccinimide (NIS) activation of thioglycoside **2** in acetone was found to be extremely slow.
12 The use of the ketone as the solvent is not essential. A trial reaction involving NISAc mediated glycosylation of **2** with **5** in dichloroethane at −40 °C, in the presence of 5 equivalents of acetone, produced an inseparable mixture of the trapped material **6**, plus the expected disaccharide (interestingly as mainly the α-anomer) in an approximate 1:1 ratio, in an overall 60% yield.
13 L. F. Tietze, R. Fischer, M. Lögers and M. Beller, *Carbohydr. Res.*, 1989, **194**, 155; L. F. Tietze and M. Lögers, *Liebigs Ann. Chem.*, 1990, 261; L. F. Tietze and M. Beller, *Liebigs Ann. Chem.*, 1990, 587.
14 H. K. Chenault, A. Castro, L. F. Chafin and J. Yang, *J. Org. Chem.*, 1996, **61**, 5024.

CHEMCOMM Communication
www.rsc.org/chemcomm

On a new catalyzed silylation of alcohols by phenylhydrosilanes

Franck Le Bideau,*[a] Thibaud Coradin,[b] Josette Hénique[a] and Edmond Samuel[a]

[a] *UMR 7576 CNRS, Ecole Nationale Supérieure de Chimie de Paris, 11 rue Pierre et Marie Curie 75231 Paris Cedex 05, France. E-mail: lebideau@ext.jussieu.fr; Fax: +33 1 43 26 00 61; Tel: +33 1 44 27 66 98*

[b] *UMR 7574 CNRS, Université Pierre et Marie Curie 75252 Paris Cedex 05, France*

Received (in Cambridge, UK) 5th April 2001, Accepted 14th June 2001
First published as an Advance Article on the web 4th July 2001

KOH–18-crown-6 ether is a valuable system for the catalyzed dehydrocoupling of alcohols with phenylhydrosilanes (Ph_3SiH and $PhMe_2SiH$).

The importance of silyl ethers in organic synthesis as protecting groups for alcohols has been discussed.[1,2] The most common route to these compounds involves the reaction of a silyl chloride (or the corresponding triflate for hindered alcohols) with an alcohol in the presence of an amine (pyridine, triethylamine, imidazole…). The stoichiometric amounts of ammonium salts produced as well as the cost[3] of the silylating reagents has led chemists to study the dehydrocoupling process involving hydrosilanes. This reaction has been reported using a wide range of catalytic species such as transition metal complexes, Lewis acids[4] and salts.[5,6] In this work, we show that a new method involving KOH–18-crown-6 ether is simple, inexpensive and is valuable for the catalyzed silylation of alcohols with phenylhydrosilanes.

When hydrosilanes **1** were added to a mixture of KOH (9% mol)–18-crown-6 ether (3% mol) and alcohols **2** in CH_2Cl_2 (Scheme 1), a gas evolution occurred. Apart from the desired silyl ether **3**, small amounts of siloxanes **4** were produced so that a slight excess of hydrosilanes (1.4 eq.) was therefore required for the total conversion of the alcohols.† It is noteworthy that the reactions are generally clean as judged by the ^1H NMR spectra of the crude reaction mixtures and that under the same reaction conditions, no conversion of the starting materials in the absence of 18-crown-6 ether was observed. Dichloromethane was chosen because of its low boiling point and for being a good solvent for the reagents used, but other solvents such as THF, benzene or ether are also appropriate.

We found that Et_3SiH is less reactive under these conditions than the phenylhydrosilanes as shown by its reaction with 4-methylbenzyl alcohol, which led to only 33% conversion. Among the phenylhydrosilanes, Ph_3SiH is more reactive than $PhMe_2SiH$ judging from their different abilities to transform tertiary alcohols (Table 1, entry 1). The reactions of other hindered alcohols such as 2-methylpropan-2-ol or 2-methylpentan-2-ol were also unsuccessful using $PhMe_2SiH$ even in boiling THF.

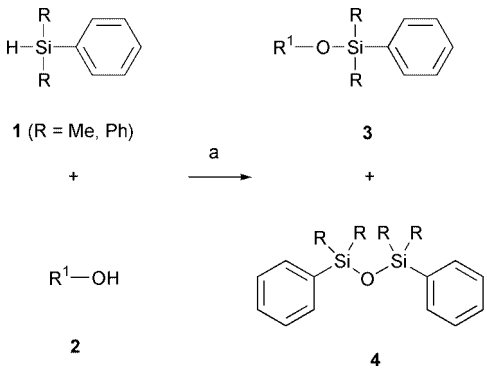

Scheme 1 a. KOH–18-crown-6 ether (9% : 3%), argon, 18 h, CH_2Cl_2, rt or CH_2Cl_2, Δ, 3 h.

A better knowledge of the course of this reaction was provided by examining different alcohols (Table 1). The presence of a strong withdrawing group close to the hydroxy function inhibits the reaction. For instance, 2-chloroethanol is not reactive under the conditions used to transform 6-chlorohexan-1-ol into the corresponding silyl ethers (Table 1, entry 2). Phenol or 4-methoxyphenol, which show a poor nucleophilic character in comparison with aliphatic alcohols, are not reactive while benzylic alcohols (Table 1, entries 3 and 4) or 2-phenylpropan-1-ol (Table 1, entry 5) are converted into the desired products in good yields. Saturated alcohols (entry 6) are good substrates for the reaction, as long as they do not provide a strong steric hindrance as mentioned above (entry 1). Compared to other transition metal catalysts,[7] the KOH–18-crown-6 ether system has the advantage of being compatible with unsaturated alcohols (entries 7 and 8). Furthermore, this system is convenient for the protection of hydroxy epoxide glycidol (entry 9) since it does not lead to the loss of the oxirane ring as mentioned for Lewis acid catalyzed reactions.[4]

This reaction when performed on a larger scale (20 mmol of glycidol) gave the same yield of the desired product with $PhMe_2SiH$ as the silylating agent.

We have recently shown that KOH–18-crown-6 ether was an efficient system for catalyzed hydrosilylation and the

Table 1 Silylation of a number of alcohols in the presence of a catalytic amount of KOH–18-crown-6 ether: reactions were performed in CH_2Cl_2 at rt under argon for 18 h and isolated yields calculated following flash chromatography, unless otherwise stated.

	2	R	**3** (cond.)
1	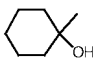	Me	—[a]
		Ph	87%
2	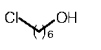	Me	73%
		Ph	100%[b]
3	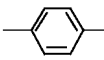	Me	94%
		Ph	100%[b]
4	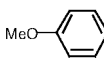	Me	80%[c]
		Ph	78%
5	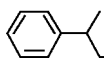	Me	90%
		Ph	100%[b]
6	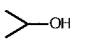	Me	90%
		Ph	100%[bd]
7	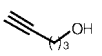	Me	68%
		Ph	57%
8	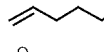	Me	72%
		Ph	100%[d]
9	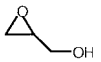	Me	50%[c]
		Ph	93%

[a] No reaction even with THF, Δ.[b] Inseparable mixture of **3** and **4**, total conversion of **2** according to the ^1H NMR spectrum of the crude reaction mixture.[c] CH_2Cl_2, Δ, 3 h.[d] Reaction performed in CD_2Cl_2, rt, 18 h.

 DOI: 10.1039/b103130a

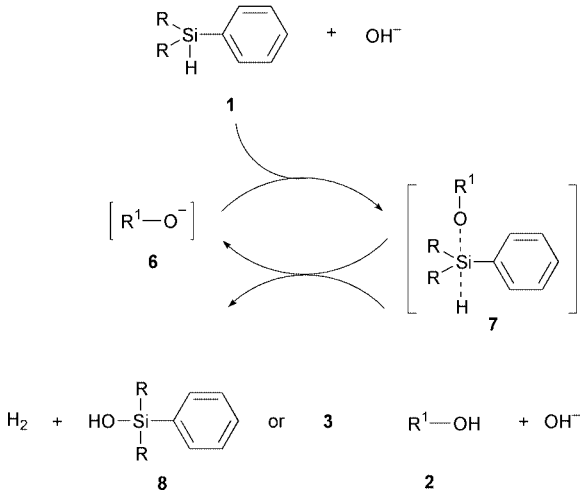

Scheme 2 A possible mechanism for the catalyzed silylation of alcohols.

Tishchenko reaction of aromatic aldehydes.[8] The KOH–18-crown-6 ether catalyzed reaction of 4-methylbenzyl alcohol with $PhMe_2SiH$ was therefore conducted with a stoichiometric amount of *p*-anisaldehyde, a good substrate in the hydrosilylation process.[8] The ^1H NMR spectrum of the crude reaction mixture showed 12% conversion of the aldehyde and 82% of the alcohol, thus demonstrating that the dehydrocoupling reaction predominates over hydrosilylation.

From a mechanistic standpoint, the catalytic cycle could be easily explained in terms of the anionic activation of the Si–H bond first reported by Corriu *et al.* for various salts.[5] Thus, it can be proposed that the Si–H bond is labilized by anionic coordination of the alcoholate **6** (or OH^-) to give the pentacoordinate intermediate **7** (Scheme 2). This activated species could give the desired product **3** or the silanol **8**, a possible precursor for the isolated siloxane **4**.

Thus we show above that KOH–18-crown-6 ether is an efficient system for the catalyzed silylation of nucleophilic alcohols with Ph_3SiH and $PhMe_2SiH$. The lack of reactivity towards non-nucleophilic and hindered alcohols could be profitable for the use of these phenylsilyl ethers as selective protecting groups in organic synthesis. Compared to most other catalyzed silylation reactions, this method has the advantage of being compatible with double or triple bonds, carbonyl functions, chlorine and oxirane.

A mechanistic study of this reaction is being undertaken. The role of OH^- in the catalytic cycle remains to be elucidated.

Notes and references

† *Typical procedure*: reaction vessels were dried under vacuum and the reactions carried out under argon. The silane (1.4 mmol) was added at rt to a solution of the alcohol (1 mmol) and KOH–18-crown-6 ether (5 mg : 6 mg) in CH_2Cl_2 (0.75 mL). After stirring for 18 h, the reaction mixture was concentrated and the residue was purified by flash chromatography or crystallization to give the silyl ether (see Table 1). All products were characterized by the usual spectroscopic techniques or compared with data reported in the literature.

1 T. W. Greene and P. G. M. Wutz, *Protective Groups in Organic Synthesis*, Wiley, 2nd edn., New York, 1991, p. 50.
2 P. J. Kocienski, *Protecting Groups*, ed. D. Enders, R. Noyori and B. M. Trost, Thieme, Stuttgart, New York, 1994, p. 28.
3 For instance, the cost (Aldrich) per mmol of Ph_3SiCl (respectively $PhMe_2SiCl$) is 1.46 euros (respectively 1.18 euros for $PhMe_2SiH$) compared with 0.60 euros for Ph_3SiH (respectively 0.50 euros for $PhMe_2SiH$)
4 J. M. Blackwell, K. L. Foster, V. H. Beck and W. E. Piers, *J. Org. Chem.*, 1999, **64**, 4887 and references cited therein.
5 R. J. P. Corriu, R. Perz and C. Reye, *Tetrahedron*, 1983, **39**, 999.
6 Y. Tanabe, H. Okumura, A. Maeda and M. Murakami, *Tetrahedron Lett.*, 1994, **35**, 8413.
7 Schubert *et al.* recently reported a good copper hydride complex which allows the hydrosilylation of alcohols without reduction of double or triple bonds present in the molecule: C. Lorenz and U. Schubert, *Chem. Ber.*, 1995, **128**, 1267.
8 F. Le Bideau, T. Coradin, D. Gourier, J. Henique and E. Samuel, *Tetrahedron Lett.*, 2000, **41**, 5215.

CHEMCOMM Communication
www.rsc.org/chemcomm

Decarboxylative acylation approach of thiohydroxamate esters

Sunggak Kim,*[a] Chae Jo Lim,[a] Sang-Eun Song[b] and Han-Young Kang[b]

[a] *Center for Molecular Design and Synthesis and Department of Chemistry, School of Molecular Science, Korea Advanced Institute of Science and Technology, Taejon 305-701, Korea. E-mail: skim@mail.kaist.ac.kr*

[b] *Department of Chemistry, Chungbuk National University, Cheongju 361-763, Korea*

Received (in Cambridge, UK) 4th May 2001, Accepted 20th June 2001
First published as an Advance Article on the web 12th July 2001

A decarboxylative acylation approach is achieved with thiohydroxamate ester 6, which is less reactive and more stable than Barton's ester 1.

Since *O*-acyl thiohydroxamates were introduced in radical chemistry by Barton,[1] they have attracted a great deal of attention among synthetic chemists as useful radical precursors of alkyl[2] and aminyl radicals.[3] Radical chemistry of *O*-acyl thiohydroxamates **1** were further applied not only to the introduction of synthetically useful functional groups such as a halide[4] and a nitrile[5] but also to the formation of carbon-carbon bonds.[6] However, a highly reactive trapping agent is normally required because the alkyl radical could attack the thiocarbonyl group of **1** concurrently.

In connection with our recent interest in tin-free radical reactions,[7,8] we have studied the feasibility of decarboxylative acylation approaches of carboxylic acids *via O*-acyl thiohydroxamates **1** using phenylsulfonyl oxime ether **2a** as an acylating trapping agent (eqn. (1)).[9] Irradiation of a solution of **1** and **2a**

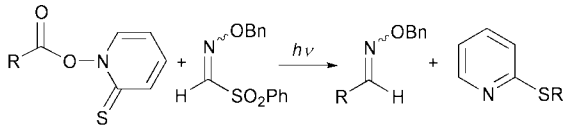

(1)

in benzene with a tungsten sun lamp (300 W) for 12 h gave a mixture of oxime ether **3** (32%) and pyridyl sulfide **4** (36%) in a roughly equal ratio, which was anticipated from the previously reported kinetic data.[10] Thus, the key feature for the success of the decarboxylative acylation approach is to reduce the rate of the alkyl radical additions onto the thiocarbonyl group to suppress the formation of **4**.

Our attention was given to somewhat less reactive thiohydroxamate esters that would not undergo aromatization upon radical-mediated fragmentation.[11] In this regard, we expected that a thiohydroxamate ester **6** would be well suited for our purpose. It is noteworthy that a very similar type of the reagent (RCO_2–NMe(C=S)SPh) was previously reported and would have similar properties.[2b] Thiohydroxamate ester **6** was obtained in high yield by treatment of a carboxylic acid with *N*-methylhydroxydithiocarbamate **5**, diethyl azodicarboxylate, and triphenylphosphine in THF and was stable thermally and hydrolytically (eqn. (2)). When **6** was treated with **2b** using 1,1′-

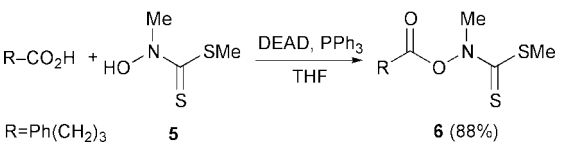

(2)

azobis(cyclohexanecarbonitrile) (V-40) as an initiator in octane at 120 °C for 10 h, a 71 : 16 mixture of oxime ether **3** and **7** was obtained, indicating the addition of the alkyl radical onto **2b** was much faster than the rearrangement to afford **8** (eqn. (3)).

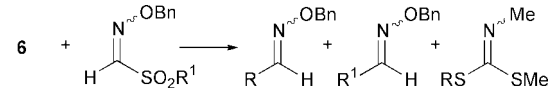

R=Ph(CH$_2$)$_3$	**3**	**7**	**8**
2a: R^1= Ph (100 °C)	78%	0%	0%
= Ph (300 nm)	65%	0%	0%
2b: R^1= Me (120 °C)	71%	16%	0%

(3)

Furthermore, it is evident that a methyl radical, generated from thermal decomposition of a methanesulfonyl radical, attacked **2b** to some extent to yield **7**.[8] Thus, we performed the same reaction with **2a** and it was gratifying to find that thermal reaction of **6** with **2a** and V-40 in refluxing heptane afforded **3** in 78% yield without the formation of **7** and **8**. Furthermore, the decarboxylative acylation approach could be performed under photochemically initiated conditions. Unlike Barton's ester **1**, **6** required irradiation at 300 nm. Irradiation of a benzene solution of **6** with **2a** at 300 nm for 9 h afforded **3** in 65% yield. Thus, the remaining reactions were carried out with **2a** in refluxing heptane (0.25 M) for 12 h. Table 1 summarizes some experimental results and illustrates the efficiency of the decarboxylative acylation approaches. Primary and secondary aliphatic carboxylic acids worked well, yielding the corresponding oxime ethers in high yields. Sterically hindered tertiary

Table 1 Preparation of oxime ethers from thiohydroxamate esters

Substrate X = (CO_2–NMe-(C=S)SMe)	Product		Yield[a] (%)
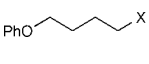	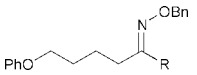	R = H R = COOMe	76 (64) 62
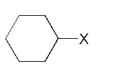	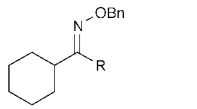	R = H R = COOMe	75 (68) 68
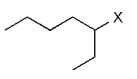	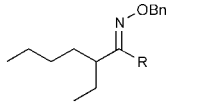	R = H R = COOMe	82 68
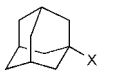	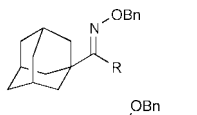	R = H R = COOMe	88 (76) 70
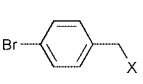	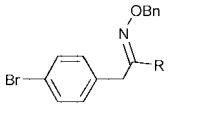	R = H R = COOMe	87 74
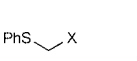	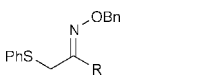	R = H R = COOMe	84 71

[a] The numbers in parentheses indicate the yields at 300 nm.

 DOI: 10.1039/b104025c

carboxylic acids underwent the decarboxylative acylation cleanly.

Thermal conditions gave somewhat higher yields than photochemical conditions and required 12 h for completion of the reaction. The major advantage of the present method is a sequential cyclization and acylation approach, which was demonstrated successfully in the present study (eqn. (4)).

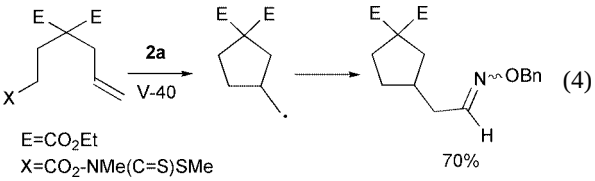

(4)

To obtain an oxime ester, a synthetic equivalent of a α-keto ester,[12] when we repeated the reaction with methoxycarbonyl oxime ether **9** in refluxing heptane for 12 h, the desired oxime ester **10** was isolated in 54% yield along with a significant amount of the rearranged product **8** (31%) (eqn. (5)). Apparently,

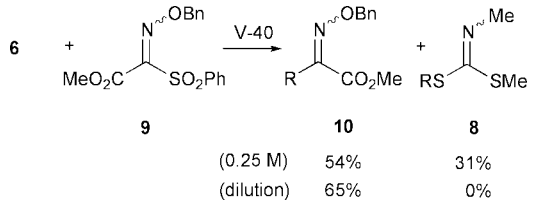

(5)

the addition of the alkyl radical onto **9** was slowed down to some extent, thereby allowing the alkyl radical to attack **6**. The problem of the formation of the rearranged product was solved by the addition of **6** into **9** with a syringe pump. Thus, the addition of a 0.05 M chlorobenzene solution of **6** to a 0.1 M chlorobenzene solution of **9** at 120 °C by a syringe pump over 8 h with additional stirring for 2 h afforded the desired **10** in 65% yield without the formation of **8**. Similarly, the formation of several oxime esters worked equally well under highly diluted conditions as shown in Table 1.

In conclusion, we have developed a new thiohydroxamate ester, which is much less reactive and more stable than Barton's ester and demonstrated the first examples of decarboxylative acylation approaches under tin-free conditions.

We thank the Center for Molecular Design and Synthesis (CMDS) and BK21 project for financial support.

Notes and references

1 For reviews, see: D. Crich and L. Quintero, *Chem. Rev.*, 1989, **89**, 1413; D. H. R. Barton, *Tetrahedron*, 1992, **48**, 2529; S. Z. Zard, *Angew. Chem., Int. Ed. Engl.*, 1997, **36**, 672.

2 (*a*) D. H. R. Barton, D. Crich and W. B. Motherwell, *Chem. Commun.*, 1983, 939; (*b*) D. H. R. Barton, D. Crich and P. Potier, *Tetrahedron Lett.*, 1985, **26**, 5943.

3 M. Newcomb, S.-U. Park, J. Kaplan and D. J. Marquardt, *Tetrahedron Lett.*, 1985, **26**, 5651; M. Newcomb and T. M. Deeb, *J. Am. Chem. Soc.*, 1987, **109**, 3163; M. Newcomb, T. M. Deeb and D. J. Marquardt, *Tetrahedron*, 1990, **46**, 2317; J. Esker and M. Newcomb, *Tetrahedron Lett.*, 1992, **33**, 5913.

4 D. H. R. Barton, D. Crich and W. B. Motherwell, *Tetrahedron*, 1985, **41**, 3901.

5 D. H. R. Barton, J. S. Jaszberenyi and E. A. Theodorakis, *Tetrahedron*, 1992, **48**, 2613.

6 D. H. R. Barton, H. T. Togo and S. Z. Zard, *Tetrahedron Lett.*, 1985, **26**, 6349; D. H. R. Barton, D. Crich and G. Kretzschmar, *Tetrahedron Lett.*, 1984, **25**, 1055.

7 S. Kim, C. J. Lim, S.-E. Song and H.-Y. Kang, *Synlett*, 2001, 688.

8 S. Kim, H.-J. Song, T.-L. Choi and Y.-J. Yoon, *Angew. Chem., Int. Ed. Engl.*, 2001, **40**, 2524.

9 S. Kim, I. Y. Lee, J.-Y. Yoon and D. H. Oh, *J. Am. Chem. Soc.*, 1996, **118**, 5138.

10 S. Kim and I. Y. Lee, *Tetrahedron Lett.*, 1998, **39**, 1587; M. Newcomb and S. U. Park, *J. Am. Chem. Soc.*, 1986, **108**, 4132; M. Newcomb and J. Kaplan, *Tetrahedron Lett.*, 1987, **28**, 1615; D. P. Curran, A. A. Martin-Esker, S.-B. Ko and M. Newcomb, *J. Org. Chem.*, 1993, **58**, 4691.

11 D. H. R. Barton and G. Kretzschmar, *Tetrahedron Lett.*, 1983, **24**, 5889; D. H. R. Barton, D. Crich and G. Kretzschmar, *J. Chem. Soc., Perkin Trans. 1*, 1986, 39; D. H. R. Barton, P. Blundell and J. C. Jaszberenyi, *Tetrahedron*, 1992, **48**, 7121.

12 S. Kim, J.-Y. Yoon and I. Y. Lee, *Synlett*, 1997, 475.

CHEMCOMM
Communication
www.rsc.org/chemcomm

Novel synthesis of 1-aryl-3-chloro-3-phenylazetidin-2-one-4-spiro-5′-4′-chloro-5′*H*-1′,2′,3′-dithiazoles and bis(2-oxo-azetidin-4-yl) trisulfides†

Moon-Kook Jeon, Kyongtae Kim*[a] and Yung Ja Park[b]

[a] *School of Chemistry and Molecular Engineering, Seoul National University, Seoul 151-742, Korea. E-mail: kkim@plaza.snu.ac.kr; Fax: 82 2874 8858; Tel: 82 2880 6636*
[b] *Department of Chemistry, Sook Myung Women's University, Seoul 140-724, Korea*

Received (in Cambridge, UK) 3rd May 2001, Accepted 13th June 2001
First published as an Advance Article on the web 12th July 2001

Treatment of 5-arylimino-4-chloro-5*H*-1,2,3-dithiazoles with *in situ* generated (chloro)phenylketene in CH_2Cl_2 at rt gave azetidin-2-one-4-spiro-5′-(1′,2′,3′-dithiazoles) as major products, which reacted with primary and secondary alkylamines in CH_2Cl_2 at rt to afford bis(2-oxo-azetidin-4-yl) trisulfides in good to excellent yields.

Azetidin-2-ones have been one of the most attractive classes of organic compounds due to their potential biological applications.[1] Numerous methods for the synthesis of azetidin-2-ones are known and these are well-documented in the literature.[1] In connection with our ongoing project for exploring the potential synthetic utility of 5-arylimino-4-chloro-5*H*-1,2,3-dithiazoles **1**,[2] we are interested in investigating the reactivity of the N=C-5 imine bond of **1** toward cycloaddition reactions with a ketene because a [2 + 2] cycloaddition with a ketene would give azetidin-2-one-4-spiro-5′-(1′,2′,3′-dithiazoles) **2**, which, to the best of our knowledge, has never been reported. Compound **2** is

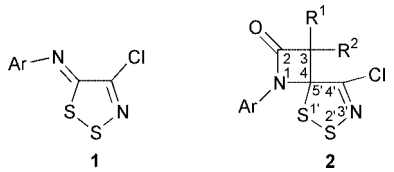

1 **2**

of interest with respect to the stereochemistry at C-3 and C-4. In addition, it may be utilized as a precursor for the synthesis of hitherto unknown azetidin-2-ones created by cleaving the bond between S-1′ and S-2′ with nucleophiles, as shown in the ready conversion of **1** to diverse products.[3] With this in mind, **1** was treated with various ketenes which were generated *in situ*. This paper describes the preliminary results we have obtained.

For the generation of a ketene, a method involving acid chlorides and Et_3N[4] in CH_2Cl_2 at rt was employed since neither reagent reacts with **1** under conditions for the generation of ketenes. When Et_3N (1.22–2.87 mmol) in CH_2Cl_2 (30 ml) was added dropwise to a mixture of **1b** (Ar = 4-$MeOC_6H_4$) (0.773–0.935 mmol) and acid chlorides **3** (1.20–2.89 mmol) in CH_2Cl_2 (20 ml) at rt, followed by stirring for 0.5–1 h, only a small amount of **4a** (Y = Cl), **4c** (Y = MeO), and **4e** (Y = AcO), which comprised a single isomer in view of the ^1H and ^{13}C NMR spectroscopic data, and most of the unreacted **1b** were isolated (Scheme 1).

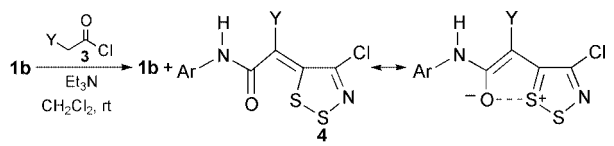

Ar = 4-$MeOC_6H_4$ **a**, Y = Cl, 26% **d**, Y = PhO, 0%
b, Y = Ph, 0% **e**, Y = AcO, 17%
c, Y = MeO, 2%

Scheme 1

Compounds **4a**, **4c**, and **4e**, derivatives of 5-(phenylcarbamoyl)methylidene-5*H*-1,2,3-dithiazole,[5] are all new. The (*E*)-stereochemistry of **4** was assigned based on the IR absorptions of the carbonyl group at 1603, 1613, and 1619 cm^{-1}, respectively, which suggests the possible interaction of the carbonyl oxygen with electron deficient S-1.[2] Surprisingly, the reactions of **1** with 2-chloro-2-phenylacetyl chloride (**3f**) under the foregoing conditions gave the desired compound **2** (R^1 = Cl, R^2 = Ph) in good to excellent yields (Scheme 2). Yields and mps of **2** are summarized in Table 1.

The structures of **2** were determined based on spectroscopic (^1H and ^{13}C NMR, IR, MS) and analytical data. The X-ray single crystal structure of **2d**‡ (Fig. 1) clearly shows *cis*-stereochemistry with *S* and *R* configurations at C-3 and C-4, respectively. The *cis*-stereochemistry of **2** may be ascribed to the avoidance of severe electronic repulsions between lone pair electrons on the two chlorine atoms at C-3 and C-4′.

Treatment of **2** (0.23–0.38 mmol) in CH_2Cl_2 (10 ml) with a slightly excessive molar amount of primary and secondary alkylamines at rt gave bis(2-oxo-azetidin-4-yl) trisulfides **5** along with alkylamino 2-oxo-azetidin-4-yl disulfides **6** and a considerable amount of unreacted **2** (Scheme 2). However, by employing 4 molar equivalents of alkylamines, **5** were obtained as major products along with **6** and a small amount of isothiazol-3-ones **7**, which were obtained only from the reactions of **2c** and

Table 1 Yields and mps of **2**[a]

Compound	Ar	Yield[b] (%)	Mp[c]/°C
2a	4-MeO-2-$MeOC_6H_3$	97	142–146 (dec.)
2b	4-$MeOC_6H_4$	96	122–124
2c	4-MeC_6H_4	95	73–76
2d	4-ClC_6H_4	86	147–149
2e	4-$MeCOC_6H_4$	74	156–160 (dec.)
2f	4-$O_2NC_6H_4$	44	139–144 (dec.)

[a] Time for dropwise addition of Et_3N: 2–3 h; time stirred: 0.5–1 h. [b] Isolated yields. [c] Recrystallized from a mixture of *n*-hexane and CH_2Cl_2.

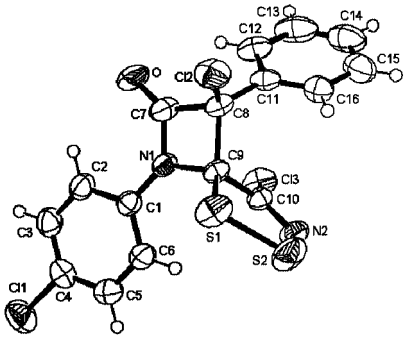

Fig. 1 ORTEP drawing of (3*S*,4*R*)-3-chloro-1-(4-chlorophenyl)-3-phenylazetidin-2-one-4-spiro-5′-(4′-chloro-5′*H*-1′,2′,3′-dithiazole) **2d**.

† Electronic supplementary information (ESI) available: spectral and analytical data for **2** and **4**–**8**. See http://www.rsc.org/suppdata/cc/b1/b103974c/

 DOI: 10.1039/b103974c

Table 2 Reaction times and yields of compounds **5**, **6** and **7**

Entry	Compound	Ar	R^3R^4NH	Time (*t*/h)	Yield[a] (%) **5**	**6**	**7**
1	**2b**	4-$MeOC_6H_4$	*n*-$PrNH_2$	0.7	**b** 93 (93–98)[c]		
2	**2b**	4-$MeOC_6H_4$	*t*-$BuNH_2$	42	**b** 77	**b** 7	
3	**2c**	4-MeC_6H_4	*n*-$PrNH_2$	0.7	**c** 80 (103–107)[c]	**c** 4	
4	**2c**	4-MeC_6H_4	*t*-$BuNH_2$	4	**c** 77	**d** 6	
5	**2c**	4-MeC_6H_4	*n*-Pr_2NH	2	**c** 61	**e** 16	**c** 6 (170–171)[d]
6	**2c**	4-MeC_6H_4	$PhNH_2$	24[b]			
7	**2d**	4-ClC_6H_4	*n*-$PrNH_2$	0.2	**d** 69 (110–115)[c]	**f** 10	**d** 19 (181–182)[d]
8	**2d**	4-ClC_6H_4	*t*-$BuNH_2$	16	**d** 73	**g** 8	
9	**2f**	4-$O_2NOC_6H_4$	*n*-$PrNH_2$	0.2	**e** 90 (160–165)[d]		

[a] Isolated yields. [b] Reflux time. [c] Recrystallized from a mixture of CH_2Cl_2 and EtOH. [d] Recrystallized from a mixture of *n*-hexane and CH_2Cl_2.

2d. Trisulfides of azetidin-2-ones have never been reported despite the existence of numerous methods for the synthesis of a variety of trisulfides.[6] Compounds **6** and **7** are also new. The stereochemistry at C-3 and C-4 of **5** and **6** are believed to be intact. Reaction times and yields of trisulfides **5**, disulfides **6**, and isothiazol-3-ones **7** are summarized in Table 2.

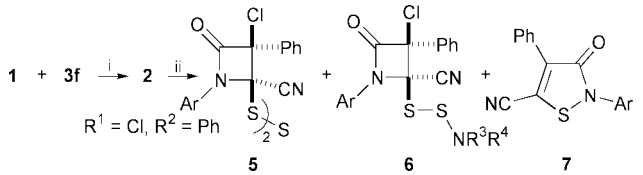

Scheme 2 *Reagents and conditions*: i, Et_3N, CH_2Cl_2, rt; ii, R^3R^4NH, CH_2Cl_2, rt.

Table 2 shows that **2** react with both primary (entries 1–4 and 7–9) and secondary (entry 5) alkylamines to give **5** but not with arylamine even at reflux temperature over a prolonged reaction time (entry 6). Among primary alkylamines, *i.e.* *n*-$PrNH_2$ and *t*-$BuNH_2$, the reactions with *n*-$PrNH_2$ proceeded more rapidly than those with *t*-$BuNH_2$, presumably due to the steric effect of a bulky *tert*-butyl group.

For a mechanistic study, a mixture of equal molar amounts of **2b** (0.253 mmol) and **2c** (0.253 mmol) was treated with *n*-$PrNH_2$ (2.07 mmol) for 3 h under the foregoing conditions. From the reaction were isolated **5b** (44%), **5c** (46%), and unsymmetrical trisulfide **8** (87%) (Scheme 3). The isolation of unsymmetrical trisulfide **8** coupled with its yield, which is approximately twice of that of either **5b** or **5c**, indicates that trisulfides **5** are formed *via* an intermolecular reaction. Furthermore, when the mixture of **2b** (0.070 mmol) and **2c** (0.069 mmol) was treated with a large exccss of *n*-$PrNH_2$ (1.1 mmol) for 24 h under the same conditions, isothiazol-3-ones **7b** (58%) and **7c** (62%) along with unknown mixtures were obtained. No trisulfides **5b** and **5c** were detected. The results indicate that **2** are converted to **7** *via* **5** in the presence of a large excess of *n*-$PrNH_2$ over a prolonged reaction time. In addition, the fact that **7c** (78%) together with an unknown mixture as obtained from the reaction of disulfide **6c** (Ar = 4-MeC_6H_4, R^3 = H, R^4 = *n*-Pr) (0.11 mmol) with *n*-$PrNH_2$ (0.49 mmol) in CH_2Cl_2 for 26 h indicates that **6** also act as intermediates for the formation of **7**.

In conclusion we have found that 5-arylimino-4-chloro-5*H*-1,2,3-dithiazoles reacted with (chloro)phenylketene in CH_2Cl_2 at rt to give spiro compound **2**, which undergoes a decomposition reaction in the presence of primary and secondary alkylamines in CH_2Cl_2 at rt, giving bis(2-oxo-azetidin-4-yl) trisulfides as major products. Study of the mechanism and scope of the reactions is in progress.

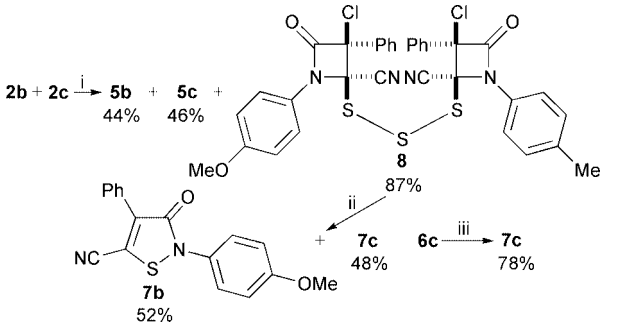

Scheme 3 *Reagents and conditions*: i, *n*-$PrNH_2$ (8 equiv.), CH_2Cl_2, rt, 3 h; ii, *n*-$PrNH_2$, (8 equiv.), CH_2Cl_2, rt, 24 h; iii, *n*-$PrNH_2$ (4 equiv.), CH_2Cl_2, rt, 26 h.

This work was supported by a Korea Research Foundation Grant (DP-0261).

Notes and references

‡ *Crystal data* for **2d**: $C_{16}H_9Cl_3N_2OS_2$, M = 415.72, monoclinic, a = 16.946(2), b = 7.4460(5), c = 15.026(3) Å, β = 113.080(10)°, U = 1744.2(4) Å^3, T = 293 K, $P2/k$, Z = 4, μ(Mo-Kα) = 0.770 mm^{-1}, λ = 0.71070 Å, 3189 reflections measured, 3057 unique (R_{int} = 0.0088) which were used in all calculations. Final R indices [$I > 2\sigma(I)$]: $R1$ = 0.0455, $wR2$ = 0.1156. CCDC 165871. See http://www.rsc.org/suppdata/cc/b1/b103974c/ for crystallographic data in CIF or other format.

Spectral data for **2d**: ν(neat)/cm^{-1} 3056, 1782, 1490, 1442, 1366, 1158, 1117, 1109, 1051, 1010; δ_H(300 MHz, $CDCl_3$) 7.36 (s, 4H), 7.38-7.44 (m, 3H), 7.59 (br, 2H); δ_C(75 MHz, $CDCl_3$) 82.9, 102.1, 119.2, 126.6, 129.2, 129.8, 130.2, 131.8, 132.9, 133.1, 142.0, 160.3.

1 D. E. Davies and R. C. Storr, in *Comprehensive Heterocyclic Chemistry*, A. R. Katritzky and C. W. Rees, ed., Pergamon, Oxford, 1984, vol. 7, pp. 237–362; N. De Kimpe, in *Comprehensive Heterocyclic Chemistry II*, A. R. Katritzky, C. W. Rees and E. F. V. Scriven, ed., Pergamon, Oxford, 1996, vol. 1B. pp. 507–720.

2 M.-K. Jeon and K. Kim, *Tetrahedron*, 1999, **55**, 9651; H.-S. Lee, Y.-G. Chang and K. Kim, *J. Heterocycl. Chem.*, 1998, **35**, 659.

3 K. Kim, *Sulfur Rep.*, 1998, **21**, 147.

4 R. S. Ward, in *The Chemistry of ketenes, allenes and related compounds*, Part 1, S. Patai, ed., John Wiley and Sons, New York, 1980, ch. 7, pp. 223–277.

5 Refer to ref. 2 for other 5-alkylidene-5*H*-1,2,3-dithiazoles.

6 B. D. Vineyard, *J. Org. Chem.*, 1966, **31**, 601; H. Bohme and H.-P. Steudel, *Liebigs Ann. Chem.*, 1969, **730**, 121; D. N. Harpp and A. Granata, *Tetrahedron Lett.*, 1976, **35**, 3001; A. Banerji and G. P. Kalena, *Tetrahedron Lett.*, 1980, **21**, 3003; A. L. Schroll and G. Barany, *J. Org. Chem.*, 1986, **51**, 1866; G. Capozzi, A. Capperucci, A. Del'Innocenti, R. D. Duce and S. Menichetti, *Tetrahedron Lett.*, 1989, **30**, 2991; M. Ghadimi and R. R. Hill, *J. Chem. Soc., Chem. Commun.*, 1991, 903; G. Derbesy and D. N. Harpp, *Tetrahedron Lett.*, 1994, **35**, 5381; I. A. Abu-Yousef and D. N. Harpp, *J. Org. Chem.*, 1998, **63**, 8654.

CHEMCOMM
Communication
www.rsc.org/chemcomm

Diastereomeric separation of $[\{M(Cp^*)(ado)\}_3]^{3+}$ (M = Rh^{III}, Ir^{III}; ado = adenosinato): crystal structure of an inclusion compound $[\{Rh(Cp^*)(ado)\}_3](CF_3SO_3)_3\cdot MeOH$

Kazuaki Yamanari,* Rie Ito, Shiori Yamamoto and Akira Fuyuhiro

Department of Chemistry, Graduate School of Science, Osaka University, 1-16 Machikaneyama-cho, Toyonaka, Osaka 560-0043, Japan. E-mail: yamanari@ch.wani.osaka-u.ac.jp

Received (in Cambridge, UK) 28th March 2001, Accepted 21st June 2001
First published as an Advance Article on the web 12th July 2001

A diastereomer with a C_3 cyclic trimer $[\{Rh(adenosine)(Cp^*)\}_3](CF_3SO_3)_3$, which was obtained selectively by a second-order asymmetric transformation, can include one methanol molecule into its triangle dome-like cavity.

Adenosine (Hado, **1**) is an important DNA/RNA nucleoside. In

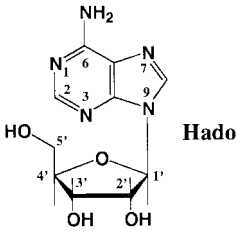

Hado

1992 Fish and coworkers reported the synthesis of an interesting C_3 cyclic trimer complex containing the ligand $[\{Rh(Cp^*)(ado)\}_3](CF_3SO_3)_3$ **2** ($Cp^* = \eta^5$-C_5Me_5).[1] However this complex was a mixture of two diastereomers (**2a** and **2b**) due to chiralities of the ribose group in **1** and the pure diastereomers had not been isolated. Hence the structure of **2** was deduced from NMR spectroscopy and the crystal structure $[\{Rh(Cp^*)(Me\text{-}ade)\}_3](CF_3SO_3)_3$ (Me-ade = 9-methyladeninato).[1]

Here we report diastereomeric separations of **2** and the corresponding Ir^{III} complex $[\{Ir(Cp^*)(ado)\}_3](PF_6)_3$ **3** (**3a** and **3b**) and a novel crystal structure of an inclusion compound $[\{Rh(Cp^*)(ado)\}_3](CF_3SO_3)_3\cdot MeOH$ (**2a**·MeOH). The absolute configurations of all complexes can be assigned based on circular dichroism (CD) spectra.

A self-assembling reaction between $[Rh(Cp^*)(H_2O)_3]^{2+}$ and **1** gave **2**† in high yield. Fig. 1(a) shows the ^1H NMR spectrum of the reaction solution, which indicates the presence of two diastereomers. However fractional crystallization of this reaction solution gave only one diastereomer **2a** up to the end of evaporation [Fig. 1(b)]. This phenomenon, the selective crystallization of one of the diastereomers under conditions of relatively rapid isomer equilibration in solution, is denoted second-order asymmetric transformation,[2] as observed in fac(*S*)-[Co{(*R*)-cysteinato-*N*,*S*}$_3$]$^{3-}$.[3] Though shifts of the diastereomeric equilibria have been known in many organometallic systems, the above phenomenon is quite rare.[4] The electrospray ionization (ESI) mass spectrum of **2a** showed dominant peaks at *m/z* 504.1, 830.7 and 1811.1, which correspond to the ions $[3M-3X]^{3+}$, $[3M-2X]^{2+}$ and $[3M-X]^{+}$, respectively, where 3M and X represent the complex and $CF_3SO_3^-$, respectively. The result indicates that **2** has a cyclic trinuclear structure.

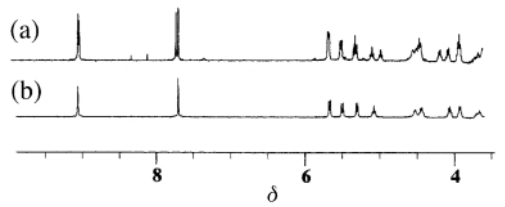

Fig. 1 Proton NMR spectra of **2** (a) and **2a** (b) in $(CD_3)_2SO$.

Fig. 2 shows a view of $[\{Rh(Cp^*)(ado)\}_3][CF_3SO_3]_3\cdot 2.5H_2O\cdot MeOH$ (**2a**·MeOH).‡ This complex has a trinuclear structure. Three Rh^{III} ions are crystallographically independent and form an almost equilateral triangle: Rh(1)···Rh(2) 5.6037(6), Rh(1)···Rh(3) 5.6353(6) and Rh(2)···Rh(3) 5.6285(6) Å. The ado ligand adopts a μ-1κN^1:2κ$^2N^6$,N^7 bridging mode: it coordinates to one Rh^{III} ion in a bidentate manner *via* the NH^6 and N(7) donors which form a five-membered chelate ring and bridges to another Rh^{III} ion through the N(1) donor. The three purine rings are located at the same side and form a triangular dome-like cavity. Interestingly one molecule of methanol just fits this cavity, forming an inclusion compound. There are two O–H···O hydrogen bonds between the oxygen of methanol and the hydroxyl groups of ribose [O(102)···O(401) 2.782(8) and O(205)···O(401) 2.748(8) Å]. Moreover three CH–π interactions are found: the three distances between the carbon atom of the methyl group and each of the least-square planes of the three purine rings are 3.53, 3.63 and 3.72 Å. These two types of interactions stabilize the inclusion of the methanol. The side length of the triangle formed by C(6), corresponding to a bottom of the cavity in Fig. 2, is 3.86 Å (av.) and the length by C(1′), at the top of the cavity, is 8.18 Å (av.). Three ribose groups close the cavity by acting as a cap. The side stereoview and the space-filling structure in Fig. 3 clearly show this triangle dome-like cavity. Fish and

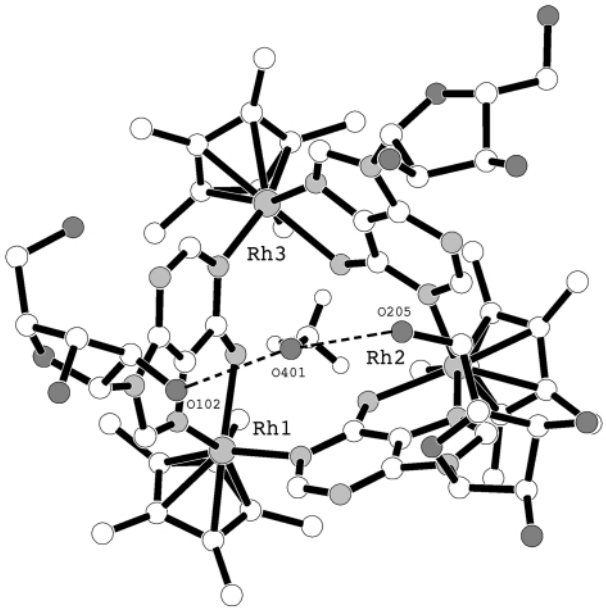

Fig. 2 The structure of the cation in $[\{Rh(Cp^*)(ado)\}_3][CF_3SO_3]_3\cdot 2.5H_2O\cdot MeOH$ (**2a**·MeOH): Selected average bond distances (Å) and angles (°) Rh–N(6) 2.161, Rh–N(7) 2.159, Rh–N(1′) 2.155, C(6)–N(6) 1.306; N(6)–Rh–N(7) 79.1, N(6)–Rh–N(1′) 89.9, N(7)–Rh–N(1′) 84.5, N(6)–C(6)–C(5) 115.6, Rh–N(7)–C(5) 106.5, Rh–N(6)–C(6) 113.4.

 DOI: 10.1039/b102870g

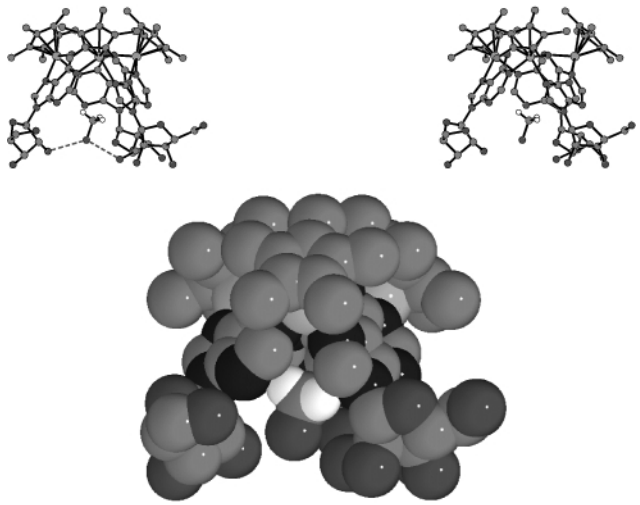

Fig. 3 Side stereoview (top) and the space-filling structure (bottom) of **2a**·MeOH.

coworkers have reported that **2** and analogous cyclic trimer complexes are useful hosts for molecular recognition of aromatic amino acid guests.[5] The present study gives the structural support for such investigations.

Since the central Rh^{III} ions become chiral each unit complex has chirality C (clockwise) or A (anticlockwise).[6] **2a** has a chiral array of CCC, and the CD spectrum is shown in Fig. 4. The CD intensity is considerably stronger than those reported for nucleosido complexes which are mixtures of two diastereomers.[7] It should be noted that the present Rh^{III} system contains only the C_3 CCC diastereomer. A D_2O solution of **2a** produced 30% of **2b** at room temperature in ten days.

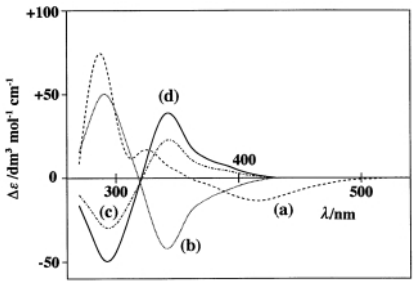

Fig. 4 CD spectra of $[\{Rh(Cp^*)(ado)\}_3](CF_3SO_3)_3$ (a) and $[\{Ir(Cp^*)(ado)\}_3](PF_6)_3$ (b, c and d). The pure CD spectrum (d) of **3b** was calculated from the spectra.

The corresponding Ir^{III} complex $[\{Ir(Cp^*)(ado)\}_3](PF_6)_3$ **3**§ was prepared in the same manner and showed a very similar ^1H NMR spectrum to that of **2** which is characteristic for a trimer.[1] Upon fractional crystallization, both diastereomers **3a** and **3b** were obtained as almost pure isomers (Fig. 5). The ESI mass spectrum of **3a** showed dominant peaks corresponding to the ions $[3M - 3X]^{3+}$ and $[3M - 2X]^{2+}$. Therefore we concluded that **3** has the same C_3 cyclic trinuclear structure as **2**. As shown in Fig. 4, both CD spectra (b) and (d) are almost enantiomeric. To our knowledge, this is the first example of isolating two diastereomers for nucleosido complexes. The CD spectra of the Ir^{III} complexes is blue-shifted by *ca.* 5000 cm^{-1} compared with those of Rh^{III} complexes. **3a** showed (−) and (+) CD peaks

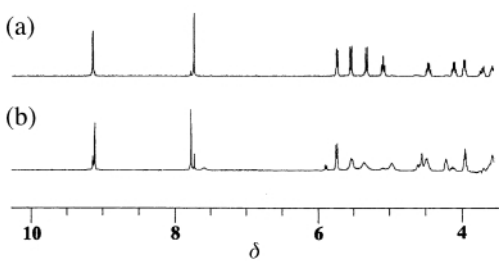

Fig. 5 Proton NMR spectra of **3a** (a) and **3b** (b) in $(CD_3)_2SO$.

from the lower energy side, the pattern of which is similar to that of the Rh^{III} complex **2a**. The ^1H NMR patterns of H^2 and H^8 are also analogous for **2a** and **3a**. Hence **3a** can be assigned as a CCC cyclic trinuclear structure and **3b** as AAA.

Notes and references

† For **2** (**2a**)**:** to a suspension of $[\{Rh(Cp^*)Cl_2\}_2]$[8] (0.2 g, 0.32 mmol) in water (30 cm^3) was added silver triflate (0.33 g, 1.3 mmol) and the mixture stirred at 40 °C for 1 h. The resulting silver chloride precipitate was removed by filtration and to the filtrate was added an aqueous solution (50 cm^3) of **1** (0.18 g, 0.64 mmol) adjusted to *ca.* pH 7 by adding aqueous NaOH. The mixed solution was stirred at room temp. for 1 d and then the resultant solution **2** was evaporated. Fractional crystallization of **2** always gave one diastereomer **2a** until the end of evaporation: that is, a second-order asymmetric transformation was found in this Rh^{III} system; hence the isolation of **2b** is impossible using $CF_3SO_3^-$. The yield was 70–85%. Found: C, 36.72; H, 4.49; N, 10.12. Calc. for $[\{Rh(Cp^*)(ado)\}_3][CF_3SO_3]_3\cdot 6H_2O$ **2a** ($C_{63}H_{93}F_9N_{15}O_{27}Rh_3S_3$): C, 36.58; H, 4.53, N, 10.16%. UV–VIS (H_2O): λ_{max}/nm (ε/dm^3 mol^{-1} cm^{-1}) 450sh (300) 385 (7470) 305sh (*ca.* 26000) 275 (32400). NMR: δ_H (DMSO-d_6) 9.081(H^8; s, 1H), 7.716(H^2; s, 1H), 5.687($H^{1'}$; d, 1H), 5.467($OH^{2'}$; d, 1H), 5.254($OH^{3'}$; d, 1H), 5.052($OH^{5'}$; t, 1H), 4.531(NH^6; s, 1H), 4.462($H^{2'}$; q, 1H), 4.092($H^{3'}$; q, 1H), 3.948($H^{4'}$; q, 1H), 3.703($H^{5'}$; m, 1H), 3.551($H^{5'}$; m, 1H), 1.827(Cp*; s, 15H); δ_C (dmso-d_6) 158.91(C6), 156.83(C2), 143.47(C4), 140.02(C8), 125.58(C5), 121.73(CF_3SO_3), 119.60(CF_3SO_3), 96.12(Cp*), 89.37(C1′), 85.68(C4′), 73.33(C2′), 69.48(C3′), 60.81(C5′), 9.27(Cp*). ESI MS (MeOH): *m/z* 504.1($[3M - 3X]^{3+}$), 830.7($[3M - 2X]^{2+}$), 1811.1 ($[3M - X]^+$). Crystals for X-ray crystal structure analysis were obtained from a methanol–ether solution.

‡ *Crystal data* for $[\{Rh(Cp^*)(ado)\}_3][CF_3SO_3]_3\cdot 2.5H_2O\cdot$MeOH **2a** were collected on a Rigaku RAXIS-RAPID Imaging Plate with graphite-monochromated Mo-Kα radiation (λ = 0.71069 Å); $C_{64}H_{90}F_9N_{15}O_{24.5}Rh_3S_3$, M_r = 2037.38, crystal size 0.15 × 0.15 × 0.35 mm; T = 23 °C; orthorhombic, space group $P2_12_12_1$ (no. 19), a = 21.0185(4), b = 21.3660(4), c = 19.4924(3) Å, V = 8753.7(3) Å^3, Z = 4, μ = 7.26 cm^{-1}, $F(000)$ = 4156, D_c = 1.546 g cm^{-3}, $2\theta_{max}$ = 55.0°. 20037 reflections were collected. Final $R1$ = 0.044 (wR = 0.137) for 13527 reflections with $I > 2\sigma(I)$ (993 parameters). All calculations were performed using the TEXSAN[9] crystallographic software package. CCDC reference number 157281. See http://www.rsc.org/suppdata/cc/b1/b102870g/ for crystallographic data in CIF or other electronic format.

§ For **3** (**3a** and **3b**): the corresponding Ir^{III} complex was prepared in the same manner but without adding aqueous NaOH. The reaction solution was stirred at room temperature for 6 d and then the resultant solution was evaporated. Since the desired complex is too soluble, an excess of NH_4PF_6 was added leading to crystals of **3** (85% yield). When an aqueous solution of **3** was fractionally recrystallized, **3a** was obtained first as the less soluble diastereomer (37% yield) and the more soluble diastereomer **3b** was obtained as a second crop (10% yield; 20% **3a** and 80% **3b**). The second-order asymmetric transformation in the Rh^{III}–CF_3SO_3 system was not observed in the Ir^{III}–PF_6 system. Found: C, 31.37; H, 3.77; N, 9.17. Calc. for $[\{Ir(Cp^*)(ado)\}_3][PF_6]_3\cdot 4H_2O$ **3a** ($C_{60}H_{89}F_{18}Ir_3N_{15}O_{16}P_3$): C, 31.50; H, 3.92, N, 9.18%. UV–VIS (H_2O): λ_{max}/nm (ε/dm^3 mol^{-1} cm^{-1}) 340sh (*ca.* 10600) 285(23400). NMR: δ_H (DMSO-d_6) 9.142(H^8; s, 1H), 7.731(H^2; s, 1H), 5.746($H^{1'}$; d, 1H), 5.523($OH^{2'}$; d, 1H), 5.296($OH^{3'}$; d, 1H), 5.081($OH^{5'}$; t, 1H), 4.651(NH^6; s, 1H), 4.469($H^{2'}$; q, 1H), 4.119($H^{3'}$; q, 1H), 3.972($H^{4'}$; q, 1H), 3.728($H^{5'}$; m, 1H), 3.568($H^{5'}$; m, 1H), 1.815(Cp*; s, 15H); δ_C (dmso-d_6) 161.38(C6), 157.93(C2), 144.19(C4), 139.36(C8), 128.06(C5), 93.80(CF_3SO_3), 89.65(C1′), 87.77(Cp*), 85.64(C4′), 73.55(C2′), 69.30(C3′), 60.62(C5′), 9.09(Cp*). ESI MS (MeCN): *m/z* 594.7($[3M - 3X]^{3+}$), 963.4($[3M - 2X]^{2+}$). **3b**: NMR: δ_H (dmso-d_6) 9.115(H^8; s, 1H), 7.775(H^2; s, 1H), 5.742($H^{1'}$; d, 1H), 5.541(s, 1H), 5.352(s, 1H), 4.970(s, 1H), 4.611(s, 1H), 4.555(s, 1H), 4.488(s, 1H), 4.220(s, 1H), 3.967(d, 1H), 1.808(Cp*; s, 15H). The concentration of **3b** for CD measurement was determined from the molar absorption coefficients of **3a**.

1 D. P. Smith, E. Bruce, B. Morales, M. M. Olmstead, M. F. Maestre and R. H. Fish, *J. Am. Chem. Soc.*, 1992, **114**, 10647.
2 E. E. Turner and M. M. Harris, *Quart. Rev. (London)*, 1947, **1**, 299.
3 M. Kita and K. Yamanari, *J. Chem. Soc., Dalton Trans.*, 1999, 1221.
4 H. Brunner, *Angew. Chem., Int. Ed.*, 1999, **38**, 1194.
5 H. Chen, M. F. Maestre and R. H. Fish, *J. Am. Chem. Soc.*, 1995, **117**, 3631.
6 *Nomenclature of Inorganic Chemistry, Recommendation 1990*, ed. G. J. Leigh, Blackwell Scientific Publications, Oxford, UK, 1990.
7 D. P. Smith, E. Kohen, M. F. Maestre and R. H. Fish, *Inorg. Chem.*, 1993, **32**, 4119.
8 C. White, A. Yates and P. M. Maitlis, *Inorg. Synth.*, 1992, **29**, 228.
9 TEXSAN-TEXRAY Structure Analysis Package, Molecular Structure Corporation, Houston, TX, 1985 and 1992.

CHEMCOMM
Communication
www.rsc.org/chemcomm

Comment on 'Self-assembled multiporphyrin arrays mediated by self-complementary quadrupole hydrogen bond motifs'†‡

Gianfranco Ercolani*

Dipartimento di Scienze e Tecnologie Chimiche, Università di Roma Tor Vergata, Via della Ricerca Scientifica, 00133 Roma, Italy. E-mail: ercolani@uniroma2.it

Received (in Cambridge, UK) 20th February 2001, Accepted 4th June 2001
First published as an Advance Article on the web 12th July 2001

The self-assembly of discrete linear tapes claimed by the title communication is questioned on the basis of a rigorous thermodynamic analysis; moreover the reported thermodynamic data are not consistent with self-assembly of the square.

There is currently much interest in the preparation and isolation of monodisperse oligomers because of their technological applications.[1] In a recent communication in this journal,[2] Drain, Shi, Milic and Nifiatis (DSMN) reported ^{1}H NMR experiments aimed at supporting a strong bias in favour of well defined linear oligomers in solution simply by changing the stoichiometric ratio between monofunctional and bifunctional reactants capable of reacting with each other in a reversible addition reaction. In particular they claimed that mixing 5-[2,6-bis(acetylamino)-pyridin-4-yl]-10,15,20-tris(4-*tert*-butylphenyl)porphyrin and 5,15-bis[2,6-bis(acetylamino)pyridin-4-yl]-10,20-bis(4-*tert*-butylphenyl)porphyrin in a 2:1 stoichiometry leads essentially to a linear trimer (Scheme 1, $i = 1$) whereas using a 2:2 ratio a linear tetramer ($i = 2$) is formed in prevalence.

This approach which seems to be self-evident, would have a profound influence on the preparation of monodisperse linear oligomers, also in view of the fact that end-terminated oligomers would inhibit the competitive formation of cyclic species.[3] Owing to the importance of the observation, I believe that a warrant based on rigorous thermodynamic grounds is required.

At first consider a monomer A–A (L_1) bearing two identical functional groups, capable of reacting with each other in a reversible addition reaction. If rings are assumed to be completely absent, a system initially composed of monomer units L_1, after equilibration, contains in principle an infinite number of linear oligomers L_i, i being the polymerisation degree. Let K be the equilibrium constant for the dimerisation of a monofunctional reactant R–A, if the association between end groups is independent of the length of the chain, then the oligomer distribution can be expressed as follows:†

$$[L_i] = (\sigma K)^{-1} x^i \quad (1)$$

where σ is a symmetry number, that in the present case is equal to 4,§ and x is the fraction of reacted end-groups. Eqn. (1) is of course equivalent to the classical Flory distribution valid in the case of polycondensation.[4] The mass balance equation is given by eqn. (2)†

$$[L_1]_0 = (\sigma K)^{-1} x (1 - x)^{-2} \quad (2)$$

where $[L_1]_0$ is the initial monomer concentration. Solving eqn. (2) for x, the weight fraction w_i of the oligomer L_i, can be easily evaluated.† In Fig. 1 are reported plots of the weight fraction of the first five oligomers as a function of $\sigma K[L_1]_0$. Extensive polymerisation occurs at high values of the product $K[L_1]_0$, whereas for the highest yield of a specific oligomer a specific $K[L_1]_0$ value is required. By inspection of Fig. 1, it results that with simple oligomerisation the yield of the dimer can be 30% at best, that of the trimer 19%, that of the tetramer 14% and that of the pentamer 11%. It would be very useful if by addition of appropriate amounts of a chain terminator R–A one could selectively increase the yield of a specific oligomer as suggested by DSMN.

A mixture of a monofunctional reactant R–A (A) and of a bifunctional reactant A–A (L_1) will generate in solution the dimer of R–A (N_0) and three families of oligomers, namely L_i having both ends free, M_i having only one end free, and N_i having both ends terminated as the species shown in Scheme 1.¶ The oligomer distribution of L_i is still given by eqn. (1) whereas those of M_i and N_i are given by eqn. (3) and (4), respectively.†

$$[M_i] = [A] x^i \quad (3)$$

$$[N_i] = K [A]^2 x^i \quad (4)$$

It is useful to consider the total concentration of the oligomers with the same polymerisation degree, $[R_i]$, obtained by summing eqn. (1), (3), and (4)

$$[R_i] = \{(\sigma K)^{-1} + [A] + K[A]^2\} x^i \quad (5)$$

Let us define the term in parentheses as $(\sigma K_{app})^{-1}$, where K_{app} is an apparent constant at a given concentration of $[L_1]_0$ and $[A]_0$, then eqn. (5) can be rewritten as eqn. (6)

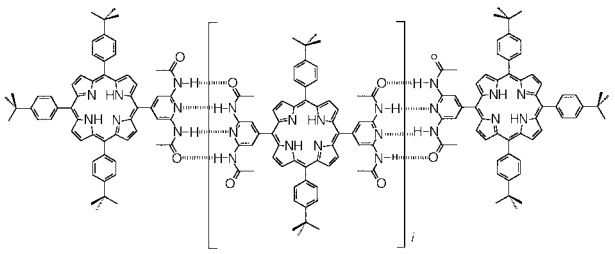

Scheme 1

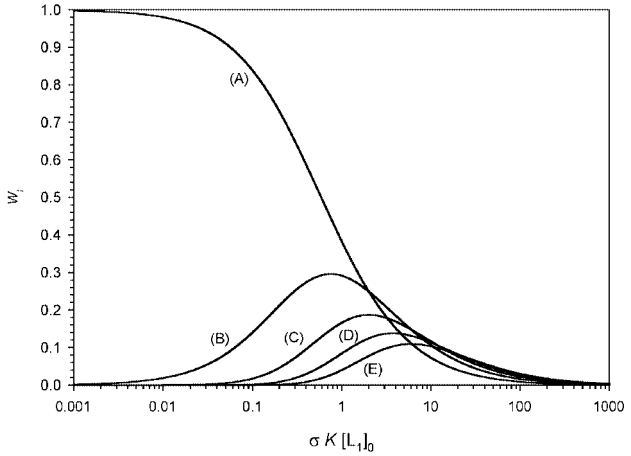

Fig. 1 Weight fraction of monomer, dimer, trimer, tetramer, and pentamer (curves from A to E, respectively) *vs.* $\sigma K[L_1]_0$.

† Electronic supplementary information (ESI) available: formal derivation of eqn. (1), (2), (3) and (4), and details about the construction of Figs. 1 and 2, and self-assembly of the square. See http: //www.rsc.org/suppdata/cc/b1/b101678b/

 DOI: 10.1039/b101678b

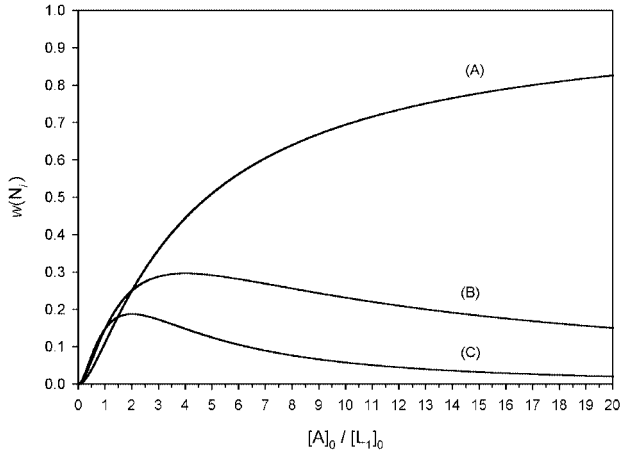

Fig. 2 Weighted fraction of N_0, N_1, and N_2 (curves A, B and C, respectively) *vs.* $[A]_0/[L_1]_0$ with K set very high.

$$[R_i] = (\sigma K_{app})^{-1} x^i \quad (6)$$

which has the same form as eqn. (1). It is easy to show that now the mass balance equation has the same form as eqn. (2) with K replaced by K_{app}, therefore Fig. 1 can now be used to predict the weight fraction of R_i. Of course in no case can the weight fraction of the end terminated oligomer N_i, which is a part of R_i, be greater than the weight fraction of R_i, thus disproving the idea that specific stoichiometric ratios between $[L_1]_0$ and $[A]_0$ can drive the reaction toward a certain oligomer, as suggested by DSMN. An increase of $[A]_0$, of course, will cause an increase of [A], and consequently a decrease of the K_{app} value. This involves a shift to the left in the abscissa of Fig. 1, *i.e.* depolymerisation. An increase of [A] will also cause a change of the relative weight of each oligomer type within R_i disfavouring the L_i type; thus in the limit of $[A]_0$ tending to infinity only N_1 will be present in solution, apart of course from A and N_0. To further illustrate the extent of polydispersity, in Fig. 2 is reported the fraction of N_0, N_1, and N_2, weighted according to the content of functional groups, against the ratio $[A]_0/[L_1]_0$, with K set very high so that $[L_i] = [M_i] = 0$ and $[R_i] = [N_i]$.† It is evident from Fig. 2 that, although DSMN realised that linear self-assembly does not give pure N_1 and N_2, they certainly undervalued the extent of polydispersity. It also appears that the best $[A]_0/[L_1]_0$ value to obtain N_i is not $2/i$ but $4/i$.

It should be noted that the equilibrium constants reported by DSMN for the formation of the trimer and the tetramer (Scheme 1, $i = 1$ and 2, respectively), 110 dm^6 mol^{-2} and 70 dm^9 mol^{-3}, respectively, are certainly wrong. Considering the value of the equilibrium constant for the dimerisation given by DSMN (K = 160 dm^3 mol^{-1}) as a *bona fide* value, the constant for the formation of the trimer should be equal to $4K^2$, *i.e.* of the order of 10^5 dm^6 mol^{-2}, and that of the tetramer $16K^3$, *i.e.* of the order of 10^8 dm^9 mol^{-3}. In fact ^{1}H NMR cannot be used to assess the distribution of linear oligomer ; ^{1}H NMR records the average chemical shift of bound and unbound end groups, and since all the associations between end groups have the same probability of occuring, any experiment in which the total concentration of end groups is identical, no matter if they come from monofunctional or bifunctional reactants, will give the same chemical shift even if the distribution of the species actually present in solution are very different. This is demonstrated by the fact that DSMN found very similar $C_{1/2}$ values (the concentration at the half maximum increase in the chemical shift) for different linear self-assembly experiments. DSMN also reported that 5,10-bis[2,6-bis(acetylamino)pyridin-4-yl]-15,20-bis(4-*tert*-butylphenyl)porphyrin undergoes self-assembly to form a cyclic tetramer (a square), however the equilibrium constant they reported for the formation of the square (K_{square} = 2400 dm^9 mol^{-3}) is not consistent with the reported $C_{1/2}$ value (0.8 mM). By assuming that the square and the monomer are the only species present in solution, a K_{square} value of 3.9×10^9 dm^9 mol^{-3} can be estimated.† It appears therefore that DSMN made some serious computational error in the evaluation of K_{square}. If the value of K_{square} were that indicated by DSMN, self-assembly of the square would not occur.

I have reported a treatment for self-assembly macrocyclisations of a monomer of the type A–B.[5] One of the principal results of my treatment is that in order for self-assembly to be virtually complete in a certain range of initial monomer concentration the following condition must be verified [eqn. (7)], where EM is the effective molarity[6] of the self-assembled

$$\mathrm{EM}\ \sigma K \geqslant 185\ n \quad (7)$$

ring, K is the equilibrium constant for the intermolecular model reaction, and n is the number of monomer units constituting the ring. Since $K_{square} = \mathrm{EM}(\sigma K)^4$, from a K_{square} value of 3.9×10^9 dm^9, an EM of $\approx$0.02 mol dm^{-3} can be calculated. According to eqn. (7) this value is too low to be compatible with complete self-assembly of the square. An approximate calculation indicates that the maximum molar fraction that can be reached by the square is about 67%.†

Another point regards the claimed quadruple hydrogen bonding. There is a general consensus that the most stable conformation of the amide linkage in 2,6-bis(acylamino)pyridines is *anti* and not *syn*,[7] as reported by DSMN; thus the subunits are probably just double hydrogen bonded. An example of a reversible polymer formed by a genuine quadruple hydrogen bond shows that such a bond can be very strong indeed ($K > 10^6$ dm^3 mol^{-1}).[8]

In conclusion the formation of discrete linear tapes by changing the stoichiometric ratio between monofunctional and bifunctional reactants is not supported by a rigorous thermodynamic analysis; the self-assembly of the cyclic tetramer should be re-examined in the light of actual knowledge in order to provide consistent thermodynamic data.

I thank both the referees for their helpful suggestions.

Notes and references

‡ Part 3 of the series Physical Basis of Self-Assembly. Part 2: G. Ercolani, D. Monti and M. Ioele, *New J. Chem.*, 2001, **25**, 783.

§ For the oligomerisation of a monomer A–B bearing two different functional groups the same equations hold but with $\sigma = 1$.

¶ Note that the species that DSMN call the dimer, the trimer and the tetramer are here defined as N_0, N_1, and N_2, respectively.

1 *Reactive Oligomers, (ACS Symposium Series, 282)*, ed. F. W. Harris and H. J. Spinelli, ACS, Washington, DC, 1985; C. V. Uglea and I. I. Negulescu, *Synthesis and Characterization of Oligomers*, CRC Press LLC, Boca Raton, FL, 1991; C. V. Uglea, *Oligomers Technology and Applications*, Marcel Dekker, New York, 1998; *Electronic Materials: The Oligomer Approach*, ed. K. Müllen and G. Wegner, Wiley-VCH, Weinheim, 1998.

2 C. M. Drain, X. Shi, T. Milic and F. Nifiatis, *Chem. Commun.*, 2001, 287.

3 G. Ercolani, L. Mandolini, P. Mencarelli and S. Roelens, *J. Am. Chem. Soc.*, 1993, **115**, 3901 and references therein.

4 P. J. Flory, *Principles of Polymer Chemistry*, Cornell University Press, Ithaca, 1953.

5 G. Ercolani, *J. Phys. Chem. B*, 1998, **102**, 5699.

6 A. J. Kirby, *Adv. Phys. Org. Chem.*, 1980, **17**, 183; L. Mandolini, *Adv. Phys. Org. Chem.*, 1986, **22**, 1.

7 F. H. Beijer, R. P. Sijbesma, J. A. J. M. Vekemans, E. W. Meijer, H. Kooijman and A. L. Spek, *J. Org. Chem.*, 1996, **61**, 6371.

8 R. P. Sijbesma, F. H. Beijer, L. Brunsveld, B. J. B. Folmer, J. H. K. K. Hirschberg, R. F. M. Lange, J. K. L. Lowe and E. W. Meijer, *Science*, 1997, **278**, 1601.

Typeset and printed by Black Bear Press Limited, Cambridge, England

CHEMCOMM
Feature Article
www.rsc.org/chemcomm

Antisense molecules and furanose conformations—is it really that simple?

Lisbet Kværnø†[a] and Jesper Wengel*[b]

[a] *Center for Synthetic Bioorganic Chemistry, Department of Chemistry, University of Copenhagen, Universitetsparken 5, DK-2100 Copenhagen, Denmark*
[b] *Department of Chemistry, University of Southern Denmark, Campusvej 55, DK-5230 Odense M, Denmark. E-mail: jwe@chem.sdu.dk; Fax: +45 66 15 87 80*

Received (in Cambridge, UK) 25th May 2001, Accepted 13th June 2001
First published as an Advance Article on the web 26th July 2001

Selected nucleic acid mimics are discussed in the context of the antisense therapeutic strategy with focus on furanose conformation, RNA-binding affinity, and activation of the RNA-cleaving enzyme RNase H.

Introduction

In order to inhibit gene expression by targeting RNA with short antisense oligonucleotides, multiple chemically modified nucleoside and oligonucleotide analogues have been synthesized and evaluated during the last 15 years.[1,2] Selected examples of modified nucleic acids are described here with the emphasis on their hybridization properties and capability to activate RNase H, an RNA-degrading enzyme, in relation to their conformational and structural characteristics. The focus is on important recent developments and their prospects towards the realization of the antisense therapeutic strategy.

The antisense strategy

The carriers of all genetic information in living organisms are 2′-deoxyribonucleic acid (DNA) and ribonucleic acid (RNA), polymers consisting of repetitive units of nucleotide monomers. Each nucleotide contains a phosphate group, a carbohydrate moiety and a nucleobase (Fig. 1). The natural nucleobases in

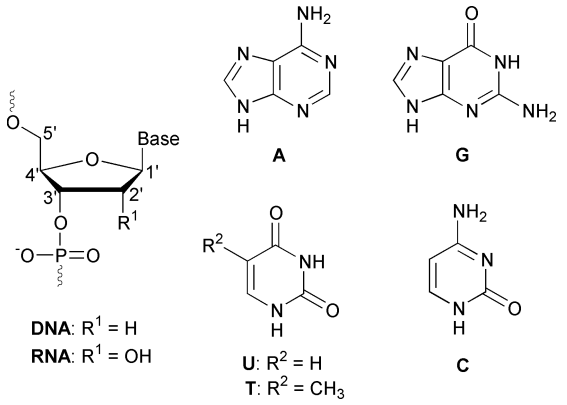

Fig. 1 Structures of a nucleotide monomer (left) and the nucleobases adenine (A), guanine (G), uracil (U), thymine (T), and cytosine (C).

DNA (R^1 = H) are A, G, T and C while U replaces T in RNA (R^1 = OH). Two complementary polymeric or oligomeric single strands hybridize in an anti-parallel fashion forming a right-handed duplex with the specific Watson–Crick base-pairing of G to C and A to T or U.

As depicted schematically in Fig. 2, the genetic information is transcribed from double-stranded DNA, located in the cell

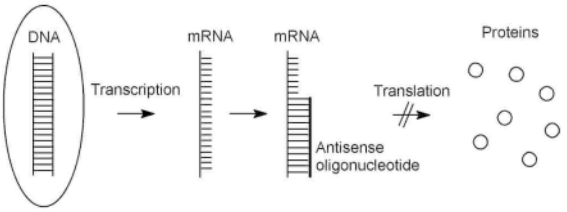

Fig. 2 Schematic overview of the antisense strategy.

nucleus, to single-stranded messenger-RNA (mRNA) which functions as a carrier of genetic information from the cell nucleus to the ribosomes in the cytoplasm. The principle of the antisense strategy is to target mRNA by duplex formation using a short (10–20 nucleotides long) antisense oligonucleotide, thereby preventing the translation of the mRNA into proteins. In principle, any genetic sequence, and thus any disease with a genetic origin, should be subject to selective targeting by varying the nucleotide sequence of an antisense oligonucleotide approximately 18 nucleotides long. This makes the antisense strategy general and attractive compared with the individual development of traditional drugs acting at the protein level. An antisense oligonucleotide has to fulfil several functional requirements, *e.g.* high binding affinity toward the RNA binding strand, resistance towards nucleases, low toxicity, and efficient delivery to the desired target site, *in vivo*, rendering

Lisbet Kværnø (b. 1974) received her BSc and MSc degrees in 1998 and 2000, respectively, from The University of Copenhagen under the supervision of Professor Jesper Wengel. She is currently pursuing a PhD within the field of total synthesis of natural products in the group of Professor David Tanner, The Technical University of Denmark.

Jesper Wengel (b. 1963) obtained his PhD within the field of nucleoside chemistry in the group of Dr Erik B. Petersen, University of Southern Denmark, Odense (formerly Odense University) in 1991 and joined the faculty immediately afterwards as an assistant professor. In 1996, he was appointed as a full professor in bioorganic chemistry at The University of Copenhagen. He returned to The University of Southern Denmark, Odense, also as a full professor, in August 2000. His main research interests are the synthesis and properties of chemically modified nucleosides and oligonucleotides, and the use of branched and functionalized oligonucleotides within supramolecular chemistry.

† Current address: Department of Chemistry, The Technical University of Denmark, Building 201, DK-2800, Lyngby, Denmark.

chemical modification of the natural nucleic acid structures needed.

Nucleic acid structure and furanose conformations

The pseudorotational circle[3] depicted in Fig. 3 describes the possible furanose conformations of the nucleotide monomers.

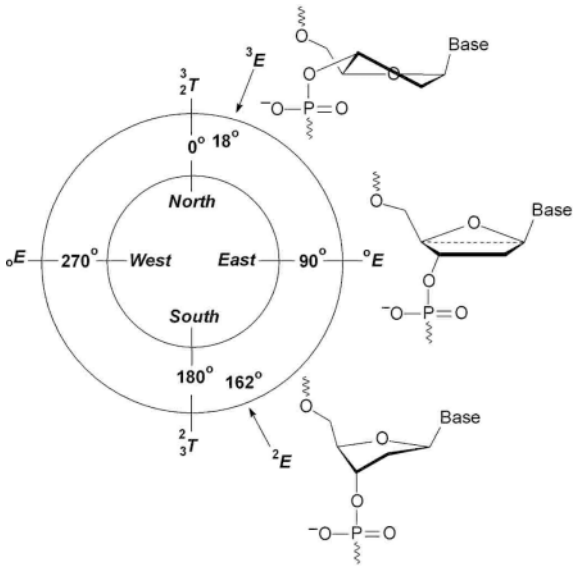

Fig. 3 The pseudorotation cycle showing the relation between the pseudorotation angle *P* (0–360°; calculated from the five torsional angles of the furanose ring[3]) and furanose ring conformations.

All distinct conformations (*i.e.* envelope, *E*, and twist, *T*, conformations) are separated by 18° with a superscript designating an atom above the plane described by the remaining three or four atoms of the furanose ring, and a subscript designating an atom below.

The two dominating furanose conformations for DNA and RNA generally give rise to two different duplex forms, as depicted in Fig. 4. Apart from having all furanose conformations in an *S*-type (*south*-type, C2′-*endo*, ^2E) conformation, the B-type helix seen in solution for DNA is characterized by 10 base-pairs almost perpendicular to the helix axis per helix turn, and a distinct difference in width of the major and the minor grooves.[4,5] In contrast, RNA adopts an A-type helix in which the furanose conformations are all *N*-type (*north*-type, C3′-*endo*, ^3E) with 11 base-pairs tilted 20° with respect to the helix axis per helix turn, and the minor and major grooves being almost equally wide.[4,5]

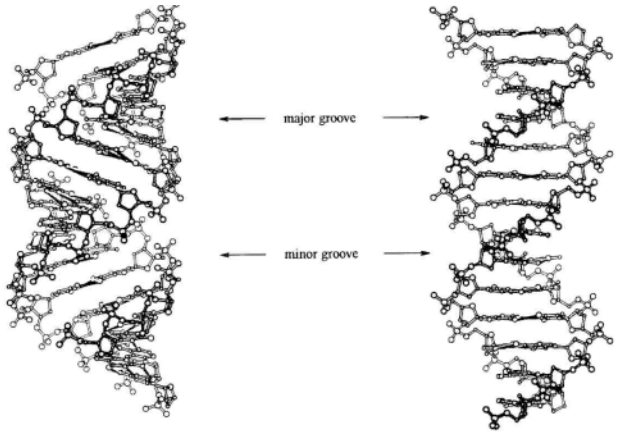

Fig. 4 Globular conformations of an A-type duplex (left) and a B-type duplex (right) generally seen for RNA:RNA and DNA:DNA duplexes, respectively.

Modes of action and conformational requirements of antisense molecules

An antisense oligonucleotide has basically two possible modes of action both depending on the duplex formation between the RNA target and the antisense oligonucleotide. One is a simple steric blocking of the mRNA, the other recognition of the RNA–antisense duplex as a substrate for the enzyme RNase H which cleaves the RNA strand of an RNA–DNA duplex. In the latter scenario, one antisense oligonucleotide is able to pacify multiple mRNA strands. A high binding affinity towards RNA is crucial, especially for the steric blocking approach. Conformational restriction of the single-stranded antisense oligonucleotides is believed to favour duplex formation entropically by diminishing the loss of conformational degrees of freedom upon duplex formation, and conformational restriction of the furanose rings of oligonucleotides has been successfully applied to the field in the recent years.[6–8] Studies of a large number of oligonucleotide analogues have been generalized to the hypothesis that oligonucleotides restricted into *N*-type furanose conformations, thus yielding A-type duplexes when hybridized to RNA, effect the highest duplex stabilities.[1,9]

However, no fully modified antisense oligonucleotide with restricted *N*-type furanose conformations has been reported to be able to activate RNase H. The RNA–DNA heteroduplexes being substrates of RNase H which has been reported to bind in the minor groove, adopt an intermediate duplex form with a minor groove width also intermediate between that of the A form and the B form.[10–14] The furanose conformations in the RNA strand are still *N*-type (3′-*endo*) while hybridization to the RNA strand causes the furanose conformations of the DNA strand to change from the typical *S*-type (C2′-*endo*) into *E*-type conformations (O4′-*endo* range, see Fig. 3).[10,11,14] Thus, the activation of RNase H proposedly requires antisense oligonucleotides with furanose rings able to adopt *E*-type (O4′-*endo*), or perhaps *S*-type (C2′-*endo*), conformations, and *not* the duplex-stabilizing *N*-type conformations.

An appealing way to circumvent the lack of RNase H activation is the introduction of chimeric structures consisting of high-affinity nucleotide modifications in the terminal regions of the antisense oligonucleotide around a ‘gap’ of RNase H-activating nucleotides in the central part. To activate the mammalian RNase H, a gap size of five[15] to seven[16] unmodified 2′-deoxynucleotides has been suggested.

Selected oligonucleotide analogues

A number of the more promising nucleic acid mimics for the development of successful antisense oligonucleotides are discussed in the following. Emphasis is given to analogues in which the furanose ring is restricted into a distinct conformation by either stereoelectronical or constitutional (sterical) means. Average duplex stabilities for hybridization towards complementary RNA targets are reported as the change in the melting temperature per modified nucleotide (°C per mod.) relative to the corresponding unmodified DNA–RNA reference duplex, the melting temperature being defined as the temperature at which half of the duplex is dissociated as measured by the associated hyperchromic shift at 260 nm.

Phosphorothioates

In 1998, the first antisense drug, Vitravene™ (ISIS-2922), was approved by the FDA for the treatment of cytomegalovirus retinitis in immunocompromised patients.[17] This antisense oligonucleotide consists of phosphorothioate (thiophosphate) nucleotides, in which one of the non-bridging phosphate oxygens is substituted by sulfur (**5**, Fig. 5) resulting in improved nuclease stability while the capability to activate RNase H remains intact. Phosphorothioates are, however, considered as

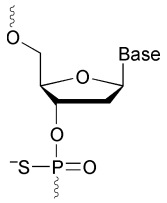

5

Fig. 5 Structure of phosphorothioates.

only 'first generation' antisense oligonucleotides due to less desirable features such as lowered duplex stabilities (approximately −0.8 °C per mod.), the existence of diastereomeric mixtures because of the chirality of the phosphorus atoms, and significant toxicity caused, *e.g.* by non-specific binding to proteins.[18]

Selected 2′-*O*-alkylated RNA derivatives

For 2′-*O*-alkylated RNA derivatives, the *gauche* effect between O2′ and O4′ (along the C1′–C2′ bond) induces a conformational shift towards an *N*-type (C3′-*endo*) furanose conformation resulting in A form duplexes as also seen for unmodified RNA. Provided that the 2′-*O*-alkyl group is not too sterically demanding (*i.e.* alkyls smaller than hexyl),[19] increased duplex stability is observed. A 2′-*O*-Me-RNA monomer (**6A**, Fig. 6)

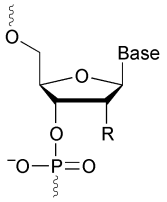

6A R = OCH_3
6B R = $OCH_2CH_2OCH_3$ (MOE)
6C R = $OCH_2CH_2CH_2NH_2$ (AP)

Fig. 6 Structures of selected 2′-*O*-alkylated RNA derivatives.

induces an increase in the melting temperature of *ca.* +0.5 to +1.0 °C per mod.,[20] while 2′-*O*-(methoxyethyl)- (MOE, **6B**) and 2′-*O*-aminopropyl- (AP, **6C**) monomers effect increases of *ca.* +1.0 to +1.5 °C per mod.[20,21] and *ca.* +1.0° C per mod.,[22] respectively. The nuclease stability of the 2′-*O*-Me derivatives is insufficient for antisense purposes,[9] which suggests the use of the more resistant MOE[21] or AP[22] modifications. Because of their preorganization into an *N*-type furanose conformation, none of the 2′-*O*-alkylated derivatives activate RNase H unless a gap-mer strategy is applied.[23]

N3′ → P5′-Phosphoramidates

Replacing the 3′-hydroxy group with an amino group introduces a non-chiral nuclease-resistant phosphoramidate internucleoside linkage. Such a modification (**7A**, Fig. 7) increases duplex

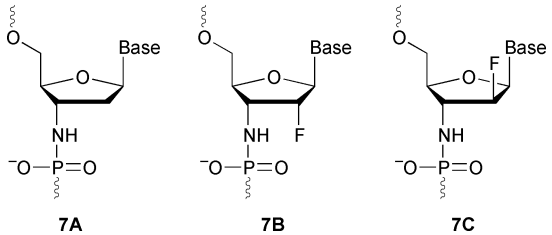

7A **7B** **7C**

Fig. 7 Structures of N3′ → P5′-phosphoramidates.

stabilities by +2.3 to +2.6 °C per mod.[24–26] which has been explained by the diminished *gauche* effect from the 3′-nitrogen atom preorganizing the furanose ring into an *N*-type (C3′-*endo*) conformation thus furnishing A-type duplexes with RNA targets as also shown by NMR[27,28] and X-ray studies.[29] Hybridized to RNA, fully modified phosphoramidates do not activate RNase H,[30] but this problem can be circumvented by the use of a gap-mer sequence with unmodified DNA monomers in the central gap[31] and also of a phosphoramidate mix-mer with alternating phosphoramidate and unmodified phosphordiester nucleotides.[32] The gap-mer phosphoramidates showed a lack of antisense activity which might be ascribed to the endonucleolytic degradation of the deoxynucleotide gap[9] while only fully modified phosphoramidates showed an RNase H-independent antisense activity.[31]

2′-Substitution with a *ribo*-configured fluorine atom (**7B**, *ribo*-configuration, Fig. 7) constrains the furanose ring entirely to a C3′-*endo* conformation due to the strong *gauche* effect from fluorine and induces increased duplex stabilities with as much as +4 to +5 °C per mod.[33] The RNA analogue of **7B** (a 2′-OH group instead of the fluorine atom) likewise afforded increased duplex stabilities (*ca.* +0.5 °C per mod.) relative to the parent phosphoramidates **7A**.[34] The *arabino*-configured 2′-fluoro phosphoramidate **7C**, too, displayed increased duplex stabilities (*ca.* +0.5 °C per mod.) relative to phosphoramidates **7A**, and, despite the opposing *gauche* effect from the 2′-fluoro substituent, a preorganized C3′-*endo* conformation, as shown by the analysis of coupling constants for trimers, still accounts for the improved hybridization properties.[35]

The results obtained for the various phosphoramidates convincingly demonstrate that stereoelectronic preorganization into a C3′-*endo* furanose conformation can be applied to induce increased duplex stabilities. It should be mentioned, though, that a considerable sequence-variation has been observed and that, *e.g.* increases as small as +0.6 °C per mod. have been reported for fully modified unsubstituted phosphoramidates **7A**.[36] A point of concern with phosphoramidates is their more difficult incorporation into oligonucleotides with step-wise coupling yields in the range of 94–97%.[25,33,35]

Arabino nucleic acids and 2′-fluoroarabino nucleic acids (ANA and 2′-F-ANA)

The inversion of the configuration around C2′ of natural RNA gives arabino nucleic acids (**8A**, Fig. 8) which show decreased

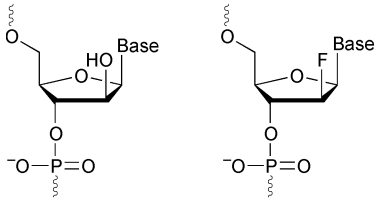

8A **8B**

Fig. 8 Structures of arabino nucleic acids.

duplex stabilities when hybridized to RNA while the corresponding 2′-fluoroarabino nucleic acids (**8B**), by contrast, enhance duplex stabilities by *ca.* +1.0 °C per mod.[37,38] The very interesting feature of both these modifications is that they were the first fully modified oligonucleotides with a chemically modified carbohydrate moiety to act as substrates for RNase H.[37–39] Their conformational similarity with natural DNA might account for this since duplexes, when hybridized to RNA, resemble an intermediate DNA–RNA duplex form as shown by CD spectroscopy.[38] The 2′-fluoro analogue **8B** adopts the O4′-*endo* furanose conformation when incorporated into DNA as shown by X-ray structure analysis.[40,41] In addition, molecular modelling[39,41] and NMR studies[39] of a fully modified 2′-F-ANA strand hybridized to RNA have confirmed an intermediate duplex form with a minor groove width intermediate between the minor groove widths of the standard A- and B-forms. The nuclease stability of the ANAs is improved compared with unmodified DNA though not as much as for the phosphorothioates.[37,39]

Hexitol nucleic acids (HNA)

Pyranose derivatives in general adopt one predominant conformation due to higher energy barriers for interconversion of ring conformers relative to furanose derivatives. To date, the 1′,5′-anhydrohexitol nucleic acids (HNA, **9A**, Fig. 9) and

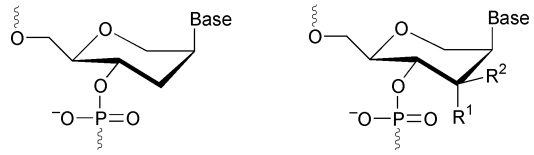

9A **9B** R^1 = OH, R^2 = H
9C R^1 = H, R^2 = OH

Fig. 9 Structures of hexitol nucleic acids.

derivatives constitute the most promising antisense candidates based on a pyranose moiety. Structurally, their substitution pattern makes them very good mimics of nucleotides preorganized into an *N*-type (C3′-*endo*) furanose conformation thus yielding A-type duplexes when hybridized to RNA as shown by CD spectroscopy,[42] molecular dynamics simulations,[43] and NMR studies.[44] Fully modified HNA displays enhanced duplex stabilities (typically +3.0 °C per mod.)[45] while sequence-specific variations of increases of duplex stabilities ranging between +0.9[45] and +5.8[42] °C per mod. have been observed. HNA acts only as a very poor substrate for RNase H,[42] while its nuclease-resistance[45] still allows it to display antisense effects ascribed to a mechanism of steric blocking.[46]

Interesting derivatives of HNA are the 1,5-anhydro-2-deoxy-D-altritol nucleic acids with an additional axial hydroxy group in the 3′-position (**9B**, Fig. 9) which show slightly enhanced duplex stabilities relative to HNA.[47] The altritol nucleic acids were designed to increase the surface hydrophilicity of the duplex thereby favouring duplex formation by improved hydratization.[8] In contrast, the inversion of configuration at the 3′-position, affording the corresponding 1,5-anhydro-2-deoxy-D-mannitol nucleic acids, leads to significantly reduced stability of duplexes with RNA[48] and obviously imposes a restricted conformation unfavourable for duplex formation.

Cyclohexene nucleic acids (CeNA)

Noteworthy results have been obtained for the conformationally rather flexible cyclohexene nucleic acids (CeNA, **10**, Fig. 10)

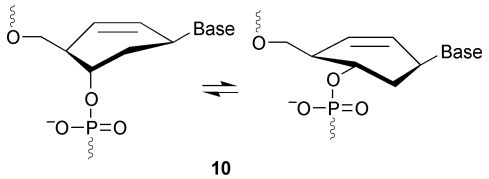

10

(*S*-type mimic) (*N*-type mimic)

Fig 10 Structure and conformational equilibrium of cyclohexene nucleic acids.

with a conformational equilibrium shifted towards *N*-type at the nucleoside level as shown by NMR and modelling studies (Fig. 10).[49] When incorporated into DNA strands, cyclohexene nucleotide monomers **10** induce increased duplex stabilities (+0.8 to +1.7 °C per mod.). Fully modified CeNA are nuclease-resistant and activate RNase H. The latter property establishes CeNA, next to ANA (Fig. 8), as the second fully modified oligonucleotide analogue with an altered carbohydrate part able to induce an RNase H cleavage of the target RNA strand.[50] This has been explained by the flexible conformational behaviour of the cyclohexane nucleotides allowing a $^2H_3$ (*S*-type mimic) conformation when hybridized to DNA and a $^3H_2$ (*N*-type mimic) conformation when hybridized to RNA as supported by CD spectroscopy, NMR studies of DNA duplexes with one cyclohexene nucleotide in each strand, and molecular dynamics simulations.[50]

Locked nucleic acids (LNA)

The synthesis of nucleosides and oligonucleotides containing furanose rings efficiently locked into a C3′-*endo* conformation has been accomplished by the introduction of an oxymethylene linkage between the C2′ and C4′ atoms generating the bicyclic locked nucleic acid (LNA, **11A**, Fig. 11). The incorporation of

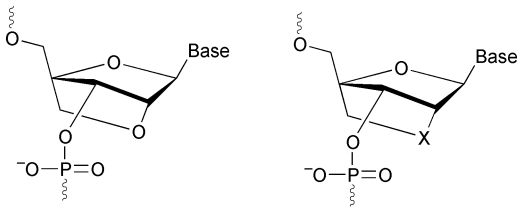

11A **11B** X = NH
11C X = S

Fig. 11 Structures of locked nucleic acids (LNA), 2′-amino LNA and 2′-thio LNA.

one or more LNA monomers, or the use of fully modified LNA, induces unprecedented increases in duplex stabilities (typically +3.0 to +11.0 °C per mod.).[51–54] The preorganization into a C3′-*endo* furanose conformation has been demonstrated at the nucleoside level by X-ray crystallography[55] as well as NMR studies[51,52] and also by NMR studies at the oligonucleotide level both when hybridized to DNA[56–58] and RNA, the latter yielding the expected A-type duplexes.[59] LNA monomers in partly modified strands were shown to strongly preorganize flanking unmodified DNA nucleotides into *N*-type–C3′-*endo* furanose conformations and single-stranded LNA into an RNA-like conformation.[58,59] Fully modified[51] and mix-mer LNA consisting of alternating LNA and DNA monomers[60] have proved to be nuclease-resistant, and an antisense effect has been demonstrated in living rats.[60] LNA activates RNase H as gapmers[60] but not as fully modified strands.[60,61]

The LNA-type constitution leads in general to efficient C3′-*endo* preorganization and favoured duplex formation which has been demonstrated by the hybridization properties (+3.0 to +8.0 °C per mod.) obtained for the heteroatom derivatives 2′-amino-LNA[62] (**11B**, Fig. 11) and 2′-thio-LNA[63] (**11C**). A related C2′-methylene extended bicyclic nucleoside (thus containing a 2-oxapropylene linker between the O2′ and O4′ atoms), shown by X-ray crystallography and NMR studies at the nucleoside level likewise to be restricted into a C3′-*endo* furanose conformation,[64] induced less dramatic but still significantly increased duplex stabilities (+1.9 to +3.3 °C per mod.).[65]

α-L-LNA—a selected LNA stereoisomer

The inversion of the configuration around C3′ and/or C2′ and C4′ of LNA afforded three LNA stereoisomers which have been evaluated with respect to RNA binding.[66] Of these, 'α-L-LNA' (α-L-*ribo* configured LNA, **12**, Fig. 12) with inverted config-

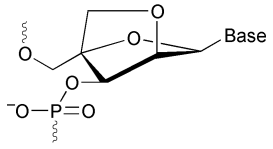

12

Fig. 12 Structure of α-L-LNA.

uration around C2′, C3′ and C4′ compared to LNA, showed the most promising properties with respect to duplex formation as

shown by increased duplex stabilities of +4.3 to +5.7 °C per mod. for both partly and fully modified strands.[66–68] NMR and molecular modelling studies on duplexes of partly or fully modified α-L-LNA hybridized to DNA or RNA have established α-L-LNA as a DNA mimic and, in addition, that an α-L-LNA–RNA duplex adopts an overall conformation intermediate between the A and B form.[69–71] The possibility of RNase H activity has therefore been evaluated. Fully modified and mixmeric (consisting of alternating α-L-LNA and unmodified DNA nucleotides) α-L-LNA showed cleavage, albeit very slow, of the RNA targets at high enzyme concentrations.[61]

Summary and outlook

For efficient antisense action by the steric blocking mechanism, the use of antisense oligonucleotides containing preorganized furanose rings with *N*-type (C3′-*endo*, RNA-like) conformations and high binding affinities towards RNA target strands appears optimal. In contrast, the mechanism involving activation of RNase H demands analogues adopting *S*-type (C2′-*endo* or O4′-*endo*, DNA-like) furanose conformations.[2,41] It therefore appears impossible to take advantage of both mechanisms effectively with only one single nucleotide modification.

Despite the above points, the necessary armamentarium of chemically modified building blocks for development of efficient antisense therapeutics appears at hand. LNA, α-L-LNA and phosphoramidates, among others, offer excellent binding affinities towards RNA targets. In addition, as shorter strands (*e.g.* 10–14 nucleotides long) can be applied, good to excellent pairing selectivities are in general obtained. The binding affinity and pharmacokinetic properties are tuneable by combining these affinity-enhancing key nucleotide building blocks with, *e.g.* DNA, RNA, phosphorothioate-DNA, phosphorothioate-LNA, 2′-amino-LNA (or conjugated derivatives thereof), and 2′-*O*-alkyl-RNA nucleotides which have all been demonstrated to be applicable in DNA–LNA duplexes.[62,63,69] Whether the recruitment of RNase H is essential for efficient and general antisense action with these strongly RNA-binding nucleic acid mimics is currently not established. If RNase H activity turns out to be needed or beneficial, it is foreseen that the combination of one or more segment(s) of conformationally restricted or conformationally locked high-affinity *N*-type oligonucleotide(s) with a segment of nuclease-resistant, RNase H-activating *S*-type nucleotides with lower affinities should be ideal. A gap-mer structure is of course one possibility, but with the discovery of LNA and other extreme RNA-binders alleviating the need for binding cooperativity between the different segments, many other architectures appear possible. However, biological studies and pharmacological developments are needed to confirm these predictions.

The results obtained with ANA (**8**, Fig. 8), HNA (**9**, Fig. 9) and α-L-LNA (**12**, Fig. 12) are remarkable and need consideration. Firstly, very efficient RNA-binding is evidently possible for analogues based on a furanose skeleton with a non-natural stereochemical structure, or on an RNA-mimicking hexitol scaffold. Especially noteworthy is the dramatic RNA-binding of the α-L-*ribo* configured α-L-LNA in which the configuration at three out of the four chirality centers is inverted compared with RNA (or LNA). In addition, fully modified HNA and fully modified or mix-meric α-L-LNA have been demonstrated to induce very weak, but significant, RNase H activity. Results like these leave ample room for further curiosity-driven chemistry-based research on modified nucleic acids.

Notes and references

1 S. M. Freier and K. H. Altmann, *Nucleic Acids Res*., 1997, **25**, 4429.
2 E. Uhlmann, *Curr. Opin. Drug Discovery Dev*., 2000, **3**, 203.
3 C. Altona and M. Sunderalingam, *J. Am. Chem. Soc*., 1972, **94**, 8205.
4 W. Saenger, *Principles of Nucleic Acid Structure*, Springer-Verlag, New York, 1984.
5 M. Egli, *Antisense Nucleic Acid Drug Dev*., 1998, **8**, 123.
6 P. Herdewijn, *Liebigs Ann. Chem*., 1996, 1337.
7 E. T. Kool, *Chem. Rev*., 1997, **97**, 1473.
8 P. Herdewijn, *Biochim. Biophys. Acta*, 1999, **1489**, 167.
9 D. Cook, *Nucleosides Nucleotides*, 1999, **18**, 1141.
10 M. Salazar, O. Y. Fedoroff, J. M. Miller, N. S. Ribeiro and B. R. Reid, *Biochemistry*, 1993, **32**, 4207.
11 O. Y. Fedoroff, M. Salazar and B. R. Reid, *J. Mol. Biol*., 1993, **233**, 509.
12 J. I. Gyi, G. L. Conn, A. N. Lane and T. Brown, *Biochemistry*, 1996, **35**, 12 538.
13 H. Nakamura, Y. Oda, S. Iwai, H. Inoue, E. Ohtsuka, S. Kanaya, S. Kimura, C. Katsuda, K. Katayanagi, K. Morikawa, H. Miyashiro and M. Ikehara, *Proc. Natl. Acad. Sci. USA*, 1991, **88**, 11 535.
14 A. T. Daniher, J. Xie, S. Mathur and J. K. Bashkin, *Bioorg. Med. Chem*., 1997, **5**, 1037.
15 B. P. Monia, E. A. Lesnik, C. Gonzalez, W. F. Lima, D. McGee, C. J. Guinosso, A. M. Kawasaki, P. D. Cook and S. M. Freier, *J. Biol. Chem*., 1993, **268**, 14 514.
16 W. F. Lima and S. T. Crooke, *Biochemistry*, 1997, **36**, 390.
17 S. T. Crooke, *Antisense Nucleic Acid Drug Dev*., 1998, **8**, vii–viii.
18 S. T. Crooke, *Handb. Exp. Pharmacol*., 1998, **131**, 1.
19 E. A. Lesnik, C. J. Guinosso, A. M. Kawasaki, H. Sasmor, M. Zounes, L. L. Cummins, D. J. Ecker, P. D. Cook and S. M. Freier, *Biochemistry*, 1993, **32**, 7832.
20 P. Martin, *Helv. Chim. Acta*, 1995, **78**, 486.
21 K.-H. Altmann, N. M. Dean, D. Fabbro, S. M. Freier, T. Geiger, R. Häner, D. Hüsken, P. Martin, B. P. Monia, M. Müller, F. Natt, P. Nicklin, J. Phillips, U. Pieles, H. Sasmor and H. E. Moser, *Chimia*, 1996, **50**, 168.
22 R. H. Griffey, B. P. Monia, L. L. Cummins, S. Freier, M. J. Greig, C. J. Guinosso, E. Lesnik, S. M. Manalili, V. Mohan, S. Owens, B. R. Ross, H. Sasmor, E. Wancewicz, K. Weiler, P. D. Wheeler and P. D. Cook, *J. Med. Chem*., 1996, **39**, 5100.
23 M. Manoharan, *Biochim. Biophys. Acta*, 1999, **1489**, 117.
24 S. Gryaznov and J. K. Chen, *J. Am. Chem. Soc*., 1994, **116**, 3143.
25 J. K. Chen, R. G. Schultz, D. H. Lloyd and S. M. Gryaznov, *Nucleic Acids Res*., 1995, **23**, 2661.
26 S. M. Gryaznov, D. H. Lloyd, J. K. Chen, R. G. Schulz, L. A. Dedionisio, L. Ratmeyer and W. D. Wilson, *Proc. Natl. Acad. Sci. USA*, 1995, **92**, 5798.
27 D. Ding, S. M. Gryaznov and W. D. Wilson, *Biochemistry*, 1998, **37**, 12 082.
28 D. Y. Ding, S. M. Gryaznov, D. H. Lloyd, S. Chandrasekaran, S. J. Yao, L. Ratmeyer, Y. Q. Pan and W. D. Wilson, *Nucleic Acids Res*., 1996, **24**, 354.
29 V. Tereshko, S. Gryaznov and M. Egli, *J. Am. Chem. Soc*., 1998, **120**, 269.
30 L. Dedionisio and S. M. Gryaznov, *J. Chromatogr. B*, 1995, **669**, 125.
31 O. Heidenreich, S. Gryaznov and M. Nerenberg, *Nucleic Acids Res*., 1997, **25**, 776.
32 N. Mignet and S. M. Gryaznov, *Nucleic Acids Res*., 1998, **26**, 431.
33 R. G. Schultz and S. M. Gryaznov, *Nucleic Acids Res*., 1996, **24**, 2966.
34 S. M. Gryaznov and H. Winter, *Nucleic Acids Res*., 1998, **26**, 4160.
35 R. G. Schultz and S. M. Gryaznov, *Tetrahedron Lett*., 2000, **41**, 1895.
36 T. J. Matray and S. M. Gryaznov, *Nucleic Acids Res*., 1999, **27**, 3976.
37 M. J. Damha, C. J. Wilds, A. Noronha, I. Brukner, G. Borkow, D. Arion and M. A. Parniak, *J. Am. Chem. Soc*., 1998, **120**, 12 976.
38 C. J. Wilds and M. J. Damha, *Nucleic Acids Res*., 2000, **28**, 3625.
39 A. M. Noronha, C. J. Wilds, C. N. Lok, K. Viazovkina, D. Arion, M. A. Parniak and M. J. Damha, *Biochemistry*, 2000, **39**, 7050.
40 I. Berger, V. Tereshko, H. Ikeda, V. E. Marquez and M. Egli, *Nucleic Acids Res*., 1998, **26**, 2473.
41 G. Minasov, M. Teplova, P. Nielsen, J. Wengel and M. Egli, *Biochemistry*, 2000, **39**, 3525.
42 C. Hendrix, H. Rosemeyer, B. DeBouvere, A. Van Aerschot, F. Seela and P. Herdewijn, *Chem. Eur. J*., 1997, **3**, 1513.
43 H. De Winter, E. Lescrinier, A. Van Aerschot and P. Herdewijn, *J. Am. Chem. Soc*., 1998, **120**, 5381.
44 E. Lescrinier, R. Esnouf, J. Schraml, R. Busson, H. A. Heus, C. W. Hilbers and P. Herdewijn, *Chem. Biol*., 2000, **7**, 719.
45 C. Hendrix, H. Rosemeyer, I. Verheggen, F. Seela, A. V. Aershot and P. Herdewijn, *Chem. Eur. J*., 1997, **3**, 110.
46 M. Vandermeeren, S. Preveral, S. Janssens, J. Geysen, E. Saison-Behmoaras, A. Van Aerschot and P. Herdewijn, *Biochem. Pharmacol*., 2000, **59**, 655.

47 B. Allart, K. Khan, H. Rosemeyer, G. Schepers, C. Hendrix, K. Rothenbacher, F. Seela, A. Van Aerschot and P. Herdewijn, *Chem. Eur. J.*, 1999, **5**, 2424.
48 N. Hossain, B. Wroblowski, A. Van Aerschot, J. Rozenski, A. De Bruyn and P. Herdewijn, *J. Org. Chem.*, 1998, **63**, 1574.
49 J. Wang and P. Herdewijn, *J. Org. Chem.*, 1999, **64**, 7820.
50 J. Wang, B. Verbeure, I. Luyten, E. Lescrinier, M. Froeyen, C. Hendrix, H. Rosemeyer, F. Seela, A. Van Aerschot and P. Herdewijn, *J. Am. Chem. Soc.*, 2000, **122**, 8595.
51 S. K. Singh, P. Nielsen, A. A. Koshkin and J. Wengel, *Chem. Commun.*, 1998, 455.
52 A. A. Koshkin, S. K. Singh, P. Nielsen, V. K. Rajwanshi, R. Kumar, M. Meldgaard, C. E. Olsen and J. Wengel, *Tetrahedron*, 1998, **54**, 3607.
53 S. Obika, D. Nanbu, Y. Hari, J. Andoh, K. Morio, T. Doi and T. Imanishi, *Tetrahedrom Lett.*, 1998, **39**, 5401.
54 J. Wengel, A. Koshkin, S. K. Singh, P. Nielsen, M. Meldgaard, V. K. Rajwanshi, R. Kumar, J. Skouv, C. B. Nielsen, J. P. Jacobsen, N. Jacobsen and C. E. Olsen, *Nucleosides Nucleotides*, 1999, **18**, 1365.
55 S. Obika, D. Nanbu, Y. Hari, K. Morio, Y. In, T. Ishida and T. Imanishi, *Tetrahedron Lett.*, 1997, **38**, 8735.
56 C. B. Nielsen, S. K. Singh, J. Wengel and J. P. Jacobsen, *J. Biomol. Struct. Dyn.*, 1999, **17**, 175.
57 K. E. Nielsen, S. K. Singh, J. Wengel and J. P. Jacobsen, *Bioconjugate Chem.*, 2000, **11**, 228.
58 M. Petersen, C. B. Nielsen, K. E. Nielsen, G. A. Jensen, K. Bondensgaard, S. K. Singh, V. K. Rajwanshi, A. A. Koshkin, B. M. Dahl, J. Wengel and J. P. Jacobsen, *J. Mol. Recognit.*, 2000, **13**, 44.
59 K. Bondensgaard, M. Petersen, S. K. Singh, V. K. Rajwanshi, R. Kumar, J. Wengel and J. P. Jacobsen, *Chem. Eur. J.*, 2000, **6**, 2687.
60 C. Wahlestedt, P. Slami, L. Good, J. Kela, T. Johnsson, T. Hökfeldt, C. Broberger, F. Porreca, J. Lai, K. Ren, M. Ossipov, A. Koshkin, N. Jakobsen, J. Skouv, H. Oerum, M. H. Jacobsen and J. Wengel, *Proc. Natl. Acad. Sci. USA*, 2000, **97**, 5633.
61 M. D. Sørensen, L. Kværnø, T. Bryld, A. E. Håkansson, G. Gaubert, B. Verbeure, P. Herdewijn and J. Wengel, manuscript in preparation.
62 S. K. Singh, R. Kumar and J. Wengel, *J. Org. Chem.*, 1998, **63**, 10035.
63 R. Kumar, S. K. Singh, A. A. Koshkin, V. K. Rajwanshi, M. Meldgaard and J. Wengel, *Bioorg. Med. Chem. Lett.*, 1998, **8**, 2219.
64 G. Y. Wang, J. L. Girardet and E. Gunic, *Tetrahedron*, 1999, **55**, 7707.
65 G. Y. Wang, E. Gunic, J. L. Girardet and V. Stoisavljevic, *Bioorg. Med. Chem. Lett.*, 1999, **9**, 1147.
66 V. K. Rajwanshi, A. E. Håkansson, M. D. Sørensen, S. Pitsch, S. K. Singh, R. Kumar, P. Nielsen and J. Wengel, *Angew. Chem., Int. Ed.*, 2000, **112**, 1722.
67 V. K. Rajwanshi, A. E. Hakansson, B. M. Dahl and J. Wengel, *Chem. Commun.*, 1999, 1395.
68 V. K. Rajwanshi, A. E. Hakansson, R. Kumar and J. Wengel, *Chem. Commun.*, 1999, 2073.
69 J. Wengel, M. Petersen, K. E. Nielsen, G. A. Jensen, A. E. Håkansson, R. Kumar, M. D. Sørensen, V. K. Rajwanshi, T. Bryld and J. P. Jacobsen, *Nucleosides Nucleotides Nucleic Acids*, in press.
70 M. Petersen, A. E. Håkansson, J. Wengel and J. P. Jacobsen, *J. Am. Chem. Soc.*, in press.
71 K. E. Nielsen, A. E. Håkansson, J. Wengel and J. P. Jacobsen, manuscript in preparation.

CHEMCOMM Communication
www.rsc.org/chemcomm

The pentadecadentate phosphazenate $[\{2\text{-}(MeO)C_6H_4N\}_6P_3N_3]^{6-}$: chelation of twelve lithium ions by a single ligand

Frederic Rivals and Alexander Steiner*

Department of Chemistry, University of Liverpool, Crown Street, Liverpool, UK L69 7ZD. E-mail: a.steiner@liv.ac.uk

Received (in Cambridge, UK) 10th May 2001, Accepted 21st June 2001
First published as an Advance Article on the web 19th July 2001

The hexaprotic phosphazene $\{2\text{-}(MeO)C_6H_4NH\}_6P_3N_3$ reacts with 12 equivalents of Bu^nLi in thf to give the monomeric dodecanuclear complex $(thf)_6Li_{12}[\{2\text{-}(MeO)C_6H_4N\}_6P_3N_3](CH_2{=}CHO)_6$ which contains six enolate anions resulting from fragmentation of thf; the hexaanionic pentadecadentate phosphazenate ligand $[\{2\text{-}(MeO)C_6H_4N\}_6P_3N_3]^{6-}$ accommodates a total of twelve lithium ions in bidentate chelation sites.

Ligands able to carry a high metal load (> 10 metal centres) have scarcely been investigated, although such systems bear the potential to stabilise well-defined multinuclear metal arrays. In contrast, a multinuclear metal arrangement held together by several counter ions in an oligomeric complex usually shows pronounced dynamic behaviour. Particularly, alkaline metal complexes are highly fluxional and their oligomerisation grades strongly depend on the nature of donor additives.[1] Recently, we have shown that cyclophosphazenes equipped with primary amino groups act as multiprotic acids in the presence of organometallic reagents yielding multianionic phosphazenates, highly charged ligands which complex multinuclear metal arrangements.[2–5] We observed that lithiated phosphazenates attract excess lithium ions and accommodate them by either dimer formation[3,4] or insertion of lithium enolate that is generated by fragmentation of thf.[5]

With the aim to increase the maximum metal load of phosphazenates we equipped the ligand with additional donor sites. The hexaanionic phosphazenate $\mathbf{A}^{6-}$ presented here

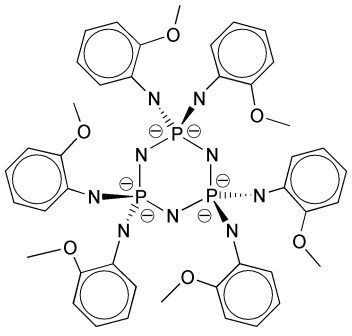

$\mathbf{A}^{6-}$

carries six *ortho*-anisidyl substituents and features an overall pentadecadentate ligand surface comprising nine N and six O donor functions. The ligand precursor $H_6\mathbf{A}$ (**1**) was synthesised by reaction of excess *ortho*-anisidine with hexachlorocyclotriphosphazene in the presence of triethylamine.† We have reacted **1** with 12 equivalents of Bu^nLi in thf in order to both deprotonate all six NH-functions and incorporate the excess Bu^nLi or lithium enolate into the ligand sphere of $\mathbf{A}^{6-}$. The reaction yields a white precipitate that re-dissolves upon heating. Crystallisation occurs on leaving the solution to cool to room temperature.‡ Spectroscopic data and X-ray structure analysis§ reveal the formation of the monomeric complex $(thf)_6Li_{12}\mathbf{A}(CH_2{=}CHO)_6$ **2** (Fig. 1), which contains six enolate and twelve lithium ions.

$$\underset{\mathbf{1}}{H_6\mathbf{A}} + 12\ Bu^nLi + 12\ thf \longrightarrow \underset{\mathbf{2}}{(thf)_6Li_{12}\mathbf{A}(CH_2{=}CH\text{-}O)_6} + 12\ C_4H_{10} + 6\ C_2H_4$$

^{31}P NMR spectroscopy shows a single peak at δ 16.4 and the P–N-ring stretching frequency appears as a very strong and broad band with a maximum at 1077 cm^{-1} in the IR spectrum which is considerably red shifted compared to that of **1** (1186 cm^{-1}). The ligand $\mathbf{A}^{6-}$ accommodates a total of twelve lithium ions in bidentate chelation sites. To our knowledge this is the largest number of s-block metal ions being chelated by a single ligand in a molecular complex.

Complex **2** crystallises in space group $R\bar{3}c$ with eight lattice bound thf molecules per formula unit and exhibits D_3 symmetry. The central P_3N_3 ring is arranged around the three-fold axis and each phosphorus along with the opposite ring N atom is located on a two-fold axis. The nine anionic N-centres and six O-donor atoms of the ligand form two large, bowl shaped, nonadentate cavities on either side of the central P_3N_3 ring providing an ideal coordination geometry for the accommodation of twelve lithium ions: six lithium ions (Li1) reside at 'inner' coordination sites represented by six N_{exo}–P–N_{endo} chelates. The other six lithium ions (Li2) occupy the 'outer' sites, which are the N_{exo}–O chelates of the anisidyl groups. The negative charge of the hexaanion is distributed over all nine N-atoms, each binds two lithium ions, the N_{endo} atom (N1) two 'inner' lithium ions and the N_{exo} atom (N2) one 'inner' and one 'outer' lithium ion, respectively. In addition, each 'inner' lithium is coordinated by one thf molecule (O3) and one enolate ion (O1); each 'outer' lithium by the O-donor function of the ligand (O2) and two enolate ions. All lithium ions are coordinated in a tetrahedral fashion. The ^7Li NMR spectrum of **2** recorded in thf at room temperature exhibits two signals at δ 2.15 and 2.81. This suggests that the presence of two non-equivalent lithium ions is retained in solution.

Bond lengths and angles of the P_3N_9 core in **2** are in agreement with those we found in other lithium phosphaze-

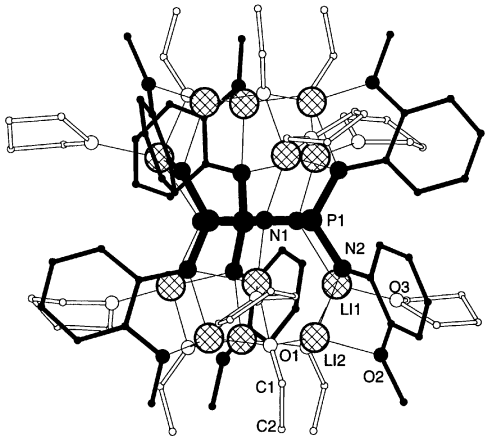

Fig. 1 X-Ray crystal structure of **2**. The $\mathbf{A}^{6-}$ ligand is drawn in black, thf and enolate moieties in white and lithium ions hatched.

 DOI: 10.1039/b104124j

nates.[3,4] P–N_{endo} and P–N_{exo} bonds are of similar length [1.638(2) and 1.637(3) Å, respectively], and the N_{exo}–P–N_{exo} angle [115.0(2)°] is similar to the N_{endo}–P–N_{endo} angle [113.4(3)°], showing equal P–N_{endo} and P–N_{exo} bond orders and distribution of negative charge over all nine N-atoms. In contrast, the neutral precursor **1** exhibits long P–N_{exo} bonds (av. 1.65 Å) and short P–N_{endo} bonds (av. 1.59 Å); and *endo* angles (av. 115°) are wider than *exo* angles (av. 104°) indicating a higher bond order in the P_3N_3 ring of **1**.§ Surprisingly, the central P_3N_3 ring in **2** is planar, which is in contrast to all other lithiated cyclotriphosphazenates we have investigated so far. All contain highly puckered central P_3N_3 rings of chair conformation. The P–N–P angle of **2** is 126.6(3)° and thus considerably wider than those observed in hexaanionic $[(CyN)_6P_3N_3]^{6-}$,[3] trianionic $[(CyNH)_3(CyN)_3P_3N_3]^{3-}$, $[(PhNH)_3(PhN)_3P_3N_3]^{3-}$,[4] and neutral H_6**A**, which are all around 120°. This shows that the P–N–P angle is rather flexible allowing a planar configuration of the central P_3N_3 ring in hexaanionic **2**.

We monitored the reaction of **1** with Bu^{n}Li in thf using ^{31}P NMR spectroscopy. Addition of 3 equivalents of Bu^{n}Li exclusively gives trianionic H_3**A**$^{3-}$ as indicated by a single peak at δ 8.7. Addition of 6 equivalents of Bu^{n}Li leads to three broad peaks at δ 13.1, 19.1 and 22.2 suggesting that the fully deprotonated species **A**$^{6-}$ is not present so far. However, **A**$^{6-}$ begins to form after addition of around 8 equivalents of Bu^{n}Li, as shown by the appearance of a sharp single peak at δ 16.4 amongst a pattern of broader signals. Finally there is only one single peak at δ 16.4 after addition of 12 equivalents Bu^{n}Li. This implies that both deprotonation of NH functions and enolate formation occur simultaneously once 3 equivalents of Bu^{n}Li are added.

The fragmentation of thf by Bu^{n}Li, which produces lithium ethenolate and ethylene, is well known[6] and also adduct formation of LiO–CH=CH_2 was observed in solid state structures of lithium complexes containing tetraanionic ligands.[5,7] However, the inclusion of six lithium enolate moieties into a molecular complex is unprecedented. We assume, once the ligand acquires a certain charge it acts as a 'Li$^+$ sponge': Bu^{n}Li is dragged into an 'outer' *N,O*-chelation site, which contains an already deprotonated *N*-function, and fragments a thf molecule, which is coordinated to a neighbouring 'inner' lithium ion. The resulting enolate ions are not sufficiently basic to deprotonate H_xA^{x-6} (x = 1, 2) any further, but remain within the complex by forming μ_3-bridges between one 'inner' and two 'outer' lithium ions.

Summarising, the generation of a ligand system with high metal loading capacity has been accomplished by combining the features of a multianionic ligand core with a multidentate ligand surface. The hexaanionic pentadecadentate phosphazenate ligand **A**$^{6-}$ accommodates twelve lithium ions in bidentate chelation sites. Currently, we are investigating self-assembly properties of this new ligand system in the presence of LiX, where X represents a monodentate monoanion (*e.g.* halide, alkoxide, amide, carbanion), potentially leading to complexes $Li_{12}A_6X_6$. Such systems promise interesting template effects, due to the potentially well-defined array of both lithium ions and counter ions X. In addition, the straightforward introduction of a variety of substituents into phosphazenes[8,9] might facilitate the generation of a wide range of other high metal loading ligands based on multidentate phosphazenates.

This work was supported by the EPSRC (GR/M17280) and the Royal Society.

Notes and references

† *Preparation* of **1**: to a solution of 10 g hexachlorocyclotriphosphazene in 100 ml of toluene was added 40 ml of *ortho*-anisidine and 100 ml of triethylamine. The mixture was refluxed for several days (^{31}P NMR control). The solution was allowed to cool to room temperature, separated by filtration from the precipitate, which was washed with toluene. All volatile components of combined filtrates were removed *in vacuo*. The resulting residue was washed with hot hexane to give a white powder, which was re-crystallised from thf–hexane. Yield: 19.7 g (79%), mp 175 °C, ^{1}H NMR (300 MHz, d_8-thf) δ 3.55 (s, 18H, OCH_3), 5.72 (m, 6H, NH), 6.55 (m, 6H, aryl-H), 7.42 (m, 18H, aryl-H); ^{13}C{^{1}H} NMR (75.46 MHz, d_8-thf) δ 56.4 (OCH_3), 111.29, 119.10, 121.44, 121.90, 132.59, 149.72 (aromatic C); ^{31}P NMR (101.25 MHz, d_8-thf, 85% H_3PO_4 in D_2O ext.) δ 5.1; IR (Nujol) ν/cm^{-1} 3385 (N–H), 1596, 1247, 1186 (P–N-ring), 1111, 1026, 870, 734.

‡ *Preparation* of **2**: to a solution of **1** (300 mg, 0.345 mmol) in 20 ml of thf was added Bu^{n}Li (2.6 ml, 1.6 M in hexane, 4.14 mmol). The solution was stirred overnight at room temperature forming a white precipitate, which was re-dissolved by gentle heating. On cooling to room temperature colourless crystals formed, which disintegrated in the absence of mother-liquor by losing lattice bound thf to give a white powder. Yield: 340 mg (88%), decomp. >180 °C; ^{1}H NMR (300 MHz, d_8-thf) δ 3.79 (s, 18H, OCH_3), 3.41 (d, 6H, $^3J_{cis}$ 5.4 Hz, HC=), 3.96 (d, 6H, $^3J_{trans}$ 13.9 Hz, HC=), 6.05–6.47 (m, 18H, aryl-H), 6.51 (dd, 6H, $^3J_{cis}$ 5.4, $^3J_{trans}$ 13.9, =CHO), 7.55 (dd, 6H, aryl-H); ^{13}C{^{1}H} NMR (75.46 MHz, d_8-thf) δ 56.3 (OCH_3), 86.1 (=CH_2), 109.5, 114.2, 120.0, 123.1, 144.3, 150.9 (aromatic C), 159.2 (OCH=); ^{31}P NMR (101.25 MHz, thf, 85% H_3PO_4 in D_2O ext.) δ 16.43; ^{7}Li NMR (97.16 MHz, thf, LiCl in D_2O ext) δ 2.15, 2.81; IR (Nujol) ν/cm^{-1} 1621, 1590, 1377, 1316, 1282, 1258, 1216, 1178, 1077 (P–N-ring), 1056, 1030, 826, 781, 736, 634.

§ Crystallographic data were recorded on a Stoe-IPDS using Mo-Kα radiation (λ = 0.71073 Å), T = 200 K, structures were solved by direct methods and refined by full-matrix least squares against F^2 using all data (SHELX-97).

Crystal data: for **1**·0.5thf: M = 903.96, triclinic, $P\bar{1}$, a = 11.570(2), b = 12.059(2), c = 18.076(3) Å, α = 77.42(2), β = 79.85(2), γ = 67.35(2)°, U = 2259.4(5) Å^3, Z = 2, D_c = 1.329, μ(Mo-Kα) = 0.148, 6717 unique reflections. R_1 [$I > 2\sigma(I)$] = 0.037, wR_2 (all data) = 0.068.

For **2**·8thf: M = 2212.76, rhombohedral, $R\bar{3}c$, a = 14.506(8), c = 100.883(11) Å, U = 18384(2) Å^3, Z = 6, D_c = 1.199, μ(Mo-Kα) = 0.119, 2647 unique reflections, R_1 [$I > 2\sigma(I)$] = 0.069, wR_2 (all data) = 0.205. C-positions of coordinated thf are disordered and were split in two positions. There are 1⅓ lattice bound thf molecules per asymmetric unit: thf on general site is disordered and its C and O atoms were split in three positions, thf on 3 is disordered around the 3-axis generating three positions per atom. Disordered groups were refined using similar distance and similar U restraints and site occupancy factors. All non-H atoms were refined anisotropically, except lattice bound thf molecules, which were treated isotropically. H atoms were fixed in calculated positions on the parent C atoms.

CCDC 152011–152012. See http://www.rsc.org/suppdata/cc/b1/b104124j/ for crystallographic data in CIF or other electronic format.

1 See for example: M. A. Beswick and D. S. Wright, in *Comprehensive Organometallic Chemistry II*, ed. E. W. Abel, F. G. A. Stone and G. Wilkinson, Pergamon, Oxford, 1995, vol. 1, pp. 1–34; W. N. Setzer and P. v. R. Schleyer, *Adv. Organomet. Chem.*, 1985, **24**, 353; K. Gregory, P. v. R. Schleyer and R. Snaith, *Adv. Inorg. Chem.*, 1991, **37**, 47; R. E. Mulvey, *Chem. Soc. Rev.*, 1991, **20**, 167; G. Boche, *Angew. Chem., Int. Ed. Engl.*, 1989, **28**, 277; R. Snaith and D. S. Wright, in *Lithium Chemistry: A Theoretical and Experimental Overview*, ed. A.-M. Saspe and P. v. R. Schleyer, John Wiley & Sons, 1995, p. 227–293; C. Schade and P. v. R. Schleyer, *Adv. Organomet. Chem.*, 1987, **27**, 169; D. S. Smith, *Adv. Organomet. Chem.*, 1998, **43**, 267; K. Bode and U. Klingebiel, *Adv. Organomet. Chem.*, 1996, **40**, 1; R. E. Mulvey, *Chem. Soc. Rev.*, 1998, **27**, 339; L. Lochmann, *Eur. J. Inorg. Chem.*, 2000, 1115.

2 G. T. Lawson, C. Jacob and A. Steiner, *Eur. J. Inorg. Chem.*, 1999, 1881.

3 A. Steiner and D. S. Wright, *Angew. Chem., Int. Ed. Engl.*, 1996, **35**, 636.

4 G. T. Lawson, F. Rivals, M. Tascher, C. Jacob, J. F. Bickley and A. Steiner, *Chem. Commun.*, 2000, 341.

5 A. Steiner and D. S. Wright, *Chem. Commun.*, 1997, 283.

6 M. E. Jung and R. B. Blum, *Tetrahedron Lett.*, 1977, **43**, 3794.

7 S. De Angelis, E. Solari, C. Floriani, A. Chiesi-Villa and C. Rizzoli, *J. Chem. Soc., Dalton Trans.*, 1994, 2467.

8 C. W. Allen, *Chem. Rev.*, 1991, **91**, 119.

9 H. R. Allcock, *Chem. Rev.*, 1972, **72**, 315.

CHEMCOMM Communication
www.rsc.org/chemcomm

Macrocyclic multi-telluranes with hypervalent Te–O apical linkages†

Kenji Kobayashi,*[a] Hiroyuki Izawa,[a] Kentaro Yamaguchi,[b] Ernst Horn[c] and Naomichi Furukawa[a]‡

[a] *Department of Chemistry, University of Tsukuba, Tsukuba, Ibaraki 305-8571, Japan. E-mail: kenjinor@staff.chem.tsukuba.ac.jp*
[b] *Chemical Analysis Center, Chiba University, Inage-ku, Chiba 263-8522, Japan*
[c] *Department of Chemistry, Rikkyo University, Nishi-Ikebukuro, Toshima-ku, Tokyo 171-8501, Japan*

Received (in Cambridge, UK) 24th April 2001, Accepted 20th June 2001
First published as an Advance Article on the web 19th July 2001

Two types of macrocyclic multi-telluranes with hypervalent Te–O apical linkages in the main chain were prepared by the reaction of a telluronium salt or a cationic ditelluroxane with phthalate *via* [3 + 3] and [2 + 2] assembly, respectively.

One of the characteristics of organic heteroatom chemistry is the formation of hypervalent compounds.[1] Telluranes have the trigonal bipyramidal geometry, in which the two apical ligands and the central Te atom construct a three-center–four-electron hypervalent bond with *ca.* 180° bond angle. A strategy for the formation of hypervalent telluranes is the use of n→σ* orbital interaction, where the σ* orbital of the Te–X bond of a telluronium salt interacts with the n orbital of a lone pair of electrons of a ligand.[1] In supramolecular chemistry, the field of macrocycles has advanced to the stage where self-assembly through transition-metal coordination has proved to be a reliable tool.[2] Hypervalent bonds *via* n→σ* orbital interactions in heteroatoms may also be a viable alternative for self-assembled macrocycles.[3–7] Recently, we have found that the cationic ditelluroxane **2** interacts with triflate as a counter ion in the solid state and with telluroxide in solution to form a pseudo-macrocyclic multi-tellurane and oligotelluroxanes, respectively, with hypervalent Te–O apical linkages *via* n→σ* orbital interaction.[8] Herein we report the synthesis of the macrocyclic multi-telluranes **4** and **5** by the reaction of the telluronium salt **1** or the cationic ditelluroxane **2** as building blocks with phthalate **3** as a convergent bidentate ligand. This is the first example of macrocycles composed of only hypervalent apical linkages in the main chain for group 13–17 elements, which are fully characterized both in solution and in the solid state.

The generation of the telluronium salt **1** *in situ* by the reaction of bis(4-methylphenyl) telluroxide with 1 equiv. of triflic anhydride in MeCN at −40 °C followed by the addition of 1 equiv. of sodium phthalate **3** at room temperature gave the hypervalent macrocycle **4** in 76% yield after recrystallization [Scheme 1(a)].§ Treatment of the cationic ditelluroxane **2** with 1 equiv. of **3** in MeCN at room temperature produced the hypervalent macrocycle **5** in 14% yield after recrystallization [Scheme 1(b)].§

The ^{125}Te NMR spectra of **4** and **5** in CD_2Cl_2 showed singlets at δ 997.0 and 1044.4, respectively, which are in the region of telluranes with hypervalent Te–O_2C apical bonds.[9] The ^{1}H NMR spectra of **4** and **5** exhibited doublet, double-doublet, double-doublet, and doublet peaks in the aromatic region in the integration ratios of 2 : 1 : 1 : 2 and 4 : 1 : 1 : 4, respectively. The IR spectrum of **5** showed the characteristic Te–O–Te stretching band at ν 639 cm^{-1}.[10] These data imply that **4** is the result of [3 + 3] assembly of **1** and **3** to give a 21-membered ring, and **5** is the result of [2 + 2] assembly of **2** and **3** to form an 18-membered ring; both structures are composed of the hypervalent Te–O apical linkages in the main chain. The FAB-MS spectra of **4** and **5** showed a parent peak at *m/z* 1423 ([M + H]$^+$) and at 1601 ([M + H]$^+$), respectively, the isotopic distribution patterns of which are consistent with the calculated ones. Distinctive fragment peaks also appeared at *m/z* 801 and 477 in both cases and at *m/z* 1509 and 1275 in **5**.

The ^{1}H and ^{125}Te NMR spectra of **4** and **5** in CD_2Cl_2 and CD_3CN remained unchanged in the range −90 to 80 °C. NOE experiments on **4** and **5** indicated −24 and −19% NOEs, respectively, at the *ortho*-hydrogens of the phthalate unit upon irradiation of the *ortho*-hydrogens of the *para*-tolyl unit. These results indicate that the cyclic structures of **4** and **5** are maintained in solution.

The molecular structures of the hypervalent macrocycles **4** and **5** were determined by X-ray crystallographic analysis, as shown in Fig. 1 and 2, respectively.¶‖ The macrocycle **4** is composed of three Te atoms and three phthalates, and possesses Te–O_2C bond lengths of 2.133–2.166 Å, CO_2–Te–O_2C bond angles of 161.8–168.3° and C–Te–C bond angles of 96.2–100.3°. The macrocycle **5** consists of two ditelluroxanes and two phthalates, and the unit cell contains four independent molecules.‖ The respective average bond lengths and angles are in the range of 2.23–2.29 Å for Te–O_2C, 1.99–2.03 Å for Te–O, 166.1–168.7° for O–Te–O_2C, 96–101° for C–Te–C and 114–126° for Te–O–Te. These data clearly indicate that both **4** and **5** have trigonal bipyramidal geometry for the Te atoms and hypervalent Te–O apical bonds.[11] In both cases, all the atoms of the respective macrocyclic rings are roughly coplanar. The halves of the carbonyl O atoms and the tolyl groups are directed inward and outward, respectively, to the respective macrocyclic rings. By contrast, the other halves of the carbonyl O atoms and the tolyl groups are vertically directed to the respective

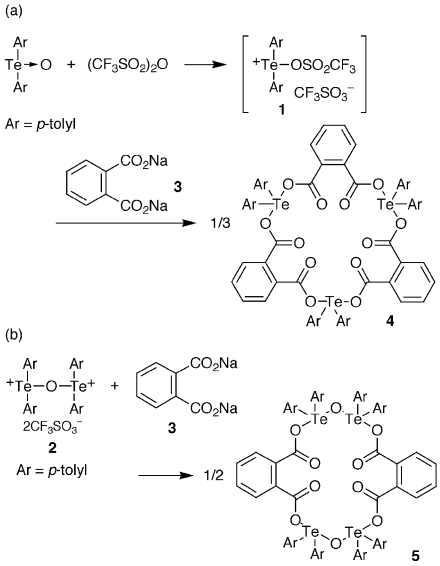

Scheme 1 Synthesis of macrocyclic multi-telluranes (a) **4** and (b) **5**.

† Electronic supplementary information (ESI) available: characterization data and ORTEP diagrams for **4** and **5**. See http://www.rsc.org/suppdata/cc/b1/b103676a/

‡ Present address: Foundation for Advancement of International Science, 586-9 Akatsuka-Ushigahuchi, Tsukuba, Ibaraki 305-0062, Japan.

 DOI: 10.1039/b103676a

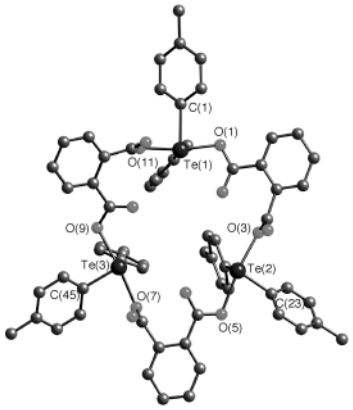

Fig. 1 Structure of **4** in the crystal; hydrogen atoms are omitted for clarity. Selected bond lengths (Å) and angles (°): Te(1)–O(1) 2.166(4), Te(1)–O(11) 2.133(4), Te(2)–O(3) 2.141(4), Te(2)–O(5) 2.163(4), Te(3)–O(7) 2.151(4), Te(3)–O(9) 2.144(4); O(1)–Te(1)–O(11) 161.8(2), O(3)–Te(2)–O(5) 168.3(2), O(7)–Te(3)–O(9) 165.6(2), C(1)–Te(1)–C(8) 100.3(2), C(23)–Te(2)–C(30) 96.2(2), C(45)–Te(3)–C(52) 98.9(2).

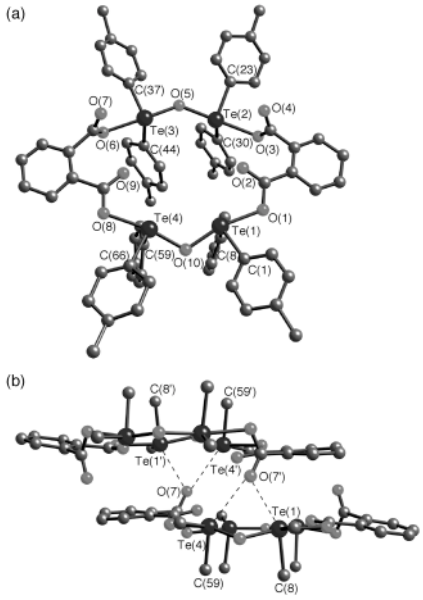

Fig. 2 (a) Structure of **5** and (b) its dimeric structure in the crystal; hydrogen atoms in (a) and (b) and *p*-tolyl groups in (b) are omitted for clarity. Selected average bond lengths (Å) and angles (°): Te(1)–O(1) 2.28(2), Te(2)–O(3) 2.23(2), Te(3)–O(6) 2.27(2), Te(4)–O(8) 2.29(2), Te(1)–O(10) 2.03(2), Te(4)–O(10) 2.01(2), Te(2)–O(5) 2.01(2), Te(3)–O(5) 1.99(2), O(7′)···Te(1) 2.95, O(7′)···Te(4) 3.20; O(1)–Te(1)–O(10) 166.6(7), O(3)–Te(2)–O(5) 167.2(7), O(5)–Te(3)–O(6) 168.7(7), O(8)–Te(4)–O(10) 166.1(8), C(1)–Te(1)–C(8) 96(1), C(23)–Te(2)–C(30) 101(1), C(37)–Te(3)–C(44) 98(1), C(59)–Te(4)–C(66) 98(1), Te(1)–O(10)–Te(4) 114(1), Te(2)–O(5)–Te(3) 126(1), O(7′)···Te(1)–C(8) 153, O(7′)···Te(4)–C(59) 149.

macrocyclic ring planes so as to be placed at the opposite side. It is noted that the Te(1) and Te(4) atoms in **5** interact with the carbonyl O(7′) atom of the adjacent molecule [O(7′)···Te(1) 2.95 and O(7′)···Te(4) 3.20 Å; O(7′)···Te(1)–C(8) 153 and O(7')···Te(4)-C(59) 149°],[12] the contact distances of which are shorter than the sum of the van der Waals radii (3.60 Å) of the Te and O atoms. Thus, **5** forms a head-to-head type of dimeric structure in the solid state [Fig. 2(b)].

In summary, we have demonstrated the synthesis of macrocyclic multi-telluranes **4** and **5** with hypervalent Te–O apical linkages in the main chain. Hypervalent bonds *via* n→σ* orbital interaction in heteroatoms can serve as a new supramolecular synthon for molecular assembly. Studies on the synthesis of hypervalent polymers using the building blocks **1** and **2** with divergent bidentate ligands are underway.

Notes and references

§ *Representative data*: for **4**: mp 199–200 °C (decomp); ^{1}H NMR (270 MHz, CD_2Cl_2, 23 °C) δ 2.35 (s, 18H), 7.31 (d, *J* 8.3 Hz, 12H), 7.38 (dd, *J* 3.2 , 5.9 Hz, 6H), 7.48 (dd, *J* 3.2, 5.9 Hz, 6H), 7.78 (d, *J* 8.3 Hz, 12H); ^{125}Te NMR (85.2 MHz, CD_2Cl_2, 23 °C) δ 997.0; FAB-MS (2-nitrophenyl octyl ether matrix) *m/z* (%) 1423 (4, $[M + H]^+$), 801 (7, $[M - Ar_2Te - 2C_6H_4(CO_2)_2 + OH]^+$), 477 (43, $[1/3M + H]^+$), 329 (79, $[Ar_2TeO + H]^+$), 312 (100, $[Ar_2Te]^+$). For **5**: mp 172–174 °C (decomp); ^{1}H NMR (270 MHz, CD_2Cl_2, 23 °C) δ 2.32 (s, 24H), 7.13 (d, *J* 8.1 Hz, 16H), 7.31 (dd, *J* 3.2, 5.7 Hz, 4H), 7.50 (dd, *J* 3.2, 5.7 Hz, 4H), 7.76 (d, *J* 8.1 Hz, 16H); ^{125}Te NMR (85.2 MHz, CD_2Cl_2, 23 °C) δ 1044.4; FAB-MS (2-nitrophenyl octyl ether matrix) *m/z* (%) 1601 (8, $[M + H]^+$), 1509 (8, $[M - Ar]^+$), 1275 (18, $[M - Ar_2TeO + H]^+$), 801 (18, $[1/2M + H]^+$), 477 (37, $[1/2M - Ar_2TeO + H]^+$), 329 (98, $[Ar_2TeO + H]^+$), 312 (100, $[Ar_2Te]^+$).

¶ *Crystal data*: for **4**·0.5(*p*-xylene)·3(CH_3CN): $C_{76}H_{68}O_{12}N_3Te_3$, M = 1598.19, triclinic, space group $P\bar{1}$, a = 13.2525(8), b = 15.1873(9), c = 19.937(1) Å, α = 76.682(1), β = 75.167(1), γ = 65.688(1)°, U = 3499.3(4) Å^3, Z = 2, D_c = 1.517 g cm^{-3}, Bruker CCD/Smart 1000, μ(Mo-Kα) = 13.06 cm^{-1}, T = 173 K. Of 20229 measured and 14907 unique reflections (R_{int} = 0.062), the final least-squares refinement based on F for 12760 observed reflections with $I > 2.5\sigma(I)$ (767 variables) converged with R = 0.055 and R_w = 0.082. For **5**·1.5(*p*-xylene): $C_{84}H_{79}O_{10}Te_4$, M = 1758.94, triclinic, space group $P\bar{1}$, a = 18.150(2), b = 28.698(3), c = 30.804(3) Å, α = 86.630(2), β = 89.491(2), γ = 77.613(2)°, U = 15644(3) Å^3, Z = 8, D_c = 1.494 g cm^{-3}, Bruker CCD/Smart 1000, μ(Mo-Kα) = 15.33 cm^{-1}, T = 123 K. Of 93535 measured and 68077 unique reflections (R_{int} = 0.082), the final least-squares refinement based on F for 19579 observed reflections with $I > 3.0\sigma(I)$ (3527 variables) converged with R = 0.088 and R_w = 0.134. CCDC reference numbers 159004 and 159005. See http://www.rsc.org/suppdata/cc/b1/b103676a/ for crystallographic data in CIF or other electronic format.

‖ Compound **4** has some high thermal parameters for the solvent molecules. The structural parameters for compound **5** reported here are still preliminary. Even from the data collected at −150 °C we have not yet obtained satisfactory parameters because of the severe disorder. Although the final level of refinement has not yet been reached, we believe the data obtained here is significant enough to demonstrate the molecular structure of **5**.

1 J. Bergman, L. Engman and J. Sidén, in *The Chemistry of Organic Selenium and Tellurium Compounds*, ed. S. Patai and Z. Rappoport, Wiley, Chichester, 1986, vol. 1, p. 517; *Chemistry of Hypervalent Compounds*, ed. K.-y. Akiba, Wiley-VCH, New York, 1999; N. Furukawa, K. Kobayashi and S. Sato, *J. Organomet. Chem.*, 2000, **611**, 116.

2 *Comprehensive Supramolecular Chemistry*, ed. J.-P. Sauvage and M. W. Hosseini, Pergamon, Oxford, 1996, vol. 9; S. Leininger, B. Olenyuk and P. J. Stang, *Chem. Rev.*, 2000, **100**, 853.

3 For hypervalent pseudo-macrocyclic multi-telluranes with apical and equatorial linkages in the solid state *via* n→σ* orbital interactions, see: J. Jeske, W.-W. du Mont and P. G. Jones, *Angew. Chem., Int. Ed. Engl.*, 1997, **36**, 2219; P. D. Boyle, W. I. Cross, S. M. Godfrey, C. A. McAuliffe, R. G. Pritchard, S. Sarwar and J. M. Sheffield, *Angew. Chem., Int. Ed.*, 2000, **39**, 1796.

4 For hypervalent multi-iodonium macrocycles with apical and equatorial linkages, see: P. J. Stang and V. V. Zhdankin, *J. Am. Chem. Soc.*, 1993, **115**, 9808.

5 For a macrocyclic multi-tellurane with equatorial linkages, see: Y. Takaguchi, E. Horn and N. Furukawa, *Organometallics*, 1996, **15**, 5112.

6 For a tellurium-containing macrocycle, see: S. C. Menon, H. B. Singh, R. P. Patel and S. K. Kulshreshtha, *J. Chem. Soc., Dalton Trans.*, 1996, 1203.

7 For macrocyclic imidazolylboranes with the sp^3-hybridized boron atoms *via* n→p$_\pi$ orbital interactions, see: A. Weiss, H. Pritzkow and W. Siebert, *Angew. Chem., Int. Ed.*, 2000, **39**, 547.

8 K. Kobayashi, N. Deguchi, E. Horn and N. Furukawa, *Angew. Chem., Int. Ed.*, 1998, **37**, 984; K. Kobayashi, N. Deguchi, O. Takahashi, K. Tanaka, E. Horn, O. Kikuchi and N. Furukawa, *Angew. Chem., Int. Ed.*, 1999, **38**, 1638.

9 Y. Takaguchi, H. Fujihara and N. Furukawa, *J. Organomet. Chem.*, 1995, **498**, 49.

10 N. W. Alcock and W. D. Harrison, *J. Chem. Soc., Dalton Trans.*, 1982, 1421; K. V. Domasevitch, V. V. Skopenko and E. B. Rusanov, *Z. Naturforsch, Teil B*, 1996, **51**, 832.

11 N. W. Alcock, W. D. Harrison and C. Howes, *J. Chem. Soc., Dalton Trans.*, 1984, 1709.

12 G. Schatte, T. Chivers, C. Jaska and N. Sandblom, *Chem. Commun.*, 2000, 1657.

CHEMCOMM Communication
www.rsc.org/chemcomm

Low viscosity ionic liquids based on organic salts of the dicyanamide anion

Douglas R. MacFarlane,* Jake Golding, Stewart Forsyth, Maria Forsyth and Glen B. Deacon

Centre for Green Chemistry, School of Chemistry, PO Box 23, Victoria 3800, Australia.
E-mail: dmacfarlane@sci.monash.edu.au

Received (in Cambridge, UK) 4th April 2001, Accepted 20th June 2001
First published as an Advance Article on the web 6th July 2001

New families of salts *viz*. quaternary ammonium, *N*-alkyl-*N*-methylpyrrolidinium or 1-alkyl-3-methylimidazolium dicyanamides, $Cat^+N(CN)_2^-$, are low melting compounds, most being liquid at rt, water-miscible and have low (for ionic liquids) viscosity at rt, *e.g.* η = 21 cP for 1-ethyl-3-methylimidazolium dicyanamide.

Currently, many chemically inert ionic liquids, which are of interest as media in Green Chemistry,[1] have viscosities much higher than those of solvents normally used in synthesis. Thus the search for new, more versatile ionic liquids is driven in part by the need for materials of lower viscosity. High viscosities not only lead to handling difficulties *e.g.* in filtration, decantation, and dissolution, but may also lead to reduced reaction rates and competitive unimolecular side reactions. One of the most fluid, inert of families of ionic liquids is that based on the bis(trifluoromethanesulfonyl)amide, $N(Tf)_2^-$ ion,[2] for example, 1-ethyl-3-methylimidazolium bis(trifluoromethanesulfonyl)-amide (**1**) (η = 34 cP 20 °C;[2a] *cf.* H_2O, 1 cP; toluene 0.59 cP).

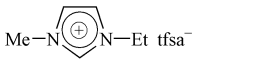

1 $N(Tf)^-_2 = N(SO_2CF_3)_2$

There is also a need for donor solvent characteristics. We now report several new series of salts based on the dicyanamide (dca) anion, *viz*. quaternary ammonium, pyrrolidinium, and imidazolium dicyanamides (**2**–**4**), most of which are liquids at rt. These have a different solubility profile from the corresponding bis(trifluoromethanesulfonyl)amides, potential donor characteristics as the anion is a powerful ligand,[3] and, in representative cases, lower viscosity.

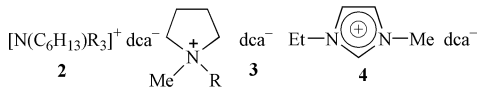

2 **3** **4**

dca = $N(CN)_2$

Quaternary iodide salts of triethylamine, tributylamine, *N*-methylpyrrolidine, and 1-methylimidazole were prepared by reported methods,[2,4] and were converted into the corresponding dicyanamides by reaction with a slight excess of silver dicyanamide in water or ethanol (Scheme 1).

Filtration to remove AgI and evaporation of water under vacuum gave the ionic liquid. Preparative details for two examples are provided;† more extensive details and discussion of properties will be published elsewhere.[5] Identification was by ^{1}H NMR and positive and negative electrospray MS.† The possible presence of residual I^- and Ag^+ were examined *via* inspection of the appropriate mass regions of the respective mass spectra. The sensitivity of the MS measurement to trace amounts of I^- was determined by spiking the ionic liquids with known iodide concentrations; the noise limited detection limit was thereby found to be 0.5% (w/w) I^-. No discernable I mass peaks were found in the dca salts, therefore indicating a residual I content of < 0.5% (w/w). The same considerations and lack of a detectable signal indicate residual Ag < 0.5% (w/w). It is known[6] that impurities such as halides and water can have an effect on properties such as viscosity, though the effect of water in particular is expected to be more dramatic when the viscosity differs greatly from that of pure water (*e.g.* emim BF_4[6]). After rigorous final drying, compounds were handled in a nitrogen drybox during preparation of thermal analysis samples. Viscosity measurements were carried out in a drybox.

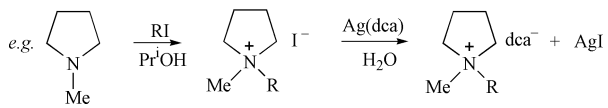

Scheme 1

Thermal properties of the salts were investigated by differential scanning calorimetry. All of the dca salts, except the *N*,*N*-dimethylpyrrolidinium compound, are liquids at rt with well defined mps below 0 °C (Table 1), providing a large liquid range. Notably, the mps are 20–30 °C or even more below those of the corresponding salts,[2a] perhaps an unexpected result since charge delocalisation could be expected to be greater for dca, producing weaker ion–ion interactions. Many of the dca salts are glass forming, with very low glass transition temperatures, T_g (Table 1), and only very sluggish crystallization kinetics at any temperature. The dimethylpyrrolidinium compound shows evidence of multiple solid phases, with a solid–solid thermal transition around −6 °C (Table 1) which consumes a large fraction of the total entropy of melting. This behaviour is indicative of plastic crystal phase formation and in the case of these ionic compounds, the plastic phases are often highly conductive.[7]

The viscosities of representative compounds at 25 °C (Table 1) are lower than those of the corresponding salts, *e.g.* 1-ethyl-3-methylimidazolium dca (η = 21 cP) and (η = 34 cP); *N*-butyl-*N*-methylpyrrolidinium dca (η = 50 cP) and (η = 85 cP).[2c] This rather useful trend is possibly related to the smaller size of the anion and parallels the lower mps of the dca compounds. In practical terms, it is possible to filter at rt a precipitate from a suspension in the lower viscosity dca salt with a sintered glass frit under vacuum.

Table 1 Thermal properties of dicyanamide salts[a]

Compound[b]	T_g/ °C ±2	T_{s-s}/ °C ±2	Mp/ °C ± 2	ρ/gcm^{-3} ±5% (25 °C)	Viscosity/ cP ±5% (25 °C)
P_{11}(dca)		−6	115	—	
P_{12}(dca)			−10	—	
P_{13}(dca)			−35	0.92	45
P_{14}(dca)	−106		−55[c]	0.95	50
P_{16}(dca)	−100		−11	0.92	45
N_{6222}(dca)	−82				
N_{6444}(dca)			−43[c]		
emim(dca)	−104		−21	1.06	21

[a] T_g = glass transition temperature, T_{s-s} = solid–solid transition temperature. [b] P = *N*,*N*-dialkylpyrrolidinium, N = tetraalkylammonium, subscripts refer to the number of carbons in the alkyl chains. [c] In these cases the melting transition is weak and the reported value only approximate.

 DOI: 10.1039/b103064g

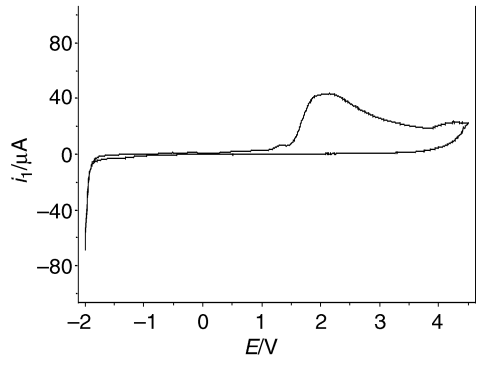

Fig. 1 Cyclic voltammetry of neat 1-ethyl-3-methylimidazolium dicyanamide (emim(dca)) carried out at 100 °C under a nitrogen atmosphere (dry box), on a glassy carbon microelectrode, with a platinum counter electrode and Ag/Ag^+ pseudo reference electrode.

The dca compounds which are liquid at rt are hygroscopic and are completely miscible with water, by contrast with the water-immiscible analogues.[2] The compounds also appear to absorb carbon dioxide readily. Extended periods at temperatures in excess of 100 °C have produced no evidence of breakdown. Qualitative tests showed that a number of hydrated cobalt(II), and copper(II) salts are appreciably soluble in 1-ethyl-3-methylimidazolium dca at rt with enhanced solubility on heating to 75 °C, whereas little dissolution of nickel salts and CuCl occurs. By contrast, the dca-soluble $CuCl_2{\cdot}2H_2O$ and $CoCl_2{\cdot}6H_2O$ are insoluble in the corresponding liquid at rt and only dissolved slightly at 75 °C. The solubility of the salts in the dca solvent may be due to its donor ligand properties, consistent with the rich coordination chemistry that is known of the anion,[3] though the inert behaviour of nickel salts is surprising. Of further interest is that glucose is soluble in the dca ionic liquid but not in the salt. Thus, the corresponding dca and salts show complementary solvent properties.

The electrochemical behaviour of these salts is illustrated by the example of the cyclic voltammogram in Fig. 1. The liquid is stable to quite low potentials, around −2 V *vs.* Ag/Ag^+, in common with other salts of this cation; the reductive limit presumably reflecting a reduction reaction of the cation. The stability in the oxidative range is reduced as compared to the analogue[2] but still leaves a large (>3.5 V) window for electrochemical use. The irreversible oxidation observed at *ca.* 1.5 V *vs.* Ag/Ag^+ may be indicative of the formation of a neutral dimer, $[N(CN)_2]_2$, a compound of theoretical interest but which has not been characterized.[8]

Thus new low melting, water-miscible, ionic liquids of relatively low viscosity which have considerable potential as a reaction medium and with a coordinating anion have been produced.

We are grateful for support from the Australian Research Council through the Centre for Green Chemistry.

Notes and references

† *Representative syntheses: 1-ethyl-3-methylimidazolium dicyanamide*: [emim(dca)]. Ag(dca)[9] (2.0 g, 11 mmol) was added to a solution of emimI (2.60 g, 11 mmol) in water (30 ml), and the resulting suspension was stirred overnight. Filtration and evaporation under vacuum gave the crude title compound, which was then dissolved in DCM and the solution dried over anhydrous $MgSO_4$. Evaporation under vacuum gave emim(dca) which was finally dried under vacuum over SiO_2 (yield, 1.51 g, 96%). Anal. Calcd for $C_8H_{11}N_5$: C, 54.2; H, 6.3; N, 39.5%. Found C, 52.7; H, 6.3; N, 38.6%. IR (liquid film): 3489 (w), 3150 (s), 3106 (s), 2988 (s), 2365 (w), 2232 (v.s), 2195 (v.s), 2132 (v.s), 1637 (w), 1573 (s), 1466 (m), 1427 (w), 1388 (w), 1131 (s), 1170 (s), 1088 (w), 1030 (w), 959 (w), 905 (w), 844 (w), 802 (w), 753 (m), 701 (w), 648 (m), 622 (s) cm^{-1}. ^1H NMR (300 MHz, d_6-DMSO): δ 1.42 (t, CH_3), 3.84 (s, n-CH_3), 4.19 (q, N-CH_2), 7.67 (s, CH), 7.76 (s, CH), 9.10 (s, N-CH-N) ppm. ^{13}C NMR (JMOD) (75 MHz, d_6-DMSO): δ 14.5 (s, CH_3), 35.2 (s, CH_3), 35.2 (s, CH_3), 43.6 (s, CH_2), 121.4 (s, CH), 123.0 (s, CH) ppm, $N(CN)_2^-$ and N–CH–N not cited. Electrospray MS(+ve): *m/z* 111 (100% − $emim^+$) MS (−ve) *m/z* 66 (100% dca^-), 243 (5% $[emim(dca)_2]^-$.

N-butyl-N-methylpyrrolidinium dicyanamide: $[P_{14}(dca)]$ Ag(dca) (2.10g, 12 mmol) and $P_{14}I$ (2.70g, 10 mmol) gave $[P_{14}(dca)]$ (yield 1.73g, 83%). IR (liquid film): 3488 (m), 2964 (m), 2876 (w), 2227 (s), 2191 (m), 2131 (v.s), 1466 (m), 1340 (m), 1306 (m), 1004 (v.w), 929 (w), 902 (v.w), 830 (v.w) cm^{-1}. ^1H NMR (300 MHz, d_6-DMSO): δ 0.92 (t, CH_3), 1.31 (m, CH_2), 1.67 (m, CH_2), 2.06 (br-t, 2 × CH_2), 2.96 (s, CH_3), 3.24 (q, CH_2), 3.43 (br-m, 2 × CH_2) ppm. ^{13}C NMR (75 MHz d_6-DMSO): δ 13.8 (s, CH_3), 19.6 (s, 2 × CH_2), 21.5 (s, CH_2), 25.3 (s, CH_2), 47.9 (t, CH_3), 63.3 (s, CH_2), 63.8 (t, 2 × CH_2) ppm, $N(CN)_2$- not observed. Electrospray MS (+ve): *m/z* 142 (100%, P_{14}^+); MS (−ve) *m/z* 66 (100%, dca^-).

1 (*a*) K. R. Seddon, *J. Chem. Tech. Biotechnol*., 1997, **68**, 351; (*b*) T. Welton, *Chem. Rev*., 1999, **99**, 2071; (*c*) J. L. Scott, D. R. MacFarlane, C. L. Raston and C. Mei Teoh, *Green Chem*., 2000, **2**, 123.

2 (*a*) P. Bonhote, A.-P. Dias, N. Papageorgio, K. Kalyanasundaram and M. Gratzel, *Inorg. Chem*., 1996, **35**, 1168; (*b*) J. Sun, D. R. MacFarlane and M. Forsyth, *Ionics*, 1997, **3**, 356; (*c*) J. Sun, M. Forsyth and D. R. MacFarlane, *J. Phys. Chem. B*, 1998, **102**, 8858.

3 S. R. Batten, P. Jensen, B. Moubaraki, K. S. Murray and R. Robson, *Chem. Commun*., 1998, 439; M. Kurmoo and C. J. Kepert, *New J. Chem*., 1998, 1515; J. L. Manson, C. R. Kmety, Q. Huang, J. W. Lynn, G. M. Bendel, S. Pagola, P. W. Stephens, L. M. Liable-Sands, A. L. Rheingold, A. J. Epstein and J. S. Miller, *Inorg. Chem*., 1999, **38**, 2552; S. R. Batten, P. Jensen, B. Moubaraki and K. S. Murray, *Chem. Commun*., 2000, 2331; P. Jensen, S. R. Batten, G. D. Fallon, D. C. R. Hockless, B. Moubaraki, K. S. Murray and R. Robson, *J. Solid State Chem*., 1999, **145**, 387.

4 D. R. MacFarlane, P. Meakin, J. Sun, N. Amini and M. Forsyth, *J. Phys. Chem*., 1999, **103**, 4164.

5 (*a*) D. R. MacFarlane, G. B. Deacon, S. Forsyth and J. Golding, to be published; (*b*) D. R. MacFarlane, J. Golding and G. B. Deacon, *Aust. Prov. Patent Application*, March 2001.

6 (*a*) J. T. Hamill, C. Hardaere, M. Nieuwenhuyzen, K. R. Seddon, S. A. Thompson and B. Ellis, *Chem. Commun*., 2000, 1929; (*b*) M. Torres, A. Stark and K. R. Seddon, *Pure Appl. Chem*., 2000, **72**, 2275.

7 (*a*) J. Huang, M. Forsyth and D. R. MacFarlane, *Solid State Ionics*, 2000, **136**, 447; (*b*) M. Forsyth, J. Huang and D. R. MacFarlan, *J. Mater. Chem*., 2000, **10**, 2259; (*c*) D. R. MacFarlane, J. Huang and M. Forsyth, *Nature*, 1999, **402**, 792.

8 (*a*) M. Sana and G. Leroy, *Ann. Soc. Sci. Bruxelles*, 1987, **101**, 23; G. Leroy, M. Sana and C. Wilante, *Belg. Theochem*., 1987, **38**, 249; A. M. Golub, H. Köhler and V. V. Skopenko, *Chemistry of Pseudohalides*, Elsevier, Berlin, 1986.

9 D. Britton and Y. M. Chow, *Acta Crystallogr., Sect. B*, 1977, **33**, 697.

CHEMCOMM Communication
www.rsc.org/chemcomm

Topological isomerism in coordination polymers†

Alexander J. Blake,[a] Neil R. Brooks,[a] Neil R. Champness,*[a] Marcello Crew,[a] Anne Deveson,[b] Dieter Fenske,[b] Duncan H. Gregory,[a] Lyall R. Hanton,*[c] Peter Hubberstey[a] and Martin Schröder*[a]

[a] *School of Chemistry, University of Nottingham, University Park, Nottingham, UK NG7 2RD. E-mail: M.Schroder@nottingham.ac.uk; Neil.Champness@nottingham.ac.uk*
[b] *Institut für Anorganische Chemie, Universität Karlsruhe, Engesserstr. Geb-Nr. 30.45, 76128 Karlsruhe, Germany*
[c] *Department of Chemistry, University of Otago, PO Box 56, Dunedin, New Zealand. E-mail: lhanton@alkali.otago.ac.nz*

Received (in Cambridge, UK) 23rd April 2001, Accepted 20th June 2001
First published as an Advance Article on the web 19th July 2001

Three coordination polymers formed between CuI and bpds [bpds = bis(4-pyridyl)disulfide] have been prepared and fully characterised illustrating rare examples of solvent dependent topological isomerism in $[(CuI)_2(bpds)]_\infty$; tetrahedral Cu_4I_4 cubane junctions are linked to give either necklace or tubular polymers.

The study of inorganic coordination frameworks has received increasing attention over recent years with a growing range of structural motifs being discovered.[1–4] Many of these studies have heightened awareness of the influence not only of metal ion and ligand[2] but also of anion[3] and solvent.[4,5] Many of the architectures reported to date are based upon rigid linear linker ligands,[1–4] with only recent efforts focusing on the use of ligands showing conformational flexibility.[5–7] The term 'supramolecular isomerism' has been used by Zaworotko and coworkers[5] to describe the two forms of the coordination polymer $[Co(NO_3)_2(L)_{1.5}]_\infty$ obtained from the reaction of $Co(NO_3)_2$ with 1,2-bis(4-pyridyl)ethane (L). The two isomers differ due to the conformational flexibility of L which is *gauche* in one isomer and *anti* in the other.[5] More recently, the various different isomers of T-shaped metal–ligand building blocks have been recognised.[8] We prefer the term topological isomerism as we believe that this describes the differences in the topology and connectivity of the coordination polymer. We report herein an unusual example of topological isomerism in which both isomers (**2** and **3**) have the same stoichiometry, the same metal-fragment and ligand-linker combinations, the same ligand conformations, and the same metal ion stereochemistry. Compounds **2** and **3** differ purely in their metal to ligand coordinative connectivity to give isomers of different topology.

We were interested in developing neutral metal–organic networks and chose to investigate metal–halide aggregation with heterocyclic ligands.[9] The coordination polymers

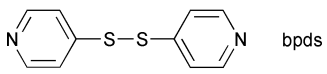

$[CuI(bpds)]_\infty$ and $[(CuI)_2(bpds)]_\infty$ [bpds = bis(4-pyridyl)disulfide] can be prepared systematically as yellow powders. Bulk quantities of the compounds are obtained by the stoichiometric reaction of CuI with the ligand in MeCN or EtCN. Crystals of the compounds were grown by slow diffusion between CuI solutions in EtCN (or MeCN) and bpds in CH_2Cl_2. Regardless of the metal : ligand ratios used, crystals of both compounds were found in the same reaction solution. Over the period of a week, yellow needles of $[CuI(bpds)]_\infty$ **1** grew in the ligand-rich region of the solution while pale-yellow blocks of $[(CuI)_2(bpds)]_\infty$, **2** or **3**, grew in the metal-rich region.‡

Although the structure of $[CuI(bpds)]_\infty$ **1** consists of Cu_2I_2 cores connected by bpds to form a planar ribbon of known topology[10] (whether grown from MeCN–CH_2Cl_2 **1a** or EtCN–CH_2Cl_2 **1b**), the single crystal X-ray structure determinations of the 2 : 1 complex $[(CuI)_2(bpds)]_\infty$ revealed two different structural motifs depending upon the solvent used in crystallisation. In both cases the $[(CuI)_2(bpds)]_\infty$ consists of Cu_4I_4 cubane tetramers which are linked by two bpds ligands to form a square-shaped cavity (Fig. 1). Crystals of **2** grown from EtCN–CH_2Cl_2 reveals tetrahedral Cu_4I_4 cubane junctions§ linked by bpds ligands [C–S–S–C 77.4(2)°] to give a necklace structure (Fig. 1). However, in this case the tetrahedral geometry of the Cu_4I_4 cubane results in alternating square-shaped units being orientated perpendicular to each other in adjacent links of the necklace. The square-shaped cavities are packed to give channels which run parallel to the *b*-axis (potential solvent accessible volume 21.5%)[11] that accommodate EtCN molecules.

Using MeCN–CH_2Cl_2 as the crystallisation solvent results in a different structural isomer of $[(CuI)_2(bpds)]_\infty$ **3**. As in **2**, Cu_4I_4 cubane tetramers are linked by two bpds ligands to form a square-shaped cavity. However, the tetrahedral junctions§ of these cubane units now allow these squares to interlink *via* two further bpds ligands forming a tubular polymer[6] (Fig. 2). The conformation adopted by the bpds ligands is similar to that observed for the 1 : 1 compound [within the square C–S–S–C 78.4(3)°, interlinkers C–S–S–C 88.3(3)°]. In **3** the spaces between the bands of the square-shaped cavities are interdigitated by the bands of two adjacent tubes translated by half the repeat unit (Fig. 3). Despite the interdigitation this packing arrangement allows the formation of two criss-crossed channels parallel to the *a* and *b* axes, giving a potential solvent accessible volume of 14.4%.[11] Both of these channels run diagonally through the square-shaped cavities of adjacent tubes and are occupied by MeCN solvent molecules (Fig. 4).

Powder X-ray diffraction studies of **2** and **3** were used to study whether each solvent mixture results exclusively in a single isomer. Compound **2** was found to undergo irreversible and rapid desolvation during the period of the diffraction

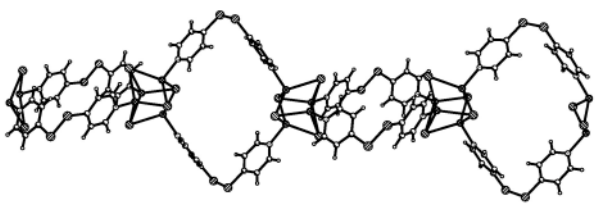

Fig. 1 The necklace isomer **2** of $[(CuI)_2(bpds)]_\infty$ showing alternating square-shaped units perpendicular to each other.

† Electronic supplementary information (ESI) available: full experimental details. See http://www.rsc.org/suppdata/cc/b1/b103612m/

 DOI: 10.1039/b103612m

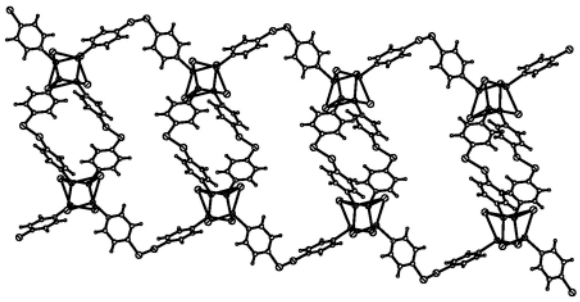

Fig. 2 The tubular isomer **3** of $[(CuI)_2(bpds)]_\infty$ illustrating the alternative linking of (Cu_4I_4) cubane units compared to its topological isomer **2**.

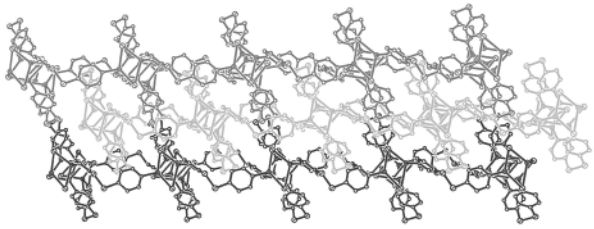

Fig. 3 Interdigitation of adjacent $[(CuI)_2(bpds)]_\infty$ tubes in **3** resulting in the formation of solvent-filled channels.

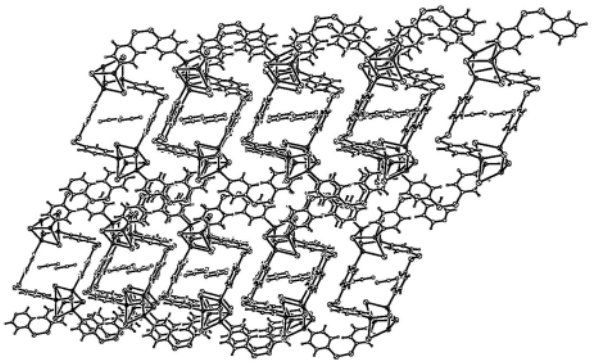

Fig. 4 The solvent-filled channels formed in **3** viewed down the *b*-axis illustrating the positioning of the MeCN solvent molecules.

experiment giving a new diffraction pattern that was not consistent with the single crystal X-ray structure. In contrast, bulk samples of **3** were found to give diffraction patterns in good agreement with that expected from the single crystal studies. No evidence for the presence of the desolvated form of **2** was found in the diffraction pattern of **3** and *vice versa*. Thus, we conclude that the formation of each isomer is exclusively dependent on solvent of crystallisation, and that due to interdigitation **3** is a more robust framework for potential reversible solvent inclusion. Indeed upon heating single crystals of **3** to 100 °C for 10 h *in vacuo* up to 58% of the guest MeCN molecules can be removed as evidenced by single crystal X-ray diffraction experiments. Further details of the desolvation processes of compound **3** will form part of a future study.

As both isomers of $[(CuI)_2(bpds)]_\infty$ form under similar reaction conditions, but with a change in the nitrile solvent, it is reasonable to conclude that there are only minor energy differences in the formation of the two polymers. The two isomers of $[(CuI)_2(bpds)]_\infty$ **2** and **3** are very rare examples of metal–organic architectures which exhibit topological isomerism, and illustrate the profound effect of solvent-template effects in their formation.[5,8] We prefer the description 'topological isomerism' rather than 'polymorphism'[12] in this case to reflect the different coordinative connectivities between **2** and **3** rather than the different crystal packing.

This work was supported by the EPSRC (UK), the University of Nottingham, the Nuffield Foundation and by the University of Otago (L. R. H.). D. H. G. thanks the EPSRC for the award of an Advanced Research Fellowship. We thank Professor Graham A. Bowmaker (University of Auckland, NZ) for helpful discussions.

Notes and references

‡ *Crystal data*: $\{[CuI(bpds)](MeCN)\}_\infty$ **1a**: $C_{12}H_{11}CuIN_3S_2$, M = 451.8, triclinic, space group $P\bar{1}$ (no. 2), yellow needles, a = 8.745(2), b = 8.955(4), c = 10.636(3) Å, α = 94.48(4), β = 96.63(3), γ = 106.11(4)°, U = 789.5(5) Å^3, Z = 2, D_c = 1.900 g cm^{-3}, μ(Mo-$K\alpha$) = 3.591 mm^{-1}, T = 150(2) K. 2775 unique reflections [R_{int} = 0.00] [2415 with $I \geqslant 2\sigma(I)$]. Final R = 0.0400, wR_2(all data) = 0.0982.

$\{[CuI(bpds)](CH_2Cl_2)\}_\infty$ **1b**: $C_{11}H_{10}Cl_2CuIN_2S_2$, M = 495.67, triclinic, space group $P\bar{1}$ (no. 2), yellow needles, a = 8.425(2), b = 10.318(2), c = 10.670(2) Å, α = 113.92(3), β = 97.23(3), γ = 92.21(3)°, U = 837.0(3) Å^3, Z = 2, D_c = 1.967 g cm^{-3}, μ(Mo-$K\alpha$) = 3.704 mm^{-1}, T = 193(2) K. 3415 unique reflections [R_{int} = 0.039] [3255 with $I > 2\sigma(I)$]. Final R = 0.0541, wR_2(all data) = 0.1496.

$\{[(CuI)_2(bpds)]\cdot 0.5EtCN\}_\infty$ **2**: $C_{11.5}H_{10.5}Cu_2I_2N_{2.5}S_2$, M = 628.72, orthorhombic, space group *Pccn* (no. 56), yellow block, a = 19.493(4), b = 10.760(2), c = 17.334(4) Å, U = 3635.7(13) Å^3, Z = 8, D_c = 2.297 g cm^{-3}, μ(Mo-$K\alpha$) = 5.957 mm^{-1}, T = 193(2) K. 3999 unique reflections [R_{int} = 0.036] [3475 with $I > 2\sigma(I)$]. Final R = 0.0336, wR_2(all data) = 0.0949.

$\{[(CuI)_2(bpds)]\cdot 0.5MeCN\}_\infty$ **3**: $C_{22}H_{19}Cu_4I_4N_5S_4$, M = 1243.43, triclinic, space group $P\bar{1}$ (no. 2), yellow column, a = 8.878(1), b = 10.212(1), c = 19.307(2) Å, α = 90.249(2), β = 103.023(2), γ = 92.796(2) °, U = 1703.2(3) Å^3, Z = 2, D_c = 2.419 g cm^{-3}, μ(Mo-$K\alpha$) = 6.356 mm^1, T = 150(2) K. 7690 unique reflections [R_{int} = 0.024] [6494 with $I \geqslant 2\sigma(I)$]. Final R = 0.0255, wR_2(all data) = 0.0643.

CCDC reference numbers 116866 and 164101–164103. See http://www.rsc.org/suppdata/cc/b1/b103612m/ for crystallographic data in CIF or other electronic format.

§ Considering the centre of the Cu_4 tetrahedron to be the 'centre' of the cubane, junction angles between the nitrogen donors range between 108.0 and 110.7° for **2** and 103.8 and 119.7° for **3**.

1 S. R. Batten and R. Robson, *Angew. Chem., Int. Ed.*, 1998, **37**, 1460; A. J. Blake, N. R. Champness, P. Hubberstey, W.-S. Li, M. Schröder and M. A. Withersby, *Coord. Chem. Rev.*, 1999, **183**, 117; B. Moulton and M. J. Zaworotko, *Chem. Rev.*, 2001, **101**, 1629.

2 B. F. Hoskins, R. Robson and D. A. Slizys, *Angew. Chem., Int. Ed. Engl.*, 1997, **36**, 2336; A. J. Blake, N. R. Champness, S. S. M. Chung, W.-S. Li and M. Schröder, *Chem. Commun.*, 1997, 1005; L. Carlucci, G. Ciani, P. Macchi and D. M. Proserpio, *Chem. Commun.*, 1998, 1837.

3 M. A. Withersby, A. J. Blake, N. R. Champness, P. Hubberstey, W.-S. Li and M. Schröder, *Angew. Chem., Int. Ed. Engl.*, 1997, **36**, 2327; L. Ballester, I. Baxter, P. C. M. Duncan, D. M. L. Goodgame, D. A. Grachvogel and D. J. Williams, *Polyhedron*, 1998, **17**, 3613.

4 M. A. Withersby, A. J. Blake, N. R. Champness, P. A. Cooke, P. Hubberstey, W.-S. Li and M. Schröder, *Inorg. Chem.*, 1999, **38**, 2259; M. A. Withersby, A. J. Blake, N. R. Champness, P. A. Cooke, P. Hubberstey and M. Schröder, *J. Am. Chem. Soc.*, 2000, **122**, 4044; A. J. Blake, N. R. Champness, P. A. Cooke, J. E. B. Nicolson and C. Wilson, *J. Chem. Soc., Dalton Trans.*, 2000, 3811.

5 T. L. Hennigar, D. C. MacQuarrie, P. Losier, R. D. Rogers and M. J. Zaworotko, *Angew. Chem., Int. Ed. Engl.*, 1997, **36**, 972.

6 L. Carlucci, G. Ciani, D. W. v. Gudenberg and D. M. Proserpio, *Inorg. Chem.*, 1997, **36**, 3812.

7 M. Fujita, O. Sasaki, K. Yamaguchi and K. Ogura, *J. Am. Chem. Soc.*, 1995, **117**, 7287; M. Fujita, O. Sasaki, K. Watanabe, K. Ogura and K. Yamaguchi, *New J. Chem.*, 1998, 189.

8 H. Gudbjartson, K. Biradha, K. M. Poirier and M. J. Zaworotko, *J. Am. Chem. Soc.*, 1999, **121**, 2599; M. A. Withersby, A. J. Blake, N. R. Champness, P. A. Cooke, P. Hubberstey and M. Schröder, *New J. Chem.*, 1999, **23**, 573.

9 A. J. Blake, N. R. Brooks, N. R. Champness, L. R. Hanton, P. Hubberstey and M. Schröder, *Pure Appl. Chem.*, 1998, **70**, 2351 and references therein. See also: M. Munakata, T. Kurodasowa, M. Maekawa, A. Honda and S. Kitagawa, *J. Chem. Soc., Dalton Trans.*, 1994, 2771.

10 M. Fujita, Y. J. Kwon, M. Miyazawa and K. Ogura, *J. Chem. Soc., Chem. Commun.*, 1994, 1977; M. L. Hernandez, M. G. Barandika, M. K. Urtiaga, R. Cortes, L. Lezama, M. I. Arriortua and T. Rojo, *J. Chem. Soc., Dalton Trans.*, 1999, 1401.

11 PLATON, A. L. Spek, *Acta Crystallogr., Sect. A*, 1990, **46**, C-34.

12 R. A. Heintz, H. Zhao, X. Ouyang, G. Grandinetti, J. Cowen and K. R. Dunbar, *Inorg. Chem.*, 1999, **38**, 144; J. D. Dunitz, in *The Crystal as a Supramolecular Entity*, ed. G. R. Desiraju, Wiley, Chichester, UK, 1996.

CHEMCOMM Communication
www.rsc.org/chemcomm

Cationic surfactant mediated hybridization and hydrophobization of DNA molecules at the liquid/liquid interface and their phase transfer

Murali Sastry,*[a] Ashavani Kumar,[a] Mrunalini Pattarkine,[b] Vidya Ramakrishnan[a] and Krishna N. Ganesh*[a]

[a] *Materials Division, National Chemical Laboratory, Pune 411 008, India. E-mail: sastry@ems.ncl.res.in and kng@ems.ncl.res.in; Fax: +91 20 5893044 and 5893153; Tel: +91 20 5893044 and 5893153*
[b] *Organic Chemistry (Synthesis) Division, National Chemical Laboratory, Pune 411 008, India*

Received (in Cambridge, UK) 1st February 2001, Accepted 20th June 2001
First published as an Advance Article on the web 19th July 2001

Hybridization of complementary oligonucleotides mediated by a cationic surfactant at the water/hexane interface leads to hydrophobic, double-helical DNA which may be readily phase transferred to the organic phase and cast into thin films on solid substrates.

The development of synthetic, virus-like DNA vectors is a topical problem of considerable interest. Following the report of Felgner *et al.*[1] demonstrating that DNA pre-complexed with a cationic surfactant leads to its enhanced uptake by eucaryotic cells, DNA–cationic liposome complexes are being investigated in great detail as non-viral DNA vectors.[2]

Many studies have dealt with DNA–surfactant complexes in an aqueous environment.[3] In aqueous solutions containing equimolar amounts of DNA and the cationic surfactant, the complex formed was water-insoluble but soluble in low-polarity organic solvents.[3a,d] Reimer *et al.*[4] have shown that DNA molecules may be hydrophobized by complexation with cationic surfactants in a Bligh and Dyer monophase[5] and thereafter transferred into the organic phase by partitioning the monophase. We describe herein a simple method for the hybridization of complementary oligonucleotides employing electrostatic complexation with a cationic lipid, octadecylamine (ODA), at the water/hexane interface followed by phase transfer of duplex DNA into the non-polar organic environment. Furthermore, films of the DNA–ODA complexes may be easily deposited on solid surfaces by solvent evaporation. To the best of our knowledge, this is the first report on the surfactant-mediated hybridization of complementary oligonucleotides at the interface between two liquids.

Oligonucleotides of the sequences GGAAAAAACTTCGTGC (ssDNA1), GCAC-GAAGTTTTTTCC (ssDNA2) and AGAAGAAGAAAAGAA (ssDNA3) were synthesized as described elsewhere.[6] ssDNA1 and ssDNA2 are complementary oligonucleotides while ssDNA3 is non-complementary to both ssDNA1 and ssDNA2. In typical experiments, 10 mL of a 10^{-4} M solution of ODA (Sigma USA) in hexane was added to: (a) 10 mL of 10^{-6} M aqueous solution of ssDNA1 and ssDNA2 taken in an equimolar ratio (experiment **A**); (b) 10 mL of 10^{-6} M preformed duplex DNA constituted from complementary pairs ssDNA1 and ssDNA2 in water[7] (experiment **B**) and (c) 10 mL of 10^{-6} M aqueous solution of non-complimentary pairs ssDNA1 and ssDNA3 in an equimolar ratio (experiment **C**). The pH of the DNA solutions in all cases was 6.8. The hybridization of the complementary oligonucleotides ssDNA1 and ssDNA2 and the intactness of the duplex structure after phase transfer of the preformed duplex DNA was followed using the fluorescent intercalator, ethidium bromide, added to the aqueous solutions at a concentration of 10^{-5} M along with the DNA molecules. Vigorous mixing of the biphasic mixture was carried out at room temperature using a motor-driven overhead stirrer operating at 3000 rpm immersed in the liquid phase for 20 min. During the mixing process, a uniform and milky microemulsion-like phase was observed to form which, within one minute of cessation of stirring, resulted in a rapid separation of two clear layers.

Fig. 1A shows UV-vis spectra recorded from the hexane phase before and after the mixing protocols described in experiments **A** and **B**.[8] There is no indication of the presence of DNA in the organic layer before mixing (Fig. 1A, curve 3) but a strong resonance at 270 nm is induced in the hexane phase by the mixing process in experiments **A** and **B** (curves 2 and 1 respectively, Fig. 1A) and indicates phase transfer of the DNA molecules into hexane.[9] The mixing procedure resulted in the formation of a microemulsion-like phase which is clearly indicative of formation of extremely small droplets of hexane stabilized in the aqueous phase by the ODA molecules. This is likely given that hexane has a finite solubility in water (0.0138 g per 100 mL of water).[10] These droplets would increase the interfacial area between the water and hexane phases facilitating the interaction of DNA with the ODA molecules at the interface. At pH 6.8, the ODA molecules are positively charged (pK_B of ODA = 10.8) and the negatively charged DNA are thus electrostatically bound to the cationic ODA molecules. The DNA molecules are rendered hydrophobic upon complexation with ODA resulting in their phase transfer into hexane. The relative molar ratio of DNA–ODA is important in achieving a minimum critical hydrophobicity to accomplish the phase transfer. Equimolar ratios of DNA–ODA did not result in a detectable phase transfer of the DNA molecules into hexane. In the experiments described herein, a nearly 100-fold molar excess of ODA molecules (over DNA) was taken in the hexane phase.

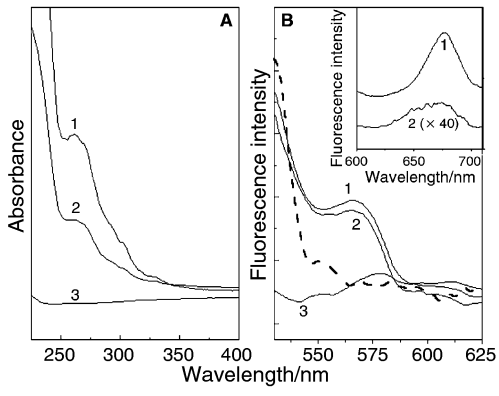

Fig. 1 (A) UV-vis spectra of the hexane phase before (curve 3) and after shaking biphasic mixtures of 10^{-4} M ODA in hexane and aqueous solutions of **A** (curve 2) and **B** (curve 1). (B) Fluorescence spectra of the hexane phase after transfer of DNA from aqueous solutions of experiment **A** (curve 1) and experiment **B** (curve 2). The fluorescence spectrum from the hexane phase in experiment **C** is also shown (curve 3). The dashed curve corresponds to the fluorescence spectrum from a mixture of ssDNA1–ODA and ssDNA2–ODA separately phase-transferred into hexane. The inset shows fluorescence spectra recorded from DNA–ODA complex films cast from the hexane phase on quartz substrates from experiments **A** (curve 1) and **B** (curve 2).

 DOI: 10.1039/b101110n

Fig. 1B shows the fluorescence spectra[11] from the hexane phase after transfer of DNA from aqueous solutions in experiments **A** (curve 1) and **B** (curve 2). A strong fluorescence signal at *ca.* 570 nm is seen in both cases. Ethidium bromide intercalates between the base pairs of DNA double helical structures and this process is detected by enhanced fluorescence.[12] The fluorescence results thus clearly indicate that the preformed double helical DNA molecules are phase transferred into hexane with retention of their double helical structure (curve 2, Fig. 1B). More importantly, the results show that not only have the single-stranded oligonucleotides ssDNA1 and ssDNA2 been transferred to the organic phase by complexation with ODA molecules, *they have hybridized into a duplex* (curve 1, Fig. 1B). No fluorescence was detected in the organic phase after the phase transfer of mixtures of ssDNA1 and ssDNA3 (non-complementary oligonucleotides, experiment **C**) even though the presence of the single-stranded DNA molecules was indicated by UV-vis measurements. To distinguish whether the transfer of DNA occurs in single-strand form followed by duplexation in hexane or directly as a duplex, hexane solutions of ssDNA1 and ssDNA2 separately phase transferred by complexation with ODA were mixed and the fluorescence measured (dashed curve, Fig. 1B). It is observed that there is no fluorescence in this experiment either. Thus, the hybridization inferred by the fluorescence measurements shown in Fig. 1B (curve 2) is clearly due to recognition of the complementary base sequences and occurs only at the hexane/water interface. In the absence of any added salts, the cationic ODA molecules act like counterions and screen the repulsive electrostatic interactions between the individual DNA strands to facilitate the hybridization process. The formation of double helical structures of ssDNA1 and ssDNA2 does not occur in the bulk of the aqueous phase in the absence of salt and these results clearly imply an interfacial process mediated by the cationic lipid molecules.

An exciting aspect of this is the possibility of depositing films of ODA-stabilized DNA by simple solvent evaporation. The fluorescence spectra obtained from films of DNA–ODA complexes cast from hexane solution onto quartz from experiments **A** and **B** are shown in the inset of Fig. 1B as curves 1 and 2 respectively. Strong emission signals from ethidium bromide are observed in both the films with an emission at *ca.* 675 nm. A large red shift in the emission wavelength is seen in the DNA–ODA films relative to the solution wavelength (main part of Fig. 1B). This is likely to be a consequence of the large increase in polarity of the intercalator environment in the film form and has support from the literature.[12] The low intensity fluorescence spectrum from the preformed DNA–ODA (curve 2, inset of Fig. 1B) is perhaps a consequence of non-uniformity of the film during evaporation of hexane and not due to a deterioration of the degree of hybridization of the DNA double helices.

Fig. 2 shows UV-melting curves from DNA–ODA complex films cast onto quartz from experiments **A** (curve 2) and **B** (curve 1). The preformed duplex DNA complexed with ODA shows a single melting transition at 55 °C (curve 1, Fig. 2) which is higher than the aqueous solution melting transition temperature of 41 °C[3b] indicating significant thermal stabilization of the duplex structure by the ODA molecules. The UV–melting transition curve for the DNA hybridized at the hexane/water interface-ODA film shows two T_M values at 39 and 61 °C (curve 2, Fig. 2). Such behaviour has been recently observed by Pattarkine and Ganesh in aqueous DNA–lipid complexes[3b] and was attributed to phase separation of lipid-free DNA double helical structures (lower T_M) and DNA double helices capped with a layer of surfactant molecules (higher T_M). DNA cannot exist in the organic phase without some degree of hydrophobization provided by electrostatically complexed ODA molecules. The above result may be attributed to two phase-transferred components wherein the degree of complexation of the DNA duplex with ODA molecules is different.

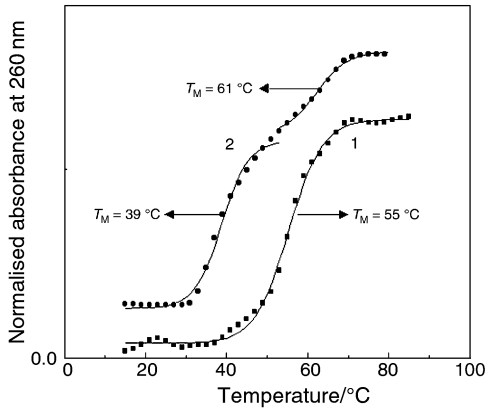

Fig. 2 UV-temperature plots of films of DNA–ODA complexes on quartz substrates in experiment **A** (curve 2) and experiment **B** (curve 1).

In conclusion, electrostatic complexation of DNA molecules with cationic lipid molecules at the organic/water interface and phase transfer of DNA into the organic phase has been demonstrated. An important finding is the surfactant-facilitated hybridization (and consequent hydrophobization and phase transfer) of complementary single-stranded DNA molecules at the liquid/liquid interface under conditions where the hybridization to form double helical structures does not occur in the bulk of the aqueous phase. The DNA molecules may be conveniently cast in the form of thin films onto any solid support by solvent evaporation. This approach is expected to facilitate the generation of lipid–DNA complexes for possible application in gene-transfer systems *etc.*

Three of us, AK, VR and MP, thank the Council of Scientific and Industrial Research (CSIR), Government of India, for financial support.

Notes and references

1 P. L. Felgner, T. R. Gadek, M. Holm, M. Roman, M. Wentz, J. P. Northrop, M. Ringold and H. Danielsen, *Proc. Natl. Acad. Sci. USA*, 1987, **84**, 7413.
2 J. O. Radler, I. Koltover, A. Jamieson, T. Salditt and C. R. Safinya, *Langmuir*, 1998, **14**, 4272; D. D. Lasic, H. Strey, M. C. A. Stuart, R. Podgornik and P. M. Frederik, *J. Am. Chem. Soc.*, 1997, **119**, 832.
3 (*a*) K. Tanaka and Y. Okahata, *J. Am. Chem. Soc.*, 1996, **118**, 10679; (*b*) M. V. Pattarkine and K. N. Ganesh, *Biochem. Biophys. Res. Comm.*, 1999, **263**, 41; (*c*) P. S. Kuhn, M. C. Barbosa and Y. Levin, *Physica A.*, 1999, **269**, 278.
4 D. L. Reimer, Y. Zhang, S. Kong, J. J. Wheeler, R. W. Graham and M. B. Bally, *Biochemistry*, 1995, **34**, 12877.
5 The Bligh and Dyer monophase is a solution of chloroform–methanol–water in the ratio of 1 : 2.1 : 1. Partitioning of the monophase into a two-phase system is accomplished by further addition of water and chloroform (see ref. 4 for details).
6 M. Sastry, V. Ramakrishnan, M. Pattarkine, A. Gole and K. N. Ganesh, *Langmuir*, 2000, **16**, 9142.
7 Pre-hybridization of DNA was carried out by heating an equimolar mixture of ssDNA1 and ssDNA2 (10^{-6} M concentration) to 90 °C in an aqueous solution of 1 mM NaCl followed by slow cooling.
8 UV-vis spectroscopy measurements were performed on a HP8542A diode array spectrophotometer operated at a resolution of 2 nm.
9 C. R. Cantor and P. R. Schimmel, *Biophysical Chemistry, Part II*, W. H. Freeman, New York, 1980.
10 *Handbook of Chemistry and Physics (42nd Edition)*, C. D. Hodgman, Editor-in-Chief, The Chemical Rubber Publishing Co., Cleveland, Ohio, 1960, p. 1030–1031.
11 Fluorescence measurements were carried out on a Perkin Elmer model LS 50-B spectrofluorimeter at 25 °C, with slit widths of 5 nm for excitation at 460 nm and 10 nm for the emission monochromators.
12 J. B. LePecq and C. Paoletti, *J. Mol. Biol.*, 1967, **27**, 87.

CHEMCOMM Communication
www.rsc.org/chemcomm

Copolymerization of carbon monoxide and aziridine†

Li Jia,* Errun Ding and William R. Anderson

Department of Chemistry, Lehigh University, 6 E. Packer Avenue, Bethlehem, PA 18015, USA. E-mail: lij4@lehigh.edu; Fax: +1 610-758-6536; Tel: +1 610-758-5715

Received (in Cambridge, UK) 1st May 2001, Accepted 15th June 2001
First published as an Advance Article on the web 19th July 2001

Alternating copolymerization of carbon monoxide with aziridine was realized, which serves as a prototype of a novel route for synthesis of poly-β-peptides.

Rational discovery of new catalytic reactions is an important scientific challenge for synthetic chemists. We are interested in designing new catalytic polymerization reactions which involve reaction and incorporation of heteroatoms in the polymer chain to produce functional polymers. In light of the successful examples of carbonylation of aziridines and epoxides and alternating copolymerization of CO and alkenes,[1–4] we set out to develop metal-catalyzed alternating copolymerization of CO with aziridines [eqn. (1)].[5] This reaction in principle provides an

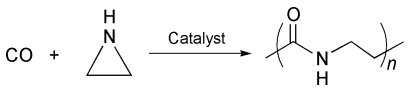

(1)

attractive route to poly-β-peptides, which have received considerable current attention as biomimetic materials.[7,8] Prior to this work, Sen and Arndtsen independently suggested the possibility of copolymerization of imines with CO to produce poly-α-peptides and demonstrated the first examples of imine insertion into Pd–acyl bonds.[9,10] We report here the initial identification of a catalyst for CO–aziridine copolymerization and that alternating polymerization can be achieved under carefully controlled experimental conditions.

At the onset of this project, we conceived a catalytic cycle leading to the copolymerization. First of all, CO insertion and aziridine insertion into a metal–carbon bond are inevitable steps in any catalytic cycle that one might design for the copolymerization of CO and aziridine. Examples of the latter reaction are absent in organometallic chemistry to our knowledge. However, an interesting reaction of aziridine insertion into acetyl chloride was reported [eqn. (2)].[11] It is well established

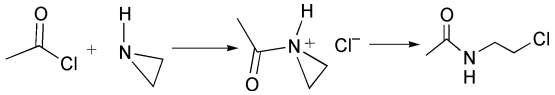

(2)

that some metal–acyl species resemble organic acyl chlorides and undergo nucleophilic cleavage by alcohols and amines to afford esters and amides. By such analogy, insertion of aziridine into metal–acyl bonds might also occur. The aziridine insertion coupled with CO insertion into a metal–alkyl bond then forms a reasonable catalytic cycle leading to the alternating copolymerization (Scheme 1).

Under the above hypothesis, we screened a number of potential catalysts and arrived at Heck's complex $CH_3COCo(CO)_3PPh_3$ **1**. In the presence of 10 mol% of **1** under 1000 psi CO in THF solution, aziridine and CO was copolymerized to produce a crystalline, hot-water soluble polymer in good yield (entry 1, Table 1). The FT-IR and NMR spectra together confirm that the product is poly-β-alanine. In the IR spectrum, two prominent amide bands are present at 1645 and 1539 cm^{-1}.† The ^1H NMR spectrum reveals two triplet resonances (**a** and **b**) at δ 3.25 and 2.26 ppm (J = 6.5 Hz) (Fig. 1a), in agreement with the chemical shifts reported for poly-β-alanine prepared from acrylamide.[12] Additional fine features (labeled with asterisks) are present overlapping with or in close vicinities of **a** and **b**. The small differences in chemical shifts between them and the main peaks **a** and **b** lead us to believe that they belong to β-alanine units located at or close to the end of the chain. These resonances are not due to amine microstructures, which would possibly be present if repetitive aziridine insertions occurred (see below), because they do not move downfield in acid solutions in contrast to what should be expected for amines upon protonation. Work is in progress in our laboratory to positively identify these resonances. A resonance (**c**) at δ 1.80 ppm is observed due to the acetyl end group that originates from

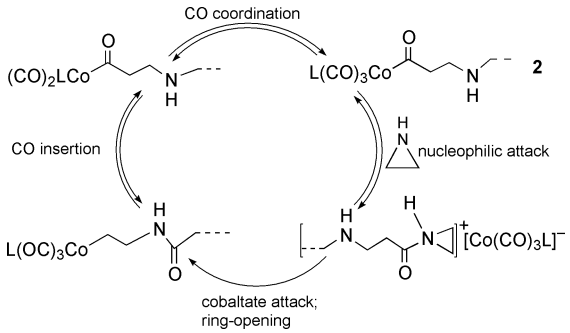

Scheme 1 Working model for alternating copolymerization of CO with aziridine (L = PPh_3).

† Electronic supplementary information (ESI): NMR spectra, GPC summary, elemental analyses, experimental procedure of polymerization, and a scheme rationalizing the imperfect alternating enchainment. See http://www.rsc.org/suppdata/cc/b1/b103899k/

Table 1 Copolymerization of CO with aziridine using **1** as the catalyst[a]

Entry	[Cat]/mM	Aziridine/g	Aziridine–**1** (molar ratio)	CO pressure/psi	Reaction time/h	Yield/g	Amine units/mol%[b]	M_w[c]/10^3	PDI[c]
1	5.8	0.25	10	1000	12	0.25 (60%)	<2	14.1	4.85
2	5.8	0.25	10	500	12	0.25 (60%)	<2	—	—
3	5.8	0.25	10	250	12	0.17 (41%)	<2	—	—
4	5.8	0.75	30	1000	12	0.98 (79%)	~8	36.6	2.52
5	5.8	1.25	50	1000	12	1.84 (89%)	~12	57.8	11.56
6[d]	5.8	0.25 × 3	30	1000	12 × 3	1.06 (86%)	~2	36.6	5.67
7[d]	5.8	0.25 × 5	50	1000	12 × 5	1.92 (93%)	~2	63.3	9.32

[a] In 100 mL THF at 80 °C. [b] Amine defects estimated by ^1H NMR. [c] Determined by GPC in 1,1,1,3,3,3-hexafluoropropan-2-ol with 0.01 M sodium triflate, light scattering–viscometry–refractive index triple detector. [d] Aziridine was added in portions.

 DOI: 10.1039/b103899k

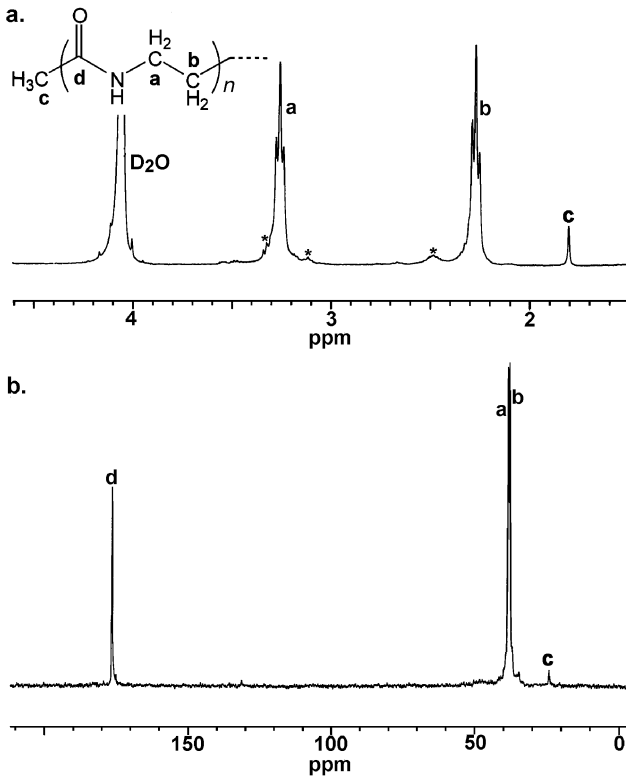

Fig. 1 a. ^{1}H NMR (360 MHz, D_2O, 95 °C) of poly-β-alanine produced from copolymerization of CO and aziridine (entry 1, Table 1). Integral ratio of **a**–**b**–**c** = 100:100:6. b. $^{13}C\{^1H\}$ NMR (90 MHz, D_2O, 95 °C, THF in D_2O as external standard) of the same sample.

1. Such assignment is consolidated by the observation that this peak disappeared when the methyl-deuterated **1** $CD_3COCo(CO)_3PPh_3$ was used for the copolymerization. In the ^{13}C spectrum (Fig. 1b), the amide carbonyl peak (**d**) is clearly shown at δ 176.2 ppm. The methylene ^{13}C resonances appear at δ 38.3 and 37.7 ppm. The peak at 24.2 ppm (**c**) in the ^{13}C spectrum is assigned to the methyl of the acetyl end group. All ^{13}C assignments are supported by ^1H–^{13}C HMQC and HMBC experiments.†

Varying CO pressure exerted little effect on the selectivity of the polymerization (entries 2 and 3, Table 1). However, the polymer yield decreased when the reaction was run under 250 psi of CO. The lower yield was likely caused by catalyst decomposition, not decrease of the reaction rate, as quadrupling the reaction time did not result in any alteration of yield.

When the initial aziridine concentration was increased (entries 4 and 5, Table 1), the selectivity of the reaction reduced, and additional peaks appeared in the ^1H spectrum.† The chemical shifts of these resonances and that they move downfield when the aqueous solution is acidified suggest that they belong to amines, which apparently arise from repetitive aziridine insertion. Extraction of the products using a wide range of solvents including methanol, ethanol, THF, and chloroform did not significantly change the relative amount of amine units, suggesting that the amine and β-alanine units are in the same chains. The problem of repetative aziridine insertion can be partially solved by slow addition of aziridine. When aziridine was added in portions under 1 atm of CO after the previously added aziridine was estimated to have been consumed, the selectivity was considerably improved without sacrifice of the yield (entries 6 and 7, Table 1).

The molecular weights and molecular weight distributions of the products are measured by gel-permeation chromatography (GPC) coupled with a light scattering-refractive index-viscometry triple detector (Table 1). The weight average molecular weights are determined with reproducibilities within 6%. The molecular weight distributions are complex and spread over a wide range, hampering accurate determination of the number average molecular weights. Thus, the polydispersities (PDI) listed in Table 1 should be taken as approximate values.

In regard to the mechanism of the polymerization, the complexity of molecular weight distribution profiles indicates that it is apparently not a simple one. However, the presence of the acetyl end group argues that complex **1** is indeed the catalyst.

The possibility that azetidin-2-one was the intermediate of the polymerization was ruled out by two parallel experiments. In the first experiment, equal molar amounts of azetidin-2-one and aziridine were subjected to the polymerization conditions. In the other experiment, only aziridine was added. The same amounts of polymer were produced in the two experiments. The requirement for high catalyst loading in order to achieve good selectivity for alternating enchainment indicates that the barriers for alternating enchainment and repetitive enchainment are not significantly different for the catalyst employed here. We are currently engaged in searching for catalyst systems that provide improved selectivity toward alternating enchainment and in elucidating the chain propagation/termination mechanisms.

This work was supported by the ACS-Petroleum Research Fund. We thank Dr Mark A. Scialdone of Du Pont Central R&D for GPC analyses and Professor James E. Roberts of Lehigh University for solid state ^{13}C NMR measurements of the polymers. L. J. thanks the Christian R. & Mary F. Lindback Foundation for a Minority Junior Faculty Award.

Notes and references

1 E. Drent and P. H. M. Budzelaar, *Chem. Rev*., 1996, **96**, 663; A. Sen, *Acc. Chem. Res*., 1993, **26**, 303.
2 P. Davoli, I. Moretti, F. Prati and H. Alper, *J. Org. Chem*., 1999, **64**, 518 and references therein.
3 E. Drent, Shell Oil Company, patent application: US 926,534, 1992.
4 G. L. Bata and K. P. Singh, Union Carbide Canada Ltd. patent application: CA 19670818, 1969.
5 I. Hiroshi, J. Furukawa, T. Mieda and F. Hiroyasu, Bridgestone Tire Co., Ltd. patent application: JP 19641103, 1968.
6 γ-Ray and azoisobutyronitrile initiated CO-aziridine: T. Kagiya, I. Maruta, T. Ichida, S. Narisawa and K. Fukui, *J. Polym. Sci., Polym. Chem. Ed*., 1967, **5**, 1645; T. Kagiya, S. Narisawa, T. Ichida and K. Fukui, *J. Polym. Sci., Part A1*, 1966, **4**, 293.
7 S. H. Gellman, *Acc. Chem. Res*., 1998, **31**, 173.
8 D. Seebach and J. L. Matthews, *Chem. Commun*., 1997, 2015.
9 S. Kacker, S. J. Kim and A. Sen, *Angew. Chem., Int. Ed*., 1998, **37**, 1251.
10 R. D. Dghaym, K. J. Yaccato and B. A. Arndtsen, *Organometallics*, 1998, **17**, 4.
11 I. Okada, T. Takahama and R. Sudo, *Bull. Chem. Soc. Jpn*., 1970, **43**, 2591.
12 J. D. Glickson and J. Applequist, *J. Am. Chem. Soc*., 1971, **93**, 3276.

CHEMCOMM Communication
www.rsc.org/chemcomm

Hierarchical design of mixed metal oxides: novel macroporous VPO phases

Moises A. Carreon and Vadim V. Guliants*

Department of Chemical Engineering, University of Cincinnati, Cincinnati, OH 45221-0171 USA. E-mail: Vadim.Guliants@uc.edu

Received (in Cambridge, UK) 5th April 2001, Accepted 20th June 2001
First published as an Advance Article on the web 19th July 2001

Macroporous vanadium–phosphorus–oxide phases (macro-VPO) displaying ordered 0.2–0.4 μm pores and unprecedented high surface areas (44–75 m^2 g^{-1}) have been synthesized using colloidal arrays of polystyrene spheres as a template.

Mixed metal oxides possess promising catalytic properties for the selective oxidation of lower alkanes (C_2–C_5).[1] For example, Mo–V–Nb and Sb–V oxides are catalytically active in selective oxidation of ethane and propane[2] and propane ammoxidation and vanadium–phosphorus–oxides (VPOs) are selective in the oxidation of *n*-butane to maleic anhydride.[3]

The conventional synthesis methods, both wet chemistry and solid-state, offer limited control over the phase, bulk and surface compositions of mixed metal oxides, preferential exposure of active and selective surface planes, surface areas and pore architectures, which define their catalytic properties in selective oxidation of lower alkanes. There is a critical need for novel routes of assembling hierarchically designed mixed metal oxides, which display remarkable ordering on micro- (<3 nm for the surface region structure and composition), nano- (3–100 nm for the bulk and phase compositions) and macro- (>100 nm for pore architectures) scales.

Macroscale-templated synthesis of nanocrystalline mixed metal oxides represents an attractive approach for the synthesis of hierarchically designed catalytic materials. Several single-element macroporous oxides with very interesting structural properties have been synthesized by self-assembly using colloidal sphere templates.[4–9] However, macroporous mixed metal oxides for applications in oxidation catalysis have not, as yet, been reported. We report here the first successful example of a hierarchically designed macroporous mixed vanadium–phosphorus–oxide (macro-VPO) with desirable structural and compositional properties for selective oxidation of *n*-butane.

Macro-VPO phases were assembled using close-packed arrays of colloidal polystyrene (PS) spheres (0.4 μm diameter) as a template. Monodispersed PS spheres were synthesized by an emulsion polymerization process described elsewhere.[7] The ordered arrays of PS spheres were obtained by either centrifugation or filtration of PS sphere suspensions. Fig. 1 shows the SEM image (Hitachi, Model S-3200N) of colloidal PS spheres used as the template.

In a typical synthesis, an array of PS spheres was first impregnated with a phosphoric or phosphorous acid solution in ethanol. Then a solution of a vanadium-(IV) or -(V) source in ethanol or isobutyl alcohol was introduced into the voids of the array, where it reacted with a phosphorus source and condensed into a macro-VPO framework upon drying. It was found that the initial surface treatment with a phosphorus source was critical for the nucleation and growth of macro-VPO phases in the voids of the PS sphere arrays. In all experiments the P/V molar ratio was 1:1, which provides the optimal surface and bulk composition for selective oxidation of *n*-butane.[3] The PS spheres were removed from as-synthesized macro-VPO by either calcination in air at 723 K or Soxhlet extraction using a mixture of acetone and tetrahydrofuran (1:1 volume ratio). Typical synthesis conditions, crystallographic phases determined by powder XRD (Siemens D-500) and the BET surface areas (Micromeritics Gemini 2360) for selected calcined and Soxhlet-extracted macro-VPO phases are given in Table 1.

The ordered pore structure of the macro-VPO phases after the template removal is evident in Fig. 2. Interconnected pores appear as dark spots (*ca.* 0.2 μm diameter) inside spherical 0.4 μm cavities left after the removal of the PS spheres. The walls of the macropore structure are formed by the $(VO)_2P_2O_7$ nanocrystals. The wall thickness was estimated from the SEM images to be *ca.* 90 nm. The average nanocrystal size determined using the Scherrer formula[10] was *ca.* 20 nm, which indicated that the wall was only four crystals thick. Relatively large size of the nanocrystal building blocks explains the

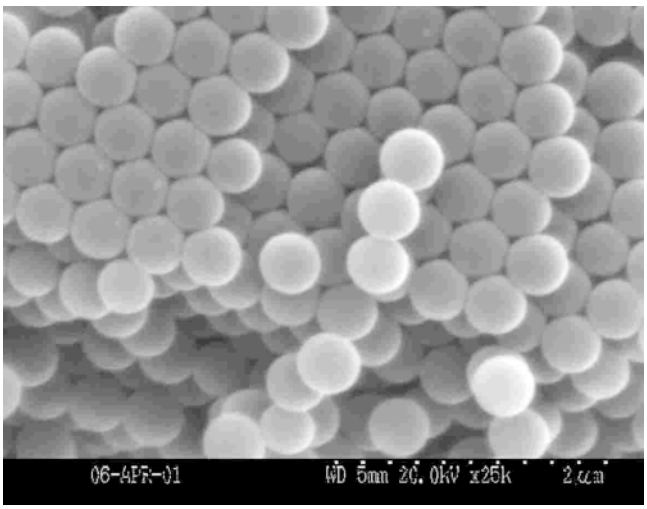

Fig. 1 SEM image of the synthesized monodispersed polystyrene spheres used as templates for the formation of macroporous VPO.

Table 1 Selected properties of macroporous VPOs

VPO sources	General description	Specific surface area/m^2 g^{-1}	Crystalline phase
$VO[CHO(CH_3)_2]_3$, H_3PO_3	Calcined in air at 723 K	64	$VOPO_4{\cdot}2H_2O$
$VO[CHO(CH_3)_2]_3$, H_3PO_3	Soxhlet extracted	50	$VOPO_4{\cdot}2H_2O$
V_2O_5, H_3PO_3	Calcined in air at 723 K	41	$VOPO_4{\cdot}2H_2O$
V_2O_5, H_3PO_3	Soxhlet extracted	75	$VOHPO_4{\cdot}4H_2O$/β-$VOHPO_4{\cdot}2H_2O$
V_2O_5, H_3PO_4	Calcined in air at 723 K	44	$(VO)_2P_2O_7$

 DOI: 10.1039/b103131g

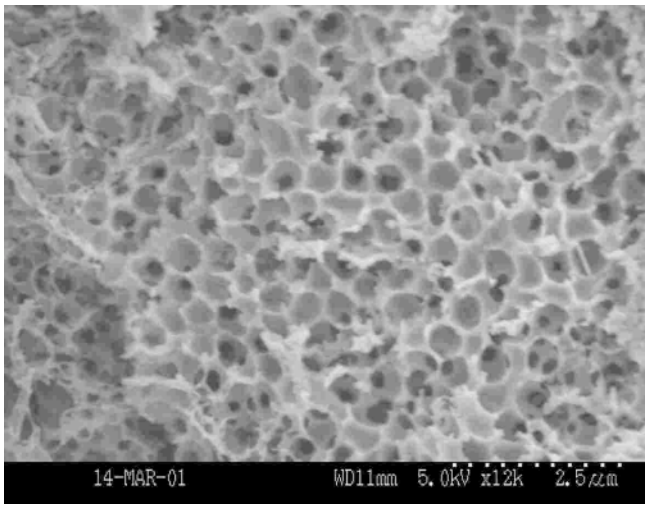

Fig. 2 SEM image for macroporous VPO.

somewhat rough and disordered appearance of the macropore structure in SEM images (Fig. 2).

The macroscale-templated synthesis produced the VPO phases with unprecedented high surface areas after the removal of the PS spheres. The macro-VPO phases displayed *ca*. 44–75 $m^2\ g^{-1}$ surface areas (Table 1) and the optimal bulk compositions (P/V *ca*. 1.05 by ICP elemental analysis). By comparison, the surface areas of VPO phases synthesized by conventional methods are in the range 5–20 $m^2\ g^{-1}$.[1,3] The surface areas of the macro-VPO phases are consistent with a theoretical estimate for 20 nm cubic crystals of $(VO)_2P_2O_7$ (90 $m^2\ g^{-1}$).

The present method of macroscale-templated synthesis of mixed metal oxides yielded $(VO)_2P_2O_7$ which preferentially exposed the active and selective surface (100) planes for the oxidation of *n*-butane. $(VO)_2P_2O_7$, which is the active and selective phase in *n*-butane oxidation to maleic anhydride,[1,3] was synthesized using the V(IV) and P(III) sources (Table 1). The intensity ratio of the interplanar (100) and in-plane (042) X-ray reflections of $(VO)_2P_2O_7$ (I_{100}/I_{042}) has been previously used to determine the prefential exposure and the stacking order of the surface (100) planes proposed to contain the active and selective catalytic sites.[3] The conventional VPO phases typically exhibited low intensity ratios, I_{100}/I_{042} *ca*. 0.4, indicating that the surface (100) planes were not dominant in these phases.[3] The macro-VPO phases are characterized by much higher intensity ratios, I_{100}/I_{042} *ca*. 2.48 suggesting that these phases preferentially expose the surface (100) planes of $(VO)_2P_2O_7$.

To the best of our knowledge, the hierarchical design of the mixed metal oxide phases with ordered macropore architectures, record high surface areas, as well as the phase compositions and the surface plane exposures critical for selective oxidation catalysis is achieved for the first time. This study demonstrated that the macroscale self-assembly route holds a great promise as a general method for the rational design of mixed metal oxides with desirable structural and compositional properties.

Further studies will focus on the catalytic performance of the novel macroporous mixed metal oxides in the oxidation of lower alkanes.

Notes and references

1 F. Trifiro, *Catal. Today*, 1998, **41**, 21.
2 S. A. Holmes, J. N. Al-Saeedi, V. V. Guliants, P. Boolchand, D. Georgiev, U. Hackler and E. Sobkow, *Catal. Today*, 2001, **67**, 403.
3 V. V. Guliants, J. B. Benziger, S. Sundaresan, I. E. Wachs, J. M. Jehng and J. E. Roberts, *Catal. Today*, 1996, **28**, 275.
4 Y. Xia, B. Gates, Y. Yin and Y. Lu, *Adv. Mater.*, 2000, **12**, 693.
5 B. T. Holland, C. F. Blanford and A. Stein, *Science*, 1998, **281**, 538.
6 B. T. Holland, L. Abrams and A. Stein, *J. Am. Chem. Soc.*, 1999, **121**, 4308.
7 B. T. Holland, C. F. Blanford, T. Do and A. Stein, *Chem. Mater.*, 1999, **11**, 795.
8 J. E. Wijnhoven and W. L. Vos, *Science*, 1998, **281**, 802.
9 A. Imhof and D. J. Pine, *Nature*, 1997, **389**, 948.
10 B. D. Cullity, *Elements of X-Ray Diffraction*, Addison Wesley Publishing Company, Inc., New York, 1978.

CHEMCOMM Communication
www.rsc.org/chemcomm

Control on the organized structure of monoalkylethylenediamine copper(II) coordinated bilayer membranes by counter ions

Chun Li, Xianchun Lu, Xuzhong Luo and Yingqiu Liang*

Lab of Mesoscopic Materials and Chemistry and State Key Lab of Coordination Chemistry, Nanjing University, Nanjing 210093, People's Republic of China. E-mail: yqliang@nju.edu.cn

Received (in Cambridge, UK) 23rd April 2001, Accepted 28th June 2001
First published as an Advance Article on the web 19th July 2001

The organized structure of Cu^{2+}-coordinated bilayer membranes formed by monoalkyl derivatives of ethylenediamine can easily be modulated by varying the counter ions, and their physical properties change correspondingly.

The design and construction of supramolecular organized assemblies utilizing non-covalent intermolecular interactions, such as hydrogen bondings, metal–ligand interactions, van der Waals interactions, π–π stackings *etc*. has become a topic of increasing interest in recent years, due to their fascinating structures and novel functionalities.[1–4] It is well-known that the structure and properties of these aggregates are determined not only by the chemical structures of the component molecules, but also by environmental factors, including pH variation, metal-ion complexation, heat, light *etc*. Recently, much work has focused on the control of the macroscopic morphology and microscopic structure of self-organized materials by changing physical or chemical environments.[5]

In our previous papers, we have reported that complexed bilayer membranes are formed from a series of single-chain amphiphiles $C_nH_{2n+1}NHC_2H_4NH_2$ dispersed in dilute aqueous $Cu(NO_3)_2$.[6] In the present work, our investigation has been concentrated on the control of the organized structure of monoalkylethylenediamine in dilute aqueous CuX_2 by changing the counter ions (X^- = Cl^-, Br^-, NO_3^- and ClO_4^-).†

Fig. 1 shows the typical transmission electron micrographs for amphiphilic aggregates of $C_nH_{2n+1}NHC_2H_4NH_2$ (n = 12, 14, 16, 18) in aqueous CuX_2 (X^- = Cl^-, Br^-, NO_3^- and ClO_4^-), which all revealed the presence of vesicular morphologies. However, there are drastic differences between the samples with Cl^-, Br^- on the one hand and NO_3^-, ClO_4^- on the other as counter ions in the appearance of the dispersion. In the former case the aggregates are blue while the latter are purple. Obviously for these four systems, the only difference lies in the X^- anion type and size, therefore, it can be inferred that the type of counter ion is of vital importance to the determination of the organized structures, and the amphiphilic aggregates can be categorized into two structurally differing types.

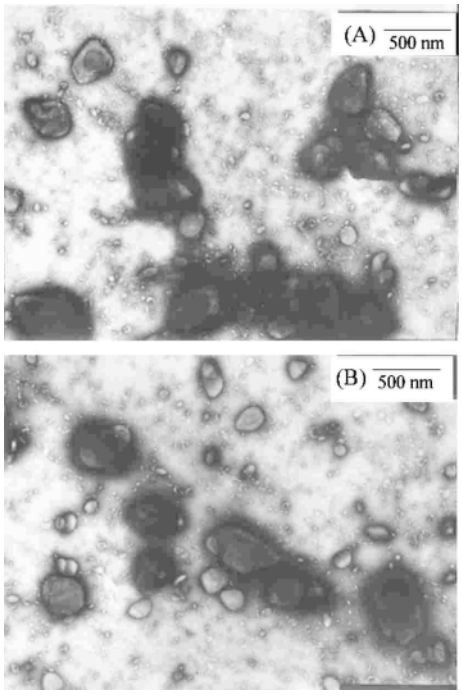

Fig. 1 Typical TEM morphologies of complexed bilayer membranes of $[Cu(C_nH_{2n+1}NHC_2H_4NH_2)_2]X_2$: (a) X^- = Cl^-, n = 14; (b) X^- = ClO_4^-, n = 14.

The differences between the two kinds of assemblies in solution colour and in their solid-state electronic spectra reveal configurational diversities in the structures of the Cu^{2+}-coordinated headgroups. Typical results (n = 14) are shown in Table 1. For asymmetric derivatives of ethylenediamine, ML_2 type complexes of Cu^{2+}-coordinated amphiphiles usually adopt planar CuN_4 structures with *cis*- and *trans*-isomers.[7] It has been established that complexes with *cis*-configuration show higher σ–σ* transition energies than those with *trans*-arrangement.[8] Additionally, square-coplanar CuN_4 complexes show d–d transition energies in the range (18–20) × 10^3 cm^{-1} while the range for tetrahedral CuN_4 is (12–16) × 10^3 cm^{-1}.[9] From the d–d and σ–σ* transition energies in Table 1, it can be deduced that when X^- = Cl^- or Br^-, the Cu^{2+}-coordinated headgroups adopt a *trans*-configuration which give a compressed tetrahedral CuN_4 environment, and the two tails in the $[Cu(C_nH_{2n+1}NHC_2H_4NH_2)_2]X_2$ (X^- = Cl^-, Br^-, n = 12–18) complexes adopt an approximately diagonal position [see Fig. 3(a)]; while for X^- = NO_3^- or ClO_4^- ions, a *cis*-configuration is adopted with the copper square-coplanar, with the two tails located at the same side of the plane and parallel to each other [see Fig. 3(b)]. Clearly the headgroup structures greatly influence the packing fashion of the hydrocarbon tails in the organized aggregates.

It has been demonstrated by many experiments that in cast films the self-aggregated structure of the amphiphiles in dilute aqueous dispersions is well preserved.[10] In order to elucidate the structural features of the assemblies in aqueous solution, small-angle XRD was applied to study the long spacing of the cast bilayer membranes. Powder diffraction experiments carried out on cast films of the complexed aggregates showed periodic peaks corresponding to bilayers with ordered structures, which are similar to those reported in the literature.[10] Fig. 2(a) shows

Table 1 The appearance of $C_{14}H_{29}NHC_2H_4NH_2$ aggregates in aqueous CuX_2, along with electronic transitions of their cast films

Counter ion (X^-)	Solution appearance	d–d Transition (10^{-3} $\tilde{\nu}$/cm^{-1})	σ–σ* Transition (10^{-3} $\tilde{\nu}$/cm^{-1})	
			I	II
Cl^-	Emulsion, blue	16.78	35.21	42.37
Br^-	Emulsion, blue	17.48	33.33	42.78
NO_3^-	Emulsion, purple	18.05	35.71	44.44
ClO_4^-	Emulsion, purple	19.23	36.50	43.10

 DOI: 10.1039/b103614a

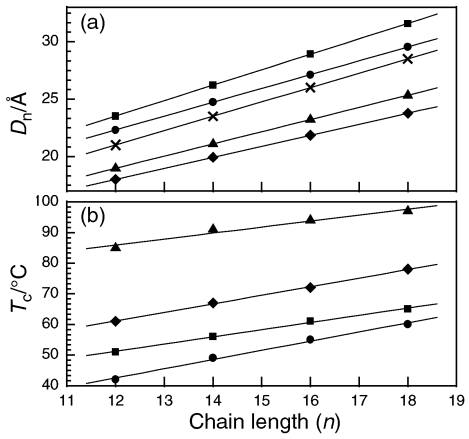

Fig. 2 (a) Bilayer thickness (D_n) values and the evaluated molecular length (L_n) as function of the tail length (n); (b) phase transition temperature (T_c) dependence on the tail length (n): X^- = (●) Cl^-; (■) Br^-; (▲) NO_3^-; (◆) ClO_4^-; (×) L_n.

the tail length (n) dependence of the bilayer thickness, *i.e.* the long spacing (D_n) of the cast bilayer membranes. As can be seen for each system the bilayer thickness shows good linearity with tail length (n = 12, 14, 16 and 18):

D_n (Cl^-) = 1.34n + 7.39
D_n (Br^-) = 1.21n + 7.83
D_n (NO_3^-) = 1.06n + 6.24
D_n (ClO_4^-) = 0.97n + 6.24

The cast bilayer thickness, for X^- = Cl^-, Br^- ions, falls between the monomolecular and bimolecular length of the amphiphile, while for X^- = NO_3^-, ClO_4^- ions the bilayer thickness is smaller than the corresponding evaluated molecular length (L_n) (CPK model). These results indicated that the amphiphilic molecules probably assume either a tail-to-tail chain packing mode or an interdigitated packing mode in the bilayer membranes.

Differential scanning calorimetry experiments of the complexed bilayer dispersions showed endothermic peaks (not shown here), indicating gel-to-liquid crystal phase transitions, one of the basic physicochemical properties of bilayer membranes. The value of the phase transition temperature (T_c) for each system exhibits fairly good linearity with n, as depicted in Fig. 2(b), indicating similar lateral packing in the membrane structure of each system. It is clear from Fig. 2(b), for X^- = Cl^-, Br^- samples, the T_c values are < 65 °C, which are similar to those of bilayer membranes showing tail-to-tail packing reported in the literature.[11] By contrast, for X^- = NO_3^-, ClO_4^-, the T_c values are > 60 °C. It has been shown that in many cases the extensively tilted tail-to-tail type bilayer assemblages possess relatively fluid chain packing and exhibit relatively low T_c, whereas interdigitated type bilayer membranes have tighter chain packing and display higher T_c values than tail-to-tail ones.[11] Thus, by combining XRD and DSC results, it can be inferred that for X^- = NO_3^-, ClO_4^- dispersions the amphiphiles adopt the partially interdigitated chain packing mode in the bilayer membranes. Two quite different structures in cast films from complexed bilayer membranes with different counter ions are thus observed. Based on the packing model of aliphatic chains in the bilayer membranes, the chain tilt angles (with respect to the bilayer normal) for each system, calculated from the slope of the linear equations[12] are 58.2° (Cl^-), 61.6° (Br^-), 33.4° (NO_3^-) and 40.2° (ClO_4^-).

In summary, this study shows a very simple method, changing the counter ion can modulate the headgroup configuration and packing mode of the aliphatic chains in synthetic bilayer membranes formed by monoalkylethylenediamines $C_nH_{2n+1}NHC_2H_4NH_2$ (n = 12–18) in dilute aqueous CuX_2 (Fig. 3). Furthermore, this molecular-level modification arising from the change of counter ions is amplified by the self-assembly process through cooperative effects of metal–ligand interactions and van der Waals interactions, on their macroscopic properties leading to variations in appearance and gel-to-liquid transition temperatures of the dispersions.

We acknowledge the National Natural Science Foundation of China (20073019) for financial support of this work.

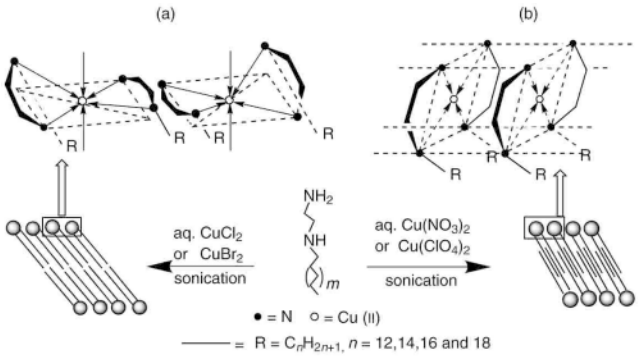

Fig. 3 Schematic representation of bilayer formation from $C_nH_{2n+1}NHC_2H_4NH_2$ (n = 12, 14, 16 and 18) in aqueous CuX_2: (a) X = Cl^- or Br^-; bilayer showing tail-to-tail packing mode, coordinated headgroups adopt a *trans*-configuration in a compressed tetrahedral CuN_4 environment with two tails in the $[Cu(C_nH_{2n+1}NHC_2H_4NH_2)_2]X_2$ complexes located at approximately diagonal positions. (b) X = NO_3^- or ClO_4^-; bilayer showing a partially interdigitated chain packing mode, coordinated headgroups adopt a *cis*-configuration in a square-coplanar environment with the two tails located at the same side of the plane and parallel to each other.

Notes and references

† Samples were prepared and characterized as described in the literature.[6]

1 J. H. Fendler, in *Membrane Mimetic Chemistry*, Wiley, New York, 1980; H. Ringsdorf, B. Schlarb and J. Venzmer, *Angew. Chem., Int. Ed. Engl.*, 1988, **27**, 113; T. Kunitake, *Angew. Chem., Int. Ed. Engl.*, 1992, **31**, 709.
2 J. M. Lehn, *Angew. Chem., Int. Ed. Engl.*, 1988, **27**, 89; J. M. Lehn, *Supramolecular Chemistry*, VCH, Weinheim, 1995.
3 J. H. Fuhrhop and W. Helfrich, *Chem. Rev.*, 1993, **93**, 1565.
4 P. Terech and R. G. Weiss, *Chem. Rev.*, 1997, **97**, 3133; D. J. Abdallah and R. G. Weiss, *Adv. Mater.*, 2000, **12**, 1237.
5 See for example: N. A. J. M. Sommerdijk, P. J. J. A. Buynsters, D. G. Geurts, A. M. A. Pistorius, M. C. Feiters, R. J. M. Nolte and B. Zwanenburg, *Chem. Eur. J.*, 1998, **4**, 127; N. A. J. M. Sommerdijk, K. J. Booy, A. M. A. Pistorius, M. C. Feiters, R. J. M. Nolte and B. Zwanenburg, *Langmuir*, 1999, **15**, 7008; U. Jonas, K. Shah, S. Norvez and D. H. Charych, *J. Am. Chem. Soc.*, 1999, **121**, 4580; K. Aoki, M. Nakagawa and K. Ichimura, *J. Am. Chem. Soc.*, 2000, **122**, 10 997; Y. Ikeda, T. Imae, M. Iida, N. Koine and S. Kaizaki, *Langmuir*, 2001, **17**, 361.
6 X. Lu, Z. Zhang and Y. Liang, *J. Chem. Soc., Chem. Commun.*, 1994, 2731; X. Lu, Z. Zhang and Y. Liang, *Langmuir*, 1997, **13**, 533.
7 B. P. Kennedy and A. B. P. Lever, *J. Am. Chem. Soc.*, 1973, **95**, 6907.
8 G. J. Leigh and D. M. P. Mingos, *J. Chem. Soc. A*, 1970, 587; M. Textor and W. Ludwig, *Helv. Chim. Acta*, 1972, **55**, 184.
9 B. J. Hathaway, *J. Chem. Soc., Dalton Trans.*, 1972, 1196.
10 M. Shimomura, R. Ando and T. Kunitake, *Ber. Bunsen-Ges. Phys. Chem.*, 1983, **87**, 1134; Y. Ishikawa and T. Kunitake, *J. Am. Chem. Soc.*, 1986, **108**, 8300; S. Asakuma, H. Okada and T. Kunitake, *J. Am. Chem. Soc.*, 1991, **113**, 1749; M. Shimomura, S. Aiba, N. Tajima, N. Inoue and K. Okuyama, *Langmuir*, 1995, **11**, 969; N. Kimizuka, T. Kawasaki, K. Hirata and T. Kunitake, *J. Am. Chem. Soc.*, 1998, **120**, 4094.
11 T. Kunitake, N. Kimizuka, N. Higashi and N. Nakashima, *J. Am. Chem. Soc.*, 1984, **106**, 1978; M. Kodama, T. Kunitake and S. Seki, *J. Phys. Chem.*, 1990, **94**, 1550; L. Streefland, F. Yun, P. Rand, D. Hoekstra and J. B. F. N. Engberts, *Langmuir*, 1992, **8**, 1715; P. Ghosh, S. Sengupta, P. K. Bharadwaj and D. Hoekstra, *Langmuir*, 1998, **14**, 5712.
12 J. Umemura, T. Kamata, T. Kawai and T. Takenaka, *J. Phys. Chem.*, 1990, **94**, 62; X. Lu, Ph. D. Thesis, Nanjing University, 2000.

CHEMCOMM
Communication
www.rsc.org/chemcomm

Formation of robust mesoscopic ring structures by self-assembly of $SiCl_3$-terminated dendrimers

Zhongdang Xiao, Chengzhi Cai* and Xiaobin Deng

Department of Chemistry, University of Houston, Houston, Texas 77204-5003, USA. E-mail: cai@uh.edu

Received (in Cambridge, UK) 16th May 2001, Accepted 28th June 2001
First published as an Advance Article on the web 19th July 2001

Robust sub-micrometer ring structures are easily prepared using $SiCl_3$-terminated dendrimers.

The formation of submicrometer-scale structures *via* the self-assembly of molecules is of great current interest.[1] Recently, several groups have reported the formation of mesoscopic ring structures on solid surfaces using a variety of materials, including porphyrin derivatives, nanoparticles, and carbon nanotubes.[2–6] These ring structures were easily formed after the evaporation of a dilute solution of the materials deposited on substrate surfaces, through an intermediate morphology featuring droplets or holes. Unfortunately, the molecules/particles in these structures were held together only through weak intermolecular interactions. Consequently, the structures possess a limited stability that restricts their potential applications. During the course of systematic investigation of the chemisorption of a series of $SiCl_3$-terminated dendrimers on flat surfaces, we observed that the films of **1** deposited on mica spontaneously

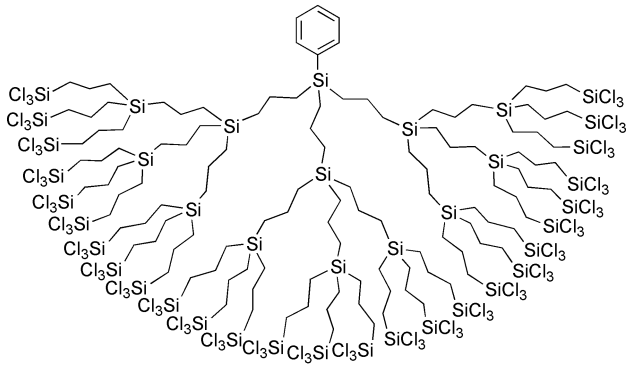

1

adopted well-defined sub-micrometer ring structures across the surface. Notably, the dendrimers in the films polymerize upon curing, thereby affording robust and highly stable ring structures.

The ring structures were easily and reproducibly prepared by spin coating of a 10^{-5} M solution of **1**[7] in anhydrous THF on a freshly cleaved mica substrate. As revealed by AFM (Fig. 1), the isolated rings are randomly located over the entire substrate surface. Most of the rings possess an inner diameter of 450–550 nm. Although rings dominate the film surface, separated islands with a bottom diameter of 110–230 nm and a height of 2.0–3.5 nm are also present; these are located predominately outside the rings and on the rims. Root mean square roughness (R_q) measurements show that the film surface inside the rings (R_q = 0.160 nm) is much flatter than outside (R_q = 0.530 nm). Fig. 2 depicts a typical ring and a cross sectional plot of the ring diameter (R), height (h), and width (L) of the rim. Notably, the rims of all the rings possess a similar average width ($L \approx 150$ nm) and height ($h \approx$ 4–6 nm). Interestingly, the layer outside the rings is higher than that inside by $D \approx 1.1$ nm (Fig. 2). To measure the thickness of the layer inside the rings, part of the film was shaved by AFM using a square pyramid Si_3N_4 probe with a loading force of *ca.* 190 nN. Fig. 3 shows an AFM image of the region containing the shaved area. The average thickness of the flat layers outside and inside the rings was then measured

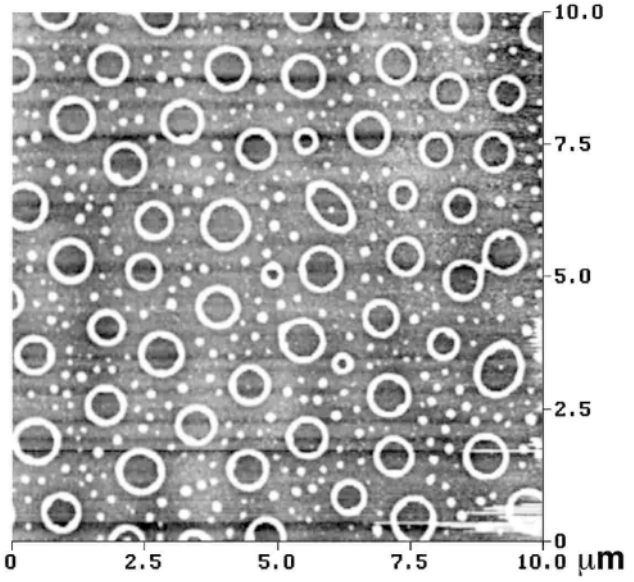

Fig. 1 An AFM image of a thin film formed by spin-coating of a THF solution of **1** onto a mica surface. The contrast covers height variations in the 0–15 nm range.

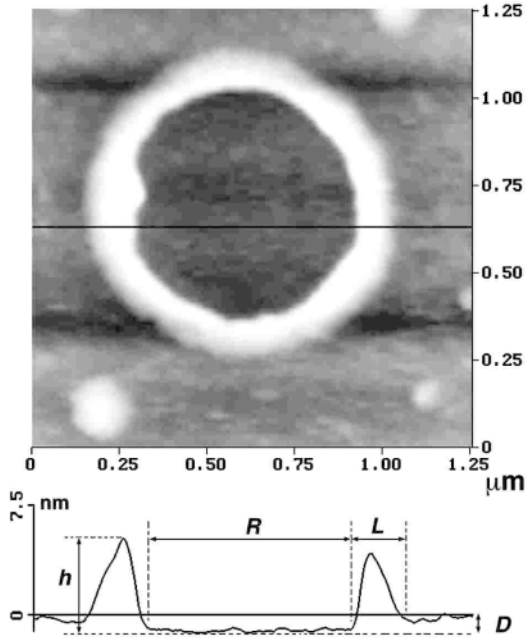

Fig. 2 An AFM image of a ring and a line scan for measurement of the ring diameter (R), height (h), and width (L) of the rim.

 DOI: 10.1039/b104306b

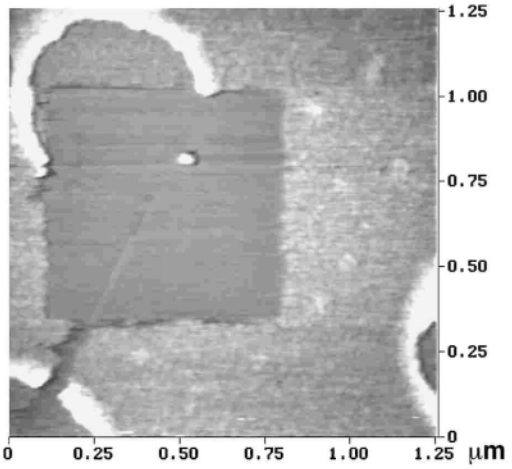

Fig. 3 Tapping mode AFM image of a film region containing an area shaved by contact mode AFM.

by AFM to be 2.2 ± 0.4 nm and 1.3 ± 0.3 nm, respectively. The former corresponds to a monolayer of densely packed dendrimers, as the height of **1** is calculated to be *ca.* 2.2 nm by molecular mechanics (MM2). The latter could correspond to a monolayer of flattened dendrimers. It is well known that flexible dendrimers can substantially flatten on a surface when their interaction with the surface is strong.[8]

Upon deposition of **1** (dissolved in THF) on mica in air, the $SiCl_3$ groups of **1** should be completely hydrolyzed to $Si(OH)_3$ groups by surface-bound and absorbed water.[9] Intermolecular condensation of the $Si(OH)_3$-terminated dendrimers may occur at room temperature, but apparently only to a limited extent. In fact, films that were kept at room temperature in air for two weeks can still be shaved by AFM. Although they cannot covalently bond to the mica surface which does not contain OH groups, the dendrimers can undergo substantial condensation to form a cross-linked network of Si–O–Si groups at elevated temperatures.[9] Indeed, after curing at 115 °C for 12 h, the unchanged ring structures became robust; they could no longer be scratched by AFM tips, even under a loading force as high as 250 nN. In addition, they remained intact after storage in air for months, and after repeated washing with water and organic solvents such as THF and chloroform.

Despite the presence of a large number of hydrophilic Si–O–Si groups in the dendrimers after hydrolysis and curing, the surface of the cured films possessed a surprisingly high water contact angle (advancing: 103°; receding: 92°; static: 100°) and hexadecane contact angle (advancing: 38°; receding: 31°; static: 35°). These contact angles are similar to those for a smooth solid surface exposing closely packed $–CH_2–$ or $–CH{=}CH_2$ groups.[10] In addition, force measurements by AFM showed that the attraction forces between the Si_3N_4 tip and the film were nearly the same inside and outside the rings, indicating a similar composition for both surfaces. These results suggest that the dendrimer molecules fully cover the hydrophilic mica surface with all of their SiOR groups (R = H, OSi), leading to a hydrophobic film surface composed mostly of $–CH_2–$ groups.

Based on the above results, it appears that the ring structures and islands ('dots') are formed on an underlying layer of the dendrimers physisorbed on mica. Preliminary results also indicated the absence of ring structures at a monolayer coverage.† During spin coating, when the liquid film of the excess dendrimers and the solvent (THF) on top of the monolayer thins below a critical thickness by evaporation, the instability of the film may cause film rupture into small droplets.[3] Some of the small droplets coalesce into larger ones, and the remaining isolated small droplets dry to form the observed islands ('dots'). AFM imaging of freshly prepared films showed that the rings were developed from larger droplets,† in agreement with the mechanism proposed by others.[3] The process involves a radial flow outward from the center of the droplet.[3,11] This outward flow of liquid can carry virtually all of the dissolved dendrimers as well as some of the dendrimers physisorbed on the substrate surface to the rim. The reduced number of dendrimers in the layer on the interior of the ring then flatten to cover the substrate surface. The observed similar heights and widths of the rims regardless of the ring diameters might be required for 'pinning' of the rim.[5]

In conclusion, we have described the preparation of robust submicrometer ring structures on mica surfaces using **1**. AFM studies revealed that the isolated mesoscopic ring structures and islands were grown on an underlying self-assembled layer of the dendrimers. The surface inside the rings is much flatter than ouside. Prior to curing, polymerization of the hydrolyzed dendrimers, if any, occurred only to a limited extent. Scanning probe lithography of the pre-cured films can be used to generate patterns (*e.g.* Fig. 3) on the film.[12] The structures become robust upon curing. Similar to the demonstrated application of graphite etch pits (3.5 Å high),[13] such ring structures (*ca.* 50 Å high) may be used to isolate ensembles of macromolecules or nanoparticles for study by scanning probe microscopy. We will explore the growth of ring structures using analogs of **1** that possess functional groups at the phenyl group.

This work was supported by the Texas Advanced Research Program under Project No.003652-0365-1999. We thank Dr C. M. Yam for contact angle measurements and Professors T. R. Lee and S. Perry for helpful discussions.

Notes and references

† Z. Xiao, A. Milenkovic and C. Cai, unpublished results.

1 D. A. Tomalia, Z. G. Wang and M. Tirrell, *Curr. Opin. Colloid Interface Sci.*, 1999, **4**, 3.
2 A. P. H. J. Schenning, F. B. G. Benneker, H. P. M. Geurts, X. Y. Liu and R. J. M. Nolte, *J. Am. Chem. Soc.*, 1996, **118**, 8549.
3 L. Latterini, R. Blossey, J. Hofkens, P. Vanoppen, F. C. De Schryver, A. E. Rowan and R. J. M. Nolte, *Langmuir*, 1999, **15**, 3582.
4 P. C. Ohara, J. R. Heath and W. M. Gelbart, *Angew. Chem., Int. Ed. Engl.*, 1997, **36**, 1078.
5 P. C. Ohara and W. M. Gelbart, *Langmuir*, 1998, **14**, 3418.
6 T. Vossmeyer, S. W. Chung, W. M. Gelbart and J. R. Heath, *Adv. Mater.*, 1998, **10**, 351.
7 D. Terunuma, T. Kato, R. Nishio, K. Matsuoka, H. Kuzuhara, Y. Aoki and H. Nohira, *Chem. Lett.*, 1998, 59.
8 V. V. Tsukruk, *Adv. Mater.*, 1998, **10**, 253.
9 A. Ulman, *Chem. Rev.*, 1996, **96**, 1533; S. R. Wasserman, Y.-T. Tao and G. M. Whitesides, *Langmuir*, 1989, **5**, 1074; C. P. Tripp and M. L. Hair, *Langmuir*, 1995, **11**, 149; M. J. Stevens, *Langmuir*, 1999, **15**, 2773; A. G. Lambert, D. J. Neivandt, R. A. McAloney and P. B. Davies, *Langmuir*, 2000, **16**, 8377.
10 C. D. Bain, J. Evall and G. M. Whitesides, *J. Am. Chem. Soc.*, 1989, **111**, 7155.
11 R. D. Deegan, O. Bakajin, T. F. Dupont, G. Huber, S. R. Nagel and T. A. Witten, *Nature*, 1997, **389**, 827.
12 D. C. Tully, K. Wilder, J. M. J. Frecht, A. R. Trimble and C. F. Quate, *Adv. Mater.*, 1999, **11**, 314.
13 D. L. Patrick, V. J. Cee and T. P. Beebe, *Science*, 1994, **265**, 231; J. D. McBride, B. van Tassell, R. C. Jachmann and T. P. Beebe, Jr., *J. Phys. Chem. B*, 2001, **105**, 3972.

CHEMCOMM Communication
www.rsc.org/chemcomm

The first metamagnetic one-dimensional molecular material with nickel(II) and end-to-end azido bridges†

Partha Sarathi Mukherjee,[a] Sudipta Dalai,[a] Ennio Zangrando,[b] Francesc Lloret[c] and Nirmalendu Ray Chaudhuri*[a]

[a] *Department of Inorganic Chemistry, Indian Association for the Cultivation of Science, Jadavpur, Calcutta-700032, India. E-mail: icnrc@mahendra.iacs.res.in*
[b] *Dipartimento de Scienze Chimiche, University of Trieste, Via Giorgieri 1, 34127 Trieste, Italy*
[c] *Department de Quimica Inorganica, Universitat de Valencia, Dr. Moliner 50, E-46100 Burjassot, Spain*

Received (in Cambridge, UK) 29th May 2001, Accepted 27th June 2001
First published as an Advance Article on the web 19th July 2001

A novel single azido bridged one-dimensional Ni(II) chain, which represents the first metamagnetic one-dimensional metal–azido system with only end-to-end azido bridges, has been synthesised and characterised by a low temperature magnetic study.

In the last decade chemists have dedicated their efforts to the study of molecular-based magnetic materials owing to the need to understand the fundamental science associated with magnetic interactions between the paramagnetic metal ions and the bridging ligand to develop magneto–structural correlation enabling the designed synthesis of interesting magnetic materials.[1] One strategy for the design of molecular-based magnets involves assembling of paramagnetic metal ions in one-, two- and three-dimensional networks using suitable bridging ligands.[1,2] The azido ligand has been widely used because of its diverse binding modes which yield different types of molecules such as dimers, tetramers, one-, two-, and three-dimensional arrays *etc*.[3] The prime coordination motif for bridging azido is end-on with ferromagnetic interaction and end-to-end having antiferromagnetic coupling.[4] To the best of our knowledge all compounds of Ni^{II} with end-to-end azido bridges are antiferromagnetic with the exception of two compounds which are weakly ferromagnetic: one is a dimer[5] and the other a one-dimensional chain of Ni^{II} using a non-chelating capping ligand.[6] Examples of metamagnetic molecular materials in the metal–azido system with only end-to-end bridging azido mode are still lacking. Here, we report the synthesis,‡ crystal structure and magnetic properties of a new one-dimensional compound, $[Ni(L)(N_3)_2]_n$ **1** (L is a tridentate Schiff base obtained by condensation of pyridine-2-aldehyde and *N*,*N*,2,2-tetramethylpropane-1,3-diamine) which represents the first example of a metamagnetic molecular material of Ni^{II} with only end-to-end azido bridges.

A crystal structure determination§ reveals that complex **1** is a single azido bridged one-dimensional Ni^{II} chain. A perspective view of the polymeric chain of complex **1** with the atom numbering scheme is shown in Fig. 1. Each nickel atom in the chain has an octahedral coordination environment with a NiN_6 core. In the chain, all nickel atoms are linked to one pendant azido in their axial positions. One nitrogen atom, N(7), of the bridging azido is linked to an equatorial position of one nickel while the other nitrogen atom N(9′) of the same azido is coordinated to an axial position of the neighbouring nickel centre. The equatorial least-square planes of the two Ni^{II} centres are not parallel and form a dihedral angle of 31.3(1)°. The deviation of Ni^{II} from the best fit square plane towards N(4) is 0.042(3) Å. The two Ni–N–N bond angles of the end-to-end azido group are different [N(8)–N(7)–Ni 133.3(4), $N(8)^{II}$–N(9)–Ni 124.5(4)]. The Ni–N_3–Ni torsion angle of 106.8(4)° is large for an azido Ni^{II} compound.[6,7] The intrachain distance between adjacent nickel centres is 5.662(1) Å.

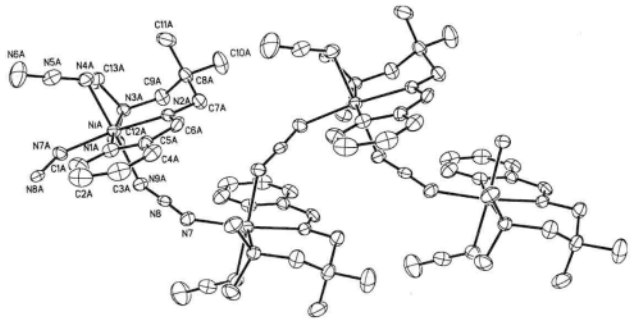

Fig. 1 View of the polymeric chain (40% thermal ellipsoids) with atom numbering scheme of complex **1** and selected bond lengths (Å) and angles (°): Ni–N(1) 2.126(5), Ni–N(2) 2.030(5), Ni–N(3) 2.179(5), Ni–N(4) 2.072(5), Ni–N(7) 2.091(6), Ni–N(9) 2.130(5), N(4)–N(5) 1.172(9), N(5)–N(6) 1.159(11); N(1)–Ni–N(2) 78.5(2), N(1)–Ni–N(3) 172.8(2), N(1)–Ni–N(7) 97.7(2), N(1)–Ni–N(9) 89.8(2), N(2)–Ni–N(9) 85.9(2), N(3)–Ni–N(4) 93.76(19), N(4)–Ni–N(7) 90.3(2), N(4)–N(5)–N(6) 178.4(8).

The thermal variation of $\chi_M T$ is shown in Fig. 2. The nature of the $\chi_M T$ *vs.* T plot is a signature of global intrachain ferromagnetic interaction. The solid line corresponds to the best fit obtained by considering an uniform ferromagnetically coupled chain of spin triplets (Fig. 2).[8] The best fitting parameters are $J = +13.5\ cm^{-1}$, $g = 2.08$ and $R = 2.3 \times 10^{-4}$. To the best of our knowledge this is the highest positive J value for end-to-end azido bridged complexes reported to date.[6] Fig. 2 indicates that it is only possible to fit the data from $T > 40$ K and below this temperature interchain magnetic interactions are present. In fact, the susceptibility curve shows a maximum at $T = 5$ K indicating that an antiferromagnetic ordering is present

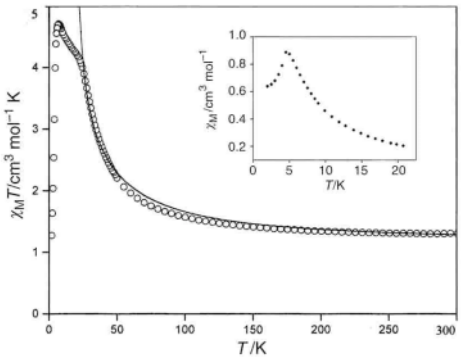

Fig. 2 Plot of $\chi_M T$ *vs.* T for **1**. Solid lines show the best fit indicated in the text. Inset: plot of χ_M *vs.* T at low temperature.

† Electronic supplementary information (ESI) available: Fig. S1: magnetisation *vs.* temperature curves at different magnetic fields. Fig. S2: AC susceptibility measurements. See http://www.rsc.org/suppdata/cc/b1/b104649g/

 DOI: 10.1039/b104649g

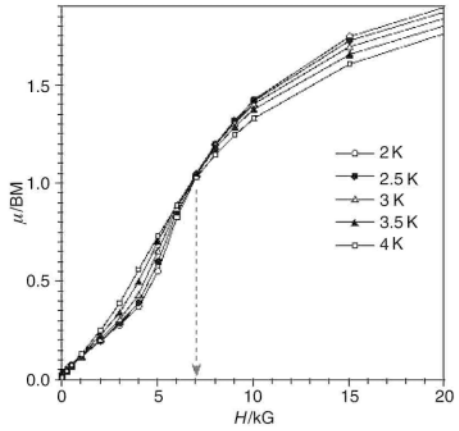

Fig. 3 Magnetization *vs.* applied field curves at different temperatures exhibiting sigmoidal shape with a common crossing point at $H = 7$ kG.

(see inset of Fig. 2). The magnetization curves for different temperatures (Fig. 3) exhibit a sigmoidal shape with a common crossing point for $H = 7$ kG. All these facts clearly indicate a metamagnetic behaviour of the complex with a critical temperature (T_c) of 5 K and critical field (H_c) of 7 kG. This magnetic order can be understood by considering that a spin canting structure may be involved, that is the interchain antiferromagnetic coupling does not imply a total antiparallel arrangement of the local spins but that a very weak canted angle should occur. The unusual intrachain ferromagnetic interaction is mainly due to the large deviation of Ni–N–N angles from 108°, the very high Ni–N_3–Ni torsion angle and the unusual axial–equatorial bridging mode of the azido. All these structural factors in complex **1** diminish the antiferromagnetic interaction to a greater extent to favour ferromagnetic interaction[9] as observed. The antiferromagnetic interactions operate between Ni^{II} of adjacent chains probably by means of electrostatic (dipolar) interactions between the aromatic ring of the coordinating Schiff base ligand due to a close contact between the parallel aromatic rings from two adjacent chains (the closest distance is 3.41 Å).[9] When present interchain hydrogen bonding interactions also play a vital role in intermolecular antiferromagnetic interaction. In our system, no classical hydrogen bonds are present, but only C–H···N bonds in which *d*(H–N) is *ca*. 2.5 Å (av.) and *d*(C–N) is 3.1 Å (av.), and so in our system the contribution of interchain hydrogen bonding interactions to interchain antiferromagnetic interaction is weak.

Previously reported results show that end-to-end azido bridged metal complexes are always antiferromagnetic.[10] However, two recently published results show the possibility of ferromagnetic materials with such bridging.[5,6] Our present result shows the possibility of a metamagnetic molecular material with only end-to-end azido bridged complexes. The present example is thus a new demonstration of the versatility of azido bridges for building molecular-based magnetic materials. In order to complete the magnetic studies, further experiments along with the DFT calculations and other theoretical calculations are in progress.

We wish to thank the Council of Scientific and Industrial Research, New Delhi for financial support (granted to N. R. C) and Prof. Joan Ribas, Universitat de Barcelona, Spain, for fruitful scientific discussion.

Notes and references

‡ The tridentate Schiff base was prepared by refluxing pyridine-2-aldehyde (2 mmol, 0.214 g) and *N*,*N*,2,2-tetramethylpropane-1,3-diamine (2 mmol, 0.260 g) in methanol (10 mL), according to the literature method.[11] A methanolic solution (10 mL) of nickel(II) perchlorate hexahydrate (2 mmol, 0.730 g) was added to the hot methanolic solution (10 mL) of the tridentate Schiff base ligand (2 mmol). The resulting solution was cooled to room temperature and an aqueous solution (5 mL) of sodium azide (4 mmol, 0.260 g) was added dropwise with continuous stirring. Suitable green single crystals for structure determination were obtained (50% yield) by slow evaporation of this solution. Anal. for $C_{13}H_{21}N_9Ni$: C, 43.15; H, 5.80; N, 34.85. Found: C, 43.60; H, 5.65; N, 34.80; IR: ν 2105 cm^{-1} [ν_a(azide)], 2095 cm^{-1}(pendant azide).

§ *Crystal data* for **1**: $C_{13}H_{21}N_9Ni$, monoclinic, space group $P2_1/n$, a = 11.922(3), b = 8.360(2), c = 17.121(5) Å, β = 101.42(2)°, V = 1672.6(8) $Å^3$, $Z = 4$, $T = 293$ K, μ(Mo-Kα) = 1.174 mm^{-1}, D_c = 1.438 g cm^{-3}, $R1$ = 0.061 based on F, $wR2$ = 0.160 based on F^2. Maximum and minimum heights in the final difference Fourier map are 0.910 and −0.360 e $Å^{-3}$. Intensity data collected on an Enraf-Nonius CAD-4 single crystal diffractometer employing the ω–2θ scan method; absorption correction was applied. The structure was refined using a full matrix refinement procedure (SHELXL 97), with anisotropic thermal parameters assigned to all non-hydrogen atoms. All hydrogen atoms were observed in the difference map.

CCDC reference number 155222. See http://www.rsc.org/suppdata/cc/b1/b104649g/ for crystallographic data in CIF or other electronic format.

1 J. S. Miller and A. Epstein, *Angew. Chem., Int. Ed. Engl.*, 1994, **33**, 385; D. Gatteschi, *Adv. Mater.*, 1994, **6**, 635; P. S. Mukherjee, T. K. Maji, G. Mostafa, T. Mallah and N. Ray Chaudhuri, *Inorg. Chem.*, 2000, **39**, 5147; G. Viau, M. G. Lombardi, G. De Munno, M. Julve, F. Lloret, J. Faus, A. Caneschi and J. M. Clemente-Juan, *Chem. Commun.*, 1997, 1195; C. Ruiz-Perez, J. Sanchiz, M. H. Molina, F. Lloret and M. Julve, *Inorg. Chem.*, 2000, **39**, 1363.

2 A. Escuer, R. Vicente, J. Ribas and X. Solans, *Inorg. Chem.*, 1995, **34**, 1793; J. Ribas, M. Monfort, C. Diaz, C. Bastos and X. Solans, *Inorg. Chem.*, 1996, **35**, 6386.

3 J. Ribas, M. Monfort, R. Costa and X. Solans, *Inorg. Chem.*, 1993, **32**, 695; R. Vicente, A. Escuer, J. Ribas, M. S. El Fallah, X. Solans and M. Font-Bardia, *Inorg. Chem.*, 1995, **34**, 1278; M. Monfort, J. Ribas and X. Solans, *J. Chem. Soc., Chem. Commun.*, 1993, 350.

4 E. Ruiz, J. Cano, S. Alvarez and P. Alemany, *J. Am. Chem. Soc.*, 1998, **120**, 11122.

5 A. Escuer, C. J. Harding, Y. Dussart, J. Nelson, V. Mckee and R. Vicente, *J. Chem. Soc., Dalton Trans.*, 1999, 223.

6 S. Hong and Y. Do, *Angew. Chem., Int. Ed.*, 1999, **38**, 193.

7 A. Escuer, R. Vicente, J. Ribas, M. S. El Fallah, X. Solans and M. Font-Bardia, *Inorg. Chem.*, 1994, **33**, 1842.

8 C. Dupas and J. P. Renard, *J. Chem. Phys.*, 1974, **61**, 3871.

9 A. Escuer, R. Vicente, J. Ribas, M. S. El Fallah, X. Solans and M. Font-Bardia, *Inorg. Chem.*, 1993, **32**, 3727; N. Matsumoto, Y. Sunatsaki, H. Miyasaka, Y. Hashimoto, D. Luneau and J. P. Tuchagues, *Angew. Chem., Int. Ed.*, 1999, **38**, 171.

10 J. Ribas, M. Monfort, C. Diaz, C. Bastos, C. Mer and X. Solans, *Inorg. Chem.*, 1995, **34**, 4986.

11 G. Zakrzewski and E. C. Lingafelter, *Inorg. Chim. Acta*, 1970, **4**, 251.

CHEMCOMM Communication
www.rsc.org/chemcomm

Templated photochemical synthesis of a uracil *vs*. thymine receptor

Dario M. Bassani,* Xavier Sallenave, Vincent Darcos and Jean-Pierre Desvergne

Laboratoire de Chimie Organique et Organométallique, CNRS UMR 5802, Université Bordeaux 1, 33505. Talence, France. E-mail: d.bassani@lcoo.u-bordeaux.fr

Received (in Cambridge, UK) 5th April 2001, Accepted 15th June 2001
First published as an Advance Article on the web 20th July 2001

The first templated photochemical synthesis of a receptor capable of differentiating between thymine and uracil is described.

Supramolecular self-assembly can be used to build structures of controlled size, shape, and functionality.[1] Of particular interest is the application of such processes to construct molecular receptors by moulding small fragments containing molecular recognition elements around a given substrate.[2] However, a means by which the reversibly-bound adduct can be captured to allow the isolation and identification of the receptor (lock-in) is invariably required. We have recently described a system in which the photoinduced dimerisation of cinnamates appended with molecular recognition units was affected by the presence of a template molecule.[3] A salient feature appeared to be the possibility to consolidate supramolecular assemblies *via* light-triggered photoreactions through a process analogous to the topochemical control achieved in the solid.[4] It therefore seemed interesting to further explore the use of light to trigger the covalent capture of reversibly-formed supramolecular receptors. The binding properties of this new class of hydrogen-bonding receptors, incorporating a diphenylcyclobutane scaffold, were investigated. In particular, their ability to discriminate between analogues of the naturally-occurring pyrimidine bases thymine and uracil makes them potential candidates in the development of RNA *vs*. DNA targeting agents.

Compound **2** was synthesised by Heck coupling between styrene and **1**(Scheme 1), prepared by sequential substitution of cyanuric chloride† according to literature procedures.[5] The binding of **2** to the template molecule, 5,5-dihexylbarbituric acid (**3**), was investigated[6] by ^{1}H NMR spectroscopy. In principle, one may expect the formation of five distinct (two 1 : 1 and three 2 : 1) complexes (Fig. 1), only one of which places the stilbene chromophores in close proximity. Because the interconversion between the hydrogen-bonded complexes is fast on the NMR timescale, the observed binding isotherm only allows determination of the overall 1 : 1 and 2 : 1 association constants. Binding of **2** to **3** in $CDCl_3$ is accompanied by a 2 ppm downfield shift of the N–H resonance of **3**, from which association constants $K_1 = 1200 \pm 60$ M^{-1} and $K_2 = 250 \pm 12$ M^{-1} can be extracted. A good fit to the experimental data was obtained only for a model comprised of sequential 1 : 1 and 2 : 1 complex formation.

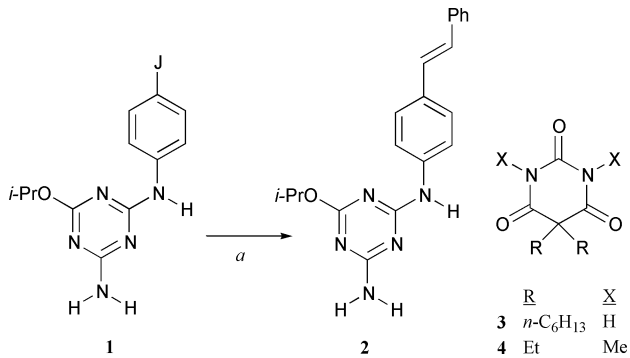

Scheme 1 (a) Styrene, Et_3N, $Pd_2(dba)_3$ (5 mol%), acetonitrile, 85 °C, 24 h (71%).

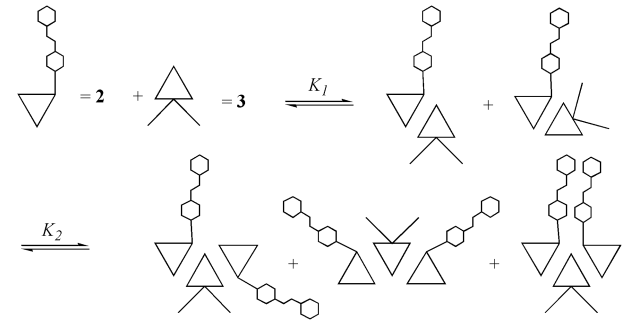

Fig. 1 Various hydrogen-bonded assemblies may be formed between **2** and **3**, only one of which places two stilbene chromophores in close proximity, favouring the formation of *syn* photodimers.

Irradiation of dilute (10^{-2} M) CH_2Cl_2 solutions of **2** results in rapid *E*, *Z* photoisomerisation of the stilbene chromophore leading to a photostationary equilibrium mixture enriched in the *Z* isomer (*Z*:*E* = 5.5), known to be unreactive towards cyclodimerisation.‡ Upon prolonged irradiation, slow grow-in of five additional products is observed by HPLC (Fig. 2). Isolation of four photoproducts by preparative HPLC allowed their characterisation by ^{1}H NMR and mass spectroscopy, which identified them as [2 + 2] cycloadducts. The structures of the isolated photoproducts **5a**–**5d** were assigned on the basis of their spectral properties by comparison with known stilbene dimers described in the literature.[7] The major cycloadducts are the head-to-head and head-to-tail dimers (**5a** and **5d**), accounting for roughly two thirds of the total dimer formation.

Under identical irradiation conditions, the presence of 0.5 eq. of **3** was found to enhance the formation of three of the photoproducts (**5b**, **5c**, and **5d**), while inhibiting the formation of **5a**. This difference in reactivity is attributed to the formation of a ternary supramolecular complex in which the stilbene moieties are held in a face-to-face geometry that is favourable to dimerisation. The preference for photodimers in which the

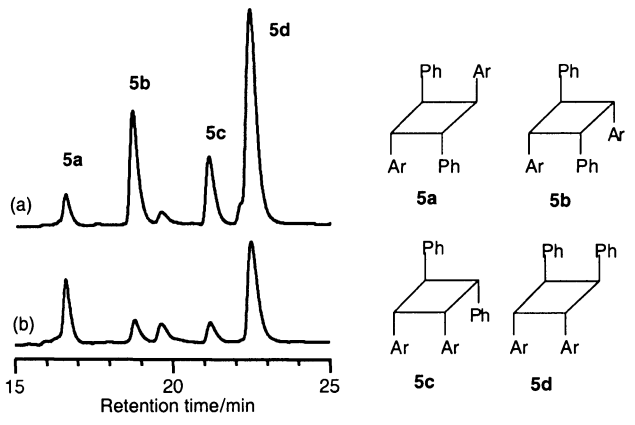

Fig. 2 Portion of the HPLC chromatograms showing the formation of photodimers in the presence (a) and absence (b) of **3** upon irradiation, and the proposed structures of dimers **5a**–**5d**.

 DOI: 10.1039/b103116n

Table 1 Quantum yields[a] of photodimers × 10^3

Dimer	**2** Alone	0.5 eq. **3**	0.5 eq. **4**
5a	0.7	0.5	0.7
5b	0.1	1.6	0.1
5c	0.1	0.6	0.1
5d	0.6	2.4	0.6

[a] In degassed dichloromethane, [**2**] = 0.01 M.

triazine units are oriented *syn* is in agreement with the involvement of **3** as a template during the dimerisation reaction. This is further supported by the lack of activity of **4**, in which the hydrogen bonding sites are blocked by methylation. The reduced yield of **5a** is consistent with the inability of **3** to promote structures that are not suitable receptors for barbiturate derivatives. Quantum yields for the formation of dimers **5a**–**5d** in the presence and absence of **3** or **4** are given in Table 1. From the measured association constants, and assuming a statistical distribution of 1:1 and 1:2 complexes, one can estimate the quantum yield for the formation of dimer **5d** *within* the supramolecular assembly to be 0.1, approximately a 170-fold increase with respect to solution. A rationalization of the catalysis and product distribution for an analogous cinnamate derivative has already been described,[3] and will therefore not be discussed further.

Molecular modelling of **5d** indicates that it has a tweezer-like geometry, with both the aminotriazine groups oriented in the same direction. Concomitant binding of a substrate to both triazines is therefore restricted both by the hydrogen-bonding pattern of triazine and by the size and shape of the cavity. Titration of **5d** with Barbital (5,5-diethylbarbituric acid, **6**) in $CDCl_3$ was monitored using NMR spectroscopy by observing the barbiturate N–H protons, which underwent a large downfield shift (> 4 ppm) upon complexation. The association constant was found to be 2400 M^{-1}, much higher than the binding of **2** to **3**, for which the microscopic binding constant is calculated to be 300 M^{-1}.[8] The increase in the association constant is attributed to the binding of **6** within the cleft formed by the triazine groups in **5d**, resulting in the formation of multiple hydrogen bonds. *In this respect, **5d** is an example of substrate-induced receptor synthesis*. The magnitude of the binding constant between **6** and **5d** is very similar to that of an analogous recently synthesised Barbital receptor containing a ferrocene unit,[9] though smaller than those previously reported by Hamilton and co-workers.[10] Thus, the preparation of receptors *via* light-induced capture of supramolecular assemblies can lead to functional receptors, of similar binding affinity as those obtained by conventional synthetic methodologies.

The rigid structure of **5d** is the basis for the observed selectivity in the binding of uracil *vs*. thymine or adenine. NMR titration ($CDCl_3$) of **5d** by 5-(4-*tert*-butylbenzyl)uracil (**7**) results in a binding isotherm indicating the formation of a 1:1 complex with a binding constant of 960 ± 120 M^{-1}.§ Molecular modelling using semi-empirical PM3 calculations (Fig. 3) reveals that uracil can bind within the diaminotriazine cleft with formation of 4 hydrogen bonds. In contrast, the presence of the methyl substituent in thymine is expected to prevent it from entering the binding cleft, and should therefore result in a lower binding affinity. This is indeed the case, and the binding of 5-(4-*tert*-butylbenzyl)thymine (**8**) to dimer **5d** can only be fitted to a model comprised of sequential 1:1 and 1:2 complex formation. This is rationalised by the binding of a thymine molecule to **5d** following partial rotation about the C–C bond connecting the diaminotriazine unit to the cyclobutane scaffold. The binding constants (K_1 = 1980 ± 65 M^{-1}, K_2 = 150 ± 5 M^{-1}) reflect a more favourable statistical weighting for binding the first thymine molecule, and a modest anticoopertive effect towards binding of the second thymine, presumably due to steric interactions. To adequately compare the binding of **7** or **8** to **5d**, one must take into consideration that whereas in the case of thymine four distinct 1:1 complexes may be formed, only one complex can be formed between **5d** and uracil. Thus, the microscopic binding constant of thymine is actually only one half that of uracil (500 *vs*. 960 M^{-1}). An upper limit of 50 M^{-1} was estimated for the association constant between **5d** and 9-ethyladenine, suggesting the formation of a rather labile complex. This is consistent with the binding of adenine in a fashion similar to that of thymine, but involving only two hydrogen bonds.

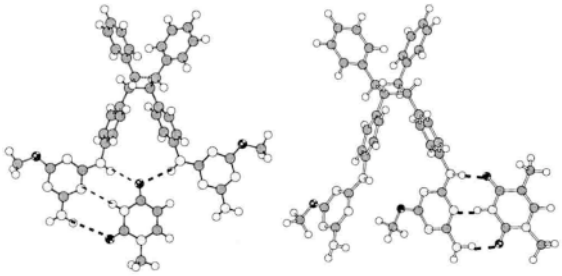

Fig. 3 Energy minimised (PM3) structures of complexes formed between **5d** and uracil (left) and thymine (right).

The methyl group in thymine has been recently recognized to play an important role in the recognition and suppression of DNA sequences by certain bacteria,[11] and receptors capable of mimicking this form of recognition would be of interest. The ability to differentiate between uracil and thymine may be further enhanced by preventing rotation of the binding site in **5d**, and this may open new possibilities for the selective recognition of RNA *vs*. DNA fragments.

We are indebted to Professor M. J. Hynes for making his program EQNMR available to us, and to the Conseil Régional Aquitaine and the MRT for supporting this work.

Notes and references

1 J.-M. Lehn, *Supramolecular Chemistry-Concepts and Perspectives*, VHC, 1995.
2 (*a*) V. Berl, I. Huc, J.-M. Lehn, A. DeCian and J. Fischer, *Eur. J. Org. Chem*., 1999, 3089; (*b*) V. Berl, M. J. Krische, I. Huc, J.-M. Lehn and M. Schmutz, *Chem. Eur. J*., 2000, **6**, 1939; (*c*) I. Huc, M. J. Krische, D. Funeriu and J.-M. Lehn, *Eur. J. Inorg. Chem*., 1999, 1415; (*d*) J. C. Adrian and C. G. Wilcox, *J. Am. Chem. Soc*., 1992, **114**, 1398; (*e*) T. Hayashi, T. Asai, H. Hokazono and H. Ogoshi, *J. Am. Chem. Soc*., 1993, **115**, 12210.
3 D. M. Bassani, V. Darcos, S. Mahony and J.-P. Desvergne, *J. Am. Chem. Soc*., 2000, **122**, 8795.
4 (*a*) Y. Ito, *Synthesis*, 1998, 1, and references therein; (*b*) D. G. Whitten, L. Chen, H. C. Geiger, J. Perlstein and X. Song, *J. Phys. Chem. B*, 1998, **102**, 10098.
5 J. A. Zerkowski, J. C. MacDonald, C. T. Seto, D. A. Wierda and G. M. Whitesides, *J. Am. Chem. Soc*., 1994, **116**, 2382.
6 M. J. Hynes, *J. Chem. Soc., Dalton Trans*., 1993, 311.
7 H. Schechter, W. J. Link and G. V. D. Tiers, *J. Am. Chem. Soc*., 1963, **85**, 1601; H. Ulrich, D. V. Rao, F. A. Stuber and A. A. R. Sayigh, *J. Org. Chem*., 1970, **35**, 1121.
8 K. A. Connors, *Binding Constants*, Wiley Interscience, London, 1987.
9 S. R. Collinson, T. Gelbrich, M. B. Hursthouse and J. H. R. Tucker, *Chem. Commun*., 2001, 555.
10 S. K. Chang, D. Van Engen, E. Fan and D. A. Hamilton, *J. Am. Chem. Soc*., 1991, **113**, 7640.
11 C. S. Chen, A. White, J. Love, J. R. Murphy and D. Ringe, *Biochemistry*, 2000, **39**, 10397.

CHEMCOMM Communication
www.rsc.org/chemcomm

Influence of low-barrier hydrogen bonds on solid state ^{17}O NMR spectra of labelled phthalate species

A. P. Howes,[a] R. Jenkins,[b] M. E. Smith,[a] D. H. G. Crout[b] and R. Dupree*[a]

[a] *Department of Physics, University of Warwick, Coventry, UK CV4 7AL. E-mail: nmrd@spec.warwick.ac.uk*
[b] *Department of Chemistry, University of Warwick, Coventry, UK CV4 7AL*

Received (in Cambridge, UK) 16th May 2001, Accepted 25th June 2001
First published as an Advance Article on the web 11th July 2001

The first ^{17}O solid state NMR study of a low barrier hydrogen bond (LBHB) is reported which shows that very strong hydrogen bonds strongly affect both the quadrupole interaction and the isotropic chemical shift reducing both.

Hydrogen bonding plays a vital role in both chemical and biological systems. Non-covalent forces are important in determining the secondary, tertiary and quaternary structures of proteins. Changes in hydrogen bonding interactions between ground and transition states can also make an important contribution to enzyme catalysis.[1] The proposal that short strong hydrogen bonds (SSHBs) can contribute up to 20 kcal mol^{-1} stabilisation energy to transition states[1–3] has provoked a vigorous debate in which the validity of this concept has been challenged.[4–6] SSHBs have been taken as synonymous with low barrier hydrogen bonds (LBHBs).[7] In such bonds, the potential energy barrier between the two possible states of a hydrogen bond, in which the hydrogen atom is associated with either one or other of the donor or acceptor atoms, is lowered so that a single well potential energy system results. The monoanions of carboxylic acids have been the focus of most studies of LBHBs with examples reported of both centred and non-centred hydrogen atoms.[8] In these systems the O–O bond is short (~ 2.4 Å) but the concept that such short bonds should be associated with exceptional hydrogen bond strength has been disputed.[4,6,9]

Solid state ^{17}O NMR can be used, in principle, to study hydrogen bonding since oxygen is directly involved in the bonds of interest. The ^{17}O isotropic chemical shift (δ_{iso}), the quadrupole coupling constant (C_Q)[10] and the asymmetry parameter (η) are very sensitive to the bonding state.[11] Despite the low natural abundance (0.037%) and consequent necessity for enrichment in ^{17}O the number of solid state NMR studies in recent years has increased rapidly because of the high sensitivity of the ^{17}O NMR parameters to local structural details and its ability to probe directly structurally significant environments.[12,13] Most work to date concerning application of ^{17}O NMR to study hydrogen bonding has been in solution. In recent solution work the relaxation times of the ^{17}O have been used to determine the quadrupole interaction which has subsequently been related, *via ab initio* calculations, to the bonding state.[11] There have recently been some preliminary solid state ^{17}O measurements in a hydrogen bonded environment,[14] however the current study is the first report of ^{17}O in a SSHB. Solid state NMR spectra are presented from ^{17}O-labelled phthalic acid[15] and three alkali metal mono- and di-anion phthalates.[16–18]

^{17}O solid state NMR spectra were accumulated at a resonance frequency of 81.35 MHz on a Varian-Chemagnetics Infinity 600 spectrometer. Fast magic angle spinning (MAS) of ~ 20 kHz was used in a Chemagnetics 3.2 mm probe. Short excitation pulses were applied of 0.6 μs (corresponding to a tip angle of π/6) and 1.2 μs in a spin-echo sequence. The echo spacing was approximately an integral number of rotation periods. Typically 100–500k acquisitions were co-added using a recycle delay of ~ 1 s. Spectra were referenced to H_2O at 0 ppm. The MAS NMR spectra together with simulations are shown in Fig. 1.

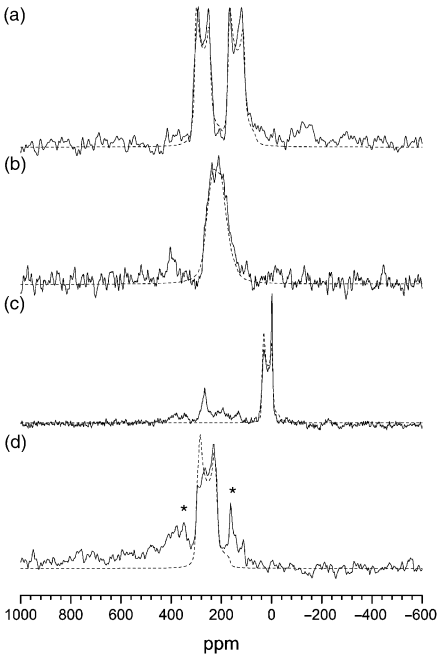

Fig. 1 ^{17}O 14.1 T MAS NMR spectra of (a) phthalic acid, (b) dilithium phthalate hemihydrate, (c) lithium hydrogen phthalate dihydrate and (d) potassium hydrogen phthalate dihydrate. [Note that the spinning speed in (d) was lower so that the spinning sidebands (*) are more prominent.]

Phthalic acid shows two completely resolved well defined second-order quadrupolar lineshapes[10] [Fig. 1(a)] with similar C_Q values but with δ_{iso} values that differ by ~ 130 ppm (Table 1). The dilithium salt gives a broader line intermediate in position to the two resonances of phthalic acid [Fig. 1(b)]. A single set of parameters provides a good simulation of both the MAS and static spectra (latter not shown) and this was confirmed by repeating the experiment at a different applied magnetic field. The monolithium salt has a well defined second-order quadrupolar lineshape with a large decrease in the isotropic chemical shift [Fig. 1(c), Table 1]. (The very sharp feature on this line at ~ 0 ppm is due to a small amount of fluid-like water in the sample.) There is also some weak intensity in the region 200–300 ppm. The monopotassium salt shows a

Table 1 ^{17}O NMR parameters from simulation of the MAS NMR spectra

Sample	δ_{iso}(ppm) ± 5	C_Q/MHz ± 0.1	η ± 0.05
Phthalic acid			
Site 1	312	7.2	0
Site 2	180	7.4	0
Lithium hydrogen phthalate dihydrate	46	5.9	0.21
Dilithium phthalate hemihydrate	272	7.6	0.44
Potassium hydrogen phthalate dihydrate	305	8.4	0.2

 DOI: 10.1039/b104308k

quadrupolar lineshape [Fig. 1(d)] with NMR parameters that are similar (Table 1) to the dilithium salt and phthalic acid, but are very different from the monolithium salt.

The ^{17}O NMR parameters observed in these four compounds show a very wide variation compared to previous studies, covering a chemical shift range $\geqslant$250 ppm with C_Q differences of ~40%. Recently there have been the first reports of high resolution ^{17}O NMR studies of solid organic materials. In poly(L-alanine) the α-helix and β-sheet show a difference in δ_{iso} for ^{17}O of 33 ppm, which is related to the different hydrogen bonding of these different units.[19] In potassium hydrogen benzoate the distinct oxygen sites show a difference in parameters of C_Q = 8.5 MHz, δ_{iso} = 290 ppm for the carbonyl group oxygen atom, and C_Q = 6.3 MHz and δ_{iso} = 230 ppm for the hydroxy group oxygen atom.[20] The limited data that currently exist for such materials indicate that as the hydrogen bond strength increases the shielding increases, so that both the chemical shift and C_Q decrease. Phthalic acid has two oxygen sites in the ratio 1 : 1. From comparison with solution ^{17}O NMR studies, the peak with a shift of 312 ppm can be assigned to the carbonyl group oxygen atom. The shift difference between the two observed peaks results from the different chemical nature of these species. However the similarity of C_Q indicates that the degree of hydrogen bonding is similar and this is confirmed by the similar O–O distance[21] of these sites. The equality of the signal intensity indicates that the two sites were equally enriched, as expected. The dilithium salt showed a chemical shift of ~280 ppm, comparable with phthalic acid. A single set of parameters simulates the line well, hence either the notionally different sites are in fact very similar, or on the NMR timescale there is some averaging of the environments. Neutron diffraction studies of lithium hydrogen phthalate monohydrate[17] have revealed that it exhibits a very short hydrogen bond with the structural properties associated with LBHBs (O–O distances of 2.4 Å). The oxygen resonance observed in the spectrum of lithium hydrogen phthalate hemihydrate in the present study provides strong evidence for a LBHB since it has a low isotropic chemical shift (the *lowest* yet reported for such a compound) and a much smaller C_Q than the other salts. The NMR spectrum reveals only one site with some additional minor intensity. Observation of a single site could indicate that locally the sites are structurally the same or alternatively there is some averaging for the NMR that is not seen by diffraction, highlighting the caution needed when the term equivalence is invoked since it depends on the timescale. This is likely to be especially true when small, mobile atoms such as hydrogen and lithium are present. The single line implies that in lithium hydrogen phthalate hemihydrate all the oxygen sites are equivalent on the NMR timescale, a result that may be attributable to electronic equivalence. Alternatively, it may be attributed to dynamic proton disorder, as has been proposed to explain an analogous equivalence in the ^{17}O solid state NMR spectrum of the benzoic acid dimer.[20] The monopotassium salt of phthalic acid contains an intermolecular hydrogen bond according to an X-ray determination and not a strong symmetric intramolecular hydrogen bond.[22] A single site simulation consistent with the MAS data is shown (and is also consistent with static and multiple field data). The ^{17}O NMR interaction parameters are similar to the dilithium salt with an isotropic chemical shift of ~305 ppm and C_Q = 8.4 MHz. There is *no* evidence of a second environment with a smaller quadrupole interaction and there is certainly no intensity at the shift seen in the monolithium salt. Hence as expected from the crystal structure there is no ^{17}O resonance characteristic of an SSHB environment. The contrast between the ^{17}O NMR spectra of these monoanionic salts is striking since the resonance of the lithium with the SSHB salt is shifted by a large amount compared to the potassium salt where the hydrogen bonding is weaker. As more data is collected it will become important to establish the exact nature of the correlation between the NMR parameters and the hydrogen bond strength.

This communication shows that ^{17}O NMR is a direct and sensitive probe of the hydrogen bonding state in solid organic compounds, easily identifying low barrier hydrogen bonds. The data indicates that the quadrupole interaction and in particular the chemical shift are strongly affected by hydrogen bonding. ^{17}O NMR should find widespread application as a probe of hydrogen bonding state, identifying other SSHBs, and determining the protonation states of proteins.

RD, APH and MES thank EPSRC for funding the solid state NMR equipment within the Physics Department at Warwick. MES thanks the Royal Society for funding work on ^{17}O NMR of hydrogen bonding. Dr C. Gervais and D. Padro are thanked for help in simulating the spectra.

Notes and references

1 W. W. Cleland and M. M. Kreevoy, *Science*, 1994, **264**, 1887.
2 J. A. Gerlt and P. G. Gassman, *J. Am. Chem. Soc*., 1993, **115**, 11552.
3 P. A. Frey, S. A. Whitt and J. B. Tobin, *Science*, 1994, **264**, 1927.
4 J. P. Guthrie, *Chem. Biol*., 1996, **3**, 163.
5 S. Scheiner and T. Kar, *J. Am. Chem. Soc*., 1995, **117**, 6970.
6 S. Shan, S. Loh and D. Herschlag, *Science*, 1996, **272**, 97.
7 C. L. Perrin and J. B. Nielson, *Annu. Rev. Phys. Chem*., 1997, **48**, 511.
8 C. L. Perrin and J. B. Nielson, *J. Am. Chem. Soc*., 1997, **119**, 12734; and references cited therein.
9 J. A. Gerlt, M. M. Kreevoy, W. W. Cleland and P. A. Frey, *Chem. Biol*., 1997, **4**, 259.
10 M. E. Smith and E. R. H. van Eck, *Prog. NMR Spectrosc*., 1999, **34**, 159.
11 A. Bagno, S. Gerard, J. Kevalam, E. Menna and G. Scorrano, *Chem. Eur. J*., 2000, **6**, 2915.
12 P. J. Dirken, S. C. Kohn, M. E. Smith and E. R. H. van Eck, *Chem. Phys. Lett*., 1997, **266**, 568.
13 L. M. Bull, B. Bussemer, T. Anupold, A. Reinhold, A. Samoson, J. Sauer, K. Cheetham and R. Dupree, *J. Am. Chem. Soc*., 2000, **122**, 4948.
14 G. Wu, K. Yamada, S. Dong and H. Grondey, *J. Am. Chem. Soc*., 2000, **122**, 4215.
15 Samples were prepared by hydrolysis of phthalic anhydride using 35 at% ^{17}O-enriched water
16 W. Gonschorek and H. Küppers, *Acta Crystallogr., Sect. B*, 1975, **31**, 1068.
17 H. Küppers, F. Takusagawa and T. F. Koetzle, *J. Chem. Phys*., 1985, **82**, 5636.
18 H. Küppers, A. Krick and I. Olovsson, *Acta Crystallogr., Sect. B*, 1981, **37**, 1203.
19 K. Yamauchi, S. Kuroki, I. Ando, T. Ozaki and A. Shoji, *Chem. Phys. Lett*., 1999, **302**, 331.
20 S. Dong, K. Yamada and G. Wu, *Z. Naturforsch., Teil A*, 2000, **55**, 21.
21 W. Nowacki and H. Jaggi, *Z. Kristallogr*., 1957, **109**, 272.
22 Y. Okaya, *Acta Crystallogr*., 1965, **19**, 879.

CHEMCOMM Communication
www.rsc.org/chemcomm

Synthesis of a new polyaniline/nanotube composite: "*in-situ*" polymerisation and charge transfer through site-selective interaction

Murielle Cochet,[a] Wolfgang K. Maser,*[a] Ana M. Benito,[a] M. Alicia Callejas,[a] M. Teresa Martínez,[a] Jean-Michel Benoit,[b] Joachim Schreiber[b] and Olivier Chauvet[b]

[a] *Instituto de Carboquímica, CSIC, Miguel Luesma Castán 4 E-50015. Zaragoza, Spain. E-mail: wmaser@carbon.icb.csic.es*
[b] *Institut des Matériaux Jean Rouxel, LPC, 2 rue de la Houssinière F-44322. Nantes Cedex 3, France*

Received (in Cambridge, UK) 4th May 2001, Accepted 25th June 2001
First published as an Advance Article on the web 11th July 2001

A new polyaniline/multi-wall carbon nanotube (PANI/MWNT) composite has been successfully synthesized by an "*in-situ*" polymerisation process; Raman studies indicate a site-selective interaction between the quinoid ring of the polymer and the MWNTs opening the way for charge transfer processes; transport measurements clearly reveal drastic changes in the electronic behaviour confirming the formation of a true composite material with enhanced electronic properties.

Carbon nanotubes have unique electronic[1] and mechanical[2] properties and are of great interest for the fabrication of new classes of advanced materials. Here, composites based on polymers and nanotubes especially offer the possibility of obtaining materials with superior characteristics.[3] Polyaniline (PANI), a particular conducting polymer[4] with a high application potential,[5] is a promising candidate for the synthesis of such nanotube composites suitable for improved structural or functional applications. In this article we report, for the first time, the synthesis of this new material by an "*in-situ*" polymerisation process.

The composites were synthesized by polymerisation of aniline with MWNTs. The MWNTs are prepared in an arc discharge experiment by sublimation of pure graphite rods under an helium atmosphere of 660 mbar, using a current of 100 A and a voltage of 25 V. After the experiment, MWNTs were collected from the inner core of the formed cathodic deposit. A solution of HCl 1 M, containing MWNTs, was sonicated at room temperature to disperse the carbon nanotubes. The aniline monomer, in HCl 1 M, was added to the MWNTs suspension. A solution of HCl 1 M containing the oxidant $(NH_4)_2S_2O_8$ was slowly added with a constant sonication at a temperature of about −3 °C. After a few minutes, the dark suspension became green indicating good polymerisation of aniline, and then was sonicated in an ice bath for 2 h. The composite is obtained by filtering and rinsing the suspension with HCl 1 M followed by drying of the remaining powder under vacuum at room temperature for 24 h. In this process, the PANI exists in its primary doped form called the "emeraldine salt"[4] in which coexist two structures: the polaronic form and the bipolaronic structure[6] (Fig. 1).

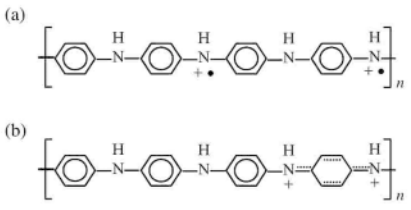

Fig. 1 Schematic structure of the emeraldine salt: (a) the polaronic form, (b) the bipolaronic structure.

† Electronic supplementary information (ESI) available: electron micrographs of PANI/MWNT composites. See http://www.rsc.org/suppdata/cc/b1/b104009j/

Different composites were synthesised by this process, using 10, 20, 30 and 50 wt% of MWNTs (in weight of monomer). In order to compare with the *in-situ* polymerised material, additionally, an "*ex-situ*" polymerised composite has been prepared by only mixing the doped PANI with 30 wt% of MWNTs by two hours of sonication.

The structural characteristics of the composites and its constituents have been analysed by X-ray powder diffraction measurements and is shown in Fig. 2. While the diffractogram of the pure MWNTs exhibits the typical peaks at 3.42, 2.13, 2.05, 1.71 and 1.23 Å corresponding to the graphite (002), (100), (101), (004) and (110) reflections, respectively, the one of PANI shows the highly pronounced oscillation structure characteristic of the doped form (emeraldine salt) with an oxidation degree of 0.5.[7] On the other hand, the diffractograms of the composites (10 and 30 wt%) display the typical peaks of the emeraldine salt as well as the strong peaks of MWNTs which are superposed and whose heights increase proportionally to their weight percentage. Therefore, it is clear that, from a structural point of view, no additional order has been introduced. This observation has also been confirmed by microscopy studies.†

On the other hand, Raman spectroscopy (Fig. 3) reveals that the electronic behaviour of the composites varies significantly from the one of its constituents. The Raman spectrum of the PANI shows the typical bands of the doped polymer in good agreement with a previous paper.[8] The spectra of pure nanotubes exhibit the three usual bands of MWNTs: the D-line at 1350 cm^{-1} (amorphous carbon and disorder induced line), the G-line at 1580 cm^{-1} (in-plane stretching E_{2g} mode) and a shoulder around 1600 cm^{-1} assigned to the D′-line (disorder line).[9] While the spectrum of the 10 wt% composite (not shown) is still identical to that of PANI, from 20 wt% on, the composite spectra clearly display different characteristics. Here, it is worth noting the remarkable decrease of the intensity of the PANI 1485 cm^{-1} band with respect to the 1161 cm^{-1} band. This band at 1485 cm^{-1} has been assigned to an in-plane deformation of

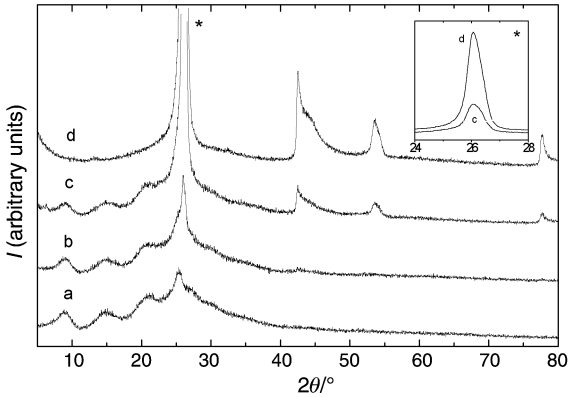

Fig. 2 X-Ray diffractograms (Cu-K_α) of doped PANI (a), composites containing 10 wt% (b) and 30 wt% (c) of MWNTs, and MWNTs (d).

 DOI: 10.1039/b104009j

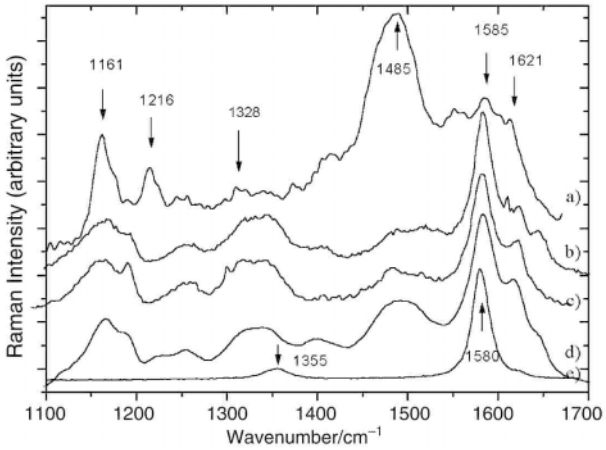

Fig. 3 Raman spectra (λ_{exc} = 514.5 nm) of doped polyaniline (a), composite using 20 (b), 30 (c) and 50 wt% (d) of MWNTs, and pure MWNTs (e).

the C–C bond of the quinoid ring of the doped PANI.[8] Therefore this pronounced decrease gives evidence that a site-selective interaction between the quinoid ring of the doped polymer and the nanotubes occurs as a consequence of the *in-situ* polymerisation. This interaction then may facilitate charge-transfer processes between the two components of the system and thus influence the transport properties of the composite.

Consequently, the transport behaviour (4 point-measurements between 300 and 1.25 K) has been studied on the MWNTs, the PANI, the *in-situ* polymerised composites (10, 20, 30 and 50 wt%) as well as on the *ex-situ* 30 wt% composite (Fig. 4). PANI shows a typical room temperature resistivity of 0.3 Ω cm.[10] It increases by 7 orders of magnitude following a $T^{-1/4}$-hopping law upon cooling to 1.7 K. The MWNTs resistivity is 2 Ω cm at room temperature and increases up to 15 Ω cm at low temperature.

The transport properties of the highly filled composites obtained by *in-situ* polymerisation exhibit the following remarkable facts. i) The room temperature resistivity is decreased by one order of magnitude as compared to PANI. ii) The low temperature resistivity is much smaller than both that of PANI as well as MWNTs (1.1 Ω cm for both the 50 and the 30 wt%, 2 Ω cm for the 20 wt% composites). iii) The temperature dependence of the resistivity is weaker than that of PANI. Regarding point iii), we can propose the following explanation. In this composite system, both the matrix and the filler (MWNTs) are conducting. At high temperatures, the conductivity is dominated by the polymer. Decreasing the temperature, the matrix becomes more and more resistive. On the other hand, the filler network which shows a very weak temperature dependence becomes more conducting than the matrix at low temperature. This means that the low temperature conductivity is due to the MWNTs. Actually this consideration is supported by the *ex-situ* polymerised 30 wt% composite (curve f) for which the low temperature resistivity shows the characteristic plateau due to MWNTs conduction.

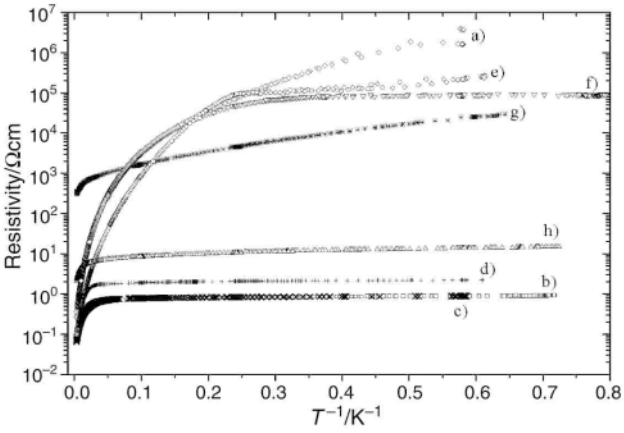

Fig. 4 Temperature dependence of the resistivity in polymer/MWNTs composite: PANI (a), *in-situ* PANI/MWNTs composites with 50 (b), 30 (c), 20 (d) and 10 wt% (e) of MWNTs, the *ex-situ* 30 wt% PANI/MWNTs composite (f), the *ex-situ* 30 wt% PMMA/MWNTs composite (g) and MWNTs (h).

Looking in more detail at the *in-situ* polymerised samples (curves b to d), the points i) and ii) further show that both the conductivity of PANI and of MWNTs has increased during the *in-situ* polymerisation process. This behaviour indicates that the electrical contacts between the MWNTs and the PANI grains have been improved. In accordance with the Raman observations, this suggests that *in-situ* polymerisation favours the charge transfer between PANI and MWNTs resulting in an overall material which is more conducting than the starting components. On the other hand, the apparent saturation of the resistivity decrease as well as of the increase of Raman intensity at 1485 cm^{-1} between the 30 and 50 wt% samples may be related to both the problems of achieving a homogeneous dispersion of large quantities of MWNTs in a matrix and the use of a microprobe in Raman spectroscopy. For the sake of comparison, additionally, a poly(methyl methacrylate) PMMA/MWNTs composite was prepared by mixing the insulating PMMA polymer with 30 wt% of MWNTs. In contrast to the PANI composites, the electronic behaviour of this material is completely different, especially in what concerns the temperature dependence of the resistivity, which is much stronger. Therefore, this observation further underlines the existence of a particular behaviour in case of the PANI/MWNTs composites. Further enhancement of the observed effects may be expected by using purified MWNTs, provided that the conducting path would include polyhedral particles as well.

Summarising, we have demonstrated the synthesis of a new PANI/MWNTs composite with enhanced electronic properties. Here, Raman and transport measurements show that the synthesis by an *in-situ* process leads to effective site-selective interactions between the quinoid ring of the PANI and the MWNTs facilitating charge-transfer processes between the two components. More detailed studies on the electronic behaviour along with the exploitation of the mechanical properties are currently carried out.

This work was supported by the EC RTN contract NANOCOMP (HPRN-CT-2000-00037).

Notes and references

1 J. W. Mintmire, B. I. Dunlop and C. T. Carter, *Phys. Rev. Lett.*, 1992, **73**, 2468.
2 G. Overney, W. Zhong and D. Tománek, *Z. Phys. D*, 1993, **27**, 93.
3 J. N. Coleman, S. Curran, A. B. Dalton, A. P. Davy, B. McCarthy, W. Blau and R. C. Barklie, *Phys. Rev. B*, 1998, **58**, 7492.
4 A. G. MacDiarmid, N. L. D. Somasiri, W. R. Salaneck, I. Lundström, B. Liedberg, M. A. Hasan, R. Erlandsson and P. Konrasson, *Springer Ser. Solid State Sci.*, 1985, **63**, 218.
5 *Handbook of Conducting Polymers*, eds. T. A. Skotheim, R. L. Elsenbaumer and J. R. Reynolds, 2nd edn., Dekker, New York, 1998, pp. 823–961
6 G. Louarn, M. Lapkowski, S. Quillard, A. Pron, J. P. Buisson and S. Lefrant, *J. Phys. Chem.*, 1996, **100**, 6998.
7 J. P. Pouget, M. E. Jozefowicz, A. J. Epstein, X. Tang and A. G. MacDiarmid, *Macromolecules*, 1991, **24**, 779.
8 M. Cochet, G. Louarn, S. Quillard, J. P. Buisson and S. Lefrant, *J. Raman Spectrosc.*, 2000, **31**(12), 1041.
9 J. Kastner, T. Pichler, H. Kuzmany, S. Curran, D. N. Weldon and W. Blau, *Chem. Phys. Lett.*, 1994, **53**, 221.
10 S. K. Jeong, J. S. Suh, E. J. Oh, Y. W. Park, C. Y. Kim and A. G. MacDiarmid, *Synth. Met.*, 1995, **69**, 171.

CHEMCOMM Communication
www.rsc.org/chemcomm

First asymmetric synthesis of dihydrobenzo[*c*]phenanthrene-1,4-quinones with helical chirality†

M. Carmen Carreño,* Susana García-Cerrada, M. Jesús Sanz-Cuesta and Antonio Urbano*

Departamento de Química Orgánica (C-I), Universidad Autónoma, Cantoblanco, 28049-Madrid, Spain. E-mail: carmen.carrenno@uam.es; antonio.urbano@uam.es; Fax: +34 91397 3966; Tel: +34 91397 3924

Received (in Cambridge, UK) 18th April 2001, Accepted 26th June 2001
First published as an Advance Article on the web 19th July 2001

The first enantioselective synthesis of 12-*tert*-butyl substituted 7,8-dihydrobenzo[*c*]phenanthrene-1,4-quinones having helical chirality is achieved with good chemical and optical yields through a domino Diels–Alder reaction–sulfoxide elimination–oxidation process starting from enantiopure (*S*)-2-(*p*-tolylsulfinyl)-1,4-benzoquinone and 5-*tert*-butyl substituted 3-vinyl-1,2-dihydronaphthalenes as dienes.

Compounds with the benzo[*c*]phenanthrene framework, [4]-helicenes, posess helical chirality due to the distortion of the planarity caused by overcrowding of the substituents at 1 and 12 positions of the terminal rings.[1] When such substituents are large enough, these molecules can be resolved into their corresponding enantiomers. The first configurationally stable 1,12-dimethyl substituted [4]-helicene was prepared and resolved by Newman[2] in 1956. Since then, only a few derivatives have been resolved into their optical isomers either by chemical[3–6] or chromatographic[4,7] methods. Some of them have shown interesting properties in chiral catalysis,[5] chiral recognition in complexation with cyclodextrins,[8] chiral Langmuir Blodgett film formation,[9] charge-transfer complexation,[10] chiral macrocyclic anhydride and amide formation,[11] and as a part of the first rationally designed chemically powered molecular motor.[12] Moreover, a recent report has shown that a high non-planarity of helical benzo[*c*]phenanthrenes induced by a methyl group at C-12 lowers their DNA-damaging effects compared with the unsubstituted derivative.[13] Although the interest in synthesizing these helicenes in optically active form is evident, to the best of our knowledge, only a single asymmetric approach has been described so far for the enantioselective construction of a lactone-type chiral tetrahelicene.[14]

In connection with a program devoted to asymmetric synthesis mediated by sulfoxides,[15] we have recently described the first asymmetric approach to [5]-helicenediquinones[16] based on the domino cycloaddition–sulfoxide elimination–oxidation process between enantiopure (*S*)-2-(*p*-tolylsulfinyl)-1,4-benzoquinone and vinyl phenanthrenes. Nevertheless, due to the poor reactivity of these aromatic derivatives as dienes, Diels–Alder reactions took place only in reflux of solvents with high boiling points or under high pressure conditions, with low chemical and optical yields. Taking into account the low racemization barriers of [4]-helicenes (< 16 kJ mol^{-1} for tetrahelicene),[17] such an asymmetric approach would not be applicable unless milder conditions conducive to the formation of the tetracyclic skeleton could be found. Thus, we thought of using more reactive non-aromatic dienes such as vinyldihydronaphthalenes which would probably allow the cycloaddition step to proceed under milder conditions, thus avoiding the racemization processes. We also reasoned that the introduction of a bulky substituent such as the *tert*-butyl group at C-1 or C-12 positions of the [4]-helicene could notably increase the racemization barrier as well as induce a higher non-planarity of these helical molecules. In this communication, we report the first enantioselective approach to configurationally stable helically chiral 12-*tert*-butyl substituted 7,8-dihydrobenzo[*c*]-phenanthrene-1,4-quinones based on this strategy.

As outlined in Scheme 1, the synthesis of vinyldihydronaphthalene **5** started with the addition of *tert*-butyl magnesium chloride to commercially available 7-methoxy-1-tetralone (**1**),‡ followed by dehydration of the resulting tertiary carbinol with 10% H_2SO_4 (48% yield for the two steps). The dihydronaphthalene **2** obtained was fully aromatized to naphthalene **3** with DDQ in 99% yield. Birch reduction of **3** with Na in refluxing EtOH followed by acid hydrolysis of the resulting

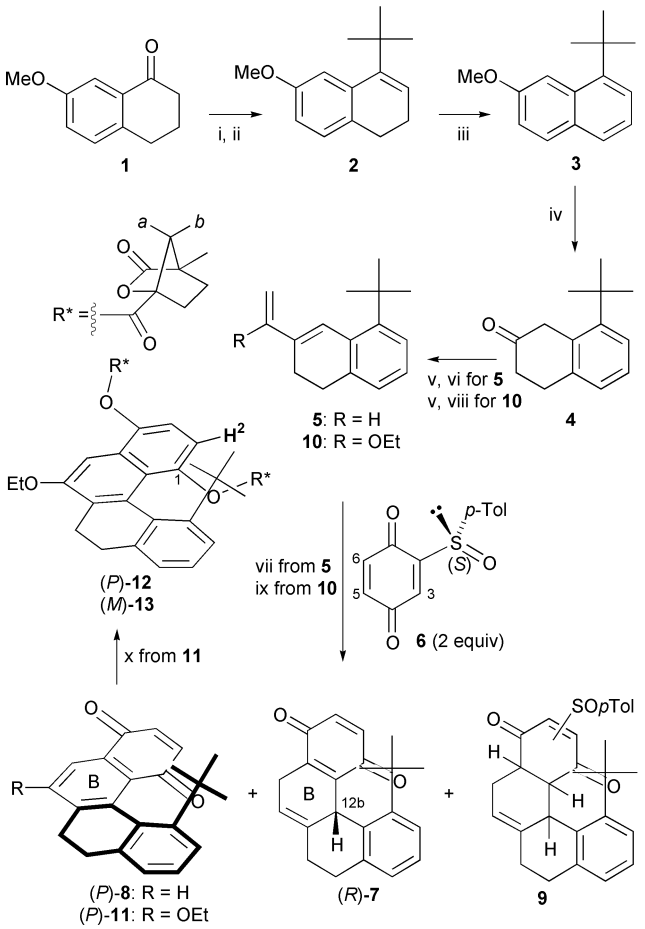

Scheme 1 *Reagents and conditions*: i, *t*-BuMgCl 2 M, Et_2O, rt, 48 h, 56%; ii, 10% H_2SO_4, benzene, reflux, 1 h, 85%; iii, DDQ, CH_2Cl_2, rt, 10 min, 99%; iv, Na, EtOH, reflux, 5–8 h, 35% HCl, 99%; v, Tf_2NPh, KHMDS, THF, −78 °C, 2 h, 91%; vi, CH_2=$CHSnBu_3$, $Pd(PPh_3)_4$, LiCl, THF, reflux, 2 h, 44%; vii, CH_2Cl_2, rt, 7 d, 54%; viii, CH_2=$C(OEt)SnBu_3$, $Pd(PPh_3)_4$, LiCl, THF, reflux, 2 h, 50%; ix, CH_2Cl_2, −20 °C, 3 d, 57% for **11**; x, Zn, (−)-camphanoyl chloride, DMAP, Et_3N, CH_2Cl_2, reflux, 1 h, 42% for (*P*)-**12** and 40% for (*M*)-**13** from (±)-**11**, 78% for (*P*)-**12** from (+)-(*P*)-**11**.

† Electronic supplementary information (ESI) available: experimental procedures. See http://www.rsc.org/suppdata/cc/b1/b103447m/

 DOI: 10.1039/b1003447m

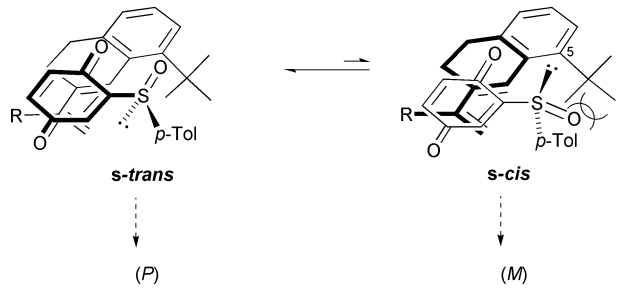

Fig. 1 *Endo* approaches of vinyldihydronaphthalenes on the s-*trans* and s-*cis* conformations of (*S*)-**6**.

vinyl ether gave 8-*tert*-butyl-2-tetralone (**4**) in 99% yield. Transformation of **4** into the corresponding enol triflate and Stille coupling with tributylvinylstannane afforded 5-*tert*-butyl-3-vinyl-1,2-dihydronaphthalene (**5**) in 40% yield for the two last steps.

The cycloaddition between diene **5** and enantiopure (*S*)-2-(*p*-tolylsulfinyl)-1,4-benzoquinone (**6**)[18] at room temperature afforded a 25:15:60 mixture of **7**, **8** and **9** which could be separated by flash chromatography (54% overall yield). Compound **7** was formed by *endo*-cycloaddition of **5** to the sulfinyl substituted C-2=C-3 double bond of **6** followed by elimination of the sulfoxide. This derivative, having a stereogenic center at C-12b, showed a 72% ee§ {$[\alpha]_D^{20} = -240$ (*c* 0.024, $CHCl_3$)}. Compound **8**, resulting from full aromatization of the B ring of **7**, was isolated in optically active form {$[\alpha]_D^{20} = +371$ (*c* 0.017, $CHCl_3$)} with a 72% ee,§ confirming the expected helical chirality for this type of quinone. Although the dienophile **6** was used in excess (2 equiv.) to achieve the aromatization of the B ring of **7**, only a small amount of the desired derivative **8** was formed under these conditions. The major component of the crude reaction mixture was characterized as a mixture of regio- and diastereoisomers **9**, resulting from the cycloaddition of diene **5** to the unsubstituted C-5=C-6 double bond of **6**.¶

In accordance with our previous findings,[19] the increasing electron donating effects of diene substituents favored cycloadditions through the more polarized sulfinyl substituted C-2=C-3 double bond of **6**. We thus thought of using a more reactive diene such as **10**, bearing an oxygenated substituent at the vinylic moiety, with the aim of increasing the yield of the desired [4]-helicenequinone. Compound **10** was prepared in a similar way as derivative **5**, by using 1-ethoxyvinyltributylstannane for the Stille coupling step (46% yield for two steps from **4**, Scheme 1). Cycloaddition between **10** and **6** could be conducted at –20 °C, affording in 57% yield helically chiral derivative **11** showing an optical rotation value of $[\alpha]_D^{20} = +1077$ (*c* 0.019, $CHCl_3$) and 88% ee.§ Compound **11** resulted from the exclusive attack of **10** on the sulfinyl substituted C-2=C-3 double bond of **6**, elimination of the sulfoxide and full aromatization of the B ring. This result evidenced that the use of the electron rich diene **10** not only completely reversed the chemoselectivity of the process, but also facilitated the aromatization of the B ring of the non-isolated intermediate, the 6-EtO derivative of (*R*)-**7**. Moreover, the lower temperature used in the cycloaddition step improved the diastereoselectivity of the whole process.[20]

The (*R*) absolute configuration at C-12b, the only stereogenic center of **7**, as well as the (*P*) absolute configuration of helical quinones **8** and **11** were initially established considering the preferred formation of a Diels–Alder adduct resulting from the *endo*-approach of **5** and **10** to the lower face of (*S*)-**6** adopting the s-*trans* conformation (Fig. 1). This should be the most favoured situation from the steric point of view since, when the dienophile reacts through the most stable s-*cis* rotamer, the approach of the diene from the less encumbered upper face gives rise to a transition state where a severe unfavourable interaction between the bulky *tert*-butyl group at C-5 of dienes and the sulfinylic oxygen of (*S*)-**6** appears. This configurational assignment was confirmed for **11** by applying, for the first time for a [4]-helicene, the methodology described by Katz[21] based on the different O=C–C–O conformations of (*M*)- and (*P*)-helicenyl camphanates‖ which bring about a different polarity and NMR behaviour of each diastereoisomer. Thus, we prepared di-(−)-camphanates (*P*)-**12** and (*M*)-**13** from racemic **11** and diastereoisomer (*P*)-**12** from enantiomerically enriched (+)-**11** (Scheme 1). The lower R_f (0.34) shown by diastereoisomer (*P*)-**12** on silica gel (eluent EtOAc–hexane 1:2) with respect to that of (*M*)-**13** (R_f = 0.42), as well as the existence of differentiated NOESY enhancements between H-2 and the methyl groups *a* and *b* of the inside camphanates (OR* at C-1, Scheme 1) in (*M*) and (*P*) isomers are consistent with the data reported[21] for determining the absolute configuration of these derivatives.

In summary, we have synthesized for the first time helically chiral 12-*tert*-butyl-substituted tetrahelicenequinones under very mild conditions from enantiopure (*S*)-2-(*p*-tolylsulfinyl)-1,4-benzoquinone and vinyldihydronaphthalenes. The presence of the bulky *tert*-butyl group at C-12 makes the system stable enough to be isolated in optically active form.

We thank DGICYT (PB98-0062) for financial support and Comunidad Autónoma de Madrid for a fellowship to S. G.-C.

Notes and references

‡ The IUPAC name for 1-tetralone is 3,4-dihydronaphthalene-1-(2*H*)-one.

§ The ee were determined by HPLC using chiral columns *Daicel Chiralpack* AS for **7** and **8**, and *Daicel Chiralcel* OD for **11**. The racemic derivatives necessary for such evaluation were prepared from racemic **6**.

¶ The major isomer of this mixture could be isolated pure by crystallysation, but its exact structure has not been elucidated.

‖ The IUPAC name for camphanic acid is 4,7,7-trimethyl-3-oxo-2-oxabicyclo[2.2.1]heptane-1-carboxylic acid.

1 M. S. Newman and W. B. Wheatley, *J. Am. Chem. Soc.*, 1948, **70**, 1913.
2 M. S. Newman and R. M. Wise, *J. Am. Chem. Soc.*, 1956, **78**, 450.
3 M. S. Newman, R. G. Mentzer and G. Slomp, *J. Am. Chem. Soc.*, 1963, **85**, 4018.
4 J. Cheung, L. D. Field, T. W. Hambley and S. Sternhell, *J. Org. Chem.*, 1997, **62**, 62.
5 H. Okubo, M. Yamaguchi and Ch. Kabuto, *J. Org. Chem.*, 1998, **63**, 9500.
6 G. Bringmann, M. Heubes, M. Breuning, L. Göbel, M. Ochse, B. Schöner and O. Schupp, *J. Org. Chem.*, 2000, **65**, 722.
7 H. Scherübl, U. Fritzsche and A. Mannschreck, *Chem. Ber.*, 1984, **117**, 336.
8 K. Kano, H. Kamo, S. Negi, T. Kitae, R. Takaoka, M. Yamaguchi, H. Okubo and M. Hirama, *J. Chem. Soc., Perkin Trans. 2*, 1999, 15.
9 F. Feng, T. Miyashita, H. Okubo and M. Yamaguchi, *J. Am. Chem. Soc.*, 1998, **120**, 10166; H. Okubo, F. Feng, D. Nakano, T. Hirata, M. Yamaguchi and T. Miyashita, *Tetrahedron*, 1999, **55**, 14855.
10 H. Okubo, D. Nakano, S. Anzai and M. Yamaguchi, *J. Org. Chem.*, 2001, **66**, 557.
11 H. Okubo and M. Yamaguchi, *Heterocycles*, 2000, **52**, 863; H. Okubo and M. Yamaguchi, *J. Org. Chem.*, 2001, **66**, 824.
12 T. R. Kelly, R. A. Silva, H. De Silva, S. Jasmin and Y. Zhao, *J. Am. Chem. Soc.*, 2000, **122**, 6935.
13 M. K. Lakshman, P. L. Kole, S. Chaturvedi, J. H. Saugier, H. J. C. Yeh, J. P. Glusker, H. L. Karrell, A. K. Katz, C. E. Afshar, W. M. Dashwood, G. Kenniston and W. M. Baird, *J. Am. Chem. Soc.*, 2000, **122**, 12629.
14 G. Bringmann, J. Hinrichs, J. Kraus, A. Wuzik and T. Schulz, *J. Org. Chem.*, 2000, **65**, 2517.
15 Overview: M. C. Carreño, *Chem. Rev.*, 1995, **95**, 1717. Recent references: M. C. Carreño, A. Urbano and J. Fischer, *Angew. Chem., Int. Ed. Engl.*, 1997, **36**, 1621; M. C. Carreño, A. Urbano and C. Di Vitta, *J. Org. Chem.*, 1998, **63**, 8320; M. C. Carreño, A. Urbano and C. Di Vitta, *Chem. Commun.*, 1999, 817; M. C. Carreño, A. Urbano and C. Di Vitta, *Chem. Eur. J.*, 2000, **6**, 906.
16 M. C. Carreño, R. Hernández-Sánchez, J. Mahugo and A. Urbano, *J. Org. Chem.*, 1999, **64**, 1387.
17 S. Grimme and S. D. Peyerimhoff, *Chem. Phys.*, 1996, **204**, 411.
18 M. C. Carreño, J. L. García Ruano and A. Urbano, *Synthesis*, 1992, 651.
19 M. C. Carreño and A. Urbano, unpublished results.
20 M. C. Carreño, J. L. García Ruano, M. A. Toledo, A. Urbano, C. Z. Remor, V. Stefani and J. Fischer, *J. Org. Chem.*, 1996, **61**, 503.
21 T. Thongpanchang, K. Paruch, T. J. Katz, A. L. Rheingold, K. Lam and L. Liable-Sands, *J. Org. Chem.*, 2000, **65**, 1850.

CHEMCOMM Communication
www.rsc.org/chemcomm

Crystal engineering using very short and linear C(sp)–H···N hydrogen bonds: formation of head-to-tail straight tapes and their assembly into nonlinear optical polar crystals

Masakazu Ohkita,*[a] Takanori Suzuki,[a] Keitaro Nakatani[b] and Takashi Tsuji*[a]

[a] *Division of Chemistry, Graduate School of Science, Hokkaido University, Sapporo 060-0810, Japan. E-mail: ohkita@sci.hokudai.ac.jp and tsuji@sci.hokudai.ac.jp*

[b] *Département de Chimie, Ecole Normale Supérieure de Cachan, 61, Avenue du Préridant Wilson, 94235Cachan Cedex, France*

Received (in Cambridge, UK) 24th April 2001, Accepted 26th June 2001
First published as an Advance Article on the web 19th July 2001

The crystallization of 4-ethynylpyridine (1) and 4-(4-ethynylphenyl)ethynylpyridine (2) leads to C(sp)-H···N hydrogen bonded straight tapes that further assemble into polar crystals, in the case of 2, and show intense powder SHG response, 8 times more efficient than crystalline urea.

The aims of crystal engineering are to design crystal structures of molecular solids with specific topological features, chemical function, or physical properties.[1] One area of particular endeavor in this field is the design of non-centrosymmetric polar crystals[2] because of their importance for physical properties of bulk assemblies such as non-linear optical (NLO) activity.[3] In this study we introduce a new class of polar crystals in which the molecules are directed in a completely parallel orientation through C(sp)–H···N hydrogen bonds. Here we

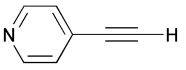

1

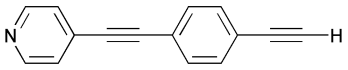

2

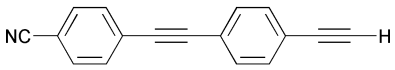

3

report the X-ray crystal structures of 4-ethynylpyridine (**1**) and 4-(4-ethynylphenyl)ethynylpyridine (**2**) as well as NLO properties of the polar crystals of **2**.

The crystal structural analysis† for **1**[4] revealed the formation of a linear tape structure formed by very short and linear C(sp)–H···N contacts (Fig. 1); the H···N distance (2.33 Å) found in the structure is about 0.4 Å shorter than the sum of their van der Waals (vdW) radii (2.75 Å) and is one of the shortest C–H···N contacts reported.[5] The C(sp)–H–N angle is 180° and the molecules in the tape are located on a crystallographic two-fold axis. The head-to-tail polar tapes of **1** are arranged in antiparallel fashion in the crystal, resulting in a centrosymmetric packing with space group *C*2/*c*.

The crystal structure analysis‡ for **2**§ also shows the formation of a tape structure through very short and linear C(sp)–H···N contacts (Fig. 2). Molecule **2** is almost planar in the crystal with the largest deviation of 0.21 Å from the least-square plane; the dihedral angle between the two aromatic rings is 19.0°. Interestingly, further packing analysis reveals that the unit cell of the crystal contains eight molecules of **2** in a non-centrosymmetric packing with space group *Fdd*2. Since the majority of achiral organic compounds tend to pack into centrosymmetric crystals,[3] this observation is rather unusual. Moreover, the dipole moments of the molecules are arranged perfectly in a parallel orientation in the crystal and, therefore, the vector parts of the first hyperpolarizabilities of the molecules are directed in a completely parallel orientation, which make this compound attractive for second-order NLO materials. In fact, the crystals of **2** show a strong second-harmonic generation (SHG) signal, 8 times more intense than that of crystalline urea, in the Kurtz powder test at 1907 nm. With this finding, we explored the SHG response in related compounds and found that the crystals of 4-(4-ethynylphenyl)-ethynylbenzonitrile (**3**)¶ also exhibit an intense SHG signal, 16 times more efficient than crystalline urea, in the Kurtz powder test at 1907 nm. We surmise that molecules of **3** are also arranged linearly in the crystal, in a head-to-tail fashion directed by the C(sp)–H···N hydrogen bond.[6] Although it is not clear at present what factors are responsible for the polar organization of **2** and **3**, it can be pointed out that the *p*-phenylene units in **2** and **3**, which is absent in **1**, should play an important role in the polar assembly process.‖

In conclusion, we have found a unique assembly of directed polar crystals based on the C(sp)–H···N hydrogen bond, which has been little exploited in crystal engineering so far. The present results clearly demonstrate that the C–H···N weak

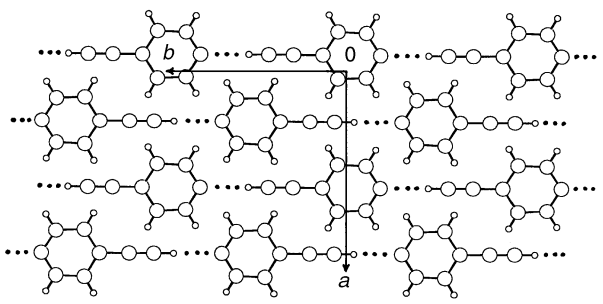

Fig. 1 Packing arrangement of **1** in the crystal. Short C(sp)–H···N contacts are shown by dotted lines; H···N 2.33 Å, C···N 3.28 Å, C–H–N 180°.

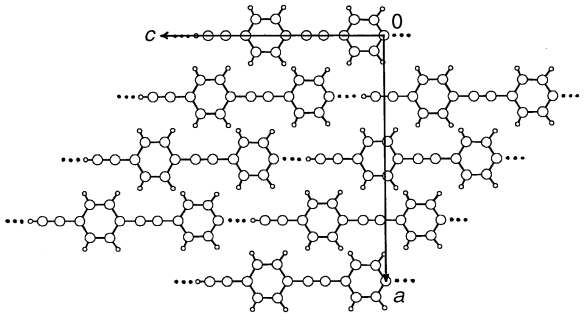

Fig. 2 Packing arrangement of **2** in the crystal. Short C(sp)–H···N contacts are shown by dotted lines; H···N 2.32 Å, C···N 3.27 Å, C–H–N 180°.

 DOI: 10.1039/b103689k

hydrogen bond is capable of not only constructing well-defined crystal structures but also inducing functional properties (SHG response) to the resulting bulk assemblies.

This work was supported in part by a Grant-in-Aid for Scientific Research (No. 12640508) from the Ministry of Education, Science, Sports and Culture of Japan. We thank Professor Tamotsu Inabe (Hokkaido University) for the use of X-ray analytical facilities.

Notes and references

† *Crystal data* for **1**: C_7H_5N, M = 103.12, colorless rod, 0.60 × 0.20 × 0.20 mm, monoclinic, space group $C2/c$, a = 9.800(5), b = 8.684(5), c = 7.334(4) Å, β = 116.90(4)°, V = 556.6(6) Å^3, Z = 4, ρ_{calcd} = 1.231 g cm^{-3}, T = 193 K, Mo-Kα radiation. A total of 577 unique reflections ($2\theta_{max}$ = 54.2°) were collected, of which 456 observed reflections [$I > 3\sigma(I)$] were used in the structure solution (direct methods) and refinement (full-matrix least-squares) to give final R = 0.085 and R_w = 0.114. Residual electron density is 0.42 e Å^{-3}. CCDC 153071. See http://www.rsc.org/suppdata/cc/b1/b103689k/ for crystallographic data in .cif or other format.

‡ *Crystal data* for **2**: $C_{15}H_9N$, M = 203.24, colorless prism, 0.20 × 0.20 × 0.15 mm, orthorhombic, space group $Fdd2$, a = 17.491(1), b = 7.748(1), c = 15.5880(9) Å, V = 2112.5(4) Å^3, Z = 8, ρ_{calcd} = 1.278 g cm^{-3}, T = 123 K, Mo-Kα radiation. A total of 595 unique reflections ($2\theta_{max}$ = 55°) were collected, of which 513 observed reflections [$I > 3\sigma(I)$] were used in the structure solution (direct methods) and refinement (full-matrix least-squares) to give final R = 0.056 and R_w = 0.072. Residual electron density is 0.30 e Å^{-3}. CCDC 164007.

§ Compound **2** was prepared by successive Sonogashira coupling of 4-bromoiodobenzene with **1** and trimethylsilylacetylene followed by desilylation using Bu_4NF. *Spectroscopic data* for **2**; mp 180–181 °C (Found: M$^+$, 203.0733. $C_{15}H_9N$ requires M, 203.0735); ν_{max} (KBr)/cm^{-1} 3148, 2216, 2088, 1592, 1502, 1408 and 838; δ_H (300 MHz, $CDCl_3$) 3.21 (1 H, s), 7.38 (2 H, AA′XX′), 7.50 (4 H, s) and 8.61 (2 H, AA′XX′); δ_C (75 MHz, CDCl3) 79.53, 83.06, 88.49, 93.27, 122.55, 123.02, 125.56, 131.17, 131.81, 132.24 and 149.89; m/z (FD) 203 (M$^+$, 100%).

¶ Compound **3** was prepared by successive Sonogashira coupling of 4-bromoiodobenzene with 4-ethynylbenzonitrile and trimethylsilylacetylene followed by desilylation using Bu_4NF. *Spectroscopic data* for **3**; mp 196–198 °C (Found: M$^+$, 227.0753. $C_{17}H_9N$ requires M, 227.0735); ν_{max} (KBr)/cm^{-1} 3236, 2212, 1600, 1504 and 840; δ_H (300 MHz, $CDCl_3$) 3.21 (1 H, s), 7.49 (4 H, s), 7.60 (2 H, AA′BB′) and 7.64 (2 H, AA′BB′); δ_C (75 MHz, CDCl3) 79.45, 82.98, 89.48, 93.02, 111.73, 118.41, 122.58, 122.81, 127.82, 131.62, 132.56, 132.16 and 133.13; m/z (FD) 227 (M$^+$, 100%).

‖ Connection of the tapes of **2** by C(sp^2)–H···π contacts between the pyridine α-proton and the terminal acetylene moiety (H···π centroid distance 2.86 Å) might play a significant role in the polar assembly process. Although there are face-to-face overlaps between the pyridine ring and the *p*-phenylene unit of **2** in the crystal, the interplanar distance (3.80 Å) beyond the sum of vdW radii (3.40 Å), so that the π-stacking interaction would play a less important role in determining the packing.

1 G. R. Desiraju, *Crystal Engineering: The Design of Organic Solids*, Elsevier, Amsterdam, 1989; J.-M. Lehn, *Supramolecular Chemistry*, VCH, Weinheim, 1995; G. R. Desiraju and T. Steiner, *The Weak Hydrogen Bond in Structural Chemistry and Biology*, Oxford University Press, Oxford, 1999; M. J. Calhorda, *Chem. Commun*., 2000, 801.

2 B. Gong, C. Zheng, H. Zeng and J. Zhu, *J. Am. Chem. Soc*., 1999, **121**, 9766; J. Kawamata, K. Inoue and T. Inabe, *Bull. Chem. Soc. Jpn*., 1998, **71**, 2777; K. D. M. Harris and M. D. Hollingsworth, *Nature*, 1989, **341**, 19 and references cited therein.

3 R. W. Boyd, *Nonlinear Optics*, Academic Press, New York, 1992; *Novel Optical Materials and Applications*, Eds. I.-C. Khoo, F. Simoni and C. Umeton, John Wiley, New York, 1997; *Nonlinear Optical Properties of Organic Molecules and Crystals*, Eds. D. S. Chemla and J. Zyss, Academic Press, Boston, 1987; *Molecular Nonlinear Optics: Materials, Physics and Devices*, Ed. J. Zyss, Academic Press, Boston, 1994.

4 N. R. Champness, A. N. Khlobystov, A. G. Majuga, M. Schröder and N. V. Zyk, *Tetrahedron Lett*., 1999, **40**, 5413.

5 Examples for the C–H···N interaction: R. Taylor and O. Kennard, *J. Am. Chem. Soc*., 1982, **104**, 5063; D. S. Reddy, B. S. Goud, K. Panneerselvam and G. R. Desiraju, *J. Chem. Soc., Chem. Commun*., 1993, 663; D. S. Reddy, D. C. Craig and G. R. Desiraju, *J. Am. Chem. Soc*., 1996, **118**, 4090; F. A. Cotton, L. M. Daniels, G. R. Jordan, IV and C. A. Murillo, *Chem. Commun*., 1997, 1673; M. Mascal, *Chem. Commun*., 1998, 303; A. N. M. M. Rahman, R. Bishop, D. C. Craig and M. L. Scudder, *Chem. Commun*., 1999, 2389; T. Steiner and G. R. Desiraju, *Chem. Commun*., 1998, 891; V. R. Thalladi, A. Gehrke and R. Boese, *New J. Chem*., 2000, **24**, 463.

6 For the crystal structures of related SHG active cyano compounds: G. R. Desiraju and R. L. Harlow, *J. Am. Chem. Soc*., 1989, **111**, 6757; P. J. Langley, J. Hulliger, R. Thaimattam and G. R. Desiraju, *New. J. Chem*., 1998, 1307.

CHEMCOMM Communication
www.rsc.org/chemcomm

A squaramide fluorescent ensemble for monitoring sulfate in water

Rafel Prohens, Gabriel Martorell, Pablo Ballester and Antoni Costa*

Departament de Química, Universitat de les Illes Balears 07071. Palma de Mallorca, Illes Balears, Spain. E-mail: antoni.costa@uib.es; Fax: +34 971 173426; Tel: +34 971 173266

Received (in Cambridge, UK) 11th May 2001, Accepted 18th June 2001
First published as an Advance Article on the web 20th July 2001

A simple molecular sensor that uses the exclusive quenching and binding abilities of two squaramide units included within an anionic recognition site is proposed for monitoring sulfate in water.

Squaramides are ideal components for molecular sensing devices due to their quenching and binding abilities. We recently described a fluorescent molecular probe,[1] showing the classical covalent arrangement of a fluorophore close to the recognition site that takes advantage of the quenching ability of squaramides. In addition, squaramides feature two hydrogen bond donor atoms that, in extended conformation, bind carboxylate anions tighly.[2] Furthermore, it is possible to achieve strong and selective binding of oxoanions by combining electrostatics together with more directional hydrogen bonding interactions, as in a related streptavidin-2-iminobiotin sulfate complex.[3] On this basis, using the hydrogen bond donor capabilities of squaramides, we describe herein a competitive strategy for sensing sulfate based on a simple macrocyclic charge-assisted squaramide receptor.

In contrast to the usual high dilution conditions required for macrocyclization, receptor **1** was obtained on a gram scale, in 60% overall yield after three steps (Scheme 1). Despite its apparent flexibility, the rigidifying effect provided by the two squaramide rings and a charge repulsion avoid the collapse of **1** and, at the same time, generates a concave cavity lined with two quaternary ammonium groups and four hydrogen bond donors useful for binding. The resulting bowl-shaped receptor is well suited for recognising tetrahedral anions as it matches the spatial and charge requirements of a target guest like sulfate placed at the centre of the cavity.

The formation of a **1**–SO_4^{2-} association complex was evidenced from the observation of characteristic association-induced shifts (CIS) on both, the squaramide and cyclophane hydrogens of **1**. Additional support was obtained from HOESY experiments performed in methanol on a related **1**–$^{13}C_2O_4^{2-}$ complex. In this case, diagnostic ^1H to ^{13}C NOE intermolecular contacts between the oxalate carboxylate at 176.8 ppm and H_a, H_b hydrogens in **1**, were observed, in accordance with the proposed localisation of the anion in **1**.

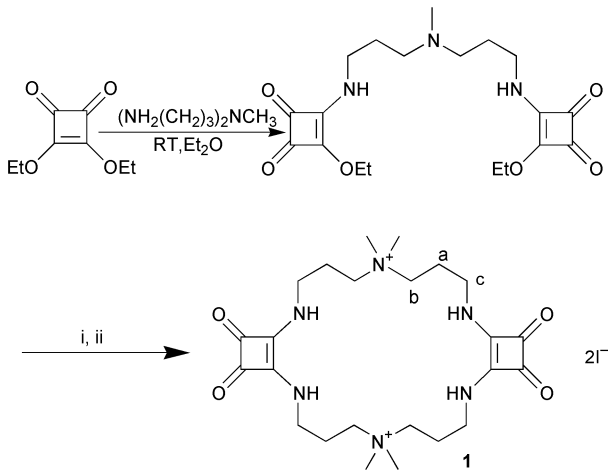

Scheme 1 Synthesis of **1**, (i) 3,3′-diamino-*N*-methyldipropylamine (1.0 equiv.) EtOH, 7 h, rt; (ii) MeI (7 equiv.), DMF, 70 °C, 12 h.

Host–guest association was fully characterized by isothermal titration calorimetry (ITC).[4] This technique is a valuable resource for investigating the energetics of host–guest processes[5] as it allows the determination of association constants larger than 10^5 M^{-1} that are clearly out of the possibilities of the standard NMR direct titration methods. In the present case, for the complexes with SO_4^{2-}, $PhOPO_3^{2-}$, $C_2O_4^{2-}$ and **1**, respectively, the value of the experimental stoichiometry parameter "n" was always in the range $0.95 < n < 1.05$ in good agreement with a 1 : 1 mode of binding.

The results obtained with selected oxodianions, show that the association is endothermic and entropically driven in all cases. The binding model emerging from the calorimetric data is consistent with an exchange equilibrium between **1** and the anionic guests. Upon formation of the complex both, **1** and the guest, must break their bonds with methanol and the release of solvent bound molecules to the bulk solvent would outweigh the entropic cost of the association.[6] Remarkably, the binding of monoanions such as halides, nitrate, acetate, and others is negligible owing to the electroselectivity imposed by the tetraalkylammonium groups. On the other hand, the preference for tetrahedral sulfate is accounted for by the structural constraints of the hydrogen bond donor array of the squaramide units in **1**, favouring the binding of sulfate over other divalent anions.

Addition of **1** to a solution of fluorescein disodium salt (FNa_2)† in MeOH–H_2O mixtures (9 : 1 v/v) produced a non-fluorescent self-assembled ensemble as a consequence of the effective quenching of the fluorescein emission band in the complex. The observed fluorescence quenching is probably due to photo-induced electron transfer (PET) from the donor squaramide rings of **1** to the fluorescein excited singlet state. This effect, namely an increase of fluorescence on binding the anion due to the suppression of PET that occur when the **1**–FNa_2 complex dissociates, is formally equivalent to the well-known cation promoted suppression of PET widely used for cation recognition. In the present case, the system is not a fluorescent chemosensor, defined as an integrated fluorophore–receptor species,[7] but merely a mixture of a receptor and a fluorophore in which the latter competes with the target ion in complexation.

Table 1 Thermodynamic parameters for the interaction of **1** with key dianions[a]

Guest	K_a/M^{-1}	$\Delta G°$/ kJ mol^{-1}	$\Delta H°$/ kJ mol^{-1}	$T\Delta S°$/ kJ mol^{-1}
$C_2O_4^{2-}$	$(3.2 \pm 0.3) \times 10^5$	−31.0	+12.2	+43.2
$PhOPO_3^{2-}$	$(1.5 \pm 0.2) \times 10^4$	−23.5	+12.5	+36.0
SO_4^{2-}	$(4.6 \pm 1.0) \times 10^6$	−37.5	+11.3	+48.7

[a] Titration conditions: 30–40 injections (5 μL each) of a 5–10 mM solution of the anion, as sodium or tetramethylammonium salt, were introduced into a sample cell at 294 K containing 1.5 mL of a 0.8 mM solution of **1** in methanol. The heats of dilution were subtracted prior to data analysis by Origin MicroCal software. In all cases the c parameter,[4] defined as $c = K_a$ [**1**]$_t n$, was kept between 10 and 1000. Errors were calculated at a confidence level of 95%.

 DOI: 10.1039/b104172j

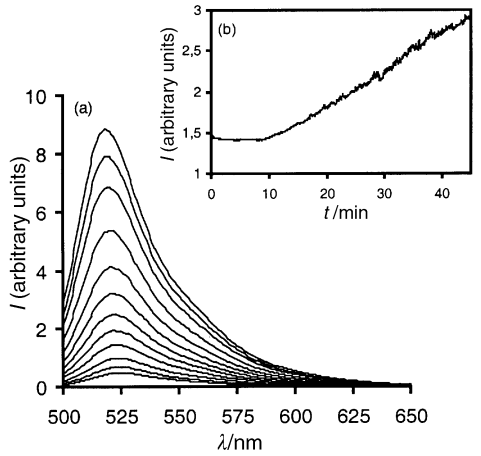

Fig. 1 (a) Fluorescence emission band ($\lambda_{exc.}$ 490 nm) of fluorescein, [FNa_2] = 1.4×10^{-5} M before (upper band) and after addition of **1**, [**1**] = 2.0×10^{-4} M (lowest band). Fluorogenic emission response with several concentrations of sulfate, [SO_4^{2-}] = 4.6, 6.5, 8.4, 10.0, 11.7, 13.3, 14.8, 15.9×10^{-5} M. The subset reflects the response of the **1**–FNa_2 ensemble to sulfate addition. (b) In this experiment, after an approximate 10 min period, the sulfate concentration of a water solution was continuously increased from 0 to 200 ppm and mixed at 0.10 mL min^{-1} together with a stream of [**1**] = 2.6×10^{-4} M and [FNa_2] = 7.4×10^{-4} M in MeOH–H_2O (90 : 10 v/v) at a flow rate 0.90 mL min^{-1}. Fluorescence was measured at 2 s intervals.

The association constant of the measuring **1**–FNa_2 ensemble (K_{ass} = $4.7 \pm 0.6 \times 10^4$ M^{-1}) was obtained by measuring the change in the fluorescence intensity of FNa_2 in the presence of an increasing amount of **1**.[8] In the same solvent system, the association constant for SO_4^{2-} (K_{ass} = $5.2 \pm 1.2 \times 10^6$ M^{-1}) estimated by competitive spectrophotometry[9] was clearly higher. In accordance, upon competitive addition of SO_4^{2-}, fluorescein was displaced[10] restoring the original fluorescence of FNa_2 (Fig. 1) and effectively signalling the presence of sulfate anion. This ensemble is also adequate for real time on-line determination of sulfate in water (pH ≥ 10). To this end, a stock solution of the sensing ensemble **1**–FNa_2 is mixed together at a 9 : 1 v/v ratio with an incoming water stream that contains an increasing concentration of sulfate. The result, shown in Fig. 1(b), shows a linear response within a wide range of sulfate concentration.

In conclusion, we have developed a squaramide-based receptor useful for sensing sulfate. In this ensemble the effective fluorescence quenching of the squaramides combined with an adequate hydrogen bond pattern are valuable resources that will be exploited in the future for sensing other targets.

Financial support from the Spanish DGESIC (PB98-0129) is gratefully acknowledged. R. P. thanks the Spanish Ministry of Education for a fellowship.

Notes and references

† The IUPAC name for fluorescein is 9-(2-carboxyphenyl)-6-hydroxy-3*H*-xanthen-3-one.

1 S. Tomás, R. Prohens, G. Deslongchamps, P. Ballester and A. Costa, *Angew. Chem., Int. Ed.*, 1999, **38**, 2208.
2 R. Prohens, S. Tomás, J. Morey, P. M. Deyà, P. Ballester and A. Costa, *Tetrahedron Lett.*, 1998, **39**, 1063.
3 B. A. Katz, *J. Mol. Biol.*, 1997, **274**, 776.
4 I. Jelesarov and H. R. Bosshard, *J. Mol. Recognit.*, 1999, **12**, 3; M. J. Blandamer, P. M. Cullis and J. B. F. N. Engberts, *J. Chem. Soc., Faraday Trans.*, 1998, **94**, 2261; I. Wadsö, *Chem. Soc. Rev.*, 1997, 79.
5 B. Linton and A. D. Hamilton, *Tetrahedron Lett.*, 1999, **55**, 6027; D. G. Lonergan, G. Deslongchamps and S. Tomás, *Tetrahedron Lett.*, 1998, **39**, 7861; C. De Stefano, O. Giuffre and S. Sammartano, *J. Chem. Soc., Faraday Trans.*, 1998, **94**, 2395.
6 M. Berger and F. P. Schmidtchen, *Angew. Chem., Int. Ed.*, 1998, **37**, 2694; M. Berger and F. P. Schmidtchen, *J. Am. Chem. Soc.*, 1999, **121**, 9986; M. Czekalla, H. Stephan, B. Haberman, J. Trepte, K. Gloe and F. P. Schmidtchen, *Thermochim. Acta*, 1998, **313**, 137.
7 P. de Silva, H. Q. N. Gunaratne, T. Gunnlaugsson, A. J. M. Huxley, C. P. McCoy, J. T. Rademacher and T. E. Rice, *Chem. Rev.*, 1997, **97**, 1515 and references therein.
8 H. Szmacinnski and J. R. Lakowicz, *Topics in Fluorescence Spectroscopy*, ed. J. R. Lakowicz, Plenum Press, New York, 1994, vol. 4, pp. 295–334.
9 K. A. Connors, *Binding Constants. The Measurement of Molecular Complex Stability*, John Wiley, New York, 1987, pp. 172–183
10 J. J. Lavigne and E. V. Anslyn, *Angew. Chem., Int. Ed.*, 1999, **38**, 3666; A. Metzger and E. V. Anslyn, *Angew. Chem., Int. Ed.*, 1998, **37**, 649.

CHEMCOMM Communication
www.rsc.org/chemcomm

First example of electroassisted biomimetic activation of molecular oxygen by a (salen)Mn epoxidation catalyst in a room-temperature ionic liquid

Laurent Gaillon[a] and Fethi Bedioui*[b]

[a] *Laboratoire d'Electrochimie et Chimie Analytique, UMR CNRS-ENSCP n° 7575, UPMC, Bat F., 4 place Jussieu, 75252 Paris cedex 05, France*
[b] *ENSCP, 11 rue Pierre et Marie Curie, 75231 Paris cedex 05, France. E-mail: bedioui@ext.jussieu.fr*

Received (in Cambridge, UK) 19th March 2001, Accepted 2nd July 2001
First published as an Advance Article on the web 19th July 2001

A first example of electroassisted activation of molecular oxygen by Jacobsen's epoxidation catalyst in an ionic liquid at room temperature has been achieved and showed the formation of the postulated high-valent manganese–oxo active intermediate.

Over the past few years, room temperature ionic liquids have re-attracted a wide range of sections of chemistry and generated much excitement and interest for various applications.[1] This renewed vigour is principally linked to the fact that these liquids have simple physical properties making them 'green friendly solvents' (easy to recycle, non-volatile and non-flammable). Thus, they offer potential alternatives for a large variety of disciplines, especially organic and inorganic chemistries. Recently, the discovery of enzyme activity in these media[1c] extends their potential use to bioinorganic applications. This context fits well with the desire to mimic enzymatic systems involving synthetic models (porphyrins and Schiff bases), especially for monooxygenases of the cytochrome P-450 family.[2]

Indeed, analysis of comparative studies dealing with the selectivity, efficiency, stability and recovery for both synthetic models and natural systems have shown that efficiency arises from the control of the environment of the enzyme active site and the development of practical immobilisation methods for catalysts, such as clay-intercalation,[3] zeolite-encapsulation,[4] covalent attachment to an organic polymeric matrix[5] and the use of two-phase systems.[6] Although relatively few efficient examples have been reported they constitute an important contribution to the development of efficient chemical systems operating according the catalytic cycle of substrate oxidation by cytochrome P-450, which involves a supposed high valent metal–oxo intermediate.[7] In the last decade, we have shown the first and rare examples involving electroassisted activation of molecular oxygen to generate metal–oxo active species for biomimetic oxidation of various hydrocarbons by immobilised enzyme models.[8,9]

Recently, Song and Roh[10] reported on the use of ionic liquids as practical recycling media for Jacobsen's catalyst {[*N*,*N*′-bis(3,5-di-*tert*-butylsalicylidene)-1,2-cyclohexanediamine)]-manganese(III) chloride, the so-called chiral (salen)Mn epoxidation catalyst and denoted here **[Mn(III)]$^+$**, Fig. 1}, for the asymmetric epoxidation of alkenes by aqueous NaOCl (as the oxidant) in the air-and moisture-stable ionic liquid [bmim][PF_6] at 0 °C, ([bmim]$^+$ = 1-butyl-3-methylimidazolium cation, Fig. 1). Our interest in electroassisted biomimetic reactions encourages us to explore a further extension of our clean chemistry concept, involving molecular oxygen and electrochemistry, into the field of a non-aqueous and polar two-phase process alternative, to provide not only simple recycling of the catalyst without modification of its structure, but also an increase in its activity. Herein, we report for the first time the electrochemical analysis of the biomimetic activation of molecular oxygen with the electrochemically reduced catalyst **[Mn(III)]$^+$** (in the presence of benzoic anhydride and 1-methylimidazole) in the ionic liquid [bmim][PF_6]. This study constitutes the first approach demonstrating the possible existence of the key steps responsible for the electroassisted formation, from molecular oxygen, of the highly reactive [Mn(V)=O]$^+$ manganese–oxo intermediate in these conditions.

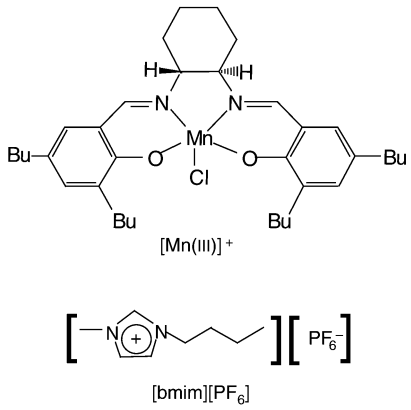

Fig. 1 Structures of **[Mn(III)]$^+$** and [bmim][PF_6].

Electrochemical experiments were carried out at a vitreous carbon electrode of area 0.07 cm^2 in [bmim][PF_6], conveniently prepared,[11] in the presence of **[Mn(III)]$^+$** catalyst and 1-methylimidazole (in the presence/absence of benzoic anhydride and molecular oxygen).† Fig. 2(a) shows the cyclic voltammogram of **[Mn(III)]$^+$** in a deaerated solution of the ionic liquid [bmim][PF_6] containing 1-methylimidazole. It exhibits a pair of well-defined peaks at $E \approx -0.460$ V *vs.* SCE corresponding to

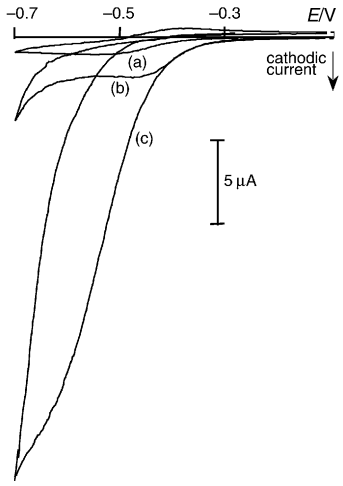

Fig. 2 Cyclic voltammograms of **[M(III)]$^+$** catalyst (2 mM) in [bmim][PF_6] ionic liquid in presence of 1-methylimidazole (10 mM) at room temperature (potential scan rate = 50 mV s^{-1}): (a): deaerated solution; (b) in the presence of molecular oxygen (saturated solution); (c) in the presence of benzoic anhydride (0.1 M) and molecular oxygen.

 DOI: 10.1039/b102526k

the reversible Mn^{III}/Mn^{II} redox process, by reference to the electrochemical behaviour of similar models in several organic solvents.[9,12,13] This was confirmed by rotating disk electrode voltammetry (data not shown). In presence of molecular oxygen, three main features related to the Mn^{III}/Mn^{II} reduction peak appear [Fig. 2(b)]: (i) its potential shifts to a higher potential value, *(ii)* its intensity is enhanced and *(iii)* its associated re-oxidation peak disappears. Such modification of the cyclic voltammogram is similar to that previously reported with related manganese catalysts under various conditions (dissolved or immobilised on solid supports and in organic solvents).[8,9,12,13] and is consistent with the first two steps of the catalytic cycle shown in Scheme 1.[12] Indeed, the reductive peak observed in Fig. 2(b) is representative of the reaction between the catalyst **[Mn(III)]**$^+$ (in the presence of 1-methylimidazole as an axial coordinating ligand, not shown in the cycle of Scheme 1) and molecular oxygen O_2, leading to a doubly reduced complex–oxygen adduct $[Mn–O_2]^-$, that can be interpreted as an 'electron transfer–chemical step–electron transfer' process.[9,12,13]

Fig. 2(c) shows the cyclic voltammogram of **[Mn(III)]**$^+$ in $[bmim][PF_6]$ containing both 1-methylimidazole and benzoic anhydride upon addition of molecular oxygen. A very large enhancement of the Mn^{III}/Mn^{II} reduction current peak is clearly observed. By reference to previously reported studies of similar complexes in several organic solvents, the modification of the cyclic voltammogram shows the occurrence of the expected reaction of the above mentioned $[Mn–O_2]^-$ adduct with anhydride $[(RCO)_2O]$ to give the high-valent manganese–oxo $[Mn(V)=O]^+$ intermediate, followed by its reduction and the steady state electrocatalytic regeneration of **[Mn(III)]**$^+$ (Scheme 1).[8,9,12,13] It is important to note that this reduction occurs competitively with the reaction of transfer of an oxygen to hydrocarbon in solution. However, we observed that the inclusion of olefin (*cis*-cyclooctene) did not produce a significant modification of the voltammograms, implying that the reaction is fast enough to be competitive with the rate of formation of the oxo complex.[9a,12] Finally, we have verified that the direct reduction of molecular oxygen takes place at *ca.*−0.8 V *vs.* SCE, outside the potential range investigated in this study, and that the presence of benzoic anhydride does not induce any electrochemical interference. Rotating disk voltammetry confirms all the above observations (data not shown).

In summary, this result shows for the first time the electroassisted biomimetic activation of molecular oxygen by Jacobsen's epoxidation catalyst in an ionic liquid and clearly demonstrates the possible existence of the key steps responsible for the formation of the highly reactive $[Mn(V)=O]^+$ manganese–oxo intermediate in the ionic liquid $[bmim][PF_6]$. This unique observation, combined with the immobilisation of the catalyst by using the ionic liquid, allows us to confidently explore this clean chemistry concept involving molecular oxygen and electrochemistry. Detailed studies are now in progress to extend this investigation to the preparative scale, for the epoxidation of selected olefins which may offer, for the first time to our knowledge, a possible extension of electrocatalysis and electrosynthesis to ionic liquid solvents.

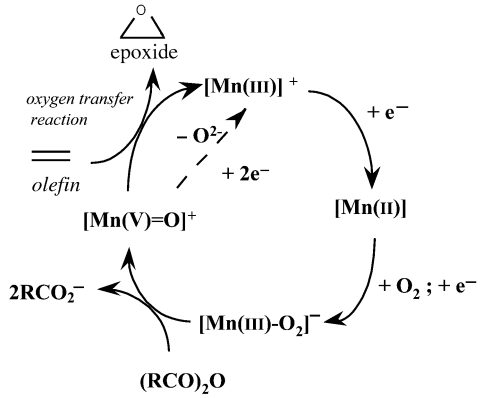

Scheme 1 Proposed scheme for the electroassisted activation of molecular oxygen by **[M(III)]**$^+$ catalyst for olefin epoxidation reaction.

We are grateful to Prof. P. Letellier and Dr J. Devynck for helpful discussion and interest in this work.

Notes and references

† *Representative procedure* for the electrochemical study: all electrochemical studies were performed with a standard three-electrode potentiostatic system (Taccussel). The potentials are referred to an aqueous saturated Calomel electrode, (SCE), placed in a separate compartment. All the experiments were performed under atmospheric pressure and at ambient temperature. Jacobsen's catalyst was purchased from Aldrich and used as received while the ionic liquid $[bmim][PF_6]$ was prepared and purified as previously reported.[11]

1 Reviews: (*a*) T. Welton, *Chem. Rev.*, 1999, **99**, 2071; (*b*) M. Freemantle, *C&EN*, 2000, 37; (*c*) M. Freemantle, *C&EN*, 2001, 21.
2 D. Mansuy and P. Battioni, *Cytochrome P-450 Model Systems in Metalloporphyrins in Catalytic Oxidations*, ed. R. A. Sheldon, Marcel Dekker, New York, 1994, p. 99.
3 For review: F. Bedioui, *Coord. Chem. Rev.*, 1995, **144**, 39 and references therein.
4 N. Herron, *J. Coord. Chem.*, 1988, **19**, 25; R. Parton, D. De Vos and P. A. Jacobs, *Enzyme Mimicking with Zeolites in Zeolite Microporous Solids: Synthesis, Structure, and Reactivity*, ed. G. A. Derouane, Kluwer Academic Publishers, Amsterdam, 1992, p. 555; K. J. Balkus Jr., A. K. Khanmamedov, K. M. Dixon and F. Bedioui, *Appl. Catal.*, 1996, **143**, 159 and references therein.
5 F. Bedioui, J. Devynck and C. Bied-Charreton, *Acc. Chem. Res.*, 1995, **28**, 30 and references therein; F. Bedioui, J. Devynck and C. Bied-Charreton, *J. Mol. Catal.*, 1996, **113**, 3 and references therein.
6 G. Oehme, *Catalyst Immobilization: Two-Phase Systems*, in *Comprehensive Asymmetric Catalysis III*, ed. E. N. Jacobsen, A. Pfaltz and H. Yamamoto, Springler-Verlag, Berlin–Heidelberg–New York, 1999, p. 1378.
7 *Cytochrome P-450: Structure, Mechanism and Biochemistry*, ed. P. R. Ortiz de Montenallo, Plenum Press, New York, 1986; B. Meunier, *Chem. Rev.*, 1992, **92**, 1411.
8 L. Gaillon, F. Bedioui, P. Battioni and J. Devynck, *J. Mol. Catal.*, 1993, **78**, L23.
9 (*a*) F. Bedioui, S. Gutierrez Granados, C. Bied-Charreton and J. Devynck, *New J. Chem.*, 1991, **15**, 939; (*b*) F. Bedioui, S. Gutierrez Granados, L. Gaillon, C. Bied-Charreton and J. Devynck, *Stud. Surf. Sci. Catal.*, 1991, **66**, 221; (*c*) F. Bedioui, P. Moisy, J. Devynck, L. Salmon and C. Bied-Charreton, *J. Mol. Catal.*, 1989, **56**, 267; (*d*) P. Moisy, F. Bedioui, Y. Robin and J. Devynck, *J. Electroanal. Chem.*, 1988, **250**, 191.
10 C. E. Song and E. J. Roh, *Chem. Commun.*, 2000, 837.
11 J. G. Huddleston, H. D. Willauer, R. P. Swatloski, A. E. Visser and R. D. Rogers, *Chem. Commun.*, 1998, 1765.
12 S. E. Creager, S. Raybuck and R. W. Murray, *J. Am. Chem. Soc.*, 1986, **108**, 4225; C. P. Horwitz, S. E. Creager and W. R. Murray, *Inorg. Chem.*, 1990, **29**, 1006.
13 S. Gutierrez Granados, F. Bedioui and J. Devynck, *Electrochim. Acta*, 1993, **38**, 1747.

CHEMCOMM Communication
www.rsc.org/chemcomm

Ab initio structure determination of a peptide β-turn from powder X-ray diffraction data†

Emilio Tedesco,[a] Kenneth D. M. Harris,*[a] Roy L. Johnston,[a] Giles W. Turner,[a] K. Muruga Poopathi Raja[b] and Padmanabhan Balaram[b]

[a] *School of Chemistry, University of Birmingham, Edgbaston, Birmingham, UK B15 2TT. E-mail: K.D.M.Harris@bham.ac.uk; Fax: +44-121-414-7473; Tel: +44-121-414-7474*
[b] *Molecular Biophysics Unit, Indian Institute of Science, Bangalore 560012, India*

Received (in Cambridge, UK) 30th April 2001, Accepted 26th June 2001
First published as an Advance Article on the web 20th July 2001

***Ab initio* crystal structure determination of the peptide Piv-Pro-Gly-NHMe directly from powder X-ray diffraction data, using the genetic algorithm technique for structure solution, has allowed the complete structural characterization of the Type II β-turn conformation and the intermolecular interactions in this structure, and highlights the opportunities that now exist for structure determination of peptide systems when single crystals appropriate for single crystal X-ray diffraction experiments cannot be prepared.**

Knowledge of the conformational properties and interactions in model peptide systems can yield important insights concerning the structural properties of polypeptide sequences in proteins. An example concerns β-turns, which are structural elements that permit polypeptide chain reversals in proteins.[1] Tight turns in proteins and peptides, involving two residues as folding nuclei, have been very widely investigated,[2–5] and the understanding of β-turn stereochemistry that now exists has been facilitated by extensive high resolution structure determination of peptides[4] and proteins[2,3] from *single crystal* X-ray diffraction data. However, an intrinsic limitation of this technique is the requirement to prepare a crystal of sufficient size, quality and stability to allow single crystal diffraction data of appropriate quality to be measured. To circumvent this problem, progress has been made recently[6–10] in the development of new techniques for determining crystal structures directly from *powder* diffraction data, particularly with regard to the structure solution stage of the structure determination process. In the field of molecular crystals, the direct-space strategy[10,11] for powder structure solution has been a particularly important development. This paper reports the application of a genetic algorithm (GA) technique for *ab initio* structure determination of the peptide *N*-pivaloyl-L-prolyl-glycyl-*N*′-methylamide (Piv-Pro-Gly-NHMe) from powder X-ray diffraction data.

In the direct-space strategy for powder structure solution, trial structures are generated in direct space, with the quality of each trial structure assessed by comparing the powder diffraction pattern calculated for the trial structure and the experimental powder diffraction pattern (this comparison is made here using the powder profile R-factor R_{wp}, which implicitly takes peak overlap into consideration). In this work, direct-space structure solution was carried out using our GA method[12–19] to locate the trial structure corresponding to the global minimum in R_{wp}. In the GA method,[12–21] a population of trial structures is allowed to evolve subject to rules and operations (mating, mutation and natural selection) analogous to those that govern evolution in biological systems. Each structure is specified by its 'genetic code', which represents, for each molecule in the asymmetric unit, the position $\{x, y, z\}$ and orientation $\{\theta, \phi, \psi\}$ of the molecule, and the molecular conformation (defined by variable torsion angles $\{\tau_1, \tau_2, ..., \tau_n\}$). New structures are generated by the mating and mutation operations, and in our implementation used here,[16] each new structure is subjected to local minimization of R_{wp}. In natural selection, only the structures of highest 'fitness' (*i.e.* lowest R_{wp}) are allowed to pass from one generation to the next generation. Details of our GA methodology for powder structure solution[12–16] and examples of its application[17–19] are given in the cited refs.

The peptide Piv-Pro-Gly-NHMe was prepared by standard procedures,[22] purified by reverse phase HPLC on a C_{18} column and fully characterized by ^{1}H NMR (500 MHz) and electrospray mass spectrometry. The powder X-ray diffraction pattern of a lightly ground sample was recorded at ambient temperature on a Siemens D5000 diffractometer [transmission; $CuK_{\alpha 1}$ (Ge-monochromated); linear position-sensitive detector covering 8° in 2θ]. The 2θ range was 5 to 60°, measured in steps of 0.02° over 12 hours. The powder diffraction pattern was indexed by the program ITO,[23] giving a triclinic unit cell [final refined unit cell parameters following Rietveld refinement: a = 7.9747(3); b = 9.1814(3); c = 5.8456(2) Å; α = 97.020(2); β = 99.429(2); γ = 114.801(2)°]. Density considerations suggested that there is one molecule in the unit cell, and the space group was assigned as $P1$. Lineshape and linewidth parameters were determined using the POWDERFIT program,[24] which uses a modified Pawley fitting procedure.[25]

The GA structure solution calculation was carried out using the program EAGER.[26] The structural fragment (Scheme 1) comprised all non-hydrogen atoms of the molecule (with standard bond lengths and angles). For each structure, the genetic code comprised 9 variables $\{\theta, \phi, \psi, \tau_1, \tau_2, ..., \tau_6\}$, with the variable torsion angles allowed to take any value, except τ_5 which was allowed to take only the values 0 or 180°. We note that the position of the structural fragment $\{x, y, z\}$ is fixed arbitrarily in space group $P1$. The O–C–N–H torsion angle between τ_3 and τ_4 was fixed[27] at 180°. The population comprised 100 structures, and in each generation 100 offspring (50 pairs of parents) and 20 mutants were produced. The calculation was carried out for 50 generations.

The best structure solution (*i.e.* with lowest R_{wp} in the final generation) was taken as the starting structure for Rietveld refinement,[28] which was carried out using the GSAS program.[29] Standard restraints were applied to bond lengths and angles, and hydrogen atoms were inserted in calculated positions. Three common isotropic displacement parameters were refined, for

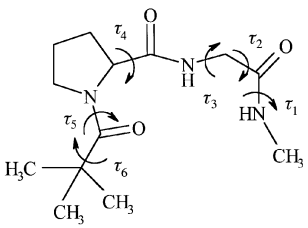

Scheme 1 Structural fragment used in the GA structure solution calculation for Piv-Pro-Gly-NHMe, with variable torsion angles indicated by arrows.

† Electronic supplementary information (ESI) available: fractional coordinates and isotropic displacement parameters for atoms in the final refined crystal structure. See http://www.rsc.org/suppdata/cc/b1/b103876c/

 DOI: 10.1039/b103876c

atoms of the main peptide chain, atoms of the ring system and oxygen atoms, respectively. For hydrogen atoms, a fixed common isotropic displacement parameter was used. In the final stages of refinement, a preferred orientation parameter was refined. The final Rietveld refinement (Fig. 1; supplementary information) gave R_{wp} = 4.14, R_p = 5.78 and R_F = 8.97% (75 variables; 269 reflections; 2857 data points).

Fig. 2 shows the final refined structure of Piv-Pro-Gly-NHMe. As shown in Fig. 2a, the molecule adopts a Type II β-turn conformation[30] (ϕ_{Pro} = −58.3; ψ_{Pro} = 127.2; ϕ_{Gly} = 71.4; ψ_{Gly} = 26.1°) stabilized by an intramolecular 4 → 1 hydrogen bond between the C=O group of the Piv residue and the methylamide N–H group (N···O, 2.99 Å; N···O–C, 140.6°). The conformation found here for Piv-Pro-Gly-NHMe is similar to those in other structures containing Type II β-turns, determined previously from single crystal X-ray diffraction data.[31] We note that Pro-Gly sequences in proteins and peptides

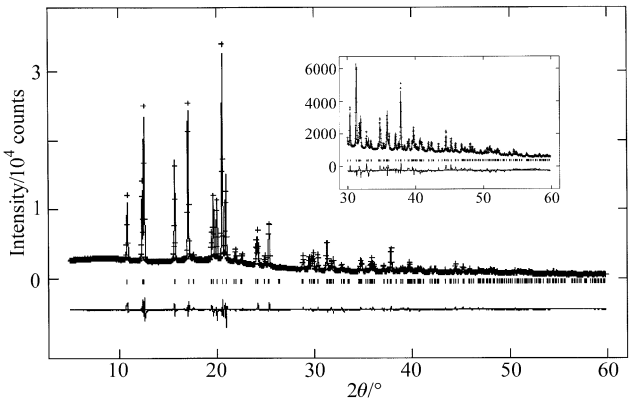

Fig. 1 Experimental (+ marks), calculated (solid line) and difference (lower line) powder X-ray diffraction profiles for the final Rietveld refinement of Piv-Pro-Gly-NHMe. The inset shows an expanded plot for 2θ = 30–60°.

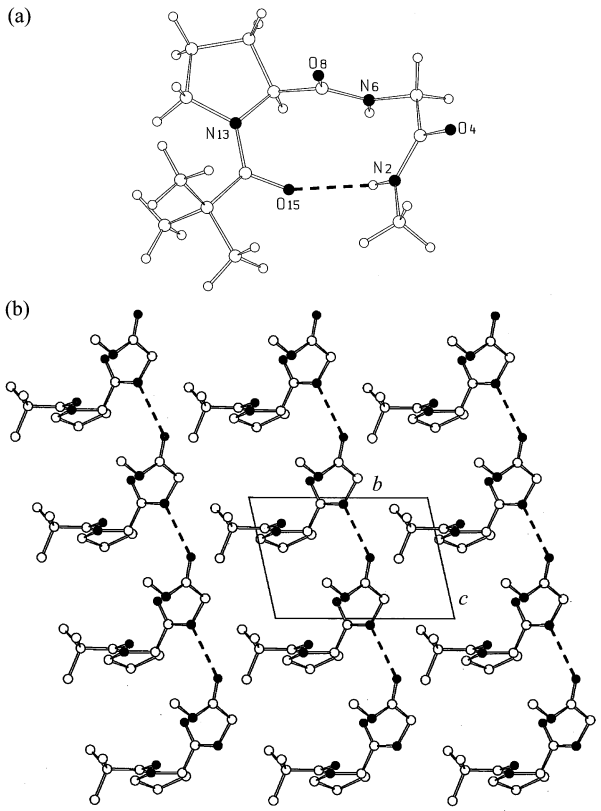

Fig. 2 (a) Molecular geometry of Piv-Pro-Gly-NHMe in the crystal structure, with the intramolecular hydrogen bond shown as a dashed line. (b) Crystal structure of Piv-Pro-Gly-NHMe viewed along the *a*-axis, with N–H···O hydrogen bonds shown as a dashed lines. Hydrogen atoms are omitted for clarity.

may alternatively adopt a Type I β-turn conformation, which is related to the Type II β-turn by a flip of the central peptide unit without disrupting the 4 → 1 hydrogen bond.[5] As shown in Fig. 2b, adjacent molecules in the crystal structure of Piv-Pro-Gly-NHMe are linked along the *c*-axis by intermolecular N–H···O hydrogen bonds (N···O, 2.87 Å; N···O–C, 135.3°).

Our *ab initio* determination of the crystal structure of Piv-Pro-Gly-NHMe from powder X-ray diffraction data has allowed the complete structural characterization of the Type II β-turn conformation as well as the intermolecular interactions in this structure, demonstrating that the direct-space approach for powder structure solution, with the molecular conformation treated as almost completely flexible, is well suited to applications in the field of polypeptides. The potential for applying powder diffraction techniques in this field is clearly important in cases that do not yield single crystals of suitable size and quality for single crystal diffraction studies.

We thank EPSRC, University of Birmingham, Wyeth-Ayerst plc and Ciba Specialty Chemicals for financial support.

Notes and references

1 J. S. Richardson, *Adv. Protein Chem.*, 1981, **34**, 167.
2 G. D. Rose, L. M. Gierasch and J. A. Smith, *Adv. Protein Chem.*, 1985, **37**, 1.
3 C. M. Wilmot and J. M. Thornton, *J. Mol. Biol.*, 1988, **203**, 221.
4 C. Toniolo, *CRC Crit. Rev. Biochem.*, 1980, **9**, 1.
5 K. Gunasekaran, L. Gomathi, C. Ramakrishnan, J. Chandrasekhar and P. Balaram, *J. Mol. Biol.*, 1998, **284**, 1505.
6 A. K. Cheetham and A. P. Wilkinson, *Angew. Chem., Int. Ed. Engl.*, 1992, **31**, 1557.
7 K. D. M. Harris and M. Tremayne, *Chem. Mater.*, 1996, **8**, 2554.
8 D. M. Poojary and A. Clearfield, *Acc. Chem. Res.*, 1997, **30**, 414.
9 A. Meden, *Croat. Chim. Acta*, 1998, **71**, 615.
10 K. D. M. Harris, M. Tremayne and B. M. Kariuki, *Angew. Chem., Int. Ed.*, 2001, **40**, 1626.
11 K. D. M. Harris, M. Tremayne, P. Lightfoot and P. G. Bruce, *J. Am. Chem. Soc.*, 1994, **116**, 3543.
12 B. M. Kariuki, H. Serrano-González, R. L. Johnston and K. D. M. Harris, *Chem. Phys. Lett.*, 1997, **280**, 189.
13 K. D. M. Harris, R. L. Johnston, B. M. Kariuki and M. Tremayne, *J. Chem. Res. (S)*, 1998, 390.
14 K. D. M. Harris, R. L. Johnston and B. M. Kariuki, *Acta Crystallogr. Sect. A*, 1998, **54**, 632.
15 K. D. M. Harris, R. L. Johnston and B. M. Kariuki, *Anal. Quím., Int. Ed.*, 1998, **94**, 410.
16 G. W. Turner, E. Tedesco, K. D. M. Harris, R. L. Johnston and B. M. Kariuki, *Chem. Phys. Lett.*, 2000, **321**, 183.
17 B. M. Kariuki, P. Calcagno, K. D. M. Harris, D. Philp and R. L. Johnston, *Angew. Chem., Int. Ed.*, 1999, **38**, 831.
18 B. M. Kariuki, K. Psallidas, K. D. M. Harris, R. L. Johnston, R. W. Lancaster, S. E. Staniforth and S. M. Cooper, *Chem. Commun.*, 1999, 1677.
19 E. Tedesco, G. W. Turner, K. D. M. Harris, R. L. Johnston and B. M. Kariuki, *Angew. Chem., Int. Ed.*, 2000, **39**, 4488.
20 K. Shankland, W. I. F. David and T. Csoka, *Z. Kristallogr.*, 1997, **212**, 550.
21 K. Shankland, W. I. F. David, T. Csoka and L. McBride, *Int. J. Pharm.*, 1998, **165**, 117.
22 B. N. N. Rao, A. Kumar, H. Balaram, A. Ravi and P. Balaram, *J. Am. Chem. Soc.*, 1983, **105**, 7423.
23 J. W. Visser, *J. Appl. Crystallogr.*, 1969, **2**, 89.
24 G. E. Engel, S. Wilke, O. König, K. D. M. Harris and F. J. J. Leusen, *J. Appl. Crystallogr.*, 1999, **32**, 1169.
25 G. S. Pawley, *J. Appl. Crystallogr.*, 1981, **14**, 357.
26 S. Habershon, K. D. M. Harris, R. L. Johnston, B. M. Kariuki, O. J. Lanning, E. Tedesco and G. W. Turner, *EAGER*, University of Birmingham, 2000 (an extended version of the program *GAPSS*, K. D. M. Harris, R. L. Johnston and B. M. Kariuki, University of Birmingham, 1997).
27 G. Fischer, *Chem. Soc. Rev.*, 2000, **29**, 119.
28 H. M. Rietveld, *J. Appl. Crystallogr.*, 1969, **2**, 65.
29 A. C. Larson and R. B. Von Dreele, Los Alamos Lab. Report No. LA-UR-86-748, 1987.
30 Standard notation is defined in: IUPAC-IUB Commission on Biochemical Nomenclature, *Biochemistry*, 1970, **9**, 3471.
31 P. A. Aubry, J. Protas, G. Boussard and M. Marraud, *Acta Crystallogr. Sect. B*, 1980, **36**, 2822.

CHEMCOMM Communication
www.rsc.org/chemcomm

The first molecular charge transfer salt containing proton channels

Samina Rashid,[a] Scott S. Turner,[a] Peter Day,*[a] Mark E. Light,[b] Michael B. Hursthouse,[b] Steven Firth[c] and Robin J. H. Clark[c]

[a] *Davy Faraday Research Laboratory, The Royal Institution of Great Britain, 21 Albemarle Street, London, UK W1S 4BS. E-mail: pday@ri.ac.uk*
[b] *Department of Chemistry, University of Southampton, Southampton, UK SO17 1BJ*
[c] *Chemistry Department, University College London, 20 Gordon Street, London, UK WC1H 0AJ*

Received (in Cambridge, UK) 30th April 2001, Accepted 27th June 2001
First published as an Advance Article on the web 20th July 2001

We report the first molecular charge transfer salt containing channels of H_3O^+/H_2O within its lattice; it is formulated β″-(BEDT-TTF)$_4$[$(H_3O)Cr(C_2O_4)_3$]$_2$[$(H_3O)_2$(18-crown-6)]·5H_2O [BEDT-TTF = bis(ethylenedithio)tetrathiafulvalene], deduced from the crystal structure and C=C and C–S bond lengths and Raman stretching frequencies.

Molecular charge transfer salts based on organo-chalcogen donors, especially those containing bis(ethylenedithio)tetrathiafulvalene (BEDT-TTF) have provided examples of most of the collective electronic ground states known to condensed matter science, such as semiconductors, metals, superconductors, antiferromagnets, spin-Peierls systems *etc*.[1] Because of their layered structures, in which organic donor cations and inorganic anions are segregated from one another (what we have called 'organic–inorganic composites' or 'chemically constructed multilayers'[2]), they are also a fruitful source of compounds combining two different types of functionality, like paramagnetic superconductors[3] or ferromagnetic metals.[4] However, with one exception,[5] there have been no reports of efforts to combine electronic with ionic conductivity in this class of compound. In that context we now report the first BEDT-TTF salt containing crown ether molecules and both H_3O^+ and H_2O in the lattice, organised in such a way as to suggest the possibility of easy proton migration.

100 mg $(NH_4)_3[Cr(C_2O_4)_3]\cdot 3H_2O$, 200 mg 18-crown-6 ether, and 1 g pyrazine in a mixture of freshly distilled 25 ml of dichloromethane and 25 ml acetonitrile was stirred overnight, and filtered into an electrochemical cell. On applying a current of 1 μA across the cell, crystals first began to appear after 5 days and were harvested after 4 weeks. Two phases were obtained, long thin rectangular needles, whose structure was not resolved, and a small quantity of very thin dark brown plates. The structure of the latter was determined as β″-(BEDT-TTF)$_4$[$Cr(C_2O_4)_3$]$_2\cdot C_{12}O_6H_{24}\cdot 9H_xO$ **1** (where x = 2, 3). Single crystal X-ray diffraction data were collected using an Enraf Nonius Kappa CCD diffractometer mounted at the window of an Mo rotating anode generator with an Oxford Cryosystems N_2 open flow cryostat. The structure was solved by direct methods and refined anisotropically on F^2 using the SHELX97 program. H atoms were placed in idealised positions and refined using a riding model. Raman spectra were measured at room temperature with a Renishaw Ramascope System 1000 microscope equipped with a He–Ne laser (632.8 nm), using a slitwidth of 10 μm and a 10% neutral density filter.

Compound **1** crystallises in the triclinic space group $P\bar{1}$.† The structure consists of alternating layers of BEDT-TTF, and layers comprising $[Cr(C_2O_4)_3]^{3-}$, 18-crown-6 and water molecules. The packing of the layers follows the sequence ABCDABCDA, where A contains only BEDT-TTF, B contains $[Cr(C_2O_4)_3]^{3-}$ in either Δ or Λ configuration and an H_3O^+ molecule, as in the superconducting compound β″-(BEDT-TTF)$_4$[$(H_3O)Cr(C_2O_4)_3$]·PhCN,[6] while layer C contains the 18-crown-6 molecule and the remainder of the H_xO molecules (where x = 2, 3); layer D is a further $[(H_3O)Cr(C_2O_4)_3]^{2-}$ layer with the anions having opposite stereo-configuration to those in the B layer. Fig. 1 shows the packing of the successive layers projected onto the *bc* plane.

The BEDT-TTF molecules are arranged parallel to each other, in the β packing motif. There are two crystallographically independent BEDT-TTF molecules with similar charges of +0.4 ± 0.1 and +0.5 ± 0.1, as estimated from the C=C and C–S bond lengths,[7] which are close to those found in the β"-(BEDT-TTF)$_4$[$(H_3O)M(C_2O_4)_3$]·solv superconductors (solv being a solvent molecule). Since the $[Cr(C_2O_4)_3]^{3-}$ ions contribute a total charge of −6, this implies that four of the H_xO molecules must be H_3O^+ to maintain charge neutrality. By analogy with the superconductors two of these may be located in layers B and D. The terminal CH_2–CH_2 groups of the BEDT-TTF are both twisted, with one of the C atoms above the plane of the TTF

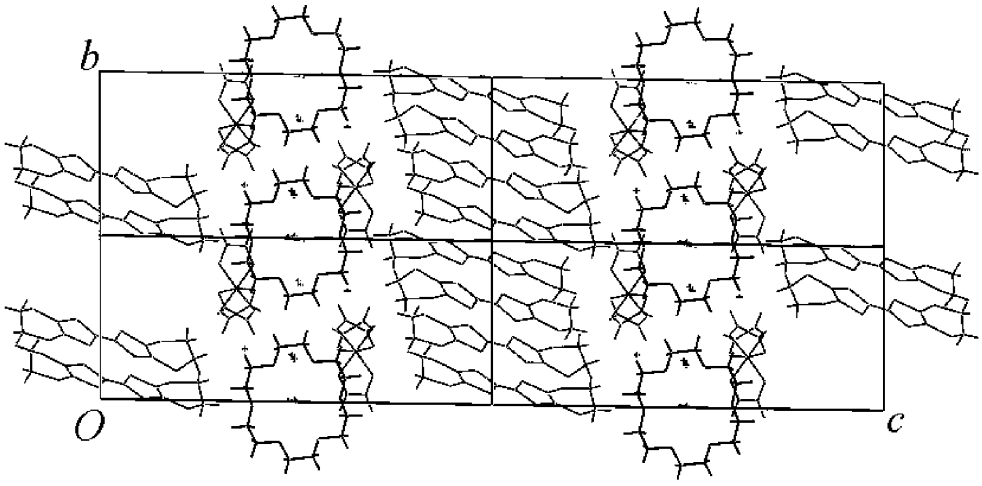

Fig. 1 The crystal structure of **1** showing the overall packing of the cationic and anionic layers.

 DOI: 10.1039/b103877j

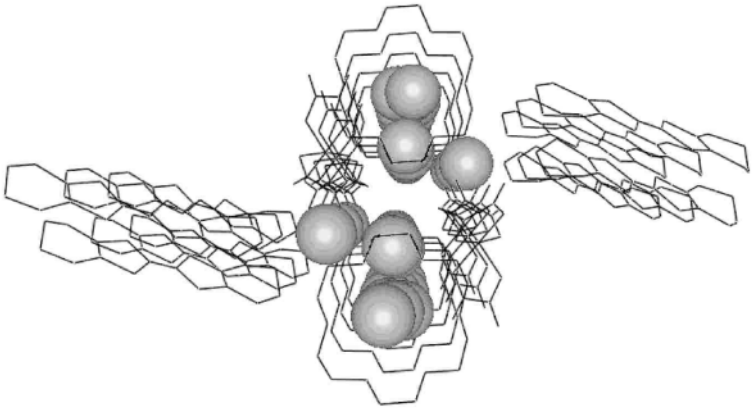

Fig. 2 The crystal structure of **1** showing the channels formed by the 18-crown-6 molecules and H_3O^+/H_2O.

moiety and the other below, but eclipsed with respect to the other end of the donor molecule. The two shortest S···S contacts between the crystallographically independent BEDT-TTF molecules average to 3.70 Å, although these are longer than the S···S van der Waals distance of 3.6 Å. The torsion angles of the CH_2–CH_2 groups of the BEDT-TTF indicate that one of the groups on one of the molecules is under more strain than the others, and the thermal ellipsoids show that this CH_2–CH_2 group is disordered. In fact it is the one located directly next to the Cr^{3+} centre of a tris(oxalato)Cr(III) ion. The other CH_2–CH_2 group, which has a more normal conformation, is closest to the 18-crown-6 ether.

Fig. 1 shows that, in contrast to the superconducting β″-BEDT-TTF tris(oxalato)metallate(III) salts,[8] the anion layer in **1** is almost as thick as two $[Cr(C_2O_4)_3]^{3-}$ and a molecule of 18-crown-6 ether. The latter separates the Δ and Λ forms of $[Cr(C_2O_4)_3]^{3-}$, between each of which there is one H_3O^+ cation, as in the superconducting phases. Thus there are two $[(H_3O)Cr(C_2O_4)_3]^{2-}$ layers, with crown ether and H_xO layers between them. One water molecule resides within each molecule of crown ether, the other forming a H-bonded chain to the next crown ether molecule along the *a* axis. The O···O contacts between these four water molecules are 1.84, 1.97 and 1.47 Å, the latter appearing short because one of the O atoms is disordered over two sites. In this way the 18-crown-6 ether molecules form an ion channel within the inorganic layer, as shown in Fig. 2. In this figure the O atoms of H_3O^+/H_2O are emphasised in space filling format, those on either side of the central chains being the H_3O^+ that form part of the $[(H_3O)Cr(C_2O_4)_3]^{2-}$ layers.

The Raman spectrum of **1** contains two peaks in the region of the totally symmetrical C=C vibrations at 1492 ± 2 and 1467 ± 2 cm^{-1} corresponding to ν_3 and ν_4 of BEDT-TTF. From the established correlation between stretching frequency and cation charge,[9] charges of +0.54 and +0.46 are indicated, in close agreement with the charges indicated by the BEDT-TTF bond lengths in the crystal structure. On the assumption that the two anion layers B and D are formulated as $[(H_3O)Cr(C_2O_4)_3]^{2-}$ as in the superconducting phases, charge neutrality requires that two of the remaining seven H_xO in the formula unit must be H_3O^+, the remaining five being H_2O. In the absence of evidence to the contrary, it can be assumed that the two H_3O^+ correspond to the water molecules closest to the rings of the crown ether molecules, with the remaining H_2O forming a H-bonded channel between neighbouring crown ether rings as described above.

In conclusion, we have found a new kind of organic–inorganic layer architecture in a molecular charge transfer salt, in which layers of $BEDT\text{-}TTF^{0.5+}$ with the classical β″-stacking arrangement, are interleaved with two layers of $[(H_3O)Cr(C_2O_4)_3]^{2-}$ honeycomb layers. The latter have the same topology as in the paramagnetic superconductors β″-$(BEDT\text{-}TTF)_4[(H_3O)M(C_2O_4)_3]\cdot solv$[2,6,8,10] but in the present case, instead of alternate anion layers consisting exclusively either of Δ or Λ-$[Cr(C_2O_4)_3]^{3-}$ separated by BEDT-TTF layers, we find alternate $[(H_3O)Cr(C_2O_4)_3]^{2-}$, again with exclusively Δ or Λ stereo-configurations, but separated by crown ether/H_3O^+/H_2O layers. The present small size and fragility of the crystals has inhibited detailed variable temperature transport measurements. However, a preliminary two-probe room temperature measurement gave a conductivity of 0.95 S cm^{-1} parallel to the plate long axis, which is in the range expected for a semiconductor. We could expect that four-probe measurements, where the contact resistances are discounted, would be higher and even metallic in nature like other β″-BEDT-TTF salts. Therefore, the possibility exists to combine both electronic and ionic conductivity in a molecular lattice which is important in fields as diverse as solid-state batteries[11] and electroluminescent displays.[12]

This work has been supported by the U.K. Engineering and Physical Sciences Research Council and the European Commission TMR Network on Molecular Magnets.

Notes and references

† *Crystal data*: β″-$(BEDT\text{-}TTF)_4[Cr(C_2O_4)_3]_2\cdot C_{12}H_{24}O_6\cdot 9H_xO$ (x = 2 or 3) $C_{32}H_{33}CrO_{19}S_{16}$, M = 1289.50, triclinic, space group $P\bar{1}$, a = 10.2212(5), b = 11.2266(5), c = 20.0998(15) Å, α = 88.433(3), β = 88.391(2), γ = 63.780(3)°, V = 2479.6(2) Å^3, T = 150 K, Z = 2; λ (Mo-Kα) = 0.71073 Å μ = 0.973 mm^{-1}, reflections collected 19985, independent reflections 8722, final R indices [$F^2 > 2\sigma(F^2)$]: R_1 = 0.0605, wR_2 = 0.1222.

CCDC reference number 166475. See http://www.rsc.org/suppdata/cc/b1/b103877j/ for crystallograpic data in CIF or other electronic format.

1 P. Day and M. Kurmoo, *J. Mater. Chem.*, 1997, **7**, 1291.
2 P. Day, *Philos. Trans. R. Soc. London A*, 1985, **314**, 145.
3 M. Kurmoo, A. W. Graham, P. Day, S. J. Coles, M. B. Hursthouse, J. L. Caulfield, J. Singleton, F. L. Pratt, W. Hayes, L. Ducasse and P. Guionneau, *J. Am. Chem. Soc.*, 1995, **117**, 12 209.
4 E. Coronado, J. R. Galan-Mascaros, C. J. Gomez-Garcia and V. Laukhin, *Nature*, 2000, **408**, 447.
5 T. Nakamura, T. Akutagawa, K. Honda, A. E. Underhill, A. Treeve Coomber and R. H. Friend, *Nature*, 1998, **394**, 159.
6 L. Martin, S. S. Turner, P. Day, F. E. Mabbs and E. J. L. McInnes, *Chem. Commun.*, 1997, 1367.
7 P. Guionneau, C. J. Kepert, D. Chasseau, M. R. Truter and P. Day, *Synth. Met.*, 1997, **86**, 1973.
8 L. Martin, S. S. Turner, P. Day, P. Guionneau, J. A. K. Howard, K. M. A. Malik, M. B. Hursthouse, M. Uruichi and K. Yakushi, *Inorg. Chem.*, in press.
9 H. H. Wang, J. R. Ferraro, J. M. Williams, V. Geiser and J. A. Schlueter, *J. Chem. Soc., Chem. Commun.*, 1994, 1893.
10 S. Rashid, S. S. Turner, P. Day, J. A. K. Howard, P. Guionneau, E. J. L. McInnes, F. E. Mabbs, R. J. H. Clark, S. Firth and T. Biggs, *J. Mater. Chem.*, in press.
11 D. Fauteux, A. Massucco, M. Mclin, M. Vanburen and J. Shi, *Electrochim. Acta.*, 1995, **40**, 2185.
12 Q. Pei, G. Yu, C. Zhang, TY. Yang and A. Heeger, *Science*, 1995, **269**, 1086.

CHEMCOMM Communication
www.rsc.org/chemcomm

DNA recognition by the first *tail-to-tail* linked distamycin-like oligopeptide dimers†

Santanu Bhattacharya*‡ and Mini Thomas

Department of Organic Chemistry, Indian Institute of Science, Bangalore, India-560 012. E-mail: sb@orgchem.iisc.ernet.in; Fax: +91-80-360-0529

Received (in Cambridge, UK) 1st February 2001, Accepted 24th May 2001
First published as an Advance Article on the web 20th July 2001

Sequence-specific bidentate binding to double-stranded (*ds*)-DNA by '*tail-to-tail*' linked dimeric distamycin analogues is described; compared to their monomeric analogues, these dimers exhibit greater affinity and longer binding site size and open up a novel avenue in the design of minor groove binders that overcome the phasing problem.

Design of molecules with low molecular mass (M_w *ca.* 10^3) that bind with high affinity and specificity to pre-determined DNA sequences that are 10–16 base pairs long is a key issue in chemical biology. For instance, a unique site within the 3 billion base pair human genome is defined by a minimum of 15–16 contiguous base pairs.[1] Natural products such as distamycin and netropsin which exert their biological activity by competing with the TATA box binding protein (TBP) for the target site on DNA serve as the 'lead compounds' for the design of such 'lexitropsins' (information reading oligopeptides).[2] Some of the compounds developed on the basis of these principles have indeed exhibited interesting biological properties.[3]

Distamycin (Dst)-type polyamides with $(n - 1)$ *N*-methylpyrrole rings and n amide groups bind preferentially to the minor groove sites containing $(n + 1)$ successive AT base pairs of *ds*-DNA. The repeating *N*-methylpyrrole-2-carboxamide unit, however, is ~20% longer than is required to match the base pair rise along the minor groove of the DNA helix. As a result longer polyamides ($n > 6$) are out of phase with DNA.[4,5] An over-wound curvature of longer polyamides is an added disadvantage. These factors result in a sub-optimal contact between DNA and the ligand leading to the manifestation of lower binding affinities. To reset an optimum fit of long polyamides with the DNA double-helix, flexible β-alanine or glycine residues have in fact been inserted.[4]

In an alternative strategy, two netropsin-like or distamycin-like cationic peptides have been connected in a 'head-to-head' (*N*-terminus-to-*N*-terminus) fashion using flexible or rigid linkers.[5] These bis(lexitropsins) were shown to adopt monodentate or bidentate modes of DNA binding depending upon the nature of the linker unit. Importantly those bound to DNA in a dimeric fashion also exhibited higher affinities.[1,6]

† Dedicated to the memory of Dr D. Ranganathan.

‡ Corresponding author and Swannajayanti Fellow (DST, Government of India); also at the Chemical Biology Unit, JNCASR, Bangalore 560012, India.

Herein we report a new approach to the design of dimeric lexitropsins such that optimum contacts between the successive amide units and the DNA helix are allowed. The following notable features characterize the present design. Firstly the dimers were constructed by linking the C-terminus of the individual monomers ('*tail-to-tail*' linkage). Secondly the positive charge necessary for optimizing the DNA affinity and water solubility is provided by the presence of a tertiary amine based linker which remains protonated at physiological pH.§ Significantly, these tail-to-tail linked *bis-Dst*s (**3**–**5**) bear only a single positive charge unlike the previously reported 'head-to-head' linked dimers which carry two positive charges. These bis-Dsts also lack the leading formamide unit at the *N*-termini.[7]

DNA binding abilities of the Dsts [**1**(**D3**) and **2**(**D4**)] and the corresponding bis-Dsts [**3**(**D33**), **4**(**D34**) and **5**(**D44**)] were examined for their ability to modify duplex DNA helix-to-coil transition temperature (T_m), induced circular dichroism (ICD) measurements, salt-dependence of ICD and fluorescence probe displacement assay.

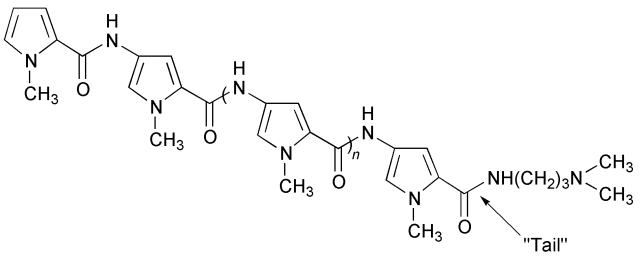

1: n = 0 (**D3**); **2**: n = 1 (**D4**)

Dst and related minor groove binders are known to enhance the T_m of *ds*-DNA. This has been attributed to the stabilization of the double-helix.[8] Table 1 summarizes the results of the T_m measurements of DNA with the dimers **D33**, **D34** and **D44** along with those for the corresponding monomers, **D3** and **D4**. The ΔT_m is higher in the case of poly d(A.T) compared to calf thymus DNA (CT DNA, ~50% AT rich) indicating that these bis-Dsts have retained the AT-specific mode of DNA binding. The ΔT_m values are significantly higher for the complexes of the bis-Dsts compared to those of the corresponding monomers. This is notable, since the positive charge is not 'doubled' for the dimers compared with the monomers. The observed enhance-

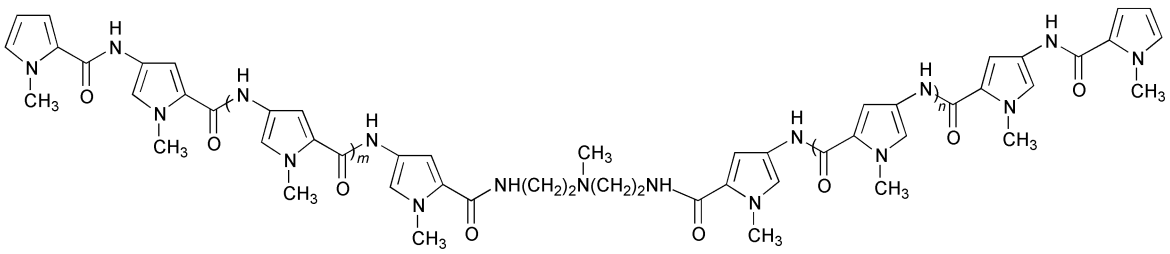

3: m = 0, n = 0 (**D33**); **4**: m = 0, n = 1 (**D34**); **5**: m = 1; n = 1 (**D44**)

 DOI: 10.1039/b101105g

Table 1 Summary of melting temperature measurements[a]

Oligopeptide	ΔT_m/°C	
	Poly d(A.T)	CT-DNA
D3	0.5	0
D4	11.0	1.6
D33	12.5	1.6
D34	21.5	5.0
D44	27.5	6.5

[a] 40 mM NaCl, 10 mM Tris·HCl (pH = 7.4), [D]/[P] = 0.2.

ment in T_m could be entirely due to specific H-bonding and van der Waals interactions. The ΔT_m was also found to increase as a function of the length of the oligopeptides. For instance, the $\Delta(\Delta T_m)$ between the complexes of **D34** and **D33** with poly d(A.T) was ~9 °C and that between the complexes of **D44** and **D34** was ~6 °C. These results would be possible only if both the 'arms' of the dimeric distamycins are in contact with *ds*-DNA implying the effectiveness of the bidentate mode of binding.

The induced Cotton effect (ICD) produced at 25 °C upon the binding of Dst and its analogues to DNA that appear in the 280–380 nm region is distinct from the intrinsic CD spectrum of DNA.[8] The intensity of the ICD signal is proportional to the strength of binding and also on the number of the *N*-methylpyrrolecarboxamide units present in the oligopeptides. All the three bis-Dsts produced intense ICD signals upon binding to poly d(A.T) and CT-DNA (not shown). The ICD was higher in the case of poly d(A.T) compared to CT-DNA and the ICD intensity increased in the order **D33** < **D34** < **D44**.

Monotonous increase was observed in the ICD signal with [ligand] until saturation at [D]/[P] ratios {ratio of [ligand] *vs.* [DNA] (in base molarity)} characteristic of each ligand/duplex type. Importantly, a single set of isodichroic points was seen in each case (not shown) implying the existence of equilibrium between the bound and the free forms of the ligand. Molar ellipticity (θ) observed in the case of the dimers was found to be at least twice as high as that for the monomers. Taken together these results suggest that both the 'arms' of the dimeric Dsts bind to DNA at all [D]/[P] ratios.

Salt-induced complex dissociation experiments are often used for comparing the relative binding affinities of ligands towards DNA.[8] The higher the binding affinity, the lower should be the complex dissociation with increasing salt concentration. Plots of the relative intensities of the positive ICD bands at the respective ICD λ_{max} as a function of [NaCl] are presented in Fig. 1. It is seen that the ICD spectra of the bis-Dsts are less susceptible to high [NaCl] compared to their respective monomers. The most dramatic difference was observed in the case of **D33**. These results clearly show that the dimers bind to AT-rich DNA stronger than their monomeric

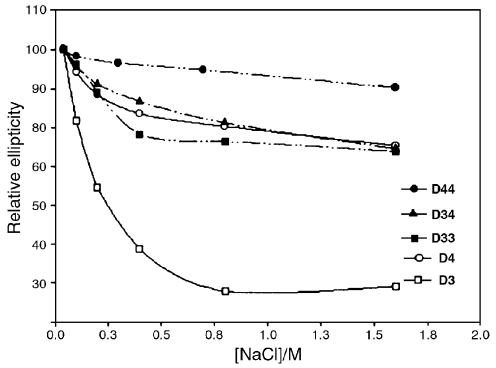

Fig. 1 Effect of NaCl on the ICD spectra of the complexes of **D33**, **D34**, **D44** and the monomers **D3** and **D4**.

counterparts, which would be possible only if the bidentate mode of binding is operational.

The binding site sizes of **1–5** were assessed from the saturation [D]/[P] values obtained from the CD titration plots. It was inferred that during DNA binding, each of the dimer arms overlap in a head-to-tail dimeric fashion with an equivalent arm from two neighboring dimers that lie on either side. The above arrangement is repeated throughout the DNA leading to 'multimeric' arrangement on the polymer. The *actual* number of bp covered by individual molecules of **3–5** may be assumed to be *ca*. 8–10 bp.

Finally, to estimate the relative binding constants (K_{app}) of these bis-Dsts and the corresponding monomers we also studied the competition between compounds **D3**, **D4**, **D33**, **D34**, **D44** and the well known AT specific DNA minor groove binder Hoechst-33258 for binding sites on poly d(A.T).[9] Displacement of Hoechst from poly d(A.T) was accompanied by a decrease in the fluorescence intensity measured at 460 nM (λ_{ex} = 355 nm). The apparent binding constants (K_{app}) were calculated from the concentration of the compounds required for 50% quenching of Hoechst fluorescence and the known values of [Hoechst] and binding constant[9] {[Hoechst-33258] = 230.4 nM, [poly d(AT)] = 4.6×10^{-6} M, $K_a = 5 \times 10^7$ M^{-1} (base molarity), 50 mM Tris·HCl buffer containing 100 mM NaCl)}. The K_{app} values for **D3**, **D4**, **D33**, **D34** and **D44** calculated this way were 6×10^5, 9.3×10^6, 2.0×10^7, 4.1×10^7 and 4.9×10^7 M^{-1} respectively. The highest enhancement in K_{app} compared to the corresponding monomer was observed in the case of **D33** (33-fold). The value of K_{app} for **D44** was 5 times that for the corresponding monomer **D4**.

In summary the present systems, which represent the first examples of 'tail-to-tail' linked dimeric lexitropsins, form a novel class of minor groove binders that bind to *ds*-DNA in a bidentate fashion and exhibit significantly greater affinity for *ds*-DNA compared to the respective monomers. These bind poly d(A.T) in a nearly 2:1 overlapped fashion and individual molecules seem to cover 8–10 bp and provide a significant step forward in the design of minor groove binders towards overcoming the phasing problem.

Notes and references

§ All the compounds were characterized by FT-IR, ^{1}H-NMR, and mass spectroscopy.

1 P. B. Dervan, *Science*, 1986, **232**, 464.
2 P. B. Dervan and R. W. Burli, *Curr. Opin. Chem. Biol.*, 1999, **3**, 688; C. Bailly and J. B. Chaires, *Bioconjugate Chem.*, 1998, **9**, 513.
3 T. C. Bruice, H.-H. Mei, G.-X. He and V. Lopez, *Proc. Natl. Acad. Sci. USA*, 1992, **89**, 1700; M. E. Filipovsky, M. L. Kopa, M.-B. Zion, J. W. Lown and R. E. Dickerson, *Biochemistry*, 1996, **35**, 1539; A. K. Mapp, A. Z. Ansari, M. Ptashne and P. B. Dervan, *Proc. Natl. Acad. Sci. USA*, 2000, **95**, 3930.
4 B. H. Geierstanger, M. Mrksich, P. B. Dervan and D. E. Wemmer, *Nat. Struct. Biol.*, 1996, **3**, 321.
5 G. Burckhardt, H. Simon, K. Strol, H. Triebel, A. Walter, J. W. Lown and C. Zimmer, *J. Biomol. Struct. Dyn.*, 1997, **15**, 81; A. I. Kalaf, A. R. Pitt, M. Scobie, C. J. Suckling, J. Urwin, R. D. Waigh, R. V. Fishleigh, S. C. Young and W. A. Wylie, *Tetrahedron*, 2000, **56**, 5225.
6 A. N. Surovaya, G. Burckardt. S. L. Grokhovsky. E. Birch-Hirschfeld, G. V. Gursky and C. Zimmer, *J. Biomol. Struct. Dyn.*, 1997, **14**, 595; N. Boitte. N. Pommey, P. Colson, C. Houssier, M. J. Waring, J. P. Henichart and C. Bailly, *Anti-Cancer Drug Des.*, 1997, **12**, 481.
7 S. Bhattacharya and M. Thomas, *Tetrahedron. Lett.*, 2000, **41**, 5571; S. Bhattacharya and M. Thomas, *Biochem. Biophys. Res. Commun.*, 2000, **267**, 139.
8 G. Buchardt, Ch. Zimmer and B. Baguley, *J. Biomol. Struct. Dyn.*, 1987, **4**, 814; C. Zimmer, G. Luck, H. Thrum and C. Pitra, *Eur. J. Biochem.*, 1972, **26**, 81; G. Luck, C. Zimmer, K.-E. Reinert and F. Arcamone, *Nucleic Acids Res.*, 1977, **4**, 2655.
9 F. G. Loontiens, P. Regenfuss, A. Zechel, L. Dumortier and R. M. Clegg, *Biochemistry*, 1990, **29**, 9029; K. A. Browne, G.-X. He and T. C. Bruice, *J. Am. Chem. Soc.*, 1993, **115**, 7072.

CHEMCOMM Communication
www.rsc.org/chemcomm

New room-temperature ionic liquids with C_2-symmetrical imidazolium cations†

Sergei V. Dzyuba and Richard A. Bartsch*

Department of Chemistry and Biochemistry, Texas Tech University, Lubbock, Texas 79409-1061, USA. E-mail: richard.bartsch@ttu.edu; Fax: +1(806) 742 1289; Tel: +1(806) 742 3069

Received (in Corvallis, OR, USA) 16th May 2001, Accepted 18th June 2001
First published as an Advance Article on the web 23rd July 2001

New 1,3-dialkylimidazolium hexafluorophosphates with two butyl, pentyl, octyl, nonyl or decyl groups are room temperature ionic liquids.

Room-temperature ionic liquids (RTILs),[1] such as 1-alkyl-3-methylimidazolium hexafluorophosphates, are finding ever-expanding applications as alternative reaction media for organic synthesis[2,3] and separation science.[4–6] Although our understanding of why these salts have such low melting points is incomplete, the unsymmetrical nature of the cation is believed to play a major role.[1,7] Thus, the 100 °C lower melting points of 1-ethyl-3-methylimidazolium salts than their *N*-butylpyridinium analogues have been attributed to the C_2 symmetry of the latter.[1]

By extension of such reasoning, 1,3-dialkylimidazolium salts that also have C_2 symmetry would seem to be poor candidates as RTILs. In agreement, 1,3-dialkylimidazolium hexafluorophosphates are reported to be solids at room temperature when the two alkyl groups are hexadecyl.[8] The salts with elongated alkyl groups are of interest because they exhibit liquid crystalline behavior above their melting points.[8,9]

We now report the synthesis of ten 1,3-dialkylimidazolium hexafluorophosphates $[(C_n)_2\text{-Im}]PF_6$ with dialkyl moieties ranging from dimethyl to didecyl and their phase transition behavior. Surprisingly, 1,3-dialkylimidazolium hexafluorophosphates with dibutyl, dipentyl, dioctyl, dinonyl, and didecyl substituents are found to be RTILs.

The $[(C_1)_2\text{-Im}]PF_6$ was prepared by reaction of commercially available 1-methylimidazole with iodomethane to form $[(C_1)_2\text{-Im}]I$[10] followed by its metathesis with potassium hexafluorophosphate in water.‡ Since higher homologues of 1-methylimidazole are not available commercially, a method was sought to convert imidazole directly into a 1,3-dialkylimidazolium halide. (Reported methods for the preparation of 1,3-dialkylimidazolium halides require multiple steps, long reactions times, and/or special precautions.[8,9,11,12]) We have found that reaction of imidazole with one equivalent of sodium hydride in THF followed by addition of two equivalents of a 1-bromoalkane and refluxing (Scheme 1) gives high yields (75–89%) of $[(C_n)_2\text{-Im}]Br$ with n = 2–10. Metathesis of the imidazolium bromide salts with potassium hexafluorophosphate in water gave high yields (89–95%) of $[(C_n)_2\text{-Im}]PF_6$ with n = 2–10.†‡

The phase transition temperatures (mid-points of glass transitions and/or melting points) for $[(C_n)_2\text{-Im}]PF_6$ with n = 1–10 as determined by differential scanning calorimetry (DSC)§ are presented in Table 1. As the alkyl groups are changed from methyl to ethyl to propyl, the melting point drops from 89 to 70 to 43 °C. This suggests poorer packing into the crystal lattice as the alkyl group is elongated. With dibutyl and dipentyl substituents, the salts are RTILs with glass transitions, but no melting points. In sharp contrast when the alkyl groups are elongated to hexyl, a melting point of 73 °C, but no glass transition, is observed. There is a remarkable, greater than 140 °C difference between the phase transition temperatures for $[(C_5)_2\text{-Im}]PF_6$ and $[(C_6)_2\text{-Im}]PF_6$. Apparently the hexyl groups pack into the crystal lattice almost as well as methyl and ethyl groups. As the alkyl groups are lengthened from hexyl to heptyl, the 73 °C melting point for the former diminishes to 47 °C. For octyl and nonyl groups, both glass transitions and melting points are observed. When the alkyl groups are decyl, there are two melting points. Since their melting points are below room temperature, $[(C_8)_2\text{-Im}]PF_6$, $[(C_9)_2\text{-Im}]PF_6$, and $[(C_{10})_2\text{-Im}]PF_6$ are also RTILs. Studies are currently underway to compare the other physical properties of these readily accessible $[(C_n)_2\text{-Im}]PF_6$ RTILs with the more common 1-alkyl-3-methylimidazolium hexafluorophosphates.

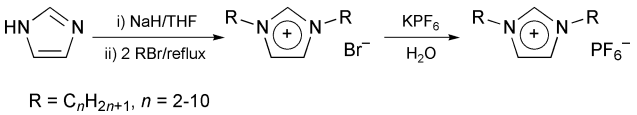

R = C_nH_{2n+1}, n = 2-10

Scheme 1 Synthesis of 1,3-dialkylimidazolium bromides and hexafluorophosphates.

Table 1 Structure and phase transition temperatures of 1,3-dialkyimidazolium ionic liquids

IL	Alkyl group	Phase transition temperature T/°C (ΔC_p/J g^{-1} K^{-1})	Phase transition temperature T_m/°C (ΔH/kJ mol^{-1})
1	CH_3	—	89 (6.8)
2	C_2H_5	—	70 (6.6)
3	C_3H_7	—	43 (6.3)
4	C_4H_9	−69 (0.3)	—
5	C_5H_{11}	−72 (0.2)	—
6	C_6H_{13}	—	73 (8.8)
7	C_7H_{15}	—	47 (5.2)
8	C_8H_{17}	−80 (0.2)	19 (5.2)
9	C_9H_{19}	−70 (0.2)	11 (5.4)
10	$C_{10}H_{21}$	—	−27 (0.4) 16 (6.7)

We thank the Texas Advanced Research Program for support of this research under Grant No. 003644-0395-1999, Professor Dominick J. Casadonte, Jr. for sharing the DSC equipment, and Professor Sindee L. Simon for helpful discussions.

Notes and references

† Electronic supplementary information (ESI) available: ^{1}H NMR and IR spectra and elemental analysis results consistent with the indicated structures for all of the $[(C_n)_2\text{-Im}]Br$ and $[(C_n)_2\text{-Im}]PF_6$ compounds. See http://www.rsc.org/suppdata/cc/b1/b104512c/

‡ Representative procedures for the preparation of $[(C_n)_2\text{-Im}]Br$ and $[(C_n)_2\text{-Im}]PF_6$. *Synthesis of 1,3-dinonylimidazolium bromide*. A flask containing a magnetically stirred mixture of 95% sodium hydride powder (0.75 g, 29.4 mmol) in THF (20 ml) was cooled in an ice bath and a solution of imidazole (2.00 g, 29.4 mmol) in THF (20 ml) was added dropwise. The ice bath was removed and the mixture was stirred for 2 h at room temperature. Following dropwise addition of 1-bromononane (11.23 ml, 58.8 mmol) at room temperature, the mixture was refluxed for 7 h and filtered. The precipitate was thoroughly rinsed with THF. The filtrate was evaporated *in vacuo* and the residue was dissolved in dichloromethane. The mixture was filtered and the filtrate was evaporated *in vacuo*. The residue was rinsed with diethyl ether (20 ml) and dried *in vacuo* to give 10.40 g (82% yield) of the product as a waxy-like solid. *Synthesis of 1,3-dinonylimidazolium hexafluor-*

 DOI: 10.1039/b104512c

ophosphate. To a magnetically stirred solution of the imidazolium bromide prepared above (1.17 g, 3.69 mmol) in water (20 ml) was added potassium hexafluorophosphate (0.68 g, 3.39 mmol). After 30 min, the lower ionic liquid layer was separated and dissolved in dichloromethane (20 ml). The dichloromethane solution was washed with water (2 × 40 mL) and evaporated *in vacuo*. Benzene was added to the residue and the solution was dried using a Dean–Stark apparatus. After removal of the benzene *in vacuo*, the residue was dried *in vacuo* (0.5 Torr) at 100 °C overnight to give 1.27 g (90%) of $[(C_9)_2\text{-Im}]PF_6$.

For the synthesis of $[(C_2)_2\text{-Im}]Br$ and $[(C_3)_2\text{-Im}]Br$, 3.0 and 1.5 molar excess of ethyl bromide and propyl bromide were used, respectively.

§ Phase transition measurements. A Shimadzu DSC-50 differential scanning calorimeter with a LTC low temperature assembly was utilized. The sample (5–25 mg), that had been stored at room temperature before analysis, was sealed in an aluminum pan under air and cooled to about −130 °C by pouring liquid nitrogen into the LTC unit under helium (30 ml min^{-1}). Cooling to this temperature usually took 20–25 min. As soon as all of the liquid nitrogen had evaporated from the LTC unit and the temperature started to rise spontaneously, heating was initiated at 30 °C min^{-1}. Heating was continued to 70 °C for liquid samples and to 130 °C for solid samples.

1 K. R. Seddon, *J. Chem. Technol. Biotechnol.*, 1997, **68**, 351.
2 T. Welton, *Chem. Rev.*, 1999, **99**, 2071.
3 P. Wasserscheid and W. Keim, *Angew. Chem., Int. Ed.*, 2000, **39**, 3772.
4 J. G. Huddleston, H. D. Willauer, R. P. Swatloski, A. E. Visser and R. D. Rogers, *Chem. Commun.*, 1998, 1765.
5 L. Blanchard, D. Nancu, E. J. Bechman and J. F. Brennecke, *Nature*, 1999, **399**, 28.
6 A. E. Visser, R. P. Swatloski, W. M. Reichert, S. T. Griffin and R. D. Rogers, *Ind. Eng. Chem. Res.*, 2000, **39**, 3596.
7 A. S. Larsen, J. D. Holbrey, F. S. Tham and C. A. Reed, *J. Am. Chem. Soc.*, 2000, **122**, 7264.
8 K. M. Lee, C. K. Lee and I. J. B. Lin, *Chem. Commun.*, 1997, 899.
9 C. M. Gordon, J. D. Holbrey, A. R. Kennedy and K. R. Seddon, *J. Mater. Chem.*, 1998, **8**, 2627.
10 B. K. M. Chan, H.-H. Chang and M. R. Grimmett, *Aust. J. Chem.*, 1977, **30**, 2005.
11 K. J. Harlow, A. F. Hill and T. Welton, *Synthesis*, 1996, 697.
12 A. J. Arduengo, III, R. Krafczyk, R. Schmutzler, H. A. Craig, J. R. Goerlich, W. J. Marshall and M. Unverzagt, *Tetrahedron*, 1999, **55**, 14 523.

CHEMCOMM Communication
www.rsc.org/chemcomm

Phase-transfer catalyst separation and re-use by solvent resistant nanofiltration membranes†

Satinder S. Luthra,*[a] Xiaojin Yang,[a] Luisa M. Freitas dos Santos,[b] Lloyd S White[c] and Andrew G. Livingston[a]

[a] *Department of Chemical Engineering and Chemical Technology, Imperial College of Science, Technology and Medicine, University of London, UK, SW7 2BY, E-mail: satinder.Luthra@ic.ac.uk*
[b] *GlaxoSmithKline, Old Powder Mills, Leigh, Tonbridge, Kent, UK, TN11 9AN*
[c] *W.R. Grace & Co.-Conn., 7500 Grace Drive, Columbia, Maryland 21044, USA*

Received (in Cambridge, UK) 24th April 2001, Accepted 15th June 2001
First published as an Advance Article on the web 23rd July 2001

This communication describes the use of nanofiltration (NF) membranes for efficient separation and recycling of phase-transfer catalysts, using the conversion of bromoheptane into iodoheptane with tetraoctylammonium bromide as the PT catalyst, as an example; a solvent flux of > 10 L m^{-2} h^{-1} was achieved with > 99% catalyst recycle and no loss in PT catalyst activity over a cycle of three consecutive reactions.

Phase-transfer (PT) catalysis, introduced by Starks,[1] is an alternative to the use of polar aprotic solvents (DMF, DMSO) for reactions involving a water-soluble nucleophilic reagent and an organic soluble electrophilic reagent (*e.g.* anions and organic substrates). However, one of the major technical problems inhibiting the use of phase-transfer catalysis in industrial applications is the need to separate the product and the phase-transfer catalyst.[2]

NF is a relatively new membrane process with a nominal molecular weight cut-off[3] (MWCO) in the range from 200–1000 Da. Recently NF membranes capable of performing separations in organic solvents have become available.[4] The molecular weight of many phase-transfer catalyts is in the range of 300–1000 Da. Therefore, it is of interest to investigate the potential application of NF membranes to separation of lipophilic phase-transfer catalysts from reaction mixtures, and subsequent recycling of the catalysts. We demonstrate the successful recycle and re-use of a catalyst in consecutive reactions using a solvent resistant NF membrane.

The model phase-transfer catalytic reaction employed in this study is given in eqn. (1), where PTC stands for phase-transfer

$$Br - C_7H_{15org} + KI_{aq} \xrightarrow{PTC} I - C_7H_{15org} + KBr_{aq} \quad (1)$$

catalyst. The model reaction involves the conversion of bromoheptane into iodoheptane using an aqueous phase containing potassium iodide[5] and is a classic example of a nucleophilic, aliphatic substitution reaction. Toluene, a common solvent in industry and a typical solvent used in phase-transfer catalysis, was used as the organic solvent. The PTC used was tetraoctylammonium bromide (TOABr). At the conclusion of the reaction, the lipophilic TOABr and the iodoheptane product both partition entirely into the organic phase.

Firstly, separation of PTC from a synthetic 'post-reaction' solution containing 0.1 M bromoheptane, 0.1 M iodoheptane and 0.01 M TOABr in toluene was studied using two polyimide solvent resistant NF membranes (142A and 142C, nominal MWCO of 220 and 400 Da respectively; W. R. Grace, USA).[6] The retention of the PTC, and the passage of the product molecule through the membrane, is necessary in order for the separation of product and catalyst to occur. Results are summarised in Table 1 and show that any residual reactant and the product pass through both membranes, which retain the catalyst for re-use. The 20–22% rejection[7] of reactant and product by 142A does not constitute a significant fraction of product being retained, and so 142A was chosen for further experiments involving repeated reactions. The flux in the presence of the reaction mixture is lower than for pure toluene, suggesting some degree of membrane fouling.

Two series of reactions were carried out, which differed only in the details of the process used to separate and recycle the PTC. In Case 1[8] a new membrane disc was used for each separation. In Case 2,[9] the same membrane disc was used for the series of separations. This latter procedure, with multiple membrane use, mimics more closely the likely procedure which would be used industrially. The time profiles for reactant (bromoheptane) and product (iodoheptane) during the Case 1 series of reactions, is shown in Fig. 1. After 5 h at 50 °C, with vigorous stirring, the yield was 97%. The phases were then separated, and the organic phase was filtered using 142A. After 35 mL of the original 40 mL of organic liquid had passed through the membrane, the residual 5 mL containing the PTC was recycled to the next reaction.

At the conclusion of the second reaction, this cycle was repeated, giving a total of three reactions and three catalyst separations. With pleasure we observed that the conversions of bromoheptane after 5 h in the second and third reactions were 90 and 96% respectively, indicating that the catalyst was recycled without any loss of activity.[10] Similar data were obtained in a second reaction cycle with catalyst recovery as per Case 2. A control confirmed no conversion of bromoheptane was observed in 6 hours in the absence of TOABr.

Flux data for filtrations from the two reaction cycles is summarised in Table 2. The permeate flux of the reaction mixture decreased to between 7 and 15 L m^{-2} h^{-1} by the end of the nanofiltration step, where a film of viscous material, assumed to be TOABr, was observed attached to the membrane surface. The solubility of TOABr in toluene is 380 g L^{-1}, and the starting concentration in the reaction mixture is 27 g L^{-1}, so it is expected that after 35 mL of organic phase has been removed, a maximum concentration of 218 g L^{-1} will result. This should be below the solubility limit of TOABr in toluene. However, it is possible that effects of the counter ion and the

Table 1 Separation of catalyst from a synthetic solution [Br–C_7H_{15} (0.1 M) + I–C_7H_{15} (0.1 M) + TOABr (0.01 M) + toluene]

		Flux/L m^{-2} h^{-1}		Rejection (%)		
Membrane	Nominal MWCO	Pure	Solution	Br–C_7H_{15} (MW 179)	I–C_7H_{15} (MW 226)	TOABr (MW 546)
142A	220	65	25	20	22	> 99
142C	400	88	32	8	5	> 99

† Electronic supplementary information (ESI) available: experimental procedures and results. See http://www.rsc.org/suppdata/cc/b1/b103645a/

 DOI: 10.1039/b103645a

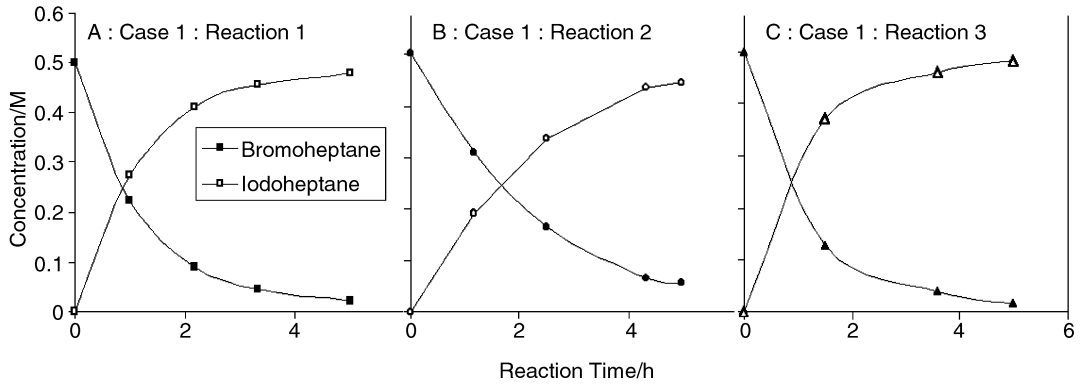

Fig. 1 Evolution of bromoheptane and iodoheptane concentration over time in the reaction in the presence of 0.05 M TOABr at 50 °C. The aqueous phase: 40 ml 0.5 M KI; the organic phase: 40 ml 0.5 M bromoheptane + 0.05 M TOABr. Stirring speed: 400 rpm. (A) Reaction 1; (B) Reaction 2 with the TOABr separated from the Reaction 1 mixture; (C) Reaction 3 with the TOABr separated from the Reaction 2 mixture.

Table 2 Separation of catalyst from reaction product mixture by 142A (MWCO = 220) membrane

						Rejection (%)					
		Conversion (%)[a]		Solution flux/L m^{-2} h^{-1}		TOABr MW 546)		$1–C_7H_{15}$ (MW 226)		$Br–C_7H_{15}$ (MW 179)	
	Reaction time/h	Case 1	Case 2	Case 1	Case 2	Case 1	Case 2	Case 1	Case 2	Case 1	Case 2
Reaction 1	5	97	98	12	9.1	>99	>99	12	11	10	11
Reaction 2	5	90	97	14	8.5	>99	>99	18	15	14	18
Reaction 3	5	96	96	15	7.0	>99	>99	5	8	13	7

[a] Case 1: the 5 ml of retentate was washed out with pure toluene and then recovered by toluene evaporation; each filtration was carried out with a fresh membrane disc. Case 2: the retentate was washed out each time with fresh organic reactant solution containing no catalyst, and consecutive filtrations were carried out with the same membrane disc.

reactant/product in the system lower the TOABr solubility, causing the catalyst to come out of solution at the membrane surface.

For both reaction and filtration, Case 1 and Case 2 gave similar results with no noticeable difference. In Case 2, (in which the same membrane disc is used for all filtrations) the membrane is effectively 'washed' at the end of each filtration with the reaction mixture going into the next batch. In Case 1, the membrane is washed with pure toluene at the end of each filtration. Subsequently, prior to each separation, the pure toluene flux was measured and found to be between 50 and 60 L m^{-2} h^{-1}. Mass balances on the PTC over each separation cycle showed that effectively all of the PTC was recovered during separation and subsequent membrane washing. We conjecture that the decrease in flux during a post-reaction filtration is due to PTC which precipitates out on the surface of the membrane, as described above possibly due to concentration effects. Apparently this flux can be restored, and the catalyst reclaimed, by simple washing with the reaction solvent. This is likely to be an important factor in making catalyst recovery by NF a viable process.

Using the polyimide solvent resistant nanofiltration membranes, it is possible to retain essentially all the PTC and to repeat reactions in a cycle of at least 3 reactions, without adding any further catalyst. Membrane fouling occurs during filtration of the catalyst, but appears to be reversible when the membrane is washed with the reaction solvent. Finally, we conclude that the membrane retention of homogenous phase-transfer catalysts is feasible and offers exciting opportunities for further work in coupling of NF membrane separators with phase-transfer catalysis reactors.

This work was supported by the UK Engineering and Physical Sciences Research Council grant No. GR/M 50751, and support in kind from W. R. Grace, Colombia, USA, and GlaxoSmithKline, Tonbridge, UK, is gratefully acknowledged.

Notes and references

1 C. M. Starks, *J. Am. Chem. Soc.*, 1997, **93**, 195.
2 B. Zaldman, Y. Sasson and R. Neumann, *Ind. Eng. Chem. Prod. Des. Dev.*, 1985, **44**, 390; S. D. Naik and L. K. Doraiswamy, *AIChE J.*, 1998, **44**, 612.
3 Molecular weight cut-off is defined by the molecular weight for which 90% rejection of the solute is achieved by the membrane.
4 J. A. Whu, B. C. Baltzis and K. K. Sirkar, *J. Membr. Sci.*, 2000, **170**, 159; L. S. White and A. R. Nitsch, *J. Membr. Sci.*, 2000, **179**, 267.
5 Reaction details: the reaction was carried out in a glass vessel of 100 mL with 40 mL aqueous phase (2 M KI) and 40 mL organic phase (0.5 M bromoheptane + 0.05 M TOABr in toluene). The temperature was kept at 50 ± 1 °C using an oil bath and stirring speed was 400 rpm. After the reaction was completed, the organic phase (40 mL) was transferred into a SEPA filtration cell and the cell was pressurized to 30 bar at room temperature. The SEPA cell was stirred at 300 rpm.
6 Values stated are supplied by W. R. Grace, Colombia, Maryland, USA, using various alkane solutes in toluene.
7 R_x defines the rejection of component x, this can be obtained from the following eqn. $1 - (C_{p,x}/C_{r,x})$ where $C_{p,x}$ is the concentration of x in the permeate and $C_{r,x}$ is the concentration of x in the retentate.
8 Case 1: the 5 ml of retentate left in the cell was washed out with pure toluene and the toluene was evaporated at 50 ± 1 °C (overnight in fume cupboard). This catalyst was then added to 35 mL 0.5 M bromoheptane in toluene (no fresh TOABr added) and mixed with 40 mL of 2 M KI aqueous phase. The reaction and nanofiltration were carried out as the above.
9 Case 2: the 5 ml of retentate left in the cell was washed out with 35 mL of 0.5 M bromoheptane in toluene to form the organic phase for the subsequent reaction. This organic phase was then mixed with 40 mL of 2 M KI aqueous phase. The reaction and nanofiltration were carried out as for the first reaction.
10 Reactants, products and catalyst were analysed using GC.

CHEMCOMM
Communication
www.rsc.org/chemcomm

Crystal structure of the two-dimensional framework $[Mn(salen)]_{4n}[Re_6Te_8(CN)_6]_n$ [salen = *N,N′*-ethylenebis(salicylideneaminato)]

Youngmee Kim, Seon-Mi Park, Wonwoo Nam and Sung-Jin Kim*

Department of Chemistry, Ewha Womans University, Seoul 120-750, Korea. E-mail: sjkim@mm.ewha.ac.kr

Received (in Cambridge, UK) 15th May 2001, Accepted 27th June 2001
First published as an Advance Article on the web 23rd July 2001

The first complex-bridged cyano–rhenium cluster framework material $[Mn(salen)]_{4n}[Re_6Te_8(CN)_6]_n$, with a two-dimensional layered structure is prepared by the reaction of a methanol solution of $[Mn(salen)]ClO_4$ with an aqueous solution of $Na_4[Re_6Te_8(CN)_6]$.

The design of extended structures based on molecular complexes has received much attention. Recently, there have been many studies on developing engineered-supramolecular networks in an effective manner and designing highly dimensional molecular systems with adjustable structures.[1,2] One way to obtain an extended structure is to utilize a molecular precursor that consists of multi-binding sites such as hexacyanoiron(III). For example, in MnL^+ (L = 3-MeO-salen,[3] 5-Cl-salen[4,5] or acacen[6]) linkage occurs *via* hexacyanoiron(III) to form two-dimensional layers. These cyano-bridged mixed-metal compounds with ferromagnetic and antiferromagnetic interactions are two-dimensional network structures. There have also been extensive studies on the face-capped octahedral rhenium cluster, $[Re_6Te_8(CN)_6]^{4-}$, which is analogous to hexacyanoiron(III). Cluster-expanded materials such as $Fe_4[Re_6Te_8(CN)_6]_3{\cdot}27H_2O$, $Ga_4[Re_6Se_8(CN)_6]_3{\cdot}38H_2O$, $[Cd_2(H_2O)_4][Re_6S_8(CN)_6]{\cdot}14H_2O$, and Cs_2[*trans*-$Fe(H_2O)_2]_3[Re_6Se_8(CN)_6]_2{\cdot}18H_2O$, where simple metal ions link the Re clusters to form bigger cavities, resemble the Prussian Blue $Fe_4[Fe(CN)_6]_3{\cdot}14H_2O$.[7–9] These three-dimensional frameworks include plenty of water molecules as well as metal ions within their cavities. $[Re_6S_8(CN)_6]^{4-}$ also coordinates to Mn(II) centers to form a neutral three-dimensional framework with isopropyl alcohol molecules.[10] In order to develop new framework materials with a potential to create new spatial or chemical functions, we designed a new extended solid system based on the Re cluster. For our linking material, we chose the $[Mn(salen)]^+$ complex instead of a simple metal ion since $[Mn(salen)]^+$ is paramagnetic with a high-spin d^4 electronic configuration of Mn(III). Futhermore, it also has axial sites to which the cyano–rhenium clusters can link up. We report here the preparation of the first cyano–rhenium cluster which is linked to an Mn complex to provide an extended framework with a unique layered structure.

The face-capped octahedral rhenium cluster $Na_4[Re_6Te_8(CN)_6]$ was prepared by a previous procedure.[11] The orange-red solid $Na_4[Re_6Te_8(CN)_6]$ was purified by recrystallization using methanol–diethyl ether. After an aqueous solution of $Na_4[Re_6Te_8(CN)_6]$ was carefully layered with a methanol solution of $[Mn(salen)]ClO_4$, black crystals of $[Mn(salen)]_{4n}[Re_6Te_8(CN)_6]_n$ **1** formed directly at the interface. A quantitative yield[12] of **1** was obtained by mixing an aqueous solution of $Na_4[Re_6Te_8(CN)_6]$ with a methanol solution of $[Mn(salen)]ClO_4$. Compound **1** was not soluble in common solvents such as methanol, ethanol, water, diethyl ether, acetone, acetonitrile, or THF. The structure of **1** was determined by X-ray crystallography.[13]

The asymmetric unit contains half of an Re cluster, a bridged $[Mn(salen)]^+$ unit, and a dangling $[Mn(salen)]^+$ unit. The complete two-dimensional layered structure is generated by the symmetry operations, $(-x + 3/2, y - 1/2, -z + 1/2)$, $(-x + 2, -y + 2, -z + 1)$, and $(-x + 3/2, y + 1/2, -z + 1/2)$. Four cyano groups of the Re cluster with C–N distances of 1.17(2)–1.18(2) Å are linked to $[Mn(salen)]^+$ units, forming a two-dimensional layer. The remaining two cyano groups with C–N distance of 1.13(2) Å are bound to a $[Mn(salen)]^+$ unit dangling outside the layer. The IR spectrum (KBr) of this compound showed two CN stretching peaks at 2073 and 2090 cm^{-1}, whereas the starting Re cluster had only one CN stretching peak at 2081 cm^{-1}. This result is consistent with the X-ray crystallographic data which shows two different types of cyano groups. Fig. 1(a) shows the rhenium cluster $[Re_6Te_8(CN)_6]^{4-}$, surrounded by six $[Mn(salen)]^+$ units. The Re–Re and Re–Te bonds range from 2.6842(7) to 2.7004(7) Å and from 2.685(1) to 2.703(1) Å, respectively. These are not significantly different from the starting rhenium cluster [The mean values of the Re–Re and Re–Te distances of the cyano–rhenium cluster are 2.681(3) and 2.694(2) Å, respectively]. The Mn(bridging

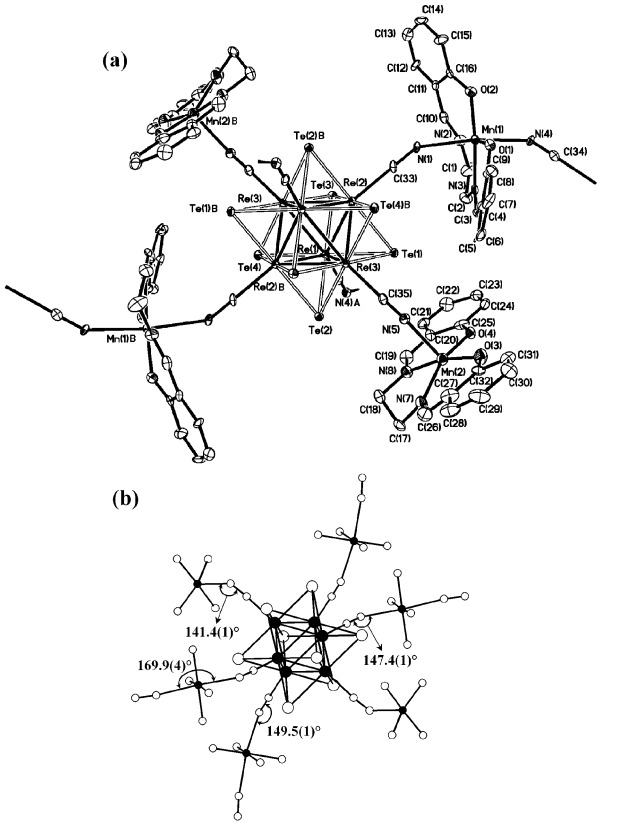

Fig. 1 (a) ORTEP drawing of the rhenium cluster $[Re_6Te_8(CN)_6]^{4-}$ surrounded by six $Mn(salen)^+$ units. Among the six $Mn(salen)^+$ units bound to six rhenium atoms, only four are shown. (b) A simplified drawing with some bond angles around the rhenium cluster. All carbon atoms of the salen molecules have been omitted for clarity. Symmery operations: A $(-x + 3/2, y - 1/2, -z + 1/2)$, B $(-x + 2, -y + 2, -z + 1)$.

 DOI: 10.1039/b104276a

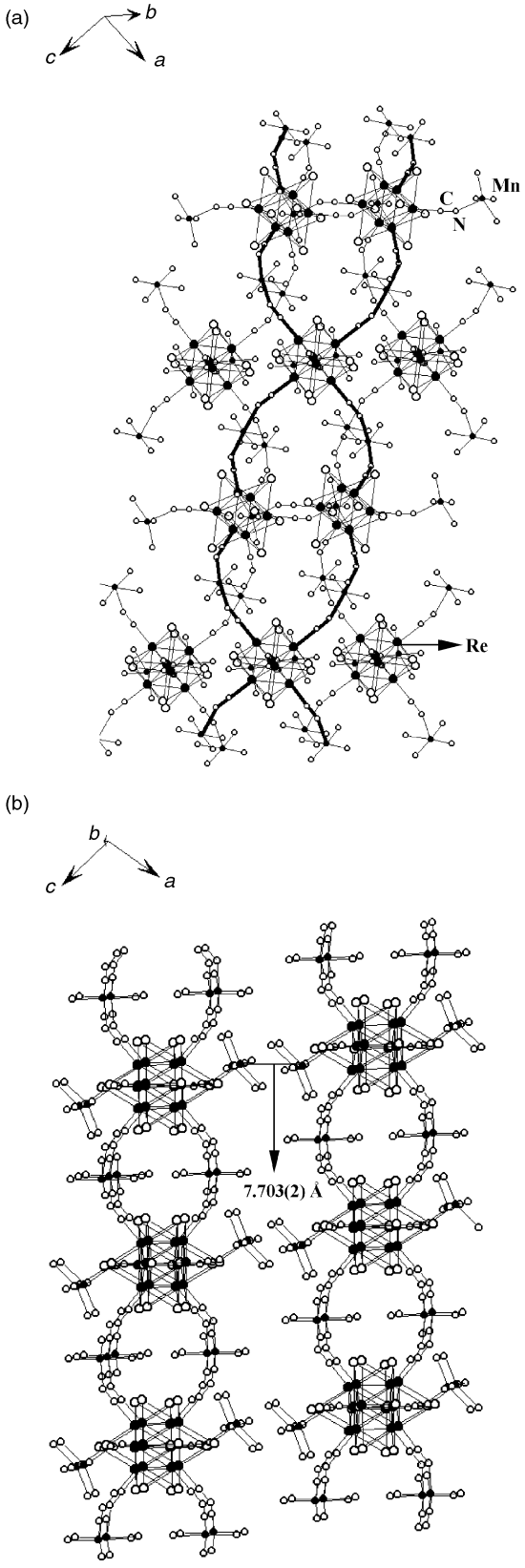

Fig. 2 (a) A two-dimensional layer containing [Mn(salen)]$^+$ units linked by cyano–rhenium clusters. The twisted ropes interconnected by Re_6Te_8 clusters are shown. (b) Side view of two layers. All carbon atoms of the salen molecules are omitted for clarity.

Mn unit)–N(cyano group) distances are 2.27(1) and 2.28(1) Å, while the Mn(dangling Mn unit)–N(cyano group) distance is 2.14(1) Å. Fig. 2(a) shows a two-dimensional layer containing [Mn(salen)]$^+$ units linked by cyano–rhenium clusters, while Fig. 2(b) shows a side view of two layers stacked perpendicular to the (1 0 1) direction. This layer is not a flat sheet, since the angle of the bridging elements N(cyano group)–Mn–N(cyano group) is 169.9(4)° and the angles C(cyano group)–N(cyano group)–Mn are 147.4(1) and 149.5(1)°. The unlinked dangling [Mn(salen)]$^+$ units are directed toward the outside of the layers, and the C(cyano group)–N(cyano group)–Mn(dangling Mn unit) angle is 141.4(1)° [Fig. 1(b)]. Two neighboring chains of –Mn(salen)–NC–Re_6Te_8–CN–Mn(salen)– run akin to a twisted rope, such ropes being interconnected by Re_6Te_8 clusters forming two-dimensional sheets. The intermolecular distances between the Mn units *via* the Re cluster are 14.490(9) and 14.38(1) Å, while the distance between the dangling Mn units *via* the Re cluster is 13.788(8) Å. The interlayer distance between the neighboring Mn (dangling Mn unit) atoms is 7.703(2) Å.

This system with cyano–rhenium clusters linked by Mn(salen) complexes is the first complex-bridged cyano–rhenium cluster framework material. Remarkably, this compound shows a unique thick-layered structure which opens the possibility of developing a new class of materials through crystal engineering of appropriate molecular complexes. We are currently investigating other transition metal complexes with high-spin systems which could provide extended network structures with cyano–rhenium clusters.

Y. Kim acknowledges financial support from the Basic Research Program of the Korean Science & Engineering Foundation. S.-J Kim acknowledges financial support from Korea Research Foundation Grant (KRF-2000-015-DP0224). We thank Dr Alan J. Lough in University of Toronto, Canada for X-ray data collection.

Notes and references

1 W. P. Fehlhammer and M. Fritz, *Chem. Rev*., 1993, **93**, 1243; K. R. Dunbar and R. A. Heintz, *Prog. Inorg. Chem*., 1997, **45**, 283.
2 H. Vahrenkamp, G. Andreas and G. N. Richardson, *J. Chem. Soc., Dalton Trans*., 1997, 3643 and references therein.
3 H. Miyasaka, N. Matsumoto, H. Okawa, N. Re, E. Gallo and C. Floriani, *Angew. Chem. Int. Ed., Engl*., 1995, **34**, 1446; H. Miyasaka, N. Matsumoto, H. Okawa, N. Re, E. Gallo and C. Floriani, *J. Am. Chem. Soc*., 1996, **118**, 981.
4 H. Miyasaka, H. Okawa, A. Miyazaki and T. Enoki, *J. Chem. Soc., Dalton Trans*., 1998, 3991.
5 H. Miyasaka, N. Matsumoto, N. Re, E. Gallo and C. Floriani, *Inorg. Chem*., 1997, **36**, 670.
6 H. Miyasaka, H. Okawa, A. Miyazaki and T. Enoki, *Inorg. Chem*., 1998, **37**, 4878.
7 M. P. Shores, L. G. Beauvais and J. R. Long, *J. Am. Chem. Soc*., 1999, **121**, 775.
8 M. P. Shores, L. G. Beauvais and J. R. Long, *Inorg. Chem*., 1999, **38**, 1648.
9 L. G. Beauvais, M. P. Shores and J. R. Long, *Chem. Mater*., 1998, **10**, 3783.
10 N. G. Naumov, D. V. Soldatov, J. A. Ripmeester, S. B. Artemkina and V. E. Fedorov, *Chem. Commun*., 2001, 571 and references therein.
11 Y. V. Mironov, J. A. Cody, T. E. Albrecht-Schmitt and J. A. Ibers, *J. Am. Chem. Soc*., 1997, **119**, 493.
12 Yield: 39.1%. Anal. Calc. for $C_{70}H_{56}Mn_4N_{14}O_8Re_6Te_8$: C, 23.49; H, 1.58; N, 5.48. Found: C, 23.48; H, 1.51; N, 5.42%.
13 The X-ray diffraction data were collected on a Nonius Kappa-CCD diffractometer using Mo-Kα radiation (λ = 0.71071 Å) at 150 K; crystal size 0.40 × 0.12 × 0.06 mm. The CCD data were integrated and scaled using the DENZO-SMN software package, and the structure was solved and refined using SHEXTL V5.0. All non-hydrogen atoms were located in the calculated positions. *Crystal data*: $C_{70}H_{56}Mn_4N_{14}O_8Re_6Te_8$, M = 3579.05, monoclinic, space group $P2_1/n$ (no. 14) a = 15.8104(7), b = 13.5732(7), c = 18.9822(5) Å, β = 101.738(3)°, V = 3988.4(3) Å^3, Z = 2, μ(Mo-Kα) = 12.603 mm^{-1}, 34426 reflections measured, 7847 unique (R_{int} = 0.115) which were used in all calculations, final R = 0.0552 (R_w = 0.1241) with reflections having intensities greater than 2σ, GOF(F^2) = 1.030. CCDC reference number 152818. See http://www.rsc.org/suppdata/cc/b1/b104276a/ for crystallographic data in CIF or other electronic format.

CHEMCOMM Communication
www.rsc.org/chemcomm

Folding and dimerization of resorcarene tetrasulfonates†

Alexander Shivanyuk‡

Department of Chemistry, University of Jyväskylä, P.O. Box 35, FIN-40351, Jyväskylä, Finland

Received (in Columbia, MO, USA) 1st May 2001, Accepted 25th May 2001
First published as an Advance Article on the web 23rd July 2001

In the solid state and in $CDCl_3$ resorcarene tetramesitylsulfonates fold by intramolecular S=O···H–O hydrogen bonds and dimerise *via* intermolecular O–H···OH hydrogen bonding.

Intramolecular folding and intermolecular association of several sub-units are key properties of biologically important macromolecules.[1] A few synthetic compounds also exhibit these features. For instance, the bowl shaped crown conformers of resorcarene octols[2] formed by intramolecular hydrogen bonds lead to hydrogen bonded dimeric and hexameric aggregates.[3] A seam of intramolecular hydrogen bonds in the calix[4]arene tetraurea derivatives was shown to change considerably the stability and binding properties of self-assembled dimeric capsules.[4] The dimer of an artificial β-sheet[5] is also an example of self-assembly involving both intra- and inter-molecular hydrogen bonds.

Novel hydrogen bonded self-assembly of tetramesityl sulfonates **1a, b**[6] is reported here which is a combination of folding and dimerization.

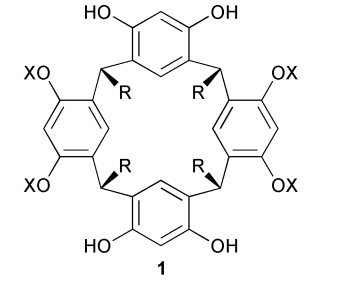

1

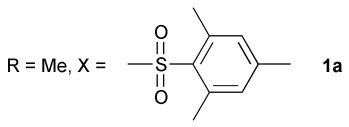

1a

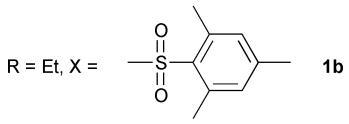

1b

In the crystalline state§ the molecule of **1a** adopts a strongly pinched and twisted boat conformation with almost parallel unsubstituted resorcinol rings (Fig. 1). Two of mesitylsulfonyl fragments oriented clock- or counter-clockwise form short intramolecular S=O···H–O hydrogen bonds to the neighboring hydroxy groups making the whole conformation inherently chiral. The asymmetric unit contains two crystallographically independent molecules (A and B) which are different mainly in the arrangement of one *non*-hydrogen bonded mesitylsulfonyl residue (Fig. 1).

Two molecules of **1a** form a cross-shaped dimer linked by four intermolecular O–H···OH hydrogen bonds (Fig. 2). Short intra- and inter-molecular contacts between hydroxy and *ortho*-methyl groups of the mesityl residues (O···C 3.2–3.4 Å) clearly indicate the C–H···O interactions which may additionally stabilize the assembly. The unsubstituted resorcinol rings of

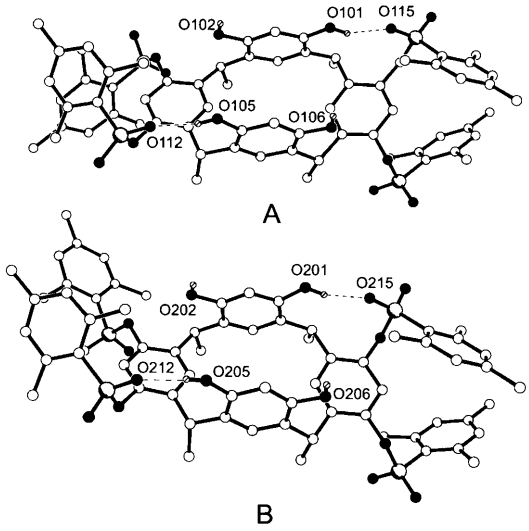

Fig. 1 Two crystallographically independent molecules of **1a**. C–H-hydrogen atoms are omitted for clarity. Hydrogen bonds are shown in dotted lines. O···O distances (Å) and O–H···O angles for intramolecular hydrogen bonds (°): O101···O115 2.590(5) (148.3), O105···O112 2.611(5) (148.1), O201···O215 2.510(5) (148.1), O205-O212 2.513(4) (145.3).

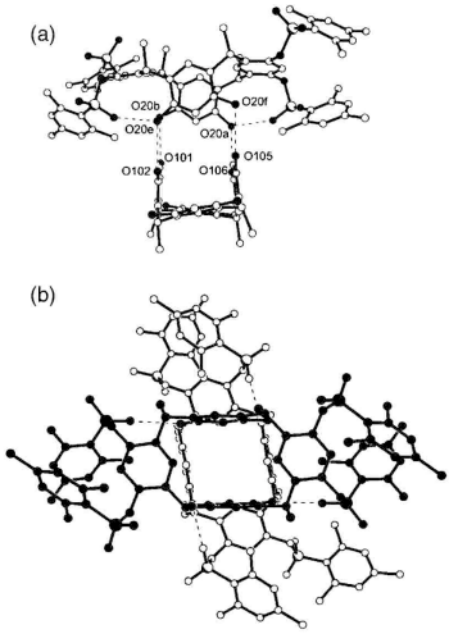

Fig. 2 Hydrogen bonded dimer of **1a**. (a) Side view. Mesitylsulfonyl groups of one molecule are omitted for clarity. (b) Top view. Molecule A is darkened. Selected intermolecular distances (Å): O101···O20B 2.808, O102···O20E 2.836, O105···O20F 2.829, O106···O20A 2.774.

† Dedicated to Volker Böhmer on the occasion of his 60th Birthday.

‡ Current address: The Skaggs Institute for Chemical Biology, The Scripps Research Institute, MB-26, 10550 North Torrey Pines Rd., La Jolla, CA 92037, USA. E-mail: shivan@scripps.edu

 DOI: 10.1039/b104076f

molecule A are nearly perpendicular both to diacylated and unsubstituted resorcinol rings of molecule B. Such a geometry leaves no space for the encapsulation of guest species within the dimer so that the solvent molecules are included in voids of the crystal.

In the dimer the molecules of **1a** have an opposite orientation of hydrogen bonded mesitylsulfonyl groups obviously owing to the requirements of complementarity. A simple consideration reveals that the molecules of **1a** having the same sense of inherent chirality cannot form the dimer.

The ^{1}H NMR spectrum of **1a**, **b** measured in $CDCl_3$ at 303 K contains four singlets for the protons of resorcinol rings, one singlet for the protons of hydroxy groups (δ 7.0) and one set of signals for other protons in accordance with C_{2v}-symmetric structure. 2D NOESY (t_m = 300 ms) and long range COSY ($CDCl_3$, 500 MHz) techniques showed that the molecules of **1** exist in the boat conformation with *parallel* unsubstituted resorcinol rings.[7] At 223 K a double set of ^{1}H NMR signals corresponds to the protons of the methyne bridges [Fig. 3(a), (b)], hydroxy groups and the aromatic protons of the mesitylene residues while the protons of the resorcinol rings emerge again as four singlets. This pattern can be ascribed to the slow exchange between two enantiomeric C_2-symmetric conformations having clock- or counter-clockwise orientation of two hydrogen bonded mesitylsulfonyl groups similar to that found in the solid state (Fig. 1). The signals of methyne bridges undergo a clear coalescence at 247 K corresponding to ΔG^* of 11.7 kcal mol^{-1}. The mixing of **1a** and **1b** in 1 : 1 molar ratio results in additional set of ^{1}H NMR signals for both resorcarenes [Fig. 3(c)]. This can be explained only by the formation of hetero-associate **1a** · **1b** which co-exists with **1a** · **1a** and **1b** · **1b** in a statistical 2 : 1 : 1 ratio. This is in accordance with the MALDI-TOF mass spectra of **1a** and **1b** which showed the peaks of both the monomer and the dimer.

The ^{1}H NMR spectrum of **1a** measured at 223 K in a 1 : 1 mixture of **1a**, **b** in CD_3OD–$CDCl_3$ (1 : 1) exhibits a sharp C_{2v}-symmetric pattern which presumably corresponds to the monomer. Furthermore, in less competing mixtures of $CDCl_3$ and acetonitrile-d_3 both C_{2v}- and C_2-symmetrical pattern are observed simultaneously, in a ratio proportional to the polarity of the medium. Since no signals of the monomer were observed at 223 K in $CDCl_3$ the dimerization constant should be $> 10^5$ M^{-1}.

The NOESY (t_m = 300 ms) spectrum of **1a** in $CDCl_3$ at 223 K reveals close proximity of the protons in 5-positions of diacylated resorcinol rings to the protons in 2-positions of unsubstituted resorcinol rings as found in the solid state dimer [Fig. 2(a)]. The singlet of hydroxy groups at δ 7.5 shows intense cross-peaks to the signal of the protons in 2-positions of unsubstituted resorcinol rings and to the OH resonance at δ 7.0. This is in accordance with the geometry of *intermolecular* O–H···O–H hydrogen bonding in the solid state dimer (Figs. 1 and 2). On the other hand, the correlation between *one* signal of the methyne bridges (δ 4.5) and the OH resonance at δ 7.0 is in keeping with the *intramolecular* S=O···H–O hydrogen bonds (Fig. 1).

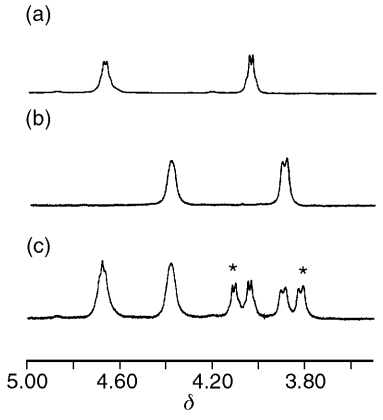

Fig. 3 The ^{1}H NMR signals of the methyne protons of the bridges at 223 K ([**1a**] = [**1b**] = 10 mM, 500 MHz, $CDCl_3$): (a) **1a**, (b) **1b**, (c) **1a** + **1b**. Signals of the heterodimer are indicated by an asterisk.

The above results strongly suggest the structural similarity of $\mathbf{1a}_2$ in $CDCl_3$ and in the solid state. The fact that only one C_2-symmetrical pattern is observed in the NMR spectra of $\mathbf{1a}_2$, $\mathbf{1b}_2$ and **1a**·**1b** reflects, most probably, the regioselective formation of one dimer—a feature predicted from the crystal structure of $\mathbf{1a}_2$.

In conclusion, the dimerization described above provides a novel structural motif for molecular self-assembly which is based on the interplay of intra- and inter-molecular hydrogen bonds. Obviously, the aggregation of resorcarene tetramesityl sulfonates characterized by cation and anion binding sites, hydrogen bonding, photochemically and/or electrochemically active groups could give novel polyfunctional molecular assemblies. Such systems are being investigated and will be reported in due course.

Professor Kari Rissanen (University of Jyväskylä) and Professor Dmitry Rudkevich (TSRI) are acknowledged for helpful discussions and Mr R. Kauppinen (University of Jyväskylä) for assistance with the NMR measurements. This work was supported by the Finnish Academy.

Notes and references

§ *Crystal data*: the data was recorded with a Kappa CCD diffractometer using graphite monochromatised Mo-Kα radiation [λ(Mo-Kα) = 0.71073 Å]. The data was processed with Denzo-SMN v0.93.0 (Z. Otwinowski and W. Minor, *Processing of X-Ray Diffraction Data Collected in Oscillation Mode; Methods Enzymol*, 1997, **276**, 307). The structures were solved by direct methods (G. M. Sheldrick, SHELXS-97, *Acta Crystallogr., Sect. A.* 1990, **46**, 467) and refinements, based on F^2, were made by full-matrix least-squares techniques (G. M. Sheldrick, SHELXL-97: A program for crystal structure refinement, University of Göttingen, Germany, 1997).

$\mathbf{1a}_2$·4EtOH·2H_2O: crystal size 0.5 × 0.3 × 0.2 mm, monoclinic, space group *Pn*, a = 18.1461(3), b = 14.8718(1), c = 23.3306(4) Å, β = 92.654(1)°, V = 6289.3(2) Å^3, Z = 2, D_c = 1.403 g cm^{-3}, μ = 0.228 mm^{-1}, $F(000)$ = 2797, 1760 parameters, $R1$ = 0.0696, $wR2$ = 0.1746 [for 20725 reflections with $I > 2\sigma(I)$], $R1$ = 0.0968, $wR2$ = 0.1980 (for 26601 unique reflections), S = 1.077, $\Delta\rho$ = −0.43/0.72 e Å^{-3}.

CCDC reference number 163620. See http://www.rsc.org/suppdata/cc/b1/b104076f/ for crystallographic data in CIF or other electronic format.

1 L. Stryer, *Biochemistry*, Freeman, New York, 4th edn., 1995, pp. 28–30.
2 P. Timmerman, W. Verboom and D. N. Reinhoudt, *Tetrahedron*, 1996, **52**, 2663.
3 K. N. Rose, L. J. Barbour, G. W. Orr and J. L. Atwood, *Chem. Commun.*, 1998, 407; K. Murayama and K. Aoki, *Chem. Commun.*, 1998, 607; L. R. MacGillivray and J. L. Atwood, *Nature*, 1997, **389**, 469; T. Gerkensmeier, W. Iwanek, C. Agena, R. Frölich, S. Kotila, C. Näther and J. Mattay, *Eur. J. Org. Chem.*, 1999, 2257.
4 Y. L. Cho, D. M. Rudkevich, A. Shivanyuk, K. Rissanen and J. Rebek Jr., *Chem. Eur. J.*, 2000, **6**, 3788.
5 J. C. Nowick, J. H. Tsai, Q.-C. D. Bui and S. Maitra, *J. Am. Chem. Soc.*, 1999, **121**, 8409.
6 O. Lukin, A. Shivanyuk, V. V. Pyrozhenko, I. F. Tsymbal and V. I. Kalchenko, *J. Org. Chem.*, 1998, **63**, 9510.
7 A. Shivanyuk, E. F. Paulus, K. Rissanen, E. Kolehmainen and V. Böhmer, *Chem. Eur. J.*, 2001, **7**, 1944.

CHEMCOMM Communication
www.rsc.org/chemcomm

Platinum colloids stabilized by bifunctional ligands : self-organization and connection to gold†

Silvia Gomez,[a] Laurent Erades,[a] Karine Philippot,[a] Bruno Chaudret,*[a] Vincent Collière,[a] Olivier Balmes[b] and Jan-Olov Bovin [b]

[a] *Laboratoire de Chimie de Coordination du CNRS, 205, route de Narbonne, 31077 Toulouse Cédex 04, France. E-mail: chaudret@lcc-toulouse.fr*
[b] *Lund University, Inorganic Chemistry 2, P.O. Box 124, 22100 Lund, Sweden*

Received (in Cambridge, UK) 26th April 2001, Accepted 28th June 2001
First published as an Advance Article on the web 23rd July 2001

Platinum nanoparticles accomodating bifunctional thiolate ligands self-assemble into regular superstructures or organize around a large gold particle; the shape of the superstructures can be modulated by addition of water.

There is presently a substantial interest for the study and the use of the novel properties of metal nanoparticles.[1] Complexation of ligands at the surface of the nanoparticles may allow a good control of both their physical and chemical properties.[2] Furthermore, the use of polyfunctional ligands may lead to connection between particles, to their self-assembly and the formation of monolayers on surfaces, as recently described.[1g,3,4] However, the coordination chemistry of the surface of nanoparticles has been relatively little developed, probably because of the lack of adequate methods for synthesizing particles of controlled surface state. CO coordination at the surface of metal particles has often been used as a probe of the surface state[5] whereas thiol or amine coordination has been used to stabilize metal particles.

In our group, we have been interested for some time in the synthesis of metal nanoparticles from organometallic precursors.[6] Two main reasons for this interest were the possibilities to access to monodisperse particles of very small size (1–2 nm) and to perform coordination chemistry at their surface. In this respect, we have been able to prepare platinum particles of small size (*ca.* 1.5 nm) protected by various ligands such as CO, THF, PPh_3, TOPO (trioctylphosphine oxide), thiols and amines. In the presence of thiols, we have shown the absence of ligand exchange at the NMR time scale between free and complexed thiol.[6c–f]

Having demonstrated the possibility to control the growth and the stability of nanoparticles with ligands, the next step is the organization of the particles in two or three dimensions. This can be achieved by self-organization (In/TOPO[6e]) or by connection of the particles in a way similar to that used in molecular techtonics.[7] We report in this communication our first attempts in this direction using both the coordination ability of dithiols and the formation of hydrogen bonded networks.

The reaction of $Pt_2(dba)_3$ with CO (1 bar) in THF leads to the formation of platinum nanoparticles of uniform size centered near 1.2 nm (colloid **1**). Addition of alkanedithiol ligands proceeds similarly as previously described for octanethiol,[6c] and leads to new platinum particles (alkane = propane, colloid **2a**; octane, colloid **2b**). The reaction can be followed by IR spectroscopy in which a shift to lower frequency of surface CO stretches is observed from 2050, 1808 cm^{-1} to 2046, *ca.* 1800 cm^{-1} upon addition of 0.1 eq./Pt dithiol. The particles have been characterized by HREM and, for some samples, by WAXS (wide angle X-ray scattering) which both demonstrate their fcc structure. Their mean size is *ca.* 1.6 nm, similar to octanethiol stabilized particles.[6c] However, in contrast to the results observed with octanethiol, the particles agglomerate into large superstructures which do not evidence any crystalline arrangement but in which the inter-particle distances is regular (Scheme 1; experimental and characterization details are given as ESI†).

In order to determine whether this aggregation was due to the presence of coordination links between the particles, a solution of colloid **2b** was reacted with large gold particles prepared by the Turkevich method.[8] According to the density of platinum particles, the organization observed around gold particles [concentric circles, Fig. 1(b)] may lead to long range ordering. In each case, a regular inter-particle distance of *ca.* 1 nm can be measured. This result therefore demonstrates the possibility to use a linker for connecting two particles, of different or of same nature.

Another approach for connecting nanoparticles consists in trying to organize them through hydrogen bonds.[9] In our case, we chose to organize platinum nanoparticles by employing bifunctional thiophenol derivatives. As the thiolate groups display high affinity for platinum, the anchoring of the ligands at the surface of the particles occurs through the thiolate functions leaving free the *para* substituents for hydrogen bonding. This leads to a new series of platinum particles accommodating respectively *p*-hydroxythiophenol (colloid **3a**), *p*-aminothiophenol (colloid **3b**), and *p*-mercaptobenzoic acid (colloid **3c**). The addition of each ligand to compound **1** can be followed as before by IR spectroscopy. The terminal CO stretch shifts upon addition of 0.15 eq./Pt substituted thiophenol to a value of *ca.* 2040 cm^{-1}. The compounds were characterized by microanalysis, TEM and HREM. In all cases, the products were found to consist of severely agglomerated nanoparticles, the

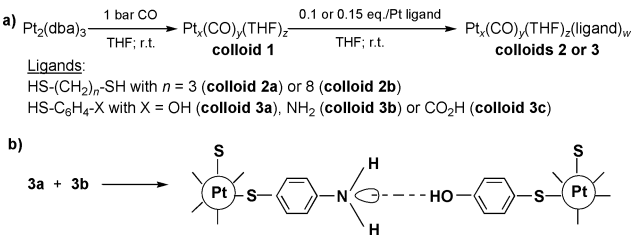

Scheme 1 Synthesis of bifunctional ligand stabilized Pt nanoparticles (a) and $[Pt]^0$ self-assemblies (b).

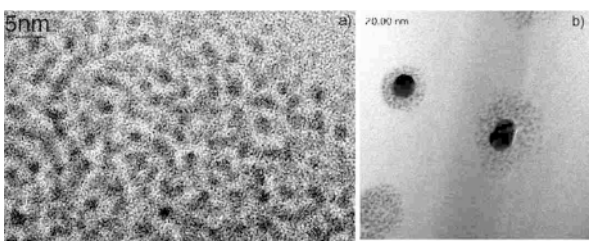

Fig 1 HREM micrograph of Pt particles stabilized by propanedithiol (a) and of $[Pt]^0$(S–S)$[Au]^0$ assemblies (b).

† Electronic supplementary information (ESI) available: experimental and characterization details; Schemes 1 and 2; Figs. 1–4; Graphical Abstract. See http://www.rsc.org/suppdata/cc/b1/b103781c/

 DOI: 10.1039/b103781c

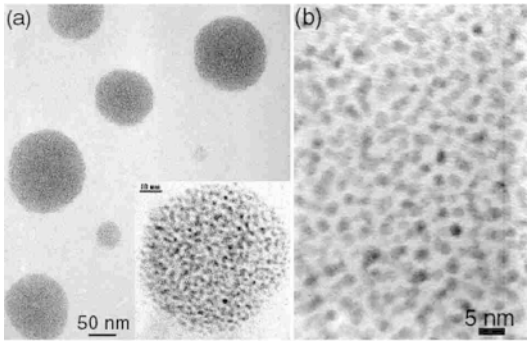

Fig 2 TEM (a) and HREM (b) micrographs of disks resulting from the condensation of **3a** and **3b** in the presence of water.

distance between which appears regular (near 1.5 nm). In most cases (Fig. 4, ESI†), the agglomerates adopt a compact shape, spherical or distorted spherical as also observed by Boal *et al.*[9] Since water may modify the hydrogen bonding network, the reaction was also carried out in the presence of water. In this case, disks composed of a monolayer of platinum particles were observed [Fig. 2(a)]. HREM analysis of these agglomerates [Fig. 2(b)] shows the presence of well-crystallized fcc platinum particles of uniform size near 1.6 nm, indicating the absence of modification of the particles upon complexation and reaction with water. Similar results were found with compounds **3b** and **3c**. In the latter case, the distance between the particles seems to be slightly shorter (1 nm) which may arise from strong hydrogen bonds between carboxylic groups.

In order to favour the organization of the particles, we mixed together fresh solutions of **3a** and **3b** containing hydroxy and amino pendent groups, respectively. XRD analysis of the samples is in accord with the presence of small fcc platinum with additional peaks at small angles possibly resulting from organization of the particles. TEM micrographs of **3a**/**3b** evidence the organization of the particles into systems showing an unidirectional anisotropy and resembling nanocrystals (Fig. 3, graphical abstract). Moreover in several cases we observe the formation of nanotubes which are hollow and may accommodate some 'pseudocrystals'. However, HREM analysis demonstrates that the 'pseudocrystals' or the walls of the tubes consist of fcc Pt nanoparticles of intact mean size and structure. As for the superstructures observed with **3a** alone, the addition of water to the system releases the hydrogen bonded network, leading to a monolayer organization.

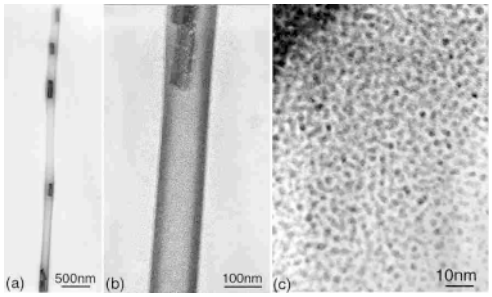

Fig 3 TEM and HREM micrographs of platinum nanotubes at different magnifications (a) ×15000 (b) ×100000 (c) ×600000.

In conclusion, functionalised platinum nanoparticles may be used as individual blocks for the growth of 2D or 3D superstructures through coordination bonds or hydrogen bonding networks. Although the chosen systems are very simple, several points appear nevertheless of interest : (1) the fact that water can control the shape of the hydrogen bonded agglomerates and favours the formation of monolayers is promising as far as the deposition of nanoparticles exhibiting controlled interparticle distance is concerned and may lead to selected electronic measurements or applications; (2) the shape of the obtained agglomerates are not yet predictable but some systems reproducibly display a preferred axis of growth to form 'pseudo-crystals' or nanotubes leading to possible access of nanowires comprised of nanoparticles; (3) connecting nanoparticles appears easy and may lead to interesting chemical and physical properties which will be studied in the future.

We thank CNRS and EC (TMR network CLUPOS) for support, and the TEMSCAN service of the 'Université Paul Sabatier' for electron microscopy facilities.

Notes and references

1 (*a*) G. Schmid, *Chem. Rev*., 1992, **92**, 1709; (*b*) J. D. Aiken III and R. G. Finke, *J. Mol. Catal. A: Chem*., 1999, **145**, 1; (*c*) T. Oku and K. Suganuma, *Chem. Commun*., 1999, 2355; (*d*) M. P. Pileni, *New J. Chem*., 1998, **22**, 693; (e) M. D. Musick, C. D. Keating, M. H. Keefe and M. J. Natan, *Chem. Mater*., 1997, **9**, 1499; (*f*) D. Bethell, M. Brust, D. J. Schiffrin and C. Kiely, *J. Elecroanal. Chem*., 1996, **409**, 137; (*g*) M. Brust, D. Bethell, D. J. Schiffrin and C. J. Kiely, *Adv. Mater*., 1995, **7**, 795.

2 C. Yee, M. Scotti, A. Ulman, H. White, M. Rafailovich and J. Sokolov, *Langmuir*, 1999, **15**, 4314; M. J. Hostetler, J. E. Wingate, C.-J. Zhong, J. E. Harris, R. W. Vachet, M. R. Clark, J. D. Londono, S. J. Green, J. J. Stokes, G. D. Wignall, G. L. Glish, M. D. Porter, N. D. Evans and R. W. Murray, *Langmuir*, 1998, **14**, 17; F. Tian and K. J. Klabunde, *New J. Chem*., 1998, **22**, 1275.

3 T. Zhu, X. Fu, T. Mu, J. Wang and Z. Liu, *Langmuir*, 1999, **15**, 5197; S. R. Johnson, S. D. Evans and R. Brydson, *Langmuir*, 1998, **14**, 6639; M. Brust, J. Fink, D. Bethell, D. J. Schiffrin and C. Kiely, *J. Chem. Soc., Chem. Commun*., 1995, 1655; X. Peng, T. E. Wilson, A. P. Alivisatos and P. G. Schultz, *Angew. Chem., Int. Ed. Engl*., 1997, **36**, 145; M. Bartz, N. Weber, J. Küther, R. Seshadri and W. Tremel, *Chem. Commun*., 1999, 2085; R. C. Mucic, J. J. Storhoff, C. A. Mirkin and R. L. Letsinger, *J. Am. Chem. Soc*., 1998, **120**, 12674; J. Küther, R. Seshadri, G. Nelles, W. Assenmacher, H.-J. Butt, W. Mader and W. Tremel, *Chem. Mater*., 1999, **11**, 1317

4 C. A. Mirkin, R. L. Letsinger, R. C. Mucic and J. J. A. Storhoff, *Nature*, 1996, **382**, 607; S. J. Park, A. A. Lazarides, C. A. Mirkin, P. W. Brazis, C. R. Kannewurf and R. L. Letsinger, *Angew. Chem., Int. Ed*., 2000, **39**, 3845; A. P. Alivisatos, K. P. Johnsson, X. Peng, T. E. Wilson, C. J. Loweth, M. P. Bruchez Jr and P. G. Schultz, *Nature*, 1996, **382**, 609; G. Schmid and N. Beyer, *Eur. J. Inorg. Chem*., 2000, 835; S. Guo, L. Konopny, R. Popovitz-Biro, H. Cohen, H. Porteanu, E. Lifshitz and M. Lahav, *J. Am. Chem. Soc*., 1999, **121**, 9589.

5 D. de Caro and J. S. Bradley, *New J. Chem*., 1998, 1267

6 (*a*) A. Rodriguez, C. Amiens, B. Chaudret, M.-J. Casanove, P. Lecante and J. S. Bradley, *Chem. Mater*., 1996, **8**, 1978; (*b*) M. Bardaji, O. Vidoni, A. Rodriguez, C. Amiens, B. Chaudret, M.-J. Casanove and P. Lecante, *New J. Chem*., 1997, **21**, 1243; (*c*) F. Dassenoy, K. Philippot, T. Ould Ely, C. Amiens, P. Lecante, E. Snoeck, A. Mosset, M.-J. Casanove and B. Chaudret, *New J. Chem*., 1998, **22**, 703; (*d*) S. Gomez, K. Philippot, V. Collière, B. Chaudret, F. Senocq and P. Lecante, *Chem. Commun*., 2000, 1945; (*e*) K. Soulantica, A. Maisonnat, M.-C. Fromen, M.-J. Casanove, P. Lecante and B. Chaudret, *Angew. Chem., Int. Ed*., 2001, **40**, 448; (*f*) C. Pan, K. Pelzer, K. Philippot, B. Chaudret, F. Dassenoy, P. Lecante and M.-J. Casanove, *J. Am. Chem. Soc*., in press.

7 M. V. Hosseini and A. de Cian, *Chem. Commun*., 1998, 727.

8 J. Turkevich, P. C. Stevenson and J. Hillier, *Discuss. Faraday Soc*., 1951, **11**, 55.

9 A. K. Boal, F. Ilhan, J. E. DeRouchey, T. Thurn-Albrecht, T. P. Russell and V. M. Rotello, *Nature*, 2000, **404**, 746; A. K. Boal and V. M. Rotello, *Langmuir*, 2000, **16**, 9527.

CHEMCOMM Communication
www.rsc.org/chemcomm

Tandem isomerisation–carbonylation catalysis: highly active palladium(II) catalysts for the selective methoxycarbonylation of internal alkenes to linear esters

Robert I. Pugh,[a] Eite Drent*[b] and Paul G. Pringle*[a]

[a] *School of Chemistry, University of Bristol, Cantocks Close, Bristol, UK, BS8 1TS. E-mail: paul.pringle@bristol.ac.uk*

[b] *Shell Research and Technology Centre, Amsterdam, PO Box 38000, 1030 BN Amsterdam, The Netherlands*

Received (in Cambridge, UK) 25th April 2001, Accepted 11th June 2001
First published as an Advance Article on the web 23rd July 2001

Fast, selective conversion of internal olefins to linear esters is catalysed by Pd(II) complexes of chelating bis(phospha-adamantyl)diphosphines and the catalysis is acutely sensitive to the ligand backbone and even to the diastereomer used; the results are compared with those for the PBu^t_2 analogue.

The palladium(II) catalysed methoxycarbonylation of olefins to esters has attracted much attention.[1] Recently, complexes of bulky alkyl diphosphines such as d^tbpp[2] and d^tbpx[3] have been

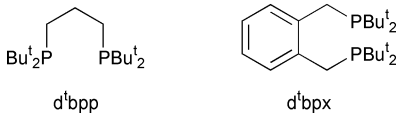

d^tbpp d^tbpx

reported to give excellent catalysts for the carbonylation of ethene to methyl propanoate (MeP) [eqn. (1)].

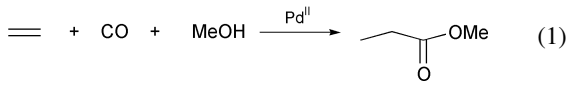

(1)

We have previously shown that adamantyl cage diphosphines *meso*/*rac*-**1** and *meso*/*rac*-**2** and their complexes are readily

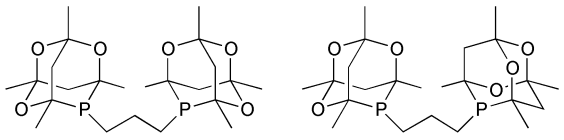

meso-**1** *rac*-**1**

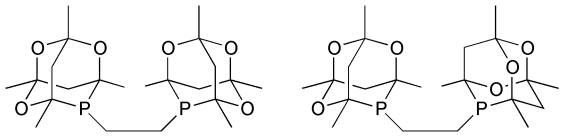

meso-**2** *rac*-**2**

prepared.[4] We report here that *in situ* generated palladium(II) complexes of *meso*/*rac*-**1** and **2** catalyse the carbonylation of ethene and terminal olefins with comparable activity and selectivity to their PBu^t_2 substituted analogues; more importantly internal alkenes are selectively converted to linear esters, a discovery of potential application in the synthesis of detergents and nylon intermediates.[5]

Diastereomerically enriched *meso*-**1** (80%) and *rac*-**1** (96%) were separated by recrystallisation from MeOH of the *ca.* 1:1 diastereomeric mixture. Selected results from the carbonylation catalysis [eqn. (2)] are shown in Table 1.

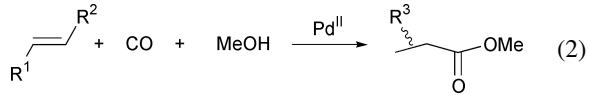

(2)

Entry 1 shows that the catalyst from *meso*/*rac*-**1** and $Pd(OAc)_2$ quantitatively forms MEP at a slightly lower rate than its d^tbpp analogue.[2,3,5] The effect of the diphosphine backbone is beautifully illustrated by comparison of entries 1 and 2; the C_2-bridged *meso*/*rac*-**2** affords a catalyst for alternating CO/C_2H_4 polymerisation, yielding polyketone of a relatively low molecular weight. Normally the most active catalysts for polyketone formation are based on C_3-diphosphines,[7] but the sterically demanding phosphaadamantyl moiety renders the C_2-diphosphine more capable of copolymerision of ethene and CO.[8]

The most significant results were obtained with the carbonylation of 1-tetradecene (entry 3) and internal isomers of tetradecene (entry 4). The catalyst derived from *meso*/*rac*-**1** gave similar selectivities to linear esters for *both* substrates; the activity for the isomerisation/carbonylation of the internal olefins is *ca.* 0.4 that of the linear olefins, indicating that isomerisation is rate limiting and the high product linearity is a consequence of the increased rate of carbonylation at the terminal olefinic position. The analogous catalyst with d^tbpp (entry 5) showed hardly any activity for this isomerisation/carbonylation reaction. Our results on methoxycarbonylation of internal olefins also compare favourably with traditional cobalt[9] and more recent phosphorus(III)–rhodium systems for related hydroformylation catalysis, which suffer from relatively poor isomerisation activity[10] or low product linearity.[11]

The most unexpected result was the factor of two difference in activity between enriched catalysts from *meso*-**1** and *rac*-**1** for methoxycarbonylation of propene (entries 6 and 7). A similar difference in activity is observed in the conversion of internal C_{11}/C_{12} olefins to linear C_{12}/C_{13} esters (entries 8 and 9). Our results demonstrate that very subtle changes in the structure of the palladium catalyst can have a large influence on catalytic activity. Activity differences between diastereomeric Pd catalysts for CO/olefin copolymerisation have been reported recently.[12]

The difference in performance between the catalysts derived from the ostensibly similar bulky alkyl diphosphines *meso*/*rac*-**1** and d^tbpp, may be associated with the unusual stereoelectronic characteristics of the cage ligand. We have previously shown that the Tolman cone angle[13] for *meso*/*rac*-**1** (θ = 173°) is even larger than that of d^tbpp (θ = 155°).[14] The σ/π-bonding ability of *meso*/*rac*-**1** can be assessed from the ν(CO) of the A_1 band for the $[Ni(CO)_2(diphos)]$ chelates. When diphos = *meso*/*rac*-**1**, ν(CO) is 2002 cm^{-1} which is much higher than its PBu^t_2 analogue (1976 cm^{-1}) and even higher than its PPh_2 analogue (1997 cm^{-1}). The inference from these IR data is that the P-atom in the phosphatrioxaadamantane cage is electronically more akin to that in a $P(aryl)_2$ than a $P(alkyl)_2$ moiety. The low σ-basicity/high π-acidity of ligands *meso*/*rac*-**1** may be

 DOI: 10.1039/b103754b

Table 1 Palladium catalysed methoxycarbonylation of olefins[6]

Entry	Ligand[a]	Olefin[b]	*P*co/bar	*T*/°C	Rate[c]	Product (yield (%))
1	*meso*/*rac* **1**	Ethene	30	90	10000	MeP (>99)
2	*meso*/*rac* **2**	Ethene	30	90	4000	Polyketone, M_n = 2000
3	*meso*/*rac* **1**	α-C_{14} olefin	30	115	310	*n*-C_{15} ester (80)
					(95)	*br*-C_{15} esters[e] (20)
4	*meso*/*rac* **1**	Internal[d] C_{14} olefins	30	115	120	*n*-C_{15} ester (78)
					(93)	*br*-C_{15} esters[e] (22)
5	d^tbpp	Internal[d] C_{14} olefins	30	115	5	*n*-C_{15} ester (75)
					(10)	*iso*-C_{15} esters (25)
6	*rac* (96%) **1**	Propene	20	60	1000	*n*-Butyrate (81)
						Isobutyrate (19)
7	*meso* (80%) **1**	Propene	20	60	2000	*n*-butyrate (77)
						Isobutyrate (23)
8	*rac* (96%) **1**	Internal[d] C_{11}/C_{12} olefin	15	115	100	*n*-C_{12}/C_{13} esters (82)
					(93)	*br*-C_{12}/C_{13} esters[e] (18)
9	*meso* (80%) **1**	Internal[d] C_{11}/C_{12} olefin	15	115	160	*n*-C_{12}/C_{13} esters (80)
					(97)	*br*-C_{12}/C_{13} esters[e] (20)

[a] *meso*/*rac*-**1** and **2** is *ca*. 1 : 1 mixture of diastereomeric diphosphines. [b] 20 Bar ethene, 20 ml liquid propene or 20 ml olefin feed. [c] mol(mol) Pd h^{-1}; average activity over conversion (% in parentheses) after 5 h (entries 3 and 4), 10 h (entries 5, 8 and 9) or after complete consumption of olefin (ethylene and propylene experiments). [d] Thermodynamically equilibrated internal olefin mixture (<0.2% α-olefins). [e] Of which typically *ca*. 65% α-methyl, 35% higher alkyl branching.

traced to a combination of the effect of the electronegative oxygen atoms α to phosphorus and, perhaps more importantly, the effect of the acute (*ca*. 90°) C–P–C angle imposed by the cage.[15] Palladium–dppp isomerisation–carbonylation catalysts are known,[16] but the rate of hydroformylation of internal octenes was shown to be a factor of eight lower than the initial rate observed with 1-octene[17] and thus we cannot rationalise the observed catalysis on a purely electronic basis.

We thank Jan-Karel Buijink and Guido Batema for their contributions and Shell for financial support.

Notes and references

1 H. M. Colquhoun, D. J. Thompson and M. V. Twigg, *Carbonylation*, Plenum Press, New York, 1991.
2 E. Drent and E. Kragtwijk, *Eur. Pat*., EP 495 548, 1992 (to Shell).
3 G. R. Eastham, R. P. Tooze, X. L. Wang and K. Whiston, *World Pat*., 96/19434, 1996 (to ICI); W. Clegg, G. R. Eastham, M. R. J. Elsegood, R. P. Tooze, X. L. Wang and K. Whiston, *Chem. Commun*., 1999, 1877; G. R. Eastham, B. T. Heaton, J. A. Iggo, R. P. Tooze, R. Whyman and S. Zacchini, *Chem. Commun*., 2000, 609.
4 V. Gee, A. G. Orpen, H. Phetmung, P. G. Pringle and R. I. Pugh, *Chem. Commun*., 1999, 901.
5 J. C. L. J. Suykerbuyk, E. Drent and P. G. Pringle, *World. Pat*., 98/42717, 1998 (to Shell).
6 Typical reaction conditions: 0.1 mmol (22.5 mg) $Pd(OAc)_2$, 0.15 mmol (71 mg) diphosphine and 0.25 mmol (17.2 μL) methanesulfonic acid were dissolved in 50 ml methanol in a 250 ml Hastelloy C autoclave. After flushing the closed autoclave three times with 40 bar N_2, it was first pressurised with 20 bar of C_2H_4 and secondly with 30 bar CO. After 30 min the autoclave was heated to reaction temperature, and kept at this temperature by a Thermo-Electric 100 temperature control unit. The pressure was continuously recorded by using a Transamerica Instruments pressure transducer, series 2000. Activity data during the experiment were calculated from the pressure decrease with time and from the GLC analysis of the reaction product at the end of the reaction period, performed on a Perkin-Elmer 8500 equipped with two capillary columns, DBI 30 m and FFAP 50 m.
7 E. Drent and P. H. M. Budzelaar, *Chem. Rev*., 1996, **96**, 663.
8 S. J. Dosset, A. Gillon, A. G. Orpen, J. S. Fleming, P. G. Pringle, D. Wass and M. Jones, *Chem. Commun*., 2001, 699.
9 C. D. Frohning and C. W. Kohlpainter, in *Applied Homogeneous Catalysis with Organometallic Compounds*, Wiley-VCH, New York, 1996.
10 L. A. van der Veen, P. C. J. Kamer and P. W. N. M. van Leeuwen, *Angew. Chem., Int. Ed*., 1999, **38**, 336.
11 D. Selent, D. Hess, K.-D. Wiese, D. Röttger, C. Kunze and A. Börner, *Angew. Chem. Int. Ed*., 2001, **40**, 1696
12 C. Bianchini, H. M. Lee, A. Meli, S. Moneti, F. Vizza, M. Fontani and P. Zanello, *Macromolecules*, 1999, **32**, 4183; B. Sesto and G. Consiglio, *J. Am. Chem. Soc*., 2001, **123**, 4097.
13 C. A. Tolman, *Chem. Rev*., 1977, **77**, 313.
14 M. Harada, Y. Kai, N. Yasuoka and N. Kasai, *Bull. Chem. Soc. Jpn*., 1979, **52**, 390.
15 B. J. Dunne, R. B. Morris and A. G. Orpen, *J. Chem. Soc., Dalton Trans*., 1991, 653.
16 E. Drent, *Pure Appl. Chem*., 1990, **62**, 661.
17 E. Drent and P. H. M. Budzelaar, *J. Organomet. Chem*., 2000, **593–594**, 211.

CHEMCOMM Communication
www.rsc.org/chemcomm

Direct functionalisation of σ-aryl ligands: preparation of homoleptic functionalised aryls of osmium(IV)†

Man-Kit Lau,[a] Qian-Feng Zhang,[a] Joyce L. C. Chim,[a] Wing-Tak Wong[b] and Wa-Hung Leung*[a]

[a] *Department of Chemistry, The Hong Kong University of Science and Technology, Clear Water Bay, Kowloon, Hong Kong, P. R. China. E-mail: chleung@ust.hk*
[b] *Department of Chemistry, The University of Hong Kong, Pokfulam Road, Hong Kong, P. R. China*

Received (in Cambridge, UK) 9th May 2001, Accepted 26th June 2001
First published as an Advance Article on the web 23rd July 2001

The osmium(IV) tetraaryl complex $[Os(C_8H_9)_4]$ (C_8H_9 = 2,5-dimethylphenyl) reacts with pyridinium tribromide in the presence of Fe powder to give $[Os(C_8H_8Br)_4]$, which undergoes Suzuki coupling with arylboronic acids to afford a series of homoleptic functionalised aryls of osmium(IV).

Transition metal complexes of σ-aryl ligands bearing reactive functional groups are of interest because they may serve as structure building units for organometallic polymers that exhibit interesting electrical, magnetic or catalytic properties.[1] There are, however, relatively few reports on chemical functionalisation of σ-aryl ligands. Functionalised arylmetal complexes have been previously prepared by using mercury transmetallation reagents[2] or oxidative addition of aryl halides to low-valent metal centres.[3] Recently Roper and Wright and their coworkers reported the direct functionalisation of aryl[4] and 2-(2′-pyridyl)phenyl[5] groups σ-bound to ruthenium and osmium, demonstrating that these metal aryls are sufficiently inert to undergo a wide range of transformations. This prompted us to investigate the functionalisation of homoleptic aryls of osmium(IV), which are known to be remarkably stable.[6] The use of homoleptic functionalised aryls of osmium as metalloligands is of interest because of their tetrahedrally directing property, and the fact that they can be readily oxidised to paramagnetic Os^V species.[7] We here report on the acylation and bromination of an osmium tetraaryl, and the Suzuki cross-coupling reactions of the resulting osmium bromoaryl complex.

The osmium tetraaryl complex $[Os(C_8H_9)_4]$ **1** (C_8H_9 = 2,5-dimethylphenyl) was synthesised by alkylation of $[OsO_4]$ with C_8H_9MgBr in diethyl ether, as described elsewhere.[6,8] Scheme 1 summarises the reactions that lead to functionalisation of the aryl groups in **1**.

As reported previously, the electron-rich σ-aryl groups in osmium tetraaryls are prone to electrophilic attack, *e.g.* Friedel–Crafts acylation.[9] Thus, treatment of **1** with MeCOCl in the presence of Al_2Cl_6 afforded a mixture of $[Os(C_8H_8COMe)_3(C_8H_9)]$ **2** and $[Os(C_8H_8COMe)(C_8H_9)_3]$ **3** in 40 and 30% yield, respectively. The solid-state structure of complex **2** is shown in Fig. 1.‡ The geometry around Os in **2** is approximately tetrahedral (average C–Os–C′ angle of 109.5°) and the average Os–C distance is 1.99(1) Å. The MeCO group in each aryl ligand is situated at the *para* position relative to Os, indicative of the *para*-directing property of the Os centre. Bromination of **1** by pyridinium tribromide in the presence of Fe powder afforded the tetrabromide compound $[Os(C_8H_8Br)_4]$ **4** in 52% yield. Fig. 2 shows the molecular structure of **4**.‡ The geometry around Os in **4** is approximately tetrahedral [average C–Os–C′ angle of 109.5°] and the average Os–C distance of 2.00(2) Å. Complex **4** in CH_2Cl_2 exhibits a reversible Os^V–Os^{IV} couple at 0.45 V *vs.*. the ferrocenium–ferrocene couple, which is about 0.21 V more anodic than that for complex **1**[7] due to the inductive effect of the bromo substitutents.

† Electronic supplementary information (ESI) available: preparations of osmium tetraaryl complexes. See http://www.rsc.org/suppdata/cc/b1/b104075h/

The tetrabromide **4** has proved to be a good starting material for metal-catalysed cross-coupling reactions. For example, complex **4** underwent Suzuki coupling with 4-$XC_6H_4B(OH)_2$ in

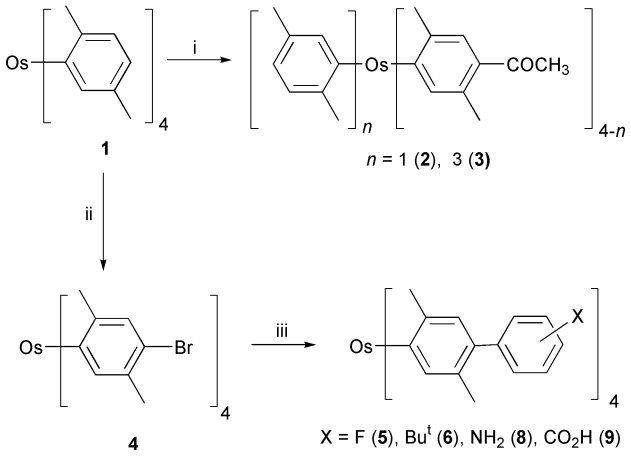

Scheme 1 *Reagents and conditions*: i, MeCOCl, Al_2Cl_6, CH_2Cl_2, −40 °C; ii, pyridinium tribromide, Fe powder, CH_2Cl_2, room temp; iii, 6 equivalents of arylboronic acids, $[Pd(PPh_3)_4]$, K_2CO_3, dmf, 110 °C.

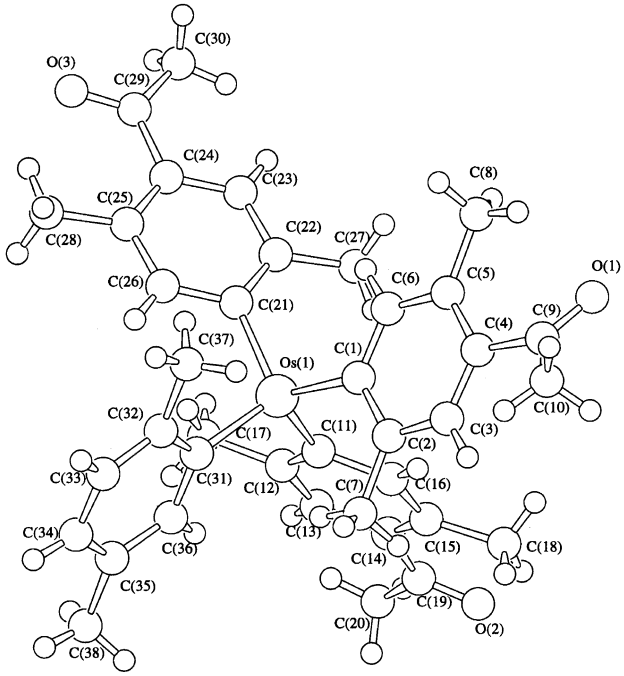

Fig. 1 Molecular structure of $[Os(C_8H_8COMe)_3(C_8H_9)]$ **2**. Selected bond lengths (Å) and angles (°): Os(1)–C(1) 2.011(9), Os–C(11) 1.975(9), Os(1)–C(21) 1.991(8), Os(1)–C(31) 1.985(10); C(1)–Os(1)–C(11) 107.9(3), C(1)–Os(1)–C(21) 111.7(3), C(1)–Os(1)–C(31) 110.7(4), C(11)–Os(1)–C(21) 108.0(4), C(11)–Os(1)–C(31) 110.0(4), C(21)–Os(1)–C(31) 108.5(4).

 DOI: 10.1039/b104075h

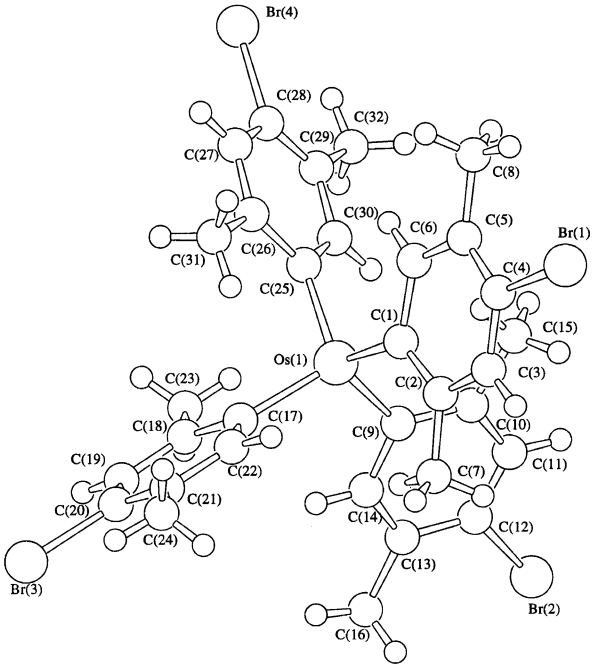

Fig. 2 Molecular structure of $[Os(C_8H_8Br)_4]$ **4**. Selected bond lengths (Å) and angles (°): Os(1)–C(1) 1.98(2), Os(1)–C(9) 2.01(2), Os(1)–C(17) 2.03(2), Os(1)–C(25) 1.98(1); C(1)–Os(1)–C(9) 107.3(6), C(1)–Os(1)–C(17) 111.6(6), C(1)–Os(1)–C(25) 109.5(6), C(9)–Os(1)–C(17) 110.8(6), C(9)–Os–C(25) 110.3(6), C(17)–Os(1)–C(25) 107.4(6).

the presence of $[Pd(PPh_3)_4]$ and K_2CO_3 to afford the respective homoleptic osmium biaryl $[Os(C_8H_8–C_6H_4X)_4]$ (X = F **5**, Bu^t **6**).§ Complexes **5** and **6** are highly soluble, lipophilic materials, which could be obtained as analytically pure dark solids after chromatography and recrystallisation. Oxidation of **5** with $AgBF_4$ gave a blue species, presumably $[Os(C_8H_8–C_6H_4F)_4]^+$, which exhibits an isotropic EPR signal at 77 K at g = 2.025 characteristic of Os^V species.[7] It appears that the Pd-catalysed cross coupling reaction involved oxidative addition of the aryl bromide ligand with Pd(0) followed by reductive elimination of the biaryl. The stoichiometric reaction between **4** and $[Pd(PPh_3)_4]$ afforded a blue solid analysed as $[Os(C_8H_8Br)_3\{C_8H_8PdBr(PPh_3)_2\}]$ **7**. Similarly, Pd-catalysed coupling of **4** with 3-$H_2NC_6H_4B(OH)_2$ and 4-$HO_2CC_6H_4$-$B(OH)_2$ afforded the tetraamine $[Os(C_8H_8–C_6H_4NH_2)_4]$ **8**, which seems to contain a very small amount of unknown impurity since the N analysis is not satisfactory at the moment, and the tetracarboxylic acid $[Os(C_8H_8–C_6H_4CO_2H)_4]$ **9**, respectively. Complex **9** is soluble both in organic solvents and in aqueous medium (pH $\geqslant$ 10), indicative of the inertness of the Os–C σ bonds. The homoleptic functionalised aryls of osmium can be used as starting materials for preparations of organometallic oligomers/polymers. For example, cyclic voltammetry indicated that complex **8** could be polymerised on a graphite electrode by anodic oxidation. A preliminary result showed that homo-coupling of the tetrabromide **4** by $[Ni(cod)_2]$ (cod = cycloocta-1,5-diene) yielded oligomers of **1**.[10]

In summary, we have demonstrated that the aryl groups in osmium tetraaryl complex **1** could be functionalised by electrophilic attack, *e.g.* acylation and bromination, without cleavage of the Os–C σ bonds. Suzuki coupling of the osmium bromoaryl complex with arylboronic acids provides convenient access to a wide range of homoleptic functionalized aryls of osmium, which can be used as starting materials for organoosmium oligomers/polymers.

This work has been supported by The Research Grants Council of Hong Kong, China (project no.: HKUST 6189/00P).

Notes and references

‡ *Crystal data*: for **2**: $C_{38}H_{42}O_3Os·½C_6H_{12}$, M = 779.03, triclinic, space group $P\bar{1}$ (no. 2), a = 12.424(2), b = 17.168(3), c = 9.184(2) Å, α = 91.71(2), β = 106.76(1), γ = 95.82(2)°, U = 1862.3(6) Å^3, T = 298 K, Z = 2, D_c = 1.389 g cm^{-3}, μ(Mo-Kα) = 3.456 mm^{-1}. 5289 reflections measured, 5016 unique (R_{int} = 0.033). The final R and $R_w(F)$ were 0.042 and 0.044, respectively, on 3843 reflections with $I > 1.5\sigma(I)$.

For **4**: $C_{32}H_{32}Br_4Os$, M = 926.42, monoclinic, space group $C2/c$ (no. 15), a = 37.556(8), b = 9.256(6), c = 18.856(7) Å, β = 97.13(3)°, U = 6503(4) Å^3, T = 298 K, Z = 8, D_c = 1.892 g cm^{-3}, μ(Mo-Kα) = 8.867 mm^{-1}. 6205 reflections measured, 6101 unique (R_{int} = 0.071). The final R and $R_w(F)$ were 0.067 and 0.051, respectively, on 3117 reflections with $I > 1.5\sigma(I)$. Empirical absorption corrections (on ψ-scans) were applied for **2** and **4**.

CCDC reference numbers 164948 and 164949. See http://www.rsc.org/suppdata/cc/b1/b104075h/ for crystallographic data in CIF or other electronic format.

§ *Typical procedure* for Suzuki coupling of **4** with arylboronic acids: to a solution of **4** (100 mg, 0.1 mmol) in *N*,*N*-dimethylformamide (20 cm^3) were added 6 equivalents of arylboronic acid, K_2CO_3 (83 mg, 0.6 mmol) and $[Pd(PPh_3)_4]$ (12 mg). The reaction mixture was heated at 110 °C for 2 h, evaporated to dryness *in vacuo*, and extracted with CH_2Cl_2. The products were purified by column chromatography [silica gel, eluent: CH_2Cl_2–hexane (1:5)] and further recrystallised from hexane (yield: 40–60%).

1 See, for example: P. Nguyen, P. Gomez-Elipe and I. Manners, *Chem. Rev.*, 1999, **99**, 1515 and references therein.
2 J. Vicente, J.-A. Abad, J. Gil-Rubio, P. G. Jones and E. Bembenek, *Organometallics*, 1993, **12**, 4151.
3 J. Vicente, J. A. Abad and J. A. Sachez, *J. Organomet. Chem.*, 1988, **352**, 257; W. A. Herrmann, C. Broßmer, T. Priermeier and K. Öfele, *J. Organomet. Chem.*, 1994, **481**, 97; J. Vicente, J. A. Abad, A. D. Frankland and M. C. Ramírez de Arellano, *Chem. Eur. J*, 1999, **5**, 3066.
4 G. R. Clark, C. E. L. Headford, W. R. Roper, L. J. Wright and V. P. D. Yap, *Inorg. Chim. Acta*, 1994, **220**, 261; G. R. Clark, C. E. F. Rickard, W. R. Roper, L. J. Wright and V. P. D. Yap, *Inorg. Chim. Acta*, 1996, **251**, 74.
5 M. Clark, C. E. F. Rickard, W. R. Roper and L. J. Wright, *Organometallics*, 1999, **18**, 2813; A. M. Clark, C. E. F. Rickard, W. R. Roper and L J. Wright, *J. Organomet. Chem.*, 2000, **598**, 262.
6 P. Starvopoulos, P. D. Savage, R. P. Tooze, G. Wilkinson, B. Hussain, M. Motevalli and M. B. Hursthouse, *J. Chem. Soc., Dalton Trans.*, 1987, 557.
7 J. Arnold, G. Wilkinson, B. Hussain and M. B. Hursthouse, *J. Chem. Soc., Dalton Trans.*, 1989, 2149.
8 M.-K. Lau, J. L. C. Chim, W.-T. Wong, I. D. Williams and W.-H. Leung, *Can. J. Chem.*, 2001, **79**, 000. in press.
9 P. D. Savage, PhD Thesis, Imperial College of Science and Technology, London, UK, 1987.
10 M.-K. Lau, W.-T. Wong, B. Tang and W.-H. Leung, results to be published.

CHEMCOMM Communication
www.rsc.org/chemcomm

Linear fluorescent oligonucleotide probes with an acridine quencher generate a signal upon hybridisation

Rohan T. Ranasinghe,[a] Lynda J. Brown[b] and Tom Brown*[a]

[a] *Department of Chemistry, University of Southampton, Highfield, Southampton, UK SO17 1BJ. E-mail: tb2@soton.ac.uk; Fax: +44 (0)23 80592991; Tel: +44 (0)23 80592974*

[b] *Oswel Research Products Ltd., Medical and Biological Sciences Building, University of Southampton, Bassett Crescent East, Southampton, UK SO16 7PX. E-mail: oswel@compuserve.com; Fax: +44 (0)23 80592982/3; Tel: +44 (0)23 80592984/5*

Received (in Cambridge, UK) 18th May 2001, Accepted 26th June 2001
First published as an Advance Article on the web 23rd July 2001

Linear, single stranded probes incorporating a fluorophore and an acridine moiety are weakly fluorescent until hybridised to a complementary target nucleic acid whereupon fluorescence increases due to reduced quenching.

In recent years interest in the detection of nucleic acid sequences in homogeneous solution has soared due to major developments in molecular genetics. Fluorescent moieties are the reporter groups of choice in these applications. Typically, an oligonucleotide probe is labelled with a fluorophore and a quencher. A reduction in quenching is caused by hybridisation of the probe to its target nucleic acid, leading to signal generation. Examples of such methods are scorpion primers,[1] TaqMan™ probes[2] and molecular beacons.[3]

These methods rely upon changes in secondary structure upon hybridisation, or subsequent enzymatic degradation of the probe for signal generation. Here, we describe a novel linear dual-labelled fluorescent probe capable of detecting specific nucleic acids in homogeneous solution that is not reliant on either of these mechanisms. The unhybridised linear probe is essentially non-fluorescent due to energy transfer between the fluorophore and the acridine quencher. However, formation of a probe–target duplex allows the acridine moiety to interact with the double strand—it can no longer act as an efficient quencher and a fluorescent signal is generated (Fig. 1). An acridine derivative has been used previously in an oligonucleotide probe as the donor in a fluorescence resonance energy transfer (FRET) system.[4] The mechanism of action leads to a *decrease* in fluorescent signal upon hybridisation. In contrast, the system we describe utilises the acridine moiety as a quencher – leading to an *increase* in fluorescence.

The probe is synthesised with the fluorophore 6-carboxy fluorescein (FAM), (Fig. 2i) at the 5′-end† linked to the intercalator 9-amino-6-chloro-2-methoxyacridine[5] (Fig. 2ii).

The advantages of the method lie in its simplicity: the probes are free of secondary structure, relatively short and inexpensive to synthesise (commercially available phosphoramidite monomers are used, Fig. 2), and the acridine stabilises probe–target hybrids.

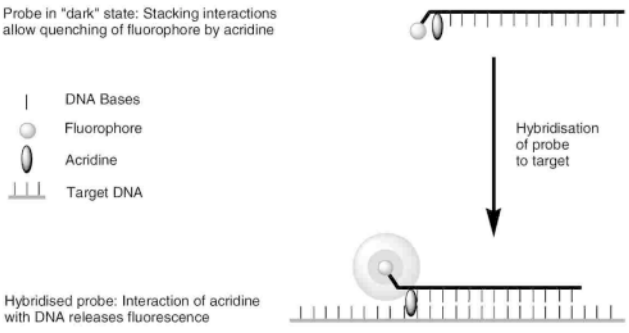

Fig. 1 Mechanism of action of the dual-labelled probe.

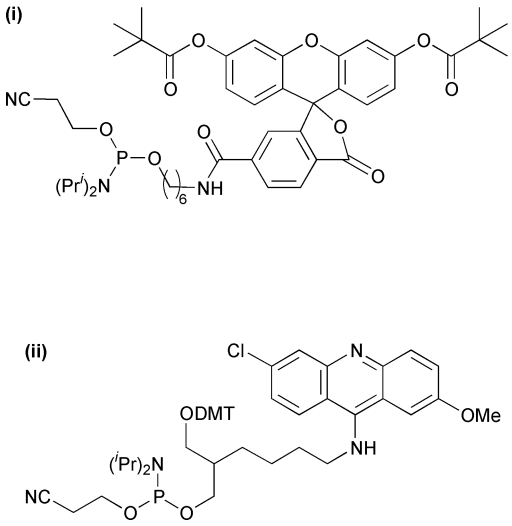

Fig. 2 Monomers used in probe synthesis (i) *O*-[(3′,6′-dipivaloyl-fluorescein-6-ylcarboxamidohexyl] *O*′-(2-cyanoethyl) (*N*,*N*-diisopropyl) phosphoramidite (PE Biosystems) (ii) *O*-[1-dimethoxytrityloxy-2-(*N*-acridin-1-yl-4-aminobutyl)propyl] *O*′-(2-cyanoethyl) (*N*,*N*,-diisopropyl)phosphoramidite (Glen Research).

The 14-mer probe (P1) used in this study was designed to hybridise to the wild type N1303K locus[6]‡ of the ABCC7 gene on chromosome 7 that produces the cystic fibrosis transmembrane conductance regulator (CFTR) protein. The probe sequence is:

5′-FAM-acridine-AAAAACTTGGATCC-octanediol-3′ (P1)

In the current studies we used a synthetic oligodeoxynucleotide version of a 24-nucleotide section of the target locus:

5′- TAGGGATCCAAGTTTTTTCTAAAT-3′ (T1)

The probe was synthesised as a 2′-*O*-methyl oligoribonucleotide. 2′-*O*-Methyl oligoribonucleotides are not generally substrates for hydrolysis by DNase enzymes, and the probes were assembled from 2′-*O*-methyl RNA phosphoramidites (Glen Research) to avoid a TaqMan-like cleavage[2] in any subsequent PCR assay. Octanediol (phosphoramidite was a gift from Oswel Research Products Ltd.) was incorporated at the 3′ end of the probe to avoid extension of the probe by *Taq* polymerase during PCR. In preliminary studies we have shown that the observed effect (Fig. 1) also occurs with oligodeoxynucleotide probes with unmodified sugars, and that the optimum position for attachment of the acridine is directly adjacent to the fluorophore.

The dual-labelled probe (210 nM) P1 was added to a suitable hybridisation buffer (100 mM sodium phosphate, 1 mM EDTA, 100 mM NaCl, pH 7.0) at room temperature, and the emission spectrum recorded on an LS 50B Luminescence Spectrometer

 DOI: 10.1039/b104421b

Table 1 T_m results of UV melting experiments

T_m of P1 with T1/ °C	T_m of C1 with T1/°C	ΔT_m °C
54.0[a]	52.3[a]	+1.7

[a] All experiments were run in triplicate, and the average reading reported.

(Perkin Elmer), from excitation at 495 nm. The synthetic target (T1, 1050 nM) was then added and the emission spectrum re-recorded with excitation at 495 nm.

On addition of T1 and excitation at 495 nm the fluorescence intensity at 520 nm rose from 61.6 units to 250.3 units (a 4.5-fold increase).

In order to investigate the mechanism of fluorescence enhancement we performed UV melting experiments to determine the T_m value of probe–target hybrids. Intercalators such as acridine are known to stabilise duplexes by participating in π-stacking and electrostatic interactions with the nucleobases.[7] A control unlabelled 2′-*O*-methyl oligoribonucleotide was synthesised with a sequence analogous to the probe:

5′-AAAAACTTGGATCC-octanediol-3′ (C1)

The probe P1 (963 nM) and the synthetic target (T1, 1260 nM) were added to the hybridisation buffer (100 mM sodium phosphate, 1 mM EDTA, 100 mM NaCl, pH 7.0). The sample was heated (75 °C, 1 min), cooled (15 °C, 1 min), then melted by heating for 3880 s, at 1 °C min^{-1}. The ultraviolet absorbance was continuously monitored at 260 nm on a Perkin Elmer Lambda 15 UV/VIS Spectrophotometer. T_m values were calculated using the PECSS 2 software (Perkin Elmer). The experiment was repeated, with unlabelled probe C1 (963 nM) in place of P1. The results are shown in Table 1.

The labelled probe–target hybrid exhibited a higher T_m than the analogous unlabelled probe–target hybrid suggesting that the acridine moiety intercalates into, or stacks on the end of the duplex upon hybridisation. Further experiments are necessary to confirm the precise interaction.

The lack of any probe secondary structure simplifies design, and enables the use of very short probes, since hybridisation to the target does not have to compete with any intramolecular structures. This can be a problem with molecular beacons.

To investigate the ability of the probes to discriminate between fully matched targets and those containing a single mismatch we prepared a further three oligodeoxynucleotides designed to form duplexes with a single base pair mismatch in the highlighted position:

5′-TAGGGATCCAA**C**TTTTTTCTAAAT-3′ (T2)

5′-TAGGGATCCAA**T**TTTTTTCTAAAT-3′ (T3)

5′-TAGGGATCCAAA**A**TTTTTTCTAAAT-3′ (T4)

P1 (0.5 μM) and the complement (5 μM T1, T2, T3, T4 or water) were added to a Roche LightCycler™ capillary containing a buffer (20 mM $(NH_4)_2SO_4$, 75 mM tris–HCl, 0.01% Tween, 4 mM $MgCl_2$, 250 ng μL^{-1} bovine serum albumin). Each tube was subjected to denaturation (95 °C, 30 s), cooled (25 °C), and then immediately heated (95 °C, 0.2 °C s^{-1}), whilst monitoring fluorescence in Channel 1 ($\lambda_{em} \approx 520$ nm) of the LightCycler™ (Roche). T_m values were calculated using the LightCycler™ software (Roche). The results are shown in Table 2.

In samples containing the synthetic targets (T1, T2, T3 or T4), the fluorescence intensity decreased with melting of the probe–target hybrid (Fig. 3). The first derivative of the melting curves allowed calculation of the T_m of probe–target hybrids (Table 2). Analysis of this data shows excellent discrimination between matched and mismatched probe–target hybrids, with the T_m values differing by up to 18.3 °C.

Table 2 T_m results of fluorescent melting experiments

Complement	Description of complement	T_m/°C	ΔT_m/°C
T1	Matched	56.8[a]	—
T2	C:C mismatch	38.5[a]	−18.3
T3	C:T mismatch	40.6[a]	−16.2
T4	C:A mismatch	40.9[a]	−14.9

[a] All experiments were run in triplicate, and the average reading reported.

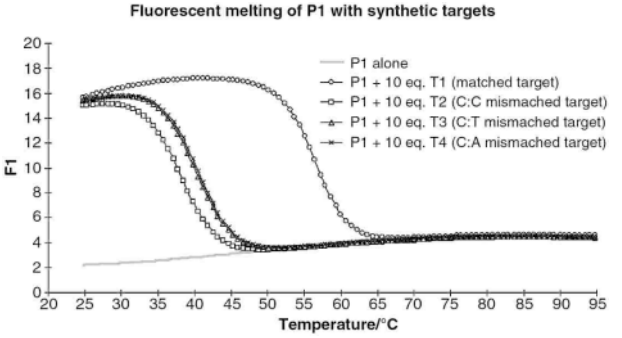

Fig. 3 Melting curves obtained from melting P1 with T1–T4.

We attribute the small rise of fluorescence with increasing temperature to thermal disruption of the fluorophore–quencher pair; in particular by increased molecular motion of the fluorescein moiety, although we have not investigated the phenomenon further.

In summary, we have developed a novel technique for detecting nucleic acid sequences that has advantages over existing methods.[8] The lack of probe secondary structure in this system allows the use of shorter probes with enhanced mismatch discrimination. At present, we are investigating the use of probes of this type in real time PCR and have shown that in this context P1 is capable of detecting a 103 base pair amplicon of the N1303K locus. We also expect the low activation barrier to probe hybridisation in this type of system to be advantageous in microarray technology.

Notes and references

† All oligonucleotides were synthesised on an ABI 394 DNA synthesiser using standard solid phase chemistry and commercially available phosphoramidites at Oswel Research Products Ltd. (Fig. 2).

‡ GenBank accession number M55128.

1 D. Whitcombe, J. Theaker, S. P. Guy, T. Brown and S. Little, *Nat. Biotechnol.*, 1999, **17**, 804; N. Thelwell, S. Millington, A. Solinas, J. A. Booth and T. Brown, *Nucleic Acids Res.*, 2000, **28**, 3752.

2 P. M. Holland, R. D. Abramson, R. Watson and D. H. Gelfand, *Proc. Natl. Acad. Sci. USA*, 1991, **88**, 7276; T. H. S. Woo, B. K. C. Patel, L. D. Smythe, M. A. Norris, M. L. Symonds and M. F. Dohnt, *Anal. Biochem.*, 1998, **256**, 132.

3 S. Tyagi and F. R. Kramer, *Nat. Biotechnol.*, 1996, **14**, 303; S. Tyagi, D. P. Bratu and F. R. Kramer, *Nat. Biotechnol.*, 1998, **16**, 49; L. G. Kostrikis, S. Tyagi, M. M. Mhlanga, D. D Ho and F. R. Kramer, *Science*, 1998, **279**, 1228.

4 K. Shinozuka, Y. Seto and H. Sawai, *J. Chem. Soc., Chem. Commun.*, 1994, 1377.

5 D. E. Comings, J. Limon, A. Ledochowski and K. C. Tsou, *Exp. Cell Res.*, 1978, **117**, 451.

6 L. Osborne, G. Santis, M. Schwarz, K. Klinger, T. Dork, I. McIntosh, M. Schwartz, V. Nunez, M. Macek and J. Reiss *et al.*, *Hum. Genet.*, 1992, **89**, 653.

7 H. M Berman and P. R. Young, *Annu. Rev. Biophys. Bioeng.*, 1981, **10**, 87.

8 L. J. Brown and T. Brown, Patent Pending, (patent applicaton no. 0111833.0), 2001.

CHEMCOMM
Communication
www.rsc.org/chemcomm

Beyond Fe-only hydrogenases: *N*-functionalized 2-aza-1,3-dithiolates $Fe_2[(SCH_2)_2NR](CO)_x$ (x = 5, 6)

Joshua D. Lawrence, Hongxiang Li and Thomas B. Rauchfuss*

Department of Chemistry, University of Illinois, 601 S. Goodwin Ave., Urbana, IL 61801, USA. E-mail: rauchfuz@uiuc.edu

Received (in Cambridge, UK) 14th May 2001, Accepted 26th June 2001
First published as an Advance Article on the web 23rd July 2001

Primary amines undergo chloromethylation with CH_2O/$SOCl_2$ to give $RN(CH_2Cl)_2$, which in turn react with $Li_2[Fe_2S_2(CO)_6]$ to give $Fe_2[(SCH_2)_2NR](CO)_6$; in the case of R = $CH_2CH{=}CH_2$ and CH_2CH_2SMe, Me_3NO-induced decarbonylation afforded pentacarbonyl derivatives wherein the pendant functionality is coordinated to Fe.

The Fe-only hydrogenases are a topical class of proteins with organometallic reaction centers of the formula $[Fe_2(SR)_2(CN)_2(CO)_3\{Fe_4S_4(\mu\text{-}SR)(SR)_3\}(X)]$ (X = H_2O, CO, H^-/H_2).[1,2] Significant progress has been achieved in characterizing the first coordination shell of the diiron core,[3–5] including high quality crystal structures of the dicyanides $[Fe_2(SR)_2(CN)_2(CO)_4]^{2-}$ **1**.[3] It has recently been proposed that the dithiolate ligand is an azadithiolate $SCH_2NH_xCH_2S$,[6] and we have used $(ClCH_2)_2NMe$ to introduce this novel functionality (Scheme 1).[7]

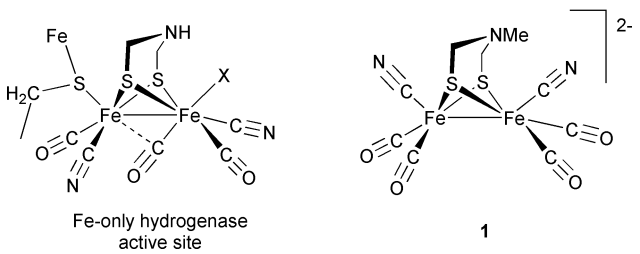

Fe-only hydrogenase active site

1

Scheme 1

Because the azadithiolate cofactor defines an unprecedented coordination motif, we sought to explore its scope. The only known bis(chloromethyl)amine, $(ClCH_2)_2NMe$, is however prepared *via* an uninviting degradation of triazine $[CH_2NMe]_3$ using PCl_5.[8]

We have found that many primary amines undergo efficient chloromethylation upon treatment with a solution of paraformaldehyde followed by 2× excess of $SOCl_2$ (Scheme 2). The reactions occur under mild conditions, and the chloromethylated amines are isolated as the free bases. In some cases the amines were further purified by vacuum distillation, but usually evaporation of ether extracts provided the targeted species. These compounds were identified by ^1H NMR spectroscopy (characteristic NCH_2Cl singlet at δ 5.5–5.2) as well as elemental analysis or high resolution mass spectrometry. The following derivatives were prepared: allyl (**2a**), *tert*-butyl (**2b**), methylcarboxylethyl (**2c**), benzyl (**2d**), 4-nitroaniline (**2e**), and 2-(methylthio)ethyl (**2f**).† Compounds **2a–f** are stable under anhydrous conditions at 0 °C.

Iron thiolate carbonyl dimers were prepared from bis(chloromethyl)amines **2a**, **2b**, **2c**, **2f** by treatment with $Li_2[Fe_2(S)_2(CO)_6]$ (Scheme 2), as for the synthesis of **1**.[7] Recrystallization from hexanes gave analytically pure samples with isolated yields of *ca.* 50% for $Fe_2[(SCH_2)_2NR](CO)_6$, **3a**, **3b**, **3c**, (**3f** was generated *in situ* and used immediately, see below).‡ We found that these alkylations proceeded more efficiently when the crude product mixture is treated with Et_3N at −78 °C to complex the BEt_3 coproduct.[9]

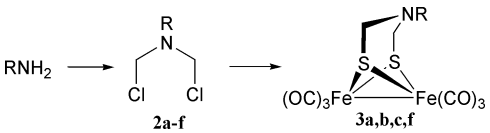

2a-f **3a,b,c,f**

Scheme 2

Suitable substituents on the amine nitrogen should be capable of coordinating to one of the two Fe centers. Decarbonylation of **3a** with Me_3NO afforded a single new derivative. Recrystallization afforded *ca.* 50% yield of the deep red pentacarbonyl $Fe_2[(SCH_2)_2N\text{-}\eta^2\text{-}CH_2CH{=}CH_2](CO)_5$ **4a**.§ ^1H NMR measurements indicate that the alkene is coordinated, *e.g.*, the $CH_2CH{=}CH_2$ signals show greatly increased coupling and chemical shift range (2.5 ppm) relative to the hexacarbonyl **3a**. Furthermore the 2-D ^1H NMR spectrum demonstrated that all methylene hydrogen atoms are diastereotopic indicative of lowered symmetry. The IR spectrum for **4a** was characteristic of a $Fe_2(SR)_2(CO)_5L$ species.[10]

Crystallographic characterization¶ shows that **4a** adopts a cage-like structure with one Fe center bound to a pair of S atoms and the alkene (Fig. 1). The alkene is approximately *trans* to the Fe–Fe bond. The remaining Fe–Fe and Fe–C and Fe–S distances are normal, indicating that the chelation does not impose strain on the Fe_2S_2 core. Alkene adducts of iron thiolates are not widely known, the closest examples being (1) $Fe_2(SMe)_2(CO)_6C_2F_4$, which results from the oxidative addition of tetrafluoroethene across the Fe–Fe bond,[11] and (2) $Fe_2(SPh)(CH_2{=}CHCHCHCH_2)(CO)_5$, which contains both alkene and allyl ligands.[12]

Analogously to the preparation of **4a**, MeCN solutions of **3c** and **3f** were subjected to Me_3NO-induced decarbonylation. We were unable to effect coordination of the ester group in **3c**, but the thioether did cyclise to give $Fe_2[(SCH_2)_2NCH_2CH_2SMe](CO)_5$ **4f** (Scheme 3). Crystallographic

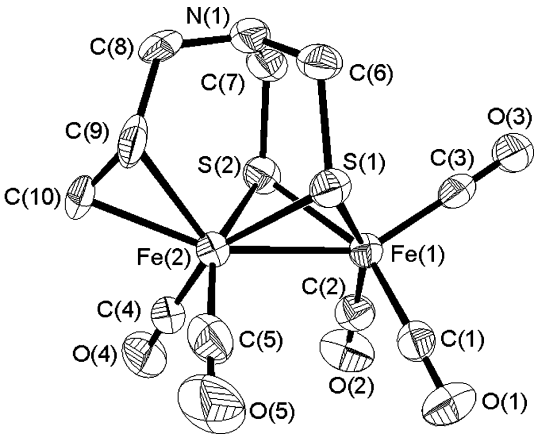

Fig. 1 Structure of $Fe_2[(SCH_2)_2NCH_2CH{=}CH_2](CO)_5$ **4a** with thermal ellipsoids set at the 50% probability level. Selected distances (Å) and angles (°): Fe(1)–Fe(2), 2.5132(6); Fe(2)–C(9), 2.185(10); Fe(2)–C(10), 2.149(8); C(9)–C(10), 1.401(11); S(1)–C(6), 1.851(3); S(2)–C(7), 1.858(3); C(6)–N1–C(7), 113.6(3); C(7)–N(1)–C(8), 123.1(7); C(6)–N(1)–C(8), 107.0(7).

 DOI: 10.1039/b104195a

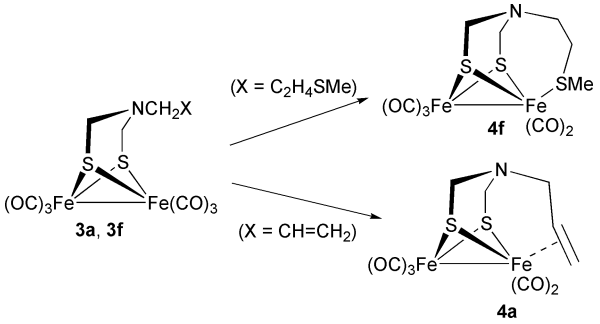

Scheme 3

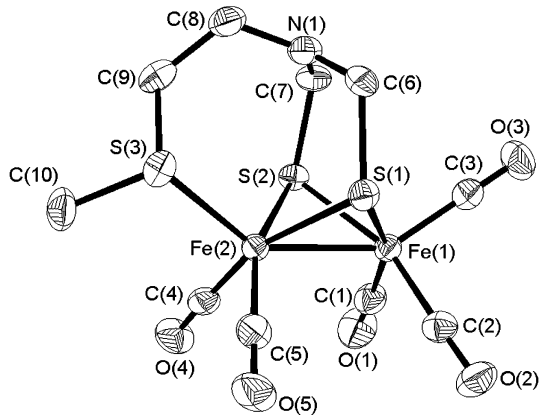

Fig. 2 Structure of $Fe_2[(SCH_2)_2NCH_2CH_2SMe](CO)_5$ **4f** with thermal ellipsoids set at the 50% probability level. Selected distances (Å) and angles (°): Fe(1)–Fe(2), 2.5144(14); Fe(2)–S(3), 2.2703(15); S(1)–C(6), 1.870(3); S(2)–C(7), 1.865(3); C(6)–N1–C(7), 115.4(3); C(7)–N(1)–C(8), 121.3(3); C(6)–N(1)–C(8), 118.3(3).

characterization showed that the thioether is coordinated in **4f** (Fig. 2). Pickett and coworkers have recently reported a similar complex $Fe_2[(SCH_2)_2CHCH_2SMe](CO)_5$.[13] For **4a**, and to an even greater extent, **4f**, C–S distances are lengthened and C–N–C angles are increased due to the anomeric effect.[7]

In summary, a new route to bis(chloromethyl)amines allows general access to a broad class of *N*-functionalized azadithiolato complexes. Independent of any biological relevance, azadithiolates could be applied more generally, especially as bridging ligands with functionality.[14]

This research was supported by the U.S. National Institute of Health.

Notes and references

† *Representative procedure*: a mixture of 1.8 g (0.025 mol) Bu^tNH_2, 1.95 g (0.065 mol) paraformaldehyde, and 30 mL CH_2Cl_2 was stirred for *ca*. 3 h; the resulting suspension was treated dropwise with 11.9 g (0.1 mol) of $SOCl_2$. After gas evolution had ceased, solvent and unreacted $SOCl_2$ were removed under vacuum and the products were purified by extraction into Et_2O. **CAUTION**: chloromethylamines resemble mustards and should be handled cautiously. **2a**: Colorless oil; bp 40 °C (0.6 mm Hg); yield: 70%. Anal. Calc. for $C_5H_9Cl_2N$: C, 38.99; H, 5.89; N, 9.09. Found: C, 38.98; H, 6.27; N, 9.16%. ^{1}H NMR ($CDCl_3$): δ 5.75 (1H, m, CH_2=C*H*), 5.30–5.32 (2H, m, CH_2=CH), 5.18 (4H, s, NCH_2Cl), 3.48 (2H, m, CHCH_2N). MS (EI): 153 (M). **2b**: Colorless oil; bp 50 °C (0.8 mm Hg); yield: 60%. Anal. Calc. for $C_6H_{13}Cl_2N$: C, 42.37; H, 7.70; N, 8.24; Cl, 41.69. Found: C, 42.22; H, 7.85; N, 8.01; Cl, 41.62%. ^{1}H NMR ($CDCl_3$): δ 5.42 (4H, s, NCH_2Cl), 1.34 (9H, s, (CH_3)$_3$C). MS (EI): 169 (M^+). **2c**: Colorless solid; mp 51 °C; yield: 33%. Anal. Calc. for $C_5H_9Cl_2NO_2$: C, 32.28; H, 4.88; N, 7.53. Found: C, 32.62; H, 5.36; N, 7.67%. ^{1}H NMR ($CDCl_3$): δ 5.20 (4H, s, NCH_2Cl), 3.76 (2H, s, NCH_2CO_2), 3.75 (3H, s, CO_2CH_3). **2d**: Colorless oil; bp 80 °C (0.05 mm Hg); yield: 50%. ^{1}H NMR ($CDCl_3$): δ 7.40 (5H, m, C_6H_5), 5.22 (4H, s, NCH_2Cl), 4.15 (2H, s, $C_6H_5CH_2$N). HR-EIMS: Calc. for $C_9H_{11}Cl_2N$, *m*/*z* 202.018731 (M − 1). Found: 202.019030 (M − 1). **2e**: pale yellow solid; mp 99 °C; yield: 85%. ^{1}H NMR ($CDCl_3$): δ 7.28–8.29 (4H, dd, C_6H_4), 5.54 (4H, s, NCH_2Cl). HR-EIMS: Calc. for $C_8H_8Cl_2N_2O_2$, *m*/*z* 233.995973. Found: 233.996283. **2f**: Colorless oil; yield: 70%. ^{1}H NMR ($CDCl_3$): δ 5.24 [s, 4H, N(CH_2Cl)$_2$], 3.24 (t, 2H, CH_2CH_2N), 2.76 (t, 2H, CH_3SCH_2), 2.18 (s, 3H, CH_3SCH_2).

‡ **3a**: Red crystals after chromatography on silica gel and recrystallization from hexanes; yield: 58%. Anal. Calc. for $C_{11}H_9Fe_2NO_6S_2$: C, 30.94; H, 2.12; N, 3.28. Found: C, 30.84; H, 1.97; N, 3.43%. ^{1}H NMR (C_6D_6): δ 5.22 (m, 1H, CH_2=CH), 4.77 and 4.66 (ddq, 2H, NCH_2CH=CH_2), 2.55 (s, 4H, NCH_2S), 2.38 (d, 2H, NCH_2CH=CH_2). IR (hexanes): ν_{co} 2076, 2038, 2003, 1999 cm^{-1}. **3b**: Red crystals from hexanes; yield: 58%. Anal. Calc. for $C_{12}H_{13}Fe_2NO_6S_2$: C, 32.53; H, 2.96; N, 3.16. Found: C, 32.42; H, 3.10; N, 3.20%. ^{1}H NMR (CD_3CN): δ 3.29 (br, 4H, NCH_2S), 0.97 (s, 9H, CH_3). IR (hexane): ν_{co} 2074, 2036, 2003, 1995 cm^{-1}. **3c**: Red crystals from hexanes; yield: 31%. ^{1}H NMR (CD_3CN): δ 3.12 (s, 3H, CO_2CH_3), 2.85 (s, 4H, NCH_2S), 2.68 (s, 2H, NC$H_2CO_2CH_3$). IR (hexane): ν_{co} 2076, 2044, 2037, 2004, 1996 cm^{-1}, ν_{ester} 1752 cm^{-1}.

§ **4a**: An orange solution of 0.150 g (0.35 mmol) **3a** in 10 mL of MeCN was treated with 0.026 g (0.35 mmol) $ONMe_3$ in MeCN. The resulting red–purple solution was evaporated and the product crystallized from cold hexane. Yield: 45%. Anal. Calc. for $C_{10}H_9Fe_2NO_5S_2$: C, 30.10; H, 2.27; N, 3.51. Found: C, 29.94; H, 2.10; N, 3.41%. ^{1}H NMR (C_6D_6): δ 4.17 (m, 1H, NCH_2CH=CH_2), 3.69 and 3.06 (dd, 2H, NCH_2CH=CH_2), 3.07 and 2.40 (s and AA′BB′, 4H, NCH_2S), 2.77 and 1.48 (dd and dd, 2H, NCH_2CH=CH_2). IR (hexanes): ν_{CO} 2062, 2009, 1998, 1982, 1967 cm^{-1}. **4f**: Dark red crystals from hexanes; yield: 32%. Anal. Calc. for $C_{10}H_{11}Fe_2NO_5S_3$: C, 27.71; H, 2.54; N, 3.23. Found: C, 27.78; H, 2.55; N, 3.23%. ^{1}H NMR (CD_3CN): δ 4.10 and 4.01 (dd, 4H, SH_2CNCH_2S), 3.12 (b, 4H, NCH_2CH_2SMe), 2.66 (s, 3H, SCH_3). IR (hexane): ν_{CO} 2053, 1990, 1970, 1943 cm^{-1}.

¶ *Crystal data*: for **4a** $C_{10}H_9Fe_2NO_5S_2$, M = 399.0, monoclinic, $P2_1/n$, a = 10.7450(13), b = 9.4727(11), c = 14.1176(16) Å, β = 91.324(2)°, V = 1436.6(3) Å^3, T = 193 K, Z = 4, max. min. transmission: 0.9990, 0.7248, D_c = 1.845 g cm^{-3}, 11960 reflections collected, 3222 unique, R_{int} = 0.0763, $R1$ = 0.0384, $wR2$ = 0.0548 [$I > 2\sigma(I)$]. For **4f** $C_{20}H_{22}Fe_4N_2O_{10}S_6$, M = 866.16, monoclinic, $P2_1/n$, a = 17.341(11), b = 10.489(7), c = 18.338(12) Å, β = 110.020(12)°, V = 3134(3) Å^3, T = 193 K, Z = 4, max. min. transmission: 0.9918, 0.7477, D_c = 1.863 g cm^{-3}, 28546 reflections collected, 7566 unique, R_{int} = 0.0489, $R1$ = 0.322, $wR2$ = 0.0709 [$I > 2\sigma(I)$].

CCDC reference numbers 163360 and 163361. See http://www.rsc.org/suppdata/cc/b1/b104195a/ for crystallographic data in CIF or other electronic format.

1 M. W. W. Adams and E. I. Stiefel, *Curr. Opin. Chem. Biol.*, 2000, **4**, 214.
2 Y. Nicolet, B. J. Lemon, J. C. Fontecilla-Camps and J. W. Peters, *Trends Biochem. Sci.*, 2000, **25**, 138.
3 M. Schmidt, S. M. Contakes and T. B. Rauchfuss, *J. Am. Chem. Soc.*, 1999, **121**, 9736.
4 A. Le Cloirec, S. P. Best, S. Borg, S. C. Davies, D. J. Evans, D. L. Hughes and C. J. Pickett, *Chem. Commun.*, 1999, 2285.
5 E. J. Lyon, I. P. Georgakaki, J. H. Reibenspies and M. Y. Darensbourg, *Angew. Chem., Int. Ed.*, 1999, **38**, 3178.
6 Y. Nicolet, A. L. de Lacey, X. Vernède, V. M. Fernandez, E. C. Hatchikian and J. C. Fontecilla-Camps, *J. Am. Chem. Soc.*, 2001, **123**, 1596.
7 J. D. Lawrence, H. Li, T. B. Rauchfuss, M. Bénard and M.-M. Rohmer, *Angew. Chem., Int. Ed.*, 2001, **40**, 1768.
8 E. Fluck and P. Meiser, *Chem. Ber.*, 1973, **106**, 69.
9 D. Seyferth, R. S. Henderson and L. C. Song, *Organometallics*, 1982, **1**, 125.
10 P. C. Ellgen and J. N. Gerlach, *Inorg. Chem.*, 1973, **12**, 2526.
11 J. J. Bonnet, R. Mathieu, R. Poilblanc and J. A. Ibers, *J. Am. Chem. Soc.*, 1979, **101**, 7487.
12 D. Seyferth, L. L. Anderson, F. Villafane and W. M. Davis, *J. Am. Chem. Soc.*, 1992, **114**, 4594.
13 M. Razavet, S. C. Davies, D. L. Hughes and C. J. Pickett, *Chem. Commun.*, 2001, 847.
14 S. H. Park, A. J. Lough, G. P. A. Yap and R. H. Morris, *J. Organomet. Chem.*, 2000, **609**, 110; R. H. Crabtree, J. A. Loch, K. Gruet, D. H. Lee and C. Borgmann, *J. Organomet. Chem.*, 2000, **600**, 7.

CHEMCOMM Communication
www.rsc.org/chemcomm

Highly efficient copper-catalysed oxidation of ascorbic acid by peroxynitrite

Yurii V. Geletti, Alan J. Bailey, Eric A. Boring and Craig L. Hill*

Department of Chemistry, Emory University, 1515 Pierce Drive, Atlanta, Georgia, 30322, USA. E-mail: chill@emory.edu

Received (in Cambridge, UK) 10th May 2001, Accepted 29th June 2001
First published as an Advance Article on the web 26th July 2001

The simple salt $CuCl_2{\cdot}2H_2O$, and the new Cu-substituted polyoxometalate (POM), $Na_7[CuCoW_{11}O_{39}]{\cdot}5H_2O$ 1 are highly efficient catalysts for the oxidation of ascorbic acid by peroxynitrite.

The chemistry and reactivity of the biologically important inorganic toxin peroxynitrite† is not yet fully understood.[1,2] Antioxidants are believed to reduce the toxic effects of peroxynitrite[3] and ascorbic acid is the most common antioxidant *in vivo*. The reaction between ascorbic acid and peroxynitrite is relatively slow (k = 42–47 M^{-1} s^{-1} at 25 °C, pH 7.4).[4,5] Transition metals are known to catalyse the decomposition of peroxynitrite and other peroxo species.[1,2,6] There are a number of reports in the literature of copper complexes that catalyse the oxidation of ascorbic acid using dioxygen[7] and peroxo species.[8] We report here the highly efficient catalytic oxidation of ascorbic acid by peroxynitrite in the presence of the simple aqueous cupric ion (henceforth Cu^{2+}), formed by dissolution of $CuCl_2{\cdot}2H_2O$, and the new Cu-substituted Co-centred polyoxometalate (POM), $Na_7[CuCoW_{11}O_{39}]{\cdot}5H_2O$ **1**.

Peroxynitrite was prepared by the reaction of nitrite and acidified hydrogen peroxide solution followed by quenching with NaOH in a simple flow reactor.[9] The concentrations of these solutions were determined by UV–VIS spectroscopy [ε_{302} = 1.7 × 10^3 M^{-1} cm^{-1}].[10] The new POM, **1**, was prepared by the slow addition of $K_9[CoW_{11}O_{39}]{\cdot}14H_2O$[11] to a solution containing an excess of $CuCl_2$.‡

Phosphate buffer solutions (pH 7.4) of Cu^{2+} show highly efficient catalysis of ascorbic acid oxidation by peroxynitrite. We also prepared and characterised **1**, a new type of mixed-metal POM, and compared its catalytic properties to those of Cu^{2+}. The kinetics of peroxynitrite decay are exponential§ and follow the rate law in eqn. (1) where k_{obs} increases linearly with [Cu^{2+}] (Fig. 1).

$$-d[ONOO^-]/dt = k_{obs}[ONOO^-] \quad (1)$$

The addition of EDTA completely inhibits the catalytic activity of Cu^{2+} and even results in a decrease of the reaction rate in the blank reaction (due to chelation of residual Cu^{2+}). The rate remains constant until [Cu^{2+}] ≈ 1.5 μM (in the presence of EDTA, Fig. 1) and then increases linearly with [Cu^{2+}]. The slope of k_{obs} *vs.* [Cu^{2+}] is the same in the presence and absence of EDTA (Fig. 1). The amount of residual Cu^{2+} in the solutions can be estimated from the interception of the straight lines (shown by the arrow in Fig. 1) at negative [Cu^{2+}]. The intercept of the plot with EDTA and the *y*-axis is linearly proportional to [ascorbic acid]. From this value the reaction rate constant for the bimolecular reaction of peroxynitrite and ascorbic acid is (51 ± 5) M^{-1} s^{-1} and is in good agreement with the literature value of 42–47 M^{-1} s^{-1}.[4,5] Thus, the reaction rate law can be written [eqn. (2)]:

$$-d[ONOO^-]/dt = (k_o + k_a[\text{ascorbic acid}] + k_{cat}[Cu^{2+}])[ONOO^-] \quad (2)$$

where k_o = the rate constant of unimolecular peroxynitrite self-decay (k_o = 0.4 s^{-1} [1,2]), k_a = the rate constant for the bimolecular reaction of ascorbic acid with peroxynitrite (k_a = 51 M^{-1} s^{-1}), and k_{cat} = the rate constant for the catalytic pathway. k_{cat} values for both Cu^{2+} and **1** depend on [ascorbic acid] (Fig. 2). This dependence is complex, and the activities of the two Cu species are very similar.¶

Similar reactions using other transition metal-containing species ($CoCl_2{\cdot}6H_2O$, $K_7[CoAlW_{11}O_{39}]{\cdot}13H_2O$,[12] $Fe(NO_3)_2{\cdot}6H_2O$, $MnCl_2{\cdot}4H_2O$ and $NiNO_3{\cdot}6H_2O$) in aqueous solution at pH 7.4 (25 °C, 75 mM phosphate buffer, 12 mM ascorbic acid and 0.1 mM initial peroxynitrite) were investigated, and the reaction rates (k_{cat}) compared to those catalysed by Cu^{2+} and **1**. While Fe^{2+} and Ni^{2+} are inactive, Mn^{2+} exhibits slight activity ($k_{cat} \leqslant 0.05 \times 10^6$ M^{-1} s^{-1}). Both Co^{2+} and $K_7[CoAlW_{11}O_{39}]$ showed significant catalytic activity[12] (k_{cat} = 0.13 ± 0.03 × 10^6 and 0.15 ± 0.03 M^{-1} s^{-1}, respectively) but were still over 30 times slower than either Cu^{2+} or **1** (k_{cat} = 3.65 ± 0.2 × 10^6 and 3.15 ± 0.2 × 10^6 M^{-1} s^{-1}, respectively). This catalytic system is one of the most efficient reported thus far. At physiological concentrations of ascorbic acid (1 mM), Cu^{2+} catalysis of peroxynitrite-based oxidation proceeds with k_{cat}

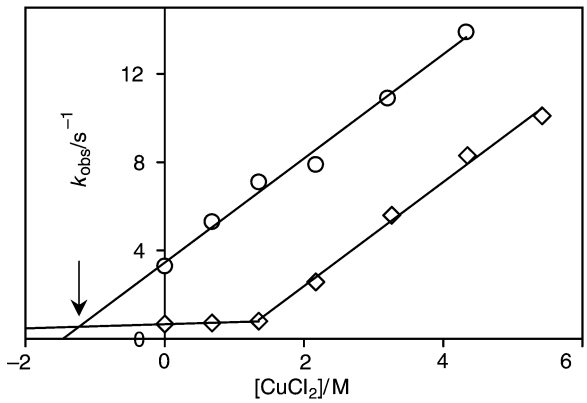

Fig. 1 Dependence of k_{obs} [eqn. (1)] *vs.* [Cu^{2+}]. *Reagents and conditions*: 25 °C, pH 7.4, 75 mM phosphate buffer, 12 mM ascorbic acid and 0.1 mM initial [peroxynitrite]. (○) No EDTA added. (◇) 2.5 μM EDTA added.

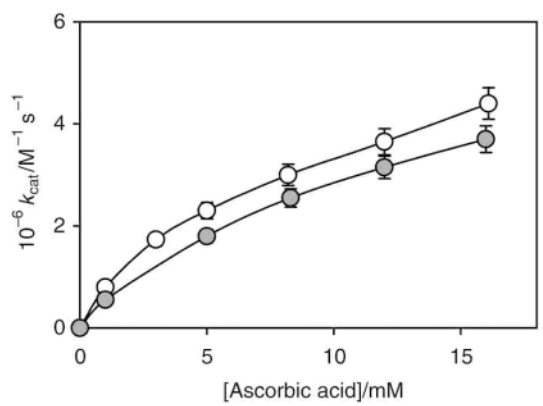

Fig 2 Dependence of k_{cat} [eqn. (2)] *vs.* [ascorbic acid]. *Reagents and conditions*: 25 °C, pH 7.4, 75 mM phosphate buffer and 0.1 mM initial [peroxynitrite]. (○): k_{cat} data for Cu^{2+}. (●): k_{cat} data for **1**.

 DOI: 10.1039/b104159m

values of 0.8×10^6 or 1.6×10^6 M^{-1} s^{-1} (at 25 and 37 °C, respectively), which is slightly slower than for Mn porphyrins (1.6×10^6 M^{-1} s^{-1} for MnTMPyP at 23 °C).[13]

In order to assess the possible relevance of Cu-catalysed ascorbic acid oxidation by peroxynitrite *in vivo*, the activity of Cu^{2+} was evaluated in the presence of biologically important Cu-binding chelates, Gly-Gly-His (GGH), bovine serum albumin (BSA), cysteine and ceruloplasmin. The effect of the abiological chelates *o*-phenanthroline and nitrilotriacetic acid was also evaluated. At a 2:1 GGH:Cu ratio ([ascorbic acid] = 12 mM), $k_{cat} = 3.0 \pm 0.2 \times 10^6$ M^{-1} s^{-1}, which is slightly lower than that for the reaction catalysed by Cu^{2+} and similar to that exhibited by **1**. Further increases in the GGH:Cu ratio decreased the rate until rate was that of the background reaction at a ratio higher than 6:1. BSA also decreased the rate. At a BSA:Cu ratio = 0.5 (the molecular weight of BSA was taken as 66429),[14] the reaction rate dropped to 60% of that in the absence of the chelate. However, at a BSA:Cu ratio >10 the activity decreased to 10% that of Cu^{2+}. Pure Cu-loaded ceruloplasmin purified from non-specifically bound Cu^{2+} was catalytically inactive. However, addition of up to 8 μM Cu^{2+} to this ceruloplasmin is a catalytic system with 50% of the activity of free Cu^{2+}. Cysteine strongly inhibits the catalytic activity of Cu^{2+} at a cysteine:Cu ratio >1.0, but the kinetics are more complex than eqn. (1). The non-biological chelates *o*-phenanthroline and nitrilotriacetic acid substantially inhibit the reaction (to approximately the background level) when they are added in a chelate:Cu ratio of 2 and 3, respectively. Most of the biologically important Cu-chelates do not greatly affect the catalytic activity. It is evident that at least one coordination site of the Cu^{2+} is required for catalytic activity. Significantly, the data suggest that Cu-catalysed peroxynitrite oxidation of ascorbic acid may constitute a minor but probable pathway for ascorbic acid depletion *in vivo*.

Detailed kinetic studies showed the oxidation of $Cu^{I}(GGH)_n$ to $Cu^{II}(GGH)_n$ (soluble models of Cu^+/Cu^{2+} suitable for kinetic studies) and subsequent reduction by ascorbic acid are both too slow under our experimental conditions to account for the observed overall reaction rate. The mechanism therefore may involve the formation of copper-peroxynitrito intermediate complex [eqn. (3)] which is subsequently trapped by ascorbic acid [eqn. (4)]:

$$Cu^{II}(H_2O) + ONOO^- \rightleftharpoons Cu^{II}(OONO^-) + H_2O \quad (3)$$

$$Cu^{II}(OONO^-) + H^+ + HA^- \rightarrow Cu^{II}(H_2O) + NO_2^- + A \quad (4)$$

where HA^- is the ascorbate anion and A is dehydroascorbic acid (the product of ascorbic acid oxidation). An alternative mechanism [eqns. (5) and (6)] may involve the formation of a complex between ascorbate and Cu(II) which is then oxidised by peroxynitrite:

$$Cu^{II}(H_2O) + HA^- \rightleftharpoons Cu^{II}(HA^-) + H_2O \quad (5)$$

$$Cu^{II}(HA^-) + H^+ + ONOO^- \rightarrow Cu^{II}(H_2O) + NO_2^- + A \quad (6)$$

Either of these mechanisms results in the rectangular hyperbolic rate law (7):

$$-d[ONOO^-]/dt = a[Cu(II)][ONOO^-][HA^-]/(b + c[HA^-]) \quad (7)$$

where $a = k_3k_4$, $b = k_{-3}$, $c = k_4$ for eqns. (3) and (4), or $a = k_6K_5$, $b = 1$, $c = K_5$ for eqns. (5) and (6). Eqns. (3) and (4) are likely to operate at low [ascorbic acid], while eqns. (5) and (6) are likely to operate at high [ascorbic acid] which is consistent with the data in Fig. 2.

We gratefully acknowledge funding by the NSF (C. L. H.) and INTAS (grant 99-209, to Y. V. G.).

Notes and references

† The term peroxynitrite is used to refer to the peroxynitrite anion O=NOO$^-$, and peroxynitrous acid, ONOOH, unless otherwise indicated. The IUPAC recommended names are oxoperoxonitrate(−1) and hydrogen oxoperoxonitrate, respectively.

‡ *Synthesis* of $Na_7[CuCoW_{11}O_{39}]\cdot 5H_2O$ **1**: $CuCl_2\cdot 2H_2O$ (0.12 g, 0.7 mmol) was dissolved in H_2O (20 mL) and $K_9[CoW_{11}O_{39}]\cdot 14H_2O$[11] (2.0 g, 0.6 mmol) was added over 30 min in small aliquots with each being allowed to dissolve before further POM was added. The resulting brown solution was stirred for a further 20 min, and KCl (10 g, 0.13 mol) was added. The solution was cooled at 5 °C overnight and the resulting brown precipitate filtered off, washed with cold H_2O (3 × 25 mL) and purified by dissolving in warm H_2O and passing a 0.1 M solution 3 times through an Amberlite® resin ion-exchange column charged with 1 M NaCl. The solution was concentrated and cooled overnight at 5 °C and the resulting solid was filtered and dried *in vacuo*. Analytical data: Calc. (found) for $Na_7CuCoW_{11}O_{44}H_{10}$: Na, 5.3 (5.2); Cu, 2.1 (2.1); Co 2.0 (2.0); W 67.0 (66.8%); IR data (cm^{-1}): 942m, 878s, 773vs, 750s, 697m, 530w, 450m.

§ Kinetics were monitored at 302 nm using a SF-61 stop flow instrument (Hi-Tech Scientific, UK). A deviation from exponential decay for the first 5–10% conversion of peroxynitrite was observed. The reaction proceeded more slowly than expected. In consequence, the first 10–15% of the kinetic curve was omitted for fitting the data. There are three possible explanations for this rate retardation. First, Cu^{2+} could be reduced by ascorbic acid to Cu^+ (in the stock solution), and subsequent reoxidation to the catalytically active Cu^{2+} is slow. Second, at high [peroxynitrite] the equilibrium in eqn. (3) can be shifted to the right and thus all the Cu^{2+} is in the form of the peroxynitrite complex. In this case, the reaction rate is zero-order with respect to peroxynitrite and proceeds slower than the projected first-order reaction. Third, at high [peroxynitrite], eqn. (5) can be rate-limiting again resulting in zero-order with respect to peroxynitrite.

¶ In aqueous solution **1** may dissociate to Cu^{2+} and lacunary POM (POM_{lac}). However, the observed activity of **1** is *not* due to this dissociation. The catalytic activities of mixtures of Cu^{2+} and POM_{lac} were investigated. The addition of POM_{lac} to Cu^{2+} slightly decreased the reaction rate. However, at a $[POM_{lac}] : [Cu^{2+}] > 1$ the catalytic activity was the same as for solutions of **1**. Moreover, the addition of POM_{lac} to **1** did not inhibit its activity.

1 W. H. Koppenol, in *Metal Ions in Biological Systems*, ed. A. Sigel and H. Sigel, Marcel Dekker, Inc., 1999, p. 597.
2 M. Trujillo, M. Naviliat, M. N. Alvarez, G. Peluffo and R. Radi, *Analusis*, 2000, **28**, 518.
3 G. E. Arteel, K. Briviba and H. Sies, *Nitric Oxide: Biology and Pathobiology*, ed L. J. Ignorro, Academic Press, 2000, 343.
4 D. Bartlett, D. F. Church, P. L. Bounds and W. H. Koppenol, *Free Radical Biol. Med.*, 1995, **18**, 85.
5 G. L. Squadrito, X. Jin and W. A. Pryor, *Arch. Biochem. Biophys.*, 1995, **322**, 53.
6 I. A. Salem, M. El-Maazawi and A. B. Zaki, *Int. J. Chem. Kinet.*, 2000, **32**, 643.
7 For an example of O_2-oxidation, see: M. Scarpa, F. Vianello, L. Signor, L. Zennaro and A. Rigo, *Inorg. Chem.*, 1996, **35**, 5201.
8 For an example of H_2O_2-oxidation, see: Yu. Skurlatov, *Int. J. Chem. Kinet.*, 1980, **12**, 347.
9 W. H. Koppenol, R. Kissner and J. S. Beckman, *Methods Enzymol.*, 1996, **269**, 296.
10 D. S. Bohle, B. Hansert, S. C. Paulson and B. D. Smith, *J. Am. Chem. Soc.*, 1994, **116**, 7423.
11 J. Bas-Serra, I. Todorut, N. Casan-Pastor, J. Server-Carrio, L. C. W. Baker and R. Acerete, *Synth. React. Inorg. Met.-Org. Chem.*, 1995, **25**, 869.
12 Yu. V. Geletii, A. J. Bailey, J. J. Cowan, I. A. Weinstock and C. L. Hill, *Can. J. Chem.*, 2001, **17**, 792.
13 J. Lee, J. A. Hunt and J. T. Groves, *J. Am. Chem. Soc.*, 1998, **120**, 6053.
14 Y. Wada, *J. Mass Spectrom.*, 1996, **31**, 263.

CHEMCOMM Communication
www.rsc.org/chemcomm

Synthesis of pure polymorph C of Beta zeolite in a fluoride-free system

Avelino Corma,* Mª Teresa Navarro, Fernando Rey and Susana Valencia

Instituto de Tecnología Química, UPV-CSIC, Universidad Politécnica de Valencia, Avda. de los Naranjos s/n, 46022 Valencia, Spain. E-mail: acorma@itq.upv.es; Fax: +34(96)3877809; Tel: +34(96)3877800

Received (in Cambridge, UK) 10th May 2001, Accepted 28th June 2001
First published as an Advance Article on the web 18th July 2001

Pure polymorph C (denoted ITQ-17) resulting from the intergrowth of zeolite Beta has been synthesized in the presence of Ge from a fluoride-free synthesis mixture; this shows that fluoride is not necessary to obtain structures containing D4MR units that were believed to be stabilised by fluoride; on the other hand, the presence of Ge directs the synthesis towards the formation of pure polymorph C.

Zeolites are porous crystalline aluminosilicates that have found important applications in catalysis, adsorption and as ion exchangers. For many of these applications, it would be interesting to carry out an *a priori* design of zeolites. Unfortunately, despite the efforts made by several groups,[1,2] the existing knowledge on nucleation and crystallization mechanisms at the molecular level is limited, and the synthesis of new structures has advanced mainly by accumulated experience using different structure directing agents (SDAs) and synthesis conditions. More specifically, in the case of high silica/alumina large pore three-dimensional zeolites, the number of existing structures is quite limited[3] and up to now only Beta zeolite has found commercial applications.[4] Zeolite Beta is a highly faulted intergrowth of two polymorphs A and B. Newsam *et al.*[5] described a hypothetical framework, denoted as polymorph C, which is related to polymorphs A and B of zeolite Beta, and could be generated from polymorph A simply by the recurrent application to the building layers of a shear operation along both *a* and *b* axes. The structure of polymorph C has a three-dimensional system of 12MR channels that intersect perpendicularly, and in contrast with polymorphs A and B, all the channels in the structure C are linear.[5] Furthermore, polymorph C contains double four-membered ring (D4MR) cages as secondary building units [two D4MR cages per unit cell (u.c.)], while polymorphs A and B do not contain such secondary building units.

It has been reported[6] that, among a large number of pure silica structures, those that contain mainly triple 4-MRs are the least stable frameworks with enthalpies of transition for quartz $\rightarrow$ molecular sieve (ΔH^{298}_{trans}) $\geq$ 10.8 kJ mol^{-1}, indicating that the presence of large fractions of multiple 4-MRs seems to lead to a destabilization of the framework, at least for less dense structures such as CHA, ISV, FAU and AST. It is apparent from this point of view that structure C which presents D4MRs should be less stable than zeolite Beta formed by polymorphs A and B. Then, while it is true that purely thermodynamic data cannot answer questions about the kinetics of zeolite synthesis, they can nevertheless help to rationalize driving forces for synthesis.[6] On this basis it is not surprising that the polymorph C has been elusive, whereas zeolite Beta has been synthesized with several SDAs.[7–9] However, it has been shown[10] that fluoride ions can stabilize D4MR small cages and, consequently, a synthesis procedure in fluoride media, in principle, could favour the synthesis of polymorph C. Very recently, Liu *et al.*[11] have found polymorph C as an impurity of the pure silica Beta zeolite, when this was synthesized in fluoride media using tetramethylenebisquinuclidinium diquaternary cation (M_4BQ^{2+}) as structure directing agent. It was suggested that the presence of fluoride ions was required for the formation of the observed impurity. However, pure polymorph C (ITQ-17) was not obtained until Corma *et al.*[12] showed that in the presence of fluoride ions this structure is formed when Ge is also introduced in the synthesis media. Then, it appears that both F^- and Ge stabilise the presence of double four-membered rings in the structure and then it is possible to prepare the pure polymorph C of Beta with a large number of organic structure directing agents.

Unfortunately, the presence of F^- in the synthesis media is not desirable from an industrial point of view and, therefore, it is of interest to find a fluoride-free synthesis of the pure polymorph C, not only for practical reasons but also from a conceptual point of view in order to establish whether the presence of F^- anions is mandatory for the stabilization of D4MR units, which are present in that structure.

Here, we will show that the synthesis of pure polymorph C (ITQ-17) of the intergrowth of Beta zeolite has now been achieved in the absence of fluoride ions.

The synthesis was carried out in OH^- media, using 1-methyl-4-aza-1-azoniabicyclo[2,2,2]octane hydroxide (DABMe(OH)) as the structure directing agent. The 1-methyl-4-aza-1-azoniabicyclo[2,2,2]octane cation ($DABMe^+$) was synthesised in its iodide form in the following way: a solution of iodomethane (Aldrich) (3.7 g) in tetrahydrofuran (THF, 15 ml) was added dropwise to a solution of 1,4-diazabicyclo[2,2,2]octane (DABCO) (Aldrich) (5.6 g) in THF (200 ml) at room temperature, and the mixture was stirred for 20 h. The resulting solid was filtered off and washed with diethyl ether. Finally the salt, DABMeI, was exchanged into its hydroxide form using an anion-exchange resin (Amberlite IRN-78, Supelco). More specifically, a synthesis gel with the following composition was prepared:

$$0.666\ SiO_2 : 0.333\ GeO_2 : 0.5\ DABMe(OH) : 3.5\ H_2O.$$

This was obtained by adding GeO_2 (powder) and TEOS (tetraethylorthosilicate) to an aqueous solution of DABMe(OH). The homogenized mixture was stirred vigorously at room temperature in order to eliminate the ethanol produced during the hydrolysis of TEOS and to adjust the water content to that of the gel composition. The resulting gel was introduced

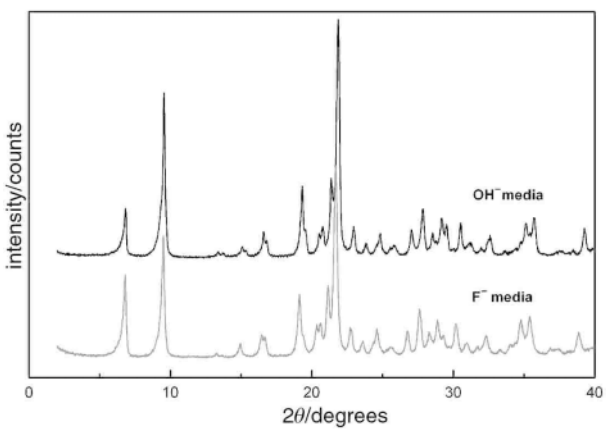

Fig. 1 X-Ray diffraction patterns of as-synthesized ITQ-17 zeolites prepared in fluoride-free media (top) and in the presence of fluoride[12] (bottom).

 DOI: 10.1039/b104114m

into new, Teflon-lined autoclaves that had never been in contact with a solution containing F^-, and were heated at 150 °C under static conditions. The fluoride-free gel after 12 days gives a sample, the X-ray diffractogram of which is given in Fig. 1. This is compared with a sample of ITQ-17 obtained in a fluoride system and whose structure was found to correspond to that of the pure polymorph C of zeolite Beta.[12] From the comparison, it becomes evident that well crystallized pure polymorph C has been obtained in OH^- media and in the absence of F^-. Elemental analysis of this sample gives a C/N atomic ratio of 3.5, as would be expected, which indicates that the SDA must be intact inside of the pores of the zeolite. A Si/Ge ratio of 2.5 was found for this sample when analysed whereas F^- anions were not detected by chemical analysis or by ^{19}F MAS NMR spectroscopy. Pure ITQ-17 samples with higher Si/Ge ratios have been obtained by this procedure. It should be remarked that even if pure polymorph C can be synthesized in the absence of F^- when Ge is introduced, the combination of both F^- and Ge accelerates the synthesis of this zeolite (Fig. 2).

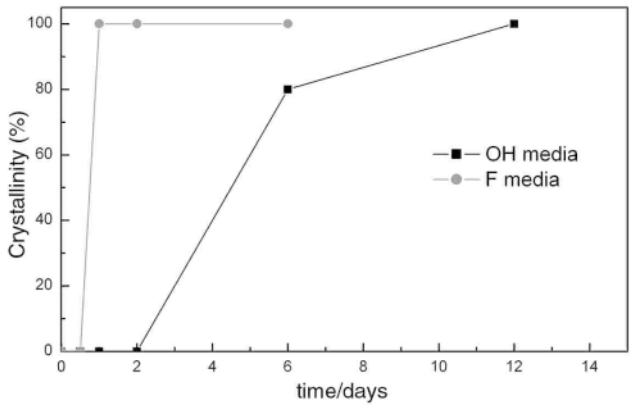

Fig. 2 Crystallization curves of ITQ-17 zeolite synthesized in fluoride-free media (■) and in the presence of fluoride (◍).

The results presented here clearly prove that pure polymorph C of Beta intergrowth can be obtained in the absence of F^- anions. Ge seems to direct the synthesis towards the formation of this structure due to the stabilization effect of D4MR units present in ITQ-17 materials. These results are in line with the fact that the presence of Ge in the synthesis media strongly accelerates the nucleation of Ti-ITQ-7[13] and Al-ITQ-7[14] zeolites that also contain D4MRs in the structure.

We thank the Spanish CICYT for financial support (Project MAT2000-1392). M. T. N. thanks the Fundación José y Ana Royo for a postdoctoral fellowship.

Notes and references

1 D. W. Lewis, D. J. Willock, C. R. A. Catlow and J. M. Thomas, *Nature*, 1996, **382**, 604.
2 D. W. Lewis, C. R. A. Catlow and J. M. Thomas, *Faraday Discuss.*, 1997, **106**, 451.
3 Atlas of Zeolite Structure Types, *Zeolites*, 1996, **17**.
4 C. Flego, G. Pazzuconi, E. Bencini and C. Perego, *Stud. Surf. Sci. Catal.*, 1999, **126**, 461.
5 J. M. Newsam, M. M. J. Treacy, W. T. Koetsier and C. B. de Gruyter, *Proc. R. Soc. London A*, 1988, **420**, 375.
6 P. M. Piccione, Ch. Laberty, S. Yang, M. A. Camblor, A. Navrotsky and M. E. Davis, *J. Phys. Chem. B*, 2000, **104**, 10001.
7 R. L. Wadlinger, G. T. Kerr and E. J. Rosinski, *US Pat.,* 3 308 069, 1967.
8 J. C. van der Waal, M. S. Rigutto and H. van Bekkum, *J. Chem. Soc., Chem. Commun.*, 1994, 1241.
9 K. Tsuji, L. W. Beck and M. E. Davis, *Microporous Mesoporous Mater.*, 1999, **28**, 519.
10 H. Kessler, J. Patarin and C. Schott-Darie, *Stud. Surf. Sci. Catal.*, 1994, **85**, 75.
11 Z. Liu, T. Ohsuna, O. Terasaki, M. A. Camblor, M. J. Díaz-Cabañas and K. Hiraga, *J. Am. Chem. Soc.*, 2001, **123**, 5370.
12 A. Corma, M. T. Navarro, F. Rey, J. Rius and S. Valencia, *Angew. Chem., Int. Ed.*, 2001, **40**, 2277.
13 A. Corma, M. J. Díaz-Cabañas, M. E. Domine and F. Rey, *Chem. Commun.*, 2000, 1725.
14 A. Corma, M. J. Díaz-Cabañas and V. Fornés, *Angew. Chem., Int. Ed.*, 2000, **39**, 2346.

CHEMCOMM Communication
www.rsc.org/chemcomm

Dendritic catalysts for asymmetric transfer hydrogenation†

Ying-Chun Chen,[a] Tong-Fei Wu,[a] Jin-Gen Deng,*[a] Hui Liu,[a] Yao-Zhong Jiang,[a] Michael C. K. Choi[b] and Albert S. C. Chan[b]

[a] *Union Laboratory of Asymmetric Synthesis, Chengdu Institute of Organic Chemistry, the Chinese Academy of Sciences, Chengdu 610041, China. E-mail: jgdeng@cioc.ac.cn*
[b] *Open Laboratory of Chirotechnology and Department of Applied Biology and Chemical Technology, The Hong Kong Polytechnic University, Hong Kong, China*

Received (in Cambridge, UK) 10th May 2001, Accepted 27th June 2001
First published as an Advance Article on the web 26th July 2001

The synthesis of chiral diamine based dendritic ligands and their ruthenium complex catalysed asymmetric transfer hydrogenation is described.

Since the pioneer works reported in 1994,[1] dendritic catalysts with well-defined nanostructures have triggered increasing attention because in principle they have the potential to combine the advantages of homogeneous and heterogeneous catalysts in one system.[2] Although a number of dendritic catalysts have been described,[3] so far, relatively few reports on catalytic asymmetric synthesis are available.[4] Also, chiral ligands and metal catalysts are very expensive and the finding of the recyclable catalysts becomes increasingly important.

Noyori *et al*. discovered an excellent ligand, (*S*,*S*)-*N*-(*p*-tolylsulfonyl)-1,2-diphenylethylenediamine [(*S*,*S*)-TsDPEN], for the ruthenium catalysed transfer hydrogenation reactions.[5] The chiral DPEN is available in our laboratory on the kilogram scale. Moreover, the polymeric catalysts, in which the chiral TsDPEN was incorporated in a polymeric matrix or bound to the insoluble polymers, were reported to be detrimental to the catalytic activity and selectivity in varying degrees.[6] Herein we report the first use of soluble and recyclable dendritic catalysts for the enantioselective transfer hydrogenation of prochiral ketones. The amino-functionalised chiral ligand (*S*,*S*)-**1** was synthesized in three steps from (*S*,*S*)-DPEN, and subsequent condensation with Fréchet's polyether dendritic wedges[7] and the final deprotection of the Boc-group readily gave the dendritic chiral ligands.‡

Asymmetric transfer hydrogenation reactions were studied using acetophenone as the model substrate.§ Compared to the monomer Ru[(*S*,*S*)-**2**] complex, a slightly enhanced reactivity was observed for the dendritic catalysts with the high enantioselectivity (>96% ee), in which the first and third generation catalysts possess higher reactivity (Table 1).

Another unique feature of these dendritic catalysts was that they completely maintained the enantioselectivity with only slight loss of activity in successive use. Using the third and fourth generation catalysts Ru[(*S*,*S*)-**5**] and Ru[(*S*,*S*)-**6**], (*S*)-1-phenylethanol was formed after ~30 h for the fourth use with 88, 85% conversions and 96.4, 96.7% ee, respectively (entries 8 and 12), and high enantioseletivities (>95% ee) remained even for the fifth use (entries 9 and 13). Further addition of $[RuCl_2(cymene)]_2$ into the Ru[(*S*,*S*)-**6**] complex could not regain the reactivity and selectivity (entry 14), and subsequent TLC analysis of the recovered catalyst confirmed that this mostly resulted from the decomposition of the dendritic ligand. For the heterogeneous polymer immobilised catalysts,[6] the reactivity has been mostly lost after the third use. Moreover, the fourth generation catalyst was more active than the third one for the fifth use with 73 *vs*. 52% conversions, respectively (entries 13 and 9), although it is less active than the third generation

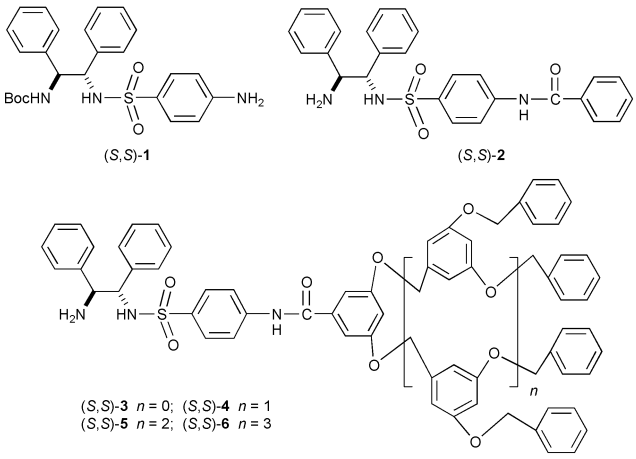

catalyst (entries 5 and 4). Thus, we refer the relatively robust activity of the dendritic catalysts to the "dendrimer effects" on stability of the catalytically active complex on the dendron, which had been observed in bis(μ-oxo)dicopper species toward oxidative self-decomposition.[8]

In conclusion, various generations of chiral diamine based dendritic catalysts encapsulated within the matrix have been synthesized and demonstrated good recyclable catalytic activity and enantioselectivity in transfer hydrogenation of an aromatic ketone. Current work is aiming at a detailed insight of the nature

Table 1 Dendritic TsDPEN–Ru(II) complex catalysed asymmetric transfer hydrogenation of acetophenone[a]

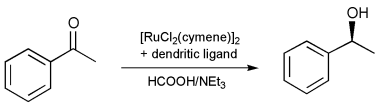

Entry	Ligand	*t*/h	Conv.[b] (%)	TOF[c]/h^{-1}	Ee[d] (%)
1	**2**	20	95	8.6	96.5
2	**3**	20	>99	11.9	96.6
3	**4**	20	98	9.5	96.5
4	**5**	20	>99	11.0	96.5
5	**6**	20	98	9.6	96.5
6	**5** (2nd use)[e]	20	93	—	96.7
7	**5** (3rd use)[e]	25	86	—	96.7
8	**5** (4th use)[e]	31	88	—	96.4
9	**5** (5th use)[e]	40	52	—	95.0
10	**6** (2nd use)[e]	20	92	—	96.6
11	**6** (3rd use)[e]	25	87	—	96.8
12	**6** (4th use)[e]	30	85	—	96.7
13	**6** (5th use)[e]	40	73	—	96.3
14	**6** (6th use)[e,f]	40	52	—	87.0

[a] (*S*)-Alcohol was obtained. [b] Based on GC and ^{1}H NMR analysis. [c] Average turn-over frequency calculated over the 5 h reaction time. [d] Determined by GC with a Chrompack CP Chrasil-dex column (25 mm × 0.25 mm). [e] Recovered catalyst was used. [f] Additional $[RuCl_2(cymene)]_2$ was supplemented.

† Electronic supplementary information (ESI) available: synthesis details, recycling procedure and a graph of time-dependent conversion of acetophenone by the catalysts. See http://www.rsc.org/suppdata/cc/b1/b104160f/

 DOI: 10.1039/b104160f

of the dendritic wedge stabilizing effect on the catalyst and the exploration of these catalysts in other asymmetric transfer hydrogenation reactions.

We are grateful for the financial support of the National Science Fund for Distinguished Young Scholars of China (No. 20025205) and The Hong Kong Polytechnic University, ASD Fund.

Notes and references

‡ ESI-HRMS data for the dendritic ligands: (*S*,*S*)-**3** calcd for $C_{41}H_{37}N_3O_5S$ 683.2454, found 684.2429 $[M + H]^+$; (*S*,*S*)-**4** calcd for $C_{69}H_{61}N_3O_9S$ 1107.4129, found 1108.4179 $[M + H]^+$; (*S*,*S*)-**5** calcd for $C_{125}H_{109}N_3O_{17}S$ 1955.7478, found 1956.7929 $[M + H]^+$; (*S*,*S*)-**6** (MALDI-TOF-MS) calcd for $C_{237}H_{205}N_3O_{33}S$ + Na 3675.41, found 3676.03.

§ General procedure: 1 mol% catalyst was prepared *in situ* by mixing 2 equivalents of triethylamine, a dendritic ligand and $[RuCl_2(cymene)]_2$ (1.1 : 0.5 molar ratios) in a 2 M DCM solution for 1 h under argon at 28 °C. Then an acetophenone and formic acid–triethylamine azeotrope (0.5 ml per mmol ketone) was added and the mixture was stirred at 28 °C.

1 J. W. J. Knapen, A. W. van der Made, J. C. de Wilde, P. W. N. M. van Leeuwen, P. Wijkens, D. M. Grove and G. van Koten, *Nature*, 1994, **372**, 659; A. Miedaner, C. J. Curtis, R. M. Barkley and D. L. DuBois, *Inorg. Chem*., 1994, **33**, 5482; J.-J. Lee, W. T. Ford, J. A. Moore and Y. Li, *Macromolecules*, 1994, **27**, 4632; H. Brunner and S. Altmann, *Chem. Ber*., 1994, **127**, 2285.

2 For a recent review on dendrimers, see: S. Hecht and J. M. J. Fréchet, *Angew. Chem., Int. Ed*., 2001, **40**, 74. For some new solutions to dendritic catalyst recovery other than solvent precipitation, see: N. J. Hovestad, E. B. Eggeling, H. J. Heidbüchel, J. T. B. H. Jastrzebski, U. Kragl, W. Keim, D. Vogt and G. van Koten, *Angew. Chem., Int. Ed*., 1999, **38**, 1655; C. Schlenk, A. W. Kleij, H. Frey and G. van Koten, *Angew. Chem., Int. Ed*., 2000, **39**, 3445; M. T. Reetz and D. Giebel, *Angew. Chem., Int. Ed*., 2000, **39**, 2498; H. Sellner and D. Seebach, *Angew. Chem., Int. Ed*., 1999, **38**, 1918; S. C. Bourque, H. Alper, L. E. Manzer and P. Arya, *J. Am. Chem. Soc*., 2000, **122**, 956; P. Arya, G. Panda, N. V. Rao, H. Alper, S. C. Bourque and L. E. Manzer, *J. Am. Chem. Soc*., 2001, **123**, 2889.

3 For later reports on achiral dendritic catalysts, see: H.-F. Chow and C. C. Mak, *J. Org. Chem*., 1997, **62**, 5116; M. T. Reetz, G. Lohmer and R. Schwickardi, *Angew. Chem., Int. Ed. Engl*., 1997, **36**, 1526; M. Petrucci-Samija, V. Guillemette, M. Dasgupta and A. K. Kakkar, *J. Am. Chem. Soc*., 1999, **121**, 1968; C. Francavilla, F. V. Bright and M. R. Detty, *Org. Lett*., 1999, **1**, 1043; G. E. Oosterom, R. J. van Haaren, J. N. H. Reek, P. C. J. Kamer and P. W. N. M. van Leeuwen, *Chem. Commun*., 1999, 1119; A. W. Kleij, R. A. Gossage, J. T. B. H. Jastrzebski, J. Boersma and G. van Koten, *Angew. Chem., Int. Ed*., 2000, **39**, 176; S. B. Garber, J. S. Kingsbury, B. L. Gray and A. H. Hoveyda, *J. Am. Chem. Soc*., 2000, **122**, 8168.

4 For later examples of chiral dendritic catalysts, see: C. Köllner, B. Pugin and A. Togni, *J. Am. Chem. Soc*., 1998, **120**, 10 274; S. Yamago, M. Furukawa, A. Azuma and J. Yoshida, *Tetrahedron Lett*., 1998, **39**, 3783; A. Schmitzer, E. Perez, I. Rico-Lattes and A. Lattes, *Tetrahedron Lett*., 1999, **40**, 2947; R. Schneider, C. Köllner, I. Weber and A. Togni, *Chem. Commun*., 1999, 2415; C. Bolm, N. Derrien and A. Seger, *Chem. Commun*., 1999, 2087; P. B. Rheiner and D. Seebach, *Chem. Eur. J*., 1999, **5**, 3221; I. Sato, T. Shibata, K. Ohtake, R. Kodaka, Y. Hirokawa, N. Shirai and K. Soai, *Tetrahedron Lett*., 2000, **41**, 3123; Q.-H. Fan, Y.-M. Chen, X.-M. Chen, D.-Z. Jiang, F. Xi and A. S. C. Chan, *Chem. Commun*., 2000, 789; R. Breinbauer and E. N. Jacobsen, *Angew. Chem., Int. Ed*., 2000, **39**, 3604.

5 R. Noyori and S. Hashiguchi, *Acc. Chem. Res*., 1997, **30**, 97.

6 R. ter Halle, E. Schulz and M. Lemaire, *Synlett*, 1997, 1257; D. J. Bayston, C. B. Travers and M. E. C. Polywka, *Tetrahedron: Asymmetry*, 1998, **9**, 2015.

7 C. J. Hawker and J. M. J. Fréchet, *J. Am. Chem. Soc*., 1990, **112**, 7638.

8 M. Enomoto and T. Aida, *J. Am. Chem. Soc*., 1999, **121**, 874.

CHEMCOMM Communication
www.rsc.org/chemcomm

Highly specific oxidative damage of double-strand DNA by copper aminoglycosides†

Anjali Patwardhan and J. A. Cowan*

Evans Laboratory of Chemistry, The Ohio State University, 100 West 18th Avenue, Columbus, Ohio 43210, USA. E-mail: cowan@chemistry.ohio-state.edu

Received (in Cambridge, UK) 26th April 2001, Accepted 22nd June 2001
First published as an Advance Article on the web 23rd July 2001

Oxidative cleavage of double-strand DNA, mediated by either Cu^{2+}-neamine 1 or Cu^{2+}-kanamycin A 2, is shown to follow a highly specific C-4′ H mediated pathway and suggests a mechanism for efficient double-strand scission of duplex DNA.

Oxidative degradation of DNA has been demonstrated to follow a number of pathways, depending on the cleavage agent.[1] Proton abstraction from one of the C-1′, C-2′, C-3′, C-4′ or C-5′ ribose carbons is followed by a series of elimination reactions that afford a variety of small molecule products characteristic of the specific cleavage pathway. Fe–bleomycin mediated cleavage shows evidence of both a major C-4′H cleavage path and for C-1′H abstraction.[2,3] While copper phenanthroline and copper desferal had previously been assigned a major C-1′H cleavage path,[4–8] more recent work has indicated that C-4′H and C-5′H abstractions are the only routes that lead to backbone scission.[9] Enediynes, oxochromium reagents and manganese porphyrin derivatives have also been shown to mediate C-1′H, C-4′H, and C-5′H abstraction.[10,11] An example of C-2′H abstraction has been reported for 5-iodouracil.[12] With the exception of Barton's rhodium complexes, which mediate photocleavage *via* C-3′H abstraction,[13] most cleavage agents typically yield a mixture of products, indicative of relatively non-specific cleavage pathways.

Previously we have synthesized and characterized copper derivatives of aminoglycosides (**1** and **2**) and have demonstrated these compounds to be highly efficient catalysts for cleavage of both RNA and DNA under physiological conditions.[14,15] Here we characterize the mechanism for oxidative cleavage of DNA mediated by **1** or **2**, and demonstrate a highly specific C-4′H mediated pathway (Fig. 1). This observation provides an explanation for the efficient conversion of closed circular to linear plasmid DNA, following the double-strand cleavage path identified in our earlier work.[14]

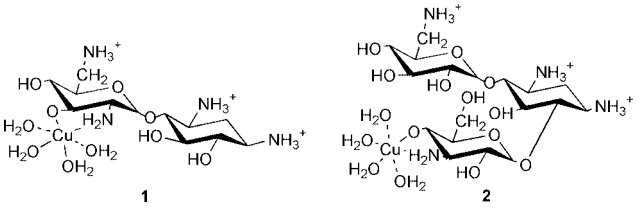

1 **2**

The HPLC profile for Cu^{2+}–kan cleaved plasmid DNA (Fig. 2A) shows the release of cytosine (C), guanine (G), thymine (T), and adenine (A) following residual DNA and larger product fragments. An additional peak corresponding to 5-methylene furanone (5-MF) (Fig. 2) appears when the reaction mixture is heated at 85 °C for 20 min following incubation. C-1′H abstraction generates a C-1′ radical that is further oxidized to a carbocation and forms either a 2′-deoxyribonolactone[6] or a 1′,2′-dehydronucleotide intermediate after subsequent attack by H_2O.[8] Both intermediates are stable at pH 7.4 and 37 °C, the conditions of our cleavage reaction, and the HPLC elution profile corroborates heat treatment to be a prerequisite for the release of 5-MF (Fig. 2). Thus C-1′H abstraction leads to the formation of abasic sites with no apparent strand cleavage, confirming the recent observation by Sugiyama *et al.*[12]

C-4′H abstraction yields distinct reaction products, depending on the attacking species following formation of the radical intermediate. In the presence of dioxygen, base propenals (detected by the TBA assay, ESI†) and 3′-phosphoglycolate terminae are generated (Fig. 1; products C and D, respectively). When water is the attacking species the pathway again does not give rise to direct strand cleavage, but base release is observed. Under anaerobic conditions the TBA assay was negative,

† Electronic supplementary information (ESI) available: experimental section and complete HPLC trace for the truncated version shown in Fig. 2B. See http://www.rsc.org/suppdata/cc/b1/b103789g/

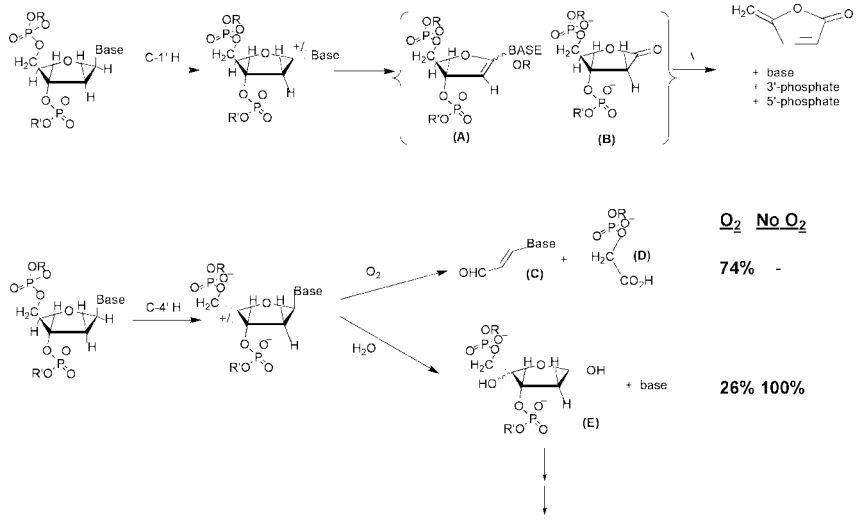

Fig. 1 Porposed radical mediated cleavage mechanisms for oxidative degradation of DNA. (A) 1′,2′-dehydronucleotide; (B) 2′-deoxyribonolactone; (C) base propenal; (D) 3′-phosphoglycolate; (E) hydroxyabasic site.

 DOI: 10.1039/b103789g

indicating the absence of a C-4′H (O_2) path. None of the expected products for C-2′H, C-3′H and C-5′H degradation paths were observed,[10–13] consistent with C-4′H abstraction paths as the only route leading to plasmid cleavage.

A C-1′H path was observed only in the case of supercoiled plasmid with peroxide as coreactant and the fraction of C-1′H abstraction was never found to be more than 12% of the C-4′H path, based on quantitation of the 5-MF released (ESI†). Reaction with ascorbate/O_2 appears to proceed *via* an intermediate copper species that does not mediate C-1′H abstraction. Neither linear plasmid, nor general polynucleotide duplex DNA (discussed below) show evidence for C-1′H loss, whereas C-4′H chemistry is observed with both substrates, and also using either H_2O_2 or ascorbate/O_2 as coreactants. This difference most likely reflects structural perturbations of the supercoiled strands that make C-1′H accessible for abstraction (Fig. 3 illustrates the close proximity of the C-1′ and C-4′ H's).

The reactivity of Cu^{2+}–kan A and Cu^{2+}–neamine toward two DNA duplexes, poly(dA)–poly(dT) and poly(dG)–poly(dC), was also examined in the presence of either hydrogen peroxide or ascorbate, under reaction conditions that were similar to those used for plasmid DNA. Base release was observed and quantitated by HPLC analysis (ESI†), and the occurrence of base propenals was confirmed with the thiobarbituric acid assay. Neither 5-MF (following heat treatment), nor products for other decay paths were observed, and so again the duplexes exhibit exclusive C-4′H abstraction chemistry in the presence of copper neamine or copper kanamycin in the presence of either H_2O_2 or ascorbate/O_2. C-4′H abstraction is normally associated with minor groove binding, and such a binding mode is consistent with our studies conducted in the presence of netropsin or Hoechst 33258 (minor groove binding drugs) which inhibit the cleavage of DNA duplexes (ESI†). Quantitation of the ratio of C-4′H (O_2) to C-4′H (H_2O) paths (ESI†) revealed a preference for the C-4′H (O_2) path, both for the polynucleotide duplexes (74 *vs.* 26%), and for a plasmid DNA (59 *vs.* 41%). These two pathways have previously been observed for $Cu(phen)_2^+$ cleavage of plasmid and duplex sequences,[6] although the factors that favor one path over another are not clear. Base release following peroxide mediated cleavage of either plasmid or duplex DNA by 1 or 2 also shows no obvious trend, other than a variable tendency for release of pyrimidine over purine.

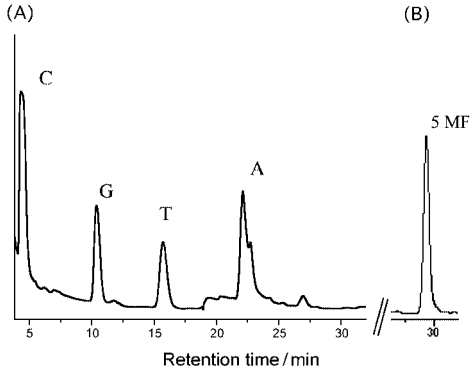

Fig. 2 HPLC profile for the reaction, 100 μg plasmid + 0.5 mM Cu–kan + 5 mM H_2O_2, incubated at 37 °C for 1 h (A) and 100 μg plasmid + 0.5 mM Cu–kan + 5 mM H_2O_2, incubated at 37 °C for 1 h followed by 20 min at 85 °C (B). Excess complex was used to promote rapid reaction, but multiturnover cleavage with sub-stoichiometric complex has been documented.[16]

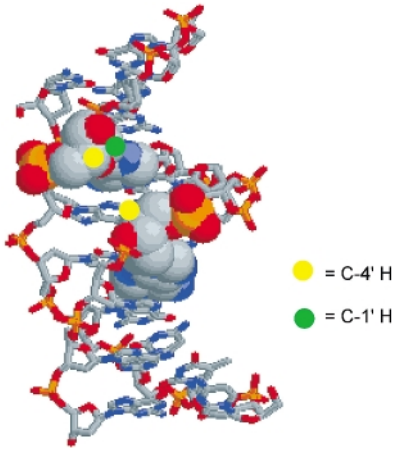

Fig. 3 The proximity of the ribose C-4′H's on opposing strands (*x*, *x* + 3 base positions) in the minor groove of B-conformer DNA suggests a pathway for double-strand scission of duplex DNA by formation of reactive oxygen intermediates in the vicinity of proximal ribose hydrogens. CPK coloring has been used and the two nucleotides on opposing strands are highlighted.

Under hydrolytic conditions,[16] in the absence of added H_2O_2 or ascorbate, treatment of DNA with either 0.5 mM $CuSO_4$ or 0.5 mM aminglycoside, under otherwise similar reaction conditions, produced neither free base, nor 5-MF, nor other products normally observed for the oxidative degradation of duplex or plasmid DNA. Reaction of $CuSO_4$ and a ten-fold excess of either H_2O_2 or ascorbate, again all other conditions being maintained, showed minimal (< 10%) base release, as compared to treatment with either **1** or **2**, but without the production of base propenals. The latter observation suggests an alternative path for production of nucleotide base. With increasing amounts of free Cu^{2+} (maintaining ten times excess of ascorbate or H_2O_2) the concentration of released bases increased. However, base release was found to be random with free Cu^{2+} and coreactant, and did not show any preference for either pyrimidines or purines, consistent with a distinct reaction path. No reaction was observed with H_2O_2 or ascorbate (with or without added neamine or kanamycin A) in the absence of Cu^{2+} (aq), **1** or **2**.

In contrast to other DNA cleavage agents that follow an oxidative path (cited earlier), copper aminoglycosides (**1** and **2**) follow a highly specific route mediated by abstraction of the C-4′H. Close proximity of C-4′H's on opposing strands separated by two additional base-paired nucleotides (Fig. 3) also provides a rational explanation for the observed linearization of plasmid (or double-strand cleavage of duplex DNA). A reactive copper moiety placed in the minor groove would be well placed to execute a double-strand scission with minor structural rearrangement between cleavage reactions. Taken with the unique enzyme-like character of these reagents,[16] these results demonstrate copper aminoglycosides to possess several valuable traits for a metallonuclease mimetic.

Notes and references

1 K. D. Sugden and K. E. Wetterhahn, *Chem. Res. Toxicol.*, 1997, **10**, 1397.
2 R. M. Burger, A. R. Berkowitz, J. Peisach and S. B. Horwitz, *J. Biol. Chem.*, 1980, **255**, 11832.
3 R. J. Duff, E. de Vroom, A. Geluk and S. M. Hecht, *J. Am. Chem. Soc.*, 1992, **115**, 3350.
4 L. M. Pope K. A. Reich, D. R. Graham and D. S. Sigman, *J. Biol. Chem.*, 1982, **257**, 12121.
5 T. E. Goyne and D. S. Sigman, *J. Am. Chem. Soc.*, 1986, **109**, 2846.
6 M. Meijler, O. Zelenko and D. S. Sigman, *J. Am. Chem. Soc.*, 1997, **119**, 1135.
7 R. R. Joshi, S. M. Likhite, K. Kumar and K. N. Ganesh, *Biochim. Biocphys. Acta*, 1993, **1199**, 285.
8 T. Chen and M. M. Greenberg, *J. Am. Chem. Soc.*, 1998, **120**, 3815.
9 T. Oyoshi and H. Sugiyama, *J. Am. Chem. Soc.*, 2000, **122**, 6313.
10 M. Pitié, J. Bernadou and B. Meunier, *J. Am. Chem. Soc.*, 1994, **117**, 2935.
11 I. H. Goldberg, *Acc. Chem. Res.*, 1991, **24**, 191.
12 H. Sugiyama, Y. Tsutsumi, K. Fujimoto and I. Saito, *J. Am. Chem. Soc.*, 1992, **115**, 4443.
13 A. Sitlani, E. C. Long, A. M. Pyle and J. K. Barton, *J. Am. Chem. Soc.*, 1991, **114**, 2303.
14 The synthesis and characterization of the chloride and sulfate salts of **1** and **2**, respectively, are described in A. Sreedhara, J. D. Freed and J. A. Cowan, *J. Am. Chem. Soc.*, 2000, **122**, 8814.
15 A. Sreedhara, A. Patwardham and J. A. Cowan, *Chem. Commun.*, 1999, 1147.
16 A. Sreedhara and J. A. Cowan, *Chem. Commun.*, 1998, 1737.

CHEMCOMM Communication
www.rsc.org/chemcomm

Electronic transduction of biocatalytic transformations on nucleic acid-functionalized surfaces†

Lital Alfonta and Itamar Willner*

Institute of Chemistry, The Hebrew University of Jerusalem, Jerusalem 91904, Israel.
E-mail: willnea@vms.huji.ac.il; Fax: +972-2-6527715; Tel: +972-2-6585272

Received (in Cambridge, UK) 16th May 2001, Accepted 21st June 2001
First published as an Advance Article on the web 23rd July 2001

Electronic transduction of enzyme-catalyzed transformations on nucleic acids associated with surfaces such as ligation, polymerization or restriction, is accomplished.

The use of nucleic acid interactions to construct organized nanostructures,[1,2] circuits[3] and nanomachines,[4] the use of the encoded information in nucleic acids for the assembly of DNA-based computers,[5,6] and the electronic transduction of DNA detection processes[7,8] represent major research efforts in the rapidly developing area of DNA bioelectronics. The hybridization of nucleic acids, and the biocatalyzed ligation, replication and scission of DNA are basic tools to detect nucleic acid interactions and to generate DNA structures. Recently, Faradaic impedance spectroscopy[9] and microgravimetric quartz-crystal-microbalance (QCM) measurements[10] were used as electronic transduction means for the nucleic acid recognition events on conductive supports. Here we report on the novel electronic transduction of a series of biocatalyzed transformations involving nucleic acids that include the surface-stimulated ligation, replication and the specific scission of nucleic acids by a restriction enzyme.

The 18-mer oligonucleotide, **1**, was assembled on an Au-electrode or on an Au/quartz piezoelectric crystal (9 MHz, AT-cut) by the association of the thymine thiophosphate-tag to the gold supports.[11] The surface coverage of the oligonucleotide **1** was estimated by QCM to be $(5.0 \pm 0.7) \times 10^{-11}$ mol cm^{-2}. The resulting **1**-functionalized surfaces were reacted with polynucleotide kinase, PNK, in the presence of ATP to phosphorylate the 5′ termini of the oligonucleotide-monolayer.† The resulting interface was reacted with **2** in the presence of ligase,† Scheme 1, to induce the ligation of **2** to the base oligonucleotide associated with the surface. Fig. 1(A) shows the Faradaic impedance spectra observed upon performing the biocatalyzed transformations on the nucleic acids associated with the electrode, whereas Fig. 1(B) shows the respective frequency changes occurring on the piezoelectric crystal as a result of the chemical transformations occurring on the crystal.† The ligation of **2** results in an increase in the interfacial electron transfer resistance from $R_{et} = 0.44$ kΩ to $R_{et} = 1.33$ kΩ (Fig. 1(A), curve (b)). This is consistent with the fact that the increase of the negative charge associated with the electrode, as a result of ligation, enhances the electrostatic repulsion of the redox-label, $Fe(CN)_6^{3-}/Fe(CN)_6^{4-}$, thus increasing the interfacial electron transfer resistance. The frequency of the Au/quartz crystal changes upon ligation by $\Delta f = -100$ Hz, a value that translates to a surface coverage of the ligated product corresponding to $(5.1 \pm 0.8) \times 10^{-11}$ mol cm^{-2}.† No frequency changes of the Au/quartz crystal were observed upon an attempt to ligate **2** to the **1**-functionalized crystal without the primary phosphorylation of the interface by PNK. Also no frequency changes of the crystal were observed upon interacting the phosphorylated functionalized crystal with **2** in the absence of ligase. The resulting nucleic acid associated with the interface was hybridized with **3**, that is complementary to a part of the nucleic acid associated with the solid supports. The interfacial electron transfer resistance increases as a result of the hybridization of **3**, $R_{et} = 1.9$ kΩ, Fig. 1(A), curve (c), consistent with the increase of the negative charge associated with the electrode. The frequency of the quartz crystal changes by $\Delta f = -31$ Hz, that corresponds to a surface coverage of the hybridized assembly of $(2.2 \pm 0.4) \times 10^{-11}$ mol cm^{-2}. The incomplete hybridization is attributed to steric constraints on the electrode support that eliminate the formation of dsDNA with all of the nucleic acid components.

The resulting assembly was then reacted with the mixture of nucleotides, dNTP, in the presence of polymerase (Klenow fragment, DNA polymerase I).† This yields an increase in the interfacial electron transfer resistance, $R_{et} = 3.1$ kΩ, as a result of the higher negative charge associated with the interface, Fig. 1(A), curve (d). The change in the frequency of the piezoelectric crystal as a result of polymerization is $\Delta f = -26$ Hz, indicates a surface coverage of $(2.6 \pm 0.4) \times 10^{-11}$ mol cm^{-2} for the replicated product.† Reaction of the assembly with the endonuclease restriction enzyme *Dra*I that stimulates the

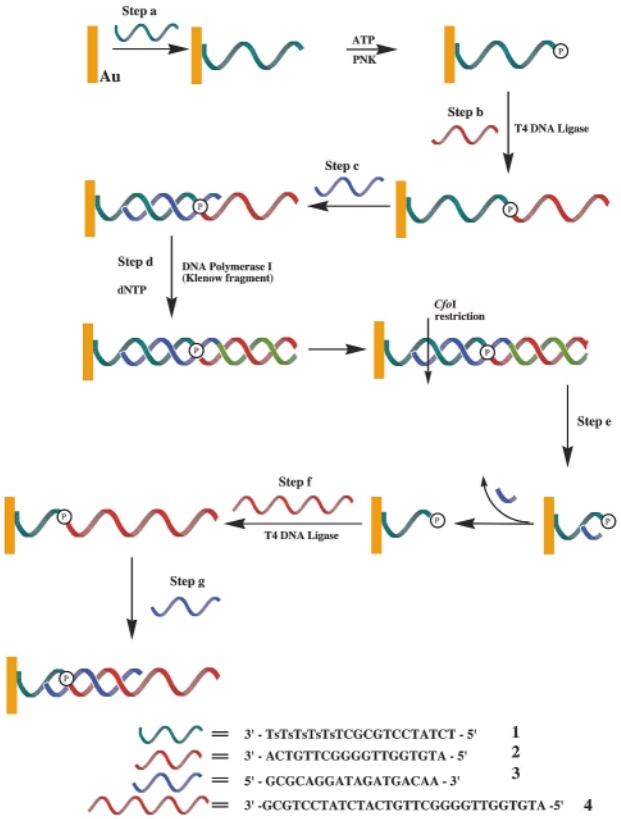

Scheme 1 Biocatalyzed ligation, replication and scission of single and double stranded DNA on electronic transducers (Ts = thymine thiophosphate).

† Electronic supplementary information (ESI) available: details of the experimental conditions for the biocatalytic transformations on the electrodes and a histogram of the frequency changes observed in a series of different experiments. See http://www.rsc.org/suppdata/cc/b1/b104335h/

 DOI: 10.1039/b104335h

specific scission of 5′TTT/AAA3′ sequence does not yield any change in the impedance spectrum of the assembly. Reaction of the resulting assembly with the endonuclease restriction enzyme *Cfo*I (*Hha*I) that induces the specific scission of the 5′GCG/C3′ sequence results, however, in the cleavage of the ds-assembly,† *cf.* Scheme 1. The resulting Faradaic impedance spectrum is shown in Fig. 1(A), curve (e). The interfacial electron transfer resistance decreases to R_e = 0.9 kΩ. This is consistent with the fact that removal of a major part of the ds-assembly and the negative charge associated with it, by the endonuclease activity, reduces the barrier for electron transfer between the redox-label and the electrode. The frequency change in the Au/quartz crystal as a result of the endonuclease activity is Δf = +75 Hz, implying a decrease in the mass associated with the crystal, Fig. 1(B). From the frequency change we estimate that *ca.* $(1.5 \pm 0.2) \times 10^{-11}$ mol cm^{-2} of the hybridized nucleic acid underwent scission. The scission of the double-stranded DNA yields a 5′-phosphorylated primer on the electrode. Note that the interfacial electron transfer resistance of the resulting electrode is higher than the electron transfer resistance of the **1**-functionalized electrode despite the fact that the endonuclease cleavage generates a shorter oligonucleotide than **1** on the electrode. This is explained by the fact that the *Cfo*I cleavage proceeds with partial efficiency, thus leaving a substantial surface coverage of the ds-replicated DNA on the electrode support (*ca.* 1.1×10^{-11} mol cm^{-2}). The resulting interface was then reacted with the oligonucleotide **4** in the presence of ligase to yield the original surface, Fig. 1(A), curve (f), exhibiting an electron transfer resistance of R_{et} = 2.2 kΩ. Further hybridization of **3** with the ligated interface results in an additional increase in the electron transfer resistance to R_{et} = 2.6 kΩ, Fig. 1(A), curve (g).‡ The ligation of **4** to the interface, and the hybridization of **3** with the interface yield, however, higher interfacial electron transfer resistances than those observed for the originally functionalized electrodes, curves (b) and (c), respectively. This is consistent with the fact that endonuclease-induced scission proceeds with partial efficiency, and thus the secondary ligation and hybridization occurs on an interface that includes a partial coverage of the polymerase-induced replicated double-stranded DNA. The negative charge associated with these latter components introduces the higher interfacial electron transfer resistances observed in the second cycle of the biocatalytic transformations. The QCM analyses, Fig. 1(B) confirm this explanation. Ligation of **4** to the interface results in a frequency change of $\Delta f = -42$ Hz, corresponding to a surface coverage of *ca.* $(1.4 \pm 0.3) \times 10^{-11}$ mol cm^{-2} of the coupled product. It should be noted that no significant changes in the interfacial electron transfer resistances, upon the performance of the set of biocatalyzed transformations outlined in Scheme 1, are observed in the presence of the neutral ferrocene methanol redox-label. This supports the conclusion that the changes in the impedance spectra originate from the electrostatic repulsions of the redox-label $Fe(CN)_6^{3-/4-}$. Also, it should be noted that the Faradaic impedance spectra results reveal an excellent reproducibility (±5%) whereas the QCM results reveal a larger experimental diversity due to a different roughness of the Au/quartz crystals.

In conclusion, the electronic transduction of different biocatalytic transformations that include nucleic acids on surfaces was accomplished. This enables the quantitative assay of DNA building blocks on surfaces, and the characterization of nanoengineered DNA structures on surfaces.

This research is supported by the Israel Ministry of Science as an Israel-Japan Binational Cooperation. The support of the Eshkol Fellowship, Israel Ministry of Science (L. A.) is acknowledged. We thank A. Lichtenstein for his assistance in the [γ-^{32}P]ATP labeling experiments.

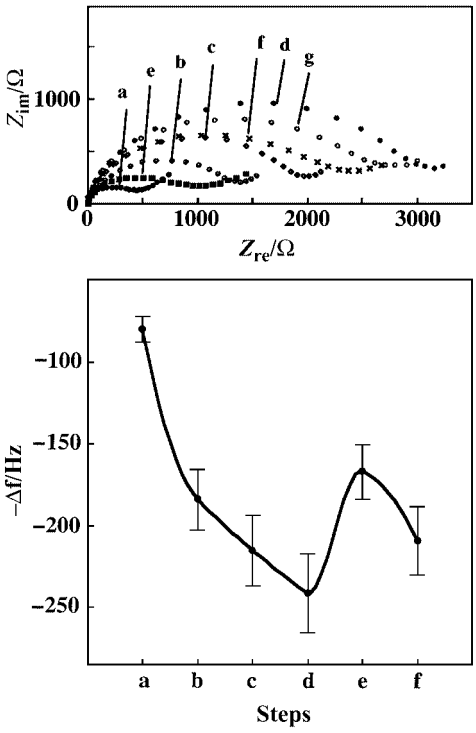

Fig. 1 (A) Faradaic impedance spectra corresponding to the biocatalytic transformation of nucleic acid-functionalized electrode: (a) **1**-functionalized electrode; (b) after ligation of **2**, 3×10^{-5} M, with the **1**-functionalized electrode in the presence of ligase, 20 units, 37 °C, 30 min; (c) after hybridization of the resulting electrode with **3**, 2.5×10^{-5} M, 2 h; (d) after replication of the double-stranded assembly in the presence of dNTP, 1×10^{-3} M, and DNA polymerase, 3 units, 37 °C, 30 min; (e) after scission of the resulting assembly with endonuclease, *Cfo*I, 10 units, 37 °C 1 h; (f) after ligation of the resulting interface with **4**, 6.5×10^{-5} M, in the presence of ligase, 20 units, 37 °C, 30 min; (g) after hybridization of the assembly with **3**, 1×10^{-4} M, for 2 h. (B) Frequency changes of an Au/quartz crystal (9 MHz, AT-cut) upon the assembly of the **1**-functionalized interface and as a result of the biocatalyzed transformations/processes occurring on the surface. Steps (a)–(f) correspond to the steps and preparation protocols outlined in (A).

Notes and references

‡ The different Faradaic impedance spectra of the DNA assemblies on the electrodes can be theoretically fitted with an equivalent circuit composed of a block of an electron transfer resistor element that is linked in series to the Warburg element in parallel to a capacitor element.

1 J. J. Storhoff and C. A. Mirkin, *Chem. Rev.*, 1999, **99**, 1849; J. J. Storhoff, R. Elghanian, R. C. Mucic and C. A. Mirkin, *J. Am. Chem. Soc.*, 1998, **120**, 1959.
2 C. A. Mirkin, R. L. Letsinger, R. C. Mucic and J. J. Storhoff, *Nature*, 1996, **382**, 607; F. Patolsky, K. T. Ranjit, A. Lichtenstein and I. Willner, *Chem. Commun.*, 2000, 1025; P. G. Schultz, *Nature*, 1996, **382**, 609.
3 N. C. Seeman, *Angew. Chem., Int. Ed.*, 1998, **37**, 3220; C. Mao, W. Sun, Z. Shen and N. C. Seeman, *Nature*, 1999, **397**, 144; C. M. Niemeyer, W. Bürger and J. Peplies, *Angew. Chem., Int. Ed.*, 1998, **110**, 2391.
4 B. Yurke, A. J. Turberfield, A. P. Mills, Jr., F. C. Simmel and J. L. Neumann, *Nature*, 2000, **406**, 605.
5 A. G. Frutos, L. M. Smith and R. M. Corn, *J. Am. Chem. Soc.*, 1998, **120**, 10 277.
6 Q. G. Liu, L. M. Wang, A. G. Frutos, A. E. Condon, R. M. Corn and L. M. Smith, *Nature*, 2000, **403**, 175.
7 J. Wang, E. Palecek, P. E. Nielsen, G. Rivas, X. H. Cai, H. Siraishi, N. Doutha, D. B. Luo and P. A. Farias, *J. Am. Chem. Soc.*, 1996, **118**, 7667; H. Korri-Youssoufi, F. Garnier, P. Srivastava, P. Godillot and A. Yassar, *J. Am. Chem. Soc.*, 1997, **119**, 7388; K. M. Millan, A. Saraulo and S. R. Mikkelsen, *Anal. Chem.*, 1994, **66**, 2943; S. Takenaka, K. Yamashita, M. Takagi, Y. Uto and M. Kondo, *Anal. Chem.*, 2000, **72**, 1334.
8 A. Bardea, A. Dagan, I. Ben-Dov and I. Willner, *Chem. Commun.*, 1998, 839; T. de Lumley-Woodyear, C. N. Campbell and A. Heller, *J. Am. Chem. Soc.*, 1996, **118**, 5504; S. R. Mikkelsen, *Electroanalysis*, 1996, **8**, 15.
9 A. Bardea, F. Patolsky, A. Dagan and I. Willner, *Chem. Commun.*, 1999, 21; F. Patolsky, A. Lichtenstein and I. Willner, *Angew. Chem., Int. Ed.*, 2000, **39**, 940.
10 F. Patolsky, A. Lichtenstein and I. Willner, *J. Am. Chem. Soc.*, 2000, **122**, 418.
11 T. Ihara, M. Nakayama, M. Murata, K. Nakano and M. Maeda, *Chem. Commun.*, 1997, 1609.

CHEMCOMM Communication
www.rsc.org/chemcomm

New, efficient electroluminescent materials based on organometallic Ir complexes†‡

Vladimir V. Grushin,* Norman Herron, Daniel D. LeCloux, William J. Marshall, Viacheslav A. Petrov* and Ying Wang*

Central Research and Development, E. I. DuPont de Nemours and Co., Inc., Experimental Station, Wilmington, DE 19880-0328, USA. E-mail: vlad.grushin-1@usa.dupont.com

Received (in Cambridge, UK) 18th April 2001, Accepted 26th June 2001
First published as an Advance Article on the web 23rd July 2001

Reaction of $IrCl_3$ with fluorinated 2-arylpyridines in the presence of AgO_2CCF_3 affords *fac*-tris-cyclometalated arylpyridine Ir complexes exhibiting excellent processing and electroluminescent properties which can be fine-tuned *via* systematic control of the nature and position of the substituents on the aromatic rings.

Low cost, lightweight, flexible, ultra-thin flat panel display devices with miserly power consumption are being fabricated using a new generation of materials' chemistry aimed at exploiting the phenomenon of electroluminescence (EL). Molecule-based 'organic' light-emitting diodes (OLEDs) represent a promising approach for just these applications.[1–4] Suitable materials for OLEDs still need to be developed. A key goal of materials' research in this area is achieving very high power efficiency, which translates into enhanced operating lifetimes and longer battery life.

An important breakthrough was reported recently[5] with the use of materials displaying phosphorescence-like EL and having theoretical efficiency four times that of devices based on fluorescence (assuming electron–hole recombination is statistically controlled). Initial reports of electroluminescence from the Ir complex of 2-phenylpyridine ($[Ir(ppy)_3]$)[6] doped into a charge-transporting matrix, 4,4′-bis(carbazol-9-yl)biphenyl,[6–8] emphasized its dramatically increased power efficiency, 19 lm W^{-1} (26 cd A^{-1}) with a Mg/Ag cathode.

We now report on the synthesis and characterization of a series of highly efficient LED materials based on fluorinated organometallic iridium compounds.[9] Fluorinated substituents in the aromatic ligand result in markedly reduced concentration-quenching of luminescence, and in excellent volatility which aids device processing.

New tris-cyclometalated arylpyridine complexes were prepared by a novel one-step method [eqn. (1)]. Reaction (1) is run

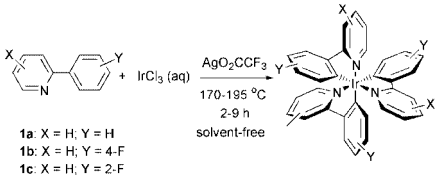

(1)

1a: X = H; Y = H
1b: X = H; Y = 4-F
1c: X = H; Y = 2-F
1d: X = H; Y = 3-CF_3
1e: X = 5-NO_2; Y = 3-CF_3
1f: X = 5-CF_3; Y = H
1g: X = 5-CF_3; Y = 3-CF_3
1h: X = 5-CF_3; Y = 4-F
1i: X = 5-CF_3; Y = 3-F
1j: X = 5-CF_3; Y = 2-F
1k: X = 5-CF_3; Y = 4-CH_3O
1l: X = 5-CF_3; Y = 3-CH_3O
1m: X = 5-CF_3; Y = 4-CF_3O
1n: X = 3-Cl, 5-CF_3; Y = H
1o: X = 3-(N), 5-CF_3; Y = 4-F

in excess arylpyridine[10] which is easily recovered and reused. Complexes **2a–o** were characterized by elemental analysis, ^1H and ^{19}F NMR data, and cyclic voltammetry (CV). Nearly all of the complexes exhibited fully reversible reduction and oxidation waves (Table 1). Single-crystal X-ray structures were obtained for **2g**, **h**, **j**, and **l**.†§ Only *fac* configuration was observed in all cases,[11] as exemplified by the structure of **2h** (Fig. 1). Importantly, trifluoromethylated complexes **2d–o** sublime more easily than **2a** and thus exhibit processing properties superior to those of $[Ir(ppy)_3]$ (Table 1).

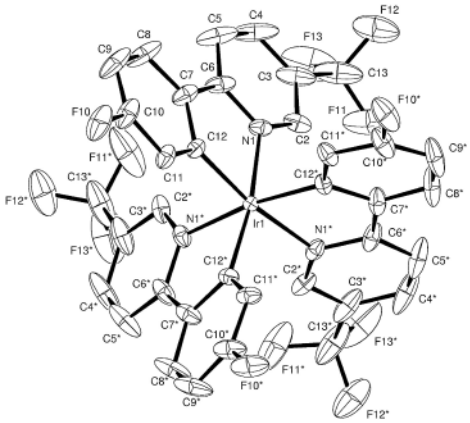

Fig. 1 An ORTEP drawing of **2h**

OLED devices were fabricated with **2a–o** by the thermal evaporation technique, and characterized by measuring current–voltage (*I–V*) curves, EL radiance *vs.* voltage, and EL spectra *vs.* voltage. A typical five-layer device employed ITO (indium doped tin oxide) as the anode, bis[4-(*N*,*N*-diethylamino)-2-methylphenyl](4-methylphenyl)methane (MPMP) as the hole transport material, **2a–o** as the luminescent material, 4,7-diphenyl-1,10-phenanthroline (DPA) or 2,9-dimethyl-4,7-diphenyl-1,10-phenanthroline (DDPA) as the electron transport material, and Al as the cathode (Table 1).

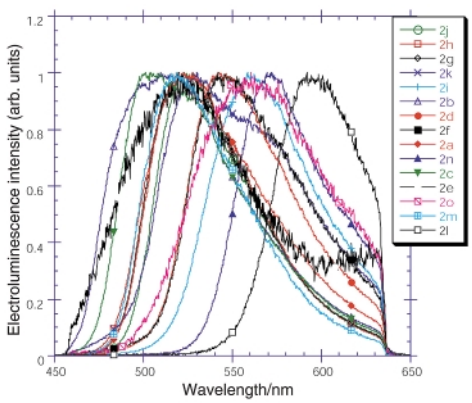

Fig. 2 Normalized EL spectra of Ir compounds shown in Table 1.

† Electronic supplementary information (ESI) available: details of the crystallographic studies, electrochemical measurements and device configuration. See http://www.rsc.org/suppdata/cc/b1/b103490c/
‡ Contribution No. 8150.

 DOI: 10.1039/b103490c

Table 1 Electroluminescent, thermal and electrochemical properties of **2a–o**

Emitter	Yield[a] (%)	Device configuration[b]	LED peak efficiency/[c] cd A^{-1}	LED peak radiance/ cd m^{-2}	$\lambda_{em\ max}$/ nm	TGA[d]/ °C	$E_{\frac{1}{2}}$ (Red)[e]/V	$E_{\frac{1}{2}}$ (Ox)[f]/V
2a	25	MPMP (523 Å), **2a** (402 Å), DDPA (406 Å), Al (742 Å), ITO-2	3.8	570	522	425	−2.77; −2.95; −3.19	0.26
2b	26	MPMP (643 Å), **2b** (409 Å), DDPA (112 Å), AlQ (361 Å), Al (737 Å), ITO-1	1.9	800	514	453	−2.74	0.48
2c	44	MPMP (603 Å), **2c** (415 Å), DDPA (111 Å), AlQ (303 Å), Al (732 Å), ITO-1	3.8	1150	506, 526	417	−2.64; −2.83; −3.12	0.46
2d[g]	14	MPMP (539 Å), **2d** (430 Å), DDPA (109 Å), AlQ (318 Å), Al (725 Å), ITO-1	2	1200	517	382	−2.56; −2.78; −2.99	0.62
2e[g]	16	MPMP (525 Å), **2e** (406 Å), DDPA (106 Å), AlQ (341 Å), Al (762 Å), ITO-1	0.013	7.6	521, ⩾630	392	−1.30; −1.46	Irrev. Ox.[h]
2f	60	MPMP (547 Å), **2f** (412 Å), DDPA (105 Å), AlQ (300 Å), Al (730 Å), ITO-1	4	400	545	383	−2.31	0.55
2g[g]	40	MPMP (553 Å), **2g** (417 Å), DDPA (439 Å), Al (714 Å), ITO-1	9.5	1500	525	345	−2.06; −2.37	0.91
2h	82	MPMP (508 Å), **2h** (428 Å), DPA (461 Å), Al (731 Å), ITO-2	20	4800	525	370	−2.24	0.77
2i[i]	52	MPMP (545 Å), **2i** (462 Å), DDPA (111 Å), AlQ (319 Å), Al (741 Å), ITO-1	2.2	514	560	305	−2.17	0.67
2j	49	MPMP (551 Å), **2j** (465 Å), DDPA (106 Å), AlQ (313 Å), Al (730 Å), ITO-1	2.1	340	525	336	−2.16	0.76
2k	9	MPMP (570 Å), **2k** (441 Å), DDPA (107 Å), AlQ (339 Å), Al (742 Å), ITO-1	1.8	175	530, 563	372	−2.47	0.52
2l[g]	22	MPMP (504 Å), **2l** (417 Å), DPA (407 Å), Al(744 Å), ITO-2	1.4	360	595	384	−2.29	0.33; 0.51; 0.69[j]
2m	72	MPMP (520 Å), **2m** (405 Å), DDPA (410 Å), AlQ (730 Å), ITO-1	5	400	520	315	−2.16; −2.53	0.84
2n	8	MPMP (532 Å), **2n** (457 Å), DDPA (108 Å), AlQ (306 Å), Al (730 Å), ITO-1	3.3	190	575	280	−1.56[k]	0.68
2o	14	MPMP (553 Å), **2o** (417 Å), DDPA (439 Å), Al (714 Å), ITO-1	9.5	1500	525	376	−1.91; −2.27	0.89

[a] Most yields are not optimized. [b] See ESI† for details. [c] LED device efficiency is dependent on the ITO substrate used and emitter purity; **2a** and **2h** received more purification effort. [d] At point of 50% weight loss (1 atm, N_2, 10 °C min^{-1}). [e] In THF, *vs.* Cp_2Fe/Cp_2Fe^+. Only fully reversible 2nd and 3rd reduction waves are listed. [f] In CH_2Cl_2, *vs.* Cp_2Fe/Cp_2Fe^+. [g] Substituent on the Ph ring *para* to Ir. [h] No return wave observed. [i] Mixture of isomers containing F *ortho* or *para* to Ir. [j] Multiple oxidation waves were only observed for **2l**; the second and third waves are tentatively assigned to ligand-based redox processes. [k] E_{pc}.

Most complexes **2a–o** show good EL efficiency on the order of a few cd A^{-1} (Table 1). A non-optimized device based on **2h** with an Al cathode yields a peak radiance of *ca.* 4800 cd m^{-2} and a peak external efficiency of 20 cd A^{-1} (*ca.* 16 lm W^{-1}). Improvement in the device is expected with a low work function cathode (*e.g.*, Mg/Ag or LiF/Mg) and further optimization.

Forrest and coworkers[6] used $[Ir(ppy)_3]$ as a 6% dopant in a charge-transporting host, in order to achieve highest efficiency. This is presumably due to the self-quenching effect in pure **2a**.[6] Measuring the relative luminescence quantum yield of **2h** *vs.* **2a** in the form of a solid state thin film under N_2 showed that the photoluminescence efficiency of pure **2h** was 10 times that of **2a**. Preliminary studies demonstrated comparable photoluminescence quantum yields of *ca.* 0.5–0.6 for **2a** and **2h** in toluene solution. The marked reduction of the self-quenching effect for some of the fluorinated iridium complexes (compare **2a** with **2b–d**, **f–o** in Table 1) obviates the need to dope them into a host material.

By changing the substituents and their position, the peak wavelength of the LED can be tuned from *ca.* 500 to 595 nm (Fig. 2). The peak wavelength is sensitive not only to the nature but also to the position of the substituent. Thus, **2l** with a MeO group *para* to Ir exhibits yellow–orange EL at 595 nm, whereas its *meta* isomer **2k** is green electroluminescent (530 and 565 nm). With fluorine *meta* to Ir (**2h** and **2j**) EL is at 525 nm, while the *ortho*/*para* isomers (**2i**) show EL at 560 nm. These changes are likely due to the strong π-donating effect of both F and MeO.[12] The F and MeO groups may π-interact with either Ir (**2i**, **2l**) or the pyridine ring (**2h**, **2j**, **2k**), leading to destabilization of the HOMO (Ir) and stabilization of the LUMO (Py). These findings raise the exciting possibility of color tuning all the way from blue to red *via* systematic control of the nature and position of the substituents. If material efficiencies can be maintained as this tuning occurs (as intimated by unoptimized results in Table 1) then these materials will provide a unique platform for full color display devices of the future.

Notes and references

§ CCDC reference numbers 161821–161824. See http://www.rsc.org/suppdata/cc/b1/b103490c/ for crystallographic data in CIF or other electronic format.

1 For most recent reviews, see: V. Bulovic, P. E. Burrows and S. R. Forrest, *Semicond. Semimetal.*, 2000, **64**, 255; Y. Sato, *Semicond. Semimetal.*, 2000, **64**, 209; V. Bulovic and S. R. Forrest, *Semicond. Semimetal.*, 2000, **65**, 1.
2 C. W. Tang and S. A. VanSlyke, *Appl. Phys. Lett.*, 1987, **51**, 913.
3 J. H. Burroughes, D. D. C. Bradley, A. R. Brown, R. N. Marks, K. Mackay, R. H. Friend, P. L. Burn and A. B. Holmes, *Nature*, 1990, **347**, 539.
4 M. Bernius, M. Inbasekaran, E. Woo, W. Wu and L. Wujkowski, *Thin Solid Films*, 2000, **363**, 55.
5 M. A. Baldo, D. F. O'Brien, Y. You, A. Shoustikov, S. Sibley, M. E. Thompson and S. R. Forrest, *Nature*, 1998, **395**, 151.
6 M. A. Baldo, S. Lamansky, P. E. Burrows, M. E. Thompson and S. R. Forrest, *Appl. Phys. Lett.*, 1999, **75**, 4; C. Adachi, M. A. Baldo, S. R. Forrest and M. E. Thompson, *Appl. Phys. Lett.*, 2000, **77**, 904.
7 M.-J. Yang and T. Tsutsui, *Jpn. J. Appl. Phys. 2*, 2000, **39**, L828.
8 P. I. Djurovich, S. A. Lamansky, M. R. Nugent, D. L. Murphy, R. C. Kwong and M. E. Thompson, *Polym. Prep.*, 2000, **41**, 770.
9 Y. Wang, V. A. Petrov and V. V. Grushin, *Pat. Appl. (DuPont)*, 2000.
10 O. Lohse, P. Thevenin and E. Waldvogel, *Synlett*, 1999, 45.
11 K. A. King, P. J. Spellane and R. J. Watts, *J. Am. Chem. Soc.*, 1985, **107**, 1431; M. G. Colombo, T. C. Brunold, T. Riedener, H. U. Güdel, M. Fortsch and H.-B. Bürgi, *Inorg. Chem.*, 1994, **33**, 545; K. Dedeian, P. I. Djurovich, F. O. Garces, G. Carlson and R. J. Watts, *Inorg. Chem.*, 1991, **30**, 1685.
12 C. Hansch, A. Leo and R. W. Taft, *Chem. Rev.*, 1991, **91**, 165.

CHEMCOMM Communication
www.rsc.org/chemcomm

Design of an adsorbent with an ideal pore structure for methane adsorption using metal complexes

Kenji Seki

Department of Research and Development, Osaka Gas Co., Ltd., 6-19-9 Torishima, konohana-ku, Osaka 554-0051, Japan. E-mail: ken@osakagas.co.jp

Received (in Cambridge, UK) 14th May 2001, Accepted 28th June 2001
First published as an Advance Article on the web 26th July 2001

Three-dimensional metal complexes synthesized from copper dicarboxylates and triethylenediamine (TED), which have an ideal pore size for methane adsorption, have higher methane adsorption capacity than the theoretical maximum for activated carbons.

Methane is a primary component of natural gas, which is an important candidate for clean transportation fuels. The storage of methane on adsorbents has been pursued actively as an alternative to high pressure compressed gas storage. However, it was concluded that none of the conventional adsorbents tested showed sufficient methane storage to meet that required for commercial viability.[1–5] The analysis of pore structure of adsorbents indicated that for even carbons as the best methane adsorbent, there is a large percentage of mesopores and macropores where methane adsorption does not occur sufficiently.[2] Therefore, to achieve higher adsorption capacity, it is essentially necessary that the micropore volume must be maximized, while the mesopore and macropore volume must be minimized as far as possible.

Recently, a great deal of attention has been directed toward the use of metal complexes in the design and synthesis of new porous materials.[6–11] Because of their structural controllability, these porous materials will be attractive adsorbents for methane storage. However previously reported complexes are not suitable owing to low adsorption capacities. Herein, a new type of methane adsorbent with ideal pore structure and sufficient adsorption capacity is reported.

Novel metal complexes $[\{Cu(O_2CRCO_2)\cdot 1/2TED\}_n]$ (R = 4,4′-$C_6H_4C_6H_4$ **1** or *trans*-$C_6H_4CH{=}CH$ **2**) were synthesized by a heterogeneous reaction between porous copper dicarboxylates[6] and TED.† The temperature dependence of the magnetic susceptibilities for the metal complexes obtained indicates that the existence of the same dinuclear structure as that of copper(II) acetate monohydrate and porous copper(II) dicarboxylates *i.e.* a two-dimensional structure of dicarboxylic acids bridging central copper ions. Based on these results and elemental analysis, it is suggested that the two-dimensional layer bridging the copper(II) ions with dicarboxylate ions are linked with TED as pillar ligands to give a three-dimensional structure (Fig. 1).

The stability of this network structure was studied by X-ray powder diffraction (XRPD) and thermal gravimetric (TG) analysis. The TG curve of **1** illustrates the release of the adsorbed molecules up to *ca.* 373 K, followed by thermal decomposition of the structure at 513 K. No chemical decomposition was observed between 373 and 513 K. The structure of this stable phase was studied by measuring the XRPD pattern at room temp., 473 K and 513 K. These results demonstrate that the porous network structure is retained up to 513 K in the absence of the included guest molecules. Similarly the network structure of **2** is retained up to 473 K in the absence of the included guest molecules.

Fig. 2 shows that the observed XRPD pattern of **1** is in very good accordance with a simulated pattern of the optimized plausible structure generated using Cerius2, indicating that the structure of **1** is similar to that shown in Fig. 1.

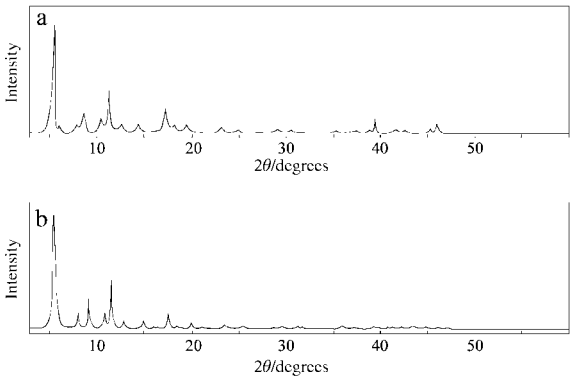

Fig. 2 X-Ray diffraction patterns of **1**. (a) Experimental X-ray powder diffraction after removal of the included guest molecules. (b) Simulated X-ray powder diffraction of the optimized structure using Cerius2.

To examine the porosity of **1** and **2**, high-resolution adsorption isotherms of Ar at 87.3 K were measured in a relative pressure (P/P_0) range from 10^{-6} to 1 using ASAP 2000M volumetric adsorption equipment from Micromeritics. These adsorption isotherms of **1** and **2** (Fig. 3) show typical isotherms of Langmuir type, confirming the presence of micropores without mesopores. Analyses of these isotherms yielded BET surface areas of 3265 and 3129 $m^2\ g^{-1}$, micropore volumes of 1.18 and 1.07 $cm^3\ g^{-1}$ and effective pore sizes of 10.8 and 9.5 Å for **1** and **2**, respectively (using Dubinin–Radushkevitch methods[12] and Horvath–Kawazoe methods[13]).

The pore size distributions are sharp with one sharp peak at 9.5 Å for **2**, indicating that the obtained metal complexes have uniform micropores. On the other hand, for **1**, the pore size distributions exhibit two peaks. This result does not indicate the existence of two kinds of pores, but rather the existence of two adsorption sites having different values of adsorption potential

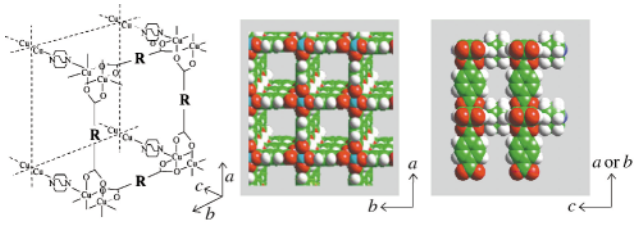

Fig. 1 A plausible three-dimensional structure for the complexes.

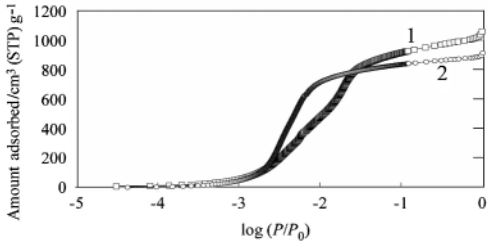

Fig. 3 Ar adsorption isotherms at 87.3 K for the coordination polymers.

 DOI: 10.1039/b104204c

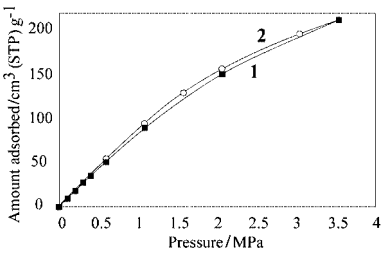

Fig. 4 High-pressure adsorption isotherms of methane at 298 K on metal complexes.

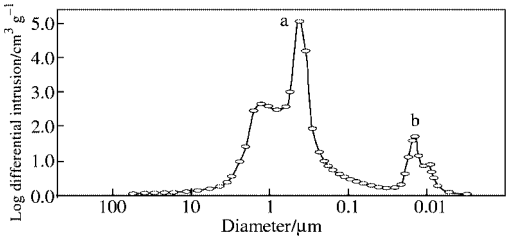

Fig. 6 Mercury penetration curve for **2** (differential intrusion *vs.* pore diameter).

in one pore. These sites are the corner and the edge of the square pore. HK methods can not be used to calculate the pore size distributions for pores of the more than >8 Å width.[14] To compare experimental values of the pore size with calculated values, the plausible structures were optimized by molecular mechanic (MM) and molecular dynamics (MD) of Cerius2 and the pore sizes were calculated. The effective pore size calculated from the optimized structure of **2** was *ca.* 9.4 Å (Fig. 1). This calculated value is in good agreement with the experimental HK value indicating the structure of the obtained complexes is as suggested. The bigger the size of dicarboxylic acid as a ligand, the larger the porosity and pore size, indicating that the porosity and pore size can be controlled by the starting materials. These surface areas and pore volumes are much larger compared with those of other coordination polymers, zeolites and commercial activated carbons already reported, and are the same as those of special high surface area activated carbons. These coordination polymers have adequate porosity to adsorb methane as well as a suitable pore size distribution which is nearly ideal for methane adsorption.

The adsorption isotherms of methane were measured gravimetrically up to 3.5 MPa. Fig. 4 shows methane adsorption isotherms of **1** and **2** at 298 K. The adsorption isotherms are of Langmuir type. Approximately 212 cm^3 (STP) and 213 cm^3 (STP) of methane were adsorbed per g of dried samples of **1** and **2** at 3.5 MPa. These values are much higher than that of zeolite 5A [*ca.* 83 cm^3 (STP) g^{-1} at 3.5 MPa] and nearly the same as that of the high surface area activated carbon AX-21, a methane adsorbent with the highest capacity among conventional materials.[2]

The samples were characterized by scanning electron microscopy (SEM) and atomic force microscopy (AFM). Fig. 5(a) and (b) show SEM image of particles of **2**, indicating that the particles are plate forms of *ca.* 0.2 μm in width, these particles aggregate and particles of *ca.* 7 μm in size are formed. Fig. 5(c) shows a surface AMF image of **2**. Nanocrystallites of *ca.* 100 nm in size were observed on the surface, considered to be the primary particles.

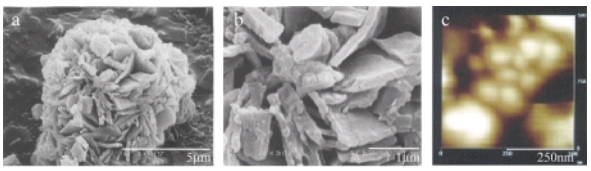

Fig. 5 SEM and AFM images of coordination polymer **2**.

Moreover, in order to characterize pore structures and material density, mercury intrusion penetration was measured from 1 to 60 000 psia with a Micromeritics instrument. Fig. 6 shows the result of mercury porosimetry for **2**, which is in good accordance with those of SEM and AFM, with regard to voids between particles, *i.e.* the voids between the secondary particles (plate forms) correspond to peak a of 0.1–5 μm and the voids between the primary particles correspond to peak b of 6–20 nm. The apparent density (0.983 g cm^{-3}) of the primary particles is calculated from the result of mercury porosimetry by assuming that peaks a and b are derived from voids between particles. The practical parameter, v/v, expressing the gas storage capacity [v/v is the volume of gas (at 298 K and 0.1013 MPa) divided by the volume of the tank] was estimated to be 225 from the density and the amount of adsorbed methane per weight of dried sample. On the other hand, adsorption simulations predict that the theoretical maximum for methane storage capacity of carbon, the structure of which consists of parallel planes of graphite with an optimum slit width 11.4 Å, is v/v = 198, for void-free monolithic carbon.[15] Thus the amount of adsorbed methane for **2** surpasses the theoretical maximum storage capacity of carbon calculated under the same conditions due to the high density of the complex.

The results of the present work have important implications since practical utilization of the coordination polymer for new adsorptive gas storage may be feasible.

I thank Dr Y. Yokomichi for simulation of structures, and Professor W. Mori and Professor S. Kitagawa for guidance and advice in the synthesis.

Notes and references

† **1**: An ethanol solution (15 cm^3) of copper(II) acetate monohydrate (0.095 g) was added to a dimethylformamide solution (30 cm^3) of stylene dicarboxylic acid (0.096 g) and formic acid (0.3 cm^3). After the mixture was allowed to stand for several days at 313 K, a toluene solution (12.5 cm^3) of triethylenediamine was added to the mixture, which was then allowed to react at 373 K in an autoclave for 1 h. A light blue precipitate was collected, washed with methanol, and dried at 373 K *in vacuo*. Anal. Found: C, 49.34; H, 2.70; N, 4.42. Calc. for $Cu(O_2CC_6H_4CO_2)\cdot 1/2C_6H_{12}N_2$: C, 50.90; H, 2.96; N, 4.42%.

2: This complex was prepared using the procedure described for **1**. Anal. Found: C, 56.52; H, 3.55; N, 3.52. Calc. for $Cu(O_2CC_6H_4CO_2)\cdot 1/2C_6H_{12}N_2$: C, 57.22; H, 3.11; N, 3.93%.

1 R. A. Innes, F. E. Lutinski, M. L. Occelli and J. V. Kennedy, *Proceedings of the 22nd Automotive Technology Development Contractors' Coordination Meeting*, 1985, p. 73.
2 D. F. Quinn and J. A. F. MacDonald, *Carbon*, 1992, **29**, 1097.
3 J. A. F. MacDonald and D. F. Quinn, *Fuel*, 1998, **77**, 61.
4 O. Talu, *4th Proc. Fundam. Adsorpt.*, 1992, **4**, 655.
5 A. Golovoy, *Compressed Nat. Gas. Conf. Proc.*, 1983, p. 39.
6 K. Seki, S. Takamizawa and W. Mori, *Chem. Lett.*, 2001, 122.
7 S. S.-Y. Chui, S. M.-F. Lo, J. P. H. Charmant, A. G. Orpen and I. D. Williams, *Science*, 1999, 1148.
8 H. Li, M. Eddaoudi, M. O'Keeffe and O. M. Yaghi, *Nature*, 1999, **402**, 276.
9 H. Li, M. Eddaoudi, T. L. Groy and O. M. Yaghi, *J. Am. Chem. Soc.*, 1998, **120**, 8571.
10 M. Kondo, M. Shimamura, S. Noro, S. Minakoshi, A. Asami, K. Seki and S. Kitagawa, *Chem. Mater.*, 2000, **12**, 1288.
11 S. Noro, S. Kitagawa, M. Kondo and K. Seki, *Angew. Chem., Int. Ed.*, 2000, **39**, 2081.
12 S. J. Gregg and K. S. W. Sing, *Adsorption, Surface Area and Porosity*, Academic Press, London, UK, 2nd edn. 1982.
13 G. Horvath and K. Kawazoe, *J. Chem. Eng. Jpn.*, 1983, **16**, 470.
14 M. Kruk, M. Jaroniec and J. Choma, *Adsorption, Shimizu*, 1997, **3**, 209.
15 K. R. Matranga and A. L. Myers, *Chem. Eng. Sci.*, 1992, **47**, 156.

CHEMCOMM Communication
www.rsc.org/chemcomm

Diastereospecific synthesis of amino-acid substituted 2,2′-bipyridyl complexes

Shane G. Telfer,[a] Gérald Bernardinelli[b] and Alan F. Williams*[a]

[a] *Département de Chimie minérale, analytique et appliquée, Université de Genève, 30 quai Ernest Ansermet, CH 1211 Genève 4, Switzerland. E-mail: Alan.Williams@chiam.unige.ch*
[b] *Laboratoire de Cristallographie aux Rayons-X, Université de Genève, 24 quai Ernest Ansermet, CH 1211 Genève 4, Switzerland*

Received (in Cambridge, UK) 22nd May 2001, Accepted 4th July 2001
First published as an Advance Article on the web 26th July 2001

The L-valine substituted 2,2′-bipyridyl ligand 1 forms Δ-M(1)$_3$ (M = Fe^{II}, Co^{II}, Co^{III}) complexes diastereospecifically, with the L-valinate arms forming a chiral anion-binding pocket in the solid state.

Tris(2,2′-bipyridyl) metal complexes are among the most studied in coordination chemistry. Although the complexes are inherently chiral, simple bipyridines invariably lead to mixtures of enantiomers. To achieve stereoselectivity at the metal centre, the ligands must be modified to introduce an element of chirality as discussed recently by Knof and von Zelewsky.[1] For some years we have been interested in the synthesis of triple helicates using octahedral metal ions binding to multibidentate ligands, and the stereoselective synthesis of such complexes is an obvious challenge. With a view to combining stereoselectivity and the synthesis of heteronuclear helicates we conceived the ligand valabipy, **1**, comprising three bidentate

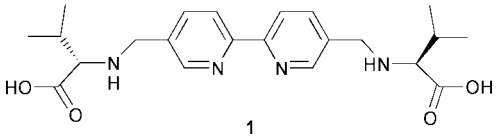

1

sites, one bipyridyl and two amino acids. The amino acid moiety could induce stereoselectivity in the coordination of metal ions, as demonstrated by Bernauer's group for mononuclear complexes of pyridine-amino acid ligands,[2] and the different ligating powers of bipyridyl and amino acids should allow the binding of different metal ions in the two sites. Ligand **1** is a rare example of a chiral 5,5′-substituted bipyridyl ligand and here we report the surprising observation of diastereospecificity when *only* the achiral bipyridyl chelating unit is occupied, and the observation of anion binding at the amino acid site in the solid state.

Valabipy **1** is prepared in three steps from diethyl-2,2′-dipyridyl-5,5′-dicarboxylate[3] by reduction of this ester to the corresponding alcohol, formation of the chloro derivative, and substitution of the chloride by L-valine in basic methanol.† The neutral ligand is sparingly soluble in water, but dissolves readily in slightly acid solution. If a solution of three equivalents of **1** in dilute HCl is treated with one equivalent of iron(II) perchlorate, a red–violet solution is obtained, indicating complexation of low spin iron(II) in the bipyridyl site. The composition [Fe(**1**)$_3$]$^{2+}$ was confirmed by electrospray mass spectrometry. The ^{1}H NMR spectrum of the diamagnetic complex showed it to be a mixture of diastereomers, most clearly revealed by the signals due to the α proton of the amino acid and the 6,6′-protons of the bipyridyl moiety. The initial ratio of diastereomers was 2:1, but on warming to 60 °C or on standing overnight, the weaker set of signals completely disappeared, indicating a thermodynamically controlled diastereospecificity. On the basis of the sign of the CD bands arising from the exciton coupling of the π–π* transitions, we can assign the Δ configuration to the thermodynamically stable diastereomer (Fig. 1).[4,5]

If the labile cobalt(II) ion was used instead of iron(II), the complex was less stable in acid solution than [Fe(**1**)$_3$]$^{2+}$ but in the pH range 4–5 the paramagnetic ^{1}H NMR spectrum showed a set of 9 peaks corresponding to [Co(**1**)$_3$]$^{2+}$. The sign of the exciton couplet in the CD spectrum again indicated a Δ-configuration at the metal centre (Fig. 1). [Co(**1**)$_3$]$^{2+}$ could be oxidised by hydrogen peroxide to give the corresponding cobalt(III) complex. The ^{1}H NMR spectrum of the crude product showed predominantly one diastereomer, with traces of some minor products easily removed by crystallisation. The CD spectrum indicated that the oxidation reaction was stereoretentive, yielding Δ-[Co(**1**)$_3$]$^{3+}$ (Fig. 1).[4,6]

If valabipy is synthesised using D-valine, instead of natural L-valine, the enantiomeric ligand **2** is obtained. As expected, the CD spectrum of [Co(**2**)$_3$]$^{2+}$ was the mirror image of that seen for [Co(**1**)$_3$]$^{2+}$, indicating that the Λ configuration is favoured for [Co(**2**)$_3$]$^{2+}$. Interestingly, when three equivalents of **1**, three equivalents of **2** and two equivalents of cobalt(II) were mixed, the ^{1}H NMR spectrum was identical to that of [Co(**1**)$_3$]$^{2+}$. This demonstrates that the ligands undergo a homochiral self-recognition process, preferentially forming Δ-[Co(**1**)$_3$]$^{2+}$ and Λ-[Co(**2**)$_3$]$^{2+}$ over any mixed ligand species.

Crystals suitable for an X-ray structure determination were obtained from a solution of [Fe(**1**)$_3$]$^{2+}$ in 1 M HCl with added sodium perchlorate.‡ The crystal structure of [Fe(**1**H)$_2$(**1**H)Cl$_2$](ClO$_4$)$_4$Cl·14H$_2$O confirmed the Δ-configuration for the [Fe(bipy)$_3$] unit, and revealed, to our surprise, the binding of two chloride ions by the complex. The cation may be regarded as a helicate in which the helical axis is defined by the Cl–Fe–Cl direction [angle Cl–Fe–Cl 179.50(6)] and the **1** ligands twist around the axis (Fig. 2 and 3).

The structure is held together by coordinate bonds between the iron and the bipyridyls, and hydrogen bonds and electro-

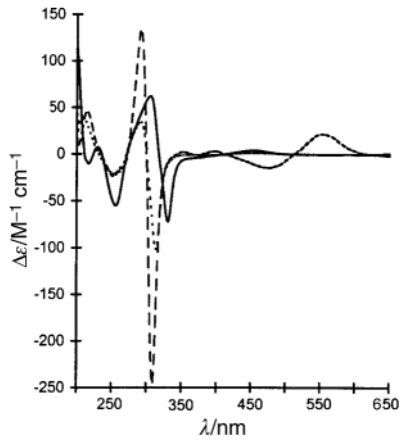

Fig. 1 CD spectra of [Fe(**1**)$_3$]$^{2+}$ (-----), [Co(**1**)$_3$]$^{2+}$ (pH 4.2) (·····), and [Co(**1**)$_3$]$^{3+}$ (—) in aqueous solution.

 DOI: 10.1039/b104520m

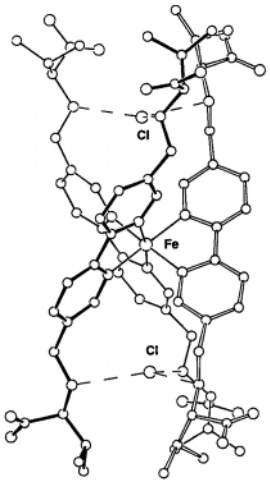

Fig. 2 View of the solid state structure of the $[Fe(\mathbf{1}H)(\mathbf{1}H_2)_2Cl_2]^{5+}$ cation showing the threefold hydrogen bonding of the chloride ions.

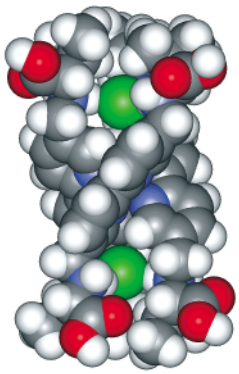

Fig. 3 Space filling view of the structure of the $[Fe(\mathbf{1}H)(\mathbf{1}H_2)_2Cl_2]^{5+}$ cation perpendicular to the pseudo-threefold axis. The iron atom is hidden by the bipyridyl unit; the chloride ions are shown in green and the carboxylate oxygens in red.

static interactions between the chlorides and the protonated amino residues of the ligand. The geometry of the $Fe(bipy)_3$ unit is normal[7] with an average Fe–N distance of 1.968 Å, interplane torsional angles for the bipyridyl units between 4 and 8°, and approximate D_3 symmetry. The isopropyl side chains of **1** are oriented so that they are clustered together around the helical axis, while the carboxylates are directed away from the axis to form a hydrophilic surface. The crystal packing of the cations shows an ABCABC packing of layers with the pseudo-threefold axis of the cation perpendicular to the layers and parallel to the [1 1 1] direction. The amino acid moieties are protonated on all the amino groups, and on five of the carboxylates, although the deprotonated carboxylate is delocalised between two sites. One of the N–H protons of each amino group is directed towards the helical axis and is available to hydrogen bond the chloride ions, with average N···Cl distances of 3.16 Å, typical of N–H···Cl hydrogen bonding. Each chloride forms three hydrogen bonds in an approximately trigonal arrangement, but is displaced slightly out of the N_3 plane towards the iron atom which is 4.98 Å away.

Whilst this manuscript was in preparation, a ruthenium(II) complex with amide-substituted 2,2′-bipyridyl ligands was shown by Beer and coworkers to encapsulate chloride ions in both the solid state and in solution ($MeOH–CH_2Cl_2$).[8] The anion binding site is very similar, though in the case of **1** the cationic ammonium units form significantly shorter N–H···Cl bonds, and both the chloride ions form three hydrogen bonds in the solid state, whereas in ref. 8 one chloride ion formed two hydrogen bonds and the other three hydrogen bonds.

It is interesting that for $[M(\mathbf{1})_3]^{n+}$, the stereoselective organisation of **1** around the metal ion leads to the generation of a chiral receptor site at each end of the complex. The nature of this site may be modified by changes in the chelating side arms used to construct the ligand and thus these complexes have promise as tunable selective chiral anion sensors—an area of much current interest.[9]

The diastereospecific formation of Δ-$[Fe(\mathbf{1})_3]^{2+}$ is initially surprising when the distance of the chiral centres of the ligand from the iron atom is considered. The fact that the complex may be crystallised from strongly acid (1 M HCl) solution implies that an additional stabilising element is present since α-diimine complexes such as $[Fe(phen)_3]^{2+}$ or [Fe(diethyl-2,2′-dipyridyl-5,5′-dicarboxylate)$_3$]$^{2+}$ are rapidly decomposed under these conditions. The observation that the labile Co^{II} ion shows immediate diastereoselectivity, whereas the kinetically more inert Fe^{II} ion takes longer for the ^1H NMR and CD spectra to stabilise indicates that the selectivity is thermodynamic rather than kinetic. Current investigations in this laboratory are focussing on the precise origins of the observed diastereoselectivity and the behaviour of the anion receptor site in solution.

Notes and references

† Ligand **1** was fully characterised by ^1H NMR, ^{13}C NMR, mass spectrometry and elemental analysis.

‡ *Crystal data*: $[Fe(C_{22}H_{31.667}N_4O_4)_3Cl_2](ClO_4)_4Cl{\cdot}14H_2O$: triclinic, space group $P1$, a = 12.2214(9), b = 13.0213(10), c = 15.5397 Å , V = 2361.3(2) Å^3, α = 85.007(9), β = 79.818(9), γ = 76.218(9)°, Z = 1, D_c 1.449 g cm^{-3}. 32169 reflections were collected using a STOE IPDS system at 200 K with Mo-Kα radiation. 17362 unique reflections (R_{int} = 0.041), Data correction for Lorentzian polarisation and absorption (μ = 0.45 mm^{-1}, T_{min} = 0.9289, T_{max} = 0.9539). The structure was solved by direct methods,[10] and refined against $|F|$ using anisotropic atomic displacement parameters for all non-hydrogen atoms. Ligand hydrogen atoms were calculated, and OH groups were attributed on the basis of the associated C–O distances. Inclusion and refinement of the water hydrogen atoms gave no improvement. The final R factor for 11445 reflections ($|F_o| > 4\sigma(F_o)$) with 1151 variables was 0.039 (R_w = 0.040) and the absolute structure parameter −0.04(2). Residual electron density peaks: min. −0.67, max. 0.52 e Å^{-3}. Calculation used the XTAL[11] programs.

CCDC reference number 154157. See http://www.rsc.org/suppdata/cc/b1/b104520m/ for crystallographic data in CIF or other electronic format.

1 U. Knof and A. von Zelewsky, *Angew. Chem., Int. Ed.*, 1999, **38**, 302.
2 K. Bernauer, H. Stoeckli-Evans, D. Hugi-Cleary, H. J. Hilgers, H. Abd-el-Khalek, J. Porret and J.-J. Sauvain, *Helv. Chim. Acta*, 1992, **75**, 2327.
3 G. R. Newkome, J. Gross and A. K. Patri, *J. Org. Chem.*, 1997, **62**, 3013.
4 M. Ziegler and A. von Zelewsky, *Coord. Chem. Rev.*, 1998, **177**, 257.
5 J. Hidaka and B. E. Douglas, *Inorg. Chem.*, 1964, **3**, 1180.
6 J. Ferguson, C. J. Hawkins and N. A. P. Kane-Maguire, *Inorg. Chem.*, 1969, **8**, 771.
7 P. C. Healy, B. W. Skelton and A. H. White, *Aust. J. Chem.*, 1983, **36**, 2057.
8 L. H. Uppadine, M. G. B. Drew and P. D. Beer, *Chem. Commun.*, 2001, 291.
9 P. D. Beer and D. K. Smith, *Prog. Inorg. Chem.*, 1997, **46**, 1; P. D. Beer and P. A. Gale, *Angew. Chem., Int. Ed.*, 2001, **40**, 486.
10 P. Main, S. J. Fiske, S. E. Hull, L. Lessinger, D. Germain, J. P. Declercq and M. M. Woolfson, Universities of York, England and Louvaine-La-Neuve, Belgium, 1987.
11 S. R. Hall, H. D. Flack and J. M. Stewart, *XTAL 3.2 User's Manual*, Universities of Western Australia, Geneva and Maryland, 1992.

CHEMCOMM Communication
www.rsc.org/chemcomm

Substituent effects on aromatic interactions in the solid state

Harry Adams,[a] Pablo L. Bernad Jr.,[a] Drake S. Eggleston,[b] R. Curtis Haltiwanger,[b] Kenneth D. M. Harris,*[d] Guy A. Hembury,[ad] Christopher A. Hunter,*[a] David J. Livingstone,[c] Benson M. Kariuki[d] and James F. McCabe[a]

[a] *Centre for Chemical Biology, Krebs Institute for Biomolecular Science, Department of Chemistry, University of Sheffield, Sheffield, UK S3 7HF. E-mail: C.Hunter@sheffield.ac.uk*
[b] *SmithKline Beecham Pharmaceuticals, 709 Swedeland Road, PA 19406, USA*
[c] *ChemQuest, Delamere House, 1 Royal Crescent, Sandown, Isle of Wight, UK PO36 8LZ*
[d] *School of Chemistry, University of Birmingham, Edgbaston, Birmingham, UK B15 2TT. E-mail: K.D.M.Harris@bham.ac.uk*

Received (in Cambridge, UK) 16th February 2001, Accepted 26th June 2001
First published as an Advance Article on the web 26th July 2001

A systematic series of structural studies has led to an understanding of how to use hydrogen-bonding and steric interactions to control two aromatic rings to interact in a well-defined and predictable manner in the solid state.

The study of non-covalent interactions in the solid state can be a rather hit or miss pursuit, as subtle changes in molecular structure can have dramatic effects on the way in which molecules organise in the crystal.[1] Indeed, the arrangement of molecules observed in a crystal structure is governed by maximising favourable intermolecular interactions and minimising unfavourable intermolecular interactions throughout the whole crystal, and the fact that the molecular packing arrangement arises from the interplay of several different factors calls for considerable caution in attempting to interpret, to rationalize and even to identify specific intermolecular interactions simply on the basis of inspecting known crystal structures. For example, there is an unfortunate tendency to attribute as a favourable interaction any situation in which two functionalities happen to be found close to each other in a crystal structure—however, the two groups involved may be unwillingly forced into close contact as the result of a stronger interaction involving neighbouring groups. To make progress in understanding and controlling specific interactions in the solid state requires investigations on families of materials designed such that the effects of different factors on the resultant structural properties may be systematically delineated. In this communication, we describe systematic studies of this type, which have led to an understanding of how to use hydrogen-bonding and steric interactions to control two aromatic rings to interact in a well-defined and predictable manner.[2]†

Using a combination of edge-to-face aromatic interactions and H-bonds to assemble double-stranded 'zipper' complexes from oligomeric amides, we have been able to quantify the magnitudes of a range of aromatic interactions in solution.[3] The key non-covalent structural motif is shown in Fig. 1(a). Simple aromatic amides of this general structure are self-complementary on both faces and should therefore self-assemble to give linear hydrogen bonded chains in the solid state (Fig. 1(b)).[3a,4] This system provides an interesting framework for probing the properties of aromatic interactions in the solid state, and so we have investigated the degree of control that can be achieved over the geometry of the interactions between the aromatic rings and the sensitivity of these interactions to the nature of the substituents on these rings.[5]

We synthesised the fifteen compounds shown in Fig. 2(a).[6] This series allows us to probe the influence of the size of the aniline *ortho* substituents (R^1 and R^2) and the effects of strongly polarising substituents (X and Y) on the edge-to-face aromatic interaction. For all but one of these compounds, crystals of appropriate size and quality for single crystal X-ray diffraction studies were obtained. It is found that, when there are no aniline *ortho* substituents (*i.e.* $R^1 = R^2 = H$), the molecules are more planar, and although linear H-bonded chains are formed, the molecules are arranged in a head-to-head fashion with stacking interactions between like aromatic rings (not shown). All of the other compounds except **12** adopt a conformation in which the benzoyl and aniline groups are orthogonal (in an intramolecular sense), and the crystal structures contain H-bonded chains with head-to-tail dimers of the type depicted in Fig. 1(a)—*i.e.* with

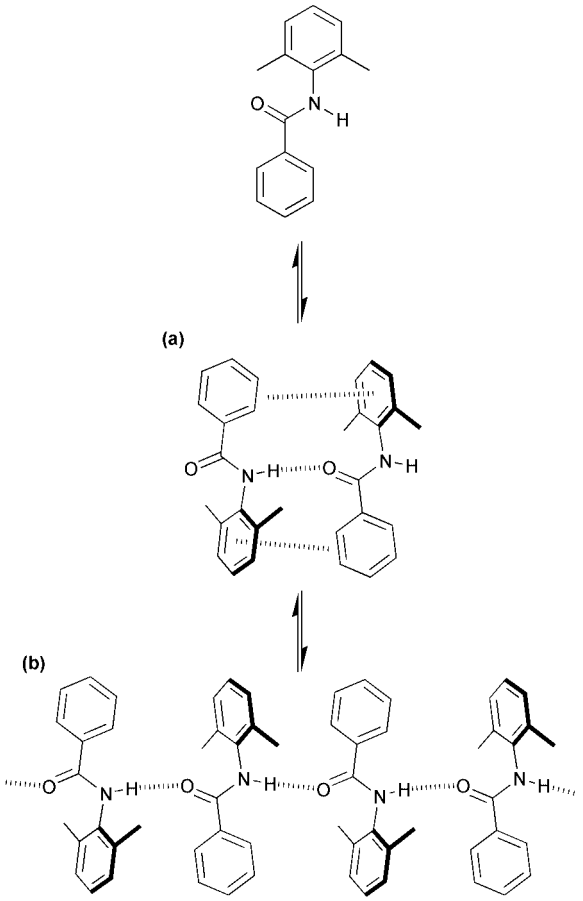

Fig. 1 (a) The key non-covalent structural motif used to assemble oligomeric zipper complexes in solution. (b) Extending this motif yields linear H-bonded chains for aromatic amides of the general structure shown. The term 'head-to-tail dimer' is used to refer to the situation shown, in which the aniline ring of one molecule is adjacent to the benzoyl ring of the neighbouring molecule along the chain (and *vice versa*). In the alternative situation (not shown), the aniline ring of one molecule is adjacent to the aniline ring of the neighbouring molecule along the chain, which is described as a 'head-to-head dimer'.

 DOI: 10.1039/b101575n

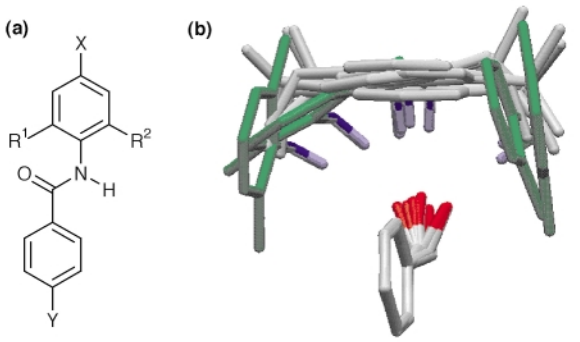

Fig. 2 (a) Compounds used to probe the influence of the aniline *ortho* substituents on the geometry of the aromatic interactions in the solid state.

X	Y	R^1 = R^2 =	H H	H Me	Me Me	Et Et	iPr iPr
H	^{t}Bu		**1**	**2**	**3**	**4**	**5**
H	NO_2		**6**	**7**	**8**	**9**	**10**
NO_2	^{t}Bu		**11**	**12**	**13**	**14**	**15**

(b) The aromatic interactions in the head-to-tail dimers found in the crystal structures of **2**–**5**, **8**–**10**, **13**–**15** are shown, with the benzoyl rings superimposed and the *para* substituents deleted for clarity.[5] Aniline rings with ethyl and isopropyl substituents are coloured grey, and anilines with methyl substituents are coloured green. The H-bonded chains in the crystal structures of **1**, **6**, **11** and **12** contain head-to-head dimers and are not shown. We have not yet been able to obtain a crystal structure of **7**.

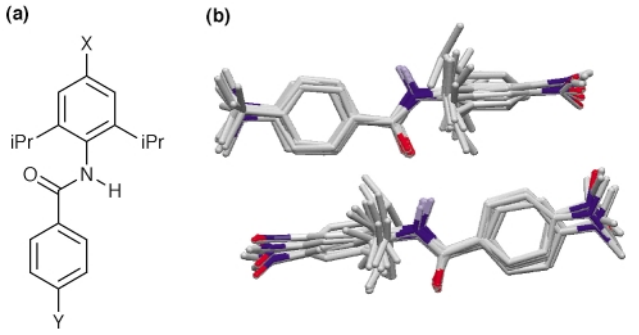

Fig. 3 (a) Compounds used to probe the influence of the polarising substituents on the geometry of the aromatic interactions in the solid state.

X	Y =	NMe_2	^{t}Bu	NO_2
NMe_2		**16**	**17**	**18**
H		**19**	**5**	**10**
NO_2		**20**	**15**	**21**

(b) The head-to-tail dimers found in the crystal structures of **16**, **17**, **19**, **5**, **10**, **20**, and **15** are shown as a least squares overlay of the amide group (C, N and O), the aniline ring (six C atoms) and benzoyl ring (six C atoms).[5] We have not yet been able to obtain the crystal structures of **18** and **21**.

interactions between the benzoyl and aniline rings of adjacent molecules.

Fig. 2(b) shows an overlay of the aromatic interactions in all of the crystal structures that contain head-to-tail dimers. The behaviour of the aniline rings with *ortho* methyl groups is clearly different from those with *ortho* ethyl and *ortho* isopropyl groups. The bulkier substituents strictly enforce edge-to-face interactions between the two π-systems, such that the geometry of these interactions is essentially identical for all of the structures with ethyl and isopropyl groups. As shown in Fig. 2(b) (grey structures), the benzoyl group fits into a groove which runs along the face of the aniline ring, sandwiched between the two alkyl substituents which project above the plane of the aniline π-system.

For the smaller *ortho* methyl groups, the molecules still adopt a conformation in which the benzoyl and aniline rings are orthogonal to each other, but the intermolecular interactions are significantly different. Now the geometric relation between adjacent molecules is distorted such that intermolecular aromatic stacking interactions are observed (Fig. 2(b), green structures). The major distortion concerns the geometry of the H-bonding interaction which allows the two π-systems to become parallel, improving the packing efficiency of the dimer.

For X = NO_2, alternating head-to-tail and head-to-head dimers are found within the H-bonded chain for the dimethyl and diethyl aniline derivatives, and for the mono-methyl derivative only head-to-head dimers are found. There appears to be a strong driving force for the nitroanilines to stack with themselves, and this is only prevented in the presence of bulky isopropyl groups which disrupt stacking of the aniline groups.

These results suggest that we can rigorously control the geometry of the aromatic interactions in this system by using isopropyl aniline derivatives, and that the packing, at least within a chain, is insensitive to the nature of the terminal substituents (X and Y). It should therefore be possible to use this system as a scaffold to set up geometrically well-defined intermolecular aromatic interactions with a variety of different substituents. To explore this potential, we have synthesised the wider series of compounds containing isopropyl substituents shown in Fig. 3(a), and crystal structures have been obtained for seven of these compounds (three structures were available from our studies of the series shown in Fig. 2(a) and four additional structures were obtained). In all cases, the crystals contain H-bonded chains containing the expected head-to-tail dimers of the type shown in Fig. 1(a).[7] Fig. 3(b) shows an overlay of the aromatic interactions in the head-to-tail dimers found in these crystal structures. These structures are essentially identical, supporting the view that the H-bonded motif in Fig. 1 represents a robust framework for the study of edge-to-face aromatic interactions in the solid state.

We thank SmithKline Beecham (JFM), BBRSC (GAH), the Lister Institute (CAH) and EPSRC (BMK) for funding.

Notes and references

† CCDC 158573–158589. See http://www.rsc.org/suppdata/cc/b1/b101575n/ for crystallographic data in CIF or other electronic format for compounds **1**–**4**, **6**, **8**–**17**, **19** and **20**. The crystal structure of **5** was reported previously.[2a]

1 (*a*) G. R. Desiraju, *Crystal Engineering*, Elsevier, Amsterdam, 1989; (*b*) *The Crystal as a Supramolecular Entity*, ed. G. R. Desiraju, Wiley, Chichester, 1996.
2 (*a*) H. Takahashi, S. Tsuboyama, Y. Umezawa, K. Honda and M. Nishio, *Tetrahedron*, 2000, **56**, 6185; (*b*) J. P. Glusker, *Top. Curr. Chem.*, 1998, **198**, 1; (*c*) A. Gavezzotti, *Curr. Opin. Solid State Mater. Sci.*, 1996, **1**, 501.
3 (*a*) H. Adams, F. J. Carver, C. A. Hunter, J. C. Morales and E. M. Seward, *Angew. Chem., Int. Ed. Engl.*, 1996, **35**, 1542; (*b*) H. Adams, K. D. M. Harris, G. A. Hembury, C. A. Hunter, D. Livingstone and J. F. McCabe, *Chem. Commun.*, 1996, 2531; (*c*) F. J. Carver, C. A. Hunter and E. M. Seward, *Chem. Commun.*, 1998, 775.
4 N. E. C. Duke and P. W. Codding, *J. Med. Chem.*, 1992, **35**, 1806.
5 We emphasize that some of the measured diffraction data were of intrinsically poor quality as a consequence of comparatively poor crystal quality. In spite of this fact, significant new structural insights have been obtained, and the structural results are discussed at a level compatible with the quality of the data. Disorder is a factor in structures **12**, **13**, **15** and **16**, and a serious factor in the latter two, where it leads to alternative orientations for the H-bonded chains. These factors do not affect the overall findings reported here and will be fully discussed in a full paper on this topic.
6 All new compounds gave satisfactory spectroscopic data.
7 For compound **16** (X = Y = NMe_2), head-to-head dimers were also found within the H-bonded chain.

CHEMCOMM
Communication
www.rsc.org/chemcomm

A cross-shaped Ag_5Ti_4 molecule based on a $[Ag(C{\equiv}N)_4]^{3-}$ core

Thomas Stein and Heinrich Lang*

Technische Universität Chemnitz, Fakultät für Naturwissenschaften, Institut für Chemie, Lehrstuhl für Anorganische Chemie, Straße der Nationen 62, D-09111 Chemnitz, Germany. E-mail: heinrich.lang@chemie.tu-chemnitz.de

Received (in Cambridge, UK) 4th June 2001, Accepted 29th June 2001
First published as an Advance Article on the web 26th July 2001

$K_3[Ag(C{\equiv}N)_4]$ (2) reacts with $\{[Ti](C{\equiv}CR)_2\}AgOClO_3$ {R = $SiMe_3$, 1a; R = Ph, 1b; [Ti] = $(\eta^5\text{-}C_5H_4SiMe_3)_2Ti$} in a 1 : 4 molar ratio to produce the nonametallic Ag_5Ti_4 species $[Ag(C{\equiv}N{\rightarrow}Ag\{(RC{\equiv}C)_2[Ti]\})_4](ClO_4)$ (R = $SiMe_3$, 3a; R = Ph, 3b) in which four heterobimetallic titanium(IV)–silver(I) tweezer units, $[\{[Ti](C{\equiv}CR)_2\}Ag]^+$, are bridged by a $[Ag(C{\equiv}N)_4]^{3-}$ core; the reaction chemistry of 3 is reported.

Recently, oligonuclear cyanide bridged transition metal complexes have attracted much attention, since they possess interesting chemical as well as physical properties.[1,2]

In this context, we here describe a straightforward method for the preparation of, *e.g.* the cross-shaped structured Ag_5Ti_4 species $[Ag(C{\equiv}N{\rightarrow}Ag\{(RC{\equiv}C)_2[Ti]\})_4](ClO_4)$ by introduction of a group-11 metal cyanide core, $[Ag(C{\equiv}N)_4]^{3-}$, as linking component for heterobimetallic early–late organometallic building blocks, *e.g.* $[\{[Ti](C{\equiv}CR)_2\}Ag]^+$.

Treatment of orange $\{[Ti](C{\equiv}CR)_2\}AgOClO_3$ {R = $SiMe_3$, **1a**;[3] R = Ph, **1b**;[4] [Ti] = $(\eta^5\text{-}C_5H_4SiMe_3)_2Ti$} with $K_3[Ag(C{\equiv}N)_4]$[5] in a 4 : 1 molar ratio in tetrahydrofuran as solvent affords nonametallic orange-brown (**3a**) or red (**3b**) $[Ag(C{\equiv}N{\rightarrow}Ag\{(RC{\equiv}C)_2[Ti]\})_4](ClO_4)$ (R = $SiMe_3$, **3a**; R = Ph, **3b**) in excellent yields (Scheme 1).†

The most striking feature of **3a** and **3b** is the bridging cyano–argentate core $[Ag(C{\equiv}N)_4]^{3-}$, which links the four heterobimetallic early–late transition metal units $[\{[Ti](C{\equiv}CR)_2\}Ag]^+$, giving rise to the formation of the novel nonametallic Ag_5Ti_4 species **3a** or **3b**, respectively.

In **3** each cyano ligand of the $[Ag(C{\equiv}N)_4]^{3-}$ core is datively bonded to the silver(I) center of the respective end-grafted titanium–silver tweezer fragment $[\{[Ti](C{\equiv}CR)_2\}Ag]^+$. While, the core silver(I) center possesses a tetrahedral environment, the silver atoms of the corresponding tweezer moieties are trigonal-planar coordinated.[6]

Although $[Fe(C{\equiv}N)_6]^{4-}$ can successfully be used for the preparation of, *e.g.* heptametallic cationic $\{Fe[C{\equiv}N{\rightarrow}Cu(tpa)]_6\}^{8+}$ [tpa = tris(2-pyridylmethyl)amine],[7] surprisingly no reaction seems to take place when $K_4[Fe(C{\equiv}N)_6]$ is reacted with **1a** or **1b**, even though various reaction conditions were applied.

Complexes **3a** and **3b** are readily soluble in polar organic solvents, such as acetone and tetrahydrofuran.

However, **3a** and **3b** decompose, even in the dark, in solution within several days. Besides the formation of elemental silver,

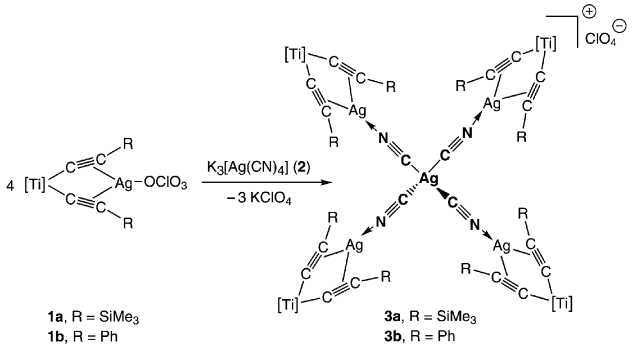

Scheme 1

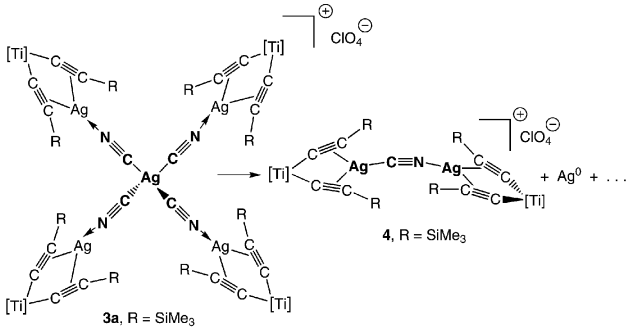

Scheme 2

the tetranuclear Ag_2Ti_2 complex **4** along with other undefined products is produced (Scheme 2).

A further possibility for the preparation of **4** is *via* reacting equimolar amounts of $\{[Ti](C{\equiv}CSiMe_3)_2\}AgOClO_3$ **1a** and $\{[Ti](C{\equiv}CSiMe_3)_2\}AgC{\equiv}N$ **6**.[4] In this reaction the cyano moiety in the latter molecule replaces the $OClO_3$ group in **1a**, thus yielding **4**.[4]

Tetranuclear **4** features a bent Ag–C≡N→Ag array as was demonstrated by single X-ray structure analysis (Fig. 1).‡

The molecular structure of **4** in the solid state shows that each of the two silver(I) centers possesses a trigonal-planar surrounding, caused by two η^2-coordinated alkynyl moieties [Ag(1): Ti(1)–C(1)–C(2)–Si(1), Ti(1)–C(6)–C(7)–Si(2); Ag(2): Ti(2)–C(27)–C(28)–Si(5); Ti(2)–C(32)–C(33)–Si(6)] and the μ-bridging C≡N unit C(53)–N(1) (Fig. 1). A *cis*-bending of the central Ag(1)–N(1)–C(53)–Ag(2) assembly is observed [Ag(1)–N(1)–

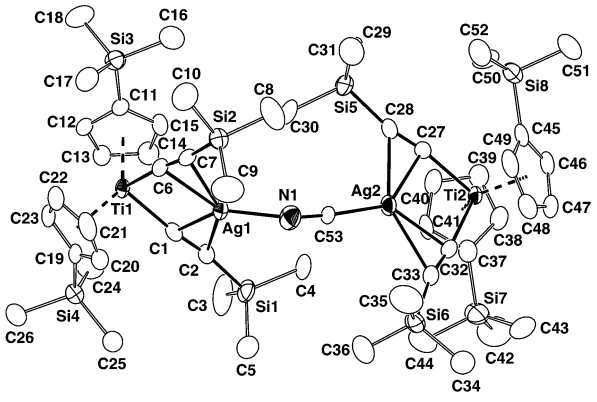

Fig. 1 ZORTEP drawing (50% probability level) of **4**. Selected interatomic bond distances (Å) and angles (°): Ti(1)···Ag(1) 3.1585(10), Ti(2)···Ag(2) 3.1705(9), Ag(1)–N(1) 2.152(5), Ag(1)–C(1) 2.279(5), Ag(1)–C(2) 2.445(5), Ag(1)–C(6) 2.313(5), Ag(1)–C(7) 2.442(5), Ag(2)–C(53) 2.106(5), Ag(2)–C(27) 2.290(5), Ag(2)–C(28) 2.443(5), Ag(2)–C(32) 2.309(5), Ag(2)–C(33) 2.434(5), Ti(1)–C(1) 2.133(5), Ti(1)–C(6) 2.112(5), Ti(2)–C(27) 2.135(5), Ti(2)–C(32) 2.124(5), C(1)–C(2) 1.216(6), C(6)–C(7) 1.248(6), C(27)–C(28) 1.223(7), C(32)–C(33) 1.236(6); Ag(1)–N(1)–C(53) 156.3(4), Ag(2)–C(53)–N(1) 158.5(5), C(1)–Ti(1)–C(6) 93.14(18), C(27)–Ti(2)–C(32) 92.85(18), Ti(1)–C(1)–C(2) 173.6(4), Ti(1)–C(6)–C(7) 171.3(4), Ti(2)–C(27)–C(28) 171.9(4), Ti(2)–C(32)–C(33) 171.2(4), C(1)–C(2)–Si(1) 164.9(4), C(6)–C(7)–Si(2) 169.5(4), C(27)–C(28)–Si(5) 163.3(5), C(32)–C(33)–Si(6) 167.4(5).

 DOI: 10.1039/b104841b

C(53) 156.3(4)°, Ag(2)–C(53)–N(1) 158.5(5)°; Fig. 1]. The planes, comprised of the atoms Ti(1), C(1), C(2), Si(1), C(6), C(7), Si(2) and Ag(1) (rms deviation of fitted atoms 0.02 Å) as well as Ti(2), C(27), C(28), Si(5), C(32), C(33), Si(6) and Ag(2) (rms deviation of fitted atoms 0.04 Å), respectively, are at 87.3°, almost perpendicularly orientated to each other.

The structural features of the organometallic π-tweezer part {[Ti](C≡CSiMe$_3$)$_2$}Ag are in accordance with this type of molecule: (i) the lengthening of the C≡C triple bonds, (ii) *trans*-bending of the Ti–C≡C–Si units and (iii) decreasing of the bite angle $_{C\equiv C}$C–Ti–C$_{C\equiv C}$, as a result of the η^2-coordination of both C≡C triple bonds of the [Ti](C≡CSiMe$_3$)$_2$ moieties to the corresponding silver centers.[6]

IR spectroscopy is a suitable method to prove the formation of **3a** and **3b**. While, in the starting material K$_3$[Ag(C≡N)$_4$] **2**, the $\nu_{C\equiv N}$ frequency is found at 2097 cm^{-1}, it is shifted to 2152 cm^{-1} in **3a** and **3b**. This behaviour is common for cyanide complexes in which the C≡N moiety bridges two transition metal atoms.[8,9b] The counter-ion ClO$_4^-$ in **3a** and **3b** is non-coordinated, since only one absorption band is found for the ν_{Cl-O} stretching vibrations at 1097 cm^{-1} (**3a**) or 1100 cm^{-1} (**3b**) which differs from the starting materials **1a** and **1b** in which the perchlorate entities OClO$_3$ are σ-bonded *via* the formation of a Ag–O bond to the corresponding silver(I) center, giving rise to two (**1a**: 1122, 1032 cm^{-1})[4] or three (**1b**: 1120, 1107, 1067 cm^{-1})[4] bands.[9]

^{13}C{^{1}H} NMR studies on **3a** and **3b** show only minor changes with respect to the chemical shifts of **1a** and **1b**, however, ^{1}H NMR measurements reveal conspicious differences for the protons of the cyclopentadienyl ligands. While **1a** and **1b** display the characteristic AA′XX′ pattern with two pseudo-triplets at δ 6.38 and 6.68 for **1a**[3,4] or δ 6.49 and 6.63 for **1b**,[4] in **3b** two singlets at δ 6.77 and 6.87 and in **3a** only one singlet at δ 6.56 are observed, probably due to the fact that dynamic processes are involved. However, variable temperature ^{1}H NMR measurements could not be carried out, since **3a** and **3b** start to precipitate on cooling during the measurements.

This work was supported in part by the Fonds der Chemischen Industrie and the Deutsche Forschungsgemeinschaft.

Notes and references

† *Experimental details*: as an example, the synthesis of **3a** is presented: to a tetrahydrofuran solution (80 mL) containing 500 mg (0.69 mmol) of {[Ti](C≡CSiMe$_3$)$_2$}AgOClO$_3$ **1a**,[3] 57 mg (0.17 mmol) of K$_3$[Ag(C≡N)$_4$][5] was added in one portion at 25 °C. The reaction mixture was stirred in the dark for 8 h. After filtration through a pad of Celite all volatiles were removed *in vacuo* (oil-pump) and the orange–brown residue washed twice with 20 mL of *n*-pentane (yield: 435 mg, 91%). **CAUTION**: Perchlorates of silver(I) can be explosive. Care has to be taken with all safety precautions followed.

Anal. Calc. for C$_{108}$H$_{176}$Ag$_5$ClN$_4$O$_4$Si$_{16}$Ti$_4$ (2810.28): C, 46.16; H, 6.31; N, 1.99. Found: C, 45.78; H, 6.44; N, 1.69%. Mp: 147 °C (decomp.). IR (KBr, cm^{-1}): [$\nu_{C\equiv N}$] 2152w; [$\nu_{C\equiv C}$] 1949w; [ν_{Cl-O}] 1099s. ^{1}H NMR (d$_6$-acetone), 250.130 MHz, δ 0.29 (s, 72 H, SiMe$_3$), 0.37 (s, 72 H, SiMe$_3$), 6.56 (br s, 32 H, C$_5$H$_4$). ^{13}C{^{1}H} NMR (d$_6$-acetone, 62.902 MHz), δ 0.4 (SiMe$_3$), 1.1 (SiMe$_3$), 118.0 (CH/C$_5$H$_4$), 120.6 (CH/C$_5$H$_4$), 128.0 (^{i}C/C$_5$H$_4$), 138.8 (C≡*C*Si), 156.3 (Ti*C*≡C); owing to the low solubility of **3a** in acetone the ^{13}C{^{1}H} NMR signals for the C≡N units could not be assigned.

‡ *Crystal data* for **4**: C$_{57}$H$_{96}$Ag$_2$ClNO$_5$Si$_8$Ti$_2$, orange rods, 0.60 × 0.15 × 0.10 mm, M_r = 1446.06, triclinic, space group $P\bar{1}$, a = 12.6070(2), b = 16.9396(2), c = 18.5179(3) Å, V = 3695.49(9) Å^3, α = 99.1690(10), β = 100.4600(10), γ = 103.5460(10), Z = 2, D_c = 1.300 g cm^{-3}, F(000) = 1504, T = 173 K, Bruker Smart CCD, Mo-Kα radiation (λ = 0.71073 Å), μ = 0.936 mm^{-1}, min., max. transmission 0.821695, 0.481409, ω-scans, θ_{max} = 30.27°, 18810 unique data, final $R1$ = 0.0562 and $wR2$ = 0.0881 [$I \geqslant 2\sigma(I)$], 709 refined parameters, structure solution by least square methods.

CCDC reference number 165761. See http://www.rsc.org/suppdata/cc/b1/b104841b/ for crystallographic data in CIF or other electronic format.

1 For examples: W. P. Fehlhammer and M. Fritz, *Chem. Rev*., 1993, **93**, 1243; O. Kahn, *Adv. Inorg. Chem*., 1995, **43**, 179; V. Balzani, A. Juris, M. Venturi, S. Campagna and S. Serroni, *Chem. Rev*., 1996, **96**, 759; K. R. Dunbar and R. A. Heintz, *Prog. Inorg. Chem*., 1997, **45**, 283; C. A. Bignozzi, J. R. Schoonover and F. Scandola, *Prog. Inorg. Chem*., 1997, **44**, 1; F. W. Vance, L. K. Karki, J. K. Reigle, J. T. Hupp and M. A. Ratner, *J. Phys. Chem. A*, 1998, **102**, 8320; M. D. Robin and P. Day, *Adv. Inorg. Chem. Radiochem*., 1967, **10**, 247; H. Taube, *Electron Transfer Reactions of Complex Ions in Solution*, Academic Press, New York, 1970; C. Creutz, *Prog. Inorg. Chem*., 1983, **30**, 1; A. Vogler, A. H. Osman and H. Kunkely, *Coord. Chem. Rev*., 1985, **64**, 159; K. Kalyanasundaram and M. K. Nazeeruddin, *Inorg. Chim. Acta*, 1994, **226**, 213; B. J. Coe, T. J. Meyer and P. S. White, *Inorg. Chem*., 1995, **34**, 3600; N. G. Connelly, G. R. Lewis, M. T. Moreno and A. G. Orpen, *J. Chem. Soc., Dalton Trans*., 1998, 1905; H. Vahrenkamp, A. Geiss and G. N. Richardson, *J. Chem. Soc., Dalton Trans*., 1997, 3643; A. Geiss and H. Vahrenkamp, *Inorg. Chem*., 2000, **39**, 4029; R. Argazzi, C. A. Bignozzi, C. G. Garcia, T. J. Meyer, F. Scandola and J. R. Schoonover, *J. Am. Chem. Soc*., 1992, **114**, 8727; C. Chang, D. Ludwig and A. Bocarsly, *Inorg. Chem*., 1998, **37**, 5467.

2 For physical properties, see for example: M. Verdaguer, A. Bleuzen, V. Marvaud, J. Vaissermann, M. Seuleiman, C. Desplanches, A. Scuiller, C. Train, R. Garde, G. Gelly, C. Lomenech, I. Rosenman, P. Veillet, C. Cartier and F. Villain, *Coord. Chem. Rev*., 1999, **192**, 1023; R. Lescouezec, F. Lloret, M. Julve, J. Vaissermann, M. Verdaguer, R. Llusar and S. Uriel, *Inorg. Chem*., 2001, **40**, 2065; C. C. dit Moulin, F. Villain, A. Bleuzen, M.-A. Arrio, P. Sainctavit, C. Lomenech, V. Escax, F. Baudelet, E. Dartyge, J.-J. Gallet and M. Verdaguer, *J. Am. Chem. Soc*., 2000, **122**, 6653; A. Bleuzen, C. Lomenech, V. Escax, F. Villain, F. Varret, C. C. dit Moulin and M. Verdaguer, *J. Am. Chem. Soc*., 2000, **122**, 6648; Z. J. Zhong, H. Seino, Y. Mizobe, M. Hidai, M. Verdaguer, S.-i. Ohkoshi and K. Hashimoto, *Inorg. Chem*., 2000, **39**, 5095.

3 H. Lang, M. Herres and L. Zsolnai, *Organometallics*, 1993, **12**, 5008.

4 T. Stein, Ph.D. Thesis, Technische Universität Chemnitz, 2001.

5 H. Bassett and A. S. Corbet, *J. Chem. Soc*., 1924, **125**, 1660; L. H. Jones and R. A. Pennemann, *J. Chem. Phys*., 1954, **22**, 965; E. Staritzky and F. H. Ellinger, *Anal. Chem*., 1956, **28**, 423.

6 H. Lang, D. S. A. George and G. Rheinwald, *Coord. Chem. Rev*., 2000, **206–207**, 101; H. Lang and G. Rheinwald, *J. Prakt. Chem*., 1999, **341**, 1; H. Lang and M. Weinmann, *Synlett*, 1996, **1**, 1; H. Lang, K. Köhler and S. Blau, *Coord. Chem. Rev*., 1995, **143**, 113; Th. Stein and H. Lang, *Abhath Yarmouk J*., 2001, in press.

7 R. J. Parker, D. C. R. Hockless, B. Moubaraki, K. S. Murray and L. Spiccia, *Chem. Commun*., 1996, 2789.

8 A. G. Sharpe, *The Chemistry of Cyano Complexes of the Transititon Metals*, Academic Press, London, 1976; A. G. Sharpe, *Comprehensive Coordinaton Chemistry*, Pergamon Press, Oxford, 1987, vol. 2, p. 7.

9 (*a*) M. R. Rosenthal, *J. Chem. Ed*., 1973, **150**, 331; (*b*) K. Nakamoto, *Infrared and Raman Spectra of Inorganic and Coordination Compounds*, John Wiley and Sons, New York, 4th edn., 1986.

CHEMCOMM Communication
www.rsc.org/chemcomm

The first organo-tungsten pyrylium salt and structural characterization of its pseudobase

Pierre Haquette,[a] Michèle Salmain,[a] Yann Marchal,[a] Yoann Marsac,[a] Gérard Jaouen,*[a] Desmond Cunningham,[b] Darren P. Egan[b] and Patrick McArdle*[b]

[a] *Laboratoire de Chimie Organométallique, UMR CNRS 7576, Ecole Nationale Supérieure de Chimie de Paris, 11, rue Pierre et Marie Curie F-75231. Paris cedex 05, France. E-mail: jaouen@ext.jussieu.fr*
[b] *Department of Chemistry, National University of Ireland, Galway, Ireland*

Received (in Cambridge, UK) 18th May 2001, Accepted 28th June 2001
First published as an Advance Article on the web 18th July 2001

The first example of an organo-tungsten pyrylium complex (4-cyclopentadienyl-2,6-diphenylpyrylium)$W(CO)_3CH_3$ has been prepared, fully characterized and transformed in an aqueous basic medium to the corresponding pseudobase (3-cyclopentadienyl-1,5-diphenylpent-2-ene-1,5-dione)W-$(CO)_3CH_3$ which is the first X-ray structure analysed organometallic pseudobase.

It has been shown recently[1–3] that pyrylium salts bearing an organometallic fragment are very promising candidates for the labeling of biological molecules. Due to their electrophilicity, this family of compounds could be attractive for the selective introduction of heavy atoms into protein crystals by means of covalent bond formation with protein side chains carrying a primary amine. Since such heavy metal protein derivatives are required for crystallographic phase determination when using, for example, the multiple isomorphous replacement method (MIR),[4] organometallic pyrylium salts could potentially be of great use for three-dimensional protein structure determination by X-ray crystallography. Several synthetic approaches have been suggested for the preparation of organometallic pyrylium salts bearing benchrotrenyl,[1,5] ferrocenyl,[6] cyclopentadienyl-tricarbonyl-manganese[1,7] or -rhenium[1] fragments at the 4-position of the heterocyclic ring. Reactivity studies using benchrotrenyl pyrylium salts with primary amines, amino acids or proteins have shown that labeling was observed even using crystalline protein.[8] Nevertheless, X-ray diffraction experiments indicated the need for heavier atoms with larger electronic densities. We therefore sought to develop derivatives of the $CpW(CO)_3CH_3$ system which are both air and light stable and provide a heavy metal in a suitable organometallic environment.

We now report the synthesis of the first pyrylium salt containing a tungsten organometallic moiety and the X-ray structural analysis of the pseudobase obtained from its hydrolysis under basic conditions.

The tungsten pyrylium complex **3** was obtained by reaction of deprotonated starting material **1** with preformed 2,6-diphenylpyrylium salt followed by hydride abstraction from the resulting pyran derivative with trityl cation (Scheme 1).†

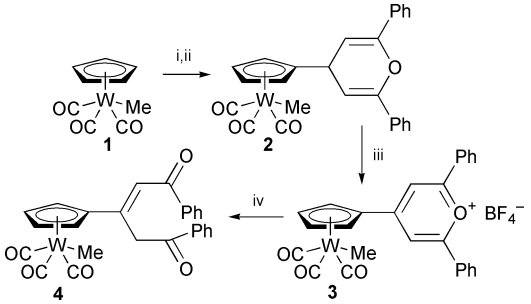

Scheme 1 *Reagents and conditions*: i, Bu^nLi, THF, −78 °C; ii, 2,6-diphenylpyrylium salt, THF, −78 °C to RT; iii, $Ph_3C^+BF_4^-$, CH_3CN, RT; iv, Na_2CO_3, acetone/H_2O/ether, RT.

Complex **3** was isolated as a deep purple air stable solid in 30% overall yield and characterized by elemental analysis, IR and ^1H and $^{13}C\{^1H\}$ NMR spectroscopies. In the ^1H NMR spectrum, a characteristic resonance at 8.79 (s) ppm was assigned to the two pyrylium protons. The $^{13}C\{^1H\}$ NMR spectrum exhibited three signals at 113.5, 164.1 and 171.2 ppm assignable to C^β, C^γ and C^α, respectively, of the heterocycle. These data are very similar to those of 2,4,6-triphenylpyrylium salt[9] and show no significant influence of the organometallic fragment on the heterocycle carbon chemical shifts.

The mechanism of pyrylium to pyridinium conversion has been thoroughly studied.[10] Kinetic measurements using UV–visible spectroscopy performed on a series of 4-benchrotrenyl pyrylium salts indicated that in aqueous media, and especially at basic pH, the hydrolysis of the pyrylium salt is very fast and that the pseudobase form (open chain diketone form) resulting from the addition of OH^- to the pyrylium salt is in fact the reactive species that undergoes the nucleophilic addition by the protein amino group (Scheme 2).[3] Thus, knowledge of the structure and reactivity of the pseudobase form of pyrylium complex **3** is important for the understanding of the mechanism of protein labelling by these species.

Treatment of the tungsten pyrylium salt **3** with Na_2CO_3 in an acetone–water mixture and subsequent extraction with diethyl ether led to the corresponding pseudobase ((3-cyclopentadienyl-1,5-diphenylpent-2-ene-1,5-dione)$W(CO)_3CH_3$) **4** in 92% yield (Scheme 1) as a moderately air stable yellow solid.†

The structure of **4** was established by ^1H NMR analysis which revealed the presence of methylenic and vinylic protons at 4.51 and 7.24 ppm, respectively. The carbon atoms of the pent-2-ene-1,5-dione chain gave signals at 195.7 (C=O), 190.3 (conjugated C=O), 144.4 and 121.2 (C=C) and 41.7 (CH_2) ppm

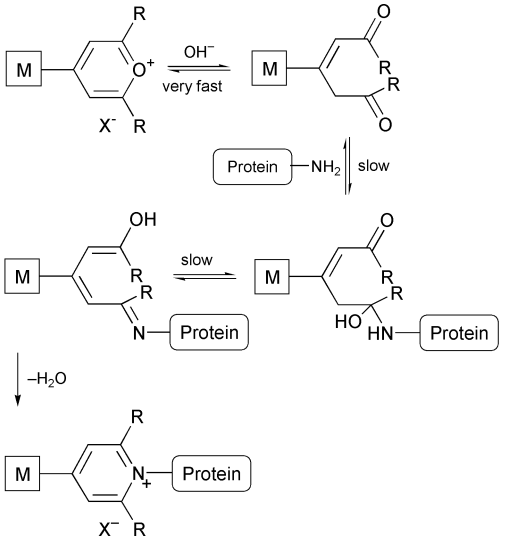

Scheme 2 Reaction of a protein with a pyrylium salt in basic aqueous medium.

 DOI: 10.1039/b104419m

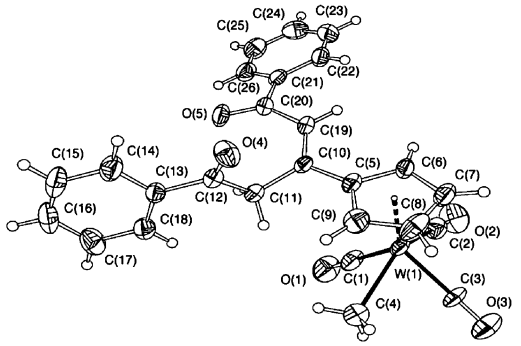

Fig. 1 The molecular structure of **4**. Selected bond lengths (Å) and angles (°); C(5)–C(10) 1.424(9), C(10)–C(19) 1.325(10), C(19)–C(20) 1.473(9), C(20)–O(5) 1.227(9), C(20)–C(21) 1.484(10); C(6)–C(5)–C(10) 126.5(7), C(5)–C(10)–C(19) 119.3(6), C(10)–C(19)–C(20) 124.7(6), C(19)–C(20)–O(5) 122.4(7), C(19)–C(20)–C(21) 118.1(6), C(5)–C(10)–C(11) 117.0(6), C(10)–C(11)–C(12) 112.6(6), C(11)–C(12)–O(4) 120.8(8), C(11)–C(12)–C(13) 118.4(6).

in the $^{13}C\{^{1}H\}$ NMR spectrum. These spectroscopic data are very similar to those of the corresponding compound bearing a phenyl group instead of the organo-tungsten fragment[11] except for the carbon C^3 signal which is shifted 8 ppm upfield.

The structure of pseudobase **4** was confirmed by X-ray crystallography (Fig. 1).‡ The complex exhibits a four-legged piano stool geometry with the methyl group on tungsten and the substituent on the Cp in perpendicular vertical planes. Bond distances within the diketone chain are in agreement with those reported for the only structurally characterized pseudobase $PhC(O)CH{=}C(CF_3)CH_2C(O)Ph$[12] which bears a CF_3 substituent in place of the Cp-tungsten fragment. The dihedral angles along the conjugated chain (C(6)–C(5)–C(10)–C(19) 18.6°; C(10)–C(19)–C(20)–O(5) 21.2°; O(5)–C(20)–C(21)–C(26) 18.7°) show significant deviation from planarity and the two phenyl end groups are almost perpendicular to each other.

The kinetics of reaction of complex **3** with *n*-butylamine in acetonitrile was studied spectrophotometrically. Conversion to the *N*-butylpyridinium salt followed a pseudo-first order reaction rate with $k_{obs} = 5.4 \times 10^{-4}$ s^{-1}. The structure of the final product was confirmed by ^{1}H NMR. For comparison, in the same experimental conditions, a k_{obs} of 0.58×10^{-4} s^{-1} and 0.32×10^{-4} s^{-1} was measured for 4-benchrotrenyl-2,6-diphenylpyrylium tetrafluoroborate and 2,4,6-triphenylpyrylium tetrafluoroborate, respectively.[3,13]

This synthesis may help provide a new approach in X-ray structural determination of proteins.

This work was supported by the European COST D8/0016 action.

Notes and references

† *Synthetic procedure for* **3**: to a solution of the pyran complex **2** (232 mg, 0.4 mmol) in acetonitrile (10 mL) was added $Ph_3C^+BF_4^-$ (170 mg, 0.45 mmol). The solution was stirred for 0.5 h at RT. On addition of diethyl ether (30 ml), complex **3** precipitated as a deep purple solid (205 mg, 0.29 mmol, 72%). *Selected data for* **3**: $\nu(CH_2Cl_2)$/cm^{-1} 1936, 2026 (C≡O); δ_H(200 MHz, d_6-acetone): 0.54 (s, 3H, CH_3), 6.28 (t, 2H, J = 2.4 Hz, Cp), 6.93 (t, 2H, J = 2.4 Hz, Cp), 7.93–7.75 (m, 6H, Ph), 8.54 (m, 4H, Ph), 8.79 (s, 2H, $H^{3,5}$-pyr); δ_C(100 MHz, d^6-acetone) −30.8 (CH_3), 93.8 ($C^{2,2'}$-Cp), 98.3 (C^1-Cp), 99.6 ($C^{3,3'}$-Cp), 113.50 ($C^{3,5}$-pyr), 129.3 (C_{ortho}-Ph), 130.1 (C_{ipso}-Ph), 130.8 (C_{meta}-Ph), 135.9 (C_{para}-Ph), 164.1 (C^4-pyr), 171.2 ($C^{2,6}$-pyr), 214.5 (C≡O), 226.1 (C≡O); Elemental anal. Calc. for $C_{26}H_{19}BF_4O_4W$: C, 46.87; H, 2.85. Found: C, 46.76; H, 2.91%. *Synthetic procedure for* **4**: to a solution of the pyrylium complex **3** (143 mg, 0.2 mmol) in acetone (5 ml) and ether (5 ml) was added K_2CO_3 (70 mg, 2 mmol) in water (3 ml). The mixture was stirred for 10 min at RT during while the organic phase turned orange. After extraction with diethyl ether (10 ml), evaporation and addition of pentane to the resulting oil, the pseudobase **4** was obtained as a yellow powder (110 mg, 0.184 mmol, 92%). *Selected data for* **4**: $\nu(CH_2Cl_2)$/cm^{-1} 1922, 2017 (C≡O); δ_H(200 MHz, $CDCl_3$): 0.51 (s, 3H, CH_3), 4.51 (s, 2H, CH_2), 5.49 (t, 2H, J = 2.4 Hz, Cp), 5.59 (t, 2H, J = 2.4 Hz, Cp), 7.24 (s, 1H, –CH=), 7.67–7.43 (m, 6H, Ph), 7.91 (d, 2H, J = 8.5 Hz, Ph), 8.09 (d, 2H, J = 8.5 Hz, Ph); δ_C(100 MHz, $CDCl_3$): −30.9 (CH_3), 41.7 (C^4), 90.1 ($C^{2,2'}$-Cp), 92.5 ($C^{3,3'}$-Cp), 109.4 (C^1-Cp), 121.2 (C^2), 128.3, 128.4, 128.7, 128.9 ($C_{ortho,meta}$-Ph), 133.0, 133.6 (C_{para}-Ph), 136.5 (C_{ipso}-Ph), 138.8 (C_{ipso}-Ph), 144.4 (C^3), 190.3 (C^1), 195.7 (C^5), 215.1 (C≡O), 227.6 (C≡O); Elemental anal. Calc. for $C_{26}H_{20}O_5W$: C, 52.36; H, 3.36. Found: C, 52.84; H, 3.54%.

‡ *Crystal data for* $C_{26}H_{20}O_5W$ (**4**): The compound crystallises in the triclinic space group $P\bar{1}$; M_r = 596.27, a = 9.952(2), b = 10.753(3), c = 12.567(3) Å, α = 66.63(2), β = 71.183(19), γ = 63.35(2)°, U = 1086.2(4) Å^3, Z = 2, T = 293(2) K, μ = 5.353 mm^{-1}, D_c = 1.823 Mg m^{-3}, $F(000)$ = 580, Of a total of 6921 collected reflections, 6315 were unique (R(int) = 0.0325) and used in all calculations. The final wR_2 = 0.1622 (all data), R_1 [$I > 2\sigma(I)$] = 0.0755. The structure was solved by direct methods, SHELXS-97,[14] and refined by full matrix least squares using SHELXL-97.[15] SHELX operations were automated using ORTEX which was also used to obtain the drawings.[16] Data were corrected for Lorentz, polarization effects and for absorption by the method of Ψ scans. The minimum transmission was 74%.[17] Hydrogen atoms were included in calculated positions with thermal parameters 30% larger than the atom to which they are attached. The non-hydrogen atoms were refined anisotropically. All calculations were performed on a Pentium PC. CCDC reference number number 166487. See http://www.rsc.org/suppdata/cc/b1/b104419m/ for crystallographic data in CIF or other electronic format.

1 K. L. Malisza, S. Top, J. Vaissermann, B. Caro, M.-C. Sénéchal-Tocquer, D. Sénéchal, J.-Y. Saillard, S. Triki, S. Kahlal, J. F. Britten, M. J. McGlinchey and G. Jaouen, *Organometallics*, 1995, **14**, 5273.
2 M. Salmain, K. L. Malisza, S. Top, G. Jaouen, M.-C. Sénéchal Tocquer, D. Sénéchal and B. Caro, *Bioconjugate Chem.*, 1994, **5**, 655.
3 B. Caro, F. Le Guen-Robin, M. Salmain and G. Jaouen, *Tetrahedron*, 2000, **56**, 257.
4 T. L. Blundell and L. N. Johnson, *Protein Crystallography*, Academic Press, New York, 1976, pp. 173–259.
5 B. Caro, M.-C. Sénéchal-Tocquer, D. Sénéchal and P. Marrec, *Tetrahedron Lett.*, 1993, **34**, 7259.
6 (*a*) G. N. Dorofeenko, V. V. Krasnikov and A. I. Pyshchev, *Khim. Geterotskl. Soedin.*, 1977, 599; *Chem. Abstr.*, 1977, **87**, 85121; L. Yu. Ukhin, A. I. Pyshchev, V. V. Krasnikov, Zh. I. Orlova and G. N. Dorofeenko, *Dokl. Akad. Nauk SSSR*, 1977, **234**, 1351; *Chem. Abstr.*, 1977, **87**, 168162; (*c*) V. V. Krasnikov, Yu. P. Andreichikov, N. V. Kholodova and G. N. Dorofeenko, *Zh. Org. Khim.*, 1977, **13**, 1566; *Chem. Abstr.*, 1977, **87**, 152357.
7 (*a*) V. V. Krasnikov and G. N. Dorofeenko, *Khim. Geterotsikl. Soedin.*, 1979, 21; *Chem. Abstr.*, 1979, **80**, 168702 (*b*) G. N. Dorofeenko and V. V. Krasnikov, *Zh. Org. Khim.*, 1972, **8**, 2620; *Chem. Abstr.*, 1973, **78**, 97785; A. G. Milaev and O. Yu. Okhlobystin, *Khim. Geterotsikl. Soedin.*, 1985, 593; *Chem. Abstr.*, 1986, **104**, 68978.
8 D. P. Egan, P. McArdle, M. Salmain and G. Jaouen, unpublished work.
9 A. R. Katritzky, R. T. C. Brownlee and G. Musumarra, *Heterocycles*, 1979, **12**, 775.
10 A. T. Balaban, G. W. Fischer, A. Dinulescu, A. V. Koblik, G. N. Dorofeenko, V. V. Mezhritski and W. Schroth, *Adv. Heterocycl. Chem., Suppl. II*, ed. A. R. Katritzky, Academic Press, New York, 1982.
11 A. R. Katritzky, R. T. C. Brownlee and G. Musumarra, *Tetrahedron Lett.*, 1980, 1643.
12 R. G. Pritchard, S. Tajammal and A. E. Tipping, *Acta Crystallogr., Sect. C* , 1994, **50**, 294.
13 A. R. Katritzky and R. H. Manzo, *J. Chem. Soc., Perkin Trans.*, 1981, **2**, 571.
14 G. M. Sheldrick, *Acta Crystallogr., Sect. A*, 1990, **46**, 467.
15 G. M. Sheldrick, *SHELXL-97: a computer program for crystal structure determination*, University of Göttingen, 1997.
16 P. McArdle, *J. Appl. Crystallogr.*, 1995, **28**, 65.
17 A. C. T. North, D. C. Phillips and F. S. Mathews, *Acta Crystallogr., Sect. A*, 1968, **24**, 351.

CHEMCOMM Communication
www.rsc.org/chemcomm

Carbon–sulfur bond activation of thiophenes by [W(NPh){*o*-$(Me_3SiN)_2C_6H_4$}$(pyridine)_2$]†

R. C. Mills, K. A. Abboud and J. M. Boncella*

Department of Chemistry and Center for Catalysis, University of Florida, Gainesville, FL 32611-7200, USA. E-mail: boncella@chem.ufl.edu

Received (in Irvine, CA, USA) 1st March 2001, Revised version received 20th June 2001, Accepted 26th June 2001
First published as an Advance Article on the web 26th July 2001

Addition of thiophene, 2-methylthiophene, benzothiophene or 3-methylthiophene to [W(NPh){*o*-$(Me_3SiN)_2C_6H_4$}-$(C_5H_5N)_2$] 1 affords the metallathiacycle complexes [{*o*-$(Me_3SiN)_2C_6H_4$}(NPh)W(SC_4H_4)] 2, [{*o*-$(Me_3SiN)_2C_6H_4$}-(NPh)W(SC_5H_6)] 3, [{*o*-$(Me_3SiN)_2C_6H_4$}(NPh)W(SC_8H_6)] 4 and [{*o*-$(Me_3SiN)_2C_6H_4$}(NPh)W(SC_5H_6)] 5a and 5b, providing the first example of thiophene C–S bond activation by a W(IV) metal complex.

Hydrodesulfurization (HDS), the process by which sulfur is removed from petroleum feedstocks, represents one of the largest-scale industrial processes that utilizes transition metal catalysts. The process involves treatment of crude oil with a high pressure of hydrogen gas (up to 200 atm) in the presence of an alumina-supported catalyst, typically Mo/Co, at elevated temperatures (300–450 °C).[1–5] Of the sulfur containing impurities present in petroleum feedstocks, thiophene and its derivatives are among the most difficult to desulfurize. In order to improve the efficiency of the HDS process, a better understanding of the interaction of thiophenes with transition metal complexes is necessary. As a result, homogeneous modeling of HDS has become an active area of research during the past decade.[4]

Many research groups have studied the coordination and activation of thiophenes, which are believed to be the initial steps in HDS. A variety of thiophene complexes have been prepared and studied possessing, η^1(S)-coordinated, η^4 and η^5 bound thiophenes.[6–10] In addition, several metal complexes have been found to promote direct C–S bond activation of thiophenes.[4] Surprisingly, thiophene complexes of group 6 metals (Mo and W), an integral component of an industrial HDS catalyst, have been almost non-existent. A recent report by Parkin and coworkers[11] of thiophene and benzothiophene C–S bond activation by the molybdocene complexes $[Me_2Si(C_5Me_4)_2]MoH_2$ and $[Me_2Si(C_5Me_4)_2]Mo(Ph)H$ represents the first homogeneous example of such chemistry with molybdenum. The analogous tungsten system has also been shown to facilitate the C–S bond activation of thiophene.[12]

Recently, we have prepared a series of coordinatively unsaturated [W(NPh){*o*-$(Me_3SiN)_2C_6H_4$}L_2] (L = pyridine, 4-picoline or quinoline) complexes.[13] Our investigation of ligand substitution reactions of the W(IV)L_2 complexes with unsaturated substrates has demonstrated the propensity of the W metal center to reduce the coordinated substrate ligand, thereby increasing the W(VI) character of the resulting compounds. These results have prompted us to examine the activity of these W(IV)L_2 complexes towards substrate oxidative addition, specifically the activation of the C–S bonds of thiophene and its derivatives.

Thermolysis (65 °C, 8–12 h) of a toluene solution containing [W(NPh){*o*-$(Me_3SiN)_2C_6H_4$}$(C_5H_5N)_2$] **1** and 2 equivalents of thiophene, 2-methylthiophene or benzothiophene afforded the carbon–sulfur bond activation products [{*o*-$(Me_3SiN)_2C_6H_4$}(NPh)W(SC_4H_4)] **2**, [{*o*-$(Me_3SiN)_2C_6H_4$}(NPh)-W(SC_5H_6)] **3** and [{*o*-$(Me_3SiN)_2C_6H_4$}(NPh)W(SC_8H_6)] **4**, respectively, as a dark red solid in 60–80% isolated yield for **2** and **3**, Scheme 1.‡ Isolation of a pure sample of compound **4** has proved difficult because the complex slowly decomposes during the work-up procedure. As determined by ^{1}H NMR spectroscopy, compound **4** is formed in *ca.* 50% yield.

Characterization of the reaction products by ^{1}H NMR spectroscopy was straightforward due to the distinct resonances and coupling constants associated with the thiophene ring protons, which are similar for all three compounds. For example, the ^{1}H NMR spectrum of **2** displays two resonances (δ 0.39 and 0.50), which correspond to the inequivalent Me_3Si groups. The metallathiacycle protons are shifted downfield with respect to free thiophene and appear as a doublet of doublets (δ 6.70, $^3J_{HH}$ 7, 9 Hz) corresponding to the β-CH, a doublet (δ 8.01, $^3J_{HH}$ 9 Hz) with ^{183}W satellites ($^2J_{WH}$ 8 Hz) for the α-CH, a doublet of doublets (δ 8.20, $^3J_{HH}$ 13, 7 Hz) for the γ-CH, and a doublet (δ 9.00, $^3J_{HH}$ 13 Hz) for the δ-CH adjacent to the S atom.

Compound **4** displays two doublet resonances corresponding to the α (δ 8.50, $^3J_{HH}$ 13 Hz) and β (δ 8.65, $^3J_{HH}$ 13 Hz) protons, respectively. The resonance at δ 8.50 has ^{183}W satellites ($^2J_{WH}$ 10 Hz), confirming the suggested C(vinyl)–S insertion product. The absence of a proton resonance in the ^{1}H NMR spectrum of **3** with ^{183}W satellites or in the vicinity of that observed for the α-CH proton of compound **2** suggests preferential activation of the (Me)C–S bond in the reaction of **1** with 2-methylthiophene. The observed downfield shift of the metallathiacycle protons for compounds **2**, **3** and **4** contrasts with the reported upfield shift with respect to free thiophene found for the complex $(C_5H_5)_2W(SC_4H_4)$.[12] This is presumably due to the increased electron deficiency of the d^0 W(VI) center in compounds **2**, **3** and **4** relative to the d^2, Cp_2W(IV) system.

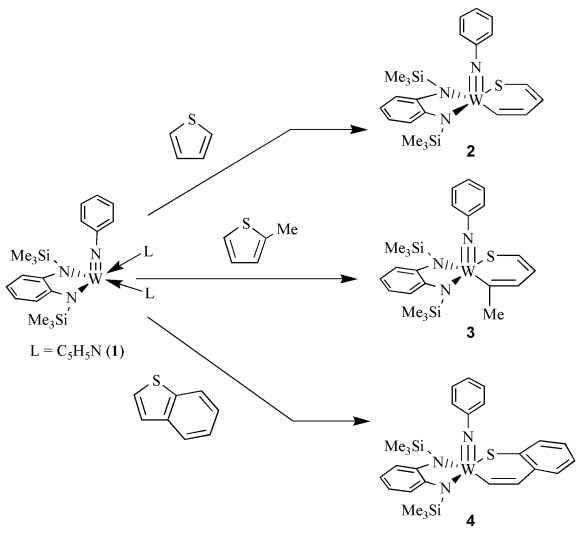

Scheme 1 C–S bond activation products.

† Electronic supplementary information (ESI) available: experimental section, proton NMR spectra for **2**, **3** and **5a**,**b** and crystallography. See http://www.rsc.org/suppdata/cc/b1/b101955b/

 DOI: 10.1039/b101955b

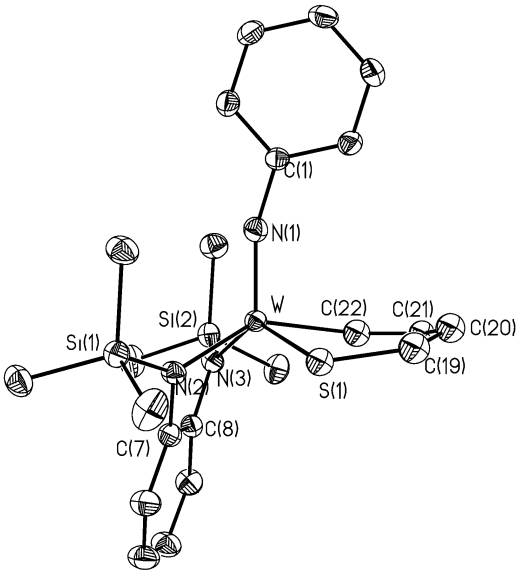

Fig. 1 Molecular structure of **2**, showing 50% thermal ellipsoids and the atom labeling scheme. The H atoms and the minor part of the disordered metallathiacycle are removed for clarity. Selected bond distances (Å) and angles (°): W–N(1) 1.734(3), W–N(2) 2.016(3), W–N(3) 2.008(3), W–S(1) 2.371(3), W–C(22) 2.196(9), S(1)–C(19) 1.722(12), C(19)–C(20) 1.192(16), C(20)–C(21), 1.600(16), C(21)–C(22) 1.289(14); W–N(1)–C(1) 162.4(3), N(1)–W–N(2) 116.06(13), N(1)–W–N(3) 117.02(14), N(1)–W–S(1) 104.49(13), N(1)–W–C(22) 98.0(3), C(22)–W–S(1) 83.7(3).

An X-ray diffraction study of a single crystal of **2** grown from a concentrated pentane solution at −40 °C confirmed the nature of the C–S bond activation product. Due to disorder in S1 and C22, the positions of the metallathiacycle atoms were solved independently in two parts. A molecular drawing of **2** with selected bond lengths and angles for the major part are shown in Fig. 1.§ Compound **2** adopts a five-coordinate, distorted square pyramidal geometry with the imido ligand occupying the apical position. The short W–N(imido) bond length of 1.734(3) Å, consistent with a W–N triple bond and the W–N(amido) bond lengths of 2.016(3) and 2.008(3) Å are similar to that observed for other W(VI) complexes.[14] The average bond lengths for the thiophene fragment of the complex suggest localized bonding within the metallathiacycle.

Thiophenes are known to interact with a metal center in a number of different modes however; a η^1-S-bound thiophene[6–10] is believed to be a prerequisite for C–S bond activation. Although the initial interaction of thiophene and its derivatives with compound **1** has not been directly observed, the ability of **1** to accommodate additional ligands has been demonstrated.[13] Compound **1** rapidly forms octahedral complexes with the addition ligands such as CO and PMe_3. For the reaction of the σ-donor ligand PMe_3 with **1**, the complex $[W(NPh)\{o\text{-}(Me_3SiN)_2C_6H_4\}(C_5H_5N)(PMe_3)_2]$ is the preferred product, suggesting labilization of one of the pyridine ligands upon coordination of the first PMe_3 ligands. Although thiophenes are weaker donor ligands than PMe_3, under the thermolysis conditions for the reaction of thiophenes with **1**, labilization of a pyridine ligand would generate the open coordination site necessary for C–S bond activation. Although no direct evidence for such a mechanism has been observed, it must be considered given the reactions of **1** with PMe_3.

Compound **1** also reacts with 2 equivalents of 3-methylthiophene. Unlike the previously described examples, 3-methylthiophene generates a mixture of the two possible C–S bond activation products, $[\{o\text{-}(Me_3SiN)_2C_6H_4\}(NPh)W(SC_5H_6)]$ **5a** and **5b**, Scheme 2.‡ As determined by ^{1}H NMR spectroscopy, the products are formed in a 60:40 ratio with **5a** as the major component. A similar product mixture was observed for the reaction of $Cp^*Rh(Ph)(H)(PMe_3)$ with 3-methylthiophene.[15] The observed product selectivity in the reaction of **1** with benzothiophene arises from steric congestion on one side of the thiophene ring, whereby C–S bond activation opposite the substituent is preferred. For the reaction of 3-methylthiophene with **1**, both C–S bonds are accessible as demonstrated by the formation of both **5a** and **b**.

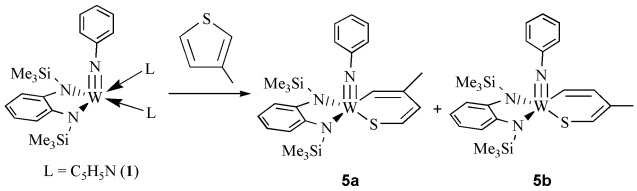

Scheme 2 Product mixture generated from 3–methylthiophene C–S bond activation.

In summary, we have demonstrated that the chelate stabilized W(IV)L_2 complex $[W(NPh)\{o\text{-}(Me_3SiN)_2C_6H_4\}(C_5H_5N)_2]$ **1** facilitates the C–S bond activation of both thiophene and substituted thiophenes. To our knowledge, this reactivity is the first example of thiophene C–S bond activation by a W(IV) species. Currently we are investigating other substrates, such as more highly substituted thiophenes and nitrogen and oxygen containing heterocycles, to determine the scope of this reactivity.

We thank the National Science Foundation (CHE 9523279 and CHE 0094404) for funding of this work and the NSF and the University of Florida for funding X-ray equipment purchases.

Notes and references

‡ All reactions and manipulations were carried out using standard Schlenk techniques or in a dry box under atmospheres of argon or nitrogen. *Synthesis* of compounds **2**–**5a**,**b**: to a purple toluene solution of **1** were added 2 equivalents of the appropriate thiophene. Thermolysis (65 °C) of the reaction mixtures for 8–12 h resulted in a color change from purple to red. After removal of the reaction solvent *in vacuo*, the crude products were extracted with cyclohexane and dried *in vacuo*.

§ *Crystal data* for **2**: $C_{22}H_{31}N_3SSi_2W$, M = 609.59, triclinic, space group $P\bar{1}$, a = 9.4647(4), b = 11.7141(5), c = 12.4830(5) Å, α = 101.246(1), β = 111.655(1), γ = 93.904(1)°, V = 1246.64(9) Å^3, Z = 2, T = 173(2) K, final $R1$ = 0.0264, $wR2$ = 0.0647, GOF (on F^2) = 1.024.

The structure was solved by the Direct Methods in SHELXTL5, and refined using full-matrix least squares.[16] The non-H atoms, except the disordered, were treated anisotropically, whereas the methyl hydrogen atoms were calculated in ideal positions and were riding on their respective carbon atoms. The S1–C22 chain is found to be disordered by a 180° rotation and was refined in two parts; the major part is represented by the S1–C22 chain and the minor part by S1′–C22′. Their site occupation factors were dependently refined to 0.55(1) for the major part and, consequently, 0.45(1) for the minor part. All atoms of the disorder were refined with isotropic thermal parameters. The W–S1 and W–S1′ bonds were constrained to be equivalent during refinement. Similarly, W–C22 and W–C22′ were also constrained to remain equivalent.

CCDC reference number 162416. See http://www.rsc.org/suppdata/cc/b1/b101955b/ for crystallographic data in CIF or other electronic format.

1 H. Topsøe, B. S. Clausen and F. E. Massoth, *Hydrotreating Catalysis in Catalysis: Science and Technology*, Springer-Verlag, New York, 1996, vol. 11.
2 D. D. Whitehurst, T. Isoda and I. Mochida, *Adv. Catal.*, 1998, **42**, 345.
3 C. Bianchini and A. Meli, *Acc. Chem. Res.*, 1998, **31**, 109.
4 R. J. Angelici, *Polyhedron*, 1997, **16**, 3073.
5 R. A. Sanchez-delgado, *J. Mol. Catal.*, 1994, **86**, 287.
6 R. J. Angelici, *Coord. Chem. Rev.*, 1990, **105**, 61.
7 R. J. Angelici, *Organometallics*, 2001, **20**, 1259.
8 R. J. Angelici, *Bull. Soc. Chim. Belg.*, 1995, **104**, 265.
9 T. B. Rauchfuss, *Prog. Inorg. Chem.*, 1991, **39**, 259.
10 L. Dong, S. B. Duckett, K. F. Ohman and W. D. Jones, *J. Am. Chem. Soc.*, 1992, **114**, 151.
11 D. G. Churchill, B. M. Bridgewater and G. Parkin, *J. Am. Chem. Soc.*, 2000, **122**, 178.
12 W. D. Jones, R. M. Chin, T. W. Crane and D. M. Baruch, *Organometallics*, 1994, **13**, 4448.
13 R. C. Mills, K. A. Abboud and J. M. Boncella, *Inorg. Chem.*, in press.
14 J. M. Boncella, S. Y. S. Wang, D. D. Vanderlende, R. L. Huff, K. A. Abboud and W. M. Vaughn, *J. Organomet. Chem.*, 1997, **530**, 59.
15 W. D. Jones and L. Dong, *J. Am. Chem. Soc.*, 1991, **113**, 559.
16 G. M. Sheldrick, SHELXTL5, Bruker-AXS, Madison, WI, USA, 1998.

CHEMCOMM
Communication
www.rsc.org/chemcomm

Ring, polymer and network structures in silver(I) complexes with dipyridyl and diphosphine ligands

Marie-Claude Brandys and Richard J. Puddephatt*

Department of Chemistry, University of Western Ontario, London, Canada, N6A 5B7.
E-mail: pudd@uwo.ca

Received (in Cambridge, UK) 4th June 2001, Accepted 4th July 2001
First published as an Advance Article on the web 26th July 2001

Interesting molecular architectures are obtained by self-assembly from silver(I) trifluoroacetate with a combination of the diphosphine ligands [$Ph_2P(CH_2)_nPPh_2$, n = 1–6] and *trans*-1,2-bis(4-pyridyl)ethylene (bipyen); in complexes with stoichiometry $Ag_2(O_2CCF_3)_2\{Ph_2P(CH_2)_nPPh_2\}$(bipyen), the complexes crystallize in the form of macrocyclic rings $[Ag_4(O_2CCF_3)_4\{\mu\text{-}Ph_2P(CH_2)_nPPh_2\}_2(\mu\text{-bipyen})_2]$ when n = 1 or 5, but as a one-dimensional polymer $[\{Ag_2(O_2CCF_3)_2\{\mu\text{-}Ph_2P(CH_2)_nPPh_2\}(\mu\text{-bipyen})\}_x]$ when n = 6. The complex $[\{Ag\{\mu\text{-}Ph_2P(CH_2)_3PPh_2\}(\mu\text{-bipyen})\}_x](CF_3CO_2)_x$ has a novel network structure.

There is intense current interest in polymeric coordination networks,[1] but there are surprisingly few examples containing silver(I) or phosphine ligands, and very few architectures with mixed bridging ligands.[2,3] Given the interesting electronic,[4] medicinal,[5] and structural[4–6] properties of silver(I) phosphine complexes, the synthesis of polymeric diphosphine bridged silver(I) complexes was attempted. The strategy was to form mixed ligand complexes, using the rigid linear dipyridyl ligand *trans*-1,2-bis(4-pyridyl)ethylene (bipyen) in conjunction with the more flexible diphosphine ligands $Ph_2P(CH_2)_nPPh_2$, since the diphosphines alone tend to give chelate complexes or other ring structures with silver(I).[4–6] This article shows that linear and network polymers, as well as ring complexes, can be formed by this strategy and that the variable coordination number of silver(I) is a key feature in allowing formation of a particularly interesting series of compounds.[7]

The new silver(I) complexes were prepared by reaction of silver(I) trifluoroacetate with the appropriate ligand $Ph_2P(CH_2)_nPPh_2$ (n = 1–6) followed by reaction with *trans*-1,2-bis(4-pyridyl)ethylene (bipyen).† Studies of the reaction solutions by ^1H or ^{31}P NMR spectroscopy indicated that mixtures of products were formed but, in favourable cases, it was possible to crystallize pure products for structure determination and these are representative of major components of the equilibrium system.‡

Three complexes were crystallized having the formula $Ag_2(O_2CCF_3)_2\{Ph_2P(CH_2)_nPPh_2\}$(bipyen) of which two formed macrocyclic ring structures (**1**, n = 1; **2**, n = 5) and one formed a one-dimensional polymer (**3**, n = 6). The structures are shown in Figs. 1 and 2. In the 30-membered ring complex **1** two of the trifluoroacetate ions bridge silver atoms in the ring while two are not coordinated, so the complex is formulated as $[Ag_4(\mu\text{-}O_2CCF_3)_2(\mu\text{-}Ph_2PCH_2PPh_2)_2(\mu\text{-bipyen})_2]^{2+}$, with each silver(I) ion having distorted trigonal planar stereochemistry. There is a short intramolecular silver–silver distance Ag(1)–Ag(2) 3.0479(8) Å, which is about equal to the distance P(1)–P(2) 3.051(2) Å but significantly shorter than N(11)–N(21) 3.507(4) Å, so indicating the presence of a secondary Ag···Ag bond.[4,8] In the related 38-membered ring structure **2**, all trifluoroacetate ions are close enough to silver(I) to influence the stereochemistry so **2** is formulated as $[Ag_4(\mu\text{-}O_2CCF_3)_4\{\mu\text{-}Ph_2P(CH_2)_5PPh_2\}_2(\mu\text{-bipyen})_2]$. The longer Ag···O bonds are shown in Fig. 1 as broken lines; if all are considered bonds, then each silver(I) ion is four-coordinate. The transannular distance Ag(1)–Ag(4) 3.936(1) Å is too long for a bonding interaction

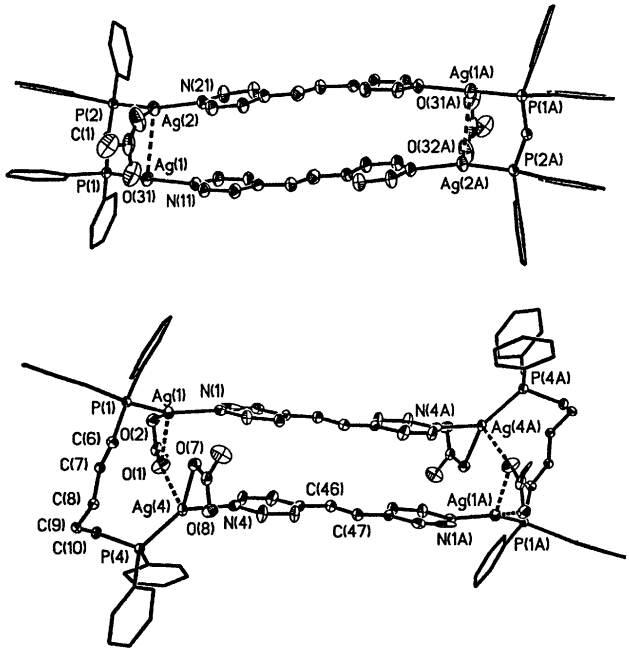

Fig. 1 Views of the structures of the macrocyclic ring complexes **1** (above) and **2** (below). Thermal ellipsoids for phenyl carbon atoms, and fluorine atoms of the trifluoroacetate groups, are not shown for clarity. Selected geometrical parameters (Å, °) for **1**: Ag(1)–P(1) 2.360(1), Ag(2)–P(2) 2.366(1), Ag(1)–N(11) 2.199(4), Ag(2)–N(21) 2.217(5), Ag(1)–O(31) 2.506(7), Ag(2)–O(32) 2.496(7); N(11)–Ag(1)–P(1) 157.5(1), N(21)–Ag(2)–P(2) 155.3(1). For **2**: Ag(1)–P(1) 2.348(3), Ag(4)–P(4) 2.363(3), Ag(1)–N(1) 2.20(1), Ag(4)–N(4) 2.23(1), Ag(1)–O(1) 2.63(1), Ag(1)–O(2) 2.63(1), Ag(4)–O(7) 2.379(9), Ag(4)–O(1) 2.63(1); N(1)–Ag(1)–P(1) 149.5(3), N(4)–Ag(4)–P(4) 130.1(3).

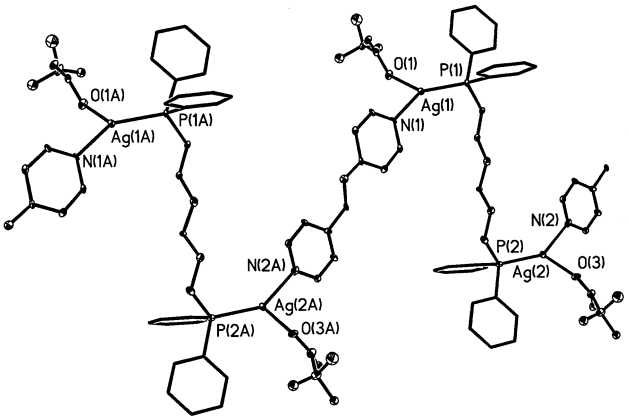

Fig. 2 A view of the structure of the polymeric complex **3**. Thermal ellipsoids for phenyl carbon atoms are not shown for clarity. Selected geometrical parameters (Å, °): Ag(1)–P(1) 2.377(6), Ag(2)–P(2) 2.367(7), Ag(1)–N(1) 2.18(2), Ag(2)–N(2) 2.31(3), Ag(1)–O(1) 2.38(2), Ag(2)–O(3) 2.46(2); N(1)–Ag(1)–P(1) 143.5(6), N(2)–Ag(2)–P(2) 143.4(6).

 DOI: 10.1039/b104857k

and the conformation may be controlled by the weakly bridging trifluoroacetate ligand and by π-stacking of the bipyen groups (the transannular distance between centroids of pyridyl rings in **2** is 3.86 Å).

Part of the polymeric chain structure of complex **3** is shown in Fig. 2. All trifluoroacetate ions are coordinated so the complex is formulated as $[Ag_2(O_2CCF_3)_2\{\mu\text{-}Ph_2P(CH_2)_6PPh_2\}(\mu\text{-bipyen})]_x$. The change in structure is attributed to the preference for the *syn* or *anti* conformation of the phosphorus donors when there is an odd or even number of methylene bridges in $Ph_2P(CH_2)_nPPh_2$,[7] leading naturally to ring structures **1** and **2**, when $n = 1$ and 5, but a polymer **3** when $n = 6$. This conformational change is clear from a comparison of Fig. 1 and 2. The polymer could be considered to be formed by ring-opening polymerization of the corresponding ring complex.

With higher ligand:silver ratios, more complex product mixtures were formed and only in one case ($n = 3$) was a pure complex crystallized. The complex **4** is formulated as $[\{Ag\{\mu\text{-}Ph_2P(CH_2)_3PPh_2\}(\mu\text{-bipyen})\}_x]^{x+}$, isolated as the trifluoroacetate salt, and its network structure is shown in Fig. 3, illustrating the presence of channels that are occupied by the anions and by solvent molecules. Each silver(I) ion is roughly tetrahedral with AgP_2N_2 coordination, and all silver centres are identical, but the overall structure is more complex. One view would be to consider the structure as spiral chains $[\{Ag(\mu\text{-dppp})\}_x]^{x+}$ [dppp = $Ph_2P(CH_2)_3PPh_2$], running roughly perpendicular to the plane in Fig. 3 crosslinked by μ-bipyen ligands. The smallest rings incorporated into these units are 46-membered $\{-Ag(\mu\text{-dppp})Ag(\mu\text{-dppp})Ag(\mu\text{-bipyen})\}_2$. Another view is to consider the structure to be formed from crossing zigzag polymers $[\{Ag(\mu\text{-bipyen})\}_x]^{x+}$ crosslinked by μ-dppp ligands. The conformation of the diphosphine is neither *syn* nor *anti* but intermediate such that the diphosphine links chains that are roughly orthogonal. The smallest ring structure is 56-membered $\{-Ag(\mu\text{-bipyen})Ag(\mu\text{-bipyen})Ag(\mu\text{-dppp})\}_2$ and they lie roughly in the plane of Fig. 3.

This work shows that combination of flexible diphosphine and linear dipyridyl ligands with silver(I) can give interesting new molecular architectures that are significantly different from those obtained with only nitrogen-donor ligands,[1,2] and that factors such as the preferred conformation of the diphosphine ligand[7] and the variable coordination number of silver(I)[1–6] can determine the preferred structure. There is clear potential for design of still more complex molecular topologies by application of these principles.

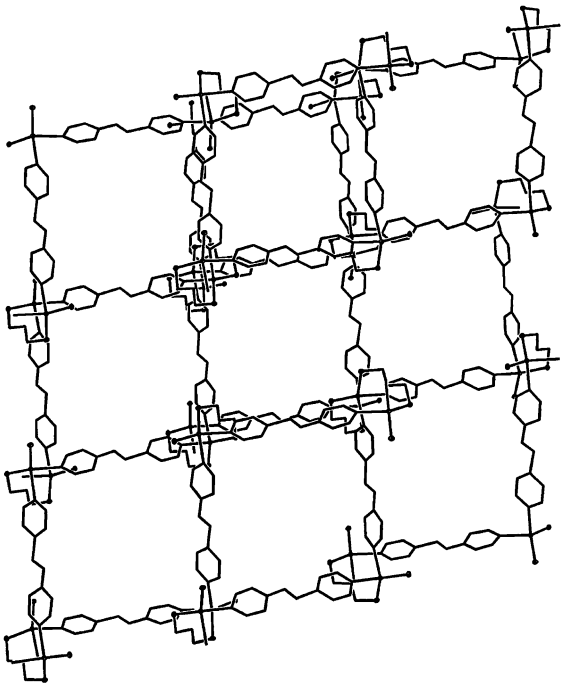

Fig. 3 A view of the structure of the network polymeric complex **4**. Phenyl carbon atoms are not shown for clarity. Selected geometrical parameters (Å, °): Ag–P(1) 2.444(3), Ag–P(2) 2.448(3), Ag–N(1) 2.425(8), Ag–N(2) 2.370(7); N(1)–Ag–N(2) 90.4(2), P(1)–Ag–P(2) 123.36(5), N(1)–Ag–P(1) 121.6(2), N(1)–Ag–P(2) 98.4(2), N(2)–Ag–P(1) 98.0(2), N(2)–Ag–P(2) 121.9(2).

We thank the NSERC (Canada) for financial support and for a scholarship to M.-C. B, and Dr M. C. Jennings for X-ray data collection. R. J. P. thanks the Government of Canada for a Canada Research Chair.

Notes and references

† *Typical synthetic procedure*: $[Ag_4(\mu\text{-}O_2CCF_3)_2(\mu\text{-}Ph_2PCH_2PPh_2)_2(\mu\text{-}NC_5H_4CH{=}CHC_5H_4N)_2](CF_3CO_2)_2$, **1**: bis(diphenylphosphino)methane (0.107 g, 0.278 mmol) was added to a solution of CF_3CO_2Ag (0.123 g, 0.556 mmol) in THF (15 mL) and after 1 h *trans*-1,2-bis(4-pyridyl)ethylene (0.051 g, 0.279 mmol) was added. After 1.5 h, the volume was reduced until the product formed as a white precipitate, which was collected by filtration, washed with diethyl ether and pentane and dried *in vacuo*. Yield: 0.17 g (60%). Anal. Calc. for $C_{41}H_{32}N_2O_4F_6P_2Ag_2$: C, 48.84; H, 3.20, N, 2.78. Found: C, 49.26; H, 3.03, N, 2.82%.

‡ *Crystal data*: for **1**·2THF: $C_{87}H_{69}Ag_4F_{12}N_4O_9P_4$, $M = 2097.82$, 296 K, triclinic, space group $P\bar{1}$, $a = 10.4879(2)$, $b = 15.2385(5)$, $c = 19.7575(5)$ Å, $\alpha = 99.008(1)$, $\beta = 95.106(2)$, $\gamma = 96.283(2)°$, $V = 3081.8(1)$ Å^3, $Z = 1$, $\mu = 0.737$ mm^{-1}, 21543 reflections, $R1 = 0.0836$, $wR2 = 0.2891$.

For **2**: $C_{90}H_{80}Ag_4F_{12}N_4O_8P_4$, $M = 2128.94$, 200 K, triclinic, space group $P\bar{1}$, $a = 15.079(3)$, $b = 17.850(4)$, $c = 20.232(4)$ Å, $\alpha = 80.72(3)$, $\beta = 86.72(3)$, $\gamma = 75.02(3)°$, $V = 5191(2)$ Å^3, $Z = 2$, $\mu = 0.875$ mm^{-1}, 29338 reflections, $R1 = 0.1168$, $wR2 = 0.3223$.

For **3**: $C_{48}H_{50}Ag_2F_6N_2O_6P_2$, $M = 1142.58$, 150 K, triclinic, space group, $P\bar{1}$, $a = 9.747(2)$, $b = 9.588(2)$, $c = 15.104(3)$ Å, $\alpha = 83.85(3)$, $\beta = 73.80(3)$, $\gamma = 62.91(3)°$, $V = 1206.5(4)$ Å^3, $Z = 1$, $\mu = 0.950$ mm^{-1}, 4358 reflections, $R1 = 0.0604$, $wR2 = 0.1410$.

For **4**: (CH_2Cl_2, MeOH solvate), $C_{43}H_{43}AgCl_2F_3N_2O_3P_2$, $M = 933.50$, 150 K, orthorhombic, space group $Fdd2$, $a = 31.5201(7)$, $b = 39.636(1)$, $c = 13.9957(4)$ Å, $V = 17485.5(8)$ Å^3, $Z = 16$, $\mu = 0.709$ mm^{-1}, 9871 reflections, $R1 = 0.0699$, $wR2 = 0.1961$.

CCDC reference numbers 165406–165409. See http://www.rsc.org/suppdata/cc/b1/b104857k/ for crystallographic data in CIF or other electronic format.

1 A. J. Blake, N. R. Champness, P. Hubberstey, W.-S. Li, M. Schroder and M. A. Withersby, *Coord. Chem. Rev.*, 1999, **183**, 117; S. R. Batten and R. Robson, *Angew. Chem., Int. Ed.*, 1998, **37**, 1460.

2 A. J. Blake, N. R. Champness, P. A. Cooke, J. E. B. Nicolson and C. Wilson, *J. Chem. Soc., Dalton Trans.*, 2000, 3811; L. Carlucci, G. Ciani, P. Macchi, D. M. Proserpio and S. Rizzato, *Chem. Eur. J.*, 1999, **5**, 237; K. A. Hirsch, S. R. Wilson and J. S. Moore, *Inorg. Chem.*, 1997, **36**, 2960.

3 G. K. H. Shimizu, G. D. Enright, C. I. Ratcliffe, J. A. Ripmeester and D. D. M. Rayner, *Angew. Chem., Int. Ed. Engl.*, 1997, **37**, 1407.

4 F. B. Xu, L. H. Weng, L. J. Sun, Z. Z. Zhang and Z. F. Zhou, *Organometallics*, 2000, **19**, 2658; C. M. Che, M. C. Tse, M. C. W. Chan, K. K. Cheung, D. L. Phillips and K. H. Leung, *J. Am. Chem. Soc.*, 2000, **122**, 2464; V. J. Catalano, H. M. Kar and B. L. Bennett, *Inorg. Chem.*, 2000, **39**, 121; D. A. Edwards, R. M. Harker, M. F. Mahon and K. C. Molloy, *J. Mater. Chem.*, 1999, **9**, 1771.

5 D. Affandi, S. J. Berners-Price, Effendy, P. J. Harvey, P. C. Healy, B. E. Ruch and A. H. White, *J. Chem. Soc., Dalton Trans.*, 1997, 1411; S. J. Berners-Price, R. J. Bowen, P. J. Harvey, P. C. Healy and G. A. Koutsantonis, *J. Chem. Soc., Dalton Trans.*, 1998, 1743; K. Nomiya, R. Noguchi, T. Shigeta, Y. Kondoh, K. Tsuda, K. Ohsawa, N. Chikaraishi-Kasuga and M. Oda, *Bull. Chem. Soc. Jpn.*, 2000, **73**, 1143.

6 S. P. Crabtree, A. S. Batsanov, J. A. K. Howard and M. Kilner, *Polyhedron*, 1998, **17**, 367; B. Heuer, S. J. A. Pope and G. Reid, *Polyhedron*, 2000, **19**, 743; M. Bardaji, O. Crespo, A. Laguna and A. K. Fischer, *Inorg. Chim. Acta*, 2000, **304**, 7; G. A. Bowmaker, J. V. Hanna, C. E. F. Rickard and A. S. Lipton, *J. Chem. Soc., Dalton Trans.*, 2001, 20; T. C. Deivaraj and J. J. Vittal, *J. Chem. Soc., Dalton Trans.*, 2001, 329; S. Kitagawa, M. Kondo, S. Kawata, S. Wada, M. Maekawa and M. Munakata, *Inorg. Chem.*, 1995, **34**, 1455; F. Caruso, M. Camalli, H. Rimml and L. M. Venanzi, *Inorg. Chem.*, 1995, **34**, 673.

7 M. J. Irwin, J. J. Vittal, G. P. A. Yap and R. J. Puddephatt, *J. Am. Chem. Soc.*, 1996, **118**, 13 101; M. C. Brandys, M. C. Jennings and R. J. Puddephatt, *J. Chem. Soc., Dalton Trans.*, 2000, 4601.

8 S. Attar, N. W. Alcock, G. A. Bowmaker, J. S. Frye, W. H. Bearden and J. H. Nelson, *Inorg. Chem.*, 1991, **30**, 4166; A. Del Zotto, P. Di Bernardo, M. Tolazzi, G. Tornat and P. Zanonato, *J. Chem. Soc., Dalton Trans.*, 1993, 3009.

CHEMCOMM Communication
www.rsc.org/chemcomm

Is MCM-41 really advantageous over amorphous silica? The case of grafted titanium epoxidation catalysts†

José M. Fraile,[a] José I. García,[a] José A. Mayoral,*[a] Eugenio Vispe,[a] D. R. Brown[b] and M. Naderi[b]

[a] *Departamento de Química Orgánica, Instituto de Ciencia de Materiales de Aragón, Facultad de Ciencias, Universidad de Zaragoza-C.S.I.C., E-50009 Zaragoza, Spain. E-mail: mayoral@posta.uniza.es*

[b] *Department of Chemical and Biological Sciences, University of Huddersfield, Huddersfield, UK HD1 3DH*

Received (in Cambridge, UK) 4th April 2001, Accepted 28th June 2001
First published as an Advance Article on the web 26th July 2001

MCM-41 can be used in the same way as amorphous silica for the preparation of supported titanium catalysts; MCM-41 does not show clear advantages over silica in epoxidation reactions with either TBHP or H_2O_2; only in one case is a positive effect observed and this involves the recycled catalyst with H_2O_2.

Catalysts based on mesoporous crystalline silicas, especially MCM-41, have been widely applied in recent years.[1] Among the advantages proposed for this type of solid are the presence of a regular porous system, and the large pore size. In many cases comparisons have only been made regarding the behaviour of zeolites and MCM-41, and comparisons with amorphous silica are generally ignored.

Titanium catalysts are among the most important oxidation catalysts[2] and titanium centres can be incorporated in MCM-41[3,4] or amorphous silica[6–9] either within the framework, by substitution of silicon atoms,[3] or by grafting titanium species onto the surface. Several of these catalysts have been used in the epoxidation of alkenes with dilute hydrogen peroxide.[10–12] In the case of MCM-41, grafting has been described as being more efficient than framework substitution.[10,13,14] However, no direct comparison has been made between amorphous and crystalline mesoporous silicas. In this communication we report the behaviour of MCM-41 as a support for $Ti(OPr^i)_4$ using the same methodology employed for amorphous silica.

The synthesis of pure siliceous MCM-41[15] and titanium grafting[7] were carried out as previously described. The titanium loading onto MCM-41 (Table 1) is in good agreement with the surface area of the support (802 $m^2\ g^{-1}$) and the reported density of hydroxy groups[16] (*ca.* 2 OH nm^{-2}). In the case of amorphous silica, this agreement (1.07 mmol g^{-1}, 475 $m^2\ g^{-1}$, 3.7 hydrogen-bridged OH nm^{-2}) is also observed. Treatment of the catalyst with tartaric acid was carried out as described for silica.[12] The Ti content of MCM-Ti(TA) was found to be very similar to that found in the silica counterpart (Table 1).

Si-Ti(OPr^i) has previously been characterised by MAS-NMR,[7] EXAFS[18] and IR.[12] The similarity of the IR spectra of the solids (ESI†), together with the agreement observed in the titanium loading, seem to indicate that the surface species' are similar irrespective of the structure of the silica. The exclusion of water in the preparation method prevents the formation of titania (anatase) on the silica surface, as demonstrated by the absence of a UV absorption above 300 nm.

All the catalysts were tested in the epoxidation of cyclohexene with 30% hydrogen peroxide in *tert*-butyl alcohol at 353 K (Scheme 1). The active hydroperoxotitanium species is able to epoxidise directly cyclohexene with hydrogen peroxide and also to produce free radicals, which give rise to an allylic hydroperoxide. This compound can also be involved in titanium-catalysed epoxidation of cyclohexene, leading to cyclohex-2-en-1-ol as a by-product. Finally, the acidity of the catalyst promotes the hydrolysis of cyclohexene oxide to the corresponding diol. The results of this study are gathered in Table 1.

As far as catalysts prepared with $Ti(OPr^i)_4$ are concerned, MCM-41 leads to a solid that is less active than the silica-based one in terms of both hydrogen peroxide conversion and turnover number to epoxidation products. Moreover, the epoxidation/allylic oxidation selectivity is also slightly lower, indicating a lower contribution of the direct epoxidation. The main advantage of MCM-41 comes from the reusability of the catalyst, in fact the turnover number for epoxidation products is nearly constant up to the third run. However, the epoxidation/allylic oxidation selectivity is almost 50/50, which indicates that only

† Electronic supplementary information (ESI) available: experimental details of preparation and characterisation of the catalysts, IR spectra and results of the cyclohexene epoxidation with TBHP. See http://www.rsc.org/suppdata/cc/b1/b103057b/

Table 1 Results obtained in the epoxidation of cyclohexene with dilute H_2O_2 in the presence of titanium catalysts[a]

Catalyst	Run	Ti content[b]	H_2O_2/Ti	Conv. H_2O_2[c]	Yield[d] (24 h) ep	diol	enol	chhp	TON (ep + diol)	(ep + diol)/enol	ep/diol
Si-Ti(OPr^i)	1	1.07	58.4	72	9	21	12	15	17.2	71/29	29/71
	3[e]	0.74	86.7	75	2	2	7	32	3.6	36/64	50/50
MCM-Ti(OPr^i)	1	1.25	50.0	56	9	14	13	10	11.4	64/36	37/63
	3[e]	1.01	61.9	67	3	12	18	17	9.3	44/56	20/80
Si-Ti(TA)	1	0.99	63.0	92	9	32	15	18	25.3	73/27	22/78
	3[e]	0.56	111.6	108	19	28	35	13	52.8	57/43	40/60
MCM-Ti(TA)	1	1.01	61.9	37	5	18	12	1	14.3	66/34	22/78
	3[e]	0.94	66.5	38	10	7	13	4	10.6	56/44	59/41

[a] *Reaction conditions*: 200 mg catalyst, 250 mmol cyclohexene, 12.5 mmol H_2O_2 (30%), 25 mL *tert*-butyl alcohol 353 K, 24 h. [b] mmol g^{-1} [c] % conversion to cyclohexene oxidation products. [d] Determined by gas chromatography. ep = cyclohexene oxide; diol = *trans*-cyclohexane-1,2-diol; enol = cyclohex-2-en-1-ol; chhp = cyclohexenyl hydroperoxide. [e] Ti content after the third run. Ratios are referred to this value.

 DOI: 10.1039/b103057b

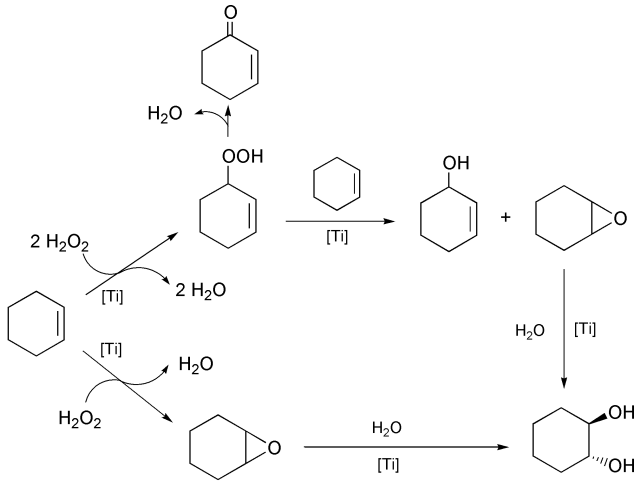

Scheme 1

the radical mechanism takes place with the recovered catalyst. The presence of different titanium species, with either two or three bonds to the surface, or the higher titanium dispersion due to the larger surface area of MCM-41 could be responsible for these differences in behaviour.

Treatment with tartaric acid improves the activity of the silica-based catalyst without causing a modification in the epoxidation/allylic oxidation selectivity. This higher activity is reflected in the higher hydrogen peroxide conversion and the higher turnover number for epoxidation products. It has been shown that some of the titanium species generated in the treatment with tartaric acid are able to pass into solution.[12] However, some other more active species remain on the solid, as shown by the higher turnover number attained with the recovered catalyst. Even with this recovered catalyst the epoxidation/allylic oxidation selectivity is > 50/50, signifying a contribution of the direct epoxidation with hydrogen peroxide. Similar treatment with tartaric acid does not cause the same beneficial effect in the case of the MCM-41 catalyst. This solid is much less active in terms of the productive conversion of hydrogen peroxide and turnover numbers and, in addition, the selectivities are very similar to those obtained with the parent MCM-Ti(OPr^i) catalyst. In this case the species are more strongly bonded to the surface, as demonstrated by the lower degree of titanium leaching.

A particularly interesting point concerns the stability of these catalysts in comparison to other similar systems described in the literature. One of the few studies regarding the stability of grafted titanium species on MCM-41 describes a titanium loss of 50–61% after two reactions, with a total H_2O_2/Ti ratio in the range 228–686.[10] However, this leaching does not seem to be proportional to either the H_2O_2/Ti ratio or the catalytic activity. In our case, titanium loss is 7–19% for MCM catalysts after three runs, with a total H_2O_2/Ti ratio in the range 150–200. These values indicate that the solids described here have a higher stability. The solids described here also show a higher stability in comparison with related silica-based catalysts.[8] This stability is demonstrated by the the fact that catalysts prepared with TiF_4 or tetraneopentyltitanium cannot be used with dilute hydrogen peroxide.

The IR spectra of the recovered catalysts (ESI†) show that some by-products remain adsorbed on the surface.

Another interesting feature of these systmes is the lower content of cyclohexenyl hydroperoxide (chhp) in the final reaction mixture when MCM-41-based catalysts are used. This may be due to a higher activity of these catalysts in the epoxidation with alkyl hydroperoxides or to a more rapid deactivation of the silica-based catalysts. In order to clarify this point, the four catalysts were compared in the epoxidation of cyclohexene with *tert*-butyl hydroperoxide (TBHP). The results (ESI†) show that the catalysts with isopropoxy groups have nearly the same catalytic activity and selectivity. Treatment with tartaric acid noticeably reduces the activity, irrespective of the type of support, but Si-Ti(TA) is clearly more active than MCM-Ti(TA). Thus, the hypothesis regarding the higher activity of MCM-catalysts is not confirmed.

In conclusion, the three factors studied (support, titanium environment and nature of the oxidant) have a significant influence on both the results of the reaction and the stability of the catalyst. Furthermore, the three factors are not completely independent and a careful selection of each parameter is necessary to optimise the behaviour of this kind of catalyst.

Treatment of MCM-41 with tartaric acid has a detrimental effect with both oxidants used (H_2O_2 and TBHP) in such a way that silica-grafted systems become far more active. On using amorphous silica, treatment with tartaric acid leads to a catalyst that is more active in the epoxidation with dilute hydrogen peroxide but is less active with TBHP. Ti(OPr^i) species immobilised on amorphous silica are only slightly more active than those grafted onto MCM-41. However, the use of the crystalline MCM-41 leads to more stable catalysts.

It is clear that none of the supports are particularly advantageous over the others and that the choice of one or other is influenced by other factors concerning the titanium environment and the reaction conditions.

This work was made possible by the generous financial support of the CICYT (project MAT99-1176).

Notes and references

1 A. Sayari, *Chem. Mater.*, 1996, **8**, 1840.
2 R. A. Sheldon, M. Wallau, I. W. C. E. Arends and U. Schuchardt, *Acc. Chem. Res.*, 1998, **31**, 485; M. Dusi, T. Mallat and A. Baiker, *Catal. Rev.-Sci. Eng.*, 2000, **42**, 213.
3 T. Blasco, A. Corma, M. T. Navarro and J. Pérez Pariente, *J. Catal.*, 1995, **156**, 65.
4 T. Maschmeyer, F. Rey, G. Sankar and J. M. Thomas, *Nature*, 1995, **378**, 159.
5 R. Hutter, T. Mallat and A. Baiker, *J. Catal.*, 1995, **153**, 177.
6 H. P. Wulff, *US Pat.*, 3923843, 1975.
7 J. M. Fraile, J. I. García, J. A. Mayoral, L. C. de Mènorval and F. Rachdi, *J. Chem. Soc., Chem. Commun.*, 1995, 539; C. Cativiela, J. M. Fraile, J. I. García and J. A. Mayoral, *J. Mol. Catal. A*, 1996, **112**, 259.
8 E. Jorda, A. Tuel, R. Teissier and J. Kervennal, *J. Catal.*, 1998, **175**, 93; S. A. Holmes, F. Quignard, A. Choplin, R. Teissier and J. Kervennal, *J. Catal.*, 1998, **176**, 173.
9 M. C. Capel-Sánchez, J. M. Campos-Martin, J. L. G. Fierro, M. P. de Frutos and A. Padilla Polo, *Chem. Commun.*, 2000, 855.
10 L. Y. Chen, G. K. Chuah and S. Jaenicke, *Catal. Lett.*, 1998, **50**, 107.
11 H. Kochkar and F. Figueras, *J. Catal.*, 1997, **171**, 420.
12 J. M. Fraile, J. I. García, J. A. Mayoral and E. Vispe, *J. Catal.*, 2000, **189**, 40.
13 R. D. Oldroyd, J. M. Thomas, T. Maschmeyer, P. A. MacFaul, D. W. Snelgrove, K. U. Ingold and D. D. M. Wayner, *Angew. Chem., Int. Ed. Engl.*, 1996, **35**, 2787.
14 C. Berlini, M. Guidotti, G. Moretti, R. Psaro and N. Ravasio, *Catal. Today*, 2000, **60**, 219.
15 C. F. Cheng, D. H. Park and J. Klinowski, *J. Chem. Soc., Faraday Trans.*, 1997, **93**, 193.
16 L. Marchese, E. Gianotti, V. Dellarocca, T. Maschmeyer, F. Rey, S. Coluccia and J. M. Thomas, *Phys. Chem. Chem. Phys.*, 1999, **1**, 585.
17 C. G. Armistead, A. J. Tyler, F. H. Hambleton, S. A. Mitchell and J. A. Hockey, *J. Phys. Chem.*, 1969, **73**, 3947; K. Schrijnemakers, P. van der Voort and E. F. Vansant, *Phys. Chem. Chem. Phys.*, 1999, **1**, 2569.
18 J. M. Fraile, J. García, J. A. Mayoral, M. G. Proietti and M. C. Sánchez, *J. Phys. Chem.*, 1996, **100**, 19484.

CHEMCOMM Communication
www.rsc.org/chemcomm

Selective complexation of uranium(III) over cerium(III) by 2,6-bis(5,6-dialkyl-1,2,4-triazin-3-yl)pyridines: ^{1}H NMR and X-ray crystallography studies

Peter B. Iveson,[a] Christelle Rivière,[a] Denis Guillaneux,[b] Martine Nierlich,[a] Pierre Thuéry,[a] Michel Ephritikhine*[a] and Charles Madic[c]

[a] *CEA/Saclay, DSM/DRECAM/SCM, CNRS URA 331, 91191 Gif-sur-Yvette, France. E-mail: ephri@drecam.cea.fr*
[b] *CEA/Valrhô, DEN/DRCP/SPCS/LCAM, 30207 Bagnols-sur-Cèze, France*
[c] *CEA/Saclay, DEN, 91191 Gif-sur-Yvette, France*

Received (in Cambridge, UK) 23rd April 2001, Accepted 26th June 2001
First published as an Advance Article on the web 26th July 2001

Addition of 2,6-bis(5,6-dialkyl-1,2,4-triazin-3-yl)pyridines (btp) to UI_3 and CeI_3 in anhydrous pyridine gave the 1:3 complexes $[M(btp)_3]I_3$, the terdentate nitrogen ligand being completely selective for U^{III} over Ce^{III}, as shown by ^{1}H NMR competition experiments; crystal structures of analogous btp complexes of U^{III} and Ce^{III} revealed that the U–N bond distances are significantly shorter than the corresponding Ce–N distances.

Much attention is currently paid to the separation of trivalent minor actinides (americium and curium) from trivalent lanthanides, which represents a challenging goal for the definition of new methods in the management of nuclear wastes.[1] A number of multidentate nitrogen extractants have been designed for the selective complexation of the actinides, and the recently discovered 2,6-bis(5,6-dialkyl-1,2,4-triazin-3-yl)pyridines (btp) are the most effective so far.[2] The high separation factors have been attributed to the very weakly basic nature of these ligands which results in the formation of stronger actinide–nitrogen bonds with increased covalent character. However, no actinide complex with btp ligands has been isolated and characterized. We have studied the complexation of the triiodides UI_3 and CeI_3 with two btp molecules, Mebtp and Pr^{n}btp (Fig. 1) in anhydrous pyridine; U^{III} was used as an actinide analogue of the highly radiotoxic Am^{III} and Cm^{III}, and the similarly sized Ce^{III} was chosen as representative of the lanthanides. For the first time, btp complexes of 4f and 5f elements have been studied both in solution and in the solid state, and the remarkably better affinity of actinides(III) *vs.* lanthanides(III) for such multidentate ligands has been revealed by ^{1}H NMR competition experiments and also by X-ray crystallography, with the direct comparison of the crystal structures of the analogous complexes $[M(Pr^nbtp)_3]I_3$ (M = U, Ce).

A 2×10^{-2} M solution of UI_3 in [$^2H_5$]pyridine was titrated with Mebtp in the presence of cyclohexane as internal standard. The ^{1}H NMR spectra† showed that, whatever the number n of ligand equivalents, only the 1:3 complex $U^{III}(Mebtp)_3$ was formed in an immediate and quantitative manner. For $n > 3$, free Mebtp was observed in solution, without exchanging with coordinated ligands. The four resonances in the intensity ratio of 18:18:6:3 indicate that the three Mebtp ligands are equivalent in a D_3 symmetrical arrangement. Complexation of CeI_3 with Mebtp exhibited some differences since for $n < 3$, the 1:2 and 1:3 complexes $Ce^{III}(Mebtp)_2$ and $Ce^{III}(Mebtp)_3$ were formed together. This result is a first indication that Ce^{III} has a lesser affinity for Mebtp than U^{III}. However, the 1:3 complex was the major species for $n > 2$ and the sole present in solution for $n \geqslant 3$. It is also interesting to note that addition of Pr^{n}btp to $Ln(NO_3)_3$ in a 1:1 ratio in ethanol resulted in the crystallization of 1:3 complexes containing the $[Ln(Pr^nbtp)_3]^{3+}$ cations (Ln = Sm, Tm and Yb) with a variety of anions.[3] However, this work did not demonstrate, in contrast to the present study, that the 1:3 complexes were actually the dominant species in solution, while crystallization alone implies exceptional stability of the 1:3 complexes. The strong preference for the formation of the 1:3 complexes with respect to the 1:1 and 1:2 complexes is quite exceptional in coordination chemistry,[4] but some 1:3 complexes between lanthanide ions and terdentate nitrogen ligands have been reported.[5]

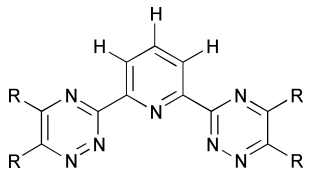

Fig. 1 The Rbtp ligands (R = Me and Pr^n).

Even more striking was the competition reaction of U^{III} and Ce^{III} with Mebtp. Only the 1:3 complex $U^{III}(Mebtp)_3$ was observed in pyridine solution on addition of 1–3 mol equivalents of Mebtp to 1 mol equivalent of both UI_3 and CeI_3; no cerium complex could be detected. The two Ce^{III} complexes $Ce^{III}(Mebtp)_2$ and $Ce^{III}(Mebtp)_3$ then appeared as more ligand was added (3–6 mol equivalents) and finally, only $U^{III}(Mebtp)_3$ and $Ce^{III}(Mebtp)_3$ were observed with an excess of ligand. Similar observations were made when Mebtp was replaced with Pr^{n}btp, and these results clearly demonstrate that these very efficient complexants are completely selective for uranium(III) over cerium(III). By considering that 5% of the cerium complex could be easily detected in solution by ^{1}H NMR, the selectivity factor is certainly higher than 20. This value can be compared with those obtained for the actinide(III)–lanthanide(III) separation (Am^{III}/Eu^{III}) with btp ligands from aqueous nitric acid solutions, which lie between 50 and 150 and are ten times greater than those observed with other terdentate nitrogen ligands such as 2,2′:6′,2″-terpyridine or 2,4,6-tri(2-pyridyl)-1,3,5-triazine.[2]

Single crystals of $[Ce(Mebtp)_3]I_3 \cdot 9C_5H_5N$ (red), $[Ce(Pr^nbtp)_3]I_3 \cdot 3C_5H_5N$ (orange) and $[U(Pr^nbtp)_3]I_3 \cdot 4C_5H_5N$ (brown) were obtained by slow diffusion of pentane into pyridine solutions and their structures were determined.‡ The crystals are composed of discrete $[M(btp)_3]^{3+}$ cations, iodide anions and pyridine molecules. The structures of the cations are very similar; those of $[Ce(Mebtp)_3]^{3+}$ and $[U(Pr^nbtp)_3]^{3+}$ are shown in Figs. 2 and 3, respectively, together with selected data. The metal centres are nine coordinate in a slightly distorted tricapped trigonal prismatic configuration, each btp ligand being attached *via* the nitrogen atom of the pyridine fragment (N_p or N1 in Figures) which occupies the capping position and the nitrogen atoms at the 2 position of the triazine rings (N_t or N3 and N6 in Figures). These structures are equivalent to those found in the lanthanide cations $[Ln(Pr^nbtp)_3]^{3+}$ (Ln = Sm, Tm, Yb).[3] Of special interest is the comparison of the metal–nitrogen bond distances in these cations. The Ce–N_p distances

 DOI: 10.1039/b103606h

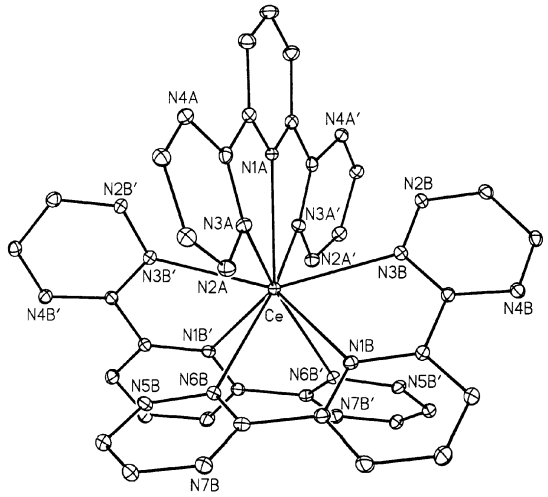

Fig. 2 Crystal structure of the cation $[Ce(Mebtp)_3]^{3+}$. Methyl groups and hydrogen atoms are omitted for clarity. Selected bond lengths (Å) and angles (°): Ce–N1A 2.641(6), Ce–N1B 2.624(4), Ce–N3A 2.613(5), Ce–N3B 2.598(5), Ce–N6B 2.625(5); N1A–Ce–N1B 120.7(1), N1B–Ce–N1B′ 118.7(2). Primed atoms are related to unlabelled atoms by the two-fold axis.

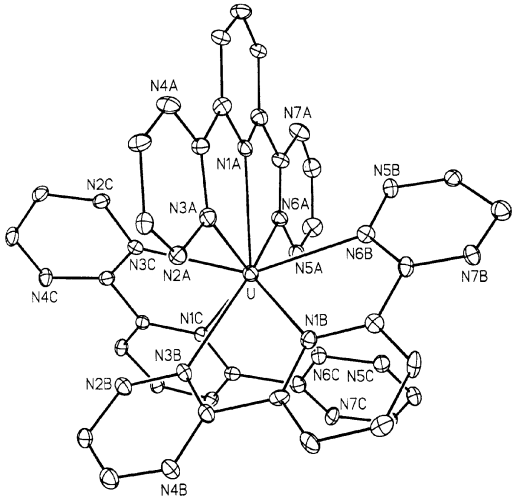

Fig. 3 Crystal structure of the cation $[U(Pr^nbtp)_3]^{3+}$. Propyl groups and hydrogen atoms are omitted for clarity. Selected bond lengths (Å) and angles (°); the corresponding values in the analogous cerium cation are given in square brackets: U–N1A 2.56(2) [2.63(2)], U–N1B 2.53(2) [2.65(2)], U–N1C 2.56(2) [2.65(2)], U–N3A 2.54(2) [2.57(2)], U–N6A 2.57(3) [2.64(2)], U–N3B 2.56(2) [2.66(2)], U–N6B 2.53(3) [2.61(2)], U–N3C 2.52(3) [2.54(2)], U–N6C 2.53(3) [2.59(2)]; N1A–U–N1B 122.1(8) [116.9(7)], N1A–U–N1C 118.6(8) [121.9(5)], N1B–U–N1C 119.4(8) [121.2(6)].

in $[Ce(Mebtp)_3]^{3+}$ are equal to 2.624(4) and 2.641(6) Å with an average value of 2.63(1) Å whereas the Ce–N_t bond lengths range from 2.598(5) to 2.625(5) Å with a mean value of 2.61(2) Å. Very similar distances are found in $[Ce(Pr^nbtp)_3]^{3+}$ [$<$Ce–$N_p$$>$ = 2.64(1) Å and $<$Ce–$N_t$$>$ = 2.60(4) Å], indicating that the different alkyl groups at the 5 and 6 positions of the triazine moiety have no significant effect on the metal coordination sphere. These average Ce–N_p and Ce–N_t distances appear longer than the corresponding distances in the other $[Ln(Pr^nbtp)_3]^{3+}$ cations: 2.57(3) and 2.57(3) Å (Sm), 2.49(2) and 2.50(2) Å (Tm), 2.46(2) and 2.48(2) Å (Yb); this order is in agreement with the variation of the ionic radii of the metals.[6] In the cation $[U(Pr^nbtp)_3]^{3+}$, the U–N_p bond lengths vary from 2.53(2) to 2.56(2) Å and the U–N_t distances range from 2.52(3) to 2.57(3) Å. These metal–nitrogen distances are shorter than those found in the cerium analogue, by 0.09 and 0.06 Å, if the average values are considered, while U^{III} and Ce^{III} have similar ionic radii.[6] Such a difference, which has never been observed in other pairs of analogous uranium and lanthanide complexes with neutral N-donor ligands,[4,7] could reflect some uranium to nitrogen π-back bonding[8] and some degree of covalency in the U–N bond. The distinctive structural features of the $[U(Pr^nbtp)_3]^{3+}$ cation, in comparison with its Ce^{III} counterpart, should be related to the outstanding capacity of btp molecules to coordinate trivalent actinides in preference to trivalent lanthanides, and can be attributed to the much softer character of the N atoms in this weakly basic ligand.

Notes and references

† ^1H *NMR spectra* (200 MHz, 30 °C in $[^2H_5]$pyridine): $[Ce(Mebtp)_2]I_3$, δ 0.42 (6 H, s, Me), 1.33 (6 H, s, Me), 11.36 (1 H, t, 4-py), 12.06 (2 H, d, 3,5-py); $[Ce(Mebtp)_3]I_3$, δ −0.41 (6 H, s, Me), 0.55 (6 H, s, Me), 11.91 (1 H, t, 4-py), 12.28 (2 H, d, 3,5-py); $[U(Mebtp)_3]I_3$, δ −18.04 (6 H, s, Me), 4.59 (6 H, s, Me), 5.64 (1 H, t, 4-py), 33.95 (2 H, d, 3,5-py). The coupling constants are equal to 6–8 Hz; 4-py and 3,5-py denote the H atoms at the 4 and 3,5 positions of the pyridine ring, respectively.

‡ *Crystal data*: for $[Ce(Mebtp)_3]I_3{\cdot}9C_5H_5N$: $C_{90}H_{90}I_3N_{30}Ce$, M = 2112.74, monoclinic, space group $P2/n$, a = 14.078(3), b = 13.889(3), c = 24.741(5) Å, β = 101.94(3)°, V = 4732.9(16) Å^3, Z = 2, D_c = 1.483 g cm^{-3}, μ = 1.520 mm^{-1}, $F(000)$ = 2114. R_1 = 0.052, wR_2 = 0.117, S = 1.026 for 7635 observed reflections with $I > 2\sigma(I)$ (R_{int} = 0.075) and 508 parameters.

For $[Ce(Pr^nbtp)_3]I_3{\cdot}3C_5H_5N$: $C_{84}H_{108}I_3N_{24}Ce$, M = 1974.76, monoclinic, space group Pc, a = 13.576(2), b = 19.695(2), c = 16.643(2) Å, β = 95.095(4)°, V = 4432.4(8) Å^3, Z = 2, D_c = 1.480 g cm^{-3}, μ = 1.615 mm^{-1}, $F(000)$ = 1994. R_1 = 0.093, wR_2 = 0.158, S = 0.956 for 12500 observed reflections with $I > 2\sigma(I)$ (R_{int} = 0.117) and 974 parameters. The structure was refined as corresponding to a racemic twin with x = 0.25(4).

For $[U(Pr^nbtp)_3]I_3{\cdot}4C_5H_5N$: $C_{89}H_{113}I_3N_{25}U$, M = 2151.77, triclinic, space group $P\bar{1}$, a = 13.431(1), b = 16.509(1), c = 21.140(2) Å, α = 80.601(4), β = 88.755(4), γ = 83.588 (5)°, V = 4595.4(6) Å^3, Z = 2, D_c = 1.555 g cm^{-3}, μ = 2.832 mm^{-1}, $F(000)$ = 2146. R_1 = 0.084, wR_2 = 0.174, S = 0.990 for 15377 observed reflections with $I > 2\sigma(I)$ (R_{int} = 0.093) and 1011 parameters.

The data were collected at 123 K on a Nonius Kappa-CCD area detector diffractometer using graphite monochromated Mo-Kα radiation (λ = 0.71073 Å). The structures were solved by direct methods. Absorption effects were empirically corrected, except in $[Ce(Mebtp)_3]I_3{\cdot}9C_5H_5N$, with the program DELABS from PLATON.[9] Some pyridine molecules in all three compounds were found to be disordered as well as the propyl groups and two iodide ions in $[U(Pr^nbtp)_3]I_3{\cdot}4C_5H_5N$. Hydrogen atoms were included at calculated positions as riding atoms, except those of the disordered fragments or molecules. All non-hydrogen atoms were refined anisotropically, except those of the disordered fragments and some pyridine molecules. The structures were refined by full-matrix least-squares on F^2 with SHELXTL.[10]

CCDC reference numbers 161597–161599. See http://www.rsc.org/suppdata/cc/b1/b103606h/ for crystallographic data in CIF or other electronic format.

1 NEA/OECD Report, 1999, *Actinides and Fission Products Partitioning and Transmutation. Status and Assessment Report*, NEA/OECD Report, 1999; *Actinides and Fission Products Partitioning and Transmutation*, Proceedings of the Fifth International Information Exchange Meeting, Mol, Belgium, 25–27 Nov. 1998.

2 Z. Kolarik, U. Mullich and F. Gassner, *Solv. Extr. Ion Exch.*, 1999, **17**, 23; Z. Kolarik, U. Mullich and F. Gassner, *Solv. Extr. Ion Exch.*, 1999, **17**, 1155.

3 M. G. B. Drew, D. Guillaneux, M. J. Hudson, P. B. Iveson, M. L. Russell and C. Madic, *Inorg. Chem. Commun.*, 2001, **4**, 12.

4 R. Wietzke, M. Mazzanti, J. M. Latour and J. Pécaut, *J. Chem. Soc., Dalton Trans.*, 2000, 4167.

5 H. R. Mürner, E. Chassat, R. P. Thummel and J. C. G. Bünzli, *J. Chem. Soc., Dalton Trans.*, 2000, 2809; L. I. Semenova, A. N. Sobolev, B. W. Skelton and A. H. White, *Aust. J. Chem.*, 1999, **52**, 519; S. Petoud, J. C. G. Bünzli, F. Renaud, C. Piguet, K. J. Schenk and G. Hopfgartner, *Inorg. Chem.*, 1997, **36**, 5750; C. Piguet, J. C. G. Bünzli, G. Bernardinelli, G. Hopfgartner and A. F. Williams, *J. Am. Chem. Soc.*, 1993, **115**, 8197.

6 R. D. Shannon, *Acta Crystallogr., Sect. A*, 1976, **32**, 751.

7 J. G. Brennan, S. D. Stults, R. A. Andersen and A. Zalkin, *Organometallics*, 1988, **7**, 1329; R. Wietzke, M. Mazzanti, J. M. Latour and J. Pécaut, *J. Chem. Soc., Dalton Trans.*, 1998, 4087.

8 N. Kaltsoyannis and P. Scott, *Chem. Commun.*, 1998, 1665.

9 A. L. Spek, PLATON, University of Utrecht, 2000.

10 G. M. Sheldrick, SHELXTL, Version 5.1, University of Göttingen, distributed by Bruker-AXS Inc., Madison, WI, 1999.

CHEMCOMM Communication
www.rsc.org/chemcomm

Synthesis of a linear-shaped tetramer and trimers of rhenium(I) diimine complexes†

Osamu Ishitani,* Keiko Kanai, Yoshinori Yamada and Kazuhiko Sakamoto

Graduate School of Science and Engineering, Saitama University, 255 Shimo-Okubo, Saitama 338-8570, Japan. E-mail: ishitani@apc.saitama-u.ac.jp

Received (in Cambridge, UK) 15th May 2001, Accepted 25th June 2001
First published as an Advance Article on the web 18th July 2001

First examples of a linear-shaped tetramer and non-symmetrical trimers of rhenium(I) diimine complexes have been synthesized in good yields, and their UV–vis absorption and emission spectra are reported.

Linear-shaped multinuclear complexes have excited much interest as electron or photon relays.[1,2] However, only certain kinds of metal complexes, for example, ruthenium(II) bisterpyridine derivatives[3] and *meso*-linked metalloporphyrins,[4,5] can be used as building blocks.[6] Also, rhenium(I) diimine complexes *fac*-[Re(LL)(CO)$_3$X]$^{n+}$ (LL = diimine ligand, X = monodentate ligand), for which the photophysics and photochemistry have been intensively studied,[7,8] have been used only as 'L-shaped' bent building blocks for supramolecules, such as molecular squares,[9–11] since only the ligands LL and X in positions *cis* to one another are easily modified.[12] In fact, only two 'linear-shaped' rhenium(I) diimine trimers, both having a symmetrical structure [{[Re(bpy)(CO)$_3$](dppene)}$_2$Re(LL)(CO)$_2$]$^{3+}$, have been reported so far because of the lack of general synthetic methods.[13]

We report here new synthetic routes for 'linear-shaped' but non-symmetrical trimers of rhenium(I) diimine complexes. This new synthesis strategy is also successfully applied to obtain for the first time a 'linear-shaped' rhenium(I) tetrameter [{Re(bpy)(CO)$_3$(dppe)Re(bpy)(CO)$_2$}$_2$(py–py)]$^{4+}$ **1**$^{4+}$ (Scheme 1).

As a typical example, the synthetic procedure for [Re(bpy)(CO)$_3$(dppe)Re(bpy)(CO)$_2$(py–py)Re{(CF$_3$)$_2$bpy}(CO)$_3$]$^{3+}$ **2a**$^{3+}$, where bpy = 2,2′-bipyridine, dppe = 1,2-bis(diphenylphosphino)ethane, py–py = 4,4′-bipyridine, and X$_2$bpy = 4,4′-X$_2$-2,2′-bipyridine, is now reported. An acetonitrile (MeCN) solution (50 dm^3) of the PF_6^- salts of [{Re(bpy)(CO)$_3$}$_2$(dppe)]$^{2+}$ **3**$^{2+}$ (0.04 mmol) was irradiated under an argon atmosphere using a high-pressure mercury lamp with a glass filter (> 330 nm) for 40 min, giving [Re(bpy)(CO)$_3$(dppe)Re(bpy)(CO)$_2$(MeCN)]$^{2+}$ **4**$^{2+}$ [eqn. (1)].

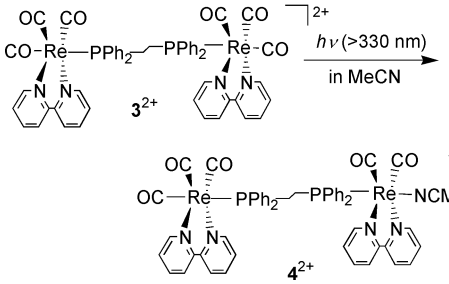

(1)

After evaporation of the MeCN solvent, [Re{(CF$_3$)$_2$bpy}(CO)$_3$(py–py)]$^+$(PF_6^-) and tetrahydrofuran (5 dm^3) were added and the solution was refluxed under an argon atmosphere for 3 h. A red–orange solid consisting of (**2a**$^{3+}$)(PF_6^-)$_3$ was precipitated in 72% yield [eqn. (2)]

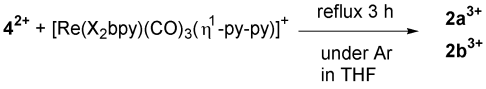

(2)

The further trimer [Re(bpy)(CO)$_3$(dppe)Re(bpy)(CO)$_2$(py–py)Re(bpy)(CO)$_3$]$^{3+}$ **2b**$^{3+}$ was also synthesized by a similar procedure in 78% yield. This photochemical method should be applicable for the synthesis of various rhenium(I) trimers [Re(X$_2$bpy)(CO)$_3$(PP)Re(X$_2$bpy)(CO)$_2$(BL)Re(LL)(CO)$_3$]$^{3+}$ (PP = diphosphorus ligand; BL = bridge ligand), because photoexcitation of rhenium(I) diimine complexes with a phosphorus ligand generally gives a good yield of the *cis*,*trans*-[Re$^{\mathrm{I}}$(LL)(CO)$_2$(PR$_3$)(L′)]$^{n+}$ type complexes.[14]

The tetranuclear complex **1**$^{4+}$ was also synthesized using the same photochemical product **4**$^{2+}$. This product was dissolved in THF containing half molar concentration of py–py. The solution was refluxed for 3 h to give (**1**$^{4+}$)(PF_6^-)$_4$ at 60% yield, based on **3**$^{2+}$ used [eqn. (3)]

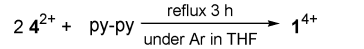

(3)

The symmetrical dimers [{Re(LL)(CO)$_2$(MeCN)}$_2$(dppe)]$^{2+}$ are good candidates for synthetic building blocks for longer rhenium diimine oligomers because they have thermally-active acetonitrile ligands at both ends. Photochemical ligand substitution of **4**$^{2+}$ was much slower than for **3**$^{2+}$ because of the efficient energy transfer reaction from the excited state of the [Re(bpy)(CO)$_3$(dppe)–] group to the other group (specified below), but then proceeded to give [{Re(bpy)(CO)$_2$(MeCN)}$_2$(dppe)]$^{2+}$. Attempts to synthesize longer rhenium diimine oligomers are in progress.

The electrospray ionization mass spectra of the complexes essentially show just a parent peak, and the elemental analysis

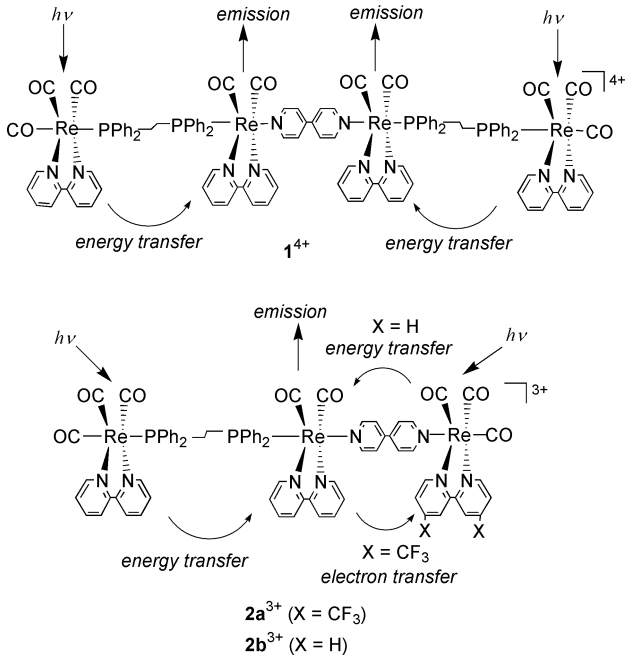

Scheme 1 Linear-shaped Re(I) oligomers.

† Electronic supplementary information (ESI) available: IR and ^{1}H NMR data. See http://www.rsc.org/suppdata/cc/b1/b104220n/

 DOI: 10.1039/b104220n

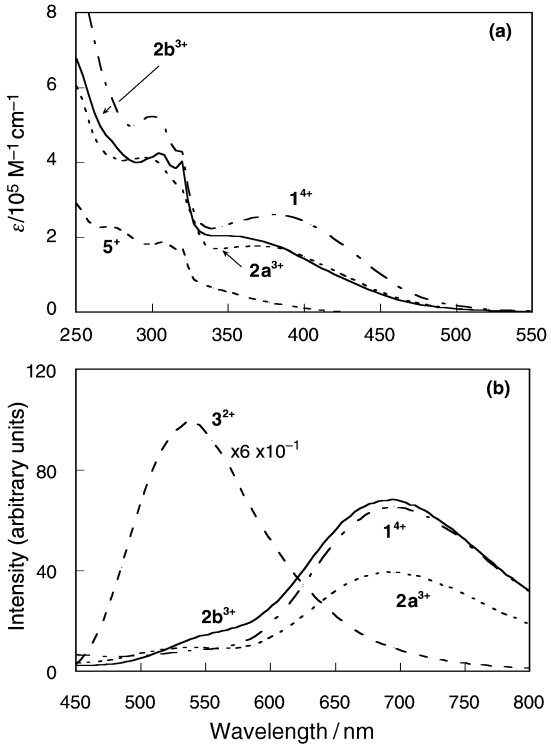

Fig. 1 (a) UV–vis absorption and (b) emission spectra (350 nm excitation) of $\mathbf{1}^{4+}$, $\mathbf{2b}^{3+}$, $\mathbf{3}^{2+}$ and $\mathbf{5}^{+}$ in acetonitrile.

data were in good agreement with the calculated values. The ^{1}H NMR spectra clearly indicate that the two pyridine rings of all the bpy and $(CF_3)_2$bpy ligands are magnetically equivalent and that the bridged ligands are in positions *trans* to one another, so that all the synthesized trimers and the tetrameter are linear-shaped.

We report preliminary spectroscopic data for the complexes synthesized. The UV–vis absorption spectra are shown in Fig. 1(a). The difference in the absorption maxima at 360–390 nm, due to metal-to-ligand charge transfer (MLCT), arises mainly from the differences in the constituent groups and their number. We chose two excitation wavelengths for emission measurements, at 350 and 440 nm: the higher energy photons can excite all the rhenium–complex groups in the oligomers while the other light is absorbed mainly by the central biscarbonyl group(s) [–{(dppe)Re^{I}(bpy)(CO)$_2$}$_2$(py–py)–] and one of the terminal tricarbonyl groups [Re^{I}{(CF$_3$)$_2$bpy}(CO)$_3$ (py–py)–].

Fig. 1(b) illustrates the emission spectra of both the tetramer $\mathbf{1}^{4+}$ and the corresponding dimer $\mathbf{3}^{2+}$ under 350 nm excitation; these differ greatly even though both complexes have the same emissive group, [Re^{I}(bpy)(CO)$_3$(dppe)–]. The strong emission of $\mathbf{3}^{2+}$, which arises from the triplet MLCT excited state (^{3}MLCT) of the [Re^{I}(bpy)(CO)$_3$(dppe)–] groups, was observed at 540 nm. The emission of $\mathbf{1}^{4+}$ at the same wavelength was much weaker, whereas another emission was observed at 695 nm, arising from ^{3}MLCT on the central groups [–(dppe)-Re^{I}(bpy)(CO)$_2$]$_2$(py–py)–]. This assignment is supported by the following experimental results: excitation of $\mathbf{1}^{4+}$ using 440 nm light absorbed mostly by the central groups gave emission only at 695 nm, and a model complex of the central groups [Re^{I}(bpy)(CO)$_2$(PPh$_2$Pr)(η^1-py–py)]$^+$ emits at 710 nm. The strength of the 695 nm emission stimulated by the 440 nm excitation, normalized using the absorbance, was only 1.3 times greater than that stimulated by the 350 nm excitation. These results clearly show that efficient energy transfer occurs from the excited state of the terminal [Re^{I}(bpy)(CO)$_3$(dppe)–] groups to the central [–{(dppe)Re^{I}(bpy)(CO)$_2$}$_2$(py–py)–] groups in $\mathbf{1}^{4+}$ as shown in Scheme 1.

The trimer $\mathbf{2b}^{3+}$ has a different emission property: excitation using 350 nm light causes dual emission, at 540 and 670 nm [Fig. 1(b)], whereas 690 nm emission alone was observed with 440 nm excitation. The emission at 540 nm arises from ^{3}MLCT of the [Re^{I}(bpy)(CO)$_3$(py–py)–] group, because the corresponding mononuclear complex [Re^{I}(bpy)(CO)$_3$(η^1-py–py)]$^+$ $\mathbf{5}^{+}$ emits at 570 nm and the excitation of another terminal [Re^{I}(bpy)(CO)$_3$(dppe)–] group should cause efficient energy transfer to the central group, as described above. Energy transfer from the excited [Re^{I}(bpy)(CO)$_3$(py–py)–] group to the central group is expected to occur (Scheme 1) because the emission strength from the [Re^{I}(bpy)(CO)$_3$(py–py)–] group was much less than that of the model complex.

Emission from $\mathbf{2a}^{3+}$ using either 350 or 440 nm light was weaker than that from $\mathbf{2b}^{3+}$. It follows that the ^{3}MLCT state of the central [–{(dppe)Re^{I}(bpy)(CO)$_2$}$_2$(py–py)–] group should be quenched by the terminal [Re^{I}{(CF$_3$)$_2$bpy}(CO)$_3$(py–py)–] group. There are two possible quenching mechanisms: energy transfer and electron transfer. Energy transfer might not occur because the ^{3}MLCT energy of the central group is lower than that of the [Re^{I}{(CF$_3$)$_2$bpy}(CO)$_3$(py–py)–] group, of which the model complex [Re^{I}{(CF$_3$)$_2$bpy}(CO)$_3$(η^1-py–py)]$^+$ emits at 660 nm.

Further study of the intramolecular electron- and/or energy-transfer processes of rhenium(I) oligomers is in progress using laser flash photolysis.

Notes and references

1 M. C. Petty, M. R. Bryce and D. Bloor, *An Introduction to Molecular Electronics*, Edward Arnold, London, 1995.
2 R. F. Ziessel, *J. Chem. Educ.*, 1997, **74**, 673.
3 V. Grosshenny, A. Harriman, J. P. Gisselbrecht and R. Ziessel, *J. Am. Chem. Soc.*, 1996, **118**, 10 315.
4 B. W. Jiang, S. W. Yang, D. C. Barbini and W. E. Jones, *Chem. Commun.*, 1998, 213.
5 A. Osuka and H. Shimidzu, *Angew. Chem., Int. Ed. Engl.*, 1977, **36**, 135.
6 V. Balzani, A. Juris, M. Ventyri, S. Campagna and S. Serroni, *Chem. Rev.*, 1996, **96**, 759.
7 D. J. Stufkens, *Comments Inorg. Chem.*, 1992, **13**, 359.
8 K. Kalyanasundaram, *Photochemistry of Polypiridine and Porphyrin Complexes*, Academic Press Limited, London, 1992.
9 R. V. Slone, K. D. Benkstein, S. Béanger, J. T. Hupp, I. A. Guzei and A. L. Rheingold, *Coord. Chem. Rev.*, 1998, **171**, 221.
10 T. Rajendran, B. Manimaran, F.-Y. Lee, G.-H. Lee, S.-M. Peng, C. M. Wang and K.-L. Lu, *Inorg. Chem.*, 2000, **39**, 2016.
11 S. M. Woessner, J. B. Helms, J. F. Houlis and B. P. Sullivan, *Inorg. Chem.*, 1999, **38**, 4380.
12 R. Ziessel, A. Juris and M. Venturi, *Inorg. Chem.*, 1998, **37**, 5061.
13 S. M. Woessner, J. B. Helms, K. M. Lantzky and B. P. Sullivan, *Inorg. Chem.*, 1999, **38**, 4378.
14 K. Koike, J. Tanabe, S. Toyama, H. Tsubaki, K. Sakamoto, J. R. Westwell, F. P. A. Johnson, H. Hori, H. Saitoh and O. Ishitani, *Inorg. Chem.*, 2000, **39**, 2777.

CHEMCOMM Communication
www.rsc.org/chemcomm

Biodegradable thermoreversible gelling PLGA-g-PEG copolymers†

Byeongmoon Jeong,* Li-Qiong Wang and Anna Gutowska*

Pacific Northwest National Laboratory (PNNL), 902 Battelle Boulevard, P.O. Box 999, K2-44, Richland, WA 99352, USA. E-mail: byeong.jeong@pnl.gov; Anna.Gutowska@pnl.gov

Received (in Columbia, MO, USA) 14th March 2001, Accepted 11th May 2001
First published as an Advance Article on the web 26th July 2001

The thermogelling aqueous solution of poly(DL-lactic acid-*co*-glycolic acid) grafted with poly(ethylene glycol)s is developed, and the elegant instrumental methods to determine sol–gel transition temperature and the method to control gel duration are reported.

Self-assembly of polymers by external stimuli has been studied extensively over the past decade.[1,2] *In situ* gelling systems have recently generated attention as promising biomaterials.[3–6] To apply *in situ* gelling systems for drug delivery and tissue engineering, the aqueous polymer solution should be free flowing at a certain temperature and form a gel at the physiological temperature. The resultant gel must have reasonable mechanical strength to persist as a drug-releasing depot over the designed lifetime.

The synthesis of thermogelling poly(ethylene glycol-*b*-(DL-lactic acid-*co*-glycolic acid)-*b*-ethylene glycol) (PEG-PLGA-PEG) triblock copolymers by Jeong *et al*. required two steps.[7,8] The ring-opening polymerization of DL-lactide and glycolide on methoxy poly(ethylene glycol), followed by the coupling of the PEG-PLGA diblock with hexamethylene diisocyanate (HMDI) requires strict anhydrous conditions. The resulting triblock copolymer contains two urethane linkages, which might affect the degradation profile of the polymer. However, there is a limitation of molecular weight for PEG-PLGA-PEG copolymers by a triblock topology. Because the sol–gel transition temperature strongly depends on the PEG length, the total molecular weight of PEG-PLGA-PEG triblock copolymers should be 4000–5000, if aqueous solutions are to show a sol–gel transition below 37 °C.[7]

In this paper, thermogelling aqueous solutions of biodegradable graft copolymers, poly(DL-lactic acid-*co*-glycolic acid) grafted with poly(ethylene glycol)s (PLGA-g-PEG) are reported and we will show that such a molecular weight limitation can be overcome by graft copolymer systems.

PLGA-g-PEG copolymers were synthesized by one-step ring opening polymerization of DL-lactide, glycolide, and epoxy terminated poly(ethylene glycol) (PEG; M = 600) using stannous octanoate, as a catalyst.[9] The final DL-lactic acid/glycolic acid/ethylene glycol mol ratio of 3.2/1/2.8 was determined by ^{1}H NMR spectroscopy. Therefore, the grafting frequency of PEG is 4.7 mol%. Gel permeation chromatography (GPC) using light scattering and refractive index detectors in series has been used to determine the absolute molecular weight of polymers.[10] GPC results found a unimodal distribution for our polymers. The number average molecular weight (M_n) and polydispersity (M_w/M_n) of the polymers determined by GPC using tetrahydrofuran (THF) as an eluting solvent were 9300 Daltons and 1.5, respectively. Therefore, the 4–5 PEGs are grafted onto the PLGA backbone.

At 23 °C, the viscosity of the aqueous solution (25 wt%) was *ca*. 0.3 P (g m^{-1} s^{-1}). This viscosity is suitable for injecting the solution through a 25-gauge syringe needle. With increasing temperature, the aqueous solution (25 wt%) of PLGA-g-PEG undergoes a sol–gel transition at 30 °C. In the practical application, the gel should keep its equilibrium-swollen state in an excess amount of water. Further increase in temperature above 50 °C of the PLGA-g-PEG aqueous solution results in a macroscopic phase separation between gel and water. The entire phase diagram will be reported elsewhere.[11] The gel state has been traditionally defined as a non-flowing semisolid in a test-tube inversion test. The method is controversial in its simplicity and lack of scientific rigidity.

To address this issue, the sol–gel transition of the graft copolymer aqueous solution was investigated using dynamic rheometry (Rheometric Scientific: SR 2000).[12] The polymer solution was placed between parallel plates of 25 mm diameter and a gap of 0.5 mm. The data were collected under a controlled stress (4.0 dyn cm^{-2}) and a frequency of 1.0 radian s^{-1}. The heating and cooling rate was 0.2 °C min^{-1}. According to dynamic rheometry, the sol–gel transition was identified in a more reproducible and quantitative manner than by the test-tube inversion method.

The storage moduli (G') of PLGA-g-PEG aqueous solutions varying from 22 to 29 wt% were measured at a heating rate of 0.2 °C min^{-1}. As the temperature increased, the storage modulus increased abruptly at the sol–gel transition temperature. The gels have a modulus of *ca*. 50 dyn cm^{-2} and are slightly affected by concentration in the range of 22–29 wt%. The sol–gel transitions occur at *ca*. 30 °C, suggesting easy formulation at room temperature.

To confirm the reversibility of the sol–gel transition, a 25 wt% PLGA-g-PEG aqueous solution was studied. The real part (η') of complex viscosity of the polymer solution, which is a measure of dissipated energy when cyclic deformation is applied to a material, is shown as a function of temperature in Fig. 1(a). During the first heating cycle (H1), η' increased 1000 times upon the sol–gel transition. The cooling curve (C1) shows that the gel phase persisted over the temperature range of 43–20 °C during the experiment. This fact results from the difficulty in molecular motion to occur in the gel phase; once the solution forms a gel, the gel resists rehydration. η' abruptly decreased at 15 °C due to the gel–sol transition during the cooling of the system. The second heating curve (H2) shows the sol–gel transition at practically the same temperature as the first heating curve (H1).

The storage modulus (G') of the PLGA-g-PEG aqueous solution (25 wt%), which is a measure of stored energy when a cyclic deformation is applied to a material, approaches zero in the sol state and is not shown in the heating curve [Fig. 1(b); H1]. G' sharply increased during the sol–gel transition at 32 °C as shown in the heating curves. The maximum value for G' was observed in the temperature range 35–39 °C, indicating a promising material for *in vivo* (37 °C) applications. During the cooling cycle (C1), the gel modulus increased over the temperature range 43–20 °C, exhibiting similar behavior to typical elastic materials, and dropped abruptly at 15 °C due to the gel–sol transition. During the first (H1) and second (H2) heating cycle, practically the same transition curve was measured for G', indicating reversible gelation. The decrease in G' at temperatures above 40–45 °C can be expected due to an increase in thermal motion. This trend was also observed in the ^{13}C NMR spectra (see ESI†).

† Electronic supplementary information (ESI) available: ^{1}H NMR spectrum of PLGA-g-PEG in $CDCl_3$. ^{13}C NMR (75 MHz) spectra of 25 wt% PLGA-g-PEG copolymer in D_2O as a function of T. See http://www.rsc.org/suppdata/cc/b1/b102819g/

 DOI: 10.1039/b102819g

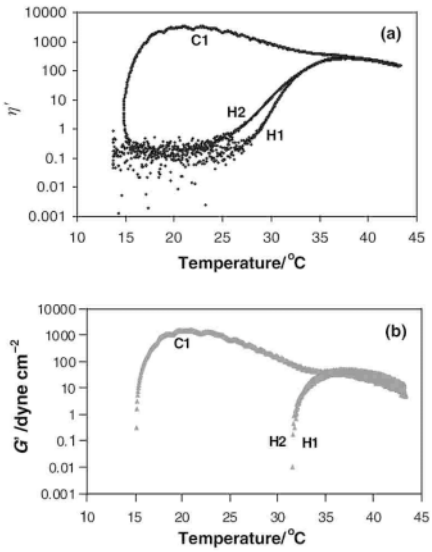

Fig. 1 Rheological study of PLGA-g-PEG copolymer aqueous solutions (25 wt%). The thermogram was obtained while heating and cooling with a rate of 0.2 °C min^{-1}. Temperature programming sequence was heating → cooling → heating. H1, C1 and H2 indicate the first heating cycle, cooling cycle and the second heating cycle, respectively. The real part (η') of complex viscosity, (a), and the storage modulus (G'), (b), of the copolymer solution were measured as a function of temperature.

The ^{13}C NMR spectra of a 25 wt% copolymer solution in D_2O were recorded with increasing temperatures. In the sol state (20 °C), the methyl peak of the hydrophobic PLGA (δ 18) is collapsed and broadened compared with PEG peak (δ 72) whereas that in $CDCl_3$ appears as a sharp peak, indicating a core–shell structure of this polymer in water. The core–shell structure of these amphiphilic copolymers was also confirmed by micelle formation in dilute aqueous solutions. The critical micelle concentration (CMC) determined by a dye solubilization method was 0.03 wt% at 20 °C.[13]

Just above the sol–gel transition temperature (33 °C) of an aqueous PLGA-g-PEG solution (25 wt%), the ^{13}C NMR peak shapes of both the hydrophobic PLGA methyl peak and the hydrophilic PEG peak are preserved except that the PEG peak is shifted down field about 0.3 ppm. With a further increase in temperature, the peak height of the PLGA methyl peak increases, and the PEG peak is split into two peaks, a sharp one at δ 72.4 and a broad one at δ 72.7. These behaviors are thought to be caused by an increase in molecular motion of the hydrophobic backbone and phase mixing between PEG and PLGA. Phase mixing between PEG and PLGA or PLLA has been previously reported.[14] A further increase in temperature resulted in macrophase separation between water and the polymer.

The reversibility of the sol–gel transition is also confirmed by deuterium NMR spectroscopy (Fig. 2). The peak at δ 4.8 at 20 °C (sol state) shifted to δ 4.6 at 33 °C (just above sol–gel transition), δ 4.58 at 37 °C (gel state), δ 4.56 at 40 °C, and δ 4.5 at 50 °C (syneresis). The change in chemical shift was most pronounced during the sol–gel transition (δ 0.2). When the system is cooled to 20 °C, the deuterium peak reappears at δ 4.8, indicating the reversibility of the transition. In a sol state, water moves more freely than in a gel state. During the sol–gel transition, PEG becomes more hydrophobic due to dehydration and the extent of hydrogen bonding between water molecules and polymers changes. Therefore, the time average environment around deuterium nuclei will be affected, leading to the changes in chemical shift of water during the sol–gel transition. This finding suggests that the deuterium NMR can be a good method for the determination of the sol–gel transition.

The sol–gel transition temperature could be controlled from 20 to 40 °C by changing PEG length and composition. When the PEG molecular weight of PLGA-g-PEG was increased from 600 to 1000 the sol–gel transition occurred at 40 °C, whereas the sol–gel transition occurred at 20 °C when the PEG composition was decreased by 20 mol%.[11]

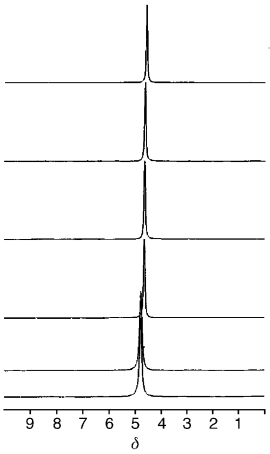

Fig. 2 Deuterium NMR showing reversibility of the sol–gel transition. The deuterium NMR spectra of PLGA-g-PEG in D_2O (25 wt%) were recorded at 20 (5th row from the top), 33 (4th row), 37 (3rd row), 40 (2nd row), 50 (1st row) °C, and after cooling to 20 °C (6th row). The sample was held at each temperature for 30 min.

To conclude, an aqueous PLGA-g-PEG system showing a reversible sol–gel transition at slightly elevated temperatures is developed and a dynamic mechanical test and deuterium NMR confirm the reversibility of this process. These tools can be suggested as standard methods to determine the sol–gel transition temperature than the more empirical test-tube inverting method reported most often.

The system developed in this study is very promising for injectable local delivery of pharmaceutical agents. *In vitro* study shows that the duration of gels could be controlled from one week to three months by mixing slow degrading PLGA-g-PEG and fast degrading PEG-g-PLGA in different ratios.[15] Both polymer aqueous solutions undergo a sol–gel transition around 30 °C. This is very important for applications in drug delivery and tissue engineering, which need the control of gel duration as a matrix or carrier.

This work was supported by Battelle Memorial Institute Independent Research and Development funds.

Notes and references

1 V. Bulmus, Z. Ding, C. J. Long, P. S. Stayton and A. S. Hoffman, *Bioconjugate Chem.*, 2000, **11**, 78.
2 J. J. Marler, A. Guha, J. Rowley, R. Koka, D. Mooney, J. Upton and J. P. Vacanti, *Plast. Reconstr. Surg.*, 2000, **105**, 2049.
3 W. A. Petka, J. L. Harden, K. P. McGrath, D. Wirtz and D. A. Tirrell, *Science*, 1998, **281**, 389.
4 M. Malmsten and B. Lindman, *Macromolecules*, 1992, **25**, 5440.
5 W. Mingvanish, S. M. Mai, F. Heatley and C. Booth, *J. Phys. Chem. B*, 1999, **103**, 11 269.
6 B. Jeong, Y. H. Bae and S. W. Kim, *J. Controlled Release*, 2000, **63**, 155.
7 B. Jeong, Y. H. Bae and S. W. Kim, *Macromolecules*, 1999, **32**, 7064.
8 B. Jeong, Y. H. Bae and S. W. Kim, *Colloids Surf.: B. Biointerfaces*, 1999, **16**, 185.
9 K. Cho, C. H. Kim, J. W. Lee and J. K. Park, *Macromol. Rapid Commun.*, 1999, **20**, 598.
10 P. J. Wyatt, *Anal. Chim. Acta*, 1993, **272**, 1.
11 B. Jeong and A. Gutowska, 2001, in preparation.
12 G. Wanka, H. Hoffmann and W. Ulbricht, *Colloid Polym. Sci.*, 1990, **268**, 101.
13 P. Alexandridis, J. F. Holzwarth and T. A. Hatton, *Macromolecules*, 1994, **27**, 2414.
14 S. S. Shah, K. J. Zhu and C. G. Pitt, *J. Biomater. Sci. Polym. Ed.*, 1994, **5**, 421.
15 B. Jeong, M. R. Kibbey, J. C. Birnbaum, Y. Y. Won and A. Gutowska, *Macromolecules*, 2000, **33**, 8317.

CHEMCOMM Communication
www.rsc.org/chemcomm

Synthesis and characterization of hollow clay microspheres through a resin template approach

A. B. Bourlinos,[a] M. A. Karakassides[b] and D. Petridis*[a]

[a] *Institute of Materials Science, NCSR "Demokritos", Ag. Paraskevi Attikis, Athens 15310, Greece. E-mail: dpetrid@ims.demokritos.gr*
[b] *Department of Materials Science and Engineering, University of Ioannina, 45110 Ioannina, Greece*

Received (in Cambridge, UK) 5th June 2001, Accepted 4th July 2001
First published as an Advance Article on the web 26th July 2001

Hollow clay microspheres of high thermal stability were easily fabricated by the adsorption of colloidal clay layers onto the surfaces of a spherical anion exchange resin and calcination of the resulting resin–clay composite.

Hollow spheres of nanometer to micrometer dimensions define an important class of shape-fabricated materials in which the shell of the hollow sphere can be constructed by a variety of materials of high scientific interest and technological importance; magnetic, semiconducting, ceramic, metallic, polymer, composite *etc*.[1–3] Owing to their low density, large specific area, stability and surface permeability, hollow spheres are widely used as controlled release capsules for drugs, dyes, cosmetics and inks, artificial cells, catalysts and fillers. Engineering hollow spheres from porous solids, such as mesoporous silica[4–6] and zeolites,[7] constitutes an important advance in materials, because of the unique properties of these well organized superstructures. Recently, the fabrication of hollow laponite submicrometer spheres (laponite is a synthetic smectite clay) based on the layer-by-layer self-assembly technique, was reported.[8] In this communication we report another approach for easy construction of hollow inorganic spheres, and in particular, describe the synthesis and characterization of thermally stable hollow smectite clay spheres in the micrometer range. In general, the production of clay spheres is expected to be of great value since smectite clays define a known class of layered aluminosilicate minerals that possess unique swelling, intercalative and cation exchange properties.[9] In addition, their thermal stability and chemical inertness make them suitable materials for particle engineering (clay ceramics) and for use as fillers in many industrial applications.[10,11] The method proposed for the morphogenesis of hollow clay microspheres, simply comprises the adsorption of colloidal acid clay layers onto the surfaces of a spherical anion exchange resin (carbonated form), followed by removal of the resin's organic backbone by calcination in air. In principle, our synthetic strategy resembles that of the sacrificial core–shell technique in which hollow spheres are assembled by a controlled adsorption, involving precipitation reactions, sol–gel condensations and layer-by-layer depositions of the desirable material onto the surfaces of an appropriately modified colloidal template (usually a polymer) and subsequent removal of the template by thermal or chemical treatment.[12–15]

In this work, a strongly basic anion exchange resin of a quaternary ammonium chloride type and spherical morphology (Dowex 2, x8 100/200 mesh) was used. The resin was initially treated with 1 M Na_2CO_3 aqueous solutions in order to obtain its carbonated form. Two sources of clay were used. The first, was a naturally occurring montmorillonite from the island of Milos, Greece, denoted Zenith-N. The montmorillonite was fractionated to <2 μm by gravity sedimentation and purified by standard methods to obtain its sodium saturated form with a CEC of 0.8 meq. g^{-1}. The second was a synthetic sodium hectorite (laponite, monovalent cation exchange capacity: CEC = 0.74 meq. g^{-1}) supplied by Laporte Industries Ltd. The resin–clay products were obtained as follows: 1 g of each clay sample was dispersed in 100 ml of deionized water. To each colloidal dispersion, 1–2 drops of concentrated HCl (37%) were added (pH of the mixture *ca*. 3) and the gelatinous mixtures were vigorously stirred for 1 min. After centrifugation of the solids, the supernatant liquids were discarded and the same procedure was repeated twice. Finally, the acid clays were washed once with water, centrifuged and redispersed in 100 ml of deionized water. Each acid clay colloidal dispersion was then slowly added to 4 g of carbonated resin in 20 ml of deionized water and the mixture was heated under vigorous stirring at 80 °C for 30–45 min. During the addition of the acid clay dispersions to the carbonated resin and the thermal treatment, evolution of gas (CO_2) was observed, indicating the binding of the negatively charged clay layers to the positively charged resin surfaces according to eqn. (1) where $Resin^+]$

$$Resin^+]CO_3^{2-} + 2H^+[^-Clay \rightarrow Resin^+][^-Clay + CO_2 + H_2O \quad (1)$$

denotes the positively charged surfaces of the resin and $[^-Clay$ denotes the negatively charged clay layers. After the thermal treatment, the resin–clay mixtures were centrifuged (4000 rpm, 1 min), washed twice with commercial acetone and dried at 60 °C for 20 min in an oven. Observation of the resin–clay samples under an optical microscope did not reveal the presence of any discrete clay phase but only the presence of transparent resin spheres, suggesting a homogeneous coverage of the resin surfaces by a thin clay coating. The as obtained resin–clay samples were finally calcined in air at 600 °C for 7 h *via* steps of 1 °C min^{-1} to give pure hollow clay microspheres as evidenced by the lack of organic absorptions in IR spectra. The final samples were studied by optical microscopy, SEM and XRD techniques.

Optical microscopy images of the parent anion exchange resin as well as the Zenith-N and laponite clay samples derived after calcination of the corresponding resin–clay composites are shown in Fig. 1. The XRD patterns of the clay samples are also included as inset photos. The parent amorphous resin particles possess a spherical morphology with a non-uniform size distribution of small and large spheres in the range 100–200 μm. On the other hand, both clay samples also consist of spherical particles (Zenith-N spheres: opaque and with rough surfaces, laponite spheres: transparent and with smooth surfaces) with a non-uniform size distribution in the range 20–50 μm. Therefore, the clay samples inherit the shape morphology and size non-uniformity of the parent resin throughout the synthetic process. Accordingly, by controlling the size distribution of the starting resin particles, *e.g*. by sieving the resin, the problem of the size non-uniformity can be eliminated. As far as the observed size shrinkage of the clay samples is concerned, this can be attributed to the removal of the large resin core (at least 100 μm) after calcination of the resin–clay composites. The spheres based on Zenith-N show a weak (001) XRD reflection with a basal spacing (d_{001} = 9.8 Å) characteristic for the collapsed state of the layers in the prime clay particles. In contrast to Zenith-N, the laponite based spheres do not exhibit any (001) reflection that may be attributed to a turbostatic stacking of the

 DOI: 10.1039/b104922b

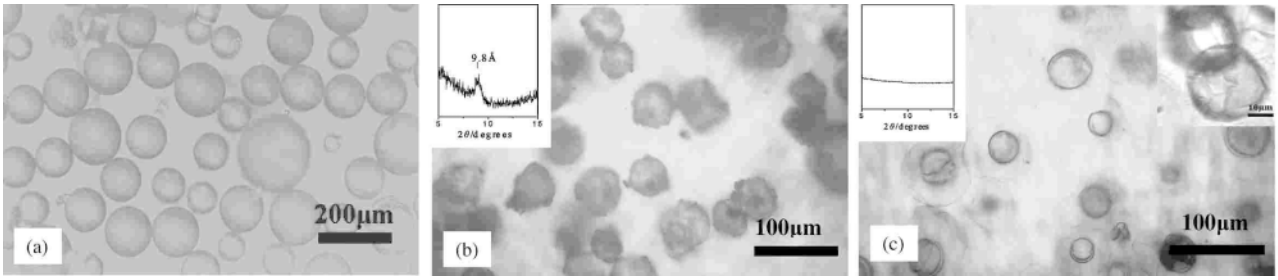

Fig. 1 Optical microscopy pictures of (a) parent resin spheres, (b) Zenith-N clay spheres and (c) laponite clay spheres (the inset photos show XRD patterns of the given clay samples).

layers in the clay particles due to their very small size (*ca.* 0.1 μm *cf. ca.* 1 μm for Zenith-N).

The SEM examination of Zenith-N and laponite samples reveals the presence of compact and intact spheres which are smoother in the latter, Fig. 2. The inset photo, Fig. 2(a), shows a broken sphere that reveals the hollow structure of the spheres. The wall thickness of the spherical cells is rather uniform and varies between 3 and 5 μm for both clay samples. Note that the large majority of the hollow clay spheres are intact at their surfaces. In contrast to this observation, when the clay samples were prepared using the sodium form of Zenith-N and laponite instead of the acid forms, and the chloride form of the resin instead of carbonated form, clay samples consisting primarily of broken specimens with irregular shape and morphology were obtained, features that were more pronounced for the laponite sample. It seems that the resin surfaces are not sufficiently covered by clay layers to form a thick enough coating that remains intact after calcination. This probably arises from the strong electrostatic binding of chloride ions by the positively charged surface of the resin thus making their efficient replacement by the negatively charged clay layers difficult.

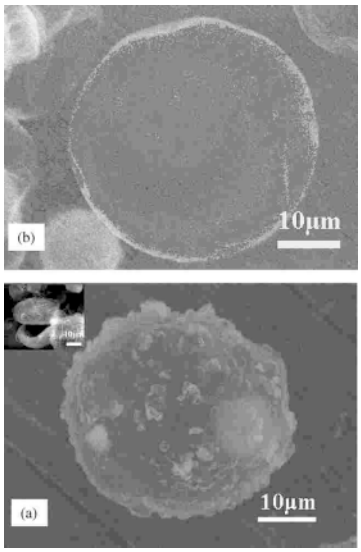

Fig. 2 SEM micrographs of a Zenith-N (a) and laponite (b) hollow clay sphere (the inset photo shows a broken Zenith-N hollow specimen).

Fig. 3 shows XRD patterns of Zenith-N clay spheres before (a) and after (b) treatment with trimethylamine vapor at 80 °C for 3 h. After vapor treatment, the basal spacing of the collapsed clay (d_{001} = 9.8 Å) increased to 12.8 Å due to the insertion of trimethylamine molecules into the gallery space of the clay layers *via* interlayer protonation of the base. The results show that the hollow clay spheres can be easily reconstructed to other clay derivatives *via* intercalative patterning of their interlayer space. For laponite, insertion of trimethylamine into the galleries does not alter the amorphous state of the clay shell, even after prolonged exposure. In this case, the lack of layer re-stacking may be attributed to some chemical sintering occurring after calcination, between laponite layers through cross-linking of adjacent broken sites (much greater in number than for

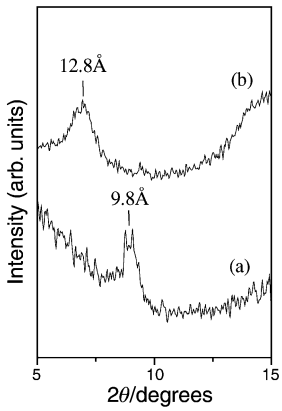

Fig. 3 XRD patterns of Zenith-N hollow spheres (a) before and (b) after trimethylamine vapor treatment.

Zenith-N due to the smaller size of the layers) near their edges.[8] It should be noted that the morphology of the clay samples was preserved after the above mentioned treatments.

In conclusion, thermally stable hollow microspheres (size: 20–50 μm, wall thickness: 3–5 μm) of a naturally occurring and of a synthetic clay were prepared using the sacrificial core–shell technique, in which an anion exchange resin played the role of the core/template and the clay particles the role of the building units of the shell. Intact hollow spheres were obtained only when a carbonated resin and an acid clay were used, as this combination provides an efficient way to sufficiently cover the resin surfaces with the clay layers without screening effects from the counter ions of the resin. The template approach described here can also apply to fabrication of micrometer sized analogues of clay colloidal systems, *e.g.* zeolites and magnetic particles. In a forthcoming publication the ability to synthesize a variety of hollow inorganic microspheres by simply exploiting the exchange properties of the resin will be described.

Notes and references

1 D. L. Wilcox, M. Berg, T. Bernat, D. Kellerman and J. K. Cochran, *Hollow and Solid Spheres and Microspheres: Science and Technology Associated with Their Fabrication and Application*, Materials Research Society Proceedings, Pittsburgh, NJ, 1995, vol. 372.
2 F. Caruso, *Chem. Eur. J.*, 2000, **6**, 413.
3 D. E. Bergbreiter, *Angew. Chem., Int. Ed.*, 1999, **38**, 2870.
4 S. Schacht, Q. Huo, I. G. Voigt-Martin, G. D. Stucky and F. Schuth, *Science*, 1996, **273**, 768.
5 P. J. Bruinsma, A. Y. Kim, J. Liu and S. Baskaran, *Chem. Mater.*, 1997, **9**, 2507.
6 H. Lin, Y. Cheng and C. Mou, *Chem. Mater.*, 1998, **10**, 3772.
7 X. D. Wang, W. L. Yang, Y. Tang, Y. J. Wang, S. K. Fu and Z. Gao, *Chem. Commun.*, 2000, 2161.
8 R. A. Caruso, A. Susha and F. Caruso, *Chem. Mater.*, 2001, **13**, 400.
9 T. J. Pinnavaia, *Science*, 1983, **220**, 365.
10 P. H. Nadeau, *Appl. Clay Sci.*, 1987, **2**, 83.
11 R. E. Kirk and D. F. Othmer, ed., *Encyclopedia of Chemical Technology*, Interscience, New York, 1954, vol. 4, pp. 24–86.
12 N. Kawahashi and H. Shiho, *J. Mater. Chem.*, 2000, **10**, 2294.
13 Z. Zhong, Y. Yin, B. Gates and Y. Xia, *Adv. Mater.*, 2000, **12**, 206.
14 G. Decher, *Science*, 1997, **277**, 1232.
15 F. Caruso, R. A. Caruso and H. Mohwald, *Science*, 1998, **282**, 1111.

CHEMCOMM Communication
www.rsc.org/chemcomm

Polyamines containing naphthyl groups as pH-regulated molecular machines driven by light†

M. Teresa Albelda,[a] M. Alexandra Bernardo,[b] Pilar Díaz,[a] Enrique García-España,*[a] J. Seixas de Melo,[c] Fernando Pina,*[b] Conxa Soriano,[d] and Santiago V. Luis.[e]

[a] *Departament de Química Inorgànica, Facultat de Química, Universitat de València, C/ Dr. Moliner 50, 46100 Burjassot (València), Spain. E-mail: enrique.garcia-es@uv.es*
[b] *Departamento de Química, Centro de Química Fina e Biotecnologia, Universidade Nova de Lisboa, Quinta da Torre 2825 Monte de Caparica, Portugal. E-mail: fjp@dq.fct.unl.pt*
[c] *Departamento de Química, Faculdade de Ciências e Tecnologia, Universidade de Coimbra, 3000 Coimbra, Portugal*
[d] *Departament de Química Orgànica, Facultat de Farmàcia, Universitat de València, Avda Vicent Andrés Estellés s/n, 46100 Burjassot (València), Spain*
[e] *Departament de Química Inorgànica i Orgànica, Universitat Jaume I, C/ Borriol s/n 12080, Castellón, Spain*

Received (in Cambridge, UK) 16th May 2001, Accepted 27th June 2001
First published as an Advance Article on the web 26th July 2001

A series of compounds made up by linking methylnaphthalene fragments at both ends of different polyamine chains have shown to behave as pH-regulated molecular machines driven by light and fluorescence emission studies have proved the formation of an excimer between the two naphthalene units whose appearance, fluorescence intensity and decay times depend on the pH value of the media.

Many biological systems can be considered as more or less complex molecular machines operated by chemical or physical stimuli. Examples of this behaviour are found in the triggering effect of many calcium binding proteins or in the astonishing ATP synthase molecular rotor.[1,2] Therefore, in the last few years a lot of research effort has been devoted to identifying systems able to perform molecular motions following chemical or physical inputs.[1–9] Herewith, we communicate on a family of very simple compounds whose molecular movements driven by light can be controlled and even modulated by inputs like the concentration of hydrogen ions and/or metal ions. Compounds L1–L5 have been prepared in good yields by reaction of the

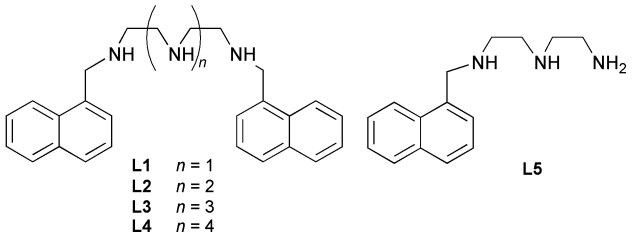

elected polyamine with naphthalene-1-carbaldehyde in ethanol followed by reduction with sodium borohydride.[10]

While the absorption spectra of these compounds do not change significantly with pH, the fluorescence emission intensity dramatically depends on their protonation state (see Fig. 1A for L1). As described for related compounds,[10] the fully protonated forms of L1–L5 exhibit the most intense fluorescence emission. Unprotonated amines are efficient electron transfer quenchers of the aromatic excited state and depending on the distance to the fluorophore can produce a partial or complete quenching. This trend is illustrated in Fig. 1B, where the fluorescence emission intensity monitored at 334 nm is plotted together with the mole fraction distribution of the different protonated species calculated from the protonation constants determined potentiometrically.[11] In order to have a full picture of the situation, the protonation sequence established for L1 by means of the ^{1}H and ^{13}C NMR data has to be taken into account. As shown in Fig. 1B, the first deprotonation that occurs on the central nitrogen atom leads to a partial quenching, *ca.* 80% of the emission of the fully protonated form. Total quenching takes place only upon removing the second proton from one of the side nitrogens. However, the most remarkable feature in the emission spectra of these compounds is the presence of a red-shifted and non-structured band attributable to excimer formation (Fig. 1A). This red shitted band does not appear in the case of the compound containing a single terminal naphthalene (L5), or in the case of an analogue receptor possessing a reinforcing piperazine ring (L6, see ESI). This absence in L5 excludes the possibility of a charge transfer (CT) state involving the deprotonated amine and the fluorophore.[12]

Excimer formation is only observed for the H_2L1^{2+} species. Neither the fully protonated species H_3L1^{3+} nor the species with lower protonation degrees yield such association. In the case of H_3L1^{3+}, this can be ascribed to the large electrostatic repulsion at this stage which prevents the required bending movement while the total quenching of the emission produced in the low protonated species would avoid observing any excimer formation.

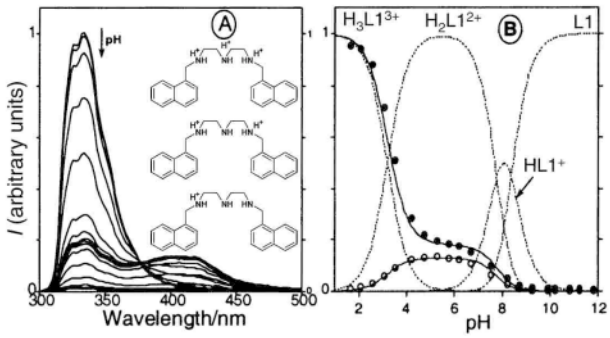

Fig. 1 A—pH dependence of the fluorescence emission of compound L1 at λ_{exc} = 287 nm. Protonation sequence determined by ^{1}H NMR is shown in the inset. B—Mole fraction distribution of the protonation states of compound L1 (-----); fluorescence emission at λ_{exc} = 287 nm and λ_{em} = 334 nm (●); fluorescence emission at λ_{exc} = 287 nm and λ_{em} = 418 nm (○).

† Electronic supplementary information (ESI) available: synthesis and characterisation data for L1–L4, protonation constants and spectra. See http://www.rsc.org/suppdata/cc/b1/b104311k/

 DOI: 10.1039/b104311k

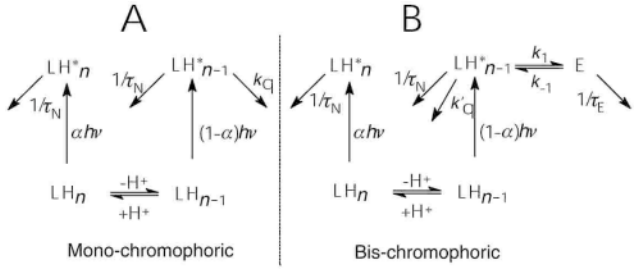

Scheme 1

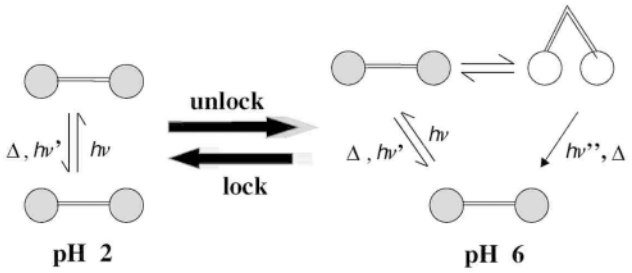

Scheme 2

Intramolecular excimer formation was studied by nanosecond time-resolved fluorescence. Fluorescence decays were monitored at λ_{em} = 315 nm, where the fluorescence emission is essentially due to the excited monomer, and at λ_{em} = 418 nm, where the excimer emits. Global analysis of the decays can only be properly fitted with sums of two or three exponentials. The fluorescence emission behaviour of the mono-chromophoric and bis-chromophoric systems can be interpreted as depicted in Schemes 1A and 1B for the triaza receptors L5 and L1, respectively. In both cases, a ground-state equilibrium exists between the fully protonated species (H_3L^{3+}) and the mono-unprotonated one (H_2L^{2+}). Simultaneous excitation of both H_3L^{3+} and H_2L^{2+}, leads to H_3L^{3+*} and H_2L^{2+*} excited species; the relative proportion of these species will depend on the pH (Fig. 1B). While H_3L^{3+*} decays with a rate constant equal to the reciprocal of τ_N, H_2L^{2+*} presents an additional direct quenching to the ground-state by the CT state with k_q (rate constant due to amine quenching); the overall decay for the H_2L^{2+*} species is equal to $1/\tau_N + k_q$.

The question arising now is the correct attribution of the observed components of the decay times to the species shown in Fig. 1B for L1. At pH = 4.6, the H_3L1^{3+} and H_2L1^{2+} species coexist with the excimer. At pH = 2.3, where practically no excimer is observed, we have obtained a double-exponential decay with decay times equal to 29.6 and 2.9 ns, and pre-exponential factors, a_i, of respectively 0.93 for H_3L1^{2+} and 0.07 for the small amount of the H_2L1^{2+} species present at this pH. At pH = 3.2 the two monomers coexist with the excimer. While H_2L1^{2+*} with a decay time of 3.4 ns gives rise to the excimer (τ_E = 15.8 ns), the more protonated monomer is found uncoupled with the other emissive species and must unequivocally be attributed to the H_3L1^{3+} species. Also it is worth noting that the negative pre-exponential at λ_{em} = 418 nm is associated with the shorter lifetime (H_2L1^{2+}) and that no negative amplitude is associated with the longer lifetime (H_3L1^{3+}). This once more shows that the H_3L^{3+} species decays with a lifetime identical to the one obtained at pH = 2.3 and to the one of L5 (where no intramolecular excimer formation occurred).[10] For pH = 6.1 the system is now reduced to a bi-exponential decay law since the H_3Ll^{3+} species is absent (see ESI). The H_2L1^{2+*} species will have at this pH two additional deactivation channels: i) electron quenching promoted by unprotonated amino groups, k_q, and ii) excimer formation, k_1. This situation does not apply to the case of H_3L1^{3+*} because excimer formation is forbidden and the only possible deactivation route occurs *via* its natural fluorescence lifetime ($\approx$31 ns). Comparison with the excited state behaviour of L5, where only a double-exponential fit is required, clearly supports the above considerations.

Another interesting aspect is the existence of excited state reversibility of the excimer leading to delayed fluorescence emission because, as reported above, the intermediate lifetime emission can also be detected at 315 nm.

Although the behaviour of L2, L3 and L4 is analogous to that of L1, several aspects deserve comment. The quenching processes and the efficiency of excimer formation are strongly affected by the length of the chain and the protonation states of the molecules. Indeed, the protonation degree for which the ratio excimer–monomer emission is maximum increases proton by proton from one receptor to the following in size; for L2 it is H_2L2^{2+}, for L3 it would be H_3L3^{3+} and for L4, H_4L4^{4+}. In all these species the central nitrogens are unprotonated facilitating the delocalisation of the positive charges along the chain.

All these data clearly point out that the compounds here described are examples of elementary molecular movements driven by light and switched on/off by pH. Scheme 2 for compound L1 illustrates this concept. At pH values below 2, the system is rigid and no bending movement occurs upon light absorption; in this state the system is locked. The unlock step takes place following a pH jump to 6. For this pH value, light absorption by the monomer leads to excimer formation as well as to the back reaction responsible for the delayed fluorescence.

Financial support from Fundação para a Ciência e Tecnologia project 32442/99 (Portugal), PRAXIS/QUI/10137/98, HPRN-CT-2000-29 (EC), and DGICYT project BQU2000-1424 (Spain) are gratefully acknowledged. M. T. A. and P. D. want to thank Generalitat Valenciana and Ministerio de Ciencia y Tecnología for their respective PhD grants.

Notes and references

1 P. D. Boyer, *Angew. Chem., Int. Ed.*, 1998, **37**, 2296; J. E. Walker, *Angew. Chem., Int. Ed.*, 1998, **37**, 2308.
2 W. Junge, *Proc. Natl. Acad. Sci. USA*, 1999, **96**, 4735.
3 V. Balzani, M. G-López and J. F. Stoddart, *Acc. Chem. Res.*, 1998, **31**, 405; V. Balzani, A. Credi, F. M. Raymo and J. F. Stoddart, *Angew. Chem., Int. Ed.*, 2000, **39**, 3348.
4 A. P. Davies, *Angew. Chem., Int. Ed.*, 1998, **37**, 909.
5 A. P. de Silva, H. Q. Gunaratne, T. Gunnlaugsson, A. J. M. Huxley, C. P. McCoy, J. T. Rademacher and T. E. Rice, *Chem. Rev.*, 1997, **97**, 1515; T. R. Kelly, H. Silva and R. A. Silva, *Nature*, 1999, **401**, 150; T. R. Kelly, M. C. Bowyer, K. V. Bhaskar, D. Bebbington, A. Garcia, F. Lang, M. H. Kim and M. P. Jette, *Angew. Chem., Int. Ed. Engl.*, 1997, **36**, 1866; T. R. Kelly, R. A. Silva and G. Finkenbeiner, *Tetrahedron Lett.*, 2000, **41**, 9651.
6 E. Kimura and T. Koike, *Chem. Commun.*, 1998, 1495; M. Shionoya, E. Kimura and M. Shiro, *J. Am. Chem. Soc.*, 1993, **115**, 6730.
7 B. König, M. Pelka, H. Zieg, T. Ritter, H. Bouas-Laurent, R. Bonneau and J. P. Desvergne, *J. Am. Chem., Soc.*, 1999, **121**, 1681.
8 F. McLaren, P. Moore and A. M. Wynn, *J. Chem. Soc., Chem. Commun.*, 1989, 798.
9 L. Fabbrizzi, *Coord. Chem. Rev.*, 2000, **205**, 3.
10 M. A. Bernardo, S. Alves, F. Pina, J. Seixas de Melo, M. T. Albelda, E. García-España, J. M. Llinares, C. Soriano and S. V. Luis, *Supramol. Chem.*, 2001, in press; F. Pina, M. A. Bernardo and E. García-España, *Eur. J. Inorg. Chem.*, 2000, 2143.
11 Potentiometric measurements were carried out in 0.15 mol dm^{-3} NaCl at 298.1 ± 0.1 K The program HYPERQUAD (A. Sabatini, A. Vacca and P. Gans, *Coord. Chem. Rev.*, 1992, **120**, 389) was used to derive the values of the protonation constants. Stepwise constants calculated for L1 are: log $K_{HL/H\cdot L}$ = 8.38(2), log $K_{H_2L/HL\cdot H}$ = 7.81(1) and log $K_{H_3L/H_2L\cdot H}$ = 3.81(3); for L2: log $K_{HL/H\cdot L}$ = 9.12(2), log $K_{H_2L/HL\cdot H}$ = 8.22(2), log $K_{H_3L/H_2L\cdot H}$ = 6.01(3) and log $K_{H_4L/H_3L\cdot H}$ = 3.18(3); for L3: log $K_{HL/H\cdot L}$ = 9.32(1), log $K_{H_2L/HL\cdot H}$ = 8.58(1), log $K_{H_3L/H_2L\cdot H}$ = 7.39(2), log $K_{H_4L/H_3L\cdot H}$ = 4.77(3) and log $K_{H_5L/H_4L\cdot H}$ = 2.68(3); for L4 (see ref. 10): log $K_{HL/H\cdot L}$ = 10.04(4), log $K_{H_2L/HL\cdot H}$ = 8.94(3), log $K_{H_3L/H_2L\cdot H}$ = 8.29(3), log $K_{H_4L/H_3L\cdot H}$ = 6.82(4) and log $K_{H_5L/H_4L\cdot H}$ = 4.58(4) and log $K_{H_6L/H_5L\cdot H}$ = 2.23(1); for L5: log $K_{HL/H\cdot L}$ = 9.72(1), log $K_{H_2L/HL\cdot H}$ = 8.21(1) and; log $K_{H_3L/H_2L\cdot H}$ = 3.94(2).
12 E. A. Chandross and H. T. Thomas, *Chem. Phys. Lett.*, 1971, **9**, 393.

Typeset and printed by Black Bear Press Limited, Cambridge, England

CHEMCOMM
Feature Article
www.rsc.org/chemcomm

Recent developments in the chemistry, biology and medicine of the epothilones†

K. C. Nicolaou,* Andreas Ritzén and Kenji Namoto

Department of Chemistry and The Skaggs Institute for Chemical Biology, The Scripps Research Institute, 10550 North Torrey Pines Road, La Jolla, California 92037, USA and Department of Chemistry and Biochemistry, University of California San Diego, 9500 Gilman Drive, La Jolla, California 92093, USA. E-mail: kcn@scripps.edu

Received (in Cambridge, UK) 5th June 2001, Accepted 19th June 2001
First published as an Advance Article on the web 15th August 2001

The epothilones have occupied center stage on the scenes of total synthesis, chemical biology and medicine for the last five years, no doubt because of their intriguing mode of action and unusually high potency against tumor cells, including multi-drug-resistant cell lines. This article highlights the most recent advances within this exciting field. Thus, an overview of recent synthetic endeavors culminating in a new generation of total syntheses and analogues, some with higher potencies than the naturally occurring substances, will be given, and the chemical biology, in particular the current understanding of structure–activity relationships of the epothilones, will also be discussed in light of the latest biological results. In addition, the recently elucidated biosynthetic machinery of the natural epothilone-producing myxobacterium *Sorangium cellulosum*, as it is now understood, will be described. Finally, some preclinical and clinical studies will be summarized.

† Dedicated to Drs Margaret Harris and Muriel Hall of Bedford College, London, for their dedicated and inspiring teachings and research contributions in celebration of their retirement.

K. C. Nicolaou, born in Cyprus and educated in England and the US, is currently Chairman of the Department of Chemistry at The Scripps Research Institute where he holds the Darlene Shiley Chair in Chemistry and the Aline W. and L. S. Skaggs Professorship in Chemical Biology as well as Professor of Chemistry at the University of California, San Diego. His impact on chemistry, biology and medicine flows from his works in organic synthesis described in over 500 publications and 65 patents and his dedication to chemical education resulted in the training of over 300 graduate students and postdoctoral fellows. His recent book titled Classics in Total Synthesis, *which he co-authored with Erik J. Sorensen, is used around the world as a teaching tool and source of inspiration for students and practitioners of the art of organic synthesis.*

Andreas Ritzén was born in Nicosia, Cyprus, in 1973. After completing a BSc in Organic Chemistry with Professor Rolf Carlson at Umeå University, Sweden, in 1994, he received his PhD degree in Organic Chemistry under the supervision of Professor Torbjörn Frejd at Lund University, Sweden, in 2000. He is currently a Research Associate at The Scripps Research Institute with Professor K. C. Nicolaou.

Kenji Namoto was born in 1973 in Chiba, Japan, and received his BSc in 1997 from Waseda University, Tokyo. In the same year, he joined a PhD program in chemistry at the Scripps Research Institute, La Jolla, California, where he currently conducts graduate research under the guidance of Professor K. C. Nicolaou. His major research interest is design and synthesis of biologically active compounds.

Introduction

Cancer claims approximately one death per minute in the United States alone. As such, this dreaded disease has stimulated enormous efforts directed at curative and preventive strategies to combat its menacing effects on society. Chemistry and biology provide most unique platforms for addressing this problem as evidenced by the several chemotherapeutic agents discovered and developed through endeavors in these disciplines. Prominent among them are Taxol® and Taxotere™, two tubulin binding anticancer drugs[1] whose combined sales exceed the 2 billion dollar mark. As a new class of potent tubulin polymerizing and microtubule stabilizing compounds, the epothilones[2] have received a great deal of attention over the last few years from chemists, biologists and clinicians. Research activities in this area span from isolation of natural products to genetic engineering of new producing organisms for fermentation purposes, from total synthesis to chemical synthesis of designed analogues, and from chemical biology to clinical studies. Despite the several reviews[3–6] covering the great strides made in the epothilone area, the fast pace of research surrounding these molecules necessitates this update which aims at summarizing and placing in perspective the latest developments in the field.

Recent total syntheses of epothilones and analogues thereof

Many groups have reported the total or partial syntheses of epothilone family members (Fig. 1) during the past years, and

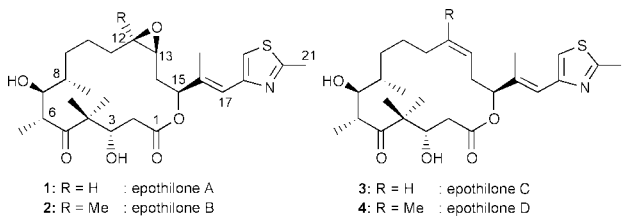

Fig. 1 The epothilones.

this subject has been extensively reviewed.[3–6] Within this section we will highlight the most recent developments with particular emphasis on the new generation total syntheses in the field of epothilones and analogues thereof.

Although we had previously reported two different total synthesis strategies leading to epothilones and a large number of

analogues,[3] there was still room for improvements, particularly with regards to the stereoselectivity at some key points. Through our most recent work, these deficiencies have now been corrected, for the most part, so that a highly efficient, stereoselective, and flexible approach towards the epothilones has been established. Our general strategy is outlined retrosynthetically in Scheme 1. Key improvements include the introduction of the C12–C13 epoxide *via* a Sharpless asymmetric epoxidation directed by a C26 hydroxy group, and a highly efficient and reproducible protocol for the aldol coupling which creates the C6–C7 bond and simultaneously sets the stereochemistry at these centers with > 10 : 1 diastereoselectivity. A high degree of convergence was achieved, as the synthesis proceeds through the union of three fragments (**6**–**8**) of similar size and complexity, to afford the advanced intermediate **5**. This vinyl iodide (**5**) had already been proved to be highly versatile, as it allowed the synthesis of a large number of epothilones with aromatic side chains through our Stille coupling methodology,[7,8] and, in addition, enabled the synthesis of various C26-modified analogues.[7a]

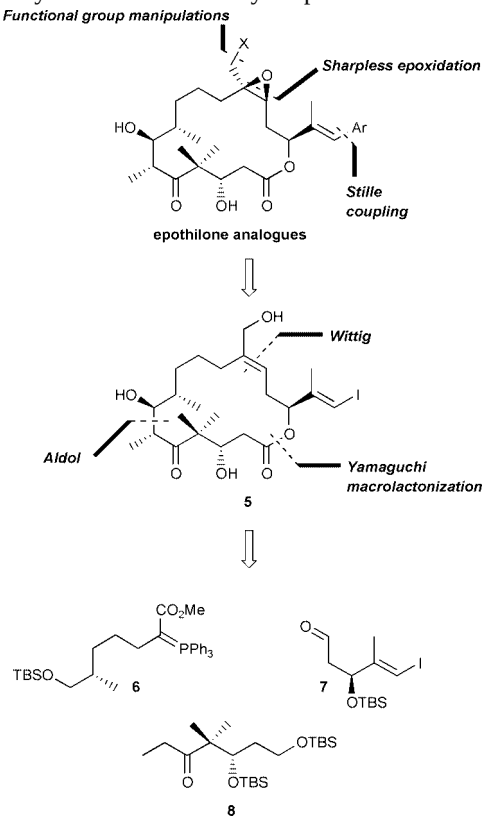

Scheme 1 Nicolaou's retrosynthetic analysis of epothilones.

The synthesis of vinyl iodide **5**[7b] is summarized in Scheme 2. Starting from the commercially available bromoalcohol **9** (optically active), protection and conversion to the iodide **10** was followed by an alkylation with but-4-enylmagnesium bromide to yield terminal olefin **11**. Through standard methodology, this was converted to the ylide **6**, which participated in a Wittig coupling with iodoaldehyde **7** to yield fragment **15**, which corresponds to the C7–C17 region of the epothilones. Functional group manipulations furnished aldehyde **19** in short order. When this derivative was subjected to our optimized aldol coupling protocol (enolate generation at −78 °C, then −40 °C for 1 h, then rapid addition of aldehyde at −78 °C followed by rapid quenching after 5 min with HOAc in THF)[7b,9] with ketone **8**,[10] a 74% yield of the desired aldol diastereomer **20** was realized. Moreover, the diastereoselectivity before purification was better than 10 : 1. With all the carbon atoms in place in **20**, straight-forward functional group manipulations and a Yamaguchi macrolactonization[10] afforded the desired vinyl iodide **5**.

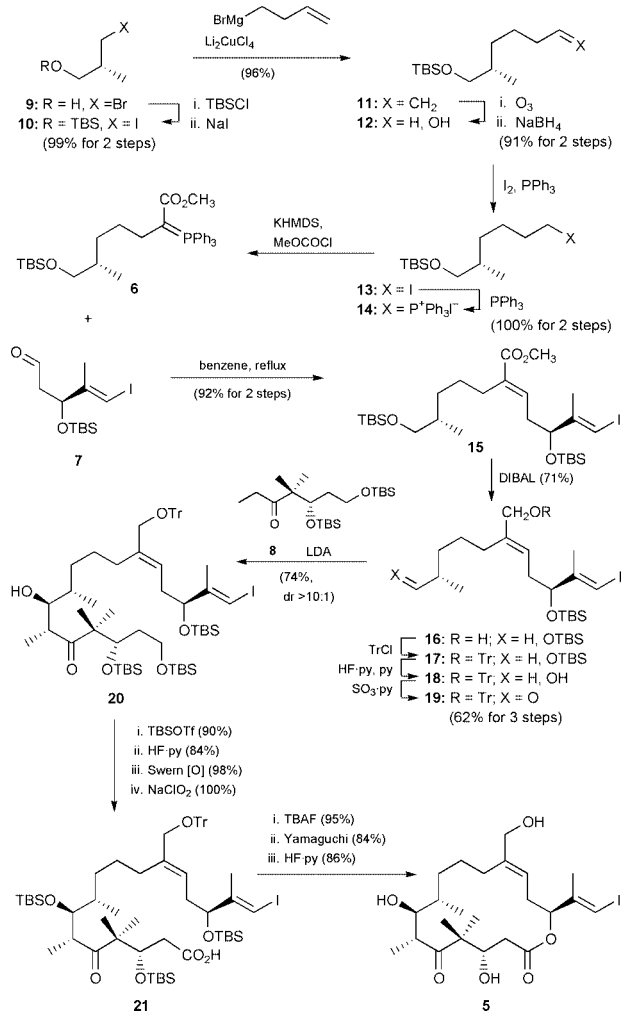

Scheme 2 Nicolaou's synthesis of the advanced intermediate **5**.

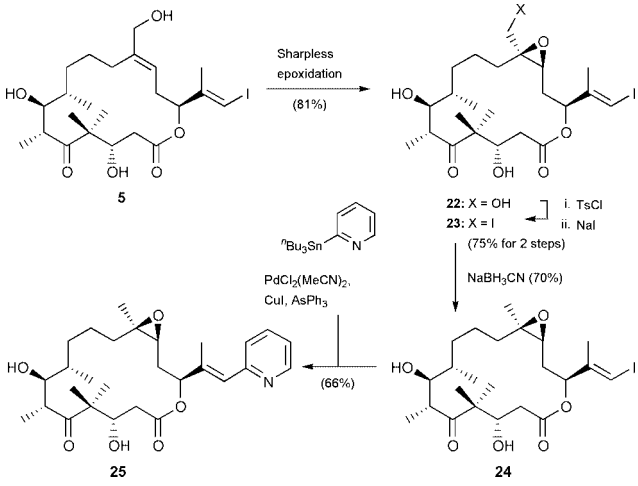

Scheme 3 Nicolaou's synthesis of side chain-modified analogues.

The vinyl iodide **5** was converted into the epothilone B precursor **24** by a Sharpless epoxidation, followed by a mild deoxygenation protocol (Scheme 3). This vinyl iodide (**24**) was used to construct a series of aromatic side chain-modified epothilones (see Fig. 2). Notable among them are several pyridine derivatives (**25**–**28**, Fig. 2), some of which proved to possess remarkable biological activities (*vide infra*). Using analogous chemistry, 26-fluoroepothilone B (**37**)[11] and 16-desmethylepothilone B (**38**)[7b,9] were also constructed (see Fig. 2).

In order to probe the significance of the epoxide oxygen atom, a novel class of epothilones in which the epoxide was replaced by a cyclopropyl or cyclobutyl moiety was targeted for

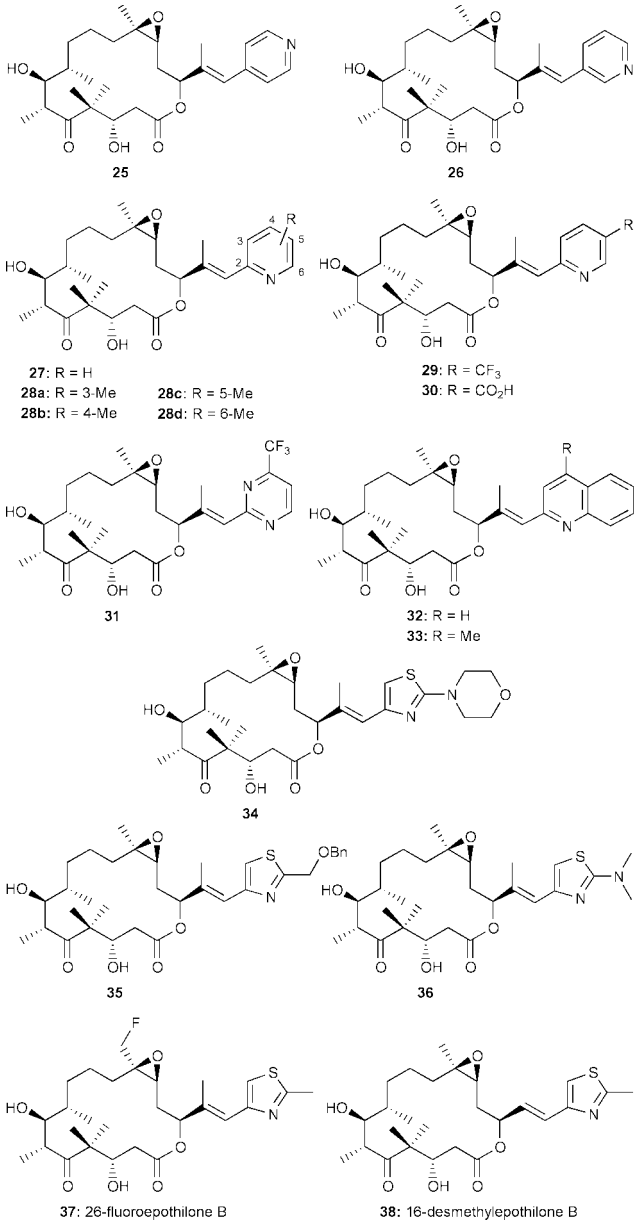

Fig. 2 Selected epothilone analogues.

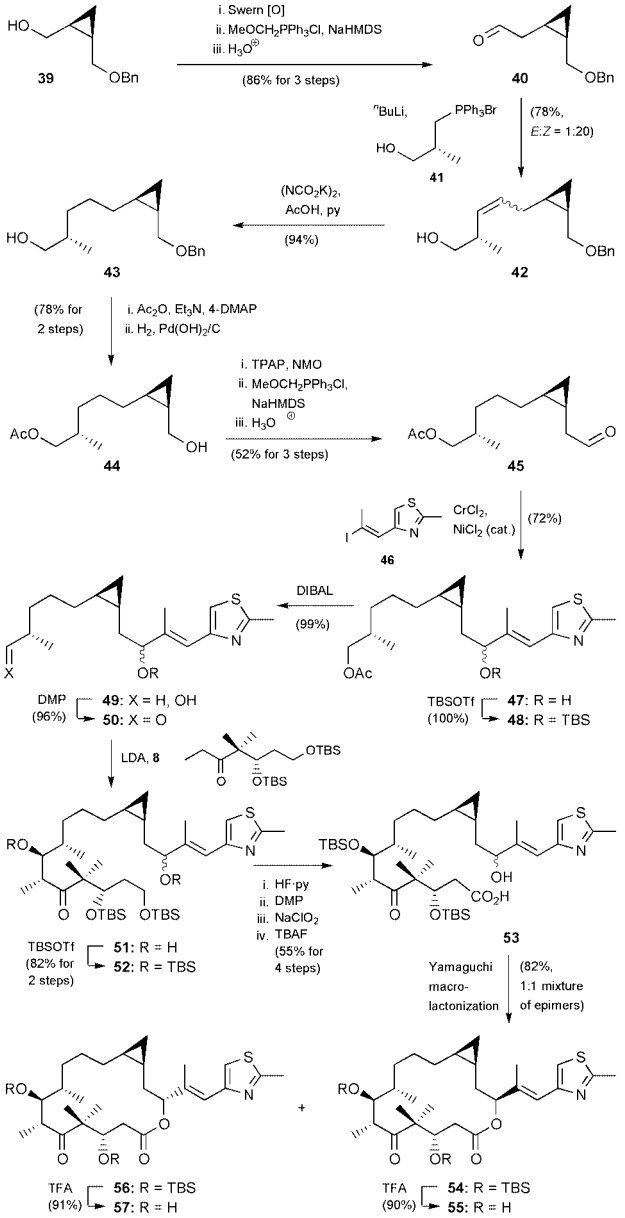

Scheme 4 Nicolaou's synthesis of cyclopropylepothilone A (**55**).

synthesis. Our original studies[12] with cyclopropyl epothilones probing this question were plagued by stereochemical ambiguities. Specifically, our original assignments[12] of the C12–C13 stereochemistries of cyclopropyl epothilones A were proven incorrect[13,14*a*] (the correct structures of these compounds are shown in Fig. 3, structures **58** and **59**). We therefore embarked on a new program directed at clarifying this issue. To this end, a new total synthesis had to be developed, which allowed for the incorporation of the requisite cycloalkyl moieties in a stereoselective manner at an early stage, in order to assure that no stereochemical ambiguity would exist in the final products.

The total synthesis of 12,13-cyclopropylepothilone A (**55**) serves to exemplify the approach to these compounds (Scheme 4).[14] This synthesis starts from the known cyclopropyl alcohol **39**, readily obtained by enantioselective Charette cyclopropanation[15] of *cis*-4-benzyloxybut-2-enol in 94% ee. Homologation and Wittig olefination with the commercially available chiral phosphonium bromide **41** afforded alkene **42**, predominantly as the *cis* isomer. Diimide reduction followed by hydrogenolysis of the benzyl ether and a second homologation yielded aldehyde **45**. At this point, a Nozaki-Kishi coupling with vinyl iodide **46**[14] afforded a 1:1 mixture of C15 epimers of the C7–C21 fragment **47**. Standard manipulations afforded aldehyde **50**, which smoothly underwent aldol coupling with ketone **8** to yield open-chain derivative **52** as a single diastereomer after TBS protection of the secondary alcohol. The same sequence of operations, *i.e.* protecting group manipulations, oxidation at C1 and Yamaguchi macrolactonization, as was described in Scheme 2, was then applied to complete the synthesis. After macrolactonization, the C15 epimers were separated and individually desilylated to afford the desired *cis*-12,13-cyclopropylepothilones **55** and **57**. This synthetic route also allowed the preparation of several other cycloalkylepothilone derivatives (**60**–**67**, Fig. 3) of various stereochemistries.[14*b*]

The Danishefsky group has made major contributions in the epothilone field, not only with regards to their total synthesis and their analogues, but also by extensive *in vitro* and *in vivo* studies.[4] A recent development from this camp is a new and highly efficient synthesis of epothilone D (**4**, Schemes 5 and 6),[16] and a closely related total synthesis of 12,13-desoxyepothilone F (**90**, Scheme 7),[17] which promise to secure sufficient quantities of these interesting compounds for ongoing biological and clinical investigations.

Danishefsky's 'new-generation synthesis' of epothilone D (**4**) is summarized in Scheme 6.[16,18] This new venture into the epothilone class features a newly developed *anti*-Felkin–Ahn selective aldol coupling of the (*Z*)-lithium enolate of **72**, an

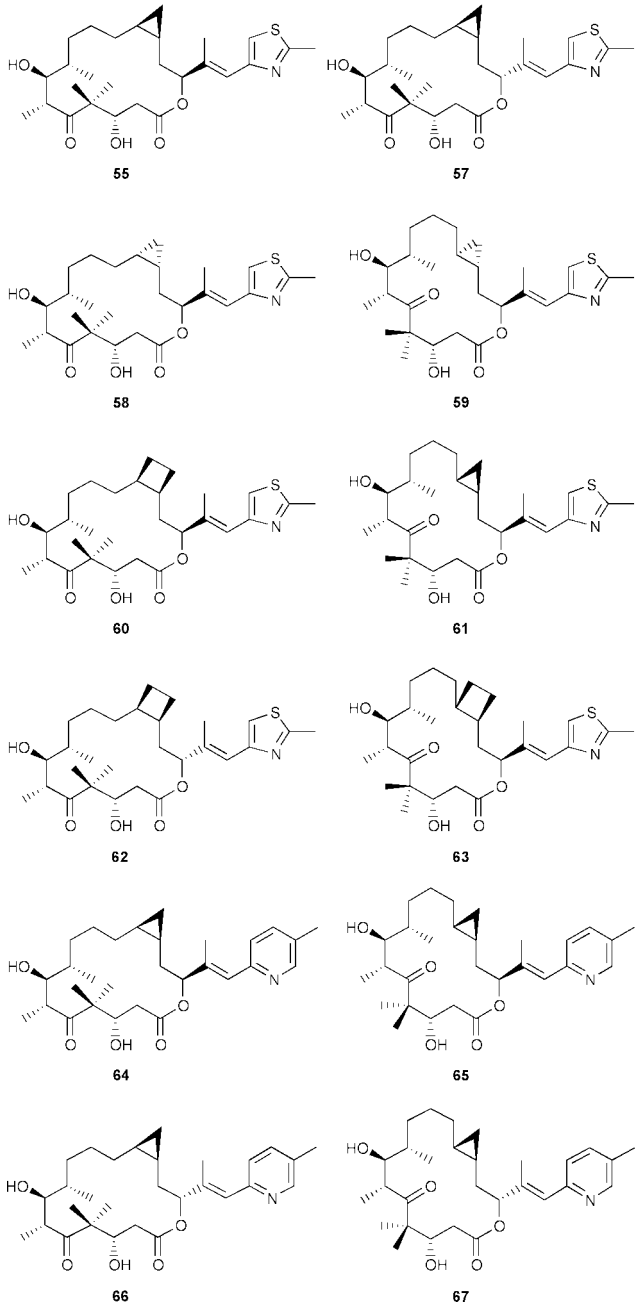

Fig. 3 Cyclopropyl and cyclobutylepothilones.

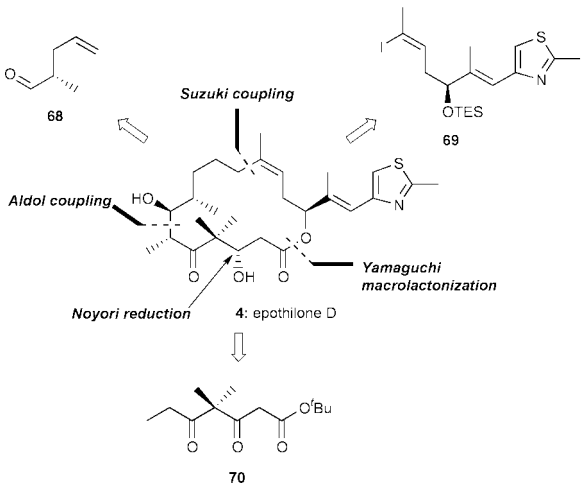

Scheme 5 Danishefsky's new retrosynthetic analysis of epothilones.

alkylborane Suzuki coupling of advanced intermediates **75** and **69**, and a stereoselective Noyori reduction of the C3 carbonyl group at a late stage of the synthesis. To this end, the requisite aldol coupling precursor **72** was assembled from the known β-ketoester **71** in two steps, and the chiral aldehyde **68** was derived from isoprene *via* asymmetric epoxidation. After extensive experimentation, good diastereoselectivity, 5–6 : 1 with the *syn*-(C6,C7)/*anti*-(C7,C8) compound **73** as the major isomer, was achieved in the aldol coupling between **68** and **72**. This outcome was rationalized by postulating neighboring-group participation by the olefinic moiety of **68**. Straightforward manipulations converted aldol **73** into olefin **75**. The vinyl iodide **69**, derived from propyne (**76**) *via* vinyl iodide **77** by an efficient protocol,[18] was joined with alkene **75** *via* the alkylborane Suzuki coupling, which proceeded smoothly to afford the open-chain ester **82**. After deprotection leading to alcohol **83**, the crucial Noyori reduction afforded the C3 alcohol **85** in > 95 : 5 diastereoselectivity, and in 82–88% yield. Protecting group manipulations and Yamaguchi macrolactonization, followed by global deprotection, finally afforded the desired epothilone D (**4**). By closely analogous routes, see Scheme 7, the Danishefsky group also prepared 12,13-deoxyepothilone F (**90**),[17] aza-epothilone D (**93**)[19] (both C15 epimers of **93** were prepared), and aza-epothilone B (**94**),[19b] the latter of which had previously been synthesized and shown to be very promising by the Bristol-Myers Squibb company (BMS), *vide infra*.

Using their reactive immunization technology,[20] the Lerner–Sinha group set out to devise a new synthesis of epothilones, where key intermediates would be generated by aldolase-like antibody catalysts. These efforts culminated in the syntheses of epothilones A–F,[21–23] as shown in Scheme 8. Thus, monoclonal antibodies, generated by reactive immunization against a β-diketone hapten, were used to prepare enantiomerically enriched key intermediates for epothilone A synthesis, either by kinetic resolution of racemic substrates through a retro-aldol reaction, or by enantioselective aldol reactions with prochiral substrates. The so obtained building blocks were elaborated to the target molecules, epothilones A–F. Remarkably, in their most recent work,[22,23] these authors report aldolase-type antibodies capable of resolving racemic aldols with 95–99% ee at 50% conversion, and with as little as 0.003 mol % of the antibody catalyst.

The C15 stereocenter of epothilones is arguably one of the most challenging to install, and many different solutions to this problem have been reported. In their first-generation synthesis,[21] the Lerner–Sinha group used their 38C2 antibody to catalyze the addition of acetone to aldehyde **95** (see Scheme 8a). At 51% conversion, an ee of 75% for **96** was realized for this tranformation. Using a new hapten, more efficient aldolase antibodies were raised, which allowed a retro-aldol kinetic resolution of (±)-**96**, affording **96** in > 97% ee and 45% isolated yield.[22,23] Moreover, the aldehyde **95** could be recovered and recycled back to (±)-**96**. Furthermore, it was possible to generate a host of closely related thiazoles, including **97**, which was subsequently elaborated into epothilone E. The team's total synthesis of epothilones started with a retro-aldol kinetic resolution of (±)-**98** to afford (–)-**98** in 98% ee. This operation set the stereocenters at C6 and C7 of epothilones. Hydrogenation afforded a 1:1 mixture of C8 epimers (**99**), and the desired epimer **99b** was taken on to the aldols **101a** and **101b**, obtained as a 1:2 mixture of diastereomers favoring the desired isomer **101b**. Further standard manipulations afforded acid **102**, which was esterified with alcohol **104**, obtained from **96** *via* a seven-step sequence. Ring-closing metathesis and deprotection afforded epothilone C (**3**) which was epoxidized to epothilone A (**1**) using a sequence of steps analogous to those previously reported in related works.[3–5] The Lerner-Sinha group also reported a related synthesis of epothilones A (**1**) and C (**3**)[21] *via* the macrolactonization approach,[10] as well as syntheses of epothilones B (**2**), D (**4**), E (**184** in Scheme 16) and F (**185** in Scheme 16).[21–23]

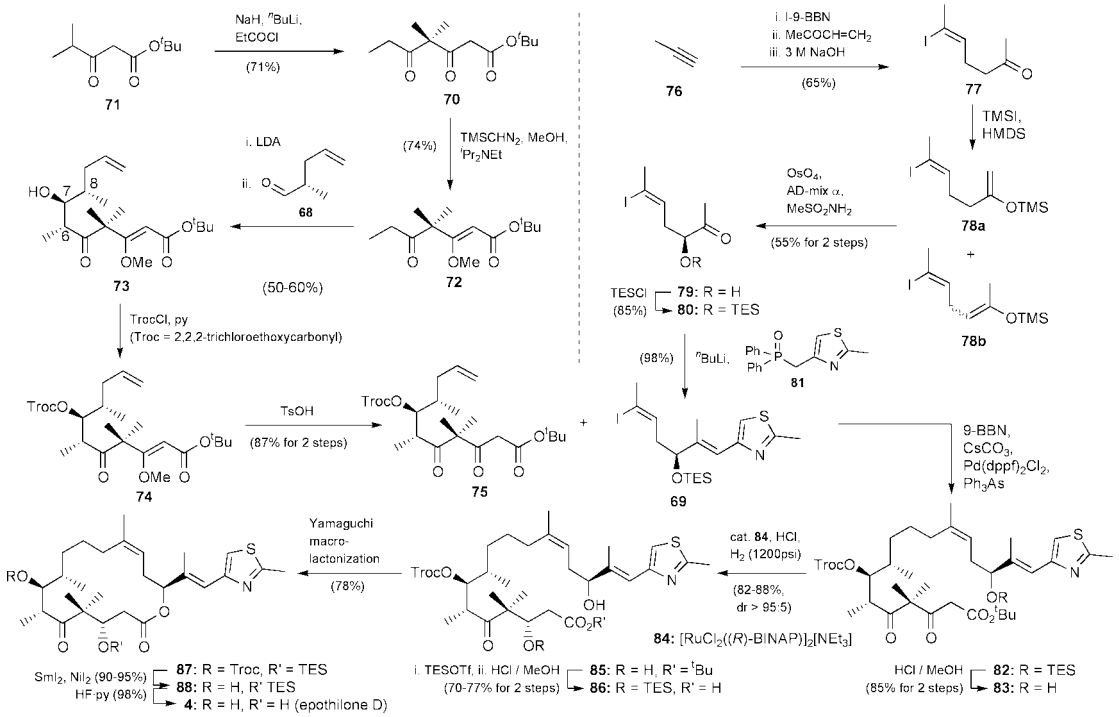

Scheme 6 Danishefsky's synthesis of epothilone D (**4**).

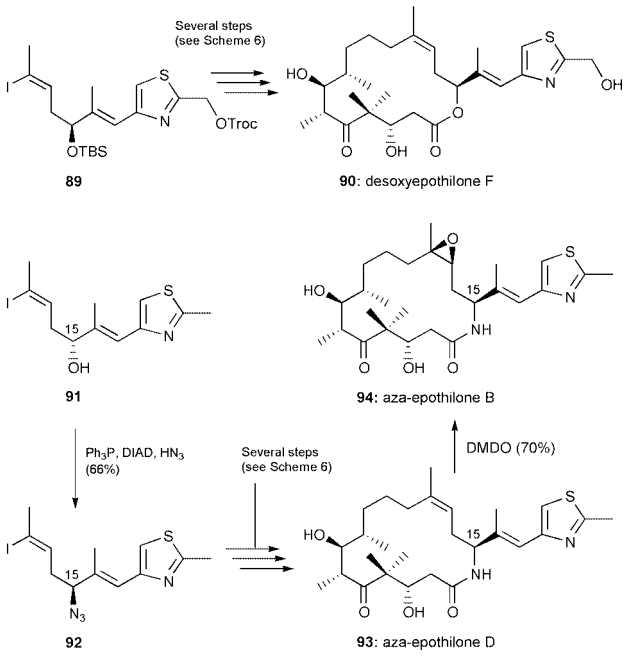

Scheme 7 Danishefsky's synthesis of selected epothilone analogues.

The Shibasaki group's syntheses of epothilones A and B addressed the stereochemical challenges posed by these target molecules by employing their recently developed Lewis acid–Lewis base bifunctional asymmetric polyheterometallic catalysts for cyanosilylation, aldol coupling and asymmetric protonation.[24,25] Thus, in their preparation of the C12–C21 fragment **111** (see Scheme 9), a catalytic asymmetric cyanosilylation using a bis(phosphine oxide)binaphthol–aluminum complex (**106**) as a chiral Lewis acid–Lewis base catalyst was successfully applied to the α,β-unsaturated aldehyde **105** to furnish, after acidic workup, the corresponding chiral cyanohydrin **107** in 97% yield and 99% ee. Straight-forward manipulations, including homologation, Wittig olefination and iodination, afforded the desired vinyl iodide **111**.

Two other multifunctional asymmetric catalysts, previously developed by the Shibasaki group, were applied to the preparation of the C1–C11 fragment **120** (see Scheme 10). In the first-generation approach,[24] the oxime ether epoxide **114** was constructed by a short sequence of steps from diol **112** using standard methodology. A cyanocuprate-based addition of a methyl group to **114** yielded the racemic *anti*-aldol **115**, by a process representing a new general approach to *anti*-aldols. Reductive cleavage of the O–N bond followed by regioselective alkylation of the resulting ketone furnished ketone **116**. The latter compound was reduced with good diastereoselectivity, and the resulting 1,3-diol was subjected to acetonide formation and other manipulations, ultimately leading to racemic aldehyde **118**. At this point, resolution by enantioselective aldol addition of acetophenone, catalyzed by the heteropolymetallic catalyst (*R*)-$LaLi_3$tris(binaphthoxide), afforded the desired aldol **119a** in 30% yield and 89% ee, together with its diastereomer **119b** (29%, 88% ee), which could be removed chromatographically. Standard transformations eventually afforded the desired fragment **120**. Noting the low efficiency of their resolution-based scheme, the Shibasaki group proceeded to develop a second generation synthesis,[25] starting with a catalytic asymmetric protonation of the enolate of thioester **121** (Scheme 10b). In the event, treatment of **121** with 5 mol % of $SmNa_3$tris(binaphthoxide) in the presence of 4-*tert*-butylthiophenol afforded the Michael adduct **122** in 92% yield and 88% ee. This intermediate was then elaborated into aldehyde **123**, which smoothly underwent an aldol coupling with the required ketone **124** to afford aldol **125** (dr = 4:1). Standard chemistry finally furnished the advanced intermediate **120** *via* **126**. The total synthesis of epothilone B (**2**) was completed by the joining of fragments **111** and **120** through a Suzuki coupling, macrolactonization and protecting group removal. The Shibasaki group also completed the synthesis of epothilone A (**1**) using closely related chemistry.[25]

Although several of the reported epothilone syntheses form the macrocycle by ring-closing metathesis, poor *E/Z* selectivities are generally observed.[3–5] To circumvent this problem, the Kalesse group's formal total synthesis[26] of epothilone A (**1**) employed the metathesis ring closure to form a smaller, 10-membered lactone, which would be expected to favor the *Z* geometry on the basis of lower ring strain as opposed to the *E* arrangement. To this end (see Scheme 11), chiral aldehyde **127** was allylated and the product was esterified with hept-6-enoic acid to afford the cyclization precursor **129**. Ring-closing

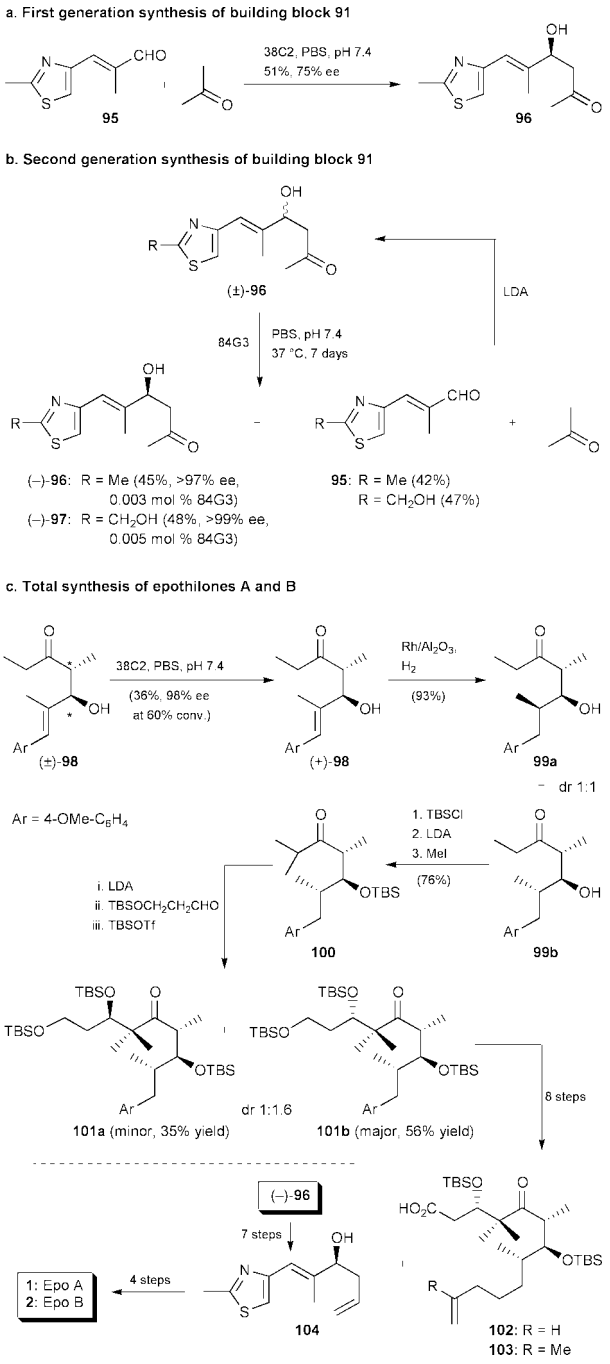

Scheme 8 Lerner–Sinha's synthesis of epothilones A (**1**) and B (**2**).

metathesis of this diene system yielded 63% of the desired lactone **130**, with an *E*:*Z* ratio of 1 : 12; and furthermore, the *E* isomer could be separated and recycled, in 60% yield, to afford additional amounts of the desired *Z* lactone (*Z*)-**130** (see Scheme 11). Alkylation of the lactone enolate derived from (*Z*)-**130** with methyl iodide then afforded methylated lactone **131** (as a single diastereomer), the configuration of which was confirmed by independent synthesis using Evans' oxazilidinone technology. Elaboration of this intermediate (**131**), including installation of the thiazole side chain, ultimately yielded the aldehyde **136**. Since this aldehyde had previously been converted to epothilone A (**1**) by Nicolaou *et al.*[10] *via* coupling to ketoacid **137**, the formal total synthesis was complete. The Kalesse group also reported an independent synthesis of carboxylic acid **137**.[26]

The Panek group's synthesis of epothilone A (see Scheme 12) utilizes a lipase resolution to establish the stereochemistry at C15 of key fragment **111**, a Suzuki coupling between **111** and olefin **138** to form the C11–C12 carbon–carbon bond, a

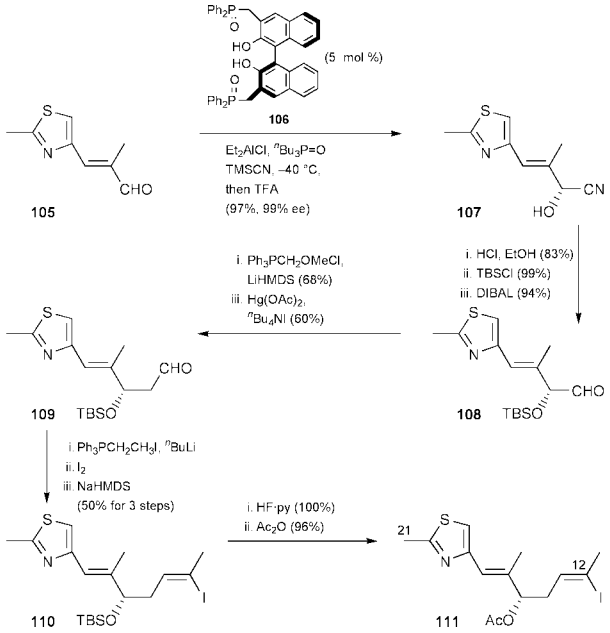

Scheme 9 Shibasaki's synthesis of vinyl iodide **111**.

Mukaiyama–type aldol coupling with **139** to construct the C2–C3 bond, and finally Yamaguchi macrolactonization and epoxidation.[27]

The Carreira group's synthesis of epothilones A (**1**) and B (**2**) features a unique nitrile oxide cycloaddition approach to the solution of the stereochemical problems at C12, C13 and C15 (see Scheme 13).[28] The highly diastereoselective cycloaddition of allylic alcohol **141** or **143** and nitrile oxide **145**, generated from phosphonate **140**, gave a single isoxazoline diastereomer (**142** and **146**, respectively), thus creating the C14–C15 bond while simultaneously establishing the correct stereochemistry at C12 and C13. A Horner–Emmons olefination with aldehyde **147** next installed the side chain, while reduction of the isoxazoline moiety of the resulting compound **148** yielded diol **149** stereoselectively. This intermediate was then conveniently converted to the key epoxide **150** *via* 1,3-cyclic sulfite formation and TBAF-mediated C12 desilylation. The latter compound (**150**) was then elaborated into epothilone A (**1**) following Mulzer's general strategy.[5] In a similar manner, the isoxazoline **142** was employed to synthesize epothilone B (**2**).

The Fürstner group's total synthesis of epothilone C (**3**), and formal total synthesis of epothilone A (**1**), features a novel ring-closing alkyne metathesis reaction as the key step (see Scheme 14).[29] The C1–C6 fragment **154** was prepared from ketone **151** through a Noyori asymmetric hydrogenation, protection and Grignard addition of an ethyl group to ester **153**. An aldol coupling was then employed to join the ketone **154** with the aldehyde **155** in a stereoselective manner to yield intermediate **156**. Straight-forward manipulations yielded carboxylic acid **157**, which was esterified with the side chain alcohol **158**, derived from the aldehyde **95** *via* a Brown asymmetric allylboration. The so obtained cyclisation precursor **159** was treated with 10 mol % of the metathesis catalyst **161** to afford the desired macrocycle **160**. Lindlar reduction and deprotection finally afforded the desired epothilone C (**3**).

An ongoing research program at Novartis Pharma AG, led by Altmann, has resulted in a number of highly potent epothilone derivatives.[30,31] Thus, following a convergent route, several heterocyclic epothilone derivatives were prepared (see Scheme 15).[31] The required C1–C11 fragment **165** was reached by a short sequence of steps from **162** and **163**. This olefin was coupled to a series of vinyl iodides (**169**), which were synthesized using the Oppolzer sultam aldol reaction starting with sultam **166** and aldehyde **167**. Stille coupling of **169** with **165** followed by straight-forward manipulations and macro-

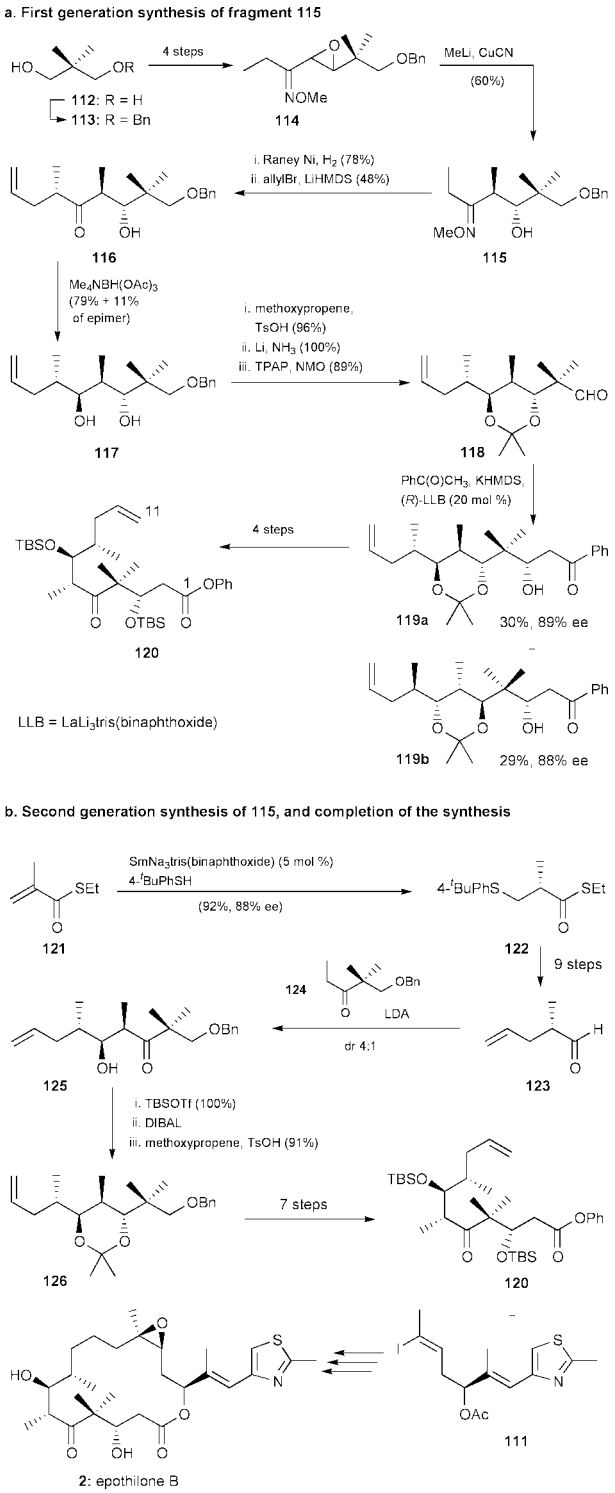

Scheme 10 Shibasaki's synthesis of epothilone B (**2**).

cyclization yielded the epothilone D derivatives **170**–**173**. Epoxidation of the latter compounds afforded epothilone B analogues **174**–**177**. Using similar methodology, a number of C12–C13 modified epothilones were also prepared.[30]

Many other groups, in particular those of Grieco,[32] Schinzer,[33] Mulzer[34] and White,[35] also made significant contributions to the epothilone field, and these efforts have been reviewed recently.[3,5] The Schinzer group, together with Altmann's group at Novartis, also reported a total synthesis of two 'aza-epothilone C' derivatives (epothilone lactams) using a ring-closing metathesis strategy.[36] An interesting biocatalytic method for the generation of intermediates for epothilone synthesis has been reported by Wong.[37]

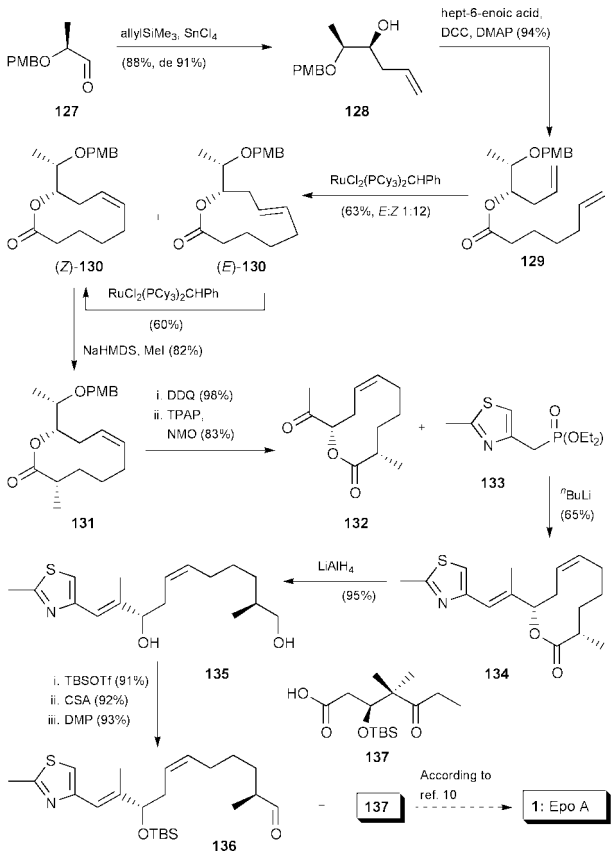

Scheme 11 Kalesse's formal synthesis of epothilone A (**1**).

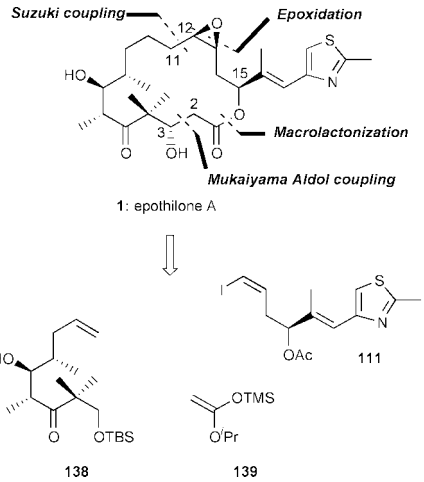

Scheme 12 Panek's retrosynthetic analysis of epothilone A (**1**).

Partial syntheses of epothilone analogues

From an industrial standpoint, and despite the progress outlined above, fermentation followed by partial synthesis may still hold certain advantages over total synthesis. With such advantages in mind, a number of groups initiated programs directed at semisynthesis of epothilone analogues. Particularly notable are the reports from the Höfle[38] and Bristol-Myers Squibb[13,39] groups.

Thus, several interesting epothilone tranformations have been carried out by Höfle (see Scheme 16).[38] Ozonolysis and silylation of epothilone A (**1**) or B (**2**) afforded the versatile methyl ketone **178** (R = H, Me). Although Wittig-type reactions with this substrate were largely unsuccessful, probably due to enolization of the methyl ketone, aldol condensations with aromatic aldehydes produced the side chain modified epothilones **179**, none of which, however, exhibited any tubulin polymerization activity or cytotoxicity. Alternatively, ketone **178** could be converted into the vinyl boronic acid **180** (*E*:*Z* =

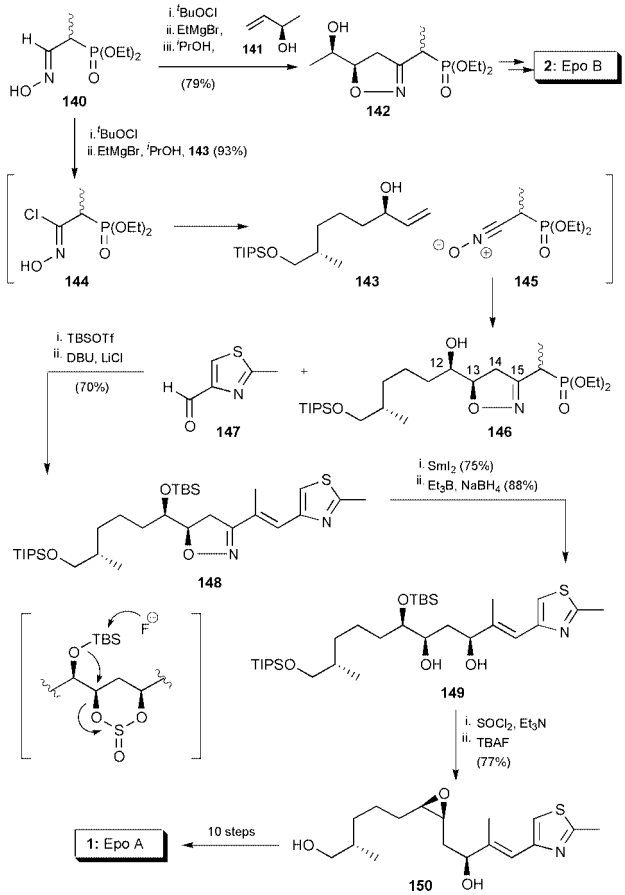

Scheme 13 Carreira's synthesis of epothilones A (**1**) and B (**2**).

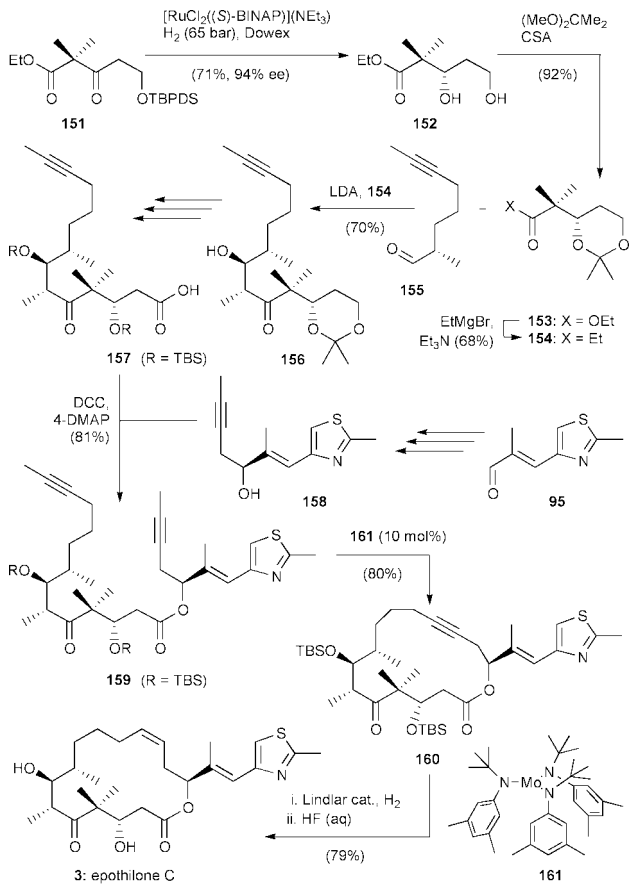

Scheme 14 Fürstner's synthesis of epothilone C (**3**).

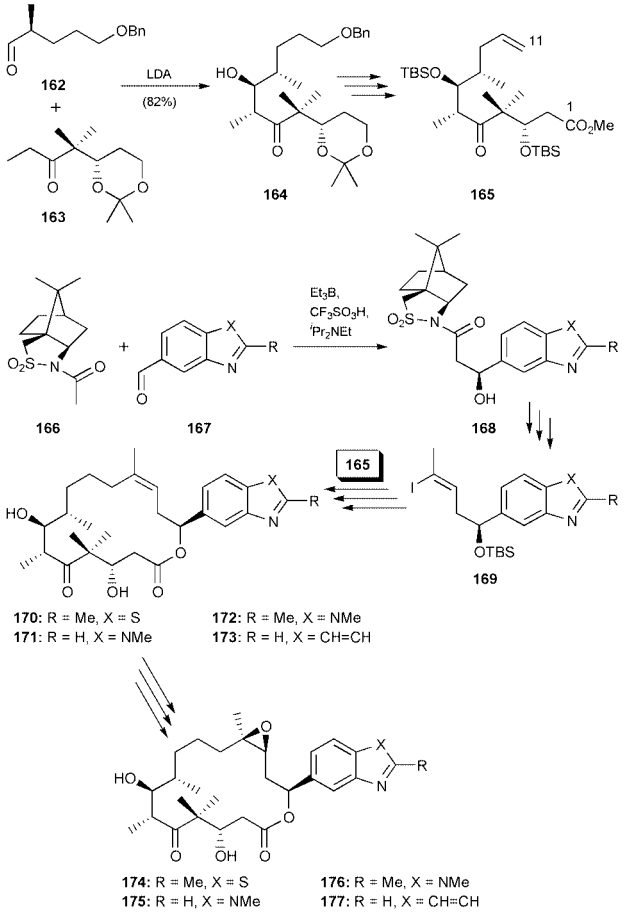

Scheme 15 Altmann's synthesis of side chain-modified analogues.

7:3), the *E* isomer of which could be transformed into vinyl iodide **181**, which bears considerable similarity to the highly versatile intermediate **24** (see Scheme 3) used by the Nicolaou group to generate a number of analogues *via* Stille coupling methodology.[3] Höfle also discovered that epothilones could be *N*-oxidized in fair yields by MCPBA. Upon acetylation, the *N*-oxides underwent a Polonovsky-type rearrangement to yield, after hydrolysis, the side chain oxidized epothilones E (**184**) and F (**185**) (see Scheme 16).[38]

A partial synthesis of a number of cyclopropylepothilones has been disclosed by a Bristol-Myers Squibb group[13] (see Scheme 17). Thus, deoxygenation protocols to convert epothilones A (**1**) and B (**2**) into the C12–C13 olefinic epothilones C (**3**) and D (**4**) were developed. Epothilone C (**3**) could be cyclopropanated in 12% yield using dibromocarbene, generated from bromoform and aqueous base under phase-transfer conditions, to form the protected derivative **186**. Dehalogenation with $^{n}Bu_3SnH$ afforded silyl ether **187** which was deprotected to yield cyclopropylepothilone A (**55**). Using similar chemistry, cyclopropylepothilones **188**, **189** and **190** were also prepared (Scheme 17).

The Bristol-Myers Squibb (BMS) group developed a very convenient three-step, one-pot procedure for the conversion of epothilones into the corresponding macrolactams (aza-epothilones)[39] (see Scheme 17). To this end, treatment of epothilone B (**1**) with $Pd(PPh_3)_4$ in the presence of NaN_3 afforded the corresponding azide (**192**) with complete retention of stereochemistry at C15. Reduction of this azide with PMe_3 followed by macrolactamization afforded aza-epothilone B (**94**, BMS-247550) in moderate yield, and without the need to isolate any intermediates.

Chemical biology of epothilones

Biological evaluation

As more and more experimental data have accumulated, a fairly good understanding of what modifications to the epothilone

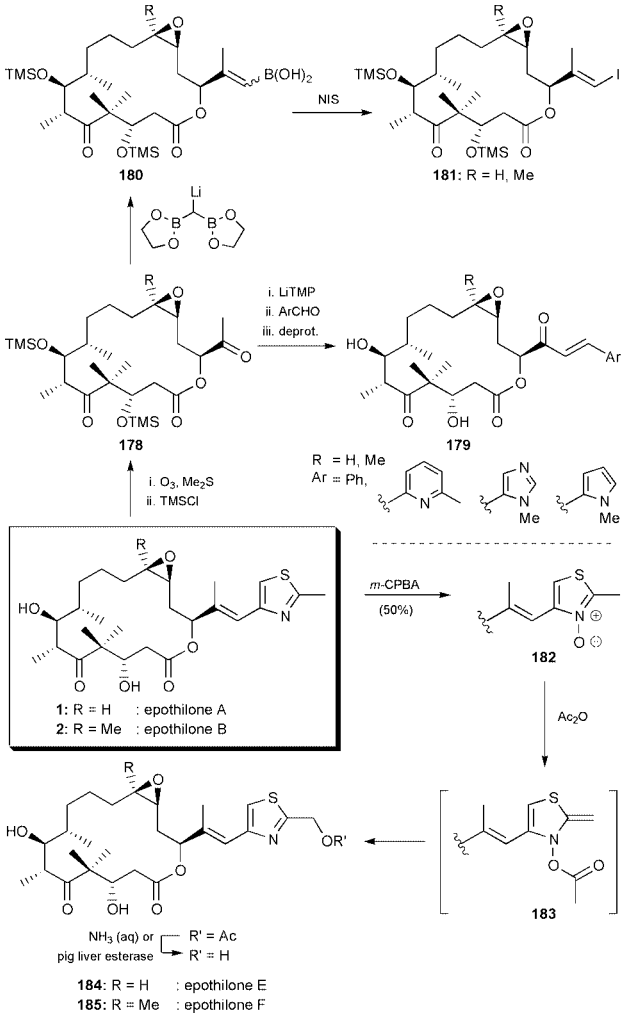

Scheme 16 Höfle's partial syntheses of side chain-modified analogues.

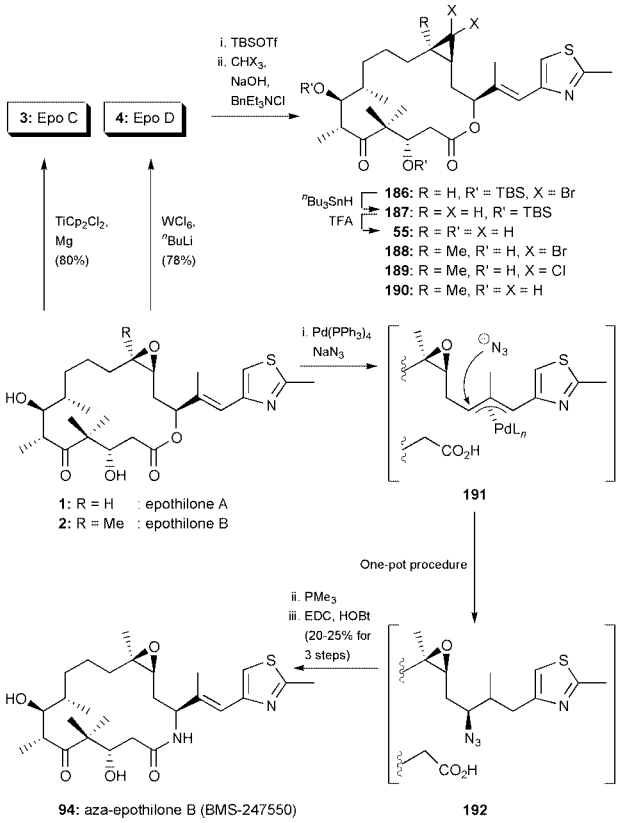

Scheme 17 BMS's partial syntheses of cyclopropyl and aza analogues.

structure might produce active analogues has developed. This section aims to survey some of the most recent progress in this area. Several excellent reviews have appeared,[3–6] and most of the data published in these works will not be repeated here.

Some difficulty in evaluating the results from different studies do arise as a result of the use of many different cell lines, and even differences in experimental protocols may lead to considerable variability between seemingly identical experiments. The *in vitro* experimental data generally fall into two categories, namely tubulin polymerization assays using purified tubulin, and cytotoxicity assays employing various cancer cell lines. Although there is generally some degree of correlation between the results from these two assays, factors such as uptake into and retention by cells obviously play a part in determining the observed effect on cell proliferation, in addition to the effects caused by the tubulin polymerization properties of a given agent. In fact, the concentrations needed to induce tubulin polymerization are two to three orders of magnitude higher than the medium concentrations which will induce cell death. This observation is rationalized by the fact that epothilones, like Taxol®, readily accumulate in cells, so that the relatively high concentrations necessary for tubulin polymerization are finally reached.[6] Because of differences in protocols and cell lines, it will be convenient to first discuss the contributions from the different research groups separately, and then compare the results in order to draw some general conclusions.

We have recently reported two new classes of epothilone analogues with potent biological activities, namely epothilones with pyridine or related side chains (Fig. 2, Table 1),[8] and derivatives of epothilone A (**1**) where the epoxide group has been replaced by a cyclopropyl or a cyclobutyl moiety (Fig. 3, Table 2).[14] A systematic substitution study[8] of pyridine epothilones where the nitrogen atom was "walked" around the ring (**25**–**27**) revealed its crucial position adjacent to the macrocycle attachment site in **27** (Fig. 2, Table 1). A second study "walked" a methyl group around the most active pyridine epothilone analogue (**27**) revealing the C4 and C5 methyl derivatives (**28b**, **28c**, Fig. 2, Table 1) as the most active. Interestingly, the latter compounds (**28b**,**c)** are more active than natural epothilone B (**2**) itself (see Table 1), and they are in fact among the most active derivatives reported to date, with IC_{50} values on the order of 10^{-10} M.

Remarkably, some of the prepared epothilone A cyclopropanes and cyclobutanes (**55**, **57**–**67**) were also active (Fig. 3, Table 1), in some cases even more active than the parent epoxide epothilone A (**1**).[14] In particular, the hybrid epothilones **64** and **65** with pyridine side chains and cyclopropyl moieties at C12–C13 (Fig. 3) were found to be highly active. On the other hand, all derivatives with the unnatural C15 (*R*) configuration (**57**, **62**, **66**, **67**, Fig. 3, Table 1) were essentially inactive. In addition, we have previously reported that *cis*- and *trans*-cyclopropyl epothilones **58** and **59** (Fig. 3, Table 1), with the configuration at C13 opposite to that of the natural series, were inactive.[12,14] From these results, it became clear that in the epothilone A series the stereochemistry at C13 and C15 is critical to the activity. Specifically, the configurations at these centers must match those of the natural compound. On the other hand, the C12 stereocenter appears to play a minor role, as both *cis*- and *trans*-cyclopropanes exhibited similar activity. Several other epothilone B derivatives with heteroaromatic side chains were also prepared (Fig. 2, Table 2; unpublished results). For example, the quinoline derivatives **32a** and **32b** retain significant activity, indicative of the fact that relatively large side chains are tolerated, as long as the basic nitrogen atom is present at the right position.

The Novartis group has also made major contributions to the field, and an excellent review on the biology of epothilones reporting up to the end of 1999 has been published by Altmann.[6] Notable among the many analogues reported by the Novartis group are a series of bicyclic aromatic side chain analogues of epothilones D (**170**–**173**) and B (**174**–**177**) where the aromatic moiety replaces the C16–C17 double bond in the native

Table 1 Induction of tubulin polymerization[a] and cytotoxicity[b] towards human cancer cell lines of selected epothilone analogues from the Nicolaou group and Novartis

Cpd.	% TP	KB-31	KB-8511	1A9	A8	PTX10	PTX22	Ref.
2	85	0.18	0.18	0.2	5.4	0.6	0.2	8
25	35	11.8	34.7	5.75	38	180	25	8
26	42	4.32	16.5	1.7	23	35	8	8
27	80	0.30	0.3	0.1	3	1	0.15	8
28a	12	39.3	50.5	> 300	> 300	> 300	> 300	8
28b	90	0.16	0.16	0.1	2.5	0.36	0.1	8
28c	89	0.11	0.1	0.15	1.5	0.6	0.15	8
28d	30	9.05	10.6	9	180	72	18	8
37	93	*nd*	*nd*	0.2	*nd*	0.4	0.2	3
1	69[c]	2.15[c]	1.91[c]	2.37	117	23.4	5.21	14*b*
2	90[c]	0.19[c]	0.18[c]	0.095	2.14	0.55	0.16	14*b*
Txl	49[c]	2.92[c]	626[c]	1.77	18.0	52.8	28.5	14*b*
55	83	0.84	0.41	1.60	23.4	10.9	2.6	14*b*
57	26	160	66.7	> 300	> 300	> 300	> 300	14*b*
58	2	*nd*	*nd*	> 100	*nd*	> 100	> 100	12
59	2	*nd*	*nd*	> 100	*nd*	> 100	> 100	12
60	79	60.7	29.7	8.8	196	62	20	14*b*
61	29	378	156	> 300	> 300	> 300	*nd*	14*b*
62	100	0.97	0.64	2.7	48	14.4	3.7	14*b*
63	82	23.1	11.5	25.5	> 300	146	63	14*b*
64	100	0.62	0.45	1.40	53.5	8.15	1.17	14*b*
65	94	0.84	0.68	0.63	9.5	3.49	0.39	14*b*
66	6	> 10^3	> 10^3	> 300	> 300	> 300	> 300	14*b*
67	< 10	930	> 10^3	> 300	> 300	> 300	> 300	14*b*

Abbreviations: Cpd. = compound, *nd* = not determined, Txl = Taxol®. [a] %TP = percent tubulin polymerized after incubation of tubulin with a known concentration of compound (typically 3 μM). [b] Cytotoxicity (nM) towards human cancer cell lines. KB-31: epidermoid Taxol®-sensitive, KB-8511: epidermoid Taxol®-resistant (due to P-gp overexpression), 1A9: ovarian Taxol® sensitive, A8: ovarian epothilone-resistant (due to β-tubulin mutations), PTX10 and PTX22: ovarian Taxol®-resistant (due to β-tubulin mutations). [c] Data from ref. 31.

Table 2 Induction of tubulin polymerization[a] and cytotoxicity[b] towards human epidermoid cancer cell lines of selected epothilone analogues from the Nicolaou group and Novartis

Compound	% TP	KB-31	KB-8511	Ref.
1: EpoA	69	2.15	1.91	31
2: EpoB	90	0.19	0.18	31
4: EpoD	83	2.70	1.44	31
Taxol®	49	2.92	626	31
29	77	32	31	[c]
30	49	184	351	[c]
31	70	25	25	[c]
32	78	0.58	0.47	[c]
33	80	0.49	0.37	[c]
34	75	123	302	[c]
35	74	64	132	[c]
36	82	38	41	[c]
38	84	0.45	0.53	[c]
170	76	0.45	0.23	31
171	86	0.46	0.91	31
172	94	0.21	0.73	31
173	90	0.59	0.38	31
174	83	0.13	0.09	31
175	97	0.13	0.46	31
176	99	0.14	0.38	31
177	78	0.11	0.10	31

[a] %TP = percent tubulin polymerized after incubation of tubulin with a known concentration of compound (typically 3 μM). [b] Cytotxicity (nM) towards human cancer cell lines. KB-31: epidermoid Taxol®-sensitive, KB-8511: epidermoid Taxol®-resistant (due to P-gp overexpression). [c] Unpublished results.

epothilones, while retaining the overall shape and, most importantly, the position of the crucial nitrogen atom (see Scheme 15).[31] These compounds are also among the most active analogues reported to date (see Table 2), and they are indeed of comparable activity to our pyridine analogues **28b** and **28c** (*vide supra*).

The BMS group has reported an interesting, one-pot transformation which converts epothilones into their potentially more metabolically stable lactam congeners (*vide supra*).[39] While most of these lactams were found to be significantly less active than their parent lactones,[19,36,39] one compound, 'aza-epothilone B' (**94**: BMS-247550), with good activity was selected as a drug candidate and is currently in clinical trials (see Table 3).[39] The BMS group also reported the partial synthesis of cyclopropyl epothilones A (**55**) and B (**190**) and their potent biological activities (see Table 3).[13]

Table 3 Induction of tubulin polymerization[a] and cytotxicity towards human colon carcinoma cells of selected epothilone analogues from BMS

Compound	Tubulin $EC_{0.01}$ (μM)	HCT-116 IC_{50} (nM)	Ref.
1: EpoA	2.0	4.4	13
2: EpoB	1.8	0.8	13
Taxol®	4.6	2.3	13
3: EpoC	3.9	63	13
4: EpoD	0.6	6.0	13
55: cpEpoA	1.4	1.4	13
188: Br_2cpEpoB	1.6	3.8	13
189: Cl_2cpEpoB	1.7	1.9	13
190: cpEpoB	2.1	0.7	13
1: EpoA	2.3	3.2	39
2: EpoB	1.4	0.42	39
Taxol®	5.0	2.3	39
184: EpoE	17	6.0	39
185: EpoF	1.8	0.77	39
94: azaEpoB	3.8	3.6	39

[a] Tubulin $EC_{0.01}$ (effective concentration) is defined as the interpolated concentration of compound capable of inducing an initial slope of 0.01 OD min^{-1} rate of polymerization.

The Danishefsky group has pursued an extensive synthesis and screening program, which led to a number of interesting results.[4] These authors reported that initial animal studies using the highly potent epothilone B (**2**) were plagued by the high toxicity of this compound. Specifically, it was difficult to achieve high enough doses to effect tumor regression in mice with human tumor xenografts without simultaneously causing lethal toxicity. This led the group to propose epothilone D (**4**), and later desoxyepothilone F (**90**),[17] as more viable drug candidates. Treatment efficacy of these compounds was demonstrated *in vivo*, again using mouse xenograft models.[17,40] The potency of these epothilones is about one order of

magnitude less than that of epothilone B (**2**), but this is apparently more than compensated for by their much lower toxicities to the animals used. Table 4 summarizes the observed

Table 4 Cytotoxicity[a] towards human leukemia cell lines of selected epothilone analogues from the Danishefsky group

Compound	CCRF-CEM	CCRF-CEM/VBL_{100}	CCRF-CEM/VM_1	CCRF-CEM/Taxol®	Ref.
1: EpoA	3.0	200	*nd*	*nd*	17
2: EpoB	0.2	1.0	*nd*	*nd*	17
Taxol®	2.1	4140	6.6	120	17
3: EpoC	22	12	*nd*	*nd*	17
4: EpoD	9.5	17	14	16	17
90: dEpoF	2.7	47	4.9	5.3	17
93: azaEpoD	27.8	997	*nd*	791	19*b*
94: azaEpoB	2.1	2990	39	171	19*b*

Abbreviations: *nd* = not determined. [a] Cytotxicity (nM) towards human T-cell acute lymphoblastic leukemia cell lines. CCRF-CEM: parental cell line, CCRF-CEM/VBL_{100}: vinblastin resisistant, multidrug-resistant (due to P-gp overexpression), CCRF-CEM/VM_1: teniposide-resistant (due to mutated topoisomerase II), CCRF-CEM/Taxol®: Taxol®-resistant.

cytotoxicities for these compounds against some sensitive and multidrug-resistant human leukemia cell lines.

Structure–activity relationships

As a result of the extensive chemical synthesis–chemical biology studies of hundreds of epothilone analogues, structure–activity relationships could be established quite rapidly.[3] An electron crystallographic structure of the tubulin αβ dimer with bound Taxotere™ at 3.7 Å resolution has been disclosed, and although the resolution is too low to pinpoint the exact conformation of bound ligand, it clearly identifies its binding site.[41] The solution conformations of epothilones have been investigated by NMR methods,[42] and by purely computational techniques.[43] Several pharmacophore models have been advanced,[44–48] generally incorporating not only epothilones, but also taxoids and other tubulin binding molecules, under the assumption that they all bind to a common binding site on the tubulin dimer. This assumption was based on the similar biological effects of these various substances, the competitive and mutually exclusive binding of different compounds to tubulin, and the partial cross-resistance acquired by tubulin mutants with amino acid replacements at the proposed binding site. Although there are many differences between these studies, particularly as to the proposed binding conformations, there seems to be some level of consensus as to what features are of importance to binding (see Fig. 4).

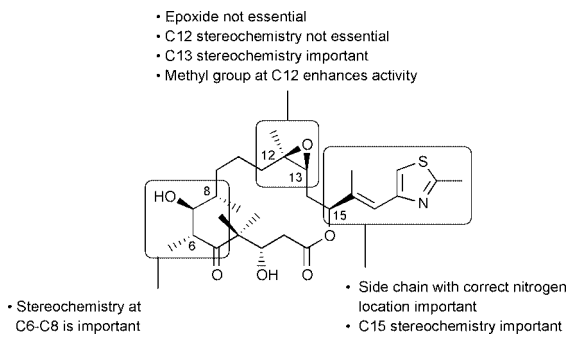

Fig. 4 Structure–activity relationships for the epothilones.

The configurations at C6–C8 are vital for the biological activity, probably because this region strongly influences the overall conformation of the macrocycle through steric and/or stereoelectronic effects.[42] There was initially some speculation that the epoxide oxygen of epothilone played a role as a hydrogen bond acceptor, but after independent reports by several groups[13,14,40*b*] it became clear that the epoxide moiety is not essential for biological activity. However, a substituent at C12, particularly a methyl group, consistently enhances the activity. Interestingly, both *cis*- and *trans*-epoxides and cyclopropanes are of comparable activity, so that as long as the configuration at C13 agrees with that of the native epothilones, the C12 stereochemistry is of relatively little importance. This is most probably due to the flexible C9–C11 trimethylene element, which allows both stereoisomers to be accomodated within the binding site. The side chain is also highly important for biological activity, with 4- or 5-methylpyridine or related derivatives being the optimum choice so far, about two-fold more active than the native 2-methylthiazole analogues.[8] Even quinoline side chains resulted in very active analogues, indicative of the fact that considerable steric bulk is tolerated in the side chain. Finally, the stereochemistry at C15 is very important, with C15 epimers being largely devoid of any biological activity.[14,19]

Biosynthesis

The biosynthetic pathway leading to the epothilones has been elucidated in some detail (Fig 5). Two independent reports, originating from Novartis[49] and KOSAN Biosciences,[50] on the gene cluster responsible for epothilone production in different *Sorangium cellulosum* strains have appeared with essentially identical results and conclusions. Both epothilones A and B are produced by the same polyketide synthase (PKS), which includes a non-ribosomal peptide synthase (NRPS) domain for the formation of the thiazole side chain from cysteine. One of the C4 gem-dimethyl groups is introduced by an (*S*)-adenosylmethionine-dependent methyltranferase domain which is also part of the PKS. It appears that the acyltransferase domain responsible for the installation of the C11–C12 fragment is rather unselective for malonyl-CoA *vs.* methylmalonyl-CoA, and can incorporate either of these units, ultimately giving rise to epothilones C and D, respectively. Both of these latter compounds are the end products of the same PKS, and the epothilones A and B are formed by post-PKS oxidation by a cytochrome P450 oxygenase, which is also part of the epothilone gene cluster. Additional biosynthetic studies have been performed by the Höfle group, and their results confirm the findings discussed above.[51,52] Using labeling techniques, it was confirmed that the epothilones are indeed synthesized from acetate and propionate units, one cysteine unit (C17–C19 of the thiazole side chain), and the methyl group of methionine (incorporated as one of the C4 methyls). It was further shown that epothilones C and D are the final products of the same PKS, and these are oxidized by a separate enzyme to epothilones A and B. Although only trace amounts of epothilones C and D are produced by the native strain of *S. cellulosum*, mutants with defects which render the oxygenase enzyme inactive have been created and shown to produce only epothilones C and D.[52] It has also been suggested that by replacing the C11–C12 acyltransferase domain with a methylmalonyl-CoA-specific one should lead to a PKS specific for epothilone D.[50] Impressively, it has already been possible to produce a mixture of epothilones A (**1**) and B (**2**) by cloning of the entire epothilone gene cluster and expressing it in *Streptomyces coelicolor*, a much better understood organism, and with a ten-fold faster rate of growth as compared to *S. cellulosum*.[50]

Preclinical and clinical studies

In contrast to the extensive chemistry and *in vitro* biological studies discussed above, relatively scarce data have been disclosed on the *in vivo* efficacy of the epothilones. To date, published results only exist for natural epothilones B (**2**)[6,40] and D (**4**),[40] aza-epothilone B (**94**: BMS-247550, Scheme 7),[19*b*,53] desoxyepothilone F (**90**, Scheme 7),[17] and 26-fluoroepothilone B (**37**, Fig. 2).[54] Danishefsky's group initially reported promising activity against subcutaneously implanted tumors in SCID mice for epothilone B (**2**),[40*a*] but they later encountered severe toxicity problems with this compound.[40*b*] On the other hand, it was claimed that epothilone D (**4**) was much less toxic, and this compound was found to be superior to both epothilone B (**2**) and Taxol® in a variety of mouse tumor models.[40*b*,40*c*] In some cases, epothilone D (**4**) was found to be curative against

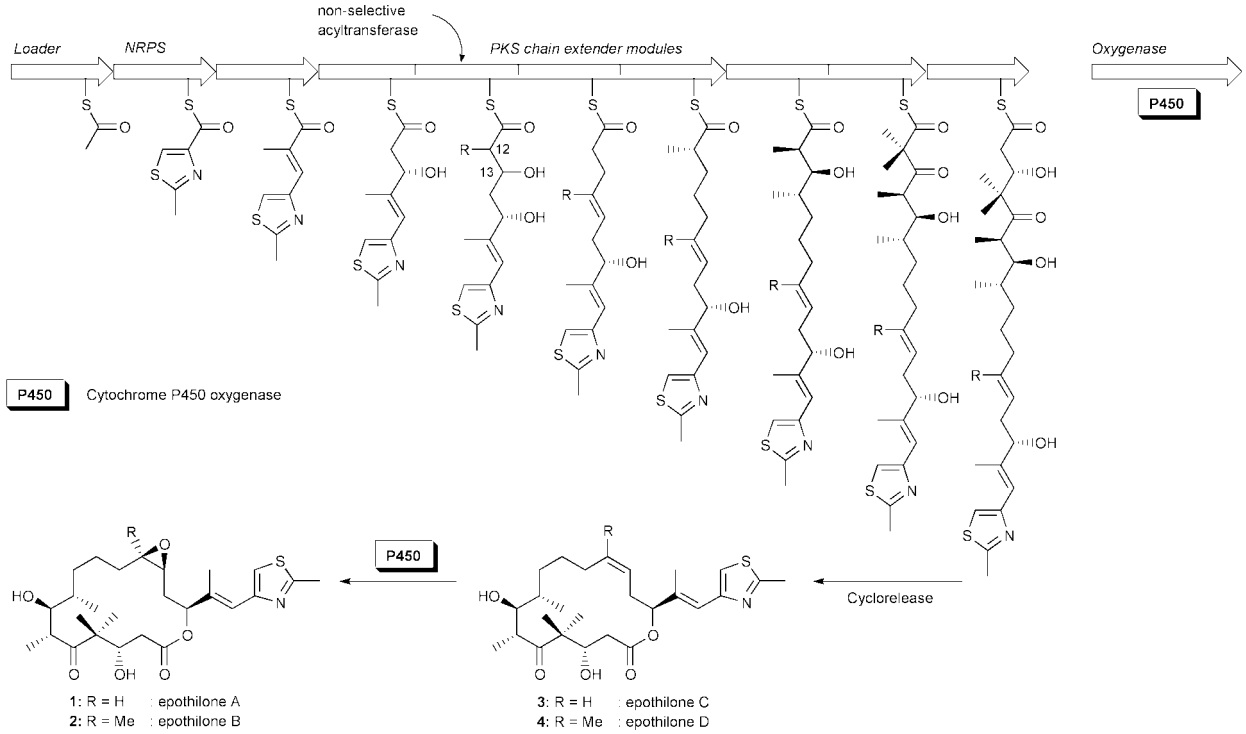

Fig. 5 Structure of the epothilone biosynthetic gene cluster from *Sorangium cellulosum*. NRPS = non-ribosomal peptide synthase, PKS = polyketide synthase.

human tumor xenografts, even when these were unresponsive to Taxol®.[40c] Preliminary results for desoxyepothilone F (**90**)[17] showed that this compound is highly potent in the mouse tumor models employed, while preliminary data for aza-epothilone B (**94**) showed that this compound appeared to be less effective in reducing tumor growth.

The BMS team also encountered difficulties with natural epothilone B (**2**) not only due to its toxicity in mice and lower primates, but also because of its low metabolic stability towards various esterases. To ameliorate these problems, aza-epothilone B (**94**: BMS-247550) was targeted and it was found to possess a very promising pharmacological profile, despite its lower *in vitro* activity compared to epothilone B (**2**).[53] In fact, even when orally administered, **94** was found to be highly effective against a range of human tumor xenografts in mice and rats, including taxol-resistant tumors.[53]

Phase I clinical trials with this compound have been conducted by BMS, and the results are so far very promising.[55] It was found that although the toxicity of **94** was similar to that of Taxol®, **94** did show evidence of being effective in patients with taxane-resistant tumors. Clinical trials with this compound are currently entering phase II.

Contrary to the results above, through tumor graft studies in mice, the Novartis group found epothilone B (**2**) itself to be a viable drug candidate,[6] and this compound is also currently in phase II clinical trials, having successfully been evaluated in clinical phase I trials.[56] The Novartis group has also carried out extensive preclinical studies with a number of our designed epothilone analogues. In collaboration with the Logothesis–Navone group, we have also carried out comparative *in vivo* studies with Taxol®, epothilone B (**2**) and 26-fluoroepothilone B (**37**),[54] and we found that the latter compound was more active than Taxol® in inhibiting growth of human prostate cancer xenografts in mice, and the tolerated dose of this agent was higher than that for either Taxol® or epothilone B (**2**). These observations were attributed to lower overall toxicity of the fluoroepothilone analogue **37**.

Conclusion

With a number of epothilones (from both the natural and designed categories) in clinical trials as potential anticancer agents, the anticipation regarding this class of compounds is climaxing. Indeed their emergence as top candidates for cancer chemotherapy was rapid, being greatly facilitated by chemical synthesis and chemical biology studies. Carried out by many groups around the world, these investigations ensured the availability of not only the naturally occurring substances, but also of thousands of analogues which allowed elucidation of structure–activity relationships. While more results from the clinical trials of this first generation epothilone drug candidates are eagerly awaited, the basic research efforts that brought these molecules thus far will no doubt continue unabated for some time to come.

Addendum

Since the submission of this manuscript relevant publications have appeared in the literature.[57–65]

Acknowledgements

It is with great pride and pleasure that we wish to thank our collaborators whose names appear in the references and whose contributions made the described work possible and enjoyable. We also wish to express our many thanks to our collaborators Dr Karl-Heinz Altmann (Novartis) and Dr Paraskevi Giannakakou (Emory University) for their contributions and for valuable discussions. We gratefully acknowledge the National Institutes of Health (USA), Merck & Co., DuPont, Schering Plough, Pfizer, Hoffmann-La Roche, GlaxoWellcome, Rhone-Poulenc Rorer, Amgen, Novartis, Abbott Laboratories, Bristol-Myers Squibb, Boehringer Ingelheim, Zeneca, CaPCURE, the George E. Hewitt Foundation, and the Skaggs Institute for Chemical Biology for supporting our research programs. This work was also supported by a fellowship to A. Ritzén (STINT).

Notes and references

1 K. C. Nicolaou, D. Hepworth, N. P. King and M. R. V. Finlay, *Pure Appl. Chem.*, 1999, **71**, 989.

2 (*a*) G. Höfle, N. Bedorf, K. Gerth and H. Reichenbach, German patent DE 4138042, May 5, 1993; (*b*) K. Gerth, N. Bedorf, G. Höfle, H. Irschik and H. Reichenbach, *J. Antibiot.*, 1996, **49**, 560; (*c*) G. Höfle, N. Bedorf,

H. Steinmetz, D. Schomberg, K. Gerth and H. Reichenbach, *Angew. Chem., Int. Ed. Engl.*, 1996, **35**, 1567; (*d*) D. M. Bollag, P. A. McQueney, J. Zhu, O. Hensen, L. Koupal, J. Liesch, M. Goetz, E. Lazarides and C. A. Woods, *Cancer Res.*, 1995, **55**, 2325.
3 K. C. Nicolaou, F. Roschangar and D. Vourloumis, *Angew. Chem., Int. Ed.*, 1998, **37**, 2014.
4 C. R. Harris and S. J. Danishefsky, *J. Org. Chem.*, 1999, **64**, 8434.
5 J. Mulzer, *Monatsh. Chem.*, 2000, **131**, 205.
6 K.-H. Altmann, M. Wartmann and T. O'Reilly, *Biochim. Biophys. Acta*, 2000, **1470**, M79.
7 (*a*) K. C. Nicolaou, N. P. King, M. R. V. Finlay, Y. He, F. Roschangar, D. Vourloumis, H. Vallberg, F. Sarabia, S. Ninkovic and D. Hepworth, *Bioorg. Med. Chem.*, 1999, **7**, 665; (*b*) K. C. Nicolaou, D. Hepworth, N. P. King, M. R. V. Finlay, R. Scarpelli, M. M. A. Pereira, B. Bollbuck, A. Bigot, B. Werschkun and N. Winssinger, *Chem. Eur. J.*, 2000, **6**, 2783.
8 K. C. Nicolaou, R. Scarpelli, B. Bollbuck, B. Werschkun, M. M. A. Pereira, M. Wartmann, K.-H. Altmann, D. Zaharevitz, R. Gussio and P. Giannakakou, *Chem. Biol.*, 2000, **7**, 593.
9 K. C. Nicolaou, D. Hepworth, M. R. V. Finlay, N. P. King, B. Werschkun and A. Bigot, *Chem. Commun.*, 1999, 519.
10 (*a*) K. C. Nicolaou, F. Sarabia, S. Ninkovic and Z. Yang, *Angew. Chem., Int. Ed. Engl.*, 1997, **36**, 525; (*b*) K. C. Nicolaou, S. Ninkovic, F. Sarabia, D. Vourloumis, Y. He, H. Vallberg, M. R. V. Finlay and Z. Yang, *J. Am. Chem. Soc.*, 1997, **119**, 7974.
11 K. C. Nicolaou, M. R. V. Finlay, S. Ninkovic and F. Sarabia, *Tetrahedron*, 1998, **54**, 7127.
12 K. C. Nicolaou, M. R. V. Finlay, S. Ninkovic, N. P. King, Y. He, T. Li, F. Sarabia and D. Vourloumis, *Chem. Biol.*, 1998, **5**, 365.
13 J. Johnson, S.-H. Kim, M. Bifano, J. DiMarco, C. Fairchild, J. Gougoutas, F. Lee, B. Long, J. Tokarski and G. Vite, *Org. Lett.*, 2000, **2**, 1537.
14 (*a*) K. C. Nicolaou, K. Namoto, J. Li, A. Ritzén, T. Ulven, M. Shoji, D. Zaharevitz, R. Gussio, D. L. Sackett, R. D. Ward, A. Hensler, T. Fojo and P. Giannakakou, *Chem Bio Chem.*, 2001, **2**, 69; (*b*) K. C. Nicolaou, K. Namoto, A. Ritzén, J. Li, T. Ulven, M. Shoji and P. Giannakakou, *J. Am. Chem. Soc.*, in the press.
15 A. B. Charette, H. Juteau, H. Lebel and C. Molinaro, *J. Am. Chem. Soc.*, 1998, **120**, 11943.
16 C. R. Harris, S. D. Kuduk, A. Balog, K. Savin, P. W. Glunz and S. J. Danishefsky, *J. Am. Chem. Soc.*, 1999, **121**, 7050.
17 C. B. Lee, T.-C. Chou, X.-G. Zhang, Z.-G. Wang, S. D. Kuduk, M. D. Chappell, S. J. Stachel and S. J. Danishefsky, *J. Org. Chem.*, 2000, **65**, 6525.
18 M. D. Chappell, S. J. Stachel, C. B. Lee and S. J. Danishefsky, *Org. Lett.*, 2000, **2**, 1633.
19 (*a*) S. J. Stachel, M. D. Chappell, C. B. Lee, S. J. Danishefsky, T.-C. Chou, L. He and S. B. Horwitz, *Org. Lett.*, 2000, **2**, 1637; (*b*) S. J. Stachel, C. B. Lee, M. Spassova, M. D. Chappell, W. G. Bornmann, S. J. Danishefsky, T.-C. Chou and Y. Guan, *J. Org. Chem.*, 2001, **66**, 4369.
20 P. Wirsching, J. A. Ashley, C.-H. L. Lo, K. D. Janda and R. A. Lerner, *Science*, 1995, **270**, 1775.
21 S. C. Sinha, C. F. Barbas, III and R. A. Lerner, *Proc. Natl. Acad. Sci. USA*, 1998, **95**, 14603.
22 S. C. Sinha, J. Sun, G. Miller, C. F. Barbas, III, and R. A. Lerner, *Org. Lett.*, 1999, **1**, 1623.
23 S. C. Sinha, J. Sun, G. P. Miller, M. Wartmann and R. A. Lerner, *Chem. Eur. J.*, 2001, **7**, 1691.
24 D. Sawada and M. Shibasaki, *Angew. Chem., Int. Ed.*, 2000, **39**, 209.
25 D. Sawada, M. Kanai and M. Shibasaki, *J. Am. Chem. Soc.*, 2000, **122**, 10521.
26 M. Kalesse, M. Quitschalle, E. Claus, K. Gerlach, A. Pahl and H. H. Meyer, *Eur. J. Org. Chem.*, 1999, 2817.
27 B. Zhu and J. S. Panek, *Org. Lett.*, 2000, **2**, 2575.
28 J. W. Bode and E. M. Carreira, *J. Am. Chem. Soc.*, 2001, **123**, 3611.
29 A. Fürstner, C. Mathes and K. Grela, *Chem. Commun.*, 2001, 1057.
30 K.-H. Altmann, G. Bold, G. Caravatti, N. End, A. Flörshemier, V. Guagnano, T. O'Reilly and M. Wartmann, *Chimia*, 2000, **54**, 612.
31 K.-H. Altmann, G. Bold, G. Caravatti, A. Flörsheimer, V. Guagnano and M. Wartmann, *Bioorg. Med. Chem. Lett.*, 2000, **10**, 2765.
32 S. A. May and P. A. Grieco, *Chem. Commun.*, 1998, 1597.
33 (*a*) D. Schinzer, A. Bauer, O. M. Böhm, A. Limberg and M. Cordes, *Chem. Eur. J.*, 1999, **5**, 2483; (*b*) D. Schintzer, A. Bauer and J. Schieber, *Chem. Eur. J.*, 1999, **5**, 2492.
34 (*a*) H. J. Martin, M. Drescher and J. Mulzer, *Angew. Chem., Int. Ed.*, 2000, **39**, 581; (*b*) J. Mulzer, A. Mantoulidis and E. Öhler, *J. Org. Chem.*, 2000, **65**, 7456; (*c*) J. Mulzer, G. Karig and P. Pojarliev, *Tetrahedron Lett.*, 2000, **41**, 7635.
35 (*a*) J. D. White, R. G. Carter and K. F. Sundermann, *J. Org. Chem.*, 1999, **64**, 684; (*b*) J. D. White, K. F. Sundermann and R. G. Carter, *Org. Lett.*, 1999, **1**, 1431.
36 D. Schinzer, K.-H. Altmann, F. Stuhlmann, A. Bauer and M. Wartmann, *Chem. Bio. Chem.*, 2000, **1**, 67.
37 T. D. Machajewski and C.-H. Wong, *Synthesis*, 1999, 1469.
38 (*a*) G. Höfle, N. Glaser, T. Leibold and M. Sefkow, *Pure Appl. Chem.*, 1999, **71**, 2019; (*b*) G. Höfle, N. Glaser, M. Kiffe, H.-J. Hecht, F. Sasse and H. Reichenbach, *Angew. Chem., Int. Ed.*, 1999, **38**, 1971; (*c*) M. Sefkow and G. Höfle, *Heterocycles*, 1998, **48**, 2485; (*d*) M. Sefkow, M. Kiffe, D. Schummer and G. Höfle, *Bioorg. Med. Chem. Lett.*, 1998, **8**, 3025; (*e*) M. Sefkow, M. Kiffe and G. Höfle, *Bioorg. Med. Chem. Lett.*, 1998, **8**, 3031.
39 R. M. Borzilleri, X. Zheng, R. J. Schmidt, J. A. Johnson, S.-H. Kim, J. D. DiMarco, C. R. Fairchild, J. Z. Gougoutas, F. Y. F. Lee, B. H. Long and G. D. Vite, *J. Am. Chem. Soc.*, 2000, **122**, 8890.
40 (*a*) D.-S. Su, A. Balog, D. Meng, P. Bertinato, S. J. Danishefsky, Y.-H. Zheng, T.-C. Chou, L. He and S. B. Horwitz, *Angew. Chem., Int. Ed. Engl.*, 1997, **36**, 2093; (*b*) T.-C. Chou, X.-G. Zhang, A. Balog, D.-S. Su, D. Meng, K. Savin, J. R. Bertino and S. J. Danishefsky, *Proc. Natl. Acad. Sci. USA*, 1998, **95**, 9642; (*c*) T.-C. Chou, X.-G. Zhang, C. R. Harris, S. D. Kuduk, A. Balog, K. A. Savin, J. R. Bertino and S. J. Danishefsky, *Proc. Natl. Acad. Sci. USA*, 1998, **95**, 15798.
41 E. Nogales, S. G. Wolf and K. H. Downing, *Nature*, 1998, **391**, 199.
42 R. E. Taylor and J. Zajicek, *J. Org. Chem.*, 1999, **64**, 7224.
43 P. Ballone and M. Marchi, *J. Phys. Chem. A*, 1999, **103**, 3097.
44 M. Wang, X. Xia, Y. Kim, D. Hwang, J. M. Jansen, M. Botta, D. C. Liotta and J. P. Snyder, *Org. Lett.*, 1999, **1**, 43.
45 I. Ojima, S. Chakravarty, T. Inoue, S. Lin, L. He, S. B. Horwitz, S. D. Kuduk and S. J. Danishefsky, *Proc. Natl. Acad. Sci. USA*, 1999, **96**, 4256.
46 P. Giannakakou, R. Gussio, E. Nogales, K. H. Downing, D. Zaharevitz, B. Bollbuck, G. Poy, D. Sackett, K. C. Nicolaou and T. Fojo, *Proc. Natl. Acad. Sci. USA*, 2000, **97**, 2904.
47 L. He, P. G. Jagtap, D. G. I. Kingston, H.-J. Shen, G. A. Orr and S. B. Horwitz, *Biochemistry*, 2000, **39**, 3972.
48 K. W. Lee and J. M. Briggs, *J. Computer-Aided Mol. Design*, 2001, **15**, 41.
49 I. Molnár, T. Schupp, M. Ono, R. E. Zirkle, M. Milnamow, B. Nowak-Thompson, N. Emgel, C. Toupet, A. Stratmann, D. D. Cyr, J. Gorlach, J. M. Mayo, A. Hu, S. Goff, J. Schmid and J. M. Ligon, *Chem. Biol.*, 2000, **7**, 97.
50 L. Tang, S. Shah, L. Chung, J. Carney, L. Katz, C. Khosla and B. Julien, *Science*, 2000, **287**, 640.
51 K. Gerth, H. Steinmetz, G. Höfle and H. Reichenbach, *J. Antibiot.*, 2000, **53**, 1373.
52 K. Gerth, H. Steinmetz, G. Höfle and H. Reichenbach, *J. Antibiot.*, 2001, **54**, 144.
53 F. Y. F. Lee, R. Borzilleri, C. R. Fairchild, S.-H. Kim, B. H. Long, C. Reventos-Suarez, G. D. Vite, W. C. Rose and R. A. Kramer, *Clin. Cancer Res.*, 2001, **7**, 1429.
54 R. A. Newman, J. Yang, M. R. V. Finlay, F. Cabral, D. Vourloumis, C. Stevens, P. Troncoso, X. Wu, C. J. Logothetis, K. C. Nicolaou and N. M. Navone, *Cancer Chemother. Pharm.*, 2001, in the press.
55 (*a*) B. Damle, S. Letrent, G. Duncan, V. Litwin, L. Panting, D. Lebwohl, S. Johnes, H. Burris and D. Spriggs, ASCO 2001 Annual Meeting Abstract; (*b*) D. Spriggs, S. Soignet, B. Bienvenu, S. Letrent, D. Lebwohl, S. Jones and H. Burris, III, ASCO 2001 Annual Meeting Abstract; (*c*) S. Mani, H. McDaid, Heng-Jia, J. S. Sparano, A. Hamilton, C. Runowicz, H. Hochster, F. Muggia, A. Fields, G. Duncan, D. Lebwohl and S. B. Horwitz, ASCO 2001 Annual Meeting Abstract.
56 K.-H. Altmann, Novartis Pharma AG, personal communication.
57 A. Regueiro-Ren, R. M. Borzilleri, X. Zheng, S.-H. Kim, J. A. Johnson, C. R. Fairchild, F. Y. F. Lee, B. H. Long and G. D. Vite, *Org. Lett.*, 2001, ASAP.
58 K.-H. Altmann, *Curr. Opin. Chem. Biol.*, 2001, **5**, 424.
59 T.-C. Chou, O. A. O'Connor, W. P. Tong, Y. Guan, Z.-G. Zhang, S. J. Stachel, C. Lee and S. J. Danishefsky, *Proc. Natl. Acad. Sci. USA*, 2001, **98**, 8113.
60 A. Flörsheimer and K.-H. Altmann, *Expert Opin. Ther. Pat.*, 2001, **11**, 951.
61 R. E. Taylor and Y. Chen, *Org. Lett.*, 2001, **3**, 2221.
62 I. H. Hardt, H. Steinmetz, K. Gerth, F. Sasse, H. Reichenbach and G. Höfle, *J. Nat. Prod.*, 2001, **64**, 847.
63 H. J. Martin, P. Pojarliev, H. Kahlig and J. Mulzer, *Chem. Eur. J.*, 2001, **7**, 2261.
64 B. Zhu and J. S. Panek, *Eur. J. Org. Chem.*, 2001, **9**, 1701.
65 J. D. White, R. G. Carter, K. F. Sundermann and M. Wartmann, *J. Am. Chem. Soc.*, 2001, **123**, 5407.

CHEMCOMM Communication
www.rsc.org/chemcomm

A new palladium-catalysed synthesis of 1,1-dialkylbuta-1,3-dienes *via* organoboron intermediates†

Paolo Balma Tivola,[a] Annamaria Deagostino,[a] Cristina Prandi*[b] and Paolo Venturello*[a]

[a] *Dipartimento di Chimica Generale ed Organica Applicata dell'Università, Corso M. D'Azeglio, 48, I 10125 Torino, Italy. E-mail: venturello@ch.unito.it; Fax: 0039 0116707642; Tel: 0039 0116707646*
[b] *Dipartimento di Scienze e Tecnologie Avanzate dell'Università, Corso Borsalino, 54, I 15100 Alessandria, Italy*

Received (in Cambridge, UK) 21st May 2001, Accepted 26th June 2001
First published as an Advance Article on the web 31st July 2001

Iodobenzene and tetrakis(triphenylphosphine)palladium(0) $[(C_6H_5)_3P]_4Pd$ catalyse a new synthesis of 1,1-dialkylbuta-1,3-dienes, starting from 1,1-diethoxybut-2-ene and trialkylboranes, in the presence of Schlosser's superbase LIC–KOR.

The synthesis of polienic structures has been of great interest to organic chemistry owing not only to their presence in natural products,[1] but also to their importance as useful chemicals in the perfume industry and other fields.[2] Our interest in the synthesis of stereodefined substituted dienes required the development of diverse organometallic reagents and protocol for the preparation of key building blocks.[3] In the course of these studies we have set up a new synthesis of 1,1-dialkyl substituted buta-1,3-dienes, resorting to the reactivity of organoboron compounds.[4] Treatment of crotonaldehyde diethyl acetal (**1**) at −95 °C with LIC–KOR base (LIC: butyllithium, KOR: potassium *tert*-butoxide)[5] readily gives α-metalated 1-ethoxybuta-1,3-diene (**2**). Subsequent reaction with trialkylboranes leads to the immediate disappearance of the deeply red colour of the metalated diene. An intermediate 'ate' complex **3**[6] (Scheme 1) is probably formed that undergoes different reactions according to experimental conditions.

Treatment of complex **3** at −95 °C with H_2O–THF leads to the corresponding 1-alkoxy-1-alkylbuta-1,3-dienes **4**, that can be, like all enol ethers, smoothly converted to the corresponding

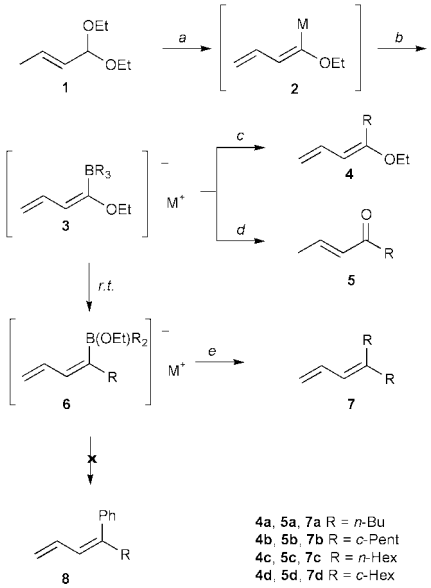

Scheme 1 *Reagents and conditions*: *a*: LIC–KOR, THF, −95 °C; *b*: BR_3, THF, −95 °C; *c*: −95 °C, H_2O; *d*: $BF_3{\cdot}OEt_2$, H_2O_2, −95 °C; *e*: C_6H_5I, $[(C_6H_5)_3P]_4Pd$, THF, 25 °C.

† Dedicated to Professor Iacopo Degani on the occasion of his 70th birthday.

α,β-unsaturated ketones **5** (Scheme 1: path *c*). Moreover, derivatives **5** can be directly obtained from **3** upon treatment with a Lewis acid ($F_3B{\cdot}OEt_2$) in an oxidative milieu (Scheme 1: path *d*). More interestingly, a new and intriguing result comes from the reaction with iodobenzene in the presence of catalytic amounts of $[P(C_6H_5)_3]_4Pd$, according to the procedure of the Suzuki–Miyura cross-coupling reaction. Thus, when intermediate **3** was warmed to room temperature and treated with a THF solution of iodobenzene and $[P(C_6H_5)_3]_4Pd$ no coupling product **8** was detected, while the *gem*-dialkyl substituted buta-1,3-diene **7** was isolated in good yield (Scheme 1: path *e*).[7,8] In contrast, treatment of **3** with $[P(C_6H_5)_3]_4Pd$ in the absence of iodobenzene afforded only traces of product **7**.[9] Moreover, also when intermediate **3** undergoes the iodination reaction[6] or treatment with iodobenzene in the absence of a palladium complex no trace of product **7** was detected and only ketone **5** was recovered. The results obtained with different alkylboranes are reported in Table 1.

Table 1 Synthesis of 1-alkyl-1-ethoxybuta-1,3-dienes and 1,1-dialkylbuta-1,3-dienes[a]

1-Alkyl-1-ethoxybuta-1,3-dienes			1,1-Dialkylbuta-1,3-dienes		
R	Product	Yield (%)	R	Product	Yield (%)
n-C_4H_9	**4a**	86	*n*-C_4H_9	**7a**	79
c-C_5H_{11}	**4b**	87	*c*-C_5H_{11}	**7b**	86
n-C_6H_{13}	**4c**	82	*n*-C_6H_{13}	**7c**	68
c-C_6H_{11}	**4d**	71	*c*-C_6H_{11}	**7d**	77

[a] For experimental details, see note 7. The spectral data for new compounds **4a–4d** and **7a–7d** are consistent with the structures proposed.

The formation of compound **7** suggests the intermediate formation of the rearranged borate complex **6**, and in Scheme 2 a possible reaction mechanism is reported that may account for the formation of a *gem* substituted diene. According to this hypothesis vinylborate interacts with the Pd catalyst and undergoes transfer of an alkyl group, which promotes the

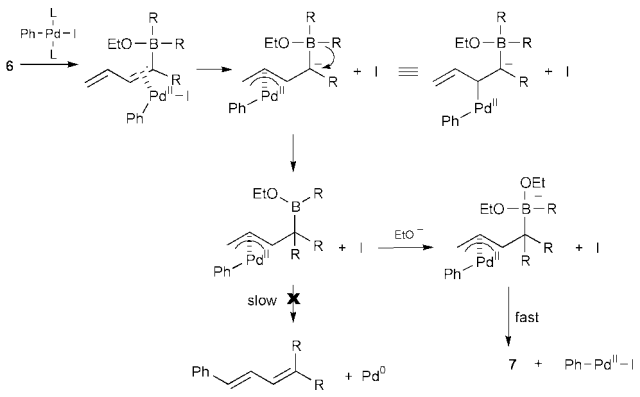

Scheme 2 Proposed reaction mechanism.

 DOI: 10.1039/b104449b

formation of a new π allyl complex. At this stage a new 'ate' complex forms that undergoes the elimination reaction much faster than the phenyl transfer process.

In conclusion, these results indicate that depending on the experimental conditions 1,1-dialkyl substituted buta-1,3-dienes, 1-ethoxy-1-alkylbuta-1,3-dienes and α,β-unsaturated ketones can be selectively prepared. Extension to other organoboron intermediates (asymmetric ones, in particular) and synthetic applications for these functionalized synthons, as well as mechanistic studies to check the role of the palladium complex and iodobenzene, are currently in progress in our group.[10]

This work was supported by grants from Italian MURST. We thank Dr Arnaud Gauthier and Dr Jacques Maddaluno (Université de Rouen) for helpful criticism, and CNR-CNRS for a grant for cultural exchange.

Notes and references

1 R. Baker and J. W. S. Bradshaw, in *Aliphatic and Related Natural Product Chemistry*, ed. F. D. Gunstone, Specialist Periodical Report, Royal Society of Chemistry, London, 1983, vol. 3; K. C. Nicolau, J. Y. Ramphal, N. A. Petasis and C. N. Serhan, *Angew. Chem., Int. Ed. Engl.*, 1991, **30**, 1100; V. Launay, I. Beaudet and J.-P. Quintard, *Bull. Soc. Chim. Fr.*, 1997, **134**, 937; B. Dominguez, B. Iglesia and A. R. de Lera, *J. Org. Chem.*, 1998, **63**, 4135; B. H. Lipshutz, B. Ullman, C. Lindsley, S. Pecchi, D. J. Buzard and D. Dickson, *J. Org. Chem.*, 1998, **63**, 6092.

2 M. Goldbach, E. Jäkel and M. P. Schneider, *J. Chem. Soc., Chem. Commun.*, 1987, 1434.

3 P. Venturello, *J. Chem. Soc., Chem. Commun.*, 1992, 1032; P. Balma Tivola, A. Deagostino, C. Prandi and P. Venturello, *J. Chem. Soc., Perkin Trans. 1*, 2001, 437, and refs. therein.

4 N. Miyaura and A. Suzuki, *Chem. Rev.*, 1995, **95**, 2457; A. Suzuki, *J. Organomet. Chem.*, 1999, **576**, 147.

5 M. Schlosser, *J. Organomet. Chem.*, 1967, **8**, 9; M. Schlosser, *Mod. Synth. Methods*, 1992, **6**, 227; A. Mordini, *Advances in Carbanion Chemistry*, ed. V. Snieckus, JAI Press Inc., Greenwich CT, 1992, vol. 1, pp. 1–45; M. Schlosser, F. Faigl, L. Franzini, H. Geneste, G. Katsoulos and G. Zhong, *Pure Appl. Chem.*, 1994, **66**, 1439; L. Lochmann, *Eur. J. Inorg. Chem.*, 2000, 1115.

6 A. B. Levy and S. J. Schwartz, N. Wilson and B. Christie, *J. Organomet. Chem.*, 1978, **156**, 123; H. C. Brown, J. A. Sinclair and M. M. Midland, *J. Org. Chem.*, 1986, **51**, 4507.

7 Typical run: to a cooled solution (−95 °C) of *t*-BuOK (1.4 g, 12.5 mmol) in anhydrous THF (10 ml) acetal **1** (0.72 g, 5.0 mmol) and BuLi (7.8 ml, 12.5 mmol) were consecutively added dropwise under stirring. After 2 h the purple–red solution was treated with tributylborane (5.0 mmol, 5 ml, 1.0 M in THF). The solution was allowed to warm to 25 °C and then added to a THF solution of C_6H_5I (4.0 mmol)–$[(C_6H_5)_3P]_4Pd$ (0.058 g, 1 mol%). The reaction mixture was allowed to react for 8 h. After standard work up the crude product was purified by column chromatography to afford pure **7a**. δ_H (400 MHz; $CDCl_3$) 0.87 (t, *J* 6.5, 3 H), 0.90 (t, *J* 6.5, 3 H), 1.2–1.5 (m, 8 H), 2.05 (t, *J* 6.2, 2 H), 2.15 (t, *J* 6.2, 2 H), 4.95 (dd, *J* 10.0, 1.0, 1 H), 5.10 (dd, *J* 16.0, 10.0, 1 H), 5.85 (d, *J* 10.0, 1 H), 6.60 (dt, *J* 16.0, 10.0, 1 H); δ_C (100.4 MHz; $CDCl_3$) 14.1, 22.7, 22.9, 29.8, 30.4, 30.5, 31.1, 37.0, 114.4, 125.3, 128.3, 133.4, 144.6.

8 Organoboron reagents have been used in the preparation of alkylidenecycloalkanes and *trans* disubstituted alkenes. See, G. Zweifel and R. P. Fisher, *Synthesis*, 1972, 557, and E. Negishi, J.-J. Katz and R. C. Brown, *Synthesis*, 1972, 555, respectively. Moreover, to our knowledge substituted and *gem*-dibutyl substituted buta-1,3-dienes have only been prepared in aqueous medium by the reaction of aldehydes and ketones with 1-chloro-3-iodopropene in the presence of zinc powder. See, T.-H. Chan and C.-J. Li, *Organometallics*, 1990, **9**, 2649.

9 We have carried out some control reactions (R = *n*-C_4H_9 and R = *c*-C_6H_{11}) in the presence of catalytic amounts (ranging from 5 to 10% with respect to acetal **1**) of PhI. The reactions proceed in good yields, but longer reaction times are needed.

10 In order to assess the role of the catalyst, in accordance with the suggestion of one of the referees, we have carried out a reaction in the presence of a Pd(II) complex. In particular we have repeated the synthesis of compound **7d** (R = *c*-C_6H_{11}) using $Pd(AcO)_2$ as a catalyst. The reaction takes place, but the product was obtained with a quite lower yield (by GC).

CHEMCOMM
Communication
www.rsc.org/chemcomm

Direct observation of light induced spin transitions in new 3,5-bis(2-pyridyl)pyrazolato bridged thiocyanato diirion(II) complexes by monitoring variable temperature laser Raman spectra†

Naohiko Suemura, Mitsuo Ohama and Sumio Kaizaki*

Department of Chemistry, Graduate School of Science, Osaka University, Toyonaka, Osaka, 560-0043, Japan. E-mail: kaizaki@chem.sci.osaka-u.ac.jp

Received (in Cambridge, UK) 10th May 2001, Accepted 4th July 2001
First published as an Advance Article on the web 31st July 2001

The light induced excited spin state trapping LIESST and the reverse LIESST-like phenomena are observed below and above the spin transition temperature, respectively, for new dinuclear diirion(II) complexes and familiar Fe(II) complexes with thiocyanate ligands by monitoring the Raman spectra where only excitation light of various wavelengths for the spectroscopy was used without extra excitation light sources.

There have been a number of investigations concerning spin-crossover phenomena accompanying the spin state transition between the high-spin quintet and the low-spin singlet states of iron(II) complexes.[1] Among them, much attention has recently been paid to light induced excited spin state trapping (LIESST)[2] in relation with molecular switching or information storage from a viewpoint of molecular devices.[3] The thermal spin-crossover and LIESST by temperature variation and irradiation into the d–d or charge transfer transition regions are mainly observed by monitoring magnetic susceptibilities, optical spectra and Mössbauer spectroscopy.[2] On the other hand, there have been several studies of the spin-crossover on the basis of temperature variable vibrational spectroscopy. The Fe–N(NCS) or –N(phen) stretching bands for far IR[4] and the NC(NCS) band for IR[5] and FTIR[6] could be monitored to reveal the spin transitions for *cis*-$[Fe(NCS)_2(phen)_2]$ or related complexes. By monitoring the imine stretching band for Raman spectra, the Schiff base complexes were found to exhibit spin equilibrium. Meanwhile, the LIESST of *cis*-$[Fe(NCS)_2(phen)_2]$ has been detected by variable temperature FTIR measurement for the NC(NCS) stretching bands.[6] This occurs by irradiation of a low power 632.8 nm He–Ne laser for the calibration of the FTIR spectrophotometer. However, this method utilizes a limited radiation source with a low power and only one wavelength. Much advance in this field is expected to be made by overcoming this disadvantage of limited excitation sources. One of the candidates for easy access to LIESST could be laser Raman spectroscopy with excitation radiation of various wavelengths and variable powers for the spectroscopy itself, but without using any extra light source. Raman spectroscopy has been applied only to differentiating between high- and low-spin Fe(II) complexes[7,8] or estimating the entropy contributions.[8]

This paper reports a successful attempt to observe light induced spin transitions by measuring Raman spectra as a convenient and easily accessible probe. The complexes concerned are new dinuclear diiron(II) complexes bridged by two 3,5-bis(2-pyridyl)pyrazolates (bpypz) ligands with thiocyanate and pyridine derivatives in the Fe(II) unit, *trans*-(NCS, py-x)-$[Fe_2(NCS)_2(\mu\text{-bpypz})_2(py\text{-}x)_2]$ [py complex (**1**) and 3-Br-py complex (**2**)]‡ together with *cis*-$[Fe(NCS)_2(phen)_2]$ **3**§ and *cis*-$[Fe(NCS)_2(picen)]$ (picen = bis(2-pyridylmethyl)ethylenediamine) **4**.§ For complexes **1**–**4**, one or two Raman bands are observed around 2070 and 2100 cm^{-1} due to the C–N stretching of the NCS^- ligand. The lower and higher frequency bands correspond to the high- and low-spin complexes **1**–**4**, respectively, and their intensities vary with temperature [Fig. 1 (Figs. S1 and S2†)].¶ The high-spin fractions are approximated as $n_{HS} = I_{HS}/(I_{HS} + I_{LS})$ where I_{HS} of the high-spin species around 2070 cm^{-1} and I_{LS} of the low-spin one around 2100 cm^{-1} are Raman integrated band intensities at the observed temperatures. Plots of the high-spin fraction from the Raman band intensities *vs. T* do not always behave in a similar manner to those obtained from the magnetic susceptibility ($\chi_M T$) as seen in Figs. 2 and 3 (Fig. S3†). At temperatures just below T_c for complexes **1**–**3**, almost only the low-spin complexes exist as is evident from the $\chi_M T$ values; *ca.* 140–80 K for **1**, *ca.* 120–100

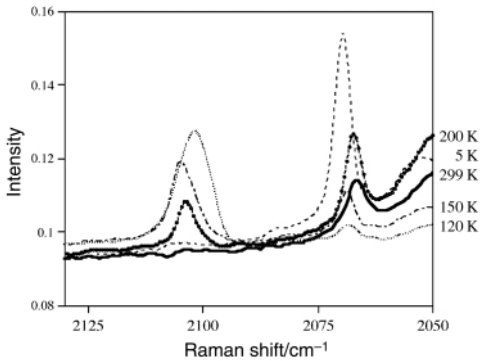

Fig. 1 Variable temperature Raman spectra of complex **1** with excitation of 514.5 nm radiation. (—) 299 K; (--·--·--·--) 200 K; (-·-·-·-·-·-·) 150 K; (·····) 120 K; (---------) 5 K.

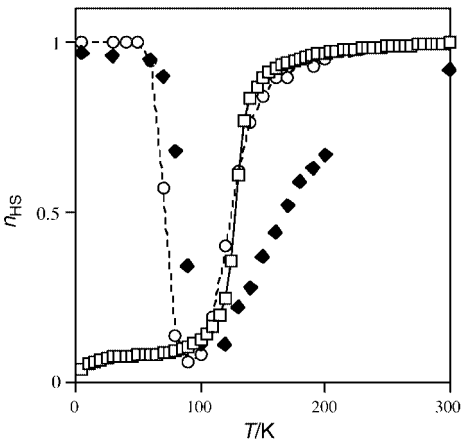

Fig. 2 Plots of the mole fraction of the high-spin state (n_{HS}) of complex **1** obtained from the magnetic susceptibility (—□—) and from Raman integrated intensities *vs. T*: (---○---) with 632.8 nm radiation, (◆) 514.5 nm radiation.

† Electronic supplementary information (ESI) available: Fig. S1: variable temperature Raman spectra of complex **2** (Ar laser). Fig. S2: variable temperature Raman spectra of complexes **3** and **4**. Fig. S3: plots of n_{HS} of complex **2** from magnetic susceptibility and Raman measurements. Fig. S4: plots of n_{HS} of complex **3** from magnetic susceptibility and Raman measurements. See http://www.rsc.org/suppdata/cc/b1/b104121p/

 DOI: 10.1039/b104121p

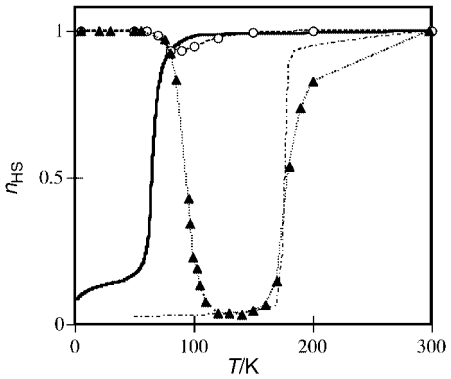

Fig. 3 Plots of the mole fraction of the high-spin state (n_{HS}) obtained from magnetic susceptibility measurements: **3** (-·-·-·-) and **4** (—) and from Raman intensities *vs.* *T*: **3** (···▲···) and **4** (---○---). The magnetic susceptibility and Raman measurements for complex **4** were conducted at a cooling rate of 0.06 K min^{-1}.

K for **2** and *ca*. 170–120 K for **3**. On further cooling, the low-spin fraction decreases and the high-spin state increases as shown in Figs. 2 and 3 (Fig. S3†). This observation of the spin transition from low- to high-spin demonstrates the LIESST. The LIESST occurs at the higher temperature with use of shorter wavelength irradiation light (Fig. 2 and Fig. S4†). In contrast to a deep drop to 100% of the low-spin fraction between the transition temperatures for **1**–**3**, complex **4** exhibits a shallow dip below T_c as shown in Fig. 3. This shallow dip might result from a slow relaxation from high- to low-spin[9b] or could be related to the anomalous spin-crossover phenomenon with hysteresis depending on cooling and heating rates.[9a] This observation suggests that the Raman spectra provide information on the spin-crossover dynamics. For the LIESST of complex **4**, the high-spin fraction was found to be *ca.* 40% by Mössbauer spectroscopy using broad-band (350–650 nm) excitation with a Xe arc lamp at 10 K,[9b] whereas the high-spin population is 100% according to Raman spectroscopy with a 632.8 nm He–Ne laser around 60 K.

It is noted that the low-spin complexes **1**–**4** exist even at temperatures above T_c. This phenomenon is more clearly recognized for the complexes **1** and **2** on measuring the Raman spectra with 514.5 nm Ar laser excitation (Fig. 1 and Fig. S2†). The low spin fraction for **1** is *ca.* 30% around 200 K (Fig. 2), and that for **2** is 15 and 50% at 300 and 118 K, respectively, (Fig. S3†). In contrast, almost 100% of the high-spin fraction is found to remain unchanged from the FT-IR[6] of **3** as well as the Raman measurements of **1** and **2** with 632.8 nm He–Ne laser irradiation at this temperature range. This light induced spin transition appears to be a kind of reverse LIESST.[10] However, the experimental conditions of temperature and radiation wavelength are definitely different from each other; the reverse LIESST occurs below T_c with 820 nm irradiation,[10] whereas the present phenomenon (reverse LIESST-like) is observed above T_c with 514.5 nm irradiation. This anomalous phenomenon is not clearly elucidated so far. Since both the Raman spectra and LIESST occur for a finite number of molecules[7] or a single molecule,[6c,11] the present Raman measurement may not be associated with light induced thermal hysteresis (LITH)[11] where the cooperative character affects the relaxation rate.[11b] To our knowledge, this is the first observation of LIESST and reverse LIESST-like phenomena in such a way that the high- and low-spin complexes are spontaneously trapped, respectively, below and above T_c by irradiation with a Raman spectral excitation laser. These discoveries by Raman spectroscopy will confer advantages to reveal new aspects of the light induced spin transitions by only one radiation source without an extra one.

We acknowledge support of this research by a Grant-in-Aid for Scientific Research on Priority Areas 'Metal-assembled Complexes' (No. 11136228) from the Ministry of Education, Science and Culture.

Notes and references

‡ These complexes were newly prepared from *trans*-[Fe(NCS)$_2$(py)$_4$] and Hbpypz with py-x and characterized to be *trans*-(NCS,py-x)-[(NCS)-(py-x)Fe(μ-bpypz)$_2$Fe(NCS)(py-x)] [x = H (**1**) and Br (**2**)] belonging to C_{2h} [*anti*(NCS)] or C_{2v} [*syn*(NCS)] point group by the elemental analysis of **1** and **2**, ^{1}H NMR, and magnetic susceptibility measurement of the analogous complex, *trans*-(NCS,dmso)-[(NCS)(dmso)Fe(μ-bpypz)$_2$Fe(NCS)(dmso)].
§ Complexes **3** and **4** were prepared by the methods detailed in ref. 4(*d*) and 9(*a*), respectively.
¶ These assignments are made according to ref. 5. Raman spectra were recorded for powdered samples using a Raman excitation He–Ne, Ar or Dye CW unfocused laser beam (ϕ = 1 mm; *ca*. 3 mW) with 32 scans accumulating at 20 s intervals by a Jasco NR-1800 Raman spectrophotometer. Variable-temperature Raman measurements were performed using an Oxford CF1204 cryostat.

1 H. Toflund, *Coord. Chem. Rev.*, 1989, **94**, 67; P. Gütlich, Y. Garcia and H. A. Goodwin, *Chem. Soc. Rev.*, 2000, **29**, 419.
2 S. Decuritins, P. Gütlich, C. P. Koler, H. Spiering and A. Hauser, *Chem. Phys. Lett.*, 1984, **105**, 1; P. Gütlich and A. Hauser, *Coord. Chem. Rev.*, 1990, **97**, 1; A. Hauser, *Coord. Chem. Rev.*, 1991, **111**, 275; P. Gütlich, A. Hauser and H. Spiering, *Angew. Chem., Int. Ed. Engl.*, 1994, **33**, 2024.
3 O. Kahn and C. J. Martinez, *Science*, 1998, **279**, 44; O. Kahn, *Chem. Br.*, 1999, 24.
4 (*a*) J. H. Takemoto and B. Hutchinson, *Inorg. Nucl. Chem. Lett.*, 1972, **8**, 769; (*b*) J. H. Takemoto and B. Hutchinson, *Inorg. Chem.*, 1973, **12**, 705; (*c*) J. R. Ferraro and J. H. Takemoto, *Appl. Spectrosc.*, 1974, **28**, 66; (*d*) S. Savage, Z. Jia-Long and A. G. Maddock, *J. Chem. Soc., Dalton Trans.*, 1985, 991.
5 W. A. Baker, Jr. and G. J. Long, *Chem. Commun.*, 1965, 368.
6 (*a*) R. Herber and L. M. Casson, *Inorg. Chem.*, 1986, **25**, 847; (*b*) R. H. Herber, *Inorg. Chem.*, 1987, **26**, 173; (*c*) D. C. Figg and R. H. Herber, *Inorg. Chem.*, 1990, **29**, 2170; (*d*) D. C. Figg, R. H. Herber and J. A. Potenza, *Inorg. Chem.*, 1992, **31**, 2111.
7 W. H. Batschelet and N. J. Rose, *Inorg. Chem.*, 1983, **22**, 2083.
8 A. Bousseksou, J. J. McGarvey, F. Varret, J. A. Real, J.-P. Tuchagues, A. C. Dennis and M. Boilloy, *Chem. Phys. Lett.*, 2000, **318**, 409.
9 (*a*) H. Toflund, E. Pedersen and S. Yde-Andersen, *Acta Chem. Scand., Part A*, 1984, **38**, 693; (*b*) T. Buchen, H. Toflund and P. Gütlich, *Chem. Eur. J.*, 1996, **2**, 1129.
10 A. Hauser, *Chem. Phys. Lett.*, 1986, **124**, 543.
11 (*a*) J.-F. Létard, P. Guionneau, L. Rabardel, J. A. K. Howard, A. E. Goeta, D. Chasseau and O. Kahn, *Inorg. Chem.*, 1998, **37**, 4432; (*b*) A. Desaix, O. Roubeau, J. Jeftic, J. G. Haasnoot, K. Boukheddaden, E. Codjovi, J. Linarès, M. Noguès and F. Varret, *Eur. Phys. J.*, 1998, **B6**, 183.

CHEMCOMM Communication
www.rsc.org/chemcomm

Highly active catalysts for the Suzuki coupling of aryl chlorides

Robin B. Bedford* and Catherine S. J. Cazin

School of Chemistry, University of Exeter, Exeter, UK EX4 4QD. E-mail: r.bedford@ex.ac.uk

Received (in Cambridge, UK) 20th June 2001, Accepted 6th July 2001
First published as an Advance Article on the web 20th July 2001

Simple tricyclohexylphosphine adducts of palladium complexes with orthometallated *N*-donor ligands show by far the highest activity yet reported in the Suzuki coupling of aryl chlorides, even under aerobic conditions.

The ability to use aryl chlorides as substrates in Suzuki biaryl coupling reactions (Scheme 1), rather than the far more commonly employed aryl bromides, is advantageous for two reasons. Firstly there are many more commercially available aryl chlorides than bromides and secondly they are much cheaper. These considerations are particularly important for industrial applications. Consequently the search for catalysts that can activate these substrates is a highly topical field of study. Recent notable advances in the use of aryl chlorides in Suzuki reactions have been made by the groups of Buchwald,[1] Guram[2] and Nolan.[3] Most of these catalyst systems rely on the use of complexes derived from di- or tri-alkyl substituted phosphine ligands which are either laborious to synthesise or are commercially available but comparatively expensive. The expense is compounded by the fact that the catalysts have to be used in relatively high loadings. These factors coupled with the current high cost of palladium detract from the appeal of using aryl chloride substrates when far cheaper ligands can be used in ultra-high dilutions for the activation of aryl bromides.[4]

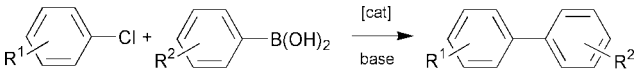

Scheme 1 The Suzuki biaryl coupling reaction.

By comparison with other phosphine ligands currently used in the activation of aryl chlorides, tricyclohexylphosphine is relatively cheap, readily available and easily handled. Littke and Fu have shown that palladium catalysts formed *in situ* with tricyclohexylphosphine show reasonable activity,[5] whilst Beller and coworkers have demonstrated that pre-formed Pd(0) complexes of the type [Pd(diene)(PCy_3)], **1**, are far more active.[6] Unfortunately, the synthesis and handling of the pre-formed complexes **1** are not particularly facile. It can be envisaged that an ideal catalyst for the Suzuki coupling of aryl chlorides would be one that: contains tricyclohexylphosphine; is easy to synthesise from cheap, commercially available materials; is easy to handle and shows good activity at low loadings.

We have previously obtained results that suggest that triphenylphosphine adducts of palladium complexes with orthometallated *N*-donor ligands act as precursors for low coordinate 'Pd–PPh_3' species in the Suzuki coupling of aryl bromides and that it is these low coordinate species that are the true active catalysts.[7] We were therefore interested to see whether analogous tricyclohexylphosphine adducts would show good activity in the Suzuki coupling of aryl chlorides. The preliminary findings of this study are reported below.[8]

The orthometallated amine complex **2** was used as a precursor as it is readily accessible from *N*,*N*-dimethylbenzylamine, which is commercially available and inexpensive and because we and later others have shown that the chloride-bridged analogue of **2** can be used in C–C bond forming processes.[9] Complex **2** readily reacts with tricyclohexylphosphine in dichloromethane to generate the adduct **3** in 60% yield after recrystallisation from dichloromethane–ethanol (Scheme 2). Complex **3** shows good air- and moisture-stability: ^{31}P NMR spectroscopy of a $CDCl_3$ solution shows only **3** and trace amounts of a second species after one month under aerobic conditions. For comparison purposes we also synthesised complex **4** by an analogous route from the metallated imine complex **5**. Complexes related to the precursor **5** have been found to give good activity in C–C coupling reactions with aryl bromides and iodides.[10]

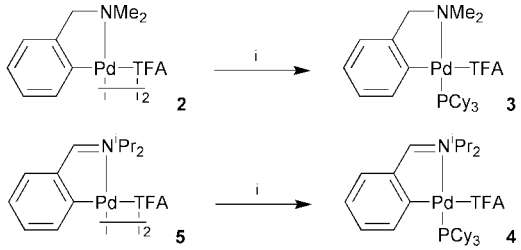

Scheme 2 *Reagents and conditions*: i, PCy_3, CH_2Cl_2, r.t., 30 min.

4-Chloroanisole was chosen as the main test substrate for the optimisation studies as it is electronically deactivated and thus resistant to oxidative addition and consequently very reluctant to enter a catalytic manifold. Therefore any catalyst that can activate this challenging substrate would be expected to be active with a broad spectrum of aryl chlorides. The results of the coupling of 4-chloroanisole with phenylboronic acid are summarised in Table 1. A brief optimisation of solvents and bases (entries 1–8) showed that the activity of the catalyst was profoundly affected by reaction conditions and demonstrated that dioxane/Cs_2CO_3 mixtures gave the highest activity, although good activity was seen when K_3PO_4 was used as a base. We were delighted to see that complex **3** gave essentially complete conversion at 0.1 mol% catalyst loading and very high turnover numbers (TONs) of up to 8000 at 0.01 mol% loading. Astonishingly, no loss in activity was observed when coupling reactions were performed under air. The observed activity is over seven times higher than that of the catalysts **1** which give a maximum TON of 1120 for this reaction under similar conditions and an inert atmosphere.[6] To the best of our knowledge, the highest reported TON for any aryl chloride in the Suzuki reaction is 4600 for the comparatively easy to couple substrate 4-chloroacetophenone.[1*b*] Even at 60 °C catalyst **3** shows excellent conversion in the coupling of 4-chloroanisole at 1.0 mol% loading.

Whilst the parent dimer **2** shows virtually no activity in the coupling of 4-chloroanisole, catalysts prepared *in situ* from **2** and one equivalent of PCy_3 show essentially identical activity to **3**. However in this case the dilute solutions of the phosphine need to be made up under nitrogen whereas no special precautions are required with **3**. Increasing the amount of PCy_3 in *in situ* formed catalysts appears to have a deleterious effect on the activity. The complex **4** shows somewhat lower activity than **3**, in addition the need to pre-synthesise the imine ligand detracts from its appeal.

Encouraged by these results we investigated the use of **3** in the Suzuki coupling reactions of a range of aryl chlorides (entries 17–23). The reactions with the electron deficient substrates 4-chloroacetophenone, 4-chloronitrobenzene and

 DOI: 10.1039/b105394a

Table 1 Suzuki coupling of aryl chlorides with phenylboronic acid. *Reaction conditions*: aryl chloride (2.0 mmol), $PhB(OH)_2$ (3.0 mmol), base (6.0 mmol), solvent (20 ml), 17 h

Entry	Substrate	Catalyst ([Pd]/mol% Pd)	Base	Solvent	*T*/°C[a]	Conversion (%)[b]	TON/mol product (mol Pd)$^{-1}$
1	4-Chloroanisole	**3** (1.0)	K_2CO_3	Toluene	110	6	6
2	4-Chloroanisole	**3** (1.0)	KF	Toluene	110	18	18
3	4-Chloroanisole	**3** (1.0)	KF	NMP	130	1	1
4	4-Chloroanisole	**3** (1.0)	KF	DMA	130	8	8
5	4-Chloroanisole	**3** (1.0)	NaO_2CMe	Dioxane	100	25	25
6	4-Chloroanisole	**3** (1.0)	KF	Dioxane	100	22	22
7	4-Chloroanisole	**3** (1.0)	K_3PO_4	Dioxane	100	60	60
8	4-Chloroanisole	**3** (1.0)	Cs_2CO_3	Dioxane	100	100	100
9	4-Chloroanisole	**3** (0.1)	Cs_2CO_3	Dioxane	100	> 99	> 990
10	4-Chloroanisole	**3** (0.01)	Cs_2CO_3	Dioxane	100	74	7400
11	4-Chloroanisole	**3** (0.01)[c]	Cs_2CO_3	Dioxane	100	80	8000
12	4-Chloroanisole	**3** (1.0)	Cs_2CO_3	Dioxane	60	97	97
13	4-Chloroanisole	**2** (1.0)	Cs_2CO_3	Dioxane	100	< 0.2	< 0.2
14	4-Chloroanisole	**2** (0.01) + PCy_3	Cs_2CO_3	Dioxane	100	80	8000
15	4-Chloroanisole	**2** (0.01) + 2 PCy_3	Cs_2CO_3	Dioxane	100	24.5	2450
16	4-Chloroanisole	**4** (0.01)	Cs_2CO_3	Dioxane	100	26	2600
17	4-Chloroacetophenone	**3** (0.01)	Cs_2CO_3	Dioxane	100	100	10000
18	4-Chloronitrobenzene	**3** (0.01)	Cs_2CO_3	Dioxane	100	100	10000
19	4-Chlorobenzaldehyde	**3** (0.001)	Cs_2CO_3	Dioxane	100	99	99000
20	2-Chlorotoluene	**3** (0.1)	Cs_2CO_3	Dioxane	100	100	1000
21	2-Chloroanisole	**3** (0.1)	Cs_2CO_3	Dioxane	100	100	1000
22	2-Chlorotoluene	**3** (0.01)	Cs_2CO_3	Dioxane	100	100	10000
23	2-Chloroanisole	**3** (0.01)	Cs_2CO_3	Dioxane	100	96	9600

[a] Approximate internal temperature. [b] Determined by GC against hexadecane internal standard, based on aryl chloride. [c] Under air.

4-chlorobenzaldehyde all showed quantitative conversions at 0.01 mol% catalyst loading. Further reducing the catalyst loading gave a TON of at least 99 000 in the coupling of 4-chlorobenzaldehyde—over twenty times higher activity than observed previously in any aryl chloride coupling reaction.[1b] In order to evaluate the performance of **3** with more sterically demanding substrates, the reactions of 2-chlorotoluene and 2-chloroanisole were investigated. Both substrates were coupled with ease, the catalyst **3** again showing considerably higher activity than any other reported previously.

With respect to the mechanism, it seems highly unlikely that a Pd(II)/Pd(IV) catalytic cycle operates when complex **3** is used as a pre-catalyst, particularly when 4-chloroanisole, which is relatively resistant to oxidative addition reactions, is used as the substrate. It is far more likely that the active catalyst is a low-coordinate palladium(0) species. Such a species may conceivably be formed by a process involving nucleophilic attack of the phenylboronic acid at the metal centre followed by reductive elimination of the phenyl and metallated *N*,*N*-dimethylbenzylamine functions from the putative intermediate **6** (Scheme 3). Indeed GC and GC-MS analysis of the reaction mixture for the coupling of 4-chloroanisole at 60 °C showed the presence of substantial amounts of **7** (~63%) indicating that such a process almost certainly occurs under catalytic conditions. Mono-coordinate phosphine complexes have been implicated previously as catalysts in coupling reactions and it seems likely that they are the active species here.[6,11] This may help explain why doubling the concentration of PCy_3 in catalysts formed *in situ* drastically reduces the catalytic activity—effectively the Pd becomes over-ligated.

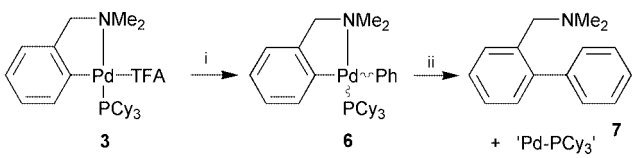

Scheme 3 *Reagents and conditions*: i, $PhB(OH)_2$, base; ii, reductive elimination.

Interestingly, regardless of the precise nature of the active catalyst species derived from **3** or from mixtures of **2** and PCy_3, they show far greater activity than preformed palladium(0) complexes of the type **1** or complexes formed *in situ* from PCy_3 and either $[Pd_2(dba)_3]$ or palladium acetate.[5,6] This demonstrates that the choice of palladium precursor can have a profound influence on the activity of the catalyst and that the orthopalladated *N*,*N*-dimethylbenzylamine moiety represents the most efficient source of active palladium species yet reported.

In summary we have found that the very easily synthesised, comparatively inexpensive complex **3** shows by far the highest activity yet reported in the Suzuki coupling of aryl chlorides, regardless of whether the substrates are electron rich or poor. Additionally this high activity is observed with catalysts formed *in situ* and when the reactions are performed under air.

We thank the University of Exeter for the provision of a student bursary (for C. S. J. C.).

Notes and references

1 (*a*) D. W. Old, J. P. Wolfe and S. L. Buchwald, *J. Am. Chem. Soc.*, 1998, **121**, 9722; (*b*) J. P. Wolfe, R. A. Singer, B. H. Yang and S. L. Buchwald, *J. Am. Chem. Soc.*, 1999, **121**, 9550.
2 X. Bei, H. W. Turner, W. H. Weinberg and A. S. Guram, *J. Org. Chem.*, 1999, **64**, 6797.
3 C. Zhang, J. Huang, M. L. Trudell and S. P. Nolan, *J. Org. Chem.*, 1999, **64**, 3804.
4 R. B. Bedford and S. L. Welch, *Chem. Commun.*, 2001, 129.
5 A. F. Littke and G. C. Fu, *Angew. Chem., Int. Ed.*, 1998, **37**, 3387.
6 M. G. Andreu, A. Zapf and M. Beller, *Chem. Commun.*, 2000, 2475.
7 R. B. Bedford, C. S. J. Cazin, M. B. Hursthouse, M. E. Light, K. J. Pike and S. Wimperis, *J. Organomet. Chem.*, in press.
8 *UK Pat. Appl.*, 0116093.6, 2001
9 D. A. Albisson, R. B. Bedford and P. N. Scully, *Tetrahedron Lett.*, 1998, **39**, 9793; S. Iyer and C. Ramesh, *Tetrahedron Lett.*, 2000, **41**, 8981; I. P. Beletskaya, A. N. Kashin, N. B. Karltedt, A. V. Mitin, A. V. Cheprakov and G. M. Kazankov, *J. Organomet. Chem.*, 2001, **622**, 89.
10 H. Weissman and D. Milstein, *Chem. Commun.*, 1999, 1901; M. Ohff, A. Ohff and D. Milstein, *Chem. Commun.*, 1999, 357.
11 F. Paul, J. Patt and J. F. Hartwig, *J. Am. Chem. Soc.*, 1994, **116**, 5969.

CHEMCOMM
Communication
www.rsc.org/chemcomm

Tuning metal coordination number by ancillary ligand steric effects: synthesis of a three-coordinate iron(II) complex

Jeremy M. Smith, Rene J. Lachicotte and Patrick L. Holland*

Department of Chemistry, University of Rochester, Rochester NY 14627, USA.
E-mail: holland@chem.rochester.edu

Received (in Cambridge, UK) 24th April 2001, Accepted 9th July 2001
First published as an Advance Article on the web 31st July 2001

The coordination number of the metal in iron(II) β-diketiminate complexes can be tuned through the size of the alkyl substituents on the ligand backbone.

Low coordinate transition metal complexes are of much interest for their ability to achieve unusual and difficult transformations.[1] Biological interest stems from the low coordinate iron centres found in the iron–molybdenum cofactor of nitrogenase.[2] The high reactivity of coordinatively unsaturated sites on iron surfaces may also be imitated by these complexes.[3]

The chelating β-diketiminate ligands (Fig. 1) have experienced a renaissance in interest recently, in part for their ability to stabilise low-coordinate metal complexes.[4] Here we show how a simple modification of these ligands at a position away from the immediate site of coordination results in dramatic changes to the geometry of the metal atom.

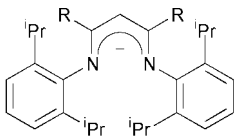

L R = Me
L′ R = ^{t}Bu

Fig. 1 β-Diketiminate ligands used in this study.

Reaction of equimolar amounts of the lithium salt of 2,4-bis(2,6-diisopropylphenylimido)pentane[5] (LiL) and $FeCl_2(THF)_{1.5}$[6] in THF results in the formation of a yellow solution, from which a yellow air-sensitive solid **1a** can be isolated by crystallisation from THF.† The molecular structure of crystals grown from pentane solution was determined by X-ray diffraction, revealing the product to be the 'ate' complex, $LFe(\mu\text{-}Cl)_2Li(THF)_2$ **1a**.‡ The complex crystallises with two molecules in the asymmetric unit (Fig. 2, only one molecule shown). The iron atom is four-coordinate, and distorted from ideal tetrahedral geometry. Thus, for example, the N(11)–Fe(1)–N(21) bond angle is relatively acute at 93.21(14)°, while the N(11)–Fe(1)–Cl(11) bond angle is relatively obtuse at 114.00(10)°. The bond lengths to iron do not significantly differ from typical values.[7] Interestingly, a second crystal form **1b**‡§ can be grown from THF at −35 °C; it crystallises with 3 molecules in the asymmetric unit. The gross structural features of all the unique molecules in both polymorphs are similar. The analogous diethyl ether solvated complex, $LFe(\mu\text{-}Cl)_2Li(Et_2O)_2$ **1c** can be obtained by crystallisation from diethyl ether at −35 °C.

The solid state magnetic moment is 5.4 μ_B, consistent with tetrahedral high spin iron(II).[8] More complicated behaviour is observed in solution. An unexpectedly large number of signals are observed in the ^{1}H NMR spectrum of **1a** in C_6D_6, although the correct number of resonances are observed in THF-d_8 solution. The solution magnetic moment[9] in either solvent is 4.4 μ_B. No changes in the spectrum or magnetic moment are observed in either solvent on addition of excess LiCl. Complexes **1a** and **1b** give identical ^{1}H NMR spectra in C_6D_6.

To determine the effect of the source of the β-diketiminate ligand on the coordination environment at iron, we used the magnesium complex LMg(Cl)(THF),¶ prepared from L and MeMgCl in THF. Reaction of this complex with $FeCl_2(THF)_{1.5}$ in THF solution results in the yellow complex $Mg(THF)_4[LFeCl(\mu\text{-}Cl)]_2$ **2** (Fig. 3).‖ The complex, which is insoluble in less polar solvents, can be isolated in moderate yield by multiple crystallisations from THF at −35 °C. An X-ray diffraction study‡ revealed the product to have an unusual structure, with the two iron centres bridged by a magnesium atom lying on a crystallographic inversion centre. Once again the iron is approximately tetrahedral, with bond lengths and angles similar to those in **1**.

Use of a slightly modified ligand resulted in a completely different product. Thus, refluxing a mixture of toluene, $FeCl_2(THF)_{1.5}$, and one molar equivalent of LiL′,[10] in which the ligand backbone methyls have been replaced by *tert*-butyl groups, results in the formation of a red solution from which a

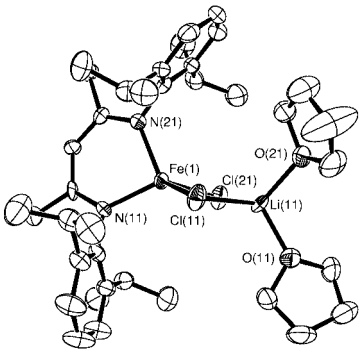

Fig. 2 Molecular structure of $LFe(\mu\text{-}Cl)_2Li(THF)_2$ **1a**. Hydrogen atoms not shown, thermal ellipsoids at 50% probability. Selected bond lengths (Å) and angles (°): Fe(1)–N(11) 2.006(3); Fe(1)–N(21) 2.021(4), Fe(1)–Cl(11) 2.324(1) Fe(1)–Cl(21) 2.338(1), Cl(11)–Li(11) 2.357(11), Cl(21)–Li(11) 2.363(8); N(11)–Fe(1)–N(21) 93.21(14), N(11)–Fe(1)–Cl(11) 114.00(10).

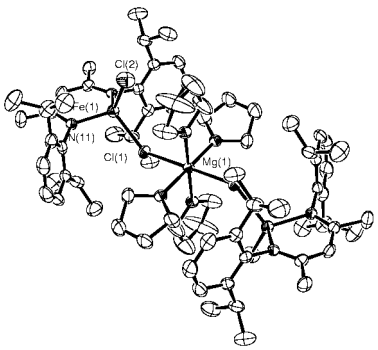

Fig. 3 Molecular structure of $[LFe(\mu\text{-}Cl)_2]Mg(THF)_4$ **2**. Hydrogen atoms not shown, thermal ellipsoids at 50% probability. Selected bond lengths (Å) and angles (°): Fe(1)–N(11) 2.011(3), Fe(1)–N(21) 2.014(3), Fe(1)–Cl(1) 2.377(1), Fe(1)–Cl(2) 2.267(1), Cl(1)–Mg(1) 2.5201(9); N(11)–Fe(1)–N(21) 92.15(12), N(11)–Fe(1)–Cl(1) 110.25(9).

 DOI: 10.1039/b103635c

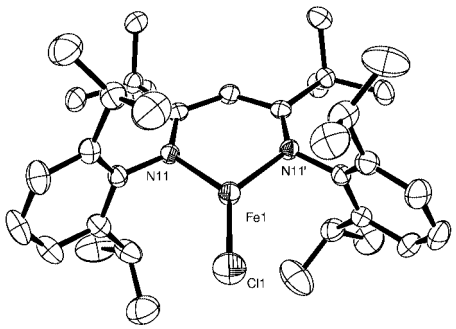

Fig. 4 Molecular structure of L′FeCl **3**. Hydrogen atoms not shown, thermal ellipsoids at 50% probability. Selected bond lengths (Å) and angles (°): Fe(1)–N(11) 1.948(2), Fe(1)–Cl(1) 2.172(1); N(11)–Fe(1)–N(11)′ 96.35(11), N(11)–Fe(1)–Cl(1) 131.83(5).

highly air-sensitive red solid **3** can be isolated.** The molecular structure of the product L′FeCl **3** was determined by X-ray crystallography (Fig. 4).‡ The iron and chlorine atoms are on a crystallographic mirror plane. The iron atom lies in a planar ring formed with the ligand; the bond angles around the metal reveal a planar geometry (sum of angles = 360°). The N(11)–Fe(1)–N(11)′ bond angle is compressed to 96.35(11)°, while the N(11)–Fe(1)–Cl(1) angle opens up to 131.83(5)°. As expected, the lower coordination number of the iron atom in **3** causes the bond lengths to the metal to decrease as compared to **1** and **2**. Both the solution (μ_{eff} = 5.5 μ_B) and solid state (μ_{eff} = 5.9 μ_B) magnetic moments confirm the high-spin iron(II) oxidation state. The ^{1}H NMR spectrum is relatively simple, consisting of seven paramagnetically shifted resonances.

While the effect of the ligand backbone groups on the coordination number of iron may not be immediately obvious, it can be understood by examining the C–N–C bond angles in the three complexes. In **1** they are in the range 118.6–120.3°, while in **3** they are 128.4(2)°. Thus, the *tert*-butyl groups on the ligand backbone in L′ force the aryl rings to close in on the metal, limiting the space available at the iron centre for more ligands.

In most three-coordinate complexes of Fe(II),[1,11] functionalisation, if it is achieved, is usually at the expense of the low coordination number. In contrast, complex **3** presents many viable pathways for further functionalisation by reactions with the chloride ligand while maintaining the low coordination number.

The University of Rochester is gratefully acknowledged for funding of this work. We would like to thank Kevin Mooney (University at Buffalo) for recording the SQUID data.

Notes and references

† **1a**: Yield 90% based on $FeCl_2(THF)_{1.5}$, mp 310 °C (decomp.) (Anal. Found: C, 63.88; H, 8.37; N, 4.11. $C_{37}H_{57}Cl_2FeLiN_2O_2$ requires C, 63.89; H, 8.25; N, 4.02%), δ_H(400 MHz, C_6D_6, 23 °C) 17.08, 15.33, 9.19, 6.42, 5.15, 2.67, 1.99, 1.14, 0.93, 0.31, −12.89, −13.14, −16.93, −24.25, −35.43, −40.44, −44.60, −65.39; δ_H(THF-d_8, 23 °C) 15.28, 6.98, −16.77, −43.60, −64.68.

‡ *Crystal data* For **1a**: $C_{37}H_{57}Cl_2FeLiN_2O_2$, M = 695.54, orthorhombic, space group $Pna2_1$, a = 23.1015(12), b = 9.9748(5), c = 35.9530(18), U = 7786.4(7) Å^3, T = 193(2) K, Z = 8, μ(Mo-Kα) = 0.556 mm^{-1}, 32164 reflections measured, 10201 unique (R_{int} = 0.0307), R_1 = 0.0478, wR_2 = 0.0967 [$I > 2\sigma(I)$].

For **1b**: orthorhombic, space group $P2_12_12_1$, a = 16.7761(8), b = 19.0238(9), c = 36.8905(19), U = 11773.4(10) Å^3, T = 193(2) K, Z = 12, μ(Mo-Kα) = 0.556 mm^{-1}, 53706 reflections measured, 16937 unique (R_{int} = 0.0520), R_1 = 0.0447, wR_2 = 0.0822 [$I > 2\sigma(I)$]. The ratio of the two enantiomorphic components was refined to a value of 0.461(13).

For **2**: $C_{42}H_{70}Cl_2FeMg_{0.5}N_3$, M = 1545.71, monoclinic, space group $P2_1/c$, a = 12.6469(8), b = 13.0103(8), c = 26.414(2), β = 102.853(1), U = 4237.3(5) Å^3, T = 193(2) K, Z = 2, μ(Mo-Kα) = 0.526 mm^{-1}, 18679 reflections measured, 6069 unique (R_{int} = 0.0551), R_1 = 0.0546, wR_2 = 0.1361 [$I > 2\sigma(I)$].

For **3**: $C_{35}H_{53}ClFeN_2$, M = 593.09, monoclinic, space group $C2/c$, a = 16.9014(11), b = 9.3514(6), c = 22.7756(15), β = 107.237(1), U = 3428.0(4) Å^3, T = 193(2) K, Z = 4, μ(Mo-Kα) = 0.540 mm^{-1}, 7361 reflections measured, 2463 unique (R_{int} = 0.0256), R_1 = 0.0398, wR_2 = 0.0704 [$I > 2\sigma(I)$].

CCDC reference numbers 167176–167180. See http://www.rsc.org/suppdata/cc/b1/b103635c/ for crystallographic data in CIF or other electronic format.

§ **1b**: μ_{eff} = 4.4 μ_B (Evans), μ_{eff} = 5.4 μ_B (SQUID, 5000 G, 50–300 K).

¶ LMgCl(THF): Yield 75%, δ_H(400 MHz, C_6D_6, 23 °C) 7.2–7.3 (br s, 6H, Ar-H), 4.95 (s, 1H, CH), 3.63 (br s, 4H, CH_2), 3.94 (br s, 4H, C*H*$(CH_3)_2$), 1.78 (s, 6H, CH_3), 1.48 (br s, 4H, CH_2), 1.39 (br s, 24H, C*H*$(CH_3)_2$).

‖ **2**: Yield 60% based on $FeCl_2(THF)_{1.5}$, mp 302–304 °C, δ_H(400 MHz, THF-d_8, 23 °C) 13.58, 12.95, 5.68, −0.97, −1.25, −1.74, −2.63, −20.76, −28.13, −41.02, −47.98, −69.77; μ_{eff} = 4.2 μ_B.

** **3**: Yield 88% based on $FeCl_2(THF)_{1.5}$, mp 270–272 °C (Anal. Found: C, 70.26; H, 8.86; N, 4.77. $C_{35}H_{53}ClFeN_2$ requires C, 70.69; H, 8.42; N, 4.61%); δ_H(400 MHz, C_6D_6, 23 °C) 48.78, 2.35, 1.21, 0.40, −25.84, −105.33, −115.05; μ_{eff} = 5.5 μ_B (Evans), μ_{eff} = 5.9 μ_B (SQUID, 5000 G, 50–300 K).

1 C. C. Cummins, *Prog. Inorg. Chem.*, 1998, **47**, 685; S. Alvarez, *Coord. Chem. Rev.*, 1999, **193**–**195**, 13.
2 J. Kim and D. C. Rees, *Nature*, 1992, **360**, 553; J. B. Howard and D. C. Rees, *Chem. Rev.*, 1996, **96**, 2965; D. C. Rees and J. B. Howard, *Curr. Opin. Chem. Biol.*, 2000, **4**, 559.
3 *Handbook of Heterogeneous Catalysis*, ed. G. Ertl, H. Knözinger and J. Weitkamp, Wiley-VCH, Weinheim, 1997, vol. 4.
4 P. H. M. Budzelaar, R. de Gelder and A. W. Gal, *Organometallics*, 1998, **17**, 4121; M. Cheng, E. B. Lobkovsky and G W. Coates, *J. Am. Chem. Soc.*, 1998, **120**, 11 018; P. L. Holland and W. B. Tolman, *J. Am. Chem. Soc.*, 1999, **121**, 7270; C. E. Radzewich, I. A. Guzei and R. F. Jordan, *J. Am. Chem. Soc.*, 1999, **121**, 8673; M. Cheng, A. B. Attygalle, E. B. Lobkovsky and G. W. Coates, *J. Am. Chem. Soc.*, 1999, **121**, 11 583; C. Cui, H. W. Roesky, H.-G. Schmidt, M. Noltemeyer, H. Hao and F. Cimpoesu, *Angew. Chem., Int. Ed.*, 2000, **39**, 4274; V. C. Gibson, J. A. Segal, A. J. P. White and D. J. Williams, *J. Am. Chem. Soc.*, 2000, **122**, 7120; N. J. Hardman, B. E. Eichler and P. P. Power, *Chem. Commun.*, 2000, 1991; P. J. Bailey, R. A. Coxall, C. M. Dick, S. Fabre and S. Parsons, *Organometallics*, 2001, **20**, 798; A. Akkari, J. J. Byrne, I. Saur, G. Rima, H. Gornitzka and J. Barrau, *J. Organomet. Chem.*, 2001, **622**, 190; N. J. Hardman, C. Cui, H. W. Roesky, W. H. Fink and P. P. Power, *Angew. Chem., Int. Ed.*, 2001, **40**, 2172.
5 J. Feldman, S. J. McLain, A. Parthasarathy, W. J. Marshall, J. C. Calabrese and S. D. Arthur, *Organometallics*, 1997, **16**, 1514.
6 R. J. Kern, *J. Inorg. Nucl. Chem.*, 1962, **24**, 1105.
7 A. G. Orpen, L. Brammer, F. H. Allen, O. Kennard, D. G. Watson and R. Taylor, *J. Chem. Soc., Dalton Trans.*, 1989, S1.
8 C. D. Burbridge and D. M. L. Goodgame, *J. Chem. Soc. A*, 1968, 1074.
9 M. V. Baker, L. D. Field and T. W. Hambley, *Inorg. Chem.*, 1988, **27**, 2872.
10 P. H. M. Budzelaar, A. B. van Oort and A. G. Orpen, *Eur. J. Inorg. Chem.*, 1998, 1485.
11 W. Seidel and K.-J. Lattermann, *Z. Anorg. Allg. Chem.*, 1982, **488**, 69; D. M. Roddick, T. D. Tilley, A. L. Rheingold and S. J. Geib, *J. Am. Chem. Soc.*, 1987, **109**, 945; P. P. Power and S. C. Shoner, *Angew. Chem., Int. Ed. Engl.*, 1991, **30**, 330; F. M. MacDonnell, K. Ruhlandt-Senge, J. J. Ellison, R. H. Holm and P. P. Power, *Inorg. Chem.*, 1995, **24**, 1815; S. L. Stokes, W. M. Davis, A. L. Odom and C. C. Cummins, *Organometallics*, 1996, **15**, 4521; M. A. Putzer, B. Neumüller, K. Dehnicke and J. Magull, *Chem. Ber.*, 1996, **129**, 715; U. Siemeling, U. Vorfeld, B. Neumann and H.-G. Stammler, *Inorg. Chem.*, 2000, **39**, 5159.

CHEMCOMM
Communication
www.rsc.org/chemcomm

Ultrasound promoted C–C bond formation: Heck reaction at ambient conditions in room temperature ionic liquids

Ravindra R. Deshmukh, R. Rajagopal and K. V. Srinivasan*

Organic Chemistry, Technology Division, National Chemical Laboratory, Pune - 411 008, India. E-mail: kvsri@dalton.ncl.res.in

Received (in Cambridge, UK) 22nd May 2001, Accepted 27th June 2001
First published as an Advance Article on the web 1st August 2001

Heck reaction proceeds at ambient temperature (30 °C) with considerably enhanced reaction rate (1.5–3 h) through the formation of Pd–biscarbene complexes and stabilized clusters of zero-valent Pd nanoparticles in ionic liquids under ultrasonic irradiation.

The palladium catalyzed Heck reaction involving the coupling of alkenes/alkynes with aryl and vinyl halides is one of the most powerful tools in synthetic organic chemistry.[1] The reactions which are carried out in polar solvents such as DMF and NMP generally involve long reaction times (8–72 h) at temperatures ranging from 80–140 °C.[2] In recent times, ionic liquids have gained prominence as attractive alternatives to volatile organic solvents for catalytic reactions and separation processes.[3] Heck reaction in ionic liquids, in particular those involving dialkylimidazolium salts, have been reported very recently.[4] However, even in such media, wherein the ionic liquid anion and cation can exert a marked effect on the rate of the reaction, the reaction times involved are 24–72 h at temperatures ranging from 80–100 °C. This communication reports for the first time an ultrasound promoted Heck reaction in ionic liquids at ambient temperature (30 °C) with considerably enhanced reaction rates (reaction times 1.5–3 h) than those reported so far.

The sonochemical reactions were carried out in a thermostated ultrasonic cleaning bath of frequency 50 KHz (Branson 5200). Iodobenzene and substituted iodobenzenes were reacted with various alkenes/phenylacetylene in ionic liquids 1,3-di-*n*-butylimidazolium bromide [(bbim)$^+$Br$^-$] and 1,3-di-*n*-butylimidazolium tetrafluoroborate [(bbim)$^+$BF$_4^-$][5] using $Pd(OAc)_2$ as well as $PdCl_2$ as catalyst and sodium acetate as base under ultrasonic irradiation as shown in Fig. 1.

The products could be easily separated from the catalyst by extraction with 10% ethyl acetate in petroleum ether leaving behind the palladium catalyst in the dissolved state in the immiscible ionic liquid. The catalyst thus recovered as a solution in the ionic liquid could be reused at least three times without any loss of activity. Pure products were isolated by column chromatography.

The results are summarized in Table 1. As is evident, the ultrasound assisted Heck reaction of the iodobenzenes with alkenes/alkynes proceeded smoothly at ambient temperature (30 °C) with complete conversion of iodobenzenes in just 1.5–3 h to afford the *trans* products in excellent isolated yields (73–87%). No reaction under similar sonication conditions was observed when the ionic liquid was replaced by molecular solvents such as DMF and NMP even in the presence of a ligand such as PPh_3. The reaction also did not proceed with the less reactive aryl chlorides (chlorobenzene, *p*-nitrochlorobenzene and 2,4-dinitrochlorobenzene) and aryl bromides (bromobenzene) under the sonochemical conditions of the present work. Obviously, no reaction even in traces could be observed under ambient conditions in the absence of ultrasound.

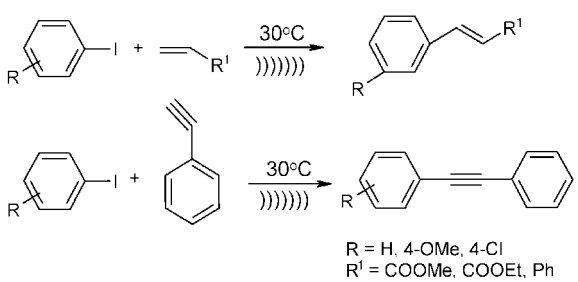

Fig. 1

Phosphine ligands, ammonium and phosphonium halides and quarternary ammonium salts have been found to stabilize the Pd-catalysts probably *via* formation of zero-valent Pd species and accelerate the olefination reaction.[6,7] In particular, Pd–carbene complexes with alkylimidazol-2-ylidenes have been reported very recently to be active in the Heck reaction.[4b] In the present work, the formation of such a complex was studied by subjecting a mixture of $Pd(OAc)_2$ or $PdCl_2$ and NaOAc in [bbim] + Br$^-$ and [bbim] + BF$_4^-$ respectively to ultrasound irradiation for 1 h. The complex was extracted into chloroform from the ionic liquid, the chloroform evaporated and the resulting crude product purified by column chromatography [petroleum ether–EtOAc, 1 : 1]. Indeed, the formation of the complex A was established and characterized by ^{1}H-NMR by the appearance of N–CH vinylic protons at δ 6.85 as a multiplet in the complex similar to the value reported by Xiao *et al.*[4b] and by the conspicuous absence of the N_2CH protons which appears as a singlet at δ 8.82 in the parent ionic liquid. The complexes were also characterized by MS which showed the respective molecular ion peaks. It is highly probable that complex A could be the immediate precursor for the likely active catalyst which could lead to a zero-valent Pd-species whose *in situ* generation by reduction of the divalent Pd–carbene complex is accelerated by electron transfer reactions under the sonochemical conditions primarily through the phenomenon of cavitation. It is well known that sonochemical processes proceed through SET mechanistic pathway by means of formation and adiabatic collapse of transient cavitation bubbles.[8,9] It is also highly probable that the Pd complexes formed *in situ* will experience secondary reactions in the liquid phase after the bubble collapses. Moreover, such Pd carbene complexes have been shown to be the precursors for active catalysts for the Heck and related C–C bond forming reactions in both molecular solvents and ionic liquids.[10–12] Detailed investigation of the mechanistic pathways as regards the formation/decomposition of the Pd–carbene complex under the sonochemical conditions is in progress and will form part of a full paper.

It has long been known that chemical or electrochemical reduction of transition metal salts in the presence of ammonium salts leads to $R_4N^+X^-$ stabilized colloids.[13] A recent study points to the involvement of intermediary colloidal Pd-nanoparticles generated under thermolytic conditions for the catalysis of the Heck reaction.[14] The formation of such Pd-nanoparticles was investigated in the present work by subjecting the reaction mixture, after successful Heck reaction of iodobenzene with ethyl acrylate in [bbim]$^+$BF$_4^-$ under sonochemical conditions, for '*in situ*' TEM analysis.

TEM analysis was carried out in Transmission Electron Microscope Model JEOL-1200 EX operated at 100 kV with a magnification of 200 K. The sample after appropriate dilution with isopropyl alcohol was directly deposited on carbon film

 DOI: 10.1039/b104532f

Table 1 Heck reaction of iodobenzenes with activated alkenes/alkyne under sonication in [bbim]$^+$ Br$^-$/[bbim]$^+$ BF_4[a]

No.	Aryl halide	Olefin/alkyne	Time/h	Product	% Yield[b] (Isolated)
1.		Methyl acrylate	2.0	Methyl cinnamate	81
		Ethyl acrylate	1.5	Ethyl cinnamate	87
		Styrene	1.5	Stilbene	82
		Phenylacetylene	2.0	Diphenylacetylene	78
2.	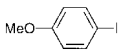	Methyl acrylate	3.0	4-Methoxymethyl cinnamate	82
		Ethyl acrylate	3.0	4-Methoxyethyl cinnamate	79
		Styrene	3.0	4-Methoxystilbene	80
		Phenylacetylene	2.0	(4-Methoxyphenyl)phenylacetylene	77
3.	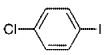	Methyl acrylate	1.5	4-Chloromethyl cinnamate	79
		Ethyl acrylate	1.5	4-Chloroethyl cinnamate	77
		Styrene	1.5	4-Chlorostilbene	73
		Phenylacetylene	2.0	(4-Chlorophenyl)phenyl acetylene	78

[a] *Reaction conditions*: a mixture of iodoarene (2 mmol), alkene/alkyne (2.1 mmol), sodium acetate (0.2 g), $Pd(OAc)_2$ (0.02 mmol) and ionic liquid (1.5 ml) sonicated in an atmosphere of argon. [b] Yields are based on iodobenzenes. All the products were *trans* and fully characterized by ^{1}H-NMR, IR, MS and elemental analysis.

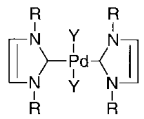

A

R = n-butyl
Y = Br, BF_4

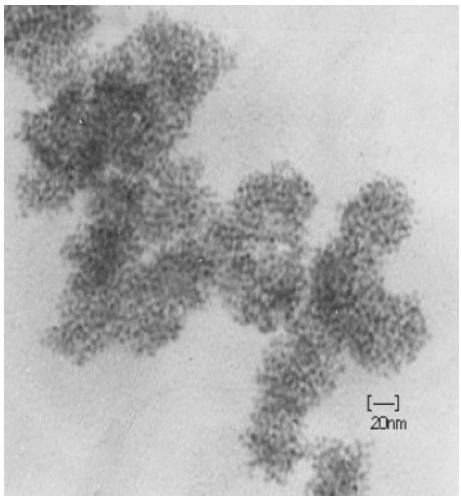

Fig. 2 TEM image of palladium clusters formed in the sonolytic Heck reaction.

coated TEM grids forming a thin film of colloidon. The TEM image (Fig. 2) shows the presence of monodispersed grains nearly spherical in shape. The average size of the grains obtained from the TEM picture is about 20 nm. The porous grains show that they are composed of dispersed particles of approximately 1 nm size. The clusters of Pd^0 nanoparticles in ionic liquids were found to be stable even after storage for a week since no change in the TEM picture was observed after this period, the ionic liquid obviously contributing to the stability. Further work is in progress in investigating the structural details of the nano-assembly of metallic palladium and its dispersion in ionic liquids under sonolytic conditions.

In conclusion, the Heck reaction has been performed at ambient temperature with considerably enhanced reaction rates by the combined use of ultrasonic irradiation and ionic liquids as solvent. Under the sonochemical conditions, the formation of Pd–biscarbene complex as a precursor and its subsequent sonolytic conversion to a highly stabilized cluster of zero-valent Pd nanoparticles has been established by NMR/MS and *in situ* TEM analyses respectively. Further work is in progress to elaborate these findings to other C–C bond formations such as Suzuki and Stille coupling reactions.[6]

R. R. D. and R. R. thank CSIR, New Delhi for the award of a Senior Research Fellowship. We thank Dr M. Bhadbhade and Dr Rajesh Gonnade for help in TEM analysis.

Notes and references

1 (*a*) H. A. Dieck and R. F. Heck, *J. Org. Chem.*, 1975, **40**, 1083; (*b*) T. Jeffery, *J. Chem. Soc., Chem. Commun.*, 1984, 1287.
2 (*a*) J. I. i. Kim, B. A. Patil and R. F. Heck, *J. Org. Chem.*, 1981, **46**, 1067; (*b*) D. D. Bender, I. G. Stakem and R. F. Heck, *J. Org. Chem.*, 1982, **47**, 1278.
3 (*a*) T. Welton, *Chem. Rev.*, 1999, **99**, 2071; (*b*) P. Wasserschied and W. Keim, *Angew. Chem., Int. Ed.*, 2000, **39**, 3772.
4 (*a*) A. J. Carmichael, M. J. Earle, J. D. Holbrey, P. B. McCormac and K. R. Seddon, *Org. Lett.*, 1999, **1**, 997; (*b*) L. Xu, W. Chem and J. Xiao, *Organometallics*, 2000, **19**, 1123.
5 [bbim]$^+$ Br $^-$ was prepared by heating 1-butylimidazole with 1-bromobutane at 70 °C for 2 h and distilling off excess 1-bromobutane under high vacuum to afford a thick brownish yellow liquid having density, 1.228 g cm^{-3}. [bbim]$^+$ BF_4^- was obtained by the metathesis of [bbim]$^+$ Br$^-$ with $NaBF_4$ in water to give a pale yellow free flowing liquid having density, 1.152 g cm^{-3}. Both the ionic liquids were well characterized by IR, ^{1}H and ^{13}C NMR, and elemental analysis.
6 (*a*) S. Brase and A. de Meijere, *Metal catalyzed cross coupling reactions*, ed. F. Diederich and P. J. Stang, Wiley-VCH, Chichester, 1998; (*b*) J. Tsuji, *Palladium Reagents and Catalyst-Innovations in Organic Synthesis*, Wiley, Chichester, 1995.
7 (*a*) T. Jeffery, *Tetrahedron Lett.*, 1985, **26**, 2267; (*b*) C. Amatore, M. Azzahi and A. J. Juand, *J. Am. Chem. Soc.*, 1991, **113**, 8375.
8 J. L. Luche, *Ultrasonics*, 1992, **30**, 156.
9 A. Henglein, *Advances in Sonochemistry*, ed. T. J. Mason, JAI Press, London and Greenwich, 1993, vol. 3, pp. 17–83.
10 W. A. Herrmann and C. Kocher, *Angew. Chem., Int. Ed. Engl.*, 1997, **36**, 2163.
11 W. A. Herrmann, V. P. W. Bohm and C. J. Reisinger, *J. Organomet. Chem.*, 1999, **576**, 23.
12 C. Zhang, J. Huang, M. L. Trudell and S. P. Nolan, *J. Org. Chem.*, 1999, **64**, 3804.
13 (*a*) H. Bonnemann, W. Brijoux, R. Brinkmann, E. Dinjus, T. Joussen and B. Korall, *Angew. Chem., Int. Ed. Engl.*, 1991, **30**, 1312; (*b*) M. T. Reetz and S. A. Quaiser, *Angew. Chem., Int. Ed.*, 1995, **34**, 2240.
14 M. T. Reetz and E. Westermann, *Angew. Chem., Int. Ed.*, 2000, **39**, 165.

CHEMCOMM Communication
www.rsc.org/chemcomm

Asymmetric trialkylaluminium addition to aldehydes catalyzed by titanium complexes of *N*-sulfonylated amino alcohols with two stereogenic centers

Jing-Song You,† Sheng-Hsiang Hsieh and Han-Mou Gau*

Department of Chemistry, National Chung-Hsing University, Taichung, Taiwan 402. E-mail: hmgau@dragon.nchu.edu.tw

Received (in Cambridge, UK) 23rd April 2001, Accepted 20th June 2001
First published as an Advance Article on the web 1st August 2001

The asymmetric methylation, ethylation and allylation of aldehydes using trialkylaluminium reagents catalyzed by titanium(IV) complexes of *N*-sulfonylated amino alcohols gave excellent enantioselectivities of up to 99% ee.

Catalytic asymmetric carbon–carbon bond formation has been one of the most studied subjects in the past 10 years.[1] In these studies, the enantioselective additions of organozinc to aldehydes are one of the most reliable processes and thus gain much attention from chemists.[2–6] For alkylation reagents, trialkylaluminium reagents are more interesting since they are economically obtained in industrial scale.[7] Therefore the successful alkylation of aldehydes by trialkylaluminium should have great potential for practical applications. Unlike the diethylzinc addition to aldehydes which is extremely slow in the absence of a catalyst, trialkylaluminium reagents themselves are known to add to aldehydes at room temperature within hours. Due to competing reactions, the development of enantioselective catalysts for trialkylaluminium addition becomes much more challenging. Recently, Chan *et al.* reported the first example of asymmetric $AlEt_3$ addition to aldehydes employing titanium–BINOL systems with excellent ee's.[8] Subsequently, two papers dealing with the asymmetric methylation[9] and ethylation[10] of aldehydes by trialkylaluminium reagents were also reported.

Following our recent interest in titanium chemistry,[11] we herein report the synthesis of a family of amino alcohol derivatives **1**–**4** with one or two stereogenic centers. For *N*-sulfonylated amino alcohol derivative (*S*)-**1a** or (*S*)-**1b** as a chiral ligand, the asymmetric triethylaluminium addition to benzaldehyde was examined to afford low ee values of 29% (*R*) and 2% (*S*), respectively. The above results prompted us to synthesize a series of amino alcohols with two stereogenic centers, hoping to learn more about the structural factors that influence the enantioselectivity. Based on the route described by Reetz *et al.*,[12] amino alcohols **2** with two stereogenic centers starting from (*S*)-amino acids were synthesized. Compound **2** further reacted with arylsulfonyl chloride to give *N*-sulfonylated amino alcohol derivatives (*R*,*S*)-**3a**, (*R*,*S*)-**4a**–**c**, and (*S*,*S*)-**4a**.

Asymmetric triethylaluminium additions to benzaldehyde catalyzed by titanium(IV) complexes were conducted [eqn. (1)],

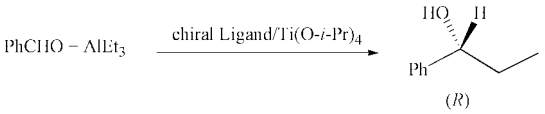

(1)

and the results are listed in Table 1.‡ While using 10 mol% of *N*-sulfonylated β-amino alcohol (*S*)-**1a** or (*S*)-**1b**, the reaction gave low ee values (entries 1 and 2). In using bidentate (*R*,*S*)-**3a** with two stereogenic centers, the ee value dramatically improved to 70% (entry 3). From entries 4–6, the tridentate ligands (*R*,*S*)-**4a** were examined with variation of the amount of $Ti(O\text{-}i\text{-}Pr)_4$ added. Without the addition of $Ti(O\text{-}i\text{-}Pr)_4$, the yield of 1-phenylpropanol is 44% with ee value of only 4% (*R*) (entry 4). With the addition of 0.05 mmol $Ti(O\text{-}i\text{-}Pr)_4$ (10 mol%), which gives a molar ratio of 1 : 1 of $Ti(O\text{-}i\text{-}Pr)_4$–(*R*,*S*)-**4a**, the ee value improves to 45% (*R*) (entry 5). Similar to previous studies of asymmetric diethylzinc addition to aldehydes, excess $Ti(O\text{-}i\text{-}Pr)_4$ is required in order to obtain the best enantioselectivity and, in this study, the best ee value of 96% was obtained for a catalytic system with a $Ti(O\text{-}i\text{-}Pr)_4$–(*R*,*S*)-**4a** ratio of 18 (entry

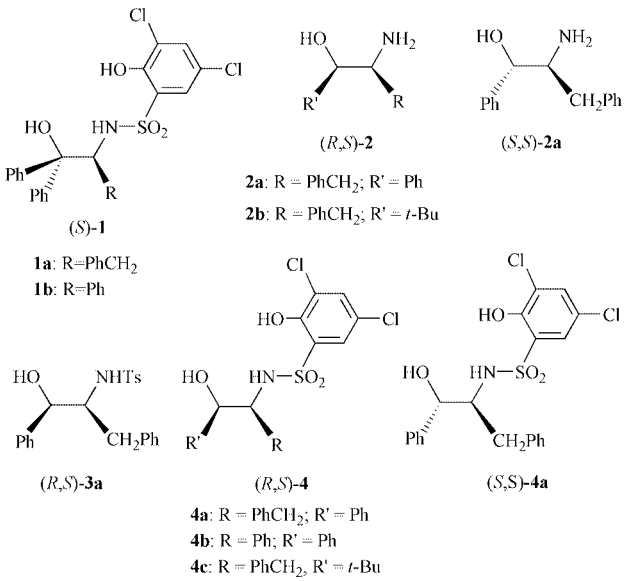

† Postdoctoral research fellow from Department of Chemistry, Sichuan University, P. R. China.

Table 1 Enantioselective addition of trialkylaluminium to benzaldehyde catalyzed by *in Situ*-formed chiral ligand–$Ti(O\text{-}i\text{-}Pr)_4$ catalytic systems in THF[a]

Entry	Compd. (mol%)	AlR_3	$Ti/O\text{-}i\text{-}Pr)_4$/mmol	Yield (%)	% ee[b]
1	(*S*)-**1a** (10)	$AlEt_3$	0.9	90	29 (*R*)
2	(*S*)-**1b** (10)	$AlEt_3$	0.9	84	2 (*S*)
3	(*R*,*S*)-**3a** (10)	$AlEt_3$	0.9	97	70 (*R*)
4	(*R*,*S*)-**4a** (10)	$AlEt_3$	0	44	4 (*R*)
5	(*R*,*S*)-**4a** (10)	$AlEt_3$	0.05	49	45 (*R*)
6	(*R*,*S*)-**4a** (10)	$AlEt_3$	0.9	98	96 (*R*)
7	(*R*,*S*)-**4a** (5)	$AlEt_3$	0.45	97	95 (*R*)
8	(*S*,*S*)-**4a** (10)	$AlEt_3$	0.9	70	26 (*S*)
9	(*R*,*S*)-**4b** (10)	$AlEt_3$	0.9	94	75 (*R*)
10	(*R*,*S*)-**4c** (10)	$AlEt_3$	0.9	66	8 (*S*)

[a] Benzaldehyde, 0.5 mmol; trialkylaluminium, 1.25 mmol; reaction temperature, 0 °C; reaction time, 12 h. [b] The ee values were determined by HPLC with a chiral OD column.

 DOI: 10.1039/b103618c

Table 2 Enantioselective addition of trialkylaluminium to aldehydes catalyzed by *in situ*-formed 10 mol% (*R*,*S*)-**4a**–Ti(O-*i*-Pr)$_4$ catalytic systems in THF[a]

Entry	Aldehyde	AlR_3	Ti(O-*i*-Pr)$_4$/ mmol	Yield (%)	% ee[b]
1	Benzaldehyde	$AlEt_3$	0.9	98	96 (*R*)
2	4-Chlorobenzaldehyde	$AlEt_3$	0.9	100	94 (*R*)
3	1-Naphthaldehyde	$AlEt_3$	0.9	94	92 (*R*)
4	2-Naphthaldehyde	$AlEt_3$	0.9	100	92 (*R*)
5	*E*-Cinnamaldehyde	$AlEt_3$	0.9	100	88 (*R*)
6	Cyclohexanecarboxaldehyde	$AlEt_3$	0.9	54	91 (*R*)[c]
7	Benzaldehyde	$AlMe_3$	0.9	100	98 (*R*)
8	1-Naphthaldehyde	$AlMe_3$	0.9	95	96 (*R*)
9	Cyclohexanecarboxaldehyde	$AlMe_3$	0.9	100	91 (*R*)[c]
10	(*E*)-Cinnamaldehyde	$AlMe_3$	0.9	99	> 99 (*R*)
11	Benzaldehyde	(Allyl)$AlEt_2$	0.9	100	90 (*R*)
12	2-Naphthaldehyde	(Allyl)$AlEt_2$	0.9	100	96 (*R*)

[a] Aldehyde, 0.5 mmol; trialkylaluminium, 1.25 mmol; Ti(O-*i*-Pr)$_4$, 0.9 mmol; reaction temperature, 0 °C; reaction time, 12 h. [b] The ee values were determined by HPLC with a chiral OD column. [c] Determined by HPLC with a chiralcel AS column after protecting as a benzoyl ester.

6). Even with the use of as little as 5 mol% of (*R*,*S*)-**4a**, 95% ee was still obtained (entry 7). For chiral ligand (*S*,*S*)-**4a** which is a diastereomer of (*R*,*S*)-**4a**, a much lower ee value of 26% was obtained (entry 8). When the substituent on the amino carbon was replaced with a phenyl group ((*R*,*S*)-**4b**), the ee value decreases to only 75% (entry 9). For (*R*,*S*)-**4c** with a *tert*-butyl substituent instead of a phenyl group on the chiral alcoholic carbon in (*R*,*S*)-**4a**, an ee value of 8% of *S*-configuration was observed (entry 10). In the initial study of triethylaluminium addition to benzaldehyde, a profound solvent effect was observed, and only a coordinating solvent such as THF prompted high enantioselectivities.

The enhanced unique reactivity of the *N*-sulfonylated amino alcohol (*R*,*S*)-**4a** is suggested to arise from the following two factors: (1) phenoxides are known to form strong bonds to group 4 transition metals, and with electron withdrawing halogen groups, the phenoxide moiety may lead to enhance Lewis acidity at the metal centre; (2) the phenolic ring provides conformational rigidity which may be an important factor in the transfer of asymmetry.

For examining the substrate generality, the best performing (*R*,*S*)-**4a**–Ti(O-*i*-Pr)$_4$ catalytic system was used (Table 2). Ee values ranging from 92–96% (*R*) (entries 1–4) were recorded for aromatic aldehydes with the best result observed for benzaldehyde as a substrate. For the (*E*)-cinnamaldehyde, the ee value is somewhat lower at 88% (entry 5). Interestingly, the catalytic system catalyzed the ethylation of the aliphatic cyclohexanecarboxaldehyde with an ee value of 91% (entry 6). Though not many aldehydes were examined, the catalytic system generally seems to work well for both aromatic and aliphatic aldehydes.

In addition, other trialkylaluminium reagents such as $AlMe_3$ and $AlEt_2$(allyl)[13] were also examined. $AlMe_3$ was added to aldehydes, to give exceptional ee values from 91 to 99% (entries 7–10). More interestingly, when allyldiethylaluminium was used as an alkylation reagent, the allyl group rather than the ethyl group selectively added to aldehydes to give the secondary homoallyl alcohol with excellent ee values of 90% for benzaldehyde (entry 11) and 96% for 2-naphthaldehyde (entry 12). For catalytic allylation reactions, this is the first example of catalytically enantioselective allylation of aldehydes employing the allyldialkylaluminium reagent, to the best of our knowledge.

In summary, a family of *N*-sulfonylated amino alcohols have been developed for asymmetric alkylation reactions. The (*R*,*S*)-**4a**–Ti(O-*i*-Pr)$_4$ system is an excellent catalyst for trialkylaluminium addition to aldehydes at a convenient temperature of 0 °C. Furthermore, the (*R*,*S*)-**4a**/Ti(O-*i*-Pr)$_4$ catalytic system shows a wide generality of trialkylaluminum reagents such as $AlEt_3$, $AlMe_3$, or even (allyl)$AlEt_2$.

We would like to thank the National Science Council of Taiwan for financial support (NSC 89-2113-M-005-024).

Notes and references

‡ *General procedures for the addition of trialkylaluminium reagents to aldehydes*. Under a dry dinitrogen atmosphere, the ligand and Ti(O-*i*-Pr)$_4$ were mixed in 1.5 mL of dry THF at room temperature. After 1 hour, 1.25 mmol of $AlEt_3$, $AlMe_3$ or allyldiethylaluminum was added at 0 °C. After the mixture was stirred for 30 min, the orange-colored solution was treated with aldehyde (0.5 mmol) at 0 °C, kept at this temperature for 10 h, and quenched with 1 M HCl. The aqueous phase was extracted with ethyl acetate (3 × 5 mL), dried over $MgSO_4$, filtered and concentrated. Chromatography of the residue on silica gel (elution with 5:1 hexane–ethyl acetate) gave the alcohol. The enantiomeric purity of the product was determined by HPLC.

1 R. Noyori, *Asymmetric Catalysis in Organic Synthesis*, Wiley, New York, 1994.
2 R. O. Duthaler and A. Hafner, *Chem. Rev.*, 1992, **92**, 807; K. Soai and S. Niwa, *Chem. Rev.*, 1992, **92**, 833.
3 For amino alcohols as ligands: M. Kitamura, S. Suga, K. Kawai and R. Noyori, *J. Am. Chem. Soc.*, 1986, **108**, 6071; P. I. Dosa and G. C. Fu, *J. Am. Chem. Soc.*, 1998, **120**, 445; B. Goldfuss and K. Houk, *J. Org. Chem.*, 1998, **63**, 8998; W. A. Nugent, *Chem. Commun.*, 1999, 1369; M. R. Paleo, I. Cabeza and F. J. Sardina, *J. Org. Chem.*, 2000, **65**, 2108; D. E. Frantz, R. Fässler and E. M. Carreira, *J. Am. Chem. Soc.*, 2000, **122**, 1806; I. Sato, T. Saito and K. Soai, *Chem. Commun.*, 2000, 2471.
4 For diols as ligands: D. Seebach, A. K. Beck, B. Schmidt and Y. M. Wang, *Tetrahedron*, 1994, **50**, 4363; N. Oguni, N. Satoh and H. Fujii, *Synlett*, 1995, 1043; H. Sellner and D. Seebach, *Angew. Chem., Int. Ed. Engl.*, 1999, **38**, 1918; D. Seebach, A. Pichota, A. K. Beck, A. B. Pinkerton, T. Litz, J. Karjalainen and V. Gramlich, *Org. Lett.*, 1999, **1**, 55.
5 For binaphthols as ligands: M. Mori and T. Nakai, *Tetrahedron Lett.*, 1997, **38**, 6233; F. Y. Zhang and A. S. C. Chan, *Tetrahedron: Asymmetry*, 1997, **8**, 3651; X. W. Yang, J. H. Sheng, C. S. Da, H. S. Wang, W. Su, R. Wang and A. S. C. Chan, *J. Org. Chem.*, 2000, **65**, 295.
6 For disulfonamides as ligands: H. Takahashi, T. Kawakita, M. Ohno, M. Yoshioka and S. Kobayashi, *Tetrahedron*, 1992, **48**, 5691; C. Lutz and P. Knochel, *J. Org. Chem.*, 1997, **62**, 7895; J. Qiu, C. Guo and X. Zhang, *J. Org. Chem.*, 1997, **62**, 2665; L. A. Paquette and R. Zhou, *J. Org. Chem.*, 1999, **64**, 7929; J. Balsells and P. J. Walsh, *J. Am. Chem. Soc.*, 2000, **122**, 1802; J. Balsells and P. J. Walsh, *J. Am. Chem. Soc.*, 2000, **122**, 3250.
7 F. A. Cotton and G. Wilkinson, *Advanced Inorganic Chemistry*, 4th edn., Wiley, New York, 1980, p. 342.
8 A. S. C. Chan, F. Y. Zhang and C. W. Yip, *J. Am. Chem. Soc.*, 1997, **119**, 4080.
9 B. L. Pagenkopf and E. M. Carreira, *Tetrahedron Lett.*, 1998, **39**, 9593.
10 J.-F. Lu, J.-S. You and H.-M. Gau, *Tetrahedron: Asymmetry*, 2000, **11**, 2531.
11 M.-Y. Shao and H.-M. Gau, *Organometallics*, 1998, **17**, 4822; J.-S. You, M.-Y. Shao and H.-M. Gau, *Organometallics*, 2000, **19**, 3368; J.-S. You, H.-M. Gau and M. C. K. Choi, *Chem. Commun.*, 2000, 1963.
12 M. T. Reetz, M. W. Drewes and A. Schmitz, *Angew. Chem., Int. Ed. Engl.*, 1987, **26**, 1141.
13 T. Mukaiyama, N. Minowa, T. Oriyama and K. Narasaka, *Chem. Lett.*, 1986, 97.

CHEMCOMM Communication
www.rsc.org/chemcomm

A comparison of the pentaammine(pyridyl)ruthenium(II) and 4-(dimethylamino)phenyl groups as electron donors for quadratic non-linear optics

Benjamin J. Coe,*[a] James A. Harris,[a] Koen Clays,[b] André Persoons,[b,c] Kurt Wostyn[b] and Bruce S. Brunschwig[d]

[a] *Department of Chemistry, University of Manchester, Oxford Road, Manchester, UK M13 9PL. E-mail: b.coe@man.ac.uk*
[b] *Department of Chemistry, University of Leuven, Celestijnenlaan 200D, B-3001 Leuven, Belgium*
[c] *Optical Sciences Center, University of Arizona, Tucson, Arizona, AZ 85721, USA*
[d] *Chemistry Department, Brookhaven National Laboratory, P.O. Box 5000, Upton, New York 11973-5000, USA*

Received (in Cambridge, UK) 19th April 2001, Accepted 13th June 2001
First published as an Advance Article on the web 1st August 2001

Hyper-Rayleigh scattering and Stark spectroscopic studies show that the complex salts [1–4]PF_6 have larger static first hyperpolarizabilities β_0 than [5–8]PF_6, because the higher HOMO energy of a $\{Ru^{II}(NH_3)_5\}^{2+}$ centre more than offsets the superior π-orbital overlap in the purely organic chromophores.

Recent years have witnessed great interest in molecular materials having non-linear optical (NLO) properties, due to their potential for applications in nascent optoelectronic/photonic technologies.[1] Most such materials are purely organic, but organotransition metal complexes also exhibit NLO effects.[2] Our contribution to this field has focused on the quadratic NLO properties of dipolar Ru^{II} ammine complexes.[3]

Molecules with large quadratic NLO activities contain electron donor and acceptor groups connected via polarisable π-systems. Molecular quadratic NLO behaviour arises from first hyperpolarizabilities β, and static first hyperpolarizabilities β_0 are used for comparison purposes. Perhaps surprisingly, quantitative, systematic comparisons of the electron donor/acceptor properties of metal centres with those of more traditional organic groups are very scarce. Indeed, the only such study appears to be a ZINDO analysis of β values which showed that the ferrocenyl and 4-(methoxy)phenyl donor groups are essentially interchangeable.[4] Here we report an experimental study of the complex salts [**1**–**4**]PF_6 and the organics [**5**–**8**]PF_6 which allows a comparison of the $\{Ru^{II}(NH_3)_5(py)\}^{2+}$ (py = pyridyl) and 4-(dimethylamino)phenyl π-electron donors.

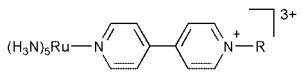

R = Me (**1**), Ph (**2**), 2,4-DNPh (**3**), 2-Pym (**4**)

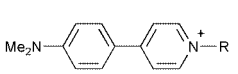

R = Me (**5**), Ph (**6**), 2,4-DNPh (**7**), 2-Pym (**8**)

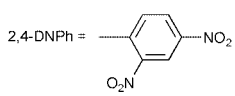

[**1**–**4**]PF_6[3b,c] and [**5**–**7**]Cl[5] were synthesized as described previously, and [**5**–**7**]Cl were metathesised to [**5**–**7**]PF_6 by precipitation from H_2O–NH_4PF_6.† [**8**]PF_6 was prepared from 4-(dimethylaminophenyl)pyridine[6] and 2-chloropyrimidine, followed by precipitation from H_2O–NH_4PF_6.†

Selected spectroscopic and electrochemical data for [**1**–**8**]PF_6 are given in Table 1. The visible absorptions of [**1**–**4**]PF_6 are due to $d_\pi(Ru^{II}) \rightarrow p_{\pi^*}$(pyridinium) charge-transfer (CT) excitations,[3b,c] whilst those of [**5**-**8**]PF_6 arise from $p_\pi(NMe_2) \rightarrow p_{\pi^*}$(pyridinium) CTs. The CT energies E_{max} of [**5**–**8**]PF_6 are higher than those of [**1**–**4**]PF_6, but the organic *vs.* complex energy difference decreases from 0.85 to 0.72 eV as R changes in the order Me > Ph > 2,4-DNPh > 2-Pym. Also, the molar extinction coefficients of the CT bands of [**5**–**8**]PF_6 are *ca.* 2–3 times larger than those of [**1**–**4**]PF_6. Within both series, E_{max} decreases as R changes in the order Me > Ph > 2,4-DNPh > 2-Pym, the differences between the extremes being 0.26 eV for [**1**–**4**]PF_6 and 0.39 eV for [**5**–**8**]PF_6.

The cyclic voltammetric data show that the $\{Ru^{II}(NH_3)_5\}^{2+}$ moiety is much easier to oxidise than the $–NMe_2$ group, and the pyridinium groups in the complexes are easier to reduce than those in the organics. These observations are consistent with the lower E_{max} values, due to smaller HOMO–LUMO gaps, for [**1**–**4**]PF_6 compared with [**5**–**8**]PF_6. Furthermore, the E_{red} values show that the $–C_6H_4NMe_2$-4 group exerts a greater electron-donating influence on the acceptors than does the $\{Ru^{II}(NH_3)_5(py)\}^{2+}$ moiety, despite the fact that the $\{Ru^{II}(NH_3)_5\}^{2+}$ centre is more electron-rich than the $–NMe_2$ group. E_{ox} does not change greatly within each series, but E_{red} becomes less negative as R changes in the order Me < Ph < 2-Pym < 2,4-DNPh. This trend almost parallels the decreasing CT energies and reflects the increasing electron-deficiency of the acceptor group. The NMR data show that the protons *ortho* to the pyridinium N atoms are more shielded in [**5**–**8**]PF_6, consistent with the greater net electron-donating effect of the $–C_6H_4NMe_2$-4 group *vs.* $\{Ru^{II}(NH_3)_5(py)\}^{2+}$.

The greater electron-donating influence of a $–C_6H_4NMe_2$-4 group compared with $\{Ru^{II}(NH_3)_5(py)\}^{2+}$ can be traced to two

Table 1 Visible absorption, cyclic voltammetric and proton NMR data for salts [**1**–**8**]PF_6

Salt	E_{max}/eV[a] (ε/dm^3 mol^{-1} cm^{-1})	*E*/V (*vs.* Ag–AgCl)[b] E_{ox}[d]	E_{red}[e]	δ/ppm[c] py-H[f]
[**1**]PF_6[g]	2.10 (15 800)	0.48	−0.89	9.15
[**2**]PF_6[g]	1.97 (19 300)	0.48	−0.73	9.33
[**3**]PF_6[g]	1.88 (16 900)	0.48	−0.38	9.37
[**4**]PF_6[h]	1.84 (18 000)	0.51	−0.43	10.17
[**5**]PF_6	2.95 (40 200)	1.14	−1.35	8.76
[**6**]PF_6	2.77 (50 100)	1.18	−1.11	9.01
[**7**]PF_6	2.64 (45 300)	1.27	−0.55	9.23
[**8**]PF_6	2.56 (55 600)	1.22	−0.81	9.78

[a] Using acetonitrile solutions (*ca.* 10^{-5} mol dm^{-3}). [b] Measured in acetonitrile solutions *ca.* 10^{-3} mol dm^{-3} in analyte and 0.1 mol dm^{-3} in $NBu^n_4PF_6$ at a platinum-bead/disc working electrode with a scan rate of 200 mV s^{-1}. $E_{1/2}$ values are given for [**1**]PF_6, [**2**]PF_6 and [**4**]PF_6; E_{pa} or E_{pc} values are given for [**3**]PF_6 and [**5**–**8**]PF_6 (return waves are also observed in some cases). Ferrocene internal reference $E_{1/2}$ = 0.43 V. [c] Chemical shift at 200 MHz with respect to $SiMe_4$ in CD_3COCD_3. [d] Potential for first oxidation of HOMO. [e] Potential for first reduction of LUMO. [f] Doublet signal for protons *ortho* to pyridinium N atom. [g] Ref. 3(*b*). [h] Ref. 3(*c*).

 DOI: 10.1039/b103543f

Table 2 Visible absorption, Stark and HRS data for salts [**1**–**8**]PF_6

Salt	E_{max}/eV[a]	f_{os}[b]	$\|\mu_{12}\|$/D	$\|\Delta\mu_{12}\|$/D	$\Delta\mu_{ab}$/D	c_b^2	$H_{ab}/10^3$ cm^{-1}	$\beta_0/10^{-30}$ esu[c]	$\beta/10^{-30}$ esu[d]	$\beta_0/10^{-30}$ esu[e]
[**1**]PF_6	1.92	0.20	5.2	13.8	17.3	0.10	4.7	60	750[f]	123[f]
[**2**]PF_6	1.78	0.22	5.7	15.3	19.1	0.10	4.3	93	858[f]	220[f]
[**3**]PF_6	1.70	0.22	5.8	16.3	20.0	0.09	4.0	113	871[f]	289[f]
[**4**]PF_6	1.64	0.28	6.7						640[g]	230[g]
[**5**]PF_6	2.93	0.66	7.7	13.2	20.3	0.17	9.0	54		
[**6**]PF_6	2.74	0.79	8.7	12.7	21.6	0.21	8.9	75	50	23
[**7**]PF_6	2.64	0.66	8.1						70	29
[**8**]PF_6	2.52	0.88	9.6	12.4	22.9	0.23	8.5	106	75	29

[a] Butyronitrile glasses at 77 K (*ca*). 10^{-5} mol dm^{-3}). [b] Oscillator strength determined by numerical integration of the digitized absorption spectra. [c] Static first hyperpolarizability calculated from eqn. (1). [d] First hyperpolarizability measured in acetonitrile at 298 K using a ns 1064 nm laser for [**1**–**4**]PF_6 and a fs 1300 nm laser for [**5**–**8**]PF_6. [e] Static first hyperpolarizability estimated from β *via* the two-state model.[9] [f] Ref. 3(*b*). [g] Ref. 3(*c*).

factors. Firstly, the latter is a σ-electron acceptor, as well as a π-donor, whilst the former is only a π-donor. The second, and perhaps more important, factor is more effective p(N)–p(C) compared with p(N)–d(Ru) π-orbital overlap. Such an effect also explains differences between mixed-valence ions containing $–C_6H_4NMe_2$-4 or $\{Ru^{II}(NH_3)_5(py)\}^{2+}$ groups.[7]

We have obtained β values for [**1**–**8**]PF_6 by using hyper-Rayleigh scattering (HRS) studies;[8] β_0 values were derived *via* the two-state model[9] and results are shown in Table 2. The previously reported β_0 values of [**1**-**4**]PF_6 were derived from nanosecond 1064 nm HRS,[3b,c] whilst [**5**-**8**]PF_6 were studied using femtosecond 1300 nm HRS,[10] incorporating fluorescence demodulation.[11] Unfortunately, the 650 nm HRS signal from [**5**]PF_6 was too weak to allow determination of β. Two conclusions can be drawn from the HRS data: *(i)* the β_0 values of the complexes appear to be much larger than those of their organic counterparts (but note that comparison of HRS β_0 values obtained under different experimental conditions may be of limited validity),[12] and (*ii*) decreasing E_{max} generally corresponds with increasing β_0 within both series.

Stark spectroscopy affords dipole moment changes upon CT excitation $\Delta\mu_{12}$.[13] According to the two-state model, $\Delta\mu_{12}$ can be used to calculate β_0 by using eqn. (1)[9]

$$\beta_0 = \frac{3\Delta\mu_{12}(\mu_{12})^2}{2(E_{max})^2} \quad (1)$$

where μ_{12} is the transition dipole moment. The results of Stark studies on [**1**–**8**]PF_6, carried out at 77 K as previously described,[14] are given in Table 2. Unfortunately, the data fits for [**4**]PF_6 and [**7**]PF_6 were unsatisfactory. The μ_{12} values, diabatic dipole moment changes $\Delta\mu_{ab}$, mixing coefficients c_b^2 and electronic coupling matrix elements H_{ab} for the diabatic states were calculated as previously described.[14]

The CT f_{os} and μ_{12} values of [**5**–**8**]PF_6 are larger than those of [**1**–**4**]PF_6. Furthermore, μ_{12} generally increases as E_{max} decreases within each series. [**1**–**8**]PF_6 show relatively large $\Delta\mu_{12}$ values, with [**1**]PF_6 and [**2**]PF_6 having larger values than [**5**]PF_6 and [**6**]PF_6, respectively. For the complexes, $\Delta\mu_{12}$ increases as R changes in the order Me < Ph < 2,4-DNPh, but a similar trend is not shown by the organics. The values of c_b^2 and H_{ab} for the organics are about twice those for the complexes, consistent with the less effective d(Ru)–p(N) *vs.* p(N)–p(C) π-orbital overlap indicated by the electrochemical and NMR data. The β_0 values derived from eqn. (1) are in agreement with the HRS results in as much as they increase as E_{max} decreases within each series. However, in contrast with HRS, the Stark data indicate that the β_0 values of [**1**]PF_6 and [**2**]PF_6 are only slightly larger than those of their organic counterparts. This is because the β_0-enhancing effects of decreasing E_{max} and increasing $\Delta\mu_{12}$ are largely offset by decreasing μ_{12} when moving from organic to complex.

In conclusion, a $\{Ru^{II}(NH_3)_5(py)\}^{2+}$ centre is more electron-rich than a $–C_6H_4NMe_2$-4 group, but the latter exerts a greater electron-donating effect on pyridinium units due in part to more effective π-orbital overlap. HRS data show that [**1**–**4**]PF_6 have much larger β_0 values than their organic counterparts, but Stark spectroscopy indicates that the increase in β_0 between the complexes and organics is much smaller. Nevertheless, the complexes do have the added attraction that their CT absorption and NLO responses are redox-switchable.[15]

We thank the EPSRC for a PhD studentship (J. A. H.). Studies at Brookhaven National Laboratory were carried out under contract DE-AC02-98CH10886 with the US Department of Energy and supported by its Division of Chemical Sciences, Office of Basic Energy Sciences. K. W. is a research assistant with the Fund for Scientific Research-Flanders.

Notes and references

† [**5**–**8**]PF_6 were characterised by C,H,N analyses and proton NMR spectroscopy.

1 *Nonlinear Optics of Organic Molecules and Polymers*, ed. H. S. Nalwa and S. Miyata, CRC Press, Boca Raton, FL, 1997.
2 N. J. Long, *Angew. Chem., Int. Ed. Engl.*, 1995, **34**, 21.
3 (*a*) B. J. Coe, M. C. Chamberlain, J. P. Essex-Lopresti, S. Gaines, J. C. Jeffery, S. Houbrechts and A. Persoons, *Inorg. Chem.*, 1997, **36**, 3284; (*b*) B. J. Coe, J. A. Harris, L. J. Harrington, J. C. Jeffery, L. H. Rees, S. Houbrechts and A. Persoons, *Inorg. Chem.*, 1998, **37**, 3391; (*c*) B. J. Coe, J. A. Harris, I. Asselberghs, A. Persoons, J. C. Jeffery, L. H. Rees, T. Gelbrich and M. B. Hursthouse, *J. Chem. Soc., Dalton Trans.*, 1999, 3617.
4 D. R. Kanis, M. A. Ratner and T. J. Marks, *J. Am. Chem. Soc.*, 1992, **114**, 10338.
5 M. G. Hutchings, *Tetrahedron*, 1984, **40**, 2061.
6 A. N. Kost, A. K. Sheinkman and N. F. Kazarinova, *J. Gen. Chem. USSR*, 1964, **34**, 2059.
7 S. F. Nelsen, H. Q. Tran and M. A. Nagy, *J. Am. Chem. Soc.*, 1998, **120**, 298.
8 E. Hendrickx, K. Clays and A. Persoons, *Acc. Chem. Res.*, 1998, **31**, 675.
9 J. Zyss and J. L. Oudar, *Phys. Rev. A*, 1982, **26**, 2016.
10 G. Olbrechts, K. Wostyn, K. Clays and A. Persoons, *Opt. Lett.*, 1999, **24**, 403.
11 G. Olbrechts, R. Strobbe, K. Clays and A. Persoons, *Rev. Sci. Instrum.*, 1998, **69**, 2233.
12 P. Kaatz and D. P. Shelton, *J. Chem. Phys.*, 1996, **105**, 3918.
13 G. Bublitz and S. G. Boxer, *Ann. Rev. Phys. Chem.*, 1997, **48**, 213.
14 Y. K. Shin, B. S. Brunschwig, C. Creutz and N. Sutin, *J. Phys. Chem.*, 1996, **100**, 8157.
15 B. J. Coe, S. Houbrechts, I. Asselberghs and A. Persoons, *Angew. Chem., Int. Ed.*, 1999, **38**, 366; B. J. Coe, *Chem. Eur. J.*, 1999, **5**, 2464.

CHEMCOMM Communication
www.rsc.org/chemcomm

A new stabilised form of isobenzofuran, rack-mounted on an alicyclophane

Ronald N. Warrener,* Muhong Shang and Douglas N. Butler

Centre for Molecular Architecture, Central Queensland University, Rockhampton, Queensland, 4702, Australia. E-mail: r.warrener@cqu.edu.au; Fax: +61 7 4930 9919; Tel: +61 7 4930 9917

Received (in Cambridge, UK) 18th May 2001, Accepted 20th June 2001
First published as an Advance Article on the web 1st August 2001

New stable, crystalline isobenzofurans 9a and 9b linked through the 1,3-positions and incorporated into alicyclophanes have been prepared from the related furano-alicyclophane 5 in three steps (i) addition of benzyne or 4,5-bis(trimethylsilyl)benzyne (ii) hydrogenation of the π-bond (iii) ejection of ethylene by flash vacuum pyrolysis, and shown to yet retain high 1,3-diene character and form adducts with dienophiles, *e.g.* dimethyl acetylenedicarboxylate or *N*-methyl maleimide; the corresponding off-rack 1,3-dimethylisobenzofurans were too unstable for isolation.

Many cyclic polyene compounds that resist isolation in monomeric form, do so because of their propensity to react with themselves, *e.g.* dimerisation of cyclobutadiene[1] or polymerisation of isobenzofuran.[2] Specialised techniques to generate the monomer species in a controlled environment have been reported, *e.g.* flash vacuum pyrolysis or matrix isolation at liquid helium temperatures. The most ingenious way to isolate such a highly reactive monomer, however, was reported by Cram and co-workers who were able to corral cyclobutadiene inside a hemicarcerand (**1**, Fig. 1), study its chemistry and even record its NMR spectrum.[3] This method succeeded since it kept the cyclobutadiene molecules separated from each other, and confirmed the inherent stability of cyclobutadiene itself. In principle, this technique should be suitable for the study of isobenzo-systems, a class of unstable monomeric compounds characterised by the presence of the *o*-xylylidene chromophore.[4] In practice, our efforts to achieve this goal using the Cram technique have been unrewarding because of the difficulty in preparing hemicarcerand hosts large enough to encase photosubstrates currently required for such isobenzo-system generation.[5]† Accordingly, we have sought ways to stabilise these highly reactive monomers other than having them so heavily substituted that their natural chemistry could be compromised.[6]

We report herein a new technique for stabilising isobenzofurans (rack-IBFs) by incorporating them into an alicyclophane macrocycle (**2**, Fig. 1).[7] The concept depends on the rack section of the alicyclophane acting as a steric shield (6.65 × 6.81 Å in rack **3**, X-ray data[8]) that by its presence in rack-IBFs **9a** and **9b** inhibits intermolecular self-dimerisation or polymerisation processes. This motif should be applicable to other isobenzo-systems (isoindoles, isoindenes and isobenzofulvenes) as well as elusive monomers such as cyclobutadiene and cyclopentadienones. The new rack-IBFs **9a** and **9b** are stable, high melting solids that could be isolated, handled as regular compounds and stored in solution for several days at 5 °C and for many months in the solid state.

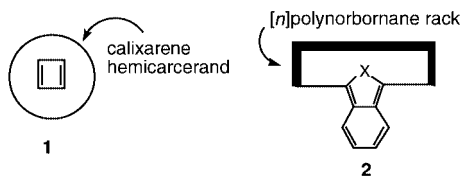

Fig. 1

The synthesis of the parent rack-IBF **9a** commenced from the bis(succinimide) rack **3**[7] which was reacted with 2,5-bis-(bromomethyl)furan **4** in dimethylformamide containing solid potassium carbonate to produce the furano-alicyclophane **5**[9] in 84% yield (Scheme 1). Reaction of rack-furan **5** with benzyne **6a**, generated by diazotisation of anthranilic acid, gave the 1,4-epoxy-1,4-dihydronaphthalene derivative **7a** which was hydrogenated (Pd/C, H_2, 50 psi, 3 days) to the 2,3-dihydro compound **8a** and this subjected to flash vacuum pyrolysis (FVP, 500 °C, 0.001 mbar) to afford the rack-IBF **9a**, mp 199–201 °C, in 98% yield.[10]‡ The stability of rack-IBF **9a** contrasted strikingly with the structurally similar 1,3-dimethylisobenzofuran **12a** which, when generated under the same FVP conditions from **11a**, was found to form a polymer upon attempted isolation.§

The ^{1}H NMR spectrum of rack-IBF **9a** revealed that the rack *endo*-protons Ha, Hb were equivalent (δ 1.70) and upfield-shifted relative to those in rack-IBF **3** (δ 2.30) owing to the ring-current of the 10π-isobenzofuran while the other rack protons occurred as overlapping resonances at δ 3.01 (bridgehead, succinimide) and an AB doublet (δ 2.19, δ 1.33 J = 11 Hz) for the methano bridges. Also, the aromatic protons appeared as an AA′BB′ pattern at δ 6.99 and 7.59 while the *N*-methylene protons displayed a singlet resonance at δ 4.93 indicative of a rapid, pendulum motion of the IBF ring about the long σ-plane of the molecule.¶

While the isobenzofuran component of rack-IBF **9a** was stabilised against polymerisation (or homocycloadditions) by incorporation into the rack, it still retained the ability to react as a 4π-diene with small 2π-dienophiles to form [4π + 2π] Diels–Alder cycloadducts, *e.g.* reaction with *N*-methylmaleimide **13** was complete in 2 minutes (quantitative yield) and gave exclusively the *endo*-adduct (*N*-Me δ 2.25). In contrast, *N*-methylmaleimide **13** reacted more slowly (1 hour, RT) with the unstable 1,3-Me_2IBF **12a** and produced a 1:5 mixture of *exo*-(*N*-Me δ 3.03) and *endo*- (*N*-Me δ 2.23) isomers of **14** in 55% yield.

This rack-mounting strategy was general and FVP (500 °C, 0.001 mbar) of **8b** yielded rack-$(TMS)_2$IBF **9b**‖ [^{1}H NMR δ 7.93 (s, 2H), 4.93, (s, 4H), 3.02, (s, 8H), 2.19 (d, J = 11 Hz, 2H), 1.73 (s, 4H), 1.56 (s, 4H), 1.28 (d, J = 11 Hz, 2H), 0.42 (s, 18H)], isolated as a stable crystalline product (96% yield), mp 312–314 °C. In a model study, 5,6-$(TMS)_2$-1,3-Me_2IBF **12b** was prepared by FVP (620 °C, 0.001 mbar) of the 1,4-epoxy-1,2,3,4-tetrahydro $(TMS)_2$ naphthalene **11b**. The non-crystalline product **12b** [^{1}H NMR δ 7.55 (s, 2H), 2.57 (s, 6H), 0.35 (s, 18H)] rapidly decomposed in $CDCl_3$ solution but could be characterised by treating the pyrolysate immediately after deposition with a solution of *N*-methyl maleimide **13** in $CDCl_3$ as its *endo*-adduct **14b** (67% yield).

In conclusion, we have demonstrated that incorporation of isobenzofurans into alicyclophanes to produce rack-IBFs dramatically increases their stability, yet achieves this without compromising the Diels–Alder capacity of the IBF component. This strategy should be applicable to other reactive monomers with a propensity for self-dimerisation, and experiments to test

 DOI: 10.1039/b104383h

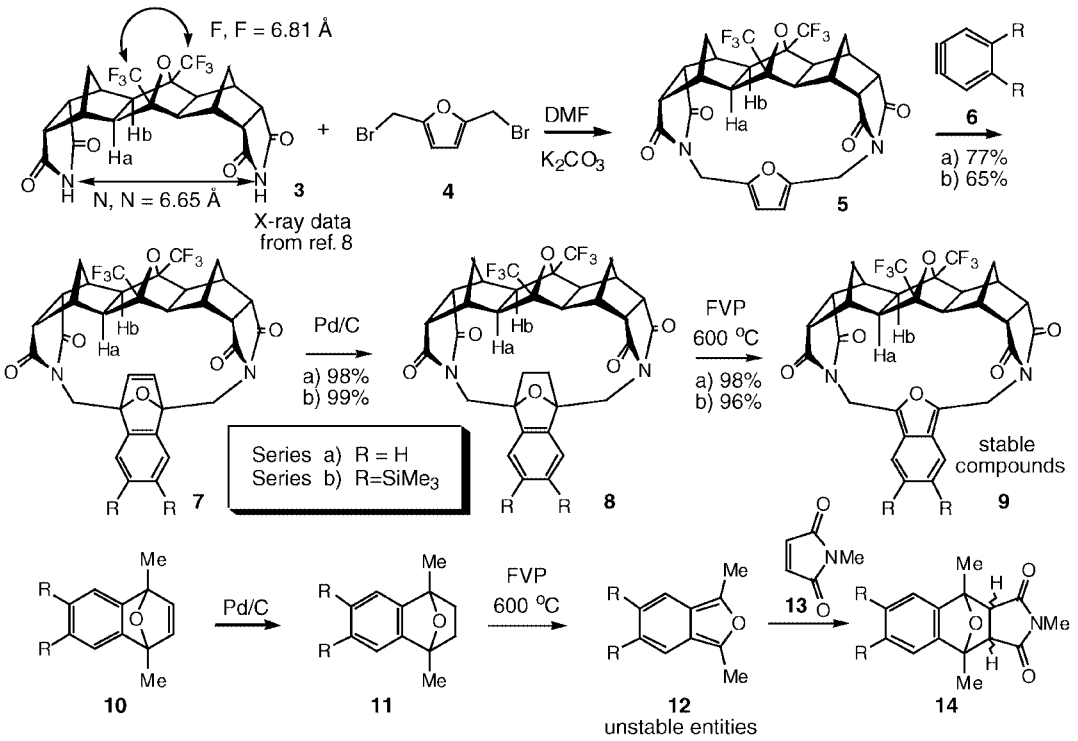

Scheme 1

this proposal are currently being undertaken and results will be reported in due course.

Notes and references

† We have conducted a theoretical study (AM1) on the size compatibility of guests with Cram-type hemicarcerands as an aid to selecting hemicarcerands for photosubstrate incorporation (ref. 7).

‡ The incorporation of trifluoromethyl substituents into the alicyclophane improved their volatility and thermal stability, key factors required for application of this FVP technique.

§ Substituents at the 1,4-positions of 1,4-epoxy-1,4-dihydronaphthalene are known to restrict access of 3,6-di-2-pyridyl-s-tetrazine (ref. 11) to the π-bond and often preclude the use of this route to produce the corresponding IBF (ref. 12) in this study, attempts to prepare rack-IBF **9a** from **7** failed (too crowded), yet it is known that 1,3-Me_2IBF **12a** can be formed from **10a**. Removal of one or both 1,4-substituents allows the reaction to proceed, *e.g.* Wong and co-workers used the method successfully for the preparation of 5,6-$(TMS)_2$IBF and trapped it with *N*-phenylmaleimide (ref. 13).

¶ Protons Ha, Hb are non-equivalent in **7** and **8**, but are equivalent in **5** and **9**. The significance of these observations will be discussed elsewhere, (ref. 14).

‖ The 4,5-bis(trimethylsilyl)benzyne **6b** required for the formation of **7b** from **5b** was generated from 1,2,3,4-tetra(trimethylsilyl)benzene by treatment with diacetoxyiodobenzene (ref. 15).

1 G. Maier, *Angew. Chem.*, 1988, **100**, 317.
2 D. Wege, *Adv. Theor. Interesting Mol.*, 1998, **4**, 1.
3 D. J. Cram, M. E. Tanner and R. Thomas, *Angew. Chem., Int. Ed. Engl.*, 1991, **30**, 1024.
4 J. L. Segura and N. Martin, *Chem. Rev.*, 1999, **99**, 3199.
5 M. Liddell, D. Margetic, A. Mitchell and R. N. Warrener, unpublished.
6 *inter alia* 2,3-dimethyl-1,3-diphenylisoindene: K. Alder and M. Fremery, *Tetrahedron*, 1961, **14**, 190. 8-(dimethylamino)-1,3-diphenylisobenzofulvene: K. Hafner and W. Bauer, *Angew. Chem., Int. Ed. Engl.*, 1968, **7**, 297.
7 D. N. Butler, M. Shang and R. N. Warrener, *Tetrahedron Lett.*, 2000, **41**, 5985.
8 R. N. Warrener, M. Shang and D. N. Butler, *Tetrahedron Lett.*, 2001, **42**, 159.
9 All new compounds gave high-resolution mass spectra, ^{1}H and ^{13}C NMR spectra corresponding to their assigned structures. Compound, mp (°C): **5**, >350; **7**, >350; **8**, >350; **9a**, 199–201; **9b**, 312–314; **14a** (*exo*), 105–106; **14a** (*endo*), 122–123; **14b** (*endo*) 186–187.
10 This reaction sequence was modelled on the synthesis of isobenzofuran reported by U. E. Wiersum and W. J. Mijs, *J. Chem. Soc., Chem. Commun.*, 1972, 347.
11 R. N. Warrener, D. A. C. E Evans, M. N. Paddon-Row and R. A. Russell, *Aust. J. Chem.*, 1982, **35**, 757.
12 L. Lui and R. N. Warrener, *Electronic Conference on Heterocyclic Chemistry '98*, ed. H. S. Rzepa and O. Kappe, Imperial College Press, ISBN 981-02-3594-1 (http://www.ch.ic.ac.uk/ectoc/echet98/pub/095/index.htm).
13 C.-Y. Yick, S.-H. Chan and H. N. C. Wong, *Tetrahedron Lett.*, 2000, **41**, 5957.
14 D. N. Butler and M. R. Johnston, unpublished results.
15 A. Winling and R. A. Russell, *J. Chem. Soc., Perkin Trans. 1*, 1998, 3921.

CHEMCOMM
Communication
www.rsc.org/chemcomm

Synthetic study of phomoidride B (CP-263,114); utilization of the oxidopyrylium [5 + 2] cycloaddition

Naoki Ohmori

Department of Chemistry, Graduate School of Science, Hiroshima University, 1-3-1 Kagamiyama, Higashi-Hiroshima 739-8526, Japan. E-mail: d1174001@hiroshima.u.ac.jp

Received (in Cambridge, UK) 15th May 2001, Accepted 28th June 2001
First published as an Advance Article on the web 1st August 2001

The highly functionalized core structure of phomoidride B (CP-263,114) was pursued by using intermolecular oxidopyrylium–alkene cyclization as one of the key steps.

In 1997, the group of Kaneko reported the structure of phomoidride B (**1**) and its hydrolysed derivatives, both showing inhibitory activity towards farnesyl transferase[1] with IC_{50} values in the micromolar range.[2] A great many synthetic organic chemists have been attracted by its fascinating structural features and so far four groups have achieved elegant complete total syntheses.[3] Retrosynthetic analysis suggested that **1** could be accessed from **2** by introducing side chains followed by minimal functional group manipulations. Bicyclic **2** in turn could be constructed from modestly functionalized seven-membered ring **3**, which could easily be obtained by treating the oxidopyrylium ylide[4] **4** with fumarate ester or its variants thus providing easy access to the maleic anhydride moiety of the CP-core (Scheme 1).

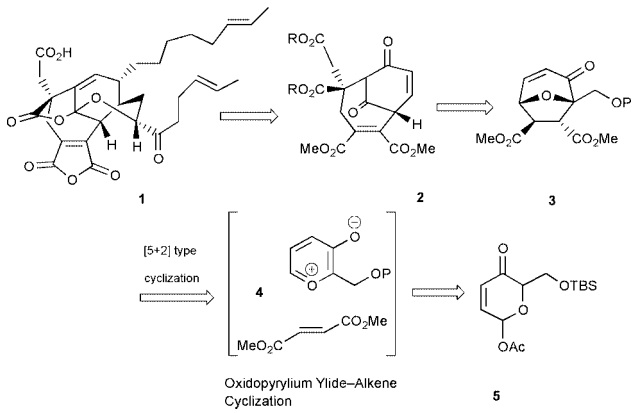

Scheme 1 Strategy for the total synthesis of phomoidride B (**1**).

The synthesis began with the protection of but-2-ene-1,4-diol with TBSCl (Scheme 2). Oxidopyrylium precursor **8** was easily prepared in 5 steps (39% from but-2-ene-1,4-diol). When using dimethyl fumarate as the alkene, cyclization took place quite efficiently in the presence of Et_3N to deliver oxabicycles **9a** and **9b** (13 : 1) in 77% combined yield. Hydrogenation of **9a** followed by the removal of the silyl protecting group and iodination gave **12** (Scheme 3). Of several attempts to cleave the ether bridge in reductive fashion, Zn proved to be the most suitable, yielding *exo*-enone **13** in 96% yield. Homologation of the *exo* olefin seemed reasonable for introducing the lacking two carbon unit required for construction of the bicyclo-[4.3.1]decene core. To this end, **13** was treated with TBSOTf in the presence of 2,6-lutidine to give a separable mixture of TBS-protected acetal **14** (49%) and enone **15** (5%). Acetal **14** was next converted to **16**† in two steps by allylation in the presence of $TiCl_4$ followed by reprotection of the liberated alcohol with TBSOTf. Ketone **16** was subjected to ozonolysis to yield a keto-aldehyde, which was subsequently treated with DBU to promote the intramolecular aldol reaction.[6] The crude aldol adduct was oxidized with PCC to deliver diketones **17a** and **17b** (4 : 1, 82% yield over 2 steps). Oxidation of **17a** to enone **18** under Saegusa's conditions[7] proceeded in 35% yield. Improved yields were obtained using the recently reported Nicolaou method using IBX (IBX = 2-iodylbenzoic acid),[8] giving enone **18** in 30% yield along with recovery of the starting material (42%). Repeated oxidation of recovered **17a** resulted in a combined yield of 42% (52%, based on recovered **17a**). Lewis acid catalyzed allylation of **18** gave a 1,4-adduct as a single stereoisomer. Further allylation utilizing palladium chemistry

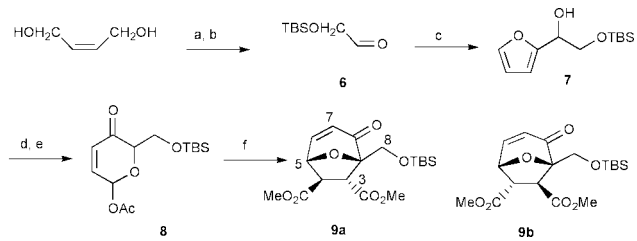

Scheme 2 *Reagents and conditions*: (a) TBSCl, Et_3N, DMAP, THF, rt; (b) O_3, MeOH, −78 °C, then $NaHCO_3$, Me_2S, −78 °C → rt, quant. (2 steps); (c) 2-lithiofuran, Et_2O, −78 °C → rt; (d) MCPBA, CH_2Cl_2, 0 °C → rt; (e) Ac_2O, pyridine, rt, 39% (3 steps); (f) dimethyl fumarate, Et_3N, CH_3CN, reflux, 77% (**9a** : **9b**, 13 : 1).

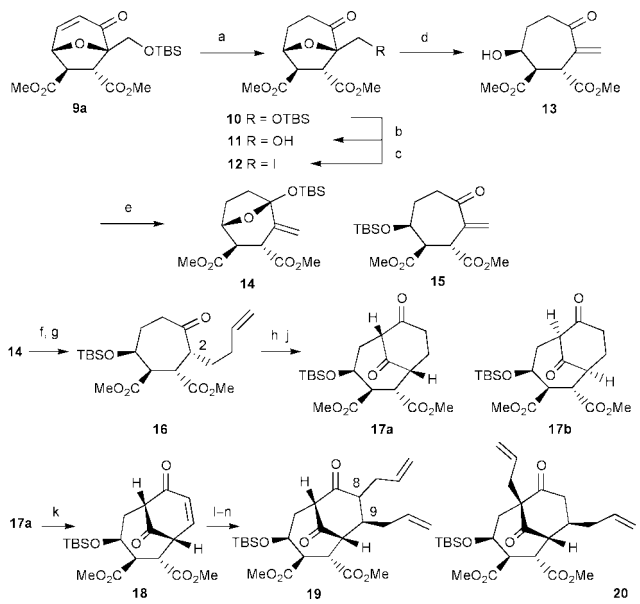

Scheme 3 *Reagents and conditions*: (a) H_2, Pd/C, MeOH, rt; (b) aq. HCl, rt; (c) I_2, PPh_3, imidazole, benzene, reflux, 64% (3 steps); (d) Zn, MeOH, reflux, 96%; (e) TBSOTf, 2,6-lutidine, CH_2Cl_2, −78 °C, 54% (**14** : **15**, 10 : 1); (f) allyltrimethylsilane, $TiCl_4$, CH_2Cl_2, −78 °C; (g) TBSOTf, 2,6-lutidine, CH_2Cl_2, rt, 66% (2 steps); (h) O_3, MeOH, then $NaHCO_3$, Me_2S, −78 °C → rt, 81%; (i) DBU, CH_2Cl_2; (j) PCC, CH_2Cl_2, 4 Å MS, rt, 82% (2 steps, **17a** : **17b**, 4 : 1); (k) IBX, DMSO–PhMe (1 : 2), 80 °C, 52%; (l) allyltrimethylsilane, $TiCl_4$, CH_2Cl_2, −78 °C, 57%; (m) KHMDS, allyl chloroformate, THF, −78 °C, 63%; (n) $Pd_2(dba)_3$·$CHCl_3$, PPh_3, THF, rt, 81% (**19** : **20**, 2 : 1).

 DOI: 10.1039/b104268h

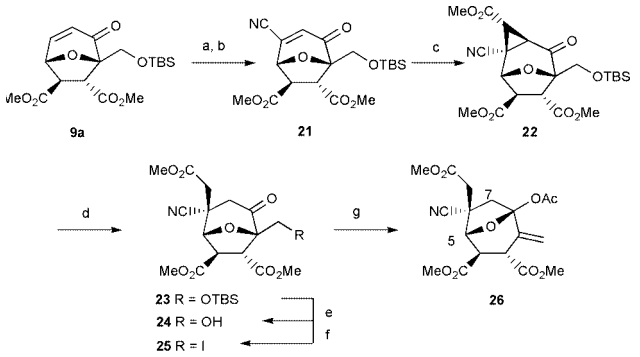

Scheme 4 *Reagents and conditions*: (a) Br_2, CH_2Cl_2, −40 °C, then Et_3N, −40 °C → rt; 99%; (b) NaCN, Bu_4NI, CH_2Cl_2—H_2O, rt, then Et_3N, rt, 97%; (c) $Me_2S{=}CHCO_2Me$, THF, 0 °C → rt, 61%; (d) SmI_2, THF, −78 °C, 79%; (e) aq. HCl, 0 °C → rt; (f) I_2, PPh_3, imidazole, benzene, reflux, 64% (2 steps); (g) Zn, Ac_2O, 50 °C, 25%.

delivered **19**‡ (19% yield from **18**) a highly advanced bicyclic intermediate with the required relative stereochemistry between the bridging carbonyl group and the hydrophobic side-chain at C9 along with **20** (10% yield from **18**).

Having established a method for the construction of the bicyclic framework, we then focussed upon the quaternary carbon centre adjacent to the bridgehead. To this end **9a** was first converted to **21** in 2 steps (96%) (Scheme 4). Various attempts to produce directly the desired quaternary centre with organometal reagents were unsuccessful, probably due to the highly functionalized nature of **21**. Only by using a sulfonium ylide did the reaction take place without any problems, furnishing a cyclopropane product **22**. Reductive cleavage of **22** with SmI_2 proceeded with complete regioselectivity to generate the required quaternary centre.§ Compound **23** was next deprotected under acidic conditions followed by iodination to give **25**. Zinc reduction and protection of the resultant hydroxy group with an acetyl group gave **26**.¶

We are currently exploring methods to complete the fully functionalized core and modify the side chains *en route* to phomoidride B.

I am grateful to Professor K. Ohkata for his valuable advice and to Dr S. Kojima for prereading of the manuscript. I am also grateful to Drs Y. Hiraga and R. Takagi for assistance in NMR.

Notes and references

† In this reaction **16** was obtained stereoselectively at the C2 centre. While the reason for this selectivity is unclear, it may be due to the proton delivering effect of the hydroxy group in the intermediate silyl enol ether during work-up (ref. 5).

‡ Although the C8 stereochemistry of **19** is not certain, **19** was obtained as the sole stereoisomer.

§ Although SmI_2 has previously been used for cyclopropane opening (ref. 10), to our knowledge, regioselective opening of cyclopropane bearing electron stabilizing groups on all three carbons with SmI_2 is unprecedented.

¶ *Data* for **9a**: R_f = 0.39 (silica gel, EtOAc–hexane 1:2); mp 92–94 °C (CH_2Cl_2); ν_{max}(neat)/cm^{-1} 2955, 1740, 1695; δ_H (500 MHz, $CDCl_3$) 7.34 (dd, *J* 9.8, 4.6, 1H, H-6), 6.02 (d, *J* 9.8, 1H, H-7), 5.19 (d, *J* 4.6, 1H, H-5), 4.25 (d, *J* 11.9, 1H, H-8), 4.22 (d, *J* 4.3, 1H, C*H*CO_2Me), 4.01 (d, *J* 11.9, 1H, H-8), 3.76 (s, 3H, CO_2CH_3), 3.66 (s, 3H, CO_2CH_3), 3.61 (d, *J* 4.3, 1H, C*H*CO_2Me), 0.90 (s, 9H, Si-*t*-*Bu*), 0.11 (s, 3H, Si-*Me*) 0.70 (s, 3H, Si-*Me*); δ_C (125 MHz, $CDCl_3$) 193.6, 171.0, 170.3, 150.7, 127.3, 91.7, 75.9, 60.3, 52.6, 52.4, 50.6, 46.6, 25.6, 18.1, −5.5, −5.7. HRMS (EI): calc. for $C_{18}H_{28}O_7Si$ (M^+): 384.1604. Found: 384.1588. Anal calc: C 56.23, H 7.34. Found: C 56.13, H 7.43%. For **26**: R_f = 0.53 (silica gel, EtOAc–hexane 1:1); ν_{max}(neat)/cm^{-1} 2955, 1740, 1440; δ_H (500 MHz, $CDCl_3$) 5.59 (br s, 1H, *exo*-CH_2=), 5.09 (s, 1H, *exo*-CH_2=), 4.99 (s, 1H, H-5), 4.23 (d, *J* 7.0, 1H, C*H*CO_2Me), 3.81 (s, 3H, CO_2CH_3), 3.79 (s, 3H, CO_2CH_3), 3.77 (s, 3H, CO_2CH_3), 3.66 (dd, *J* 7.0, 1.8, 1H, C*H*CO_2Me), 3.08 (d, *J* 17.4, 1H, CH_2CO_2Me), 3.00 (d, *J* 17.4, 1H, CH_2CO_2Me), 2.89 (d, *J* 13.7, 1H, H-7), 2.62 (d, *J* 13.7, 1H, H-7), 2.11 (s, 3H, acetyl); δ_C (125 MHz, $CDCl_3$) 171.8, 171.5, 169.4, 167.6, 141.4, 119.8, 113.3, 104.9, 80.9, 53.1, 52.8, 52.3, 45.9, 45.5, 44.6, 43.1, 40.9, 21.6. HRMS (EI) calc. for $C_{18}H_{21}O_9Si$ (M^+): 395.1216. Found: 395.1212.

1 Review: D. M. Leonard, *J. Med. Chem.*, 1997, **40**, 2971; K. Hinterding, D. Alonso-Díaz and H. Waldmann, *Angew. Chem., Int. Ed.*, 1998, **37**, 688.
2 T. T. Dabrah, T. Kaneko, W. Massefski, Jr. and E. B. Whipple, *J. Am. Chem. Soc.*, 1997, **119**, 1594; T. T. Dabrah, H. J. Harwood, Jr., L. H. Huang, N. D. Jankovich, T. Kaneko, J.-C. Li, S. Lindsey, P. M. Moshier, T. A. Subashi, M. Therrien and P. C. Watts, *J. Antibiot.*, 1997, **50**, 1.
3 K. C. Nicolaou, P. S. Baran, Y.-L. Zhong, H.-S. Choi, W. H. Yoon, Y. He and K. C. Fong, *Angew. Chem., Int. Ed.*, 1999, **38**, 1669; K. C. Nicolaou, P. S. Baran, Y.-L. Zhong, K. C. Fong, Y. He, W. H. Yoon and H.-S. Choi, *Angew. Chem., Int. Ed.*, 1999, **38**, 1676; K. C. Nicolaou, J. K. Jung, W. H. Yoon, Y. He, Y.-L. Zhong and P. S. Baran, *Angew. Chem., Int. Ed.*, 2000, **39**, 1829; C. Chen, M. E. Layton, S. M. Sheehan and M. D. Shair, *J. Am. Chem. Soc.*, 2000, **122**, 7424; N. Waizumi, T. Itoh and T. Fukuyama, *J. Am. Chem. Soc.*, 2000, **122**, 7825; Q. Tan and S. J. Danishefsky, *Angew. Chem., Int. Ed.*, 2000, **39**, 4509.
4 J. B. Hendrickson and J. S. Farina, *J. Org. Chem.*, 1980, **45**, 3359; P. A. Wender, K. D. Rice and M. E. Schnute, *J. Am. Chem. Soc.*, 1997, **119**, 7897.
5 R. Hara, T. Furukawa, Y. Horiguchi and I. Kuwajima, *J. Am. Chem. Soc.*, 1996, **118**, 9186.
6 J. R. Tagat, M. S. Puar and S. W. McCombie, *Tetrahedron Lett.*, 1996, **37**, 8463.
7 Y. Ito, T. Hirato and T. Saegusa, *J. Org. Chem.*, 1978, **43**, 1011.
8 K. C. Nicolaou, Y.-L. Zhong and P. S. Baran, *J. Am. Chem. Soc.*, 2000, **122**, 7596.
9 J. Tsuji, I. Minami and I. Shimizu, *Tetrahedron Lett.*, 1983, **24**, 1793.
10 R. A. Batey and W. B. Motherwell, *Tetrahedron Lett.*, 1991, **32**, 6211.

CHEMCOMM
Communication
www.rsc.org/chemcomm

Self-assembled nanoscale capsules between resorcin[4]arene derivatives and Pd(II) or Pt(II) complexes

Seong Jin Park and Jong-In Hong*

School of Chemistry and Molecular Engineering, Seoul National University, Seoul 151-747, Korea. E-mail: jihong@plaza.snu.ac.kr

Received (in Cambridge, UK) 4th June 2001, Accepted 5th July 2001
First published as an Advance Article on the web 1st August 2001

Nanoscale molecular capsules have been prepared by self-assembly of resorcin[4]arene derivatives and Pd(II) or Pt(II) complexes; the positively charged *N*-alkylpyridinium derivatives are encapsulated inside capsules due to strong cation–π interactions.

The formation of self-assembled superstructures has received a great deal of attention in recent years. Two main approaches have been widely used to construct supermolecules using intermolecular interactions between building blocks. One involves using hydrogen bonding interactions between the complementary binding sites.[1] The other approach is to employ metal–ligand interactions. Metal-induced self-assembly is a flourishing area of study in the field of host–guest and supramolecular chemistry. There are many examples of metal-mediated self-assembly to form squares,[2] helices,[3] grids,[4] catenanes,[5] cylinders,[6] circular helicates[7] and cages.[8]

Recently we reported that an intramolecularly assembled structure **2** was constructed by addition of two equivalents of $(en)Pd(NO_3)_2$ to a suspension of **1** in aqueous solution (Scheme 1).[9] Molecular models show that pyridyl groups of **3** with one fewer carbon compared to **1**, however, cannot easily get close enough to form an intramolecularly organized structure *via* Pd(II) or Pt(II) complexation. Herein we describe the formation of nanoscale cage-like complexes composed of two resorcin[4]arene derivatives and four Pd^{II} or Pt^{II} square planar precursors, and the complexation of *N*-alkylpyridinium derivatives in the organic phase.

Capsules are instantly formed by simple addition of two equivalents of $Pd(dppp)(OTf)_2$ to acetone, CH_2Cl_2 or $CHCl_3$ solutions of resorcin[4]arene derivatives **3a–c**† having four pyridine units as pendent groups (Scheme 1). For **2**, the bridge methylene protons split into two sets of signals in the ^1H NMR spectrum since $H_{i'}$ and $H_{o'}$ exist in the shielding region between two pyridine ligands interacting with a Pd(II) ion and move far upfield compared to H_i and H_o.[9] In the present case, however, the bridge methylene protons ($H_{in'}$ and $H_{out'}$) do not divide into two sets [Fig. 1(e)]. Both ^1H and ^{13}C NMR spectra are in accord with the D_{4h} symmetric structure of **5** and the assignments are fully supported by two-dimensional NMR measurements. In particular, a ^1H NMR titration study clearly shows capsule formation. When **3a** and **4a** are mixed in a 1 : 1 molar ratio, a mixture of the capsule **5a**† and free **3a** is obtained. Moreover, when an excess amount of **4a** is added, **5a** and unreacted **4a** are present (Fig. 1). This means that a 1 : 2 adduct is formed as the sole product.

The molecular weight estimated by vapor pressure osmometry (VPO) of a CH_2Cl_2 solution containing **3a** and **4a** in a 2 : 4 molar ratio (6230 ± 590) is consistent with the molecular weight for the dimer **5a** (6426). Moreover, electrospray ionization mass spectrometry (ESI-MS) clearly shows the formation of **5b** when a $CHCl_3$ solution containing **2b** and **3b** in a 2 : 4 molar ratio was examined: $[M - 2CF_3SO_3^-]^{2+}$ (2961.99), $[M - 3CF_3SO_3^-]^{3+}$ (1928.83) and $[M - 4CF_3SO_3^-]^{4+}$ (1406.44).‡ Molecular modeling shows that the cavity of **5** has nanoscale dimensions of 16 × 20 Å.[10]

Several neutral guest molecules such as adamantane, anthracene, phenanthrene and pyrene show no ^1H NMR spectroscopic signs of encapsulation within the capsule. This indicates either that there is no driving force for the guest encapsulation or the guests are too small to be encapsulated due to the large portals of the capsule through which these guests can permeate. However, addition of a positively charged guest such as 1-methyl-4-phenylpyridinium (OTf^- salt) **6** and methylviologen ($2OTf^-$ salt) **7** to an acetone-d_6 solution of **3a** followed by addition of 2 equivalents of **4a** to the resulting mixture gave two sets of separate ^1H NMR peaks for the free and bound

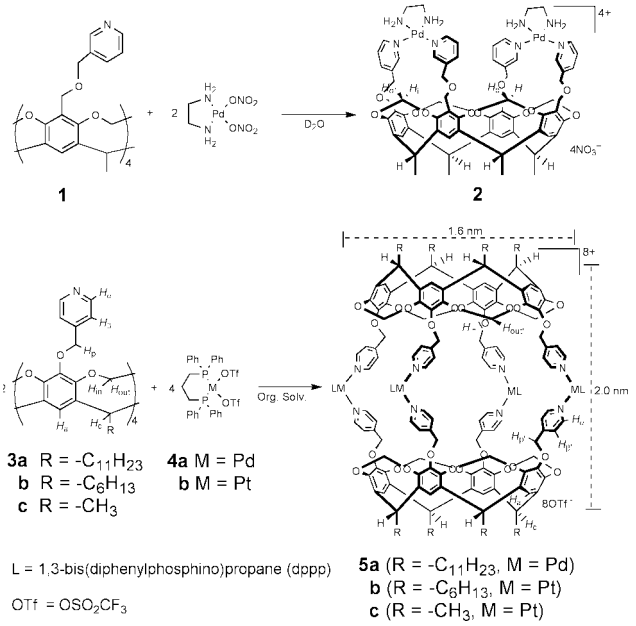

Scheme 1

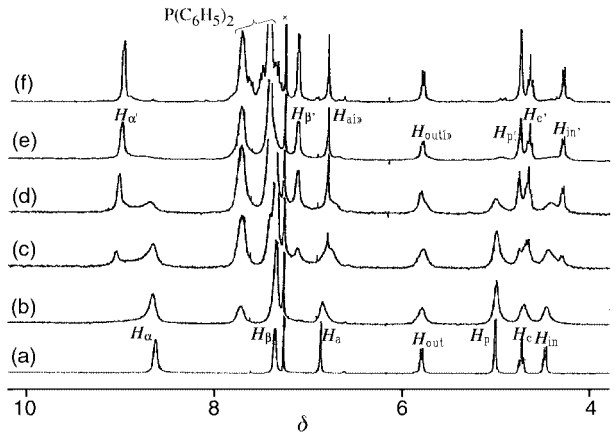

Fig. 1 Monitoring capsule formation by ^1H NMR spectroscopy (300 MHz, $CDCl_3$, 300 K). (a) free **3a**; (b) **3a**:**4a** = 2:1; (c) **3a**:**4a** = 2:2; (d) **3a**:**4a** = 2:3; (e) **3a**:**4a** = 2:4; (f) **3a**:**4a** = 2:5 molar ratio. A signal at δ 7.28 from $CDCl_3$ is marked by an asterisk.

 DOI: 10.1039/b104897j

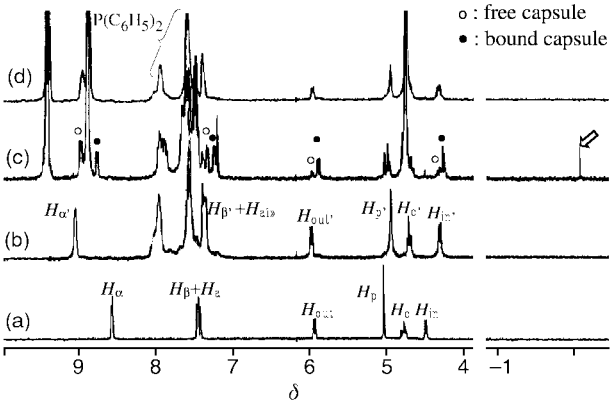

Fig. 2 Portion of the ^{1}H NMR spectra (300 MHz, acetone-d_6, 300 K); (a) free **3a**; (b) capsule **5a** formed from **3a**:**4a** = 2:4; (c) *ca.* 10 equiv. **7** added to **3a** and then 2 equiv. **4a** was added; (d) *ca.* 10 equiv. **7** was added to **5a**. The methyl group of the encapsulated guest is indicated by an arrow.

capsules.[11] This peak separation indicates that the decomplexation or guest-exchange rate is slow with respect to the ^{1}H NMR time scale. In addition, the integration ratio of the bound capsule and encapsulated guest resonances indicated a highly symmetric 1:1 complex. Particularly, NCH_3 protons of **7** move *ca.* 6.8 ppm upfield, appearing at δ −2.08,§ which presumably indicates that **7** is encapsulated such that the methyl group points towards the shielding region of the aromatic cavity at the end of the long axis of the capsule. As expected from the nearly irreversible Pd–pyridine bond formation in organic solvents, when **7** was added after the capsule formation, no spectroscopic signs of encapsulation were detected except that the pyridine's α-proton shifted slightly in the upfield direction (Fig. 2).¶ In order to investigate the behavior of the counter ions, the ^{19}F NMR spectrum was examined and showed only one signal at δ −77 in the spectra of **5a** and **5a** containing **7**; this indicates that there is not a slow exchange between triflate ions inside and outside of the cage. We also observed the release of the encapsulated **7** from the capsule in acetone-d_6 upon heating at 35 °C in the sealed NMR tube. The first-order approximation gives a guest-releasing rate constant of 4.5×10^{-6} s^{-1}. This means that guest release occurs slowly with a half-life of 43 h at 308 K. These phenomena indicate that **7** was complexed inside **3a**, most probably due to the cation–π interaction, and then if **4a** was added, properly positioned **7** was entrapped in the forming capsule **5a**.¶

In summary, we have constructed nanoscale self-assembled molecular capsules instead of an intramolecularly organized structure between properly designed resorcin[4]arene derivatives having relatively rigid pendent pyridine groups and square planar metal complexes. The positively charged *N*-methylpyridinium derivatives turn out to be encapsulated by cation–π interactions. Further studies will explore the potential for the use of nanoscale capsules as selective reaction chambers for chemical reaction catalysis.¶

We are grateful to the CMDS (KOSEF) for support of this work. S. J. P. thanks the Ministry of Education for the BK 21 fellowship.

Notes and references

† **3a**: δ_H (300 MHz, $CDCl_3$) 8.61 (d, *J* 5.89 Hz, 8H), 7.32 (d, *J* 5.89 Hz, 8H), 6.88 (s, 4H), 5.79 (d, *J* 7.11 Hz, 4H), 5.01 (s, 4H), 4.75 (t, *J* 7.92 Hz, 4H), 4.49 (d, *J* 7.12 Hz, 4H), 2.22 (br, 8H) 1.4–1.1 (br m, 72H), 0.90 (t, *J* 6.58 Hz, 12H); δ_C (75 MHz, $CDCl_3$) 149.69, 147.97, 147.01, 144.09, 139.07, 121.39, 114.69, 99.45, 73.37, 36.91,31.92, 29.83, 29.71, 29.40, 27.91, 22.68, 14.11; FAB-MS (NBA) *m*/*z* 1581.9962 (M + H$^+$) (calc. 1581.9920).

3b: δ_H (300 MHz, $CDCl_3$) 8.61 (d, *J* 5.18 Hz, 8H), 7.33 (d, *J* 5.37 Hz, 8H), 6.88 (s, 4H), 5.79 (d, *J* 7.12 Hz, 4H), 5.01 (s, 4H), 4.75 (t, *J* 7.93 Hz, 4H), 4.49 (d, *J* 7.13 Hz, 4H), 2.22 (br, 8H) 1.4–1.1 (br m, 32H), 0.92 (t, *J* 6.47 Hz, 12H); δ_C (75 MHz, $CDCl_3$) 149.62, 147.98, 146.99, 144.08, 139.10, 122.00, 113.98, 99.44, 73.36, 36.37, 31.85, 29.78, 29.44, 27.84, 22.62, 14.34 ; ESI-MS *m*/*z* 1301.6 (M + H$^+$).

3c: δ_H (300 MHz, $CDCl_3$) 8.61 (d, *J* 5.85 Hz, 8H), 7.33 (d, *J* 5.71 Hz, 8H), 7.02 (s, 4H), 5.81 (d, *J* 7.12 Hz, 4H), 5.1–4.9 (m, 12H), 4.50 (d, *J* 7.13 Hz, 4H), 2.22 (br, 8H) 1.78 (t, *J* 7.42 Hz, 12H); δ_C (75 MHz, $CDCl_3$) 149.56, 147.66, 147.15, 143.97, 139.99, 121.54, 114.18, 99.45, 73.40, 31.23, 15.82; FAB-MS (NBA) *m*/*z* 1021.3663 (M + H$^+$) (calc. 1021.3660).

5a: δ_H (300 MHz, $CDCl_3$) 8.95 (d, *J* 5.12 Hz, 16H), 7.72 (br, 32H), 7.42 (br, 48H), 7.12 (d, *J* 5.36 Hz, 16H), 6.80 (s, 8H), 5.79 (d, *J* 6.96 Hz, 4H), 4.76 (s, 16H), 4.60 (t, *J* 7.60 Hz, 8H), 4.30 (d, *J* 7.04 Hz, 8H), 3.22 (br, 16H), 2.32 (m, 8H), 2.15 (br, 16H), 1.23 (br, 144H), 0.85 (t, *J* 6.56 Hz, 24H); δ_C (75 MHz, $CDCl_3$) 150.9, 150.2, 147.6, 144.3, 138.9, 133.2, 132.2, 129.5, 125.7, 122.8, 121.0 (q, *J* 318 Hz, CF_3), 114.6, 99.5, 72.3, 36.9, 31.9, 29.8, 29.7, 29.6, 29.4, 27.9, 22.7, 21.6, 17.7, 14.1.

‡ When **5c** formed from gentle heating of a $CHCl_3$–MeOH (10:1, v/v solution of **3c** and **4b** in 1:2 molar ratio was examined by ESI-MS, [M − *n*$CF_3SO_3^-$]$^{n+}$ (*n* = 2,3,4) ion peaks were also clearly observed at *m*/*z* 2682.21, 1739.52 and 1266.74, respectively.

§ NCH_3 protons of the encapsulated guest **6** appear at δ −2.09.

¶ Addition of 1,4-dimethylpyridinium triflate, which is small enough to freely pass in and out of the cavity, either before or after capsule formation, results in two sets of separate ^{1}H NMR peaks for the free and bound capsules. NCH_3 protons of the encapsulated 1,4-dimethylpyridinium triflate also appear at δ −2.08. This constitutes strong evidence for cation–π interactions in the encapsulation process. According to molecular modeling[10] and ^{1}H NMR integration, the interior of **5a** can accommodate two molecules of 1,4-dimethylpyridinium triflate. The association constant (K_a) can be estimated from the ratio of peak intensity of free and bound to be 1180 dm^6 mol^{-2}.

1 M. M. Conn and J. Rebek, Jr. *Chem. Rev.*, 1997, **97**, 1647; *Comprehensive Supramolecular Chemistry*, ed. J.-M. Lehn (Chair); J. L. Atwood, J. E. D. Davies, D. D. MacNicol and F. Vögtle, Pergamon, Oxford, 1996, vol. 9.
2 S. B. Lee, S. Hwang, D. S. Chung, H. Yun and J.-I. Hong, *Tetrahedron Lett.*, 1998, **39**, 873; P. J. Stang, J. Fan and B. Olenyuk, *Chem. Commun.*, 1997, 1453; M. Fujita, J. Yazaki and K. Ogura, *J. Am. Chem. Soc.*, 1990, **112**, 5645.
3 M. Scherer, D. L. Caulder, D. W. Johnson and K. N. Raymond, *Angew. Chem., Int. Ed.*, 1999, **38**, 1587; C. Piguet, G. Bernardinelli and G. Hopfgartner, *Chem. Rev.*, 1997, **97**, 2005.
4 P. N. W. Baxter, J.-M. Lehn, G. Baum and D. Fenske, *Chem. Eur. J.*, 2000, **6**, 4510; A. M. Garcia, F. J. Romero-Salguero, D. M. Bassani, J.-M. Lehn, G. Baum and D. Fenske, *Chem. Eur. J.*, 1999, **5**, 1803; L. R. MacGillivray, R. H. Groeneman and J. L. Atwood, *J. Am. Chem. Soc.*, 1998, **120**, 2676.
5 F. Ibukuro, M. Fujita, K. Yamaguchi and J.-P. Sauvage, *J. Am. Chem. Soc.*, 1999, **121**, 11 014; M. Fujita, *Acc. Chem. Res.*, 1999, **32**, 53; D. B. Amabilino, C.-O. Dietrich-Buchecker, A. Livoreil, L. Pérez-García, J.-P. Sauvage and J. F. Stoddart, *J. Am. Chem. Soc.*, 1996, **118**, 3905.
6 Y. Yamanoi, Y. Sakamoto, T. Kusukawa, M. Fujita, S. Sakamoto and K. Yamaguchi, *J. Am. Chem. Soc.*, 2001, **123**, 980; M. Aoyagi, K. Biradha and M. Fujita, *J. Am. Chem. Soc.*, 1999, **121**, 7457.
7 O. Mamula, F. J. Monlien, A. Porquet, G. Hopfgartner, A. E. Merbach and A. von Zelewsky, *Chem. Eur. J.*, 2001, **7**, 533; B. Hasenknopf, J.-M. Lehn, B. O. Kneisel, G. Baum and D. Fenske, *Angew. Chem., Int. Ed. Engl.*, 1996, **35**, 1838.
8 O. D. Fox, M. G. B. Drew, E. J. S. Wilkinson and P. D. Beer, *Chem. Commun.*, 2000, 391; S. Hiraoka, Y. Kubota and M. Fujita, *Chem. Commun.*, 2000, 1509; B. Olenyuk, J. A. Whiteford, A. Fechtenkötter and P. J. Stang, *Nature*, 1999, **398**, 796; A. Ikeda, M. Yoshimura, H. Udzu, C. Fukuhara and S. Shinkai, *J. Am. Chem. Soc.*, 1999, **121**, 4296; P. Jacopozzi and E. Dalcanale, *Angew. Chem., Int. Ed. Engl.*, 1997, **36**, 613.
9 C. W. Lim and J.-I. Hong, *Tetrahedron Lett.*, 2000, **41**, 3113.
10 Molecular modeling was carried out using MacroModel 7.0 and the modified Amber* force field: F. Mohamadi, N. G. J. Richards, W. C. Guida, R. Liskamp, M. Lipton, C. Caufield, G. Chang, T. Hendrickson and W. C. Still, *J. Comput. Chem.*, 1990, **11**, 440.
11 Hydrogen-bonded capsules that encapsulate *N*-alkyl pyridinium derivatives *via* ion–dipole interactions have been reported recently: Y. L. Cho, D. M. Rudkevich and J. Rebek, Jr. *J. Am. Chem. Soc.*, 2000, **122**, 9868.

CHEMCOMM
Communication
www.rsc.org/chemcomm

Self-assembled organogels formed by mono-chain L-alanine derivatives

Xuzhong Luo, Bin Liu and Yingqiu Liang*

Lab of Mesoscopic Materials and Chemistry and State Key Lab of Coordination Chemistry, Nanjing University, Nanjing 210093, P. R. China. E-mail: yqliang@netra.nju.edu.cn

Received (in Cambridge, UK) 18th May 2001, Accepted 26th June 2001
First published as an Advance Article on the web 1st August 2001

The mono-chain L-alanine derivatives self-assemble into bilayer aggregates in a number of organic liquids and gelatinize the liquids.

Recent discoveries of low molecular weight gelators have stimulated considerable interest not only in academic investigations but also technological applications.[1–9] Although dozens of different categories of gelators have so far been identified, it is difficult to select a molecule that will definitely gel a selected liquid. Previous reports reveal that some oligomers of α-amino acids[2a,b,8] and bolaform amides derived from amino acids[2c] can gel a number of organic liquids, while the reports relating mono-amino acid derivatives are relatively few.[2d,e] Bhattacharya and co-workers reported recently that mono-amino acid derivatives can gelate selectively oil from oil–water mixtures.[9] Herein, we report simple compounds, mono-chain L-alanine derivatives, which form bilayer aggregates in a number of organic liquids and gelate the liquids.

The L-alanine derivatives, **1**–**8**,† used here were prepared in our laboratory. A typical procedure for studying gel formation

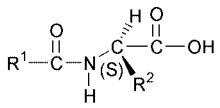

1 $R^1 = C_9H_{19}$, $R^2 = CH_3$ **2** $R^1 = C_{11}H_{23}$, $R^2 = CH_3$
3 $R^1 = C_{13}H_{27}$, $R^2 = CH_3$ **4** $R^1 = C_{17}H_{35}$, $R^2 = CH_3$
5 $R^1 = (CH_3)_3COCO$, $R^2 = CH_3$ **6** $R^1 = C_6H_5$, $R^2 = CH_3$
7 $R^1 = C_{11}H_{23}$, $R^2 = H$ **8** $R^1 = C_{11}H_{23}$, $R^2 = C_6H_5CH_2$

ability is as follows: a weighed sample was mixed with an organic liquid (1 mL) in a sealed test tube and the mixture was heated until the solid dissolved. The resulting solution was cooled at 20 °C for 2 h and then the gelation was studied. Upon formation the organogel is stable and the tube can be inverted without any change of shape of the organogel.

The results of gelation tests of **1**–**3** are summarized in Table 1,‡ in which the values denote the minimum gel concentrations (g L^{-1}) necessary for gelation. From Table 1, it is clear that compounds **1**–**3** can form a stable physical organogel and gelatinize a number of organic fluids even at a very low concentration. For example, the amounts of **2** necessary to gel 1 L of CCl_4, PhH, PhMe, *o*-xylene and mesitylene are 7, 4, 5, 5 and 4 g, respectively. Weiss and co-workers' studies reveal that the size of organogel colloids depends upon the nature of the liquid.[1c] The amphiphiles **1**–**3**, which form transparent or translucent organogels in different liquids, may be due to the different size of their colloids.

Table 1 Gelation test of **1**–**3** and minimum gel concentration necessary for gelation at 20 °C. Values refer to the minimum gel concentration in g L^{-1} (gelator/liquid)

	Gel concentration/g L^{-1}		
Organic liquids	**1**	**2**	**3**
Carbon tetrachloride	6 (translucent)	7 (translucent)	6 (translucent)
Benzene	5 (transparent)	4 (transparent)	4 (transparent)
Toluene	5 (transparent)	5 (transparent)	4 (transparent)
o-Xylene	6 (transparent)	5 (transparent)	5 (transparent)
Mesitylene	5 (transparent)	4 (transparent)	4 (transparent)
1,1,2,2-Tetrachloroethane	6 (translucent)	6 (translucent)	5 (translucent)
Tetrachloroethylene	6 (transparent)	6 (transparent)	5 (transparent)
Tetralin	6 (translucent)	5 (translucent)	5 (translucent)
n-Octane	4 (translucent)	4 (translucent)	4 (translucent)
1,1,2-Trichloroethane	7 (translucent)	7 (translucent)	6 (translucent)
Cyclohexane	5 (transparent)	5 (transparent)	5 (transparent)

Fig. 1 shows the FT-IR spectra for the CCl_4 gel and the $CHCl_3$ solution of **2**. The FT-IR spectrum of the translucent CCl_4 gel of **2** is characterized by bands attributed to intermolecular hydrogen bonding, *i.e.* 3349 (νN–H of amide), 1704 (νC=O of −COOH), and 1640 cm^{-1} (νC=O of amide), whereas the isotropic solution of **2** in $CHCl_3$ affords bands at 3450 (νN–H), 1740 (νC=O of carboxylic acid), and 1660 cm^{-1} (νC=O of amide), indicative of non-hydrogen bonding stretching vibrations. The FT-IR spectrum of the KBr pellet of **2** is similar to that of the CCl_4 gel of **2,** suggesting that the pattern of hydrogen bonding in the gel is close to that in the crystal. The sharp peak near 1704 cm^{-1} is ascribed to the C=O stretching mode of CO_2H groups, characteristic of the formation of carboxylic acid dimers.[10] These results imply that in the gel the intermolecular hydrogen bonds have been formed between the neighboring molecules of **2** and thus they form a hydrogen bond network.

The TEM image of a CCl_4 gel of **2** is shown in Fig. 2. It reveals a number of fibers, juxtaposed and intertwined by several long slender aggregations with width of *ca*. 30–100 nm. The X-ray diffraction pattern (Fig. 3) of the gel cast film from the CCl_4 gel of **2** show periodical diffraction peaks, indicating

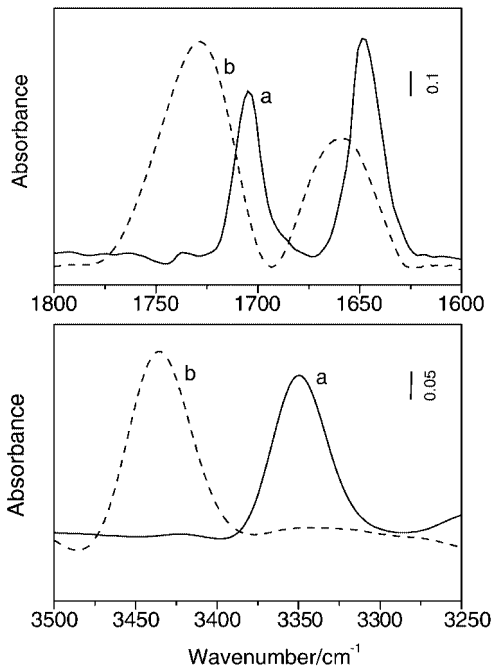

Fig. 1 FTIR spectra of **2** a) as a CCl_4 gel, b) in $CHCl_3$ solution (dashed line).

 DOI: 10.1039/b104428c

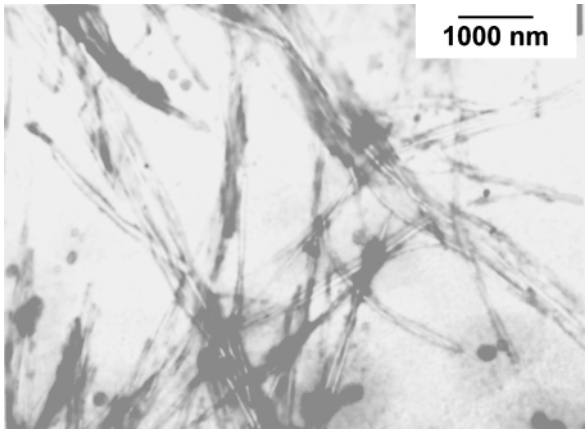

Fig. 2 TEM image of a CCl_4 gel of **2** (7 g L^{-1}). The sample was prepared by picking up the gel on a carbon grid and post-stained by uranyl acetate.

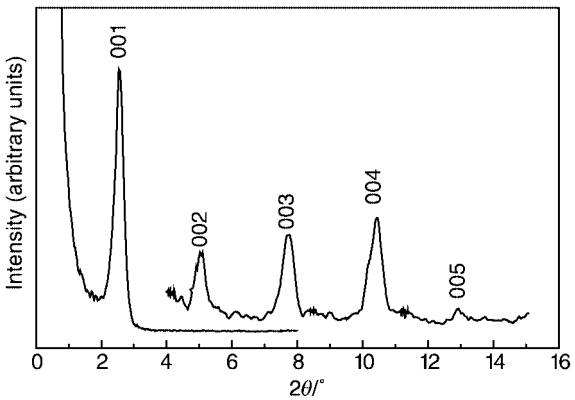

Fig. 3 X-ray diffraction patterns of a cast film from CCl_4 gel of **2**.

that **2** indeed assembles into an ordered structure. The long spacing (*D*) of the aggregate obtained by the XRD method is about 3.43 nm, which is much smaller than twice the evaluated molecular length of **2** (2.14 nm, by the CPK model), but much larger than the length of one molecule of **2**. From the XRD and FT-IR results, it can be deduced that that the gel aggregates consist of a repeating bilayer unit, which bears the head-to-head packing model with highly tilted alkyl chains relative to the bilayer normal. Within the bilayer unit, the amphiphiles are connected by intra- and inter-layer hydrogen bonds to form a hydrogen bond network and then develop the superstructure that is schematically shown in Fig. 4.

The gelling abilities of some structurally related compounds **4**–**8** (non-gel-forming) have been inspected. Comparing the molecular structure of **4**–**6** with **1**–**3**, it can be inferred that suitable length of the tail chain is essential for gelation since organogels fail to form when the tail chain is lengthened to 18 C atoms (**4**) or is substituted by *tert*-butoxycarbonylcarbonyl (**5**) and benzoyl (**6**). In experiment, we also find that the racemes of *N*-dodecanoylalanine do not induce any gelation, which is similar to that for *N*-dodecanoylglycine (**7**). The findings imply that the homochiral effect plays an important role in the gel formation. *N*-Dodecanoyl-L-phenylalanine (**8**), a compound containing a chiral center, does not exhibit gelling ability, which may be due to the relatively large steric hindrance effect of the benzyl group of the L-phenylalanine which weakens the intermolecular hydrogen bonding between neighboring molecules. Therefore the intermolecular hydrogen bonding is unable to meet the need for gelation. From these observations and analyses, it can be concluded that (i) gelling ability strongly depends on the L-alanine group, (ii) the hydrophile–lypophile balance is a significant factor for gelation, the suitable length of the tail chain is in the range of 8 to 14 C atoms, (iii) the formation of the bilayer aggregates and the homochiral effect play important roles in gel-forming.

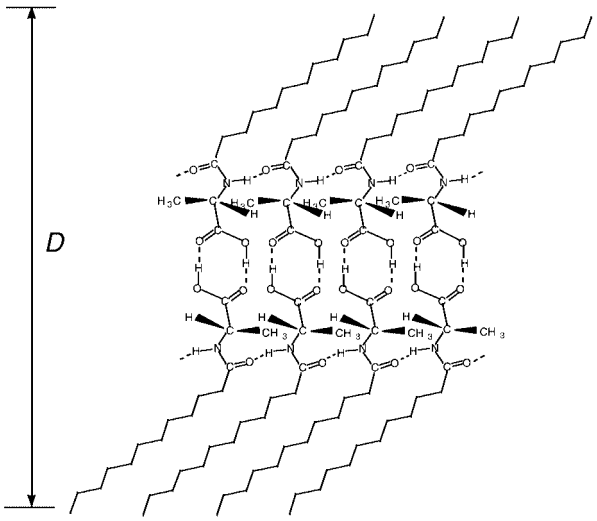

Fig. 4 Local microstructure of the bilayer aggregates of **2** in organogel.

In conclusion, this paper has shown that simple mono-chain L-alanine derivatives can self-assemble into bilayer aggregates through intermolecular hydrogen bonding and the homochiral effect in a number of organic liquids, which are juxtaposed and interlocked by van der Waals interaction, and finally gelate the organic liquids.

This work was financially supported by the National Natural Science Foundation of China (NSFC, NO. 20073019).

Notes and references

† Amino acid (0.05 mol) is placed in a three-necked round-bottomed flask, filled with an efficient stirrer, and dissolved in 50 mL of 1 M NaOH. The flask is then almost completely immersed in a bath of ice and water (*T ca.* +3 °C) and the stirrer is now set in very rapid motion. To the solution are added, dropwise, 0.10 mol of pure acyl chloride and 80 mL of 1 M NaOH at the same rate. When the reaction is complete, the suspension is acidified carefully with 2 M HCl. The residue obtained after filtration is extracted with petroleum ether to remove the fatty acid. The final amino acid derivative is chromatographed on a silica gel column empolying appropriate solvent. Satisfactory ^{1}H NMR, IR, element analysis and optically activity data were obtained for the corresponding amino acid derivatives.

‡ The minimum gel concentration was calculated as described in the literature.[8] The gels were stable in a sealed tube for over two weeks. On re-heating, the physical gelation is reversible.

1 (*a*) D. J. Abdallah and R. G. Weiss, *Adv. Mater.*, 2000, **12**, 1237; (*b*) T. Pierre and R. G. Weiss, *Chem. Rev.*, 1997, **97**, 3133; (*c*) Y. C. Lin, B. Kachar and R. G. Weiss, *J. Am. Chem. Soc.*, 1989, **111**, 5542.

2 (*a*) K. Hanabusa, Y. Naka, T. Koyama and H. Shirai, *J. Chem. Soc., Chem. Commun.*, 1994, 2683, (*b*) K. Hanabusa, J. Tange, Y. Taguchi, T. Koyama and H. Shirai, *J. Chem. Soc., Chem. Commun.*, 1993, 390; (*c*) K. Harabusa, R. Tanaka, M. Suzuki, M. Kimura and H. Shirai, *Adv. Mater.*, 1997, **9**, 1095; (*d*) K. Hanabusa, H. Nakayama, M. Kimura and H. Shirai, *Chem. Lett.*, 2000, 1070; (*e*) K. Hanabusa, J. Tange, Y. Taguchi, T. Koyama and H. Shirai, *J. Chem. Soc., Chem. Commun.*, 1992, 1371.

3 R. Oda, I. Huc and S. J. Candau, *Angew. Chem., Int. Ed.*, 1998, **37**, 2689.

4 (*a*) J. H. Jung, Y. Ono, K. Hanabusa and S. Shinkai, *J. Am. Chem. Soc.*, 2000, **122**, 5008; (*b*) J. H. Jung, Y. Ono and S. Shinkai, *Angew. Chem., Int. Ed.*, 2000, **39**, 1862; (*c*) J. H. Jung, M. Amaike and S. Shinkai, *Chem. Commun.*, 2000, **23**, 2342.

5 M. d. Loos, J. v. Esch, I. Stokroos, R. M. Kellogg and B. L. Feringa, *J. Am. Chem. Soc.*, 1997, **119**, 12 675, and references cited therein.

6 K. Murata, M. Aoti, T. Suzuki, T. Harada, H. Kawabata, T. Komori, F. Ohseto, K. Ueda and S. Shinkai, *DIC Tech. Rev.*, 1996(2), 39, and references cited therein.

7 C. M. Garner, P. Terech, J.-J. Allegraud, B. Mistrot, P. Nguyen, A. de Geyer and D. Rivera, *J. Chem. Soc., Faraday Trans.*, 1998, **94**, 2173.

8 H. T. Stock, N. J. Turner and R. McCague, *J. Chem. Soc., Chem. Commun.*, 1995, 2063.

9 S. Bhattacharya and Y. K. Ghosh, *Chem. Commun.*, 2001, 185.

10 Y. Fujimoto, Y. Ozaki, T. Kato, N. Matsumoto and K. Iriyama, *Chem. Phys. Lett.*, 1992, **196**, 347.

CHEMCOMM Communication
www.rsc.org/chemcomm

A regioselective cycloaddition route to isoxazoleboronic esters†

Mark W. Davies,[a] Robert A. J. Wybrow,[a] Christopher N. Johnson[b] and Joseph P. A. Harrity*[a]

[a] *Department of Chemistry, University of Sheffield, Sheffield, UK S3 7HF. E-mail: j.harrity@Sheffield.ac.uk; Fax: +44 (0)114 273 8673; Tel: (0)114 222 9496*
[b] *Medicinal Chemistry, GlaxoSmithKline, New Frontiers Science Park, Harlow, Essex, UK CM19 5AW*

Received (in Cambridge, UK) 12th April 2001, Accepted 26th June 2001
First published as an Advance Article on the web 1st August 2001

Alkynylboronates participate in 1,3-dipolar cycloaddition reactions with nitrile oxides to provide isoxazoleboronic esters with excellent levels of regiocontrol; additionally, these potentially valuable synthetic intermediates have been shown to participate efficiently in Suzuki coupling reactions.

Aromatic boronic esters are amongst the most valuable and widely used synthetic intermediates in modern organic chemistry due to their ability to participate in functional group transformations and carbon–carbon bond forming reactions.[1] These compounds are generally accessed *via* a functional group interconversion strategy from a starting aryl halide or triflate.[2] However, the requirement of these precursors can prove problematic when more highly substituted or heavily functionalised boronic ester products are required. Accordingly, in an effort to develop novel and efficient routes to complex arylboronates, we have recently been exploring the possibility of employing cycloaddition/benzannulation reactions of boron containing alkynes.[3] In connection with this study, we wish to report herein our recent findings on the [3+2] cycloaddition reaction of alkynylboronates with nitrile oxides towards the assembly of highly substituted isoxazoleboronic esters.

The cycloaddition reaction of nitrile oxides with alkynylboronates has received scant attention in the literature to-date. Indeed, we are aware of only a single report whereby dibutyl ethynylboronate provided the corresponding isoxazole as a single regioisomer.[4] However and importantly, only this terminal alkynylboronate was examined and the effect of acetylenic alkyl substituents on regioselectivity was not described. In contrast, the employment of alkynylstannanes is well documented.[5] However, this approach suffers from ready protodestannylation of the heterocyclic product, as well as the associated problems of handling toxic organotin species. In an effort to further clarify the effectiveness of alkynylboronates as precursors to isoxazoleboronic esters, to examine the regiochemistry of substituted boron containing alkynes and to establish the utility of isoxazoleboronic esters in carbon–carbon bond forming processes, we undertook a study of the scope of the cycloaddition reaction as outlined in Table 1.

We decided to initiate our studies on the scope of alkynylboronate [3+2] cycloaddition reactions with mesitylenecarbonitrile oxide **1** (R^1 = Mes), which is known to be stable towards dimerisation.[6] As outlined in Entry 1, we were pleased to find that 2-ethynyl-4,4,5,5-tetramethyl-1,3,2-dioxaborolane[7] **2** (R^2 = H), underwent a smooth cycloaddition reaction to provide the isoxazole **4a** bearing the boronic ester unit in the 5-position in 59% yield, with only 23% of the alternative regioisomer **3a**. On changing the alkyne substituent R^2 = H to R^2 = Me (Entry 2) the reaction proceeded cleanly to provide a *single regioisomer* of **3b**, remarkably, with complete reversal in regiochemistry. Finally, the use of longer chain alkyl and phenyl substituents also provided the 4-substituted boronic esters as single regioisomers in good yield.[8] We briefly examined the scope of nitrile oxides in the cycloaddition process and were pleased to find that this technique was applicable to phenyl and alkyl substituted 1,3-dipole substrates (Entries 5–7), the isoxazole

Table 1 1,3-Dipolar cycloadditions[a]

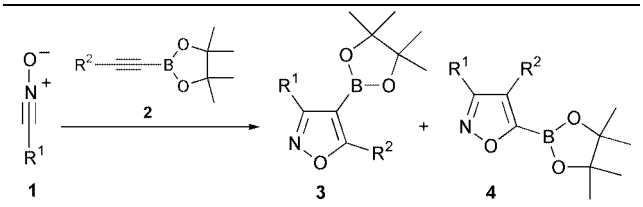

Entry[b]	R^1	R^2	Product	Yield (%)
1	Mes	H	**4a**	59%[c]
2	Mes	Me	**3b**	90%
3	Mes	Bu	**3c**	73%
4	Mes	Ph	**3d**	64%
5	Ph	H	**4e**	53%[c]
6	Ph	Me	**3f**	54%
7	*t*-Bu	Me	**3g**	27%[e]

[a] Regiochemical assignments made on the basis of diagnostic ^{13}C resonances. Additionally, these assignments have been supported by X-ray data for compounds **3b** and **3c**, which will be the subject of a future disclosure. [b] For experimental conditions, see ref. 8. [c] 23% of **3a** was isolated. [d] 6% of **3e** was islolated. [e] Estimated by ^1H NMR.[9]

† Electronic supplementary information (ESI) available: full experimental procedures. See http://www.rsc.org/suppdata/cc/b1/b103319k/

 DOI: 10.1039/b103319k

products **4e**, **3f–g**, were again formed with excellent levels of regioselectivity and followed the same insertion pattern established with the mesitylenecarbonitrile oxide in Entries 1–4. Notably, and in contrast to the stannylated isoxazoles, boronic esters **3** and **4** were isolated as white crystalline solids which could be readily purified by standard chromatographic techniques without problematic protodeboronation side reactions.

The regiochemical outcomes outlined in Table 1 are consistent with literature reports of electron deficient alkyne [3+2] cycloaddition reactions with nitrile oxides. Specifically, whereas terminal propiolates generally give a mixture of regioisomers which favours that bearing the ester moiety in the 5-position,[10] substituted propiolates and alkynyl ketones provide the regioisomeric products with the electron withdrawing group in the 4-position with high levels of selectivity.[11] Nonetheless, from a synthetic standpoint, this methodology provides a quick and direct method for the assembly of isoxazoleboronic esters which avoids problematic metallation of the heterocyclic nucleus.[12]

With a rapid and efficient entry into isoxazoleboronic esters in hand, we decided to confirm their effectiveness as synthetic intermediates for Suzuki coupling reactions. As outlined in Scheme 1, isoxazoles **3b** and **3d** were found to undergo smooth and efficient Pd-catalysed coupling with bromobenzene and allyl bromide to give **5** and **6** respectively in excellent yields. We therefore anticipate that this efficient two step procedure holds great promise for the regioselective assembly of a range of functionalised highly substituted isoxazole products.[13] Additionally, as exemplified in Scheme 2, attempts to prepare **5** by direct [3+2] cycloaddition of prop-1-ynylbenzene failed to produce any of the cycloaddition product, even after prolonged reaction times. Therefore, not only does the cycloaddition–coupling technique permit the regioselective formation of highly substituted isoxazole products, it also circumvents limitations associated with preparing 4,5-dialkyl or -diaryl substituted isoxazoles through the employment of unactivated alkyne substrates.

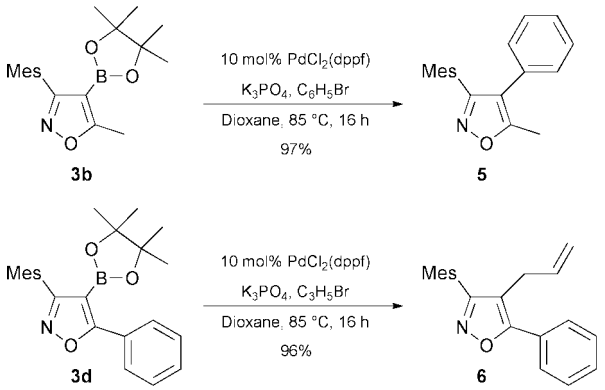

Scheme 1 Suzuki coupling reactions.

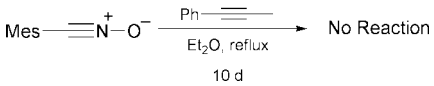

Scheme 2

In conclusion, we report a novel and flexible approach to highly substituted isoxazoles through a key [3+2] cycloaddition reaction of nitrile oxides with alkynylboronates. The investigation of related cycloaddition reactions is currently underway in our laboratories and will be reported in due course.

The authors are grateful to the EPSRC for a studentship (M. W. D.) and to GlaxoSmithKline and the University of Sheffield for generous financial support.

Notes and references

1 For comprehensive reviews, see: A. Suzuki, *Pure Appl. Chem.*, 1994, **66**, 213; N. Miyaura and A. Suzuki, *Chem. Rev.*, 1995, **95**, 2457.
2 M. Valtier and B. Carboni, in *Comprehensive Organometallic Chemistry II*, ed. E. W. Abel, F. G. A. Stone and G. Wilkinson, Pergamon, Oxford, 1995, Vol. 11, p. 191; T. Ishiyama, Y. Itoh, T. Kitano and N. Miyaura, *Tetrahedron Lett.*, 1997, **38**, 3447; M. Murata, T. Oyama, S. Watanabe and Y. Masuda, *J. Org. Chem.*, 2000, **65**, 164.
3 M. W. Davies, C. N. Johnson and J. P. A. Harrity, *Chem. Commun.*, 1999, 2107; M. W. Davies, C. N. Johnson and J. P. A. Harrity, *J. Org. Chem.*, 2001, **66**, 3525.
4 G. Bianchi, A. Cogoli and P. Grünanger, *J. Organomet. Chem.*, 1966, **6**, 598.
5 T. N. Mitchell, A. El-Faragy, S. N. Moschref and E. Gourzoulidou, *Synlett*, 2000, 223; T. Sakamoto, Y. Kondo, D. Uchiyama and H. Yamanaka, *Tetrahedron*, 1991, **47**, 5111.
6 C. Grundman and J. M. Dean, *J. Org. Chem.*, 1965, **30**, 2809.
7 Prepared according to the procedure developed by Brown: H. C. Brown, N. G. Bhat and M. Srebnik, *Tetrahedron Lett.*, 1988, **29**, 2631.
8 Typical experimental procedure as exemplified by the synthesis of **3d**: a solution of 2,4,6-trimethylbenzonitrile *N*-oxide (0.50 g, 3.1 mmol) and 4,4,5,5-tetramethyl-2-phenylethynyl-1,3,2-dioxaborolane (1.41 g, 6.2 mmol) in Et_2O (50 ml) was heated at reflux for 64 h. The reaction mixture was filtered through Celite and concentrated by rotary evaporation. Purification of the resulting residue by silica gel chromatography provided isoxazole **3d** (0.78 g, 64%) as a white crystalline solid; mp 87.7–88.2 °C; δ_H (250 MHz, $CDCl_3$) 1.11 (12H, s, C*H*$_3$), 2.13 (6H, s, Ar-C*H*$_3$), 2.32 (3H, s, Ar-C*H*$_3$), 6.89 (2H, s, Ar-*H*), 7.43–7.48 (3H, m, Ar-*H*), 8.05–8.13 (2H, m, Ar-*H*); δ_C (62.9 MHz, $CDCl_3$) 20.1, 21.2, 24.3, 83.8, 127.1, 127.5, 127.6, 128.5, 128.6, 130.3, 137.2, 138.1, 166.9, 174.4; υ_{max}/cm^{-1} 3054 (w), 2981 (m), 1570 (m), 1144 (m). (Calc. for $C_{24}H_{28}BNO_3$: C, 74.05; H, 7.25; N, 3.60. Found C, 73.94; H, 7.23; N, 3.45%). For full experimental procedure see Supplementary Information.
9 Product could not be separated from the nitrile oxide dimer by silica gel chromatography.
10 V. P. Sandanayaka and Y. Yang, *Org. Lett.*, 2000, **2**, 3087
11 R. R. Sauers, L. M. Hadel, A. A. Scimone and T. A. Stevenson, *J. Org. Chem.*, 1990, **55**, 4011; M. Hojo, K. Tomita and A. Hosomi, *Tetrahedron Lett.*, 1993, **34**, 485; F. A. Fouli, M. M. Habashy, A. F. El-Kafrawy, A. J. A. Youseef and M. M. El-Adly, *J. Prakt. Chem.*, 1987, **329**, 1116.
12 For an excellent review on the metallation of isoxazoles, see: B. Iddon, *Heterocycles*, 1994, **37**, 1263.
13 Disubstituted alkynes have been shown to undergo incorporation with low levels of regioselectivity: P. Pevarello, R. Amici, M. Colombo and M. Varasi, *J. Chem. Soc., Perkin Trans. 1*, 1993, **18**, 2151.

CHEMCOMM
Communication
www.rsc.org/chemcomm

Cerium masquerading as a Group 4 element: synthesis, structure and computational characterisation of [CeCl{N(SiMe$_3$)$_2$}$_3$]†

Odile Eisenstein,[a] Peter B. Hitchcock,[b] Alexander G. Hulkes,[b] Michael F. Lappert*[b] and Laurent Maron*[c]

[a] *Laboratoire de Structure et de Dynamique des Systèmes Moléculaires et Solides (CNRS UMR 5636), CC 14, Université de Montpellier II, Place Eugène Bataillon, 34095 Montpellier cedex 5, France. E-mail: odile.eisenstein@lsd.univ-montp2.fr*

[b] *The Chemistry Laboratory, University of Sussex, Brighton, UK BN1 9QJ. E-mail: M.F.Lappert@sussex.ac.uk*

[c] *Laboratoire de Physique Quantique - IRSAMC (CNRS UMR 5626), Université Paul Sabatier, 118 route de Narbonne, 31062 Toulouse, France. E-mail: laurent.maron@irsamc.ups-tlse.fr*

Received (in Cambridge, UK) 24th April 2001, Accepted 28th June 2001
First published as an Advance Article on the web 2nd August 2001

Oxidation of the three-coordinate cerium amide [Ce{N(SiMe$_3$)$_2$}$_3$] with TeCl$_4$ in toluene solution yields purple, diamagnetic [CeCl{N(SiMe$_3$)$_2$}$_3$], whose structure has been examined by X-ray crystallographic and computational methods.

Cerium occupies an unusual position in the periodic table, providing a bridge between Group 3 and the lanthanides, but rather than combining the useful characteristics of both families it often fails to fulfil expectations. Were it not for the fact that at atomic number 58 electrons begin to occupy the 4f shell,[1] cerium would behave more like a member of Group 4, and would presumably warrant study as intensive as that devoted to titanium, zirconium and hafnium.[2] Nature is, however, not that accommodating, and while cerium is abundant, cheap and readily available, it is very much a lanthanide element, is commonly encountered as Ce^{III}, and is thus often consigned to the backwaters of the Periodic Table.

When seen from the point of view of the other lanthanides, its standing is reversed, and it becomes potentially the most interesting of those elements as it is the only one so far proven to have chemically accessible (II),[3] (III) and (IV)[4] oxidation states. High-valent cerium chemistry (excluding *O*-donor complexes, where there is a more obvious convergence in behaviour between cerium and Group 4) is still very much under-developed, but an important contribution has been made in this area by Scott and co-workers,[5] who have reported the oxidation of the trisamidoamine complex [Ce(NN′$_3$)] [NN′$_3$ = N(CH$_2$CH$_2$NSiMe$_2$Bu^t)$_3$] with molecular halogens, which in the case of iodine produces the mononuclear Ce^{IV} amide [CeI(NN′$_3$)].

We wish to report that it is possible to oxidise the prototypical cerium amide [Ce(NR$_2$)$_3$] (R = SiMe$_3$)[6] **1** (eqn. 1), and to

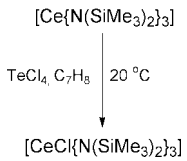

(1)

isolate a well-defined cerium(IV) compound from the reaction. Notwithstanding the fact that the Ce^{III} amide is known to be unreactive towards Cl$_2$,[5] we find that the addition of 0.25 equivalents of TeCl$_4$[7] to a toluene solution of **1** results in an immediate change in colour from yellow to deep purple.‡ Very dark, almost black, needles, which are characterised as [CeCl(NR$_2$)$_3$] **2** by ^{1}H NMR, EI-MS, microanalysis and an X-ray crystallographic study,§ are isolable in—admittedly low—yields of 24–30%. The diamagnetic nature of the complex (and by implication the cerium(IV) oxidation state) is apparent from the proton NMR spectrum in C$_6$D$_6$ which shows a sharp singlet at δ 0.42. The haloamide **2** has marginal stability in solvents other than thf, decomposing over a few hours into small amounts of [Ce(NR$_2$)$_3$] **1**, and other, unidentified, products. This instability is reflected in the absence of a parent ion and the paucity of chlorine-containing fragments in its mass spectrum, the highest *m/z* peak being assigned as [M − Me]$^+$. A representation of the molecular structure is shown in Fig. 1.

The molecule is C_3 symmetric about the Ce–Cl axis, while the geometry at the metal is intermediate between tetrahedral and trigonal pyramidal (although closer to the latter) the angles Cl–Ce–N and N–Ce–N′ being 99.48(7) and 117.34(4)° respectively. The cerium ion protrudes 0.36 Å out of the plane formed by the three nitrogen atoms, which is around 0.05 Å further than is the case for the parent Ce^{III} species **1**.[8] These features may be contrasted with those of the superficially similar Group 4 complexes [MCl(NR$_2$)$_3$] (M = Ti, Zr, Hf)[9] which are tetrahedral (despite their shorter M–N bonds) although distorted significantly from the ideal. The Ce–N and Ce–Cl bonds of 2.217(3) and 2.597(2) Å in **2** are all relatively short, as a consequence both of the presence of a contracted metal ion and the adoption of a lower coordination number than is normally found for Ce^{IV} species; we estimate from our data that Ce^{IV} has a radius of *ca*. 0.77 Å in four-coordination. There

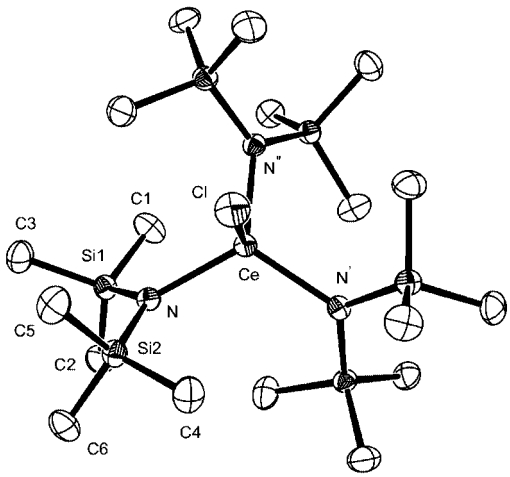

Fig. 1 Molecular structure of [CeCl{N(SiMe$_3$)$_2$}$_3$] **2**. Ce–N 2.217(3), Ce–Cl 2.597(2), Si(1)–N 1.752(3), Si(2)–N 1.750(3) Å, N–Ce–N′ 117.34(4), Cl–Ce–N 99.48(7), Si(1)–N–Si(2) 120.13(16)°.

† Electronic supplementary information (ESI) available: further details of calculations relating to **3**. See http://www.rsc.org/suppdata/cc/b1/b103634n/

 DOI: 10.1039/b103634n

is a notable elongation of the N–Si bonds to around 1.751 Å, 0.05 Å longer than those found in **1** (see below).

In order to investigate the factors which determine the overall geometry of **2**, we have undertaken a computational study, using methods previously described,[10] on the hypothetical complex [CeCl{N(SiH$_3$)$_2$}$_3$] **3**. The optimised model has C_3 symmetry, with the Ce–Cl bond coincident with the C_3 axis, and in general its geometrical features are very close to those of the experimental complex **2**, although the Ce–L separations are slightly longer (Ce–Cl 2.589; Ce–N 2.246 Å) than those determined by X-ray methods, all L–Ce–L′ bond angles are around 109°, and the dihedral angle Cl–Ce–N–Si is smaller in **2** (40°) than it is in **3** (55°). These latter, more substantial, angular differences may be ascribed to imperfect modelling of steric bulk in the periphery of the amide ligands; however, even in their absence the lengthening of the N–Si bond is reproduced very well (1.762 Å *vs*. 1.75 Å experimental) indicating that the effect is electronic in origin.

The calculated structure **3** may in turn be compared to that of the model cation [Ce{N(SiH$_3$)$_2$}$_3$]$^+$ **4**.[11] It is apparent that the N–Si bonds are significantly elongated in those complexes containing an additional chloride ligand, apparently irrespective of the metal oxidation state,¶ unperturbed bonds being 1.70 Å by our initial calculations on the Ce^{IV} centre **4** and 1.702(2) Å by X-ray analysis on the parent Ce^{III} amide **1**,[8] both of which are nominally three-coordinate. It is surprising to find that the presence of an additional ligand appears to exert a greater influence on the geometry within the amido ligand than on the Ce–N distances themselves (Ce–N in **4** is calculated to be 2.22 Å, similar to equivalent bonds in **2** and **3**).

In summary, we have accomplished the isolation of [CeCl(NR$_2$)$_3$] **2**, a cerium analogue of the familiar [M(anion)(amido)$_3$] family of complexes perhaps best known for M = Ti, Zr and Hf. Its structural characterisation has revealed an elongation of the N–Si bonds in the hexamethyldisilylamido ligands, which, when the continued uncertainty over the existence or otherwise of N(p_π)–Si(d_π) bonding is considered, invites further study of its origin. Preliminary steps towards this end have been taken in the computational characterisation of [CeCl{N(SiH$_3$)$_2$}$_3$] **3**, which reproduces the effect very well even in the absence of significant steric crowding.

We wish to thank the EPSRC (M. F. L., A. G. H.) and CNRS (O. E., L. M.) for support.

Notes and references

‡ *Synthesis of* [CeCl(NR$_2$)$_3$] **2**: [Ce(NR$_2$)$_3$][6] **1** (1.0 g, 1.6 mmol) was dissolved in toluene (25 mL) at room temperature and TeCl$_4$ (0.11 g, 0.25 eq.) was added in one portion with vigorous stirring. The solution immediately turned purple, although stirring was continued for 2 h; its volume was reduced under vacuum to *ca*. 2 mL, hexane (*ca.* 15 mL) was added, and the resulting mixture was filtered and stored overnight at −25 °C to produce well-formed purple–black needles of **2**, which were isolated by filtration (0.25 g, 24%). Found: C, 32.4; H, 8.2; N, 6.5. $C_{18}H_{54}CeClN_3Si_6$ requires C, 32.92; H, 8.29; N, 6.40%. Mp, 119–121 °C (decomp.). ^{1}H NMR (300 MHz, [D$_6$]benzene, 20 °C): δ 0.42. EI-MS: *m/z* (%) 640 (4) [M − Me]$^+$, 620 (54) [Ce(NR$_2$)$_3$]$^+$, 605 (14) [Ce(NR$_2$)$_3$ − Me]$^+$, 459 (78) [Ce(NR$_2$)$_2$]$^+$, 444 (24) [Ce(NR$_2$)$_2$ − Me]$^+$, 299 (73) [Ce(NR$_2$)]$^+$, 284 (57) [Ce(NR$_2$)−Me]$^+$.

§ Crystals from thf–hexane at −25 °C; $C_{18}H_{54}CeClN_3Si_6$, M = 656.75, rhombohedral (on hexagonal axes), a = b = 18.4508(7) Å, c = 16.8934(7) Å, V = 4980.6(3) Å^3, space group $R3c$, Z = 6, μ(Mo-Kα) = 1.68 mm^{-1}, 173(2) K, 1781 independent reflections, 1693 reflections with $I > 2\sigma I$, refined using SHELXL-97[12] with 88 parameters, $R1$ = 0.023 and $wR2$ (all data) = 0.057, max./min. residual electron density = 0.62 and 0.41 e Å^{-3}.

CCDC reference number 162978. See http://www.rsc.org/suppdata/cc/b1/b103634n/ for crystallographic data in CIF or other electronic format.

¶ We have been unable to synthesise the [CeCl(NR$_2$)$_3$]$^-$ anion to test this hypothesis further.

1 It should be noted that like Ti^{4+} and Zr^{4+}, but in contrast to Hf^{4+}, the Ce^{4+} ion has no 4f electrons, and so in one way deserves to be associated with Group 4. While a re-ordering of the Periodic Table is clearly not appropriate in this case, see W. B. Jensen, *J. Chem. Educ.*, 1982, **59**, 634 for an interesting and persuasive discussion of the relative positioning of La and Lu.

2 Notably absent from the literature of cerium chemistry, but pivotal in Group 4, are the metallocene dihalides [MCl$_2$Cp$_2$]. With respect to claims on their synthesis: see B. L. Kalsotra, R. K. Multani and B. D. Jain, *J. Inorg. Nucl. Chem.*, 1972, **34**, 2679 and references therein, see also ref. 4 and references herein.

3 Yu. K. Gun'ko, P. B. Hitchcock and M. F. Lappert, *Organometallics*, 2000, **19**, 2832.

4 [CeCp$_3$O^{t}Bu]: W. J. Evans, T. J. Deming and J. W. Ziller, *Organometallics*, 1989, **8**, 1581; [CeCp$_3$O^{i}Pr]: A. Gulino, M. Casarin, V. P. Conticello, J. G. Gaudiello, H. Mauermann, I. Fragala and T. J. Marks, *Organometallics*, 1988, **7**, 2360.

5 C. Morton, N. W. Alcock, M. R. Lees, I. J. Munslow, C. J. Sanders and P. Scott, *J. Am. Chem. Soc.*, 1999, **121**, 11 255.

6 D. C. Bradley, J. S. Ghotra and F. A. Hart, *J. Chem. Soc., Dalton Trans.*, 1973, 1021.

7 (*a*) A. F. Hill, A. G. Hulkes, A. J. P. White and D. J. Williams, *Angew. Chem., Int. Ed.*, 1999, **38**, 512; (*b*) similarly, reaction of **1** with TeBr$_4$ yields [CeBr(NR$_2$)$_3$] in low yield. We have found [PBr$_2$Ph$_3$] to be a more effective oxidant: A. G. Hulkes and M. F. Lappert, to be submitted.

8 W. S. Rees Jr., O. Just and D. S. Van Derveer, *J. Mater. Chem.*, 1999, **9**, 249.

9 C. Airoldi, D. C. Bradley, H. Chudzynska, M. B. Hursthouse, K. M. Abdul Malik and P. R. Raithby, *J. Chem. Soc., Dalton Trans.*, 1980, 2010.

10 L. Maron and O. Eisenstein, *J. Phys. Chem. A*, 2000, **104**, 7140.

11 L. Maron and O. Eisenstein, *New J. Chem.*, 2000, **25**, 255; additional calculations are in progress on this hypothetical species.

12 SHELXL-97, Program for structural refinement, G. M. Sheldrick, University of Göttingen, Germany, 1997.

CHEMCOMM Communication
www.rsc.org/chemcomm

Mono- and di-nickellaazaphosphiranes of mono- and bis-(amido)cyclodiphosph(III)azanes†

Graham R. Lief,[a] Christopher J. Carrow,[a] Lothar Stahl*[a] and Richard J. Staples[b]

[a] *Department of Chemistry, University of North Dakota, Grand Forks, ND 58202-9024, USA. E-mail: lstahl@chem.und.edu*

[b] *Department of Chemistry and Chemical Biology, Harvard University, Cambridge, MA, 02138, USA. E-mail: staples@chemistry.harvard.edu*

Received (in Purdue, IN, USA) 14th June 2001, Accepted 6th July 2001
First published as an Advance Article on the web 3rd August 2001

The syntheses and solid-state structures of the first three-membered nickel–phosphorus–nitrogen ring compounds, having anionic four-electron P=N moieties are reported.

Most modern homogeneous catalysts, which polymerize olefins to macromolecules with predictable properties, are mixtures of early-transition metal compounds and Lewis-acidic Group 13 cocatalysts.[1] Recently Brookhart and Gibson demonstrated that similar mixtures of late-transition metal complexes, particularly those with chelating bis(imino) ligands, also polymerize olefins with excellent activities.[2] Even more promising are single-component, late transition-metal alkyls, because they are both active in the absence of the expensive cocatalyst and they polymerize polar olefins.[3] The unusual properties of these neutral compounds and their polymers have rekindled interest in transition metals, especially iron, cobalt and nickel, that were once considered unlikely candidates for polyolefin catalysis.

We previously reported bis(amido)cyclodiphosph(III)azane complexes **A** of group 4 metals, which form polyethylene, but

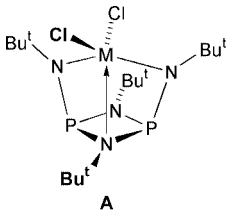

A

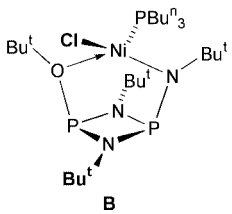

B

have comparatively short lifetimes.[4] Follow-up studies showed that the Lewis-acidic medium deactivates the catalyst by the ring opening of the cyclodiphosph(III)azane. This caused us to test the suitability of these heterocycles as ligands for neutral late-transition metal catalysts. To synthesize such complexes we modified the cyclodiphosph(III)azane to a monoanionic version, because one chloride ligand is required for polymer-chain growth.

By treating $NiCl_2(PBu^n_3)_2$ with *cis*-[$Bu^tOP(\mu\text{-}NBu^t)_2PN\text{-}Bu^t$]$^-$ (Scheme 1) we hoped to obtain precatalyst **B** and activate it by alkylation. Although both, tetrahedral and planar, coordination geometries were conceivable, the diamagnetism of the orange–red product **2**‡ indicated that the nickel atom was planar or almost planar. The uncommon chemical shift of one of the heterocycle's phosphorus atoms (−53.1 ppm and *ca*. 170 ppm upfield of that of pristine ligand), however, suggested an unusual ligand coordination.

This suspicion was confirmed by an X-ray analysis, Fig. 1, which showed that in **2**§ the amidocyclodiphosph(III)azane is not the expected *N,O*-chelate, but an η^2-*P,N* ligand, instead. Compound **2** is a spirocycle of three- and four-membered rings, whose crystallographic *m* symmetry implies a perfectly-planar

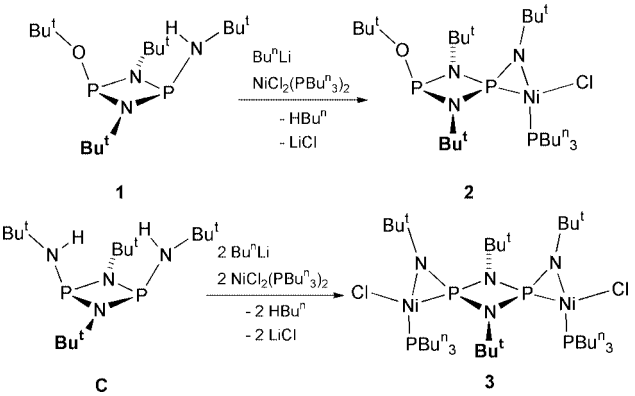

Scheme 1

nickel environment, although some of the bond angles [*e.g.* P1–Ni–N1 45.62(9)°] are far from ideal square planar. The Ni–Cl [2.2175(10) Å] and Ni–P3 [2.1522(12) Å] bond lengths, however, are quite similar to those in related nickel–chloro–amido–phosphine complexes.[5]

To test the generality of the reaction we repeated it with the bifunctional bis(amino)cyclodiphosph(III)azane **C** (Scheme 1), for which *N,N* chelation seemed a distinct plausibility. Treatment of {$NiCl_2[P(Bu^n)_3]_2$} with dianionic **C** afforded again a dark-red, diamagnetic complex **3**.‡ The X-ray analysis, Fig. 2,§ confirmed that **3** was an almost C_2-symmetric, dinuclear analogue of **2**, whose nickel atoms exhibited bond parameters that are isometric with each other and those of **2**.

A survey of the bond lengths of **2** and **3** reveals that the amidocyclodiphosph(III)azanes are not simple amido ligands with auxiliary nickel–phosphorus interactions. Thus, the metal-

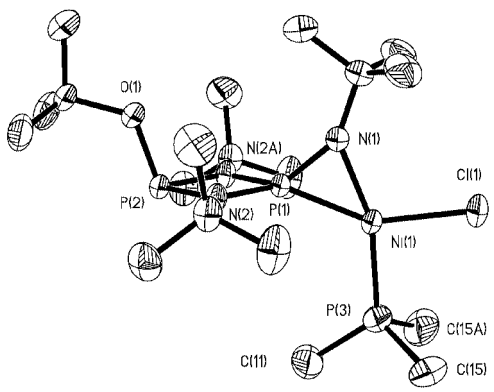

Fig. 1 Thermal ellipsoid (35% probability) plot of **2**. The *n*-butyl substituents of PBu^n_3 have been truncated to the first methylene carbons. Selected bond lengths (Å) and angles (°): Ni(1)–Cl(1) 2.2175(10), Ni(1)–P(1) 2.0796(9), Ni(1)–N(1) 1.925(3), Ni(1)–P(3) 2.1522(12) P(1)–N(1) 1.559(3); P(3)–Ni(1)–Cl(1) 92.95(5), N(1)–Ni(1)–Cl(1) 105.55(9), P(1)–Ni(1)–N(1) 45.62(9), P(1)–Ni(1)–P(3) 115.88(5).

† Electronic supplementary information (ESI) available: experimental section and crystallography. See http://www.rsc.org/suppdata/cc/b1/b105359k/

 DOI: 10.1039/b105359k

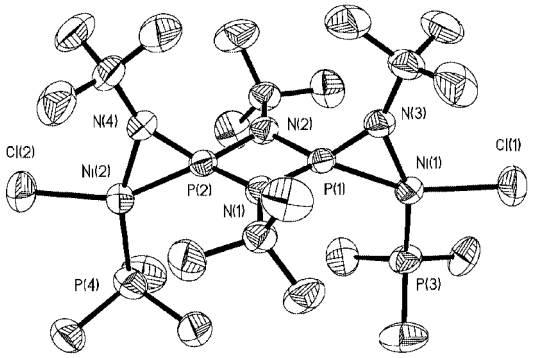

Fig. 2 Thermal ellipsoid (35% probability) plot of **3**. The *n*-butyl substituents of both PBu^n_3 ligands have been truncated to the first methylene carbons. Selected bond lengths (Å) and angles (°): Ni(1)–Cl(1) 2.2001(16), Ni(2)–Cl(2) 2.1996(17), Ni(1)–P(1) 2.0759(13), Ni(2)–P(2) 2.0739(14), Ni(1)–N(3) 1.939(4), Ni(2)–N(4) 1.944(4), Ni(1)–P(3) 2.1551(16), Ni(2)–P(4) 2.1584(18), P(1)–N(3) 1.556(4), P(2)–N(4) 1.551(4); P(3)–Ni(1)–Cl(1) 95.64(7), N(3)–Ni(1)–Cl(1) 105.27(13), P(1)–Ni(1)–N(3) 45.44(12), P(1)–Ni(1)–P(3) 113.76(6), P(4)–Ni(2)–Cl(2) 95.24(7), N(4)–Ni(2)–Cl(2) 105.72(13), P(2)–Ni(2)–N(4) 45.27(12), P(2)–Ni(2)–P(4) 113.91(6).

lacyclic P–N bonds [av. 1.555(5) Å] are substantially shorter than in pristine **C** [1.664(3) Å],[6] and consistent with P=N double bonds. This electron distribution places a formal negative charge on the phosphorus atoms, thereby reversing the polarity in the phosphorus–nitrogen bonds. The very short Ni–P [av. 2.0796(9) Å] and normal Ni–N [av. 1.925(3) Å] bonds reflect this as well, suggesting that canonical form **D** best describes the bonding in these mono- and di-nuclear species. The title compounds are thus planar, 16-electron nickel(II) complexes with anionic four-electron P=N ligands.

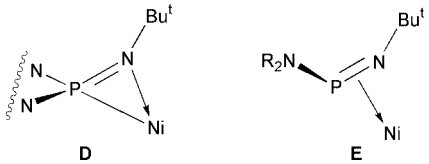

Only two nickellaazaphosphiranes have previously been structurally characterized, but in these nickel(0) species (**E**) the iminophosphine is a neutral π-donor ligand.[7] Diagnostic for this type of coordination is the lengthening of the P=N bond from 1.544(4) Å[8] in the free iminophosphine to 1.646(2) Å in the complexes, as would be expected from the removal of π-bonding electron density. The nickel–phosphorus bonds in such compounds are also substantially longer [2.23(1)–2.409(3) Å] than those in **2** and **3**.

Nickellaazaphosphiranes with anionic P=N moieties have, to our knowledge, not been fully characterized, although their existence has been confirmed by NMR spectroscopy.[9] The closest crystallographically characterized analogue of the title compounds is a zirconium phosphinomethanide complex with a three-membered P–Zr–C ring, the $P{=}CR_2$ unit being isoelectronic with P=NR.[10]

The easy syntheses and remarkable stabilities of these three-membered metallacycles suggest that it may be possible to extend these metallations to related heterocyclic and perhaps even acyclic primary aminophosphines. Despite their unexpected structures, **2** and **3** exhibit the expected reactivity and are readily alkylated. They may thus still serve as the targeted neutral, single-component catalysts. Our investigations into the generality of these metallaazaphosphirane formations and potential uses of the title compounds in olefin catalysis are continuing.

We thank the Chevron Phillips Chemical Company for financial support.

Notes and references

‡ Anal. Found for **2**: C, 52.46; H, 9.96; N, 6.64. Calc. for $C_{28}H_{63}ClN_3NiOP_3$: C, 52.15; H, 9.85; N, 6.52%. Mp 176–179 °C. δ_H (C_6D_6, 298 K) 1.626 (9 H, s), 1.592 (30 H, s), 1.349 [6 H, q, *J*(HH) 7.0 Hz], 1.200 (9 H, s, NBu^t), 0.918 [9 H, t, *J*(HH) 7.4 Hz]. δ_C (C_6D_6, 298 K) 76.82 [d, *J*(PC) 8.8 Hz], 54.25 [d, *J*(PC) 27.5 Hz], 53.08 [dd, *J*(PC) 7.6, 3.1 Hz], 32.79 [d, *J*(PC) 4.1 Hz], 32.33 [t, *J*(PC) 5.6 Hz], 31.30 [d, *J*(PC) 8.8 Hz], 27.09 (s), 25.94 [dd, *J*(PC) 25.5, 1.7 Hz], 25.01 [d, *J*(PC) 12.9 Hz], 14.25 (s). δ_P (C_6D_6, 298 K) 109.6 [d, *J*(PP) 24.7 Hz, PO], 15.2 [d, *J*(PP) 85.3 Hz, PBu^n_3], −53.6 [dd, *J*(PP) 84.2, 24.7 Hz, P=N].

Anal. Found for **3**: C, 51.29; H, 10.16; N, 5.97. Calc. for $C_{40}H_{90}Cl_2N_4Ni_2P_4$: C, 51.15; H, 9.66; N, 5.96%. Mp 164 °C. δ_H (C_6D_6, 298 K) 1.88 (18 H, s, NBu^t), 1.67 (12 H, m, Bu^n), 1.52 (12 H, m, Bu^n), 1.46 (18 H, s, NBu^t), 1.35 [12 H, q, *J*(HH) 7.2 Hz, Bu^n], 0.89 [18 H, t, *J*(HH) 7.3 Hz, Bu^n]. δ_C (C_6D_6, 298 K) 54.97 (s, NBu^t), 53.84 [t, *J*(PC) 14.1 Hz, NBu^t], 32.95 (s, NBu^t), 32.70 [t, *J*(PC) 4.6 Hz, NBu^t], 27.21 (s, Bu^n), 25.05 [d, *J*(PC) 11.9 Hz, Bu^n], 24.45 [d, *J*(PC) 25.0 Hz, Bu^n], 14.12 (s, Bu^n). δ_P (C_6D_6, 298 K) 12.19 [dm, *J*(PP) 84.5 Hz, PBu^n_3], −82.43 [dt, *J*(PP) 85.4, 21.6 Hz, P=N].

§ *Crystal data*: for **2**: $C_{28}H_{63}ClN_3NiOP_3$, M = 644.88; orthorhombic, space group *Pnma*, a = 20.538(2), b = 13.6862(15), c = 13.1024(14) Å, U = 3682.8(7) Å^3, T = 212 K, Z = 4, μ(Mo-Kα) = 0.753 mm^{-1}. 24068 reflections measured, 4736 unique (R_{int} = 0.0355) which were used in all calculations. The final $wR(F^2)$ was 0.1549 (all data). For **3**: $C_{40}H_{90}Cl_2N_4Ni_2P_4$, M = 939.36; monoclinic, space group $P2_1/c$, a = 13.905(3), b = 18.186(4), c = 21.592(4) Å, β = 98.13(3)°, U = 5405.3(19) Å^3, T = 293 K, Z = 4, μ(Mo-Kα) = 0.942 mm^{-1}. 8647 reflections measured, 7028 unique (R_{int} = 0.0876) which were used in all calculations. The final $wR(F^2)$ was 0.1486 (all data).

CCDC reference numbers 166955 and 166956. See http://www.rsc.org/suppdata/cc/b1/b105359k/ for crystallographic data in CIF or other electronic format.

1 *Metalorganic Catalysts for Synthesis and Polymerization*, ed. W. Kaminsky, Springer Verlag, Berlin, 1999; M. J. Bochmann, *J. Chem. Soc., Dalton Trans.*, 1996, 225; H. H. Brintzinger, D. Fischer, R. Mülhaupt, B. Rieger and R. M. Waymouth, *Angew. Chem., Int. Ed. Engl.*, 1995, **34**, 1143.
2 S. D. Ittel, L. K. Johnson and M. Brookhart, *Chem. Rev.*, 2000, **100**, 1169; G. J. P. Britovsek, M. Bruce, V. C. Gibson, B. S. Kimberley, P. J. Maddox, S. Mastroianni, S. J. McTavish, C. Redshaw, G. A. Solan, S. Strömberg, A. J. P. White and D. J. Williams, *J. Am. Chem. Soc.*, 1999, **121**, 8728.
3 L. S. Boffa and B. M. Novak, *Chem. Rev.*, 2000, **100**, 1479; T. R. Younkin, E. F. Connor, J. I. Henderson, S. K. Friedrich, R. H. Grubbs and D. A. Bansleben, *Science*, 2000, **287**, 460.
4 L. Grocholl, L. Stahl and R. J. Staples, *Chem. Commun.*, 1997, 1465.
5 M. D. Fryzuk, P. A. MacNeil, S. J. Rettig, A. S. Secco and J. Trotter, *Organometallics*, 1982, **1**, 918.
6 I. Schranz, L. Stahl and R. J. Staples, *Inorg. Chem.*, 1998, **37**, 1493.
7 O. J. Scherer, R. Walter and W. S. Sheldrick, *Angew. Chem., Int. Ed. Engl.*, 1985, **24**, 525; O. J. Scherer, R. Walter and W. S. Sheldrick, *Angew. Chem., Int. Ed. Engl.*, 1985, **24**, 115.
8 S. Pohl, *Angew. Chem., Int. Ed. Engl.*, 1976, **15**, 687.
9 D. Gudat and E. Niecke, *J. Chem. Soc., Chem. Commun.*, 1987, 10; J. P. Majoral, N. Dufour, F. Meyer, A.-M. Caminade, R. Choukroun and D. Gervais, *J. Chem. Soc., Chem. Commun.*, 1990, 507.
10 H. H. Karsch, B. Deubelly, J. Hofmann, U. Pieper and G. Müller, *J. Am. Chem. Soc.*, 1988, **110**, 3654.

CHEMCOMM
Communication
www.rsc.org/chemcomm

NMR evidence of pentaoxo organosilicon complexes in dilute neutral aqueous silicate solutions

Stephen D. Kinrade,*[a] Andrew S. Schach,[a] Robin J. Hamilton[a] and Christopher T. G. Knight[b]

[a] *Department of Chemistry, Lakehead University, Thunder Bay, ON P7B5E1, Canada. E-mail: Stephen.Kinrade@lakeheadu.ca*
[b] *School of Chemical Sciences, University of Illinois at Urbana-Champaign, Urbana IL 61801, USA*

Received (in Cambridge, UK) 30th May 2001, Accepted 2nd July 2001
First published as an Advance Article on the web 3rd August 2001

Silicon-29 NMR spectra of a neutral, dilute aqueous silicic acid solution, with a pH and Si concentration typical of soil solutions, reveal that a significant fraction of the silicon is incorporated in two five-coordinated organosilicon complexes when sodium gluconate is present.

The solubility of silica in aqueous solution is markedly pH dependent above pH 8.0, although it is nearly constant across the pH range typical of groundwater and soil solutions, varying from *ca.* 5 ppm for α-quartz to 130 ppm for amorphous silica at pH 7.[1] At these concentrations, silica exists primarily as tetravalent monosilicic acid, $Si(OH)_4$, although some also occurs as disilicic acid, $(OH)_3SiOSi(OH)_3$.[2] Indeed, small quantities of higher oligomers are also expected since the speciation of aqueous silicates is governed by the rules of polymer chemistry, and monomeric silicic acid is always in dynamic equilibrium with more condensed species.[3–5] No other silicon containing species have ever been identified in neutral aqueous solutions, and there has never been any evidence to suggest that silicic acid reacts with organic species at these pH values and concentrations. Although it has often been proposed that organosilicon compounds are key to molecular level processes underpinning the weathering of minerals and biosilicification in plants, such claims have always been speculative.

We have shown elsewhere,[6,7] however, that silicon–carbohydrate compounds readily form in aqueous solution, although at pH values and silica concentrations much greater than are generally found in nature. Surprisingly, the Si centres in such complexes are not tetravalent, but instead exist with either pentaoxo or hexaoxo coordination, or both.[6] Such hypervalent species only form when the carbohydrate ligand contains four or more adjacent hydroxy groups, with two in *threo* configuration, and are especially stable if the ligand also contains a carboxylic acid end group.[7] Accordingly, simple sugar acids like gluconic, saccharic and glucoheptonic acid show great affinity for aqueous silicate anions at high pH.

Here we present evidence for the existence of stable silicon–carbohydrate compounds in *neutral* solution. This represents the first observation of an organosilicon compound forming at biologically relevant Si concentrations and pH. Indeed, with the exception of the well attested monosilicic and disilicic acid species, no other Si-containing molecule has ever been observed in neutral aqueous solution.

Fig. 1 shows the ^{29}Si-{^{1}H} NMR spectrum of an aqueous sodium gluconate solution which has been tumbled with amorphous silica (enriched to 75 atom% in the NMR active ^{29}Si nuclide) for 4 weeks at 311 K. The solution has a measured pH of 7.0† and a silicon concentration of 1.4×10^{-3} mol kg^{-1}, a figure that is consistent with Si levels in soil solutions. As expected, most of the silicon is present as monosilicic and disilicic acid, and the corresponding signals at −71.0 and −80.2 ppm, respectively, are labeled in the figure. Two additional signals are seen at −101.3 and −102.0 ppm, in the region characteristic of five-coordinated Si,[8] and account for 31% of the silicon in solution. Analogous signals appear in the ^{29}Si spectra of high pH silicate solutions that contain gluconic acid or other aliphatic carbohydrate molecules having the requisite hydroxy group configuration.[6,7] Analysis of ^{29}Si–^{1}H scalar coupling and the corresponding ^{13}C NMR spectra for those solutions showed unequivocally that the ^{29}Si signals originate from Si centres coordinated to two or more carbohydrate –OC≡ linkages.[6,7] Since a –OC≡ group is significantly less shielding than –OSi≡, the peaks at −101.3 and −102.0 ppm almost

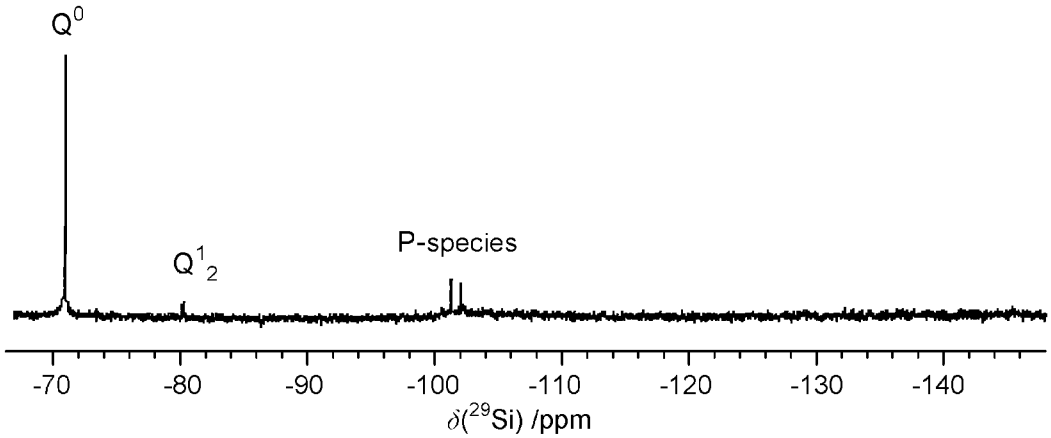

Fig. 1 Silicon-29 NMR ^{1}H-decoupled spectrum (99.36 MHz) at 270 K of a 3.35 mol kg^{-1} sodium D-gluconate solution in which amorphous SiO_2 (75% ^{29}Si-enriched) was tumbled for 4 weeks at 311 K, followed by 0.1 μm filtration. The final solution composition was 1.4×10^{-3} mol kg^{-1} Si (by ICAP), with a measured pH of 7.0 (298 K). The spectrum was recorded using 8414 π/2 pulses with an interpulse delay of 47 s, and processed using 2 Hz artificial line broadening. Spectral integration shows that 66 ± 2% of the dissolved silicon exists as the four-coordinated silicate monomer [$Si(OH)_4$, Q^0; −71.0 ppm, $\Delta\nu_{\frac{1}{2}}$ = 2.5 Hz], 3 ± 1% as the dimer [$(OH)_3SiOSi(OH)_3$, $Q^1{}_2$; –80.2 ppm, $\Delta\nu_{\frac{1}{2}}$ = 2.5 Hz], and 31 ± 2% as one of two five-coordinated silicon (denoted 'P' for pentafunctional[6]) complexes that correspond to the signals at −101.3 ($\Delta\nu_{\frac{1}{2}}$ = 8.2 Hz) and −102.0 ppm ($\Delta\nu_{\frac{1}{2}}$ = 3.7 Hz).

 DOI: 10.1039/b104713m

certainly arise from pentaoxosilicon complexes rather than from those containing either tetrahedral $Si(OSi\equiv)_4$ or $(\equiv CO)_nSi(O\text{-}Si\equiv)_{4-n}$ sites.

The spectrum remains unchanged over time, indicating that the complexes are thermodynamically stable. Indeed, the complexes are so energetically favoured that they re-assemble within the time required to obtain an NMR spectrum if the sample constituents are broken down by heating the sample to boiling.

The actual molecular structure of these complexes cannot be deduced with certainty from our spectra. The low Si concentrations involved place these experiments at the very edge of the spectrometer detection limits, even using isotopically enriched materials. The spectrum shown in Fig. 1 required 8 days to acquire. Nevertheless, our work on concentrated alkaline samples[7] would suggest that pentavalent organosilicon complexes **1**, **2** and **3** occur when silicate anions combine with gluconate ligands. Based then on the chemical shifts of signals identified at higher pH, we tentatively assign the peak at −101.3 ppm in Fig. 1 to species **2** and that at −102.0 ppm to species **3**.

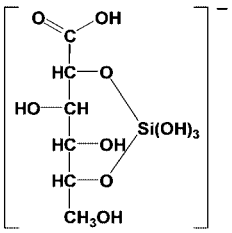

1

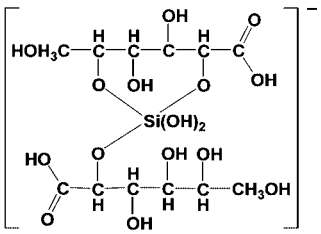

2

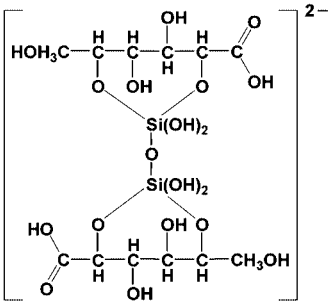

3

Evidence that gluconic acid is effective at sequestering silicate anions in dilute neutral solution suggests that simple sugar acids, or molecules containing structurally related subunits, could indeed play a role in isolating and trapping silicate anions in groundwater and biofluids, thus contributing to the functionality of silicon in nature.

This work was supported in part by the National Institutes of Health (USA; PHS 1 S10 RR 10444-01, GM-42208, RR01811) and the Natural Sciences and Engineering Research Council of Canada.

Notes and references

† pH measurements were performed on two non-isotopically enriched solutions prepared under conditions identical to those used for the ^{29}Si enriched sample in Fig. 1 (also yielding the same 1.4×10^{-3} mol kg^{-1} Si concentration), using an Orion ROSS glass pH electrode. The calculated pH for a 3.35 mol kg^{-1} gluconate ($K_b = 4.0 \times 10^{-11}$) solution is 9.0, which indicates that 4 weeks exposure to atmospheric CO_2 and amorphous silica had an appreciable neutralizing effect.

1 R. K. Iler, *The Chemistry of Silica*, Wiley, New York, 1979, pp. 40–46; J. D. Rimstidt, *Geochim. Cosmochim. Acta*, 1997, **61**, 2553.
2 L. W. Cary, B. H. W. S. De Jong and W. E. Dibble, *Geochim. Cosmochim. Acta*, 1982, **46**, 1317.
3 C. T. G. Knight and S. D. Kinrade, in *Silicon in Agriculture*, ed. L. E. Datnoff and G. H. Snyder, Elsevier, Amsterdam, 2001, pp. 57–84.
4 C. T. G. Knight, *J. Chem. Soc., Dalton Trans.*, 1988, 1457.
5 S. D. Kinrade and T. W. Swaddle, *Inorg. Chem.*, 1988, **27**, 4253; S. D. Kinrade and T. W. Swaddle, *Inorg. Chem.*, 1988, **27**, 4259.
6 S. D. Kinrade, J. W. Del Nin, A. S. Schach, T. A. Sloan, K. L. Wilson and C. T. G. Knight, *Science*, 1999, **285**, 1542.
7 S. D. Kinrade, R. J. Hamilton, A. S. Schach and C. T. G. Knight, *J. Chem. Soc., Dalton Trans.*, 2001, 961.
8 B. Herreros, S. W. Carr and J. Klinowski, *Science*, 1994, **263**, 1585.

CHEMCOMM Communication
www.rsc.org/chemcomm

Non-catalytic and selective alkylation of phenol with propan-2-ol in supercritical water

Takafumi Sato, Gaku Sekiguchi, Tadafumi Adschiri and Kunio Arai*

Department of Chemical Engineering, Tohoku University, Aoba 07 Aramaki-Aza, Aoba-ku, Sendai 980-8579, Japan. E-mail: karai@arai.che.tohoku.ac.jp; Fax: +81-22-217-7246; Tel: +81-22-217-7245

Received (in Cambridge, UK) 14th May 2001, Accepted 28th June 2001
First published as an Advance Article on the web 25th July 2001

Phenol can be alkylated with propan-2-ol without catalyst in supercritical water at 673 K with mainly *ortho* substituted alkylphenols being obtained and alkylation reaction rate increasing with increasing water density.

The Friedel–Crafts reaction is the most widely used in chemistry and industry for the alkylation of aromatics. This reaction is promoted by strong acid catalysts such as Lewis acids ($AlCl_3$ and BF_3) and mineral acids (HF, H_2SO_4),[1] and is frequently conducted in organic solvents, which requires considerable waste treatment. Because of increased awareness towards our environment, research has been directed towards alternative solvents and non-catalytic pathways.

The reactivity of the hydroxy group of phenol strongly activates the ring substituents, especially at the *ortho* and *para* positions. Thus, in the alkylation of phenol through the Friedel–Crafts reaction, it is difficult to alkylate only one position. If the alkylating agents are propan-1-ol or propan-2-ol, the condensation between alcohol and hydroxy group yields isopropyl phenoxy ether, in addition to the alkylation.[2] Solid catalysts have been used for *ortho*-selective alkylation of phenol.[3,4] Gray *et al.* reported that the etherification and alkylation of phenol could be controlled and the *ortho* alkylphenol obtained was over 3 times larger than that for *para* substituents in supercritical CO_2 with a solid catalyst.[4]

High temperature water can possibly provide an alternative pathway for formation of C–C bonds.[5,6] In the alkylation of phenol, Chandler *et al.*[7,8] studied non-catalytic alkylation of phenol with several alcohols in high temperature water at 523–573 K. They reported that alkylation of phenol with propan-2-ol occurred almost only at the *ortho* position of phenol. However, the reaction rate and alkylphenol yield obtained were low being about 20% after 120 hours reaction time.

Supercritical water (T_c = 647 K, P_c = 22.1 MPa) shows some unique properties and has been considered for the decomposition of organics.[5] It is completely miscible with many organics and can provide a homogeneous reaction field. Solvent properties such as density and relative permittivity can be varied by manipulating temperature and pressure. The reaction rate in supercritical water is expected to be much higher than that in sub-critical water due to not only the higher temperature but also to the homogeneous reaction environment[9] and the chemical effects caused by the relative permittivity.[10] In this study, we conducted non-catalytic alkylation of phenol with propan-2-ol in supercritical water at 673 K and water densities ranging from 0 to 0.5 g cm^{-3} and determined the reaction pathway. We show that high reaction rate, high alkylphenol yields and *ortho* selectivity are possible in high temperature dense water.

Reactions were conducted with 6 cm^3 stainless 316 tube bomb reactors. Phenol (99.0% purity, Wako Pure Chemical Industries, Ltd.) and propan-2-ol (99.5% purity, Wako Pure Chemical Industries, Ltd.) were loaded into the reactors and then a given amount of water was added. The air in the reactor was exchanged with argon gas by successive purgings and the reactor was sealed. The molar ratio of propan-2-ol to phenol was 1 : 5, which corresponded to a concentration of 0.33 mol L^{-1} for propan-2-ol and 1.65 mol L^{-1} for phenol. Water was loaded from 0 to 0.5 g cm^{-3} of water density corresponding to a range of concentration from 0 to 27.7 mol L^{-1}. The reactors were submerged into a sand bath controlled at 673 K. After 10–60 minutes, the reactors were quenched. Products were identified by GC-MS and by comparison of the GC retention time with standards. Quantitative analysis of products was conducted with GC-FID. For some cases, we conducted experiments for the analysis of gas products using a reactor that was connected to a valve. For these cases, the gas compositions were analyzed by GC-TCD. The product yield was defined on a propan-2-ol basis, as: yield (%) = (moles of carbon atom of the alkyl chain except benzene ring) / (moles of carbon atom in propan-2-ol loaded) × 100.

Fig. 1 shows the yield of main products for the alkylation of phenol with propan-2-ol in supercritical water at 0.5 g cm^{-3} of water density and 673 K. The main liquid products were 2-isopropylphenol, 2-propylphenol and 2,6-diisopropylphenol, and their maximal yields were 57.9, 6.9 and 5.9%, respectively. Other liquid products obtained were 2-isopropyl-6-propylphenol and 4-isopropylphenol, and their maximal yields were 1.7 and 2.4%, respectively. From 10 to 60 minutes reaction time, the gas product was almost all propylene, whose molar proportion to all gases was always above 90%. In particular, the proportion of propylene was above 95.9% before 30 minutes reaction time. After that, the proportion of hydrogen, methane and propane slightly increased up to 4.7, 1.5 and 3.4%, respectively. Propylene yields shown in Fig. 1 were obtained by the carbon balance and so include other gas products as well. The yield of propan-2-ol rapidly decreased and the conversion of propan-2-ol was above 90% at 20 minutes of reaction time. The yield of propylene was 52.1% at 10 minutes of reaction time and decreased with reaction time down to 25.8%. The yield of 2-isopropylphenol increased with time up to 57.9% and that of 2-propylphenol increased up to 6.9%. The yield of 2,6-diisopropylphenol increased up to 5.9% at 45 minutes and subsequently decreased to 5.2% at 60 minutes reaction time. After 45 minutes, the reaction appeared to be at equilibrium. In contrast, Chandler *et al.*[7] reported that the reaction did not reach equilibrium even after 120 hours of reaction time at 548 K.

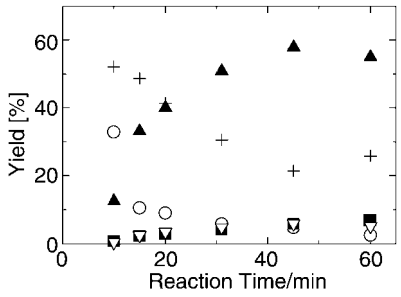

Fig. 1 Yield of (+) propylene, (▲) 2-isopropylphenol, (■) 2-propylphenol and (▽) 2,6-diisopropylphenol for reaction of phenol with propan-2-ol (○) at 0.5 g cm^{-3} of water density and 673 K.

 DOI: 10.1039/b104184n

The dehydration of propan-2-ol yielded propylene at the early reaction times. Alkylphenols dissociate in its aqueous solution, as shown by Xiang *et al.*[11] who reported that β-naphthol dissociates even in supercritical water. For example, the dissociation constant of β-naphthol is 1.26×10^{-11} mol kg^{-1} at 673 K and 0.5 g cm^{-3} of water density. At room temperature and pressure, the dissociation constant of phenol (pK_a = 9.89) at 293 K and 0.1 MPa was similar to that of β-naphthol (pK_a = 9.51) at 298 K and 0.1 MPa.[12] Phenol probably dissociates in supercritical water. Antal *et al.*[13] reported that the acid-catalyzed dehydration of propan-2-ol yielded propylene in high temperature water at 593 K.

Considering these experimental findings, the reaction pathway shown in Scheme 1 was developed. The dehydration of propan-2-ol (**1**) probably yields propylene (**2**), following alkylation of phenol with propylene to 2-isopropylphenol (**3**), 2-propylphenol (**4**) and 2,6-diisopropylphenol (**5**). It is probable that phenol acts as an acid catalyst and promotes the dehydration of propan-2-ol at supercritical conditions.

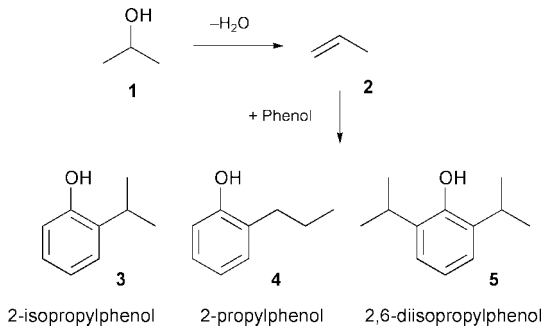

Scheme 1

The alkylation of phenol with propylene yielded 2-isopropylphenol, 2-propylphenol and 2,6-diisopropylphenol and this reaction was the rate-determining step. Phenoxyether was not produced, probably because hydrolysis of ethers occurs readily in supercritical water.[5] Phenol was alkylated almost solely at the *ortho* position of the hydroxy group even in the homogeneous system as obtained in high temperature water by Chandler *et al.*[7] The hydroxy group of phenol and several water molecules can construct a ring structure formed by hydrogen-bonds[14] and the distance between hydroxy oxygen and hydrogen increases with increasing the number of water molecules in a ring structure.[15] In supercritical carbon dioxide, specific solvation around the hydroxy group of phenol can occur.[16] Taking these results into account, water molecules probably locate around the hydroxy group of phenol at supercritical conditions and construct a ring structure with the hydroxy group of phenol. Then, the dissociation of the hydroxy group is promoted locally around it. This makes the reaction field limited only around the hydroxy group, which results in mainly the *ortho* position being alkylated.

The data reported above were measured at 0.5 g cm^{-3} of water density. At these conditions, the phase in the reactor was probably homogeneous and phenol was dissociated to a certain extent as discussed previously. In order to determine the effect of phase behavior and the dissociation of phenol, we conducted the experiment at various water densities from 0 g cm^{-3} (in Ar atmosphere) to 0.5 g cm^{-3} and at reaction times of 60 minutes. The sum of the yield of alkylphenol was less than 2.4% below 0.3 g cm^{-3} of water density. Table 1 shows the yield of propan-2-ol (**1**), 2-isopropylphenol (**3**), 2-propylphenol (**4**) and 2,6-diisopropylphenol (**5**) at 673 K and more than 0.3 g cm^{-3} of water density. The yields of all alkylphenols increased with increasing water density at more than 0.4 g cm^{-3} of water density, compared with the yield of propan-2-ol. This result clearly shows that alkylation was accelerated with increasing water density. We consider that phase behavior and the concentration of protons can affect the reaction. At low water density, the reactants were separated into two phases. Phenol would probably be mainly distributed in the liquid phase while the propan-2-ol would be distributed in the gas phase. With increasing water density, the phase in the reactor probably became homogeneous. In addition, the dissociation constant of β-naphthol increases with increasing water density in supercritical water.[11] This trend seems to be applicable to the dissociation of phenol. If the dissociation constant of phenol increased with increasing water density, the concentration of protons also increased. Then, dehydration and alkylation was promoted with increasing water density, because the proton catalyzed both reactions.

Table 1 Yield of propan-2-ol and alkylphenols with water density for 60 minutes of reaction time at 673 K, [propan-2-ol]$_0$ = 0.33 mol L^{-1}, [phenol]$_0$ = 1.65 mol L^{-1}

Water density/ g cm^{-3}	Yield (%)			
	1	**3**	**4**	**5**
0.3	75.9	3.1	0.3	0
0.4	58.5	18.0	2.2	0.6
0.42	13.7	45.5	5.8	3.7
0.46	4.5	55.1	7.1	5.1
0.48	3.6	58.8	7.5	5.4
0.5	2.6	55.0	6.9	5.1

In summary, phenol was alkylated with propan-2-ol without catalyst in supercritical water at 673 K. The alkylphenols obtained were mainly *ortho* substituted compounds and the maximum yield of 2-isopropylphenol was 58.8%. The sum of *ortho* alkylphenols yield was 71.7%. Further, alkylation was enhanced with increasing water density. Our results show that supercritical water can provide a unique reaction field for the alkylation, which is non-catalytic and highly selective.

The authors thank a Grant-in-Aid for Scientific Research on Priority Areas (09450281, 10555270, 11450295 and 11694921) the Ministry of Education, Culture, Sports, Science and Technology, for support of this research.

Notes and references

1 G. A. Olah, *Friedel–Crafts and related reactions*, Interscience Publishers, New York, 1963, vol I.
2 F. J. Sowa, G. F. Hennion and J. A. Nieuwland, *J. Am. Chem. Soc.*, 1935, **57**, 709.
3 S. Sato, R. Takahashi, T. Sodesawa, K. Matsumoto and Y. Kamimura, *J. Catal.*, 1999, **184**, 180.
4 W. K. Gray, F. R. Smail, M. G. Hitzler, S. K. Ross and M. Poliakoff, *J. Am. Chem. Soc.*, 1999, **121**, 10711.
5 P. E. Savage, *Chem. Rev.*, 1999, **99**, 603.
6 M. Siskin and A. R. Katritzky, *J. Anal. Appl. Pyrolysis*, 2000, **54**, 193.
7 K. Chandler, F. Deng, A. K. Dillow, C. L. Liotta and C. A. Eckert, *Ind. Eng. Chem. Res.*, 1997, **36**, 5175.
8 K. Chandler, C. L. Liotta, C. A. Eckert and D. Schiraldi, *AIChE J.*, 1998, **44**, 2080.
9 M. Sasaki, Z. Fang, Y. Fukushima, T. Adschiri and K. Arai, *Ind. Eng. Chem. Res.*, 2000, **39**, 2883.
10 P. E. Savage, S. Gopalan, T. I. Mizan, C. J. Martino and E. E. Brock, *AIChE J.*, 1995, **41**, 1723.
11 T. Xiang and K. P. Johnston, *J. Phys. Chem.*, 1994, **98**, 7915.
12 D. R. Lide, *CRC Handbook of Chemistry and Physics 73rd Edition*, CRC Press, Inc., Boca Raton, 1992–1993.
13 M. J. Antal, M. Carlsson, X. Xu and D. G. M. Anderson, *Ind. Eng. Chem. Res.*, 1998, **37**, 3820.
14 N. Mikami, *Bull. Chem. Soc. Jpn.*, 1995, **68**, 683.
15 Y. Dimotrova, *J. Mol. Struct. (THEOCHEM)*, 1998, **455**, 9.
16 N. Wada, M. Saito, D. Kitada, R. L. Smith, H. Inomata, K. Arai and S. Saito, *J. Phys. Chem. B*, 1997, **101**, 10918.

CHEMCOMM Communication
www.rsc.org/chemcomm

Rhodizonate and croconate dianions as divergent hydrogen-bond acceptors in the self-assembly of supramolecular structures†

Chi-Keung Lam and Thomas C. W. Mak*

Department of Chemistry, The Chinese University of Hong Kong, Shatin, New Territories, Hong Kong SAR, P. R. China. E-mail: tcwmak@cuhk.edu.hk

Received (in Cambridge, UK) 18th May 2001, Accepted 9th June 2001
First published as an Advance Article on the web 9th August 2001

The $C_5O_5^{2-}$ and relatively unstable $C_6O_6^{2-}$ dianions, each serving as a hub for binding with a set of convergent NH donor groups of four phenylurea molecules, have been generated *in situ* and stabilized in nearly isostructural hydrogen-bonded host lattices.

Recently we initiated a program to explore the use of the non-benzenoid aromatic oxocarbons $C_nO_n^{2-}$ (n = 3, deltate; n = 4, squarate; n = 5, croconate; n = 6, rhodizonate),[1] each bearing a planar set of divergent hydrogen-bond acceptor sites, in combination with urea or thiourea, for the construction of anionic host frameworks that accommodate quaternary ammonium cations. In the series of inclusion complexes $[Et_4N^+]_2C_4O_4^{2-}\cdot 2Et_4N^+\cdot HCO_3^-\cdot 4(NH_2)_2CO\cdot 6H_2O$,[2] $[Pr^n{}_4N^+]_2C_4O_4^{2-}\cdot 6(NH_2)_2CO\cdot 2H_2O$,[3] $[Et_4N^+]_2C_4O_4^{2-}\cdot 4(NH_2)_2CS\cdot 2H_2O$,[4] $[Et_4N^+]_2C_4O_4^{2-}\cdot 6(NH_2)_2CS$[6] and $[Et_4N^+]_2C_4O_4^{2-}\cdot 2(NH_2)_2CS\cdot 2H_2O$,[6] direct linkages between squarate and urea/thiourea exhibit the hydrogen bonding patterns I–IV shown in Fig. 1, which are further connected with the commonly occurring infinite urea/thiourea chains or ribbons[5] to generate two- or three-dimensional host networks.

Attempts to obtain analogous croconate and rhodizonate inclusion complexes with urea (and thiourea) have so far been unsuccessful. We then proceeded on the hypothesis that an oxocarbon dianion could be stabilized by surrounding it with the maximum number of convergent NH donor sites, and to do so it would be necessary to disrupt the intermolecular association between urea molecules. We therefore decided to replace urea with phenylurea, whose bulky and hydrophobic substituent is expected to prevent, or at least suppress, the formation of urea ribbons. Furthermore, the rhodizonate dianion readily undergoes oxidative ring contraction through an α-oxo alcohol rearrangement,[6] which is related to the well known benzil–benzylic acid rearrangement,[7] to produce the croconate ion. Accordingly we developed a simple method to generate the rhodizonate ion *in situ* and incorporate it and its ring-contracted croconate product into the host lattices of new inclusion compounds $[Bu^n{}_4N^+]_2C_6O_6^{2-}\cdot 4PhNHCONH_2$ **1** and $[Bu^n{}_4N^+]_2C_5O_5^{2-}\cdot 4PhNHCONH_2$ **2**, respectively.‡

In the crystal structure of **1**,§ four crystallographically independent phenylurea molecules are directly connected to the rhodizonate ion *via* separate pairs of strong N–H$_{anti}$···O hydrogen bonds in the range of 2.834–2.933 Å [ring motifs **A**, **B**, **C** and **D**; graph set $N_2 = R_2^2(9)$][8] to form a pseudo-centrosymmetric, slightly twisted X-shaped pentamer (Fig. 2). One pair of opposite phenylurea molecules (designated as type A) are nearly coplanar with the rhodizonate ion, as shown by the relevant torsion angles C46–N5···O3–C3 0.6°, C46–N6···O4–C4 18.9°, C60–N9···O6–C6 23.5° and C60–N10···O1–C1 −8.2°, while the other pair (type B) are inclined to it at about 45°. Adjacent pentamers are joined together by pairs of strong N–H$_{syn}$···O hydrogen bonds between urea fragments (N5···O10 2.913 Å and N9···O8 2.969 Å) in a complementary manner [**E**, $N_2 = R_2^2(8)$] to generate a wide rhodizonate–phenylurea ribbon, which is further strengthened by additional strong N–H$_{anti}$···O hydrogen bonds (N3···O10 3.063 Å and N7···O8 3.083 Å) to produce two other ring motifs [**F** and **G**, $N_2 = R_4^2(8)$]. This wide ribbon runs parallel to the [110] direction, and the hydrophilic amido fragment of the type A phenylurea molecule participates in the construction of its zigzag 'pseudo rhodizonate–urea' backbone in a 'chain of rings' pattern $C_3^3(12)[R_2^2(9)R_2^2(8)\ R_2^2(9)]$. The phenyl rings of type A urea molecules and whole urea molecules of type B protrude outward from the backbone, and stacking of the wide ribbons leads to a system of grated, broken-walled channels each accommodating two parallel columns of well ordered tetra-*n*-butylammonium cations (Fig. 3).

The hydrogen bonding pattern in the crystal structure of **2**§ (Fig. 4) is very similar to that in **1** (Fig. 2), and the cyclic pentameric structural unit with an oxocarbon core is basically retained, so that the pair of inclusion compounds exhibit an interesting isostructurality relationship.[9] However, the croconate ion is disordered about an inversion center, and it adopts two equally populated orientations. Consequently, there are only two independent phenylurea molecules in the asymmetric unit of **2**, and the length of the *c*-axis is about half of that in **1**. In addition to the conventional N–H···O hydrogen bonds, the croconate-based pentamers are consolidated by the charged-assisted C–H···O hydrogen bonds, whose metric parameters (C19···O5 3.282 Å, H19···O5 2.497 Å, C19–H19···O5 142.3°, H19···O5–C5 135.6°; C8···O2 3.341 Å, H8···O2 2.568 Å, C8–

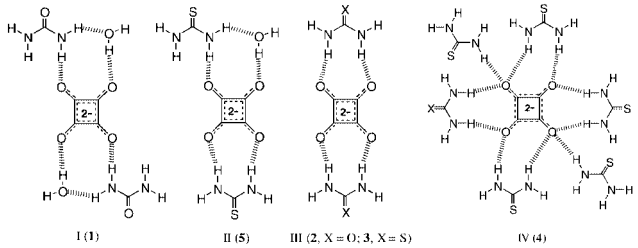

Fig. 1 Hydrogen bonding interaction between squarate ions and urea/thiourea molecules in some inclusion complexes.

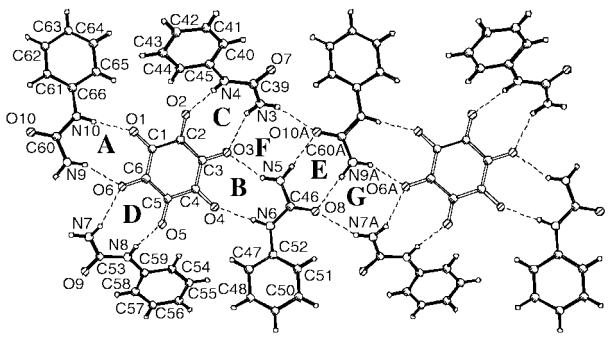

Fig. 2 Hydrogen bonding scheme of **1** showing a portion of the rhodizonate–phenylurea wide ribbon consolidated by strong N–H···O hydrogen bonds. The phenyl rings lie on opposite sides of the zigzag ribbon; half of them are nearly co-planar with the ribbon, and the other half are inclined at 45°. The orientation of these two kinds of phenyl rings is further illustrated in Fig. 2. Symmetry transformation: A ($-x$, $-y$, $-z$).

† Dedicated to Dr. Tze-Lock Chan on the occasion of his retirement.

 DOI: 10.1039/b104386m

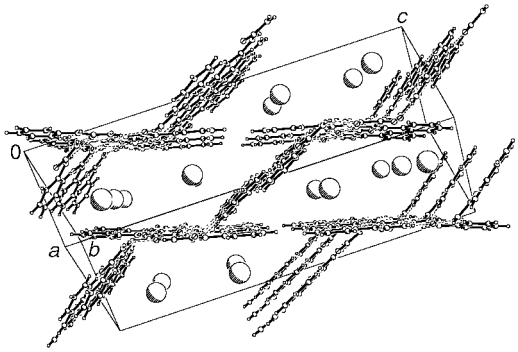

Fig. 3 The crystal structure of **1** showing the one-dimensional 'broken-walled' channel system. The well ordered tetra-*n*-butylammonium cations (represented by large shaded circles for clarity) are arranged in two parallel columns in the [1$\bar{1}$0] direction. Half of the phenylurea molecules reach out of the plane of each rhodizonate–phenylurea ribbon, functioning as spacers which effectively separate the double cationic columns. The cross-section of the parallelogram-shaped channel is *ca.* 11.6 × 19.2 Å.

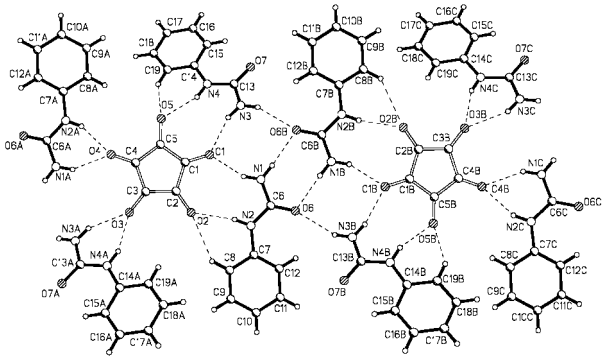

Fig. 4 Hydrogen bonding scheme of **2**, showing a wide croconate–phenylurea ribbon running parallel to the *b*-axis. The disordered croconate dianion lies at an inversion center; for clarity, one orientation is shown on the left and the other on the right. Symmetry transformations: A ($1 - x$, $-y$, $1 - z$), B ($1 - x$, $1 - y$, $1 - z$) and C (x, $1 + y$, z).

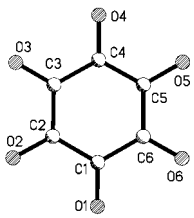

Fig. 5 Structure of $C_6O_6^{2-}$ in **1**. Bond lengths (Å) and angles (°) with esds in parentheses: O(1)–C(1) 1.234(4), O(2)–C(2) 1.247(4), O(3)–C(3) 1.252(4), O(4)–C(4) 1.251(4), O(5)–C(5) 1.258(4), O(6)–C(6) 1.250(4), C(1)–C(2) 1.449(5), C(1)–C(6) 1.458(5), C(2)–C(3) 1.443(5), C(3)–C(4) 1.421(5), C(4)–C(5) 1.424(5), C(5)–C(6) 1.447(5); O(1)–C(1)–C(2) 120.1(4), O(1)–C(1)–C(6) 120.5(4), C(2)–C(1)–C(6) 119.4(4), O(2)–C(2)–C(3) 120.0(4), O(2)–C(2)–C(1) 120.8(4), C(3)–C(2)–C(1) 119.2(4), O(3)–C(3)–C(4) 120.4(4), O(3)–C(3)–C(2) 119.2(4), C(4)–C(3)–C(2) 120.5(4), O(4)–C(4)–C(3) 119.7(4), O(4)–C(4)–C(5) 118.9(4), C(3)–C(4)–C(5) 121.4(4), O(5)–C(5)–C(4) 120.8(4), O(5)–C(5)–C(6) 120.1(3), C(4)–C(5)–C(6) 119.1(4), O(6)–C(6)–C(5) 119.5(4), O(6)–C(6)–C(1) 120.4(4), C(5)–C(6)–C(1) 120.1(4).

H8···O2 140.9°, H8···O2–C2 164.4°) are comparable to those in the most probable ranges (C···O 3.3–3.4 Å, H···O 2.2–2.6 Å, C–H···O 150–160° and H···O–C *ca.* 120°).[10]

The present study provides the first reasonably precise molecular dimensions of the rhodizonate dianion, which lends support to the aromaticity of this non-benzenoid cyclic oxocarbon. Notably, the measured C–C bond lengths [1.421(5)–1.458(5) Å; see Fig. 5] of the rhodizonate in **1**, which exhibits approximate D_{6h} molecular symmetry, are significantly shorter than the corresponding values (1.488 and 1.501 Å) in $Rb_2C_6O_6$[11] and the calculated values (1.500 and 1.501 Å) for the C_2 structure of this dianion.[12] Compound **1** provides yet another example of the use of urea and its derivatives for stabilizing elusive molecular anions such as allophanate[13] and dihydrogen borate[14] in a hydrogen-bonded host lattice.

In summary, we have shown that the supramolecular approach to the synthesis of solids may lead to the stabilization, by way of crystal engineering, of a reactive covalent species, and this strategy holds good promise for further development.

This work was supported by Hong Kong Research Grants Council Earmarked Grant Ref. No. CUHK 4206/99P.

Notes and references

‡ *Synthesis*: phenylurea[15a] and tetrahydroxy-1,4-quinone hydrate[15b] were prepared according to literature procedures. For **1**, tetrahydroxy-1,4-quinone hydrate was dissolved in a small amount of absolute ethanol (E-Merck, 99.8%) in a stoppered flask, to which two molar equivalents of aqueous tetra-*n*-butylammonium hydroxide solution (40 wt% in water, Aldrich) were added. The solution was stirred until all solid material had completely dissolved. Five molar equivalent of phenylurea was then added and stirred for a while. The solution was concentrated under vacuum to yield a brownish orange solid. The solid was next re-dissolved in a minimum amount of absolute ethanol. After filtration, the deep orange red solution was evaporated in a dessicator charged with anhydrous calcium chloride. Rose-red polyhedral crystals of **1** (yield *ca.* 50%) were obtained after about one week. Mp 125.4–130.6 °C. IR (KBr): 3390, 3338, 3271, 3205, 3075, 2956, 2871, 1696, 1652, 1598, 1545, 1500, 1444, 1343, 1247, 756, 696 cm^{-1}. It was found that when **1** was exposed in air, its reddish color gradually faded and completely turned to pale yellow in *ca.* 3 h, therefore, a selected crystal from a freshly prepared sample was sealed in a 0.5 mm glass capillary for X-ray analysis. For **2**, having noticed the color change of **1** in air, a small amount of warm absolute ethanol was added to re-dissolve the immersed crystals. After the solution was kept inside a locker for another three weeks, a crop of brownish yellow rectangular prisms of **2** was deposited in *ca.* 60% yield. Compound **2** proved to be stable in air for an indefinite period. Mp 128.3–134.5 °C. IR (KBr): 3339, 3271, 3201, 3076, 2957, 2874, 1695, 1595, 1545, 1509, 1445, 1343, 1250, 755, 698 cm^{-1}.

§ CCDC reference numbers 163266 and 163267. See http://www.rsc.org/suppdata/cc/b1/b104386m/ for crystallographic data in CIF or other electronic format.

1 *Oxocarbons*, ed. R. West, Academic Press, New York, 1980; R. West, *Isr. J. Chem.*, 1980, **20**, 300; R. West and J. Niu, in *The Chemistry of the Carbonyl Group*, ed. J. Zabicky, Interscience, London, 1970, vol. II, ch. 4; R. West and J. Niu in *Non-benzenoid Aromatics*, ed. J. P. Snyder, Academic Press, New York, 1969, vol. I, ch. 6; F. Serratosa, *Acc. Chem. Res.*, 1983, **16**, 170; G. Seitz and P. Imming, *Chem. Rev.*, 1992, **92**, 1227.

2 C.-K. Lam and T. C. W. Mak, *Russ. J. Chem. (Zh. Strukt. Khim.)*, 1999, **40**, 883.

3 C.-K. Lam and T. C. W. Mak, *Cryst. Eng.*, 2000, **3**, 33.

4 C.-K. Lam and T. C. W. Mak, *Tetrahedron*, 2000, **56**, 6657.

5 Q. Li and T. C. W. Mak, *Inorg. Chem.*, 1999, **38**, 4142; T. C. W. Mak and Q. Li, in *Advances in Molecular Structure and Research*, ed. M. Hargittai and I. Hargittai, JAI Press, Stamford, Connecticut, 1998, vol. IV, pp. 151–225.

6 R. Nietzki, *Ber.*, 1887, **20**, 1617, R. Nietzki, *Ber.*, 1887, **20**, 2114; O. Gelormini and N. E. Artz, *J. Am. Chem. Soc.*, 1930, **52**, 2483; F. Arcamone, C. Prevost and P. Souchay, *Bull. Soc. Chim. Fr.*, 1953, 891; J. Fatiadi, H. S. Isbell and W. F. Sager, *J. Res. Natl. Bur. Std. A*, 1963, **67**, 153; J. D. Dunitz, P. Seiler and W. Czechtizky, *Angew. Chem., Int. Ed. Engl.*, 2001, **40**, 1779.

7 S. Selman and J. F. Eastham, *Quart. Rev.*, 1960, **14**, 221.

8 M. C. Etter, J. C. MacDonald and J. Bernstein, *Acta Crystallogr., Sect. B*, 1990, **46**, 256; M. C. Etter, *Acc. Chem. Res.*, 1990, **23**, 120; J. Bernstein, R. E. Davis, L. Shimoni and N.-L. Chang, *Angew. Chem., Int. Ed. Engl.*, 1995, **34**, 1555.

9 A. Kálmán, L. Párkányi and Gy. Argay, *Acta Crystallogr., Sect. B*, 1993, **49**, 1039; A. Kálmán and L. Párkányi, in *Advances in Molecular Structure and Research*, ed. M. Hargittai and I. Hargittai, JAI Press, Stamford, Connecticut, 1997, vol. III, pp. 189-226.

10 G. R. Desiraju and T. Steiner, *The Weak Hydrogen Bond in Structural Chemistry and Biology*, Oxford University Press, New York, 1999.

11 Ref. 1; M. A. Neuman, *Dissertation Abstr.*, 1966, **26**, 6394.

12 P. v. R. Schleyer, K. Najafian, B. Kiran and H. Jiao, *J. Org. Chem.*, 2000, **65**, 426.

13 T. C. W. Mak, W. H. Yip and Q. Li, *J. Am. Chem. Soc.*, 1995, **117**, 11 995.

14 Q. Li, F. Xue and T. C. W. Mak, *Inorg. Chem.*, 1999, **38**, 4142.

15 (*a*) A. I. Vogel, *Vogel's Textbook of Practical Organic Chemistry*, 5th edn., rev. by B. S. Furniss, A. J. Hanndaford, P. W. G. Smith and A. R. Tatchell, Longman, Harlow, Essex, 1989; (*b*) *Org. Synth. Collect.*, 1973, **Collect. vol. 5**, 1011.

CHEMCOMM
Communication
www.rsc.org/chemcomm

A remarkable temperature-dependent, accidental degeneracy of ^{31}P NMR chemical shifts in Ru(II) diphosphine/diimine complexes

Paul W. Cyr, Brian O. Patrick and Brian R. James*

Department of Chemistry, The University of British Columbia, Vancouver, British Columbia V6T 1Z1, Canada. E-mail: brj@chem.ubc.ca

Received (in Cambridge, UK) 18th April 2001, Accepted 28th June 2001
First published as an Advance Article on the web 2nd August 2001

Several *cis*-RuX_2((*R*)-BINAP)(diimine) complexes have been prepared, and many of these exhibit an unusual temperature-dependent, accidental degeneracy of the ^{31}P shifts in their solution NMR spectra.

There is on-going research in this laboratory on Ru(II) complexes possessing one chelating, ditertiary phosphine (P–P) per Ru atom, because of their proven ability as hydrogenation catalysts,[1] especially for enantioselective catalysis when P–P is a chiral diphosphine ligand;[2] of such ligands, the C_2-symmetric BINAP (2,2′-bis(diphenylphosphino)-1,1′-binaphthyl) and its derivatives have been employed very successfully in asymmetric catalysis.[3,4] We have also studied Ru(II) complexes with mixed P- and N-donor ligand sets, where the N-donor is either incorporated into the phosphine ligand,[5] or with separate P- and N-donor ligands,[6] and the use of Ru(II) systems with tetradentate 'P_2N_2' ligands for catalytic hydrogenation[7] and epoxidation[8] reactions has been explored recently. Of particular note, spectacular success has been achieved in the use of chiral Ru(II) complexes with phosphine (either mono- or bidentate) and diamine ligands in catalytic enantioselective hydrogenation.[4] We report here a warning concerning interpretation of the ^{31}P NMR spectra of such systems: 'apparent complications' can result from a remarkable temperature-dependent degeneracy of ^{31}P NMR chemical shifts. More specifically, some systems, where two P atoms are *trans* to different ligands (an N-donor, and a halogen), generate a singlet ^{31}P{^{1}H} signal resulting from an authentic, accidental degeneracy.

Complexes of formula *cis*-RuCl_2((*R*)-BINAP)(L_2), where L_2 = a bidentate (N–N) ligand,† were prepared by reaction of L_2 with RuCl_2((*R*)-BINAP)(PPh_3),‡ and halide metathesis using NaX (X = Br, I) in acetone afforded the corresponding *cis*-RuX_2((*R*)-BINAP)(L_2) complexes. The structure of *cis*-RuBr_2((*R*)-BINAP)(bipy) (**1b**) is shown in Fig. 1.§ The crystallographic and solution ^{31}P{^{1}H} NMR data (Table 1) indicate that these complexes are formed stereoselectively. For example, the pseudo-octahedral structure of **1b** has the expected[3b] λ-conformation of the (*R*)-BINAP chelate ring, and only the *R*,Λ diastereomer is seen (where Λ refers to the chirality about the Ru atom; a parallel structural refinement was carried out for both Λ and Δ isomers, but only the Λ structure refined to convergence). Further, the solution ^{31}P spectra reveal the presence of only one set of signals at any given temperature, while diastereomeric Ru(II) BINAP complexes have been differentiated by ^{31}P NMR data.[6b,9] *Cis*-**3a** is seen solely as the *R*,Δ diastereomer; whether the halide metathesis reaction occurs with retention or inversion of stereochemistry at Ru remains to be established.[10] The solution ^{31}P NMR behaviour is

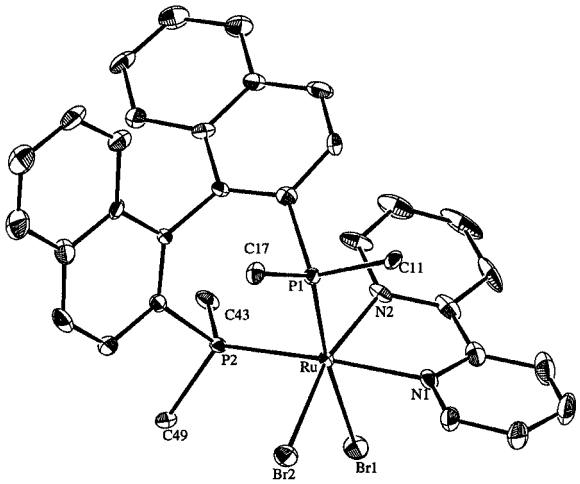

Fig. 1 ORTEP representation (50% probability ellipsoids) of *cis*-RuBr_2((*R*)-BINAP)(bipy) (**1b**). Solvates and H-atoms have been omitted for clarity. Selected bond distances (Å) and angles (°): Ru–Br(1), 2.6175(6); Ru–Br(2), 2.5476(7); Ru–P(1), 2.305(1); Ru–P(2), 2.317(2); Ru–N(1), 2.128(4); Ru–N(2), 2.091(4); Br(1)–Ru–Br(2), 89.42(2); P(1)–Ru–P(2), 93.13(5); N(1)–Ru–N(2), 77.7(2). Only the *ipso* carbon atoms (C(11), C(17), C(43) and C(49)) of the phenyl groups are shown.

Table 1 ^{31}P{^{1}H} NMR spectroscopic data for *cis*-RuX_2((*R*)-BINAP)(L_2)[a]

	δ_A, δ_B [$^2J_{AB}$/Hz][b]		
Complex	C_6D_6	$CDCl_3$	CD_2Cl_2
cis-RuCl_2((*R*)-BINAP)(bipy) **1a**	48.0, 46.0 [32.3]	47.1, 46.6 [33.5][c]	47.2[d]
cis-RuBr_2((*R*)-BINAP)(bipy) **1b**	47.8, 45.2 [32.1]	47.3, 46.7 [33.3][e]	47.2, 46.9 [33.7][f]
cis-RuI_2((*R*)-BINAP)(bipy) **1c**	49.4, 42.5 [30.0]	48.8, 44.2 [30.6]	48.4, 44.6 [31.7]
cis-RuCl_2((*R*)-BINAP)(dmbipy) **2**	47.5, 47.2 [33.4][g]	48.3, 47.4 [34.6]	48.0, 47.5 [34.4]
cis-RuCl_2((*R*)-BINAP)(phen) **3a**	48.4, 46.2 [34.0]	47.2[h]	47.9, 47.5 [34.4][i]
cis-RuBr_2((*R*)-BINAP)(phen) **3b**	48.7, 45.7 [32.8]	48.0, 47.0 [33.1][j]	47.5, 46.9 [34.0][k]
cis-RuI_2((*R*)-BINAP)(phen) **3c**	50.8, 42.6 [29.7]	49.6, 44.6 [31.3]	49.3, 45.2 [31.5]
cis-RuCl_2((*R*)-BINAP)(batho) **4**	47.8, 45.5 [33.4]	47.6, 46.9 [33.6]	47.4, 47.1 [33.7][l]
cis-RuCl_2((*R*)-BINAP)(bpa) **5**	50.7, 47.1 [33.3]	50.0, 47.6 [33.5]	49.5, 48.0 [33.6]

[a] Satisfactory elemental analyses were obtained for all the complexes listed.[10] [b] At room temperature (~20 °C) except where noted (121 MHz spectrometer frequency). [c] At 50 °C: δ 47.2 (s). [d] At −30 °C: δ_A = 47.8, δ_B = 47.4 [33.8]; at 35 °C: δ_A = 47.4, δ_B = 47.0 [34.5]. [e] At −60 °C: δ 47.3 (s). [f] At 10 °C: δ 47.2 (s); at −20 °C: δ_A = 47.6, δ_B = 47.2 [32.9]. [g] At 25 °C: δ 47.3 (s); at 40 °C: δ_A = 47.4, δ_B = 47.0 [33.6]. [h] At −30 °C: δ_A = 47.8, δ_B = 47.2 [34.4]; at 60 °C: δ_A = 47.2, δ_B = 46.9 [33.9]. [i] At 0 °C: δ 47.9 (s); at −90 °C: δ_A = 48.4, δ_B = 48.1 [34.9]. [j] At −40 °C: δ 47.7 (s). [k] At −10 °C: δ 47.6 (s); at −20 °C: δ_A = 47.6, δ_B = 47.2 [32.9]. [l] At 25 °C: δ 47.2 (s).

 DOI: 10.1039/b103473c

remarkable in that the expected AB pattern is sometimes 'lost' (Table 1). Thus, **3a** in $CDCl_3$ shows a singlet (δ47.2) in its room temperature spectrum, while in CD_2Cl_2 an AB pattern (δ_A = 47.9, δ_B = 47.5, $^2J_{AB}$ = 34.4 Hz) is present; **1a** demonstrates the opposite behaviour (an AB pattern in the $CDCl_3$ spectrum and a singlet in CD_2Cl_2).

Variable temperature (VT) NMR studies, conducted on all the complexes, are exemplified by the data shown in Fig. 2. From 0 to 10 °C, the spectrum of **1b** consists of a sharp singlet, while an AB pattern is observed either side of this range with increasing separation of the signals; there is clearly no dynamic exchange process between, for example, two species giving a time-averaged singlet. A temperature-dependent, accidental degeneracy of the two signals of the 4-line AB pattern gives rise to the singlet. At a specific solvent and temperature combination, an A_2 pattern is observed, the ^{31}P nuclei having become isochronous. This degeneracy occurs in at least one solvent studied (usually chlorinated) for most of the *cis*-RuX_2((*R*)-BINAP)(L_2) complexes, while *cis*-$RuCl_2$((*R*)-BINAP)(dmbipy) (**2**) is the only complex exhibiting degeneracy in C_6D_6 and not in $CDCl_3$ or CD_2Cl_2. The dibromo complexes **1b** and **3b** exhibit degeneracy at lower temperatures than the corresponding dichloro analogues (**1a** and **3a**); the diiodo complexes (**1c** and **3c**) show no degeneracy from −90 to 60 °C. Changing from the planar bipy- or phen-based ligand systems (**1**–**4**) to that with bis(*o*-pyridyl)amine (**5**) sufficiently separates the two ^{31}P shifts that degeneracy is not seen (Table 1). The related *cis*-$RuCl_2$(DPPB)(L_2) complexes (DPPB = 1,4-bis(diphenylphosphino)butane) possess well separated ($\Delta\delta$ > 10) signals in their ^{31}P NMR spectra.[6c]

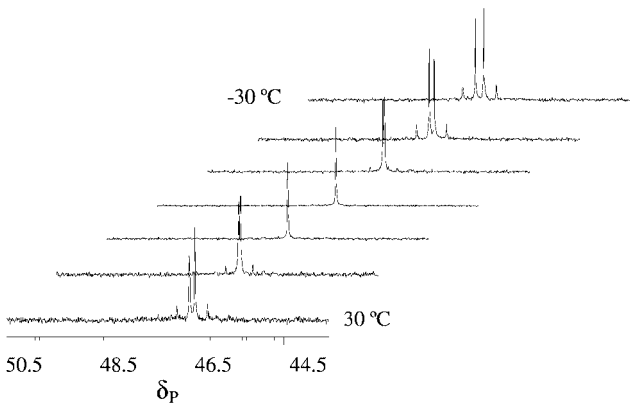

Fig. 2 VT ^{31}P{^{1}H} NMR spectra (CD_2Cl_2, 121 MHz) of *cis*-$RuBr_2$((*R*)-BINAP)(bipy) (**1b**) from 30 to −30 °C. Spectra are plotted in 10 °C increments.

Such accidental degeneracy is likely involved in some 'anomalies' in earlier work from this laboratory. Within the L(DPPB)Ru(μ-Cl)$_3$*Ru*Cl(DPPB) complexes (L = nitrile), a ^{31}P{^{1}H} singlet, rather than the expected AB (or AX) pattern, is seen for the two P atoms at *Ru* at 20 °C in CD_2Cl_2 (*i.e.* a singlet and 2 doublets are observed), while the expected 4 doublets are seen in C_6D_6 or $CDCl_3$;[6b] at −40 °C in CD_2Cl_2 the 2 sets of AB patterns are seen.[11] When L is Me_2S, the AB pattern is seen at 20 °C in C_6D_6, but not in $CDCl_3$, while the reverse holds true when L is tetrahydrothiophene, although VT NMR experiments were not performed.[12]

The temperature-dependence of ^{31}P NMR shifts is well documented, and indeed has been used for measuring sample temperature in VT work; *e.g.* the δ_P values for PPh_3 and O=PPh_3 change linearly with temperature (~1.3 Hz °C).[13] Further, the temperature-dependence of the δ_P values for the dimetallic, mixed-halide ClPd(μ-DPPM)$_2$PdI species (DPPM = bis(diphenylphosphino)methane) formed *in situ* varies with solvent, and the A_2B_2 pattern observed in $CDCl_3$ at −20 °C 'collapses' to a singlet at 35 °C, and reemerges above 45 °C,[14] behaviour similar to that of our Ru complexes.

To our knowledge, the *cis*-RuX_2((*R*)-BINAP)(L_2) complexes are the first isolated complexes to exhibit temperature-dependent degeneracy of ^{31}P NMR shifts. These data, particularly the observance of the degeneracy at room temperature in common NMR solvents, indicate that caution should be taken in the analysis of ^{31}P NMR data, especially for the widely studied chiral P–P systems, where such spectra remain a major characterization technique. The 'impossible' observation of a singlet NMR signal *must* be interrogated further by variation of temperature *and* variation of solvent.

We thank Colonial Metals Inc. for a loan of $RuCl_3 \cdot 3H_2O$, Dr S. King (formerly of Merck Research) for a gift of (*R*)-BINAP, and NSERC of Canada for financial support.

Notes and references

† Abbreviations used are: bipy (2,2′-bipyridine), dmbipy (4,4′-dimethyl-2,2′-bipyridine), phen (1,10-phenanthroline), batho (4,7-diphenyl-1,10-phenanthroline, or bathophenanthroline) and bpa (bis(*o*-pyridyl)-amine).

‡ A representative synthesis is as follows: $RuCl_2$((*R*)-BINAP)(PPh_3)[1b] (0.19 g, 0.18 mmol) and bipy (0.37 g, 0.24 mmol) were dissolved in 7 mL of C_6H_6 and the solution was refluxed for 3 h. The orange product (**1a**, L_2 = bipy), precipitated by the addition of 30 mL hexanes, was washed with hexanes and dried *in vacuo*. Yield: 0.11 g (65%). Anal. Calc. for $C_{54}H_{40}N_2Cl_2P_2Ru$: C, 68.21; H, 4.24; N, 2.95. Found: C, 68.24; H, 4.23; N, 3.01%.

§ *Crystal data* for **1b**: $C_{54}H_{40}N_2Br_2P_2Ru \cdot 3C_6D_6$, M = 1292.09, monoclinic, space group $P2_1$, a = 13.3564(7), b = 14.2879(7), c = 15.4367(9) Å, β = 98.448(4)°, V = 2913.9(2) Å^3, Z = 2, D_c = 1.473 g cm^{-3}, μ = 17.45 cm^{-1}, T = −100 °C, 25153 reflections measured, 6590 unique (R_{int} = 0.089), R (R_w) = 0.079 (0.092) on all data. X-ray crystal data are also available for **3a** and **5**.

CCDC reference number 164469. See http://www.rsc.org/suppdata/cc/b1/b103473c/ for crystallographic data in CIF or other electronic format.

1 For example: (*a*) B. R. James, R. S. MacMillan, R. H. Morris and D. K. W. Wang, in *Transition Metal Hydrides*, ed. R. Bau, ACS Symposium Series 167, Washington, DC, 1978, p. 122; (*b*) A. M. Joshi, I. S. Thorburn, S. J. Rettig and B. R. James, *Inorg. Chim. Acta*, 1992, **198**–**200**, 283; (*c*) D. E. Fogg, B. R. James and M. Kilner, *Inorg. Chim. Acta*, 1994, **222**, 85.

2 (*a*) K. S. MacFarlane, I. S. Thorburn, P. W. Cyr, D. E. K.-Y. Chau, S. J. Rettig and B. R. James, *Inorg. Chim. Acta*, 1998, **270**, 130; (*b*) K. S. MacFarlane, S. J. Rettig, Z. Liu and B. R. James, *J. Organomet. Chem.*, 1998, **557**, 213.

3 For example: (*a*) R. Noyori and H. Takaya, *Acc. Chem. Res.*, 1990, **23**, 345; (*b*) R. Noyori, *CHEMTECH*, 1992, **22**, 360; (*c*) R. Noyori, *Acta Chem. Scand.*, 1996, **50**, 380.

4 (*a*) R. Noyori and T. Ohkuma, *Angew. Chem., Int. Ed.*, 2001, **40**, 40; (*b*) K. Abdur-Rashid, A. J. Lough and R. H. Morris, *Organometallics*, 2001, **20**, 1047.

5 For example: (*a*) C. R. S. M. Hampton, I. R. Butler, W. R. Cullen, B. R. James, J.-P. Charland and J. Simpson, *Inorg. Chem.*, 1992, **31**, 5509; (*b*) E. S. F. Ma, S. J. Rettig and B. R. James, *Chem. Commun.*, 1999, 2463; (*c*) R. P. Schutte, S. J. Rettig, A. M. Joshi and B. R. James, *Inorg. Chem.*, 1997, **36**, 5809; (*d*) N. D. Jones, K. S. MacFarlane, M. B. Smith, R. P. Schutte, S. J. Rettig and B. R. James, *Inorg. Chem.*, 1999, **38**, 3956.

6 (*a*) A. A. Batista, E. A. Polato, S. L. Queiroz, O. R. Nascimento, B. R. James and S. J. Rettig, *Inorg. Chim. Acta*, 1995, **230**, 111; (*b*) D. E. Fogg and B. R. James, *Inorg. Chem.*, 1997, **36**, 1961; (*c*) S. L. Queiroz, A. A. Batista, G. Oliva, M. T. P. Gambardella, R. H. A. Santos, K. S. MacFarlane, S. J. Rettig and B. R. James, *Inorg. Chim. Acta*, 1998, **267**, 209.

7 J.-X. Gao, T. Ikariya and R. Noyori, *Organometallics*, 1996, **15**, 1087.

8 R. M. Stoop, S. Bachmann, M. Valentini and A. Mezzetti, *Organometallics*, 2000, **19**, 4117.

9 (*a*) H. Doucet, T. Ohkuma, K. Murata, T. Yokozawa, M. Kozawa, E. Katayama, A. F. England, T. Ikariya and R. Noyori, *Angew. Chem., Int. Ed.*, 1998, **37**, 1703; (*b*) C.-C. Chen, T.-T. Huang, C.-W. Lin, R. Cao, A. S. C. Chan and W. T. Wong, *Inorg. Chim. Acta*, 1998, **270**, 247.

10 P. W. Cyr, PhD Dissertation, University of British Columbia, Vancouver, 2001.

11 D. E. Fogg, PhD Dissertation, Univeristy of British Columbia, Vancouver, 1994.

12 K. S. MacFarlane, A. M. Joshi, S. J. Rettig and B. R. James, *Inorg. Chem.*, 1996, **35**, 7304.

13 F. L. Dickert and S. W. Hellmann, *Anal. Chem.*, 1980, **52**, 966.

14 C. T. Hunt and A. L. Balch, *Inorg. Chem.*, 1982, **21**, 1641.

CHEMCOMM
Communication
www.rsc.org/chemcomm

Assembling the biosynthetic puzzle of crucifer metabolites: indole-3-acetaldoxime† is incorporated efficiently into phytoalexins but glucobrassicin is not

M. Soledade C. Pedras,* Sabine Montaut, Yiming Xu, Abdul Q. Khan and Ali Loukaci

Department of Chemistry, University of Saskatchewan, 110 Science Place, Saskatoon SK S7N 5C9, Canada. E-mail: soledade.pedras@usask.ca

Received (in Cambridge, UK) 18th April 2001, Accepted 27th June 2001
First published as an Advance Article on the web 9th August 2001

First biosynthetic studies utilizing tetradeuterated precursors indicate that the indole glucosinolate glucobrassicin is not a precursor of the phytoalexin brassinin, and that indole-3-acetaldoxime is an efficient precursor.

Plants have a complex arsenal of defense mechanisms to fight pathogen attack. A significant aspect of these defense mechanisms involves secondary metabolites, which may be either constitutive or biosynthesized *de novo* in response to diverse forms of stress, *i.e.* phytoalexins.[1] The plant family Cruciferae comprises a large number of economically important oilseed crops as well as vegetables. Besides their economic importance, crucifers are also interesting plant model-systems, containing the first and only example to date of a completely sequenced plant genome.[2] Chemical characterization of secondary metabolites from crucifers has unraveled a remarkable array of phytoalexins (*e.g.* **1**–**4**),[3] and a group of structurally related secondary metabolites known as glucosinolates (*e.g.* **6**).[4] This structural connection becomes more transparent considering that methoxy derivatives of brassinin **1** (*e.g.* R = OMe, R^1 = H) and glucobrassicin **6** (*e.g.* R = OMe, R^1 = H, R^2 = β–D–glucosyl) are naturally occurring within the same species and that their levels increase simultaneously in plants subjected to stress.[5] Furthermore, unambiguous biosynthetic studies have demonstrated that (*S*)-tryptophan is the precursor of both metabolites **1** and **6**.[3,6] In this connection a number of suggestions and attempts to establish a biogenetic relationship between indole glucosinolates such as glucobrassicin **6** and cruciferous phytoalexins have been reported.[3,7] Furthermore, a number of studies[8] have demonstrated that (*S*)-tryptophan is converted to **6** *via* indole-3-acetaldoxime **5** (Scheme 1).

Paradoxically, because glucosinolates are considered an undesirable group of metabolites in brassicas,[8] a large number of oilseed breeding programs are directed at obtaining plants containing low levels of glucosinolates. However, if indole glucosinolates such as glucobrassicin **6** are precursors of phytoalexins **1**–**4** (Scheme 1), then lowering glucosinolate contents in these oilseeds may pose a substantial ecological risk from a plant defense perspective. Nonetheless, despite a number of biosynthetic studies in crucifers, this biogenetic relationship has not been demonstrated.[3] Thus we became interested in establishing the possible biogenetic relationship between indole glucosinolate **6** and brassinin **1**, as well as the biosynthetic pathway to the phytoalexin brassilexin **3**.[9] Here we establish for the first time a biosynthetic relationship between indole-3-acetaldoxime **5** and phytoalexins **1**–**4** which, contrary to previous speculations,[3] do not appear to be derived from indole glucosinolate **6**.

To investigate the possible biogenetic relationship between phytoalexins and indole glucosinolates, [4,5,6,7-$^2H_4$]-compounds **1a**–**3a** were synthesized as previously reported;[9] [4,5,6,7-$^2H_4$]glucobrassicin **6a** was synthesized according to the previously reported route[10] but utilizing **7a**[9] as the starting material.[11] Initially, the cruciferous brown mustard (*Brassica juncea*) was selected to determine the proposed biosynthetic relationship because it produces phytoalexins **1**–**4** and indole glucosinolate **6**. Thus, [4,5,6,7-$^2H_4$]glucobrassicin **6a** was administered to leaves of brown mustard; after solution uptake the leaves were elicited with a spore suspension of the fungus *Phoma lingam* (perfect stage *Leptosphaeria maculans*), were incubated, and extracted.[9,12] HPLC analysis of the extracts indicated the presence of phytoalexins **2**–**4**; the extracts were fractionated by HPLC and the identity of each phytoalexin was confirmed by ^{1}H NMR and HRMS-EI. Deuterium incorporation in **2**–**4** (≤0.1% relative to a natural abundance control sample by HRMS-EI) was too small to establish **6a** as a precursor. Similar results were obtained when leaves were elicited with UV light instead of the fungal spores. This lack of deuterium incorporation was thought to be partly due to the substrate not reaching the appropriate cell site.

Subsequently, it was thought that a different plant tissue where precursors could be in contact with the tissue for a longer period (*i.e.* no uptake of the substrate solution *via* the plant vascular system) might lead to higher deuterium incorporation levels. Thus, [4,5,6,7-$^2H_4$]glucobrassicin **6a** was administered to UV-irradiated turnip root slices (*B. rapa*)[6] followed by incubation. Similar experiments were conducted with non-irradiated turnip roots. Extraction of the turnip tissue, fractionation, and HPLC analysis of extracts and fractions indicated the presence of phytoalexins **1**–**4**. Once again HRMS-EI analysis indicated that deuterium incorporation in **1**–**4** was too low to allow a reliable conclusion (≤0.1%). However, two additional compounds containing deuterium were separated and identified unambiguously as indole-3-carbaldehyde **7a** (34% ^{2}H incorporation) and methyl indole-3-carboxylate **8a** (26% ^{2}H

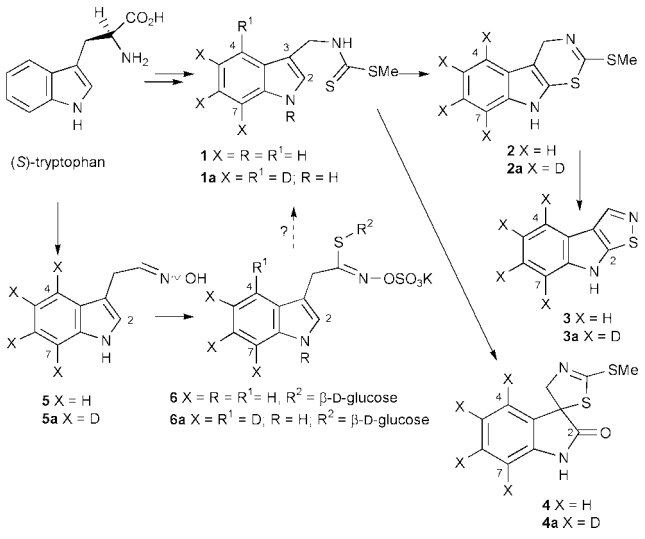

Scheme 1 Biosynthetic pathway from (*S*)-tryptophan to phytoalexins **1**–**4** and indole glucosinolate **6**.

† The IUPAC name for an acetaldoxime is acetaldehyde oxime.

 DOI: 10.1039/b103442c

incorporation**)**. These results indicated that metabolism of **6a** to **7a** and **8a** occurred in turnip roots and that the metabolism was unrelated to phytoalexin biosynthesis (Scheme 2).[13] These results also revealed for the first time that **3** was produced in turnip roots.[14]

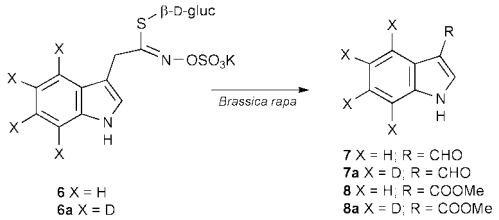

Scheme 2 Metabolism of [4,5,6,7-$^2H_4$]glucobrassicin (**6a**) in turnip roots (*B. rapa*).

Next, to confirm that turnip root was an appropriate tissue to study phytoalexin pathways, [4,5,6,7-$^2H_4$]brassinin **1a** was added to roots, the tissues were incubated, extracted, analyzed, and the extracts fractionated to yield phytoalexins **3** and **4**. HRMS-EI and ^{1}H NMR analysis indicated substantial deuterium incorporation into both spirobrassinin **4a** (15% ^{2}H incorporation) and **3a** (9% ^{2}H incorporation).[13] The incorporation level of deuterium into brassilexin was substantially higher than our early work utilizing *B. carinata* leaves,[9] thus demonstrating for the first time that in turnip, **1a** is also a precursor of **3a** and confirming that turnip root tissue is an adequate system for biosynthetic studies.[6]

Because of our unsuccessful attempt to demonstrate that **6a** is a precursor of **1a** or related phytoalexins **2a**–**4a**, we investigated the potential biogenetic relationship between **5a** and **1a**. Thus, tetradeuterated **5a** was administered to UV-irradiated turnip roots;[15] after incubation of the tissues, extraction, and fractionation of the extracts, **2**–**4** were obtained. HRMS-EI analysis indicated significant deuterium incorporation into **2a** (10% ^{2}H incorporation), **4a** (14% ^{2}H incorporation) and **3a** (2% ^{2}H incorporation). Furthermore, three additional compounds, subsequently established to be tryptophol **9a** and oxindoles **10a** and **11a**, were isolated and analyzed by HRMS-EI. Deuterium incorporation levels suggested that metabolites **9a**–**11a** were fully derived from metabolism of **5a** (Scheme 3, deuterium incorporation ⩽98%). This conclusion was consistent with the absence of compounds **9a**–**11a** in elicited control tissues. Additional studies indicated that oxime **10a** dehydrated upon standing to yield nitrile **11a**, suggesting that turnip tissue contained the enzyme system required to oxidize oxime **5a** to **10a**, and that **11a** might be an artifact of the isolation process.[16] Note that **11** was previously isolated from *B. oleracea*,[17] however its precursor oxindole oxime **10** has not been described to date.

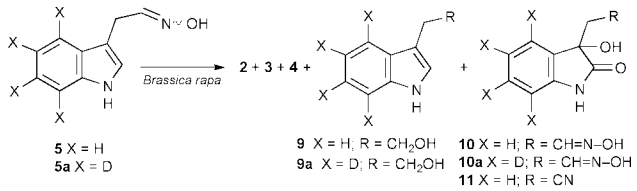

Scheme 3 Metabolism of [4,5,6,7-$^2H_4$]indole-3-acetaldoxime (**5a**) in turnip roots (*B. rapa*).

In conclusion, our results established a most important biogenetic relation between phytoalexins **1**/**1a**–**4**/**4a** and aldoxime **5**/**5a**, whereas the postulated relationship between indole glucosinolate **6**/**6a** and these phytoalexins was not demonstrated. Thus, considering that **5** is also a precursor of **6**,[8] it is likely that the pathway to phytoalexins follows the tryptophan–aldoxime route and will branch out from the indole glucosinolate pathway a step(s) earlier than previously proposed.[3] Nonetheless, our results have strong implications on plant breeding to produce low glucosinolate content oilseed brassicas, *i.e.* it is essential not to delete the indole acetaldoxime formation steps, as aldoxime **5** is a close precursor of important cruciferous phytoalexins (*e.g.* **1**–**4**). Otherwise, ecologically unfit plants with higher disease susceptibility may be produced. Further work is necessary to find additional intermediates between aldoxime **5** and brassinin **1** as well as the branch point between the tryptophan pathway to indole glucosinolates and to phytoalexins.

Support for the authors' work was obtained from the Natural Sciences and Engineering Research Council of Canada (Individual Research grant and NRC-NSERC Research Partnership grant to M. S. C. P.) and the University of Saskatchewan. We would like to acknowledge the technical assistance of Ken Thoms, Department of Chemistry, for mass spectroscopic determinations.

Notes and references

1 C. J. Smith, *New Phytol.*, 1996, **132**, 1; C. J. B. Brooks and D. G. Watson, *Nat. Prod. Rep.*, 1985, 427, and references therein.
2 A. Theologis *et al.*, 'The Arabidopsis Genome Initiative' *Nature (London)*, 2000, **408**, 796.
3 For a review on cruciferous phytoalexins, see: M. S. C. Pedras, F. I. Okanga, I. L. Zaharia and A. Q. Khan, *Phytochemistry*, 2000, **53**, 161.
4 For a recent review on glucosinolates, see: J. W. Fahey, A. T. Zalcmann and P. Talalay, *Phytochemistry*, 2001, **56**, 5.
5 K. Monde, M. Takasugi, J. E. Lewis and G. R. Fenwick, *Z. Naturforsch., Teil C*, 1991, **46**, 189.
6 K. Monde, M. Takasugi and T. Ohnishi, *J. Am. Chem. Soc.*, 1994, **116**, 6650.
7 A. B. Hanley, K. R. Parsley, J. A. Lewis and G . R. Fenwick, *J. Chem. Soc., Perkin Trans. 1*, 1990, 2273.
8 For a recent review on the biosynthesis of glucosinolates, see: B. A. Halkier and L. Du, *Trends in Plant Science*, 1997, **2**, 425.
9 M. S. C. Pedras, A. Loukaci and F. I. Okanga, *Bioorg. Med. Chem. Lett.*, 1998, **8**, 3037.
10 M. C. Viaud and P. Rollin, *Tetrahedron Lett.*, 1990, **10**, 1417; S. Chevolleau, B. Joseph, P. Rollin and J. Tulliez, *J. Labelled Compd. Radiopharm.*, 1993, **33**, 671.
11 All compounds gave satisfactory spectroscopic data; in each case the percentage of tetradeuterated synthetic compound was ⩾99%.
12 Experiments were carried out as reported in ref. 9; each incorporation experiment was repeated at least twice. All compounds administered to plant tissues were tetradeuterated at concentrations of 6×10^{-4}–10^{-3} M.
13 Indole glucosinolate **6**/**6a** was stable on standing in solution. The % of deuterium incorporation was determined by HRMS-EI using the expression: $[M + 4]^+/([M]^+ + [M + 4]^+) \times 100$ (HRMS data indicated that $[M + 4]^+$ is not present in natural abundance samples).
14 In previous work we attributed lower incorporation of deuterated **2a** into **3a** to factors such as the low solubility and high phytotoxicity of **2a**,[9] however these factors are not likely to account for the absence of incorporation of **6a** into any of the phytoalexins **2a**–**4a**; **6**/**6a** was soluble in aqueous solution and did not show phytotoxicity to leaves of *B. juncea*.
15 Spectroscopic data of **5a**: δ_H (300 MHz, CD_3OD): 7.08 (s, 1H, H-2), 6.80 (t, *J* 5.3, 1H, CH_2-CH=N-OH), 3.80 (d, *J* 5.4, 2H, CH_2-CH=N-OH). δ_C (75.5 MHz, CD_3OD): 152.2, 138.3, 128.7, 123.8, 122.2 (t, $^1J_{C\text{-}D}$ 24), 119.4 (t, $^1J_{C\text{-}D}$ 24), 118.9 (t, $^1J_{C\text{-}D}$ 24), 112.4 (t, $^1J_{C\text{-}D}$ 24 Hz), 111.2, 22.5. HRMS-EI *m/z*: calcd. for $C_{10}H_6D_4N_2O$ 178.1044, found 178.1040. Synthesis to be published elsewhere.
16 In the absence of turnip cells acetaldoxime **5**/**5a** was stable in solution for the duration of the experiments.
17 K. Monde, K. Sasaki, A. Shirata and M. Takasugi, *Phytochemistry*, 1991, **9**, 2915.

CHEMCOMM Communication
www.rsc.org/chemcomm

Dual-mode electrochromism switched by proton transfer: dynamic redox properties of bis(diarylmethylenium)-type dyes†

Takanori Suzuki,* Hiroki Higuchi, Masakazu Ohkita and Takashi Tsuji

Division of Chemistry, Graduate School of Science, Hokkaido University, Sapporo 060-0810, Japan. E-mail: tak@sci.hokudai.ac.jp

Received (in Cambridge, UK) 31st May 2001, Accepted 28th June 2001
First published as an Advance Article on the web 3rd August 2001

Upon oxidative dimerization of pale yellow Ar_2C=CHPh 1 (Ar = 4-$Me_2NC_6H_4$), deep blue 1,4-dication 2^{2+} was obtained as a stable salt, which was transformed into 1 by reductive C–C bond fission; deprotonation of 2^{2+} gave intense yellow diene 3, which was interconvertible with violet dication 4^{2+} by two-electron transfer, thus exhibiting two distinct modes of electrochromism before and after proton transfer.

Recently, much attention has been focused on electrochromic dyes[1,2] for use as optical memories or electrochemical switches.[3] The representative examples are a series of open-chain violenes[4] shown by the redox couple of **C** and **D** in Scheme 1. Diene **C** can be prepared by oxidative dimerization of olefin **A**,[2a] and the similar procedure has been widely used to synthesize novel TTF vinylogues.[5,6] Although the oxidation reactions are believed to proceed *via* unconjugated 1,4-dication **B**, this intermediate has never been isolated nor even detected spectroscopically probably due to its instability by rapid deprotonation to **C** under the reaction conditions.

In our continuing efforts to develop new electrochromic systems endowed with bistability by reversible C–C bond making/breaking[7] or drastic structural changes[8] upon electron transfer (dynamic redox properties), we have found here that the dication **B** possessing two dye chromophores [X = $(4\text{-}Me_2NC_6H_4)_2C$] and two aryl groups (R = aryl) can be isolated as stable salts. By the selective transformation of **B** to **A** by reduction and **B** to **C** by deprotonation, novel dual-mode electrochromism shown in Scheme 1 could be realized, where proton transfer alters the mode from one to another.

The voltammetric analysis‡ indicated that olefin **1**§ undergoes irreversible oxidation at +0.55 V *vs.* SCE in MeCN. The corresponding reduction wave appeared in the far cathodic region (−0.38 V), which is rather close to the reduction potential of $(4\text{-}Me_2NC_6H_4)_2CH^+$ (−0.54 V). Such a large shift of redox peaks can be accounted for by assuming oxidative dimerization of **1** (Scheme 2).

In fact, dication $\mathbf{2}^{2+}$ was isolated as deep blue I_3^- salt§ in 97% yield by the reaction of yellow olefin **1**§ with 1.5 eq. of I_2 in CH_2Cl_2. Mechanistically, there can be two pathways to produce $\mathbf{2}^{2+}$ from **1**: (a) dimerization of $\mathbf{1}^{+\cdot}$ to $\mathbf{2}^{2+}$, and (b) reaction of $\mathbf{1}^{+\cdot}$ with neutral **1** to form $\mathbf{2}^{+\cdot}$ followed by further one-electron

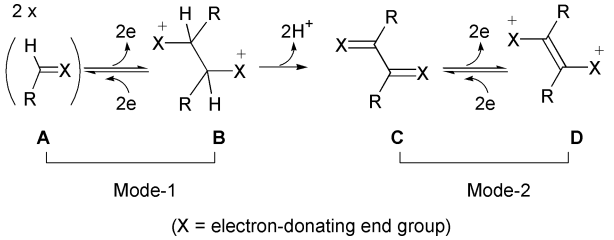

Scheme 1

† Electronic supplementary information (ESI) available: spectral data for new compounds. See http://www.rsc.org/suppdata/cc/b1/b104742f/

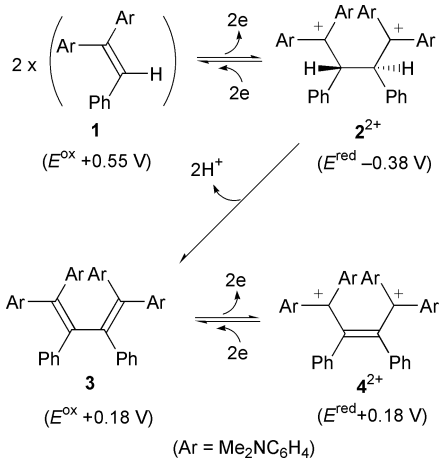

Scheme 2

oxidation. In the present case, path (a) is plausible because $\mathbf{2}^{2+}$ $(I_3^-)_2$ was obtained in 92% yield by the reaction of **1** with 1.5 eq. I_2 under the presence of Ph_2C=CHPh (2 eq.) which remained intact and was recovered quantitatively.

The 1,4-dication $\mathbf{2}^{2+}$ is surprisingly stable with no sign of spontaneous deprotonation; its methine proton appears at 6.02 ppm as a sharp singlet in the ^{1}H NMR spectrum measured in CD_3CN. Upon reduction of this salt with Zn powder in MeCN, olefin **1** was regenerated in 100% yield. Such high-yield interconversion indicates that **1** and $\mathbf{2}^{2+}$ can be considered as a 'reversible' redox pair even though C–C bond making and breaking are accompanied by two-electron transfer.[7,10]

When $\mathbf{2}^{2+}$ $(I_3^-)_2$ was treated with $Bu^n{}_4NF$ in THF–MeCN, deprotonation proceeded smoothly to give intense yellow diene **3**§ in 75% yield, which is a stronger donor [E^{ox} +0.18 V (2e, rev.)]‡ than **1**. Attempted deprotonation of $\mathbf{2}^{2+}$ $(I_3^-)_2$ with Et_3N [E^{ox} +0.85 V (irrev.)] resulted in formation of olefin **1** in quantitative yield by electron transfer, and deprotonation with pyridine was very slow.

Upon treatment of **3** with 3 eq. of I_2 in CH_2Cl_2, deep violet dication salt $\mathbf{4}^{2+}$ $(I_3^-)_2$§ was obtained in 98% yield, which regenerated diene **3** in 100% yield upon reduction with Zn in MeCN. According to the X-ray analyses,¶ the diene unit in **3** adopts a nonplanar geometry with a large torsion angle of 59.1° around the C^2–C^3 bond (Fig. 1a), which is undoubtedly due to steric congestion among six aryl groups. It is likely that lack of effective conjugation in diene **3** as well as steric shielding against the base in the hindered C–H acid $\mathbf{2}^{2+}$ are the reasons for reluctant deprotonation of $\mathbf{2}^{2+}$ to **3**. On the other hand, all of the diene carbons lie nearly on the same plane in $\mathbf{4}^{2+}$ (Fig. 1b), thus confirming drastic geometrical changes by twisting motions[2,6,8] during interconversion between **3** and $\mathbf{4}^{2+}$.

In this way, two types of dynamic structural changes are presented by the redox couples of **1**–$\mathbf{2}^{2+}$ and **3**–$\mathbf{4}^{2+}$, which can be switched by proton transfer. Furthermore, the novel dual-mode electrochromism can be realized by these couples since each pair exhibits distinct spectral changes upon electrolyses

 DOI: 10.1039/b104742f

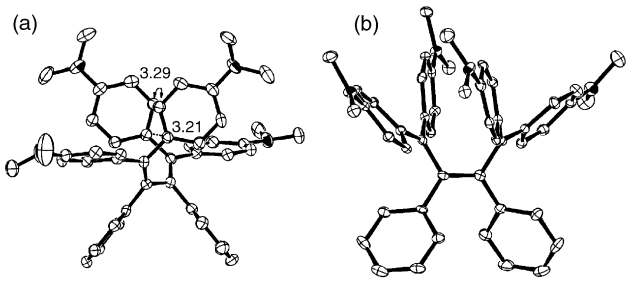

Fig. 1 (a) ORTEP drawing of diene **3** determined by X-ray at −163 °C. Torsion angle of diene unit is 59.1°. Two aryl groups are arranged in a face-to-face manner (dihedral angle 7.9°). Short intramolecular C···C contacts (3.21 and 3.29 Å) are shown by dotted line. (b) ORTEP drawing of dication $\mathbf{4}^{2+}$ determined by X-ray at −176 °C on I_3^- salt. The four carbon atoms of C^+–C=C–C^+ lie nearly on the same plane (the largest deviation from the least-squares plane, 0.09 Å).

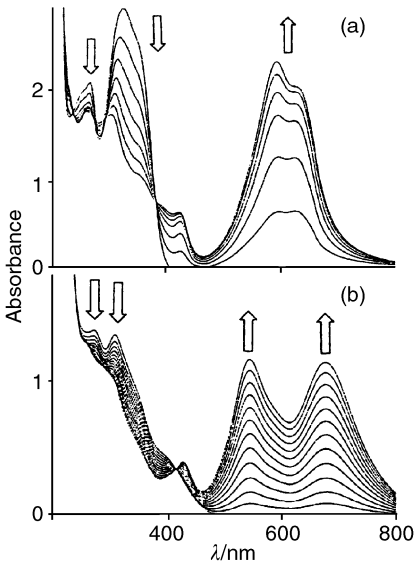

Fig. 2 Two modes of electrochromism. a) Mode-1; changes in the UV-VIS spectrum of **1** (3.5 mL, 1.1×10^{-4} mol dm^{-3} in MeCN) upon constant-current electrochemical oxidation (32 μA, 4 min interval) to $\mathbf{2}^{2+}$. (b) Mode-2; changes in the UV-VIS spectrum of **3** (3.5 mL, 2.6×10^{-5} mol dm^{-3} in MeCN) upon constant-current electrochemical oxidation (31 μA, 2 min interval) to $\mathbf{4}^{2+}$. Note the presence of isosbestic points in both transformation.

(Fig. 2), which opens up a way to construct a molecular device where two independent inputs (e^- and H^+) are transduced into a unified two-dimensional output (ε *vs.* λ in UV-VIS).

This work has revealed that the 1,4-dication **B** in Scheme 1 can exist as stable species (as in $\mathbf{2}^{2+}$)‖ when deprotonation is not feasible due to steric shielding in **B** and/or prohibited full-conjugation in diene **C** by twisted geometry. In such an appropriate case, all of the species of **A**–**D** (as in **1**–$\mathbf{4}^{2+}$) are stable enough to realize the dual-mode optical response. The present electrochromism modulated by proton transfer provides a new successful entry into the proton–electron cooperating functions.[11]

This work was supported by the Ministry of Education, Science, and Culture, Japan (No. 13440184). Financial support from the Iwatani Naoji Foundation is gratefully acknowledged. We thank Professor Tamotsu Inabe (Hokkaido University) for use of the X-ray structure analysis system.

Notes and references

‡ All of the redox potentials shown in the text were measured under the same conditions: *E*/V *vs.* SCE, 0.1 mol Et_4NClO_4 in MeCN, Pt electrode, scan rate 100 mV s^{-1}. Values for E^{ox} and E^{red} were calculated as $E_p - 0.03$ and $E_p + 0.03$ V, respectively, in the cases of irreversible processes.

§ Olefin **1** was prepared in 95% yield by Wittig–Horner reaction of PhCHO and Ar_2CH-$PO(OMe)_2$/Bu^nLi in THF, and its physical data are identical to those reported in ref. 9. Stereochemistry of $\mathbf{2}^{2+}$ was determined to be *dl* by X-ray analysis of $\mathbf{I}_3^-$ salt.¶ All new compounds show satisfactory analytical values. λ_{max} (MeCN)/nm (log ε): **1**, 345 sh (4.38), 322 (4.43), 266 (4.30), 255 (4.28); $\mathbf{2}^{2+}$ $(I_3^-)_2$, 619 (4.83), 595 (4.84), 423 (4.47), 361 (4.80), 293 (5.04); **3**, 397 sh (4.27), 345 sh (4.59), 312 (4.71), 277 (4.65); $\mathbf{4}^{2+}$ $(I_3^-)_2$, 679 (4.86), 545 (4.91), 426 (4.48), 358 (4.83), 292 (5.14).†

¶ *Crystal data* for $\mathbf{2}^{2+}$ $(I_3^-)_2$: $C_{48}H_{52}N_4I_6$, *M* 1446.39, monoclinic, $P2_1/n$, a = 10.054(2), b = 17.393(3), c = 28.880(5) Å, β = 92.970(9)°, U = 5043(1) Å^3, D_c (Z = 4) = 1.905 g cm^{-1}, μ(Mo-Kα) = 37.43 cm^{-1}, T = 123 K. The final R value is 0.062 for 4842 independent reflections with $I > 3\sigma I$ and 263 parameters. For **3**: $C_{48}H_{50}N_4$, *M* 682.95, monoclinic, $P2_1/c$, a = 14.612(3), b = 16.076(2), c = 17.1807(7) Å, β = 91.792(1)°, U = 4034.0(10) Å^3, D_c (Z = 4) = 1.124 g cm^{-1}, μ(Mo-Kα) = 0.66 cm^{-1}, T = 110 K. The final R value is 0.065 for 3614 independent reflections with $I > 3\sigma I$ and 469 parameters. For $\mathbf{4}^{2+}$ $(I_3^-)_2$: $C_{48}H_{50}N_4I_6$, *M* 1444.38, monoclinic, $P2_1/n$, a = 9.6884(8), b = 23.432(1), c = 22.8948(4) Å, β = 107.5794(4)°, U = 4954.9(5) Å^3, D_c (Z = 4) = 1.936 g cm^{-1}, μ(Mo-Kα) = 37.99 cm^{-1}, T = 97 K. The final R value is 0.026 for 7707 independent reflections with $I > 3\sigma I$ and 526 parameters. CCDC/164961–164963. See http://www.rsc.org/suppdata/cc/b1/b104742f/ for electronic files in .cif or other electronic format.

‖ Similarly, 2,2′-bis[2,2-bis(4-dimethylaminophenyl)ethenyl]biphenyl undergoes oxidative cyclization to give another isolable 1,4-dication framed in a 9,10-dihydrophenanthrene skeleton, which will be reported in a full paper.

1 P. M. S. Monk, R. J. Mortimer and D. R. Rosseinsky, *Electrochromism: Fundamentals and Applications*, VHC, Weinheim, 1995.
2 (*a*) S. Hünig, M. Kemmer, H. Wenner, F. Barbosa, G. Gescheidt, I. G. Perepichka, P. Bäuerle, A. Emge and K. Peters, *Chem. Eur. J.*, 2000, **6**, 2618; (*b*) S. Hünig, M. Kemmer, H. Wenner, I. F. Perepichka, P. Bäuerle, A. Emge and G. Gescheid, *Chem. Eur. J.*, 1999, **5**, 1969.
3 V. Balzani, M. Gómez-López and J. F. Stoddart, *Acc. Chem. Res.*, 1998, **31**, 405; J.-P. Sauvage, *Acc. Chem. Res.*, 1998, **31**, 611; P. L. Boulas, M. Gómez-Kaifer and L. Echegoyen, *Angew. Chem., Int. Ed. Engl.*, 1998, **37**, 216.
4 K. Deuchert and S. Hünig, *Angew. Chem., Int. Ed. Engl.*, 1978, **17**, 875.
5 R. Mayer and K. Kröber, *J. Prakt. Chem.*, 1974, **316**, 907; U. Schöberl, J. Salbech and J. Daub, *Adv. Mater.*, 1992, **4**, 41; D. Lorcy, R. Carlier, A. Robert, A. Tallec, P. Le Maguerés and L. Ouahav, *J. Org. Chem.*, 1995, **60**, 2443; P. Hapiot, D. Lorcy, A. Tallec, R. Carlier and A. Robert, *J. Phys. Chem.*, 1996, **100**, 14 823; A. Benahmed-Gasmi, P. Frére, J. Roncali, E. Elandaloussi, J. Ordun, J. Garin, M. Jubault and A. Gorgues, *Tetrahedron Lett.*, 1995, **36**, 2983; A. J. Moore, M. R. Bryce, P. J. Skabara, A. S. Datsanov, L. M. Goldenberg and J. A. K. Howard, *J. Chem. Soc., Perkin Trans. 1*, 1997, 3443; P. Hascoat, D. Lorcy, A. Robert, R. Carlier, A. Tallec, K. Boubekeur and P. Batail, *J. Org. Chem.*, 1997, **62**, 6086.
6 A. Ohta and Y. Yamashita, *J. Chem. Soc., Chem. Commun.*, 1995, 1761; Y. Yamashita, M. Tomura, M. B. Zaman and K. Imaeda, *Chem. Commun.*, 1998, 1657.
7 T. Suzuki, J. Nishida and T. Tsuji, *Angew. Chem., Int. Ed. Engl.*, 1997, **36**, 1329; *Chem. Commun.*, 1998, 2193; T. Suzuki, H. Takahashi, J. Nishida and T. Tsuji, *Chem. Commun.*, 1998, 1331; T. Suzuki, M. Kondo, T. Nakanura, T. Fukushima and T. Miyashi, *Chem. Commun.*, 1997, 2325; T. Suzuki, T. Yoshino, M. Ohkita and T. Tsuji, *J. Chem. Soc., Perkin Trans. 1*, 2000, 3417; T. Suzuki, J. Nishida, M. Ohkita and T. Tsuji, *Angew. Chem., Int. Ed. Engl.*, 2000, **39**, 1804.
8 T. Suzuki, H. Shiohara, M. Monobe, T. Sakimura, S. Tanaka, Y. Yamashita and T. Miyashi, *Angew. Chem., Int. Ed. Engl.*, 1992, **31**, 455; T. Suzuki, Y. Yoshino, J. Nishida, M. Ohkita and T. Tsuji, *J. Org. Chem.*, 2000, **65**, 5514.
9 M. Matsui, M. Tsuge, K. Shibata and H. Muramatsu, *Bull. Chem. Soc. Jpn.*, 1994, **67**, 1753.
10 M. Horner and S. Hünig, *J. Am. Chem. Soc.*, 1977, **99**, 6122; R. Rathore, P. Le Magueres, S. V. Lindeman and J. K. Kochi, *Angew. Chem., Int. Ed. Engl.*, 2000, **39**, 809.
11 K. Nakasuji, K. Sugiura, J. Toyoda, Y. Morita, H. Okamoto, K. Okaniwa and T. Mitani, *Mol. Cryst. Liq. Cryst.*, 1992, **216**, 213; G. De Santis, L. Fabbrizzi, M. Licchelli and P. Pallavicini, *Inorg. Chim. Acta*, 1994, **225**, 239; V. A. Ozeryanskii, A. F. Pozharskii, G. R. Milgizina and S. T. Howard, *J. Org. Chem.*, 2000, **65**, 7707.

CHEMCOMM
Communication
www.rsc.org/chemcomm

Efficient radical addition of tertiary amines to electron-deficient alkenes using semiconductors as photochemical sensitisers

Siniša Marinković and Norbert Hoffmann*

Laboratoire des Réactions Sélectives et Applications, UMR CNRS et Université de Reims Champagne-Ardenne, UFR Sciences, B.P. 1039, F-51687 Reims, Cedex 02, France.
E-mail: norbert.hoffmann@univ-reims.fr

Received (in Cambridge, UK) 18th May 2001, Accepted 9th July 2001
First published as an Advance Article on the web 3rd August 2001

Tertiary amines can be added to electron-deficient alkenes with yields up to 98% in a radical chain reaction initiated by a photochemical electron transfer using inorganic semiconductors like TiO_2 as sensitiser.

Radical reactions have become a valuable tool in preparative organic chemistry.[1] Among radicals having a nucleophilic character which can be considered for addition reactions with electron deficient alkenes, α-aminoalkyl radicals seem very attractive.[2] Recently, we described an efficient procedure involving a photochemical electron transfer to initiate the intermolecular radical addition of tertiary amines to electron deficient alkenes.[3] Under the same conditions, radical tandem reactions could also be carried out efficiently.[4]

In principle, photochemical excited semiconductors like TiO_2 could initiate the radical addition of tertiary amines. Photochemical reactions with TiO_2 were studied, for instance, for detoxification of waste water,[5] oxidations and reductions,[6] solar energy havesting[7] or in the context of organic synthesis.[8] Metal sulfides like ZnS and CdS have been used for the formation of dehydrodimers of olefins or enol/allyl ethers and for the addition of allyl radicals to imines or diazo compounds.[9]

During photochemical excitation, an electron is transferred from the valence band into the conduction band.[10] The resulting electron hole h^+ of the valence band can be filled by electron transfer from a reductive species such as a tertiary amine (Scheme 1) with the formation of a radical cation and of nucleophilic α-aminoalkyl radicals by deprotonation.

We started our investigations by irradiating a suspension of SiC, TiO_2 (anatase) or ZnS in a solution containing (5*R*)-menthyloxy-2[5*H*]furanone **1a** and *N*-methylpyrrolidine **2a** in acetonitrile (Table 1, entries 1–3). Low conversion rates were observed for TiO_2 and ZnS while no transformation could be detected for SiC. The yields based on conversion were rather low. Much faster conversions was observed when the reaction was carried out in **2a** as solvent (Table 1, entries 4–7) and yields increased under these conditions. The concentration of **1a** was changed and it turned out that 5×10^{-2} mol L^{-1} with a corresponding quantity of TiO_2 is the optimal concentration (Table 1, entries 4, 6 and 7). Under these reaction conditions, *N*-*tert*-butylpyrrolidine **2b** was added to **1a** with the same efficiency (entry 8). As mentioned previously, the addition of the amine took place exclusively from the less-hindered side of the furanone **1a**.[3] Unfortunately, little selectivity was observed for the asymmetric carbon in the α-position of the nitrogen.

Under the optimised conditions,† the reaction of various α,β-unsaturated lactones with methylpyrrolidine **2a** was examined (Table 2). Generally, high conversion rates and high yields were observed. However, in the case of lactone **1e** possessing two substituents in the 4-position, the conversion rate was low. A low reactivity for β-disubstituted enones is also observed when homogeneous reaction conditions were applied.[3]

When TiO_2 was used as sensitiser for the addition of *N*-methylpiperidine **2c**, only a slow reaction was observed and

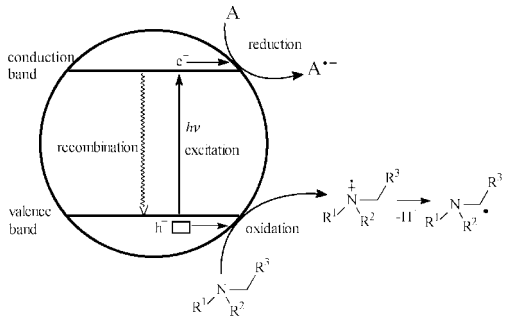

Scheme 1 Formation of α-aminoalkyl radicals by single electron transfer to an electronically excited semiconductor particle.

Table 1 Reaction of (5*R*)-menthyloxy-2[5*H*]furanone **1a** with *N*-methylpyrrolidine **2a** and *tert*-butylpyrrolidine **2b** under different reaction conditions; 0.1 equivalent of the semiconductor (SC) with respect to **1a** was added

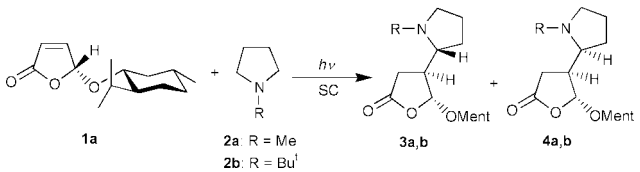

1a **2a**: R = Me, **2b**: R = Bu^t **3a,b** **4a,b**

Entry	Semiconductor	c(**1a**)/mol L^{-1}	c(**2a,b**)/mol L^{-1}	R	Irradiation time/h	Conversion (%)	Yield[a] (%)	Ratio c(**3**)/c(**4**)
1	SiC	10^{-2}	4×10^{-1}	Me	8	—	—	—
2	TiO_2	10^{-2}	4×10^{-1}	Me	9	59	25	47/53
3	ZnS	10^{-2}	4×10^{-1}	Me	9	68	28	45/55
4	TiO_2	10^{-2}	Solvent	Me	2.5	100	53	45/55
5	ZnS	10^{-2}	Solvent	Me	2.5	100	59	45/55
6	TiO_2	5×10^{-2}	Solvent	Me	2.5	73	90	45/55
7	TiO_2	10^{-1}	Solvent	Me	2.5	50	39	45/55
8	TiO_2	5×10^{-2}	Solvent	Bu^t	3.5	83	88	45/55

[a] Based on conversion of **1a**.

 DOI: 10.1039/b104387k

Table 2 Reaction of different α,β-unsaturated lactones with methylpyrrolidine **2a** under different reaction conditions; 0.1 equivalent of the semiconductor with respect to **1a** was added

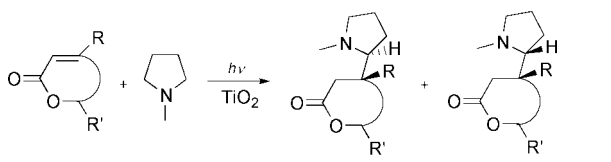

1b-e 2a 3c-f 4c-f

1		Irradiation time/h	Conversion (%)	Yield[a] (%)	Ratio *c*(**3**)/*c*(**4**)
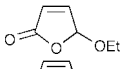	**1b**	2	90	64	45/55
	**1c**	2	100	98	43/57
	**1d**[b]	3.5	100	90	44/56
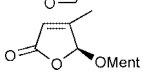	**1e**	13	20	76	44/56

[a] Based on conversion of **1**. [b] The starting concentration was 10^{-2} mol L^{-1}.

Table 3 Reaction of (5*R*)-menthyloxy-2[5*H*]furanone **1a** with *N*-methylpiperidine **2c** under different reaction conditions; 0.1 equivalent of the semiconductor (SC) with respect to **1a** was added

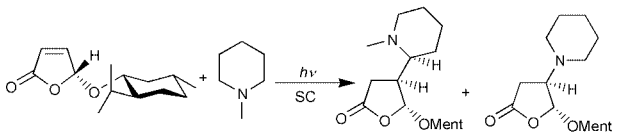

1a 2c 4g 5

Entry	Semiconductor	*c*(**1a**)/mol L^{-1}	Conversion (%)	Yield[a] **4g**	Yield[a] **5**
1	TiO_2	5×10^{-2}	72	—	74
2	TiO_2[b]	5×10^{-2}	15	Trace	90
3	TiO_2	10^{-2}	34	28	62
4	ZnS	10^{-2}	94	23	Trace

[a] Based on conversion of **1a**. [b] The amine was distilled over CaH_2 under argon and the semiconductor was kept at 100 °C for 48 h.

product **5** resulting from a Michael addition of piperidine to **1a** was isolated (Table 3, entry 1). Due to their lower reactivity of α-aminoalkyl radicals derived from *N*-methylpiperidine, the oxidation of these radicals became competitive and demethylation occurred.[11] Even under strictly anhydrous conditions, this side reaction took place (entry 2). However, when the concentration of compound **1a** was reduced, the radical addition could be observed and product **4g** was isolated with moderate yield (entry 3). This result indicates that **1** or, more likely, the oxoallyl radical **6** might participate in the demethylation process *via* an electron transfer from the radical cation to **7** (Scheme 2). It should be noted that the radical addition always takes place on the ring of **2a**,**c** and never at the methyl group. Therefore, we propose a tautomeric equilibrium of the iminium ions **7** and **8**.[11] As described previously, only one diastereomer was isolated.[3] Such a bimolecular reaction between two reactive intermediates appears more realistic if the overall reaction takes place near the surface of the semiconductor.

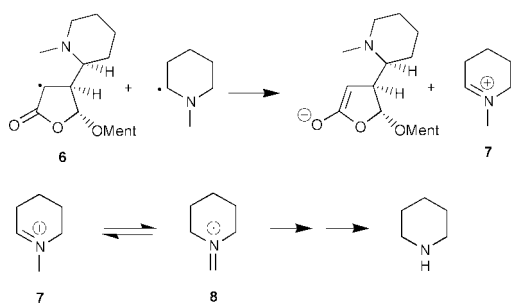

Scheme 2 Possible mechanism of the oxidation of an α-aminoalkyl radical by an oxoallyl radical introducing the demethylation of **2c**.

Oxidation of an α-aminoalkyl radical by excited TiO_2 is also possible. Therefore, we searched to diminish the two-electron oxidation by changing the semiconductor (Table 3, entry 4). When ZnS was used as sensitiser, only product **4g** could be isolated. Despite the more rapid conversion, the yield of the desired product **4g** remained low. Probably, this semiconductor is less oxidative due to the higher energy level of its valence band edge[12] and its surface properties.

The most apparent difference between the reaction conditions of the homogeneous and the heterogeneous catalysis is the concentration of the tertiary amine. In the case of homogeneous catalysis, acetonitrile must be used as solvent to obtain the best results[3] and the reaction is slower and less chemoselective when the tertiary amine is used as solvent. These results might be explained by the higher polarity of acetonitrile solutions which stabilise the radical ion pairs formed by electron transfer and decrease the rate of the back electron transfer. In the case of heterogeneous catalysis, the electron transfer from the amine to the sensitiser takes place at the surface of the semiconductor. Molecules at interfaces are less mobile than the same molecules in solution. Therefore, the back electron transfer can be slowed down only by enhancement of the subsequent deprotonation step. This acid–base reaction is facilitated by the presence of a large excess of tertiary amine. A higher concentration of the tertiary amine favours also the hydrogen abstraction of the oxoallyl radical **6** in the chain propagation.

We thank Professor J. P. Pete for his support and for helpful discussions. S. M. thanks the Ministère de la Recherche for a doctoral fellowship.

Notes and references

† *Experimental*: a Rayonet photochemical chamber reactor equipped with lamps emitting at $\lambda = 350$ nm was used as the light source.

A suspension of the substrate (7.5 mmol) and the semiconductor (0.15 mmol) in 150 ml of the tertiary amine was irradiated in Pyrex-tubes (outside diameter: 4 cm) under vigorous stirring with a magnetic stir bar. The mixture was filtered through Celite and the solvent was recycled by distillation under reduced pressure. The residue was purified by flash chromatography (silica gel, eluent: light petroleum–ethyl acetate: 2:1)

1 B. Giese, *Radicals in Organic Synthesis: Formation of Carbon–Carbon Bonds*, Pergamon Press, Oxford, 1986; J. Fossey, D. Lefort and J. Sorba, *Free Radicals in Organic Chemistry*, Wiley, Chichester, 1995; D. P. Curran, N. A. Porter and B. Giese, *Stereochemistry of Radical Reactions*, VCH, Weinheim, 1996.
2 P. Renaud and L. Giraud, *Synthesis*, 1996, 913.
3 S. Bertrand, N. Hoffmann and J. P. Pete, *Eur. J. Org. Chem.*, 2000, 2227.
4 S. Bertrand, N. Hoffmann, S. Humbel and J. P. Pete, *J. Org. Chem.*, 2000, **65**, 8690.
5 O. Legrini, E. Oliveros and A. M. Braun, *Chem. Rev.*, 1993, **93**, 671.
6 M. A. Fox and M. T. Dulay, *Chem. Rev.*, 1993, **93**, 341.
7 M. Grätzel, *Photoinduced Electron Transfer, Part D*, ed. M. A. Fox and M. Chanon, Elsevier, Amsterdam, 1988, ch. 6.3.
8 Y. Li, *Organic Photochemistry*, ed. V. Ramamurthy and K. S. Schanze, Marcel Dekker Inc., New York, 1997, p. 295; P. Pichat, *Catal. Today*, 1994, **19**, 313; L. Cermenati, C. Richter and A. Albini, *Chem. Commun.*, 1998, 805.
9 W. Schindler, F. Knoch and H. Kisch, *Chem. Ber.*, 1996, **129**, 925; R. Künnerth, C. Feldmer, F. Knoch and H. Kisch, *Chem. Eur. J.*, 1995, **1**, 441.
10 J. Eriksen, *Photoinduced Electron Transfer, Part A*. ed. M. A. Fox and M. Chanon, Elsevier, Amsterdam, 1988, ch 1.10; P. V. Kamat, *Chem. Rev.*, 1993, **93**, 267.
11 C. Ferroud, P. Rool and J. Santamaria, *Tetrahedron Lett.*, 1998, **39**, 9423; G. Pandey, *Synlett*, 1992, 546; X. Zhang, Y. S. Jung, P. Mariano, M. A. Fox, P. S. Martin and J. Merkert, *Tetrahedron Lett.*, 1993, **34**, 5239; M. Bietti, A. Cuppoletti, C. Dagostin, C. Florea, C. Galli, P. Gentili, H. Peride and C. R. Caia, *Eur. J. Org. Chem.*, 1998, 2425.
12 T. Sakata, *Photocatalysis*, ed. N. Serpone and E. Pelizzetti, J. Wiley & Sons, New York, 1989, p. 311.

CHEMCOMM Communication
www.rsc.org/chemcomm

The structure dependent electrochemical-response of novel 1-(4-mercaptobutyl)-4-(2-ferrocenylvinyl)pyridinium bromide SAMs on an Au electrode

Tong Xie,[a,b] Yong-Min Liang,[a] Wan-Yi Liu,[a] Bang-Jing Li[a] and Yong-Xiang Ma*[a]

[a] *National Laboratory of Applied Organic Chemistry, Lanzhou University, Lanzhou 730000, People's Republic of China. E-mail: mayx@lzu.edu.cn*
[b] *Qinghai Institute of Salt Lakes, Chinese Academy of Science, Xining, Qinghai 810008, People's Republic of China*

Received (in Cambridge, UK) 5th February 2001, Accepted 27th June 2001
First published as an Advance Article on the web 6th August 2001

The 1-(4-mercaptobutyl)-4-(2-ferrocenylvinyl)pyridinium bromide {1-HS$(CH_2)_4$-4-[(*E*)-FcCH=CH]C_5H_4N}$^+Br^-$ and its hydrogenated product [1-HS$(CH_2)_4$-4-(-FcCH_2CH_2)C_5H_4N]$^+Br^-$ were synthesized and assembled on an Au electrode to form self-assembled monolayers which showed a structure-dependent electrochemical-response in phosphate buffer aqueous solutions (pH = 7).

Self-assembled monolayers (SAMs) of alkanethiols and their derivatives with functionalized terminal groups have been studied intensively on gold electrodes due to their stability, organization, and potential application in many fields such as surface chemistry, biochemistry, electroanalytical chemistry, *etc.*[1] Motivated by Chidsey's novel work,[2] many research groups have investigated SAMs of ω-ferrocenylalkanethiols on gold because the ferrocenyl group is expected to exchange electrons readily with gold in the monolayer and the system can be considered as a model for the formation of electronic devices by self-assembly.[3–6] The advantage of electrochemically-active (*e.g.* ferrocene) monolayers is that the redox signal can be used as an internal readout. A linear porphyrin–ferrocene–alkanethiol was recently shown to be both sensitive and electrochemically-active.[7] A mixed acid–ferrocene self-assembled sulfide monolayer on gold shows a pH-dependent electrochemical-response by through-space communication between the receptor and ferrocene readout unit.[8] In addition, Marder reported that the compound incorporating a ferrocenyl moiety as a donor and a pyridinium as an acceptor connected by a CH=CH bridge, which is similar to our compound **1**, has excellent NLO properties.[9]

Here we primarily discuss a novel kind of 1-(4-mercaptobutyl)-4-(2-ferrocenylvinyl)pyridinium bromide and its structure-dependent electrochemical-response in phosphate buffer solution.

Compounds **1** and **2** can be conveniently prepared following the steps shown in Scheme 1.[10,11] Electrochemical measurement was conducted in a three-electrode cell with a CHI660A electrochemical workstation (Covarda, USA). Ag/AgCl and Pt foil were used as reference and counter electrodes, respectively. A gold disk electrode (CHI101) was employed as the working electrode (its apparent area S = 0.0314 cm^2), which was subjected to the same pre-treatment procedure before each experiment. The polished gold electrode (with 0.05 μm Al_2O_3) was rinsed with water. Thereafter, it was cleaned thoroughly in an ultrasonic cleaner with 1:1 nitric acid, 1:1 alcohol and distilled water, respectively. The cleaned gold electrode was washed with ethanol, dried by N_2 stream, then put into 0.1 mmol **1** or **2** ethanol solution and self-assembled in 12 h. After assembling, the monolayers were rinsed with ethanol and dried under a stream of purified N_2. The electrochemistry of the SAMs modified Au electrodes was tested by cyclic voltammetry in 0.1 mol L^{-1} phosphate buffer aqueous solution. The scan rates were 50, 100, 200, 300 and 400 mV s^{-1}, respectively.

Fig. 1(A) and (B) show a typical cyclic voltammogram obtained from the SAMs of **1** and **2** modified gold electrodes in 0.1 mol L^{-1} phosphate aqueous solution (pH = 7.0).

In each voltammogram, the electrode potential was cycled between −0.1 and 0.7 V. One electron reversible oxidation of the surface-confined ferrocenyl tail group was observed. The peak currents (i_{pa}, i_{pc}) were found to increase linearly with scan rate (v) as expected for a surface-confined redox system. The currents do not show decrease after repeated cycling in buffer solution, indicating that the ferrocene SAMs are very stable. Hence, it can be considered that the redox centers of these SAMs are fully solvated by aqueous electrolyte and the local environment around each redox center is quite uniform. The surface coverage of each thiolate was estimated from the charge passed for the oxidation of the ferrocene redox center during the anodic sweep. Values of Q_{Fc} were obtained by integration of the area under the anodic wave and were corrected for any charging-current contributions. The surface coverage of **1** was 6.4×10^{-11} mol cm^{-2}, and **2** was 7.1×10^{-11} mol cm^{-2}. This coverage is somewhat lower than the value of *ca.* 4.5×10^{-10} mol cm^{-2}, which is typically reported for a complete monolayer of uncharged ferrocenylalkanethiolates.[2] However, a decrease in packing efficiency is to be expected in this case, considering the steric effects of the pyridinium ion, ethylene band and the cationic charge on the nitrogen. The electrostatic repulsion of the adjacent cationic charges and the need to accommodate a counterion at each positively charged site would necessarily prevent the formation of a tightly packed monolayer. In a study carried out by Creager and co-workers a low monolayer coverage was reported for a charged thiol on gold, and this was

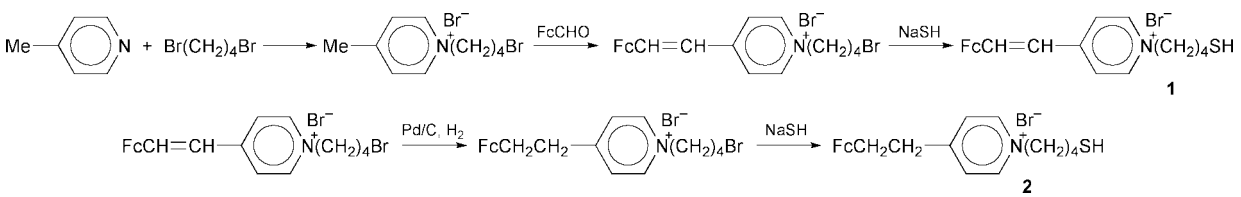

Scheme 1

 DOI: 10.1039/b101154p

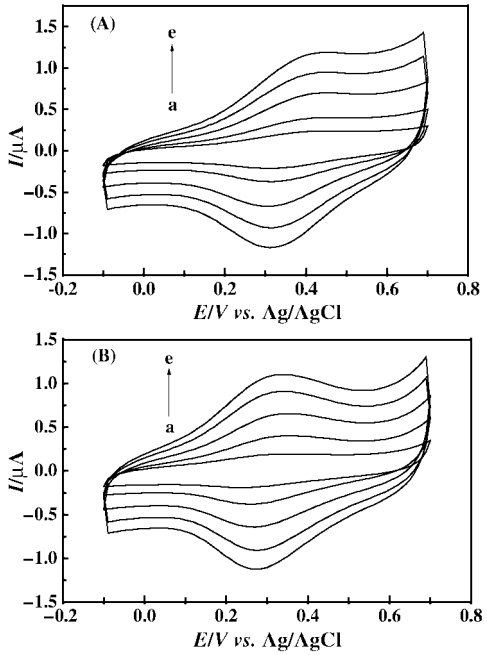

Fig. 1 The cyclic voltammograms of **1** and **2** SAMs modified Au electrode in 0.1 mol L^{-1} phosphate buffer electrolyte (pH = 7). (A) **1**; (B) **2**. The scan rate from **a** to **e** was 50, 100, 200, 300, 400 mV s^{-1}.

attributed to the strength and nature of the coulombic forces relative to dipolar and dispersion of forces within the monolayer.[12]

The location of the electron-withdrawing ethylene band and the electron-donating pyridinum group had a pronounced effect on the formal potential of the modified electrodes. The formal potential for the surface-bound ferrocenyl species was estimated from the average of the anodic (E_{pa}) and cathodic (E_{pc}) peak potentials, $E^{0\prime} = 1/2(E_{pa} + E_{pc})$. Monolayers of **1** displayed the more positive formal potential of 0.37 V, whereas monolayers of **2** exhibited the less positive potential of 0.30 V. This can be expected because the electroactive ferrocenyl moiety is located adjacent to the strong electron-withdrawing ethylene band in **1**, thus making it more stable and slightly harder for the ferrocene to undergo oxidation. It is well known that ferrocene monolayers are pH-independent. Fig. 2 shows the redox signal for **1** at pH 5.0, 6.0 and 7.0. The electrochemical response of the **1** monolayer is influenced by the pH of the electrolyte solution.

The electron transfer rate of these SAMs can be estimated from the peak separation ΔE_p. A surface-confined species participating in a reversible electron transfer process would be expected to exhibit a value of $\Delta E_p = 0$ mV. The experimental ΔE_p values obtained from the voltammograms show that the peak potential separation is independent of the scan rate, which implies that the electron transfer is relatively fast. However, the nonzero ΔE_p values (for **1** $\Delta E_p = 120$ mV, for **2** $\Delta E_p = 60$ mV) for separation between the oxidation and reduction peak

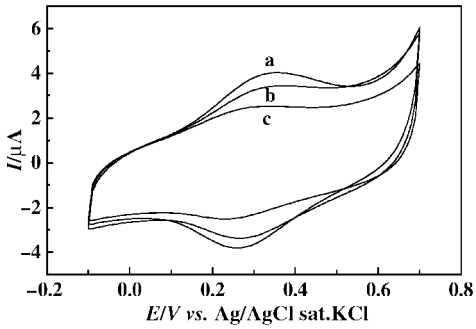

Fig. 2 Electrochemical response of **1** in phosphate electrolyte: (a). pH = 7.0; (b). pH = 6.0; (c). pH = 5.0.

potentials of Fc/Fc^+ indicated that the presence of the pyridinium ion with positive charge and the ethylene band slowed the electron transfer rate to some extent. The apparent electrochemical reversibility of the monolayers of ferrocene derivatives of the alkanethiolate has been tentatively attributed to the rapid lateral transport of the electrons from one ferrocene unit to an adjacent ferrocene unit, following electron shuttling from the conducting gold surface to the ferrocene plane.[2]. Here, the electron may be entrapped by the pyridinium ion, so the ΔE_p values became large.

The authors are grateful to the NSF (QT program) and the foundation of the University Key Teacher by the Ministry of Education of China for suport.

Notes and references

1 A. Ulman, *Chem. Rev.*, 1996, **96**, 1533.
2 C. E. D. Chidsey, C. R. Bertozzi, T. M. Putvinski and A. M. Mujsce, *J. Am. Chem. Soc.*, 1990, **112**, 4301.
3 S. W. Han, H. Seo, Y. K. Chung and K. Kim, *Langmuir*, 2000, **16**, 9493.
4 Y. Sato, B. L. Fiey, R. M. Corn and K. Uosaki, *Bull. Chem. Soc. Jpn.*, 1994, **67**, 21.
5 Y. Sato, H. Itoigawa and K. Uosaki, *Bull. Chem. Soc. Jpn.*, 1993, **66**, 1032.
6 K. Uosaki, *Electrochem.*, 1999, **66**, 1105.
7 K. Uosaki, T. Kondo, X.-Q. Zhang and M. Yanagida, *J. Am. Chem. Soc.*, 1997, **119**, 8367.
8 W. J. Benlen, J. M. van Veggel and D. N. Reinhoudt, *Chem. Commun.*, 1999, 503.
9 S. R. Marder, J. W. Perry and B. G. Tiemann, *Organometallics*, 1991, **10**, 1896.
10 Data for **1**: ^{1}H NMR (200 MHz, $CDCl_3$), δ: 9.17 (s, 2H, C***H***N), 7.91 (s, 2H, C***H***CHN), 7.70 (d, J = 16.0 Hz, 1H, (η-C_5H_4)C***H***), 6.71 (d, J = 15.6 Hz, 1H, (η-C_5H_4)CHC***H***), 4.81 (s, 2H, −NC***H***$_2$), 4.66, 4.56 (each s, 4H, η-C_5***H***$_4$), 4.20 (s, 5H, η-C_5***H***$_5$), 2.84 (m, 2H, -C***H***$_2$SH), 2.17–1.68 (m, 4H); MS (FAB) *m*/*e*: 378 (M – Br)$^+$.
11 Data for **2**: ^{1}H NMR (200 MHz, $CDCl_3$), δ: 9.76 (s, 2H, C***H***N), 7.72 (s, 2H, C***H***CHN), 4.96 (s, 2H, -NC***H***$_2$), 4.06–3.93 (t, 9H, η-C_5***H***$_4$, η-C_5***H***$_5$), 2.99 (s, 2H, (η-C_5H_4)C***H***$_2$), 2.81 (s, 2H, (η-C_5H_4)CH_2C***H***$_2$), 2.74 (m, 2H, -C***H***$_2$SH), 2.20–1.83 (m, 4H); MS (FAB) *m*/*e*: 380 (M – Br)$^+$.
12 S. E. Creager and G. K. Rome, *J. Electroanal. Chem.*, 1994, **370**, 203.

CHEMCOMM Communication
www.rsc.org/chemcomm

Disruption of protein–protein interactions: design of a synthetic receptor that blocks the binding of cytochrome *c* to cytochrome *c* peroxidase

Yen Wei,*[ab] George L. McLendon,*[a] Andrew D. Hamilton,*[c] Martin A. Case,[a] Cherie B. Purring,[a] Qing Lin,[c] Hyung Soon Park,[c] Chang-Sun Lee[c] and Tianning Yu[a]

[a] *Department of Chemistry, Princeton University, Princeton, New Jersey 08544, USA. E-mail: glm@princeton.edu; Fax: 609-258-6746; Tel: 609-258-1595*
[b] *Department of Chemistry, Drexel University, Philadelphia, Pennsylvania 19104, USA. E-mail: weiyen@drexel.edu; Fax: 215-895-1265; Tel: 215-895-2650*
[c] *Department of Chemistry, Yale University, New Haven, Connecticut 06520, USA. E-mail: ahamilton@ursula.chem.yale.edu; Fax: 203-432-3221; Tel: 203-432-5570*

Received (in Cambridge, UK) 1st May 2001, Accepted 14th June 2001
First published as an Advance Article on the web 6th August 2001

Synthetic receptor 1 has been found *via* fluorescence titration to compete effectively with cytochrome *c* peroxidase for binding cytochrome *c* (Cc), forming 1:1 Cc:1 complex with a binding constant of (3 ± 1) × 10^8 M^{-1}, and to disrupt Cc:Apaf-1 complex, a key adduct in apoptosis.

Protein–protein recognition is critical to virtually all cellular processes. Consequently, molecules which could specifically disrupt the high affinity natural protein complexes found physiologically could provide an important route to modulate cellular processes. However, there are few examples of such a modulation.[1] Since high affinity protein–protein complexes generally involve large surface areas,[2] it has been argued that small synthetic molecules which bind at the interaction surface are unlikely to compete with high affinity natural protein partners. Here, we show that a synthetic receptor molecule of structure **1** can bind cytochrome *c* (Cc) with a sufficiently high

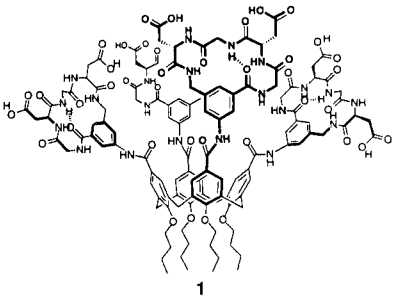

1

affinity to displace a natural high affinity protein partner, cytochrome *c* peroxidase (CcP). Cytochrome *c* provides an important model for such studies for several reasons. First, the structure of Cc is well characterized.[3] Second, the Cc:CcP complex is unusually well characterized, both from structural and thermodynamic viewpoints.[4,5] Finally, the key role of Cc in mediating apoptosis[6–8] makes it a particularly interesting target.

Several previous studies have explored the binding of small molecules to Cc.[3,9] However, in few previous cases was the binding sufficiently strong and specific to be shown to compete with the binding of natural partner proteins at relevant concentrations ($< 10^{-6}$ M). Preliminary data on Cc binding by **1** suggested the possibility of specific and high affinity binding.[10] To test this possibility, we have carried out a series of spectroscopic studies and established that the synthetic receptor **1** is indeed capable of disrupting the physiological complex of Cc with CcP by binding competitively to Cc. From the concentration of **1** needed to disrupt the Cc:CcP binding, we can estimate that the dissociation constant (K_d) for the Cc:**1** complex is near the nanomolar level ($\sim 10^{-8}$ M) in a phosphate buffer (10 mM, pH 6.0). Furthermore, the competitive displacement of CcP from its natural protein partner by **1** suggests that they share a similar binding site on the surface of Cc.

The competitive binding experiments were based on the quenching of strong fluorescence of magnesium(II) CcP (MgCcP) by Cc and the reversal of that quenching by addition of receptor **1**. The reaction schemes are illustrated in eqns. (1) and (2). It has been demonstrated that the magnesium substitution of iron in the native CcP does not alter the binding characteristics of CcP with Cc.[5] The use of MgCcP is advantageous because of its strong, interference-free fluorescence signals. In a typical experimental procedure, 3.0 mL of 0.077 μM solution of MgCcP[5] in 10 mM degassed potassium phosphate buffer (KPhos, pH 6.0) was prepared in a quartz cuvette of 1 cm pathlength equipped with magnetic stirrer. The fluorescence spectrum of the solution was recorded on a PTI fluorimeter (Photon Technology International, NJ) with an excitation wavelength of 556 nm and a scan rate of 1 nm s^{-1} at 15.0 °C (Fig. 1a). The solution was titrated *in situ* with a 3.5 μM solution of yeast Cc (Sigma) to an equivalent point [CcP]:[Cc] = 1. Upon Cc:CcP complex formation, the fluorescence signals of MgCcP at 598 and 653 nm were quenched by resonant energy transfer (Fig. 1b). Then a 4.48 μM solution of receptor **1**[10] in 10 mM KPhos (pH 6.0) was added in aliquots of 10 to 20 μL. The fluorescence spectrum was measured after each addition until the [**1**]:[Cc] molar ratio reached 5 or higher (Figs. 1c and 1d). Upon addition of receptor **1**, the intensity of the fluorescence signals of MgCcP increased, indicating that CcP is gradually freed from the Cc:CcP complex.

$$\mathrm{Cc} + \mathrm{CcP} \leftrightharpoons \mathrm{Cc{:}CcP} \quad (1)$$

$$\mathrm{Cc{:}CcP} + \mathbf{1} \leftrightharpoons \mathrm{Cc{:}}\mathbf{1} + \mathrm{CcP} \quad (2)$$

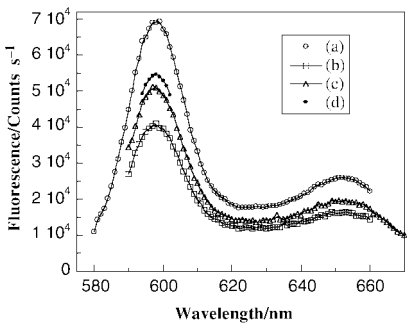

Fig. 1 Representative fluorescence spectra of (a) MgCcP (0.075 μM), (b) MgCcP (0.075 μM) with 0.077 μM of Cc, and the MgCcP:Cc complex titrated with (c) 0.11 and (d) 0.28 μM of **1**. Excitation at 556 nm at 15.0 °C in 10 mM KPhos buffer (pH 6.0).

 DOI: 10.1039/b104142h

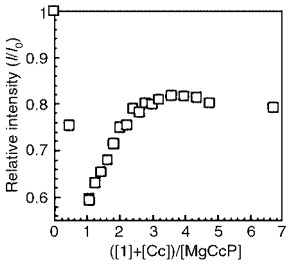

Fig. 2 Plots of the relative fluorescence intensity (I/I_o) at 598 nm against the normalized concentration ([Cc] + [**1**])/[CcP] (ex. 556 nm). [Cc] = 0.077 μM, [MgCcP] = 0.075 μM in 10 mM KPhos buffer (pH 6.0) at 15.0 °C.

Fig. 2 shows the plots of relative intensity of the fluorescence at 598 nm against the normalized concentration, ([Cc] + [**1**])/[CcP]. At [Cc]/[CcP] = 1 and before addition of **1**, the fluorescence intensity (I) of MgCcP was reduced to ~57% of the initial value (I_o), which is in agreement with that reported in the literature.[5] Addition of **1** resulted in a sharp increase in the relative intensity (I/I_o) until ([Cc] + [**1**])/[CcP] reached about 2, *i.e.* [**1**]/[Cc] ≈ 1, after which the intensity levelled off, suggesting the formation of 1:1 Cc:**1** complex. The intensity does not increase to the original level because of partial photodegradation of MgCcP. The recovery of fluorescence suggests that receptor **1** effectively disrupts the Cc:CcP complex at nanomolar concentrations (*i.e.* ~0.08 μM), and releases CcP free into solution. Under these conditions, the interaction between **1** and Cc appears stronger than that between CcP and Cc, with a K_d value < 100 nM.

The binding constant (K_b) for Cc:**1** complex can be estimated from the competitive titration results using a standard nonlinear curve-fitting. The competition equilibrium constant K_c for eqn. (2) can be expressed [eqn. (4)] in terms of the K_b's for eqn. (1) ($K_{b1} = 2 \times 10^7$ M^{-1})[5] and for eqn. (3) (K_{b2}). Assuming that the concentration of free Cc in eqn. (3) at equilibrium is negligible, a quadratic equation can be derived as shown in eqn. (5), where $A = [Cc]_{Total}$, $B = [CcP]_{Total}$, $x = [\mathbf{1}]_{Total}$, and $y = (I_{obs} - I_f)/(I_i - I_f)$ with I_i and I_f being the fluorescence intensities at ([Cc] + [**1**])/[CcP] of 1 and of ⩾2, respectively. From the solution for y in eqn. (5), K_c was obtained. A set of typical results are shown in Fig. 3, from which K_{b2} was estimated to be $(3 \pm 1) \times 10^8$ M^{-1}.

$$Cc + \mathbf{1} \leftrightharpoons Cc{:}\mathbf{1} \quad (3)$$

$$K_c = K_{b2}/K_{b1} \quad (4)$$

$$(B^2K_c - B^2)y^2 + (K_cBx - ABK_c + AB + B^2)y - AB = 0 \quad (5)$$

The titration of the MgCcP solution with **1** in the absence of Cc showed little change in the fluorescence of MgCcP in the range of [**1**]/[MgCcP] from 0 to 5, indicating that there is no significant interaction between **1** and CcP. The region of Cc

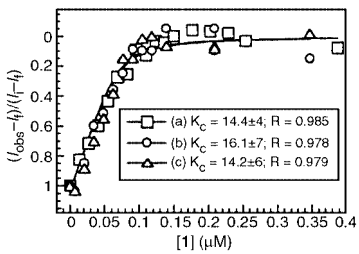

Fig. 3 Typical curve-fitting results for the fluorescence titration of 1:1 Cc:CcP complex with the receptor **1**. The values of $y = (I_{obs} - I_f)/(I_i - I_f)$ for emissions at (a) 598 nm at 15.0 °C, (b) 598 nm at 25.0 °C and (c) 653 nm at 25.0 °C are plotted against the concentration of **1**. The experimental data are fitted according eqn. (5) to estimate K_c values. Excitation at 556 nm, [MgCcP] = 0.076 μM, [Cc] = 0.077 μM in 10 mM KPhos buffer (pH 6.0).

involved in binding to CcP contains an array of positively charged residues that interacts with a complementary patch of negative residues on CcP.[4] The polyanionic receptor **1** competes successfully with CcP, presumably by binding to a similar site on the surface of Cc. The CcP molecules are freed from the interactions with Cc, leading to the observed recovery of fluorescence.

The binding of **1** with Cc has been independently confirmed by direct fluorescence titration of **1**. Receptor **1** exhibits a broad fluorescence peak at ~432–443 nm with excitation wavelength of 298 nm. Addition of Cc results in a rapid decrease in the fluorescence intensity, which levels off as Cc concentration increases. Further quantitative interpretations of such data are precluded at the present time, since the receptor molecules (**1**), due to their surfactant-like structure, tend to aggregate, which interferes with the determination of binding stoichiometry. Reducing the concentration of **1** prevents the aggregation but the decrease in fluorescence signal to noise ratio impedes quantitative analysis.

The ability to bind to Cc with high affinity is of great interest, given the major role of Cc as a signal protein for activating Apaf-1 (the apoptosis protease activating factor-1) protein in apoptosis.[6–8] The binding constant for the 2:1 Cc:Apaf-1 complex was estimated to be ~10^{11} M^{-1} from the fluorescence polarization titration measurements, in which Apaf-1 was added to nanomolar concentrations of horse heart zinc(II) Cc and the increase in polarization was monitored.[8] Upon formation of the Cc:Apaf-1 complex, receptor **1** was added to the system. At a [**1**]/[Cc:Apaf-1] molar ratio of ~200, the relative fluorescence polarization decreased significantly from 1.9 to 1.3. The preliminary data indeed suggest that **1** can disrupt the Cc:Apaf-1 interactions. More detailed results of further studies will be reported in due course.

In conclusion, we have demonstrated that the physiological complex of Cc with CcP can be disrupted by a synthetic receptor (**1**). Receptor **1** competes effectively with CcP for binding Cc, forming 1:1 Cc:**1** complex with a binding constant of ~10^8 M^{-1}. Investigation is in progress to evaluate the effects of the structure of synthetic receptors on their competitive binding with various proteins, including Apaf-1, and protein–protein complexes.

Y. Wei thanks Drexel University for granting him a sabbatical leave at Princeton University and Drs V. Lai, S. Springs and S. Hatch for many helpful discussions.

Notes and references

1 (*a*) D. W. Banner, *Nature*, 2000, **404**, 449; (*b*) W. E. Stites, *Chem. Rev.*, 1997, **97**, 1233.
2 (*a*) C. Branden and J. Tooze, *Introduction to Protein Structure*, Garland, New York, 1991, p. 187; (*b*) D. R. Davies, E. A. Padlan and S. Sheriff, *Annu. Rev. Biochem.*, 1990, **59**, 439; (*c*) H. S. Park, Q. Lin and A. D. Hamilton, *J. Am. Chem. Soc.*, 1999, **121**, 8.
3 R. A. Scott and A. G. Mauk, *Cytochrome c—A Multi-disciplinary Approach*, U. Sci. Books, Sausalito, CA, USA, 1996.
4 H. Pelletier and J. Kraut, *Science*, 1992, **258**, 1748.
5 G. McLendon, Q. Zhang, S. A. Wallin, R. M. Miller, V. Billstone, K. G. Spears and B. M. Hoffman, *J. Am. Chem. Soc.*, 1993, **115**, 3665.
6 H. Zou, W. J. Henzel, X. Liu, A. Lutschg and X. Wang, *Cell*, 1997, **90**, 405.
7 P. Li, D. Nijhawan, I. Budihardjo, S. M. Srinivasula, M. Ahmad, E. S. Alnemri and X. Wang, *Cell*, 1997, **91**, 479.
8 C. Purring, H. Zou, X. Wang and G. McLendon, *J. Am. Chem. Soc.*, 1999, **121**, 7435.
9 (*a*) M. Marjatta and P. K. Kinnunen, *Biochem.*, 1996, **35**, 4529; (*b*) T. E. Meyer, Z. G. Zhao, M. A. Cusanovich and G. Tollin, *Biochem.*, 1993, **32**, 4552; (*c*) M. Antalik, M. Bona, Z. Gazova and A. Kuchar, *Biochim. Biophys. Acta*, 1992, **1100**, 155; (*d*) D. W. Concar, D. Whitford and R. J. P. Williams, *Eur. J. Biochem.*, 1991, **199**, 553; (*e*) K. K. Clark-Ferris and J. Fisher, *J. Am. Chem. Soc.*, 1985, **107**, 5007.
10 Y. Humuro, M. C. Calama, H. S. Park and A. D. Hamilton, *Angew. Chem., Int. Ed. Engl.*, 1997, **36**, 2680.

CHEMCOMM
Communication
www.rsc.org/chemcomm

Design and post-functionalisation of ordered mesoporous zirconia thin films†

Eduardo L. Crepaldi,[a] Galo J. de A. A. Soler-Illia,[a] David Grosso,[a] Pierre-Antoine Albouy[b] and Clément Sanchez*[a]

[a] *Laboratoire Chimie de la Matière Condensée, Université Pierre et Marie Curie, 4 Place Jussieu, 75252 Paris Cedex 05, France. E-mail: clems@ccr.jussieu.fr.*
[b] *Laboratoire de Physique des Solides, Université Paris-Sud, 91405 Orsay Cedex, France*

Received (in Cambridge, UK) 25th May 2001, Accepted 13th July 2001
First published as an Advance Article on the web 6th August 2001

Bidimensional hexagonal or centred-rectangular mesoporous zirconia thin films have been reproducibly prepared by evaporation-induced self-assembly (EISA), which are stable up to 300 °C, with pore size around 35 Å; the films can be post-functionalised with organic ligands presenting different functions, opening a land of opportunities for the design of new hybrid mesostructured materials, based on the synergy of a transition metal oxide network and organic groups.

Since Beck and coworkers[1] demonstrated the use of arrays of amphiphilic species as 'supramolecular templates', mesoporous materials have been receiving increasing attention.[2,3] However, the hydrothermal treatment usually applied in the synthesis procedures is not adequate for the processing of mesoporous films, fibres or monoliths. The evaporation-induced self-assembly (EISA)[4] process represents an alternative way to design mesostructured organic–inorganic hybrids, which are precursors for mesoporous solids. By this process, silica based mesoporous materials have been prepared as powders, fibres, monoliths and thin films in a variety of structural arrangements (2D- and 3D-hexagonal, cubic and lamellar phases).[1,5] This same process has been applied to obtain transition metal oxide-based materials, such as mesoporous TiO_2,[6] ZrO_2, Nb_2O_5, Al_2O_3, SnO_2, WO_3, Ta_2O_5 and many mixed metal oxides.[7] For these systems, this approach has been applied mainly to the preparation of powders, or even titania mesoporous films.[8]

Here, we report for the first time to the best of our knowledge, the preparation of oriented mesostructured zirconium oxide-based hybrids and mesoporous oxide films. The post-functionalisation of the zirconia mesoporous films is also reported. Zirconia mesoporous films are particularly interesting because of the high chemical stability of this oxide, being potentially applicable as catalyst support, adsorbent, heavy duty membranes and chemical sensors.

Films were prepared by dip-coating glass or silicon substrates at a constant withdrawal speed ranging from 0.08 to 0.4 cm s^{-1} at room temperature (20–23 °C). The dipping solutions contain 1 $ZrCl_4$: 0.05 Brij-58 [$C_{16}H_{33}(CH_2CH_2O)_{20}OH$] : 40 EtOH : 0–20 H_2O.[9] The relative humidity (RH) inside the dip-coater chamber is a parameter of paramount importance, and was thus controlled between 10 and 80%. After drying, the as-prepared films were submitted to a sequence of treatments in order to stabilise the structure and remove the surfactant: drying overnight at low humidity (< 10%), 12 h at 60 °C, ammonia atmosphere (30 min), and calcination in air at temperatures ranging from 150 to 500 °C for 2 h (ramp of 1 °C min^{-1}).

Two-dimensional XRD patterns in transmission mode demonstrate that a hexagonal (*p*6*m*) mesophase is obtained upon dip-coating, the organised domains are mono-oriented, as previously observed in silica and titania mesoporous films.[8,10] Fig. 1(a)–(c) shows representative 2D-XRD patterns of films treated at 60, 220 and 300 °C, respectively. The observed spots can be indexed in all cases in a 2D-centred-rectangular cell

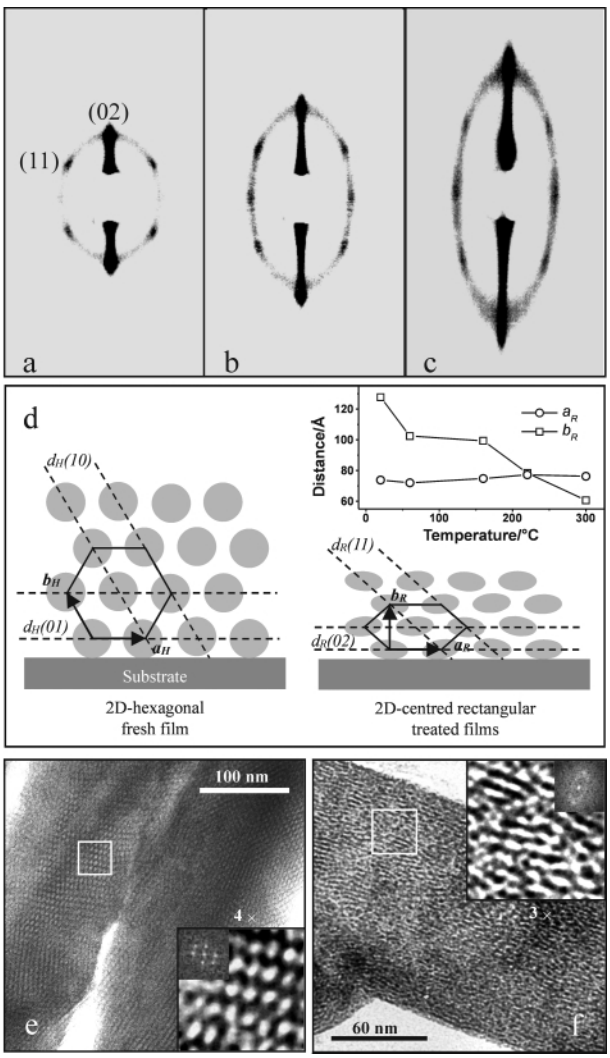

Fig. 1 Two-dimensional XRD patterns obtained by transmission for films treated at (a) 60, (b) 220 and (c) 300 °C. Schematic representation of the relationship between 2D-hexagonal (*p*6*m*) and 2D-centred rectangular (*c*2*m*) cells (d), the inset showing the observed variation of the parameters a_R and b_R of the 2D-centred rectangular cell with temperature. TEM images along the [001] zone axis of Brij 58-templated mesostructured zirconia films treated at (e) 60, and (f) 300 °C. Inset in parts (e) and (f) are reconstructed images and moduli of the Fourier transform of the indicated regions.

† Electronic supplementary information (ESI) available: XRD and SEM data showing the influence of water content in solution and atmospheric relative humidity in the organisation and optical quality of the films, and details about the post-functionalisation. See http://www.rsc.org/suppdata/cc/b1/b104623n/

 DOI: 10.1039/b104623n

(space group *c*2*m*), resulting from a preferential contraction of the hexagonal mesophase in the direction normal to the substrate.[8,10] Low-angle XRD analysis in θ–2θ mode (graphite-monochromated Cu-Kα_1 radiation, λ = 1.5406 Å) of the as-prepared films only showed the presence of a single peak at d = 63.9 Å, corresponding to the d_{02} spot of the bidimensional rectangular (*c*2*m*) lattice [equivalent to the d_{01} distance of the hexagonal (*p*6*m*) structure, see Fig. 1(d)]. The uniaxial contraction in the direction normal to the substrate upon thermal treatment is clearly observed by θ–2θ and 2D-XRD [see inset in Fig. 1(d)], the a_R parameter remaining almost constant (*ca*. 76 Å).

TEM images of films (detached from the substrate, embedded in epoxy resin and ultramicrotomed) support the XRD data, showing almost circular pores for films treated between 60 and 160 °C, and elliptical pores for films treated between 200 and 300 °C, clearly a consequence of the uniaxial contraction. Representative examples are shown in Fig. 1(e) and 1(f). Moreover, images obtained for films treated at low temperatures (60–160 °C) display regular long-range ordered patterns, in accord with XRD data that showed narrow, intense diffraction peaks (or spots, in the 2D-XRD pattern). The partial degradation of the structure can be clearly visualised from Fig. 1(e), that shows broad diffractions for films treated at temperatures > 200 °C, and the presence of an ellipse (characteristic of entangled worm-like channels[10]), the intensity of which increases with temperature. The wall thickness was estimated from TEM to be *ca*. 37 Å for the film treated at 60 °C, decreasing to *ca*. 20 Å upon treatment at 300 °C, probably as a consequence of further condensation, as showed by TGA–DSC analysis. The pore diameter was estimated to be *ca*. 35 Å for films treated between 60 and 160 °C; thermal treatment at 300 °C results in *ca*. 14 × 36 Å pores. N_2 adsorption data (scratched films treated at 220 °C followed by UV/O_3 treatment) showed an average pore diameter of 28 Å (BJH) and specific surface (BET) of 192 $m^2\ g^{-1}$.

Films were prepared in different conditions by varying the water contents in the solution ($h = H_2O/Zr = 0$–20) and the relative humidity (RH 10–80%) (ESI†). In general, 'dry' conditions (low h and RH) lead to non-organised coatings, confirming the essential role of water in solution and evaporation rate.[6] The organisation increases for higher h values, and in most cases, with increasing relative humidity. However, the highest degree of organisation was observed with h = 20 and 10% RH. This result confirms the importance of the evaporation rate, relatively fast (drying within 1 min) at 10% RH and very slow at high humidity conditions.

Despite the high degree of organisation attained for high water contents, the optical quality of the coatings is poor, due to a phase segregation (observed by SEM) (ESI†). In order to obtain transparent films, a two-step process was developed. Submitting fresh films (h = 20; RH% = 10) to a high humidity atmosphere (RH > 80%) for a short time (5–10 s) resulted in the incorporation of water. A second drying process led to transparent and homogeneous films. A SEM image of a film submitted to this treatment shows a completely smooth surface, and the corresponding XRD diagram presents a narrow, intense peak with a *d*-spacing of 63.9 Å. These results indicate that the as-prepared films are quasi-liquid, showing a liquid crystal behaviour, as shown before by Brinker *et al.* for silica films.[4,11] The post-processing (submission to high humidity for few seconds) facilitates homogeneous texture, and leads to better organised domains in the mesostructure, indicated by the narrowing and increasing in intensity of the XRD peak. The thickness of such films as estimated by SEM was 700 nm, and can be tailored by varying the withdrawal speed and the ethanol content in the solution without any noticeable variation in the structure or optical quality.

Following drying overnight at low humidity and room temperature, the *d*-spacing slightly contracted from 63.9 to 63.0 Å while subsequent ammonia vapour treatment resulted in a *d*-spacing of 57.3 Å, indicating further condensation of the zirconium oxide network. From this point on, the films were submitted to thermal treatment, in order to increase the stability of the inorganic network and to remove the surfactant. TGA–DSC analysis of detached films (1 °C min^{-1}, air flow) shows that surfactant decomposition occurs from 150 to 350 °C (26.5 mass%). A crossed XRD-FTIR analysis showed that contraction is small [$(d_0 - d)/d_0 < 22\%$] up to 200 °C; in this range, the surfactant is not removed. From 200 °C on, a strong contraction was observed (40–52% in the range 200–300 °C) coinciding with the decomposition of the surfactant. By 350 °C the mesostructure is lost. However, organic or carboxylate species (detected by FT-IR bands at *ca*. 1618 and 1378 cm^{-1}) cannot be removed, even at 400 °C. An alternative combination of UV light and ozone at room temperature was thus performed,[12] giving rise to pure zirconia mesoporous films.

In order to tailor the nature of the pore surfaces, organic molecules were grafted on the mesoporous zirconia films. Three grafting functions were selected, known by their ability of complexing Zr(IV): β-diketonate, carboxylate and phosphonate. The probe molecules were chosen because of their different properties: dibenzoylmethane, (DBM) and phenylphosphonic acid, (PPA) carrying hydrophobic groups, can be used to impart hydrophobic properties to the pore surface. Methyl red dye, (MTR) is well known as a pH indicator. Finally, ferrocenecarboxylic acid (FCA), is interesting due to its redox properties. FT-IR and UV–VIS data clearly show the grafting of the probes (ESI†). The possibility of ready post-functionalisation of the film, leading to pores with a tailored surface, is a very interesting result, since functionalised films can be applied in many fields, depending on the nature of the grafted species.

Financial support from the French Ministry of Research, CNRS, CNPq (Brazil, grant # 200635/00-0), CONICET and Fundación Antorchas (Argentine Republic) is gratefully acknowledged.

Notes and references

1 C. T. Kresge, M. E. Leonowicz, W. J. Roth, J. C. Vartuli and J. S. Beck, *Nature*, 1992, **359**, 710; J. S. Beck, J. C. Vartuli, W. J. Roth, M. E. Leonowicz, C. T. Kresge, K. D. Schmitt, C. T.-W. Chu, D. H. Olson, E. W. Sheppard, S. B. McCullen, J. B. Higgins and J. L. Schlenker, *J. Am. Chem. Soc.*, 1992, **114**, 10834.
2 C. Göltner and M. Antonietti, *Adv. Mater.*, 1997, **9**, 431.
3 S. Mann, S. L. Burkett, S. A. Davis, C. E. Fowler, N. H. Mendelson, S. D. Sims, D. Walsh and N. T. Whilton, *Chem. Mater.*, 1997, **9**, 2300.
4 C. J. Brinker, Y. Lu, A. Sellinger and H. Fan, *Adv. Mater.*, 1999, **11**, 579.
5 N. K. Raman, M. T. Anderson and C. J. Brinker, *Chem. Mater.*, 1996, **8**, 1682; H. Yang, N. Coombs, I. Sokolov and G. A. Ozin, *Nature*, 1996, **381**, 589; H. Yang, A. Kuperman, N. Coombs, S. Mamicheafara and G. A. Ozin, *Nature*, 1996, **379**, 703; D. Zhao, Q. Huo, J. Feng, B. F. Chmelka and G. D. Stucky, *J. Am. Chem. Soc.*, 1998, **120**, 6024; P. J. Bruinsma, A. Y. Kim, J. Liu and S. Baskaran, *Chem. Mater.*, 1997, **9**, 2507; N. Melosh, P. Lipic, F. S. Bates, F. Wudl, G. D. Stucky, G. H. Frederickson and B. F. Chmelka, *Macromolecules*, 1999, **32**, 4332; D. Zhao, P. Yang, N. Melosh, J. Feng, B. F. Chmelka and G. D. Stucky, *Adv. Mater.*, 1998, **10**, 1380; D. Grosso, A. R. Balkenende, P.-A. Albouy, M. Lavergne, L. Mazerolles and F. Babonneau, *J. Mater. Chem.*, 2000, **10**, 2085.
6 G. J. A. A. Soler-Illia, E. Scolan, A. Louis, P. A. Albouy and C. Sanchez, *New J. Chem.*, 2001, **25**, 156.
7 (*a*) P. Yang, D. Zhao, D. I. Margolese, B. F. Chmelka and G. D. Stucky, *Nature*, 1998, **395**, 583; (*b*) P. Yang, D. Zhao, D. I. Margolese, B. F. Chmelka and G. D. Stucky, *Chem. Mater.*, 1999, **11**, 2813.
8 D. Grosso, G. J. de A. A. Soler-Illia, F. Babonneau, C. Sanchez, P.-A. Albouy, A. Brunet-Bruneau and A. R. Balkenende, *Adv. Mater.*, 2001, **13**, 1085.
9 Care must be taken during the addition of the anhydrous metal chloride into the surfactant alcoholic solution, since the reaction is exothermic and HCl is released.
10 M. Klotz, P.-A. Albouy, A. Ayral, C. Ménager, D. Grosso, A. Van der Lee, V. Cabuil, F. Babonneau and C. Guizard, *Chem. Mater.*, 2000, **12**, 1721.
11 Y. Lu, R. Ganguli, C. Drewien, M. Anderson, C. Brinker, W. Gong, Y. Guo, H. Soyez, B. Dunn, M. Huang and J. Zink, *Nature*, 1997, **389**, 364.
12 T. Clark Jr., J. D. Ruiz, H. Fan, C. J. Brinker, B. I. Swanson and A. N. Parikh, *Chem. Mater.*, 2000, **12**, 3879.

CHEMCOMM
Communication
www.rsc.org/chemcomm

Synthesis and structure of the novel mixed anion–dianion lithium cage compound $[(6\text{-}LiCH_2Py\text{-}2\text{-}OLi)_4(6\text{-}CH_3Py\text{-}2\text{-}OLi)_2(THF)_9]$

Stephen T. Liddle and William Clegg*

Department of Chemistry, University of Newcastle upon Tyne, Newcastle upon Tyne, UK NE1 7RU. E-mail: w.clegg@ncl.ac.uk

Received (in Cambridge, UK) 30th May 2001, Accepted 9th July 2001
First published as an Advance Article on the web 6th August 2001

The title compound crystallises as a novel homometallic mixed anion–dianion cage incorporating two four-coordinate diorgano lithiate centres, in addition to eight lithium centres coordinated only by oxygen and nitrogen atoms.

The past two decades have witnessed considerable interest in organolithium chemistry. Within this realm the formation of complexes containing 'ate' centres is still comparatively rare, despite the overwhelming number of organolithium complexes reported to date. The first example was reported by Eaborn *et al.*,[1] and some closely related complexes subsequently followed.[2] There are only a handful of other examples,[3] including the recently reported dibenzyl lithiate complex by Bildmann and Müller, which contains the first example of a four-coordinate diorganolithiate.[3c] Examples of ate complexes with nitrogen donors have also been reported.[4]

We are currently interested in aspects of the structural chemistry of 2-hydroxy-6-methylpyridine (Hhmp) and other substituted 2-pyridones. Hhmp has been employed extensively in transition metal chemistry where the similarity of its anion hmp^- to the carboxylate group has been exploited to probe the nature of multiple metal–metal bonds in dinuclear complexes.[5] Such complexes are frequently synthesised *via* an alkali metal salt; these are notable by their relative lack of structural characterisation. Indeed, a search of the Cambridge Structural Database[6] reveals, with the exception of some heterobimetallic alkali metal–transition metal complexes,[7] only two related compounds, both produced in aqueous media, namely the monohydrated potassium salt of 2-pyridone $[2\text{-}KOPy\cdot H_2O]$[8] and the caesium salt of the more highly substituted 2-pyridone $[2\text{-}CsO\text{-}3\text{-}CN\text{-}4\text{-}CF_3\text{-}6\text{-}Ph\text{-}Py\cdot H_2O]$.[9] Consequently we have sought to characterise alkali metal complexes of hmp, as they promise to be more structurally diverse than 'pure' alkoxides or aryloxides due to the additional coordination possibilities provided by the pyridyl nitrogen. Although our principal goal has been to synthesise monometallated complexes, we find that subsequent lithiation at the methyl site occurs readily, thus allowing facile access to the synthesis of mixed anion–dianion complexes. Indeed, it is possible to control precisely the extent of metallation from monometallated through to dimetallated by addition of the appropriate amount of butyllithium. It is consequently possible to synthesise aggregates with varying degrees of anion/dianion character and we have synthesised a range of such complexes, which will be elaborated on in a full account of this work. As revealed herein, we describe the synthesis and solid state structure of the title compound **1**, which is notable for being a rare example of a Group I mixed anion–dianion complex containing two four-coordinate organolithiate centres.

In a Schlenk tube under dry nitrogen, Hhmp (10 mmol) in dry THF (50 mL) was lithiated by Bu^nLi (10 mmol) to afford a dark orange solution. Addition of an additional 2/3 equivalent of Bu^nLi (6.67 mmol) affords a dark red solution with evolution of gas clearly visible [eqn. (1)]. Concentration and layering with *n*-hexane at −30 °C affords highly air-sensitive orange crystals of

$$6\text{-}CH_3Py\text{-}2\text{-}OH + 10\ Bu^nLi \xrightarrow{THF} [(6\text{-}LiCH_2Py\text{-}2\text{-}OLi)_4(6\text{-}MePy\text{-}2\text{-}OLi)_2(THF)_9] + 10\ Bu^nH \quad (1)$$

the title compound **1** in 82.4% isolated yield, which rapidly degrade to a yellow powder when removed from solvent or exposed to vacuum. Despite repeated attempts, it was not possible to obtain satisfactory microanalysis for **1**, due to the extremely air- and moisture-sensitive nature of this complex and loss of coordinated THF. Analyses obtained were consistent with variable loss of non-integral amounts of coordinated THF (typically between two and four molecules).

The structure of **1** (Fig. 1)† consists of an alkoxo cage with two diorgano lithiate centres. There are ten lithium centres, two anionic and four dianionic hmp ligands (deprotonated at the hydroxy *and* methyl sites), and nine THF molecules. Each lithium centre, with the exception of the three-coordinate Li(2), which is distinctly pyramidal [sum of angles 343.5(6)°], displays a distorted tetrahedral environment. Setting aside the C–Li bonds, four of the hmp ligands are tetra-coordinating [N(1), N(2), N(4) and N(6)] (with μ_3-oxygen atoms) and two [N(3) and N(5)] are penta-coordinating (with μ_4-oxygen atoms).

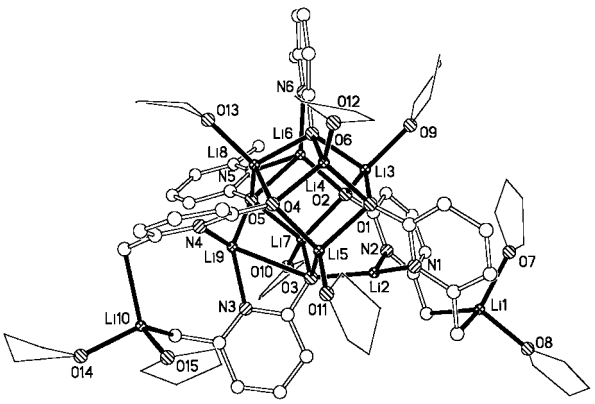

Fig. 1 Molecular structure of **1**. Hydrogen atoms and parentheses in atom labels have been omitted for clarity. Selected bond lengths (Å): Li(1)–O(7) 1.998(15), Li(1)–O(8) 1.994(15), Li(1)–C(6) 2.198(16), Li(1)–C(12) 2.230(16), Li(2)–N(1) 1.996(15), Li(2)–N(2) 2.015(15), Li(2)–O(3) 1.957(14), Li(3)–O(1) 1.937(13), Li(3)–O(2) 1.898(15), Li(3)–O(6) 2.034(16), Li(3)–O(9) 1.961(16), Li(4)–O(1) 1.959(15), Li(4)–O(4) 1.916(15), Li(4)–O(6) 1.982(14), Li(4)–O(12) 1.991(15), Li(5)–O(1) 2.036(15), Li(5)–O(3) 1.938(15), Li(5)–O(4) 1.948(15), Li(5)–O(11) 1.937(14), Li(6)–O(2) 1.907(15), Li(6)–O(5) 2.267(15), Li(6)–N(5) 2.043(15), Li(6)–N(6) 2.070(17), Li(7)–O(2) 1.979(14), Li(7)–O(3) 1.927(14), Li(7)–O(5) 2.063(15), Li(7)–O(10) 2.010(15), Li(8)–O(4) 1.956(15), Li(8)–O(5) 2.004(15), Li(8)–O(6) 1.974(16), Li(8)–O(13) 1.933(16), Li(9)–O(3) 2.580(16), Li(9)–O(5) 1.970(16), Li(9)–N(3) 1.984(18), Li(9)–N(4) 1.996(18), Li(10)–O(14) 1.994(16), Li(10)–O(15) 1.934(16), Li(10)–C(18) 2.243(18), Li(10)–C(24) 2.300(20).

 DOI: 10.1039/b104680m

Both these bonding modes are, to the best of our knowledge, unprecedented with this ligand; only mono-, di- and tri-coordination modes are known. The core of the cage may be thought of as a stack of two six-membered $(LiO)_3$ rings [ring 1: Li(3)–O(1)–Li(5)–O(3)–Li(7)–O(2); ring 2: O(6)–Li(4)–O(4)–Li(9)–O(5)–Li(6)], of similar architecture to the hexameric complex $[\{Li(OPh)(THF)\}_6]$,[10] which has been distorted by the presence of the four extra lithium centres [Li(1), Li(2), Li(8) and Li(10)]. The chiral cage crystallises in the non-centrosymmetric space group *P*1.

Turning to bond lengths, excluding the four long Li–O contacts of 2.267(15), 2.580(16), 2.613(15) and 2.655(17) Å [Li(6)–O(5), Li(9)–O(3), Li(6)–O(6) and Li(9)–O(4) respectively], the $Li–O_{hmp}$ bond lengths span the range 1.898(15)–2.063(15) Å. This compares with a range of 1.856–2.063 Å in the heterometallic cluster $[(Bu^tOLi)_6(Bu^tOK)_2(Li_2O)(TMEDA)_2]$,[11] and a range of 1.830–2.101 Å in the heterometallic cluster $[\{(Bu^tOLi)_5(Bu^tORb)_4(Li_2O_2)(TMEDA)_2\}_\infty]$,[12] and agrees well with a recently reported series of lithium phenoxides.[13] The overall larger range observed in **1** reflects the various coordination modes adopted by the hmp ligands. The $Li–O_{THF}$ bond lengths span the range 1.933(16)–2.010(15) Å, which is in good agreement with previously reported values for neutral oxygen donor co-ordinated organolithium complexes.[14] The Li–N bond lengths span the range 1.996(15)–2.678(16) Å, reflecting the distorted nature of the cage and, discounting the longest Li(9)–N(4) contact of 2.678(16) Å, compare well with values previously reported for tertiary amine coordinated organolithium complexes.[15] The Li–C bond lengths are distinctly longer than the Li–O and Li–N average bond lengths in accord with periodic considerations, spanning the range 2.198(16)–2.300(20) Å; this is in good agreement with Li–C bond lengths reported previously.[3c,14] The bond angles around the benzylic carbons span the range 99.9(7)–108.3(8)°, indicating geometries more in keeping with sp^3 hybridised centres. This relatively wide range of bonding angles implies a complicated situation in terms of the electronic environment of the hmp dianion ligand, and is in keeping with the highly polar nature of bonding exhibited by Group I metals. This is also indicated by inspection of the $O–C_{ipso}$ bond lengths, which span the range 1.284(9)–1.343(9) Å; this range is in between values generally quoted for C–O (1.43 Å) and C=O (1.20 Å) bond lengths, and indicates a bond order greater than one.

Recorded in $[^2H]_8$THF solution at 298 K, the ^1H NMR (200 MHz) spectrum consists of multiplets at 1.40 and 3.61 ppm characteristic of THF, a broad multiplet at 2.35–2.85 ppm attributed to the methyl and benzylic protons, and three broad multiplets centred at 5.47, 6.43 and 7.46 ppm attributed to the three pyridyl protons. Integration indicated an average loss of approximately three THF. The broad appearance of these signals implies that a dynamic process is operating in solution. Dynamic exchange in solution is a process for which alkoxides are notorious, and alkali metal complexes are also well known for their partial to full deaggregation in solution. However, no coalescence was observed in a variable temperature study over the range 200–323 K, indicating that this dynamic process continues to operate over that temperature range. The ^7Li NMR (116.6 MHz) spectrum in $[^2H]_8$THF at 298 K exhibits six identifiable signals at 1.92, 1.67, 0.66, −0.04, −1.02 and −1.17 ppm. No further signals were apparent from a variable temperature study over the range 200–323 K.

In conclusion, we have demonstrated that 2-hydroxy-6-methylpyridine can be deprotonated not only at the hydroxy site, but also subsequently at the methyl site. This allows the possibility of preparing structurally diverse alkoxo clusters with varying degrees of alkyl character, and thus the possibility of tuning the properties such clusters may display. Further work will explore such avenues and will also investigate hetero-bimetallic complexes of hmp with higher alkali metals. These should prove to be interesting as it is likely that the lithiate centres will be the first to be substituted by higher alkali metals.

We thank EPSRC for equipment funding.

Notes and references

† *Crystal data* for **1**: $C_{80}H_{120}Li_{10}N_6O_{17}$, M = 1507.2, triclinic, space group *P*1, a = 12.1861(12), b = 13.4120(12), c = 14.5875(14) Å, α = 106.156(2), β = 99.760(2), γ = 104.451(2)°, U = 2143.1(4) Å^3, Z = 1, D_c = 1.168 g cm^{-3}, μ = 0.08 mm^{-1}, (Mo-Kα, λ = 0.71073 Å), T = 160 K, $R(F^2 > 2\sigma)$ = 0.093, $R_w(F^2$, all data) = 0.210, for all 12522 unique data (13722 measured, R_{int} = 0.028, $2\theta < 50°$, CCD diffractometer) and 932 refined parameters. Programs: standard Bruker AXS control and integration software and SHELXTL.[16] Structure solution was accomplished by SIR 97.[17] Uncoordinated THF solvent was too highly disordered for individual atoms to be resolved; this was treated by the SQUEEZE procedure of PLATON,[18] which indicated the correct total electron density and void volume for two molecules of THF per cluster molecule.

CCDC reference number 160559. See http://www.rsc.org/suppdata/cc/b1/b104680m/ for crystallographic data in CIF or other electronic format.

1 C. Eaborn, P. B. Hitchcock, J. D. Smith and A. C. Sullivan, *J. Chem. Soc., Chem. Commun.*, 1983, 827.

2 C. Eaborn, S. M. El-Hamruni, P. B. Hitchcock and J. D. Smith, *Chem. Commun.*, 1998, 1277; C. Eaborn, Z. R. Lu, P. B. Hitchcock and J. D. Smith, *Organometallics*, 1996, **15**, 1651; C. Eaborn, P. B. Hitchcock, K. Izod and J. D. Smith, *Angew. Chem., Int. Ed. Engl.*, 1995, **34**, 2679; A. Avent, C. Eaborn, P. B. Hitchcock, G. A. Lawless, P. D. Lickiss, M. Mallien, J. D. Smith, A. D. Webb and B. Wrackmeyer, *J. Chem. Soc., Dalton Trans.*, 1993, 3259; N. H. Buttrus, C. Eaborn, P. B. Hitchcock, J. D. Smith, J. G. Stamper and A. C. Sullivan, *J. Chem. Soc., Chem. Commun.*, 1986, 969; C. Eaborn, P. B. Hitchcock, J. D. Smith and A. C. Sullivan, *J. Organomet. Chem.*, 1984, **263**, C23.

3 (*a*) S. Harder and M. Prosenc, *Angew. Chem., Int. Ed. Engl.*, 1994, **33**, 1744; (*b*) U. Schümann and E. Weiss, *Angew. Chem., Int. Ed. Engl.*, 1988, **27**, 584; (*c*) U. J. Bildmann and G. Müller, *Organometallics*, 2001, **20**, 1689.

4 S. T. Liddle and W. Clegg, *J. Chem. Soc., Dalton Trans.*, 2001, 402; H. Gornitzka and D. Stalke, *Organometallics*, 1994, **13**, 4398; H. Gornitzka and D. Stalke, *Angew. Chem., Int. Ed. Engl.*, 1994, **33**, 693; F. Pauer, J. Rocha and D. Stalke, *J. Chem. Soc., Chem. Commun.*, 1991, 1477.

5 J. M. Rawson and R. E. P. Winpenny, *Coord. Chem. Rev.*, 1995, **139**, 313.

6 F. H. Allen and O. Kennard, *Chem. Des. Autom. News*, 1993, **8**, 31.

7 E. K. Brechin, L. M. Gilby, R. O. Gould, S. G. Harris, S. Parsons and R. E. P. Winpenny, *J. Chem. Soc., Dalton Trans.*, 1998, 2657; A. J. Blake, S. Parsons, J. M. Rawson and R. E. P. Winpenny, *Polyhedron*, 1995, **14**, 1895; S. McConnell, M. Motevalli and P. Thornton, *Polyhedron*, 1995, **14**, 459.

8 A. J. Blake, P. E. Y. Milne and R. E. P. Winpenny, *Acta Crystallogr., Sect. C*, 1991, **47**, 2461.

9 A. F. Mishnev, S. V. Belyakov, Y. Y. Bleidelis, S. K. Apinitis and E. Y. Gudrinietse, *Kristallografiya*, 1986, **31**, 297.

10 L. M. Jackmann, D. Cizmeciyan, P. G. Willard and M. A. J. Nichols, *J. Am. Chem. Soc.*, 1993, **115**, 6262.

11 F. M. MacKenzie, R. E. Mulvey, W. Clegg and L. Horsburgh, *Polyhedron*, 1998, **17**, 993.

12 W. Clegg, A. M. Drummond, R. E. Mulvey and S. T. Liddle, *Chem. Commun.*, 1998, 2391.

13 T. J. Boyle, D. M. Pedrotty, T. M. Alam, S. C. Vick and M. A. Rodriguez, *Inorg. Chem.*, 2000, **39**, 5133.

14 For examples, see: W. Setzer and P. von R. Schleyer, *Adv. Organomet. Chem.*, 1985, **24**, 353.

15 For examples, see: K. Gregory, P. von R. Schleyer and R. Snaith, *Adv. Inorg. Chem.*, 1991, **37**, 47.

16 SMART, SAINT and SHELXTL software, Bruker AXS Inc., Madison, WI, USA, 1997.

17 A. Altomare, M. C. Burla, M. Camalli, G. Cascarano, C. Giacovazzo, A. Guagliardi and G. Polidori, *J. Appl. Crystallogr.*, 1994, **27**, 435.

18 A. L. Spek, PLATON, University of Utrecht, The Netherlands, 2000.

CHEMCOMM Communication
www.rsc.org/chemcomm

Novel octahedral tungsten sulfidocyanide cluster anion $[W_6S_8(CN)_6]^{6-}$†

Song Jin and Francis J. DiSalvo*

Baker Laboratories, Department of Chemistry and Chemical Biology, Cornell University, Ithaca, NY 14853, USA. E-mail: fjd3@cornell.edu

Received (in Cambridge, UK) 10th May 2001, Accepted 13th July 2001
First published as an Advance Article on the web 6th August 2001

Novel tungsten octahedral sulfidocyanide cluster compounds $Na_6[W_6S_8(CN)_6]\cdot18DMSO$ 1 and $K_6[W_6S_8(CN)_6]$ 2 have been synthesized and characterized by X-ray crystallography and NMR spectroscopy.

Chevrel phases,[1] $M_xMo_6Q_8$, (M = metal, Q = chalcogen) are a class of cluster compounds extensively studied for their superconductivity,[2] fast ion conductivity[3] and catalytic activity.[4] The building block of the Chevrel phases is an octahedral molybdenum cluster face-capped by eight chalcogenide atoms (Q). Although no tungsten analogues of the Chevrel phases are known, the molecular tungsten clusters $W_6Q_8L_6$ (L = neutral Lewis base ligand) have been synthesized in solution,[5–10] as have the $Mo_6S_8L_6$ clusters.[11,12] Our investigation of $W_6S_8L_6$ clusters,[10,13–15] particularly the finding of strong bonding to the W_6S_8 cluster by isocyanide,[15] suggested cyanide might also be a good ligand. It would be interesting to explore such chemistry, given the diverse structural chemistry of cyanides,[16] in particular, $[Re_6Q_8(CN)_6]^{4-}$ clusters have been exploited to prepare a number of extended structure coordination compounds.[17,18] It was reported recently that molecular $[Mo_6Se_8(CN)_6]^{7-/6-}$ clusters could be synthesized through 'excision' of clusters from the Chevrel phase with molten KCN,[19] however, such synthesis could be achieved from simple non-cluster starting materials as well.[20] We report here the synthesis and characterization of the first W_6S_8 cluster compounds with anionic cyanide ligand: $Na_6[W_6S_8(CN)_6]\cdot18DMSO$ **1** and $K_6[W_6S_8(CN)_6]$ **2**. Our preliminary study indicates that $[W_6S_8(CN)_6]^{6-}$ have different redox behavior from $[Mo_6Se_8(CN)_6]^{6-}$.

Reaction of $W_6S_8(4\text{-Bu}^t\text{py})_6$[10] with NaCN (slightly more than 1:6 equiv.) in DMSO at 100 °C for 1 day resulted in a brown-red crystalline precipitate which was filtered off as product **1**‡ from a brown–red solution (yield of the product: 84%). Slow cooling of a hot DMSO solution of **1** yielded suitable single crystals for X-ray structural analysis.§ The identity of the cluster anion is apparent and shown in Fig. 1(a). The W_6S_8 cluster core is a quite regular octahedron with an average W–W distance of 2.685(3) Å, similar to that found in $W_6S_8(C{\equiv}NBu^t)_6$ [2.681(3) Å].[15] The N terminal of each CN^- ligand is coordinated to a Na^+ ion in a roughly collinear fashion and each Na^+ ion is also coordinated by 3 O atoms from DMSO solvent molecules [Fig. 1(b)]. The overall crystal structure can be described as approximately "ABC" close packing of the cluster complexes including Na^+ ions and DMSO [Fig. 1(c)]. Based on the stoichiometry, the charge of the cluster anion is −6 and the metal electron count (MEC) of the cluster is 20.

Reaction of $W_6S_8(4\text{-Bu}^t\text{py})_6$ with $K^{13}CN$ (slightly more than 1:6 equiv.) in DMSO at 100 °C for 1 day resulted in a lustrous crystalline precipitate which was filtered off as product **2**¶ from a nearly colorless solution (yield of the product: 91%). Insoluble in any organic solvents, **2** is apparently not isostructural to **1** as the PXRDs are different. Layering deoxygenated water solutions of **2** with methanol yielded dark red single crystals suitable for X-ray structural analysis.§ Shown in Fig. 2, the refined cubic structure of $K_6[W_6S_8(CN)_6]\cdot10H_2O$ (**2**·$10H_2O$) shows *fcc* packing of the $[W_6S_8(CN)_6]^{6-}$ cluster anion. The K^+ ions and solvent water molecules reside, often with partial occupancies, in octahedral, tetrahedral and other interstitial sites. The cluster has the ideal O_h symmetry with a slightly shorter W–W distance [2.6772(7) Å] than that of **1**.

These syntheses are facilitated by the sparing solubility of both $W_6S_8(4\text{-Bu}^t\text{py})_6$ and NaCN (or KCN) in DMSO and simplified by the insolubility of product **2** or the low solubility of **1** at RT. Cyanide can replace the more weakly bonded ligands (L) on $W_6S_8L_6$ clusters, such as *n*-butylamine,[13] more readily, but phosphine ligands on $W_6S_8(PEt_3)_6$[10] can not be completely replaced by cyanide even in considerable excess. Therefore, the binding free energy of CN^- is estimated to be, not surprisingly, close to that of *tert*-butyl isocyanide.[15]

The PXRD of the bulk sample of **1** is identical to the simulated pattern from the single crystal structure (both

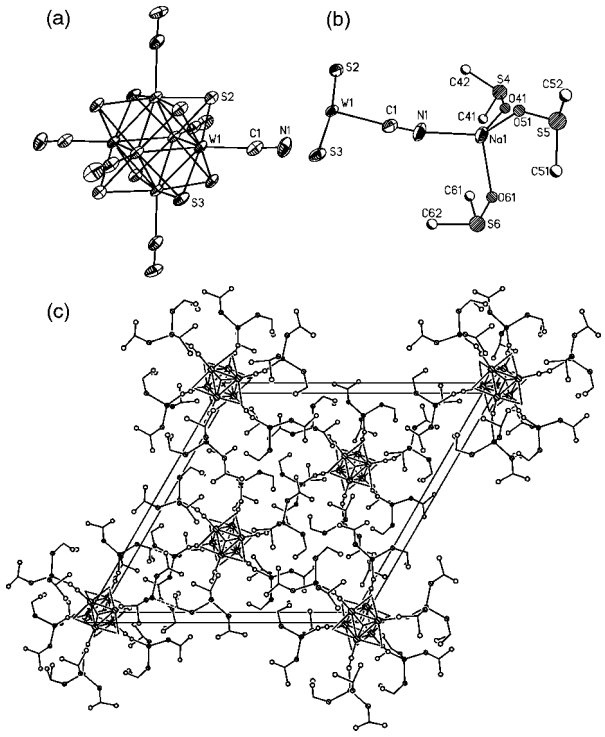

Fig 1 (a) ORTEP drawing of the $[W_6S_8(CN)_6]^{6-}$ cluster anion in **1** at 50% probability level; (b) asymmetric unit in **1** emphasizing the tetrahedral environment around the Na^+ cation (DMSO molecules are disordered, but not shown for clarity); (c) packing diagram of $Na_6[W_6S_8(CN)_6]\cdot18DMSO$ **1** along the *c* axis. Selected bond lengths (Å) and angles (°): W1–W1A 2.6875(4), W1–W1C 2.6818(4), W1–S2 2.4518(15), W1–S3 2.4571(12), W1–S3A 2.4587(11), W1–S3B 2.4667(11), W1–C1 2.196(5), C1–N1 1.158(6), N1–Na1 2.327(4), Na1–O range 2.118(13)–2.378(8); W1–C1–N1 176.6(4), C1–N1–Na1 164.2(4). Symmetry transformations used to generate equivalent atoms: A *y*, $-x+y$, $-z+2$; B $x-y$, *x*, $-z+2$; C $-y$, $x-y$, *z*.

† Electronic supplementary information (ESI) available: Fig. S1: observed and simulated XRPD patterns for **1**. Fig. S2: observed XRPD pattern for **2**. Fig. S3: TGA for **1**. See http://www.rsc.org/suppdata/cc/b1/b104161b/

 DOI: 10.1039/b104161b

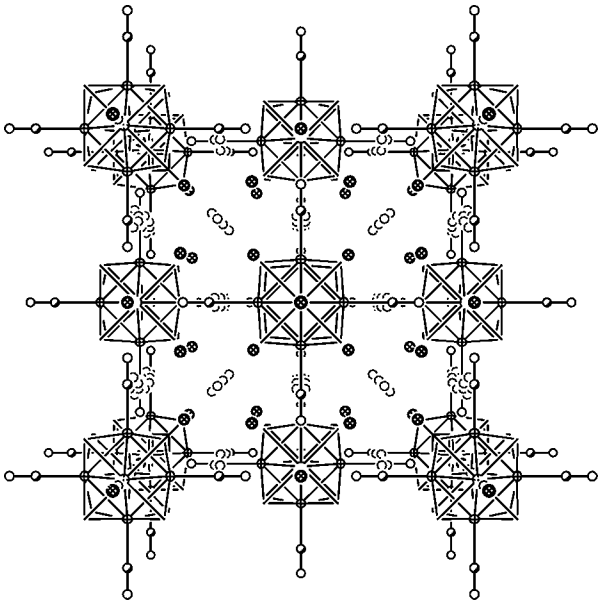

Fig 2 Unit cell (*fcc*) packing structure of $K_6[W_6S_8(CN)_6]\cdot 10H_2O$ (**2**·$10H_2O$). The circles of S atoms are omitted for clarity, K^+ ions are shown as cross-hatched circles, oxygen atoms of solvent water are shown as open circles with dotted boundaries. Selected bond lengths (Å): W–W 2.6772(7), W–S 2.452(2), W–C 2.152(16), C–N 1.162(19), N–K 2.447(13), 3.139(5).

available as ESI†). The stoichiometry was also confirmed by elemental analysis‡ and TGA analysis in which all of the DMSO solvent molecules (46 wt%) were lost upon heating. For **2**, the crystallographic refinements alone can not determine the stoichiometry or cluster oxidation state since K^+ and H_2O are disordered. Interestingly, the reported *blue* crystal of $K_7[Mo_6Se_8(CN)_6]\cdot 8H_2O$[19] is isotypic to this structure. However, elemental analysis¶ and ^{13}C NMR (*vide infra*) of the as prepared compound **2** establishes the 6− charge for the cluster anion.

It proved to be extremely difficult to observe the ^{13}C NMR signal from $[W_6S_8(CN)_6]^{6-}$ anions due to the low receptivity and tertiary nature of ^{13}C in CN^-.[21] Using ^{13}C labeled KCN enabled such observation and thus provides convenient means to monitor the chemistry in solution. A ^{13}C NMR spectrum of cluster **2** in D_2O is shown in Fig. 3. The chemical shift, δ 146.8, is different from that of free CN^- in water (δ 165) and falls into the general range for C-bonded cyanide ligands.[21] Satellite peaks with $J_{W\text{-}C}$ 107 Hz caused by coupling to ^{183}W isotope (14.3%)[21] confirms C terminal bonding to the W atom in the cyanide. The *sharp* NMR signal indicates a closed shell electron configuration. *If* the cluster was oxidized or reduced, the paramagnetic cluster would have severely broadened the NMR peak(s).[14]

In deoxygenated D_2O, the NMR spectrum of the clear brown–red solution of **2** does not change for at least a week. Upon exposure to air, the solution becomes darker and the ^{13}C NMR peak diminishes to half of the original intensity within 20 days accompanied by some new upfield peaks, suggesting that the cluster has been oxidized. This behavior is different from that of $[Mo_6Se_8(CN)_6]^{7-/6-}$ anions: the *reduced* cluster $[Mo_6Se_8(CN)_6]^{7-}$ (MEC = 21) was found to be the product of

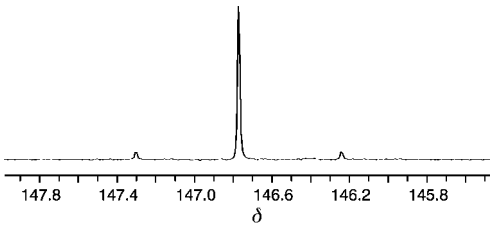

Fig 3 ^{31}C NMR spectrum of $K_6[W_6S_8(CN)_6]$ **2** in deoxygenated D_2O with dioxane as internal reference.

reactions with molten KCN (though the reducing agent has yet to be identified) and this cluster is oxidized in air to the *'normal'* closed shell cluster $[Mo_6Se_8(CN)_6]^{6-}$.[19,20] The stability of the $[W_6S_8(CN)_6]^{6-}$ cluster in deoxygenated water should allow the exploration of its aqueous solution chemistry.

When excess NaCN is present in the DMSO solutions, the $[W_6S_8(CN)_6]^{6-}$ cluster anion is stable at least up to 180 °C. This suggests that $[W_6S_8(CN)_6]^{6-}$ might be synthesized by direct reaction of NaCN, W and S.

We thank the Department of Energy (Grant No. DE-FG02-87ER45298) for support of this work. This study made use of the Polymer Characterization Facility of the Cornell Center for Materials Research supported through the NSF Material Research Science and Engineering Centers program (grant DMR-0079992).

Notes and references

‡ Elemental analysis for **1**: found (calc.): C 16.58 (16.49), H 3.37 (3.56), N 2.86 (2.91), W 35.84 (36.05), Na 4.37 (4.51)%. IR: ν(C≡N), 2083; DMSO, 2990, 1435, 1313, 1037, 954 cm^{-1}.

§ *Crystal data*: for **1**: $C_{42}H_{108}N_6Na_6O_{18}S_{26}W_6$, M = 3059.94, rhombohedral, space group $R\bar{3}$ (no. 148), a = 26.497(3), c = 12.1761(19) Å, U = 7403.3(15) Å^3, T = 165 K, Z = 3, D_c = 2.059 g cm^{-3}, μ(Mo-Kα) = 7.593 mm^{-1}, F(000) = 4416, 17304 reflections measured, 3370 unique (R_{int} = 0.0328) which were used in refinements, 166 parameters. The final refinements converge to R_1 = 0.0249, wR_2 = 0.0563 [for $I > 2\sigma(I)$] and R_1 = 0.0314, wR_2 = 0.0576 for all data.

For **2**·$10H_2O$: $C_6H_{20}K_6N_6O_{10}S_8W_6$, M = 1930.46, cubic, space group $Fm\bar{3}m$ (no. 225), a = 15.3084(15) Å, U = 3587.5(6) Å^3, T = 165 K, Z = 4, D_c = 3.574 g cm^{-3}, μ(Mo-Kα) = 20.369 mm^{-1}, F(000) = 3456, 2749 reflections measured, 327 unique (R_{int} = 0.0445) which were used in refinements, 27 parameters. The final refinements converge to R_1 = 0.0348, wR_2 = 0.0453 [for $I > 2\sigma(I)$] and R_1 = 0.0385, wR_2 = 0.0457 for all data.

CCDC reference numbers 163699 and 163700. See http://www.rsc.org/suppdata/cc/b1/b104161b/ for crystallographic data in CIF or other electronic format.

¶ Elemental analysis for **2**: found (calc.): C 4.48 (4.13), H 0.58 (0), N 4.77 (4.78), W 62.86 (62.81), K 13.28 (13.35)%. IR: ν(C≡N), 2038 cm^{-1}.

1 R. Chevrel, M. Sergent and J. Prigent, *J. Solid State Chem.*, 1971, **3**, 515.
2 R. Chevrel and M. Sergent, in *Topics in Current Physics*, ed. O. Fischer and M. B. Maple, Heidelberg, 1982.
3 P. J. Mulhern and R. R. Haering, *Can. J. Phys.*, 1984, **62**, 527.
4 S. J. Hilsenbeck, R. E. McCarley, R. K. Thompson, L. C. Flanagan and G. L. Schrader, *J. Mol. Catal. A: Chem.*, 1997, **122**, 13 and references therein.
5 T. Saito, A. Yoshikawa and T. Yamagata, *Inorg. Chem.*, 1989, **28**, 3588.
6 X. Zhang and R. E. McCarley, *Inorg. Chem.*, 1995, **34**, 2678.
7 X. B. Xie and R. E. McCarley, *Inorg. Chem.*, 1995, **34**, 6124.
8 X. B. Xie and R. E. McCarley, *Inorg. Chem.*, 1997, **36**, 4665.
9 G. M. Ehrlich, C. J. Warren, D. A. Vennos, D. M. Ho, R. C. Haushalter and F. J. DiSalvo, *Inorg. Chem.*, 1995, **34**, 4454.
10 D. Venkataraman, L. L. Rayburn, L. I. Hill, S. Jin, A.-S. Malik, K. J. Turneau and F. J. DiSalvo, *Inorg. Chem.*, 1999, **38**, 828.
11 T. Saito, N. Yamamoto, T. Yamagata and H. Imoto, *J. Am. Chem. Soc.*, 1988, **110**, 1646.
12 S. J. Hilsenbeck, V. G. Young, Jr. and R. E. McCarley, *Inorg. Chem.*, 1994, **33**, 1822.
13 S. Jin, D. Venkataraman and F. J. DiSalvo, *Inorg. Chem.*, 2000, **39**, 2747.
14 L. I. Hill, S. Jin, R. Zhou, D. Venkataraman and F. J. DiSalvo, *Inorg. Chem.*, 2001, **40**, 2660.
15 S. Jin, R. Zhou, E. M. Scheuer, J. Adamchuk, L. L. Rayburn and F. J. DiSalvo, *Inorg. Chem.*, 2001, **40**, 2666.
16 K. R. Dunbar and R. A. Heintz, *Prog. Inorg. Chem.*, 1997, **45**, 283.
17 L. G. Beauvais, M. P. Shores and J. R. Long, *J. Am. Chem. Soc.*, 2000, **122**, 2763 and references therein.
18 N. G. Naumov, S. B. Artemkina, V. E. Fedorov, D. V. Soldatov and J. A. Ripmeester, *Chem. Commun.*, 2001, 571 and references therein.
19 Y. V. Mironov, A. V. Virovets, N. G. Naumov, V. N. Ikorskii and V. E. Fedorov, *Chem.–Eur. J.*, 2000, **6**, 1361.
20 C. Magliocchi, X. Xie and T. Hughbanks, *Inorg. Chem.*, 2000, **39**, 5000.
21 J. Mason, *Multinuclear NMR*, Plenum Press, New York, 1987.

CHEMCOMM
Communication
www.rsc.org/chemcomm

Photoreactivity of ETS-10

Russell F. Howe* and Yuni K. Krisnandi

Chemistry Department, University of Aberdeen, Aberdeen, Scotland, UK AB24 3UE.
E-mail: r.howe@abdn.ac.uk

Received (in Cambridge, UK) 4th June 2001, Accepted 9th July 2001
First published as an Advance Article on the web 6th August 2001

Irradiation of H-ETS-10 in the presence of adsorbed methanol or ethene causes photoreduction of Ti(IV) to Ti(III); photoreduction does not occur for Na, K-ETS-10, but a photoinduced polymerization of ethene is observed.

ETS-10 is a titanosilicate zeolite with a novel structure comprising one-dimensional chains of corner-linked TiO_6 octahedra surrounded by tetrahedral silicate units, generating a three-dimensional 12-ring pore system.[1] There is particular interest in the O–Ti–O–Ti–O chains, which have been described as semiconductor nanowires within an insulating sheath.[2] Titanium in ETS-10 can be chemically reduced by adsorbing sodium vapour into ETS-10,[3] suggesting that electronic communication can occur between the semiconductor chains and species in the pores. There is also an early report of photocatalytic activity of ETS-10 in the oxidation of organic alcohols,[4] which likewise implies that electron transfer can occur through the silicate 'insulation'. The photoreactivity of conventional anatase photocatalysts has been extensively studied; band gap irradiation of anatase in the presence of adsorbed organic compounds causes photoreduction of Ti(IV) to Ti(III), due to trapping of holes by the adsorbed organic and consequent trapping of electrons at Ti(IV) sites.[5] We have begun a study comparing the photoreactivity of anatase with that of ETS-10, and report here that the photoreduction of ETS-10 depends on the presence of defects in the structure.

Two ETS-10 samples were studied: a hydrogen exchanged material provided by Engelhard,[6] and a sample synthesized in-house following established procedures[7] which contains sodium and potassium as the charge balancing cations. Both samples gave X-ray powder diffraction patterns characteristic of ETS-10;[1] the higher angle peaks of the H-ETS-10 sample were however substantially broadened relative to Na,K-ETS-10, indicating a higher degree of disorder in the proton exchanged sample (chemical analysis of this sample showed the extent of proton exchange to be H/(H + Na + K) = 0.78). SEM showed average crystallite sizes to be around 2 μm for Na,K-ETS-10, but 0.3 μm for H-ETS-10. Indications of greater disorder in the O–Ti–O–Ti–O chains in the proton exchanged material came from the absence of the intense Raman band at 732 cm^{-1} attributed to Ti–O stretching vibrations in the chains[8] which is present in the Na,K-ETS-10, and substantially increased Debye–Waller factors in the Ti K-edge EXAFS of H-ETS-10 compared with Na,K-ETS-10.[9] ^{29}Si NMR spectra of the H-ETS-10 were similar to those previously reported,[6] showing retention of Si–O–Ti bonds. A commercial (Degussa P25) anatase sample was used for comparison with ETS-10.

Photoreduction experiments were performed in a vacuum EPR cell; samples were outgassed *in vacuo* at 573 K, then exposed to either methanol or ethene vapour and irradiated at room temperature with a 125 W mercury arc lamp. Irradiation of anatase in the presence of methanol or ethene produces a dark blue colour and an intense broad EPR signal of Ti(III), with parameters $g_\perp$ = 1.973, $g_\parallel$ = 1.949 (measured at 77 K). This signal could not be detected at room temperature. Similar signals have been previously attributed to Ti(III) cations on lattice sites distributed through the bulk of anatase, or to surface Ti(III) cations, in both cases with distorted octahedral coordination.[10] The Ti(III) signal was removed when the sample was evacuated then exposed to oxygen, but no new signals were formed.

Fig. 1 shows EPR signals recorded at room temperature following irradiation of H-ETS-10 in the presence of ethene. The sample turns grey and the new signal which appears is shifted significantly to higher field relative to that obtained with anatase ($g_{av} \approx 1.95$). The other important difference from anatase is that this signal could be observed at room temperature. Subsequent exposure to oxygen (5 Torr) gave weak new signals in the vicinity of g = 2.010, but evacuation followed by exposure to 5 Torr of oxygen totally removed the Ti(III) signal (and the grey colour) and enhanced the new signals [Fig. 1(c)]. Closer examination of the new signals reveals that one component is the superoxide ion O_2^- adsorbed on Ti(IV) sites (g_{zz} = 2.022, g_{yy} = 2.011, g_{xx} = 2.004).[11] Identification of the other species is less certain, but the lower field shoulders may be the g_{zz} components of superoxide species adsorbed on sites of lower formal charge.[12] Similar spectra were obtained when H-ETS-10 was irradiated in the presence of adsorbed methanol and subsequently exposed to oxygen.

The Ti(III) signal formed on irradiation of H-ETS-10 in the presence of the adsorbed ethene or methanol differs from that formed in anatase under the same conditions. This is not unexpected if the Ti(III) is in a one-dimensional O–Ti–O–Ti–O chain rather than the three-dimensional anatase lattice. However it is clear from the reactivity of this species towards oxygen, and in particular from the observation of O_2^- adsorbed on Ti(IV)

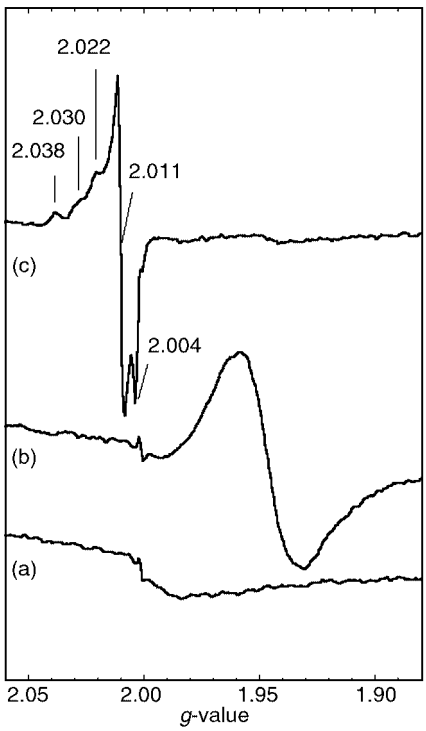

Fig. 1 EPR signals from H-ETS-10: (a), exposed to ethene prior to irradiation; (b), irradiated for 2 h; (c), evacuated at room temperature then exposed to 5 Torr of oxygen.

 DOI: 10.1039/b104870h

sites, that H-ETS-10 contains exposed titanium sites which should not be present in a defect free ETS-10 structure.

This conclusion is supported by the observation that when the same experiments were conducted with Na,K-ETS-10 in which the spectroscopic evidence indicates that the O–Ti–O–Ti–O chains are relatively defect free, no photoreduction was observed; *i.e.* no colour changes occurred on irradiation in the presence of methanol or ethene, and no Ti(III) signals were detected by EPR.

Nevertheless, *in situ* FTIR studies of Na,K-ETS-10 in the presence of adsorbed ethene show that a photoinduced reaction of ethene with the ETS-10 does occur. Fig. 2 shows IR spectra recorded in an *in situ* cell of Na,K-ETS-10 following adsorption of ethene and subsequent irradiation (these are difference spectra from which the spectrum of the dehydrated ETS-10 prior to admission of ethene has been subtracted, and ratioed against a background containing the gas phase ethene to remove gas phase contributions to the spectra).

On irradiation bands due to adsorbed ethene (*e.g.* 3083, 1613, 1445 and 1338 cm^{-1}) are reduced in intensity, and new bands appear and grow in the ν(OH) region (3660, 3580 cm^{-1}), in the ν(CH) region (2926 and 2856 cm^{-1}), at 1632 cm^{-1} and at 1468 cm^{-1}. Evacuation at room temperature removes the adsorbed ethene bands but leaves the new bands unchanged.

The bands appearing at 2926, 2856 and 1468 cm^{-1} are characteristic of saturated CH_2 groups,[13] suggesting that polymerization of ethene has occurred to form $(CH_2)_n$ chains. On the other hand, the bands at 3660, 3580 and 1632 cm^{-1} are close to those expected for isolated (non-hydrogen bonded) water molecules.[14] This experiment thus suggests that in Na,K-ETS-10 holes and electrons formed on irradiation both react with adsorbed ethene. A free radical polymerization of ethene may be initiated by electrons generated in the O–Ti–O–Ti–O chains, while the formation of adsorbed water may occur as a result of oxidation of adsorbed ethene by positive holes (involving reaction of lattice oxide ions). The sharpness of the bands due to adsorbed water indicates that these are isolated water molecules. It is important to note also that no reaction occurred in the absence of irradiation.

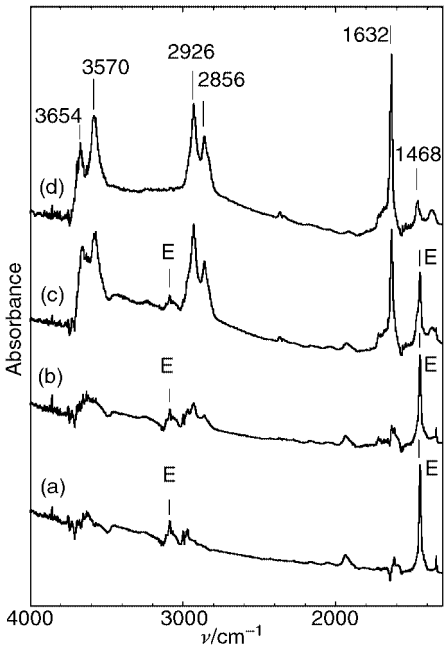

Fig. 2 *In situ* FTIR spectra of ethene in Na,K-ETS-10 (gas phase and background spectrum of ETS-10 subtracted): (a) exposed to ethene (70 Torr) at room temperature; (b), irradiated 90 min; (c), irradiated 300 min; (d), evacuated at room temperature. (E denotes bands due to physisorbed ethene).

This chemistry is different from that occurring in H-ETS-10, where electron trapping occurs preferentially at Ti(IV) sites associated with defects. An IR experiment similar to that described above was performed on ethene adsorbed in H-ETS-10. In this case irradiation caused a similar reduction in intensity of the bands due to physisorbed ethene, but the only new bands appearing were broad bands due to hydrogen bonded adsorbed water, at *ca.* 3300 and 1630 cm^{-1}. In particular, no new bands due to polyethene were detected in H-ETS-10.

Further work is needed to establish details of the photoreduction and photoinduced polymerization mechanisms. Further characterization of the defect sites in H-ETS-10 is also in progress. It is clear however that the defect sites are important in the photoreactivity of these novel materials. Our observation of photoinduced ethene polymerization in Na,K-ETS-10 also confirms that electron transfer can occur between the semiconductor chains and molecules adsorbed in the ETS-10 pores. This has important consequences for the potential use of ETS-10 as a photocatalyst.

This work was carried out in the School of Chemistry, University of New South Wales, and supported by a grant from the Australian Research Council. Y. K. acknowledges an AUSAID postgraduate scholarship.

Notes and references

1 M. W. Anderson, O. Terasaki, T. Ohsuna, P. J. O'Malley, A. Philippou, S. P. Mackay, A. Ferreira, J. Rocha and S. Lidin, *Philos. Mag.*, 1995, **71**, 813; X. Q. Wang and A. J. Jacobson, *Chem. Commun.*, 1999, 973.
2 C. Lamberti, *Microporous Mesoporous Mater.*, 1999, **30**, 155.
3 S. Bordiga, G. T. Palomino, A. Zecchina, G. Ranghini, E. Giamello and C. Lamberti, *J. Chem. Phys.*, 2000, **112**, 3589.
4 M. A. Fox, K. E. Doan and M. T. Dulay, *Res. Chem. Intermed.*, 1994, **20**, 711.
5 R. F. Howe and M. Grätzel, *J. Phys. Chem.*, 1985, **89**, 4495.
6 X. Yang and P. W. Blosser, *Zeolites*, 1996, **17**, 237.
7 S. M. Kuznicki, *US. Pat.*, 1990, 4 938 989.
8 Y. Su, M. L. Balmer and B. C. Bunker, *J. Phys. Chem. B*, 2000, **104**, 8160.
9 Y. Krisnandi, MSc Thesis, University of New South Wales, Sydney, Australia, 2001.
10 R. D. Iyengar and M. Codell, *Adv. Colloid Interface Sci.*, 1972, **3**, 365.
11 P. Meriadeau and J. C. Vedrine, *J. Chem. Soc., Faraday Trans. 2*, 1976, **72**, 472.
12 J. H. Lunsford, *Catal. Rev.*, 1973, **8**, 135.
13 L. J. Bellamy, *The Infrared Spectra of Complex Molecules*, Chapman and Hall, London, 3rd edn., 1975.
14 G. Herzberg, *Molecular Spectra and Molecular Structure, II Infrared and Raman Spectra of Polyatomic Molecules*, Van Nostrand, Princeton, NJ, 1959.

CHEMCOMM
Communication
www.rsc.org/chemcomm

Design and synthesis of a new bicyclic dipeptide isostere

Franca M. Cordero,* Silvia Valenza, Fabrizio Machetti and Alberto Brandi*

Dipartimento di Chimica Organica 'Ugo Schiff', Centro di Studio C.N.R. sulla Chimica e la Struttura dei Composti Eterociclici e loro Applicazioni (CSCEA), Università di Firenze, via G. Capponi 9, I-50121 Firenze, Italy. E-mail: cordero@chimorg.unifi.it; Fax: +39-055-2476964

Received (in Cambridge, UK) 21st February 2001, Accepted 27th June 2001
First published as an Advance Article on the web 6th August 2001

The synthesis of a new Gly-Pro turn mimetic and the computational study of its ability to induce β-turn is reported.

In recent years several strategies have been adopted to limit the conformational space of peptide chains[1] and many efforts have been made to develop β-turn mimetics.[2]

It is known that a *cis* peptide moiety is geometrically suited for inducing the peptide chain to bend and that β-turns of type VI are characterized by a *cis*-Pro in the *i* + 2 position.[3] The control of the *cis*-prolyl amide geometry has been effectively achieved by tethering the α-carbon of the *N*-terminal amino acid residue to the proline 2-position.[4] Particularly, the bicyclic dipeptide analogues **1**, in which the α positions are joined by a two (X = $–CH_2CH_2–$) or three (X = $–CH_2NHCO–$) atom bridge, have been synthesized[4] to serve as mimetics of dipeptide *cis*-Xxx-Pro (Fig. 1). To reduce the conformational freedom of dipeptide mimetics like **1**, a shorter link could be introduced. In this way the pyrrolizidine amino acids **1** (X = $–CH_2–$), containing the *cis*-Xxx-Pro residue, would result (Fig. 1).

In this communication we report the synthesis of the GPTM (Gly-Pro Turn Mimetic) **2** (Fig. 1) either in racemic or enantiomerically pure form and its successful coupling with L-Boc-Phe-OH.

The 1,3-dipolar cycloaddition (1,3-DC) of nitrone **3**[5] and an acrylic acid derivative, followed by reductive opening of the isoxazolidine ring and intramolecular cyclization was envisaged as a rapid route to afford the bicyclic lactam **9**.

The 1,3-DC reaction was performed under different conditions and the best results were obtained from **3** and acrylamide (**4**) in water at 60 °C (Scheme 1) which afforded the 2-aminocarbonylhexahydropyrrolo[1,2-*b*]isoxazoles **5** and **6** and their 3-aminocarbonyl isomers **7** in 4 : 1 ratio and excellent yield (98%). Although the *endo–exo* selectivity of the cycloaddition was very low (6% de) this approach was synthetically convenient because both the diastereomeric adducts **5** and **6** could be transformed into **9**.

The pyrrolizidine **9** was obtained from **6** through the domino process N–O bond hydrogenolysis/intramolecular trans-amidation. Moreover, the *cis* substituted pyrrolizidine **8**, analogously derived from **5**, could be quantitatively isomerized to the corresponding *trans* hydroxy ester **9** by treatment with NaOH–MeOH at 70 °C followed by methylation with CH_2N_2. Therefore, the intermediate **9**, possessing the bicyclic skeleton of the GPTM **2**, was achieved in 55% overall yield starting from **3** and **4** (Scheme 1).

The *trans* alcohol **9** was easily transformed into the corresponding *cis* amine **2** by mesylation followed by a nucleophilic displacement with NaN_3 and reduction of the azido group with Ni-Raney (Scheme 1). The lactam **2**, was immediately coupled with an amino acid such as Boc-L-Phe, to test the reactivity of the amino group towards the peptide synthesis and to avoid the possible epimerization to the thermodynamically more stable *trans* isomer. The two diastereomeric tripeptides **10a** and **10b** were separated by chromatography on silica gel and fully characterized.

To assign the absolute configuration of **10a** and **10b**, a sample of the racemic *cis* alcohol **8** was resolved through the formation of the corresponding diastereomeric esters of *R*-Mosher acid, and one of the separated esters was analyzed by single crystal X-ray crystallography.† Consequently, both the diastereomeric esters were assigned their absolute configuration. After hydrolysis and treatment with CH_2N_2 the enantiomerically pure alcohols (2*R*,7a*R*)-**8** and (2*S*,7a*S*)-**8** were obtained, and transformed into **10a** and **10b**, respectively, through the previously described procedure.

The investigation of the turn-inducing potential of both the enantiomers (2*R*,7a*R*)-**2** and (2*S*,7a*S*)-**2** has been carried out through a simulation procedure run on model hexapeptides according to the criteria recently proposed by Müller *et al.*[6]

The model hexapeptides Ac-Ala-Ala-GPTM-Ala-Ala-NHMe **11** and **12** (Fig. 2), containing in the central position *RR*-GPTM and *SS*-GPTM respectively, were examined for their conformational freedom by Monte Carlo (global search

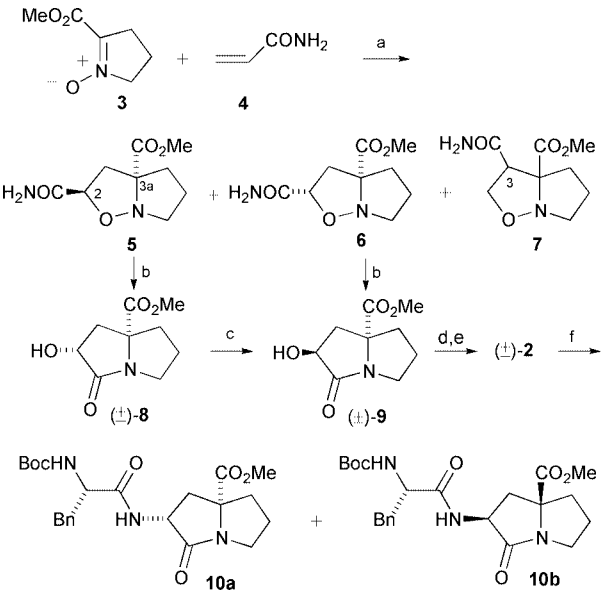

Scheme 1 a: H_2O, 60 °C, 14 h (**5**: 37%, **6:** 42%, **7**: 19%). b: $Pd(OH)_2$ (cat), MeOH, AcOH, H_2, 12 h (98%). c: (i) NaOH, MeOH, 70 °C, 2 h; (ii) Dowex 50; (iii) CH_2N_2; (60%). d: (i) MsCl, py; (ii) NaN_3, DMF; (87%). e: Ni-Raney (80%). f: L-Boc-Phe-OH, PyBroP, DiPEA, CH_2Cl_2 (55%).

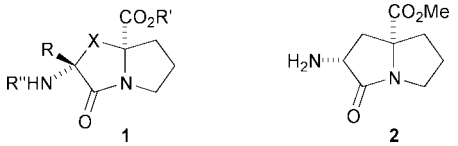

Fig. 1 Mimetics of *cis*-Xxx-Pro dipeptide and Gly-Pro turn mimetic.

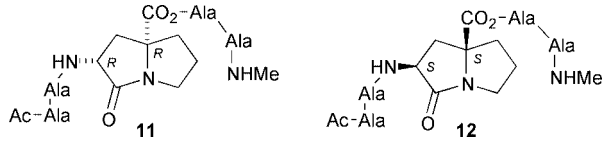

Fig. 2 Model hexapeptides.

 DOI: 10.1039/b101692j

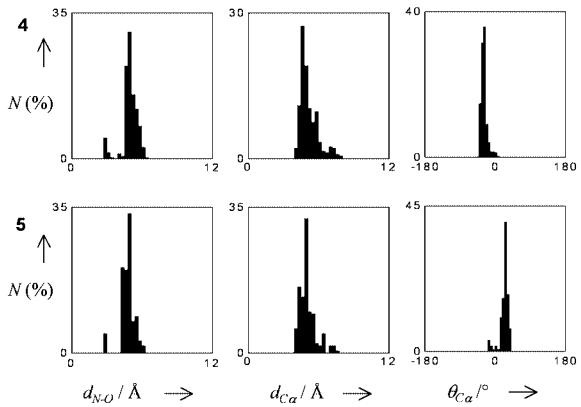

Fig. 3 Percentage distribution N of $d_{N\text{-}O}$, $d_{C\alpha}$ and $\theta_{C\alpha}$ values in the conformers of **4** and **5** within 6 kcal mol^{-1} of the global minimum. (Each column spans 0.3 Å or 6°.)

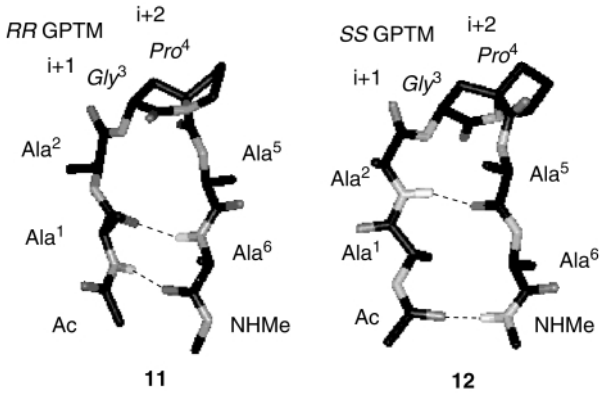

Fig. 4 Structures of two low energy conformers of **11** and **12**. Legend: C: black, N: pale grey, O: grey, H: white. For reasons of clarity only the H atoms involved in hydrogen bondings (--) were depicted.

MCMM) procedure.[7] The following parameters were used to establish the presence of a reverse turn: the donor–acceptor NH_{Ala5}–CO_{Ala2} distance $d_{N\text{-}O}$, the $C\alpha_{Ala2}$–$C\alpha_{Ala5}$ distance $d_{C\alpha}$ and the virtual torsion angle $\theta_{C\alpha}$ (defined by $C\alpha_{Ala2}$–$C\alpha_{Gly3}$–$C\alpha_{Pro4}$–$C\alpha_{Ala5}$).[3,6] The percentage distribution of $d_{N\text{-}O}$, $d_{C\alpha}$ and $\theta_{C\alpha}$ values in the calculated conformations within 6 kcal mol^{-1} of the global minimum of **11** and **12** (318 and 170 conformers respectively) were reported in Fig. 3. The histograms showed a substantial restriction of the occupied conformational space of hexapeptides incorporating GPTMs **2**. Moreover, a very good portion of conformers possessed the $d_{C\alpha}$ and $\theta_{C\alpha}$ values characteristic of β-turn. In particular the percentages of conformers of **11** and **12** with $d_{C\alpha}$ less than 5 Å (one definition of a tight β-turn) were 55 and 58%, respectively, while almost all structures showed $d_{C\alpha}$ less than 7 Å (**11**: 94%, **12**: 96%).[3] All conformers had $|\theta_{C\alpha}|$ under 50°, and $|\theta_{C\alpha}|$ under 30° present in 54 and 75% conformers of **11** and **12**, respectively.

On the contrary, the presence of the hydrogen bonding characteristic of classical β-turn ($d_{N\text{-}O}$ < 3.5 Å) was found in a small fraction of conformers (**11**: 7%; **12**: 5%). However, the intramolecular hydrogen bond was not found critical for the stability of a β-turn,[3] and seems not to be necessary in peptides incorporating mimics **2**, because the three torsion angles (ψ_{Gly3}, ω_{Pro4} and φ_{Pro4}) embedded in the 5,5-bicyclic structure and the spatial orientation of the terminal amino and carboxylic groups (on the same face of the bicyclic ring system) force the peptide chain to fold back upon itself.

The whole set of computational data clearly showed that bicyclic lactams like (2*R*,7a*R*)-**2** and (2*S*,7a*S*)-**2** were effective turn restraints when incorporated in the hexapeptides **11** and **12**.

The spatial arrangement of side chains is generally critical to recognition and bioactivity of peptides and its control is one of the goals of peptidomimetics. GPTMs (2*R*,7a*R*)-**2** and (2*S*,7a*S*)-**2** were shown to promote complementary relative orientation of the side chains of the residues near the reverse-turn.

As shown in Fig. 3, the $\theta_{C\alpha}$ values were prevalently negative in the conformers of **11**, but positive in those of **12** because of the enantiomeric relationship between the incorporated GPTMs. The presence of opposite reverse turns resulted also in an opposite orientation of the amino acid side chains as illustrated by a structural comparison of two representative low energy conformers of **11** and **12** (Fig. 4).

Both the selected structures were characterized by the presence of two intramolecular hydrogen bonds which indicated the initiation of an antiparallel β-sheet interaction between the two half-strands. In **11** the β-sheet hydrogen bonds were contiguous (between NH_{Ala6}–CO_{Ala1} and NH_{Ala1}–CO_{Ala6}) while in **12** were more distant (between NH_{Ala2}–CO_{Ala5} and NH_{NHMe}–CO_{Ac}). In **11** the methyl groups of Ala^2 and Ala^5 were situated under the back-bone plane (when the peptide chain was oriented as shown in Fig. 4) and those of Ala^1 and Ala^6 over the plane, while in **12** the opposite orientations occurred.

In conclusion both the enantiomers of GPTMs **2** were shown to be potentially useful reverse turn mimics. Attractive features of these new dipeptide surrogates were the reduced flexibility compared to analogous bicyclic systems, the complementary behavior of the two enantiomers in controlling the side-chain orientation, the rapid access to these systems starting from easily available compounds, the possibility of extending the process to the synthesis of other Xxx-Pro analogues (XPTMs) through the cycloaddition of nitrone **3** to 2-substituted acrylic acid derivatives.

Some structural modifications of GPTMs **2** for their use in solid phase syntheses and their incorporation into selected bioactive peptides for structure–activity relationship studies are currently under investigation in our laboratories.

This work was supported by the Ministry of University and Scientific and Technological Research, Italy (Cofin 2000 Project *Synthesis of Mimics and Analogs of Bioactive Natural Compounds*). S. V. acknowledges the receipt of a PhD stipend from Menarini Ricerche S.p.A.

Notes and references

† *Crystallographic data* for (2*S*,7a*S*)-3-oxo-2-[(2*R*)-3,3,3-trifluoro-2-methoxy-2-phenylpropionyloxy]tetrahydro-1*H*-pyrrolizine-7a(5*H*)-carboxylic acid methyl ester: $C_{19}H_{20}F_3NO_6$, M = 415.36, orthorhombic, a = 8.2726(3), b = 11.9643(6), c = 19.746(2) Å, U = 1954.7(2) Å^3, T = 293 K, space group $P2_12_12_1$, Z = 4, μ(Cu-K$_\alpha$) = 1.067 mm^{-1}, 2168 reflections collected, 1992 independent (R_{int} = 0.0318) which were used in all calculations. The final $R1$ was 0.0399 and $wR2$ 0.1177 (all data).

CCDC 166488. See http://www.rsc.org/suppdata/cc/b1/b101692j/ for crystallographic data in .cif or other electronic format.

1 J. Gante, *Angew. Chem., Int. Ed. Engl.*, 1994, **33**, 1699; A. Giannis and T. Kolter, *Angew. Chem., Int. Ed. Engl.*, 1993, **32**, 1244.
2 For a recent review see S. Hanessian, G. McNaughton-Smith, H.-G. Lombard and W. D. Lubell, *Tetrahedron*, 1997, **53**, 12 789.
3 G. D. Rose, L. M. Gierasch and J. A. Smith, *Adv. Protein Chem.*, 1985, **37**, 1; J. S. Richardson, *Adv. Protein Chem.*, 1981, **34**, 167; P. N. Lewis, F. A. Momany and H. A. Scheraga, *Biochim. Biophys. Acta*, 1973, **303**, 211; J. B. Ball, R. A. Hughes, P. F. Alewood and P. R. Andrews, *Tetrahedron*, 1993, **49**, 3467.
4 D. Gramberg, C. Weber, R. Beeli, J. Inglis, C. Bruns and J. A. Robinson, *Helv. Chim. Acta*, 1995, **78**, 1588; K. Kim, J.-P. Dumas and J. P. Germanas, *J. Org. Chem.*, 1996, **61**, 3138; K. Kim and J. P. Germanas, *J. Org. Chem.*, 1997, **62**, 2847; T. P. Curran and P. M. McEnaney, *Tetrahedron Lett.*, 1995, **36**, 191.
5 S.-I. Murahashi and T. Shiota, *Tetrahedron Lett.*, 1987, **28**, 2383.
6 G. Müller, G. Hessler and H. Y. Decornez, *Angew. Chem., Int. Ed.*, 2000, **39**, 894.
7 The conformational search (61000 steps for each structure) was performed with MacroModel v. 6.5 on Silicon Graphics O2 R10000 workstation using the AMBER* force field for energy minimization, the GB/SA continuum model for water and the Polak-Ribiere conjugate gradient (PRCG) minimization mode with the derivative convergence criteria of 0.05 kJ Å^{-1} mol^{-1}. F. Mohamadi, N. G. J. Richards, W. C. Guida, R. Liskamp, M. Lipton, C. Caufield, G. Chang, T. Hendrickson and W. C. Still, *J. Comput. Chem.*, 1990, **11**, 440.

CHEMCOMM
Communication
www.rsc.org/chemcomm

Self-assembly of a bis-urea macrocycle into a columnar nanotube

Linda S. Shimizu,* Mark D. Smith, Andrew D. Hughes and Ken D. Shimizu

University of South Carolina, Department of Chemistry and Biochemistry, Columbia, SC 29208, USA. E-mail: shimizul@mail.chem.sc.edu

Received (in Columbia, MO, USA) 20th December 2000, Accepted 30th April 2001
First published as an Advance Article on the web 7th August 2001

A bis-urea macrocycle 1 was synthesized and shown to form extended nanotubular columns by X-ray crystallography.

There has been great interest in the development of new molecular building blocks that predictably self-assemble into three-dimensional nanoscale structures.[1] In particular, columnar or tube shaped structures have been sought for applications as sensors, templates for directed reactions, and in ion and small molecule transport systems.[2] A common design motif has been to identify macrocyclic building blocks that stack to form cylindrical assemblies (Fig. 1). The interior cavity size and integrity of the columns are ensured by the rigidity of the macrocyclic building blocks. Excellent examples in this regard are Ghadiri's cyclic peptides, Stang's molecular squares, and Moore's macrocyclic polyphenylenethynylenes.[3] We have designed a series of bis-urea macrocycles that are readily synthetically accessible and similarly self-assemble into columnar nanotubes. We report, herein, the synthesis and assembly of the first and smallest member of this family.

The guiding interaction in macrocycle **1** is the urea self-association. The topology of urea assembly is well understood. The ureas commonly form head-to-tail arrays based on 3-center hydrogen bonds from the NH's of the urea in one molecule to the carbonyl of the urea in the adjacent molecule which position the ureas 4.6 Å apart.[4] This strong hydrogen-bonding interaction has been used in self-assembled materials,[5] supramolecular assemblies,[6] and organic gelators.[7] Most of these have been acyclic systems and only a single demonstration of a macrocyclic assembly has been reported in which the ureas are part of the cyclic framework.[8]

In macrocycle **1**,† two *meta*-xylenes serve as rigid spacers. The macrocycle **1** was readily synthesized (Scheme 1). First the urea functionality was protected as a triazinanone **2**, inhibiting over-alkylation and premature self-assembly. Reaction of 5-*tert*-butyl-1,3,5-triazinan-2-one **2** with *meta*-dibromoxylene yielded the protected bis-urea **3**.[9] The enhanced solubility of the protected bis-urea **3** enabled facile isolation and purification. Deprotection with diethanolamine in methanol yielded bis-urea macrocycle **1**. Proton NMR analysis in DMSO of the deprotected **1** showed two broad peaks for the benzyl CH_2 groups centered at 4.6 and 3.8 ppm, consistent with slow flipping of the 16-membered ring. This dynamic conformational behavior is consistent with studies of the protected macrocyclic precursor **3** by Dave *et al.*[10]

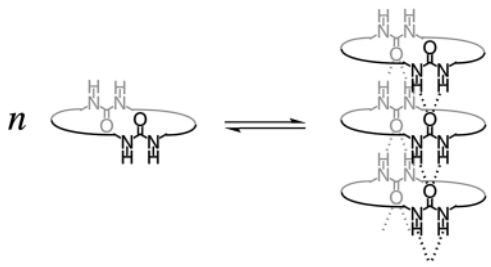

Fig. 1 Schematic representation of the self-assembly of rigid macrocyclic bis-ureas.

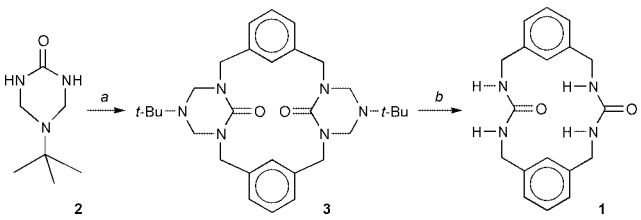

Scheme 1 Synthesis of bis-urea macrocycle **1**. *Reagents and conditions*: (a) *meta*-dibromoxylene, NaH, THF, 20%, (b) 20% diethanolamine, MeOH, reflux, 66%.

The solid-state molecular and assembled structures of bis-urea **1**‡ were examined by X-ray crystallographic analysis. The self-association of **1** was immediately apparent by its poor solubility characteristics. Single crystals suitable for X-ray diffraction were ultimately obtained upon slow cooling of **1** (135 °C to 25 °C) in a sealed tube of glacial acetic acid (100 mg/15 mL). The crystal structure of **1** reveals the expected bis-urea macrocycle (Fig. 2). The opposing urea functionalities are parallel but oriented oppositely, presumably to minimize the dipole moment. Most importantly, the ureas are not intramolecularly hydrogen-bonded and thus are free to form the designed macrocyclic stacks. The phenyl rings are tilted slightly out of the plane of the macrocycle, one pointing above and the other pointing below the plane of the macrocycle. The protons on C4 point inward, with an intramolecular H···H distance of 3.5 Å, filling most of the interior cavity.

The extended structure reveals that bis-urea units **1**§ stack on top of each other to form the desired supramolecular tubular structure. The bis-urea monomers are held together by the head-to-tail urea hydrogen-bonding motif extending along on both sides of the tube (Fig. 3). The three-centered hydrogen bonds have an N···O distance of between 2.82 and 3.01 Å and an H···O distance of 1.98 to 2.21 Å. This generates a spacing of 4.614 Å between the urea groups, consistent with other urea hydrogen-bonding systems. The urea monomers are aligned parallel but off-centered. The stacks are tilted 26° off of perpendicular as measured by the tilt in the ureas with respect to the macrocycle. This brings the aryl rings in adjacent macrocycles closer together within π-stacking distance (3.568 Å) while maintaining the longer urea–urea distance of 4.614 Å. The tilt also serves to orient the adjacent aryl rings in the more favorable offset aryl π-stacking geometry.[11]

In conclusion, the simple, symmetric bis-urea macrocycle **1**, assembles as designed into columnar structures. These extended

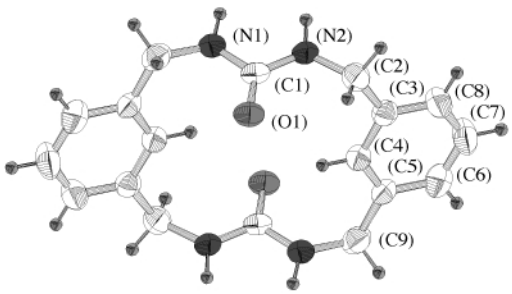

Fig. 2 ORTEP representation of bis-urea **1**.

 DOI: 10.1039/b102159c

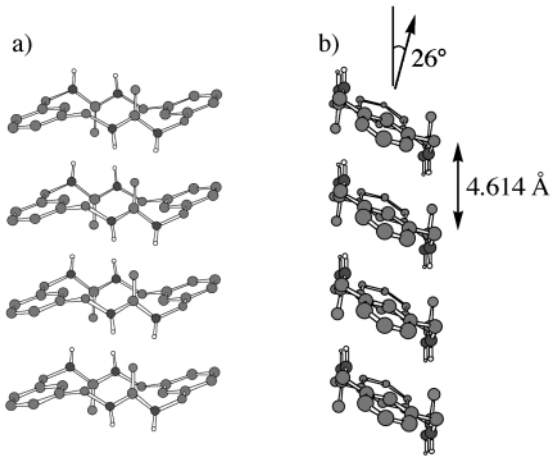

Fig. 3 X-Ray structures of bis-urea macrocycle **1**. The hydrogens have been omitted for clarity. Views alongside the tube showing (a) the 3-centered hydrogen bonding patterns and (b) the skewed orientation of monomers.

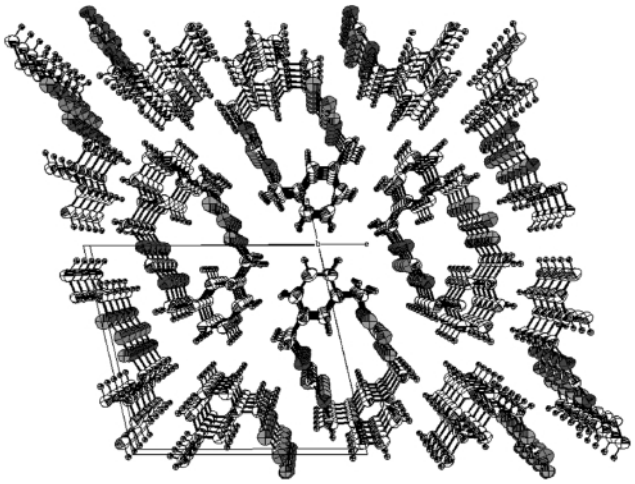

Fig. 4 Packing of the individual tubes highlights the potential channels that could be formed with macrocycles that have significant cavities.

tubes are held together by the urea–urea 3-centered hydrogen bonds and by aryl stacking interactions. Fig. 4 highlights the potential channels that may form with larger bis-urea macrocycles. We are currently focused on the synthesis and crystallization studies of larger analogues that would contain channels upon nanotubular assembly.

This work is supported by the National Science Foundation under Grant No. 9973132. In addition, A. D. H. thanks the Howard Hughes Foundation for support.

Notes and references

† Synthesis of the protected bis-urea macrocycle: the triazone protected macrocycle was prepared from the *tert*-butyl triazone and *meta*-α,α′-dibromoxylylene according to the method described by Dave *et al.*[10]

‡ Synthesis of the bis-urea macrocycle **1**: the triazone protected macrocycle (0.26 g, 0.55 mmol) was stirred in MeOH (10 mL) and 20% diethanolamine (10 mL aqueous, pH 3) was added. The solution was heated at reflux overnight. A white precipitate formed. The reaction mixture was cooled and the crystals were collected by filtration and washed with water to yield 0.12 g (66%) of the urea cleft (**1**). The material was purified by crystallization from glacial acetic acid. ^{1}H NMR (300 MHz, DMSO) δ 7.30 (s, 2H), 7.16 (t, 2H, J = 7.4 Hz), 7.0 (d, 4H, J = 6.9 Hz), 6.46 (br s, 4H), 4.6 (v br m, 4H), 3.8 (v br m, 4H). ^{13}C NMR (75 MHz, DMSO) δ 158.0, 141.8, 127.5, 124.9, 123.3, 42.4. CHN analysis: C (calc.) 66.65 (found) 66.54, H (calc.) 6.21 (found) 6.25, N (calc.) 17.27 (found) 16.94%.

§ *Crystallographic data*: for **1**, 293 K $C_{18}H_{20}N_4O_2$, M = 324.38, monoclinic, space group $P2_1/n$, a = 12.808, b = 4.6145, c = 13.950 Å, β = 103.193°, U = 802.7 Å^3, Z = 2, D_c = 1.342 Mg m^{-3}, λ = 0.71073 Å (Mo-Kα), F(000) = 344. Bruker SMART APEX CCD-based diffractometer system, crystal size 0.22 × 0.03 × 0.02 mm^3, Θ_{max} = 23.29°, 4211 reflections measured, 1155 unique (completeness = 100%, R_{int} = 0.0686) and 618 were greater than 2σ(I). Corrections for Lorentz and polarization effects were also applied by SAINT. Final R_w = 0.0695 (all atoms). Conventional R = 0.0386.

CCDC reference number 166911. See http://www.rsc.org/suppdata/cc/b1/b102159c/ for crystallographic data in CIF or other electronic format.

1 (*a*) V. A. Russell and M. D. Ward, *Chem. Mater.*, 1996, **8**, 1654; (*b*) R. Bishop, *Chem. Soc. Rev.*, 1996, **25**, 311; (*c*) G. R. Desiraju, *Angew. Chem., Int. Ed. Engl.*, 1995, **34**, 2311.
2 B. Konig, *Angew. Chem., Int. Ed. Engl.*, 1997, **36**, 1833.
3 (*a*) M. R. Ghadiri, J. R. Granja, R. A. Milligan, D. E. McRee and N. Khazanovich, *Nature*, 1993, **366**, 324; (*b*) B. Olenyuk and P. J. Stang, *Acc. Chem. Res.*, 1997, **30**, 502; (*c*) A. S. Shetty, J. S. Zhang and J. S. Moore, *J. Am. Chem. Soc.*, 1996, **118**, 1019.
4 (*a*) M. C. Etter, Z. Urbanczyk-Lipkowska, M. Zia-Ebrahimi and T. W. Panuto, *J. Am. Chem. Soc.*, 1990, **112**, 8415; (*b*) M. C. Etter and T. W. Panunto, *J. Am. Chem. Soc.*, 1988, **110**, 5896.
5 (*a*) X. Shao, Y.-L. Chang, F. W. Fowler and J. W. Lauher, *J. Am. Chem. Soc.*, 1990, **112**, 6627; (*b*) C. L. Schauer, E. Matwey and F. W. Fowler, *J. Am. Chem. Soc.*, 1997, **119**, 10 245; (*c*) M. D. Hollingsworth, M. E. Brown, B. D. Satarsiero, J. C. Huffman and C. R. Goss, *Chem. Mater.*, 1994, **61**, 1227.
6 K. D. Shimizu and J. Rebek, *Proc. Natl. Acad. Sci. USA*, 1995, **92**, 12 403.
7 (*a*) D. Ranganathan, S. Kurur, K. P. Madhusudanan and I. L. Karle, *Tetrahedron Lett.*, 1997, **38**, 4659; (*b*) J. van Esch, S. DeFeyter, R. M. Kellogg, F. DeSchryver and B. L. Feringa, *Chem.-Eur. J.*, 1997, **3**, 1238; (*c*) A. J. Carr, R. Melendez, S. J. Geib and A. D. Hamilton, *Tetrahedron Lett.*, 1998, **39**, 7447.
8 (*a*) D. Ranganathan, C. Lakshmi and I. L. Karle, *J. Am. Chem. Soc.*, 1999, **121**, 6103; (*b*) for an example of self-assembly of exocyclic urea macrocyclics, see: J. van Esch, F. Schoonbeek, M. de Loos, H. Koijman, A. L. Spek, R. M. Kellogg and B. L. Feringa, *Chem.-Eur. J.*, 1999, **5**, 937.
9 A. R. Mitchell, P. F. Pagoria, C. L. Coon, E. S. Jessop, J. F. Poco, C. M. Tarver, R. D. Breithaupt and G. L. Moody, *Propellants, Explos. Pyrotech.*, 1994, **19**, 232.
10 P. R. Dave, G. Doyle, T. Axenrod, H. Yazdekhasti and H. L. Ammon, *J. Org. Chem.*, 1995, **60**, 6946.
11 C. A. Hunter, *Chem. Soc. Rev.*, 1994, **23**, 101.

CHEMCOMM Communication
www.rsc.org/chemcomm

A multi-component coupling approach to benzo[*b*]furans and indoles†

Jason H. Chaplin and Bernard L. Flynn*

Department of Chemistry, The Faculties, Australian National University, Canberra ACT, 0200, Australia. E-mail: flynn@rsc.anu.edu.au

Received (in Cambridge, UK) 25th May 2001, Accepted 28th June 2001
First published as an Advance Article on the web 6th August 2001

A single step access to multiply substituted benzo[*b*]furans and indoles has been developed.

Indoles, benzo[*b*]furans and benzo[*b*]thiophenes are structural cores to a host of bioactive compounds in pharmaceutical use or development. Recently, we described a novel, concise approach to benzo[*b*]thiophenes.[1] This synthesis was used to prepare the tubulin polymerisation inhibitor (TPI) **1**.[1,2] TPIs are valued for

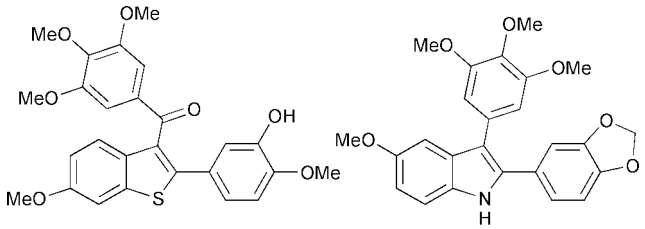

1 **2**

their capacity to inhibit the proliferation of cancer cells and to target tumour vascular endothelial cells.[2c] Medarde *et al.* recently described some cytotoxic 2,3-diarylindole systems, *e.g.* **2**, that were also believed to be TPIs.[3] In our ongoing examination of the structure–activity relationship (SAR) of TPIs such as **1** and **2**,[1,4] we required a concise, flexible access to 2,3-diaryl (and aroyl) benzo[*b*]furans and indoles to complement our access to benzo[*b*]thiophenes. Here we describe a palladium mediated, one-pot, multi-component coupling process that gives direct access to 2,3-disubstituted benzo[*b*]furans and indoles.

Cacchi and co-workers previously reported a two step synthesis of 2,3-disubstituted indoles from *o*-iodotrifluoroacetanilides **3** (Scheme 1).[5] This involves initial Sonogashira coupling of **3** to a terminal alkyne **4** to give an *o*-alkynyltrifluoroacetanilide **5**, which undergoes heteroannulative coupling to aryl iodides and alkenyl triflates to give indoles **6** (R^3 = aryl or alkenyl respectively). The trifluoroacyl group is lost during the coupling process. When performed under an atmosphere of CO gas, heteroannulation proceeds in a carbonylative fashion to provide the corresponding 3-acylindoles **7**.

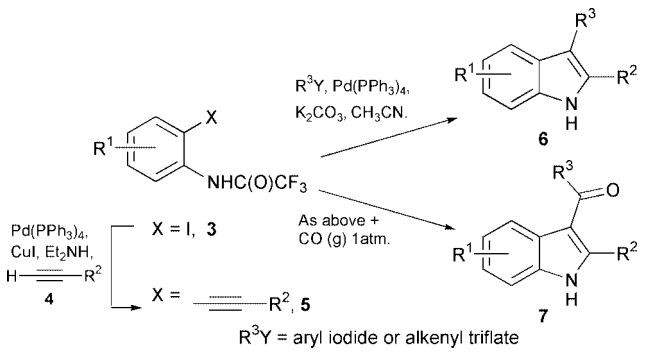

Scheme 1

This access to indoles **6** and **7** was generally quite efficient. However, extending this approach to the synthesis of 2,3-disubstituted benzo[*b*]furans from *o*-iodophenols proved problematic.[6] The propensity of intermediate *o*-alkynylphenols **8** to undergo cyclisation to simple 2-substituted benzo[*b*]furans **9**, particularly in the presence of palladium, required that the phenolic hydroxy be protected during the initial coupling of the alkyne to the *o*-iodophenol [eqn. (1)].[6] Cyclisation of **8** to **9** was

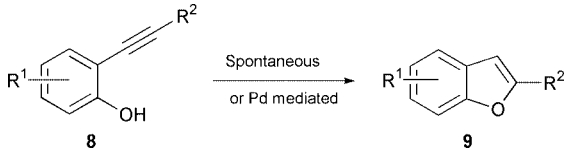

(1)

also a problem during deprotection and attempted heteroannulative coupling. As a result the overall yield of 2,3-disubstituted benzo[*b*]furan obtained from this multi-step sequence was generally very low. The process was also quite specific to the use of alkenyl triflates as substrates in the heteroannulative coupling reaction and for electron withdrawing groups in the *o*-alkynylphenol.[6]

We sought to improve this access to benzo[*b*]furans by removing any possibility of cyclisation of the *o*-alkynylphenols **8** to 2-substituted benzo[*b*]furans **9** and by reducing the number of steps required. This led to our development of a one-pot, multi-component coupling procedure (Scheme 2). This involves initial deprotonation of a mixture of *o*-iodophenol **10** and terminal alkyne **4** with MeMgCl to give the corresponding magnesium phenolate and magnesium acetylide respectively (not shown). Addition of $Pd(PPh_3)_2Cl_2$ (3 mol%) and heating leads to a coupling to give *o*-alkynylphenoxy magnesium chloride **12** (X = O). Dilution with an equal volume of DMSO and addition of a suitable coupling partner R^3Y (**13**) then gives the heteroannulatively coupled product **14** (X = O) or **15** (X = O) (under carbonylative conditions).

Alkenyl bromides, alkenyl iodides, and aryl iodides all proved to be effective coupling partners in heteroannulation (Table 1, entries 1–5).† The low yield of the product involving

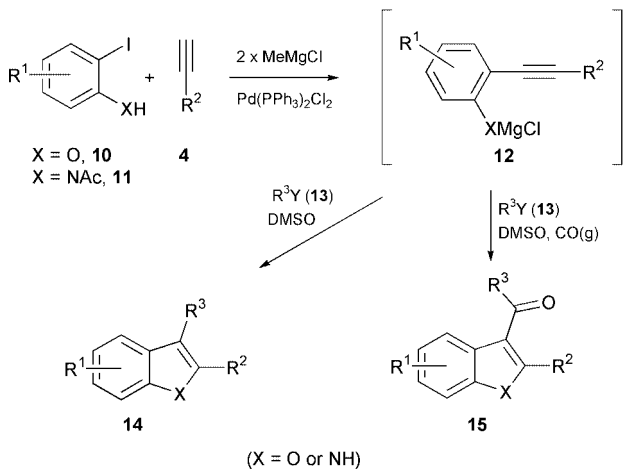

Scheme 2

† Electronic supplementary information (ESI) available: experimental procedures and spectroscopic data for **14a–h**, **15a** and **16**. See http://www.rsc.org/suppdata/cc/b1/b104624c/

 DOI: 10.1039/b104624c

Table 1 Multi-component coupling reaction for the formation of benzo[*b*]furans and indoles (see also Scheme 1)[a]

	Components					Components			
Entry	**10**	**4**	**13**	Product (yield (%))	Entry	**10/11**	**4**	**13**	Product (yield (%))
1	 **10a**	 **4a**	 **13a**	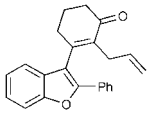 **14a** (78%)	6	**10a**	 **4d**	 **13d**	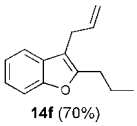 **14f** (70%)
2	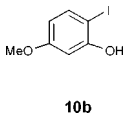 **10b**	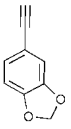 **4b**	 **13b**	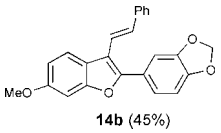 **14b** (45%)	7[b]	**10a**	**4a**	 **13e**	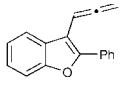 **14g** (64%)
3	**10b**	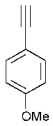 **4c**	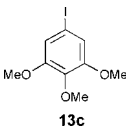 **13c**	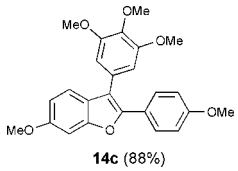 **14c** (88%)	8[c]	**10b**	**4c**	**13c** + CO(g)	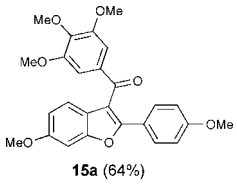 **15a** (64%)
4	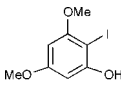 **10c**	**4b**	**13c**	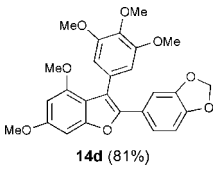 **14d** (81%)	9[c]	**10c**	**4b**	**13b** + CO(g)	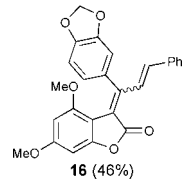 **16** (46%)
5	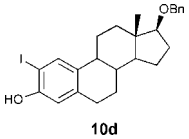 **10d**	**4b**	**13c**	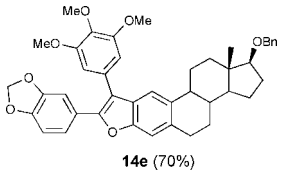 **14e** (70%)	10	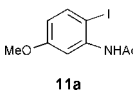 **11a**	**4c**	**13c**	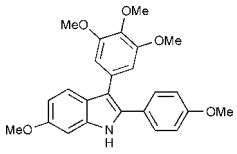 **14h** (85%)

[a] All reactions were performed as follows (unless otherwise stated): (i) **10** (or **11**), **4**, 2 × MeMgCl in THF, 0 °C; (ii) $Pd(PPh_3)_2Cl_2$ 3 mol%, 65 °C, 1–2 h; (iii) cool to 18 °C, add **13**, dilute with an equal volume of DMSO and heat to 80–95 °C, 4–19 h. [b] CH_3CN was used as a solvent in place of DMSO and a further 1.3 equiv. of **12e** was added after 2 h. [c] CO (g) 1 atm was introduced upon addition of **13** and DMSO and the reaction heated to 80–95 °C for 20 h.

the styrenyl iodide **13b** is expected to have resulted from the instability of this iodide under the reaction conditions, that is, in the presence of palladium at elevated temperatures. Good yields were also obtained when allyl acetate **13d** and propargyl tosylate **13e** (gives an allenic product) were used as coupling partners (entries 6 and 7).

When the coupling reaction that gave rise to **14c** was repeated, using a carbon monoxide atmosphere at the point of introduction of **13c**, the heteroannulative coupling proceeded in a carbonylative fashion to give **15a** in good yield (entry 8). There were no signs of formation of significant quantities of ester (esterification of the *o*-alkynylphenol) or the simple 2-substituted benzo[*b*]furan **9**, which dominated under the reaction conditions employed by Cacchi and co-workers.[6] Heteroannulative coupling involving the styrenyl iodide **13b** under such carbonylative conditions gave rise to the 3-alkylidenebenzo[*b*]furan-2-one **16** as the major product (entry 9). Benzo[*b*]furanone **16** has clearly resulted from an alternative coupling pathway. Arcadi *et al*. recently described a similar reaction involving vinyl triflates with *o*-ethynylphenols and proposed a mechanism of formation of the benzo[*b*]furanones.[7]

Although the two step process developed by Cacchi for the synthesis of indoles was quite efficient we were gratified to find that our approach to benzo[*b*]furans could also be extended to a one-pot access to indoles as is exemplified by our efficient preparation of **14h** (entry 10).

The authors thank the Australian Research Council for financial support including an ARC Australian Research Fellowship to B. L. F.

Notes and references

1 B. L. Flynn, P. Verdier-Pinard and E. Hamel, *Org. Lett.*, 2001, **3**, 651.
2 (*a*) K. G. Pinney, A. D. Bounds, K. M. Dingeman, V. P. Mocharla, G. R. Pettit, R. Bai and E. Hamel, *Bioorg. Med. Chem. Lett.*, 1999, **9**, 108; (*b*) K. G. Pinney, G. R. Pettit, V. P. Mocharla, P. M. M. Del and A. Shirali, PCT Int. Appl. WO 9839323, 1998; *Chem. Abstr.*, 1998, **129**, 245 037; (*c*) Z. Chen, V. P. Mocharla, J. M. Farmer, G. R. Pettit, E. Hamel and K. G. Pinney, *J. Org. Chem.*, 2000, **65**, 8811 and refs. therein.
3 M. Medarde, A. C. Ramos, E. Caballero, R. Pelaez-Lamamie de Clairac, J. L. Lopez, D. G. Gravalos and A. San Feliciano, *Bioorg. Med. Chem. Lett.*, 1999, **9**, 2303.
4 B. L. Flynn, G. P. Flynn, E. Hamel and M. K. Jung, *Bioorg. Med. Chem. Lett.*, in the press.
5 (*a*) A. Arcadi, S. Cacchi and F. Marinelli, *Tetrahedron Lett.*, 1992, **33**, 3915; (*b*) A. Arcadi, S. Cacchi, V. Carnicelli and F. Marinelli, *Tetrahedron*, 1994, **50**, 437.
6 A. Arcadi, S. Cacchi, M. Del Rosario, G. Fabrizi and F. Marinelli, *J. Org. Chem.*, 1996, **61**, 9280.
7 A. Arcadi, S. Cacchi, G. Fabrizi and L. Moro, *Eur. J. Org. Chem.*, 1999, 1137.

CHEMCOMM Communication
www.rsc.org/chemcomm

Enantioselective Michael addition of β-keto esters to methyl vinyl ketone employing a chiral *N,N′*-dioxide–scandium trifluoromethanesulfonate complex as a catalyst

Makoto Nakajima,* Yukiko Yamaguchi and Shunichi Hashimoto

Graduate School of Pharmaceutical Sciences, Hokkaido University, Sapporo 060–0812, Japan. E-mail: nakajima@pharm.hokudai.ac.jp

Received (in Cambridge, UK) 4th June 2001, Accepted 16th July 2001
First published as an Advance Article on the web 6th August 2001

An enantioselective Michael addition of β-keto esters to methyl vinyl ketone exploiting a chiral *N,N′*-dioxide–scandium trifluoromethanesulfonate complex as a catalyst affords the corresponding Michael adducts in high yields and with enantioselectivities of up to 80% ee.

Enantioselective catalytic Michael additions are one of the most important carbon–carbon bond formation reactions because of the versatility of the products as chiral building blocks.[1] Various chiral catalysts have been reported for the Michael addition of prochiral β-keto esters to α,β-unsaturated carbonyl compounds including cinchona alkaloids,[2a–c] chiral crown ether–metal alkoxide complexes,[2d] chiral amine–transition metal complexes,[2e–g] chiral alkoxide complexes,[2h] and chiral bimetallic lanthanoid complexes[1b].

The *N*-oxide functional group is known to form complexes with a variety of metals[3] due to its strong electron donating ability, and as such could be considered useful in potential catalysts. However, only a limited number of attempts to employ *N*-oxides in chiral catalysts have been reported.[4] As part of our program of developing *N*-oxide-mediated reactions,[5] herein we describe an enantioselective Michael addition of β-keto esters to methyl vinyl ketone catalyzed by a chiral *N,N′*-dioxide–scandium trifluoromethanesulfonate complex.

We have recently reported enantioselective conjugate addition of thiols to cyclic enones and acyclic enals catalyzed by the complex between **1** and cadmium iodide.[6] This prompted an investigation of the Michael addition of dimethyl malonate to cyclohexenone employing the **1**–cadmium complex, however, no Michael adduct was obtained with the cadmium complex. A study of the Michael addition of methyl 1-oxoindan-2-carboxylate (**2a**) to methyl vinyl ketone, a reaction frequently investigated as a probe for enantioselective Michael addition, was then undertaken. The reaction proceeded smoothly with the **1**–cadmium iodide complex, but the observed enantiomeric excess of the adduct was low (75% yield, 13% ee). After screening complexes prepared *in situ* from **1** and various metal salts, we found that 5 mol % of a 1:1 complex of **1** and scandium trifluoromethanesulfonate in dichloromethane at room temperature catalyzed the Michael addition to generate the adduct **3a** in quantitative yield with moderate enantioselectivity of 39% ee (Table 1, entry 1).

Introduced by Kobayashi *et al.*, scandium trifluoromethanesulfonate[7] is known as a versatile Lewis acid, yet only a few chiral scandium complexes as catalysts for enantioselective reactions have been reported, scandium trifluoromethanesulfonate–BINOL–amine complexes[8,9] and bimetallic complexes.[1b] Scandium trifluoromethanesulfonate is not soluble in dichloromethane, while its complex with **1** and **2a** dissolves in dichloromethane to give a yellow solution. Other solvents examined in the Michael addition were found to generate products in lower enantiomeric excess than dichloromethane (toluene: 99% yield, 8% ee; propionitrile: 99% yield, 19% ee, tetrahydrofuran: 99% yield, 10% ee). Lower selectivities were obtained at both higher and lower temperatures (0 °C: 91% yield, 5% ee; 40 °C: 98% yield, 20% ee). The enantioselectivity also strongly depended on the ratio of *N*-oxide to scandium (2.5; 99% yield, 19% ee, 1.0: 99% yield, 39% ee, 0.5: 94% yield, 30% ee with 0.5 mM scandium trifluoromethanesulfonate), as well as the catalyst concentration (0.1 mM: 85% yield, 35% ee; 0.5 mM: 99% yield, 39% ee; 2.5 mM: 93% yield, 6% ee with the ratio of *N*-oxide to scandium 1.0). These results suggest a variety of aggregation states for the complexes of scandium and *N*-oxide, though the details of these complexes are beyond the scope of this work.

As a Michael acceptor, acrolein generates a product with similar enantioselectivity (rt, 2 h, 75% yield, 30% ee after conversion of aldehyde into methyl ester), while chalcone

Table 1 Enantioselective Michael addition of β-keto ester **2** to methyl vinyl ketone catalyzed by **1**–$Sc(OTf)_3$ complex

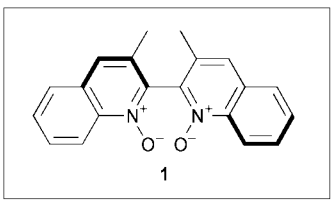

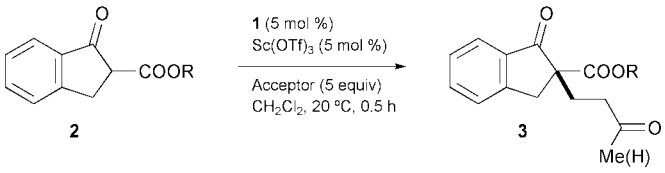

Entry	Donor	R	Acceptor	Adduct	Yield(%)	Ee (%)[a]	Confgn	$[\alpha]_D^{25}$ (*c* 1, benzene)
1	**2a**	Me	CH_2=CHCOMe	**3a**	98	39	*R*[b]	+27.1
2	**2b**	CH_2Ph	CH_2=CHCOMe	**3b**	85	38	*R*[c]	+17.5
3	**2c**	*i*-Pr	CH_2=CHCOMe	**3c**	94	47	*R*[d]	+31.9
4	**2d**	$CH(i\text{-Pr})_2$	CH_2=CHCOMe	**3d**	98	69	*R*[d]	+20.4
5	**2e**	*t*-Bu	CH_2=CHCOMe	**3e**	93	80	*R*[e]	+46.6
6	**2e**	*t*-Bu	CH_2=CHCHO	**3f**	73[f]	75[f]	*R*[d]	+38.3[g]

[a] Determined by HPLC analysis employing Daicel Chiralpak AD or Chiralcel OJ (hexane–isopropyl alcohol = 9:1, 1 mL min^{-1}). [b] Assigned by optical rotation ($[\alpha]_{577}^{25}$+29.8 (*c* 1, benzene), lit. 2*b*: $[\alpha]_{578}^{rt}$ −77 (*c* 2, benzene) for (*S*)-**3a**). [c] Assigned by optical rotation of **3b** prepared from **3a**. [d] Assigned by analogy. [e] Assigned by optical rotation after conversion to **3a**. [f] Determined after conversion of aldehyde into methyl ester. [g] Optical rotation of diester.

 DOI: 10.1039/b104876g

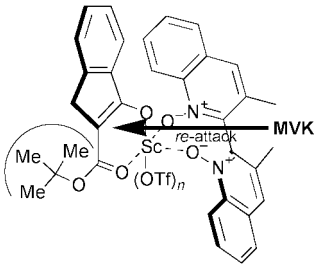

Fig. 1

generates a complex mixture of products. No reaction was observed using methyl acrylate as an acceptor. A variety of β-keto esters were then evaluated as Michael donors employing methyl vinyl ketone as an acceptor. Benzyl 2-oxocyclopentanecarboxylate, methyl 1-oxo-1,2,3,4-tetrahydronaphthalene-2-carboxylate, and methyl 2-methyl-3-oxopropanoate produced racemic mixtures, which suggests the importance of the indan skeleton in directing the enantiocontrol.

Enantioselective Michael additions of various esters of 1-oxoindan-2-carboxylic acid to methyl vinyl ketone were then investigated. The bulkiness of the ester substituent was found to have a pronounced effect on the observed enantioselectivity. As shown in Table 1, the enantioselectivities increased with the bulkiness of the ester. *tert*-Butyl ester **2e** exhibits the highest enantioselectivity of 80% ee (entry 5), while the Michael addition of *tert*-butyl ester **2e** to acrolein also produces notably better enantioselectivity (entry 6) than that of methyl ester **2a**.

The predominant formation of (*R*)-**3e** may be explained by the transition state model shown in Fig. 1. The bulky *tert*-butyl ester moiety should be located on the *si*-face of the keto ester plane in order to avoid steric repulsion with the quinoline moiety, which leads the attack of methyl vinyl ketone at the *re*-face preferentially.

A representative procedure for the enantioselective Michael addition catalyzed by the scandium trifluoromethanesulfonate–**1** complex is as follows. A mixture of *N*,*N*′-dioxide **1** (8.0 mg, 0.026 mmol), scandium trifluoromethanesulfonate (15 mg, 0.026 mmol) and β-keto ester **2e** (120 mg, 0.52 mmol) in dichloromethane (5 ml) was sonicated for 5 min to generate a yellow solution. Methyl vinyl ketone (0.2 mL, 2.6 mmol) was added to the solution and the mixture was stirred at room temperature for 0.5 h. After standard work-up followed by silica gel chromatography, **3e** (145 mg, 93%) was isolated as needles. *N*,*N*′-Dioxide **1** was recovered by elution with 10% ethanol in dichloromethane without a loss of optical purity. The enantiomeric excess of the adduct was determined by chiral HPLC.

In conclusion, we have demonstrated the potentiality of a chiral *N*,*N*′-dioxide–scandium trifluoromethanesulfonate complex to act as a catalyst for enantioselective Michael additions of β-keto esters to methyl vinyl ketone. The present reaction provides the first example of a chiral *N*-oxide–scandium complex acting as a catalyst in an enantioselective reaction. Studies into design modifications of chiral *N*,*N*′-oxides to further enhance enantioselectivity, and into the refinement of the mechanism of the reaction are currently in progress.

This work was partly supported by a Grant-in-Aid for Scientific Research from the Ministry of Education, Science, Sports and Culture of Japan and Otsuka Chemical Award in Synthetic Organic Chemistry, Japan.

Notes and references

1 (*a*) B. E. Rossiter and N. M. Swingle, *Chem. Rev.*, 1992, **92**, 771; (*b*) M. Shibasaki, H. Sasai and T. Arai, *Angew. Chem., Int. Ed. Engl.*, 1997, **36**, 1236; (*c*) J. Christoffers, *Eur. J. Org. Chem.*, 1998, 1259; (*d*) J. Leonard, E. Díez-Barra and S. Merino, *Eur. J. Org. Chem.*, 1998, 2051.

2 (*a*) H. Wynberg and R. Helder, *Tetrahedron Lett.*, 1975, 4057; (*b*) K. Hermann and H. Wynberg, *J. Org. Chem.*, 1979, **44**, 2238; (*c*) N. Kobayashi and K. Iwai, *J. Am. Chem. Soc.*, 1978, **100**, 7071; (*d*) D. J. Cram and G. D. J. Sogah, *J. Chem. Soc., Chem. Commun.*, 1981, 625; (*e*) H. Brunner and H. Benedikt, *Angew. Chem., Int. Ed. Engl.*, 1984, **23**, 312; (*f*) G. Desimoni, P. Quadrelli and P. P. Righetti, *Tetrahedron*, 1990, **46**, 2927; (*g*) C. Botteghi, S. Paganelli, A. Schionato, C. Boga and A. Fava, *J. Mol. Catal.*, 1991, **66**, 7; (*h*) Y. Tamai, A. Kamifuku, E. Koshiishi and S. Miyano, *Chem. Lett.*, 1995, 957.

3 N. M. Karayannis, L. L. Pytlewski and C. M. Mikulski, *Coord. Chem. Rev.*, 1973, **11**, 93.

4 (*a*) M. B. Diana, M. Marchetti and G. Melloni, *Tetrahedron: Asymmetry*, 1995, **6**, 1175; (*b*) I. A. O'Neil, C. D. Turner and S. B. Kalindjian, *Synlett*, 1997, 777; (*c*) G. Dyker, B. Hölzer and G. Henkel, *Tetrahedron: Asymmetry*, 1999, **10**, 3297; (*d*) V. Derdau, S. Laschat, E. Hupe, W. A. König, I. Dix and P. G. Jones, *Eur. J. Inorg. Chem.*, 1999, 1001; (*e*) K. Miura and T. Katsuki, *Synlett*, 1999, 783.

5 (*a*) M. Nakajima, Y. Sasaki, M. Shiro and S. Hashimoto, *Tetrahedron: Asymmetry*, 1997, **8**, 341; (*b*) M. Nakajima, Y. Sasaki, H. Iwamoto and S. Hashimoto, *Tetrahedron Lett.*, 1998, **39**, 87; (*c*) M. Nakajima, M. Saito, M. Shiro and S. Hashimoto, *J. Am. Chem. Soc.*, 1998, **120**, 6419; (*d*) M. Nakajima, M. Saito and S. Hashimoto, *Chem. Pharm. Bull.*, 2000, **48**, 306.

6 (*a*) M. Saito, M. Nakajima and S. Hashimoto, *Chem. Commun.*, 2000, 1851; (*b*) M. Saito, M. Nakajima and S. Hashimoto, *Tetrahedron*, 2000, **56**, 9589.

7 S. Kobayashi, *Eur. J. Org. Chem.*, 1999, 15.

8 (*a*) S. Kobayashi, M. Araki and I. Hachiya, *J. Org. Chem.*, 1994, **59**, 3758; (*b*) S. Kobayashi, H. Ishitani, M. Araki and I. Hachiya, *Tetrahedron Lett.*, 1994, **35**, 6325.

9 H. Kodama, J. Ito, K. Hori, T. Ohta and I. Furusawa, *J. Organomet. Chem.*, 2000, **603**, 6.

CHEMCOMM
Communication
www.rsc.org/chemcomm

Intercalation of a pendant-arm tetraazamacrocycle into molybdenum disulfide

Rabin Bissessur,*[a] Robert I. Haines,*[a] Dean R. Hutchings[a] and Ralf Brüning[b]

[a] *Department of Chemistry, University of Prince Edward Island, Charlottetown, PEI, Canada C1A 4P3. E-mail: rabissessur@upei.ca; rhaines@upei.ca*
[b] *Department of Physics, Mount Allison University, Sackville, New Brunswick, Canada E4L 1E6*

Received (in Cambridge, UK) 3rd May 2001, Accepted 6th July 2001
First published as an Advance Article on the web 31st July 2001

A novel macrocycle-MoS_2 nanocomposite has been synthesized and characterized using the exfoliation/restacking properties of $LiMoS_2$, providing the first of a new family of intercalation compounds.

There is significant interest in the properties of polyazamacrocycles bearing pendant-arms, particularly those having arms attached at the nitrogen atoms of the macrocycles. Interest in these complexes has focussed on applications to catalysis, ion-selectivity[1] and their use as radioimmunotherapy agents.[2] Transition metal macrocycles find utility as electrocatalysts in fuel cells,[3] or as catalysts for decomposition of environmentally important small molecules (NO_x, SO_x and CO_2).[4] Cobalt macrocycles will bond sulfur directly to the metal[5] and these complexes, which are also extremely stable in aggressive environments, provide excellent candidates for both fundamental and applied studies of hydrodesulfurization (HDS) of fossil fuels. Thus macrocycles may provide a portal to a completely unique class of intercalation compounds, that may prove to be robust, efficient HDS catalysts.

While the synthesis of nanocomposite materials is an important area of research and there have been a number of reports of intercalation of, for example, crown ethers into phyllosilicates[6] and inorganic hosts,[7] there have been no reports to date of intercalation of tetraazamacrocyclic compounds, particularly of the pendant-arm variety. This class of compound is particularly interesting, given its ability to form extremely stable redox active transition metal complexes. Molybdenum disulfide is a very attractive host material for nanocomposites and has already been shown in its own right to be an effective catalyst in the hydrodesulfurization (HDS) process.[8] It also finds application as a solid lubricant[9] and as a cathode material in high energy density lithium batteries.[10] Despite the importance of MoS_2 in industrial applications, formation of its intercalation compounds using redox techniques is usually limited to those of alkali and alkaline earth metals dissolved in liquid ammonia,[11] or to organolithium reagents such as *n*-butyllithium.[12] However, intercalation compounds of MoS_2 may be produced by utilizing the exfoliation and restacking properties of $LiMoS_2$. Complete exfoliation of $LiMoS_2$ occurs upon reaction with water. Addition of guest species such as organic molecules and polymers to the de-laminated layers can afford a wide range of intercalation compounds of MoS_2.[13] These include the intercalation of crown ethers and polyethylene oxides.[14] In this case, however, washing the intercalation compounds containing alkali metal complexes of the guest ethers caused progressive elimination of the intercalated compounds, giving solids of variable stoichiometry. We have chosen to exploit the $LiMoS_2$ exfoliation technique to attempt to prepare a series of intercalation compounds containing tetraazamacrocycles that should provide new, stable intercalation compounds with novel, useful properties.

We report here the formation and characterization of the first MoS_2 intercalation compound containing a pendant-arm tetraazamacrocycle, 5,5,7,12,12,14-hexamethyl-1,4,8,11-tetraazacyclotetradecane-1-acetic acid, (L).

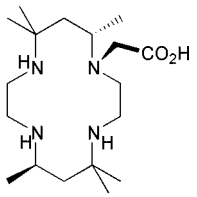

The macrocycle L was prepared by following the literature procedure.[15] $LiMoS_2$ was prepared by reacting MoS_2 with 3 equivalents of Bu^nLi[12] and was exfoliated by reaction with water. Addition of an ethanol solution of L to the delaminated layers resulted in its encapsulation in between the disulfide sheets.

Evidence for the intercalation of L into MoS_2 was obtained by powder X-ray diffraction (XRD)† which clearly shows the first eight (00*l*) reflections, indicative of a lamellar structure (Fig. 1). The observed *d*-spacing of the intercalated compound is 11.48 Å, showing an interlayer expansion of 5.3 Å with respect to pristine MoS_2, which has a *d*-spacing value of 6.15 Å. This expansion is consistent with a monolayer of L lying virtually co-planar with the MoS_2 sheets.

The stoichiometry of the sandwiched compound was determined by thermogravimetric analysis under air. This method has been shown previously[13] to give reliable results that agree closely with elemental analysis data. Examination of the thermogram showed that the inclusion compound is stable up to 308 °C. Thereafter, a major weight loss was observed up to 450 °C, followed by the formation of MoO_3, which was stable up to 650 °C. The identity of the MoO_3 phase was confirmed by XRD. From the thermogram, the composition of the intercalated material was found to be $L_{0.11}MoS_2$. It was also found that 0.11 is the maximum loading of L into MoS_2. Increasing the molar ratio of L : MoS_2 from 0.11 to 1.0 during the intercalation process had no effect. The average particle size of $L_{0.11}MoS_2$ was calculated from its powder pattern by using the Scherrer formula[16] and was found to be 80 Å, which may be compared

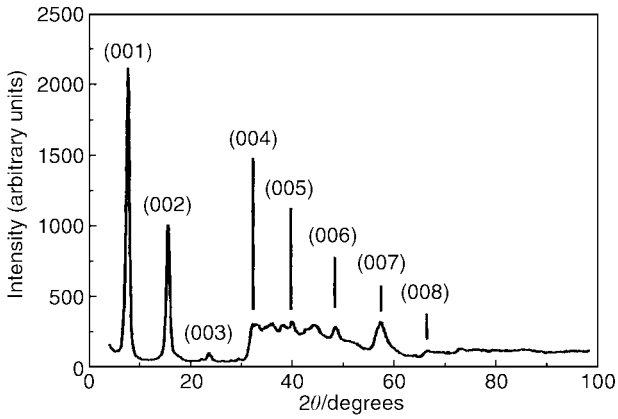

Fig. 1 Powder X-ray diffraction pattern for $L_{0.11}MoS_2$.

 DOI: 10.1039/b103965m

with an average particle size of 129 Å for the pristine MoS_2 used in this study. The decrease in particle size of MoS_2 upon intercalation corresponds to a significant loss in crystallinity of the material since upon exfoliation it does not restack quite as well as in its initial state.

The room temperature electronic conductivity of $L_{0.11}MoS_2$ was assessed by the two-probe technique on a pressed pellet of the sample. The measured conductivity value is 2.5×10^{-3} S cm^{-1}, which shows a 250-fold increase with respect to pristine MoS_2. The latter, which is in the 2H form, is a semiconductor with a room temperature electrical conductivity of 10^{-5} S cm^{-1}. This increase in electrical conductivity is explained by a structural transformation of the MoS_2 which takes place during the intercalation process. In 2H-MoS_2, the molybdenum atoms are bonded to the sulfur atoms in a trigonal prismatic arrangement. Upon treatment of 2H-MoS_2 with Bu^nLi, reduction of the layers takes place forming $LiMoS_2$ that contains molybdenum atoms octahedrally coordinated to six sulfurs. The reaction of $LiMoS_2$ with water is fast, where oxidation of the layers results in the formation of single layers trapped in the octahedral geometry. When the single layers restack with L sandwiched in between, the octahedral geometry of the MoS_2 is retained. Band structure calculations by Matthesis showed that MoS_2 in the octahedral (O_h) form is metallic.[17] However, this form is metastable and reverts to the thermodynamically more stable 2H state. This is consistent with the observed continuous decrease in conductivity of our samples over a period of time. This effect is currently being examined as well as the effect of temperature and pressure on the conductivity of $L_{0.11}MoS_2$, and will be the subject of a future paper. The structural conversion of MoS_2 in $L_{0.11}MoS_2$ has also been probed by differential scanning calorimetry which shows a broad exothermic peak with a peak maximum at 200 °C. This is consistent with the structural transformation of MoS_2 from the O_h to the 2H form. The observed transition was found to be irreversible. restacked MoS_2 (*d*-spacing 6.15 Å) has been reported to show a similar transition at 100 °C.[18] It seems that an increase in *d*-spacing leads to an increase in the transition temperature and we are currently exploring this effect by using macrocycles of different sizes and with differing number and bulk of substituents. A detailed study of the steric effects of pendant-arm macrocycles on the properties of their MoS_2 intercalation compounds is currently underway. This work provides the first evidence that pendant-arm macrocycles are viable guests in intercalation compounds hosted by MoS_2, which may lead to materials with unique and useful properties.

We are grateful to the Natural Sciences and Engineering Research Council (NSERC) of Canada, and the UPEI Senate Committee on Research for financial support. Thanks go to Dr J. Dahn, Physics Department, Dalhousie University for the thermogravimetric measurements.

Notes and references

† A diffractometer equipped with a graphite monochromator and an analyzer crystal was used, along with a scintillation detector. Cu-Kα radiation (λ = 1.542 Å) was utilized and the data collection was carried out at 22 °C. Samples were run under vacuum with a scan range of 4–100°.

1 J.-P. Collin and J.-P. Sauvage, *J. Chem. Soc., Chem. Commun,*, 1987, 1075; E. Kimura, T. Koike and M. Takahashi, *J. Chem. Soc., Chem. Commun.*, 1985, 385.
2 J. P. L. Cox, K. J. Jankowski, R. Kataky, D. Parker, N. R. A. Beeley, B. A. Boyce, M. A. W. Eaton, K. Miller, A. T. Millian, A. Harrison and C. Walker, *J. Chem. Soc., Chem. Commun.*, 1989, 797.
3 B. W. Clauberg and G. Sandstede, *J. Electroanal. Chem.*, 1976, **74**, 393.
4 (*a*) J. P. Collman, M. Marrocco, P. Deisevich, C. Kooval and F. C. Anson, *J. Electroanal. Chem.*, 1979, **101**, 117; (*b*) M. M. Burley, M. R. Rhodes and T. Meyer, *Inorg. Chem.*, 1987, **26**, 1746.
5 J. Burgess, J. Fawcett, R. I. Haines, K. Singh and D. R. Russell, *Transition Met. Chem.*, 1999, **24**, 355.
6 E. Ruiz-Hitzky and B. Casal, *Nature*, 1978, **276**, 596; B. Casal, P. Aranda, J. Sanz and E. Ruiz-Hitzky, *Clay Miner.*, 1994, **29**, 191; P. Aranda, B. Casal, J. J. Fripiat and E. Ruiz-Hitzky, *Langmuir*, 1994, **10**, 1207.
7 R. H. Herber and R. A. Cassell, *J. Chem. Phys.*, 1981, **75**, 4669; D. S. Glueck, A. R. Brough, P. Mountford and M. L. H. Green, *Inorg. Chem.*, 1993, **32**, 1893.
8 O. Weisser and S. Landa, *Sulfided Catalysts: Their Properties and Applications*, Pergamon, New York, 1973.
9 P. D. Fleischauer, *Thin Solid Films*, 1987, **154**, 309.
10 C. Julian, S. I. Saikh and G. A. Nazri, *Mater. Sci. Eng. B*, 1992, **15**, 73; H. Tributsch, *Faraday Discuss. Chem. Soc.*, 1980, **70**, 190.
11 R. Schollhorn and A. Weiss, *J. Less-Common Met.*, 1974, **36**, 229; R. B. Somoano, V. Hadek, A. Rembaum, S. Samson and J. A. Woollam, *J. Chem. Phys.*, 1975, **62**, 1068; R. B. Somoano and A. Rembaum, *Phys. Rev. Lett.*, 1971, **27**, 402.
12 M. S. Whittingham and F. R. Gamble, Jr., *Mater. Res. Bull.*, 1975, **10**, 363.
13 W. M. R. Divigalpitiya, S. Morrison and R. F. Frindt, *Thin Solid Films*, 1990, **186**, 177; L. Kosiodowski and A. V. Powell, *Chem. Commun.*, 1998, 2201; R. Bissessur, M. G. Kanatzidis, J. L Schindler and C. R. Kannewurf, *J. Chem. Soc., Chem. Commun.*, 1993, **20**, 1582.
14 N. Lara and E. Ruiz-Hitzky, *J. Braz. Chem. Soc.*, 1996, **7**, 193.
15 X. Ji-De, N. Shi-Sheng and L. Yu-Juan, *Inorg. Chim. Acta*, 1986, **111**, 61.
16 P. Scherrer, *Nachr. Ges. Wiss. Gottingen, Math.-Phys.*, 1918, **Kl**. 2, 96.
17 L. F. Matthesis, *Phys. Rev.*, 1973, **8**, 3179; M. A. Py and R. R. Haering, *Can. J. Phys.*, 1983, **61**, 76.
18 M. G. Kanatzidis, R. Bissessur, D. C. Degroot, J. L. Schindler and C. R. Kannewurf, *Chem. Mater.*, 1993, **5**, 595.

CHEMCOMM Communication
www.rsc.org/chemcomm

Tandem anionic Michael addition/radical cyclizations: a new and efficient strategy for the synthesis of functionalized cyclopentanes†

Ullrich Jahn

Institut für Organische Chemie, TU Braunschweig, Hagenring 30 D-38106 . Braunschweig, Germany. E-mail: u.jahn@tu-bs.de; Fax: 49-531-391-5388; Tel: 49-531-391-7371

Received (in Cambridge, UK) 18th May 2001, Accepted 2nd July 2001
First published as an Advance Article on the web 1st August 2001

The combination of anionic Michael addition of lithium ester enolates with radical 5-*exo* cyclizations through SET oxidation gives highly functionalized cyclopentanes.

Radical reactions have developed into a valuable tool in organic synthesis. Especially radical cyclizations are widely used since one of their advantages is the versatility to design tandem processes.[1] However, this advantage is offset by tedious precursor preparation. Radical addition/cyclization sequences are conceptually attractive since the gain in complexity from simple precursors is high. However, this strategy suffers from drawbacks: 1) radical additions (Giese reactions) obey complex kinetics, requiring an excess of one precursor (often a α,β-unsaturated carbonyl compound).[2] This excess, however, may interfere with the following reaction steps in the tandem processes thus limiting overall efficiency. 2) The radical acceptor should be unsubstituted in the β-position to achieve useful addition rates.[2,3]

A promising alternative to radical addition/cyclization cascades should be one in which the addition step is performed on the anionic oxidation stage allowing better reactivity/selectivity control. An attractive approach is the anionic Michael addition[4] proceeding with stoichiometric amounts of reagents, but the resulting enolate is normally not able to undergo anionic cyclization to unpolar functionalities.[5] However, by oxidizing the adduct enolate, radical cyclizations may be induced.[6]

Here, efficient tandem Michael addition/radical cyclizations[7] are reported. Cyclopentane derivatives with up to five stereocenters can be created from simple precursors.

An initial study of the Michael addition revealed that (*Z*)-enolates **1a**–**e** generated by deprotonation of the ester with LDA–THF–HMPA underwent a useful *anti*-selective addition to Michael acceptors **2a**–**c** providing good yields of **3** [Scheme 1, dr > 6.6 : 1 except for **1e**/**2b** (4.6 : 1), see Table 2 in the ESI†]. Enolates (*E*)-**1a**,**d** (generated with LDA–THF) gave *syn*-**3** with a very moderate selectivity. Additions of **1** to **2a**,**b** provided **3** directly while those of **1** to **2c** formed the aldol adduct at −78 °C that rearranged to **3** on warming to 0 °C.[4a,b]

With these results in hand, the Michael addition/radical cyclizations were studied (Scheme 2, Table 1). Addition of **2a** or **2c** to (*Z*)-**1** in THF–HMPA at −78 °C followed by warming to 0 °C generated the enolates **4** that were treated with a thoroughly homogenized solid mixture of SET oxidant ferrocenium hexafluorophosphate **5**–TEMPO **6** as oxygenation/termination reagent at −40 °C (Scheme 2, Table 1). For 5-unsubstituted **1a** and **2a**,**c** oxygenated cyclopentane derivatives **7aa**‡ and **7ac** were formed with good to excellent diastereoselectivity (entries 1,2). 5-Monosubstituted **1b** gave an inseparable 1.6 : 1 diastereomeric mixture of **7ba**‡ and **8ba** in 87% yield with good control of the exocyclic stereocenter (entry 3). More bulky ester **1c** improved the cyclization diastereoselectivity **7ca**/**8ca** only slightly, but induced excellent diastereoselectivity at the exocyclic stereocenter (entry 4). Even a fifth stereocenter can be controlled with reasonable efficiency. Applying **1c** and **2c** provided 61% (75% based on **1c**) of a partly separable 13.5:3.3:1 mixture of **7cc**/**8cc**/**9cc** (entry 5). The *cis*/*trans*-cyclization diastereoselectivity for *anti*-**4** amounted to 4.1 : 1. Michael addition/radical cyclization of **1d**/**2a** gave a 2 : 1 diastereomeric mixture of **7da** and **8da** in good yield (entry 6).

The protected alcohol function in **7** can be regenerated by reductive N–O bond cleavage[6,8] as exemplified for **7aa** providing **11aa** in 63% yield (Scheme 3).

The sequences are not limited to TEMPO trapping of the cyclized radical (Scheme 4). If Michael donors **1d**,**e** were coupled with **2a,b** followed by addition of 2.5–3 equiv. of **5**, isopropenylcyclopentanes **12** were formed as the major products together with minor amounts of **13**–**18**. The sequence of methyl ester **1d**/**2a** in the absence of additives gave **12da** in 51% yield as a 3:1 diastereomeric mixture accompanied by **14da**–**16da**. Alcohol α-**15da** lactonized to **17da** during purification. The more bulky ester **1e** and addition of 3 equiv. of KO*t*Bu

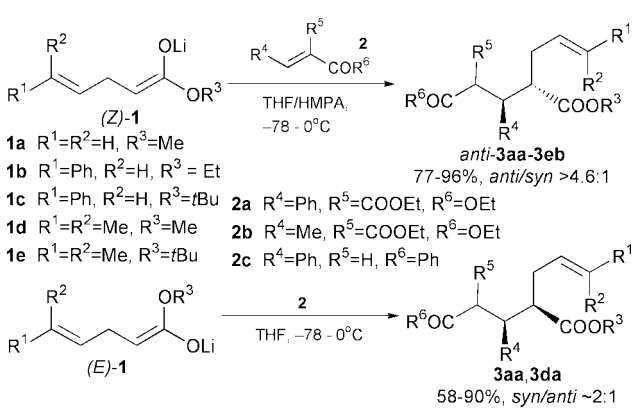

Scheme 1

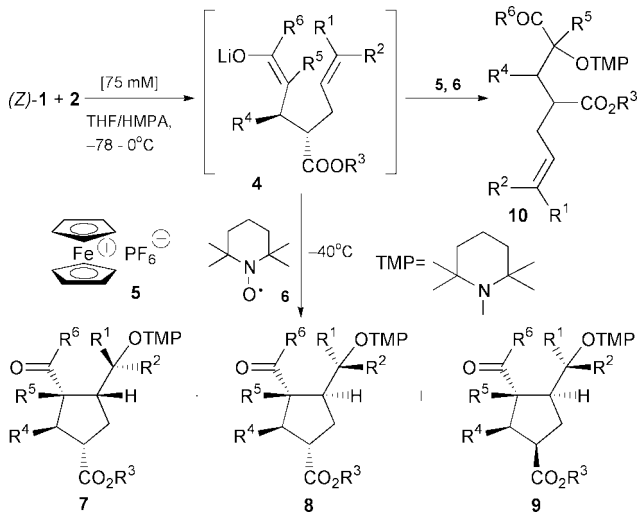

Scheme 2

† Electronic supplementary information (ESI) available: further experimental and spectral data. See http://www.rsc.org/suppdata/cc/b1/b104415j/

 DOI: 10.1039/b104415j

Table 1 Tandem Michael addition/radical cyclizations of **1**/**2**

Entry	1	2	Yield (%) 7+8+9	dr: 7 : 8 : 9 7(βR¹:αR¹)[a]	8(αR¹:βR)[a]	9	10 (%)
1	**a**	**a**	71	100(−)	0	0	—
2	**a**	**c**	53[b]	7.5(−)	1(−)	0	25[c]
3	**b**	**a**	87	1.6(6:1)	1(>20:1)	0	—
4	**c**	**a**	86	2.3(22:1)	1(>20:1)	0	—
5	**c**	**c**	61(75)[d]	13.5(5.4:1)	3.3(2:1)	1	—
6	**d**	**a**	82	1.8(−)	1(−)	0	—

[a] Configuration at exocyclic stereocenter. [b] A cyclized dimer was also formed in 4.7% yield. [c] Mixture of four diastereomers (not assigned). [d] Yield in parentheses represents yield based on recovered **1c**.

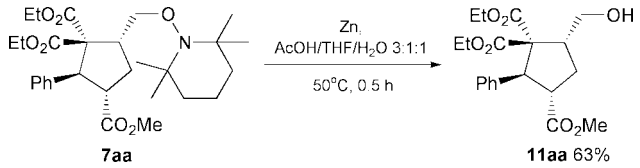

Scheme 3

improved the product distribution and the diastereoselectivity of the sequence to **12ea**. Some **14ea**, **16ea**, **17ea** and **18ea**, but almost no **15ea**, were formed. From ethylidenemalonate **2b** and **1e**, all four diastereomers of **12eb**/**13eb** were isolated in 54% yield in a 26:6:3:1 ratio due to the lower *anti*-selectivity of the Michael addition (4.6:1). Although not that interesting from the synthetic point of view, this example strengthened the configuration assignment to all products and indicated that *syn*-**4** may cyclize as efficiently as *anti*-**4**.

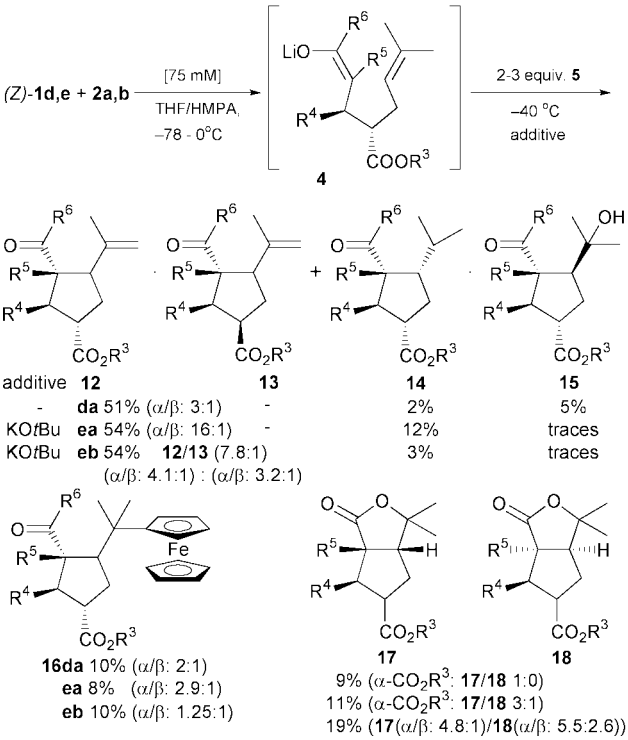

Scheme 4

The tandem processes can be rationalized by assuming a chelation controlled Michael addition step *via* **A** to *anti*-**4**[9] (Scheme 5). SET oxidation of **4** by **5** occurs predictably to radicals **B**. The cyclization diastereoselectivity to **C** can be explained by a preferred Beckwith–Houk chair transition state **B**[10] depending on the substitution pattern of the alkene in **1** followed by combination with TEMPO **6** to the major diastereomer **7**. TEMPO trapping of radical **B** does not play a significant role except for the **1a**/**2c** combination. Tertiary radicals **C** are predominately oxidized to carbenium ions **D**

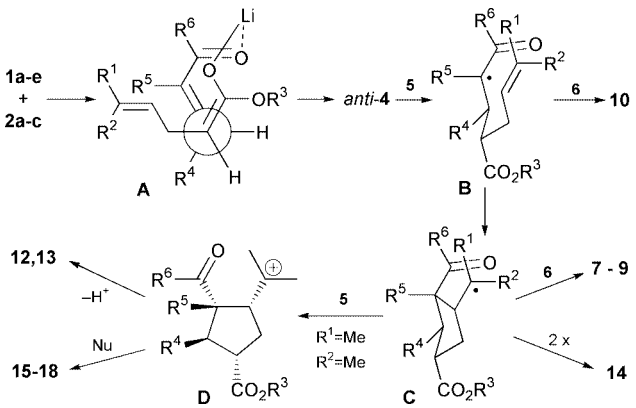

Scheme 5

giving **12**(**13**) and **15**–**18** *via* deprotonation and nucleophilic trapping, respectively, while **14** and **16** may be formed from **C** *via* disproportionation or ligand transfer with ferrocenium/ferrocene, respectively.

In summary, it was shown that Michael addition/radical cyclization cascades are a convenient strategy to overcome limitations of purely radical or anionic addition/cyclization sequences. The results may have many implications for the design of heterointermediate strategies since other enolate generating reactions such as conjugate additions or anionic rearrangements can be envisaged to be coupled with radical reactions thus expanding the opportunities of organic synthesis.

I thank Deutsche Forschungsgemeinschaft and Dr Otto Röhm-Gedächtnisstiftung for generous financial support. Professor H. Hopf's support is gratefully acknowledged.

Notes and references

‡ Configuration determination by X-ray crystal structure analysis.

1 Reviews: B. Giese, B. Kopping, T. Göbel, J. Dickhaut, G. Thoma, K. J. Kulicke and F. Trach, *Org. React.*, 1996, **48**, 301; D. P. Curran, *Comprehensive Organic Synthesis*, ed. B. M. Trost and I. Fleming, Pergamon Press, Oxford, 1991, vol. 4, p. 779G. G. Melikyan, *Org. React.*, 1997, **49**, 427.
2 D. P. Curran, *Comprehensive Organic Synthesis*, ed. B. M. Trost and I. Fleming, Pergamon Press, Oxford, 1991, vol. 4, p. 715M. P. Sibi, J. Ji, J. B. Sausker and C. P. Jasperse, *J. Am. Chem. Soc.*, 1999, **121**, 7517.
3 H. Fischer and L. Radom, *Angew. Chem., Int. Ed.*, 2001, **40**, 1340.
4 Reviews: D. A. Oare and C. H. Heathcock, *Top. Stereochem.*, 1989, **19**, 227; C. H. Heathcock, *Modern Synthetic Methods*, ed. R. Scheffold, Verlag Helvetica Chimica Acta, Basel, 1992, vol. 6, p. 1; A. Bernardi, *Gazz. Chim. Ital.*, 1995, **125**, 539; E. N. Gorobets, M. S. Miftakhov and F. A. Valeev, *Usp. Khim.*, 2000, **69**, 1091.
5 I. Marek, *J. Chem. Soc., Perkin Trans. 1*, 1999, 535.
6 U. Jahn and P. Hartmann, *Chem. Commun.*, 1998, 209.
7 Another approach: T. Cohen, K. McNamara, M. A. Kuzemko, K. Ramig, J. J. Landi, Jr. and Y. Dong, *Tetrahedron*, 1993, **49**, 7931.
8 D. L. Boger, R. M. Garbaccio and Q. Jin, *J. Org. Chem.*, 1997, **62**, 8875.
9 D. A. Oare and C. H. Heathcock, *J. Org. Chem.*, 1990, **55**, 157.
10 D. P. Curran, N. A. Porter and B. Giese, *Stereochemistry of Radical Reactions*, VCH, Weinheim, 1996

CHEMCOMM
Communication
www.rsc.org/chemcomm

Synthesising protease-stable isopeptides by proteases: an efficient biocatalytic approach on the basis of a new type of substrate mimetics†

Nicole Wehofsky,[a] Mandy Alisch[b] and Frank Bordusa*[ab]

[a] *Max-Planck Society, Research Unit 'Enzymology of Protein Folding', Weinbergweg 22, D-06120 Halle/Saale, Germany. E-mail: bordusa@enzyme-halle.mpg.de; Fax: +49 345 551 1972; Tel: +49 345 552 2806*

[b] *University of Leipzig, Department of Biochemistry, Talstr. 33, D-04103 Leipzig, Germany*

Received (in Cambridge, UK) 2nd July 2001, Accepted 19th July 2001
First published as an Advance Article on the web 9th August 2001

A biocatalytic route to the 'post-synthesis' formation of Asp/Glu-derived isopeptides is illustrated on the basis of the *Staphylococcus aureus* V8 protease used as the biocatalyst, a new type of substrate mimetics as the donor peptides, and several acceptor peptides varying in length and sequence.

The trifunctional structure of Asp and Glu allows both amino acids to be incorporated in the backbone of polypeptides by the side-chain and the C^{α}-carboxyl moiety as well. While the latter results in the formation of normal linear peptides, the involvement of the side-chain carboxyl group in the peptide backbone leads to the corresponding isopeptides. Isopeptides are ubiquitously found in nature and are considered to be one of the most common forms of non-enzymatic degradation of linear polypeptides under physiological conditions.[1] Rearrangement of normal peptides into isopeptides is catalysed by bases as well as acids, and starts with the formation of cyclic succinimide intermediates following dehydration. Re-opening of the ring finally leads to a mixture of normal peptides and isopeptides in a typical ratio that ranges from 40 : 60 to 15 : 85 along with small amounts of D-isopeptides.[2] Since isopeptide formation involves the addition of extra carbon atoms to the polypeptide backbone, its presence in a functional protein domain has profound effects on biological activity and its susceptibility to proteolytic degradation.[3] Recent findings have demonstrated that widespread accumulation of isopeptide linkages in cellular proteins greatly increases the immunogenicity and disrupts a wide range of important biochemical pathways by competitively displacing normal proteins in protein–protein or protein–ligand interactions.[4] Because of this function, isopeptides were found to be highly useful to study complex biological phenomena and for the development of therapeutic agents resulting in a great interest in their synthesis.

Although isopeptide bond formation is often an undesired side reaction during the chemical synthesis of normal linear peptides due to the need for strong bases and acids for deprotection steps and peptide release,[5] the directed synthesis of isopeptides is difficult and strictly limited by competitive cyclisation reactions. Like bases and acids, the use of coupling reagents to yield side-chain activation of Glu- and Asp-containing peptides further reinforces the formation of unwanted cyclic products and finally leads to a crude synthesis product with substantial amounts of undesired material. A few enzymes, *i.e.* protein carboxyl methyltransferases,[6] isopeptidases,[7] and transglutaminases,[8] are known to be active on the side-chain of Glu and Asp and, therefore, may be interesting biocatalysts for the synthesis of isopeptide bonds. However, due to the highly restricted substrate and reaction specificity, none of these enzymes is capable of catalysing the synthesis of isoAsp- or isoGlu-Xaa bonds. Therefore, the development of alternative catalytic and mild approaches to improve the current synthesis methods of isopeptides is a challenging task.

This account reports on the use of a normal peptidase, *i.e.* the Glu-specific endopeptidase from *Staphylococcus aureus* strain V8 (V8 protease), that acts as an efficient biocatalyst for the formation of isopeptides. The key feature of this approach is the use of a novel type of substrate mimetics that directs the synthesis activity of the protease to the side-chain carboxyl moiety of Asp and Glu (Scheme 1). Similar to classical substrate mimetics, the novel type donors bear a site-specific ester leaving group that mediates the acceptance of non-specific acyl moieties by the protease.[9] To direct the activity of the enzyme to the side-chain, the specific ester group, however, is linked to the ω-carboxyl moiety of Asp and Glu instead of being at the C-terminus of the peptide donor. This different architecture was shown to lead to a shift in the synthetic activity of the protease from the C^{α}-carboxyl group towards the side-chain moiety of the two amino acids finally resulting in the synthesis of isopeptides.

The general function of this biocatalytic approach was proved by the use of several Asp- and Glu-containing peptides that were esterified by carboxymethylthiol at their side-chain carboxylates. The carboxymethyl thioester functionality (SCm, *cf.* Scheme 1) itself was selected due to its function as a mimic which was already shown to mediate the acceptance of non-specific (non-Asp- and Glu-containing) linear donor peptides by V8 protease and other highly Glu-specific peptidases as well.[10] The influence of the length of the donor peptide on the synthesis reaction was investigated by using donor esters derived from single amino acids up to pentapeptides. Furthermore, the effect of the position of the Asp and Glu moieties within the donor peptide on the acceptance by the enzyme was studied by using peptides with either N-/C-terminal or endogenous Glu/Asp-residues. The resulting 14 peptide esters have served as donor components in V8 protease-catalysed isopeptide syntheses using amino acid amides, dipeptide amides, and

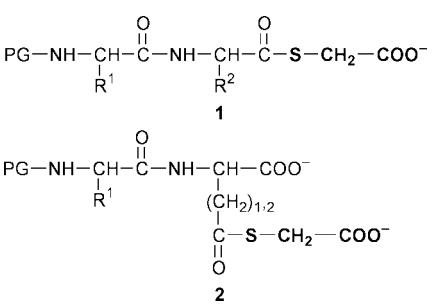

Scheme 1 General structures of classical linear (**1**) and new type (**2**) substrate mimetics. The site-specific carboxymethyl thioester group is emphasized by bold letters. PG, protecting group; R^1, R^2, individual side chains.

† Electronic supplementary information (ESI) available: complete details for experimental procedures. See http://www.rsc.org/suppdata/cc/b1/b105752a/

 DOI: 10.1039/b105752a

Table 1 Yields (%) of the V8 protease-catalysed synthesis of isopeptides. [donor]: 2 mM, [acceptor]: 15 mM, [V8 protease]: 3.61–10.33 μM

	Acceptor peptide				
Donor peptide	H-Met-NH_2	H-Gly-Leu-NH_2	H-Leu-Gly-NH_2	Ile-Ala-Ala-Ala-Gly	Leu-Ala-Ala-Ala-Gly
Z-Glu/*Asp*(SCm)-OH	41.2/*41.5*	40.3/*41.6*	47.7/*48.5*	49.8/*49.3*	50.5/*52.2*
Z-Ala-Glu/*Asp*(SCm)-NH_2	41.3/*59.5*	39.8/*56.9*	47.0/*60.3*	47.2/*67.9*	50.3/*65.9*
Z-Ala-Ala-Glu/*Asp*(SCm)-NH_2	44.9/*53.9*	45.1/*56.6*	50.4/*61.9*	49.4/*62.3*	51.0/*61.8*
Z-Glu/*Asp*(SCm)-Ala-NH_2	39.0/*51.7*	39.6/*54.2*	46.5/*59.7*	48.6/*66.8*	49.3/*64.3*
Z-Glu/*Asp*(SCm)-Ala-Ala-NH_2	44.7/*58.7*	45.4/*55.8*	52.6/*61.7*	54.6/*67.5*	54.9/*64.8*
Z-Ala-Glu/*Asp*(SCm)-Ala-NH_2	42.5/*60.9*	43.9/*62.8*	50.2/*65.7*	50.1/*67.4*	51.6/*68.0*
Z-Ala-Ala-Glu/*Asp*(SCm)-Ala-Ala-NH_2	40.8/*59.1*	41.5/*61.9*	51.9/*64.0*	52.4/*66.4*	52.8/*65.0*

pentapeptides as the amino components. The reactions themselves were performed under identical conditions at pH and temperature optimal to the enzyme.[11] As a control for spontaneous hydrolysis and aminolysis of the peptide esters that may interfere with the enzymatic syntheses, parallel reactions without enzyme were analysed. On the basis of these control experiments, non-enzymatic aminolysis could be ruled out and the extent of spontaneous hydrolysis was found to be less than 5%. The results observed for the enzyme-catalysed syntheses are summarised in Table 1. Generally, the data document that all donor peptides show productive binding at the active site of the biocatalyst resulting in isopeptide bond formation. In contrast, model reactions using donor components lacking the specific ester moiety, *i.e.* Z-Glu(SMe)-OH and Z-Asp(SMe)-OH (SMe, methylthiol), gave no reaction. This finding indicates that the negative charge of the SCm-leaving group is essential to mediate the acceptance by V8 protease. Accordingly, the lack of this charge causes a complete loss of specificity that inevitably leads to a loss of synthesis activity of the enzyme. On analysis of the efficiency of syntheses, yields of isopeptide products within a range of about 40–70% were obtained that roughly correspond with those of comparable reactions using normal linear substrate mimetics.[10] Interestingly, apart from the formation of the respective hydrolysed donor peptides no further side products could be detected. Addressing the moderate variations in the yields, the Asp- and Glu-residue itself appears to affect the efficiency of synthesis to the highest extent. While the use of Z-Glu(SCm)-OH and Z-Asp(SCm)-OH led to practically the same yields, the chain elongation of the Asp ester either in the C- or N-terminal direction resulted in an increase in the product yields of around approximately 10–20%. This increase makes the Asp-containing peptides more efficient donor components than those derived from glutamic acid. Interestingly, the individual position of both the Asp and Glu residue within the donor peptide does not affect the course of isopeptide synthesis significantly. In the same way, there is only a minor influence of the length of the donor peptide on the reaction. Surprisingly, this also holds for the acceptor peptide as it is reflected by the similar product yields which are less affected by the sequence and the chain length of the respective peptide. This atypical behaviour is in contrast to reactions using classical linear substrate mimetics as the donor peptides that generally displayed a more pronounced influence of the acceptor peptide on the course of synthesis.[10] Accordingly, in particular, N-terminal Gly and Met residues usually led to a decrease in product yield; an effect that can not be found for the synthesis of isopeptides. The synthesis of glutathione (γ-glutamylcyteinylglycine) starting from Z-Glu(SCm)-OH and Cys-Gly, which proceeds with a yield of about 62%, gave a further hint to the small influence of the acceptor peptide on the efficiency of catalysis. From a synthetic point of view, this broad tolerance towards the sequence and chain length of both the acceptor and donor peptide should make the approach presented a rather general one for the synthesis of a wide variety of isoaspartyl- and isoglutamyl-containing peptides. Furthermore, due to the mild reaction conditions, the weak carboxyl activation, and abandoning the use of additional bases and acids, the risk of undesired cyclisation reactions is reduced to a minimum. The synthetic utility of the method is even not narrowed by proteolytic side reactions. Model syntheses with elongated reaction times up to several days do not gave any hints to an undesired cleavage activity of V8 protease towards the formed isoGlu- and isoAsp-bonds indicating an irreversible course of the enzymatic ligation reaction (data not shown). Only the presence of further Glu and Asp residues additional to those that are to be modified may lead to undesired peptide cleavages. In such cases, freezing of the reaction mixture, which was shown to repress the proteolytic activity of enzymes closely related to V8 protease while retaining their synthesis activity,[12] may represent an efficient resource. From a biocatalytic point of view, the approach presented broadens the scope of proteases in organic synthesis and opens up a new field of synthetic applications of these enzymes for the synthesis of isopeptides. Finally, because of the universal applicability of substrate mimetics it can be further expected that other proteases may also be useful biocatalysts for isopeptide synthesis. Studies in this direction are presently under investigation.

Generous financial support by the DFG (Innovationskolleg 'Chemisches Signal und biologische Antwort') and Fonds der Chemischen Industrie (Liebig-scholarship, F. B.) is gratefully acknowledged. The authors thank Professor K. Burger and co-workers for helpful discussions and technical support and Professors G. Fischer and A. Beck-Sickinger for hosting.

Notes and references

1 L. Gráf, S. Bajusz, A. Patthy, E. Barát and G. Cseh, *Acta Biochim. Biophys. Acad. Sci. Hung.*, 1971, **6**, 415; B. A. Johnson, J. M. Shirokawa, W. S. Hancock, M. W. Spellmann, L. J. Basa and D. W. Aswad, *J. Biol. Chem.*, 1989, **264**, 14262.
2 T. Geiger and S. Clarke, *J. Biol. Chem.*, 1987, **262**, 785; B. A. Johnson, E. D. Murray, Jr., S. Clarke, D. B. Glass and D. W. Aswad, *J. Biol. Chem.*, 1987, **262**, 5622.
3 D. W. Aswad, M. V. Paranandi and B. T. Schurter, *J. Pharm. Biomed. Anal.*, 2000, **21**, 1129.
4 M. J. Mamula, *Immunol. Rev.*, 1998, **164**, 231; M. J. Mamula, R. J. Gee, J. I. Elliot, A. Sette, S. Southwood, P.-J. Jones and P. R. Blier, *J. Biol. Chem.*, 1999, **274**, 22321.
5 M. Bodanszky and J. Z. Kwei, *Int. J. Pept. Protein Res.*, 1978, **12**, 69; M. Bodanszky, J. C. Tolle, S. S. Deshmane and A. Bodanszky, *Int. J. Pept. Protein Res.*, 1978, **12**, 57; G. Barany and R. B. Merrifield, in *The Peptides*, ed. E. Gross and J. Meienhofer, Academic Press, New York, 1979, 193.
6 E. D. Murray, Jr. and S. Clarke, *J. Biol. Chem.*, 1984, **259**, 10722; P. N. McFadden and S. Clarke, *J. Biol. Chem.*, 1986, **261**, 11503; I. M. Ota and S. Clarke, *J. Biol. Chem.*, 1989, **264**, 54.
7 A. G. Loewy, J. K. Blodgett, F. R. Blase and M. H. May, *Anal. Biochem.*, 1997, **246**, 111.
8 M. L. Fink and J. E. Folk, *Methods Enzymol.*, 1983, **94**, 347.
9 V. Schellenberger, H.-D. Jakubke, N. P. Zapevalova and Y. V. Mitin, *Biotechnol. Bioeng.*, 1991, **38**, 104; H. Sekizaki, K. Itoh, E. Toyota and K. Tanizawa, *Chem. Pharm. Bull.*, 1996, **44**, 1585; F. Bordusa, D. Ullmann, C. Elsner and H.-D. Jakubke, *Angew. Chem. Int. Ed. Engl.*, 1997, **36**, 2473; M. Thormann, S. Thust, H.-J. Hofmann and F. Bordusa, *Biochemistry*, 1999, **38**, 6056.
10 N. Wehofsky and F. Bordusa, *FEBS Lett.*, 1999, **443**, 220; N. Wehofsky, J.-D. Wissmann, M. Alisch and F. Bordusa, *Biochim. Biophys. Acta*, 2000, **1479**, 114.
11 G. R. Drapeau, Y. Boily and J. Houmard, *J. Biol. Chem.*, 1972, **247**, 6720.
12 N. Wehofsky, S. W. Kirbach, M. Haensler, J.-D. Wissmann and F. Bordusa, *Org. Lett.*, 2000, **2**, 2027.

CHEMCOMM
Communication
www.rsc.org/chemcomm

Catalytic asymmetric synthesis of 1,1′-spirobi[indan-3,3′-dione] *via* a double intramolecular C–H insertion process

Teruki Takahashi, Hideyuki Tsutsui, Masafumi Tamura, Shinji Kitagaki, Makoto Nakajima and Shunichi Hashimoto*

Graduate School of Pharmaceutical Sciences, Hokkaido University, Sapporo 060-0812, Japan. E-mail: hsmt@pharm.hokudai.ac.jp

Received (in Cambridge, UK) 25th April 2001, Accepted 12th July 2001
First published as an Advance Article on the web 9th August 2001

A highly efficient one-pot construction of optically active 1,1′-spirobi[indan-3,3′-dione] derivative (up to 80% ee) has been achieved by exploiting the double intramolecular C–H insertion reaction of dimethyl 2,2′-methylenebis(α-diazo-β-oxobenzenepropanoate) under the influence of dirhodium (II) tetrakis[*N*-phthaloyl-(*R* or *S*)-*tert*-leucinate] as a catalyst.

The development of efficient chiral metal complexes in the field of asymmetric synthesis has focused mainly on the design and synthesis of novel chiral ligands. BINAP, BINOL and related ligands based on the axially chiral 1,1′-binaphthyl skeleton have achieved significant success in asymmetric catalysis.[1] In this context, certain bifunctional chiral spirans with C_2-symmetry may be regarded as promising ligands, as they contain a totally rigid spiro backbone which creates an effective asymmetric environment. Although chiral *cis*,*cis*-spiro[4.4]nonane-1,6-diol has recently shown potential either as a chiral ligand itself[2] or as a precursor to other useful chiral ligands,[3] the widespread application of this class of spiran ligands has received relatively little attention.[4] Clearly, a major obstacle is the difficulty in obtaining enantiomerically pure spiran molecules, which generally involves a tedious resolution of racemates *via* fractional crystallization[5] or chromatography[6] of the diastereomeric mixtures. Thus, the development of a catalytic asymmetric synthesis of C_2-symmetrical chiral spirans would represent significant improvement over current methodologies for obtaining these ligands.[7,8]

Recently, Aburel and Undheim reported a new synthetic approach to generate racemic spiro[4.4]nonane-2,7-dione derivatives from acyclic bis(α-diazoketone) using a $Rh_2(OAc)_4$-catalyzed double intramolecular C–H insertion reaction, though the product yields are found to be only 27–35%.[9] Inspired by their pioneering work, and taking advantage of our continuing research in this field,[10] we turned our attention to the feasibility of a high-yielding and enantioselective synthesis of C_2-symmetrical chiral 1,1′-spirobiindan systems. Herein we report

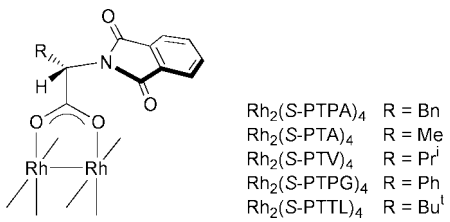

Rh_2(*S*-PTPA)$_4$ R = Bn
Rh_2(*S*-PTA)$_4$ R = Me
Rh_2(*S*-PTV)$_4$ R = Pr^i
Rh_2(*S*-PTPG)$_4$ R = Ph
Rh_2(*S*-PTTL)$_4$ R = Bu^t

a facile path to optically pure 1,1′-spirobi[indan-3,3′-dione] **1**,[5b] a potential intermediate in the synthesis of the hitherto unknown *cis*,*cis*-1,1′-spirobi[indan-2,2′-diol], *via* an enantioselective double intramolecular C–H insertion process with up to 80% ee.

At the outset of this work, we explored the double cyclization of bis(α-diazo-β-keto ester) **2** in the presence of 2 mol % of $Rh_2(OAc)_4$.† While the use of DCM as solvent gave a complex mixture of products, the catalysis of **2** in toluene was found to proceed sluggishly at rt to produce spirobiindanone derivative

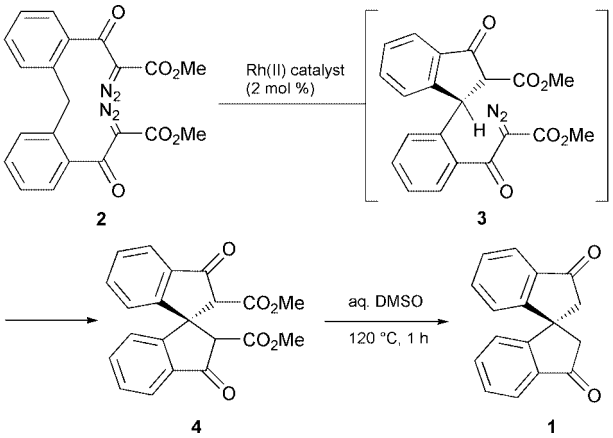

4, which, without purification, was transformed by demethoxycarbonylation to give spirobiindanone **1**. As might be expected from the results of Undheim,[9] a product yield of only 29% was found. The use of $Rh_2(O_2CC_7H_{15})_4$, $Rh_2(O_2CCPh_3)_4$[12] or $Rh_2(O_2CC_3F_7)_4$ also resulted in low yields.‡ Thus, we were gratified to find that the reaction proceeded smoothly at 0 °C with the aid of chiral dirhodium(II) carboxylates, Rh_2(*S*-PTPA)$_4$, Rh_2(*S*-PTA)$_4$, Rh_2(*S*-PTV)$_4$, Rh_2(*S*-PTPG)$_4$, and Rh_2(*S*-PTTL)$_4$, derived from *N*-phthaloyl-(*S*)-phenylalanine, -alanine, -valine, -phenylglycine, and -*tert*-leucine, respectively,[10] to give synthetically useful product yields (Table 1). Although no explanation for the striking contrast between the achiral and chiral dirhodium(II) carboxylates can be offered at present, the advantage of our catalysts extends beyond stereocontrol in this system.§ While the formation of (*R*)-1,1′-spirobi[indan-3,3′-dione] (*R*)-**1** was favored in all cases, Rh_2(*S*-PTTL)$_4$ characterized by an exceptionally bulky *tert*-butyl group proved to be the catalyst of choice for displaying a reasonable degree of enantioselectivity (68% ee, entry 5).¶ Further screening of solvents confirmed that the use of toluene was the superior choice for allowing smooth insertion at −10 °C to provide (*R*)-**1** in 78% yield with 80% ee (entry 6), which, upon a single recrystallization from ethanol, produced the optically pure sample, mp 212–213 °C, $[\alpha]_D^{25}$ −237.0 (*c* 0.69, $CHCl_3$) [lit.,[5b] $[\alpha]_D^{24}$ +238.7 (*c* 0.64, $CHCl_3$) for (*S*)-**1**], in 67% yield. The use of Rh_2(*R*-PTTL)$_4$ also generated (*S*)-**1** with 79% ee (entry 7). Thus, both enantiomers of **1** are equally available. The use of DCM provided (*R*)-**1** with 60% ee (entry 8), however, 0 °C was found to be the temperature limit for allowing smooth cyclization. It is of particular interest that the use of benzotrifluoride (α,α,α-trifluorotoluene)[14] greatly accelerated the insertion rate, though the largest ee was found to be 72% at −23 °C (entry 9).

The stereochemical outcome observed here suggests that the chiral rhodium(II) carbene intermediate generated *via* Rh_2(*S*-PTTL)$_4$-catalyzed decomposition of **2** preferentially inserts into a methylene C–H*s* bond to give (3*S*)-indan-1-one derivative **3**, which undergoes a second C–H insertion at the methine C–H bond with well-established retention of configuration[15] to

 DOI: 10.1039/b103747c

Table 1 Enantioselective double C–H insertion reaction of **2** catalyzed by chiral dirhodium(II) complexes[a]

Entry	Catalyst	Solvent	Temp./°C	Time/h	Yield of **1** (%)[b]	Ee of **1** (%)[c]
1	Rh_2(*S*-PTPA)$_4$	Toluene	0	0.5	71	25
2	Rh_2(*S*-PTA)$_4$	Toluene	0	1	68	23
3	Rh_2(*S*-PTV)$_4$	Toluene	0	0.5	66	24
4	Rh_2(*S*-PTPG)$_4$	Toluene	0	1	67	21
5	Rh_2(*S*-PTTL)$_4$	Toluene	0	0.5	83	68
6	Rh_2(*S*-PTTL)$_4$	Toluene	−10	1	78	80
7	Rh_2(*R*-PTTL)$_4$	Toluene	−10	1	76	−79[d]
8	Rh_2(*S*-PTTL)$_4$	CH_2Cl_2	0	1	72	60
9	Rh_2(*S*-PTTL)$_4$	$CF_3C_6H_5$	−23	1	66	72

[a] Reactions were carried out as follows: 2 mol % of catalyst was added to a stirred solution of diazo compound **2** (0.20 mmol) in the indicated solvent (2 ml) at the indicated temperature under argon. After the reaction proceeded to completion, the solvent was evaporated *in vacuo* and the residue was treated with 90% aqueous DMSO (1.5 ml) at 120 °C for 1 h. Standard workup followed by chromatography provided (*R*)-**1**. [b] Overall isolated yield. [c] Determined by HPLC (column, Daicel chiralcel OD; 4.6 × 250 mm × 2; eluent, 15% propan-2-ol in hexane; flow rate, 1.0 ml min^{-1}; retention time, 31.2 min [(*R*)-**1**] and 35.1 min [(*S*)-**1**]). [d] (*S*)-**1** was preferentially formed.

provide (*R*)-**1** after demethoxycarbonylation. Thus, the sense and magnitude of enantioselection indicates the level of differentiation between methylene C–H bonds during the first C–H insertion. In accordance with the order of reactivity of the target C–H bond (methine C–H > methylene C–H),[16] we could not observe the first insertion product **3**,[9] which makes it possible to conduct this one-pot reaction under the constant conditions.

In summary, we have achieved the first catalytic, enantioselective synthesis of 1,1′-spirobi[indan-3,3′-dione] (**1**) of up to 80% ee, in which the use of Rh_2(*R* or *S*-PTTL)$_4$ as a catalyst is crucial to the success of the double C–H insertion process. The present protocol has the advantages of operational simplicity as well as a facile entry to optically pure **1** *via* a single recrystallization, thus providing great potential for large-scale preparation. Elaboration of (*R*)- or (*S*)-**1** to hitherto unexplored chiral ligands such as 1,1′-spirobi[indan-2,2′-diol] for metal catalyzed enantioselective reactions is currently in progress.

This research was supported in part by a Grant-in-Aid (No.11470465) from the Ministry of Education, Science, Sports and Culture, Japan. We thank Ms S. Oka of the Center for Instrumental Analysis at Hokkaido University, for mass measurements.

Notes and references

† Bis(α-diazo-β-keto ester) **2** was prepared from diphenylmethane-2,2′-dicarboxylic acid[11] in 70% yield by the following three-step sequence: i, $SOCl_2$, toluene, reflux; ii, $LiCH_2CO_2Me$, THF, −78 °C; iii, MsN_3, Et_3N, MeCN.

‡ Overall isolated yield: $Rh_2(O_2CC_7H_{15})_4$, 28%; $Rh_2(O_2CCPh_3)_4$, 13%; $Rh_2(O_2CC_3F_7)_4$, 17%.

§ While reaction of the corresponding bis(α-diazoketone) with $Rh_2(OAc)_4$ in CH_2Cl_2 provided 52% yield of **1**, Rh_2(*S*-PTTL)$_4$ gave a complex mixture of products under the same conditions.

¶ Rh_2(*S*-DOSP)$_4$ developed by Davies[13] was found to be less reactive than our catalysts; catalysis of **2** with 2 mol % of Rh_2(*S*-DOSP)$_4$ in toluene proceeded at rt sluggishly to afford, after demethoxycarbonylation, (*S*)-**1** in 48% yield with 8.3% ee.

1 R. Noyori, *Asymmetric Catalysis in Organic Synthesis*, Wiley, New York, 1994; *Catalytic Asymmetric Synthesis*, ed. I. Ojima, Wiley-VCH, New York, 2000.
2 N. Srivastava, A. Mital and A. Kumar, *J. Chem. Soc., Chem. Commun.*, 1992, 493.
3 A. S. C. Chan, W. Hu, C.-C. Pai, C.-P. Lau, Y. Jiang, A. Mi, M. Yan, J. Sun, R. Lou and J. Deng, *J. Am. Chem. Soc.*, 1997, **119**, 9570; W. Hu, M. Yan, C.-P. Lau, S. M. Yang, A. S. C. Chan, Y. Jiang and A. Mi, *Tetrahedron Lett.*, 1999, **40**, 973.
4 Y. Jiang, S. Xue, K. Yu, Z. Li, J. Deng, A. Mi and A. S. C. Chan, *J. Organomet. Chem.*, 1999, **586**, 159; M. A. Arai, T. Arai and H. Sasai, *Org. Lett.*, 1999, **1**, 1795.
5 (*a*) S. Hagishita, K. Kuriyama, M. Hayashi, Y. Nakano, K. Shingu and M. Nakagawa, *Bull. Chem. Soc. Jpn.*, 1971, **44**, 496; (*b*) J. H. Brewster and R. T. Prudence, *J. Am. Chem. Soc.*, 1973, **95**, 1217; (*c*) R. K. Hill and D. A. Cullison, *J. Am. Chem. Soc.*, 1973, **95**, 1229; (*d*) H. Falk, W. Fröstl and K. Schlögl, *Tetrahedron Lett.*, 1974, 217; (*e*) E. Dynesen, *Acta Chem. Scand., Ser. B*, 1975, **29**, 77; (*f*) N. Harada, N. Ochiai, K. Takada and H. Uda, *J. Chem. Soc., Chem. Commun.*, 1977, 495.
6 (*a*) H. Gerlach, *Helv. Chim. Acta*, 1968, **51**, 1587; (*b*) J. A. Nieman, M. Parvez and B. A. Keay, *Tetrahedron: Asymmetry*, 1993, **4**, 1973; (*c*) J. A. Nieman and B. A. Keay, *Tetrahedron: Asymmetry*, 1995, **6**, 1575; (*d*) V. B. Birman, A. L. Rheingold and K.-C. Lam, *Tetrahedron: Asymmetry*, 1999, **10**, 125.
7 For asymmetric synthesis of 4,9-dimethylspiro[4.4]nonane-2,7-dione using Rh(I)-catalyzed hydroacylation twice, see: M. Takahashi, M. Tanaka, E. Sakamoto, M. Imai, A. Matsui, K. Funakoshi, K. Sakai and H. Suemune, *Tetrahedron Lett.*, 2000, **41**, 7879.
8 For synthesis of enantiomerically pure *trans,trans*-spiro[4.4]nonane-1,6-diol by asymmetric reduction of racemic spirodiketone, see: C.-W. Lin, C.-C. Lin, Y.-M. Li and A. S. C. Chan, *Tetrahedron Lett.*, 2000, **41**, 4425.
9 P. S. Aburel and K. Undheim, *Tetrahedron Lett.*, 1998, **39**, 3813; P. S. Aburel and K. Undheim, *J. Chem. Soc., Perkin Trans. 1*, 2000, 1891.
10 M. Anada and S. Hashimoto, *Tetrahedron Lett.*, 1998, **39**, 79; M. Anada, N. Watanabe and S. Hashimoto, *Chem. Commun.*, 1998, 1517; M. Anada and S. Hashimoto, *Tetrahedron Lett.*, 1998, **39**, 9063; M. Anada, O. Mita, H. Watanabe, S. Kitagaki and S. Hashimoto, *Synlett*, 1999, 1775.
11 R. N. Renaud, R. B. Layton and R. R. Fraser, *Can. J. Chem.*, 1973, **51**, 3380.
12 S. Hashimoto, N. Watanabe and S. Ikegami, *Tetrahedron Lett.*, 1992, **33**, 2709.
13 H. M. L. Davies, *Aldrichim. Acta*, 1997, **30**, 107.
14 A. Ogawa and D. P. Curran, *J. Org. Chem.*, 1997, **62**, 450; S. Kitagaki, M. Anada, O. Kataoka, K. Matsuno, C. Umeda, N. Watanabe and S. Hashimoto, *J. Am. Chem. Soc.*, 1999, **121**, 1417.
15 D. F. Taber, E. H. Petty and K. Raman, *J. Am. Chem. Soc.*, 1985, **107**, 196.
16 D. F. Taber and R. E. Ruckle, Jr., *J. Am. Chem. Soc.*, 1986, **108**, 7686.

CHEMCOMM
Communication
www.rsc.org/chemcomm

A tandem allylsilane–vinylsilane difunctionalization by silylcupration of allene followed by reaction with α,β-unsaturated nitriles

Asunción Barbero, Yolanda Blanco and Francisco J. Pulido*

Departamento de Química Orgánica, Universidad de Valladolid, 47011 Valladolid, Spain. E-mail: pulido@qo.uva.es

Received (in Cambridge, UK) 17th April 2001, Accepted 10th July 2001
First published as an Advance Article on the web 9th August 2001

Silylcupration of allene using phenyldimethylsilylcopper 1 followed by BF_3-mediated reaction with α,β-unsaturated nitriles at −40 °C affords allylsilane–vinylsilane-containing ketones resulting from consecutive addition (1,2 and 1,4) of the intermediate allyl- and vinylcopper species formed in the silylcupration of allene.

We recently reported[1–3] that addition of phenyldimethylsilylcopper ($PhMe_2SiCu{\cdot}LiCN$, **1**) to propa-1,2-diene leads to a silylated copper intermediate, which can be imprecisely formulated as a mixture of the allylsilane–vinylcopper species **2** and the vinylsilane–allylcopper species **3**. The reversibility of the reaction is one of its features. Quenching of the intermediate copper species with different electrophiles results in formation of compounds of type **4** or **5** (Scheme 1).

The reaction is temperature dependent and the presence of species **2** and **3** can be demonstrated by protonation of the reaction mixture at different temperatures. Thus, at −40 °C (or lower temperature) only formation of **4** (E = H) was observed, whereas **5** (E = H) was the major product obtained near to 0 °C.

In general, for most of the reported work[1] the reactive species at low temperature is **2**. Thus, at −40 °C, α,β-unsaturated ketones or aldehydes react with **2** giving exclusively 1,4-addition. However, at temperatures around −40 °C, simple ketones are unreactive toward species **2**, but they are readily attacked by **3** as the temperature increases to 0 °C, giving hydroxymethyls bearing the vinylsilane moiety.[1] In this case, conversion of species **2** into species **3** seems to occur rapidly as the temperature increases, which probably accounts for the observed result.

We now report an interesting and unusual tandem diaddition-hydrolysis process by successive addition (1,2 and 1,4) of species **3** and **2** to α,β-unsaturated nitriles. Protonation of the intermediate adduct, gives products that have both allylsilane and vinylsilane functionality.

Reaction of α,β-unsaturated nitriles with organocopper compounds has not been widely explored. Yamamoto[4] reported that the reaction of α,β-unsaturated nitriles with $RCu{\cdot}BF_3$ was not satisfactory; yields were low, and mixtures of monoalkylated and dialkylated products were obtained. Alexakis *et al.*[5] showed that introduction of an additive like TMSCl in the reaction of Me_2CuLi with some α,β-unsaturated nitriles gave the dialkylated ketone, whereas Lipshutz *et al.*[6] found that $Me_2CuCNLi_2$ slowly produced a poor yield of the methyl ketone resulting from 1,2 addition.

Silylcupration of allene (2 eq., following our usual protocol[1]) followed by addition of $BF_3{\cdot}Et_2O$ (2 equiv.) and subsequent slow addition of nitriles **6**–**9** (1 eq., THF, −40 to 0 °C) afforded, after hydrolysis at 0 °C, the ketones **10**–**13**, which seem to be produced by addition of the vinylsilane–allylcopper species **3** to the nitrile group and conjugate addition of the allylsilane–vinylcopper species **2** to the β position (Table 1).[7] The reaction (one pot) is clean and high yielding. Monoaddition products were not found. Remarkably, when this reaction is carried out with one equivalent each of allene and **1**, BF_3 and nitrile, the same diaddition products were formed, and almost half of the nitrile was wasted, which suggests that the second stage of the overall addition occurs quickly. It should be also noted that silylcupration of allene and further reaction with **8**, **9** (nitrile–organocopper; 1:2) at 0 °C, in the absence of BF_3, gives exclusively the 1,2-adducts **14** and **15** (Table 1).

The order in which the two steps (1,2 and 1,4) of addition take place and the mechanistic pathway are not certain. Weiberth and Hall[8] have proposed the intervention of Cu(III) intermediates in the copper-activated reaction of benzonitriles with Grignard reagents. Although we defer any definitive statement about the mechanism, it seems feasible—in view of the absence of 1,4-monoaddition products—that the reaction proceeds by initial addition of species **3** to the nitrile group followed by BF_3-catalyzed conjugate addition of species **2** to the intermediate α,β-unsaturated ketimine (Scheme 2). The chemoselectivity observed and the preference for the attack of **3** to the nitrile and of **2** to the conjugate position can be related to the different hardness of the nucleophilic species.

A completely different pattern of reaction is observed when the bulky *tert*-butyldiphenysilyl group is used instead of $PhMe_2Si$. Silylcupration of propa-1,2-diene with *tert*-$BuPh_2Si$-$Cu{\cdot}LiCN$[9] followed by addition of BF_3 and reaction with **6** and **8**—under the same conditions used before—affords selectively the 1,4-adducts **16** and **17** as the only products (Table 1). We have noted before[1] that species of type **2**, but carrying the bulky *tert*-butyldiphenysilyl group, are regiochemically stable at any temperature between −40 °C and 0 °C.

The one-pot tandem diaddition-hydrolysis process reported here could be of importance in synthetic work since the allylsilane and vinylsilane moieties are versatile synthons for organic synthesis. Thus, the diadducts undergo selective intramolecular allylsilane terminated cyclization,[1] while the vinylsilane unit remains unchanged, as shown in Scheme 3 with the conversion of **10**–**12** into **18**–**20**.

In summary, silylated organocopper reagents, like those used in this work, react well with α,β-unsaturated nitriles, giving

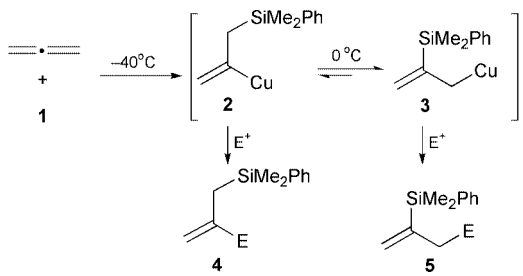

Scheme 1

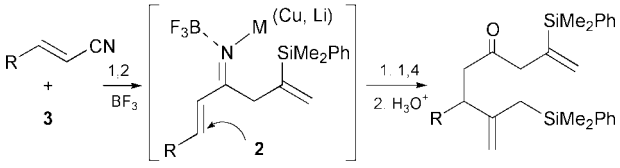

Scheme 2

 DOI: 10.1039/b103387p

Table 1 Reaction of α,β-unsaturated nitriles with silicon containing allyl- and vinylcopper reagents

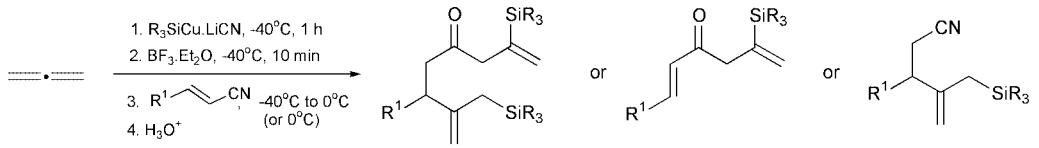

Nitrile	Ratio nitrile : organocopper	R_3Si	Temp.	Product (yield)[a]
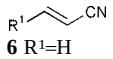 **6** R^1=H **7** R^1=Me **8** R^1=Ph	1:2	$PhMe_2Si$	−40 to 0 °C	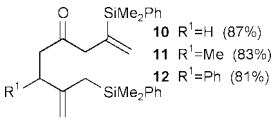 **10** R^1=H (87%) **11** R^1=Me (83%) **12** R^1=Ph (81%)
 **9**	1:2	$PhMe_2Si$	−40 to 0 °C	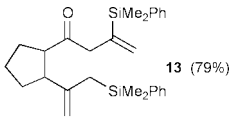 **13** (79%)
8	1:1	$PhMe_2Si$	0 °C[b]	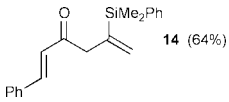 **14** (64%)
9	1:1	$PhMe_2Si$	0 °C[b]	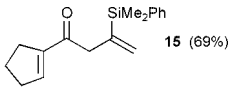 **15** (69%)
6 R^1=H **8** R^1=Ph	1:2	$^tBuPh_2Si$	−40 to 0 °C	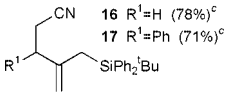 **16** R^1=H (78%)[c] **17** R^1=Ph (71%)[c]

[a] Yields refer to isolated pure compounds. [b] Reaction was carried out in the absence of BF_3. [c] Yield refers to the starting nitrile.

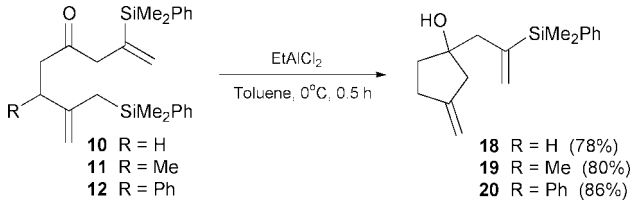

Scheme 3

1,2-adducts, 1,4-adducts or diaddition adducts, depending on the reaction conditions and on the nature of the silyl group.† We are not totally clear why we succeeded where others did not, but most probably it is connected with the nature of the equilibrium mixture of species and with the fact that a Lewis acid (BF_3)-activated organocopper is used. The effects of Lewis acid on cuprates have been examined recently, and they show that a strong chemoselectivity enhancement is frequently observed when Lewis acid-modified organocopper reagents are used.[10]

We gratefully acknowledge financial support from the Ministry of Science and Technology (BQU2000-0867 project).

Notes and references

† Satisfactory analytical data were obtained for the new compounds. The purity and structure of all new compounds were confirmed by ^1H and ^{13}C NMR, IR and GC-MS.

1 A. Barbero, C. García and F. J. Pulido, *Tetrahedron*, 2000, **56**, 2739, and references therein.

2 A. Barbero, C. García and F. J. Pulido, *Tetrahedron Lett.*, 1999, **40**, 6649.

3 F. J. Blanco, P. Cuadrado, A. M. González, F. J. Pulido and I. Fleming, *Tetrahedron Lett.*, 1994, **35**, 8881.

4 Y. Yamamoto, S. Yamanoto, H. Yatagai, Y. Ishibara and K. Maruyama, *J. Org. Chem.*, 1982, **47**, 119.

5 A. Alexakis, J. Berlan and Y. Besace, *Tetrahedron Lett.*, 1986, **27**, 1047.

6 B. H. Lipshutz, R. S. Wilhelm and J. A. Kozlowski, *J. Org. Chem.*, 1984, **49**, 3938.

7 *Typical procedure*: a solution of 6 mmol of $PhMe_2SiCu{\cdot}LiCN$ (see ref. 1) in THF (16 ml) was cooled to −40 °C and a slight excess of propa-1,2-diene was added from a balloon. The mixture was stirred for 1 h at this temperature, then $BF_3{\cdot}Et_2O$ (6 mmol) was added at −40 °C and the solution stirred for an additional period of 10 min. The nitrile (3 mmol) in THF (3 ml) was slowly dropped in at −49 °C, and the resulting mixture stirred at this temperature for 1 h. The reaction mixture was left to warm to 0 °C and was quenched with saturated ammonium chloride solution. Purification by flash-chromatography gave the ketones **10**–**13** (Table 1).

6-Phenyl-2-[dimethyl(phenyl)silyl]-7-{[dimethyl(phenyl)silyl]-methyl}octa-1,7-dien-4-one (**12**): ^1H NMR (300 MHz, $CDCl_3$): 7.53–7.02 (m, 15H), 5.58 (d, J = 2.5, 1H), 5.52 (d, J = 2.5, 1H), 4.64 (d, J = 0.7, 1H), 4.62 (d, J = 0.7, 1H), 3.52 (dd, J = 6.7 and 7.9, 1H), 2.98 (d, J = 14.7, 1H), 2.93 (d, J = 14.7, 1H), 2.69 (dd, J = 16.5 and 6.7, 1H), 2.54 (dd, J = 16.5 and 7.9, 1H), 1.66 (d, J = 13.8, 1H), 1.44 (d, J = 13.8, 1H), 0.41 (s, 6H), 0.34 (s, 6H); ^{13}C NMR (75 MHz, $CDCl_3$): 206.6, 148.2, 143.2, 142.6, 138.9, 137.3, 133.9, 133.6, 130.6, 129.1, 128.9, 128.3, 128.1, 127.7, 127.6, 126.4, 107.6, 50.4, 47.8, 47.2, 25.7, −2.9, −3.2; CIMS: m/z 483 (M + 1).

8 F. J. Weiberth and S. S. Hall, *J. Org. Chem.*, 1987, **52**, 3901.

9 P. Cuadrado, A. M. González, B. González and F. J. Pulido, *Synth. Commun.*, 1989, **19**, 275. See also ref. 1.

10 *Comprehensive Organic Synthesis*, eds. B. Trost and I. Fleming, Pergamon Press, Oxford, 1991, Vol. 4, pp. 148 and 179.

CHEMCOMM
Communication
www.rsc.org/chemcomm

Alizarin Red S. as a general optical reporter for studying the binding of boronic acids with carbohydrates

Greg Springsteen and Binghe Wang*

Department of Chemistry, North Carolina State University, Raleigh, NC 27695-8204, USA. E-mail: binghe-wang@ncsu.edu

Received (in Cambridge, UK) 4th June 2001, Accepted 16th July 2001
First published as an Advance Article on the web 9th August 2001

Alizarin Red S. displays a dramatic change in fluorescence intensity and color in response to the binding of a boronic acid and can be used as a general reporter for studying carbohydrate–boronic acid interactions, both quantitatively and qualitatively.

Boronic acids are known to bind diol moieties with high affinities through reversible boronate formation.[1] Consequently, boronic acid compounds have been widely used for the synthesis of artificial receptors for sugars with great success.[2–4] In addition, boronic acid compounds have been used for the development of protease inhibitors and other biologically important agents.[5,6] However, the examination of the binding of boronic acids to the target compounds is often difficult. Detection of boronate ester formation can sometimes be achieved by appending a fluorophore directly to the boronic acid.[4,7] In cases without a readily detectable and sensitive signal associated with the binding events, nuclear magnetic resonance, circular dichroism, and pH titration have been used for the examination of the binding.[1,8] In our research, we are interested in the design and synthesis of boronic acid compounds with highly selective affinities for saccharides,[9] especially certain cell surface carbohydrates. In such studies, the incorporation of fluorophores onto the boronic acid could greatly affect the binding affinity of the artificial receptor for the target sugar in a negative fashion, and could significantly increase the difficulty of the synthesis. Non-fluorescent assays using NMR and absorbance techniques often lack the desired sensitivity. Therefore, we wish to develop a general fluorescence assay method that allows us to monitor the binding of an unmodified boronic acid compound with its target carbohydrate.

Conceivably, the binding between boronic acids and their target carbohydrates can be monitored with the inclusion of a separate reporter fluorophore whose fluorescence is sensitive to the binding event. This type of fluorescence assay system requires two competing equilibria (Scheme 1). The first equilibrium, between the boronic acid and a fluorescent reporter compound (**1**), will be directly measured. To this end, we have worked on the synthesis of sensors that detect free boronic acids.[10] Alizarin Red S. (ARS) (**1**, Scheme 1) has been used as a reagent for the fluorimetric determination of boric acid concentrations.[11] Although the mechanism of the fluorescence increase was not elucidated, it is known that the active protons of hydroxyanthraquinones are responsible for a large fluorescence quenching.[12] Conceivably, binding of a boronic acid to the catechol diol of ARS would remove the active protons and, therefore, abolish the fluorescence quenching (**2**, Scheme 1). The addition of a carbohydrate (**3**) sets up a second equilibrium between the boronic acid and the diol moiety of the carbohydrate to give complex (**4**). This perturbs the reporter–boronic acid equilibrium, resulting in a change in fluorescence intensity. The fluorescence intensity changes in a three-component system can be used for the determination of binding constants using well-known literature procedures.[3,13,14]

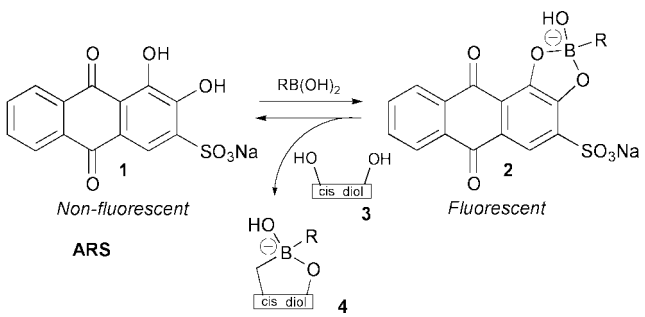

Scheme 1 Competitive binding of a boronic acid with Alizarin Red S. and a *cis*-diol.

To test the feasibility of this assay method, we first examined the effect of added boronic acid on the spectroscopic and fluorescence properties of ARS in aqueous solution at physiological pH. ARS shows a color change, from deep red to yellow, and an increase in fluorescence intensity by 20–80 fold in the presence of a wide variety of arylboronic acids in aqueous solution at pH 7.4 (data not shown). All of the boronic/boric acids tested induced significant fluorescence increases, indicating the general applicability of this method. It should also be noted that ARS has reasonable water solubility, up to 10^{-3} M, which makes it a good candidate as a reporter compound in an aqueous assay.

In order to determine the applicability of using ARS for the determination of the binding between a boronic acid and a carbohydrate in a three-component system, we used fructose as a model compound. D-Fructose is known to bind to phenylboronic acid (PBA) with high affinity.[1] When D-fructose was added to the mixture of PBA and ARS, significant fluorescence intensity changes were observed. Titrating fructose into an aqueous solution of 10^{-4} M ARS and 10^{-3} M PBA caused an eight-fold drop in fluorescence intensity (at 100 mM), and a measurable change down to the 100 μM level (Fig. 1). The fructose–PBA complex forms immediately upon mixing, and can also be monitored by UV absorption and a corresponding change in solution color from yellow to red (Fig. 2).

The ARS system also allows the quantitative determination of association constants (K_a) of diol–boronic acid complexes.

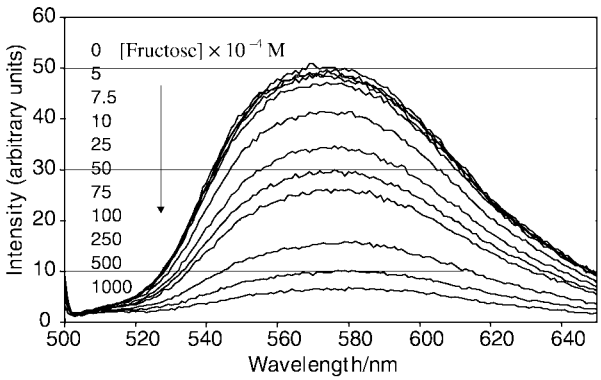

Fig. 1 Titration of fructose into a solution of ARS (10^{-4} M) and PBA (10^{-3} M). Fluorescence decreases with added fructose (0 through 0.1 M), aqueous 0.1 M phosphate buffer, pH 7.4, Exc. λ = 495 nm.

 DOI: 10.1039/b104895n

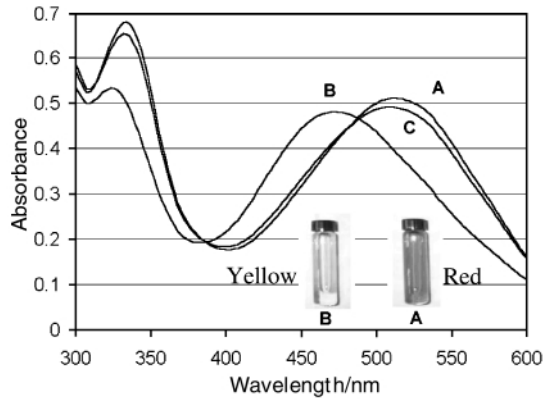

Fig. 2 A, Absorbance of ARS at 10^{-4} M in pH 7.4, 0.1 M phosphate buffer. B, ARS at 10^{-4} M with PBA at 10^{-3} M. C, Alizarin Red S. at 10^{-4} M with PBA at 10^{-3} M and fructose at 10^{-1} M.

Monitoring the fluorescence of ARS at different concentrations of boronic acid allows the calculation of the K_a of the boronic acid–ARS complex by the Benesi–Hildebrand method.[15] The boronic acid–diol association constant can then be measured in a separate titration with all three components using well-established literature procedures.[14] Using the ARS system, we have determined the binding constant between PBA and sialic acid (K_a, 21; pH 7.4 in 0.1 M phosphate buffer), one of the carbohydrates that we are interested in making a specific sensor for because of its important roles in biological systems.

In order to gain a greater understanding of the causes of the fluorescence change, the pH profile of the PBA–ARS complex was studied (Fig. 3). The profile shows that the largest response to PBA is centered on pH 7. The shape of the profile is likely a result of both the stability of the ARS–PBA complex, and the intrinsic fluorescence of the three ionic forms of ARS (pK_a = 5.3 and 10.9 by UV titration). It is well known that boronate ester complexes have decreased stability under acidic conditions.[16] This results in a high concentration of the quenched, free form of the dye at low pH (< 5). At medium pH (5–9), the boronate ester becomes stable, and therefore the quenching

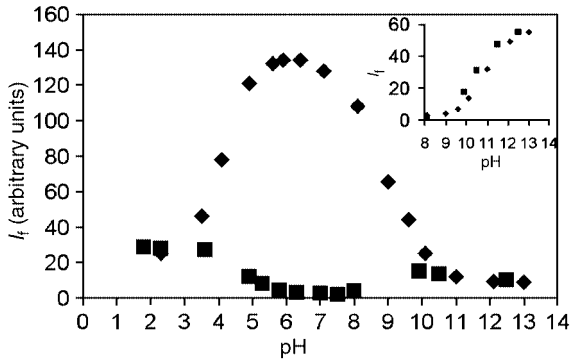

Fig. 3 (■)–pH titration of the fluorescence intensity (I_f) of ARS (10^{-4} M). (◆)–ARS (10^{-4} M) in the presence of PBA (10^{-2} M). Em. λ = 565 nm, Exc., λ = 495 nm, 0.1 M phosphate buffer. Inset–Em. λ = 633 nm, Exc. λ = 600 nm.

active protons are removed from the system. Association constants determined using the Benesi–Hildebrand method support this view (K_a = 190 at pH 4.6, and 1100 at pH 7.4). At high pH, there is also a considerable drop-off in the stability of the ester (K_a = 274 at pH 9.1). Although the uncomplexed dianion form has no active protons, there is a shift in fluorescence to longer wavelength (Fig. 3 inset), resulting in a sharp decrease in intensity at the shorter excitation and emission wavelengths (Fig. 3). Methylation of the 2′-hydroxyl of ARS causes an increase in the intrinsic fluorescence of the molecule, but removes virtually all response to phenylboronic acid at neutral pH (data not shown).

The absorption shift to lower wavelength upon complexation with phenylboronic acid (Fig. 2) is likely due to a decreased electron density on the ARS oxygens caused by the electron deficient boron. Acetyl and benzoyl substitution on hydroxy-anthraquinones results in similar shifts.[17]

ARS can be used as a general fluorescent reporter for studying the binding events between boronic acids and carbohydrates. It needs to be emphasized that there is no intrinsic specificity to the ARS system, and this is vital for its application as a general fluorescent reporter. There are many examples in the literature of boronic acids designed to specifically bind a particular analyte.[18,19] The ARS system will allow researchers a general and sensitive method to study the binding events of any boronic acid–diol interaction both quantitatively and qualitatively. This will aid in the further development of carbohydrate sensors and other biologically important boronic acid compounds.

Financial support by the National Institutes of Health (DK55062 and CA88343) is gratefully acknowledged.

Notes and references

1 J. P. Lorand and J. O. Edwards, *J. Org. Chem.*, 1959, **24**, 769.
2 T. D. James, P. Linnane and S. Shinkai, *Chem. Commun.*, 1996, 281.
3 L. Cabell, M. Monahan and E. Anslyn, *Tetrahedron Lett.*, 1999, **40**, 7753.
4 J. Yoon and A. W. Czarnik, *J. Am. Chem. Soc.*, 1992, **114**, 5874.
5 H. Suenaga, H. Yamamoto and S. Shinkai, *Pure Appl. Chem.*, 1996, **68**, 2179.
6 Z. Q. Tian, B. B. Brown, D. P. Mack, C. A. Hutton and P. A. Bartlett, *J. Org. Chem.*, 1997, **62**, 514.
7 T. James, S. Samankumara, R. Iguchi and S. Shinkai, *J. Am. Chem. Soc.*, 1995, **117**, 8982.
8 M. Takeuchi, T. Mizuno, H. Shinmori, M. Nakashima and S. Shinkai, *Tetrahedron.*, 1996, **52**, 1195.
9 W. Wang, S. Gao and B. Wang, *Org. Lett.*, 1999, **1**, 1209.
10 W. Wang, G. Springsteen, S. Gao and B. Wang, *Chem. Commun.*, 2000, 1283.
11 L. Szebellady and S. Tomay, *Z. Anal. Chem.*, 1936, **107**, 26.
12 D. Palit, H. Pal, T. Mukherjee and J. Mittal, *J. Chem. Soc., Faraday Trans.*, 1990, **86**, 3861.
13 J. Corkill, R. Foster and D. Hammick, *J. Chem. Soc.*, 1955, 1202.
14 K. Connors, *Binding Constants*, John Wiley and Sons, New York, 1987.
15 H. A. Benesi and J. Hildebrand, *J. Am. Chem. Soc.*, 1949, **71**, 2703.
16 X. Liu and W. Scouten, *J. Chromatogr., A.*, 1994, **687**, 61.
17 A. Diaz, *J. Photochem. Photobiol., A*, 1990, **53**, 141.
18 Y. Shiomo, M. Saisho, K. Tsukagoshi and S. Shinkai, *J. Chem. Soc., Perkin Trans. 1*, 1993, 2111.
19 S. Sandanayake, T. James and S. Shinkai, *Pure Appl. Chem.*, 1996, **68**, 1207.

CHEMCOMM
Communication
www.rsc.org/chemcomm

Electrochemical evidence for electronic interactions through the *para*-carborane skeleton in the novel tricluster $[\{Co_2C_2(SiMe_3)(CO)_4(dppm)\}_2(\mu\text{-}CB_{10}H_{10}C)]$

Mark A. Fox,[a] Michael A. J. Paterson,[a] Carlo Nervi,[b] Francesco Galeotti,[b] Horst Puschmann,[a] Judith A. K. Howard[a] and Paul J. Low*[a]

[a] *Department of Chemistry, University of Durham, South Road, Durham, UK DH1 3LE. E-mail: p.j.low@durham.ac.uk*
[b] *Dipartmento di Chimica IFM, via P. Giuria, 10125 Torino, Italy. E-mail: nervi@ch.unito.it*

Received (in Cambridge, UK) 16th May 2001, Accepted 13th July 2001
First published as an Advance Article on the web 9th August 2001

The electrochemical properties of the title compound reveal electronic interactions between two dicobalt–dicarbon clusters *via* a 1,12-*para*-carborane cage.

Conjugated molecular and polymeric compounds with delocalised π-electron frameworks and rigid-rod geometries are a source of immense contemporary interest, with potential for application in the construction of photonic and molecular electronic devices.[1] The unusual electronic properties of *closo*-carborane cages, which display three-dimensional aromaticity,[2] and the abilities of *para*-carboranes to form rod-like structures have raised considerable interest in the synthesis of novel conjugated materials that contain this motif.[3–7] The capacity for polyhedral transition metal clusters to act as 'electron sinks', accepting or releasing electrons in response to the demands of the environment (*i.e.* an electrode) or pendant groups, suggests molecular assemblies which feature these moieties may be of use in molecular electronics applications.[8]

However, compounds which feature both carborane and transition metal clusters are rare,[9] and the transmission of electronic effects between these different types of polyhedra has not yet been demonstrated. We have taken advantage of the availability of 1,12-bis(trimethylsilylethynyl)-*para*-carborane **1**[10] and the redox properties of Co_2(alkyne) complexes[11,12] to demonstrate, using electrochemical methods, the capacity for the 12-vertex *para*-carborane fragment to transmit electronic information between two transition metal clusters. Aryl, alkynyl and ferrocenyl based spacing groups have already been shown to permit such interactions between cobalt-containing tetrahedral clusters.[12]

The reaction of **1** with $[Co_2(CO)_6(dppm)]$[13] in refluxing benzene afforded a dark red solution from which the novel tricluster compound **2** was isolated as the major product (60 mg, 40%) by preparative TLC and crystallisation (CH_2Cl_2–MeOH) (Scheme 1). The composition of the complex was established from the spectroscopic data,† and confirmed by X-ray analysis.‡ The structure (Fig. 1) clearly shows the *para*-C_2B_{10} icosahedron and the two Co_2C_2 tetrahedra, which are related by a crystallographic inversion centre at the centre of the carborane cage. The carborane cage in **2** is the most spherical example of a *para*-carborane structurally characterised to date, with a cage C···C separation of 3.176 Å and an average tropical B–B bond length of 1.776 Å. This contrasts sharply with the distorted cage geometry found in 1,12-bis(ethynyl)-*para*-carborane [C···C 3.104(2) Å, tropical B–B 1.793(3) Å].[10] These variations in the geometry of the carborane cage are probably a consequence of the different interactions between the carborane C_{sp} atom and the carbon centre of the pendant ethynyl group [C_{sp}, C–C 1.451(2) Å] or cobalt cluster [**2**, C_{sp^3}, C(1)–C(2) 1.497(2) Å]. The parameters associated with the cobalt(alkyne) cluster cores fall in the range established for aryl substituted clusters.[14] While the description of carborane clusters as analogues of benzene is not intended to be literal, we note here that the C(1)–C(2) bond in **2** is longer than the C(aryl)–C(cluster) separations in conjugated $Co_2(\mu\text{-}\eta^2\text{-}RC_2C_6H_4\text{-}X\text{-}p)(CO)_4(dppm)$ systems [1.458(3)–1.463(3) Å],[14] due to the high coordination number of the carborane cage carbon atoms.

The Co_2C_2 tetrahedral cluster core offers a filled a_2-type fragment orbital suitable for interaction with π-systems of adjacent groups bonded at a carbon vertex of the tetrahedron.[15] The carbon atoms of the carborane cage offer tangential fragment orbitals with considerable p-character suitable for such an interaction.[16] Of course, good orbital overlap requires matching of fragment orbital energy as well as symmetry. The concept of a degree of π-bonding between the cobalt/carbon and boron/carbon cluster cores in the neutral tricluster **2** is supported, although by no means proven, by the geometry adopted by the complex in the solid state. Semi-empirical MO calculations (LANL2MB)[17] revealed the frontier orbitals (HOMO and LUMO) of **2** to be largely centred on the cobalt clusters.

The cyclic voltammogram of complex **2** revealed both oxidation and reduction processes which were better resolved using semi-derivative[18] and square wave voltammetry (SWV) (Fig. 2). Digital simulation of the CV and SWV responses was employed to confirm the four redox potentials [+0.87, +0.77, −1.58, −1.66 V (*vs.* decamethylferrocene, Fc*/Fc*$^+$ 0.084 V); ΔE^0(ox) *ca.* 105 mV, $K_C = e^{\Delta E^\circ F/RT} = 60$; ΔE^0(red) *ca.* 80

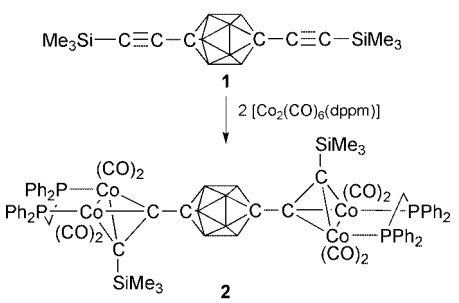

Scheme 1

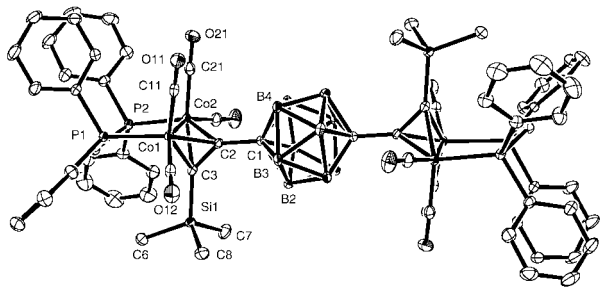

Fig. 1 Molecular structure of **2**. Selected bond lengths (Å) and angles (°): C(1)–C(2) 1.497(2), C(2)–C(3) 1.359(2), C(1)–B(av.) 1.728(3), B–B(av.) 1.771(3), Co(1)–Co(2) 2.4804(4), C(1)–C(2)–C(3) 139.3(2), C(2)–C(3)–Si(1) 138.9(1), Co(1)–Co(2)–P(2) 98.41(2), Co(2)–Co(1)–P(1) 95.14(2).

 DOI: 10.1039/b104307m

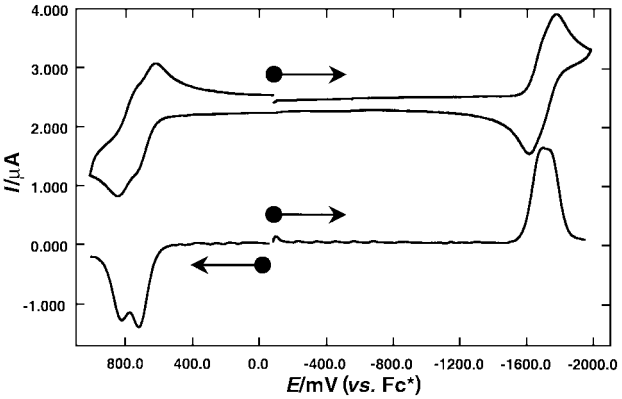

Fig. 2 Cyclic voltammogram (upper trace) and corresponding semi-derivative voltammogram of a THF solution of **2** (0.5 mM), containing 0.1 M $[NBu_4]PF_6$ as supporting electrolyte, at 0.2 V s^{-1}. Data obtained at 298 K, glassy carbon working electrode *vs.* SCE reference electrode.

mV, K_C = 5].[19] No redox processes were found within the accessible potential window when **1** was subjected to a similar electrochemical study. For comparison, the phenyl-bridged complex $[\{Co_2C_2(H)(CO)_4(dppm)\}_2(\mu\text{-}1,4\text{-}C_6H_4)]$ gave also gave two oxidation and reduction processes with ΔE^0(ox) 110 mV, ΔE^0(red) 80 mV.[12c]

The splitting of redox waves associated with otherwise chemically identical redox sites contained within a single molecular unit is often cited as evidence of electronic interaction (or communication) between these sites.[11,12,20] These interactions may be transmitted between the bonding framework or through-space.[21] While ion-pairing effects may be expected to play a role in the magnitude of the coulombic interaction between remote intramolecular sites, a through-space interaction should affect both oxidation and reduction processes more or less equally. In the present example, the difference in oxidation potentials observed is significantly large, especially given the > 6 Å separation of the cobalt cluster cores, and is indicative of a moderate degree of extended electronic communication between the cobalt clusters in the radical cation $\mathbf{2}^{\cdot+}$. The separation of the reduction events is somewhat smaller, but is still larger than the statistical limit (*ca.* 36 mV at 298 K) predicted for non-interacting redox centres.[20] The voltammetric studies reported here therefore suggest that the unpaired electron in both the radical cation $\mathbf{2}^{\cdot+}$ and the radical anion $\mathbf{2}^{\cdot-}$ is delocalised through the bonding framework. These studies clearly indicate that the bonding framework of the *para*-carborane cage can offer an efficient conduit for electronic effects, and may participate in π-type delocalised bonding with substituents in the 1 and 12 positions. Further studies on the scope of these interactions and a thorough molecular orbital description of assemblies derived from *para*-carboranes, including $\mathbf{2}^{\cdot+}$ and $\mathbf{2}^{\cdot-}$ are in progress.

We gratefully acknowledge financial support from the EPSRC, the Department of Chemistry, Durham University and MURST (Rome, COFIN-99). J. A. K. H. holds an EPSRC Senior Research Fellowship. M. A. F. thanks the EPSRC for an Advanced Research Fellowship. Assistance from the EPSRC National Mass Spectrometry Service Centre (Swansea) is gratefully acknowledged. We thank Prof. K. Wade for encouraging this work, and helpful comments.

Notes and references

† *Selected spectral data*: NMR ($CDCl_3$): ^{1}H, δ 7.10–6.30 (m, 20H, Ph), 3.09, 3.25 (2 dt, $J_{HP} = J_{HH} = 11$ Hz, 2 × 1H, CH_2), 1.28 (br, 5H, BH), 0.00 (s, 9H, $SiMe_3$). ^{11}B, δ −11.0. FAB-MS (*m*/*z*) 1454, 1426, 1342 $[M - nCO]^+$ (n = 4, 5, 7). IR (cyclohexane): ν(BH) 2659; ν(CO) 2026m, 2002s, 1976s, 1964m cm^{-1}. Found: C, 52.15; H, 4.56. $C_{70}H_{72}B_{10}O_8Si_2P_4Co_4{\cdot}0.5CH_2Cl_2$ requires C, 52.64; H, 4.42%.

‡ *Crystal data*: $C_{73}H_{78}B_{10}O_8Si_2P_4Cl_6Co_4$, M = 1819.93, triclinic, space group $P\bar{1}$, a = 12.287(2), b = 13.004(2), c = 13.545(2) Å, α = 103.15(1), β = 95.82(1), γ = 96.04(1)°, V = 2078.1(6) Å^3, T = 100(2) K, Z = 1, μ(Mo-Kα) = 1.135 mm^{-1}, 23469 reflections measured, 9578 unique (R_{int} = 0.0396) which were used in all calculations. The final $wR(F^2)$ = 0.0789 (all data). All phenyl group hydrogen atoms were placed in calculated positions and refined using a riding model. Three disordered molecules of CH_2Cl_2 were found per formula unit. CCDC reference number 167400. See http://www.rsc.org/suppdata/cc/b1/b104307m/ for crystallographic data in CIF or other electronic format.

1 P. F. H. Schwab, M. D. Levin and J. Michl, *Chem. Rev.*, 1999, **99**, 1863.
2 J. Aihara, *J. Am. Chem. Soc.*, 1978, **100**, 3339; A. J. Stone and M. J. Alderton, *Inorg. Chem.*, 1982, **21**, 22971; R. B. King, *Russ. Chem. Bull.*, 1993, **42**, 1283; B. M. Gimarc and M. Zhao, *Inorg. Chem.*, 1996, **35**, 825; G. A. Olah, G. K. S. Prakash, R. E. Williams, L. E. Fidd and K. Wade, *Hypercarbon Chemistry*, Wiley, New York, 1987; P. v. R. Schleyer and K. Najafion, *Inorg. Chem.*, 1998, **37**, 3454.
3 S. Pakhomov, P. Kaszynski and V. G. Young Jr., *Inorg. Chem.*, 2000, **39**, 2243.
4 P. Kaszynski and A. G. Douglas, *J. Organomet. Chem.*, 1999, **581**, 28.
5 M. A. Fox, J. A. H. MacBride, R. J. Peace and K. Wade, *J. Chem. Soc., Dalton Trans.*, 1998, 401.
6 C. Mazal, A. J. Paraskos and J. Michl, *J. Org. Chem.*, 1998, **63**, 2116.
7 X. Yang, W. Jiang, C. B. Knobler and M. F. Hawthorne, *J. Am. Chem. Soc.*, 1992, **114**, 9719; J. M ller, K. Base, T. F. Magnera and J. Michl, *J. Am. Chem. Soc.*, 1992, **114**, 9721.
8 W. E. Geiger and N. G. Connelly, *Adv. Organomet. Chem.*, 1985, **24**, 87; U. Simon, in *Metal Clusters in Chemistry*, ed. P. Braustein, L. A. Oro and P. R. Raithby, Wiley-VCH, Weinham, 1999, vol. 3, ch. 4.4, pp. 1342–1363.
9 R. N. Grimes, *Coord. Chem. Rev.*, 2000, **200-202**, 773; M. Heberhold, U. Bertholdt, W. Milius, A. Gloeckle and B. Wrackmeyer, *Chem. Commun.*, 1996, 1219.
10 A. S. Batsanov, M. A. Fox, J. A. K. Howard, J. A. H. MacBride and K. Wade, *J. Organomet. Chem.*, 2000, **610**, 20.
11 R. P. Aggarwal, N. G. Connelly, M. C. Crespo, B. J. Dunne, P. M. Hopkins and A. G. Orpen, *J. Chem. Soc., Dalton Trans.*, 1992, 655; P. J. Low, R. Rousseau, P. Lam, K. A. Udachin, G. D. Enright, J. S. Tse, D. D. M. Wayner and A. J. Carty, *Organometallics*, 1999, **18**, 3885.
12 (*a*) C. J. McAdam, N. W. Duffy, B. H. Robinson and J. Simpson, *Organometallics*, 1996, **15**, 3935; (*b*) N. Duffy, J. McAdam, C. Nervi, D. Osella, M. Ravera, B. Robinson and J. Simpson, *Inorg. Chem. Acta.*, 1996, **247**, 99; (*c*) D. Osella, L. Milone, C. Nervi and M. Ravera, *Eur. J. Inorg. Chem.*, 1998, 1473; (*d*) C. J. McAdam, J. J. Brunton, B. H. Robinson and J. Simpson, *J. Chem. Soc., Dalton Trans.*, 1999, 2487; (*e*) L.-A. Hore, C. J. McAdam, J. L. Kerr, N. W. Duffy, B. H. Robinson and J. Simpson, *Organometallics*, 2000, **19**, 5039; (*f*) M. L. Marcos, M. J. Macazaga, R. M. Medina, C. Moreno, J. A. Castro, J. L. Gomez, S. Delgado and J. Gonzalez-Velasco, *Inorg. Chim. Acta.*, 2001, **312**, 249.
13 L. S. Chia and W. R. Cullen, *Inorg. Chem.*, 1975, **14**, 482.
14 T. J. Snaith, P. J. Low, R. Rousseau, H. Puschmann and J. A. K. Howard, *J. Chem. Soc., Dalton Trans.*, 2001, 292.
15 D. M. Hoffman, R. Hoffmann and C. R. Fisel, *J. Am. Chem. Soc.*, 1982, **104**, 3858.
16 K. Wade, *Adv. Inorg. Radiochem.*, 1976, **18**, 1.
17 Gaussian 94, Revision E.2, M. J. Frisch, G. W. Trucks, H. B. Schlegel, P. M. W. Gill, B. G. Johnson, M. A. Robb, J. R. Cheeseman, T. Keith, G. A. Petersson, J. A. Montgomery, K. Raghavachari, M. A. Al-Laham, V. G. Zakrzewski, J. V. Ortiz, J. B. Foresman, J. Cioslowski, B. B. Stefanov, A. Nanayakkara, M. Challacombe, C. Y. Peng, P. Y. Ayala, W. Chen, M. W. Wong, J. L. Andres, E. S. Replogle, R. Gomperts, R. L. Martin, D. J. Fox, J. S. Binkley, D. J. Defrees, J. Baker, J. P. Stewart, M. Head-Gordon, C. Gonzalez and J. A. Pople, Gaussian, Inc., Pittsburgh, PA, 1995.
18 J. C. Myland and K. B. Oldham, *Anal. Chem.*, 1988, **60**, 62.
19 The simulation program ESP (C. Nervi) is available *via the* Internet at http://lem.ch.unito.it/chemistry/esp_manual.htm
20 D. E. Richardson and H. Taube, *Inorg. Chem.*, 1981, **20**, 1278.
21 K. Bowden and E. J. Grubbs, *Chem. Soc. Rev.*, 1996, **25**, 171.

CHEMCOMM Communication
www.rsc.org/chemcomm

A remarkable rate acceleration of the Baylis–Hillman reaction

Wei-Der Lee, Kung-Shuo Yang and Kwunmin Chen*

Department of Chemistry, National Taiwan Normal University, 88 Sec. 4 TingChow Road, Taipei, Taiwan 116, ROC. E-mail: kchen@scc.ntnu.edu.tw; Fax: +886-2-29324249; Tel: +886-2-89315831

Received (in Cambridge, UK) 24th April 2001, Accepted 28th June 2001
First published as an Advance Article on the web 9th August 2001

Treatment of α-naphthyl acrylate with both aliphatic and aromatic aldehydes in the presence of DABCO (30 mol%) afforded the desired (α-methylene-β-hydroxy)esters with reasonable chemical yields (51–88%) within 20 min.

Increasing interest has been focused on the coupling of an aldehyde with acrylate in the presence of DABCO (Baylis–Hillman reaction).[1] The resulting (α-methylene-β-hydroxy)-esters are versatile intermediates that allow for further functional group manipulation. One of the major drawbacks of this transformation is the poor reaction rates which limits the range of substrates that are tolerated.[2] Many aromatic aldehydes and branched aliphatic aldehydes are reluctant to serve as substrates. It is not surprisingly that numerous methods including physical as well as chemical attempts have been made to increase the reaction rate.[3] Modest increases in rates have been obtained under modified reaction conditions. No practical methods have been developed so far. We wish to report here that an extremely rapid rate can be achieved using α-naphthyl acrylate as the Michael acceptor for the Baylis–Hillman reaction.

A plausible mechanism for the Baylis–Hillman reaction is proposed and the addition of ammonium enolate with an aldehyde is believed to be the rate-determining step.[4] Stabilization of the enolate species would shift the equilibrium forward and therefore to accelerate the rates. The use of Lewis acid to catalyze this transformation is a common strategy. The use of lanthanides and group III metal triflates to accelerate the Baylis–Hillman reaction have been studied.[3e–g] However structural variants of acrylates for this transformation have not been studied systematically.[5] This promoted us to screen a range of substituted acrylates **1a**–**g** as Michael acceptor. The substituted acrylates may provide stereo- and/or stereoelectronic effects to stabilize the oxy anion intermediate and subsequently accelerate the following aldol reaction. To test this hypothesis various acrylates **1a**–**g** with diverse steric, geometric and electronic properties were prepared and benzaldehyde was used as a probe electrophile (Table 1). Reaction of methyl acrylate (1.0 equiv.) with benzaldehyde (1.0 equiv.) in CH_3CN in the presence of DABCO (50 mol%) at room temperature gave the corresponding product **2a** in 62% yield for 48 h (entry 1). The use of *tert*-butyl acrylate affords a similar result (entry 2). The use of phenyl acrylate **1c** gave the desired product **2c** with 86% yield in 2 h (entry 3). Treatment of benzyl acrylate with benzaldehyde under the same reaction conditions provided **2d** with 80% yield in 15 h (entry 4). The desired product **2e** was isolated in 34% yield when the commercial available 1,1,1,3,3,3-hexafluoroisopropyl acrylate[6] **1e** was used (entry 5). The use of β-naphthyl acrylate **1f** gave **2f** with 70% yield in 5 h (entry 6). A significant rate acceleration was observed when α-naphthyl acrylate **1g** was employed. Thus, treatment of **1g** with benzaldehyde in the presence of DABCO affords the desired product with 88% yield in 20 min (entry 7). The unexpected rate acceleration using α-naphthyl acrylate for the Baylis–Hillman reaction is amazing and was studied in more detail.

To further determine the feasibility of this system, various aldehydes were then studied using α-naphthyl acrylate under the optimum conditions and the results are tabulated in Table 2. Thus, treatment of **1g** with acetaldehyde affords **3a** with 70% yield at room temperature in 20 min (entry 1). Similar results were observed with different chain aldehydes (entries 2–4). The reaction was slightly less effective when α-branched aldehyde was used (entry 5). *trans*-Cinnamaldehyde was employed to give the desired product with 60% yield in 20 min (entry 6). Next, substituted aromatic aldehydes were subjected to the same reaction conditions. Reaction of *p*-nitrobenzaldehyde and *p*-fluorobenzaldehyde with **1g** under the same conditions

Table 1 Reaction of benzaldehyde with various acrylates **1a**–**g** in the presence of DABCO[a]

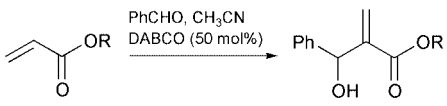

1 **2**

a R = Me
b R = t-Bu
c R = Ph
d R = Bn
e R = $CH(CF_3)_2$
f R = β-Naphthyl
g R = α-Naphthyl

Entry	Acrylate	*t*/h	Product	Yield (%)[b]
1	**1a**	48 (4)[c]	**2a**	62 (68)
2	**1b**	15 (28 days)[d]	**2b**	50 (90)
3	**1c**	2 (3)[e]	**2c**	86 (78)
4	**1d**	15	**2d**	80
5	**1e**	48	**2e**	34
6	**1f**	5	**2f**	70
7	**1g**	1/3	**2g**	88

[a] All reactions were conducted using 1:1 ratio of acrylate and aldehyde in CH_3CN at room temperature in the presence of DABCO (50 mol%). [b] Isolated yield. [c] Numbers in parentheses are reported data. For experimental details see ref. 3*j*. [d] Ref. 2. [e] Ref. 5.

Table 2 Reaction of **1g** with various aldehydes[a]

1g **3a-k**

Entry	RCHO (R=)	*t*/min	**3** (% yield)[b]
1	CH_3	20	70
2	CH_3CH_2	20	77
3	$(CH_3)_2CHCH_2$	20	62
4	$PhCH_2CH_2$	20	65
5	$(CH_3)_2CH$	20	51
6	*trans*-$C_6H_4CH{=}CH$	20	60
7	*p*-$NO_2C_6H_4$	10	82
8	*p*-FC_6H_4	20	65
9	*p*-MeC_6H_4	20	71
10	*p*-$OMeC_6H_4$	20 h	35
11	*p*-$OMeC_6H_4$	96 h	71
12	3-Pyridyl	20	72

[a] All reactions were conducted using 1:1 molar ratio of acrylate and aldehyde in CH_3CN at room temperature. The amounts of DABCO used was reduced to 30 mol% to minimize the formation of the cyclic acetates **4**. [b] Isolated yield.

 DOI: 10.1039/b103644k

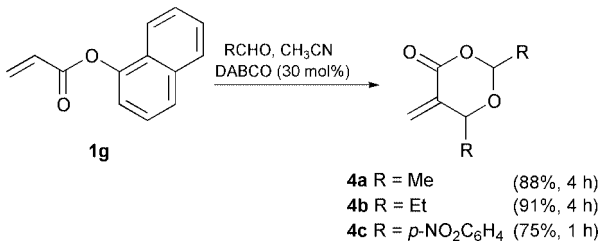

Scheme 1 The synthesis of 1,3-dioxan-4-ones **4a**–**c**.

provide the desired products with 82 and 65% yield, respectively (entries 7 and 8). Although the use of *p*-methylbenzaldehyde gave a similar result, the use of *p*-methoxybenzaldehyde requires 96 h to obtain comparable yield (entries 9 and 11). This may be due to the relatively strong electron donating ability of the methoxy group that deaccelerates the reaction rate. The detailed mechanistic speculation is premature at this stage and work is underway to study this phenomenon in more detail.

The reaction of various aldehydes with α-naphthyl acrylate **1g** was very fast as mentioned above. In addition to the conventional Baylis–Hillman products isolated, small quantities (3–10%) of cyclic acetates were identified dependent upon the substrates used. The minor product may come from the addition of the initial product with the unreacted aldehyde followed by elimination of α-naphthol anion.[5] The cyclic acetal products are of great synthetic interest.[7] The preparation of various 1,3-dioxan-4-ones under several different reaction systems have been reported.[3k,5,6] In this study, the use of excess amounts of aldehydes (4.0 equiv.) under prolonged reaction time gave 1,3-dioxan-4-ones **4a**–**c** with good to high chemical yields (Scheme 1).

In summary, we have developed an efficient method for the synthesis of highly functionalized acrylates. Reaction of α-naphthyl acrylate **1g** with both aliphatic and aromatic aldehydes in the presence of DABCO (30 mol%) provided the corresponding α-methylene β-hydroxy carbonyl derivatives with reasonable material yields within 20 min. *This represents, to the best of our knowledge, one of the best rate acceleration systems for wide ranges of aldehydes in Baylis–Hillman reactions under atmospheric pressure*. The pronounced acceleration of this reaction further extends the Baylis–Hillman reaction into a viable transformation. The asymmetric version of the Baylis–Hillman reaction using this reaction system is underway in our laboratory.

We thank the National Science Council (NSC) for financial support of this work.

Notes and references

1 For reviews of the Baylis–Hillman reaction, see: (*a*) P. Langer, *Angew. Chem.*, 2000, **39**, 3049; (*b*) E. Ciganek, *Org. React.*, 1997, **51**, 201; (*c*) D. Basavaiah, D. P. Rao and R. S. Hyma, *Tetrahedron*, 1996, **52**, 8001; (*d*) S. E. Drewes and G. H. P. Roos, *Tetrahedron*, 1988, **44**, 4653.
2 Y. Fort, M. C. Berthe and P. Caubere, *Tetrahedron*, 1992, **48**, 6371.
3 (*a*) M. K. Kundu, S. B. Mukherjee, N. Balu, R. Padmakumar and S. V. Bhat, *Synlett*, 1994, 444; (*b*) R. J. W. Schuurman, A. Linden, R. P. F. Grimbergen, R. J. M. Nolte and H. S. Scheeren, *Tetrahedron*, 1996, **52**, 8307; (*c*) M. Shi and Y.-S. Feng, *J. Org. Chem.*, 2001, **66**, 406; (*d*) M. Kawamura and S. Kobayashi, *Tetrahedron Lett.*, 1999, **40**, 1539; (*e*) V. K. Aggarwal, G. J. Tarver and R. McCague, *J. Chem. Soc., Chem. Commun.*, 1996, 2713; (*f*) V. K. Aggarwal, A. Mereu, G. J. Tarver and R. McCague, *J. Org. Chem.*, 1998, **63**, 7183; (*g*) V. K. Aggarwal and A. Mereu, *J. Chem. Soc., Chem. Commun.*, 1999, 2311; (*h*) J. Auge, N. Lubin and A. Lubineau, *Tetrahedron Lett.*, 1994, **35**, 7947; (*i*) Y. M. A. Yamada and S. Ikegami, *Tetrahedron Lett.*, 2000, **41**, 2165; (*j*) S. Rafel and J. W. Leahy, *J. Org. Chem.*, 1997, **62**, 1521; (*k*) L. J. Brzezinski, S. Rafel and J. W. Leahy, *J. Am. Chem. Soc.*, 1997, **119**, 4317.
4 J. S. Hill and N. S. Issacs, *J. Phys. Org. Chem.*, 1990, 285.
5 P. Perlmutter, E. Puniani and G. Westman, *Tetrahedron Lett.*, 1996, **37**, 1715.
6 Y. Iwabuchi, M. Nakatani, N. Yokoyama and S. J. Hatakeyama, *J. Am. Chem. Soc.*, 1999, **121**, 10 219 and also footnote 8.
7 J. Zimmermann and D. Seebach, *Helv. Chim. Acta*, 1987, **70**, 1104.

CHEMCOMM Communication
www.rsc.org/chemcomm

Positive and negative photopatterning of metal oxides on silicon *via* bipolar electrochemical deposition†

Hee Cheul Choi and Jillian M. Buriak*

Department of Chemistry, 1393 Brown Laboratories, Purdue University, West Lafayette, IN 47907-1393, USA. E-mail: buriak@purdue.edu

Received (in Cambridge, UK) 24th May 2001, Accepted 13th July 2001
First published as an Advance Article on the web 9th August 2001

Negative and positive microscale patterning of metal oxides is efficiently and rapidly carried out on flat Si(100) surfaces *via* a simple white light assisted bipolar electrochemical process.

The importance of transparent or semi-transparent thin films of high band gap metal oxide semiconductors is rapidly increasing due to a wide range of applications,[1] such as inexpensive photovoltaic cells,[2,3] electrochromic smart windows,[4] ultrafast color displays,[5] and as a base material for room temperature dilute magnetic oxides (DMO).[6] Various techniques such as simple sol–gel preparation followed by dip or spin coating,[7] radio frequency magnetron sputtering,[8] chemical vapor deposition,[9] or laser ablation[10] have been used for many years to prepare metal oxide thin films. Electrochemical deposition has, however, been the focus of much recent interest due its comparable simplicity of required apparatus, and the possibility for either kinetic or thermodynamic control of products *via* galvanostatic or potentiostatic modes.[11] Since Switzer introduced an electrosynthetic technique for preparation of metal oxides in 1987,[12] there have been many reports outlining electrochemical deposition of different metal oxides on various types of conducting substrates.[11] Generally, metal oxide deposition can be accomplished by either anodic or cathodic bias, depending on the desired oxide.[11,13–17] Patterning of metal oxide thin films is central to their application in technological devices to allow for spatial definition.[18] Here we describe a general white light promoted electrochemical metal oxide photopatterning procedure on n- or p-type Si(100) that allows, in a very straightforward and efficient manner, both negative and positive masking, as shown in Fig. 1.

A number of electrochemical deposition parameters were systematically varied to determine the requirements for positive and negative pattern formation on Si(100) substrates, as summarized in Table 1. In addition, the influence of different procedures on the metal oxide structures was determined by X-ray diffraction (XRD) and scanning electron microscopy (SEM). The first four processes, 1P–4P, are illuminated through a grid mask with white light, and the second four, processes 1–4, do not involve photopatterning and are used as reference samples. Only processes 3P and 4P lead to positive and negative photopatterning, depending upon the doping of the silicon. Processes 1P and 2P, on the other hand, lead to homogeneous deposition of metal oxides across the entire face of the exposed silicon surface. Fig. 2 shows the results of positive and negative photopatterning experiments formed *via* process 3P with zinc nitrate on n-type (left) and p-type (right) silicon substrates as visualized by optical microscopy (similar patterns of CeO_2 and Cr_2O_3 are shown in the ESI†). The dark areas in Fig. 2 are underivatized Si, and the light areas the metal oxide, as determined by XRD (*vide infra*). The metal oxides deposit in the shaded region when the substrate is n-type Si, and exclusively in the illuminated area on p-type Si. Process 4P, involving *in situ* heating and elimination of the secondary sintering step, yields similar results and indicates that metal oxides can be successfully patterned regardless of the heating process. Earlier work has shown that in the case of metal oxides

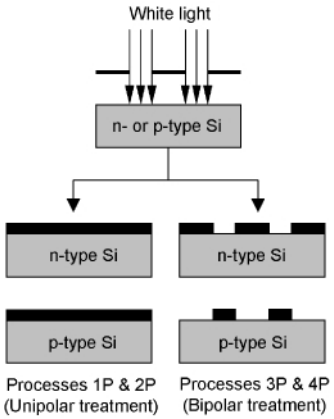

Fig. 1 Schematic view of electrochemical patterning of ZnO on Si(100) substrates with white light illumination through a photomask. Positive and negative patterning can be achieved through bipolar electrochemical treatment.

† Electronic supplementary information (ESI) available: experimental details, XRD profiles, optical and SEM micrographs. See http://www.rsc.org/suppdata/cc/b1/b104586p/

Table 1 Outline of the 8 different metal oxide deposition approaches for synthesis of ZnO, CeO_2 and Cr_2O_3 on Si(100). Processes 1–4 do not involve patterning, while processes 1P–4P differ only in that they are patterned *via* simultaneous white light illumination with a photomask

Method	Treatment
Photopatterning of metal oxides on Si	
Process 1P	Unipolar (cathodic) → *ex situ* sintering at 350 °C
Process 2P	Unipolar (cathodic) → *in situ* heating at 60 °C
Process 3P	Bipolar (anodic followed by cathodic) → *ex situ* sintering at 350 °C
Process 4P	Bipolar (anodic followed by cathodic) → *in situ* heating at 60 °C
Non-photopatterned deposition of metal oxides on Si	
Process 1	Unipolar (cathodic) → *ex situ* sintering at 350 °C
Process 2	Unipolar (cathodic) → *in situ* heating at 60 °C
Process 3	Bipolar (anodic followed by cathodic) → *ex situ* sintering at 350 °C
Process 4	Bipolar (anodic followed by cathodic) → *in situ* heating at 60 °C

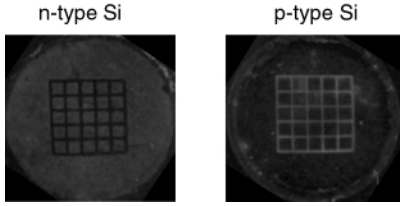

Fig. 2 Optical micrographs of the patterned ZnO films on n- and p-type Si. The diameter of the circular area is 1.0 cm. The light areas correspond to the metal oxide deposits while the dark areas correspond to underivatized Si surfaces.

 DOI: 10.1039/b104586p

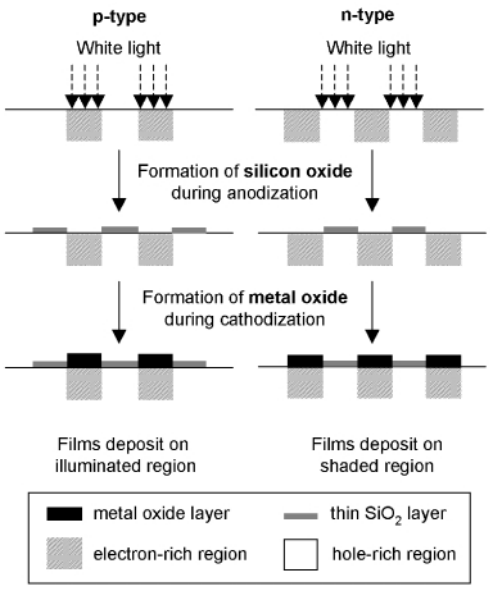

Fig. 3 Schematic illustration of the effect of light illumination, allowing selective photopatterning of various metal oxides on n- and p-type silicon, outlining the importance of doping type. Illumination coupled with application of an anodic bias induces holes to localize in the illuminated areas for n-type Si, and in the shaded areas for p-type Si. Therefore, silicon oxide formation occurs in positive and negative areas, relative to the photomask. The insulating characteristics of the SiO_2 layer prevent metal oxide deposition during the subsequent cathodic step.

which can be formed *via* anodic oxidation on silicon (Tl_2O_3 for example), photopatterning occurs only in the illluminated area of n-type silicon.[14] The bipolar electrochemical deposition approach therefore demonstrates excellent and unique selectivity for both negative and positive photopatterning of different metal oxides on silicon substrates.

While unipolar cathodic metal oxide deposition with either *ex situ* sintering[19] or *in situ* heating[15] is known in the literature, bipolar deposition, on the other hand, is not. Processes 1–4 were examined to prepare large areas of metal oxide for characterization, and to ensure that the same material is produced under photopatterning conditions (processes 1P–4P). XRD experiments reveal that the ZnO film deposited by cathodic unipolar treatment (processes 1 and 2), with or without illumination, is of a wurtzite crystal structure (JCPDS table 35–1451).[20] The XRD patterns of ZnO deposited through processes 3 and 4 on n-type Si are identical to processes 1 and 2, also of a wurtzite structure, and little difference in the crystal structure between *in situ* (process 3) and *ex situ* heating (process 4) is noted. The XRD spectra of the photopatterned metal oxides indicate that the crystal structures formed under these conditions (processes 3P and 4P) are the same as processes 1–4, and thus the photopatterning process does not have a major influence on the nature of the metal oxide. The details of XRD studies of all the metal oxides studied here are included in the ESI†. SEM studies revealed that a porous granular thin film is formed *via* all of these electrodeposition procedures ESI†. The mechanism for cathodic metal oxide formation is most likely nitrate reduction, forming OH^- which precipitates the metal hydroxide/oxide.[15]

The bipolar electrochemical deposition technique that leads to patterning requires application of a short period of anodic current to the silicon surface (+ 5 mA cm^{-2}) for 5 s, prior to cathodization (−5 mA cm^{-2}) for 5 min. As a control experiment, the silicon surface (both n- and p-type) was illuminated through a photomask during application of a cathodic current for 5 min, without the preceding short anodic pulse. Under these conditions, only homogeneous deposition of metal oxides occurs over the entire substrate surface; no patterning is observed, confirming the importance of the short anodic pretreatment for patterning ZnO, CeO_2 and Cr_2O_3. Another control experiment involved cathodic treatment after light illumination on n- or p-type Si in the deposition solution for 10–60 s without any applied current. Again, only a homogeneous thin film was achieved, as observed under cathodic unipolar treatment. These results clearly show that the deposition of metal oxides and their patterning is not controlled by the generation of excess holes during the electrochemical metal oxide deposition process.

On the n-type Si electrode, hole migration under positive bias to the illuminated area takes place, leading to patterned silicon oxide formation which requires holes at the surface; the holes are provided by electron tunneling from the valence band to the conduction band. Therefore, the applied current will flow preferentially through the illuminated areas, giving rise to selective silicon oxide growth in these regions. The silicon oxide formed is expected to act as an electronic barrier. Thus, upon application of cathodic current, metal oxide deposition will take place only in the dark areas because the SiO_2 layer blocks current in the illuminated regions, as shown schematically in Fig. 3. On the p-type Si electrode, on the other hand, holes are the majority charge carriers and thus charge separation upon the illumination is not expected at a low bias of +5 mA cm^{-2}, *i.e.* the whole area should be oxidized. In this case, however, the onset of the photocurrent may be at a more positive potential than the breakdown potential of the bulk silicon band gap (electron tunneling from the valence band to the conduction band at the surface), leading to metal oxide deposition only in the illuminated areas. Further investigation is presently being performed in order to elucidate these mechanisms more clearly.

We gratefully acknowledge support from NSF, the Purdue Research Foundation (fellowship to H. C. C.) and Purdue University. J. M. B. is holder of a Sloan Research Fellowship (2002–2002) and is a Cottrell Teacher-Scholar of Research Corporation (2000–2002).

Notes and references

1 C. Feldmann and H.-O. Jungk, *Angew. Chem., Int. Ed.*, 2001, **40**, 359.
2 T. Yoshida and H. Minoura, *Adv. Mater.*, 2000, **12**, 1219.
3 T. Yoshida, K. Terada, D. Schlettwein, T. Oekermann, T. Sugiura and H. Minoura, *Adv. Mater.*, 2000, **12**, 1214.
4 C. G. Granqvist, *Handbook of Inorganic Electrochromic Materials*, Elesevier, Amsterdam, 1995.
5 M. Grätzel, *Nature*, 2001, **409**, 575; F. Campus, P. Bonhôte, M. Grätzel, S. Heinen and L. Walder, *Sol. Energy Mater. Sol. Cells*, 1999, **56**, 281.
6 Y. Matsumoto, M. Murakami, T. Shono, T. Hasegawa, T. Fukumura, M. Kawasaki, P. Ahmet, T. Chikyow, S.-Y. Koshihara and H. Koinuma, *Science*, 2001, **291**, 854.
7 N. Özer, D.-G. Chen and T. Büyüklimanli, *Sol. Energy Mater. Sol. Cells*, 1998, **52**, 223.
8 O. Takai, M. Futsuhara, G. Shimizu, C. P. Lungu and J. Notue, *Thin Solid Films*, 1998, **318**, 117.
9 J. Hu and R. G. Gordon, *J. Appl. Phys.*, 1992, **71**, 880.
10 S. V. Prasad, S. D. Walck and J. S. Zabinski, *Thin Solid Films*, 2000, **360**, 107.
11 G. H. A. Therese and P. V. Kamath, *Chem. Mater.*, 2000, **12**, 1195.
12 J. A. Switzer, *Am. Ceram. Soc. Bull*, 1987, **66**, 1521.
13 R. Chaim, S. Almaleh-Rockman and L. Gal-Or, *J. Am. Ceram. Soc.*, 1994, **77**, 3202.
14 R. J. Phillips, M. J. Shane and J. A. Switzer, *J. Mater. Res.*, 1989, **4**, 923; J. A. Switzer, *J. Electrochem. Soc.*, 1986, **133**, 722.
15 M. Izaki and T. Omi, *J. Electrochem. Soc.*, 1996, **143**, L53; M. Izaki, *J. Electrochem. Soc.*, 1999, **146**, 4517.
16 K. J. Stevenson, G. J. Hurtt and J. T. Hupp, *Electrochem. Solid State*, 1999, **2**, 175.
17 C. Natarajan and G. Nogami, *J. Electrochem. Soc.*, 1996, **143**, 1547; E. A. Meulenkamp, *J. Electrochem. Soc.*, 1997, **144**, 1664.
18 D. Gal, G. Hodes, D. Lincot and H.-W. Schock, *Thin Sold Films*, 2000, **361**–**362**, 79.
19 V. Srinivasan and J. W. Weidner, *J. Electrochem. Soc.*, 1997, **144**, L210.
20 *Joint Committee on Powder Diffraction Standards*, Set 36, No 1451, International Center for Diffraction Data, Swarthmore, PA, 1986.

CHEMCOMM Communication
www.rsc.org/chemcomm

The effect of the primary structure of the polypeptide catalyst on the enantioselectivity of the Juliá–Colonna asymmetric epoxidation of enones

Paul A. Bentley,[a] Robert W. Flood,[a] Stanley M. Roberts,*[a] John Skidmore,[a] Corina B. Smith[a] and John A. Smith[b]

[a] *Department of Chemistry, University of Liverpool, Liverpool, UK L69 7ZD. E-mail: smrsm@liv.ac.uk*
[b] *School of Biological Sciences, University of Liverpool, Liverpool, UK L69 7ZB*

Received (in Cambridge, UK) 10th May 2001, Accepted 13th July 2001
First published as an Advance Article on the web 1st August 2001

Epoxidation of chalcone (1), using basic hydrogen peroxide, catalysed by polypeptides with defined primary structures demonstrates that the residues in the chain near to the *N*-terminus determine the stereochemical outcome of the reaction.

In recent years there has been an increase in the application of peptides as catalysts for asymmetric reactions.[1] One of the first reported examples was the asymmetric epoxidation of chalcones, catalysed by polyamino acids in a triphasic system, discovered and developed by Juliá and Colonna.[2] Advances in this field have been made through the introduction of biphasic protocols, leading to an expansion in the range of enones which can be epoxidised with good stereoselectivity.[3] These methodologies have been successfully applied to reach various synthetic targets.[4]

For such synthetic work, the preferred catalyst is polyleucine prepared by the polymerisation of leucine *N*-carboxyanhydride (Leu-NCA), in an organic solvent, using a nucleophilic initiator (typically 1,3-diaminopropane or cross-linked aminomethyl polystyrene).[5] This polymerisation generates a mixture of oligomers with a distribution of chain lengths. Epoxidation of chalcone (**1**) using a catalyst prepared from L-Leu-NCA (15 equivalents compared to the initiator) at the start of the process followed by D-Leu-NCA (5 equivalents) provided the first indication that the *N*-terminal region of the chain has a disproportionately large influence on the stereochemical outcome of the reaction.[6]

In order to investigate more thoroughly the influence of the primary structure of a given polypeptide on its activity as an epoxidation catalyst, selected oligoleucines were prepared using an automated peptide synthesiser. It was shown that H-(L-Leu)$_{20}$-R† catalyses the epoxidation of chalcone (**1**), to afford the (2*R*, 3*S*)-epoxide **2**, in a similar manner to the NCA-derived polymer having an *average* chain length of twenty residues.[7] A peptide was then prepared in which the five *N*-terminal L-Leu residues were replaced by D-Leu: H-(D-Leu)$_5$-(L-Leu)$_{15}$-R. This material catalysed the epoxidation of chalcone (**1**) to give the antipodal (2*S*, 3*R*)-epoxide **3** with 85% conversion and 45% ee after 32 hours under the Juliá–Colonna triphasic conditions (Scheme 1).[8] In this last catalyst, the D-Leu residues make up only 25% of the total polyamino acid, however they dictate the stereochemical outcome of the reaction.

In this paper the use of other polypeptides as epoxidation catalysts is reported, in order to investigate in detail which residues in the *N*-terminal region are responsible for determining the origin of the stereocontrol exhibited by these catalysts.

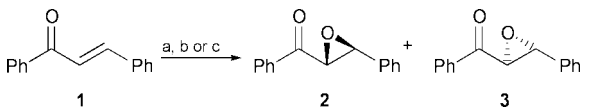

Scheme 1 *Reagents and conditions*: (a) aq. NaOH, aq. H_2O_2, catalyst, toluene; (b) DBU, urea–H_2O_2, catalyst, THF; (c) $Na_2CO_3{\cdot}1.5H_2O_2$, catalyst, DME, water.

First, in order to determine whether the terminal amine group plays a defining role in the action of the peptide catalyst, three derivatives of H-(L-Leu)$_{20}$-R were prepared. In the first, one of the terminal amine hydrogens was substituted by an acetyl group [Ac-(L-Leu)$_{20}$-R]. The second oligomer had the same hydrogen replaced by a methyl group [Me-(L-Leu)$_{20}$-R] while the third had both amine hydrogens replaced by methyl groups [Me$_2$-(L-Leu)$_{20}$-R].‡ The peptides were tested as catalysts for the epoxidation of chalcone (**1**) under mild reaction conditions in order to minimise the possible cleavage of the sterically unhindered acetyl moiety (Table 1). The biphasic conditions[3a] utilise urea–H_2O_2 and DBU in THF, whilst the percarbonate conditions[3b] employ sodium percarbonate as both base and oxidant, in a DME–water solvent mixture.

Table 1 Epoxidation of chalcone (**1**) using selected catalysts

Catalyst[a]	Conditions[b]	Time/h	Conversion[c] (%)	Ee[d] (%)
H-(L-Leu)$_{20}$-R	Percarbonate	7	94	88
Ac-(L-Leu)$_{20}$-R	Percarbonate	5	96	50
Me-(L-Leu)$_{20}$-R	Percarbonate	5	98	67
Me$_2$-(L-Leu)$_{20}$-R	Percarbonate	6	82	58
H-(L-Leu)$_{20}$-R	Biphasic	1.07	100	92
Me$_2$-(L-Leu)$_{20}$-R	Biphasic	1.5	78	78

[a] For the reactions under the biphasic conditions the catalyst was activated before use by stirring with toluene–aq. NaOH for 18 h, filtered and then washed with water, acetone and hexane. [b] Ref. 3. [c] Determined by HPLC. [d] Determined by chiral HPLC.

All three polymers gave significant enantioselectivities (50–78% ee). The polymer Ac-(L-Leu)$_{20}$-R gave the lowest ee but clearly this modification (which markedly reduces the basicity and nucleophilicity of the terminal nitrogen atom) does not render the catalyst wholly inactive. This result is in agreement with the observation by Ohkata[9] that a 20-mer of L-Leu, protected at the amino-terminus with a Boc group and at the carboxylate end as a benzyl ester, when used as an epoxidation catalyst, affords chalcone epoxide **2** in 41% ee.

Next, a series of five peptides, H-(L-Leu)$_n$-(D-Leu)$_5$-(L-Leu)$_{15-n}$-R where n = 1–5 was prepared (these are referred to as *n*L/5D/(15 − *n*)L). These peptides were used to catalyse the epoxidation of chalcone (**1**) under the triphasic conditions[2] and the results are summarised in Table 2. On using the peptide L/5D/14L as a catalyst, the major product was epoxide **3** (*i.e.* that normally generated under poly-D-leucine catalysis), with an ee somewhat greater than that observed for the 5D/15L polymer.[8] In contrast, utilisation of the polymer 2L/5D/13L led to a sharp drop in the ee of the product; however the major enantiomer was still the epoxide **3**. Moving the block of five D-Leu residues one step further away from the amino terminus had another dramatic effect on the outcome of the epoxidation. Thus the 3L/5D/12L catalyst provided the epoxide **2** (normally generated using the

 DOI: 10.1039/b104123c

Table 2 Epoxidation of chalcone (**1**) using mixed D- and L-Leu catalysts under triphasic[a] conditions over 32 h

Catalyst	Major product	Conversion[b] (%)	Ee[c] (%)
1L/5D/14L	**3**	99	67
2L/5D/13L	**3**	96	11
3L/5D/12L	**2**	100	89
4L/5D/11L	**2**	99	86
5L/5D/10L	**2**	99	88

[a] Ref. 2. [b] Determined by HPLC. [c] Determined by chiral HPLC.

poly-L-leucine catalyst) in 89% ee; the oligomers 4L/5D/11L and 5L/5D/10L gave very similar results. From this study it appears that the penultimate and antepenultimate residues from the *N*-terminus play a dominant role in determining the stereoselectivity of the Juliá–Colonna reaction.

We reasoned that, given the above results, the inclusion of glycine residues close to the *N*-terminus might have a significant effect on the catalytic activity of the peptide. Three catalysts H-(L-Leu)-Gly-(L-Leu)$_{18}$-R, H-(L-Leu)-Gly$_2$-(L-Leu)$_{17}$-R and H-(L-Leu)-Gly$_3$-(L-Leu)$_{17}$-R were prepared. Inclusion of three glycine residues reduces the ee of the epoxide **2** significantly; the effect of incorporating two glycine residues is more modest and the substitution of Gly for L-Leu in the penultimate position has relatively little effect, when compared to the polymer containing only L-Leu residues (Table 3). Interestingly, incorporation of the glycine residues results in a reduced conversion to the epoxide as well as diminishing the enantioselectivity.

Table 3 Epoxidation of chalcone (**1**) using selected catalysts under triphasic[a] conditions over 24 h

Catalyst	Conversion[b] (%)	Ee[c] (%)
H-(L-Leu)$_{20}$-R	97	88
H-(L-Leu)-Gly-(L-Leu)$_{18}$-R	90	70
H-(L-Leu)-Gly$_2$-(L-Leu)$_{17}$-R	79	52
H-(L-Leu)-Gly$_3$-(L-Leu)$_{17}$-R	60	29

[a] Ref. 2. [b] Determined by HPLC. [c] Determined by chiral HPLC, in each case epoxide **2** was the major enantiomer.

Finally, on the evidence that the residues close to the amino terminus of the polypeptide chain have the primary influence on the stereochemistry of the oxidation reaction, the peptides H-(L-Leu)$_n$-(D-Leu- L-Leu)$_8$-R, where n = 3–6, were prepared. These have an equal mixture of the two enantiomers of leucine in the bulk of the peptide chain and a different number of residues of the L-enantiomer at the amino terminus.

Table 4 shows that the polymers with five or six consecutive L-Leu residues at the amino terminus are excellent catalysts. Surprisingly, even the polymer with just three L-Leu residues at the amino terminus generates **2** with significant ee. It is noteworthy that this polymer has only one change (D- to L-Leu) from a polymer with residues of alternating stereochemistry, adding a little more weight to the postulate that polyamino acids could potentially have been prebiotic catalysts,[10] in as much as these results show that even a small excess of one enantiomer in an oligomeric structure, when correctly assembled, can lead to an amplification and a diversification of chirality.

Overall, it appears that the enone substrate and/or the peroxide reagent binds to the polyleucine near the *N*-terminus. It may well be pertinent that the final four N–H groups of an α-helical peptide are not able to act as hydrogen bond donors to carbonyl groups within the helix, thus providing a possible explanation for the differentiation between the terminal region and the bulk of the peptide. Kinetics and spectroscopy experiments are being undertaken (using PEG-bound polyamino acids that are soluble in organic solvents[11]) to ascertain which species is complexed to the chiral environment of the polymer. Such experimentation seems prudent before more detailed modelling can commence.

Table 4 Epoxidation of chalcone (**1**) using selected catalysts under triphasic[a] conditions over 18 h

Catalyst	Conversion[b] (%)	Ee[c] (%)
H-(L-Leu)$_3$-(D-Leu-L -Leu)$_8$-R	55	64
H-(L-Leu)$_4$-(D-Leu-L -Leu)$_8$-R	52	64
H-(L-Leu)$_5$-(D-Leu-L -Leu)$_8$-R	95	92
H-(L-Leu)$_6$-(D-Leu-L -Leu)$_8$-R	98	91

[a] Ref. 2. [b] Determined by HPLC. [c] Determined by chiral HPLC, in each case epoxide **2** was the major enantiomer.

We thank the EPSRC and BBSRC for studentships (R. W. F., P. A. B. and C. B. S.) and the EPSRC for a fellowship (J. S.).

Notes and references

† The oligoleucines were linked *via* a hydroxymethylphenoxyacetic acid linker to PEG and thence to polystyrene resin (loading 0.18 mmol g^{-1}). These oligomers are represented as H-(Leu)$_n$-R where R = linker–PEG-resin.

‡ Strictly speaking this material is Me$_2$NCH(CH$_2$CHMe$_2$)CO(L-Leu)$_{19}$R, the nomenclature Me$_2$-(L-Leu)$_{20}$-R is used for convenience.

1 P. A. Bentley, *Biotransformations*, ed. D. R. Kelly, VCH, Weinheim, 2000, vol. 8b, ch. 12.

2 The triphasic system consists of a solution of the substrate in an organic solvent (typically toluene), aq. NaOH–H_2O_2 and the insoluble catalyst, see S. Juliá, J. Masana and J. C. Vega, *Angew. Chem., Int. Ed. Engl.*, 1980, **19**, 929; S. Juliá, J. Guixer, J. Masana, J. Rocas, S. Colonna, R. Annuziata and H. Molinari, *J. Chem. Soc., Perkin Trans. 1*, 1982, 1317.

3 (*a*) P. A. Bentley, S. Bergeron, M. W. Cappi, D. E. Hibbs, M. B. Hursthouse, T. C. Nugent, R. Pulido, S. M. Roberts and L. E. Wu, *Chem. Commun.*, 1997, 739; (*b*) J. V. Allen, K. H. Drauz, R. W. Flood, S. M. Roberts and J. Skidmore, *Tetrahedron Lett.*, 1999, **40**, 5417.

4 B. M. Adger, J. V. Barkley, S. Bergeron, M. W. Cappi, B. E. Flowerdew, M. P. Jackson, R. McCague, T. C. Nugent and S. M. Roberts, *J. Chem. Soc., Perkin Trans. 1*, 1997, 3501; W. P. Chen and S. M. Roberts, *J. Chem. Soc., Perkin Trans. 1*, 1999, 103; L. Carde, D. H. Davies and S. M. Roberts, *J. Chem. Soc., Perkin Trans. 1*, 2000, 2455.

5 H. R. Kricheldorf, *α-Aminoacid-N-Carboxy-Anhydrides and Related Heterocycles: Syntheses, Properties, Peptide Synthesis, Polymerisation*, Springer-Verlag, Berlin, 1987; S. Itsuno, M. Sakakura and K. Ito, *J. Org. Chem.*, 1990, **55**, 6047.

6 P. A. Bentley, W. Kroutil, J. A. Littlechild and S. M. Roberts, *Chirality*, 1997, **9**, 198.

7 M. W. Cappi, W.-P. Chen, R. W. Flood, Y.-W. Liao, S. M. Roberts, J. Skidmore, J. A. Smith and N. M. Williamson, *Chem. Commun.*, 1998, 1159.

8 P. A. Bentley, M. W. Cappi, R. W. Flood, S. M. Roberts and J. A. Smith, *Tetrahedron Lett.*, 1998, **39**, 9297.

9 R. Takagi, T. Manabe, A. Shiraki, A. Yuneshige, Y. Hiraga, S. Kojima and K. Ohkata, *Bull. Chem. Soc. Jpn.*, 2000, **73**, 2115.

10 S. M. Roberts and J. Skidmore, *Chem. Br.*, 2000, **36**, 31.

11 R. W. Flood, T. P. Geller, S. A. Petty, S. M. Roberts, J. Skidmore and M. Volk, *Org. Lett.*, 2001, **3**, 683.

CHEMCOMM Communication
www.rsc.org/chemcomm

A novel precipitating auxiliary approach to the purification of Baylis–Hillman adducts†

Todd Bosanac and Craig S. Wilcox*

Department of Chemistry and The Combinatorial Chemistry Center, University of Pittsburgh, Pittsburgh, PA 15260, USA. E-mail: daylite@pitt.edu

Received (in Cambridge, UK) 3rd May 2001, Accepted 27th June 2001
First published as an Advance Article on the web 9th August 2001

Diaryl alkene alcohol 1 is a 'precipiton', a precipitating auxiliary that is used to aid the isolation of Baylis–Hillman adducts.

There is a need for new methods of product isolation which rely on simple purification procedures, eliminate the need for distillation or chromatography, and can be easily automated and used for parallel chemical syntheses.[1] While solid-phase organic synthesis (SPOS) remains the most popular method, there are several disadvantages associated with SPOS: the supports can be expensive; loading capacities can be low (0.1–1.0 mmol g^{-1}); solid-phase reactions often require extensive optimization of reaction conditions; and monitoring of reaction progress is difficult. To address the shortcomings of SPOS, molecules can be attached to 'phase-tags'. Fluorous synthesis,[2] soluble polymer-supported organic synthesis (SPSOS),[3] dendrimer-supported organic synthesis,[4] and acid/base tags[5] are examples of this approach. With these methods, tagged compounds can be easily separated from untagged compounds by a phase-transfer event (precipitation or liquid–liquid partition).

We recently introduced an approach to product isolation based on a solubility switch activated by structural isomerization.[6] Diaryl alcohol **1** is a 'precipiton', a group of atoms

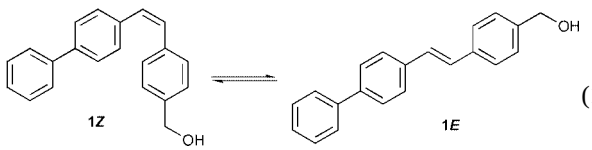

(1)

(molecular fragment) that is purposefully attached to a reactant molecule and that can be activated {in this case isomerized [equilibrium (1)]} after the reaction in order to cause precipitation of the attached product. Our method has been applied to the synthesis and isolation of isoxazolines[6] and α-substituted β-ketoesters.[7] In this communication, we describe the precipiton approach for the synthesis of pure Baylis–Hillman adducts.

The Baylis–Hillman reaction[8] is a C–C bond forming reaction between an activated alkene and an aldehyde in the presence of a tertiary amine, tertiary phosphine, or chalcogenide.[9] This reaction provides useful multifunctional intermediates that can be used for subsequent transformations. One of the drawbacks associated with the Baylis–Hillman reaction is that one of the components must be used in an excess to drive the reaction to completion.[10] This often leads to a need to use chromatography to separate the desired product from the excess reactant. In order to avoid chromatography we sought to use our methodology to isolate pure Baylis–Hillman adducts.

Alcohol **1*Z*** was prepared as previously described from 4-biphenylcarbaldehyde and *p*-bromobenzyl alcohol *via* a Negishi coupling.[7] Acrylate **2*Z*** was then readily prepared by treatment of **1*Z*** with acryloyl chloride in the presence of NEt_3.[6]

† Electronic supplementary information (ESI) available: full experimental details. See http://www.rsc.org/suppdata/cc/b1/b103969p/

The precipiton Baylis–Hillman reactions were performed on a 0.52 to 2.43 mmol scale with respect to the acrylate. The acrylate **2*Z*** was treated with a catalytic amount of DABCO and an excess of aldehyde at room temperature.[11] Upon completion of the reaction (depending upon the nature of the aldehyde, reactions were complete in 1 to 10 days) the crude mixture was diluted with a suitable solvent and treated with I_2 and dibenzoyl peroxide or PhSSPh.[12] The isomerization process was monitored by ^{1}H NMR (isomerizations were complete in 4–24 h). Upon completion of the isomerization event, the crude reaction mixture was diluted with $CHCl_3$. Aqueous work-up with bisulfite, followed by evaporation of the organic layer, gave a crude product, that was then purified simply by trituration with hexanes, ether, or MeOH, followed by filtration. This protocol afforded Baylis–Hillman adducts in good yields and with purities of ≥95% (Table 1).[13]

The precipiton-bound products were cleaved from the precipiton by hydrolysis (LiOH in THF–H_2O).[14] These reactions were performed on a 22 to 188 μmol scale. The acids were isolated by filtration of the insoluble precipiton, acidification of the solution, followed by extraction with EtOAc. Removal of the EtOAc furnished the desired acids in good yields and with purities of ≥95% (Table 2).[13] Several other conditions,

Table 1 Precipiton Baylis-Hillman reaction with acrylate **2*Z***

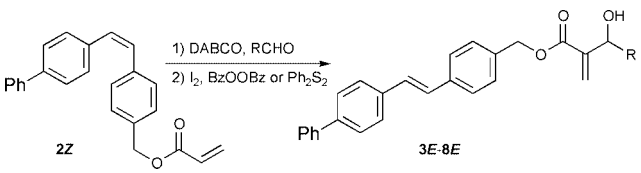

Entry	R	Time/d	Isomerization catalyst(s)	Product	Yield (%)
1		20	I_2/BzOOBz	**3*E***	70
2	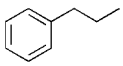	5	I_2/BzOOBz	**4*E***	58
3	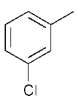	5	I_2/BzOOBz	**5*E***	78
4	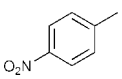	3	I_2/BzOOBz	**6*E***	76
5	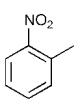	4	I_2/BzOOBz	**7*E***	76
6		1	I_2/BzOOBz	**8*E***	81
7		2	Ph_2S_2	**8*E***	75

 DOI: 10.1039/b103969p

Table 2 Hydrolytic removal of product from the precipiton

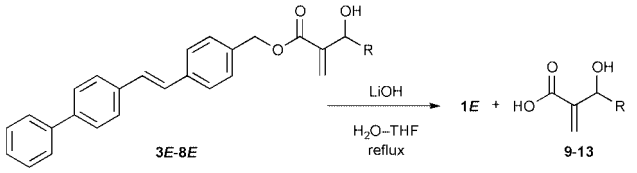

Entry	Starting material	R	Product	Yield (%)
1	**3*E***		9	72
2	**4*E***	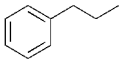	10	74
3	**5*E***		11	85
4	**6*E***	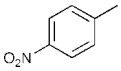	12	83
5	**7*E***		13	72

methanolysis and the Weinreib aminolysis, were examined for cleavage of the precipiton but were found ineffective. The acid derived from compound **8*E*** is a zwitterionic compound which could not be conveniently isolated.

These experiments demonstrate an application of the precipiton approach to product isolation. This method does not require chromatography, which is often a necessity in the Baylis–Hillman reaction. This process can be automated and has been successfully applied to very small scale reactions. It therefore may be found useful for preparing small quantities of pure compound for biological screening. We expect the method will be equally useful for large-scale preparations of compounds.

Notes and references

1 D. P. Curran, *Angew. Chem., Int. Ed.*, 1998, **37**, 1174.
2 A. Studer, S. Hadida, R. Ferritto, S.-Y. Kim, P. Jeger, P. Wipf and D. P. Curran, *Science*, 1997, **275**, 823; A. Studer, P. Jeger, P. Wipf and D. P. Curran, *J. Org. Chem.*, 1997, **62**, 2917; P. Wipf and J. T. Reeves, *Tetrahedron Lett.*, 1999, **40**, 5139; Z. Luo, Q. Zhang, Y. Oderaotoshi and D. P. Curran, *Science*, 2001, **291**, 1766.
3 D. J. Gravert and K. D. Janda, *Chem. Rev.*, 1997, **97**, 489; P. H. Toy and K. D. Janda, *Acc. Chem. Res.*, 2000, **33**, 546.
4 R. M. Kim, M. Manna, S. M. Hutchins, P. R. Griffin, N. A. Yates, A. M. Bernick and K. T. Chapman, *Proc. Natl. Acad. Sci. USA*, 1996, **93**, 10 012; N. J. Hovestd, A. Ford, J. T. B. H. Jastrzebski and G. van Koten, *J. Org. Chem.*, 2000, **65**, 5338.
5 H. Perrier and M. Labelle, *J. Org. Chem.*, 1999, **64**, 2110; J. Yoshida, K. Itami, K. Mitsudo and S. Suga, *Tetrahedron Lett.*, 1999, **40**, 3403.
6 T. Bosanac, J. Yang and C. S. Wilcox, *Angew. Chem., Int. Ed.*, 2001, **40**, 1875.
7 T. Bosanac and C. S. Wilcox, *Tetrahedron Lett.*, 2001, **42**, 4309.
8 A. B. Baylis and M. E. D. Hillman, GP 2155113, 1972; *Chem. Abstr.*, 1972, **77**, 34174q.
9 D. Basavaiah, P. D. Rao and R. S. Hyma, *Tetrahedron*, 1996, **52**, 8001.
10 Y. Fort, M. C. Berthe and P. Caubere, *Tetrahedron*, 1992, **48**, 6371.
11 L. J. Brzezinski, S. Rafel and J. W. Leahy, *Tetrahedron*, 1997, **53**, 16423.
12 The isomerization using I_2 and benzoyl peroxide was effected by dilution of the crude residue with Et_2O or CCl_4 followed by irradiation with a 250 W sunlamp. The isomerization conditions with PhSSPh involved dilution of the crude residue with THF followed by heating at reflux.
13 All products were fully characterized. Reactions were monitored by TLC or ^{1}H NMR. Purities were determined by ^{1}H NMR and were $\geqslant$95% for all isolated compounds. Experimental procedures are presented in the supporting information.
14 S. E. Drewes, N. D. Emslie, J. S. Field, A. A. Khan and N. Ramesar, *Tetrahedron: Asymmetry*, 1992, **3**, 255.

CHEMCOMM
Communication
www.rsc.org/chemcomm

Attenuation of Hofmeister bias in ion-pair extraction by a disulfonamide anion host used in strikingly effective synergistic combination with a calix-crown Cs^+ host

Konstantinos Kavallieratos† and Bruce A. Moyer*

Chemical Separations Group, Chemical and Analytical Sciences Division, Oak Ridge National Laboratory, Bldg. 4500S/MS-6119, P.O. Box 2008, Oak Ridge, TN 37831-6119 USA. E-mail: moyerba@ornl.gov

Received (in Columbia, MO, USA) 11th February 2001, Accepted 13th July 2001
First published as an Advance Article on the web 9th August 2001

A calix-crown/disulfonamide dual-host combination in 1,2-dichloroethane exhibits markedly enhanced ion-pair extraction of caesium salts, with the observed synergism following an anti-Hofmeister order.

Ion-pair recognition and extraction by synthetic hosts is an area of intense interest. Design of early prototype ion receptors has mainly focused on cation complexation, the co-extracted anion selectivity being determined by non-specific solvation effects. Consequently, salt extractability generally increases in the direction of larger, more charge-diffuse anions, consistent with the well-known Hofmeister selectivity.[1] Hence arises the question as to the extent to which one may perturb this bias-type *vs*. recognition-type of selectivity.[2] This question has gained particular relevance in connection with the need to separate radiocaesium from nuclear waste,[3] where recent attention has been focusing on certain calix-crowns.[4] Although elegant heteroditopic hosts which are able to complex both the anion and the Cs cation have been reported,[5] the use of dual-host systems remains rare, despite their apparent simplicity and versatility.[6,7] We recently demonstrated that simple carboxamides enhance extraction of the $CsNO_3$ ion pair *via* binding of the co-extracted anion, when used together with a crown-ether cation host.[6a,b] These encouraging results prompted us to examine the question of anion selectivity in such systems.[6c] Herein, we report that synergism in the dual-host system involving disulfonamides **1** or **2** as anion hosts,[8] and the Cs^+ selective calix-crown **4** as cation host[4b] is strongly biased toward small anions, with remarkably uniform dependence on the standard Gibbs energies of partitioning for the anions OAc^-, Cl^-, Br^-, I^-, NO_3^- and ClO_4^-. In addition, this particular dual-host system is shown to be strikingly effective, generating the largest synergistic effects yet observed.

The anion-binding properties of disulfonamide **1**, the di(*tert*-butyl) disulfonamide **2**, and the monosulfonamide **3** (Scheme 1) were initially investigated in 1,2-dichloroethane-d_4 by ^{1}H NMR titrations of receptor solutions with ^{n}Bu$_4$NX salts (X = Cl^-, Br^-, I^-, OAc^-, NO_3^-, ClO_4^-). The observed large downfield chemical shift changes for the sulfonamide N–H protons, as well as for the α-C–H protons (Scheme 1) were analyzed *via* non-linear regression methods.[8a,9,10] The results confirm the observations of Crabtree and coworkers indicating a predominant 1:1 complex formation in CD_2Cl_2 for all anions plus a weaker 1:2 complexation mode for OAc^-, Cl^-, Br^- and NO_3^-.[8a] The association constants (Table 1) are generally higher for the more charge-dense Cl^- and OAc^- and much smaller for the large and more hydrophobic, NO_3^-, ClO_4^- and I^-. This general order is what one would expect for a strong non-specific hydrogen-bond receptor.[2,8a] It follows that synergistic enhancements on combining **1** or **2** with a cation receptor should also follow this general order.

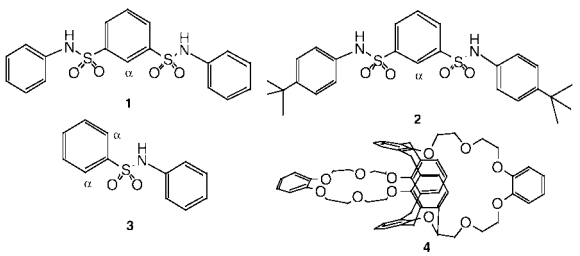

Scheme 1 Ion receptors used in this study.

Table 1 Association constants K (M^{-1}) for the formation of 1:1 and 1:2 complexes of **1**, **2** and **3** with anions in 1,2-dichloroethane-d_4 at 295 K. Tetrabutylammonium salts were used as anion sources

Anion X^-		**1**	**2**	**3**
OAc^-	K_{11}	19 500 (± 1400)	13 500 (± 400)	750 (± 80)
	K_{12}	73 (± 1)	70 (± 1)	
Cl^-	K_{11}	50 000 (± 4000)	32 500 (± 2000)	410 (± 9)
	K_{12}	5.8 (± 0.2)	3.6 (± 0.1)	
Br^-	K_{11}	10 600 (± 500)	8 900 (± 600)	150 (± 5)
	K_{12}	1.7 (± 0.7)	1.2 (± 0.3)	
NO_3^-	K_{11}	4 300 (± 100)	1 800 (± 20)	55 (± 5)
	K_{12}	2 (± 0.2)	1.2 (± 0.7)	
I^-	K_{11}	1 400 (± 13)	690 (± 27)	19 (± 2.5)
ClO_4^-	K_{11}	81 (± 1)	48 (± 1)	< 3

The ^{137}Cs tracer distribution experiments were performed by methodology described earlier,[4b] using aqueous phases containing 0.10 M NaX (inextractable)[11] and 5×10^{-6} M CsX (X = Cl^-, Br^-, I^-, OAc^-, NO_3^-, ClO_4^-) and organic phases containing 0.010 M of calix[4]arene-bis(benzo-18-crown-6) **4** with 0.035 M of **1**, **2** or **3**. Based on previous results[4b] and ion-pairing theory,[12] these experimental conditions are expected to minimize ion-pairing and its role in anion selectivity. In particular, at the low maximum concentration of CsX that could be extracted, estimated ion-pairing in the organic phase would at most be 5%. Control experiments were also performed with organic phases containing (1) no sulfonamide, (2) no crown ether, and (3) solvent only. The results summarized in Table 2

Table 2 Caesium distribution ratios for calixarene **4** only (D_4) and for calixarene **4** plus sulfonamides **1**–**3** (D_{4+R}, R = **1**–**3**). Last column shows the synergistic factors observed for **1**, expressed as the ratio D_{4+1}/D_4[a]

Anion	D_4	D_{4+1}	D_{4+2}	D_{4+3}	D_{4+1}/D_4
OAc^-	0.471	291	62.3	1.45	618
Cl^-	0.357	42.2	11.8	0.88	118
Br^-	2.64	125	48.5	6.32	47.3
NO_3^-	8.44	180	73.0	17.0	21.3
I^-	77.6	644	284	113	8.3
ClO_4^-	850	1770	1070	1020	2.1

[a] D_1 is negligible in relation to D_4.

† Current address: Department of Chemistry, Florida International University, University Park, FL 33199 USA.

 DOI: 10.1039/b102152b

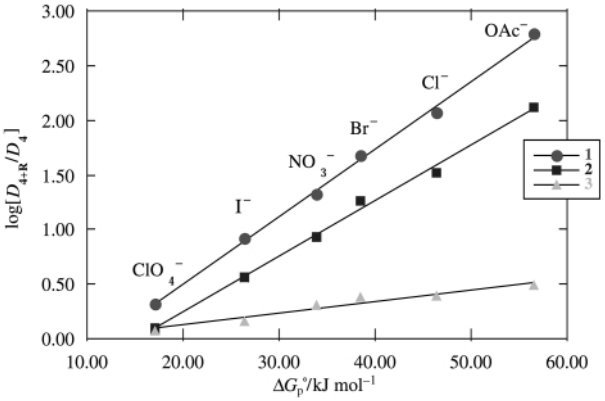

Fig. 1 Plot of the logarithm of the synergistic factor (D_{4+R}/D_4) for sulfonamides (**R** = **1**–**3**) *vs*. the standard Gibbs energy of partitioning $\Delta G°_p$ for various anions.

and Fig. 1 show that receptors **1** and **2** dramatically enhance Cs^+ ion extraction by the calix-crown. The synergism is stronger for the more charge-dense OAc^- and Cl^-, and weaker for the more hydrophobic I^- and ClO_4^-, as expected by the corresponding anion-receptor binding affinities. It is noteworthy that the extraction selectivity is higher for OAc^-, while K_{11} is higher for Cl^-, possibly reflecting a contribution of 1:2 complexation or anion-hydration effects.[13] For NO_3^- the observed synergism is in good agreement with data previously obtained using tetrabenzo-24-crown-8 as a cation receptor.[13] This observation implies weak if any ion-pairing effects and no significant role of the nature of the cation hosts.

One of the remarkable and unexpected aspects of this system is the excellent correlation between the synergistic effect and the standard Gibbs energy of anion partitioning $\Delta G_p°$.[11,14] Plotting the logarithm of the synergistic factor *vs*. $\Delta G_p°$ gave straight lines (Fig. 1) with a higher slope for the stronger anion receptor **1**. This correlation reveals that, whereas the bidentate nature of the disulfonamide receptor confers a strong interaction, the extraction enhancement is remarkably non-specific in breaking the simple bias-type dependence on anion size. Since the magnitude of enhancement reflects the strength of anion complexation in the organic phase,[7a,b] the strict correlation with $\Delta G_p°$ suggests that the anion receptor functions by non-specific solvation in a manner fundamentally resembling the partitioning process.

In conclusion, a potent disulfonamide anion receptor strongly synergizes the extraction of Cs salts when used together with a calix-crown cation host. The synergistic effects, as well as the anion binding affinities, are anti-Hofmeister, and thus these compounds and derivatives represent a new, valuable tool for tuning selectivity for anions in ion-pair extraction.

We thank Drs Jeffrey C. Bryan and Richard A. Sachleben for useful discussions. This research was sponsored by the Division of Chemical Sciences, Geosciences, and Biosciences, Office of Basic Energy Sciences, U.S. Department of Energy under contract DEAC0500OR22725 with Oak Ridge National Laboratory, managed and operated by UT-Battelle, LLC. The participation of K. K. was made possible through a appointment to the U.S. Department of Energy Postgraduate Research Program, administered by Oak Ridge Associated Universities.

Notes and references

1 F. Hofmeister, *Arch. Exp. Pathol. Pharmakol.*, 1888, **24**, 247.
2 B. A. Moyer and P. V. Bonnesen, in *The Supramolecular Chemistry of Anions*, ed. A. Bianchi, K. Bowman-James and E. García-España, Wiley-VCH, New York, 1997, pp. 31–33.
3 *Science and Technology for Disposal of Radioactive Tank Wastes*, ed. W. W. Schultz and N. J. Lombardo, Plenum, New York, 1998.
4 (*a*) P. Thuéry, M. Nierlich, E. Lamare, J.-F. Dozol, Z. Asfari and J. Vicens, *J. Inclusion Phenom. Macrocycl. Chem.*, 2000, **36**, 375; (*b*) T. J. Haverlock, P. V. Bonnesen, R. A. Sachleben and B. A. Moyer, *J. Inclusion Phenom. Macrocycl. Chem.*, 2000, **36**, 21.
5 M. T. Reetz, in *Comprehensive Supramolecular Chemistry*, ed. F. Vögtle, Pergamon, Oxford, 1996, vol. 2, pp. 553-562 and references therein; M. M. G. Antonisse and D. N. Reinhoudt, *Chem. Commun.*, 1998, 443 and references therein; M. J. Deetz, M. Shang and B. D. Smith, *J. Am. Chem. Soc.*, 2000, **122**, 6201; P. D. Beer, P. K. Hopkins and J. D. McKinney, *Chem. Commun.*, 1999, 1253.
6 (*a*) K. Kavallieratos, R. A. Sachleben, G. J. Van Berkel and B. A. Moyer, *Chem. Commun.*, 2000, 187; (*b*) K. Kavallieratos, A. Danby, G. J. Van Berkel, M. A. Kelly, R. A. Sachleben and B. A. Moyer, K. Bowman-James, *Anal. Chem.*, 2000, **72**, 5258; (*c*) C. K. Chambliss, S. Key, K. Kavallieratos, P. V. Bonnesen, J. C. Bryan and B. A. Moyer, Presented at the 219th National Meeting of the American Chemical Society, San Francisco, CA, March 2000.
7 (*a*) L. A. J. Chrisstoffels, F. de Jong, D. N. Reinhoudt, S. Sivelli, L. Gazzola, A. Casnati and R. Ungaro, *J. Am. Chem. Soc.*, 1999, **121**, 10 142; (*b*) M. M. Murad, T. Hayashita, K. Shigemori, S. Nishizawa and N. Teramae, *Anal. Sci.*, 1999, **15**, 1185.
8 (*a*) K. Kavallieratos, C. M. Bertao and R. H. Crabtree, *J. Org. Chem.*, 1999, **64**, 1675; (*b*) K. Kavallieratos and R. H. Crabtree, *Chem. Commun.*, 1999, 2109.
9 K. A. Connors, *Binding Constants*, Wiley, New York, 1987, pp. 189–215.
10 Binding constants have ±5% precision and are within the upper limit of the technique (10^5 M^{-1}).[9]
11 T. G. Levitskaia, T. J. Haverlock and B. A. Moyer, unpublished results.
12 R. M. Fuoss, *J. Am. Chem. Soc.*, 1958, **80**, 5059.
13 K. Kavallieratos, J. C. Bryan, G. J. Van Berkel and B. A. Moyer, manuscript in preparation.
14 J. Chapkiewicz and B. Czapkiewicz-Tutaj, *J. Chem. Soc., Faraday Trans. 1*, 1980, **76**, 1663: values employ the tetraphenylarsonium tetraphenylborate assumption.

CHEMCOMM
Communication
www.rsc.org/chemcomm

Selective recovery of solutes from ionic liquids by pervaporation—a novel approach for purification and green processing

Thomas Schäfer, Carla M. Rodrigues, Carlos A. M. Afonso and João G. Crespo*

Department of Chemistry-CQFB, Faculdade de Ciências e Tecnologia, Universidade Nova de Lisboa, 2825-114 Caparica, Portugal. E-mail: jgc@dq.fct.unl.pt

Received (in Cambridge, UK) 14th May 2001, Accepted 18th July 2001
First published as an Advance Article on the web 9th August 2001

Non-porous membranes with the selective layer consisting of hydrophilic or hydrophobic polymers have been applied for the quantitative and selective recovery of solutes with different physico-chemical properties from a room-temperature ionic liquid, ([bmim][PF_6]).

Room-temperature ionic liquids are fluids that consist entirely of organic cations and inorganic or organic anions and, as a consequence, they lack a measurable partial pressure.[1] This feature of ionic liquids permits their repeated use as benign solvents for green chemical syntheses without solvent loss to the environment due to evaporation.[2] The challenge for the equally benign recovery of solutes from ionic liquids remains and has been identified.[3] Conventional separation techniques for solute recovery either apply energy non-specifically to the bulk (distillation), or employ volatile organic solvents for extraction, thus cancelling out one of the ionic liquid's major advantages. 'Cleaner' and energy-efficient technologies for solute recovery from ionic liquids have recently been summarised to comprise supercritical carbon dioxide extraction and liquid–liquid extraction using aqueous systems or crown ether extractants.[4] Although supercritical carbon dioxide extraction is an efficient separation technique applicable to a wide range of separation problems, it remains technically demanding.[5] Here we demonstrate that pervaporation, as a highly selective and versatile membrane separation process, is capable of quantitatively recovering volatile solutes directly from ionic liquids, more effectively and under milder operating conditions than distillation. Choosing the appropriate membrane for the individual separation problem, pervaporation may prove more versatile than solvent extraction processes as well as more efficient and energetically more advantageous than evaporative techniques.

The separation principle of pervaporation is based on the preferential partitioning of a solute from a liquid feed phase into a dense, non-porous membrane through which it diffuses according to its chemical potential gradient.[6] This gradient is the driving force for the solute transport across the membrane. It is in general established by maintaining a low vacuum on the membrane downstream side, while keeping the membrane upstream side, which is in contact with the liquid feed, at ambient pressure. According to the solution-diffusion model, the partial flux J_i of a solute i across the membrane is given by eqn. (1):

$$J_i = \frac{S_i D_i}{z_m} \Delta\mu_i = \frac{S_i D_i}{z_m} (\mu_i^{\mathrm{f}} - \mu_i^{\mathrm{p}}) \qquad (1)$$

with S_i the partitioning coefficient of solute i between the feed liquid phase and the membrane; D_i the diffusion coefficient of i in the membrane; z_m the membrane thickness; $\Delta\mu_i$ the chemical potential gradient of i over the membrane; μ_i^{f} and μ_i^{p} are the chemical potential of i in the liquid feed phase and the permeate, respectively.

Any compound partitioning between the bulk solvent and the membrane can be recovered by pervaporation once there exists a chemical potential gradient over the membrane. For the same chemical potential gradient, pervaporation can be more effective than distillation for solute recovery.[7] The solute partitions from the bulk solvent into the membrane polymer where it sorbs. Due to the chemical potential gradient it then diffuses through the membrane polymer and subsequently desorbs on the membrane downstream side into the vacuum. This explains why pervaporation can also be applied to the recovery of low-volatile, high-boiling compounds at relatively moderate temperature: unlike distillation, pervaporation is not governed by the vapour–liquid equilibrium, but by solute–polymer interactions.[8] For an individual separation problem, it is therefore crucial to choose or develop the membrane polymer such that it exhibits a high selectivity for the target compounds under the separation process operating conditions. Otherwise, the process is not efficient.[9]

Energy consumption in pervaporation stems mainly from establishing the vacuum and condensing the solutes permeated. Specific to coupling pervaporation to ionic liquids is the fact that energy is spent very efficiently on the permeating solute only because no bulk solvent permeates the membrane. In contrast, during distillation energy is spent non-specifically on heating both the non-volatile bulk solvent and the solutes, with the latter often being present in minor concentrations.

Four case studies were chosen to test the promising concept of removing volatile solutes from ionic liquids by pervaporation: (1) water as a possible reaction product during, for example, condensations or esterifications, whose removal shifts the reaction equilibrium toward higher product yields; (2) ethyl hexanoate as a possible product of low volatility from a heat sensitive biotransformation; (3) chlorobutane as a possible residue stemming from the synthesis of the ionic liquid, whose removal increases significantly the purity of the latter; (4) naphthalene as a low-boiling compound.

Laboratory-scale pervaporation experiments were carried out using a range of binary solutions of the ionic liquid, 1-butyl-3-methylimidazolium hexafluorophosphate [bmim][PF_6], and model solutes all of which differ strongly in their physico-chemical properties. The ionic liquid was synthesised in our laboratory using a procedure reported.[10] The model solutes used were naphthalene, ethyl hexanoate, chlorobutane and water with initial feed concentrations of 15, 3.5, 20 and 17 kg m^{-3}, respectively. Different dense hydrophilic and hydrophobic polymeric membranes, namely poly(octylmethylsiloxane) (POMS) polyether block amide (PEBA) and poly(vinyl alcohol) (PVA) were chosen for the solute recovery based on their selectivity for the individual model solute. All experiments with results depicted in Figs. 1 and 2 were carried out at 323.15 K and a permeate pressure of 10 Pa, using a standard laboratory pervaporation set-up with an effective membrane area of 0.01 m^2.[11] The feed volume used was 110 cm^3 throughout all experiments. No ionic liquid was detected in any of the permeates, with the detection limit being 74 μg kg^{-1} using inductively coupled plasma (ICP) spectroscopy and phosphorus as the reference atom for the hexafluorophosphate anion of [bmim][PF_6]. Organic model solute concentrations in the feed and the permeate were determined by gas chromatography after extraction from the ionic liquid with diethyl ether. Water

 DOI: 10.1039/b104191f

concentration in the ionic liquid was determined using an automated Karl–Fischer titrator.

Fig. 1 depicts the successful, quantitative recovery (> 99.2%) of all solutes tested by pervaporation. It should be noted that recovery rates apply for the small membrane area used in the laboratory and therefore appear uneconomically long. Because membrane area is relatively inexpensive, large-scale pervaporation units will employ larger membrane area/feed volume ratios, thus diminishing the time for quantitative solute recovery manifold, as can be simulated on the basis of the partial fluxes presented in Fig. 2.

Water exhibited the highest flux, using a hydrophilic PVA-composite membrane. Because of their hydrophilicity, PVA-membranes are highly permeable for water, while hindering the permeation of hydrophobic molecules.[12] This is particularly interesting for reversible condensation reactions or biocatalytic esterifications carried out in ionic liquids, during which the selective and continuous removal of the water formed shifts the equilibrium to higher yields of the target product.[12] The target product, such as esters formed by esterification, can then be recovered using an appropriate hydrophobic membrane, with an example being the pervaporation of ethyl hexanoate utilising a POMS-composite membrane (Figs. 1 and 2). It should be pointed out that especially with regard to biotransformations carried out in ionic liquids, pervaporation is the only separation technique that can be applied without either degrading the biocatalyst or interfering with the bioconversion: it can be efficiently operated at a moderate temperature, and does not require any extraction aid detrimental to the performance of the biocatalyst that, in turn, can be reused without loss of activity.[13]

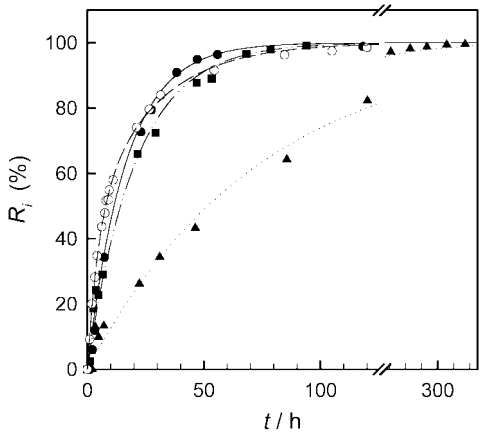

Fig. 1 Recovery of water by a PVA (4 μm)-composite membrane (○); chlorobutane (●) and ethyl hexanoate (■) by POMS (25 μm)-composite membrane; naphthalene by a homogeneous PEBA (30 μm)-membrane (▲). All solutes were recovered to a degree > 99.2% (limit of the analytical sensitivity) of their initial feed concentration.

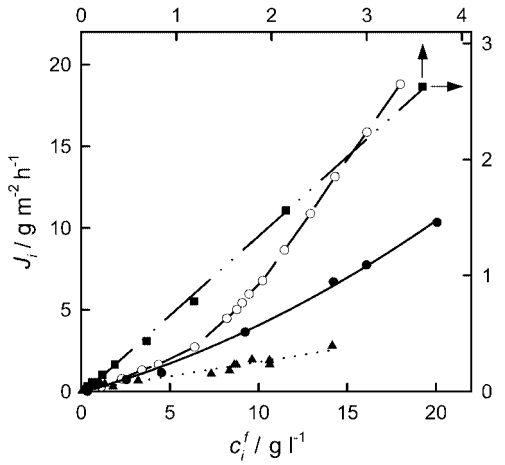

Fig. 2 Partial fluxes of the solutes recovered from [bmim][PF_6] as a function of their respective feed concentration. Experimental conditions and symbol legend are as reported in Fig. 1; for graphical reasons, the *x*- and *y*-axes for ethyl hexanoate are depicted on the top and on the right of the plot (indicated by arrows).

Once prepared, ionic liquids still contain solvent/reactant originating from their synthesis or the subsequent purification procedure. Commonly, these solvent residues are removed using evaporative techniques under high vacuum and/or an elevated temperature.[10] Utilising a POMS-composite membrane, chlorobutane as a solvent/reactant during synthesis of [bmim][PF_6] was recovered as depicted in Figs. 1 and 2, respectively. Pervaporation can hence be integrated in the production and purification process of ionic solvents for the recovery of volatile solvent residues, enabling a closed-loop production process for obtaining a pure ionic liquid at mild operating conditions.

The low-volatile model solute, naphthalene, was recovered quantitatively at 323 K, 168 K below its boiling point of 491 K (Figs. 1 and 2) using a homogenous PEBA-membrane. A homogenous membrane was chosen for this separation because in composite membranes the pressure loss in the porous support can be sufficient to cause undesired condensation of the low-volatile solute on the membrane downstream face. Although the rate of recovery was lower than that of the other solutes, owing to a smaller driving force, this example illustrates the potential pervaporation has for the recovery of high-boiling compounds.

In conclusion, pervaporation is a non-evaporative process that can be integrated in the production and purification process of ionic solvents for the selective recovery of volatile solvent residues at mild, and therefore energetically favourable, operating conditions. For the recovery of volatile solutes from heat sensitive reactions carried out in ionic liquids, such as bioconversions, pervaporation may be superior to other techniques.

We thank Elf Atochem, Portugal, and GKSS, Germany, for the kind donations of membranes, and João N. Rosa and Luis C. Branco for the preparation of the ionic liquid. T. S. gratefully acknowledges financial support from FCT, Portugal.

Notes and references

1 C. L. Hussey, *Pure Appl. Chem.*, 1988, **60**, 1763; T. Welton, *Chem. Rev.*, 1999, **99**, 2071; P. Wasserscheid and W. Keim, *Angew. Chem., Int. Ed.*, 2000, **39**, 3772.
2 K. R. Seddon, *J. Chem. Tech. Biotechnol.*, 1997, **68**, 351.
3 M. Freemantle, *Chem. Eng. News*, 2000, May 15, 37; M. J. Earle, P. B. McCormac and K. R. Seddon, *Green Chem.*, 1999, 23.
4 A. E. Visser, R. P. Swatloski and R. D. Rogers, *Green Chem.*, 2000, 1; L. A. Blanchard, D. Hancu, E. J. Beckman and J. F. Brennecke, *Nature*, 1999, **399**, 28; L. A. Blanchard and J. F. Brennecke, *Ind. Eng. Chem. Res.*, 2001, **40**, 287; S. G. Cull, J. D. Holbrey, V. Vargas-Mora, K. R. Seddon and G. J. Lye, *Biotechnol. Bioeng.*, 2000, **69**, 227; S. Dai, Y. H. Ju and C. E. Barnes, *J. Chem. Soc., Dalton Trans.*, 1999, 1201; R. A. Brown, P. Pollet, E. McKoon, C. A. Eckert, C. L. Liotta and P. G. Jessop, *J. Am. Chem. Soc.*, 2001, **123**, 1254.
5 G. Brunner, *Gas extraction*, Steinkopf, Darmstadt, Springer, New York, 1994.
6 J. Néel, in *Pervaporation Membrane Separation Processes*, ed. R. Y. Huang, Elsevier, Amsterdam, 1991.
7 A. Baudot and M. Marin, *Trans. Inst. Chem. Eng.*, 1997, **75C**, 117.
8 K. W. Böddeker, I. L. Gatfield, J. Jahnig and C. Schorm, *J. Membr. Sci.*, 1997, **137**, 155.
9 A. G. Fadeev and M. M. Meagher, *Chem. Commun.*, 2001, 295.
10 J. G. Huddleston, H. D. Willauer, R. P. Swatloski, A. E. Visser and R. D. Rogers, *Chem. Commun.*, 1998, 1765.
11 T. Schäfer, G. Bengtson, H. Pingel, K. W. Böddeker and J. G. Crespo, *Biotechnol. Bioeng.*, 1999, **62**, 412.
12 M. Mulder, *Basic Principles of Membrane Technology*, Kluwer, Dordrecht, 1996.
13 S. H. Schöfer, N. Kaftzik, P. Wasserscheid and U. Kragl, *Chem. Commun.*, 2001, 425.

CHEMCOMM Communication
www.rsc.org/chemcomm

The hetero Diels–Alder reactions of masked *o*-benzoquinones with nitroso compounds

Ken-Ching Lin and Chun-Chen Liao*

Department of Chemistry, National Tsing Hua University, Hsinchu, Taiwan 300. E-mail: ccliao@mx.nthu.edu.tw; Fax: +886-3-5728123

Received (in Cambridge, UK) 24th April 2001, Accepted 2nd July 2001
First published as an Advance Article on the web 9th August 2001

The first examples of hetero Diels–Alder reaction of masked *o*-benzoquinones with nitroso dienophiles leading to novel and highly functionalized heterocycles, which are potential intermediates for nitrogenous natural products are reported.

The hetero Diels–Alder reaction represents a powerful strategy for the stereoselective construction of highly functionalized heterocyclic systems.[1] A nitroso function that is directly linked with an electron-withdrawing group acts as an efficient dienophile as a result of extremely low LUMO energy and weak π-bond.[2] Acyl nitroso compounds have been used as dienophiles in both intermolecular and intramolecular versions of hetero Diels–Alder reactions to produce highly functionalized cycloadducts that provide valuable synthetic intermediates to a variety of biologically interesting molecules.[1,3]

Masked *o*-benzoquinones (MOBs),[4] a highly reactive class of 2,4-cyclohexadienones with extensive utility can be generated by the oxidation of easily available 2-methoxyphenols using hypervalent iodine reagents such as diacetoxyiodobenzene (DAIB) and phenyliodonium(III) bis(trifluoroacetate) (PIFA) in MeOH. In the course of our investigations on MOB chemistry, we have developed methods for their *in situ* generation and studied their inter-[5] and intramolecular[6] carbo-Diels–Alder reactions. The synthetic potential of this methodology has been demonstrated in the total/formal syntheses of several natural products by us[7] and others.[8] Very recently, MOBs were shown to drive heteroaromatics such as furans,[9] pyrroles[10] and indoles[11] as 2π-components in the carbo-Diels–Alder reaction. In continuation of our efforts to broaden the versatility of MOBs, we contemplated their hetero Diels–Alder reaction with nitroso dienophiles to generate functionalized bicyclo[2.2.2]octenone derivatives that are possible intermediates for several biologically active natural products such as aminocyclitols,[12] pancratistatin[13] and tetrodotoxin[14] (Scheme 1).

Owing to their highly reactive nature, both MOB (diene) and nitroso dienophile were transiently generated in the reaction medium. Thus, at the outset of our study, we examined the reaction of MOB **1a**, obtained from the parent 2-methoxyphenol *i.e.* guaiacol (**2a**), with nitroso compound **3a**. The oxidation of **2a** with DAIB in MeOH produced MOB **1a** and the periodate oxidation of *tert*-butyl *N*-hydroxycarbamate (**4a**) produced **3a**. When the reaction was performed with an equimolar ratio of **2a** and **4a**, the two transient intermediates reacted very efficiently at 0 °C to furnish the Diels–Alder adduct **5a** in 80% yield. However, use of two equivalents of **4a** under the same conditions increased the yield to 90%. This overwhelming result prompted us to extend this reaction to other 2-methoxyphenols. Thus, a variety of phenols **2b–j** in the reaction with **4a** were examined as summarized in Scheme 2 and Table 1.† The MOBs **1b–g** reacted very smoothly with nitroso compound **3a** at 0 °C resulting in the formation of adducts **5b–g** in good to excellent yields (entries 1, 3, 5, 7, 9, 11 and 13). However, the reactions of phenols **2h–j** bearing electron-releasing substituents at C-4 did not proceed at 0 °C. A workable solution was found by the slow addition of hydroxamic acid **4a** to a mixture of phenol **2h** and oxidants in MeOH–CH_2Cl_2 at 50 °C and continuing the reaction at the same temperature. Under these

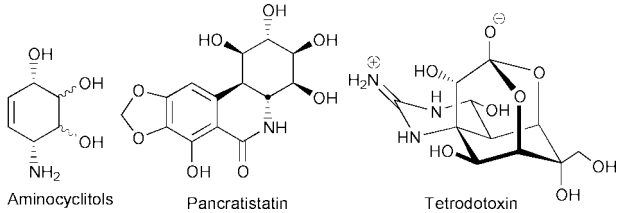

Scheme 1

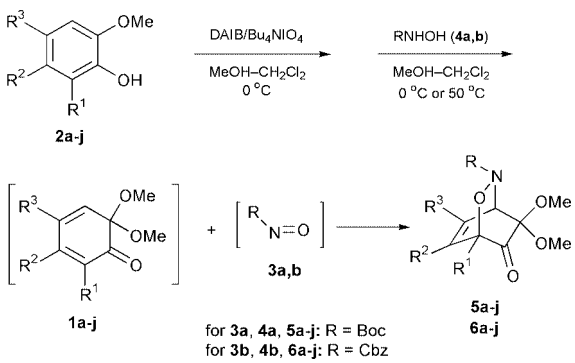

Scheme 2

Table 1 Hetero Diels–Alder reaction of masked *o*-benzoquinones **1a–j** with BocNO (**3a**) and CbzNO (**3b**)

Entry	MOB				Nitroso compd	Temp.[a]/ °C	Time[b]/ h	Adduct (Yield (%))[c]
		R^1	R^2	R^2				
1	**1a**	H	H	H	**3a**	0	1	**5a** (90)
2					**3b**	0	1	**6a** (96)
3	**1b**	H	CO_2Me	H	**3a**	0	1	**5b** (71)
4					**3b**	0	1	**6b** (81)
5	**1c**	H	Me	H	**3a**	0	1	**5c** (93)
6					**3b**	0	1	**6c** (95)
7	**1d**	H		H	**3a**	0	1	**5d** (92)
8					**3b**	0	1	**6d** (96)
9	**1e**	Me	H	H	**3a**	0	1	**5e** (69)
10					**3b**	0	1	**6e** (81)
11	**1f**	H	H	CO_2Me	**3a**	0	1	**5f** (70)
12					**3b**	0	1	**6f** (74)
13	**1g**	H	H	COMe	**3a**	0	1	**5g** (57)
14					**3b**	0	1	**6g** (52)
15	**1h**	H	H	Me	**3a**	50	3	**5h** (84)
16					**3b**	50	3	**6h** (90)
17	**1i**	H	H		**3a**	50	12	**5i** (71)
18					**3b**	50	12	**6i** (92)
19	**1j**	H	H	Br	**3a**	50	12	**5j** (91)
20					**3b**	50	12	**6j** (90)

[a] Reaction temperature. [b] Reaction time after the addition of RNHOH. [c] Yields of pure and isolated adducts.

 DOI: 10.1039/b103649c

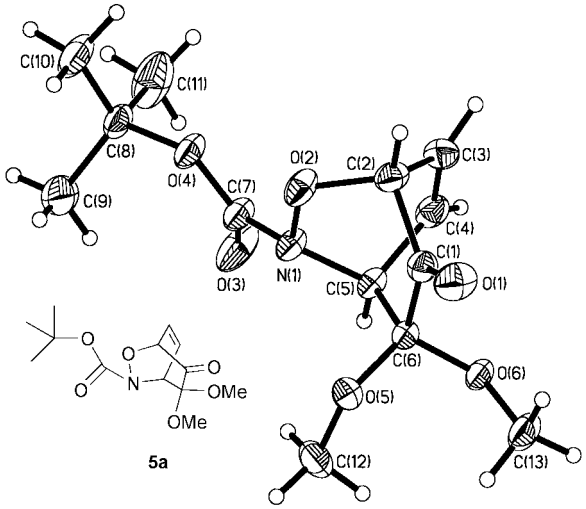

Fig. 1 ORTEP plot of the crystal structure of cycloadduct **5a** (numbering is arbitrary).

conditions, phenols **2h**–**j** afforded the cycloadducts **5h**–**j** in high to excellent yields (entries 15, 17 and 19).

In an effort to ascertain whether the *N*-substitution of nitroso compound has influenced the reaction, we have evaluated the Diels–Alder reaction of MOBs **1a**–**j** with (*N*-carbobenzyloxy)nitroso compound **3b** (Scheme 2). These cycloadditions were found to be quite efficient and the adducts **6a**–**j** were obtained in very good to excellent yields. These results are summarized in Table 1.

The structures of all the cycloadducts were based on the IR, ^{1}H (400 MHz) and ^{13}C (100 MHz) NMR, DEPT, low-, and high-resolution mass spectral analyses. The regiochemistry of the adduct **5a** was confirmed by its single crystal X-ray structure (Fig. 1)‡ and that of the adducts **5b**–**j** and **6a**–**j** is derived by comparing the chemical shifts of their ^{1}H NMR spectra with that of **5a**.

The excellent regioselectivity of this Diels–Alder reaction is in full agreement with our earlier studies on Diels–Alder reactions of MOBs.[5,9–11] The moderately stable MOBs such as **1i**,**j** require higher temperature and prolonged reaction times for the reaction as reflected by the reaction conditions employed for phenols **2i**,**j** (entries 17–20), which is in accordance with our earlier findings.[15]

In conclusion, bicyclo[2.2.2]octenone derivatives embedded with heteroatoms—types of substrate that are useful in the total syntheses of natural products possessing an aminopolyhydroxycyclohexane or cyclohexene moiety—are accessed in a highly regioselective manner from simple 2-methoxyphenols. The simplicity of the experimental procedure and the ready accessibility of masked *o*-benzoquinones and nitroso dienophiles thus renders this an experimentally attractive method for the preparation of nitrogenous heterocycles. Currently, we are actively pursuing the transformation of such cycloadducts to pertinent targets including conduramines and natural products such as pancratistatin and tetrodotoxin.

We gratefully acknowledge financial support from the National Science Council of the Republic of China. We thank Mr G.-H. Lee of the Department of Chemistry, National Taiwan University for X-ray diffraction studies and Dr R. K. Peddinti for helpful discussions.

Notes and references

† *General procedure for phenols **2a**–**g** and* N-*hydroxycarbamates **4a**,**b***: to a stirred mixture of DAIB (1.1 mmol) and Bu_4NIO_4 (2 mmol) in MeOH (5 mL) at 0 °C, was added phenol **2** (1 mmol) in CH_2Cl_2 (5 mL) at once. After 10 min of stirring at 0 °C, was added carbamate **4** (2 mmol) in a 1 : 1 mixture of MeOH–CH_2Cl_2 (5 mL) at once and the reaction was continued for 1 h at the same temperature. Then the solvent and other volatiles were removed under reduced pressure and the residue was subjected to silica gel column chromatography (ethyl acetate–hexanes) to obtain pure cycloadducts **5a**–**g** and **6a**–**g**.

*General procedure for phenols **2h**–**j** and* N-*hydroxycarbamates **4a**,**b***: To a stirred mixture of DAIB (1.1 mmol) and Bu_4NIO_4 (2 mmol) in MeOH (5 mL) at 0 °C, was added phenol **2** (1 mmol) in CH_2Cl_2 (5 mL) at once. After 10 min of stirring at 0 °C, the reaction flask was moved to a preheated oil bath (50 °C), and carbamate **4** (2 mmol) in a 1 : 1 mixture of MeOH–CH_2Cl_2 (5 mL) was added dropwise using a syringe pump (addition time: 1 h for entries 15 and 16, 4 h for entries 17 and 18, and 8 h for entries 19 and 20) and the reaction was continued [for 3 h (entries 15 and 16) or 12 h (entries 17–20)] at the same temperature. Thus formed adducts **5h**–**j** and **6h**–**j** were isolated as described in the above procedure.

‡ *Crystal data* for **5a**: $C_{13}H_{19}NO_6$, M = 285.29, triclinic, a = 12.035(2), b = 6.288(2), c = 19.541(2) Å, α = 90, β = 100.71(2), γ = 90°, V = 1453.0(6) Å^3, T = 295(2)K, space group $P2_1$, Z = 4, μ(Mo-Kα) = 0.103 mm^{-1}, 3344 reflections collected, independent reflections (R_{int} = 0.0000), final R indices [$I > 2\sigma(I)$], $R1$ = 0.0418, $wR2$ = 0.1249. CCDC 161113. See http://www.rsc.org/suppdata/cc/b1/b103649c/ for crystallographic data in CIF or other electronic format.

1 (*a*) D. L. Boger and S. M. Weinreb, *Hetero-Diels–Alder Methodology in Organic Synthesis*, Academic Press, San Diego, 1987; (*b*) D. L. Boger, *Comprehensive Organic Synthesis*, Vol. 5, ed. B. M. Trost and I. Fleming, Pergamon, New York, 1991, pp. 451–551; (*c*) H. Waldmann, *Synthesis*, 1994, 535; (*d*) L. F. Tietze and G. Kettschau, *Top. Curr. Chem.*, 1997, **189**, 1.
2 M. A. McCarrick, Y.-D. Wu and K. N. Houk, *J. Org. Chem.*, 1993, **58**, 3330.
3 (*a*) J. Strieth and A. Defoin, *Synthesis*, 1994, 1107; (*b*) C. Kibayashi and S. Aoyagi, *Synlett*, 1995, 873; (*c*) P. F. Vogt and M. J. Miller, *Tetrahedron*, 1998, **54**, 1317.
4 (*a*) C.-C. Liao, *Modern Methodology in Organic Synthesis*, Kodansha, Tokyo, 1992, p. 409; (*b*) S. Quideau and L. Pouysegu, *Org. Prep. & Proc. Int.*, 1999, **31**, 617.
5 (*a*) C.-C. Liao, C.-S. Chu, T.-H. Lee, P. D. Rao, S. Ko, L.-D. Song and H.-C. Shiao, *J. Org. Chem.*, 1999, **64**, 4102; (*b*) D.-S. Hsu, P. D. Rao and C.-C. Liao, *Chem. Commun.*, 1998, 1795; (*c*) S.-Y. Gao, S. Ko, Y.-L. Lin, R. K. Peddinti and C.-C. Liao, *Tetrahedron*, 2001, **57**, 297.
6 (*a*) P.-Y. Hsiu and C.-C. Liao, *Chem. Commun.*, 1997, 1085; (*b*) C.-S. Chu, T.-H. Lee, P. D. Rao, L.-D. Song and C.-C. Liao, *J. Org. Chem.*, 1999, **64**, 4111.
7 (*a*) C.-C. Liao and C.-P. Wei, *Tetrahedron Lett.*, 1989, **30**, 2255; (*b*) C.-S. Chu, C.-C. Liao and P. D. Rao, *Chem. Commun.*, 1996, 1537; (*c*) T.-H. Lee and C.-C. Liao, *Tetrahedron Lett.*, 1996, **37**, 6869; (*d*) W.-C. Liu and C.-C. Liao, *Synlett*, 1998, 912; (*e*) W.-C. Liu and C.-C. Liao, *Chem. Commun.*, 1999, 117; (*f*) D.-S. Hsu, P.-Y. Hsiu and C.-C. Liao, *Org. Lett.*, 2001, **3**, 263.
8 (*a*) R. Carlini, K. Higgs, C. Older, S. Randhawa and R. Rodrigo, *J. Org. Chem.*, 1997, **62**, 2330; (*b*) R. Carlini, K. Higgs, R. Rodrigo and N. Taylor, *Chem. Commun.*, 1998, 65.
9 (*a*) C.-H. Chen, P. D. Rao and C.-C. Liao, *J. Am. Chem. Soc.*, 1998, **120**, 13 254; (*b*) P. D. Rao, C.-H. Chen and C.-C. Liao, *Chem. Commun.*, 1999, 713.
10 M.-F. Hsieh, R. K. Peddinti and C.-C. Liao, *Tetrahedron Lett.*, in press.
11 M.-F. Hsieh, P. D. Rao and C.-C. Liao, *Chem. Commun.*, 1999, 1441.
12 M. Balci, Y. Sütbeyaz and H. Seçen, *Tetrahedron*, 1990 **46**, 3715.
13 J. H. Rigby, U. S. M. Maharoof and M. E. Mateo, *J. Am. Chem. Soc.*, 2000, **122**, 6624.
14 Y. Kishi, T. Fukuyama, M. Aratani, F. Nakatsubo, T. Goto, S. Inoue, H. Tanino, S. Sugiura and H. Kakoi, *J. Am. Chem. Soc.*, 1972, **94**, 9219.
15 C.-F. Yen, R. K. Peddinti and C.-C. Liao, *Org. Lett.*, 2000, **2**, 2909.

CHEMCOMM
Communication
www.rsc.org/chemcomm

An *ab initio* study of the influence of crystal packing on the host–guest interactions of calix[4]arene crystal structures

Mark I. Ogden,*[a] Andrew L. Rohl[a] and Julian D. Gale[b]

[a] *School of Applied Chemistry, Curtin University of Technology, GPO Box U1987, Perth, 6845, Australia. E-mail: mark@crystallization.curtin.edu.au; Fax: +618 9266 2300; Tel: +618 9266 2483*
[b] *Department of Chemistry, Imperial College of Science, Technology and Medicine, South Kensington, London, UK SW7 2AY*

Received (in Cambridge, UK) 14th June 2001, Accepted 16th July 2001
First published as an Advance Article on the web 9th August 2001

We report the first quantum mechanical calculations of *p-tert*-butylcalix[4]arene inclusion complexes in the crystalline state with geometrical aspects demonstrating good agreement with experiment, while comparison of the configurations calculated for an isolated complex and in the crystal, illustrate that crystal packing forces contribute to the observed structure of the host–guest assembly.

The solid-state structures of calix[*n*]arene host–guest complexes have been studied intensively since the archetypal *p-tert*-butylcalix[4]arene·toluene structure was reported.[1] The structural and dynamic features of this particular system have been studied using a range of experimental methods revealing a remarkably complex structure.[2,3] To complement experimental studies of this and other host–guest complexes, we have used *ab initio* methods, within the framework of density functional theory, to calculate the structures and energetics of calixarene complexes in the crystalline state. Through the use of an appropriate method it has been possible to treat both the periodic crystal structure and gas phase molecular systems at the same level. This allows the influence of crystal packing on the host–guest chemistry of calixarenes to be assessed. To this end, geometry optimisations for *p-tert*-butylcalix[4]arene **1** with the guests toluene and carbon disulfide have been performed.

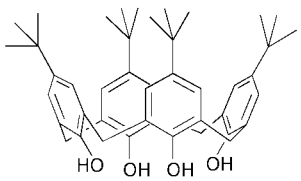

1

All calculations were performed using the *ab initio* program SIESTA[4] which is capable of determining the electronic structure and properties of molecules, surfaces and bulk materials based on density functional theory. For this work, all runs were performed using the non-local density functional of Perdew, Burke and Ernzerhoff.[5] The core electrons for all elements were represented by norm-conserving non-local pseudopotentials, while the valence orbitals were described using a double-zeta basis set, with polarisation functions included for non-hydrogens. Here the basis set is a numerical one, consisting of the exact solutions of the pseudopotential for the atomic state, except that a radial confinement is included to localise the orbital corresponding to an energy shift of 0.001 Rydberg.[4,6] The energy shift used in the present work is smaller than typical values used in many studies. This is necessary to reduce the basis set superposition error (BSSE) that arises due to the radial confinement. Residual BSSE present in binding energies was accounted for using the counterpoise correction. Selected calculations with lower energy shift values verified that the binding configurations are not significantly influenced by further reduction in orbital confinement. A real space mesh equivalent to a planewave cut-off of 150 Rydberg was used for the evaluation of the Hartree and exchange-correlation energies. Optimisations performed on the solid-state structures were constrained at the experimental unit cell dimensions, while all other degrees of freedom were free to relax with no symmetry restrictions.

The results for *p-tert*-butylcalix[4]arene·CS_2 (Fig. 1 and Table 1) show that the guest is less deeply included in the calixarene cavity in the calculated crystal structure as compared to experiment,[7] although other structural parameters are in reasonable agreement (the two complexes in the calculated unit cell were essentially identical). For comparison, results for the previously reported *ab initio* RHF/6-31G* calculation[8] of the gas phase complex are given in Table 1. In this case, the host–guest intermolecular forces are underestimated to a greater extent, although some parameters, such as the C–S bond length are in better agreement with experiment than the present DFT study due to the tendency of the Hartree–Fock calculations to yield shorter bonds. A key finding is that the binding of the guest is weaker in the gas phase (3.2 kJ mol^{-1}) than in the solid

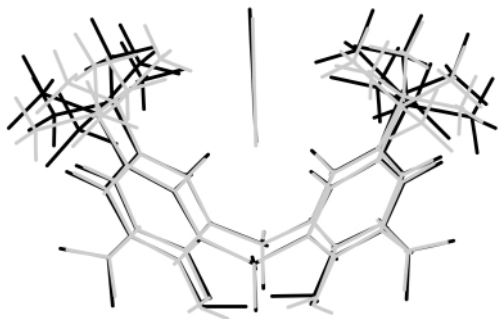

Fig. 1 Superposition of the *p-tert*-butylcalix[4]arene·CS_2 structure calculated in the solid-state (in black), and that determined by crystallography (in grey).

Table 1 Comparison between calculated structural parameters in the isolated *p-tert*-butylcalix[4]arene·CS_2 assembly and crystal structure, the RHF/6-31G* calculated structure and the experimental crystal structure (Ar refers to each of the four phenyl rings, and O_4 represents the plane defined by the four phenol O atoms in the calixarene)

	SIESTA–gas phase	SIESTA–crystal	RHF/6-31G*[a]	Crystal structure[b]
Ar–O_4 angles (°)	125.6 125.6 125.6 125.9	124.6, 124.8 124.7, 125.1 124.5, 124.9 124.5, 124.4	124.7	123.5
C (CS_2)–O_4 distances (Å)	5.93	5.75, 5.80	6.51	5.34
C–S distance (Å)	1.587, 1.596	1.583, 1.597	1.55	1.55
O_4-CS_2 tilt (°)	1.2	0.93, 1.24	0	0

[a] Ref. 8. [b] Ref. 7.

 DOI: 10.1039/b104193m

Table 2 Comparison between calculated structural parameters in the isolated *p-tert*-butylcalix[4]arene·toluene assembly and crystal structure, in addition to the experimental crystal structure (Ar refers to each of the four phenyl rings, and O_4 represents the plane defined by the four phenol O atoms in the calixarene)

		SIESTA–gas phase	SIESTA–crystal	Crystal structure[a]
Ar–O_4 angles (°)	1	123	123, 121	118
	2	132	127, 128	126
	3	124	122, 123	
	4	127	126, 126	
CH_3(tol)–O_4 distance (Å)		3.93	3.64, 3.66	3.65
Toluene tilt (°)		3.5	1.1, 3.8	7

[a] Ref. 2; coordinates obtained from G. D. Enright and J. A. Ripmeester, personal communication.

state (7.7 kJ mol^{-1}), consistent with the fact that the cavity in the crystal is defined and influenced by neighbouring calixarene molecules, as well as the main host. However, the absolute binding energies will be underestimated due to the absence of dispersion forces.

Experimental data suggest that the *p-tert*-butylcalix[4]arene·toluene complex has a C_2-elliptical calixarene cavity that is dynamically disordered to give an average 4-fold symmetry.[2] This disorder is associated with rotational disorder of the toluene guest molecule. While inclusion of statistical sampling, typically *via* dynamical calculations, will be required to study these processes, geometry optimisation gives preliminary results consistent with some aspects of the experimental data. In this case, the two complexes in the calculated crystal structure were slightly different (Table 2). The most striking difference between the calculated structures of the complex in the crystal and the isolated system is the orientation of the guest toluene molecule, along the *pseudo* 4-fold axis of the host calixarene (Fig. 2). In the isolated assembly, the toluene molecule lies on the *pseudo* mirror plane intersecting two of the methylene C atoms (the interplanar angle is 1.5°). In the calculated crystal structure, the same interplanar angle is 19.9 and 24.8°, in good agreement with the experimental crystal structure (22.5°). It is likely that the *tert*-butyl groups of neighbouring calixarenes, which lie 'above' the host calixarene, are inducing this change in orientation. It is also noteworthy that experimental data suggest that the toluene molecule is tilted relative to the calixarene 4-fold axis by 7°; the calculated results are 1.1 and 3.8° in the crystal, and 3.5° in the isolated complex. As observed for the CS_2 guest, the toluene is more deeply included in the calculated crystal structure than in the isolated complex (Table 2).

The results presented here clearly demonstrate that crystal packing can have a significant effect on the geometries of host–guest assemblies and that periodic density functional calculations can accurately reproduce this effect. Molecular dynamics calculations will be the next step in studying the disorder observed in the experimental crystal structures.

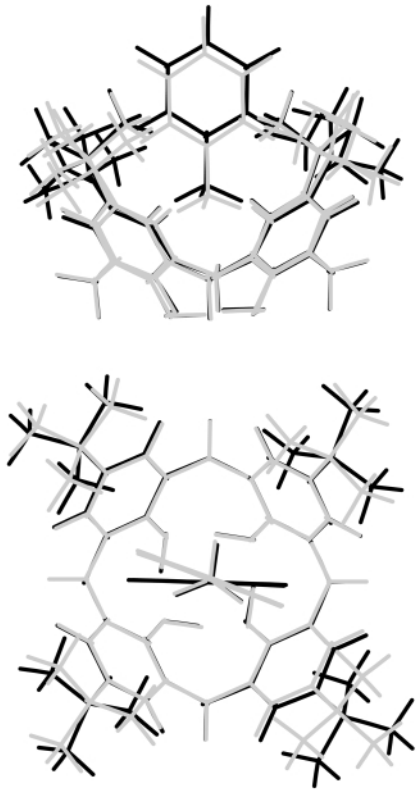

Fig. 2 Side and top views of the superposition of the *p-tert*-butylcalix[4]-arene.toluene structure calculated in the solid-state (in grey), and in the gas phase (in black).

Notes and references

1 G. D. Andreetti, R. Ungaro and A. Pochini, *Chem. Commun.*, 1979, 1005.
2 E. B. Brouwer, G. D. Enright, C. I. Ratcliffe and J. A. Ripmeester, *Supramol. Chem.*, 1996, **7**, 79.
3 E. B. Brouwer, J. A. Ripmeester and G. D. Enright, *J. Inclusion Phenom. Mol. Recognit.*, 1996, **24**, 1; R. Caciuffo, R. Galeazzi, A. J. Horsewill, A. Ikram and F. Ugozzoli, *Phys. Rev. B*, 1999, **60**, 11 867; A. Arduini, R. Caciuffo, S. Geremia, C. Ferrero, F. Ugozzoli and F. Zontone, *Supramol. Chem.*, 1998, **10**, 125.
4 E. Artacho, J. D. Gale, A. Garcia, P. Ordejon and D. Sanchez-Portal, SIESTA Version 1.0.51, 2001; E. Artacho, D. Sanchez-Portal, P. Ordejon, A. Garcia and J. M. Soler, *Phys. Stat. Sol. B*, 1999, **215**, 809; D. Sanchez-Portal, P. Ordejon, E. Artacho and J. M. Soler, *Int. J. Quantum Chem.*, 1997, **65**, 453.
5 J. P. Perdew, K. Burke and M. Ernzerhof, *Phys. Rev. Lett.*, 1996, **77**, 3865.
6 O. F. Sankey and D. J. Niklevski, *Phys. Rev. B*, 1989, **40**, 3979.
7 J. Schatz, F. Schildbach, A. Lentz, S. Rastatter, J. Schilling, J. Dormann, A. Ruoff and T. Debaerdemaeker, *Z. Naturforsch., Teil B*, 2000, **55**, 213.
8 J. Schatz, A. C. Backes and H. U. Siehl, *J. Chem. Soc., Perkin Trans. 2*, 2000, **4**, 609.

CHEMCOMM
Communication
www.rsc.org/chemcomm

Synthesis and properties of novel bis(triarylamines) based on a 3,3′-diphenyl-2,2′-bithiophene core

Ken-Tsung Wong,*[a] Tsung Hsi Hung,[a] Shen C. Kao,[b] Chung Hsien Chou[a] and Yuhlong Oliver Su[a]

[a] *Department of Chemistry, National Taiwan University, Taipei 106, Taiwan. E-mail: kenwong@ccms.ntu.edu.tw; Fax: +886 2 23636359; Tel: +886 2 23630231 ext. 3315*
[b] *Advance Instrumentation Center, National Taiwan University, Institute of Organic and Materials, National Taipei University of Technology, Taiwan*

Received (in Cambridge, UK) 10th April 2001, Accepted 28th June 2001
First published as an Advance Article on the web 3rd August 2001

An efficient synthesis of 3,3′-diphenyl-2,2′-bithiophene based bis(triarylamines) and their physical properties are reported.

Amorphous triarylamines with high glass transition temperatures (T_g) are widely used as hole-transporting materials in organic light-emitting devices (OLED).[1] Thiophene and oligothiophene-linked triarylamines and bis(triarylamines), with phenyl rings separating the thiophene system from the terminal diarylamino groups were first introduced by Shirota *et al.*[2] These amorphous materials form thin films with high morphological stability and also show interesting hole-transporting properties, resulting in their successful use as colour-tunable emitting materials for OLED devices. Triarylamines with diarylamino group(s) directly attached to thiophene are one of the least exploited class of hole-transporting materials.[3,4] Recently, Watanabe and co-workers[5] have accomplished a systematical study on Pd-catalysed amination for the synthesis of 2-diarylaminothiophenes and 2,5-bis(diarylamino)thiophenes. In addition to this, a new synthetic strategy involving transition-metal free cyclization followed by thermal decarboxylation has also been introduced for the synthesis of triarylamines bearing a thiophene moiety.[6] However, the physical properties of thiophene based triarylamines are still limited.[5,6] In this communication, we report the synthesis and physical properties of a new class of bis(triarylamines) based on 3,3′-diphenyl-2,2′-bithiophene as a central linkage. It is well documented that the physical properties of oligothiophenes and polythiophenes strongly depend on the nature of the substituents. However, the similar oxidation potential and absorption λ_{max} of bithiophene and 3,3′-diphenyl-2,2′-bithiophene have been attributed to counterbalancing the resonance effect of phenyl substituents by the steric effect.[7] Interestingly, polythiophenes with phenyl substituent(s) at its 3- and 4-position exhibit higher thermal stability and lower oxidation potentials.[8] Accordingly, the resulting new class of bis(triarylamines) based on 3,3′-diphenyl-2,2′-bithiophene could enhance the thermal and morphological stability, which are crucial for their application in optoelectronic devices.

Cu-promoted Ullman reaction for the synthesis of 3,3′-diphenyl-2,2′-bithiophene was first reported by Johnson in 1976.[9] Further synthetic efforts based on the Ni-catalysed Kumada coupling reaction of 2-halo-3-phenylthiophene with 2-magnesium-3-phenylthiophene gave 3,3′-diphenyl-2,2′-bithiophene in poor yields.[7,8] We report herein a more efficient synthetic pathway (Scheme 1). In the presence of a catalytic amount of $Pd(PPh_3)_4$, 3,3′-dibromo-2,2′-bithiophene **1**[10] was treated with phenylboronic acid in DME to afford 3,3′-diphenyl-2,2′-bithiophene (**2**) in 86% yield. Regioselective bromination[11] of **2** was accomplished by treating **2** with bromine in AcOH–$CHCl_3$ (1:2) solution, which afforded 5,5′-dibromo-3,3′-diphenyl-2,2′-bithiophene **3** in 95% yield. Six different diarylamines were screened to react with **3** respectively in the presence of a catalytic amount of $Pd(OAc)_2$ and PBu^t_3 in toluene[12] at reflux temperature, resulting in compounds **4a**–**4f** as bright yellow solids in moderate yields (Table 1). For a comparative study of the influences of phenyl

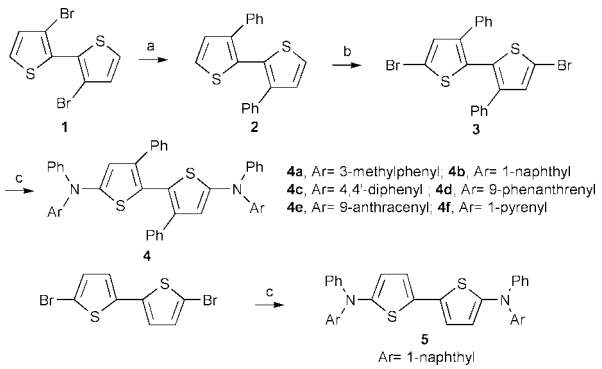

Scheme 1 Reagents and conditions: a, $PhB(OH)_2$, $Pd(PPh_3)_4$, Na_2CO_3, DME, reflux 2 d, 86%; b, Br_2, AcOH–$CHCl_3$ (1:2), 0 °C to rt 98%; c, diarylamine, $Pd(OAc)_2$, PBu^t_3, $NaOBu^t$, toluene, reflux overnight.

† Electronic supplementary information (ESI) available: experimental details and NMR spectra. See http://www.rsc.org/suppdata/cc/b1/b103194p/

Table 1 Chemical yields and physical properties of 5,5′-bis(diarylamino)-3,3′-diphenyl-2,2′-bithiophenes **4** and model compound **5**

Compound	Yield (%)[a]	λ_{max}/nm, log ε[b]	λ_{em}/nm[c]	E_{pa}, E_{pc} /mV[d]	T_g/°C[e]
4a	62	263 (4.59), 367 (4.12)	535	550, 430	55
4b	56	262 (4.69), 365 (4.26)	535	595, 440	85
4c	60	260 (4.96), 317 (4.87)	538	570, 465	83
4d	52	254 (4.90), 363 (4.09)	539	605, 470	114
4e	51	256 (4.99), 376 (4.54)	494	(545, 455), (650, 570)	119
4f	53	265 (4.94), 381 (4.48)	458, 503	600, 500	124
5	62	273 (4.38), 392 (4.42)	480	(460, 385), (695, 610)	67

[a] Isolated yield by column chromatography on SiO_2 (hexane–CH_2Cl_2 = 4:1) with satisfactory spectral analyses (^1H, ^{13}C, mass, HRMS, and IR). [b] Recorded in EtOAc; units of ε mol^{-1} dm^3 cm^{-1}. [c] Recorded in EtOAc and excited at λ_{max}. [d] Performed in 0.1 M solution of n-Bu_4NPF_6 in CH_2Cl_2, carbon electrode was used as the working electrode, scan rate 100 mV s^{-1}, Ag/AgCl as reference electrode. [e] Analyzed by differential scanning calorimetry (DSC), T_g was recorded from heating (10 °C min^{-1}) a liquid nitrogen quenched melt-sample.

 DOI: 10.1039/b103194p

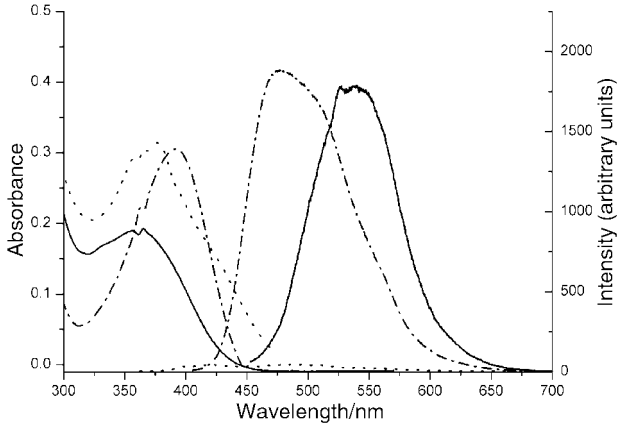

Fig. 1 Absorption and photoluminescence spectra of **4b** (solid), **4e** (dot), and **5** (dash-dot) in EtOAc (1.0×10^{-5} M)

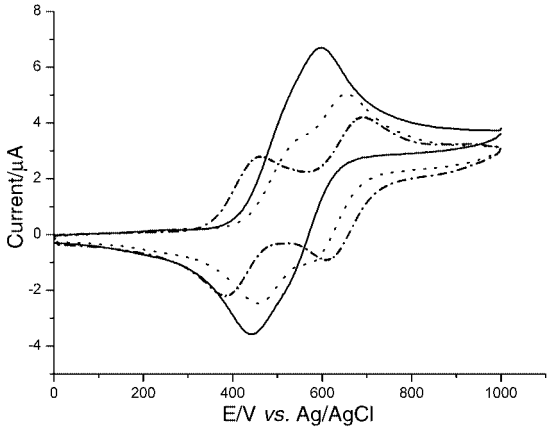

Fig. 2 Cyclic voltammogram of **4b** (solid), **4e** (dot), and **5** (dash-dot) in CH_2Cl_2.

substituents on the physical properties, model compound **5** was also synthesized by the Pd-catalysed amination of 5,5′-dibromo-2,2′-bithiophene.

The absorption spectra of **4a**–**4f** in ethyl acetate showed similar behaviour, displaying two absorption maxima (Table 1). The second bands of **4e** and **4f** were slightly red-shifted compared to that of **4a**–**4d**. Compound **4a**–**4d** were highly fluorescent. These results indicate that the absorption λ_{max} is relatively insensitive to the nature of the diarylamino substitutents. However, the photoluminescence efficiency and emission maxima are strongly dependent on the structural feature of the terminal diarylamino groups. Thus, bis(triarylamines) (**4a**–**4d**) with less conjugated diarylamino substituents showed more efficient photoluminescence than when compared with those bearing more conjugated terminal diarylamino groups (**4e**–**4f**). The significant Stokes shift (*ca*. 170 nm for **4a**–**4d**) reveals that the 3,3′-diphenyl-2,2′-bithiophene linkage may be highly twisted in the ground state. The emission maxima with relatively long wavelength could be attributed to the relaxation from an excited state with a more coplanar conformation. The influence of phenyl substituents of the bithiophene linkage on the photophysical properties are demonstrated by a comparison of the UV-Vis and photoluminescent spectra of **4b**, **4e**, and **5** (Fig. 1). Bis(triarylamine) **5** exhibited a sharper, red-shifted absorption and a blue-shifted emission compared to that of **4b**. The longer emission wavelength of **4b** further confirms a more conjugated excited state.

Compounds **4a**–**4f** exhibited only quasi-reversible anodic oxidation (Table 1). The onset of oxidation and E_{pa} (V *vs*. Ag/AgCl) varied with the nature of the terminal diarylamino groups. Differing from the conventional bis(triarylamines),[13] only one redox couple (E_{pa} 550 mV, E_{pc} 430 mV *vs*. Ag/AgCl) was detected for **4a** and **4c**. Coulometry in a thin layer cell showed the redox process of **4a** to be a two-electron oxidation. The lack of co-planarity of the central 3,3′-diphenyl-2,2′-bithiophene linkage prevents the extension of π-conjugation along the molecular axis. The rate of second oxidation in **4a** may be faster than the conformational change reaching a more coplanar conformation. Therefore, the first radical cation can not efficiently delocalise in the whole molecule, the two triarylamine systems behave independently but are oxidized simultaneously without any communication. Fig. 2 shows a comparison of the cyclic voltammogram of **4b, 4e**, and **5**. Two partially resolved redox processes (E_{pa} 545 mV, E_{pc} 455 mV and E_{pa} 650 mV, E_{pc} 570 mV *vs*. Ag/AgCl) of **4e** were detected, which were assigned to be a two-step one-electron redox couple corresponding to removal of an electron from each triarylamine system. The redox potential difference (110 mV) of **4e** indicates that the second oxidation could occur *via* a radical cation with more coplanar conformation. **4b**, **4d**, and **4f** showed similar redox behaviour but were less resolved when compared with that of **4e**. The model compound **5** exhibited two well-resolved redox couples (E_{pa} 460 mV, E_{pc} 385 mV and E_{pa} 695 mV, E_{pc} 610 mV *vs*. Ag/AgCl). The lower oxidation onset and larger potential difference (230 mV) reveal that the the central bithiophene linkage is in a coplanar conformation.

All the compounds in this study exhibited an amorphous nature evidenced by the presence of the glass transition temperature (Table 1). The asymmetric diarylamino substituent and the diphenyl substituted central bithiophene linkage significantly contribute to the high T_gs. Compounds (**4d**, **4e**, **4f**) with higher molecular weight aryl groups showed higher T_gs compared to that of **4a**, **4b** and **4c** bearing a lower molecular weight aryl group in the terminal diarylamino substituents.

In summary, we have successfully established an efficient method for the synthesis of a new class of bis(triarylamines) bearing 3,3′-diphenyl-2,2′-bithiophene as a central linkage. The introduction of phenyl substituents on the central linkage apart from improving the morphological stability, twists the conformation of the central bithiophene linkage in the ground state, which results in interesting photophysical and electrochemical properties. Further studies on the modification of the central bithiophene linkage by introducing bulkier aryl groups and their applications in OLED are under way and will be reported in due course.

We thank the National Science Council of Taiwan for providing financial support (NSC-89-2113-M002-053).

Notes and references

1 C. H. Chen, J. Shi and C. W. Tang, *Macromol. Symp.*, 1997, **125**, 1; Y Shirota, *J. Mater. Chem.*, 2000, **10**, 1.
2 T. Noda, I. Imae and Y. Shirota, *Adv. Mater.*, 1997, **9**, 239; T. Noda, H. Ogawa, N. Noma and Y. Shirota, *Adv. Mater.*, 1997, **9**, 720; T. Noda, H. Ogawa, N. Noma and Y. Shirota, *J. Mater. Chem.*, 1999, **9**, 2177.
3 E. Ueta, H. Nakano and Y. Shirota, *Chem. Lett.*, 1994, 2397.
4 I.-Y. Wu, J. T. Lin, Y.-T. Tao and E. Balasubramaniam, *Adv. Mater.*, 2000, **12**, 668.
5 M. Watanabe, T. Yamamoto and M. Nishiyama, *Chem. Commun.*, 2000, 133.
6 H. Hartmann, P. Gerstner and D. Rohde, *Org. Lett.*, 2001, **3**, 1673.
7 É. Naudin, N. E. Mehdi, C. Soucy, L. Breau and D. Bélanger, *Chem. Mater.*, 2001, **13**, 634.
8 M. Ueda, T. Ito, Y. Seino, Y. Ohba and T. Sone, *Polym. J.*, 1992, **24**, 693; R. J. Waltman, A. J. Diaz and J. Bargon, *J. Electrochem. Soc.*, 1984, **131**, 740.
9 A. L. Johnson, *J. Org. Chem.*, 1976, **41**, 1320.
10 U. Dahlmann and R. Neidlein, *Helv. Chim. Acta*, 1996, **79**, 755.
11 H. Meng and W. Huang, *J. Org. Chem.*, 2000, **65**, 3894.
12 T. Yamamoto, M. Nishiyama and Y. Koie, *Tetrahedron Lett.*, 1998, **39**, 2367.
13 B. E. Koene, D. E. Loy and M. E. Thompson, *Chem. Mater.*, 1998, **10**, 2235.

CHEMCOMM
Communication
www.rsc.org/chemcomm

Highly diastereoselective dihydride formation by activation of methanol with IrCl{(*S*)-binap}(PPh_3)

Kazuhide Tani,* Kouji Nakajima, Aika Iseki and Tsuneaki Yamagata

Department of Chemistry, Graduate School of Engineering Science, Osaka University, Toyonaka, Osaka 560-8351, Japan. E-mail: tani@chem.es.osaka-u.ac.jp; Fax: +81-6-6850-6245

Received (in Cambridge, UK) 13th March 2001, Accepted 13th July 2001
First published as an Advance Article on the web 3rd August 2001

Reaction of [IrCl{(*S*)-binap}(PPh_3)] {(*S*)-3} with methanol gave one of the diastereomers of the *cis,mer*-dihydride, *cis,mer-OC*-6-44-*A*-[$IrCl(H_2)$\{(*S*)-binap}(PPh_3)] {(*S*)-4a} stereoselectively, the structure of which was determined crystallographically, whereas the reaction of (*S*)-3 with H_2 produced a 1:1 mixture of the diastereomers of the *cis,mer*-dihydride, (*S*)-4a and *cis,mer-OC*-6-44-*C*-[$IrCl(H_2)$\{(*S*)-binap}(PPh_3)] {(*S*)-4b}.

Although the stereochemistry for the formation of the dihydrides of rhodium and iridium carrying chiral ligands is of great interest in connection with their potential as asymmetric hydrogenation and its mechanism,[1] only very rare cases of detection of diastereoselective formation of dihydrides have been reported.[2–6] Even in such cases the absolute configuration of the hydride was only estimated based on spectroscopic results. Here we report a highly diastereoselective formation of the dihydride (*S*)-**4a** by reaction of [IrCl{(*S*)-binap}(PPh_3)] {(*S*)-**3**}[7] with methanol, the absolute configuration of which was determined by X-ray analysis. Oxidative addition of dihydrogen to (*S*)-**3** gave also the same *cis,mer*-dihydrides **4** but as a 1:1 mixture of the diastereomers **4a** and **4b**.

Recently we have reported that iridium(I) complexes bearing peraryldiphosphines [IrCl(diphosphine)]$_2$ (**1**) can activate O–H bonds easily at room temperature. For example, [IrCl(binap)]$_2$ (**1a**) reacted easily with methanol at room temperature to give the hydrido(methoxo) complex, [{Ir(H)(binap)}$_2$(μ-OMe)$_2$(μ-Cl)]Cl (**2**) in good yield,[8] which becomes an efficient catalyst precursor for transfer hydrogenation of alkynes using methanol as a hydrogen source.[9] During the studies on the reactivity of complex **1**, we have found that [IrCl(binap)]$_2$ (**1a**) reacted with 2 equiv. of PPh_3 to give a square-planar complex, [IrCl(binap)(PPh_3)] (**3**) selectively as a red solid.[7] The molecular structure of (*R*)-**3** is shown in Fig. 1.† In contrast to complex **1a**, complex **3** was fairly stable in the solid state. Heating a toluene solution of complex (*S*)-**3** with large excess of methanol at 70 °C during 6 h, however, gave pale-red precipitates (67% yield) of the dihydride (*S*)-**4a**[10] as a single diastereomer. The crude reaction mixture obtained after removal of the all solvents showed almost quantitative and selective formation of the dihydride **4** containing a small amount of the other diastereomer (*S*)-**4b**[11] {(*S*)-**4a**:(*S*)-**4b** = 92:8}. The reaction of (*S*)-**3** with methanol proceeded even at room temperature in toluene and after 45 h gave selectively the *cis,mer*-dihydride (*S*)-**4a** in about 90% yield {(*S*)-**4a** : (*S*)-**4b** = 96:4} (Scheme 1). The reaction, however, is very much suppressed when excess triphenylphosphine is present. Complex (*S*)-**4a** was fully characterized by elemental analyses and spectroscopic studies. The ^{1}H NMR spectrum showed two characteristic hydride signals at δ −19.56 and –9.97; the latter signal showed one large P–H coupling indicating that the hydride is situated *trans* to one phosphorus atom while the former signal does not show any couplings larger than *ca.* 20 Hz, indicating the hydride situates *cis* to all the phosphorus atoms. The ^{31}P NMR spectrum measured at 35 °C showed three phosphorus signals at δ −4.7 (br m), 14.9 (dd, J = 16, 358 Hz) and 19.6 (dd, J = 11, 358 Hz) in a 1:1:1 ratio; the signal pattern indicates that the three phosphorus atoms

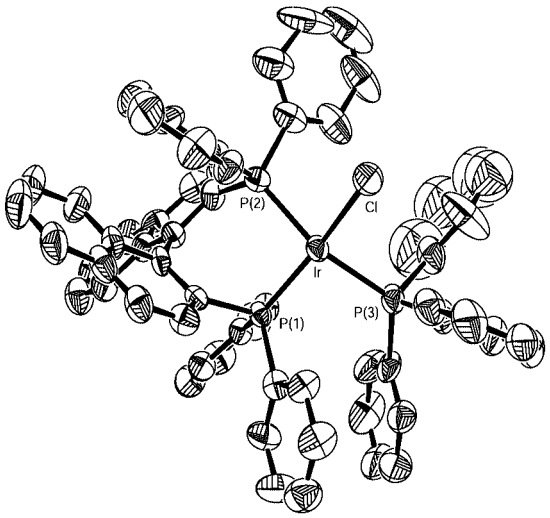

Fig. 1 View of (*R*)-**3** showing the labeling of the heteroatoms. Displacement ellipsoids are drawn at the 50% probability level. Selected bond distances (Å) and angles (°): Ir–P(1) 2.1998(19), Ir–P(2) 2.277(2), Ir–P(3) 2.305(2), Ir–Cl 2.394(2); P(1)–Ir–P(2) 91.58(7), P(1)–Ir–P(3) 99.20(8), P(2)–Ir–P(3) 157.11(8), P(1)–Ir–Cl 159.23(10), P(2)–Ir–Cl 87.76(9), P(3)–Ir–Cl 89.09(9).

coordinate to the central atom in a *mer* configuration. The dihydride complex showed two Ir–H stretchings (Nujol) at 2207 (*trans* to Cl) and 2083 cm^{-1} (*trans* to P). Suitable crystals for X-ray analysis were obtained by recrystallization from toluene-methanol. The absolute configuration of the dihydride was concretely determined by X-ray crystallography.† The ORTEP drawing is depicted in Fig. 2. The predominant diastereomer (*S*)-**4a** obtained by the reaction of (*S*)-**3** with methanol was revealed to be the (*S*)-*OC*-6-44-*A* isomer. The long bond distance (2.363(2) Å) of Ir–P(2) indicates a strong *trans* influence of the hydride ligand. Similarly, the Ir(III)–Cl bond distance (2.505(3) Å) is long and even longer than the Ir(I)–Cl distance (2.394(2) Å) in the Ir(I) complex (*R*)-**3**. The acute P(1)–Ir–P(3) angle (167.30(9)°) reflects also the small hydride ligand. The same diastereomeric dihydride (*S*)-**4a** was also obtained selectively by the reaction of (*S*)-**2** with 2 equiv. of PPh_3 in a mixed solvent of methanol and toluene under reflux

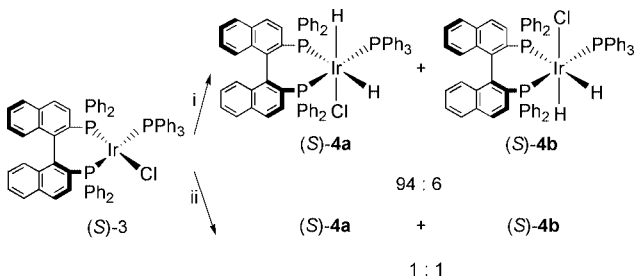

Scheme 1 *Reagents and conditions*: i, MeOH–toluene, room temp.; ii, H_2 (1 atm)/toluene, room temp.

 DOI: 10.1039/b102395k

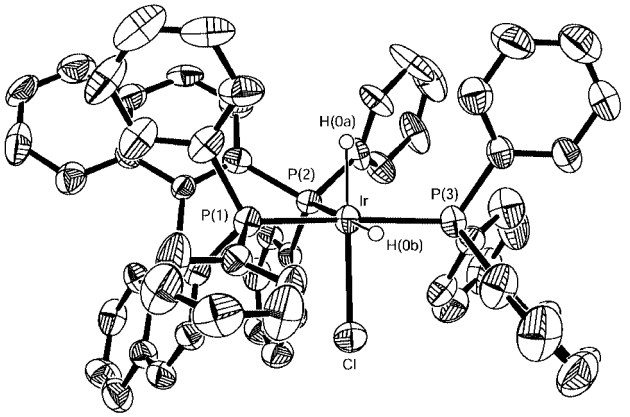

Fig. 2 View of (*S*)-**4a** showing the labeling of the heteroatoms and the hydride hydrogen atoms. Displacement ellipsoids are drawn at the 50% probability level. Selected bond distances (Å) and angles (°): Ir–P(1) 2.299(3), Ir–P(3) 2.326(3), Ir–P(2) 2.363(2), Ir–Cl 2.505(3); P(1)–Ir–P(3) 167.30(9), P(1)–Ir–P(2) 92.70(16), P(3)–Ir–P(2) 100.00(16), P(1)–Ir–Cl 88.81(10), P(3)–Ir–Cl 88.38(10), P(2)–Ir–Cl 102.98(10).

but accompanied by small amounts of several unidentified hydrides [eqn. (1)]. Hydrogenation of complex (*S*)-**3** with dihydrogen in toluene at room temperature also yielded the same *cis*,*mer*-dihydride **4** but as an almost 1 : 1 mixture of the two diastereomers (*S*)-**4a** and (*S*)-**4b**. These dihydrides are obtained by a concerted *cis* addition of H_2 along the P–Ir–Cl axis of the square planar complex (*S*)-**3**. In the reaction products obtained by oxidative addition of H_2 to (*S*)-**3** substantial amounts of *cis*,*fac*-isomer **5** resulted from *cis* addition of H_2 along the P–Ir–P axis of complex (*S*)-**3** and the other possible dihydride **6** could not be detected.

$$[(\text{ir(H)}\{(S)\text{-binap}\})_2(\mu\text{-OMe})_2(\mu\text{-Cl})]\text{Cl} + 2\text{PPh}_3 \xrightarrow[\text{MeOH/toluene (v/v = 1/1)}]{\text{reflux, 39 h}} (S)\text{-}\mathbf{4a} \quad (1)$$

(*S*)-**5a** (*S*)-**5b** (*S*)-**6**

Although the detailed mechanism for diastereoselective formation of (*S*)-**4a** by the reaction of (*S*)-**3** with methanol is not clear at present, the large difference of the selectivity between methanol and hydrogen may be explained as follows. Dihydride formation from the reaction of **3** with methanol could be explained by β-hydrogen elimination from the Ir–OMe group of the initial oxidative addition product of methanol, a hydrido-(methoxo) complex, 'IrCl(H)(OMe)(binap)(PPh_3)', which is not detected in the reaction mixture. Such iridium dihydride formation from the H–Ir–OMe species has been reported.[12] Because methanol is much larger than dihydrogen, methanol approaches also only along the P–Ir–Cl axis to complex (*S*)-**3** and in addition can discriminate efficiently between the two diastereotopic planes of (*S*)-**3**, above and below the Ir(I) square plane. By inspection of a CPK model, approach of methanol from above the square plane of (*S*)-**3** described in Scheme 1 is more preferable and leads to the highly stereoselective formation of dihydride (*S*)-**4a**.[13] In contrast, the small dihydrogen molecule can not efficiently discriminate between the diastereotopic planes.

This work was partly supported by the Grant-in Aid for Scientific Research from the Ministry of Education, Science, Sports, and Culture of Japan.

Notes and references

† *Crystal data* for (*R*)-**3**: $C_{62}H_{47}ClIrP_3$, M = 1112.56, trigonal, space group $P3_1$ (no. 144), a = 18.579(5), b = 18.579(5), c = 13.368(6) Å, α = 90, β = 90, γ = 120°, U = 3996(2) Å^3, T = 296(2) K, Z = 3, D_c = 1.387 Mg m^{-3}, λ(Mo-Kα) = 0.71069 Å, μ = 2.684 mm^{-1}, $2\theta_{max}$ = 55.0°, absorption corrections[14] (T_{min} = 0.2958, T_{max} = 0.4998), a linear correction was applied (24.9% decay), 12250 unique reflections including Friedel pairs (R_{int} = 0.0426), direct methods (SIR97),[15] full-matrix least-squares methods (SHELXL-97),[16] refined on F^2. The aromatic H-atoms were included in the refinement on calculated positions riding on their carrier atoms (C(sp^2)–H = 0.93 Å, U_{iso}(H) = 1.2U_{eq}(C) Å^2). *R*1/*wR*2 (for 9697 reflections with $I > 2.0\sigma(I)$) = 0.0455/0.1288, *R*1/*wR*2 (for 12550 reflections with all data) = 0.0739/0.1429 for 581 parameters and 5 restraints, χ (Flack parameter) = −0.005(7), GOF = 1.040, $\Delta\rho$ (max./min.) = 1.513/−0.745 e Å^{-3}.

For (*S*)-**4a**: $C_{62}H_{49}ClIrP_3$, M = 1114.57, monoclinic, space group $P2_1$ (no. 4), a = 11.070(3), b = 21.979(4), c = 11.788(3) Å, β = 96.50(2)°, U = 2849.7(12) Å^3, T = 296(2) K, Z = 2, D_c = 1.299 Mg m^{-3}, λ(Mo-Kα) = 0.71069 Å, μ = 2.509 mm^{-1}, $2\theta_{max}$ = 65.0°, absorption corrections[14] (T_{min} = 0.4023, T_{max} = 0.8168), a linear correction was applied (9.2% decay), 21894 reflections measured, 20525 unique reflections including Friedel pairs (R_{int} = 0.0693), direct methods (SIR97),[15] full-matrix least-squares methods (SHELXL-97),[16] refined on F^2. Non-hydrogen atoms were anisotropically refined. The aromatic H-atoms were included in the refinement on calculated positions riding on their carrier atoms (C(sp^2)–H = 0.93 Å, U_{iso}(H) = 1.2U_{eq}(C) Å^2). Probable hydride-ligand positions were calculated at the minima of the potential energy by the program HYDEX[17] and were included as fixed contributions. *R*1 = 0.0578, *wR*2 = 0.1483, (for 8479 reflections with $I > 2.0\sigma(I)$), *R*1 = 0.2305, *wR*2 = 0.1953, (for 20525 reflections with all data), parameters = 603, χ (Flack parameter) = −0.050(9), GOF = 0.964.

CCDC reference numbers 168686 and 168687.

See http://www.rsc.org/suppdata/cc/b1/b102395k/ for crystallographic data in CIF or other electronic format.

1 P. P. Deutsch and R. Eisenberg, *Chem. Rev.*, 1988, **88**, 1147.
2 I. D. Grindnev, N. Higashi, K. Asakura and T. Imamoto, *J. Am. Chem. Soc.*, 2000, **122**, 7183.
3 B. F. M. Kimmich, E. Somsook and C. R. Landis, *J. Am. Chem. Soc.*, 1998, **120**, 10115.
4 A. Harthun, R. Kadyrov, R. Selke and J. Bargon, *Angew. Chem., Int. Ed.*, 1997, **36**, 1103.
5 A. J. Kunin, R. Farid, C. E. Johnson and R. Eisenberg, *J. Am. Chem. Soc.*, 1985, **107**, 5315.
6 J. M. Brown and P. J. Madox, *J. Chem. Soc., Chem. Commun.*, 1987, 1278.
7 T. Yamagata, A. Iseki and K. Tani, *Chem. Lett.*, 1997, 1215.
8 K. Tani, A. Iseki and T. Yamagata, *Angew. Chem., Int. Ed.*, 1998, **37**, 3381.
9 K. Tani, A. Iseki and T. Yamagata, *Chem. Commun.*, 1999, 1821.
10 *OC*-6-44-*A* isomer **4a**: ^{1}H NMR (C_6D_6, 35 °C): δ −19.56 (m, 1H), −9.97 (dddd, J = 5.2, 11.2, 22.1, 132.9 Hz, 1H), 6.3–8.1 (m, 44H), 8.20 (t, J = 8.4 Hz, 1H), 8.87 (t, J = 8.4 Hz, 2H). ^{31}P NMR (C_6D_6, 35 °C): δ −4.7 (br m, 1P), 14.9 (dd, J = 16, 358 Hz, 1P), 19.6 (dd, J = 11, 358 Hz). IR(Nujol): 2207 ($\nu_{Ir–H}$), 2083 cm^{-1} ($\nu_{Ir–H}$), Anal. Calc. for $C_{62}H_{49}ClIrP_3$: C, 66.81; H, 4.43. Found: C, 66.73; H, 4.54%.
11 *OC*-6-44-*C* isomer **4b**: ^{1}H NMR (C_6D_6, 35 °C): δ −20.03 (m, 1H), −10.56 (dddd, J = 5.1, 16.9, 22.2, 136.8 Hz, 1H); ^{31}P NMR (C_6D_6, 35 °C): δ 1.0 (m, 1P), 4.6 (dd, J = 13, 356 Hz, 1P), 7.0 (dd, J = 16, 356 Hz). IR(Nujol): 2274 ($\nu_{Ir–H}$), 2119 cm^{-1} ($\nu_{Ir–H}$).
12 O. Blum and D. Milstein, *Angew. Chem., Int. Ed. Engl.*, 1995, **34**, 229; O. Blum and D. Milstein, *J. Am. Chem. Soc.*, 1995, **117**, 4582.
13 As one referee pointed out, a possibility that the high diastereoselectivity arises during the β-hydrogen elimination from methoxide cannot be excluded at present.
14 A. C. T North, D. C. Phillips and F. S. Mathews, *Acta. Crystallogr., Sect. A*, 1968, **24**, 351.
15 A. Altomare, M. C. Burla, M. Camalli, G. L. Cascarano, C. Giacovazzo, A. Guagliardi, A. G. G. Moliterni, G. Polidori and R. Spagna, *J. Appl. Crystallogr.*, 1999, **32**, 115.
16 G. M. Sheldrick, , SHELXL 97, Programs for Crystal Structure Analysis (Release 97-2), University of Göttingen, Germany, 1997.
17 A. G. Orpen, *J. Chem. Soc., Dalton Trans.*, 1980, 2509.

CHEMCOMM
Communication
www.rsc.org/chemcomm

The binding of difunctional neutral guest molecules by novel bis(tripyrrolyl) cryptands†

O. Danny Fox,[a] Toby D. Rolls,[a] Michael G. B. Drew[b] and Paul D. Beer*[a]

[a] *Department of Chemistry, Inorganic Chemistry Laboratory, University of Oxford, Oxford, UK OX1 3QR. E-mail: paul.beer@chem.ox.ac.uk*
[b] *Department of Chemistry, University of Reading, Whiteknights, Reading, UK RG6 6AD*

Received (in Cambridge, UK) 9th May 2001, Accepted 5th July 2001
First published as an Advance Article on the web 14th August 2001

Bis(tripyrrolyl) cryptands are prepared *via* a [2 + 3] Schiff base condensation of formyltripyrrolyls with diamines; an ethyl-spaced hexapyrrole cryptand is shown to bind strongly ethane-1,2-diamine and ethane-1,2-diol in chloroform solution.

Cryptand ligands and carcerand hosts display fascinating coordination and host–guest chemistry due to their ability to wholly encapsulate their guest atoms or molecules.[1,2] Novel and versatile building blocks possessing multiple and convergent donor atoms from which to prepare these cage-like molecular hosts are currently in particular demand. From a practical perspective, the ease with which a building block can be prepared and modified contributes significantly to its degree of future exploitation. Recent developments in calixarene-[3] and more recently porphyrinogen/calixpyrrole-[4] chemistry are prime examples of how simple-to-prepare and robust macrocycles can be skilfully exploited for the coordination of cations[5] and anions.[6]

We were quite surprised therefore that given the recent attention accorded to the chemistry of cyclic, oligomeric pyrrole compounds that the coordination and supramolecular chemistry of tripyrrolylmethane **1** appears to have been sparsely studied.[7] In addition, three-dimensional cryptand-like pyrrole compounds have also remained largely unexplored.[8,9] Herein we report our initial findings on the synthesis of substituted tripyrrolyls and demonstrate the ease with which such molecules can be incorporated into cryptand-like ligands *via* a Schiff base condensation reaction. An ethyl-spaced bis(tripyrrolyl) host **6** is shown to bind strongly ethane-1,2-diamine and ethane-1,2-diol in chloroform solution.

Attempts to formylate tripyrrolylmethane[10] **1** employing a variety of modifications to the Vilsmeier–Haack reaction were unsuccessful. However, adaptation of Bruce's method[11] employing triethyl orthoacetate or triethyl orthopropanoate yielded the methyl and ethyl tripyrrolyls **2** (59%) and **3** (60%) respectively (see Scheme 1). These were easily formylated employing standard Vilsmeier–Haack conditions ($POCl_3$ and DMF) to give the triformylpyrrolyls **4** (84%) and **5** (70%) in good yields. The use of two different triethyl orthoalkanoates demonstrates the generality of this reaction and also illustrates a convenient route to the preparation of further apically-substituted tripyrrolyls.

Treatment of **5** with 1.5 eq. of ethane-1,2-diamine (**en**) or butane-1,4-diamine (**bn**) in THF afforded the cryptand-like Schiff base pyrrole cages **6** and **7**. Recrystallisation from DCM–hexane afforded large, yellow, prismatic crystals of the butyl-spaced cage **7**. Confirmation of the structure was provided by X-ray crystallography‡ (Fig. 1) and also showed the fortuitous inclusion of a molecule of butane-1,4-diamine (**bn**) within **7**. The diaminobutane guest is encapsulated within the cavity *via* 7 hydrogen bonds between the two nitrogen atoms in the guest and 7 different nitrogen atoms in the host. Each nitrogen head of the **bn** molecule is held in place by host hydrogen-bonding

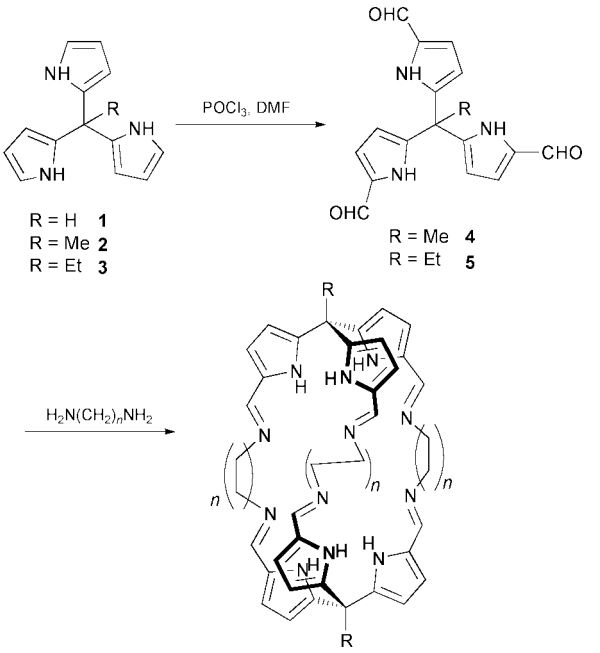

Scheme 1

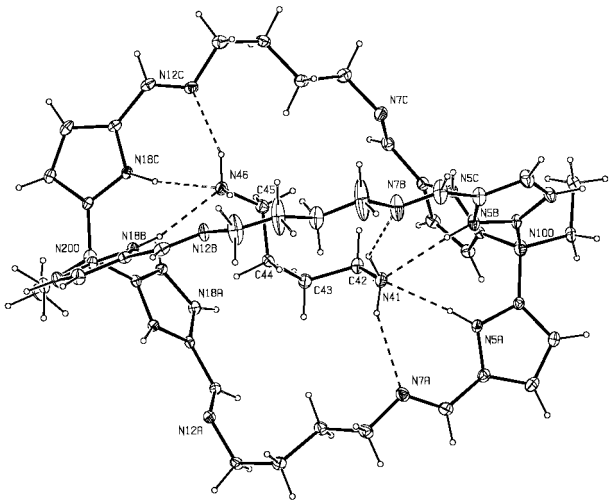

Fig. 1 The structure of **7**·**bn**. Ellipsoids are shown at 10% probability. The 7 hydrogen bonds are shown as dotted lines. Distances for donor hydrogen bonds from the guest are N(46)···N(12C), 3.19; N(41)···N(7A) 2.99; N(41)···N(7B) 3.01 and acceptor hydrogen bonds are N(46)–N(18B) 3.00; N(46)–N(18C) 3.09; N(41)–N(5A) 3.16 and N(41)–N(5B) 3.22 Å.

† Electronic supplementary information (ESI) available: experimental procedures, spectroscopic data and titration protocol. See http://www.rsc.org/suppdata/cc/b1/b104077b/

 DOI: 10.1039/b104077b

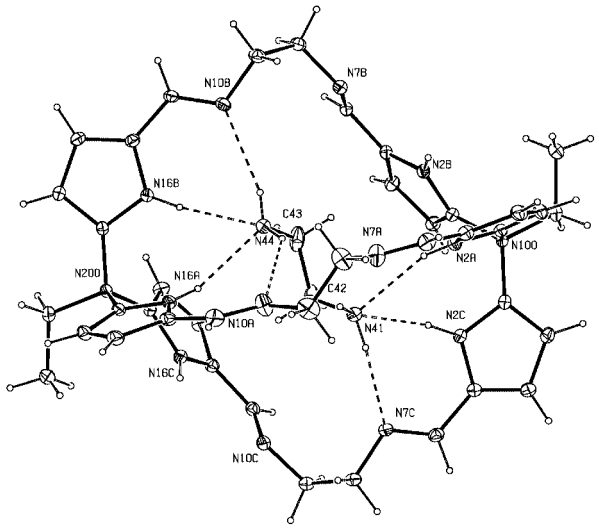

Fig. 2 The structure of **6·en**. Ellipsoids are shown at 10% probability. The 7 hydrogen bonds are shown as dotted lines. Distances for donor hydrogen bonds from the guest are N(41)···N(7c), 3.20; N(44)···N(10b), 3.17; N(44)···N(10a), 3.29 and acceptor hydrogen bonds are N(41)–N(2C), 3.05; N(41)–N(2a), 3.06; N(44)–N(16a), 3.04 and N(44)–N(16b), 3.06 Å.

acceptor interactions to the pyrrole nitrogen atoms and donor interactions to the Schiff base nitrogens. There are seven typical hydrogen bonding N···N distances which range between 2.99 and 3.22 Å (see Fig. 1). In the crystal structure of **7·bn** only two of the three pyrrole moieties at each end of the macrocycle are orientated with their NHs towards the guest **bn**. The remaining two pyrroles are both turned away and only participate in the binding interaction with the **bn** through weak $C–H_{bn}\cdots\pi_{pyrrole}$ contacts at 2.97 and 2.66 Å. Interestingly, in order to fit into the cavity the guest molecule **bn** takes up a *gauche, gauche, trans* conformation rather than the more energetically favourable *trans, trans, trans* conformation. Overall, inspection of the **7·bn** complex illustrates the excellent complementarity of the host's shape and hydrogen bonding capabilities which hold the guest in place through multiple co-operative binding interactions.

Further evidence for the binding of **bn** by **7** was provided by ^{1}H and ^{13}C NMR in $CDCl_3$ solution.[12] In the ^{1}H NMR spectrum of **7·bn** the two resonances for the methylene chain of the coordinated **bn** were observed to be shifted upfield, at δ 2.24 and 0.92 compared to their unbound values, 2.72 and 1.42 ppm. Peaks at δ 40.2 and 29.9 ppm in the ^{13}C of **7·bn** are assigned to the methylene carbons of the guest **bn**. The inclusion and identity of the guest was further qualified by ^{1}H COSY and ^{1}H–^{13}C HETCOR experiments. A very broad resonance at approximately δ 5 is attributed to both the pyrrolic and **bn** amine protons; this peak is lost upon addition of D_2O.

In a similar manner the preparation of **6** in THF produced the ethane-1,2-diamine (**en**) included complex **6·en**. The crystal structure of which was also determined and is shown in Fig. 2. The structure of **6·en** closely resembles that of **7·bn** with very similar hydrogen-bonding distances from the host's donor pyrrole and acceptor Schiff base nitrogen atoms to the guest **en**. Notably, the bound guest **en** adopts the *gauche* conformation. Weak contacts attributable to $C–H_{en}\cdots\pi_{pyrrole}$ interactions are again observed. The identity of the guest was supported by ^{1}H, ^{13}C and 2D NMR experiments with the incarcerated **en** molecule assigned to resonances at δ 2.12 (^{1}H), and 43.6 ppm (^{13}C).

The inclusion of the reactant diamine inside the Schiff base suggests that the formation of the tripyrrolyl cages is templated by the diamine. The preparation of **6** and **7** was performed in acetonitrile using 2 eq. but again yielded **6·en** (81%) and **7·bn** (73%). It is noteworthy that using 2 eq. of diamine does significantly improve the yield of tripyrrolyl cryptands. Considering the high yields of cages **6** and **7** it is quite likely that the guest diamine is involved, in some shape or form, in templating the formation of the bis(tripyrrolyl) cryptands.

The guest **en** could be simply removed from **6·en** by stirring with MeOH. ^{1}H NMR titration experiments in $CDCl_3$ of the diamine-free bis(tripyrrolyl) cryptand **6** were performed to confirm diamine binding and determine a stability constant. Titration of **en** with **6** produced identical ^{1}H, ^{13}C and 2D NMR spectra as for **6·en** and a binding constant, *K*, of 1500 ± 140 M^{-1} was calculated using EQNMR.[13]† Titration experiments showed **6** binds ethane-1,2-diol (**eg**) strongly, K = 1060 ± 29 M^{-1}; the resonance attributed to the **eg** methylene protons being shifted upfield from 3.74 to 3.32 ppm. However, no significant shift in the resonance of the methylene protons of 1,2-ethanedithiol (**es**) was observed under the same titration conditions. That no binding was observed for **es** can be attributed to a number of factors such as the reduced hydrogen bonding abilities of thiols, the larger size of the dithiol guest and the significantly lower stability of the *gauche* conformation in **es** compared to **en** and **eg**. Macrocyclic calix[4]pyrroles have been shown to bind neutral guest molecules in d_6-benzene solution.[12] The large binding constants for the binding of difunctional neutral guest molecules by the pyrrole cryptands reported here demonstrates the enhancement in molecular recognition that can be achieved by the use of three dimensional host molecules that encompass their guest. Further studies with neutral guest molecules are in progress.

In summary, bis(tripyrrolyl) cryptand-like cages have been prepared in excellent yields and preliminary studies demonstrate neutral guest molecule binding. The ease and scale with which the formylated tripyrrolylalkanes can be prepared offers plenty of opportunity for the future exploitation of these building blocks in the construction of new cryptands. We are currently exploring the cation and anion coordination chemistry of these bis(tripyrrolyl) cryptands and routes to further cages based on metal-assembled strategies.[14]

We thank the EPSRC for a post-doctoral fellowship (O. D. F.) and the University of Reading and EPSRC for funds for the Image Plate diffractometer.

Notes and references

‡ *Crystal data* for **7·bn**: $C_{50.5}H_{72}ClN_{16}O_{0.5}$, M 946.69, triclinic, space group $P\bar{1}$, a = 10.955(12), b = 14.307(17), c = 17.45(2) Å, α = 100.85(1), β = 99.17(1), γ = 91.80(1)°, U = 2646 Å^3, Z = 2, μ = 0.123 mm^{-1}, l = 1.184 gm cm^{-3}. **6·en**: $C_{44}H_{54}N_{14}$, M 779.02, triclinic, space group $P\bar{1}$, a = 11.983(15), b = 13.283(15), c = 14.765(17) Å, α = 72.41(1), β = 81.74(1), γ = 77.62(1)°, U = 2180 Å^3, Z = 2, μ = 0.075 mm^{-1}, l = 1.187 gm cm^{-3}. CCDC 167338, 167339. See http://www.rsc.org/suppdata/cc/b1/b104077b/ for crystallographic data in CIF or other format. The structures were refined on F^2 using SHELXL[15] to respectively $R1$ 0.0881, $wR2$ 0.2231 for 4360 reflections and $R1$ 0.0756, $wR2$ 0.2107 for 3602 reflections with $I > 2\sigma(I)$.

1 X. X. Zhang, R. M. Izatt, J. S. Bradshaw and K. E. Krakowiak, *Coord. Chem. Rev.*, 1998, **174**, 179.
2 A. Jasat and J. C. Sherman, *Chem. Rev.*, 1999, **99**, 931.
3 C. D. Gutsche, *Calixarenes Revisited, Monographs in Supramolecular Chemistry*, Royal Society of Chemistry, Cambridge, 1998.
4 C. Floriani, *Chem. Commun.*, 1996, 1257; P. A. Gale, J. L. Sessler and V. Král, *Chem. Commun.*, 1998, 1.
5 L. Bonomo, O. Dandin, E. Solari, C. Floriaini and R. Scopelliti, *Angew. Chem., Int. Ed.*, 1999, **38**, 914.
6 P. A. Gale, J. L. Sessler, V. Kral and V. Lynch, *J. Am. Chem. Soc.*, 1996, **118**, 5140.
7 M. Tayebani, S. Conoci, K. Feghali, S. Gambarotta and G. P. A. Yap, *Organometallics*, 2000, **19**, 4568.
8 J. L. Sessler, M. C. Hoehner, D. W. Johnson, A. Gebauer and V. Lynch, *Chem. Commun.*, 1996, 2311.
9 Q. Lu, V. McKee and J. Nelson, *Chem. Commun.*, 1994, 649.
10 C.-H. Lee and J. S. Lindsey, *Tetrahedron*, 1994, **50**, 11 427.
11 Q. M. Wang and D. W. Bruce, *Synlett*, 1995, 1267.
12 W. E. Allen, P. A. Gale, C. T. Brown, V. M. Lynch and J. L. Sessler, *J. Am. Chem. Soc.*, 1996, **118**, 12 471.
13 M. J. Hynes, *J. Chem. Soc., Dalton Trans.*, 1993, 311.
14 O. D. Fox, M. G. B. Drew and P. D. Beer, *Angew. Chem., Int. Ed.*, 2000, **39**, 135; O. D. Fox, M. G. B. Drew, E. J. S. Wilkinson and P. D. Beer, *Chem. Commun.*, 2000, 391.
15 SHELXL, G. M. Sheldrick, 1993, Program for Crystal Structure Refinement, University of Göttingen, Germany.

CHEMCOMM
Communication
www.rsc.org/chemcomm

Formation of the monoanion $[Ar^*P(BH_3)(\mu\text{-}BH_2)_2H]^-$ with a symmetrically bridging hydride from the attempted synthesis of the dianion $[Ar^*P(BH_3)_3]^{2-}$†

Valentyn L. Rudzevich, Heinz Gornitzka, Vadim D. Romanenko* and Guy Bertrand

Laboratoire d'Hétérochimie Fondamentale et Appliquée, UMR CNRS 5069, Université Paul Sabatier, 118, route de Narbonne, F-31062 Toulouse Cédex 04, France. E-mail: gbertran@chimie.ups-tlse.fr

Received (in Cambridge, UK) 7th June 2001, Accepted 23rd July 2001
First published as an Advance Article on the web 14th August 2001

Addition of an excess of Bu^nLi to the bis(borano)phosphide complex $[Ar^*PH(BH_3)_2]^-Li^+$ 1 (Ar^* = 2,4,6-tri-*tert*-butylphenyl) and subsequent treatment with BH_3, gives the anionic complex $[Ar^*P(BH_3)(\mu\text{-}BH_2)_2H]^-Li^+$ 2 instead of the expected tris(borano)phosphide dilithium, $[Ar^*P(BH_3)_3]^{2-}2Li^+$ 3.

Borane complexes of trivalent organophosphorus derivatives have been extensively used in organic synthesis.[1] In particular, borane-stabilized phosphide anions of the type $[R^1R^2PBH_3]^-$, which are readily available by deprotonation of the corresponding secondary phosphine– or phosphinite–borane adducts, have been found to be valuable intermediates for the preparation of enantiomerically pure phosphines with chiral carbon skeletons or stereogenic phosphorus centres.[2] It may be assumed that application of a conceptually similar approach (P–H deprotonation/P–B complexation) to primary phosphines and PH_3 would lead to a series of reactive anions $[R_nH_{3-n-m}P(BH_3)_{m+1}]^{m-}$ (n = 1, m = 1, 2 or n = 0, m = 1–3). However, surprisingly, few investigations of borane-stabilized RP^{2-} and P^{3-} anions have been reported to date. An early ^1H NMR spectroscopic study claimed that stepwise removal of protons from $[H_2P(BH_3)_2]^-$ followed by complexation of intermediates with BH_3 afforded $[HP(BH_3)_3]^{2-}$ and $[P(BH_3)_4]^{3-}$ anions. Yet, the observed formation of $LiBH_4$ leaves some doubts as to the true structure of the anionic products.[3]

The Cambridge Structural Database reveals that trivalent phosphorus derivatives in which the phosphorus is bonded to two or three boron atoms have rarely been characterized in the solid state, and those identified are limited to polyhedral compounds,[4] neutral diborylphosphines[5] and various heterocyclic systems.[6] No poly(borane)phosphide anions have so far been characterized by X-ray crystallography. Here we report the synthesis of the $[Ar^*PH(BH_3)_2]^-$ anion (Ar^* = 2,4,6-tri-*tert*-butylphenyl) and its subsequent deprotonation and complexation with BH_3.

The $[Ar^*HP(BH_3)_2Li]$ complex **1** was prepared in 95% yield by metallation of Ar^*PH_2 with an equimolar amount of Bu^nLi in thf solution and subsequent addition of BH_3 (2 equiv.).‡ An alternative route to **1**, based on the preparation of the $Ar^*PH_2{\cdot}BH_3$ adduct and its subsequent deprotonation, led to the formation of a complex mixture of products. The ^{31}P NMR spectrum of **1** in C_6D_6 displays a broad doublet at δ −53 [^1J(PH) 340 Hz]. The resonance is considerably shifted toward low field compared to that of $Ar^*P(H)Li$ [δ −108, ^1J(PH) 172 Hz]. The signal observed by ^{11}B NMR spectroscopy (δ −30.6) was very broad ($W_{1/2}$ ~ 350 Hz) in both the ^{11}B proton-coupled and decoupled spectra, with no observable ^{11}B–^{31}P coupling. Furthermore, the signal attributable to BH_3 units in ^1H-{^{11}B} and ^1H-{^{31}P} spectra is not resolved and appeared as a broad singlet at δ 1.54.

The molecular structure of **1** is depicted in Fig. 1.§ The compound crystallizes with three molecules of thf and can be described by the formula $[Ar^*HP(BH_3)_2Li(thf)_3]$. Two different BH_3 units are found in the crystal: one shows contacts of two hydridic hydrogen atoms with Li through a μ_2-type interaction, while the hydridic hydrogen atoms of the other are not involved in the Li–H bonding. The bond distance between phosphorus and boron engaged in B–H···Li coordination [P(1)–B(1), 1.955 Å] is shorter than that found for the 'free' BH_3 group [P(1)–B(2) 1.984 Å]. It is apparent that the sterically demanding Ar* group has no significant influence on the molecular geometry of **1** since the Li(1)–B(1) distance (2.430 Å) is quite similar to those found in $Li\cdots(H)_2BH_2$ complexes in which the BH_4^- group acts as a μ_2 donor.[7]

In marked contrast to the PH-acid type behaviour generally shown by secondary phosphine–borane complexes, $R^1R^2(H)PBH_3$, compound **1** does not react with KH at room temperature in thf. The reaction with Bu^nLi in a 1 : 1 molar ratio only proceeds partially; complete deprotonation of **1** requires an excess of Bu^nLi (*ca.* 2.0 equiv., toluene, −50 °C), according to ^{31}P NMR spectroscopy. Removal of the solvent and extraction of the residue with pentane gave a pale yellow moisture-sensitive oil that exhibits strong, basic properties (on addition of $CHCl_3$ the complex **1** is regenerated immediately). Both ^{11}B– and ^{31}P–^1H coupled NMR spectra show a single broad resonance (δ_P −143.9 , δ_B −27.8), indicating the absence of a PH bond. Addition of excess borane to a toluene solution of the deprotonated product at −50 °C results in the formation of a mixture of the complex **2**‡ (δ_P −161.8 , δ_B −28.4) and $LiBH_4$ (δ_B −42.1) (Scheme 1). After crystallization from toluene–pentane solution, single colourless crystals of the phosphorus-containing complex were obtained, suitable for the determination of its molecular structure in the solid state.§ Compound **2** crystallizes as a dimer and can be described by the formula $[Ar^*P(BH_3)(\mu\text{-}BH_2)_2HLi(thf)_2]_2$ (Fig. 2). The most prominent feature of **2** is the presence of both a four-membered heterocyclic ring with a symmetrically bridging hydride P(μ-

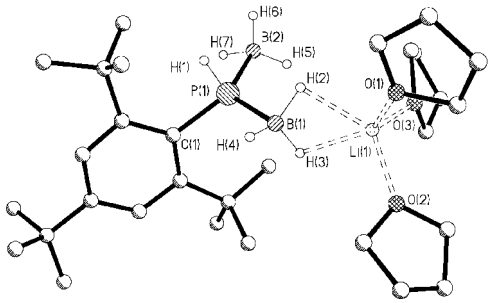

Fig. 1 Molecular structure of **1**. Selected bond lengths (Å) and angles (°): B(1)–P(1) 1.955(3), B(2)–P(1) 1.984(3), P(1)–C(1) 1.860(2), B(1)–Li(1) 2.430(5), B(1)–H(2) 1.12(3), B(1)–H(3) 1.06(3), B(1)–H(4) 1.08(3), B(2)–H(5) 1.02(3), B(2)–H(6) 1.02(4), B(2)–H(7) 1.18(4); B(1)–P(1)–B(2) 121.52(14), P(1)–B(1)–Li(1) 139.2(2), C(1)–P(1)–B(1) 113.05(11), C(1)–P(1)–B(2) 117.88(12).

† Electronic supplementary information (ESI) available: crystallographic details and colour ORTEP views of **1** and **2**. See http://www.rsc.org/suppdata/cc/b1/b105030n/

 DOI: 10.1039/b105030n

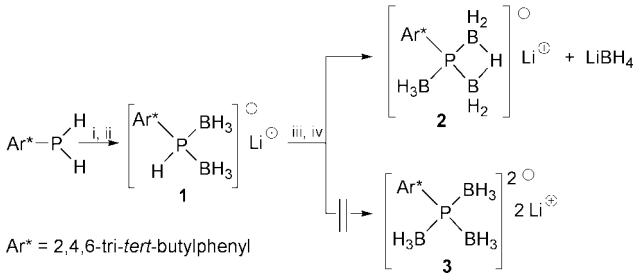

Scheme 1 Synthesis of the borane–phosphide complexes **1** and **2**. *Reagents and conditions*: i, Bu^nLi (1 equiv.), thf, −50 °C; ii, BH_3·thf (2 equiv.), thf, −40 °C, 2 h; iii, Bu^nLi (2 equiv.), toluene, −50 °C, 2 h; iv, BH_3·thf (2 equiv.), toluene, −30 °C, 1 h.

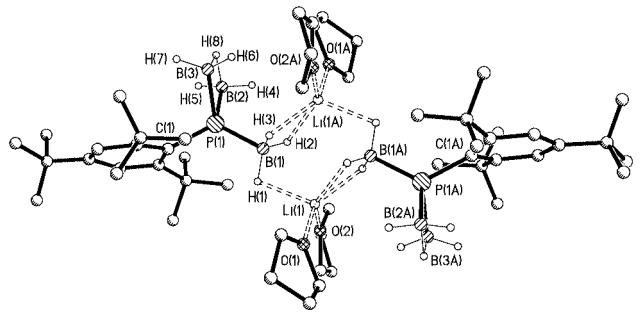

Fig. 2 Molecular structure of **2**. Selected bond lengths (Å) and angles (°): B(1)–P(1) 1.961(2), B(2)–P(1) 1.924(2), B(3)–P(1) 1.913(2), B(1)–H(1) 1.12(2), B(1)–H(2) 1.13(2), B(1)–H(3) 1.09(2), B(2)–H(4) 1.12(2), B(2)–H(5) 1.12(2), B(3)–H(6) 1.11(2), B(3)–H(7) 1.11(2), P(1)–C(1) 1.845(1), B(1)–Li(1) 2.563(3), B(1)–Li(1A) 2.548(3); B(2)–P(1)–B(3) 62.91(10), B(1)–P(1)–B(2) 118.27(9), B(1)–P(1)–B(3) 115.26(9), P(1)–B(1)–Li(1) 154.39(11), P(1)–B(1)–Li(1A) 114.66(11), C(1)–P(1)–B(1) 123.45(7), C(1)–P(1)–B(3) 110.68(8), C(1)–P(1)–B(2) 110.94(8). The molecule of toluene has been omitted for clarity.

$BH_2)_2H$, and a BH_3 unit. The P(1)–B(2) and P(1)–B(3) bonds in the four-membered ring are slightly shorter than the exocyclic P(1)–B(1) bond distances, indicating that, as expected, B(2) and B(3) are stronger electron acceptors than B(1). The B(2)–B(3) distance in **2** is 2.00 Å, approximately 0.1 Å larger than in neutral μ-aminodiboranes $[R_2N(\mu\text{-}BH_2)_2H]$.[8] Two H atoms of the BH_3 group coordinate through a μ_1-interaction to two different Li cations forming an eight-membered ring. The Li···B(1) distances (2.548–2.563 Å) compare well with those found in other H_3B–H···Li interactions.[7] The coordination sphere of each Li atom is completed by two molecules of thf. In solution, no evidence for or against the dimeric structure can be found, but the presence of the hydride bridging two boron atoms is strongly suggested by the presence of an upfield broad doublet at δ −0.65 [^2J(PH) 36 Hz] in the ^{1}H NMR spectrum.

In conclusion, we have demonstrated that accumulation of negative charge on phosphorus by H^+/Li^+ replacement in complex **1** resulted in a considerable increase in the reduction properties of BH_3 groups. This results in the formation of the monoanionic bridging complex **2** observed along with $LiBH_4$, instead of the expected dianionic tris(borano)phosphide complex **3**. Compound **2** does not react with KH in the presence of 18-crown-6 (thf, 20 °C, 24 h), despite the presence of the electron deficient 3c–2e B–H–B bond. Thus, it appears that the anionic μ-(boratophosphino)diboranes are considerably more stable than previously described neutral μ-phosphinodiboranes, $[R_2P(\mu\text{-}BH_2)_2H]$.[9]

Thanks are due to the CNRS for financial support of this work, to the University Paul Sabatier for a grant to V. L. R.

Notes and references

‡ *Selected NMR data* for $Ar^*(H)_2PBH_3$: ^{31}P($CDCl_3$): δ −61.5 (t, $^1J_{PH}$ 371 Hz); ^{11}B($CDCl_3$): δ −33.6 (br s). For **1**, ^{31}P(C_6D_6): δ −53.3 (d, $^1J_{PH}$ 340 Hz); ^{11}B(C_6D_6): δ −30.6 (br s); ^{1}H (C_6D_6): δ 1.41 (s, 9H, *p*-Bu^t), 1.48 (br s, thf), 1.54 (br s, 6H, BH_3), 1.99 (s, 18H, *o*-Bu^t), 3.72 (br s, thf), 5.96 (d, $^2J_{PH}$ 371 Hz, 1H, PH), 7.72 (s, 2H, H_{arom}). ^{13}C ($CDCl_3$): δ 25.5 (s, thf), 31.4 [s, *p*-$C(CH_3)_3$], 34.2 [s, *o*-$C(CH_3)_3$], 34.7 [s, *p*-$C(CH_3)_3$], 38.8 [s, *o*-$C(CH_3)_3$], 68.6 (s, thf), 122.8 (d, $^3J_{PC}$ 8.3 Hz, *m*-C_{arom}), 129.7 (d, $^1J_{PC}$ 28.7 Hz, *ipso*-C_{arom}), 148.3 (d, $^4J_{PC}$ 2.8 Hz, *p*-C_{arom}), 154.9 (d, $^2J_{PC}$ 3.7 Hz, *o*-C_{arom}). For **2**, ^{31}P (C_6D_6): δ −161.8 (br s); ^{11}B(C_6D_6): δ −28.4 (br s); ^{1}H{^{11}B} (C_6D_6): δ −0.65 (d, $^2J_{PH}$ 36 Hz, 1H, BHB), 1.39 (s, 9H, *p*-Bu^t), 1.49 (thf), 1.61 (br s, 7H, BH_3 and BH_2), 2.12 (s, 18H, *o*-Bu^t), 3.68 (thf), 7.67 (d, 2H, $^4J_{PH}$ 2.8 Hz, H_{arom}). ^{13}C ($CDCl_3$): δ 25.45 (s, (thf), 31.26 [s, *p*-$C(CH_3)_3$], 34.45 [s, *p*-$C(CH_3)_3$], 38.82 [s, *o*-$C(CH_3)_3$], 39.88 [d, $^3J_{CP}$ 2.8 Hz, *o*-$C(CH_3)_3$], 68.75 (s, thf), 122.92 (d, $^3J_{CP}$ 9.2 Hz, *m*-C_{arom}), 127.13 (d, $^1J_{CP}$ 49 Hz, *ipso*-C_{arom}), 148.03 (d, $^4J_{CP}$ 2.8 Hz, *p*-C_{arom}), 157.73 (d, $^2J_{CP}$ 4.6 Hz, *o*-C_{arom}).

§ *X-Ray structure analysis*: *Crystal data for*: **1**: $C_{30}H_{60}B_2LiO_3P$, M = 528.31, orthorhombic, space group $P2_12_12_1$, a = 9.4853(5), b = 11.0044(5), c = 32.8968(16) Å, V = 3433.8(3) Å^3, Z = 4, μ(Mo-Kα) = 0.105 mm^{-1}, T = 193(2) K, final $R1$ = 0.0505, $wR2$ = 0.1299, GOF (on F^2) = 1.078.

For **2**: $C_{33}H_{61}B_3LiO_2P$, M = 560.16, triclinic, space group $P\bar{1}$, a = 9.8395(8), b = 11.2345(9), c = 16.5435(13) Å, α = 96.708(2), β = 98.842(2), γ = 91.449(2)°, V = 1792.9(2) Å^3, Z = 2, μ(Mo-Kα) = 0.102 mm^{-1}, T = 193(2) K, final $R1$ = 0.0499, $wR2$ = 0.1379, GOF (on F^2) = 1.036.

Both structures were solved using the direct methods option on SHELXS.[10] Full matrix least-squares refinements based on F^2 were subsequently performed using SHELXL-97.[11]

CCDC reference numbers 167806 and 167807. See http://www.rsc.org/suppdata/cc/b1/b105030n/ for crystallographic data in CIF or other electronic format.

1 A. Pelter, K. Smith and H. C. Brown, *Borane Reagents*, Academic Press, London, 1988.
2 For reviews, see: J. Holz, M. Quirmbach and A. Börner, *Synthesis*, 1997, 983; M. Ohff, J. Holz, M. Quirmbach and A. Börner, *Synthesis*, 1998, 1391; see also: B. Wolfe and T. Livinghouse, *J. Am. Chem. Soc.*, 1998, **120**, 5116; M. Al-Masum and T. Livinghouse, *Tetrahedron Lett.*, 1999, **40**, 7731; K. Nagata, S. Matsukawa and T. Imamoto, *J. Org. Chem.*, 2000, **65**, 4185.
3 E. Mayer, *Angew. Chem., Int. Ed. Engl.*, 1971, **10**, 416; see also: N. R. Thompson, *J. Chem. Soc.*, 1965, 6290; R. W. Rudolph, R. W. Parry and C. F. Farran, *Inorg. Chem.*, 1966, **5**, 723; J. W. Gilje, K. W. Morse and R. W. Parry, *Inorg. Chem.*, 1967, **6**, 1761; E. Mayer and A. W. Laubengayer, *Monatsh. Chem.*, 1970, **101**, 1138.
4 L. J. Todd, I. C. Paul, J. L. Little, P. S. Welcker and C. R. Peterson, *J. Am. Chem. Soc.*, 1968, **90**, 4490; T. D. Getman, H.-B. Deng, L.-Y. Hsu and S. G. Shore, *Inorg. Chem.*, 1989, **28**, 3612; S. R. Bunkhall, X. L. R. Fontaine, N. N. Greenwood, J. D. Kennedy and M. Thornton-Pett, *J. Chem. Soc., Dalton Trans.*, 1990, 73; F. Meyer, P. Paetzold and U. Englert, *Chem. Ber.*, 1994, **127**, 93.
5 See, for example: R. A. Barlett, H. V. Rasika Dias and P. P. Power, *Inorg. Chem.*, 1988, **27**, 3913; D. Dou, G. L. Wood, E. N. Duesler, R. T. Paine and H. Nöth, *Inorg. Chem.*, 1992, **31**, 1695.
6 G. J. Bullen and P. R. Mallinson, *J. Chem. Soc., Dalton Trans.*, 1973, 1295; G. R. Clark and G. J. Palenik, *Aust. J. Chem.*, 1975, **28**, 1187; B. Kaufmann, R. Jetzfellner, E. Leissring, K. Issleib, H. Nöth and M. Schmidt, *Chem. Ber.*, 1997, **130**, 1677.
7 N. Edelstein, *Inorg. Chem.*, 1981, **20**, 197; W. Lippert, H. Nöth, W. Ponikwar and T. Seifert, *Eur. J. Inorg. Chem.*, 1999, 817.
8 A. F. Wells, *Structural Inorganic Chemistry*, University Press, Oxford, 1986.
9 H. Hofstötter and E. Mayer, *Angew. Chem., Int. Ed. Engl.*, 1973, **12**, 413; H. Hofstötter and E. Mayer, *Monatsh. Chem.*, 1974, **105**, 712.
10 G. M. Sheldrick, *Acta Crystallogr., Sect. A*, 1990, **46**, 467.
11 SHELXL-97, Program for Crystal Structure Refinement, G. M. Sheldrick, University of Göttingen, 1997.

CHEMCOMM
Communication
www.rsc.org/chemcomm

A novel bimetallic cage complex constructed from six V_4Co pentatomic rings: hydrothermal synthesis and crystal structure of $[(2,2'\text{-}Py_2NH)_2Co]_3V_8O_{23}$†

Cai-Ming Liu,[a] Song Gao,*[a] Huai-Ming Hu[b] and Zhe-Ming Wang[a]

[a] *State Key Laboratory of Rare Earth Materials Chemistry and Applications & PKU-HKU Joint Laboratory on Rare Earth Materials and Bioinorganic Chemistry, Peking University, Beijing 100871, P. R. China. E-mail: gaosong@pku.edu.cn.*

[b] *Center for Molecular Science, Institute of Chemistry, Chinese Academy of Sciences, Beijing 100080, P. R. China.*

Received (in Cambridge, UK) 15th May 2001, Accepted 19th July 2001
First published as an Advance Article on the web 14th August 2001

A bimetallic cluster complex, $[(2,2'\text{-}Py_2NH)_2Co]_3V_8O_{23}$ ($2,2'\text{-}Py_2NH$ = 2,2′-dipyridylamine) 1, has been hydrothermally synthesized; X-ray crystallography reveals that 1 possesses a novel cage topology structure in which the metal cluster core is constructed from six V_4Co pentatomic rings.

The hydrothermal synthesis of organic–inorganic hybrid vanadium oxides and polyvanadate clusters is of great interest due to their intriguing structural diversity and their potential functions as microporous solids for molecular adsorption, ion exchange and heterogeneous catalysis,[1–3] and as anode candidates in secondary lithium batteries and electrochromic devices.[4,5] Besides acting as a charge-compensating and space-filling constituent, the organic structure-directing component of such hybrid materials may also function as a ligand, the resulting transition metal complexes or fragments are then covalently bonded to metal framework or polyanion clusters.[6] Up to now, the study of vanadium solid state complexes has largely focused on infinite chains and layer structures.[7–10] Only a few discrete clusters have been reported, they are limited to $V_4O_{12}^{4-}$, [11] and $V_{10}O_{29}^{8-}$,[12] the latter formed through combination of two $V_4O_{12}^{4-}$ and one $V_2O_7^{4-}$ building unit by sharing oxygen atoms. Herein, we report the structure of a novel bimetallic cage complex, $[(2,2'\text{-}Py_2NH)_2Co]_3V_8O_{23}$ ($2,2'\text{-}Py_2NH$ = 2,2′-dipyridylamine**) 1**, which is based upon a new vanadium cluster $V_8O_{23}^{6-}$. To our knowledge, **1** is the first heterometallic cage complex composed of six pentatomic rings.

Complex **1** was obtained as red blocks in 20% yield by a hydrothermal reaction. A mixture of V_2O_5, 2,2′-dipyridylamine, $Co(OAc)_2{\cdot}4H_2O$ and H_2O in the mol ratio of 1 : 2 : 1 : 889 was stirred for 20 min, then transferred to a 25 ml Teflon-lined stainless steel bomb, which was kept at 140 °C under autogenous pressure for three days.‡ The IR spectrum of **1** exhibits characteristic bands at 922vs cm^{-1} for the terminal V=O stretch and at 800–770 cm^{-1} for the V–O–V stretch.

As shown in Fig. 1, the crystal structure§ of **1** consists of isolated neutral undecanuclear heterometallic clusters $[(2,2'\text{-}Py_2NH)_2Co]_3V_8O_{23}$ which are built up from a $V_8O_{23}^{6-}$ cluster and three $[(2,2'\text{-}Py_2NH)_2Co]^{2+}$ fragments. The cobalt atom has a distorted octahedral environment. It coordinates to four N atoms from two 2,2′-dipyridylamine ligands and two oxygen atoms from vanadium oxides, which adopt *cis*-orientation.

The core of **1** is $V_8O_{23}^{6-}$, which can be regarded as a pseudo-cube octanuclear vanadium cluster though there are three V–O–V edges replaced with three V–O–Co–O–V long edges (Fig. 2). The anionic vanadium cluster is composed of corner-sharing VO_4 tetrahedra, all VO_4 tetrahedra have one terminal oxygen atom. There are two crystallographically independent vanadium atoms: the V1 atom shares oxygen atoms with one CoN_4O_2 octahedron and two VO_4 tetrahedra while the V2 atom only shares oxygen atoms with three VO_4 tetrahedra. The cobalt atoms connect with neighboring vanadium atoms *via* O1 and its symmetry equivalents to finish the empty 'edges' of the pseudo-cube, thus a unique cage topology structure is formed, which is constructed from six V_4Co pentatomic rings. This cage topology feature has not been described in other heterometallic clusters to date.[11,12]

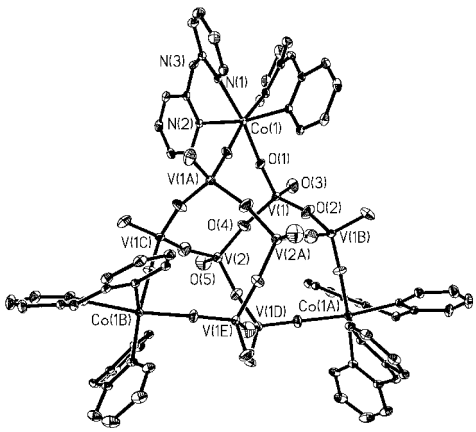

Fig. 1 A diagram showing the molecular structure of **1** with 10% thermal ellipsoids.

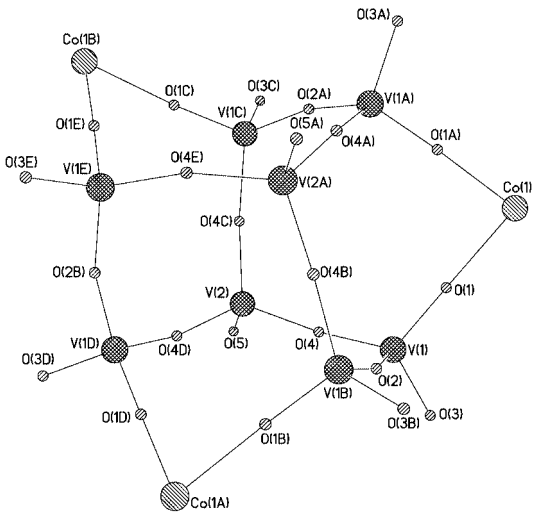

Fig. 2 The metal cluster core in **1**.

† Electronic supplementary information (ESI) available: rotatable 3-D crystal structure diagrams of **1** in CHIME format. Fig. S1: another view of the packing of cage **1** in three-dimensional space. See http://www.rsc.org/suppdata/cc/b1/b104273b/

 DOI: 10.1039/b104273b

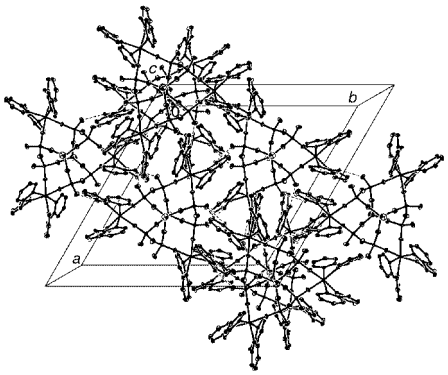

Fig. 3 The three-dimensional supramolecular array formed through intermolecular hydrogen bonding interactions in the solid state of **1**.

It is noteworthy that there is a C_3 symmetry axis along the O5=V2···V2A=O5A vector, the cluster, therefore, looks like a paddle with six 2,2′-dipyridylamine ligands corresponding to the paddles. The Co···Co separation along the edge of the cobalt triangle is 8.832 Å while the V2···V2A separation is 5.765 Å. The intermolecular hydrogen bonds play a significant role in stabilization of the structure of **1**. Each uncoordinated amino group of the 2,2′-dipyridylamine ligand links to O3 or its symmetry equivalents of the neighboring $V_8O_{23}^{6-}$ clusters *via* hydrogen bonding with a corresponding N···O distance of 2.787 Å. These hydrogen bonding interactions force the undecanuclear cages $[(2,2'\text{-}Py_2NH)_2Co]_3V_8O_{23}$ into an interesting three-dimensional supermolecular array, as shown in Fig. 3.

The cube-based cage compounds related to silsesquioxanes have been studied extensively for modeling framework metal zeolite centers.[13,14] This work demonstrates that a hydrothermal method is another optional route for obtaining new metal oxide cage materials. The formation of this type of heterometallic cage suggests that there will be many potential implications of such materials as new candidates for models of zeolites or catalyst.

This work was supported by the Visiting Scholar Foundation of Key Lab. in University (sponsored by the Education Ministry of China) and grants from the State Key Project for Fundamental Research (G1998061305).

Notes and references

‡ The other product is very thin yellow plate. *Anal. Calc.* for $C_{60}H_{54}N_{18}O_{23}Co_3V_8$ **1**: C, 36.41; H, 2.75; N, 12.74. Found: C, 36.20; H, 2.91; N, 12.53%; IR(KBr, cm^{-1}) for **1**: 1638m, 1582m, 1528w, 1475vs, 1434m, 1420w, 1362w, 1238w, 1158w, 922vs, 879s, 863s, 790s, 773s, 752m, 741m, 672w, 665w.

§ *Crystal data* for **1**: $C_{60}H_{54}N_{18}O_{23}Co_3V_8$, rhombohedral, space group $R\bar{3}c$, M_r = 1979.52, a = 22.596(3), b = 22.596(3), c = 27.515(6) Å, $\alpha = \beta$ = 90, γ = 120°, V = 12167(3) $Å^3$, Z = 6, D_c = 1.621 g cm^{-3}, T = 293(2) K, μ = 1.551 mm^{-1}, R_1 = 0.0532, wR_2 = 0.1397 for 2259 observed reflections [$I > 2\sigma(I)$] from 3107 independent reflections, GOF = 1.055. The data were collected on a Nonius Kappa CCD with Mo-Kα radiation (λ = 0.71073 Å). The structure was solved by direct methods and refined by a full matrix least-squares technique based on F^2 using the SHELXL 97 program. The V2 atom and O5 atom are disordered over 90:10 sites. All non-hydrogen atoms except V2′ and O5′ were refined anisotropically and hydrogen atoms were allowed for as riding atoms.

CCDC reference number 167670. See http://www.rsc.org/suppdata/cc/b1/b104273b/ for crystallographic data in CIF or other electronic format.

1 G. Centi, F. Trifiro, J. R. Ebner and V. M. Franchetti, *Chem. Rev.*, 1988, **88**, 55.
2 Louis C. W. Baker and D. C. Glick, *Chem. Rev.*, 1998, **98**, 3.
3 P. Gouzerh and A. Proust, *Chem. Rev.*, 1998, **98**, 77.
4 C. R. Walk, in *Lithium Batteries*, ed. J. P. Gabano, Academic Press, New York, 1983.
5 B. E. Koene, N. J. Taylor and L. F. Nazar, *Angew. Chem., Int. Ed.*, 1999, **38**, 2888.
6 P. J. Hagrman and J. Zubieta, *Inorg. Chem.*, 2000, **39**, 3252.
7 Y. Zhang, J. R. D. DeBord, C. J. O'Connor, R. C. Haushalter, A. Clearfield and J. Zubieta, *Angew. Chem., Int. Ed. Engl.*, 1996, **35**, 989; J. R. D. DeBord, Y. Zhang, R. C. Haushalter, J. Zubieta and C. J. O'Connor, *J. Solid State Chem.*, 1996, **122**, 251.
8 Z. Shi, L.-R. Zhang, G.-S. Zhu, G.-Y. Yang, J. Hua, H. Ding and S.-H. Feng, *Chem. Mater.*, 1999, **11**, 3565; L.-R. Zhang, Z. Shi, G.-Y. Yang, X.-M. Chen and S.-H. Feng, *J. Chem. Soc., Dalton Trans.*, 2000, 275.
9 L.-M. Zheng, J.-S. Zhao, K.-H. Lii, L.-Y. Zhang, Y. Liu and X.-Q. Xin, *J. Chem. Soc., Dalton Trans.*, 1999, 939.
10 C.-M. Liu, S. Gao and H.-Z. Kou, *Chem. Commun.*, 2001, in press.
11 Y. Zhang, P. J. Zapf, L. M. Meyer, R. C. Haushalter and J. Zubieta, *Inorg. Chem.*, 1997, **36**, 2159.
12 X.-M. Zhang, M.-L. Tong and X.-M. Chen, *Chem. Commun.*, 2000, 1817.
13 L. A. Neville, T. R. Spalding and G. Ferguson, *Angew. Chem., Int. Ed.*, 2000, **39**, 3598.
14 F. Liu, K. D. John, B. L. Scott, R. T. Baker, K. C. Ott and W. Tumas, *Angew. Chem., Int. Ed.*, 2000, **39**, 3127.

CHEMCOMM
Communication
www.rsc.org/chemcomm

Bidentate carbenoid ester coordination in ruthenium(II) Schiff-base complexes leading to excellent levels of diastereo- and enantioselectivity in catalytic alkene cyclopropanation†

Ian J. Munslow, Kevin M. Gillespie, Robert J. Deeth and Peter Scott*

Department of Chemistry, University of Warwick, Coventry, UK CV4 7AL.
E-mail: peter.scott@warwick.ac.uk

Received (in Cambridge, UK) 5th June 2001, Accepted 12th July 2001
First published as an Advance Article on the web 14th August 2001

Exceptionally high stereoselectivity (ee ⩽ 98%, dr ⩽ 99 : 1) in the cyclopropanation of alkenes with ethyl diazoacetate using a non-planar ruthenium(II) Schiff-base precatalyst is a result of η^2*C,O* binding of the carbenoid ester intermediate, according to DFT calculations.

The design of selective methods for the catalytic enantioselective synthesis of cyclopropanes remains of great interest to organic chemists, not least because of the importance of the compounds in biological and medicinal chemistry.[1] The asymmetric addition of carbenes to electron rich alkenes[2] (alkene cyclopropanation) represents a conceptually simple approach,[3] but typical reactions, such as that of styrenes with α–diazoacetates in the presence of a chiral metal catalyst, give a total of six organic products (Scheme 1).

Chemoselectivity for cyclopropanes over carbene dimerisation products (diethyl malonate and fumarate) is achieved through use of an excess of alkene and slow addition of the carbene source *e.g.* ethyl diazoacetate (EDA) to the reaction mixture.[4,5] For *trans*-selective catalysts, excellent enantiomeric excesses have been obtained,[6] but most exhibit only moderate *trans*/*cis*- *i.e.* diastereoselectivity. For example, Evans' bis(oxazoline) copper system gave 99% ee in the *trans* product which was formed with a dr of 73 : 27.[6] This and other results are consistent with Pfaltz's analysis that the *cis/trans* selectivity for a given metal depends almost exclusively on the structure of the alkene and diazo compound; the effect of the ligand is relatively unimportant.[7] Correspondingly, the use of bulkier diazo ester substituents such as *tert*-butyl and 2,6-di-*tert*-butyl-4-methylphenol leads to much higher diastereoselectivities.[6,8,9] An exception here is found in Che's D_4-symmetric Ru porphyrin system (dr 97 : 3, ee 98% at −40 °C) where the four sterically-demanding chiral substituents strongly orient alkene approach.[10] Highly *cis* selective catalysts based on Co and Ru using *tert*-butyl diazoacetate have recently been reported (*e.g.* dr 7 : 93 and ee 99%).[11]

We have been interested in the use of biaryldiimine complexes in enantioselective catalysis,[12] and have discovered

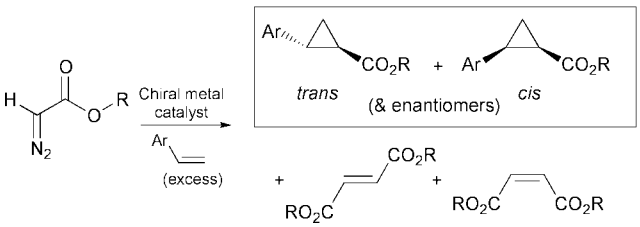

Scheme 1 Products typically formed in metal catalysed cyclopropanation *via* intermolecular carbene transfer to alkene.

† Electronic supplementary information (ESI) available: experimental and theoretical details, structures of [RuL^1(CH$_3$CN)$_2$] and [RuL^1(η^2-CHCO$_2$Et)] (.pdb). CCDC 167600. See http://www.rsc.org/suppdata/cc/b1/b104964j/

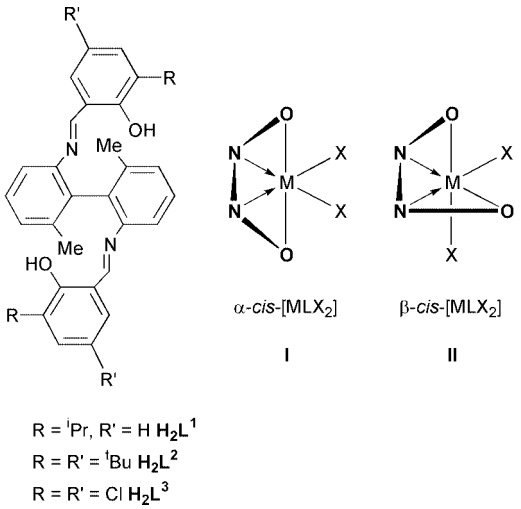

R = ^{i}Pr, R' = H **H_2L^1**
R = R' = ^{t}Bu **H_2L^2**
R = R' = Cl **H_2L^3**

that unlike salen-derived ligands, the system L in its early transition metal complexes gives the α-*cis* topology **I** or occasionally the β-*cis* structure **II**;[13] both arrangements dictate that the co-ligands X are placed in mutually *cis* coordination sites. This has important consequences for alkene cyclopropanation by the complexes M = Ru as described herein.

The reaction of Na_2L^n with [{RuCl(μ-Cl)(η-C$_6$H$_6$)}$_2$] in acetonitrile gave the Ru^{II} complexes of ligands L^n in high yield.

The molecular structure of one example β-*cis*-[RuL^1(CH$_3$CN)$_2$] is shown in Fig. 1.† This, and analogous complexes of L^2 and L^3 retain the β-*cis* structure **II** in solution as evidenced by NMR spectroscopy.

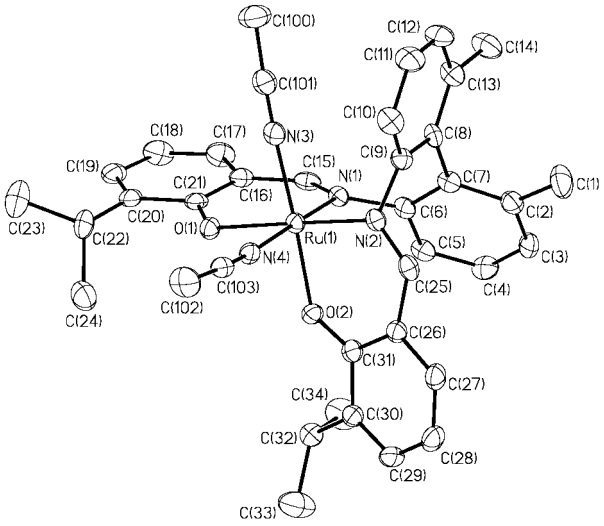

Fig. 1 Molecular structure of the precatalyst β-*cis*-[RuL^1(CH$_3$CN)$_2$].

 DOI: 10.1039/b104964j

Table 1 Enantioselective cyclopropanation catalysed by (*R*)-β-*cis*-[RuL^1(CH$_3$CN)$_2$][a]

Entry	Product	Yield/(%)[b]	dr/(%)	ee/(%)[c]
1	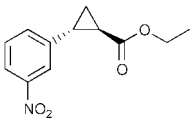	92	99:1	98
2	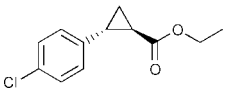	88	99:1	97
3	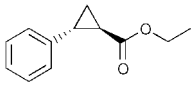	94	98:2	95
4	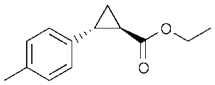	90	96:4	86
5	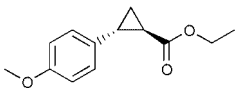	89	96:4	86
6	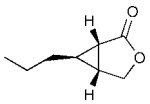	80	—	91
7	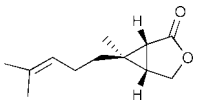	98	—	85

[a] Entries 1–5; 5 mol% of (*R*)-β-*cis*-[RuL^n(CH$_3$CN)$_2$] in toluene, 4/5 equiv. of styrene, 2 h at rt. [b] Isolated yield after flash chromatography (yield based on EDA for entries 1–5). [c] Absolute configuration of *trans* isomer (1*R*,2*R*) by comparison of optical rotations with literature values (ref. 15) for entries 1–5.

The results of addition of EDA over 2 h to solutions of styrenes at rt in the presence of pure precatalyst (*R*)-β-*cis*-[RuL^1(CH$_3$CN)$_2$] are summarised in Table 1 (entries 1–5).‡ The chemoselectivity (yield), *trans*:*cis* ratios (dr) and ee are arguably the best yet attained.[10,11] The ligand L^1 appears to be close to optimal for the cyclopropanation of styrenes; preliminary experiments with the bulky system L^2 and the electron withdrawing L^3 gave significantly lower selectivities. Mechanistic details for the catalytic reaction are currently under investigation.§

The selectivity determining step in alkene cyclopropanation involves the transfer of a metal bound carbene to the substrate,[14] and we set out to investigate this crucial step for the current system using Density Functional Theory (DFT) calculations. A fully optimised DFT structure of the precatalyst β-*cis*-[RuL^1(CH$_3$CN)$_2$] was found to be virtually superimposable on the molecular structure shown in Fig. 1. Minimisation of a structure arising from the removal of the CH$_3$CN groups and addition of the carbene derived from EDA (*i.e.* :CH-CO$_2$Et) led spontaneously to formation of a chelate, reminiscent of η^2-carboxylate, with both carbene C atom and carbonyl oxygen atom bound to Ru (Fig. 2). This structure with the carbene C atom *trans* to phenolate is *ca.* 30 kJ mol^{-1} more stable than that with the carbene *trans* to imine; an observation in accord with the expected order of *trans* influence of the two groups (N > O).

Hence the electronically controlled placement of the carbene *trans* to phenolate and the subsequent ester binding determines which diastereomeric face of the carbenoid is presented to the incoming alkene. The sense of asymmetric induction is as predicted by this model.¶ Also as a result of tight binding of the carbenoid ester, the orientation of approach of the alkene toward the reaction centre is exceptionally well directed by the chiral biaryldiimine ligand (Fig. 2); this leads to the high diastereoselectivity observed.

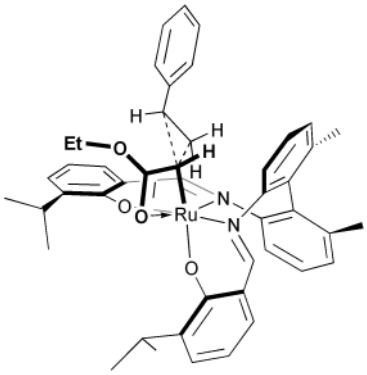

Fig. 2 Calculated structure of the carbene catalyst [RuL^1(η^2-CHCO$_2$Et)] showing the preferred orientation of approach of styrene.

P. S. wishes to thank EPSRC for a postdoctoral fellowship (K. M. G.) and Pfizer Ltd for a CASE award (I. J. M.). R. J. D. acknowledges the use of the EPSRC UK Computational Chemistry Facility.

Notes and references

‡ This complex also efficiently catalyses the intramolecular cyclopropanation/cylisation of a range of allylic diazoacetates. For example, *trans*-hex-2-enyl and geranyl diazoacetates were converted to the corresponding oxabicyclohexanones (entries 6 and 7) in a similar manner to Doyle *et al.*,[3] with the exception that *slow addition of substrate was not required* and the reaction proceeded at rt in under 2 h.

§ Attenuated selectivity in polar solvents, particularly for more electron rich alkenes, suggests significant polarity in the transition state. This will be investigated by Hammett methods. Preliminary kinetic experiments have indicated that the reaction is first order in catalyst.

¶ The (*S*)-catalyst shown in Fig. 2 gives rise to 1*S*-2*S* cyclopropanes, hence (*S*)-β-*cis*-[RuL^1(CH$_3$CN)$_2$] used in the experimental study is predicted to yield 1*R*-2*R* isomers (Table 1).

1 J. Salaün, *Top. Curr. Chem.*, 2000, **207**, 1; J. Salaun and M. S. Baird, *Curr. Med. Chem.*, 1995, **2**, 511; C. J. Suckling, *Angew. Chem., Int. Ed.*, 1988, **27**, 537.
2 For cyclopropanation of electron poor alkenes see V. K. Aggarwal, H. W. Smith, G. Hynd, R. V. H. Jones, R. Fieldhouse and S. E. Spey, *J. Chem. Soc., Perkin Trans. 1*, 2000, 3267; A.-H. Li, L.-X. Dai and V. K. Aggarwal, *Chem. Rev.*, 1997, **97**, 2341.
3 M. P. Doyle and D. C. Forbes, *Chem. Rev.*, 1998, **98**, 911.
4 M. P. Doyle, D. V. Leusen and W. H. Tamblyn, *Synthesis*, 1981, 787.
5 H.-L. Kwong, L.-S. Cheng, W. -S. Lee, W.-L. Wong and W.-T. Wong, *Eur. J. Inorg. Chem.*, 2000, 1997; M. M. Díaz-Requejo, T. R. Belderrain, M. C. Nicasio, F. Prieto and P. J. Pérez, *Organometallics*, 1999, **18**, 2601.
6 D. A. Evans, K. A. Woerpel, M. M. Hinman and M. M. Faul, *J. Am. Chem. Soc.*, 1991, **113**, 726.
7 H. Fritschi, U. Leutenegger and A. Pfaltz, *Helv. Chim. Acta.*, 1988, **71**, 1553.
8 T. Fukuda and T. Katsuki, *Tetrahedron*, 1997, **53**, 7201; S.-B. Par, N. Sakata and H. Nishiyama, *Chem. Eur. J.*, 1996, **2**, 303.
9 R. Rios, J. Liang, M. M.-C. Lo and G. C. Fu, *Chem. Commun.*, 2000, 377.
10 C.-M. Che, J.-S. Huang, F.-W. Lee, Y. Li, T.-S. Lai, H.-L. Kwong. P.-F. Teng, W.-S. Lee W.-C. Lo, S.-M. Peng and Z.-Y. Zhou, *J. Am. Chem. Soc.*, 2001, **123**, 4119.
11 T. Uchida, R. Irie and T. Katsuki, *Tetrahedron*, 2000, **56**, 3501; T. Niimi, T. Uchida, R. Irie and T. Katsuki, *Tetrahedron Lett.*, 2000, **41**, 3647.
12 C. J. Sanders, K. M. Gillespie, D. Bell and P. Scott, *J. Am. Chem. Soc.*, 2000, **122**, 7132; K. M. Gillespie, E. J. Crust, R. J. Deeth and P. Scott, *Chem. Commun.*, 2001, 785.
13 P. R. Woodman, N. W. Alcock, I. J. Munslow, C. J. Sanders and P. Scott, *J. Chem. Soc., Dalton Trans.*, 2000, 3340; P. R. Woodman, I. J. Munslow, P. B. Hitchcock and P. Scott, *J. Chem. Soc., Dalton Trans.*, 1999, 4069; P. R. Woodman, C. J. Sanders, N. W. Alcock, P. B. Hitchcock and P. Scott, *New J. Chem.*, 1999, **23**, 815.
14 M. Brookhart, Y. Liu, E. W. Goldman, D. A. Timmers and G. D. Williams, *J. Am. Chem. Soc.*, 1991, **113**, 927.
15 A. Nakamura, A. Konishi, R. Tsujitani, M. Kudo and S. Otsuka, *J. Am. Chem. Soc.*, 1978, **100**, 3449.

CHEMCOMM
Communication
www.rsc.org/chemcomm

The inverse podant $[Li_3(NBu^t)_3S\}]^+$ stabilises a single ethylene oxide $OCH{=}CH_2$ anion as a high- and low-temperature polymorph of $[(thf)_3Li_3(OCH{=}CH_2)\{(NBu^t)_3S\}]$

Bernhard Walfort,[a] Sushil K. Pandey[b] and Dietmar Stalke*[a]

[a] *Institut für Anorganische Chemie der Universität Würzburg, Am Hubland, D-97074 Würzburg, Germany. E-mail: dstalke@chemie.uni-wuerzburg.de*
[b] *Department of Chemistry, University of Jammu, New Campus, Jammu-180006, India*

Received (in Cambridge, UK) 20th June 2001, Accepted 25th July 2001
First published as an Advance Article on the web 14th August 2001

A single ethylene oxide anion derived from the ether cleavage reaction of thf with Bu^{t}Li is stabilised by the inverse podant $[Li_3(NBu^t)_3S\}]^+$ to give a high- and a low-temperature polymorph with a considerable difference in conformation and packing.

The ether cleavage reaction is one of the most common side reactions in organometallic chemistry as the RLi starting material is often dissolved in ethers.[1] Apart from the mostly unintended reaction to side products, cyclic ethers are deliberately employed in this reaction[2–5] as they give synthetically important lithium enolates[6] by an α-metalation followed by a [π4s + π2s]-cycloreversion. In this reaction the most common cyclic ether tetrahydrofuran (thf) gives lithium ethylene oxide and ethene (Scheme 1).

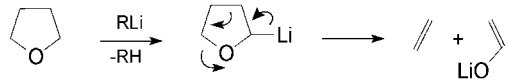

Scheme 1 Ether cleavage reaction of thf by lithium organics: α-metalation is followed by a [π4s + π2s]-cycloreversion to give lithium ethylene oxide and ethene.[1]

Recently it was found that ethene can insert in the Li–C bond of non-reacted Bu^{t}Li, to give *n*-hexyllithium $[(thf)LiCH_2\text{-}CH_2Bu^t]_4$.[7] Because the ionic character of the Li–O bond lithium enolates tend to aggregate in the solid state as solvated dimers, tetramers or even hexamers.[6] Although heteroatoms, like in the mixed lithium enolate/chiral amide structures[8] or adjacent double bonds,[9] help to coordinate the lithium atoms and to decrease the degree of aggregation, structurally characterised ethylene oxides generally form complex cage like structures.[2–5,10] The S_4 symmetric tetrasolvated tetramer $[(Me_2O)(LiOCH{=}CH_2)]_4$ was computed to be the most stable oligomer (Scheme 2(a)).[11]

Here we report the solid state structure of $[(thf)_3Li_3(OCH{=}CH_2)\{(NBu^t)_3S\}]$ **1**. Formally it derives from the tetramer $[(Me_2O)(LiOCH{=}CH_2)]_4$ by replacement of the top $[(Me_2O)(LiOCH{=}CH_2)_3]^{2-}$ dianionic fragment by the diimido sulfite dianion $[S(NBu^t)_3]^{2-}$(Scheme 2(b)). This tripodal dianion templates the Li_3 triangle required for the oxygen atom of the single ethylene oxide ion to be η^3 metal coordinated. By analogy to Mulvey's inverse crowns[12] like $[M_2Mg_2(NR_2)_4]^{2+}$, M = Li, Na, K, the $[Li_3(NBu^t)_3S\}]^+$ cationic motif in **1** can be regarded an inverse podant, capable of single-anion coordination to *e.g.* methanide.[13] In the attempted coordination of *tert*-butanide from Bu^{t}Li we isolated and crystallised **1** in a high-temperature (**1a**; D_c = 1.036 Mg m^{-3}) and a low-temperature phase (**1b**; D_c = 1.073 Mg m^{-3}).† For the first time an *in situ* generated, industrial important product is stabilised by the diimido sulfite dianion.

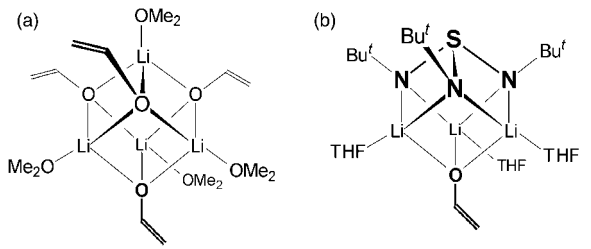

Scheme 2 The computed S_4 symmetric cubic tetramer $[(Me_2O)\text{-}(LiOCH{=}CH_2)]_4$ is the most stable lithium enolate solvate (a).[11] $[(thf)_3Li_3(OCH{=}CH_2)\{(NBu^t)_3S\}]$ **1** mimics the same aggregation by replacement of the top $[(Me_2O)(LiOCH{=}CH_2)_3]^{2-}$ dianionic fragment by the triimido sulfite dianion $[S(NBu^t)_3]^{2-}$ (b).

Both phases contain the cap shaped triimido sulfite dianion coordinated to three lithium atoms close to the SN_2 bisectors. The single ethylene oxide anion is η^3 coordinated *via* the oxygen atom to those three metal centres (Fig. 1). Thus, the oxygen atom forms one corner of a SN_3Li_3O cube. In both polymorphs the $H_2C{=}CHO$ group is disordered. In **1a** it slots in between the three thf molecules with a 0.8/0.1/0.1 site occupation factor (SOF) each. In **1b** the ethylene group is only disordered over two positions: staggered between Li2 and Li3 (0.8 SOF) and eclipsed to Li1 (0.2 SOF). The average S–N bond lengths of 165.3 and 166.4 pm for **1a** and **1b**, respectively, are almost identical. The Li_3N_3 array is not a regular chair-shaped ring but shows alternating long and short Li–N bonds. The average Li···Li distances in the cap shaped $[Li_3(NBu^t)_3S]^+$ cation are 264.3 pm in **1a** and 265.5 pm in **1b** and are only marginally longer than the distances found in parent tetrameric lithium organics (241 ($[Bu^tLi]_4$),[14a] 253 ($[EtLi]_4$),[14b] 259 pm ($[MeLi]_4$)).[14c] The bond lengths similarities in both structures indicate that the different phases are not a result of severe changes in bond distances. However, the conformation of both molecules changes quite dramatically.‡

The most obvious difference between **1a** and **1b** is the more dense packing of the molecules in the low-temperature phase

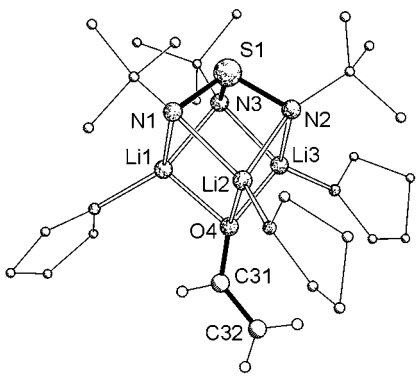

Fig. 1 Solid-state structure of $[(thf)_3Li_3(OCH{=}CH_2)\{(NBu^t)_3S\}]$ **1**. Selected average bond lengths (pm) and angles (°) [**1b** in square brackets]: S–N 165.3(3) [166.4(2)], long Li–N 210.9(7) [211.0(5)], short Li–N 202.3(7) [200.4(5)], Li–OCH=CH$_2$ 195.7(8) [196.4(11)], Li···Li 264.3(10) [265.5(6)], C31–O4 135.8(6) [133.1(6)], C31–C32 136.5(13) [132.1(5)]; N–S–N 100.4(2) [100.38(11)].

 DOI: 10.1039/b105429p

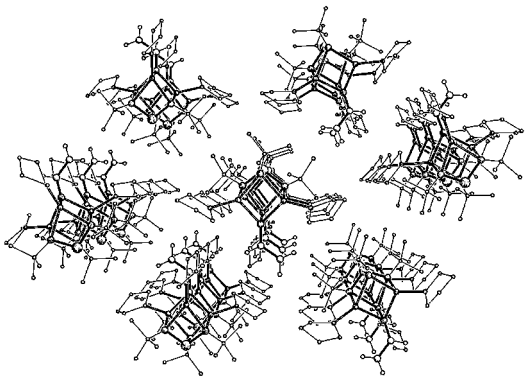

Fig. 2 Wide packing of the molecules in the high-temperature polymorph of **1a** with no interlocking at the periphery.

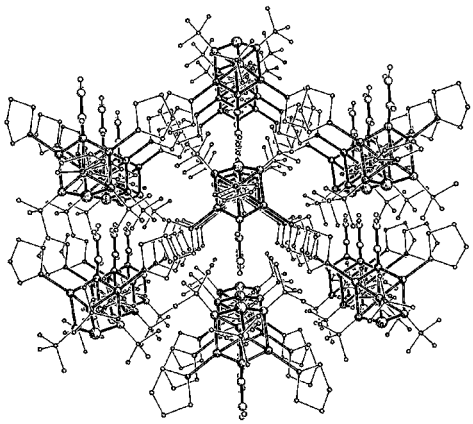

Fig. 3 Dense packing of the low-temperature polymorph **1b**, with the thf donors zipping the molecular rods. The ethylene oxide moiety is locked in a groove provided by an adjacent rod.

compared to the high-temperature polymorph.[15] The average intermolecular distances in **1a** give the molecules considerably more room than in **1b**. Virtually no interlocking of the molecular periphery in the packing of **1a** tolerates the disordered orientation of the ethylene oxide over three positions, although the depicted one is favoured by eight of ten molecules (Fig. 2). In the packing of **1b** the molecular rods are zipped together by interlocking thf molecules (Fig. 3). This causes the ethylene oxide to slot in to the groove formed by two *tert*-butyl groups of an adjacent rod. The channel permits only two disordered orientations of the ethylene oxide group in **1b**. The position with the smaller SOF is disfavoured by the orientation of the CH_2 group eclipsed towards Li1.

Evidently the beginning of the chain of cause and effect between the change in conformation and different packing can not be identified. The question whether the different packing causes the conformation or *vice versa* remains open. However, at temperatures lower than −36 °C the ethylene oxide group clicks into the space between two thf molecules while it has more rotational freedom at higher temperatures.[15c]

We gratefully acknowledge the continued financial support of the Deutsche Forschungsgemeinschaft and the Fonds der Chemischen Industrie.

Notes and references

† *Preparation* of $[(thf)_3Li_3(OCH{=}CH_2)\{(NBu^t)_3S\}]$ **1**: to a solution of 5.0 g $[(thf)Li_2\{(NBu^t)_3S\}]_2$ (8.46 mmol) in 20 mL thf, 4.97 mL of a 1.7 M solution of *tert*-butyllithium (16.92 mmol) were slowly added at −78 °C and stirred for 1 h. The mixture was stirred for 2 h at room temperature. The solvent was reduced by half under vacuum. Crystallisation at room temperature gives colourless pyrophoric crystals of the high temperature phase **1a**. Storage of the solution at −36 °C for several days affords colourless pyrophoric crystals of **1b**; destructive phase transition from **1b** to **1a** was observed at −30 °C; spectroscopic data for both phases are identical (2.6 g, 78%). ^{1}H NMR (400.4 MHz, C_6D_6): δ 1.37 (12H, thf), 1.54 [s, 27H, $C(CH_3)$], 3.71 (12 H, thf), 4.03 [d, 2 H, $OCHCH_2$], 7.45 (t, 1 H, $OCHCH_2$); ^{13}C NMR (100 MHz, C_6D_6): δ 25.52, 68.40 (thf), 33.89 [$C(CH_3)_3$], 52.99 [$C(CH_3)_3$] 82.15 ($OCHCH_2$), 159.68 ($OCHCH_2$); ^{7}Li NMR (155.5 MHz, ext. sat. LiCl solution) δ 1.35, (br s, 3 Li).

‡ *Crystal data* were collected from shock-cooled crystals on a STOE IPDS (**1a**) or a Bruker SMART-APEX CCD diffractometer (**1b**) (Mo-Kα radiation, λ = 71.073 pm) at 193(2) and 173(2) K, respectively (D. Stalke, *Chem. Soc. Rev.*, 1998, **27**, 171). The structure of **1a** was solved by direct methods (SHELXS-97) and refined by full-matrix least squares methods against F^2 (SHELXL-97); (G. M. Sheldrick, *Acta Crystallogr., Sect. A*, 1990, **46**, 467; G. M. Sheldrick, SHELXL-97, program for crystal structure refinement, 1996, Göttingen). The low-temperature phase **1b** crystallised as a non-merohedral twin. The matrices of both domains were determined and every domain was integrated independently. Subsequently, the structure was solved with the data of one domain by direct methods; *R* values defined as $R1 = \Sigma||F_o| - |F_c||/\Sigma|F_o|$, $wR2 = [\Sigma w(F_o^2 - F_c^2)^2/\Sigma w(F_o^2)^2]^{0.5}$, $w = [\sigma^2(F_o^2) + (g_1P)^2 + g_2P]^{-1}$, $P = 1/3[\max(F_o^2,0) + 2F_c^2]$.

1a: $C_{26}H_{54}Li_3N_3O_4S$, M = 525.60, monoclinic, space group $P2_1/n$, a = 1003.5(2), b = 2331.1(5), c = 1469.6(3) pm, β = 101.55(3), U = 3.3683(12) nm^3, Z = 4, D_c = 1.036 Mg m^{-3}, μ = 0.126 mm^{-1}, F(000) = 1152, 22142 reflections measured, 5718 unique, R_{int} = 0.0558, $wR2$ (all data) = 0.1949, $R1[I > 2\sigma(I)]$ = 0.0747, 520 parameters and 718 restraints.

1b: $C_{26}H_{54}Li_3N_3O_4S$, M = 525.60, monoclinic, space group $P2_1/c$, a = 1586.05(11), b = 1371.07(10), c = 1497.29(11) pm, β = 91.444(2), U = 3.2550(4) nm^3, Z = 4, D_c = 1.073 Mg m^{-3}, μ = 0.130 mm^{-1}, F(000) = 1152, 18299 reflections measured, 6989 unique, R_{int} = 0.0647, $wR2$ (all data) = 0.2113, $R1[I > 2\sigma(I)]$ = 0.0775, 426 parameters and 305 restraints.

The disordered ethylene oxide moiety was refined with distance and ADP restraints to split occupancies of 0.79/0.10/0.11 (**1a**) and 0.79/0.21 (**1b**). The disordered thf molecules were refined with distance and ADP restraints to split occupancies. All hydrogen atom positions were refined using a riding model.

CCDC reference numbers 165029 and 165030. See http://www.rsc.org/suppdata/cc/b105429p/ for crystallographic data in CIF or other electronic format.

1 Review: A. Maercker, *Angew. Chem., Int. Ed. Engl.*, 1987, **26**, 972.
2 C. Hilf, F. Bosold, K. Harms, M. Marsch and G. Boche, *Chem. Ber./Recl.*, 1997, **130**, 1213.
3 H. C. Aspinall and M. R. Tillotson, *Inorg. Chem. Commun.*, 1996, **35**, 2163.
4 J. Jubb, S. Gambarotta, R. Duchateau and J. H. Teuben, *J. Chem. Soc., Chem. Commun.*, 1994, 2641.
5 S. De Angelis, E. Solari, C. Floriani, A. Chiesi-Villa and C. Rizzoli, *J. Chem. Soc., Dalton Trans.*, 1994, 2467.
6 D. Seebach, *Angew. Chem., Int. Ed. Engl.*, 1988, **27**, 1624.
7 T. Kottke, R. J. Lagow, D. Hoffmann and R. D. Thomas, *Organometallics*, 1997, **16**, 789.
8 C. Sun and P. G. Williard, *J. Am. Chem. Soc.*, 2000, **122**, 7829.
9 K. Sorger, P. v. R. Schleyer, R. Fleischer and D. Stalke, *J. Am. Chem. Soc.*, 1996, **118**, 6924.
10 A. Steiner and D. S. Wright, *Chem. Commun.*, 1997, 283.
11 A. Abbotto, A. Streitwieser and P. v. R. Schleyer, *J. Am. Chem. Soc.*, 1997, **119**, 11255.
12 R. E. Mulvey, *Chem. Commun.*, 2001, 1049.
13 B. Walfort, L. Lameyer, W. Weiss, R. Herbst-Irmer, R. Bertermann, J. Rocha and D. Stalke, *Chem. Eur. J.*, 2001, **7**, 1417.
14 (*a*) T. Kottke and D. Stalke, *Angew. Chem., Int. Ed. Engl.*, 1993, **32**, 580; (*b*) H. J. Dietrich, *J. Organomet. Chem.*, 1981, **205**, 291; (*c*) E. Weiss, T. Lambertsen, B. Schubert, J. K. Cockcroft and A. Wiedemann, *Chem. Ber.*, 1990, **123**, 79.
15 Polymorphism is a challenging phenomenon in crystal engineering, drug design and theory; see *e.g.* (*a*) G. R. Desiraju, *Crystal Engineering–The Design of Organic Solids*, Elsevier, Amsterdam, 1989; (*b*) J. Wouters and F. Ooms, *Curr. Pharm. Des.*, 2001, **7**, 529; (*c*) J. Starbuck, R. Docherty, M. H. Charlton and D. Buttar, *J. Chem. Soc., Perkin Trans. 2*, 1999, 677.

CHEMCOMM
Communication
www.rsc.org/chemcomm

An unusual six-co-ordinate platinum(II) complex containing a neutral I_2 ligand

Rie Makiura,[b] Isoroku Nagasawa,*[a] Noriyoshi Kimura,[c] Shin'ichi Ishimaru,[b] Hiroshi Kitagawa[b] and Ryuichi Ikeda[b]

[a] *Department of Chemistry, Fukuoka University of Education, Akama 729-1, Munakata, Fukuoka 811-4192, Japan. E-mail: isoroku@fukuoka-edu.ac.jp*
[b] *Department of Chemistry, University of Tsukuba, Tennodai 1-1-1, Tsukuba, Ibaraki 305-8571, Japan. E-mail: ikeda@staff.chem.tsukuba.ac.jp*
[c] *Department of Chemistry, Faculty of Education, Wakayama University, Sakaedani 930, Wakayama 640-8510, Japan. E-mail: nkimura@center.wakayama-u.ac.jp*

Received (in Cambridge, UK) 24th April 2001, Accepted 20th July 2001
First published as an Advance Article on the web 7th August 2001

The present paper deals with a rare platinum(II) complex containing the κ-I_2 ligand, which is an unusual example of a six-co-ordinated octahedral platinum(II) complex.

Platinum(II) strongly demands a square-planar co-ordination geometry and very few six-co-ordinate complexes have so far been characterized.[1] *Trans*-[PtI_2(diars)$_2$] (diars = *o*-phenylenebis(dimethylarsine)) has been the only example of a six-co-ordinate platinum(II) complex determined by X-ray study.[1b] However, Pt–I bonds in this complex seem to be weak because of long Pt–I distances of 3.50 Å. Here, we present a novel octahedral platinum(II) complex, [PtI(dmpe)$_2$(κ-I_2)]I_3 (dmpe = 1,2-bis(dimethylphosphino)ethane) in which the neutral molecular iodine co-ordinates to the platinum(II) ion. This is a quite rare example of the platinum(II) complex having clearly short Pt–I bond distances.

Treatment of [Pt(dmpe)$_2$](SCN)$_2$ **1**[2] with a 3 molar amount of iodine gave black needle crystals formulated as [PtI(dmpe)$_2$(κ-I_2)]I_3 **2** (Scheme 1, yield 21%).†

The molecular structure of complex **2** is displayed in Fig. 1, with partial labeling.‡ Complex **2** is a mononuclear complex with Pt1, I1, I2, and I3 atoms located on a crystallographic mirror plane that is coincident with mirror symmetry of the complex. The I4, I5 and I6 atoms of I_3^- anion are located on a crystallographic mirror. The co-ordination geometry around the platinum atom is octahedral with 4P and 2I donor atoms, with two iodine atoms having *trans* geometry. The bond distances between platinum and iodine atoms are 2.811(1) and 2.817(1) Å for Pt1–I1 and Pt1–I2, respectively. These values are considerably shorter than those in the complex *trans*-[PtI_2(diars)$_2$] **3** (here the bond length of Pt–I is 3.50 Å).[1b] Compared to **3**, complex **2** can be undoubtedly considered to be a six-co-ordinate octahedral platinum(II) complex. Furthermore, it is worthy of note that the neutral molecular iodine co-ordinates to the platinum(II) ion by end-on type (Pt1–I2–I3 = 171.58(3)°), and the I2–I3 bond distance of 3.061(1) Å is much longer than that of 2.715(6) Å in free diiodine molecules.[3] This means that the electrons on the central platinum(II) flow into the κ-I_2 ligand, which is attributable to a d_{z^2} (Pt) to σ* (I_2) donation.[4]

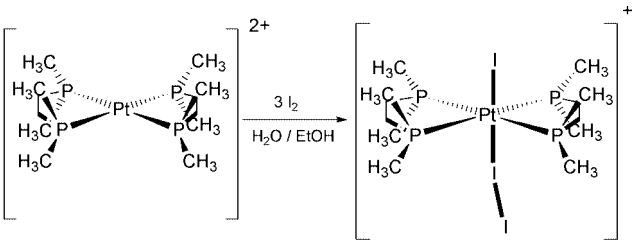

Scheme 1

Van Koten and coworkers have reported five-co-ordinate platinum(II) complexes containing the κ-I_2 ligand, [PtI{C_6H_3(CH_2NMe_2)$_2$-2,6}(κ-I_2)] **4a** and [Pt(κ-I_3)(κ-I_2){C_6H_3(CH_2N(*t*-Bu)Me)$_2$-2,6}] **4b**.[5] The Pt–I_2 bond distances of 2.895(1) and 2.906(2) Å in **4a** and **4b**, respectively,[5d] are longer than 2.817(1) Å in **2**, showing that a stronger platinum–molecular iodine bond is realised in **2**. The I–I bond distances in these complexes show a marked difference: the I2–I3 distance of 3.061(1) Å in **2** is much longer than that of 2.822(1) and 2.793(1) Å in **4a** and **4b**, respectively. This elongation is attributable to the existence of the ligand on a *trans* position of the κ-I_2 ligand. The bond distances between platinum and co-ordinated phosphorus in **2** are 2.369(2) and 2.374(2) Å for Pt1–P1 and Pt1–P2, respectively. These values are longer than that of starting square-planar complex **1** with a Pt–P of 2.317(1) Å.[6]

The formal oxidation state of the platinum ion in **2** is expected to be +2. To confirm this, X-ray photoelectron spectroscopy (XPS) measurements were performed.§ Binding energies of the Pt 4f region given in Table 1 were determined by a conventional deconvolution procedure. The XPS spectrum of **2** shows a doublet, whose binding energies are coincident with the values of Pt(II) binding energies.[5c,7] From XPS measurements, the platinum ion in complex **2** was found to have the +2 oxidation state.

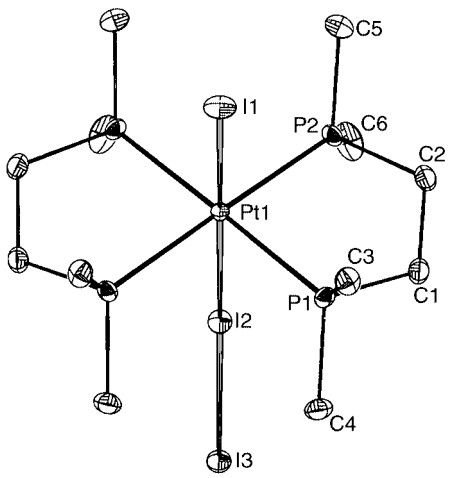

Fig. 1 The structure of **2**. Selected bond distances (Å) and angles (°): Pt1–I1 2.811(1), Pt1–I2 2.817(1), Pt1–P1 2.369(2), Pt1–P2 2.374(2), I2–I3 3.061(1), P1–C1 1.82(1), P1–C3 1.80(1), P1–C4 1.80(1), P2–C2 1.82(1), P2–C5 1.82(1), P2–C6 1.80(1), C1–C2 1.52(1); I1–Pt1–I2 177.75(3), I1–Pt1–P1 89.73(5), I1–Pt1–P2 92.45(5), I2–Pt1–P1 91.78(5), I2–Pt1–P2 86.04(5), P1–Pt1–P2 84.46(6), Pt1–I2–I3 171.58(3).

 DOI: 10.1039/b103648n

Table 1 Binding energies (eV) for the 4f region of platinum

Compound	$4f_{5/2}$	$4f_{7/2}$
1	76.0	72.7
2	76.0	72.6

The ^{31}P MAS NMR spectral data for **1** and **2** in the solid state and in CD_3CN or D_2O solution are given in Table 2. In the ^{31}P MAS NMR spectrum of **2**, a signal appeared at δ 11.9 ppm with satellites due to the coupling with ^{195}Pt (1758 Hz). The smaller coupling constant $^1J_{Pt-P}$ in **2** compared with 2173 Hz in **1**, is explained by the difference in the co-ordination number.[8] $^1J_{Pt-P}$ of 2173 Hz in **1** is a normal value compared with analogous platinum(II) square-planar co-ordinate complexes.[9] On the other hand, in CD_3CN solution, the observed $^1J_{Pt-P}$ of 2172 Hz in **2** was very close to 2162 Hz observed in D_2O solution for **1**. This result indicates that complex **2** has a square-planar geometry caused by the dissociation of iodine in CD_3CN solution.

Table 2 ^{31}P NMR spectroscopic data

Compound	$\delta_{^{31}P}$/ppm	$^1J(^{195}Pt-^{31}P)$/Hz
1	32.75[a]	21 273[a]
	33.06[b]	2162[b]
2	11.85[a]	1758[a]
	28.95[c]	2172[c]

[a] MAS NMR spectrum in the solid state with a spinning rate of 4–5 kHz. [b] In D_2O. [c] In CD_3CN solution.

This work was partly supported by Grant-in Aid for Scientific Research No.(B) 12440192 from the Ministry of Education, Science, Sports and Culture. The authors are grateful to Dr Y. Yokoyama and Mr H. Nakazono, the Chemical Analysis Center, University of Tsukuba, for JEOL EX-270 NMR spectral and elemental analysis measurements. We thank Dr H. Kuma and Dr T. Kawamoto, Osaka University, for discussion of X-ray data.

Notes and references

† In this reaction, two electrons are gained, but the fully balanced equation was not understood. The authors consider that the reaction is related to the redox systems of Pt(II) with Pt(IV) and of $2I^-$ with I_2.

‡ *Crystal data* for **2**: $C_{12}H_{32}I_6P_4Pt$, M = 1256.8, orthorhombic, *Pnma*, a = 8.6718(4), b = 10.7317(5), c = 30.9849(3) Å, U = 2883.6(3) Å^3, D_c = 2.89 g cm^{-3}, Z = 4, $F(000)$ = 2240, μ(Mo-Kα) = 11.51 mm^{-1}, graphite monochromator, room temperature, 4933 reflections measured, 2734 observed [$I > 3\sigma(I)$], 115 parameters. Empirical absorption corrections (ψ-scan) were applied. Final R factor = 0.033, R_w = 0.040. Hydrogen atoms were included in fixed positions with isotropic thermal parameters, while all other atoms were refined by anisotropic thermal parameters.

CCDC reference number 155325. See http://www.rsc.org/suppdata/cc/b1/b103648n/ for crystallographic data in CIF or other electronic format.

§ XPS spectra were carried out on an Ulvac Phi 5600ci with monochromated Al-Kα X-rays (1487 eV). Binding energies were measured relative to the Au $4f_{7/2}$ peak of the gold fine powder mixed with the sample.

1 (*a*) C. M. Harris, R. S. Nyholm and D. J. Phillips, *J. Chem. Soc.*, 1960, 4379; (*b*) N. C. Stephenson, *J. Inorg. Nucl. Chem.*, 1962, **24**, 791.
2 D. J. Gulliver, W. Levason and K. G. Smith, *J. Chem. Soc., Dalton Trans.*, 1981, 2153.
3 F. van Bolhuis, P. B. Koster and T. Migchelsen, *Acta Crystallogr.*, 1967, **23**, 90.
4 F. M. Bickehaupt, E. J. Baerends and W. Ravenek, *Inorg. Chem.*, 1990, **29**, 350.
5 (*a*) J. A. M. van Beek, G. van Koten, W. J. J. Smeets and A. L. Spek, *J. Am. Chem. Soc.*, 1986, **108**, 5010; (*b*) J. A. M. van Beek, G. van Koten, G. P. C. M. Dekker, E. Wissing, M. C. Zontberg and C. H. Stam, *J. Organomet. Chem.*, 1990, **394**, 659; (*c*) J. C. Muijsers, J. W. Niemantsverdriet, I. C. M. Wehman-Ooyevaar, D. M. Grove and G. van Koten, *Inorg. Chem.*, 1992, **31**, 2655; (*d*) R. A. Gossage, A. D. Ryabov, A. L. Spek, D. J. Stufkens, J. A. M. van Beek, R. van Eldik and G. van Koten, *J. Am. Chem. Soc.*, 1999, **121**, 2488.
6 I. Nagasawa and R. Ikeda, unpublished work.
7 J. Moulder, W. F. Stickle, P. E. Sobel and K. D. Bomben, *Handbook of X-Ray Photoelectron Spectroscopy*, ed. J. Chastain, Perkin-Elmer Co., 1992, pp.180, 234.
8 J. F. Nixon and A. Pidcock, *Annual Review of NMR Spectroscopy*, ed. E. F. Mooney, Academic Press, London, 1969, vol. 2, p 374.
9 E. G. Hope, W. Levason and N. A. Powell, *Inorg. Chim. Acta*, 1986, **115**, 187; V. S. Reddy, K. V. Katti and C. L. Barnes, *Inorg. Chim. Acta*, 1995, **240**, 367.

CHEMCOMM Communication
www.rsc.org/chemcomm

Nickel porphyrin nanotweezers†

Stéphanie Gazeau, Jacques Pécaut and Jean-Claude Marchon*

Laboratoire de Chimie Inorganique et Biologique (CEA, CNRS, UJF), Département de Recherche Fondamentale sur la Matière Condensée, CEA-Grenoble, 38054 Grenoble cedex 9, France. E-mail: jcmarchon@cea.fr

Received (in Cambridge, UK) 30th May 2001, Accepted 9th July 2001
First published as an Advance Article on the web 7th August 2001

A strapped chiroporphyrin free base with two 8-methylene chains linking two adjacent meso-substituents was synthesized as the α⁴ conformer; insertion of Ni(II) triggered a complete conversion to the αβαβ complex, and demetallation totally regenerated the strapped free base in the α⁴ conformation.

Metalloporphyrin compounds which have a rigid concave shape can trap molecular guests by coordinative or non-covalent interactions; recognition of the guest is due to complementarity in size, shape and functional groups.[1] A 'Venus flytrap' zinc porphyrin that reversibly swings between an open and a closed form upon binding and dissociation of pyridine has also been reported.[2] We have now designed a strapped chiroporphyrin whose shape can be controlled at will by exploiting the specific coordination requirements of nickel(II). The forces which operate this molecular metamorphosis might be useful in the design of nanoscale tweezers.

Deprotonation of (1*R*)-cis-hemicaronaldehyde **1** by sodium hydride, followed by nucleophilic attack[3] on 1,8-diiodooctane, led to the diester-strapped dialdehyde **2** in 99% yield (Scheme. 1). The latter was reacted with pyrrole according to a literature method[4] to afford the bis-strapped chiroporphyrin **3** in 5% yield.‡ In contrast to the first-generation chiroporphyrins devoid of straps, which are always obtained as the αβαβ atropisomer,[5] **3** shows an α⁴ conformation with the two 8-methylene straps linking adjacent *meso* substituents on the same face of the porphyrin. This unusual conformation is apparent in the C_2 symmetry of the NMR spectra of **3** [*e.g.* two AB systems for the pyrrole protons, Fig. 1(a)], and in the large upfield shifts of the methylene groups of the straps. The zinc complex **4** exhibits the same spectral symmetry [Fig. 1(b),§ and its α⁴ conformation was confirmed by its X-ray structure shown in Fig. 2.[6]

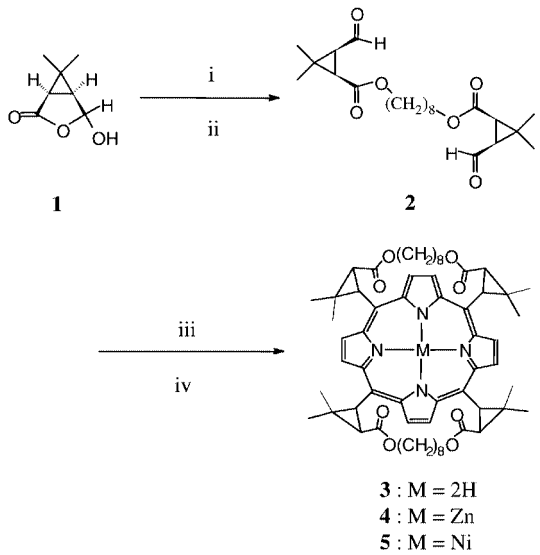

Scheme 1 *Reagents and conditions:* i, NaH, THF, 10 °C, 30 min under Ar; ii, 1,8-diiodooctane in DMF, 25 °C, 24 h under Ar (99%); iii, pyrrole, TFA, CH_2Cl_2, 25 °C, 6 days; iv, DDQ, 4 h (5%).

† Electronic supplementary information (ESI) available: spectroscopic data for **3**–**6**. See http://www.rsc.org/suppdata/cc/b1/b104715a/

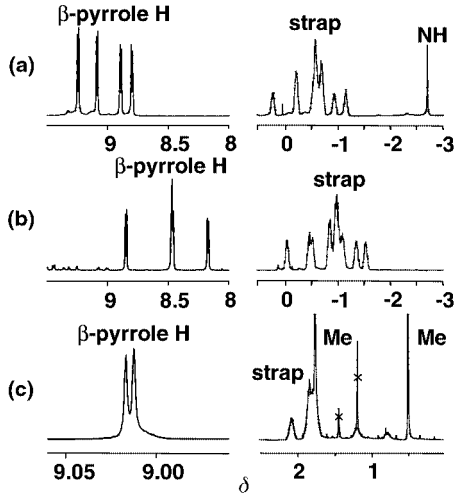

Fig. 1 ¹H NMR spectra (400 MHz, $CDCl_3$, 298 K) for (*a*) the free base chiroporphyrin **3** with two 8-methylene straps in the α⁴ conformation; (*b*) its α⁴ zinc(II) complex **4**; and (*c*) its αβαβ nickel(II) complex **5**; crossed peaks correspond to $CDCl_3$ solvent impurities.

Much to our surprise, metallation of α⁴-**3** by Ni(II) triggered a major conformational change. The nickel complex **5** shows a D_2-symmetric ¹H NMR spectrum [*e.g.* two singlets for the pyrrole proton resonances, Fig. 2(*c*) in which the chemical shifts of the methylene protons are in the normal alkyl range, unambiguously indicating an αβαβ conformation in which the straps now link the adjacent *meso* substituents on opposite faces of the porphyrin.¶ The conversion was complete, and no intermediate could be detected. This unprecedented conformation of a strapped porphyrin[4] was confirmed by the X-ray structure of **5** illustrated in Fig. 3.

Several experiments were carried out to try and remove the nickel(II) center from the porphyrin, in the view of examining

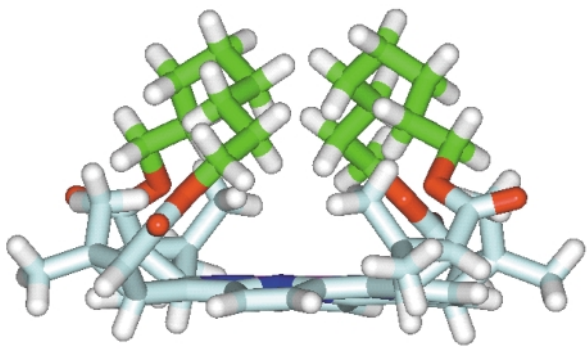

Fig. 2 Stick representation of the X-ray structure of the zinc(II) chiroporphyrin complex **4** showing the α⁴ conformation and the two straps (green) linking adjacent *meso* substituents on the same face of the porphyrin (light blue).

 DOI: 10.1039/b104715a

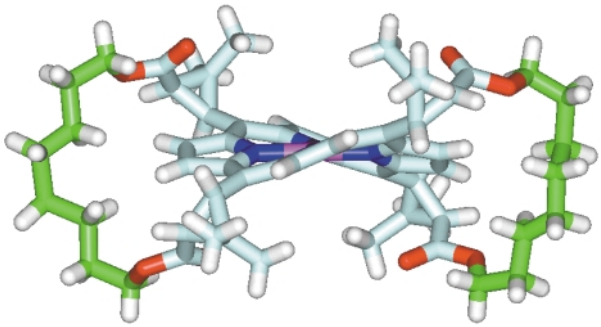

Fig. 3 Stick representation of the X-ray structure of the nickel(II) chiroporphyrin complex **5** showing the αβαβ conformation and the two straps (green) linking adjacent *meso* substituents on opposite faces of the porphyrin (light blue).

the conformation of the resulting free base. Among several acids which were tried, only trifluoromethanesulfonic acid was found strong enough to transfer protons to the very weakly basic nitrogen atoms of **5** and release the nickel(II) ion. Short reaction times (15 min, resulting in *ca*. 50% demetallation) were required with such a strong reagent, which also hydrolyzes the ester groups upon prolonged contact. The resulting free base exhibited α^1H NMR spectrum identical to that of the starting material **3**, indicating the same α^4 conformation. Thus the $\alpha^4 \rightarrow$ αβαβ conformation change is entirely reversible upon nickel(II) insertion and extrusion (see Graphical Abstract).

Metal insertion in a porphyrin generally induces modest distortions of the core, such as the *sad*, *ruf*, *dom*, *wav* and *pro* types or combinations thereof,[7] but usually it does not affect the orientation of the macrocycle substituents. The intriguing $\alpha^4 \rightarrow$ αβαβ conformation change which is observed upon Zn(II) → Ni(II) substitution in the strapped chiroporphyrin may be related to the coordination requirements of the two metals and to the constraints induced by the short straps. While Zn(II) with its full d^{10} complement shows long Zn-N bonds (average 2.036(5) Å for the two independent molecules) compatible with the flat porphyrin core of α^4-**4**, square-planar d^8 Ni(II) with its vacant antibonding $d_{x^2-y^2}$ orbital requires short Ni–N bonds [average 1.916(5) Å for the two independent molecules] which are obtained by ruffling of the core of **3**. In this distorted core conformation, the 8-methylene straps apparently are too short to stride over their adjacent cyclopropyl substituent, which are forced to rotate toward the opposite face of the porphyrin. The low rotation barrier usually observed in ruffled nickel(II) porphyrins[8] may facilitate this motion, which results in the αβαβ complex **5**.

Nearly complete conversion to a paramagnetic piperidine adduct **6** was obtained by dissolution of **5** in neat $C_5D_{10}ND$, as judged from the UV–VIS spectrum.[9,10] The 500 MHz ^{1}H NMR spectrum of the resulting solution showed a broad peak near 40 ppm at room temperature for the pyrrole protons of the high-spin Ni(II) complex **6**, typical of a $d_{z^2}{}^1\, d_{x^2-y^2}{}^1$ configuration.[9,11] A pair of singlets was also observed at δ 7.44 and 7.61 for the pyrrole protons of the residual diamagnetic species **5**. The fact that **5** and **6** are not in fast exchange on the NMR time scale stands in contrast to the rapid equilibrium between Ni(TPP) and its high-spin piperidine adduct which has been observed earlier.[9] These observations suggest that **5** and **6** have quite different conformations, and they are consistent with the expected structural consequences of the singly occupied $d_{x^2-y^2}$ orbital in **6**. High-spin nickel(II) porphyrins usually exhibit an expanded core [average Ni–N bond length 2.04–2.07 Å] and reduced non planar distortion relative to their parent low-spin complex (average Ni–N bond length 1.89–1.93 Å).[12] The expanded porphyrin core of the piperidine adduct **6** is incompatible with the αβαβ conformation which imparts short Ni-N bonds. Thus this adduct is prone to undergo a structural change to the α^4 conformation which allows near planarity of the porphyrin core similar to that of the zinc complex **3**. The piperidine ligand located between the two straps is probably held by mechanical forces in addition to the coordination bond.

The strong effects of $d_{x^2-y^2}$ orbital occupancy on molecular shape and dynamics in this system could be exploited in the design of molecular machines such as motors and switches.

We thank Nathalie Gon, Colette Lebrun and Pierre-Alain Bayle for assistance, and Dr Pierrette Battioni for experimental details on the use of trifluoromethanesulfonic acid.

Notes and references

‡ *Selected spectroscopic data* for **3**: MS (ES) *m/z* 979 (MH^+); UV–VIS (CH_2Cl_2) λ_{max}/nm 426, 526, 561, 605, 666; δ_H(200 MHz, $CDCl_3$) 8.52, 8.66, 8.81 and 9.02 (4d, 8H, *J* 4.9 Hz), 4.02 (2d, 4H, *J* 8.8 Hz), 3.37 (m, 4H), 2.89 (m, 4H), 2.73 (2d, 4H, *J* 8.8 Hz), 1.87 and 1.85 (2s, 12H), 1.28 and 1.18 (2s, 12 H), 0.13 (m, 2H), −0.3 (m, 4H), −0.7 (m, 14H), −1.1 (m, 2H), −1.32 (m, 2H), −3.07 (s, 2H).

§ *Selected spectroscopic data* for **4**: MS (ES) *m/z* 1040.5 ($M^{+\cdot}$); UV–VIS (CH_2Cl_2) λ_{max}/nm 429, 563, 613; δ_H(200 MHz, $CDCl_3$) δ 8.83, 8.44, and 8.14 (3d, 8H, *J* = 4.4 Hz), 3.77 (2d, 4H, *J* 9.3 Hz), 3.21 (m, 4H), 2.70 (2d, 6H, *J* 9.3 Hz), 2.50 (m, 2H), 1.92 and 1.88 (2s, 12H), 1.04 and 0.94 (2s, 12 H), −0.05 (m, 2H), −0.46 (m, 4H), −1.03 (m, 14H), −1.38 (m, 2H), −1.58 (m, 2H).

¶ *Selected spectroscopic data* for **5**: MS (ES) *m/z* 1034.2 ($M^{+\cdot}$); UV–VIS (CH_2Cl_2) λ_{max}/nm 427, 548, 583; δ_H(200 MHz, $CDCl_3$) 9.03 and 8.99 (2s, 8H), 4.59 (d, 4H, *J* 9.3 Hz), 4.06 (m, 4H), 3.75 (m, 4H), 2.66 (d, 4H, *J* 9.3 Hz), 2.14 and 1.88 (2s, 24H), 1.83 (s, 12 H), 0.67 (s, 12H).

1 Y. Le Mest, M. L'Her, J. Courtot-Coupez, J. P. Collman, E. R. Evitt and C. S. Bencosme, *J. Chem. Soc., Chem. Commun.*, 1983, 1286; M. J. Crossley, T. W. Hambley, L. G. Mackay, A. C. Try and R. Walton, *Chem. Commun.*, 1995, 1077; T. Hayashi, M. Nonoguchi, T. Aya and H. Ogoshi, *Tetrahedron Lett.*, 1997, **38**, 1603; A. Vidal-Ferran, N. Bampos and J. K. M. Sanders, *Inorg. Chem.*, 1997, **36**, 6117; M. Ikeda, S. Shinkai and A. Osuka, *Chem. Commun.*, 2000, 1047; M. Sirish and H.-J. Schneider, *J. Am. Chem. Soc.*, 2000, **122**, 5881; D. Sun, F. S. Tham, C. A. Reed, L. Chaker, M. Burgess and P. D. W. Boyd, *J. Am. Chem. Soc.*, 2000, **122**, 10 704; J. Brettar, J.- P. Gisselbrecht, M. Gross and N. Solladié, *Chem. Commun.*, 2001, 733.

2 M. Mazzanti, J.-C. Marchon, M. Shang, W. R. Scheidt, S. Jia and J. A. Shelnutt, *J. Am. Chem. Soc.*, 1997, **119**, 12 400.

3 P. E. Pfeffer and L. S. Silbert, *J. Org. Chem.*, 1976, **41**, 1373.

4 R. W. Wagner, T. E. Johnson and J. N. Lindsey, *Tetrahedron*, 1997, **53**, 6755.

5 C. Pérollier, M. Mazzanti, J.- P. Simonato, F. Launay, R. Ramasseul and J.-C. Marchon, *Eur. J. Org. Chem.*, 2000, 583.

6 *Crystal data* for **4**: $C_{60}H_{72}N_4O_8Zn{\cdot}1.5CHCl3$, M = 1221.64, triclinic space group $P\bar{1}$, a = 14.1554(17), b = 14.795(3), c = 16.406(3) Å, α = 84.311(14), β = 77.063(10), γ = 65.296(10)°, V = 3042.2(8) Å^3, T = 193 K, Z = 2, μ(Mo-Kα) = 0.658 mm^{-1}, 11 286 independent reflections (R_{int} = 0.0297) which were used in all calculations. The final R was 0.0565, the final $wR(F^2)$ was 0.1425 [$I > 2\sigma(I)$]. For **5**: $C_{60}H_{72}N_4O_8Ni{\cdot}0.25CH_3CN{\cdot}H_2O$, M = 1064.21, monoclinic, space group $P2_1$, a = 16.8288(8), b = 19.5869(9), c = 20.0979(9) Å, β = 110.3270(10)°, V = 6212.2(5) Å^3, Z = 4, μ(Mo-Kα) = 0.366 mm^{-1}, 17 805 independent reflections (R_{int} = 0.0490) which were used in all calculations. The final R was 0.0637, the final $wR(F^2)$ was 0.1649 [$I > 2\sigma(I)$]. CCDC reference numbers 167256 and 167257. See http://www.rsc.org/suppdata/cc/b1/b104715a/ for crystallographic data in CIF or other electronic format.

7 W. R. Scheidt and Y. J. Lee, *Struct. Bonding (Berlin)*, 1987, **64**, 1; W. Jentzen, M. C. Simpson, J. D. Hobbs, X. Song, T. Ema, N. Y. Nelson, C. J. Medforth, K. M. Smith, M. Veyrat, M. Mazzanti, R. Ramasseul, J.-C. Marchon, T. Takeuchi, W. A. Goddard III and J. A. Shelnutt, *J. Am. Chem. Soc.*, 1995, **117**, 11 085.

8 M. Veyrat, R. Ramasseul, I. Turowska-Tyrk, W. R. Scheidt, M. Autret, K. M. Kadish and J.-C. Marchon, *Inorg. Chem.*, 1999, **38**, 1772.

9 G. N. La Mar and F. A. Walker, in *The Porphyrins*, ed. D. Dolphin, Academic Press, New York, 1978, vol. 4, ch. 2, pp. 129–135.

10 S. L. Jia, W. Jentzen, M. Shang, X. Z. Song, J. G. Ma, W. R. Scheidt and J. A. Shelnutt, *Inorg. Chem.*, 1998, **37**, 4402.

11 T. La, R. A. Richards, R. S. Lu, R. Bau and G. M. Miskelly, *Inorg. Chem.*, 1995, **34**, 5632; K. Ozette, P. Leduc, M. Palacio, J. F. Bartoli, K. M. Barkigia, J. Fajer, P. Battioni and D. Mansuy, *J. Am. Chem. Soc.*, 1997, **119**, 6442.

12 H. Duval, V. Bulach, J. Fischer and R. Weiss, *Inorg. Chem.*, 1999, **38**, 5495; W. R. Scheidt, in *The Porphyrin Handbook*, ed. K. M. Kadish, K. Smith, R. Guilard, Academic Press, San Diego, CA and Burlington, MA, 1999, vol. 3, ch. 16.

CHEMCOMM Communication
www.rsc.org/chemcomm

Local ordering of hydroxy groups in hydroxyapatite

N. H. de Leeuw

Department of Chemistry, University of Reading, Whiteknights, Reading, UK RG6 5XE. E-mail: n.h.deleeuw@reading.ac.uk

Received (in Cambridge, UK) 4th June 2001, Accepted 11th July 2001
First published as an Advance Article on the web 7th August 2001

Density functional theory calculations of hydroxyapatite identified the oxygen and hydrogen positions of the hydroxy groups in the crystal structure to be well defined, alternating in a column in the *c*-direction, and we predict that the experimentally found oxygen and hydrogen disorder is due to the presence in the crystal of differently oriented locally ordered domains, a finding which is important for studies of crystal growth and surface reactivity.

Apatites $Ca_{10}(PO_4)_6(F,Cl,OH)_2$ are a diverse class of minerals, which are becoming increasingly important as likely candidates for use as biomaterials. They are the most abundant phosphorus-bearing minerals and are found extensively in igneous, metamorphic and sedimentary rocks, mainly in the form of fluor- or chlor-apatite.[1] More recently, hydroxyapatite has increased its prominence due to its biological role as one of the main constituents of mammalian bones and teeth enamel.[2] As such, hydroxyapatite may be immensely valuable in the manufacture of artificial bones, while another possible application is to use ceramic implants as a support for the crystallisation and layer growth of hydroxyapatite, which can then bond to living bone, aiding the acceptance by the body of the implant material. It is necessary for the success of these and other applications, such as the replacement of the hydroxy groups by fluorine ions to strengthen tooth enamel and prevent caries,[3] that we obtain a detailed knowledge of the structure of hydroxyapatite. Although crystallographic studies of the mineral have elucidated the locations of the heavier atoms in the hexagonal crystal structure,[4,5] the oxygen and hydrogen ions of the hydroxy groups are found to be disordered, each partially occupying two possible sites, and little is known about the hydroxy group environment in the crystal structure, *e.g.* whether the constituent atoms are completely disordered over the positions or whether there is local ordering of the groups within domains. It is important for the investigation of hydroxyapatite surfaces, *i.e.* in studies of crystal growth, interfacial bone/ceramic behaviour and interactions between natural bone material and organic matrices, that we have a good understanding of the sites and interactions of the hydroxy groups within the apatite crystal.

Computational methods are well placed to calculate at the atomic level the geometry and relative energies of the various possible hydrogen locations in apatite, investigations which are at present inaccessible with experimental techniques. The approach we have used is to employ quantum mechanical calculations based on density functional theory (DFT) to study the hydroxy groups in hydroxyapatite. The DFT methodology, often used within the generalized gradient approximation (GGA) and employing pseudo-potentials, is well established and has been successfully applied to the study of structural and electronic properties of complex materials, *e.g.* magnesium silicates[6] and microporous aluminium phosphates.[7] The VASP program[8–10] was employed to calculate the structure and total energies of a number of hydroxyapatite structures with different configurations for the hydroxy groups. We used a cut-off for the planewave energy of 500 eV, together with a $2 \times 2 \times 2$ k-point mesh, which led to a convergence of the total energy to within 0.01%.

Although a monoclinic form of hydroxyapatite is known, biological and synthetic hydroxyapatite has a hexagonal crystal structure with space group $C6_3/m$ and $a = b = 9.432$, $c = 6.881$ Å, $\alpha = \beta = 90$, $\gamma = 120°$.[1,2] After full electronic and ionic optimisation, the structure with the lowest energy configuration of the hydroxy groups relaxed to $a = b = 9.563$, $c = 6.832$ Å, $\alpha = \beta = 90$, $\gamma = 120°$, in excellent agreement with the experiment (discrepancy $\leqslant$1.5%). The F^- or OH^- ions in apatite structures are located one above each other in a column parallel to the *c*-axis (into the paper in Fig. 1), where the F^- ions in fluorapatite are located at a crystallographic symmetry position (0, 0, 0.25), while the hydroxy groups in hydroxyapatite are located either above or below the symmetry position in the *c*-direction (oxygen at 0, 0, 0.2008, hydrogen at 0, 0, 0.0617). The deviation of the hydroxy group away from the symmetry position, leading to four possible locations in the unit cell, on either side of two symmetry positions, causes disorder of the oxygen and hydrogen ions. In this work, we investigated whether the occupancy of the oxygen and hydrogen sites is likely to be completely random or whether we could identify local ordering in domains. To this end, we calculated four possible configurations for the oxygen and hydrogen ions in hydroxyapatite, shown in Table 1, where for clarity the (Cartesian) symmetry positions are identified together with the hydroxy group positions above and below the symmetry position in the *c*-direction. Table 1 further shows which of the oxygen and hydrogen positions are occupied in the different calculations with their final coordinates in the *c*-direction, where the unit cell shown is periodically repeated in three dimensions. In configuration 1, both hydroxy groups are located at the two sites corresponding to one symmetry position, while configurations 2 and 3 have the hydroxy groups located at sites corresponding to both symmetry positions. In configuration 2, all hydroxy groups are lined up with the hydrogen and oxygen ions alternating along the *c*-axis, whereby each OH^- group forms one O–H bond of 0.957 Å and one rather long O···H hydrogen bond of 2.483 Å, while configuration 3 forms a column of pairs of OH^- groups, with the hydrogen ions pointing towards each other at a separation of only 0.849 Å and an O···O separation of 4.117 Å. Finally, in configuration 4 we investigated whether the oxygen and hydrogen ions of hydroxy groups were likely to be found separated in the apatite structure, by splitting up one OH^- group into its constituent atoms, whereby the hydrogen atom of the remaining hydroxy group

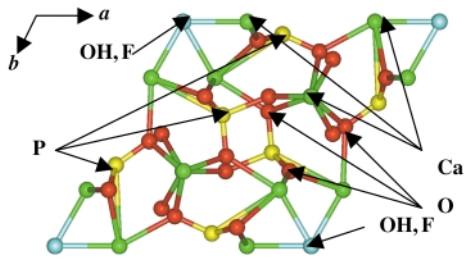

Fig. 1 Structure of the hexagonal apatite unit cell, showing the position of the fluoride or hydroxy anions in the *c*-direction into the plane of the paper [O = red, Ca = green, P = yellow, F(OH) = pale blue].

 DOI: 10.1039/b104850n

Table 1 The experimental and calculated Cartesian coordinates (*c*-direction) of four different hydroxy group configurations in the hydroxyapatite structure, together with the calculated total energies

Symmetry position		Hydroxy sites		Configuration 1		Configuration 2		Configuration 3		Configuration 4	
F	1.720	H(1)	0.425	H(1)	—	H(1)	0.456			H(1)	0.520
		O(1)	1.382	O(1)	—	O(1)	1.453				
		O(2)	2.059	O(2)	—			O(2)	1.728	O(2)	1.518
		H(2)	3.016	H(2)	—			H(2)	2.722		
F	5.160	H(3)	3.865			H(3)	3.873	H(3)	4.146	H(3)	3.853
		O(3)	4.822			O(3)	4.871	O(3)	5.140	O(3)	4.851
		O(4)	5.499								
		H(4)	6.456								
Total energy/eV				Not converged		−311.171		−310.740		−311.175	

can form a hydrogen bond to the separated oxygen atom at 1.806 Å, while the separated hydrogen is in a position to form one short and one long hydrogen bond with the oxygen atoms at 1.634 and 2.483 Å.

After electronic and ionic relaxation, the total energies of the structures are compared (Table 1). We find that starting configuration 1, where two hydroxy groups were located either side of a single symmetry position, did not lead to a stable structure. Configuration 3 led to a stable structure, but the positions of the hydroxy groups had shifted away from the experimental locations by about 0.3 Å to the positions shown in Table 1, due to repulsion between the two neighbouring hydrogen ions, which leads to an increase in the distance between the hydroxy groups of 0.65 Å. The structure has somewhat expanded from the experimental structure in the *a* and *b* directions to $a = b = 9.551$ Å and contracted in the *c*-direction, $c = 6.868$ Å. Configurations 2 and 4 are the most stable structures, with practically identical energies ($\Delta E < 0.4$ kJ mol^{-1}). On inspection of Table 1, we see that the hydrogen and oxygen ions in configuration 2 remain virtually at their initial positions with lengthening of the O–H bond lengths from 0.957 to 0.998 Å. The *a* and *b* vectors increase to $a = b = 9.564$ Å, but contraction occurs again in the *c*-direction, $c = 6.831$ Å, which causes the apparent shift of the oxygen and hydrogen ions away from their initial position. In configuration 4 ($a = b = 9.563$, $c = 6.832$ Å), the dissociated hydroxy group in the initial structure has recombined upon geometry optimisation, and is located at the same site as in configuration 2, with a final O–H bond length of 0.998 Å, forming a series of hydrogen-bonded interactions down the *c*-axis at alternating O···H distances of 2.335 and 2.500 Å. If we compare these hydrogen bonds to configuration 2 (Fig. 2), where we find all O···H interactions down the *c*-axis at 2.42 Å, it is clear that configuration 2 is a more regular structure even though energetically identical. Contour plots of the electron density in the plane of the hydroxy groups (Fig. 2) show that the O–H bond has covalent character, but bonding of its oxygen atom to neighbouring calcium ions is fully ionic, as is the interaction between calcium ions and the oxygen atoms of the phosphate groups. Bonding within the phosphate groups is found to be covalent in character, in agreement with quantum chemical calculations of aluminium phosphates.[11]

Our calculations of different possible configurations of hydroxy groups within the hydroxyapatite structure have shown that there is a preferred arrangement of the hydroxy groups, where the energetically most favourable configurations (2 and 4) have all OH$^-$ groups lined up with oxygen and hydrogen ions alternating in a column parallel to the *c*-axis (Fig. 2). These columns of aligned OH$^-$ groups can of course be found in two directions, either up or down the *c*-axis, and hence we predict that the hydroxyapatite structure will consist of local domains of these well-ordered OH$^-$ columns. When the OH$^-$ groups have

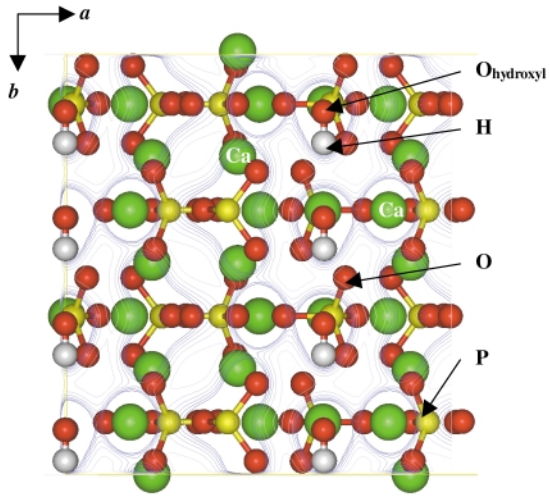

Fig. 2 Relaxed apatite crystal with OH$^-$ configuration 2, showing electron density contour plots in blue (O = red, Ca = green, P = yellow, H = white, contour levels from 0.05 to 0.30 e Å^{-3} at 0.05 e Å^{-3} intervals).

neighbouring oxygen ions (configuration 1) the structure is not stable, while introducing a pair of hydroxy groups with hydrogen ions in neighbouring positions (configuration 3) costs approximately 42 kJ mol^{-1} (0.436 eV/OH pair). A change in the ordering of the hydroxy groups within columns is therefore not energetically impossible, and may be promoted by the presence of anionic impurities such as F$^-$.

N. H. d L. thanks the Mineral Physics and Materials Consortia for provision of computer time on the Cray T3E.

Notes and references

1 W. A. Deer, R. A. Howie and J. Zussman, *An introduction to the rock-forming minerals*, Longman, UK, 1992.
2 T. S. B. Narasaraju and D. E. Phebe, *J. Mater. Sci.*, 1996, **31**, 1.
3 A. Knappwost, *Angew. Chem.*, 1956, **68**, 371.
4 A. S. Posner, A. Perloff and A. F. Diorio, *Acta Crystallogr.*, 1958, **11**, 308.
5 M. I. Kay, R. A. Young and A. S. Posner, *Nature*, 1964, **204**, 1050.
6 J. P. Brodholt and K. Refson, *J. Geophys. Res. [Solid Earth]*, 2000, **105**, 18 977.
7 C. R. A. Catlow, F. Cora and A. A. Sokol, *Comput. Mater. Sci.*, 2000, **17**, 312.
8 G. Kresse and J. Hafner, *Phys. Rev. B*, 1993, **47**, 558; G. Kresse and J. Hafner, *Phys. Rev. B*, 1994, **49**, 14 251.
9 G. Kresse and J. Furthmüller, *Comput. Mater. Sci.*, 1996, **6**, 15.
10 G. Kresse and J. Furthmüller, *Phys. Rev. B*, 1996, **54**, 11 169.
11 F. Cora, C. R. A. Catlow and A. d'Ercole, *J. Mol. Catal. A: Chem.*, 2001, **166**, 87.

CHEMCOMM
Communication
www.rsc.org/chemcomm

$Cs_{1-x}Sn_{1-x}Bi_{9+x}Se_{15}$ and $Cs_{1.5-3x}Bi_{9.5+x}Se_{15}$: members of the homologous superseries $A_m[M_{1+l}Se_{2+l}]_{2m}[M_{1+2l+n}Se_{3+3l+n}]$ (A = alkali metal, M = Sn and Bi) allowing structural evolution in three different dimensions

Antje Mrotzek, Lykourgos Iordanidis and Mercouri G. Kanatzidis*

Department of Chemistry and Center for Fundamental Materials Research, Michigan State University, East Lansing, MI 48824, USA. E-mail: kanatzid@cem.msu.edu

Received (in Cambridge, UK) 21st March 2001, Accepted 13th June 2001
First published as an Advance Article on the web 16th August 2001

$Cs_{1-x}Sn_{1-x}Bi_{9+x}Se_{15}$ and $Cs_{1.5-3x}Bi_{9.5+x}Se_{15}$ crystallize in a new structure type which does not belong to but is closely related to the members of the homologous series $A_m[M_6Se_8]_m[M_{5+n}Se_{9+n}]$; the new phases reveal a third dimension of structural evolution for this series according to the formula $A_m[M_{1+l}Se_{2+l}]_{2m}[M_{1+2l+n}Se_{3+3l+n}]$.

Recent efforts[1] in our laboratory aimed at defining new chemical concepts[2] identified the grand homologous series of phases $A_m[M_6Se_8]_m[M_{5+n}Se_{9+n}]$ (A = alkali metal, M = heavy group IV or V element). Members of this series include β-$K_2Bi_8Se_{13}$,[3] $K_{2.5}Bi_{8.5}Se_{14}$,[4] $K_{1+x}Sn_{4-2x}Bi_{7+x}Se_{15}$,[5] $K_{1-x}Sn_{4-x}Bi_{11+x}Se_{21}$[6] and $K_{1-x}Sn_{5-x}Bi_{11+x}Se_{22}$,[7] which exhibit a close structural and compositional relationship. This homology has predictive properties leading to charge-balanced hypothetical members that can be easily generated by the general formula. In fact, the following members of this series, $K_{1+x}Sn_{3-2x}Bi_{7+x}Se_{14}$,[8] $K_{1-x}Sn_{3-x}Bi_{11+x}Se_{20}$,[8] and $K_{1-x}Sn_{9-x}Bi_{11+x}Se_{26}$,[9] have been successfully targeted for synthesis *after* their compositions and structures had been predicted. The construction of each member of the homologous series is modular and assembled by two different modules, $[M_{5+n}Se_{9+n}]$ ($NaCl^{111}$-type) and $[M_6Se_8]_m$ ($NaCl^{100}$-type)[10] of variable dimensions defined by *n* and *m*, which are linked to an anionic framework with tunnels that accommodate the alkali ions (A_m). The terminology of 'homologous series' was given by Magnèli[11] to characterize chemical series that are expressed by general formulae and built on common structural principles, that are found in transition metal oxides.[12] The Aurivillius phases $Bi_2A_{n-1}B_nO_{3n+3}$ (A = Na, K, Ca, Sr, Ba, Pb. Ln, Bi, U, Th *etc* and B = Fe, Cr, Ga, Ti, Zr, Nb, Ta, Mo, W *etc.*)[13] and the Jacobson–Dion phases $A[A'_{n-1}B_nO_{3n+1}]$ (A = Li, Na, K, Rb, Cs, Tl, NH_4; A′ = Ca, Nd, B = Nb)[14] are examples of known homologous series in solid state chemistry. The structures of the lamellar oxides are related to the rutile and perovskite type, where the integer *n* determines the thickness of the slabs.

In contrast to these homologies which evolve in only one dimension, the above mentioned series presents two integers *n* and *m* that can be changed independently and therefore cause evolution of the structure in two different dimensions. While the thickness of the $NaCl^{100}$-type units is controlled by *m*, the shape of the $NaCl^{111}$-type units is induced by *n*. Interestingly, the width of the $NaCl^{100}$-type modules in $A_m[M_6Se_8]_m[M_{5+n}Se_{9+n}]$ is constant for all members. Here we report $Cs_{1-x}Bi_{9+x}Se_{15}$ and its isostructural ternary analog, $Cs_{1.5-3x}Bi_{9.5+x}Se_{15}$, both revealing a novel structure type that is closely related to the known members of the grand homologous series but are not members themselves because they differ in the *width* of the $NaCl^{100}$-type modules. In fact, $Cs_{1-x}Sn_{1-x}Bi_{9+x}Se_{15}$ represents structural evolution of the series in a *third* dimension. Therefore the general formula has to be expanded to the superseries $A_m[M_{1+l}Se_{2+l}]_{2m}[M_{1+2l+n}Se_{3+3/+n}]$ where now the additional integer *l* determines the width of the building modules. The mineral cannizzarite, $Pb_{46}Bi_{54}S_{127}$, represents one end member of this new homologous series with $l = \infty$, $m = 1$ and $n = 5$. $Cs_{1-x}Sn_{1-x}Bi_{9+x}Se_{15}$ shows the same motif of assembling the fundamental building units that is found for the members of the homologous series (now a sub-series) we described earlier. Therefore we had to introduce a third integer to account for the structural evolution by changing the width of the $NaCl^{100}$- and $NaCl^{111}$-type units. In order to achieve the next step of the evolutionary ladder in this new direction two MSe equivalents and one M_2Se_3 have to be added. For $l = 2$ this formula is reduced to $A_m[M_6Se_8]_m[M_{5+n}Se_{9+n}]$. This homologous superseries predicts the structure and composition of countless compounds by modifying the three independent integers *l*, *m* and *n*. Fig. 1 depicts the different ways the structure can develop. $Cs_{1-x}Sn_{3-x}Bi_{11+x}Se_{20}$ ($l = 2$, $m = 1$, $n = 3$) evolves by changing only one integer at a time leading to $Cs_{1-x}Sn_{1-x}Bi_{9+x}Se_{15}$ ($l = 1$, $m = 1$, $n = 3$), $Cs_{1+x}Sn_{3-2x}Bi_{7+x}Se_{14}$ ($l = 2$, $m = 2$, $n = 3$) and $Cs_{1-x}Sn_{9-x}Bi_{11+x}Se_{26}$ ($l = 2$, $m = 1$, $n = 9$). It will be interesting to attempt to prepare further compounds that can be predicted, for example $CsSn_7Bi_9Se_{21}$ ($l = 1$, $m = 1$, $n = 9$),

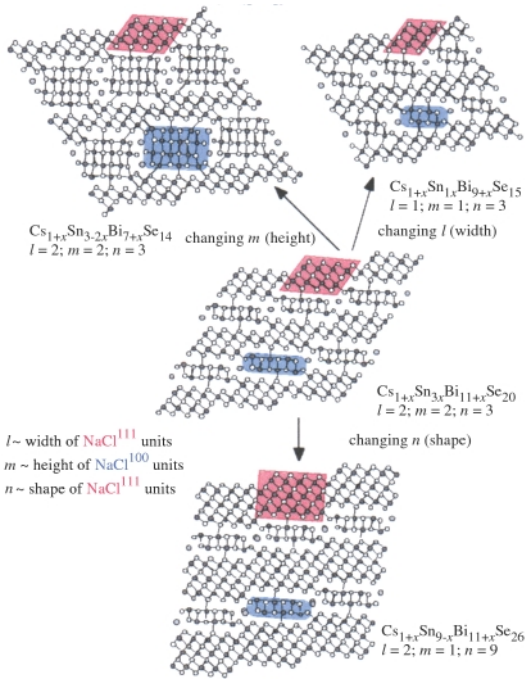

Fig. 1 Structural evolution of the homologous superseries $A_m[M_{1+l}Se_{2+l}]_{2m}[M_{1+2l+n}Se_{3+3l+n}]$ (A = alkali metal, M = heavy group IV or V element) in three different dimensions by varying the independent integers *l*, *m* and *n*. The $NaCl^{111}$-type units are highlighted in red and the $NaCl^{100}$-type units in blue. Small white spheres: Se, large light-gray spheres: A medium-gray spheres: M.

 DOI: 10.1039/b103870m

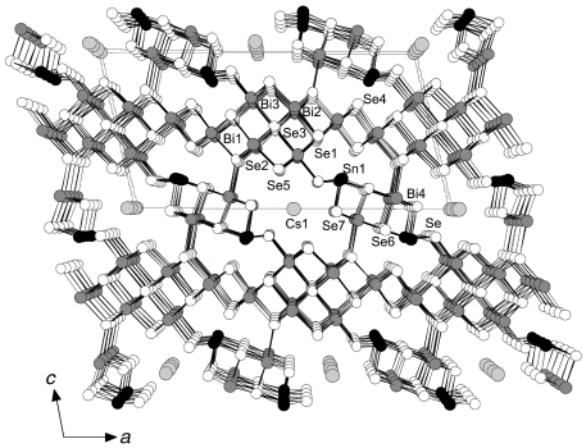

Fig. 2 Projection of the structure of $Cs_{0.65}Sn_{0.65}Bi_{8.35}Se_{15}$ with atom labeling. The tunnels in the anionic framework accommodate the Cs ions in distorted tri-capped trigonal prismatic sites. In $Cs_{1.5-3x}Bi_{9+x}Se_{15}$ the Sn1 site is occupied by Cs and Bi.

$Cs_2Sn_2Bi_{12}Se_{21}$ (l = 1, m = 2, n = 3) and $CsSn_6Bi_{12}Se_{25}$ (l = 3, m = 1, n = 3).

$Cs_{1-x}Sn_{1-x}Bi_{9+x}Se_{15}$ was prepared involving Cs_2Se, Bi_2Se_3, Sn and Se (ratio 1 : 2 : 11 : 2) in a sealed evacuated carbon coated quartz ampoule. The tube was heated within 24 h to 800 °C and kept at this temperature for 24 h, followed by slow cooling to 400 °C at a rate of 0.1 °C min^{-1} and then to 50 °C in 10 h resulting in a silver, shiny, polycrystalline ingot of $Cs_{1-x}Sn_{1-x}Bi_{9+x}Se_{15}$ as the major phase with $Cs_{1-x}Sn_{3-x}Bi_{11+x}Se_{20}$ as impurity (about 10%). EDS analyses of selected needles gave the average composition $Cs_{1.1}Sn_{0.9}Bi_{9.3}Se_{15}$. The ternary phase $Cs_{1.5-3x}Bi_{9.5+x}Se_{15}$ was obtained as follows. A mixture of 0.040 g (0.116 mmol) Cs_2Se and 0.380 g (0.580 mmol) was transferred to a silica tube which was flame-sealed under vacuum. The tube was placed under the flame of a natural gas-oxygen torch until the mixture melted and then was removed from the flame and let to solidify. The product consisted of a silvery chunk with needles growing across its surface. $Cs_{1.5-3x}Bi_{9.5+x}Se_{15}$ is the main phase with $CsBi_{3.67}Se_6$[15] as a minor phase as evidenced by X-ray powder diffraction.

The isostructural $Cs_{1.5-3x}Bi_{9.5+x}Se_{15}$ and $Cs_{1-x}Sn_{1-x}Bi_{9+x}Se_{15}$ crystallize in a new structure type as expected from $A_m[M_{1+l}Se_{2+l}]_{2m}[M_{1+2l+n}Se_{3+3l+n}$.[16] The crystal structure is shown in Fig. 2. Similar to the known members of the homologous series (l = 2) the structure is assembled by two distinct building units of the $NaCl^{111}$-type and $NaCl^{100}$-type, respectively, forming a three-dimensional anionic framework with tunnels running along the b axis which are filled by Cs ions. In $Cs_{1-x}Sn_{1-x}Bi_{9+x}Se_{15}$ three $BiSe_6$ octahedra wide and two octahedra thick fragments of the $NaCl^{111}$-type form a step-shaped layer by two adjacent units sharing an octahedra face. The distorted 3 + 3 coordination of Bi with interatomic distances in the range 2.74–3.07 Å is caused by the lone pair of Bi. In contrast to $A_{1-x}M_{3-x}Bi_{11+x}Se_{20}$ which shows the same linkage of the $NaCl^{111}$-type units to a step-shaped layer, the units in $Cs_{1-x}Bi_{9+x}Se_{15}$ represent a narrower cut out of a Bi_2Se_3-layer. In order to adjust to the narrower $NaCl^{111}$-type $[M_6Se_9]$ blocks in $Cs_{1-x}Sn_{1-x}Bi_{9+x}Se_{15}$ the $NaCl^{100}$-type $[M_4Se_6]$ units are shorter as well. They are two $(Bi,Sn)Se_6$ octahedra wide parallel to the direction of the $NaCl^{111}$-type layers and one octahedron high perpendicular to this direction while these units are three octahedra wide in $A_{1-x}Sn_{3-x}Bi_{11+x}Se_{20}$. M–Se interactions between the $NaCl^{100}$-type blocks and the stepped-shaped $NaCl^{111}$-type layers cause the formation of a three-dimensional anionic framework with tunnels along the b-direction that accommodate the Cs ions. Besides positional disorder a high thermal displacement parameter indicates possible 'rattling' of Cs ions in their partly occupied sites.

Preliminary charge transport measurements on polycrystalline ingots of $Cs_{1-x}Sn_{1-x}Bi_{9+x}Se_{15}$ reveal moderate electrical conductivity (370 S cm^{-1}) and Seebeck coefficient (−70 μV K^{-1}) at room temperature. The negative sign indicates electrons as the main charge carriers. The compound is a narrow gap n-type semiconductor with a band gap of *ca.* 0.53 eV.

In summary, $Cs_{1-x}Sn_{1-x}Bi_{9+x}Se_{15}$ and $Cs_{1.5-3x}Bi_{9.5+x}Se_{15}$ help reveal a new superseries $A_m[M_{1+l}Se_{2+l}]_{2m}[M_{1+2l+n}Se_{3+3l+n}]$ that presents three different and independent compositional variables. The new integer l controls the width of both building units, while the shape of the $NaCl^{111}$-type block is given by n and the thickness of the $NaCl^{100}$-type fragment by m. According to our results the systems A/M/Bi/Se, M = Sn, Pb, seems to be *infinitely adaptive*[17] and the identification of this broad series will permit considerable control in the design of new compounds based on phase homologies.

Financial support from the Office of Naval Research (Grant No. N00014-98-1-0443) and the Deutsche Forschungsgemeinschaft is gratefully acknowledged.

Notes and references

1 M. G. Kanatzidis, *Semicond. Semimet.*, 2001, **69**, 51.
2 G. A. Slack, in *CRC Handbook of Thermoelectrics*, ed. D. M. Rose, CRC Press, Boca Raton, FL, 1995, p. 407.
3 M. G. Kanatzidis, D.-Y. Chung, L. Iordanidis, K.-S. Choi, P. Brazis, M. Rocci, T. Hogan and C. R. Kannewurf, *Mater. Res. Soc. Symp. Proc.*, 1998, **545**, 233.
4 D.-Y. Chung, K.-S. Choi, L. Iordanidis, J. L. Schindler, P. W. Brazis, C. R. Kannewurf, B. Chen, S. Hu, C. Uher and M. G. Kanatzidis, *Chem. Mater.*, 1997, **9**, 3060.
5 K.-S. Choi, D.-Y. Chung, A. Mrotzek, P. W. Brazis, C. R. Kannewurf, C. Uher, W. Chen, T. Hogan and M. G. Kanatzidis, *Chem. Mater.*, 2001, **13**, 756.
6 A. Mrotzek, D.-Y. Chung, N. Ghelani, T. Hogan and M. G. Kanatzidis, *Chem. Eur. J.*, 2001, **7**, 1915.
7 A. Mrotzek, D.-Y. Chung, T. Hogan and M. G. Kanatzidis, *J. Mater. Chem.*, 2000, **10**, 1667.
8 A. Mrotzek, L. Iordanidis and M. G. Kanatzidis, *Inorg. Chem.*, in press.
9 A. Mrotzek and M. G. Kanatzidis, submitted.
10 $NaCl^{111}$ is meant to indicate that this fragment derives from a section of the NaCl lattice perpendicular to the (111) direction. $NaCl^{100}$ refers to a section of the NaCl lattice perpendicular to the (100) direction. In previous publications,[6–8] we addressed the ($NaCl^{111}$) and ($NaCl^{100}$) fragments as Bi_2Te_3-type and NaCl-type, respectively. We now realize this is inadequate for large values of n as for $K_{1-x}Sn_{9-x}Bi_{11+x}Se_{26}$.
11 A. Magnèli, *Acta Crystallogr.*, 1953, **6**, 495.
12 S. Andersson, A. Sundholm and A. Magnèli, *Acta Chem. Scand.*, 1959, **13**, 989.
13 B. Aurivillius, *Ark. Kemi*, 1949, **1**, 463; B. Frit and J. P. Mercurio, *J. Alloys Compd.*, 1992, **188**, 27.
14 M. Dion, M. Ganne and M. Tournoux, *Mater. Res. Bull.*, 1981, **16**, 1429; M. Dion, M. Ganne, M. Tournoux and J. Ravez, *Rev. Chim. Miner.*, 1984, **21**, 92; A. J. Jacobson, J. W. Johnson and J. T. Lewandowski, *Inorg. Chem.*, 1985, **24**, 3727.
15 L. Iordanidis, P. W. Bravis, T. Kyratsi, J. Ireland, M. Lane, C. R. Kannewurf, J. S. Dyck, C. Uher, N. A. Ghelani, T. Hogan and M. G. Kanatzidis, *Chem. Mater.*, 2001, **13**, 622.
16 *Crystal data* (Bruker, CCD, T = 273, *173* K) for $Cs_{1-x}Sn_{1-x}Bi_{9+x}Se_{15}$ and $Cs_{1.5-3x}Bi_{9.5+x}Se_{15}$ [in italics]: M_w = 3303.18; *3344.41*, monoclinic, space group C2/*m*; a = 27.287(8); *27.547(9)*, b = 4.116(1); *4.162(1)*, c = 14.004(4); *14.132(5)* Å, β = 103.346(5); *103.350(6)*, Z = 2, λ = 0.71073 $Å^3$, D_c = 7.168, *7.046* g cm^{-3}, μ(Mo-Kα) = 72.544; *72.112* mm^{-1}, 2020; *2087* independent reflections, unique data with $I > 2\sigma(I)$, 1531; *1735*, $R1$ = 0.0403; *0.0524*, $wR2$ = 0.0911; *0.1423*, number of variables 84; *88*. Structure solved and refined using the SHELXTL-Plus program suite. Crystal dimensions 0.06 × 0.08 × 0.32; *0.10 × 0.12 × 0.25* mm. Absorption corrections were applied to the data. Both structure refinements of $Cs_{1.5-3x}Se_{15}$ and $Cs_{1-x}Sn_{1-x}Bi_{9+x}Se_{15}$ revealed unusual thermal displacement parameters for the Bi5 and Cs1 sites which introduced a disorder model with mixed Bi/Cs occupancies and mixed Bi/Sn occupancies, respectively, in the same crystallographic site for Bi5 and statistical disorder in the Cs1 site. Their occupancies were constrained to give charge balance and resulted in the formulae $Cs_{1.11}Bi_{9.63}Se_{15}$ and $Cs_{0.65}Sn_{0.65}Bi_{9.35}Se_{15}$. CCDC reference numbers 165415 and 165416. See http://www.rsc.org/suppdata/cc/b1/b103870m/ for crystallographic data in CIF or other electronic format.
17 For definition see: J. S. Anderson, *J. Chem. Soc., Dalton Trans.*, 1973, **10**, 1107; J. S. Swinnea and H. Steinfink, *J. Solid State Chem.*, 1982, **41**, 114.

CHEMCOMM
Communication
www.rsc.org/chemcomm

Heteroanionic intercalation into positively charged inorganic hosts: the first nitride mixed halides†

Amy Bowman, Pamela V. Mason and Duncan H. Gregory*

School of Chemistry, University of Nottingham, Nottingham, UK NG7 2RD.
E-mail: Duncan.Gregory@Nottingham.ac.uk

Received (in Cambridge, UK) 21st June 2001, Accepted 25th July 2001
First published as an Advance Article on the web 15th August 2001

The first nitride mixed halides have been synthesised by disordered intercalation of anions between the positively charged layers of subnitride hosts.

Intercalation reactions are used extensively in solid state chemistry not only to access new compounds or polymorphs, but also in the synthesis of a wide range of commercially important materials such as zeolites and layered transition metal oxides and sulfides. The dominating pattern in this area of chemistry is the insertion of cationic guests into neutral or ostensibly negatively charged 2D or 3D hosts. The ability to intercalate negatively charged species is restricted to a relatively small and exclusive group of host materials, of which graphite and its intercalation compounds (GICs) are well-known examples. In fact, graphite is exceptional in its capacity to act as both electron acceptor (*e.g.* C_8K) and electron donor (*e.g.* C_8Br).[1] Furthermore, the hydrotalcite group of clays are unusual examples of 2D hosts containing formally positively charged layers.[1,2]

Intercalation in nitride chemistry is relatively undeveloped and is largely limited to the insertion of lithium and other alkali metals. Most notable has been the intercalation of Li^+ into Zr(Hf)NCl to induce superconductivity at *ca* 25 K,[3] although other isolated examples exist (*e.g.* 3D insertion in the $Na_xTa_3N_5$ system).[4] One interesting aspect of nitride chemistry, however, is the propensity for compounds to form *anti*-structures; frameworks that are the antithesis of some of the most common 'normal' structures seen in oxide chemistry (*e.g. anti*-perovskites, M_3NX; *anti*-fluorites $(Li,M)_2N$ *etc.*).[5] These *anti*-structures can be exploited for new synthetic and materials chemistry. Here we report our initial investigations of mixed *anion* intercalation in subnitride hosts with layered *anti*-$CdCl_2$ structures to produce the first examples of nitride mixed halides.

Nitride halides $A_2N(X,X')$ (A = Ca, Sr; X, X′ = Cl, Br, I) were synthesised by reaction of the binary alkaline earth nitrides (Ca_3N_2, Ca_2N or Sr_2N), AX_2 and AX'_2 at elevated temperatures (typically 800–1200 °C) under anaerobic conditions. Binary nitrides were prepared first by reaction of the alkaline earth metals under nitrogen in liquid sodium solvent as described previously.[6,7] We also observed that A_2NX species spontaneously form at lower temperatures by reaction of the subnitride with halogen (*e.g.* shaking together Sr_2N and I_2) or an anhydrous transition metal halide salt (*e.g.* grinding Ca_2N and $FeCl_3$ in a mortar in an Ar-filled glove box). Both these processes begin at room temperature and are highly exothermic. The former process leads to a crystalline powder with a powder X-ray diffraction (PXD) pattern that cannot yet be indexed, the latter to microcrystalline Ca_2NCl and iron powder.

Nitride halides were initially characterised by PXD using a Philips Xpert diffractometer with Cu-Kα radiation.‡ Analysis and subsequent indexing of powder data revealed continuous solid solutions existing in the A_2N(Cl, Br) systems (A = Ca, Sr). The hexagonal *anti*-α-$NaFeO_2$ structure (filled *anti*-$CdCl_2$ structure) is retained across the entire solubility range ($A_2NCl_{1-y}Br_y$; $0 \leqslant y \leqslant 1$) with no evidence of superstructure reflections (Table 1). We see no evidence of staging or ordering in these $A_2N(X,X')$ compounds and Cl and Br statistically occupy the 3a (0,0,0) site within the van der Waals type gap of the subnitrides.

Preliminary Rietveld refinement of PXD data collected for $Sr_2NCl_{1-y}Br_y$ (y = 0, 0.33, 1) compounds using the GSAS package[7] confirms that the nitride halides crystallise in space group $R\bar{3}m$ with the *anti*-α-$NaFeO_2$ structure with Cl^- and Br^- disordered on the 3a site between $[Sr_2N]^+$ layers in the y = 0.33 compound. The Sr–N 2D ionic framework does not change dramatically as a function of intercalant concentration. Sr–N bond length increases slightly [2.618(1) to 2.626(1) Å] and $[Sr_2N]^+$ layer thickness decreases (*via* angular compression of NSr_6 octahedra) from 2.68 Å in Sr_2NCl (R_{wp} = 11.51%, R_p = 8.26%, χ^2 = 2.91) to 2.63 Å in Sr_2NBr (R_{wp} = 11.29%, R_p = 8.04%, χ^2 = 2.81). The ionic layers thus separate to accommodate the larger anion and the interlayer gap increases (from 4.31 Å in Sr_2NCl to 4.65 Å in Sr_2NBr).

A detailed structural description of the Ca_2N(Cl,Br) system was obtained by GSAS[8] refinement of time of flight (ToF) powder neutron diffraction (PND) data collected using the high intensity diffractometer POLARIS at ISIS, Rutherford Appleton Laboratory. Diffraction data were collected for $Ca_2NCl_{1-y}Br_y$ (y = 0, 0.6, 1) at 298 K and additionally at 150 and 75 K for $Ca_2NCl_{0.6}Br_{0.4}$. Full details of the refinements of these and other related compounds will be presented elsewhere. A profile plot for $Ca_2NCl_{0.6}Br_{0.4}$ data collected at 75 K is shown in Fig. 1. Ca_2NCl and Ca_2NBr crystallise with the *anti*-α-$NaFeO_2$ structure as previously reported in a single crystal X-ray diffraction study.[9] $Ca_2NCl_{0.6}Br_{0.4}$ (Fig. 2) also adopts this structure, with Cl^- and Br^- disordered on the 3a site at 298 K and there is no evidence for a phase transition to an ordered halide anion arrangement at lower temperature. The structure is one of $[Ca_2N]^+$ layers of edge sharing NCa_6 octahedra lying parallel to the *ab* plane stacked along the *z*-direction between which are inserted halide anions $(Cl,Br)^-$. This thus creates

Table 1 Lattice parameters of $A_2N(X,X')$ nitride halides from PXD data

Compound[a]	*a*/Å	*c*/Å	*V*/Å^3	*c*/*a*
Ca_2NCl	3.6678(1)	19.718(2)	229.7(1)	5.38
$Ca_2NCl_{0.833}Br_{0.167}$	3.6732(7)	19.843(4)	231.8(2)	5.40
$Ca_2NCl_{0.667}Br_{0.333}$	3.6800(3)	19.973(2)	234.2(1)	5.43
$Ca_2NCl_{0.5}Br_{0.5}$	3.6937(3)	20.179(1)	238.4(1)	5.46
$Ca_2NCl_{0.333}Br_{0.667}$	3.699(1)	20.199(8)	239.3(3)	5.46
$Ca_2NCl_{0.167}Br_{0.833}$	3.7096(8)	20.401(6)	243.1(2)	5.50
Ca_2NBr	3.7171(4)	20.547(3)	245.9(1)	5.53
$Ca_2NBr_{0.5}I_{0.5}$	3.752(1)	21.113(5)	257.4(2)	5.63
Sr_2NCl	3.8944(2)	20.991(1)	275.7(1)	5.39
$Sr_2NCl_{0.67}Br_{0.33}$	3.9052(2)	21.232(2)	280.4(1)	5.44
$Sr_2NCl_{0.5}Br_{0.5}$	3.916(1)	21.490(9)	285.4(3)	5.49
Sr_2NBr	3.9341(3)	21.853(2)	292.9(1)	5.55

[a] Nominal stoichiometry.

† Electronic supplementary information (ESI) available: OCD profile plots for data from each POLARIS detector bank. See http://www.rsc.org/suppdata/cc/b1/b105448c/

 DOI: 10.1039/b105448c

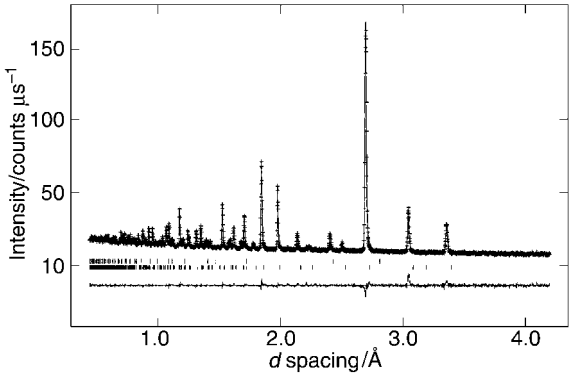

Fig. 1 Observed (crosses), calculated (solid line) and difference (below) profile plot for $Ca_2NCl_{0.6}Br_{0.4}$ PND data collected from the 90° detector bank at 75 K. Tick marks denote the major phase and CaO impurity.

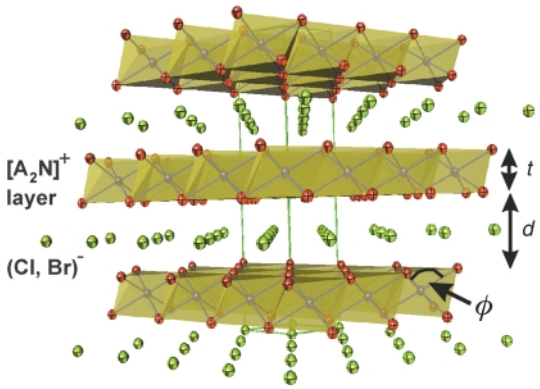

Fig. 2 Structure of $Ca_2N(X,X')$ indicating layer thickness (t), interplanar distance (d) and Ca–N–Ca angle, ϕ.

alternating edge sharing layers of NCa_6 and $(Cl,Br)Ca_6$ octahedra.

The Ca–N bond lengths in the $Ca_2NCl_{1-y}Br_y$ nitride halides are typical of the distances found in Ca containing nitrides. These are 2.4462(2), 2.4574(2) and 2.4679(2) Å for y = 0, 0.6 and 1 respectively, compared to 2.46 Å in α-Ca_3N_2 and 2.4426(4) Å in the subnitride host itself, Ca_2N.[7,10] As in the $Sr_2N(X,X')$ compounds, the $[Ca_2N]^+$ framework is fairly robust. As the average size of the anionic intercalant increases, so the $[Ca_2N]^+$ layer compresses along z through angular distortion of the N–Ca octahedra. The Ca–N–Ca angle, ϕ (see Fig. 2) increases from 97.09(1)° in Ca_2NCl to 97.77(1)° in Ca_2NBr. As a result the intralayer Ca–Ca distances increase [to 3.7187(1) Å along layers and 3.246(1) Å across layers in Ca_2NBr] but remain shorter than that in Ca metal (3.94 Å).[11] In turn the layers separate to accommodate the larger halide and Ca–X distances increase; y = 0: 2.9542(3) Å, y = 0.4: 3.0226(2) Å, y = 1: 3.0818(2) Å. The ratio of layer thickness, t, to interlayer distance, d thus changes from 0.65 in Ca_2N[7] through 0.59 (Ca_2NCl) and 0.57 ($Ca_2NCl_{0.6}Br_{0.4}$) to 0.55 in Ca_2NBr.

Whereas mixed halide compounds themselves are quite prevalent [*e.g.* $Sr(Br,I)_2$, $InBrI_2$ *etc.*][12] and disorder of multiple halides is seen in oxyhalides [*e.g.* $BaCuO_2(Br,I)$, $WOCl_3Br$],[13] these compounds are the first examples of nitride mixed halides. The $A_2N(X,X')$ nitrides are also, more generally, the first examples of heteroanionic intercalation of any sort in A_2N subnitride hosts. The $[A_2N]^+\cdot(e^-)$ formulation describing ionic layers constraining free electrons within van der Waals gaps suggests a highly reactive environment for intercalation. The potential electron donor properties of these hosts are obvious and the ready incorporation of halides at room temperature is testament to the stability of the filled structures (both relative to the hosts and to AX_2). Interestingly, despite the rigidity of the A–N framework with respect to Cl, Br and I intercalation and in contrast to many examples of cation substitution in normal structured 2D chalcogenides, reaction with smaller spherical anions (*e.g.* H^-) or non-spherical species (*e.g.* CN_2^{2-}) can lead to a collapse of A–N layers and formation of 3D structures.[14] This is in contrast however to incorporation of gold (Ca_2NAu) or diazenide (SrN) where more subtle modifications of the A_2N framework allow retention of 2D structure.[15,16]

The electronic properties of the A_2N subnitrides and their intercalates are by no means well elucidated, although the expectation is that the subnitrides are 2D metals which become more insulating (less conducting) with increased intercalation of X^- (X=H, halide). Preliminary magnetic measurements were performed on powders of Ca_2N, Ca_2NCl and Ca_2NBr using a Cryogenic S100 SQUID magnetometer in the range 4–298 K. Data show weak temperature independent paramagnetism, indicating apparently little difference in magnetic behaviour between intercalated compounds and their Pauli paramagnetic hosts. More comprehensive studies of the (de)intercalation chemistry, crystal structures, magnetic and transport properties of these and other A_2N derived nitrides will be published elsewhere.

We thank Dr R. I. Smith for assistance in collecting PND data, Dr M. O. Jones for SQUID data and Dr P. Hubberstey for useful discussions. D. H. G. would like to thank the EPSRC for the award of an Advanced Research Fellowship and for funding this work and the Nuffield Foundation for the award of an undergraduate bursary to P. V. M.

Notes and references

‡ All PND data collected at 298 K unless otherwise stated. Samples were loaded into V cans with In seals in a N_2-filled glovebox before data collection. Data were collected at 145, 90 and 35° detector banks. All compounds crystallise in hexagonal space group $R\bar{3}m$ with Z = 3, X occupying the 3a site, N the 3b site and Ca the 6c (0,0,z) site. Ca_2NCl, M = 224.3, a = 3.6665(1), c = 19.7187(2) Å, V = 229.57(1) Å^3, z(Ca) = 0.2288(1), 12645 observations, 57 parameters, R_{wp} = 2.93%, R_p = 5.65%, χ^2 = 5.89. $Ca_2N(Cl,Br)$, M = 447.2, a = 3.6937(1), c = 20.1780(2) Å, V = 238.42(1) Å^3, z(Ca) = 0.2272(1), SOF(Cl) = 0.56(1), 12847 observations, 59 parameters, R_{wp} = 2.26%, R_p = 4.24%, χ^2 = 2.88. Ca_2NBr, M = 522.23, a = 3.7186(1), c = 20.5668(1) Å, V = 246.30(1) Å^3, z(Ca) = 0.2258(1), 12011 observations, 55 parameters, R_{wp} = 2.31%, R_p = 3.58%, χ^2 = 2.76. $Ca_2N(Cl,Br)$ at 150 K, a = 3.6871(1), c = 20.1295(2) Å, V = 236.99(1) Å^3, z(Ca) = 0.2273(1), 13090 observations, 54 parameters, R_{wp} = 1.39%, R_p = 2.31%, χ^2 = 3.32. $Ca_2N(Cl,Br)$ at 75 K, a = 3.6851(1), c = 20.1130(1) Å, V = 236.54(1) Å^3, z(Ca) = 0.2273(1), 12756 observations, 57 parameters, R_{wp} = 1.43%, R_p = 2.36%, χ^2 = 3.60.

1 See, for example: *Intercalation Chemistry*, ed. M. S. Whittingham and A. J. Jacobson, Academic Press, New York 1982.
2 F. Cavani, *Catal. Today*, 1991, **11**, 173; V. Rives and M. A. Ulibarri, *Coord. Chem. Rev.*, 1999, **181**, 61.
3 S. Yamanaka, K. Hotehama and H. Kawaji, *Nature*, 1998, **392**, 580.
4 S. J. Clarke and F. J. DiSalvo, *J. Solid State Chem.*, 1997, **132**, 394.
5 M. Y. Chern, D. A. Vennos and F. J. DiSalvo, *J. Solid State Chem.*, 1992, **96**, 415; R. Juza, K. Langer and K. v. Benda, *Angew. Chem., Int. Ed. Engl.*, 1968, **7**, 360.
6 M. G. Barker, M. J. Begley, P. P. Edwards, D. H. Gregory and S. E. Smith, *J. Chem. Soc., Dalton Trans.*, 1996, 1.
7 D. H. Gregory, A. Bowman, C. F. Baker and D. P. Weston, *J. Mater. Chem.*, 2000, **10**, 1635.
8 A. C. Larson and R. B. von Dreele, *The General Structure Analysis System*, Los Alamos National Laboratories, Report LAUR 086-748, LANL, Los Alamos, NM, 1999.
9 C. Hadenfeldt and H. Herdejürgen, *Z. Anorg Allg. Chem.*, 1987, **545**, 177.
10 Y. Laurent, J. Lang and M. Th. Le Bihan, *Acta Crystallogr., Sect. B*, 1968, **24**, 494.
11 W. B. Pearson, *The Crystal Chemistry and Physics of Metals and Alloys*, Wiley-Interscience, New York, 1972.
12 S. A. Hodorowicz and H. A. Eick, *J. Solid State Chem.*, 1983, **46**, 313; R. Kniep and P. Blees, *Angew. Chem.*, 1984, **96**, 782.
13 A. Böhlke and Hk. Müller-Buschbaum, *J.Less-Common Met.*, 1990, **158**, 33; P. M. Boorman, N. N. Greenwood and H. J. Whitfield, *J. Chem. Soc. A*, 1968, 2256.
14 T. Sichla and H. Jacobs, *Eur. J. Solid State Inorg. Chem.*, 1995, **32**, 49; O. Reckeweg and F. J. DiSalvo, *Angew. Chem., Int. Ed.*, 2000, **39**, 412.
15 P. F. Henry and M. T. Weller, *Angew. Chem., Int. Ed.*, 1998, **37**, 2855.
16 G. Auffermann, Y. Prots and R. Kniep, *Angew. Chem., Int. Ed.*, 2001, **40**, 547.

CHEMCOMM
Communication
www.rsc.org/chemcomm

Self-assembly of a novel macrotricyclic Pd(II) metallocage encapsulating a nitrate ion†

Dillip K. Chand, Kumar Biradha and Makoto Fujita*

Department of Applied Chemistry, Graduate School of Engineering, Nagoya University and CREST, Japan Science and Technology Corporation (JST), Chikusaku, Nagoya 464-8603, Japan. E-mail: mfujita@apchem.nagoya-u.ac.jp

Received (in Cambridge, UK) 4th June 2001, Accepted 13th July 2001
First published as an Advance Article on the web 15th August 2001

Complexation of the ligand 1 with $Pd(NO_3)_2$ leads to the self-assembly of a very stable M_2L_4 type macrotricyclic cage that encapsulates a nitrate ion inside its cavity.

Construction of discrete and well-defined molecular architectures using organic ligands and cleverly selected metal ions through the self-assembly route has received much attention during the last decade.[1] Desired species having predetermined structural and functional properties can be obtained by simply mixing the participating components under suitable conditions.[2] The self-assembled structures formed *via* a metal-driven self-assembly path can be classified logically under M_xL_y types (where M and L denote metal ions and ligands involved, respectively) with varying values of *x* and *y*. While previously reported cage structures are mostly formulated as M_3L_2,[3] M_6L_4,[4] or M_4L_6,[5] there is a scarcity in the series of M_2L_4 type cages[6] in the literature. Atwood and coworkers have reported an early example of a M_2L_4 cage[6a] where two octahedral copper(II) ions are bridged by four units of a bidentate ligand. While all the four equatorial positions of each copper ions are coordinated with the terminal pyridyl groups of the ligand strands, the axial positions are occupied by water molecules. Dinuclear copper(II) complexes of the M_2L_4 family having twisted structures and including chloride[6c] and perchlorate[6d] anions in between the metal centers are also reported. Another analogus structure is a dinuclear Pd(II) cage,[6b] with inclusion of hexafluorophosphate ion inside the cavity. However, in none of the cases the complexation reaction leading to the cage was directly monitored using NMR spectroscopy unlike our study in this work. Herein, we report the self-assembly of a novel macrotricyclic

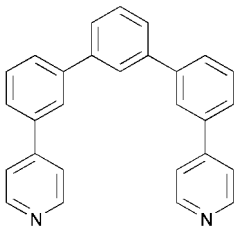

1

cage molecule from ligand **1** and $Pd(NO_3)_2$, the pivotal positions of the cage being occupied by Pd(II) ions. A nitrate ion is included inside the cavity in a cascade fashion bridging both the metal centers.

Ligand **1** was synthesized by Suzuki coupling of 1,3-bis(3-bromophenyl)benzene with 2-(4-pyridyl)-4,4,5,5-tetramethyl-1,3-dioxaborolane[7] using K_3PO_4 as base and $Pd(PPh_3)_4$ as catalyst.‡ The ligand **1** was mixed with $Pd(NO_3)_2$ at a ratio of 2:1 in DMSO and stirred at 90 °C for 1 day. Subsequently, addition of diethyl ether precipitated a pale yellow powder which was separated by filtration, washed with MeOH, and

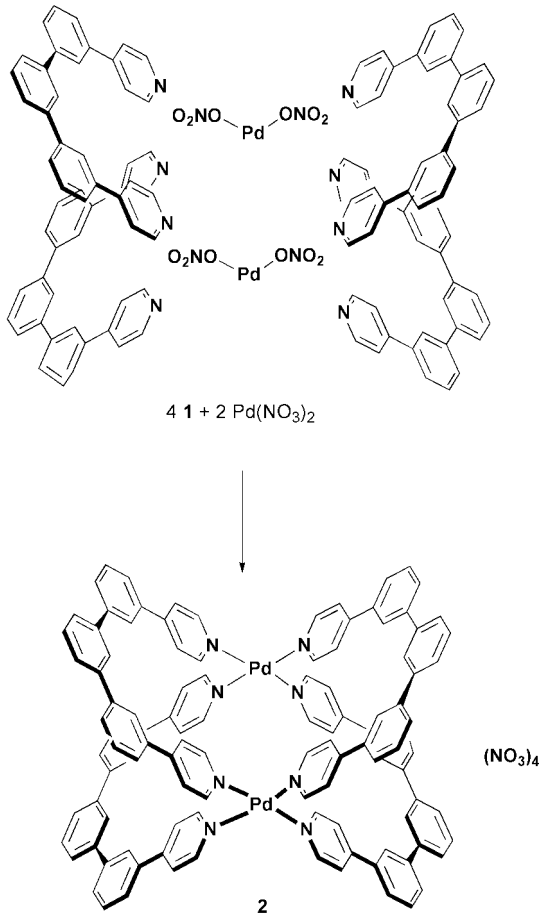

Scheme 1

dried *in vacuo* to obtain the complex $[(Pd)_2(\mathbf{1})_4(NO_3)_4]$ **2**§ as a white solid in 74% yield (Scheme 1).

Ligand **1** and complex **2** were characterised by ^1H and ^{13}C NMR. All the peaks were further completely assigned using H–H COSY and C–H COSY techniques. The signals for complex **2** as compared to ligand **1** in its proton NMR spectrum, particularly for py_α and py_β protons, were remarkably downfield shifted due to the complexation. A simple pattern of the spectrum suggests the formation of a discrete species (Fig. 1). Similarly ^{13}C NMR data also supports the assumed structure.¶ All the findings indicate that the four arms in complex **2** are equivalent and that four-fold symmetry axes pass through the metal centers in solution.

The same complexation reaction was also carried out in DMSO-d_6 and the solution was directly monitored by NMR spectroscopic means without isolating the complex. The spectrum obtained matched exactly that of the isolated complex. No peaks other than due to complex **2** were observed which establishes the quantitative self-assembly of **2**. When the metal

† Electronic supplementary information (ESI) available: Crystallography section; Figs. S1–8: ^1H, ^{13}C, H–H and C–H COSY NMR spectra for **1** and **2**. See http://www.rsc.org/suppdata/cc/b1/b104853h/

 DOI: 10.1039/b104853h

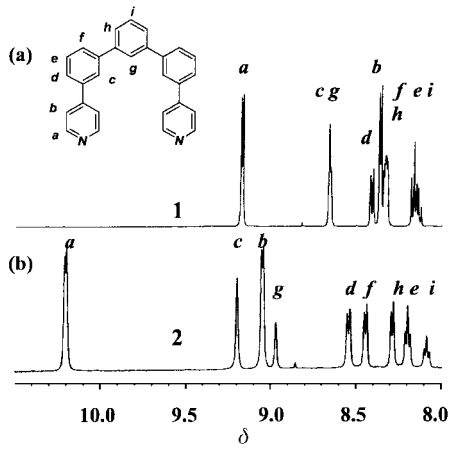

Fig. 1 ^{1}H NMR spectra of (a) ligand **1** and (b) macrotricyclic cage **2** (500 MHz, DMSO-d_6, 25 °C, TMS as an external standard).

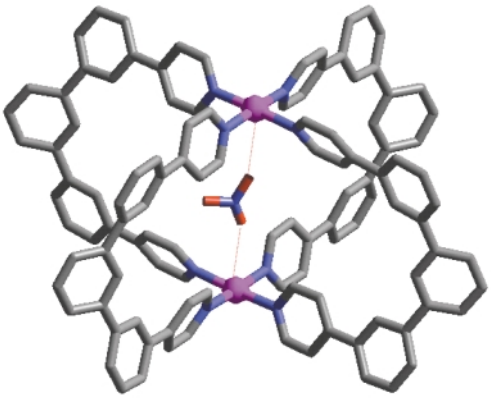

Fig. 2 Representation of $[(Pd)_2(\mathbf{1})_4(NO_3)]^{3+}$ in the crystal structure of **2** (Pd: ball mode and others: cylinder mode). The disorder of the nitrate anion is not shown. Key: palladium (magenta); nitrogen (blue); oxygen (red); carbon (gray).

salt was added in a lesser amount than the required stoichiometry for the complexation, all the signals of complex **2** were still observed, without any indication of any impurity, along with additional signals corresponding only to the uncomplexed free ligand. Also, by adding excess of the metal salt, no other new structures were suggestive from the NMR pattern. All these findings support the remarkable thermodynamic stability of **2**.

Finally, the structure of complex **2** was determined unambiguously from an X-ray diffraction study.‖ Needle-shaped crystals, suitable for X-ray diffraction analysis, were obtained in 2 days by layering diethyl ether over a solution of **2** in DMSO. A perspective view of the molecule is shown in Fig. 2. The crystal structure consists of the complexed cation $[(Pd)_2(\mathbf{1})_4(NO_3)]^{3+}$, three nitrate anions, nine DMSO and two diethyl ether molecules. Each Pd(II) has a square planar geometry with Pd–N bond distances in the range 2.024(7)–2.030(6) Å. The size of the 3-D cavity is *ca.* 11.1 × 10.2 × 8.4 Å which is defined by the arms of the rectangular array formed from four hydrogen centers, H_g (see Fig. 1 for labelling and Fig. 2 for comparison) and Pd–Pd separation. The cavity size after correcting for the van der Waals radius of the H centers is 8.7 × 7.8 × 6.0 Å . While three out of four nitrate ions stay outside of the cavity, one nitrate ion is encapsulated inside by ionic interactions, the Pd–O distance being 3.135(7) Å.

Analysis of crystal packing displayed the extension of intermolecular interactions in a linear manner, where three DMSO molecules lie in the intermolecular cavity formed in between two consecutive $[(Pd)_2(\mathbf{1})_4(NO_3)]^{3+}$ units (Fig. 3). The Pd–Pd axes of adjacent cages adopt a perpendicular geometry to each other making a hydrophobic pocket.

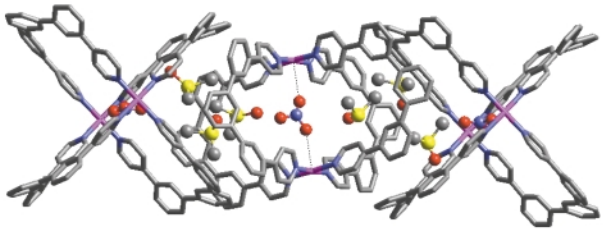

Fig. 3 Linear chain in the crystal structure of **2**. Three DMSO molecules are trapped in each of the intermolecular cavities. Key: palladium (magenta); nitrogen (blue); oxygen (red); sulfur (yellow); carbon (gray). The disorders of the nitrate anions and DMSO molecules are not shown.

D. K. C. thanks the Japan Society for the Promotion of Science (JSPS) for a postdoctoral fellowship.

Notes and references

‡ Ligand **1**: a mixture of 1,3-bis(3-bromophenyl)benzene (0.3881 g, 1.0 mmol), 2-(4-pyridyl)-4,4,5,5-tetramethyl-1,3-dioxaborolane (0.5126 g, 2.5 mmol), K_3PO_4 (0.7429 g, 3.5 mmol), and $Pd(PPh_3)_4$ (0.1155 g, 0.1 mmol), was refluxed in 1,4-dioxane (25 mL) for 2 days at 100 °C under an argon atmosphere. After usual aqueous work-up the residue was chromatographed over silica gel to obtain a white soild, which was recrystallized from methanol affording **1** as white needles in 65% yield. δ_H (500 MHz, DMSO-d_6,TMS): 9.17 (d, 4H, a), 8.66(s, 2H, c), 8.65 (s, 1H, g), 8.41(d, 2H, d), 8.36 (d, 4H, b), 8.32–8.34 (m, 4H, f & h), 8.16 (t, 2H, e), 8.13 (t, 1H, i).δ_C (125 MHz, DMSO-d_6,TMS): 151.04 (a), 147.92 (C_q), 142.04(C_q), 141.51(C_q), 138.84(C_q), 130.70(e), 130.47(i), 128.86(d), 127.41(h), 126.97(f), 126.64(g), 126.45(c), 122.47(b); mp 192–193 °C, Anal. Calc. for $C_{28}H_{20}N_2{\cdot}0.3CH_3OH$: C, 86.12; H, 5.44; N, 7.09. Found: C, 86.17; H, 5.16, N, 7.07%.

§ Cage **2**: δ_H (500 MHz, DMSO-d_6,TMS): 10.18 (d, 16H, a), 9.20(s, 8H, c), 9.04 (d, 16H, b), 8.96(s, 4H, g), 8.53(d, 8H, d), 8.44 (d, 8H, f), 8.27 (d, 8H, h), 8.19 (t, 8H, e), 8.06 (t, 4H, i). δ_C (125 MHz, DMSO-d_6,TMS): 152.39 (a), 151.17 (C_q), 141.77(C_q), 140.58(C_q), 135.71(C_q), 131.12(e), 130.74(i), 130.25(f), 127.28(h), 127.19(c & d), 126.88(g), 125.61(b); mp decomp. at 289 °C), Anal. Calc. for $C_{112}H_{80}N_{12}O_{12}Pd_2{\cdot}6(CH_3)_2SO$: C, 60.36; H, 4.74; N, 6.81. Found: C, 60.12; H, 4.59, N, 6.80%.

¶ In the ^{13}C NMR spectrum of **2**, instead of 13 peaks only 12 peaks were observed. Here the signals of carbons c and d (see Fig. 1 for nomenclature) overlapped with each other as confirmed by the C–H COSY spectrum.

‖ *Crystal data* for **2**: $C_{112}H_{80}N_{12}O_{12}Pd_2{\cdot}9(CH_3)_2SO{\cdot}2(C_2H_5)_2O$, M = 2850.07, monoclinic, space group $C2/c$, a = 23.510(4), b = 22.229(3), c = 27.394(5) Å, β = 104.216(3)°, U = 13878(4) Å^3, T = 193 K, Z = 4, D_c = 1.364 g cm^{-3}, λ = 0.71073 Å, 36208 reflections measured, 12216 unique (R_{int} = 0.2039) which were used in all calcutations. $R1$ = 0.0766 and $wR2$ = 0.1676. Two of the nitrates and seven DMSO molecules were disordered.

CCDC reference number 164966. See http://www.rsc.org/suppdata/cc/b1/b104853h/ for crystallographic data in CIF or other electronic format.

1 *Templating, Self-Assembly and Self-Organization*, Exec. ed. J.-P. Sauvage and M. W. Hosseini, *Comprehensive Supramolecular Chemistry*, ed. J.-M. Lehn (Chair), Pergamon Press, Oxford, 1995, vol. 9.
2 M. Fujita, K. Umemoto, M. Yoshizawa, N. Fujita, T. Kusukawa and K. Biradha, *Chem. Commun.*, 2001, 509; S. Leininger, B. Olenyuk and P. J. Stang, *Chem. Rev.*, 2000, **100**, 853; R. W. Saalfrank, E. Uller, B. Demleitner and I. Bernt, *Struct. Bonding (Berlin)*, 2000, **96**, 149; D. L. Caulder and K. N. Raymond, *Acc. Chem. Res.*, 1999, **32**, 975.
3 M. Fujita, S. Nagao and K. Ogura, *J. Am. Chem. Soc.*, 1995, **117**, 1649.
4 M. Fujita, D. Oguro, M. Miyazawa, H. Oka, K. Yamaguchi and K. Ogura, *Nature*, 1995, **378**, 469; P. J. Stang, B. Olenyuk, D. C. Muddiman and R. D. Smith, *Organometallics*, 1997, **16**, 3094; C. M. Hartshorn and P. J. Steel, *Chem. Commun.*, 1997, 541.
5 R. W. Saalfrank, A. Stark, K. Peters and H. G. Von Schnering, *Angew. Chem., Int. Ed. Engl.*, 1988, **27**, 851; T. Beissel, R. E. Powers and K. N. Raymond, *Angew. Chem., Int. Ed. Engl.*, 1996, **35**, 1084.
6 (*a*) L. J. Barbour, G. William Orr and J. L. Atwood, *Nature*, 1998, **393**, 671; (*b*) D. A. McMorran and P. J. Steel, *Angew. Chem., Int. Ed.*, 1998, **37**, 3295; (*c*) T. D. Owens, F. J. Hollander, A. G. Oliver and J. A. Ellman, *J. Am. Chem. Soc.*, 2001, **123**, 1539; (*d*) C.-Y. Su, Y.-P. Cai, C.-L. Chen, H.-X. Zhang and B.-S. Kang, *J. Chem. Soc., Dalton Trans.*, 2001, 359.
7 C. Coudret, *Synth. Commun.*, 1996, **26**, 3543.

CHEMCOMM Communication
www.rsc.org/chemcomm

The activation of molecular oxygen by horseradish peroxidase with sodium sulfite†

Shin-ichi Ozaki,* Seiko Watanabe, Sachiko Hayasaka and Megumi Konuma

Faculty of Education, Yamagata University, Kojirakawa, Yamagata 990-8560, Japan. E-mail: ozaki@ke-sci.kj.yamagata-u.ac.jp

Received (in Cambridge, UK) 22nd May 2001, Accepted 23rd July 2001
First published as an Advance Article on the web 16th August 2001

Horseradish peroxidase (HRP) utilizes molecular oxygen (O_2) with sodium sulfite (Na_2SO_3) to oxidize thioanisole and styrene at the exterior of the heme pocket.

Horseradish peroxidase (HRP) bearing iron protoporphyrin (IX) as the prosthetic group normally utilizes hydrogen peroxide (H_2O_2) as an oxidant to generate an oxoferryl species ($O{=}Fe^{IV}$) paired with porphyrin radical cation, so-called compound **I**.[1] Compound **I** is reduced back to the ferric state by either sequential one-electron transfer from typical phenolic substrates such as guaiacol or by ferryl oxygen transfer to thioethers.[2–4] Since HRP is known to react with racemic hydroperoxides to afford chiral hydroperoxides and alcohols in high enantioselectivity, the enzyme is also used for kinetic resolutions.[5–9] In contrast to P450 monooxygenases, HRP does not efficiently activate O_2 with a reductase and NADH or NADPH because the peroxidase does not mediate the electron transfer from external electron sources on the protein surface to the heme iron buried inside.[10] However, the direct electron transfer from sulfite (SO_3^{2-}) to the ferric heme iron would produce $SO_3^{\cdot}$ (step 1 in Scheme 1), which could initiate the activation of O_2 to oxidize the substrates.[11,12] In order to explore transition metal promoted oxidative reactions with sulfite, we have investigated one- and two-electron oxidation by HRP with SO_3^{2-} and O_2.

Thioanisole is oxidized to methyl phenyl sulfoxide by HRP in the presence of sodium sulfite and ambient O_2 at a rate more than four times faster than the value obtained in the incubation with H_2O_2 as an oxidant (Table 1). Not more than a trace amount of the sulfoxide product is detected when the reaction is performed under anaerobic conditions. The results clearly indicate that HRP together with sulfite can activate molecular oxygen to produce a potential oxidant for the monooxygenation reaction. Interestingly, sulfoxidation with SO_3^{2-} and O_2 does not proceed enantioselectively as observed in the reaction with H_2O_2 (Table 1); therefore, compound **I** does not seem to be a catalytic species in the HRP–SO_3^{2-}–O_2 system (*i.e.* pathway step 3 → 4 → 5 in Scheme 1 is not dominant). Since the oxidation of thioanisole with monoperoxysulfate (HSO_5^-) has been found to afford a racemic mixture of sulfoxide in the presence or absence of HRP, we speculated that monoperoxysulfate released from the heme pocket would be involved in sulfoxidation with sulfite and molecular oxygen.

In order to investigate the mechanism further, we have performed the sulfoxidation reaction in the presence of superoxide dismutase (SOD) and catalase. The reaction is subject to significant inhibition (97%) although SOD and catalase do not decelerate the chemical sulfoxidation by monoperoxysulfate (Table 2). By contrast, the rate of sulfoxidation is reduced by < 18% in the presence of $OH^{\cdot}$ radical scavengers such as methanol or *tert*-butyl alcohol and $SO_4^{\cdot-}$ radical quenchers like ethanol (Table 2). The results imply that (a) superoxide ($O_2^{\cdot-}$) is involved in the production of monoperoxysulfate and (b) the lack of inhibition observed in the presence of ethanol, methanol or *tert*-butyl alcohol argues against the involvement of $SO_4^{\cdot-}$ or $OH^{\cdot}$ radicals in the catalysis. The ferrous–dioxygen and ferric–superoxide complex of HRP are in equilibrium (step 8 in Scheme 1). Thus, the recombination of $O_2^{\cdot-}$ and $SO_3^{\cdot-}$ generated in step 9 and 1 (Scheme 1), respectively, could produce SO_5^{2-}, which is subsequently protonated to produce monoperoxysulfate (HSO_5^-). The release of HSO_5^- from the intermediate by Fe–O

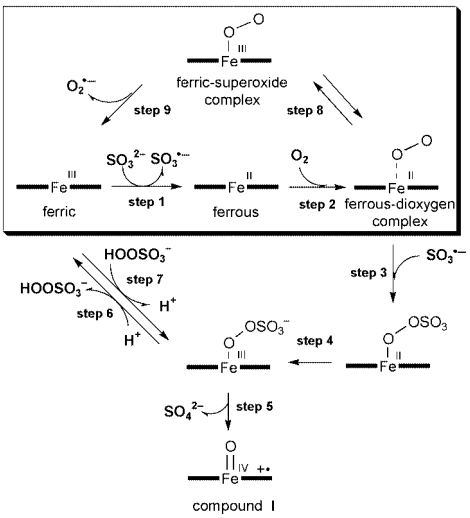

Scheme 1 Reaction scheme for the HRP–SO_3^{2-}–O_2 system. The catalytic cycle postulated by our results is indicated inside the square; $SO_3^{\cdot-}$ and $O_2^{\cdot-}$ generated by step 1 and 9, respectively, would mediate the oxidation reaction outside of the active site under the conditions described here.

† Electronic supplementary information (ESI) available: plots of pH *vs.* rate of sulfoxidation. See http://www.rsc.org/suppdata/cc/b1/b104529f/

Table 1 Oxidation of thioanisole[a]

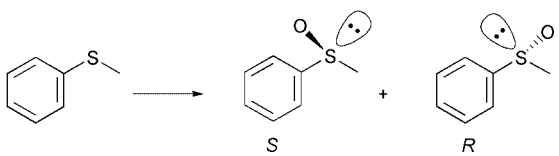

Protein	Oxidant	Initial rate/ turnover min^{-1}	%ee
HRP	H_2O_2	1.1	77[b]
HRP	sulfite and O_2	1.2	0

[a] The reaction mixture containing HRP (5 μM) and thioanisole (2 mM) was incubated with either H_2O_2 (0.6 mM) or sodium sulfite (0.6 mM) at 25 °C in sodium phosphate buffer (50 mM, pH 7.0). The sulfoxide product extracted with CH_2Cl_2 was analyzed by HPLC equipped with a Dicel OD chiral column as reported in ref. 4. The reported values are the average of two independent experiments. For anaerobic experiments, the vessel containing the reaction mixture was frozen, evacuated and then filled with nitrogen. The procedure was repeated three times to remove dissolved oxygen. Sulfoxidation was then performed under a nitrogen atmosphere. [b] The *S* isomer is the major product.

 DOI: 10.1039/b104529f

Table 2 Inhibition of thioanisole oxidation by additives[a]

Additive	Relative activity (%)
—[b]	100
SOD and catalase[c]	3
Methanol[d]	96
Ethanol[d]	82
tert-Butyl alcohol[d]	96

[a] Reactions were conducted with HRP (5 μM), thioanisole (2 mM), sodium sulfite (0.6 mM) and additive(s) in sodium phosphate buffer (50 mM, pH 7.0) at 25 °C for 10 min. The reported values are the average of two independent experiments. SOD and catalase did not inhibit chemical oxidation of thioanisole by monoperoxysulfate (0.6 mM). [b] No additive. [c] SOD (10 units) and catalase (11 units) added to the reaction mixture. [d] The concentration of additive is 25 mM.

bond cleavage (step 6 in Scheme 1) is excluded because superoxide is not involved in the catalytic cycle (step 1 → 2 → 3 → 6 in Scheme 1) and the observed inhibition in the presence of SOD and catalase can not be rationalized.

Plots of sulfoxidation rate *vs.* pH examined in the range pH 5–10 reveal that the reaction with sulfite does not proceed below pH 5, and the optimum pH is found to be 7 (see ESI†). The trend here is similar to that observed for nickel-catalyzed oxidative deamination with sulfite under aerobic conditions[13] but differs from the pH profile for the HRP–H_2O_2 system, which can produce sulfoxide even below pH 6. The result is consistent with our hypothesis that the oxidation mechanism is altered when SO_3^{2-}–O_2 instead of H_2O_2 is utilized.

Styrene and guaiacol oxidations by HRP with sulfite and oxygen provide further support for the proposed reaction scheme (Scheme 1). In contrast to sulfoxidation, the epoxidation reaction by compound **I** requires interactions of the two vinyl carbons with a ferryl oxygen atom. Since the active site of HRP is sterically hindered, it was previously reported that compound **I** of HRP could not efficiently oxidize styrene.[2,4] However, styrene oxide is detected in the mixture of HRP–styrene–SO_3^{2-}–O_2 (Table 3) although the rate of oxidation is slow. In addition, phenylacetaldehyde, which is normally observed as a side product of compound **I** mediated epoxidation by other hemoproteins, is not produced.[14–18] The results indicate that monooxygenation reactions in the HRP–SO_3^{2-}–O_2 system do not proceed *via* compound **I** but occur outside of the heme pocket by monoperoxysulfate. Significantly, slow one-electron oxidation of guaiacol exhibited by HRP with SO_3^{2-} and O_2 also indicates that the intermediate formation

Table 3 Epoxidation of styrene

Experiment	Protein	Oxidant	Rate
1[a]	HRP	H_2O_2	ND[c]
2[a]	HRP	Sulfite and O_2	200[b]
3[d]	—	Monoperoxysulfate	250[b]
4[e]	—	Sulfite and O_2	ND[c]

[a] Styrene (1 μL) was added to HRP (5 μM) in 0.5 mL of sodium phosphate buffer (50 mM, pH 7.0). The concentration of styrene was expected to be 17 mM, but the reaction mixture appeared to be slightly turbid. To the styrene-saturated solution, either H_2O_2 (0.6 mM) or sodium sulfite (0.6 mM) was added to initiate the reaction at 25 °C. Products were extracted with CH_2Cl_2 and analyzed by GC on a Shimadzu CBP1 capillary column. The reaction time varied from 20 to 120 min to obtain the time *vs.* epoxide formation plot. A linear relationship was observed for 120 min, and the rate was determined as the slope of the plot. The quoted values are the average of two independent experiments. [b] pmol of epoxide min^{-1}. [c] Not detected.[d] The reaction was performed with monoperoxysulfate (0.6 mM) in the absence of HRP. Since the exact concentration of monoperoxysulfate in the HRP–sulfite–O_2 solution can not be determined, direct comparison of the rates in experiments 2 and 3 would not be appropriate, however, the results indicated that the epoxide could be produced from styrene with monoperoxysulfate. [e] Oxidation was also performed with sodium sulfite (0.6 mM) with styrene aerobically in the absence of HRP, but the epoxide product was not detected.

(step 3 in Scheme 1) or/and the heterolytic cleavage of the O–O bond in Fe(III)–SO_5^{2-} species (step 5 in Scheme 1) is not an efficient process since guaiacol can not be oxidized by monoperoxysulfate but only by compound **I**. The addition of an excess of monoperoxysulfate to ferric HRP (step 7 in Scheme 1) somewhat facilitates compound **I** formation to improve the one-electron oxidation activity (4.1 turnover min^{-1}); however, the rate is 6500-fold slower than the value obtained in guaiacol oxidation with H_2O_2. It was previously reported that high valent metal–oxo species generated from water-soluble porphyrins and oxygen atom donors ($KHSO_5$, H_2O_2, … *etc.*) mediate the oxidation of alcohols, olefins or DNA,[19–23] but the active site of HRP may not be large enough to accommodate HSO_5^- as a good oxidant.

In summary, we report that HRP can utilize SO_3^{2-} and O_2 to oxidize thioanisole and styrene, but the catalytic species is not compound **I** as established in the oxidation with H_2O_2. Our mechanistic studies imply that monoperoxysulfate (HSO_5^-) generated from $O_2^{\cdot-}$ and $SO_3^{\cdot-}$ mediates the oxidation reaction outside of the heme pocket. A similar mechanism might be involved in the metalloprotein associated biological toxicity of sulfite inhaled from industrial emissions or ingested as a preservative in foods.[24]

We thank Drs Naohiko Masuda, Minoru Ishii and Yoshihito Watanabe for their technical support. Financial support of this work by Grant-in-Aid for Scientific Research (No. 10680575) and Mitsubishi Chemical Corporation Fund for S. O. is gratefully acknowledged.

Notes and references

1 H. B. Dunford, *Heme Peroxidases*, Wiley-VCH, New York, 1999.
2 R. Z. Harris, S. L. Newmyer and P. R. Ortiz de Montellano, *J. Biol. Chem.*, 1993, **268**, 1637.
3 S. Ozaki and P. R. Ortiz de Montellano, *J. Am. Chem. Soc.*, 1994, **116**, 4487.
4 S. Ozaki and P. R. Ortiz de Montellano, *J. Am. Chem. Soc.*, 1995, **117**, 7056.
5 E. Hoft, H. J. Hamann, A. Kunath, W. Adam, U. Hoch, C. R. Sahamoller and P. Schreier, *Tetrahedron: Asymmetry*, 1995, **6**, 603.
6 W. Adam, U. Hoch, M. Lazarus, C. R. Sahamoller and P. Schreier, *J. Am. Chem. Soc.*, 1995, **117**, 11 898.
7 W. Adam, R. T. Fell, U. Hoch, C. R. Sahamoller and P. Schreier, *Tetrahedron: Asymmetry*, 1995, **6**, 1047.
8 W. Adam, U. Hoch, H. U. Humpf, C. R. SahaMoller and P. Schreier, *Chem. Commun.*, 1996, 2701.
9 W. Adam, C. R. Saha-Moller and K. S. Schmid, *J. Org. Chem.*, 2000, **65**, 1431.
10 P. R. Ortiz de Montellano, *Cytochrome P450*, Plenum Press, New York, 2nd edn., 1995.
11 J. F. Perez-Benito and C. Arias, *Collect. Czech. Chem. Commun.*, 1991, **56**, 1552.
12 Y. Song, C.-M. Yang and R. Kluger, *J. Am. Chem. Soc.*, 1993, **115**, 4365.
13 J. Levine, J. Etther and I. Apostol, *J. Biol. Chem.*, 1999, **274**, 4848.
14 C. E. Catalano and P. R. Ortiz de Montellano, *Biochemistry*, 1987, **26**, 8373.
15 V. P. Miller, G. DePillis, D. J. C. Ferrer, A. G. Mauk and P. R. Ortiz de Montellano, *J. Biol. Chem.*, 1992, **267**, 8936.
16 S. Ozaki, T. Matsui and Y. Watanabe, *J. Am. Chem. Soc.*, 1996, **118**, 9784.
17 S. Ozaki, T. Matsui and Y. Watanabe, *J. Am. Chem. Soc.*, 1997, **119**, 6666.
18 T. Matsui, S. Ozaki and Y. Watanabe, *J. Am. Chem. Soc.*, 1999, **121**, 9952.
19 S. VilainDeshayes, A. Robert, P. Maillard, B. Meunier and M. Momenteau, *J. Mol. Catal. A: Chem.*, 1996, **113**, 23.
20 K. Wietzerbin, B. Meunier and J. Bernadou, *Chem. Commun.*, 1997, 2321.
21 R. J. Balahura, A. Sorokin, J. Bernadou and B. Meunier, *Inorg. Chem.*, 1997, **36**, 3488.
22 J. M. An, S. J. Yang, S. Y. Yi, G. J. Jhon and W. Nam, *Bull. Korean Chem. Soc.*, 1997, **18**, 117.
23 K. Wietzerbin, J. G. Muller, R. A. Jameton, G. Pratviel, J. Bernadou, B. Meunier and C. J. Burrows, *Inorg. Chem.*, 1999, **38**, 4123.
24 C. Brandit and R. van Eldik, *Chem. Rev.*, 1995, **95**, 119.

CHEMCOMM Communication
www.rsc.org/chemcomm

Reversible *trans–cis* photoisomerization of azobenzene-attached bipyridine ligands coordinated to cobalt using a single UV light source and the Co(III)/Co(II) redox change

Shoko Kume, Masato Kurihara and Hiroshi Nishihara*

Department of Chemistry, School of Science, The University of Tokyo, 7-3-1 Hongo, Bunkyo-ku, Tokyo 113-0033, Japan. E-mail: nisihara@chem.s.u-tokyo.ac.jp

Received (in Cambridge, UK) 18th May 2001, Accepted 25th July 2001
First published as an Advance Article on the web 16th August 2001

The *trans*/*cis* ratio of the azobenzene-attached bipyridine ligands in a cobalt complex is reversibly altered by a combination of photoirradiation with a single UV light source and the reversible redox change between Co(II) and Co(III).

The photoisomerization of organic azobenzenes is a subject of current research interest with regard to information storage and photo-switching molecular devices.[1] Molecular motion induced by isomerization of the azo group can be controlled by a combination of UV- and visible-light irradiation, where the former (π–π* transition) achieves the *trans*-to-*cis* isomerization and the latter (n–π* transition) promotes the reverse isomerization.[2] Thus, use of two different light sources to achieve reversible molecular motion is an essential factor in the development of molecular devices.[3] An exception, which made use of a photochemical–electrochemical hybrid system, has been reported by Fujishima and coworkers.[4] Transition metal-conjugated azo compounds[5,6] can provide new advanced molecular functions utilizing combination of the photoisomerization and redox change of the metal center. In this communication, we report the first example of reversible *trans–cis* isomerization of the azo group achieved through a combination of photoirradiation and a redox cycle between Co(II) and Co(III), that makes possible both forward and backward isomerization in response to irradiation with a single light source (Scheme 1). A novel tris(azobenzene-attached bipyridine)cobalt complex was employed in this system, since both the Co(II) and Co(III) complexes are fairly stable in air under ambient conditions.

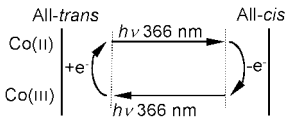

Scheme 1

A tolylazophenylbipyridine ligand, azobpy, was synthesized through the coupling of 4-(4″-anilino)-2,2′-bipyridine and 4-nitrosotoluene.[7] The Co(II) complex of azobpy, $[Co^{II}(azobpy)_3](BF_4)_2$, was obtained by reaction of $Co^{II}(NO_3)_2$ with azobpy in dichloromethane at room temperature, followed by exchange of the counter ion with NEt_4BF_4. The oxidation of $[Co^{II}(azobpy)_3]^{2+}$ was carried out with $AgCF_3SO_3$ and $[Co^{III}(azobpy)_3](BF_4)_3$ was precipitated through the addition of an excess amount of NH_4BF_4.† In the ^1H NMR spectrum, two distinct signals of the terminal methyl group and complicated signals of aromatic ring protons were derived from a mixture of *mer*- and *fac*-isomers of $[Co^{III}(azobpy)_3]^{3+}$ with respect to three tolylazophenyl groups.

In a cyclic voltammogram of $[Co^{II}(azobpy)_3](BF_4)_2$, a reversible Co(III)/(II) redox wave and a quasi-reversible Co(II)/(I) redox wave were observed at −0.15 and −1.27 V *vs.* ferrocenium/ferrocene (Fc^+/Fc) in dichloromethane, respectively.

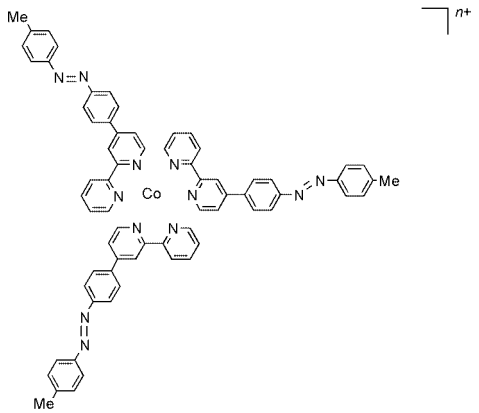

UV–VIS absorption spectra of azobpy, $[Co^{II}(azobpy)_3](BF_4)_2$ and $[Co^{III}(azobpy)_3](BF_4)_3$ showed π–π* bands due to the azo group at λ_{max} = 345 nm ($\varepsilon = 3.5 \times 10^4$ mol^{-1} dm^3 cm^{-1}), 360 (1.1×10^5) and 374 (9.7×10^4), respectively. An increase in the electron-withdrawing effect on the azo group in response to the oxidation of Co(II) to Co(III) resulted in a lower energy of the π–π* band.[8] Upon irradiation to the dichloromethane solution of azobpy with UV light at 366 nm,‡ the π–π* band decreased and the n–π* band of the azo group at 445 nm increased in intensity, showing a typical *trans*-to-*cis* isomerization of the azobenzene moiety [Fig. 1(a)]. The molar ratio of the *cis*-form reached 92% in the photostationary state (PSS). The spectral change of $[Co^{II}(azobpy)_3](BF_4)_2$ in dichloromethane is essentially similar to that of azobpy upon irradiation with the 366 nm light, and 40% of the *trans*-azobenzene moiety was found to be changed into the *cis*-form in PSS [Fig. 1(b)]. The irradiation with 438 nm light reversed the spectral change, indicating a *cis*-to-*trans* isomerization. Intriguingly, almost no decrease in absorbance of the π–π* band of $[Co^{III}(azobpy)_3](BF_4)_3$ was observed under the same 366 nm light irradiation, suggesting that the *cis*-to-*trans* back-reaction of the Co(III) complex is much more effective than that of the Co(II) complex in PSS (*vide infra*).

The difference in the *cis*-form concentrations in PSS between Co(II) and Co(III) described above indicates the possibility of a reversible *trans–cis* conversion with single monochromatic light irradiation by changing the redox state between Co(II) and Co(III). To test this hypothesis, we carried out the following experiments. A dichloromethane solution of the *trans*-form of $[Co^{II}(azobpy)_3](BF_4)_2$ was irradiated with 366 nm light to reach PSS, and the resulting mixture of *trans*- and *cis*-forms was oxidized with a stoichiometric amount of 1,1′-dichloroferrocenium hexafluorophosphate, $[Fe(\eta^5\text{-}C_5H_4Cl)_2]PF_6$ ($E^{0\prime}$ = 0.19 V *vs.* Fc^+/Fc).[5] The ratio of the *cis*-form remained constant after the oxidation, the thermal isomerization to the *trans*-form proceeding very slowly in the dark [the recovery of absorbance of the π–π* band was not pronounced in intensity over 30 min

 DOI: 10.1039/b104381c

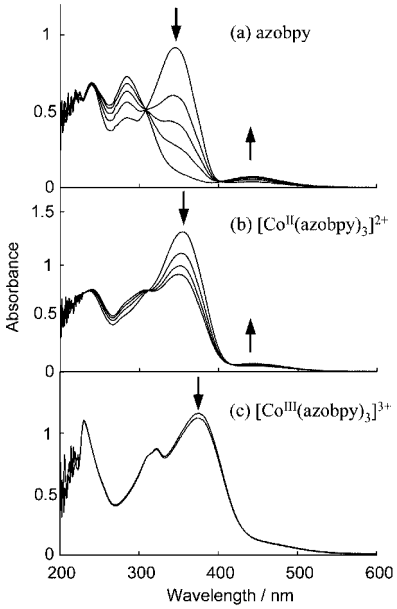

Fig. 1 UV–VIS absorption spectral change of azobpy (2.62×10^{-5} mol dm^{-3}) (a), [Co^{II}(azobpy)](BF$_4$)$_2$ (1.17×10^{-5} mol dm^{-3}) (b), and [Co^{III}(azobpy)](BF$_4$)$_3$ (1.20×10^{-5} mol dm^{-3}) (c), in dichloromethane upon irradiation with 366 nm light.

Fig. 2(b)]. When the oxidized solution was exposed again to 366 nm light, the *cis*-to-*trans* photoisomerization promptly occurred to create the *trans*-rich PSS which is characteristic of the Co(III) state, accompanied by a fast increase in the absorbance of the π–π* band within a few minutes [Fig. 2(a)]. The Co(III) complex in PSS upon irradiation with 366 nm light was re-reduced with a stoichiometric amount of 1,1′-acetylcobaltocene, [Co(η^5-C$_5$H$_4$COMe)$_2$] ($E^{0\prime}$ = −0.76 V *vs.* Fc$^+$/Fc)[9] and the exposure to the same 366 nm light resulted in a *trans*-to-*cis* isomerization to reach the different PSS that is characteristic of the Co(II) state. These results suggest that a reversible *trans–cis* isomerization can be achieved by a combination of the reversible redox change between Co(II) and Co(III) and irradiation with a single UV light source, which is a novel route differing from the reversible isomerization of general organic azobenzenes with a combination of π–π* and n–π* excitation employing UV and visible light, respectively (Scheme 1).

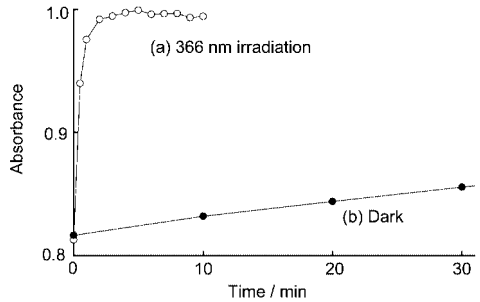

Fig. 2 Change in absorbance at 360 nm with time upon irradiation with 366 nm light (○) and in the dark (●) after a dichloromethane solution of [Co^{II}(azobpy)$_3$](BF$_4$)$_2$ (1.04×10^{-5} mol dm^{-3}) was first irradiated with 366 nm light to reach PSS and then oxidized with [Fe(η^5-C$_5$H$_4$Cl)$_2$]PF$_6$.

The redox-coupled photoisomerization system described above may enable continuous control of total conversion to the *cis*-form of azobenzene moieties in PSS by means of a continuous change in Co(II) to Co(III) complex molar ratio upon irradiation with monochromatic 366 nm light. Solutions consisting of various molar ratios of the Co(III) complex, *x*, were prepared by the addition of *x* equivalents of [Fe(η^5-C$_5$H$_4$Cl)$_2$]PF$_6$ to the solution of [Co^{II}(azobpy)$_3$](BF$_4$)$_3$, which was then irradiated with 366 nm light. After reaching PSS within a few minutes, the Co(II) component was oxidized with

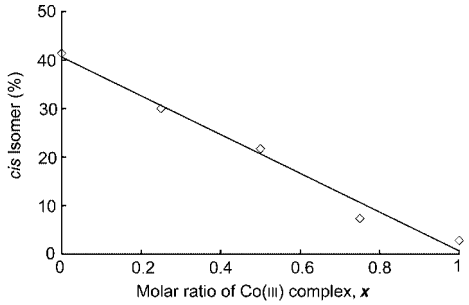

Fig. 3 Correlation between the conversion ratio of the *cis*-form and the molar ratio, *x*, of the Co(III) complex.

$1 - x$ equivalents of [Fe(η^5-C$_5$H$_4$Cl)$_2$]PF$_6$ to estimate the total formation ratio of the *cis*-azobenzene moiety by using the absorbance of the π–π* band normalized as the Co(III) complex (Fig. 3). The contribution of thermal *cis*-to-*trans* isomerization to the *cis* ratio can be neglected, as the process proceeds very slowly compared to the photo-process, as already mentioned. The conversion ratio of the *cis*-form was found to linearly correlate with the ratio *x* within 0–40%. A similar continuous control of the conversion ratio of the *cis*-form for organic azobenzenes can be achieved by tuning the relative intensities of two different monochromatic light sources or by selection of a suitable excitation wavelength closely associated with overlapping of the π–π* and n–π* bands. Compared with these photochemical methods, the combination of the photoisomerization and the redox processes of the metal complex-conjugated azobenzene is a more facile and precise pathway to adjust the *cis* conversion ratio.

In conclusion, reversible *trans–cis* isomerization has been achieved by a combination of the reversible redox reaction between Co(II) and Co(III) and single UV-light irradiation. This method should provide a new design for photochemical and electrochemical hybrid molecular devices. We are currently expanding the method developed in the present study to a modified electrode system in which the redox state of Co can be controlled electrochemically.

This work was supported by Grants-in-Aid for scientific research (Nos. 10149102, 11167217 and 11209003) from the Ministry of Culture, Education, Science, Sports and Technology, Japan, the Ogasawara Foundation, and the Tokyo Ohka Foundation.

Notes and references

† *Characterisation data*: [Co^{II}(azobpy)$_3$](BF$_4$)$_2$; ESI-MS: *m/z* 554.7 ([M − 2BF$_4$]$^{2+}$). Anal. Calc. for C$_{69}$H$_{542}$CoF$_8$N$_{12}$·3.5H$_2$O: C, 61.53; H, 4.56; N, 12.48. Found C, 61.55, H, 4.50; N, 12.34%. [Co^{III}(azobpy)$_3$](BF$_4$)$_3$; ESI-MS: *m/z* 1283 ([M − BF$_4$]$^+$). Anal. Calc. for C$_{69}$H$_{54}$B$_3$CoF$_{12}$N$_{12}$·3H$_2$O: C, 58.17; H, 4.24; N, 11.80. Found C, 58.11, H, 4.27; N, 11.62%.

‡ The light source was a super-high-pressure mercury lamp (500 W, USHIO Electronic. Inc.) and the wavelength was selected with a monochromator (Jasco CT-10).

1 T. Ikeda and O. Tsutsumi, *Science*, 1995, **268**, 1873; S. Kawata and Y. Kawata, *Chem. Rev.*, 2000, **100**, 1777.
2 H. Rau, in *Photochromism: Molecules and Systems*, ed. H. Dürr and H. B.-Laurent, Elsevier, Amsterdam, 1990, pp. 165–192.
3 K. Ichimura, S.-K. Oh and M. Nakagawa, *Science*, 2000, **288**, 1624.
4 Z. F. Liu, K. Hashimoto and A. Fujishima, *Nature*, 1990, **347**, 658.
5 M. Kurosawa, T. Nankawa, T. Matsuda, K. Kubo, M. Kurihara and H. Nishihara, *Inorg. Chem.*, 1999, **38**, 5113.
6 M. Kurihara, T. Matsuda, A. Hirooka, T. Yutaka and H. Nishihara, *J. Am. Chem. Soc.*, 2000, **122**, 12 373; T. Yutaka, M. Kurihara, K. Kubo and H. Nishihara, *Inorg. Chem.*, 2000, **39**, 3438; S. Tsuchiya, *J. Am. Chem. Soc.*, 1999, **121**, 48.
7 H. D. Anspon, *Org. Synth.*, 1945, **25**, 86; F. Kröhnke, *Synthesis*, 1976, **1**, 1.
8 M.-S. Ho, A. Natansohn, C. Barrett and P. Rochon, *Can. J. Chem.*, 1995, **73**, 1773.
9 W. P. Hart, D. W. Macomber and M. D. Rausch, *J. Am. Chem. Soc.*, 1980, **102**, 1196.

CHEMCOMM Communication
www.rsc.org/chemcomm

A novel luminescent copper(I) complex containing an acetylenediide-bridged, butterfly-shaped tetranuclear core

Hai-Bin Song,[a] Quan-Ming Wang,[a] Zheng-Zhi Zhang[b] and Thomas C. W. Mak*[a]

[a] *Department of Chemistry, The Chinese University of Hong Kong, Shatin, New Territories, Hong Kong SAR, P. R. China. E-mail: tcwmak@cuhk.edu.hk*

[b] *State Key Laboratory of Elemento-Organic Chemistry, Nankai University, Tianjin, P. R. China*

Received (in Cambridge, UK) 23rd March 2001, Accepted 11th July 2001
First published as an Advance Article on the web 16th August 2001

A novel luminescent acetylenediide-bridged tetranuclear copper(I) complex $[Cu_4(\mu\text{-}Ph_2Ppypz)_4(\mu_4\text{-}\eta^1,\eta^2\text{-}C{\equiv}C)](ClO_4)_2$ [Ph_2Ppypz = 2-(diphenylphosphino-6-pyrazol-1-yl)pyridine] has been synthesized and structurally characterized by X-ray crystallography.

Metal acetylides have been subjected to intensive study for many years.[1] The interest mainly stems from: (i) the ability of the acetylide group to bond to transition metals, forming a growing number of mono- and poly-nuclear complexes that display an unusually rich variety of structures; (ii) the versatile reactivity of the coordinated acetylide group in its complexes, which serve as useful precursors for the synthesis of other target organometallic compounds. In contrast to the plethora of ethynyl complexes containing acetylenide ligands of the type R–C≡C$^-$, ethynediyl complexes containing the acetylenediide ligand, C_2^{2-}, that exhibits the known coordination modes[2] shown in Fig. 1 are relatively rare.

The group 11 metal acetylides M_2C_2 exhibit properties that are characteristic of covalent polymeric solids. They are insoluble in many common solvents, and highly explosive and sensitive to mechanical shock when completely dried. Some examples of (μ-C≡C)bis[(phosphine)gold(I)] complexes have been reported.[3] In these complexes, the C_2^{2-} anion coordinates a pair of gold atoms by σ-bonding to form a linear molecule. Double salts of silver(I) acetylide were studied over half a century ago,[1a] and recently several novel triple and quadruple salts have been synthesized.[5d,e] Their structures exhibit a variety of polyhedral silver cages each encapsulating a C_2^{2-} anion ($C_2@Ag_n$, n = 6, 7, 8, 9).[5] In the context of the chemistry of copper(I) acetylide, development has been hampered by its insolubility in common solvents and the lack of general methods for the synthesis of its derivatives. To date, there is only one known ethynediyl copper(I) complex, namely $[Cu_4(\mu\text{-}dppm)_4(\mu_4\text{-}\eta^1,\eta^2\text{-}C{\equiv}C)](BF_4)_2$ [dppm = bis(diphenylphosphino)methane] **1** where the C_2^{2-} anion coordinates four rectangularly arranged copper atoms by distinct σ and π bonding, and this planar **D**(1) coordination mode is illustrated in Fig. 1.[6a] Here we report the synthesis, structure and luminescence properties of a related complex $[Cu_4(\mu\text{-}Ph_2Ppypz)_4(\mu_4\text{-}\eta^1,\eta^2\text{-}C{\equiv}C)](ClO_4)_2$ [Ph_2Ppypz = 2-(diphenylphosphino-6-pyrazol-1-yl)pyridine] **2**, in which the coordination mode of C_2^{2-} is **D**(2), with the metal atoms arranged about it in a butterfly configuration.

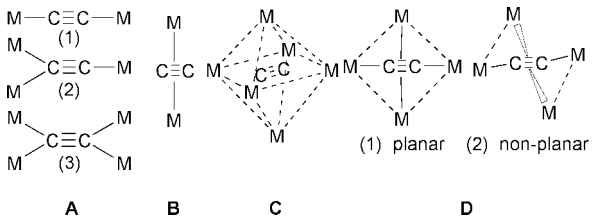

Fig. 1 Coordination modes of C_2^{2-} to metal atoms. In mode **A**, the metal centers are bridged by the C_2^{2-} anion through σ bonds.[1g,2b,c,3] In mode **B**, the C_2^{2-} anion is π-bonded to a pair of metal atoms.[4] In mode **C**, the C_2^{2-} species is encapsulated in a polyhedral metal cage.[5] In modes **D**(1) and **D**(2), the metal atoms are bridged by the C_2^{2-} anion through distinct σ and π bonds in a planar[6] and non-planar[5b] configuration, respectively.

The synthesis of **2** is shown in Scheme 1. In the first method, 1 equiv. Bu^{n}Li was added at room temperature to a solution of 0.5 equiv. $Me_3SiC{\equiv}CH$ in pre-dried, degassed THF under an inert nitrogen atmosphere, and 1 equiv. $[Cu_2(\mu\text{-}Ph_2Ppypz)_2(MeCN)_2](ClO_4)_2$ was then introduced with stirring. After evaporation to dryness, the resulting solid was extracted with CH_2Cl_2. Subsequent diffusion of diisopropyl ether into the concentrated solution gave air-stable orange crystals of **2**·3CH_2Cl_2. In the second method, 0.45 equiv. NaC≡CH was added to a solution of 1 equiv. $[Cu_2(\mu\text{-}Ph_2Ppypz)_2(MeCN)_2](ClO_4)_2$[7a] in degassed THF at −78 °C under an inert atmosphere of nitrogen, and the solution was stirred for 24 h at room temperature. The work-up was similar to that in the first method. However, the yield of the second method is very low (< 10%) due to formation of Cu_2C_2 as the major product. The much higher yield by the first method (60%) is attributable to the gradual release of C_2^{2-} from $Me_3SiC{\equiv}C^-$. Complex **2** gave satisfactory C,H,N analyses, and was subsequently characterized by $^{13}C\{^1H\}$ NMR spectroscopy and X-ray crystallography.† In the $^{13}C\{^1H\}$ NMR (CD_2Cl_2) spectrum, the resonance for carbon in the –C≡C– group appeared at δ 68.65, comparable with that in C_2H_2 (δ 71.90). Although the C≡C stretching vibration is IR active in coordination mode **D**(2), the intensity is weak and scarcely observable in the IR spectrum.

Fig. 2 shows a perspective drawing of the tetranuclear cation in **2**·3CH_2Cl_2 with the atomic numbering scheme. The cation has crystallographic C_2 symmetry. Its structure consists of a butterfly-shaped tetranuclear Cu_4C_2 core in which the acetylenediide anion bridges a pair of Cu_2 sub-units in both η^1 and η^2 bonding modes. The normal electron count requires that the C_2^{2-} anion acts as a six-electron donor according to the covalent model. While the interaction of the C_2^{2-} anion with each Cu_2 sub-unit resembles that found in other μ-η^1,η^2-acetylido complexes, best overlap of the two π orbitals of the C_2^{2-} ligand with the metal orbitals would require that the two Cu_2 sub-units be orthogonal to each other. As shown in Fig. 2, the Cu(2)–C(1)–C(1A)–Cu(2A) system is approximately linear, and the dihedral angle between the planes Cu(1)–C(1)–C(1A) and Cu(1A)–C(1)–C(1A) is 129.0(3)°, which is very distinct

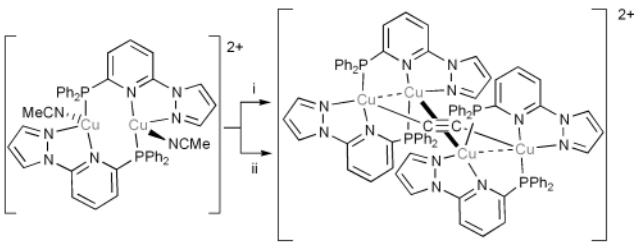

Scheme 1 Synthesis of acetylenediide-bridged tetranuclear copper(I) complex. *Reagents and conditions*: i 1 equiv. Bu^{n}Li and 0.5 equiv. HC≡CSiMe$_3$, THF, 0 °C; ii 0.45 equiv. NaC≡CH (18 wt% slurry in xylene oil), THF, −78 °C.

 DOI: 10.1039/b102717b

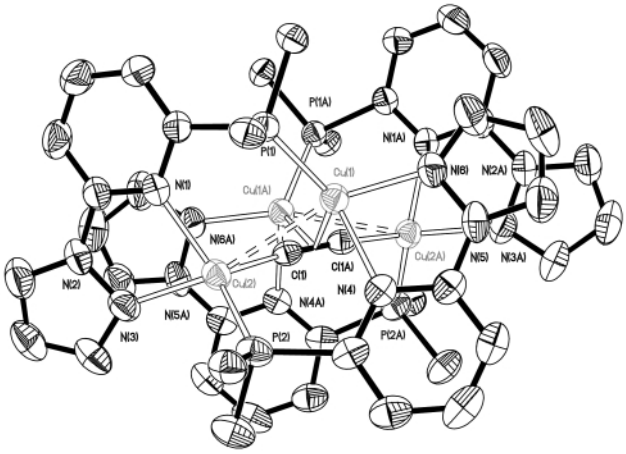

Fig. 2 Perspective drawing (thermal ellipsoids at 35% probability level) of the tetranuclear copper(I) cation in **2**·3CH_2Cl_2 with the atomic numbering scheme. Hydrogen atoms and phenyl rings have been omitted for clarity. Selected bond lengths (Å) and angles (°): Cu(1)–C(1) 2.143(6), Cu(1)–C(1A) 2.215(6), Cu(2)–C(1) 1.931(6), Cu(1)–Cu(2) 2.843(1), C(1)–C(1A) 1.26(1), Cu(1)–P(1) 2.220(2), Cu(1)–N(4) 2.244(5), Cu(1)–N(6) 2.050(5), Cu(2)–P(2) 2.217(2), Cu(2)–N(1) 2.116(5), Cu(2)–N(3) 2.104(5), Cu(1)–C(1)–C(1A) 76.3(5), Cu(2)–C(1)–C(1A) 160.9(7), dihedral angle between planes Cu(1)–C(1)–C(1A) and Cu(1A)–C(1A)–C(1) 129.0(3)°. Symmetry code: A $-x, y, \frac{1}{2} - z$.

from the planar Cu_4C_2 core in **1**. A plausible reason is that the pyridinopyrazole group has less steric hindrance than the dppm group. The C≡C bond in **2** [1.26(1) Å] is identical to that in **1** but longer than those (1.15–1.22 Å) in the ethynediyl silver and gold complexes. The shortest copper–copper distance Cu(1)–Cu(2) 2.843(1) Å lies between those in $[Cu_2(\mu\text{-}Ph_2Ppypz)_2(\mu\text{-}C{\equiv}CPh)](ClO_4)$ [2.516(1) Å] and **1** [3.264(2) and 3.245(2) Å], which is suggestive of cuprophilic interaction between the copper(I) centers.[8] The coordination number of each copper atom in **2** is four, in contrast to the coordination number of three in **1**. The reason can also be attributed to the difference in steric bulk of the two ligands. The dppm ligand is soft and bulky, and the binuclear complex $[Cu_2(MeCN)_4(dppm)_2](BF_4)_2$ readily reacts with halide or $RC{\equiv}C^-$ to form a trinuclear complex.[9] On the other hand, Ph_2Ppypz is more rigid and $[Cu_2(MeCN)_2(Ph_2P\text{-}pypz)_2](ClO_4)_2$ reacts with halide or $RC{\equiv}C^-$ to form other binuclear products.[7]

The electronic absorption and emission spectra of complex **2** in CH_2Cl_2 are shown in Fig. 3.‡ The electronic spectrum exhibits absorption bands at *ca.* 340–400 nm (λ_{max}^{abs}/nm (ε_{max}/dm^3 mol^{-1} cm^{-1}), 345sh (100 000), 364sh (63 827), 373 (37 675), 396 (28 400)). A similar band is also observed in **1** at 374 nm. Such bands most likely involve the Cu_4C_2 core, so they are assigned to LMCT bands of $[(C{\equiv}C)^{2-}{\rightarrow}Cu_4]$. Excitation of

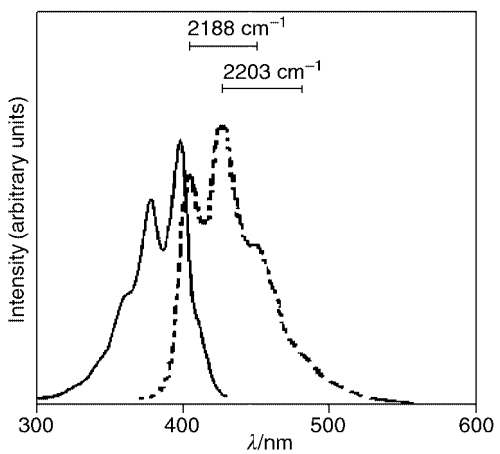

Fig. 3 Excitation spectrum (left, ——) and emission spectrum (right, - - - -) of **2** in CH_2Cl_2 at 298 K.

2 in dichloromethane at λ > 350 nm produces blue–green luminescence (408, 430, 448sh, 475sh nm). Vibronically structured bands with two progressional spacings at 2188 and 2203 cm^{-1}, characteristic of the ν(C≡C) stretch,[9b–d] were observed. The appearance of vibrational progressions is suggestive of involvement of the C_2^{2-} unit in the excited state. The overlap of the emission bands with the low-energy excitation bands and a quite small Stokes shift, quite distinct from the case in **1**, are assigned to the rigid and unsubstituted aromatic ring of Ph_2Ppypz. A possible origin of the emission involves emissive states derived from $[(C{\equiv}C)^{2-}{\rightarrow}Cu_4]$ LMCT mixed with d→s character. Similar assignments have been proposed for other alkynyl/alkynediyl copper(I)/silver(I) systems.[9]

This project is supported by Hong Kong Research Grants Council Earmarked Grant CUHK 4022/98P.

Notes and references

† *Crystal data* for compound **2**: $C_{82}H_{64}Cl_2Cu_4N_{12}O_8P_4{\cdot}3CH_2Cl_2$, M = 2049.17, monoclinic, space group $C2/c$ (no. 15), a = 21.343(9), b = 17.303(8), c = 26.26(1) Å, β = 97.79(1)°, V = 9607(7) Å^3, Z = 4, D_c = 1.417 Mg m^{-3}, $F(000)$ = 4160, μ(Mo-Kα) = 1.22 mm^{-1}, 25902 reflections measured, 8484 unique (R_{int} = 0.061), final $R1$ = 0.055, $wR2$ = 0.152 for 8484 independent reflections [$I > 2\sigma(I)$]. Data collection was performed at 293 K on a Bruker SMART 1000 CCD diffractometer using frames of oscillation range 0.3°, with 1.5 < θ < 25°. CCDC reference number 160440.

See http://www.rsc.org/suppdata/cc/b1/b102717b/ for crystallographic data in CIF or other electronic format.

‡ The emission and excitation spectra were obtained with a RF-540 fluorimeter (conc. 10^{-5} mol dm^{-3}, CH_2Cl_2). The excitation wavelength was 368 nm.

1 (*a*) R. Vestin and E. Ralf, *Acta Chem. Scand.*, 1949, **3**, 101; (*b*) R. Nast, *Coord. Chem. Rev.*, 1982, **47**, 89; (*c*) M. F. Lappert, R. Pearce and P. I. W. Yarrow, *Chem. Rev.*, 1983, **83**, 135; (*d*) M. Akita, M. Terada and Y. Morooka, *Organometallics*, 1992, **11**, 1825; (*e*) F. Paul and C. Lapinte, *Coord. Chem. Rev.*, 1998, **178**–**180**, 431; (*f*) R. E. Martin and F. Diederich, *Angew. Chem., Int. Ed.*, 1999, **38**, 1350; (*g*) T. Ren, G. Zou and J. C. Alvarez, *Chem. Commun.*, 2000, 1197.

2 (*a*) W. Kockelmann and U. Ruschewitz, *Angew. Chem., Int. Ed.*, 1999, **38**, 3492; (*b*) D. Miguel, M. Moreno, J. Pérez and V. Riera, *J. Am. Chem. Soc.*, 1998, **120**, 417; (*c*) S. B. Falloon, A. M. Arif and J. A. Gladysz, *Chem. Commun.*, 1997, 629.

3 (*a*) T. E. Müller, D. M. P. Mingos and D. J. Williams, *J. Chem. Soc., Chem. Commun.*, 1994, 1787; (*b*) J. Vicente, M. T. Chicote, M. D. Abrisqueta and P. G. Jones, *Organometallics*, 1997, **16**, 5628; (*c*) J. Vicente, M. T. Chicote, M. D. Abrisqueta and P. G. Jones, *Organometallics*, 2000, **19**, 2629; (*d*) M. I. Bruce, K. R. Grundy, M. J. Liddell, M. R. Snow and E. R. T. Tiekink, *J. Organomet. Chem.*, 1988, **344**, C49.

4 (*a*) E. Ruiz and P. Alemany, *J. Phys. Chem.*, 1995, **99**, 3114; (*b*) B. Goldfuss, P. v. R. Schleyer and F. Hampel, *J. Am. Chem. Soc.*, 1997, **119**, 1072.

5 (*a*) G.-C. Guo, G.-D. Zhou, Q.-G. Wang and T. C. W. Mak, *Angew. Chem., Int. Ed.*, 1998, **37**, 630; (*b*) G.-C. Guo, Q.-G. Wang, G.-D. Zhou and T. C. W. Mak, *Chem. Commun.*, 1998, 339; (*c*) G.-C. Guo, G.-D. Zhou and T. C. W. Mak, *J. Am. Chem. Soc.*, 1999, **121**, 3136; (*d*) Q.-M. Wang and T. C. W. Mak, *J. Am. Chem. Soc.*, 2000, **122**, 7608; (*e*) Q.-M. Wang and T. C. W. Mak, *J. Am. Chem. Soc.*, 2001, **123**, 1501; (*f*) Q.-M. Wang and T. C. W. Mak, *Angew. Chem., Int. Ed.*, 2001, **40**, 1130; (*g*) Q.-M. Wang and T. C. W. Mak, *Chem. Commun.*, 2001, 807.

6 (*a*) V. W.-W. Yam, W. K.-M. Fung and K.-K. Cheung, *Angew. Chem., Int. Ed. Engl.*, 1996, **35**, 1100; (*b*) M. I. Bruce, M. R. Snow, E. R. T. Tiekink and M. L. Williams, *J. Chem. Soc., Chem. Commun.*, 1986, 701.

7 (*a*) S.-M. Kuang, Z.-Z. Zhang and T. C. W. Mak, *J. Chem. Soc., Dalton Trans.*, 1998, 1115; (*b*) S.-M. Kuang, Z.-Z. Zhang, Q.-G. Wang and T. C. W. Mak, *J. Organomet. Chem.*, 1998, **558**, 131.

8 C.-M. Che, Z. Mao, V. M. Miskowski, M.-C. Tse, C.-K. Chan, K.-K. Cheung, D. L. Phillips and K. H. Leung, *Angew. Chem., Int. Ed.*, 2000, **39**, 4084.

9 (*a*) V. W.-W. Yam, W.-K. Lee, K.-K. Cheung, B. Crystall and D. Phillips, *J. Chem. Soc., Dalton Trans.*, 1996, 3283; (*b*) V. W.-W. Yam, W. K.-M. Fung and M.-T. Wong, *Organometallics*, 1997, **16**, 1772; (*c*) V. W.-W. Yam, W. K.-M. Fung and K.-K. Cheung, *Organometallics*, 1997, **16**, 2032; (*d*) V. W.-W. Yam, W. K. M. Fung and K.-K. Cheung, *Chem. Commun.*, 1997, 963; (*e*) P. C. Ford, E. Cariati and J. Bourassa, *Chem. Rev.*, 1999, **99**, 3625.

CHEMCOMM
Communication
www.rsc.org/chemcomm

Subtlety in the reactivity of a diketo phosphorus ylide towards mercuric halides: the unprecedented O-coordination of α-acetyl-α-benzoylmethylenetriphenylphosphorane to Hg(II)†

Parthasarathi Laavanya,[a] Ulaganathan Venkatasubramanian,[a] Krishnaswamy Panchanatheswaran*[a] and Jeanette A. Krause Bauer[b]

[a] *Department of Chemistry, Bharathidasan University, Tiruchirappalli 620 024, India. E-mail: pan@bdu.ernet.in*
[b] *Department of Chemistry, University of Cincinnati, OH 45221-0172, USA. E-mail: Jeanette.Krause@UC.edu*

Received (in Cambridge, UK) 9th May 2001, Accepted 20th July 2001
First published as an Advance Article on the web 6th August 2001

The reactions of the title ylide with HgX_2 (X = Cl, Br or I) lead to the regiospecific binding of the acetyl oxygen to soft Hg(II), producing a chloro complex with (2 + 2) coordination and isostructural dimeric bromo and iodo complexes containing halogen bridges with tetrahedral configurations around the metal centres.

The ambidentate resonance stabilized ylide, $Ph_3PCHCOPh$ coordinates through carbon and oxygen to Hg(II)[1,2] and U(VI),[3] respectively. The diketo ylide, α-acetyl-α-benzoylmethylenetriphenylphosphorane (ABPPY) has an additional oxygen site for coordination and can utilize different bonding modes. The symmetrical bidentate O-coordination of the carbonyl groups had been recently observed by us in its reaction with uranyl nitrate.[3] We present herein the regiospecific coordination of the diketo ylide to the soft metal center, Hg(II) *via* the acetyl oxygen. This paper represents the first report of O-coordination of any keto phosphorus ylide to Hg(II).

The parent ylide was prepared by the action of acetic anhydride on $Ph_3PCHCOPh$ and spectrally characterized as published.[4] The action of HgX_2 on an equimolar methanolic solution of the ylide afforded the complexes $HgCl_2(ABPPY)_2$ (**1**), $[HgBr_2(ABPPY)]_2$ (**2**) and $[HgI_2(ABPPY)]_2$ (**3**) which were formed as crystals, on cooling the concentrated solution. Elemental analyses of the products revealed their stoichiometry. In the FTIR spectra of the products, the ν_{CO} for the COMe group observed at 1537 cm^{-1} for ABPPY is shifted to 1526, 1573 and 1575 cm^{-1} in **1**, **2** and **3**, respectively. The corresponding frequencies for the COPh group occur at 1566, 1568, 1600 and 1596 cm^{-1} in the above molecules. It is significant that the ν_{CO} values are very similar in **2** and **3** as expected for the identical environment of their two carbonyl groups. In the $^{13}C\{^1H\}$ NMR spectra of the products in $CDCl_3$, the resonance due to the ylidic carbon at δ 86.35 as well as the $^1J_{PC}$ of 101.8 Hz observed for the free ylide is not very much shifted in the products. The ^{31}P NMR spectra contain a single signal around δ 17 for the ylide and each of the complexes. This suggests the presence of a single isomer in all the complexes, with the oxygen being bonded to the metal. In contrast, the C-coordination which implies a change in the hybridization for the ylidic carbon is characterized by its upfield ^{13}C chemical shifts[5] and also by the downfield shifts of ^{31}P NMR signals.[1] That the bonding of the ylide to Hg(II) in the chloro complex is much weaker than in the bromo and the iodo complexes is indicative in the ^1H NMR spectra in which the methyl group resonances appear at δ 1.80, 1.81, 1.70 and 1.71 for the free ylide and complexes **1**, **2** and **3**, respectively.

In order to establish the region and mode of coordination, single crystal X-ray analysis‡ of the complexes has been undertaken. The solid state structure of **1** shows that it adopts a square planar geometry with two collinear strong covalent Hg–Cl bonds referred to as 'characteristic coordination.' The preference for a characteristic coordination number of two for mercury in its complexes with electronegative ligands, as observed in **1** has been attributed to relativistic effects.[6] The Hg–O bond lengths are distinctly longer in the chloro complex and denoted[7] as 'secondary bonds.' The importance of such inter-species interactions has been realized in solid state architecture, molecular recognition, prototype 'ionic liquids' and biological chemistry.[8] Semiempirical calculations at the PM3 level[9] corroborate the geometry and bond parameters of **1**, discerned from X-ray crystallography. In particular, the calculated values, 173.9 and 179.2°, for O–Hg–O and Cl–Hg–Cl angles, respectively, are comparable to the experimental values (Fig. 1). Mulliken population analysis[10] on the title ylide shows that the oxygen of the COMe group possesses a higher negative charge (−0.47) than the oxygen of the COPh group (−0.38). The linear disposition of secondary bonds in **1** is traceable to the electrostatic interactions caused by the bulky ylide ligands precluding any weak covalent interactions involving p orbitals. The latter type of interactions is indicated by B3LYP[11]/LANL2DZ[12] calculations for the identical Hg–O bonds in $HgCl_2(HCHO)_2$[13] and likely to be present in the crystal structure of $HgCl_2$(chd) (chd = cyclohexane-1,4-dione) complex[14] with an observed O–Hg–O angle of 86°. The Hg(II) in each of the molecules **2** and **3** has a tetrahedral coordination environment with two unsymmetrically bridging Hg–X bonds. The oxygen of the acetyl group is oriented *cis* to the phosphorus

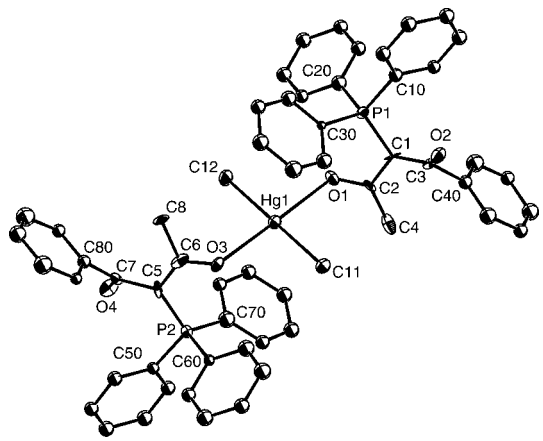

Fig. 1 ZORTEP view of **1** with 50% probability thermal ellipsoids and selected atom labelling scheme. The hydrogen atoms are omitted for clarity. Selected bond lengths (Å) and angles (°): Hg1–O1 2.707(2), Hg1–O3 2.735(2), Hg1–Cl1 2.283(4), Hg1–Cl2 2.297(3); O1–C2 1.275(11), O2–C3 1.227(11), O3–C6 1.249(12), O4–C7 1.247(11), P1–C1 1.788(8), P2–C5 1.731(10), Cl1–Hg1–Cl2 179.8(2), O1–Hg1–O3 179.0(2), Hg1–O1–C2 118.4(7), Hg1–O3–C6 123.5(7).

† Electronic supplementary information (ESI) available: analytical and spectroscopic data for **1**–**3**. See http://www.rsc.org/suppdata/cc/b1/b104082k/

 DOI: 10.1039/b104082k

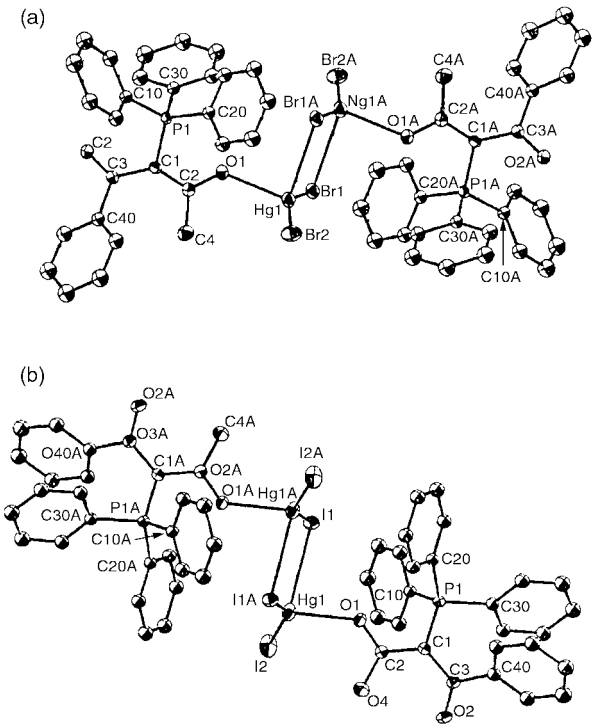

Fig. 2 ZORTEP view of **2** and **3** with 50% probability thermal ellipsoids and selected atom labelling scheme. The hydrogen atoms are omitted for clarity. Selected bond lengths (Å) and angles (°): for **2**: Hg1–O1 2.397(3), Hg1–Br1 2.4693(5), Hg1–Br2 2.4420(5), Hg1–Br1A 2.9997(5), O1–C2 1.270(5), O2–C3 1.239(5), P1–C1 1.770(4); O1–Hg1–Br1 100.86(7), O1–Hg1–Br2 105.87(7); O1–Hg1–Br1A 87.67(7), Br1–Hg1–Br1A 90.76(2), Hg1–O1–C2 128.9(3). For **3**: Hg1–O1 2.370(3), Hg1–I1 3.120(1), Hg1–I2 2.615(1), Hg1–I1A 2.676(1), O1–C2 1.269(5), O2–C3 1.223(5), P1–C1 1.766(4); O1–Hg1–I1 81.37(8), O1–Hg1–I2 104.05(8), O1–Hg1–I1A 102.80(8), I1–Hg1–I1A 92.49(1), Hg1–O1–C2 129.6(3).

in all the three complexes as is evident from the P–C–C–O torsion angles of 0.0 and 6.1° in **1**, 0.8° in **2** and 8.31° in **3**.

We conclude that novel bonding modes to Hg(II) could be mediated by the flexidentate ylide, ABPPY. It is significant that $HgCl_2$ prefers to form the 1:2 complex, *albeit* with secondary Hg··O interactions. The coordination of the ylide to mercury in **2** and **3** through the lone pair on the unpolarized acetyl oxygen is shown by the C2–O1 and C1–C2 bond lengths, by the bond angles around the trigonal acetyl oxygen (Fig. 2) and also by the upward shifts for the ν_{CO} of COMe group in the IR spectra of the products. This type of bonding that involves the canonical keto form of the ylide contrasts with the enolate bonding of $Ph_3PCHCOMe$.[15] We ascribe this keto-coordination of the ylide found in both **2** and **3** to the symbiotic effects of the softer halogens.

P. L. thanks the Council of Scientific and Industrial Research, Government of India for the award of Senior Research Fellowship [9/475(92)/99-EMRI]. The authors thank the Ohio Crystallographic Consortium, funded by the Ohio Board of Regents 1995 Investment Fund [(CA)-075] located at the University of Toledo, Instrumentation Center in A&S, Toledo, OH 43606, USA for X-ray data collection, the Sophisticated Instruments Facility, Indian Institute of Science, Bangalore, India, for recording ^{13}C NMR spectra for the samples and Dr Mariappan Manoharan, Post-Doctoral Fellow, Centre for Computational Quantum Chemistry, University of Georgia, Athens, GA 30602-2525, USA for DFT calculations.

Notes and references

‡ *Crystal data*: for **1**: $C_{56}H_{46}Cl_2HgO_4P_2$, a = 13.4399(2), b = 10.0105(3), c = 17.9576(4) Å, β = 100.525(2)°, V = 2375.37(10) Å^3, space group $P2_1$, Z = 2, D_c = 1.561 Mg m^{-3}, μ(Mo-Kα) = 3.467 mm^{-1}, reflections collected/unique 25177/11404, refinement method: full-matrix least-squares on F^2; data/restraints/parameters 11403/1/254, goodness-of-fit on F^2 1.025. Final R indices [$I > 2\sigma(I)$] R_1 = 0.0267, wR_2 = 0.0587; R indices (all data) R_1 = 0.0430, wR_2 = 0.0645.

For **2**: $C_{28}H_{23}Br_2HgO_2P$, a = 9.5287(6), b = 11.6425(8), c = 12.3992(8) Å, α = 94.835(2)°, β = 98.281(2), γ = 102.172(2)°, V = 1321.22(15) Å^3, space group $P1$, Z = 2, D_c = 1.968 Mg m^{-3}, μ(Mo-Kα) = 8.933 mm^{-1}, reflections collected/unique 13906/6329, refinement method: full-matrix least-squares on F^2, data/restraints/parameters 6329/0/142, goodness-of-fit on F^2 1.041. Final R indices [$I > 2\sigma(I)$] R_1 = 0.0310, wR_2 = 0.0743; R indices (all data) R_1 = 0.0371, wR_2 = 0.0766.

For **3**: $C_{28}H_{23}I_2HgO_2P$, a = 8.9528(2), b = 11.7157(3), c = 13.8223(2) Å, α = 107.6152(12), β = 91.6914(4), γ = 99.4180(4)°, V = 1358.37(5) Å^3, space group $P1$, Z = 2, D_c = 2.144 Mg m^{-3}, μ(Mo-Kα) = 8.020 mm^{-1}, reflections collected/unique 14475/6554, refinement method: full-matrix least-squares on F^2, data/restraints/parameters 6554/0/142, goodness-of-fit on F^2 1.019. Final R indices [$I > 2\sigma(I)$] R_1 = 0.0313, wR_2 = 0.0637; R indices (all data) R_1 = 0.0401, wR_2 = 0.0669.

The intensity data, collected at 150 K on a standard Siemens SMART 1K CCD diffractometer were corrected for decay, Lorentz and polarization effects. Non-hydrogen atoms anisotropic; hydrogen atoms in idealized positions. *Programs used*: SAINT[16] (X-ray data processing), SADABS[17] (absorption correction), MOPAC6.0[18] (semiempirical PM3 calculations) SIR-97, (structure solution) SHELX-97 (structure refinement), PARST96 (geometrical calculations) and ZORTEP (molecular Graphics).

CCDC reference numbers 167767–167769. See http://www.rsc.org/suppdata/cc/b1/b104082k/ for crystallographic data in CIF or other electronic format.

1 M. Kalyanasundari, K. Panchanatheswaran, W. T. Robinson and Huo Wen, *J. Organomet. Chem.*, 1995, **491**, 103.
2 B. Kalyanasundari, K. Panchanatheswaran, V. Parthasarathi and W. T. Robinson, *Bull. Chem. Soc. Jpn.*, 1999, **72**, 33.
3 M. Kalyanasundari, Ph.D. Thesis, Bharathidasan University, Tiruchirapalli, India, 1998.
4 P. A. Chopard, R. J. G. Searle and F. H. Devitt, *J. Org. Chem.*, 1965, **30**, 1015.
5 G. Facchin, R. Bertani, M. Calligaris, G. Nardin and M. Mari, *J. Chem. Soc., Dalton Trans.*, 1987, 1381.
6 M. Kaupp and H. G. von Schnering, *Inorg. Chem.*, 1994, **33**, 2555.
7 N. W. Alcock, *Adv. Inorg. Chem. Radiochem.*, 1972, **15**, 1.
8 W. Clegg, M. R. J. Elsegood and N. C. Norman, *J. Mater. Chem.*, 1994, **4**, 891; G. M. Whitesides, J. P. Mathias and C. T. Seto, *Science*, 1991, **254**, 1312; J. J. Golding, D. R. MacFarlane, L. Spiccia, M. Forsyth, B. W. Skelton and A. H. White, *Chem. Commun.*, 1998, 1593; D. H. Williams and M. S. Westwell, *Chem. Soc. Rev.*, 1998, **27**, 57.
9 J. J. P. Stewart, *J. Comput. Chem.*, 1989, **10**, 221.
10 R. S. Mulliken, *J. Chem. Phys.*, 1955, **23**, 1833.
11 A. D. Becke, *J. Chem. Phys.*, 1993, **98**, 5648.
12 M. J. Frish, G. W. Trucks, H. B. Schlegel, P. M. W. Gill, B. G. Johnson, M. A. Robb, J. R. Cheeseman, T. Keith, G. A. Petersson, J. A. Montgomery, K. Raghavachari, M. A. Alhaham, V. G. Zakrewski, J. W. Wong, J. L. Andres, E. S. Replogle, R. Gomperts, R. L. Matin, D. J. Fox, J. S. Binkley, D. J. Defrees, J. Baker, J. J. P. Stewart, M. H. Gordon, C. Gonzalez and J. A. Pople, GAUSSIAN94, revision B.3, Gaussian, Pittsburgh, PA, 1995.
13 Calculated parameters for $HgCl_2(HCHO)_2$: Hg–O 2.571 Å, C–O 1.248 Å, Hg–Cl 2.472, 2.542 Å; O–Hg–O 96.8, Cl–Hg–Cl 156.9°.
14 P. Groth and O. Hassel, *Acta Chem. Scand.*, 1964, **18**, 1327.
15 L. R. Falvello, S. Fernandez, R. Navarro and E. P. Urriolabeitia, *Inorg. Chem.*, 1996, **35**, 3064.
16 Siemens, SMART V5.051 and SAINT V5.A06, Area Detector Control and Integration Software, BRUKER-AXS Inc., Madison, WI, USA, 1994.
17 G. M. Sheldrick, SADABS, University of Göttingen, Germany, 1996.
18 J. J. P. Stewart, MOPAC6.0, QCPE No. 455, Indiana University, Bloomington, IN, 1990.

CHEMCOMM Communication
www.rsc.org/chemcomm

The effect of diethylamine on Stille alkylations with tetraalkylstannanes†

M. Teresa Barros,[a] Christopher D. Maycock,*[b] Mariana I. Madureira[b] and M. Rita Ventura[b]

[a] *Faculdade de Ciências e Tecnologia da, Universidade Nova de Lisboa, Departamento de Química 2825. Monte da Caparica, Portugal*
[b] *Instituto de Tecnologia Química e Biológica, Universidade Nova de Lisboa, Apartado 127 2780. Oeiras, Portugal. E-mail: maycock@itqb.unl.pt; Fax: +351 21 4469789; Tel: +351 21 4469775*

Received (in Cambridge, UK) 4th April 2001, Accepted 11th July 2001
First published as an Advance Article on the web 6th August 2001

The addition of diethylamine to Stille alkylation reactions using stannanes improves yields by reducing β-hydride elimination and reduction reactions, it also serves as a substitute for other additives such as Cu(I)I.

The Stille reaction is a member of a large family of palladium-catalysed cross-coupling reactions. However, its generality and high degree of success have made it popular among synthetic chemists. One obvious reason for such popularity is the reaction's versatility.[1] It is frequently used in the total syntheses of large polyfunctional molecules for the coupling of complex subunits.[2,3] However, it is sometimes found that it is not universally applicable and that many substrates require specific reaction conditions for cross-coupling to be successful.[1–5]

There are relatively few examples of the successful introduction of alkyl groups employing Stille cross-coupling reactions described in the literature,[6] and for α-iodocyclohexenones the reported yields are only moderate. This is probably due to failure resulting from competing β-hydride elimination when employing stannanes with alkyl groups bearing β-hydrogens and to the low reactivity of the system. A further problem often encountered is the competing reduction of vinylic or aromatic halides to the corresponding hydrocarbon. This can be a serious problem where the halide is unreactive.

Several reports have appeared relating to the importance of intramolecular participation by amino groups in Stille cross-coupling reactions. For example, it has been reported that alkyl derivatives of 1-aza-5-stannabicyclo[3.3.3]undecane were reactive in Stille couplings with aryl and alkenyl halides,[7,8] without β-hydride elimination. It was suggested that intramolecular tin–nitrogen coordination could be the reason.

A difficult case for Stille coupling is represented in Scheme 1 (Table 1) where the highly substituted aryl iodide **1** having an amido group reacted readily with allyl triphenylstannane in the presence of Pd to form the expected product **3** in good yield (95%). The ester **2** under a wide range of normally successful conditions afforded a maximum of 36% of **4**.

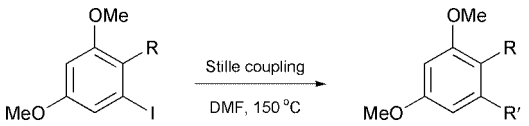

1 R = $CONEt_2$
2 R = CO_2Me

3 R = $CONEt_2$, R′ = $CH_2CH{:}CH_2$
4 R = CO_2Me, R′ = $CH_2CH{:}CH_2$

Scheme 1 Stille coupling at a polysusbstituted aromatic compound.

Table 1 Stille coupling at polysubstituted aromatic compounds **1** and **2**[a]

Cpd	Pd cat	Ligand	LiCl	Et_2NH	Prod.	Time	Yield
1	$Pd(PPh_3)_2Cl_2$	PPh_3	Yes	No	**3**	2 h	95%
2	$Pd(PPh_3)_2Cl_2$	PPh_3	Yes	No	**4**	1 h	36%
2	$Pd(PPh_3)_2Cl_2$	PPh_3	Yes	Yes	**4**	1 h	87%

[a] The solvent employed was DMF.

† Electronic Supplementary Information (ESI) available: Tables—Stille coupling of α-iodoenone **5** with Et_4Sn and Me_4Sn, and general procedure. See http://www.rsc.org/suppdata/cc/b1/b103072h/

Assuming that the nitrogen atom of the amide was facilitating the aryl transfer process for **1** by intramolecular chelation,[9] we added diethylamine to the reaction mixture, containing ester **2**, to ascertain if the corresponding intermolecular process was possible. This resulted in a 87% isolated yield of the expected allyl compound **4**. No amination[10] or amidification products were isolated. We next applied these findings to other cases.

Alkylation of the iodoenone **5** under 'normal' Stille conditions with tetrabutylstannane gave none of the expected butylated compound **6** but high yields of the reduced product **9** (Scheme 2). The addition of diethylamine to this reaction

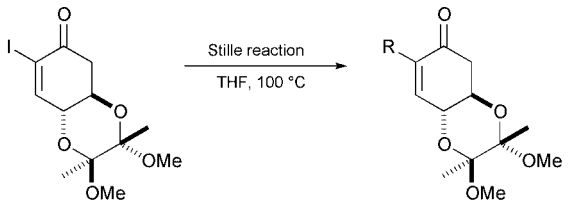

5

6 R = Bu
7 R = Et
8 R = Me
9 R = H
10 R = $(CH_2)_9CH_3$

Scheme 2 Stille coupling at a substituted α-iodoenone.

Table 2 Stille coupling of α-iodoenone **5** with Bu_4Sn under several conditions[a]

Pd catalyst	Ligand	CuI	Et_2NH	Prod	Time	Yield
$Pd_2(dba)_3{\cdot}CHCl_3$	$AsPh_3$	Yes	No	**9**	24 h	99%
$Pd_2(dba)_3{\cdot}CHCl_3$	$AsPh_3$	Yes	Yes	**6**	48 h	96%
$Pd_2(dba)_3{\cdot}CHCl_3$	$AsPh_3$	No	No	**9**	24 h	98%
$Pd_2(dba)_3{\cdot}CHCl_3$	$AsPh_3$	No	Yes	**6**	48 h	97%
$Pd_2(dba)_3{\cdot}CHCl_3$	PPh_3	Yes	No	**9**	48 h	60%
$Pd_2(dba)_3{\cdot}CHCl_3$	PPh_3	Yes	Yes	**9**	48 h	63%
$Pd_2(dba)_3{\cdot}CHCl_3$	PPh_3	No	No	**9**	48 h	54%
$Pd_2(dba)_3{\cdot}CHCl_3$	PPh_3	No	Yes	**9**	48 h	61%
$Pd(P(o\text{-tol})_3)_2Cl_2$	$P(o\text{-tol})_3$	No	Yes	**6**	48 h	99%
$Pd(P(o\text{-tol})_3)_2Cl_2$	$P(o\text{-tol})_3$	No	No	**9**	24 h	96%

[a] The solvent employed was THF.

Table 3 Effect of adding diethylamine to the Stille coupling of α-iodoenone **5** with $[CH_3(CH_2)_9]_4Sn$[a]

Pd catalyst	Ligand	CuI	Et_2NH	Prod	Time	Yield
$Pd_2(dba)_3{\cdot}CHCl_3$	$AsPh_3$	Yes	No	**9**	24 h	99%
$Pd_2(dba)_3{\cdot}CHCl_3$	$AsPh_3$	Yes	Yes	**10**	48 h	86%

[a] The solvent employed was THF.

 DOI: 10.1039/b103072h

Table 4 Stille coupling of methyl 2-iodobenzoate **11** with Bu_4Sn under several conditions

Pd Catalyst	Ligand	Solvent	LiCl	Et_2NH	Prod	Time	Yield
$Pd(P(o\text{-tol})_3)_2Cl_2$	$P(o\text{-tol})_3$	THF	No	No	**11**	24 h	70%
$Pd(P(o\text{-tol})_3)_2Cl_2$	$P(o\text{-tol})_3$	THF	No	Yes	**11**	24 h	99%
$Pd(P(o\text{-tol})_3)_2Cl_2$	$P(o\text{-tol})_3$	DMF	No	No	**12**	24 h	68%
$Pd(P(o\text{-tol})_3)_2Cl_2$	$P(o\text{-tol})_3$	DMF	Yes	Yes	**11**	48 h	96%
$Pd(P(o\text{-tol})_3)_2Cl_2$	$P(o\text{-tol})_3$	DMF	No	Yes	**12** + **11**[a]	48 h	96%
$Pd(PPh_3)_2Cl_2$	PPh_3	DMF	Yes	No	**12** + **13**[b]	48 h	97%
$Pd(PPh_3)_2Cl_2$	PPh_3	DMF	Yes	Yes	**12** + **11**[c]	48 h	99%
$Pd(PPh_3)_2Cl_2$	PPh_3	DMF	No	Yes	**12** + **11**[d]	48 h	98%

[a] 2.3:1. [b] 1.5:1. [c] 1:4. [d] 3.6:1.

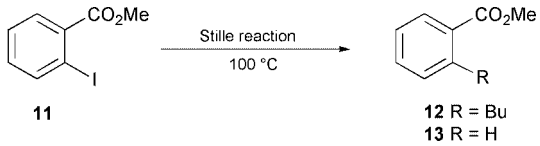

11 **12** R = Bu
13 R = H

Scheme 3

resulted in the formation of the butylated compound **6** in good yield (Table 2). This was also the case for tetraethylstannane and for tetradecylstannane. The products **7** and **10** were obtained in good yield. Without added diethylamine, the reduced product **9** was formed exclusively.

Having shown that diethylamine did influence the outcome of these reactions we next proceeded to approach optimisation by studying several variables for this reaction (Tables 2, 3). Thus, the influence of using Pd(0) or Pd(II) as catalyst sources, the effect of the Pd ligands (PPh_3, $P(o\text{-Tol})_3$ and $AsPh_3$), the presence of CuI as cocatalyst and the additon of LiCl for the aromatic substrates were analysed. We have concluded that both Pd(0) and Pd(II) were equally effective, as expected. The catalytic role of the Pd species was largely influenced by the ligand. $AsPh_3$ and $P(o\text{-Tol})_3$ were found to be the best ligands tested while PPh_3 was considerably less effective. Remarkably, we have observed that for the Stille coupling of iodoenone **5** with tetramethyltin, CuI could effectively be replaced by diethylamine. When this reaction was carried out in the presence of diethylamine the workup was considerably simplified and the yields consequently higher. Analogous reactions reported in the literature used involatile NMP as the solvent.

Studies on the electron poor aromatic substrate **11** were also carried out. For this compound the reaction conditions as used for the iodoenone, had to be changed and DMF became the solvent of choice. The use of diethylamine again prevented reduction, as seen for the reaction of **11** with tetrabutyltin. The yield of the coupling product **12** was not improved over that of the same reaction without added amine but starting material was recovered when Et_2NH was present, whereas several other products were formed in its absence (Scheme 3 and Table 4). The addition of LiCl[11] alone simplified the product distribution but did not avoid reduction and the yield of coupling product was zero or low. When both LiCl and Et_2NH were included in the mixture the coupling product **12** was produced in low yield and starting halide **11** was recovered as the only other product.

The function of the amine is not yet clear but we suspect that it augments the activity of the phosphine ligand in maintaining the Pd(0) in solution. This complexation with the Pd atom of intermediates may also reduce the ability to undergo β-hydride elimination reactions, once it has bonded with the alkyl group by exchanging with the tin.

In conclusion, the addition of diethylamine clearly prevented β-hydride elimination/reduction in the Stille alkylation reactions tested when employing alkylstannanes with β-hydrogens, a problem frequently reported in the literature.[1] Its addition permits the use of more volatile less polar solvents in some cases and can reduce reaction times, as is well exemplified in the case of tetramethyltin.† In this case too the work up and purification of the reaction products was facilitated and the need to use cocatalytic CuI was eliminated. This method permits the efficient introduction of alkyl side chains into the synthetically useful α-iodoenones,[12] which are particularly difficult substrates for this kind of Stille cross-coupling[13] reaction.

Recent reports[14] highlighting the use of organozincs and organoboranes for the alkylation of α-iodoenones and vinyl halides have been described. Reduction and/or β-hydride elimination not a problem in these cases. The mechanism of Pd catalysed coupling reactions[15] may change with the type of coupling reaction depending upon the metal or non-metal present.

We thank Fundação para a Ciência e a Tecnologia for generous financial support (PCTI/1999/QUI/36536) and for grants (Praxis XXI) awarded to M. R. V. and M. I. M.

Notes and references

1 V. Farina, V. Krishnamurthy and W. J. Scott, *The Stille Reaction*, Wiley Interscience, New York, 1998, and references therein
2 K. C. Nicolau, T. K. Chakraborty, A. D. Piscopio, N. Minowa and P. Bertinato, *J. Am. Chem. Soc.*, 1993, **115**, 4419.
3 D. A. Evans and W. C. Black, *J. Am. Chem. Soc.*, 1993, **115**, 4497.
4 T. N. Mitchell, *Metal-catalysed Cross-coupling Reactions*, Organotin Reactions in Cross Coupling, Wiley-VCH, Germany, 1998, 167–197.
5 X. Han, B. M. Stoltz and E. J. Corey, *J. Am. Chem. Soc.*, 1999, **121**, 7600.
6 F. Bellina, A. Carpita, D. Ciucci, M. De Santis and R. Rossi, *Tetrahedron*, 1993, **49**, 4677.
7 E. Vedejs, A. R. Haight and W. O. Moss, *J. Am. Chem. Soc.*, 1992, **114**, 6556.
8 M. S. Jensen, C. Yang, Y. Hsiao, N. Rivera, K. M. Wells, J. Y. L. Chung, N. Yasuda, D. L. Hughes and P. J. Reider, *Org. Lett.*, 2000, **2**, 1081.
9 J. M. Brown, M. Pearson, J. T. B. H. Jastrzebski and G. van Koten, *J. Chem. Soc., Chem. Commun.*, 1992, 1440.
10 M. H. Ali and S. L. Buchwald, *J. Org. Chem.*, 2001, **66**, 2560.
11 LiCl is known to inhibit coupling reactions in some circumstances, E. Piers, R. W. Friesen and B. A. Keay, *Tetrahedron*, 1991, **47**, 4555.
12 M. T. Barros, C. D. Maycock and M. R. Ventura, *Chem. Eur. J.*, 2000, **6**, 3991.
13 Stille coupling in ionic liquids has recently been reported, S. T. Handy and X. Zhang, *Org. Lett.*, 2001, **3**, 233.
14 E. Negishi, Z. Tan, S-Y Liou and B. Liao, *Tetrahedron*, 2000, **56**, 10197; A. Kamatani and L. E. Overman, *Org. Lett.*, 2001, **3**, 1229.
15 A. L Casado and P. Espinet, *J. Am. Chem. Soc.*, 1998, **120**, 8978.

CHEMCOMM
Communication
www.rsc.org/chemcomm

A new Hg^{2+}-selective chromoionophore based on calix[4]arenediazacrown ether†

Mi Jung Choi, Mi Yee Kim and Suk-Kyu Chang*

Department of Chemistry, Chung-Ang University, Seoul 156-756, Korea. E-mail: skchang@cau.ac.kr; Fax: +82 2 825 4736; Tel: +82 2 820 5199

Received (in Cambridge, UK) 1st February 2001, Accepted 12th July 2001
First published as an Advance Article on the web 6th August 2001

A new azophenol type chromogenic ionophore based on the *p-tert*-butylcalix[4]arenediazacrown ether was prepared: the ionophore exhibited a pronouncedly selective chromogenic behaviour toward Hg^{2+} ions among the surveyed guests of alkali, alkaline earth, transition and heavy metal ions in liquid–liquid extraction experiments.

Selective signaling of heavy metal ions is a very important topic for the detection and treatment of the toxic metal ions in various chemical systems including living systems.[1,2] There are, however, relatively few examples of designed sensors for the heavy metal ions in comparison with the variety of compounds developed for the alkali and alkaline earth metal ions.[3] For the selective recognition of soft heavy metal ions, nitrogen binding sites might be a choice as is well exemplified with classical azacrown ethers.[4] Obviously, a suitably designed calix[4]-areneazacrown ether derivative might be a good candidate. This can be realized by combining the azacrown ether moiety as a binding site with the molecular framework of a calix[4]arene as a handle for the elaborate further functionalization to endow the signaling properties.[5] Recently, sensitive ionophores having chromogenic and fluorogenic functions have begun to be devised for heavy metal ions.[6–11] Azophenol groups are one of the most frequently employed functions as a signaling device for the design of chromogenic ionophores and a lot of derivatives based on the crown ethers and calixarenes showed unique chromogenic behaviours toward a variety of guest species.[12] Here, we report the synthesis of a new chromogenic ionophore having 2,4-dinitrophenylazophenol functions derived from the *p-tert*-butylcalix[4]arenediazacrown ether and its selective chromoionophoric behaviour toward Hg^{2+} ions in liquid–liquid extraction systems.

The azophenol derivative was prepared from diazacrown ether **1**,[13] as shown in Scheme 1. Oxidation of the diazacrown ether **1** with $Tl(CF_3CO_2)_3$ in TFA gave the diquinone **2** (61%).‡ Reaction of the resulting diquinone **2** with 2,4-dinitrophenylhydrazine (EtOH–$CHCl_3$, with trace H_2SO_4)[14] afforded 2,4-dinitrophenylazophenol derivative **3** (44%). The resulting product was purified by column chromatography (silica gel, CH_2Cl_2–MeOH, 9:1) followed by recrystallization from CH_2Cl_2–MeOH.

The chromoionophoric properties of the azophenol **3** were investigated by the liquid–liquid extraction of metal ions from buffered aqueous solution into chloroform. The azophenol **3** itself showed a typical UV spectral behaviour of 2,4-dinitrophenylazophenol derivatives and revealed a distinct colour change from yellow (λ_{max} = 424 nm) to blue (λ_{max} = 619 nm) around pH 8.5 as the pH of the aqueous phase increases. The metal ion extraction experiments were performed at pH 6 buffered with morpholin-4-ylethanesulfonic acid (MES) to prevent the possible complications in chromogenic responses of **3**. The aqueous solution containing varying amounts of target metal ions (up to 0.05 mol dm^{-3}) was extracted with the chloroform solution containing azophenol ionophore ([**3**] = 2 × 10^{-5} mol dm^{-3}) at 25 °C. After extraction, the organic phase

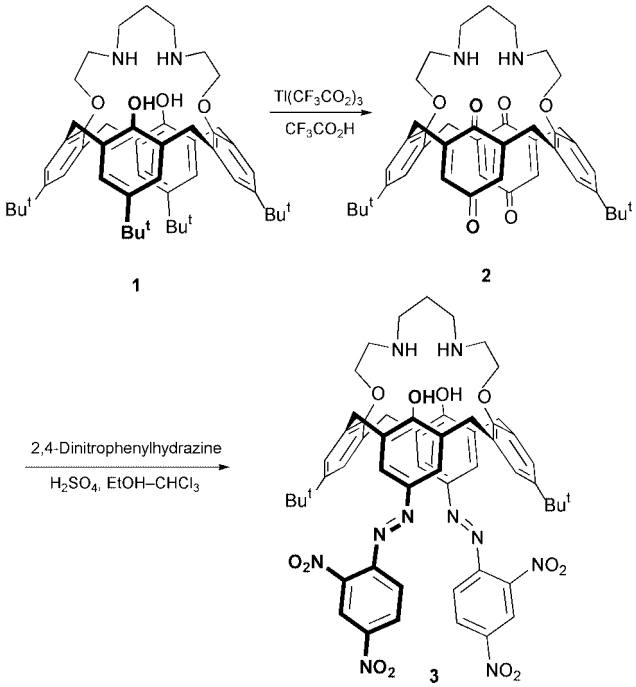

Scheme 1

was separated and the UV spectra of the solution were measured. The guest ions surveyed were representative alkali (Li^+, Na^+, K^+, Rb^+), alkaline earth (Mg^{2+}, Ca^{2+}, Ba^{2+}), transition metal (Co^{2+}, Ni^{2+}, Cu^{2+}, Zn^{2+}) and heavy metal ions (Cd^{2+}, Hg^{2+}, Pb^{2+}) in perchlorate.

The ionophore showed pronounced chromogenic responses to Hg^{2+} and Cd^{2+} ions among the tested metal ions (Fig. 1). Upon interaction with 100 equiv. of Hg^{2+} ions, the colour of the ionophore solution changed distinctly from yellow (λ_{max} = 424 nm) to red (λ_{max} = 500 nm). With Cd^{2+} ions, a more dramatic change in the UV spectrum was observed and the λ_{max} of **3** was significantly red-shifted and transformed into two bands (from

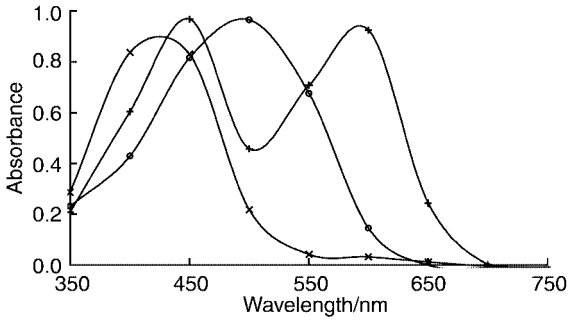

Fig. 1 Absorption spectra of **3** in $CHCl_3$ upon extraction with aqueous metal ion solution. [**3**] = 2 × 10^{-5} mol dm^{-3} in $CHCl_3$. [M^{2+}] = 2 × 10^{-3} mol dm^{-3} in MES buffer at pH 6: (×) **3**, (+) **3** with Cd^{2+} and (○) **3** with Hg^{2+}.

† Dedicated to Professor Iwhan Cho on the occasion of his 65th birthday.

 DOI: 10.1039/b101112j

Table 1 Spectral responses of **3** upon interaction with varying chemical stimuli

Initial form[a]	Reagent added[b]	Final form
3–Hg^{2+}	Cd^{2+}	**3**–Hg^{2+}
3–Hg^{2+}	EDTA	**3**[c]
3–Cd^{2+}	Hg^{2+}	**3**–Hg^{2+}
3–Cd^{2+}	EDTA	**3**

[a] Formed by the extraction with 50 equiv. of guest metal ions. [**3**] = 2×10^{-5} mol dm^{-3} in $CHCl_3$. [b] Concentration of reagents added = 5×10^{-3} mol dm^{-3}. [c] Transforms relatively sluggishly compared with **3**–Cd^{2+}–EDTA system.

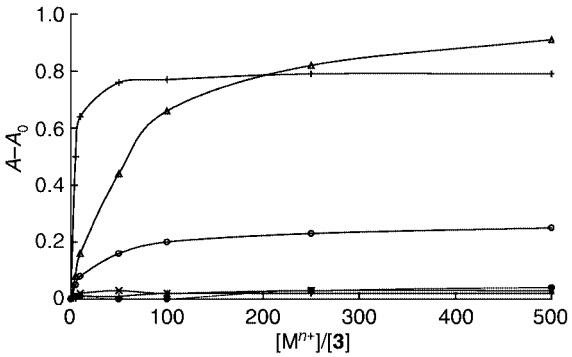

Fig. 2 Changes in absorbance of **3** induced by metal ions. ΔAbs at 500 nm with the addition of (×) Na^+, (*) Mg^{2+}, (●) Zn^{2+}, (○) Cd^{2+} and (+) Hg^{2+} ions. (△) ΔAbs at 591 nm with Cd^{2+} ion addition. [**3**] = 2×10^{-5} mol dm^{-3}. ΔAbs = (Abs of **3** in the presence of metal ion − Abs of **3**).

424 to 457 and 591 nm). Interestingly, the changes in spectral pattern induced by Cd^{2+} ions are quite different from Hg^{2+} ions, which suggests that the two metal ions can be discriminated, even visually, with the present chromogenic ionophore system. Other guest ions of alkali, alkaline earth, and transition metal ions revealed almost no changes in the chromogenic behaviour of **3** at the present extraction conditions of pH 6.

The selective chromogenic behaviour of **3** toward Hg^{2+} ions was further evidenced by the competitive extraction experiments. The ionophore **3** showed a pronounced Hg^{2+}-selectivity even in the presence of a large excess of other metal ions. For example, the absorption spectrum of **3**–Hg^{2+} (obtained by the extraction of 2×10^{-5} mol dm^{-3} of **3** with 50 equiv. Hg^{2+} ions) in $CHCl_3$ was almost unaffected by the addition of 500 equiv. of alkali, alkaline earth, transition metal, and Pb^{2+} ions. Even with Cd^{2+} as competitive guest ion, the chromogenic behaviour of the **3**–Hg^{2+} system was retained up to 250 equiv. of Cd^{2+} ions (Table 1). In contrast to this, the spectral behaviour of **3**–Cd^{2+} was changed upon addition of 2 equiv. of Hg^{2+} ions, and the spectrum was progressively converted into almost that of **3**–Hg^{2+} system by treatment with 30 equiv. of Hg^{2+} ions. These observations clearly showed that the ionophore **3** has much higher affinity toward Hg^{2+} than Cd^{2+} ions, that is in good agreement with the transport results of parent calix[4]-arenediazacrown compound **1** reported earlier.[13]

To have more insight for the selectivity and sensitivity of the present ionophore system, the effects of metal ion concentration in aqueous phase on the absorption spectrum of **3** were investigated. Fig. 2 shows the changes in absorbance of **3** induced by the most responding ions among the surveyed alkali, alkaline earth, transition and heavy metal ions. The selectivity ratios for Hg^{2+} over other representative metal ions, estimated from the ratio of the metal ions required for the same ΔAbs value at 500 nm, were as follows: Na^+, 830; Mg^{2+}, 480; Zn^{2+}, 250; Cd^{2+}, 28. Upon interaction with as low as 4 equiv. of Hg^{2+} ions, visibly discernible changes in chromogenic behaviour were observed for **3**. With Cd^{2+} ions, similar colour change from yellow to violet was observed with around 10 equiv. of guest ions, that can also be easily detected visually. From these measurements the detection limits of **3** for Hg^{2+} and Cd^{2+} ions were estimated to be 1×10^{-5} mol dm^{-3} (at 500 nm) and 8×10^{-5} mol dm^{-3} (at 591 nm), respectively. One more thing to note is the facile regeneration of the ionophore by simple treatment with EDTA solution, that suggests the reusability of the compound as a reversible sensor material. The ionophore solution **3**–Hg^{2+} and **3**–Cd^{2+} fully restored the spectrum of free **3** by the back extraction of extracted guest metal ions with 0.1 mol dm^{-3} EDTA solution at pH 6 (Table 1). In this case, however, the **3**–Hg^{2+}–EDTA system restores the free **3** spectrum relatively sluggishly compared with the **3**–Cd^{2+}–EDTA system, which also implies that Hg^{2+} interacts more strongly with **3** than Cd^{2+} ions.

In conclusion, we have developed a new azophenol type chromogenic ionophore having high selectivity toward Hg^{2+} and possibly Cd^{2+} ions *via* metal ion induced deprotonation of the azophenol moieties. Although ionophore **3** needs more optimization for the practical applications in terms of selectivity and sensitivity, we believe that this compound can be utilized, along with many intriguing systems developed up to now,[15,16] for the detection of toxic Hg^{2+} and Cd^{2+} ions which are of general interest in the treatment of industrial waste streams.

This work was supported by a fund from KOSEF, Korea (1999-2-123-001-3) and gratefully acknowledged.

Notes and references

‡ *Selected data for* **2**: ^{1}H NMR ($CDCl_3$, 300 MHz) δ 6.92 (s, 4H, quinone-H), 6.69 (s, 4H, ArH), 4.01 (br t, 4H, OCH_2CH_2N), 3.91 and 3.29 (d, 4H each, J = 13.5 Hz, $ArCH_2Ar$), 3.03 (br t, 4H, OCH_2CH_2N), 2.96 (br t, 4H, $NCH_2CH_2CH_2N$), 1.72 (br m, 2H, $NCH_2CH_2CH_2N$), 1.12 (s, 18H, CMe_3); FAB MS (*m*-NBA), *m*/*z* 691 (M + 1)$^+$. For **3**: ^{1}H NMR ($CDCl_3$, 300 MHz) δ 8.78 (s, 2H, ArH), 8.48 and 7.82 (d, 2H each, J = 9 Hz, ArH), 7.78 and 7.08 (s, 4H each, ArH), 4.37 and 3.57 (d, 4H each, J = 13.2 Hz, $ArCH_2Ar$), 4.28 (br t, 4H, OCH_2CH_2N), 3.33 (br t, 4H, OCH_2CH_2N), 3.13 (br t, 4H, $NCH_2CH_2CH_2N$), 2.08 (br m, 2H, $NCH_2CH_2CH_2N$), 1.11 (s, 18H, CMe_3); FAB MS (*m*-NBA), *m*/*z* 1051.5 (M + 1)$^+$.

1 *Chemosensors of Ion and Molecule Recognition*, ed. J. P. Desvergne and A. W. Czarnik, Kluwer, Dordrecht, 1997.
2 *Fluorescent Chemosensors for Ion and Molecule Recognition*, ed. A. W. Czarnik, American Chemical Society, Washington, DC, 1993.
3 A. P. de Silva, H. Q. N. Gunaratne, T. Gunnlaugsson, A. J. M. Huxley, C. P. McCoy, J. T. Rademacher and T. E. Rice, *Chem. Rev.*, 1997, **97**, 1515.
4 J.-M. Lehn and F. Montavon, *Helv. Chim. Acta*, 1978, **61**, 67.
5 C. D. Gutsche, *Calixarenes Revisited*, The Royal Society of Chemistry, Cambridge, 1998.
6 G. G. Talanova, N. S. A. Elkarim, V. S. Talanov and R. A. Bartsch, *Anal. Chem.*, 1999, **71**, 3106.
7 L. Prodi, C. Bargossi, M. Montalti, N. Zaccheroni, N. Su, J. S. Bradshaw, R. M. Izatt and P. B. Savage, *J. Am. Chem. Soc.*, 2000, **122**, 6769.
8 G. G. Talanova, H.-S. Hwang, V. S. Talanov and R. A. Bartsch, *Chem. Commun.*, 1998, 1329.
9 K. Rurack, M. Kollmannsberger, U. Resch-Genger and J. Daub, *J. Am. Chem. Soc.*, 2000, **122**, 968.
10 J. Yoon, N. E. Ohler, D. H. Vance, W. D. Aumiller and A. W. Czarnik, *Tetrahedron Lett.*, 1997, **38**, 3845.
11 B. Vaidya, J. Zak, G. J. Bastiaans, M. D. Porter, J. L. Hallman, N. A. R. Nabulsi, M. D. Utterback, B. Strzelbicka and R. A. Bartsch, *Anal. Chem.*, 1995, **67**, 4101.
12 T. Hayashita and M. Takagi, *Comprehensive Supramolecular Chemistry, Vol. 1*, ed. G. W. Gokel, Pergamon, Oxford, 1996, pp. 635–669.
13 M. J. Choe, M. Y. Kim and S.-K. Chang, *Chem. Lett.*, 2000, 1432.
14 N. Y. Kim and S.-K. Chang, *J. Org. Chem.*, 1998, **63**, 2362.
15 O. Brümmer, J. J. La Clair and K. D. Janda, *Org. Lett.*, 1999, **1**, 415.
16 L. Prodi, M. Montalti, N. Zaccheroni, J. S. Bradshaw, R. M. Izatt and P. B. Savage, *Tetrahedron Lett.*, 2001, **42**, 2941.

CHEMCOMM Communication
www.rsc.org/chemcomm

The first bis-Rh(I) metal complex of *N*-confused porphyrin†

Alagar Srinivasan,[a] Hiroyuki Furuta*[ab] and Atsuhiro Osuka*[a]

[a] *Department of Chemistry, Graduate School of Science, Kyoto University, Kyoto 606-8502, Japan. E-mail: hfuruta@kuchem.kyoto-u.ac.jp; osuka@kuchem.kyoto-u.ac.jp*
[b] *PRESTO, Japan Science and Technology Corporation (JST), Japan*

Received (in Cambridge, UK) 4th May 2001, Accepted 20th July 2001
First published as an Advance Article on the web 15th August 2001

An inner- and outer-*N* coordinated bis-Rh(I) metal complex was obtained from the reaction of *N*-confused porphyrin and $[Rh(CO)_2Cl]_2$ in CH_2Cl_2 and the structure was confirmed by a single crystal X-ray analysis.

N-Confused porphyrin (NCP) is a porphyrin isomer in which one of the pyrrole rings is *confused* or *inverted*.[1,2] Because of the unique NCP structure, which has peripheral nitrogen and inner core carbon atoms, entirely different coordination chemistry from the parent porphyrin system has been expected and revealed gradually.[3–5] Recently, we reported a new type of double-decker Pd NCP dimer complex that used both the inner- and outer-N coordination sites with the help of a carbon–metal bond from an *ortho*-position of a *meso*-aryl ring (**A**).[6] At that

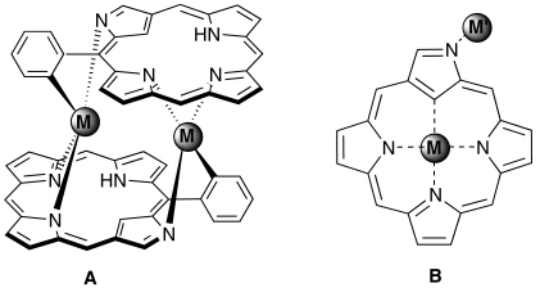

point, it was really a question whether outer-*N* coordination was general and whether the complex formed could be stabilized without any assistance from the surroundings (**B**). Such coordination, if manipulated easily, would be of particular interest for potential use in metal catalysts.[7] Herein, we report the X-ray structure of a bis-Rh(I) NCP complex where the Rh(I) metal atoms are coordinated to the inner- and the outer-nitrogen atoms. For comparison, the X-ray structure of the bis-Rh(I) tetraphenylporphyrin (TPP) complex is also presented.[8] To the best of our knowledge, the structures are the first examples of bis-Rh(I) complexes of *meso*-phenylporphyrin and NCP.

When *N*-confused tetraphenylporphyrin (NCTPP, **1**) was treated with 1 equiv. of $[Rh(CO)_2Cl]_2$ in the presence of 10 equiv. of sodium acetate in refluxing CH_2Cl_2 for 2 h, bis-Rh(I) NCTPP complex **2** was obtained as a blue-greenish solid in 53% yield. Using the same procedure with TPP (**3**), bis-Rh(I) TPP complex **4** was obtained as a purple solid in 36% yield (Scheme 1). FAB mass spectra of **2** and **4** showed molecular ion peaks at *m/z* 967.5 and 930.6, respectively, indicating the presence of two Rh metal ions connected with a chloride and four carbonyl ligands in **2** and the absence of the chloride ligand in **4**. ^{1}H NMR spectral peaks of complex **2** in $CDCl_3$ appeared distinctly in the region from −4 ppm to 9 ppm. The appearance of peaks corresponding to inner β-CH, outer α-CH and an inner NH at −3.83, 8.89 and 1.06 ppm, respectively, proved that they do not participate in the metal coordination and further confirms that only two pyrrolic nitrogens are coordinated to the Rh metal in

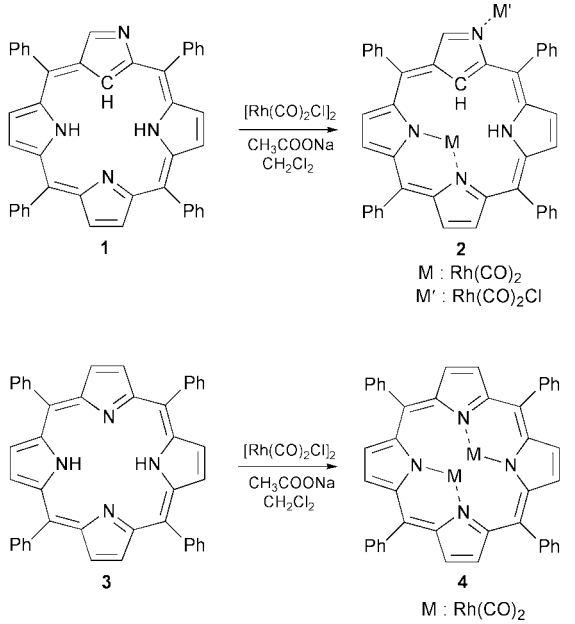

Scheme 1 Syntheses of bis-Rh(I) metal complexes.

the cavity. Relative to NCTPP (**1**), there is significant shielding of the inner α-CH and the outer β-CH signals ($\Delta\delta$ = 1.28 and 0.11 ppm) suggesting that the peripheral nitrogen also participates in the metal coordination. In contrast, the absence of NH signals for complex **4** inferrs that all four nitrogens are involved in the metal coordination.

The absorption spectrum of **2** in CH_2Cl_2 displays a Soret-like band at 488 nm and four Q-type bands in the region of 545–780 nm (Fig. 1). In general, the metal complexation is accompanied by a red-shift of both the Soret and Q-type bands.[9] The bis-metallic complex of **2** also shows 50 nm and 44 nm red-shifts of the Soret and the Q-type bands, respectively, as compared to **1**. This proves that the peripheral nitrogen coordination should not perturb the π electron delocalization much, while the Rh coordinated inside the cavity is expected to perturb the

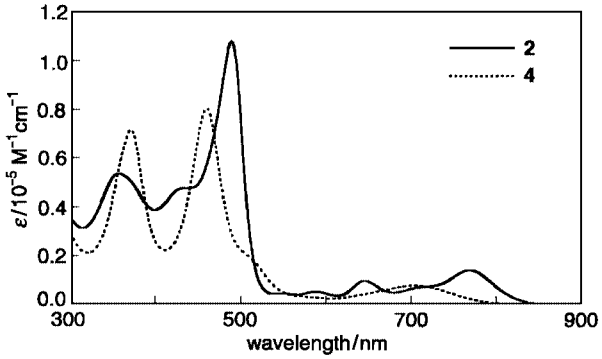

Fig. 1 Electronic absorption spectra of **2** and **4** in CH_2Cl_2.

† Electronic supplementary information (ESI) available: synthetic procedures and X-ray structure information for **2** and **4**. See http://www.rsc.org/suppdata/cc/b1/b104004a/

 DOI: 10.1039/b104004a

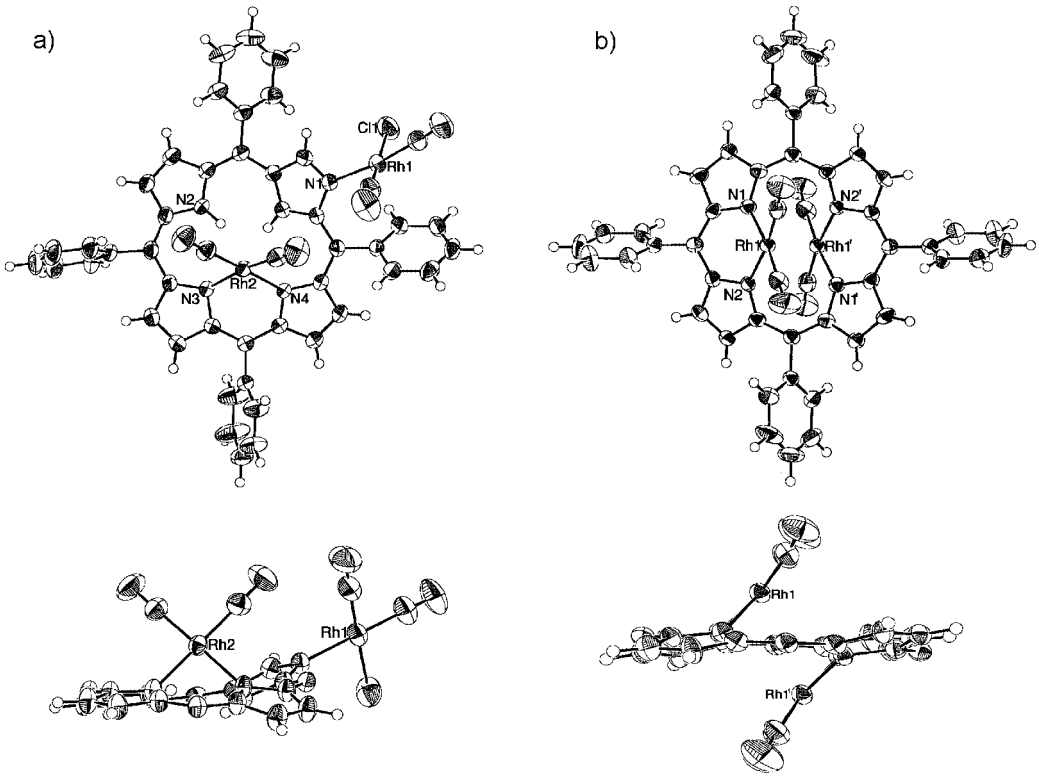

Fig. 2 X-Ray structures of (a) **2** and (b) **4**. The *meso*-aryl rings are omitted for clarity in the side views (bottom). Selected bond lengths (Å) for **2**: Cl1–Rh1, 2.349(3); Rh1–N1, 2.104(6); Rh2–N3, 2.099(6); Rh2–N4, 2.0877(6); and for **4**: Rh1–N1, 2.067(6), Rh1–N2, 2.074(6).

delocalization pathway, and this is reflected in the larger optical absorption band shifts. This trend is further confirmed by the absorption spectrum of **4** where both the Rh are coordinated inside the cavity leading to strong distortion of the molecule and resulting in bands at 371, 460 and 704 nm (Fig. 1).

The explicit structural details of the bis-Rh(I) complexes **2** and **4** were derived from the single crystal X-ray diffraction analyses (Fig. 2).[10] As predicted from the above observations, in the bis-metallic complex of **2**, there are two Rh atoms attached in the NCP skeleton. One imino (N3) and one amino (N4) nitrogen of the macrocycle are coordinated to the Rh2 ion and the other two coordination sites are occupied by the carbonyl ligands. The other Rh1 ion is coordinated to the periphery nitrogen (N1) and the remaining coordination sites are occupied by a chloride and the two carbonyl ligands. Both the Rh(I) ions are located above the NCP plane and the geometry around the metal centers is close to square planar (Cl1–Rh1–N1, 87.6(2)°; N3–Rh2–N4, 85.7(2)°). The angles between the planes containing the Rh1 and the Rh2 with their coordinated atoms and the mean NCP plane are 117.29° and 61.30°, respectively, and the distance between the two Rh metal centers is 6.286 Å.

On the other hand, the metalloporphyrin of **4** is centrosymmetric and the two Rh(I) metal ions are bonded to two dipyrromethene units, one above and one below the macrocyclic plane. Like **2**, the geometry around the metal centers is close to square planar (N1–Rh1–N2, 84.9(2)°). The angle between the plane containing the Rh(1) with its coordinated atoms and the mean TPP plane is 131.59° and the distance between the two metal centers is 3.166 Å, which is considerably longer than the Rh(I)–Rh(I) single bond (2.617–2.705 Å).[11] These results are comparable with the bis-Rh(I) octaethylporphyrin (OEP) complex.[8]

In conclusion, we have synthesized two new bis-Rh(I) metal complexes and disclosed their solid state structures. Inner- and outer-metallation is characteristic of NCP ligands, thus, for **2**, rich and diverse coordination chemistry similar to the parent porphyrin (**1**) can be expected. The present study has also exploited the interaction of only Rh(I) metal ions, but other metal ions are likely to interact with the macrocycle, especially at the peripheral nitrogen. Studies on the synthesis of such hetero bis-metal NCP complexes are currently underway.

Notes and references

1 H. Furuta, T. Asano and T. Ogawa, *J. Am. Chem. Soc.*, 1994, **116**, 767.

2 P. J. Chmielewski, L. Latos-Grażyński, K. Rachlewicz and T. Głowiak, *Angew. Chem., Int. Ed. Engl.*, 1994, **33**, 779.

3 L. Latos-Grażyński, in *The Porphyrin Handbook*, ed. K. M. Kadish, K. M. Smith and R. Guilard, Academic Press, San Diego, 1999, vol. 2, ch. 14.

4 P. J. Chmielewski, L. Latos-Grażyński and T. Głowiak, *J. Am. Chem. Soc.*, 1996, **118**, 5690; P. J. Chmielewski, L. Latos-Grażyński and I. Schmidt, *Inorg. Chem.*, 2000, **39**, 5475; P. J. Chmielewski and L. Latos-Grażyński, *Inorg. Chem.*, 2000, **39**, 5639.

5 H. Furuta, T. Ogawa, Y. Uwatoko and K. Araki, *Inorg. Chem.*, 1999, **38**, 2676; T. Ogawa, H. Furuta, M. Takahashi, A. Morino and H. Uno, *J. Organomet. Chem.*, 2000, **611**, 551; H. Furuta, H. Maeda and A. Osuka, *J. Am. Chem. Soc.*, 2000, **122**, 803.

6 H. Furuta, N. Kubo, H. Maeda, T. Ishizuka, A. Osuka, H. Nanami and T. Ogawa, *Inorg. Chem.*, 2000, **39**, 5424.

7 J. Tsuji, *Palladium Reagents and Catalysts*, Wiley, Chichester, 1995, p. 87.

8 The crystal structure of bis-Rh(I)OEP was reported. A. Takenaka, Y. Sasada, T. Omura, H. Ogoshi and Z. Yoshida, *J. Chem. Soc., Chem. Commun.*, 1973, 792.

9 M. Gouterman, in *The Porphyrins*, ed. D. Dolphin, Academic Press, New York, 1978, vol. 3, pp. 1–165.

10 Bis-Rh(I)NCP (**2**): green prism, $C_{48.5}H_{31}N_4Rh_2O_{4.5}Cl_2$, M_w 1018.52, monoclinic, space group *C*2/*c* (#15), a = 18.0381(3), b = 31.4290(5), c = 17.1686(3) Å, β = 111.3050(6)°, V = 9068.0(2) Å^3, Z = 8, $D_{calc.}$ = 1.492 g cm^{-3}, T = 23 °C. Final R = 0.039 (GOF = 0.49) for 7278 observed reflections with $I > 3.00\sigma(I)$, R_w = 0.072 for 10611 all unique data. Bis-Rh(I)TPP (**4**): brown prism, $C_{49}H_{30}N_4Rh_2O_4Cl_2$, M_w 1015.52, monoclinic, space group *C*2/*c* (#15), a = 21.695(2), b = 11.1778(7), c = 21.600(1) Å, β = 120.957(3)°, V = 4492.0(5) Å^3, Z = 4, $D_{calc.}$ = 1.501 g cm^{-3}, T = 23 °C. Final R = 0.046 (GOF = 1.91) for 3014 observed reflections with $I > 3.00\sigma(I)$, R_w = 0.0763 for 5415 all unique data. CCDC reference numbers 164092 and 164093. See http://www.rsc.org/suppdata/cc/b1/b104004a/ for crystallographic data in CIF or other electronic format.

11 O. S. Mills and E. F. Paulus, *J. Organomet. Chem.*, 1967, **10**, 331; O. S. Mills and J. P. Nice, *J. Organomet. Chem.*, 1967, **10**, 337.

CHEMCOMM Communication
www.rsc.org/chemcomm

Photoluminescence of open-framework phosphates and germanates

Pingyun Feng

Department of Chemistry, University of California, Riverside, CA 92521, USA.
E-mail: pingyun.feng@ucr.edu

Received (in West Lafayette, IN, USA) 27th June 2001, Accepted 9th July 2001
First published as an Advance Article on the web 16th August 2001

Upon excitation by long wavelength UV radiation, strong room temperature luminescence is observed in a family of metal-activator-free zeolite-type materials; the luminescent output from the large cage UCSB-8Mg structure is independent of temperature from 298 K until at least 77 K.

The development of less-expensive and non-toxic luminescent materials for lighting and display technology represents a research area that could have significant commercial impact. In particular, efficient phosphors that could convert low energy UV radiation (340 to 400 nm) into visible light may lead to the replacement of toxic mercury widely used in fluorescent lamps. So far, the synthetic design of inorganic phosphors usually involves the doping of crystalline host lattices with metal activators that can be either expensive or toxic.[1]

Open-framework materials have been known for several decades and have undergone an explosive growth since the discovery of zeolite-type aluminophosphates.[2] Previous efforts to generate luminescent materials using crystalline porous materials were either by incorporating organic dyes or by doping with metal activators.[3] For example, laser action was observed when organic laser dye molecules, pyridine 2 {1-ethyl-4-[4-(*p*-dimethylaminophenyl)-1,3-butadienyl]pyridinium perchlorate}, were inserted into the pores of $AlPO_4$-5 crystals.[4] To our knowledge, dye-free or metal-activator-free open-framework phosphates or germanates that display luminescent properties have not been reported. Furthermore, no open-framework materials were previously known to display both fluorescence and phosphorescence. Here, a class of efficient luminescent crystalline open-framework materials that do not contain metal activators are described.† Some of these phosphors can display visually observable green afterglow with a lifetime up to 15 s.

One particularly interesting example is UCSB-8Mg (Fig. 1 and Table 1).[5] UCSB-8Mg is built from stacking of large cages, each of which has as many as 64 tetrahedral atoms (*i.e.* Mg, Al, P) and 128 oxygen atoms. Clear, transparent square plates of UCSB-8Mg can be synthesized by the low temperature hydrothermal synthesis. When illuminated with a long wavelength UV lamp (365 nm), the sample displays a strong bluish color. Surprisingly, the luminescent output from UCSB-8Mg is independent of temperature until at least 77 K, suggesting that there might be no thermal non-radiative decay, even at room temperature. The lack of thermal non-radiative decay, could lead to a reasonably high quantum efficiency for UCSB-8Mg. The method of using the temperature dependence of the light output of a luminescent material to estimate the quantum efficiency was described earlier.[6] For open-framework materials, in addition to the possible intensity increase at lower temperatures, the luminescence bands also show a noticeable blue-shift (Fig. 2).

Another example is UCSB-10Mg (Table 1) with large cages and a framework topology closely related to that of faujasite.[5] Excited at 340 nm, the room temperature luminescence of UCSB-10Mg gives an emission band at λ_{max} = 402 nm (Fig. 1). The fit to a biexponential equation gives τ = 7.2 ns and 2.0 ns. The strong luminescence of UCSB-10Mg is persistent even at

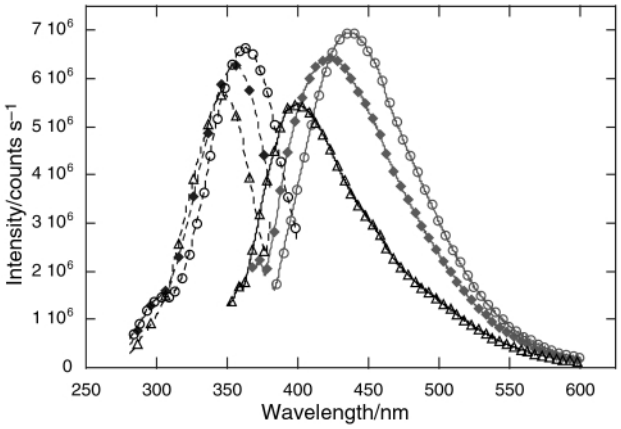

Fig. 1 The excitation (dashed curves) and emission spectra (solid curves) for selected open-framework materials. (△): UCSB-10Mg; (◆): UCSB-7AlGe; (○): UCSB-8Mg. Intensity data for UCSB-10Mg and UCSB-8Mg are multiplied by 5 and 3, respectively. Fluorescent spectra were measured on a SPEX Fluorolog-3 Tau3 system equipped with a 450 W xenon lamp and double monochromators on both excitation and emission sides. Data were collected with a step size of 1 Å and an integration time of 1 s per step.

Table 1 Photoluminescent properties of selected open-framework materials

Name	Framework composition	Guest type[a]	Structure type[b]	Emission λ_{max}/nm
UCSB-10Mg	$MgAlP_2O_8$	R4710	SBT	402
UCSB-10Zn	$ZnAlP_2O_8$	R4710	SBT	407
UCSB-6Mg	$MgAlP_2O_8$	R17	SBS	410
UCSB-6Zn	$ZnAlP_2O_8$	R17	SBS	408
UCSB-8Mg	$MgAlP_2O_8$	R19	SBE	436
UCSB-10ZnGa	$ZnGaP_2O_8$	R4710	SBT	415
UCSB-7AlGe	$Al_{1-x}Ge_{1+x}O_4$	R33	UCSB-7	421
UCSB-7GaGe	$Ga_{1-x}Ge_{1+x}O_4$	R1	UCSB-7	396
UCSB-7K	$GaGeO_4$	K^+, H_2O	UCSB-7	Zero emission
ZnGaP-SOD	$ZnGa_2P_3O_{12}$	$(CH_3)_4N^+$	SOD	Zero emission

[a] R4710 = 1,13-diamino-4,7,10-trioxatridecane; R17 = 1,7-diaminoheptane; R19 = 1,9-diaminononane; R33 = 3,3′-diamino-*N*-methyldipropylamine; R1 = *N*-(2-aminoethyl)-1,3-propanediamine. [b] The three-letter codes are assigned by the Structure Commission of the International Zeolite Association (http://www.iza-structure.org/).

 DOI: 10.1039/b105715b

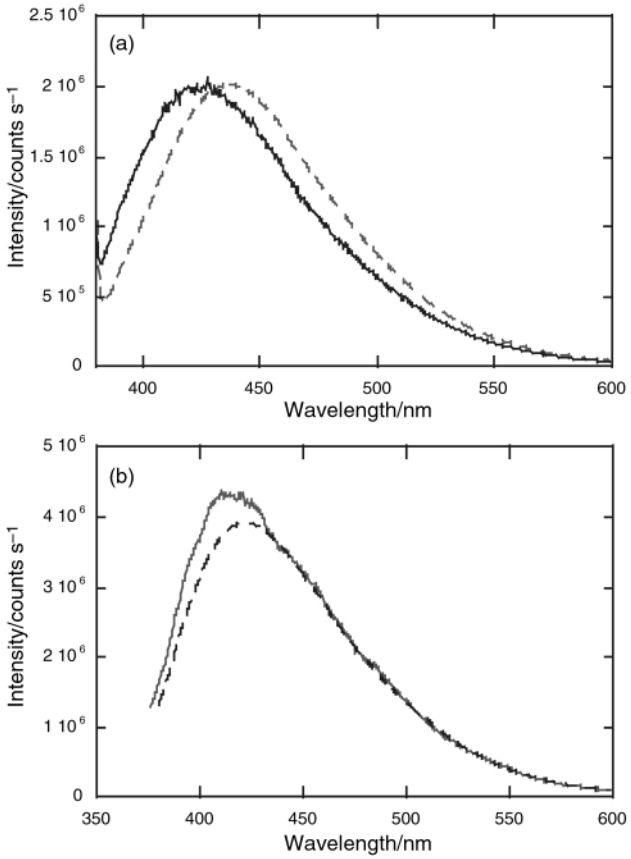

Fig. 2 The emission spectra at room temperature (dashed curves) and at liquid nitrogen temperature (solid curves). (a) UCSB-8Mg (excited at 360 nm); (b) UCSB-7AlGe (excited at 355 nm). Low temperature spectra were collected with the sample tube immersed in a quartz liquid nitrogen Dewar.

high temperatures, *e.g.* 200 °C, below or at which crystalline microporous materials are usually synthesized. Whether the observed photoluminescent phenomena can be used in a screening method for the rapid detection of crystalline open-framework materials represents an interesting question for further studies. In our synthesis, we have frequently found it convenient to detect crystalline open-framework phases with a UV lamp even in the presence of a large amount of amorphous phases because amorphous gel phases are generally not photoluminescent.

Other open-framework materials with efficient luminescence include UCSB-7GaGe and UCSB-7AlGe (Table 1) that are amine-templated gallo- or aluminogermanates with two sets of continuous helical channels separated by a gyroid minimal surface.[7–9] Strong bluish luminescence has also been observed for other open-framework materials with different guest amines, framework compositions and topologies (Table 1). The compositional diversity is advantageous because less expensive and more environmentally benign starting materials may be selected for the synthesis of phosphors reported here and it also offers opportunities for the fine tuning of emission wavelength and bandwidth.

The luminescent mechanism for these open framework materials is not unambiguously known at this stage. For insulating solids without metal activators, the luminescence is often attributed to the presence of various kinds of lattice defects such as oxygen vacancies. Such a defect mechanism is also possible for materials reported here. However, it is also observed that some closely related open-framework materials do not exhibit any photoluminescence. For example, gallogermanate UCSB-7 can be synthesized with either alkali metal cations or different organic amines. Fluorescence measurements show that purely inorganic UCSB-7 structures[7] (those templated with either K or Na cations) do not exhibit luminescence at all while those directed by protonated amine molecules show visible photoluminescence. In addition, it is noteworthy that open-framework materials templated by TMA (TMA = $N(CH_3)_4^+$) such as $(TMA)ZnGa_2X_3O_{12}$ (X = P or As) sodalites[10] do not have any observable photoluminescence when measured on a spectrofluorometer. These preliminary results suggest that the luminescence may also be related to the highly negatively charged inorganic framework and the presence of protonated guest amine molecules.

Considering the great variety of open-framework materials,[11] it is anticipated that additional novel properties will be discovered in the future, which might make it possible to use open framework materials for applications beyond traditional catalytic or adsorptive areas. The interesting luminescent phenomenon observed in open-framework oxides suggests that the investigation of non-oxide open-frameworks such as sulfides, selenides, halides, cyanides *etc*. might be desirable in order to achieve a broader range of emission spectral characteristics.

The financial support of this work by UC Riverside Startup Fund is appreciated. Samples of UCSB-7K and ZnGaP-SOD were prepared by Thurman E. Gier at Prof. Galen D. Stucky's laboratory at University of California, Santa Barbara.

Notes and references

† The following is a typical synthesis procedure, using UCSB-10Mg as an example. Slurry A was prepared by adding aluminium isopropoxide (1.40 g, 98%, Aldrich) and H_3PO_4 (1.43 g, 85 wt% in water) into ethylene glycol (7.52 g). The mixture was stirred for 1 week. Solution B was prepared by mixing 1.19 g magnesium hydrogenphosphate trihydrate (99%, Aldrich) with H_2O (7.16 g) and H_3PO_4 (0.84 g, 85 wt% in water) and was stirred for 1 h. To the mixture of A and B, 3.01 g of 1,13-diamino-4,7,10-trioxatridecane was slowly added with stirring. The final pH of the mixture was 8.12. The mixture was stirred for 5 h at room temperature, transferred into a 23 mL autoclave, and heated in an oven at 170 °C for 4 days. The product was filtered off, washed with distilled H_2O and ethanol, and further purified by repeated sonication of the sample in deionised water and decanting off the cloudy solution. Hexagonal-shaped clear crystals were obtained.

1 G. Blasse and B. C. Grabmaier, *Luminescent Materials*, Springer-Verlag, New York, 1994.
2 S. T. Wilson, B. M. Lok, C. A. Messina, T. R. Cannan and E. M. Flanigen, *J. Am. Chem. Soc.*, 1982, **104**, 1146.
3 P. Behrens and G. D. Stucky, in *Comprehensive Supramolecular Chemistry*, ed. G. Albert and T. Bein, Elsevier, New York, 1996, vol. 7, pp. 721–772.
4 I. Braun, G. Ihlein, F. Laeri, J. U. Nockel, G. Schulz-Ekloff, F. Schuth, U. Vietze, O. Weiss and D. Wohrle, *Appl. Phys. B: Lasers Opt.*, 2000, **70**, 335.
5 X. Bu, P. Feng and G. D. Stucky, *Science*, 1997, **278**, 2080.
6 D. R. Vij, *Luminescence of Solids*, Plenum Press, New York, 1998.
7 T. E. Gier, X. Bu, P. Feng and G. D. Stucky, *Nature*, 1998, **395**, 154.
8 P. Feng, X. Bu and G. D. Stucky, *Nature*, 1997, **388**, 735.
9 X. Bu, P. Feng, T. E. Gier, D. Zhao and G. D. Stucky, *J. Am. Chem. Soc.*, 1998, **120**, 13 389.
10 X. Bu, T. E. Gier, P. Feng and G. D. Stucky, *Microporous Mesoporous Mater.*, 1998, **20**, 371.
11 A. K. Cheetham, G. Ferey and T. Loiseau, *Angew. Chem., Int. Ed.*, 1999, **38**, 3268.

CHEMCOMM
Communication
www.rsc.org/chemcomm

Dehydrogenative coupling of phenanthroline under hydrothermal conditions: crystal structure of a novel layered vanadate complex constructed of 4,8,10-net sheets: [(2,2′-biphen)Co]$V_3O_{8.5}$

Cai-Ming Liu,† Song Gao* and Hui-Zhong Kou

State Key Laboratory of Rare Earth Materials Chemistry and Applications & PKU-HKU Joint Laboratory on Rare Earth Materials and Bioinorganic Chemistry, College of Chemistry and Molecular Engineering, Peking University, Beijing 100871, P. R. China. E-mail: gaosong@pku.edu.cn

Received (in Cambridge, UK) 12th April 2001, Accepted 17th July 2001
First published as an Advance Article on the web 8th August 2001

2,2′-Biphenanthroline (2,2′-biphen) formed from 1,10-phenanthroline when a new two-dimensional layered vanadium oxide metal coordination complex, [(2,2′-biphen)Co]$V_3O_{8.5}$, which contains novel 4,8,10-net sheets, was hydrothermally synthesized.

Increasing attention has been paid to organic–inorganic hybrid materials due not only to their intriguing structure diversity but also their potential applications in areas of molecular adsorption, catalysis, electromagnetism and photochemistry.[1] The role of organic components in hybrid materials is of great interest. Usually, organic amines act as structural directors to construct inorganic frameworks, compensating charges and filling space; on the other hand, they may also function as ligands, coordinated directly to the oxide scaffolding or to the secondary metal centers. [2] As examples of the latter, many hybrid organic–inorganic vanadium oxides have recently been found to be coordinated by transition metal complexes,[3–7] which have discrete cluster, one-dimensional (1D) chain and layer structures. However, few examples involving the self-reaction of the organic component have been reported. Herein, we present a novel two-dimensional (2D) layered vanadium solid state complex [(2,2′-biphen)Co]$V_3O_{8.5}$ **1**, where 2,2′-biphenanthroline (2,2′-biphen) formed automatically from 1,10-phenanthroline (phen) under hydrothermal reaction conditions. To our knowledge, the dehydrogenative coupling of 1,10-phenanthroline during hydrothermal reaction has not been described to date though there are hybrid organic–inorganic structures reported in which 1,10-phenanthroline coordinates to metal centers.[7,8] Complex **1** is the first vanadate complex containing a tetradentate ligand.

Dark red block crystals of **1** were synthesized hydrothermally from a mixture of NH_4VO_3, H_3BO_3, $Co(NO_3)_2{\cdot}6H_2O$, phen and H_2O (molar ratio 1:1.5:1:2:1000) in a polyfluoroethylene-lined stainless steel bomb (25 ml capacity) under autogenous pressure heated to 160 °C for five days (yield 50% based on vanadium).‡ H_3BO_3 is necessary for this reaction though boron is not incorporated into the structure of **1**. H_3BO_3 might have adjusted the pH value of the mixture (the pH value changed from 6 to *ca.* 5 after adding of H_3BO_3), however, **1** did not form in the presence of other acids such as $H_2C_2O_4$ or HCl instead of H_3BO_3.

The formation mechanism for 2,2′-biphenanthroline is not yet known, but probably arises from the polymerization catalysis role of the cobalt complex.[9] High temperature and pressure have also been proved to be effective for the dehydrogenation of pyridine when suitable transition metal salts are present,[10] but require strictly anhydrous conditions[10*a*] or dioxygen as oxidant.[10*b*] Gillard and Hall suggested the 2-(or 4-) position of pyridine becomes polarized upon coordination to metal ions and so facilitating oxidition.[10*b*] A similar situation may occur in the formation of 2,2′-biphenanthroline in our reaction system. Interestingly, no 2,2′-biphenanthroline was observed in the products when $Ni(NO_3)_2$ instead of $Co(NO_3)_2$ was used under the same hydrothermal conditions.[11]

The coordination sphere of the cobalt(II) site in **1** is defined by four nitrogen donors of a biphen ligand and two vanadate oxygen donors in the apical position leading to a distorted CoN_4O_2 octahedron (Fig. 1).§ The two phenanthroline planes of the 2,2′-biphenanthroline ligand are coplanar (mean deviation from the plane defined by N1, C12, C11, N2, C10, C13, N3, C24, C23 and N4 is 0.0209 Å; all 2,2′-biphenanthroline planes are parallel to the *ab* plane) with a C10–C13 bond distance of 1.459(7) Å. The N1–Co1, N4–Co1 bond distances (2.197(2) and 2.189(2) Å, respectively) are slightly larger than those for N2–Co1 (2.111(2) Å) and N3–Co1 (2.110(2) Å), and the bond angle of N1–Co1–N4 (135.40(9)°) is larger than that of N2–Co1–N3 (72.49(10)°) for the tetradentate 2,2′-biphenanthroline ligand. Similar bond angle trends have also been observed in tetradentate Schiff base complexes.[12]

The structure of **1** consists of a 2D neutral framework, where (2,2′-biphen)Co units are covalently linked to the vanadium oxide V_6O_{17} chains (Fig. 2). Each V_6O_{17} chain is constructed from V_4O_{12} tetramer rings and V_2O_7 units arranged alternately by edge- and corner-sharing interactions, while (2,2′-biphen)Co units connect, in a *trans* fashion, V_4O_{12} tetramer rings and V_2O_7 units of neighboring V_6O_{17} chains to form an extended 2D network structure with a unique 4,8,10-net as shown in Fig. 3. It is noteworthy that **1** is the first 2D layered vanadium oxide metal coordination complex constructed of 4,8,10-net sheets.

$[(bipy)_2Zn]_2V_6O_{17}$ also possesses a $V_6O_{17}^{4-}$ component but this exhibits a quite different 2D layer structure,[3*a*] where within each VO layer there are roughly circular rings, defined by

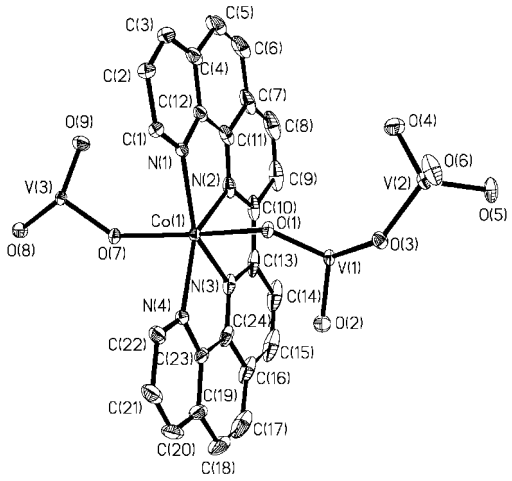

Fig. 1 A fragment of the net with the atomic labeling scheme (30% probability ellipsoids) in complex **1**.

† Permanent address: Organic Solids Laboratory, Center for Molecular Science, Institute of Chemistry, Chinese Academy of Sciences, Beijing 100080, P.R. China.

 DOI: 10.1039/b103304m

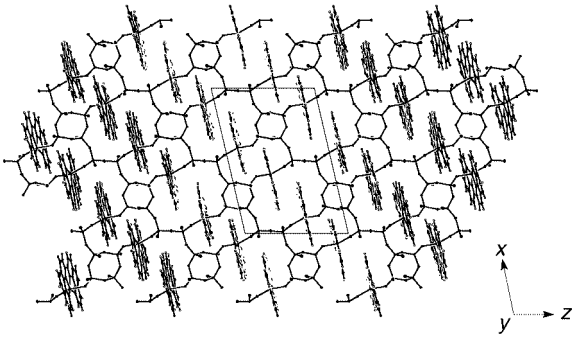

Fig. 2 View of the 2D layer in **1** along the *b*-axis direction.

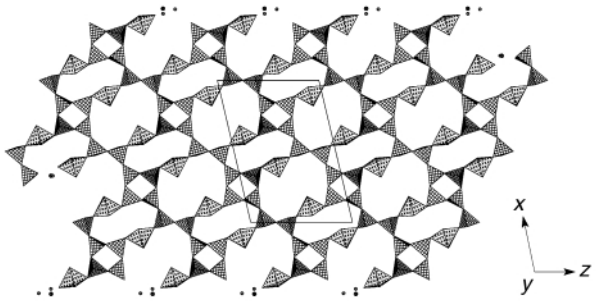

Fig. 3 Polyhedral representation of complex **1** packed along the *b*-axis; all C and H atoms are omitted for clarity.

fourteen corner-sharing VO_4 tetrahedra and two $Zn(bpy)_2$ moieties which are bonded in a *cis* fashion to two second-nearest neighbor VO_4 groups on opposite sides of each ring. It is clear that two oxygen atoms of vanadate connected to the $Zn(bpy)_2$ moiety adopting *cis*- rather than *trans*-orientation give rise to the structure difference of $[(bipy)_2Zn]_2V_6O_{17}$ from **1**. Another quite recently reported vanadium solid state complex with a $V_6O_{17}^{4-}$ component is $[Co_4(2\text{-pzc})_4(V_6O_{17})]\cdot xH_2O$ (2-pzc is the anion of 2-pyrazinecarboxylic acid),[13] where $V_6O_{17}^{4-}$ forms double chains, and each chain connects four $[Co_4(2\text{-pzc})_4]$ chains to form a 3-D chiral structure.

In conclusion, this study illustrates that even organic ligands can undergo self-reaction under hydrothermal conditions, which suggests more novel structures can be obtained by hydrothermal or solvothermal methods even with common ligands.

This work was supported by Visiting Scholar Foundation of Key Lab. in University (sponsored by Education Ministry of China) and grants from State Key Project for Fundamental Research (G1998061305).

Notes and references

‡ Other products are amorphous materials. Anal. Calc. for $C_{24}H_{14}N_4O_{8.5}CoV_3$ **1**: C, 40.82; H, 2.00; N, 7.93. Found: C, 40.50; H, 2.03; N, 7.80%. IR (KBr, cm^{-1}) for **1**: 1674(w), 1608(m), 1517(w), 1425(m), 968(s), 946(m), 894(s), 853(s), 835(s), 796(m), 727(s), 667(vs).

§ *Crystal data* for **1**: $C_{24}H_{14}N_4O_{8.5}CoV_3$, monoclinic, space group *C*2/*c*, M_r = 706.14, a = 19.660(4), b = 18.430(4), c = 13.640(3) Å, β = 103.20(3)°, V = 4811.7(17) $Å^3$, Z = 8, D_c = 1.950 g cm^{-3}, T = 293(2) K, Mo-Kα radiation (λ = 0.71073 Å), μ = 1.870 mm^{-1}, R_1 = 0.0420, wR_2 = 0.1046 for 5750 observed reflections from 6778 independent reflections, GOF = 1.014, Nonius Kappa-CCD diffractometer.

CCDC reference number 163766.

See http://www.rsc.org/suppdata/cc/b1/b103304m/ for crystallographic data in CIF or other electronic format.

1 (*a*) P. J. Hagrman, D. Hagrman and J. Zubieta, *Angew. Chem., Int. Ed.*, 1999, **38**, 2638; (*b*) G. Centi, F. Trifro, J. R. Ebbner and V. M. Franchetti, *Chem. Rev.*, 1988, **88**, 55.

2 P. J. Hagrman and J. Zubieta, *Inorg. Chem.*, 2000, **39**, 3260.

3 (*a*) Y. Zhang, J. R. D. DeBord, C. J. O'Connor, R. C. Haushalter, A. Clearfield and J. Zubieta, *Angew. Chem., Int. Ed. Engl.*, 1996, **35**, 989; (*b*) Y. Zhang, P. J. Zapf, L. M. Meyer, R. C. Haushalter and J. Zubieta, *Inorg. Chem.*, 1997, **36**, 2159; (*c*) J. R. D. DeBord, Y. Zhang, R. C. Haushalter, J. Zubieta and C. J. O'Connor, *J. Solid State Chem.*, 1996, **122**, 251.

4 (*a*) Z. Shi, L.-R. Zhang, G.-S. Zhu, G.-Y. Yang, J. Hua, H. Ding and S.-H. Feng, *Chem. Mater.*, 1999, **11**, 3565; (*b*) L.-R. Zhang, Z. Shi, G.-Y. Yang, X.-M. Chen and S.-H. Feng, *J. Chem. Soc., Dalton Trans.*, 2000, 275.

5 L.-M. Zheng, J.-S. Zhao, K.-H. Lii, L.-Y. Zhang, Y. Liu and X.-Q. Xin, *J. Chem. Soc., Dalton Trans.*, 1999, 939.

6 (*a*) S. Aschwanden, H. W. Schmalle, A. Reller and H. R. Oswald, *Mater. Res. Bull.*, 1993, **28**, 45; (*b*) P. J. Ollivier, J. R. D. DeBoard, P. J. Zapf, J. Zubieta, L. M. Meyer, C.-C. Wang, T. E. Mallouk and R. C. Haushalter, *J. Mol. Struct.*, 1998, **470**, 49.

7 X.-M. Zhang, M.-L. Tong and X.-M. Chen, *Chem. Commun.*, 2000, 1817.

8 C.-Y. Duan, Y.-P. Tian, Z.-L. Lu and X.-Z. You, *Inorg. Chem.*, 1995, **34**, 1.

9 (*a*) B. L. Small, M. Brookhart and A. M. A. Bennett, *J. Am. Chem. Soc.*, 1998, **120**, 4049; (*b*) G. J. P. Britovsek, M. Bruce, V. C. Gibson, B. S. Kimberley, P. J. Maddox, S. Mastroianni, S. J. McTavish, C. Redshaw, G. A. Solan, S. Strömberg, A. J. P. White and D. J. Williams, *J. Am. Chem. Soc.*, 1999, **121**, 8728.

10 (*a*) G. T. Morgan and F. H. Burstall, *J. Chem. Soc.*, 1932, 20; (*b*) R. D. Gillard and D. P. J. Hall, *J. Chem. Soc., Chem. Commun.*, 1988, 1163.

11 $[Ni(phen)_2]_2V_6O_{17}$ and $[Ni(phen)_2]V_4O_{11}$ are products: C.-M. Liu, S. Gao, Y.-L. Hou and J. Zhang, *Inorg. Chem.*, submitted

12 (*a*) C.-M. Liu, R.-G. Xiong, X.-Z. You, Y.-J. Liu and K.-K. Cheung, *Polyhedron*, 1996, **15**, 4565; (*b*) C.-M. Liu, R.-G. Xiong, X.-Z. You, H.-K. Fun and K. Sivakumar, *Polyhedron*, 1997, **16**, 119; (*c*) J. Lange, H. Elias, H. Paulus, J. Müller and U. Weser, *Inorg. Chem.*, 2000, **39**, 3342.

13 L.-M. Zheng, T. Whitfield, X. Wang and A. J. Jacobson, *Angew. Chem., Int. Ed.*, 2000, **39**, 4528.

CHEMCOMM Communication
www.rsc.org/chemcomm

Naphthalene formation by allylation of zirconaindenes in the ZnX_2–$Pd(PPh_3)_4$ system

Zheng Duan,[a] Kiyohiko Nakajima[b] and Tamotsu Takahashi*[a]

[a] *Catalysis Research Center and Graduate School of Pharmaceutical Sciences, Hokkaido University, and CREST, Science and Technology Corporation (JST), Sapporo 060-0811, Japan. E-mail: tamotsu@cat.hokudai.ac.jp*

[b] *Department of Chemistry, Aichi University of Education, Igaya, Aichi 448-8542, Japan*

Received (in Cambridge, UK) 24th April 2001, Accepted 10th July 2001
First published as an Advance Article on the web 16th August 2001

Zirconaindenes reacted with allyl halides in the presence of ZnX_2 (X = Cl or Br) and a catalytic amount of $Pd(PPh_3)_4$ to give naphthalene derivatives in good yield.

It has been believed for a long time that zirconacyclopentadienes are inert toward C–C bond formation reactions. Recently, we found that transmetalation reactions of zirconacyclopentadienes to copper,[1] nickel[2] and lithium[3] could open a way to various carbon–carbon bond formation reactions. In this paper we would like to report the novel naphthalene formation reaction[4] of zirconaindenes in the presence of ZnX_2 and a catalytic amount of $Pd(PPh_3)_4$.[5]

When we investigated novel transmetalation to Zn, we tried the allylation reaction of zirconacyclopentadienes, since double allylation of zirconacyclopentadienes[1] proceeded in the presence of either a catalytic or stoichiometric amount of CuCl.[1] When only the zinc salts were used, the reactions were very sluggish. However in the presence of a catalytic amount of $Pd(PPh_3)_4$ the reaction dramatically changed. Monoallylation products were clearly formed. The formation of double allylation products was not observed [eqn. (1)].

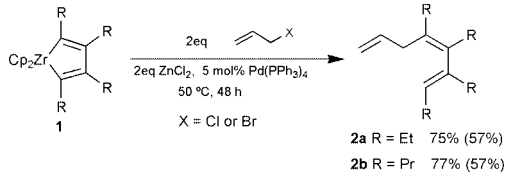

(1)

This is in sharp contrast to the allylation in the presence of CuCl.[1] Then our attention was turned to the allylation reaction of zirconaindenes. It is interesting to note that, when zirconaindene[6] **3a** was used, substituted naphthalene **4a** was clearly formed as a single product [eqn. (2)].† The formation of

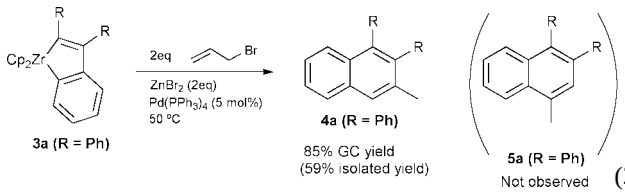

(2)

regioisomer **5a** was not observed. The use of only a catalytic amount of $Pd(PPh_3)_4$ without zinc salt did not give a clean reaction, although **4a** was formed in 33% GC yield.

The structure of the compound **4a** was confirmed by X-ray analysis.‡ It clearly shows that the allylation reaction proceeded selectively at the benzene-carbon attached to Zr. When $MeOC_6H_4$- and MeC_6H_4- were used as substituents instead of the Ph group, the similar perfect regiocontrol was observed as shown in Table 1. This perfect regioselectivity is attributed to the high reactivity of the benzene-carbon attached to Zr compared with the carbon of the –C(Ph)=C(Ph) group attached to Zr. It is interesting to note that when the nucleophilic property

Table 1 The formation of naphthalene derivatives

Zirconacyclopentadienes	Product	Yield (%)[a]
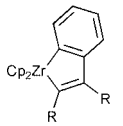	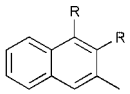	
3a R = Ph	**4a** R = Ph	85(59)
3b R = C_6H_4OMe	**4b** R = C_6H_4OMe	61(42)
3c R = C_6H_4Me	**4c** R = C_6H_4Me	68(40)
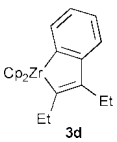	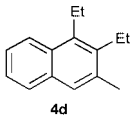	
3d	**4d** + **5d**	79(47) 1.9:1
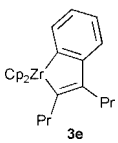	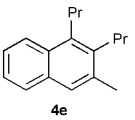	
3e	**4e** + **5e**	77(51) 3:1

[a] GC yields. Isolated yields are given in parentheses.

of the carbon in the –C=C group attached to Zr was enhanced by introducing alkyl groups such as the Et group and the Pr group instead of the Ph groups, carbon–carbon bond formation with allyl halides at the –C(R)=C(R), R = Et or Pr, was observed. The isomers **5d** and **5e** were obtained in the case of **3d** and **3e**, respectively.

A possible mechanism of the naphthalene formation involves (i) transmetalation of the Zr-phenyl carbon bond to Zn giving **6**, (ii) transmetalation of **6** with an allylpalladium halide formed by oxidative addition of allyl halide to a Pd^0 complex, (iii) reductive elimination to give allylated intermediate **7**, (iv) transmetalation of the second Zr–C bonds to Pd forming **8**, (v) insertion of the vinyl group into the Pd–C bond (vi) β-hydrogen elimination to give *exo*-methylene derivative **10** that isomerizes to the corresponding naphthalene **4** (Scheme 1).

Further investigations on mechanism and selectivity are currently in progress.

 DOI: 10.1039/b103674m

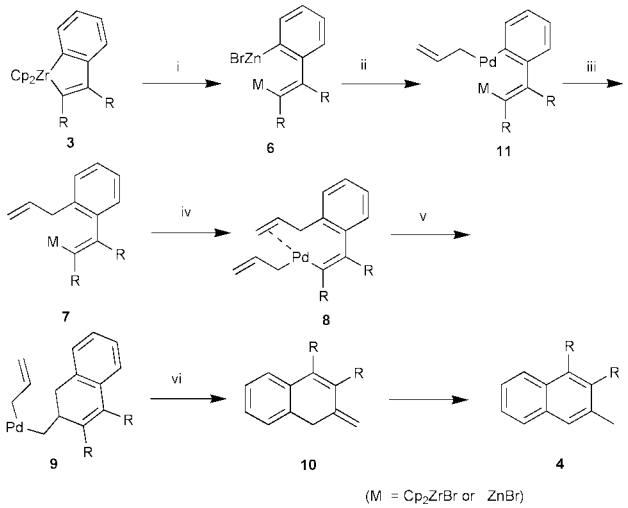

Scheme 1

Notes and references

† *Typical procedure*: to zirconaindene **3a** prepared according to the literature were added 2 eq. of $ZnBr_2$, a catalytic amount of $Pd(PPh_3)_4$ (5 mol%) and 2 eq. allyl bromide. The mixture was stirred at 50 °C for 12 h. Only **4a** was formed in 85% GC yield. After isolation and purification by column chromatography, **4a** was obtained in 59% isolated yield.

‡ *Crystallographic data of* **4a**: colorless prisms, monoclinic, space group *C*2/*c*, a = 21.312(1), b = 10.6981(6), c = 16.2781(8) Å, β = 117.713(4)°, Z = 8, R = 0.044, GOF = 1.84. CCDC 165561. See http://www.rsc.org/suppdata/cc/b1/b103674m/ for crystallographic files in .cif or other electronic format.

1 T. Takahashi, M. Kotora, K. Kasai and N. Suzuki, *Organometallics*, 1994, **13**, 4183.

2 T. Takahashi, F.-Y. Tsai, Y. Li., K. Nakajima and M. Kotora, *J. Am. Chem. Soc.*, 1999, **121**, 11093.

3 T. Takahashi, S. Q. Huo, R. Hara, Y. Noguchi, K. Nakajima and W.-H. Sun, *J. Am. Chem. Soc.*, 1999, **121**, 1094.

4 For a recent review of naphthalene formation from benzyne complexes, see M. A. Bennett and E. Wenger, *Chem. Ber.*,1997, **130**, 1029.

5 For recent examples of naphthalene formation using transition metal compounds, see D. Peña, D. Pérez, E. Guitián and L. Castedo, *J. Am. Chem. Soc.*, 1999, **121**, 5827; E. Yoshikawa and Y. Yamamoto, *Angew. Chem., Int. Ed.*, 2000, **39**, 173; E. Yoshikawa, K. V. Radhakrishnan and Y. Yamamoto, *J. Am. Chem. Soc.*, 2000, **122**, 7280; T. Takahashi, R. Hara, Y. Nishihara and M. Kotora, *J. Am. Chem. Soc.*, 1996, **118**, 5154; T. Takahashi, Z. F. Xi, A. Yamazaki, Y. H. Liu, K. Nakajima and M. Kotora, *J. Am. Chem. Soc.*, 1998, **120**, 1672; R. C. Larock, M. J. Doty, Q. P. Tian and J. M. Zenner, *J. Org. Chem.*, 1997, **62**, 7536; N. Iwasawa, M. Shido, K. Maeyama and H. Kusama, *J. Am. Chem. Soc.*, 2000, **122**, 10226.

6 For transmetalation of acyclic organozirconium to Zn, see E. Negishi, D. E. Van Horn, T. Yoshida and C. L. Rand, *Organometallics*, 1983, **2**, 563.

7 G. Erker, *J. Organomet. Chem.*, 1977, **134**, 189; K. Kropp and G. Erker, *Organometallics*, 1982, **1**, 1246; S. L. Buchwald and B. T. Watson, *J. Am. Chem. Soc.*, 1986, **108**, 7411.

CHEMCOMM Communication
www.rsc.org/chemcomm

Powerful Claisen condensation and Claisen–aldol tandem reaction of α,α-dialkylated esters promoted by $ZrCl_4$–$^iPr_2NEt$

Yoo Tanabe,* Ryota Hamasaki and Syunsuke Funakoshi

School of Science, Kwansei Gakuin University, 1-1-155 Uegahara, Nishinomiya, Hyogo 662-8501, Japan

Received (in Cambridge, UK) 14th May 2001, Accepted 19th July 2001
First published as an Advance Article on the web 7th August 2001

Powerful Claisen ester condensations of α,α-dialkylated esters mediated by $ZrCl_4$–$^iPr_2NEt$ were performed to give the corresponding thermodynamically unfavorable α,α-dialkylated β-ketoesters, and Claisen–aldol tandem reactions between an intermediary Zr-enolate of a α,α-dialkylated β-ketoester and aldehydes also proceeded.

The Claisen ester condensation is recognized as a fundamental and useful C–C bond-forming reaction.[1] Traditional Claisen condensations using alkali-metal basic reagents such as NaOR, NaH, LDA and LiHMDS are widely applied to α-monoalkylated esters **1** giving the corresponding dimeric β-ketoesters **3** (Scheme 1). However, α,α-dialkylated esters **4** could not undergo this type of the condensation, because **4** lacks the ability to force the formation of a stable enolate.[1,2] Actually, the reversible equilibrium barely shifts from **4** to the unfavorable production of the β-ketoesters **5**. Thermodynamics dictate that the starting α,α-dialkylated esters **4** are more stable than the desired β-ketoesters **5**, namely, the retro-Claisen condensation of esters **5** should predominate.[1,2] Although two methods for the Claisen condensation of alkyl 2-methylpropanoate using strong bases ($Ph_3C^-\cdot Na^+$ or KH)[3,4] have been reported, the yields were moderate to low (~35%).† In addition, these methods describe the sole example of the condensation of alkyl 2-methylpropanoate.

Recently, Ti–Claisen condensations were demonstrated[5–9] and proved to be more reactive and practical between α-monoalkylated esters than the representative method using NaH or LDA.‡ However, this method is unfortunately limited to the case of α-monoalkylated esters **1**. Here we introduce the powerful Claisen ester condensation of α,α-dialkylated esters **4** promoted by the $ZrCl_4$–$^iPr_2NEt$ reagent and its extension to the Claisen–aldol tandem reaction.

First, the Claisen condensation of α,α-dialkylated esters is described. Although ethyl 2-methylpropanoate was inert (no reaction) to $ZrCl_4$–amine (Et_3N, Bu_3N, or $^iPr_2NEt$) reagent, successful results were obtained using a slightly more acidic substrate, phenyl 2-methylpropanoate (**4a**). Treatment of **4a** with $ZrCl_4$–$^iPr_2NEt$ afforded the desired phenyl 2,2,4-trimethyl-3-oxopentanoate (**5a**) in 72% yields under optimized conditions.§ Table 1 summarizes the results of the Zr–Claisen condensation of α,α-dialkylated esters **4a**–**e**. Replacement of phenyl ester **4b** for 4-chlorophenyl analog **4e** increased the yield. On the other hand, $TiCl_4$–Bu_3N agent (with or without cat. TMSCl *or* cat. TMSOTf) failed to drive the reaction (no reaction).

Phenyl esters are readily prepared by several methods and, in addition, are smoothly hydrolyzed under milder conditions compared with alkyl esters.[10] A little higher acidity of phenyl esters than that of alkyl esters is suggested by the following two experiments: (a) ^1H NMR chemical shifts of α-hydrogen of **4a**

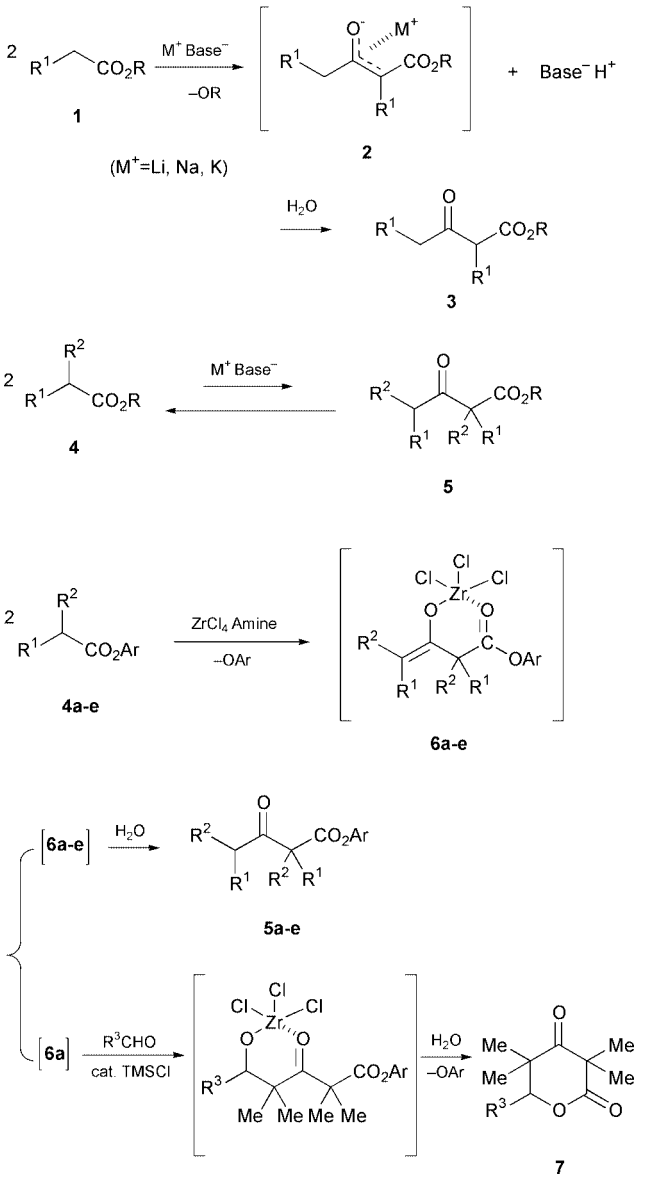

Scheme 1

Table 1 Claisen condensations of α,α-dialkylated esters promoted by $ZrCl_4$–amine[a]

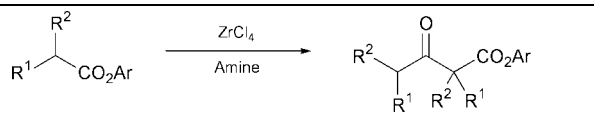

4	R^1	R^2	Ar	Amine	Yield (%)
4a	Me	Me	Ph	Et_3N	6
4a	Me	Me	Ph	Bu_3N	19
4a	Me	Me	Ph	TMEDA	Trace
4a	Me	Me	Ph	$^iPr_2NEt$	72
4b	Me	Et	Ph	$^iPr_2NEt$	44
4c	Me	Et	2-Cl-Ph	$^iPr_2NEt$	29
4d	Me	Et	2-MeO-Ph	$^iPr_2NEt$	22
4e	Me	Et	4-Cl-Ph	$^iPr_2NEt$	55

[a] In CH_2Cl_2 at −15 to −20 °C for 3 h. Molar ratio; **4**–$ZrCl_4$–amine = 1.0:2.0:3.0.

 DOI: 10.1039/b104185c

Table 2 Claisen–aldol tandem reactions of phenyl 2-methylpropanoate (**4a**) with aldehydes promoted by ZrCl–$^{i}Pr_2NEt$–(catalytic TMSCl)[a]

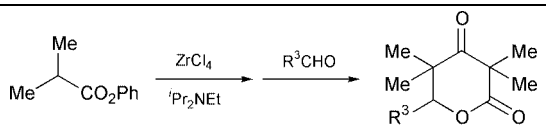

4a **7**

R^3	Product	Yield	R^3	Product	Yield[b] (%)
Ph	**7a**	71	PhCH=CH	**7e**	57
4-Cl-Ph	**7b**	59	2-Naphthyl	**7f**	43 (54)
4-NO_2-Ph	**7c**	61	*n*-Pr	**7g**	54 (74)
4-MeO-Ph	**7d**	57	^{i}Pr	**7h**	31 (61)

[a] In CH_2Cl_2 at −15 to −20 °C for 3 h. Molar ratio; **4a**–$ZrCl_4$–amine–aldehyde = 1.0:2.0:3.0:1.0. [b] Parentheses indicate the yields using catalytic TMSCl (0.05 equiv.).

and ethyl 2-methylpropanoate were located at 2.80 and 2.53 ppm, respectively; and (b) when equimolar mixtures of **4a** and ethyl 2-methylpropanoate in THF were treated with 1 equiv. of LDA at 0–5 °C for 1 h, followed by quenching with D_2O, the ratio of α-deuterated esters was *ca*. 9:1 by the ^{1}H NMR measurement.

The successful results using the Zr reagent suggest that the strong chelation effect of zirconium toward two carbonyl oxygens and longer bond length between Zr–O than that between Ti–O contribute to drive the reactions, releasing steric constraint around the crowded Zr-intermediate **6**.

Next, the intermediary Zr-enolate **6a** was utilized for further C–C bond formation. Namely, the first Claisen–aldol tandem reaction between 2 equiv. of phenyl 2-methylpropanoate **4a** and several aldehydes successfully proceeded in a one-pot manner through intermediary Zr-enolate **6a**, eventually affording pyran-2,4-diones **7** with a concomitant lactonization.¶ Table 2 summarizes these results. It should be noted that catalytic TMSCl significantly affects the second aldol addition step for some aldehydes.[7]

Thus, we achieved an efficient, powerful and practical Zr–Claisen condensation and the first Claisen–aldol tandem reaction of α,α-dialkylated esters **4**.

This work was partially supported by a Grant-in-Aid for Scientific Research on Priority Areas (A) "Exploitation of Multi-Element Cyclic Molecules" and on Basic Areas (C) from the Ministry of Education, Culture, Sports, Science and Technology, Japan.

Notes and references

† In the first method,[3] preparation of the $Ph_3C^{-}\cdot Na^{+}$ reagent includes a tedious procedure from a practical and green chemical standpoint: *ca*. 9.3 g of 1% Na(Hg) *vs*. 0.28 g (1 mmol) of Ph_3CCl is used for ethyl 2-methylpropanoate (0.21 g, 1.8 mmol). The second method[4] using KH lacks generality; this reaction failed to proceed in several of our experiments when ethyl 2-methylpropanoate was employed as the substrate.

‡ For an example of the Claisen condensation of methyl dec-9-enoate using NaH by the reported method,[11] the desired β-ketoester was obtained in *ca*. 75% (DME, reflux, 20 h). The Ti–Claisen condensation proceeded with a 93% yield (toluene, 0–5 °C, 1 h).[8] Accordingly, the Ti–Claisen condensation clearly has the advantage of a high yield, mild conditions and a shorter reaction time. Related Dieckmann condensation using $AlCl_3$ is also reported.[12]

§ A typical procedure is as follows. $^{i}Pr_2NEt$ (388 mg, 3.0 mmol) in CH_2Cl_2 (0.5 cm^3) was added to a stirred suspension of $ZrCl_4$ (466 mg, 2.0 mmol) and phenyl 2-methylpropanoate (164 mg, 1.0 mmol) in CH_2Cl_2 (2.5 cm^3) at −15 to −20 °C. After stirring at the same temperature for 3 h, the mixture was quenched with water (5 cm^3) and extracted twice with ether. The combined organic phase was washed with water, brine, dried (Na_2SO_4) and concentrated. The obtained crude oil was purified by SiO_2-column chromatography (hexane–ether = 30:1) to give phenyl 2,2,4-trimethyl-3-oxopentanoate (84 mg, 72%). Colorless oil. ^{1}H NMR (400 MHz, $CDCl_3$) δ 1.17 (6H, d, J = 7.2 Hz), 1.53 (6H, s), 3.01–3.11 (1H, m), 7.05–7.09 (2H, m), 7.22–7.26 (2H, m), 7.37–7.41 (2H, m). ^{13}C NMR (100 MHz, $CDCl_3$) δ 20.42, 21.85, 36.98, 56.33, 121.11, 126.08, 129.51, 150.51, 172.35, 212.12. IR (film) 2980, 2938, 1763, 1717, 1196, 1121 cm^{-1}.

¶ A typical procedure is as follows. In place of quenching with water, TMSCl (0.006 cm^3, 0.05 mmol) and isobutyraldehyde (72 mg, 1.0 mmol) were successively added to a stirred reaction mixture at 0–5 °C. The mixture was stirred for 2 h, and was then quenched with water (5 cm^3) and extracted twice with AcOEt. The combined organic phase was washed with water, brine, dried (Na_2SO_4) and concentrated. The obtained crude crystals were purified by SiO_2-column chromatography (hexane–AcOEt = 20:1 → 10:1) to give 3,3,5,5-tetramethyl-6-(1-methylethyl)pyran-2,4-dione (65 mg, 61%). Colorless crystals; mp 34.0–34.5 °C. ^{1}H NMR (400 MHz, $CDCl_3$) δ 1.08 (3H, d, J = 6.8 Hz), 1.13 (3H, s), 1.14 (3H, d, J = 6.8 Hz), 1.22 (3H, s), 1.43 (3H, s), 1.44 (3H, s), 2.08–2.16 (1H, m), 4.12 (1H, d, J = 3.2 Hz). ^{13}C NMR (100 MHz, $CDCl_3$) δ 17.15, 18.21, 20.60, 22.50, 23.88, 25.63, 28.93, 47.59, 50.03, 83.97, 174.79, 211.36. IR (film) 2978, 2942, 1750, 1711, 1290, 1152, 1024 cm^{-1}.

1 J. March, *Advanced Organic Chemistry*, Benjamin, New York, 4th edn., 1992, p. 491.
2 For example,K. P. C. Vollhardt and N. E. Schore, *Organic Chemistry*, 3rd edn., Freeman, New York, 1999, p. 1039.
3 C. R. Hauser and W. B. Renfrow, Jr., *J. Am. Chem. Soc.*, 1937, **59**, 1823.
4 C. A. Brown, *Synthesis*, 1975, 326.
5 Y. Tanabe, *Bull. Chem. Soc. Jpn.*, 1988, **62**, 1917.
6 Y. Yoshida, R. Hayashi, H. Sumihara and Y. Tanabe, *Tetrahedron Lett.*, 1997, **38**, 8727.
7 Y. Yoshida, N. Matsumoto, R. Hamasaki and Y. Tanabe, *Tetrahedron Lett.*, 1999, **40**, 4227.
8 R. Hamasaki, S. Funakoshi, T. Misaki and Y. Tanabe, *Tetrahedron*, 2000, **56**, 7423.
9 W. Oppolzer and I. Rodriguez, *Helv. Chem. Acta*, 1993, **76**, 1275.
10 T. W. Green and P. G. M. Wuts, *Protective Groups in Organic Synthesis*, 3rd edn., Wiley, New York, 1999, p. 414.
11 J. E. McMurry, M. P. Fleming, K. L. Kees and L. R. Krepski, *J. Org. Chem.*, 1978, **17**, 3255.
12 S. Tamai, H. Ushirogochi, S. Sano and Y. Nagao, *Chem. Lett.*, 1955, 295.

CHEMCOMM Communication
www.rsc.org/chemcomm

Niobium and vanadium iminophosphinimide complexes†

Justin K. Brask, Michael G. Fickes, Preeyanuch Sangtrirutnugul, Víctor Durà-Vilà, Aaron L. Odom and Christopher C. Cummins*

Department of Chemistry, Room 2-227, Massachusetts Institute of Technology, Cambridge, MA 02139-4307, USA. E-mail: ccummins@mit.edu

Received (in Purdue, IN, USA) 25th June 2001, Accepted 18th July 2001
First published as an Advance Article on the web 16th August 2001

The iminophosphinimide complexes $[Ar(R)N]_3M(NPNBu^t)$ (M = V, Nb) were prepared from the corresponding anionic nitride species $\{[Ar(R)N]_3M{\equiv}NNa\}_2$ by way of a four-step synthetic strategy.

Unusually stable Group 5 arylazide complexes were recently isolated and their reactivity probed, *e.g.* $Cp_2Ta(Me)N_3Ph$[1] and $[Ar_F(Bu^t)N]_2V(I)N_3Mes$ (Ar_F = 2-F-5-MeC_6H_3).[2] Upon heating, these species gradually lose N_2 to form the corresponding arylimido complexes.[1,2] An iminophosphinimide ligand resembles the organoazide functionality, with substitution of phosphorus in the β-position. Although several main group compounds with an iminophosphinimide framework have been reported, *e.g.* [Li][Mes*NPNMes*][3] and $[Bu^tNP(\mu\text{-}NBu^t)_2PNBu^t]Ga(Bu^tNPNBu^t)$,[4] this ligand-type has not been supported on a transition-metal platform, *i.e.* $L_nM(N–P{=}NR)$ (R = organic group). Of particular interest is the possibility of N≡P extrusion as a consequence of organoimide formation. Herein we report characterization of the Group 5 iminophosphinimide derivatives $[Ar(R)N]_3M(NPNBu^t)$ [Ar = 3,5-$Me_2C_6H_3$; M = Nb, R = $C(CD_3)_2CH_3$; M = V, R = Bu^t], as constructed in several steps from the corresponding anionic nitride complexes (Scheme 1).

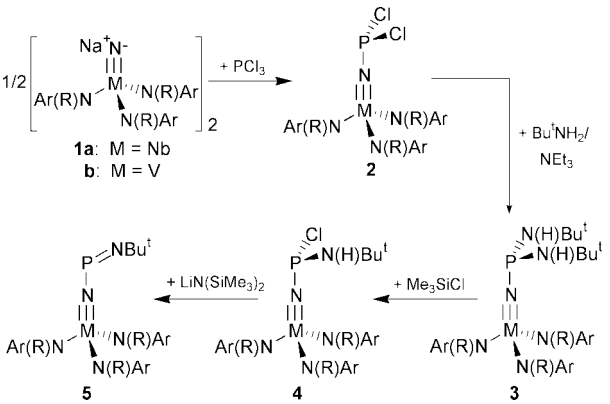

Scheme 1

In a demonstration of the versatility and controlled reactivity of the nitride dimer $\{[Ar(R)N]_3NbNNa\}_2$ (**1a**), reported previously by us in this journal,[5] the addition of PCl_3 to a THF solution of **1a** gave the pale yellow dichlorophosphine complex $[Ar(R)N]_3Nb(NPCl_2)$ (**2a**) in 86% isolated yield. The ^{31}P NMR spectrum for **2a** consists of a broad resonance at 158 ppm ($\Delta\nu_{1/2}$ = 160 Hz).‡ It is important to note that although **2a** was obtained exclusively upon addition of ⩾ 1 equiv. PCl_3, a second substitution reaction of the niobium nitride on phosphorus occurred cleanly when **1a** was added to **2a**.

Employing the synthon **2a**, design of a primary aminochlorophosphinimide functionality, *i.e.* –NP(Cl)($NHBu^t$), was pursued, since dehydrohalogenation of said species would deliver the desired iminophosphinimide ligand. The addition of 1 equiv. Bu^tNH_2 (10% solution in NEt_3) to **2a**, however, did not result in the formation of $[Ar(R)N]_3Nb[NP(Cl)(NHBu^t)]$ (**4a**), but rather a 1 : 1 mixture of $[Ar(R)N]_3Nb[NP(NHBu^t)_2]$ (**3a**) and unreacted **2a**. The yield of yellow di-*tert*-butylaminophosphinimide **3a**, for which the ^{31}P NMR spectrum contains a singlet at 101 ppm ($\Delta\nu_{1/2}$ = 85 Hz), was optimized (92%) upon addition of excess (*ca.* 4.4 equiv.) Bu^tNH_2/NEt_3 to **2a**. In an alternative approach, **4a** was generated by treating **3a** with a large excess of Me_3SiCl. As a caveat, however, the selective substitution of one *tert*-butylamino group on **3a** by chloride, as monitored by ^{31}P NMR spectroscopy, has characteristics of an equilibrium. The ratio of **3a**:**4a** decreased asymptotically when the number of silane equivalents was increased, but partial regeneration of **3a** occurred upon removal of all volatile materials *in vacuo*. This behavior is presumably due to the presence of the by-product $Me_3Si(Bu^t)NH$, which likely drives the equilibrium back towards **3a**. Treatment of **3a** with Me_3SiCl in three stages, between which all volatiles were removed *in vacuo*, conquered this dilemma and yielded **4a** as a yellow microcrystalline solid (73%). The ^{31}P NMR spectrum for **4a** consists of a single resonance at 146 ppm ($\Delta\nu_{1/2}$ = 101 Hz) and the ^1H NMR spectrum exhibits a doublet for the *tert*-butylamino protons, due to 1.5 Hz coupling with the ^{31}P center.

Dehydrohalogenation of **4a** was indeed achieved by treatment with 1 equiv. $LiN(SiMe_3)_2$ in pentane, yielding the *tert*-butyliminophosphinimide complex $[Ar(R)N]_3Nb(NPNBu^t)$ (**5a**) as bright yellow microcrystals in 66% yield. Interestingly, **5a** exhibits a 1 : 1 : 1 triplet centered at 318 ppm ($^1J_{14N–31P}$ = 61 Hz) in its ^{31}P NMR spectrum, due to coupling with one of the adjacent nitrogen atoms.‡ As this phenomenon was not observed for compounds **2a**–**4a**, it is speculated that the imino nitrogen experiences a more symmetric electric field gradient than its imido counterpart and is therefore the more likely source of $^{14}N–^{31}P$ coupling.[6] During recrystallization of **5a** from pentane it was observed that an orange solid started to form, with complete conversion in 24 h at 23 °C. A singlet at 240 ppm ($\Delta\nu_{1/2}$ = 72 Hz) in the ^{31}P NMR spectrum was recorded for this new orange species.‡ X-Ray diffraction analysis revealed the complex $[Ar(R)N]_3NbNP(\mu\text{-}NBu^t)_2PNNb[N(R)Ar]_3$ (**6**), the product of a [2 + 2] cycloaddition reaction involving two molecules of **5a** (Fig. 1).§ The two halves of dimeric **6** are related by a center of inversion, with a planar P_2N_2 core containing pyramidal phosphorus centers and nearly planar nitrogen centers. Selected bond distances and angles are provided in the caption to Fig. 1.

Main group iminophosphinimide compounds tend to form oligomers when lacking sufficiently bulky substituents.[4a] In the case of **5a**, the $[Ar(R)N]_3Nb$ platform apparently does not provide enough steric protection to totally encumber dimerization. It was anticipated that the vanadium analogue of **5a**, with an expected shorter metal–imide bond, would be less susceptible to oligomerization. In order to employ the same synthetic procedure as used for **5a**, however, we set out first to prepare the vanadium nitride complex $\{[Ar(Bu^t)N]_3VNNa\}_n$ (**1b**). Two related anionic vanadium(v) nitride species, $\{[(Me_3SiNCH_2CH_2)_3N]VNLi\}_n$[7] and $(Ph_2N)_3VNLi(THF)_3$,[8] were previously produced *via* deprotection or deprotonation strategies,

† Electronic supplementary information (ESI) available: Synthetic, spectroscopic, analytical, and theoretical data for all new complexes. See http://www.rsc.org/suppdata/cc/b1/b105584b/

 DOI: 10.1039/b105584b

respectively, involving neutral imide precursors. Another approach involved the reductive cleavage of dinitrogen.[9] In the present case, treatment of the readily available vanadium(III) trisanilide $[Ar(Bu^t)N]_3V$[10] with NaN_3 in THF, and subsequent dissolution in pentane followed by drying *in vacuo*, yielded bright yellow **1b** in 88% yield. By analogy with **1a**, unsolvated **1b** is thought to be dimeric (n = 2) in the solid state, with intramolecular solvation of the Na^+ ions provided by the aryl substituents of the –N(Bu^t)Ar groups.[5]

The vanadium iminophosphinimide $[Ar(R)N]_3V(NPNBu^t)$ (**5b**) was indeed successfully generated from **1b** by the methodology illustrated in Scheme 1, with yields for complexes **2b**–**4b** similar to those obtained for their niobium counterparts. The ^{31}P NMR chemical shift values for these intermediates are also similar to those recorded for **2a**–**4a** (*vide supra*), but the resonances are considerably broader, likely due to unresolved long-range ^{51}V coupling.‡ Complex **5b** was isolated from diethyl ether as red crystals in 56% yield. The ^{31}P and ^{51}V NMR spectra for **5b** in D_6-benzene both consist of single broad resonances at 341 ($\Delta\nu_{1/2}$ = 332 Hz) and −151 ($\Delta\nu_{1/2}$ = 123 Hz) ppm, respectively.‡ In contrast to **5a**, coupling with a ^{14}N nucleus was not resolved in the ^{31}P NMR spectrum. An X-ray structure determination confirmed the monomeric nature of **5b**, but is not of publishable quality due to severe disorder in the –N(Bu^t)Ar groups.§ Significantly, dimerization of **5b** to form the vanadium analogue of **6** was not observed, even upon heating to 60 °C in hexane for a period of 18 h.‡ Shortening of the $V–N_{imide}$ bond in **5b**, as compared with **5a**, presumably draws the iminophosphinimide functionality deeper into the sterically protective pocket formed by the three anilide ligands at the metal center,[11] hindering P_2N_2 ring formation.

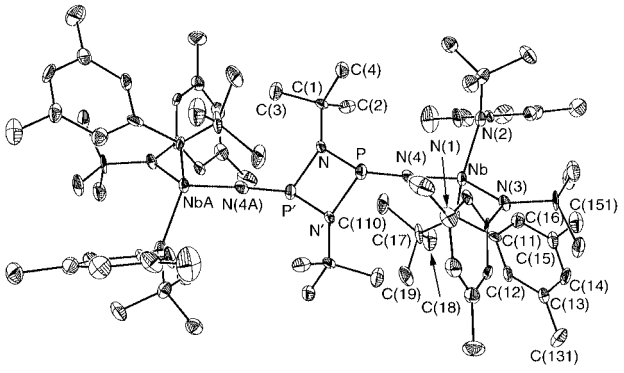

Fig. 1 Molecular structure of $[Ar(R)N]_3NbNP(\mu\text{-}NBu^t)_2PNNb[N(R)Ar]_3$ **6** (35% probability ellipsoids). Hydrogen atoms are omitted for clarity. Selected bond distances (Å) and bond angles (°): Nb–N(1) 2.005(8), Nb–N(2) 2.050(8), Nb–N(3) 2.037(7), Nb–N(4) 1.790(7), P–N 1.734(7), P–N′ 1.727(8); Nb–N(4)–P 167.0(5), N(4)–P–N 108.7(4), N(4)–P–N′ 105.1(4), N–P–N′ 79.9(4), P–N–P′ 100.1(4).

In summary, two examples of a transition-metal supported iminophosphinimide ligand have been prepared by way of a dehydrohalogenation strategy. In the case of **5a**, dimerization occurs *via* cycloaddition of this moiety while a monomer is retained for **5b**, making possible an exploration of the reactivity of the novel M(NPNR) functionality. It is noteworthy that N≡P extrusion to give the corresponding imides was not observed for either complex, illustrating the robust nature of this ligand.

For financial support we gratefully acknowledge the National Science Foundation (CAREER Award CHE-9988806), the Alfred P. Sloan Foundation, the National Science Board (1998 Alan T. Waterman award to C. C. C.), and the David and Lucile Packard Foundations. J. K. B. thanks NSERC (Canada) for a post-doctoral fellowship.

Notes and references

‡ ^{31}P NMR chemical shift values were calculated (DFT) for models of the complexes **2a**, **5a**, **6**, and **2b**–**5b**. Remarkably good agreement between the experimental and theoretical values lends further support to the structural assignments of these species. Additionally, the chemical shift calculated for **5b** compared with that derived for the hypothetical product of dimerization of **5b**, *i.e.* the vanadium analogue of **6**, substantiates designation of this complex as a monomer. See ESI for details.†

§ *Crystal data*: **6**: $C_{40}H_{63}N_5NbP$, M = 737.83, triclinic, space group $P\bar{1}$, a = 10.584(7), b = 12.626(10), c = 17.968(13) Å, α = 116.92(4), β = 90.52(6), γ = 114.37(4)°, V = 2069(3) Å^3, T = 183(2) K, Z = 2, μ(Mo-K$_\alpha$) = 0.361 mm^{-1}, D_c = 1.184 g cm^{-3}, 6162 reflections measured, 3802 unique (R_{int} = 0.0675), 3490 observed [$I > 2\sigma(I)$]. The final R_1 and $wR_2(F^2)$ were 0.0736 [$I > 2\sigma(I)$] and 0.1678 (all data), respectively.

5b: a = 13.7960(2), b = 15.0337(3), c = 20.0772(4) Å, $\alpha = \beta = \gamma$ = 90°, V = 4164.1 Å^3, Z = 4.

CCDC reference number 167617. See http://www.rsc.org/suppdata/cc/b1/b105584b/ for crystallographic data in CIF or other electronic format.

1 G. Proulx and R. G. Bergman, *J. Am. Chem. Soc.*, 1995, **117**, 6382.
2 M. G. Fickes, W. M. Davis and C. C. Cummins, *J. Am. Chem. Soc.*, 1995, **117**, 6384.
3 (*a*) J. K. Brask, T. Chivers, M. L. Krahn and M. Parvez, *Inorg. Chem.*, 1999, **38**, 290; (*b*) P. B. Hitchcock, H. A. Jasim, M. F. Lappert and H. D. Williams, *J. Chem. Soc., Chem. Commun.*, 1986, 1634.
4 (*a*) L. Stahl, *Coord. Chem. Rev.*, 2000, **210**, 203; (*b*) I. Schranz, D. F. Moser, L. Stahl and R. J. Staples, *Inorg. Chem.*, 1999, **38**, 5814.
5 M. G. Fickes, A. L. Odom and C. C. Cummins, *Chem. Commun.*, 1997, 1993.
6 J. G. Verkade and L. D. Quin, *Phosphorus-31 NMR Spectroscopy in Stereochemical Analysis*, VCH Publishers, Inc., Deerfield Beach, FL, vol. 8, 1987.
7 C. C. Cummins, R. R. Schrock and W. M. Davis, *Inorg. Chem.*, 1994, **33**, 1448.
8 J.-I. Song and S. Gambarotta, *Chem. Eur. J.*, 1996, **2**, 1258.
9 G. K. B. Clentsmith, V. M. E. Bates, P. B. Hitchcock and F. G. N. Cloke, *J. Am. Chem. Soc.*, 1999, **121**, 10 444.
10 M. G. Fickes, Ph.D. Thesis, Massachusetts Institute of Technology, MA, 1998.
11 C. C. Cummins, *Chem. Commun.*, 1998, 1777.

CHEMCOMM
Communication
www.rsc.org/chemcomm

Trimagnesium-bridged trinuclear ferrocenophanes cocomplexed with solvated mononuclear alkali metal amide molecules†

Kenneth W. Henderson, Alan R. Kennedy, Robert E. Mulvey,* Charles T. O'Hara and René B. Rowlings

Department of Pure and Applied Chemistry, University of Strathclyde, Glasgow, UK G1 1XL. E-mail: r.e.mulvey@strath.ac.uk

Received (in Cambridge, UK) 6th June 2001, Accepted 25th July 2001
First published as an Advance Article on the web 16th August 2001

Three prototypes of the remarkable new class of compound referred to in the title have been synthesised by treating ferrocene with the same mixed lithium (or sodium)–magnesium amide recipes as those used previously to make s-block metal inverse crowns.

A recent feature article[1] highlighted the special synergistically driven chemistry that can be activated by pairing two distinct metal atom types (Li, Na or K from Group 1 with Mg or Zn from Group 2 or 12) within the same molecular amide environment. Arene molecules such as toluene can undergo selective dideprotonation at thermodynamically unfavourable ring sites to generate dianions which are locked within the central cavities of these so-called 's-block metal inverse crowns'. A representative example germane to the new work described herein is **1**.[2]

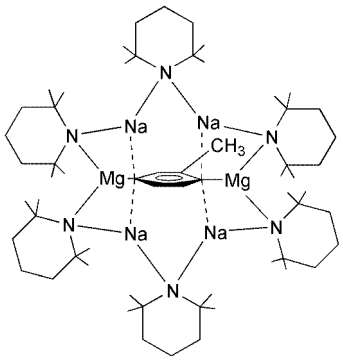

1

Derived from the sterically demanding amine 2,2,6,6-tetramethylpiperidine (TMPH) and formulated as $[Na_4Mg_2(TMP)_6\{C_6H_3(CH_3)\}]$, **1** displays a twelve-membered polymetallic ring, comprising alternate NaNMg and NNaN units, which stabilises the encapsulated arenediide through a combination of Mg–C σ bonds and Na–C π bonds (aligned parallel and perpendicular, respectively, to the arene ring plane). This interplay of σ and π bonding prompted the possibility of introducing cyclopentadienyl-based ligands into this developing area of heterometallic chemistry. Here, as a first attempt towards this goal we have subjected ferrocene to the same mixed sodium–magnesium amide recipe as that used to prepare **1**. The surprising product of this reaction is the trinuclear ferrocenophane disodium trimagnesium amide $[\{Fe(C_5H_4)_2\}_3\{Na_2Mg_3(TMP)_2\cdot(TMPH)_2\}]$ **2**. We have also been successful in synthesising two lithium analogues $[\{Fe(C_5H_4)_2\}_3\{Li_2Mg_3(TMP)_2\cdot(TMPH)_2\}]$, **3** and $[\{Fe(C_5H_4)_2\}_3\{Li_2Mg_3(TMP)_2\cdot(pyridine)_2\}]$ **4**, and so herein report the prototypes of a remarkable new class of structure.

In the preparation of **2**, freshly prepared Bu^nNa and commercial Bu_2Mg (10 mmol of each) were stirred together in a hexane–heptane mixture in an argon-filled Schlenk tube. The congealed brown mass obtained was then treated with TMPH (30 mmol) and the mixture was stirred until complete dissolution had occurred. Next, ferrocene (5 mmol) was introduced and the mixture was heated to reflux for 90 min. This produced a red powder which only partially dissolved on addition of hot toluene (40 ml), so what remained was collected by filtration. Left to cool overnight in a Dewar flask of hot water, the filtrate deposited a crop of red crystals. Both the powder and crystals were identified as **2**.‡ Substituting Bu^nLi for Bu^nNa in a similar procedure afforded the lithium analogue **3**.‡ Note that TMPH is available as a ligand here because it is the byproduct of ferrocene deprotonation by amido anions (TMP). Isolated **3** can be smoothly converted to **4**‡ by re-dissolving it in toluene solution and adding several molar equivalents of the stronger donor pyridine.

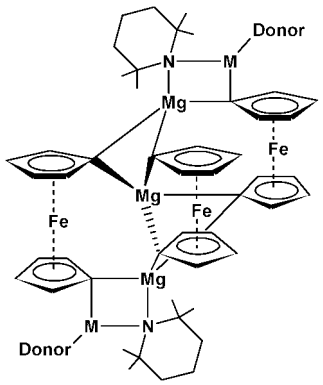

2/3/4

Each Mg atom independently stitches together the three ferrocene-1,1′-diyl units of **2** (Fig. 1). The distorted tetrahedral coordination sphere of centric Mg(1) comprises four C atoms, belonging to the 'top', 'bottom', and 'top' and 'bottom' C_5H_4 rings attached to Fe(1A), Fe(1) and Fe(2), respectively. This unique third ferrocenyl unit is disordered over two sites. Unfortunately this disorder would prejudice any discussion of dimensions pertaining to **2**, though it has no bearing on the connectivities within the structure which are unambiguous. A crystallographic C_2 axis runs through Mg(1) and Fe(2). The fourth coordination site of symmetry partners Mg(2)/Mg(2A) is filled by an amido N atom [N(1)/N(1A)]. Essentially planar (CMgNNa) rings, solvated at Na by TMPH molecules, complete the architecture. Of special significance therein is the Na(1)–C(1) bond [length 2.526(4) Å] as, to the best of our knowledge, it represents the first direct contact between Na and a ferrocenyl unit.

Detailed discussion of the structure is confined to that of **4** (Fig. 2) because there is no disorder within its molecular structure though there are disordered solvent molecules in the extended structure. Its connectivity pattern follows that of **2**, though the C_2 symmetry about the Mg(2)···Fe(2) axis is only approximate in this case. Mimicking the role of the TMPH

† Dedicated to Professor P. L. Pauson on the 50th anniversary of the landmark discovery of ferrocene.

 DOI: 10.1039/b105009p

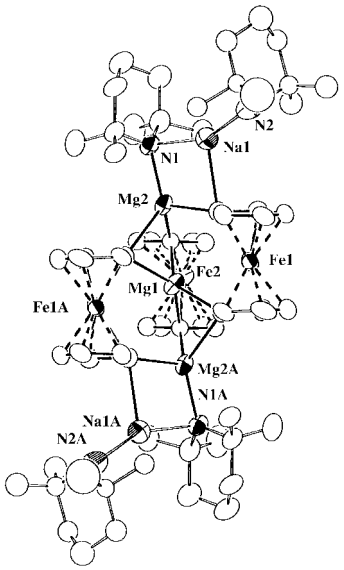

Fig. 1 Molecular structure of **2** without H atoms and disorder component.

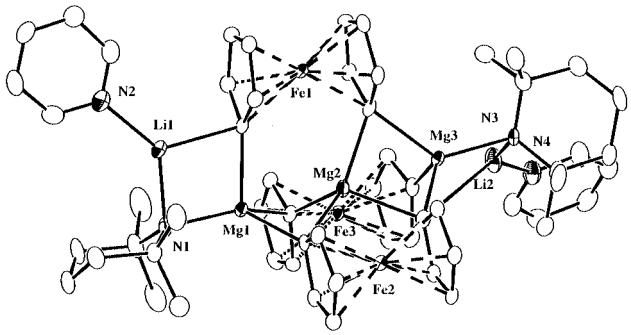

Fig. 2 Molecular structure of **4** from an alternative view to that given for **2** in Fig. 1. H atoms and solvent molecules of crystallisation have been omitted. Key dimensions (Å): Li1–N1 2.031(8), Li1–N2 2.050(8), Li1–C1 2.279(8), Li2–N3 2.027(8), Li2–N4 2.049(8), Li2–C26 2.243(8), Mg1–N1 2.072(3), Mg1–C1 2.187(4), Mg1–C11 2.224(4), Mg1–C21 2.344(4), Mg3–N3 2.094(3), Mg3–C6 2.304(4), Mg3–C16 2.221(4), Mg3–C26 2.194(4), Mg2–C6 2.224(4), Mg2–C11 2.352(4), Mg2–C16 2.307(4), Mg2–C21 2.219(4).

molecules in **2**, pyridine molecules bind terminally to Li at the periphery of the structure. Centric Mg(2) bonds asymmetrically to the ferrocenyl units: the pair of Mg–C bridging bonds to the Fe(2) unit are longer than their single terminal counterparts to the Fe(1) and Fe(3) units (mean lengths, 2.339 and 2.234 Å respectively). Significantly the shortest such bonds in the structure [Mg(1)–C(1) 2.187(4) Å, Mg(3)–C(26) 2.194(4) Å] lie almost parallel with their attached C_5H_4 ring [torsion angles: Mg(1)–C(1)–C(2)–C(3) 176.6(3)°, Mg(3)–C(26)–C(27)–C(28) −176.3(3)°] implying a high degree of σ character. All three Mg atoms deviate substantially from a tetrahedral geometry, with distortion most pronounced for the exclusively ferrocenyl-bound Mg(2) [range of bond angles 90.04(14)–140.42(15)°]. Another salient feature is the near-planarity of the four-element (CMgNLi) rings (sum of endocyclic bond angles, 359.05 or 360.05°). The quasi perpendicular approach of the Li atoms towards the C_5H_4 ring [*e.g.* Li1–C1–C2–C3, 103.6(3)°] signifies a large π contribution to the Li–C bonding. Finally it should be noted that each ferrocenyl unit has essentially eclipsed C_5H_4 rings, and that the staggered positioning of the three ferrocenyl ligands with respect to the Mg···Mg axis gives each molecule a chiral nature.

No precedent exists for this extraordinary class of hetero-trimetallic complex, either in terms of composition or structure. The closest analogy, also reported in 2001,[3] is the homo-main group-metallic gallium-bridged species $[\{Fe(C_5H_4)_2\}_3\{Ga\cdot(pyridine)\}_2]$. Made by a condensation reaction from a methylgallium precursor as opposed to the novel synergic metallation approach used here, it possesses a similar chiral 'carousel' arrangement of ferrocenyl units linked by two end-positioned Ga atoms [*à la* Mg(1) and Mg(3) in **4**], but is 'missing' a centric metal atom and metal amide component. A trinuclear ferrocenyl unit was first observed in the homometallic lithium-bridged species $[\{Fe(C_5H_4)_2\}_3Li_6\cdot(TMEDA)_2]$,[4] but the bridges are exclusively μ_2-Li–C in this case. While no other trinuclear examples are known, there has been a recent report[5] of a dinuclear ferrocenyl complex containing both lithium and magnesium; however, $[(FcN)_2Li_2Mg(Br)_2\cdot(OEt_2)]$ (where FcN is a dimethylaminomethylferrocenyl unit) bears little structural resemblance to **4**.

Returning to the original theme of the work, while **2**, **3** and **4** are clearly not inverse crown ring systems (*à la* **1**) they do nonetheless contain component parts thereof. In particular, their bimetallic MNMg (where M is an alkali metal) fragments are essential building blocks of all the known 8-, 12- and 24-membered inverse crown ring systems. Furthermore the ferrocene-diyl units can be likened to the arene-diyl units encountered in the 12-membered inverse crown **1**. Where **2**, **3** and **4** are truly unique in the context of heterometallic s-block chemistry, is in having a (centric) Mg atom stripped naked of amido ligands. With this atom acting as a fulcrum for supporting the three ferrocenyl units, it should be possible to build supramolecular assemblies of multiple trinuclear ferrocenophane molecules by exploiting the metathetical reactivity of the peripheral alkali metal amide fragments. Such redox-active assemblies could possess a range of interesting electrochemical, electronic and magnetic properties.

We thank the EPSRC for funding this research (through grant award no. GR/M78113).

Notes and references

‡ **2**: Yield (based on ferrocene consumption) 49%; mp decomp. from 200 °C; pyrophoric; satisfactory C, H, N analyses; δ_H (400 MHz, C_5D_5N), 4.83/4.77 (α- or β-H, C_5H_4), 1.58 (γ-H, TMP/H), 1.30 (β-H, TMP/H), 1.12 (α-Me, TMP/H), NH resonance was not observed. **3**: Yield, 68%; mp 174–176 °C; non-pyrophoric, satisfactory C, H, N analyses; δ_H (400 MHz, C_5D_5N). 4.85/4.80 (α- or β-H, C_5H_4), 1.57 (γ-H, TMP/H), 1.29 (β-H, TMP/H), 1.12 (α-Me, TMP/H), NH resonance was not observed. **4**: Yield, 63%; mp 166–168 °C; non-pyrophoric, satisfactory C, H, N analyses; δ_H (400 MHz, C_5D_5N), 8.74 (α-H, pyr), 7.59 (γ-H, pyr), 7.23 (β-H, pyr), 4.84/4.80 (α- or β-H, C_5H_4), 1.58 (γ-H, TMP), 1.29 (β-H, TMP), 1.12 (α-Me, TMP). All samples are extremely sensitive to hydrolysis as shown by trace amounts of ferrocene at δ 4.20. Note that solubility problems were encountered when the reactions were repeated using the stoichiometry consistent with the formulas of **2**, **3** and **4**. However, in all cases the same products were again observed.

Crystal data: for **2**: $C_{66}H_{98}Fe_3Mg_3N_4Na_2$, M = 1233.94, monoclinic, space group $P2/c$, a = 16.6871(3), b = 10.3932(2), c = 18.5237(4) Å, β = 102.392(1)°, U = 3137.8(1) Å^3, Z = 2, λ = 0.71073 Å, μ = 0.77 mm^{-1}, T = 150 K, R = 0.062 for 4553 observed reflections, $wR2$ = 0.1705 for 6166 unique reflections for 355 parameters refined to convergence on F^2.

For **4**·$C_6H_5CH_3$: $C_{65}H_{78}Fe_3Li_2Mg_3N_4$, M = 1169.66, triclinic, space group $P\bar{1}$, a = 15.402(5), b = 16.552(2), c = 11.622(3) Å, α = 98.651(11), β = 100.01(2), γ = 94.796(14)°, U = 2866.2(11) Å^3, Z = 2, λ = 0.71069 Å, μ = 0.83 mm^{-1}, T = 123 K, R = 0.0499 for 6837 observed reflections, $wR2$ = 0.1350 for 8991 unique reflections and 696 parameters refined to convergence on F^2.

CCDC reference numbers 165404 and 165405. See http://www.rsc.org/suppdata/cc/b1/b105009p/ for crystallographic data in CIF or other electronic format.

1 R. E. Mulvey, *Chem. Commun.*, 2001, 1049.
2 D. R. Armstrong, A. R. Kennedy, R. E. Mulvey and R. B. Rowlings, *Angew. Chem.*, 1999, **111**, 231; D. R. Armstrong, A. R. Kennedy, R. E. Mulvey and R. B. Rowlings, *Angew. Chem., Int. Ed.*, 1999, **38**, 131.
3 P. Jutzi, N. Lenze, B. Neumann and H.-G. Stammler, *Angew. Chem.*, 2001, **113**, 1470; P. Jutzi, N. Lenze, B. Neumann and H.-G. Stammler, *Angew. Chem., Int. Ed.*, 2001, **40**, 1424.
4 I. R. Butler, W. R. Cullen, J. Ni and S. J. Rettig, *Organometallics*, 1985, **4**, 2196.
5 N. Seidel, K. Jacob, A. K. Fischer, C. Pietzsch, P. Zanello and M. Fontani, *Eur. J. Inorg. Chem.*, 2001, 145.

CHEMCOMM
Communication
www.rsc.org/chemcomm

Crystal growth, structure determination and magnetism of a new hexagonal rhodate: $Ba_9Rh_8O_{24}$

K. E. Stitzer,[a] M. D. Smith,[a] J. Darriet*[b] and H.-C. zur Loye*[a]

[a] *Department of Chemistry and Biochemistry, University of South Carolina, Columbia, SC, 29208, USA. E-mail: zurloye@sc.edu*

[b] *Institut de Chimie de la Matière Condensée de Bordeaux (ICMCB-CNRS), Avenue du Dr. Schweitzer, 33608 Pessac Cedex, France. E-mail: darriet@icmcb.u-bordeaux.fr*

Received (in Cambridge, UK) 25th May 2001, Accepted 23rd July 2001
First published as an Advance Article on the web 16th August 2001

Single crystals of $Ba_9Rh_8O_{24}$, grown from a molten potassium carbonate flux, crystallize in the spacegroup $R\bar{3}c$ with lattice parameters of a = 10.0899(4) and c = 41.462(2) Å. Magnetic measurements on oriented single crystals reveal the existence of magnetic anisotropy.

During recent years, there has been much interest in the preparation and investigation of oxides structurally related to the 2H hexagonal perovskites, the prototype of which, Sr_4PtO_6, was first prepared by Randall and Katz[1] and forms in the K_4CdCl_6 structure type. As shown by Darriet and Subramanian,[2] and more recently by Darriet and Perez-Mato,[3] the structures of these oxides can all be described as resulting from stacking sequences of $m[A_3O_9]$ layers and $n[A_3A'O_6]$ layers, with the subsequent filling of the interstitial octahedral sites. The general formula that can be derived from the stacking of such layers is: $A_{3n+3m}A'_nB_{3m+n}O_{9m+6n}$ (n, m = integers, A = alkaline earth; A′, B = large assortment of metals including alkali, alkaline earth, transition, main group, and rare earth metals). The structures are characterized by one-dimensional chains of face-sharing trigonal prisms and octahedra along the *c*-axis of the hexagonal unit cell.

Sr_4PtO_6 is the n = 1, m = 0 member of this family and consists of chains of alternating face-sharing octahedra and trigonal prisms. While many n = 1, m = 0 members are known, for example Sr_3NaRhO_6,[4] $Ca_3Co_2O_6$,[5,6] and Ca_3CuIrO_6,[7] far fewer oxides with higher integer values of n and m have been prepared and structurally characterized. In addition, until recently, most structure determinations were based on Rietveld refinements of polycrystalline powders and few single crystals of any members, and in particular very few members with higher integer values of n and m, have been grown and structurally characterized. A recent example of the latter type includes $Ba_8CoRh_6O_{21}$ corresponding to the m = 5, n = 3 member.[8] Other examples include $Ba_6Ni_5O_{15}$,[9] $Sr_4Ru_2O_9$,[10] and the incommensurate phases of $Ba_{1+x}(Cu_xRh_{1-x})O_3$ (x = 0.1605 and 0.1695) whose average structure is that of the n = 3, m = 4 member with a repeat sequence of five octahedra and one trigonal prism.[11] In this communication we report the first structural characterization of the m = 2, n = 1 member $Ba_9Rh_8O_{24}$ and the investigation of its magnetic properties.

Single crystals of $Ba_9Rh_8O_{24}$ were grown from a molten potassium carbonate flux. $BaCO_3$ and Rh metal powder (6:1 molar ratio) were mixed with a 10 fold mass excess of K_2CO_3. The alumina crucible was heated in air to 1050 °C, held for 48 h, and then quickly cooled to room temperature. The crystals were isolated manually by dissolving the flux in water.

An approximate [110] view is shown in Fig. 1. The structure is characterized by infinite chains containing groups of seven face-sharing RhO_6 octahedra separated by one face-sharing RhO_6 trigonal prism. These chains are in turn separated from one another by chains of Ba cations. The metal–oxygen bond distances [Rh1–O1 2.020(6), Rh2–O2 2.008(6), Rh2–O1 2.035(6), Rh3–O3 2.003(7), Rh3–O2 2.035(6), Rh4–O4 1.969(10), Rh4–O3 2.048(7), Rh5–O4 2.012(12) Å] are typical for oxides of this type. Intrachain Rh–Rh bond distances [Rh1–Rh2 2.523(1), Rh2–Rh3 2.455(1), Rh3–Rh4 2.637(2), Rh4–Rh5 2.750(1) Å] can be considered non-bonding.

$Ba_9Rh_8O_{24}$ represents the first structurally characterized m = 2, n = 1 member of this family, and more interestingly one of only a few single crystal compositions which are commensurate and not of the n = 1, m = 0 structure type. It is worth noting that this compound consists of the longest octahedra repeat sequence structurally characterized to date and structurally approaches the other end member of this family, n = 0, m = 1, the $BaNiO_3$ hexagonal perovskite structure. Compounds with chains consisting of 5 ($Sr_6Rh_5O_{15}$[12]) and 6 ($Ba_8CoRh_6O_{21}$) face-sharing octahedra separated by one face-sharing trigonal prism are known. In these and related oxides,[6] large magnetic anisotropies have been observed as a function of crystal orientation. To investigate the magnetic behavior of $Ba_9Rh_8O_{24}$, susceptibility measurements were obtained using a large single crystal weighing 5.53(1) mg.†

The plot of susceptibility as a function of crystal orientation measured at 2 K is shown in Fig. 2. A beautiful regular sinusoidal variation in the susceptibility is clearly evident. The maxima in the susceptibility correspond to a parallel alignment of the hexagonal *c*-axis (*i.e.* the $[Rh_8O_{24}]_\infty$ chain direction) with the applied field and the minima correspond to a 90 degree rotation from that position, or a perpendicular orientation of the *c*-axis relative to the magnetic field. Susceptibility measurements with the crystal oriented parallel and perpendicular with respect to the magnetic field are shown in Fig. 3, where the two curves diverge below *ca.* 100 K, indicating the onset of the

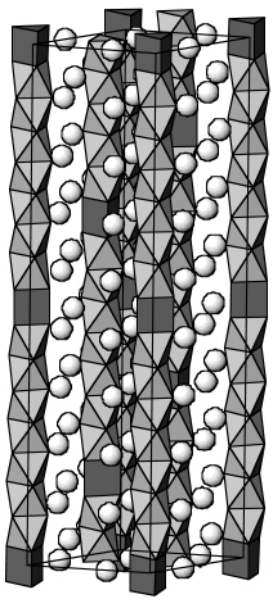

Fig. 1 Approximate [110] view of the structure of $Ba_9Rh_8O_{24}$. Dark grey: RhO_6 trigonal prisms; grey: RhO_6 octahedra; light grey: Ba atoms.

 DOI: 10.1039/b104513j

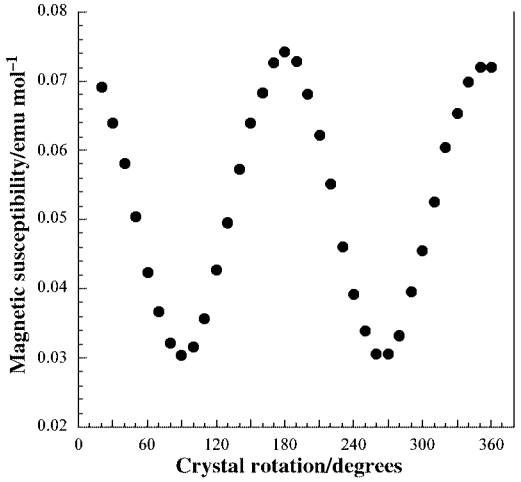

Fig. 2 Magnetic susceptibility of a single crystal of $Ba_9Rh_8O_{24}$ as a function of crystal orientation with respect to the applied magnetic field measured at 2 K and 5 kG. The maxima occur for the crystal's *c*-axis aligned parallel with the applied field.

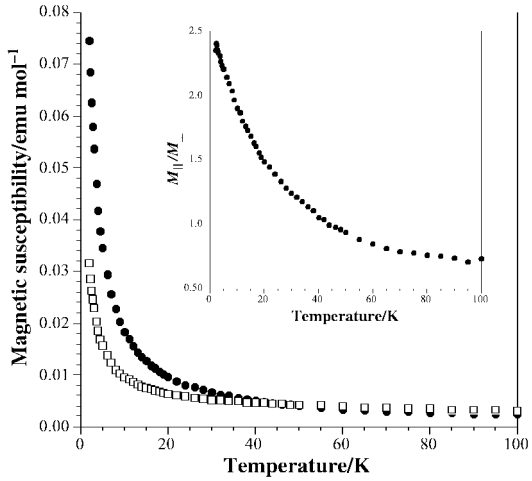

Fig. 3 Temperature dependence of the magnetic susceptibility of a single crystal of $Ba_9Rh_8O_{24}$ oriented parallel (●) and perpendicular (□) with respect to the applied field at 5 kG. Inset: temperature dependence of the magnetic anisotropy (defined as the ratio between the susceptibility of a single crystal oriented parallel and perpendicular with respect to the applied field).

magnetic anisotropy. The inset in Fig. 3 is a plot of the magnitude of the magnetic anisotropy, $M_{\|}/M_{\perp}$, as a function of temperature.‡

The issue of oxidation states for the rhodium and their location in this chain structure is currently not possible to resolve. In order to charge balance $Ba_9Rh_8O_{24}$, oxidation states can be distributed as six Rh^{4+} and two Rh^{3+}. A bond valence analysis proved inconclusive, and so one might hope to gain insight into the oxidation states from the magnetic susceptibility data. Assuming low spin rhodium in octahedral coordination, the Rh^{4+}, d^5, would each contribute one unpaired electron, while Rh^{3+}, d^6, would contribute no unpaired electrons. Unfortunately, the magnetic data cannot be fit to Curie-type behavior, making it impossible to check the above assignment.

Finally, the presence of the non-magnetic Rh^{3+} in the chain, would break any exchange interactions between Rh^{4+} sites, leading to a disruption of magnetic interactions within the chain. This should result in the formation of small magnetic units along the chain. The anisotropy that is observed at low temperature can potentially be due to an anisotropy in the exchange interaction between rhodium atoms in these small units or, alternatively, by irregular Rh^{4+} octahedra, resulting in different *g*-factors for $g_{\|}$ and $g_{\perp}$. This is an area of further investigation and beyond the scope of this communication.

Financial support from the National Science Foundation through Grant DMR:9873570 is gratefully acknowledged.

Notes and references

† *Crystal data*: A black hexagonal prism was epoxied onto the end of a thin glass fiber. X-Ray intensity data were measured at 293 K using a Bruker SMART APEX CCD-based diffractometer system using Mo-Kα radiation (λ = 0.71073 Å). $Ba_9Rh_8O_{24}$, M = 2443.34 g mol^{-1}, rhombohedral, space group $R\bar{3}c$ (no. 167), a = 10.0899(4), c = 41.462(2) Å, V = 3655.6(3) Å^3, Z = 6, D_c = 6.659 Mg m^{-3}, μ(Mo-Kα) = 19.622 mm^{-1}, crystal size: 0.24 × 0.11 × 0.10 mm, θ range 2.38–33.16°, independent reflections 1551 (R_{int} = 0.0312), data/restraints/parameters 1551 / 0 / 66. Structure solved and refined using SHELXTL Version 5.1. An empirical absorption correction based on the multiple measurement of equivalent reflections was applied with the program SADABS (min., max. transmission = 0.1341, 0.2694). Final $R1$ (all data) = 0.0524, $wR2$ (all data) = 0.0992.

Atomic coordinates and equivalent isotropic displacement parameters:

Atom	*x*	y	*z*	U_{eq}/Å^2
Ba(1)	0.3223(1)	0.9932(1)	0.0273(1)	0.012(1)
Ba(2)	0.3519(1)	0	1/4	0.010(1)
Rh(1)	0	0	0	0.006(1)
Rh(2)	0	0	0.9392(1)	0.008(1)
Rh(3)	0	0	0.8800(1)	0.006(1)
Rh(4)	0	0	0.8163(1)	0.011(1)
Rh(5)	0	0	3/4	0.014(1)
O(1)	0.1581(7)	0.1566(7)	0.0301(2)	0.010(1)
O(2)	0.8377(7)	0.9935(8)	0.9101(1)	0.008(1)
O(3)	0.8518(9)	0.8438(9)	0.8490(2)	0.022(2)
O(4)	0.8417(13)	0.9600(20)	0.7839(3)	0.080(6)

CCDC reference number 164826. See http://www.rsc.org/suppdata/cc/b1/b104513j/ for crystallographic data in CIF or other electronic format.

‡ *Magnetism*: Magnetic measurements were collected on a single crystal of $Ba_9Rh_8O_{24}$ weighing 5.53(1) mg using a Quantum Design MPMS XL SQUID magnetometer. Aligned crystal measurements were performed using a Quantum Design Single Crystal Rotator attachment. The crystal was affixed to the rotator using standard vacuum grease. The crystal was rotated in 10° steps through 360° at 2 K with an applied field of 5 kG; knowing the initial orientation makes it possible to correlate the maxima and minima to the crystal alignment. Temperature dependence measurements were taken at a position corresponding to a maximum and a minimum in susceptibility at 5 kG. The moment of the sample holder was corrected for using the Automatic Background Subtraction software by Quantum Design.

1 J. J. Randall and L. Katz, *Acta Crystallogr.*, 1959, **12**, 519.
2 J. Darriet and M. A. Subramanian, *J. Mater. Chem.*, 1995, **5**, 543.
3 J. M. Perez-Mato, M. Zakhour-Nakhl, F. Weill and J. Darriet, *J. Mater. Chem.*, 1999, **9**, 2795.
4 B. A. Reisner and A. M. Stacy, *J. Am. Chem. Soc.*, 1998, **120**, 9682.
5 H. Fjellvag, E. Gulbrandsen, S. Aasland, A. Olsen and B. C. Hauback, *J. Solid State Chem.*, 1996, **124**, 190.
6 A. Maignan, C. Michel, A. C. Masset, C. Martin and B. Raveau, *Eur. Phys. J.* B, 2000, **15**, 657.
7 A. Tomaszewska and Hk. Müller-Buschbaum, *Z. Anorg. Allg. Chem.*, 1993, **619**, 534.
8 H.-C. zur Loye, K. E. Stitzer, M. D. Smith, A. El Abed and J. Darriet, *Inorg. Chem.*, in press.
9 J. A. Campa, E. Gutierrez-Puebla, M. A. Monge, I. Rasines and C. Ruiz-Valero, *J. Solid State Chem.*, 1994, **108**, 230.
10 C. Dussarrat, J. Fompeyrine and J. Darriet, *Eur. J. Solid State Inorg. Chem.*, 1995, **32**, 3.
11 M. Zakhour-Nakhl, J. B. Claridge, J. Darriet, F. Weill, H.-C. zur Loye and J. M. Perez-Mato, *J. Am. Chem. Soc.*, 2000, **122**, 1618.
12 K. E. Stitzer, A. El Abed, J. Darriet and H.-C. zur Loye, *J. Am. Chem. Soc.*, in press.

CHEMCOMM Communication
www.rsc.org/chemcomm

Oxidative cyclisation of cinnamyl ethers mediated by CAN: a stereoselective synthesis of 3,4-*trans* disubstituted tetrahydrofuran derivatives

Vijay Nair,*[a] Lakshmi Balagopal,[a] V. Sheeba,[a] Sreeletha B. Panicker[a] and Nigam P. Rath[b]

[a] *Organic Chemistry Division, Regional Research Laboratory (CSIR), Trivandrum 695 019, India. E-mail: gvn@csrrltrd.ren.nic.in; Fax: +91-471-491712*
[b] *Department of Chemistry, The University of Missouri, St Louis, MO 63121-4499, USA*

Received (in Cambridge, UK) 5th April 2001, Accepted 6th July 2001
First published as an Advance Article on the web 16th August 2001

The oxidative cyclisation of cinnamyl ethers mediated by cerium(IV) ammonium nitrate results in the stereospecific formation of 3,4-*trans* disubstituted tetrahydrofuran derivatives in moderate to good yields.

Cerium(IV) ammonium nitrate (CAN) has been found to be a very efficient reagent for carbon–carbon bond formation especially in reactions involving the oxidative addition of 1,3-dicarbonyl compounds to alkenes.[1a,b] In spite of its success in this and a variety of other highly efficient intermolecular reactions of value in organic synthesis,[1] CAN has found very little use in intramolecular C–C bond formation;[2] this is in contrast to the general acceptance of Mn(III) in intramolecular cyclisations.[3] In view of this and prompted by our recent observation of CAN induced dimerisation of alkoxy styrenes,[4] we surmised that appropriately tethered alkoxy cinnamyl ethers would undergo CAN mediated cyclisation leading to tetrahydrofuran derivatives. It is noteworthy that a chemical electron transfer mediated intramolecular cyclobutanation of dicinnamyl ethers using triarylaminium salts has been reported by Bauld *et al*.[5]

Our studies were initiated by the reaction of 2-methoxycinnamyl cinnamyl ether **1a** with CAN in methanol under an oxygen atmosphere. In the event, the reaction afforded a tetrahydrofuran derivative **2a**, in moderate yield. The reaction was found to be general and applicable to similar substrates (Scheme 1).

Interestingly, when the reaction of **1a** with CAN was carried out under argon atmosphere, instead of the ketone, a mixture of the methoxy and nitrato derivatives **3a**, in the ratio 2:1, was obtained in high yield. Similar results were obtained with other substrates (Scheme 2).

Catalytic hydrogenation of the mixture of methoxy and nitrato derivatives **3a** effected the selective conversion of the latter to the corresponding alcohol **5a** (Scheme 3).

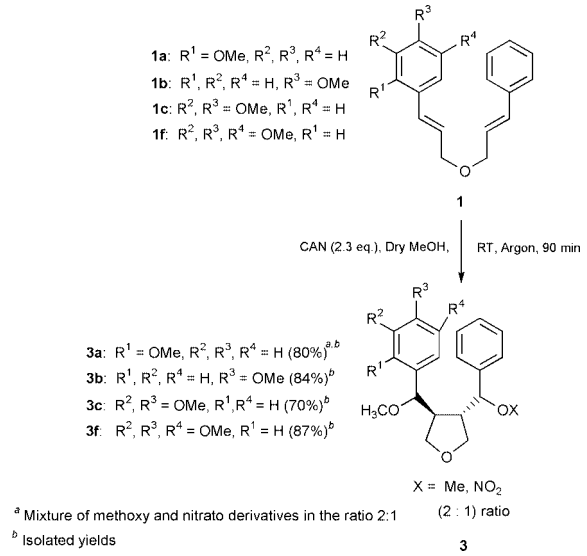

Scheme 2

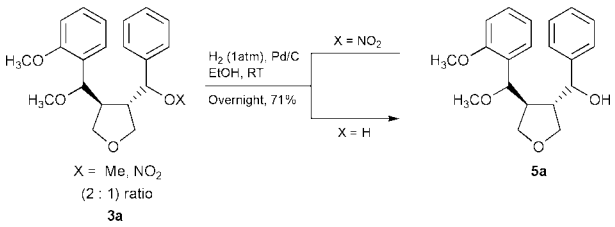

Scheme 3

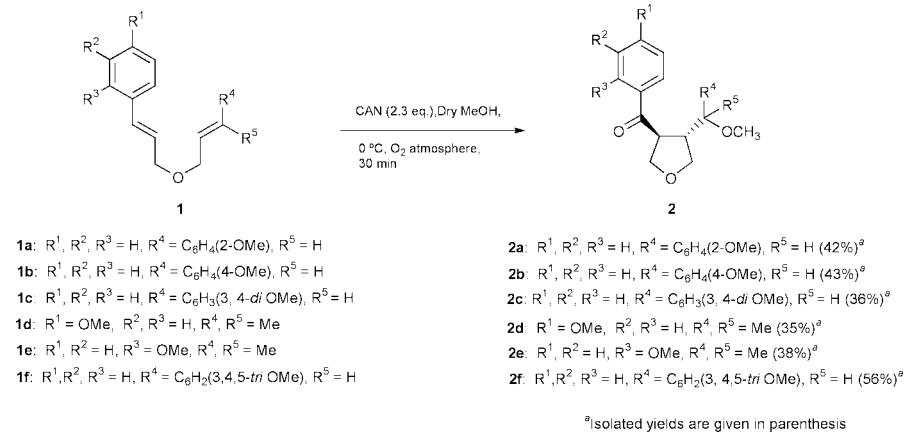

Scheme 1

 DOI: 10.1039/b103111m

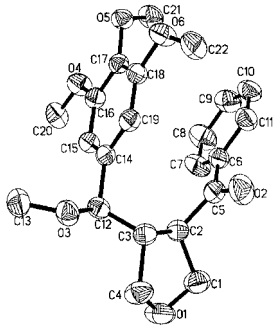

Fig. 1 X-Ray crystal structure of compound **2f**.

Relevant spectral data (IR, ^{1}H NMR, ^{13}C NMR, DEPT-135 NMR) of the products are in good agreement with structures assigned.† The stereochemistry of the 3,4-disubstituted-tetrahydrofuran derivative has been confirmed to be *trans* with the aid of single crystal X-ray analysis of compound **2f** (Fig. 1).‡

A mechanistic rationale for the formation of the product can be depicted along the following lines (Scheme 4).

A radical cation initially formed from the methoxy styrene unit of the substrate can add in an intramolecular fashion to the adjacent styrene moiety to form a distonic radical cation. The cationic center is quenched by methanol, whereas the radical center is prone to two different transformations.[1c,d] Under oxygen atmosphere, the radical site is quenched by molecular oxygen yielding the keto product *via* the initially formed peroxy radical. Under argon atmosphere, the radical site is quenched by nitrate by ligand transfer from CAN; alternatively, it can undergo oxidation by CAN to the benzylic cation with subsequent addition of methanol yielding the dimethoxy product.

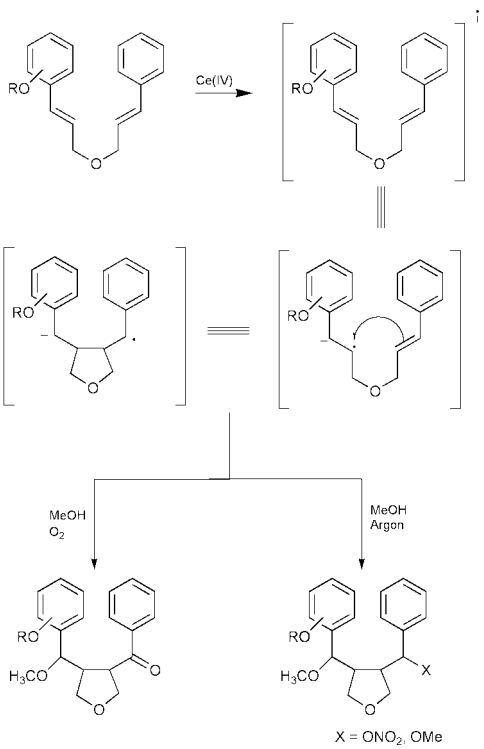

Scheme 4

In conclusion, we have devised a novel and efficient route towards the stereospecific construction of 3,4-*trans* substituted tetrahydrofurans from relatively simple precursors, which assumes importance in view of the fact that substituted tetrahydrofurans feature in many natural products of biological importance,[6] especially lignans. Further studies are currently in progress.

L. B., V. S. and S. B. P. thank CSIR, New Delhi, for research fellowships. The authors also thank Ms Soumini Mathew for high-resolution NMR spectra and Mrs S. Viji for elemental analysis.

Notes and references

† Experimental procedure and selected data for **2f** : A solution of CAN (740 mg, 1.33 mmol) in dry methanol (15 ml) was added dropwise with stirring to a solution of **1f** (200 mg, 0.58 mmol) in dry methanol (10 ml) under oxygen atmosphere. After 30 minutes the reaction mixture was diluted with 50 ml water and extracted with DCM (3 × 25 ml). The combined organic extracts were washed with water, saturated brine and dried over sodium sulfate. After the removal of the solvent, chromatographic separation on silica gel using 80 : 20 hexane–ethyl acetate gave the THF derivative **2f** (128 mg) in 56% yield as a colorless crystalline solid. Mp: 115–117 °C (recrystallised from CH_2Cl_2–hexane). (Elemental analysis; Calcd for $C_{22}H_{26}O_6$ C, 68.38; H, 6.78. Found: C, 68.00; H, 6.75%) ν_{max}/cm^{-1} 2940, 2853, 1720, 1664, 1589, 1496, 1458, 1328, 1234, 1128, 1085, 1004. δ_H (300 MHz; $CDCl_3$) 7.54–7.46 (m, 3H, ArH), 7.35–7.30 (m, 2H, ArH), 6.42 (s, 2H, ArH), 4.23–4.17 (m, 1H), 4.09–3.92 (m, 3H), 3.84–3.72 (m, 11H, 3 × OCH_3 embedded in this multiplet), 3.19 (s, 3H, OCH_3), 3.1–3.06 (m, 1H); δ_C 198.96, 153.29, 136.47, 135.27, 133.02, 128.34, 127.90, 104.33, 85.36, 71.32, 71.27, 60.56, 56.70, 55.91, 50.67, 49.19; DEPT-135: (CH_2 negative) 71.32, 71.27. All new compounds were fully characterized.

‡ *Crystal data* for **2f**: $C_{22}H_{26}O_6$, FW 386.43, 0.30 × 0.20 × 0.14 mm, monoclinic, space group $P2_1/n$, unit cell dimensions: a = 10.8619(4) Å, α = 90°; b = 12.9527(4) Å, β = 99.570°; c = 14.2988(5) Å, γ = 90°. R indices (all data) $R1$ = 0.0656, $wR2$ = 0.1131. v = 1983.71(12) Å^3, Z = 4. D_{calc} = 1.294 Mg m^{-3}. F(000) = 824. Absorption coefficient 0.094 mm^{-1}; reflections collected 42489 (G. M. Sheldrick, Siemens, Analytical X-ray Division, Madison, WI, USA, 1995). CCDC 163141. See http://www.rsc.org/suppdata/cc/b1/b103111m/ for crystallographic data in .cif or other electronic format.

1 (*a*) V. Nair, J. Mathew and J. Prabhakaran, *Chem. Soc. Rev.*, 1997, 127; (*b*) T. Linker, K. Hartmann, T. Sommermann, D. Scheutzow and E. Ruckdeschel, *Angew. Chem., Int. Ed. Engl.*, 1996, **35**, 1730; (*c*) V. Nair and J. Mathew, *J. Chem. Soc., Perkin Trans. 1*, 1995, 1881; (*d*) V. Nair, J. Mathew and L. G. Nair, *Synth.Commun.*, 1997, **27**, 3053; (*e*) V. Nair, L. G. Nair, T. G. George and A. Augustine, *Tetrahedron*, 2000, **56**, 7607; (*f*) E. Baciocchi, A. Casu and R. Ruzziconi, *Synlett*, 1990, 679; (*g*) T. Linker and U. Linker, *Angew. Chem., Int. Ed. Engl.*, 2000, **39**, 902.

2 (*a*) B. B. Snider and T. Kwon, *J. Org. Chem.*, 1990, **55**, 4786; (*b*) E. Baciocchi, A. B. Paolobelli and R. Ruzziconi, *Tetrahedron*, 1992, **48**, 4617; (*c*) H. J. Kim, U. C. Yoon, Y. Jung, N. S. Park, E. M. Cederstorm and P. S. Mariano, *J. Org. Chem.*, 1998, **63**, 860; (*d*) Y. Takemoto, S. Yamagata, S. I. Furuse, H. Hayase, T. Echigo and C. Iwata, *J. Chem. Soc., Chem. Commun.*, 1998, 651; (*e*) A.-C. Durand, J. Rodriguez and J.-P. Dulcere, *Synlett*, 2000, 731 and references cited therein.

3 (*a*) G. G. Melikyan, *Synthesis*, 1993, 833; (*b*) B. B. Snider, *Chem. Rev.*, 1996, **96**, 339; (*c*) A. D'Annibale, D. Nanni, C. Troglo and F. Umani, *Org. Lett.*, 2000, 401.

4 (*a*) V. Nair, J. Mathew, P. P. Kanakamma, S. B. Panicker, V. Sheeba, S. Zeena and G. K. Eigendorf, *Tetrahedron Lett.*, 1997, **38**, 2191; (*b*) V. Nair, V. Sheeba, S. B. Panicker, T. G. George, R. Rajan, L. Balagopal, M. Vairamoni and S. Prabhakar, *Tetrahedron*, 2000, **56**, 2461.

5 (*a*) T. Kim, G. A. Mirafzal, J. Liu and N. L. Bauld, *J. Am. Chem. Soc.*, 1993, **115**, 7653; (*b*) N. P. Schepp, D. Shukla, H. Sarker, N. L. Bauld and L. J. Johnston, *J. Am. Chem. Soc.*, 1997, **119**, 10325.

6 (*a*) H. Yoda, T. Shimojo and K. Takabe, *Synlett*, 1999, 1969 and references cited therein.

CHEMCOMM
Communication
www.rsc.org/chemcomm

Three component synthesis of oxa-bridged tetracyclic tetrahydroquinolines

Eduardo González-Zamora,† Aude Fayol, Michèle Bois-Choussy, Angèle Chiaroni and Jieping Zhu*

Institut de Chimie des Substances Naturelles, CNRS, 91198 Gif-sur-Yvette Cedex, France. E-mail: zhu@icsn.cnrs-gif.fr; Fax: +33 1 69 07 72 47; Tel: +33 1 69 82 31 31

Received (in Cambridge, UK) 16th May 2001, Accepted 11th July 2001
First published as an Advance Article on the web 16th August 2001

Bridged tetracyclic tetrahydroquinoline is synthesized by a novel one-pot three component condensation of an *ortho*-amino cinnamate, α-isocyano acetamide and an aldehyde.

Maximizing synthetic efficiency by designing complexity-generating multicomponent domino processes is gaining more and more importance in organic synthesis and in drug discovery endeavour.[1–4] In connection with our ongoing project, a novel one-pot three component synthesis of tetracyclic tetrahydroquinoline[5] was envisaged. The sequence of events, hinged upon our recently developed synthesis of 5-aminooxazole,[6] is outlined in Scheme 1. Thus, reaction of an aniline, an aldehyde and an α-isocyano acetamide should give the aminooxazole *via* an iminium, then a nitrilium ion intermediate. Cycloaddition of oxazole as an aza-diene with a properly predisposed dienophile would then produce a bridged tetrahydroquinoline-containing polycycle that, *a priori*, would undergo further fragmentation to provide phenanthroline.[7] While domino Ugi/Diels–Alder cycloadditions starting from diene- and dienophile-containing building blocks have been elegantly developed,[8] the multi-component reaction (MCR)/cycloaddition sequence involving *en route* generation of a transient diene, to the best of our knowledge, was unknown.[9] The realization of this concept as well as the documentation of the remarkable thermostability of cycloadduct **1** is the subject of this communication.

Using *ortho*-amino methyl cinnamate (**2a**), heptanal (**3a**) and α-isocyano α-benzyl acetamide (**4a**) as inputs, reaction conditions were surveyed varying the solvent (MeOH, CF_3CH_2OH, benzene, toluene), the temperature (rt to 110°C), and the promotor (LiBr, $BF_3{\cdot}OEt_2$, $Yb(OTf)_3$, $Sc(OTf)_3$, $MgSO_4$). After a considerable number of experiments, conditions were worked out for the domino 3 component reaction (3CR)/intramolecular Diels–Alder cycloaddition process. Thus, under the optimal conditions (**2a** and **3a**, LiBr, in toluene, 2h then **4a**, 70 °C), tetracyclic tetrahydroquinoline **1** was isolated in 94% yield as a mixture of two separable diastereomers (ratio of **1a**:**1a′** = 3:1, Scheme 2). Without LiBr, **1a** and **1a′** were isolated in less than 6% yield under otherwise identical conditions.[10] The identification of 5-aminooxazole intermediate **7** (where NR^5R^6 = NEt_2) provided evidence that the reaction indeed proceeded as programmed. It is worthy of note that one C–N, one C–O and three C–O bonds were formed with the concomitant creation of five asymmetric centers in this one-pot process. The efficiency of this reaction was thus truly remarkable if one looks at the yield per bond formation.

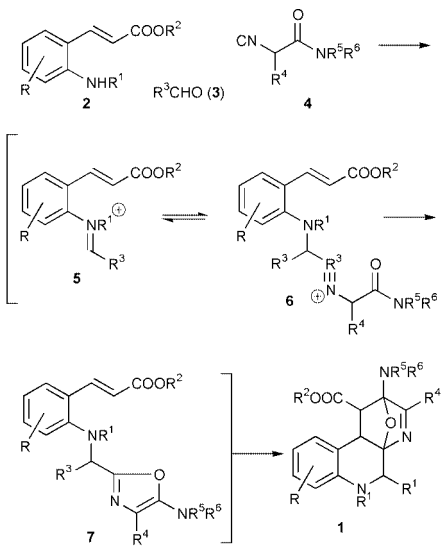

Scheme 1

The stereochemistry of compound **1a** and **1a′** was deduced from both mechanistic consideration and NMR studies. The observed coupling constant between H_a and H_b ($J_{Ha\text{-}Hb}$ = 4.6 Hz for **1a** and 4.4 Hz for **1a′**) indicated a *gauche* relationship of these two protons in both compounds. For the inherent ring strain imposed by the connecting bridge, only the aryl-*exo*-ester-*endo* mode of cycloaddition was possible leading to the observed compounds. This model of ring formation is also indicative of a concerted rather than a stepwise process, since one could expect the formation of aryl-*exo*-ester-*exo* diastereomers if the latter mechanism was operating. The relative stereochemistry of the major adduct **1a** was deduced from the observation of a strong NOE cross peak between H_b and H_c in its NOESY spectrum and corroborated by X-ray analysis (Fig. 1).‡

Control experiments showed that the observed stereoselectivity was a thermodynamically controlled process. Indeed, re-submitting the diastereomerically pure compound **1a** to the reaction conditions led to the formation of a mixture of **1a** and **1a′** with the ratio identical to that resulting from the reaction mixture. The same is true for **1a′**. While the thermo-equilibrium can be interpreted by a sequence of heterocycloreversion/

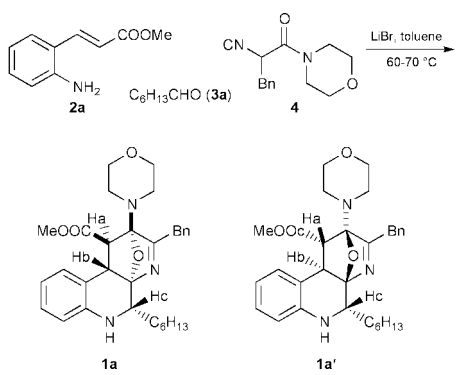

Scheme 2

† E. González-Zamora is a visiting Professor from Universidad Autónoma Metropolitana-Iztapalapa, 09340 México D. F.

 DOI: 10.1039/b104317j

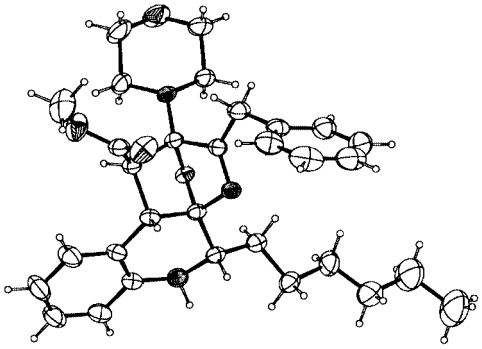

Fig. 1 X-ray structure of **1a**.

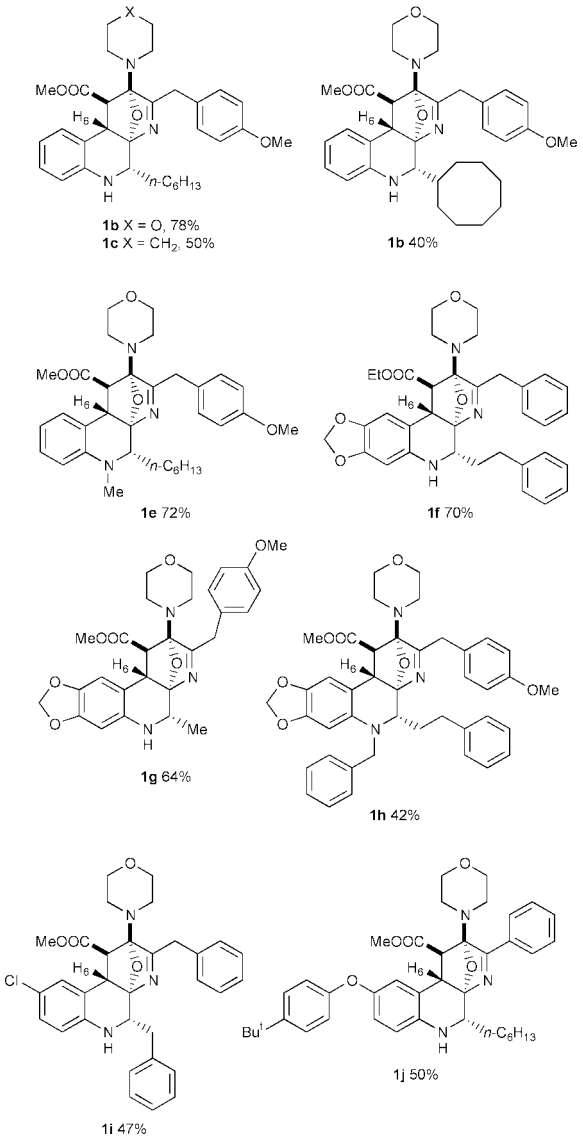

Fig. 2 Selected tetrahydroquinolines synthesized.

cycloaddition, the relatively high stability of compound **1** with a strained aminal function was nevertheless intriguing.

Selected structures synthesized in this preliminary study are listed in Fig. 2.§ The reaction conditions have not been individually optimized. As is seen, all substituents at the periphery of the tetracyclic ring system can be varied. The *ortho*-amino cinnamate with either electron donating or electron withdrawing group participated in the reaction, as did the *N*-alkylated derivatives. The α-branched aldehydes, as well as the α-alkyl and α-aryl substituted α-isocyano acetamides took part in this reaction. When cyclooctyl aldehyde was used, a single diastereomer was isolated. Since the nitrogen bearing the asymmetric center was the one that controlled the facial selectivity of the subsequent aza-Diels–Alder cycloaddition, the observation is thus understandable. As expected for Ugi type reaction, racemic tetrahydroquinoline was obtained even when enantiomerically pure isonitrile **4** (R = Bn, or phenyl) was used as input. At this stage of the development, the failure of aromatic aldehyde to enter the reaction cascade constituted the limitation of the present methodology.

In conclusion, we have developed a novel multicomponent domino process for the synthesis of oxa-bridged tetrahydroquinoline starting from simple and readily accessible linear precursors. Besides its synthetic efficiency and potential application in diversity oriented synthesis, we demonstrated, to the best of our knowledge, for the first time that Ugi-type condensations can be performed in toluene in the presence of LiBr without concurrent occurrence of a Passerini-type reaction.

Financial support from CONACYT (E. G.-Z.) and CNRS are gratefully acknowledged. We thank Mr M. De Paolis for helpful discussion.

Notes and references

‡ *Crystal data for* **1a**: pale yellow crystal (0.32 × 0.37 × 0.40 mm). $C_{31}H_{39}N_3O_4$, M_w = 517.65. Monoclinic system, space group $P2_1/n$, Z = 4, a = 14.049 (5), b = 9.982 (5), c = 20.886 (8) Å, β = 97.64 (3)°, V = 2903 Å^3, D_C = 1.184 g cm^{-3}, $F(000)$ = 1112, λ(Mo Kα) = 0.71073 Å, T = 293 K, μ = 0.08 mm^{-1}; 8306 data measured (θ range: 2.12 to 27.47°) on a Nonius Kappa-CCD area-detector diffractometer. Refinement with *SHELXL93*. $R_1(F)$ = 0.0755 for the 3303 $F_o \geq 4\,\sigma(F_o)$ and $wR_2(F^2)$ = 0.2294 for all the 4665 unique data. *GOF S* = 1.101. Residual electron density between −0.24 and 0.71 e Å^{-3}. CCDC 164901. See http://www.rsc.org/suppdata/cc/b1/b104317j/ for crystallographic data in .cif or other electronic format.

§ For the sake of convenience, only one diastereomer is shown.

1 Recent review on MCR, see: A. Dömling and I. Ugi, *Angew. Chem., Int. Ed.*, 2000, **39**, 3168.

2 Recent review on domino process, see: L. F. Tietz and A. Modi, *Med. Res. Rev.*, 2000, **20**, 304.

3 Reviews discussing diversity-oriented synthesis: (*a*) S. L. Schreiber, *Science*, 2000, **287**, 1964; (*b*) P. Arya, D. T. H. Chou and M. G. Baek, *Angew. Chem., Int. Ed.*, 2001, **40**, 339.

4 (*a*) L. Weber, K. Illgen and M. Almstetter, *Synlett*, 1999, 366; (*b*) H. Bienaymé, C. Hulme, G. Oddon and P. Schmidtt, *Chem. Eur. J.*, 2000, **6**, 3321.

5 A broad range of bioactivities have been described for quinoline derivatives. For recent syntheses by MCR, see: (*a*) P. A. Grieco and A. Bahsas, *Tetrahedron Lett.*, 1988, **29**, 5855; (*b*) J. M. Mellor and G. D. Merriman, *Tetrahedron*, 1995, **51**, 6115; (*c*) S. Kobayashi and S. Nagayama, *J. Am. Chem. Soc.*, 1996, **118**, 8977; (*d*) B. Crosse, J. P. Bégué and D. Bonnet-Delpon, *J. Org. Chem.*, 2000, **65**, 5009.

6 (*a*) X. Sun, P. Janvier, G. Zhao, H. Bienaymé and J. Zhu, *Org. Lett.*, 2001, **3**, 877; (*b*) G. Zhao, X. Sun, H. Bienaymé and J. Zhu., *J. Am. Chem. Soc.*, 2001, **123**, 6700.

7 Reviews on the chemistry of oxazole, see: (*a*) A. Hassner and B. Fischer, *Heterocycles*, 1993, **35**, 1441; (*b*) I. J. Turchi and M. J. S. Dewar, *Chem. Rev.*, 1975, **75**, 389; (*c*) R. Lakhan and B. Ternai, in *Adv. Heterocycl. Chem.*, 1974, **17**, 99.

8 (*a*) K. Paulvannan, *Tetrahedron Lett.*, 1999, **40**, 1851; (*b*) D. Lee, J. K. Sello and S. L. Schreiber, *Org. Lett.*, 2000, **2**, 709.

9 Representative examples of intramolecular cycloaddition of oxazole, see: (*a*) J. L. Levin and S. M. Weinreb, *J. Org. Chem.*, 1984, **49**, 4325; (*b*) M. E. Jung and L. J. Street, *J. Am. Chem. Soc.*, 1984, **106**, 8327; (*c*) C. Subramanyam, M. Noguchi and S. M. Weinreb, *J. Org. Chem.*, 1989, **54**, 5580; (*d*) J. I. Levin, *Tetrahedron Lett.*, 1989, **30**, 2355; (*e*) M. E. Jung and S. M. K. Dansereau, *Heterocycles*, 1994, **39**, 767; (*f*) E. Vedejs, D. W. Piotrowski and F. C. Tuci, *J. Org. Chem.*, 2000, **65**, 5498; (*g*) A Padaw M. Dimitroff and B. Liu, *Org. Lett.*, 2000, **2**, 3233 and references cited therein.

10 As a mild Lewis acid, lithium bromide may activate the imine intermediate and thus facilitating the subsequent nucleophilic attack. Control experiements showed that the strong Lewis acids such as $BF_3{\cdot}OEt_2$ decomposed both the tetrahydroisoquinoline and the amino-oxazole intermediate.

CHEMCOMM Communication
www.rsc.org/chemcomm

Synthesis of diphenylmethane from formalin and benzene in a biphasic system with 12-tungstophosphoric acid

Zhaoyin Hou and Toshio Okuhara*

Graduate School of Environmental Earth Science, Hokkaido University, Sapporo 060-0810, Japan. E-mail: oku@ees.hokudai.ac.jp

Received (in Cambridge, UK) 16th May 2001, Accepted 23rd July 2001
First published as an Advance Article on the web 16th August 2001

Heteropoly acids such as $H_3PW_{12}O_{40}$ are exceptionally active catalysts in the synthesis of diphenylmethane from benzene and formalin (aqueous formaldehyde) in a biphasic system and can be recycled simply by drying the aqueous phase at room temperature.

Diphenylmethane ($PhCH_2Ph$) is an important intermediate in spices, pharmaceutics and other fine chemicals[1] and its alkylated compounds can be used as insulators in place of PCB.[2] $PhCH_2Ph$ has commercially been synthesized by the Friedel–Crafts reaction with benzyl chloride and benzene, using aluminium-amalgam, $AlCl_3$, or $ZnCl_2$ as catalyst.[3] However, both the materials and the catalysts are environmentally unfriendly. Moreover, harmless solid acids like HY zeolite,[4] H-ZSM-5,[5] and sulfated ZrO_2[6] were reported to be of insufficient activity.

Synthesis of $PhCH_2Ph$ by condensation of benzene with formalin [eqn. (1)] is very attractive, since the direct use

$$2C_6H_6 + HCHO\ (\text{in water}) \rightarrow PhCH_2Ph + H_2O \qquad (1)$$

of formalin is economical and the only by-product of the reaction is water. There are several reports describing reactions between aromatic compounds and paraformaldehyde (water-free oligomers of HCHO) catalysed by liquid acids,[7] solid acids like HY zeolite,[8] and SiO_2-composites of polymer resins.[9] However, when formalin was used instead of paraformaldehyde, no reaction occurred under the same conditions,[7,9] due to serious inhibition by water. There is no report detailing a catalyst effective for the reaction of benzene with formalin. In this communication, we report that $H_3PW_{12}O_{40}$ is unusually active and recyclable for this reaction in a biphasic system. Similar biphasic catalytic systems have been reported for cyclotrimerization of propionaldehyde catalysed by heteropoly acid[10] and for nitration of benzene by lanthanide triflates.[11]

The reaction was performed at 433 K in a stainless steel autoclave (*ca*. 100 cm^3, TAIATSU TECHNO, Japan) with 40 cm^3 of benzene (450 mmol), 6.72 cm^3 of formalin (Wako Chem. Co., HCHO 90 mmol, H_2O 222 mmol, methanol (as stabilizer) 18.2 mmol), and the catalyst (2.3–16.6 mol% with respect to HCHO). The vapor phase was analyzed with a TCD gas chromatograph (Shimadzu, GC-8A) with an active carbon column. Each liquid phase was analyzed with an FID gas chromatograph (Shimadzu, GC-14B) with a 15 m capillary column of cross-linked 5% PhMe siloxane (HP-5, USA) for the aromatic compounds and a Porapak P column for methyl formate and methanol. The TCD-GC with an APS-201 (Flusin T) column was also used for HCHO, HCOOH, and H_2O. All liquid acids (except for *para*-toluenesulfonic acid) were exclusively present in the aqueous phase. When the reaction solution was cooled to room temperature after the reaction (2 h), the solution consisted of two phases, a benzene phase (the upper) and an aqueous phase (the lower), and a phase boundary was apparent.

As Table 1 shows, the conversions of HCHO reached over 93 mol% with $H_3PW_{12}O_{40}$ and $Sc(CF_3SO_3)_3$. It should be emphasized that only $H_3PW_{12}O_{40}$ gave an appreciable amount of $PhCH_2Ph$ (the yield was 35.3% under these conditions), which accumulated in the benzene phase. In addition, dibenzylbenzene ($(PhCH_2)_2C_6H_4$), methyl benzyl ether ($PhCH_2OMe$), and methyl formate (HCOOMe) were detected in the benzene phase, and formic acid, methanol, and excess HCHO in the aqueous phase. For the formation of $PhCH_2Ph$, the following steps are considered:[8] $H_2{}^+COH$ is generated from HCHO and the proton attacks the benzene ring to form, initially, benzyl alcohol. Benzyl alcohol can be transformed to the benzyl cation *via* protonation and dehydration. $PhCH_2Ph$ is produced by the attack of the benzyl cation on the benzene ring. With $H_3PW_{12}O_{40}$ as catalyst, two competitive reactions of HCHO proceeded: (i) attack of the benzyl cation on benzene to form $PhCH_2Ph$ and (ii) dimerization of HCHO to HCOOMe (Tichenko reaction).

On the other hand, $Sc(CF_3SO_3)_3$ efficiently catalysed dimerization of HCHO to HCOOMe, but was inactive for the formation of $PhCH_2Ph$. *para*-Toluenesulfonic acid (PTS) was also active for the dimerization of HCHO, but less active than $H_3PW_{12}O_{40}$ for $PhCH_2Ph$ formation. Mineral acids like H_2SO_4, H_3PO_4, and HNO_3 showed no activity for the formation of $PhCH_2Ph$ and CF_3COOH was also inactive for this reaction. It was confirmed that HCOOMe did not react with benzene under these conditions with any of these catalysts.

A series of other heteropoly acids were examined as catalysts for the synthesis of $PhCH_2Ph$ from benzene and formalin (Table 2). All these heteropoly acids showed activities: $H_4SiW_{12}O_{40}$ and $H_3PMo_{12}O_{40}$ were effective, but $H_6P_2W_{18}O_{62}$ and H_4Si-

Table 1 Conversion and selectivity of diphenylmethane synthesis from benzene and formalin with various liquid acids

Catalyst	(mmol)	Conversion[a] (mol%)	Yield[b] (mol%)	Selectivity[a] (mol%)							MB[c] (%)
				CO	HCOOMe	MeOH	HCOOH	$PhCH_2Ph$	$(PhCH_2)_2CH_2$	$PhCH_2OMe$	
$H_3PW_{12}O_{40}$	(4.2)	93.2	35.3	3.3	35.1	5.4	5.3	38.7	11.4	0.8	97.0
$Sc(CF_3SO_3)_3$	(2.1)	95.1	0.0	0.2	83.0	12.3	4.6	0.0	0.0	0.0	100.0
PTS[d]	(12.6)	82.2	4.1	4.2	71.8	7.2	6.3	5.9	1.5	3.0	79.8
HNO_3	(12.6)	24.4	0.0	10.0	90.0	0.0	0.0	0.0	0.0	0.0	100.0
H_3PO_4	(4.2)	18.7	0.0	0.2	68.8	12.0	19.0	0.0	0.0	0.0	100.0
H_2SO_4	(6.3)	33.7	0.0	0.6	92.0	4.0	4.0	0.0	0.0	0.0	101.0

Reaction conditions: benzene 40 cm^3 (450 mmol), formalin 6.72 cm^3 (HCHO 90 mmol, H_2O 222 mmol, methanol 18.2 mmol), 160 °C for 2 h. [a] On the basis of HCHO. [b] $PhCH_2Ph$ (on the basis of HCHO) [c] Mass balance; 100 × (total amount of products and remaining HCHO)/(the initial amount of HCHO) [d] *para*-Toluenesulfonic acid.

 DOI: 10.1039/b104321h

Table 2 Conversion and selectivity of diphenylmethane synthesis from benzene and formalin with heteropoly acids

Catalyst	(mmol)	Conversion (mol%)	Yield (mol%)	Selectivity[a] (mol%)		TON[b]
				HCOOMe	$PhCH_2Ph$	
$H_3PW_{12}O_{40}$	(4.2)	93.2	35.3	34.3	37.9 (79.9)	7.1
$H_4SiW_{12}O_{40}$	(4.2)	92.8	25.4	43.6	27.4 (79.7)	5.1
$H_3PMo_{12}O_{40}$	(4.2)	93.5	23.4	54.8	25.1 (71.1)	4.7
$H_6P_2W_{18}O_{62}$	(2.1)	72.4	9.2	68.8	12.7 (76.1)	2.8
$H_4SiMo_{12}O_{40}$	(4.2)	92.0	3.6	77.1	3.9 (33.9)	0.7

Reaction conditions were the same as given in the footnotes of Table 1. [a] On the basis of HCHO. The figures in parentheses are the selectivities for $PhCH_2Ph$ among the aromatic compounds ($PhCH_2Ph$ + $(PhCH_2)_2CH_2$ + $PhCH_2OMe$). [b] Turnover number defined as (mol of $PhCH_2Ph$)/(mol of catalyst).

Table 3 Recycled $H_3PW_{12}O_{40}$[a]

Run	Conversion (%)	Total yield of aromatics[b] (mmol)	Selectivity (mol%)[c]	
			$PhCH_2Ph$	TON[d]
1	83.5	31.4	79.1	4.5
2	74.7	23.8 (75.6%)	76.2	2.9
3	72.2	21.1 (68.4%)	73.4	2.4
4	64.1	17.8 (56.7%)	70.6	1.7
5	63.1	17.6 (56.1%)	66.7	1.6

Reaction conditions: benzene 40 cm^3 (450 mmol), formalin 6.72 cm^3 (HCHO 90 mmol, H_2O 222 mmol, methanol 18.2 mmol), $H_3PW_{12}O_{40}$ 4.2 mmol, 160 °C, and 30 min. [a] Between the runs, the aqueous phase of $H_3PW_{12}O_{40}$ was dried in the ambient atmosphere. The recovered solid $H_3PW_{12}O_{40}$ was reused without any treatment. [b] Total yield of $PhCH_2Ph$, $(PhCH_2)_2CH_2$ and $PhCH_2OMe$. The figures in parentheses are the percentage yield relative to that of the first run. [c] Selectivity for $PhCH_2Ph$ among the aromatic products on the basis of HCHO. [d] Turnover number defined as (mol of $PhCH_2Ph$)/(mol of catalyst).

$Mo_{12}O_{40}$ were less efficient. With $H_3PW_{12}O_{40}$ as catalyst, when the ratio of HCHO/benzene was reduced from 1:5 to 1:10, keeping the amount of benzene (450 mmol) the same, the yield of $PhCH_2Ph$ became higher (42%) with 43% selectivity and 97% conversion. However, the amount of $PhCH_2Ph$ produced was still higher at 1:5 ratio.

IR spectroscopy showed that, while the Keggin structure of $SiMo_{12}O_{40}^{4-}$ decomposed to some extent after the reaction, the structures of the other polyanions were retained. The pH values of the aqueous phases of these heteropoly acids (pH = 0.10, 0.58, 0.61, 0.79, and 0.96 for $H_3PW_{12}O_{40}$, $H_4SiW_{12}O_{40}$, $H_3PMo_{12}O_{40}$, $H_6P_2W_{18}O_{62}$, and $H_4SiMo_{12}O_{40}$, respectively) were close to those of $Sc(CF_3SO_3)_3$ (pH = 0.90), H_3PO_4 (pH = 1.25), HNO_3 (pH = 0.65), and H_2SO_4 (pH = 0.19). Thus the exceptionally high activities of the heteropoly acids are due to not only the strong acidity of the solution, but also the soft basicity of the heteropoly anion, which has been proposed by Izumi *et al.*[12] The cationic intermediates are probably stabilized by the heteropoly anions.

The results of five successive reactions are summarized in Table 3, where used $H_3PW_{12}O_{40}$ was recovered simply by drying the aqueous solution at room temperature. The recovered $H_3PW_{12}O_{40}$ was found to be active in the repeated runs, although the conversion of HCHO and yield of aromatics decreased somewhat. As shown in Table 3, the conversion and the total yield of aromatics reached plateaus after the fourth run. These changes in the conversion, yield, and selectivity are due to the remaining carbonaceous species on the heteropoly acid. Elemental analysis showed that the amount of carbon on the used $H_3PW_{12}O_{40}$ was 2.1%, which corresponds to 0.4 molecules of $PhCH_2Ph$ per heteropoly anion at the fifth run. IR spectroscopy of $H_3PW_{12}O_{40}$ revealed that the Keggin structure was completely retained after repeating the reaction five times.

In conclusion, $H_3PW_{12}O_{40}$ is a highly active and recyclable catalyst for use in the synthesis of diphenylmethane from benzene and formalin in a biphasic system. This is a novel example for direct use of formalin in clean organic synthesis with solid acid.

Notes and references

1 S. I. Okada, K. Tanaka and Y. Nakahara, *Bull. Chem. Soc. Jpn.*, 1992, **65**, 2833.
2 *Encyclopedic Dictionary of Chemistry*, ed. M. Ohki, T. Osawa, M. Tanaka and H. Chihara, Tokyo Kagaku, Dojin, 1989, p. 1032.
3 G. A. Olah, *Friedel–Crafts Chemistry*, Wiley, New York, 1973.
4 B. Coq, V. Gourves and F. Figueras, *Appl. Catal. A*, 1993, **100**, 69.
5 V. R. Choudhary, S. K. Jana and B. P. Kiran, *Catal. Lett.*, 1999, **59**, 217.
6 S. N. Koyande, R. G. Jaisswal and R. V. Jayaram, *Ind. Eng. Chem. Res.*, 1998, **37**, 908.
7 J. Machida, T. Mitsui, K. Shindo and S. Ishikawara, *Riken Rep.*, 1977, **53**, 186.
8 M. J. Climent, A. Corma, H. Garcia and J. Primo, *Appl. Catal. A*, 1989, **51**, 113.
9 Z. Hou and T. Okuhara, *Appl. Catal. A*, 2001, **216**, 147.
10 S. Sato, C. Sakura, H. Furuta, T. Sodesawa and F. Nozaki, *J. Chem. Soc., Chem. Commun.*, 1991, 1327.
11 F. J. Waller, A. G. M. Barrett, D. C. Braddock and D. Ramprasad, *Chem. Commun.*, 1997, 613.
12 Y. Izumi, K. Matsuo and K. Urabe, *J. Mol. Catal.*, 1983, **18**, 299.

CHEMCOMM Communication
www.rsc.org/chemcomm

Novel self-assembled monolayers of disulfides with bicyclo[2.2.2]octane moieties on Au(111)

Shintaro Fujii, Uichi Akiba and Masamichi Fujihira*

Department of Biomolecular Engineering, Tokyo Institute of Technology, 4259 Nagatsuta Midori-ku, Yokohama, 226-8501, Japan. E-mail: mfujihir@bio.titech.ac.jp

Received (in Cambridge, UK) 30th May 2001, Accepted 26th July 2001
First published as an Advance Article on the web 16th August 2001

A series of disulfides containing bicyclo[2.2.2]octane moieties have been synthesised and their self-assembled monolayers (SAMs) on Au(111) have been characterized using scanning tunnelling microscopy (STM).

SAMs consisting of thiols and disulfides chemisorbed on Au(111) have been extensively studied owing to their stability and ease of preparation. Among organosulfurs on gold, *n*-alkanethiols and their substituted analogues are considered the simplest case due to their linear structure of saturated hydrocarbon chain and degree of freedom in the process of self-assembling.[1,2] The first structural study of alkanethiols having a bulky end group was reported in 1992.[3] STM topographs of these SAMs exhibited a ($\sqrt{3} \times \sqrt{3}$)R30° lattice in spite of the bulky end group that sterically hinders the ($\sqrt{3} \times \sqrt{3}$)R30° structure. Later study of other bulky thiols showed incommensurate lattices.[4] Furthermore, new classes of SAMs consisting of spiro-alkanethiols[5] (organic) or polyhedral borane derivatives[6] (inorganic) have been recently investigated. In these reports, the authors attempted to control the film properties by designing the molecular structure of adsorbates. Detailed microscopic structures, however, remain unsolved.

In the present work, we focused on the preparation of well-defined thin rigid films. As a new class of adsorbates, structurally simple and symmetric molecules (bicyclo[2.2.2]octane derivatives) were synthesized. In comparison with *n*-alkanethiols and their substituted analogues, sulfur compounds with bicyclo[2.2.2]octane moieties are expected to have unique properties. First, the overall shape of the molecule is roughly spherical and the size is *ca*. 0.60 nm, which is larger than the nearest neighbour spacing (0.50 nm) of the ($\sqrt{3} \times \sqrt{3}$)R30° structure. Owing to the bulkiness of the bicyclo[2.2.2]octane moieties, they are expected to be oriented perpendicularly to the surface and thus the formation of domain structure due to the tilt of adsorbates can be avoided.[1,2] Second, three ethylene chains are linked at both terminals of this moiety and the structure of the bulky end group itself is rigid. Third, formation of rigid thin films is expected due to the stronger van der Waals interactions between bicyclo[2.2.2]octane moieties compared to those of *n*-butane moieties of *n*-alkanethiols with the same height. The chain ordering in the films with such short *n*-alkane chains is known to be disturbed appreciably by their vigorous thermal motion at room temperature.[1]

Compounds **1a** and **1b** (Fig. 1) were derived from 4-methoxybicyclo[2.2.2]octane-1-carboxylic acid[7] in 20–30% overall yields by a 6–7 steps procedure.† As desired adsorbates, disulfides were synthesized taking their stability and ease of purification into account. Au(111) surfaces for STM studies were prepared by thermal evaporation of gold (99.99%) onto freshly cleaved mica *in vacuo* with a background pressure of $< 5 \times 10^{-7}$ Torr. SAMs [**1**/Au(111) in Fig. 1] were prepared by dipping the Au substrates for 10–72 h in 0.5 mM ethanol solutions of **1a**, **1b**, or **1a** + **1b**. All STM measurements were performed using a constant-current mode with a tungsten tip in the atmosphere at room temperature and the images were unfiltered.

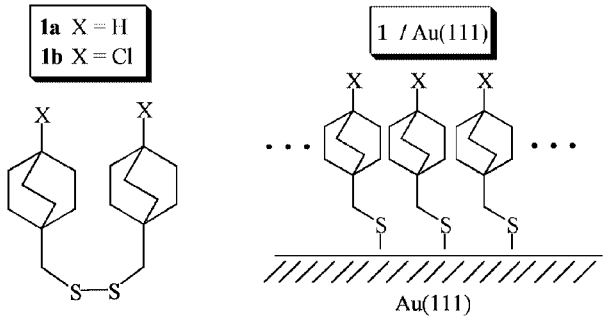

Fig. 1 Bicyclo[2.2.2]octane derivatives (**1a** and **1b**) synthesized in this study and schematic structure of their SAMs [**1**/Au(111)].

Fig. 2 shows a constant-current STM image of a 20 × 20 nm area of a SAM of **1a**/Au(111). In the same way as with *n*-alkanethiols, single Au atom deep pit defects and a hexagonal close-packed lattice were found as shown in Fig. 2. We also investigated a SAM image of a short chain *n*-alkenethiol (pentanethiol) with a carbon number in the vertical direction equal to that of **1**. In the pentanethiol SAM, disordered structure and domains including a *c*(4 × 2) superlattice of a hexagonal lattice[1,2] were found. Periodicities of topographic differences found in the superlattice are considered to reflect the difference in azimuthal orientation. In Fig. 2, such periodicities of topographic differences are not seen and the nearest spacing is 0.59 ± 0.03 nm. This spacing is larger than the ($\sqrt{3} \times \sqrt{3}$)-R30° structure (Au spacing is 0.288 nm). It is also clear from Fig. 2 that rows of molecules are not always straight and that such deviations are not due to thermal drifts.

We also imaged the underlying Au(111) lattice by mechanically removing part of the SAM with the STM tip. It was found that the hexagonal lattice of the adsorbate was rotated *ca*. 30°

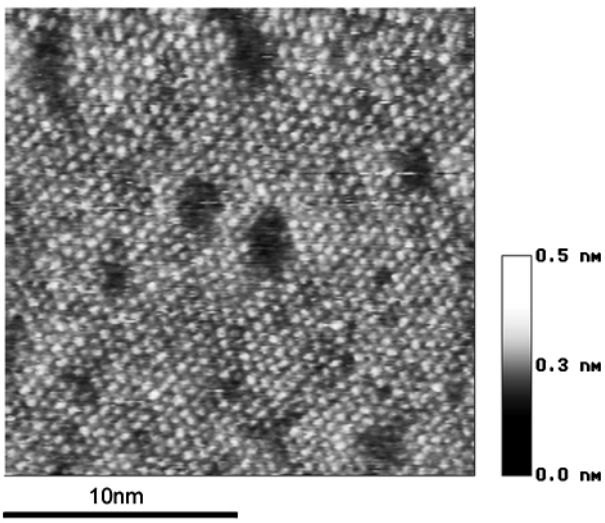

Fig. 2 Constant-current STM image of a 20 × 20 nm area of a SAM of **1a** (tunnelling current = 50 pA, sample bias voltage = +1 V).

 DOI: 10.1039/b104703p

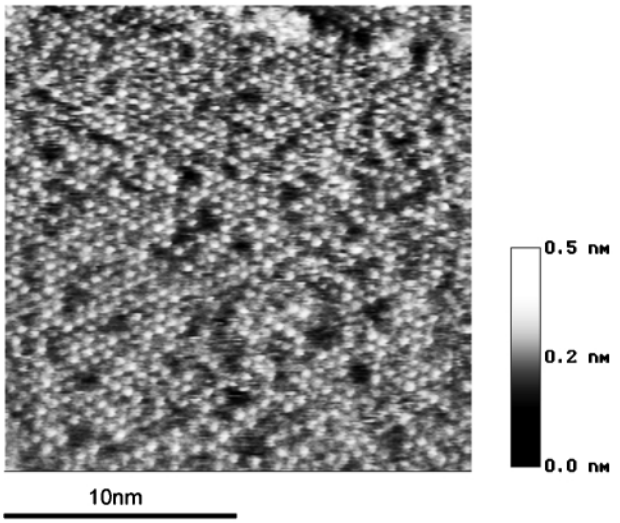

Fig. 3 Constant-current STM image of a 20 × 20 nm area of a SAM of **1b** (tunnelling current = 30 pA, sample bias voltage = +1 V).

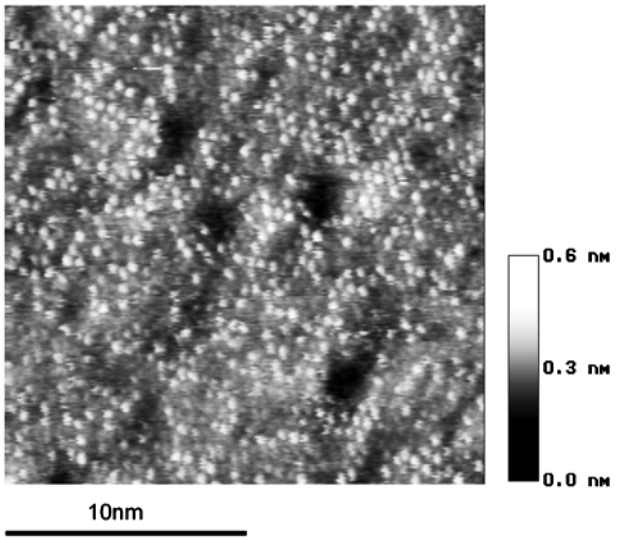

Fig. 4 Constant-current STM image of a 20 × 20 nm area of a SAM of **1a** + **1b** (tunnelling current = 50 pA, sample bias voltage = +1 V).

over that of Au(111). The molecular rows in the same direction went across steps and pits.

Although the shape of a bicyclo[2.2.2]octane moiety is roughly spherical as stated above, it also possesses a three-fold axis. A shorter distance of closest approach between the two bicyclo[2.2.2]octane moieties may be achieved when an ethylene chain of one moiety is located between two chains of the other moiety. We are now undertaking a study of annealing effects to obtain detailed information on the unit cell.

Fig. 3 shows a constant-current STM image of a 20 × 20 nm area of a SAM of **1b**/Au(111). This film shows a slightly different feature. The depressions (pits), that are usually observed in SAMs of *n*-alkanethiols and also in a SAM of **1a**/Au(111) in Fig. 2, are not observed clearly in Fig. 3. Instead, the organic overlayer itself is more poorly ordered. Since there are tip convolution problems for imaging small size depressions, we should take care when discussing this result. This feature probably results from strong short-range interaction, *i.e.* dipole–dipole interactions among C–Cl end groups on the bicyclo[2.2.2]octane moieties, oriented perpendicularly to the Au(111) surface [**1b**/Au(111) in Fig. 1]. For this upright orientation of the terminal groups, the bridgeheads of the moieties play an important role.

Finally, we carried out adsorption of a mixture of two components (compounds **1a** and **1b**). We prepared an ethanol solution of a 1:1 mixture of **1a** + **1b**. Fig. 4 shows a constant-current STM image of a 20 × 20 nm area of a SAM of the mixture on Au(111). The two components were molecularly dispersed. We assigned bright features (*ca*. 0.1 nm protrusions) to chloride end groups on the basis of insertion experiments of **1b** to the matrix containing **1a** carried out separately. This result clearly indicates that dots on the lattice of the STM image correspond to individual molecules and a distinction of the small difference between the H and Cl terminal atoms can be possible by STM. The observed distinction is afforded by the high structural order in the organic surface film which is, in turn, the result of interactions between the rigid sphere-shaped molecules. Most of the bright features seemed to be pairing, indicating that lateral diffusion of dissociated thiolates occured upon chemisorption of **1a** and **1b** from the 0.5 mM mixed solution was slow.

In summary, we have investigated the structure of novel bicyclo[2.2.2]octane derivatives chemisorbed onto Au(111) from 0.5 mM ethanol solutions using STM. Owing to their rigid structure, small differences between the end groups, *e.g.* between H and Cl, were distinctive. This distinction of individual molecules, to the best of our knowledge, represents one of the highest resolutions of organic monolayers on solid surfaces.[8] Although our knowledge of SAMs of these novel adsorbates is still limited in comparison with that of the widely used *n*-alkanethiols, the well-defined structure and the ease of detection and distinction described above will be useful for further investigation of these adsorbates and their substituted analogues. For example, their application to rigid bases for oriented dipoles, rigid spacers for molecular single electron devices, hexagonally close-packed host matrices for insertion experiments, markers for lateral diffusion dynamics, *etc*. are expected. As spacers, dimers and trimers of the bicyclo[2.2.2]octane unit will be useful.

Notes and references

† 4-Methoxybicyclo[2.2.2]octane-1-carboxylic acid was synthesized according to a previously reported procedure.[8] Disulfides used for SAM formation were characterized by ^{1}H and ^{13}C NMR spectra and elemental analysis giving satisfactory results. Details of the syntheses will be reported elsewhere.

1 F. Schreiber, *Prog. Surf. Sci.*, 2000, **65**, 151; A. Ulman, *Chem. Rev.*, 1996, **96**, 1533.
2 G. E. Poirier, *Chem. Rev.*, 1997, **97**, 1117.
3 Y.-T. Kim, R. L. McCarley and A. J. Bard, *J. Phys. Chem.*, 1992, **96**, 7416.
4 H. Wolf, H. Ringsdorf, E. Delamarche, T. Takami, H. Kang, B. Michel, Ch. Gerber, M. Jaschke, H.-J. Butt and E. Bamberg, *J. Phys. Chem.*, 1995, **99**, 7102; E. Delamarche and B. Michel, *Thin Solid Films*, 1996, **273**, 54.
5 Y.-S. Shon, S. Lee, S. S. Perry and T. R. Lee, *J. Am. Chem. Soc.*, 2000, **122**, 1278; Y.-S. Shon, S. Lee, R. Colorado, Jr., S. S. Perry and T. R. Lee, *J. Am. Chem. Soc.*, 2000, **122**, 7556.
6 L. J. Yeager, F. Saeki, K. Shelly, M. F. Hawthorne and R. L. Carrell, *J. Am. Chem. Soc.*, 1998, **120**, 9961.
7 W. Adcock and A. N. Abeywickrema, *J. Org. Chem.*, 1982, **47**, 2951.
8 T. Takami, E. Delamarche, B. Michel and Ch. Gerber, *Langmuir*, 1995, **11**, 3876.

CHEMCOMM
Communication
www.rsc.org/chemcomm

Dynamic equilibration of η¹-carbene and η²-alkyne moieties within an alkynylcarbene dimanganese complex†

Yannick Ortin, Yannick Coppel, Noël Lugan,* René Mathieu and Michael J. McGlinchey‡

Laboratoire de Chimie de Coordination du CNRS, 205 route de Narbonne, 31077 Toulouse Cedex 4, France. E-mail: lugan@lcc-toulouse.fr

Received (in Cambridge, UK) 30th May 2001, Accepted 24th July 2001
First published as an Advance Article on the web 16th August 2001

The coordination of an additional [$Cp(CO)_2Mn$] fragment to the alkyne linkage of an alkynylcarbene complex of the type $Cp(CO)_2Mn{=}C(R')C{\equiv}CR''$ yields a highly fluxional molecule, in which the [η¹-carbene] and [η²-alkyne] moieties are seen to exchange rapidly on the NMR time scale.

The energy surface of the C_3H_2 system continues to attract considerable attention.[1] Among the numerous possible isomers that can exist and interconvert are propynylidene **A**, cyclopropenylidene **B**, and allenylidene **C**, and many such species have

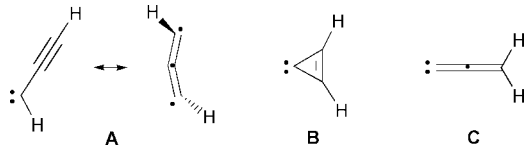

been isolated as stable organometallic complexes. In continuation of our studies on manganese carbene complexes,[2] our current work has focussed on non-heteroatom-substituted alkynylcarbenes of the type $(RC_5H_4)Mn{=}C(R')C{\equiv}CR''$, where R = H, Me.[3,4] A recent report by Casey *et al.*[4] that related rhenium systems undergo a fascinating dimerization[4] prompts us to present our own findings in this area.

The alkynylcarbene complexes $(RC_5H_4)Mn{=}C(R')C{\equiv}CR''$ **1** shown in Scheme 1 were synthesised in a straightforward manner and in high yields (81–85%) upon treatment of the corresponding carbyne complexes $[(RC_5H_4)Mn{\equiv}CR'][BPh_4]$ with the appropriate alkynyllithium reagents $LiC{\equiv}CR''$.† With the general idea of inducing remote activation of the carbene carbon atom by coordination of a transition metal to the alkyne function in alkynylcarbene complexes, **1a** was treated with $Cp(CO)_2Mn(THF)$ **2a**, at room temperature. This yielded **3a**, whose IR spectrum showed four bands in the *ν*CO region, strongly indicative of a polymetallic structure.

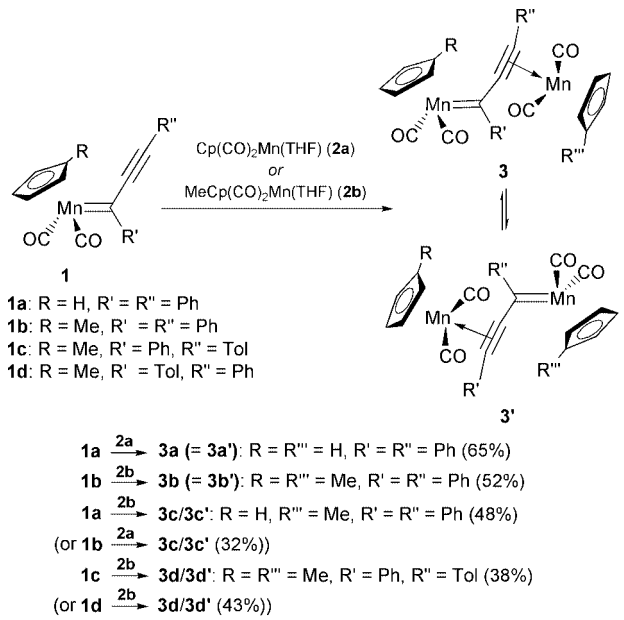

Scheme 1

The structure of **3a**, as determined by X-ray diffraction§ (Fig. 1) shows that, as anticipated, the molecule consists of a Mn alkynylcarbene complex in which the alkyne is coordinated to an additional $Cp(CO)_2Mn$ fragment. Both $Cp(CO)_2Mn$ units are bonded in the conventional fashion so as to maximise the overlap between the frontier orbitals of the metal fragments and of the carbene and alkyne units, respectively.[5] Indeed, the interplanar angle {cent1–Mn1–C3}–{Mn1–C3–C4} is 2.4° (ideal 0°), whereas the corresponding value for {cent2–Mn2–cent3}–{Mn2–C4–C5} is 83.6° (ideal 90°) [cent1 and cent2 are the centroids of the Cp rings attached to Mn1 and Mn2, respectively, and cent3 is the middle of the C4–C5 vector]. The angle between the plane containing the two alkyne carbon atoms and Mn2, and the plane of the carbene unit attached to Mn1 is 74.6°. The Mn1–C3 distance compares well with the Mn=C bond distance found in mononuclear non-heteroatom-substituted Mn carbene complexes.[6] The alkyne moiety is coordinated to Mn2 in an unsymmetrical fashion, whereby the Mn2–C4 and the Mn2–C5 distances represent, respectively, the longest and the shortest Mn–C bonds ever reported for an alkyne η²-coordinated to a $Cp(CO)_2Mn$ fragment.[7]

The variable-temperature $^{13}C\{^1H\}$ NMR spectra of **3a** are particularly informative. At 183 K, the spectrum is in full agreement with the X-ray crystal structure; in particular, the carbene carbon atom, C3, and two carbon atoms of the alkyne moiety, C4 and C5, are observed at δ 317.9, and 76.9 and 106.3,

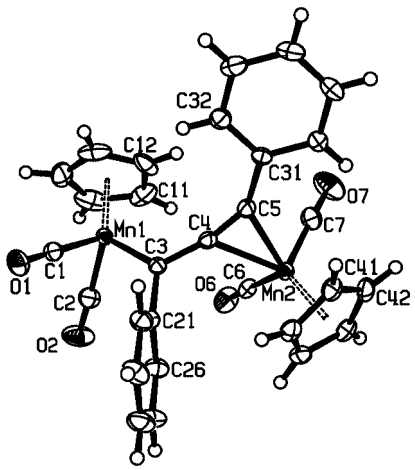

Fig. 1 A perspective view of complex $[Cp(CO)_2Mn]_2[\mu\text{-}\eta^3\text{-}PhCCCPh]$ **3a**. Selected bond distances (Å) and angles (°): Mn1–C3 1.888(2), Mn2–C4 2.186(2), Mn2–C5 2.082(2), C3–C4 1.411(3), C4–C5 1.261(3); C3–C4–C5 166.7(2), C4–C5–C31 145.5(2).

† Electronic supplementary information (ESI) available: details of synthesis and spectral characterisation of the new complexes. See http://www.rsc.org/suppdata/cc/b1/b104712b/

‡ On sabbatical leave from: Department of Chemistry, McMaster University, Hamilton, Ontario, Canada L8S 4M1.

 DOI: 10.1039/b104712b

respectively. As a consequence of the lack of symmetry, the Cp rings appear as two sharp singlets at δ 91.9 and 85.9, the CO ligands give rise to four resonances at δ 235.6, 235.4, 232.6 and 231.4, and the signals due to each of the Ph rings are clearly differentiated. However, as the temperature is gradually raised, the signals for the two Cp rings coalesce (T_c = 213 K), as do the pairs of Ph ring absorptions as well as the four CO resonances. Over the same temperature range, the signals attributed to the C3 and C5 sites rapidly collapse, ultimately giving a barely observable broad resonance centred at δ 212 at 298 K. Clearly, the molecule executes a dynamic process that averages the two Mn environments. Additional spin saturation transfer experiments, performed at 188 K, confirmed the exchange between the C3 and C5 sites. In other words, the results indicate that equilibration of the [η^1-carbene] and the [η^2-alkyne] moieties in **3a** occurs readily on the NMR time-scale, as depicted in Scheme 1. The coalescence behaviour of the Cp ring resonances (both ^{13}C and ^{1}H) yields an activation energy barrier of 9.3 ± 0.5 kcal mol^{-1}.

The MeCp analogue, **3b**, behaved similarly, and the non-dissociative character of the exchange was established by a crossover experiment, whereby no trace of the mixed Cp/MeCp product was detected when **3a** and **3b** were mixed. In fact, the mixed Cp/MeCp complex can be obtained by reaction of *either* **1a** with **2b**, *or* **1b** with **2a**, as a mixture of interconverting isomers **3c**/**c′**, and this provides additional support for the equilibration process shown in Scheme 1.

Likewise, complexes **3d**/**d′**, in which an η^3-PhCCCTol ligand bridges two MeCp(CO)$_2$Mn fragments, is preparable by reaction of *either* **1c** *or* **1d** with **2b**. Gratifyingly, subsequent reaction of **3d**/**d′** with carbon monoxide gave a 1 : 1 mixture of **1c** *and* **1d** through loss of the alkyne-bonded Mn fragment in each isomer, as shown in eqn. (1).

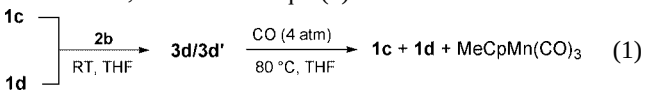

(1)

These observations raise the possibility of alkynylcarbene transfer from a metal fragment to an other one upon a bond shift isomerism within a transient bimetallic bridging η^3-alkynylcarbene complex. We now report that this can be realized in the case of (CO)$_5$Cr=C(OEt)C≡CPh **4**, for which treatment with **2b** yields MeCp(CO)$_2$Mn=C(Ph)C≡COEt **6**, through the intermediacy of **5** (Scheme 2). This rearrangement is readily accounted for by the same mechanism that gives rise to fluxionality in the **3**/**3′** system; the difference lies in the fact that the MeCp(CO)$_2$Mn=C linkage is favored over the (OC)$_5$Cr=C moiety, and that (OC)$_5$Cr[η^2-alkyne] complexes are unstable, thus rendering the isomerization irreversible.

This may also be relevant to the postulated alkynyl carbenoid rearrangement observed in the Rh(II)-catalysed cyclisation reaction of dialkynyl-substituted α-diazoketones, reported by Padwa *et al.*[8] Moreover, it is not inconceivable that the slow equilibrium between isomeric monometallic Re alkynylcarbene complexes briefly mentioned by Casey *et al.*[4] may be mediated by traces of a dirhenium complex analogous to the Mn systems described here.

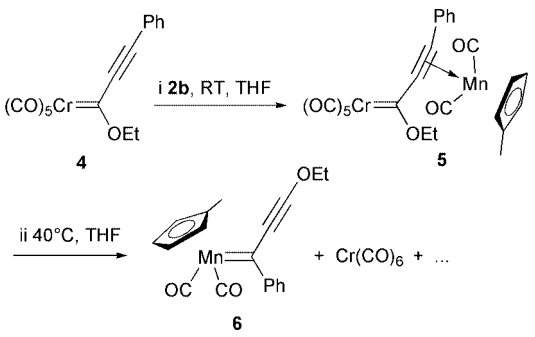

Scheme 2

A more complete analysis of the transition state for these processes must await the full DFT study that is currently under way, however, the variable-temperature NMR data provide some insight. At the low-temperature limit, the ^{13}C spectrum of **3a** exhibits *four* different CO environments but, as the temperature is raised, these signals coalesce into a *single* peak. This implies that the molecule passes through a highly symmetrical conformation allowing the pairs of carbonyls bonded to each manganese to lose their diastereotopic character. Planar transition states of C_{2h} or C_{2v} symmetry, such as those shown below, in which the central carbon possesses carbene character with some stabilisation provided by the two manganese fragments, would be consistent with the NMR data. We favour the C_{2h} conformation on steric grounds, and hypothesize that the reaction proceeds by a stretching of the alkyne-bonded manganese fragment—evidenced by the elongated Mn2–C4 bond in the X-ray structure of **3a**—while the carbene-bonded Cp(CO)$_2$Mn unit approaches the central carbon atom. We emphasise, however, that unlike a conventional organic S_N2 process in which the incoming nucleophile and the leaving group maintain a rectilinear relationship, this process involves a quasi-helical, twisting motion since in the initial and final structures, the planes bisecting the Cp(CO)$_2$Mn fragments adopt mutually almost orthogonal orientations.

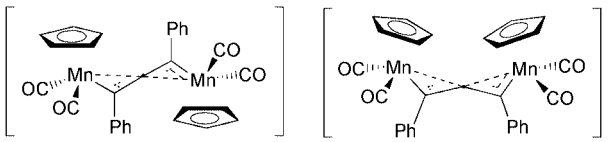

[**3a**]$^{\#}$ (C_{2h}) [**3a**]$^{\#}$ (C_{2v})

Notes and references

§ *Crystal data*: $C_{29}H_{20}Mn_2O_4$, M = 542.33, monoclinic, space group $P2_1/c$ (no. 14), a = 12.843(2), b = 8.358(1), c = 22.265(6) Å, U = 2368.8(8) Å^3, T = 160 K, Z = 4, μ(Mo-K$_\alpha$) = 1.10 mm^{-1}, 14485 reflections measured, 3520 unique (R_{int} = 0.039) which were used in all calculations. The final $wR(F^2)$ was 0.0628 (all data).

CCDC reference number 168123. See http://www.rsc.org/suppdata/cc/b1/b104712b/ for crystallographic data in CIF or other electronic format.

1 M. Rubio, J. Stalring, A. Bernhardsson, R. Lindh and B. O. Roos, *Theor. Chem. Acc.*, 2000, **105**, 15 and references therein; A. M. Mebel, W. M. Jackson, A. H. H. Chang and S. H. Lin, *J. Am. Chem. Soc.*, 1998, **120**, 5751; R. A. Seburg, E. V. Patterson, J. F. Stanton and R. J. McMahon, *J. Am. Chem. Soc.*, 1997, **119**, 5847; M. Noro, T. Masude, A. S. Ichimura, N. Koga and H. Iwamura, *J. Am. Chem. Soc.*, 1994, **116**, 6179.

2 A. Rabier, N. Lugan and R. Mathieu, *J. Organomet. Chem.*, 2001, **617**–**618**, 681.

3 For other non-heteroatom-stabilised alkynylcarbene complexes, see for instance: M. A. Esteruelas, A. V. Gomez, A. M. Lopez, J. Modrego and E. Onate, *Organometallics*, 1997, **16**, 5826; M. R. Terry, C. Kelley, N. Lugan, G. L. Geoffroy, B. S. Haggerty and A. L. Rheingold, *Organometallics*, 1993, **12**, 3607.

4 C. P. Casey, S. Kraft and D. R. Powell, *J. Am. Chem. Soc.*, 2000, **122**, 3771.

5 N. M. Kostic and R. F. Fenske, *J. Am. Chem. Soc.*, 1982, **104**, 3979; B. E. R. Schilling, R. Hoffmann and D. L. Lichtenberger, *J. Am. Chem. Soc.*, 1979, **101**, 585.

6 W. A. Herrmann, J. L. Hubbard, I. Bernal, J. D. Korp, B. L. Haymore and G. L. Hillhouse, *Inorg. Chem.*, 1984, **23**, 2878 and references therein.

7 C. Lowe, H.-U. Hund and H. Berke, *J. Organomet. Chem.*, 1989, **378**, 211; G. G. Cash and R. C. Pettersen, *J. Chem. Soc., Dalton Trans.*, 1979, 1630.

8 A. Padwa, D. J. Austin, Y. Gareau, J. M. Kassir and S. L. Xu, *J. Am. Chem. Soc.*, 1993, **115**, 2637.

CHEMCOMM Communication
www.rsc.org/chemcomm

Ruthenium catalysed cross metathesis with fluorinated olefins

Sonia Imhof, Stefan Randl and Siegfried Blechert*

Institut für Chemie, Technische Universität Berlin, Strasse des 17. Juni 135, D-10623 Berlin, Germany. E-mail: Blechert@chem.tu-berlin.de

Received (in Cambridge, UK) 7th June 2001, Accepted 25th July 2001
First published as an Advance Article on the web 16th August 2001

The *E*-selective cross metathesis (CM) of fluorinated olefins with various functionalised alkenes in good to excellent yields is reported.

In the last decade ruthenium catalysed olefin metathesis has emerged as a powerful synthetic tool for the formation of carbon–carbon bonds.[1] There is growing interest in fluorinated molecules, with their particularly interesting chemical, biological and physical properties.[2] For instance, a high electronegativity together with an atomic size close to hydrogen have made these compounds useful components of both pharmaceuticals and agrochemicals. This, in addition to the selective solubilities of perfluorinated molecules and the advent of new possibilities with fluorinated phases,[3] encouraged us to prepare fluorine-substituted olefins *via* a CM methodology. There has been one report concerning this subject, however the yield of the cross product was modest.[4] Recently we have demonstrated[5,6] that reactivity and selectivity in Ru-catalysed CM reactions depend strongly on the electronic properties of both the ligand and Ru–carbene complex. In line with this earlier work, we

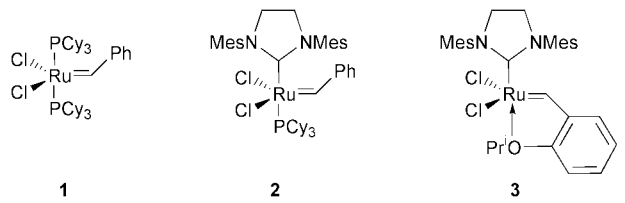

1 **2** **3**

Cy = cyclohexyl Mes = 2,4,6-trimethylphenyl

expected that phosphine-free catalyst **3**[6,7] would show superior activity and stability in CM reactions involving electron deficient fluoroalkenes than either **1** or **2**.[8]

Herein we report the CM of various functionalised olefins with 3,3,3-trifluoropropene **4**† and 3,3,4,4,5,5,6,6,6-nonafluorohexene **5**,‡ as models for molecules with varying degrees of fluorine substitution using catalysts **1**, **2** and **3**. Preliminary experiments using terminal olefins **6**–**12**[9] (Scheme 1) with up to five equivalents of **4** in a closed flask at 45 °C under atmospheric pressure, resulted in quantitative dimerisation of the more electron rich substrates. In order to suppress the dimerisation reaction in the presence of **4**, the flask was equipped with a balloon containing 10 equivalents of **4**. In the case of **5**, 10 equivalents of nonafluorohexene were used as a solvent to achieve good yields of the products **20**–**26**. It was found that α,α,α-trifluorotoluene could be used successfully as an additive to overcome the insolubility of **1**, **2** and **3** in **5**. Using **2**, best results were achieved stirring the reaction mixture at 60 °C for 4 h, whereas reactions catalysed by **3** gave higher yields of CM products under milder conditions (45 °C, 3 h). The results of these experiments are presented in Table 1.

Using substrates **6**–**10** with ester, carboxylic acid, ketone and hydroxy functionalities (Scheme 1), general conversions to CM products (**13**–**17** and **20**–**24**) and dimers were good to excellent. CM reactions with the fluoroolefin were generally favoured over dimerisation, except where the substrate contained a hydroxy group; this effect could be due to the poor solubility of these substrates in the fluorinated media. The nitrile derivatives **11** and **12**, which contain both electron deficient and relatively electron rich terminal double bonds, were chosen to investigate chemoselectivity. Irrespective of the catalyst, fluoroalkene substrates or reaction conditions, the nitrile derivatives with an unprotected hydroxy group were not converted to CM products, giving only starting materials in all cases. The corresponding acetylated derivatives **11** and **12** gave good to excellent conversions, however **11** showed disappointing yields of CM products (**18**, **25**) due to competitive ring-closing metathesis (RCM), giving a ratio of about 50% of RCM in three cases and 6% of RCM using the combination of catalyst **2** and fluorinated olefin **5**. In the case of the larger homologue **12**, formation of the eleven membered RCM product is unfavourable, and hence

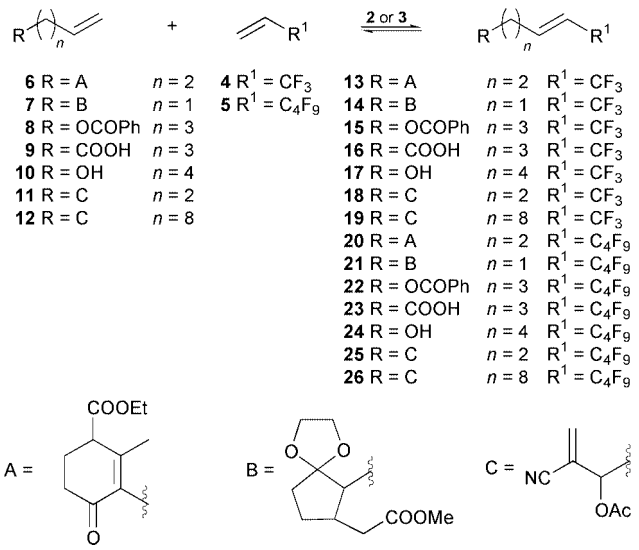

Scheme 1

Table 1 CM reactions of fluorinated olefins using **2** and **3**

		Yield[a] (%)		Dimer[a] (%)	
Substrate	Product	Cat. **3**	Cat. **2**	Cat. **3**	Cat. **2**
6	**13**	⩾95[b]	41	0	33
7	**14**	⩾95[b]	77	0	10
8	**15**	⩾95[b]	85	0	5
9	**16**	70	58	19	23
10	**17**	75	50	18	50
11	**18**	50	16	0	19
12	**19**	⩾95[b]	⩾95[b]	0	0
6	**20**	90	40	10	45
7	**21**	79	38	21	42
8	**22**	⩾95[b]	⩾95[b]	0	0
9	**23**	59	42	41	56
10	**24**	7	21	79	73
11	**25**	57	13	0	47
12	**26**	⩾95[b]	24	0	35

[a] CM product and dimer yields determined by ^{1}H NMR. [b] Only CM product detected by ^{1}H NMR.

 DOI: 10.1039/b105031c

higher yields of the CM products **19** and **26** could be obtained.

These CM reactions proved to be chemoselective, *i.e.* only coupling between the fluorinated olefins and the more electron rich, monosubstituted double bond was observed in all cases.

No difference in reactivity or selectivity was found when the fluoroolefin was varied from **4** to **5**, with the exception of when **10** was used as the CM partner. In this case the poor solubility of **10** in **5** (also observed with the unprotected forms of **11** and **12)** possibly explains the lack of activity with this substrate.

Consistent with our earlier findings,[6] **3** gave superior conversions and higher yields of CM products than **2**. Bisphosphine complex **1** proved inactive in these systems, giving neither CM nor dimerisation products regardless of the reaction conditions.

CM processes are generally known to exhibit a moderate *E*-selectivity,[10] favoured when the substrates contain bulky substituents.[4] We found that all CM products (**13**–**26**) had an *E*/Z ratio of $\geqslant 20:1$. The stereoselectivity of fluorinated olefins with a variety of functionalised alkenes should further increase the synthetic utility of this reaction.

In summary, we have shown that stereoselective CM reactions between **4** and **5** with a variety of alkenes are possible in good yields. With the exception of hydroxy substrates, catalysts **2** and **3** both gave good conversions to CM, dimerisation and RCM products, whereas **1** proved unsuitable for these purposes. Product ratio analyses show that **3** is a better catalyst for CM than **2** in this system.[6]

Further studies in the use of selective CM reactions are underway in our laboratories. The results of these investigations will be reported in due course.

Support for this work from the 'Freiwillige Akademische Gesellschaft, Basel' (S. I.) and the 'Graduiertenkolleg: Synthetische, mechanistische und reaktions-technische Aspekte von Metallkatalysatoren of the TU Berlin' (S. R.) is gratefully acknowledged. We would also like to thank Dr S. Connon for useful comments and suggestions.

Notes and references

† Procedure for CM reactions with **4** and **2** or **3**: to a solution (0.05 M) of **6** (78 mg, 0.410 mmol) and catalyst **3** (12.6 mg, 5 mol%) in trifluorotoluene (10 mL) under N_2 was added gaseous **4** (100 mL, 4.46 mmol) *via* a needle, the atmosphere being maintained by a balloon. The resulting solution was stirred at 45 °C for 3 h (60 °C for 4 h for **2**). Removal of the solvent *in vacuo* gave a brown oil which could be purified by flash chromatography (hexane–EtOAc).

‡ Procedure for CM reactions with **5** and **2** or **3**: to a mixture of **6** (80 mg, 0.420 mmol) and **5** (1.033 g, 4.200 mmol) was added catalyst **3** (12.9 mg, 10 mol%) in trifluorotoluene (61.3 mg, 0.420 mmol) under N_2. The resulting solution was stirred at 45 °C for 3 h (60 °C for 4 h for **2**). Removal of the solvent *in vacuo* gave a brown oil which could be purified by flash chromatography (hexane–EtOAc). The excess of **5** could be recovered by distillation.

1 M. Schuster and S. Blechert, *Angew. Chem.*, 1997, **109**, 2124; M. Schuster and S. Blechert, *Angew. Chem., Int. Ed. Engl.*, 1997, **36**, 2036; S. Chang and R. H. Grubbs, *Tetrahedron*, 1998, **54**, 4413; H. E. Blackwell, D. J. O'Leary, A. K. Chatterjee, R. A. Washenfelder, D. A. Bussmann and R. H. Grubbs, *J. Am. Chem. Soc.*, 2000, **122**, 58; A. Fürstner, *Angew. Chem.*, 2000, **112**, 3140; A. Fürstner, *Angew. Chem., Int. Ed.*, 2000, **39**, 3012.

2 *Organofluorine Chemicals and their Industrial Applications*, ed. R. E. Banks, Ellis Horwood, Chichester, UK, 1979; *Preparation, Properties and Industrial Application of Organofluorine Compounds*, ed. R. E. Banks, Ellis Horwood, Chichester, UK, 1982; *Organofluorine Chemistry, Principles and Commercial Applications*, ed. R. E. Banks, B. E. Smart and J. C. Tatlow, Plenum Press, New York, 1994; *Chem. Rev.*, 1996, **96**, 1555.

3 M Cavazzini, F. Montanari, G. Pozzi and S. Quici, *J. Fluorine Chem.*, 1999, **94**, 183.

4 A. K. Chatterjee, J. P. Morgan, M. Scholl and R. H. Grubbs, *J. Am. Chem. Soc.*, 2000, **122**, 3783.

5 S. Randl, S. Gessler, H. Wakamatsu and S. Blechert, *Synlett*, 2000, **3**, 430.

6 S. Gessler, S. Randl and S. Blechert, *Tetrahedron Lett.*, 2000, **41**, 9973.

7 S. B. Garber, J. S. Kingsbury, B. L. Gray and A. Hoveyda, *J. Am. Chem. Soc.*, 2000, **122**, 8168.

8 M. Scholl, S. Ding, C. W. Lee and R. H. Grubbs, *Org. Lett.*, 1999, **1**, 953.

9 E. Ciganek, *Org. React.*, 1977, **51**, 201; S. E. Drewes and G. H. P. Roos, *Tetrahedron*, 1988, **44**, 4653; D. Basaviah, P. D. Rao and R. S. Hyma, *Tetrahedron*, 1996, **52**, 8001.

10 D. J. O'Leary, H. E. Blackwell, R. A. Washenfelder and R. H. Grubbs, *Tetrahedron Lett.*, 1998, **39**, 7427; A. K. Chatterjee and R. H. Grubbs, *Org. Lett.*, 1999, **1**, 1751.

CHEMCOMM
Communication
www.rsc.org/chemcomm

Complex of polyelectrolyte network with surfactant as novel shape memory networks

Ying Guan,[a] Yiping Cao,[a] Yuxing Peng,*[a] Jian Xu[b] and Albert S. C. Chen*[c]

[a] *Institute of Organic Chemistry, Chinese Academy of Sciences, Chengdu 610041, China. E-mail: yxpeng@cioc.ac.cn*
[b] *Polymer Physics Laboratory, Center for Molecular Science, Institute of Chemistry, Chinese Academy of Sciences, Beijing 100080, China*
[c] *Department of Applied Biology and Chemical Technology, Hong Kong Polytechnic University, Hung Hom Kowloon, Hong Kong, China*

Received (in Cambridge, UK) 17th January 2001, Accepted 6th July 2001
First published as an Advance Article on the web 15th August 2001

Poly(acrylic acid-*co*-methyl methacrylate)–cetyltrimethylammonium bromide (P(AA-*co*-MMA)–C_{16}TAB) complex has shape memory behavior due to the formation of crystalline aggregates among the long alkyl chains of C_{16}TAB in the complex, and can be regarded as a novel shape memory network.

During recent years, shape memory materials have received increasing attention on account of their interesting properties and potential applications, especially thermally stimulated shape memory materials.[1–3] The mechanism of shape memory behavior with temperature can be schemed briefly as outlined below where L is the initial state of material and L′ is the

$$\mathrm{L}\xrightarrow[\text{deformation}]{T > T_g \text{ or } T > T_m}\mathrm{L}+\mathrm{L}'\xrightarrow[\text{fixation}]{T < T_g \text{ or } T < T_m}\mathrm{L}+\mathrm{L}'\xrightarrow[\text{recovery}]{T > T_g \text{ or } T > T_m}$$

deformation of material. These materials have a two phase structure, namely, the fixing phase remembers the initial shape and the reversible phase shows a reversible soft and rigid transition with temperature. Based on this principle, some polymers were discovered that had shape memory behavior.[4–9]

Among shape memory materials, copolymer networks[6,7] containing long alkyl side chains were reported due to a reversible order–disorder transition of long alkyl side chains. Below the transition temperature, these side chains form a crystalline aggregate structure, and behave as hard plastic. While above this temperature they transfer to the amorphous state and the material abruptly becomes soft and flexible.

It is well known that many beneficial properties of polyelectrolyte–surfactant complexes[10,11] result from the highly ordered structures[12–14] formed by the self-assembly of surfactant molecules inside the complexes. The supermolecular formation was driven by both electrostatic interactions between charged components and hydrophobic interactions between the polymer backbones and the surfactant alkyl chains.

The research works mentioned above served as a great source of inspiration to us in designing the polyelectrolyte network–surfactant complexes for shape memory networks. Up to now, any similiar research work has not been reported. Hence the polyelectrolyte network–surfactant complexes may broaden the list of shape memory polymers. In this paper, we synthesized poly[(acrylic acid)-*co*-(methyl methacrylate)] (P(AA-*co*-MMA)) networks and the complex of P(AA-*co*-MMA)–(cetyltrimethylammonium bromide) (P(AA-*co*-MMA)–C_{16}TAB). The composition and the structure of the network and complex were characterized. And the surface microstructure before and after deformation was also studied.

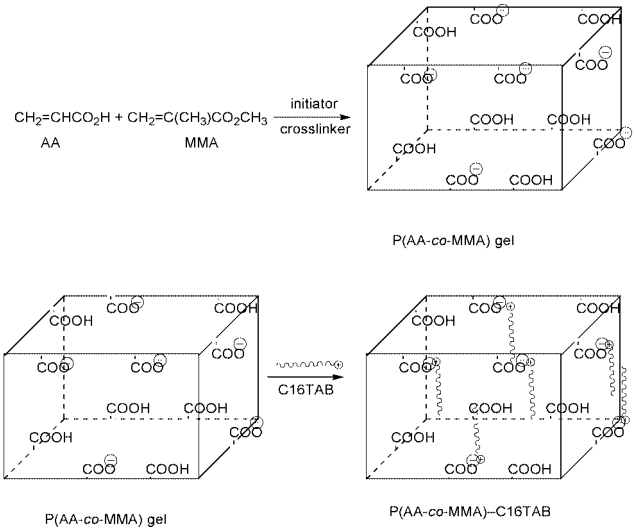

Scheme 1 Synthesis of P(AA-*co*-MMA)–C_{16}TAB complex.

Scheme 1 shows the synthesis and the expected structure of P(AA-*co*-MMA)–C_{16}TAB. The crosslinked P(AA-*co*-MMA) network was designed as the fixed phase, while C_{16}TAB was designed as the reversible phase for shape memory networks. Fig. 1 is the FTIR spectra of P(AA-*co*-MMA) before and after complexation with C_{16}TAB. The curves of P(AA-*co*-MMA) and P(AA-*co*-MMA)–C_{16}TAB both give a wide peak from 3100 to 3600 cm^{-1} indicating the stretching of –OH groups of polyacrylic acid (PAA). The relative intensity of the peak at 2955 cm^{-1} due to the stretching of the $-CH_2$ groups of P(AA-*co*-MMA)–C_{16}TAB is slightly higher than that of P(AA-*co*-

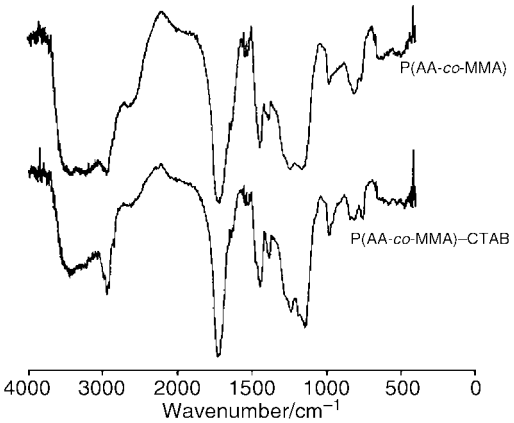

Fig. 1 FTIR spectra of P(AA-*co*-MMA) and P(AA-*co*-MMA)–C_{16}TAB complex.

 DOI: 10.1039/b100625h

MMA). Comparing the C or H content between P(AA-*co*-MMA) and P(AA-*co*-MMA)–C_{16}TAB, the C_{16}TAB : AA ratio can be calculated from eqn. (1) where n_{CTAB} and n_{AA} is the mole content of C_{16}TAB and AA in the complex, respectively.

$$n_{CTAB}/n_{AA} = 0.432 \times [(\%_{complex} - \%_{P(AA\text{-}co\text{-}MMA)})/(\%_{CTAB} - \%_{complex})] \times 100\% \quad (1)$$

$\%_{complex}$, $\%_{P(AA\text{-}co\text{-}MMA)}$ and $\%_{CTAB}$ are the C or H content of P(AA-*co*-MMA)–C_{16}TAB, P(AA-*co*-MMA) and C_{16}TAB, respectively. The calculated value of n_{CTAB}/n_{AA} was 15.4%, which is higher than the pK_a of the PAA segment which is *ca.* 5.[15] Hence, the complexation of C_{16}TAB with P(AA-*co*-MMA) was driven not only by electrostatic interactions but hydrophobic interactions among long alkyl chains of C_{16}TAB and between C_{16}TAB and polymer chains of the network.

The most important key to a shape memory network for P(AA-*co*-MMA)–C_{16}TAB is whether the long alkyl chain of C_{16}TAB could form a highly ordered structure or crystalline phase in the P(AA-*co*-MMA) network. Table 1 gives the DSC data for P(AA-*co*-MMA) and P(AA-*co*-MMA)–C_{16}TAB. A glass transition temperature (T_g) attributed to the PAA segment was obtained for both the polymer network and complex. A melting point (T_m) and crystalline point (T_c) was found only in complex. These facts mean the long alkyl side chains of C_{16}TAB form a crystalline phase in P(AA-*co*-MMA)–C_{16}TAB. This is the necessary condition for P(AA-*co*-MMA)–C_{16}TAB to adopt a shape memory network.

The T_g should be greater than or equal to the melting point of P(AA-*co*-MMA)–C_{16}TAB, 98.26 °C. Hence, 100 °C was chosen to observe the deformation and recovery of the complex. Fig. 2 shows the shape memory phenomenon of P(AA-*co*-MMA)–C_{16}TAB. The straight strip sample was heated to 100 °C, deformed as an 'e' shape and then cooled to rt. The complex is rigid and retains the 'e' shape. On heating again to 100 °C, the complex becomes soft and recovers it's original strip shape. This phenomenon may be attributed to the formation of crystalline aggregates among the long alkyl chains of C_{16}TAB in the complex that locks the new shape. When the deformed complex is heated again above T_g, the crystalline aggregates become amorphous and the complex recovers its original size and shape.

In order to give further support for the shape memory behavior of P(AA-*co*-MMA)–C_{16}TAB, the surface variation of P(AA-*co*-MMA) and P(AA-*co*-MMA)–C_{16}TAB before and after deformation were also observed on an optic microscope and recorded by a PC digital camera. Fig. 3 shows the microphotographs of P(AA-*co*-MMA) and P(AA-*co*-MMA)–C_{16}TAB under different conditions. The initial surface of P(AA-*co*-MMA)–C_{16}TAB is rougher than that of P(AA-*co*-MMA). Those concavo-convex flecks on the surface of P(AA-*co*-MMA)-C_{16}TAB are due to the shrinkage caused by the complexation of P(AA-*co*-MMA) with C_{16}TAB. The surface of P(AA-*co*-MMA) after deformation shows many tiny streaks, while the surface of P(AA-*co*-MMA)-C_{16}TAB shows the extension flecks along the tensile direction. The surface of P(AA-*co*-MMA) is significantly different after recovery from the initial state, which means P(AA-*co*-MMA) cannot recover its initial microstructure. In contrast, the surface of P(AA-*co*-MMA)–C_{16}TAB is very similiar in both the initial and recovery states. In other words, the complex can recover its initial microstructure. The recovery ratio is about 85%, calculated from the difference in length of the test sample in the initial and recovered states.

Table 1 DSC data of P(AA-*co*-MMA) and P(AA-*co*-MMA)–C_{16}TAB

Sample	T_m[a]/°C	T_c[b]/°C	T_g[c]/°C
P(AA-*co*-MMA)	—	—	115.54
P(AA-*co*-MMA)–C_{16}TAB	98.26	68.98	128.12

[a] Melting point. [b] Crystalline point. [c] Glass transition temperature.

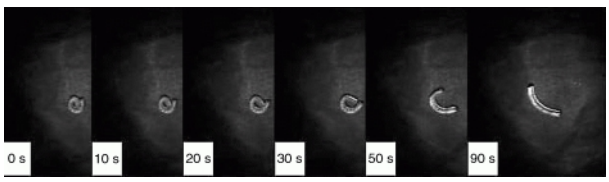

Fig. 2 Shape memory phenomenon of P(AA-*co*-MMA)–C_{16}TAB. (The initial straight stripe was heated to 100 °C and deformed as an 'e' alphabet, then cooled to room temperature under constrained conditions. After withdrawal of the external force, the 'e' shape sample was put into a glass container and kept at a constant temperature of 100 °C. At the same time the snapshot was captured by a digital camera every 2 s.)

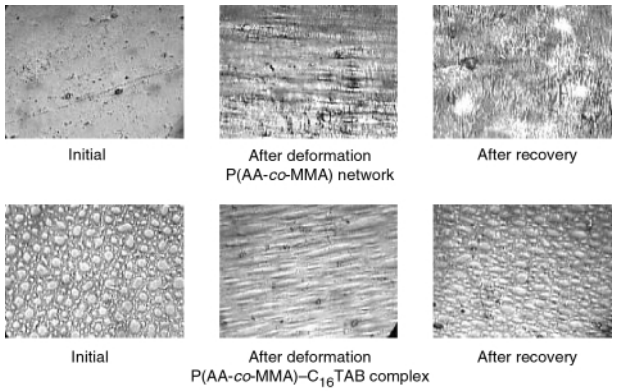

Fig. 3 Microphotographs of the surface of (a) P(AA-*co*-MMA) and (b) P(AA-*co*-MMA)–C_{16}TAB under different conditions at rt. (The enlargement multiple was 160. Initial: initial state of sample. After deformation: sample were drawn at 100 °C under a constant tensile force of 0.05 N until the elongation rate was 150% and then cooled to room temperature. After recovery: samples after deformation were heated to 100 °C and kept at constant temperature for 30 min, then cooled to room temperature.)

In conclusion, although the reversible temperature is high, 100 °C, and the recovery ratio is not 100%, the shape memory phenomenon of P(AA-*co*-MMA)–C_{16}TAB shows that the well designed polyelectrolyte network–surfactant complex can be considered as a kind of novel shape memory network.

The National Natural Science Foundation of China is gratefully acknowledged for the financial support of this work (Grant No. 59773019 and 29774036).

Notes and references

1 *Proceedings of the International Symposium on Shape Memory Effect and its Applications*, ed. J. Perkins Plenum, New York, 1975.
2 S. Wang, Z. Lv, W. Zhao, X. Xu and B. Li, *Polym. Mater. Sci. Eng. (Chengdu, People's Republic of China)*, 2000, **16**(1), 1.
3 T. Takahashi, *J. Appl. Polym. Sci.*, 1996, **60**, 1061.
4 M. Xu and F. Li, *Chin. J. Polym. Sci.*, 1999, **17**(3), 203.
5 J. Lin and L. Chen, *J. Appl. Polym. Sci.*, 1999, **73**, 1305.
6 W. G. Reyntjens, F. E. Du Prez and E. J. Goethals, *Macromol. Rapid Commun.*, 1999, **20**, 251.
7 Y. Kagami, J. P. Gong and Y. Osada, *Macromol. Rapid Commun.*, 1996, **17**, 539.
8 Y. Osada and A. Matsuda, *Nature*, 1995, **376**(20), 219.
9 Z. Hu, X. Zhang and Y. Li, *Science*, 1995, **269**, 525.
10 B. Lindman and K. Thalberg, in *Interactions of Surfactants with Polymers and Proteins*, ed. E. D. Goddard and K. P. Anantha-padmanbhan, CRC Press, Boca Raton, FL, 1993, ch. 5.
11 H. Okuzabi and Y. Osada, *Macromolecules*, 1994, **28**, 4554.
12 H. Okuzaki and Y. Osada, *Macromolecules*, 1995, **28**, 380.
13 M. Antonietti and J. Conrad, *Angew. Chem., Int. Ed. Engl.*, 1994, **33**(18), 1869.
14 S. Q. Zhou, F. Yeh, C. Burger and B. Chu, *J. Phys. Chem. B*, 1999, **103**, 2107.
15 *Encyclopedia of Polymer Science and Engineering*, vol. 1, 3rd edn., ed. H. Mark, N. M. Bikales, C. G. Overberger and G. Menges, John Wiley & Sons Inc., New York, 1985, p. 228.

CHEMCOMM Communication
www.rsc.org/chemcomm

Nafion-H catalysed sulfonylation of aromatics with arene/alkenesulfonic acids for the preparation of sulfones[1a]†

George A. Olah,* Thomas Mathew and G. K. Surya Prakash*

Loker Hydrocarbon Research Institute and Department of Chemistry, University of Southern California, Los Angeles, CA 90089-1661, USA

Received (in Corvallis, OR, USA) 21st May 2001, Accepted 17th July 2001
First published as an Advance Article on the web 16th August 2001

Synthesis of both symmetric and unsymmetric diaryl/aryl alkyl sulfones is easily achieved by Friedel–Crafts type sulfonylation of aromatics with suitable arene- or alkanesulfonic acids in the presence of Nafion-H, a perfluorinated resinsulfonic acid catalyst.

The wide use of organosulfones as very versatile synthons in organic synthesis is well known for the past few decades.[1b–d]

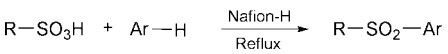

Scheme 1

Diaryl sulfones are important drugs active against malaria, leishmaniasis, infections in patients with AIDS and discoid lupus erythematosus.[2–4] Various methods for the synthesis of sulfones involve the conventional Friedel–Crafts type sulfonylation of aromatics using sulfonyl halides,[5] oxidation of the corresponding sulfides,[6] reactions of sulfonyl fluorides with organolithium compounds or Grignard reagents,[7] *etc*. Recently, effective synthesis of sulfones from aryl trifluoromethyl sulfone using Grignard reagents and sulfonyl halides and anhydrides using metal triflates and zeolites as catalysts[8] have been reported. Thus far no convenient synthetic method is available for the synthesis of sulfones using sulfonic acids directly.

In this communication, we would like to report an efficient preparation of aromatic sulfones directly from arene- or

Table 1 Nafion-H catalysed sulfonylation of aromatics using sulfonic acids

Sulfonic acid	Substrate	Time/h	Yield (%)	Sulfone
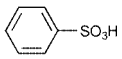	Benzene	20	48	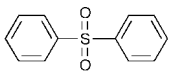
	Toluene	20	52	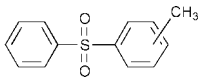
	p-Xylene	16	82	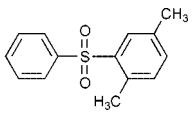
	m-Xylene	16	80	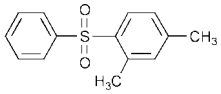
	Chlorobenzene	20	52	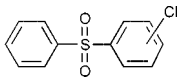
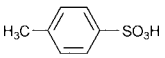	Benzene	20	50	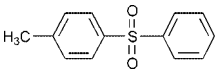
	Toluene	20	57	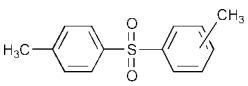
	p-Xylene	8	78	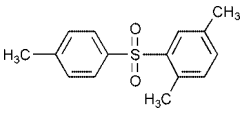
	m-Xylene	8	70	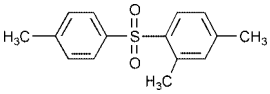
	Chlorobenzene	20	55	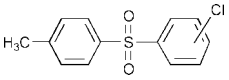
CH_3SO_3H	*p*-Xylene	8	30	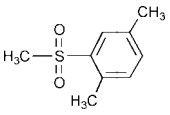

 DOI: 10.1039/b104603a

alkenesulfonic acids with the use of Nafion-H, a solid perfluorinated resinsulfonic acid polymer as a catalyst. We have previously found that Friedel–Crafts type intramolecular acylation with suitably *ortho* substituted benzoic acids in the presence of Nafion-H affords ketones in good yields.[9] Nafion membranes have also been found to allow permeation of sulfonating reagents such as SO_3 and 20% oleum during sulfonation reactions.[10] Preparation of aromatic symmetric and unsymmetric sulfones could be achieved in good yields (30–80%) by intermolecular Friedel–Crafts type sulfonylation of arenes with suitable sulfonic acids (Scheme 1).

Nafion-H has been found to be a suitable solid acid catalyst with high selectivity and catalytic activity giving good yields of sulfones. The reaction with the use of Nafion-H conveniently eliminates the use of volatile or noxious reagents. After the reactions with Nafion-H, the catalyst is easily regenerated.[11] This solid resin catalyst is more convenient and environmentally friendly in comparison with corrosive acid catalysts (liquid acids) generally used in reactions involving strong acids.

The sulfonylation reactions were carried out by refluxing a stirred mixture of the corresponding arene- or alkanesulfonic acid and excess arene in the presence of the solid Nafion-H catalyst. The arenes act as both the substrate and the solvent. The products were isolated after filtering the reaction mixture and distilling off the excess arene.[12]

The sulfonylation reactions are general for sulfonic acids such as benzenesulfonic acid, toluenesulfonic acid and methanesulfonic acid. Activated aromatics such as *p*-xylene and *m*-xylene afforded the corresponding sulfones in good yields (~ 80%). The yield of the corresponding sulfones from benzene and toluene were, however, low (5–15%) due to the insufficient activation of Nafion-H under the used relatively mild refluxing conditions. On the other hand, when the reactions with benzene and toluene were conducted under pressure at 160–165 °C, the product yields increased considerably (48–57%). Along with the product and the unreacted starting material, minor amounts of side products due to alkylation and dealkylation were also observed.

Azeotropic removal of water using a Dean–Stark trap increases the yields. As shown in Table 1, the present method provides an easy approach to sulfones with no undesired side products. Sulfonylation of toluene and chlorobenzene, afforded *para* substituted sulfones as the major product indicating a typical electrophilic aromatic sulfonylation. The method developed is simple, uses readily available arene- or alkanesulfonic acids instead of sulfonyl halides, anhydrides, *etc.*, used in Friedel–Crafts reactions. The substitution of the typical Friedel–Crafts type catalyst with this resin and its convenient regeneration bodes well for the protocol and its overall applicability.

Support of our work by Loker Hydrocarbon Research Institute is gratefully acknowledged.

Notes and references

† Dedicated to our colleague, Professor William P. Weber on the occasion of his sixtieth birthday.

1 (*a*) Considered as catalysis by solid super acids, Part 34. For Part 33, see ref. 9; (*b*) K. Tanaka and A. Kaji, *Synthetic Uses of Sulfones in The Chemistry of Sulphones and Sulphoxides*, Eds. S. Patai, Z. Rappoport and C. J. M. Stirling, Wiley-Interscience, New York, 1988, ch. 15, pp. 759; (*c*) B. M. Trost, *Bull. Chem. Soc. Jpn.*, 1988, **61**, 107; (*d*) L. Field, *Synthesis*, 1978, 713.

2 R. C. Hastings and S. G. Franzblau, *Ann. Rev. Pharmacol. Toxicol.*, 1966, **28**, 231.

3 G. Wozel, *Int. J. Dermatol.*, 1989, **28**, 17.

4 J. S. Lo, R. E. Berg and K. J. Tomecki, *Int. J. Dermatol.*, 1989, **28**, 497.

5 J. B. Hendrickson and K. W. Bair, *J. Org. Chem.*, 1977, **42**, 3875; G. A. Olah and H. C. Lin, *Synthesis*, 1974, 342.

6 G. A. Olah and B. G. B. Gupta, *J. Org. Chem.*, 1983, **48**, 3585; D. J. Procter, *J. Chem. Soc., Perkin Trans. 1*, 2000, **1**, 835.

7 Y. Shirota, T. Nagai and N. Tokura, *Tetrahedron*, 1969, **25**, 3193; L. L. Frye, E. L. Sullivan, K. P. Cusack and J. M. Funaro, *J. Org. Chem.*, 1992, **57**, 697.

8 R. W. Steensma, S. Galabi, J. R. Tagat and S. W. McCombie, *Tetrahedron Lett.*, 2001, **42**, 2281; R. P. Singh, R. M. Kamble, K. L. Chandra, P. Sravanan and V. K. Singh, *Tetrahedron*, 2001, **57**, 241; S. Repichet, C. Le Roux, P. Hernandex, J. Dubac and J. R. Desmurs, *J. Org. Chem.*, 1999, **64**, 6479; B. M. Chaudhary, N. S. Chaudhari and M. L. Kantam, *J. Chem. Soc., Perkin Trans. 1*, 2000, **16**, 2689.

9 G. A. Olah, T. Mathew, M. Farnia and G. K. S. Prakash, *Synlett*, 1999, 1067.

10 R. J. Vaughan, *US Patent*, 4308215, 1981; *Chem. Abstr.*, 1982, **96**, 87450a.

11 G. A. Olah, P. S. Iyer and G. K. S. Prakash, *Synthesis*, 1986, 513 and references therein; T. Yamato, C. Hideshima, G. K. S. Prakash and G. A. Olah, *J. Org. Chem.*, 1991, **56**, 3192; M. Hachoumy, T. Mathew, E. C. Tongo, Y. D. Vankar, G. K. S. Prakash and G. A. Olah, *Synlett*, 1999, 363; G. K. S. Prakash, T. Mathew, S. Krishnaraj, E. R. Marinez and G. A. Olah, *Appl. Catal., A*, 1999, **181**, 283.

12 Typical sulfonylation procedure is as follows: to a solution of dry benzenesulfonic acid (790 mg, 5.0 mmol) in dry *p*-xylene (40 mL), Nafion-H (400 mg, 50 wt%) was added and stirred. The flask was fitted with a Dean–Stark trap and the solution was refluxed continuously with stirring for 16 hours (water formed during the reaction was removed completely by introducing dry molecular sieves, ≈2.0 g, in the trap). The reaction mixture was filtered and washed with 10% $NaHCO_3$ solution to remove any amount of unreacted sulfonic acid. After washing with water and drying with anhydrous Na_2SO_4, excess *p*-xylene was distilled off and the residue was recrystallized from a mixture of dichloromethane and *n*-hexane (1:2) to afford 2,5-dimethylphenyl phenyl sulfone as a white crystalline solid, (1.0 g, 82%) mp 101–103 °C.

CHEMCOMM Communication
www.rsc.org/chemcomm

Lanthanide triflate-catalyzed three component synthesis of α-amino phosphonates in ionic liquids. A catalyst reactivity and reusability study

Sang-gi Lee,*[a] Jung Hwan Park,[a] Jahyo Kang[b] and Jae Kyun Lee[a]

[a] *Life Sciences Division, Korea Institute of Science and Technology, PO Box 131, Cheongryang, Seoul 130-650, Korea. E-mail: sanggi@kist.re.kr*
[b] *Department of Chemistry, Sogang University, Seoul 121-742, Korea*

Received (in Cambridge, UK) 5th June 2001, Accepted 24th July 2001
First published as an Advance Article on the web 9th August 2001

The catalyst reactivity and reusability for the lanthanide triflate-catalyzed three component synthesis of α-amino phosphonates have been examined in room temperature ionic liquids, [bmim][X], in which the catalytic activities were very dependent on the counter anion, X, as well as on the phosphorus nucleophile, and moreover, the catalyst immobilized in an ionic liquid was reused several times without any loss of activity.

The use of environmentally benign reaction media is very important in view of today's environmentally conscious attitude. In connection with this, room temperature ionic liquids that are air and moisture stable have received a good deal of attention in recent years as novel solvent systems for organic synthesis. A number of reactions such as Friedel–Crafts reactions, Diels–Alder cycloadditions, hydrogenation, and Heck reactions have employed ionic liquids as solvents.[1] More recently they have been introduced in halogenations of alkenes and alkynes[2] and in asymmetric epoxidation[3] and asymmetric hydrogenations.[4] Here we report lanthanide triflate-catalyzed three component reactions in room temperature ionic liquids, [bmim][X], to give α-amino phosphonates.

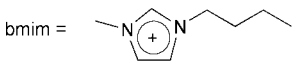

X = PF_6^-, SbF_6^-, BF_4^-, OTf^-

α-Amino phosphonates are an important class of compounds in modern pharmaceutical chemistry. Consequently, their synthesis has received an increasing amount of attention.[5] It has been recently reported that ytterbium triflates[6] and indium trichloride[7] are effective catalysts for three component reactions of aldehydes, amines, and diethyl phosphonate in organic solvents to give α-amino phosphonates. Kobayashi discovered that similar three component reactions using triethyl phosphite were also efficiently promoted by a catalytic amount of scandium-surfactant-combined catalysts in water to give α-amino phosphonates.[8] To examine the catalytic activities of lanthanide triflates as well as indium trichloride in ionic liquids, we carried out the three component reactions of benzaldehyde, aniline and diethyl phosphonate, $HP(O)(OEt)_2$, in the presence of 10 mol% of catalyst at 20 °C for 27 h. The results are summarized in Table 1.†

It has been found that, using anhydrous lanthanide triflates as catalysts, the reactions in [bmim][PF_6] proceeded highly efficiently (entries 1–4 in Table 1). Among the anhydrous lanthanide triflates catalysts, $Sm(OTf)_3$ is superior to other catalysts in an ionic liquid (entry 4 in Table 1) whereas $Yb(OTf)_3$ is more effective in an organic solvent.[6] More interestingly, although it has been known that the lanthanide triflates are generally stable and function well in water,[9] the yields decreased greatly with hydrated catalysts, $Yb(OTf)_3{\cdot}H_2O$ (entry 5 in Table 1) and $La(OTf)_3{\cdot}H_2O$ (entry 6 in Table 1). The catalytic activity of $Sm(OTf)_3$ was retained even at 1 mol% (95%, entry 7 in Table 1). However, the activity of the recovered catalyst immobilized in ionic liquid decreased (74%, entry 8 in Table 1) which may be due to water generated during

Table 1 The three component reactions of benzaldehyde, aniline and diethyl phosphonate in ionic liquids in the presence of lanthanide triflates and indium trichloride

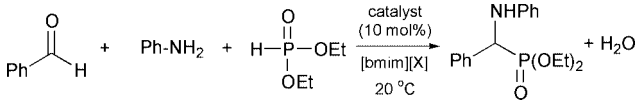

Entry	Ionic liquid	Catalyst	Yield (%)[c]
1	[bmim][PF_6]	$Yb(OTf)_3$	95
2	[bmim][PF_6]	$Sc(OTf)_3$	80
3	[bmim][PF_6]	$Dy(OTf)_3$	94
4	bmim][PF_6]	$Sm(OTf)_3$	99
5	[bmim][PF_6]	$Yb(OTf)_3{\cdot}H_2O$	63
6	[bmim][PF_6]	$La(OTf)_3{\cdot}H_2O$	39
7[a]	[bmim][PF_6]	$Sm(OTf)_3$	95
8[b]	[bmim][PF_6]	$Sm(OTf)_3$	74
9	[bmim][SbF_6]	$Sm(OTf)_3$	71
10	[bmim][BF_4]	$Sm(OTf)_3$	18
11	[bmim][OTf]	$Sm(OTf)_3$	89
12	[bmim][PF_6]	$InCl_3$	90
13	CH_2Cl_2	$Sm(OTf)_3$	70

[a] Used 1 mol% catalyst. [b] Used recovered catalyst of entry 7. [c] Isolated yield.

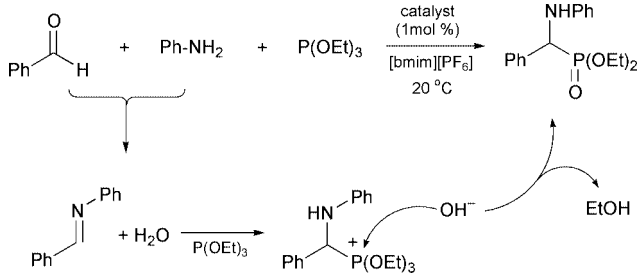

Scheme 1 Plausible mechanism of the three component reaction using $P(OEt)_3$.

Table 2 The three component reactions of benzaldehyde, aniline and triethyl phosphite in [bmim][PF_6] in the presence of 1 mol% of lanthanide triflates and recycled catalysts

Entry	Catalyst	1st[a]	2nd	3rd	4th	5th	Average
1	$Sc(OTf)_3$	97	94	97	93	> 99	96.2
2	$Yb(OTf)_3$	57	54	—	—	—	55.5
3	$Sm(OTf)_3$	87	87	—	—	—	87.0
4	$Gd(OTf)_3$	84	77	—	—	—	80.5
5	$InCl_3$	86	50	—	—	—	68.0

[a] Isolated yield.

 DOI: 10.1039/b104967b

Table 3 The three component reactions of aldehydes, aniline and triethyl phosphite in [bmim][PF_6] in the presence of $Sc(OTf)_3$ as catalyst

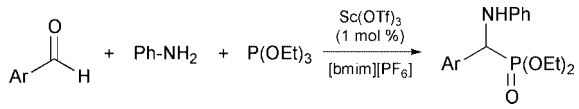

Entry	Aldehyde	Yield (%)[a]
1	Benzaldehyde	97
2	*p*-Methoxybenzaldehyde	> 99
3	*o*-Tolualdehyde	90
4	*m*-Tolualdehyde	> 99
5	*p*-Tolualdehyde	> 99
6	*p*-Fluorobenzaldehyde	93
7	α,α,α-Trifluoro-*p*-tolualdehyde	97
8	1-Naphthaldehyde	> 99
9	3-Thiophenecarboxaldehyde	93
10	3-Furaldehyde	90

[a] Isolated yield

the reaction. The counter anion of the ionic liquids affected the catalytic activity considerably (entries 9–11), thus, only 18% of product was obtained upon using BF_4 anion (entry 10 in Table 1). By employing indium trichloride as a catalyst in [bmim][PF_6], the reaction also proceeded efficiently (entry 12 in Table 1). However, the reaction in dichloromethane solvent using $Sm(OTf)_3$ afforded product only in 70% yield (entry 13 in Table 1).

We expected that employing triethyl phosphite, $P(OEt)_3$, as a phosphorus nucleophile could overcome the drawback of catalyst recycling in the three component reactions. Mechanistically, the water generated during formation of imine could be used for the hydrolysis of phosphonium intermediate[10] to give α-amino phosphonates and EtOH as shown in Scheme 1.

The use of $P(OEt)_3$ instead of $HP(O)(OEt)_2$ changed the catalytic activities of the lanthanide triflates. In this reaction system, $Sc(OTf)_3$ exhibited the highest catalytic activity (97%, entry 1 in Table 2), and the reaction was completed within 2 h. The $Sc(OTf)_3$ can be used five times without any loss of catalytic activity (entry 1 in Table 2). In second cycle reactions, as we expected, the catalytic activities of the recovered catalysts except $InCl_3$ (entry 5 in Table 2) were almost retained.

The three component reactions of various aldehydes and aniline with $P(OEt)_3$ in the presence of 1 mol% $Sc(OTf)_3$ in ionic liquid, [bmim][PF_6], gave the corresponding α-amino phosphonates in excellent yields as shown in Table 3.

In summary, the catalytic activities of various lanthanide triflates as well as indium trichloride were examined for the three component reactions of aldehydes, amines and phosphorus nuleophiles, $HP(O)(OEt)_2$ and $P(OEt)_3$, in room temperature ionic liquids. The catalytic activities were very dependent on the counter anion, X, as well as on the phosphorus nucleophile. The catalysts immobilized on ionic liquid can be reused several times without any loss of activity.

Notes and references

† *General procedure for the three component reactions and catalyst recycling*: aniline (0.25 mmol), an aldehyde (0.25 mmol) and a phosphorus nucleophile, $HP(O)(OEt)_2$ (1 mmol) or $P(OEt)_3$ (1 mmol), were successively added to a solution of catalyst (0.25×10^{-2} mmol) in an ionic liquid (1 mL) at 20 °C. The mixture was stirred at the same temperature for 27 h for $HP(O)(OEt)_2$ or 2 h for $P(OEt)_3$. The mixture was extracted with benzene (4 mL × 5) and concentrated. Purification by silica gel chromatography afforded the desired product. More reactants (aldehyde, aniline and $P(OEt)_3$) were added to the ionic liquid solution remaining in the vessel. This was the start of the second cycle.

1 P. Wasserscheid and W. Keim, *Angew. Chem., Int. Ed.*, 2000, **39**, 3772; T. Welton, *Chem. Rev.*, 1999, **99**, 2071; K. R. Seddon, *J. Chem. Technol. Biotechnol.*, 1997, **68**, 351; Y. Chauvin and H. Olivier, *CHEMTECH*, 1995, 26; and references therein.
2 C. Chiappe, D. Capraro, V. Conte and D. Pieraccini, *Org. Lett.*, 2001, **3**, 1061.
3 C. E. Song and E. J. Rho, *Chem. Commun.*, 2000, 837.
4 R. A. Brown, P. Pollet, E. McKoon, C. A. Eckert, C. L. Liotta and P. G. Jessop, *J. Am. Chem. Soc.*, 2001, **123**, 1254.
5 P. Kafarski and B. Lejczak, *Phosphorous Sulfur Silicon*, 1991, **63**, 193; and references therein.
6 C. Qian and T. Huang, *J. Org. Chem.*, 1998, **63**, 4125.
7 B. C. Ranu, A. Hajira and U. Jana, *Org. Lett.*, 1999, **1**, 1141.
8 K. Manabe and S. Kobayashi, *Chem. Commun.*, 2000, 669.
9 S. Kobayashi, *Synlett*, 1994, 689; W. Xie, Y. Jin and P. G. Wang, *CHEMTECH*, 1999, **29**, 23.
10 In ref. 8, Kobayashi stated that the phosphonium intermediate was hydrolyzed rapidly in water as solvent.

Typeset and printed by Black Bear Press Limited, Cambridge, England

CHEMCOMM
Feature Article
www.rsc.org/chemcomm

Understanding organic reactions in water: from hydrophobic encounters to surfactant aggregates

Jan B. F. N. Engberts*[a] and Michael J. Blandamer[b]

[a] *Physical Organic Chemistry Unit, Stratingh Institute, University of Groningen, Nijenborgh 4, 9747 AG Groningen, The Netherlands. E-mail: J.B.F.N.Engberts@chem.rug.nl*
[b] *Department of Chemistry, University of Leicester, Leicester, UK LE1 7RH. E-mail: mjb@le.ac.uk*

Received (in Cambridge, UK) 22nd May 2001, Accepted 6th July 2001
First published as an Advance Article on the web 9th August 2001

A crucial factor in realising a green chemical process in solution involves the choice of a safe, non-toxic and cheap solvent. Water is the obvious choice. Despite solubility problems, considerable interest has developed recently in organic chemistry in water. This interest also results from the fact that association and chemical reactions often benefit noticeably from the special properties of water, resulting mainly from its small molecular size, its three-dimensional hydrogen-bond network and hydrophobic interactions which are so unique for liquid water. Here we discuss organic reactions and assembly processes in water, largely taken from experiments performed in the authors' laboratories. We show that non-covalent interactions in water can be utilised for fine tuning organic reactions in aqueous media.

Introduction

For a very long time, water has been recognised as essential for all life processes and indeed life support on planet Earth. For example, at the dawn of western scientific thought, Thales (from Milete, B.C. 640–548) said: '*All things are produced from water*'. This statement was one of the first attempts to formulate a generalisation; *i.e.* referring all things to a common origin. In ancient Chinese thought, water was frequently used as a root metaphor for natural and civilised behaviour.[1] K'ung Tzu said: '*Water, which extends everywhere and gives everything life without acting (wuwei) is like virtue (de) . . . That is the reason that when a gentleman (junzi) sees a great river, he will always look upon it . . .*'

In all major religions and philosophies, water plays an important role. In chemical research, a long-standing interest exists in the properties of water[2,3] and in chemical reactions between solutes taking place in this fascinating liquid. However, water is rarely seen as the solvent of choice in which to carry out synthetic chemistry. In this review we illustrate some of the key features involved in understanding the role of solvent water for chemical reactions involving small molecules and then for processes involving larger molecules and large molecular assemblies including micelles and vesicles. We emphasise that water is not just a 'green' solvent, but that the special properties of the liquid give rise to intra- and intermolecular non-covalent interactions leading to novel solvation behaviour and assembly processes.

Professor Jan B. F. N. Engberts graduated with a PhD degree from the University of Groningen, The Netherlands (1967). After a stay at the University of Amsterdam with Prof. Th. J. de Boer (ESR spectroscopy) Jan returned to Groningen and was appointed as a Professor of General Chemistry in 1978 and as a Professor of Physical Organic Chemistry in 1991. Fascinated by the peculiar properties of water as a medium for organic reactions and aggregation processes, much emphasis has been placed on hydrolysis reactions in water in the presence of hydrophobic addenda, surfactant aggregation, vesicle fusion, and, most recently, development of DNA carrier systems for application in gene therapy. In these studies, thermodynamics always played an important role, and these interests brought Mike and Jan together, more years ago than both care to remember.

Professor Mike Blandamer is an Emeritus Professor at the University of Leicester, having retired in 1999. Mike graduated with BSc and PhD degrees from the University of Southampton who awarded Mike the degree of DSc in 1984. Following post-doctoral research at NRC in Ottawa (Canada), Mike joined the staff at the University of Leicester. Mike and Jan share a common interest in aqueous solution chemistry, good food, good wine and New Orleans jazz music. They were coauthors on a paper published in 1985 followed over 26 years by 50 joint papers and reviews. For part of their period of cooperation, Mike was a Visiting Professor at the University of Groningen.

Aqueous solutions: general features

Introductory chemistry textbooks reviewing the properties of water stress the importance of intermolecular hydrogen bonding, leading to the conclusion that water is an associated liquid. The high relative permittivity is consistent with the idea that water is a polar liquid and therefore a good solvent for salts such as sodium chloride. $E(T)$30-values, as defined by Reichardt, which are particularly useful microscopic solvent micropolarity reporter values, confirm that water is a polar solvent.[4] The absence of strong ion-pairing in aqueous solution allows unambiguous mechanistic studies of reactions that proceed *via* highly polar or ionic intermediates. We also note that water has one of the highest heat capacities per unit volume for a liquid; *e.g.* for water, C_p = 4.18 J K^{-1} cm^{-3}; for ethanol C_p = 1.92 J K^{-1} cm^{-3}. This high heat capacity is important in moderating possible extremes of temperature on planet Earth.

This emphasis on molecular association should be set against the fact that water has a modest (shear) viscosity; the liquid pours easily, quite different from, say, glycerol.

Granted the properties of water, including its volumetric properties (*e.g.* a temperature of maximum density near 277 K) are complicated, the expectation is that the properties of aqueous solutions are also complicated. This is indeed the case. Nevertheless important features of water and aqueous solutions can be understood in the following general terms.[2]

A cluster of non-intermolecularly hydrogen bonded, but closely packed water molecules has high density–low molar volume coupled with weak cohesion. A cluster of inter-

molecularly hydrogen-bonded water molecules has low density–large molar volume with strong cohesion. In other words, strong cohesion is coupled with large molar volume. The latter is a consequence of the structural requirements of hydrogen bond formation which for a simple dimer has a *trans*-near linear configuration. To an important extent hydrogen bonding is both cohesive and repulsive, the latter reflecting the tendency to hold apart the centres of mass of water molecules. This situation is reflected in the low internal pressure of water.[5] In the context of describing the properties of aqueous solutions, we might speculate that any process (*e.g.* chemical reaction) which enhances water–water hydrogen bonding leads to an increase in molar volume. This rather unusual situation (compared to organic solvents) accounts in part for the complexity of the properties of aqueous solutions.

Experimental

This review focuses on the results obtained in the laboratories of the two authors using two major experimental techniques: (i) chemical kinetics, and (ii) titration microcalorimetry.

Determination of rate constants for chemical reactions in aqueous solutions using spectrophotometric techniques is considerably helped by computer-based data capture and data analysis programs, coupled with good thermostatting of solutions. In recently published kinetic studies from Groningen we routinely monitor chemical reactions for up to six half-lives leading to rate constants having standard errors of better than 1%. This precision is important in the determination of standard enthalpies ($\Delta^{\ddagger}H^0$) and entropies ($\Delta^{\ddagger}S^0$) of activation as defined by Eyring transition-state theory.

Titration microcalorimetry[6] has proved an extremely important technique particularly in the context of our investigations into the properties of surfactants in aqueous solutions. In this technique (see Fig. 1 of ref. 7) a micro-syringe under computer control injects at pre-selected time intervals a small volume (*e.g.* 5×10^{-6} dm^3) of an aqueous solution into another aqueous solution held in the sample cell, volume *ca.* 1.5 cm^3. A reference cell for the systems discussed here contains water. The reference cell is heated, raising the temperature very slowly. The computer-based control system monitors the temperature of reference and sample cells, adjusting the power to heaters of both sample and reference cells in order to hold the two cells at the same temperature. The recorded quantity is the rate of heating of the sample cell over the time required to bring both sample and reference cells on to the same temperature ramp. In effect the outcome is a plot of the ratio $(q/\delta n_j^0)$ {where heat q results from adding δn_j^0 moles of chemical substance j to the solution in the sample cell} against either injection number or concentration of chemical substance j in the sample cell.

The thermodynamic analysis is based on the following set of equations. The extensive state variable enthalpy H for a closed system is defined by the three independent variables, T, p, ξ where ξ describes the composition of the system. Thus,

$$H = H[T,p,\xi] \tag{1}$$

The complete differential of eqn. (1) yields an equation for the change in enthalpy; eqn. (2)

$$\mathrm{d}H = \left(\frac{\partial H}{\partial T}\right)_{p,\xi} \cdot \mathrm{d}T + \left(\frac{\partial H}{\partial p}\right)_{T,\xi} \cdot \mathrm{d}p + \left(\frac{\partial H}{\partial \xi}\right)_{T,p} \cdot \mathrm{d}\xi \tag{2}$$

Then at constant temperature and pressure the heat q recorded by the calorimeter between injection numbers I and $(I+1)$ following injection of δn_j^0 moles of chemical substance j at injection number I is given by eqn. (3).

$$\left[\frac{q}{\delta n_j^0}\right]_I^{I+1} = \left[\left(\frac{\partial H}{\partial \xi}\right)_{T,p} \cdot \frac{\delta \xi}{\delta n_j^0}\right]_I^{I+1} \tag{3}$$

The left-hand side of eqn. (3) is the measured quantity recorded as a function of injection number. Eqn. (3) shows that the measured ratio $(q/\delta n_j^0)$ is given by the product of two terms which are not known *a priori*. We indicate below some important cases where analysis of the thermodynamic properties of the solutions in the sample cells and injected aliquots yields important information concerning a given system, *e.g.* micelle formation.[7] The thermodynamic properties commented on in this review are Gibbsian[8] in that they are generated by differentials of Gibbs energies with respect to the variables T and p.

Aqueous solutions: general properties

Enderby and coworkers[9] using neutron inelastic scattering techniques have published detailed information for the structures of hydrated metal cations and halide ions in aqueous solutions. For cations, the results are in line with the structures predicted on the basis of secondary evidence; *e.g.* ionic mobilities. Thus for Ni^{2+}, the oxygen atom is adjacent to the cation but the $Ni^{2+}\cdots$O–D(H) angle is less than 2π; the water molecules undergo a wagging motion.

For many years there was intense speculation concerning the arrangement of water molecules around, for example, chloride ions. Two models were often proposed; (i) a bifurcated structure such that the water dipole moment is co-linear with the centre of the anion, and (ii) a linear structure for $Cl^-\cdots$H–O(H). The latter turns out to be the favoured structure. However, the systems are quite dynamic in that water molecules in the primary hydration sheath exchange with water molecules in the bulk solvent although the hydrogen-bond dynamics of water molecules in the hydration shell are slow compared to those for pure water.[10]

Again the fact that water is a polar liquid is often stated to account for the fact that apolar molecules such as rare gases and hydrocarbons are sparingly soluble in water. Even here complexities emerge. The solubilities of argon, methane, ethane and butane in cold water are higher than predicted on the basis of the cohesive energy density of water.[11] For almost 50 years the low solubilities of apolar solutes in water were attributed to the loss of entropy by the solvent accompanying enhancement of water–water hydrogen bonding.[12] The structures of solid clathrate hydrates were taken as models for the H-bond structure of water around apolar solutes.

In general terms the standard enthalpy of solution for neutral solute j (*i.e.* gas phase to solution) $\Delta_{\mathrm{sln}}H^0$ is negative (*i.e.* exothermic). But the solution process is dominated by a negative $\Delta_{\mathrm{sln}}S^0$ such that $\Delta_{\mathrm{sln}}G^0 > 0$ where $\left|T\Delta_{\mathrm{sln}}S^0\right| > \left|\Delta_{\mathrm{sln}}H^0\right|$. Interestingly, thermodynamic parameters such as limiting isobaric heat capacities C_{pj}^{∞}(aq) and limiting partial molar volumes V_j^{∞}(aq) for neutral solute j in aqueous solution can be expressed in terms of group contributions, a form of analysis which seemed to support the clathrate hydrate model.[13] A similar clathrate model[14] was advanced for the hydration of alkylammonium salts, $R_4N^+X^-$.

Serious doubt was thrown on the clathrate model (and the general concept of structure making) for hydration of apolar solutes (including alkylammonium salts) by the results of neutron inelastic experiments. Neutron diffraction data for $(CH_3)_4N^+Cl^-$ in aqueous solution show no evidence for enhancement of water–water interactions over that in pure water.[15] The negative entropy change for dissolution of apolar gases apparently arises largely from a pronounced preference for tangentially oriented water O–H groups with respect to the apolar solute rather than from more or stronger H-bonds in the hydrophobic hydration shell. Apart from neutron scattering, supporting evidence comes from MD computer simulations,[16] thermodynamic analyses,[17a] and quantum chemical calculations.[17b] However, 'whether or not the H-bond structure in the

hydrophobic hydration shell is significantly different from that in water?' is a question still not fully answered.[18]

Analysis of the properties of polyfunctional solutes in aqueous solution is not straightforward. In the case of, for example, monosaccharides account must be taken of the possible multitude of conformations for these solutes. Such is the complexity that it is difficult to formulate general rules although we return in a later section to these systems. Similar complexities emerge in the case of aqueous solutions containing proteins.[19]

Intermolecular interactions in water

The properties of aqueous solutions reflect both (i) solute–water interactions, and (ii) solute–solute interactions. Certainly for concentrated solutions the two sets of interactions cannot be considered independent.

In the context of understanding solute–solute interactions the simple calculation described by Robinson and Stokes[20] has considerable merit leading to intermolecular solute–solute centre-to-centre distances d as a function of solute concentration, c_j; eqns. (4) and (5), where c_j is expressed in mol dm^{-3} and N_A is the Avogadro constant.

$$\text{neutral solutes: } d = (10^3 N_A c_j)^{1/3} \quad (4)$$

$$1:1 \text{ salts: } \quad d = (2 \times 10^3 N_A c_j)^{1/3} \quad (5)$$

The results are summarised in Table 1 for solutions prepared

Table 1 Inter-solute distances[a]

c_j/mol dm^{-3}	10^{-4}	10^{-3}	10^{-2}	0.1	1.0	10.0
Neutral solutes (*e.g.* urea) d/nm	26	12	5.4	2.6	1.2	0.55
1:1 Salts (*e.g.* NaCl) d/nm	20	9.4	4.4	2.0	0.94	0.44

[a] The distances are calculated on the basis that each solute molecule (ion) is at the centre of a cube, volume d^3. The difference between calculated distances for a neutral solute and a 1:1 salt is a consequence of the fact that each mole of a 1:1 salt yields, with complete dissociation, 2 moles of ions.

using a simple solute (*e.g.* urea) and using a 1:1 salt. Distance d provides an indication of the number of solvent molecules between solute molecules, a number which dramatically decreases with increase in solute concentration.

A useful concept was introduced by Gurney[21] who identified a cosphere of water around each solute molecule (ion). The organisation of water in the cosphere differs from that in bulk water. Then the properties of real aqueous solutions of neutral molecules (*e.g.* urea) differ from the properties of the corresponding ideal solutions as a consequence of 'communication' through the intervening water molecules between solute molecules plus their cospheres. Quantitatively this communication is described by the Gibbs–Duhem equation which requires that (at fixed T and p) for an aqueous solution containing water (1) and solute (j), the chemical potentials μ_1(aq) and μ_j(aq) are not independent but closely linked.

$$n_1 \mathrm{d}\mu_1(\text{aq}) + n_j \mathrm{d}\mu_j(\text{aq}) = 0 \quad (6)$$

In these terms the extent and nature of the differences between the properties of real and ideal aqueous solutions (at fixed T and p) are a function of the organisation of water in the cospheres. Then for a given solution, molality m_j, the differences between Gibbs energies of real and ideal solutions can be expressed in terms of an excess Gibbs energy G^E. Moreover the latter property for dilute solutions can also be expressed in terms of pairwise solute–solute interaction parameters[22] g_{jj} as shown in eqn. (7) where $m^o = 1$ mol kg^{-1}.

$$G^E = RTg_{jj}(m_j/m^o)^2 \quad (7)$$

Interaction parameter g_{jj} is a member of a family of such parameters which includes volumetric v_{jj}, enthalpic h_{jj} and entropic s_{jj} pairwise interaction parameters. For ideal solutions h_{jj} is zero and so the enthalpy of dilution of a given aqueous ideal solution is zero. This is not the case for real solutions as is readily demonstrated using a titration microcalorimeter. We can compare the recorded traces for two experiments. In both cases the sample cell at the start of the experiment contained water. In one experiment the syringe contained urea(aq); in a second experiment the syringe contained *N*-ethylurea(aq) at the same molality, 0.8 mol kg^{-1}. The point to note is that in terms of the model discussed above (*cf.* Table 1) dilution simply means that the inter-solute distance increases. We find that for urea(aq), separation is *endothermic* whereas for monoethylurea(aq) separation is *exothermic*, showing a dramatic impact on the properties of the solutions by replacing a hydrogen atom in urea by an ethyl group.[23] The latter comments signal the possibility that these pairwise solute–solute interaction parameters can be decomposed into pairwise group–group interaction parameters. Wood and coworkers[24] developed this method of analysis leading to a significant increase in the understanding of the properties of aqueous solutions containing neutral solutes (Savage–Wood Additivity of Group Interactions, SWAG, approach).

Kinetics of organic reactions in water containing inert cosolutes

If a substrate X undergoes spontaneous hydrolysis in very dilute aqueous solutions at fixed temperature and pressure, the (first-order) rate constant k(aq;id) (id = ideal, *i.e.* in the absence of a cosolute) is determined by the standard Gibbs energy of activation, $\Delta^{\ddagger}G^0$.

When an inert cosolute j is added, the rate constant changes reflecting the impact of solute j on the chemical potentials of X in both initial and transition states. The rate constant k(aq) is sensitive to the molality of added solute m_j as determined by the impact of solute j on the hydration properties of solute X in both initial and transition states. The changes in the latter two states depend on the hydration properties of solute j. In addition, account must be taken of the fact that in real solutions properties of the solvent are not ideal. The final equation[25] takes the following form where ϕ is the practical osmotic coefficient for the solvent, molar mass M_1.

$$\ln[k(\text{aq})/k(\text{aq;id})] = (2/RT)[1/m^o]^2 G_c m_j - \phi M_1 m_j \quad (8)$$

Here G_c is a compact representation of the effect of added solute j on the chemical potentials of initial and transition states for reacting solute X. For most dilute aqueous solutions it can be assumed that ϕ is unity. Then $\{\ln[k(\text{aq})/k(\text{aq;id})]\}$ is a linear function of the solute molality m_j such that if added solute lowers the rate constant, G_c is negative. This model was originally tested using kinetic data describing the effects of added monohydric alcohols on the water-catalysed hydrolysis of 1-acyl-1,2,4-triazoles[26] and the effects of added ureas on the neutral hydrolysis of *p*-methoxyphenyl dichloroethanoate,[25] Fig. 1 and 2, respectively.

In both cases kinetic data at low concentrations of cosolute followed patterns in which G_c parameters can be understood in terms of pairwise interactions describing added solute–substrate interactions. With increase in hydrophobicity of both added cosolute and reacting substrate, G_c decreases. Hence in terms of the substrate, the hydration characteristics of the initial state rather than the transition state are important. In the context of the model, interaction between added cosolvent and initial state is envisaged as taking place *via* the cooperative hydrogen-bonding interactions within the solvent; that is *via* cosphere–cosphere communication.

This kinetic analysis of the effects of added solutes is illustrated by kinetic data for the following reactions:

(i) Hydrolysis of [(*p*-nitrophenyl)sulfonyl]methyl perchlorate;[27] Fig. 3.

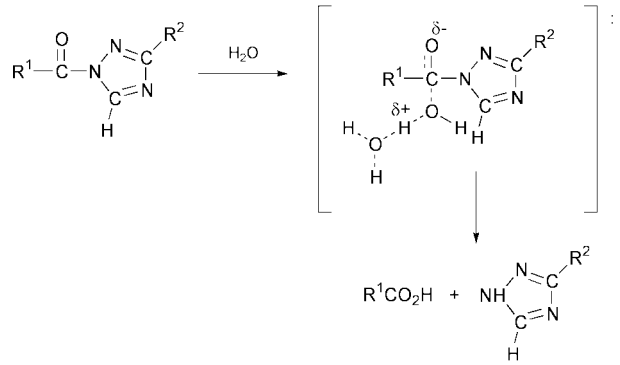

Fig. 1 Neutral hydrolysis of 1-acyl-3-substituted-1,2,4-triazoles.

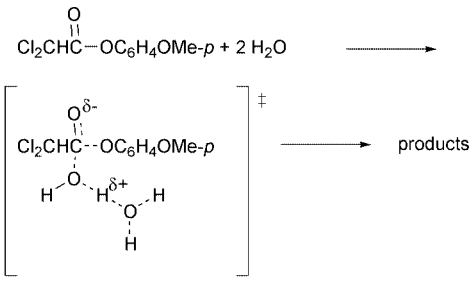

Fig. 2 Mechanism of the water-catalysed hydrolysis of acyl-activated esters.

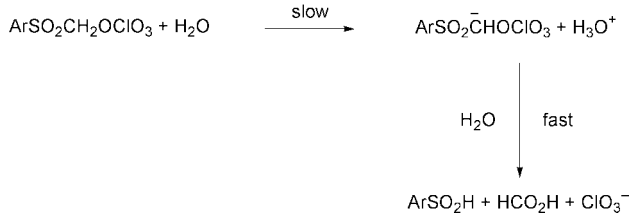

Fig. 3 Water-catalysed hydrolysis of covalent arylsulfonylmethyl perchlorates.

(ii) Hydrolysis of 1-benzoyl-3-phenyl-1,2,4-triazole in aqueous solution containing monohydric alcohols. No alcoholysis of the kinetic probes occurs under the reaction conditions. Group interaction parameters for polyhydric alcohols are strongly dependent on the positions of the hydroxyl groups in the alcohols.[28]

(iii) Hydrolysis of eighteen 1-acyl-(3-substituted)-1,2,4-triazoles in aqueous solutions containing ethanol and propan-1-ol. Although the SWAG analysis is reasonably satisfactory, stereochemical effects also play an important role.[29] The latter feature is also shown by the effects of added monosaccharides on rate constants for hydrolysis of 1-benzoyl-3-phenyl-1,2,4-triazoles.[30]

(iv) For the hydrolysis of *p*-methoxyphenyl dichloroethanoate in aqueous solutions, the elegance of the SWAG approach is shown by the additivity of G_c for carboxamides, ureas, sulfonamides and sulfoxides.[31]

(v) The kinetics of hydrolysis of 1-benzoyl-1,2,4-triazole in aqueous solutions is accounted for in terms of pairwise solute interactions in solution containing amphiphilic solutes below their critical micellar concentrations.[32]

The additivity pattern does break down if salts are added to the solutions in solvents comprising alcohol + water mixtures.

There are interesting and important exceptions to the SWAG additivity concept as shown in the dramatic retardation by added α-phenylalanine of the hydrolysis of activated amides in contrast to the rate acceleration induced by alanine.[33] Similar non-additivity is observed for the effects of isomeric aliphatic α-amino acids on the kinetics of hydrolysis of 2-(4-nitrophenoxy)tetrahydropyran and of alkylammonium salts on the hydrolysis of 1-benzoyl-1,2,4-triazole.[34]

Camouflage effects

Quite generally solutes in aqueous solutions can be classified as either hydrophilic or hydrophobic. However, we noted above that the properties of hydrophilic solutes in aqueous solutions are quite complicated. Indeed the properties of mono- and polyhydroxylated solutes point to key influences of the structure and stereochemistry of the functional groups. This conclusion is confirmed by limiting partial molar volumes and apparent molar isentropic compressions $\phi(K_{Sj};\ \mathrm{def})^{\infty}$ of carbohydrates in aqueous solutions.[35] However we note that $\phi(K_{Sj};\ \mathrm{def})^{\infty}$ is a complicated property[8,36] being for the most part based on an extrathermodynamic assumption.[37]

Hydration of carbohydrates is crucially governed by the relative positions of OH groups in a given carbohydrate. Their hydration characteristics depend on the matching fit between OH-groups in a given carbohydrate and either nearest neighbour (*e.g.* D-talose) or next nearest-neighbour oxygen; Table 2. A

Table 2 Kinetic medium effects and related properties of D-galactose and D-talose in aqueous solutions at 298.15 K

Property	D-galactose	D-talose
$G_c{}^a$/J kg mol^{-2}	−142	−280
$\phi(K_{Sj};\mathrm{def})^{\infty b}$/cm^3 mol^{-1} bar^{-1}	−20.14	−11.9
$n_S{}^c$	8.7	7.7

[a] G_c; see eqn. (6). [b] $\phi(K_{Sj};\mathrm{def})^{\infty}$; defined limiting apparent molar isentropic compression for solute *j* in aqueous solution; see ref. 37. [c] n_h; hydration number.

further feature emerges from analysis of isobaric heat capacity data which can be understood in terms of solute–solute interactions. For a 'probe' solute *j* in an aqueous solution containing a carbohydrate, we might ask how solute *j* 'reacts' to the presence of the carbohydrate. The evidence suggests that if the OH groups of a carbohydrate match into the three-dimensional hydrogen-bond structure of water, solute *j* is unaware of their presence—they have been camouflaged by the solvent. Indeed solute *j* may characterise the carbohydrate solute as hydrophobic.[38] The dependence of the hydration of monosaccharides on the detailed stereochemistry of the OH moieties has also been noted for single-tailed nonionic surfactants with sugar head groups.[39]

Hydrophobic inhibition

The thermodynamic properties of solute X in real solutions containing neutral solute *j* can be described in terms of the activity coefficient of solute X which can in turn be expressed in terms of Gibbs energy interaction parameters. This analysis leads to the description of the effects of added neutral solutes (*e.g.* alcohols) on rate constants for ester hydrolysis in terms of $G(c)$ parameters. This line of argument envisages that the chemical potential of a given solute X in aqueous solution is sensitive to the nature and hydration properties of other solutes by virtue of the communication through intervening water molecules; *i.e.* cosphere–cosphere interactions. This type of explanation is based on the proposal that the properties of a given solute molecule X in solution are perturbed by the sum of individual effects of all other solute molecules in solution.

In an alternative explanation the properties of a given solute molecule X are strongly influenced by intense interaction with a single neighbouring solute molecule *j* in a specific solute–solute interaction. The possibility that the latter model could account for the effects of added solute on the rate of ester hydrolysis was raised by a molecular dynamics simulation.[40]

The latter indicated that an encounter complex[41] involving ester and added solute could be formed. Moreover the cosolute *j* blocks the reaction centre from attack by water in the hydrolysis reaction. In these terms the first-order rate constant for ester hydrolysis $k(m_j)$ in the presence of solute *j*, molality m_j, is related to the equilibrium constant K_{ec} using eqn. (9); (ec = encounter complex).

$$k(m_j) = k(m_j = 0) / [1 + K_{ec}m_j] \quad (9)$$

In the limit that $K_{ec}m_j < 1$, $\ln[k(m_j)]$ is predicted to be a linear function of molality m_j, with slope K_{ec}. Kinetic data for the hydrolysis of three activated esters show that the model accounts satisfactorily for the observed patterns.[42]

Diels–Alder reactions in water

Relatively apolar solutes in aqueous solutions can form encounter complexes which are stabilised by hydrophobic interactions. This can occur for two solutes that can react to form a product if the orientation of both reactions in the encounter complex is suitable for bond making/bond breaking processes. An important example is provided by the formation of an encounter complex that consists of a diene/dienophile pair. The relative stability of the encounter complex in aqueous solution then leads to a rate acceleration compared to the reaction in organic solvents, primarily because the larger number of intermolecular collisions in the complex will favour the cycloaddition reaction. If, in addition to this effect, the activated complex is also stabilised by increased hydrogen-bond interaction relative to the initial state, substantial rate enhancements in water can be realised.[43]

Even in 1931 Diels and Alder used water as a solvent for their famous reaction. However it was the communication by Rideout and Breslow[44] that aroused particular interest in Diels–Alder (DA) reactions and other organic reactions in water. It was reported that the DA reaction of methyl vinyl ketone with cyclopentadiene (CP) was 290 times faster in water than in cyanomethane and that the preference for the *endo* adduct was significantly increased, Fig. 4. Later we found that the second-order rate constant for the DA reaction of 5-methoxy-naphthoquinone with CP was about 1.3×10^4 times higher in water than in *n*-hexane.[43] Detailed examination of aqueous solvent effects on the otherwise solvent-insensitive DA reactions showed that *enforced hydrophobic interactions* between diene and dienophile and *hydrogen bonding* of water to the polarised carbonyl moieties in the activated complex play a major role in the large aqueous rate acceleration.[45] The enhanced preference for the *endo* reaction product (mentioned above) is understood in terms of the smaller solvent accessible surface area for the activated complex leading to this stereoisomer. Computational studies support the interpretation of the beneficial effect of water on these electrocyclic reactions.[46] Aqueous rate acceleration for DA reactions is quite general and has been employed in many synthetic applications. Of course, the magnitude of the effect depends on the contribution of both hydrophobic and hydrogen-bonding interactions.The hydrogen-bonding effect of water can be replaced by Lewis-acid catalysts such as Cu(II) ions with particularly successful applications for bidentate dienophiles,[47] Fig. 5. Relative to the uncatalysed cycloaddition with CP, 0.01 mol dm^{-3} $Cu(NO_3)_2$ in water leads to a rate enhancement of *ca.* 8×10^4. Lewis-acids Ni^{2+}, Co^{2+} and Zn^{2+} are less effective. Water does not enhance the *endo*-selectivity for these reactions, consistent with the view that the stereochemistry is influenced by enforced hydrophobic interactions.

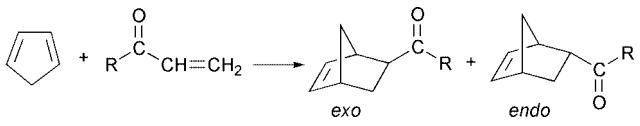

Fig. 4 Diels–Alder reaction of cyclopentadiene with alkyl vinyl ketones.

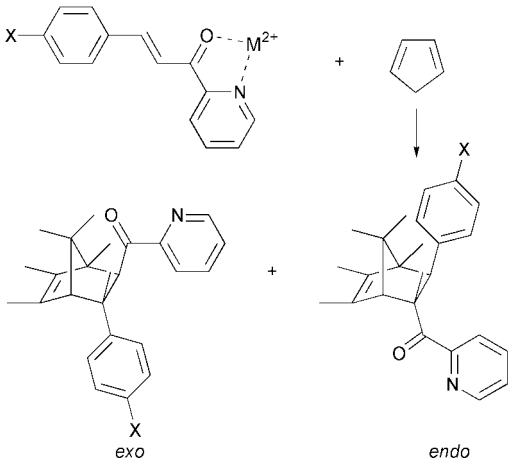

Fig. 5 Lewis-acid catalysed Diels–Alder reaction of 3-*para*-substituted-phenyl-1-(2-pyridyl)-2-propen-1-ones with cyclopentadiene to provide the *endo* (major product) and *exo* (minor product) cycloadducts. (a) X = NO_2, (b) X = Cl, (c) X = H, (d) X = CH_3, (e) X = OCH_3, (f) X = $CH_2SO_3^-$ Na^+, (g) X = $CH_2N^+(CH_3)_3Br^-$.

The same DA reactions have also been performed in the presence of diamine and α-amino acid ligands. Interestingly, ligand-accelerated catalysis of the reaction in the presence of Cu^{2+} ions was observed for a series of (chiral) aromatic α-amino acid ligands. In the case of N^{α}-methyl-L-tryptophan, 74% enantioselectivity was found. Smaller selectivities were found when organic solvents were used. The enhanced catalytic effect and the enantioselectivity are consistent with arene–arene interactions between the pyridine ring[48] of the dienophile and the aromatic ring of the α-amino acid ligand bound to Cu^{2+}, Fig. 6.

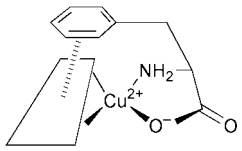

Fig. 6 Ligand-induced hydrophobic bonding of the Lewis acid to the dienophile.

Combination of Lewis-acid catalysis with micellar catalysis leads to exceptionally efficient catalysis.[49] For example, the DA reaction with copper didodecyl sulfate micelles shows a rate acceleration of 1.8×10^6, again compared to the uncatalysed cycloaddition in cyanomethane. The major factor responsible for this huge catalytic effect is the essentially complete complexation of the dienophile to the Cu^{2+} ions at the surface of the micelles. A similar vesicular-catalysed reaction is somewhat less effective (rate acceleration *ca.* 10^6), but the maximum catalytic effect is obtained at significantly lower surfactant concentration, which is important from the view point of 'green chemistry'.[50] Lewis-acid–surfactant-combined catalysts have a definite potential for green organic synthesis in aqueous media as demonstrated by Kobayashi *et al.* for several carbon–carbon bond-forming reactions.[51] The detailed studies of the aqueous rate accelerations of DA reactions have set the stage for extensive application of organic synthesis in water.[50]

Surfactant aggregation

Micelles

The story is told[52] how McBain's original proposal[53] concerning the possibility that surfactants might aggregate in water above a critical micellar concentration was met with the reply, 'Nonsense, McBain'. Of course it is now recognised that in

aqueous solutions up to 100 monomer surfactant monomers may associate to form micelles. Nevertheless the actual structure of micelles is still a matter for debate.

Interest in these systems not only stems from their use in detergent formulations but also for their general ability to solubilise chemical substances in aqueous systems and to act as catalysts for their chemical reactions. Thermodynamic description of the equilibrium between micelles and monomers in solutions is generally based on one of two models, both recognising that micelle formation is a strongly cooperative process, with hydrophobic interactions as the major driving force.[54]

According to the closed association model, a chemical equilibrium exists between monomers and micelles. This is the mass action model.[55] Thus if N is the aggregation number for surfactant S,

$$N\mathrm{S(aq)} \rightleftharpoons \mathrm{S}_N\mathrm{(aq)} \quad (10)$$

Hence, the equilibrium constant is,

$$K = [\mathrm{S}_N\mathrm{(aq)}]/[\mathrm{S(aq)}]^N \quad (11)$$

Numerical analysis shows that with an increase in aggregation number N and with increase in concentration of surfactant, the change in composition of the solution at the critical micellar concentration becomes sharper.

According to the phase separation model,[54] micelles form a separate phase in the aqueous system with surfactant in the micellar phase in equilibrium with surfactant in aqueous solution at the critical micellar concentration. Thus the equilibrium for surfactant j is described as follows; c_r = 1 mol dm^{-3}.

$$\mu^*(\mathrm{micelle};N\mathrm{S}) = N[\mu^0(\mathrm{aq}) + RT\ln(\mathrm{cmc}/c_r)] \quad (12)$$

Then the standard Gibbs energy for micelle formation $\Delta_{mic}G^o$(aq) is given by the following equation.

$$\Delta_{mic}G^o(\mathrm{aq}) = \mu^*(\mathrm{micelle};\ N\mathrm{S}) - N\mu^0(\mathrm{aq}) = NRT\ln(\mathrm{cmc}/c_r) \quad (13)$$

The right-hand site of eqn. (13) contains two important quantities, N and cmc of which only the cmc is readily determined. This point signals that there are complications in the thermodynamic analysis of micellar systems.[56] The way ahead defines a standard Gibbs energy of micelle formation per monomer, $\Delta_{mic}G^o$(aq;mon) [$= \Delta_{mic}G^o(\mathrm{aq})/N$].

Then,

$$\Delta_{mic}G^o(\mathrm{aq;mon}) = RT\ln(\mathrm{cmc}/c_r) \quad (14)$$

If the monomer surfactant is a 1:1 salt (*e.g.* hexadecyltrimethylammonium bromide; CTAB) then the standard Gibbs energy of micelle formation per monomer is given by the following equation.

$$\Delta_{mic}G^o(\mathrm{aq;mon}) = \Delta_{mic}H^o(\mathrm{aq;mon}) - T\Delta_{mic}S^o(\mathrm{aq;mon}) = 2RT\ln(\mathrm{cmc}/c_r) \quad (15)$$

Here $\Delta_{mic}H^o$(aq;mon) is the standard enthalpy of micelle formation per monomer. We have used the latter two equations in an extensive study of the thermodynamics of micelle formation using a titration microcalorimeter. In these experiments the syringe contains an aqueous solution of, for example, CTAB, at a concentration above the cmc whereas the sample cell contains, initially, water. Over the first set of injections of aliquots, the calorimeter records the heat associated with the break up (*i.e.* deaggregation) of the injected micelles to form monomers.[57] However gradually the concentration of surfactant in the sample cell increases, eventually approaching the cmc. At this stage the recorded heat is close to zero in that a micellar solution is being injected into a micellar solution. The resulting plot, an enthalpogram, of the ratio $[q/\delta n_j^0]$ against injection number I is step-shaped such that the ratio $[q/\delta n_j^0]$ effectively yields the enthalpy of micelle formation because $[q/\delta n_j^0]$ at high injection numbers is close to zero. A more detailed analysis takes account of the fact that CTAB is a 1:1 salt. The cmc is calculated using the van Os method[58] in which $\sum_{I=1}^{I=N}[q/\delta n_j^0]$ is plotted against the concentration of CTAB in the sample cell at injection number N. The points generate two straight lines which intersect at a point corresponding to the cmc.

With decreasing alkyl chain length (*e.g.* C_{16} to C_{10} trimethylammonium bromide) the enthalpograms become more complicated indicating that account has to be taken of the thermodynamic properties of the monomer salt and ionic micelles together with the extent of counter ion binding.[59]

An interesting study exploited the structural variations in the cation using 1-alkyl-4-pyridinium surfactants in aqueous solutions.[60] For 1-alkyl-4-methylpyridinium halides, the standard enthalpy of micelle formation becomes more exothermic with an increase in alkyl chain length by -2.6 ± 0.2 kJ mol^{-1} per CH_2 group at 303 K. For 1-methyl-4-*n*-dodecylpyridinium surfactants prepared using aromatic counter ions, the enthalpograms point to different degrees of penetration of the counter anions into the cationic micelles.[61]

Interpretation of the enthalpograms generated by different surfactants is often complicated by the fact that enthalpies of micelle formation are strongly temperature dependent leading in some cases to a change in sign of the standard enthalpy of micelle formation.

In fact there are further complications as shown by the change in sign of the enthalpy of micelle deaggregation of CTAB(aq) when pentanol is added.[62] Titration calorimetric data for non-ionic carbohydrate-derived surfactants[63] show interesting but complicated patterns in the contributions to standard Gibbs energies and enthalpies of micelle formation. A similar comment applies to aqueous solutions containing alkylpolyoxyethylene glycol ethers.[64] The enthalpograms are complicated by the presence of two processes when aliquots are injected into the sample cell, namely micelle deaggregation and declustering of micellar aggregates. The impact of additional methylene groups in the alkyl chain on going from CTAB to octadecyltrimethylammonium bromide is dramatic. The enthalpograms show that the sign of deaggregation changes with a change in concentration of surfactant in the injected aliquots, again pointing to the influence of micellar aggregation.

Analysis of the enthalpograms for mixed alkyltrimethylammonium bromide surfactants turns out not to be straightforward.[65] The effective cmc of a given mixture, as signalled by an enthalpogram, is a function of the mixture concentration. The mixed micellar phase is treated as resembling a binary liquid mixture characterised by rational activity coefficients for both components together with enthalpic interaction parameters treated along the lines used in the treatment of binary liquid mixtures.[66] Monomer–monomer surfactant interaction in both aqueous solution and mixed micellar phase are important in determining the properties of a mixed surfactant. For solutions containing high concentrations of surfactants, the presence of large aggregates is confirmed by a DSC scan for concentrated aqueous solutions of hexadecyltrimethylammonium bromide and chloride.[67]

Vesicles

Whether a surfactant molecule preferentially undergoes molecular assembly to form a micelle or a (closed) bilayer, depends, in a first approximation, on the architecture of the amphiphilic molecule.[68] This shape-dependent association signals a tendency for the most efficient intermolecular overlap of hydrophobic hydration shells with a maximum release of these water molecules to the bulk aqueous solution. The thermodynamics of vesicle formation have also been examined using a titration microcalorimeter.[69] The results emphasise the importance of the nature of the counter ion and reveal a large temperature dependence of the enthalpy of vesiculation as anticipated for a

process involving hydration shell overlap.Gel-to-liquid crystalline phase transitions in vesicular bilayers can be studied using a differential scanning microcalorimeter.[70] The design of the latter is similar to that for a titration microcalorimeter except that the syringe system is absent and the sample cell sealed under nitrogen gas. Both cells are gradually heated from 5 to 90 °C under computer control. The system records the differential amounts of heat required to raise together the temperatures of sample and reference cells. A plot is obtained of the relative isobaric heat capacity of a given vesicular aqueous system as a function of temperature. These scans are extremely informative concerning the factors controlling the thermal characteristics of vesicular bilayers. We have concentrated attention on two classes of vesicular systems, dialkyldimethylammonium bromides[71] (*e.g.* DOAB = di-*n*-octadecyldimethylammonium bromide) and sodium dialkylphosphates[72] (*e.g.* DDP = sodium di-*n*-dodecyl phosphate).

The DSC experiments show that the transitions responsible for extrema in isobaric heat capacities involve patches of between 100 and 200 monomers which melt cooperatively. The extent of cooperative melting in each patch involves but a small fraction of the total number of monomers in each vesicle. The melting temperature (as revealed by the maximum in isobaric heat capacity) depends on the vesicle both in terms of the dialkyl component and the counter ion.[72] The melting has a dynamic feature. For some vesicular systems no extremum in isobaric heat capacity is detected in the second scan if the latter is recorded shortly after the first. In other words there is an element of kinetic control to the repacking of the dialkyl chains forming the gel state from the liquid crystal state.[73]

DSC scans for mixed vesicular systems indicate that when the differences in alkyl chain lengths are small, the chains can assemble in reasonably ordered fashion leading to well defined features in the DSC scans. When the lengths of the dialkyl chains differ considerably, the DSC scans are complicated indicative of domains having different compositions; *cf.* partial miscibility.[74]

For vesicles formed by a series of three sodium dialkylphosphates having identical chain lengths, their thermal stability is strongly dependent on the degree of unsaturation in the alkyl chains. In general, vesicles are stabilised by alkyl–alkyl group cohesion and destablised by charge–charge interactions in the ionic head groups. The thermal stability of the bilayers is very sensitive to added salt,[75a] and other cosolutes including surfactants,[75b] α-amino acids,[75c] sodium dipicolinate[75d] and poly(sodium acrylate)s.[75e]

Conclusion and outlook

Chemical reactions and aggregation processes in water are strongly determined by the properties of the aqueous medium, *i.e.* by the three-dimensional hydrogen-bond network that combines strongly intermolecular interactions with low density. Because water molecules are small and each molecule can form up to four hydrogen bonds (twice as a donor and twice as an acceptor), changes in the H-bond network are associated with large entropy changes (often largely compensated by changes in enthalpy) and with large temperature effects. There appears to be little doubt that in the coming years the unique solvent properties of water will be frequently employed for tuning of desired chemical processes. In particular hydrophobic interactions provide rich possibilities for this purpose. Mother Nature was the first to recognise the potential of such medium-induced control of chemical reactivity.

Acknowledgements

We are much indebted to our coworkers, mentioned in the references, for their enthusiasm and important contributions to the work discussed herein. Special thanks are due to Niek Buurma for his help in processing the manuscript.

Notes and references

1 S. Allan, *The Way of Water and Sprouts of Virtue*, State University of New York Press, Albany, New York, 1997, p. 24.
2 *Water: A Comprehensive Treatise*, ed. F. Franks, Vol. 1–7, 1973–1982, Plenum Press, New York.
3 D. Eisenberg and W. Kauzmann, *The Structure and Properties of Water*, Oxford University Press, 1969.
4 Ch. Reichardt, *Chem. Rev*., 1994, **94**, 2319; a useful discussion of linear solvation energy relationships, allowing a sensible comparison of water with organic solvents, is given in: M. J. Kamlet, J. L. M. Abboud, M. H. Abraham and R. W. Taft, *J.Org.Chem*., 1983, **48**, 2877.
5 M. J. R. Dack, *Chem. Soc Rev*., 1975, **4**, 211.
6 T. Wiseman, S. Williston, J. E. Brands and L.-N. Lim, *Anal. Biochem*., 1987, **179**, 131; M. J. Blandamer, *Biocalorimetry: Applications of Calorimetry in the Biological Sciences*, ed. J. Ladbury and B. Z. Chowdhry, Wiley, Chichester, 1998, ch.1.
7 M. J. Blandamer, P. M. Cullis and J. B. F. N. Engberts, *J. Chem. Soc., Faraday Trans*., 1998, **94**, 2261.
8 J. C. R. Reis, M. J. Blandamer, M. I. Davis and G. Douheret, *Phys. Chem. Chem. Phys*., 2001, **3**, 1465.
9 J. Enderby, *Chem. Soc. Rev*., 1995, **95**, 159; G. W. Neilson and J. E. Enderby, *Adv. Inorg. Chem*., 1989, **34**, 195; J. E. Enderby and G. W. Neilson, *Rep. Prog. Phys*., 1981, **44**, 38.
10 N. A. Hewish, J. E. Enderby and W. S. Howells, *J. Phys. C. Solid State Phys*., 1983, **16**, 1777; M. F. Kropman and H. J. Baker, *Science*, 2001, **291**, 2118.
11 D. Mirejovsky and E. M. Arnett, *J. Am. Chem. Soc*., 1983, **105**, 1112.
12 H. S. Frank and W.-Y. Wen, *Discuss. Faraday Soc*., 1957, **24**, 133; For another extensive set of data and an interesting analysis, see: M. H. Abraham, *J. Am. Chem. Soc*., 1982, **104**, 2085.
13 S. Cabani, P. Gianni, V. Mollica and L. Lepori, *J. Solution Chem*., 1981, **10**, 563; G. Perron and J. E. Desnoyers, *Fluid Phase Equilib*., 1979, **2**, 239; E. M. Arnett, W. B. Kover and J. V. Carter, *J. Am. Chem. Soc*., 1969, **91**, 4028.
14 R. McMullan and G. A. Jeffrey, *J. Chem. Phys*., 1959, **31**, 1231.
15 J. Turner, A. K. Soper and J. L. Finney, *Mol. Phys*., 1992, **77**, 441.
16 B. Guillot, Y. Guissani and S. Bratos, *J. Chem. Phys*., 1991, **95**, 3643.
17 (*a*) G. Graziano, *J. Chem. Soc., Faraday Trans*., 1998, **94**, 3345; (*b*) A. Bagno, *J. Chem. Soc., Faraday Trans*., 1998, **94**, 2501.
18 K. A. T. Silverstein, A. D. J. Haymet and K. A. Dill, *J. Am. Chem. Soc*., 2000, **122**, 8037.
19 T. H. Lilley, *Water Sci. Rev*., 1990, **5**, 137.
20 R. A. Robinson and R. H. Stokes, *Electrolyte Solutions*, Butterworth, London, 1959, 2nd revised edn., p. 15.
21 R. W. Gurney, *Ionic Processes in Solution*, McGraw-Hill, New York, 1953.
22 W. McMillan and J. Mayer, *J. Chem. Phys*., 1945, **13**, 176.
23 M. J. Blandamer, M. D. Butt and P. M. Cullis, *Thermochim. Acta*, 1992, **211**, 49.
24 J. J. Savage and R. H. Wood, *J. Solution Chem*., 1976, **5**, 733; S. K. Suri and R. H. Wood, *J. Solution Chem*., 1986, **15**, 705 and references therein.
25 W. Blokzijl, J. B. F. N. Engberts, J. Jager and M. J. Blandamer, *J. Phys. Chem*., 1987, **91**, 6022.
26 W. Blokzijl, J. Jager, J. B. F. N. Engberts and M. J. Blandamer, *J. Am. Chem. Soc*., 1986, **108**, 6411.
27 S. A. Galema, M. J. Blandamer and J. B. F. N. Engberts, *J. Org. Chem*., 1989, **54**, 1227.
28 W. Blokzijl, J. B. F. N. Engberts and M. J. Blandamer, *J. Am. Chem. Soc*., 1990, **112**, 1197.
29 J. B. F. N. Engberts and M. J. Blandamer, *J. Phys. Org. Chem*., 1998, **11**, 841.
30 S. A. Galema, M. J. Blandamer and J. B. F. N. Engberts, *J. Org. Chem*., 1992, **57**, 1995.
31 R. P. V. Kerstholt, J. B. F. N. Engberts and M. J. Blandamer, *J. Chem. Soc., Perkin Trans. 2*, 1983, 49.
32 W. H. Noordman, W. Blokzijl, J. B. F. N. Engberts and M. J. Blandamer, *J. Org. Chem*., 1993, **58**, 7111.
33 L. Streefland, M. J. Blandamer and J. B. F. N. Engberts, *J. Phys. Chem*., 1995, **79**, 5769.
34 L. Streefland, M. J. Blandamer and J. B. F. N. Engberts, *J. Chem. Soc., Perkin Trans. 2*, 1997, 769; P. Hol, L. Streefland, M. J. Blandamer and J. B. F. N. Engberts, *J. Chem. Soc., Perkin Trans. 2*, 1997, 485.
35 S. A. Galema, J. B. F. N. Engberts, H. Hoiland and G. M. Forland, *J. Phys. Chem*., 1993, **87**, 6885.

36 M. J. Blandamer, M. I. Davis, G. Douheret and J. C. R. Reis, *Chem. Soc. Rev*., 2001, **30**, 8.
37 M. J. Blandamer, *J. Chem. Soc., Faraday Trans*., 1998, **94**, 1057.
38 S. A. Galema, E. Howard, J. B. F. N. Engberts and J. R. Grigera, *Carbohydrate Res*., 1994, **265**, 215.
39 H. A. van Doren, S. A. Galema and J. B. F. N. Engberts, *Langmuir*, 1995, **11**, 687.
40 M. F. Lensink, J. Mavri and H. J. C. Berendsen, *J. Comput. Chem*., 1999, **20**, 886.
41 W. Blokzijl and J. B. F. N. Engberts, *Angew. Chem., Int. Ed. Engl*., 1993, **32**, 1545.
42 N. J. Buurna, L. Pastorello, M. J. Blandamer and J. B. F. N. Engberts, submitted for publication.
43 W. Blokzijl, M. J. Blandamer and J. B. F. N. Engberts, *J. Am. Chem. Soc*., 1991, **113**, 4241; W. Blokzijl and J. B. F. N. Engberts, *J. Am. Chem. Soc*., 1992, **114**, 5440.
44 R. Breslow and D. Rideout, *J. Am. Chem. Soc*., 1980, **102**, 7816.
45 S. Otto and J. B. F. N. Engberts, *Pure Appl. Chem*., 2000, **72**, 1365.
46 J. F. Blake and W. L. Jorgensen, *J. Am. Chem. Soc*., 1991, **113**, 7430; J. F. Blake, L. Dongchul and W. L. Jorgensen, *J. Org. Chem*., 1994, **59**, 803; S. Kong and J. D. Evanseck, *J. Am. Chem. Soc*., 2000, **122**, 10418.
47 S. Otto, F. Bertoncin and J. B. F. N. Engberts, *J. Am. Chem. Soc*., 1996, **118**, 7702.
48 S. Otto and J. B. F. N. Engberts, *J. Am. Chem. Soc*., 1999, **121**, 6798.
49 S. Otto, J. B. F. N. Engberts and J. C. T. Kwak, *J. Am. Chem. Soc*., 1998, **120**, 9517.
50 T. Rispens and J. B. F. N. Engberts, *Org. Lett*., 2001, 941; for general references, see: (i) *Organic Synthesis in Water*, ed. P. A. Grieco, Blackie, Thomson Science, London, 1998; (ii) C.-J. Li and T.-H. Chan, *Organic Reactions in Aqueous Media*, Wiley, New York, 1997.
51 K. Manabe, Y. Mori, T. Wakabayashi, S. Nagayama and S. Kobayashi, *J. Am. Chem. Soc*., 2000, **122**, 7202.
52 F. M. Menger, *Acc. Chem. Res*., 1979, **12**, 111.
53 J. W. McBain, *Trans. Faraday Soc*., 1913, **9**, 99.
54 D. F. Evans and H. Wennerstrom, *The Colloidal Domain*, VCH, New York, 1994.
55 A. H. Roux, D. Hetu, G. Perron and J. E. Desnoyers, *J. Solution Chem*., 1984, **13**, 1.
56 M. J. Blandamer, P. M. Cullis, L. G. Soldi, J. B. F. N. Engberts, A. Kacperska, N. M. van Os and M. C. S. Subha, *Adv. Colloid Interface Sci*., 1995, **58**, 171.
57 M. J. Blandamer, P. M. Cullis and J. B. F. N. Engberts, *Pure Appl. Chem*., 1996, **68**, 1577.
58 N. M. van Os, G. J. Daane and G. Haandrikman, *J. Colloid Interface Sci*., 1991, **141**, 199.
59 K. Bijma, J. B. F. N. Engberts, M. J. Blandamer, P. M. Cullis, P. M. Last, K. D. Irlam and L. G. Soldi, *J. Chem. Soc., Faraday Trans*., 1997, **93**, 1579.
60 K. Bijma, J. B. F. N. Engberts, G. Haandrikman, N. M. van Os, M. J. Blandamer, M. D. Butt and P. M. Cullis, *Langmuir*, 1994, **10**, 2578.
61 K. Bijma, M. J. Blandamer and J. B. F. N. Engberts, *Langmuir*, 1998, **14**, 79.
62 T. Mehhrian, A. de Keizer, A. J. Korteweg and J. Lyklema, *Colloids Surf., A. Physiochem. Eng. Asp*., 1993, **71**, 255.
63 J. M. Pestman, J. Kevelam, M. J. Blandamer, H. A. van Doren, R. M. Kellogg and J. B. F. N. Engberts, *Langmuir*, 1999, **15**, 2009.
64 M. J. Blandamer, B. Briggs, P. M. Cullis, J. B. F. N. Engberts and J. Kevelam, *Phys. Chem. Chem. Phys*., 2000, **2**, 4369.
65 M. J. Blandamer, B. Briggs, P. M. Cullis and J. B. F. N. Engberts, *Phys. Chem. Chem. Phys*., 2000, **2**, 5146.
66 E. A. Guggenheim, *Mixtures*, Clarendon Press, Oxford, 1952.
67 M. J. Blandamer, B. Briggs, H. R. Brown, J. Burgess, M. D. Butt, P. M. Cullis and J. B. F. N. Engberts, *J. Chem. Soc., Faraday Trans*.,1992, **88**, 979.
68 For a detailed discussion, see: J. Israelachvili, *Intermolecular and Surface Forces*, Academic Press, London, 2nd edn., 1992, p. 380.
69 J. M. de Gooyer, J. B. F. N. Engberts and M. J. Blandamer, *J. Colloid Interface Sci*., 2000, **224**, 4.
70 M. J. Blandamer, B. Briggs, P. M. Cullis and J. B. F. N. Engberts, *Chem. Soc. Rev*., 1995, 253.
71 M. J. Blandamer, B. Briggs, P. M. Cullis, J. A. Green, M. Waters, L. G. Soldi, J. B. F. N. Engberts and D. Hoekstra, *J. Chem. Soc., Faraday Trans*., 1992, **88**, 3431.
72 M. J. Blandamer, B. Briggs, P. M. Cullis, J. B. F. N. Engberts, A. Wagenaar, E. Smits, D. Hoekstra and A. Kacperska, *Langmuir*, 1994, **10**, 3507.
73 M. J. Blandamer, B. Briggs, P. M. Cullis, S. D. Kirby and J. B. F. N. Engberts, *J. Chem. Soc., Faraday Trans*., 1997, **93**, 453.
74 M. J. Blandamer, B. Briggs, P. M. Cullis, J. B. F. N. Engberts, A. Wagenaar, E. Smits, D. Hoekstra and A. Kacperska, *J. Chem. Soc., Faraday Trans*., 1994, **90**, 2709.
75 (*a*) M. J. Blandamer, B. Briggs, P. M. Cullis, J. B. F. N. Engberts and D. Hoekstra, *Thermochim. Acta*, 1994, **247**, 341; (*b*) M. J. Blandamer, B. Briggs, P. M. Cullis, J. B. F. N. Engberts and A. Kacperska, *J. Chem. Soc., Faraday Trans*., 1995, **91**, 4275; (*c*) M. J. Blandamer, B. Briggs, P. M. Cullis, K. D. Irlam, J. B. F. N. Engberts and L. Streefland, *Thermochim. Acta*, 2000, **364**, 173; (*d*) M. J. Blandamer, B. Briggs, M. D. Butt, P. M. Cullis, M. Waters, J. B. F. N. Engberts and D. Hoekstra, *J. Chem. Soc., Faraday Trans*., 1994, **90**, 727; (*e*) J. Kevelam, J. B. F. N. Engberts, M. J. Blandamer, B. Briggs and P. M. Cullis, *Colloid Polym. Sci*., 1998, **276**, 190.

CHEMCOMM Communication
www.rsc.org/chemcomm

Difluoromethylene analogues of aspartyl phosphate: the first synthetic inhibitors of aspartate semi-aldehyde dehydrogenase

Russell J. Cox,*[a] Andrea T. Hadfield[b] and M. Belén Mayo-Martín[a]

[a] *School of Chemistry, University of Bristol, Cantock's Close, Bristol BS8 1TS, UK. E-mail: r.j.cox@bris.ac.uk*
[b] *Department of Biochemistry, University of Bristol, Bristol BS8 1TD, UK*

Received (in Cambridge, UK) 3rd May 2001, Accepted 12th July 2001
First published as an Advance Article on the web 10th August 2001

The difluoromethylene analogue of aspartyl phosphate 6 has been prepared by the fluoride catalysed coupling of diethyl trimethylsilyldifluoromethyl phosphonate with an appropriate aldehyde followed by Dess–Martin oxidation and deprotection; the deprotected compound inhibited (K_I 95 μM) aspartate semi-aldehyde dehydrogenase, a key enzyme involved in bacterial amino acid and peptidoglycan biosynthesis.

Bacterial resistance to current classes of antibacterial compounds is increasing alarmingly.[1,2] Many successful antibiotics target bacterial cell wall biosynthesis, and the efforts of our group have concentrated on attempts to design and synthesise inhibitors of enzymes from this pathway.[3] We have focussed on inhibitors of L-lysine **1** biosynthesis since L-lysine and its precursor, diaminopimelic acid (DAP), form the strength bearing cross-links of the peptidoglycan layer of bacterial cell walls (Scheme 1).[4] One of the earliest enzymes on the pathway, aspartate semi-aldehyde dehydrogenase (ASA-DH, EC 1.2.1.11) forms the key intermediate L-aspartate semi-aldehyde **2** the precursor of DAP and also L-threonine **3** and L-methionine **4**. Inhibitors of ASA-DH would therefore block dual key bacterial metabolic processes forming proteins and peptidoglycan.

The mechanism of ASA-DH is believed to involve an active site nucleophilic cysteine.[5] γ-Aspartyl phosphate **5**, is bound at the active site. Thiolester formation then occurs with concomitant loss of phosphate. NADPH then transfers its 4-*proS* hydride to reduce the thiolester, releasing the aspartate semi-aldehyde **2** and regenerating the nucleophile (Scheme 1). The 3D crystal structure of ASA-DH has recently been solved, but as no substrates were bound in the structure little information is available regarding the active site geometry and potential binding sites.[6] We decided to synthesise specific ASA-DH inhibitors. Ideally these compounds would mimic the natural substrate and contain an electrophillic centre for covalent attachment to the active site nucleophile.

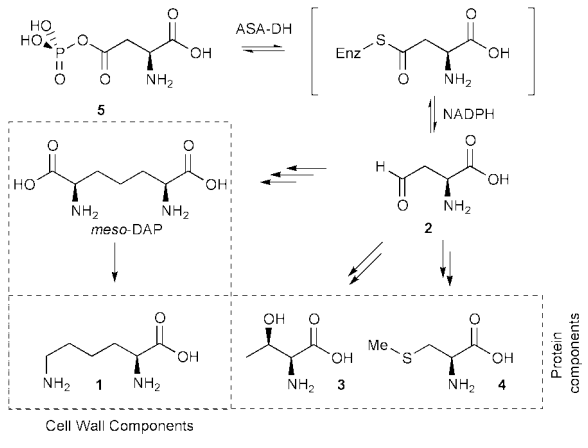

Scheme 1 Bacterial pathways to cell wall and protein components.

Difluoromethylene phosphonates have found use as phosphate mimics in numerous applications.[7] The difluoromethylene unit effectively mimics oxygen and the pK_a of difluoromethylene phosphonates closely matches that of the analogous phosphates.[8] Compounds such as **6** could form effective inhibitors of ASA-DH. Additionally the difluoromethylene α to the carbonyl would have the effect of making it an excellent electrophile and likely target for thiol attachment.

Berkowitz has reacted difluoromethylene anions such as **7** with methyl esters to prepare ketones directly.[9] We attempted to follow this methodology for the synthesis of **6** (Scheme 2). L-Aspartic acid **8** was selectively protected at the γ-ester using methanol and thionyl chloride to form the mono ester **9**. BOC protection to give **10** followed by formation of the α-*tert*-butyl ester then gave the required methyl ester **11**. However this ester was unreactive under the reaction conditions of Berkowitz[9] and we considered that the mono-protected amine could be the source of an acidic proton. Formation of the doubly BOC protected aspartate **12** was achieved, but this also could not be transformed to the required phosphonate. The bis(methyl ester) **13** was also synthesised by parallel methodology, but was similarly unreactive towards anion **7**.

We next attempted to add **7** to aldehydes (Scheme 3).[10] Treatment of **13** with DIBAL-H yielded a mixture of the corresponding alcohol **14** (22%) and aldehyde **15** (68%);[11] **14** could be converted to **15** by treatment with the Dess–Martin periodinane.[12,13] When **15** was treated with excess **7** (*ca.* 7.5 eq.) at −78 °C we were able to isolate the mixture of diastereomers **16a** and **16b** in very low yield—no products were

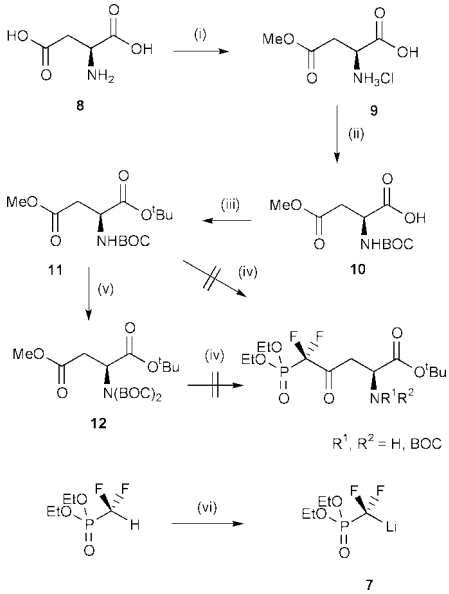

Scheme 2 *Reagents and conditions*: (i) $SOCl_2$, MeOH, −10 °C, 78%; (ii) BOC_2O, $NaHCO_3$–MeOH, 75%; (iii) $(CH_3)_3COH$, DMAP, EDCI, 64%; (iv) **7**, THF, −78 °C–0 °C; (v) NaH, BOC_2O, THF, Δ, 86%; (vi) LDA, −78 °C–0 °C.

 DOI: 10.1039/b103988c

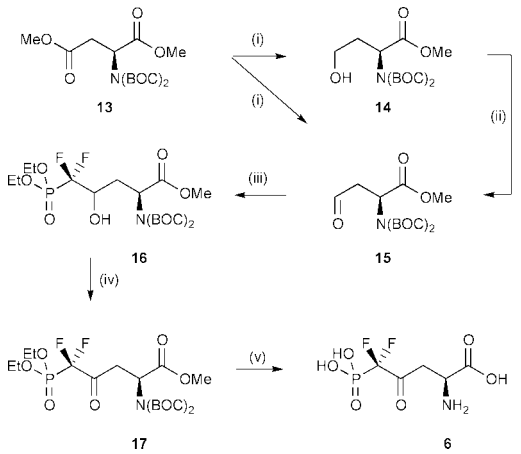

Scheme 3 *Reagents and conditions*: (i) DIBAL-H, THF, −78 °C, 68%; (ii) Dess–Martin periodinane, CH_2Cl_2, RT, 75%; (iii) $(EtO)_2P(O)CF_2SiMe_3$, THF, 10 mol% TBAF, −60 °C RT, 55%; (iv) Dess–Martin periodinane, CH_2Cl_2, RT, 69%; (v) TMSI, then aq. KOH, then Dowex AG50 WX8, 95%.

formed with lower excesses or stoichiometric amounts of **7**. Under milder conditions treatment of **15** with $(EtO)_2P(O)CF_2SiMe_3$ in THF at 0 °C in the presence of a catalytic fluoride source such as CsF, TBAF or TBAT ($Bu_4N^+SiPh_3F_2^-$) yielded the required products. The most favourable conditions required the use of 1.3 eq. of $(EtO)_2P(O)CF_2SiMe_3$, 10 mol% TBAF and one equivalent of **15**. This reaction yielded a mixture of diastereomers **16a** (2*S*,4*S*) and **16b** (2*S*,4*R*)[14] in 3 : 1 ratio in overall 55% (Scheme 3) with the remaining mass balance being unreacted aldehyde. The alcohols were smoothly converted to the ketone **17**. A two-step deprotection involving treatment of **17** with 5 eq. of TMSI (Me_3SiI) followed by KOH treatment to remove the methyl ester yielded **6** in excellent yield as a 45 : 55 mixture of keto- and hydrate forms.[15] After purification by ion exchange chromatography, **6** was used in inhibition assays using recombinant *E. coli* ASA-DH.

The ASA-DH assay (Scheme 4) requires that the enzyme be run in the 'reverse' direction as aspartyl phosphate is unavailable whereas aspartate semi-aldehyde is obtained by reductive ozonolysis of allyl glycine in 1 M aqueous HCl. In the assay, reaction is observed at 340 nm as NADPH is formed from $NADP^+$ (150 μM). In order to ensure satisfactory reaction rates the other substrates (PO_4^{3-} and ASA) must be present in large excess (15 and 0.35 mM respectively). In initial inhibition reactions under these conditions **6** showed little observable effect. However in pre-incubation reactions in which ASA-DH was incubated with **6** *prior* to addition of the other assay components clear inhibition was observable varying with time (Fig. 1A) and concentration (Fig 1B). Based on this assay a K_I of 95 μM was measured.[16] The rate of inhibition of ASA-DH by **6** was diminished in the presence of phosphate (Fig. 1B) indicating that inhibition occurs at the active site. The inhibition appears to be slowly reversible as indicated by the regeneration of activity upon dilution of the inhibited enzyme into the assay cuvette. This behaviour is consistent with that expected for a slow binding model of inhibition and is most likely caused by covalent bond formation between **6** and the active site thiol of ASA-DH.

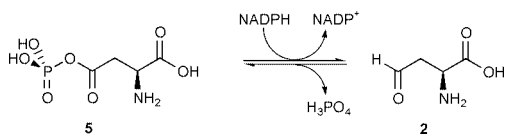

Scheme 4 Assay of ASA-DH. In the reverse reaction phosphate and ASA are present in large excess.

Thus we have shown that a rational approach can successfully be used for the design and synthesis of ASA-DH inhibitors. The route should enable the synthesis of a range of related compounds designed to probe the mechanism and active

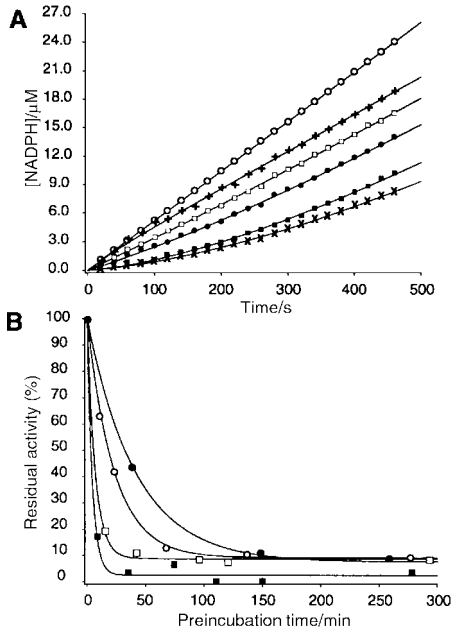

Fig. 1 A. Inhibition of ASA-DH by preincubation with **6** at 0.66mM. ○ uninhibited reaction; + preincubation with **6** for 0 min; □ preincubation with **6** for 12 min; ● preincubation with **6** for 25 min; ■ preincubation with **6** for 68 min; X preincubation with **6** for 138 min. B. Rate of inhibition of ASA-DH at varying **6** concentration (○ 0.66; □ 2.5; ■ 5.0 mM) and at ● 2.5 mM **6** in the presence of phosphate (15 mM).

site geometry of ASA-DH. The inhibited enzyme is currently undergoing crystallisation trials.

We thank Alessia Rossi for technical assistance and the University of Bristol for financial support (University Scholarship to MBM-M).

Notes and references

1 House of Lords Select Committee on Science and Technology, Seventh Report, 1998.
2 *The Management and Control of Hospital Acquired Infections in Acute NHS Trusts in England and Wales* Report by the Comptroller and Auditor General, House of Commons, 14th February 2000.
3 R. J. Cox, A. Sutherland and J. C. Vederas, *Bioorg. Med. Chem.*, 2000, **8**, 843.
4 R. J. Cox, *Nat. Prod. Rep.*, 1996, **13**(1), 29.
5 W. E. Karsten and R. E. Viola, *Biochim. Biophys. Acta*, 1991, **1077**, 209.
6 A. Hadfield, G. Kryger, J. Ouyang, G. A. Petsko, D. Ringe and R. Viola, *J. Mol. Biol.*, 1999, **289**(4), 991.
7 M. J. Tozer and T. F. Herpin, *Tetrahedron*, 1996, **52**(26), 8619.
8 G. M. Blackburn, D. E. Kent and F. Kolkmann, *J. Chem. Soc., Perkin Trans. 1*, 1984, 1119.
9 D. B. Berkowitz, M. Eggen, Q. Shen and R. K. Shoemaker, *J. Org. Chem.*, 1996, **61**, 4666.
10 S. F. Martin, D. W. Dean and A. S. Wagman, *Tetrahedron Lett.*, 1992, **33**, 1839.
11 A. Sutherland, J. F. Caplan and J. C. Vederas, *J. Chem. Soc., Chem. Commun.*, 1999, 555.
12 D. B. Dess and J. C. Martin, *J. Am. Chem. Soc.*, 1991, **113**, 7277.
13 R. E. Ireland and L. B. Liu, *J. Org. Chem.*, 1993, **58**(10), 2899.
14 R. J. Cox, M. Murray and M. B. Mayo-Martin, unpublished.
15 Selected data for **6. Hydrate:** δ_H(400 MHz, D_2O) 4.05 (1 H, dd, $^3J_{HH}$ 4.1, 8.05, αCH), 2.35 (1H, dd, $^2J_{HH}$ 15.4, $^3J_{HH}$ 4.4, βCH), 2.17 (1H, dd, $^2J_{HH}$ 15.4, $^3J_{HH}$ 8.2, βCH); δ_F(283 MHz, D_2O) −122.6 (1F, dd, $^2J_{FF}$ 301.8, $^2J_{FP}$ 90.6), −123.5 (1F, dd, $^2J_{FF}$ 300.0, $^2J_{FP}$ 90.3); δ_P(122 MHz, D_2O) 3.26 (dd, $^2J_{PF}$ 86.6, 89.1). **Ketone:** δ_H(400 MHz, D_2O) 4.05 (1H, dd, $^3J_{HH}$ 4.02, 8.05, αCH), 3.39 (1H, dd, $^2J_{HH}$ 19.8, $^3J_{HH}$ 4.1, βCH), 3.32 (1H, dd, $^2J_{HH}$ 20.1, $^3J_{HH}$ 7.8, βCH); δ_F(283 MHz, D_2O) −120.2 (br d, $^2J_{FP}$ 84.1); δ_P(122 MHz, D_2O) 0.67 (t, $^2J_{PF}$ 85.3); *m/z* (ESMS, CH_3CN–H_2O) 247.9 ([M]H^+, 100%), 265.9 ([M + H_2O]H^+, 75%), 270.0 ([M]Na^+, 50%), 289.9 ([M + CH_3CN]H^+, 45%), 494.8 ([2M]H^+, 20%).
16 *Fundamentals of Enzyme Kinetics*, ed. A. Cornish-Bowden, Portland Press, London, 1995.

CHEMCOMM Communication
www.rsc.org/chemcomm

Palladium catalysed 3-component cascade synthesis of bis(2-arylallyl) tertiary amines from aryl iodides, allene and primary amines

Xinjie Gai,[a] Ronald Grigg,*[a] Simon Collard[b] and Jayne E. Muir[b]

[a] *Molecular Innovation, Diversity and Automated Synthesis (MIDAS) Centre, School of Chemistry, Leeds University, Leeds, UK LS2 9JT. E-mail: R. Grigg@chem.leeds.ac.uk; Fax: (+44) 113-233 6501; Tel: (+44) 113 233 6501*

[b] *Johnson Matthey, Precious Metal Division, Royston, Herts, UK SG8 5HE*

Received (in Cambridge, UK) 26th June 2001, Accepted 20th July 2001
First published as an Advance Article on the web 29th August 2001

A 3-component cascade synthesis of bis(2-arylallyl) tertiary amines from aryl iodide, allene and primary aliphatic amines is described; chiral amines give analogous products with no detectable racemisation; mixtures of two different aryl iodides can be utilised to give the mixed tertiary amines as the sole, or major, product; the reaction is sensitive to stereoelectronic effects which lead to mono(2-arylallyl) secondary amines.

π-Allylpalladium species react with both carbon- and heteroatom-centred nucleophiles with formation of carbon–carbon or carbon–heteroatom bonds and catalytic versions of these processes have been widely utilized in organic synthesis.[1] Heteroatom nucleophiles, including RCO_2H,[2] H_2O,[3] ROH[4] and amines[5] (primary and secondary), have proved particularly valuable in complex molecule synthesis. The reaction of nitrogen nucleophiles with π-allylpalladium(II) species are amongst the most widely used in organic synthesis. The efficiency of intermolecular amination and its tolerance of a wide range of functional groups has encouraged extensive applications including the synthesis of carbocyclic nucleoside analogues.[6] Aryl, acyl and hydropalladation of allenes are additional versatile routes to π-allylpalladium species which have been imaginatively exploited in harness with nucleophilic attack.[7–9]

Most reported cases of reactions with amines involve one π-allylpalladium species reacting with a primary or secondary amine to form a secondary amine or tertiary amine respectively. The sequential transfer of two allyl groups from Pd(II) to a primary amine to form a tertiary amine in a one pot reaction has not, to our knowledge, been reported. Herein we report the first cases where primary amines react with π-allylpalladium(II) species, generated from allene, to form tertiary amines. The three component reaction can be carried out under mild conditions in the presence of a palladium catalyst in good yield (Scheme 1) (Table 1) and involves formation of two carbon–carbon bonds and two carbon–nitrogen bonds. The palladium(0) catalyst Pd_2dba_3 (2.5 mol%) in combination with tris(2-furyl)phosphine (TFP) together with allene gas (1 bar) proved effective at 60–90 ° C over 1–2 d.[10]

A range of aryl/heteroaryl iodides and primary amines were evaluated and good yields were obtained in all cases (Table 1). The reaction also works well for vinyl iodides (Table 1, entries 4 and 9) and for a range of primary aliphatic amines. Reaction of primary aliphatic amines with 1 : 1 mixtures of two different aryl iodides gives the desired mixed product as the major or, in some cases, the sole product. Two typical examples are provided by reaction of (−)-myrtanylamine **4** with 1 mol eq. of 4-methoxyiodobenzene and 4-(*N*,*N*-diethylaminocarbonyl)iodobenzene which affords **5** (56%) as the sole product whilst amine **6** reacts with 4-methoxycarbonyliodobenzene and 3,5-di-

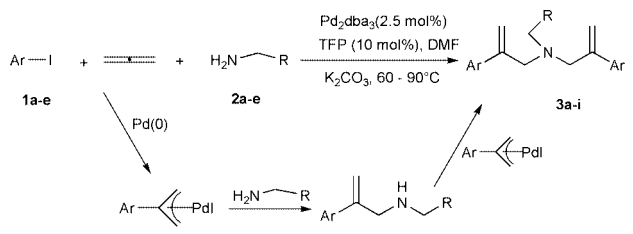

Scheme 1

Table 1 3-Component cascade synthesis of symmetrical bis(2-arylallyl) tertiary amines (**3a–i**)[a]

Entry	Ar-I	Amine	Temp/°C[b]; Time/d	Product	Yield[c] (%)
1	 1a	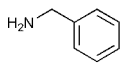 2a	85; 2	**3a**	82
2	 1b	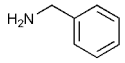 2a	60; 2	**3b**	82
3	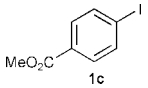 1c	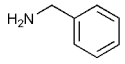 2a	90; 1	**3c**	70
4	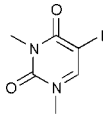 1d	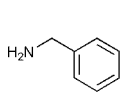 2a	90; 2	**3d**	80
5	 1a	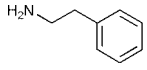 2b	90; 1.5	**3e**	78
6	 1a	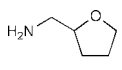 2c	80; 2	**3f**	70
7	 1a	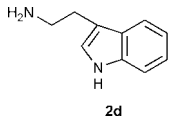 2d	80; 1	**3g**	62
8	 1a	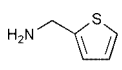 2e	85; 2	**3h**	72
9	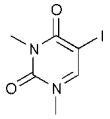 1d	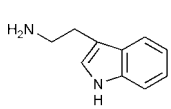 2d	80; 2	**3i**	71

[a] All reactions were run in DMF at 60–90 °C over 1–2 days in the presence of 2.5 mol% Pd_2dba_3, 10 mol% $(2\text{-furyl})_3P$, allene (1 bar) and K_2CO_3(4 mol eq.) in a Schlenk tube. [b] Oil bath temperature. [c] Isolated yield.

 DOI: 10.1039/b105567b

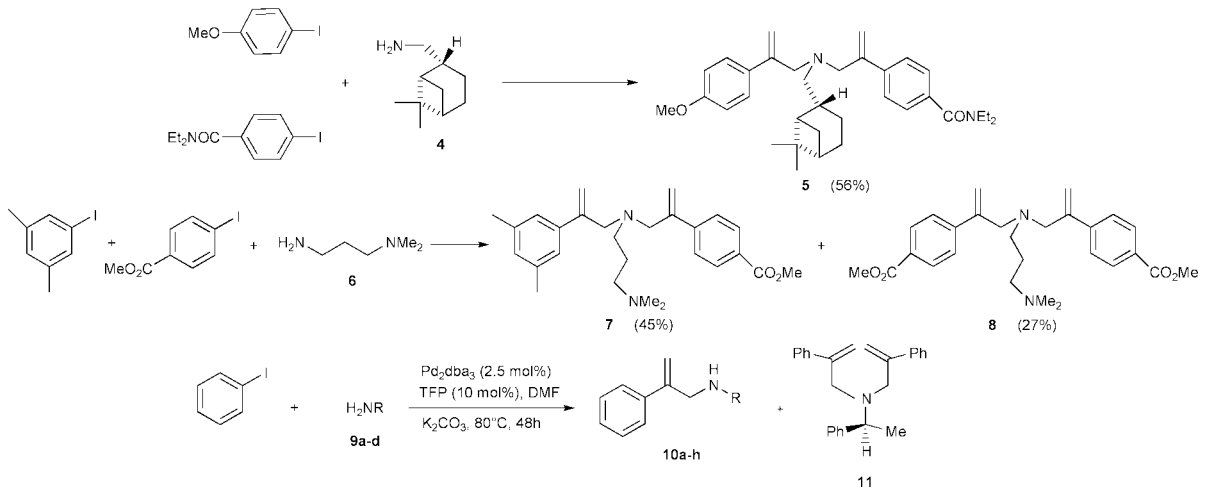

Scheme 2

Table 2 3-Component cascade synthesis of 2-arylallyl secondary amines (**5a–h**)[a]

Entry	Amine	Product	Yield(%)
1	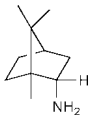 **9a** (·)	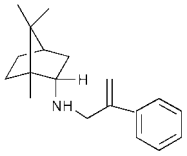 **10a**	92
2	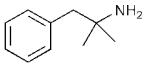 **9b**	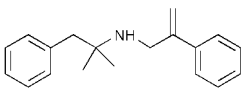 **10b**	88
3	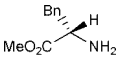 **9c** (S) –	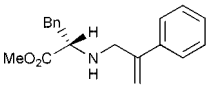 **10c**	72
4	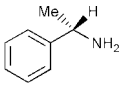 **9d** (S)	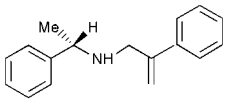 **10d**	73[b]
5	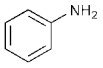 **9e**	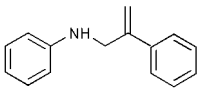 **10e**	73
6	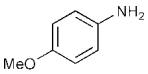 **9f**	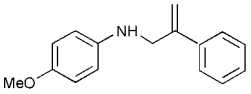 **10f**	95
7	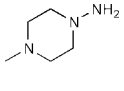 **9g**	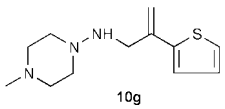 **10g**	48[c]
8	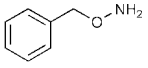 **9h**	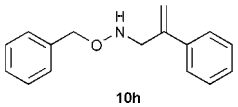 **10h**	83

[a] All reactions were run in DMF at 80 °C for 48 h. Catalyst and additive as for Table 1. Iodobenzene was the aryl iodide unless otherwise noted. [b] In addition the tertiary amine **6** was obtained. [c] 2-Iodothiophene replaced iodobenzene.

methylbenzene to afford a mixture of **7** and **8**. Clearly there is scope for considerable optimisation in these cases.

The reaction is also sensitive to stereoelectronic factors as demonstrated by Scheme 2 and Table 2.

The monoallylated α-branched primary amines **10a–d** (Table 2, entries 1–4) fail to undergo a second allylation due to substantial steric hindrance. The primary amines **9e–h** (Table 2) are orders of magnitude less basic [11] and nucleophilic than **2a–d** and are also sterically more hindered. These two factors conspire to prevent the second allylation under the specified conditions.

The secondary and tertiary amine products of these cascades are unusual derivatives of the bioactive β-aryl/heteroaryl-(ethyl)amine pharmacophore. Bis(2-arylallyl) tertiary amines have also found applications as additives in copolymer latexes[12] and in endoperoxide[13] chemistry.

We thank the ORS and Tetley and Lupton for scholarships (to X. Gai) and Johnson Matthey and Leeds University for support.

Notes and references

1 For reviews, see: R. Zimmer, C. U. Dinesh, E. Nandana and F . A. Khan, *Chem. Rev*., 2000, **100**, 3067; L. S. Hegedus, *Transition Metal in the Synthesis of Complex Organic Molecules*, University Science Books, 1999, ch. 9.
2 M. Al-Masum and Y. Yamamoto, *J. Am. Chem. Soc*., 1998, **120**, 3809.
3 G. D. Shier, *J. Organomet. Chem*., 1967, **10**, 15.
4 Y. Inoue, Y. Ohtsuka and H. Hashimoto, *Bull. Chem. Soc. Jpn*., 1984, **57**, 3345.
5 X. Gai, R. Grigg, M. I. Ramzan, V. Sridharan, S. Collard and J. E. Muir, *Chem. Commun*., 2000, 2053; M. Gardiner, R. Grigg, V. Sridharan and N. Vicker, *Tetrahedron Lett*., 1998, **39**, 435.
6 H. F. Ohno and J. Yu, *J. Chem. Soc., Perkin Trans. 1*, 1998, 391.
7 R. Grigg, V. Sridharan and C. Terrier, *Tetrahedron Lett*., 1996, **37**, 4221.
8 R. Grigg, A. Liu, D. Shaw, S. Suganthan, D. E. Woodall and G. Yoganathan, *Tetrahedron Lett*., 2000, **41**, 7125; R. Grigg, S. Brown, V. Sridharan and M. D. Uttley, *Tetrahedron Lett*., 1997, **38**, 5031.
9 R. Grigg, M. Monteith, V. Sridharan and C. Terrier, *Tetrahedron*, 1998, **54**, 3885.
10 General procedure: a mixture of aryl iodide (2.2–2.5 mol eq.), amine (1 mmol), Pd_2dba_3 (24 mg, 0.025 mmol), TFP (25 mg, 0.10 mmol) and K_2CO_3 (556 mg, 4 mmol) was stirred in DMF (10 ml) and heated at 80–90 °C for 1–2 days in a Schlenk tube under allene (1 bar). On completion of the reaction, the tube was cooled, vented, H_2O (30 ml) was added and the mixture was extracted with ether (3 × 20 ml). The combined organic layer was dried ($MgSO_4$), concentrated under reduced pressure and the residue purified by flash chromatography.
11 The following pK_a values were calculated with ACD/p*K*a v4.56 using the ACD/I-Lab service: **9e** (4.61), **9f** (5.21), **9g** (7.35) and **9h** (4.63).
12 V. A. Belyaev, I. M. Patanova, E. P. Kopylov, L. V. Kosmodem'yanskii, V. P. Bugrov, S. G. Yukhnovich and A. S. Doronin, *USSR Patent*, 1982, URXXAF SU 899531 A1 19820123. (*Chem. Abstr*., 1982, **97**, 24760b).
13 H. G. Posner, D. Wang, L. Gonzalez, X. Tao, J. N. Cumming, D. Klinedinst and T. A. Shapiro, *Tetrahedron Lett*., 1996, **37**, 815.

CHEMCOMM Communication
www.rsc.org/chemcomm

A dramatic improvement of epoxide selectivity of [Ti,Al]-beta by ion-exchange with quaternary ammonium salts

Yasuhide Goa,[a] Peng Wu[b] and Takashi Tatsumi*[b]

[a] *Department of Applied Chemistry, Graduate School of Engineering, The University of Tokyo, 7-3-1, Hongo, Bunkyo-ku, Tokyo, 113-8656, Japan*
[b] *Division of Materials Science & Engineering, Graduate School of Engineering, Yokohama National University, 79-5, Tokiwadai, Hodogaya-ku, Yokohama, 240-8501, Japan. E-mail: ttatsumi@ynu.ac.jp*

Received (in Cambridge, UK) 11th June 2001, Accepted 30th July 2001
First published as an Advance Article on the web 29th August 2001

Ion-exchange of [Ti,Al]-beta with quaternary ammonium acetates greatly enhances the epoxide selectivity in the oxidation of alkenes with hydrogen peroxide; this is due to the selective poisoning of the acid sites without suppressing the oxidation activity of Ti sites.

Since the first report of TS-1 by Taramasso *et al*. in 1983, titanosilicates have attracted the attention of many researchers.[1] Ti-beta zeolite has a three-dimensionally connected pore system with 12-membered-ring channels and is verified to be more active towards bulky substances such as branched and cyclic alkanes and alkenes using aqueous H_2O_2 or *tert*-butyl hydroperoxide (TBHP) as an oxidant than medium pore TS-1 because of the reduced diffusion restriction imposed by the large pores. A small amount of Al (Si/Al < 200), as crystallization-promoting agent, is generally needed in the conventional hydrothermal synthesis method for Ti-beta using tetraethylammonium hydroxide (TEAOH) as a structure-directing agent (SDA).[2,3] The presence of Al leads to the formation of acid sites, which promotes the successive ring-opening solvolysis of the epoxide generated in the catalytic reactions to lower its selectivity extensively.[4] Afterwards, several novel synthesis methods for Al-free or low-Al Ti-beta were also developed, such as the seeding method,[5] cogel method,[6] fluoride method[7,8] and dry-gel conversion method;[9,10] however none of these were very efficient for enhancing epoxide selectivity in alcoholic solvents. This is probably because the very complex, severely intergrown nature of the beta structure results in high concentration of weak acid sites such as silanol groups at defect sites. Although ion-exchange with alkaline or alkaline earth metal cations inhibits the acidity of titanosilicates, it also suppresses the oxidation activity of Ti species.[11,12] We report here a new method for dramatically enhancing the yield of epoxide in the alkene oxidation reactions catalyzed by Ti-beta even in protic alcoholic solvents without losing its oxidation activity.

[Ti,Al]-beta zeolite was hydrothermally synthesized by modifying the method reported by Camblor *et al*.[2,3] Tetrabutyl orthotitanate [$Ti(OBu)_4$] was employed as a Ti source instead of tetraethyl orthotitanate [$Ti(OEt)_4$] and was hydrolyzed in aqueous H_2O_2 before adding to the SDA solution to suppress the formation of extraframework anatase TiO_2. The mother gel composition was SiO_2:0.33 TiO_2:0.005 Al_2O_3:0.56 TEAOH:12.5 H_2O. The crystallization was carried out by agitating the gel in a Teflon-lined stainless steel autoclave at 413 K for 4 days. The resultant [Ti,Al]-beta was calcined at 793 K for 10 h in a stream of O_2 (30 ml min^{-1} g-$solid^{-1}$) to remove the SDA. Calcined [Ti,Al]-beta was treated with 1 M aqueous solutions of various ammonium acetates (NR_4OAc, R = Me, Et, Pr and H) or 1 M aqueous potassium acetate (KOAc) solution at 353 K for 4 h and then filtered off, washed, dried and finally calcined of 473 K for 10 h. The liquid phase epoxidation of alkenes with H_2O_2 was performed in a flask.

Table 1 shows the results of epoxidation of alkenes. Calcined [Ti,Al]-beta exhibited a low selectivity to epoxide for oxidation reactions of cyclohexene and hex-2-ene (entries 1 and 2). The products were mainly diol and monomethyl glycol ether produced by the acid-catalyzed solvolysis of epoxide, together with a small amount of allylic oxidation products. The negligible formation of epoxide strongly indicates that there were a considerable amount of acid sites in [Ti,Al]-beta, which contributed to the solvolysis of epoxide.

When the catalyst ion-exchanged with tetramethylammonium acetate was employed (entries 4 and 5), the epoxide selectivity was greatly enhanced owing to the suppression of ring-opening reactions, and the selectivity to the allylic oxidation did not change significantly. The enhancement was more obvious for hex-2-ene which gave an epoxide/glycol ratio of 28. Solvent effects were also tested. It is generally known that aprotic solvents such as acetonitrile enhance the selectivity to the epoxide. Employment of the weakly basic solvent, acetoni-

Table 1 Catalytic oxidation of cyclohexene and hex-2-ene[a]

Entry	Ion-exchange	Substrate	N^+/Al	Maximum conv. (mol%)	Selectivity[b] (mol%)			H_2O_2 (mol%)	
					Epox.	Glyc.	Allyl	Conv.	Efficiency
1	No	Cyclohexene	–	76.1	0.0	97.6	2.4	83	90
2	No	Hex-2-ene[c]	–	49.5	0.2	98.0	0.0	76	64
3[d]	No	Cyclohexene	–	30.4	69.3	14.9	15.8	81	41
4	NMe_4OAc	Cyclohexene	1.8	75.2	55.1	43.2	1.8	95	79
5	NMe_4OAc	Hex-2-ene[c]	1.8	60.7	92.4	3.3	4.1	78	72
6[d]	NMe_4OAc	Cyclohexene	1.8	57.1	88.5	5.3	6.1	86	69
7	NEt_4OAc	Cyclohexene	1.8	47.2	71.6	26.5	1.9	69	67
8	NPr_4OAc	Cyclohexene	1.5	24.5	51.4	46.6	2.0	42	59
9	NH_4OAc	Cyclohexene	1.6	57.4	0.1	96.9	3.0	60	97
10	KOAc	Cyclohexene	2.2[e]	18.7	63.5	34.2	2.3	48	40

[a] *Reaction conditions*: 333 K, 3 h, 8.25 mmol of alkene, 2.5 mmol of H_2O_2 (31 wt% in water), 50 mg of catalyst (Si/Ti = 35, Si/Al = 38) and 5 ml of methanol. [b] Epox. = cyclohexene oxide or 2,3-epoxyhexane; Glyc. = cyclohexanediol or hexane-2,3-diol and their monomethyl ethers; Allyl = alcohol and ketone formed by oxidation. [c] *cis*/*trans* Isomer ratio = 41/59. [d] Acetonitrile was employed as solvent. [e] K^+/Al.

 DOI: 10.1039/b105088p

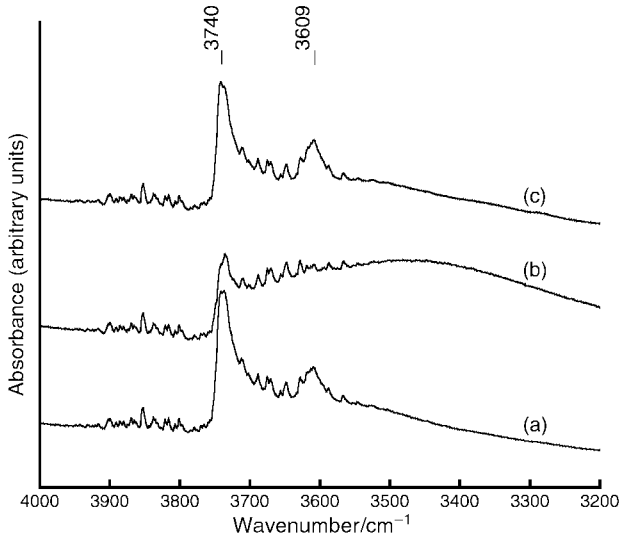

Fig. 1 FTIR spectra of Ti-beta in the OH region; (a) without ion-exchange after evacuation at 773 K, (b) ion-exchanged with NMe_4OAc and evacuated at 473 K, (c) ion-exchanged and evacuated at 773 K.

trile, further enhanced the epoxide selectivity (entries 3 and 6).

Use of larger quaternary ammonium cations led to decreased activity, probably because the bulky cations hinder the reactant molecules from approaching the Ti sites (entries 4, 7 and 8). Ammonium acetate treatment led to no enhancement of the epoxide selectivity (entry 9). FT-IR spectra of the ion-exchanged [Ti,Al]-beta taken before and after the catalytic runs indicated that NH_4^+ was oxidatively degradated while NMe_4^+ remained intact. Ion-exchange with KOAc also increased the selectivity to the epoxide; however the oxidation activity was adversely affected (entry 10). This is consistent with the observations that ion-exchange with sodium carbonate (Na_2CO_3) or sodium azide (NaN_3) on Al-containing TS-1 gave rise to a higher epoxide selectivity but a very low activity in allyl alcohol oxidation,[11] that ion-exchange with potassium carbonate severely lowered the oxidation turnover in unsaturated alcohol oxidation[12] and that TS-1 synthesized in the presence of large amounts of alkali and alkaline earth ions showed low oxidation activity.[13] Elemental analyses indicated that ion-exchanged catalyst contained NMe_4^+ cations in excess of Al, which suggests that the NMe_4^+ blocks not only all the bridging hydroxy groups but also other less acidic sites.

Calcined [Ti,Al]-beta exhibited two bands in its FTIR spectra in the OH vibration region [Fig. 1(a)]. A peak at 3609 cm^{-1} is assigned to bridged hydroxy groups [Si–(OH)–Al] and the other peak around 3740 cm^{-1} to terminal silanols (SiOH) composed of several types of silanol groups:[14] silanols of amorphous silica–alumina species (3747 cm^{-1}), silanols of amorphous silica (3745 cm^{-1}) and terminal silanols attached to the zeolite lattice (3736 cm^{-1}) After ion-exchange with NMe_4OAc followed by calcination at 473 K, the bridged hydroxy groups band disappeared and the silanol bands significantly decreased in intensity [Fig. 1(b)]. When the ion-exchanged sample was calcined at 773 K, the intensities of these bands were almost recovered [Fig. 1(c)]. The pH of aqueous NMe_4OAc used for the ion-exchange was high enough (pH ~ 9) to allow the silanol groups to be exchanged with NMe_4^+ cations since the isoelectric point of SiO_2 is 1.0–2.0. These findings indicate that a part of silanol groups with weaker acidity as well as all of the bridged hydroxy groups with strong acidity were ion-exchanged with NMe_4^+.

The pH of the NMe_4OAc solution was varied from 8 to 12 to control the ion-exchange ratio. The oxidation activity gradually increased with increasing pH. Treatment at high pH resulted in the formation of mesopores, as revealed by N_2 adsorption measurements, which could promote the diffusion of the substances. However, the catalyst ion-exchanged at high pH exhibited low selectivity for epoxide; probably the zeolite framework dissolves to form silanol groups, which would catalyze undesirable reactions.

When the ion-exchanged [Ti,Al]-beta catalyst was reused for the oxidation of cyclohexene after the catalyst was calcined at 473 K for 10 h, the epoxide selectively was retained, although the oxidation activity gradually decreased to 37% for the third run probably because of the blocking of the Ti species by unremovable reaction products such as polymers with high boiling points. Nevertheless, after re-calcination at 793 K and repeated ion-exchange of the deactivated catalyst with NMe_4OAc, both the oxidation activity and the epoxide selectivity were recovered to the initial value, which strongly indicates that the present method is effective in developing an active, selective and reusable catalyst.

Notes and references

1 M. Taramasso, G. Perego and B. Notari, *US Pat*., 4,410,501, 1983.
2 M. A. Camblor, A. Corma, A. Martínez and J. Pérez-Pariente, *Chem. Commun*., 1992, 589.
3 M. A. Camblor, A. Corma and J. Pérez-Pariente, *Zeolites*, 1993, **13**, 83.
4 A. Corma, P. Esteve, A. Martínez and S. Valencia, *J. Catal*., 1995, **152**, 18.
5 M. A. Camblor, M. Constantini, A. Corma, L. Gilbert, P. Esteve, A. Martínez and S. Valencia, *Chem. Commun*., 1996, 1339.
6 M. A. Camblor, M. Constantini, A. Corma, P. Esteve, L. Guilbert, A. Martínez and S. Valencia, *Appl. Catal*., 1995, **133**, L185.
7 T. Blasco, M. A. Camblor, A. Corma, P. Esteve, A. Martínez, C. Prieto and S. Valencia, *Chem. Commun*., 1996, 2367.
8 T. Blasco, M. A. Camblor, A. Corma, P. Esteve, J. M. Guil, A. Martínez, J. A. Perdigon-Melon and S. Valencia, *J. Phys. Chem. B*, 1998, **102**, 7126
9 N. Jappar, Q.-H. Xia and T. Tatsumi, *J. Catal*, 1998, **180**, 132.
10 T. Tatsumi and N. Jappar, *J. Phys. Chem. B*, 1998, **102**, 7126.
11 G. J. Hutchings, D. F. Lee and A. R. Minihan, *Catal. Lett*., 1996, **39**, 83.
12 T. Tatsumi, K. A. Koyano and Y. Shimizu, *Appl. Catal. A*, 2000, **200**, 125.
13 C. B. Khouw and M. E. Davis, *J. Catal*., 1995, **151**, 71.
14 A. Janin, M. Maache, J. C. Lavalley, J. F. Joly, F. Raatz and N. Szydlowsky, *Zeolites*, 1991, **11**, 391.

CHEMCOMM Communication
www.rsc.org/chemcomm

Catalyst-free reactions under solvent-free conditions: microwave-assisted synthesis of heterocyclic hydrazones below the melting points of neat reactants†

Marjan Ješelnik,[a] Rajender S. Varma,*[b] Slovenko Polanc[a] and Marijan Kocevar*[a]

[a] *Faculty of Chemistry and Chemical Technology, University of Ljubljana, Aškerceva 5, SI-1000 Ljubljana, Slovenia. E-mail: marijan.kocevar@Uni-Lj.si*

[b] *Clean Processes Branch, National Risk Management Research Laboratory, U.S. Environmental Protection Agency, MS 443, 26 W. Martin Luther King Drive, Cincinnati, OH 45268, USA. E-mail: varma.rajender@epa.gov*

Received (in Corvallis, OR, USA) 17th May 2001, Accepted 27th June 2001
First published as an Advance Article on the web 29th August 2001

The reaction of neat 5- or 8-oxobenzopyran-2(1*H*)-ones, 1–3, with a variety of aromatic and heteroaromatic hydrazines, 4, is remarkably accelerated upon irradiation in a household microwave oven in the absence of any catalyst, solid support or solvent thus providing an environmentally friendly route to several heterocyclic hydrazones.

Microwave (MW) irradiation has been used for the rapid synthesis of a variety of compounds.[1] Chemical reactions can be accelerated because of selective absorption of microwave energy by polar molecules, non-polar being inert to the MW dielectric loss. Heterogeneous reactions facilitated by supported reagents on various inorganic surfaces have received special attention in recent years.[2] However, relatively little attention is paid to solventless reactions with neat reactants in the absence of a catalyst or solid support.

From the synthetic point of view hydrazones are important synthons for several transformations[3a–d] and their synthesis from various precursors is well documented.[3a,b] Recently, some hydrazones have been prepared from carbonyl compounds and hydrazine hydrate in ethylene glycol[4a] and toluene[4b] by the application of MW irradiation while some others are synthesized in the presence of silica gel and NaOH.[5]

We report here a general synthesis of several hydrazones **5–15**, which in some earlier preparations required relatively strenuous reaction conditions namely heating substrates for several hours in the presence of an acidic catalyst.[6] The synthetic efforts for these compounds have been previously directed for the selective design of the benzopyran-2-one ring at the positions 5 and 8 as well as for the new transformation into the corresponding quinoline derivatives. The conformational analysis has been accomplished for some of these derivatives by applying molecular modelling techniques based on experimentally determined NOE distance restraints in order to determine their structure in solution.[6a,d] These studies have been stimulated, in part, due to potentially significant biological activity associated with a variety of 2*H*-1-benzopyrans and quinolines.[6d] For the above reasons and in view of our general interest in the development of environmentally friendlier synthetic alternatives using microwaves,[2] we became interested in an expeditious synthesis of these compounds. In all the reactions reported in this paper we worked with neat starting materials, 1-benzopyran-2(2*H*)-ones **1**,[7a,b] **2**,[7a,b] **3**[7c] and hydrazines, **4**, wherein the reactions are completed within minutes and in high yields (61–98%, Scheme 1, Table 1)‡ using an unmodified household MW oven. Remarkably, reactions proceeded well even when both the starting reactants were solids and the reaction temperature was maintained below the melting points of both components; recently some comments have been made on the preparation of phthalimides starting from solid components, phthalic anhydride and amino compounds.[8a] In view of the unprecedented nature of this reaction, we examined the synthesis of the products **10** and **14** in detail. Since a conventional household MW oven is used with no accurate temperature control,§ we decided to measure the temperature of the alumina bath (used for housing the reaction vessel in the MW oven) with a calibrated thermometer immediately after completion of the reaction. In a controlled experiment, concurrently, we also heated the lower melting reactant in a second glass beaker to obtain visual information about the integrity of the solid materials upon exposure to microwaves.

For the synthesis of **10**, the starting benzopyran **2**[7a,b] (mp 179–179.5 °C) and 3-chloro-6-hydrazinopyridazine[9a] (mp 135–137 °C), were admixed in the ratio 1 : 2 (Table 1). When the reaction mixture was irradiated with MW for 5.5 min the highest temperature of the alumina recorded was 120–122 °C. The reaction mixture remained solid and no reaction was observed. After heating for 6 min, however, the temperature of the bath reached 130–132 °C and the reaction mixture was completely in

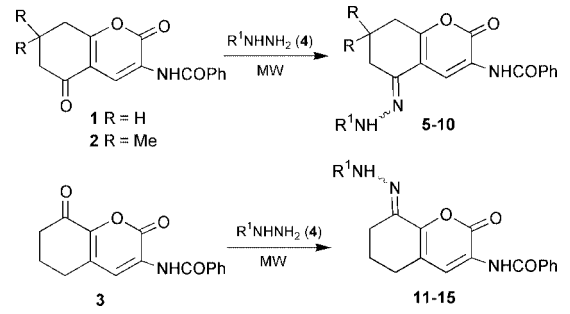

Scheme 1

Table 1 Solvent-free preparation of hydrazones, **5–15**, using microwaves

Starting benzopyran	Hydrazine **4** R¹=	(mmol)	React. time/ min	Product (yield, %)
1	Ph	(1.2)	6	**5** (83)
1	2,5-Difluorophenyl	(3.0)	8	**6** (69)
1	3-CF_3-C_6H_4	(1.5)	8	**7** (75)
2	Ph	(2.0)	8	**8** (61)
2	3-CF_3-C_6H_4	(3.0)	10	**9** (62)
2	6-Chloropyridazin-3-yl	(2.0)	6	**10** (85)
3	Ph	(3.0)	3	**11** (95)
3	3-CF_3-C_6H_4	(1.5)	8	**12** (92)
3	Pyridin-2-yl	(3.0)	5	**13** (65)
3	4-Nitrophenyl	(~2.6)[a]	9	**14** (98)
3	2,5-Difluorophenyl	(3.0)	8	**15** (96)

[a] Reagent contains 10–15% of water for stabilization.

† Dedicated with deep respect to Professor Miha Tišler, University of Ljubljana, Slovenia on the occasion of his 75th birthday.

 DOI: 10.1039/b104508n

liquefied form affording hydrazone **10** in 85% isolated yield (see Table 1). The 3-chloro-6-hydrazinopyridazine kept in the same bath barely melted (~5% as estimated visually) at that temperature. With the critical temperature information in hand, we embarked on a comparative study and heated the above reaction mixture in the same proportions using a preheated oil bath. Heating for 12 min at 133 °C gave a mixture (liquid with some suspended solid material). NMR analysis revealed that the molar ratio between hydrazone **10** and starting benzopyran **2** was approximately 3.3:1. Prolonged heating of the reaction mixture for 1 h at 133 °C resulted in the formation of the liquid with no suspended solids. The work-up (as in general procedure) and NMR analysis revealed that the ratio between **10** and **2** in the isolated product was 92:8. Obviously, the unreacted benzopyran derivative contaminated product **10**, while under MW conditions we observed complete conversion to a single product (Table 1).

For the synthesis of **14** starting from **3**[7c] (mp 248–250 °C) and 4-nitrophenylhydrazine[9b] (mp ~157 °C with decomp.) we performed an experiment with the reactants in the ratio 1:2.6 respectively. The commercially obtained hydrazine derivative, however, contained 10–15% of water for stabilization and as such slightly melted at 130 °C. Upon MW irradiation for 5.5 min the same temperature (120–122 °C) was attained and the reaction mixture was completely melted while the 4-nitrophenylhydrazine in the second beaker was only barely melted. NMR analysis of the crude mixture showed no presence of the benzopyran derivative **3**, and the work-up resulted in hydrazone **14** in 94% yield. On the other hand, heating the same reaction mixture for 1 h at 128 °C in an oil bath resulted in a mixture of product **14** and starting **3** in the ratio 4.3:1, as discerned from the ^{1}H NMR spectrum of the crude reaction mixture. It should be mentioned that in this case the reaction mixture at the end of the heating period remained solid but attained a brownish color presumably as a result of partial decomposition.

This comparative study of the reactions taking place in an oil bath in the absence of MW heating revealed a substantial rate enhancement for reactions conducted under MW irradiation conditions, presumably due to the increase in polarity after change from the solid to the liquid phase.[8a] Such bimolecular reactions[2d,e] will have polarity enhancement as a result of ensuing intermediate transition state and consequently may display a pronounced microwave effect.[8b] Further, the reactions could be visibly monitored since no reaction occurs without formation of a melt. This methodology allows for performing rapid syntheses of a variety of hydrazones¶ below melting points of starting materials used. This could be explained by the lowering of the melting point by the formation of the eutectic;[10] such methodology seems to be especially useful when starting from substrates, which decompose at the normal melting point.

In conclusion, we have shown an expeditious, easy-to-handle and environmentally friendlier approach to the synthesis of a variety of non-easily-available hydrazones using MW irradiation that can be extended to other systems.

The authors wish to thank the Ministry of Education, Science and Sport of the Republic of Slovenia for financial support (P0-0503-103). Dr B. Kralj and Dr D. Žigon ('Jožef Stefan' Institute, Ljubljana) are acknowledged for mass spectra.

Notes and references

‡ The starting benzopyran-2(2*H*)-ones, **1**–**3**, and 3-chloro-6-hydrazinopyridazine were prepared as described in the literature.[7,9a] A household microwave oven operating at 2450 MHz was used at its full power, 650 W, for all the experiments.

*General procedure for the synthesis of hydrazones **5**–**15***: a neat mixture of benzopyran derivative **1**–**3** (1 mmol) and hydrazine **4** (1.2–3 mmol; see Table 1) in a 10 mL glass beaker was thoroughly mixed for about 5 min, then it was placed in an alumina bath inside the household microwave oven and irradiated. Maximum temperature reached in the alumina after 10 min was about 150 °C. After cooling, methanol (~4 mL) was added to the mixture and the separated solid was filtered off and washed with a small amount of methanol. Reaction conditions and yields are given in Table 1 for products, **5**–**15**, which conform to the NMR and elemental analyses.

§ There are commercial microwave devices available that provide adequate mixing and control of reaction parameters such as temperature, pressure.

¶ *N*-(5,6,7,8-Tetrahydro-2-oxo-5-phenylhydrazono-2*H*-1-benzopyran-3-yl)benzamide (**5**): mp 213–216 °C (DMF–MeOH); lit.[6c] 216–220 °C.

N-[5-(2,5-Difluorophenyl)hydrazono-5,6,7,8-tetrahydro-2-oxo-2*H*-1-benzopyran-3-yl]benzamide (**6**): mp 248–249 °C, decomp. (DMF–MeOH).

N-[5,6,7,8-Tetrahydro-2-oxo-5-(3-trifluoromethyl)phenylhydrazono-2*H*-1-benzopyran-3-yl]benzamide (**7**): mp 222–223 °C (DMF–MeOH).

N-(5,6,7,8-Tetrahydro-7,7-dimethyl-2-oxo-5-phenylhydrazono-2*H*-1-benzopyran-3-yl)benzamide (**8**): mp 223–226 °C (DMF–MeOH); lit.[6c] 223–226 °C.

N-[5,6,7,8-Tetrahydro-7,7-dimethyl-2-oxo-5-(3-trifluoromethyl)phenylhydrazono-2*H*-1-benzopyran-3-yl]benzamide (**9**): mp 221–223 °C (DMF).

N-[5,6,7,8-Tetrahydro-7,7-dimethyl-2-oxo-5-(6-chloropyridazin-3-yl)-hydrazono-2*H*-1-benzopyran-3-yl]benzamide (**10**): mp 259–261 °C (DMF–MeOH); lit.[6a] 260–263 °C.

N-(5,6,7,8-Tetrahydro-2-oxo-8-phenylhydrazono-2*H*-1-benzopyran-3-yl)benzamide (**11**): mp 258–262 °C (DMF–MeOH); lit.[6f] 257–260 °C.

N-[5,6,7,8-Tetrahydro-2-oxo-8-(3-trifluoromethyl)phenylhydrazono-2*H*-1-benzopyran-3-yl]benzamide (**12**): mp 113–114.5 °C (DMF–MeOH).

N-[5,6,7,8-Tetrahydro-2-oxo-8-(pyridin-2-yl)hydrazono-2*H*-1-benzopyran-3-yl]benzamide (**13**): mp 226–229 °C (DMF–MeOH).

N-[5,6,7,8-Tetrahydro-2-oxo-8-(4-nitrophenyl)hydrazono-2*H*-1-benzopyran-3-yl]benzamide (**14**): mp 290 °C (DMSO).

N-[5,6,7,8-Tetrahydro-2-oxo-8-(2,5-difluorophenyl)hydrazono-2*H*-1-benzopyran-3-yl]benzamide (**15**): mp 238–239 °C (DMSO).

1 (*a*) S. Caddick, *Tetrahedron*, 1995, **51**, 10 403; (*b*) R. S. Varma, *Green Chem*., 1999, **1**, 43; (*c*) R. S. Varma, *J. Heterocycl. Chem*., 1999, **36**, 1565; (*d*) A. Loupy, A. Petit, J. Hamelin, F. Texier-Boullet, P. Jacquault and D. Mathe, *Synthesis*, 1998, 1213; (*e*) A. de la Hoz, A. Díaz-Ortis, A. Moreno and F. Langa, *Eur. J. Org. Chem*., 2000, 3659.

2 (*a*) R. S. Varma, in *ACS Symposium Series No. 767/ Green Chemical Syntheses and Processes*, ed. P. T. Anastas, L. Heine and T. Williamson, American Chemical Society, Washington DC, 2000, Chapter 23, pp. 292–313; (*b*) R. S. Varma, in *Green Chemistry: Challenging Perspectives*, ed. P. Tundo and P. T. Anastas, Oxford University Press, Oxford, 2000, pp. 221–244; (*c*) R. S. Varma, *Pure Appl. Chem*., 2001, **73**, 193; (*d*) R. S. Varma, R. Dahiya and S. Kumar, *Tetrahedron Lett*., 1997, **38**, 2039; (*e*) A. Vass, J. Dudas and R. S. Varma, *Tetrahedron Lett*., 1999, **40**, 4951; (*f*) R. S. Varma, *Clean Products and Processes*, 1999, **1**, 132.

3 (*a*) J. S. Clark, in *Comprehensive Organic Functional Group Transformations*, ed. A. R. Katritzky, O. Meth-Cohn and C. W. Rees, Pergamon, Oxford, 1995, Vol. 3, pp. 443–490; (*b*) D. E. Bergbreiter and M. Momongan, in *Comprehensive Organic Synthesis*, ed. B. M. Trost and I. Fleming, Pergamon Press, Oxford, 1991, Vol. 2, pp. 503–526; (*c*) W. Sucrow, *Org. Prep. Proced. Int*., 1982, **14**, 93; (*d*) R. Fusco and F. Sannicolo, *Tetrahedron*, 1980, **36**, 161.

4 (*a*) B. K. Banik, K. J. Barakat, W. R. Wagle, M. S. Manhas and A. K. Bose, *J. Org. Chem*., 1999, **64**, 5746; (*b*) S. Gadhwal, M. Baruah and J. S. Sandhu, *Synlett*, 1999, 1573.

5 A. R. Hajipour, I. Mohammadpoor-Baltork and M. Bigdeli, *J. Chem. Res., (S)*, 1999, 570.

6 (*a*) P. Trebše, S. Polanc, M. Kocevar, T. Šolmajer and S. Golic Grdadolnik, *Tetrahedron*, 1997, **53**, 1383; (*b*) P. Trebše, B. Recelj, M. Kocevar and S. Polanc, *J. Heterocycl. Chem*., 1997, **34**, 1247; (*c*) P. Trebše, B. Recelj, T. Lukanc, S. Golic Grdadolnik, A. Petric, B. Vercek, T. Šolmajer, S. Polanc and M. Kocevar, *Synth. Commun*., 1997, **27**, 2637; (*d*) S. Golic Grdadolnik, P. Trebše, M. Kocevar and T. Šolmajer, *J. Chem. Inf. Comput. Sci*., 1997, **37**, 489; (*e*) M. Kocevar, *Chem. Listy*, 1997, **91**, 610; (*f*) P. Trebše, L. Vranicar, I. Mušic, S. Polanc, W. C. Stevens and M. Kocevar, *Heterocycles*, 2000, **53**, 1111.

7 (*a*) M. Kocevar, S. Polanc, M. Tišler and B. Vercek, *Synth. Commun*., 1989, **19**, 1713; (*b*) V. Kepe, M. Kocevar, S. Polanc, B. Vercek and M. Tišler, *Tetrahedron*, 1990, **46**, 2081; (*c*) V. Kepe, M. Kocevar, A. Petric, S. Polanc and B. Vercek, *Heterocycles*, 1992, **33**, 843.

8 (*a*) T. Vidal, A. Petit, A. Loupy and R. N. Gedye, *Tetrahedron*, 2000, **56**, 5473; (*b*) S. Paul, M. Gupta, R. Gupta and A. Loupy, *Tetrahedron Lett*., 2001, **42**, 3827.

9 (*a*) N. Takahayashi, *J. Pharm. Soc. Jpn*., 1955, **75**, 778; *Chem. Abstr*., 1956, **50**, 4970c; (*b*) The Merck Index, 12th edn., Merck & Co., Inc., Whitehouse Station, 1996, p. 1138 (Monograph number 6721).

10 C. F. Most, *Experimental Organic Chemistry*, J. Wiley & Sons, New York, 1988, pp. 53–62.

CHEMCOMM
Communication
www.rsc.org/chemcomm

Iron polynitroporphyrins bearing up to eight β-nitro groups as interesting new catalysts for H_2O_2-dependent hydrocarbon oxidation: unusual regioselectivity in hydroxylation of alkoxybenzenes

Jean-François Bartoli, Karine Le Barch, Magali Palacio, Pierrette Battioni and Daniel Mansuy*

UMR 8601, Université Paris V, 45 Rue des Saints-Pères, 75270 Paris Cedex 06, France.
E-mail: daniel.mansuy@biomedicate.univ-paris5.fr

Received (in Cambridge, UK) 11th June 2001, Accepted 26th July 2001
First published as an Advance Article on the web 29th August 2001

A series of iron porphyrins bearing one to eight β-nitro substituents were synthesized and evaluated as catalysts for hydrocarbon oxidation with H_2O_2; iron porphyrins bearing five or six β-nitro groups were the best catalysts for cyclooctene epoxidation and adamantane or anisole hydroxylation without need of a cocatalyst, and led to very different regioselectivities with either H_2O_2 or PhIO as oxidants, as shown by an unusual *ortho*-hydroxylation of alkoxybenzenes highly favored in the H_2O_2-dependent oxidations.

Three successive generations of Fe(III) porphyrins have been developed during the last fifteen years as catalysts mimicking cytochromes P450.[1–3] Recently, iron porphyrins bearing electronegative substituents have been shown to catalyze olefin epoxidation and alkane hydroxylation with H_2O_2 in aprotic solvents without cocatalysts.[4] However, iron porphyrin–H_2O_2 systems efficient for other difficult P450-type monooxygenations, such as aromatic hydroxylation, remain to be found.

Quite recently, we have reported a new general method for selective polynitration of a Zn(II) porphyrin which affords a full series of zinc porphyrins bearing one through to eight β-nitro groups in high yields.[5] This opens the way towards metalloporphyrins with a remarkably wide span of redox potentials.[5] This communication reports a first comparison of the catalytic properties of a full series of new iron(III) β-polynitroporphyrins, that became available by this method,[6] in oxidations of hydrocarbons with H_2O_2. It shows that some of them catalyze not only alkene epoxidation but also alkane and aromatic hydroxylation with H_2O_2, without the need of any cocatalyst, and with chemo- and regio-selectivities very different from those of the corresponding oxidations with PhIO.

Eqn. (1) shows the procedure that was used for preparing the

$$\text{Zn(TDCPP)} \xrightarrow[\text{HNO}_3,\ \text{CF}_3\text{SO}_3\text{H}]{(\text{CF}_3\text{SO}_2)_2\text{O}} \text{Zn(TDCPN}x\text{P)} \xrightarrow[\text{iii } \text{O}_2,\ \text{HCl}]{\text{i } \text{H}^+ \text{ ii } \text{FeBr}_2} \text{Fe(TDCPN}x\text{P)Cl} \quad (1)$$

eight iron porphyrins, Fe(III)(TDCPN*x*P)Cl bearing one through to eight β-nitro substituents (x = 1–8), from Zn(TDCPP).[7] The key step is a reaction of Zn(TDCPP) with increasing amounts of a HNO_3–CF_3SO_3H–$(CF_3SO_2)_2O$ mixture which leads to each compound of the Zn(TDCPN*x*P) series with yields between 50 and 95%.[5] All Zn(II) and Fe(III)Cl complexes of the TDCPN*x*PH_2 porphyrins were completely characterized by mass spectrometry, UV–VIS, ^{1}H NMR and EPR (for the iron complexes) spectroscopy; their detailed synthesis and characteristics will be published elsewhere. The reduction potential of the Fe(III)Cl complexes vary from −225 (for x = 0) to +660 mV (for x = 8) (*vs.* SCE[7]).

As shown in Table 1, Fe(TDCPP)Cl is a poor catalyst for cyclooctene expoxidation with H_2O_2 in CH_2Cl_2–MeCN, in accord with previous literature data.[3] Increasing the number of β-NO_2 substituents of the porphyrin led to a spectacular increase of the epoxidation yield from 5 to 90%. This optimal yield was obtained with Fe(TDCPN$_5$P)Cl, a further increase of the number of β-NO_2 substituents leading to much lower yields. Fe(TDCPN$_5$P)Cl was also the best catalyst for hydroxylation of adamantane with H_2O_2 with a total yield (1- and 2-adamantanols) of 35% based on starting H_2O_2. For this alkane, very low yields were found for Fe(TDCPP)Cl, with a progressive increase of the yield with catalysts bearing one through to four β-nitro groups and optimum yields for Fe(TDCPN$_5$P)Cl and Fe(TDCPN$_6$P)Cl.

A similar trend was observed for aromatic hydroxylation of anisole with H_2O_2 catalyzed by this iron porphyrin series. Fe(TDCPP)Cl is almost inactive for this reaction, whereas iron porphyrins bearing from three to six β-NO_2 substituents led to the formation of *ortho*- and *para*-hydroxylated products with total yields between 13 and 17% (Table 1). Interestingly, the regioselectivity of these Fe(TDCPN*x*P)Cl-catalyzed aromatic hydroxylations varies significantly as a function of x (Table 1). The *ortho*:*para* ratio is in favor of *para*-hydroxylation for x = 0, 1 and 2, whereas it progressively increases to values up to 5.5 for Fe(TDCPN$_6$P)Cl. This remarkable change of regioselectivity as a function of x should be due to a change in the nature and/or reactivity of the active species formed in these reactions. Possible involvement of further oxidations of *o*- and *p*-phenols in determining the *ortho*:*para* ratio is unlikely because of the

Table 1 Oxidation of cyclooctene, adamantane and anisole with H_2O_2 in the presence of the Fe(TDCPN$_x$P)Cl catalysts

Catalyst Fe(TDCPN*x*P)Cl		x = 0	1	2	3	4	5	6	7	8
Reaction		Yield[d] (%)								
Cyclooctene epoxidation[a]		5	20	48	68	80	90	15	6	2
Hydroxylation	ol-1	1.5	3	1.5	2	7	26	25	17	4
of adamantane[b]	ol-2	1	1.5	1	0.5	2.5	9	10	7	2
Hydroxylation	*p*-OH	1	2	3	5	6	3	2	1	2
of anisole[c]	*o*-OH	<1	<1	1.5	9.5	11	13.5	11	3	9
	o/*p*			0.5	1.9	1.8	4.5	5.5	3	4.5

[a] *Conditions*: catalyst:H_2O_2:cyclooctene molar ratio = 1:300:100 in CH_2Cl_2–MeCN (1:1) for 2 h at 20 °C, with [catalyst] = 1 mM. [b] *Conditions*: catalyst:H_2O_2:adamantane molar ratio = 1:40:300 in CH_2Cl_2–MeCN (1:1) for 2 h at 20 °C; [catalyst] = 1 mM. Small amounts of adamantan-2-one were also detected (yield < 1%). [c] *Conditions*: catalyst:H_2O_2:anisole molar ratio = 1:20:3000 in H_2O–MeCN (1:9); [catalyst] = 2 mM. *p*-OH and *o*-OH are used for *p*- and *o*-hydroxyanisole. [d] Yields are based on starting H_2O_2 except for cyclooctene epoxidations for which H_2O_2 was used in excess relative to substrate; yields for cyclooctene epoxidation were thus based on cyclooctene.

 DOI: 10.1039/b105101f

Table 2 Comparison of the Fe(TDCPN$_5$P)Cl-catalyzed oxidations of various substrates either with H_2O_2 or with PhIO

Substrate	Oxidant	Products (yield in %)[d]				
Adamantane[a]		ol-1	ol-2	one-2	ol-1/ol-2	
	PhIO	62	30	2	2.1	
	H_2O_2	26	9	< 1	2.9	
Limonene[b]		1,2-Oxide	8,9-Oxide	Oxide ratio	Carveols	Carvone
	PhIO	35	18	1.9	8	4
	H_2O_2	24	9	2.7	2	< 1
Anisole[c]		*o*-OH	*p*-OH	*o*/*p*	Phenol	
	PhIO	< 1	7	< 0.1	2	
	H_2O_2	11	4	2.75	4	
Ethoxybenzene[c]		*o*-OH	*p*-OH	*o*/*p*	Phenol	
	PhIO	< 1	8	< 0.1	2	
	H_2O_2	14	5	2.8	7	

[a] *Conditions*: Fe(TDCPN$_5$P)Cl : oxidant : adamantane molar ratio = 1 : 40 : 300 in CH_2Cl_2–MeCN (1 : 1) for 2 h at 20 °C; [catalyst] = 2 mM; o1-1, ol-2 and one-2 denote adamantan-1-ol, -2-ol and -2-one. [b] *Conditions*: Fe(TDCPN$_5$P)Cl : oxidant : limonene = 1 : 40 : 800 in CH_2Cl_2–MeCN (1 : 1). Carveols and carvone are the products resulting from allylic hydroxylation of limonene (at position 6).[3a] [c] *Conditions*: Fe(TDCPN$_5$P)Cl : oxidant : alkoxybenzene = 1 : 20 : 3000 in CH_2Cl_2–MeCN (1 : 1). *o*-OH and *p*-OH are used for the *ortho*- and *para*-hydroxylation products. [d] Yields are based on starting H_2O_2 or PhIO. All the experiments described in Tables 1 and 2 were usually performed under aerobic conditions. However, it is noteworthy that many experiments were also done under anaerobic conditions (under Ar) and gave almost identical results, showing that the observed regioselectivities were not affected by the presence of O_2.

huge excess of substrate used in these reactions (catalyst : H_2O_2 : substrate = 1 : 20 : 3000). Moreover, identical experiments performed under stoichiometric conditions (iron porphyrin : H_2O_2 : substrate = 1 : 1 : 3000) led to almost identical regioselectivities for anisole hydroxylation. It is noteworthy that the Fe(TDCPN*x*P)Cl catalysts were stable under the conditions described in Table 1. This was shown by their visible spectra that were found to be unchanged at the end of the reactions, and by their catalytic activity that remained almost identical after a further addition of H_2O_2 in the reaction medium.

The aforementioned results show the particular efficiency of iron porphyrins bearing around five β-nitro substituents to catalyze alkene epoxidation and alkane and aromatic hydroxylations with H_2O_2 in the absence of a cocatalyst. In order to have a first idea of the nature of the major active species responsible for these oxidations, we compared the oxidations of several substrates with H_2O_2 and Fe(TDCPN$_5$P)Cl to those performed with PhIO and the same catalyst under identical conditions. Table 2 clearly shows marked differences in the chemo- and regio-selectivities of the H_2O_2- and PhIO-dependent oxidations. This changes from small significant albeit small differences in the regioselectivity of adamantane hydroxylation (ol-1/ol-2 molar ratio of 2.9 with H_2O_2 *cf.* 2.1 with PhIO) and in the regioselectivity of limonene epoxidation (1,2 oxide/8,9 oxide = 2.7 *cf.* 1.9) to more dramatic differences in the regioselectivity of anisole and ethoxybenzene hydroxylations (major formation of *ortho*-hydroxylated products with H_2O_2 instead of almost exclusive *para* hydroxylation with PhIO).

Several years ago, a similar comparison between the chemo- and regio-selectivities of the oxidations of alkenes and alkanes with either PhIO or H_2O_2, in the presence of the Mn(TDCPP)Cl catalyst and imidazole cocatalyst, led to the conclusion that both systems involve the same active oxygen species, presumably a high-valent Mn=O complex.[3a] The results of Table 2 strongly suggest that the Fe(TDCPN$_5$P)Cl–H_2O_2 and Fe(TDCPN$_5$P)Cl–PhIO systems involve different active oxygen species. If one assumes that the active species formed with PhIO is a (por$^{+\cdot}$)Fe(IV)=O intermediate, as has been proposed for many other iron porphyrins,[1] one is led to the conclusion that different active species are involved in the H_2O_2-dependent oxidations. Several authors have already mentioned the possible formation of a ferric–hydroperoxo complex as an intermediate towards the high-valent iron–oxo species, in reactions of H_2O_2 with iron porphyrins[1,8] [eqn. (2)]. *Ortho*-hydroxylation of anisole from

$$(por)Fe^{III} + H_2O_2 \xrightarrow{-H^+} [(por)Fe^{III}\text{–}OOH] \xrightarrow[-H_2O]{+H^+} [(por^{+\cdot})Fe^{IV}{=}O] \quad (2)$$

transfer of the terminal oxygen atom of such a ferric–hydroperoxo complex should be less sterically restricted than the transfer of the oxygen atom of a high-valent (TDCPN*x*P) iron–oxo intermediate.[9] Preferential involvement of a Fe(III)–OOH intermediate in reaction of H_2O_2 with iron–β-polynitroporphyrins, which should be less prone to stabilize high-valent iron–oxo species, is likely and could explain the surprising regioselectivity observed in the hydroxylation of anisole and ethoxybenzene. However, additional experiments are necessary to determine the nature of the active intermediate(s) involved in reactions using H_2O_2 and iron–β-polynitroporphyrins. Nonetheless, the preliminary results reported here indicate that the Fe(TDCPN*x*P)Cl complexes with $x \geqslant 4$ are interesting catalysts for alkane and aromatic hydrocarbon oxidation with H_2O_2 without need of a cocatalyst, that lead to new regioselectivities, especially in the hydroxylation of aromatic molecules.

Notes and references

1 For a recent review, see: B. Meunier, A. Robert, G. Pratviel and J. Bernardou, in *The Porphyrin Handbook*, ed. K. M. Kadish, K. M. Smith and R. Guilard, Academic Press, New York, 1999, vol. 4, p. 119.

2 T. G. Traylor, C. Kim, K. L. Richards, F. Xu and C. L. Perrin, *J. Am. Chem. Soc.*, 1995, **117**, 3468.

3 P. Battioni, J. P. Renaud, J. F. Bartoli, M. Reina-Artiles, M. Fort and D. Mansuy, *J. Am. Chem. Soc.*, 1988, **110**, 8462.

4 (*a*) J. F. Bartoli, P. Battioni, W. R. De Foor and D. Mansuy, *J. Chem. Soc., Chem. Commun.*, 1994, 23; (*b*) S. Tsuchiya and M. Seno, *Chem. Lett.*, 1989, 263; (*c*) W. Nam, Y. M. Goh, Y. J. Lee, M. H. Lim and C. Kim, *Inorg. Chem.*, 1999, **38**, 3238; (*d*) E. Porhiel, A. Bondon and J. Leroy, *Tetrahedron Lett.*, 1998, **39**, 4829.

5 M. Palacio, V. Mansuy-Mouries, G. Loire, K. Le Barch-Ozette, P. Leduc, K. M. Barkigia, J. Fajer, P. Battioni and D. Mansuy, *Chem.Commun.*, 2000, 1907.

6 The only Fe(III)(β-polynitroporphyrin)complexes described so far[4a] have been obtained from a nitration method that only led to a mixture of penta- and hexa-nitroporphyrin derivatives.

7 TDCPP and TDCPN*x*P represent tetrameso(2,6-dichlorophenyl)porphyrin dianion and TDCPP bearing x β-NO_2 substituents ($1 \leqslant x \leqslant 8$) respectively; SCE = saturated calomel electrode.

8 W. Nam, M. H. Lim, H. J. Lee and C. Kim, *J. Am. Chem. Soc.*, 2000, **122**, 6641.

9 Previous literature data indicate that hydroxylation of anisole by Fe(TDCPP)Cl-based systems, that are believed to involve iron–oxo active species, mainly leads to *para*-hydroxyanisole: M. N. Carrier, C. Scheer, P. Gouvine, J. F. Bartoli, P. Battioni and D. Mansuy, *Tetrahedron Lett.*, 1990, **31**, 6645.

CHEMCOMM Communication
www.rsc.org/chemcomm

ITQ-16, a new zeolite family of the beta group with different proportions of polymorphs A, B and C

Avelino Corma,* Mª Teresa Navarro, Fernando Rey and Susana Valencia

Instituto de Tecnología Química, UPV-CSIC, Universidad Politécnica de Valencia, Avda. de los Naranjos s/n, 46022 Valencia, Spain. E-mail: acorma@itq.upv.es

Received (in Cambridge, UK) 13th June 2001, Accepted 1st August 2001
First published as an Advance Article on the web 29th August 2001

ITQ-16 is a new zeolite family formed by polymorphs A, B and C of the beta intergrowth in which the proportion of polymorph C can be controlled by changing the organic structure directing agent and/or by changing the Ge content of the synthesis gel; ITQ-16 can be synthesised either in fluoride or fluoride-free medium and Al can be introduced in the framework giving a material with very strong Brönsted acidity.

Beta is the only high silica zeolite with a three-dimensional system of 12-membered ring pores (MRP) that has found commercial applications up to now.[1] Zeolite beta is formed by an intergrowth of polymorphs A and B which gives the typical XRD pattern of this zeolite (Fig. 1).

Over 20 years ago, Newsam *et al*.[2] predicted that a third polymorph with a closely related structure should also exist. We have showed that polymorph C not only exists, but can be synthesised as a unique phase by working in either fluoride[3] or in OH^- fluoride free media.[4] The structure of polymorph C is formed by a three-dimensional system of rectilineous 12 MRP channels, and the corresponding XRD pattern is shown in Fig. 1.

In the present work, we show that it is possible now not only to synthesise the pure polymorph of C (ITQ-17), but also a new family of materials (ITQ-16) can be prepared where the three polymorphs A, B and C exist and the ratio C/(A + B) can be varied as desired. This can be achieved by using different organic structure directing agents (OSDAs) in the synthesis, and also by working in different ranges of gel compositions and crystallization conditions. It will be shown here that ITQ-16 can be synthesised in fluoride as well as in a fluoride-free media.

The general synthesis conditions employed in this work for the experiments in fluoride media were as follows:

$(1 - x)\ SiO_2 : x\ GeO_2 : 0.5\ R^1OH : 0.5\ HF : 8\ H_2O$ and
$(1 - x)\ SiO_2 : x\ GeO_2 : 0.25\ R^2(OH)_2 : 0.5\ HF : 8\ H_2O$

where R^1 and R^2 are the OSDAs shown in Scheme 1 and x was varied between 0.0196 and 0.1667. The OSDAs were prepared according to methods reported in the literature.[5] ITQ-16 zeolite was also synthesised in alkaline media, starting with the following gel compositions:

$(1 - y)\ SiO_2 : y\ GeO_2 : 0.5\ BzDOH : 3.5\ H_2O$ and
$0.8333\ SiO_2 : 0.1667\ GeO_2 : 0.25\ p\text{-}XydD(OH)_2 : 3.5\ H_2O$

where y was 0.0625 and 0.1667. For ITQ-16 synthesised by the alkaline route, 3 wt% (with respect to the total weight of SiO_2 and GeO_2) seeds of pure ITQ-17 zeolite were added to the synthesis gel in order to promote crystallisation.

The gels were autoclaved at 150 °C for different crystallisation times and the solids were recovered by filtration and then were extensively washed with distilled water and dried at 100 °C, overnight. Table 1 shows the synthesis conditions studied in this work as well as the crystalline phase obtained in the final solids.

Syntheses 1–5 show that the level of polymorph C present in the final solid obtained from the same starting synthesis gel can be varied by using different organic structure directing agents. In this way, p-$XydD^{2+}$ (sample 2) and BzD^+ (sample 1) give pure polymorph C, while BzQ^+ (sample 3) gives a mixture of the three polymorphs (Fig. 2). ITQ-16 can also be obtained with other OSDAs, such as $dPyrrP^{2+}$ and in this case a different ratio of C/(A+B) polymorphs is observed (Fig. 2, sample 4). It is noted that polymorph C is not detected when using TEA^+ (sample 5) as the OSDA in the same synthesis conditions.

The ratio of the three polymorphs in ITQ-16 can also be controlled by modifying the cation composition of the synthesis gel. For instance, when using BzD^+ as the OSDA, it can be seen in Fig. 3 that the proportion of polymorph C increases when increasing the Ge content of the synthesis gel (Table 1; samples 1, 6–9).

ITQ-16 can also be synthesised in fluoride-free alkaline media. In this case, highly concentrated gels and longer crystallisation periods are required for the synthesis of ITQ-16 (Table 1; samples 10–12). The formation of ITQ-16 in alkaline

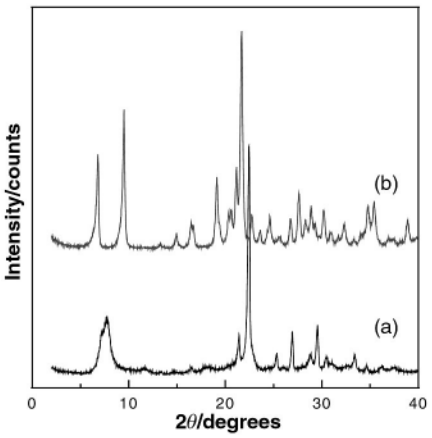

Fig. 1 X-Ray diffraction patterns of as-prepared zeolite beta (a) and pure polymorph C (ITQ-17) (b).

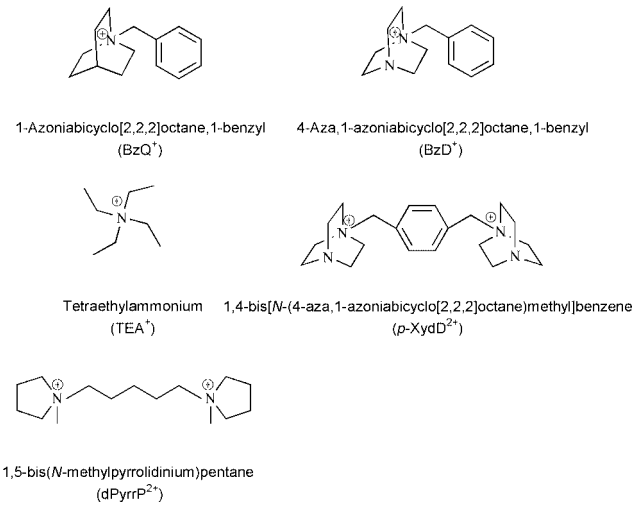

Scheme 1

 DOI: 10.1039/b105206n

Table 1 Synthesis conditions and zeolitic structures obtained using different OSDAs and Ge contents in the crystallisation gel

Sample	Crystallisation time	OSDA	Ge/(Si + Ge)	Structure	Percentage of polymorph C[a]
1	13 h	BzD^+	0.0625	ITQ-17	100
2	19 h	*p*-$XydD^{2+}$	0.0625	ITQ-17	100
3	20 h	BzQ^+	0.0625	ITQ-16	46
4	12 d	$dPyrrP^{2+}$	0.0625	ITQ-16	31
5	24 h	TEA^+	0.0625	Beta	0
6	14 h	BzD^+	0.1667	ITQ-17	100
7	15 h	BzD^+	0.0385	ITQ-16	85
8	48 h	BzD^+	0.0278	ITQ-16	52
9	13 h	BzD^+	0.0196	ITQ-16	27
10[b]	5 d	*p*-$XydD^{2+}$	0.1667	ITQ-16	66
11[b]	6 d	BzD^+	0.1667	ITQ-16	48
12[b]	7 d	BzD^+	0.0625	ITQ-16	40

[a] The percentage of polymorph C was estimated from the XRD patterns as the integrated area below the characteristic peaks at *ca.* 7.0 and 9.5° with respect to the total area in the range 5–12°. [b] Syntheses carried out in alkaline fluoride-free gels.

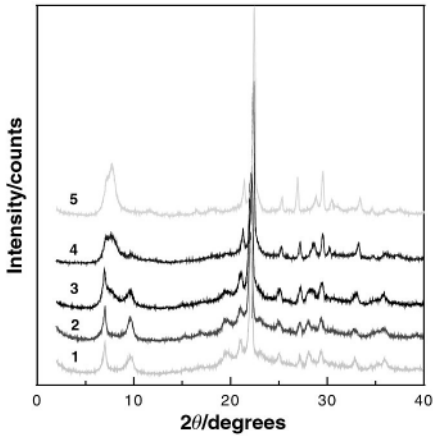

Fig. 2 X-Ray diffraction patterns of as-prepared ITQ-16 zeolites synthesised with different OSDAs (samples of Table 1).

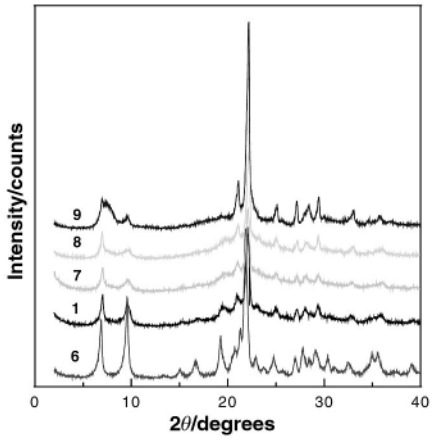

Fig. 3 X-Ray diffraction patterns of as-prepared ITQ-16 zeolites synthesised from gels with different Ge content (samples of Table 1).

media requires lower Si/Ge ratios than when the synthesis was carried out in fluoride media. Thus, it appears that Ge plays a very important role in driving the synthesis towards the formation of polymorph C between the other possible polymorphs which constitute the beta zeolite intergrowth.

For practical catalytic uses it is interesting to introduce acidity in the samples. We have succeeded in incorporating isomorphically Al into the ITQ-16, and one of the possible synthesis gel compositions is given below.

$$0.9375\ SiO_2 : 0.0625\ GeO_2 : 0.5\ BzDOH : 0.5\ HF : 20\ H_2O : 0.02\ Al_2O_3$$

An Al-ITQ-16 material was obtained after 10 days of crystallisation at 150 °C. The resulting Al-ITQ-16 shows a unique resonance peak at 53 ppm in the ^{27}Al MAS NMR spectrum assigned to the presence of Al in tetrahedral coordination.

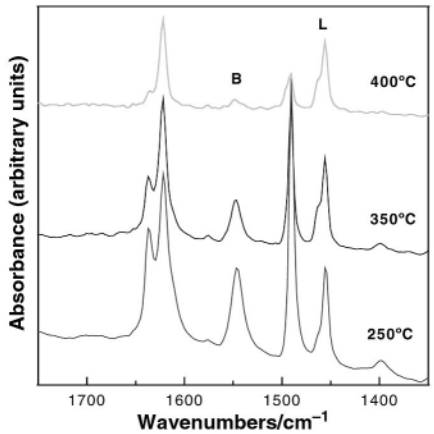

Fig. 4 IR spectra of adsorbed pyridine of the Al-ITQ-16 sample at different desorption temperatures (B and L indicate the characteristic IR bands of pyridine adsorbed on Brönsted and Lewis acid sites, respectively).

Acidity was measured after calcination of the sample at 500 °C, by means of pyridine adsorption–desorption. The IR spectra of adsorbed pyridine (Fig. 4) indicate the formation of pyridinium ions (*ca.* 1545 cm^{-1}) associated with the presence of Brönsted acid sites, as well as a band of pyridine coordinated to extraframework or partially dislodged Lewis acid Al atoms generated upon calcination (*ca.* 1450 cm^{-1}). It can be seen in Fig. 4 that Brönsted acid sites have been generated by the introduction of framework Al, and some of these sites can retain pyridine upon desorption at 350 and 400 °C and 10^{-2} Torr, indicating the presence of very strong acid sites in Al-ITQ-16.

In conclusion, ITQ-16 is formed by polymorphs A, B and C, and the proportion of polymorph C in the sample can be controlled by changing the organic structure directing agent and/or by changing the Ge content of the synthesis gel. ITQ-16 can be synthesized either in fluoride or fluoride-free medium and Al can be introduced in the framework giving a material with very strong Brönsted acidity.

Notes and references

1 C. Flego, G. Pazzuconi, E. Bencini and C. Perego, *Stud. Surf. Sci. Catal.*, 1999, **126**, 461.

2 J. M. Newsam, M. M. J. Treacy, W. T. Koetsier and C. B. de Gruyter, *Proc. R. Soc. London A*, 1988, **420**, 375.

3 A. Corma, M. T. Navarro, F. Rey, J. Rius and S. Valencia, *Angew. Chem., Int. Ed.*, 2001, **40**, 2277.

4 A. Corma, M. T. Navarro, F. Rey and S. Valencia, *Chem. Commun.*, 2001, 1486.

5 J. March, *Advanced Organic Chemistry, Reactions, Mechanisms and Structure*, John Wiley & Sons, New York, 4th edn., 1992, pp. 411 and references therein.

CHEMCOMM Communication
www.rsc.org/chemcomm

Enantioselective deprotonation reactions using polymer-supported chiral magnesium amide bases†

Kenneth W. Henderson,* William J. Kerr* and Jennifer H. Moir

Department of Pure and Applied Chemistry, University of Strathclyde, 295 Cathedral Street, Glasgow, Scotland, UK G1 1XL. E-mail: w.kerr@strath.ac.uk

Received (in Cambridge, UK) 18th May 2001, Accepted 25th July 2001
First published as an Advance Article on the web 28th August 2001

Novel and readily accessible polymer-supported chiral magnesium amide reagents have been prepared and shown to be effective in the asymmetric deprotonation of a series of prochiral cyclohexanones, affording good to excellent levels of both conversion and enantiomeric ratio (up to 93:7); the Merrifield-based chiral amine species has been shown to be readily recyclable.

The application of chiral lithium amide base reagents within asymmetric organic synthesis is widespread.[1] Additionally we have recently disclosed the preparation of a novel homochiral magnesium amide base and have shown it to be particularly effective in the desymmetrisation of both 4-substituted and 2,6-disubstituted cyclohexanones; the initially reported processes afforded the corresponding silyl enol ethers in up to 95:5 er.[2] Consequently, with a view to gaining the practical and economic advantages offered by solid phase chemistry,[3] we envisioned that tethering the chiral amine, and ultimately the Mg-amide, to a polymer support[4] would provide a convenient and potentially recyclable enantioselective reaction source. Furthermore and at least as importantly, based on our drive to alter the nature of the base itself, we believed that this approach would also allow the establishment of a library of supported chiral amines and, in turn, resin-bound Mg-amides, which would enable an effective assessment of the key structural requirements for the optimisation of such enantioselective reagents. Herein, we report our initial studies in this area and, more specifically, the first use of a polymer-supported chiral Mg-amide base to mediate enantioselective deprotonation processes.

At the outset of this programme, the simple and readily accessible Merrifield resin **1**[5] formed an attractive starting point for direct functionalisation with (*R*)-α-methylbenzylamine. The process shown in Scheme 1 cleanly afforded the supported chiral amine (*R*)-**2**.‡

Having established a practically efficient approach to the preparation of (*R*)-**2**, its use as a Mg-amide derivative was then evaluated in the enantioselective deprotonation of **3a**. Optimum formation of the requisite Mg-amide species occurred following reflux of (*R*)-**2** with dibutylmagnesium for 90 min in THF.§ On cooling the resin-bound base to −78 °C, we were pleased to observe the first asymmetric deprotonations with our new supported reagent. As shown in Scheme 2, in the presence of 0.5 mol equiv. of DMPU and excess TMSCl, good levels of both conversion of **3a** to (*S*)-**4a** (78%) and enantiomeric ratio (74:26 er) were achieved.†

Based on this experimental protocol, we moved on to consider the desymmetrisation reaction of a series of alternative prochiral cyclohexanones **3** using our Merrifield-based chiral

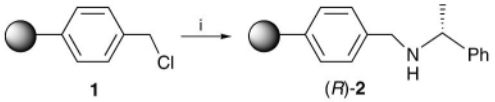

1 (*R*)-**2**

Scheme 1 *Reagents and conditions*: i, (*R*)-α-methylbenzylamine (3 eq.), NaI (1 eq.), DMF, 48 h.

† Electronic supplementary information (ESI) available: representative experimental procedure. See http://www.rsc.org/suppdata/cc/b1/b104417f/

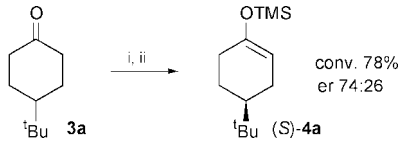

Scheme 2 *Reagents and conditions*: i, (*R*)-**2** (2 eq.), Bu_2Mg (1 eq.), THF, reflux, 90 min; ii, TMSCl (4 eq.), DMPU (0.5 eq.), THF, −78 °C, 4 h.

amine resin (*R*)-**2** (Table 1). At −78 °C the 4-substituted cyclohexanones **3a–d** all showed good levels of conversion and gave enol ethers (*S*)-**4a–d** with enantiomeric ratios of up to 75:25. With the 2,6-disubstituted substrates, higher temperatures were required to achieve acceptable levels of conversion. However, when all ketones (**3a–f**) employed here are considered, it should be noted that at room temperature higher conversions were achieved in almost every instance with, at worst, only small reductions in the recorded enantiomeric ratios. Indeed, the enantioselection observed upon reaction of *cis*-**3e** and *cis*-**3f** appears largely independent of temperature. Furthermore reaction of *cis*-diisopropylcyclohex-

Table 1 Enantioselective deprotonations using Merrifield-based amine (*R*)-**2**[a]

Ketone	Product	Temp.	*t*/h	Conversion (%)[b]	er[c]
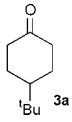	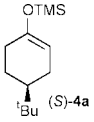	−78 °C	4	78	74:26
		rt	2	91	65:35
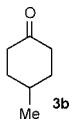	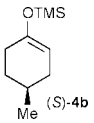	−78 °C	4	74	68:32
		rt	2	94	64:36
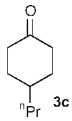	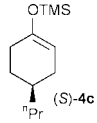	−78 °C	4	85	74:26
		rt	2	91	68:32
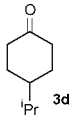	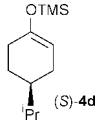	−78 °C	4	89	75:25
		rt	2	88	69:31
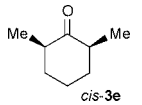	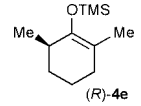	−78 °C	43	7	76:24
		−40 °C	24	86	73:27
		rt	2	98	75:25
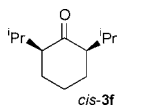	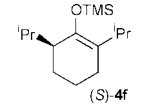	−78 °C	19	2	—
		−40 °C	68	69	91:9
		rt	2	97	93:7

[a] *Reagents and conditions*: i, (*R*)-**2** (2 eq), Bu_2Mg (1 eq.), THF, reflux, 90 min; ii, TMSCl (4 eq), DMPU (0.5 eq.), ketone (0.8 eq.), THF.† [b] Conversions were determined by GC analysis. [c] See footnote¶.

 DOI: 10.1039/b104417f

Table 2 Enantioselective deprotonation of **3a** using recycled amine (*R*)-**2**

Cycle	Temp.	*t*/h	Conversion (%)	er (*S*):(*R*)
1	rt	2	91	65:35
2	rt	2	97	65:35
3	rt	2	86	65:35
4	rt	2	91	66:34
5	rt	2	92	66:34
6	−78 °C	4	71	73:27

anone *cis*-**3f** gives a 97% conversion and an outstanding er of 93:7 even at room temperature. As such, this method affords us a practically convenient method by which to generate high levels of asymmetric induction in the deprotonation of specific 2,6-disubstituted cyclohexanones.¶

In addition to establishing the initial deprotonation strategies using our Merrifield-based Mg-amide, we were also keen to develop an efficient recycling protocol. In this respect, following completion of reaction, the parent polymer-bound chiral amine (*R*)-**2** was readily regenerated by consecutively washing the resin with a 2:1 mixture of THF–HCl (1 M) and then, to liberate the amine from the HCl salt, with 10% $^{i}Pr_2NEt$ in DMF. This process opened up the possibility of re-using the supported chiral amine and, as such, we can now report that (*R*)-**2** can, indeed, be recycled up to and over 5 times. More specifically, in a series of deprotonations of **3a** to afford (*S*)-**4a**, no appreciable drop in conversion was noted and the enantiomeric ratio remained consistent throughout (Table 2). Furthermore, after 5 cycles at room temperature, the resin was also able to show a return to the enhanced levels of asymmetric induction observed at −78 °C (Cycle 6), thus demonstrating the durability of the tethered amine.‖

Having successfully optimised our deprotonation strategy using the accessible and readily recyclable Merrifield-based chiral amine resin (*R*)-**2**, we moved on to explore the effects of alternative polystyrene supports on the enantioselective potential of the resin-bound Mg-amide, In this respect, a soluble polystyrene resin[8] was prepared and, subsequently, functionalised with (*R*)-α-methylbenzylamine to afford the supported amine (*R*)-**5** (Scheme 3).‡ With this material in hand, we went on to assess the performance of (*R*)-**5**, as the Mg-amide, in the enantioselective deprotonation reaction of a selection of ketones. Pleasingly, as can be seen in Table 3, with **3a** and **3d** this new soluble resin-bound species provided excellent reaction conversions and, moreover, delivered enhanced levels of enantiomeric ratio at both room temperature and at −78 °C. One again, (*S*)-**4f** was formed in excellent er and with no appreciable difference in enantioselection being observed between room temperature and −40 °C.

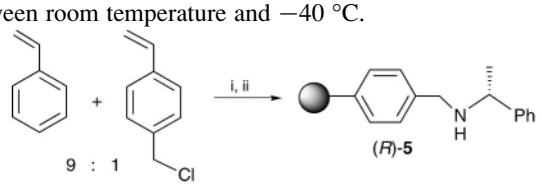

Scheme 3 *Reagents and conditions*: i, AIBN, toluene, 70 °C, 40 h; ii, (*R*)-α-methylbenzylamine (3 eq.), NaI (1 eq.), DMF, 48 h.

In conclusion, we have successfully prepared two distinct polymeric species posessing chiral amino functionality and, in turn, chiral Mg-amide units and both of these have been shown to be effective in the enantioselective deprotonation reaction of a variety of 4-substituted and, more particularly, 2,6-disubstituted cyclohexanones. Moreover, moderate to high levels of asymmetric induction (up to 93:7 er) were observed, even during reactions performed at room temperature. In addition, the supported chiral amine derived from Merrifield resin was found to be efficiently recycled for further use within the

Table 3 Enantioselective deprotonations using soluble supported amine (*R*)-**5**[a]

Ketone	Product	Temp.	*t*/h	Conversion (%)	er
3a	(*S*)-**4a**	−78 °C	4	91	83:17[b]
		rt	2	>99	70:30
3d	(*S*)-**4d**	−78 °C	4	82	80:20
		rt	2	96	71:29
cis-**3f**	(*S*)-**4f**	−40 °C	24	67	93:7
		rt	2	>99	93:7

[a] *Reagents and conditions*: i, (*R*)-**2** (2 eq.), Bu_2Mg (1 eq.), THF, reflux, 90 min; ii, TMSCl (4 eq.), DMPU (0.5 eq.), ketone (0.8 eq.), THF. [b] This result is comparable with that observed in our unsupported base studies (−78 °C, 6 h; 89% conv., 90:10 er); see ref. 2.

deprotonation protocols. Indeed, it is envisaged that this facet of the supported Mg-amide chemistry disclosed here will be of considerable benefit when employing more precious chiral amines, which are either commercially unavailable or have required multi-step generation. The application of this methodology to the preparation of a library of chiral Mg-amide reagents and the use of other resins is underway and will be reported in due course.

We gratefully acknowledge The Carnegie Trust for the Universities of Scotland for a postgraduate studentship (J. H. M.) and The Royal Society of a University Research Fellowship (K. W. H.). We also thank Dr J. Cai and Dr W. B. Wathey at Organon Laboratories, for many helpful discussions and the generous donation of materials, and the EPSRC Mass Spectrometry Service, University of Wales, Swansea for analyses.

Notes and references

‡ The amine loading level was established by derivatisation with FmocCl, followed by UV analysis of the subsequent cleavage reaction.[6] This routinely showed an amine loading of 1.30–1.40 mmol g^{-1} for (*R*)-**2** and 1.00 mmol g^{-1} for (*R*)-**5**.

§ It should be noted that whilst the production of a resin-bound Mg-bisamide reagent is supposed, the possible formation of some alkyl(Bu)-Mg-amide species must also be recognised. A control experiment performed between Bu_2Mg and **3a** gave no reaction, even at room temperature. Based on this observation, it is believed that the presence of such an alkyl–Mg intermediate would have no adverse affect on the deprotonation process.

¶ Enantiomeric ratios were determined by GC analysis. Additionally, the absolute configuration of the major and minor enantiomers for **4a**, **4b**, **4d**, and **4e** were assigned by correlation of optical rotation measurements with those of Koga and co-workers (ref. 7); for **4c** and **4f** the major and minor isomer configurations were tentatively assigned by comparison with **4a**, **b**, and **d**, and **4e**, respectively. All compounds also exhibited satisfactory analytical and spectral data.

‖ It should be noted that resin (*R*)-**2** was also effectively recycled following the initial reaction of *cis*-**3f** at room temperature, and afforded a >99% conversion and 93:7 er.

1 For recent reviews, see: P. O'Brien, *J. Chem. Soc., Perkin Trans. 1*, 2001, 95; P. O'Brien, *J. Chem. Soc., Perkin Trans. 1*, 1998, 1439.
2 K. W. Henderson, W. J. Kerr and J. H. Moir, *Chem. Commun.*, 2000, 479.
3 S. V. Ley, I. R. Baxendale, R. N. Bream, P. S. Jackson, A. G. Leach, D. A. Longbottom, M. Nesi, J. S. Scott, R. I. Storer and S. J. Taylor, *J. Chem. Soc., Perkin Trans. 1*, 2001, 3815; R. H. Drewry, D. M. Coe and S. Poon, *Med. Res. Rev.*, 1999, **19**, 97; S. J. Shuttleworth, S. M. Allin and P. K. Sharma, *Synthesis*, 1997, 1217.
4 M. Majewski, A. Ulaczyk and F. Wang, *Tetrahedron Lett.*, 1999, **40**, 8755.
5 Polymer Laboratories Ltd, Essex Road, Church Stretton, Shropshire, UK SY6 6AX; loading: 1.88 mmol g^{-1}; 1% cross-linking.
6 E. Atherton and R. C. Sheppard, *Solid Phase Peptide Synthesis, A Practical Approach*, IRL Press, Oxford, 1989.
7 K. Aoki, H. Noguchi, K. Tomioka and K. Koga, *Tetrahedron Lett.*, 1993, **34**, 5105; H. Kim, R. Shirai, H. Kawasaki, M. Nakajima and K. Koga, *Heterocycles*, 1990, **30**, 307.
8 M. Narita, *Bull. Chem. Soc. Jpn.*, 1978, **51**, 1477. For a review on soluble polymer-supported reagents in organic synthesis, see: P. H. Toy and K. D. Janda, *Acc. Chem. Res.*, 2000, **33**, 546.

CHEMCOMM Communication
www.rsc.org/chemcomm

Generation of chromioenamines by reduction of *O*-acetyloximes with chromium(II) and their application†

Kazuhiko Takai,* Noriko Katsura and Yuji Kunisada

Department of Applied Chemistry, Faculty of Engineering, Okayama University, Tsushima, Okayama 700-8530, Japan. E-mail: ktakai@cc.okayama-u.ac.jp

Received (in Cambridge, UK) 19th June 2001, Accepted 24th July 2001
First published as an Advance Article on the web 13th August 2001

Chromioenamines can be generated by treatment of *O*-acetyloximes with chromium(II) *via* two steps of one-electron reduction and successive isomerization, and the species react with aldehydes to give γ-amino alcohols after reduction with $LiAlH_4$.

Treatment of *O*-acetyloximes **1** with low valent metals such as Cr(II) and Ti(III) under aqueous conditions is a mild deoximation procedure.[1] The process includes the reductive cleavage of N–O bonds leading to *N*-metal imines **3**[2] *via* iminyl radicals **2**,[3] and the hydrolysis of the formed imines to obtain ketones [eqn. (1)].

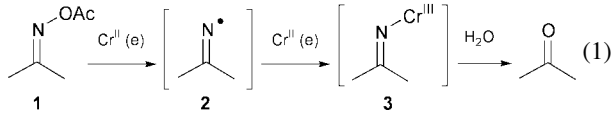

1 2 3 (1)

In order to examine the utilization of the formed reactive species **2** or **3** for carbon–carbon formation, we conducted the chromium(II)-mediated deoximation in aprotic solvents.[4]

The *O*-acetyloxime **4** was treated with 2 equiv. of chromium(II) chloride in the presence of 10 equiv. of methyl acrylate to give the corresponding deoximated ketone **5** in 88% yield after hydrolysis [eqn. (2)]. Nitrogen-containing five-membered

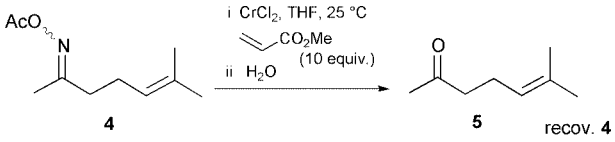

4 5 recov. 4

$CrCl_2$	2.0 equiv.	88%	0%
	1.0 equiv.	44%	44%

(2)

ring compounds derived *via* intramolecular radical cyclization were not observed,[3] and no coupling product between **4** and the acrylate was obtained. When the amount of chromium(II) chloride was reduced to 1 equiv. of the oxime **4**, the ketone **5** was obtained in 44% yield and **4** was recovered in 44% yield. These results suggest that the second one-electron reduction of the iminyl radical **2** to the *N*-chromium imine **3** proceeds faster than the first reduction of **1** to **2**.

Trapping of the formed *N*-chromium imine **3** was examined. Although the reduction of the cyclohexanone *O*-acetyloxime **6** with $CrCl_2$ in the presence of Me_3SiCl resulted only in deoximation leading to cyclohexanone, the reduction in the presence of the benzoyl chloride gave **7** in 70% yield along with benzamide in 8% yield [eqn. (3)].[1b] The expected *N*-acyl imine

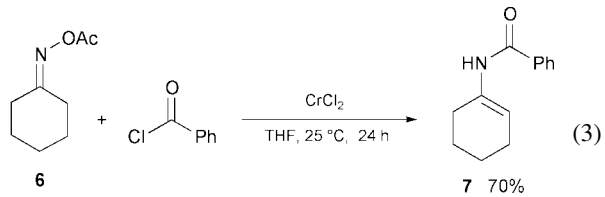

6 7 70% (3)

† Electronic supplementary information (ESI) available: experimental section. See http://www.rsc.org/suppdata/cc/b1/b105357b/

derived from *N*-chromium imine **3** was not obtained, and instead a chromioenamine was trapped as **7**.

Thus, carbon–carbon bond formation with this chromioenamine[5] was investigated in the presence of an aldehyde in the aprotic solvent. Treatment of a mixture of acetone *O*-acetyloxime (**8**, 2 equiv.) and benzaldehyde with $CrCl_2$ (8 equiv.) in THF at 25 °C for 24 h followed by hydrolysis with water gave 4-phenyl-4-hydroxybutan-2-one (**9**) in 23% yield. The quenching procedure affected the yields considerably, probably due to the strong chelation of the adducts to chromium(III). The yield was improved to 88% by quenching with aqueous NaF solution (Table 1 run 2).[6–8] Although the reaction proceeded more slowly in the case of aliphatic aldehydes, addition of a catalytic amount of $NiCl_2$ accelerated the reaction rate and improved the yields.[9]

A possible mechanism is shown in Scheme 1. One electron reduction of an *O*-acetyloxime with chromium(II) gives the

Table 1 Aldol reactions between *O*-acetyloximes and aldehydes with chromium(II)[a]

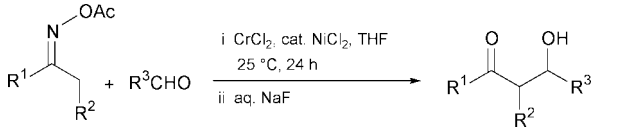

Run	R^1	R^2	R^3	Yield (%)[b]	*syn*–*anti*[c]
1	Me	H (**8**)	Ph	84[d] (**9**)	—
2		**8**	Ph	88[e]	—
3		**8**	n-C_8H_{17}	67	—
4		**8**	c-C_6H_{11}	74	—
5		-$(CH_2)_4$- (**6**)	Ph	81[ef]	36:64
6		**6**	$Ph(CH_2)_2$	54[e]	6:94

[a] Reaction conditions as in typical procedure (ESI) unless otherwise stated. [b] Isolated yields. [c] Isomer ratios were determined by isolation and/or NMR. [d] The reaction was completed in 8 h. [e] The reaction was conducted without addition of $NiCl_2$. [f] 8 mol of $CrCl_2$ was used per mol of benzaldehyde.

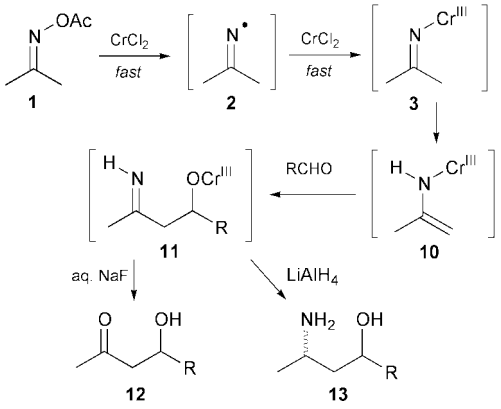

Scheme 1 A possible mechanism for the coupling reaction.

 DOI: 10.1039/b105357b

imine radical **2**,[3] which is then subjected to the second one electron reduction to give **3**. The imine **3** is isomerized to chromioenamine **10**,[1d,10] and the chromioenamine reacts with an aldehyde to give **11**.[11] Hydrolysis of **11** gives the aldol adduct **12**. Metalloenamines are usually prepared by deprotonation of imine derivatives with strong bases,[5] however, the procedure does not require such bases. Attempts to reduce the amount of chromium(II) with manganese and Me_3SiCl resulted in deoximation probably due to the fast trapping of the chromium imine **3** or the chromioenamine **10** with Me_3SiCl.[12]

When *anti*- and *syn*-**4** were employed in the reaction, almost the same product distributions were observed [eqn. (4)]. The

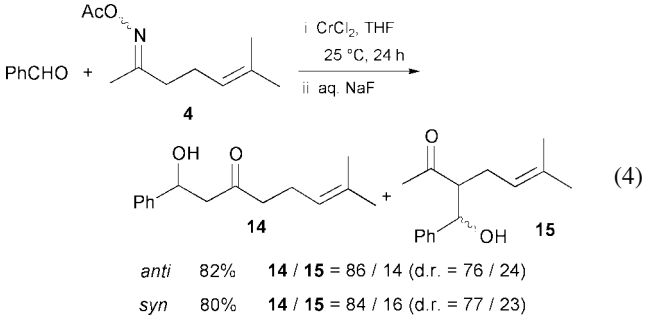

(4)

major product was an aldol adduct **14** at the less hindered carbon. This result supports the proposed Scheme 1, in which the two reactions involve the same iminyl radical as the intermediate.

In order to utilize the nitrogen-containing adduct **11**, reduction of **11** leading to a γ-amino alcohol **13** was examined.[13] A mixture obtained from **8** and benzaldehyde was treated with $LiAlH_4$ (10 equiv.) at −78 °C, and the temperature of the mixture was gradually raised to 0 °C. Quenching of the mixture with alkaline NaF solution followed by acetylation gave the acetylated γ-amino alcohol **16** in 79% yield [eqn. (5)].[14,15] The yield was increased by addition of a catalytic

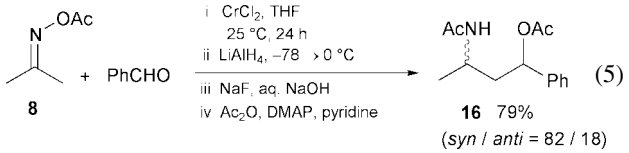

(5)

amount of $NiCl_2$. The results of the preparation of γ-amino alcohols from *O*-acetyloximes and aldehydes with $CrCl_2$ and $NiCl_2$ are summarized in Table 2.

In conclusion, chromioenamines are generated by treatment of *O*-acetyloximes with chromium(II) *via* sequential reduction and isomerization. These react with aldehydes to obtain γ-amino alcohols after reduction with $LiAlH_4$. The reaction proceeds under mild conditions and does not require strong bases such as LDA.

This work was supported by a Grant-in-Aid from the Ministry of Education, Culture, Sports, Science and Technology of Japan.

Table 2 Preparation of γ-amino alcohols from *O*-acetyloximes and aldehydes[a]

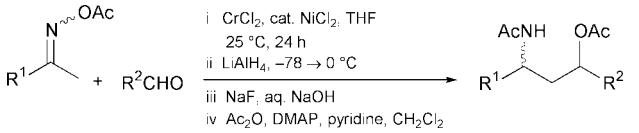

Run	R^1	R^2	Yield (%)[b]	*syn–anti*[c]
1	Me (**8**)	Ph	86 (**16**)	70:30
2	**8**	Ph	79[d]	82:18
3	**8**	$Ph(CH_2)_2$	65	69:31
4	**8**	c-C_6H_{11}	71	69:31
5	Ph (**17**)	Ph	88	42:58
6	**17**	$Ph(CH_2)_2$	70	53:47
7	**17**	c-C_6H_{11}	71	54:46

[a] Reaction conditions as in typical procedure (ESI) unless otherwise stated. [b] Isolated yields. [c] Isomer ratios were determined by isolation and/or NMR. [d] The reaction was conducted without addition of $NiCl_2$.

Notes and references

1 (*a*) Cr: E. J. Corey and J. E. Richman, *J. Am. Chem. Soc*., 1970, **92**, 5276; (*b*) R. B. Boar, J. F. McGhie, M. Robinson, D. H. R. Barton, D. Horwell and R. V. Stick, *J. Chem. Soc., Perkin Trans. 1*, 1975, 1237; (*c*) Ti: G. H. Timms and E. Wildsmith, *Tetrahedron Lett*., 1971, 195; (*d*) D. H. R. Barton and S. Z. Zard, *J. Chem. Soc., Perkin Trans. 1*, 1985, 2191.

2 H. Tsutsui and K. Narasaka, *Chem. Lett*., 1999, 45.

3 Ni: J. Boivin, A.-M. Schiano, S. Z. Zard and H. Zhang, *Tetrahedron Lett*., 1999, **40**, 4531; J. Boivin, E. Fouquet and S. Z. Zard, *Tetrahedron Lett*., 1990, **31**, 3545.

4 We thank Mr Shigeki Nakatsukasa of Kyoto University for conducting an initial investigation of chromioenamines.

5 For metalloenamines, see: S. F. Martin, *Comprehensive Organic Synthesis*, ed. B. M. Trost and I. Fleming, Pergamon, Oxford, 1991, vol. 2, ch. 1.16, p. 475.

6 The yield was improved to 92% when the mixture was quenched with aq. NaF solution for 48 h.

7 Among the oxime derivatives examined, *O*-acetyl gave the best result. Results with the other oxime derivatives are as follows: *O*-benzoyloxime, 58%; *O*-mesyloxime, 75%; *O*-tosyloxime, 47%; *O*-trimethylsilyloxime, 12%.

8 Although the amounts of *O*-acetyloxime and chromium(II) chloride can be reduced to 1.2 and 3.6 equiv., respectively, without affecting the yield, the couplings required longer reaction times.

9 (*a*) K. Takai, M. Tagashira, T. Kuroda, K. Oshima, K. Utimoto and H. Nozaki, *J. Am. Chem. Soc*., 1986, **108**, 6048; (*b*) S. Py, C. W. Harwig, S. Banerjee, D. L. Brown and A. G. Fallis, *Tetrahedron Lett*., 1998, **39**, 6139.

10 (*a*) J. V. Braun and W. Rudolph, *Ber*., 1934, **67B**, 269; (*b*) For reverse isomerization, see: K. A. Miller, T. W. Watson, J. E. Bender IV, M. M. Banaszak-Hall and J. F. Kampf, *J. Am. Chem. Soc*., 2001, **123**, 982.

11 J.-E. Dubois, G. Axiotis and E. Bertounesque, *Tetrahedron Lett*., 1985, **26**, 4371; L. Wessjohann and T. Gabriel, *J. Org. Chem*., 1997, **62**, 3772.

12 A. Fürstner and N. Shi, *J. Am. Chem. Soc*., 1996, **118**, 12349.

13 K. Narasaka, Y. Ukaji and S. Yamazaki, *Bull. Chem. Soc. Jpn*., 1986, **59**, 525.

14 Because chromium(III) salts can be reduced with $LiAlH_4$, an excess amount of the hydride source was required to complete the reduction. See: Y. Okude, S. Hirano, T. Hiyama and H. Nozaki, *J. Am. Chem. Soc*., 1977, **99**, 3179.

15 The following reducing agents were examined: i-Bu_2AlH (51% yield, *syn–anti* = 72:28), $Na(MeOCH_2CH_2O)_3AlH$ (10%, 33:67); $LiEt_3BH$ (10%, 68:32), Li(*sec*-Bu)$_3$BH (35%, 63:37).

CHEMCOMM Communication
www.rsc.org/chemcomm

Synthesis and application of novel catalytically active polymers containing 1,4,7-triazacyclononanes†

Achim Grenz, Simona Ceccarelli and Carsten Bolm*

Institut für Organische Chemie der RWTH Aachen, Professor-Pirlet-Straße 1, D-52056 Aachen, Germany. E-mail: Carsten.Bolm@oc.rwth-aachen.de; Fax: +49 (0)241 8888391; Tel: +49 (0)241 804675

Received (in Cambridge, UK) 26th June 2001, Accepted 30th July 2001
First published as an Advance Article on the web 29th August 2001

New polymers containing 1,4,7-triazacyclononanes have been synthesised by means of ring opening metathesis polymerisation (ROMP); their complexes with Mn(II) catalyse the oxidation of simple olefins by hydrogen peroxide.

The ongoing interest in environmentally benign processes for oxidations of simple organic molecules has led to the development of various catalytic systems for the activation of H_2O_2. Among these, manganese–triazacyclononane complexes have received considerable attention in recent years.[1] Simple protocols allow epoxidations to be performed in water–cosolvent mixtures using catalytic amounts of such complexes and hydrogen peroxide as stoichiometric oxidant. However, separation and recycling of the catalysts are still major challenges, and several strategies have already been investigated. For example, triazacyclononanes (TACNs) have been linked to silica affording heterogeneous systems, which can easily be recovered by filtration.[2] Alternatively, perfluorinated side chains were introduced onto the TACN in order to allow for fluorous biphasic catalysis (FBC).[3] Unfortunately, most of these approaches led to systems with reduced catalytic activity and lower product selectivity. Thus, a feasible immobilization strategy which allows maintenance of the positive attributes of the 'free' triazacyclononane–manganese system is still missing. In this work, we now present the synthesis of polymeric structures bearing a dense arrangement of 1,4,7-triazacyclononane moieties by application of ROMP.[4] With hydrogen peroxide as terminal oxidant manganese complexes of such polymeric ligands efficiently catalyse epoxidations of simple olefins exhibiting activities and selectivities which are comparable to those of the monomeric systems. Allylic and benzylic alcohols are also oxidised. In the case of conjugated alkenes, other oxidation products (*e.g.* diols) are formed as well.

Monomer **4** containing a polymerisable norbornene‡ element and a 1,4,7-triazacyclonane unit was readily assembled from norbornenylmethylamine (**2**) following a well-established bis-(chloroacetamide) cyclisation–reduction sequence (Scheme 1).[5]

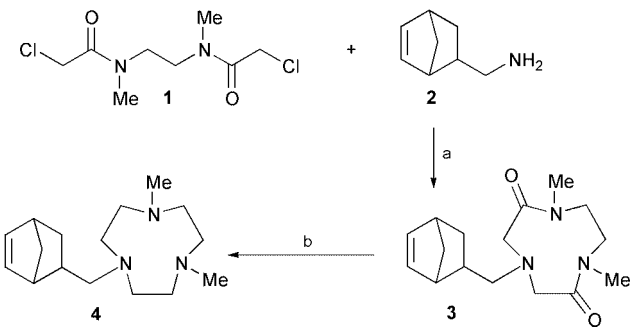

Scheme 1 Synthesis of the monomer **4**. *Reagents and conditions*: (a) Na_2CO_3, LiBr, CH_3CN, reflux, 12 h; (b) $LiAlH_4$, THF, reflux, 6 h.

† Electronic supplementary information (ESI) available: experimental details. See http://www.rsc.org/suppdata/cc/b1/b105560g/

Purification *via* column chromatography or high-vacuum distillation afforded **4** in 15% overall yield.

Attempted polymerisation of monomer **4** with Grubbs's catalyst[6] failed, probably due to interference of the multiple amine groups present in the molecule. Protonated **4** gave polycationic polymers, which, unfortunately, only showed negligible catalytic activity in the epoxidation of olefins when combined with manganese salts and hydrogen peroxide. To our delight, Schrock's molybdenum based catalyst[7] reacted with the free triamine **4** rapidly and efficiently, allowing the preparation of desired polymer **5** in quantitative yield (Scheme 2). In these preliminary studies, 5 mol% of the catalyst was employed in all runs, setting the number of triazacyclononane units per molecule (*n*) at about 20. The terminal ends of the polymer were capped by treatment of the reaction mixture with pivaldehyde after complete consumption of the monomer. Diimide mediated hydrogenation afforded saturated polymer **6** (with a degree of hydrogenation of *ca.* 86%) in 70% yield.

The performance of manganese catalysts derived from polymers **5** and **6** in olefin oxidations with hydrogen peroxide was investigated under the conditions indicated in eqn. (1).§

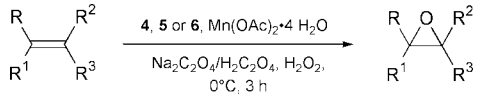

(1)

In all runs, 1 mol% of active catalyst (based on 3.7 mmol TACN units per g of polymer) formed *in situ* from $Mn(OAc)_2{\cdot}4H_2O$ and **4**, **5**, or **6** was employed. Both the ligand and the manganese complexes were soluble in aqueous acetone–methanol–H_2O_2 mixtures. The presence of sodium oxalate as co-ligand proved essential for the efficiency of the reaction.[8] Noteworthy is the fact that the conversion of the substrates was negligible in the absence of the triazacyclononane-containing polymers. The most significant results of this study are summarised in Table 1.

The performance of the polymeric systems in catalysing the oxidation reactions was in most cases comparable or even superior to that of the corresponding monomeric azacycle. Simple aromatic olefins were converted efficiently to the corresponding epoxides (entries 1–4). In the cases of α-methylstyrene and indene notable amounts of diols were

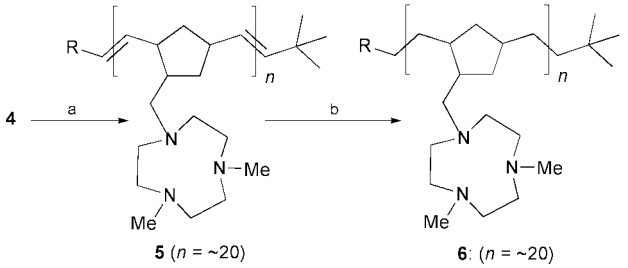

Scheme 2 Preparation of polymers **5** and **6**. *Reagents and conditions*: (a) i. Schrock's catalyst (5 mol%), toluene, RT, 4 h; ii. Pivaldehyde; (b) *p*-tolylsulfonylhydrazide, NaOH, di(ethylene glycol) methyl ether, 120–130 °C, 1.5 h.

 DOI: 10.1039/b105560g

Table 1 Oxidation of organic substrates with manganese catalysts prepared from **4** and polymeric 1,4,7-triazacyclononanes **5** and **6**

Entry	Substrate	Monomer **4**: Conv. (%) (Epoxide selectivity (%)[a])	Polymer **5** Conv. (%) (Epoxide selectivity (%)[a])	Polymer **6** Conv. (%) (Epoxide selectivity (%)[a])
1	Styrene	75 (87)	88 (91)	78 (92)
2	β-Methylstyrene	43 (93)	48 (83)	40 (83)
3	α-Methylstyrene	88 (86)	92 (62)[b]	86 (69)
4	Indene	98 (63)[c]	80 (64)[c]	70 (61)
5	Cyclohexene	100 (83)	100 (90)	94 (92)
6	Cyclooctene	32 (87)	41 (85)	49 (92)
7	Hex-1-ene	58 (100)	66 (100)	50 (95)
8	(*E*)-Hex-3-ene	58 (71)	29 (100)	23 (100)
9	(*Z*)-Hex-3-ene	100 (71)[d]	100 (91)[e,f]	83 (90)[e]
10	Methyl acrylate	4 (100)	12 (83)	7 (100)
11	Methyl cinnamate	16 (100)	23 (91)	18 (94)
12	3-Phenylpropenol[g]	100 (72)	76 (50)	54 (55)
13	1-Hydroxymethylcyclohexene[h]	96 (73)	80 (67)	68 (75)
14	Benzyl alcohol[i]	73	69	52
15	2-Phenylethanol	41	31	21

[a] Calculated as the ratio of epoxide yield and conversion. [b] A notable amount (11–27%) of the corresponding diol is produced. Other byproducts include benzophenone and 2-phenylpropionaldehyde. [c] The main byproduct is indan-2-one (10–24%). A notable quantity (6–11%) of the corresponding *cis*-diol is also produced. [d] + 17% of the corresponding *trans*-epoxide. [e] + 8% of the corresponding *trans*-epoxide. [f] 0.03 M oxalic buffer was employed. [g] A considerable amount (21–27%) of the corresponding α,β-unsaturated aldehyde is formed in this reaction. [h] Notable amounts (13–17%) of the corresponding α,β-unsaturated aldehyde are formed in this reaction. [i] The main products are benzaldehyde (18–29%) and benzoic acid (22–55%).

formed. Most probably this result is due to a subsequent epoxide hydrolysis under these reaction conditions.¶ Aliphatic alkenes were also epoxidised. In particular, internal (*Z*) systems reacted more effectively than terminal or (*E*) olefins (entries 5–9). In the case of (*Z*)-hex-3-ene, a significant amount of *trans*-epoxide was produced. α,β-Unsaturated carbonyl compounds showed poor reactivity (entries 10, 11). Hydroxy groups in the allylic or benzylic position were oxidised. In the case of allylic alcohols, both the epoxy alcohol and the corresponding α,β-unsaturated aldehyde were formed (entries 12, 13), with the epoxidation being the main reaction pathway. The two products did not undergo further transformations. The possibility of converting alcohols to conjugated systems was demonstrated by the oxidation of benzyl alcohol to benzaldehyde and benzoic acid (entry 14) as compared to the relatively less efficient transformation of 2-phenylethanol, which gave the corresponding aldehyde in low yield (7–11% of the reaction mixture) (entry 15). Finally, the procedure described herein was successfully performed of a 100 mmol scale with styrene as substrate, and no variation in conversion or selectivity was observed.

In conclusion, the possibility of generating polymeric systems with a high density of 1,4,7-triazacyclononane units by ROMP has been demonstrated. The corresponding manganese complexes are catalytically active in oxidation reactions with hydrogen peroxide as terminal oxidant. Currently, we are studying alternative polymeric systems based on the model presented with improved characteristics regarding catalyst stability and recovery.

This research was supported by the Fonds der Chemischen Industrie. We thank the Commission of the European Union for a postdoctoral fellowship to S. C. (Marie Curie grant HPMFCI-2000-00430).

Notes and references

‡ The IUPAC name for norbornene is bicyclo[2.2.1]hept-2-ene.

§ General experimental procedure: a solution of 1 mmol of substrate in acetone (GC quality, 1 mL) is cooled to 0–2 °C and treated with the ligand (for **4**: 2.7 mg in 48 μL of MeOH, 0.01 mmol; for **5** or **6**: 2.7 mg in 48 μL of MeOH, 0.5 μmol) and $Mn(OAc)_2{\cdot}4\,H_2O$ (2.5 mg in 141 μL of H_2O, 0.01 mmol). The mixture is stirred for 15 min. Oxalic buffer (0.15 M, 0.133 mL, 0.02 mmol) is added, followed within 1–2 min by H_2O_2 (30%, 0.4 mL, 4 mmol). After stirring for 1.5 h at 0–2 °C, another aliquot of H_2O_2 is added (0.2 mL, 2 mmol). After a reaction time of 2.5–3 h, the excess oxidant is destroyed by adding a small quantity of MnO_2, the reaction mixture is diluted with approx. 2 mL of CH_2Cl_2 and the organic phase is separated and analysed by gas-chromatography (see ESI).

¶ Samples of pure α-methylstyrene oxide were converted to the corresponding diol when exposed to the reaction conditions.

1 R. Hage, J. E. Iburg, J. Kerschner, J. H. Koek, E. L. M. Lempers, R. J. Martens, U. S. Racherla, S. W. Russell, T. Swarthoff, M. R. P. van Vliet, J. B. Warnaar, L. van der Wolf and B. Krijnen, *Nature*, 1994, **369**, 637; V. C. Quee-Smith, L. DelPizzo, S. H. Jureller, J. L. Kerschner and R. Hage, *Inorg. Chem.*, 1996, **35**, 6461; D. De Vos and T. Bein, *J. Organomet. Chem.*, 1996, **520**, 195; C. Zondervan, R. Hage and B. L. Feringa, *Chem. Commun.*, 1997, 419; C. Bolm, D. Kadereit and M. Valacchi, *Synlett*, 1997, 687; W.-H. Fung, W.-Y. Yu and C.-M. Che, *J. Org. Chem.*, 1998, **63**, 2873; D. H. R. Barton, W. Li and J. A. Smith, *Tetrahedron Lett.*, 1998, **39**, 7055; A. Berkessel and C. A. Sklorz, *Tetrahedron Lett.*, 1999, **40**, 7965; G. B. Shul'pin, G. Süss-Fink and J. R. L. Smith, *Tetrahedron*, 1999, **55**, 5345; C. Bolm, N. Meyer, G. Raabe, T. Weyhermüller and E. Bothe, *Chem. Commun.*, 2000, 2435.

2 V. V. Subba Rao, D. E. De Vos, T. Bein and P. A. Jacobs, *Chem. Commun.*, 1997, 355; D. E. De Vos, S. de Wildeman, B. F. Sels, P. J. Grobet and P. A. Jacobs, *Angew. Chem., Int. Ed.*, 1999, **38**, 980.

3 J.-M. Vincent, A. Rabion, V. K. Yachandra and R. H. Fish, *Angew. Chem., Int. Ed. Engl.*, 1997, **37**, 2346.

4 C. Bolm, C. L. Dinter, A. Seger, H. Höcker and J. Brozio, *J. Org. Chem.*, 1999, **64**, 5730.

5 J. S. Bradshaw, K. E. Krakowiak and R. M. Izatt, *Tetrahedron Lett.*, 1989, **30**, 803; K. E. Krakowiak, J. S. Bradshaw and R. M. Izatt, *J. Heterocycl. Chem.*, 1989, **26**, 1431.

6 T. M. Trnka and R. H. Grubbs, *Acc. Chem. Res.*, 2001, **34**, 1.

7 R. R. Schrock, *Acc. Chem. Res.*, 1990, **23**, 158.

8 D. E. De Vos, B. F. Sels, M. Reynaers, Y. V. Subba Rao and P. A. Jacobs, *Tetrahedron Lett.*, 1998, **39**, 3221.

CHEMCOMM Communication
www.rsc.org/chemcomm

Novel synthesis of cyclobutanone derivatives *via* dimetalation of iminium ions with the $TiCl_4$–trialkylamine reagent system†

Mariappan Periasamy,* K. Natarajan Jayakumar and Pandi Bharathi

School of Chemistry, University of Hyderabad, Central University P. O. Hyderabad–500 046, India. E-mail: mpsc@uohyd.ernet.in

Received (in Cambridge, UK) 5th April 2001, Accepted 24th July 2001
First published as an Advance Article on the web 28th August 2001

Iminium salts are generated *in situ*, react with $TiCl_4$–trialkylamines, and diaryl ketones to produce 3,3-diarylcyclobutanones in moderate to good yields.

The $TiCl_4$–R_3N combination is well-known to mediate aldol type condensation reactions[1] and oxidative coupling of certain ester enolates.[2] We have reported that the $TiCl_4$–R_3N reagent system is useful for the oxidative coupling of aryl methyl ketimines to 2,5-diarylpyrroles,[3a] for the direct metalation of alk-1-ynes,[3b] for the reductive coupling of imines and aromatic aldehydes,[3c] and for the oxidative coupling of *N,N*-dialkylarylamines.[3d] Also, it was observed that trialkylamines are oxidized to iminium ions by $TiCl_4$ with concomitant formation of $TiCl_3$.[3c,4] Herein, we wish to report that the iminium ions generated *in situ*,[5] undergo metalation followed by reaction with diaryl ketones to produce the corresponding 3,3-diarylcyclobutanones in moderate to good yields.

Metalation of iminium ions using $TiCl_4$ and its further reaction with PhCOPh produce α,β-unsaturated aldehydes (Scheme 1).[4]

We have examined the reaction of *N,N*-diisopropyl-*N*-ethylamine under these conditions. In this case, an inseparable mixture of the corresponding α,β-unsaturated aldehyde derivative and the cyclobutanone derivative was obtained. The use of *N,N*-diisopropyl-*N*-octylamine produced a better yield of the product mixture (Scheme 2).

Fortunately, the corresponding cyclobutanol could be readily separated after the reduction of the product mixture with $NaBH_4$–MeOH–H_2O (overall yield 12%). Attempts to optimize the reaction conditions to obtain better yields of the cyclobutanones using various *N,N*-diisopropyl-*N*-alkylamines were not fruitful. Therefore, we have examined the reactions of iminium ions prepared *in situ* using other methods. It was found that the iminium ions prepared through the oxidation of *N,N*-diisopropyl-*N*-benzylamine with I_2 gave better results. For example, in the reaction of the iminium ions with $TiCl_4$–*N,N*-diisopropyl-*N*-benzylamine and PhCOPh, the cyclobutanone derivative was obtained in 76% yield (Scheme 3).[6]

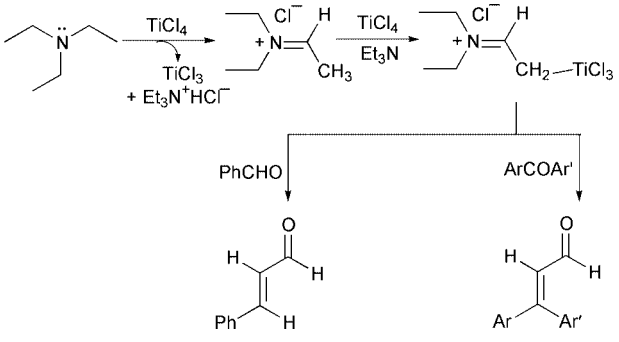

Scheme 1

† Electronic supplementary information (ESI) available: ^{13}C NMR spectra of compounds **1a**, **2a**, **3a**, **4a**, **5a**, **6a**, **7a** and **7b**. See http://www.rsc.org/suppdata/cc/b1/103112k/

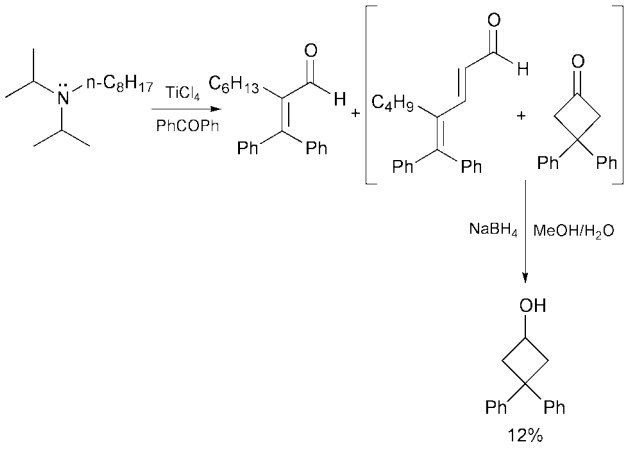

Scheme 2

When benzaldehyde was used as electrophile, the expected 3-arylcyclobutanone was not formed. Instead, only the dihydroxy ketone **7a** and the divinyl ketone **7b** were obtained in 58 and 11% yields respectively, besides some unidentified products. Earlier, such a reactivity was reported when the (2-siloxyallyl)silane was used as synthetic equivalent of acetone α,α′-dianion in the $TiCl_4$ mediated reaction with aromatic aldehydes.[7]‡

We have carried out several experiments to examine the scope and limitations of this transformation (Table 1). It was observed that the use of TMEDA in the place of *N,N*-diisopropyl-*N*-benzylamine gave the cyclobutanone derivative in poor yields (6%). Addition of PhCOPh initially or after the formation of the iminium ion gave no significant change to the results. Though the reaction works well at 25 °C, the yields of cyclobutanone are slightly better (10 to 20% more) under refluxing conditions. Dichloroethane was found to be the best solvent compared to CH_2Cl_2 and $CHCl_3$. When acetophenone was used as substrate, a complex mixture of products was obtained, possibly due to competing aldol type reactions.[8]

The formation of a cyclobutanone derivative may be tentatively explained by a mechanism involving the dimetalated iminium ion intermediate (Scheme 3). The reaction of 2 eq. of 3° amine and 1 eq. of I_2 would give the iminium iodide.[5] Deprotonation of the β-hydrogen atoms of the iminium ion using *N,N*-diisopropyl-*N*-benzylamine and further metalation with $TiCl_4$ could give the 1,3-dititanated iminium ion intermediate. The reaction of 1,3-dimetalated species with diarylketone would give the corresponding cyclobutanone (Scheme 3). However,

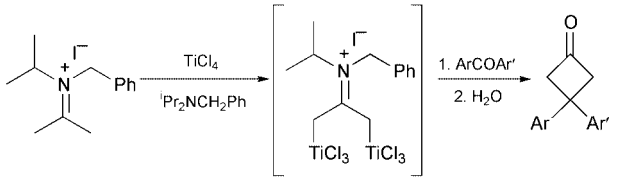

Scheme 3

 DOI: 10.1039/b103112k

Table 1 Reaction of iminium ions (Scheme 3) with $TiCl_4$–R_3N and ArCOAr′ or PhCHO

Entry	Substrate	Product[a]	Yield[b] (%)
		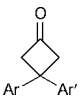	
1	Ar=Ar′=Ph **1**	**1a**	76
2	Ar=Ar′=4-MeC_6H_4 **2**	**2a**	71
3	Ar=Ar′=4-ClC_6H_4 **3**	**3a**	86
4	Ar=Ph Ar′=4-MeC_6H_4 **4**	**4a**	73
5	Ar=Ph Ar′=Ferrocenyl **5**	**5a**	51
6	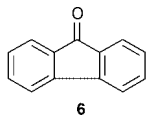 **6**	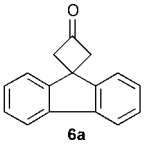 **6a**	56
7	 **7**	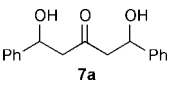 **7a**	58
		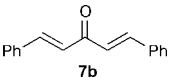 **7b**	11

[a] The products were identified by ^1H, ^{13}C NMR, mass spectral and physical constant data and comparison with the reported data.[8] [b] The yields are based on the amount of ketone/aldehyde used.

the possibility of an alternative mechanism involving sequential metalation–addition reactions cannot be ruled out.

In conclusion, simple one pot methods of conversion of diaryl ketones to 3,3-diarylcyclobutanones from readily available starting materials have been developed. Previously, syntheses of such cyclobutanone derivatives have been reported *via* methods such as (i) the 2 + 2 cycloaddition of ketenes to diazomethane,[9] (ii) the 2 + 2 cycloaddition of dichloroketene to olefins,[10] and (iii) the 2 + 2 cycloaddition of ketiminium salts to olefins.[11] The one pot conversions described here involving a 1,3-dimetalated iminium ion intermediate, is a simple alternative to hitherto known methods of synthesis of cyclobutanone derivatives.[12] Moreover, it is anticipated that the interesting reactivity pattern of the titanium intermediates reported here should stimulate further research activities in this area.

We are grateful to the UGC and DST (New Delhi, India) for financial support. KNJ thanks CSIR and PB thanks UGC for fellowships. We are also thankful to the UGC for support under Special Assistance Program.

Notes and references

‡ ^1H NMR (200 MHz) and ^{13}C NMR (50 MHz) spectra were recorded in $CDCl_3$ unless otherwise stated and TMS was used as reference (δ = 0 ppm). The chemical shifts are reported in ppm on the δ scale relative to $CDCl_3$ (77.0 ppm). Melting points are uncorrected.

1 C. R. Harrison, *Tetrahedron Lett*., 1987, **28**, 4135; D. A. Evans, J. S. Clark, R. Metternich, V. J. Novack and G. S. Sheppard, *J. Am. Chem. Soc*., 1990, **112**, 866; D. A. Evans, D. L. Rieger, M. T. Bilodeau and F. Urpi, *J. Am. Chem. Soc*., 1991, **113**, 1047; M. T. Crimmins, B. W. King and E. A. Tabet, *J. Am. Chem. Soc*., 1997, **119**, 7883; Y. Yoshida, R. Hayashi, H. Sumihara and Y. Tanabe, *Tetrahedron Lett*., 1997, **38**, 8727, and references cited therein.

2 Y. Matsumura, M. Nishimura, H. Hiu, M. Watanabe and N. Kise, *J. Org. Chem*., 1996, **61**, 2809; N. Kise, K. Tokioka, Y. Aoyama and Y. Matsumura, *J. Org. Chem*., 1995, **60**, 1100; N. Kise, K. Kumuda, Y. Terao and N. Ueda, *Tetrahedron*, 1998, **54**, 2697.

3 (*a*) M. Periasamy, G. Srinivas and P. Bharathi, *J. Org. Chem*., 1999, **64**, 4204; (*b*) P. Bharathi and M. Periasamy, *Organometallics*, 2000, **19**, 5511; (*c*) M. Periasamy, G. Srinivas, G. V. Karunakar and P. Bharathi, *Tetrahedron Lett*., 1999, **40**, 7577; (*d*) M. Periasamy, K. N. Jayakumar and P. Bharathi, *J. Org. Chem*., 2000, **65**, 3548.

4 P. Bharathi and M. Periasamy, *Org. Lett*., 1999, **1**, 857.

5 D. H. Wadsworth, M. R. Detty, B. J. Murray, C. H. Weidner and N. F. Haley, *J. Org. Chem*., 1984, **49**, 2676.

6 *Representative procedure for the reaction of diaryl ketones*: to dichloroethane (25 mL) benzophenone (0.456 g, 2.5 mmol) and I_2 (0.63 g, 2.5 mmol) were added at 25 °C under N_2. *N*,*N*-diisopropyl-*N*-benzylamine (0.955 g, 5 mmol) was added and the mixture was refluxed at 95–100 °C for 2 h and brought to rt under N_2. $TiCl_4$ (1.65 mL of 1 : 1 solution of $TiCl_4$–CH_2Cl_2, 7.5 mmol) was added at 0 °C followed by *N*,*N*-diisopropyl-*N*-benzylamine (1.433 g, 7.5 mmol). It was stirred at 0 °C for 10 min and then refluxed at 95–100 °C for 6 h. The contents were brought to rt, then a saturated NH_4Cl solution (20 mL) was added and stirred for 0.5 h. The organic layer was separated, and the aqueous layer was extracted with CH_2Cl_2 (2 × 25 mL). The combined organic extract was washed with 5 M HCl (2 × 20 mL) to remove the unreacted amine, followed by water and brine solution (10 mL) and dried over anhydrous $MgSO_4$. The solvent was removed and the residue was chromatographed on a silica gel column. Unidentified less polar compounds and the unreacted ketone were eluted using 1 : 99 EtOAc–hexane mixture. The 3,3-diphenylcyclobutanone **1a** was eluted using 2 : 98 EtOAc–hexane (0.258 g, 76%). *Procedure for the reaction of benzaldehyde*: to dichloroethane (25 mL) I_2 (0.63 g, 2.5 mmol) was added at 25 °C under N_2. *N*,*N*-diisopropyl-*N*-benzylamine (0.955 g, 5 mmol) was added and the mixture was refluxed at 95–100 °C for 2 h and brought to rt under N_2. $TiCl_4$ (1.65 mL of 1 : 1 solution of $TiCl_4$–CH_2Cl_2, 7.5 mmol) was added at 0 °C followed by *N*,*N*-diisopropyl-*N*-benzylamine (1.433 g, 7.5 mmol). It was stirred at 0 °C for 10 min and then benzaldehyde (0.51 mL, 5 mmol) was added. The mixture was refluxed at 95–100 °C for 6 h. The contents were brought to rt, then a saturated NH_4Cl solution (20 mL) was added and stirred for 0.5 h. The organic layer was separated, and the aqueous layer was extracted with CH_2Cl_2 (2 × 25 mL). The combined organic extract was washed with 5 M HCl (2 × 20 mL) to remove the unreacted amine, followed by water and brine solution (10 mL) and dried over anhydrous $MgSO_4$. The solvent was removed and the residue was chromatographed on a silica gel column. Unidentified less polar compounds and the unreacted benzaldehyde were eluted using 1 : 99 EtOAc–hexane mixture. The divinyl ketone **7b** was eluted using 3 : 97 EtOAc–hexane mixture (0.054 g, 11%). The dihydroxy ketone **7a** was eluted using 6 : 94 EtOAc–hexane mixture (0.372 g, 58%).

7 A. Hosomi, H. Hayashida and Y. Tominaga, *J. Org. Chem*., 1989, **54**, 3254.

8 **1a**: mp 83–84 °C (lit.[9] mp 84–85 °C); IR (cm^{-1}): $\nu_{C=O}$ 1786; ^{13}C NMR δ 205.29, 147.29, 128.72, 126.76, 126.52, 60.57, 42.06; ^1H NMR δ 7.4–7.2 (m, 10H), 3.8 (s, 4H). **2a**: mp 71–73 °C; IR (cm^{-1}): $\nu_{C=O}$ 1786; ^{13}C NMR δ 205.65, 144.64, 136.02, 129.39, 126.65, 60.57, 41.43, 20.98; ^1H NMR δ 7.3–7.18 (m, 8H), 3.8 (s, 4H), 2.4 (s, 6H); mass: M^+ (*m*/*e*) 250. **3a**: mp 110–112 °C; IR (cm^{-1}): $\nu_{C=O}$ 1790, 1770; ^{13}C NMR δ 203.73, 145.23, 132.75, 128.95, 128.08, 60.49, 41.39; ^1H NMR δ 7.32–7.2 (m, 8H), 3.77 (s, 4H); mass: M^+ (*m*/*e*) 291. **4a**: mp 64–65 °C; IR (cm^{-1}): $\nu_{C=O}$ 1790; ^{13}C NMR δ 205.29, 147.59, 144.39, 136.10, 129.41, 128.70, 126.72, 126.45, 60.57, 41.76, 20.97; ^1H NMR δ 7.4–7.2 (m, 9H), 3.85 (s, 4H), 2.4 (s, 3H); mass: M^+ (*m*/*e*) 236. **5a**: mp 153–155 °C; IR (cm^{-1}): $\nu_{C=O}$ 1784, 1768; ^{13}C NMR δ 207.42, 147.34, 128.32, 126.55, 126.36, 98.44, 68.65, 68.28, 66.64, 61.42, 37.03; ^1H NMR δ 7.4–7.2 (m, 5H), 4.2 (s, 9H), 4.0–3.7 (m, 4H); mass: M^+ (*m*/*e*) 330. **6a**: mp 145–147 °C; IR (cm^{-1}): $\nu_{C=O}$ 1786; ^{13}C NMR δ 205.68, 150.05, 140.13, 128.04, 127.84, 121.85, 120.14, 58.95, 41.41; ^1H NMR δ 7.8–7.35 (m, 8H), 3.66 (s, 4H); mass: M^+ (*m*/*e*) 220. **7a**: mp 56–57 °C (lit.[13] mp 58–59 °C); IR (cm^{-1}): $\nu_{C=O}$ 1709, ν_{O-H} 3410; ^{13}C NMR δ 205.94, 140.89, 128.71, 128.12, 125.74, 78.95, 49.72; ^1H NMR δ 7.5–7.3 (m, 10H), 4.85 (dd, 2H), 2.8–2.6 (m, 4H). **7b**: mp 108–110 °C (lit.[14] mp 107–110 °C); IR (cm^{-1}): $\nu_{C=O}$ 1651, 1626; ^{13}C NMR δ 189.00, 143.32, 135.00, 130.51, 129.00, 128.42, 125.46; ^1H NMR δ 7.75 (d, 2H, J = 16 Hz), 7.65–7.4 (m, 10H), 7.09 (d, 2H, J = 16 Hz).

9 C. J. Michejda and R. W. Comnick, *J. Org. Chem*., 1975, **40**, 1046.

10 L. R. Krepski and A. Hassner, *J. Org. Chem*., 1978, **43**, 2879, and references cited therein.

11 J. Marchand-Brynaert and L. Ghosez, *J. Am. Chem. Soc*., 1972, **94**, 2870; A. Sidani, J. Marchand-Brynaert and L. Ghosez, *Angew. Chem., Int. Ed. Engl*., 1974, **13**, 267.

12 For a comprehensive review of cyclobutanones, see D. Seebach, S. Beckman and H. Geiger, in *Houben-Weyl, Methoden der Organischen Chemie*, Vol. IV/4, ed. E. Mueller, George Thieme Verlag, Stuttgart, 1971; For elegant examples of the synthetic utility of cyclobutanones, see B. M. Trost, *Top. Curr. Chem*., 1973, **41**, 1; B. M. Trost, *Acc. Chem. Res*., 1974, **7**, 85; B. M. Trost, *Pure Appl. Chem*., 1975, **43**, 563.

13 E. Hasegawa, K. Ishiyama, T. Kato, T. Horaguchi, T. Shimizu, S. Tanaka and Y. Yamashita, *J. Org. Chem*., 1992, **57**, 5352.

14 R. C. Larock and S. S. Hershberger, *J. Org. Chem*., 1980, **45**, 3840.

CHEMCOMM
Communication
www.rsc.org/chemcomm

The first 1,3-digermyla-2-nickela-carboranylene and the Ni-catalyzed double germylation of unsaturated organic substrates

Junghyun Lee,[a] Chongchan Lee,[a] Shim Sung Lee,[b] Sang Ook Kang[a] and Jaejung Ko*[a]

[a] *Department of Chemistry, Korea University, Chochiwon, Chungnam 339-700, Korea. E-mail: jko@tiger.korea.ac.kr*

[b] *Department of Chemistry, and Institute of Natural Science, Gyeong-sang University, Chinju 660-701, Korea*

Received (in Cambridge, UK) 7th June 2001, Accepted 23rd July 2001
First published as an Advance Article on the web 29th August 2001

The reaction of *o*-bis(dimethylgermyl)carborane with $Ni(PEt_3)_4$ in pentane affords the reactive intermediate, $[o\text{-}(GeMe_2)_2C_2B_{10}H_{10}]Ni(PEt_3)_2$ 2: the facile double germylation of unsaturated organic substrates catalyzed by 2 is reported.

Although the transition metal-catalyzed double silylation of unsaturated organic substrates has been well documented for three decades,[1] metal-catalyzed double germylation is quite limited.[2–5] Reactions were carried out mainly in the presence of $[Pd(PPh_3)_4]$ as a catalyst. In the catalytic cycle, bis(germyl)-complexes have been implicated as important intermediates. However, there are only a few precedents for such species[6] and only bis(chlorogermyl)platinum has been structurally characterized by Tanaka and coworkers.[7] However, the reactivity towards unsaturated organic substrates was not studied. We found that the bis(germyl)nickel complex is the most efficient and reactive catalyst for the double germylation reaction. We now describe (i) the isolation of the most reactive intermediate cyclic bis(germyl)nickel compound with a bulky *o*-carborane unit; (ii) the facile double germylation of alkyne catalyzed by the intermediate under mild conditions; and (iii) the double germylation of an alkene, aldehyde and nitrile by stoichiometric reacion with the intermediate.

Addition of 1.1 equiv. of *o*-bis(dimethylgermyl)carborane, prepared from $1,2\text{-}Li_2C_2B_{10}H_{10}$ and 2 equiv. of $GeMe_2Cl_2$, followed by reduction by $NaB(CN)H_3$, to $Ni(PEt_3)_4$ in pentane gave a red solution. Standard work-up and crystallization from toluene–pentane gave $[o\text{-}(GeMe_2)_2C_2B_{10}H_{10}]Ni(PEt_3)_2$ **2** as a spectroscopically pure, red crystalline solid very sensitive to air and water in 60% yield [eqn. (1)].†

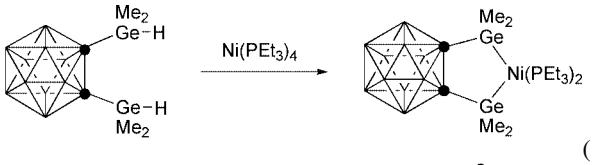

1 **2** (1)

The ^1H, ^{13}C and ^{31}P NMR spectra for **2** support the proposed structure. The structure of **2** was unambiguously established by a single-crystal X-ray analysis (Fig. 1).‡ Complex **2** has a distorted tetrahedral geometry with the dihedral angle between Ge(1)–Ni–Ge(2) and P(1)–Ni–P(2) being 84.60°. This bis(germyl)nickel complex is the first as indicated by a search of the Cambridge Crystallographic Database. As expected, the average Ni–Ge bond length [2.3290(5) Å] is slightly longer than that of 2.248(1) Å in $CpNi(PPh_3)GeCl_3$.[8] The Ni–P bond distance [2.2188(10) Å] is consistent with those observed in other phosphine nickel compounds.

Intermediate **2** was found to be an efficient reactant for the double germylation reaction under mild conditions. The reaction of *o*-bis(dimethylgermyl)carborane **1** with hex-1-yne (1 equiv.) in the presence of a catalytic amount of **2** (0.03 equiv.) at room temperature for 14 h afforded the double-germylated

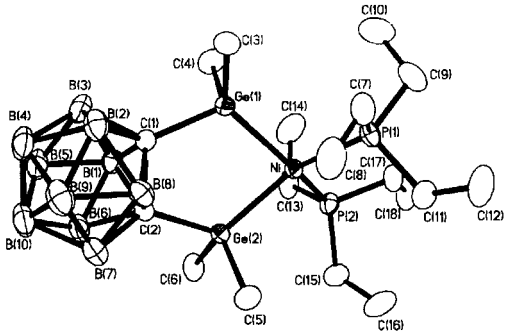

Fig. 1 Molecular structure of **2**. Selected bond lengths (Å) and angles (°): Ge(1)–C(1) 2.028(3), Ge(2)–C(2) 2.035(3), Ge(1)–Ni 2.3316(5), Ge(2)–Ni 2.3264(5), Ni–P(1) 2.2146(10), Ni–P(2) 2.2230(10); C(1)–Ge(1)–Ni 116.01(10), C(2)–Ge(2)–Ni 116.52(9), P(1)–Ni–P(2) 103.10(4), P(1)–Ni–Ge(2) 146.73(3), P(2)–Ni–Ge(2) 92.08(3), Ge(2)–Ni–Ge(1) 84.231(8).

product **3** in 62% yield. All the spectral data of **3** were consistent with the proposed formulation.§ A key feature in the ^1H NMR spectrum includes a singlet at δ 6.24 assigned to the vinyl proton. A characteristic high-field ^{13}C NMR signal at δ 142.82 provides evidence for a tethered carbon atom of the two germanium moieties. Formation of the digermyl ring compound **3** can be related to nickel-catalyzed double silylation.[9]

The reaction of **2** with 1 equiv. of 4-vinylanisole takes place at room temperature and affords a moderate yield of the five-membered digermyl ring compound **4** (Scheme 1). One doublet (δ 2.80) in the ^1H NMR spectrum of **4** is assigned to the methine proton. A low-frequency ^{13}C NMR resonance at δ 55.41 provides evidence for the tethered carbon atom of the two germanium moieties. The structure of **4** has been determined by X-ray crystallography (Fig. 2).‡ The formation of **4** may

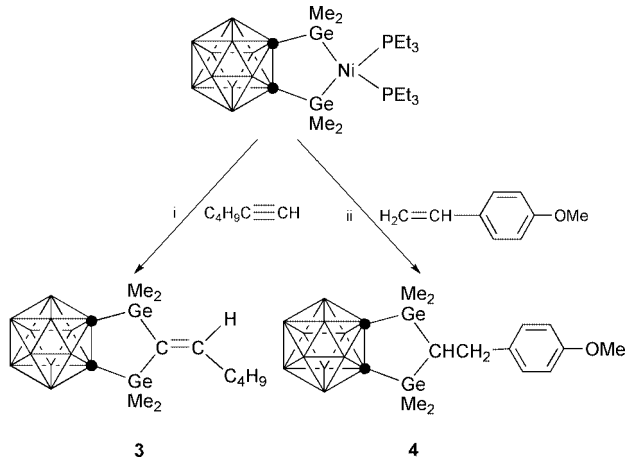

3 **4**

Scheme 1 *Reagents and conditions*: i, $HCCC_4H_9$ (1 equiv.), **1** (0.5 equiv.), **2** (0.03 equiv.), toluene, 25 °C; ii, $H_2CCHC_6H_4OMe$ (1 equiv.), **2** (1 equiv.), toluene, 80 °C.

 DOI: 10.1039/b105026p

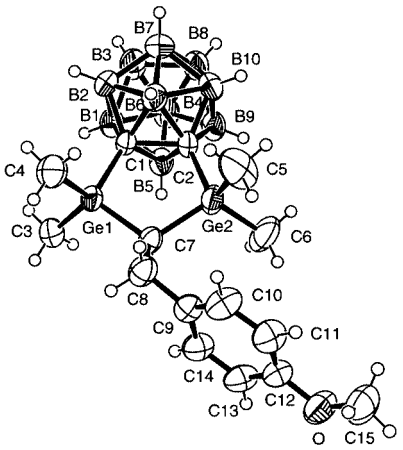

Fig. 2 Molecular structure of **4**. Selected bond lengths (Å) and angles (°): Ge(1)–C(1) 1.990(3), Ge(2)–C(2) 1.997(3), Ge(1)–C(7) 1.967(3), Ge(2)–C(7) 1.954(3), C(1)–C(2) 1.679(3); Ge(1)–C(7)–Ge(2) 110.04(14), Ge(1)–C(1)–C(2) 112.30(16).

involve an initial oxidative addition reaction of an olefinic C–H bond to the nickel center, followed by the shift of a phenyl group from the nickel atom to one of two germanium atoms. Such a C–H activation has been observed in Ni-catalyzed double silylation.[10] Treatment of **2** with 1 equiv. of *trans*-cinnamaldehyde at room temperature gave the 1,2-double germylation product **5** (Scheme 2). The ^{1}H NMR spectrum of **5**¶ contained a distinguishing low-field methine resonance (δ 4.61) as a doublet of doublets which was used to monitor its formation. This result is in contrast with that of double silylation which gave the insertion product of two carbonyl ligands into the C–Si bond.[11]

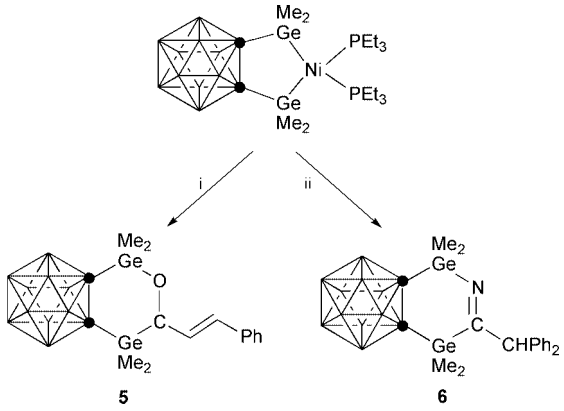

Scheme 2 *Reagents and conditions*: i, PhCH=CHCHO (1 equiv.), **2** (1 equiv.), toluene, 25 °C, 70%; ii, Ph_2CHCN (1.3 equiv.), **2** (1 equiv.), toluene, 25 °C, 66%.

When diphenylacetonitrile is employed in the reaction with **1**, the six-membered digermyl ring compound **6** is isolated as colorless crystals in 74% yield. All the spectral data of **6** were consistent with the proposed formulation.‖

In summary, we have isolated a reactive intermediate, a cyclic bis(germyl)nickel complex, which readily reacts with unsaturated organic substrates such as alkynes, alkenes, aldehydes and nitriles, generating a new class of heterocyclic compounds. This potential has been further exploited in a series of novel chemical transformations with this system.

We are grateful to KOSEF (2001) for generous financial support.

Notes and references

† *Experimental procedure*: for **2**: compound **1** (0.14 g, 0.38 mmol) in 5 ml of pentane was added to a stirred solution of $Ni(PEt_3)_4$ (0.1 g, 0.37 mmol) in 10 ml of pentane at −15 °C. The solution was warmed to room temperature and stirred for 2 h. The solution was then evaporated *in vacuo* and the residue extracted with toluene (8 ml) and then the solution was covered with a layer of pentane (10 ml) at −5 °C. Red crystals of **2** were formed over a period of several days (0.14 g, 60% yield). ^{1}H NMR (C_6D_6): δ 1.14 (dq, J_{HP} 7.42, J_{HH} 5.48 Hz, CH_2), 0.86 (dt, J_{HP} 7.04, J_{HH} 5.48 Hz, CH_3) and 0.21 (s, $GeCH_3$). ^{31}P{^{1}H} NMR (C_6D_6): δ 6.18.

‡ *Crystal data*: for **2**: $C_{18}H_{52}B_{10}P_2Ge_2Ni$, M = 641.52, monoclinic, space group $P2_1/n$, a = 11.28880(10), b = 14.2049(3), c = 20.6930(4) Å, β = 104.7760(10)°, V = 3208.52(10) Å^3, Z = 4, D_c = 1.328 g cm^{-3}, μ(Mo-Kα) = 2.550 mm^{-1}, 5038 reflections observed [$I > 2\sigma(I)$], 338 parameters, final R, R_w on [$I > 2\sigma(I)$] data were 0.0339, 0.0809, goodness of fit on F^2 = 1.059.

For **4**: $C_{15}H_{32}B_{10}Ge_2O$, M = 481.69, orthorhombic, space group *Pbca*, a = 16.6363(9), b = 15.3576(8), c = 18.9404(10) Å, V = 4839.2(4) Å^3, Z = 8, D_c = 1.322 g cm^{-3}, μ(Mo–Kα) = 2.488 mm^{-1}, 5992 reflections observed [$I > 2\sigma(I)$], 253 parameters, final R, R_w on [$I > 2\sigma(I)$] data were 0.0378, 0.0781, goodness of fit on F^2 = 0.951. CCDC reference numbers 166073 and 168186. See http://www.rsc.org/suppdata/cc/b1/b105026p/ for crystallographic data in CIF or other electronic format.

§ **3**: ^{1}H NMR ($CDCl_3$): δ 6.24 (s, C=C*H*), 2.13 (t, J_{HH} 9.40 Hz, CH_2), 1.59–1.27 (m, CH_2CH_2), 0.92 (t, J_{HH} 4.46 Hz, CH_3), 0.48 (s, $GeCH_3$) and 0.45 (s, $GeCH_3$). ^{13}C{^{1}H} NMR ($CDCl_3$): δ 159.20 (C=*C*H), 142.82 (Si-*C*=CH), 41.00, 31.49, 22.69, 14.22, −0.68 and −0.84.

¶ **5**: ^{1}H NMR ($CDCl_3$): δ 7.34–7.25 (m, Ph), 6.52 (dd, J_{HH} 15.88, J_{HH} 1.82 Hz, C=C*H*Ph), 6.22 (dd, J_{HH} 15.88, J_{HH} 5.44 Hz, CH=C), 4.61 (dd, J_{HH} 5.44 Hz, J_{HH} 1.82 Hz, OCH), 0.75 (s, $GeCH_3$), 0.73 (s, $GeCH_3$), 0.44 (s, $GeCH_3$) and 0.42 (s, $GeCH_3$). ^{13}C{^{1}H} NMR ($CDCl_3$): δ 137.04, 131.64, 128.74, 128.43, 127.44, 127.21, 126.26, 70.01, −0.07, −1.85, −3.63 and −6.91.

‖ **6**: ^{1}H NMR ($CDCl_3$): δ 7.35–7.06 (m, Ph), 4.75 (s, C*H*), 0.64 (s, $GeCH_3$) and 0.61 (s, $GeCH_3$). ^{13}C{^{1}H} NMR ($CDCl_3$): δ 143.54, 132.86, 130.22, 128.58, 128.34, 128.22, 125.92, 54.59, 5.85 and 1.29.

1 I. Beletskaya and C. Moberg, *Chem. Rev.*, 1999, **99**, 3435; H. K. Sharma and K. H. Pannell, *Chem. Rev.*, 1995, **95**, 1351.
2 T. Tsumuraya and W. Ando, *Organometallics*, 1989, **8**, 2286.
3 T. Hayashi, H. Yamashita, T. Sakakura, Y. Uchimaru and M. Tanaka, *Chem. Lett.*, 1991, 245.
4 K. Mochida, C. Hodota, H. Yamashita and M. Tanaka, *Chem. Lett.*, 1992, 1635.
5 H. Komoriya, M. Kako, Y. Nakadaira and K. Mochida, *Organometallics*, 1996, **15**, 2014.
6 J. Barrau, G. Rima, V. Cassano and J. Satgé, *Inorg. Chim. Acta*, 1992, **198**, 461; J. Barrau, G. Rima, V. Cassano and J. Satgé, *Organometallics*, 1995, **14**, 5700; H. Komoriya, M. Kako, Y. Nakadaira and K. Mochida, *J. Organomet. Chem.*, 2000, **611**, 420.
7 H. Yamashita, T. Kobayashi and M. Tanaka, *Organometallics*, 1992, **11**, 2330.
8 F. Glockling, A. Mcgredor, M. L. Schneiber and H. M. M. Shearer, *J. Inorg. Nucl. Chem.*, 1970, **32**, 3101.
9 Y. Kang, J. Lee, Y. K. Kong, S. O. Kang and J. Ko, *Organometallics*, 2000, **19**, 1722.
10 M. Ishikawa, S. Okazaki, A. Naka, A. Tachibana, S. Kawauchi and T. Yamabe, *Organometallics*, 1995, **14**, 114.
11 Y. Kang, S. O. Kang and J. Ko, *Organometallics*, 2000, **19**, 1216.

CHEMCOMM Communication
www.rsc.org/chemcomm

Direct NO group transfer from *S*-nitrosothiols to iron centres

Anthony R. Butler,*[a] Susie Elkins-Daukes,[a] David Parkin[b] and D. Lyn H. Williams*[b]

[a] *Department of Chemistry, University of St. Andrews, St. Andrews, Fife, UK KY16 9ST*
[b] *University of Durham, South Road, Durham, UK DH1 3LE. E-mail: D.L.H.Williams@durham.ac.uk*

Received (in Cambridge, UK) 21st June 2001, Accepted 30th July 2001
First published as an Advance Article on the web 29th August 2001

A number of *S*-nitrosothiols react rapidly with the Fe(II) complexes of 2,3-dimercapto-1-propanesulfonic acid (DMPS) and of *N*-methyl-D-glucamine dithiocarbamate (MGD), transferring the NO group directly to the iron centres.

S-Nitrosothiols (RSNO) are now widely believed to be important species in the storage and transport of nitric oxide *in vivo*.[1] Since they generally show the same physiological properties as does nitric oxide itself (notably the induction of vasodilation and inhibition of platelet aggregation[2]), it has been generally assumed that RSNO species act in this way by first releasing nitric oxide. Release of NO from an RSNO can be brought about by at least three routes: (a) a spontaneous thermal reaction, which is too slow at ambient temperatures to be important, (b) a photochemical reaction, which is also unimportant in the absence of appropriate incident radiation, and (c) a rapid copper(II) catalysed process.[3] For reaction (c) it has been shown[4] that decomposition is brought about by Cu^+ generated by thiol reduction of Cu^{2+}. Even low $[Cu^{2+}]$ at the impurity level are effective. Cu^+ can also be obtained by reduction from Cu^{2+} bound to proteins and peptides.[5] Complexation of Cu^+ in biological experiments results in loss of some biological function.[6] Low levels of [RSH] always present in equilibrium with RSNO[7] are sufficient to bring about the reduction. All three decomposition pathways initially generate nitric oxide and the corresponding disulfide, [eqn. (1)] although in the

$$2\mathrm{RSNO} \rightarrow \mathrm{RSSR} + 2\mathrm{NO} \qquad (1)$$

presence of oxygen oxidation of nitric oxide occurs and the final product in aqueous buffer is nitrite ion.

In addition, *S*-nitrosothiols react readily with many nucleophiles transferring the NO group in the NO^+ sense to, for example, amines, thiols and ascorbate[3] directly, without it ever becoming free, *i.e.* they can act as electrophilic nitrosating agents. Many of the biological properties of NO are believed to occur by activation of the enzyme guanylate cyclase, through the binding of NO to a haem iron atom in the enzyme. This leads to elevated levels of cyclic guanosine monophosphate (cGMP) which effects smooth muscle relaxation. It is an interesting and pertinent question as to whether RSNO compounds can achieve this without NO formation, *i.e.* whether they can transfer the NO group directly to an iron atom.

We have chosen initially to look at a simple non-haem iron compound. Iron(II) readily forms a complex $[Fe(DMPS)_2]^{4-}$ with 2,3-dimercaptopropane-1-sulfonate (DMPS) shown as **1**.[8]

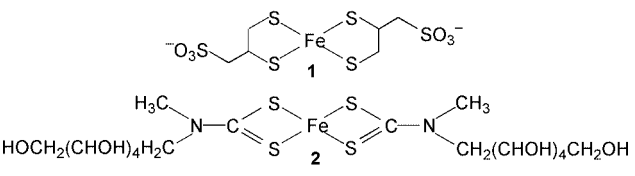

This is stable in solution under anaerobic conditions and the solution is red with absorbance maxima at 358 and 509 nm. This iron complex has a strong affinity for NO and has been used industrially as a scrubber of flue gases to remove NO. The nitrosyl complex has been characterised.[9]

The complex is readily prepared in aqueous solution from Fe^{2+} and a two-fold excess of DMPS. Addition of *S*-nitrosoglutathione (GSNO), generated in solution from equimolar quantities of nitrous acid and glutathione, to a solution of **1** at physiological pH 7.4 resulted in the rapid disappearance of the absorbance at 509 nm. The final absorbance spectrum was identical with that obtained when NO gas was reacted with $[Fe(DMPS)_2]^{4-}$ and is taken to be that of $[Fe(DMPS)_2NO]^{3-}$. Kinetic measurements, noting the decreasing absorbance at 509 nm, were made with [GSNO] >> $[Fe(DMPS)_2{}^{4-}]$. Each individual run followed the first-order law and there was also a first-order dependence on [GSNO], leading to a second-order rate constant value k [defined by eqn. (2)] of 24 $dm^3\ mol^{-1}\ s^{-1}$

$$\mathrm{Rate} = k\,[\mathrm{Fe(DMPS)_2}^{4-}]\,[\mathrm{RSNO}] \qquad (2)$$

at 25 °C. The *S*-nitroso derivatives of *N*-acetylcysteine, cysteine, homocysteine and captopril (all generated *in situ*) behaved similarly yielding comparable k values (6.1, 71, 16 and 7.5 $dm^3\ mol^{-1}\ s^{-1}$ respectively). The nitrosyl complex from *S*-nitrosocysteine was identical (spectrally) with that derived from GSNO.

An HPLC analysis of the final solution from the reaction of GSNO with the iron complex showed that the other product of reaction between GSNO and the iron complex was glutathione (GSH) in > 80% yield. This oxidised slowly to give some of the disulfide GSSG on standing in air for several hours. Initial (essentially quantitative) formation of glutathione indicates that the NO group is being transferred as NO^+ rather than as NO. That the same complex is formed by reaction with NO itself means that there must be an oxidation step in that process. It is not unknown in the synthesis of metal nitrosyls for the formal oxidation state of the nitrosyl ligand in the product to be different from that in the reactants.[10]

GSNO also reacts rapidly with the Fe^{2+} complex of *N*-methyl-D-glucamine dithiocarbamate (MGD) shown as structure **2**. The reaction is rapid and much faster than the 'spontaneous' release of NO from GSNO under the same conditions. The Fe^{2+} complex of MGD is EPR active and has been used recently as a trap for NO.[11] Reaction occurs rapidly with NO generated in solution giving the NO complex with a characteristic EPR spectrum. We find that the same UV-Visible spectrum is generated from the reactions of GSNO and NO with the Fe^{2+} complex of MGD. Strangely here in our reaction, the other product is GSSG and not GSH as in the DMPS case. This implies that with the DMPS complex NO is delivered in the NO^+ sense, whereas with the MGD complex it appears that it is in the NO sense. Our principal conclusion is that a direct bimolecular process occurs in the reactions of RSNO compounds with these two iron complexes and there is no prior release of NO. Our product studies also show that this NO-transfer reaction can occur in the NO or NO^+ sense depending presumably on which is the more favoured ligand in the resulting nitrosyl complex. Both reactions are far too rapid for the results to be explained mechanistically in terms of prior breakdown of RSNO to yield NO.

Our results indicate that when considering the reaction of an *S*-nitrosothiol with a biological target, the possibility of a direct

 DOI: 10.1039/b105460k

bimolecular process must be considered. Transfer may occur as either NO or NO^+.

We thank the EPSRC for a research studentship to D. P., and for an equipment grant.

Notes and references

1 P. R. Myers, R. L. Minor, R. Guerra, J. N. Bates and D. G. Harrison, *Nature*, 1990, **345**, 161.
2 M. W. Radomski, D. D. Rees, A. Dutra and S. Moncada, *Br. J. Pharmacol*., 1992, **107**, 745.
3 D. L. H. Williams, *Acc. Chem. Res*., 1999, **32**, 869.
4 A. P. Dicks, H. R. Swift, D. L. H. Williams, A. R. Butler, H. H. Al-Sa'doni and B. G. Cox, *J. Chem. Soc., Perkin Trans. 2*, 1996, 481.
5 A. P. Dicks and D. L. H. Williams, *Chem. Biol*., 1996, **3**, 655.
6 H. H. Al-Sa'doni, I. L. Megson, S. Bisland, A. R. Butler and F. W. Flitney, *Br. J. Pharmacol*., 1997, **121**, 1047.
7 P. H. Beloso and D. L. H. Williams, *Chem. Commun*., 1997, 89.
8 Y. Shi, D. Littlejohn and S. Chang, *Ind. Eng. Chem. Res*., 1996, **35**, 1668.
9 E. K. Pham and S. Chang, *Nature*, 1994, **369**, 139.
10 N. N. Greenwood and A. Earnshaw, *Chemistry of the Elements*, 2nd edn., 1997, Butterworth Heineman, pp. 448 and 449.
11 A. Komarov, D. Mattson, M. M. Jones, P. K. Singh and C.-C. Lai, *Biochem. Biophys. Res. Commun*., 1993, **195**, 1191.

CHEMCOMM
Communication
www.rsc.org/chemcomm

Control over directional metal–metal charge transfer in cyanide-bridged dimanganese complexes: effects of μ-CN linkage isomerism and ancillary ligand set†

Kirsty M. Anderson, Neil G. Connelly, Estefania Llamas-Rey, A. Guy Orpen and Rowena L. Paul

School of Chemistry, University of Bristol, Bristol, UK BS8 1TS. E-mail: Neil.Connelly@bristol.ac.uk

Received (in Cambridge, UK) 6th June 2001, Accepted 28th June 2001
First published as an Advance Article on the web 29th August 2001

Synthesis and characterisation of cyano-bridged complexes of the form [(η-C_5R_4Me)L(ON)Mn(μ-XY)Mn(CO)$_2$-L′(dppm)]^z (X,Y = C,N; z = 1–3) shows that systematic variation of the orientation of the CN bridge and the nature and geometric arrangement of the ancillary ligands affords control of the direction and energy of metal–metal charge transfer in the mixed valence dications.

While much of the current wide interest[1,2] in cyanide-bridged complexes centres on structural properties[1,3] deriving from the (usually linear) M(μ-CN)M′ unit, other important effects (optical,[4–6] magnetic,[1,7] *etc.*) depend on the facility with which intramolecular metal–metal charge transfer (MMCT) occurs in mixed valence complexes.

In order to understand more fully the nature of the MMCT process, and how its energy and direction (through the bridge) might be controlled, there is a need to prepare and study kinetically inert cyanide-bridged species, *i.e.* species in which linkage isomerisation, from M(μ-CN)M′ to M(μ-NC)M′, does not occur. Many systems, often constructed from classical coordination complex units, do isomerise.[1,8] However, by using low valent transition metal building blocks (*e.g.* organometallic or metal carbonyl units) we[9] and others[6,10] have isolated stable cyanide-bridged complexes and, in some cases, linkage isomers.[4,11–14]

Electrochemical studies[11,13,14] which probe the effects of linkage isomerism on redox potential are of particular relevance, especially those on the asymmetric species {$(OC)_5$Cr(μ-CN)Fe(dppe)(η^5-C_5H_5)] and [$(OC)_5$Cr(μ-NC)Fe(dppe)(η^5-C_5H_5)] (each oxidised in two one-electron steps, at $E^{\circ\prime}{}_1$ and $E^{\circ\prime}{}_2$). These isomers show quite different redox behaviour, with $E^{\circ\prime}{}_1$ and $E^{\circ\prime}{}_2$ 0.28 and 0.97 V for the former and 0.46 and 0.91 V for the latter, $\Delta E^{\circ\prime}$ ($\Delta E^{\circ\prime} = E^{\circ\prime}{}_2 - E^{\circ\prime}{}_1$) is 0.68 and 0.45 V, respectively. The difference in $\Delta E^{\circ\prime}$ for the two neutral complexes implies different MMCT behaviour for the corresponding monocations [$(OC)_5$Cr(μ-CN)Fe(dppe)(η^5-C_5H_5)]$^+$ and {$(OC)_5$Cr(μ-NC)Fe(dppe)(η^5-C_5H_5)]$^+$ although a direct comparison on the electronic properties of the two was not possible.[14]

Here we describe a new and highly versatile series of stable cyanide-bridged linkage isomers, [(η-C_5R_4Me)L(ON)Mn(μ-XY)Mn(CO)$_2$L′(dppm)]$^+$, in which the pseudo-tetrahedral unit Mn$^{\rm I}$X(NO)L(η-C_5R_4Me) (generalised as Mn$_{\rm tet}$, R = H or Me) is joined to octahedral *cis*- or *trans*-[Mn$^{\rm I}$Y(CO)$_2$L′(dppm)] (generalised as Mn$_{\rm oct}$) by the bridge XY (X,Y = C,N). The potentials for, and order of, the sequential one-electron oxidations of the two metal centres in Mn$^{\rm I}$(μ-XY)Mn$^{\rm I}$ to Mn$^{\rm I}$(μ-XY)Mn$^{\rm II}$ and Mn$^{\rm II}$(μ-XY)Mn$^{\rm II}$, vary not only with the orientation of the cyanide bridge but also with the cyclopentadienyl ring substituents R, the ancillary ligands L and L′ and the geometry of the Mn(CO)$_2$ unit (*cis* or *trans*) at Mn$_{\rm oct}$. Thus, the energy and direction of MMCT within the Mn$^{\rm I}$Mn$^{\rm II}$ species {(η-C_5H_4Me)L(ON)Mn(μ-XY)Mn(CO)$_2$L′(dppm)]$^{2+}$ can be systematically controlled.

† Electronic supplementary information (ESI) available: Table S1: IR and electrochemical data. See http://www.rsc.org/suppdata/cc/b1/b104998b/

The complexes [(η-C_5R_4Me)L(ON)Mn(μ-XY)Mn(CO)$_2$-L′(dppm)][PF_6] [X,Y = C,N; R = H or Me; L = PPh_3, $P(OPh)_3$ or CNBu^t; L′ = $P(OR')_3$ (R′ = Et or Ph); dppm = $Ph_2CH_2PPh_2$], with either *cis*- or *trans*-Mn(CO)$_2$ units, are prepared as their [PF_6]$^-$ salts by reacting [Mn(CN)(CO)$_2$-L′(dppm)] with [MnI(NO)L(η-C_5R_4Me)] or [MnBr(CO)$_2$-L′(dppm)] with [Mn(CN)(NO)L(η-C_5R_4Me)] in the presence of $TlPF_6$.‡ Representative examples are shown in Scheme 1 and Table S1 (ESI†).

The order in which the two Mn$^{\rm I}$ sites of the binuclear complexes are oxidised is indicated by cyclic voltammetry; assignment of each oxidation site is aided by observing the effects of altering the ancillary ligands L and L′ on redox potential (better donors L and L′ shift oxidation waves to less positive potentials) and noting that a *cis*-[Mn$^{\rm I}$Y(CO)$_2$L′(dppm)] unit undergoes oxidative isomerisation, giving rise to an irreversible oxidation wave coupled with a reversible oxidation wave for the *trans* product.[15] The assignments based on cyclic voltammetry are supported by the results of IR spectroelectrochemistry (see below).

The effect of CN linkage isomerism on redox behaviour is demonstrated by [(η-C_5H_4Me)(Bu^{t}NC)(ON)Mn(μ-CN)-Mn(CO)$_2${P(OEt)$_3$}(dppm)-*trans*][PF_6] **1**$^+$[PF_6]$^-$ and [(η-C_5H_4Me)(Bu^{t}NC)(ON)Mn(μ-NC)Mn(CO)$_2${P(OEt)$_3$}(dppm)-*trans*][PF_6] **2**$^+$[PF_6]$^-$, the X-ray structures of which are virtually identical; that of the cation **1**$^+$ is shown in Fig. 1, together with important bond lengths and angles for the two isomers.§

Both **1**$^+$ and **2**$^+$ show two reversible oxidation waves in their cyclic voltammograms, IR spectroelectrochemistry¶ confirming that the first oxidation occurs at Mn$_{\rm oct}$ (Table 1). Thus, on electrolysis at $E_{\rm applied}$ = 0.6 (for **1**$^+$) or 0.75 V (for **2**$^+$), ν(CO) increases by *ca.* 70–80 cm^{-1} while ν(NO) and ν(CNBu^t)

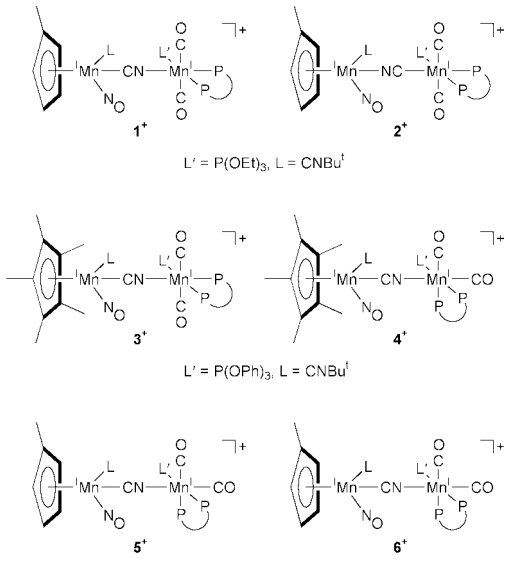

Scheme 1 P–P = dppm.

 DOI: 10.1039/b104998b

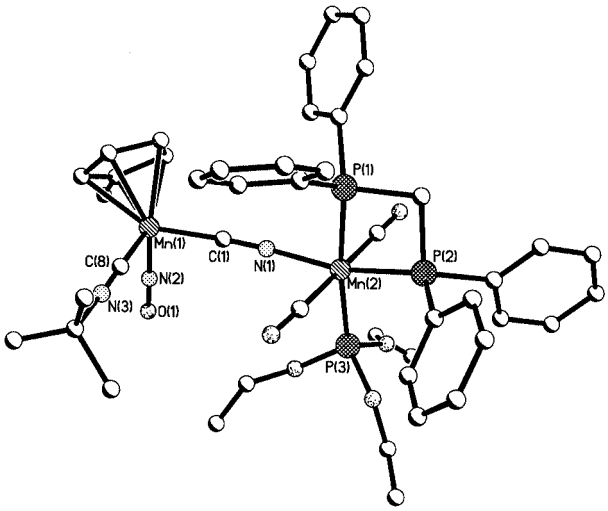

Fig. 1 Structure of the cation of $[(\eta\text{-}C_5H_4Me)(Bu^tNC)(ON)Mn(\mu\text{-}CN)Mn(CO)_2\{P(OEt)_3\}(dppm)][PF_6]$ $\mathbf{1}^+[PF_6]^-$ (hydrogen atoms omitted for clarity); the structure of $[(\eta\text{-}C_5H_4Me)(Bu^tNC)(ON)Mn(\mu\text{-}NC)\text{-}Mn(CO)_2\{P(OEt)_3\}(dppm)][PF_6]$ $\mathbf{2}^+[PF_6]^-$ is virtually identical. Important bond lengths (Å) and angles (°) for $\mathbf{1}^+$: Mn_{tet}–CN 1.951(3), Mn_{oct}–NC 2.010(3), C–N 1.153(4), Mn_{tet}–NO 1.656(3), Mn_{tet}–CNBu^t 1.916(4), Mn–P {*trans* to $P(OEt)_3$} 2.296(1), Mn–P (*trans* to $NCMn_{tet}$) 2.275(1); Mn_{tet}–C–N 176.9(3), Mn_{oct}–N–C 171.6(2). For $\mathbf{2}^+$: Mn_{tet}–NC 1.968(3), Mn_{oct}–CN 1.955(3), C–N 1.151(4), Mn_{tet}–NO 1.665(3) Mn_{tet}–CNBu^t 1.922(3), Mn–P {*trans* to $P(OEt)_3$} 2.283(1), Mn–P (*trans* to $CNMn_{tet}$) 2.290(1) Å; Mn_{tet}–N–C 173.6(2), Mn_{oct}–C–N 175.0(2).

increase by much smaller amounts (*ca.* 13–20 and 6–7 cm^{-1}, respectively), consistent with oxidation at the *trans*-$Mn(CO)_2$ terminus. [Further electrolysis of $\mathbf{1}^{2+}$, at 1.45 V, results in increases in ν(CO), ν(NO) and ν(CNBu^t) of 16, 101 and 62 cm^{-1}, this time consistent with oxidation at Mn_{tet} to give $\mathbf{1}^{3+}$]. Thus, in the isomeric mixed valence dications $\mathbf{1}^{2+}$ and $\mathbf{2}^{2+}$, Mn^I to Mn^{II} MMCT occurs in the opposite sense with respect to the cyanide bridge, *i.e.* from Mn^I to CN to Mn^{II} in the former and from Mn^I to NC to Mn^{II} in the latter.

Cyanide bridge isomerisation leads to very different values of $\Delta E^{\circ\prime}$ for $\mathbf{1}^+$ and $\mathbf{2}^+$ (0.81 and 0.49 V respectively) and thence to a large difference in the MMCT band energy for the mono-oxidised complexes. Thus, UV–VIS spectroelectrochemistry¶ shows the growth of a MMCT absorption band at 890 nm on oxidation of $\mathbf{1}^+$ to $\mathbf{1}^{2+}$ and a similar band at 1360 nm on oxidation of $\mathbf{2}^+$.

Further control of the direction (and energy) of MMCT is possible simply by varying the geometry (*cis* or *trans* dicarbonyl) of the Mn_{oct} unit. Thus, the positional isomers $[(\eta\text{-}C_5Me_5)(Bu^tNC)(ON)Mn(\mu\text{-}CN)Mn(CO)_2\{P(OPh)_3\}(dppm)\text{-}trans]^+$ $\mathbf{3}^+$ and $[(\eta\text{-}C_5Me_5)(Bu^tNC)(ON)Mn(\mu\text{-}CN)Mn(CO)_2\text{-}\{P(OPh)_3\}(dppm)\text{-}cis]^+$ $\mathbf{4}^+$ are first oxidised at Mn_{oct} and Mn_{tet} respectively, an assignment confirmed in the latter case by IR spectroelectrochemistry; electrolysis (E_{appl} = 1.0 V) leads to a large increase in enery for ν(NO) (94 cm^{-1}) and only a small increase in ν(CO) (Table S1, ESI†). Similar behaviour has been inferred from the CVs of $[(\eta\text{-}C_5H_5)(dppe)Fe(\mu\text{-}XY)(Mn(CO)_2\text{-}\{P(OPh)_3\}(dppm)][PF_6]$ (X, Y = C, N).[11]

Finally, the direction of MMCT can be controlled by varying the ligands L and L′. Thus, replacing PPh_3 at the *pseudo*-tetrahedral site of $[(\eta\text{-}C_5H_4Me)(Ph_3P)(ON)Mn(\mu\text{-}CN)Mn\text{-}(CO)_2\{P(OPh)_3\}(dppm)\text{-}cis]^+$ $\mathbf{5}^+$ by $P(OPh)_3$, giving $[(\eta\text{-}C_5H_4Me)\{(PhO_3P)(ON)Mn(\mu\text{-}CN)Mn(CO)_2\{P(OPh)_3\}\text{-}(dppm)\text{-}\ cis]^+$ $\mathbf{6}^+$, leads to the site of first oxidation changing from Mn_{tet} (first oxidation wave reversible) to Mn_{oct} [isomerisation of the *cis*-$Mn^I(CO)_2$ unit at the first oxidation step].

In summary, cyclic voltammetry and spectroelectrochemistry (IR and UV–VIS) on a range of stable linkage isomers shows that the order of oxidation of the two Mn^I sites in the $Mn^I_{tet}(\mu\text{-}XY)Mn^I_{oct}$ (X,Y = C,N) unit can be controlled by the orientation of XY, by the geometry at Mn^I_{oct} and by the ancillary ligands at either metal centre. In this way, the direction and energy of MMCT, from Mn^I to Mn^{II} through a cyanide bridge, may be systematically and selectively controlled.

We thank the University of Bristol for Postgraduate Scholarships (K. M. A., E. L.-R.), the Leverhulme Foundation for a Postdoctoral Fellowship (R. L. P.) and Professor M. D. Ward for help with the spectroelectrochemistry.

Notes and references

‡ All new complexes had satisfactory elemental analyses (C. H and N).

§ *Crystal data*: for $\mathbf{1}PF_6$: (from CH_2Cl_2–*n*-hexane): $C_{48}H_{59}F_6Mn_2N_3O_7P_4$, M = 1137.74, triclinic, space group $P\bar{1}$ (no. 2), a = 11.077(4), b = 13.608(4), c = 19.195(3) Å, α = 103.00(3), β = 100.75(3), γ = 97.00(2)°, V = 2728.9(14) Å^3, Z = 2, μ = 0.65 mm^{-1}, $R1$ = 0.049. For $\mathbf{2}PF_6$: (from CH_2Cl_2–*n*-hexane): $C_{48}H_{59}F_6Mn_2N_3O_7P_4$, M = 1137.74, triclinic, space group $P\bar{1}$ (no. 2), a = 11.092(2), b = 13.638(2), c = 19.076(4) Å, α = 102.98(1), β = 100.44(1), γ = 97.53(1)°, V = 2720.5(8) Å^3, Z = 2, μ = 0.652 mm^{-1}, $R1$ = 0.050. In each case an alternative model, with the C and N atoms of the CN bridge exchanged, was explored; there was no indication that the other linkage isomer was present in either crystal. CCDC reference numbers 166635 and 166636. See http://www.rsc.org/suppdata/cc/b1/b104998b/ for crystallographic data in CIF or other electronic format.

¶ UV–VIS spectroelectrochemistry was carried out in CH_2Cl_2 at 253 K, as described previously.[16] IR spectroelectrochemistry was carried out similarly, using a KBr microcavity cuvette, a Pt gauze working electrode and a Bruker IFS25 spectrometer. (Details will be described elsewhere.[17])

1 K. R. Dunbar and R. A Heintz, *Prog. Inorg. Chem.*, 1997, **45**, 283.
2 H. Vahrenkamp, A. Geiss and G. N. Richardson, *J. Chem. Soc., Dalton Trans.*, 1997, 3643.
3 See, for example, T. Iwamoto, S. Nishikiori, T. Kitazawa and H. Yuge, *J. Chem. Soc., Dalton Trans.*, 1997, 4127; J. L. Heinrich, P. A. Berseth and J. R. Long, *Chem. Commun.*, 1998, 1231; S. M. Contakes and T. B. Rauchfuss, *Chem. Commun.*, 2001, 553; N. G. Naumov, D. V. Soldatov, J. A. Ripmeester, S. B. Artmekina and V. E. Fedorov, *Chem. Commun.*, 2001, 571.
4 D. W. Thompson, J. R. Schoonover, T. J. Meyer, R. Argazzi and C. A. Bignozzi, *J. Chem. Soc., Dalton Trans.*, 1999, 3729.
5 B. J. Coe, *Chem. Eur. J.*, 1999, **5**, 2464.
6 W. M. Laidlaw, R. G. Denning, T. Verbiest, E. Chauchard and A. Persoons, *Nature*, 1993, **363**, 58; W. M. Laidlaw and R. G. Denning, *J. Chem. Soc., Dalton Trans.*, 1994, 1987.
7 See, for example: E. Colacio, J. M. Dominguez-Vera, M. Ghazi, R. Kivekas, J. M. Moreno and A. Pajunen, *J. Chem. Soc., Dalton Trans.*, 2000, 505; H.-Z. Kou, S. Gao, B.-Q. Ma and D.-Z. Liao, *Chem. Commun.*, 2000, 1309; G. Rogez, A. Marvilliers, E. Riviere, J.-P. Audiere, F. Lloret, F. Varret, A. Goujon, N. Menendez, J.-J. Girerd and T. Mallah, *Angew. Chem., Int. Ed.*, 2000, **39**, 2885.
8 C. A. Bignozzi, C. Chiorbili, M. T. Indelli, F. Scandola, V. Bertolasi and G. Gilli, *J. Chem. Soc., Dalton Trans.*, 1994, 2391; A. J. Deeming, G. P. Proud, H. M. Dawes and M. B. Hursthouse, *Polyhedron*, 1988, **7**, 651; J. E. House, Jr. and N. E. Kob, *Inorg. Chem.*, 1993, **32**, 1053; D. J. Darensbourg, J. C. Yoder, M. W. Hotcamp, K. K. Klausmeyer and J. B. Reibenspies, *Inorg. Chem.*, 1996, **35**, 4764.
9 G. A. Carriedo, N. G. Connelly, S. Alvarez, E. Perez-Carreno and S. Garcia-Granda, *Inorg. Chem.*, 1993, **32**, 272; F. L. Atkinson, A. Christofides, N. G. Connelly, H. J. Lawson, A. C. Loyns, A. G. Orpen, G. M. Rosair and G. H. Worth, *J. Chem. Soc., Dalton Trans.*, 1993, 1441; F. L. Atkinson, N. C. Brown, N. G. Connelly, A. G. Orpen, A. L. Rieger, P. H. Rieger and G. M. Rosair, *J. Chem. Soc., Dalton Trans.*, 1996, 1959; N. C. Brown, G. B. Carpenter, N. G. Connelly, J. G. Crossley, A. Martin, A. G. Orpen, A. L. Rieger and G. H. Worth, *J. Chem. Soc., Dalton Trans.*, 1996, 3977; N. G. Connelly, O. M. Hicks, G. R. Lewis, A. G. Orpen and A. J. Wood, *J. Chem. Soc., Dalton Trans.*, 2000, 1637; K. M. Anderson, N. G. Connelly, N. J. Goodwin, G. R. Lewis, M. T. Moreno, A. G. Orpen and A. J. Wood, *J. Chem. Soc., Dalton Trans.*, 2001, 1421 and references therein..
10 W. M. Laidlaw and R. G. Denning, *Inorg. Chim. Acta*, 1996, **248**, 51.
11 G. Barrado, G. A. Carriedo, C. Diaz-Valenzuela and V. Riera, *Inorg. Chem.*, 1991, **30**, 4416.
12 G. A. Carriedo, N. G. Connelly, M. C. Crespo, I. C. Quarmby, V. Riera and G. H. Worth, *J. Chem. Soc., Dalton Tans.*, 1991, 315.
13 G. A. Stark, A. M. Arif and J. A. Gladysz, *Organometallics*, 1997, **16**, 2909.
14 N. Zhu and H. Vahrenkamp, *Chem. Ber.*, 1997, **130**, 1241.
15 N. G. Connelly, K. A. Hassard, B. J. Dunne, A. G. Orpen, S. J. Raven, G. A. Carriedo and V. Riero, *J. Chem. Soc., Dalton Trans.*, 1988, 1623.
16 S.-M. Lee, R. Kowallick, M. Marcaccio, J. A. McCleverty and M. D. Ward, *J. Chem. Soc., Dalton Trans.*, 1998, 3443.
17 M. Marcaccio, M. D. Ward and J. A. McCleverty, unpublished work.

CHEMCOMM Communication
www.rsc.org/chemcomm

The first example of catalytic *N*-oxidation of tertiary amines by tungstate-exchanged Mg–Al layered double hydroxide in water: a green protocol†

B. M. Choudary,* B. Bharathi, Ch. Venkat Reddy, M. Lakshmi Kantam and K. V. Raghavan

Indian Institute of Chemical Technology, Hyderabad-500007, India. E-mail: choudary@iict.ap.nic.in

Received (in Cambridge, UK) 31st May 2001, Accepted 23rd July 2001
First published as an Advance Article on the web 28th August 2001

A green process, using a recyclable tungstate-exchanged Mg–Al layered double hydroxide (LDH-WO_4^{2-}) heterogenised catalyst and aqueous H_2O_2 oxidant in water, leads to *N*-oxidation of aliphatic *tert*-amines to amine *N*-oxides in quantitative yields, at a high rate at room temperature.

Aliphatic *tert*-amine *N*-oxides are essential and major components for ubiquitously used materials such as hair conditioners, shampoos, toothpaste, laundry detergent powders, fabric softeners, toilet soaps and cosmetics as well as in biomedical applications.[1] Amine oxides are compounds of increasing interest as potential cytoximes which are hypoxia-selective for the treatment of solid tumors.[2] These *N*-oxides are also used as stoichiometric oxidants to accomplish catalytic cycles in important reactions such as osmium catalysed dihydroxylation of olefins,[3a,b] ruthenium catalysed oxidation of alcohols[3c] and Mn–salen catalysed epoxidation of olefins.[3d] Amine *N*-oxides are currently prepared *via* a non-catalytic oxidation of *tert*-amines with H_2O_2 in a slow reaction.[3a,4] Other oxidants employed to hasten the oxidation of *tert*-amines include peracids,[5a] magnesium monophthalate,[5b] 2-sulfonyloxaziridines,[5c] α-azohydroperoxides[5d] and dioxiranes,[5e] which are not only expensive, but also generate large amounts of effluent during the reaction. The biomimetic oxidation of *tert*-amines is induced by 4a-hydroperoxyflavin in the presence of H_2O_2 as oxidant.[6] This forms the sole example of a catalytic reaction to the best of our knowledge. There is a strong need to develop a '*greener technology*'[7] with higher throughput, and in order to conform to the above, we accordingly designed and developed an eco-compatible process utilising a recyclable heterogeneous catalyst in aqueous medium. We report here, an efficient and heterogeneous tungstate-exchanged layered double hydroxide catalyst (LDH-WO_4^{2-}), for the oxidation of aliphatic *tert*-amines in water as solvent using aqueous H_2O_2 as oxidant which leads to excellent yields for the first time (Scheme 1).

Layered double hydroxides (LDHs)[8] have recently received much attention.[9] LDHs consist of alternating cationic $M^{II}_{1-x}M^{III}_x(OH)_2^{x+}$ and anionic $A^{n-}\cdot zH_2O$ layers. The positively charged layers contain edge-shared metal M^{II} and M^{III} hydroxide octahedra, with charges neutralized by A^{n-} located in interlayer spacings or at edges of the lamellae. Small hexagonal LDH crystals of composition $Mg_{1-x}Al_x(OH)_2Cl_x\cdot 2H_2O$ were synthesized following existing procedures (here $x = 0.25$).[9a] The anionic species tungstate, molybdate and vanadate were exchanged with LDH-Cl to give LDH tungstate, molybdate and vanadate, respectively. The Mg–Al LDH (3 : 1) tungstate (cat **1**) was prepared according to the reported procedure.[9c] 1 g of Mg–Al–Cl LDH was stirred in 100 ml of an aqueous solution of 1.87 mM (0.616 g) sodium tungstate at 293 K for 24 h. The solid catalyst was filtered off, washed with deionised and decarbonated water and lyophilized to dryness. Similarly, the Mg–Al LDH molybdate (cat **2**) and Mg–Al LDH vanadate (cat **3**) were prepared. The preparation of LDH-{$PO_4[WO(O_2)]_4$} (cat **4**) was carried out according to the literature procedure.[10] To a solution of 0.46 mmol of isolated (NBu^n_4){$PO_4[WO(O_2)_2]_4$} in acetone (3 ml) was added 1 ml of H_2O_2 [35% (w/w) aqueous solution] and 1 g of Mg–Al–Cl LDH and the mixture was stirred for 16 h at room temperature. The obtained material (cat **4**) was treated consecutively with water–acetone (1 : 1) and acetone.

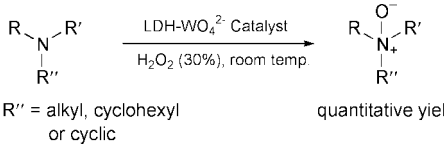

Scheme 1 Oxidation of *tert*-amines to amine *N*-oxides catalysed by tungstate-exchanged Mg–Al LDH.

All these catalysts were well characterised by powder-XRD, TGA–DTA and chemical analysis. The X-ray powder diffraction patterns of the LDH and LDH-WO_4^{2-} (cat **1**), LDH-MoO_4^{2-} (cat **2**), LDH-VO_3^- (cat **3**), LDH-{$PO_4[WO(O_2)]_4$} (cat **4**) scarcely differ in the range 2θ = 3–65°. These data clearly indicate that the above anions are not intercalated but lie on edge-on positions of LDH in the solid catalyst. Chemical analysis of the catalysts revealed the tungstate (%) content in cat **1** as 11% and cat **4** as 21% while the molybdate content in cat **2** was 9.9%, and vanadate content in cat **3** was 7.8%. The thermogravimetric profiles and the relative derivative curves (TGA and DTA) for the tungstate, molybdate and vanadate exchanged LDH catalysts cat **1**–**4** show two stages of weight loss associated with two endotherms characteristic of LDHs. These results provide evidence that there is no structural disorder after the ion-exchange.

The exchanged LDH catalysts (cat **1**–**4**) and their homogeneous analogues were evaluated in oxidation of aliphatic *tert*-amines with H_2O_2 in order to identify the best catalysts (Table 1). The *tert*-amine is oxidised with aqueous hydrogen peroxide (30% w/w) using water as a solvent in the presence of catalyst at room temperature under continuous stirring, while monitoring the progress of the reaction by TLC. The order of activity of

Table 1 Catalytic *N*-oxidation of *N*-methylmorpholine to *N*-methylmorpholine *N*-oxide catalysed using various metal ion-exchanged LDH catalysts and their homogeneous analogues

Entry	Catalyst	Time/h	Yield[c] (%)
1	LDH-WO_4^{2-} (cat **1**)		
	Procedure I[a]	1.0	96
	Procedure II[b]	1.0	96
2	LDH-MoO_4^{2-}(cat **2**)	3.5	90
3	LDH-VO_3^- (cat **3**)	3.5	40
4	LDH-{$PO_4[WO(O_2)]_4$} (cat **4**)	3.5	40
5	Na_2WO_4	3.5	75
6	$NaVO_3$	3.5	15
7	Na_2MoO_4	3.5	48
8	None	24.0	25

[a] 2 mmol of substrate, 200 mg of catalyst, 10 ml of water and 6 mmol of aq. H_2O_2 (30% w/w). [b] 6 mg of dodecylbenzenesulfonic acid sodium salt added as surfactant. [c] Isolated yield.

† IICT Communication No: 4804.

 DOI: 10.1039/b104754j

the LDH exchanged catalysts is: cat **1** > cat **2** > cat **3** = cat **4** and thus LDH-WO_4^{2-} (cat **1**) is inferred to be the best catalyst in the oxidation of *tert*-amines. The heterogeneous catalysts provide superior performance over their homogeneous counterparts. The efficacy in increasing the rate of *N*-oxidation is evident from Table 1, in which LDH-WO_4^{2-} affords 96% conversion in 1 h *cf.* 25% in 24 h in the absence of a catalyst.

In an effort to understand the scope of the reaction, several other amines having different R groups attached to the tertiary nitrogen atom were subjected for oxidation using the best catalytic LDH–WO_4^{2-}–H_2O_2 system to give excellent yields and ≅ 100% selectivity (Table 2). No other by-products were observed in these reactions. Water proved to be the best solvent in terms of activity in the *N*-oxidation of *tert*-amines. When the dodecylbenzenesulfonic acid sodium salt is employed as an additive, the rate of the *N*-oxidation reaction is increased 2–3 fold except in the case of *N*-methylmorpholine (Table 2). This may be due to the high hydrophilicity of the latter, when compared with other *tert*-amines used. The present *N*-oxidation reaction takes place under liquid–solid–liquid triphasic conditions, comprising of organic *tert*-amine, solid catalyst and aqueous phase. We assumed that the main role of the surfactant is to increase the contact area of the interface between the aqueous and organic phases and to enhance the transfer of the lipophilic amine from the organic to the aqueous phase. The amine *N*-oxides thus obtained are useful additives for the surfactants,[11,12] for example, the product in Table 2, entry 18 is sold under the trade name *Barlox 10S*.[1a] The benzylic amine *N*-oxides (Table 2, entries 14, 16 and 21) serve as substrates.[13]

Table 2 Oxidation of *tert*-amines catalysed by LDH-WO_4^{2-} (cat **1**)[a]

Entry	Tertiary amine	Procedure	Amine oxide	Time/h	Yield[b] (%)
9	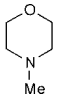	I	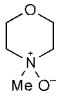	1.0	96
10		II		1.0	96
11	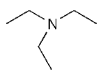	I	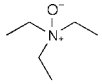	3.0	96
12		II		1.5	96
13	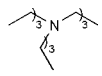	I	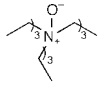	3.0	94
14	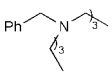	I	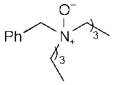	1.5	96
15		II		1.0	95
16	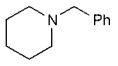	I	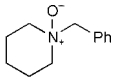	3.0	97
17		II		1.0	97
18		I		2.5	97
19		I		2.5	95
20		II		1.0	95
21		I		1.5	95
22		II		1.0	96
23	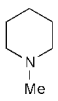	I	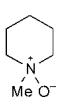	3.5	95(94)[c]
24		II		1.0	95
25	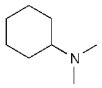	I	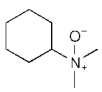	3.0	96
26		II		1.0	95

[a] Reaction conditions as in Table 1 (footnotes *a* and *b*). [b] Isolated yields (all the products were characterized by ^{1}H NMR and mass spectrometry). [c] Yield after sixth cycle.

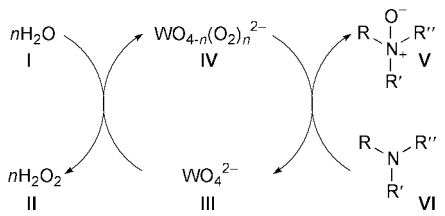

Scheme 2 Plausible catalytic cycle for the *N*-oxidation of *tert*-amines to amine *N*-oxides by tungstate-exchanged Mg–Al LDH.

Furthermore cat **1** can be reused for six cycles (see Table 2, entry 23) without loss of activity and selectivity. The reaction did not proceed when conducted with the resulting filtrate after separation of the solid catalyst from the previous batch. This indicates that the active ingredient has not leached out of the solid catalyst during the reaction.

A plausible catalytic cycle in the oxidation of amines to amine oxides as described in Scheme 2 involves formation of peroxotungstate, **IV** on interaction of tungstate LDH **III** with hydrogen peroxide **II**.[9c] A shift of λ_{max} 250 (LDH **III**) to 325 nm (**IV**) according to UV-DRS confirms the formation of peroxotungstate species. The peroxotungstate **IV** species transfers its electrophilic oxygen to an amine **VI** forming the amine *N*-oxide **V** with regeneration of the active catalyst **III**.

In conclusion, the present process represents the sole example for synthesis of *N*-oxides wherein the heterogenised tungstate-based Mg–Al LDH is used as a catalyst. The potential for its commercial application is strengthened by the high throughput of the product, lower process inventories and use of an aqueous phase reaction system.

B. B. and Ch. V. R. thank CSIR, India for SRF.

Notes and references

1 (*a*) Kirk-Othmer, *Encyclopedia of Chemical Technology*, John Wiley and Sons, Wiley-Interscience, New York, 4th edn., 1997, vol. 23, p. 524; (*b*) T. A. Isbell, T. P. Abbott, J. A. Dworak, *US Pat*., 6,051,214, 2000.

2 K. I. Priyadarsini, M. F. Dennis, M. A. Naylor, M. R. L. Stratford and P. Wardman, *J. Am. Chem. Soc*., 1996, **118**, 5648.

3 (*a*) V. Vanrheenen, D. Y. Cha and W. M. Hartley, *Org. Synth*., 1988, **Coll. Vol. VI**, 342; (*b*) M. Schroder, *Chem. Rev*., 1980, **80**, 187; (*c*) S. V. Ley, J. Norman, W. P. Griffith and S. P. Marsden, *Synthesis*, 1994, 639; (*d*) S. Cicchi, F. Cardona, A. Brandi, M. Corsi and A. Goti, *Tetrahedron Lett*., 1999, **40**, 1989.

4 A. C. Cope and E. Ciganek, *Org. Synth*., 1963, **Coll. Vol. IV**, 616.

5 (*a*) H. S. Mosher, L. Turner and A. Carismith, *Org. Synth*., 1963, **Coll. Vol. IV**, 828; (*b*) P. Brougham, M. S. Cooper, D. A. Cummerson, H. Heaney and N. Thomson, *Synthesis*, 1987, 1015; (*c*) W. W. Zajac, T. R. Walters and M. G. Darcy, *J. Org. Chem*., 1988, **53**, 5856; (*d*) A. L. Baumstark, M. Dotrong and P. C. Vasquez, *Tetrahedron Lett*., 1987, **28**, 1963; (*e*) M. Ferrer, F. Sanchez-Baeza and A. Messguer, *Tetrahedron*, 1997, **53**, 15 877.

6 K. Bergstad and J. E. Backvall, *J. Org. Chem*., 1998, **63**, 6650.

7 G.-J. ten Brink, I. W. C. E. Arends and R. A. Sheldon, *Science*, 2000, **287**, 1636.

8 F. Cavani, F. Trifiro and A. Vaccari, *Catal. Today*, 1991, **11**, 173.

9 (*a*) S. Miyata, *Clays Clay Miner*., 1975, **23**, 369; (*b*) B. M. Choudary, M. L. Kantam, A. Rahman, Ch. V. Reddy and K. K. Rao, *Angew. Chem., Int. Ed*., 2001, **40**, 763; (*c*) B. Sels, D. E. de Vos, M. Buntinx, P. Frederic, A. K. Mesmaeker and P. A. Jacobs, *Nature*, 1999, **400**, 855.

10 D. Hoegaerts, B. F. Sels, D. E. de Vos, F. Verpoort and P. A. Jacobs, *Catal. Today*, 2000, **60**, 209.

11 A. Albini, *Synthesis*, 1993, 263.

12 J. D. Sauer, *Surfactants Sci. Ser*., 1990, **34**, 275.

13 J. B. Meisenheimer, *Otsch. Chem. Ges*., 1919, **52B**, 1667.

CHEMCOMM Communication
www.rsc.org/chemcomm

Nanoparticle routes to mesoporous titania thin films

Young Kyu Hwang,[a] Kyoung-Chul Lee[b] and Young-Uk Kwon*[a]

[a] *Department of Chemistry and BK-21 School of Molecular Science, Sungkyunkwan University, Suwon 440-746, Korea. E-mail: ywkwon@chem.skku.ac.kr*
[b] *Department of Chemistry, Sungkyunkwan University, Suwon 440-746, Korea*

Received (in Cambridge, UK) 30th May 2001, Accepted 26th July 2001
First published as an Advance Article on the web 15th August 2001

Controlled aging of TiO_2 nanoparticles blended with diblock copolymers and processed into dip-coated thin films led to ordered mesostructures with cubic and hexagonal symmetries that can be transformed into mesoporous TiO_2 by calcination.

There has been much interest in porous titania for its potential applications in areas such as photocatalysis,[1] photovoltaics,[2] and proton conducting membranes.[3] However, attempted syntheses of mesoporous titania so far have achieved only limited success.[4] On the other hand, many of the possible applications of mesoporous titania require thin films with accessible pores from the film surfaces, which is not possible with the common 2D hexagonal phases that form channels parallel to the film surfaces; a bicontinuous cubic phase would be desirable. Recently, Yang *et al*. have developed a generalized method to synthesize mesoporous oxides of many non-silicon metals utilizing non-hydrolytic condensation reactions of metal halides with alcohols and Pluronic block copolymers as the structure directing agents.[5] They have synthesized mesoporous titania with a cubic structure as well as 2D hexagonal structure. However, this seemingly simple method actually involves many different reactions occurring simultaneously including condensation of metal ions and self-assembly of the block copolymer templates that are sensitively affected by the reaction conditions. Slight variations of the reaction environments often produce totally different results making this method not highly reproducible. We have sought solutions for this problem by utilizing pre-synthesized nanoparticles instead of inducing the condensation of metal halides in the presence of surfactant molecules to alleviate the system's sensitivity, and thus to make the method simpler and more reproducible. In this paper, we report our results on the synthesis of mesoporous titania films using TiO_2 nanoparticles.

The synthesis of mesoporous titania is achieved in four steps of (1) synthesis of nanoparticles, (2) blending nanoparticles with template molecules into thin films, (3) aging the blended mixtures into mesostructures under appropriate conditions, and (4) calcination to remove the organic templates. Stock solutions of TiO_2 nanoparticles were prepared according to the literature procedure with slight modifications:[6] Titanium chloride, $TiCl_4$, was dissolved in absolute ethanol to a final $TiCl_4$ concentration of 20 wt%. A mixed solution of conc. HCl and 35% H_2O_2 in a 4/1 ratio (v/v) was added and the solution was refluxed at 80 °C for 2 h. The nanoparticles so obtained have anatase structure according to electron diffraction and transmission electron microscopy (TEM, JEOL-3011, 300 keV) studies† with sizes of *ca*. 1.6–2.0 nm based on the absorption edge of 305–325 nm from UV–VIS spectroscopic data.[7] A Brij-type diblock copolymer, $C_nH_{2n+1}(OCH_2CH_2)_yOH$ (C_nEO_y) with n/y = 16/20, 16/10, or 12/4, was dissolved in the TiO_2 stock solution and stirred for 10 h at room temperature. The molar composition of the final solution was $TiCl_4/C_nEO_y/HCl/H_2O_2/EtOH/H_2O$ = 1/0.083/3.8/0.97/6.1/15. The solution was dip-coated on silicon substrates at a pulling rate of 6 cm m^{-1}. The films were dried/aged either at 10 °C for 8 d or at 18 °C for 7 d under a controlled humidity of 80%. The progress of mesostructure formation of the materials in the as-synthesized films was monitored by powder X-ray diffraction (XRD, Rigaku D/max-RC). After the film materials ordered into cubic or hexagonal mesostructures (according to XRD), the films were calcined at 450 °C for 5 h in air. The as-synthesized films had some chlorine impurity (Cl/Ti = 0.3 by EDX/TEM), which was completely removed by calcination. The film thickness was typically about 300 nm for the as-synthesized and about 100 nm for the calcined films by SEM (JEOL-35 CF) and ellipsometry (Woollam VASE instrument). The crack-free, uniform and transparent (to the naked eye) TiO_2 mesoporous thin films so obtained were characterized by XRD and TEM.

The as-synthesized film prepared with $C_{16}EO_{20}$ block copolymer formed a mesostructure after aging at 10 °C for 7 d as evidenced by the XRD peak with d = 5.8 nm [Fig. 1(a)]. The XRD patterns were featureless up to 6 d of aging, indicating the sluggish nature of the self-assembly kinetics of the film materials. The XRD peak was shifted to d = 4.1 nm upon calcination indicating a lattice contraction by about 30% [Fig. 1(b)]. Although the XRD patterns do not reveal the details of the structure with only one peak present, the TEM image of the calcined material, in Fig. 1(c), can be explained by a pseudo-cubic structure with the [100] axis parallel to the viewing direction. The repeating distance of 4.3 nm of this image is in accord with the d-value from the XRD pattern. With the limited information available from these data, we cannot determine the structure of this material. However, the coinciding d-values from the XRD and TEM data suggest that the material has a primitive cubic unit cell. The one-peak nature in the XRD

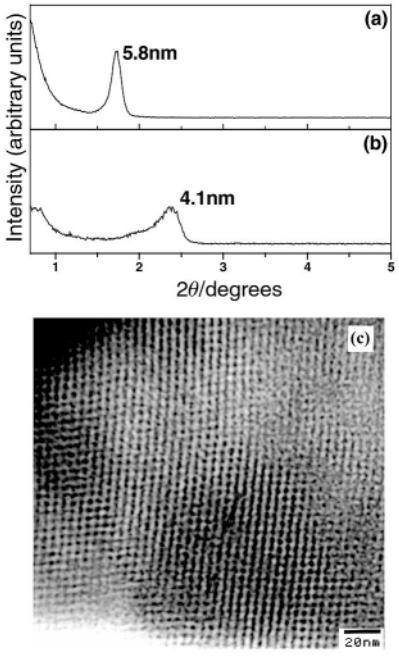

Fig. 1 XRD patterns of (a) an as-synthesized thin film prepared using $C_{16}EO_{20}$ surfactant as a structure directing agent and aged at 10°C for 7 d and (b) the calcined thin film. (c) TEM image of the calcined thin film showing pseudo-cubic symmetry.

 DOI: 10.1039/b104699n

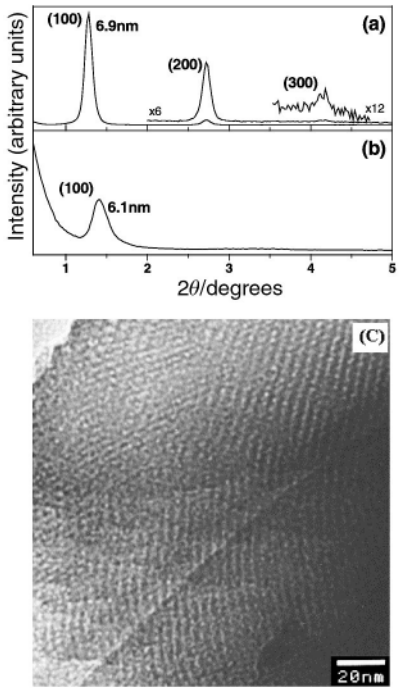

Fig. 2 XRD patterns of (a) an as-synthesized thin film prepared using using $C_{16}EO_{10}$ surfactant as the structure directing agent and aged at 18 °C for 4 d and (b) the calcined thin film. (c) TEM image of the calcined thin film that shows a 2D hexagonal structure preferentially oriented with the [100] axis parallel to the viewing direction.

pattern and the off-perpendicular axes in the TEM images suggest that the material is distorted from the ideal cubic structure, probably because the ordering of the materials is not perfect. The anisotropic lattice contraction during the calcination may also be responsible for the distorted mesostructure in the TEM image. Reflectance UV–VIS spectroscopic data on a calcined thin film shows an absorption edge of 360 nm that corresponds to a size of 3.0 nm for the anatase nanoparticles. This value agrees with the wall thickness measured from the TEM images and implies that the particle size is increased upon calcination. We have attempted to obtain better ordering of the materials by aging for longer periods of time up to 14 d, but the XRD patterns did not reveal any further peaks. Notwithstanding, it is clear that thin films of mesoporous titania with accessible pores from the film surfaces can be obtained by this procedure.

If the as-synthesized film was aged at 18 °C for 4 d instead of 10 °C for 7 d and calcined, the XRD pattern did not show any peak, indicating that a lamellar structure was not obtained. However, when $C_{16}EO_{10}$ was used instead of $C_{16}EO_{20}$ and aged at 18 °C, an XRD pattern with high order peaks that could be indexed with a 2D hexagonal or a lamellar mesostructure was obtained [Fig. 2(a)]. The XRD pattern was maintained after calcination with peaks shifted to higher angles [Fig. 2(b)] indicating a 2D hexagonal phase. The lattice parameters were a = 6.9 and 6.1 nm before and after calcination. The TEM image of the calcined sample also confirmed the hexagonal structure with channels with a repeating distance of 3.7 nm in agreement with the expected value of 3.5 nm (= $a/2$) based on the lattice parameter from XRD measurements.

Unfortunately, our TEM and XRD data did not provide any evidence of crystalline TiO_2 in the mesoporous films, probably because the particles were not well crystallized or were too small in size. Attempts to improve the crystallinity of the wall TiO_2 by calcining at higher temperatures than 450 °C caused collapse of the mesostructures, although anatase peaks were observed in the XRD patterns.

Because of the limited amount of samples available from thin films, we were not able to perform any other characterization studies such as surface area measurements. However, with the XRD and TEM data provided, it is clear that the materials we have obtained are mesoporous TiO_2.

The present system requires optimization of the reaction conditions. When different templates such as $C_{16}EO_{10}$ or $C_{12}EO_4$ were used instead of $C_{16}EO_{20}$ and aged at 10 °C, lamellar or disordered mesostructures were formed. Synthesis using $C_{12}EO_4$ and aging at 18 °C produced a lamellar structure whose lattice collapsed upon calcination. Thin films from solutions with different molar ratio of $TiCl_4/C_nEO_y$ from those given above formed poorly ordered mesostructures. However, the synthesis results are reproducible once the conditions including the composition, aging temperature and atmosphere are controlled as described. The nanoparticles in the solutions, with or without surfactant molecules, are very stable so that thin films prepared from solutions stored for up to 2 weeks under ambient conditions produce the same results.

Even after the mesostructures were formed by aging, the film materials are washed out when immersed in alcohols, indicating that the nanoparticles are not condensed into a 3D framework structure by aging alone. This observation and the strong dependency of the final mesostructure to the aging temperature resemble those of liquid crystals. Therefore, the mesostructures in the as-synthesized films can be explained by the self-assembly of the block copolymer and TiO_2 nanoparticles which, together, behave as a liquid crystal.

The method used in this paper has many advantages over those reported in the literature. First, by using block copolymers with large molecular weight and nanoparticles, the resulting mesostructures have large pores and thick walls, which can be of benefit for the utilization of semiconducting properties of transition metal oxides. Second, the results in this paper are highly reproducible as long as the conditions described are met since the complex condensation reactions of the inorganic precursors were eliminated. Third, the principles used in this work are simple and can be easily adapted to other metal oxide systems. Fourth, the mesoporous thin films of transition metal oxides with accessible pores from the film surfaces can be used for long sought applications such as photocatalysis, photovoltaics and membranes.

This research was financially supported by KOSEF (SRC, CNNC). We thank Mr J. S. Ju at Central Research Facilities, SKKU for the TEM data.

Notes and references

† For the TEM studies, the nanoparticles were embedded into a polyacrylamide matrix by refluxing with added acrylamide.

1 Y. Matsumoto, Y. Ishikawa, M. Nishida and S. Ii, *J. Phys. Chem. B*, 2000, **104**, 4204; E. Stathatos, D. Tsiourvas and P. Lianos, *Colloids Surf. A*, 1999, **149**, 49.

2 A. Hagfeldt and M. Grätzel, *Acc. Chem. Res.*, 2000, **33**, 269; F. G. Gao, A. J. Bard and L. D. Kispert, *J. Photochem. Photobiol. A: Chem.*, 2000, **130**, 49.

3 F. M. Vichi, M. I. Tejedor-Tejedor and M. A. Anderson, *Chem. Mater.*, 2000, **12**, 1762.

4 D. M. Antonelli and J. Y. Ying, *Angew. Chem., Int. Ed. Engl.*, 1995, **34**, 2014; D. M. Antonelli, *Microporous Mesoporous Mater.*, 1999, **30**, 315; V. F. Stone. Jr. and R. J. Davis, *Chem. Mater.*, 1998, **10**, 1468; D. T. On, *Langmuir*, 1999, **15**, 8561; D. Khushalani, G. A. Ozin and A. J. Kuperman, *J. Mater. Chem.*, 1999, **9**, 1491; G. de A. A. Soler-Illia and C. Sanchez, *New J. Chem.*, 2000, **24**, 493.

5 P. Yang, D. Zhao, D. I. Margolese, B. F. Chmelka and G. D. Stucky, *Nature*, 1998, **396**, 6707.

6 H. K. Park, D. K. Kim and C. H. Kim, *J. Am. Ceram. Soc.*, 1997, **80**, 743; C. Sanchez, J. Livage, M. Henry and F. Babonneau, *J. Non-Cryst. Solids*, 1988, **100**, 65.

7 L. Brus, *J. Phys. Chem.*, 1986, **90**, 2555; C. Kormann, P. W. Bahnemann and M. R. Hoffmann, *J. Phys. Chem.*, 1988, **92**, 5196.

CHEMCOMM Communication
www.rsc.org/chemcomm

Aggregation-induced emission of 1-methyl-1,2,3,4,5-pentaphenylsilole

Jingdong Luo,[a] Zhiliang Xie,[a] Jacky W. Y. Lam,[a] Lin Cheng,[a] Haiying Chen,[b] Chengfeng Qiu,[b] Hoi Sing Kwok,[b] Xiaowei Zhan,[c] Yunqi Liu,[c] Daoben Zhu[c] and Ben Zhong Tang*[a]

[a] *Department of Chemistry, Institute of Nano Science and Technology, Hong Kong University of Science & Technology (HKUST), Clear Water Bay, Kowloon, Hong Kong, China. E-mail: tangbenz@ust.hk*
[b] *Center for Display Research, HKUST, Clear Water Bay, Kowloon, Hong Kong, China*
[c] *Institute of Chemistry, Chinese Academy of Sciences, Beijing 100080, China*

Received (in Cambridge, UK) 12th June 2001, Accepted 19th July 2001
First published as an Advance Article on the web 14th August 2001

Aggregation greatly boosts emission efficiency of the silole, turning it from a weak luminophor into a strong emitter.

Many chromophoric organics and polymers are highly emissive in their dilute solutions but become weakly luminescent when fabricated into thin films.[1] This is believed to be caused by aggregate formation: in the solid state, the molecules aggregate to form less emissive species such as excimers, leading to a reduction in the luminescence efficiency. The chromophoric molecules are practically utilised in solid state commonly as thin films, and mitigation of the aggregation quenching has been a goal of research.[1,2] Many groups have attempted to obstruct aggregate formation through elaborate chemical, physical, and engineering approaches, which have, however, met with only limited success. Aggregation is in some sense inherent in film formation and it would be ideal if a molecule can emit intense light in its aggregation state. We here report such an unusual molecule, whose isolated species are faintly emissive but whose aggregates are strongly luminescent.

In our search for highly emissive linear and hyperbranched polymers,[3] we are attracted by a group of molecules called 'siloles', whose linearly drawn chemical structures appear to be conjugated, an example of which is shown in Fig. 1. During the purification process of the silole compound 1-methyl-1,2,3,4,5-pentaphenylsilole (**1**),[4] we noticed an intriguing phenomenon: when a drop of a solution of **1** was placed on a TLC plate, the wet spot could hardly be visualised with a UV lamp, but the dried spot (after solvent evaporation) was clearly visible upon UV illumination. This suggests that **1** does not luminesce when dissolved but does so upon aggregation. This rare observation prompted us to further study its luminescence behaviours.

When a dilute ethanol solution of **1** was excited at 381 nm, almost no photoluminescence (PL) signals were recorded by a spectrofluorometer (Fig. 2A). The 100-times magnified data gave a noisy spectrum; that is, **1** is indeed a weak emitter when it is molecularly dissolved in a good solvent. In contrast, when large amounts of water were added to its ethanol solutions (the final concentrations being kept unchanged at 10 μM), intense PL spectra were recorded under identical measurement conditions. Water is a non-solvent of **1** and the silole molecules must have aggregated in the solvent mixtures with high water contents. The 'solutions' were, however, macroscopically homogenous with no precipitate, suggesting that the silole aggregates are of nanodimension. A thin film of **1** prepared by vapour deposition also gave a strong PL spectrum. The spectroscopic analyses thus confirmed our visual observation described above.

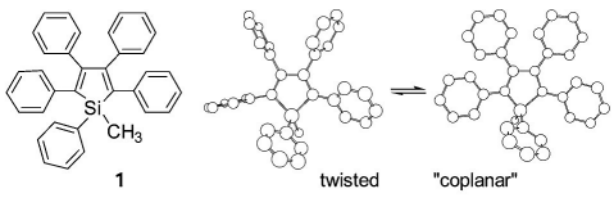

Fig. 1 Molecular structure and conformational rotamers of **1**.

To have a quantitative picture, we estimated the PL quantum yields (Φ_F) of **1** in ethanol and water–ethanol mixtures, using 9,10-diphenylanthracene as the reference. The Φ_F value for the ethanol solution was 0.63×10^{-3} (Fig. 2B), falling in the range of the literature values ($0.31–5.13 \times 10^{-3}$) of their close cousins.[5] The Φ_F value remained almost unchanged when up to 50% water was added to the ethanol solution but started to swiftly increase afterwards. When the water fraction was increased to 90%, Φ_F rose to 0.21, which is 333 times higher than that of the ethanol solution. The trajectory of the Φ_F change suggests that the molecularly dissolved **1** starts to congregate at a water fraction of 50% and the population of the aggregate continues to increase as the water fraction increases. Similar results were obtained when water was added into THF solutions of **1**. The change of the PL spectrum with solvent composition may be regarded as a special type of solvatochromism, and the sensitive on/off switching of the light emission by aggregation/deaggregation may find potential applications in optoelectronics systems.

To gain an insight into the cause of the unique PL behaviours of **1**, we checked its UV absorption spectra. The spectra of **1** in ethanol and 50% water–ethanol mixture were almost identical (Fig. 3). Its absorption bands in the 60% water–ethanol mixture, however, rose in intensity and moved to longer wavelengths. A level-off tail is seen in the visible spectral region; such tails are commonly observed in nanoparticle suspensions,[6] confirming the existence of nanoaggregates of **1** in the solvent mixture. The spectrum was further intensified as the water fraction increased. The differential spectra shown in the inset clearly manifest the growth of the red-shifted bands with an increase in the water fraction. The new peaks at ~291 and 400 nm are obviously due to the nanoaggregate absorption. When the silole molecules cluster together, its effective concentration decreases and the absorbance should also decrease. The increase in the absorbance thus indicates that the nanoaggregates are better conjugated than their counterparts of isolated species.

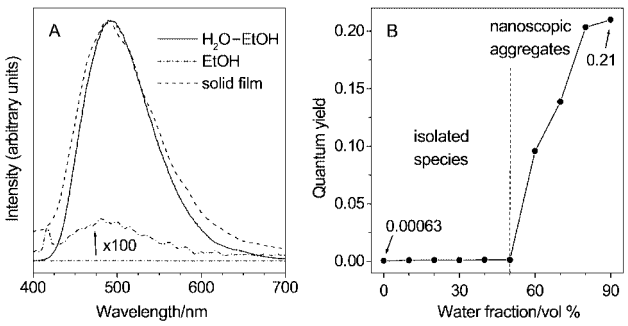

Fig. 2 (A) PL spectra of **1** in water–ethanol mixture (90 : 10 by volume), absolute ethanol, and solid film; concentration of **1**: 10 μM; excitation wavelength (nm): 381 (for solutions), 325 (for film). (B) Quantum yield of **1** *vs.* solvent composition of the water–ethanol mixture.

 DOI: 10.1039/b105159h

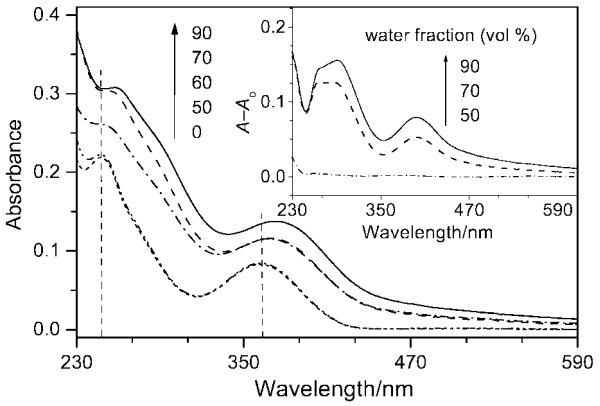

Fig. 3 UV spectra of **1** in water–ethanol mixtures (concentration of **1**: 10 μM). Inset: differential spectra of **1** (*A* and A_0 being absorbance of **1** in mixture solvent and absolute ethanol, respectively).

The silole may exist mainly as a twisted conformer when it is molecularly dissolved in a good solvent. A twisted rotamer of **1**, whose energy was minimised by the MM2 method in a CS Chem3D Pro program, is given in Fig. 1. The phenyl peripheries linked to the silole core are obviously out of coplanarity. It has been proposed that coplanarisation of chromophores can be induced by aggregation.[7] When **1** aggregates, coplanarisation of its peripheries and core may be induced to a certain extent. It is well known that coplanar and twisted conformers have different resonance energy: when the rings are on the same plane, the degree of conjugation is at a maximum; when the rings rotate to 90° to one another, the conjugation drops to a minimum. The best-known example of this is biphenyl (**2**) and its non-coplanar 2,2'-dimethyl homologue (**3**), which exhibit quite different electronic properties (*e.g.* $\varepsilon_2/\varepsilon_3 > 20$). The coplanarisation of **1** induced by the aggregation leads to a better conjugation between its peripheries and core, thus intensifying and red-shifting its absorption and emission bands. The silole molecules in the nanoaggregates cannot, however, assume a perfect coplanar conformation due to the involved steric crowdedness, and the phenyl rings may still rotate to some degree to cope with the steric repulsion. Such rotation will preclude co-facial alignment of the molecules and hinder excimer formation.[7] Aggregation quenching thus cannot operate in the luminescence process of **1**.

To further verify that aggregation quenching is not involved and to prove the usefulness of the novel luminescence property, we carried out a solid-state 'dilution' experiment and prepared a series of composite films of **1** and poly(methyl methacrylate) (PMMA). The compatibility of **1** and PMMA enabled us to cast thin films of optical quality from its chloroform solutions. The progressive red-shift of the PL spectrum with an increase in the content of **1** manifests the formation and population of the nanoaggregates in the solid 'solutions' (Fig. 4A). The linear increase of the luminance with the content of **1** testifies that the light emission is not quenched by aggregation. The composite film with 90% of **1** emitted a blue light of 492 nm with a high luminance of ~24000 cd m^{-2}. We built an electroluminescence (EL) device of ITO/CuPc/TPD/**1**/Mg-Ag,† which emitted a blue light of 496 nm. When an Alq_3† layer was introduced, the device ITO/CuPc (20 nm)/TPD (50 nm)/**1** (50 nm)/Alq_3 (10 nm)/LiF-Al showed a low turn-on voltage (3.4 V), high emission efficiencies (9234 cd m^{-2}, 12.6 lm W^{-1}, and 12 cd A^{-1}) and external quantum yield (8%). When the thickness of the Alq_3 layer was optimised (7 nm), the power efficiency was boosted to 20 lm W^{-1}. The silole is thus an excellent light-emitting material for the device application.

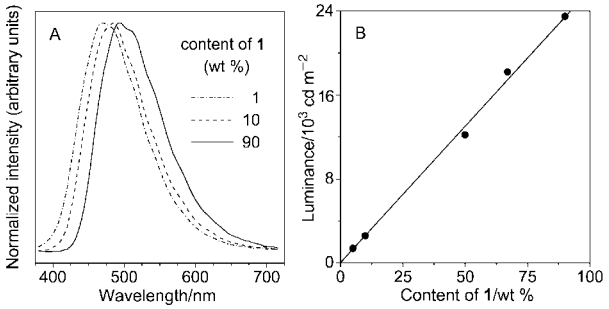

Fig. 4 (A) PL spectra of **1**–PMMA composites (excited at 325 nm). (B) Luminance of the composite film *vs.* its content of **1**.

In summary we revealed the uncommon emission behaviours of a silole (**1**) in this study. It has been a common 'law' that aggregation quenches light emission. What we observed here is exactly the opposite: light emission is induced by aggregation. The aggregation increased the emission efficiency of **1** by as high as two orders of magnitude (333 times). This is exceptionally rare, if not unprecedented, for small organic molecules.[8] Aggregation quenching has been the thorniest problem in the development of organic light-emitting diodes with high efficiencies. Our finding of aggregation-induced emission may stimulate new molecular engineering endeavours in the design of luminescent organics and polymers with highly emissive aggregation states.

We thank the Hong Kong Research Grants Council for financial support (HKUST 6187/99P and 6062/98P).

Notes and references

† ITO = indium–tin oxide, CuPc = copper phthalocyanine, TPD = *N,N'*-diphenyl-*N,N'*-bis(3-methylphenyl)-1,1'-diphenyl-4,4'-diamine, Alq_3 = tris(8-hydroxyquinolinato)aluminum.

1 R. H. Friend, R. W. Gymer, A. B. Holms, J. H. Burroughes, R. N. Marks, C. Taliani, D. D. C. Bradley, D. A. Dos Santos, J. L. Brédas, M. Lögdlund and W. R. Salaneck, *Nature*, 1999, **397**, 121.
2 B. Z. Tang, *Chem. Innov.*, 2001, **31**(5), 8.
3 Y. M. Huang, W. Ge, J. W. Y. Lam and B. Z. Tang, *Appl. Phys. Lett.*, 2001, **78**, 1652; B. Z. Tang, H. Xu, J. W. Y. Lam, P. P. S. Lee, K. Xu, Q. Sun and K. K. L. Cheuk, *Chem. Mater.*, 2000, **12**, 1446; Y. M. Huang, J. W. Y. Lam, K. K. L. Cheuk, W. Ge and B. Z. Tang, *Macromolecules*, 1999, **32**, 5976; C. W. Lee, K. S. Wong, W. Y. Lam and B. Z. Tang, *Chem. Phys. Lett.*, 1999, **307**, 67; H. Peng, K. Xu, J. Luo, D. Jia and B. Z. Tang, *Polym. Prepr.*, 2001, **42**, 560; Peng, K. Xu, J. Luo, J. A. K. Cha, D. Jia, Y. Huang, D. Zhang, Z. Xu and B. Z. Tang, *Polym. Mater. Sci. Eng.*, 2001, **84**, 643.
4 E. Braye, W. Hubel and I. Caplier, *J. Am. Chem. Soc.*, 1961, **83**, 4406; B. Z. Tang, X. Zhan, G. Yu, P. P. S. Lee, Y. Q. Liu and D. B. Zhu, *J. Mater. Chem.*, 2001, in the press.
5 S. Yamaguchi, T. Endo, M. Uchida, T. Izumizawa, K. Furukawa and K. Tamao, *Chem. Eur. J.*, 2000, **6**, 1683; S. Yamaguchi, R.-Z. Jin and K. Tamao, *J. Am. Chem. Soc.*, 1999, **121**, 2937.
6 B. Z. Tang, Y. Geng, J. W. Y. Lam, B. Li, X. Jing, X. Wang, F. Wang, A. Pakhomov and X. X. Zhang, *Chem. Mater.*, 1999, **11**, 1581.
7 M. Levitus, K. Schmieder, H. Ricks, K. D. Schimizu, U. H. F. Bunz and M. A. Garcia-Garibay, *J. Am. Chem. Soc.*, 2001, **123**, 4259.
8 Aggregation-favoured emission with 2.2–8.7 times enhancement in Φ_F was observed in a few polymer systems: R. Deans, J. Kim, M. R. Machacek and T. M. Swager, *J. Am. Chem. Soc.*, 2000, **122**, 8565; C. Belton, D. F. O'Brien, W. J. Blau, A. J. Cadby, P. A. Lane, D. D. C. Bradley, H. J. Byrne, R. Stockmann and H.-H. Horhold, *Appl. Phys. Lett.*, 2001, **78**, 1059; K. S. Wong, C. W. Y. Law, T. Sun, A. P. Monkman, M. E. Vaschetto, L. J. Hartwell, L. E. Horsburgh and M. da G. Miguel, *Synth. Met.*, 2001, **116**, 15. A cyanin dye salt was found to form superradiant aggregates in an aqueous medium: S. Özçelik and D. L. Akins, *J. Phys. Chem. B*, 1999, **103**, 8926.

CHEMCOMM Communication
www.rsc.org/chemcomm

One-step synthesis and redox properties of dodecahydro-3a,9a-diazaperylene—the most easily oxidized *p*-phenylenediamine

Abdel Monem M. Rawashdeh, Chariklia Sotiriou-Leventis,* Xuerong Gao and Nicholas Leventis*

Department of Chemistry, University of Missouri-Rolla, Rolla, MO 65409, USA.
E-mail: cslevent@umr.edu (CSL); Fax: +1 573 341 6033; Tel: +1 573 341 4353(CSL);
E-mail: leventis@umr.edu (NL); Tel: +1 573 341 4391(NL)

Received (in Corvallis, OR, USA) 29th May 2001, Accepted 17th July 2001
First published as an Advance Article on the web 29th August 2001

Dodecahydro-3a,9a-diazaperylene (DHDAP) was prepared in one step from *p*-phenylenediamine and 1-bromo-3-chloropropane, and its first redox potential is 292 mV more negative than the first redox potential of *N,N,N′,N′*-tetramethyl-*p*-phenylenediamine (TMPD), thus becoming the most easily oxidized *p*-phenylenediamine homologue.

The quest for structure–function relationships in redox chemistry finds an expression in tuning and control of redox potentials. In this context, alkylation is known to increase the electron density and render aromatic systems more easily oxidized. For example, the redox potentials of decamethylmetallocenes are shifted by about 0.5 V to more negative values relative to the corresponding metallocene–metallocenium couples.[1] Similarly, conducting polymer precursors such as *N*-methylpyrrole and 3-methylthiophene are easier to oxidize by 0.06 and 0.20 V relative to pyrrole[2] and thiophene,[3] respectively.

N,N,N′,N′-tetraalkyl-*p*-phenylenediamines, and particularly *N,N,N′,N′*-tetramethyl-*p*-phenylenediamine (TMPD), are among the most well-known redox systems, typically undergoing two well-separated (*vide infra*) chemically and electrochemically reversible one-electron oxidations.[4] Consequently, this class of compounds has been considered for fundamental studies in electrochemical[5] and photoinduced electron transfer,[6] as derivatizing agents for electrodes in conjunction with redox mediation of biological reagents,[7] as electrochromic materials,[8] and more recently as flow indicators in electrochemically generated magnetohydrodynamic convection.[9] The structures of three representative *p*-phenylenediamines pertinent to the ensuing discussion are:

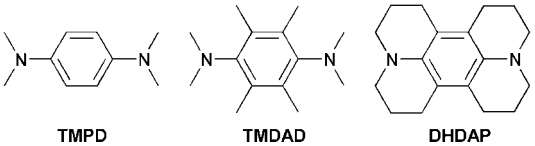

In general, the various derivatives of the parent *p*-phenylenediamine demonstrate the typical pattern of lower redox potentials as the degree of methylation increases (Table 1). TMPD has been the easiest to oxidize homologue in that series of compounds, and in fact it is one of the most easily oxidizable organic compounds. Importantly, methylation of the phenyl ring of TMPD does not lower the redox potential any further: *N,N,N′,N′*-tetramethyl-3,6-diaminodurene (TMDAD) is not only more difficult to oxidize than TMPD, but also according to Evans and Hu,[10] the second one-electron oxidation occurs at a less positive potential than the first one, so electrochemical oxidation of TMDAD yields directly the two-electron oxidized form. Evans and co-workers have proposed that this redox potential reversal is due to large conformational changes occurring during the oxidation of TMDAD, but not of TMPD. The essence of Evans' theory is that if any of the redox forms of TMDAD were planar, the H-atoms of the *N*-methyl groups would compete for space with the H-atoms of the aromatic methyl groups. The neutral form of TMDAD avoids these steric repulsions by twisting the dimethylamino groups out of planarity with the aromatic system. This is supported by the blue-shifted absorption spectrum of TMDAD relative to that of TMPD (Table 1). The two-electron oxidized form of TMDAD avoids the steric repulsions by adopting a boat-like conformation.[10] At this point, we reasoned that if the *N*-methyl and the aromatic methyl groups of TMDAD were bridged by a single atom, the competition for space by the aforementioned H-atoms would no longer exist, and the steric reasons for the abnormal behaviour of TMDAD would be eliminated. The resulting molecule, DHDAP, should demonstrate redox chemistry analogous to that of TMPD, but it should be much easier to oxidize than the latter. These expectations are justified fully by the following results.

Table 1 Redox and electronic absorption data for various *p*-phenylenediamines in acetonitrile[a]

Compound[b]	$E_{1/2}(1)$, V ($\Delta E_{p\text{-}p}$, V)	$E_{1/2}(2)$, V ($\Delta E_{p\text{-}p}$, V)	λ_{max}/nm ($\varepsilon \times 10^{-3}$/M^{-1} cm^{-1})		
p-Phenylenediamine	−0.106 (0.063)	0.429 (0.068)	321 (2.6)	251 (9.9)	
3,6-Diaminodurene	−0.259 (0.068)	0.237 (0.066)	308 (3.9)	245 (9.8)	
TMPD	−0.281 (0.062)	0.294 (0.060)	332 (2.5)	266 (17.4)	
TMDAD	−0.068 (0.443)		264 (3.6)	218 (13.0)	
DHDAP	−0.573 (0.066)	−0.037 (0.065)	338 (27.6)	280 (65.6)	220 (193)

[a] All redox data were determined by cyclic voltammetry in CH_3CN–0.1 M *n*-$Bu_4N^+ClO_4$ (applying 80% compensation for the solution resistance), and are reported *versus* ferrocene. The $E_{1/2}$ values are the mid-points between the anodic and cathodic peak currents. [b] *p*-phenylenediamine, 3,6-diaminodurene, and *N,N,N′,N′*-tetramethyl-*p*-phenylenediamine (TMPD) were commercially available and sublimed before use. *N,N,N′,N′*-tetramethyl-3,6-diaminodurene (TMDAD) was prepared according to the literature.[10] Dodecahydro-3a,9a-diazaperylene (DHDAP) was prepared in this study.†

The previously reported preparation procedure for DHDAP involves multistep synthesis.[11] Here, DHDAP was synthesized in high yield from *p*-phenylenediamine and 1-bromo-3-chloropropane in one step (Scheme 1).† DHDAP is stable as a solid,

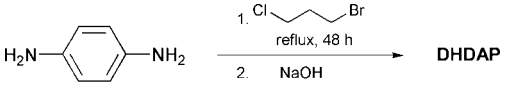

Scheme 1

and in oxygen-free solutions. Its solubility in CH_3CN is in the 2–3 mM range, but in CH_2Cl_2 is significantly higher. Like TMPD, in non-degassed solvents DHDAP is oxidized slowly, yielding blue solutions. In further analogy to TMPD, DHDAP shows two successive one-electron oxidations, but both of its

 DOI: 10.1039/b104991g

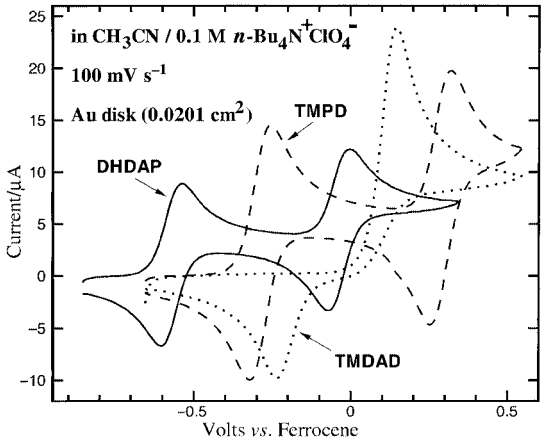

Fig. 1 Cyclic voltammograms of TMPD (1.71 mM), TMDAD (1.59 mM) and DHDAP (1.38 mM) in Ar degassed solutions.

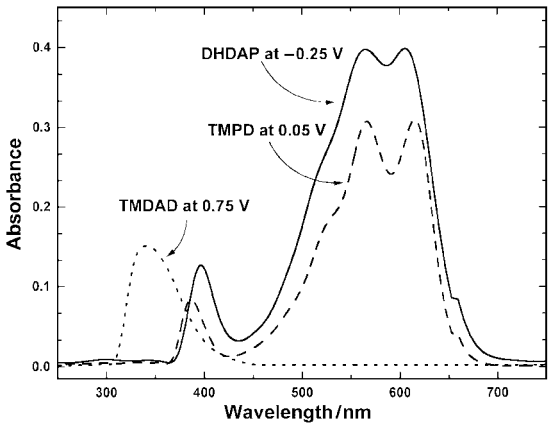

Fig. 2 Absorption spectra of TMPD (10.6 mM), TMDAD (11.1 mM), and DHDAP (7.9 mM) recorded with a dual ITO-electrode thin-layer cell in Ar degassed CH_2Cl_2–0.1 M n-$Bu_4N^+ClO_4^-$.

cyclic voltammetric (CV) waves are negative-shifted relative to those of TMPD, by 292 mV for the first and 331 mV for the second (Fig. 1). By comparison, TMDAD (its CV is also included in Fig. 1) is oxidized 0.213 V more positive than TMPD, reflecting its twisted geometry, which limits the extent of conjugation. The anodic-to-cathodic peak current ratios for both waves of DHDAP are equal to 1.0, indicating chemical reversibilty. Bulk electrolysis to $DHDAP^{\cdot+}$ and then back to DHDAP under the conditions of Fig. 1 led to 100% recovery of DHDAP (by ultramicroelectrode voltammetry), showing that $DHDAP^{\cdot+}$ is a stable species. The same experiment yielded the following diffusion coefficient data: $D_{DHDAP} = 1.52 \times 10^{-5}$ $cm^2\ s^{-1}$ and $D_{DHDAP^{\cdot+}}/D_{DHDAP} = 0.89$. By comparison, $D_{TMPD} = 2.58 \times 10^{-5}$ $cm^2\ s^{-1}$ and $D_{TMPD^{\cdot+}}/D_{TMPD} = 0.79$,[12] reflecting the somewhat smaller size of TMPD. (The different sizes of the CV waves of DHDAP and TMPD in Fig. 1 can be accounted for completely by the small differences in the concentrations and the diffusion coefficients.) Bulk electrolysis to $DHDAP^{2+}$ in CH_3CN–0.1 M $NaClO_4$ led to *ca.*. 80% recovery of DHDAP. The peak-to-peak separation of DHDAP is 66 ± 1 mV (*vs.* 59 mV for ferrocene) indicating a nearly reversible redox couple. Indeed, fitting the CV data with the Perkin–Elmer COOL™ software package we obtained as electron transfer coefficient for the first wave, $\alpha = 0.546$ (indicating an almost symmetric transition state) and a relatively high value for the standard rate constant, $k^\circ = 10.7$ cm s^{-1}.

The 292 mV negative shift of the first oxidation wave of DHDAP relative to TMPD indicates that the HOMO of the former is significantly higher in energy. Also, the two lower energy absorptions of DHDAP are red-shifted by only 7–23 mV (6–14 nm) relative to TMPD's (Table 1), suggesting that the HOMO and the LUMO of DHDAP are destabilized simultaneously by comparable amounts of energy.

The blue $DHDAP^{\cdot+}$ and $TMPD^{\cdot+}$ radicals were generated quantitatively in transparent thin layer electrochemical cells,[8] and their absorption spectra are shown in Fig. 2 alongside the spectrum of $TMDAD^{2+}$. The spectrum of $DHDAP^{\cdot+}$ is identical to the spectrum of $TMPD^{\cdot+}$, indicating analogous structures and identical chromophores. Similarly, the spectrum of the yellow $DHDAP^{2+}$ in CH_3CN–0.1 M $NaClO_4$ (not shown here) is identical to the spectrum of $TMDAD^{2+}$. Although energy minimization (AM1 method) yields a boat-like structure for $TMDAD^{2+}$,[10] and a planar structure for $DHDAP^{2+}$, the fact that their absorption spectra are identical implies that the differences in their geometry are not important. In both cases the iminium groups are electronically isolated from one another, probably due to the perturbation imposed by the positive *N*-atoms.

In summary, the preparation of DHDAP has been straightforward. DHDAP demonstrates two well-separated one-electron oxidation waves, shifted negatively by about 300 mV compared with the corresponding waves of TMPD. DHDAP is expected to render itself a main stream redox-active substance, with utility in redox staircases, and as a charge transfer quencher.

This research was supported by the Petroleum Research Fund, administered by the ACS (Grant No. 35154-AC5). A. M. M. Rawashdeh thanks ICSC-World Laboratory for a scholarship.

Notes and references

† *Synthesis of dodecahydro-3a,9a-diazaperylene*‡ *(DHDAP)*: *p*-phenylenediamine (0.50 g, 4.6 mmol, Aldrich, purified by sublimation) was added to 1-bromo-3-chloropropane (25 ml, 0.25 mol) and the resulting yellow solution was refluxed under Ar for 48 h. During this time a precipitate was formed and the color of the reaction mixture changed to orange. It was then cooled to rt, filtered under Ar and the pale orange solid was washed with diethyl ether and dried *in vacuo* to give DHDAP2H$^+$Br$^-$Cl$^-$ (1.51 g); ^{1}H NMR (400 MHz, D_2O): δ = 7.35 (s, 2H), 3.39 (t, J = 5.7 Hz, 8H,), 2.66 (t, J = 6.9 Hz, 8H), 2.10 (quint, J = 5.7 Hz, 6.9 Hz, 8H). A solution of the latter in 1 M HCl (50 ml, argon degassed) was made basic with 10% NaOH (argon degassed) and then extracted with diethyl ether (3 × 100 ml). Concentration of the pale yellow ether extracts after adding charcoal (rt) and drying over solid NaOH yielded 0.40 g (32%) of DHDAP as colorless platelets;§ mp 188–190 °C (lit.[11a] mp 190–191 °C; lit.[11b] mp 189–190 °C); ^{13}C NMR (100 MHz, argon degassed $CDCl_3$): δ = 136.4, 119.6, 50.4, 24.9, 22.9 ppm; anal. calcd. for $C_{18}H_{24}N_2$ (268.19): C, 80.55; H, 9.01; N, 10.44; found: C, 80.37; H, 9.06; N, 10.23.

‡ In ref. 11, the name of this compound was reported incorrectly as 1,2,3,3a,4,5,6,7,8,9,9a,10,11,12-tetradecahydro-3a,9a-diazaperylene.

§ The isolation of protonated DHDAP may be bypassed by extraction of the reaction mixture with water, basification and isolation of DHDAP as above.

1 J. L. Robbins, N. Edelstein, B. Spencer and J. C. Smart, *J. Am. Chem. Soc.*, 1982, **104**, 1882; D. Albagli and M. S. Wrighton, *Langmuir*, 1993, **9**, 1893.
2 A. F. Diaz, A. Martinez, K. K. Kanazawa and M. Salmón, *J. Electroanal. Chem.*, 1981, **130**, 181.
3 A. F. Diaz and J. Bargon, in *Handbook of Conducting Polymers*, ed. T. A. Skotheim, Marcel Dekker, Inc., New York, 1986, vol. 1, p 98.
4 A. Zweig, J. E. Lancaster, M. T. Neglia and W. H. Jura, *J. Am. Chem. Soc.*, 1964, **86**, 4130.
5 B. A. Kowert, L. Marcoux and A. Bard, *J. Am. Chem. Soc.*, 1972, **94**, 5538.
6 (*a*) D. G. Nocera and H. B. Gray, *J. Am. Chem. Soc.*, 1981, **103**, 7349; (*b*) C. D. Clark and M. Z. Hoffman, *J. Phys. Chem.*, 1996, **100**, 14688.
7 R. M. Buchanan, G. S. Calabrese, T. J. Sobieralski and M. S. Wrighton, *J. Electroanal. Chem.*, 1983, **153**, 129.
8 N. Leventis, M. Chen, A. I. Liapis, J. W. Johnson and A. Jain, *J. Electrochem. Soc.*, 1997, **145**, L55.
9 (*a*) N. Leventis, M. Chen, G. Xuerong, M. Canalas and P. J. Zhang, *J. Phys. Chem. B*, 1998, **102**, 3512; (*b*) N. Leventis and X. Gao, *J. Phys. Chem. B*, 1999, **103**, 5832.
10 (*a*) D. H. Evans and K. J. Hu, *Chem. Soc. Faraday Trans.*, 1996, **92**, 3983; (*b*) K. Hu and D. H. Evans, *J. Electroanal. Chem.*, 1997, **423**, 29.
11 (*a*) P. A. S. Smith and T.-Y. Yu, *J. Am. Chem. Soc.*, 1952, **74**, 1096; (*b*) W. O. Sykes, *J. Chem. Soc.*, 1960, **86**, 4583.
12 N. Leventis and X. Gao, *J. Electroanal. Chem.*, 2001, **500**, 78.

CHEMCOMM Communication
www.rsc.org/chemcomm

Enhancement of a two-photon absorption cross section (TPACS) — design and synthesis of a novel class of photochromic molecules with large TPACS

Gui-Lan Pan,[a] M. G. Fan,*[a] Ping Fan,[a] H. Z. Wang[b] and Z. C. Wei[b]

[a] *Technical Institute of Physics and Chemistry, The Chinese Academy of Sciences, Beijing 100101, People's Republic of China. E-mail: mgf206@ipc.ac.cn*

[b] *State Key Laboratory of Ultrafast Laser Spectroscopy, Zhongshan University, Guangzhou 510275, People's Republic of China*

Received (in Cambridge, UK) 28th March 2001, Accepted 4th July 2001
First published as an Advance Article on the web 28th August 2001

Two novel photochromic compounds were designed and synthesized; the two-photon absorption (TPA) cross section of both were measured with a nanosecond laser pulse; their TPACS (δ) values are around 25 $\times$ 10^{-46} cm^4 s photon^{-1} molecule^{-1} in acetonitrile; the molecular structure of the target compounds have a 3-methyl-1-benzothiophen-2-yl moiety, which can greatly enhance the two-photon absorption cross section.

In the early 1930's two-photon absorption (TPA) of an atom was introduced into the literature as a new concept by Göppert-Mayer.[1] The TPA can be defined as the simultaneous absorption of two photons through a virtual state in a molecule or medium. Theoretical studies have been done to define a unit of two-photon absorption cross section (δ) as GM.

$$1\ \mathrm{GM} = 1 \times 10^{-50}\ \mathrm{cm^4\ s\ photon^{-1}\ molecule^{-1}}$$

After that, the experimental studies were not developed very well for about forty years. In the 80's and especially in the 90's an upsurge of research on TPA followed the fast development of various lasers and advanced techniques in different fields, such as three dimensional (3D) optical storage;[2–4] the pioneer work being contributed by Rentzepis *et al.*[2] Other fields included 3D fluorescence imaging,[5,6] 3D microfabrication,[7,8] optical limiting[9–11] and two-photon photodynamic cancer therapy.[12,13] Most of the advanced techniques are interlinked between different sciences and techniques. Most of them are based on TPA or multi-photon absorption (MPA).

Studies of TPA can be carried out by nanosecond, picosecond or femtosecond laser pulses. TPA or MPA are based on nonlinear properties of a molecule or medium. The main advantage of TPA is that the excitation spatial area can be selected accurately in a volume medium through a tightly focused laser beam, so volume (3D) or multi-layer devices can be exploited.

It is well known that systematic research on photochromism was started from the 1950's. Until the end of the 1980's photochromism was studied basically on molecules and systems.[14] Two-photon induced photochromism was studied from 1989.[2] Recently, Belfield and Fan *et al.*[15] used a femtosecond laser to study one beam two-photon induced photochromism of 2-[1-(1,2-dimethyl-1*H*-indol-3-yl)ethylidene]-3-isopropylidene succinic anhydride (indolyl fulgide). The TPACS (δ) was measured through a Z-scan technique. The δ value of indolyl fulgide is 10.3 $\times$ 10^{-48} cm^4 s photon^{-1} molecule^{-1}. It is almost the same as that of the D-π-D type molecule, 1,4-bis{[4-(4-dibutylamino)phenyl]buta-1,3-dienyl}-2,5-dimethoxybenzene[7] (as large as 12.5 $\times$ 10^{-48} cm^4 s photon^{-1} molecule^{-1}), but indolyl fulgide is a D-π-A type molecule.

Unfortunately, design and synthesis for molecules with a large TPA cross section have not been well developed. It is well known that a large δ value of a medium is a fundamental property to make 3D or multilayer volume devices. The study of the relationship between molecular structure and δ value is quite important. Some molecular models are designed as D-π-D, D-π-A-π-D or A-π-D-π-A.[7,16] Kim *et al.*[17] studied π systems and they found that the dithienothiophene chromophore as the center π system can greatly enhance the TPA.

We find the connecting chromophore (D or A) can also greatly affect the TPA. Two novel kinds of photochromic compounds will be reported in this communication. The chemical structure of these compounds has been identified by NMR, MS and elemental analysis. They are 3,4-bis(3-methyl-1-benzothiophen-2-yl)-2,5-dihydrofuran (**I**) and 3,4-bis(3-methyl-1-benzothiophen-2-yl)-2,5-dihydrothiophene (**II**). The photochromic reaction is described as follows.

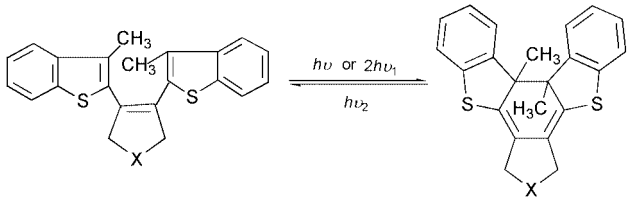

I, X = O; **II**, X = S — **C-I**, X = O; **C-II**, X = S

$h\upsilon$ is UV light; $h\upsilon_1$ is visible light, it is a 532 nm laser beam in this paper;

$h\upsilon_2$ is blue light. **C-I** and **C-II** are the colored forms of **I** and **II**.

The target compounds can be defined as 1,2-diarylethenes,[18] but the 3,4-bis(3-methyl-1-benzothiophen-2-yl)heterocyclopentene derivatives having photochromic properties have never been reported before and never studied as TPA materials.

The one-photon absorption spectra were measured by a spectrometer (Hitachi F-4500). Their maximum wavelengths (λ_{max}) are listed in Table 1.

In the transmittivity measurements, the second harmonic wave of a Q-switched Nd:YAG laser (Spectra-Physics GCR Series) with pulse duration of 10 ns was used as a pump source, and a laser energy meter (Laser Precision Corp., Model Rj-7200) with double detector was used as a recorder. The light beam from the laser was firstly divided into two beams by an optical splitter. The weaker one was used as a reference beam, which entered directly into the detector of the laser energy meter

Table 1 Maximum wavelength (λ_{max}) of absorption spectra of the target compounds and their colored forms (**C-I** and **C-II**)

	λ_{max}/nm	
Compd.	Cyclohexane (CHX)	Acetonitrile (ACN)
I	263, 310	263, 312
II	230, 264	230, 266
C-I	375	380
C-II	350	350

 DOI: 10.1039/b102876f

Table 2 TPACS values of the target compounds in different solvents under nanosecond laser pulse

Compounds Solvent	**I** CHX[a]	**I** ACN[b]	**II** ACN[b]
Concentration/10^{-2} mol L^{-1}	1.00	1.00	1.00
Pulse duration/ns	10.0	10.0	10.0
$I_{in}/10^{-2}$ GM cm^{-2}	4.433	4.822	6.178
$I_{out}/10^{-2}$ GM cm^{-2}	3.367	3.903	3.827
NLO absorption coeff. β/cm GM^{-1}	21.59	42.59	39.59
$\delta'_{TPA}/10^{-18}$ cm^4 GM^{-1}	3.585	7.053	6.575
$\delta_{TPA}/10^{-46}$ cm^4 s $photon^{-1}$ mol^{-1}	13.38	26.41	24.55

[a] CHX = cyclohexane. [b] ACN = acetonitrile.

in order to monitor the intensity of the pump beam. The other beam was focused into the solution of the compounds, and the transmitted energy was measured by another detector of the same laser energy meter. The diameter of the laser beam in the sample was 0.6 mm.

The TPACS are calculated by a method in the literature.[10] The results are collected in Table 2.

Compound **I** can be assigned as a D-π-A-π-D type molecule based on the difference of electronegativity between oxygen and sulfur. The benzothiophenyl could act as an electron donor and the oxygen as an acceptor. On the other hand, there is no difference in electronegativity of heteroatoms in compound **II**. It is difficult to say how the photoinduced electron transfer between different moieties of the molecule occurs. The δ values of studied compounds are almost the same in spite of the difference in the centre moiety between dihydrofuran and dihydrothiophene. In fact, the moieties on the left and right hand side of the target molecules are the same, 3-methyl-1-benzothiophen-2-yl.

The conclusion is that 3-methyl-1-benzothiophen-2-yl can greatly enhance the TPA cross section of a molecule. Based on papers we have checked in the literature, the δ values of the target compounds are the largest in acetonitrile. The reason for the TPA enhancement of the 3-methyl-1-benzothiophen-2-yl moiety could be owing to the lone election pairs of 3p electrons on the sulfur atom. We propose that the enhancement mechanism of dithienothiophene chromophore[17] could also be the same as that of 3-methyl-1-benzothiophen-2-yl. The magnitude of the δ value is a fundamental property of a molecule or medium in making three dimensional optical devices.

This work was supported by National Research fund for Fundamental key project of China (G1999033005) and NSFC (No. 29832030).

Notes and references

1 M. Göppert-Mayer, *Ann. Phys*., 1931, **9**, 373.
2 D. A. Parthenopoulos and P. M. Rentzepis, *Science*, 1989, **245**, 843.
3 A. S. Dvornikov and P. M. Rentzepis, *Opt. Commun*., 1995, **119**, 341.
4 A. Toriumi, S. Kawata and M. Gu, *Opt. Lett*., 1998, **23**, 1924.
5 W. Denk, J. H. Strickler and W. W. Webb, *Science*, 1990, **248**, 73.
6 A. Diaspro and M. Robello, *J. Photochem. Photobiol. B*, 2000, **55**, 1.
7 B. H. Cumpston, S. P. Anathavel, S. Barlow, D. L. Dyer, J. E. Ehrlich, L. L. Erskine, A. A. Heikal, S. M. Kueble, I.-Y. S. Lee, D. McCord-Maughon, J. Qin, H. Röckel, M. Rumi, X.-L. Wu, S. R. Marder and J. W. Perry, *Nature*, 1999, **398**, 51.
8 J. H. Strickler and W. W. Webb, *SPIE Proc*., 1990, **107**, 1398.
9 J. Oberlé, L. Bramerie, G. Jonusauskas and C. Rullière, *Opt. Commn*., 1999, **169**, 325.
10 G. S. He, G. C. Xu, P. N. Prasad, B. C. Bhatt and A. G. Dillard, *Opt. Lett*., 1995, **20**, 435.
11 J. E. Ehrlich, X. L. Wu, I.-Y. S. Lee, Z.-Y. Hu, H. Röckel, S. R. Marder and J. W. Perry, *Opt. Lett*., 1997, **22**, 1843.
12 J. D. Bhawalkar, N. D. Kumar, C. F. Zhao and P. N. Prasad, *J. Clin. Laser Med. Surg*., 1997, **15**, 201.
13 Y. P. Meshalkin, E. E. Alfimov, N. E. Vasil'ev, A. N. Denisov, V. K. Makukha and A. P. Ogirenko, *Quantum Electronics*, 1999, **29**, 1066.
14 H. Dürr and H. Bouas-Laurent, *Photochromism, Molecules and Systems*, Elsevier, Amsterdam, 1990.
15 K. D. Belfield, D. J. Hagan, Y. Liu, M. Fan and E. E. Hermandes, *Proc. SPIE's Annual Meeting, Optical Science and Technology*, San Diego, USA, 2000, 4104–4103.
16 M. Albota, D. Beljonne, J.-L. Bre'das, J. E. Ehrlich, J.-Y. Fu, A. A. Heikal, S. E. Hess, T. Kogej, M. D. Levin, S. R. Marder, D. McCord-Maughon, J. W. Perry, H. Röckel, M. Yumi, G. Subramanian, W. W. Webb, X.-L. Wu and C. Wu, *Science*, 1998, **281**, 1653.
17 O.-K. Kim, K.-s. Lee, H. Y. Woo, K.-S. Kim, G. S. He, J. Swiatkiewicz and P. N. Prasad, *Chem. Mater*., 2000, **12**, 284.
18 M. Irie, *Chem. Rev*., 2000, **100**, 1685.

CHEMCOMM Communication
www.rsc.org/chemcomm

Zeolite membrane on catalyst particles for selective formation of *p*-xylene in the disproportionation of toluene

Norikazu Nishiyama,* Manabu Miyamoto, Yasuyuki Egashira and Korekazu Ueyama

Division of Chemical Engineering, Graduate School of Engineering Science, Osaka University, 1–3 Machikaneyama, Toyonaka, Osaka 560-8531 Japan. E-mail: nisiyama@cheng.es.osaka-u.ac.jp

Received (in Cambridge, UK) 14th June 2001, Accepted 1st August 2001
First published as an Advance Article on the web 29th August 2001

The selective formation of *p*-xylene is shown in toluene disproportionation using a new catalyst which is surrounded with a permselective membrane.

New technologies using inorganic membrane reactors have become of interest with the development of preparation methods for metal and ceramic membranes. The basic concept of the membrane reactor is a coupling of a catalyst with a membrane that gives (1) selective addition of reactants to the reaction zone and (2) selective removal of products from the reaction zone. Although the preparation of zeolite membranes on porous supports has been extensively studied,[1–9] the number of reports regarding membrane reactors combined with zeolite membranes is still small.[10,11] Recently, titania plate-supported platinum catalysts covered with a silicalite layer have been developed by van der Pauil *et al.*[12–14] who used titania/Pt/silicalite composites for hydrogenation of linear and branched alkenes. They showed that the yield of the hydrogenation of linear alkenes was much higher than that of branched alkenes because of a high diffusivity (D) of linear alkenes through the silicalite layer.

In this study, we developed catalyst particles coated with a permselective membrane. The reaction models for the potential applications using this type of catalyst particle are shown in Scheme 1. In the first example, if the diffusivity of reactant A is much larger than that of B, reactant A selectively diffuses to a catalyst particle through a membrane. The undesired reaction B to S or the adsorption of B as a poison on the catalyst can be prevented. In the second example, the reaction has a limited yield or selectivity controlled by the reaction equilibrium according to thermodynamics. The selective removal of desired product R from the catalyst particle gives enhancement of selectivity when the diffusivity of product R is much greater than S.

A catalyst with a permselective membrane has a larger membrane area per unit reactor volume compared to conventional membrane reactors. This is one of the most advantageous points of this catalyst considering practical applications since the membranes with large membrane areas without pinholes or cracks are difficult to prepare in many cases.

In this study, a silica-alumina catalyst covered with a silicalite membrane was used for disproportionation of toluene to produce benzene and xylene isomers, which is an example of the reaction shown in Scheme 1(b). An amorphous acid catalyst, silica-alumina, was first used in the industrial process of toluene disproportionation.[15] Following this, zeolite catalysts such as mordenite, faujasite and ZSM-5 were reported to be very active in catalyzing toluene disproportionation. However, the selectivity of *p*-xylene production was close to the thermodynamic equilibrium. To overcome this, various improvements have been carried out using medium pore zeolites, such as dealuminated MCM-22[16] and ZSM-5[17] modified with P and Mg. The high *para*-selectivity over modified MCM-22 and ZSM-5 can be explained by 'restricted transition-state selectivity' or 'product selectivity' inside the zeolite pores.

The silica-alumina/silicalite catalyst was prepared as follows: silica-alumina particles (Nikki Chemical Co., Ltd.) with composition of 82 wt% SiO_2 and 13 wt% Al_2O_3 were crushed to *ca.* 1 mm in size. The starting sol for the zeolite coating consisted of colloidal silica (Nissan Chemical Industries, Ltd.), tetrapropylammonium bromide (TPABr) and tetrapropylammonium hydroxide (TPAOH) (Wako Pure Chemical Industries Co., Ltd.) and deionized water. The silica-alumina particles were placed in the bottom of the sol with a molar ratio of 3 SiO_2:0.3 TPABr:0.3 TPAOH:130 H_2O. The crystallization was carried out in an autoclave at 453 K for 24 h. The product was calcined in air at 773 K for 5 h with a heating rate of 0.8 K min^{-1} and characterized by X-ray diffraction (XRD), scanning electron microscopy (SEM) and catalytic tests.

XRD patterns of silica-alumina particles and zeolite-coated silica-alumina particles are shown in Fig. 1. No amorphous phase was observed in the XRD pattern of the silicalite-coated sample. The observed peaks are similar to the reported XRD patterns of silicalite powder, indicating that randomly oriented polycrystalline silicalite was formed on the silica-alumina particles. Fig. 2 shows SEM images of the obtained particles with different magnifications. The size of the silicalite crystals formed on the silica-alumina was about 5 μm.

The disproportionation of toluene was performed using a fixed-bed reactor (i.d. 4 mm) with a continuous flow system under atmospheric pressure. The feed rate of toluene was 2.16 mg min^{-1}. The catalyst weight and the flow rate of helium carrier were 1.3 g and 10 ml min^{-1}, respectively. Reaction

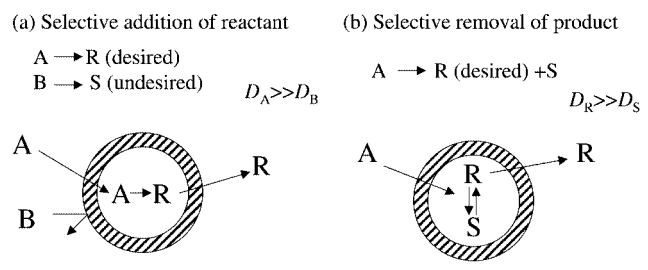

Scheme 1 Principle of operation of a catalyst particle coated with a permselective membrane.

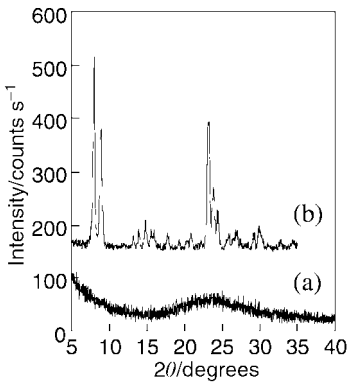

Fig. 1 XRD patterns of (a) silica-alumina particles and (b) silicalite-coated silica-alumina particles.

 DOI: 10.1039/b105256j

Table 1 Results of toluene disproportionation

Catalyst	*T*/K	WHSV[a]	Yield of xylene (%)	Fraction of xylene (%)			Ref.
				p	*m*	*o*	
Silicalite/SA[b]	673	0.1	0.08	100	0	0	This work
	823	0.1	0.4	91	5	4	This work
SA	673	0.1	1.5	23	52	25	This work
Silicalite	673	0.1	0.0	—	—	—	This work
H-MCM-22	573	0.1	7.8	85.3	14.4	0.3	16
P-ZSM-5	873	10	21	97	2	1	17
Mg-ZSM-5	823	3.5	10.9	88	10	2	17
Thermodynamic equilibrium	673		—	22	54	24	
	823		—	22	54	24	

[a] WHSV: weight hourly space velocity, (g of feed)/(g of catalyst) h^{-1}. [b] SA = silica-alumina.

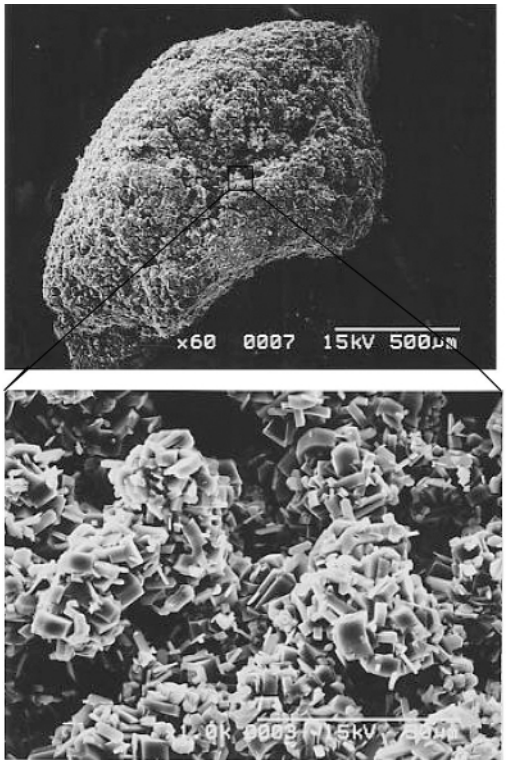

Fig. 2 SEM images of a silicalite-coated silica-alumina particle.

temperatures used were 723 and 823 K and the products were directly introduced to an FID gas chromatograph.

Table 1 lists the yields of the xylene isomers and the fraction of each xylene. The distribution of xylene isomers was very close to their equilibrium value over the silica-alumina catalyst without silicalite coating. On the other hand, the fraction of *p*-xylene in xylene isomers (*para*-selectivity) over the silicalite-coated catalyst largely exceeded the equilibrium value of about 22%. The selective permeation of *p*-xylene through silicalite membranes has been reported by several groups.[18–20] The high *para*-selectivity in the toluene disproportionation is caused by the selective removal of *p*-xylene from the silica-alumina particles, which leads to an apparent equilibrium shift between xylene isomers. The activity of the silicalite-coated catalyst was lower than that of the non-coated catalyst because of diffusion resistance through the membrane. A remarkable increase in the yield of xylenes was found at high temperature (823 K) owing to an increase in activated diffusivity of xylene through the silicalite membrane. When silicalite crystals without silica-alumina particles were used for the reaction, no catalytic activity was observed. Therefore, the silicalite membrane on the catalyst is believed to act not as a catalyst but as a separator.

High *para*-selectivity over shape-selective zeolite catalysts has been reported previously[16,17] (listed in Table 1). However, the mechanism of selective *p*-xylene production in this study is different from those observed in shape-selective zeolite catalysts. Here, the high *para*-selectivity does not result from 'product shape-selectivity' but from the selective removal of the produced *p*-xylene as seen in membrane reactors. The great potential of catalyst particles coated with a permselective membrane has been shown.

We would like to thank GHAS laboratory at Osaka University for the XRD and SEM measurements.

Notes and references

1 C. Bai, M. D. Jia, J. L. Falconer and R. D. Noble, *J. Membr. Sci.*, 1995, **105**, 79.
2 W. J. W. Bakker, F. Kapteijn, J. Poppe and J. A. Moulijn, *J. Membr. Sci.*, 1996, **117**, 57
3 E. D. Geus, M. J. Exter and H. Bekkum, *J. Chem. Soc., Faraday Trans.*, 1992, **88**, 3101.
4 K. Kita, T. Inoue, H. Asamura, K. Tanaka and K. Okamoto, *Chem. Commun.*, 1997, 45.
5 K. Kusakabe, S. Yoneshige, A. Murata and S. Morooka, *J. Membr. Sci.*, 11996, **16**, 39.
6 T. Masuda, H. Hara, M. Kouno, H. Kinoshita and K. Hashimoto, *Microporous Mater.*, 1995, **3**, 565.
7 T. Sano, H. Yanagishita, Y. Kiyozumi, F. Nizukami and K. Haraya, *J. Membr. Sci.*, 1994, **95**, 221.
8 Z. A. E. P. Vroon, K. Keizer, M. J. Gilde, H. Verweij and A. J. Burggraaf, *J. Membr. Sci.*, 1996, **113**, 293.
9 N. Nishiyama, K. Ueyama and M. Matsukata, *Microporous Mater.*, 1996, **7**, 299.
10 J. M. van de Graaf, M. Zwiep, F. Kapteijn and J. A. Moulijn, *Chem. Eng. Sci.*, 1999, **54**, 1441.
11 D. Casanave, P. Ciavarella, K. Fiaty and J. A. Dalmon, *Chem. Eng. Sci.*, 1999, **54**, 2807.
12 N. Van der Pauil, E. J. Creyghton, E. C. Rodenburg, T. S. Sie, H. van Bekkum and J. C. Jansen, *J. Chem. Soc., Faraday Trans.*, 1996, **92**, 4609.
13 N. Van der Pauil, I. B. Janto-Saputro, H. van Bekkum and J. C. Jansen, *Stud. Surf. Sci. Catal.*, 1997, **105**, 1341.
14 N. Van der Pauil, F. M. Dautzenberg, H. van Bekkum and J. C. Jansen, *Microporous Mesoporous Mater.*, 1999, **27**, 95.
15 D. C. Kieth, M. H. Dalson and W. C. Pfefferle, *US Pat.*, 3 646 236, 1972.
16 P. Wu, T. Komatsu and T. Yashima, *Microporous Mesoporous Mater.*, 1998, **22**, 343.
17 N. Y. Chen, W. W. Kaeding and F. G. Dwyer, *J. Am. Chem. Soc.*, 1979, 6783.
18 K. Keizer, A. J. Burggraaf, Z. A. E. P. Vroon and H. Verweij, *J. Membr. Sci.*, 1998, **147**, 159.
19 H. Sakai, T. Tomita and T. Takahashi, *Proc. ICIM 2000*, 2000, p. 67.
20 G. Xomeritakis and M. Tsapatsis, *Chem. Mater.*, 1999, **11**, 875.

CHEMCOMM
Communication
www.rsc.org/chemcomm

Ab initio study of oxygen atom transfer from hydrogen peroxide to trimethylamine†

Gianluca Ottolina* and Giacomo Carrea

Istituto di Biocatalisi e Biconoscimento Molecolare, Via Mario Bianco 9, 20131 Milano, Italy. E-mail: ottolina@ico.mi.cnr.it; Fax: 39 02285 0036; Tel: 39 02285 0021

Received (in Cambridge, UK) 4th June 2001, Accepted 27th July 2001
First published as an Advance Article on the web 28th August 2001

Unlike what has been theoretically proposed for ammonia oxidation with hydrogen peroxide, trimethylamine oxidation occurs with a concerted mechanism, which is favored even when an explicit water molecule is added or continuum solvent (water) is simulated.

Tertiary amines can be oxidised to their corresponding *N*-oxides using a large variety of oxidants, one of the most widely used of which is hydrogen peroxide. However, despite the simplicity of this reaction, there is a lack of published *ab initio* calculations of oxygen transfer from hydrogen peroxide to tertiary amines.

By means of such calculations, Bach *et al*. have extensively studied the transfer of an oxygen atom from organic and inorganic peroxy acids,[1] dioxiranes,[2] hydroperoxides[3] and hydrogen peroxide[4] to a broad array of substrates (reactions which involve the cleavage of an oxygen–oxygen σ bond), but the *N*-oxidation of tertiary amines by means of hydrogen peroxide is still not completely understood. Such an understanding would be extremely useful because this reaction can be considered a model for its biological counterpart, which involves the hydroperoxy-enzymes that are currently the subject of intense fundamental and applied research.[5]

Bach has also reported that the oxidation of ammonia by hydrogen peroxide is a 2-step process dominated by a 1,2-hydrogen shift, which is followed by a simple S_N2-like displacement to afford H_3NO and water: *i.e*. the transition state seems to be controlled by the formation of the water oxide (H_2OO) during the reaction.[4b] Furthermore, investigation of the role of solvation showed that a molecule of water stabilised the transition state. This differs from the generally accepted mechanism,[6] which assumes that hydrogen peroxide is attacked by the substrate with a direct nucleophilic displacement of the β-peroxy oxygen. In this study, we investigated this last mechanism by means of *ab initio* calculations, using the model reaction of trimethylamine (TMA) oxidation to the corresponding *N*-oxide (TMAO).

Table 1 shows the optimised geometries and related energies of the reagent complex (TMA–H_2O_2), transition state (TS-1) and product complex (TMAO–H_2O) obtained using the 6-31+G* basis set at different levels of theory.[7] The TMA–H_2O_2 complex was obtained through the hydrogen bond between the hydrogen of H_2O_2 and the TMA nitrogen. Differences in geometry (mainly in the torsion angle ∠HOOH) and energy can be found using HF, B3LYP or MP2 calculations. Significant differences in energy were also found in TS-1, which had only one negative eigenvalue in the Hessian matrix, and ΔE values ranging from 72.24 kcal mol^{-1} (HF) to 36.86 kcal mol^{-1} (B3LYP). Initial TS-1 geometries were obtained from several relaxed PES scans and refined with the eigenvalue-following methodology. It has been reported that the activation energy involved in the oxidation of ammonia by means of water oxide is regulated by the formation of the water oxide itself (56 kcal mol^{-1} MP4SDTQ/6-31G*//MP2/6-31G*),[4a] but our calculated activation barriers were in the range of 36–39 kcal mol^{-1} for B3LYP and MP2 (without ZPE), and thus far below the energy of water oxide formation. This suggests a concerted mechanism for the oxidation of TMA by means of hydrogen peroxide. Another important aspect for all of the transition states (TS-1) is that the hydrogen is not partially shifted towards the distal oxygen as in the concerted transition state mechanism found by Bach in the case of the oxidation of ammonia.[4a]

In our calculations, the 1,2-hydrogen shift occurs with the transfer of oxygen by cleavage of the O–O bond after the activation barrier is crossed. This was also demonstrated by far-reaching intrinsic reaction coordinate (IRC) calculations along the reaction pathway.[8]

In the TMAO–H_2O complex, the water was in staggered disposition to the methyl group in TMAO and had a strong hydrogen bond (~ 10 kcal mol^{-1} for each case), as has already been shown for the TMAO–H_2O complex.[9]

Oxidations with hydrogen peroxide are typically carried out in aqueous solution, and so specific solvent effects were calculated including one explicit water molecule. The transition state (TS-2) parameters (together with the TMA–H_2O_2–H_2O and TMAO–H_2O–H_2O complexes) are summarised in Table 2.

Table 1 Optimized geometries and energies for the *N*-oxidation of TMA with H_2O_2 (6-31+G* basis set)

	HF	B3LYP	*B3LYP*[a]	MP2[b]
	TMA–H_2O_2			
R(OO)[c]	1.398	1.462	*1.459*	1.481
R(NO)	2.914	2.790	*2.770*	2.770
R(NH)	1.953	1.787	*1.759*	1.769
∠NOO[d]	100.3	98.0	*100.4*	92.8
∠HOOH	−116.9	−122.9	*−105.6*	−126.8
E[e]	−324.05650	−326.04573	*−326.04815*	−325.00570
E_{ZPE}[f]	0.16123	0.14982	*0.14984*	0.15212
	TS-1			
R(OO)	1.915	2.018	*2.016*	2.010
R(NO)	1.759	1.826	*1.834*	1.762
∠NOO	164.2	161.1	*170.3*	164.5
∠HOOH	−122.0	−120.2	*−125.8*	−123.0
Frequencies[g]	984i	775i	*421i*	1147i
E	−323.94138	−325.98699	*−326.00338*	−324.94305
E_{ZPE}	0.15723	0.14982	*0.14684*	0.14801
ΔE[h]	72.24	36.86	*28.10*	39.31
ΔE_{IR}[i]	64.42	26.65	*18.03*	26.23
	TMAO–H_2O			
R(OO)	2.794	2.711	*2.717*	2.726
R(NO)	1.369	1.384	*1.384*	1.387
∠NOO	105.1	99.5	*142.3*	98.4
E	−324.09258	−326.08734	*−326.08493*	−325.04795
E_{ZPE}	0.16225	0.15100	*0.15031*	0.15356

[a] In bulk solvent (water). [b] MP2 frozen core. [c] Bond lengths in Å. [d] Angles in deg. [e] Total energy in hartree with geometry optimized at the level indicated. [f] Zero-point energies in hartree. [g] Frequencies in cm^{-1}. [h] Relative energy in kcal mol^{-1}. [i] Energies relative to the isolated reactants in kcal mol^{-1}.

† Electronic supplementary information (ESI) available: transition state structures and experimental data. See http://www.rsc.org/suppdata/cc/b1/b104902j/

 DOI: 10.1039/b104902j

Table 2 Optimized geometries and energies for the *N*-oxidation of TMA with H_2O_2 in the presence of one water molecule (6-31+G* basis set)

	HF	B3LYP	MP2[a]
	TMA–H_2O_2–H_2O		
R(OO)[b]	1.396	1.456	1.472
R(NH)	1.924	1.749	1.736
∠NOO[c]	104.8	106.0	103.9
∠HOOH	−109.3	−107.9	−126.8
E[d]	−400.08350	−402.48018	−401.22984
E_{ZPE}[e]	0.18721	0.17457	0.17702
	TS-2		
R(OO)	1.899	2.090	2.014
R(NO)	1.761	1.724	1.701
$R(HB_{OH-water})$	1.928	1.828	1.867
$R(HB_{water-OH})$	1.747	1.570	1.654
∠NOO	170.9	165.5	165.8
∠HOOH	−124.1	−114.8	−116.6
Frequencies[f]	883i	359i	623i
E	−399.98506	−402.43481	−401.18062
E_{ZPE}	0.18597	0.17264	0.17533
ΔE[g]	61.77	28.47	30.89
ΔE_{IR}[h]	48.18	10.81	8.79
	TMAO–H_2O–H_2O		
R(OO)	2.760	2.671	2.692
R(NO)	1.367	1.385	1.387
∠NOO	122.7	118.9	118.4
E	−400.12549	−400.51944	−401.27841
E_{ZPE}	0.18915	0.17619	0.17897

[a] MP2 frozen core. [b] Bond lengths in Å. [c] Angles in deg. [d] Total energy in hartree with geometry optimized at the level indicated. [e] Zero-point energies in hartree. [f] Frequencies in cm^{-1}. [g] Relative energy in kcal mol^{-1}. [h] Energies relative to the isolated reactants in kcal mol^{-1}.

The geometric and energy parameters obtained from the optimised structures indicate the presence of hydrogen bonds.

Comparing the energies obtained from the optimised TMA–H_2O_2 and TMA–H_2O_2–H_2O complexes with those of the isolated reactants, the energy of the water-induced hydrogen bond stabilisation was 6–9 kcal mol^{-1}, and further increased in the transition state: the ΔE values for TS-2 were 8–10 kcal mol^{-1} below the TS-1 values. The overall barrier from the isolated reactants was also reduced by about 16–20 kcal mol^{-1} (ΔE_{IR} in Tables 1 and 2) by the action of one molecule of water.

TS-2 optimisation and IRC indicated that the water molecule did not act as a proton relay, but was involved in a relatively strong hydrogen bond linking the complex. This finding is very important because it excludes the alternative mechanism of the 1,4-hydrogen shift that has been proposed for ammonia oxidation *via* hydrated water oxide.[4b] The 1,4-shift barrier for hydrated water oxide at MP4SDTQ/6-31G*//MP2/6-31G* was 37.4 kcal mol^{-1},[4b] whereas we calculated a barrier of 30.89 kcal mol^{-1} for TS-2 at MP2/6-31+G*. These results suggest that the concerted mechanism is preferred even when one molecule of water is added.

We also studied the effect of a continuum bulk solvent, and analysed its consequences on the geometric and energetic characteristics of the reaction. Our attempts to calculate the bulk solvent effect using polarised continuum model (PCM) approaches were unsuccessful,[10] and so we adopted the Onsager model.[11] The results obtained at the B3LYP level (summarised in italics in Table 1) show that the solvent induced only small geometric changes. The main effect was a decrease in the imaginary frequency associated with the transition state, which indicates that this is significantly looser in aqueous solution than in the gas phase. Despite the small difference between some of the geometric parameters optimised in the gas phase and solution, there was a significant difference in the implied energy. Comparison of the energy in the gas phase and solution clearly showed that the transition state was stabilized (8.62 kcal mol^{-1}) as a result of the electrostatic effect of the solvent. On the other hand, the TMA–H_2O_2 complex was destabilized by 0.15 kcal mol^{-1} and the TMAO–H_2O complex stabilized by 2.47 kcal mol^{-1}.

Comparison of the optimised structures in bulk solvent and with one explicit water molecule revealed that the geometric differences were mainly localised to the transition state and, to a lesser extent, to the product complex: *e.g.* in the transition state, the N–O distance was lengthened in solution by 0.110 Å and the O–O bond simultaneously shortened by 0.07 Å.

In brief, unlike what has been proposed for ammonia, our results show that the 1,2-hydrogen shift follows the oxygen transfer in the case of TMA oxidation by means of hydrogen peroxide. The concerted mechanism was favoured at the studied theoretical levels even when an explicit water molecule was added or continuum water was simulated.

We thank the BVMO project (Biotechnology Programme of the European Commission BIO4-CT98-0267) for its financial support.

Notes and references

1 R. D. Bach, A. L. Owensby, C. Gonzalez and H. B. Schlegel, *J. Am. Chem. Soc*., 1991, **113**, 2338; R. D Bach, J. E. Winter and J. J. W. McDouall, *J. Am. Chem. Soc*., 1995, **117**, 8586; R. D. Bach, M. N. Glukhovtsev and C. Canepa, *J. Am Chem. Soc*., 1998, **120**, 775.

2 R. D. Bach, J. L. Andrés, A. L. Owensby, H. B. Schlegel and J. J. W. McDouall, *J. Am. Chem. Soc*., 1992, **114**, 7207; A. G. Baboul, H. B. Schlegel, M. N. Glukhovtsev and R. D. Bach, *J. Comput. Chem*., 1998, **19**, 1353.

3 R. D. Bach, P. Y. Ayala and H. B. Schlegel, *J. Am. Chem. Soc*., 1996, **118**, 12 758.

4 (*a*) R. D. Bach, J. J. W. McDouall, A. L. Owensby and H. B. Schlegel, *J. Am. Chem. Soc*., 1990, **112**, 7065; The activation energies calculated by us for water oxide formation using the 6-31+G* basis set were the following: B3LYP 53.90, MP2 58.86 kcal mol^{-1}; (*b*) R. D. Bach, A. L. Owensby, C. Gonzalez, H. B. Schlegel and J. J. W. McDouall, *J. Am. Chem. Soc*., 1991, **113**, 6001. The activation energy calculated by us for the 1,4-hydrogen shift at MP2/6-31+G* was 41.36 kcal mol^{-1}; (*c*) R. D. Bach, M. D. Su and H. B. Schlegel, *J. Am. Chem. Soc*., 1994, **116**, 5379.

5 G. Ottolina, S. Bianchi, B. Belloni, G. Carrea and B. Danieli, *Tetraherdon Lett*., 1999, **40**, 8483; S. Colonna, N. Gaggero, P. Pasta and G. Ottolina, *Chem. Commun*., 1996, 2303.

6 J. O. Edwards, in *Peroxide Reaction Mechanisms*, ed. J. O. Edwards, Interscience, New York, 1962, pp. 67–106; D. E. Richardson, H. Yao, K. M. Frank and D. A. Bennet, *J. Am. Chem. Soc*., 2000, **122**, 1729.

7 Gaussian 98, Revision A.7, M. J. Frisch, G. W. Trucks, H. B. Schlegel, G. E. Scuseria, M. A. Robb, J. R. Cheeseman, V. G. Zakrzewski, J. A. Montgomery, R. E. Stratmann, J. C. Burant, S. Dapprich, J. M. Millam, A. D. Daniels, K. N. Kudin, M. C. Strain, O. Farkas, J. Tomasi, V. Barone, M. Cossi, R. Cammi, B. Mennucci, C. Pomelli, C. Adamo, S. Clifford, J. Ochterski, G. A. Petersson, P. Y. Ayala, Q. Cui, K. Morokuma, D. K. Malick, A. D. Rabuck, K. Raghavachari, J. B. Foresman, J. Cioslowski, J. V. Ortiz, A. G. Baboul, B. B. Stefanov, G. Liu, A. Liashenko, P. Piskorz, I. Komaromi, R. Gomperts, R. L. Martin, D. J. Fox, T. Keith, M. A. Al-Laham, C. Y. Peng, A. Nanayakkara, C. Gonzalez, M. Challacombe, P. Gill, B. Johnson, W. Chen, M. W. Wong, J. L. Andres, M. Head-Gordon, E. S. Replogle and J. A. Pople, Gaussian, Inc., Pittsburgh PA, 1998.

8 C. Gonzalez and H. B Schlegel, *J. Chem. Phys*., 1989, **90**, 2154; C. Gonzalez and H. B. Schlegel, *J. Phys. Chem*., 1990, **94**, 5523.

9 K. M. Kast, S. Reiling and J. Brickmann, *J. Mol. Struct. (THEOCHEM)*, 1998, **453**, 169.

10 At the B3LYP level PCM calculations (D-PCM, C-PCM and IEF-PCM) for TS-1 did not meet the convergence criteria. S. Miertus, E. Scrocco and J. Tomasi, *Chem. Phys*., 1981, **55**, 117; V. Barone and M. Cossi, *J. Phys. Chem. A*, 1998, **102**, 1995; M. T. Cances, B. Mennucci and J. Tomasi, *J. Chem. Phys*., 1997, **107**, 3032.

11 M. W. Wong, K. B. Wiberg and M. J. Frisch, *J. Am Chem. Soc*., 1991, **113**, 4776.

CHEMCOMM Communication
www.rsc.org/chemcomm

A new phenomenon in the induction period of the methane dehydroaromatization reaction

Lijie Men,[a] Li Zhang,*[a]† Yan Xie,[a] Zhongmin Liu,[b] Jiling Bai,[a] Guohe Sha[a] and Jinchun Xie[a]

[a] *State Key Laboratory of Molecular Reaction Dynamics, Dalian Institute of Chemical Physics, Chinese Academy of Sciences, 457 Zhongshan Road, Dalian 116023, China. E-mail: Zhangli@chem.ucla.edu*
[b] *Department of Natural Gas Chemistry & Applied Catalysts, Dalian Institute of Chemical Physics, Chinese Academy of Sciences, 457 Zhongshan Road, Dalian 116023, China*

Received (in Cambridge, UK) 5th April 2001, Accepted 1st August 2001
First published as an Advance Article on the web 28th August 2001

The induction period of dehydroaromatization of methane to benzene over Mo/HZSM-5 had been investigated in real-time by the resonant-enhanced two-photon ionization (RE2PI) technique; it is remarkable that there is a small amount of benzene formed in the early stage of the induction period; we suggest that the trace amount of benzene was caused by the reduction of the original Mo^{6+} ion during the induction period and the Mo^{6+} species has a slight catalytic activity for methane–benzene conversion.

Direct conversion of methane to higher hydrocarbons, particularly to aromatics such as benzene, toluene, and naphthalene under non-oxidative conditions has received considerable recent attention.[1–3] The dehydroaromatization reaction of methane to benzene over the Mo/HZSM-5 catalysts in flow reactors has been carried out and achieved some attractive results, such as a methane conversion of 7–8% with 70–80% selectivity to benzene. Although a similar catalytic performance has been reported by several groups[2,4–7] for methane conversion over Mo/HZSM-5, differing active sites, reaction mechanisms and reaction intermediates have been proposed by various investigators. Xu *et al.*[6] suggest that MoO_3 may be involved as the catalytically active center, and that dimerization of a CH_2=MoO_3 species occurs to produce ethylene as the reaction intermediate. Later they further proposed that the active center was partially reduced molybdenum oxide species $MoO_{(3-x)}$. Lin *et al.*[7] supposed that the activation of methane to form CH_3· radicals occurred *via* a synergistic action between MoO_x and the Brønsted acid site, and the CH_3· radicals dimerized to form ethane as the primary product. Wang *et al.*[8] reported that the reaction is characterized by an induction period, prior to the initiation of benzene formation, during which Mo_2C is formed and coke deposition occurs, as revealed by X-ray photoelectron spectroscopy (XPS) measurements. Solymosi *et al.*[9] suggested that Mo_2C–MoO_2 with an oxygen deficiency was responsible for the production of ethylene from methane, and ethylene was then converted to benzene on the acidic sites of HZSM-5 support. This reaction is characterized by an induction period, prior to the initiation of benzene production, during which the catalyst surface undergoes physical and chemical changes and gradually forms catalytic active sites, so it is without doubt that the amount of the reaction products varies with time and different detective methods will give rise to different reaction mechanisms.

The resonant-enhanced multi-photon ionization (REMPI) spectrum technique has a high sensitivity and good selectivity. It has been widely used to study spectrum structures and energy-transfer dynamics of atoms, molecules and free radicals.[10,11] In REMPI, we exploit a tunable laser to selectively ionize the product molecules and collect the signals of the resulting photoelectrons *via* electrodes. Based on the ion signals of specified reactant or products, we can instantly monitor the changes of the content of the objective species in the reaction product mixture, monitoring the course of catalytic reaction. In this paper, we investigated in real-time the induction period of the reaction by RE2PI (resonant-enhanced 2-photon ionization) technique and new phenomena have been observed.

According to the resonant-enhanced two-photon ionization spectrum of benzene, we use UV light at 259.5 nm obtained from the frequency-doubled output by the BBO crystal of a dye-laser (Lambda-Physick model FL2002) operating with Coumarin 503 dye, which is pumped by XeCl (Xe/HCl/He) excimer. A Photodiode was used to monitor the wave of laser energy. Through the amplifier and BOXCAR, ion signals produced by the two electrodes were collected by microcomputer. Typical dye laser pulse energy was attenuated to ~50 μJ, before accessing detection windows. All ionization signal measurements were an average of 6 laser pulses, in order to remove pulse to pulse signal variations caused by fluctuations of pump laser energies.

The catalyst was prepared by impregnating an aqueous solution containing the desired amount of ammonium heptamolybdate [$(NH_4)_6Mo_7O_{24}$] in a vacuum environment at rt for 24 h, followed by drying for 4 h at 120 °C and then calcining for 4 h at 500 °C in air. The calcined samples were crushed and sieved to 60/80 mesh granules. Since all of the Mo-containing solution was deposited onto HZSM-5 support during drying, the Mo content in the final catalyst was assumed to be the same as the total Mo content of the solution.

Reactions were carried out in a fixed bed continuous up-flow quartz reactor with an inter diameter of 7 mm and using 0.1 g of catalyst. The upper section of the reactor is a pair of detection electrodes and detecting windows and the middle is a catalyst bed. Temperature was measured by a type K thermocouple located inside a quartz sheath in contact with the catalyst bed. The reactor effluent was sampled using transfer lines held at 400 K, avoiding gas-product condensations. The hourly space velocity of methane was 1500 ml g^{-1} h^{-1}. Reactant and flush gases which included 50% CH_4–Ar, Ar (99.99%), respectively, were used with further purification and gas flows were regulated by mass flow controllers. The catalyst was first heated under the flow reactor in a stream of Ar from rt to 973 K for 1 h, maintained at a temperature of 973 K for 0.5 h, and then the 50% CH_4–Ar reactant gas mixture was introduced into the reactor. The reaction mixtures were also analyzed by online Gas Chromatography (Shanghai Xianchuang Instrument Factory, Model GC-8810) using a column SE-30 and hydrogen flame ionization detector. All studies were carried out at atmospheric pressure and at 973 K.

The aromatization reaction of methane over 6 wt% Mo/HZSM-5 was studied at 973 K by RE2PI techniques and experimental results are shown in Fig. 1. It is obvious to see from Fig. 1(A) that the dehydroaromation reaction of methane to benzene over Mo/HZSM-5 zeolite does have an induction period for CH_4 activation. The results of RE2PI are almost the same as the results of GC, which proves that REMPI is a reliable technique to study this reaction. But it is noteworthy that there

† *Current address*: Department of Chemistry and Biochemistry, UCLA, 405 Hilgard Avenue, Los Angeles, CA 90095-1569, USA.

 DOI: 10.1039/b103083n

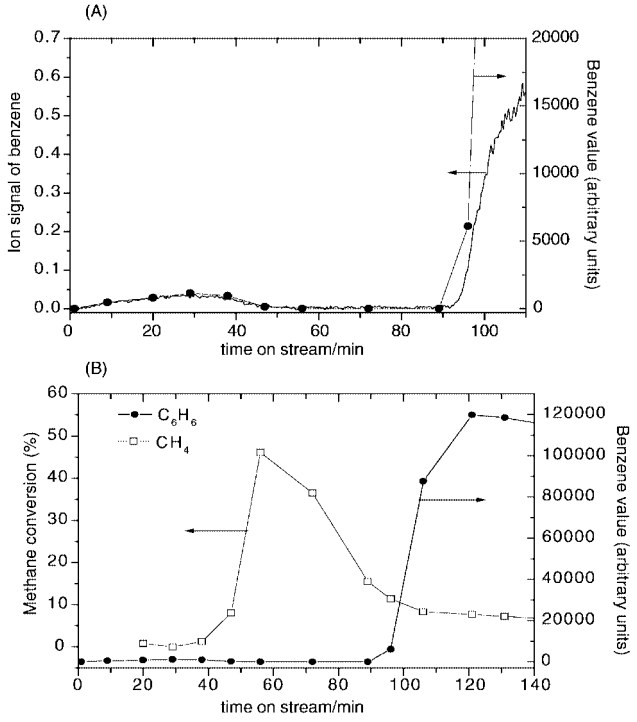

Fig. 1 (A) Benzene RE2PI and GC results *versus* reaction time over 6 wt% Mo/HZSM-5 at 973 K, 1 atm and GHSV = 1500 h^{-1}. — denotes ion signal results by RE2PI, — ● — denotes GC results. (B) Methane conversion and benzene relative peak area by GC method over 6 wt% Mo/HZSM-5 at 973 K, 1 atm, and GHSV = 1500 h^{-1}.

is a small amount of benzene formed at the very beginning of the reaction. Though compared with the amount of benzene after the induction period, the amount of benzene in the early stage of the induction period is negligible; it is an important hint for the reaction mechanism. This phenomenon has never been reported in previous studies. According to Fig. 1(A), we divided the induction period into two continuous sections; one is from 0 to 50 min and the other is from 50 to 90 min. In section one, when reactant gases were contacted with the catalyst, benzene was immediately formed. With the increase of reaction time, the benzene signal grows slowly. After reaching its highest point at about 27 min, the benzene signal began to decrease steadily. At the end of section one, there is no benzene signal. In section two, there is no signal of benzene. From Fig. 1(B), we see that the conversion of methane in these sections is totally different. In section one, the conversion of methane is 1–2%; in section two, the conversion of methane increases with time and reaches its highest point, 31%, at about 52 min, and then decreases. After section two, a significant amount of benzene was produced, while the conversion of methane almost keeps constant at ~7%. The signal of benzene from GC in Fig. 1(B) is the same with in Fig. 1(A), except the unit. Under the same reaction conditions, we repeated the experiment with 3.5 wt% Mo/HZSM-5 and 12 wt% Mo/HZSM catalysts and achieved similar results. The only differences are the lengths of induction period for the three catalysts.

As to the mechanism of methane aromatization reaction to benzene over Mo/HZSM-5 catalyst without oxidant, we suggest that the limited generation of benzene in the induction period section two was produced during the reduction of the original Mo^{6+} species. Less than 2% of the incoming methane was converted and only a trace amount of benzene was formed, showing that the Mo^{6+} species has a slight catalytic activity for methane–benzene conversion. The Mo^{6+} ion was reduced to lower oxidation state Mo species in this section. However in section two, a large amount of methane interacted with the catalyst without generation of benzene, suggesting that large amounts of carbon deposited on the catalyst in the course of high temperature methane conversion. The catalytic active sites were converted from Mo^{6+} species, which are unstable and easily reduced, to lower oxidation states of Mo species, which are very stable in a non-oxidizing atmosphere.

Notes and references

1 L. Wang, L. Tao, M. Xie, G. Xu, J. Huang and Y. Xu, *Catal. Lett.*, 1993, **21**, 35.
2 F. Solymosi, A. Erdohelyi and A. Szoke, *Catal. Lett.*, 1995, **32**, 43.
3 B. M. Weckhuysen, D. Wang, M. P. Rosynek and J. H. Lunsford, *J. Catal.*, 1998, **175**, 338.
4 D. Wang, M. P. Rosynek and J. H. Lunsford, *Top. Catal.*, 1996, **3**, 289.
5 L. Wang, Y. Xu, M. Xie, S. Liu and L. Tao, *Stud. Surf. Sci. Catal.*, 1995, **94**, 495.
6 X. Yide, L. Shetian, W. Linsheng, X. Maosong and G. Xiexian, *Catal. Lett.*, 1995, **30**, 135.
7 L. Chen, L. Lin, Z. Xu, T. Zhang and X. Li, *Catal. Lett.*, 1996, **39**, 169.
8 D. Wang, J. H. Lunsford and M. P. Rosynek, *J. Catal.*, 1997, **169**, 347.
9 F. Solymosi, J. Cserenyi, A. Szike, T. Bansagi and A. Oszko, *J. Catal.*, 1997, **165**, 150.
10 T. A. Cool, *App. Optics*, 1994, **23**, 1559.
11 C. M. Gittins, M. J. Castaldi, S. M. Senkan and E. A. Rohlfing, *Anal. Chem.*, 1997, **69**, 286.

CHEMCOMM Communication
www.rsc.org/chemcomm

Characterisation of a hydroxymandelate oxidase involved in the biosynthesis of two unusual amino acids occurring in the vancomycin group of antibiotics†

Tsung-Lin Li, Oliver W. Choroba, Elizabeth H. Charles, Alan M. Sandercock, Dudley H. Williams and Jonathan B. Spencer*

Cambridge Centre for Molecular Recognition, Department of Chemistry, Lensfield Road, Cambridge, UK CB2 1EW. E-mail: jbs20@cam.ac.uk

Received (in Cambridge, UK) 19th April 2001, Accepted 24th July 2001
First published as an Advance Article on the web 28th August 2001

ORF22 from the chloroeremomycin gene cluster has been cloned, expressed and characterised as a hydroxymandelate oxidase (HmO) that is involved in the formation of both (*S*)-4-hydroxyphenylglycine and (*S*)-3,5-dihydroxyphenylglycine.

The glycopeptide antibiotics vancomycin (**1**, Fig. 1) and teicoplanin are currently the treatment of last resort against methicillin-resistant *Staphylococcus aureus*.[1] The continued rise of vancomycin-resistant bacteria has heightened the need for new therapeutic agents. Manipulation of the biosynthetic gene cluster of glycopeptide antibiotics may be a potential route to new antibiotics. To explore this approach we have set out to elucidate the function of the genes involved in chloroeremomycin biosynthesis, another important member from the vancomycin family (**2**, Fig. 1).[2] In this communication we report the overexpression of the protein coded for by *orf*22 from the chloroeremomycin gene cluster, and its characterisation as a flavin-dependent oxidase catalysing the conversion of 4-hydroxymandelic acid and 3,5-dihydroxymandelic acid to their corresponding keto acids.

(*R*)-4-Hydroxyphenylglycine, found at positions 4 and 5 of the heptapeptide backbone of chloroeremomycin, is one of a number of rare amino acids in glycopeptide antibiotics. The peptide synthetase involved in the biosynthesis of chloroeremomycin contains epimerase domains for amino acids 2, 4 and 5, which suggests that (*S*)-4-hydroxyphenylglycine is the precursor of (*R*)-4-hydroxyphenylglycyl units at positions 4 and 5. Recently we have determined that *orf*21 codes for a dioxygenase involved in the pathway to (*S*)-4-hydroxyphenylglycine.[3] This enzyme, 4-hydroxymandelic acid synthase (HmaS), catalyses the production of 4-hydroxymandelate (**4**) (4HMA) from 4-hydroxyphenylpyruvate (**3**) (4HPP) (Fig. 2). Based on this discovery, it was postulated that ORF22, which shows homology to a known glycolate oxidase[4] (50% similarity and 40% identity) might oxidise 4-hydroxymandelic acid to its keto-acid derivative (**5**) followed by transamination, possibly by ORF17, to give (*S*)-4-hydroxyphenylglycine (**6**) (Fig. 2). During the preparation of this manuscript, Hubbard *et al.* published a paper independently establishing parts of the results presented here.[5]

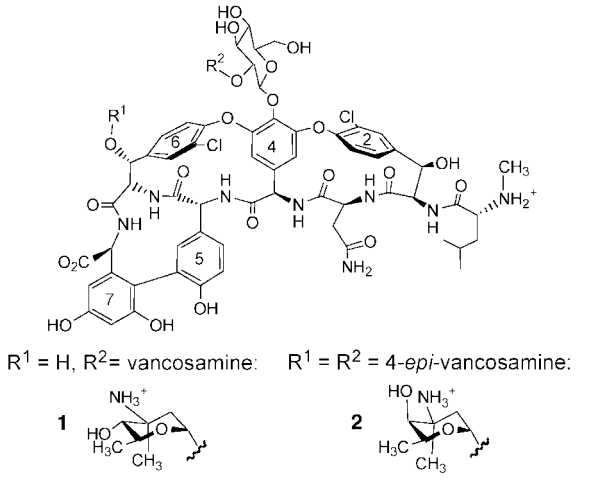

Fig. 1 Structures of vancomycin (**1**) and chloroeremomcyin (**2**).

In order to confirm the proposed pathway for the formation of 4HPG, *orf*22 was amplified by polymerase chain reaction (PCR) and cloned into the expression vector pET28a(+) (Novagen) as an *N*-terminal His_6-tagged protein. The resulting plasmid was used to transform the expression host *E. coli* BL21(DE3). Overexpression was carried out at 37 °C in 1 L 2 × YT medium with induction by isopropyl β-D-thiogalactoside (IPTG, 1 mM). The protein was recovered as an ammonium sulfate precipitate and further purified on Ni^{2+}-NTA agarose resin. The resulting protein was then transferred into 50 mM HEPES buffer, pH 7.6 using Millipore centrifugal filters. The purified protein showed a single band on a SDS-PAGE gel. The relative molecular mass was determined by ESI-MS to be 39863 ± 5 Da which was in excellent agreement with that calculated from the protein sequence (39864 Da). The enzyme contained a cofactor which was released when the protein was denatured by heat. This was determined to be FMN by HPLC analysis.

The enzyme (50 μg) was incubated with commercially available racemic 4HMA (20 mM) in HEPES buffer (50 mM, pH 7.6, 0.5 mL) in the presence of molecular oxygen, flavin mononucleotide (FMN, 0.5 mM) and catalase (1600 IU) at 25 °C for 16 h. The reaction was then quenched with 100 μL 6 M HCl and extracted with ethyl acetate (3 × 1 mL). The combined organic phases were dried with N_2 gas and the products converted to their methyl esters using diazomethane. The mixture was analysed by ammonia chemical ionisation GC-MS. The GC trace clearly shows that a new compound had been produced with a retention time of 16.0 min (Fig. 3, the substrate had a retention time of 16.0 min). The newly formed product

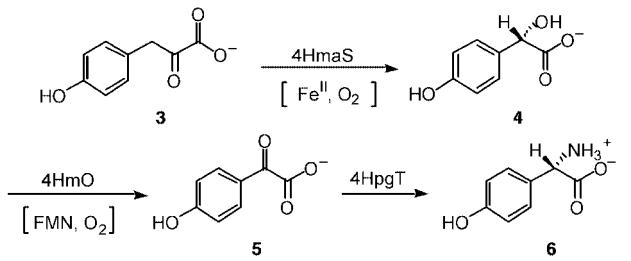

Fig. 2 Proposed biosynthetic pathway for 4-hydroxyphenylglycine (**6**): 4HmaS, 4-hydroxymandelate synthase; 4HmO, 4-hydroxymandelate oxidase; 4HpgT, 4-hydroxyphenylglyoxylate transaminase.

† Electronic supplementary information (ESI) available: SDS-PAGE analysis of HmO and molecular weight analysis of HmO protein by ESI-MS and GC/CI-MS of the enzymatic conversion of 3,5DHMA with HmO. See http://www.rsc.org/suppdata/cc/b1/b103548g/

 DOI: 10.1039/b103548g

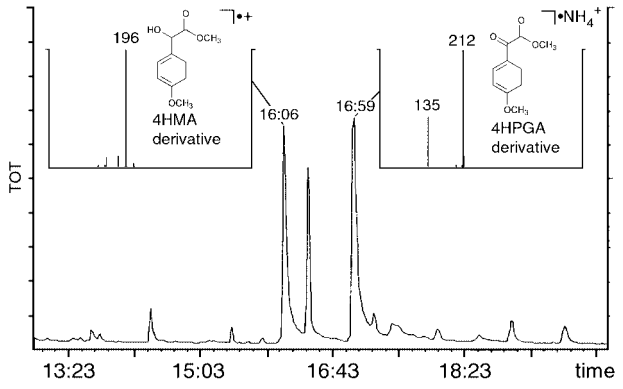

Fig. 3 GC trace and CI mass spectrum of an enzyme reaction of 4HMA with HmO after derivatisation by diazomethane showing 4-hydroxyphenylglyoxylic acid (4HPGA, product) and 4-hydroxymandelic acid (4HMA, substrate).

was identified as 4-methoxyphenylglyoxylate methyl ester (identical retention time and fragmentation pattern to standard material). This identifies *orf*22 as a hydroxymandelic acid oxidase (HmO) and strongly suggests that it is involved in the formation of (*S*)-4-hydroxyphenylglycine.

The stereochemistry of the substrate was elucidated using a racemic mixture of 4HMA and determining the optical rotation of the enantiomer remaining at the end of the incubation. Thus, the 4-hydroxymandelic acid isolated from the reaction had a negative optical rotation ($[\alpha]_D^{25}$ −5.1°, c = 2.5, ethanol) which corresponds to the same sign as synthetic (*R*)-4HMA ($[\alpha]_D^{25}$ −10.2°, c = 0.98, H_2O).[6] The enzyme was also found to oxidise commercially available (*S*)-mandelic acid but not (*R*)-mandelic acid. These combined results lead to the conclusion that (*S*)-4HMA is the natural substrate for the enzyme. Previous studies had determined that (*S*)-3,5-dihydroxyphenylglycine, another rare amino acid found in glycopeptide antibiotics, was formed from acetate *via* a polyketide pathway.[7,8] Analysis of the gene cluster reveals *orf*27 to be homologous to a number of chalcone synthases (polyketide synthases found mainly in plants). Recent work suggests that the pathway to (*S*)-3,5-dihydroxyphenylglycine involves the formation of 3,5-dihydroxyphenylacetic acid by ORF27[9a] followed by hydroxylation at the benzylic position, oxidation to the keto-acid and transamination to (*S*)-3,5-dihydroxyphenylglycine. The last two steps in this pathway are the same as those for (*S*)-4-hydroxyphenylglycine. Therefore it is tempting to suggest that ORF22 might also participate in this pathway and catalyse the oxidation 3,5-dihydroxyphenylmandelate to its keto-acid derivative. To test this, racemic 3,5-dihydroxymandelic acid[9b] was incubated with HmO as described previously (a shorter incubation time was used in this case) and the products analysed by GC-MS. The results show that 3,5-dihydroxymandelic acid is oxidised by the enzyme to give 3,5-dihydroxyphenylglyoxylic acid. This provides strong evidence that HmO is involved in the formation of both (*S*)-4-hydroxyphenylglycine and (*S*)-3,5-dihydroxyphenylglycine. The reaction catalysed by HmO can therefore be summarised as shown in Fig. 4.

Flavin-dependent enzymes are normally divided into two classes, oxidases and dehydrogenases.[10] Oxidases use molecular oxygen to oxidise the flavin after each reaction cycle with the formation of hydrogen peroxide, whereas dehydrogenases re-oxidised the flavin through electron transfer from proteins, such as ubiquinine or cytochrome b_5. To determine whether HmO is an oxidase or dehydrogenase the incubation mixtures were tested for the presence of hydrogen peroxide using a coupled assay of horseradish peroxidase (HRP) and *o*-dianisidine.[11,12] HRP generates *o*-dianisidine radicals which combine with 4HMA to give a product with an absorbance maximum at 550 nm (Fig. 5, trace a). When HmO was incubated with HRP and *o*-dianisidine an increase in absorbance at 550 nm was observed (Fig. 5, trace b). This determines that HmO is formally a flavin dependent oxidase.

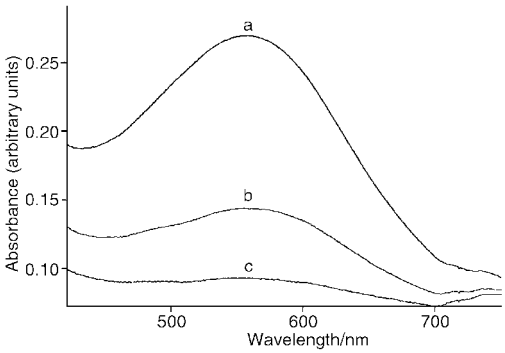

Fig. 5 Visible spectra probing the generation of H_2O_2 during HmO catalysis. a: enzymic reaction of horseradish peroxidase plus H_2O_2, *o*-dianisidine and 4HMA, b: enzymic reaction of HmO plus *o*-dianisidine and horseradish peroxidase, c: blank reaction omitting HmO.

In summary, we have identified the enzyme coded for by *orf*22, as a hydroxymandelate oxidase (HmO) which carries out the oxidation of both 4-hydroxymandelic acid and 3,5-hydroxymandelic acid. This provides strong evidence that it is involved in the pathway to both (*S*)-4-hydroxyphenylglycine and (*S*)-3,5-dihydroxyphenylglycine and sheds new light on how these important antibiotics are biosynthesised.

We thank the Royal Society for a Research Fellowship (J. B. S.), the Ministry of Education, Taiwan, for a Research Fellowship (T.-L. L.), the European Union for a TMR Marie-Curie Research Fellowship (O. W. C), St. John's College, Cambridge for a Junior Research Fellowship (O. W. C.), and the BBSRC for financial support. We thank Hwi Hong, in particular, for her help in GC-MS analysis.

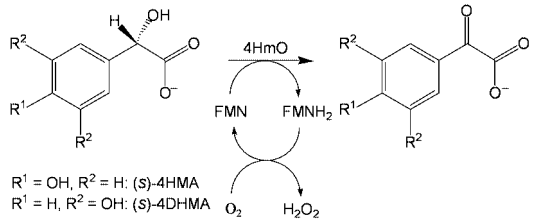

Fig. 4 Oxidation of (*S*)-4-hydroxymandelate ((*S*)-4HMA) and (*S*)-3,5-dihydroxymandelate ((*S*)-4DHMA) to 4-hydroxyphenylglyoxylate by 4HmO in the presence of FMN and molecular oxygen.

Notes and references

1 M. Foldes, R. Monro, T. C. Sorrell, S. Shankar and M. Toohey, *J. Antimicrob. Chemother*., 1983, **11**, 21.
2 A. M. v. Wageningen, P. N. Kirkpatrick, D. H. Williams, B. R. Harris, J. K. Kershaw, N. J. Lennard, M. Jones, S. J. Jones and P. J. Solenberg, *Chem. Biol*., 1998, **5**, 155.
3 O. W. Choroba, D. H. Williams and J. B. Spencer, *J. Am. Chem. Soc*., 2000, **122**, 5389.
4 P. Macheroux, V. Massey and D. J. Thiele, *Biochemistry*, 1991, **30**, 4612.
5 B. K. Hubbard, M. G. Thomas and C. T. Walsh, *Chem. Biol*., 2000, **7**, 931.
6 Y. S. Tsantrizos and K. K. Ogilvie, *Can. J. Chem*., 1991, **69**, 772.
7 S. J. Hammond, D. H. Williams and R. V. Nielsen, *J. Chem. Soc., Chem. Commun*., 1983, 116.
8 S. J. Hammond, M. P. Williamson, D. H. Williams, L. D. Boeck and G. G. Marconi, *J. Chem. Soc., Chem. Commun*., 1982, 344.
9 (*a*) T.-L. Li, O. W. Choroba, H. Hong, D. H. Williams and J. B. Spencer, *Chem. Commun*., accepted for publication; (*b*) A. M. Sandercock, E. H. Charles, W. Scaife, P. N. Kirkpatrick, S. W. O'Brien, E. A. Papageorgiou, J. B. Spencer and D. H. Williams, *Chem. Commun*., 2001, 1252.
10 R. B. Silverman, in *The Organic Chemistry of Enzyme-Catalysed Reactions*, Academic Press, San Diego, 2000.
11 T. Betsche, D. Schaller and M. Melkonian, *Plant Physiol*., 1992, **98**, 887.
12 I. G. Gazaryan, N. L. Klyachko, Y. K. Dulkis, I. V. Ouporov and A. V. Levashov, *Biochem. J*., 1997, **328**, 643.

CHEMCOMM Communication
www.rsc.org/chemcomm

Methanol to hydrocarbons: enhanced aromatic formation using a composite Ga_2O_3–H-ZSM-5 catalyst

David Freeman, Richard P. K. Wells and Graham J. Hutchings*

Department of Chemistry, Cardiff University, PO Box 912, Cardiff, UK CF10 3TB. E-mail: hutch@cardiff.ac.uk

Received (in Cambridge, UK) 4th June 2001, Accepted 17th July 2001
First published as an Advance Article on the web 28th August 2001

Addition of β-Ga_2O_3 to H-ZSM-5, as a physical mixture, enhances the formation of aromatic hydrocarbons in the methanol to hydrocarbons reaction.

Methanol conversion to hydrocarbons has been extensively studied using zeolite catalysts[1] since Chang and Silvestri reported this reaction for the zeolite H-ZSM-5.[2] The reaction has been demonstrated over a range of zeolites and microporous materials, *e.g.* zeolite Y,[3] zeolite β,[4] mordenite,[5] Me-APO-5,[6] SAPO-34,[7] as well as non-microporous catalysts e.g. WO_3–γ-Al_2O_3.[8] During these studies most attention has focussed on the reaction mechanism for the formation of the first carbon–carbon bond.[1] In addition, significant attention has been given to the control of the product distribution e.g. the formation of light alkenes or gasoline.[1] In all these previous studies it is surprising that no attention has been given to the use of composite catalysts in which an oxide and zeolite are mixed together. We have now addressed this, and we have found that the addition of β-Ga_2O_3 to H-ZSM-5 can dramatically enhance the yield of aromatic hydrocarbons and in this communication we present our preliminary results.

H-ZSM-5 (Si : Al mol ratio = 80; calcined at 350 °C, 3 h; PQ Corporation) and β-Ga_2O_3 (Aldrich, 99.99%) were obtained commercially and used without further purification or treatment. The methanol to hydrocarbons reaction was carried out using a standard laboratory microreactor. Methanol was fed using a calibrated syringe pump to a vaporisor, mixed with helium diluent (60 ml min^{-1}) and was reacted over the catalyst (0.25 g) in the heated zone of a tubular microreactor (id = 9 mm). Product analysis was carried out using on-line gas chromatography and the lines to and from the reactor were heated to avoid condensation of the products.

H-ZSM-5 and β-Ga_2O_3 were separately reacted with methanol (400 °C, 3.1 g methanol g $catalyst^{-1}$ h^{-1}) and the results are shown in Table 1. It is apparent that β-Ga_2O_3 is not active for this reaction under these conditions (experiment 3), whereas, as expected H-ZSM-5 gives complete conversion of the methanol to hydrocarbons (experiment 1).

Subsequently, the zeolite (0.125 g) and β-Ga_2O_3 (0.125 g) were mixed together as a physical mixture. This was achieved by mixing either the powders or pellets (β-Ga_2O_3, 250–300 μm; H-ZSM-5, 600–1000 μm) together in a glass tube without crushing. This simple physical mixture gave a significantly higher yield of aromatic compounds and lower yields of $C_4 + C_5$ hydrocarbons, when compared with the same mass of H-ZSM-5 alone (experiment 4). A blank experiment in which BN (0.125 g), a material that is totally unreactive for the conversion of methanol under these reaction conditions, was physically mixed in the same way with H-ZSM-5 (0.125 g) gave no enhancement in the yield of aromatic hydrocarbons (experiment 2). In a subsequent set of experiments, separate beds of β-Ga_2O_3 (0.125 g) and H-ZSM-5 (0.125 g) were reacted with methanol. In these experiments the two beds were separated by glass beads so that there was no physical contact between the two materials. The results (experiments 5 and 6, Table 1) show that no enhancement in the yield of aromatic compounds was observed. This indicates that the effect is the result of physical contact between the two materials. To demonstrate this, an experiment was carried out using a physical mixture of H-ZSM-5 pellets (0.125 g, particle diameter = 600–1000 μm, prepared by pelleting and sieving the zeolite) and β-Ga_2O_3 powder (0.125 g, particle diameter < 80 μm). The results for methanol conversion (400 °C, 3.1 g methanol g $catalyst^{-1}$ h^{-1}) are shown in Fig. 1, and a yield of aromatic hydrocarbons > 20 wt% is observed. After 270 min time on line, the flow of methanol was stopped and the catalyst was cooled in He to ambient temperature. Once cooled, the β-Ga_2O_3 (powder)–H-ZSM-5 (pellets) mixture was sieved to separate the β-Ga_2O_3 from the zeolite. Analysis of the two components by powder X-ray diffraction indicated that no changes had occurred during the reaction to the crystallinity of these materials, althouth it is recognised that this technique cannot provide information on the formation of nano-crystalline material. In addition, analysis of the zeolite pellets using atomic absorption spectroscopy confirmed that it did not contain any gallium. Both materials were retested for methanol conversion using the same conditions that had been used for the previous

Table 1 Methanol conversion to hydrocarbons over H-ZSM-5, β-Ga_2O_3 and β-Ga_2O_3–H-ZSM-5[a]

Experiment No.	Catalyst	Methanol conversion (%)	Product selectivity (%)[b]										Aromatic yield (%)
			CH_4	C_2	C_3	C_4	C_5	C_{6+}	C_6H_6	C_7H_8	C_8H_{10}	C_9H_{12}	
1	H-ZSM-5–glass beads[c]	100	0.2	8.8	38.4	27.6	10.4	5.5	2.4	1.4	3.4	2.7	10.4
2	H-ZSM-5–BN[d]	100	0.2	6.3	36.1	28.2	12.6	7.3	3.1	1.1	2.7	2.5	9.3
3	β-Ga_2O_3 –glass beads[e]	0.5	tr[f]	tr	tr	tr	tr	—	—	—	—	—	0
4	β-Ga_2O_3–H-ZSM-5[g]	100	0.3	6.5	35.5	21.9	12.7	4.9	4.6	2.2	5.9	5.5	18.2
5	β-Ga_2O_3–H-ZSM-5[h] Sandwich	100	1.5	5.1	40.8	31.1	8.9	5.1	3.8	0.7	1.6	1.4	7.5
6	H-ZSM-5–β-Ga_2O_3[i] Sandwich	100	0.2	8.0	43.9	24.9	10.2	4.3	4.0	0.8	2.1	1.6	8.5

[a] 400 °C, 3.1 g methanol g $catalyst^{-1}$ h^{-1}. [b] Selectivity for alkenes and alkanes are combined. [c] H-ZSM-5 (0.125 g, pellets) + glass beads (0.125 g) mixed. [d] H-ZSM-5 (0.125 g, pellets) + boron nitride (0.125 g, pellets) mixed. [e] β-Ga_2O_3 (0.125 g, pellets) + glass beads (0.125 g) mixed. [f] tr = trace. [g] H-ZSM-5 (0.125 g, pellets, 600–1000 μm) + β-Ga_2O_3 (0.125 g, pellets, 250–300 μm) mixed. [h] Bed of β-Ga_2O_3 (0.125 g, pellets) upstream of H-ZSM-5 (0.125 g, pellets), the two beds separated by glass beads. [i] Bed of H-ZSM-5 (0.125 g, pellets) upstream of β-Ga_2O_3 (0.125 g, pellets), the two beds separated by glass beads.

 DOI: 10.1039/b104844a

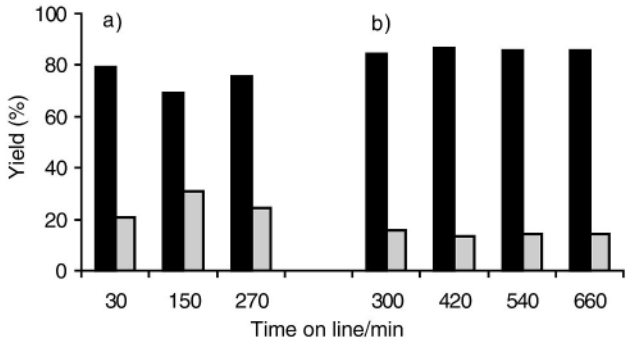

Fig. 1 Methanol conversion to hydrocarbons over (a) β-Ga_2O_3 (powder)–H-ZSM-5 (pellets) physical mixture until 270 min time-on-line and (b) H-ZSM-5 (pellets) following removal of β-Ga_2O_3 (powder) by sieving. Reaction conditions: 400 °C, 3.1 g methanol g catalyst^{-1} h^{-1}. Key: black = aliphatic hydrocarbons, grey = aromatic hydrocarbons. All data recorded at 100% methanol conversion.

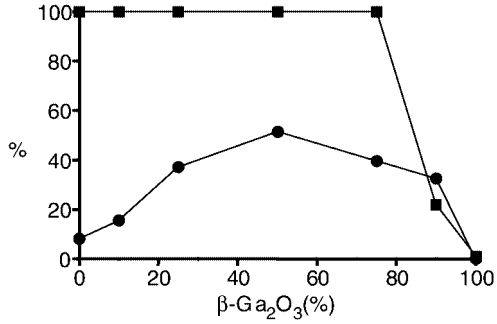

Fig. 2 Methanol conversion to hydrocarbons over β-Ga_2O_3–H-ZSM-5 physical mixtures prepared by grinding as a function of H-ZSM-5 (wt%). Reaction conditions: 400 °C, 0.7 g methanol g catalyst h^{-1}. Key: ■ methanol conversion, ● aromatic yield.

physical mixture experiment. The β-Ga_2O_3 was found to be inactive. The results for the H-ZSM-5 pellets (Fig. 1) show that the yield of aromatic hydrocarbons was now much lower (typically 13–14 wt%), and typical for that expected for H-ZSM-5 alone. This experiment demonstrates that the β-Ga_2O_3–H-ZSM-5 composite catalyst exhibits a new catalytically active site that gives enhanced yields of aromatic hydrocarbons. It is proposed that this new site involves contact synergy between the crystallites of β-Ga_2O_3 and H-ZSM-5. Furthermore, it is apparent that these sites can be removed by separating the physical mixture. To confirm this effect, a further experiment was conducted in which β-Ga_2O_3 (0.125 g) and H-ZSM-5 (0.125 g) were ground together to achieve a uniform intimate mixture. When this intimately mixed material was tested for methanol conversion (400 °C, 0.7 g methanol g catalyst^{-1} h^{-1}) the yield of aromatic hydrocarbons increased to 51.4 wt% (24.2% C_8H_{10}, 20.6% C_9H_{12}). Investigation of other ratios of Ga_2O_3–H-ZSM-5 confirmed that the 1 : 1 physical mixture gives the most marked enhancement in the yield of aromatic hydrocarbon (Fig. 2) which is consistent with the proposal of the active site for enhanced aromatic formation being at the junction of the β-Ga_2O_3 and H-ZSM-5 particles. It is proposed that at this site alkenes are dimerised and aromatised in a similar manner to the aromatisation of propane in the Cyclar process which is observed at temperatures >600 °C using Ga^{3+}-doped H-ZSM-5.[9] Indeed, recently Lunsford and co-workers[10] showed that ethene could be converted to aromatic products using a Ga–H-ZSM-5 catalyst at temperatures in the range 500–550 °C. To demonstrate the generality of the observed effect, we have also investigated β-Ga_2O_3–zeolite β and β-Ga_2O_3–WO_3–γ-Al_2O_3 physical mixture and have observed similar effects of contact synergy. It is therefore considered that composite catalysts, comprising oxides and microporous materials, may generate new types of catalyst for hydrocarbon formation from methanol and these catalysts can be used to control the product distribution.

We thank the EPSRC for financial support.

Notes and references

1 M. Stöcker, *Microporous Mesoporous Mater*., 1999, **29**, 3.
2 C. D. Chang and A. J. Silvestri, *J. Catal*., 1977, **47**, 249.
3 P. Salvador and W. Kladnig, *J. Chem. Soc., Faraday Trans. 1*, 1977, **73**, 1153.
4 G. J. Hutchings, P. Johnston, D. F. Lee, A. Warwick, C. D. Williams and M. Wilkinson, *J. Catal*., 1994, **147**, 177.
5 M. Sawa, M. Niwa and Y. Murakami, *Chem. Lett*., 1987, **8**, 1637.
6 O. V. Kikhtyanin, V. M. Mastikhin and K. G. Ione, *Appl. Catal*., 1988, **42**, 1.
7 B. V. Vora, T. L. Marker, P. T. Barger, H. R. Nilsen, S. Kvisle and T. Fuglerud, *Stud. Surf. Sci. Catal*., 1997, **107**, 87.
8 G. A. Olah, H. Doggweiler, J. D. Felberg, S. Frohlich, M. J. Grdina, K. Karpeles, T. Keumi, S. Inaba, W. M. Ip, K. Lammertsma, G. Salem and D. C. Tabor, *J. Am. Chem. Soc*., 1984, **106**, 2143.
9 G. Buckles, G. J. Hutchings and C. D. Williams, *Catal. Lett*., 1991, **11**, 89.
10 P. Qiu, J. H. Lunsford and M. P. Rosynck, *Catal. Lett*., 1998, **52**, 37.

CHEMCOMM
Communication
www.rsc.org/chemcomm

Monocarbaborane chemistry. Preparation and characterisation of $[4\text{-}CB_8H_9]^-$, the 'missing' *closo*-carbaborane anion†‡

Tomáš Jelínek,[a] Bohumil Štíbr,[b] Josef Holub,[c] Mario Bakardjiev,[c] Drahomír Hnyk,[c] Daniel L. Ormsby,[d] Colin A. Kilner,[a] Mark Thornton-Pett,[a] Hans-Jörg Schanz,[b] Bernd Wrackmeyer[b] and John D. Kennedy*[a]

[a] *School of Chemistry of the University of Leeds, West Yorkshire, UK LS2 9JT*
[b] *Laboratorium für Anorganische Chemie der Universität Bayreuth, Postfach 101251, Bayreuth, Bayern D-95440, Germany*
[c] *Institute of Inorganic Chemistry of the Academy of Sciences of the Czech Republic, 25068, Řež-by Prague, The Czech Republic*
[d] *Department of Chemistry of the Imperial College of Science, Technology and Medicine, Exhibition Road, London, UK SW7 2AY*

Received (in Cambridge, UK) 17th April 2001, Accepted 25th June 2001
First published as an Advance Article on the web 20th August 2001

Thermolysis in the solid state of $Cs^+[arachno\text{-}CB_9H_{14}]^-$, or of $Cs^+[nido\text{-}CB_9H_{12}]^-$, or the oxidation of *nido*-1-CB_8H_{12} with I_2 in THF at −78 °C in the presence of NEt_3, gives the first nine-vertex *closo* monocarbaborane, the stable [*closo*-4-CB_8H_9]$^-$ anion, in yields of 56, 61 and 75%, respectively.

Although carbaborane chemistry is the most investigated area of polyhedral boron-containing cluster chemistry,[1,2] it is dominated by dicarbaborane chemistry. Monocarbaborane chemistry, by contrast, is sparsely represented,[1] and many of the fundamental cluster types are unreported. Of the classically *closo* $[CB_nH_{n+1}]^-$ monocarbaborane anions, $[CB_5H_6]^-$ (known only as its conjugate acid CB_5H_7), together with the $[CB_9H_{10}]^-$, $[CB_{10}H_{11}]^-$ and $[CB_{11}H_{12}]^-$ anions, have been recognised for some 30 years.[3] Of these, the $[CB_9H_{10}]^-$ and $[CB_{10}H_{11}]^-$ species and their derivatives attract much current attention.[4,5] More recently, the $[CB_7H_8]^-$ species has been reported,[6] but $[CB_6H_7]^-$ and $[CB_8H_9]^-$ have remained elusive. We now report three routes for the preparation of one of these last two missing species, *viz*. the nine-vertex $[CB_8H_9]^-$ anion, in good yields. The first two routes are simple solid-state thermolyses, of $Cs^+[arachno\text{-}6\text{-}CB_9H_{14}]^-$ and of $Cs^+[nido\text{-}6\text{-}CB_9H_{12}]^-$,[7] and the third is the straightforward oxidation of the neutral monocarbaborane *nido*-1-CB_8H_{12}[8,9] with I_2 in the presence of NEt_3. The geometries and numbering systems for the ten-vertex *nido* and *arachno* cages, and for the nine-vertex *closo* and *nido* cages, are shown in Scheme 1: unlettered vertices represent BH(*exo*) units.

In the first method a sample of $Cs^+[arachno\text{-}CB_9H_{14}]^-$ (compound **1** in Scheme 1)[7] is heated at 220 °C for 3 h, followed by dissolution of the product in $(Me)_2CO$, and filtration. Examination of the solution by NMR spectroscopy showed the [*closo*-4-CB_8H_9]$^-$ anion (compound **2**; *ca*. 60%), and smaller quantities of the $[nido\text{-}CB_9H_{12}]^-$ and $[closo\text{-}CB_9H_{10}]^-$ anions (*ca*. 5 and 35% respectively); no starting anion **1** remained. Chromatographic separation on a silica column (30 cm × 2.5 cm) using MeCN–CH_2Cl_2 5:95 as the eluting phase, followed by precipitation with $[PMePh_3]^+Cl^-$, thence resulted in crystalline $[PMePh_3]^+[CB_8H_9]^-$ (56% isolated). The second method consists of a similar heating of $Cs^+[nido\text{-}CB_9H_{12}]^-$ (compound **3**)[7] at 220 °C for 3 h, again followed by dissolution of the product in $(Me)_2CO$ and filtration. Examination by NMR spectroscopy§ again showed the [*closo*-CB_8H_9]$^-$ anion (*ca*. 61% after purification as above), but now with smaller quantities of $[nido\text{-}CB_{10}H_{13}]^-$ (20%) and $[closo\text{-}CB_9H_{10}]^-$ (*ca*. 3%); no starting anion **3** remained. The by-products of the formation of $[CB_9H_{10}]^-$ by these two variants suggest a series of competing reactions. Thus, $[CB_9H_{14}]^-$ may lose H_2 to give $[CB_9H_{12}]^-$, and $[CB_9H_{12}]^-$ may lose H_2 to give $[CB_9H_{10}]^-$. Alternatively, $[CB_9H_{14}]^-$ may lose $\{BH_3\}$ to give $[CB_8H_{11}]^-$ which would be unstable to H_2 loss to give $[CB_8H_9]^-$, and $[CB_9H_{12}]^-$ may lose $\{BH_3\}$ to give $[CB_8H_9]^-$ directly. $[CB_9H_{12}]^-$ may add transient $\{BH_3\}$ to give $[CB_{10}H_{12}]^-$ *via* elimination of H_2, whereas relatively hydrogen-rich $[CB_9H_{14}]^-$ would not add $\{BH_3\}$ so readily. These considerations suggest that the thermolysis conditions may be tailorable to favour between $[CB_8H_9]^-$ or $[CB_9H_{10}]^-$ formation. We currently devise experiments to examine for this possibility.

The other, efficient and fast, route for the preparation of the [*closo*-4-CB_8H_9]$^-$ anion **2** is based on the oxidation of *nido*-1-CB_8H_{12} (compound **4**).[8,9] Treatment of neutral **4** with NEt_3 (3 mol equiv.) and I_2 (1 mol equiv.) in THF solution at −78 °C for

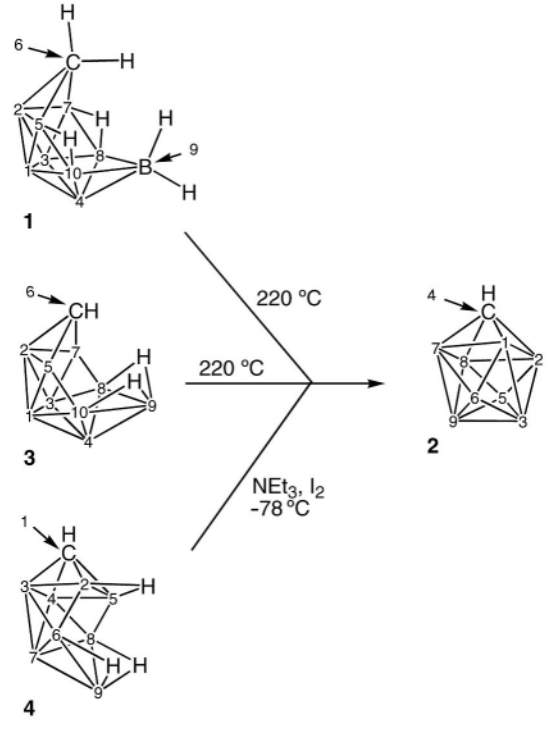

Scheme 1

† Electronic supplementary information (ESI) available: NMR spectroscopy and calculated coordinates for the B3LYP/6-31G* symmetry-locked structure for $[CB_8H_9]^-$. See http://www.rsc.org/suppdata/cc/b1/b103408c/
‡ Systematic IUPAC nomenclature: the *closo*-4-carbanonaborate(1−) anion; characterised crystallographically as its methyltriphenylphosphonium salt.

 DOI: 10.1039/b103408c

1 h, followed by stirring at room temperature for a further hour, resulted in the formation of the $[NHEt_3]^+$ salt of the [*closo*-4-$CB_8H_9]^-$ anion **2**. The reaction is consistent with the stoichiometry as in eqn. (1).

$$1\text{-}CB_8H_{12}\ \mathbf{4} + 3NEt_3 + I_2 \rightarrow 3[NHEt_3]^+ + [4\text{-}CB_8H_9]^-\ \mathbf{2} + 2I^- \qquad (1)$$

The $[NHEt_3]I$ by-product was removed by filtration, the filtrate evaporated to dryness, and then treated with aqueous KOH, followed by aqueous $[PBu^n_4]Br$. Extraction with CH_2Cl_2 and chromatographic separation of the CH_2Cl_2 extract on a silica column (25 cm × 2.5 cm) using MeCN–CH_2Cl_2 5 : 95 as eluting phase, thence gave crystalline $[PBu^n_4]^+$[*closo*-4-$CB_8H_9]^-$ (75%). Mechanistically, the formation of anion **2** as in eqn. (1) seems to agree with a deprotonation of CB_8H_{12} **4** by NEt_3 and thence oxidation of the transient [*nido*-1-$CB_8H_{11}]^-$ anion with I_2. Closure of the nine-vertex *nido* cage by joining the B(9) vertex of **4** with the B(2) and B(5) vertices (Scheme 1), would yield the product configuration of **2**.

The structure of the [*closo*-4-$CB_8H_9]^-$ anion **2** was confirmed by a single-crystal X-ray diffraction analysis of the $[PMePh_3]^+$ salt (Fig. 1).¶ It has the classical tricapped trigonal prismatic structure of $[B_9H_9]^{2-}$, but with a carbon atom in a four-connectivity 4-position. As with the $[B_9H_9]^{2-}$ anion,[10] the edges of the central trigonal prism, at 191.4(4)–200.4(4) pm, are at the longer end of typical interboron cluster bonding distances. NMR spectroscopy on a bulk sample was consistent with the structure derived from the single-crystal work.§¶ Like the $[CB_7H_8]^-$ anion,[6] the new compound is a stronger reducing agent than the $[CB_9H_{10}]^-$ and $[CB_{11}H_{12}]^-$ congeners. It is similarly iodinated at the sites distal from carbon; thus monoiodination with elemental I_2 in CH_2Cl_2 solution gives [3-I-*closo*-4-$CB_8H_8]^-$ and [5-I-*closo*-4-$CB_8H_8]^-$.

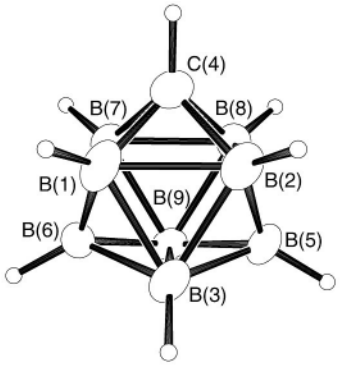

Fig. 1 Crystallographically determined molecular structure of the [*closo*-4-$CB_8H_9]^-$ anion in its $[PMePh_3]^+$ salt. The crystal had two independent $[PMePh_3]^+[CB_8H_9]^-$ units per unit cell. One anion was disordered, the other not. The anion shown here is the undisordered one. Distances (in pm throughout) from C(4) to its adjacent B atoms are in the range 162.8(5)–164.6(5), and the corresponding distances from B(5) and B(6) 'caps' are in the range 165.4(5)–177.4(5). The triangular faces of the internal trigonal prism are longer at 191.4(4)–200.4(4) than the trigonal prism edge distances at 177 6.8(5)–180.0(5); correspondingly, the angles (in degrees throughout) subtended at C(4) fall into two sets: 65.2(2)–66.2(2), and 71.9(2)–75.8(2). Similarly, angles subtended at B(5) and B(6) are in two sets: 63.3(2)–65.0(2) and 67.9(2)–72.5(2).

These results, allied with efficient routes from $B_{10}H_{14}$ to the starting monocarbaboranes **1**, **3** and **4**,[7,9,11] mean that the [*closo*-4-$CB_8H_9]^-$ anion is now one of the most readily accessible *closo*-carboranes. Long the missing link between eight- and ten-vertex [1-$CB_7H_8]^-$ and [1-$CB_9H_{10}]^-$, its chemistry should now contribute substantially to the development of carborane science. For example, the anion could act as a 'weakly coordinating anion' to complement $[CB_9H_{10}]^-$ and $[CB_{10}H_{11}]^-$, and their derivatives:[4] it is also likely to be amenable to substitution and metallacarborane chemistries. We currently work on the optimisation of its synthesis and on the development of other nine-vertex monocarbaborane chemistry.

B. Š. acknowledges an Alexander von Humboldt Stiftung (FRG) and we thank Professor Max Herberhold (University of Bayreuth) for his good offices. We acknowledge support from the UK EPSRC, the UK DTI, the Ministry of Education of the Czech Republic (Projects LN00A028 and LB98233), the Grant Agency of the Czech Academy of Sciences (Grants nos. A2032007 and A40320804) and the Grant Agencies of the Czech Republic (Grants no. 203/99/M037), as well as the Grant Agency of Charles University (Grant no. 203/00/B-CH/PrF) and the Supercomputing Centre of the Charles University in Prague for computer time.

Notes and references

§ *NMR data*, 294–297 K, ordered as: assignment $\delta(^{11}B)$/ppm, [$\delta(^1H)$, {$\delta(^{13}C)$/ppm where appropriate}], observed splitting from $^1J(^{11}B^1H)$/Hz (relative intensity in parentheses): for $[PMePh_3]^+[CB_8H_9]^-$ (CD_3CN solution): BH(5,6) +12.85, [+4.35], 145, (2BH); BH(1,2,7,8), −14.40, [+1.46], 150, (4BH); BH(3,9), −20.3, [+0.60], 135, (2BH); and CH(4), —, [+4.10], —, (1CH). For $[PBu_4]^+[CB_8H_9]^-$ ($CDCl_3$ solution): BH(5,6) +12.80, [+4.37], 145, (2BH); BH(1,2,7,8) −14.30, [+1.42], 148, (4BH); BH(3,9) −20.3, [+0.64], 136, (2BH); and CH(4), —, [+4.13, {+44.5 $J(^{13}C–^1H)$ 182 Hz], —, (1CH).

¶ *Crystal data* for $[PMePh_3][CB_8H_9]$ (colourless, from EtOH/Et_2O at 290 K, 0.46 × 0.22 × 0.11 mm): $C_{20}H_{27}B_8P$, M = 384.87, monoclinic, space group $P2_1/a$, a = 14.7338(2), b = 14.1571(3), c = 22.7377(4) Å, β = 107.7840(10)°, U = 4516.17(14) Å^3, Z = 8, Mo-Kα radiation, λ = 0.71073 Å, μ = 0.126 mm^{-1}, T = 150(2) K, $R1$ = 0.0549 for 6775 reflections with $I > 2\sigma(I)$, $wR2$ = 0.1491 for all 8821 independent data; methods and programs were standard and from the SHELX suite.[12]

CCDC 159456. See http://www.rsc.org/suppdata/cc/b1/b103408c/ for crystallographic data in CIF or other electronic format.

1 B. Štíbr, *Chem. Rev*., 1992, **92**, 225.
2 V. I . Bregadze, *Chem. Rev*., 1992, **92**, 209.
3 T. Onak, R. P. Drake and G. B. Dunks, *J. Am. Chem. Soc*., 1965, **87**, 2505; S. R. Prince and R. Schaeffer, *Chem. Commun*., 1968, 451; T. Onak, P. Matschei and E. Groszek, *J. Chem. Soc. A*, 1969, 1990; W. H. Knoth, *J. Am. Chem. Soc*., 1967, **89**, 1274; W. H. Knoth, *Inorg. Chem*., 1971, **10**, 598; W. H. Knoth, *Inorg. Chem*., 1973, **12**, 785.
4 C. Reed, *Acc. Chem. Res*., 1998, **31**, 133; S. Strauss, *Chem. Rev*., 1993, **93**, 927.
5 P. Kaszynski, *Collect. Czech. Chem. Commun*., 1999, **64**, 895; and references cited therein.
6 J. Plešek, T. Jelínek, B. Štíbr and S. Heřmánek, *J. Chem. Soc., Chem. Commun*., 1988, 348; T. Jelínek, B. Štíbr, J. Plešek, J. D. Kennedy and M. Thornton-Pett, *J. Chem. Soc., Dalton Trans*., 1995, 431.
7 B. Brellochs, *Contemporary Boron Chemistry*, ed. M. G. Davidson, A. K. Hughes, T. B. Marder and K. Wade, Royal Society of Chemistry, Cambridge, UK, 2000, pp. 212–214.
8 K. Baše, S. Heřmánek and B. Štíbr, *Chem. Ind. (London)*, 1977, 951; K. Baše, B. Štíbr, J. Dolanský and J. Duben, *Collect. Czech.Chem. Commun*., 1981, **46**, 2345.
9 T. Jelínek, I. Kanerová, J. Holub, B. Štíbr, O. Tok and B. Wrackmeyer, in preparation.
10 J. Guggenberger, *Inorg. Chem*., 1968, **7**, 2260; M. E. O'Neill and K. Wade, *Polyhedron*, 1983, **2**, 963.
11 $B_{10}H_{14}$ (12.4 g, 100 mmol) in hexane (200 cm^3) was treated with 15% aqueous NaOH (500 cm^3) with vigorous stirring at room temperature and cooled to 0 °C. 37% aqueous HCHO (containing 36.5 g HCHO, molar ratio $B_{10}H_{14}$: HCHO = 1 : 4.5) was added together with H_2O (30 cm^3) over 1 h. The aqueous layer was separated and extracted with Et_2O (3 × 100 cm^3). Addition of saturated aqueous CsCl (100 mmol) to the combined Et_2O extracts followed by evaporation of the Et_2O, filtration, and recrystallisation of the precipitate from hot H_2O gave $Cs[CB_9H_{14}]$ (44%), as used in the thermolysis. For the CB_8H_{12} route, H_2O (100 cm^3) was added, and the Et_2O removed by rotary evaporation, resulting in an aqueous solution of $Na[CB_9H_{14}]$ [at this stage, precipitation with $[NEt_4]Cl$ can be used to give $[NEt_4][CB_9H_{14}]$ (48%)], which was added dropwise to a stirred mixture of aqueous HCl (*ca*. 4.5 M; 350 cm^3), $FeCl_3·6H_2O$ (65 g) and hexane (200 cm^3), and stirred for 3 h. The hexane layer was separated and evaporated, and the resulting white solid sublimed to give CB_8H_{14} (5.4 g; 47%); which was converted to CB_8H_{12} by dehydrogenation at 350 °C as in ref. 8.
12 G. M. Sheldrick, University of Göttingen, Germany, 1997G. M. Sheldrick, Bruker AXS Inc., Madison, WI, 1994 and 1998.

CHEMCOMM Communication
www.rsc.org/chemcomm

Addition of diprotic nucleophiles to a C_{60}–tetrazine monoadduct: structural reassignment and correction of a novel rearrangement†

Glen P. Miller,*[a] Mark C. Tetreau,[a] Marilyn M. Olmstead,[b] Pamela A. Lord[b] and Alan L. Balch*[b]

[a] *Department of Chemistry, University of New Hampshire, Durham, New Hampshire 03824, USA. E-mail: gpm@cisunix.unh.edu*

[b] *Department of Chemistry, University of California, Davis, California 95616, USA*

Received (in Corvallis, OR, USA) 9th May 2001, Accepted 18th July 2001
First published as an Advance Article on the web 29th August 2001

C_{60}–tetrazine Diels–Alder adducts bearing electron deficient dihydropyridazine groups undergo chemoselective amination and hydration reactions upon addition of primary aliphatic amines and water, respectively, to form new adducts with 4,5-dihydropyrazole groups nested atop the [60]fullerene skeleton.

Recently, we reported[1] Diels–Alder reactivity between C_{60} and electron deficient 3,6-disubstituted-1,2,4,5-tetrazines. With 3,6-di-2′-pyridyl-1,2,4,5-tetrazine, the corresponding monoadduct **1** bears a 4,5-dihydro-3,6-di-2′-pyridylpyridazine group fused to the [60]fullerene skeleton. Compound **1** behaves as an isolable but reactive intermediate capable of considerable further chemistry. Previously a facile, regioselective 1,4-hydrogenation of **1** was reported.[1] Continued work on this and related compounds shows that the structure reported for the hydrogenated monoadduct was incorrect. Compound **1** does hydrogenate in a 1,4 fashion, but only in concert with a novel rearrangement which effectively converts the fused 4,5-dihydropyridazine function into a 4,5-dihydropyrazole group. The reaction is a net hydration. With the aid of an X-ray crystal structure, we are now able to redefine the chemistry of **1** as it pertains to the addition of diprotic nucleophiles. A variety of nucleophiles including water, alcohols, thiols, and primary and secondary aliphatic amines add smoothly to **1**. Chemoselective additions of the diprotic nucleophiles, primary aliphatic amines and water, are followed in each case by a novel rearrangement reaction on the [60]fullerene surface leading to new compounds bearing fused 4,5-dihydropyrazole groups.[2]

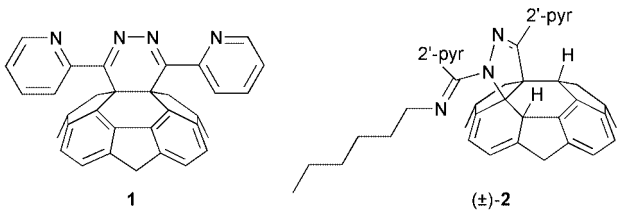

1 (±)-**2**

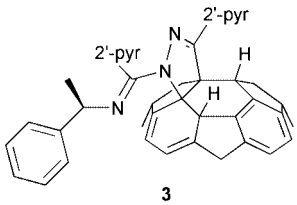

3
1 of 2 diastereomers

Monoadduct **1** was formed as previously described[1] and reacted with several diprotic nucleophiles including hexylamine and (*R*)-(+)-α-methylbenzylamine. The reactions yield new compounds, (±)-**2** and **3** (as a mixture of 2 diastereomers), respectively. Compounds (±)-**2** and **3** bear 1,3-disubstituted-4,5-dihydropyrazole groups nested atop the corresponding [60]fullerene skeletons.

The structure of **3** was obtained by single crystal X-ray diffraction. Black crystals of **3** ($C_{84}H_{19}N_5{\cdot}2CS_2$) form in the chiral space group $P2_12_12_1$ through vapor diffusion of hexane into a carbon disulfide solution of the compound.‡ The structure is disordered with both diastereomers present, but in unequal amounts. Fig. 1 shows a view of the entire molecule for the major diastereomer, which has a refined population of 0.529(3). (The minor diastereomer has an analogous structure, but the location of the [60]fullerene moiety is switched such that the positions of the 5- and 6-membered rings adjacent to C2 and C3 are reversed relative to those shown in Fig. 1. The ability of these two diastereomers to co-crystallize at a common crystallographic site is related to the orientational disorder seen in many fullerene crystals.[3,4]) Structurally the adduct can be viewed as involving addition to two adjacent 6:6 ring junctions of the fullerene, analogous to a *cis*-1 bisadduct.[5] The C2–C3–N3–N2–C61 ring spans a 6:5 ring junction, protrudes radially from the [60]fullerene skeleton, and is very nearly planar. The hydrogen atoms attached to C1 and C4 were located in a difference Fourier map for both the major and minor diastereomers. As is usual with additions to fullerenes,[6] geometric changes in the carbon cage are localized at the sites of attachment. Thus, the C1–C2 and C3–C4 bond lengths (1.670(8) and 1.712(10) Å in the major diastereomer, 1.720(8) and 1.731(11) Å in the minor diastereomer) are longer than the 1.38 Å distance found for 6:6 ring junction of C60. The C2–C3 bond, 1.622(5) Å, is also long.

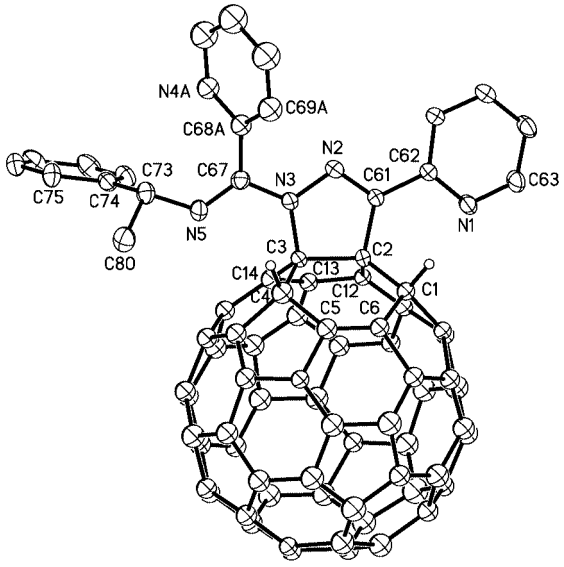

Fig. 1 A perspective view of the major diastereomer (0.529(3) occupancy) of the adduct **3**, $C_{84}H_{19}N_5$, with 50% thermal contours for all non-hydrogen atoms. Only the hydrogen atoms on C1 and C4 are shown.

† Electronic supplementary information (ESI) available: select spectroscopic data for (±)-**2**, **3** and (±)-**4**. See http://www.rsc.org/suppdata/cc/b1/b104151g/

 DOI: 10.1039/b104151g

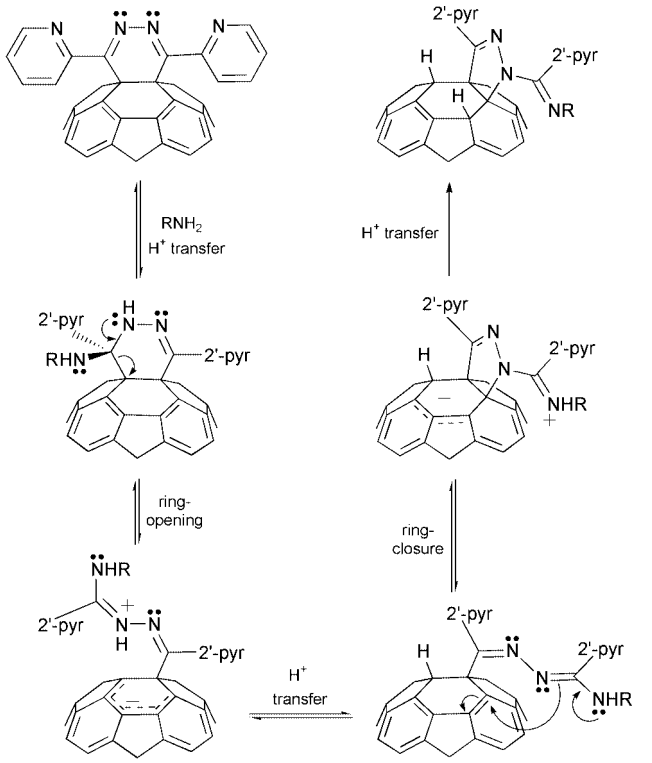

Scheme 1 Possible mechanism for amination of C_{60}–tetrazine monoadduct.

Strong spectroscopic similarities (^{1}H and ^{13}C NMR†) between (±)-**2** and **3** suggest an analogous structure for (±)-**2**.

The structures for (±)-**2** and **3** are consistent with amination across a single imine C=N bond of **1** followed by a rearrangement of the amination adducts (Scheme 1). Chemoselective amination across an imine C=N bond of **1** is somewhat surprising considering that C_{60} itself is readily aminated by primary and secondary aliphatic amines.[7] EPR and UV–VIS–NIR evidence[7a,b] suggests that the amination of C_{60} involves initial electron transfer from the amine to C_{60}. In our laboratory, the amination of C_{60} usually requires ambient light when relatively nonpolar organic solvents are employed (*e.g.* toluene, chloroform). This observation is consistent with a mechanism involving electron transfer from amine to photoexcited fullerene (for similar observations involving tertiary amine addition, see refs. 7*f* and 7*g*). However, compounds (±)-**2** and **3** are formed equally well in ambient light or darkness, consistent with but by no means specific to a mechanism involving simple nucleophilic additions (Scheme 1).

Other diprotic nucleophiles show similar reactivity. Water adds to **1** to give the analogous hydration product (±)-**4**. The reaction is catalyzed by weak acid catalysts such as silica gel and requires ambient light.

Compounds (±)-**2** and **3** are formally imine derivatives of (±)-**4**, but do not originate from (±)-**4**. Thus, addition of the appropriate amine to (±)-**4** does not produce (±)-**2** or **3** under otherwise identical reaction conditions employed for the synthesis of (±)-**2** or **3** from **1**. Consequently, (±)-**4** is not an intermediate in the amination reactions leading to (±)-**2** and **3**. Compounds (±)-**2** and **3**, however, are converted to (±)-**4** under harsh hydrolysis conditions (conc. HCl, CH_3CN, 80 °C), thereby confirming the structure of (±)-**4**.

The ^{1}H and ^{13}C NMR spectra for (±)-**4** match those reported previously for a compound assigned structure (±)-**5**.[1]

With an X-ray crystal structure now available for **3**, it is clear that the previously assigned structure (±)-**5** is incorrect and should be replaced with the structure (±)-**4**. The original assignment of structure (±)-**5** was based upon the observations that the reaction leading to hydrogenated product is photoinduced, the reaction requires water adsorbed on glass, and the NMR data are uniquely consistent with a 1,4-hydrogenation

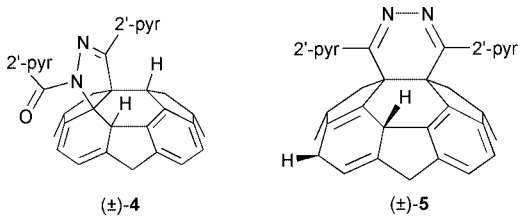

(±)-**4** (±)-**5**

pattern on the fullerene skeleton. Moreover, the completely regioselective nature of the reaction suggested new C–H bond formation in close proximity to the dihydropyridazine group. Indeed, each of these statements holds true for the hydration of **1** leading to (±)-**4**. A key shortcoming of the earlier work was the failure to recognize rearrangement of the dihydropyridazine function, as well as the erroneous incorporation of the tetrazine–dihydrotetrazine redox cycle into the proposed reaction mechanism.

Because the hydration and amination reactions produce structurally similar compounds, it is tempting to conclude that they proceed *via* similar mechanisms. However, the hydration of **1** leading to (±)-**4** requires ambient light while the amination reactions leading to (±)-**2** and **3** do not. By analogy to known photoinduced processes involving C_{60},[7f,g] at least one of the steps leading to (±)-**4** likely involves an electron transfer to a photoexcited [60]fullerene skeleton.

A. L. B., M. M. O. and P. A. L. thank the National Science Foundation (Grant CHE 0070291 to ALB) for financial support.

Notes and references

‡ *Crystal data*: black needles of **3**, $C_{84}H_{19}N_5{\cdot}2\,CS_2$, M = 1202.26, form in the orthorhombic space group $P2_12_12_1$ with a = 13.0656(9), b = 14.3786(9), c = 25.8201(17) Å, at 91(2) K with Z = 4. A total of 64323 reflections were collected with graphite monochromated Mo-Kα (λ = 0.71073 Å) radiation, μ(Mo-Kα) = 0.262 mm^{-1}, and a Brucker SMART 1000 diffractometer. Refinement of 15217 reflections (R(int) = 0.04) and 735 parameters yielded $wR2$ = 0.231 for all data and a conventional R_1 = 0.087 based on 12123 reflections with $I > 2\sigma(I)$. All non-hydrogen atoms were assigned anisotropic thermal parameters except 58 of the fullerene carbon atoms (C2 and C3 were refined anisotropically) and a disordered pyridine ring, which were refined with isotropic thermal parameters. All hydrogen atoms were located in difference maps and subsequently refined using a riding model. The largest peak and hole in the final difference map are 0.99 e Å^{-3} and −0.81 e Å^{-3}. Atomic coordinates, bond lengths and angles, and thermal parameters have been deposited at the Cambridge Crystallographic Data Centre. CCDC 168187. See http://www.rsc.org/suppdata/cc/b1/b104151g/ for crystallographic data in .cif or other format.

1 G. P. Miller and M. C. Tetreau, *Org. Lett.*, 2000, **2**, 3091.
2 This work was recently presented to the Fullerenes Group at the 199th Meeting of the Electrochemical Society: G. P. Miller and M. C. Tetreau, March 28, 2001.
3 H. B. Bürgi, E. Blanc, D. Schwarzenbach, S. Liu, Y. J. Lu, M. M. Kappes and J. A. Ibers, *Angew. Chem., Int. Ed. Engl.*, 1992, **31**, 640.
4 A. L. Balch, J. W. Lee, B. C. Noll and M. M. Olmstead, *J. Chem. Soc., Chem. Commun.*, 1993, 56.
5 A. Hirsch, *The Chemistry of the Fullerenes*, Thieme, Stuttgart, 1994, p. 69.
6 A. L. Balch, A. S. Ginwalla, M. M. Olmstead and R. Herbst-Irmer, *Tetrahedron*, 1996, **52**, 5021.
7 (*a*) F. Wudl, A. Hirsch, K. C. Khemani, T. Suzuki, P.-M. Allemand, A. Koch, H. Eckert, G. Srdanov and H. Webb, in *Fullerenes: Synthesis, Properties, and Chemistry of Large Carbon Clusters*, ACS Symposium Series 468, American Chemical Society, ed. G. S. Hammond and V. S. Kuck, Washington, D.C., p. 161, 1992; (*b*) A. Skiebe, A. Hirsch, H. Klos and B. Glotschy, *Chem. Phys. Lett.*, 1994, 397; (*c*) A. Hirsch, Q. Li and F. Wudl, *Angew. Chem., Int. Ed. Engl.*, 1991, **30**, 1309; (*d*) G. P. Miller, J. M. Millar, B. Liang, S. Uldrich and J. E. Johnston, *J. Chem. Soc., Chem. Commun.*, 1993, 897; (*e*) A. L. Balch, B. Cullison, W. R. Fawcett, A. S. Ginwalla, M. M. Olmstead and K. Winkler, *J. Chem. Soc., Chem. Commun.*, 1995, 2287; (*f*) K.-F. Liou and C.-H. Cheng, *Chem. Commun.*, 1996, 1423; (*g*) G. E. Lawson, A. Kitaygorodskiy, B. Ma, C. E. Bunker and Y.-P. Sun, *J. Chem. Soc., Chem. Commun.*, 1995, 2225.

CHEMCOMM
Communication
www.rsc.org/chemcomm

Identification of Tyr58 as the proton donor in the aspartate-α-decarboxylase reaction

S. Adrian Saldanha,†[a] Louise M. Birch,†[a] Michael E. Webb,[a] Brent K. Nabbs,[a] Frank von Delft,[b] Alison G. Smith[c] and Chris Abell*[a]

[a] *University Chemical Laboratory, Lensfield Road, Cambridge, UK CB2 1EW. E-mail: ca26@cam.ac.uk*
[b] *Department of Biochemistry, University of Cambridge, 80 Tennis Court Road, Cambridge, UK CB2 1GA*
[c] *Department of Plant Sciences, University of Cambridge, Downing Street, Cambridge, UK CB2 3EA*

Received (in Cambridge, UK) 10th July 2001, Accepted 30th July 2001
First published as an Advance Article on the web 29th August 2001

The decarboxylation of L-aspartate by *E. coli* L-aspartate-α-decarboxylase (ADC) is shown to occur with retention of configuration; analysis of the protein structure identifies Tyr58 as the proton donor in the decarboxylation mechanism.

ADC catalyses the decarboxylation of L-aspartate to β-alanine.[1] It is one of four enzymes in *E. coli* involved in the biosynthesis of pantothenate (vitamin B_5),[2] the precursor of 4′-phosphopantetheine and coenzyme A. ADC is a tetrameric protein comprising four 14 kDa subunits. The X-ray crystal structure of *E. coli* ADC has been determined, and shows that the active sites are between subunits.[3]

The mechanism of decarboxylation involves formation of an imine between the amino group of aspartate and an integral pyruvoyl group. The pyruvoyl group is formed by an autocatalytic post-translational modification which cleaves the Gly24–Ser25 bond and converts Ser25 into the pyruvoyl group. This reaction is analogous to that which occurs in histidine decarboxylase[4] and *S*-adenosylmethionine decarboxylase.[5]

The proposed enzyme mechanism is depicted in Scheme 1. After formation of the enzyme–substrate adduct (**1**), carbon dioxide is lost to form the extended enolate (**2**). This then reprotonates to form the imine adduct of the product β-alanine (**3**), which is finally released by hydrolysis to regenerate the pyruvoyl group. Evidence for this mechanism comes from trapping of the enzyme–substrate adduct and enzyme–product adduct by reduction with cyanoborohydride, and subsequent detection by electrospray mass spectrometry.[6]

In this paper we report the results of our investigation into the stereochemical course of the decarboxylation reaction catalysed by ADC. Analysis of the crystal structure of ADC suggests that the proton may come from the phenolic group of Tyr58 or the hydroxy group of Thr57, which lie above and below the face of the enzyme–intermediate adduct (**2**) respectively (Fig. 1). If the proton donor were Tyr58, the proton would be added to the *re* face (Scheme 1, path a), corresponding to decarboxylation–protonation occurring with overall retention of configuration. Conversely, decarboxylation–protonation would occur with inversion of configuration if the proton were added from Thr57 to the *si* face of (2) (path b). Alternatively, but less probable, the reprotonation could be non-stereospecific.

The stereochemical course of the reaction can be determined by using ADC to catalyse the conversion of L-aspartate into β-alanine in deuterium oxide. Stereospecific deuteriation of (**2**) will generate chirally-labelled β-alanine which can be charac-

† These authors contributed equally to this work.

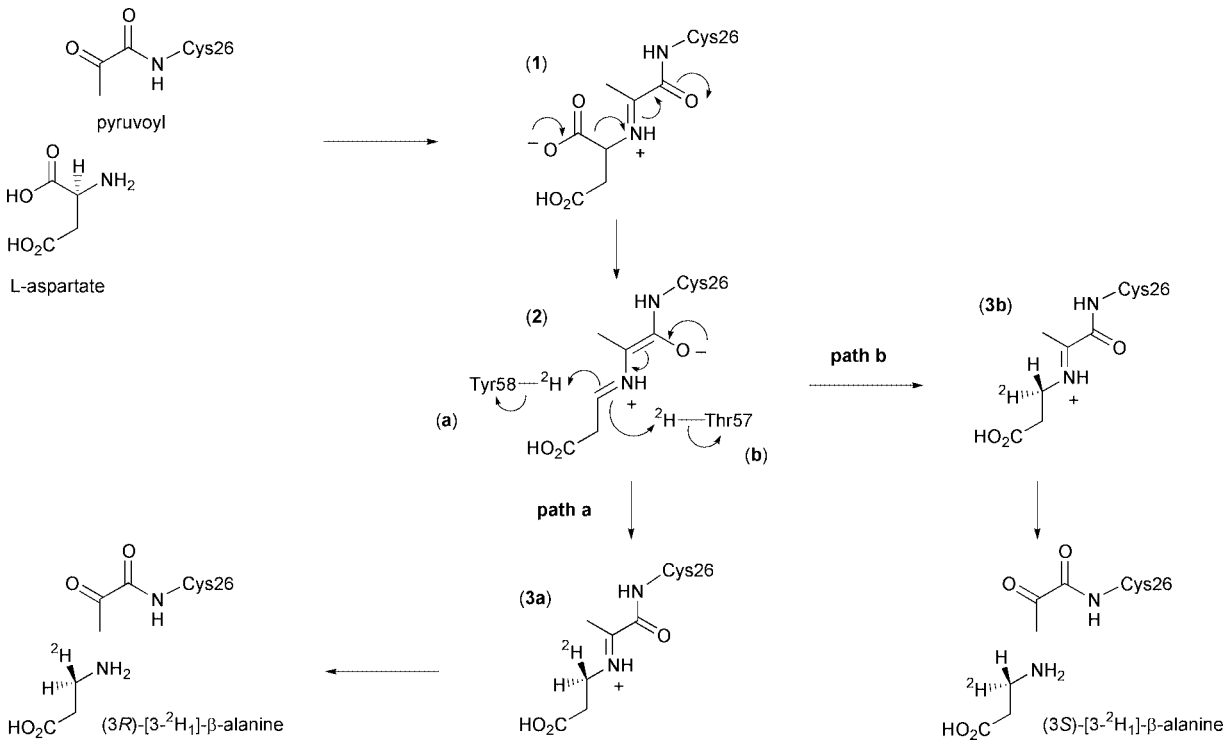

Scheme 1 Catalytic mechanism of ADC showing the possible stereochemical outcomes in the presence of ^2H_2O.

 DOI: 10.1039/b106090m

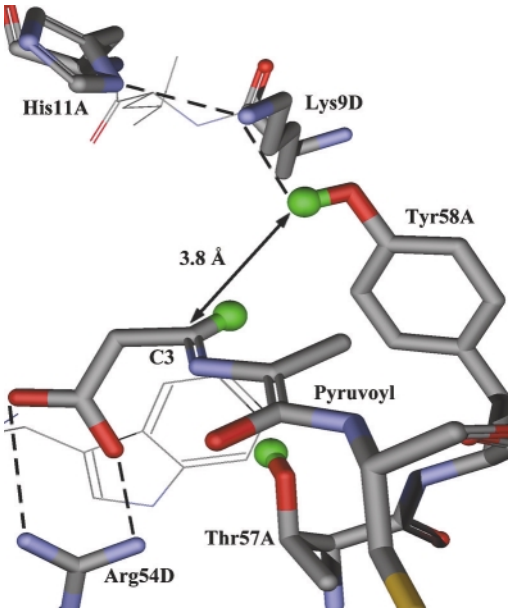

Fig. 1 Active site of ADC with the enzyme-intermediate adduct (**2**) modelled in. The active site is at the interface of subunits and is composed of residues from both subunits (in this case subunits A and D).

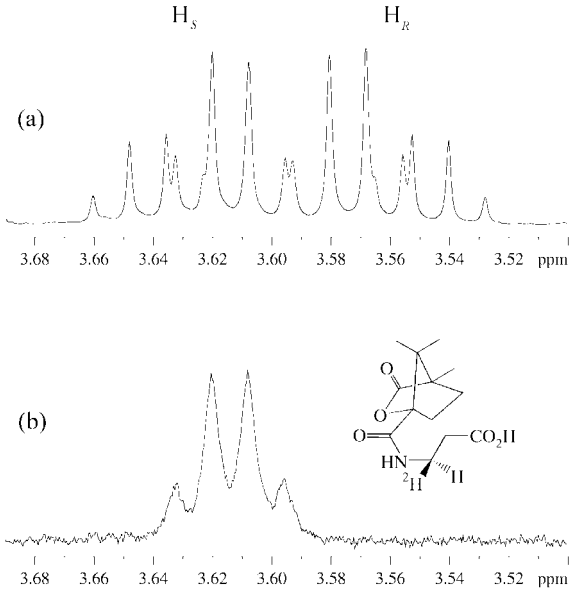

Fig. 2 ^1H NMR (500 MHz, C^2HCl_3) of the C3 protons of β-alanine in (a) *N*-camphanoyl-β-alanine and (b) camphanoyl derivative of the biotransformed material.

terised as its camphanoyl derivative by comparison with previously assigned spectra of (3*R*)- and (3*S*)-*N*-camphanoyl-[3-$^2H_1$]-β-alanine.[7]

The *panD* gene[6,8] in *E. coli* was overexpressed with an *N*-terminal hexa-histidine tag to facilitate protein purification by affinity chromatography on a nickel–nitrilotriacetic acid (Ni–NTA) column. L-Aspartate (50 mg) and His_6-ADC (6 mg) were incubated in phosphate buffer (pD = 7.6, 50 mM) in ^2H_2O for four days at 25 °C. The enzyme was removed by ultrafiltration and the solution lyophilised to dryness. The residue was derivatised with camphanoyl chloride by shaking in a biphasic mixture of 2 M NaOH and toluene for 3 h, followed by extraction with chloroform, drying with Na_2SO_4 and evaporation. Unlabelled *N*-camphanoyl-β-alanine was also synthesised by this procedure. The ^1H NMR spectra of the C3 protons of *N*-camphanoyl-β-alanine and the camphanoyl derivative of the biotransformed material are shown in Fig. 2.[9]

Comparison of the two spectra in Fig. 2 shows that a deuterium atom has been incorporated, leading to loss of the signal for one proton. The geminal ^1H coupling to the remaining proton has been replaced by a smaller ^2H coupling, causing an apparent simplification of the multiplet and broadening of the signals. This confirms that the reprotonation is stereospecific.

In order to determine the absolute stereochemistry of the labelling of β-alanine, the spectra were compared to published data on (3*R*)- and (3*S*)-*N*-camphanoyl-[3-$^2H_1$]-β-alanine, determined as part of a study on the dihydropyrimidine dehydrogenase reaction.[7] The upfield multiplet in Fig. 2a has been assigned to the 3*R* proton. The biotransformed compound, in which this proton has been replaced by a deuteron, is consequently (3*R*)-*N*-camphanoyl-[3-$^2H_1$]-β-alanine. This is the expected product if deuterium is delivered from Tyr58 to the *re* face of (**2**), with the decarboxylation–protonation steps proceeding with overall retention of configuration (Scheme 1, path a).

The enzyme–intermediate adduct (**2**) has been modelled into the crystal structure of ADC (Fig. 1). In this model the distance between the hydroxy proton of Thr57 and the C3 carbon is 3.3 Å. The corresponding distance from C3 to the phenolic proton of Tyr58 is 3.8 Å. Despite being the closest potential donor, Thr57 may not be the most appropriate. It is relatively buried in the active site, and deprotonation of the hydroxy group could destabilise the neighbouring salt bridge between the β-carboxyl of the enzyme–intermediate adduct (**2**) and Arg54. Tyr58 appears to be better placed; in particular it is part of a potential proton relay with Lys9 and His11. All three are conserved residues. As His11 is close to the surface of the protein it could acquire a proton from the solvent.

In conclusion, the stereochemical labelling study and analysis of a model of the putative intermediate bound to the enzyme (**2**), together suggest that the source of the proton in the reprotonation step is the phenolic group of Tyr58.

We would like to thank Drs Martyn Frederickson, Peter Grice and Nick Bampos and the NMR technical staff for their assistance.

Notes and references

1 J. M. Williamson and G. M. Brown, *J. Biol. Chem.*, 1979, **254**, 8074.
2 G. M. Brown and J. M. Williamson, *Adv. Enzymol. Relat. Areas Mol. Biol.*, 1982, **53**, 345.
3 A. Albert, V. Dhanaraj, U. Genschel, G. Khan, M. K. Ramjee, R. Pulido, B. L. Sibanda, F. von Delft, M. Witty, T. L. Blundell, A. G. Smith and C. Abell, *Nat. Struct. Biol.*, 1998, **5**, 289.
4 T. Gallagher, E. E. Snell and M. L. Hackert, *J. Biol. Chem.*, 1989, **264**, 12737.
5 G. D. Markham, C. W. Tabor and H. J. Tabor, *J. Biol. Chem.*, 1982, **257**, 2063.
6 M. K. Ramjee, U. Genschel, C. Abell and A. G. Smith, *Biochem. J.*, 1997, **323**, 661.
7 D. Gani and D. W. Young, *J. Chem. Soc., Perkin Trans. 1*, 1985, **7**, 1355.
8 J. E. Cronan, *J. Bacteriol.*, 1980, **141**, 1291.
9 *N*-Camphanoyl-β-alanine: ^1H NMR δ (500 MHz, C^2HCl_3, β-alanine signals) 3.63 (H, m, 3-H_S), 3.56 (H, m, 3-H_R), 2.61 (2H, t, J = 5.9 Hz, CH_2); ^{13}C NMR δ (125.8 MHz, C^2HCl_3) 178.4, 175.9, 167.4, 92.4, 55.2, 53.9, 34.6, 33.8, 30.1, 28.9, 16.6, 16.3, 9.6; HRMS (ES) calcd for $C_{13}H_{19}NaNO_5$ (MNa) *m/z* 292.1161, found *m/z* 292.1169. (3*R*)-*N*-Camphanoyl-[3-$^2H_1$]-β-alanine: ^1H NMR δ (500 MHz, C^2HCl_3, β-alanine signals) 3.61 (H, m, 3-H_S), 2.63 (2H, d, J = 5.9 Hz, CH_2); ^{13}C NMR δ (125.8 MHz, C^2HCl_3) 178.4, 176.2, 167.3, 92.4, 55.2, 53.9, 34.4, 33.9, 30.1, 29.0, 16.6, 16.4, 9.6; HRMS (ES) calcd for $C_{13}H_{18}DNaNO_5$ (MNa) *m/z* 293.1224, found *m/z* 293.1212.

CHEMCOMM Communication
www.rsc.org/chemcomm

Novel silver(I)–organic coordination polymers: conversion of extended structures in the solid state as driven by argentophilic interactions

Long Pan,[a] E. Brice Woodlock,[a] Xiaotai Wang,*[a] Kin-Chung Lam[b] and Arnold L. Rheingold[b]

[a] *Department of Chemistry, Campus Box 194, University of Colorado at Denver, P.O. Box 173364, Denver, Colorado 80217-3364, USA. E-mail: xwang@carbon.cudenver.edu*
[b] *Department of Chemistry and Biochemistry, University of Delaware, Newark, DE 19716, USA*

Received (in Columbia, MO, USA) 27th April 2001, Accepted 13th July 2001
First published as an Advance Article on the web 23rd August 2001

Structurally distinct coordination polymers [Ag(bpp)]ClO_4 1 and [Ag(bpp)]PF_6 2 [bpp = 1,3-bis(4-pyridyl)propane] have been assembled; the conversion of 1 into 2 on treatment with $NaPF_6$ is driven by argentophilic interactions and is the first such transformation reported for silver(I)–organic coordination polymers.

The field of metal–organic coordination polymers[1] has recently attracted intense interest because such supramolecular compounds have potential as smart optoelectronic,[2] magnetic,[3] microporous,[4] and biomimetic materials.[5] The design of coordination polymers takes into account factors such as the coordination nature of the metal ion, the structural characteristics of the polydentate organic ligand, the metal–ligand ratio, and the possible counter ion influence. A subtle alteration in any of these factors can lead to new extended network structures. Thus, a great variety of supramolecular architectures have been ingeniously constructed. These not only have aesthetic appeal, but occasionally exhibit interesting functions. In contrast, there has been a scarcity of information on supramolecular reactivity featuring well-defined conversions of extended structures in coordination polymers.[6] Such transformations may find applications in molecular recognition and chemical sensor technologies. For cationic networks, exchange of anions has recently been reported to induce the interconversion of several silver(I)–polynitrile coordination polymers.[6a] These changes apparently involve the breaking and forming of silver(I)–nitrile coordination bonds, but the driving force and mechanism are not well understood.

The coordination affinity of silver(I) for pyridyl-donor ligands is well known, and the argentophilic d^{10}–d^{10} bonding interactions frequently affect the extended structures of the resulting coordination polymers.[7] The commercially available 1,3-bis(4-pyridyl)propane (bpp) is a bipyridine-type ligand with a flexible $–CH_2CH_2CH_2–$ spacer, and several research groups have reported a few Ag^I–bpp cationic networks where the counter ion is $CF_3SO_3^-$ or NO_3^-.[8] Ciani and coworkers have also mentioned that bpp reacts with $AgBF_4$ or $AgClO_4$ in 2 : 1 molar ratio to form two-fold interpenetrated diamondoid networks.[8a] We have sought to generate novel cationic Ag^I–bpp networks with various counter ions and use such systems for the study of anion-induced transformations of supramolecular structures. Herein we report the assembly of [Ag(bpp)]ClO_4 **1** and [Ag(bpp)]PF_6 **2**, two coordination polymers with novel and distinct cationic network structures. We also describe the well-defined, irreversible conversion of **1** into **2** on treatment with $NaPF_6$. This conversion is unique in that it is driven by forming more and stronger Ag–Ag bonds in the polymeric cation (see below); no such transformations have been previously reported for silver(I)–organic coordination polymers.

Solution-phase reactions of bpp with $AgClO_4$ and $AgPF_6$ in 1 : 1 molar ratio generate **1** and **2**, respectively.† The structures of **1** and **2** determined *via* single crystal X-ray diffraction analysis‡ are shown in Fig. 1. In both **1** and **2**, each Ag^I ion is coordinated by two pyridyl nitrogen atoms of different bpp units in approximately linear geometry, and the Ag–N bond distances fall between 2.114(5) and 2.144(5) Å, as expected for Ag^I complexes with pyridine-type ligands . Despite this similarity in local silver(I)–pyridyl coordination, **1** and **2** have significantly different extended supramolecular structures due to differences in argentophilic interaction.

In the cationic network of **1**, there are two types of crystallographically and chemically equivalent Ag^I ions, both of which form 1-D sinusoidal chains with the bound bpp molecules where each $–CH_2CH_2CH_2–$ spacer adopts a TT conformation.[8a] Adjacent chains containing one type of Ag^I ions are cross-linked through argentophilic bonding to form 2-D layers, as evidenced by the Ag–Ag contact [3.2214(10) Å] that is well below the van der Waals diameter of silver (3.44 Å).[9] The 1-D sinusoidal chains containing the other type of Ag^I ions lack interchain Ag^I–Ag^I interactions because the shortest Ag···Ag separation (4.40 Å) is greater than the van der Waals

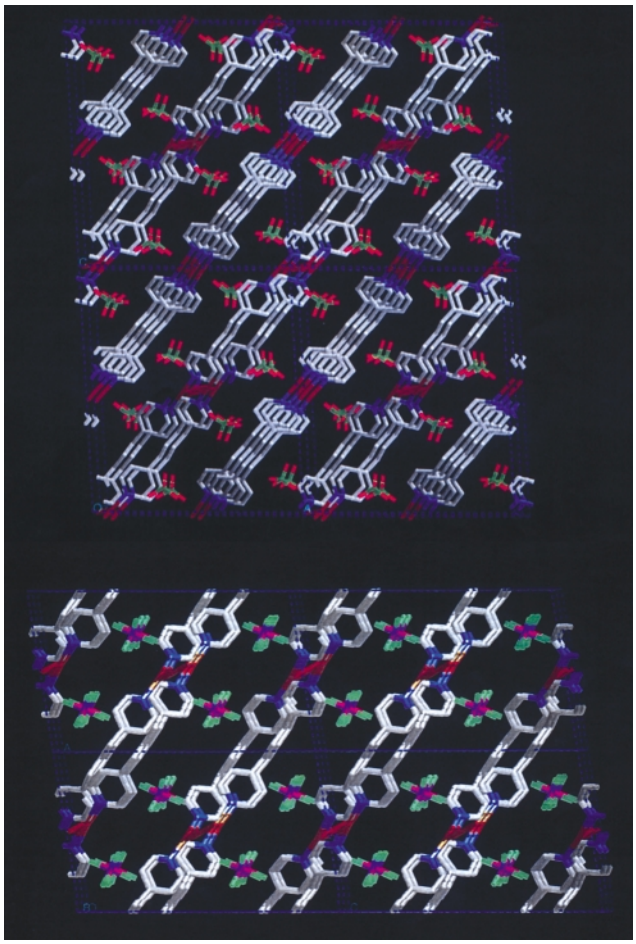

Fig. 1 Cylinder representations of the structures of **1** (top) and **2** (bottom), both viewed approximately along the crystallographic *b* axis. H atoms are omitted for clarity. Color scheme for the cationic networks: Ag, red; N, blue; and C, green.

 DOI: 10.1039/b104074j

diameter. In the entire crystal structure of **1**, the 2-D Ag^{I}–bpp layers and the 1-D Ag^{I}–bpp chains pack the space alternately. The ClO_4^- ions occupy the volume between the 2-D layers and 1-D chains, interacting with the cationic network through predominantly ionic bonding, with the shortest Ag···O(ClO_4^-) separation at 2.78 Å. To our knowledge, the polymeric cation of **1**, consisting of stacked 2-D layers separated by 1-D chains, exhibits an unprecedented structural motif in coordination polymers. Structurally, the polymeric cation of **2** is more straightforward than that of **1**. All silver(I) ions are crystallographically and chemically equivalent and are each coordinated by two pyridyl nitrogen atoms of different bpp units. The sinusoidal Ag^{I}–bpp chains are cross-linked *via* stronger and shorter Ag–Ag bonds [3.0852(9) Å] in comparison with those in **1**. The Ag–Ag bond distance in **2** is comparable to that observed in [Ag(bpy)]NO_3 (bpy = 4,4′-bipyridine).[7e,f] However, adjacent Ag^{I}–bpy chains are perpendicularly linked to afford a 3-D framework whereas the Ag^{I}–bpp chains in **2** are connected approximately in parallel to generate a 2-D layer. The known [Ag(bpp)](CF_3SO_3)·EtOH and [Ag(bpp)]NO_3 display wave-like Ag^{I}–bpp chains similar to **2**, but no interchain Ag–Ag bonds were reported.[8] The 2-D Ag^{I}–bbp layers in **2** are intercalated by the PF_6^- ions and the interaction between $[Ag(bpp)]^+$ and PF_6^- is predominantly ionic, the shortest Ag···F(PF_6^-) separation being 2.75 Å. In both **1** and **2**, π–π interactions between pyridyl rings are very weak.[10,11]

Comparing the extended structures of **1** and **2**, we reasoned that the latter is more stable than the former primarily because of the greater number and strength of Ag–Ag bonds. This rationale prompted us to study the possibility of transforming **1** into **2** *via* anion exchange. Reaction of **1** with $NaPF_6$ affords **2** in quantitative yield [eqn. (1)]:

$$[Ag(bpp)]ClO_4(s) + NaPF_6(aq) \rightarrow [Ag(bpp)]PF_6(s) + NaClO_4(aq) \quad (1)$$

The IR spectrum of the exchanged solid shows the disappearance of the ClO_4^- bands and the appearance of the intense PF_6^- adsorptions at 835 and 561 cm^{-1}. Furthermore, the X-ray powder diffraction (XRD) pattern of the exchanged solid is identical to that of [Ag(bpp)]PF_6 prepared from $AgPF_6$ and bpp (Fig. 2). According to IR and XRD monitoring, no reaction occurred between **2** and $NaClO_4$ even after a sample of **2** was immersed in a large excess of saturated aqueous solution of $NaClO_4$ (*ca.* 14 M) for five days. This result agrees with the observation that **2** has greater structural stability than does **1**.

In conclusion, we have obtained structurally distinct coordination polymers [Ag(bpp)]ClO_4 and [Ag(bpp)]PF_6. Treatment of [Ag(bpp)]ClO_4 with $NaPF_6$ affords [Ag(bpp)]PF_6, and this reactivity is well-correlated with the extended structures of the two compounds. These findings illustrate the structure–property relationship at the supramolecular level. We are currently attempting to extend this study to silver(I) complexes with other pyridyl-donor ligands.

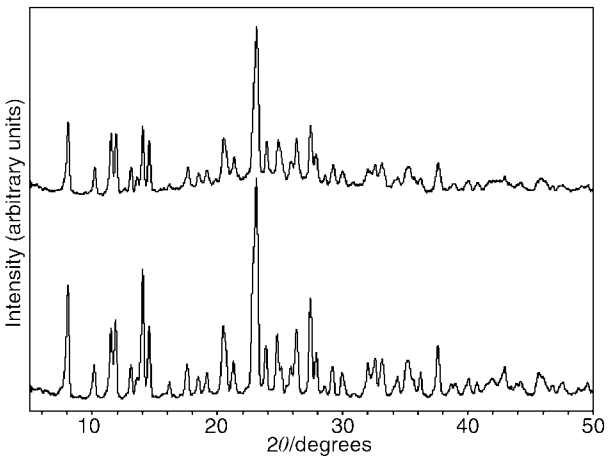

Fig. 2 The XRD patterns of the exchanged solid (top) and [Ag(bpp)]PF_6 prepared from $AgPF_6$ and bpp (bottom).

This work was supported by the University of Colorado at Denver; Research Corporation; and the donors of the Petroleum Research Fund, administered by the American Chemical Society. We thank Dr Jing Li for making X-ray powder diffraction instrumentation available to us. We also thank Drs Jing Li and Robert Damrauer for helpful discussions.

Notes and references

† Under ambient conditions, layering of a methanol solution (4 mL) of bpp (0.10 mmol) over aqueous solutions (4 mL) of $AgClO_4$ and $AgPF_6$ (0.10 mmol) produced colorless crystals of **1** and **2** in 51 and 50% yields, respectively. Compounds **1** and **2** are insoluble in water and common organic solvents. The bulk-phase purities of **1** and **2** were confirmed by comparing their observed and simulated XRD patterns. IR (KBr pellet): for **1**: ν/cm^{-1} 2925m, 2858w, 1609s, 1558w, 1500w, 1429m, 1225w, 1097vs, 808s, 626s, 514m. For **2**: ν/cm^{-1} 2923m, 2856w, 1604s, 1558w, 1500w, 1417m, 1069s, br, 835vs, 561s.

‡ *Crystal data*: for $C_{13}H_{14}AgClN_2O_4$ **1**: M = 405.58, monoclinic, space group $P2_1/n$, a = 16.8826(2), b = 8.6694(2), c = 19.9505(2) Å, β = 93.545(2)°, V = 2914.38(7) $Å^3$, Z = 8, D_c = 1.849 g cm^{-3}, T = 173(2) K, μ(Mo-Kα) = 1.583 mm^{-1}, 3568 data with $I > 2\sigma(I)$, $R(F)$ = 0.040.

For $C_{13}H_{14}AgN_2PF_6$ **2**: M = 451.10, monoclinic, space group $P2_1/c$, a = 11.0925(2), b = 8.4883(2), c = 17.6297(4) Å, β = 99.0826(6)°, V = 1639.12(8) $Å^3$, Z = 4, D_c = 1.828 g cm^{-3}, T = 173(2) K, μ(Mo-Kα) = 1.385 mm^{-1}, 2351 data with $I > 2\sigma(I)$, $R(F)$ = 0.0504.

All data were collected on a Siemens P4 diffractometer equipped with a SMART/CCD detector. The structures were solved by direct methods, completed by subsequent difference Fourier syntheses, and refined by full-matrix least-squares procedures. An absorption correction, using SADABS, was applied to the data for **1** while no absorption correction was required for **2**.

CCDC reference numbers 154893 and 154894. See http://www.rsc.org/suppdata/cc/b1/b104074j/ for crystallographic data in CIF or other electronic format.

1 M. J. Zaworotko, *Angew. Chem., Int. Ed.*, 2000, **39**, 3052; W. Mori and S. Takamizawa, *J. Solid State Chem.*, 2000, **152**, 120; A. K. Cheetham, G. Ferey and T. Loiseau, *Angew. Chem., Int. Ed.*, 1999, **38**, 3268; M. Munakata, L. P. Wu and T. Kuroda-Sowa, *Adv. Inorg. Chem.*, 1998, **46**, 174; M. J. Zaworotko, *Chem. Soc. Rev.*, 1994, **23**, 283.

2 W. Lin, Z. Wang and L. Ma, *J. Am. Chem. Soc.*, 1999, **121**, 11249; O. R. Evans, R. Xiong, Z. Wang, G. K. Wong and W. Lin, *Angew. Chem., Int. Ed.*, 1999, **38**, 536.

3 O. Kahn, *Acc. Chem. Res.*, 2000, **33**, 647.

4 P. Long, E. B. Woodlock and X. Wang, *Inorg. Chem.*, 2000, **39**, 4174; S. Noro, S. Kitazawa, M. Kondo and K. Seki, *Angew. Chem., Int. Ed.*, 2000, **39**, 2082.

5 O.-S. Jung, Y. J. Kim, Y.-A. Lee, J. K. Park and H. K. Chae, *J. Am. Chem. Soc.*, 2000, **122**, 9921.

6 (*a*) K. S. Min and M. P. Suh, *J. Am. Chem. Soc.*, 2000, **122**, 6834; (*b*) L. Pan, N. Ching, X. Huang and J. Li, *Inorg. Chem.*, 2000, **39**, 5333.

7 (*a*) S. Sailaja and M. V. Rajasekharan, *Inorg. Chem.*, 2000, **39**, 4586; (*b*) L. Carlucci, G. Ciani, P. Macchi and D. M. Proserpio, *Chem. Commun.*, 1998, 1837; (*c*) A. J. Blake, N. R. Champness, S. S. M. Chung, W.-S. Li and M. Schroder, *Chem. Commun.*, 1997, 1675; (*d*) M. A. Withersby, A. J. Blake, N. R. Champness, P. Hubberstey, W.-S. Li and M. Schroder, *Angew. Chem., Int. Ed. Engl.*, 1997, **36**, 2327; (*e*) O. M. Yaghi and H. Li, *J. Am. Chem. Soc.*, 1996, **118**, 295; (*f*) F. Robinson and M. Zaworotko, *J. Chem. Soc., Chem. Commun.*, 1995, 2413.

8 (*a*) L. Carlucci, G. Ciani, D. W. v. Gudenberg and D. M. Proserpio, *Inorg. Chem.*, 1997, **36**, 3812; (*b*) S. R. Batten, J. C. Jeffery and M. D. Ward, *Inorg. Chim. Acta*, 1999, **292**, 231.

9 A. Bondi, *J. Phys. Chem.*, 1964, **68**, 441; M. Jansen, *Angew. Chem., Int. Ed. Engl.*, 1987, **26**, 1098.

10 Within the 2-D layer in **1**, the four pyridyl rings surrounding a Ag–Ag bond form two equivalent stacking orientations. Each involves two stacked rings that are somewhat deviated from being parallel and are separated by 3.98 Å (a distance estimated by averaging the C···C and N···N separations). Similar pyridyl ring orientations occur within the 2-D layer in **2**, the corresponding separation being 3.89 Å. Between two adjacent Ag^{I}–bbp chains in **1** that lack Ag–Ag bonds, the pyridyl rings are parallel and offset and are separated by 4.30 Å.

11 C. A. Hunter and J. K. M. Sanders, *J. Am. Chem. Soc.*, 1990, **112**, 5525; G. W. Coates, A. R. Dunn, L. M. Henling, D. A. Dougherty and R. H. Grubbs, *Angew. Chem., Int. Ed. Engl.*, 1997, **36**, 248; M.-L. Tong, H. K. Lee, Y.-X. Tong, X.-M. Chen and T. C. W. Mak, *Inorg. Chem.*, 2000, **39**, 4666.

CHEMCOMM
Communication
www.rsc.org/chemcomm

Crystal engineering of microporous 'Chinese-lantern' compounds to improve their ability to reversibly adsorb sulfur dioxide†

Wendy I. Cross, Stephen M. Godfrey, Charles A. McAuliffe and Robin G. Pritchard

Department of Chemistry, UMIST, Manchester, UK M60 1QD. E-mail: Noel.McAuliffe@UMIST.ac.uk

Received (in Cambridge, UK) 8th February 2001, Accepted 4th June 2001
First published as an Advance Article on the web 3rd September 2001

Three new 'Chinese lantern' complexes [XMn(μ-dppO$_2$)$_4$MnX]$^{2+}$2X$^-$·4MeOH·Me$_2$CO [X = Cl, Br, I; dppO$_2$ = 1,3-bis(diphenylphosphinoyl)propane], have been structurally characterised using single-crystal X-ray diffraction and shown to have increasing affinity for SO$_2$ across the series Cl < Br < I *via* thermogravimetric measurements.

The discovery that dppO$_2$ and manganese isothiocyanate self-assemble to form 'Chinese-lantern' shaped macromolecules[1] (Fig. 1) emerged from research into the ability of manganese phosphine oxide complexes to capture sulfur dioxide within their lattices[2,3]

As our earlier work had shown that iodide containing monophosphine oxide compounds retained SO$_2$ more tenaciously than the corresponding isothiocyanates, dppO$_2$ complexes of manganese iodide, bromide and chloride were synthesised,‡ structurally characterised§ and subjected to SO$_2$ adsorption tests. At first sight all the lantern solids appear isostructural as they all crystallise in space group *I*4/*m* and in each case the cations are centred on crystallographic C_{4h} sites. This leads to the structures having a characteristic microporous packing, criss-crossed by tunnels in the *a* and *b* directions (Fig 2).

The tunnels house counter-ions and, in the halide compounds, acetone and methanol guest molecules too. Although, reminiscent of zeolites, whose cages contain cations and water molecules, the tunnels are not rigid and cannot therefore act as molecular sieves. However, the dppO$_2$-based structures achieve steric control by a different means. Once complexed, the dppO$_2$ conformation is locked, as indicated by the near constancy of the torsion angles in all four compounds, Table 1. Effectively, the phenyl rings that surround each manganese atom, act as a rigid calixarene type well.

The molecular shape is maintained by non-classical CH/π hydrogen bonds[4] between phenyl rings on adjacent dppO$_2$ ligands in the lantern cations. These type of bonds are also a feature of the crystal packing (Fig 2) and hence a reason for the four crystal structures being nearly identical.

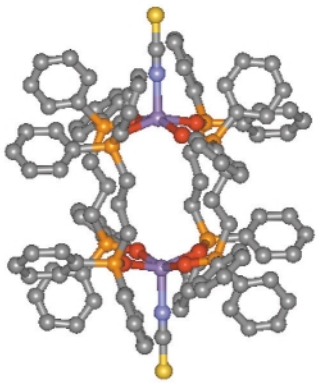

Fig. 1 The cation from [Mn$_2$(μ-dppO$_2$)$_4$(NCS)$_2$]$^{2+}$ 2(NCS)$^-$ **1**.

† Electronic supplementary information (ESI) available: full synthesis and crystal refinement details for **2**–**4**. See http://www.rsc.org/suppdata/cc/b1/b101263k/

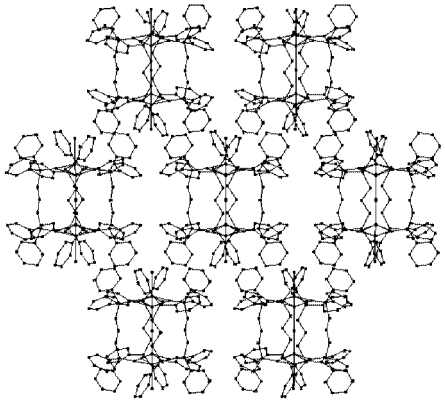

Fig. 2 Crystal packing of the lantern shaped cations, viewed down the crystallographic *b* axis.

Despite the above similarities, closer examination of the manganese and halide atoms lying along the central four-fold axis reveals striking differences between the structures. Importantly, halide anions are smaller than thiocyanate and can be accommodated within the lantern shaped central part of the complex (Cl 100%, Br 100%, I 44%). This difference has ramifications for the manganese atom, which can now occupy two types of sites *ca*. 0.5 on either side of the plane defined by the four coordinated oxygen atoms. This allows an Mn–X bond to form to the central halide atom or, alternatively, to the external capping halide (Table 1).

Table 1 Torsion angles ϕ(°) relative to P=O and Mn displacement from the oxygen plane[a]

				Mn displacement/Å	
Anio	ϕ_1	ϕ_2	ϕ_3	In	Out
NCS	−24.0	9.3	−62.9	—	0.47
C	−26.7	11.2	−68.1	−0.61	0.46
Br	−25.7	13.2	−71.7	−0.59	0.48
I	−23.9	12.6	−69.1	−0.44	0.59

[a] ϕ_1 and ϕ_2 = O=P–C–C$_{Ph}$, ϕ_3 = O=P–C–C$_{prop}$.

These features are manifested in the Cl$^-$ and Br$^-$ X-ray structures as two semi-populated manganese sites and a semi-populated external capping halide site. This leads to the straightforward interpretation that a racemic mixture of the C_4 symmetry molecule illustrated in Fig. 3 occupies each molecular site.

The structures are completed by halide counter-ions, each flanked by two methanol solvate molecules, and disordered acetone, occupying C_{4h} sites above the capping halide ligands. In the halide cases this lead to a total formulation of [Mn$_2$(μ-dppO$_2$)$_4$X$_2$]$^{2+}$2X$^-$·Me$_2$CO·4MeOH.

As the iodide central site is not fully occupied [44.3(1)%], presumably because of the bulk of I$^-$, it is tempting to assume that the molecular site contains a mixture of isothiocyanate and chloride type complexes. However a reasonable match for the crystallographically derived site occupancies cannot be ob-

 DOI: 10.1039/b101263k

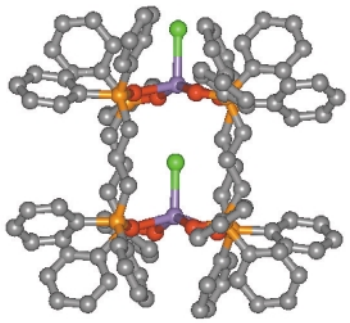

Fig. 3 The cation from $[Mn_2(\mu\text{-}dppO_2)_4Cl_2]^{2+}2Cl^-\cdot Me_2CO\cdot 4MeOH$ **2**, which is isostructural with the bromide analogue **3**.

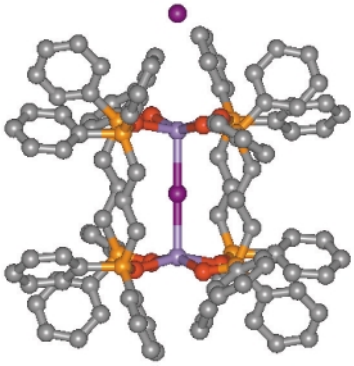

Fig. 4 The cation from $[Mn_2(\mu\text{-}dppO_2)_4I_2]^{2+}$ $2I^-\cdot Me_2CO\cdot 4MeOH$ **4**, showing the central centrosymmetric iodine atom.

tained using this model and 30% of a third molecular configuration must also be used (Fig. 4).

The manganese bonded to the externally capping iodide has flipped to the inner site, allowing the central iodide to bridge the two manganese atoms. This breaks the bond to the capping iodide, which is now held in position by dispersive forces within the calixarene well.

The ability of manganese to occupy the two types of sites is reminiscent of iron in haemoglobin, but the dynamic haemoglobin situation and static disorder cannot be distinguished crystallographically. Nevertheless, a guest molecule diffusing through the microporous tunnels in the iodide crystals would encounter an additional halide bridged Mn type of calixarene site, compared to only the non-bridged types in the bromide and chloride structures.

A series of combined thermogravimetric and X-ray powder diffraction experiments were therefore carried out in order to measure the effect of the above structural variations on SO_2 adsorption. A typical curve shows rapid and fully reversible SO_2 take-up, reminiscent of zeolites. The XRD patterns confirm that all the compounds retain their original crystal structure, although small expansions of the unit cells were observed on adsorption ($<3\%$ at maximum of 4 SO_2 molecules /lantern). Analysis of the isotherms using Hill's adaptation of Langmuir's theory provided a series of equilibrium constants, which were then used to determine the enthalpies of adsorption by means of the Van't Hoff equation. The enthalpy values obtained for the chloride, bromide, iodide and isothiocyanate lanterns were -34, -44, -54 and -39 kJ mol^{-1}, respectively.

As would be expected for compounds that adsorb SO_2 so readily, the energies straddle the physisorption/chemisorption boundary.[5] They are comparable in value to the -50 kJ mol^{-1} determined for $[K(18\text{-crown-}6)]^+[NCS\cdot SO_2]^-$ [5] and fall in the range -20 to -79 kJ mol^{-1} calculated for a series of iodosulfinates, $[I\cdot SO_2]^-$.[6] The order Cl < Br < I is the same as was found in square-planar $Ir(X)(CO)(PPh_3)_2$ complexes,[8,9] where the SO_2 binds loosely to the halide atom, suggesting that this type of interaction also influences the retention of SO_2 within the lantern crystals.

We thank the EPSRC for providing a studentship for W. I. C. and Dr Michael Ruf of Bruker AXS GmbH for collecting the iodide lantern data set.

Notes and references

‡ Synthesis of $[Mn_2(\mu\text{-}dppO_2)_4X_2]X_2\cdot Me_2CO\cdot 4MeOH$ **2**–**4**. MnX_2 (1 equiv.) and $dppO_2\cdot H_2O$ (2 equiv.) were stirred together in acetone–methanol (1 : 1) for **2** and **3** and diethyl ether for **4**. The resulting solid was filtered off under suction, washed with diethyl ether and dried *in vacuo*.

Crystals of **2** and **3** were grown by the vapor diffusion of diethyl ether onto an acetone–methanol (1 : 1) solution of the synthesized complex, and by liquid diffusion using the same solvents for **4**.

TGA measurements were carried out by means of a CAHN TG-131. Exhaust gases from this instrument were fed to an enclosed powder sample in a Scintag XDS2000 X-ray powder diffractometer for simultaneous TGA/XRD analysis.

§ *Crystal data*: for **2**: $C_{115}H_{126}O_{13}P_8Mn_2Cl_4$, tetragonal, space group *I*4/*m*, $a = b = 14.382(3)$, $c = 26.076(9)$ Å, $V = 5393(2)$ Å^3, $T = 223$ K, $\mu = 5.14$ cm^{-1}, $Z = 2$, 2441 unique ($R_{int} = 0.053$), $wR2 = 0.152$ for all reflections and $R1 = 0.070$ for 1321 reflections [$I > 2\sigma(I)$].

For **3**: $C_{115}H_{126}O_{13}P_8Mn_2Br_4$, tetragonal, space group *I*4/*m*, $a = b = 14.523(4)$, $c = 25.874(12)$ Å, $V = 5457(3)$ Å^3, $T = 223$ K. $\mu = 18.74$ cm^{-1}, $Z = 2$, 2750 unique, $wR2 = 0.158$ for all reflections and $R1 = 0.073$ for 1500 reflections [$I > 2\sigma(I)$].

For **4**: $C_{115}H_{126}O_{13}P_8Mn_2I_4$, tetragonal, space group *I*4/*m*, $a = b = 14.984(4)$, $c = 25.761(12)$ Å, $V = 5784(3)$ Å^3, $T = 223$ K, $\mu = 14.55$ cm^{-1}, $Z = 2$, 4499 unique ($R_{int} = 0.079$), $wR2 = 0.100$ for all reflections and $R1 = 0.041$ for 2103 reflections [$I > 2\sigma(I)$].

CCDC reference numbers 153090-153092. See http://www.rsc.org/suppdata/cc/b1/b101263k/ for crystallographic data in CIF or other electronic format.

1 B. Beagley, G. Dyer, C. A. McAuliffe, P. P. Macrory and R. G. Pritchard, *J. Chem. Soc., Chem. Commun.*, 1991, 965.
2 G. A. Gott, J. Fawcett, C. A. McAuliffe and D. R. Russell, *J. Chem. Soc., Chem. Commun.*, 1984, 1283.
3 K. Al-Farhan, B. Beagley, O. El-Sayrafi, G. A. Gott, C. A. McAuliffe, P. P. MacRory and R. G. Pritchard, *J. Chem. Soc., Dalton Trans.*, 1990, 1243.
4 H. Takahashi, S. Tsuboyama, Y. Umezawa, K. Honda and M. Nishio, *Tetrahedron*, 2000, **56**, 6185.
5 I. Levine, *Physical Chemistry*, McGraw Hill Inc, New York, 4th edn.
6 A. J. Downs, A. J. Edwards, R. E. Martin and S. Parsons, *J. Chem. Soc., Dalton Trans.*, 1994, 753.
7 P. G. Eller and G. J. Kubas, *Inorg. Chem.*, 1978, **17**, 894.
8 M. R. Snow and J. A. Ibers, *Inorg. Chem.*, 1973, **12**, 224.
9 E. C. Moroni, R. A. Friedel and I. Wender, *J. Organomet. Chem.*, 1970, **21**, P23.

CHEMCOMM Communication
www.rsc.org/chemcomm

A space group assignment of ZrP_2O_7 obtained by ^{31}P solid state NMR

Ian J. King,[ab] Franck Fayon,[b] Dominique Massiot,[b] Robin K. Harris[a] and John S. O. Evans*[a]

[a] *Department of Chemistry, University of Durham, Durham, UK DH1 3LE. E-mail: john.evans@durham.ac.uk*
[b] *CNRS-CRMHT, Recherche Scientifique, 1D Av 45071, Orléans Cedex 2, France. E-mail: fayon@cnrs-orleans.fr*

Received (in Cambridge, UK) 18th July 2001, Accepted 25th July 2001
First published as an Advance Article on the web 15th August 2001

2-D ^{31}P dipolar recoupling magic angle spinning NMR has been used to determine the true symmetry of the low temperature structure of ZrP_2O_7 for the first time.

ZrP_2O_7 is often considered to be the parent of the AM_2O_7 family of compounds (A = Sn, Ti, Zr *etc.*; M = P, V, As), which are of interest as several members of the family show low or even negative coefficients of thermal expansion.[1–3] A detailed knowledge of the structure of these materials is of vital importance in understanding this unusual property. The approximate structure of ZrP_2O_7 was reported as being cubic with an ~8.25 Å cell edge as long ago as 1935 by Levi and Peyronel.[4] It can be described as a network of corner-sharing ZrO_6 octahedra and PO_4 tetrahedra, the PO_4 tetrahedra themselves sharing corners to form $P_2O_7^{4-}$ pyrophosphate groups (Fig. 1). It has long been realised, however, that there are problems associated with this simple structure in that the space group symmetry requires linear P–O–P bonds, whereas the energetically preferred bond angle for these linkages is in the region 130–160°. The bending of these linear bonds (and the concomitant lowering of symmetry) is believed to be the driving force behind the phase transition to a low temperature $3 \times 3 \times 3$ superstructure which has been observed for ZrP_2O_7 (and other members of the AM_2O_7 family) by a variety of experimental techniques.[5–9]

The exact nature of these low temperature superstructures is a matter of some debate. Good quality single crystals of these materials can be hard to obtain, and the structural complexity makes detailed interpretation of powder diffraction data difficult. Symmetry considerations show that a $3 \times 3 \times 3$ material can adopt one of 12 possible space groups, containing between 11 ($Pa\bar{3}$) and 216 ($P1$) different unique P sites.[3] Several members of this family have been shown to adopt space group $Pa\bar{3}$; others are known to have lower symmetry.[10,11] In the case of ZrP_2O_7 there has been one previous NMR study, which interpreted the 12 resonances observed in terms of the 11 ^{31}P sites expected for space group $Pa\bar{3}$ and a peak due to an unspecified impurity phase.[3] However, the observation of the same impurity peak by several groups has cast some doubt on this interpretation.[12] Electron diffraction studies[13] have shown extinction conditions consistent with the presence of an *a*-glide, suggesting that the space group is either cubic $Pa\bar{3}$ or orthorhombic *Pbca*. In the former possibility the 11 crystallographically independent P sites give rise to 6 independent $P_2O_7^{4-}$ groups, 4 in general positions, 1 on a 3-fold axis and 1 on an inversion centre (such that the P atoms of the P–O–P linkage are crystallographically equivalent and the bond angle is required to be 180°). For *Pbca* one would expect 27 P sites giving rise to 13 $P_2O_7^{4-}$ groups in general positions and one on a centre of inversion. In the case of SiP_2O_7[14] and TiP_2O_7,[15] two-dimensional (2-D) homonuclear correlation NMR techniques have been shown to be very useful in assigning the space group of these $3 \times 3 \times 3$ superstructures, since they allow the phosphorus connectivity scheme to be probed[16] and give evidence of the presence of different phases in a sample.[17] In this work, we have used various 2-D ^{31}P dipolar recoupling MAS NMR experiments to characterize the ZrP_2O_7 structure.

^{31}P NMR experiments on ZrP_2O_7† were carried out on a Bruker DSX 300 spectrometer operating at a Larmor frequency of 121.48 MHz, using a standard 4 mm Bruker MAS probe. One dimensional (1-D) single-pulse MAS NMR spectra were recorded at spinning speeds of 3, 5, and 10 kHz using a small pulse angle ($\pi/8$) and recycle delay of 80 s to prevent saturation. ^{31}P 2-D MAS exchange NMR experiments were obtained at 10 kHz spinning rate using the RFDR sequence[18] during the mixing time. ^{31}P 2-D MAS double quantum spectra were recorded at a 10 kHz spinning rate using the POSTC7 sequence[19] for excitation and reconversion of double quantum coherences under MAS. The hypercomplex acquisition method[20] was used to obtain pure absorption phase 2-D spectra and the t_1 time increment was synchronised with the rotor period to avoid sidebands in the ω_1 dimension. 160 t_1 increments with 8 and 16 transients per increment were recorded for the MAS exchange NMR spectra and for the MAS double quantum experiment, respectively. The ^{31}P chemical shifts were referenced relative to a 85% H_3PO_4 solution at 0 ppm.

The ^{31}P 1-D MAS NMR spectra of ZrP_2O_7 obtained at different spinning rates are shown in Fig. 2 (centreband region only). These spectra can be seen to contain at least 13 partially overlapping ^{31}P isotropic resonances, corresponding to at least 13 different phosphorus sites. Assuming that these resonances belong to the same phase this is not consistent with space group $Pa\bar{3}$. It can be noted that the positions and linewidths of these resonances vary to different extents with the spinning fre-

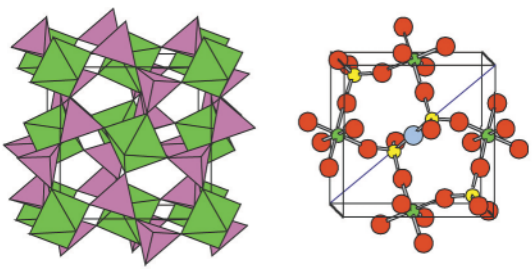

Fig. 1 The ideal cubic structure of ZrP_2O_7 containing ZrO_6 octahedra and PO_4 tetrahedra. A linear P_2O_7 group is emphasised on the right.

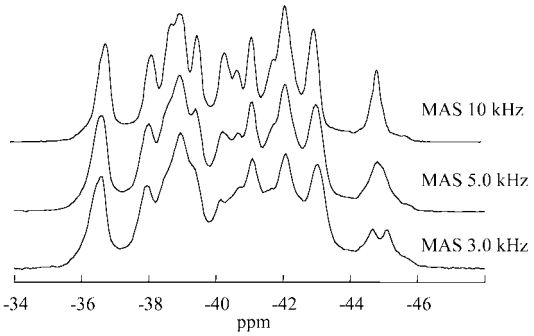

Fig. 2 ^{31}P 1-D MAS NMR spectra of ZrP_2O_7.

 DOI: 10.1039/b106379k

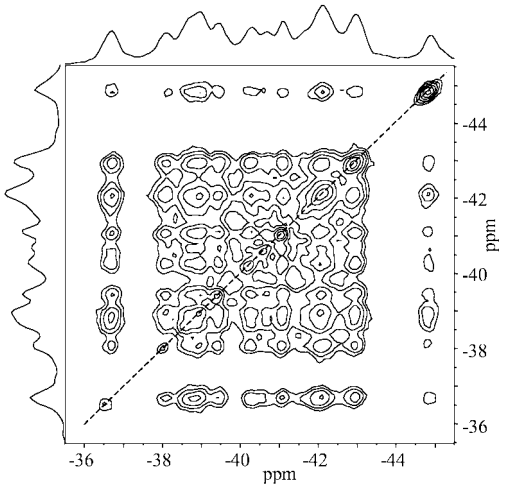

Fig. 3 ^{31}P 2-D exchange MAS spectrum of ZrP_2O_7 obtained with a mixing time of 40 ms at 10 kHz spinning rate, showing that all peaks belong to the same phase.

quency. These effects have also been reported for SiP_2O_7 and TiP_2O_7[15] and may be attributed to the presence of residual dipolar interactions under MAS conditions.

To investigate the possible presence of different phases in our ZrP_2O_7 sample, we have used 2D exchange MAS NMR spectroscopy. In this experiment, the polarisation transfer in the mixing time is driven by the dipolar interaction, allowing one to probe large intra-$P_2O_7^{4-}$ ^{31}P–^{31}P dipolar couplings at short mixing times and weaker long range dipolar couplings at long mixing times. As shown in Fig. 3, the 2-D exchange MAS spectrum of ZrP_2O_7 obtained with a mixing time of 40 ms shows cross-correlation peaks of various intensities between all the individual resonances displayed in the 1-D MAS spectrum reflecting their short and long range spatial proximities. This clearly indicates that our sample contains a single phase with at least 13 different crystallographic sites, ruling out the possibility of the $Pa\bar{3}$ space group to which the ZrP_2O_7 superstructure has previously been assigned.

As well as the number of individual ^{31}P sites, the number of $P_2O_7^{4-}$ groups in the ZrP_2O_7 structure can be used for space group assignement. To characterize the number of $P_2O_7^{4-}$ groups in the $3 \times 3 \times 3$ superstructure, we have used the 2-D MAS double quantum experiment. As shown for other crystalline phosphates,[14,15] short double quantum excitation and reconversion periods of 600 μs allow us to differentiate dipolar coupling between chemically linked PO_4 tetrahedra (~ 750 Hz) and weaker long range dipolar interactions (~ 300 Hz) and thus to identify clearly the P–O–P connectivity scheme. As shown in

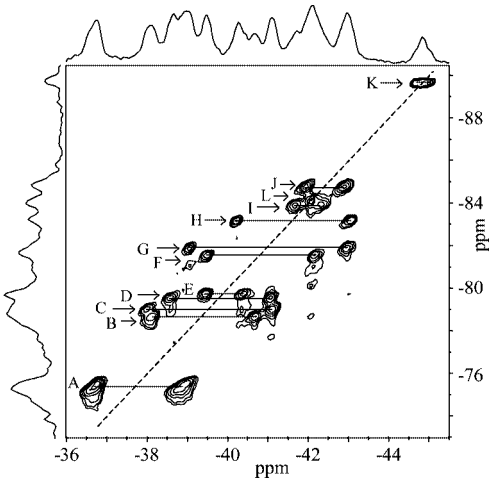

Fig. 4 ^{31}P 2-D MAS double quantum spectrum of ZrP_2O_7 at 10 kHz spinning rate. Cross-correlation peaks are labelled A–K; L is the single auto-correlation peak.

Fig. 4, the 2-D MAS double quantum spectrum of ZrP_2O_7 exhibits one intense auto-correlation peak along the diagonal (L) and 11 pairs of intense resolved cross-correlation peaks (A–K) that reflect the dipolar connectivities between chemically bound PO_4 tetrahedra. The weaker correlation peaks (two lowest contour levels in Fig. 4) correspond to weaker longer range dipolar couplings in the structure. The diagonal auto-correlation peak (L) arises from a single $P_2O_7^{4-}$ group containing two crystallographically equivalent P sites; the remaining 11 paired cross-correlation correspond to $P_2O_7^{4-}$ dimers in which the two P sites are inequivalent. Analysis of the peak intensities in Fig. 4 shows that the paired cross-peaks A are about three times higher than the remaining resonances, suggesting the presence of three overlapping cross-correlation peaks corresponding to three $P_2O_7^{4-}$ groups. Good fits (not shown) of the 2-D double quantum and 1-D MAS spectra were thus obtained with 27 distinct ^{31}P resonances of equal intensity corresponding to 13 $P_2O_7^{4-}$ units (A–K) with two inequivalent P sites, and one $P_2O_7^{4-}$ group (L) with two equivalent P sites. This is entirely consistent with space group *Pbca*.

We therefore conclude that the previously assigned space group of $Pa\bar{3}$ for the ZrP_2O_7 superstructure is incorrect. From the analysis of ^{31}P double quantum MAS NMR spectra, we suggest that the true symmetry of ZrP_2O_7 is *Pbca*. Using this space group excellent agreement with powder X-ray and neutron diffraction data can be obtained.

We gratefully acknowledge support of the EPSRC and CNRS for this work. I. J. K. would like to thank the EU for a Marie-Curie fellowship (HPMT-CT-2000-00169).

Notes and references

† High purity ZrP_2O_7 was prepared from $ZrOCl_2$ and H_3PO_4 (85%) which were mixed in a 1:2 molar ratio in a platinum crucible and heating to 350 °C for 1 h. The resultant powder was washed with distilled water, and heated to 750 °C then 1000 °C for 12 h periods. Powder X-ray and neutron diffraction measurements confirmed sample purity and the presence of $3 \times 3 \times 3$ superstructure reflections.

1 A. W. Sleight, *Annu. Rev. Mater. Sci*., 1998, **28**, 29.
2 J. S. O. Evans, *J. Chem. Soc., Dalton Trans*., 1999, 3317.
3 V. Korthuis, N. Khosrovani, A. W. Sleight, N. Roberts, R. Dupree and W. W. Warren, *Chem. Mater*., 1995, **7**, 412.
4 G. R. Levi and G. Peyronel, *Z. Kristallogr*., 1935, **92**, 190.
5 E. Tillmanns, W. Gebert and W. H. Baur, *J. Solid State Chem*., 1974, **7**, 69.
6 H. Vollenke, A. Wittmann and H. Novotny, *Monatsh. Chem*., 1963, **94**, 956.
7 R. L. Withers, J. S. O. Evans, J. Hanson and A. W. Sleight, *J. Solid State Chem*., 1998, **137**, 161.
8 J. S. O. Evans, J. C. Hanson and A. W. Sleight, *Acta. Crystallogr., Sect. B*, 1998, **54**, 705.
9 S. T. Norberg, G. Svensson and J. Albertsson, *Acta Crystallogr., Sect. C*, 2001, **57**, 225.
10 E. R. Losilla, A. Cabeza, S. Bruque, M. A. G. Aranda, J. Sanz, J. E. Iglesias and J. A. Alonso, *J. Solid State Chem*., 2001, **156**, 213.
11 J. Sanz, J. E. Iglesias, J. Soria, E. R. Losilla, M. A. G. Aranda and S. Bruque, *Chem. Mater*., 1997, **9**, 996.
12 A. M. K. Andersen and P. Norby, *Acta Crystallogr., Sect. B*, 2000, **56**, 618.
13 R. L. Withers, Y. Tabira, J. S. O. Evans, I. J. King and A. W. Sleight, *J. Solid State Chem*., 2001, **157**, 186.
14 R. J. Iuliucci and B. H. Meier, *J. Am. Chem. Soc*., 1998, **120**, 9059.
15 X. Helluy, C. Marichal and A. Sebald, *J. Phys. Chem. B*, 2000, **104**, 2836.
16 M. Feike, R. Graf, I. Schnell, C. Jager and H. W. Spiess, *J. Am. Chem. Soc*., 1996, **118**, 9631.
17 P. Hartmann, C. Jana, J. Vogel and C. Jager, *Chem. Phys. Lett*., 1996, **258**, 107.
18 A. E. Bennett, J. H. Ok, R. G. Griffin and S. Vega, *J. Chem. Phys*., 1992, **96**, 8624.
19 M. Hohwy, H. J. Jakobsen, M. Eden, M. H. Levitt and N. C. Nielsen, *J. Chem. Phys*., 1998, **108**, 2686.
20 D. J. States, R. A. Haberkorn and D. J. Ruben, *J. Magn. Reson*., 1982, **48**, 286.

CHEMCOMM Communication
www.rsc.org/chemcomm

First observation of clusters for solvated tropylium ions

Tomomi Kinoshita,*[a] Akihiro Wakisaka,[b] Chikafumi Yasumoto,[a] Ken'ichi Takeuchi,[a] Kazunari Yoshizawa,[c]† Akiya Suzuki[c] and Tokio Yamabe[c]

[a] *Department of Energy and Hydrocarbon Chemistry, Graduated School of Engineering, Kyoto University, Sakyo-ku, Kyoto 606-8501, Japan. E-mail: knst@scl.kyoto-u.ac.jp; Fax: +81-75-753-3350; Tel: +81-75-753-5710*

[b] *National Institute of Advanced Industrial Science and Technology, Onogawa 16-1, Tsukuba 305-8569, Japan. E-mail: akihiro-wakisaka@aist.go.jp; Fax: +81-298-61-8252; Tel: +81-298-61-8271*

[c] *Department of Molecular Engineering, Graduated School of Engineering, Kyoto University, Sakyo-ku, Kyoto 606-8501, Japan*

Received (in Cambridge, UK) 18th May 2001, Accepted 28th July 2001
First published as an Advance Article on the web 28th August 2001

We have first observed clusters for solvated tropylium ions ($Tr^+(ROH)_n$) which were isolated from ROH–CH_3CN (1:1 by vol.; R = Me, Et, and Pr^n) solutions by using a specially designed mass spectrometer and found the clear-cut essential features concerning the solvation structure around Tr^+.

The solvation structure around a carbocation has not thoroughly been clarified in spite of so many investigations from various aspects for a long time[1] owing to few practically available methods for direct observation.[2] Earlier than a decade ago, a specially designed mass spectrometer was devised[3] and utilized to examine the composition of clusters which were isolated from a liquid phase[3,4] and an electrospray source[3a] was introduced to the special mass spectrometer to result in direct observation of species of clusters with a positive charge.[5] Our instruments have the advantage of a splendid isolation of clusters and a hermetic way of working. Then, by using the mass spectrometer and tropylium ion as a stable carbocation, we have examined the compositions of clusters for solvated tropylium ions ($Tr^+(ROH)_n$) to find clear-cut essential features for the solvated carbocation clusters.

The Tr^+–solvent clusters were obtained from a solution containing tropylium ions, by electrospray interface. Since the experimental details on the mass spectrometric analysis of clusters including an ion isolated from solutions containing ionic species has already been reported elsewhere,[5] it is briefly explained here. A sample solution containing ionic species is injected into a five-stage differentially pumped vacuum chamber through the electrospray interface, which leads to the formation of multi-charged liquid droplet flow. The resulting multi-charged liguid droplets fly from the first room to the fifth room through the pressure difference and the electric field in the vacuum chamber. During the flight, the multi-charged liquid droplets are fragmented into the clusters and molecules through the expansion due to the decrease of pressure and the electric repulsion among the ions providing the multi-charge. After the fragmentation of the multi-charged liquid droplets, the strongly interacting cation(s)-molecules were isolated as clusters. However, weakly interacting molecules were vapourized as monomeric molecules. Herein, the clusters with positive charge, by Tr^+, were analyzed by the quadrupole mass spectrometer.

The positively charged clusters were analyzed for a solution of tropylium tetrafluoroborate ($Tr^+BF_4^-$; 4.5×10^{-3} M) in ethanol–acetonitrile (1:1 by vol.). Signals corresponded to clusters containing Tr^+, *e.g.* $Tr^+(EtOH)_2$ to $Tr^+(EtOH)_{17}$, though only up to eight solvent molecules were shown in Fig. 1. No complexes of Tr^+ with CH_3CN were detected. The signal intensity generally decreased with an increase in the number of EtOH molecules which formed clusters with Tr^+, with an exception of those from $Tr^+(EtOH)_4$ to $Tr^+(EtOH)_6$ (Fig. 1). The signals from $Tr^+(EtOH)_4$ to $Tr^+(EtOH)_6$ were somewhat larger than their neighbouring ones. Four to six are 'magic number clusters'.[6] An analogous tendency was observed for $Tr^+(MeOH)_n$, from a solution of Tr^+ ions in MeOH–CH_3CN, and $Tr^+(Pr^nOH)_n$, from a solution of Tr^+ ions in Pr^{n}OH–CH_3CN. The same feature in cluster compositions could be observed for neutral clusters which were isolated from EtOH–CH_3CN (1:1 by vol.) solutions.[7] Theoretical calculation by b$_3$lyp/6-31G** indicated that the binding constant between Tr^+ and five MeOH molecules was larger compared to that for the less or more MeOH molecules.[8]

The relative signal intensities for a solution of Tr^+ in MeOH–EtOH–CH_3CN (1:1:2, by vol.) indicated that the cluster forming ability for Tr^+ was apparently MeOH:EtOH = 1.0:5.2.[9] Similarly, the solution of Tr^+ in EtOH–Pr^{n}OH–CH_3CN was analyzed to show that the cluster forming ability for Tr^+ is EtOH:Pr^{n}OH = 1.0:14.[9] Consequently, the ability for Tr^+ should be MeOH:EtOH:Pr*n*OH = 1.0:5.2:70. The longer the alkyl chain of alcohol molecules, the stronger the cluster forming ability, *i.e.* the solvation ability for Tr^+. Such a tendency might be related to the clustering of the alcohols in acetonitrile, that is, the clustering of alcohols was promoted with an increase in the size of the alkyl group. The binding energy for Tr^+ with an alcohol molecule from theoretical calculations (by b$_3$lyp/6-31G**)[10] was consistent with the observed sequence of cluster forming ability mentioned above. Also, the calculations are in line with the work of Meot-Ner (Mautner) for other ions.[11] The binding energy has a linear relationship with donor numbers[12] for EtOH, MeOH, and CH_3CN suggesting that the Lewis basicity of the alcohol molecule might play a significant role for the carbocation.

In conclusion, we have first observed the solvated cluster compositions for Tr^+ and found that the cluster forming ability (solvation ability) increased with increasing alkyl chain length

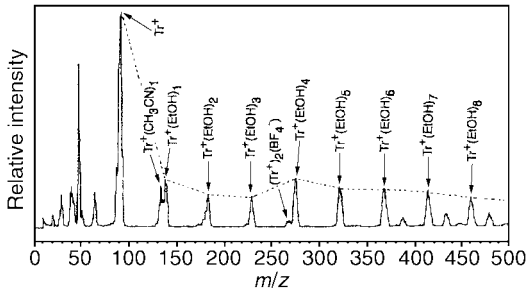

Fig. 1

† *Present address*: Institute for Fundamental Research of Organic Chemistry, Kyushu University, Higashi-ku, Fukuoka, Japan. E-mail: kazunari@ms.ifoc.kyushu-u.ac.jp; Fax: +81-92-642-2735; Tel: +81-92-642-2720.

 DOI: 10.1039/b104384f

of alcohols. Further elaboration and application of the present methodology are now in progress.

Notes and references

1 (*a*) C. Reichardt, *Solvents and Solvent Effects in Organic Chemistry*, 2nd edn, VCH Publishers, Weinheim, 1988; (*b*) N. S. Isaacs, *Physical Organic Chemistry*, chap. 5, Longman Scientific & Technical, New York, 1987.

2 For studies by high pressure mass spectrometry, see, *e.g.* P. Kebarle, in *Techniques for the Study of Ion-Molecule Reactions*, ed. J. M. Farrar and W. H. Saunders, John Wiley, New York, 1988, p. 221.

3 (*a*) M. Yamashita and J. B. Fenn, *J. Phys. Chem.*, 1984, **88**, 4451, and references cited therein; (*b*) N. Nishi and K. Yamamoto, *J. Am. Chem. Soc.*, 1987, **109**, 7353.

4 (*a*) Y. Akiyama, A. Wakisaka, F. Mizukami and K. Sakaguchi, *J. Chem. Soc., Perkin Trans. 2*, 1998, 95; (*b*) A. Wakisaka, H. Abdoul-Carime, Y. Yamamoto and Y. Kiyozumi, *J. Chem. Soc., Faraday Trans.*, 1998, **94**, 369, and references cited therein.

5 A. Wakisaka and H. Kobara, *J. Mol. Liq.*, 2000, **88**, 121.

6 *E.g.* T. M. Barlak, J. R. Wyatt, R. J. Colton, J. J. DeCorpo and J. E. Campana, *J. Am. Chem. Soc.*, 1982, **104**, 1212.

7 Another specially designed mass spectrometer for analysis of neutral clusters (see ref. 4) was used.

8 The theoretical study of the mechanism: A. Suzuki, T. Kinoshita, K. Takeuchi, A. Wakisaka and K. Yoshizawa, *J. Mol. Struct. (Theochem)*, in the press.

9 The ratios of relative signal intensities were estimated from the ones of summations of height of all detected signals corresponding to the respective alcohol molecule.

10 Binding energy calculated by $b_3$lyp/6-31G** is 9.652, 17.067, 17.331, and 17.541 kcal mol^{-1} for Tr^+–CH_3CN, Tr^+–MeOH, Tr^+–EtOH, and Tr^+–Pr^nOH, respectively.

11 (*a*) M. Meot-Ner (Mautner), *Acc. Chem. Res.*, 1984, **17**, 186; (*b*) M. Meot-Ner (Mautner), *J. Phys. Chem.*, 1987, **91**, 417; (*c*) J. M. Mestdagh, A. Binet and O. Sublemontier, *J. Phys. Chem.*, 1989, **93**, 8300.

12 (*a*) V. Gutmann, *Electrochim. Acta*, 1976, **21**, 661; (*b*) V. Gutmann and M. J. Kamlet, *Monatsch.*, 1969, **100**, 2048.

CHEMCOMM Communication
www.rsc.org/chemcomm

Enhanced activity and stability of a Cu/SiO_2 catalyst for the reverse water gas shift reaction by an iron promoter

Ching-Shiun Chen, Wu-Hsun Cheng* and Shou-Shiun Lin

Department of Chemical and Materials Engineering, Chang Gung University, Tao-Yuan 333, Taiwan, Republic of China. E-mail: cheng@mail.cgu.edu.tw

Received (in Cambridge, UK) 15th May 2001, Accepted 30th July 2001
First published as an Advance Article on the web 28th August 2001

An Fe promoter inhibits the sintering of Cu particles and oxidation of the Cu surface, resulting in high catalyst activity and stability.

Carbon dioxide has been attributed to be the main source of the greenhouse effect. The increase of carbon dioxide concentration will strongly influence the global weather. Conversion of CO_2 to CO by catalytic hydrogenation has been recognized as one of the most promising processes for CO_2 utilization. Synthesis gas, H_2 and CO, can be used to produce long-chain hydrocarbons *via* the Fischer–Tropsch reaction.[1,2] The reverse water gas shift (RWGS) reaction is one of the available methods for the production of CO.

Generally, copper catalysts are used for both the water gas shift reaction and the reverse water gas shift reaction.[3–10] There have been many papers reporting the enhanced activity by promoters and the reaction mechanism;[3–7] however, the stability of copper catalysts is little mentioned. The RWGS reaction is an endothermic reaction; therefore, high temperature will facilitate the formation of CO. Nevertheless, copper-based catalysts are not suitable for operation at high temperature because they are significantly deactivated by sintering. In this study, iron is used as a promoter for copper catalysts in order to improve the stability of the catalysts at high temperature.

The 10 wt% Cu/SiO_2 and 0.3 wt% Fe/SiO_2 samples were prepared by impregnating Cab-O-Sil M-5 SiO_2 with an aqueous solution of $Cu(NO_3)_2$ and $Fe(NO_3)_3$, respectively. The $Cu–Fe/SiO_2$ (Cu:Fe = 10:0.3) was prepared by the addition of an aqueous solution of $Fe(NO_3)_3$ to dried Cu/SiO_2 before calcination and/or reduction. These catalysts were calcined in air and reduced in pure H_2 at 873 K for 5 h before reaction. Carbon dioxide hydrogenation was carried out over a fixed bed reactor at atmospheric pressure. 0.1 g samples of catalysts were used for the RWGS reaction by feeding a stream of H_2/CO_2 at 100 ml min^{-1} in a 1:1 feed ratio. Temperature programmed reduction (TPR) of catalysts was performed at atmospheric pressure in a conventional flow system. Samples of 0.06 g of the catalysts were placed in a U-shaped tube reactor and heated in a 5% H_2/N_2 mixed gas stream flowing at 30 ml min^{-1} at a heating rate of 10 °C min^{-1} from 25 to 973 K. The area of the copper surfaces was determined by using TPR of Cu oxidized by N_2O.[11]

The dependence of CO_2 conversion on time on stream for comparison of the RWGS reaction over Cu/SiO_2, $Cu–Fe/SiO_2$ and Fe/SiO_2 are shown in Fig. 1. It was found that the reaction conversion using Cu/SiO_2 was drastically decreased within 120 h: the catalytic activity decreased from 8.5 to 0.3%. The 0.3% Fe/SiO_2 catalyst offered low catalytic activity: its conversion decreased from 2.5 to 0.4% within 120 h. However, when the same experiment was run over the $Cu–Fe/SiO_2$ (Cu:Fe = 10:0.3) catalyst, it was found that CO_2 conversion was significantly increased and initial conversion increased from 8.5 to 15%. On the other hand, the deactivation of $Cu–Fe/SiO_2$ decreased only from 15 to 12% within 120 h. After 40 h, the catalytic activity fluctuated at about 12%. This shows that the Cu-based catalyst could be kept in a stable state by the Fe promoter.

Fig. 2 shows the comparison of surface area of Cu/SiO_2 and $Cu–Fe/SiO_2$ catalysts before and after the reaction. The fresh

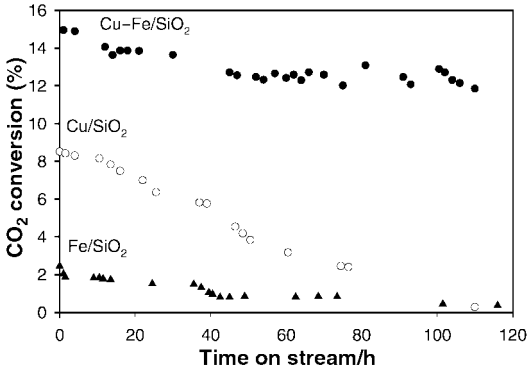

Fig. 1 The dependence of CO_2 conversion on time for H_2/CO_2 with 1:1 ratio over Cu/SiO_2, $Cu–Fe/SiO_2$ and Fe/SiO_2 catalysts at 873 K.

Cu/SiO_2 and $Cu–Fe/SiO_2$ catalysts were pretreated by calcination and reduction at 873 K for 5 h. Obviously, the copper surface area in $Cu–Fe/SiO_2$ was twice as large as that in Cu/SiO_2 [Fig. 2(a) and (b)]. When both catalysts were exposed to the H_2/CO_2 feed at 873 K for 120 h, the copper surface area in Cu/SiO_2 was significantly decreased, but $Cu–Fe/SiO_2$ retained a copper surface area as high as that of a fresh catalyst.

TPR was used to characterize the Cu/SiO_2 and $Cu–Fe/SiO_2$ after H_2/CO_2 reaction at 873 K for 120 h (see Fig. 3). The TPR profile of the Cu/SiO_2 catalyst shows a typical Cu_2O reduction peak at 503 K. A similar result was found in our previous paper, showing that copper can be oxidized in the process of the RWGS reaction.[7] Two peaks are observed in the $Cu–Fe/SiO_2$ catalysts at 723 and 853 K, respectively. The TPR profile of the Fe/SiO_2 catalyst through H_2/CO_2 reaction at 873 K for 120 h was performed to confirm the assignment of iron reduction peaks in the Cu–Fe catalyst. Two peaks are also observed at 723 and 853 K. Comparing these features with earlier literature reports,[1,12] the first peak could be due to reduction of Fe_2O_3 to Fe_3O_4. The second peak is due to reduction of Fe_3O_4 to FeO. Surprisingly, no reduction peak of copper is found in the TPR profile of $Cu–Fe/SiO_2$. The reduced copper particles in $Cu–Fe/SiO_2$ catalyst cannot be oxidized during the reaction process.

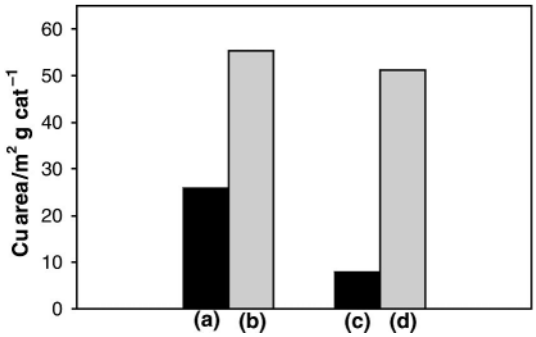

Fig. 2 The copper surface area in Cu/SiO_2 and $Cu–Fe/SiO_2$: (a) fresh Cu/SiO_2, (b) fresh $Cu–Fe/SiO_2$, (c) Cu/SiO_2 after exposure to H_2/CO_2 feed at 873 K for 120 h, (d) $Cu–Fe/SiO_2$ after exposure to H_2/CO_2 feed at 873 K for 120 h.

 DOI: 10.1039/b104279n

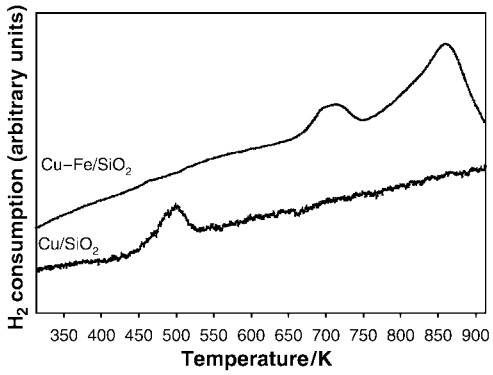

Fig. 3 TPR profiles of Cu/SiO_2 and $Cu–Fe/SiO_2$ catalysts after exposure to H_2/CO_2 feed at 873 K for 120 h.

Two models, redox and formate decomposition mechanisms, were proposed to explain the mechanism of CO formation in the RWGS reaction.[3–7] Cu^0 may be attributed to be the major active site for the RWGS reaction. The higher activity of $Cu–Fe/SiO_2$ compared with Cu/SiO_2 can be explained by the difference in copper surface area values between these two catalysts. When the pretreatment of Cu/SiO_2 was conducted at 773 K for 5 h, the copper surface area was 55 m^2 g cat^{-1}. When the temperature of calcination and reduction increased to 873 K, the surface area of copper decreased markedly due to sintering. By adding 0.3% iron onto the copper catalyst, the sintering of the copper catalyst was successfully inhibited under these high temperature conditions.

A decrease of the copper surface area together with the oxidation of copper caused the decay in catalytic activity for Cu/SiO_2. Iron additives obviously suppressed the decrease of copper surface area and catalyst deactivation. The small surface energy of copper would easily lead to migration of copper under high temperatures. The TPR study showed that iron was oxidized under the reaction conditions. Fe oxides may act as textural promoters which effectively suppress the sintering of Cu.

Instead of the oxidation of copper, an Fe species in the Cu–Fe catalyst was oxidized by the H_2/CO_2 stream. The TPR profile of an Fe_2O_3/zeolite catalyst has been reported: three reduction steps appeared at 695, 850 and 1000 K, respectively, when the catalyst was calcined at 773 K.[12] The lower temperature peak at 695 K corresponds to the reduction of Fe_2O_3 to Fe_3O_4; the middle temperature peak at 850 K is due to the reduction of Fe_3O_4 to FeO; and the higher temperature peak at 1000 K is for the reduction of FeO to Fe^0. FeO can reasonably be deduced to be the major species in the Cu–Fe catalyst after the reduction treatment at 873 K for 5 h in this study. The TPR profile of our $Cu–Fe/SiO_2$ catalyst in Fig. 3 provides strong evidence that FeO can be oxidized to Fe_3O_4 and/or Fe_2O_3 during the reaction.

In summary, we have shown that Fe-promoted Cu/SiO_2 exhibits high activity and stability for the RWGS reaction. The Cu surface area was significantly improved at high temperature by Fe additives. The Fe promoter inhibits the sintering of Cu particles and oxidation of Cu, resulting in high catalytic activity and stability.

We thank the Chinese Petroleum Corporation for financial support of this study.

Notes and references

1 T. Riedel, M. Claeys, H. Schulz, G. Schaub, S. S. Nam, K. W. Jun, M. J. Choi, G. Kishan and K. W. Lee, *Appl. Catal. A*, 1999, **186**, 201.
2 L. D. Mansker, Y. Jin, D. B. Bukur and A. K. Datye, *Appl. Catal. A*, 1999, **186**, 277.
3 K. H. Ernst, C. T. Campbell and G. Moretti, *J. Catal*., 1992, **134**, 66.
4 S. I Fujita, M. Usui and N. Takezawa, *J. Catal*., 1992, **134**, 220.
5 M. J. L. Ginés, A. J. Marchi and C. R. Apesteguía, *Appl. Catal. A*, 1997, **154**, 155.
6 D. B. Clarke and A. T. Bell, *J. Catal*., 1995, **154**, 314.
7 C. S. Chen, W. H. Cheng and S. S. Lin, *Catal. Lett*., 2000, **68**, 45.
8 M. S. Spencer, *Catal. Lett*., 1995, **32**, 9.
9 J. Nakamura, J. M. Campbell and C. T. Campbell, *J. Chem. Soc., Faraday Trans*., 1990, **86**, 2725.
10 E. Iglesia and M. Boudart, *J. Catal*., 1983, **81**, 214.
11 C. J. G. Van Der Grift, A. F. H. Wielers, B. P. J. Joghi, J. V. Beijnum, M. E. Boer, M. V. Helder and J. W. Geus, *J. Catal*., 1991, **131**, 178.
12 S. S. Nam, H. Kim, G. Kishan, M. J. Choi and K. W. Lee, *Appl. Catal. A*, 1999, **179**, 155.

CHEMCOMM
Communication
www.rsc.org/chemcomm

Penetration of pyrene and its derivatives into polystyrene latex particles as studied by fluorescence spectroscopy

Yong-Kuan Gong and Kenichi Nakashima*

Department of Chemistry, Faculty of Science and Engineering, Saga University, 1 Honjo-machi, Saga 840-8502, Japan. E-mail: nakashik@cc.saga-u.ac.jp; Fax: +81-952-28-8548; Tel: +81-952-28-8850

Received (in Cambridge, UK) 5th July 2001, Accepted 31st July 2001
First published as an Advance Article on the web 20th August 2001

Small hydrophobic pores (channels) in polystyrene latex particles were found by investigating the penetration of pyrene using fluorescence techniques.

Polystyrene latex (PSL) particles are solid nano- or microspheres with functional groups attached on the surfaces.[1] Latexes have many applications in coatings,[2] biomedical diagnostics[3] and drug delivery.[4] They are used also as model systems in colloid research because of their well-defined physicochemical characteristics.[5] Recently we used latex particles as microsubstrates for photoreactions and found that the efficiencies of the reactions are enhanced dramatically.[6,7] This effect is attributed to effective adsorption of the reactants on the particle surfaces. Although all the applications of latex are closely related to the composition and structure of the particle surfaces, some structural details, such as compactness of the polymer chains and penetration of chemicals into the particle, are still unclear.

One particular phenomenon we observed is that the efficiency of photoinduced electron transfer from pyrene (Py) to methylviologen (MV^{2+}) decreases with increase in the loading time (*i.e.* the time of storage after mixing of the reactants with PSL).[7] This result cannot be explained by considering that the reactants are adsorbed only on the surface of the particles. The decrease of the efficiency suggests that there are small channels or pores on the particle surface and Py molecules can go inside the particle to be protected from quenching.

In this work, we report the evidence for small pores in PSL by studying the penetrations of Py, pyrenemethanol (PyM) and 1-pyrenylbutyltrimethylammonium bromide (PBTAB) into PSL particles in aqueous dispersion. This finding will extend the application of PSL as a nano-scale substrate for coatings, drug delivery systems, ammunoassay and so on.

PyM and PBTAB were purchased from Molecular Probes, Inc. and used as supplied. Py was purified by vacuum sublimation. To avoid any aggregate or excimer of the probes, 0.60, 5.0 and 10.0 μM stock solutions were used to prepare samples in the penetration experiments for Py, PyM and PBTAB, respectively. The synthesis, purification and characterization methods of PSL were reported elsewhere.[7,8] The mean diameter of the latex particles used in this work is 212 nm as determined by dynamic light scattering measurements.[8]

Adsorption isotherms of the probes onto the latex particles were measured by ultra-centrifugation.[7,8] Fluorescence spectra were recorded on a Hitachi F-4000 spectrofluorometer. Steady-state fluorescence intensity is expressed in terms of peak heights. Fluorescence lifetime measurements were carried out with a Horiba NAES 1100 time-resolved spectrofluorometer. All Fluorescence measurements were carried out at room temperature with air-saturated samples.

It is well known that the microenvironment of a Py molecule can be measured by the I_1/I_3 ratio in the vibronic fine structure of its fluorescence spectrum.[9] Therefore, the location of a Py probe in a PSL aqueous dispersion can be determined by the I_1/I_3 ratio. Illustrated in Fig. 1 are the loading time effects on the relative fluorescence intensities (a) and I_1/I_3 ratios (b) of Py, PyM and PBTAB in PSL aqueous dispersions. The obvious decrease of I_1/I_3 ratio of Py indicates it was adsorbed from the environment with high polarity (aqueous phase, I_1/I_3 = 1.84)[9] to that with low polarity (polystyrene bulk, $I_1/I_3 \approx 1.05$). However, adsorption equilibrium is usually reached in minutes, the slow process of the decreasing I_1/I_3 ratio with loading time suggests that Py penetrates inside the particle. The homogeneous distribution of Py in poly(methyl methacrylate) latex particles after soaking in a methanolic solution of Py[10] also supports the penetration.

The remarkable increase of Py fluorescence intensity with loading time suggests that the quantum yield or lifetime was increased due to its microenvironmental change. Time-resolved fluorescence measurements suggest that the probes are located in two kinds of environments (Fig. 2). Environment 1 makes Py have a long lifetime (τ_1) and environment 2 makes it have a short lifetime (τ_2). The adsorption isotherm of Py onto PSL shows that more than 99.9% of Py exist in the adsorbed state

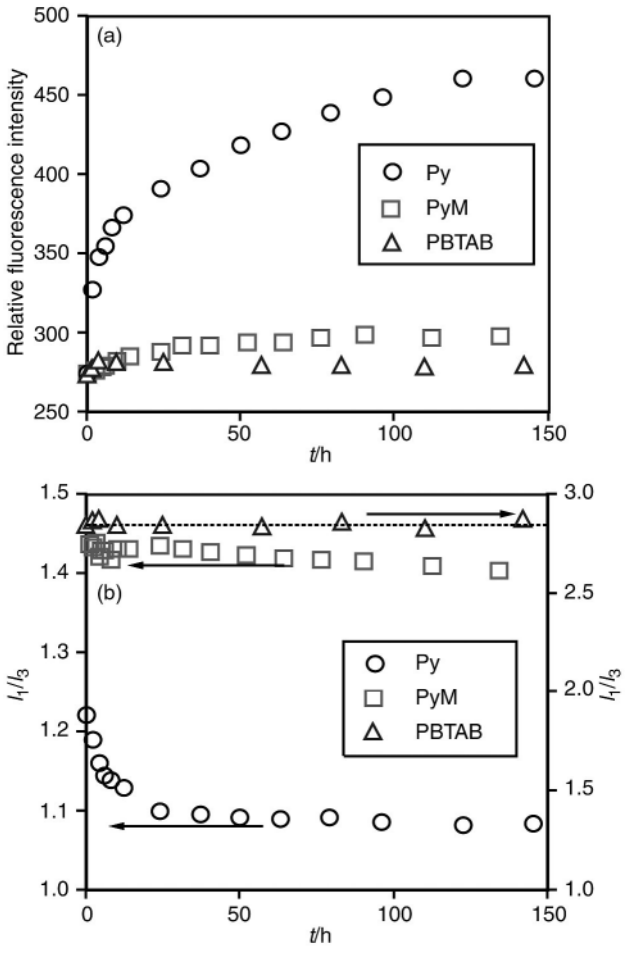

Fig. 1 Loading time effect on the relative fluorescence intensities (a), and I_1/I_3 ratios (b) of Py, PyM, and PBTAB in PSL dispersion at room temperature.

 DOI: 10.1039/b105959a

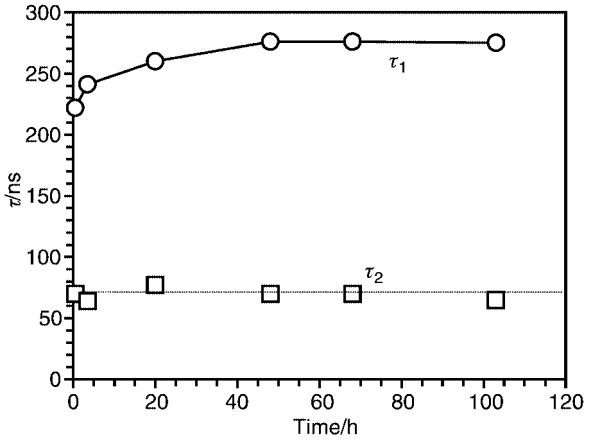

Fig. 2 Loading time effect on the fluorescence lifetimes of pyrene in PSL aqueous dispersion. [Py] = 0.40 μM, [PSL] = 0.40 g L^{-1}.

(data not shown). Therefore, the contribution from the species in aqueous phase is negligible. This means that both of the two environments locate in/on the particle.

The fluorescence lifetime of Py is mainly affected by the mobility of Py and O_2 concentration in the system. In aqueous phase, the fluorescence lifetime of Py decreases from 210 ns in O_2 free solution to 112 ns in air-saturated solution. It is expected in the PSL dispersion that the lifetime will decrease further when Py stays on the PSL surface due to adsorption of both Py and O_2.[11] Actually, we observed the decrease of fluorescence intensity within 2 min of the loading. On the other hand, when Py goes into the inner part of the particle, the lifetime increases due to the reduced mobility of Py. Thus, we ascribe environment 1 to pores or channels inside of PSL particle, and environment 2 to the adsorption sites at the liquid–solid interface.

Py molecules located in environment 2 seem to go gradually to environment 1. This is indicated by the change of fluorescence quantum yields of the two components (data not shown) and the increase of the total fluorescence intensity (Fig. 1a). The microenvironmental change with the loading time is concrete evidence for the penetration of Py.[9] In aqueous solution, the I_1/I_3 ratio of Py is 1.84. After Py was loaded onto PSL, the ratio decreased to 1.22 in 2 min. Then it decreased gradually to 1.08 in 5 d at rt (Fig. 1b). If we assume that the I_1/I_3 ratio of the adsorbed Py is 1.22 at the interface between PSL particle and water, we get some details about the particle surface structure and adsorption mechanism.

First, there are pores or channels in PSL particles through which Py penetrates into the inner part of the particle resulting in the decrease of I_1/I_3 ratio and increase of lifetime. Second, the pore or channel is small and hydrophobic. The hydrophobicity of the channel prevents water molecules and ionic species from penetrating but allows Py to go slowly into the inner part. It is known that a pyrene excimer can be easily formed in confined spaces such as polymer micelles,[12] and zeolites.[13] However, a Py aggregate or excimer was not detected even at high concentration. Thus the dimension of the pore should be slightly larger than the size of Py molecule. Thirdly, the number of the holes should be large because the uptake capacity of Py monomer can be as high as 2% (g/g).

As shown in Fig. 1, the I_1/I_3 ratio of PyM decreases slightly and that of PBTAB is almost constant during the loading. If PyM and PBTAB can go to the inside of the particle, their I_1/I_3 ratios should show obvious change because the I_1/I_3 ratios of PyM and PBTAB are also sensitive to the polarity of the environments.[14] Comparing with that of Py, we conclude that PBTAB does not go inside the particle and PyM goes slightly inside. Here the "passport" for entering into the particle seems to be mainly the polarity of the "passenger".

To confirm the existence of the pores in the latex particles, the control experiments were carried out using PSL and polystyrene cast films. The former was prepared by drying the latex dispersion, and the latter by casting from DCM solution. Both films were annealed at 150 °C for 20 min. The fluorescence intensities of Py from the films immersed in the aqueous solutions decreased and the I_1/I_3 ratio did not decrease below 1.2 as the loading time increased. These results are very different from that of the latex particles. Therefore, we conclude that there exist small hydrophobic pores in the PSL particles.

One of the authors (Y.-K. Gong) acknowledges financial support by the Sasakawa Scientific Research Grant from the Japan Science Society.

Notes and references

1 K. Nakashima, T. Miyamoto and S. Hashimoto, *Chem. Commun*., 1999, 213.
2 O. Pekcan, M. A. Winnik and M. D. Croucher, *Macromolecules*, 1990, **23**, 2673; S. T. Eckersley and A. Rudin, *J. Coatings Technol*., 1990, **62**, 89.
3 S. Slomkowski, D. Kowalczyk and M. Trznadel, *Trends Polym. Sci*., 1995, **3**, 297; M.-T. Charreyre, O. Tcherkasskaya, M. A. Winnik, A. Hiver, T. Delair, P. Cros, C. Pichot and B. Mandrand, *Langmuir*, 1997, **13**, 3103.
4 I. Ichihara, K. Sakamoto, K. Mori and M. Akagi, *Cancer Res*., 1989, **49**, 4357.
5 A. E. Larsen and D. G. Grier, *Nature*, 1997, **385**, 230; T. Palberg, J. Kottal, F. Bitzer, R. Simon, M. Würth and P. Leiderer, *J. Colloid Interface Sci*., 1995, **169**, 85; Y.-K. Gong, K. Nakashima and R. Xu, *Langmuir*, 2001, **17**, 2889.
6 K. Nakashima, N. Kido, A. Yekta and M. A. Winnik, *J. Photochem. Photobiol. A: Chem*., 1997, **110**, 207; K. Nakashima, S. Tanida, T. Miyamoto and S. Hashimoto, *J. Photochem. Photobiol. A: Chem*., 1998, **117**, 111; K. Nakashima, D. Koide and Y.-K. Gong, *Bull. Chem. Soc. Jpn*., 2000, **73**, 1507.
7 Y.-K. Gong, T. Miyamoto, K. Nakashima and S. Hashimoto, *J. Phys. Chem. B*, 2000, **104**, 5772.
8 Y.-K. Gong, K. Nakashima and R. Xu, *Langmuir*, 2000, **16**, 8546.
9 D. C. Dong and M. A. Winnik, *Photochem. Photobiol*., 1982, **35**, 17; D. C. Dong and M. A. Winnik, *Can. J. Chem*., 1984, **62**, 2560; K. Kalyanasundaram and J. K. Thomas, *J. Am. Chem. Soc*., 1977, **99**, 2039.
10 K. Sasaki, M. Koshioka and H. Masuhara, *Appl. Spectr*., 1991, **45**, 1041.
11 P. R. Crippa, *Colloids Surf. B*, 2001, **20**, 315.
12 J.-H. Kim, M. M. Domach and R. D. Tiltoni, *Colloids Surf. A*, 1999, **150**, 55; S. Lee and J. Duhamel, *Macromolecules*, 1998, **31**, 9193; M. A. Winnik, S. M. Bystryak and J. Siddiqui, *Macromolecules*, 1999, **32**, 624.
13 F. L. Cozens, M. Regimbald, H. Garcia and J. C. Scaiano, *J. Phys. Chem*., 1996, **100**, 18165.
14 Y.-K. Gong and K. Nakashima, unpublished data.

CHEMCOMM
Communication
www.rsc.org/chemcomm

1,2,4,3,5-Benzotrithiadiazepine and its unexpected hydrolysis to unusual 7*H*,14*H*-dibenzo[*d*,*i*][1,2,6,7,3,8]tetrathiadiazecine

Alexander Yu. Makarov,[a] Makhmut M. Shakirov,[a] Konstantin V. Shuvaev,[b] Irina Yu. Bagryanskaya,[a] Yuri V. Gatilov[a] and Andrey V. Zibarev*[a]

[a] *Institute of Organic Chemistry, Russian Academy of Sciences, 630090 Novosibirsk, Russia. E-mail: zibarev@nioch.nsc.ru*
[b] *Department of Natural Sciences, Novosibirsk State University, 630090 Novosibirsk, Russia*

Received (in Cambridge, UK) 6th June 2001, Accepted 2nd August 2001
First published as an Advance Article on the web 3rd September 2001

Previously unknown 1,2,4,3,5-benzotrithiadiazepine 1 was prepared by 1:1 condensation of Ph-N=S=N-SiMe$_3$ with S_2Cl_2 followed by intramolecular *ortho*-cyclization of [Ph-N=S=N-S-S-Cl] intermediate, and hydrolyzed in pyridine to unusual macrocyclic 7*H*,14*H*-dibenzo[*d*,*i*][1,2,6,7,3,8]tetrathiadiazecine 2.

Polysulfur–nitrogen π-excessive heterocycles, especially heterocyclic stable radicals (with the former frequently being precursors of the latter), are of keen interest for contemporary chemistry and materials science.[1–4] Among them, fused trithiadiazepines belong to a little studied system. While 1,3,5,2,4-benzotrithiadiazepine[5,6] **3** is described and subjected to preliminary investigation,[6–8] its non-symmetric isomer 1,2,4,3,5-benzotrithiadiazepine **1** was unknown. The present article deals with the preparation of **1** and its unexpected hydrolysis in pyridine to unusual macrocyclic 7*H*,14*H*-dibenzo-[*d*,*i*][1,2,6,7,3,8]tetrathiadiazecine **2**.

For the synthesis of **1**, the intramolecular electrophilic cyclization of Ar-N=S=N-SiMe$_3$ azathienes into 1,3,2,4-benzodithiadiazines under the action of SCl_2[6,9] was extended to S_2Cl_2. This allows the preparation† of the target heterocycle **1** from C_6H_5-N=S=N-SiMe$_3$ **4** (Scheme 1). The cyclization is also successful with 4-BrC_6H_4-N=S=N-SiMe$_3$ **5** (providing compound **6**, an 8-Br derivative of **1**) and 3-RC_6H_4-N=S=N-SiMe$_3$ (**7**, R = CH_3; **8**, R = I). In the latter case of *meta*-substituted precursors the cyclization is regioselective leading predominantly or even exclusively to 7-R substituted derivatives of **1** (Scheme 1). The ratio of the major 7-R isomer to the minor 9-R one is 65:35 for R = CH_3, as shown by ^{1}H NMR spectroscopy.† With R = I, only the 7-I isomer **11** was observed and its structure has unambiguously been confirmed by X-ray crystallography (Fig. 1).‡

Contrary to the successful synthesis of **1**, an attempt to prepare its symmetric isomer **3**[5,6] by the similar approach from C_6H_5-S-N=S=N-SiMe$_3$ and SCl_2 fails. This result agrees with previously reported[6] one.

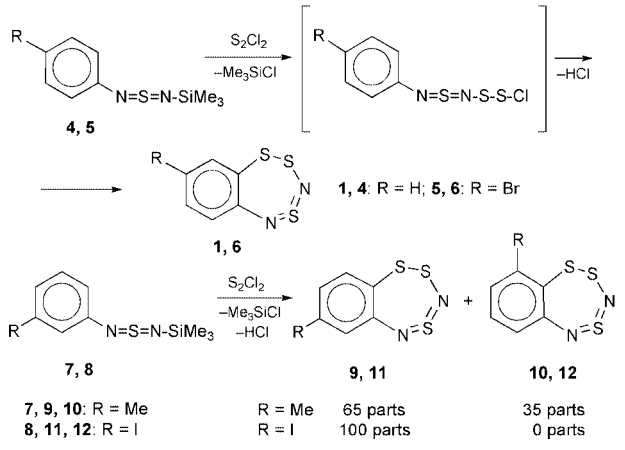

Scheme 1

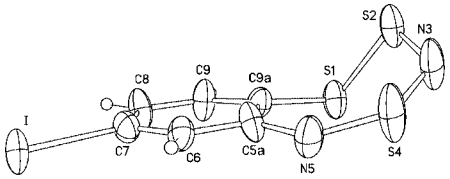

Fig. 1 The X-ray structure of molecule **11**. Selected bond lengths (Å), bond and torsion angles (°): S(1)–S(2) 2.051(6), S(2)–N(3) 1.69(2), N(3)–S(4) 1.52(2), S(4)–N(5) 1.55(1), N(5)–C(5a) 1.41(2), S(1)–C(9a) 1.76(1); C(9a)–S(1)–S(2) 104.6(5), S(1)–S(2)–N(3) 104.2(6), S(2)–N(3)–S(4) 124.6(9), N(3)–S(4)–N(5) 127.1(8), S(4)–N(5)–C(5a) 138(1), N(5)–C(5a)–C(9a) 125(1), C(5a)–C(9a)–S(1) 124(1), C(5a)–C(9a)–S(1)–S(2) −61(1), C(9a)–S(1)–S(2)–N(3) 80.2(8), S(1)–S(2)–N(3)–S(4) −48(2), S(2)–N(3)–S(4)–N(5) 8(2), N(3)–S(4)–N(5)–C(5a) −11(2), S(4)–N(5)–C(5a)–C(9a) 35(3).

According to the data of X-ray crystallography (Fig. 1)‡ and MP2/6-31G* calculations (Fig. 2),‡ the heterocycle of **1** is significantly bent (similar to that of benzopentathiepine)[10] in contrast to the perfectly planar heterocycle of **3**[5b] and its tetrafluoro derivative.[11] The heterocycle conformation (Fig. 1) features the planarity of the C(5a)-N(5)=S(4)=N(3)-S(2) fragment within ± 0.03(1) Å. The S(1) and C(9a) atoms deviate from this plane by 1.35(2) and 0.48(3) Å, respectively. It is seen (Figs. 1 and 2) that the conformation and bond lengths of the title heterocycle are practically the same for a free molecule compared to that packed in the crystal, which is in striking contrast to the situation with related 1,3,2,4-benzodithiadiazines where molecular conformation significantly changes on going from a gas phase to the solid state.[12]

The heteroatom reactivity of **1** differs from that of **3**. For example, it is reported that **3** is stable towards hydrolysis in weak bases and acids[7b] and undergoes fast transformation into 1,3,2-benzodithiazolium chloride under the action of Me$_3$SiCl (a side-product of its preparation).[7a,13] Compound **1** interacts with Me$_3$SiCl to give 1,2,3-benzodithiazolium chloride **13** (Scheme 2) extremely slowly.† However, the most interesting finding is that hydrolysis of **1** in pyridine results unexpectedly in the unusual macrocyclic compound **2** (Scheme 2).† In the absence of pyridine (for example, in THF) the hydrolysis proceeds very slowly if at all. Catalytic or even equimolar

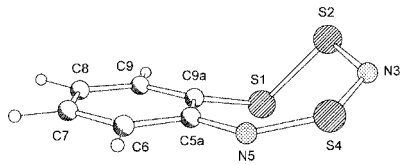

Fig. 2 The MP2/6-31G* structure of molecule **1**. Selected bond lengths (Å), bond and torsion angles (°): S(1)–S(2) 2.086, S(2)–N(3) 1.688, N(3)–S(4) 1.614, S(4)–N(5) 1.594, N(5)–C(5a) 1.381, S(1)–C(9a) 1.757; C(9a)–S(1)–S(2) 106.5, S(1)–S(2)–N(3) 105.0, S(2)–N(3)–S(4) 124.9, N(3)–S(4)–N(5) 126.9, S(4)–N(5)–C(5a) 137.8, N(5)–C(5a)–C(9a) 127.6, C(5a)–C(9a)–S(1) 122.3, C(5a)–C(9a)–S(1)–S(2)–67.1, C(9a)–S(1)–S(2)–N(3) 78.8, S(1)–S(2)–N(3)–S(4) −42.1, S(2)–N(3)–S(4)–N(5) 3.1, N(3)–S(4)–N(5)–C(5a) −2.5, S(4)–N(5)–C(5a)–C(9a) 21.9.

 DOI: 10.1039/b105001j

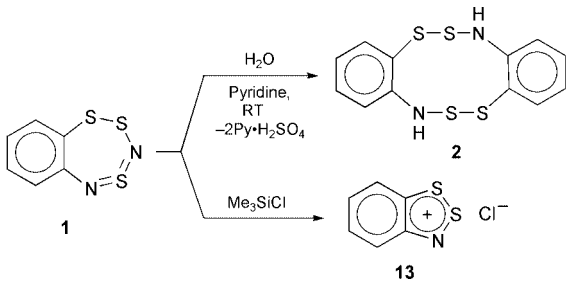

Scheme 2

amounts of pyridine facilitate the hydrolysis in THF insignificantly.

According to the X-ray diffraction data (Fig. 3) the molecule **2** possesses an inversion center. The macrocycle conformation can be described as a chair featuring two transannular N–H···S hydrogen bonds with a H···S distance of 2.60 Å.

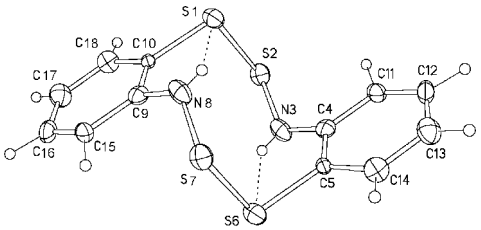

Fig. 3 The X-ray structure of molecule **2**. Selected bond lengths (Å), bond and torsion angles (°): S(1)-S(2) 2.082(5), S(2)-N(3) 1.66(1), N(3)-C(4) 1.42(2), C(4)-C(5) 1.37(2), C(5)-S(6) 1.80(1), S(6)-S(7) 2.082(5); S(1)-S(2)-N(3) 107.1(5), S(2)-N(3)-C(4) 124(1), N(3)-C(4)-C(5) 121(1), C(4)-C(5)-S(6) 121.2(9), C(5)-S(6)-S(7) 100.9(4), C(10)-S(1)-S(2)-N(3) −68.3(7), S(1)-S(2)-N(3)- C(4) −69(1), S(2)-N(3)-C(4)-C(5) 144(1), C(4)-C(5)-S(6)-S(7) −97(1). The dotted lines show N-H···S hydrogen bonds.

Thus, two novel polysulfur–nitrogen heterocyclic systems have been prepared by original approaches and structurally characterized.

The authors are grateful to the Russian Foundation for Basic Research for financial support of their work (project 99-03-33115 and grant 01-03-06190) and access to the Cambridge Structural Database (grant 99-07-90133) and to the STN International databases *via* STN Center at their Institute (grant 00-03-32721).

Notes and references

† *Syntheses. Compounds* **1–6**, **9–11**. In an argon atmosphere, solutions of 1.35 g (0.01 mol) of S_2Cl_2 and 0.01 mol of Ar-N=S=N-$SiMe_3$ (Ar = C_6H_5, 4-BrC_6H_4, 3-$CH_3C_6H_4$ and 3-IC_6H_4),[6,9] each in 30 cm³ of CH_2Cl_2, were slowly mixed by adding them dropwise to 300 cm³ of CH_2Cl_2 at 20 °C, over a period of 1 h, with stirring. After a further 1 h, the reaction solution was filtered, the solvent distilled off under reduced pressure, and the residue was chromatographed on silica (CCl_4).

Compound **1**, 10%, red oil. MS *m*/*z* 199.9534 (M^+; calculated for $C_6H_4N_2S_3$ 199.9537). NMR (Bruker DRX-500 throughout the work) δ ($CDCl_3$): ^{1}H: 7.59, 7.34, 6.98; ^{13}C: 151.1, 146.0, 132.7, 130.6, 130.4, 124.9; ^{15}N [NH_3 (liq.)]: 318.9 (s), 292.0 (d, *J* 3.3 Hz). UV (heptane) λ_{max}/nm (log ε): 457 (3.39), 322 (3.53), 272 (3.85), 267 (3.83), 258 (3.75).

Compound **6**, 4%, orange–red crystals, mp 80–81 °C (hexane). MS *m*/*z* 277.8642 (M^+; calculated for $C_6H_3BrN_2S_3$ 277.8642, ^{79}Br). NMR δ ($CDCl_3$): ^{1}H: 7.78, 7.46, 7.19; ^{13}C: 150.0, 147.6, 134.5, 133.0, 131.0, 117.1; ^{14}N [NH_3 (liq.)]: 319, 292. UV (heptane) λ_{max}/nm (log ε): 464 (3.51), 325 (3.60), 277 (3.98), 229 (4.32), 208 (4.32).

Compounds **9** and **10** (~2:1 mixture, ^{1}H NMR), 7%, red oil. MS *m*/*z* 213.9697 (M^+; calculated for $C_7H_6N_2S_3$ 213.9693). NMR δ ($CDCl_3$): ^{1}H: **9**, 7.48, 7.14, 6.80, 2.34; **10**, 7.22, 7.17, 6.91, 2.49; ^{13}C: **9**, 150.9, 142.8, 140.4, 131.9, 130.1, 125.2, 20.8; **10**, 152.1, 145.2, 140.4, 129.7, 128.0, 125.5, 21.3; ^{15}N [NH_3 (liq.)]: **9**, 319.2 (s), 292.1 (d, *J* 3.3 Hz); **10**, 319.8 (s), 292.3 (d, *J* 3.3 Hz).

Compound **11**, 3%, red crystals, mp 100–101 °C (hexane). MS *m*/*z* 325.8505 (M^+; calculated for $C_6H_3IN_2S_3$ 325.8505). NMR δ ($CDCl_3$): ^{1}H: 7.70, 7.30, 7.29; ^{13}C: 151.9, 145.5, 138.5, 133.2, 132.7, 95.5; ^{14}N [NH_3 (liq.)]: 325, 289. UV (EtOH) λ_{max}/nm (log ε): 458 (3.24), 324 (3.45), 273 (3.95), 214 (4.07).

Compound **2**. To a solution of 100 mg (5×10^{-4} mol) of **1** in 0.6 cm³ of pyridine was added 36 mg (2×10^{-3} mol) of H_2O. After 24 h the precipitate (which consisted of a mixture of **2** and pyridinium sulfate, according to the MS and IR data) was filtered off, washed with pyridine and recrystallized from toluene. Compound **2**, 5 %, colorless crystals, mp 215–217 °C. MS *m*/*z* 309.9729 (M^+; calculated for $C_{12}H_{10}N_2S_4$ 309.9727). IR ν/cm^{-1} (KBr): 3274s, 3050w, 1585m, 1470s, 1443m, 1269s, 901m, 757s, 612s, 575m, 448s. Evaporation of the filtrate under reduced pressure affords viscous oil assumed to be (GC-MS, ^{1}H and ^{13}C NMR) a mixture of 2,2′-diaminodiphenyl disulfide and related polysulfanes.

Compound **13**. To a solution of 105 mg (5.25×10^{-4} mol) of **1** in 4 cm³ of CH_2Cl_2 was added 228 mg (2.1×10^{-3} mol) of Me_3SiCl. After 21 d the precipitate was filtered off and recrystallized from $SOCl_2$–CCl_4 (3:1). Compound **13**, 10%, yellow crystals, mp 194–196 °C (decomp.) MS *m*/*z* 153.9775 ($M^+ - {}^{35}Cl$; calculated for $C_6H_4NS_2$ 153.9785). NMR δ (CF_3CO_2H): ^{1}H: 9.09, 9.00, 8.65, 8.46; ^{13}C: 164.0, 156.2, 139.1, 133.9, 128.1, 123.4; ^{14}N [NH_3 (liq.)]: 406. UV λ_{max}/nm (log ε) (CF_3CO_2H): 426 (3.25), 347 (4.38).

After evaporation of the filtrate under reduced pressure unreacted **1** was recovered in 80% yield.

‡ *X-ray crystallography and ab initio calculations. X-ray structure data for* **2** *and* **11**. *Compound* **2**: $C_{12}H_{10}N_2S_4$, M = 310.46, monoclinic, a = 8.101(2), b = 4.7156(9), c = 16.905(5) Å, β = 95.57(2)°, U = 642.7(3) Å³, space group $P2_1/c$, Z = 2, d_c = 1.604 g cm^{-3}, μ(MoKα) = 0.719 mm^{-1}, 875 reflections measured, 807 unique (R_{int} = 0.037) which were used in all calculations. The final R was 0.0873 (for 505 observed reflections).

Compound **11**: $C_6H_3IN_2S_3$, M = 326.18, monoclinic, a = 4.117(2), b = 11.048(7), c = 20.63(1) Å, β = 91.74(5)°, U = 938.2(9) Å³, space group $P2_1/c$, Z = 4, d_c = 2.309 g cm^{-3}, μ(MoKα) = 4.023 mm^{-1}, 1859 reflections measure, 1616 unique (R_{int} = 0.040) which were used in all calculations. The final R was 0.0831 (for 943 observed reflections).

CCDC 164031 (**2**) and 164032 (**11**). See http://www.rsc.org/suppdata/cc/b1/b105001j/ for electronic files in .cif or other electronic format.

The MP2/6-31G calculations* were performed using the GAMESS program.[14]

1 C. W. Rees, *J. Heterocycl. Chem.*, 1992, **29**, 639; X.-G. Duan, X.-L. Duan, C. W. Rees and T.-Y. Yue, *J. Heterocycl. Chem.*, 1996, **33**, 1419.
2 J. M. Rawson, A. J. Banister and I. Lavender, *Adv. Heterocycl. Chem.*, 1995, **62**, 137; J. M. Rawson and G. D. McManus, *Coord. Chem. Rev.*, 1999, **189**, 135; T. M. Barclay, A. W. Cordes, R. C. Haddon, M. E. Itkis, R. T. Oakley, R. W. Reed and H. Zhang, *J. Am. Chem. Soc.*, 1999, **121**, 969.
3 T. Torroba, *J. Prakt. Chem.*, 1999, **341**, 99.
4 I. V. Vlasyuk, V. A. Bagryansky, N. P. Gritsan, Yu. N. Molin, A. Yu. Makarov, Yu. V. Gatilov, V. V. Shcherbukhin and A. V. Zibarev, *Phys. Chem. Chem. Phys.*, 2001, **3**, 409.
5 (*a*) J. L. Morris, C. W. Rees and J. D. Rigg, *J. Chem. Soc., Chem. Commun.*, 1985, 55; (*b*) S. T. A. K. Daley, C. W. Rees and D. J. Williams, *J. Chem. Soc., Chem. Commun.*, 1985, 57.
6 A. W. Cordes, M. Hojo, H. Koenig, M. C. Noble, R. T. Oakley and W. T. Pennington, *Inorg. Chem.*, 1986, **25**, 1137.
7 J. L. Morris and C. W. Rees, *J. Chem. Soc., Perkin Trans. 1*, 1987, 211; J. L. Morris and C. W. Rees, *J. Chem. Soc., Perkin Trans. 1*, 1987, 217.
8 M. J. Plater and C. W. Rees, *J. Chem. Soc., Perkin Trans. 1*, 1991, 317.
9 I. Yu. Bagryanskaya, Yu. V. Gatilov, A. Yu. Makarov, A. M. Maksimov, A. O. Miller, M. M. Shakirov and A. V. Zibarev, *Heteroat. Chem.*, 1999, **10**, 113; A. Yu. Makarov, I. Yu. Bagryanskaya, Yu. V. Gatilov, T. V. Mikhalina, M. M. Shakirov, L. N. Shchegoleva and A. V. Zibarev, *Heteroat. Chem.*, 2001, **12**, in the press.
10 F. Feher and B. Engelen, *Z. Anorg. Allg. Chem.*, 1979, **452**, 37.
11 I. Yu. Bagryanskaya, H. Bock, Yu. V. Gatilov, A. Haas, M. M. Shakirov, B. Solouki and A. V. Zibarev, *Chem. Ber./Recueil*, 1997, **130**, 247.
12 F. Blockhuys, S. L. Hinchley, A. Yu. Makarov, Yu. V. Gatilov, A. V. Zibarev, J. D. Woollins and D. W. H. Rankin, *Chem. Eur. J.*, 2001, **7**, 3592.
13 A. V. Zibarev, A. V. Rogoza, S. N. Konchenko, M. A. Fedotov and G. G. Furin, *Zh. Obshch. Khim.*, 1991, **61**, 441 (*Chem. Abstr.*, **115**, 92167).
14 M. V. Schmidt, K. K. Baldridge, J. A. Boatz, S. T. Elbert, M. S. Gordon, J. J. Jensen, S. Koseki, N. Matsunaga, K. A. Nguen, S. Su, T. L. Windus, M. Dupuis and J. A. Montgomery, *J. Comput. Chem.*, 1993, **14**, 1347.

CHEMCOMM Communication
www.rsc.org/chemcomm

New high-nuclearity Ni–Pt carbonyl clusters: synthesis and X-ray structure of the ordered $[Ni_{24}Pt_{14}(CO)_{44}]^{4-}$ and the substitutionally Ni/Pt disordered $[Ni_{10}(Ni_{6-x}Pt_x)Pt_8(CO)_{30}]^{4-}$ (x = 1.92) tetraanions

Cristina Femoni, M. Carmela Iapalucci, Giuliano Longoni* and Per H. Svensson

Dipartimento di Chimica Fisica ed Inorganica, Università di Bologna, viale Risorgimento 4, 40136 Bologna, Italy. E-mail: longoni@ms.fci.unibo.it

Received (in Cambridge, UK) 23rd April 2001, Accepted 30th July 2001
First published as an Advance Article on the web 3rd September 2001

The reaction of $[N^nBu_4]_2[Ni_6(CO)_{12}]$ in THF solution with 1.5–2 equivalents of K_2PtCl_4 leads to formation of the $[Ni_{24}Pt_{14}(CO)_{44}]^{4-}$ and $[Ni_{10}(Ni_{6-x}Pt_x)Pt_8(CO)_{30}]^{4-}$ ($x \approx 2$) tetraanions, the latter presents a localised substitutional Ni/Pt disorder and an unprecedented close-packed metal structure.

Most high-nuclearity metal carbonyl clusters containing interstitial Ni or Pt atoms, *e.g.* $[Ni_{11}E_2(CO)_{18}]^{n-}$ (E = Sb, Bi),[1,2] $[H_{6-n}Ni_{38}Pt_6(CO)_{48}]^{n-}$,[3] $[H_{6-n}Ni_{36}Pt_4(CO)_{45}]^{n-}$,[4] $[Pt_{19}(CO)_{22}]^{4-}$[5] and $[Pt_{24}(CO)_{30}]^{2-}$,[6,7] display multivalence encompassing several redox changes.[5,8,9] Previously reported Ni–Pd carbonyl clusters, *viz.* $[Ni_{16}Pd_{16}(CO)_{40}]^{4-}$ and $[Ni_{26}Pd_{20}(CO)_{54}]^{6-}$,[10] contain interstitial Pd atoms and are an exception to the above rule. This probably happens because of the weakness of all bonds involving palladium atoms, which may favour fragmentation–condensation processes under redox conditions. On the other hand, it is possible that the above weakness could favour crowding of almost degenerate energy levels in the frontier region and anticipate the size-induced metal–insulator transition,[11] which for metal carbonyl clusters is expected to occur for nuclearities beyond 70.[3] In partial agreement, preliminary magnetic measurements indicate that the even-electron $[Ni_{16}Pd_{16}(CO)_{40}]^{4-}$ displays magnetic behaviour arising from the presence of four unpaired electrons.[12]

The above considerations stirred interest in platinum-rich Ni–Pt carbonyl clusters. As a result, we now report the synthesis and structure of the first examples of such compounds consisting of the substitutionally Ni/Pt crystal disordered $[Ni_{10}(Ni_{6-x}Pt_x)Pt_8(CO)_{30}]^{4-}$ ($x \approx 2$) and the ordered $[Ni_{24}Pt_{14}(CO)_{44}]^{4-}$ tetraanions.

Both compounds were obtained by reaction of $[N^nBu_4]_2[Ni_6(CO)_{12}]$ in THF with 1.5–2 equivalents of K_2PtCl_4 and from the residue obtained by evaporation of the reaction solution were separated by differential solubility of their salts. Thus, treatment of the above residue with THF gave a dark-green solution containing a mixture of $[Pt_{3n}(CO)_{6n}]^{2-}$ (n = 3, 4)[13,14] and $[Ni_{24}Pt_{14}(CO)_{44}]^{4-}$, and an insoluble dark precipitate. Extraction of the latter with acetone and precipitation with hexane afforded $[N^nBu_4]_4[Ni_{10}(Ni_{6-x}Pt_x)Pt_8(CO)_{30}]\cdot Me_2CO$ (x = 1.92) (ν_{CO} in MeCN at 2003 s, 1990 sh, 1821 m (br) cm^{-1}) as black prisms. $[N^nBu_4]_4[Ni_{24}Pt_{14}(CO)_{44}]\cdot 6THF$ (ν_{CO} in MeCN at 2008 s, 1877 mw, 1854 m and 1835 mw cm^{-1}) separated out as hexagonal black crystals from the above dark-green THF solution upon concentration. Both compounds have been characterised by elemental analysis and X-ray diffraction studies.†

The overall structures of the $[Ni_{10}(Ni_{6-x}Pt_x)Pt_8(CO)_{12}(\mu\text{-}CO)_{18}]^{4-}$ and $[Ni_{24}Pt_{14}(CO)_{26}(\mu\text{-}CO)_{18}]^{4-}$ tetraanions are shown in Fig. 1 and 2, respectively. The $[Ni_{10}(Ni_{6-x}Pt_x)Pt_8(CO)_{30}]^{4-}$ metal frame is based on an unprecedented *hcp* sequence of M_7, M_{10} and M_7 layers. Interestingly, the closely related homometallic $[Pt_{24}(CO)_{30}]^{2-}$[6,7] is based on a *ccp* fragment deriving from that of $[Pt_{38}(CO)_{44}]^{2-}$[15] by cutting two adjacent hexagonal Pt_7 faces. The metal sites (relative number of metal atoms in parentheses) of $[Ni_{10}(Ni_{6-x}Pt_x)Pt_8(CO)_{30}]^{4-}$ display rather spread metallic coordinations of 4 (4 Ni), 5 (2 Ni/Pt), 6 (1 Pt, 4 Ni/Pt), 7 (6 Ni, 4 Pt), 8 (1 Pt) and 12 (2 Pt). The Ni/Pt substitutional disorder is limited to the two middle-layer sites with metal connectivity of 5 and their adjacent atoms belonging to the top- and bottom-layer and displaying metal connectivity of 6. These were refined as a mixture of Ni and Pt atoms to obtain occupancy fractions of *ca.* 2/3 and 1/3, respectively. All other metal sites could be refined either as nickel or platinum atoms. Analysis of two other crystals, coming from different preparations of $[Ni_{10}(Ni_{6-x}Pt_x)Pt_8(CO)_{30}]^{4-}$, gave rise to slightly different Ni and Pt occupancy fractions in the same substitutionally disordered sites. However, an overall x value of *ca.* 2 was confirmed. This finding is in agreement with the presence of a stoichiometric $[Ni_{10}(Ni_4Pt_2)Pt_8(CO)_{30}]^{4-}$ species having localised substitutional Ni/Pt disorder (as, for instance, $[Fe_2Rh_4(CO)_{16}]^{2-}$).[16] A non-stoichiometric and substitutionally disordered mixture of $[Ni_{10}(Ni_{6-x}Pt_x)Pt_8(CO)_{30}]^{4-}$ species, as exemplified by the recently reported $[Au_6Pd_6(Pd_{6-x}Ni_x)Ni_{20}(CO)_{44}]^{6-}$,[17] seems less in keeping with the available data.

The metal framework of $[Ni_{24}Pt_{14}(CO)_{44}]^{4-}$ represents a fragment of *ccp* lattice identical to that displayed by the homometallic $[Pt_{38}(CO)_{44}]^{2-}$ dianion,[15] but different from that of other carbonyl clusters possessing the same metal nuclearity, *viz.* $[HNi_{38}C_6(CO)_{42}]^{5-}$,[18,19] $[Ni_{32}Au_6(CO)_{44}]^{6-}$,[17] $[Ni_{20}(Pd_{6-x}Ni_x)Pd_6Au_6(CO)_{44}]^{6-}$,[17] and $Pd_{38}(CO)_{28}$-

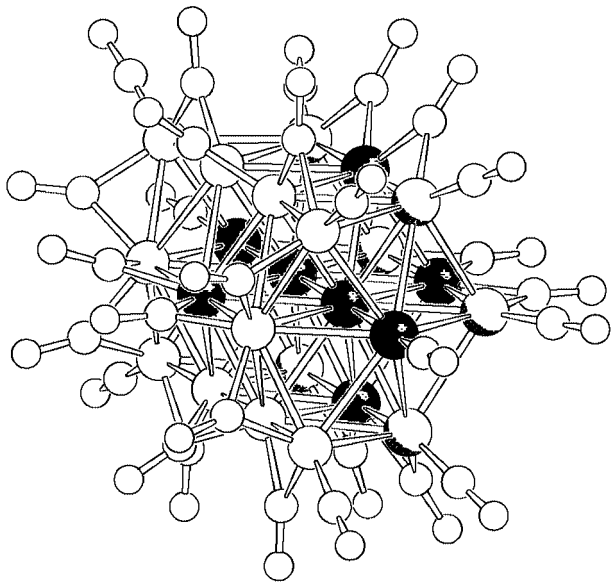

Fig. 1 The $[Ni_{10}(Ni_{6-x}Pt_x)Pt_8(CO)_{30}]^{4-}$ ($x \approx 2$) tetraanion. Pt and Ni atoms are shown as black and open spheres, respectively. Substitutional Ni–Pt disorder is limited to the sites shown as partially blackened spheres. Range of M–M distances: Pt–Pt 2.612(1)–2.817(1), Ni–Pt 2.673(2)–2.854(2), Ni–Ni 2.466(3)–2.815(3), Ni/Pt–Ni 2.705(3)–2.787(3), Ni/Pt–Pt 2.649(2)–2.796(2), Ni/Pt–Ni/Pt 2.732(3)–2.781(3) Å.

 DOI: 10.1039/b103610f

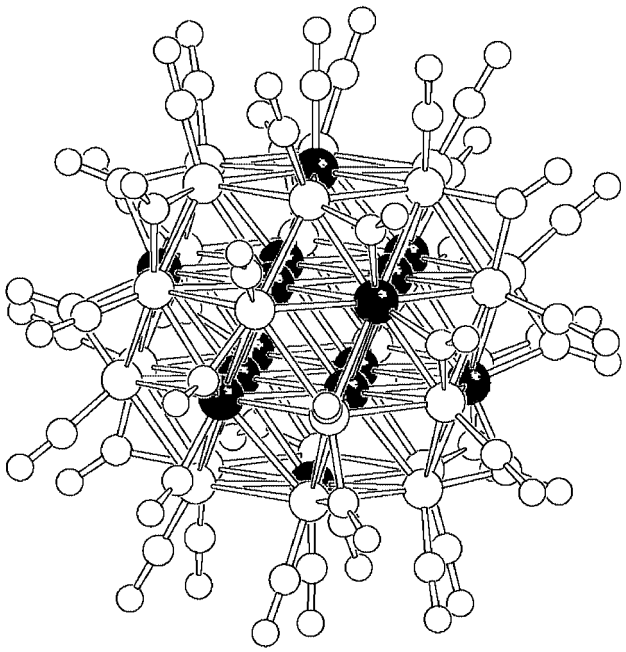

Fig. 2 The $[Ni_{24}Pt_{14}(CO)_{44}]^{4-}$ tetraanion (Pt atoms are shown as black spheres). Range of M–M and average M–C distances: Pt–Pt 2.725(1)–2.878(1), Ni–Pt 2.531(2)–2.861(2), Ni–Ni 2.524(3)–2.783(3) Å; $Pt–C_{terminal}$ 1.80(2), $Pt–C_{edge\text{-}bridging}$ 1.99, $Ni–C_{terminal}$ 1.71, $Ni–C_{edge\text{-}bridging}$ 1.85 Å.

$(PEt_3)_{12}$.[20] The 24 nickel atoms occupy the corner sites of the truncated-ν_3-octahedron,[21] whereas the 14 platinum atoms occupy the six vertices of the interstitial octahedron and the centers of the eight hexagonal faces. Such an ordered occupation is probably favoured by the substantial difference in metal coordination (6, 9 and 12) of the three kinds of geometrically equivalent metal sites of $[Ni_{24}Pt_{14}(CO)_{44}]^{4-}$.

The carbonyl stereochemistry of $[Ni_{24}Pt_{14}(CO)_{26}(\mu\text{-}CO)_{18}]^{4-}$ represents a variant of that of the non-isoelectronic $[Pt_{38}(CO)_{32}(\mu\text{-}CO)_{12}]^{2-}$ dianion.[15] The tetraanion has 26 terminal ligands (one per each nickel atom and the two platinum atoms centering two opposite Ni_6 hexagonal rings) and 18 edge-bridges (12 onto the Ni–Pt–Ni diagonals of the other six Pt-centered Ni_6 hexagonal faces and six onto one Ni–Ni edge of each Ni_4 square face). Spanning of Ni–Pt bonds rather than a second opposite Ni–Ni edge of each Ni_4 square face reduces the number of short C···C non-bonding contacts and releases the steric pressure among the carbonyl groups. Moreover, an increased number of edge-bridging carbonyl groups with respect to $[Pt_{38}(CO)_{44}]^{2-}$ is in keeping with the increased negative charge of $[Ni_{24}Pt_{14}(CO)_{44}]^{4-}$. Regeneration of the carbonyl stereochemistry of the former would only require a concerted terminal–edge site exchange of the 12 edge-bridging carbonyls spanning the Ni–Pt–Ni diagonals of 6 out of 8 hexagonal faces and six terminal ligands bonded to one of the two nickel atoms of the above diagonals.

EHMO calculations with CACAO[22] show that the frontier regions of each of $[Ni_{24}Pt_{14}(CO)_{44}]^{4-}$ and $[Ni_{10}(Ni_{6-x}Pt_x)Pt_8(CO)_{30}]^{4-}$ do not feature a well-defined HOMO–LUMO gap. Therefore, it appears possible that both compounds could exhibit a wide range of redox states as their homometallic $[Pt_{24}(CO)_{30}]^{2-}$ and $[Pt_{38}(CO)_{44}]^{2-}$ congeners.[6,7] A further hint is given by the electron counts of both $[Ni_{24}Pt_{14}(CO)_{44}]^{4-}$ and $[Ni_{10}(Ni_{6-x}Pt_x)Pt_8(CO)_{30}]^{4-}$, which exceed by two valence electrons those of the related dianions, $[Pt_{38}(CO)_{44}]^{2-}$ [15] and $[Pt_{24}(CO)_{30}]$,$^{2-}$ respectively.[6,7] Studies devoted to elucidating their magnetic and electrochemical behaviour and the eventual structural changes occurring upon reduction or oxidation are ongoing.

G. L. thanks the MURST (COFIN2000) and the University of Bologna for funding. P. H. S. acknowledges grants from The Wenner-Gren Foundation, Stiftelsen BLANCEFLOR Boncompagni-Ludovisi, född Bildt and Svenska Institutet.

Notes and references

† *Crystal data* for $[N^nBu_4]_4[Ni_{24}Pt_{14}(CO)_{44}]\cdot 6THF$: M = 6775.2, orthorhombic, a = 29.464(1), b = 18.581(1), c = 31.648(1) Å, U = 17327.0(8) Å^3, T = 298 K, space group *Pbca*, Z = 4, μ(Mo-Kα) = 50.59 cm^{-1}, reflections measured 152459, unique 15233 (R_{int} = 0.1468) which were used in all calculations. The final $R1$ and $wR2$ were 0.0487 and 0.1141 [$I > 2\sigma(I)$].

Crystal data for $[N^nBu_4]_4[Ni_{10}(Ni_{6-x}Pt_x)Pt_8(CO)_{30}]\cdot Me_2CO$ (x = 1.92): M = 4630.48, monoclinic, a = 26.716(1), b = 15.276(1), c = 31.998(1) Å, β = 98.404(1),° U = 12918.3(8) Å^3, T = 193 K, space group $P2_1/n$, Z = 4, μ(Mo-Kα) = 50.59 cm^{-1}, reflections measured 111119, unique 21957 (R_{int} = 0.1347) which were used in all calculations. The final $R1$ and $wR2$ were 0.0458 and 0.0924 [$I > 2\sigma(I)$].

CCDC reference numbers 147008 and 163767.

See http://www.rsc.org/suppdata/cc/b1/b103610f/ for crystallographic data in CIF or other electronic format.

1 V. G. Albano, F. Demartin, M. C. Iapalucci, F. Laschi, G. Longoni, A. Sironi and P. Zanello, *J. Chem. Soc., Dalton Trans*., 1991, 739.
2 V. G. Albano, F. Demartin, M. C. Iapalucci, G. Longoni, M. Monari and P. Zanello, *J. Chem. Soc., Dalton Trans*., 1992, 497.
3 C. Femoni, M. C. Iapalucci, G. Longoni, P. Zanello and A. Ceriotti, *Inorg. Chem*., 1999, **38**, 3721.
4 F. Demartin, C. Femoni, M. C. Iapalucci, G. Longoni, P. Macchi and P. Zanello, *J. Cluster Sci*., 2001, in press.
5 P. Zanello, *Stereochem. Organomet. Inorg. Compds*., 1994, **5**, 163; P. Zanello, *Struct. Bonding (Berlin)*, 1992, **79**, 101.
6 G. J. Lewis, J. D. Roth, R. A. Montag, L. K. Safford, X. Gao, S.-C. Chang, L. F. Dahl and M. J. Weaver, *J. Am. Chem. Soc*., 1990, **112**, 2831.
7 J. D. Roth, G. J. Lewis, L. K. Safford, X. Jiang, L. F. Dahl and M. J. Weaver, *J. Am. Chem. Soc*., 1992, **114**, 6159
8 G. Longoni, C. Femoni, M. C. Iapalucci and P. Zanello, in *Metal Clusters in Chemistry*, ed. P. Braunstein, L. Oro and P. Raithby, VCH, Weinheim, 1999, vol. 2, p. 1137.
9 P. Zanello, *Coord. Chem. Rev*., 1988, **83**, 199; P. Zanello, *Coord. Chem. Rev*., 1988, **87**, 1.
10 C. Femoni, M. C. Iapalucci, G. Longoni, P. H. Svensson and J. Wolowska, *Angew. Chem. Int. Ed. Engl*., 2000, **39**, 1635.
11 P. P. Edwards, R. L. Johnston and C. N. R. Rao, in *Metal Clusters in Chemistry*, ed. P. Braunstein, L. Oro and P. Raithby, VCH, Weinheim, 1999, vol. 3, p. 1454.
12 M. C. Iapalucci, G. Longoni, M. Riccò, M. Solzi, F. Bolzoni and C. Bucci, manuscript in preparation.
13 J. C. Calabrese, L. F. Dahl, P. Chini, G. Longoni and S. Martinengo, *J. Am. Chem. Soc*., 1974, **96**, 2614.
14 G. Longoni and P. Chini, *J. Am. Chem. Soc*., 1976, **98**, 7225.
15 A. Ceriotti, N. Masciocchi, P. Macchi and G. Longoni, *Angew. Chem., Int. Ed. Engl*., 1999, **38**, 3724.
16 A. Ceriotti, G. Longoni, R. Della Pergola, B. T. Heaton and D. O. Smith, *J. Chem. Soc., Dalton Trans*., 1983, 1433.
17 N. T. Tran, M. Kawano, D. R. Powell, R. K. Hayashi, C. F. Campana and L. F. Dahl, *J. Am. Chem. Soc*., 1999, **121**, 5945.
18 A. Ceriotti, A. Fait, G. Longoni, G. Piro, F. Demartin, M. Manassero and M. Sansoni, *J. Am. Chem. Soc*., 1986, **108**, 8091.
19 F. Calderoni, F. Demartin, F. Fabrizi de Biani, C. Femoni, M. C. Iapalucci, G. Longoni and P. Zanello, *Eur. J. Inorg. Chem*., 1999, 663.
20 E. G. Mednikov, N. K. Eremenko, Yu. L. Slovokhotov and Yu. T. Struchkov, *J. Chem. Soc., Chem. Commun*., 1987, 218.
21 B. K. Teo and H. Zhang, *Polyhedron*, 1990, **9**, 1985.
22 C. Mealli and D. M. Proserpio, *J. Chem. Educ*., 1990, **67**, 399.

CHEMCOMM Communication
www.rsc.org/chemcomm

Poly(distyrylbenzene-*block*-sexi(ethylene oxide)), a highly luminescent processable derivative of PPV

Franco Cacialli,[a] Richard H. Friend,[b] W. James Feast[c] and P. Wilfried Lovenich[c]

[a] *Department of Physics and Astronomy, University College London, Gower Street, London, UK WC1E 6BT*
[b] *Cavendish Laboratory, Madingley Road, Cambridge, UK CB3 OHE*
[c] *IRC in Polymer Science and Technology, Department of Chemistry, University of Durham, South Road, Durham, UK DH1 3LE. E-mail: w.j.Feast@durham.ac.uk*

Received (in Cambridge, UK) 10th July 2001, Accepted 3rd August 2001
First published as an Advance Article on the web 3rd September 2001

A block copolymer of distyrylbenzene with sexi(ethylene oxide) spacers displays high solid state photoluminescence efficiency (34%). Single layer light-emitting diodes with calcium or aluminium cathodes exhibit luminances over 2000 cd m^{-2} and efficiencies of 0.5 cd A^{-1}.

Electroluminescence in conjugated polymers was first observed in poly(*p*-phenylenevinylene),[1] PPV, which is made *via* a precursor route and has been the workhorse for investigations of the phenomenon.[2] Most unsubstituted conjugated polymers are insoluble and infusible and consequently not easily processed. Various protocols have been adopted to overcome this fundamental problem including the use of precursor routes, solubilising side chains, formation of block copolymers and polymers containing functional units in side chains.[3] Several groups have demonstrated the use of Wittig condensation as an effective route to copolymers with well-defined conjugated chromophores separated by a non-conjugated unit.[4] In this context oligo(ethylene oxide), OEO, spacers are attractive as they can provide a dramatic enhancement of solubility in both organic and aqueous solvents[5] and avoid the requirement to introduce solubilising side chains directly on the chromophore, which can disrupt planarity. In addition OEOs can provide a significant ionic conductivity that can, in principle, be exploited for fabricating light-emitting electrochemical cells, LECs. Sandman *et al.*[6] and Li *et al.*[7] have described the synthesis of copolymers of distyrylbenzene (DSB) and OEO, but found it difficult to report device characteristics owing to rapid device degradation.[6]

In contrast to these reports, we describe the synthesis and characterisation of a block copolymer of DSB with sexi-(ethylene oxide), SEO, spacers (DSB-*block*-SEO) **1** which displays high solid state photoluminescence (PL) efficiency and good electroluminescence in device structures. In our approach SEO was activated as the bis-tosylate and reacted with 4-hydroxybenzaldehyde to give the flexible linker **2**. The reaction of triphenylphosphine with α,α′-dibromoxylene gave bis(triphenylphosphonium)xylylene dibromide **3** and Wittig condensation of **2** and **3** gave the polymer **1** (see Scheme 1).

The polymer is soluble in chloroform and robust free-standing films can be cast from solution. The ^{1}H-NMR-, ^{13}C-NMR-, FTIR and UV/vis spectra and elemental analysis were consistent with the assigned structure. The ^{1}H-NMR spectrum is reproduced in Fig. 1, in the inset four AB quartets can be identified and assigned;[8] the two with J_{AB} = 16 Hz are assigned to *trans* vinylenes in *trans,trans* and *trans,cis* DSB units and the two with J_{AB} = 12 Hz to *cis* vinylenes in *cis,cis* and *cis,trans* units, the relative intensities of these signals indicating a 50:50 *cis*:*trans* distribution of double bonds.

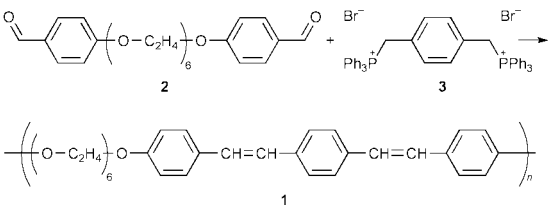

Scheme 1 Synthesis of polymer DSB-*block*-SEO **1**.

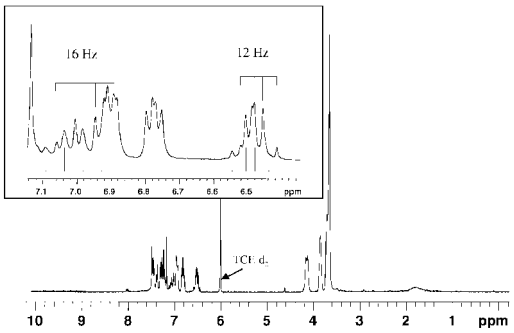

Fig. 1 ^{1}H NMR spectrum of DSB-*block*-SEO in Tetrachloroethane-d_2 (TCE-d_2).

Gel Permeation Chromatography (Viscoteck, RI detector, chloroform eluent, 2 × PL_{gel} mixed bed D 30 cm columns, polystyrene standards, we thank RAPRA for this measurement) indicated a M_n of 5600, a polydispersity of 3 and a degree of polymerisation of about 10 with respect to polystyrene calibration. Ion chromatography (Dionex, DX 120) indicated no traces of Li^+, Na^+, K^+, Mg^{2+} or Ca^{2+} and ^{31}P-NMR showed no phosphorous.

The solid state PL quantum efficiency of polymer **1** is 34%, as measured by exciting a 100 nm thick film on spectrosil inside an integrating sphere, with laser excitation at 325 nm (He-Cd laser). The solid state absorption spectrum is reported in Fig. 2 and shows a maximum at 3.71 eV (334 nm), whereas the solid state PL spectrum (Fig. 3) shows two maxima at 2.34 eV (529 nm) and 2.50 eV (496 nm), *i.e.* in the green region of the visible range. The substantial red-shift (~0.25 eV) with respect to distyrylbenzene oligomers can be explained by taking into

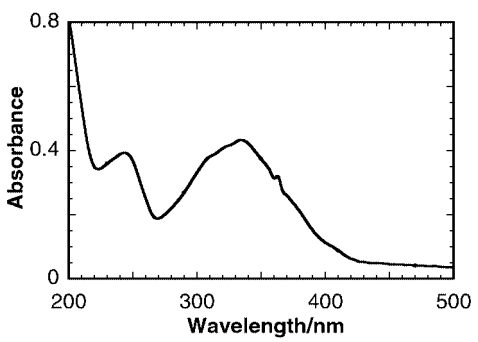

Fig. 2 Absorption spectrum of a DSB-*block*-SEO thin film (100 nm thick) on a spectrosil substrate.

 DOI: 10.1039/b106122b

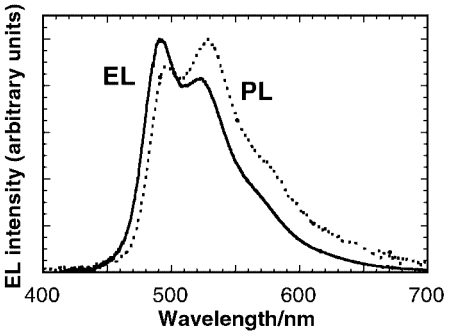

Fig. 3 EL and PL spectra of DSB-*block*-SEO. The EL spectrum is from an ITO/DSB-*block*-SEO/Al diode (2 mm^2 area; 100 nm thick layer). The PL spectrum is obtained by exciting with a He-Cd laser (325 nm) a 100 nm thick film on spectrosil. The relatively broad spectrum with respect to previous reports[6] is likely to be due to a greater disorder, induced by the significant *cis*-content.

account the electron-donating properties of the alkoxy groups in the 4 and 4′ positions.[9] The Stokes shift between absorption and emission is substantial (162 nm).

Light-emitting diodes, LEDs, were prepared on ITO substrates treated with an oxygen plasma prior to spin-coating, in order to increase the work function and surface energy.[10] The active material was spin-coated from a chloroform solution, and the device fabrication completed by thermal evaporation of a calcium and/or aluminium cathode.

Typical current density and luminance *vs*. voltage (IVL) curves for a diode with ITO and Al electrodes are reported in Fig. 4. The turn-on voltage is at 6.5 V, and we obtained luminance values over 2000 cd m^{-2} at 19 V, with luminescence efficiencies up to 0.5 cd A^{-1}. Interestingly, we observed no significant improvement when replacing Al cathodes by Ca cathodes in spite of a much lower work function (2.8 eV *vs*. 4.2–4.3 eV for Al). This is unexpected in view of the position of the frontier levels, found at 5.5 ± 0.1 eV (ionisation potential, IP) and 2.5 ± 0.1 eV (electron affinity, EA), determined by cyclic voltammetry with ferrocene as reference. Relatively high

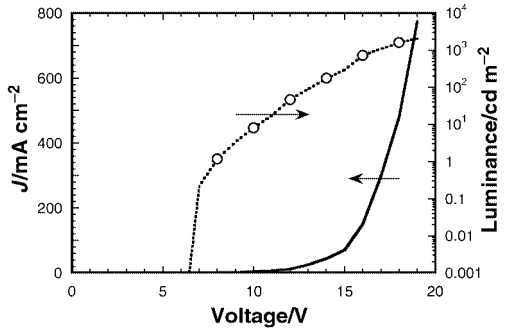

Fig. 4 Current density and luminance *vs*. voltage characteristics of the same ITO/DSB-*block*-SEO/Al device used for the EL spectrum of Fig. 3.

turn-on voltages, even when a poly(ethylenedioxythiophene)–poly(styrenesulfonic acid), PEDOT:PSS, hole-injection layer was used in order to try to increase the anode work function,[11] are consistent with the presence of a significant energy barrier at the anodic interface.

LECs use an electroluminescent polymer, an ion transporting polymer (such as poly(ethylene oxide)) and a salt in order to aid charge injection at the electrodes.[12] Since our polymer comprises both OEO and DSB within its backbone we were able to prepare LECs with active layers made of DSB-*block*-SEO blended with lithium triflate (10 wt%) (ITO/DSB-*block*-SEO(LiTf)/Al). The turn-on voltage was reduced to 3.8 V with emission, as before, in the green and we could observe electroluminescence under reverse bias.

In summary, we have prepared and characterised a solution processable polymer containing distyrylbenzene units having a 50:50 *cis*:*trans* vinylene distribution linked at the 4,4′-positions by sexi(ethylene oxide) units. In contrast to earlier reports on related materials this polymer can be used to construct very efficient LEDs.

We thank EC Network LAMINATE (HPRN-CT-2000-00135) (PWL), the Royal Society and Clare Hall College (FC), the EPSRC, and CDT.

Notes and references

1 J. H. Burroughes, D. D. C. Bradley, A. R. Brown, R. N. Marks, K. Mackay, R. H. Friend, P. L. Burns and A. B. Holmes, *Nature*, 1990, **347**, 539.
2 A. Kraft, A. C. Grimsdale and A. B. Holmes, *Angew. Chem., Int. Ed. Engl.*, 1998, **37**, 402.
3 G. Hadziioannou and P. F. van Hutten, *Semiconducting Polymers Chemistry, Physics and Engineering*, Wiley-VCH, Weinheim, Germany, 2000.
4 M. R. Pinto, B. Hu, F. E. Karasz and L. Akcelrud, *Polymer*, 2000, **41**, 2603; B. Hu and F. E. Karasz, *Synth. Met*., 1998, **92**, 157; M. Hay and F. L. Klavetter, *J. Am. Chem. Soc*., 1995, **117**, 7112.
5 A. F. M. Kilbinger and W. J. Feast, *J. Mater. Chem*., 2000, **10**, 1777.
6 N. Benfaremo, D. J. Sandman, S. Tripathy, J. Kumar, K. Yang, M. F. Rubner and C. Lyons, *Macromolecules*, 1998, **31**, 3595.
7 C. H. Yang, G. F. He, R. Q. Wang and Y. F. Li, *Mol. Cryst. Liq. Cryst*., 1999, **337**, 473.
8 NMR data: ^{1}H-NMR δ (300 MHz; TCE-d_2) 7.5–7.1 (8H, m), 7.01 (1H, AB q, J = 16 Hz), 6.97 (1H, AB q, J = 16 Hz), 6.90 (2H, m), 6.77 (2H, m), 6.49 (1H, AB q, J = 12 Hz), 6.46 (1H, AB q, J = 12 Hz), 4.13 (4H, m), 3.84 (4H, m), 3.64 (16 H, m).
9 H. S. Woo, O. Llost, S. Graham, D. D. C. Bradley, R. H. Friend, C. Quattrocchi, J. L. Brédas, R. Schenk and K. Müllen, *Synth. Met*., 1993, **59**, 13; H. Ndayikengurukiye, S. Jacobs, W. Tachelet, J. Van Der Looy, A. Pollaris, H. J. Geise, M. Claeys, J. M. Kaufmann and S. Janietz, *Tetrahedron*, 1997, **53**, 13811; J. L. Brédas and A. J. Heeger, *Chem. Phys. Lett*., 1994, **217**, 507.
10 J. S. Kim, M. Granström, R. H. Friend, N. Johansson, W. R. Salaneck, R. Daik, W. J. Feast andF. Cacialli, *J. Appl. Phys*., 1998, **84**, 6859; J. S. Kim, R. H. Friend and F. Cacialli, *J. Appl. Phys*., 1999, **86**, 2774.
11 T. M. Brown, J. S. Kim, R. H. Friend, F. Cacialli, R. Daik and W. J. Feast, *Appl. Phys. Lett*., 1999, **75**, 1679.
12 Q. B. Pei, G. Yu, C. Zhang, Y. Yang and A. J. Heeger, *Science*, 1995, **269**, 1086.

CHEMCOMM
Communication
www.rsc.org/chemcomm

Synthesis and structural characterization of a silver complex of a mixed-donor N-heterocyclic carbene linked cyclophane†

Jered C. Garrison, Richard S. Simons, William G. Kofron, Claire A. Tessier and Wiley J. Youngs*

Department of Chemistry, University of Akron, Akron, Ohio 44325, USA. E-mail: youngs@uakron.edu

Received (in Cambridge, UK) 30th June 2001, Accepted 2nd August 2001
First published as an Advance Article on the web 21st August 2001

The synthesis of a dicationic imidazolium-linked cyclophane and a dimeric silver–N-heterocyclic carbene complex, that is the first silver complex with a N-heterocyclic carbene ligand involved in a π-bonding interaction, is reported.

Our group[1] and others[2] have been exploring the chemistry of silver complexes with mixed-donor N-heterocyclic carbene ligands. Bis(carbene)–Ag complexes with monodentate N-heterocyclic carbene ligands are all structurally similar, with two carbene moieties complexed to a Ag atom in a linear fashion.[3,4] The mixed-donor N-heterocyclic carbene ligands stabilize silver complexes that are quite varied. These complexes can have a combination of Ag–Ag, donor atom–Ag, and bis(carbene)–Ag interactions.

We report herein, the synthesis of the dicationic imidazolium-linked cyclophane **1** and the dimeric silver N-heterocyclic carbene complex $[Ag_4(\mathbf{1}^*)_2][PF_6]_4$ (**2**), where **1*** denotes deprotonated **1**, a bis-carbene-linked cyclophane.[5] Complex **2** is the first silver complex that has a N-heterocyclic carbene ligand involved in a π-bonding interaction. This novel situation facilitates the stabilization of a $[Ag_4]^{4+}$ cluster with four non-coordinating PF_6 anions.

The synthesis of cyclophane **1** is outlined in Scheme 1. The 3 + 1 condensation reaction of 2,6-bis(imidazolmethyl)pyridine[6] and 1-methyl-2,5-bis(trimethylaminomethyl)pyrrole diiodide[7] in nitromethane affords the cyclophane $\mathbf{1}[I]_2$. Treatment of an aqueous solution of $[\mathbf{1}][I]_2$ with ammonium hexafluorophosphate affords $[\mathbf{1}][PF_6]_2$. The ^{1}H and ^{13}C NMR spectra for $[\mathbf{1}][PF_6]_2$ are consistent with the proposed structure of **1**. The most notable features in the ^{1}H and ^{13}C NMR spectra are the resonances for the imidizolium protons at 8.6 ppm and the corresponding imidazolium carbons at 135.4 ppm. Cyclophane **1** in acetone generates $[\mathbf{1}][PF_6]^+$ ions at *m*/*z* 491.3 upon ESI-MS conditions (calculated *m*/*z* 491.2 for $C_{20}H_{22}N_6PF_6$).

Treatment of cyclophane $[\mathbf{1}][PF_6]_2$ with Ag_2O in DMSO at 55 °C affords the N-heterocyclic carbene complex $[Ag_4(\mathbf{1}^*)_2][PF_6]_4$ (**2**) (eqn. (1)). The ^{1}H and ^{13}C NMR data are consistent with the structure of **2**. The most notable feature of the ^{1}H NMR spectrum is the absence of the resonance for the imidazolium protons at 8.6 ppm. In the ^{13}C NMR spectrum for **2**, the carbene resonance appears as two doublets centered at 163.2 ppm ($^1J_{C_\sigma–Ag}$ = 220 Hz, $^1J_{C_\pi–Ag}$ = 47 Hz).[8] The chemical shift and the coupling pattern are consistent with two bonding interactions for the carbene moiety. The larger coupling of 220 Hz is consistent with a σ-bonding interaction between the carbene and a silver atom. Carbene–silver coupling constants have been reported in the range 204–220 Hz (^{109}Ag) and 180–189 Hz (^{107}Ag).[2b,3,4a,b] The smaller coupling of 47 Hz is unprecedented in silver–carbene chemistry, and we assign this value to an unconventional π-bonding interaction between the carbene and a neighboring silver atom. The assignment of each carbene interacting with two different silver atoms, *via* a σ-bonding and a π-bonding interaction, is consistent with the solid state structure for **2**.‡

$$2\,[\mathbf{1}][PF_6]_2 + 4\,Ag_2O \longrightarrow \underset{\mathbf{2}}{[Ag_4(\mathbf{1}^*)_2][PF_6]_4} \qquad (1)$$

The structure of the tetracationic portion of **2** consists of a centrosymmetric dimer with four Ag cations (Fig. 1). The asymmetric unit consists of precisely half of the dimer leading to equivalent bond lengths and angles. With this in mind, we will confine our discussions to only the asymmetric portion of the molecule except in the cases where the inversion center produces additional non-redundant parameters. The four Ag atoms form a central planar core with two Ag cations bridging the Ag–Ag contacts between the other two. The Ag1–Ag1A cross-ring distance (2.9712(11) Å) is slightly longer than the bridging Ag1–Ag2 (2.7680(9) Å) and Ag1A–Ag2 (2.8077(16) Å) interactions. Each bridging Ag atom forms two bonding

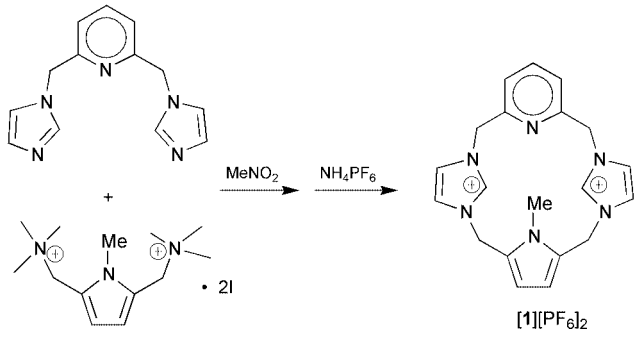

Scheme 1

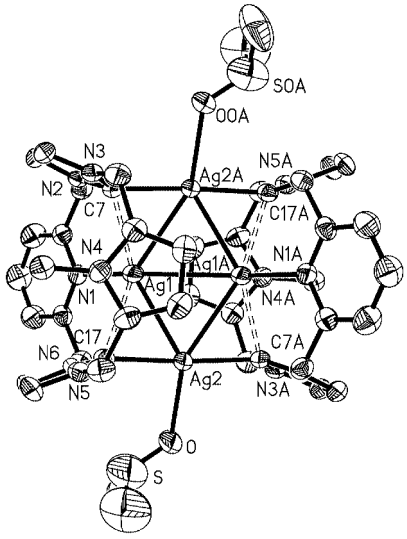

Fig. 1 Molecular structure of the tetracationic portion of $[Ag_4(\mathbf{1}^*)_2][PF_6]_4$ **2** with thermal ellipsoids drawn at 50% probability. Hydrogen atoms have been omitted for clarity. Selected bond lengths (Å) and angles (°): Ag1–Ag1A 2.9712(11), Ag1–Ag2 2.7680(9), Ag1A–Ag2 2.8077(16), Ag2–C7A 2.148(6), Ag2–C17 2.149(6), Ag1–C7 2.412(5), Ag1–C17 2.516(6); C17–Ag2–C7A 176.2(2).

† Electronic supplementary information (ESI) available: detailed experimental procedures for the syntheses of $[\mathbf{1}][PF_6]_2$ and $[Ag_4(\mathbf{1}^*)_2][PF_6]_4$ (**2**) and details of crystallography. See http://www.rsc.org/suppdata/cc/b1/b105751k

 DOI: 10.1039/b105751k

interactions with the carbene ligands of two neighboring macrocycles at Ag2–C7A (2.148(6) Å) and Ag2–C17 (2.149(6) Å) bond distances and a nearly linear C17–Ag2–C7A (176.2(2)°) bond angle. These values are quite normal when compared to the same parameters reported for other silver–bis(carbene) complexes.[1,3,4a,b] In addition, each bridging Ag atom has a DMSO molecule coordinated to it with a Ag–O distance of 2.401(5) Å. The non-bridging Ag atoms are each coordinated to the pyridine nitrogen atoms of neighboring ligands at a Ag1A–N1A bond distance of 2.360(5) Å. An interesting feature of **2** is the manner in which each carbene ligand tilts inward toward the center of the molecule and interacts with the non-bridging Ag atoms at distances of Ag1–C7 (2.412(5) Å) and Ag1–C17 (2.516(6) Å). Bonding interactions of this type are unprecedented in N-heterocyclic carbene chemistry.[9] We assign this interaction as a π-carbene–silver bond. Our assignment is supported by previously reported silver–arene π-bonding interactions which lie in the range 2.43–2.61 Å.[10] The pyrrole portion of each macrocycle is positioned such that a π–Ag interaction could be envisioned; however, the shortest contact is 3.30 Å (Ag1–N4) and they vary from 3.30–3.89 Å.

Organosilver complexes having inner $[Ag_4]^{4+}$ clusters similar to **2** have been reported.[11] In fact, the structural similarity between **2**, $[Ag(C_6H_4CH_2NMe_2\text{-}2)]_4$ **3**[11a] and $[Ag(C_5H_3CH_2NMe_2\text{-}2)Fe(C_5H_5)]_4$ **4**[11e] is remarkable. For **3**, four Ag–Ag bonds that average 2.738(2) Å are each asymmetrically bridged by an anionic $^{-}C_6H_4CH_2NMe_2$-2 ligand forming two Ag–C bonds that average 2.155(13) and 2.381(13) Å, respectively. For **4**, four Ag–Ag bonds (2.740(2) Å) form a planar core with each of the Ag–Ag bonds symmetrically bridged by an anionic ($^{-}C_5H_3CH_2NMe_2$-2)Fe(C_5H_5) ligand with Ag–C distances of 2.17(2) Å. The structural similarity between **2**, **3** and **4** can be explained in terms of the isoelectronic relationship between the anionic aryl ligands used for **3** and **4** and the N-heterocyclic carbene ligand.

We wish to thank the National Science Foundation, the University of Akron and the Ohio Board of Reagents for financial support. We thank Dr. Judith Gallucci for assistance in the collection of X-ray diffraction data for **2**.

Notes and references

‡ *Crystal data* for $C_{22}H_{26}N_6Ag_2P_2F_{12}$ (**2**)·Me_2SO: M = 928.21, triclinic, space group $P\bar{1}$, a = 10.389(2), b = 11.272(2), c = 14.104(3) Å, α = 110.21(3), β = 96.34(3), γ = 102.46(3°), V = 1482.3(5) Å^3, Z = 2, D_c = 1.125 Mg m^{-3}, μ = 0.817 mm^{-1}, T = 200 K, Refinement for data with $I > 2\sigma(I)$ (5212 reflections, R_{int} = 0.0214) gave $R1(F)$ = 0.0444 and $wR2(F^2)$ = 0.1343 for all data.

See http://www.rsc.org/suppdata/cc/b1/b105751k/ for crystallographic data in CIF or other electronic format.

1 J. C. Garrison, R. S. Simons, J. M. Talley, C. Wesdemiotis, C. A. Tessier and W. J. Youngs, *Organometallics*, 2001, **20**, 1276.

2 (*a*) A. A. D. Tulloch, A. A. Danopoulos, S. Winston, S. Kleinhenz and G. Eastham, *J. Chem. Soc., Dalton Trans*., 2000, 4499; (*b*) A. Caballero, E. Díez-Barra, F. A. Jalón, S. Merino and J. Tejeda, *J. Organomet. Chem*., 2001, **617–618**, 395; (*c*) A. M. Magill, D. S. McGuinness, K. J. Cavell, G. J. P. Britovsek, V. C. Gibson, A. J. P. White, D. J. Williams, A. H. White and B. W. Skelton, *J. Organomet. Chem*., 2001, **617–618**, 546.

3 A. J. Arduengo III, H. V. R. Dias, J. C. Calabrese and F. Davidson, *Organometallics*, 1993, **12**, 3405.

4 (*a*) B. Bildstein, M. Malaun, H. Kopacka, K. Wurst, M. Mitterböck, K. Ongania, O. Giuliana and P. Zanello, *Organometallics*, 1999, **18**, 4325; (*b*) H. M. J. Wang and I. J. B. Lin, *Organometallics*, 1998, **17**, 972; (*c*) D. S. McGuinness and K. J. Cavell, *Organometallics*, 2000, **19**, 741.

5 N-Heterocyclic carbene-linked cyclophanes have only been observed in the gas phase: E. Alcalde, N. Mesquida and M. Vilaseca, *Rapid Commun. Mass Spectrom*., 2000, **14**, 1443.

6 W. A. Herrmann, C. Kocher and L. Goossen, *US Pat*., 6 025 496, 2000

7 I. T. Kim and R. L. Elsenbaumer, *Tetrahedron Lett*., 1998, **39**, 1087.

8 ^{107}Ag and ^{109}Ag coupling constants for $^{1}J_{C-Ag}$ are within 10% of each other and were not resolvable for **2** due to broadening.

9 (*a*) D. Bourissou, O. Guerret, F. P. Gabbaï and G. Bertrand, *Chem. Rev*., 2000, **100**, 39; (*b*) W. A. Herrmann and C. Köcher, *Angew. Chem., Int. Ed. Engl*., 1997, **36**, 2162.

10 (*a*) H. C. Kang, A. W. Hanson, B. Eaton and V. Boekelheide, *J. Am. Chem. Soc*., 1985, **107**, 1979; (*b*) P. F. Rodesiler, E. A. Hall Griffith and B. L. Amma, *J. Am. Chem. Soc*., 1972, **94**, 761; (*c*) E. A. Hall Griffith and B. L. Amma, *J. Am. Chem. Soc*., 1974, **96**, 5407; (*d*) E. A. Hall Griffith and B. L. Amma, *J. Am. Chem. Soc*., 1974, **96**, 743; (*e*) I. F. Taylor, E. A. Hall and B. L. Amma, *J. Am. Chem. Soc*., 1969, **91**, 5745; (*f*) H. G. Smith and R. E. Rundle, *J. Am. Chem. Soc*., 1958, **80**, 5075.

11 (*a*) D. A. Edwards, R. M. Harker, M. F. Mahon and K. C. Molloy, *J. Chem. Soc., Dalton Trans*., 1997, 3509; (*b*) E. M. Meyer, S. Gambarotta, C. Floriani, A. Chiesi-Villa and C. Guastini, *Organometallics*, 1989, **8**, 1067; (*c*) S. Gambarotta, C. Floriani and A. Chiesi-Villa, *J. Chem. Soc., Chem. Commun*., 1983, 1087; (*d*) P. M. Jeffries, S. R. Wilson and G. S. Girolami, *J. Organomet. Chem*., 1993, **449**, 203; (*e*) A. N. Nesmeyanov, N. N. Sedova, Y. T. Struchkov, V. G. Adrianov, E. N. Stakheeva and V. A. Sazonova, *J. Organomet. Chem*., 1978, **153**, 115.

CHEMCOMM Communication
www.rsc.org/chemcomm

Production of Au–Ag alloy nanoparticles by laser ablation of bulk alloys

Inhyung Lee, Sang Woo Han and Kwan Kim*

Laboratory of Intelligent Interface, School of Chemistry and Molecular Engineering and Center for Molecular Catalysis, Seoul National University, Seoul 151-742, Korea.
E-mail: kwankim@plaza.snu.ac.kr

Received (in Cambridge, UK) 20th June 2001, Accepted 6th August 2001
First published as an Advance Article on the web 3rd September 2001

Gold–silver alloy nanoparticles can be produced by pulsed laser irradiation of bulk alloy metals in water, preserving the stoichiometry of the target metals.

The intense research activity in the field of nanoparticles that has been conducted by chemists, physicists, and material scientists is motivated by the search for new materials in order to further miniaturize electronic devices, as well as by the fundamental question of how molecular electronic properties evolve with increasing size in this intermediate region between molecular and solid-state physics.[1] In particular, nanocomposites, *i.e.*, alloy and/or core–shell particles, are attractive materials because of their composition-dependent optical and catalytic properties. Papavassiliou has successfully prepared Au–Ag alloy particles *via* evaporation of Au–Ag alloys.[2] Liz-Marzan and Philipse prepared various bimetallic colloidal nanoparticles (Au–Ag, Au–Pt, and Ag–Pt) by reducing the metal salts in aqueous, optically transparent dispersions of inorganic fibers.[3] Our research group[4] and El-Sayed *et al.*[5] employed simultaneous reduction of gold and silver salts to form Au–Ag alloy particles with 4 and 18 nm diameters, respectively. Very recently, Hodak *et al.*[6] and Chen and Yeh[7] reported the production of Au–Ag alloy nanoparticles by laser irradiation of either the Au–Ag core–shell nanoparticles or the gold and silver colloidal mixtures. This suggests that the interaction between laser light and nano/colloidal particles can result in compositional changes *via* a melting process.[6–8] Herein, we report that homogeneous alloy nanoparticles can be produced even from bulk alloys by laser ablation in water.[9] A gold–silver system is chosen as a model case since both metals are miscible in all proportions in bulk due to their comparable lattice constants. Moreover, UV-vis absorption spectroscopy can readily be applied to differentiate an alloyed structure from a core–shell one for Au–Ag bimetallic particles.[3–5]

Initially, Au–Ag bulk alloys were prepared by inductively heating two metals at high frequency; metals used were in molar ratios of Au:Ag = 3:1, 2:2, and 1:3. Hereafter, we will refer to the metal nanoparticles prepared from the Au–Ag alloys in molar ratios of 3:1, 2:2, and 1:3 as $Au_{0.75}Ag_{0.25}$, $Au_{0.5}Ag_{0.5}$, and $Au_{0.25}Ag_{0.75}$, respectively.† Silver and gold nanoparticles are known to show plasmon absorption bands in the visible region (at ~390 and ~520 nm, respectively[10]). In fact, distinct peaks are observed at 394 and 518 nm in the UV-vis spectra of the Ag and Au nanoparticles prepared from pure metals (see the spectra labeled (a) and (e) in Fig. 1). In Fig. 1 are also shown the UV-vis spectra of the $Au_{0.25}Ag_{0.75}$, $Au_{0.5}Ag_{0.5}$, and $Au_{0.75}Ag_{0.25}$ samples (see the spectra labeled (b), (c), and (d), respectively). Peaks are clearly observed at 427, 460, and 493 nm, respectively, for these samples; all these peaks are located at intermediate positions between the intrinsic Ag and Au plasmon bands. Hence, they must arise from the surface plasmon absorptions of alloyed nanoparticles. It is noteworthy that the plasmon absorptions of the gold–silver composite clusters are linearly red-shifted from that of a monometallic Ag cluster in proportion to the increase in the mol fraction of the Au content. This is demonstrated by Fig. 2, in which the UV-vis absorption peak position is plotted against the mol fraction of Au in the precursor samples. Two plasmon bands would be expected if the clusters consisted of individual Au and Ag particles or of bimetallic composites with a core–shell structure.[4,10] All these UV-vis spectral features suggest that the Au–Ag composite particles prepared in this work are neither a simple mechanical mixture of two different monometallic particles nor bimetallic nanoparticles with a core–shell structure.

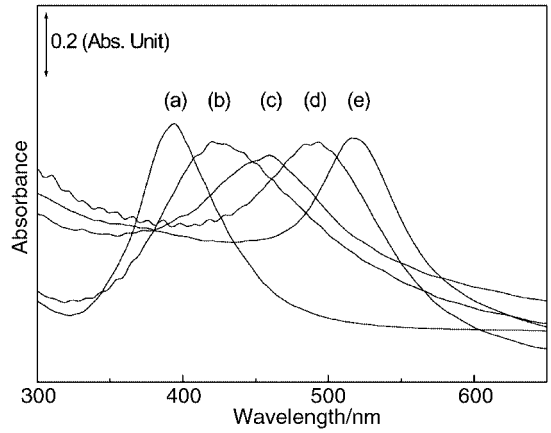

Fig. 1 UV-vis absorption spectra of Au–Ag alloy nanoparticles produced in distilled water with nominal formulae of (a) Ag, (b) $Au_{0.25}Ag_{0.75}$, (c) $Au_{0.5}Ag_{0.5}$, (d) $Au_{0.75}Ag_{0.25}$, and (e) Au.

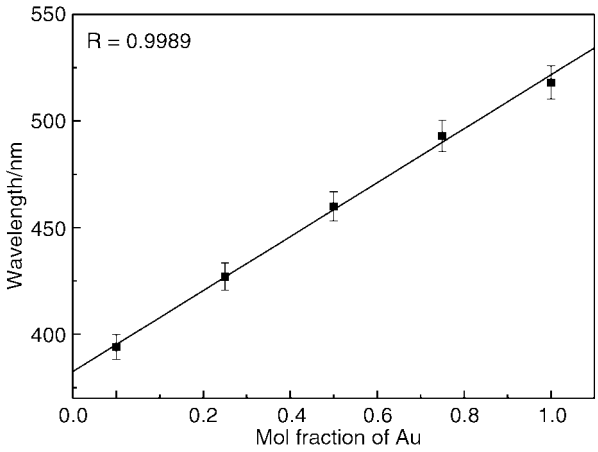

Fig. 2 Positions of surface plasmon bands plotted against the mol fractions of Au atoms in alloy nanoparticles.

Fig. 3(a) shows a typical TEM (JEM-2000 EXII, 160 kV) image taken for a $Au_{0.5}Ag_{0.5}$ sample. As can be seen in the image, most of the particles are not agglomerated and their average size is ~10 nm. Other samples showed similar TEM images. As surmised from UV-vis absorption spectroscopy, the probability of the presence of core–shell particles is proved to

 DOI: 10.1039/b105437f

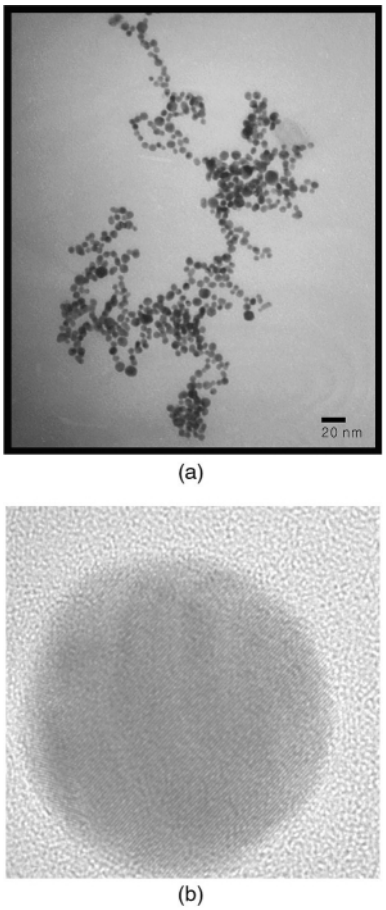

Fig. 3 (a) TEM image of Au–Ag alloy nanoparticles with a nominal formula of $Au_{0.5}Ag_{0.5}$. (b) HRTEM image of a 16 nm diameter Au–Ag alloy nanoparticle with a nominal formula of $Au_{0.5}Ag_{0.5}$.

be very low from the energy dispersive X-ray spectroscopy (EDX) analysis. In the latter analysis, peak integration and normalization were carried out to measure the Au-to-Ag ratio in individual particles, and the data were collected over 10 particles. The EDX analysis on the $Au_{0.75}Ag_{0.25}$, $Au_{0.5}Ag_{0.5}$, and $Au_{0.25}Ag_{0.75}$ particles thus yielded atomic ratios of Au : Ag = 75.79 : 24.21 (±1.65), 49.75 : 50.25 (±1.01), and 25.14 : 74.86 (±1.71), respectively. The results were always comparable to within 2%. These observations indicate that the laser-ablated products are indeed homogeneous alloyed nanoparticles.

Fig. 3(b) is a high-resolution TEM (HRTEM, JEM-3000F, 300 kV) image of the sample in Fig. 3(a). We can estimate from this image that the lattice plane spacing is about 2.35 Å. Much the same value (2.35 ± 0.01 Å) was obtained for other samples with different compositions. In fact, the value obtained herein is very close to those of pure Ag and Au, *i.e.*, 2.36 Å for Ag and 2.35 Å for Au.[11] This may be attributed to the fact that Ag and Au are miscible in all proportions due to their almost identical lattice constants. The unit cell size of Au–Ag alloys changes by less than 1% over the entire range from pure Au to pure Ag, and no superlattice reflections are observed in the alloys.[12]

Let us briefly provide a plausible mechanism for the alloyed particle formation. Immediately after the laser irradiation, the surface of a sample will reach a very high temperature by absorbing pulsed laser energy. As a consequence, atoms and/or small particles should be ejected through vaporization, followed by the build-up of a dense cloud of metal atoms (Au and Ag atoms) near the laser spot. Since the interaction between metal atoms is much greater than that between a metal atom and a solvent molecule, the metal atom(s) will aggregate to produce nanoparticles. Since Au and Ag form nearly ideal solid solutions at all compositions,[13] mixing of the two metals is a thermodynamically favorable process. Therefore, nanoparticles formed must be homogeneous alloy particles.

In summary, we found that Au–Ag alloy nanoparticles could be easily produced by laser ablation of a bulk alloy in water. Formation of homogeneous alloyed particles was clearly demonstrated by UV-vis absorption spectroscopy and TEM and EDX measurements. The simplicity of the procedure is clearly a major advantage of the present method. The size distribution of nanoparticles can be readily controlled by varying the pulse energy and time of ablation. The method is versatile with respect to the kinds of metals and/or solvents employed. The absence of chemical reagents or ions in the final preparation will also be advantageous. The particles can be derivatized with suitable amphiphiles afterwards. Currently, we are attempting to synthesize other alloyed particles such as Au–Pt, Au–Cu, and Ag–Pt.

This work was supported in part by the Korea Research Foundation (KRF, 042-D00073) and the Korea Science and Engineering Foundation (KOSEF, 1999-2-121-001-5). K. K. also acknowledges KOSEF for providing a leading-scientist grant. S. W. H. was supported by KOSEF through the Center for Molecular Catalysis at Seoul National University. I.L., is a recipient of the BK21 fellowship.

Notes and references

† For the laser ablation experiments, bulk alloys were placed at the bottom of a glass vessel filled with 10 mL triply distilled water, and then irradiated using a focused beam of a Nd : YAG laser (Continuum Surelite II-10, at 1064 nm). The typical pulse energy, repetition rate, laser pulse duration, and irradiation time were 50 mJ, 10 Hz, 6 ns, and 30 min, respectively. For reference, pure gold and silver nanoparticles were also prepared *via* the same method. Since the produced particles interfere with the subsequent laser pulses, the efficiency of the ablation process gradually decreases as a function of the irradiation time. This can be minimized by stirring the solution phase continuously during the laser ablation process. The extinction spectrum was recorded with a UV-vis absorption spectrometer (SINCO S-2130). Transmission electron microscope (TEM) images of the nanoparticles were acquired by placing drops of sample solutions on copper grids, followed by evaporation of the solvent in a vacuum desiccator.

1 See for example: (*a*) G. Schmid, *Clusters and Colloids: From Theory to Application*, VCH, Weinheim, 1994; (*b*) J. H. Fendler, *Nanoparticles and Nanostructured Films: Preparation, Characterization and Applications*, Wiley-VCH, Weinheim, 1998; (*c*) T. Sugimoto, *Fine Particles: Synthesis, Characterization, and Mechanisms of Growth*, Marcel Dekker, Inc., New York, 2000.
2 G. C. Papavassiliou, *J. Phys. F*, 1976, **6**, L103.
3 L. M. Liz-Marzan and A. P. Philipse, *J. Phys. Chem.*, 1995, **99**, 15 120.
4 S. W. Han, Y. Kim and K. Kim, *J. Colloid Interface Sci.*, 1998, **208**, 272.
5 S. Link, Z. L. Wang and M. A. El-Sayed, *J. Phys. Chem. B*, 1999, **103**, 3529.
6 J. H. Hodak, A. Henglein, M. Giersig and G. V. Hartland, *J. Phys. Chem. B*, 2000, **104**, 11 708.
7 Y.-H. Chen and C.-S. Yeh, *Chem. Commun.*, 2000, 371.
8 H. Kurita, A. Takami and S. Koda, *Appl. Phys. Lett.*, 1998, **72**, 789.
9 See for example: (*a*) A. Fojtik and A. Henglein, *Ber. Bunsen-Ges. Phys. Chem.*, 1993, **97**, 252; (*b*) M. S. Sibbald, G. Chumanov and T. M. Cotton, *J. Phys. Chem.*, 1996, **100**, 4672; (*c*) I. Srnová, M. Procházka, B. Vlčková, J. Štěpánek and P. Malý, *Langmuir*, 1998, **14**, 4666.
10 P. Mulvaney, *Langmuir*, 1996, **12**, 788.
11 P. Mulvaney, M. Griersig and A. Henglein, *J. Phys. Chem.*, 1993, **97**, 7061.
12 M. LeBlanc and W. Erler, *Ann. Phys.*, 1933, **16**, 321.
13 H. Okamoto and T. B. Massalki, *Binary Alloy Phase Diagrams*, ASM International, Ohio, 1990.

CHEMCOMM Communication
www.rsc.org/chemcomm

Asymmetric synthesis of 2-substituted piperidines using a multi-component coupling reaction: rapid assembly of (*S*)-coniine from (*S*)-1-(1-phenylethyl)-2-methyleneaziridine

Jerome F. Hayes,[a] Michael Shipman*[b] and Heather Twin[b]

[a] *GlaxoSmithKline, Old Powder Mills, Tonbridge, Kent, UK TN11 9AN*
[b] *School of Chemistry, University of Exeter, Exeter, Devon, UK EX4 4QD. E-mail: m.shipman@exeter.ac.uk; Fax: +44 1392 263434; Tel: +44 1392 263469*

Received (in Cambridge, UK) 13th July 2001, Accepted 30th July 2001
First published as an Advance Article on the web 21st August 2001

(*S*)-Coniine is made using a reaction which assembles the piperidine ring by the sequential formation of four new chemical bonds and installs the C-2 stereogenic centre with high levels of diastereocontrol (90% de).

We recently devised a new type of multi-component coupling reaction using 2-methyleneaziridines.[1] Ring opening of this stable and readily accessible heterocyclic system with a Grignard reagent in the presence of copper(I) iodide furnishes a metalloenamine in a regiocontrolled fashion by formation of a carbon–carbon bond. This methodology was originally used to make simple ketones by further *in situ C*-alkylation of the metalloenamine followed by imine hydrolysis. We imagined that by suitable modification, this multi-component coupling reaction could be used to assemble 2-substituted piperidines, important structural motifs in organic chemistry.[2] Our basic approach to these piperidines is depicted in Scheme 1. Alkylation of the initially generated metalloenamine with a 1,3-difunctionalised electrophile ($XCH_2CH_2CH_2X$) followed by reduction of the resultant imine and *in situ* cyclisation was anticipated to lead directly to the piperidine ring system by the sequential formation of two carbon–carbon bonds, one carbon–nitrogen bond and a carbon–hydrogen bond in a single transformation. Furthermore, since 2-methyleneaziridines bearing chiral, nonracemic substituents on nitrogen are known,[3] we hoped that control of the absolute stereochemistry at C-2 of the piperidine ring may be possible by effecting a diastereocontrolled reduction of the intermediate imine using an enantiomerically pure 2-methyleneaziridine starting material.[4] In this communication, we report the successful realisation of these concepts as demonstrated by the enantiocontrolled synthesis of the hemlock alkaloid (*S*)-coniine in a very concise fashion.[5]

We chose to use (*S*)-1-(1-phenylethyl)-2-methyleneaziridine **1** for this study as it is readily accessible in two steps from (*S*)-1-phenylethylamine in good overall yield.[3b] In addition to bearing a group suitable for effecting stereocontrolled reduction of the imine double bond, it possesses the additional attribute that the PhCHMe group can ultimately be removed by cleavage of the benzylic C–N bond. Treatment of (*S*)-**1** with EtMgCl and copper(I) iodide, then 1,3-diiodopropane, and finally sodium triacetoxyborohydride results in the production of piperidine **4** in 42% yield as essentially a single diastereomer (97% de) after chromatography on neutral alumina (Scheme 2).†‡ Slightly larger amounts of the (2*R*)-diastereomer can be detected {(2*S*):(2*R*) = 95:5} by GC analysis prior to chromatography. Piperidine **4** (97% de) was obtained in identical yield using sodium borohydride as the reducing agent, however, the crude diastereomeric ratio was slightly lower {(2*S*):(2*R*) = 88:12}. Metalloenamine **2** must be added to a solution of excess 1,3-diiodopropane (5 equiv.) in THF (inverse addition) to obtain these chemical yields. In this way, additional intermolecular reactions of imine **3a** are suppressed. Using a normal addition mode, quantities of *N*-(1-phenylethyl)-4-decylamine (21%) were produced as a result of displacement of the second iodide by excess ethylmagnesium chloride present in the reaction mixture. Further hydrogenolysis of **4** provides (*S*)-(+)-coniine hydrochloride in 93% yield whose physical and spectroscopic data were in good agreement with those reported previously {mp 212 °C (lit. mp 217 °C[6]); $[\alpha]_D^{25}$ +8.1 (*c* 0.6, EtOH) [lit. $[\alpha]_D^{28}$ + 5.8 (*c* 0.43, EtOH)][6]}. The enantiomeric excess of the synthetic (*S*)-coniine was established to be ⩾95% ee by preparation of the corresponding Mosher amide using (*S*)-(+)-α-methoxy-α-(trifluoromethyl)phenylacetic acid chloride.§

Interestingly, when 1-iodopropane was used as the electrophile in this multi-component coupling reaction, amine **5** was isolated in 49% yield as a 58:42 mixture of diastereomers after reduction with $NaBH_4$, indicating that the presence of the remote iodine atom has a significant influence on the diastereoselectivity of the imine reduction. To account for these differences, we suggest that imine **3a** cyclises to iminium ion **6** prior to reduction (Scheme 3). The high level of stereochemical control seen in favour of the (2*S*)-diastereomer can be

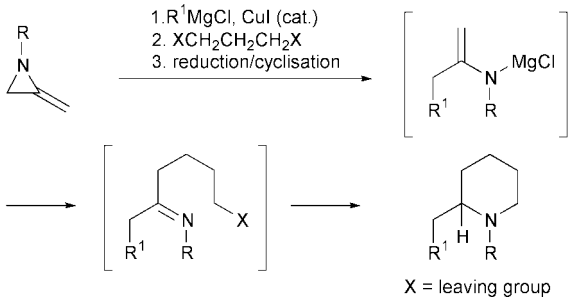

Scheme 1 Planned one-pot piperidine synthesis.

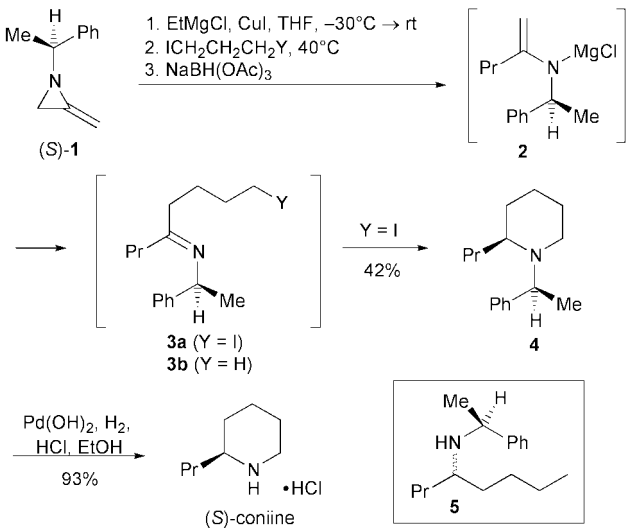

Scheme 2 Asymmetric synthesis of (*S*)-coniine.

 DOI: 10.1039/b106260n

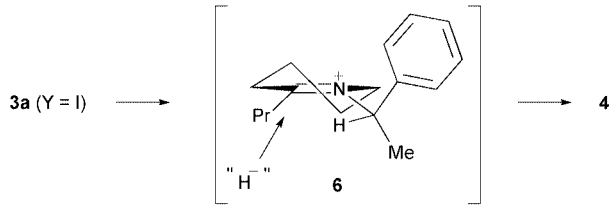

Scheme 3 Rationalisation of diastereoselectivity.

rationalised by assuming this iminium cation adopts a conformation in which allylic 1,3-strain is minimised by projecting the hydrogen atom of the benzylic carbon towards the propyl group, with subsequent hydride addition from the least hindered *Re*-face. In contrast, acyclic imine **3b** has much greater conformation freedom and is reduced in a non-selective fashion to **5**.

In conclusion, we have devised a very short and stereoselective synthesis of the piperidine alkaloid (*S*)-coniine by way of a multi-component coupling reaction. The key step forms four new chemical bonds (>80% efficiency for each) and is highly stereoselective (90% de). Since we have demonstrated that a variety of Grignard reagents (alkyl, aryl, benzyl) ring open 2-methyleneaziridines to metalloenamines,[1] this method should provide a rapid entry to a wide variety of enantiomerically enriched 2-substituted piperidines.

We are indebted to EPSRC and GlaxoSmithKline for their generous financial support of this work. We thank the EPSRC National Mass Spectrometry Centre for performing some of the mass spectral measurements and the EPSRC Chemical Database Service at Daresbury.[7]

Notes and references

† All new compounds have been fully characterised using standard spectroscopic and analytical methods.

‡ *Experimental procedure*: To CuI (72 mg, 0.378 mmol) in THF (6 ml) at −30 °C was added EtMgCl (2.0 M in THF, 2.36 ml, 4.72 mmol) dropwise. After stirring for 10 min, (*S*)-**1** (300 mg, 1.88 mmol) in THF (3 ml) was added. The reaction mixture was allowed to warm up to room temperature and stirred for 24 h. This mixture was then added to diiodopropane (1.09 mL, 9.49 mmol) in THF (2 ml) at 0 °C. A reflux condenser was fitted and the mixture was heated to 40 °C for 18 h. On cooling, the resultant dark green mixture was added to a solution of sodium borohydride (214 mg, 5.66 mmol) in glacial acetic acid (4 ml) at 10 °C. After 2 hours, water (6 ml) was slowly added, then 2 M NaOH (4 ml) and EtOAc (4 ml). After 10 min, the mixture was extracted with EtOAc then washed with aq. NH_4Cl (2 × 20 ml), aq. $NaHCO_3$ (2 × 20 ml) and brine (2 × 20 ml). The organic layer was dried ($MgSO_4$), filtered and the solvent removed *in vacuo*. Column chromatography on alumina (0.1% MeOH in CH_2Cl_2) gave **4** (183 mg, 42%, 97% de) as a pale yellow oil. $[\alpha]_D^{26}$ +14.0 (*c* 0.86, $CHCl_3$); ν_{max} (neat) 2929, 2797, 1445 cm^{-1}; δ_H (400 MHz, $CDCl_3$) 7.45–7.19 (5H, m), 4.02 (1H, q, *J* 6.7 Hz), 2.75–2.73 (1H, m), 2.41–2.36 (1H, m), 2.25–2.17 (1H, m), 1.75–1.25 (10H, m, 5 × CH_2), 1.26 (3H, d, *J* 6.7 Hz), 0.94 (3H, t, *J* 7.2 Hz); δ_C (100.9 MHz, $CDCl_3$) 146.4 (s), 128.0 (d), 127.5 (d), 126.2 (d), 56.8 (d), 55.7 (d), 45.1 (t), 31.0 (t), 29.6 (t), 25.8 (t), 22.7 (t), 18.9 (t), 14.7 (q), 14.6 (q); Observed: 231.1995 (M^+); $C_{16}H_{25}N$ requires 231.1987; Anal. calc. for $C_{16}H_{25}N$: C, 83.06; H, 10.89; N, 6.05%. Found: C, 83.15; H, 11.17; N, 5.89%.

§ *rac*-Coniine was made and used for comparison purposes.

1 J. F. Hayes, M. Shipman and H. Twin, *Chem. Commun*., 2000, 1791.
2 For recent reviews, see (*a*) P. Hammann, *Organic Synthesis Highlights II*, ed. H. Waldmannn, VCH, New York, 1995, p. 323; (*b*) P. D. Bailey, P. A. Millwood and P. D. Smith, *Chem. Commun*., 1998, 633; (*c*) S. Laschat and T. Dickner, *Synthesis*, 2000, 1781.
3 (*a*) A. T. Bottini and V. Dev, *J. Org. Chem*., 1962, **27**, 968; (*b*) J. Ince, T. M. Ross, M. Shipman, A. M. Z. Slawin and D. S. Ennis, *Tetrahedron*, 1996, **52**, 7037; (*c*) J. Ince, T. M. Ross, M. Shipman and D. S. Ennis, *Tetrahedron: Asymmetry*, 1996, **7**, 3397.
4 Diastereocontrolled [2π + 2π] cycloadditions of 2-methyleneaziridines have been reported, see T. M. Ross, M. Shipman and A. M. Z. Slawin, *Tetrahedron Lett*., 1999, **40**, 6091.
5 For recent asymmetric syntheses of coniine, see (*a*) K. Pachamuthu and Y. D. Vankar, *J. Organomet. Chem*., 2001, **624**, 359; (*b*) J. L. Terán, D. Gnecco, A. Galindo, J. Juárez, S. Bèrnes and R. G. Enríquez, *Tetrahedron: Asymmetry*, 2001, **12**, 357; (*c*) M. Eskici and T. Gallagher, *Synlett*, 2000, 1360; (*d*) F. Bois, D. Gardette and J.-C. Gramain, *Tetrahedron Lett*., 2000, **41**, 8769; (*e*) T. J. Wilkinson, N. W. Stehle and P. Beak, *Org. Lett*., 2000, **2**, 155; (*f*) J. C. A. Hunt, P. Laurent and C. J. Moody, *Chem. Commun*., 2000, 1771; (*g*) M. Shimizu, A. Arai and T. Fujisawa, *Heterocycles*, 2000, **52**, 137; (*h*) E. Jo, Y. Na and S. Chang, *Tetrahedron Lett*., 1999, **40**, 5581; (*i*) S. B. Davies and M. A. McKervey, *Tetrahedron Lett*., 1999, **40**, 1229; (*j*) A. R. Katritzky, G. Qiu, B. Yang and P. J. Steel, *J. Org. Chem*., 1998, **63**, 6699; (*k*) M. T. Reding and S. L. Buchwald, *J. Org. Chem*., 1998, **63**, 6344; (*l*) F. Sánchez-Sancho and B. Herradón, *Tetrahedron: Asymmetry*, 1998, **9**, 1951; (*m*) S. Nazabadioko, R. J. Pérez, R. Brieva and V. Gotor, *Tetrahedron: Asymmetry*, 1998, **9**, 1597; (*n*) Y. Hirai and H. Yokoyama, *J. Syn. Org. Chem. Jpn*., 1998, **56**, 50.
6 D. Enders and J. Tiebes, *Liebigs Ann. Chem*., 1993, 173.
7 D. A. Fletcher, R. F. McMeeking and D. Parkin, *J. Chem. Inf. Comp. Sci*., 1996, **36**, 746.

CHEMCOMM
Communication
www.rsc.org/chemcomm

Oxoanionic or sulfur lone pair attack? The difference in reactivity of hydrogensulfite anion and neutral dimethylsulfite towards $[Bu_4N]_2[MoO_2\{S_2C_2(CN)_2\}_2]$ in the model reductive half reaction of sulfite oxidase

Kowliki Nagarajan,[a] Pradeep K. Chaudhury,[b] Bikshandarkoil R. Srinivasan[c] and Sabyasachi Sarkar*[a]

[a] *Department of Chemistry, Indian Institute of Technology, Kanpur 208 016, India. E-mail: abya@iitk.ac.in*
[b] *Department of Chemistry, University of Pune, Pune 411 007, India*
[c] *Department of Chemistry, Goa University, Goa 403 206, India*

Received (in Cambridge, UK) 18th June 2001, Accepted 2nd August 2001
First published as an Advance Article on the web 22nd August 2001

pH dependent reactivity differences of dimethylsulfite towards the title complex 1 demonstrate the crucial need of oxo-anionic coordination of sulfite to the molybdenum centre of 1 in the model reductive half reaction of sulfite oxidase.

Sulfite oxidase catalyzes the physiologically vital oxidation of sulfite to sulfate.[1] It contains molybdenum associated with a molybdopterin dithiolene cofactor and a cytochrome *b*-type heme.[1,2] The two-electron oxidation of sulfite to sulfate occurs at the molybdenum site leading its reduction from Mo(VI) to Mo(IV) and the catalytic cycle is completed by two sequential one-electron oxidations of Mo(IV) to Mo(VI) *via* Mo(V) by cytochrome *c* through the cytochrome *b* site.[3]

The fundamental chemistry catalyzed by sulfite oxidase has been investigated using several model compounds possessing a $\{Mo^{VI}O_2\}$ moiety involving phosphines as model substrates.[4] $[Bu_4N]_2[MoO_2\{S_2C_2(CN)_2\}_2]$ **1** is shown to perform oxidation of HSO_3^- to HSO_4^- both in terms of saturation as well as anionic inhibition kinetics similar to the reductive half reaction of native sulfite oxidase.[5] The initial proposal of oxoanionic attack[5] of HSO_3^- on the Mo center of **1** has been questioned[6] based on the unique experimental results reported by Hille and Brody involving neutral dimethylsulfite as an alternate substrate of the native sulfite oxidase.[7] Nucleophilic attack on one of the Mo=O groups present in **1** by a lone pair of sulfur of HSO_3^-, similar to that of phosphorus in phosphines, have been suggested.[6] Hille and Brody have shown that the methylation of two oxoanions of sulfite reduces the affinity of dimethylsulfite for the active site of the native enzyme. Exhibition of saturation kinetics by dimethylsulfite implies the formation of a Michaelis complex which they interpreted in terms of possible electrostatic interaction between the active site and modified substrate.[7] It has also been reported that sulfite anion contributes 3.4 kcal mol^{-1}. towards the stablization of the E_{ox} S complex which is consistent with the direct coordination to Mo.† Direct oxoanionic coordination of sulfite to the Mo center has also been suggested by Rajagopalan and coworkers.[9] **1** has been shown to respond to saturation kinetics with typical anionic inhibition involving HSO_3^- as substrate.[5] In this communication we furnish proof for the importance of oxo-anionic coordination for such an enzymatic atom transfer reaction by presenting the pH dependent reactivity difference of dimethylsulfite towards **1** which is of relevance to its reaction with native protein.

In order to gain an insight into the reaction of **1** with reductants such as dimethylsulfite, PPh_3 or HSO_3^-; the reactivity of all these oxo-acceptors have separately been examined by following the absorbance change of **1** during the progress of the reaction. In the presence of an excess of dimethylsulfite, **1** in acetonitrile or in acetonitrile–water (pH, 5–7) did not show any change in its electronic spectrum suggesting the inability of dimethylsulfite to reduce **1** [Fig. 1(a)]. Interestingly, dimethylsulfite after standing at pH 8 for a few minutes was found to be capable to reduce **1**, the time-dependent progress of the reaction distinctly showed the formation of the reduced species, $[Bu_4N]_2[MoO\{S_2C_2(CN)_2\}_2]$ **2** [Fig. 1(b)].

The difference in reactivity of dimethylsulfite in the pH range 5–7 and 8 towards **1** was checked by its response to hydrolysis under similar conditions. Thus aqueous solutions of dimethylsulfite at different pH were tested with aqueous $BaCl_2$. In the pH range 5–7 there was no precipitation of $BaSO_3$ over a time period of hours but at pH 8 (and above) precipitation of $BaSO_3$ started to occur within minutes and its identity was confirmed by the standard $BaSO_4$ test.§ The reactions described above clearly demonstrate the inability of neutral dimethylsulfite to react with **1** suggesting the inability of the sulfur lone pair to initiate any redox reaction. Once the neutral dimethylsulfite is base hydrolysed (pH 8) to yield HSO_3^-, the reaction progresses smoothly [Fig. 1(b)].

Interestingly PPh_3 does reduce **1** to **2**; the time-dependent progress of the reaction is shown in Fig. 2.[6]

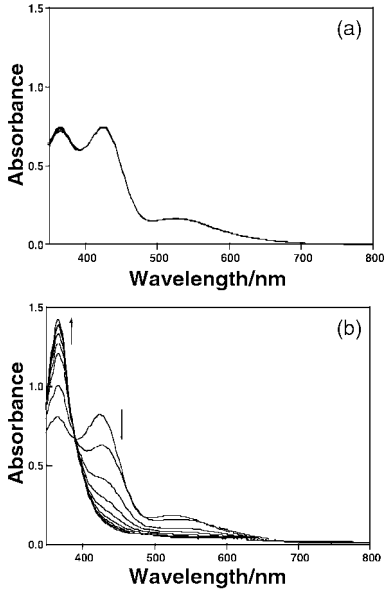

Fig. 1 (a) Spectral changes for the reaction between **1** (1×10^{-4} M) and dimethylsulfite (1.15×10^{-2} M) in acetonitrile. Spectra were taken for 150 min at intervals of 30 min. (b) Spectral changes for the reaction between **1** (1.075×10^{-4} M) and dimethylsulfite (3.4×10^{-2} M) at pH 8 in acetonitrile–water medium.‡ Spectra were taken for 14 min at intervals of 2 min.

 DOI: 10.1039/b105341h

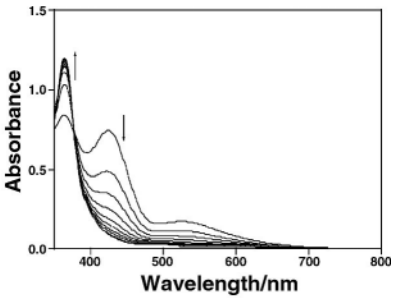

Fig. 2 Spectral changes for the reaction between **1** (1×10^{-4} M) and PPh_3 (5×10^{-3} M) in acetonitrile. Spectra were taken for 150 min at intervals of 15 min.¶

The difference in reactivity between HSO_3^- and PPh_3 should be noted in a sense that for all the reported reactions of model compounds including that of **1**, phosphines invariably respond to oxo abstraction by following second order kinetics (without the involvement of the Michaelis complex) whereas the unique reduction of **1** by HSO_3^- follows enzymatic kinetics (Michaelis complex) similar to that of the native sulfite oxidase.[5] Thus the reactivity of anionic HSO_3^- towards **1** is clearly dependent on the direct coordination of HSO_3^- to the Mo site as proposed earlier.[5] This also explains the observed competitive inhibiton by sulfate,[5] otherwise the lone pair attack of sulfur on the coordinated terminal oxo group and the direct binding of SO_4^{2-} to Mo would have resulted in mixed non-competitive inhibition. The heptacoordinated E_{ox} S type complex, $\{[Bu_4N]_2[Mo(O)(O^-)\{S_2C_2(CN)_2\}_2\{O(OH)SO\}]\}$, generated by the oxoanionic binding of HSO_3^- transforms the $\{Mo(O)_2\}$ group to $\{Mo^{VI}(O)(O^-)\{O(OH)SO\}\}$ moiety which in turn may lead to bidentate coordination of bisulfite to form $\{Mo^{VI}(O)(\mu\text{-}O)_2(OH)S(O)\}$ for the product release step (Scheme 1). This reaction may thus be viewed as being similar to the reductive elimination reaction where the Mo(VI) containing heptacoordinated[11] E_{ox} S complex‖ changed to pentacoordinated Mo(IV) in **2** with the elimination of HSO_4^-.

Funding of this work by DST (New Delhi) and IIT-Kanpur is gratefully acknowledged.

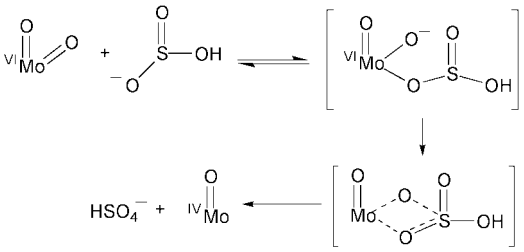

Scheme 1

Notes and references

† The possibility of direct binding of the oxoanion of HSO_3^- to Mo has not been considered in the calculation.[8]

‡ Aqueous dimethylsulfite solution was adjusted to pH 8 by sodium hydroxide and after 5 min its pH was lowered to ~6 by adding acetic acid. This was added to an acetonitrile solution of **1** to monitor the reaction.

§ Aqueous dimethylsulfite in the pH range 5–7 (adjusted by adding acetic acid) does not show any precipitation on addition of $BaCl_2$ over a time scale of hours but at pH 8 and above, precipitation started to occur within minutes. This precipitate readily dissolved in dilute HCl and on addition of Br_2 (aq) to this clear solution insoluble $BaSO_4$ was precipitated. At this point it is important to mention that the rate of hydrolysis of dimethylsulfite in water is 10^{-5} s^{-1} as quoted by Brody and Hille[7] from the work of Guthrie.[10] A careful inspection of the data mentioned in Guthrie's paper reveals that this actually refers to the hydrolysis of the methyl ester of methanesulfonic acid ($CH_3S(O)_2OCH_3$) for which the corresponding acid is CH_3SO_3H (methanesulfonic acid) with $pK_a = -1.92$. For dimethylsulfite ($CH_3OS(O)OCH_3$), the corresponding acid is sulfurous acid (HOS(O)OH) with pK_1 and pK_2 values = +1.90 and +7.25, respectively.

¶ A similar reaction using acetonitrile–water medium showed faster conversion of **1** to **2** compared to that in pure acetonitrile.

‖ Mono-oxoheptacoordinated Mo(VI) or dithiolene coordinated mono-oxoheptacoordinated W(VI) complexes in aqueous media have precedence in the literature.[12]

1 R. M. Mcleod, W. Farkas, I. Fridovitch and P. Handler, *J. Biol. Chem.*, 1961, **236**, 1841; H. L. Cohen, S. Betcher-Lange, D. L. Kessler and K. V. Rajagopalan, *J. Biol. Chem.*, 1972, **247**, 7759.
2 C. Kisker, H. Schindelin, A. Pacheco, W. A. Wehbi, R. M. Garrett, K. V. Rajagopalan, J. H. Enemark and D. C. Rees, *Cell.*, 1997, **91**, 1.
3 J. L. Johnson and K. V. Rajagopalan, *J. Biol. Chem.*, 1977, **252**, 2017; C. A. Kipke, M. A. Cusanovitch, G. Tollin, R. A. Sunde and J. H. Enemark, *Biochemistry*, 1988, **27**, 2918; E. P. Sullivan, J. T. Hazzard, G. Tollin and J. H. Enemark, *Biochemistry*, 1993, **32**, 12465.
4 R. H. Holm, *Chem.Rev.*, 1987, **87**, 1401; R. H. Holm, *Coord. Chem. Rev.*, 1990, **100**, 183; B. E. Schultz, S. F. Gheller, M. C. Muetterties, M. J. Scott and R. H. Holm, *J. Am. Chem. Soc.*, 1993, **115**, 2714; S. A. Roberts, C. G. Young, W. E. Cleland, R. B. Ortega and J. H. Enemark, *Inorg. Chem.*, 1988, **27**, 3044; Z. Xiao, C. G. Young, J. H. Enemark and A. G. Wedd, *J. Am. Chem. Soc.*, 1992, **114**, 9194.
5 S. K. Das, P. K. Chaudhury, D. Biswas and S. Sarkar, *J. Am. Chem. Soc.*, 1994, **116**, 9061; P. K. Chaudhury, S. K. Das and S. Sarkar, *Biochem. J.*, 1996, **319**, 953.
6 C. Lorber, M. R. Plutino, L. I. Elding and E. Nordlander, *J. Chem. Soc., Dalton Trans.*, 1997, 3997.
7 M. S. Brody and R. Hille, *Biochim. Biophys. Acta*, 1995, **1253**, 133; R. Hille, *J. Biol. Inorg. Chem.*, 1997, **2**, 804.
8 A. Thapper, R. J. Deeth and E. Nordlander, *Inorg. Chem.*, 1999, **38**, 1015.
9 G. N. George, R. M. Garrett, T. Graf, R. C. Prince and K. V. Rajagopalan, *J. Am . Chem. Soc.*, 1998, **120**, 4522.
10 J. P. Guthrie, *Can. J. Chem.*, 1978, **56**, 2342.
11 J. R. Bradbury and F. A. Schultz, *Inorg. Chem.*, 1986, **25**, 4416; W. E. Newton, J. W. McDonald, J. L. Corbin, L. Ricard and R. Weiss, *Inorg. Chem.*, 1980, **19**, 1997 and references therein
12 J. L. Templeton, B. C. Ward, G. J-J. Chen, J. W. McDonald and W. E. Newton, *Inorg. Chem.*, 1981, **20**, 1248; S. K. Das, D. Biswas, R. Maiti and S. Sarkar, *J. Am. Chem. Soc.*, 1996, **118**, 1387.

CHEMCOMM Communication
www.rsc.org/chemcomm

Triple linking of the decaboranyl cluster. Structure of $[(SMe_2)_2B_{10}H_{10}(B_{10}H_{13})_2]$ as determined by synchrotron X-ray diffraction analysis†

Jonathan Bould,[a] Udo Dörfler,[ab] William Clegg,[cd] Simon J. Teat,[d] Mark Thornton-Pett[a] and John D. Kennedy*[a]

[a] *The School of Chemistry of the University of Leeds, Leeds, UK LS2 9JT. E-mail: johnk@chem.leeds.ac.uk*
[b] *Institut für Organische Chemie, Universität Bremen, Postfach 330 440, Bremen, Germany D-28334.*
[c] *Department of Chemistry of the University of Newcastle, Newcastle upon Tyne, UK NE1 7RU*
[d] *CCLRC Daresbury Laboratory, Daresbury, Warrington, UK WA4 4AD*

Received (in Cambridge, UK) 26th June 2001, Accepted 1st August 2001
First published as an Advance Article on the web 3rd September 2001

In an attempt to find generic routes to multiple inter-cluster σ-linking, mild thermolysis of [6,9-$(SMe_2)_2$-*arachno*-$B_{10}H_{12}$] 1 in inert hydrocarbon solution gives the tridecaboranyl species [6,9-$(SMe_2)_2$-*arachno*-$B_{10}H_{10}$-1,5-(6′-*nido*-$B_{10}H_{13})_2$] 3 (23%).

There is current activity in the linking together of boron-containing clusters to generate (a) chains, rods and rings of σ-linked clusters,[1] (b) strings and other assemblies in which clusters join with a common metal atom,[2] and (c) macro-polyhedral assemblies of clusters fused with two or more atoms in common.[3] In this context, we have interest in the possibility of multiple σ-linking of several boron clusters to a central boron core for possible precursors to globular 'megaloboranes', of which structures would be based on central boron cluster cores of which, in turn, the peripheral valencies are σ-linked to outer boron–hydride cluster units which are themselves mutually σ-linked to form a boron–hydride skin around the central borons-only nucleus.[4] Here, we thought it useful to examine for activity of the $\{B_{10}H_{12}(SMe_2)\}$ fragment, as it has both 'reactive' and 'unreactive' forms: both forms will electrophilically add to olefins and acetylenes,[5] and thence might add to electrophilically susceptible sites of boron clusters in first steps of a possible synthetic approach involving initial assembly of boron hydride units around a central core. A 'reactive' form of $\{B_{10}H_{12}(SMe_2)\}$, of unestablished constitution, is proposed as a key intermediate in the formation of $\{C_2B_{10}\}$ dicarbaboranes from $[B_{10}H_{12}(SMe_2)_2]$ **1**.[5] A 'stable' form, [5-(SMe_2)-*nido*-$B_{10}H_{12}$] **2** is well established and is generated in yields of 40–60% by heating $[B_{10}H_{12}(SMe_2)_2]$ in the absence of other reagents, other products being unidentified.[6,7] We surmised that these other products might arise from electrophilic attack by the $\{B_{10}H_{12}(SMe_2)\}$ fragments, either 'stable' or 'unstable', on other decaboranyl residues in quasi-auto-fusion processes to generate multidecaboranyl assemblies. We here report preliminary results that are consistent with this idea.

Specifically, a solution of $[(SMe_2)_2B_{10}H_{12}]$ **1** (schematic structure **I**; 107 mg; 440 μmol) in benzene (10 mL) was heated at reflux for 6 h. TLC separation (silica G, hexane–CH_2Cl_2, 3:7) gave known [5-(SMe_2)-*nido*-$B_{10}H_{12}$] **2**[6] (R_F 0.8, 8 mg; 43 μmol, 9%). Closely following **2** on the TLC plate was a faint yellow band (R_F *ca.* 0.7) which was purified by HPLC (Lichrosorb SI 60, 25 cm × 2 cm, hexane–CH_2Cl_2 57:43, 20 mL min^{-1}). The fraction with R_T 1.3 min was the tridecaboranyl species [6,9-$(SMe_2)_2$-*arachno*-$B_{10}H_{10}$-1,5-(6′-*nido*-$B_{10}H_{13})_2$] **3**, (schematic structure **II**; 16 mg, 33 μmol, 23%), characterized by single-crystal X-ray diffraction analysis (Fig. 1)‡ and NMR spectroscopy.‡§ We hope to be able to describe other, lower-yield, by-products in due course.

† Specifically 6,9-bis(dimethylsulfide)-1,5-bis(6′-*nido*-decaboranyl)-*arachno*-decaborane (IUPAC nomenclature).

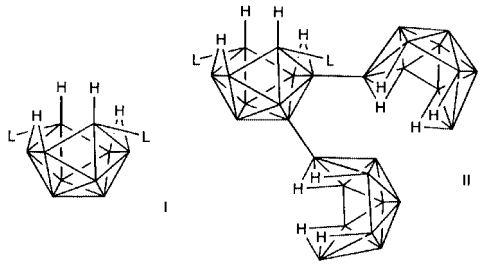

Obtainable crystals under our conditions were of *ca.* 0.02 × 0.08 mm cross section, and needed synchrotron-generated X-ray radiation for sufficient diffraction intensity for structural analysis.[8] This revealed the *arachno* $\{(SMe_2)_2B_{10}\}$ configura-

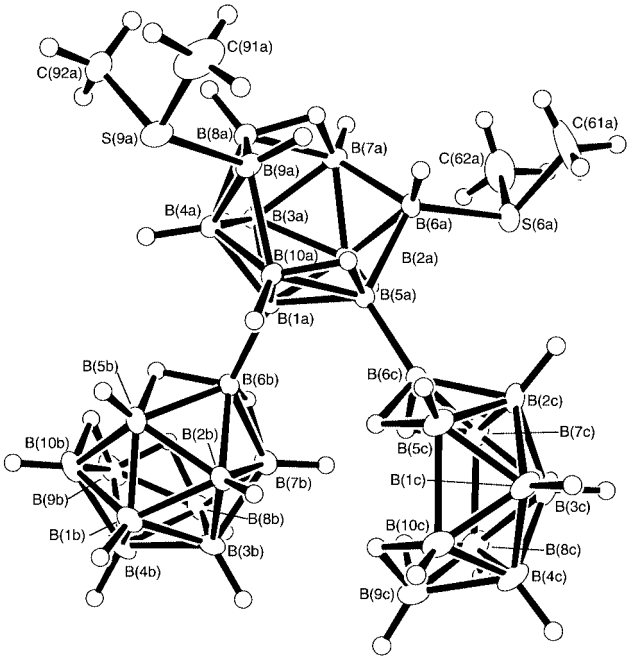

Fig. 1 Crystallographically determined molecular structure of [6,9-$(SMe_2)_2$-*arachno*-$B_{10}H_{10}$-1,5-(6′-*nido*-$B_{10}H_{13})_2$] **3**, drawn with 40% probability ellipsoids for non-hydrogen atoms, and with a small arbitrary radius for hydrogen atoms. The crystal structure had two molecules per unit cell, of which one was disordered over two positions. The undisordered molecule is drawn here. Selected interatomic distances (Å) for the undisordered molecule are as follows: B(6)–S(6) 1.924(3), B(9)–S(9) 1.927(3), B(1)–B(6′) 1.688(5), B(5)–B(6″) 1.676(5), B(5)–B(10) 1.874(5), B(7)–B(8) 1.861(5), B(5′)–B(10′) 1.969(5), B(7′)–B(8′) 1.993(5), B(5″)–B(10″) 1.980(6) and B(7″)–B(8″) 1.979(6).

 DOI: 10.1039/b105551h

tion as in compound **1**, but now with two pendant open decaboranyl groups, on the B(1) and B(5) positions. These are established as {*nido*-$B_{10}H_{13}$} moieties by their bridging hydrogen-atom positions, general *nido*-decaboranyl molecular dimensions, and NMR characteristics.‡ Compound **3** is the first tridecaboranyl specifically identified. Although bidecaboranyls are well recognized,[9] as far as we are aware this tridecaboranyl {B_{30}} framework constitutes the biggest molecular all-boron skeletal assembly yet unequivocally characterized. Although $B_{30}H_{38}$, bis(*nido*-decaboranyl)-*nido*-decaborane, [$B_{10}H_{12}$-($B_{10}H_{13}$)$_2$], is formed in the thermolysis of *nido*-$B_{10}H_{14}$ in refluxing toluene with 0.03 mol% [6,9-(SC_4H_8)$_2$-*arachno*-$B_{10}H_{12}$] (a close relative of compound **1**) as catalyst, this product is in low yield (0.2%), and is an unspecifiable mixture of isomers, of which 546 are possible.[10]

The reaction stoicheiometry and product constitution of compound **3** suggest initial dissociation of compound **1** to give {$B_{10}H_{12}(SMe_2)$}, followed by addition into B–H sites by {$B_{10}H_{12}(SMe_2)$} to give B–$B_{10}H_{13}$ units with the elimination of SMe_2 [eqn. (1)].

$$[(SMe_2)_2B_{10}H_{12}]\ \mathbf{1} + 2\ \{B_{10}H_{12}(SMe_2)\} \rightarrow [(SMe_2)_2B_{10}H_{10}(B_{10}H_{13})_2]\ \mathbf{3} + 2\ SMe_2 \qquad (1)$$

The result of one predominant isomer, from three clusters conjoined σ, in good yield for a thermolytic three-molecule conjoining reaction, has interesting auguries. Firstly, the ready attack of a {$(SMe_2)B_{10}H_{12}$} moiety at nucleophilic sites on [$(SMe_2)_2B_{10}H_{12}$] **1** suggests a more general use for compounds **1** and **2** in co-thermolysis reactions with other boranes to link the versatile *nido*-decaboranyl residue to other borane residues. Reaction with the [*closo*-$B_{12}H_{12}]^{2-}$ dianion to give [$B_{12}H_{11}(B_{10}H_{13})]^{2-}$, which might be precursive, *via* further oxidation, to the novel fused-cluster [$B_{22}H_{22}]^{2-}$ anion,[11] would be an attractive target here. Second, the high yield and site specificity for this predominant product suggest preferential activation by the first boron substituent to the addition of the second boron substituent at an adjacent site, which would augur well for the observation of further addition in this and related systems. Third, the observed multiple addition of borane residues to adjacent sites is of potential use in the synthesis of higher more condensed boranes, as mentioned above. Here, the nearness of the *nido*-decaboranyl residues on the central borane unit of compound **3** might imply that coupling reactions among them, with dihydrogen loss, may be readily effected. Thus, for example, establishment of conditions for multiple addition in this type of reaction system to generate species such as in **III**,

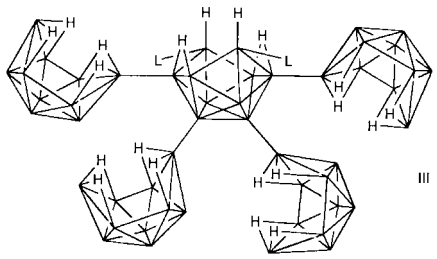

III

followed by cross-linking among the pendant $B_{10}H_{13}$ moieties, could engender the type of 'megaloborane' globular species presaged by the structures of very condensed metallaboranes such as [$(PPh_3)_2(PPh_2)Pd_2B_{20}H_{16}Pd(PPh_3)$].[4] Such big 'filled-ball' globular species with borons-only cores surrounded by boron hydride sheaths may well be those that ultimately typify much big borane chemistry.[3,4] Their 'filled-ball' constitution contrasts to the hollow-ball structures of the fullerenes.

We thank the Deutsche Forschungsgemeinschaft and the UK EPSRC (grants nos. J/56929, L/49505 and M/83360) for support and Mr Simon Barrett for assistance with NMR spectroscopy. We gratefully acknowledge the use of the UK CCLRC SRS facility.

Notes and references

‡ *Crystal data*: [6,9-(SMe_2)$_2$-*arachno*-$B_{10}H_{10}$-1,5-(6′-*nido*-$B_{10}H_{13}$)$_2$] **3** (colourless, from C_6H_{14}–CH_2Cl_2 at 245 K, 0.18 × 0.08 × 0.02 mm), $C_4H_{48}B_{30}S_2$, M = 484.84, triclinic, space group $P\bar{1}$, a = 13.693(2), b = 13.823(2), c = 17.961(3) Å, α = 90.469(3), β = 105.008(3), γ = 104.249(3)°, U = 3173.2(8) Å^3, Z = 4, synchrotron wiggler-generated radiation,[8] λ = 0.6895 Å, μ = 0.169 mm^{-1}, T = 150 K, $R1$ = 0.0785 for 10613 reflections with $I > 2\sigma(I)$, $wR2$ = 0.2099 for all 13451 independent data. Methods and programs were standard and from the SHELX suite.[12]

CCDC reference number 162053.

See http://www.rsc.org/suppdata/cc/b1/b105551h/ for crystallographic data in CIF or other electronic format.

§ *NMR data* for compound **3** ($CDCl_3$, 294–297 K): δ(^{11}B) [δ(^{1}H) of directly bound H atom] as follows: B(1) −40.5 [*conjuncto* position, no terminal H], BH(3) and BH(4′) both at *ca.* −37.5 [+0.44 and +0.31], BH(4″) −36.2 [+0.51], BH(2″) −32.8 [−0.27], BH(2′) −31.7 [+0.68], BH(9) −22.9 [+0.14], BH(6) and BH(7) both at *ca* −19.6 [+1.72 and +1.58], BH(7) and BH(8) both at *ca.* −17.5 [both at *ca.* +1.79], B(5) −14.1 [*conjuncto* position, no terminal H], BH(2) −3.2 [+2.30], BH(1″) −2.1 [+2.22], BH(5′), BH(5″) and BH(10′) all three at *ca.* −1.1 [two at *ca.* +3.00 and one at +2.87], BH(8′), BH(8″) and BH(10′) all three at *ca.* +0.5 [all three at *ca.* +3.04], BH(9′) and BH(9″) both at *ca.* +8.4 [both at *ca.* +3.77], BH(1′), BH(3′), BH(1″) and BH(3″) all four at *ca.* +11.6 [two at *ca.* +3.61{2H} and two at *ca.* +3.52{2H}], B(6′) and *B*(6″) +26.8 and +32.2 [*conjuncto* positions, no terminal H atoms]; additionally δ(^{1}H) {μ-H(5,10)} −4.17, {μ-H(7,8)} −4.26, {μ-H(5′,6′},{μ-H(6′,7′), {μ-H(5″,6″) and {μ-H(6″,7″)} −1.29, two at *ca.* −1.52, and −1.62, {μ-H(8′,9′), {μ-H 9′,10′); {μ-H 8″,9″} and {μ-H 9″,10″)} −2.15, −2.24, and two at *ca.* −2.31(2H), and δ(^{1}H)(SMe_2) +2.46. Mass spectrometry showed an isotopomer envelope centred at *m*/*z* 484 corresponding to that calculated for $C_4H_{48}B_{30}S_2$.

1 See, for example, W. Jiang, D. E. Harwell, M. D. Mortimer, C. B. Knobler and M. F. Hawthorne, *Inorg. Chem.*, 1996, **35**, 4355; J. Müller, K. Baše, T. F. Magnera and J. Michl, *J. Am. Chem. Soc.*, 1992, **114**, 9721; X. Yang, C. B. Knobler, Z. Zheng and M. F. Hawthorne, *J. Am. Chem. Soc.*, 1994, **116**, 7142.

2 R. N. Grimes, *Coord. Chem. Rev.*, 1995, **143**, 71; W. Weinmann, H. Pritzkow, W. Siebert and L. G. Sneddon, *Chem. Ber./Recl.*, 1997, **130**, 329.

3 J. Bould, W. Clegg, S. J. Teat, L. Barton, N. P. Rath, M. Thornton-Pett and J. D. Kennedy, *Inorg. Chim. Acta*, 1999, **289**, 95; J. Bould, D. L. Ormsby, H.-J. Yao, C.-H. Hu, J. Sun, R.-S. Jin, S. L. Shea, W. Clegg, T. Jelínek, N. P. Rath, M. Thornton-Pett, R. Greatrex, P.-J. Zheng, L. Barton, B. Štíbr and J. D. Kennedy, in *Contemporary Boron Chemistry*, ed. M. Davidson, A. K. Hughes, T. B. Marder and K. Wade, Royal Society of Chemistry, Cambridge, UK, 2000, pp. 171–174.

4 H.-J. Yao, C.-H. Hu, J. Sun, R.-S. Jin, P.-J. Zheng, J. Bould, R. Greatrex, J. D. Kennedy, D. L. Ormsby and M. Thornton-Pett, *Collect. Czech. Chem. Commun.*, 1999, **64**, 927.

5 W. E. Hill, F. A. Johnson and R. W. Novak, *Inorg. Chem.*, 1975, **14**, 1244; E. I. Tolpin, E. Mizusawa, D. S. Becker and J. Venzel, *Inorg. Chem.*, 1980, **19**, 1182.

6 W. Knoth and E. L. Muetterties, *J. Inorg. Nucl. Chem.*, 1961, **20**, 66; B. Štíbr, J. Plešek and S. Hermánek, *Collect. Czech. Chem. Commun.*, 1972, **37**, 2696.

7 A. N. Bridges, D. R. Powell, J. A. Dopke, J. M. Desper and D. F. Gaines, *Inorg. Chem.*, 1998, **37**, 503; H. Beall and D. F. Gaines, *Inorg. Chem.*, 1998, **37**, 1420.

8 R. J. Cernik, W. Clegg, C. R. A. Catlow, G. Bushnell-Wye, J. V. Flaherty, G. N. Greaves, I. Burrows, D. J. Taylor, S. J. Teat and M. Hamichi, *J. Synchrotron Radiat.*, 1997, **4**, 279; R. J. Cernik, W. Clegg, C. R. A. Catlow, G. Bushnell-Wye, J. V. Flaherty, G. N. Greaves, I. Burrows, D. J. Taylor, S. J. Teat and M. Hamichi, *J. Synchrotron Radiat.*, 2000, **7**, 40; W. Clegg, M. R. J. Elsegood, S. J. Teat, C. Redshaw and V. C. Gibson, *J. Chem. Soc., Dalton Trans.*, 1998, 3037.

9 J. Bould, J. D. Kennedy, W. Clegg and S. J. Teat, *Acta Crystallogr., Sect. C*, 2001, **57**, 779.

10 S. K. Boocock, N. N. Greenwood and J. D. Kennedy, *J. Chem. Res. (S)*, 1981, 50.

11 N. S. Hosmane, A. Franken, G. Zhang, R. R. Srivastava, R. Y. Smith and B. F. Spielvogel, *Main Group Met. Chem.*, 1998, **21**, 3190; O. Volkov, W. Dirk, U. Englert and P. Paetzold, in *Contemporary Boron Chemistry*, ed. M. Davidson, A. K. Hughes, T. B. Marder and K. Wade, Royal Society of Chemistry, Cambridge, England, 2000, pp. 159–162; O. Volkov, W. Dirk, U. Englert and P. Paetzold, *Z. Anorg. Allg. Chem.*, 1999, **625**, 1193.

12 G. M. Sheldrick, SHELX97, University of Göttingen, Germany, 1997; G. M. Sheldrick, SHELXTL Manual, Bruker AXS Inc., Madison, WI, USA, 1994 and 1998.

CHEMCOMM Communication
www.rsc.org/chemcomm

Monocarbaborane anion chemistry. The elusive C-arylated $[PhCB_{11}H_{11}]^-$, $[PhCB_9H_9]^-$ and $[PhCB_8H_8]^-$ anions

Tomáš Jelínek, Colin A. Kilner, Mark Thornton-Pett and John D. Kennedy

The School of Chemistry of the University of Leeds, Leeds, UK LS2 9JT. E-mail: johnk@chem.leeds.ac.uk

Received (in Cambridge, UK) 27th June 2001, Accepted 1st August 2001
First published as an Advance Article on the web 3rd September 2001

$B_{10}H_{14}$ and PhCHO yield [6-Ph-*nido*-6-CB_9H_{11}]$^-$ (94%), from which the nine-vertex C-phenyl monocarbaborane anion [4-Ph-*closo*-4-CB_8H_8]$^-$ (68%) can be obtained by heating at 200 °C, and from which the twelve- and ten-vertex analogues [1-Ph-*closo*-1-$CB_{11}H_{11}$]$^-$ (50%) and [4-Ph-*closo*-4-CB_9H_9]$^-$ (25%) can be obtained by heating at 210 °C with $BH_3(NEt_3)$.

There is much contemporary interest in the *closo* monocarbaborane monoanions [1-$CB_{11}H_{12}$]$^-$ and [1-CB_9H_{10}]$^-$, and in their derivatives. This is because their very low basicities, as manifested, for example, in their 'least coordinating anion' properties, enable the investigation and exploitation of species with very high Lewis acidities.[1,2] A considerable focus of current activity derives from the substituent chemistry of these anions, and how their low basicities can be tailored by these substituents for particular purposes. Although C-substitution of $[CB_{11}H_{12}]^-$ and $[CB_9H_{10}]^-$ has engendered a variety of derivatives,[1–3] and, although B-arylation has been achieved,[4] the important target of C-arylation has proved elusive, with no reports in the literature. Here we now report preliminary results on convenient routes to the C-phenylated twelve-vertex [1-Ph-*closo*-1-$CB_{11}H_{11}$]$^-$ anion **1**, and to its corresponding ten-vertex [1-Ph-*closo*-1-CB_9H_9]$^-$ analogue **2**. We also report the nine-vertex [4-Ph-*closo*-4-CB_8H_8]$^-$ anion **3**, which is the C-phenylated derivative of the very recently established 'missing link' [*closo*-4-CB_8H_9]$^-$ monoanion.[5] All three species are characterised crystallographically (Fig. 1),† and by NMR spectroscopy.‡

The synthesis of this series derives from Brellochs' report of the reaction of PhCHO with $B_{10}H_{14}$ in 5% aqueous ethanolic KOH,[6] which we have found to give the [6-Ph-*nido*-6-CB_9H_{11}]$^-$ anion **4** in 94% yield. The method is essentially the same as that for the synthesis of unsubstituted [*arachno*-6-CB_9H_{14}]$^-$ from HCHO and $B_{10}H_{14}$,[5,6] except that, interestingly, the *nido* rather than the *arachno* ten-vertex species is formed. The reaction may go *via* the [*arachno*-B_9H_{14}]$^-$ anion as intermediate. Thence, solid-state thermolysis of the $[NEt_4]^+$ salt of [6-Ph-*nido*-6-CB_9H_{11}]$^-$ **4** at 200 °C for 4 h, followed by column chromatographic separation (silica gel, 30 cm × 2.5 cm, MeCN–CH_2Cl_2 10:90), gave the $[NEt_4]^+$ salts of $[PhCB_8H_8]^-$ (anion **3**, 68%) and [7-Ph-*nido*-7-$CB_{10}H_{12}$]$^-$ (anion **5**, 22%), together with trace quantities of the $[NEt_4]^+$ salt of $[PhCB_9H_9]^-$ (anion **2**). A crystallographic sample of the $[NEt_4]^+$ salt of the $[PhCB_8H_8]^-$ anion **3** was obtained from dichloromethane–diethyl ether. The *nido* eleven-vertex anion $[PhCB_{10}H_{12}]^-$ **5** may be synthesised more specifically in 78% yield by treatment of $[PhCB_9H_{11}]^-$ **4** with $[BH_3(SMe_2)]$ in 1,2-$Cl_2C_2H_4$, and thence converted to the $[PhCB_{11}H_{11}]^-$ anion **1** by treatment with $[BH_3(SMe_2)]$. More conveniently, this last reagent also converts $[PhCB_9H_{11}]^-$ **4** more directly to $[PhCB_{11}H_{11}]^-$ **1**. Thus, $[NEt_4]^+[PhCB_9H_{11}]^-$ (1.65 g, 5 mmol) was suspended in $[BH_3(NEt_3)]$ (2.3 g, 20 mmol), and the mixture heated on an oil bath (210 °C) under nitrogen for 6 h. After cooling to room temperature, the mixture was extracted with benzene (2 × 30 ml), and the solid residue was then decomposed by heating at reflux for 3 h in ethanol–concentrated hydrochloric acid (1:1, 50 ml). The ethanol was evaporated, the mixture mixed with

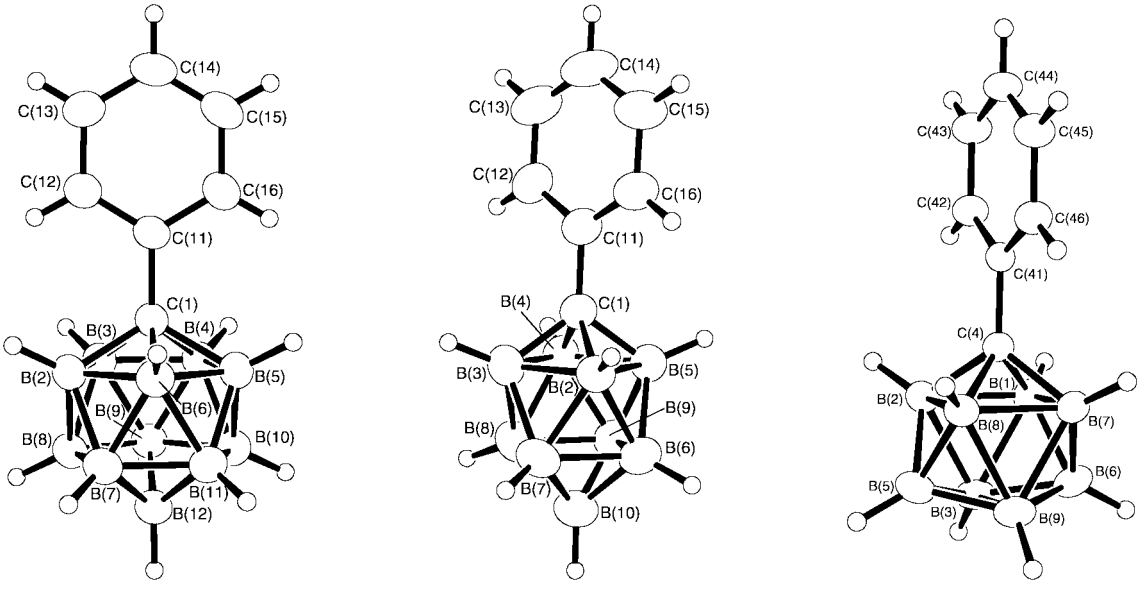

Fig. 1 From left to right, molecular structures of the $[PhCB_{11}H_{11}]^-$ twelve-vertex cluster anion **1**, and its corresponding ten- and nine-vertex $[PhCB_9H_9]^-$ and $[PhCB_8H_8]^-$ analogues, **2** and **3** respectively, as determined crystallographically for their $[NEt_4]^+$ salts.‡ Selected dimensions in Å are as follows: for anion **1**, C(1)–C(11) 1.512(3), C(1)–B(2) 1.729(4), C(1)–B(3) 1.715(3), C(1)–B(4) 1.725(4), C(1)–B(5) 1.722(4) and interboron distances 1.772(4)–1.791(4); for anion **2**, C(1)–C(11) 1.503(4), C(1)–B(2) 1.613(4), C(1)–B(3) 1.606(4), C(1)–B(4) 1.598(5) and interboron distances 1.694(6)–1.843(5); and for anion **3** C(4)–C(41) 1.490(2), C(4)–B(1) 1.623(2), C(4)–B(2) 1.622(2), C(4)–B(7) 1.620(2), C(4)–B(8) 1.623(2) and interboron distances 1.694(3)–1.975(3).

 DOI: 10.1039/b105645j

water (50 ml), and the precipitate filtered off. The latter was a mixture of the $[NEt_4]^+$ salts of $[PhCB_{11}H_{11}]^-$ and $[PhCB_9H_9]^-$ (anions **1** and **2** respectively; molar ratio 2 : 1; combined yield 1.45 g; 76%). Crystallographic samples of these $[NEt_4]^+$ salts of **1** and **2** for diffraction analysis were obtained by fractional crystallisation from dichloromethane–diethyl ether. However, bulk separation of **1** and **2** is better achieved by ion-exchange of $[NEt_4]^+$ for Cs^+, followed by fractional crystallisation of the Cs^+ salts. Thus, a solution of the mixture of the two $[NEt_4]^+$ salts (1.20 g) was dissolved in ethanol–water (4 : 1, 60 ml) and passed through of column of ionex resin (Zerolit 325 in H^+ form, 2.5 cm × 30 cm) using ethanol–water (4 : 1) as eluting liquid. Evaporation of ethanol *in vacuo* from the resulting acidic solution, followed by neutralisation by Cs[OH] to pH 7, gave a white precipitate of the Cs^+ salts of **1** and **2**. This mixture was separated by fractional crystallisation from water, starting with *ca.* 15 ml of hot solution: $Cs^+[PhCB_9H_9]^-$ is much less soluble in cold water (*ca.* 12×) than $Cs^+[PhCB_{11}H_{11}]^-$.

The synthesis of these first of a new generation of C-arylated monocarbaborane anions by simple routes in relatively good yield in two steps from the common polyhedral borane starting material $B_{10}H_{14}$ significantly augments the range of materials available for 'least-coordinating anion' chemistry; the aromatic ring/delocalised cluster conjunction may also have implications for investigation of electronic 'push–pull ' phenomena,[6] and other related interactions between the delocalised cluster and ring systems.[7] The advantage of the method is that it starts with the carbon atom pre-substituted, and thereby avoids complex synthetic carborane carbon-substitution protocols. We currently explore possibilities for other C-substituted monocarbaboranes, and for the generality of this aromatic aldehyde route.

We thank the EPSRC and the DTI for support.

Notes and references

† *Crystal data*: for **1** (CH_2Cl_2 monosolvate), $C_{16}H_{38}B_{11}Cl_2N$: M = 434.28, monoclinic (from dichloromethane–hexane), space group $P2_1/c$, a = 15.7334(5), b = 10.8812(4), c = 15.7928(6) Å, β = 110.9350(14)°, U = 2525.22(16) Å^3, D_c = 1.14 Mg m^{-3}, Z = 4, Mo-Kα, λ = 0.71073 Å, μ = 0.262 mm^{-1}, T = 150(2) K, R_1 = 0.0654 for 3750 reflections with $I > 2\sigma(I)$, and wR_2 = 0.1731 for all 4857 unique reflections; CCDC reference number 164850.

For **2**: $C_{15}H_{34}B_9N$, M = 325.72, monoclinic (from dichloromethane–hexane), space group $C2/c$, a = 24.4404(16), b = 10.5641(6), c = 16.7478(14) Å, β = 99.099(3)°, U = 4269.7(5) Å^3, D_c = 1.01 Mg m^{-3}, Z = 8, Mo-Kα, λ = 0.71073 Å, μ = 0.051 mm^{-1}, T = 150(2) K, R_1 = 0.0826 for 2212 reflections with $I > 2\sigma(I)$, and wR_2 = 0.2285 for all 4147 unique reflections; CCDC reference number 164851.

For **3**, $C_{15}H_{33}B_8N$: M = 313.90, monoclinic (from dichloromethane–hexane), space group $P2_1/n$, a = 11.6480(3), b = 10.5204(3), c = 17.5709(6) Å, β = 107.9740(10)°, U = 2048.08(11) Å^3, D_c = 1.02 Mg m^{-3}, Z = 4, Mo-Kα, λ = 0.71073 Å, μ = 0.052 mm^{-1}, T = 150(2) K, R_1 = 0.0548 for 2417 reflections with $I > 2\sigma(I)$, and wR_2 = 0.1703 for all 4011 unique reflections; CCDC reference number 164852. For all three compounds, methods and programs were standard.[8]

See http://www.rsc.org/suppdata/cc/b1/b105645j/ for crystallographic data in CIF or other electronic format.

‡ *Measured NMR data* for anions [1-Ph-*closo*-1-$CB_{11}H_{11}]^-$ **1**, [1-Ph-*closo*-1-$CB_9H_9]^-$ **2**, [4-Ph-*closo*-4-$CB_8H_8]^-$ **3** and [7-Ph-*nido*-7-$CB_{10}H_{12}]^-$ **5**, $[NEt_4]^+$ salts in CD_3CN at 294–300 K, ordered as assignment $\delta(^{11}B)$/ppm [$\delta(^1H)$/ppm]: anion **1**: BH(12) −8.0 [+2.13], BH(2,3,4,5,6) and BH (7,8,9,10,11) coincident at *ca.* −12.9 [*ca.* +1.75]; $\delta(^1H)(C_6H_5)$ +7.29 to +7.63 (multiplet). Anion **2**, BH(10) +27.1 [+5.49], BH(2,3,4,5) −16.1 [+1.79], BH(6,7,8,9) −24.4 [+0.84], $\delta(^1H)(C_6H_5)$ +7.40 to +7.98 (multiplet). Anion **3**, BH(5,6) +13.4 [+4.44], BH(1,2,7,8) −10.8 [+1.71], BH(3,9) −17.2 [+0.88], $\delta(^1H)(C_6H_5)$ +7.32 to +7.93, multiplet. Anion **5**, BH(5) −0.8 [+2.32], BH(2,3) −9.1 [+2.09], BH(8,11) −10.0 [+1.98], B(9,10) −22.6 [*ca.* +1.24], BH(1) −25.2 [*ca.* +1.24] and BH(4,6) –31.5 [+0.45]; $\delta(^1H)(C_6H_5)$ +7.25 to +7.70 (multiplet), μ-H(8,9; 10,11) −3.33.

1 S. Strauss, *Chem. Rev*., 1993, **93**, 927.
2 C. Reed, *Acc. Chem. Res*., 1998, **31**, 133.
3 See for example, together with references cited therein: Z. Xie, C.-W. Tsang, F. Xue and T. C. W. Mak, *J. Organomet. Chem*., 1999, **577**, 197; S. V. Ivanov, S. M. Ivanova, S. M. Miller, O. P. Anderson, K. N. Solntsev and S. H. Strauss, *Inorg. Chim. Acta*, 1999, **289**, 76; T. Peymann, A. Herzog, C. B. Knobler and M. F. Hawthorne, *Angew. Chem., Int. Ed*., 1999, **38**, 1062; J. H. Morris, K. W. Henderson and V. A. Ol'shevskaya, *J. Chem. Soc., Dalton Trans*., 1998, 1951; A. G. Douglas, Z. Janoušek, P. Kaszynski and V. G. Young, *Inorg. Chem*., 1998, **37**, 6361.
4 B. Grüner, Z. Janoušek, B. T. King, J. N. Woodford, C. H. Wang, V. Všetečka and J. Michl, *J. Am. Chem. Soc*., 1999, **121**, 3122.
5 T. Jelínek, B. Štíbr, J. Holub, M. Bakardjiev, D. Hnyk, D. L. Ormsby, C. A. Kilner, M. Thornton-Pett, H.-J. Schanz, B. Wrackmeyer and J. D Kennedy, *Chem. Commun*., 2001, 1756.
6 B. Brellochs, in *Contemporary Boron Chemistry*, ed. M. G. Davidson, A. K. Hughes, T. B. Marder and K. Wade, Royal Society of Chemistry, Cambridge, UK, 2000, pp. 212–214.
7 D. G. Allis and J. T. Spencer, *J. Organomet. Chem*., 2000, **614/615**, 309.
8 Z. Otwinowski and W. Minor, DENZO-SMN, Processing of X-ray Diffraction Data Collected in Oscillation Mode, *Methods Enzymol*., 1997, **276**, 307–326; COLLECT, Data Collection Strategy Program, Nonius, 1999.

CHEMCOMM Communication
www.rsc.org/chemcomm

New and easy route to primary cyclopropylamines from nitriles

Philippe Bertus and Jan Szymoniak*

Réactions Sélectives et Applications, CNRS (UMR 6519) and Université de Reims Champagne Ardenne, 51687 REIMS cedex 2 France. E-mail: jan.szymoniak@univ-reims.fr; Fax: +33 3 26 91 34 31

Received (in Cambridge, UK) 15th June 2001, Accepted 7th August 2001
First published as an Advance Article on the web 3rd September 2001

Starting from readily available substrates, we have developed a new synthesis of primary cyclopropylamines. The reaction involves a cooperative Ti(II)- and Lewis acid-mediated coupling of alkanenitriles with Grignard reagents.

Cyclopropylamines are not only versatile synthetic intermediates,[1] but also a variety of biologically active molecules contain a cyclopropylamine moiety.[2] Yet, a few synthetic methods that allow preparation of these important compounds[1,3] often require multi-step reactions. Among the available methods, the recent de Meijere adaptation[4] of the Kulinkovich hydroxycyclopropanation[5] presents a useful synthesis of *N*,*N*-dialkylcyclopropylamines from *N*,*N*-dialkylcarboxamides and Grignard reagents in the presence of $Ti(OPr^i)_4$ or $MeTi(OPr^i)_3$. Here we disclose that primary cyclopropylamines may be easily obtained in one step by a Ti(II)-mediated coupling of Grignard reagents with alkanenitriles.

The idea of transforming nitriles to cyclopropylamines directly was initially based on our recent approach to cyclopropanes from carbonyl compounds *via* Cp_2Zr chemistry.[6] This reaction involves a deoxygenative contraction of an intermediate oxazirconacycle into a carbocycle under Lewis acid activation conditions [Scheme 1, eqn. (1)]. We envisioned that, in an analogous way, nitriles might be converted to cyclopropylamines following eqn. (2).

However, attempts to perform the reaction by using Cp_2Zr(ethylene) invariably led to complex reaction mixtures. Therefore, we investigated the feasibility of the reaction using the *in situ* formed (ethylene)$Ti(OPr^i)_2$[4,5] instead of (ethylene)zirconocene. We noticed that cyclopropylamines were formed by combining the use of this reagent with the subsequent addition of a Lewis acid, $BF_3{\cdot}OEt_2$ or $TiCl_4$. After optimizing the reaction conditions, synthetically useful yields were obtained. In a representative procedure, to a solution of benzyl cyanide (1 eq.) and $Ti(OPr^i)_4$ (1.1 eq.) in Et_2O was slowly added at rt EtMgBr (2 eq., 1 M solution in ether). After stirring for 1 h, $BF_3{\cdot}OEt_2$ (2 eq.) was added, and the reaction mixture further stirred for 0.5 h at rt. Finally, basic workup (10% NaOH aq) followed by extraction with ether and flash chromatography purification afforded (1-benzyl)cyclopropylamine (**2**) in 70% yield.

The following additional observations gave an insight into the reaction: (i) $BF_3{\cdot}OEt_2$ and $TiCl_4$ gave rise to similar results. (ii) The yields of **2** in the reactions employing $BF_3{\cdot}OEt_2$ were similar in THF and in Et_2O. (iii) Cyclopropylamine **2** was also formed in the absence of the additional Lewis acid, however, in this case, the yields were markedly lower in Et_2O (31%) and negligible in THF (7%); in these reactions benzyl ethyl ketone (**3**) was the major product formed (60% yield in Et_2O and 70% yield in THF). (iv) When using more than 2 eq. of EtMgBr the yield of **2** decreased significantly to detriment of the tertiary carbinamine **4**, which was obtained solely in 67% yield with 4 eq. of EtMgBr. (v) Lowering the quantity of $Ti(OPr^i)_4$ below 1 eq. decreased the yield of **2** to the detriment of **3** and **4**.

The competing reactions to afford compounds **2**, **3** and **4** are summarized in Scheme 2. In accordance with our initial hypothesis, and by analogy with the cyclopropanation of carbonyl compounds,[6] the Lewis acid plays a crucial role for the ring contraction leading to cyclopropane **2**. The reaction differs to that of the Kulinkovich and de Meijere reactions, in which the ring contraction occurs in the absence of an additional Lewis acid, spontaneously from the intermediate oxatitanacycle. In our reaction, in the absence of $BF_3{\cdot}OEt_2$ the intermediate azatitanacycle (cyclic titanium iminate) remains unchanged to furnish the ketone **3** on hydrolysis. The minor formation of **2** in this case can be explained by assuming that weak acid species always present in solution (Mg, Ti) operate, to a significantly lower degree, however, in the more coordinating THF (7% yield of **2**) than in the less coordinating Et_2O (31% yield of **2**). In contrast, when a strong Lewis acid is used, the cyclopropanation step proceeds efficiently (70% yield) in both solvents. The competing formation of **4** also deserves some comments. It is known that simple nitriles do not undergo double alkylation by alkyl Grignard reagents.[7] In contrast, the attack of a second equivalent of EtMgBr on the C atom of the titanium iminate (Scheme 2) would be an efficient process. This reaction possibly opens a simple, general way to tertiary carbinamines.

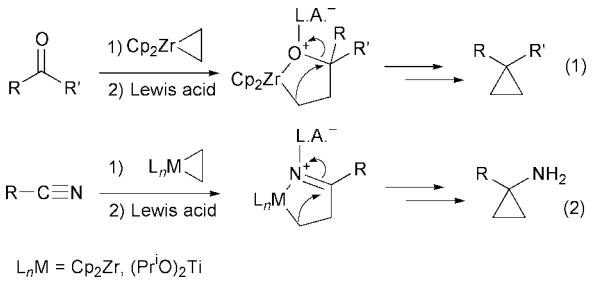

Scheme 1

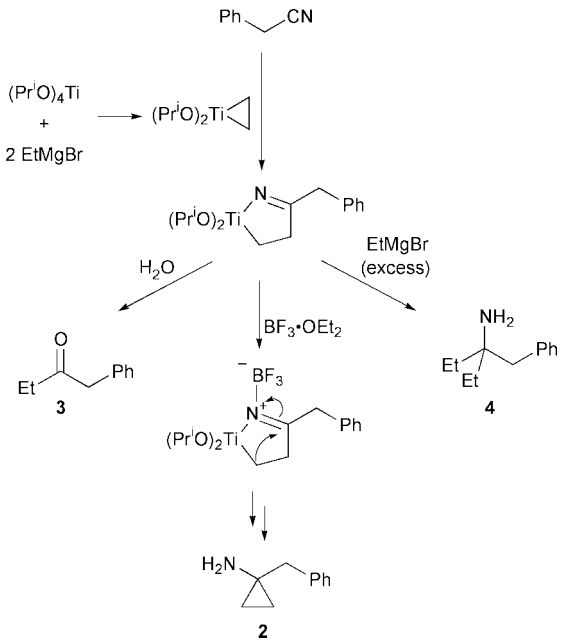

Scheme 2

 DOI: 10.1039/b105293b

Table 1 Reaction of nitriles with Grignard reagents promoted by $Ti(OPr^i)_4$ and $BF_3{\cdot}OEt_2$

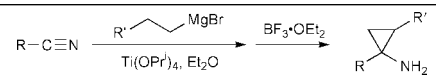

Entry	Nitrile	R′-$(CH_2)_2$-MgBr	Product	Yield[a] (%)
1	 **1**	Et-MgBr	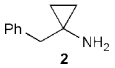 **2**	70
2	 **5**	Et-MgBr	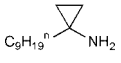 **10**	70
3	 **6**	Et-MgBr	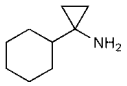 **11**	52
4	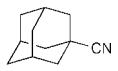 **7**	Et-MgBr	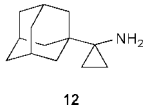 **12**	53
5	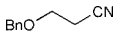 **8**	Et-MgBr	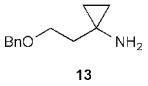 **13**	54
6	 **1**	Bu^n-MgBr	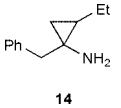 **14**	57 (64:36)[b]
7	 **1**	Bu^s-MgBr	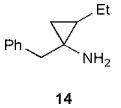 **14**	54 (55:45)[b]
8	 **1**	Ph$(CH_2)_2$-MgBr	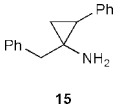 **15**	51 (68:32)[b]
9	 **9**	Ph$(CH_2)_2$-MgBr	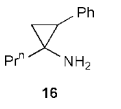 **16**	54 (68:32)[b]

[a] Yields of isolated products. [b] Mixture of diastereomers.

Furthermore, since an excess of EtMgBr strongly favours the dialkylation over the cyclopropanation reaction, the nucleophilic attack of a Grignard reagent on titanium seems not to be determining the ring contraction.[8]

To further explore the scope of the cyclopropanation reaction we tested other nitriles and Grignard reagents under the optimized reaction conditions. As shown in Table 1, the reaction employing EtMgBr proceeded smoothly from different alkanenitriles to afford the corresponding cyclopropylamines in moderate to good yields (entries 1–5). Both acyclic and cyclic nitriles were used. Particularly, the reaction took place starting from the sterically crowded adamantane-1-carbonitrile (**7**) (entry 4), and the nitrile **8** having the benzyloxy group (entry 5). Benzonitrile and acrylonitrile did not afford the corresponding cyclopropylamines under the conditions used here. The reactions employing other Grignard reagents, namely Bu^{n}MgBr, Bu^{s}MgBr and $PhCH_2CH_2MgBr$, could also be accomplished leading to 1,2-disubstituted cyclopropylamines **14**, **15** and **16** (entries 6–9). Interestingly, starting from the isomeric Grignard reagents Bu^{n}MgBr and Bu^{s}MgBr, the same compound **14** was formed solely (entries 6 and 7). A unique reaction pathway through (but-1-ene)$Ti(OPr^i)_2$ accounts for the totally regioselective formation of **14**. In all cases, a moderate diastereoselectivity of about 2:1 was observed.[9] The very easy separation by flash chromatography of diastereomeric primary cyclopropylamines (**14**, **15** and **16**) is noteworthy,[9] and should be synthetically useful.

In summary, we have presented a new method for the preparation of primary cyclopropylamines. The described reaction involves a cooperative Ti(II) and Lewis acid-mediated coupling of nitriles with Grignard reagents. Simplicity of the procedure, cheap reagents as well as readily available starting materials, and particularly different alkanenitriles, are the major advantages of this method. Studies aimed at further exploring the reaction are currently underway.

Notes and references

1 E. Vilsmaier, *The Chemistry of the Cyclopropyl Group*, ed. Z. Rappoport, Wiley, New York, 1987, ch.. 22, p. 1341.

2 For examples, see: K. Grohe, H. Zieler and K. Metzger, *Eur. Pat.* 0078362, 1983; E. S. C. Wu, T. E. Cole, T. A. Davidson, J. C. Blosser, A. R. Borrelli, C. R. Kinsolving, T. E. Milgate and R. B. Parker, *J. Med. Chem.*, 1987, **30**, 788; H. Homma, Y. Watanabe, T. Abiru, T. Murayama, Y. Nomura and A. Matsuda, *J. Med. Chem.*, 1992, **35**, 2881; M. C. Pirrung, J. Cao and J. Chen, *J. Org. Chem.*, 1995, **60**, 5790.

3 Houben-Weyl, *Methoden der Organischen Chemie*, ed. M. Regitz, Thieme, Stuttgart, 1989, 4th edn., vol. E 19b.

4 The oxatitanacyclopentane intermediate is involved in both Kulinkovich and de Meijere reactions. However, whereas the OR group of an ester further migrates to the strongly oxophilic titanium, the NR_2 group of an amide remains attached to the carbon, see: V. Chaplinski and A. de Meijere, *Angew. Chem., Int. Ed. Engl.*, 1996, **35**, 413; V. Chaplinski, H. Winsel, M. Kordes and A. de Meijere, *Synlett*, 1997, 111; J. Lee and J. K. Cha, *J. Org. Chem.*, 1997, **62**, 1584.

5 O. G. Kulinkovich, S. V. Sviridov, D. A. Vasilevski and T. S. Prityts kaya, *Zh. Org. Khim.*, 1989, **25**, 2244; Recent review: O. G. Kulinkovich and A. de Meijere, *Chem. Rev.*, 2000, **100**, 2789.

6 P. Bertus, V. Gandon and J. Szymoniak, *Chem. Commun.*, 2000, 171; V. Gandon, P. Bertus and J. Szymoniak, *Eur. J. Org. Chem.*, 2000, **22**, 3713.

7 The $Ti(OPr^i)_4$-promoted double nucleophilic addition of Grignard reagents to CN triple bond of protected cyanohydrins (chelating nitriles) has recently been reported, see: A. B. Charette, A. Gagnon, M. Janes and C. Mellon, *Tetrahedron Lett.*, 1998, **39**, 5147.

8 In contrast to the Kulinkovich reaction, for which the intermediacy of a titanium ate complex has recently been postulated, see: O. G. Kulinkovich, *Pure Appl. Chem.*, 2000, **72**, 1715.

9 Selected data for **2** and **14**: **2**: ^{1}H-NMR (250 MHz; $CDCl_3$) δ 0.6–0.7 (m, 4 H), 2.72 (s, 2 H), 3.77 (s, 2 H), 7.20–7.35 (m, 5 H); ^{13}C-NMR (63 MHz; $CDCl_3$) δ 9.1, 35.4, 39.7, 127.5, 128.8, 129.8, 134.8; IR ν (cm^{-1}) 3361, 1605, 1495, 1453; MS (70 eV) *m*/*z* 147 ($M^{+\cdot}$, 44), 132 (28), 92 (71), 91 (90), 56 (100); Analysis calculated for $C_{10}H_{13}N{\cdot}HCl$: C, 65.39; H, 7.68; N, 7.63; found C, 65.34; H, 7.61; N, 7.58%. **14**: minor isomer: R_f (ether–methanol 95:5) 0.34; ^{1}H-NMR (250 MHz; $CDCl_3$) δ 0.31 (dd, J = 5.7, 4.7 Hz, 1 H), 0.75 (dd, J = 9.4, 4.7 Hz, 1 H), 0.86–0.99 (m, 1 H), 1.05 (t, J = 7.3 Hz, 3 H), 1.20–1.38 (m, 1 H), 1.56 (br s, 2 H), 1.54–1.72 (m, 1 H), 2.72 (d, J = 14.4 Hz, 1 H), 2.87 (d, J = 14.4 Hz, 1 H),7.20–7.38 (m, 5 H); ^{13}C-NMR (63 MHz; $CDCl_3$) δ 14.2, 20.2, 23.3, 28.1, 38.1, 41.4, 126.2, 128.3, 129.3, 139.5; IR ν (cm^{-1}) 3356, 1601, 1495, 1453; MS (70 eV) *m*/*z* 175 ($M^{+\cdot}$, 11), 160 (22), 146 (76), 92 (71), 91 (100). **14**: major isomer: R_f (ether–methanol 95:5) 0.70; ^{1}H-NMR (250 MHz; $CDCl_3$) δ 0.23 (t, J = 4.9 Hz, 1 H), 0.72 (dd, J = 8.9, 4.4 Hz, 1 H), 0.77–0.88 (m, 1 H), 0.95 (t, J = 7.4 Hz, 3 H), 1.30 (br s, 2 H), 1.40–1.55 (m, 2 H), 2.62 (d, J = 14.0 Hz, 1 H), 2.78 (d, J = 14.0 Hz, 1 H), 7.22–7.38 (m, 5 H); ^{13}C-NMR (63 MHz; $CDCl_3$) δ 14.3, 19.0, 21.6, 26.7, 38.4, 47.9, 126.2, 128.2, 129.2, 139.5; IR ν (cm^{-1}) 3372, 1604, 1495, 1454; MS (70 eV) *m*/*z* 175 ($M^{+\cdot}$, 10), 160 (19), 146 (68), 92 (68), 91 (100); Analysis calculated for $C_{12}H_{17}N{\cdot}HCl$: C, 68.07; H, 8.57; N, 6.62%; found C, 67.83; H, 8.54; N, 6.38%.

CHEMCOMM
Communication
www.rsc.org/chemcomm

A remarkably stable hydrogen-bonded porphyrin·iron(terpyridine) ion pair

Tyler B. Norsten, Kelly Chichak and Neil R. Branda*†

Department of Chemistry, University of Alberta, Edmonton, AB, Canada T6G 2G2

Received (in Columbia, MO, USA) 10th May 2001, Accepted 18th July 2001
First published as an Advance Article on the web 3rd September 2001

Even in highly competitive solvents such as DMSO, strong bimolecular association and subsequent fluorescence quenching result from the combination of hydrogen bonding and ion pairing between a porphyrinic bis(carboxylate) dianion and an iron(terpyridine) bis(urea).

In naturally occurring light harvesting systems, the relative orientation and proximity of the photoactive components play fundamental roles in the effective operation of the systems. These complex molecular devices rely primarily on non-covalent interactions to place the chromophores in optimal locations to facilitate beneficial electronic communication. Accordingly, significant efforts have been devoted to develop artificial multi-component photoactive arrays, with a particular emphasis on those involving porphyrins.[1–7] Because the photochemical characteristics are ultimately governed by the assemblies' topologies, their fabrication hinges on the tailoring of productive molecular recognition interactions such as coordination bonding,[2,3] ion pairing,[4] π–π stacking[5,6] and hydrogen bonding.[3,7] The hydrogen bond is a particularly serviceable driving force to align building blocks due to its directionality and its ease of tailoring. This is especially true when several hydrogen bonds are united into a multipoint recognition site. The utility of the hydrogen bond is diminished, however, in polar competitive solvents that can better solvate the hydrogen bonding surface. The implementation of cooperative or ionic hydrogen bonding motifs, where the hydrogen bond partners are of opposite charge, can often overcome these destructive solvation effects.[8] Strong complexation is especially critical in order to study energy/electron transfer processes at the low concentrations required by luminescence spectroscopy without having to add excessive quantities of quencher.

We describe here the synthesis and characterization of the novel non-covalently bound porphyrinic assembly **1**. The building blocks were designed to harness the beneficial recognition attributes of both ion pairing and hydrogen bonding interactions. The first interaction is provided by the attraction between the Fe^{2+} dication complex **3a** and the porphyrinic bis(carboxylate) dianion **4**. The carboxylate groups on the porphyrin serve dual roles in that they also act as charged hydrogen bond acceptors for the neutral bidentate urea hydrogen bond donors on the iron(terpyridine) fragment. The result is the self-assembly of neutral complex **1**, which retains both its structural integrity and topology even at low concentrations in polar solvents such as DMSO.

Assembly **1** was prepared by mixing an equimolar mixture of building blocks **3a** and **4** in methanol (Scheme 1). The neutral complex precipitated from the solution and was easily isolated in high purity and in nearly quantitative yield. Owing to the charges balancing in the final complex, 2 equivalents of $[Bu_4N][BF_4]$ were produced in the reaction and were washed away during the filtration. The integration of signals in the ^1H NMR spectrum of the isolated solid supports the claim that the 1:1 complex is the product of the self-assembly process. Electrospray mass spectrometry confirmed this claim as peaks at *m*/*z* 1738.7 and 880.3 corresponding to $[M + Na]^+$ and $[M + 2Na]^{2+}$, respectively, were observed.

Assembly **1** is freely soluble in highly polar solvents such as DMSO and DMF, but is only sparingly soluble in all other common organic solvents. GCOSY and T-ROESY experiments aided in assigning the protons of complex **1**. The complex

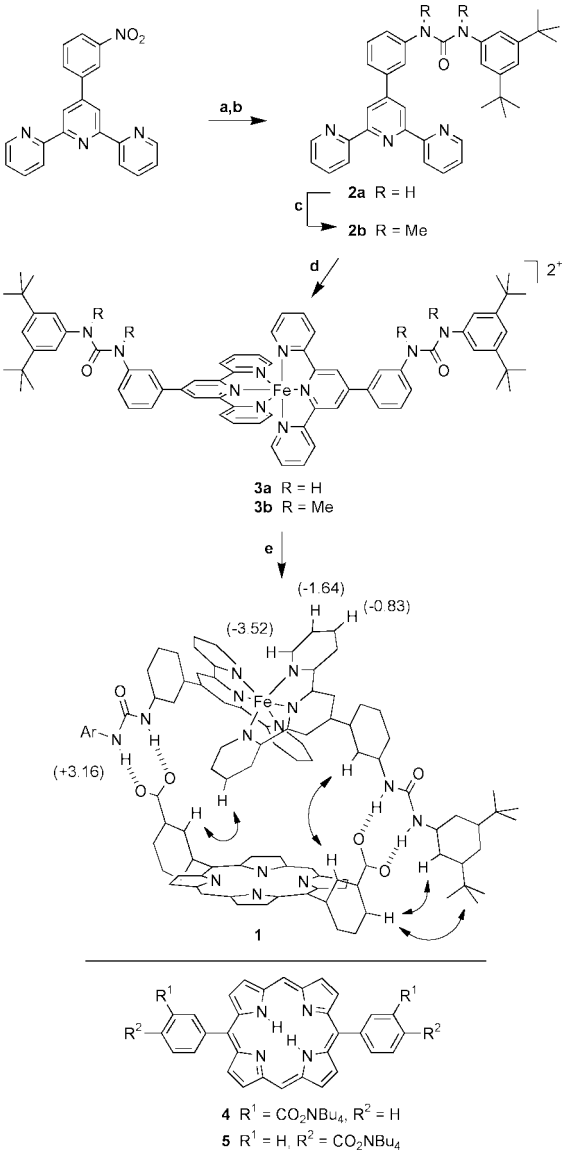

Scheme 1 *Reagents and conditions*: (a) $SnCl_2·2H_2O$, EtOH; (b) triphosgene, CH_2Cl_2, then 3,5-di-*tert*-butylaniline, 78% for three steps; (c) NaH, CH_3I, DMF, 50 °C, 99%; (d) $Fe(H_2O)_6(BF_4)_2$, acetone, quantitative; (e) **4**, MeOH, 97%. The double bonds have been removed from structure **1** for clarity. Observed intermolecular nOe's (represented as arrows) and complex induced chemical shifts in the ^1H NMR spectrum (shown in parentheses) are highlighted.

† Current address: Department of Chemistry, Simon Fraser University, 8888 University Drive, Burnaby, B.C., Canada V5A 1S6. E-mail: nbranda@sfu.ca

 DOI: 10.1039/b106430b

induced shift (CIS) values for complex **1** in the ^{1}H NMR spectrum in DMSO-d_6 and the observed intermolecular nuclear Overhauser enhancements (nOe's) are highlighted in Scheme 1. Both experiments support the proposed structure of **1**, where **3a** is straddling across the porphyrin macrocycle and is not lying to its side. The significant downfield shift ($\Delta\delta > 3$ in DMSO-d_6) observed for the urea N–H protons in assembly **1** is indicative of effective hydrogen bonding even in such a polar and competitive solvent. The role of the hydrogen bonds is also to steer the iron(terpyridine) fragment into a position where it lies directly over the porphyrin plane. This guidance is successful as diagnosed by the upfield shifts observed for the hydrogen atoms of **3a** lying directly over the porphyrin plane and within the shielding region of the macrocycle ($\Delta\delta$ are as large as -3.52). The signals for the four hydrogen atoms on the terminal pyridine ring of **3a** are unique in that they appear as broad peaks in the spectrum. We attribute this to the fact that **3a** can be thought of as a 'spit on a barbecue' in which the terpyridine can slowly rotate above the porphyrin ring. The terpyridine protons can, therefore, range in distance from 3.5 to 14.5 Å‡ from the plane of the macrocycle at any given moment affording a variety of possible conformers that can exist within the NMR time-scale. Variable temperature NMR experiments failed to alter the shape of these broadened signals.

The strength of the binding between **3a** and **4** was too large to be accurately measured by ^{1}H NMR spectroscopy even in DMSO-d_6. Isothermal titration calorimetry (ITC) experiments in DMSO, however, indicated a binding stoichiometry of 1 : 1 for **3a** and **4** and an impressive value for the association constant (K_a) of $(2.47 \pm 0.44) \times 10^6$ M^{-1}. When the ITC experiments were repeated replacing **3a** with the *N*,*N*′-dimethylated analog **3b**, that can only associate through ion pairing, the heat released upon binding was so small that the association constant was impossible to estimate. The titration of **5** with **3a** also revealed a similar trend, despite the fact that the **3a**·**5** complex can be isolated as a solid in a similar fashion as for **1**. In this case, the hydrogen bonds are not suitably positioned to operate in unison and direct the formation of a strapped 1 : 1 complex. Although the ^{1}H NMR spectrum in DMSO-d_6 does reveal a 1 : 1 stoichiometry between **3a** and **5**, the signals for the urea N–H protons shift only 1 ppm downfield, and there is no observable shift of the signals corresponding to the C–H protons on the iron(terpyridine) fragment. This indicates that **3a** does not reside over the plane of **5** and the 1 : 1 complex should really be thought of as an aggregate $(\mathbf{3a}\cdot\mathbf{5})_n$. These experiments clearly highlight that ion pairing contributes to the association of **1**; however, the cooperative hydrogen bonds aid in aligning the building blocks into close proximity so that these ion pairing attractive forces can be maximized.

The relative positioning of **3a** and **4** within **1** has a significant impact on the photophysical behavior of the final assembly. Studies using steady-state fluorescence spectroscopy to monitor the changes in the emission intensities of DMSO solutions of **4** and **5** as the porphyrins were treated with aliquots of **3a** are shown in Fig. 1. The immediate quenching of the fluorescence of **4** is most likely a direct result of the straddling nature of the iron(terpyridine) fragment which positions the two chromophores into the most intimate arrangement possible and ensures maximum through-space communication. The fluorescence quenching of porphyrin **4** by **3a** is clearly a result of both strong bimolecular association and optimal spatial positioning of the two chromophores. The *N*,*N*′-dimethylated analog **3b**, on the other hand, only slightly quenched the fluorescence of **4** presumably in a dynamic, collision-based process. A similar low level of quenching was obtained when porphyrin **5** was titrated with **3a**. Despite the fact that both hydrogen bonding and ion pairing are present in the $(\mathbf{3a}\cdot\mathbf{5})_n$ polymolecular assembly, the terpyridine fragment cannot form a strapped arrangement, and any through-space communication between the chromophores is significantly reduced. Impressively, similar photophysical behavior of assembly **1** was observed in a 10% H_2O/MeCN solution attesting to the strength of the association between building blocks **3a** and **4** even in an aqueous environment.

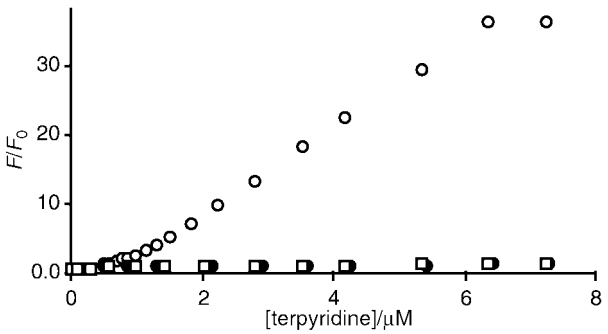

Fig. 1 Stern–Volmer quenching when a DMSO solution of **4** is titrated with **3a** (○), with **3b** (□), and when **5** is titrated with **3a** (●) (λ_{ex} = 415 nm, λ_{em} = 633 nm). Concentrations: [**4**] and [**5**] = 1.0×10^{-6} M, [**3a**] and [**3b**] = 2×10^{-5} M.

This work was supported by the Natural Sciences and Engineering Research Council of Canada and the University of Alberta. We are grateful to Pablo Ballester (Universitat de les Illes Balears) for his helpful suggestions.

Notes and references

‡ These distances were estimated from the lowest energy structure of assembly **1** using computer-assisted molecular modeling.

1 M. D. Ward, *Chem. Soc. Rev.*, 1997, **26**, 365 and references therein.
2 T. Imamura and K. Fukushima, *Coord. Chem. Rev.*, 2000, **198**, 133; R. A. Haycock, A. Yartsev, U. Michelsen, V. Sundstrom and C. A. Hunter, *Angew. Chem., Int. Ed.*, 2000, **39**, 3616; K. Ogawa and Y. Kobuke, *Angew. Chem., Int. Ed.*, 2000, **39**, 4070; K. Chichak and N. R. Branda, *Chem. Commun.*, 2000, 1211; C. C. Mak, N. Bampos and J. K. M. Sanders, *Chem. Commun.*, 1999, 1085; G. S. Wilson and H. L. Anderson, *Chem. Commun.*, 1999, 1539; J. Otsuki, K. Harada, K. Toyama, Y. Hirose, K. Araki, M. Seno, K. Takatera and T. Watanabe, *Chem. Commun.*, 1998, 1515; C. M. Drain, F. Nifiatis, A. Vasenko and J. D. Batteas, *Angew. Chem., Int. Ed.*, 1998, **37**, 2344; C. A. Hunter and R. A. Hyde, *Angew. Chem., Int. Ed. Engl.*, 1996, **35**, 1936.
3 C. A. Hunter and R. J. Shannon, *Chem. Commun.*, 1996, 1361.
4 S. Agirtas, R.-M. Ion and O. Bekaroglu, *Mater. Sci. Eng. C*, 2000, **7**, 105; J. F. Lipskier and T. H. Tran-Thi, *Inorg. Chem.*, 1993, **32**, 722.
5 K. Kano, H. Minamizono, T. Kitae and S. Negi, *J. Phys. Chem. A*, 1997, **101**, 6118.
6 H.-J. Schneider and M. Wang, *J. Org. Chem.*, 1994, **59**, 7464.
7 Examples of reports of multi-porphyrin arrays include: C. M. Drain, X. Shi, T. Milic and F. Nifiatis, *Chem. Commun.*, 2001, 287; S. Masiero, G. Gottarelli and S. Pieraccini, *Chem. Commun.*, 2000, 1995; C. Ikeda, N. Nagahara, E. Motegi, N. Yoshioka and H. Inoue, *Chem. Commun.*, 1999, 1759; C. M. Drain, K. C. Russell and J.-M. Lehn, *Chem. Commun.*, 1996, 337. Examples of porphyrinic donor–acceptor hybrid arrays include: A. J. Myles and N. R. Branda, *J. Am. Chem. Soc.*, 2001, **123**, 177; A. Berg, Z. Shuali, M. Asano-Someda, H. Levanon, M. Fuhs, K. Mobius, R. Wang, C. Brown and J. L. Sessler, *J. Am. Chem. Soc.*, 1999, **121**, 7433; A. Osuka, R. Yoneshima, H. Shiratori, T. Okada, S. Taniguchi and N. Mataga, *Chem. Commun.*, 1998, 1567; T. Hayashi, T. Miyahara, K. Norihiro, K. Tukitoshi, H. Masuda and H. Ogoshi, *J. Am. Chem. Soc.*, 1997, **119**, 7281; T. Arimura, C. T. Brown, S. L. Springs and J. L. Sessler, *Chem. Commun.*, 1996, 2293; J. P. Kirby, N. A. van Dantzig, C. K. Chang and D. G. Nocera, *Tetrahedron Lett.*, 1995, **36**, 3477; C. Turro, K. Chang, G. E. Leroi, R. I. Cukier and D. G. Nocera, *J. Am. Chem. Soc.*, 1992, **114**, 4013.
8 C. Schmuck, *Chem. Eur. J.*, 2000, **6**, 709; L. Sebo, B. Schweizer and F. Diederich, *Helv. Chim. Acta*, 2000, **83**, 80; B. Linton and A. D. Hamilton, *Tetrahedron*, 1999, 6027; T. W. Bell. N. H. Hext and A. B. Khasanov, *Pure Appl. Chem.*, 1998, **70**, 2371; E. Fan, S. A. Van Arman, S. Kincaid and A. Hamilton, *J. Am. Chem. Soc.*, 1993, **115**, 369.

CHEMCOMM Communication
www.rsc.org/chemcomm

Ring opening–cross metathesis of unstrained cycloalkenes

Stefan Randl, Stephen J. Connon and Siegfried Blechert*

Institut für Chemie, Technische Universität Berlin, Strasse des 17. Juni 135, 10623 Berlin, Germany. E-mail: blechert@chem.tu-berlin.de; Fax: +49 30 31423619

Received (in Cambridge, UK) 23rd July 2001, Accepted 3rd August 2001
First published as an Advance Article on the web 4th September 2001

Unstrained cycloalkenes undergo ruthenium-catalysed ring opening–cross metathesis reactions with simple α,β-unsaturated carbonyl compounds under mild conditions.

Over the last decade, olefin metathesis has emerged as a powerful tool for the formation of carbon–carbon double bonds.[1] Due to their excellent activity and functional group tolerance, ruthenium complexes with sterically demanding *N*-heterocyclic carbene (NHC) ligands (**1** and **2**) have proved to be

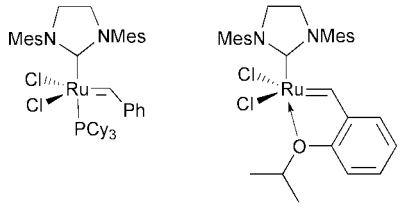

1 **2**

Cy = Cyclohexyl
Mes = 2,4,6-trimethylphenyl

an important development in this field. Our group[2] and others[3] have investigated the catalytic properties of the readily prepared phosphine-free catalyst **2**. In the case of cross metathesis (CM) with α,β-unsaturated carbonyl compounds catalysed by **1**, the formation of the relatively unstable acceptor substituted carbene species was rejected.[4] However, Grubbs *et al*. have demonstrated that β-carbonyl ruthenium carbene species generated from diazoacetate are highly active, reacting in stoichiometric quantities with cyclohexene to afford new ruthenium carbene complexes.[5] Little is known about the ring opening–cross metathesis (ROM-CM) of unstrained cycloolefins,[6] and since **1** and **2** can promote highly efficient CM reactions with α,β-unsaturated carbonyl compounds,[2] we wondered if catalytic ROM-CM reactions of low-strain cycloolefins could be accomplished *via* highly reactive β-carbonyl ruthenium carbene intermediates.

Preliminary studies were carried out with cyclohexene and various electron deficient olefins. We found that methyl vinyl ketone (**3**), methyl acrylate (**4**), acrylic acid (**5**) and acrylaldehyde (**6**) were suitable substrates for ROM-CM, whereas vinyl sulfones, nitriles and amides gave poor results. Encouraged by these findings, we investigated the ROM-CM of unstrained cycloolefins (Scheme 1) such as cyclopentene, cyclohexene and cycloheptene (3.0 eq.), with simple α,β-unsaturated carbonyl compounds **3**–**6**.† It was also decided to compare the activity of catalysts **1** and **2** in these reactions. The results of these experiments are outlined in Table 1.

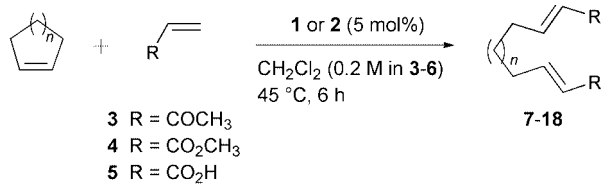

Scheme 1

In almost all cases moderate to excellent yields of ring opened double-cross products (**7**–**18**) were obtained. In addition, several trends were observed. Firstly, as expected,[2] phosphine-free catalyst **2** gave better cross product yields than **1**; secondly, the order of reactivity of the cycloalkene substrates was cycloheptene ≥ cyclopentene > cyclohexene presumably due to ring strain. In addition, acrylic acid gave especially good results over the range of substrates.

Having established that efficient ROM-CM of unstrained cycloolefins is possible, we wished to extend this methodology to both functionalised and heterocyclic compounds. Thus, **19**–**25** were subjected to ROM-CM conditions, using catalyst **2** (5 mol%) and CM partners **3**, **4** and **5** (Table 2). Given the high reactivity of cyclopentene, the failure of 5- and 6-membered *N*-heterocycles **19** and **20** to give ring-opened products was somewhat surprising. In these reactions, only dimerisation of the electron deficient olefin occurred. At this time it is not known if this lack of ROM reactivity is attributable to either an internal complexation of the heteroatom to ruthenium during the catalytic cycle, or to the electron withdrawing effect of the tosyl-protected nitrogen atom on the 'allylic' double bond. In this regard it is interesting to note that dihydrofuran **23** gave only moderate yields of double-cross product. In the case of **21**, the 7-membered analogue of **19** and **20**, this effect is obviously less important than relief from ring strain, as good CM product yields were obtained. This is supported by the fact that the yields of **32**, **33** and **34** are in good correlation with those of **35**, **36** and **37** derived from **22**, where the olefin double bond is one methylene unit further removed from the heteroatom. Epoxycyclooctene **24** also gave smooth conversion to **41**, **42** and **43**, however bicyclic lactone **25** did not react, possibly due to steric factors.

Given that neither polymeric nor terminal olefinic products were detected even in the presence of excess cycloolefin, it is clear that the first step in the catalytic cycle is reaction between **1** or **2** and the electron deficient olefin to afford reactive carbene intermediates of general type **47**, which then ring-open the substrate to form a second alkylidene **48** (Scheme 2).

Table 1 Performance of **1** and **2** in ROM-CM with electron deficient alkenes

Product[a]	Yield (%)[b] using cat. **2**	Yield (%)[b] using cat. **1**
7 n = 1, R = $COCH_3$	86	62
8 n = 1, R = CO_2CH_3	90	79
9 n = 1, R = CO_2H	83	57
10 n = 1, R = CHO	83	30
11 n = 2, R = $COCH_3$	54	26
12 n = 2, R = CO_2CH_3	66	47
13 n = 2, R = CO_2H	80	38
14 n = 2, R = CHO	45	5
15 n = 3, R = $COCH_3$	87	87
16 n = 3, R = CO_2CH_3	97	80
17 n = 3, R = CO_2H	83	70
18 n = 3, R = CHO	90	75

[a] Only the *E*-isomers were detected in all cases. [b] Determined by ^{1}H NMR using (*E*)-stilbene as an internal standard.

 DOI: 10.1039/b106558k

Table 2 ROM-CM of functionalised cycloolefins

Cycloolefin	Products with **3**, **4** and **5** (% Yield)[a,b]			
 **19**	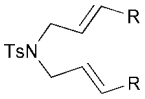	**26**	R = $COCH_3$	(0)
		27	R = CO_2CH_3	(0)
		28	R = CO_2H	(0)
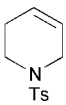 **20**	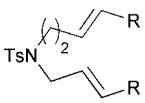	**29**	R = $COCH_3$	(0)
		30	R = CO_2CH_3	(0)
		31	R = CO_2H	(0)
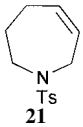 **21**	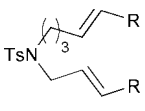	**32**	R = $COCH_3$	(79)
		33	R = CO_2CH_3	(70)
		34	R = CO_2H	(85)
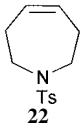 **22**	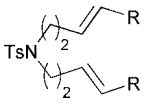	**35**	R = $COCH_3$	(75)
		36	R = CO_2CH_3	(90)
		37	R = CO_2H	(82)
 **23**	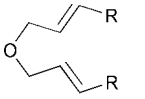	**38**	R = $COCH_3$	(42)
		39	R = CO_2CH_3	(0)
		40	R = CO_2H	(60)
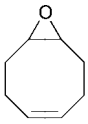 **24**	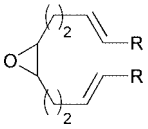	**41**	R = $COCH_3$	(84)
		42	R = CO_2CH_3	(92)
		43	R = CO_2H	(80)
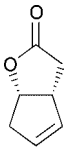 **25**	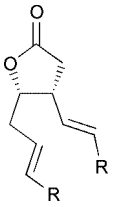	**44**	R = $COCH_3$	(0)
		45	R = CO_2CH_3	(0)
		46	R = CO_2H	(0)

[a] Only the *E*-isomers were detected in all cases. [b] Determined by ^{1}H NMR using (*E*)-stilbene as an internal standard.

The intermediacy of **48** suggested that a ring opening double cross metathesis reaction with two different CM partners could be possible. In order to test this, cyclohexene (3.0 eq.) was ring opened in the presence of **2** (5 mol%), **5** (1.0 eq) and phenyl vinyl sulfone (1.0 eq.) to give 25% yield (by ^{1}H NMR) of double cross product **49** (Scheme 3).

In summary, the novel ROM-CM of relatively unstrained carbo- and heterocycles to give ring opened bis-α,β-unsaturated carbonyl compounds has been described. Phosphine free catalyst **2** has been shown to possess a superior activity

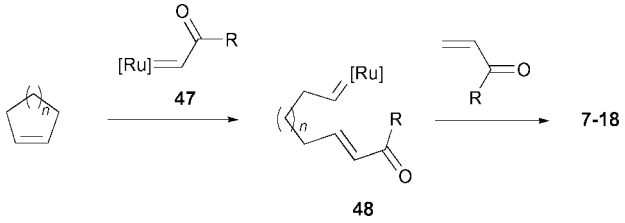

Scheme 2

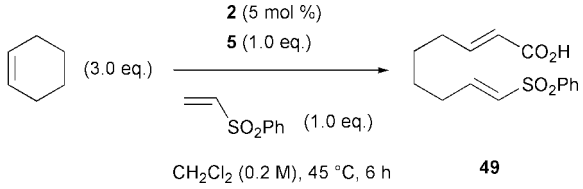

Scheme 3

compared to **1** in these reactions. The bis-functionalisation of cyclohexene with two different CM partners using a ROM-CM strategy has also been demonstrated. Further investigations along these lines are in progress in our laboratories.

We would like to thank the 'Fonds der Chemischen Industrie' for financial support. S. R. and S. J. C. thank the Graduiertenkolleg "Synthetische, mechanistische und reaktionstechnische Aspekte von Metallkatalysatoren" for their stipends.

Notes and references

† All new compounds were purified by column chromatography and fully characterised. Representative procedure: a solution of cyclohexene (0.40 mL, 3.95 mmol), **2** (125.4 mg, 0.2 mmol) and **5** (0.18 mL, 2.62 mmol) in CH_2Cl_2 (13 mL, 0.2 M in **5**) was stirred at 45 °C for 6 h under a nitrogen atmosphere, after which time the solvent was evaporated and (*E*)-stilbene added as an internal standard. The product yield was determined by ^{1}H NMR analysis of the crude mixture.

1 For recent reviews see: T. M. Trnka and R. H. Grubbs, *Acc. Chem. Res.*, 2001, **34**, 18; A. Fürstner, *Angew. Chem., Int. Ed.*, 2000, **39**, 3013; A. D. Philips, *Aldrichima Acta*, 1999, **32**, 75; S. K. Armstrong, *J. Chem. Soc., Perkin Trans. 1*, 1998, 371; R. H. Grubbs and S. Chang, *Tetrahedron*, 1998, **54**, 4413; M. Schuster and S. Blechert, *Angew. Chem. Int. Ed. Engl.*, 1997, **36**, 2036.

2 S. Gessler, S. Randl and S. Blechert, *Tetrahedron Lett.*, 2000, **41**, 9977; S. Randl, S. Gessler, H. Wakamatsu and S. Blechert, *Synlett*, 2001, **3**, 430; S. Imhof, S. Randl and S. Blechert, *Chem. Commun.*, 2001, 1692.

3 S. B. Garber, J. S. Kingsbury, B. L. Gray and A. H. Hoveyda, *J. Am. Chem. Soc.*, 2000, **122**, 8168; J. Cossy, S. BouzBouz and A. H. Hoveyda, *J. Organomet. Chem.*, 2001, **624**, 327.

4 A. K. Chatterjee, J. P. Morgan, M. Scholl and R. H. Grubbs, *J. Am. Chem. Soc.*, 2000, **122**, 3783.

5 M. Ulman, T. R. Belderrain and R. H. Grubbs, *Tetrahedron Lett.*, 2000, **41**, 4689.

6 N. B. Bespalova, M. A. Bovina, M. B. Sergeeva, V. D. Oppengeim and V. G. Zaikin, *J. Mol. Catal.*, 1994, **90**, 21.

CHEMCOMM Communication
www.rsc.org/chemcomm

Barbier reaction in the regime of metal oxide: the first example of carbonyl allylation mediated by tetragonal tin(II) oxide†

Pradipta Sinha and Sujit Roy*

Organometallics & Catalysis Laboratory, Chemistry Department, Indian Institute of Technology, Kharagpur 721302, India. E-mail: sroy@chem.iitkgp.ernet.in; Fax: +91 3222 82252; Tel: +91 3222 83338

Received (in Cambridge, UK) 22nd May 2001, Accepted 25th July 2001
First published as an Advance Article on the web 4th September 2001

Facile synthesis of homoallylic alcohols is achieved from allyl halides and aldehydes or ketones over an all-oxide heterogenous media involving β-SnO and catalytic Cu_2O.

The reaction of a carbonyl compound and an organic halide in the presence of magnesium metal, trivially known as the Barbier reaction, has carved a distinct niche in synthetic organic and pharmaceutical chemistry.[1] In the hundred years, since its original discovery,[2] this one-pot variant of the Grignard reaction has been demonstrated solely with zerovalent metals, and metal halides.[3] With specific reference to carbonyl allylation *via* tin reagents,[4] both preformed as well as *in situ* generated allylstannanes continue to evoke widespread[5] interest due to their chemo-, regio-, stereo-, and enantioselecivity aspects. Our continuing interest[6] in organotin chemistry and recent interest in heterobimetallic reagents, prompted us to explore a gateway into the Barbier reaction *via* metal oxides. We are delighted to disclose herein a facile carbonyl allylation reaction over tetragonal tin(II)oxide (β-SnO)[7] and catalytic Pt(II), Pd(II), Pd(0), Cu(I) salts/complexes in organic–aqueous or aqueous medium (Scheme 1). *Further extension to β-SnO/catalytic Cu_2O affords an all-oxide reagent in Barbier allylation*. We believe that the results provide new directions in the synthetic and mechanistic issues of Grignard type carbon–carbon bond forming reactions across metal oxides.

The model reaction of 1-bromoprop-2-ene **1a** (2 mM) and 4-chlorobenzaldehyde **2a** (1 mM) in the presence of catalytic $PtCl_2(PPh_3)_2$ **4a** (0.01 mM) and β-SnO (1.5 mM) in THF–water (9 : 1 v/v) at 70 °C for 6 h gives rise to the desired homoallylic alcohol 1-(4-chlorophenyl)but-3-ene-1-ol **3a** in 96% isolated yield (Table 1, entry 3).[8] Under identical conditions, uncatalyzed reaction affords < 15% of the product. Also important is the remarkable effect of water: reaction in the presence of catalyst **4a** but in dry THF yields < 15% of the product, while reaction in water alone gives rise to 55% of the desired alcohol. That there is no phase change of β-SnO before and after treatment with THF–water, is indicated by XRD. Among the other catalysts screened, $NiCl_2(PPh_3)_2$, $PdCl_2(PhCN)_2$ and $Pd_2(dba)_3{\cdot}CHCl_3$ are found unsatisfactory (< 25% yields), but $PdCl_2(PPh_3)_2$, $Pd_2(dba)_3$, and CuCl afford moderate to excellent yields of product. The generality of the reaction has been successfully tested with aliphatic, aromatic and heteroaromatic aldehydes and substituted allyl bromides (Table 2, entry 1–5).

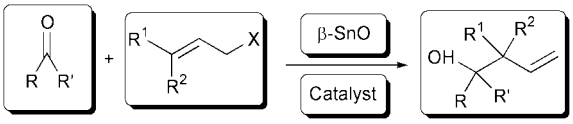

Scheme 1

Table 1 β-SnO promoted carbonyl allylation: effect of catalyst

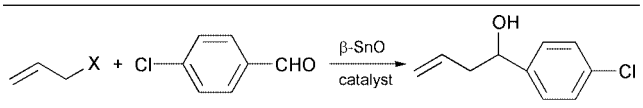

#	X	Catalyst	Solvent	Yield (%)
1	Br	NIL	THF–H_2O	15
2	Br	$PtCl_2(PPh_3)_3$ **4a**	THF	15
3	Br	**4a**	THF–H_2O	96
4	Br	$Pd_2(dba)_3$ **4b**	THF–H_2O	76
5	Br	Cu_2O **4c**	DCM–H_2O	80
6	Cl	**4c**	DCM–H_2O	52
7	Br	CuCl **4d**	THF–H_2O	33

† Electronic supplementary information (ESI) available: further experimental details, XRD and EIMS spectra. See http://www.rsc.org/suppdata/cc/b1/b104500h/

Table 2 Allylation of various carbonyl compounds with β-SnO/catalyst

#	Halide	Carbonyl	Cat	Product	Yield (%)
1	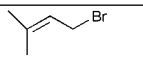 **1b**	Fc-CHO **2b**	**4a**	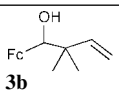 **3b**	70
2	**1b**	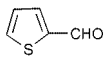 **2c**	**4a**	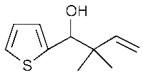 **3c**	65
3	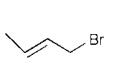 **1c**	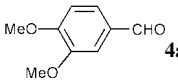 **2d**	**4a**	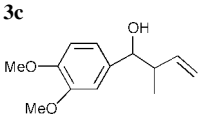 **3d**	63
4	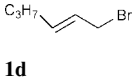 **1d**	BnCHO **2e**	**4b**	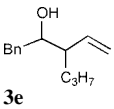 **3e**	53
5	**1d**	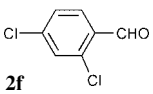 **2f**	**4b**	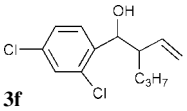 **3f**	76
6	**1c**	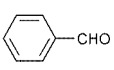 **2g**	**4c**	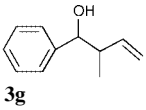 **3g**	79
7	**1c**	$Me(CH_2)_8CHO$ **2h**	**4c**	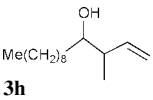 **3h**	54
8	**1a**	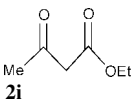 **2i**	**4c**	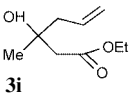 **3i**	71
9	**1a**	 **2j**	**4c**	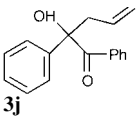 **3j**	45

 DOI: 10.1039/b104500h

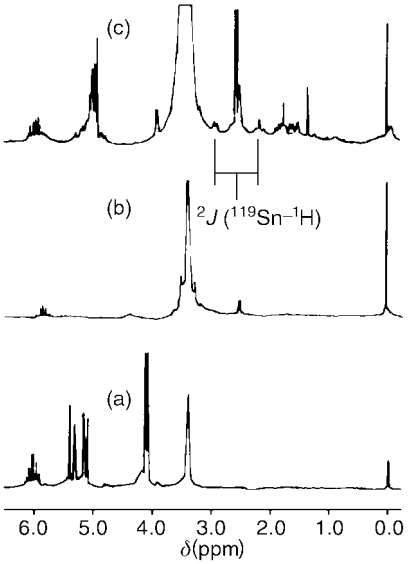

Fig. 1 ^{1}H NMR spectra in DMSO-d_6 of (a) allyl bromide; (b) residue from the reaction of β-SnO–allyl bromide; (c) residue from the reaction of β-SnO–allyl bromide–catalytic $Pd_2(dba)_3$ [dba = dibenzylideneacetone].

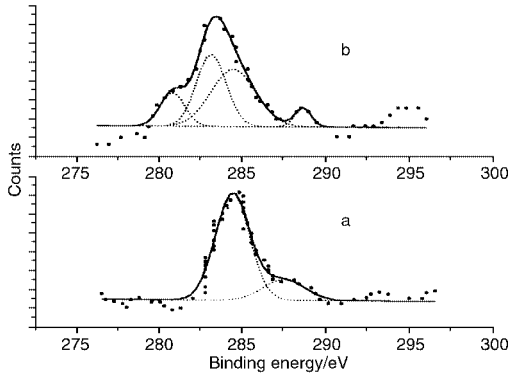

Fig. 2 XPS spectra in the C-1s region of (a) untreated β-SnO/Cu_2O—peaks at 284.5, 287.6; (b) β-SnO/Cu_2O after treatment with allyl bromide—peaks at 280.8, 283.2, 284.5, 288.9.

Triggered by the success as above, we wished to attempt *an all-oxide reagent* for carbonyl allylation. The reagent combination of β-SnO and catalytic Cu_2O in refluxing DCM–water (9 : 1 v/v) is adjudged to be the best (Table 1, entry 5–6; Table 2, entry 6–9).

While mechanistic studies are underway in our laboratory, preliminary experiments clearly establish the formation of new tin–carbon bonded species during the course of the reaction. Thus, a mixture of β-SnO (2 mM), catalytic $Pd_2(dba)_3$ (0.02 mM) and allyl bromide (4 mM) in THF–H_2O (99 : 1 v/v) was refluxed for 10 h. Following filtration under argon, and solvent removal, the residue was examined by ^{1}H NMR. The spectrum (Fig. 1, spectrum c) showed the formation of a new σ-allyl tin species[9] characterized by allylic proton signals at 2.55 ppm [^2J(^{119}Sn–^{1}H) = 154 Hz], as compared to that of allyl bromide at 4.1 ppm (spectrum a). No such species was detected in the reaction without catalyst (Fig. 1, spectrum b). On the other hand, reaction of allyl bromide with $Pd_2(dba)_3$ alone, showed signals due to known π-allylpalladium intermediate.[10] We conclude that the latter assists the formation of the σ-allyl tin species (Scheme 2).[11]

Unlike the above, we could not detect any soluble organotin species in the reaction of allyl bromide with β-SnO/catalytic Cu_2O, thereby indicating that the incipient metal–carbon intermediate is formed in the solid phase. To test this hypothesis, narrow scan XPS analysis was performed for β-SnO/Cu_2O before and after its reaction with allyl bromide. Formation of new species is indicated by major shifts in the binding energies of Sn ($3d_{5/2}$, $3d_{3/2}$), Cu ($2p_{3/2}$, $2p_{1/2}$), O (1s) and C (1s) peaks.[12] Multi-Gaussian peak analysis of carbon-1s spectra shows two new peaks at 280.8 and 283.2 eV (Fig. 2, spectrum b) indicative of metal–carbon bonded species. Prior interaction of alkene with copper(I) is likely to promote the formation of an allyltin intermediate.[13] We hope to address this and related mechanistic issues in future studies.

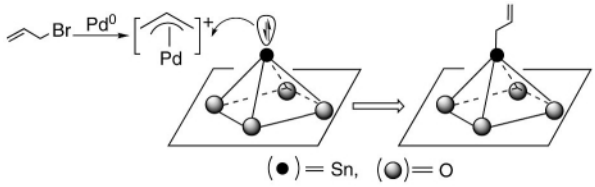

Scheme 2 π-Allylpalladium attacks tetragonal tin(II) oxide.

We thank CSIR, UGC and DST for financial support.

Notes and references

1 B. J. Wakefield, *Organomagnesium Methods in Organic Chemistry*, Academic Press, New York, 1995; R. D. Rieke, *Science*, 1989, **246**, 1260; C. J. Li and W.-C. Zhang, *J. Am. Chem. Soc.*, 1998, **120**, 9102.

2 P. Barbier, *Competus Rendus*, 1898, **128**, 110; V. Grignard, *Competus Rendus*, 1900, **130**, 1322.

3 For representative examples, please see: T. H. Chan and Y. Yang, *J. Am. Chem. Soc.*, 1999, **121**, 3228; X.-H. Yi, Y. Meng, X-G. Hua and C. J. Li, *J. Org. Chem.*, 1998, **63**, 7472; A. Yanagisawa, S. Habaue, K. Yasue and H. Yamamoto, *J. Am. Chem. Soc.*, 1994, **116**, 6130; D. P. Curran, X. Gu, W. Zhang and P. Dowd, *Tetrahedron*, 1997, **53**, 9023; F. Dubner and P. Knochel, *Angew. Chem., Int. Ed.*, 1999, **38**, 379.

4 For reviews please see: W. R. Rousch, in *Comprehensive Organic Synthesis*, eds. B. M. Trost, I. Fleming and C. H., Heathcock, Pergamon Press, Oxford, 1991, vol. 2, pp. 1–53 and related chapters; Y. Yamamoto and N. Asao, *Chem. Rev.*, 1993, **93**, 2207; J. A. Marshall, *Chem. Rev.*, 1996, **96**, 31; E. J. Thomas, *Chemtracts-Org. Chem.*, 1994, **7**, 207; Y. Masuyama, in *Advances in Metal-Organic Chemistry*, ed. L. S. Liebeskind, JAI Press, Greenwich CT, 1994.

5 For representative examples, please see: (*a*) G. E. Keck, K. H. Tarbet and L. S. Geraci, *J. Am. Chem. Soc.*, 1993, **115**, 8467; (*b*) A. Yanagisawa, H. Inoue, M. Morodome and H. Yamamoto, *J. Am. Chem. Soc.*, 1993, **115**, 10 356; (*c*) A. Ito, M. Kishida, Y. Kurusu and Y. Masuyama, *J. Org. Chem.*, 2000, **65**, 494; (*d*) J. P. Takahara, Y. Masuyama and Y. Kurusu, *J. Am. Chem. Soc.*, 1992, **114**, 2577; (*e*) T. H. Chan, Y. Yang and C. J. Li, *J. Org. Chem.*, 1999, **64**, 4452.

6 (*a*) P. Sinha, A. Kundu, S. Roy, S. Prabhakar, M. Vairamani, A. R. Sankar and A. C. Kunwar, *Organometallics*, 2001, **20**, 157; (*b*) A. Kundu and S. Roy, *Organometallics*, 2000, **19**, 105; (*c*) A. Kundu, S. Prabhakar, M. Vairamani and S. Roy, *Organometallics*, 1999, **18**, 2782; (*d*) A. Kundu, S. Prabhakar, M. Vairamani and S. Roy, *Organometallics*, 1997, **16**, 4796.

7 For chemistry of bivalent tin, please see: J. D. Donaldson, *Prog. Inorg. Chem.*, 1967, **8**, 287; P. J. Harrison, *Chemistry of Tin*, Blackie, New York, 1989, pp. 221–244.

8 Typical procedure: a mixture of **1a** (242 mg, 2 mM) and **2a** (140 mg, 1 mM) in THF (2 mL) was added slowly to a refluxing solution containing β-SnO (202 mg, 1.5 mM) and **4a** (8 mg, 0.01 mM) in THF–H_2O (2.5 mL–0.5 mL) and under argon. Upon completion (TLC monitoring: silica gel, eluent: *n*-hexane–EtOAc 9 : 1), an aqueous solution of NH_4F (15%, 10 mL) was added to the reaction mixture and the organic layer was extracted with diethyl ether (3 × 10 mL), washed with water (2 × 10 mL), brine (2 × 10 mL) and dried over magnesium sulfate. Solvent removal followed by column chromatography (eluent *n*-hexane–ethyl acetate 9 : 1) afforded pure **3a** (175 mg, 96% w.r.t. aldehyde). Similar procedure as above was followed for reactions with Cu_2O as catalyst (14 mg, 0.1 mM), the solvent used was CH_2Cl_2–H_2O (4.5 mL–0.5 mL).

9 For comparison with known σ-allyl tin NMR, please see: refs. 5*d*, 5*e* and 6*d*.

10 *The Organic Chemistry of Palladium*, ed. P. Maitilis, Vol. 1, 2, Academic Press, New York, 1971.

11 Direct injection of a reaction mixture into an EIMS probe results in major peaks at 351, 430, 478 corresponding to possible fragments $[(allyl)_2Sn_2O_2 - H]^+$, $[(allyl)_2Sn_2O_2Br - H]^+$, and $[(allyl)_2Sn_2Br_2]^+$.

12 *Handbook of X-ray Photoelectron Spectroscopy: A Reference Book of Standard Data for Use in XPS*, Perkin–Elmer Corporation Physical Electronics Division, 1979.

13 For olefin-Copper(I) interaction see: ref. 6*d*.

CHEMCOMM Communication
www.rsc.org/chemcomm

Enzymatic synthesis of pyruvic acid from acetaldehyde and carbon dioxide

Masaya Miyazaki, Mitsukuni Shibue, Kazuya Ogino, Hiroyuki Nakamura and Hideaki Maeda*

Institute for Structual and Engineering Materials, AIST Kyushu, National Institute of Advanced Industrial Science and Technology (AIST), 807-1 Shuku, Tosu Saga 841-0052, Japan.
E-mail: maeda-h@aist.go.jp; Fax: +81(942)81-3695; Tel: +81(942)81-3643

Received (in Cambridge, UK) 4th June 2001, Accepted 3rd August 2001
First published as an Advance Article on the web 22nd August 2001

A new enzymatic synthesis of pyruvic acid from acetaldehyde and carbon dioxide has been developed.

Because global environmental pollution has recently become a serious problem, it is advantageous to develop a clean chemical process, which produces low emissions and organic wastes. Biocatalytic reactions attract attention as environmentally safe catalytic reactions in organic synthesis.[1] Several enzymatic processes have been designed and used as alternative organic processes.

Pyruvate decarboxylase (EC 4.1.1.1) is known as a catalyst of the decarboxylation reaction of pyruvic acid, to produce acetaldehyde. The mechanism of catalytic reaction of pyruvate decarboxylase has been elucidated. This enzyme requires thiamin pyrophosphate as a coenzyme for catalytic activity.[2] As for other thiamin pyrophosphate dependent enzymes, this enzyme has been interesting as a catalyst for carbon–carbon bond formations.[3–5] Pyruvate decarboxylase has been intensively studied as a carboligase for synthesis of chiral α-hydroxy ketones, which are versatile building blocks for organic and pharmaceutical chemistry.

The reverse reaction of this enzyme is also of interest as a catalytic procedure for carboxylation. Several studies have been performed which imitate these enzyme reactions using CO_2 as the reactant.[6–8] A previous study using α-lactoylthiamin showed that production of pyruvate was achieved at higher pH (>10).[8] However, these reactions require organic solvents and severe conditions.

We are interested in the development of novel enzymatic reactions and reactor systems having environmentally safe chemical processes. In the present study, we demonstrate the usefulness of the reverse reaction of pyruvate decarboxylase in the production of pyruvic acid from acetaldehyde and carbon dioxide (Scheme 1).

We chose a sodium bicarbonate buffer system, because not only is this buffer suitable at higher pHs, but it also can be used as the source of carbon dioxide. A typical run was as follows. To a solution of acetaldehyde (100 μM) in sodium bicarbonate buffer (1 ml) in a 1.5 ml microcentrifuge tube, Brewer's yeast pyruvate decarboxylase (1 unit) and thiamin pyrophosphate (the final concentration was 10 μM) were added at 4 °C. The reaction mixture was warmed to 25 °C quickly, and then shaken on a vortex mixer at room temperature. After 1 h, the reaction mixture was chilled on ice, and then subjected to HPLC analysis immediately. The amount of pyruvic acid was calculated from the peak area of HPLC analysis calibrated with commercially available pyruvic acid standards. The yield was estimated based on acetaldehyde.

First, we evaluated the effect of pH on the reaction. The reaction was performed using acetaldehyde (100 μM), thiamin

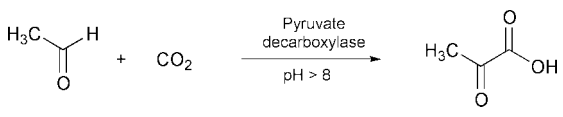

Scheme 1 Synthesis of pyruvic acid.

(0.1 μM), and pyruvate decarboxylase (1 unit) in 0.1 M $NaHCO_3$–Na_2CO_3 buffer at various pHs (pH 8.5–11.5). The result is shown in Fig. 1. Higher pHs gave a better yield of pyruvic acid. The maximum yield was obtained at pH 11 (61%). The present result agreed well with a previous observation obtained from the hydrolysis of α-lactoylthiamin. In that case, the best yield from hydrolysis was obtained at pH 12. In our case, the best yield was obtained at pH 11, but the yields decreased at much higher pH. Although the hydrolysis proceeds at a maximum rate at pH 12, the enzyme might not be stable over pH 11. Therefore, the maximum yield was obtained at pH 11. Thus, we decided to perform further experiments at pH 11.

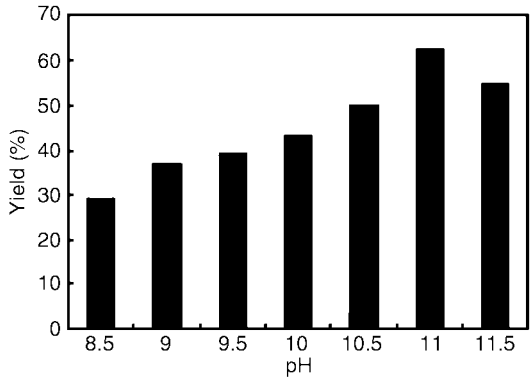

Fig. 1 Effect of pH on pyruvic acid production.

Next, we examined the effects of concentration of bicarbonate buffer on the reaction (Fig. 2). Higher ionic strength of the bicarbonate buffer strongly influenced the yield, as expected. The maximum yield of the reaction was 81% at 500 mM $NaHCO_3$–Na_2CO_3 buffer. This yield was sufficient to use as an organic process, and much higher than that obtained by the reaction in DMF under 20 atm of CO_2.[8] Not only does the latter reaction require multiple steps, but the use of the organic solvent DMF is problematic for environmental safety reasons. The enzymatic reaction does not require any organic solvent and gave a better yield. It has been reported that the thiamin itself

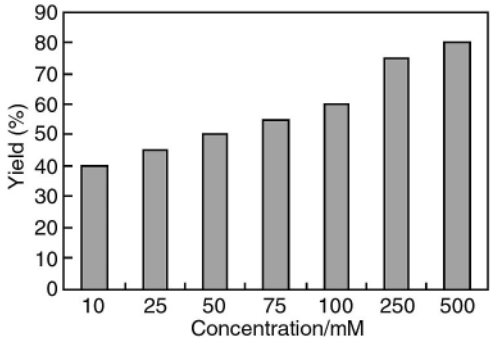

Fig. 2 Effect of ionic strength on enzyme reaction.

 DOI: 10.1039/b104873m

could catalyze a reaction analogous to that of the enzyme, but preparation of the intermediate lactoylthiamin from acetaldehyde was unsuccessful. Thus, it is difficult to reverse the reaction without an enzyme, and pyruvate decarboxylase is the best catalyst for carboxylation of acetaldehyde.

Recently, some enzymatic reactions utilizing supercritical carbon dioxide have been reported.[9,10] In our method, a higher concentration of carbon dioxide is required. The supercritical conditions might be effective at improving the yield of pyruvic acid synthesis, because they should provide a much higher carbon dioxide concentration. The reaction in supercritical carbon dioxide conditions will be our next subject.

Although the effect is much weaker than methane, carbon dioxide is considered to be a greenhouse gas, and therefore its immobilization is desired. The methods currently reported are mainly catalytic or electrochemical reactions, which require much energy.[11–13] One alternative method has been reported, which utilized carbonic anhydrase for the immobilization of carbon dioxide.[14] This biomimetic approach needs almost no energy for the reaction. However, the carbonic anhydrase just improves the solubility of carbon dioxide in aqueous media, and further treatment of dissolved gas is required. Although the reaction requires a large excess of CO_2, our approach can be useful for such a purpose. By our method, the carbon dioxide in the aqueous phase can be condensed with acetaldehyde to produce the pyruvic acid. Because pyruvic acid can easily be converted into lactic acid, which is a constituent of a biodegradable plastic, the carbon dioxide can be immobilized into the biological cycle. An enzymatic reaction by lactic dehydrogenase can be used for hydrogenation of pyruvic acid into lactic acid. Thus, it is possible to design a two-step enzymatic process as a completely environmentally safe method for CO_2 immobilization.

In summary, we have demonstrated the usefulness of the reverse reaction of pyruvate decarboxylase. This reaction might become a recommendable, environmentally safe carboxylation procedure for acetaldehyde. Further studies, such as the reaction utilizing supercritical carbon dioxide, and two-step enzymatic production of lactic acid, are in progress in our laboratories.

We thank Drs Masao Shibata, Tsuyoshi Sakaki, Hiroaki Kodama and Shoji Ando, for their continuous supports.

Notes and references

1 K. M. Koeller and C.-H. Wong, *Nature*, 2001, **409**, 232; A. Schmid, J. S. Dordick, B. Hauer, A. Kiener, M. Wubbolts and B. Witholt, *Nature*, 2001, **409**, 258.
2 R. Kluger, *Chem. Rev*., 1987, **87**, 863.
3 W.-D. Fessner, *Curr. Opin. Chem. Biol*., 1998, **2**, 85.
4 G. A. Sprenger and M. Pohl, *J. Mol. Catal. B: Enzym*., 1999, **6**, 145.
5 U. Schorken and G. A. Sprenger, *Biochim. Biophys. Acta*, 1998, **1385**, 229.
6 D. Walther, *Coord. Chem. Rev*., 1987, **79**, 135.
7 P. Braunstein, D. Matt and D. Nobel, *Chem. Rev*., 1988, **88**, 747.
8 M.-A. E. Foppen, Y. M. de Lange, F. van Rantwijk, L. Maat and A. P. G. Kieboom, *Recl. Trav. Chim. Pay-Bas*, 1990, **109**, 359.
9 A. K. Chaudhary, E. J. Bechman and A. J. Russel, *J. Am. Chem. Soc*., 1995, **117**, 3728.
10 Y. Ikushima, N. Saito, M. Arai and H. W. Blanch, *J. Phys. Chem*., 1995, **99**, 8941.
11 Y. Li, G.-H. Xu, C.-J. Liu, B. Eliasson and B.-Z. Xue, *Energy Fuels*, 2001, **15**, 299.
12 M. Aresta, A. Dibenedetto and I. Tommasi, *Energy Fuels*, 2001, **15**, 269.
13 C.-J. Liu, G.-H. Xu and T. Wang, *Fuel Process. Technol*., 1999, **58**, 119.
14 G. M. Bond, J. Stringer, D. K. Brandvold, F. Arzum Simsek, M.-G. Medina and G. Egeland, *Energy Fuels*, 2001, **15**, 309.

CHEMCOMM Communication
www.rsc.org/chemcomm

Synthesis of alkenylene-bridged macrocyclic silsesquioxanes by ruthenium or rhodium-catalyzed ring-closing reactions of bis(allyldimethylsilyl) groups†

Kenji Wada, Daisuke Izuhara, Koichi Yamada, Masashi Shiotsuki, Teruyuki Kondo and Take-aki Mitsudo*

Department of Energy and Hydrocarbon Chemistry, Graduate School of Engineering, Kyoto University, Sakyo-ku, Kyoto 606-8501, Japan

Received (in Cambridge, UK) 9th May 2001, Accepted 7th August 2001
First published as an Advance Article on the web 5th September 2001

Novel alkenylene-bridged oligosilsesquioxanes composed of half-caged structures with 16- or 17-membered rings as well as a titanium-containing molecule with a twisted 21-membered macrocycle have been synthesized by ruthenium or rhodium-catalyzed ring-closing reactions of silsesquioxanes with bis(allyldimethylsilyl) groups.

Recently, development of novel organic–inorganic hybrid materials, such as organic functionalized micro- and mesoporous materials, has attracted widespread attention because of the novel catalytic activities and physical properties of these substances.[1] Since silsesquioxanes and spherosilicates with cage-like core structures are expected to be candidates for building blocks of such materials, a number of silsesquioxanes with organic functional groups have been synthesized by various methods[2] including ruthenium or molybdenum-catalyzed cross-metathesis.[3] Porous materials are reported to be obtained by the hydrosilylative polymerization of T_8 cubes.[2d,4] Therefore, synthesis of oligosilsesquioxanes with novel core structures is of great importance. On the other hand, the synthesis of silacycloalkenes, which incorporate an alkenylene unit in the ring system, has attracted growing interest from the viewpoint of materials chemistry,[5] and various methods[6] for the synthesis of these compounds by catalytic ring-closing metathesis (RCM) reactions[7] have been developed.

Here we report the synthesis of silsesquioxanes containing novel organic–inorganic hybrid half-caged core structures. The ring-closing reactions of bis(allyldimethylsilyl)-substituted silsesquioxanes in the presence of a catalytic amount of a ruthenium or rhodium complex successfully gave novel alkenylene-bridged oligosilsesquioxanes composed of 16-, 17- and 21-membered macrocycles in high yields.

A silsesquioxane with two allyldimethylsilyl groups **1a** was prepared by the stepwise silylation of silsesquioxane disilanol $(c\text{-}C_5H_9)_7Si_7O_9(OSiMe_3)(OH)_2$ (**2**) by allylchlorodimethylsilane.[8] The RCM reaction of **1a** promoted by stepwise addition of 13 mol% of the ruthenium benzylidene complex, $\{(C_6H_{11})_3P\}_2Cl_2Ru{=}CHPh$ (**3**),[7] at 65 °C for 54 h, followed by column chromatography and reprecipitation afforded the desired novel half-caged oligosilsesquioxane with a 17-membered ring **4a** in an isolated yield of 94% as a mixture of *cis* and *trans* isomers.‡ At present, the major isomer is assigned to be *cis* on the basis of IR and ^{13}C NMR, and the ratio of *cis*:*trans* was estimated to be 4.9:1. The preliminary X-ray analysis of a single crystal of the major isomer established the structure illustrated in Scheme 1 with *cis* configuration of the butenylene bridge,§ although the complete solution of the structure was hampered by poor diffraction in the high angle region ($2\theta > 30°$) and severe disorder at trimethylsilyl and cyclopentyl groups. According to the ^1H NMR spectrum, these single crystals were composed of the major isomer. The undesired intermolecular reaction was not observed. The ^{29}Si NMR spectrum of *cis*-**4a** consists of one set of five peaks in a 1:1:2:2:1 ratio for seven silicon atoms in the silsesquioxane cage, which is in good accordance with the local C_s-symmetry of the siloxane framework. Note that the RCM reaction with a smaller amount of a ruthenium catalyst (reduced to 5 mol%) also gave **4a** in 85% yield (by ^1H NMR).

The treatment of **1b**, which has three allyldimethylsilyl groups, by stepwise addition of 10 mol% of **3** at 65 °C for 36 h afforded **4b**, a silsesquioxane containing both terminal and internal alkenyl groups, in 90% yield as a mixture of *cis* and *trans* isomers in a 5.6:1 ratio.

The synthesis of a titanium-containing silsesquioxane with a more extended alkenylene-bridged macrocycle by the RCM reaction was examined. The RCM reaction of a titanium-containing silsesquioxane having two allylic moieties **6**[8] (prepared by the reaction of an allyldimethylsilyl-substituted silsesquioxane disilanol **5** with tetrakis(diethylamino)titanium) in the presence of 15 mol% of the ruthenium catalyst **3** at 65 °C for 54 h afforded the desired silsesquioxane **7** in 74% yield (*cis*:*trans* = 4.4:1). The product (**7**) which contains an organic–inorganic hybrid 21-membered macrocycle, was fully characterized by NMR, IR, FAB-MS, and elemental analysis. ^1H and ^{13}C NMR measurements indicate the presence of one butenylene unit together with two half-caged silsesquioxane cores in **7**. The ^{29}Si NMR spectrum of *cis*-**7** consists of eight peaks of almost the same intensity for sixteen silicon atoms in the molecule, which indicates the apparent local C_2-symmetry of its siloxane framework.

On the other hand, treatment of **1a** with 10 mol% of the rhodium complex Cp*Rh(ethylene)$_2$ **9** produced a *trans*-propenylene-bridged silsesquioxane **8a** in an isolated yield of 90%, which has a 16-membered ring. There was no sign of the *cis* isomer in the crude reaction mixture. Note that the reaction in toluene instead of ethanol did not proceed at all, strongly suggesting that formation of a rhodium hydride species is crucial for the present reaction. Although the present untypical formation of (*E*)-propenylene-bridges has been reported in the $RuHCl(CO)(PPh_3)_3$ or $RuCl_2(PPh_3)_3$–catalyzed coupling or polycondensation of allylsilanes,[9–11] the use of these ruthenium catalysts in toluene at 80 °C reduced the yield of **8a** drastically (less than 25% by ^1H NMR), where considerable isomerization of **1a** to 1-propenylsilyl-substituted silsesquioxanes occurred. These reactions previously had been explained in terms of isomerization of allylsilanes to 1-propenylsilanes followed by metathesis,[9] but a mechanism including the formation of a silylmetal species *via* the silyl group transfer is now generally accepted.[11,12] Treatment of a titanium-containing silsesquioxane **6** under similar reaction conditions, however, did not give any desired propenylene-bridged product, and only the isomerization of allylic groups was observed.

In conclusion, a series of novel alkenylene-bridged silsesquioxanes with 16- to 21-membered rings were synthesized in high yields by ruthenium or rhodium complex-catalyzed reactions. These molecules are quite interesting as building blocks for new materials or a platform for novel macrocyclic

† Electronic supplementary information (ESI) available: experimental details. See http://www.rsc.org/suppdata/cc/b1/b104086n/

 DOI: 10.1039/b104086n

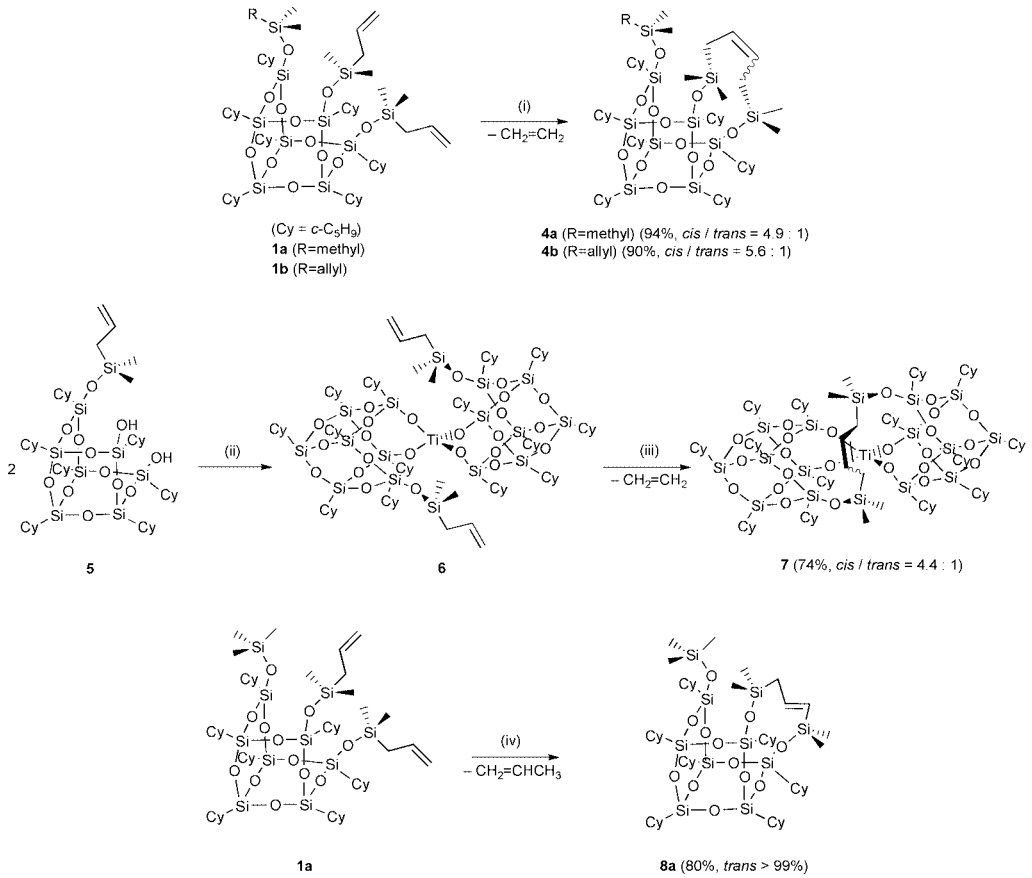

Scheme 1 *Reagents and conditions*: i, **3** (13 mol% for **1a** or 10 mol% for **1b**) in $(CH_2Cl)_2$ at 65 °C, 54 h (for **1a**) or 36 h (for **1b**); ii, $Ti(NEt_2)_4$ (0.5 equiv.) in benzene at room temperature for 18 h; iii, **3** (15 mol%) in $(CH_2Cl)_2$ at 65 °C, 54 h; iv, **9** (10 mol%) under EtOH reflux for 18 h.

hosts. The present work also provides the potential for synthesis of new organic–inorganic hybrid cage-like molecules *via* the annulation of unsaturated substituents of silsesquioxanes.

The authors are grateful to Dr M. Shiro of Rigaku Corporation for his kind help in the X-ray crystallographic study.

Notes and references

‡ All new compounds gave satisfactory NMR spectra and microanalytical data. **4a** (*cis*:*trans* = 4.9:1); Mp 239.0–242.0 °C, Anal. Calc. for $C_{46}H_{90}O_{12}Si_{10}$ (1116.05): C, 49.50; H, 8.13. Found C, 49.28; H, 8.16%. NMR data for *cis*-**4a**; ^{1}H NMR (300 MHz, $CDCl_3$, 25 °C) δ 5.35 (t, $^3J_{HH}$ = 5.6 Hz, 2H, $SiCH_2CH{=}CHCH_2Si$), 1.75–1.47 (br m, 60H, CH_2 of Cy and $SiCH_2CH{=}CHCH_2Si$), 0.99–0.89 (br m, 7H, C*H* of Cy), 0.14 (s, 6H, $Si(CH_3)_2$), 0.13 (s, 9H, $Si(CH_3)_3$), 0.10 (s, 6H, $Si(CH_3)_2$); $^{13}C\{^1H\}$ NMR (75 MHz, $CDCl_3$, 25 °C) δ 122.97 ($SiCH_2CH{=}CHCH_2Si$), 27.63, 27.58, 27.53, 27.29, 27.10, 26.99, 26.95, 26.92 (CH_2 of Cy), 24.89, 24.21, 23.80, 23.51, 22.45 (1:2:2:1:1 for CH of Cy), 19.63 ($SiCH_2CH{=}CHCH_2Si$), 1.99 ($Si(CH_3)_3$), 0.23, 0.11 ($Si(CH_3)_2$); $^{29}Si\{^1H\}$ NMR (76 MHz, $CDCl_3$, 0.02 M $Cr(acac)_3$, 25 °C) δ 8.10 ($Si(CH_3)_3$), 5.57 ($Si(CH_3)_2$), −66.28, −67.68, −67.81, −67.98, −68.37 (1:1:2:2:1).

§ Colorless single crystals of **4a** which have monoclinic space group $P2_1/c$, were obtained by slow diffusion of acetonitrile into a mesitylene solution. The unit-cell constants were a = 20.7421(5); b = 13.942(1); c = 21.0128(5) Å; β = 90.8196(7)°; V = 6075.9(5) Å^3. Data analysis revealed the structure depicted in Scheme 1 with a (*Z*)-butenylene bridge, although at present only silicon and oxygen atoms could be refined anisotropically because of poor diffraction in the high angle region of $2\theta > 30°$.

1 For example, see: S. Inagaki, S. Guan, Y. Fukushima, T. Ohsuna and O. Terasaki, *J. Am. Chem. Soc*., 1999, **121**, 9611 and references therein.

2 (*a*) F. J. Feher and T. A. Budzichowski, *Polyhedron*, 1995, **14**, 3239; (*b*) R. H. Baney, M. Itoh, A. Sakakibara and T. Suzuki, *Chem. Rev*., 1995, **95**, 1409; (*c*) R. Murugavel, A. Voigt, M. G. Walawalkar and H. W. Roesky, *Chem. Rev*., 1996, **96**, 2205; (*d*) P. Harrison, *J. Organomet. Chem*., 1997, **542**, 141.

3 F. J. Feher, D. Soulivong, A. G. Eklund and K. D. Wyndham, *Chem. Commun*., 1997, 1185.

4 (*a*) D. Hoebbel, K. Endres, T. Reinert and I. Pitsch, *J. Non-Cryst. Solids*, 1994, **176**, 179; (*b*) P. G. Harrison and R. Kannengiesser, *Chem. Commun*., 1996, 415; (*c*) C. Zhang, F. Babonneau, C. Bonhomme, R. M. Laine, C. L. Soles, H. A. Hristov and A. F. Lee, *J. Am. Chem. Soc*., 1998, **120**, 8380.

5 For example, see: H. Yamashita and M. Tanaka, *Bull. Chem. Soc. Jpn*., 1995, **68**, 403 and references therein.

6 T. Hoshi, H. Yasuda, T. Sanji and H. Sakurai, *Bull. Chem. Soc. Jpn*., 1999, **72**, 821.

7 For example, see: (*a*) P. Schwab, M. B. France, J. W. Ziller and R. H. Grubbs, *Angew. Chem., Int. Ed. Engl*., 1995, **34**, 2039; (*b*) M. Schuster and S. Blechert, *Angew. Chem., Int. Ed. Engl*., 1997, **36**, 2037.

8 K. Wada, M. Bundo, D. Nakabayashi, N. Itayama, T. Kondo and T. Mitsudo, *Chem. Lett*., 2000, 628.

9 B. Marciniec, Z. Foltynowicz and M. Lewandowski, *J. Mol. Catal*., 1994, **90**, 125.

10 B. Marciniec, M. Lewandowski and E. Kwiatkowska, *J. Polym. Sci., Part A Polym. Chem*., 1997, **35**, 3299.

11 F. Kakiuchi, A. Yamada, N. Chatani, S. Murai, N. Furukawa and Y. Seki, *Organometallics*, 1999, **18**, 2033.

12 T. Mise, Y. Takaguchi, T. Umemiya, S. Shimizu and Y. Wakatsuki, *Chem. Commun*., 1998, 699.

CHEMCOMM Communication
www.rsc.org/chemcomm

A family of highly active copper(I)–homoscorpionate catalysts for the alkyne cyclopropenation reaction

M. Mar Díaz-Requejo,[a] Miguel Angel Mairena,[a] Tomás R. Belderrain,[a] M. Carmen Nicasio,[a] Swiatoslaw Trofimenko[b] and Pedro J. Pérez*[a]

[a] *Departamento de Química y Ciencia de Materiales, Universidad de Huelva, Carretera de Palos de la Frontera s/n, E-21819 Huelva, Spain. E-mail: perez@dqcm.uhu.es; Fax: +34 959 017414; Tel: +34 959 017411*

[b] *Department of Chemistry and Biochemistry, University of Delaware, Newark, DE 19716, USA*

Received (in Cambridge, UK) 7th June 2001, Accepted 1st August 2001
First published as an Advance Article on the web 3rd September 2001

Equimolar mixtures of ethyl diazoacetate and alkynes can be converted into cyclopropenes in very high yields, at room temperature, through the intermediacy of readily available Cu(I) catalysts containing trispyrazolylborate ligands.

Carbon–carbon unsaturated bonds can be converted into three-membered rings by the intermediacy of metal-based catalysts and the appropriate carbene source.[1,2] Thus, a diazo compound and an olefin lead to cyclopropanes whereas the same carbene precursor and alkynes afford cyclopropenes (Scheme 1). Despite the obvious similarities between both reactions, most efforts have been devoted to the former transformation, the catalytic systems reported to date for the cyclopropenation reaction being reduced to a few, and mainly based on copper and rhodium. Copper bronze, Cu(I) and Cu(II) salts have been employed as catalysts for the cyclopropenation reaction, but high temperatures (90–140 °C) were required and yields were low.[3] At room temperature, $Rh_2(OAc)_4$ has been the catalyst of choice for this transformation, as reported by Hubert *et al.*[4] Related chiral derivatives of the type $Rh_2(L–L^*)_4$ have been developed by Doyle and co-workers,[5] inducing high enantiomeric excesses. However, there are two major drawbacks to address in this field. First, those rhodium catalysts do not operate with internal alkynes, or if so, yields are quite low. Secondly, and despite the use of high alkyne–EDA (ethyl diazoacetate) ratios, only moderate to high conversion yields have been achieved (40–85%), the quantitative conversion being still elusive.

The catalytic capabilities of the homoscorpionate complex Tp*Cu(C_2H_4) (**1**) (Tp* = hydrotris(3,5-dimethylpyrazol-1-yl)-borate (1), towards the alkyne cyclopropenation reaction were reported a few years ago.[6] Those preliminary results showed that both internal and alk-1-ynes could be converted into the corresponding cyclopropenes with moderate yields (40–65%). Complex Tp*Cu[7] (**2**) displays the same catalytic behaviour, with the advantage of its higher stability in comparison with **1**. Complexes **1** or **2** also catalyse the conversion of olefins into cyclopropanes[8] and epoxides,[9] both under homogeneous and heterogeneous conditions, as well as the aziridination of alkenes.[6,9] This remarkable behaviour has been now expanded to the achievement of higher degrees of alkyne cyclopropenation. It is worth mentioning that the main problem in these transformations is the formation of diazoacetate-coupling products: diethyl fumarate and maleate are also formed when EDA is employed as the carbene source. Usually, this is avoided by using a large excess of the alkyne with respect to EDA, and by adding the diazocompound by means of slow-addition devices onto the alkyne and catalyst-containing solution. As a consequence of our knowledge on the olefin cyclopropanation reaction, we have learnt that there is an enormous dependence of the three-membered ring yields on the reaction design, particularly the catalyst concentration and the carbene precursor addition rate. Fig. 1 shows the results of the hex-3-yne cyclopropenation reaction obtained from three experiments at three different concentrations of complex **2**. The initial hex-3-yne concentration was fixed at 0.45 M and EDA (0.15 M) was added with two different addition rates (0.15 and 1.5 mmol h^{-1}). The use of initial [**2**] of 0.0075 M (1:20:60 of [Cu]–[EDA]–[hex-3-yne]) induced the almost quantitative conversion into the corresponding cyclopropene, whereas a third of that value caused a 50% decrease of the product. As expected, an increase in the addition rate of EDA diminished the yields, but the same trend was observed upon varying [Cu]. These results are in accord with the reaction pathway proposed for the related cyclopropanation reaction with this type of catalyst.[10]

With this knowledge, we have tested an array of trispyrazolylborate ligands[11] (Fig. 2) in which R^1–R^3 can be modified to tune the electronic and steric effects induced to the metal centre. The catalysts of general formula $Tp^XCu(I)$ were generated *in situ* by mixing equimolar amounts of CuI and the corresponding potassium or thalium salt of the homoscorpionate ligand. These preliminary experiments were run with a [Cu]–[EDA]–[hex-3-yne] ratio of 1:30:90, that corresponds to [Cu] 0.005 in Fig. 1. As inferred from data in Table 1, the 3-neopentyl and 3-cyclohexyl derivatives showed excellent, unprecedented degrees of conversion into ethyl 2,3-diethylcyclorop-1-enecarboxylate (95 and 97%, respectively) therefore

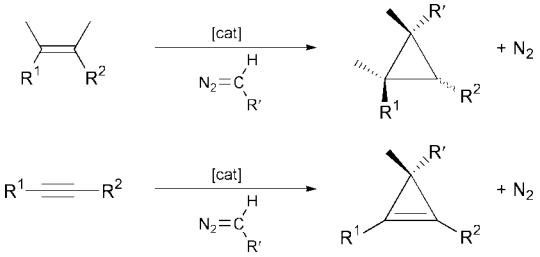

Scheme 1

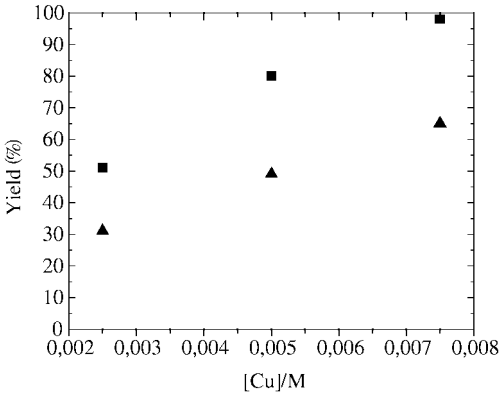

Fig. 1 Dependence of cyclopropene yields (hex-3-yne as alkyne) and the amount of catalyst (Tp*Cu, **2**). EDA addition rate: ▲ 1.5 mmol h^{-1}; ■ 0.15 mmol h^{-1}.

 DOI: 10.1039/b105020f

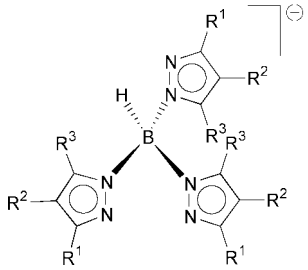

Fig. 2 Tp^X ligands.

Table 1 Cyclopropenation of hex-3-yne with Tp^X–Cu catalysts[a]

Entry	Tp^X	R^1	R^2	R^3	Yield[b]
1	Tp	H	H	H	32
2	Tp*	Me	H	Me	82
3	Tp^{rBu}	^{t}Bu	H	H	85
4	Tp^{Np}	Np	H	H	95
5	Tp^{Cy}	Cy	H	H	97
6	Tp^{Ph}	Ph	H	H	21
7	$Tp^{\alpha\text{-}Nt}$	α-Nt	H	H	27
8	Tp^{Ms}	Ms	H	H	31
9	Tp^{ClPh}	*p*-C_6H_4Cl	H	H	52
10	Tp^{An}	*p*-$C_6H_4OCH_3$	H	H	43
11	Tp^{Tol}	*p*-$C_6H_4CH_3$	H	H	49

[a] See footnote† for experimental details. [b] Percentage of cyclopropene determined by GC after total EDA consumption. Diethyl fumarate and maleate accounted for the remaining diazoacetate employed.

minimising the formation of EDA-coupling products (ethyl fumarate and maleate). We have recently reported[12] an extraordinarily active and diastereoselective (towards the *cis* isomer) catalytic system for the olefin cyclopropanation reaction, in which aromatic substituents as R^1 provided the best results in comparison with the aliphatic groups in this position. But this situation reverses in the alkyne cyclopropenation reaction, since aliphatic groups as R^1 seem to be required for high conversions. This constitutes a significant difference between these two transformations that traditionally have been described to occur in a similar way.[1,2]

After this initial screening, optimisation of the reaction conditions and expansion to other alkynes afforded more interesting features. Table 2 displays the results of the cyclopropenation reaction of hex-1-yne, 1-phenylprop-1-yne and hex-3-yne with different [Cu]–[EDA]–[alkyne] ratios using the Tp^{Cy} derivative. The observed yields show dramatic improvement over any other reported catalytic system in terms of cyclopropene formation not only for alk-1-yne derivatives, but also for internal ones: the values for hex-3-yne are >90% in all cases and 1-phenylprop-1-yne also undergoes high conversions (73–94%). This remarkable activity is confirmed by data

Table 2 Cyclopropenation of alkynes with $Tp^{Cy}Cu$[a]

Entry	Cu–EDA–alkyne[b]	Hex-1-yne[c]	Hex-3-yne[c]	1-Phenyl-prop-1-yne[c]
1	0.05:1.5:7.5	87	97	94
2	0.05:3:9	75	90	84
3	0.1:3:9	80	97	90
4	0.1:6:9	70	95	73
5	0.1:6:6	80	94	85

[a] See footnote† for experimental details. [b] In mmol. [c] Percentage of cyclopropene determined by GC after total EDA consumption. Diethyl fumarate and maleate accounted for the remaining diazoacetate employed.

in Table 2, entry 5, in which an equimolar EDA–alkyne ratio was employed: yields of cyclopropene fall in the range 80–94%. The lack of alkyne excess in these high-yield transformations has no precedent in the literature: our system has obviated the need for an excess of alkyne to achieve noticeable yields, not only with the cyclohexyl derivative but also with other Tp^X ligands (X = alkyl). Thus, the cyclopropenation of hex-3-yne using an equimolar ratio of the alkyne and ethyl diazoacetate afforded the corresponding three-membered ring in 75–94% yield (Table 3).

Table 3 Equimolar EDA–hex-3-yne cyclopropenation experiments[a]

Entry	Tp^X	Yield[b]
1	Tp*	75
2	Tp^{rBu}	72
3	Tp^{Np}	82
4	Tp^{Cy}	94

[a] [Cu]–[EDA]–[hex-3-yne] ratio of 1:60:60, 0.1 mmol of Cu employed. [b] Percentage of cyclopropene determined by GC after total EDA consumption. Diethyl fumarate and maleate accounted for the remaining diazoacetate employed.

In conclusion, we have developed an extraordinarily efficient cyclopropenation system in which terminal and internal alkynes can be converted into the corresponding unsaturated rings in very high yields. In addition, no excess of the alkyne is required for those yields to be produced. Work aimed to extend these results to a number of other unsaturated substrates is currently underway in our laboratory.

Notes and references

† Experimental procedure: CuI and an equimolar amount of the MTp^X salt were dissolved in CH_2Cl_2 and the mixture was stirred for 2–3 h. After filtration volatiles were removed under reduced pressure. The residue was dissolved in 20 mL of 1,2-dichloroethane, and the resulting solution was charged with alkyne. A solution of EDA in 1,2-dichloroethane was slowly added with the aid of an automatic syringe pump. All reactions were performed at room temperature. After complete addition, the reaction mixture was analyzed by GC, only cyclopropenes and ethyl fumarate or maleate being detected. Yields are shown in Tables 1–3.

1 M. P. Doyle, in *Comprehensive Organometallic Chemistry II*, ed. E. W. Abel, F. G. A. Stone and G. Wilkinson, Pergamon Press, Oxford, UK, 1995, vol 12, p. 387.
2 M. P. Doyle, M. A. McKervey and T. Ye, *Modern Catalytic Methods for Organic Synthesis with Diazo Compounds*, John Wiley & Sons, New York, 1998.
3 M. N. Protopopova and E. A. Shapiro, *Russ. Chem. Rev.*, 1989, **58**, 667.
4 N. Petiniot, A. J. Anciaux, A. F. Noels, A. J. Hubert and P. H. Teyssie, *Tetrahedron Lett.*, 1978, **14**, 1239.
5 M. P. Doyle, M. Protopopova, P. Müller and E. A. Shapiro, *J. Am. Chem. Soc.*, 1994, **116**, 8492; M. P. Doyle, M. Protopopova, P. Müller and D. Ene, *J. Am. Chem. Soc.*, 1992, **114**, 2755.
6 P. J. Pérez, M. Brookhart and J. L. Templeton, *Organometallics*, 1993, **12**, 261.
7 C. Mealli, C. S. Arcus, J. L. Wilkinson, T. J. Marks and J. A. Ibers, *J. Am. Chem. Soc.*, 1975, **98**, 711.
8 M. M. Díaz-Requejo, M. C. Nicasio and P. J. Pérez, *Organometallics*, 1998, **17**, 3051; M. M. Díaz-Requejo, T. R. Belderrain, M. C. Nicasio and P. J. Pérez, *Organometallics*, 2000, **19**, 285.
9 M. M. Díaz-Requejo, T. R. Belderrain and P. J. Pérez, *Chem. Commun.*, 2000, 1853; M. M. Díaz-Requejo, P. J. Pérez, M. Brookhart and J. L. Templeton, *Organometallics*, 1997, **16**, 4399.
10 M. M. Díaz-Requejo, T. R. Belderrain, M. C. Nicasio, F. Prieto and P. J. Pérez, *Organometallics*, 1999, **14**, 2601.
11 S. Trofimenko, *Scorpionates, The Coordination Chemistry of Polypyrazolylborate ligands*, Imperial College Press, London, 1999.
12 M. M. Díaz-Requejo, T. R. Belderrain, S. Trofimenko and P. J. Pérez, *J. Am. Chem. Soc.*, 2001, **123**, 3167.

CHEMCOMM Communication
www.rsc.org/chemcomm

Addition of functional vinylzinc reagents to nitrones: synthesis of (*E*)-*N*-allylhydroxylamines and their rearrangement into (*E*)-*O*-allylhydroxylamines

Shashi Urvish Pandya, Corinne Garçon, Pierre Y. Chavant, Sandrine Py and Yannick Vallée*

LEDSS, UMR 5616, Université J. Fourier, BP53, F-38041 Grenoble CEDEX 9, France. E-mail: Yannick.Vallee@ujf-grenoble.fr

Received (in Cambridge, UK) 18th May 2001, Accepted 26th July 2001
First published as an Advance Article on the web 4th September 2001

The vinylzinc reagents derived from hydrozirconation of alkynes and transmetallation add readily to nitrones to yield pure (*E*)-*N*-allylhydroxylamines; some of these rearrange into *O*-allylhydroxylamines.

In the course of our studies on nitrones,[1] we became interested in obtaining (*E*)-allylic *N*-hydroxylamines by the addition of organometallic reagents onto nitrones.

In the past, addition of organolithium or organomagnesium reagents onto C=N bonds[2] was studied to a much lesser extent than the corresponding addition onto carbonyl functions, the major reason being that imines are less prone to nucleophilic addition and more prone to deprotonation. In recent years, there has been a renewed interest in the addition of organometallics onto C=N double bonds because of both the availability of more selective organotransition reagents, and the use of more reactive C=N species. Among the latter, nitrones appear to be an interesting choice as precursors. They are reactive, readily available and stable. Indeed, recent work has dealt with the addition of alkyl,[3] allyl[4] and alkynyl[3,5] lithium, magnesium and zinc reagents onto nitrones.

Comparatively fewer examples of the addition of vinylic organometallics to C=N bonds have been described. Imines do, however, react readily with vinylzinc compounds.[6] It has also been shown that vinylmagnesium bromide adds to tosyl imines.[7] Furthermore, it was demonstrated[8] that vinylmagnesium bromide adds rapidly to nitrones. These results were extended to diastereoselective additions onto chiral nitrones[9] but the results were limited to the simplest ethenyl organometallic reagent.

For our study, we needed adducts from γ-functionalized, pure *E*, vinylmetallic species. Thus, we decided to prepare these reagents according to Wipf's procedure:[10] hydrozirconation of alkynes followed by transmetallation to the (*E*)-vinylzinc species. We found that the resultant organometallic reagents add readily onto nitrones, under mild conditions, to give secondary *N*-hydroxylamines in good yields† (Scheme 1, Table 1).

As expected, only the *E* configuration was observed in the double bond of all the products. Also, excellent conversions were obtained for the addition of the vinylzinc species derived from hex-1-yne onto a variety of nitrones **2**. Steric hindrance in the nitrone (entry **g**, 39% conversion) is a limitation. The more hindered vinylzinc reagent derived from hex-3-yne led to incomplete conversion (entry **h**), and the formation of *N*-benzyl-*N*-(1-phenylpropyl)hydroxylamine (10%), resulting from ethylzinc addition, accompanied the allylic product **3h**. Addition onto the chiral nitrone **2d** led to moderate diastereoselectivity at 0 °C. Functionalized alkynes can also be used in this protocol. The pivalate-protected but-3-yn-1-ol led readily to **3i** and **3j**. In other examples however, the ω-cyanoalkyne (entry **k**), the *O*-protected propynol[11] (entries **l**, **m**, **n**, **o**) and the

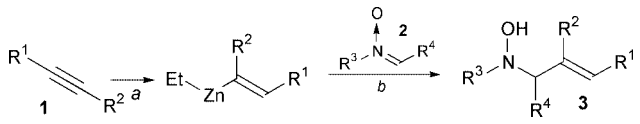

Scheme 1 *Reagents and conditions*: (*a*) Cp_2ZrHCl, CH_2Cl_2, rt, 1 h; vacuum; Et_2Zn, CH_2Cl_2, −65 to 0 °C; (*b*) CH_2Cl_2, 0 °C, 6 h.

Table 1 Preparation of *N*-allylhydroxylamines

	Alkyne **1**		Nitrone **2**			
Entry	R^1	R^2	R^3	R^4	Conv. of **2** (%)[a]	Isolated yield (%)
a	*n*-Bu	H	$PhCH_2$	Ph	>95	62
b	*n*-Bu	H	*p*-CF_3PhCH_2	Ph	>95	70
c	*n*-Bu	H	*p*-CF_3PhCH_2	Me	>95	58
d	*n*-Bu	H	$PhCH_2$	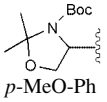	>95	83 de 72%
e	*n*-Bu	H	Ph	*p*-MeO-Ph	>95	62[c]
f	*n*-Bu	H	*p*-Tolyl	Ph	>95	50[c]
g	*n*-Bu	H	*t*-Bu	Ph	39	29[c]
h	Et	Et	$PhCH_2$	Ph	40	30
i	PivO-$(CH_2)_2$-	H	$PhCH_2$	Ph	>95	58
j	PivO-$(CH_2)_2$-	H	$PhCH_2$	*i*-Pr	>95	60[b]
k	NC-$(CH_2)_3$-	H	$PhCH_2$	Ph	75	5[b]
l	TMSO-CH_2-	H	$PhCH_2$	Ph	90	32[b]
m	TMSO-CH_2-	H	Ph	*p*-MeO-Ph	>95	30[c]
n	MeO-CH_2-	H	$PhCH_2$	Ph	50	35[b]
o	MeO-CH_2-	H	Ph	*p*-MeO-Ph	>95	40[c]
p	$(EtO)_2CH$-	H	$PhCH_2$	Ph	46	16
q	Ph	H	$PhCH_2$	Ph	90	0[d]

[a] Estimated from NMR of the crude product. [b] A significant amount of alkynyl adduct was also isolated, see text. [c] Isolated as the isomeric form **4**, see text. [d] Only alkynyl adduct, 50% yield.

 DOI: 10.1039/b104427n

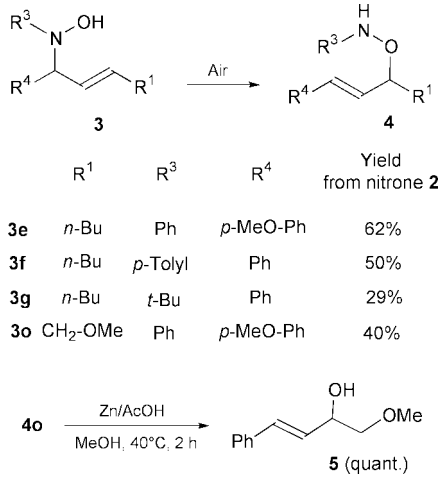

Scheme 2 Rearrangement of *N*-allylhydroxylamines **3**.

phenylacetylene (entry **q**) all yielded substoichiometric amounts of vinylzinc reagent, presumably due to a less efficient hydrozirconation step. In these runs, the conversions of nitrones **2** were incomplete, and the expected products **3** were contaminated with *N*-propargylhydroxylamines,‡ derived from the addition of the alkyne **1** onto the nitrone **2**.§

All the vinyl adducts freshly obtained from this procedure were the expected (*E*)-*N*-allylhydroxylamines **3**. Surprisingly however, we observed that on standing (at room temperature), some of the samples (neat or in $CDCl_3$ solutions) isomerized slowly, with allylic transposition, to yield (*E*)-*O*-allylhydroxylamines **4** (Scheme 2). This process occurs particularly readily for *N*-arylhydroxylamines. In these cases, the rearrangement was complete within 24 h at 20 °C and consequently, the rearranged adducts were isolated after completion of this step (entries **e**, **f**, **m**, **o**). This rearrangement also occurred in the case of *N*-*tert*-butylhydroxylamine **3g**. The structure of **4o** was confirmed by its reduction to the (*E*)-allylic alcohol **5** (Zn, AcOH–MeOH 1 : 9, 40 °C, 2 h, quant.).

To our knowledge, this rearrangement has not been previously described, although it can be related with several observations, involving allylic N–O bonds, including the Meisenheimer rearrangement of tertiary amine *N*-oxides.[12]

We observed qualitatively that the rate of this rearrangement depends strongly on the nitrogen atom substitution: Aryl > *t*-Bu >> Bn. Several observations hint at a radical mechanism. First, the reaction seems to be initiated by air: in an early experiment, we observed a 50 : 50 mixture of **3o** and **4o** 2 h after working-up the reaction. We repeated the experiment, using for the hydrolytic work-up freshly distilled solvents and freshly boiled water phases, and handling the crude materials with simple anaerobic precautions: the amount of isomer **4o** was then reduced to less than 3% (NMR) of the crude material. Thereafter, exposure to air induced the rearrangement. EPR of the crude materials during isomerization showed a strong signal, with a fine structure consistent with the aminoxyl radical derived from **3**. Obviously, this radical could be the active species, undergoing a Meisenheimer [2,3] rearrangement. We are currently investigating the mechanism, scope, and limitations of this new reaction.

It is important to note that the above isomerization amounted only to traces if the R^3 substituent on the nitrogen atom was a benzyl group: as seen in Table 1, the *N*-benzyl-*N*-allylhydroxylamines **3** can be isolated in good yields. They can be readily reduced to provide the corresponding (*E*)-*N*-benzyl-*N*-allylamines.

In conclusion, we have shown that the sequence: terminal alkyne hydrozirconation, Zr to Zn exchange and addition to nitrones, is a good method to stereoselectively synthesize (*E*)-*N*-allylhydroxylamines, under mild conditions and in good yields. It is noteworthy that this reaction occurs with no need for an external activating agent such as amino-alcohols.[13] We are currently studying an asymmetric version of this reaction by adding chiral zinc ligands to the reaction mixture.

Notes and references

† Typical experimental procedure: to a suspension of zirconocene hydrochloride (1.2 mmol) in CH_2Cl_2 (2 mL) under an N_2 atmosphere at 20 °C was added hex-1-yne (1.8 mmol) using standard Schlenk procedures. The reaction was stirred at 20 °C until a homogeneous solution was formed. All volatiles were then removed under reduced pressure at 20 °C, to give a yellow vinylchlorozirconocene reagent. To the resultant solid was added CH_2Cl_2 (2 mL) and the mixture was cooled to −65 °C. Diethylzinc (1.2 mmol, as a 1.1 M solution in toluene), was added dropwise (over 10 min) at −65 °C and allowed to stir for 15 min at −65 °C. The vessel was then immersed in an ice bath and a solution of (*N*-benzylidene)benzylamine *N*-oxide (1 mmol) in CH_2Cl_2 (2 mL) was added dropwise. After 6 h stirring at 0 °C, the reaction was quenched with saturated $NaHCO_3$ solution (2 mL), and extracted with ethyl acetate. The combined organic extracts were washed with brine, dried over Na_2SO_4, and filtered through a pad of silica. Removal of the solvents under reduced pressure and purification by chromatography (silica, cyclohexane–ethyl acetate 90 : 10) yielded the pure adduct **3**.

‡ The IUPAC name for propargyl is prop-2-ynyl.

§ We found that a mixture of alkyne **1**, nitrone **2** and diethylzinc in CH_2Cl_2 or toluene at rt leads quantitatively to *N*-propargylhydroxylamine adducts, and we are currently studying this reaction. A similar addition of species generated from the reaction of dialkylzinc with terminal alkynes onto aromatic aldehydes has been described previously.[14]

1 C. Dagoneau, A. Tomassini, J. N. Denis and Y. Vallee, *Synthesis*, 2001, **1**, 150 and references therein.

2 D. Enders and U. Reinhold, *Tetrahedron: Asymmetry*, 1997, **8**, 1895; R. Bloch, *Chem. Rev*., 1998, **98**, 1407; M. Lombardo and C. Trombini, *Synthesis*, 2000, **6**, 759.

3 A. Dondoni, D. Perrone and M. Rinaldi, *J. Org. Chem*., 1998, **63**, 9252; P. Merino, S. Franco, F. Merchan and T. Tejero, *Recent Res. Dev. Synth. Org. Chem*., 1998, **1**, 109; P. Merino, S. Franco, F. L. Merchan and T. Tejero, *Synlett*, 2000, **4**, 442; Y. Ukaji, Y. Shimizu, Y. Kenmoku, A. Ahmed and K. Inomata, *Bull. Chem. Soc. Jpn*., 2000, **73**, 447.

4 H. M. S. Kumar, S. Anjaneyulu, E. J. Reddy and J. S. Yadav, *Tetrahedron Lett*., 2000, **41**, 9311.

5 P. Merino, S. Franco, F. L. Merchan and T. Tejero, *J. Org. Chem*., 1998, **63**, 5627; P. Merino, E. Castillo, S. Franco, F. L. Merchan and T. Tejero, *Tetrahedron: Asymmetry*, 1998, **9**, 1759; J.-N. Denis, S. Tchertchian, A. Tomassini and Y. Vallee, *Tetrahedron Lett*., 1997, **38**, 5503; D. E. Frantz, R. Faessler and E. M. Carreira, *J. Am. Chem. Soc*., 1999, **121**, 11 245.

6 G. Alvaro, P. Pacioni and D. Savoia, *Chem. Eur. J*., 1997, **3**, 726.

7 M. T. Reetz, R. Jaeger, R. Drewlies and M. Hübel, *Angew. Chem., Int. Ed. Engl*., 1991, **30**, 103.

8 F. L. Merchan, P. Merino and T. Tejero, *Synth. Commun*., 1994, **24**, 2551.

9 P. Merino, S. Anoro, S. Franco, J. M. Gascon, V. Martin, F. L. Merchan, J. Revuelta, T. Tejero and V. Tunon, *Synth. Commun*., 2000, **30**, 2989; Z.-Y. Chang and R. M. Coates, *J. Org. Chem*., 1990, **55**, 3475; A. M. Palmer and V. Jäger, *Eur. J. Org. Chem*., 2001, 1293.

10 P. Wipf and S. Ribe, *J. Org. Chem*., 1998, **63**, 6454.

11 A. M. Sun and X. Huang, *Synthesis*, 2000, 775 and references therein.

12 M. T. Reetz and E. M. Lauterbach, *Tetrahedron Lett*., 1991, **32**, 4481; T. D. Lee and F. W. Keana, *J. Org. Chem*., 1976, **41**, 3237; R. L. Craig and J. S. Roberts, *J. Chem. Soc., Chem. Commun*., 1972, 1142; E. Dumez and J.-P. Dulcère, *J. Chem. Soc., Chem. Commun*., 1998, 479; S. G. Davies, S. Jones, M. A. Sanz, F. C. Teixeira and J. F. Fox, *Chem. Commun*., 1998, 2235; P. Aschwanden, D. E. Frantz and E. M. Carreira, *Org. Lett*., 2000, **2**, 23; D. Enders and H. Kempen, *Synlett*, 1994, 969; S. G. Davies and G. D. Smyth, *Tetrahedron: Asymmetry*, 1996, **7**, 1001; J. Blanchet, M. Bonin, L. Micouin and H.-P. Husson, *Tetrahedron Lett*., 2000, **41**, 8279; M. B. Gravestock, D. W. Knight, K. M. A. Malik and S. R. Thornton, *J. Chem. Soc., Perkin Trans. 1*, 2000, 3292; A. Guarna, E. G. Occhiato, M. Pizzetti, D. Scarpi, S. Sisi and M. van Sterkenburg, *Tetrahedron: Asymmetry*, 2000, **11**, 4227; J. E. H. Buston, I. Coldham and K. R. Mulholland, *J. Chem. Soc., Perkin Trans. 1*, 1999, 2327; C. S. Penkett and I. D. Simpson, *Tetrahedron Lett*., 2001, **42**, 3029.

13 K. Soai and S. Niwa, *Chem. Rev*., 1992, **92**, 833; L. Pu and H.-B. Yu, *Chem. Rev*., 2001, **101**, 757.

14 Z. Li, V. Upadhyay, A. E. DeCamp, L. DiMichele and P. J. Reider, *Synthesis*, 1999, 1453.

CHEMCOMM
Feature Article
www.rsc.org/chemcomm

Protein-based materials, toward a new level of structural control

Jan C. M. van Hest*[a] and David A. Tirrell[b]

[a] *Department of Organic Chemistry, University of Nijmegen, Toernooiveld 1, 6525ED Nijmegen, The Netherlands. E-mail: vanhest@sci.kun.nl; Fax: +31 24 3653393*
[b] *Division of Chemistry and Chemical Engineering, 210-41, California Institute of Technology, Pasadena, CA 91125 USA. E-mail: tirrell@Caltech.edu; Fax: +1 (626) 793-8472*

Received (in Cambridge, UK) 13th June 2001, Accepted 2nd August 2001
First published as an Advance Article on the web 18th September 2001

Through billions of years of evolution nature has created and refined structural proteins for a wide variety of specific purposes. Amino acid sequences and their associated folding patterns combine to create elastic, rigid or tough materials. In many respects, nature's intricately designed products provide challenging examples for materials scientists, but translation of natural structural concepts into bio-inspired materials requires a level of control of macromolecular architecture far higher than that afforded by conventional polymerization processes. An increasingly important approach to this problem has been to use biological systems for production of materials. Through protein engineering, artificial genes can be developed that encode protein-based materials with desired features. Structural elements found in nature, such as β-sheets and α-helices, can be combined with great flexibility, and can be outfitted with functional elements such as cell binding sites or enzymatic domains. The possibility of incorporating non-natural amino acids increases the versatility of protein engineering still

Jan van Hest was born in 1968 in the Netherlands. After completing his M.Sc. in polymer chemistry in 1991, he conducted his doctoral research at the Eindhoven University of Technology under supervision of Professor Dr Bert Meijer, for which the Ph.D. was granted in 1996. For this work on molecular architectures based on dendrimers he was awarded the first prize of the DSM technology and chemistry competition in 1995 and the SNS award for the best thesis in fundamental research of the Eindhoven University of Technology in 1997.

Next he investigated as a post-doctoral researcher the possibilities of protein engineering for the preparation of materials under supervision of Professor Dr D. A. Tirrell, at the University of Massachusetts in Amherst till 1997.

He then joined the chemical company DSM, where he worked in the research group New Architectures, first as research scientist and later on as group leader, on the development of innovative material concepts. Specific topics of investigation were controlled radical polymerization and integration of expertise from life sciences and materials.

In 2000 he was appointed as full professor at the University of Nijmegen to set up a new group in bio-organic chemistry. His current interests focus on translating natural structural concepts into bio-inspired materials with the aid of state of the art organic and polymeric chemistry techniques and protein engineering.

David A. Tirrell is the Ross McCollum–William H. Corcoran Professor and Chairman of the Division of Chemistry and Chemical Engineering at the California Institute of Technology. After earning the B.S. in Chemistry at MIT, Tirrell enrolled in the newly-created Department of Polymer Science and Engineering at the University of Massachusetts, where he worked in the laboratory of Otto Vogl, on the synthesis and polymerization of vinyl derivatives of salicylic acid and 2,4-dihydroxybenzophenone. He was awarded the Ph.D. in 1978. During a four-month stay with Takeo Saegusa at Kyoto University, Tirrell developed methods for the synthesis of ionomers based on polymers of ethyl glycidate. He then accepted an assistant professorship in the Department of Chemistry at Carnegie-Mellon University, where he established research programs directed toward the exploration of neighboring group effects in polymer modification reactions, and toward elucidation of mechanistic questions in radical copolymerization processes.

Tirrell returned to Amherst in 1984. He was promoted to Professor in 1987, appointed Director of the Materials Research Laboratory in 1991, and named Barrett Professor of Polymer Science and Engineering in 1992. Tirrell moved to Caltech in 1998. He has served as Visiting Professor at the University of Queensland (1987), at the Institut Charles Sadron in Strasbourg (1991), at the University of Wisconsin-Madison (1995), and at the Institut Curie in Paris. He is a Fellow of the American Institute of Medical and Biological Engineering, and serves on technical advisory boards for Dow Chemical Company and Protein Polymer Technologies, Inc. He was Editor of the Journal of Polymer Science, Part A: Polymer Chemistry from 1988 until 1999, and has served on the editorial boards of many other journals, including Macromolecules, Biopolymers, Accounts of Chemical Research, and Chemical and Engineering News. He chaired the 1994 Gordon Research Conference on Polymers in Biosystems and the 1995 Gordon Conference on Chemistry of Supramolecules and Assemblies.

Tirrell's contributions to teaching and research have been recognized in a variety of ways. He was named Outstanding Teacher in the College of Science at Carnegie-Mellon, and a Sloan Fellow in 1982. He was a Presidential Young Investigator Awardee of the National Science Foundation in 1984, and a Fulbright Senior Scholar in 1987. In 1991, he was recognized by the Carl S. Marvel Creative Polymer Chemistry Award of the American Chemical Society, in 1996 he received the Harrison Howe Award of the Rochester Section of the ACS, and in 1997 he was awarded the Chancellor's Medal of the University of Massachusetts. In 2001, he received the American Chemical Society Award in Polymer Chemistry, and the degree of Doctor honoris causa from the Eindhoven University of Technology.

Tirrell's most important contributions to chemistry have come in three areas: i). radical copolymerization mechanism, ii). biomimetic membrane chemistry, and iii). development of molecular biological approaches to new polymeric materials.

DOI: 10.1039/b105185g

further. It is expected that such methods will have large impact in the field of materials science, and especially in biomedical materials science, in the future.

Introduction

For many years materials scientists have been investigating the possibilities of obtaining higher levels of control in polymer synthesis. Although important progress has been made, especially in recent years with the advance of controlled radical polymerization techniques,[1] the level of control characteristic of biomacromolecules, such as DNA and proteins, remains unsurpassed.

In the nomenclature of polymer chemistry, organisms prepare monodisperse polymers with predetermined chain lengths. But more important is the fact that virtually complete control is achieved over the sequence of the monomeric units, the amino acids. The information stored in the primary sequence results in a three-dimensional folded structure for each protein, which is largely responsible for the most important protein properties. For every specific function, nature has refined protein structures through eons of evolution. It is striking that with the same set of amino acid building blocks such diverse products can be prepared, including globular proteins which function as enzymes as well as fibrous proteins with structural properties, such as collagen. It is the prospect of creating three-dimensional ordered structures by designing the requisite amino acid sequences that motivates much of the current interest in protein-based materials.[2]

Materials scientists have much to learn from the organizational principles employed in nature, and substantial progress has been made recently in elucidation of the three-dimensional architectures of fibrous proteins such as silks, elastins, and collagens. An important challenge, however, is to translate these concepts into synthetic or bio-inspired materials, which would lead to new kinds of high performance materials.[3] Because of the importance of control at the monomer level, the most promising approach to this target is to use the biosynthetic pathways of (micro)-organisms to synthesize macromolecular materials.

Protein engineering has been used for the design and modification of globular proteins for many years, and standard biological tools have been developed that can now be used to prepare structural proteins.[4] It is remarkable that only in the past decade, and especially in the last 5 years, has this approach to materials design become a serious topic of investigation.

This review is not meant to be comprehensive, but instead will present examples of some of the latest developments in the field of protein engineering directed toward the preparation of high performance materials. After a short explanation of the protein engineering technique, examples will be given of structural proteins found in nature and attempts to use these basic structures for the preparation of new protein-based materials. We will conclude with new methods that allow the scope of protein engineering to be extended to building blocks other than the natural amino acids, developments that promise to make this technique even more versatile in the hands of the materials chemist.

Protein engineering

Scheme 1 shows the overall process of materials synthesis *via* protein engineering.[5] Often—though not always—based on natural structures, amino acid sequences are chosen to create specific folding patterns and desired material properties. The primary amino acid sequence can then be reverse-translated into a corresponding nucleotide sequence. There are 2 methods of obtaining the needed DNA fragments. One possibility is to clone these sequences from an organism that produces the desired structural protein. The second option is to synthesize

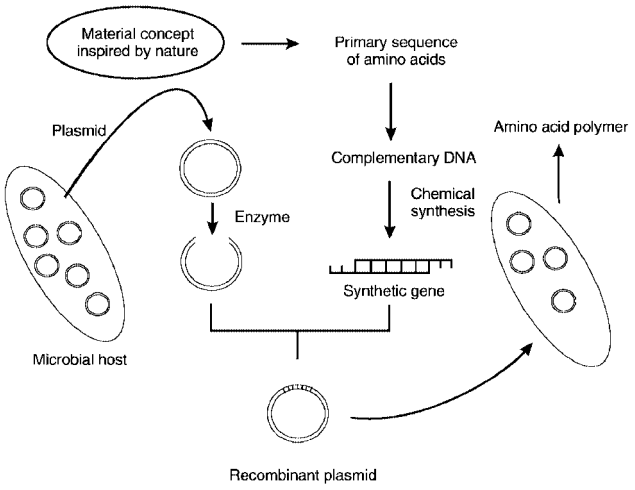

Scheme 1 Overview of the protein engineering methodology.

artificial genes by solid phase techniques. The second method of course allows maximum freedom in designing the target sequence. Because many structural proteins are characterized by repetitive amino acid sequences, it is often possible to multimerize a smaller oligonucleotide sequence to prepare an artificial gene that codes for proteins of high molecular weight.

This multimerization process can be considered as a polycondensation, which therefore results in a set of genes with different lengths. After construction of the artificial gene library, each individual gene is incorporated into circular plasmid DNA, which can be used to transform an appropriate bacterial host. Most commonly the bacterial host *E. coli* is used for these purposes. The plasmids are replicated during every division of the bacterial cells. Because there is only one type of plasmid per cell, screening of the plasmids of individual bacterial colonies leads to isolation of specific artificial genes, each encoding a protein-based material with a specific molecular weight.

The selected artificial gene is first analyzed to verify its sequence, and then cloned into a second plasmid which allows protein expression. The expression plasmid contains a promoter site for recognition by mRNA polymerase and a switch that regulates protein production from the gene of interest.

The expression plasmid is re-introduced into the bacterial host, and the host cells are allowed to grow to high cell density. During this stage the plasmid switch is turned off in order to prevent protein production from the artificial gene. Premature protein synthesis can be detrimental to cell growth. After sufficient cell density is reached the switch is turned on (a process called induction) and expression of the desired protein begins. Often the synthesis of other cellular proteins is slowed dramatically after induction.

Spider dragline silk

Among the most thoroughly studied classes of structural proteins is silk.[6] There are many forms of silk, of which that from *Bombyx mori* (Chinese silkworm silk)[7,8] and dragline spider silk of the *Nephila clavipes* (the golden orb weaver) have drawn most attention.[9] Silkworm silk of course is of interest because it is produced in large quantities and used as textile fiber. Spiders produce a large variety of types of silk, each one meant for a specific purpose, such as web construction or trapping of prey. Of all these different types of spider silk, dragline spider silk of *Nephila clavipes* is regarded as nature's high performance fiber, with a remarkable combination of strength and toughness. Values reported for its mechanical properties are an *E*-modulus of 10–50 GPa, elongation to break of 10–30% and tensile strength of 1.1–1.4 GPa. These values are

dependent on moisture content and strain rate. The effect of humidity is of utmost importance. Silk exposed to water can shrink to less than half of its original length, and the supercontracted fibers then show rubberlike behavior.[9] Although this is a desirable feature under natural conditions, because it allows spider webs to reshape in the dewy evening, it is less practical when one wants to apply this material as a high performance fiber. The large variation in properties is a result of the difficulty in maintaining constant conditions under which spiders produce their silk. In recent years important insight has been obtained into the three-dimensional structures of the different types of silk. X-ray diffraction,[10] state of the art NMR techniques[11,12] and IR and Raman spectroscopy[13] have helped to unravel the architectural reasons why this class of structural proteins has its remarkable mechanical properties. Silks from both silkworms and spiders contain repetitive sequences of crystalline and amorphous domains (Fig. 1). The crystalline

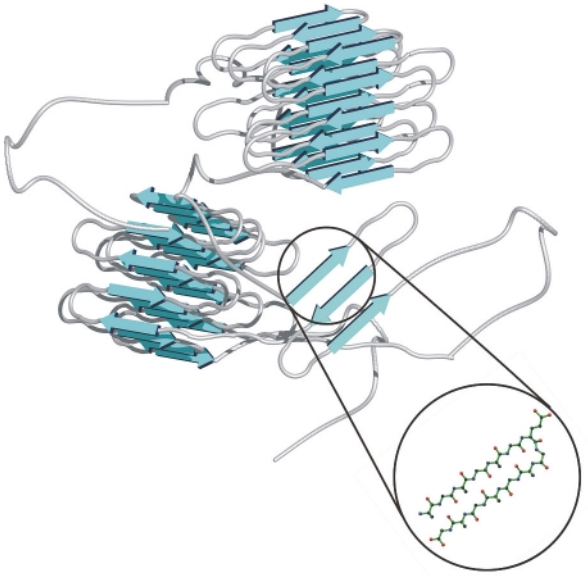

Fig. 1 Schematic representation of the organization of amorphous and crystalline domains in silk fibers. Silk has inspired protein engineers to construct β-sheet materials. A detail of a silk-like peptide sequence $((AG)_3EG)_n$[21,22] is encircled.

domains are responsible for the strength of the material, whereas the amorphous protein matrix: i) allows the crystalline domains to orient under strain to increase the strength of the material, and ii) introduces flexibility to increase the energy to break.

The crystalline domains comprise highly repetitive amino acid sequences consisting of alanine rich β-sheets. In *Bombyx mori* silk the most important repeat sequence is (Ala Gly); for *N. clavipes* dragline spider silk it is predominantly poly Ala.

In contrast to silkworm silk, there is no readily available source for spider dragline silk, and protein engineering techniques have been explored as a means of scaling up production. Furthermore, changes in the silk structure might be made to produce a material less sensitive to water. The combination of bacterial production with a synthetic processing step should allow better control of mechanical properties as compared to natural silk. On the other hand, development of methods of posttranslational silk spinning is not a straightforward process.

The first protein engineering attempts were made by using large parts of the native spider silk genes. After incorporation of these cDNA fragments into *E. coli* expression systems however, difficulties arose from gene and protein stability, and truncated proteins were produced. Clones larger than 2.5 kb proved to be unstable.[14,15] The same behavior was observed for native silkworm silk genes. An explanation for this phenomenon may lie in the highly repetitive nature of these sequences, which renders the coding sequence susceptible to genetic recombination. Differences in codon preferences between the silkworm and the bacterial host could also reduce expression efficiency.[16]

The first attempts using synthetic genes based on the native gene sequence were reported as early as 1990 by Cappello and Ferrari,[17] who used silkworm fibroin analogues. Better results were obtained than when the cDNA genes were used, although the levels of protein production remained relatively low, especially for high molecular weight variants.[18] The best results reported thus far with *E. coli* expression systems were obtained by Winkler *et al.* for spider dragline silk (25–40 mg L^{-1} cell culture)[19] and Krejchi *et al.* for an $(AG)_3EG$[20] repetitive material.[21,22] To increase protein yield, high cell density production was performed, and allowed preparation of multigram quantities of product (25 g protein/35 L culture).[23] Another approach to this problem has involved changes in the production host. O'Brien *et al.* have shown that with the yeast *Pichia pastoris* it was possible to produce spider silk-like material in larger quantity (1 g L^{-1}).[24] Even mammalian hosts are now being investigated, such as Nexia's transgenic goats, which produce milk containing spider silk protein.[25]

Protein production in large quantity is just one of the problems related to obtaining silk-like fibers. An equally difficult aspect is spinning of the polypeptide, to create a material with the correct three-dimensionally ordered structure. Recently, using micro-spinneret techniques, Jelinski *et al.* have succeeded in processing regenerated *Bombyx mori* silk fibers that show similar properties when compared to their native counterparts.[26,27]

Protein engineering can also play a role in improving processing of silk like materials. Introduction of methionine residues flanking the β-sheet domains creates a tool for chemical control of structural organization.[28] By oxidizing the methionine units, β-sheet formation was prevented, which also increased solubility, while sheet formation was restored after reduction. Enzymatic techniques have also been developed to induce this transition. The functional oligopeptide RGYSLG is a recognition site for cyclic AMP-dependent kinase, which phosphorylates the hydroxy function of the serine residue.[19] Introduction of this recognition site into the structural protein allowed Winkler *et al.* to prevent β-sheet formation upon phosphorylation. Sheet formation was restored after dephosphorylation.

Recent insights into the mechanical properties of silk[29] have shown that it is not necessary or desirable to prepare purely β-sheet sequences; a certain amount of disorder should also be introduced to allow reorientation of the β-sheet crystalline domains. With protein engineering this could be accomplished by producing multiblock copolymers of β-sheet structures flanked by random oligopeptides. Such block copolymers have been reported by Conticello *et al.*, who synthesized multiblock copolymers consisting of alanine-rich blocks and elastin-mimetic domains.[30] This method leads to good protein yield (50 mg L^{-1} culture) and a method for controlling β-sheet formation by concentration from an aqueous solution.

With respect to silk-like polymers, protein engineering is probably the only synthetic method that will allow high molecular weight materials to be prepared in sufficient quantity for materials applications. The ability to introduce switches for β-sheet formation as well as the production of multiblock copolymers will ultimately lead to materials with predictable processing behavior and mechanical properties.

Mussel byssus thread

Another masterpiece of a structural material found in nature is the mussel byssus thread. This thread is used to attach the mussel to a surface, and must be tough enough to withstand challenging marine conditions. Extensive investigations by

Waite and coworkers have shown that the thread consists predominantly of a gradient of two pentablock copolymers, which are held together by so-called dovetail proteins, and which provide a graded distribution of strength and structure (Fig. 2).[31–33]

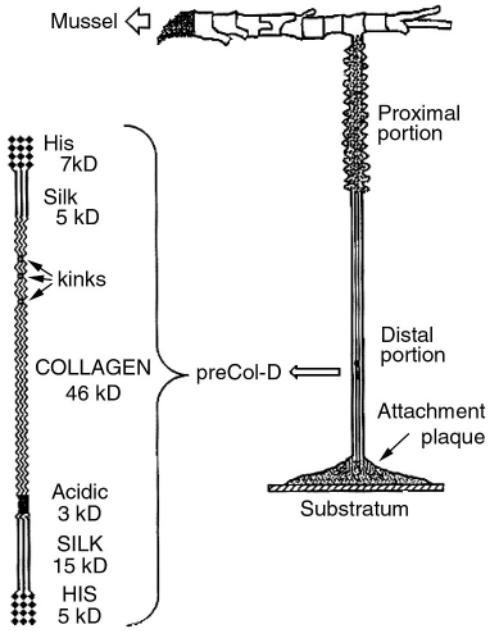

Fig. 2 Schematic view of the mussel byssus thread of *M. edulis*. The enlargement depicts the pentablock copolymer containing β-sheet domains. Reprinted with permission from (33), Copyright 1997 The American Society for Biochemistry and Molecular Biology.

The polymer that is predominant at the proximal end of the thread (*i.e.* closest to the mussel tissue) consists of a central collagen block flanked by 2 elastic domains and 2 polyhistidine sequences. The latter are expected to give rise to metal complexation between the different peptide structures. The elastin fragments introduce flexibility into the structure, whereas the collagen part is responsible for stiffness. Further down the byssus, and therefore closer to the substratum to which the mussel is attached, the elastin fragments are replaced by silk-like β-sheet domains. This structure therefore becomes much more rigid. The entire byssus is built up by a mussel within 5 minutes, and is about five times tougher and more extensible than Achilles tendon. After processing the proteins are also covalently connected. The complexity of a simple mussel byssus thread is thus far greater than that characteristic of materials produced by present-day synthetic polymer processing techniques.

Although this material would be an ideal target for protein engineering, no efforts toward this end have been reported. A possible reason could be the high content of collagen in these structures. Collagens are the most abundant family of structural proteins in the human body, and are an important constituent of ligaments, cartilage and bone. They are generally characterized by the repetitive sequence GXY, in which X is often proline and Y often hydroxyproline. Collagens form triple helices, which provide critical building blocks for higher ordered aggregates.[34] Because of their strong tendency to self-assemble, collagens become insoluble very quickly. The few protein engineering attempts reported thus far have failed for this (or perhaps other) reasons.[35] The need for a protein engineering approach for collagen is also not as pressing as for spider silk, because collagen is available in large quantities from mammalian sources. On the other hand, the repetitive sequence of collagen may be of value as an element in designed peptide-based materials, as shown by the example of the mussel byssus thread.

The mussel byssus contains more surprising peptides. The tendons have to be attached to the substrate under aqueous conditions. Nature therefore has developed a series of extraordinary protein glues, which work even in saline media. Careful analysis of these proteins, which must be done under conditions where the protein hasn't formed a network, shows that the adhesive proteins are rich in proline, tyrosine and lysine.[36] Furthermore, proline and tyrosine are posttranslationally transformed into 4-hydroxyproline and L-3,4-dihydroxyphenylalanine (DOPA), respectively. The DOPA units are expected to contribute to crosslinking *via* radical processes, in order to form networks and assist in adhesion.[37] Researchers intrigued by this phenomenon have prepared synthetic genes and expressed the corresponding $(AKPSYPPTYK)_n$ polypeptides.[38] These model peptides were treated with mushroom tyrosinase to convert the tyrosine units into DOPA, and thereby to induce crosslinking. Because expression yields were low, insufficient material was produced for a thorough evaluation. Furthermore, the question remains whether protein engineering is necessary in this case. Deming *et al*. have used NCA polymerization techniques to prepare copolypeptides consisting of lysine and DOPA residues to investigate the adhesive potential of these structures.[39] Based on the positive results obtained from this research, one can conclude that at least some of the key adhesive properties do not require the specific protein sequence; only the presence of the functional amino acids DOPA and hydroxyproline is essential. For such materials it will be more convenient to pursue the (improved) NCA polymerization routes than protein engineering.[40] More subtle effects of sequence may become apparent upon further analysis of the structure and properties of the adhesive proteins.

Elastin

One of the most versatile materials, especially from a protein engineering point of view is elastin. Elastin is a connective tissue protein that provides a combination of strength and flexibility in the extracellular matrix. Elastins are characterized by simple repeating sequences, and in contrast to silks or collagens, this family of materials does not suffer from significant solubility problems. At low temperatures elastin-like polypeptides are highly soluble in aqueous solutions and adopt random coil conformations. Elastins, however, display lower critical solution temperature (LCST) behavior, which means that the proteins form ordered structures upon raising temperature. The loss of entropy of the protein chain, when the structure folds itself into a β-helix conformation, is compensated by the release of water from the chain. A thoroughly investigated series of elastin proteins is based on the pentapeptide sequence VPGVG.[41–43] The structure and function of elastins are maintained as long as the glycine and proline residues are present, and the second valine residue can be replaced by any other amino acid. This property provides a means to control the temperature of the phase transition. When a more hydrophobic unit, such as tryptophan, replaces valine, the LCST drops significantly, and the transition temperature can be raised by introduction of more polar moieties such as glutamic acid. In the latter case, the phase transition is also made pH dependent. The pioneering work of Urry has shown that changing hydrophobicity leads to a broad spectrum of transition temperatures. The phase transition can also be induced electrochemically. For this purpose nicotinamide adenine nucleotide (NAD) is attached to glutamic acid residues within the peptide sequence. Reduction of NAD to NADH creates a more hydrophobic domain and therefore a lower transition temperature. Elastin materials have been made both by organic chemical techniques, and by microbial protein expression. Although it has been shown that one repeat unit of VPGVG is sufficient to allow the transition from random coil into an ordered β-helix structure,[44] for useful materials properties

higher molecular weight polymers are required. Protein engineering is ideally suited for this purpose, especially because production yields in bacteria are high (50–60 mg L^{-1} culture) when compared to other structural proteins.

Following up on earlier work by Urry, Conticello *et al*. have used protein engineering techniques to synthesize elastin-based block copolymers consisting of hydrophilic and hydrophobic blocks.[45] Protein engineering allows complete control of the composition, sequence and length of the blocks. By careful design, the critical micellization temperatures of these polymers could be controlled, and the resulting materials are under investigation as candidates for drug delivery. A second demonstration of the versatility of protein engineering for the preparation of elastin-based materials has been reported by the same group. Hydrogels are important products in biomedical applications. Ideally one wants to obtain control of mechanical properties by regulating crosslink density and network formation. Using protein engineering, control over monomer composition, and therefore control over distribution of crosslinkable moieties, is achieved easily. Conticello *et al*. synthesized elastin-based materials containing one specific crosslinking point (lysine) per 25 monomer units, allowing a high level of control of crosslink density after reaction with bis(sulfosuccinimidyl) suberate.[46]

Another approach, which takes advantage of additional possibilities of protein engineering was developed by Urry and extended by Panitch *et al*., who reported new materials for tissue-engineered vascular grafts.[47,48] Oligopeptides were introduced that contained either RGD (Urry) or REDV (Panitch) domains, which are known to stimulate endothelial cell binding.[49] This approach yields matrix materials that exhibit mechanical properties similar to those of the arterial wall and that support adhesion of vascular endothelial cells. An extension of the polymer design was made by introduction of lysine moieties, which allowed amine specific crosslinking of the elastin matrix without disturbing the cell binding domains.[50] The combination of structure and function in a well defined manner as demonstrated by this example is almost impossible to achieve by any method other than protein engineering.

Helical polypeptides

Leucine zipper peptides play key roles in the dimerization and DNA-binding behavior of transcriptional regulatory proteins. Related structures can be found within the keratins, the main structural protein of hair and nails. The leucine zipper motif is characterized by a consensus heptad repeat (*abdcefg*), in which *a* and *d* are hydrophobic amino acids, (*d* most frequently leucine) and the moieties at *e* and *g* are usually charged. In the helical form of the zipper peptide, the residues at *a* and *d* are arrayed along a single face of the helix. Exposure of this hydrophobic face to the aqueous environment is reduced by formation of a dimeric coiled-coil structure, while electrostatic interactions between *e* and *g* residues modulate the stability of the dimer. This feature has been exploited to prepare pH dependent peptide-based hydrogels. Triblock copolymers were constructed to comprise a central random coil $(AG_3PEG)_x$, flanked by terminal leucine zipper domains (Fig. 3).[51] These

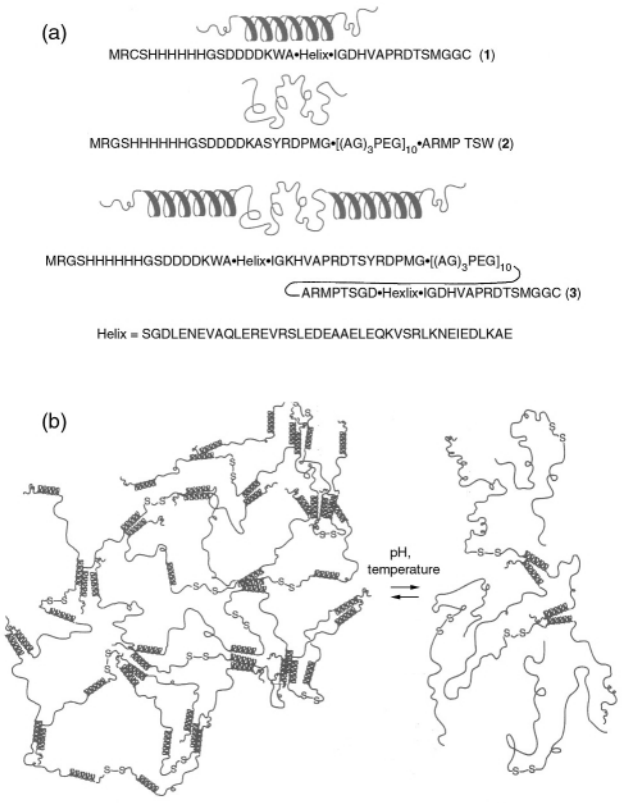

Fig. 3 (a) Amino acid sequence of the leucine zipper triblock copolymer; (b) demonstration of reversible hydrogel formation. Reprinted with permission from W. A. Petka, J. L. Harden, K. P. McGrath, D. Wirtz and D. A. Tirrell, *Science*, 1998, **281**, 389. Copyright 1998 American Association for the Advancement of Science.

domains consisted of six heptad repeats of which the choice of *a*/*d* residues was based on the *Jun* oncogene product. A database developed by Lupas *et al*.[52] was used for the selection of the residues occupying positions *b*, *c* and *f*. Nine of the 12 *e* and *g* positions were occupied by Glu residues, which allowed switching between the aggregated and dissociated states by changes in pH or temperature. At low pH and low temperature the materials formed elastic gels; increases in pH or in temperature resulted in decreased viscosity and loss of hydrogel properties.

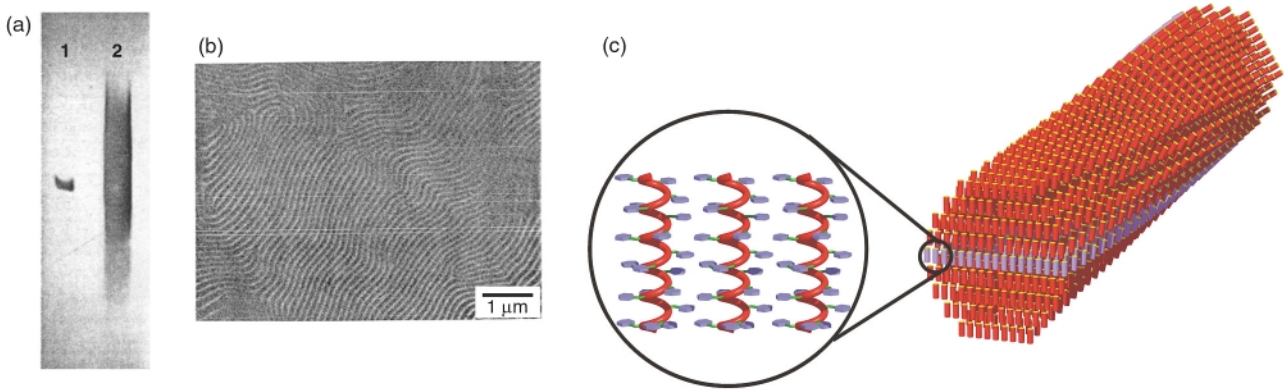

Fig. 4 (a) Difference in molecular weight distribution of protein engineered poly L-glutamic acid (1) and a conventionally prepared sample (2). Reprinted by permission from *Nature* (54), Copyright 1997 Macmillan Magazines Ltd.; (b) and (c) monodisperse poly-benzyl-L-glutamate shows a twisted smectic liquid crystalline phase. Reprinted with permission from (55), Copyright 1998 American Chemical Society.

Each of the examples examined thus far shows the need for control over composition in order to engineer the properties of the products. Molecular weight distribution is a second parameter that is of importance in polymer chemistry, though its influence on material properties is not always easy to anticipate. One striking exception however, is the synthesis of the helical polypeptide polybenzyl-L-glutamate (pBLG) (Fig. 4).

The polydisperse form, which can be prepared by NCA polymerization, has been known for many years to exhibit liquid crystalline behavior.[53] Under most conditions, pBLG forms a cholesteric phase, but certain solvents and temperatures yield a nematic. Because of the broad distribution of molecular weight a clear characterization has always been difficult. Using protein engineering, monodisperse poly L-α-glutamic acid could be synthesized, and posttranslationally modified to yield pBLG. This monodisperse sample showed distinctly different LC behavior. Instead of a nematic or cholesteric phase a twisted smectic mesophase was obtained.[54,55] The fact that all chains were of the same length resulted in ordering in layers, which was not possible in conventional polydisperse samples.

Increasing the scope of protein engineering

The foregoing examples illustrate some of the promise of protein engineering as a tool for material synthesis. Especially in cases where the information encoded in the primary amino acid sequence governs higher ordered structures, and thereby the ultimate material properties, protein engineering clearly outperforms synthetic polymerization techniques.

One of the drawbacks of protein engineering in comparison to the other techniques, however, is that the choice of building blocks might be expected to be limited to the naturally occurring amino acids. Many functional groups, which would be useful in controlling properties or postmodification efforts, such as alkenes, alkynes, or halogens, are not found in natural proteins. The chemical versatility of amino acids containing unsaturated side chains has recently been reviewed.[56] Furthermore, incorporation of halides, especially fluoride, can have dramatic effects on the physical properties of materials. Extension of the set of amino acid building blocks to unnatural analogues that can be utilized by the protein production mechanism of living systems would therefore enlarge the possibilities of protein-based materials.

This idea has intrigued several groups. A first approach is to use stop (nonsense) codons or 4-base codons[57] for the introduction of unnatural amino acids. Suppressor tRNAs can be found that overwrite these termination signals. If unnatural amino acids can be coupled to these tRNA molecules, efficient incorporation of analogues can be accomplished. This technique has been applied *in vitro* for more than a decade.[58] For this approach to succeed *in vivo* it is necessary to introduce a suppressor tRNA that is not recognized by the host enzymes that couple amino acids to tRNAs (the aminoacyl-tRNA synthetases).[59,60] This can be achieved by using a suppressor tRNA from an exogenous source such as yeast.[61,62] Next, a synthetase must be identified or developed to couple the unnatural amino acid to the suppressor tRNA. This synthetase should also be inactive toward other tRNAs. This method allows site-directed insertion of the amino acid analogue at a single position, *e.g.* in he active site of an enzyme. This method will have major impact on the design of proteins that are used for functional purposes

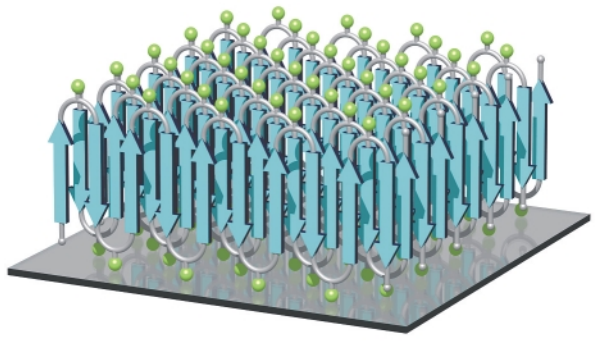

Fig. 5 Schematic representation of the lamellar crystalline phase formed by the peptide sequence $((AG)_3FG)_n$, in which phenylalanine is replaced by *p*-fluorophenylalanine. The green spots indicate amino acid side chains with unnatural functionality, in this case fluorine, at the lamellar surface.

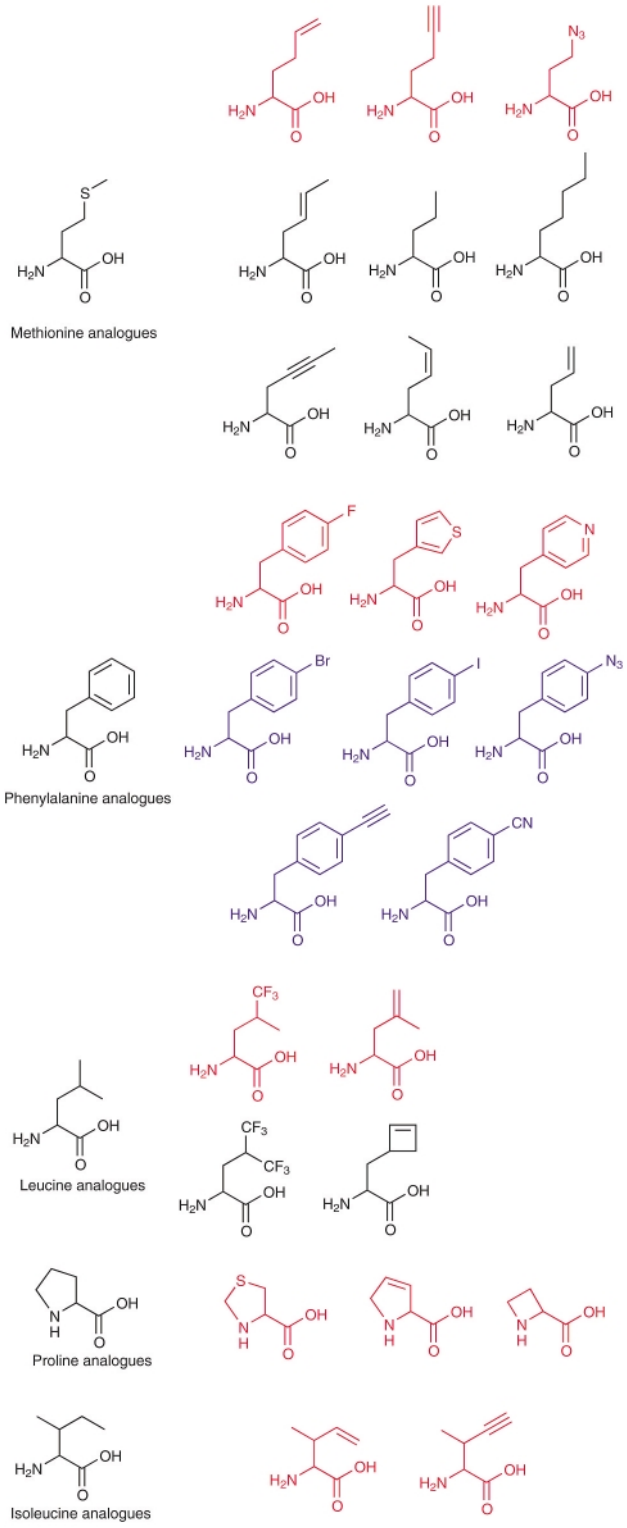

Fig. 6 An overview of the obtained results of Tirrell and coworkers with respect to *in vivo* replacement of natural amino acids by their analogues. Amino acids depicted in red are incorporated *via* standard auxotroph methodologies. Mutant aminoacyl tRNA synthetases have to be applied to be able to build in the blue amino acids. Analogues depicted in black are incorporated after boosting synthetase activity.

such as enzymes, since alteration of the overall physical properties of the macromolecule generally cannot be achieved through modification of a single site. An overview of this technique has been published recently.[63]

An alternative method has been developed by Tirrell *et al.*, based on much earlier work on substitution of natural amino acids by their close structural analogues. This method uses so-called bacterial auxotrophs, *i.e.* bacteria that have lost the ability to produce one of the natural amino acids. Such bacterial strains are dependent on the growth medium for obtaining this specific amino acid. If an analogue is added to the medium, it can be incorporated in place of the natural substrate, if it is recognized by the corresponding aminoacyl-tRNA synthetase.

In order to reduce toxicity, the cells are grown first in a medium containing all of the natural amino acids. When sufficient cell density is reached, the cells are shifted to a new medium which contains the analogue instead of the natural amino acid.

This methodology has proven successful for a large number of amino acids and derivatives thereof. Though the first publications go back for several decades,[64] only in recent years has extensive research allowed replacement of phenylalanine, proline, leucine, methionine, tyrosine and isoleucine with their respective analogues.[65–68]

An interesting application of this method is the incorporation of phenylalanine analogues into the β-sheet element $((AG)_3FG)_n$. This sequence adopts a lamellar crystalline structure, in which the phenylalanine residues are exposed to the surface. Well-defined functional surfaces can now be created. Replacement by *p*-fluorophenylalanine allowed the construction of fluorinated crystalline layers,[65] and β-sheets containing thiophene units from 3-thienylalanine[66] can be regarded as precursors for conducting polymers (Fig. 5).

Replacement of leucine by either trifluoroleucine or 2-amino-4-methylhex-4-enoic acid in leucine zippers causes marked effects on conformational stability. For example, in a leucine zipper peptide characterized by a melting temperature of 48 °C, the transition temperature was elevated to 61 °C by introduction of trifluoroleucine, whereas the native structure was destabilized by the introduction of the unsaturated analogue.[69] This simple example illustrates the extent to which incorporation of amino acid analogues expands the possibilities for engineering protein stability and protein–protein interactions.[70]

The most systematic study to date has concerned introduction of methionine analogues. Homoallylglycine and homopropargylglycine are especially effective as methionine surrogates.[68,71] Although *trans*-crotylglycine is recognized by the methionyl-tRNA synthetase, increasing the synthetase activity of the host is required for protein production.[72,73] The possibility of using mutant synthetases has also been demonstrated for *p*-bromophenylalanine[74] and azatyrosine.[75]

With the methods described in this section, some of the natural limitations of protein engineering are beginning to fade. Tailor-made materials can now be designed with pre-defined structures and properties (Fig. 6). Furthermore, protein engineering is unique in combining structural with functional elements, which can be either of natural origin, such as cell-binding domains, or introduced by incorporation of unnatural amino acids. The versatility and control of protein engineering will make this an important synthetic approach to a new generation of biomaterials.

Acknowledgement

The authors would like to thank Jurry Hannink for his assistance with the schematic representations and front cover design.

Notes and references

1 *Controlled/Living polymerization*, ed. K. Matyjaszewski, ACS Symposium series 768, Oxford University Press, Washington DC, 2000.
2 *Protein-based materials*, ed. K. McGrath and D. L. Kaplan, Birkhäuser, Boston, 1997.
3 T. J. Deming, *Adv. Mater.*, 1997, **9**, 299.
4 J. Sambrook, E. F. Fritsch and T. Maniatis, *Molecular Cloning*, Cold Spring Harbor Laboratory, Cold Spring Harbor, NY, 1986.
5 D. A. Tirrell, M. J. Fournier and T. L. Mason, *MRS Bull.*, 1991, **16**, 23.
6 D. L. Kaplan, *Polymer Degrad. Stab.*, 1998, **59**, 25.
7 J. Perez-Rigueiro, C. Viney, J. Llorca and M. Elices, *J. Appl. Polym. Sci.*, 1998, **70**, 2439.
8 S. W. Watt, I. J. McEwen and C. Viney, *Macromolecules*, 1999, **32**, 8671.
9 S. B. Warner, M. Polk and K. Jacob, *J. Macromol. Sci., Rev. Macromol. Chem. Phys.*, 1999, **C39**, 643.
10 C. Riekel, M. Muller and F. Vollrath, *Macromolecules*, 1999, **32**, 4464.
11 T. Asakura, T. Ito, M. Okudaira and T. Kameda, *Macromolecules*, 1999, **32**, 4940.
12 L. W. Jelinski, *Science*, 1996, **273**, 1481.
13 Z. Shao, F. Vollrath, J. Sirichaisit and R. J. Young, *Polymer*, 1999, **40**, 2493.
14 R. V. Lewis, M. Hinman, S. Kothakota and M. J. Fournier, *Protein Expression Purif.*, 1996, **7**, 400.
15 S. Arcidiacono, C. Mello, D. Kaplan, S. Cheley and H. Bayley, *Appl. Microbiol. Biotechnol.*, 1998, **49**, 31.
16 S. R. Fahnestock and S. L. Irwin, *Appl. Microbiol. Biotechnol.*, 1997, **47**, 23.
17 J. Cappello, J. Crissman, M. Dorman, M. Mikolajczak, G. Textor, M. Marquet and F. Ferrari, *Biotechnol. Progr.*, 1990, **6**, 198.
18 J. T. Prince, K. P. McGrath, C. M. Digirolamo and D. L. Kaplan, *Biochemistry*, 1995, **34**, 10879.
19 S. Winkler, D. Wilson and D. L. Kaplan, *Biochemistry*, 2000, **39**, 14002.
20 Amino acids are being described by a one letter code; A: alanine; G: glycine; E: glutamic acid; R: arginine; Y: tyrosine; S: serine; K: lysine; P: proline; T: threonine; V: valine; D: aspartic acid; F: phenylalanine.
21 M. T. Krejchi, E. D. T. Atkins, A. J. Waddon, M. J. Fournier, T. L. Mason and D. A. Tirrell, *Science*, 1994, **265**, 1427.
22 M. T. Krejchi, S. J. Cooper, Y. Deguchi, E. D. T. Atkins, M. J. Fournier, T. L. Mason and D. A. Tirrell, *Macromolecules*, 1997, **30**, 5012.
23 A. Panitch, K. Matsuki, E. J. Cantor, S. J. Cooper, E. D. T. Atkins, M. J. Fournier, T. L. Mason and D. A. Tirrell, *Macromolecules*, 1997, **30**, 42.
24 J. P. O'Brien, S. R. Fahnestock, Y. Termonia and K. C. H. Gardner, *Adv. Mater.*, 1998, **10**, 1185.
25 H. T. Huynh, G. Robitaille and J. D. Turner, *Exp. Cell Res.*, 1991, **197**, 191.
26 O. Liivak, A. Blye, N. Shah and L. W. Jelinski, *Macromolecules*, 1998, **31**, 2947.
27 A. Seidel, O. Liivak, S. Calve, J. Adaska, G. D. Ji, Z. T. Yang, D. Grubb, D. B. Zax and L. W. Jelinski, *Macromolecules*, 2000, **33**, 775.
28 S. Winkler, S. Szela, P. Avtges, R. Valluzzi, D. A. Kirschner and D. Kaplan, *Int. J. Biol. Macromol.*, 1999, **24**, 265.
29 L. W. Jelinski, *Curr. Opin. Solid State Mater. Sci.*, 1998, **3**, 237.
30 Y. Qu, S. C. Payne, R. P. Apkarian and V. P. Conticello, *J. Am. Chem. Soc.*, 2000, **122**, 5014.
31 K. J. Coyne, X. X. Qin and J. H. Waite, *Science*, 1997, **277**, 1830.
32 K. J. Coyne and J. H. Waite, *J. Exp. Biol.*, 2000, **203**, 1425.
33 X. X. Qin, K. J. Coyne and J. H. Waite, *J. Biol. Chem.*, 1997, **272**, 32623.
34 M. Vanderrest and R. Garrone, *Biochimie*, 1990, **72**, 473.
35 I. Goldberg, A. J. Salerno, T. Patterson and J. I. Williams, *Gene*, 1989, **80**, 305.
36 J. H. Waite, *Bioartif. Organs II*, 1999, **875**, 301.
37 M. E. Yu, J. Y. Hwang and T. J. Deming, *J. Am. Chem. Soc.*, 1999, **121**, 5825.
38 M. Kitamura, K. Kawakami, N. Nakamura, K. Tsumoto, H. Uchiyama, Y. Ueda, I. Kumagai and T. Nakaya, *J. Polym. Sci., Part A: Polym. Chem.*, 1999, **37**, 729.
39 M. E. Yu and T. J. Deming, *Macromolecules*, 1998, **31**, 4739.
40 T. J. Deming, *Nature*, 1997, **390**, 386.
41 D. W. Urry, *Biopolymers*, 1998, **47**, 167.
42 D. W. Urry, S. Q. Peng, L. C. Hayes, D. McPherson, J. Xu, T. C. Woods, D. C. Gowda and A. Pattanaik, *Biotechnol. Bioeng.*, 1998, **58**, 175.
43 D. W. Urry, *J. Phys. Chem. B*, 1997, **101**, 11 007.
44 H. Reiersen, A. R. Clarke and A. R. Rees, *J. Mol. Biol.*, 1998, **283**, 255.
45 T. A. T. Lee, A. Cooper, R. P. Apkarian and V. P. Conticello, *Adv. Mater.*, 2000, **12**, 1105.
46 R. A. McMillan and V. P. Conticello, *Abstr. Pap. Am. Chem. Soc.*, 2000, **219**, 583.

47 A. Nicol, D. C. Gowda, T. M. Parker and D. W. Urry, *Biotechnology of Bioactive Polymers*, ed. C. C. Gebelein and C. E. Carraher, Plenum Press, New York, 1994.
48 A. Panitch, T. Yamaoka, M. J. Fournier, T. L. Mason and D. A. Tirrell, *Macromolecules*, 1999, **32**, 1701.
49 M. J. Humphries, S. K. Akiyama, A. Komoriya, K. Olden and K. M. Yamada, *J. Cell. Biol.*, 1986, **103**, 2637.
50 E. R. Welsh and D. A. Tirrell, *Biomacromolecules*, 2000, **1**, 23.
51 W. A. Petka, J. L. Harden, K. P. McGrath, D. Wirtz and D. A. Tirrell, *Science*, 1998, **281**, 389.
52 A. Lupas, M. V. Dyke and J. Stock, *Science*, 1991, **252**, 1162.
53 C. Robinson and J. C. Ward, *Nature*, 1957, **180**, 1183.
54 S. J. M. Yu, V. P. Conticello, G. H. Zhang, C. Kayser, M. J. Fournier, T. L. Mason and D. A. Tirrell, *Nature*, 1997, **389**, 167.
55 S. J. He, C. Lee, S. P. Gido, S. M. Yu and D. A. Tirrell, *Macromolecules*, 1998, **31**, 9387.
56 F. Rutjes, L. B. Wolf and H. E. Schoemaker, *J. Chem. Soc., Perkin Trans. 1*, 2000, 4197.
57 T. Hohsaka, D. Kajihara, Y. Ashizuka, H. Murakami and M. Sisido, *J. Am. Chem. Soc.*, 1999, **121**, 34.
58 C. J. Noren, S. J. Anthonycahill, M. C. Griffith and P. G. Schultz, *Science*, 1989, **244**, 182.
59 L. Wang, T. J. Magliery, D. R. Liu and P. G. Schultz, *J. Am. Chem. Soc.*, 2000, **122**, 5010.
60 D. R. Liu, T. J. Magliery, M. Pasternak and P. G. Schultz, *Proc. Natl. Acad. Sci. U.S.A.*, 1997, **94**, 10092.
61 R. Furter, *Protein Sci.*, 1998, **7**, 419.
62 L. Wang, A. Brock, B. Heberic and P. G. Schultz, *Science*, 2001, **292**, 498.
63 D. A. Dougherty, *Curr. Opin. Chem. Biol.*, 2000, **4**, 645.
64 M. H. Richmond, *Bacteriol. Rev.*, 1962, **26**, 398.
65 E. Yoshikawa, M. J. Fournier, T. L. Mason and D. A. Tirrell, *Macromolecules*, 1994, **27**, 5471.
66 S. Kothakota, T. L. Mason, D. A. Tirrell and M. J. Fournier, *J. Am. Chem. Soc.*, 1995, **117**, 536.
67 T. J. Deming, M. J. Fournier, T. L. Mason and D. A. Tirrell, *J. Macromol. Sci., Pure Appl. Chem.*, 1997, **A34**, 2143.
68 J. C. M. van Hest, K. L. Kiick and D. A. Tirrell, *J. Am. Chem. Soc.*, 2000, **122**, 1282.
69 Y. Tang, G. Ghirlanda, N. Vaidehi, J. Kua, D. T. Mainz, W. A. Goddard III, W. F. DeGrado and D. A. Tirrell, *Biochemistry*, 2001, **40**, 2790.
70 C. E. MacPhee and C. M. Dobson, *J. Am. Chem. Soc.*, 2000, **122**, 12707.
71 J. C. M. van Hest and D. A. Tirrell, *FEBS Lett.*, 1998, **428**, 68.
72 K. L. Kiick, J. C. M. van Hest and D. A. Tirrell, *Angew. Chem., Int. Ed.*, 2000, **39**, 2148.
73 K. L. Kiick and D. A. Tirrell, *Tetrahedron*, 2000, **56**, 9487.
74 N. Sharma, R. Furter, P. Kast and D. A. Tirrell, *FEBS Lett.*, 2000, **467**, 37.
75 F. Hamano-Takaku, T. Iwama, S. Saito-Yano, K. Takaku, Y. Monden, M. Kitabatake, D. Soll and S. Nishimura, *J. Biol. Chem.*, 2000, **275**, 40 324.

CHEMCOMM Communication
www.rsc.org/chemcomm

Self-assembled monolayers of new dendron-thiols: manipulation of the patterned surface and wetting properties†

Li Zhang,[a] Bo Zou,[a] Bin Dong,[a] Fengwei Huo,[a] Xi Zhang,*[a] Lifeng Chi[b] and Lei Jiang[c]

[a] *Key Lab of Supramolecular Structure and Spectroscopy, Department of Chemistry, Jilin University, Changchun, 130023, P. R. China*
[b] *Physikalisches Institut, Westfälische Wilhelms-Universität, D-48149 Münster, Germany*
[c] *Institute of Chemistry, Research Center for Molecular Sciences, CAS, Beijing, 100080, P. R. China*

Received (in Cambridge, UK) 1st May 2001, Accepted 31st July 2001
First published as an Advance Article on the web 31st August 2001

SAMs based on a novel dendron-thiol system, which maintain the alkanethiols' active site, but with the –SH group connected to independently variable groups by a dendron-linker, showed a controllable surface pattern and wetting properties. The precisely tailored structure of dendron-thiols with locally controlled hydrophobic and hydrophilic peripheries allows the formation of designed surface structures on a gold surface, *e.g.* nano-stripes, honeycomb and homogeneous structures.

Self-assembled monolayers (SAMs) with macroscopic physical properties tailored by molecular-scale variation of the chemical structure and constituents are a particularly attractive field. There are two routes that are amenable to realize this goal. One is based on the chemisorption of dialkyl sulfides,[1] the other is the adsorption of an alkanethiol mixture.[2] Both methods permit local control of the surface structure of the adsorbed monolayer to some extent. But the self-assembled monolayers formed from dialkyl sulfides are significantly less densely packed and less ordered than those prepared by adsorption of alkanethiols. Moreover, the monolayers prepared from dialkyl sulfides were not stable at high temperature (*e.g.* 80 °C). As for the adsorption of mixed alkanethiols, there does exist, more or less, phase separation. So, avoiding the above problems to obtain SAMs with controllable constituents and a stable ordered surface structure is a challenge for chemists.

Dendrimers, a type of regular-branched molecule, with structures precisely controlled at the molecular level and having many unique properties,[3] are promising candidates for nano-fabrication.[4] Combining molecular self-assembly techniques and dendrimer chemistry, self-assembled monolayer formation based on the chemisorption of dendron-thiols has been addressed by several groups.[5,6] In our previous studies, we have found that SAMs of Fréchet type dendrons with a thiol group at the focal point can form patterned stripes with nanometer-sized features and long-range order. The patterned stripes were closely related to the size of dendron, and they can be improved by thermal annealing. Here we introduce two types of building blocks with different hydrophobicity into the dendron-thiols' peripheries, and expect that the SAMs formed by this type of dendron-thiol with locally controlled hydrophobicity could exhibit a stable and unique assembly structure. As Fig. 1 shows, dendron-thiols with both hydrophobic and hydrophilic groups at their peripheries have been synthesized, labelled G2REO. Heptane chains and oligo(ethylene oxide) chains were selected as hydrophobic and hydrophilic building blocks respectively. For comparison, dendron-thiols with either hydrophobic or hydrophilic groups at their peripheries were also synthesized. These are labelled G2R or G2EO, as shown in Fig. 1.

Scanning tunneling microscopy (STM) was used to observe the surface morphology of self-assembled monolayers of G2R, G2EO and G2REO on gold surfaces. For the dendron-thiols with a purely hydrophobic periphery (G2R) as the building block, the SAMs on a gold surface displayed a stripe-like ordered structure (Fig. 2a). The width of stripes is about 4 nm. It is presumed that both π–π stacking and hydrophobic interactions of hydrophobic peripheries contribute to the long-range order of G2R. In order to confirm this assumption, we also studied the SAMs of G2EO. In this case, where the dendron-thiol has a hydrophilic periphery, only uniform surface structure (except for few defects) was found on the gold surface rather than high-level ordered packing (Fig. 2b). A plausible reason is that the intermolecular interaction of dendron-thiols is weakened due to the extended conformation of the oligo(ethylene oxide) chain.

As for the case of SAMs of dendron-thiols bearing hydrophobic and hydrophilic (G2REO) groups at their peripheries on gold surface, it can be seen that a type of pore structure has been formed, and in smooth areas, the pores can further self-organize into a well-ordered structure after annealing at 70 °C for 3 h, as shown in Fig. 3. The diameter of the pore was about 5 nm, as measured from STM images. An STM image of G2REO on gold surface with a large scan area depicted the ordered structure extending over a large area. As far as we know, there are few reports concerning the formation of such patterned structures completely based on the self-assembly of organo-sulfur on gold surface. The driving force for the spontaneous formation of the 2D assembly includes chemisorption between dendron-thiols with –SH at the focal point and the gold surface, and combined intermolecular interactions among dendron-thiols. In our system, the chemisorption is similar for the series of samples. Therefore, we can deduce that the chemical structure of dendron-thiol influences greatly the intermolecular interaction, and even the molecular assembly behavior at the interface. Molecular dynamics simulations with quench dy-

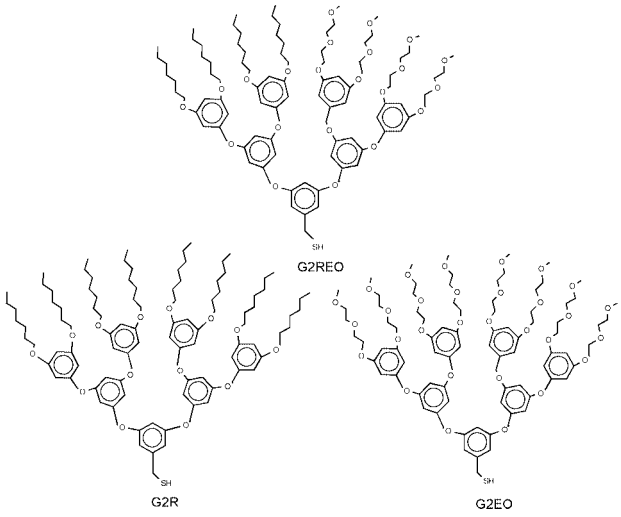

Fig. 1 Chemical structures of dendron-thiols.

† Electronic supplementary information (ESI) available: experimental details. See http://www.rsc.org/suppdata/cc/b1/b103903m/

 DOI: 10.1039/b103903m

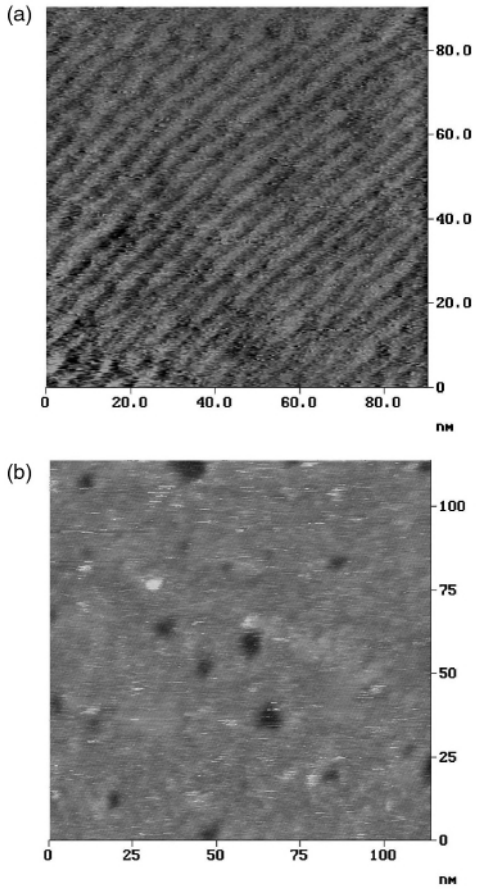

Fig. 2 STM images of self-assembled monolayers of dendron-thiols on gold surface (a) G2R; (b) G2EO.

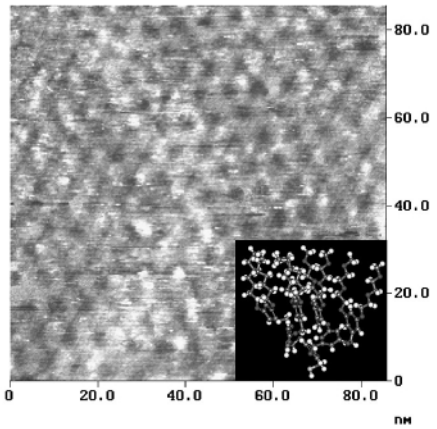

Fig. 3 STM images of self-assembled monolayers of dendron-thiols G2REO on gold surface (height mode, inset: the stable conformation of G2REO obtained by MD simulation).

namics show that the stable conformation of G2REO exhibits local aggregate behavior of the hydrophobic and hydrophilic peripheries based on the like-to-like principle. It indicates that the precisely tailored structure of dendron-thiols with local controlled hydrophobic and hydrophilic peripheries allows a nano-separation in a confined state, leading to the formation of an energetically favorable pore structure.

The process of the adsorption kinetics of dendron-thiol on gold surface was studied by contact angle measurement of water. Fig. 4 shows the relationship between contact angle and assembly time of G2R, G2REO and G2EO on gold surface. For the assembly processes of G2R or G2EO, the contact angles increased with the assembly time, and reached saturated

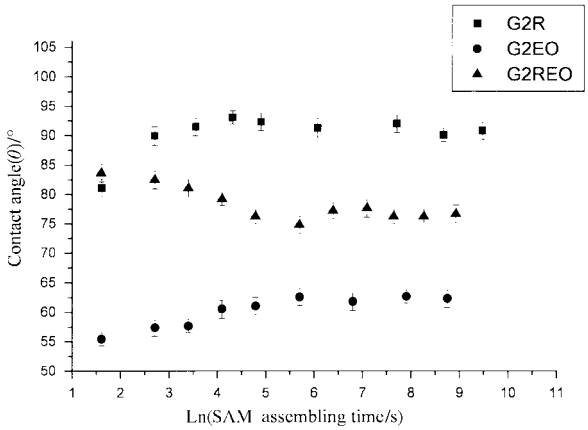

Fig. 4 Relationship between contact angles of water and assembly time of SAMs of dendron-thiols G2R, G2REO and G2EO on gold surface.

adsorption within about 7 min. The values of the contact angle at saturated adsorption were about 92° and 60° for SAMs of G2R and G2EO respectively. The process of assembly of dendron-thiols with hydrophobic and hydrophilic groups at their peripheries exhibited a special character. The contact angle decreased with assembly time at the beginning of the chemisorption and was constant after 11 min. G2REO's hydrophobic and hydrophilic peripheral group parts could both contribute to the wettability of SAMs on gold surface. The value for the contact angle of water on G2REO modified gold surface at saturated adsorption was about 75°, which was just in between the values of G2R and G2EO. The different relationship between contact angle and assembly time of G2REO as compared to that of G2R and G2EO might indicate a different 2D crystallizing process of dendron-thiols on gold surface.

In conclusion, these monolayers represent a successful example of designed modification of surface structure and properties by molecular-scale variation of the structure of molecular constituents. By taking full advantage of dendrimers with precisely controlled structures at the molecular level, many functional groups can be introduced into alkanethiol with a dendron-linker. It is expected that the interplay between dendrimer chemistry and self-assembled monolayers may open a new route for surface engineering.

We thank the support of the Major State Basic Research Development Program (Grant. No. G2000078102), Educational Ministry and National Natural Science Foundational of China. Dr Xi Zhang would like to acknowledge DFG for a one month visit to the University of Muenster in 2000.

Notes and references

1 E. Katz, N. Itzhak and I. Willner, *J. Electroanal. Chem.*, 1992, **336**, 357.
2 (*a*) K. L. Prime and G. M. Whitesides, *Science*, 1991, **252**, 1164; (*b*) K. L. Prime and G. M. Whitesides, *J. Am. Chem. Soc.*, 1993, **115**, 10714.
3 A. W. Bosman, H. M. Janssen and E. W. Meijer, *Chem. Rev.*, 1999, **99**, 1665.
4 (*a*) M. Wells and R. M. Crooks, *J. Am. Chem. Soc.*, 1996, **118**, 3988; (*b*) Y. Zhou, M. L. Bruening, D. E. Bergbreiter, R. M. Crooks and M. Wells, *J. Am. Chem. Soc.*, 1996, **118**, 3773.
5 (*a*) D. C. Tully, K. Wilder, J. M. J. Fréchet, A. R. Trimble and C. F. Quate, *Adv. Mater.*, 1999, **11**, 314; (*b*) A. Friggeri, H. Schönherr, H.-J. van Manen, B.-H. Huisman, C. J. Vancso, J. Huskens, F. C. J. M. van Veggel and D. N. Reinhoudt, *Langmuir*, 2000, **16**, 7757; (*c*) C. B. Gorman, R. L. Miller, K. Y. Chen, A. R. Bishop, R. T. Haasch and R. G. Nuzzo, *Langmuir*, 1998, **14**, 3312.
6 (*a*) Z. S. Bo, L. Zhang, X. Zhang, J. C. Shen, S. Hoeppener, L. F. Chi and H. Fuchs, *Chem. Lett.*, 1998, 1197; (*b*) L. Zhang, F. W. Huo, Z. Q. Wang, L. X. Wu, X. Zhang, S. Hoeppener, L. F. Chi, H. Fuchs, J. W. Zhao, L. Niu and S. J. Dong, *Langmuir*, 2000, **16**, 3813.

CHEMCOMM Communication
www.rsc.org/chemcomm

Ready protease-catalyzed synthesis of carbohydrate–amino acid conjugates†

Viviane Boyer,[a] Mincho Stanchev,[b] Antony J. Fairbanks*[b] and Benjamin G. Davis*[a]

[a] *Department of Chemistry, Univeristy of Durham, South Road, Durham, UK DH1 3LE. E-mail: Ben.Davis@durham.ac.uk*
[b] *Dyson-Perrins Laboratory, South Parks Road, Oxford, UK OX1 3QY*

Received (in Cambridge, UK) 10th May 2001, Accepted 6th July 2001
First published as an Advance Article on the web 12th September 2001

The protease-catalyzed synthesis of amino acid ester–carbohydrate conjugates as glycopeptide analogues has been achieved in a highly regioselective and carbohydrate-specific manner using amino acid vinyl ester acyl donors and minimally or completely unprotected carbohydrate acyl acceptors, which together probed active sites of proteases to reveal yield efficiencies that are modulated by the carbohydrate C-2 substituent, and that may be exploited to allow selective one-pot syntheses.

Many carbohydrate–peptide conjugates display a wide variety of potent biological activities of potential therapeutic and commercial value.[1,2] For example, glycoproteins act as critical cell surface communication markers,[3] glycopeptide motifs such as the Thomsen–Friedenreich (Tf) antigen are associated with cancer cell lines[4] and an oligomeric sequence of the glycopeptide motif $(AAT[Gal\beta(1,3)GalNAc\alpha])_n$ displays unusual non-colligative antifreeze properties.[5] Access to well-defined carbohydrate–peptide conjugates and their analogues to probe the nature of these properties is essential. A large number of elegant methods have been developed for the synthesis and assembly of *N*- and *O*-linked glycopeptides[2,6] but these methods may be complicated by low glycosylation efficiencies and extensive protection regimes to ensure regioselectivity. To avoid these potential problems we have investigated the utility of enzyme-catalyzed regioselective acylation of carbohydrates as a one-step method. Despite the ready construction of ester–carbohydrate linkages, there have been remarkably few syntheses of amino acid esters of carbohydrates.[7] Furthermore, although the utility of hydrolases as powerful catalysts for regioselective acylation of carbohydrates is well demonstrated,[8] their use in the transfer of amino acids to carbohydrates is, with very few exceptions,[9] neglected. This is all the more surprising given that several biofunctional molecules, such as enkephalin–carbohydrate conjugates that modulate fibroblast and melanoma growth,[10] are themselves α-amino esters of carbohydrates. Moreover, carbohydrate–peptide conjugates connected by potentially metabolisable, sacrificial linkages, such as esters, have high potential utility as prodrugs in which the glycan moiety affords both protection and specific transport properties.[11] We therefore set ourselves the goal of establishing a ready, short route for the creation of such ester-linked glycopeptides.

Initially, we chose the serine protease subtilisin *Bacillus lentus* (SBL, EC 3.4.21.14) as a powerful catalyst for ester synthesis[12] and the representative amino acids phenylalanine **1a**, aspartic acid **2a** and glutamic acid **3a**. Amino acid derivatives (Scheme 1)† were chosen to probe not only the amino acid specificity of SBL but also its tolerance for a variety of amine (Ac, Boc, Fmoc, Z) and ester (Bn) protecting groups. $Pd(OAc)_2$-mediated transesterification[13] of **1–8b** with vinyl acetate (Scheme 1) allowed the preparation of the corresponding Phe, Asp and Glu; α and side-chain vinyl esters **1–8c** as acyl donors that render transesterifications essentially irreversible.[14]

† Electronic supplementary information (ESI) available: experimental details. See http://www.rsc.org/suppdata/cc/b1/b104137c/

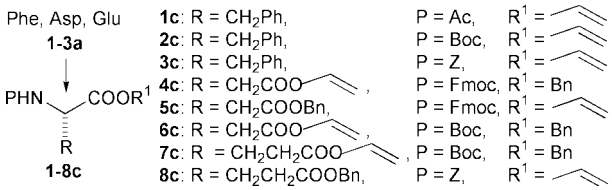

Scheme 1 For reagents and conditions, see ESI.

With these acyl donors in hand, we investigated their utility in transesterification reactions with a representative range of carbohydrate acyl acceptors **9a–20a** (Scheme 2, Table 1). After exploring a range of conditions, the use of SBL lyophilised from phosphate buffer (pH 8.0) in anhydrous pyridine at 45 °C proved optimal. Initial variation of parent carbohydrate in the completely deprotected series **9a–12a** revealed exclusive *O*-6 regioselectivity but only low isolated yields of either D-glucose **9b** or D-galactose **10b** 6-*O*-phenylalaninate esters.[15] However, a higher yield of the 6-*O*-phenylalaninate ester of D-mannose **11b** indicated an exciting preference based only on the stereochemistry of the parent carbohydrate. This crucial dependency on carbohydrate acceptor was yet more dramatically confirmed by the complete absence of product from the attempted esterification of *N*-acetylglucosamine **12a** from which only **12a** and the product of acyl donor hydrolysis **1b** were recovered. Next the effect of anomeric substituent was probed. Introduction of a methyl substituent at *O*-1 increased yield only slightly in the case of D-galactose and D-glucose acyl acceptors **13–15a**. Moreover, the near identical yields of α- and β-glucosides **13**, **14b** indicated that, at least in the D-gluco series, anomeric stereochemistry had little or no effect on overall yield. Most notably, the apparent specificity preference of SBL for D-manno acyl acceptors was further confirmed by the higher yield (76%) of ester **16b** obtained here from α-D-mannoside **16a**.

Thioglycosides and selenoglycosides are important glycosyl donors[16] and we next investigated their esterification to provide potential glycopeptide donors, in which the glycosyl unit might be further extended, and as further probes of the effect of anomeric substituent. Consistent with both their larger size and the potential for aromatic aglycones in carbohydrate substrates to interact with protein surfaces,[17] more dramatic results were obtained for the thioglycosides **17–20a**. A trend in the efficiencies of the formation of 6-*O*-phenylalaninate products in the order D-manno > D-gluco > D-galacto > *N*-acetyl-D-gluco emerged. In addition, for the first time, reduced regioselectivity was observed for D-thioglucoside **17a** (3:2, 6-*O* **17b**: 3-*O* **17c**).[18]

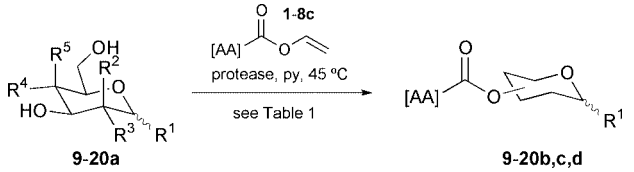

Scheme 2

 DOI: 10.1039/b104137c

Table 1 Carbohydrate–amino acid coupling reactions

Coupling pair	R^1	R^2	R^3	R^4	R^5	Yield of 6-*O*-acyl (%)[c]
9a–1c[a]	OH	H	OH	OH	H	24 **9b**
10a–1c[a]	OH	H	OH	H	OH	24 **10b**
11a–1c[a]	OH	OH	H	OH	H	49 **11b**
12a–1c[a]	OH	H	NHAc	OH	H	—
13a–1c[a]	α-OMe	H	OH	OH	H	25 **13b**
14a–1c[a]	β-OMe	H	OH	OH	H	28 **14b**
15a–1c[a]	β-OMe	H	OH	H	OH	30 **15b**
16a–1c[a]	α-OMe	OH	H	OH	H	76 **16b**
17a–1c[a]	β-SPh	H	OH	OH	H	44 **17b** + 29 **17c**[e]
18a–1c[a]	β-SPh	H	OH	H	OH	36 **18b**
19a–1c[a]	α-SPh	OH	H	OH	H	62 **19b**
20a–1c[a]	β-SePh	H	NHAc	OH	H	23 **20b**
16a–1c[b]	α-OMe	OH	H	OH	H	48 **16b**
16a–2c[a]	α-OMe	OH	H	OH	H	32 **16c**
16a–2c[d]	α-OMe	OH	H	OH	H	63 **16c** + 17 **16d**[e]
16a–3c[d]	α-OMe	OH	H	OH	H	60 **16e**

[a] 2 mg ml^{-1} of lyophilized (from pH 8.0, 0.1 M phosphate) SBL preparation, 45 °C, anhydrous pyridine, 120 h. [b] 1 mg ml^{-1} of TL-CLEC, 45 °C, 1 : 25 water–pyridine. [c] All yields are for isolated, purified, single compounds. [d] As for footnote *a* but for 500 h. [e] Yield of 3-*O*-acyl.

Next we investigated the effect of varying the amino acid acyl donor. Disappointingly, but consistent with the observed low affinity of SBL for other amino acid esters,[19] none of the aspartate or glutamate acyl donors were accepted as substrates. In all cases only vinyl esters **4**–**8c** were recovered indicating an absence of acyl–enzyme intermediate formation. This contrasted with the reactions of **1c** from which only transesterification or hydrolysis products were recovered. In order to further assess the utility of **1**, **4**–**8c** as acyl donor probes, we also screened their reactivity with CLEC-thermolysin (TL-CLEC)[20] as a protease with a different substrate specificity profile, that includes β-aspartate esters.[21] However, TL-CLEC also failed to accept **4**–**8c** and again only **1c** was accepted, allowing the preparation of **16b** from **16a** in 48% yield.

Next, the effect of *N*-protection in the acyl donor was investigated using Boc- and Z-protected phenylalanine donors **2**, **3c**, respectively. For **2c** much lower rates of reaction were observed than for **1c** and after a comparable period of time lower yields (32%) for the esterification of **16a** were obtained. However, extended reaction times gratifyingly allowed the preparation of 6-*O*-phenylalaninates **16c**, **e** from **2**, **3c** in 63 and 60% yields, respectively. The utility of **16c**, **e** as glycopeptide building blocks was confirmed through their quantitative *N*-deprotection to methyl 6-*O*-phenylalaninyl-α-D-mannopyranoside **21**, which may be extended at its *N*-terminus.

Finally, the valuable specificity information obtained in these screens was exploited to allow selective one-pot couplings. We were delighted to find that different carbohydrate acyl acceptors successfully competed in one-pot reactions to allow carbohydrate-selective esterification. Thus, in 1 : 1 mixtures of **12a** + **16a** and **19a** + **20a** (Scheme 3) mannosides reacted over *N*-acetylglucosaminides with **1c** in SBL-catalyzed acylations to yield mannoside esters **16**, **19b** exclusively. In both reactions no trace of **12b** or **20b**, respectively, was detected during this highly selective process.

In summary, we have described a ready method for the construction of glycan–peptide conjugates by exploiting a highly regioselective protease-catalyzed transesterification process. The yields for this selective carbohydrate–peptide conjugation of 23–76%, compare well with overall yields of < 34% for alternative routes employing protection–deprotection strategies.[7] The glycopeptides formed are powerful building blocks that will allow sugar reducing end (*e.g.* **17**–**20b**) or peptide *N*-terminal (*e.g.* **21**) extension. In addition, we have probed the substrate specificity of the proteases SBL and TL-CLEC in this reaction using the novel vinyl esters **1**–**8c** and this has indicated a strong preference for phenylalanine but flexibility in the *N*-protection that may be used. Furthermore, we have successfully exploited striking differences in the rate of reaction of carbohydrate acyl acceptors in this system to perform exclusively mannose over *N*-acetylglucosamine selective one-pot acylations. We have recently reported greatly broadened substrate amino acid ester specificities for glycosylated variants of SBL[22] and we are currently exploring transesterifications catalyzed by these glyco-SBLs with **4**–**8c** and other donors the results of which will be reported in due course.

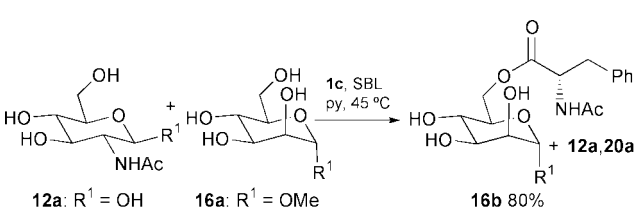

Scheme 3

We thank the BBSRC for generous funding, Genencor International for SBL, and Altus for TL-CLEC. We thank the EPSRC for access to the Mass Spectrometry Service at Swansea and the Chemical Database Service at Daresbury.

Notes and references

1 B. G. Davis, *J. Chem. Soc., Perkin Trans. 1*, 1999, 3215.
2 C. M. Taylor, *Tetrahedron*, 1998, **54**, 11 317.
3 A. Varki, *Glycobiology*, 1993, **3**, 97; R. A. Dwek, *Chem. Rev.*, 1996, **96**, 683.
4 G. F. Springer, *J. Mol. Med.*, 1997, **75**, 594.
5 T. Tsuda and S.-I. Nishimura, *J. Chem. Soc., Chem. Commun.*, 1996, 2779.
6 O. Seitz, *Chem. Bio. Chem.*, 2000, **1**, 215; M. Meldal and P. M. St Hilaire, *Curr. Opin. Chem. Biol.*, 1997, **1**, 552.
7 R. J. Tennant-Eyles and A. J. Fairbanks, *Tetrahedron: Asymmetry*, 1999, **10**, 391 and references therein.
8 N. B. Bashir, S. J. Phythian, A. J. Reason and S. M. Roberts, *J. Chem. Soc., Perkin Trans 1*, 1995, 2203.
9 S. Riva, J. Chopineau, A. P. G. Kieboom and A. M. Klibanov, *J. Am. Chem. Soc.*, 1988, **110**, 584; Y.-F. Wang, K. Yakovlevsky, B. Zhang and A. L. Margolin, *J. Org. Chem.*, 1997, **62**, 3488.
10 S. Horvat, J. Horvat, L. Vargadefterdarovic, K. Pavelic, N. N. Chung and P. W. Schiller, *Intl. J. Pept. Prot. Res.*, 1993, **41**, 399.
11 R. D. Egleton, S. A. Mitchell, J. D. Huber, J. Janders, D. Stropova, R. Polt, H. I. Yamamura, V. J. Hruby and T. P. Davis, *Brain Res.*, 2000, **881**, 37.
12 M. Dickman, R. C. Lloyd and J. B. Jones, *Tetrahedron: Asymmetry*, 1998, **9**, 4099; M. Dickman, R. C. Lloyd and J. B. Jones, *Tetrahedron: Asymmetry*, 1998, **9**, 551.
13 M. Lobell and M. P. Schneider, *Synthesis*, 1994, 375.
14 Y.-F. Wang, J. J. Lalonde, M. Momongan, D. E. Bergbreiter and C.-H. Wong, *J. Am. Chem. Soc.*, 1988, **110**, 7200. *N*-Protected vinyl ester amino acids have been used previously as non-enzymatic acyl donors with amines for peptide synthesis: F. Weygand and W. Steglich, *Angew. Chem.*, 1961, **73**, 757. In all cases, **1**–**8c** showed no non-enyzmatic reaction with **9**–**20a**.
15 Regiochemistry of *O*-X-esterification products confirmed by ^{1}H, ^{13}C NMR *e.g.* **18a** ^{1}H NMR (CD_3OD) δ 3.62 (H-6), 3.66 (H-6′); ^{13}C NMR (CD_3OD) δ 62.6 (C-6) → **18b** ^{1}H NMR (CD_3OD) δ 4.23 (H-6), 4.32 (H-6′); ^{13}C NMR (CD_3OD) δ 65.9 (C-6) and/or HMBC, HSQC; OH–H d_6-DMSO COSY; OH acylation.
16 B. G. Davis, *J. Chem. Soc., Perkin Trans. 1*, 2000, 2137.
17 S. J. Chung, S. Takayama and C.-H. Wong, *Bioorg. Med. Chem. Lett.*, 1998, **8**, 3359.
18 At the helpful suggestion of a referee, the question of whether **17c** is a direct or indirect, rearranged acylation product was investigated. Compound **17b**, under standard reaction conditions but in the absence of donor **1c**, did not yield **17c**.
19 K. Khumtaveeporn, G. DeSantis and J. B. Jones, *Tetrahedron: Asymmetry*, 1999, **10**, 2563.
20 CLECs are cross-linked enzyme crystals.
21 M. Miyanaga, M. Ohmori, K. Imamura, T. Sakiyama and K. Nakanishi, *J. Biosci. Bioeng.*, 2000, **90**, 43.
22 K. Matsumoto, B. G. Davis and J. B. Jones, *Chem. Commun.*, 2001, 903.

CHEMCOMM
Communication
www.rsc.org/chemcomm

Molybdenum-catalyzed episulfidation of (*E*)-cycloalkenes with elemental sulfur†‡

Waldemar Adam and Rainer M. Bargon*

Institut für Organische Chemie, Universität Würzburg, Am Hubland, Würzburg, Germany. E-mail: adam@chemie.uni-wuerzburg.de; Fax: +49 931 8884756; Tel: +49 931 8885340

Received (in Cambridge, UK) 18th April 2001, Accepted 13th August 2001
First published as an Advance Article on the web 4th September 2001

Episulfidation of (*E*)-cyclooctene and (*E*)-cyclononene was achieved with elemental sulfur by using a catalytic amount of a molybdenum oxo complex.

Molybdenum peroxo complexes have been utilized for the epoxidation of alkenes;[1] evidently, the analogous thioepoxidation by structurally related disulfur complexes would be of considerable synthetic value. In this context, Khan and Siddiqui claimed the first catalytic episulfidation of cyclohexene with a ruthenium persulfido complex and elemental sulfur as sulfidation source.[2] Instead of elemental sulfur, Kendall and Simpkins[3] described the rhodium-catalyzed sulfur transfer to norbornene (bicyclo[2.2.1]hept-2-ene), in which propylene sulfide was used as a sulfur source. Recently, Chandrasekaran[4] and coworkers used a molybdenum complex to transform alkyl halides into disulfides, the latter are added to Michael acceptors such as α,β-unsaturated enones.

Clearly, literature on sulfur-atom transfer to organic substrates is to date rather scarce. Since the electrophilic character of disulfur complexes has been demonstrated through the desulfuration by various nucleophiles,[5] most effectively by triphenylphosphine,[6] we have explored the feasibility of employing molybdenum disulfur complexes as sulfur-transfer agents for the episulfidation of alkenes. Herein we report the novel *catalytic* episulfidation of (*E*)-cyclooctene and (*E*)-cyclononene by elemental sulfur, mediated by the molybdenum disulfur complex **3**.

Disulfur complex **3** was obtained in three reaction steps from sodium molybdate (Scheme 1). In the first step, the molybdenum dioxo complex **1** is formed in 80% yield from sodium molybdate and sodium diethyl dithiocarbamate in an acidic medium. Deoxygenation by triphenylphosphine resulted in the isolable but air-sensitive molybdenum oxo complex **2** in 80% yield.[7] Complex **2**, when treated with elemental sulfur in refluxing acetone gave the disulfur complex **3** in 87% yield.[8]

When the disulfur complex **3** was allowed to react with two equivalents of (*E*)-cyclooctene [(*E*)-**4a**], the episulfide *trans*-**5a** was quantitatively formed, as detected by ^{1}H-NMR spectroscopy (Scheme 2). Since the oxo complex **2** was isolated in 42% yield, presumably, the molybdenum oxo complex **2** may be employed directly in a catalytic manner for the episulfidation of suitable olefinic substrates by elemental sulfur. Indeed, the catalytic sulfur-atom transfer to strained (*E*)-cycloalkenes **4** worked well in refluxing acetone (Scheme 3).

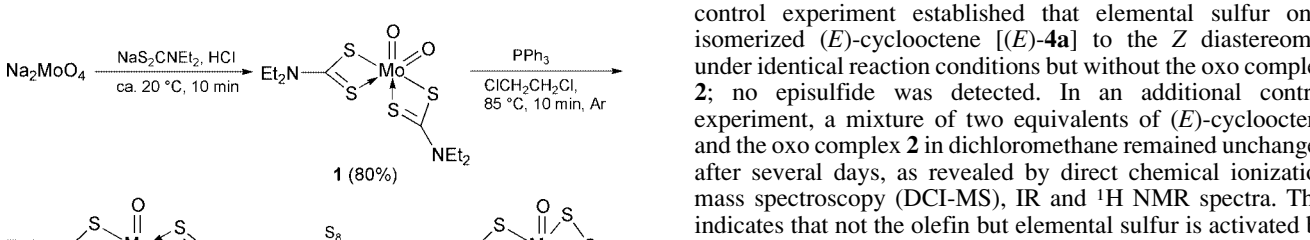

Scheme 1 Preparation of the molybdenum oxo complex **2** and its sulfuration to the disulfur complex **3**.

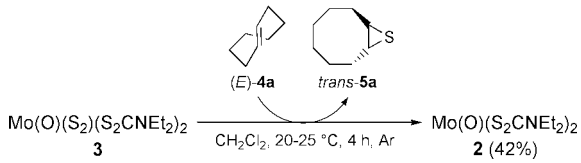

Scheme 2 Stoichiometric episulfidation of (*E*)-cyclooctene [(*E*)-**4a**].

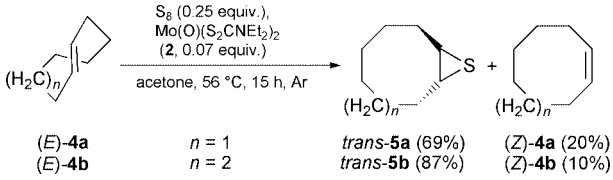

Scheme 3 Catalytic sulfur-transfer reaction with (*E*)-cyclooctene [(*E*)-**4a**] and (*E*)-cyclononene [(*E*)-**4b**].

Thus, with catalytic amounts (0.07 equiv.) of the oxo complex **2**, 69% of the *trans*-cyclooctene episulfide (*trans*-**5a**) and 87% of the *trans*-cyclononene episulfide (*trans*-**5b**) were isolated.§ When 1 mol% of catalyst **2** was used, the yield of episulfide (*trans*-**5a**) decreased to only 15%. Other less strained olefins failed to react under catalytic conditions, but could be episulfidated stoichiometrically by the disulfur complex **3**. Thus, the episulfides of (*Z*)-cyclooctene [(*Z*)-**4a**], norbornene (**4c**), bi(cyclopentadiene) (**4d**), and cyclopentene (**4e**) were isolated in 20, 50, 28 and 16% yields based on complex **3**.§ A control experiment established that elemental sulfur only isomerized (*E*)-cyclooctene [(*E*)-**4a**] to the *Z* diastereomer under identical reaction conditions but without the oxo complex **2**; no episulfide was detected. In an additional control experiment, a mixture of two equivalents of (*E*)-cyclooctene and the oxo complex **2** in dichloromethane remained unchanged after several days, as revealed by direct chemical ionization mass spectroscopy (DCI-MS), IR and ^{1}H NMR spectra. This indicates that not the olefin but elemental sulfur is activated by the molybdenum oxo complex **2**.

In Scheme 4, a mechanism is proposed for this catalytic sulfur-atom transfer, in which first sulfuration of the oxo complex **2** to the disulfur complex **3** takes place, followed by sulfur-atom abstraction from the disulfur bridge to afford the sulfido complex **A** as intermediate. Similar molybdenum monosulfido complexes have recently been isolated and characterized.[9] The subsequent sulfur-atom transfer from the sulfido complex **A** to the cycloalkene regenerates the initial oxo complex **2** and thereby the catalytic activity is sustained. In support of this mechanism for the sulfur abstraction from the

† This work was presented at the XIXth International Symposium on the Organic Chemistry of Sulfur, Sheffield, England, 25th–30th June 2000.
‡ Dedicated to Professor Manfred Christl on the occasion of his 60th birthday.

 DOI: 10.1039/b106433a

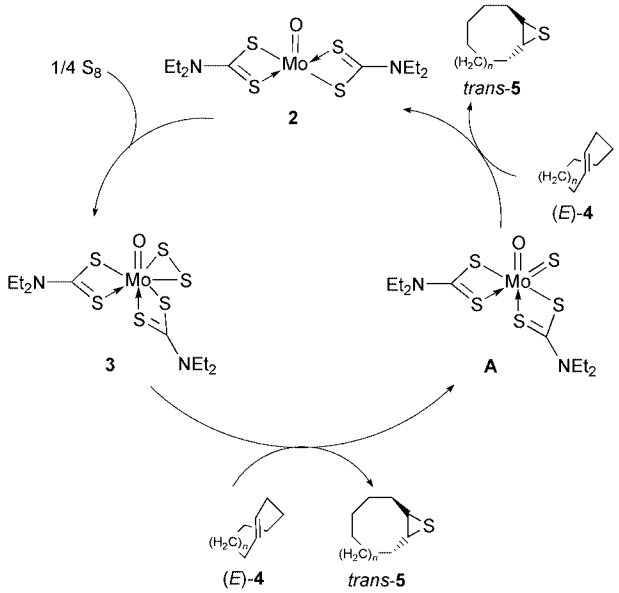

Scheme 4 Catalytic cycle for the generation of the disulfur complex **3** and the sulfuration of (*E*)-cyclooctene [(*E*)-**4a**) and (*E*)-cyclononene [(*E*)-**4b**].

disulfur complex **3** by PPh_3, the intermediary sulfido complex **A** was suggested.[10]

In view of the difficulties with the previous report,[2] presently the first catalytic episulfidation of (*E*)-cycloalkenes with elemental sulfur has been developed, in which the molybdenum oxo complex **2** functions as catalyst and the disulfur complex **3** as sulfur-transfer agent. These encouraging results should stimulate an intense search for more reactive molybdenum disulfur complexes to effect in a general manner the direct episulfidation of olefins with elemental sulfur.

We thank the Deutsche Forschungsgemeinschaft and the Fonds der Chemischen Industrie for generous financial support.

Notes and references

§ *General episulfidation procedure*: in an NMR tube were placed under argon gas 64.2 mg (2.00 mmol) of elemental sulfur and 28.6 mg (70.0 μmol) of molybdenum oxo complex **2** in 0.7 ml of oxygen-free acetone, and 130 μl (1.00 mmol) of (*E*)-cyclooctene [(*E*)-**4**] were added. The tube was sealed with a rubber septum and Parafilm®, then heated for 15 h in an oil bath to 56 °C. After cooling to room temperature, the tube was opened, the suspension transferred to a flask and the solvent evaporated (40 °C/500 mbar). The residue was subjected to silica-gel flash chromatography and 98.0 mg (69%) of *trans*-9-thiabicyclo[6.1.0]nonane (*trans*-**5a**) was isolated, R_f (silica gel, petroleum ether) = 0.33. Bis(diethylcarbamodithioato-*S*,*S*′)oxomolybdenum **2**:[7] ^{1}H NMR (200 MHz, CD_2Cl_2): 1.36 (t, ^3J = 7.18 Hz, 12 H, 4 × CH_3), 3.92 (m, 8 H, 4 × CH_2); ^{13}C NMR (50 MHz, CD_2Cl_2): 221.6 (s, CS_2), 46.2 (t, CH_2), 12.1 (q, CH_3); IR (cm^{-1}, KBr): ν 1518 [s, (CN)], 957 ($Mo^{IV}O$); DCI-MS (isobutane), *m*/*z* (isotopic abundance): 410 (59). *trans*-9-Thiabicyclo[6.1.0]nonane (*trans*-**5a**)[11]: yield 69%; mp 58–59 °C, colorless needles; ^{1}H NMR (200 MHz, $CDCl_3$): 0.95–1.20 (m, 4 H), 1.60 (m, 2 H), 1.85–2.10 (m, 4 H), 2.45 (m, 2 H), 2.68 (m, 2 H, CHS); ^{13}C NMR (50 MHz, $CDCl_3$): 26.3 (t), 29.3 (t), 29.5 (t), 41.2 (d). *trans*-10-Thiabicyclo[7.1.0]decane (*trans*-**5b**): yield 87%; mp 62.5–63 °C, colorless needles; ^{1}H NMR (200 MHz, $CDCl_3$): 0.77–1.06 (m, 2 H), 1.23–1.60 (m, 6 H), 1.62–1.82 (m, 2 H), 1.87–2.07 (m, 2 H), 2.35–2.50 (m, 2 H), 2.64–2.77 (m, 2 H); ^{13}C NMR (50 MHz, $CDCl_3$): 22.6 (t), 25.9 (t), 30.2 (t), 35.9 (t), 44.4 (d); IR (cm^{-1}, KBr): ν 2933 (s), 2849 (s), 1459(s), 1444 (s), 637 (s). Anal. calcd. for $C_9H_{16}S$: C 69.17; H 10.32; S 20.51. Found: C 69.09; H 10.38; S 20.26%. *cis*-9-Thiabicyclo[6.1.0]nonane (*cis*-**5a**)[12]: yield 20%; colorless oil; ^{1}H NMR (200 MHz, $CDCl_3$): 1.20–1.80 (m, 10 H), 2.34 (m, 2 H), 2.93 (m, 2 H); ^{13}C NMR (200 MHz, $CDCl_3$): 26.3 (t), 29.3 (t), 29.5 (t), 41.2 (d). *exo*-3-Thiatricyclo[3.2.1.0^{2,4}]octane (**5c**)[12]: yield 50%; mp 31–32 °C, colorless waxy solid; ^{1}H NMR (200 MHz, $CDCl_3$): 0.65 (d, J = 10.0 Hz, 1 H), 1.24 (m, 2 H), 1.45–1.70 (m, 3 H), 2.45 (s, 2 H), 2.74 (s, 2 H); ^{13}C NMR (50 MHz, $CDCl_3$): 27.5 (3 × t), 37.5 (2 × d), 37.6 (2 × d). *exo*-1a,2a,3,5a,6,6a-Hexahydro-2,6-methano-2*H*-indeno[5,6-*b*]thiirene (**5d**): yield 28%; colorless oil; ^{1}H NMR (200 MHz, $CDCl_3$): 0.81–0.92 (m, 1H), 1.62–1.75 (m, 1 H), 2.19–2.81 (m, 5 H), 2.87–2.93 (d, J = 4.16 Hz, 2 H), 3.22–3.33 (m, 1 H), 5.56–5.72 (m, 2H); ^{13}C NMR (200 MHz, $CDCl_3$): 30.9 (d), 31.0 (t), 34.5 (d), 37.5 (d), 39.6 (d), 41.2 (d), 42.5 (d), 54.3 (d), 130.1 (d), 132.2 (d); EI-HRMS, *m*/*z*: calcd. for $C_{10}H_{12}S$: 164.0662. Found: 164.0662. 6-Thiabicyclo[3.1.0]hexane (**5e**)[12]: yield 16%; colorless oil; ^{1}H NMR (200 MHz, $CDCl_3$): 1.42–2.15 (m, 6 H), 3.30 (m, 2 H); ^{13}C NMR (200 MHz, $CDCl_3$): 18.0 (t), 28.9 (t), 41.7 (d).

1 D. V. Deubel, J. Sundermeyer and G. Frenking, *Org. Lett*., 2001, **3**, 329; S. Ozaki, T. Takahashi and I. Sudo, Japan Patent Kokai 133309, 1974; [*Chem. Abstr*., 1975, **82**, 156973y]
2 M. M. T. Khan and M. R. H. Siddiqui, *Inorg. Chem*., 1991, **30**, 1157. All our efforts to repeat this work failed under the reported catalytic conditions with the poorly reactive cyclohexene and even the highly reactive (*E*)-cyclooctene as sulfur acceptors. Our failure to realize this claim, motivated us to develop an authentic metal-catalyzed episulfidation method with elemental sulfur.
3 J. D. Kendall and N. S. Simpkins, *Synlett*, 1998, 391; A. J. Blake, P. A. Cooke, J. D. Kendall, N. S. Simpkins and S. M. Westaway, *J. Chem. Soc., Perkin Trans. 1*, 2000, 153.
4 K. R. Prabhu, P. S. Sivanand and S. Chandrasekaran, *Angew. Chem., Int. Ed*., 2000, **39**, 4316.
5 K. Leonard, K. Plute, R. C. Haltiwanger and M. Rakowski Dubois, *Inorg. Chem*., 1979, **18**, 3246.
6 S. Xiaoqing, Y. Huixing and H. Degang, *Int. J. Chem. Kinet*., 1989, **21**, 737.
7 C. G. Young, *J. Chem. Educ*., 1995, **72**, 751.
8 J. W. McDonald and W. E. Newton, *Inorg. Chim. Acta*, 1980, **44**, L81.
9 C. G. Young, L. J. Laughlin, S. Colmanet and S. D. B. Scrofani, *Inorg. Chem*., 1996, **35**, 5368; P. D. Smith, D. A. Slizys, G. N. George and C. G. Young, *J. Am. Chem. Soc*., 2000, **122**, 2946.
10 S. Xiaoqing, Y. Huixing and H. Degang, *Int. J. Chem. Kinet*., 1989, **21**, 749.
11 W. Adam, B. Fröhling, K. Peters and S. Weinkötz, *J. Am. Chem. Soc*., 1998, **120**, 8914.
12 M. U. Bombala and S. V. Ley, *J. Chem. Soc., Perkin Trans. 1*, 1979, 3013.

CHEMCOMM Communication
www.rsc.org/chemcomm

The preparation of organically functionalised chromium and nickel nanoparticles

Mark Green†[a] and Paul O'Brien*[b]

[a] *Chemistry Department, Imperial College of Science, Technology and Medicine, South Kensington, London, UK SW7 2AY*
[b] *Chemistry Department, University of Manchester, Oxford Road, Manchester, UK M13 9PL. E-mail: paul.obrien@man.ac.uk*

Received (in Cambridge, UK) 6th August 2001, Accepted 10th August 2001
First published as an Advance Article on the web 4th September 2001

Nanoparticles of chromium or nickel have been prepared by the reduction of either $CrCl_2$ or $Ni(acac)_2$ (acac = pentane-2,4-dionate) at elevated temperatures in various Lewis base solvents; the effect of the Lewis base, which acts as both a reaction solvent and passivating ligand on morphology are apparent; the nanostructures have been analysed by NMR, IR, TEM and XRD.

Nanoparticles of metals have been known since antiquity and colloids of gold have been the subject of systematic study since 1857.[1] To date, noble metals such as gold and platinum have received most attention as they are intrinsically easier to prepare than metals such as nickel and cobalt; mainly because of their resilience to atmospheric degradation.[2–4] A popular, simple route to high quality alkylthiol passivated gold particles has been reported by Brust *et al*.[5] which has been extended to the preparation of iridium and palladium nanoparticles.[6] Heath and coworkers have also made significant advances in the preparation of noble metal colloids.[7] Nanoparticles of metals such as cobalt or nickel have interesting magnetic properties, which have potential as data storage devices and in ferrofluids. Nanoparticles of cobalt have also been prepared from oil-in-water micelles,[8] by the reduction of metal salts coupled with rapid expansion of supercritical fluid solutions.[9] Nickel nanoparticles have been prepared by the sonification of nickel tetracarbonyl.[10]

Sun and Murray have recently reported a route to high quality monodispersed passivated nanoparticulate cobalt.[11] In this work, cobalt nanoparticles were prepared by reduction of cobalt(II) chloride by superhydride in various coordinating solvents based on the tri-*n*-octylphosphine oxide (TOPO) system. Dinega and Bawendi have also prepared TOPO capped cobalt nanocrystals by thermolysis of dicobalt octacarbonyl.[12] In both cases, a new phase of cobalt was obtained, assigned ε-cobalt (space group $P4_132$), a phase similar to cubic β-manganese. This product could be used as a precursor to the more usual hexagonal close packed cobalt. Whilst single domain particles of nickel and cobalt are known to exhibit ferrimagnetism, chromium is antiferromagnetic and is not expected to have any magnetic applications. However, chromium nanostructures have been investigated.[13] The oxidation of cobalt nanoparticles to cobalt oxide once the protective ligand is removed has previously been reported,[11] and it is hoped that the controlled oxidation of chromium nanoparticles may result in the magnetic phase CrO_2, rather than the usual Cr_2O_3.

Here we report a simple preparation of alkylphosphine/alkylphosphine oxide passivated chromium and nickel nanoparticles. $Ni(acac)_2$ or $CrCl_2$ was reduced with either $LiBH_4$ or $NaBH_4$ in various Lewis base solvent systems in attempts to produce nanoparticles. Lewis bases such as tri-*n*-octylphosphine oxide (TOPO), tri-*n*-octylphosphine (TOP), tri-*n*-butylphosphine (TBP) and tri-*n*-butylphosphine oxide (TBPO) were utilised as both the reaction solvents and passivating ligands. The TOPO used in the experiments was technical grade (Aldrich, 90%), purified as described in the literature.[14] The TBPO was used as received (Aldrich, 95%), as was TOP (Aldrich, 90%) and TBP (Aldrich, 97%).

In a typical reaction, 20 g of trialkylphosphine oxide is heated to *ca*. 100 °C and degassed whilst periodically being flushed with nitrogen. The reducing agent MBH_4 (M = Na, Li) is placed in the reaction flask with the phosphine oxide, mixed, the temperature raised to between 150 and 250 °C and stabilised. (Reaction between the reducing agent and the phosphine oxide may occur. However this has not been investigated and does not appear to hinder the reduction of the metal precursors.) In a separate flask, *ca*. 0.5 g of precursor (either $CrCl_2$ or $Ni(acac)_2$) is dissolved in 5 ml of trialkylphosphine. Rapid injection of the metal precursor solution into the reaction flask results in an immediate dark colouration, consistent with reduction of the precursor. Growth is stabilised at between 150 and 250 °C for 30 min and the flask is removed from the heat and allowed to cool to *ca*. 60 °C. The nanoparticles were either dissolved straight into a solvent (toluene or pyridine) or isolated as a powder by addition of a non-solvent (methanol or light petroleum). The preferred solvent is pyridine, as this polar Lewis base solvent appears to increase the stability of the suspension.

The identity of the materials as the metals was confirmed by XRD. Both chromium and nickel nanoparticles gave reflections consistent with the cubic forms of the metals. The strongest peak in the PXRD of nanosized nickel was at 2θ *ca*. 44°, corresponding to the strongest 111 reflection of bulk nickel.[15] A weaker peak at *ca*. 51° is consistent with the 200 reflection, the second strongest reflection in bulk cubic nickel. The chromium sample gave a set of broad, weak reflections between 2θ = 40 and 50° the region of the 200, 210, 211 reflections of the metal, and another broad reflection between 55 and 70° (220, 310). These reflections are in the regions associated with the strongest reflections for bulk cubic chromium.[16]

Electron microscopy of the metal nanoparticles showed a distinct relationship between morphology and the capping agents. Preparation of chromium nanoparticles in TOPO produced highly monodispersed spherical quantum dots of *ca*. 5 nm in size (Fig. 1). Preparation of nanoparticulate nickel in TBPO showed a mixture of small (2–5 nm) particles and long nanowires up to 20 nm in length. Impurities in the mixed ligand system (TBPO/TBP) are believed to be responsible for the formation of the elongated structures (Fig. 2). The control of metal quantum dot shape and size by the capping ligand has been previously demonstrated with gold nanoparticles.[17] Alivisatos and coworkers have investigated the preparation of elongated semiconductor nanoparticles and rods by synthesis using controlled amounts of 'impurities'.[18,19]

The electronic spectra of metal colloids are well documented, especially for gold.[20] The electronic spectra of nickel and chromium colloids prepared as described above showed unusual features. Colloidal chromium displayed no absorption

† Present address: Oxonica Ltd., Begbroke Science and Business Park, Sandy Lane, Yarnton, Oxford, UK OX5 1PF.

 DOI: 10.1039/b107108b

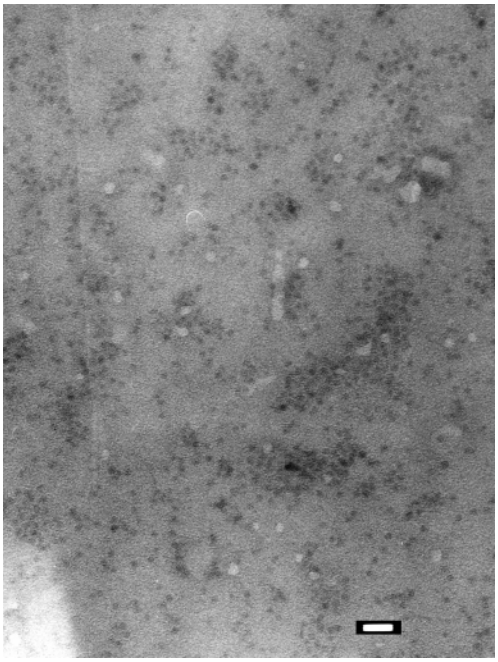

Fig. 1 TEM image of TOPO/TOP capped Cr nanoparticles, bar = 20 nm.

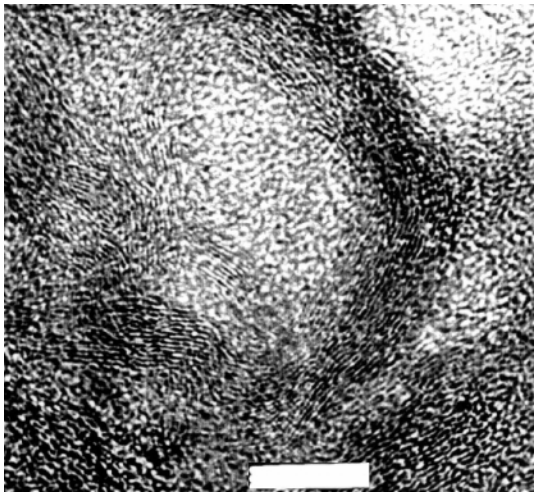

Fig. 2 HRTEM image of TBPO/TBP capped Ni nanowires, bar = 10 nm.

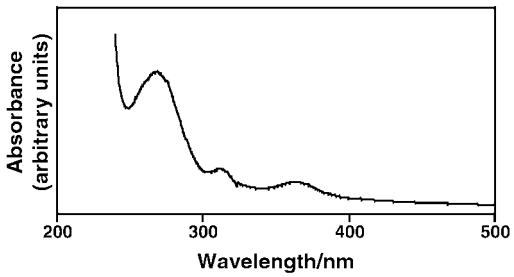

Fig. 3 Electronic spectrum of nickel nanoparticles capped with TBPO/TBP.

bands when prepared, whilst nickel displayed three peaks (Fig. 3). Altering the preparation of chromium nanoparticles by including an amine into the reaction mixture resulted in nanoparticles that displayed two plasmon resonance peaks. The origin of such effects is still under investigation. The effects of a nanoparticle's aspect ratio on optical properties, notably the surface plasmon resonance, has been investigated by El-Sayed and coworkers.[21] The presence of multiple plasmon resonances in metals has also been observed by Lutz *et al*.[22]

Solution ^{1}H and ^{31}P NMR reveals that the ligands are bound to the nanoparticle surface. The broadening of the proton spectra for all samples indicates the inhomogeneous magnetic environment due to restricted molecular motion. The phosphorus spectra reveal a shift in the resonances, consistent with surface shielding effects. TOPO capped chromium nanoparticles show a single resonance at *ca*. 45 ppm, shifted from the unattached ligand resonance at *ca*. 50 ppm.

TBPO capped nickel nanoparticles displayed a distinct resonance at *ca*. 45 ppm, shifted from the free ligand resonance at 59 ppm. Other resonances observed at −18 and −31 ppm were attributed to TBP. Unattached TBP displays resonances at −19 and −32 ppm, as well as minor features at 42, 29, −38 and −70 ppm. These may well be from impurities that encourage nanowire formation in TBPO/TBP capped Q-Ni. FTIR spectroscopy of the TOPO capped chromium particles did not show a shift in the ν(P=O) stretch at 1145 cm^{-1}, but did show a broadening in this feature, which has also been observed with TOPO capped semiconductors. TBPO capped nickel displayed the ν(P=O) stretch at 1128 cm^{-1}, shifted from the free ligand at *ca*. 1152 cm^{-1}.

In conclusion we have demonstrated a simple solution based route to passivated nanoparticulate nickel and chromium. Further work is ongoing to identify the magnetic properties of such materials.

We acknowledge Diana Zhi (Centre for Electronic Materials, Imperial College) and Keith Pell (QMW college) for electron microscopy, Richard Shepard (IC) for NMR and Richard Sweeny (IC) for XRD. P. O'B. is Sumitotmo/STS visiting Professor of Material Chemistry at ICSTM.

Notes and references

1 M. Faraday, *Philos. Trans. R. Soc. London*, 1857, **147**, 145.
2 A. Henglein and M. Giersig, *J. Phys. Chem. B*, 1999, **103**, 9533.
3 B. V. Enustun and J. Turkevich, *J. Am. Chem. Soc*., 1963, **85**, 3317.
4 J. Turkevich and G. Kim, *Science*, 1970, **169**, 873.
5 M. Brust, M. Walker, D. Bethell, D. J. Schiffrin and R. Whyman, *J. Chem. Soc., Chem. Commun*., 1994, 801.
6 C. K. Yee, R. Jordan, A. Ulman, H. White, A. King, M. Rafailovich and J. Sokolov, *Langmuir*, 1999, **15**, 3486.
7 D. V. Leff, L. Brandt and J. R. Heath, *Langmuir*, 1996, **12**, 4723.
8 N. Moumen and M. P. Pileni, *Chem. Mater*., 1996, **8**, 1128.
9 Y. P. Sun, H. W. Rollins and R. Guduru, *Chem. Mater*., 1999, **11**, 7.
10 S. Ramesh, Y. Koltypin, R. Prozorov and A. Gedanken, *Chem. Mater*., 1997, **9**, 546.
11 S. Sun and C. B. Murray, *J. Appl. Phys*., 1999, **85**, 4325.
12 D. P. Dinega and M. G. Bawendi, *Angew. Chem., Int. Ed*., 1999, **38**, 1788.
13 M. R. Fitzsimmons, J. A. Eastman, R. A. Robinson and J. W. Lynn, *Nanostruct. Mater*., 1996, **7**, 179.
14 G. W. Mason, S. McCarthy and D. F. Peppard, *J. Inorg. Nucl. Chem*., 1960, **12**, 315.
15 X-ray diffraction file 4-0850.
16 X-ray diffraction file 19-323.
17 M. Green and P. O'Brien, *Chem. Commun*., 2000, 183.
18 L. Manna, E. C. Scher and A. P. Alivisatos, *J. Am. Chem. Soc*., 2000, **122**, 12700.
19 X. G. Peng, L. Manna, W. D. Yang, J. Wickham, E. Scher, A. Kadavanich and A. P. Alivisatos, *Nature*, 2000, **404**, 59.
20 M. M. Alvarez, J. T. Khoury, T. G. Schaaff, M. N. Shafigullin, I. Vezmar and R. L. Whetten, *J. Phys. Chem. B*, 1997, **101**, 3706.
21 S. Link, M. B. Mohamed and M. A. El-Sayed, *J. Phys. Chem. B*, 1999, **103**, 3073.
22 T. Lutz, C. Estournes, J. C. Merle and J. L. Guille, *J. Alloys Compd*., 1997, **262**, 438.

CHEMCOMM Communication
www.rsc.org/chemcomm

Synthesis and photophysical properties of [3.3](3,9)carbazolophanes

Keita Tani,*[a] Yasuo Tohda,[a] Hiroyuki Takemura,[b] Hideo Ohkita,[c] Shinzaburo Ito[c] and Masahide Yamamoto[c]

[a] *Division of Natural Science, Osaka Kyoiku University, Asahigaoka, Kashiwara, Osaka 582-8582, Japan. E-mail: ktani@cc.osaka-kyoiku.ac.jp*
[b] *Department of Chemistry, Faculty of Science, Kyushu University, Ropponmatsu 4-2-1, Chuo-ku, Fukuoka 810-8560, Japan*
[c] *Department of Polymer Chemistry, Graduate School of Engineering, Kyoto University, Sakyo-ku, Kyoto 606-8501, Japan*

Received (in Cambridge, UK) 9th May 2001, Accepted 15th August 2001
First published as an Advance Article on the web 4th September 2001

syn- And _anti_-[3.3](3,9)carbazolophanes, which are suitable model compounds for sandwich and partial-overlap excimers, respectively, have been synthesized and characterized; the structures of both singlet and triplet carbazole excimer have been described.

Poly(*N*-vinylcarbazole) (PVCz) has been the subject of intense investigation because of its photoconductive and photophysical properties.[1] In particular, two kinds of excimer, sandwich and partial-overlap excimers, formed in PVCz are of high interest.[2] The excimer formation in PVCz solutions has been extensively studied using bichromophoric compounds such as 2,4-dicarbazol-9-ylpentane.[3] These excimer emissions are also observed even in PVCz solids where conformational change of carbazole (Cz) chromophores is highly restricted. In PVCz solids, electronic excitation energy of Cz monomer migrates efficiently into an excimer-forming site where conformation of two Cz chromophores are sufficiently similar to that of the excimers. Cyclophanes are some of the most attractive molecules for investigating the electronic interactions of face-to-face arranged aromatic molecules in solids as well as in solutions.[4] Here we report the synthesis and photophysical properties of *syn*- and *anti*-[3.3](3,9)carbazolophane derivatives used as model compounds of excimer-forming sites in PVCz films.

Treatment of 1,3-dicarbazol-9-ylpropane with phosphorous oxychloride and DMF gave **1**, which was reduced with sodium borohydride to afford **2** (Scheme 1). Bromination of **2** with excess conc. HBr afforded unstable dibromide **3**. The intramolecular cyclization of **3** with NH_2CN was carried out according to the method developed by one of us (H.T.)[5] to afford *syn*-isomer **4** and *anti*-isomer **5** in 3.3% and 28% yield, respectively.†

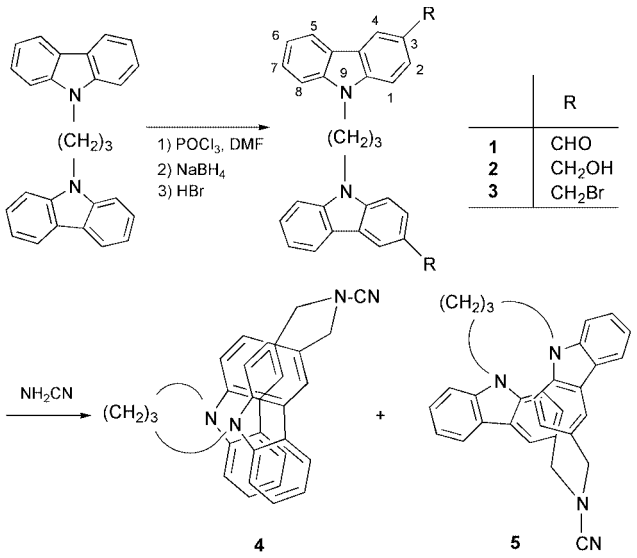

Scheme 1 Synthesis of [3.3](3,9)carbazolophanes, **4** and **5**.

The structures of carbazolophanes **4** and **5** were clearly determined by X-ray analyses.‡ Fig. 1 shows that two carbazole rings in **4** completely overlap each other. Their least-squares planes are inclined only 8.7° and the intramolecular distance between carbazole nitrogen atoms in **4** is 3.24 Å. Fig. 2 shows the X-ray analysis of **5**, which clearly indicates the overlap of only a 3-position-bridged benzene ring in the mutual Cz chromophores, just like the proposed partial overlap singlet excimer in the *tt* conformation of the syndiotactic sequence in PVCz,[2] and their least-squares planes are inclined only 6.2°. Thus, it is concluded that **4** and **5** having [3.3] linkages are suitable model compounds for investigating both sandwich and partial-overlap interactions in excimer-forming site in PVCz films, respectively.

(A) in Fig. 3 shows absorption spectra of *N*-ethylcarbazole **6**, **4**, and **5** in THF. The absorption shapes of both **4** and **5** were different from that of **6**, *i.e.*, broadening and red-shift were observed. These features were ascribed to the exciton band splitting as is commonly applied to interpret absorption spectra of cyclophanes.

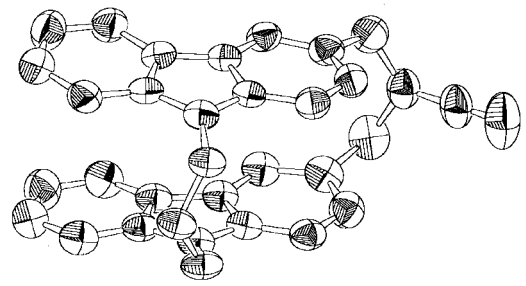

Fig. 1 Crystal structure (ORTEP representation) of **4**.

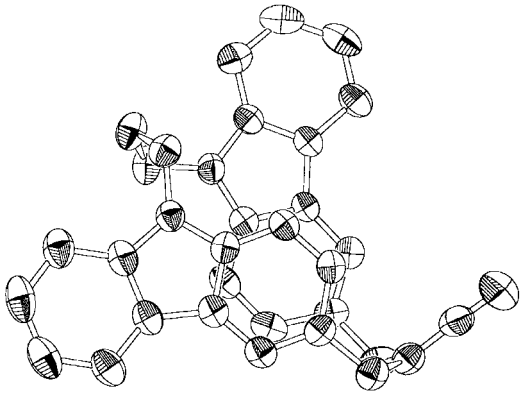

Fig. 2 Crystal structure (ORTEP representation) of **5**.

 DOI: 10.1039/b104101k

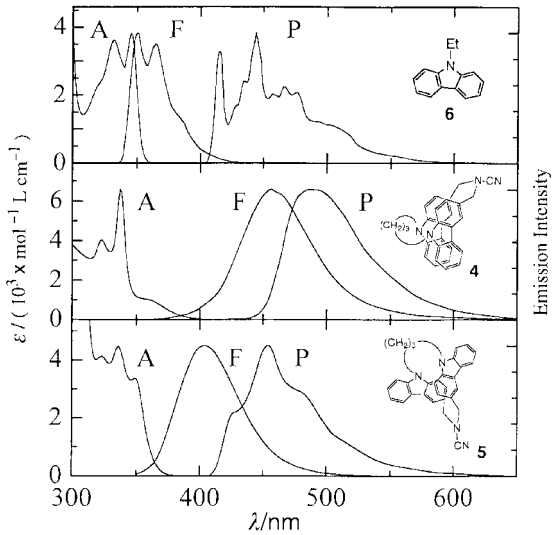

Fig. 3 Absorption (A), fluorescence (F) (λ_{ex} = 340 nm), phosphorescence (P) (λ_{ex} = 340 nm) spectra of **6**, **4**, and **5**: (A) were measured in a THF solution at room temperature; (F) in a MTHF solution at room temperature; (P) in a MTHF rigid matrix at 77 K. Emission spectra of **4** and **5** are normalized at the maximum of each spectrum peak. All samples used for fluorescence and phosphorescence measurements were degassed by the freeze–pump–thaw method. The concentrations of **4**, **5**, and **6** were *ca.* 2.0 $\times$ 10^{-5} M.

The fluorescence spectra of **4**, **5**, and **6** were measured in 2-methyltetrahydrofuran (MTHF) at room temperature indicated by (F) in Fig. 3. Both **4** and **5** exhibit broad structureless emission and large Stokes shifts (7650 cm^{-1} for **4**, 3960 cm^{-1} for **5**). These broad emissions were not due to any impurity, because the excitation spectra for the broad emission of **4** and **5** were almost the same as the absorption spectra. Therefore, two kinds of fluorescence observed from **4** (λ_{max} 457 nm) and **5** (405 nm) correspond to the emissions from the sandwich and partial-overlap excimer-forming sites in PVCz films respectively,[2] although there are slight red-shifts in the peak wavelength. The difference demonstrates that two Cz chromophores in **4** and **5** are located in a suitable geometry for the sandwich and partial-overlap excimer-forming sites in PVCz films.

The phosphorescence spectra of **4**, **5**, and **6** were measured in a MTHF rigid matrix at 77 K indicated by (P) in Fig. 3. The phosphorescence spectrum of **6** consists of a structured monomer phosphorescence with the peaks 414 and 444 nm. On the other hand, **4** exhibits a broad structureless band centered at 487 nm, which roughly agrees with that of PVCz films.[6] The phosphorescence spectrum of **5** consists of a structured band with a maximum at 454 nm, though considerable broadening and red-shift were observed. The excitation spectra for phosphorescence of **4** and **5** were almost the same as the corresponding absorption spectra. In polymeric systems, it is difficult to distinguish between triplet excimer and any impurity emission, because high concentration of the chromophores enhances photosensitization.[7] However, in our system, each carbazolophane is isolated and such sensitized phosphorescence is negligible. Therefore we ascribed the spectral change observed in the phosphorescence spectra to intramolecular electronic interaction in the excited triplet state of carbazolophanes. The structured vibrational band of **5** indicates that triplet interaction in **5** is weak. The broad emission of **4** shows that the sandwich geometry of two Cz chromophores in close proximity can surely interact in the triplet state and form a triplet excimer.

In summary, we are confident that carbazolophanes **4** and **5** will disclose interesting sandwich and partial-overlap interactions in excimer-forming sites in PVCz films. They showed definite dependence of the emission spectra upon the geometry of Cz chromophores. The most striking point of this work is that one of the geometry of triplet excimer in PVCz films is revealed for the first time.

Notes and references

† *Selected data*: for **4**: faint yellow prisms (benzene–hexane). Mp 270–271 °C. Anal. Calc. for $C_{30}H_{24}N_4$: C, 81.79; H, 5.49; N, 12.72. Found C, 82.18; H, 5.41; N, 12.66%. Crystal employed for X-ray analysis of **4** contains ½ benzene. Anal. Calc. for $C_{33}H_{27}N_4$: C, 82.64; H, 5.67; N, 11.68. Found C, 82.85; H, 5.59; N, 11.53%. For **5**: colorless columns (benzene–hexane). Mp 242–243 °C. Anal. Calc. for $C_{30}H_{24}N_4$: C, 81.79; H, 5.49; N, 12.72. Found C, 81.82; H, 5.34; N, 12.60%.

‡ *Crystal data for* **4**: $C_{30}H_{24}N_4$ + ½ C_6H_6, M = 479.6, faint yellow prism (0.20 $\times$ 0.20 $\times$ 0.40 mm, monoclinic, $P2_1/c$, a = 14.035(5), b = 11.706(4), c = 15.041(4) Å, β = 92.14(3)°, V = 2469(1) Å^3, Z = 4, D_c = 1.290 g cm^{-3}, μ = 0.77 mm^{-1}. Of 5906 reflections collected, 5680 were unique and 1675 were observed ($I > 3.00\sigma(I)$). Final R = 0.037, wR = 0.026. CCDC 151872. See http://www.rsc.org/suppdata/cc/b1/b104101k/ for crystallographic data in .cif or other format. For **5**: $C_{30}H_{24}N_4$, M = 440.5, colorless column (0.20 $\times$ 0.18 $\times$ 0.40 mm, monoclinic, $P2_1/a$, a = 7.888(8) , b = 19.486(10) , c = 14.567(7) Å, β = 91.09(6)°, V = 2238(2) Å^3, Z = 4, D_c = 1.307 g cm^{-3}, μ = 0.78 mm^{-1}. Of 5516 reflections collected, 5145 were unique and 2325 were observed ($I > 3.00\sigma(I)$). Final R = 0.040, wR = 0.031. CCDC 151873. See http://www.rsc.org/suppdata/cc/b1/b104101k/ for crystallographic data in .cif or other format.

1 J. M. Pearson and M. Stolka, *Poly(N-vinylcarbazole)*, Gordon and Breach Sci. Pub., New York, 1981, pp. 68–107

2 W. Klöpffer, *J. Chem. Phys.*, 1969, **50**, 2337; W. Klöpffer, *Ann. N. Y. Acad. Sci.*, 1981, **366**, 373; G. E. Johnson, *J. Chem. Phys.*, 1975, **62**, 4697; A. Itaya, K. Okamoto and S. Kusabayashi, *Bull. Chem. Soc. Jpn.*, 1976, **49**, 2082; H. Sakai, A. Itaya, H. Masuhara, K. Sasaki and S. Kawata, *Polymer*, 1996, **37**, 31; and references cited therein.

3 J. Vandendriessche, P. Palmans, S. Toppet, N. Boens, F. C. De Schryver and H. Masuhara, *J. Am. Chem. Soc.*, 1984, **106**, 8057; H. Masuhara, N. Tamai, N. Mataga, F. C. De Schryver and J. Vandendriessche, *J. Am. Chem. Soc.*, 1983, **105**, 7256; F. C. De Schryver, J. Vandendriessche, S. Toppet, K. Demeyer and N. Boens, *Macromolecules*, 1982, **15**, 406.

4 K. Tani, Y. Tohda, K. Hisada and M. Yamamoto, *Chem. Lett.*, 1996, 145; Y. Nakamura, M. Kaneko, N. Yamanaka, K. Tani and J. Nishimura, *Tetrahedron Lett.*, 1999, **40**, 4693.

5 G. Wen, M. Matsunaga, T. Matsunaga, H. Takemura and T. Shinmyozu, *Synlett*, 1995, 947.

6 G. Rippen, G. Kaufmann and W. Klöpffer, *Chem. Phys.*, 1980, **52**, 165.

7 As a review, W. Klöpffer, *EPA Newsl.*, 1987, **29**, 15.

CHEMCOMM Communication
www.rsc.org/chemcomm

A *green* Hunsdiecker reaction: synthesis of β-bromostyrenes from the reaction of α,β-unsaturated aromatic carboxylic acids with KBr and H_2O_2 catalysed by $Na_2MoO_4{\cdot}2H_2O$ in aqueous medium

Joy Sinha,[a] Suman Layek,[a] Gagan C. Mandal[b] and Manish Bhattacharjee*[a]

[a] *Department of Chemistry, Indian Institute of Technology, Kharagpur 721 302, India. E-mail: mxb@chem.iitkgp.ernet.in; b_manish@hotmail.com; Fax: +91-3222-82252*
[b] *Department of Chemistry, Kharagpur College, Kharagpur 721 305, India*

Received (in Cambridge, UK) 22nd May 2001, Accepted 16th August 2001
First published as an Advance Article on the web 13th September 2001

Reaction of α,β-unsaturated aromatic carboxylic acids with KBr and H_2O_2 in the presence of $Na_2MoO_4{\cdot}2H_2O$ in aqueous medium affords β-bromo alkenes in high yield.

The classical Hunsdiecker reaction and its later modifications are efficient for the synthesis of organic halides.[1] However, these reactions have major limitations, such as toxicity and hazard involving use of elemental bromine, salts of Hg(II), Tl(I), Pb(IV), Ag(I). Apart from this, very poor yields of the products are obtained in the cases of α,β-unsaturated aromatic carboxylic acids. Recently, some of these difficulties have been overcome by the use of lithium acetate as the catalyst and *N*-bromosuccinimide as the bromine source, the reaction medium being aqueous acetonitrile.[2] However, low yields were obtained in the cases of α,β-unsaturated aromatic carboxylic acids bearing electron-withdrawing groups in the aromatic ring.

Transition metal peroxo compounds have been shown to be efficient oxidising agents for various organic substrates.[3–6] Some marine organisms use a vanadium dependant enzyme, bromoperoxidase, for the bromination of organic compounds using inorganic bromides and hydrogen peroxide.[6] We have been investigating bromination of organic compounds using vanadium(V) or molybdenum(VI), potassium bromide, and hydrogen peroxide in aqueous medium.[7–9] It was observed that the transition metal peroxo complexes can oxidise inorganic bromide and produce Br_3^- species which is in equilibrium with HOBr and Br_2.

We thought that this biomimetic system could be utilised as an alternative route to the Hunsdiecker reaction. Herein we report the initial results of our studies on the reaction of α,β-unsaturated aromatic carboxylic acids with KBr and H_2O_2 in aqueous medium in the presence of $Na_2MoO_4{\cdot}2H_2O$.

When a suspension of α,β-unsaturated aromatic carboxylic acid (0.02 mol) is stirred with KBr (0.04 mol) and $Na_2MoO_4{\cdot}2H_2O$ (0.001 mol) in water (5 cm^3) and H_2O_2 (15 cm^3, 0.13 mol) is added drop-wise at room temperature (30 °C), a rapid reaction takes place and the temperature rises to 80 °C within 20 min. The reaction mixture was stirred for further 20 min and the product as well as the unreacted acid was extracted with diethyl ether. The corresponding β-bromostyrene was separated from the starting material by column chromatography in good yield (Scheme 1). The yield of the styrene is very good in the cases of α,β-unsaturated aromatic carboxylic acid bearing a substitutent in the 4-position. For example, 3-(4-methoxyphenyl)prop-2-enoic acid and 3-(4-chlorophenyl)prop-2-enoic acid yield the corresponding β-bromo alkenes in 85 and 65% yield respectively. It may be noted that for 3-(4-chlorophenyl)prop-2-enoic acid a larger amount of Na_2MoO_4 (acid–Mo, 10 : 1) is required for better yield. The unsubstituted acid also affords β-bromostyrene in good yield (65%). In the case of an acid bearing substituents in 2-positions, for example, 3-(2-chlorophenyl)prop-2-enoic acid and 3-(2-methylphenyl)-prop-2-enoic acid, the yield of the corresponding β-bromostyrene is very poor (5 and 15%, respectively). The evolution of CO_2 was detected by passing the outcoming gas through limewater. It may be noted that this is the first report of isolation of Hunsdiecker products in water. All the earlier reports deal with the reactions in non-aqueous medium.

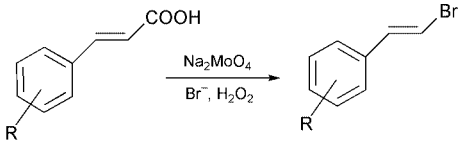

R = H or 4-OMe or 4-Cl or 2-Me or 2-Cl

Scheme 1

The solution of Na_2MoO_4 (0.001 mol) and KBr in H_2O (5 cm^3) is basic in nature (pH 10). Upon addition of solid acid, the pH of the slurry changes to 4.5. When H_2O_2 (15 cm^3) is added to the reaction mixture, the measured pH is 3.9. The pH of the reaction changes to 9 upon completion of the reaction. It has been shown by Rothenberg and Clark that a proton source is required for oxyhalogenation.[10] Thus in these reactions the proton source is the acid itself.

It has been shown earlier that, MoO_4^{2-} forms a number of peroxo species in solution in the presence of H_2O_2. The ^{95}Mo NMR spectra of a solution of Na_2MoO_4 (0.001 M) in H_2O_2 (15 cm^3) shows a major signal at −336 ppm and a relatively low intensity signal at −509 ppm. These are due to the formation of $[MoO(O_2)_3]^{2-}$ and $[Mo(O_2)_4]^{2-}$ species, respectively.[11] Upon addition of Br^- both the signals at −509 and −336 ppm disappear and two signals at −222 and −37 ppm appear. The signal at −222 ppm can be assigned to $[MoO(O_2)_2]^{2-}$.[11] The signal at −37 ppm may be assigned to a molybdate species coordinated to bromide. The slight shift in the observed ^{95}Mo NMR spectra from those of reported ones[11] may be due to the effect of pH as well as extent of hydration.

A blank reaction, which is a similar reaction without the addition of Na_2MoO_4, did not afford the brominated products. Thus, it is clear that bromide is oxidised by the peroxomolybdate species formed in solution.

The electronic spectrum of a solution (10^{-3} M) of Na_2MoO_4 in H_2O_2 (2×10^{-2} M) shows bands at 445 (ε = 162) and at 293 nm (ε = 1620 mol^{-1} dm^3 cm^{-1}). These are due to the tetraperoxo and triperoxomolybdate species.[11] When KBr is added to this solution an absorbance increase is observed in the region 700 to 290 nm. However, no new band appears. The molar extinction coefficient of the 445 nm band increases to 320 and the band at 293 nm shifts to 298 nm with increase in the molar extinction coefficient (ε = 1833). It may be noted that the oxidised bromide species, Br_2, Br_3^- and OBr^- absorb in the region, 450 to 300 nm. Meister and Butler[12] and our earlier work on the oxidation of Br^- by H_2O_2 in the presence of Mo(VI)[9] have shown that Mo(VI) first forms peroxomolybdate which then oxidises Br^- to form an equilibrium mixture of Br_2, Br_3^- and OBr^-. Thus it clear form the earlier work as well as from the present evidence that the peroxomolybdates generated

 DOI: 10.1039/b104540g

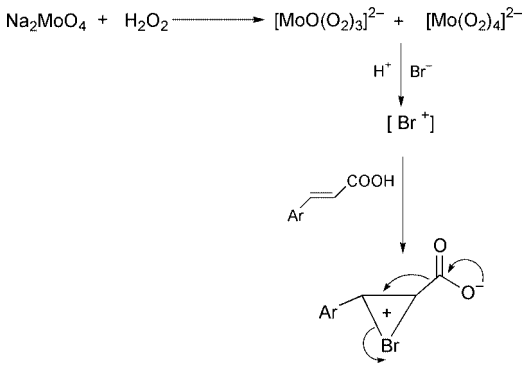

Scheme 2

from the reaction of H_2O_2 and MoO_4^{2-} react with Br^- to produce the equivalent of the Br^+ species, which then react with the unsaturated acid to give bromo alkene.

In order to identify the brominating species, reactions of Br_2 in aqueous KOH (HOBr–OBr^-) (pH = 10) as well as Br_2 in aqueous KBr (Br_3^-) with the acid in aqueous medium were carried out. But in both the cases we could only isolate the starting material. Thus, it is clear that the Mo center plays an important role, and probably the coordination of the acid is required for the conversion as observed in the case of vanadium bromoperoxidase.[13]

From the above spectral evidence, it may be inferred that, the reaction proceeds through an ionic mechanism (Scheme 2). It may be noted that a similar mechanism has been suggested by Roy *et al*. earlier.[2] The reason behind the low yield of the products in the cases of *ortho* substituted aromatic acids may be due to steric crowding of the intermediate bromonium species. The reactions described here show that the Hunsdiecker reaction can be brought about in aqueous medium, contrary to earlier reports, and also this is the greenest route to Hunsdiecker products.

The authors would like to thank Dr Sujit Roy, Department of Chemistry, Indian Institute of Technology, Kharagpur, India for helpful discussions and suggestions.

Notes and references

1 R. G. Johnson and K. R. Ingham, *Chem. Rev*., 1956, **56**, 219.
2 D. Naskar, S. Chowdhury and S. Roy, *Tetrahedron Lett*., 1998, **39**, 699.
3 H. Mimoun, M. Mignard, P. Brechot and L. Saussine, *J. Am. Chem. Soc*., 1986, **108**, 3711.
4 H. Mimoun, L. Saussine, E. Daire, M. Postal, J. Fischer and R. Weiss, *J. Am. Chem. Soc*., 1983, **105**, 3101.
5 M. Bhattacharjee, S. K. Chettri, M. K. Chaudhuri, N. S. Islam and S. Roy Barman, *J. Mol. Catal*., 1993, **78**, 143.
6 J. Rudolph, K. L. Reddy, J. P. Chiang and K. B. Sharpless, *J. Am. Chem. Soc*., 1997, **119**, 6189.
7 M. Bhattacharjee, *Polyhedron*, 1992, **11**, 2817.
8 M. Bhattacharjee, S. Ganguly and J. Mukherjee, *J. Chem. Res., (S)*., 1995, 80.
9 M. Bhattacharjee and J. Mukherjee, *J. Chem. Res., (S)*, 1995, 238.
10 G. Rothenberg and J. H. Clark, *Green Chem*., 2000, **2**, 248.
11 V. Nardello, J. Marko, G. Vermeersch and J. M. Aubry, *Inorg. Chem*., 1995, **34**, 4950.
12 G. E. Meister and A. Butler, *Inorg. Chem*., 1994, **33**, 3269.
13 R. A. Tschirret-Guth and A. Butler, *J. Am. Chem. Soc*., 1994, **116**, 411.

CHEMCOMM Communication
www.rsc.org/chemcomm

Site-selectivity in a heterotetranuclear macrocyclic complex

Sarah Cromie,[a] Frédéric Launay[b] and Vickie McKee*[a]

[a] *Chemistry Department, Loughborough University, Loughborough, UK LE11 3TU. E-mail: v.mckee@lboro.ac.uk*
[b] *Chemistry Department, Queen's University, Belfast, UK BT9 5AG*

Received (in Cambridge, UK) 17th July 2001, Accepted 17th August 2001
First published as an Advance Article on the web 13th September 2001

Site-selectivity in a heterotetranuclear macrocyclic complex is controlled by the geometry of the dinuclear intermediate.

Arrays of different interacting metal ions in controlled geometric relationships offer potential access to new reaction chemistry of exogenous ligands on such a bimetallic 'surface' and insights into heteronuclear metal–metal interactions. Synthesis of such complexes requires some mechanism for site-selectivity. Heterodinuclear complexes of phenol-based Robson[1] macrocycles are among the most studied examples[2] and the essential synthetic step is formation of a precursor containing only one type of metal ion. Most commonly, this is achieved by designing ligands with different binding sites and hence different preferences for particular metals. The metal ions are then incorporated sequentially (sometimes the first metal is selectively eliminated from one or more sites before adding the second metal[3]). Similar requirements apply to larger, tri- or tetra-nuclear systems.[4,5] Here we report the structure of a complex incorporating a heterotetranuclear macrocyclic unit in which the macrocyclic binding sites are identical. The geometric arrangement of the metal ions in the tetranuclear product is controlled by the structure of the dinuclear intermediate.

The dicopper(II) species $[Cu_2(H_3L)(OH)]^{2+}$ can be prepared directly in a metal-deficient template reaction. Reaction of

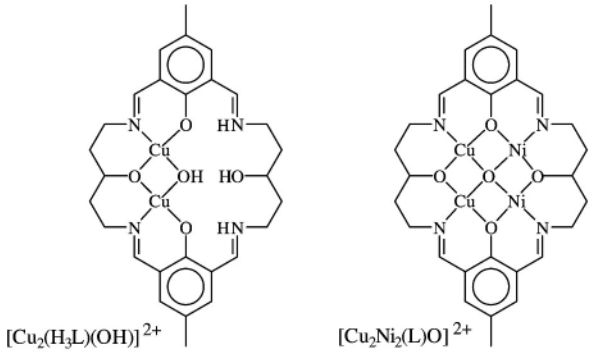

$[Cu_2(H_3L)(OH)]^{2+}$ $[Cu_2Ni_2(L)O]^{2+}$

equimolar amounts of 2,6-diformyl-4-methylphenol (Hdfmp), 1,5-diamino-3-hydroxypentane and $Cu(X)_2{\cdot}6H_2O$ (X = NO_3 or BF_4) in methanol–water (2:1) yields complexes of formula $[Cu_2(H_3L)(OH)]X_2$, each showing characteristic FAB MS spectra (in NOBA), with clusters centred on *m*/*z* values of 616 (100), 635 (20) and 653 (12%) assigned to $\{[Cu_2(H_2L)]\}^+$, $\{[Cu_2(H_3L)(OH)]\}^+$, and $\{[Cu_2(H_3L)(OH)](H_2O)\}^+$, respectively. The presence of two different imine sites is indicated by the presence of two imine stretches in the IR spectra (KBr disc), at 1636 and 1654 cm^{-1}. The stoichiometry suggests that the phenol protons have transferred to the uncoordinated imine groups, a common feature in related systems.[6,7]

The dicopper complexes dimerise on recrystallisation from methanol by slow diffusion of diethyl ether to form crystals† of formula $[Cu_2(H_3L)O]_2X_2{\cdot}nH_2O$ with IR and FAB-MS spectra very similar to the monomers. The centrosymmetric cation from $[Cu_2(H_3L)O]_2(NO_3)_2{\cdot}5H_2O$ is shown in Fig. 1, and comprises two parallel dicopper(II) macrocyclic units. The copper ions are

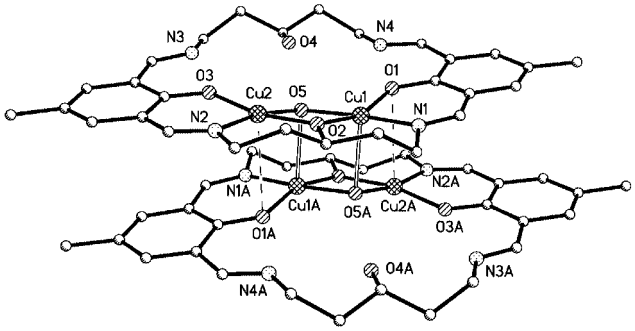

Fig. 1 Molecular structure of the $\{[Cu_2(H_3L)O]_2\}^{2+}$ cation. Selected distances (Å): Cu(1)–Cu(2) 3.0013(7), Cu(1)–O(5A) 2.413(3), Cu(2)–O(1A) 3.084(3).

bridged by one of the ligand alkoxy donors and by an exogenous oxo ligand. The two macrocycles are linked by two symmetry-related Cu–oxo bonds, supported by longer interactions between the second copper ion and a phenolate oxygen from the second ring. The structure of the dimer is markedly similar to that of the fully occupied analogue where tetranuclear and octanuclear forms are interconvertible.[8,9] In each case the dimerisation involves displacement of the OH proton by a copper(II) ion from the second macrocycle.

The alkoxide-bridged, side-by-side geometry of this intermediate complex is the key factor determining the geometry of the heterotetranuclear product described below. There are three possible arrangements of two copper ions between the four potential binding sites. The side-by-side geometry permits the copper ion to bind the largest number of deprotonated donors (an alkoxo, a hydroxo and two phenoxo donors) and is, presumably, favoured for this reason. We have never observed the conventional Robson geometry (dinuclear, bridged by two phenolate groups) in these complexes. The third possibility, a diagonal dinuclear complex in which none of the macrocyclic oxygen donors are bridging, can form[10,11] but requires different conditions.

Reaction of the dinuclear complexes with an excess of nickel(II) acetate yields heterotetranuclear complexes of formula $[Cu_2Ni_2(L)(OH)(OAc)]X_2$. These complexes are identical with those obtained *via* pyrazolate intermediates[7] and consist of olive-green powders which were readily identified from their FAB-MS spectra but which are resistant to crystallisation. However reaction of $[Cu_2(H_3L)(OH)](BF_4)_2$ with an excess of nickel(II) acetate in the presence of excess dfmp yielded small crystals† of $\{[Cu_2Ni_2(L)O(OAc)][Ni_2(dfmp)(OAc)(OH)_3]\}{\cdot}6.5H_2O$. The structure of this neutral complex is shown in Fig. 2, and the metal coordination spheres are illustrated in Fig. 3. The heterotetranuclear $[Cu_2Ni_2(L)O]$ macrocyclic unit is capped on one face by an acetate ion bridging the two nickel ions. Bound to the other face is an assembly comprising two nickel ions coordinated by a diformylmethylphenolate anion, three hydroxo ligands and a second acetate ion, also bridging two nickel ions. There are six bonds linking the macrocycle to the superstructure; four Ni–O bonds and two (longer) Cu–O interactions. The core (Fig. 3) can also be described as based on

 DOI: 10.1039/b106340p

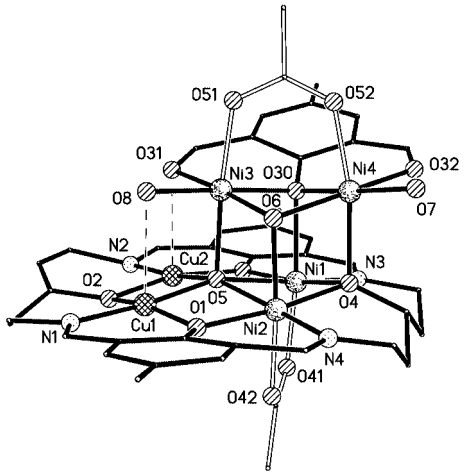

Fig. 2 Molecular structure of {[Cu_2Ni_2(L)O(OAc)][Ni_2(dfmp)(OAc)-$(OH)_3$]}.

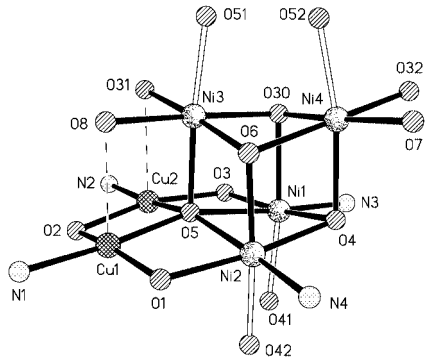

Fig. 3 Coordination spheres of the heteronuclear core. Selected distances (Å): Cu(1)–O(8) 2.592(9), Cu(2)–O(31) 2.543(8), Ni(3)–O(5) 2.079(4), Ni(2)–O(6) 2.057(7), Ni(1)–O(30) 2.172(7), Ni(4)–O(4) 2.094(4).

a Ni_4O_4 cubane. All the adjacent metal–metal distances are under 3 Å.

The X-ray data do not distinguish between the electron densities of nickel and copper ions, so assignment must be based on other factors. Firstly, the stoichiometry is consistent with the FAB-MS data, which show the presence of species containing two copper ions and four nickel ions. The spectrum (in NOBA) shows four significant clusters at *m*/*z* values of 747 (18), 807 (100), 1199 (41), and 1225 (29%) which are assigned to {[Cu_2Ni_2(L)O] − H}$^+$, {[Cu_2Ni_2(L)(OH)(OAc)]}$^+$, {[Cu_2-Ni_2(L)O(OAc)][Ni_2(dfmp)(OAc)$(OH)_3$] + H}$^+$ and {[Cu_2Ni_2-(L)O(OAc)][Ni_2(dfmp)(OAc)$(OH)_3$] + Na}$^+$, respectively. The clusters at *m*/*z* of 747 and 807 are also the principal features seen in the FAB-MS spectrum[7] of [Cu_2Ni_2(L)(OH)$(OAc)_2$]BF_4. There is no indication of scrambling of the metal ions. Secondly, the observed geometry at the metal sites, square pyramidal at copper and six-coordinate pseudo-octahedral at nickel, is consistent with the present assignment. If copper occupied the sites assigned to nickel, significant Jahn–Teller distortion would be expected and this is not observed.

The structure of the heteronuclear complex demonstrates that the macrocycle retains the metal ions in the side-by-side geometry, reflecting the structure of the dinuclear precursor. Site-selection for the heteronuclear product has been achieved based on the relative stability of one of the three possible dinuclear intermediates, without requiring different sites in the macrocyclic ligand itself.

The additional superstructure demonstrates that it is possible to use the Cu_2Ni_2 array as a platform to bind both further ligands and metal ions. Related synthetic strategies might be used to design larger mixed metal assemblies.

We are grateful to the EPSRC Mass Spectrometry Service Centre, Swansea for FAB(LSIMS) spectra and to the EPSRC for access to Station 9.8 of the SRS at Daresbury.

Notes and references

† Both crystals were too weakly diffracting for data collection using a standard laboratory sealed-tube source and so the data were collected at 150 K on Station 9.8 of the Synchrotron Radiation Source at Daresbury.[12] The structures were solved and refined using the SHELXTL[13] package.

[Cu_2(HL)O]$_2$(NO_3)$_2$·5H_2O: $C_{56}H_{80}Cu_{4.12}N_{10}O_{21}$, triclinic, space group $P\bar{1}$, a = 11.2527(7), b = 13.2136(8), c = 13.8116(9) Å, α = 104.974(1), β = 100.755(1), γ = 111.187(1)°, V = 1758.1(2) Å^3, λ = 0.68900 Å, Z = 1, 10912 reflections measured, 6465 unique (R_{int} = 0.030), $wR(F^2)$ = 0.1581 (all data), $R1$ = 0.0559 [$I > 2\sigma(I)$]. Non-H atoms were assigned anisotropic ADPs except the partial occupancy Cu(II) ions. H atoms bonded to carbon were inserted at calculated positions. The remaining protons were not located or included in the model. There is approximately 3% occupancy of the vacant Cu coordination sites, and the saturated section of the macrocyclic chain on the vacant side is disordered 70:30 between two related conformations. The lattice contains a number of severely disordered water molecules; attempts to model these were only partially successful so the PLATON SQUEEZE[14] procedure was used instead. A single void of 380 Å^3 (21.6% of the cell volume) was located between the cations, the five H_2O molecules given in the formula are based on the estimate of 88 electrons in the void.

{[Cu_2Ni_2(L)O(OAc)][Ni_2(dfmp)(OAc)$(OH)_3$]}·6.5H_2O: $C_{41}H_{61}Cu_2N_4$-$Ni_4O_{21.5}$, monoclinic, space group $C2$, a = 24.1826(1), b = 20.100(1), c = 13.9551(8) Å, β = 93.223(1)°, V = 6773.5(7) Å^3, λ = 0.69410 Å, Z = 4, 21150 reflections measured, 11931 unique (R_{int} = 0.024), $wR(F^2)$ = 0.2459 (all data), $R1$ = 0.0741 [$I > 2\sigma(I)$]. The structure could be solved and refined in either $C2/m$ or $C2$; in the $C2/m$ solution, the molecule lies on a mirror plane with the dfmp component disordered, having 50% occupancy on either side of the mirror. Since this implies that no individual molecule actually possesses mirror symmetry, the solution in $C2$ was preferred. In this space group no major disorder of the complex is exhibited but the structure behaves as a racemic twin. All non-H atoms were assigned anisotropic ADPs; hydrogen atoms bonded to carbon were inserted at calculated positions, those bonded to oxygen were not included in the model. CCDC reference numbers 169116 and 169117. See http://www.rsc.org/suppdata/cc/b1/b106340p/ for crystallographic files in CIF or other electronic format.

1 N. H. Pilkington and R. Robson, *Aust. J. Chem.*, 1970, **23**, 2225.
2 See for example: R. R. Gagné, C. L. Spiro, T. J. Smith, C. A. Hamann, W. R. Thies and A. K. Shiemke, *J. Am. Chem. Soc.*, 1981, **103**, 4073; S. Ohtsuka, M. Kodera, K. Motoda, M. Ohba and H. Ōkawa, *J. Chem. Soc., Dalton Trans.*, 1995, 2599; T. Aono, H. Wada, Y. Aratake, N. Matsumoto, H. Ōkawa and Y. Matsuda, *J. Chem. Soc., Dalton Trans.*, 1996, 25; S. Mohanta, K. N. Nanda, L. K. Thompson, U. Flörke and K. Nag, *Inorg. Chem.*, 1998, **37**, 1465; M. Yonemura, N. Usuki, Y. Nakamura, M. Ohba and H. Ōkawa, *J. Chem. Soc., Dalton Trans.*, 2000, 3624.
3 A. Hori, M. Yonemura, M. Ohba and H. Ōkawa, *Bull. Chem. Soc. Jpn.*, 2001, **74**, 495.
4 K. K. Nanda, S. Mohanta, U. Florke, S. K. Dutta and K. Nag, *J. Chem. Soc., Dalton Trans.*, 1995, 3831.
5 M. Yonemura, H. Ōkawa, M. Ohba, D. E. Fenton and L. K. Thompson, *Chem. Commun.*, 2000, 817.
6 M. G. B. Drew, O. W. Howarth, G. G. Morgan and J. Nelson, *J. Chem. Soc., Dalton Trans.*, 1994, 3149.
7 P. E. Kruger, F. Launay and V. McKee, *Chem. Commun.*, 1999, 639.
8 V. McKee and S. S. Tandon, *Inorg. Chem.*, 1989, **28**, 2901.
9 V. McKee and S. S. Tandon, *J. Chem. Soc., Dalton Trans.*, 1991, 221.
10 J. Wikaira, Ph.D. Thesis, University of Canterbury, 1996.
11 F. Launay, Ph.D. Thesis, Queen's University, 2001.
12 R. J. Cernik, W. Clegg, C. R. A. Catlow, G. Bushnell-Wye, J. V. Flaherty, G. N. Greaves, M. Hamichi, I. Burrows, D. J. Taylor and S. J. Teat, *J. Synchrotron Radiat.*, 1997, **4**, 279.
13 G. M. Sheldrick, SHELXTL version 5.1, Bruker-AXS, Madison WI, 1998.
14 P. v. d. Sluis and A. L. Spek, *Acta Crystallogr., Sect. A*, 1990, **46**, 194.

CHEMCOMM Communication
www.rsc.org/chemcomm

Directly linked dehydropurpurin–porphyrin dyads from Ag(I)-promoted oxidation of *meso*-phenylethynyl substituted zinc(II) porphyrins

Aiko Nakano, Naoki Aratani, Hiroyuki Furuta and Atsuhiro Osuka*

Department of Chemistry, Graduate School of Science, Kyoto University, Sakyo-ku, Kyoto 606-8502, Japan. E-mail: osuka@kuchem.kyoto-u.ac.jp

Received (in Cambridge, UK) 9th July 2001, Accepted 21st August 2001
First published as an Advance Article on the web 13th September 2001

Ag(I)-promoted oxidation of (5,15-diaryl-10-phenylethynylporphyrinato)zinc(II) complexes in $CHCl_3$ gave directly linked 12,13-dehydropurpurin–porphyrin dyads, the structures of which were revealed by X-ray analysis.

5,15-Diaryl metalloporphyrins without β-pyrrolic substituents have been shown to be reactive in direct coupling at the *meso*- and/or β-positions under one-electron oxidizing conditions.[1] Along this line, we reported efficient synthetic routes to *meso*–*meso* singly-linked diporphyrins,[2] *meso*–β singly-linked diporphyrins,[3] *meso*–β doubly-linked diporphyrins,[4] and *meso*–*meso*, β–β, β–β triply-linked diporphyrins[5] through the oxidation of metalloporphyrins. The observed metal-dependent coupling regioselectivities are likely to be correlated with the electronic properties of the cation radical intermediates, especially whether the SOMO is derived from the A_{2u} or A_{1u} orbital. In this respect, *meso*-ethynylated metalloporphyrins are of particular interest since their HOMO orbitals are indicated to be extending over the *meso*-ethynyl substituent.[6,7] Here, we report that Ag(I)-promoted oxidation of 5,15-diaryl-10-phenylethynyl-substituted zinc(II) porphyrins gave directly-linked dehydropurpurin–porphyrin dyads.

Treatment of **1a**–**Zn** with 1.0 equiv. of $AgPF_6$ in $CHCl_3$ at room temperature for 6 h followed by separations over size-exclusion and silica-gel columns provided a dimer of **1a**–**Zn** in 34% yield. The molecular weight of the dimer was revealed to be m/z = 2273 (calc. for $C_{144}H_{174}N_8O_8Zn_2$, 2271) by the FAB-MS measurement but its ^{1}H NMR spectrum was compatible not with the structure of symmetric *meso*–*meso* coupling product **3**[8] but with that of **2a**–**Zn**. The ^{1}H NMR spectrum revealed the presence of a symmetric 5-substituted porphyrin subunit by featuring four 2H-equivalent β-protons at 10.31, 9.43, 9.23 and 9.07 ppm, a *meso*-proton at 10.31 ppm, and a set of protons due to the two equivalent 3,5-dioctyloxyphenyl substituents, while the peripheral β-protons in the dehydropurpurin macrocycle appeared as a singlet at 7.56 ppm (H^a); three sets of mutually coupled pairs of doublets were observed of which the most high-field shifted signal appearing at 4.77 ppm was assigned to H^b because of its location in the shielding region of the neighboring porphyrin. In order to obtain an X-ray crystal structure, a similar hybrid dimer **2b**–**Zn** was prepared from **1b** in 19% yield and was converted into the bis-Cu(II) complex **2b**–**Cu**. Fig. 1 shows the X-ray crystal structure of **2b**–**Cu**,[9] which provides firm evidence for the directly-linked porphyrin–12,13-dehydropurpurin dyad. Whereas the *meso*-arylethynyl substituent in the dehydropurpurin moiety is intact, that in the porphyrin is condensed with the unsubstituted porphyrin side to form an exocyclic five-membered ring. The dehydropurpurin macrocycle is nearly flat with a mean plane deviation of 0.119 Å and is directly linked with the porphyrin ring with a dihedral angle of 90.8°. This orthogonal structure well explains the observed ^{1}H NMR spectra mentioned above. It is of interest that the two phenyl rings [designated as Ph^1 and Ph^2 in Fig. 1(a)] are nearly coplanar with the dehydropurpurin macrocycle with dihedral angles of 20.7 and 15.6°, respectively. The mechanism of this dimerization is not fully understood but may be considered to be initiated by one-electron oxidation of the zinc(II)-phenylethynylporphyrin with $AgPF_6$ followed by nucleophilic attack of another neutral porphyrin with its *meso*-position against the ethynyl-carbon adjacent to the *meso*-position.

Although tetrapyrrolic macrocycles with an exocyclic five membered ring are quite ubiquitous both in nature[10] and synthetic studies,[11] the 12,13-dehydropurpurin structure is quite

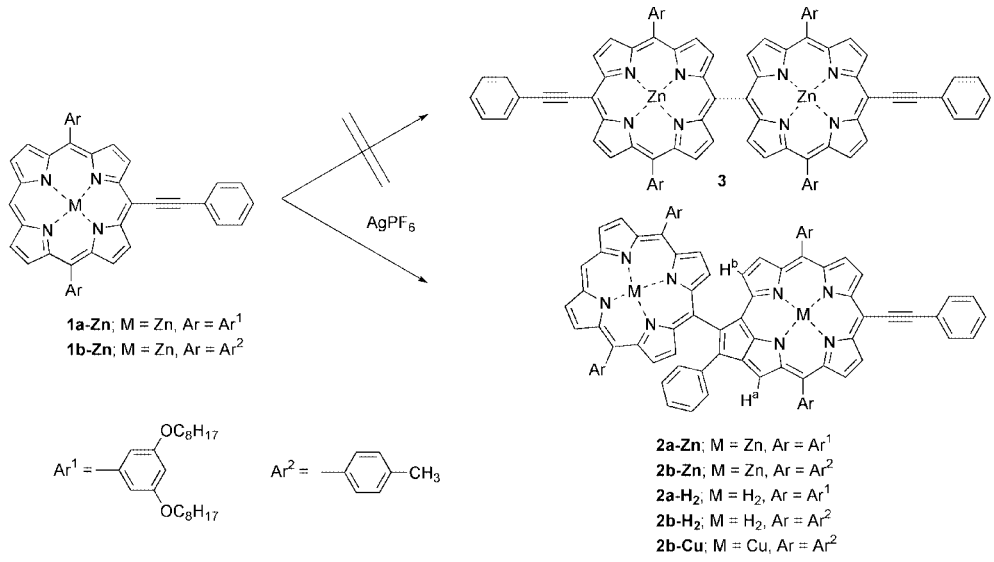

Scheme 1 Reaction of **1** and $AgPF_6$.

 DOI: 10.1039/b106050n

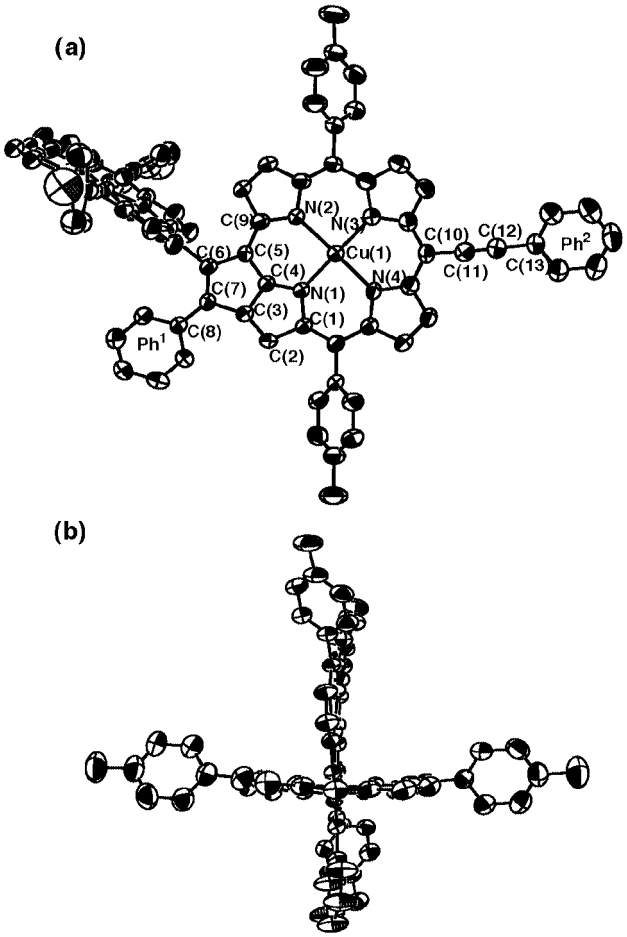

Fig. 1 Molecular structure of **2b–Cu**: (a) top view and (b) side view; solvents and hydrogen atoms are omitted for clarity. Bond lengths of C(6)–C(7) and C(6)–porphyrin *meso*-carbon are 1.38(1) and 1.50(1) Å, respectively.

rare in the literature,[12] and there is much less information on this macrocycle. The ^{1}H NMR spectrum of **2a–H$_2$** revealed the inner NH protons at 3.09 and 5.04 ppm for the dehydropurpurin ring, hence suggesting that its ring current is weaker compared with those in structurally related porphyrins and pheophorbides.

Fig. 2 shows the absorption spectra of **2a–Zn**† and **2a–H$_2$** taken in THF. It is conceivable that the direct connection leads to the strong electronic interaction between the two macrocycles and causes broadening of the absorption bands. Nevertheless, it seems likely that relatively sharp bands at 421 nm for **2a–Zn** and 415 nm for **2a–H$_2$** can be assigned to Soret bands of the porphyrin, and the broad bands at 471 and 498 nm for **2a–Zn** and 482 nm for **2a–H$_2$** can be assigned to Soret-like bands of the dehydropurpurin. In addition, broad Q-like bands are observed at 645 nm for **2a–Zn** and at 674 nm for **2a–H$_2$**. Neither **2a–Zn** nor **2a–H$_2$** exhibits fluorescence, probably reflecting strong electronic interaction between the two macrocycles. These findings may suggest the potential use of such dyads as energy- and electron-transfer functional units. Related detailed studies will be reported elsewhere.

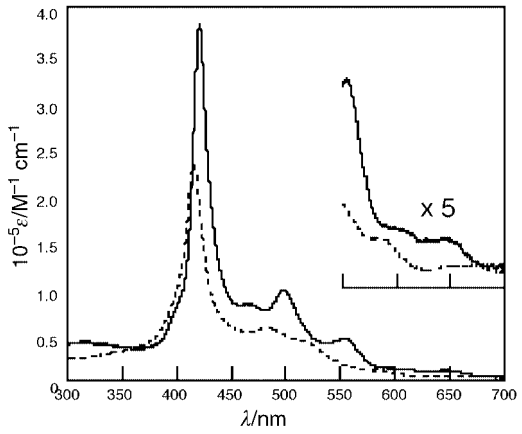

Fig. 2 Absorption spectra of **2a–Zn** (——) and **2a–H$_2$** (- - - - -) in THF.

This work was supported by a Grant-in-Aids for Scientific Research from the Ministry of Education, Science, Sports and Culture of Japan and by CREST (Core Research for Evolutional Science and Technology) of the Japan Science and Technology Corporation (JST).

Notes and references

† *Spectral data* for **2a–Zn**; δ_H(500 MHz, $CDCl_3$): 10.31 (d, *J* = 4.5 Hz, 2H, β-H), 10.31 (s, 1H, *meso*-H), 9.43 (d, *J* 4.5 Hz, 2H, β-H), 9.23 (d, *J* 4.5 Hz, 2H, β-H), 9.07 (d, *J* 4.5 Hz, 2H, β-H), 9.00 (d, *J* 4.5 Hz, 1H, β-H), 8.94 (d, *J* 4.5 Hz, 1H, β-H), 8.31 (d, *J* 4.5 Hz, 1H, β-H), 8.07 (d, *J* 5.0 Hz, 1H, β-H), 7.88 (d, *J* 7.0 Hz, 2H, Ph), 7.67 (s, 1H, β-H), 7.50 (t, *J* 7.0 Hz, 2H, Ph), 7.45 (t, *J* 7.0 Hz, 1H, Ph), 7.42 (s, 2H, Ar), 7.38 (s, 2H, Ar), 7.26 (d, *J* 2.0 Hz, 2H, Ar), 7.06 (d, *J* 8.0 Hz, 2H, Ph), 6.93 (d, *J* 4.5 Hz, 1H, β-H), 6.85 (t, *J* 2.5 Hz, 1H, Ar), 6.84 (t, *J* 2.5 Hz, 2H, Ar), 6.74 (t, *J* 8.0 Hz, 1H, Ph), 6.63 (d, *J* 2.0 Hz, 2H, Ar), 6.61 (t, *J* 8.0 Hz, 2H, Ph), 6.36 (t, *J* 2.0 Hz, 1H, Ar), 4.77 (d, *J* 5.0 Hz, 1H, β-H), 4.18 (t, *J* 6.5 Hz, 4H, octyl), 4.11 (t, *J* 6.5 Hz, 4H, octyl), 4.06 (t, *J* 6.0 Hz, 4H, octyl), 3.70 (m, 4H, octyl), 1.92 (m, 4H, octyl), 1.84 (m, 4H, octyl), 1.79 (m, 4H, octyl), 1.55–1.12 (m, 84H, octyl), 0.89 (t, *J* 8.0 Hz, 6H, octyl), 0.84 (t, *J* 8.0 Hz, 6H, octyl), 0.79 (t, *J* 8.0 Hz, 6H, octyl) and 0.75 (t, *J* 8.0 Hz, 6H, octyl). Mass (FAB): found 2273, calc. for $C_{144}H_{174}N_8O_8Zn_2$, 2271. UV–VIS (THF): λ_{max} (log ε) = 421 (5.58), 471 (4.88), 498 (5.00), 552 (4.65) and 645 (3.94) nm.

1 N. Aratani and A. Osuka, *Bull. Chem. Soc. Jpn.*, 2001, **74**, 1361.
2 A. Osuka and H. Shimidzu, *Angew. Chem., Int. Ed. Engl.*, 1997, **36**, 135; N. Aratani, A. Osuka, Y. H. Kim, D. H. Jeong and D. Kim, *Angew. Chem., Int. Ed.*, 2000, **39**, 1458; Y. H. Kim, D. H. Jeong, D. Kim, S. C. Jeoung, H. S. Cho, S. K. Kim, N. Aratani and A. Osuka, *J. Am. Chem. Soc.*, 2001, **123**, 76.
3 T. Ogawa, Y. Nishimoto, N. Yoshida, N. Ono and A. Osuka, *Angew. Chem., Int. Ed.*, 1999, **38**, 176.
4 A. Tsuda, A. Nakano, H. Furuta, H. Yamochi and A. Osuka, *Angew. Chem., Int. Ed.*, 2000, **39**, 558.
5 A. Tsuda, H. Furuta and A. Osuka, *Angew. Chem., Int. Ed.*, 2000, **39**, 2549; A. Tsuda and A. Osuka, *Science*, 2001, **293**, 79.
6 D. P. Arnold, G. A. Heath and D. A. James, *J. Porphyrins Phthalocyanines*, 1999, **3**, 5; S. M. LeCours, S. G. DiMagno and M. J. Therien, *J. Am. Chem. Soc.*, 1996, **118**, 11854; H. L. Anderson, *Chem. Commun.*, 1999, 2323.
7 A. Nakano, H. Shimidzu and A. Osuka, *Tetrahedron Lett.*, 1998, **39**, 9489; A. Nakano, Y. Yasuda, T. Yamazaki, S. Akimoto, I. Yamazaki, H. Miyasaka, A. Itaya, M. Murakami and A. Osuka, *J. Phys. Chem. A*, 2001, **105**, 4822.
8 The dimer was independently prepared from *meso–meso* linked diporphyrin through *meso,meso*-dibromination followed by bis-phenylethynylation: A. Nakano, A. Osuka, T. Yamazaki, Y. Nishimura, S. Akimoto, I. Yamazaki, A. Itaya, M. Murakami and H. Miyasaka, *Chem. Eur. J.*, 2001, **7**, 3134.
9 *Crystal data* for **2b–Cu**: red prism, $C_{84}H_{54}N_8Cu_2{\cdot}C_7H_8$, M_w = 1394.64, triclinic, space group $P\bar{1}$, *a* = 13.204(1), *b* = 24.665, *c* = 11.0879(9) Å, α = 99.737(2), β = 106.210(3), γ = 83.472(5)°, *V* = 3409.1(5) Å^3, *Z* = 2, μ(Mo-Kα) = 6.81 cm^{-1}, D_c = 1.359 g cm^{-3}, *T* = 296(1) K. Final *R* = 0.060, R_w = 0.066 for 8332 reflections with $I > 3\sigma(I)$. CCDC reference number 168237. See http://www.rsc.org/suppdata/cc/b1/b106050n/ for crystallographic data in CIF or other electronic format.
10 *Chlorophylls*, ed. H. Scheer, CRC Press, Boca Raton, FL, 1991.
11 M. D. G. H. Vicente, in *The Porphyrin Handbook*, ed. K. M. Kadish, K. M. Smith and R. Guilard, Academic Press, San Diego, CA, 2000, vol. 1, pp. 149–199.
12 C. Bauder, R. Ocampo and H. J. Callot, *Tetrahedron*, 1992, **48**, 5135; H. Klement, M. Helfrich, U. Oster, S. Schoch and W. Rüdiger, *Eur. J. Biochem.*, 1999, **265**, 862.

CHEMCOMM
Communication
www.rsc.org/chemcomm

Steric effects on the mode of aggregation and reactivity of clusters formed from the lithiation of trisamidothiophosphates

Tristram Chivers,* Mark Krahn, Masood Parvez and Gabriele Schatte

Department of Chemistry,University of Calgary, Calgary, Alberta, Canada T2N 1N4. E-mail: chivers@acs.ucalgary.ca

Received (in Purdue, IN, USA) 15th June 2001, Accepted 12th August 2001
First published as an Advance Article on the web 13th September 2001

Lithiation of $SP[N(H)R]_3$ with $LiBu^n$ produces the dimers $[(THF)LiSP(NR)(NHR)_2]_2$ (R = Pr^i) or $\{[LiSP(NR)(NHR)_2][(THF)LiSP(NR)_2(NHR)]\}_2$ (R = Bu^t) with central Li_2N_2 or Li_2S_2 rings, respectively; further lithiation yields the dianion $[SP(NR)_2(NHR)]^{2-}$ (R = Pr^i) or leads to sulfur extrusion when R = Bu^t.

The first polyimido analogues of the orthophosphate and phosphite anions, *i.e.* $[P(Nnaph)_4]^{3-}$ and $[HP(NC_6H_4OMe\text{-}2)_3]^{2-}$, were reported recently as their lithium derivatives.[1,2] Ambidentate anions involving a combination of hard (N) and soft (S or Se) donor sites attached to a P(v) centre display versatile coordination behaviour[3–6] and some of their alkali-metal derivatives form extended ladder structures.[4,5] For example, the dimers of $[EP(NBu^t)_2]^-$, isoelectronic with metaphosphate PO_3^-, adopt a different bonding mode towards Li^+ than that observed for Na^+ or K^+.[4] Heteroleptic imido/thio analogues of orthophosphate PO_4^{3-} are unknown. As a possible approach to this potentially versatile class of anionic ligands, we have now investigated the reactions of trisamidothiophosphates $SP[N(H)R]_3$ (R = Pr^i, Bu^t) with R′Li reagents. We report here that the steric bulk of R has a marked effect on both the mode of aggregation and the reactivity of partially lithiated derivatives of $SP[N(H)R]_3$.

The reaction of $SP[N(H)Pr^i]_3$ with $LiBu^n$ in a 1 : 1 molar ratio in THF produced the monolithiated derivative $\{(THF)LiSP(NPr^i)(NHPr^i)_2\}$ **1** in 61% yield.† The ^{31}P NMR spectrum of **1** in C_6D_6 showed a singlet at δ 47.9 {*cf.* δ 56.3 for $SP[N(H)Pr^i]_3$}. An X-ray analysis of **1** revealed a centrosymmetric dimer comprised of a step-shaped ladder in the transoid conformation (Fig. 1).‡ The two halves of the dimer are connected by the more polar Li–N bonds rather than the sterically unencumbered Li–S interactions. We note that lithium thioamidates $\{Li[RC(S)NR']\}_n$ invariably aggregate through Li–S bonds.[7] When the same reaction is carried out in a 1 : 2 molar ratio in THF an insoluble product is formed. In the presence of TMEDA, however, this reaction produces the dilithiated complex $\{[(TMEDA)Li]_2[SP(NPr^i)_2(NHPr^i)]\}$ **2**.† Solid state ^7Li and ^{31}P NMR spectra of **2** showed singlets at δ 1.9 and δ 45.7, respectively. An X-ray analysis showed that **2** has a monomeric structure and contains the dianion $[SP(NPr^i)_2(NHPr^i)]^{2-}$ (Scheme 1). Apparently, chelation of Li^+ ions by a TMEDA ligand prevents extensive laddering *via* Li–N interactions (*cf.* $\{[p\text{-}MeC_6H_4N(H)Li\cdot TMEDA]_2\}$);[8] the latter phenomenon may account for the insolubility of the product obtained in the absence of TMEDA.

The reaction of $SP[N(H)Bu^t]_3$ with $LiBu^n$ or $LiN(SiMe_3)_2$ in THF in a 2 : 3 molar ratio produces the complex $\{[LiSP(NBu^t)(NHBu^t)_2][(THF)LiSP(NBu^t)_2(NHBu^t)]\}_2$ **3** in an optimum yield of 82%.† In contrast to the Li–N interactions observed for **1**, an X-ray analysis showed **3** to be a dimer in which the central feature is a cisoid Li_4S_4 ladder (Fig. 2).‡ There is a crystallographic twofold axis through the middle of the central Li_2S_2 ring. The asymmetric unit of **3** is comprised of an aggregate of the mono- and di-lithiated derivatives, $LiSP(NBu^t)(NHBu^t)_2$ and $Li_2SP(NBu^t)_2(NHBu^t)$, respectively, linked by Li–S and Li–N bonds to give a distorted $Li_3PS_2N_2$ cube {bond lengths range from 1.615(6) [P(1)–N(2)] to 2.635(13) Å [Li(2)–S(2)]}. The solid-state ^{31}P NMR spectrum of **3** shows two resonances at δ 28.5 and 25.8. Complex **3** is also generated

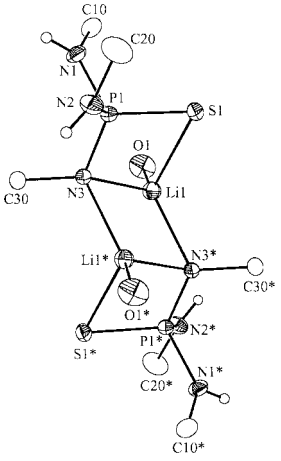

Fig. 1 X-Ray structure of **1** (30% probability ellipsoids). Only the secondary C atoms of Pr^i groups and O atoms of THF molecules are shown for clarity. Selected bond lengths (Å) and angles (°): S(1)–P(1) 1.9927(8), S(1)–Li(1) 2.526(4), P(1)–N(3) 1.6101(17), Li(1)–N(3) 2.129(4), Li(1)–N(3)* 2.104(4); P(1)–S(1)–Li(1) 75.12(8), N(3)–P(1)–S(1) 107.90(7), P(1)–N(3)–Li(1) 95.34(13), N(3)–Li(1)–S(1) 77.23(12), N(3)–Li(1)–N(3)* 110.21(17), Li(1)–N(3)–Li(1)* 69.79(17).

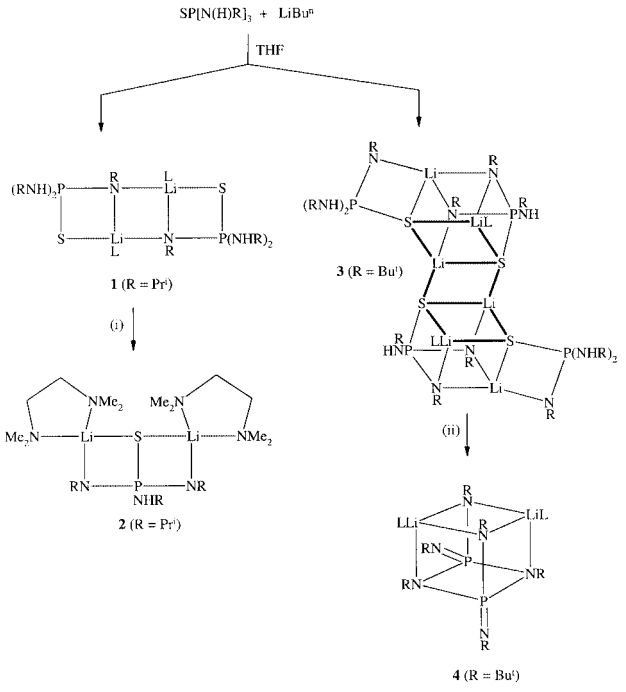

Scheme 1 *Reagents and conditions*: L = THF. (i) $LiBu^n$, TMEDA (ii) $LiBu^n$.

 DOI: 10.1039/b105360b

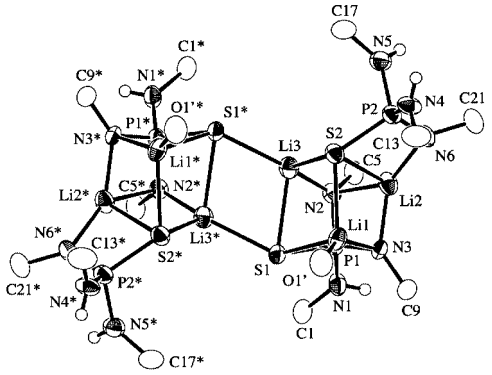

Fig. 2 X-Ray structure of **3** (40% probability ellipsoids). For clarity only α-C atoms of Bu^t groups and O atoms of THF molecules are shown. Selected bond lengths (Å): Li(1)–S(1) 2.429(12), Li(1)–S(2) 2.541(13), Li(2)–S(2) 2.635(13), Li(3)–S(1) 2.614(13), Li(3)-S(2) 2.614(13), Li(3)–S(1)* 2.449(12), P(1)–S(1) 2.077(2), P(2)–S(2) 2.036(2), P–N (amido) [mean 1.670(14), range 1.651(6)–1.683(6)], P–N (imido) [mean 1.599(24), range 1.566(7)–1.617(6)], Li–N [range 1.937(13)–2.275(13)].

when the reaction of SP[N(H)Bu^t]$_3$ with LiBu^n is carried out in a 1 : 1 molar ratio. In contrast to the behaviour of the Pr^i system, however, the use of a 1 : 2 molar ratio for this reaction results in sulfur extrusion to give the complex [(THF)LiP(NBu^t)$_3$]$_2$ **4** in *ca*. 15% yield. An X-ray analysis revealed that **4** is an $Li_2N_4P_2$ cubane with exocyclic NBu^t groups attached to P, *i.e*. the dimeric lithium derivative of the trisimidometaphosphate anion [P(NBu^t)$_3$]$^-$ (Scheme 1). Monomeric analogues of **4**, *e.g*. the ion-separated complex [Li(THF)$_4$]$^+$[P(NMes*)$_3$]$^-$, have been reported.[9] The P(III) analogue of **4** also has a cubane structure which, in the absence of THF ligands, dimerizes *via* Li–N interactions.[10,11] The facile extrusion of sulfur in this lithiation process is in marked contrast to the formation of Li$_2$[Bu^{t}N(S)P(μ-NBu^t)$_2$P(S)NBu^t] *via* lithiation with LiBu^t in boiling THF.[4b] Further details of this desulfurization process and the X-ray structures of **2** and **4** will be given in a full account of this work.

In summary, we have shown that steric effects influence the mode of aggregation and the reactivity of lithium derivatives of trisamidothiophosphates. The anions in **1** and **2** represent novel examples of multidentate ligands with hard (N) and soft (S) donor sites attached to a P(v) centre.

We thank the NSERC (Canada) for financial support and Dr R. MacDonald (University of Alberta) for the collection of the X-ray data for **1** and **2**.

Notes and references

† *Synthesis* of **1**: a solution of LiBu^n in hexanes (2.5 M, 1.69 mL, 4.21 mmol) was added to a solution of SP[N(H)Pr^i]$_3$[12] (1.00 g, 4.21 mmol) in THF (25 mL) at 23 °C. After 2 h, solvent was removed *in vacuo* and the residue washed with *n*-pentane (2 × 5 mL) to give **1** as a pale yellow solid in 61% yield. X-Ray quality crystals were obtained by layering hexane onto a THF solution at 23 °C. ^{1}H NMR (C_6D_6, 23 °C): δ 3.66 (m, THF), 2.12 (s, 2 H, NH), 1.43 (m, THF), 1.24 [br d, 18 H, CH(C*H*$_3$)$_2$], 3.45 [m, 3 H, C*H*(CH$_3$)$_2$]. ^{31}P{^{1}H} NMR (C_6D_6, 23 °C): δ 47.9 (s); (solid state): δ 55.0 (s). ^{7}Li NMR (C_6D_6, 23 °C): δ −1.2 (s).

Synthesis of **2**: a solution of LiBu^n in hexanes (2.5 M, 3.37 mL, 8.43 mmol) was added to a solution of SP[N(H)Pr^i]$_3$ (1.00 g, 4.21 mmol) in toluene (20 mL) and TMEDA (10 mL) at 23 °C. After 2 h, solvent was removed *in vacuo* and the residue washed with pentane (2 × 10 mL) to give **2** as a white solid in 56% yield. X-Ray quality crystals were obtained by layering *n*-hexane onto a TMEDA–toluene solution at 23 °C. ^{31}P{^{1}H} NMR (solid state): δ 45.7 (s). ^{7}Li NMR (solid state): δ 1.9 (br s).

Synthesis of **3**: A solution of (Et$_2$O)LiN(SiMe$_3$)$_2$ (6.82 g, 28.2 mmol) in THF (15 mL) was added slowly to a stirred solution of SP[N(H)Bu^t]$_3$[13] (5.00 g, 17.9 mmol) in THF (25 mL) at 23 °C. After 18 h solvent was removed and the residue washed with *n*-pentane (3 × 5 mL) to give **3** as a white powder in 82% yield. X-Ray quality crystals were obtained from a THF–hexane solution at 23 °C. ^{1}H NMR (d$_8$-THF, 23 °C): δ 3.61 (m, [O(C*H*$_2$)$_2$(CH$_2$)$_2$]), 1.90 (3 H, NH), 1.76 (m, [O(CH$_2$)$_2$(C*H*$_2$)$_2$]), 1.34 (36 H, Bu^t), 1.17 (18 H, Bu^t). ^{31}P {^{1}H} NMR (d$_8$-THF, 23 °C): δ 33.1 (br s); (solid state): δ 28.5 (s), 25.8 (s). IR (cm^{-1}): 3360 [ν(N–H)].

‡ *Crystal data* for **1**: $C_{26}H_{62}Li_2N_6O_2P_2S_2$, M = 630.76, monoclinic, space group $P2_1/c$ (no. 14), a = 11.0007(16), b = 17.324(3), c = 10.8355(16) Å, β = 114.463(2)°, V = 1879.6(5) Å^3, Z = 2, D_c = 1.114 g cm^{-3}, μ(Mo-Kα) = 2.56 cm^{-1}. Crystal dimensions 0.71 × 0.44 × 0.34 mm. Data were measured on a Bruker AXS P4/RA/SMART 1000 CCD diffractometer at −80 °C using Mo-Kα radiation. The structure was solved by direct methods (SHELXS-97) and the non-hydrogen atoms were refined anisotropically using data that were corrected for absorption (SHELXL97-2). 3030 of the 3837 unique reflections had $I \geqslant 2.00\sigma(I)$. The final agreement factors were R_1 = 0.0488, wR_2 = 0.1420.

Crystal data for **3**: $C_{112}H_{260}Li_{12}N_{24}O_4P_8S_8{\cdot}C_5H_{12}$, M = 2667.12, monoclinic, space group $C2/c$, a = 24.145(4), b = 16.462(4), c = 23.405(5) Å, β = 110.45(1)°, V = 8716(3) Å^3, Z = 2, D_c = 1.016 g cm^{-3}, μ(Mo-Kα) = 2.22 cm^{-1}. Crystal dimensions 0.60 × 0.50 × 0.40 mm. Data were collected at −103 °C on a Rigaku AFC 6S diffractometer and corrected for absorption. The structure was solved by direct methods (SIR92) and expanded using Fourier techniques (DIRDIF 94). One THF molecule was disordered over two sites with unequal site occupancy factors. 3940 of the 7694 unique reflections had $I \geqslant 2.00\sigma(I)$. The final agreement factors were R_1 = 0.0762, wR_2 = 0.2325. CCDC reference numbers 168972 and 168973. See http://www.rsc.org/suppdata/cc/b1/b105360b/ for crystallographic data in CIF or other electronic format.

1 P. R. Raithby, C. A. Russell, A. Steiner and D. S. Wright, *Angew. Chem., Int. Ed. Engl*., 1997, **36**, 649.
2 L. T. Burke, E. Hevia-Freire, R. Holland, J. C. Jeffery, C. A. Russell, A. P. Leedham, A. Steiner and A. Zagorski, *Chem. Commun*., 2000, 1769.
3 For reviews see: J. D. Woollins, *J. Chem. Soc., Dalton Trans*., 1996, 2893; T. Chivers and R. W. Hilts, *Coord. Chem. Rev*., 1994, **137**, 201.
4 (*a*) T. Chivers, M. Krahn and M. Parvez, *Chem. Commun*., 2000, 463; (*b*) T. Chivers, M. Krahn, M. Parvez and G. Schatte, *Inorg. Chem*., 2001, **40**, 2547; (*c*) T. Chivers, C. Fedorchuk, M. Krahn, M. Parvez and G. Schatte, *Inorg. Chem*., 2001, **40**, 1936.
5 A. M. Z. Slawin, J. Ward, D. J. Williams and J. D. Woollins, *J. Chem. Soc., Chem. Commun*., 1994, 421.
6 G. R. Lief, C. J. Carrow, L. Stahl and R. J. Staples, *Organometallics*, 2001, **20**, 1629.
7 A. Downard and T. Chivers, *Eur. J. Inorg. Chem*., 2001, 2193; T. Chivers, A. Downard and M. Parvez, *Inorg. Chem*., 1999, **38**, 5565; T. Chivers, A. Downard and G. P. A. Yap, *Inorg. Chem*., 1998, **37**, 5708.
8 Unpublished results quoted in R. E. Mulvey, *Chem. Soc. Rev*., 1998, **27**, 339.
9 E. Niecke, M. Frost, M. Nieger, V. v d Gönna, R. Ruban and W. W. Schoeller, *Angew. Chem., Int. Ed. Engl*., 1994, **33**, 2111.
10 I. Schranz, L. Stahl and R. J. Staples, *Inorg. Chem*., 1998, **37**, 1493.
11 J. K. Brask, T. Chivers, M. L. Krahn and M. Parvez, *Inorg. Chem*., 1999, **38**, 290.
12 J. D. Healy, R. A. Shaw and M. Woods, *Phosphorus, Sulfur Silicon*, 1978, **5**, 239.
13 R. R. Holmes and J. A. Forstner, *Inorg. Chem*., 1962, **2**, 380.

CHEMCOMM Communication
www.rsc.org/chemcomm

Bis[(alkoxy)benzoylsemicarbazides]—a new class of powerful organogelators

Uwe Beginn* and Bernd Tartsch

Department of Organic and Macromolecular Chemistry, Albert-Einstein-Allee 11, D-89069 Ulm, Germany. E-mail: uwe.beginn@chemie.uni-ulm.de; Fax: +49-731-502-2883; Tel: +49-731-502-2884

Received (in Cambridge, UK) 10th July 2001, Accepted 10th August 2001
First published as an Advance Article on the web 13th September 2001

Reaction of *N*-[(alkoxy)benzoyl]hydrazides and diisocyanates produces bis[(alkoxy)benzoylsemicarbazides] that allow for 'cold gelation' of organic liquids by mixing low viscous gelator solutions with a large excess of the respective solvent at ambient temperature.

'Organogels' are elastic- or viscoelastic materials consisting of solvents and low molecular weight organic 'gelators'. Most efficient gelation is found from gelators that self-assemble to networks of fibrous structures with large aspect ratios, *e.g.* rods or ribbons.[1] Though organogels have been known for a long time[2] only a few examples of designed gelators have been reported so far.[3,4]

A simple rational concept to construct gel forming molecules is to prepare nearly flat amphiphilic molecules consisting of small polar and bulky non polar parts.[4] According to this idea rod formation was found with tris(alkoxy)benzamides,[5] *N*-sorbitoyl-3,4,5-tris(alkoxy)benzamides,[6] and crown ether amphiphiles.[4] The latter have been used to generate supramolecular ion transport channels.[7] We prepared dumb-bell shaped amphiphiles to increase the thermal- and mechanical stability of the resulting gels.

Urea type hydrogen bonds are known to stabilise gelator assemblies.[8] In extension of this concept bis[(alkoxy)benzoylsemicarbazides] of the general structure **Y**–CO–NHNH–CO–NH–**X**–NH–CO–NHNH–CO–**Y** (Scheme 1) have been prepared. Y represents alkoxyphenyl units, and X denotes either an aromatic or an aliphatic moiety. Bis(semicarbazide) cores have been selected because of (i) their ability to form up to 14 hydrogen bonds per molecule, (ii) their simple preparation† and (iii) their large structural variability. Table 1 summarizes the compounds prepared so far. The thermal stability of the bis(semicarbazides) **1**–**10**, was obtained from TGA, and confirmed by thermo-optical analysis (TOA).

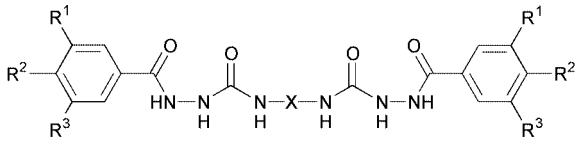

X = 1,4-phenylene, 2,4-tolylene, 2,6-tolylene, 2,6-tolylene, 1,8-naphthylene, 1,6-hexamethylene $R^i = C_nH_{2n+1}O$-, H-

Scheme 1 General formula of the bis[(alkoxy)benzoylsemicarbazides].

Compounds **2**, **3**, **6**, **8** and **9** started decomposing before melting, hence phase transition temperatures were not reproducible on repeated heating of a sample. All semicarbazides melted into optically anisotropic liquids, but isotropisation temperatures could not be obtained due to vigorous decomposition on exceeding 250 °C. The mesophase type is not yet determined.

The solubility of the semicarbazides was tested with solvents of different polarity. Mixtures of 2.5 wt% solute and 97.5 wt% of the solvent were annealed at 20 °C for 2 h, and subsequently heated to the boiling point of the solvent until a clear solution was obtained. The semicarbazides **1**–**5**, and **7**–**10** did not dissolve at ambient temperature in any of the tested solvents, only swelling of the materials was occasionally observed. Swelling most frequently occurred in the presence of THF, $CHCl_3$, styrene, toluene, and hexane. At elevated temperatures the solubilities strongly depended on the molecular structure. The derivatives with a 1,4-phenylene-core (**1**–**7**) were much less soluble than the tolylene (**8**, **9**), and the 1,8-naphthylene (**10**) compounds. With decreasing number of attached alkyl chains the solubility was reduced and the 4-decyloxy derivative **7** could only be dissolved in boiling DMF while all other solvents failed.

Thermoreversible gelation was studied as an indication for the self-ordering to supramolecular structures. Table 2 summarises qualitative tests with 2.5 wt% solutions of **1**–**10**. The hot semicarbazide–solvent mixtures were cooled at a controlled rate (< 6 K min^{-1}) to induce gelation. Three types of gels have been distinguished: (i) transparent–clear gels, (ii) turbid–translucent gels, and (iii) opaque–white gels. Opaque gels were most frequently obtained from the polar solvents, while the non-polar liquids preferably yielded clear gels.

Table 1 Synthesised bis[(alkoxy)benzoylsemicarbazides]

No.	Core	R^1	R^2	R^3	T_d/°C	T_m/°C	ΔH_m[f]
1	1,4-PDI[a]	$C_8H_{17}O$	$C_8H_{17}O$	$C_8H_{17}O$	229 ± 2	220	68.1
2	1,4-PDI	$C_{10}H_{21}O$	$C_{10}H_{21}O$	$C_{10}H_{21}O$	220 ± 2	230	73.8
3	1,4-PDI	$C_{12}H_{25}O$	$C_{12}H_{25}O$	$C_{12}H_{25}O$	223 ± 2	227	82.4
4	1,4-PDI	$C_{16}H_{29}O$	$C_{16}H_{29}O$	$C_{16}H_{29}O$	220 ± 2	209	64.0
5	1,4-PDI	$C_{10}H_{21}O$	$C_{10}H_{21}O$	H	225 ± 2	194	116.0
6	1,4-PDI	$C_{10}H_{21}O$	H	$C_{10}H_{21}O$	220 ± 2	225	66.4
7	1,4-PDI	H	$C_{10}H_{21}O$	H	250 ± 3	234	78.3
8	2,4-TDI[b]	$C_{12}H_{25}O$	$C_{12}H_{25}O$	$C_{12}H_{25}O$	212 ± 5	213	143.0
9	2,6-TDI[c]	$C_{12}H_{25}O$	$C_{12}H_{25}O$	$C_{12}H_{25}O$	202 ± 4	211	96.5
10	1,8-NDI[d]	$C_{12}H_{25}O$	$C_{12}H_{25}O$	$C_{12}H_{25}O$	208 ± 5	199	160.0
11	1,6-HMDI[e]	$C_{12}H_{25}O$	$C_{12}H_{25}O$	$C_{12}H_{25}O$	255 ± 5	95	15.0

[a] 1,4-Phenylene. [b] 2,4-Tolylene. [c] 2,6-Tolylene. [d] 1,8-Naphthylene. [e] 1,6-Hexamethylene. [f] Melting enthalpy in kJ mol^{-1}, T_d = decomposition temperature, T_m = melting temperature, T_m, and ΔH_m from DSC studies.‡

 DOI: 10.1039/b106133j

Table 2 Gelation of 2.5 wt% solution of bis(semicarbazides)

Solvent	**1**	**2**	**3**	**4**	**5**	**6**	**7**	**8**	**9**	**10**
EtOH	GO[d]	GO	GO	P	P	P	P	P	GO	GO
DMF	S	S	GO	GO	P	S	P	P	GO	GO
HEMA[a]	GO	GO	GO	GO	GO	GO	GO	P	GO	GO
THF	GO	GO	GO	GO	GT	S	P	GO	S	GO
$CHCl_3$	GC	GC	GC	GT	GC	GC	GO	GO	S	GO
tBuAc[b]	GO	GO	Sη	GC	GT	P	P	GO	GO	GO
HMA[c]	GO	GT	GO	GT	GC	GT	P	GO	GO	GO
Styrene	GT	GT	GT	GT	GC	GC	P	GT	Sη	GT
Toluene	GC	GC	GC	P	GC	GC	P	GT	Sη	Sη
n-Hexane	GC	GC	GC	P	GC	GC	P	GC	GC	GC

[a] 2-Hydroxyethyl methacrylate. [b] *tert*-Butyl acetate. [c] *n*-Hexyl methacrylate. [d] GO = opaque gel, GT = translucent gel, GC = clear–transparent gel, P = preciptate, S = solution, Sη = viscous solution.

Ethanol was a bad solvent for all bis(semicarbazides), opaque gels were formed from ethanol solutions of **2**, **3**, **9** and **10**. The critical gelation concentration was below 1 wt%.

Except for **4** and **7** all semicarbazides formed transparent–clear gels in hexane solutions. Compounds **2**, **5**, **6** and **8** formed clear solutions of high viscosity with hexane that settled to clear gels on cooling to ambient temperature. The gels could not be melted on re-heating the samples to the boiling temperature of *n*-hexane. Clear solutions of high viscosity were also found at 20 °C with **3**–*tert*-butyl acetate, **9**–toluene, **9**–styrene, and **10**–toluene (*cf.* Table 2). In $CHCl_3$ 2.5 wt% of **1** and **2** only partially dissolved, but the heterogeneous mixture gelled upon cooling. Similar observations were made with **2** in toluene and styrene. The gels from such mixtures consisted of swollen gelator particles dispersed in a gelled matrix.

It may be summarised that gelation was most pronounced with relatively non-polar solvents like $CHCl_3$, styrene, toluene, and *n*-hexane, since the solubility of the carbazides was rather limited in non-polar liquids. This orthogonality in solubility and gelation offers intriguing perspectives to induce gel formation by changing the solvent composition ('cold gelation'). Such a situation might be of practical interest as it allows to add a low viscous dissolved gelator to a solution or dispersion that should be gelled, or thickened.

An attempt was made to gel solutions of **1** in DMAc by addition of toluene or *n*-hexane as diluents of lower polarity. At 20 °C up to 33 wt% of **1** is soluble in DMAc without gelation. On diluting the concentrated DMAc solutions, gels were immediately formed. While the toluene gels were slightly turbid, clear gels emerged from *n*-hexane (*cf.* Table 3).

In a similar way hot solutions of DMF and 33 wt% of **2** were gelled by addition of toluene or hexane. Dilution of DMF solutions by means of $CHCl_3$ resulted in turbid inhomogeneous gels on exceeding 4.5 wt% of **2** that became opaque on standing for a prolonged time (> 12 h). Between 2.4 and 0.6 wt% of **2** transparent viscous liquids, containing streaky inhomogeneous regions, were obtained directly after mixing. Within 90 min the inhomogeneities vanished, and simultaneously the mixtures transformed to viscoelastic fluids. The viscoelastic properties have been recognised by the recoil of entrapped air bubbles subsequent to swirling the liquids in a vial.[9] On standing over night the fluid transformed to a turbid soft gel. Similar viscoelastic fluids arised from dilution of 1.2 wt% **2** in THF with petrol ether to an overall concentration of 0.85 wt%.

Table 3 Gelation of **1**–DMAc solutions by addition of toluene, or n-hexane at ambient temperature

[**1**][a]	+solvent	[DMAc][b]	[**1**][c]	10 min	15 h
20.0	Toluene	10.0	2.5	GT	Sη
33.3	Toluene	5.0	2.5	GT	GT
33.3	Toluene	1.7	0.8	GC	GC
33.3	*n*-Hexane	6.2	3.1	GC	GC
33.3	*n*-Hexane	2.2	1.1	GC	GC

[a] Gelator concentration prior to dilution in wt%. [b] DMAc concentration. [c] Gelator concentration of the final mixture in wt%.

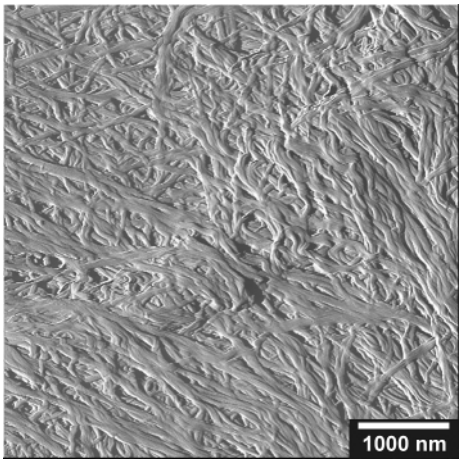

Fig. 1 SFM picture of gel fibres of **2** (0.8 wt%) in THF–PE (2 : 1).

Scanning force microscopy (Fig. 1) resolved the gel network to consist of fibre bundles 90–150 nm in diameter. The bundles contained elementary strings with diameters below 50 nm.

These few examples demonstrate the potential of bis(semicarbazides) to control the mechanical properties of organic liquids. Depending on the molecular structure of the semicarbazide and the solvent composition solid gels, viscoelastic fluids, or viscous liquids can be obtained. Future work will deal with investigation of the gel morphologies, and the kinetics of gelation.

Financial support from the German research foundation (SFB 569, A6) is gratefully acknowledged. The authors want to thank Martin Möller for helpful discussions.

Notes and references

† A solution of 10 mmol diisocyanate in 25 mL THF was added to a solution of 20 mmol *N*-[(alkoxy)benzoyl]hydrazine in 25 mL THF. After 30 min the solvent was removed, the residue taken up with DMF, and precipitated from acetone. The raw compound was crystallised from acetone.

‡ DSC was obtained with a PERKIN ELMER DSC 7 device, calibrated against cyclohexane, water, and indium standards. 5 mg samples were used, the heating rate was 10 K min^{-1}.

1 P. Terech and R. G. Weiss, *Chem. Rev.*, 1997, **97**, 3133; H.-J. Fuhrhop and J. Köning, *Membranes and Molecular Assemblies: the Synkinetic Approach*, ed. J. F. Stoddart, RSC, Oxford, 1994.

2 A. Lipowitz, *Ann. Chem. Pharm.*, 1841, **38**, 348; M. O. Foster and T. Jackson, *Trans. Chem. Soc.*, 1907, **91**, 1888.

3 J. H. van Esch and B. L. Feringa, *Angew. Chem., Int. Ed.*, 2000, **39**, 2263.

4 U. Beginn, G. Zipp and M. Möller, *J. Polym. Sci, Part A: Polym. Chem.*, 2000, **38**, 631; U. Beginn, G. Zipp and M. Möller, *Chem. Eur. J.*, 2000, **6**, 2016.

5 U. Beginn, S. S. Sheiko and M. Möller, *Macromol. Chem. Phys.*, 2000, **201**, 1008.

6 U. Beginn, S. Keinath and M. Möller, *Macromol. Chem. Phys.*, 1998, **199**, 2379.

7 U. Beginn, G. Zipp and M. Möller, *Adv. Mater.*, 2000, **12**, 510; U. Beginn, G. Zipp, A. Mourran and M. Möller, *Adv. Mater.*, 2000, **12**, 513.

8 E. A. Swakon and C. G Brannen, US Patent 2,710,839, June 14, 1955, (CA 49: 13642d); J. H. van Esch, F. S. Schoonbeek, M. de Loos, H. Kooijman, A. L. Spek, R. M. Kellogg and B. L. Feringa, *Chem. Eur. J.*, 1999, **5**, 937.

9 H. Hoffmann, *Ber. Bunsenges. Phys. Chem.*, 1994, **98**, 143.

CHEMCOMM Communication
www.rsc.org/chemcomm

Transition metal-catalysed acylation of α,β-unsaturated carbonyl compounds with acylstannanes

Eiji Shirakawa,*[a] Youko Yamamoto,[a] Yoshiaki Nakao,[b] Teruhisa Tsuchimoto[a] and Tamejiro Hiyama*[b]

[a] *Graduate School of Materials Science, Japan Advanced Institute of Science and Technology, Asahidai, Tatsunokuchi, Ishikawa 923-1292, Japan. E-mail: shira@jaist.ac.jp*
[b] *Department of Material Chemistry, Graduate School of Engineering, Kyoto University, Sakyo-ku, Kyoto 606-8501, Japan*

Received (in Cambridge, UK) 3rd July 2001, Accepted 8th August 2001
First published as an Advance Article on the web 13th September 2001

Acylstannanes were found to add to such α,β-unsaturated carbonyl compounds as enones or ynoates in the presence of a nickel or palladium catalyst to give 2-stannyl-4-oxoalk-2-enoates or 1,4-diketones, whereas the three component coupling between acylstannanes, enones and aldehydes provided 2-hydroxymethyl 1,4-diketones.

Well-documented synthetic precursors for five-membered ring compounds are 1,4-dicarbonyl compounds: furans, pyrroles or thiophenes are readily prepared by mixing with an acid,[1] an amine[2] or a sulfur nucleophile,[3] respectively, whereas treatment of 1,4-diketones with a base gives cyclopentenones.[4] On the other hand, alkenes having a carbonyl group at both of the carbon atoms behave as good dienophiles in the Diels–Alder reaction. Although addition of a C–H bond of aldehydes to α,β-unsaturated carbonyl compounds provides a straightforward way to 1,4-dicarbonyl compounds,[5] the reaction is hard to apply to synthesis of structurally complex targets. For this purpose, acylmetalation of α,β-unsaturated carbonyl compounds[6] is apparently beneficial, since metal atoms of resulting organometallic compounds can be replaced by various groups through the reaction with electrophiles. Here we report the nickel-catalysed acylstannylation of ynoates,[7] the palladium-catalysed addition of the acyl group of acylstannanes to enones, and the palladium-catalysed three component coupling between acylstannanes, enones and aldehydes to give 2-hydroxymethyl 1,4-diketones.[8]

We first examined the reaction of benzoyl(trimethyl)tin (**1a**) with methyl oct-2-ynoate (**2a**) in the presence of 5 mol% of bis(cycloocta-1,5-diene)nickel, $Ni(cod)_2$. The reaction in toluene at 30 °C for 2.5 h gave an 88 : 12 mixture of methyl (*Z*)-3-benzoyl-2-trimethylstannyloct-2-enoate (**3a**) and methyl (*E*)-2-benzoyl-3-trimethylstannyloct-2-enoate (**4a**) in 66% yield (Scheme 1 and entry 1 of Table 1). Although the reaction in a more polar solvent such as THF or DMF proceeded with a perfect preference for **3a** over **4a**, a considerable amount of the decarbonylation product, trimethyl(phenyl)tin, also was produced and the yield of **3a** was less than 40%.[9] Acylstannylation of various alkynes with the $Ni(cod)_2$ catalyst was next studied in toluene (Table 1). In addition to aliphatic ynoates, trimethylsilyl- and phenyl-substituted propiolates also can participate in the reaction with **1a** to give regioisomeric mixtures (entries 2–4). The regiochemistry was largely affected by the substituent on propiolate, where an electron-donating silyl group exhibited selectivity much higher than an electron-withdrawing phenyl

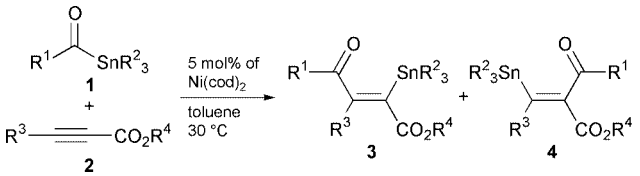

Scheme 1

Table 1 Nickel-catalysed acylstannylation of ynoates[a]

Entry	R^1	R^2	R^3	R^4	Time/h	Yield (%)[b]	**3** : **4**[c]
1	Ph	Me	$CH_3(CH_2)_4$	Me	2.5	66	88 : 12
2	Ph	Me	Me_3Si	Et	3	85	98 : 2
3	Ph	Me	Me	Me	1.5	56	91 : 9
4	Ph	Me	Ph	Et	24	58	66 : 34
5	Et	Bu	$CH_3(CH_2)_4$	Me	24	47	79 : 21

[a] The reaction was carried out in toluene (0.4 mL) at 30 °C using an acylstannane (0.30 mmol), an ynoate (0.90 mmol) and $Ni(cod)_2$ (15 μmol). [b] Isolated yield based on the acylstannane. [c] Determined by ^{119}Sn NMR.

group. Tributyl(propanoyl)tin (**1b**) also underwent acylstannylation of **2a** (entry 5).

Enones also were found to react with acylstannanes to give 1,4-diketones. However, a palladium complex showed catalytic activity higher than the nickel complex (Scheme 2). For example, the reaction of benzoyl(tributyl)tin (**1c**) with methyl vinyl ketone (**5a**) proceeded in the presence of tris(dibenzylideneacetone)dipalladium, $Pd_2(dba)_3$, in THF at 50 °C for 2 h to afford 1-phenylpentane-1,4-dione (**6a**) in 71% yield. Propanoylstannane **1b** also added to **5a** or phenyl vinyl ketone (**5b**). An aqueous additive in a stoichiometric amount accelerated the reaction considerably.

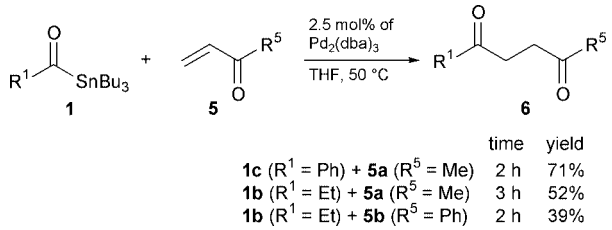

Scheme 2

Although the $SnBu_3$ group that should be definitely versatile for further construction of carbon frameworks was lost in the reaction product with enones, *in situ* trapping with an electrophile achieved three component coupling and accordingly indicated the presence of the stannyl group in the product. Thus acylstannanes, enones and aldehydes reacted in the presence of a catalytic amount of $Pd_2(dba)_3$ to give labile 2-hydroxymethyl 1,4-diketones. As the products easily underwent a retro-aldol reaction during purification by silica gel chromatography, the three component coupled products were isolated after acetylation with acetic anhydride–pyridine (Scheme 3 and Table 2).

The stannyl group of the ynoate–acylstannylation products can be easily converted into organic groups through the palladium-catalysed cross-coupling reaction with organic halides. Actually, **3a** coupled with ethyl 4-iodobenzoate in the presence of palladium and copper catalysts and gave expected product **9** with retention of configuration (Scheme 4).

 DOI: 10.1039/b105832k

Table 2 Palladium-catalysed three component coupling between acylstannanes, enones and aldehydes[a]

Entry	R^1	R^5	R^6	Time/h	Yield (%)[b]	Diastereomeric ratio
1	Ph	Me	4-$CF_3C_6H_4$	1.5	64	73:27
2	Ph	Ph	4-$CF_3C_6H_4$	24	37	55:45
3	Et	Me	4-$CF_3C_6H_4$	1	62	51:49
4	Et	Ph	4-$CF_3C_6H_4$	1.5	44	53:47
5[c]	Ph	Me	Ph	0.5	44	79:21
6[c]	Ph	Me	$PhCH_2CH_2$	1	38	69:31

[a] The reaction was carried out in THF (0.2 mL) at 50 °C using an acylstannane (0.15 mmol), an enone (0.23 mmol), an aldehyde (0.45 mmol) and $Pd_2(dba)_3$ (3.8 μmol). Then, the reaction mixture was treated with acetic anhydride (0.68 mmol) and pyridine (0.5 mL) at rt for 2 h. [b] Isolated yield based on the acylstannane. [c] The reaction was carried out in the presence of Linde molecular sieves Type 4A (60 mg).

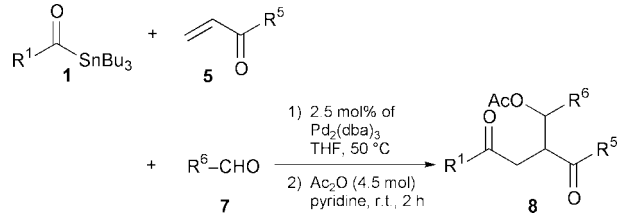

Scheme 3

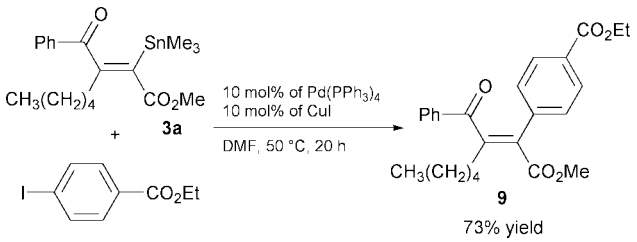

Scheme 4

The catalytic cycle should be initiated by oxidative addition of an acylstannane to a nickel(0) or palladium(0) complex as we discussed previously,[7] followed by insertion of a C–C unsaturated bond to the C–Ni bond of oxidative adduct **10** (Scheme 5). Insertion of an ynoate should afford relatively stable alkenylnickel complex **11**, which undergoes reductive elimination to give alkenylstannane **3**. In a similar manner, regioisomer **4** also would be produced. On the other hand, insertion of an enone may lead to formation of palladium enolate **12** rather than alkylpalladium complex **12′** owing possibly to relative stability of a Pd–O bond as compared with a Pd–C bond. Reductive elimination of **12** appears to be difficult, but the reaction of **12** with such an electrophile as water or an aldehyde would take place, giving **6** or **8**, respectively.

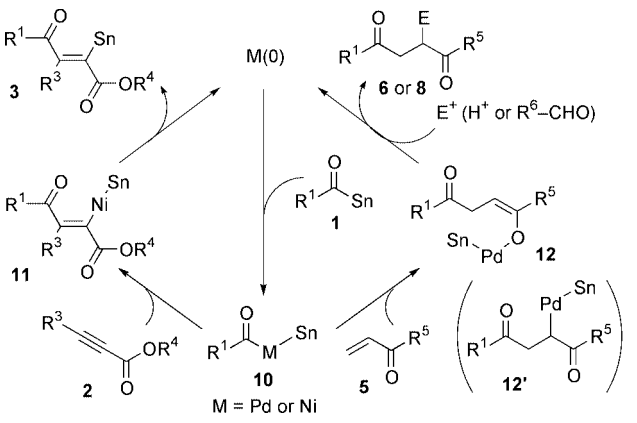

Scheme 5

In conclusion, we have demonstrated that addition of the acyl group of acylstannanes to ynoates or enones readily takes place in the presence of a nickel or palladium catalyst. The addition products are further transformed into 1,4-dicarbonyl compounds having a complicated structure in a separated step or a tandem reaction. Studies on details of the mechanism as well as synthetic applications to various unsaturated substrates and organostannanes are in progress in our laboratories.

We thank the Ministry of Education, Science, Sports and Culture, Japan, for the Grant-in-Aids for COE Research on Elements Science, No. 12CE2005 and Scientific Research, No. 12750758. E. S. thanks the Asahi Glass Foundation for financial support.

Notes and references

1 W. Friedrichsen, *Comprehensive Heterocyclic Chemistry II*, ed. A. R. Katritzky, C. W. Rees and E. F. V. Scriven, Pergamon Press, New York, 1996, vol. 2, p. 352.

2 R. J. Sundberg, *Comprehensive Heterocyclic Chemistry II*, ed. A. R. Katritzky, C. W. Rees and E. F. V. Scriven, Pergamon Press, New York, 1996, vol. 2, p. 149.

3 J. Nakayama, *Comprehensive Heterocyclic Chemistry II*, ed. A. R. Katritzky, C. W. Rees and E. F. V. Scriven, Pergamon Press, New York, 1996, vol. 2, pp. 641–644.

4 C. H. Heathcock, *Comprehensive Organic Synthesis*, ed. B. M. Trost and I. Fleming, Pergamon Press, New York, 1991, vol. 2, pp. 161 and 162.

5 The addition of aldehydes to enones or enoates catalysed by a metal cyanide or a thiazolium salt: H. Stetter and H. Kuhlmann, *Org. React.*, 1991, **40**, 407.

6 Addition reactions of the acyl group of acylmetals in the presence of a transition metal catalyst: (*a*) Y. Hanzawa, N. Tabuchi and T. Taguchi, *Tetrahedron Lett.*, 1998, **39**, 8141; (*b*) Y. Hanzawa, A. Kakuuchi, M. Yabe, K. Narita, N. Tabuchi and T. Taguchi, *Tetrahedron Lett.*, 2001, **42**, 1737; reactions without transition metal catalysts: (*c*) E. J. Corey and L. S. Hegedus, *J. Am. Chem. Soc.*, 1969, **91**, 4926; (*d*) M. P. Cooke Jr. and R. M. Parlman, *J. Am. Chem. Soc.*, 1977, **99**, 5222; (*e*) L. S. Hegedus and R. J. Perry, *J. Org. Chem.*, 1985, **50**, 4955; (*f*) M. F. Semmelhack, L. Keller, T. Sato, E. J. Spiess and W. Wulff, *J. Org. Chem.*, 1985, **50**, 5566; (*g*) M. Yamashita, H. Tashika and M. Uchida, *Bull. Chem. Soc. Jpn.*, 1992, **65**, 1257.

7 Transition metal-catalysed acylstannylation of relatively electron-rich alkynes: (*a*) E. Shirakawa, K. Yamasaki, H. Yoshida and T. Hiyama, *J. Am. Chem. Soc.*, 1999, **121**, 10221; for 1,3-dienes: (*b*) E. Shirakawa, Y. Nakao, H. Yoshida and T. Hiyama, *J. Am. Chem. Soc.*, 2000, **122**, 9030; for 1,2-dienes: (*c*) E. Shirakawa, Y. Nakao and T. Hiyama, *Chem. Commun.*, 2001, 263. Transition metal-catalysed carbostannylation of alkynes: (*d*) E. Shirakawa, H. Yoshida, T. Kurahashi, Y. Nakao and T. Hiyama, *J. Am. Chem. Soc.*, 1998, **120**, 2975; (*e*) E. Shirakawa, H. Yoshida, Y. Nakao and T. Hiyama, *J. Am. Chem. Soc.*, 1999, **121**, 4290; (*f*) E. Shirakawa, H. Yoshida, Y. Nakao and T. Hiyama, *Org. Lett.*, 2000, **2**, 2209; (*g*) H. Yoshida, E. Shirakawa, T. Kurahashi, Y. Nakao and T. Hiyama, *Organometallics*, 2000, **19**, 5671; (*h*) H. Yoshida, E. Shirakawa, Y. Nakao, Y. Honda and T. Hiyama, *Bull. Chem. Soc. Jpn.*, 2001, **74**, 637. See, also ref. 7*a*.

8 For the three component coupling between acylnickel complexes, enones and organic halides, see ref. 6*f*.

9 No carbostannylation product was obtained when 10 mol% of triphenylphosphine, tributylphosphine or pyridine was used as a ligand in a toluene solvent, and the decarbonylation from **1a** predominated.

CHEMCOMM Communication
www.rsc.org/chemcomm

Hierarchic patterning: architectures beyond 'giant molecular wheels'†

Achim Müller,*[a] Ekkehard Diemann,[a] Christoph Kuhlmann,[a] Wolfgang Eimer,[a] Claire Serain,[a] Thomas Tak,[a] Arndt Knöchel[b] and P. Klaus Pranzas[b]

[a] *Faculty of Chemistry, University of Bielefeld, D-33501 Bielefeld, Germany. E-mail: a.mueller@uni-bielefeld.de*
[b] *Institute of Inorganic and Applied Chemistry, University of Hamburg, D-20146 Hamburg, Germany*

Received (in Cambridge, UK) 24th April 2001, Accepted 16th August 2001
First published as an Advance Article on the web 13th September 2001

Based on symmetry breaking steps under one-pot conditions, simple molybdenum oxide-based building blocks initially assemble to 'giant molecular wheels' in a fast process followed by further slower assembly processes leading stepwise to more complex mesoscopic architectures including spherical ones and finally to those with a size larger than 500 nm.

Molybdenum blue solutions have fascinated chemists for more than 200 years without, however, success in identifying their true chemical nature.[1] One interesting aspect is that a structural hierarchy is obtained in a multi-step process: the initial assembly of very simple building blocks form 'giant molecular wheel' type species within seconds, and subsequent assembly leads to spherical patterns of the final complex architectures, as visualised by SEM. Equally surprising and fascinating, the whole structural hierarchy, which spans over more than four orders of magnitude is built up under one-pot conditions without changing the constituents.

We have used dynamic light scattering (DLS)‡ to characterise such solutions. The first preliminary investigations were done using the structurally characterised 'molybdenum blue' compound $Na_{24}[Mo_{144}O_{437}H_{14}(H_2O)_{56}]\cdot xH_2O$ **1** ($x \approx 250$), which contains nanoscaled wheel shaped units covalently linked to chains.[2] Surprisingly, in non-aqueous media such as methanol or acetone, we observed only a single relaxation process from which the hydrodynamic radius was calculated to be about 40 nm. In particular, it should be noted that the inverse Laplace transformation of the intensity autocorrelation function yields a rather low variance of the size distribution of the particles in solution (Fig. 1). Measurements with different solutions reveal that the variation of particle sizes is always rather small. These results are in agreement with the experiments performed in methanolic and acetonic solutions prepared from $(NH_4)_{28}[Mo_{154}(NO)_{14}O_{448}H_{14}(H_2O)_{70}]\cdot xH_2O$ **2** ($x \approx 350$),[3] which contains the same type of discrete 'giant molecular wheels' with $MoNO^{3+}$ instead of MoO^{4+} groups, and especially from $Na_{15}[Mo_{154}O_{462}H_{14}(H_2O)_{70}]_{0.5}[Mo_{152}O_{457}H_{14}(H_2O)_{68}]_{0.5}\cdot xH_2O$ **3** ($x \approx 400$) which can easily be obtained in crystalline form and high yield in a facile synthesis.[4] With DLS we do not observe an additional much faster relaxation process which would correspond to the translational motion of *monomeric* units in solution, probably due to the much lower scattering power of these particles compared to the aggregate structures. Model calculations were performed for rod-like or oblate ellipsoid particles. To achieve consistency between experimental data and theoretical predictions, we have to assume either very elongated molecules (for example rods of 4 nm diameter and 400 nm in length) or a near spherical ellipsoid shape.

Small angle X-ray scattering (SAXS) experiments‡ on such fresh solutions showed the presence of small particles as obtained from the distance distribution function [Fig. 2(a)] which corresponds clearly to the scattering of isolated single 'giant molecular wheel' units for which structure and form factors are known from the crystal structure analysis. Repeating the measurement on these solutions after about two days displayed significant changes. As shown in Fig. 2(b), the corresponding distance distribution function develops further maxima at larger distances. Supported by some preliminary simulation calculations, this implies that for **1** and **3** chain formation takes place where, within the limits of our present SAXS setup, four-membered assemblies dominate.

Therefore, we assume that the chains of **1** break in solution such that the *monomeric* unit is the 'giant molecular wheel' and a new aggregation process initiates from this particle. This corresponds to the observation that compound **3** which consists of isolated 'giant wheels' already at the beginning also shows this type of aggregation process. USAXS measurements would be required to elucidate also the presence and nature of higher aggregates with more than four members.

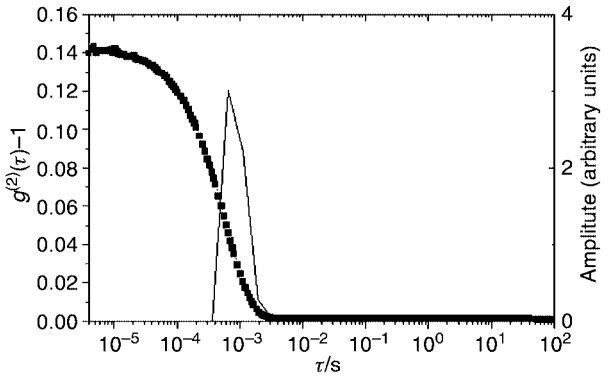

Fig. 1 Intensity autocorrelation function $g^{(2)}(\tau) - 1$ and the corresponding distribution function $G(\Gamma^{-1})$ of **1** or **3** in methanol.

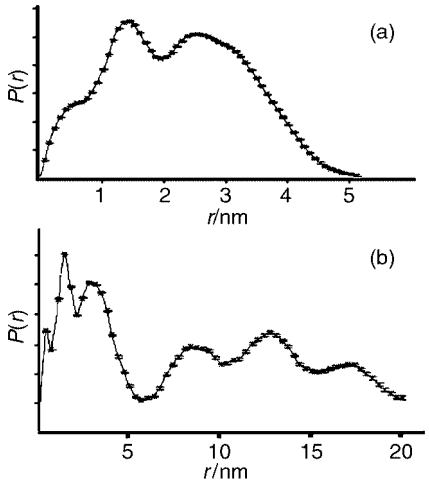

Fig. 2 Distance distribution function $P(r)$ from SAXS data (a) obtained from a fresh solution of **1** (or **3**, *cf.* text) and (b) from the same solution after two days.

† Dedicated to Professor Phillip Gütlich on the occasion of his 65th birthday.

 DOI: 10.1039/b103639b

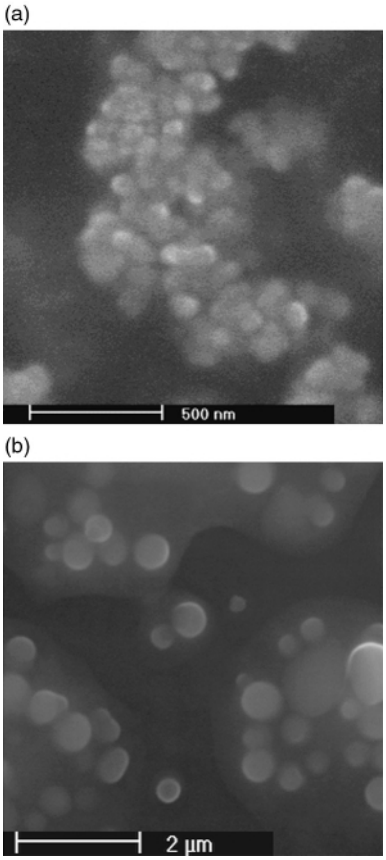

Fig. 3 ESEM images of the spherical aggregates obtained from a solution of **1**, showing further aggregation to form some more complex architecture (a); ESEM image of larger spherical units formed from an acetonic solution of **3** (b).

To obtain more information about the shape of the higher aggregated particles we examined them with an environmental scanning electronic microscope (ESEM). Fig. 3 shows ESEM micrographs‡ of residues obtained by drying off the solvent under water vapour pressure. The observed spherical particles have mainly an apparent diameter of 80–90 nm which is in reasonable agreement with the DLS results. Particularly when acetone instead of methanol is used as solvent even larger and more perfect spheres are obtained. The question whether these spherical units are filled or hollow can probably be answered from future USAXS measurements. EDAX performed on single spheres shows (*via* the carbon signal) the presence of considerable amounts of solvent inside, and, on switching the SEM from the environmental to the high vacuum mode, the spherical assemblies burst, thus implying that hollow spheres were formed. This would also explain the obviously intrinsically limited resolution of the ESEM pictures. Further studies will have to elucidate the thickness and order of the spherical walls, *e.g*. whether of onion type, and how and why they are formed from chain-like building units.

This work was supported by the Deutsche Forschungsgemeinschaft and the Fonds der Chemischen Industrie. We thank E. Krickemeyer for his contributions.

Notes and references

‡ *Experimental*: compounds **1**, **2** and **3** were dissolved in methanol (UV grade) or acetone (p.a.) (c = 0.1 mg mL^{-1} for the DLS, but higher for the SAXS). The solutions were filtered through a filter of 0.2 µm pore size and subsequently centrifuged for 30 min at *ca*. 2000 rpm to remove larger dust particles and to de-gas the solvent. All steps were performed in an Ar atmosphere.

DLS measurements: the light scattering measurements (λ = 488 nm) were performed at low sample concentration and with minimum laser power to avoid any significant heating of the sample due to absorption of the coloured material in the visible region. The experimental data were analysed using the program CONTIN.

Small angle X-ray scattering: the SAXS experiments were carried out at the instrument POLYP at beamline A2 at HASYLAB/DESY in Hamburg.[5] The solutions used for SAXS investigations were the same as those used for DLS and ESEM studies, but with higher concentrations (c = 5 mg mL^{-1}) in order to obtain sufficient scattering statistics, so that the subtraction of the solvent scattering is possible. The solutions were measured in vacuum tight sample cells with a diameter of 1 mm and Kapton windows immediately after preparation. A fixed wavelength of 0.154 nm, distances between sample and detector of 0.49 and 1.91 m and measuring times of 20 min were used.

Scanning electron microscopy: A FEI ESEM XL30 was used at an accelerating voltage of 25 kV under 4.0 mbar water vapor pressure. Acetonic and methanolic solutions were used directly. With the ESEM the sample could be examined in a wet atmosphere. Under these conditions a *fast* destruction of the aggregates is avoided.

1 A. Müller and C. Serain, *Acc. Chem. Res*., 2000, **33** and references therein.
2 A. Müller, E. Krickemeyer, H. Bögge, M. Schmidtmann, F. Peters, C. Menke and J. Meyer, *Angew. Chem., Int. Ed*., 1997, **36**, 484.
3 *Cf.* ref. 1; for the first report of the not completely crystalline material, see: A. Müller, E. Krickemeyer, J. Meyer, H. Bögge, F. Peters, W. Plass, E. Diemann, S. Dillinger, F. Nonnenbruch, M. Randerath and C. Menke, *Angew. Chem., Int. Ed*., 1995, **34**, 2122, where an error limit had been given for the anion charge.
4 Müller, S. K. Das, V. P. Fedin, E. Krickemeyer, C. Beugholt, H. Bögge, M. Schmidtmann and B. Hauptfleisch, *Z. Anorg. Allg. Chem*., 1999, **625**, 1187; see, especially: A. Müller, S. K. Das, E. Krickemeyer and C. Kuhlmann, *Inorg. Synth*., in press.
5 G. Elsner, C. Riekel and H. G. Zachmann, *Adv. Polym. Sci*., 1985, **67**, 1.

CHEMCOMM Communication
www.rsc.org/chemcomm

Inorganic–organic hybrids derived from oxovanadium sulfate motifs: synthesis and characterization of $[V^{IV}O(\mu_3\text{-}SO_4)(2,2'\text{-bpy})]_\infty$

M. Ishaque Khan,*[a] Sabri Cevik[a] and Robert J. Doedens[b]

[a] *Department of Biological, Chemical, and Physical Sciences, Illinois Institute of Technology, Chicago, IL 60616, USA. E-mail: Khan@iit.edu*

[b] *Department of Chemistry, University of California, Irvine, CA 92697, USA*

Received (in Purdue, IN, USA) 28th July 2001, Accepted 16th August 2001
First published as an Advance Article on the web 17th September 2001

The hydrothermal reaction of V_2O_5, V_2O_3, 2,2′-bpy and Na_2SO_4 in dilute sulfuric acid yields a novel hybrid, $[V^{IV}O(\mu_3\text{-}SO_4)(2,2'\text{-bpy})]_\infty$, which demonstrates the potential of constructing a new class of robust composite solids composed of a $\{V/O/SO_4\}$-based framework decorated with organic functionalities by combining appropriate vanadyl sulfate motifs with a variety of organic ligands.

The amalgamation of oxovanadate moieties with the tetrahedral $\{PO_4\}$ ligand has produced an impressive array of vanadium–oxide–phosphate based systems with fascinating electronic and structural properties.[1–8] Oxovanadiumphosphate-based porous-framework materials containing unprecedented large cavities and channels similar to those observed in conventional zeolites and solids with double-helix structure have been synthesized and characterized in recent years.[7,8] As compared to the $V/O/PO_4$, however, well-defined $V/O/SO_4$-based inorganic materials prepared from the combination of sulfate with oxovanadate units are rare.[9–11]

Since vanadium exhibits extensive coordination chemistry involving a variety of organic ligands,[12] the solids constructed from $\{V/O/SO_4\}$ system may, in principle, incorporate appropriate organic ligands. This offers opportunity for making new inorganic–organic hybrid (composite) phases containing an inorganic $\{V/O/SO_4\}$ backbone decorated with organic functionalities. Such compounds are practically unknown.[10d] We are currently exploring the potential of this approach[13] which, to our knowledge, has not been exploited for materials design and development. This report describes the synthesis and characterization by IR spectroscopy, thermogravimetry, elemental analysis, manganometric titration, bond valence sum calculations, and complete single crystal X-ray structure analysis of a new solid $[V^{IV}O(\mu_3\text{-}SO_4)(2,2'\text{-bpy})]_\infty$ **1**.

Green needle shaped crystals of **1** are prepared in ~78% yield by the hydrothermal reaction of V_2O_5, V_2O_3, Na_2SO_4, 2,2′-bpy and 1 M H_2SO_4 in the molar ratio 0.5 : 0.5 : 5 : 3 : 10 at 180 °C for 48 h.†

The crystal structure‡ of **1** is shown in Fig. 1. It may be viewed as constructed from the centrosymmetric dimer building block, $[V^{IV}_2O_2(\mu_3\text{-}SO_4)_2(2,2'\text{-bpy})_2]$, which contains two $[V^{IV}O(\mu_3\text{-}SO_4)(2,2'\text{-bpy})]$ units linked through sulfate groups. The crystal packing views, which exhibit alternating inorganic ($VOSO_4$) and organic (2,2′-bpy) layers, are aesthetically appealing. The extended structure consists of parallel running inorganic chains decorated by organic ligands. The individual chains contain $\{VO_4N_2\}$ octahedra and $\{SO_4\}$ tetrahedra joined by common vertices. Every sulfate ligand, which uses three oxygen atoms to bond three vanadium centers, bridges three $\{VO_4N_2\}$ octahedra each one of which, in turn, shares vertices with three $\{SO_4\}$ groups. This generates a series of eight-membered {–V–O–S–O–V–O–S–O–} rings that are fused to construct the entire chain. The overall geometry around sulfur is a slightly distorted tetrahedron. All O–S–O angles (105.5–112.7°) and the S–O bond distances are in the normal range. The octahedral geometry around each vanadium center is defined by a terminal oxo group, three μ-O groups from the three adjacent sulfate ligands in the chain, and two nitrogen donor atoms from a chelating 2,2′-bpy ligand. The terminal oxo groups on vanadium centers alternate such that any two adjacent vanadium atoms will have their terminal oxo groups pointing toward the opposite sides of the chain.

The structure and building block units in **1** are significantly different to those observed in our earlier reported compound $[V^{IV}_2O_2(OH)_2(\mu\text{-}SO_4)(2,2'\text{-bpy})_2]$ **2**.[13a] The structure of **2** consists of ribbons constructed from the infinite inorganic chains, $[-\{V_2O_2(\mu\text{-}OH)_2\}(\mu\text{-}SO_4)\{V_2O_2(\mu\text{-}OH)_2\}-SO_4]$, composed of pairs of edge sharing $\{VO_2(OH)_2N_2\}$ octahedra joined by $\{SO_4\}$ tetrahedra, laced by organic (2,2′-bpy) ligands. The metrical parameters of the two $V/O/SO_4$/2,2′-bpy-based hybrid materials (**1** and **2**) are comparable.

The comparison of the two structures may suggest the possible transformation of **2** into **1** by the replacement of the two μ-(OH) groups in **2** by a μ_3-SO_4 group, cleavage of {V–(OH)–V} bonds, and concomitant formation of new {V–(SO_4)–V} bonds accompanied by condensation. So far, we have not achieved the chemical interconversion between **1** and **2**. Compound **1** can, however, be prepared by the slight modification in the reaction used to synthesize **2**. The structure of **1** is strikingly similar to a recently reported compound $[Fe^{III}_2Cl_2(MoO_4)_2(2,2'\text{-bpy})_2]$ **3**[14] in which {FeCl} and tetrahedral $\{MoO_4\}$ groups occupy the positions equivalent to that of {VO} and $\{SO_4\}$ groups, respectively, in **1**. This suggests that $\{Fe^{III}Cl\}$ and $\{Mo^{VI}O_4\}$ groups are topologically equivalent to $\{V^{IV}O\}$ and $\{S^{VI}O_4\}$, respectively.[15a]

The bond valence sum§ calculations[15b] and manganometric titration (of V^{IV} sites) results are consistent with the formulation and charge balance requirements of **1**. Thermogravimetric analysis of **1** reveals its remarkable thermal stability showing no weight loss up to ~420 °C, a two-step weight loss in the range 423–488 °C corresponding to the decomposition of 2,2′-bpy and sulfate ligands, and no further weight change up to 600 °C. The IR spectrum of the black residue exhibits features [at 994w, 738m br, 699(sh), 532m and 439m cm^{-1}] of a reduced vanadium oxide phase that has not been further characterized.

This report underlines the potential of the approach for making new and robust inorganic–organic hybrid phases. In view of the spectacular progress in the design and development of $V/O/PO_4$-based materials, it is clear that many more $V/O/SO_4$-based systems remain to be discovered. The suitable combination of oxovanadate sulfate fragments and organic ligands could yield new composites (and nanocomposites) that may exhibit properties unobserved in purely organic or inorganic phases.

This work was partly supported by a grant to M. I. K. from the American Chemical Society's Petroleum Research Fund (ACS-PRF# 35591-AC5).

Notes and references

† A mixture of V_2O_5, V_2O_3, Na_2SO_4, 2,2′-bpy and 1 M H_2SO_4 in molar ratio 0.5 : 0.5 : 5 : 3 : 10 contained in a 23 ml Teflon-lined Parr autoclave was

 DOI: 10.1039/b106866k

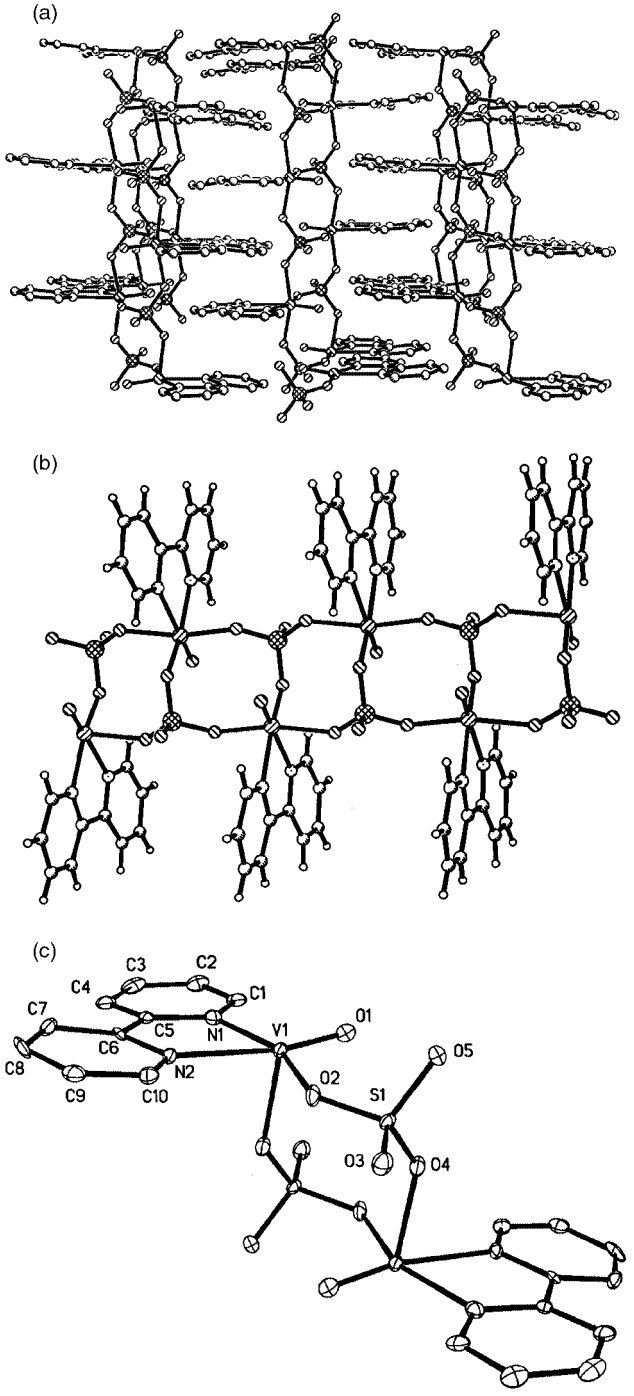

Fig. 1 (a) A view of the extended structure of $[V^{IV}O(\mu_3\text{-}SO_4)(2,2'\text{-bpy})]_\infty$. (b) Structure of a chain showing eight-membered rings. (c) The centrosymmetric building block unit in the crystal structure of **1** showing atom-labeling scheme. Hydrogen atoms are not shown. Selected bond lengths (Å): V1–O1 1.582(5), V1–O2 1.994(5), V1–O4 2.046(5), V1–O5 2.062(5), V1–N1 2.13396), V1–N2 2.259(6), S1–O3 1.442(5), S1–O4 1.479(5), S1–O5 1.484(5), S1–O2 1.499(5).

heated for 48 h at 180 °C. After cooling the autoclave for 4 h, crystals of **1** were filtered from mother-liquor, washed with water, and dried in the air at room temperature. The filtrate gave a second crop of **1**. Compound **1** could also be prepared by the hydrothermal reactions of $[VO(H_2O)_4SO_4]XSO_4$ {X = $[HN(C_2H_4)_3NH]^{2+}$ or $[H_2N(C_2H_4)_2NH_2]^{2+}$},[13b,c] 2,2′-bpy, Na_2SO_4 and 2 M sulfuric acid in the molar ratio 1.25 : 5 : 2 : 10 at 180 °C for 48 h. Crystals of **1** are stable in air, insoluble in common solvents, and analyzed satisfactorily for C, H, N and S. *Selected IR absorption bands* for **1**: (KBr pellet, 1400–500 cm^{-1}): 1315m, 1250s, 1234s, 1158s, 1124s, 1112s, 1097s, 1056s, 1044s, 1030s, 1022s, 979s, 897w, 807w, 771s, 732s, 684m, 655m, 648w, 633m, 597s, 587s, 505m cm^{-1}.

‡ *Crystal data* for **1**: $C_{10}H_8N_2O_5SV$, M = 319.18, monoclinic, space group $P2_1/n$, a = 6.4102(6), b = 16.4887(16), c = 10.2176(10) Å, β = 99.417(2)°, U = 1065.40(18) Å^3, Z = 4, T = 158(2) K, D_c = 1.99 Mg m^{-3}, μ = 1.146 mm^{-1}, $F(000)$ = 644, crystal size = 0.22 × 0.05 × 0.03 mm. A total of 7756 reflections ($2.37 \leqslant \theta \leqslant 23.27°$) were collected, of which 1530 unique reflections were used for structural elucidation (R_{int} = 0.0487). The final $R1$ was 0.0658 (all data).

CCDC reference number 167561. See http://www.rsc.org/suppdata/cc/b1/b106866k/ for crystallographic data in CIF or other electronic format.

§ 4.0 valence unit per vanadium center in the compound.

1 J. Zubieta, *Comments Inorg. Chem.*, 1994, **16**, 153.
2 R. C. Haushalter, L. M. Meyer and J. Zubieta, in *Early Transition Metal Clusters With π-Donor Ligands*, ed. M. H. Chisholm, VCH, New York, 1995, p. 217.
3 Y. Zhang, A. Clearfield and R. C. Haushalter, *Chem. Mater.*, 1995, **7**, 1221.
4 V. Soghomonian, Q. Chen, R. C. Haushalter, J. Zubieta, C. J. O'Connor and Y.-S. Lee, *Chem. Mater.*, 1993, **5**, 1690.
5 M. I. Khan, R. Haushalter, C. J. O'Connor, C. Tao and J. Zubieta, *Chem. Mater.*, 1995, **7**, 593.
6 M. Roca, D. M. Marcos, P. Amorós, A. Beltrán-Porter, A. J. Edwards and D. Beltrán-Porter, *Inorg. Chem.*, 1996, **35**, 5613.
7 M. I. Khan, L. Meyer, R. Haushalter, A. Schweitzer, J. Zubieta and J. Dye, *Chem. Mater.*, 1996, **8**, 43; V. Soghomonian, Q. Chen, R. C. Haushalter and J. Zubieta, *Angew. Chem., Int. Ed. Engl.*, 1993, **32**, 610.
8 V. Soghomonian, Q. Chen, R. C. Haushalter, J. Zubieta and C. J. O'Connor, *Science*, 1993, **259**, 1596.
9 K. Richter and R. Mattes, *Z. Anorg. Allg. Chem.*, 1992, **611**, 158; K. Richter and R. Mattes, *Inorg. Chem.*, 1991, **30**, 4367.
10 (*a*) K. M. Eriksen, K. Nielsen and R. Fehrmann, *Inorg. Chem.*, 1996, **35**, 480; (*b*) K. Nielsen, R. Fehrmann and K. M. Ericksen, *Inorg. Chem.*, 1993, **32**, 4825; (*c*) S. Fehrmann, G. N. Boghosian, G. N. Papatheodorou, K. Nielsen, R. W. Berg and N. J. Bjerrum, *Inorg. Chem.*, 1989, **28**, 1847; (*d*) K. Kanamori, E. Kameda and K. Okamoto, *Bull. Chem. Soc. Jpn.*, 1996, **69**, 2901.
11 B. I. Lazoryak, *Russ. Chem. Rev.*, 1996, **65**, 287.
12 M. I. Khan and J. Zubieta, in *Early Transition Metal Clusters With π-Donor Ligands*, ed. M. H. Chisholm, VCH, New York, 1995; M. I. Khan and J. Zubieta, *Prog. Inorg. Chem.*, 1995, **43**, 1; A. Cotton, G. Wilkinson, C. A. Murillo and M. Bochmann, *Advanced Inorganic Chemistry*, Wiley, New York, 6th edn., 1999; *Vanadium in Biological Systems*, ed. N. D. Chasteen, Kluwer Academic Publishers, Dordrecht, 1990.
13 (*a*) M. I. Khan, S. Cevik, D. Powell, S. Li and C. J. O'Connor, *Inorg. Chem.*, 1998, **37**, 81; (*b*) M. I. Khan, S. Cevik and R. J. Doedens, *Inorg. Chim. Acta*, 1999, **292**, 112; (*c*) M. I. Khan, S. Cevik and R. J. Doedens, in *Polyoxometalate Chemistry for Nanocomposite Design*, ed. T. Yamase and M. T. Pope, Plenum Publishing Corporation, New York, under review.
14 P. J. Zapf, R. P. Hammond, R. C. Haushalter and J. Zubieta, *Chem. Mater.*, 1998, **10**, 1366.
15 (*a*) Shannon ionic radii (Å): S^{6+} = 0.29; Mo^{6+} = 0.59; Fe^{3+} = 0.55 (low spin), 0.65 (high spin); V^{4+} = 0.58; Cl^- = 1.81; O^{2-} = 1.40 (R. D. Shannon, *Acta Crystallogr., Sect. A*, 1976, **32**, 751); (*b*) I. D. Brown, in *Structure and Bonding in Crystals*, ed. M O'Keefe and A. Navrotdky, Academic Press, New York, 1981, vol. II, p. 1.

CHEMCOMM
Communication
www.rsc.org/chemcomm

Stereoselective total synthesis of (+)-myriocin from D-mannose

Takeshi Oishi, Koji Ando and Noritaka Chida*

Department of Applied Chemistry, Faculty of Science and Technology, Keio University, Hiyoshi, Kohoku-ku, Yokohama 223-8522, Japan. E-mail: chida@applc.keio.ac.jp

Received (in Cambridge, UK) 4th June 2001, Accepted 21st August 2001
First published as an Advance Article on the web 4th September 2001

The stereoselective total synthesis of myriocin 1 from D-mannose is described; the carbon framework with three contiguous chiral centers including a tetra-substituted carbon with nitrogen was effectively constructed using Overman rearrangement as the key reaction.

Myriocin[1] (also known as thermozymocidin[2] and ISP-I[3]) **1** (Fig. 1) is an α,α-disubstituted α-amino acid derivative isolated from the culture broth of *Myriococcus*,[1] *Mycelia*[2] and *Isalia*,[3] and reported to show antifungal[1,2] as well as immunosuppressive activities.[3] Its promising immunosuppressive properties[4] and unique structure have attracted much synthetic interest, and several total[5] and formal syntheses[6] of **1** have been reported to date. A structural feature of **1** is the unusual α,α-disubstituted α-amino acid framework with three contiguous chiral centers including a tetra-substituted carbon with nitrogen. For construction of the tetra-substituted carbon, previous syntheses adopted the Strecker synthesis,[6a] hydrocyanation of imines,[5a] the Darzen reaction,[5b,6c] Pd-catalyzed hydroxyamination of a vinyl epoxide,[6b] asymmetric aldol reaction of chiral dilactim ethers,[5c] and Lewis acid catalyzed cyclization of an epoxytrichloroacetimidate.[5d] Our previous success in total synthesis of lactacystin, a heterocyclic natural product with an α,α-disubstituted α-amino acid framework, from D-glucose[7] suggested that the rearrangement of an allylic trichloroacetimidate (Overman rearrangement)[8] derived from a furanose with proper functionalities would generate the tetra-substituted carbon stereoselectively. This methodology was also expected to provide an efficient approach to the highly functionalized part in **1**. Here we report the realization of this plan in a total synthesis of **1** from D-mannose.

The known glycal **2**[9] derived from D-mannose in three steps (80% overall yield) (Scheme 1) was converted into α-methyl furanoside **3**† by oxymercuration-reduction followed by acid treatment in 81% yield. The primary hydroxy group in **3** was selectively *p*-methoxybenzylated[10] to afford **4** (95% yield). Swern oxidation of **4** generated ketone **5**, which was submitted to the Horner–Emmons reaction to provide an inseparable mixture of (*E*)-alkene **6** and its (*Z*)-isomer (15 : 1) in 90% yield from **4**. DIBAL-H reduction of the mixture followed by chromatographic separation afforded geometrically pure (*E*)-allyl alcohol **7** and its (*Z*)-isomer in 93 and 6% isolated yields, respectively. Compound **7** was converted into trichloroacetimidate **8**, which, without isolation, was subjected to Overman rearrangement. Thus, a xylene solution of **8** was heated at 140 °C in the presence of K_2CO_3[11] in a sealed tube for 72 h to provide an inseparable mixture of rearranged products **9** and its C(5) epimer in a ratio of 7 : 1 (determined with 300 MHz ^{1}H NMR) in 90% yield from **7**.‡ The newly formed stereochemistry in **9** was determined to be *R* by NOE experiments

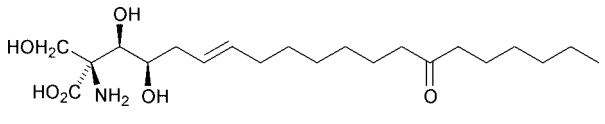

myriocin **1**

Fig. 1

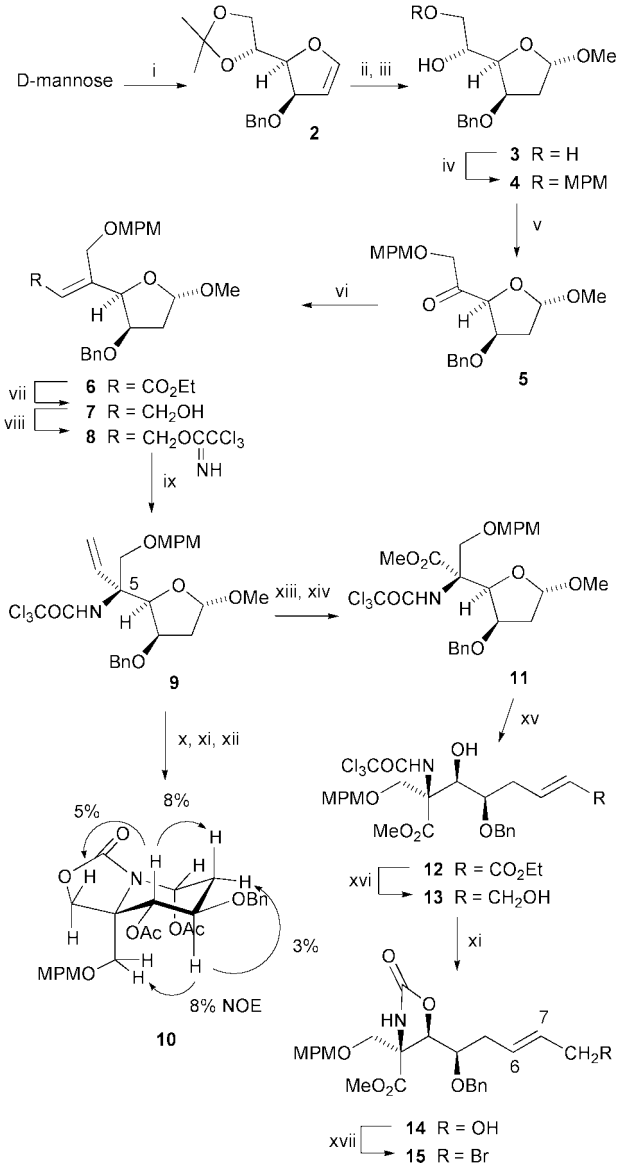

Scheme 1 Bn = –CH_2Ph, MPM = –$CH_2C_6H_4$-*p*-OMe. *Reagents and conditions*: i see ref. 9; ii $Hg(OAc)_2$, THF–H_2O, room temp., then KI, $NaBH_4$, THF–H_2O, 0 °C; iii AcOH–H_2O (3 : 2), room temp., then AcCl, MeOH, 0 °C; iv *n*-Bu_2SnO, toluene, reflux, then MPMCl, CsF, DMF, 70 °C; v $(COCl)_2$, DMSO, CH_2Cl_2, −78 °C, then Et_3N, 0 °C; vi $(MeO)_2P(O)CH_2CO_2Me$, LiBr, DBU, CH_3CN, −40 °C; vii DIBAL-H, toluene, −78 °C; viii Cl_3CCN, DBU, CH_2Cl_2, 0 °C; ix K_2CO_3, *o*-xylene, 140 °C; x O_3, MeOH, −78 °C, then $NaBH_4$, 0 °C; xi DBU, CH_2Cl_2, room temp.; xii 1 M aqueous HCl–THF (1 : 1), room temp., then Ac_2O, DMAP, pyridine, room temp.; xiii O_3, CH_2Cl_2, −78 °C, then Me_2S; xiv $NaClO_2$, NaH_2PO_4, $HOSO_2NH_2$, t-BuOH–H_2O, room temp., then Me_3SiCHN_2, MeOH, room temp.; xv 4 M aqueous HCl–THF (1 : 3), room temp., then $Ph_3P{=}CHCO_2Et$, toluene, room temp.; xvi DIBAL-H, THF–toluene, −15 °C; xvii MsCl, Et_3N, CH_2Cl_2, 0 °C, then LiBr, acetone, room temp.

 DOI: 10.1039/b104864n

of bicyclic carbamate **10** derived from **9** in four steps (46% overall yield). Ozonolysis of the mixture of **9** and its C(5) epimer (Me_2S work-up) followed by oxidation and esterification, and subsequent chromatographic separation afforded **11** in a diastereochemically pure form (82% yield from the mixture of **9** and its epimer). Acid hydrolysis of **11** provided an anomeric mixture of lactol, which was then reacted with stabilized ylide to give (*E*)-alkene **12** as a single isomer in 71% yield. When compound **12** was treated with DIBAL-H in THF–toluene at −15 °C, only the α,β-unsaturated ester function was reduced to afford allyl alcohol **13** (75% yield), which was transformed into cyclic carbamate **14** in 86% yield. The observed coupling constant in **14** ($J_{6,7}$ = 15.6 Hz) clearly supported the (*E*)-geometry of the double bond. The primary hydroxy group in **14** was converted into corresponding bromide to furnish the highly functionalized moiety, allyl bromide **15** in 92% yield.

The hydrophobic part of myriocin, sulfone **16**, was prepared by treatment of 1-bromododecan-6-one§ with $PhSO_2Na$, followed by ketalization (82% yield) (Scheme 2). Sulfone **16** was lithiated with *n*-BuLi, and then reacted with the allyl bromide **15** to afford the coupling product **17** in 80% yield. Saponification of **17** and subsequent Birch reduction gave crude carboxylic acid **18**. Removal of the ketal group and carbamate function in **18** followed by conventional acetylation provided the known γ-lactone **19** {$[\alpha]_D^{20}$ +54 (*c* 0.7, $CHCl_3$); lit.[2a] $[\alpha]_D^{24}$ +57 (*c* 1.0, $CHCl_3$)} in 47% yield from **17**. The spectral data for **19** were identical in all respects to those kindly provided by Professor Hatakeyama.[5d] Finally, according to the precedent,[5d] saponification of **19** followed by neutralization with weak acidic resin (Amberlite IRC-76, H^+ form) furnished (+)-myriocin **1** in 82% yield. The spectroscopic (^1H and ^{13}C NMR) data for synthetic **1** were fully identical with those of natural myriocin, and the physical properties of **1** {mp 168–170 °C, $[\alpha]_D^{23}$ +5.1 (*c* 0.17, MeOH); lit.[3] mp 169–171 °C, $[\alpha]_D$ +4.8 (*c* 0.286, MeOH)} showed good agreement with those reported for the natural product.

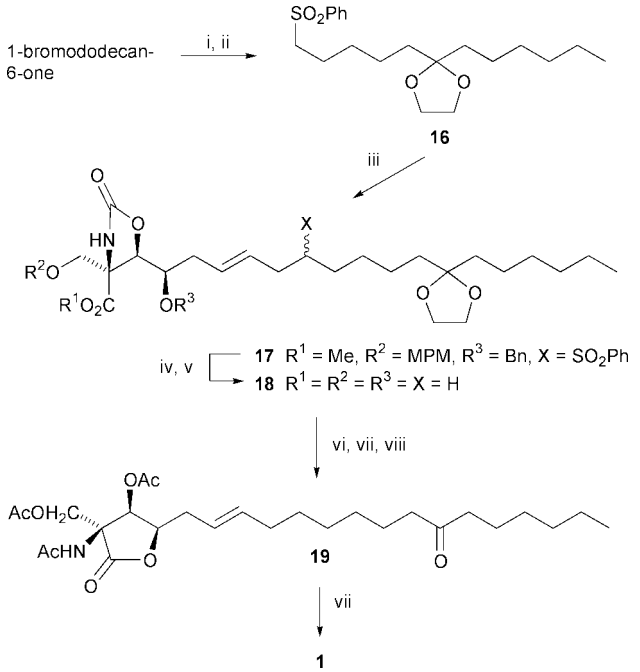

Scheme 2 *Reagents and conditions*: i $PhSO_2Na$, DMF, room temp.; ii $(TMSOCH_2)_2$, TMSOTf, CH_2Cl_2, room temp.; iii *n*-BuLi, THF, −78 °C, then **15**, −78–0 °C; iv LiOH, H_2O–MeOH, room temp.; v Li, liq. NH_3, THF, −78 °C; vi 4 M aqueous HCl–THF (1:1), room temp.; vii 10% aqueous NaOH–MeOH (1:3), reflux; viii Ac_2O, pyridine, room temp.

This synthesis established an alternative and efficient pathway to myriocin **1** (24 linear steps and 4.9% overall yield from D-mannose), which showed almost the same efficiency as previous excellent approaches (2.4–5.1% overall yield).[5b–d] In addition, this work proved that the novel methodology, Overman rearrangement on a furanose scaffold,[7] is quite effective for the chiral synthesis of both acyclic and heterocyclic natural products possessing highly functionalized α,α-disubstituted α-amino acid structures. Additional applications of this methodology in natural product synthesis are now warranted and will be reported in due course.

We thank Professor Susumi Hatakeyama (Nagasaki University, Japan) for providing us with spectral data of an authentic sample and valuable discussions. Financial support of the Grant-in-Aid for Scientific Research from the Ministry of Education, Science, Sports and Culture, Japanese Government is gratefully acknowledged.

Notes and references

† All new compounds described in this paper were fully characterized by 300 MHz ^1H NMR, 75 MHz ^{13}C NMR, IR and mass spectrometric and/or elemental analyses.

‡ Overman rearrangement of an imidate derived from (*Z*)-allyl alcohol afforded **9** and its C(5) epimer in a ratio of 1:5 in 70% yield.

§ 1-Bromododecan-6-one was synthesized by essentially the same procedure reported by Just and Payette [see ref. 6(*a*)]. In place of cyclooctanone, cyclohexanone was employed as the starting material.

1 D. Kluepfel, J. Bagli, H. Baker, M.-P. Charest, A. Kudelski, S. N. Sehgal and C. Vézina, *J. Antibiot*., 1972, **25**, 109; J. Bagli, D. Kluepfel and M. St-Jacques, *J. Org. Chem*., 1973, **38**, 1253.

2 (*a*) F. Aragozzini, P. L. Manachini, R. Craveri, R. Rindone and C. Scolastico, *Tetrahedron*, 1972, **28**, 5493; (*b*) R. Destro and A. Colombo, *J. Chem. Soc., Perkin Trans. 2*, 1979, 896.

3 T. Fujita, K. Inoue, S. Yamamoto, T. Ikumoto, S. Sasaki, R. Toyama, K. Chiba, Y. Hoshino and T. Okumoto, *J. Antibiot*., 1994, **47**, 208.

4 Y. Miyake, Y. Kozutsumi, S. Nakamura, T. Fujita and T. Kawasaki, *Biochem. Biophys. Res. Commun*., 1995, **211**, 396.

5 Total synthesis of myriocin, see: (*a*) L. Banfi, M. G. Beretta, L. Colombo, C. Gennari and C. Scolastico, *J. Chem. Soc., Chem. Commun*., 1982, 488; L. Banfi, M. G. Beretta, L. Colombo, C. Gennari and C. Scolastico, *J. Chem. Soc., Perkin Trans. 1*, 1983, 1613; (*b*) M. Yoshikawa, Y. Yokokawa, Y. Okuno and N. Murakami, *Chem. Pharm. Bull*., 1994, **42**, 994; M. Yoshikawa, Y. Yokokawa, Y. Okuno and N. Murakami, *Tetrahedron*, 1995, **51**, 6209; (*c*) S. Sano, Y. Kobayashi, T. Kondo, M. Takebayashi, S. Maruyama, T. Fuita and Y. Nagao, *Tetrahedron Lett*., 1995, **36**, 2097; (*d*) S. Hatakeyama, M. Yoshida, T. Esumi, Y. Iwabuchi, H. Irie, T. Kawamoto, H. Yamada and M. Nishizawa, *Tetrahedron Lett*., 1997, **38**, 7887.

6 Formal synthesis and synthetic approaches, see: (*a*) G. Just and D. R. Payette, *Tetrahedron Lett*., 1980, **21**, 3219; D. R. Payette and G. Just, *Can. J. Chem*., 1981, **59**, 269; (*b*) A. V. R. Rao, M. K. Gurjar, T. R. Devi and D. R. Kumar, *Tetrahedron Lett*., 1993, **34**, 1653; (*c*) S. Deloisy, T. T. Thang, A. Olesker and G. Lukacs, *Tetrahedron Lett*., 1994, **35**, 4783.

7 N. Chida, J. Takeoka, N. Tsutsumi and S. Ogawa, *J. Chem. Soc., Chem. Commun*., 1995, 793; N. Chida, J. Takeoka, K. Ando, N. Tsutsumi and S. Ogawa, *Tetrahedron*, 1997, **53**, 16287.

8 L. E. Overman, *J. Am. Chem. Soc*., 1978, **98**, 2901; L. E. Overman, *Angew. Chem., Int. Ed. Engl*., 1984, **23**, 579.

9 R. E. Ireland, D. W. Norbeck, G. S. Mandel and N. S. Mandel, *J. Am. Chem. Soc*., 1985, **107**, 3285; K. Dax, B. I. Gluänzer, G. Schulz and H. Vyplel, *Carbohydr. Res*., 1987, **162**, 13; A. Fürstner and H. Weidmann, *J. Carbohydr. Chem*., 1988, **7**, 773.

10 S. David and S. Hanessian, *Tetrahedron*, 1985, **41**, 643.

11 T. Nishikawa, M. Asai, N. Ohyabu and M. Isobe, *J. Org. Chem*., 1998, **63**, 188.

CHEMCOMM Communication
www.rsc.org/chemcomm

Synthesis of the marine natural product barbamide

Viet-Anh Nguyen,[a] Christine L. Willis*[a] and William H. Gerwick[b]

[a] *School of Chemistry, University of Bristol, Cantock's Close, Bristol, UK BS8 1TS. E-mail: chris.willis@bristol.ac.uk*
[b] *College of Pharmacy, Oregon State University, Corvallis, OR 97331, USA*

Received (in Cambridge, UK) 10th July 2001, Accepted 21st August 2001
First published as an Advance Article on the web 17th September 2001

The first total synthesis of the trichlorinated natural product barbamide is described. The convergent approach involves coupling (*S*)-3-trichloromethylbutanoyl chloride with Meldrum's acid (2,2-dimethyl-1,3-dioxane-4,6-dione) to give 15 followed by addition of the novel secondary amine *N*-methyl-(*S*)-dolaphenine 2 (prepared in 6 steps and 24% overall yield from *N*-Cbz-L-phenylalanine) to give the β-keto amide 16 which was converted directly to the required (*E*)-enol ether.

An interesting feature of many biologically active marine-derived natural products is the covalent inclusion of chlorine and bromine. Several compounds which contain a trichloromethyl group have been isolated from sponges of the genus *Dysidea* which have symbiotic association with cyanobacteria.[1] The polychlorinated natural products include, for example, the dysamides,[2] dysidin,[3] dysidenin,[4] herbacic acid[5] and herbamide A.[6] It has been suggested that sponge-based dysidenins are biosynthesised from associated cyanobacteria and indeed in 1996 a new natural product, barbamide, was found in the extracts of the cyanobacterium *Lyngbya majuscula*.[7] From extensive spectrocopic studies, it was proposed that barbamide has the structure **1** encompassing a trichloromethyl group, a thiazole ring as well as the methyl enol ether of a β-keto amide. Barbamide is an intriguing natural product in that the trichloromethyl group derives from the *pro-R* methyl group of leucine without detectable activation to facilitate a potential nucleophilic or electrophilic chlorination process. Hence, we have proposed that biochlorination occurs through a novel process, possibly involving radical chemistry.[8] In the majority of halogenated natural products the halogens are incorporated into positions which are suggestive of their biochemical reaction involving electrophilic species and indeed haloperoxidases which catalyse such reactions have been widely studied.[9]

Herein we report the first total synthesis of barbamide which confirms the structure of the natural product. Degradation studies have indicated that the configuration at C-7 is *S*.[8] Our retrosynthetic analysis is shown in Scheme 1 and involves cleavage of the amide bond to give two fragments: (*S*)-*N*-methyldolaphenine **2** which would be derived from L-phenylalanine and ketone **3** from (*S*)-3-trichloromethylbutanoic acid **4**.

The route for the synthesis of (*S*)-*N*-methyldolaphenine **2** is shown in Scheme 2. Treatment of commercially available *N*-Cbz-L-phenylalanine **5** with an excess of sodium hydride and

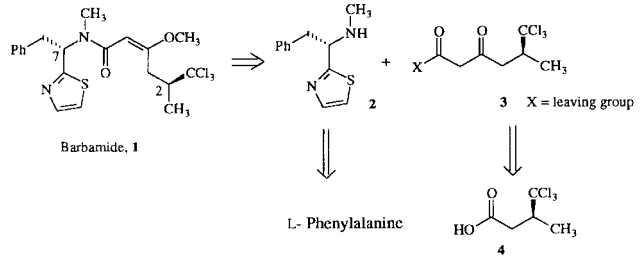

Scheme 1 Retrosynthetic analysis of barbamide.

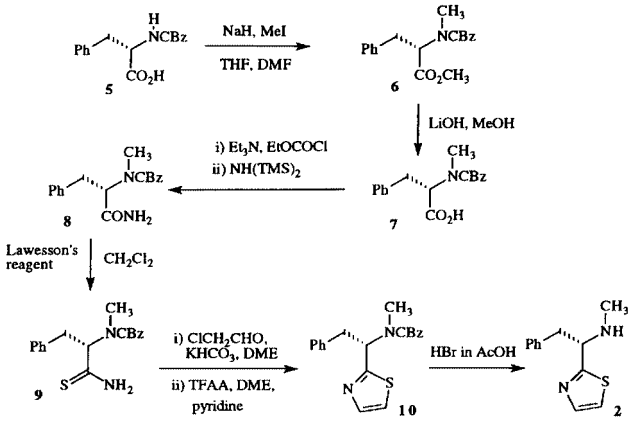

Scheme 2 Synthesis of (*S*)-*N*-methyldolaphenine.

methyl iodide gave the *N*-methyl methyl ester **6** which was hydrolysed to the corresponding acid **7** in 80% yield over the 2 steps. A modified Hantsch method was used to form the thiazole ring in which the acid **7** was first converted to an amide **8** *via* a mixed anhydride using the approach described by Pellegata and coworkers.[10] Treatment of amide **8** with Lawesson's reagent at room temperature in dichloromethane[11] gave thioamide **9** in 71% yield over the two steps from acid **7**. Reaction of **9** with α-chloroacetaldehyde (prepared from the corresponding dimethyl acetal[12]) in DME in the presence of potassium hydrogen carbonate followed by dehydration using trifluoroacetic anhydride[13] gave (*S*)-*N*-Cbz-*N*-methyldolaphenine **10** as a yellow oil. Finally removal of the Cbz protecting group with hydrobromic acid in acetic acid gave an analytically pure sample of the novel secondary amine **2** with $[\alpha]_D$ −3.02† (*c* 0.65 in $CHCl_3$). To ensure that the stereochemical integrity at C-2 of **2** had been maintained throughout the synthetic route a sample of the (*R*,*R*)-tartrate salt was prepared in $CD_3OD:D_2O$ (4:1).[14] The ^{1}H-NMR spectrum of the product showed a downfield shift of the signal assigned to 2-H from δ 4.22 for amine **2** to δ 4.97 in the salt, there was no trace of the other diastereomer which was clearly apparent in a control experiment with the (*R*,*R*)-tartrate salt of racemic amine.

With the required amine **2** in hand, we next turned our attention to the synthesis of ketone **3** for which multigram quantities of **4** were needed (Scheme 1). Several methods have been reported for the preparation of **4** and the most direct is conjugate addition of a trichloromethyl anion to the chiral crotonyl derivatives **11** and **12**.[15,16] Unfortunately, despite

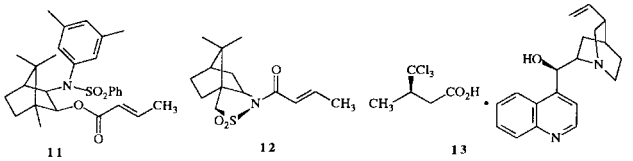

several attempts to repeat these reactions on a synthetically useful scale, in our hands generation of either trichloromethylmagnesium chloride[15] or trichloromethyllithium[16] at low temperature for reaction with **11** and **12** respectively did not

 DOI: 10.1039/b106087m

give acceptable yields of the required product. A more satisfactory approach proved to be resolution of the racemic acid.

Racemic trichloromethylbutanoic acid has been prepared previously *via* radical addition of bromotrichloromethane to crotonic acid followed by treatment of the resultant α-bromo acid with zinc.[17] The acid may then be resolved by separation of the corresponding (−)-(*R*)-α-phenylglycinol derivatives by HPLC giving **4** with 81% ee. However, there is some confusion in the literature with the sign of the optical rotation for (*S*)- and (*R*)-trichloromethylbutanoic acid.[18] Thus, in order to remove any possible ambiguity, the cinchonidine salt of **4** was prepared and repeated crystallisation of the salt from methanol and water[16] gave a single diastereomer as determined by ^{1}H- and ^{13}C-NMR spectroscopy. X-Ray crystallography revealed the (*R*)-configuration for C-3 of the trichloromethylbutanoic acid portion of the salt **13**. Treatment of the salt with potassium hydroxide followed by 2 M HCl gave, after work up, (*R*) (+)-**4** with $[\alpha]_D$ +25 (*c* 1.8 in EtOH).

For the synthesis of **4**, the (4*R*,5*S*)-4-methyl-5-phenyl-2-oxazolidinone[19] derivative of racemic trichloromethylbutanoic acid was prepared and the diastereomers were separated by column chromatography on silica. Following hydrolytic cleavage with lithium hydroxide–hydrogen peroxide the required (*S*)-**4** ($[\alpha]_D$ −28.9, *c* 0.96 in EtOH; lit.[15] −28.09, *c* 2.12 in EtOH) was isolated as well as recovered auxiliary, both in quantitative yield. From the retrosynthetic analysis shown in Scheme 1, the next stage of the synthesis of barbamide required a two carbon homologation of (*S*)-trichloromethylbutanoic acid **4** to give a β-keto acid derivative **3** with a suitable leaving group for reaction with (*S*)-*N*-methyldolaphenine **2**. Several approaches were investigated to achieve these final steps and the most direct route proved to be conversion of acid **4** to the corresponding acid chloride **14** with thionyl chloride followed by coupling **14** with Meldrum's acid to give the intermediate **15** (Scheme 3).[20] Treatment of **15** with **2** gave **16** with the framework of barbamide in 51% yield over the three steps from **4**. Finally, the (*E*)-enol ether was formed by reaction of β-keto amide **16** with sodium hydride and dimethyl sulfate in the presence of HMPA. A 1 : 1 mixture of two products was formed in this final stage of the synthesis due to epimerisation at C-7 under the basic reaction conditions. These compounds were readily separated by HPLC[21] giving the less polar product barbamide **1** and 7-epibarbamide **17**, $[\alpha]_D$ +73.4 (*c* 1.13 in CH_3OH). The ^{1}H- and ^{13}C-NMR and mass spectra of the synthetic material **1** were found to be identical with those of the natural product.[7] The optical rotation of synthetic barbamide was $[\alpha]_D$ −81.9 (*c* 0.95 in CH_3OH) whilst that of an authentic sample of the natural product gave $[\alpha]_D$ −82 (*c* 1.2 in CH_3OH).

Recently three further metabolites (pseudodysidenin **18**, dysidenamide **19** and nordysidenin **20**) containing the 3-trichloromethylbutanyl unit have been isolated from *L. majuscula*.[22] Unlike barbamide which is biosynthesised from L-trichloroleucine and a derivative of L-phenylalanine,[8] it is apparent that these metabolites are assembled from L-trichloroleucine and an L-alanine derivative (as determined by degradation studies). The 2*S*,5*S*,7*S* configurations of **18**, **19** and **20** were assigned by chiral HPLC and comparison of their optical rotations (which were all negative) to other polychlorinated natural products.[22] The synthetic studies described herein confirm that barbamide **1** isolated from extracts of *L. majuscula*, encompasses the (3*S*)-trichloromethylbutanyl unit which is in accord with the assignment of the configuration of the 2*S* and 7*S* stereocentres in these new structurally related metabolites **18**, **19** and **20** which have been isolated more recently from *L. majuscula*.

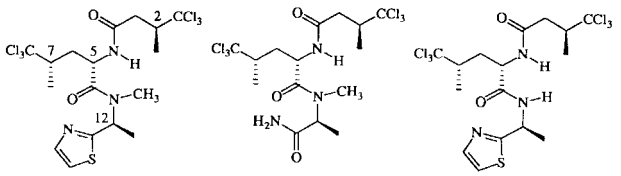

Pseudodysidenin, **18** Dysidenamide, **19** Nordysidenin, **20**

We are very grateful to Dr Clive Smith, GlaxoSmithKline for his kind assistance in the preparation of (*S*)-3-trichloromethylbutanoic acid and Dr Lee Hall for the X-ray analysis. The University of Bristol is thanked for a Scholarship (to V.-A. N.).

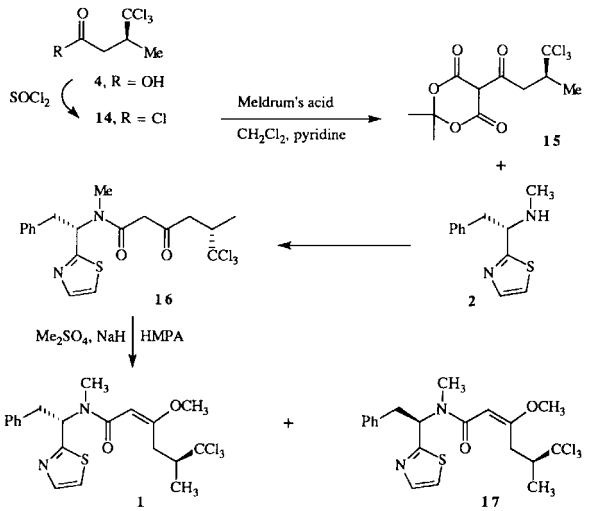

Scheme 3

Notes and references

† Units of $[\alpha]_D$ are 10^{-1} deg cm^2 g^{-1} throughout.

1 M. D. Unson, C. B. Rose, D. J. Faulkner, L. S. Brinen, J. R. Steiner and J. Clardy, *J. Org. Chem.*, 1993, **58**, 6336.
2 X. Fu, L.-M. Zeng, J.-Y. Su and M. Pais, *J. Nat. Prod.*, 1997, **60**, 695; X. Fu, M. L. G. Ferreira, F. J. Schmitz and M. Kelly-Borges, *J. Nat. Prod.*, 1998, **61**, 12 276.
3 W. Hofheinz and W. E. Oberhansli, *Helv. Chim. Acta*, 1977, **60**, 660.
4 R. Kazlauskas, R. O. Lidgard, R. J. Wells and W. Vetter, *Tetrahedron Lett.*, 1977, **18**, 3183.
5 J. B. MacMillan and T. F. Molinski, *J. Nat. Prod.*, 2000, **63**, 155.
6 W. D. Clarke and P. Crews, *Tetrahedron Lett.*, 1995, **36**, 1185.
7 J. Orjala and W. H. Gerwick, *J. Nat. Prod.*, 1996, **59**, 427.
8 N. Sitachitta, J. Rossi, M. A. Roberts, W. H. Gerwick, M. D. Fletcher and C. L. Willis, *J. Am. Chem. Soc.*, 1998, **120**, 7131; N. Sitachitta, B. L. Marquez, R. T. Williamson, J. Rossi, M. A. Roberts, W. H. Gerwick, V.-A. Nguyen and C. L. Willis, *Tetrahedron*, 2000, **56**, 9103.
9 A. Butler and J. V. Walker, *Chem. Rev.*, 1993, 1937.
10 R. Pellegata, A. Italia, M. Villa, G. Palmisano and G. Lesma, *Synthesis*, 1985, **13**, 517.
11 C. J. Moody and M. C. Bagley, *J. Chem. Soc., Perkin Trans. 1*, 1998, 601.
12 W. P. McCann, L. M. Hall and W. K. Nonidez, *Anal. Chem.*, 1983, **55**, 1454.
13 M. W. Bredenkamp, C. W. Holzapfel, R. M. Snyman and W. J. van Zyl, *Synth. Comm.*, 1992, **22**, 3029.
14 N. Irako, Y. Hamada and T. Shioiri, *Tetrahedron*, 1992, **48**, 7251.
15 G. Helmchen and G. Wegner, *Tetrahedron Lett.*, 1985, **26**, 6047.
16 S. E. Brantley and T. F. Molinski, *Org. Lett.*, 1999, **1**, 2165.
17 (*a*) R. L. Huang, *J. Chem. Soc.*, 1956, 1749; (*b*) S. E. de Laszlo and P. G. Williard, *J. Am. Chem. Soc.*, 1985, **107**, 199.
18 For example, Helmchen and Wegner refer to (+)-(*S*)-3-trichloromethylbutyric acid in the discussion section of their paper but quote $[\alpha]_D$ −31.1 (*c* 1.1, $CHCl_3$).[15] Similarly, Williard and de Laszlo quote (*R*)-(−)-3-methyl-4,4,4-trichloromethylbutanoic acid in the abstract but $[\alpha]_D$ +25.15 (*c* 1.36, $CHCl_3$) in the experimental section.[17b]
19 D. A. Evans, J. Bartroli and T. L. Shih, *J. Am. Chem. Soc.*, 1981, **103**, 2127.
20 Racemic **15** has been prepared previously: P. G. Williard and S. E. de Laszlo, *J. Org. Chem.*, 1984, **49**, 3489.
21 HPLC was performed on a Gilson Sphereclone 5μ silica column using Gilson 321 pumps with gradient control eluting with ethyl acetate–petroleum ether 5–30%; UV detection was at 254 nm.
22 J. I. Jimenez and P. J. Scheuer, *J. Nat. Prod.*, 2001, **64**, 2000.

CHEMCOMM
Communication
www.rsc.org/chemcomm

Mesopore immobilised copper bis(oxazoline) complexes for enantioselective catalysis

Richard J. Clarke and Ian J. Shannon*

School of Chemical Sciences, University of Birmingham, Birmingham, UK B15 2TT. E-mail: I.Shannon@bham.ac.uk

Received (in Cambridge, UK) 27th June 2001, Accepted 21st August 2001
First published as an Advance Article on the web 17th September 2001

New supported heterogeneous catalysts have been synthesised through the tethering of copper bis(oxazoline) complexes to the surfaces of MCM-41 and MCM-48 mesoporous materials, and the prepared catalysts shown to be highly active in the enantioselective cyclopropanation of styrene with ethyl diazoacetate.

Bis(oxazoline) complexes have been widely reported as being excellent catalysts for a broad range of organic reactions.[1] The most extensively used bis(oxazoline) ligands have been those containing a single carbon spacer between the oxazoline rings (*e.g.* **1**), enabling the ligand to chelate to a metal centre forming a stable six-membered ring. The ease with which differing bis(oxazoline) ligands may be synthesised, with stereocontrol over the C_2-symmetry of the ligand, combined with their ability to complex a variety of transition metal cations, has enabled catalysts to be tailored to give good yield and selectivity in asymmetric syntheses including Diels–Alder,[2] cyclopropanation,[3] aziridination[4] and oxidation reactions.[5]

With the success and diversity of chiral bis(oxazoline) catalysts in enantioselective reactions in the homogeneous phase, attention has also turned to the development of heterogenised systems which may be of significant industrial interest. Previous studies have seen the encapsulation of bis(oxazoline) complexes within zeolites *via* 'ship-in-a-bottle' type syntheses,[6] and layered aluminosilicate clay materials.[7,8] Both these strategies have met with some success, but have recognised the potential problem of accessibility of reactants to the catalytically active sites due to pore blocking. In both cases the interaction between the complex and the host material is through ionic interactions which, dependent on the nature of support, can lead to problems of leaching of the ligand complex into solution. An alternative strategy which prevents leaching of ligand is to covalently bind the ligand to the substrate, demonstrated for bis(oxazolines) through their attachment to dendritic cores[9] and polymers.[8,10]

We have investigated an alternative method for the development of heterogenised bis(oxazoline) catalysts through the covalent binding of the ligand to the surface of the inorganic mesoporous materials, MCM-41 and MCM-48. These MCM-type materials[11,12] are large pore silicates with high surface areas, which are ideal for use as catalyst supports. The size of the pores (*ca.* 30 Å) is sufficient that, upon catalyst immobilisation, good accessibility to isolated active sites is maintained, while also potentially enabling reactions involving larger substrates than are possible with conventional supports such as zeolites and clays. In many other studies, catalytically active species have been successfully attached to mesoporous solids,[13,14] either through ionic or covalent binding similar to that we use here. To date, however, there have been no reports of the immobilisation of the versatile bis(oxazoline) catalysts within mesoporous materials.

We have synthesised catalysts incorporating methylene-bis[(4*S*)-4-phenyl-2-oxazoline] **1** complexes, supported *via* alkyl tethers on MCM-41 and MCM-48. The mesoporous silica materials were prepared using methods derived from the literature.[12] The modified bis(oxazoline) complexes for tethering were prepared using standard Schlenk techniques in a pseudo-one-pot synthesis (Scheme 1). Typically, 0.13 mmol **1** was reacted with 0.33 mmol (2.5 equivalents) of BuLi in 5 ml dry THF in an isopropyl alcohol–dry-ice bath, before addition of 0.43 mmol of iodopropyltrimethoxysilane. After stirring for several days the colour changed to red–brown, at which point 0.135 mmol of $CuCl_2$ or $Cu(TfO)_2$ was added and the solution further stirred overnight. The solution was then added to 0.65 g of MCM-41 or MCM-48 suspended in 10 ml dry THF, and 0.5 ml Et_3N added. After overnight stirring, the resulting solid was filtered off, washed and Soxhlet extracted with THF to remove any untethered species, and dried.

Analysis by powder X-ray diffraction confirmed that the structure of the mesoporous supporting material remained intact through the tethering procedure and also after catalysis. Cu contents in the final catalysts were determined by AAS; the amount of support was selected so as to give a theoretical catalyst loading of 0.2 mmol Cu g^{-1}, however we found in practice that the true loading was much less than this value (typically 20%). IR data recorded on dehydrated samples of the supported catalysts revealed the presence of an absorption band at *ca.* 1640 cm^{-1} characteristic of the C=N double bond group of the oxazoline ligand. All compounds were pale green–blue, and comparison of the diffuse reflectance UV–VIS spectra of our catalysts with those of the corresponding untethered **1**:$CuCl_2$ and **1**:$Cu(TfO)_2$ complexes revealed that a broad absorption maximum was observed at *ca.* 740 nm, indicating further that we have synthesised the mono-bis(oxazoline) copper complex and not the di-liganded complex.[3] As final

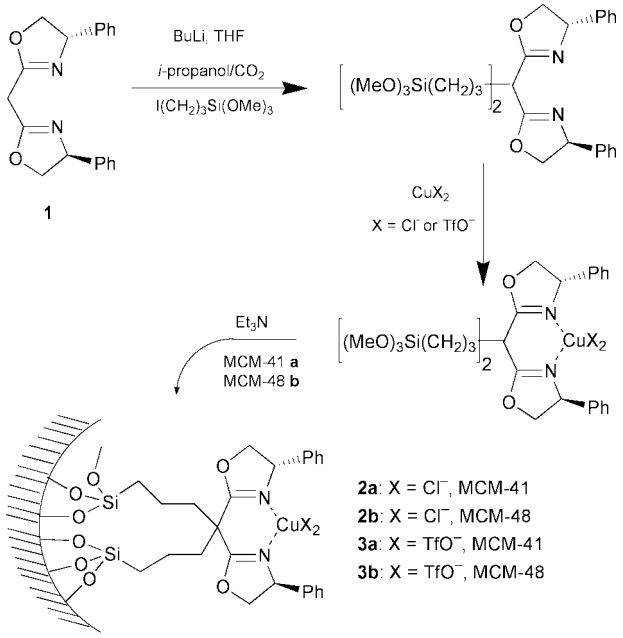

Scheme 1 Preparation of copper bis(oxazoline) catalysts tethered to the surface of mesoporous silicas through alkylsiloxane tethering groups.

 DOI: 10.1039/b105655g

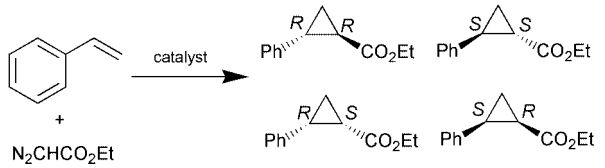

Scheme 2 Cyclopropanation reaction between styrene and ethyl diazoacetate, showing the four products obtained.

Table 1 Catalytic results for the cyclopropanation reaction involving styrene and ethyl diazoacetate[a]

Catalyst	Cu (mol%)	Run	Yield[b] (%)	*trans*/*cis*	ee (*cis*)[c](%)	ee (*trans*)[d](%)
1:$CuCl_2$ (homo)	1	1	19.5	1.99	23	21
1:$Cu(TfO)_2$ (homo)	1	1	46.3	2.05	49	58
2a	0.10	1	38.7	1.89	48	54
		2	23.7	1.80	48	52
3a	0.24	1	47.4	1.95	46	51
		2	46.6	1.78	42	45
2b	0.16	1	36.6	1.69	46	51
		2	27.8	1.63	44	46
3b	0.22	1	32.3	1.93	50	54
		2	31.0	1.79	46	48
4	0.64	1	32	1.61	1	2

[a] All reactions were run at 25 °C. To a stirred solution of 3 mmol of styrene in 2 ml of dichloroethane containing *ca.* 50 mg of catalyst, 50 μl of a 1% phenylhydrazine solution was added, and 10 μl of diethyl adipate was used as standard. 1 mmol of ethyl diazoacetate was then added and the reaction stirred for 40 h (24 h for homogeneous reactions) before filtration, solvent removal and purification by column chromatography. Analysis was carried out on a CE 2000 Series Trace GC using a Chirasil-Dex CB column. [b] Yield is percentage of cyclopropanes formed relative to the theoretical maximum expected for 100% diazoacetate conversion. [c] Major enantiomer for *cis* products is *R,S*. [d] Major enantiomer for *trans* products is *R,R*.

confirmation, ^{13}C MAS NMR of a tethered bis(oxazoline) made in the same manner as above, but to which no $CuCl_2$ or $Cu(TfO)_2$ had been added, showed peaks which matched those seen for the free ligand, with additional peaks seen corresponding to the carbons forming the alkyl chain tether to the mesopore surface. Although NMR did not show the presence of residual methoxy groups, it is known that the reaction between these and the surface silanols is incomplete, resulting in complexes attached to the surface by fewer than the maximum six Si–O–Si linkages.

The supported catalysts prepared were tested for the enantioselective cyclopropanation reaction of styrene with ethyl diazoacetate (Scheme 2). As can be seen from the results in Table 1, the supported catalysts perform favourably compared with the homogeneous catalysts operating under the same reaction conditions. The tethered Cl-catalysts, **2a** and **2b**, performed much better giving higher yield and enantioselectivity than the homogeneous mono-bis(oxazoline) complex equivalent, for significantly lower concentration of active catalyst. The supported TfO-catalysts, **3a** and **3b**, showed enantioselectivity only slightly lower than the homogeneous version.

Interestingly, when in a further comparison the **1**:$Cu(TfO)_2$ complex was immobilised directly onto the surface of MCM-41, **4** (believed to be attached *via* hydrogen bonding between the triflate anion and the surface Si–OH groups in a manner analogous to that described by de Rege *et al.*[15]), the catalyst showed respectable yield but very poor selectivity. This suggests that, for this catalyst, the triflate complex is not leached from the surface (in which case the reaction would be expected to show similar results to the homogeneous system), but that the mode of immobilisation is inferior to the covalent tethering method we have used in generating the other catalysts.

After recovery by filtration, the catalysts were washed with dichloromethane and dried and their structural integrity confirmed by XRD. On reuse, following the same catalytic procedure as above, it can be seen that those made with copper chloride (**2a** and **2b**) have deactivated faster than those from the triflate salt (**3a** and **3b**) which show very little deactivation at all, although there is an accompanying small drop in the ee values and *trans*/*cis* ratio of the products observed. In part this loss of activity and selectivity has previously been attributed to the poisoning of the system by adsorption of by-products on the catalyst's surface,[7] such as the dimer formed from diazoacetate self-reacting or excess styrene, and we are currently tuning the reaction conditions under which catalysis is carried out to further investigate this problem. Another factor under investigation for improving the efficiency of the catalysts is the removal of the residual surface silanol groups which may be acting to trap side-products in the pores.

Although further work is still required to fully optimise conditions for conversion, selectivity and recyclability in the above reaction, the general synthetic methodology proposed here provides the basis for a large family of mesopore supported bis(oxazoline) catalysts to be generated for use in a wide range of organic reactions and in particular in asymmetric syntheses.

We would like to thank EPSRC for support (studentship to R. J. C.)

Notes and references

1 A. K. Ghosh, P. Mathivanan and J. Cappiello, *Tetrahedron: Asymmetry*, 1998, **9**, 45.
2 E. J. Corey, N. Imai and H. Zhang, *J. Am. Chem. Soc.*, 1991, **113**, 728.
3 D. A. Evans, K. A. Woerpel, M. M. Hinman and M. M. Faul, *J. Am. Chem. Soc.*, 1991, **113**, 726.
4 D. A. Evans, M. M. Faul, M. T. Bilodeau, B. A. Anderson and D. M. Barnes, *J. Am. Chem. Soc.*, 1993, **115**, 5328.
5 A. S. Gokhale, A. B. E. Minidis and A. Pfaltz, *Tetrahedron Lett.*, 1995, **36**, 1831.
6 C. Langham, P. Piaggio, D. Bethell, D. F. Lee, P. McMorn, P. C. B. Page, D. J. Willock, C. Sly, F. E. Hancock, F. King and G. J. Hutchings, *Chem. Commun.*, 1998, 1601.
7 J. M. Fraile, J. I. García, M. A. Harmer, C. I. Herrerias and J. A. Mayoral, *J. Mol. Catal. A: Chem.*, 2001, **165**, 211.
8 M. J. Fernández, J. M. Fraile, J. I. García, J. A. Mayoral, M. I. Burguete, E. García-Verdugo, S. V. Luis and M. A. Harmer, *Top. Catal.*, 2000, **13**, 303.
9 H. F. Chow and C. C. Mak, *J. Org. Chem.*, 1997, **62**, 5116.
10 M. I. Burguete, J. M. Fraile, J. I. García, E. García-Verdugo, S. V. Luis and J. A. Mayoral, *Org. Lett.*, 2000, **2**, 3905.
11 C. T. Kresge, M. E. Loenowicz, W. J. Roth, J. C. Vartuli and J. S. Beck, *Nature*, 1992, **359**, 710.
12 J. S. Beck, J. C. Vartuli, W. J. Roth, M. E. Loenowicz, C. T. Kresge, K. D. Schmitt, C. T. W. Chu, D. H. Olsen, E. W. Sheppard, S. B. McCullen, J. B. Higgins and J. L. Schlenker, *J. Am. Chem. Soc.*, 1992, **114**, 10834.
13 T. Maschmeyer, *Curr. Opin. Solid State Mater. Sci.*, 1998, **3**, 71.
14 A. Stein, B. J. Melde and R. C. Schroden, *Adv. Mater.*, 2000, **12**, 1403.
15 F. M. de Rege, D. K. Morita, K. C. Ott, W. Tumas and R. D. Broene, *Chem. Commun.*, 2000, 1797.

CHEMCOMM
Communication
www.rsc.org/chemcomm

A facile, stereoselective [2 + 2] photoreaction mediated by cucurbit[8]uril

Sang Yong Jon, Young Ho Ko, Sang Hyun Park, Hee-Joon Kim and Kimoon Kim*

National Creative Research Initiative Center for Smart Supramolecules and Department of Chemistry, Division of Molecular and Life Sciences, Pohang University of Science and Technology (POSTECH), San 31 Hyojadong, Pohang 790-784, Republic of Korea. E-mail: kkim@postech.ac.kr; Fax: (+82)54-279-8129

Received (in Cambridge, UK) 12th June 2001, Accepted 14th August 2001
First published as an Advance Article on the web 4th September 2001

The [2 + 2] photoreaction of (*E*)-diaminostilbene dihydrochloride proceeds with large rate acceleration and high stereoselectivity *via* formation of a stable 1:2 host–guest complex with cucurbit[8]uril in solution.

Bringing two reactants in close proximity and the correct orientation to promote reactions between them in a regio- and/or stereoselective manner is an important research goal. Supramolecular encapsulation of two guest molecules in molecular hosts[1–3] or supramolecular hosts[4] has been studied to achieve this goal. For example, by forming host–guest complexes, cyclodextrins mediate photoreaction of aromatic guests such as anthracene,[5] coumarin[6] and stilbene[7,8] derivatives in solution as well as in the solid state.[8,9] However, few studies reported large rate acceleration and high stereo- and/or regioselectivity in [2 + 2] photoreactions mediated by cyclodextrins in solution.

Cucurbituril (CB[6]), a macrocycle comprising six glycoluril† units, forms stable host–guest complexes with small molecules.[10] Recently, we synthesized the octameric cucurbituril homologue cucurbit[8]uril (CB[8]) with a cavity comparable to that of γ-cyclodextrin. Its large cavity can accommodate two aromatic guest molecules to form 1:2 host–guest complexes,[11] or 1:1:1 ternary complexes.[12] This observation prompted us to study chemical reactions between the two guest molecules included inside the cavity of CB[8]. Here we report a facile, highly stereoselective [2 + 2] photoreaction of (*E*)-diaminostilbene dihydrochloride [(*E*)-**1**, Scheme 1] inside the cavity of CB[8] in solution.

CB[8] and (*E*)-**1** form a stable 1:2 host–guest complex in aqueous medium (D_2O) as confirmed by ^1H NMR spectroscopy (Fig. 1b). Interestingly, when the host and guest are mixed in a 1:1 stoichiometry, the 1:2 complex exists as the major product. The formation constant of the ternary complex in formic acid–water (2:3) was measured to be $(3.8 \pm 0.4) \times 10^4$ M^{-2} by isothermal titration calorimetry.‡ UV irradiation§ of an aqueous solution the 1:2 complex for 0.5 h affords **3a**, almost solely (Fig. 1c). Subsequent treatment of the reaction mixture with a small amount of base (*e.g.*, 1 M NaOH solution) produces the free [2 + 2] adduct, 1α,2α,3β,4β-tetrakis(4-aminophenyl)cyclobutane (*syn*-**4**, where α and β represent either face of the cyclobutane ring) along with a trace amount (< 5 %) of 1α,2β,3α,4β-tetrakis(4-aminophenyl)cyclobutane (*anti*-**4**). No formation of the isomerization product (*Z*)-**1** is observed. In the absence of CB[8], however, the main reaction pathway for (*E*)-**1** upon UV irradiation is the isomerization to (*Z*)-**1** as usually is the case for stilbene derivatives.[13] Therefore, the present result indicates that photodimerization is far more favorable than photoisomerization in the cavity of CB[8]. Furthermore, the facile formation (< 0.5 h) of the dimers with high stereoselectivity (*syn–anti* ratio > 95:5) in the presence of CB[8] is in contrast to the slow formation (72 h) of dimers of a similar stilbene derivative with moderate stereoselectivity (*syn–anti* ratio ≈ 4:1) in the presence of γ-CD in solution.[7]

What is the origin of the high stereoselectivity of the photodimerization mediated by CB[8]? To answer the question we carried out AM1 calculations[14] on the 1:2 host–guest complex between CB[8] and (*E*)-**1**. The most stable conformations for the ternary complex are **2a** ('*syn*') or **2b** ('*anti*') (Scheme 2), in which two guest molecules are included in the host with either '*syn*' or '*anti*' relationship of the olefinic groups. In the two equally stable conformations, half of each guest body is embedded in the host cavity while the remaining parts of the guest molecules stick out into the solution in opposite directions. The high stability of the conformations is due to ion–dipole as well as hydrogen bonding interactions between the ammonium groups of the guests and the portal oxygen atoms of the host, and hydrophobic interaction between the host cavity and the guests. For [2 + 2] photo-cycloaddition to occur, however, the two olefinic double bonds should be in close proximity as in **2a′** ('*syn*') or **2b′** ('*anti*'), which would lead to **3a** or **3b**, respectively, upon photodimerization of the guest. Although **2a′** and **2b′** would also have similar stabilization energies in solution, the concerted [2 + 2] cycloaddition of two guests in CB[8] occurs much more effectively in **2a′** than in **2b′** because of the parallel orientation of the two double bonds in **2a′**.[15] Furthermore, **3a** is more stable than **3b** ($\Delta\Delta E \approx 18$ kcal mol^{-1}) according to the gas phase calculation.[14] Although the calculated energy difference is clearly overestimated, the modeling results provide a possible explanation why the

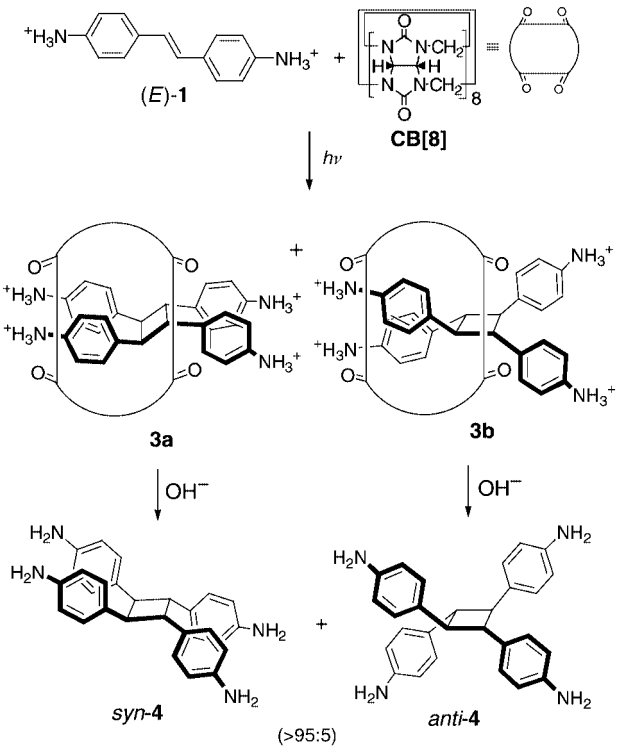

Scheme 1

 DOI: 10.1039/b105153a

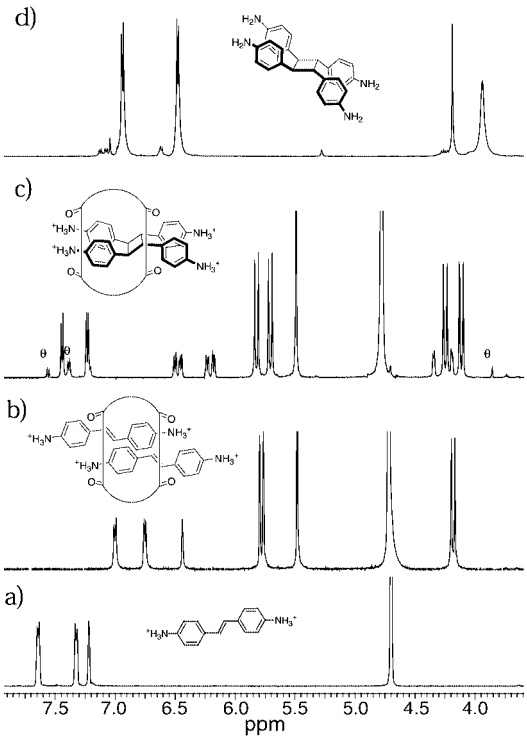

Fig. 1 (a) ^{1}H NMR spectra of (*trans*)-**1** (4×10^{-3} M) in D_2O; (b) after addition of 0.5 equiv. of CB[8]; (c) after irradiation of solution (b) for 30 min. Signals for the *anti* adduct **3b** are marked θ; (d) after isolation, *syn*-**4**–*anti*-**4** > 95:5, in CD_3CN.

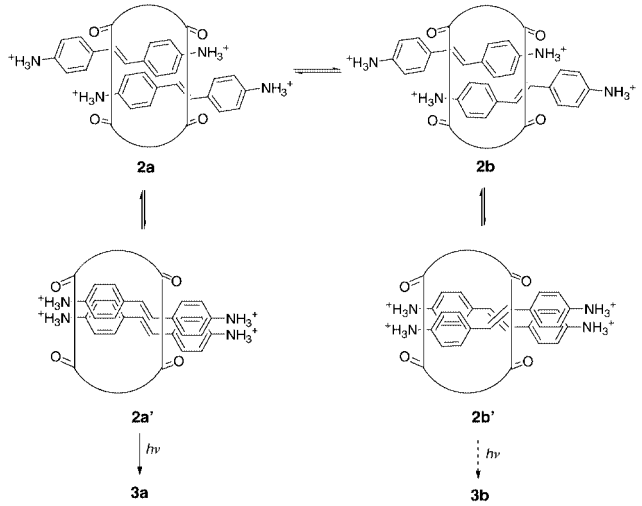

Scheme 2

photodimerization to **3a** ('*syn*') is far more favorable than to **3b** ('*anti*').

In conclusion, [2 + 2] photoreaction of (*E*)-**1** proceeds in solution with large rate acceleration and high stereoselectivity *via* formation of a stable 1:2 host–guest complex with CB[8]. The ability of the host to stabilize the two guest molecules with a parallel orientation of the olefinic groups in close proximity leads to the high stereoselectivity of the photodimerization. This work thus demonstrates a synthetic utility of CB[8] as a reaction 'vessel' in which bimolecular reactions between appropriately designed guest molecules can be facilitated with high regio- and stereoselectivity.

We thank the Korean Ministry of Science and Technology (Creative Research Initiative Program) for support of this work. We also thank Mr Eunsung Lee for synthesizing cucurbit[8]uril and Professor P. K. Bharadwaj for reading the manuscript.

Notes and references

† The IUPAC name for glycoluril is 2,4,6,8-tetraazabicyclo[3.3.0]octan-3,7-dione.

‡ The microcalorimetric titration was carried out using HCO_2H–H_2O (2:3 v/v) as solvent because CB[8] is sparingly soluble in neutral water. Therefore, the formation constant of the ternary complex in a neutral aqueous solution should be higher.

§ A solution of 2(*E*)-**1**–CB[8] complex in D_2O (4×10^{-3} M) in a NMR tube was irradiated at 300 nm in a Rayonet photochemical reactor for 0.5 h. To this solution was added several drops of dilute aqueous NaOH solution to adjust pH ~9, then excess of methanol (10 mL) was added to the mixture. After vigorous stirring for 1 h, the precipitate CB[8] was removed by filtration. The resulting solution was concentrated under reduced pressure to afford **4** in 82% yield as a pale yellow solid. The product distribution was determined by integration of the ^{1}H NMR signals of the crude product in CD_3CN. *Selected data* for *syn*-**4** δ_H (CD_3CN, 500 MHz) 6.92 (d, *J* 8.2, 2H, ArH), 6.46 (d, *J* 8.2, 2H, ArH), 4.16 (s, 1H, CH), 3.91 (br, 2H, NH_2); δ_C (CD_3CN, 125 MHz) 146.0, 130.8, 129.4, 114.9, 47.4; EI-MS: *m*/*z* 210.3 [M^+/2].

1 Review: T. Osa and I. Suzuki, in *Comprehensive Supramolecular Chemistry*, ed. J. L. Atwood, J. E. D. Davies, D. D. MacNicol and F. Vögtle, **vol. 3**, Pergamon, Oxford, 1996, p. 367
2 W. L. Mock, T. A. Irra, J. P. Wepsiec and M. Adhya, *J. Org. Chem.*, 1989, **54**, 5302; D. Turcel and J. J. G. Steike, *Chem. Commun.*, 1999, 1509.
3 L. G. Mackay, R. S. Wylie and J. K. M. Sanders, *J. Am. Chem. Soc.*, 1994, **116**, 3141; J. K. M. Sanders, *Chem. Eur. J.*, 1998, **4**, 1378.
4 J. Kang and J. Rebek, Jr., *Nature*, 1997, **385**, 50; J. Kang, G. Hilmersson, J. Santamaria and J. Rebek, Jr., *J. Am. Chem. Soc.*, 1998, **120**, 3650.
5 T. Tamaki, *Chem. Lett.*, 1984, 53; T. Tamaki, T. Kokubu and K. Ichimura, *Tetrahedron*, 1987, **43**, 1485.
6 J. N. Moorthy, K. Venkatesan and R. G. Weiss, *J. Org. Chem.*, 1992, **57**, 3292.
7 W. Herrmann, S. Wehrle and G. Wenz, *Chem. Commun.*, 1997, 1709. Their assignment of *syn* and *anti* configurations for the [2 + 2] photodimers appears to be wrong. In general, the C–H proton of a cyclobutane ring in a *syn* adduct appears at higher field than that in the corresponding *anti* adduct in ^{1}H NMR spectra. Therefore, the major product should be *syn* not *anti* (see also ref.8).
8 K. S. S. P. Rao, S. M. Hubig, J. N. Moorthy and J. K. Kochi, *J. Org. Chem.*, 1999, **64**, 8098.
9 Y. Ito, *Synthesis*, 1998, 1.
10 Review: W. L. Mock, in *Comprehensive Supramolecular Chemistry*, ed. F. Vögtle, **vol. 2**, Pergamon, Oxford, 1996, p. 477; W. L. Mock, *Top. Curr. Chem.*, 1995, **175**, 1; P. Cintas, *J. Incl. Phenom. Mol. Recognit. Chem.*, 1994, **17**, 205.
11 J. Kim, I.-S. Jung, S-Y. Kim, E. Lee, J.-K. Kang, S. Sakamoto, K. Yamaguchi and K. Kim, *J. Am. Chem. Soc.*, 2000, **122**, 540.
12 H.-J. Kim, J. Heo, W. S. Jeon, E. Lee, J. Kim, S. Sakamoto, K. Yamaguchi and K. Kim, *Angew. Chem., Int. Ed.*, 2001, **40**, 1526.
13 H. Meier, *Angew. Chem., Int. Ed. Engl.*, 1992, **31**, 1399; H. Shechter, W. J. Link and G. V. D. Tiers, *J. Am. Chem. Soc.*, 1963, **85**, 1601; M. S. Syamala and V. Ramamurthy, *J. Org. Chem.*, 1986, **51**, 3712.
14 AM1-HF calculations were carried out in gas phase: M. J. S. Dewar, E. G. Zoebisch, E. F. Healy and J. J. P. Stewart, *J. Am. Chem. Soc.*, 1985, **107**, 3902.
15 G. M. Schmidt, *J. Pure Appl. Chem.*, 1971, **27**, 647; K. Gnanaguru, N. Ramasubbu, K. Venkatesan and V. Ramamurthy, *J. Photochem.*, 1984, **27**, 355.

CHEMCOMM Communication
www.rsc.org/chemcomm

Synthesis and characterization of poly(2,3,5,6-tetrafluoro-1,4-phenylenevinylene)

Francesco Babudri,[a] Antonio Cardone,[a] Luca Chiavarone,[b] Giuseppe Ciccarella,[a] Gianluca M. Farinola,[a] Francesco Naso*[a] and Gaetano Scamarcio[b]

[a] *Centro CNR di Studio sulle Metodologie Innovative di Sintesi Organiche, Dipartimento di Chimica, Università di Bari, via Amendola 173, 70126 Bari, Italy. E-mail: naso@area.ba.cnr.it*
[b] *Dipartimento di Fisica, Università degli Studi di Bari, via Orabona 4, 70126 Bari, Italy*

Received (in Cambridge, UK) 6th June 2001, Accepted 10th August 2001
First published as an Advance Article on the web 17th September 2001

Poly(2,3,5,6-tetrafluoro-1,4-phenylenevinylene) (PTFPV) was prepared for the first time by the Stille cross-coupling reaction and the resulting material was characterized through MALDI-TOF mass spectrometry, employing a novel sample preparation protocol suitable for insoluble compounds; preliminary optical and electrooptical measurements were performed.

In recent years, conjugated organic polymers belonging to the class of poly(1,4-phenylenevinylene) (PPV) have been successfully employed as active materials in several types of devices, the most frequent use being represented by the fabrication of light emitting diodes (OLED).[1,2] However, one of the major limiting factors in the wide commercialisation of polymer based LED devices is their insufficient long term stability, mainly due to the oxidative photodegradation of the organic semiconductor layer.[3]

The replacement of carbon–hydrogen bonds by stronger and less reactive carbon–fluorine bonds has been proposed as a possible approach for increasing the chemical stability of PPVs.[4a,5] Furthermore, fluorine atoms act as electron-withdrawing groups on the π conjugated system and consequently they are expected to have important electronic effects on the light emission properties of the resulting material.[4b,5] For these reasons considerable attention has been attracted by the synthesis and optical properties of various fluorine substituted PPVs and closely related poly(arylenevinylene)s.[4,6] In particular, the synthesis of poly(2,3,5,6-tetrafluoro-1,4-phenylenevinylene) (PTFPV) has been unsuccessfully attempted by the classical soluble precursor route.[6a] The same protocol has been employed for the synthesis of copolymers containing tetrafluorophenylenevinylene with either phenylenevinylene[4a] or dialkoxyphenylenevinylene[4b] units. In the first case, upon increasing the ratio between fluorinated and unsubstituted monomers, a decrease both in the conversion to precursor polymer and in the final yield of conjugated material was observed.[4a] As a consequence, it was not practically possible to prepare PTFPV using only the fluorinated monomer. Oligomeric PTFPVs having three or four aromatic rings were obtained with very low yields, *i.e.* 7 and 0.6% respectively, in the reaction of (*E*)-2-(pentafluorophenyl)ethenyllithium with hexafluorobenzene.[6b] An alternative approach reported in the same paper was represented by a self-polycondensation of (*E*)-2-(pentafluorophenyl)ethenyllithium. However, as admitted also by the authors, it was only possible to present rough proof, *i.e.* an elemental analysis, in favour of the proposed TFPPV structure for the resulting material.

In this communication we present our successful approach to the preparation of such an elusive fluorinated polymer, together with its structural characterization and preliminary measurements of its properties. Our synthesis of PTFPV is based upon a Stille cross-coupling reaction[2a,d,7] (Scheme 1).

1,4-Diiodotetrafluorobenzene **1** and (*E*)-1,2-bis(tributylstannyl)ethene **2**[8] were suitable starting materials and $Pd(AsPh_3)_4$,[9] generated *in situ* from $Pd_2(dba)_3$ and $AsPh_3$, was found to be the most effective catalyst.†

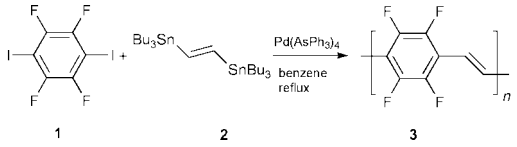

Scheme 1 Polymerization reaction.

Clear evidence that the insoluble yellow powder recovered from our reaction is PTFPV **3** is provided by the TOF mass spectrum performed in negative mode from a matrix of 2,5-dihydroxybenzoic acid after matrix-assisted laser desorption-ionization (MALDI) (Fig. 1).

Despite the complete insolubility of the material in all common organic solvents suitable for the preparation of samples for MALDI analysis, it was possible to get the spectra using a protocol recently described for polyamides.[10] The novel procedure is analogous to the preparation of a KBr sample for infrared analysis, using the matrix and the polymer in a 1:1 mixing ratio. To the best of our knowledge, the present work represents the first application of MALDI analysis to an insoluble conjugated polymer. The spectrum of PTFPV (Fig. 1) consists of peaks with masses ranging from about 500 to 4500 amu. Mass-discrimination phenomena, occurring in particular at higher molecular weight end in the MALDI-TOF spectra of polydisperse polymers,[11] allow only an approximate evaluation of the molecular weights ($M_w \approx 2400$, and $M_n \approx 1700$ with a relatively high polydispersity index $D > 1.4$). On the other hand, an analysis of the MALDI-TOF spectrum enabled us to assign the peaks to PTFPV chains with all the possible terminations as described in Fig. 2.

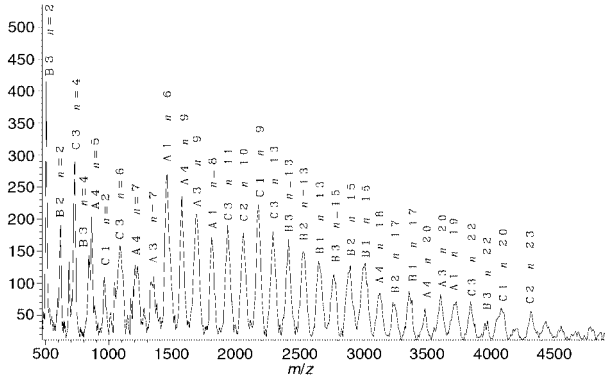

Fig. 1 MALDI-TOF mass spectrum of PTFPV. Ions are generated using a 337 nm nitrogen laser beam. The spectrum presented here is the sum of 300 shots acquired in linear mode. It was baseline corrected for presentation quality and the matrix signals are left outside the mass range reported (see also Fig. 2).

 DOI: 10.1039/b105029j

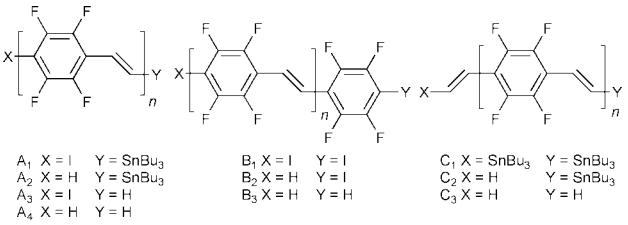

Fig. 2 PTFPV chains with all the possible terminations.

The masses calculated account for the peaks within the limit of the accuracy of about 1%, intrinsically due to the particular sample preparation technique.

As a further characterization of our material, X-ray photoelectron spectroscopy (XPS) elemental analysis was performed on a silicon-supported thin film, obtained as described below. The XPS spectrum shows the presence of carbon, fluorine, tin and iodine in the following atomic percentages: C1s = 69.09; F1s = 30.11; Sn3d = 0.44; I3d = 0.36. The C1s signal was best fitted in three components respectively due to the presence of carbon bonded to fluorine (atom% 44.19) and hydrocarbon carbon (atom% 55.81), and a third component attributable to $\pi \rightarrow \pi^*$ shake up satellites due to the aromatic rings.‡ The average polymerization degree calculated assuming statistical chain termination of an iodine atom and a tributylstannyl group is approximately 17–20 arylenevinylene units.

The Fourier transformed infrared spectrum of the material shows a strong band at 1490 cm^{-1} due to C–F stretching of the aromatic rings. A band at 963 cm^{-1}, assigned to the out of plane bending of the vinylic C–H bonds, is consistent with a *trans* geometry of the vinylene units.

In order to perform the optical and electrooptical characterization of the material, thin films of PTFPV (about 50 nm thickness) were thermally evaporated under high vacuum (10^{-6} mmHg) onto a support of quartz or commercial ITO, respectively.

Absorption and photoluminescence spectra of a PTFPV film were taken. The absorption band is centered at 347 nm. The photoluminescence (PL), in the green region, is centered at 544 nm, showing a considerable Stokes shift.

Single-layer electroluminescent devices, fabricated using PTFPV as emitting layer and aluminium and ITO as cathode and anode respectively, did not yield any emission even at high density current. According to the high electronegativity of the fluorine atom, which should increase the electron affinity of the polymer,[12] this observation can be explained in terms of a high energy barrier for hole injection from the ITO anode, while a significantly lower energy barrier is expected for electron injection from the Al cathode into the conduction band of the PTFPV.

In fact, the introduction of a layer of TPD [*N*,*N*′-bis(3-methylphenyl)-*N*,*N*′-diphenylbenzidine], a typical hole transporter,[13] between the ITO anode and the PTFPV resulted in a working device. The *I–V* and *E–V* curves, showing current density and emitted light power *versus* voltage, for an ITO/TPD/PTFPV/Al LED are reported in Fig. 3, where the inset illustrates the dependence of the light output on the injected current density. The electroluminescence (EL) threshold voltage was 6.5 eV.

The EL spectrum essentially matches the PL one suggesting that the radiative decay of the same exciton is responsible for the emission in both cases.

Summing up, we have described the first synthesis of PTFPV and performed the characterization of this insoluble material by means of MALDI-TOF mass spectrometry, using a novel sample preparation procedure that should enlarge the applications of this powerful analytical technique in the field of conjugated organic materials. Useful information was also obtained by XPS spectroscopy. Preliminary experiments have confirmed that the length and the structure of this polymer are suitable for the fabrication of electroluminescent devices.

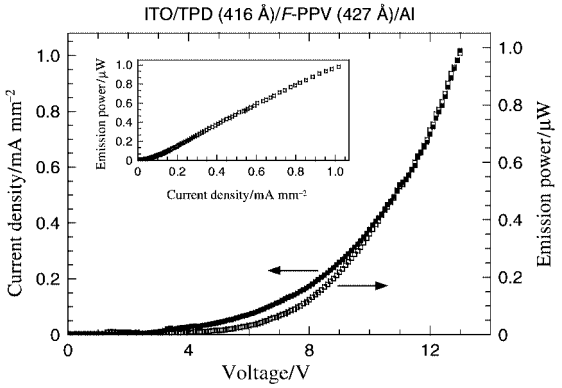

Fig. 3 *I–V* and *E–V* curves and *E–I* output of PTFPV LED. The area of device is ~9 mm^2.

This work was financially supported by Ministero dell' Università e della Ricerca Scientifica e Tecnologica, Rome (Project 'Sintesi di materiali organici per applicazioni ottiche' L.488 19/12/92, Piano 'Materiali Innovativi') and by Consiglio Nazionale delle Ricerche, Rome (National Project 'Progetto Finalizzato Materiali Speciali per Tecnologie Avanzate II').

Notes and references

† Experimental procedure: a mixture of 1,4-diiodo-2,3,5,6-tetrafluorobenzene **1** (0.600 g, 1.49 mmol), (*E*)-1,2-bis(tributylstannyl)ethene (0.905 g, 1.49 mmol) **2**, catalyst $Pd_2(dba)_3$ (0.041 g, 0.05 mmol) and ligand $AsPh_3$ (0.110 g, 0.36 mmol) in 24 ml of benzene was refluxed under a nitrogen atmosphere for 7 days. After cooling at room temperature, the solvent was evaporated under reduced pressure. The crude polymer obtained was washed twice with hexane. A greenish solid was recovered by centrifugation. Arsine and low molecular weight fractions were eliminated by extraction in a Soxhlet apparatus with ethanol (24 h) and with chloroform (12 h), respectively, leaving a yellow insoluble residue (0.260 g). The material does not melt up to 300 °C.

‡ XPS elemental analysis performed on powder gave comparable results.

1 A. Kraft, A. C. Grimsdale and A. B. Holmes, *Angew. Chem., Int. Ed.*, 1998, **37**, 402.

2 For our recent work on PPV systems see: (*a*) F. Babudri, S. R. Cicco, G. M. Farinola, F. Naso, A. Bolognesi and W. Porzio, *Macromol. Rapid Commun.*, 1996, **17**, 905; (*b*) L. Chiavarone, M. Di Terlizzi, G. Scamarcio, G. M. Farinola, F. Babudri and F. Naso, *Appl. Phys. Lett.*, 1999, **75**, 2053; (*c*) F. Naso, F. Babudri and G. M. Farinola, *Pure Appl. Chem.*, 1999, **71**, 1485; (*d*) F. Babudri, S. R. Cicco, L. Chiavarone, G. M. Farinola, L. C. Lopez, F. Naso and G. Scamarcio, *J. Mater. Chem.*, 2000, **10**, 1573; (*e*) F. Babudri, G. M. Farinola, L. C. Lopez, M. G. Martinelli and F. Naso, *J. Org. Chem.*, 2001, **66**, 3878.

3 J. Morgado, R. H. Friend and F. Cacialli, *Synth. Met.*, 2000, **114**, 189 and references therein.

4 (*a*) I. Benjamin, E. Z. Faraggi, Y. Avny, D. Davidov and R. Neumann, *Chem. Mater.*, 1996, **8**, 352; (*b*) R. Riehn, J. Morgado, R. Iqbal, S. C. Moratti, A. B. Holmes, S. Volta and F. Cacialli, *Macromolecules*, 2000, **33**, 3337; (*c*) M. R. Gurge, A. M. Sarker, P. M. Lahti, B. Hu and F. E. Karasz, *Macromol.*, 1997, **30**, 8286.

5 B. Strehmel, A. M. Sarker, J. H. Malpert, V. Strehmel, H. Seifert and D. C. Neckers, *J. Am. Chem. Soc.*, 1999, **121**, 1226.

6 (*a*) G. M. Brooke and S. D. Mawson, *J. Fluorine Chem.*, 1990, **50**, 101; (*b*) G. M. Brooke and S. D. Mawson, *J. Fluorine Chem.*, 1990, **50**, 111; (*c*) J. I. Lee, J. Y. Han, H. K. Shim, S. C. Jeoung and D. Kim, *Synth. Met.*, 1997, **84**, 261; (*d*) I. Benjamin, E. Z. Faraggi, G. Cohen, H. Chayet, D. Davidov, R. Neumann and Y. Avny, *Synth. Met.*, 1997, **84**, 401; (*e*) I.-N. Kang, H.-K. Shim and T. Zyung, *Chem. Mater.*, 1997, **9**, 746.

7 Z. Bao, W. K. Chan and L. Yu, *J. Am. Chem. Soc.*, 1995, **117**, 12426.

8 A. F. Renaldo, J. W. Labadie and J. K. Stille, *Org. Synth.*, 1989, **67**, 86.

9 V. Farina, *Pure Appl. Chem.*, 1996, **68**, 73 and references therein.

10 R. Skelton, F. Dubois and R. Zenobi, *Anal. Chem.*, 2000, **72**, 1707.

11 M. W. F. Nielen, *Mass Spectrom. Rev.*, 1999, **18**, 309 and references therein.

12 J. Cornil, D. A. dos Santos, D. Beljonne and J. L. Brédas, *J. Phys. Chem.*, 1995, **99**, 5604.

13 Z. Xie, J. S. Huang, C. N. Li, S. Y. Liu, Y. Wang, Y. Q. Li and J. C. Shen, *Appl. Phys. Lett.*, 1999, **74**, 641.

CHEMCOMM Communication
www.rsc.org/chemcomm

Preparation of highly photocatalytic active nano-sized TiO_2 particles *via* ultrasonic irradiation

Jimmy C. Yu,*[a] Jiaguo Yu,*[ab] Wingkei Ho[a] and Lizhi Zhang[a]

[a] *Department of Chemistry and Materials Science & Technology Research Center, The Chinese University of Hong Kong, Shatin, New Territories, Hong Kong, China. E-mail: jimyu@cuhk.edu.hk; yujiaguo@public.wh.hb.cn*

[b] *State Key Laboratory of Advanced Technology for Materials Synthesis and Processing, Wuhan University of Technology, Wuhan, 430070, China*

Received (in Cambridge, UK) 21st June 2001, Accepted 15th August 2001
First published as an Advance Article on the web 17th September 2001

A novel method for preparing highly photoactive nano-sized TiO_2 photocatalysts with anatase and brookite phases has been developed by hydrolysis of titanium tetraisopropoxide in pure water or a 1 : 1 EtOH–H_2O solution under ultrasonic irradiation; the photocatalytic activity of TiO_2 particles prepared by this method exceeded that of Degussa P25.

A great deal of effort has been devoted in recent years to developing heterogeneous photocatalysts with high photocatalytic activities for their applications in solving environmental problems.[1–3] In order to commercialize this treatment technique, it is of great importance to improve the preparative methods of titania, because the photocatalytic activity and phase transition behavior of TiO_2 are significantly influenced by the preparative conditions and methods.[4–8] In this study, a novel and simple method for preparing highly photoactive nano-sized TiO_2 photocatalysts with anatase and brookite phases has been developed by a sol–gel method and ultrasonic irradiation in pure water or EtOH–H_2O mixed solution. This is the first report that shows high photocatalytic activity of a photocatalyst containing an 80% anatase and 20% brookite phase.

Sonochemistry arises from acoustic cavitation, the formation, growth, and implosive collapse of bubbles in a liquid.[8–10] The use of ultrasound to enhance the rate of reaction has become a routine synthetic technique for many homogeneous and heterogeneous chemical reactions.[8–10] Sonochemistry has been used to prepare various oxides and amorphous metal powders.[8–12] In the present work, it was found that ultrasonic irradiation could not only accelerate the hydrolysis and crystallization of titania, but also enhances the photocatalytic activity.

To synthesize nano-sized TiO_2 particles, titanium tetraisopropoxide (TTIP, Aldrich) was used as a titanium source. TTIP (0.0125 mol) was added dropwise to 100 mL pure water or EtOH–H_2O mixed solution under vigorous stirring at room temperature. The molar ratio of EtOH to H_2O (R_{EtOH}) was 0, 1 or 10. Sol samples formed by the hydrolysis process were treated with and without ultrasonic irradiation in an ultrasonic cleaning bath (Bransonic ultrasonic cleaner, model 3210E DTH, 47 kHz, 120 W, USA) for 1 h, followed by ageing in a closed beaker at room temperature for 36 h in order to further hydrolyze the TTIP and form mono-dispersed TiO_2 particles. After the ageing, these samples were dried at 100 °C for *ca.* 8 h in air in order to vaporize water and alcohol in the gels and then ground to a fine powder to obtain dried gel samples. The dried gel samples were calcined at 500 °C in air for 1 h to obtain TiO_2 photocatalysts. Their synthesis conditions and physicochemical properties are summarized in Table 1.

The X-ray diffraction (XRD) patterns, obtained on a Philips MPD 18801 X-ray diffractometer using Cu-Kα radiation at a scan rate of 0.05° 2θ s^{-1}, were used to determine the identity of any phase present and its crystallite size. The phase content of titania can be calculated from the integrated intensities of anatase (101), rutile (110) and brookite (121) peaks by the method reported by Zhang.[13] The average crystallite sizes of anatase, rutile, and brookite were determined according to the Scherrer equation. Brunauer–Emmett–Teller (BET) surface areas (S_{BET}) were determined using a Micromeritics ASAP 2000 nitrogen adsorption apparatus. All the samples measured were degassed at 180 °C before the actual measurements.

The photocatalytic activity experiments on TiO_2 particles for the oxidation of acetone in air were performed at ambient temperature using a 7000 ml reactor. The detailed experimental process can be found in ref. 14. The photocatalytic oxidation of acetone is a pseudo-first-order reaction and its kinetics may be expressed as follows: $\ln(C_0/C) = kt$, where k is the apparent reaction rate constant, C_0 and C are the initial concentration and the reaction concentration of acetone, respectively.[1,2]

Fig. 1 shows XRD patterns of the as-prepared TiO_2 gel powders. The TiO_2 gel particles obtained from pure water ($R_{EtOH} = 0$) contain anatase, as the main phase along with brookite. With increasing R_{EtOH}, the intensities of anatase peaks become steadily weaker and the brookite phase disappears.

Table 1 Synthesis conditions and physicochemical properties of TiO_2 particles

Sample	R_{EtOH}[a]	Ultrasonic irradiation	Phase content[b]	Crystallite size[c]/nm	S_{BET}[d]/ m^2 g^{-1}	Porosity[e]	Pore volume[f]/ ml g^{-1}	Pore size[g]/nm
A	0	Yes	(A): 79.6 (B): 20.4	(A): 9.5 (B): 7.9	97.61	50.6	0.218	5.9
B	1	Yes	(A): 91.6 (B): 9.4	(A): 11.3 (B): 8.2	91.38	48.1	0.192	5.3
C	10	Yes	(A): 100	(A): 25.8	26.34	17.7	0.052	7.2
D	0	No	(A): 81.7 (B): 18.3	(A): 12.8 (B): 7.3	75.51	42.7	0.188	7.1
E	1	No	(A): 100	(A): 13.1	67.5	36.3	0.136	6.82
F	10	No	(A): 100	(A): 31.0	22.3	9.8	0.029	6.52

[a] Molar ratios of EtOH to H_2O. [b] Determined by XRD, (A): anatase, (B): brookite. [c] Calculated by XRD using the Scherrer equation. [d] BET surface area calculated from the linear part of the BET plot (P/P_0 = 0.1–0.2). [e] The porosity is estimated from the pore volume determined using the adsorption branch of the N_2 isotherm curve at P/P_0 = 0.995. [f] Total pore volume, taken from the volume of N_2 adsorbed at P/P_0 = 0.995. [g] Average pore diameter, estimated using the desorption branch of the isotherm and the Barrett–Joyner–Halenda (BJH) formula.

 DOI: 10.1039/b105471f

When R_w = 10, the TiO_2 gel particles appear completely amorphous. This is probably due to the fact that EtOH solvent suppresses the hydrolysis of titanium alkoxide and rapid crystallization of the TiO_2 particles by adsorbing on the surfaces of TiO_2 particles.[6,7] Usually, with increasing water content, a stronger nucleophilic reaction between water and alkoxide molecules will occur and more alkoxy groups in the alkoxide will be substituted by hydroxy groups of water.[7] Therefore, the decrease in the quantity of unhydrolysed alkyls in a precursors results in a reduction of steric hindrance by the residual alkyls, preventing crystallization to crystalline anatase. R_{EtOH} and ultrasonic irradiation also has a strong influence on the crystallization behavior of TiO_2 gels at 500 °C. Table 1 shows that with increasing R_{EtOH}, the content and crystallite size of anatase increases. This is ascribed to the fact that the heat produced by the combustion of residual alkyls will promote the transformation of the TiO_2 phase and growth of TiO_2 crystallites. Moreover, ultrasonic irradiation reduces the crystallite size of anatase. This is due to the fact that ultrasound irradiation generates many localized hot spots in the solution and within the gel. The hydrolysis of ≡Ti–OR species is enhanced and the polycondensation of ≡Ti–OH species is promoted. This further causes the homogeneous formation of a large number of seed nuclei, which leads to a smaller particle size.[11]

Fig. 2 shows the pore size distribution curve and the corresponding nitrogen adsorption–desorption isotherms (inset) of sample A. The BET surface area and pore parameters of the samples determined from the nitrogen adsorption–desorption isotherm by the BJH (Barrett–Joyner–Halenda) method are summarized in Table 1. This shows that all samples A–F have a mesoporous structure. The average pore diameter is several nm. The mesoporous structure of TiO_2 particles is attributed to pores formed between TiO_2 particles.[11] It is these mesopores

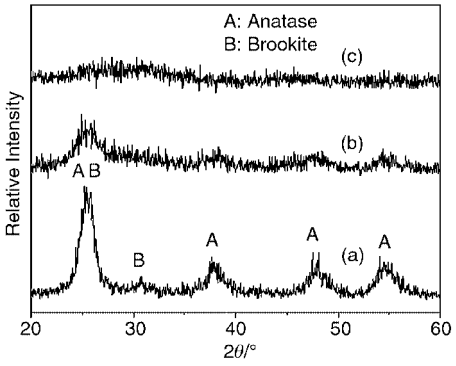

Fig. 1 XRD patterns of the TiO_2 gel powders prepared from the EtOH–H_2O mixed solutions under ultrasonic irradiation with (*a*) R_{EtOH} = 0 (pure water), (*b*) R_{EtOH} = 1 and (*c*) R_{EtOH} = 10; and dried at 100 °C for 8 h.

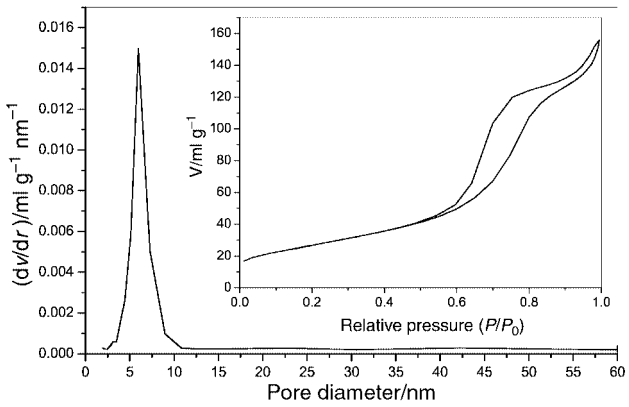

Fig. 2 Pore size distribution curve calculated from the desorption branch of the nitrogen isotherm by the BJH method. (Inset) The corresponding nitrogen adsorption–desorption isotherms of sample A.

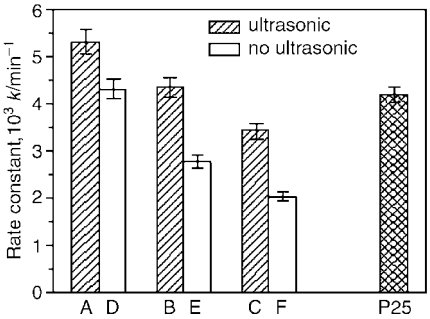

Fig. 3 Comparison of the apparent rate constants of samples A–F and P25.

that allow rapid diffusion of various reactants and products during photocatalytic reaction and enhance the speed of the photocatalytic reaction. It can also be seen from Table 1 that with increasing R_{EtOH}, BET surface area, porosity and pore volume decrease and pore diameter increases, which is attributed to the growth of TiO_2 crystallites.

Fig. 3 shows the comparison of the apparent rate constants (k/min^{-1}) of samples A–F and Degussa P25 (P25). For sample A, the k value (5.30×10^{-3}) is obviously higher than that of P25 (4.19×10^{-3}), which is well known to have a high photocatalytic activity.[1,2] This may be attributed to the fact that the former has a larger specific surface area, smaller crystallite size *etc*. With increasing R_{EtOH} (from sample A to C), the value of k decreases. For example, the k value of sample C is lower than that of P25 and sample B. This is attributed to the fact that it had a smaller specific surface area and a larger crystallite size. On the other hand, P25 and sample A or B are composed of two phases, corresponding to anatase and rutile and anatase and brookite anatase, respectively. Usually, the composite of two kinds of semiconductors or two phases of the same semiconductor is beneficial in reducing the combination of photogenerated electrons and holes and in enhancing photocatalytic activity. Fig. 3 also shows that ultrasonic irradiation obviously enhances the photocatalytic activity of TiO_2 powders whether the solvent is pure water or EtOH–H_2O. This may be ascribed to the fact that ultrasonic irradiation enhances hydrolysis of titanium alkoxide and promotes better crystallization of TiO_2 gel, since ultrasonic cavitation creates a unique environment for the hydrolysis of titanium alkoxide and the formation of seed nuclei of TiO_2.

Notes and references

1 M. R. Hoffmann, S. T. Martin, W. Choi and D. W. Bahnemann, *Chem. Rev.*, 1995, **95**, 69.
2 A. Fujishima, T. N. Rao and D. A. Tryk, *J. Photochem. Photobiol. C: Photochem. Rev.*, 2000, **1**, 1.
3 H. Tada, K. Teranishi, Y. Inubushi and S. Ito, *Chem. Commun.*, 2000, 2345.
4 K. N. P. Kumer, K. Keizer, A. J. Burggraaf, T. Okubo, H. Nagamoto and S. Morooka, *Nature*, 1992, **358**, 48.
5 M. Gopal, W. J. Moberly Chan and L. C. De Jonghe, *J. Mater. Sci.*, 1997, **32**, 6001.
6 S. Ito, S. Inoue, H. Kawada, M. Hara, M. Iwasaki and H. Tada, *J. Colloid Interface Sci.*, 1999, **216**, 59.
7 K. Terabe, K. Kato, H. Miyazaki, S. Yamaguchi, A. Imai and Y. Iguchi, *J. Mater. Sci.*, 1994, **29**, 1617.
8 K. S. Suslick, *Science*, 1990, **247**, 1439.
9 K. S. Suslick, S. B. Choe, A. A. Cichowlas and M. W. Grinstaff, *Nature*, 1991, **353**, 414.
10 T. H. Hyeon, M. M. Fang and K. S. Suslick, *J. Am. Chem. Soc.*, 1996, **118**, 5492.
11 W. Huang, X. Tang, Y. Wang, Y. Koltypin and A. Gedanken, *Chem. Commun.*, 2000, 1415.
12 X. Tang, S. Liu, Y. Wang, W. Huang, E. Sominski, O. Palchik and A. Gedanken, *Chem. Commun.*, 2000, 2119.
13 H. Zhang and J. F. Banfield, *J. Phys. Chem. B*, 2000, **104**, 3481.
14 J. Lin, J. C. Yu, D. Lo and S. K. Lam, *J. Catal.*, 1999, **183**, 368.

CHEMCOMM Communication
www.rsc.org/chemcomm

Highly efficient oligosaccharide synthesis on water-soluble polymeric primers by recombinant glycosyltransferases immobilised on solid supports

Susumu Nishiguchi,[a] Kuriko Yamada,[a] Yoshitoshi Fuji,[b] Shigeo Shibatani,[a] Atushi Toda[a] and Shin-Ichiro Nishimura*[b]

[a] *Sapporo Laboratory for Glycocluster Project, Japan Bioindustry Association, Sapporo 060-0810, Japan*
[b] *Laboratory for Bio-Macromolecular Chemistry, Division of Biological Sciences, Graduate School of Science, Hokkaido University, Sapporo 060-0810, Japan. E-mail: shin@glyco.sci.hokudai.ac.jp*

Received (in Cambridge, UK) 4th June 2001, Accepted 15th August 2001
First published as an Advance Article on the web 17th September 2001

Recombinant β-1,4-galactosyltransferase (β1,4-GalT) and α-2,6-sialyltransferase (α2,6-SiaT) immobilised covalently with activated Sepharose beads were employed for the practical synthesis of a trisaccharide derivative, Neu-5Acα(2→6)Galβ(1→4)GlcNAcβ-O-$(CH_2)_6$-NH_2, on a water-soluble primer having GlcNAc residues through a α-chymotrypsin-sensitive linker.

Synthesis of oligosaccharides using glycosyltransferases is recognized as a promising practical alternative method to chemical synthesis because enzyme-based synthesis has produced highly stereo- and regioselective glycosylations without tedious multi-step protection–deprotection procedures.[1] It has also been known that enzymatic glycosylations of polymer-supported sugars both in solid-phase[2] and in solution[3–5] greatly facilitate synthetic schemes because of easy and simple procedures for purifying products linked with macromolecules. Recently, a variety of recombinant glycosyltransferases for such a purpose are becoming practicable owing to advances in cloning studies of glycosyltransferases.[6] However, these recombinant enzymes are still very expensive and unstable as versatile reagents in chemoenzymatic synthesis, and they cannot be recovered from the reaction mixture by common work-up processes. At present, these biocatalysts are not suited for large-scale and/or combinatorial syntheses of glycoconjugates. Although immobilisation of the glycosyltransferases seems to have become a crucial step for solution of these problems,[7,8] enzymes immobilised on solid materials cannot be used for glycosylation of solid-supported sugars as glycosyl acceptors. Therefore, our interest has been focused on the feasibility of reactions between glycosyltransferases immobilised on solid phase and sugars bound on the flexible polymers showing satisfactory water-solubility as 'primers'. In the present communication, we describe highly practical synthesis of a sialooligosaccharide using immobilised recombinant-glycosyltransferases and a GlcNAc carrying primer involving an α-chymotrypsin-sensitive linker moiety.

In the course of our synthetic studies on the multivalent glycopolymers as models for glycoproteins,[9] we found that these materials can be used for polymer-assisted enzymatic synthesis as convenient 'multivalent substrates' of glycosyltransferases.[10] The success of this new strategy is critically dependent on drastically enhanced affinity of glycosyltransferases for multivalent glycopolymers.[5] Since glycosyltransferases are generally monomeric proteins with a single binding site, the mechanism for the enhancement of binding affinity observed here might be different from the cases where a 'glycoside clustering effect' is found in the proteins with multiple sugar-binding sites.[11] Although this can be explained basically by 'enhanced accessibility' of proteins to the high-density glycoclusters displayed on the flexible synthetic polymers,[12] further physicochemical analyses of the mechanism are still under way. In this study, we firstly checked the

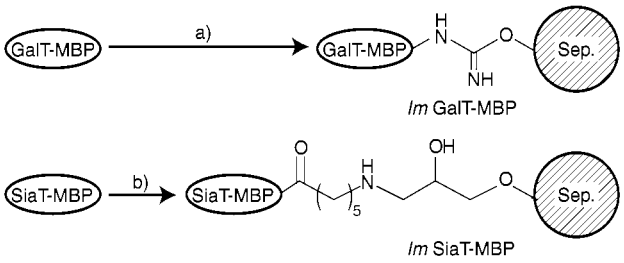

Scheme 1 Immobilisation of glycosyltransferases. (a) CNBr-activated Sepharose 4B, pH 8.0, 4 °C, 16 h, immobilisation yield 11%; (b) NHS-activated Sepharose 4FF, pH 7.0, 4 °C, 16 h immobilisation yield 17%.

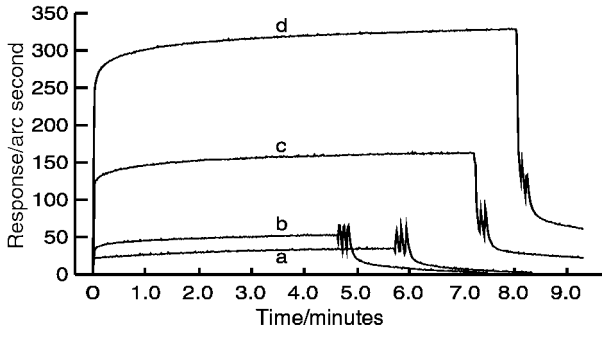

Fig. 1 Binding curves for glycopolymer to immobilised GalT. (a) 1.3 μM, (b) 2.6 μM, (c) 13 μM, and (d) 26 μM. GalT was immobilised on the activated aminosilane surface with bis(sulfosuccinimidyl) suberate.

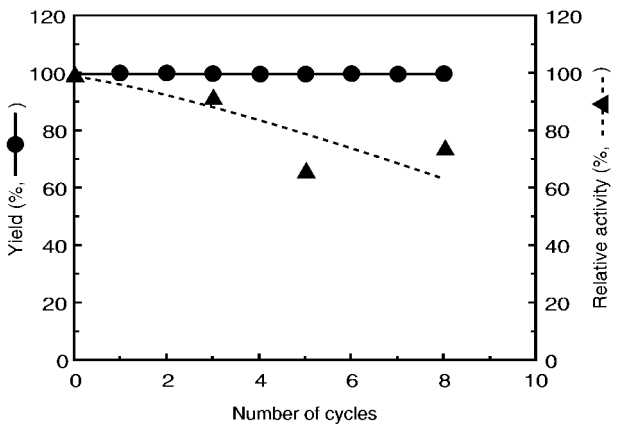

Fig. 2 Recyclability of immobilised GalT. Relative activity was determined by use of the glycosylation to 2-aminopyridyl glycoside derivative as a standard acceptor substrate. *Conditions*: primer (10 mM), UDP-Gal (13 mM), immobilised GalT (0.25 mL, 0.8 unit),† pH 7.5, 37 °C, 24 h.

 DOI: 10.1039/b104896c

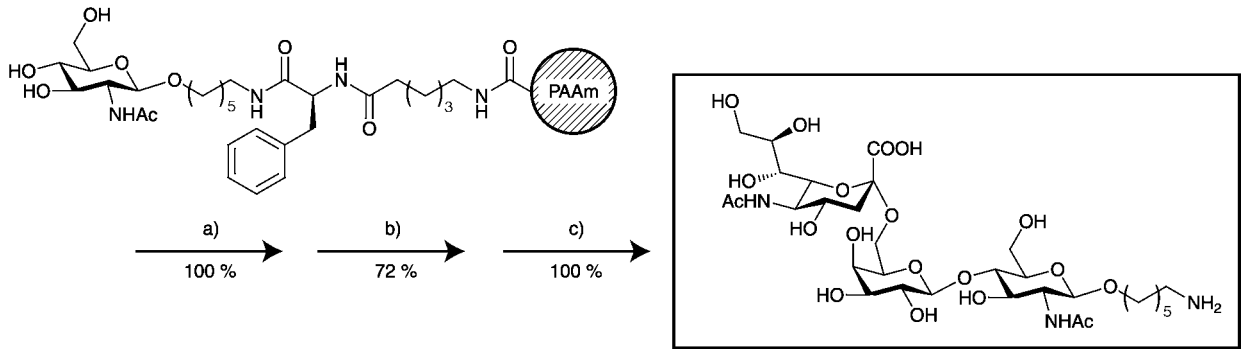

Scheme 2 (a) i, immobilized β1,4-GalT (0.2 unit, 0.3 mL),† primer (27 mg, 40 mM as GlcNAc residue), UDP-Gal (1.3 eq., 52 mM), 10 mM $MnCl_2$, 50 mM HEPES buffer (pH 7.5), 37 °C, 24 h; ii, gel filtration on Sephadex G-25 with distilled water; (b) i, immobilized α2,6-SiaT (0.08 unit, 0.3 mL),‡ polymer (19 mg, 17 mM as LacNAc residues), CMP-NeuAc (1.5 eq., 26 mM), alkaline phosphatase (40 unit), 10 mM $MnCl_2$, 0.1% Triton CF-54, 50 mM HEPES buffer (pH 7.5), 37 °C, 24 h; ii, gel filtration on Sephadex G-25 with distilled water; (c) i, α-chymotrypsin (3000 U, 1.5 mg), polymer (15 mg, 8.3 mM as SiaLacNAc residues), 10 mM $CaCl_2$, 100 mM Tris–HCl (pH 8.0), 37 °C, 24 h; ii, gel filtration on Sephadex G-25 with distilled water. PAAm: polyacrylamide copolymer (M_r > 300K, sugar–acrylamide = 1:10).

effect of immobilisation of recombinant glycosyltransferases on the affinity with glycosyl acceptor substrates by using the surface plasmon resonance (SPR, IAsys) method. As shown in Fig. 1, it was clearly suggested that recombinant β1,4-GalT immobilised on the SPR-cuvette retained a high affinity for a water-soluble primer and the affinity constant of the immobilised GalT with the glycopolymer bearing GlcNAcs was estimated to be 5.0×10^6 M^{-1}. On the contrary, the affinity of methyl 2-acetamido-2-deoxy-β-D-glucopyranoside (GlcNAc) for this GalT-conjugated SPR cuvette was estimated to be lower than 10^3 M^{-1}. This result prompted us to immobilise GalT and α2,6-SiaT on the polymer supports (Scheme 1). Thus, these glycosyltransferases expressed as fusion proteins with maltose-binding protein (MBP) in *E. coli*[13,14] were directly subjected to the coupling reactions with CNBr-activated§ Sepharose 4B (MBP-GalT) or NHS-activated¶ Sepharose 4FF (MBP-SiaT). As anticipated, immobilised GalT exhibited satisfactory sugar-elongation activity to the primer and the GalT combined beads were found to be recyclable (Fig. 2).

The versatility of oligosaccharide synthesis based on the immobilised glycosyltransferases was demonstrated by constructing a simple trisaccharide derivative that can be applied to further conjugation studies to produce glycodrugs or glycomaterials having interesting bioactivities. Galactosylation (100%) by GalT-Sepharose (0.2 unit, 0.3 mL of beads) and sialylation (72%) by α2,6-SiaT-Sepharose (0.08 unit, 0.3 mL of beads) were achieved on the primer (15.0 mg of polymer, 8.3 μmol of GlcNAc residue) and 4.6 mg of sialylα(2-6)-*N*-acetyllactosamine (72%) was finally obtained by treating the primer with α-chymotrypsin under reported conditions[4] (Scheme 2).

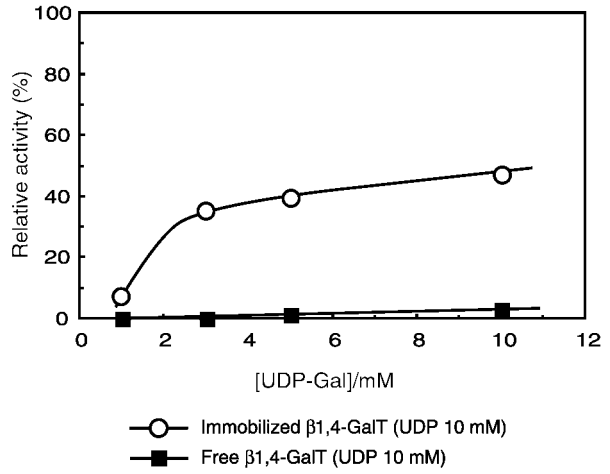

Fig. 3 The effect of UDP on the glycosylation by GalT to primer. (a) immobilised GalT; (b) free GalT. All reactions were carried out in the presence of 10 mM of UDP.

It should also be noted that glycosylation of polymer primers by glycosyltransferases conjugated with macromolecular support proceeds predominantly to afford product even in the presence of a high concentration of inhibitors (nucleotides) as shown in Fig. 3. This result indicates that the inhibitory effect of nucleotide (UDP) generated from UDP-Gal was significantly reduced by immobilisation of enzyme. The availability of the immobilised glycosyltransferases reported herein will greatly accelerate the development of an enzyme-based automated glycosynthesiser.[15]

We are grateful to Dr Fujiyama (International Center of Cooperative Research in Biotechnology, Japan, Osaka University) for gift of the cDNA coding human β1,4-GalT. This work was supported by a grant from the New Energy and Industrial Technology Development Organization (NEDO).

Notes and references

† For GalT: one unit is defined as the amount of enzyme that will transfer 1 μmole of Gal to D-glucose per minute.
‡ For SiaT: one unit is defined as the amount of enzyme that will transfer 1 μmole of Neu5Ac from CMP-Neu5Ac to asialomucin per minute.
§ CNBr = cyanogen bromide.
¶ NHS = *N*-hydroxysuccinimide.

1 C.-H. Wong, R. L. Halcomb, Y. Ichikawa and T. Kajimoto, *Angew. Chem., Int. Ed. Engl.*, 1995, **34**, 521.
2 M. Shulster, P. Wang, J. C. Paulson and C.-H. Wong, *J. Am. Chem. Soc.*, 1994, **116**, 1135.
3 U. Zehavi, S. Sadeh, M. Harchman and S. Kopper, *Carbohydr. Res.*, 1983, **124**, 23.
4 K. Yamada and S.-I. Nishimura, *Tetrahedron Lett.*, 1995, **32**, 9493.
5 K. Yamada, E. Fujita and S.-I. Nishimura, *Carbohydr. Res.*, 1998, **305**, 443.
6 M. Amado, R. Almeida, T. Schwientek and H. Clausen, *Biochem. Biophys. Acta*, 1999, **1473**, 35.
7 J. Thiem and W. Treder, *Angew. Chem., Int. Ed. Engl.*, 1986, **25**, 1096.
8 A. Lubineau, K. B. Carpentier and C. Augé, *Carbohydr. Res.*, 1997, **300**, 161.
9 S.-I. Nishimura, T. Furuike, K. Matsuoka, K. Maruyama, K. Nagata, K. Kurita, K. N. Nishi and S. Tokura, *Macromolecules*, 1994, **27**, 4876.
10 S.-I. Nishimura, K. B. Lee, K. Matsuoka and Y. C. Lee, *Biochem. Biophys. Res. Commun.*, 1994, **199**, 249.
11 Y. C. Lee and R. T. Lee, *Acc. Chem. Res.*, 1995, **28**, 321.
12 S.-I. Nishimura and Y. C. Lee, in *Polysaccharides: Structural Diversity and Functional Versatility*, Ed. S. Dumitriu, Marcel Dekker Inc., New York, 1998, pp. 523–537.
13 R. B. Kapust and D. S. Waugh, *Protein Sci.*, 1999, **8**, 1668.
14 S. Shibatani, K. Fujiyama, S. Nishiguchi, T. Seki and Y. Maekawa, *J. Biosci. Bioeng.*, 2001, **91**, 85.
15 S.-I. Nishimura, *Curr. Opin. Chem. Biol.*, 2001, **5**, 325.

CHEMCOMM
Communication
www.rsc.org/chemcomm

First crystallographic signature of amyloid-like fibril forming β-sheet assemblage from a tripeptide with non-coded amino acids

Samir Kumar Maji,[a] Michael G. B. Drew[b] and Arindam Banerjee*[a]

[a] *Department of Biological Chemistry, Indian Association for the Cultivation of Science, Jadavpur, Calcutta-700 032, India. E-mail: bcab@mahendra.iacs.res.in; Fax: +91-33-4732805*
[b] *Department of Chemistry, The University Whiteknights, Reading, UK RG6 6AD*

Received (in Cambridge, UK) 20th June 2001, Accepted 7th August 2001
First published as an Advance Article on the web 17th September 2001

The model tripeptide Boc-β-Ala(1)-Aib(2)-β-Ala(3)-OMe 1 [β-Ala: β-alanine, Aib: α-aminoisobutyric acid] forms an infinite parallel β-sheet structure through intermolecular interactions in single crystals and from the SEM diagram of this peptide, it is evident that the compound has fibrillar morphology, a characteristic of neurodegenerative disease causing amyloid aggregate.

The design of short peptide molecules that form an intermolecular β-sheet structure is a newly emerging area. The molecular basis of some fatal, neurodegenerative diseases like prion protein disease[1,2] and Alzheimer's disease[3,4] involve intermolecular β-sheet aggregation and subsequent formation of highly ordered fibrillar structure. So it is important to construct peptide β-sheet assemblage to understand the pathogenesis and therapeutics of these diseases. Until now there have been limited reports describing β-sheet stabilization in crystals and in solution by intermolecular interactions. Most of the previous reports of β-sheet stabilization include unimolecular β-hairpin formation and subsequent stabilization by only intramolecular interactions.[5] Schrader and Kirsten first established β-sheet stabilization using rigid templates like 3-aminopyrazole derivatives that promote the formation and stabilization of β-sheet structures by purely intermolecular interactions.[6] Yamada *et al*. introduced a series of model peptide derivatives that formed an amyloid-like parallel β-sheet assemblage in solution.[7] Kelly and coworkers in a recent study using 2,8-disubstituted dibenzofuran-based peptidomimetics have established that β-sheet mediated self-assembly is essential to form amyloid-like fibrils of highly ordered structures.[8] However, all previously reported peptides or peptide derivatives that participate in intermolecular β-sheet stabilization and/or amyloid-like aggregate formation, used either rigid template or long aliphatic chains. Here, we report for the first time parallel β-sheet aggregation of a short synthetic peptide containing only noncoded amino acids [*viz*. β-alanine (β-Ala) and α-aminoisobutyric acid (Aib)] in crystals and formation of amyloid-like fibrils in the solid state.

The ORTEP diagram with the atom numbering scheme is shown in Fig. 1.† The hydrogen bonding pattern (Fig. 2) in the crystal lattice shows the formation of one infinite parallel β-sheet assembly along the *c* direction. These β-sheets are themselves regularly stacked *via* van der Waals interactions as shown by the projection of the unit cells in the *c* direction (Fig. 3). The hydrogen bonding parameters for **1** are listed in Table 1. There are three intermolecular hydrogen bonds N5–H5···O4, N10–H10···O9 and N15–H15···O16 that are responsible for connecting individual molecules to form and stabilize the sheet assembly. For the peptide **1**, backbone torsions are mostly in fully extended and semi-extended conformations (Table 1), a prerequisite for individual β-strand formation. This peptide has two terminal β-Ala residues, in which inherent conformational flexibility remains and thus terminal parts of the peptide are flexible in nature and might help to adopt extended or semi-extended conformations for the two terminal β-Ala residues. The variations from extended values of torsion angles occur at the centre of the molecule, which is occupied by the conforma-

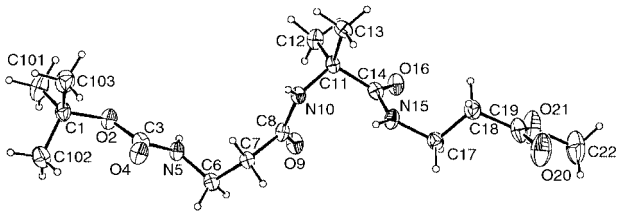

Fig. 1 An ORTEP representation of the molecular structure including atom numbering scheme of the peptide **1**. Thermal ellipsoids are shown at the level of 20% probability.

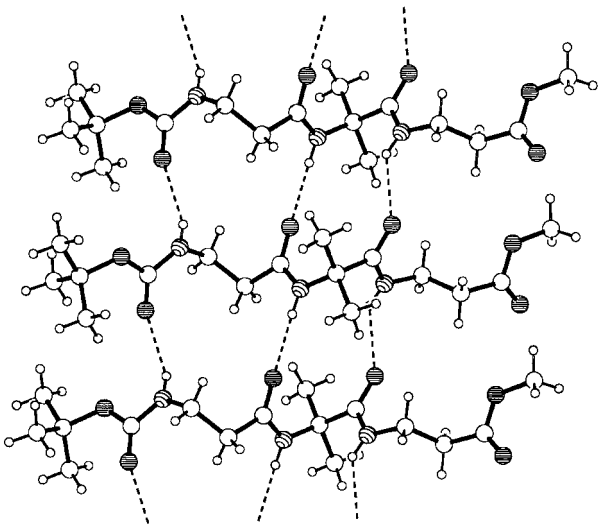

Fig. 2 Packing diagram of the peptide **1** in the *b* projection illustrating intermolecular hydrogen bonding in solid state and the formation of the β-sheets.

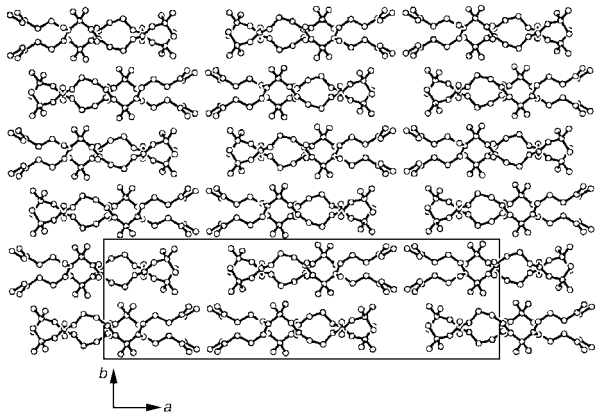

Fig. 3 Packing diagram of the peptide in the *c* direction showing the packing of the β-sheets.

 DOI: 10.1039/b105418j

Table 1 Characteristics of peptide **1** (Boc-β-Ala-Aib-β-Ala-OMe)

(a) Selected torsional angles(°)

C6-N5-C3-O2	−169.4(5)	ω_0	C8-N10-C11-C14	−57.8(6)	ϕ_2
C3-N5-C6-C7	−83.8(6)	ϕ_1	N10-C11-C14-N15	−48.5(6)	ψ_2
N5-C6-C7-C8	−77.6(6)	θ_1	C17-N15-C14-C11	−170.8(5)	ω_2
C6-C7-C8-N10	146.8(5)	ψ_1	C14-N15-C17-C18	84.1(7)	ϕ_3
C11-N10-C8-C7	178.9(5)	ω_1	N15-C17-C18-C19	−175.6(5)	θ_2
			C17-C18-C19-O21	77.5(8)	ψ_3

(b) Intermolecular hydrogen bonding parameters of **1**

D-H···A	H···A (Å)	D···A (Å)	D-H···A (°)
N5-H5···O4[a]	2.243	3.023	150.81
N10-H10···O9[b]	2.114	2.968	172.1
N15-H15···O16[a]	2.234	2.94	139.34

[a] Symmetry equivalent x, $-y+3/2$, $z+1/2$. [b] Symmetry equivalent x, $-y+3/2$, $z-1/2$.

tionally restricted α-aminoisobutyric acid (Aib) residue that is known to direct helical conformation[9] instead of β-sheet (Table 1). Here, Aib also adopts helical conformation ($\phi = -57.8°$, $\psi = -48.5°$). Some specific torsion angles along the two terminal β-Ala residues, N5–C6, C6–C7 and N15–C17, C18–C19 are in semi-extended conformations (Table 1).

The morphological similarity of the assemblage of the reported peptide with the amyloid fibrils has been studied using a scanning electron microscope (SEM). The SEM image (Fig. 4) of the dried fibrous material clearly shows that the aggregate in the solid state is a bunch of long small filaments.

The peptide **1** (containing noncoded amino acids) self-associates *via* intermolecular hydrogen bonds into a parallel β-sheet assemblage, in which all the intermolecular hydrogen bonds are present between the peptide linkages. Therefore, the present model should be a good model for β-sheet polypeptides. Morphological resemblance of this peptide with Alzheimers-associated Aβ peptides suggests that the fibril model with a parallel β-sheet assemblage will be helpful for examining the structure and function of abnormal peptides such as the prion and the Alzheimer's amyloid. Another remarkable feature of the present result is the formation of a parallel β-sheet structure in a short synthetic peptide containing the centrally-positioned, conformationally-constrained helix-forming Aib residue.

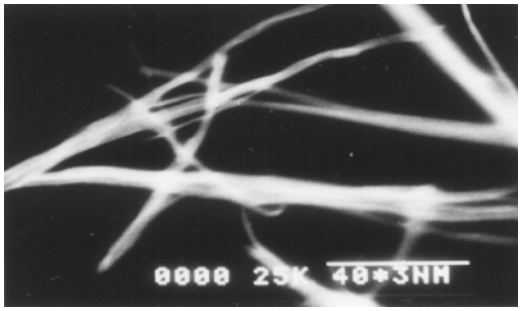

Fig. 4 A typical SEM image showing the fibril aggregate of peptide **1** in the solid state. For the SEM image, dried fibrous material was taken which was grown up from ethyl acetate solution by slow evaporation.

We thank EPSRC and the University of Reading, UK for funds for the Image Plate System. S. K. Maji wishes to acknowledge the Council for Scientific & Industrial research (C.S.I.R), New Delhi, India for financial assistance.

Notes and references

† The compound was synthesized using the fragment condensation method in solution. Single crystals were obtained from 1,2-dichlorobenzene solutions by slow evaporation.

Crystal data for **1**: $C_{16}H_{29}N_3O_6$, $M = 359.92$, orthorhombic, space group *Pccn*, $a = 37.25(4)$, $b = 11.123(19)$, $c = 9.610(14)$ Å, $U = 3981$ Å^3, $Z = 8$, $D = 1.199$ Mg m^{-3}. Intensity data were collected with MoKα radiation using the MARresearch Image Plate System. The crystal was positioned at 70 mm from the Image Plate. 100 frames were measured at 2° intervals with a counting time of 5 min to give 4684 reflections of which 1777 were independent [R(int) = 0.0506)]. Data analysis was carried out with the XDS program.[10] The structure was solved using direct methods with the SHELX86 program.[11] The non-hydrogen atoms were refined with anisotropic thermal parameters. The hydrogen atoms were included in geometric positions and given thermal parameters equivalent to 1.2 times those of the atom to which they were attached. The structure was refined on F^2 using SHELXL.[12] The final R values were $R1$ 0.0747 and $wR2$ 0.1984 for 1255 data with $I > 2\sigma(I)$. The largest peak and hole in the final difference Fourier were 0.358 and −0.317 e Å^{-3}. CCDC 167175. See http://www.rsc.org/suppdata/cc/b1/b105418j/ for crystallographic files in .cif or other electronic format.

1 S. B. Prusiner, *Science*, 1997, **278**, 245.
2 S. B. L. Ng and A. J. Doig, *Chem. Soc. Rev*., 1997, **26**, 425.
3 G. Taubes, *Science*, 1996, **271**, 1493.
4 R. Baumeister and S. Eimer, *Angew. Chem., Int. Ed*., 1998, **37**, 2978.
5 E. de Alba, J. Santoro, M. Rico and M. A. Jiménez, *Protein Sci*., 1999, **8**, 854; D. Seebach, S. Abele, K. Gademann and B. Jaun, *Angew. Chem., Int. Ed*., 1999, **38**, 1595; G. J. Sharman and M. S. Searle, *Chem. Commun*., 1997, 1955; J. D. Fisk and S. H. Gellman, *J. Am. Chem. Soc*., 2001, **123**, 343; C. Das, S. Raghothama and P. Balaram, *J. Am. Chem. Soc*., 1998, **120**, 5812.
6 T. Schrader and C. Kirsten, *Chem. Commun*., 1996, 2089.
7 N. Yamada, K. Ariga, M. Naito, K. Matsubara and E. Koyama, *J. Am. Chem. Soc*., 1998, **120**, 12 192.
8 H. L. Lashuel, S. R. LaBrenz, L. Woo, L. C. Serpell and J. W. Kelly, *J. Am. Chem. Soc*., 2000, **122**, 5262.
9 I. L. Karle and P. Balaram, *Biochemistry*, 1990, **29**, 6747; A. Banerjee, S. Dutta, A. Pramanik, N. Shamala and P. Balaram, *J. Am. Chem. Soc*., 1996, **118**, 9477; R. Kaul and P. Balaram, *Bioorg. Med. Chem*., 1999, **7**, 105; C. Toniolo, G. M. Bonora, A. Bavoso, E. Benedetti, B. DiBlasio, V. Pavone and C. Pedone, *Biopolymers*, 1983, **22**, 205.
10 W. Kabsch, *J. Appl. Cryst*., 1988, **21**, 916.
11 SHELX86, G. M. Sheldrick, *Acta Crystallogr., Sect. A: Fundam. Crystallogr*., 1990, **46**, 467.
12 SHELXL, G. M. Sheldrick, Program for Crystal Structure Refinement. University of Göttingen, Göttingen, Germany, 1993.

CHEMCOMM Communication
www.rsc.org/chemcomm

8,16,24,32,40,48-Hexamethoxy[2.6]metacyclophane-1,9,17,25,33,41-hexayne: a novel near-planar ammonium-selective ionophore

Youichi Hosokawa, Takeshi Kawase and Masaji Oda*

Department of Chemistry, Graduate School of Science, Osaka University, Toyonaka, Osaka 560-0043, Japan. E-mail: moda@chem.sci.osaka-u.ac.jp

Received (in Cambridge, UK) 16th May 2001, Accepted 7th August 2001
First published as an Advance Article on the web 17th September 2001

The titled cyclophane (cyclic [6]metaphenylacetylene) with six methoxy groups inside the cavity has a nearly planar carbon framework, forms open-channel structures in the crystal, and exhibits an ammonium-selective ionophoric property in spite of the considerably large cavity.

Recently, we have reported the synthesis of [2.4]metacyclophane-1,9,17,25-tetrayne **1** (cyclic [4]metaphenylacetylene, [4]CMPA) and its tetramethoxy derivative **2** where the methoxy groups point inside the molecule.[1,2] CMPA **2** thus has a cavity surrounded by the four methoxy oxygen atoms (1.2 Å in diameter, X-ray analysis) and was found to be a good ionophore for various alkali metal ions probably owing to its well-organized but conformationally somewhat flexible structure.[2] The good ionophoric properties of **2** are rare for this kind of molecule, because host molecules composed of anisole units have hardly shown efficient ionophoric properties except spherands and cavitands such as **3** and **4**.[3] Hexamethoxy-[6]CMPA **5**, a homologue of **2**, would also be of interest from the viewpoints of structure and ionophoric properties. While **2** has a sterically congested cavity and its carbon framework deviates from planarity, **5** would be almost free of steric congestion (PM3 calculation[4]). CMPA **5** can also be regarded as an analogue of spherand **3** extended with acetylenic bonds. Although the parent [6]CMPA and some derivatives bearing functional groups outside the molecules have been reported,[5–7] no [6]CMPAs bearing substituents inside the molecules have been described. We here report on the synthesis, structure, and host properties of **5a** and **5b**.

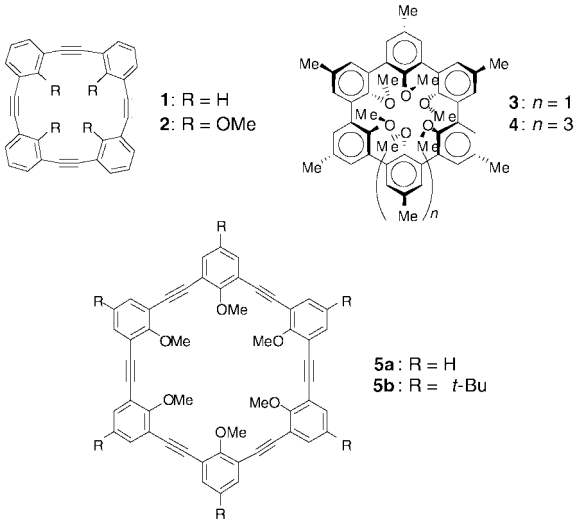

Hexamethoxy[6]CMPAs **5a** and **5b** were synthesized in a similar manner as for the synthesis of CMPAs **1** and **2**, that is, bromination–dehydrobromination of the corresponding metacyclophane-polyenes prepared by a modified McMurry coupling (Scheme 1).[1,2] The McMurry coupling of 2,2′-dimethoxy-3,3′-diformyl-(*Z*)-stilbene **6**[2] in DME–toluene (5 : 1) afforded (*EZEZ*)-tetraene **7**[2] (23% yield) and (*EZ*)[3]-hexaene **8**† (14%). Similarly, the McMurry coupling of (*Z,Z*)-1,3-bis(5-*tert*-butyl-3-formylstyryl)benzene **9**, prepared from (*Z,Z*)-1,3-bis(5-bromo-3-formylstyryl)benzene through dilithiation (BuLi) and diformylation (DMF), in THF–toluene (5 : 1) afforded (all-*Z*)-triene **10**† (4%) and (*ZEZ*)[2]-hexaene **11**† (15%). The McMurry reactions in DME or THF alone afforded **8** or **11** in poorer yield. Bromination of **8** and **11** with 9 equivalents of Br_2 in chloroform and subsequent dehydrobromination of the crude dodecabromides with 15 equivalents of *t*-BuOK in ether gave the corresponding CMPAs **5a**† (52%) and **5b**† (69%) as stable crystalline substances. Similar to the parent [6]CMPA, **5a** is poorly soluble in organic solvents, but **5b** is a little more soluble to allow the examination of complexation with metal ions and molecular cations.

^{1}H and ^{13}C NMR spectra of **5a** and **5b** are simple in agreement with the high symmetry of the molecules (C_6). The chemical shifts of their sp carbons (δ 89.92 and 89.87 respectively) are in the normal region of unstrained acetylenic carbon [δ 89.85 for bis(2-methoxyphenyl)acetylene].

A single crystal of **5b** suitable for X-ray analysis was obtained from a dichloromethane–hexane solution, and the ORTEP drawing is shown in Fig. 1.‡ The carbon framework of **5b** is nearly planar, and the six methoxy groups point up and down alternately in accord with a theoretical calculation (PM3). The distance between the diagonal oxygen atoms in *ca.* 8.1 Å which is twice as long as that in **2** (4.2 Å). Thus, **5b** (and also **5a**) has a sizable cavity of about 5 Å in diameter surrounded by six oxygen atoms. In the crystal, the molecules of **5b** form displaced sheet structures which stack so as to form open-channels with internal pores of 4.5 Å in diameter running parallel to the *c* axis (Fig. 2). There is little π–π stacking, and the inter-sheet separation is 3.7 Å. Channel formation in crystals of CMPAs has also been reported for hexahydroxy[6]CMPA **12** bearing the hydroxy groups outside the molecule.[7,8] While hydrogen bonding plays an important role in channel formation in **12**, only van der Waals interactions are operative in **5b**.

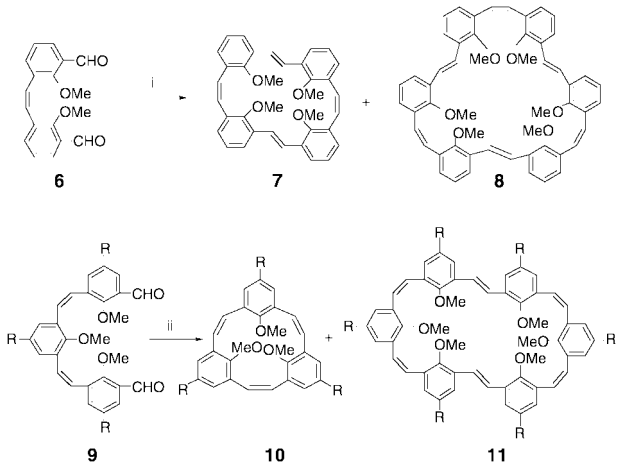

Scheme 1 *Reagents*: i, $TiCl_4$–Zn–CuI/DME–Tol 5 : 1, rt then reflux; ii, $TiCl_4$–Zn–CuI/THF–Tol 5 : 1, rt then reflux.

 DOI: 10.1039/b104325k

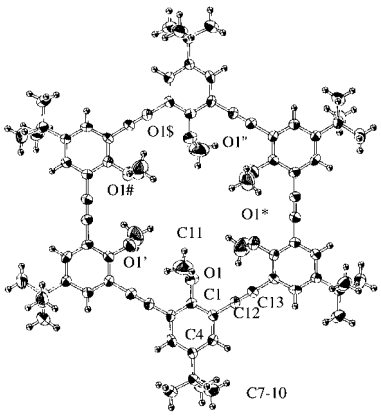

Fig. 1 ORTEP drawing of **5b** (50% probability): C1–C12, 1.457(5); C12–C13, 1.185(4); Cl–O1, 1.370(4) Å. Interatomic distance of diagonal oxygen atoms: 8.1 Å (average).

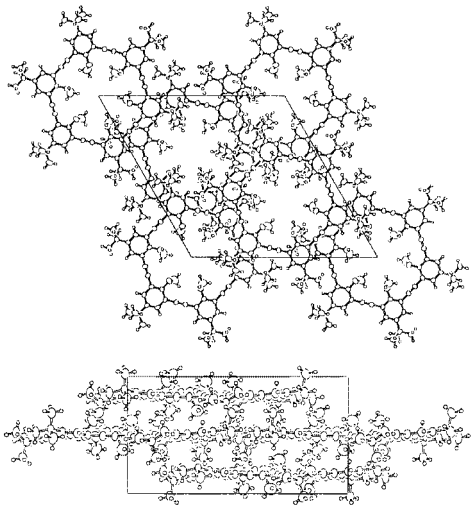

Fig. 2 Crystal packing of **5b**. Top; along *c* axis, bottom; along *a* axis.

The cavity size of **5b** is appreciably larger than the size of a caesium ion (3.4 Å), and in fact **5b** did not show any measurable complexation with alkali metal ions upon solvent extraction experiments (chloroform/aq. picrate salts; the low solubility of **5b** limits the range of detection by absorption spectroscopy). However, it was found that **5b** exhibits good ionophoric selectivity for the ammonium ion in spite of its smaller size (2.86 Å) compared with caesium ion. A plot by Shono's method shows a straight line with a slope of approximately unity, suggesting the formation of a 1 : 1 complex between **5b** and the ammonium ion in solution.[9,10] The association constant obtained for the ammonium ion (log K_a = 7.84) is smaller than that of **2** (9.51[2]) and 18-crown-6 (9.38[11]), but larger than that for the cavitand **4** (6.59[11]). On the other hand, methylammonium ion was extracted poorly (log K_a < 6.5). This large difference in K_a contrasts with small differences in the complexation of **4** with ammonium and methylammonium ion (6.66 and 6.59,[11] respectively). Cavitands have been known to be flexible enough to change the cavity for binding cationic species. The carbon framework of **5b** would be more rigid than cavitands, although some flexibility has been suggested from the low ionophoric selectivity of **2** toward alkali metal ions.

Thus, **5b** is a novel ionophore with a high selectivity for the parent ammonium ion. This selectivity is notable because other host molecules like **2**, **4** and 18-crown-6 can bind both metal cations and ammonium ions of similar size to a similar degree. According to the optimized structure of the complex of **5a** with ammonium ion by PM3 calculation,[4] the ammonium ion occupies a position where three NH bonds point to three oxygen atoms of the host.[12] Therefore, although the distance between the NH nitrogens and MeO oxygen atoms (3.5 Å) is longer than that of a usual hydrogen bond (3.0 Å), there seems weak but triple hydrogen bonding between **5b** and the ammonium ion in addition to electrostatic attraction. On the other hand, a similar structure for the complex of **5a** with methylammonium ion suffers steric repulsion between the methyl groups of the host and guest molecules and the NH bonds no longer point to the oxygen atoms of the host in the optimized structure.

In view of the present results, the phenolic molecule of **5** will be an intriguing compound and attempts to synthesize it are in progress.

We gratefully acknowledge the support of this research by a Grant-in-Aids for Scientific Research of Priority Area (No.10146102) from the Ministry of Education, Japan.

Notes and references

† *Selected spectroscopic data* [NMR: at 400 MHz (^{1}H) and 100 MHz (^{13}C) in $CDCl_3$]: Hexaene **8**: MS (FAB) *m*/*z* = 792 (M^+); δ_H 3.62 (18H, s, OMe), 6.78 (6H, s, *cis* olefin), 6.89–6.99 (12H, m, arom.), 7.17 (6H, s, *trans* olefin), 7.40 (6H, d, *J* = 7.3 Hz, arom.); δ_C 61.32, 123.74, 125.41, 125.75, 127.17, 128.34, 129.26, 131.57, 131.92, 155.40. Triene **10**: MS (FAB) *m*/*z* = 564 (M^+); δ_H 1.06 (27H, s, *t*Bu), 3.72 (9H, s, OMe), 6.68 (6H, s, *cis* olefin), 6.75 (6H, s, arom.). Hexaene **11**: MS (FAB) *m*/*z* = 1131 [$(M + H)^+$]; δ_H 1.28 (36H, s, *t*Bu), 1.54 (18H, s, *t*Bu), 3.39 (12H, s, OMe), 3.87 (6H, s, OMe), 6.70 (4H, d, *J* = 12.3 Hz, *cis* olefin), 6.72 (4H, s, arom.), 6.94 (4H, d, *J* = 12.3 Hz, *cis* olefin), 7.11 (4H, s, arom.), 7.20 (4H, m, arom. and *trans* olefin), 7.41 (4H, s, arom.). Hexayne **5a**: MS (EI) *m*/*z* 780 (M^+); δ_H 4.33 (18H, s, OMe), 7.01 (6H, t, *J* = 7.6 Hz, arom.), 7.51 (12H, d, *J* = 7.6 Hz, arom.); δ_C 61.78, 89.92 (sp C), 117.81, 123.62, 133.28; IR (KBr, cm^{-1}): ν 2220 (C≡C). Hexayne **5b**: MS (FAB) *m*/*z* = 1119 [$(M + H)^+$]; δ_H 1.34 (54H, s, *t*Bu), 4.20 (18H, s, OMe), 7.52 (12H, s, arom.); δ_C 31.28, 34.40, 61.47, 89.68 (*sp* C), 116.85, 130.96, 146.42, 159.66; UV ($CHCl_3$) λ_{max}/nm (log ε) 240 (4.64), 303 (5.22), 340 (4.73); IR (KBr, cm^{-1}) ν 2213 (C≡C); Raman (KBr) ν 2218 (C≡C).

‡ *Crystal data for* **5b**: $C_{78}H_{84}O_6$, *M* = 1117.52, trigonal, space group $R\bar{3}$ (#148), *a* = 23.604(4), *c* = 10.803(6) Å, *V* = 5212(3) Å^3, *Z* = 3, D_{calc} = 1.068 g cm^{-3}, μ = 0.66 cm^{-1}, *R* (*wR*) = 0.128 (0.135), *R*1 = 0.060 for 677 reflections.

CCDC 165271. See http://www.rsc.org/suppdata/cc/b1/b104325k/ for crystallographic data in .cif or other electronic format.

1 T. Kawase, N. Ueda, H. R. Darabi and M. Oda, *Angew. Chem., Int. Ed. Engl*., 1996, **35**, 1556; T. Kawase, N. Ueda and M. Oda, *Tetrahedron Lett*., 1997, **38**, 6681; T. Kawase, N. Ueda, T. Tanaka, Y. Seirai and M. Oda, *Tetrahedron Lett*., 2001, **42**, 5509.
2 T. Kawase, Y. Hosokawa, H. Kurata and M. Oda, *Chem. Lett*., 1999, 845.
3 D. J. Cram, T. Kaneda, R. C. Helgeson, S. B. Brown, C. B. Knobler, E. Maverick and K. N. Trueblood, *J. Am. Chem. Soc*., 1985, **107**, 3645; D. J. Cram, *Angew. Chem., Int. Ed. Engl*., 1986, **25**, 1039; D. J. Cram, R. A. Carmack, M. P. de Granodpre, G. M. Lein, I. Goldberg, C. B. Knobler, E. F. Maverick and K. N. Trueblood, *J. Am. Chem. Soc*., 1987, **109**, 7068, and references therein.
4 The calculation was performed by CAChe MOPAC ver. 94. See J. J. P. Stewart, *J. Comput. Chem*., 1989, **10**, 209.
5 H. A. Staab and K. Neunhoeffer, *Synthesis*, 1974, 424.
6 J. Zhang, D. J. Pesak, J. L. Ludwick and J. S. Moore, *J. Am. Chem. Soc*., 1994, **116**, 4227; P.-H. Ge, W. Fu, W. A. Herrmann, E. Herdtweck, C. Campana, R. D. Adams and H. F. Bunz, *Angew. Chem., Int. Ed*., 2000, **39**, 3607.
7 D. Cenkataraman, S. Lee, J. Zhang and J. S. Moore, *Nature*, 1994, **371**, 591.
8 D. T. Bong, T. D. Clark, J. R. Granja and M. R. Ghadiri, *Angew. Chem., Int. Ed*., 2001, **40**, 988.
9 K. Kimura, T. Maeda and T. Shono, *Talanta*, 1979, **26**, 945; K. E. Koenig, G. M. Lein, T. Kaneda and D. J. Cram, *J. Am. Chem. Soc*., 1979, **101**, 3553.
10 $PicNH_4$ (y = 1.023x − 5.504, R = 0.998).
11 R. M. Izatt, K. Pawlak, J. S. Bradshow and R. L. Bruenig, *Chem. Rev*., 1991, **91**, 1721, and references therein.
12 Attempts to obtain single crystals of the complex have been so far unsuccessful.

CHEMCOMM
Communication
www.rsc.org/chemcomm

A new tricyclic ring and a nitrogen–sulfur analogue of the tri-pentagon bowl. Substituted 5,6,7,7a-tetrahydropyrrolo[2,1-*b*]-1,3,4-thiadiazole-*endo*-6,7-dicarboxyimides

Richard N. Butler,* Georgina M. Smyth, Martin O. Cloonan (in part), Patrick McArdle and Desmond Cunningham

Chemistry Department, National University of Ireland, Galway, Ireland

Received (in Cambridge, UK) 13th June 2001, Accepted 15th August 2001
First published as an Advance Article on the web 7th September 2001

The first examples of a bowl-shaped tricyclic nitrogen–sulfur analogue of the tri-pentagon bowl are reported; substituted 5,6,7,7a-tetrahydropyrrolo[2,1-*b*]-1,3,4-thiadiazole-*endo*-6,7-dicarboxyimides are synthesised by a relatively simple route.

Among the fused 5,5-bicyclic heterocycles a number of simple pyrrolo systems are quite rare. One such case is the pyrrolo[2,1-*b*]-1,3,4-thiadiazole ring,[1] for which there are few reports.[1] Recently we have generated[2] the unstabilised 1,3,4-thiadiazolium-3-methanide 1,3-dipole **3** in solution by desilylation of the salts **1** with CsF, following a literature procedure[3,4] originally developed with Schiff bases (Scheme 1). If the dipole **3** were to cycloadd an alkene it should give the pyrrolo[2,1-*b*]-1,3,4-thiadiazole ring system. The 1,3-dipole **3** was unstable and could only be trapped at −60 °C using reactive electron-poor alkyne dipolarophiles. The alkyne cycloadducts were unstable and rearranged *in situ* by opening of the thiadiazole ring[2] and the likely intermediate pyrrolo-1,3,4-thiadiazole system could not be isolated or detected. Problems with the lesser reactivity and insolubility of alkene dipolarophiles in the high molar excess required at −60 °C prevented trapping with these. The difficulties have now been overcome with a number of alkene systems including *N*-substituted maleimides in reactions of the 1,3-dipoles **3** and **4**. The cycloaddition products† were the stable compounds **5**–**8** (Table 1), providing a new one-pot route to the pyrrolo [2,1-*b*]-1,3,4-thiadiazole system. The preferred stereochemistry of the cycloaddition was *endo*- and it was exclusively *endo*- for the reaction of the dipole **3** with maleimides. These reactions gave derivatives of the new tricyclic rings **5** and **6**. The bowl-shaped structure of these tricyclic products is a nitrogen–sulfur analogue of the tri-pentagon bowl-unit present in the dodecahedron.

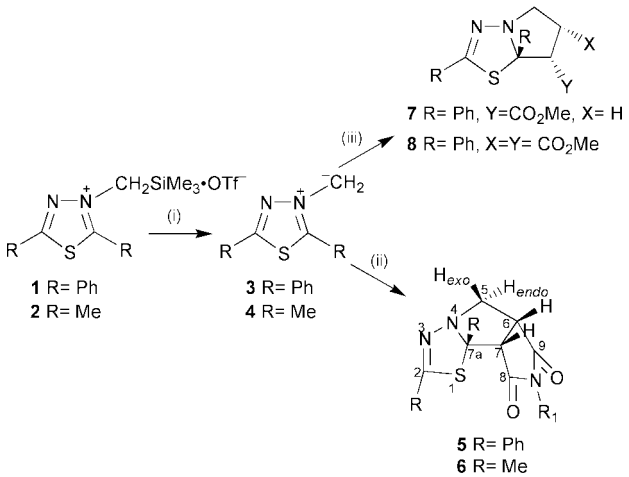

R[1] **a** Me; **b** CH_2Ph; **c** ^{t}Bu; **d** 1-admantyl; **e** Ph; **f** *p*-Me-C_6H_4; **g** *p*-Br-C_6H_4

Scheme 1 *Reagents and conditions*: (i) CsF in CH_2Cl_2 at −60 °C; (ii) *N*-substituted maleimides; (iii) methyl acrylate or dimethyl maleate.

The structures of the products were established from microanalyses, IR, ^{1}H and ^{13}C NMR spectra which showed all of the expected signals (Table 1). The 5-H$_{endo}$ proton was strongly deshielded ($\delta \approx 4.8$ ppm) relative to its geminal partner the 5-H$_{exo}$ ($\delta \approx 3.6$ ppm). NOE difference spectra showed enhancements at the 7a-substituent from H-7, H-6 and 5-H$_{exo}$ on the same face of the central ring thereby confirming the *endo*-cycloaddition. This occurred exclusively for the 1,3-dipole **3** even then R′ was a *tert*-butyl or adamantyl group. Small quantities of the *exo*-isomers were detected from cycloadditions with the dipole **4** but the *endo*–*exo* ratio was still ≥6:1. An X-ray crystal structure‡ of compound **5a** illustrates the interesting bowl-type structure of the three fused pentagons containing three nitrogens and a sulfur (Fig. 1). The system relieved strain by significant opening of the angles at the carbon fusion atoms. Thus the angles C(7)–C(7A)–S(1), C(7A)–C(7)–

Table 1 Pyrrolo[1,2-*b*]-1,3,4-thiadiazole products

Compound	Mp/°C	Yield (%)[a]	C-2	C-7a	C-5	6-CH (δ_C)	7-CH[c] (δ_C)
5a	133–135	47	148.3	94.2	54.9	3.32(46.7)	3.97(58.5)
5b	148–149	50	147.7	93.4	54.8	3.31(46.3)	3.98(58.4)
5c	148–150	54	147.1	93.9	55.5	3.15(46.30)	3.86(58.6)
5d	174–177	86	146.9	94.1	58.3	3.29(55.6)	3.94(61.1)
5e	171–173	69	147.7	94.3	55.3	3.48(46.7)	4.12(58.5)
5f	195–196	52	148.1	94.3	55.3	3.48(46.7)	4.11(58.5)
5g	201–203	57	148.1	94.5	55.4	3.47(46.8)	4.11(58.5)
6b	113–115	74	146.5	89.4	53.8	3.48(46.1)	3.20(56.7)
6e	159–161	65	164.9	90.8	54.4	3.50[b](46.3)	3.36(57.0)
6f	195–197	61	147.1	91.0	54.6	3.42[b](46.4)	3.26(57.2)
7	112–114	73	147.3	92.8	54.1	2.10(27.9)	3.70(52.2)
8	138–140	59	146.2	92.4	55.1	3.21(43.1)	3.91(58.5)

[a] Isolated yield; decomposition gums and the unreacted salts **1** and **2** (≤10%) were also recovered. [b] Overlap with 5-CH$_{exo}$. [c] All d except for compound **7** where the signal is a dd.

 DOI: 10.1039/b105190n

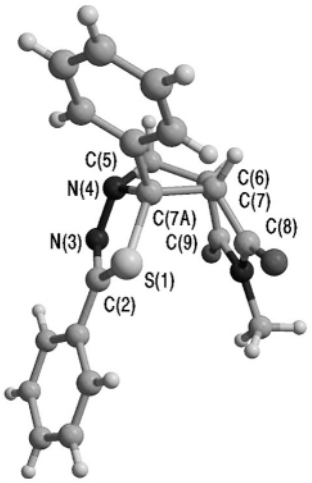

Fig. 1 X-Ray crystal structure of compound **5a**.

C(8) and C(5)–C(6)–C(9) were opened to 115.4, 113.2 and 114.6° respectively. The fusion angle at the nitrogen bridgehead, C(5)–N(4)–N(3), 110.1°, remained close to the tetrahedral value. The structure is a derivative of a 3,4,10-triaza-6-thiatricyclo[6.3.0.0^{3,7}]undecane parent.

Notes and references

† Solutions of the salts **1** or **2** (*ca.* 1 mmol) in CH_2Cl_2 (10–30 cm^3) were treated with the alkene dipolarophile (5 mmol for solids; 20 mmol for liquids), cooled to −60 °C, treated with CsF (2 mmol), stirred for 5–7 days at −60 °C, warmed to ambient temperatures and filtered. The filtrate was evaporated under reduced pressure and the residue in CH_2Cl_2 (5 cm^3) was placed on a silica-gel 60 column (230–400 mesh ASTM) and eluted with gradient mixtures of petroleum spirit (bp 40–60 °C)–CH_2Cl_2 or CH_2Cl_2–Et_2O to give the products (Table 1).

‡ *Crystal data* for **5a**: $C_{20}H_{17}N_3O_2S$, M = 363.43, monoclinic, space group $P2_1/a$, a = 12.524(2), b = 11.088(3), c = 12.935(2) Å, β = 99.75(2)°, U = 1770.3(6) Å^3, T = 298 K, Z = 4, D_c = 1.364 Mg m^{-3}, μ(Mo-Kα) = 0.203 mm^{-1}. Data collected on a CAD4 diffractometer, unique reflections = 2164, R_{int} = 0.0228, observed $I > 2\sigma I$ = 1072, data/restraints/paramaters = 2164/0/236 , obs. data R_1 = 0.0422, all data wR_2 = 0.1022, max. peak/hole 0.193 and −0.226 e Å^{-3}, software used, SHELXS,[5] SHELXL[6] and ORTEX.[7] CCDC 169186. See http://www.rsc.org/suppdata/cc/b1/b105190n/ for crystallographic files in .cif or other format.

1 The ring is not listed in *Comprehensive Heterocyclic Chemistry II* series ed. A. R. Katritzky, C. W. Rees and E. F. V. Scriven, Pergamon Press, Oxford, 1996, vol. 10, Ring Index, or *Comprehensive Heterocyclic Chemistry*, series ed. A. R. Katritzky and C. W. Rees, Pergamon, Oxford, 1984, vol. 8, part 6, ed. C. J. Drayton, Ring Index, it was reported in, M. Mühlstadt, L. Weber and P. Birner, *J. Chem. Soc., Perkin Trans. 2*, 1988, 821; and also D. M. Evans, L. Hill, D. R. Taylor and M. Myers, *J. Chem. Soc., Perkin Trans. 1*, 1986, 1499.
2 R. N. Butler, M. O. Cloonan, P. McArdle and D. Cunningham, *J. Chem. Soc., Perkin Trans. 1*, 1998, 1295.
3 E. Vedejs, S. Larsen and F. G. West, *J. Org. Chem.*, 1985, **50**, 2170.
4 R. C. F. Jones, J. R. Nichols and M. T. Cox, *Tetrahedron Lett.*, 1990, **31**, 2333.
5 G. M. Sheldrick, *Acta. Crystallogr., Sect. A*, 1990, **46**, 467.
6 G. M. Sheldrick, *SHELXL-97 a computer program for crystal structure determination*, University of Göttingen, 1997.
7 P. McArdle, *J. Appl Crystallogr.*, 1995, **28**, 65.

CHEMCOMM Communication
www.rsc.org/chemcomm

Production of ultra highly pure H_2 and higher hydrocarbons from methane in one step at mild temperatures and development of the catalyst under non-equilibrium reaction conditions

Linsheng Wang,*[ab] Kazuhisa Murata,[a] Abdelhamid Sayari,[b] Bernard Grandjean[b] and Megumu Inaba[a]

[a] *National Institute of Advanced Industrial Science and Technology, AIST Tsukuba Central 5, Tsukuba, Ibaraki 305, Japan. E-mail: linsheng.wang@aist.go.jp*
[b] *Department of Chemical Engineering, Laval University, Quebec City, Canada*

Received (in Cambridge, UK) 28th June 2001, Accepted 21st August 2001
First published as an Advance Article on the web 19th September 2001

Ultra highly pure hydrogen and more valuable hydrocarbons are produced directly from methane in one step beyond the thermodynamic equilibrium conversion by integration of the dehydrogenation reaction and hydrogen separation with a Pd–Ag based membrane reactor at mild temperatures, and a highly active catalyst is developed under the non-equilibrium reaction conditions.

Both as an alternative process for production of hydrogen and as a promising method for the production of higher hydrocarbons from natural gas, the dehydrogenation and aromatization reactions of methane on Mo/HZSM-5 and Re/HZSM-5 has attracted increasing attention since 1993. However, the maximum aromatics yield has been reported to be only 7–8% at 973 K on the catalysts by different research groups[1–9] and it seems that this is the thermodynamic equilibrium conversion at this temperature. In addition, the equilibrium reaction conditions make it difficult to develop more active catalysts. In the present communication, direct methane conversion into hydrogen and higher hydrocarbons beyond the thermodynamic equilibrium limit becomes possible by integration of the methane dehydrogenation reaction and H_2 separation with a Pd membrane reactor, and a highly active catalyst has been developed for the production of pure hydrogen and higher hydrocarbons under non-equilibrium reaction conditions.

The catalysts Re/HZSM-5 and Mo/HZSM-5 were prepared by impregnating NH_4ZSM-5 with NH_4ReO_4 and $(NH_4)_6Mo_7O_{24}{\cdot}4H_2O$ aqueous solution, respectively, followed by drying at 383 K for 4 h and calcination at 773 K for 4 h. The sample was finally pressed, crushed and sorted into 20–40 meshes. Catalytic tests were carried out in a fixed bed continuous-flow Pd–Ag based membrane reactor (5/8 inch diameter × 10 inch height). The membrane reactor contains four membrane tubes (1/8 inch diameter × 7 inch height). H_2 was continuously separated from the product by permeation through the membrane tubes and removed by a vacuum pump. A schematic diagram of the membrane reactor is shown in Fig. 1. The results for methane conversion on Re/HZSM-5 at a low temperature of 858 K and different methane space velocity (SV) values are listed in Table 1. Both hydrogen and higher hydrocarbons are produced from methane dehydrogenation on the catalyst even at such a low temperature. The major hydrocarbon products for methane dehydrogenation include benzene, naphthalene, toluene and C_2 products. When hydrogen is not separated from the dehydrogenation product by H_2 permeation through the membrane, the maximum methane conversion into aromatics and C_2 on Re/HZSM-5 is *ca.* 2.4–2.6% at 858 K (Table 1). The methane conversion changes little even for a wide methane SV range of 120–1440 ml h^{-1} g^{-1}. Therefore, under thermodynamic equilibrium reaction conditions, the yield of aromatics and C_2 is only *ca.* 2.4–2.6% at 858 K. Of most significance is that this thermodynamic equilibrium can be disturbed, leading to much higher conversions than the equilibrium conversion for methane dehydrogenation into aromatics, achieved by continuous separation of hydrogen from the product by hydrogen permeation through the membrane.

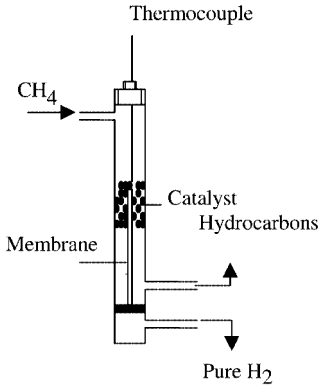

Fig. 1 Schematic illustration of the membrane reactor.

A high methane conversion of 7.5% is attained on Re/HZSM-5 at 858 K when the methane SV is 120 ml h^{-1} g^{-1} at a low temperature of 858 K. This is *ca.* twice as high as the methane equilibrium conversion at the same temperature. At the same time, ultra highly purely H_2 is produced because of the 100% selectivity of the membrane for hydrogen permeation and the pure hydrogen can be directly used in a fuel cell. Fig. 2 shows the activity profile of Re/HZSM-5 catalyst with time on stream when H_2 was separated by selective permeation. The enhanced

Table 1 Effect of hydrogen permeation on methane conversion into aromatics and C_2 on Re/HZSM-5 at 858 K

SV/ml h^{-1} g^{-1}	H_2 separation	Conversion (%)	Selectivity (%)			
			C_2	C_6H_6	C_7H_8	$C_{10}H_8$
120	No	2.5	9.6	56.0	2.4	32.0
	Yes	7.5	3.2	53.3	3.5	40.0
180	No	2.4	5.4	70.8	2.9	20.8
	Yes	5.9	4.1	64.4	4.4	27.1
240	No	2.6	6.2	69.2	3.1	23.1
	Yes	4.9	5.5	65.3	4.3	24.5
360	No	2.6	6.9	69.2	3.8	19.2
	Yes	4.2	6.4	66.7	4.8	21.4
720	No	2.4	8.8	70.8	4.6	16.7
	Yes	3.5	8.3	71.4	5.4	14.6
1440	No	2.4	11.3	62.5	4.2	22.1
	Yes	3.3	8.2	63.6	5.5	22.4

Pressure = 100 kPa; the permeability of H_2 through the membrane is *ca.* 75%.

 DOI: 10.1039/b105703k

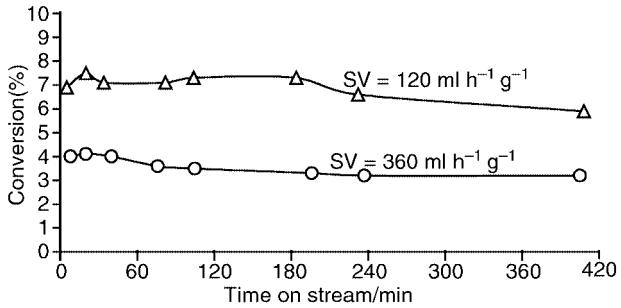

Fig. 2 Activity profile for the Re/HZSM-5 catalyst with time on stream at 858 K and different methane SV when H_2 was separated by selective permeation.

methane conversion declines from 7.5 to 5.9% after 7 h on stream at 858 K at a methane SV of 120 ml h^{-1} g^{-1} as shown in Fig. 2.

On the other hand, it is difficult to compare the activity of the catalysts under equilibrium reaction conditions and therefore, many arguments still exist about activity comparisons between Mo/HZSM-5 and Re/HZSM-5 for the methane dehydrogenation reaction. Use of non-equilibrium reaction conditions makes it more easy to develop highly active catalysts. The results in Table 2 indicate that both the catalysts show similar activity for methane conversion into higher hydrocarbons when hydrogen is not separated from the product. However, the activities of the two catalysts are quite different under non-equilibrium reaction conditions when hydrogen is continuously separated from product by selective permeation of hydrogen in the Pd–Ag based membrane reactor. Re/HZSM-5 clearly shows a higher activity than Mo/HZSM-5 under non-equilibrium reaction conditions as shown in Table 2. The evaluation of the catalysts under non-equilibrium reaction conditions is a useful method for development of highly active catalysts.

Therefore, the higher conversion of methane is dependent on hydrogen permeation and separation through the membrane. To make hydrogen permeation through the membrane and separation from the product more efficient, the effect of reaction pressure on methane conversion was investigated and some results are given in Table 3. It is clear that methane conversion is enhanced further by a small increase of the reaction pressure. This indicates that higher pressures are more favorable for hydrogen permeation through the membrane tube. Thus, a higher methane conversion of 5.8% is achieved at a higher reaction pressure of 200 kPa and a higher methane SV of 360 ml h^{-1} g^{-1} in the membrane reactor.

In conclusion, methane activation into hydrogen and more useful hydrocarbons such as aromatics and C_2 far beyond the thermodynamic equilibrium conversion has been achieved by continuous hydrogen separation from the product using a Pd–Ag based membrane reactor. The highly active Re/HZSM-5 catalyst has been developed for methane conversion at a low temperature of 858 K under non-equilibrium reaction conditions. Ultra highly pure hydrogen and aromatics are produced directly from methane in one step on the developed highly active Re/HZSM-5 catalyst by integration of the dehydrogenation reaction and a hydrogen separation process using a membrane reactor.

Table 2 Comparison of catalytic activity of Re/HZSM-5 and Mo/HZSM-5 for methane conversion into hydrogen and higher hydrocarbons under non-equilibrium reaction conditions

Catalyst	H_2 separation	Conversion (%)	Selectivity (%)			
			C_2	C_6H_6	C_7H_8	$C_{10}H_8$
Re/HZSM-5	No	2.6	6.9	69.2	3.8	19.2
	Yes	4.2	6.4	66.7	4.8	21.4
Mo/HZSM-5	No	2.4	6.7	54.2	2.9	33.8
	Yes	3.3	3.9	54.5	3.0	39.4

Temperature = 858 K; SV = 360 ml h^{-1} g^{-1}; pressure = 100 kPa; the permeability of H_2 through the membrane is *ca.* 75%.

Table 3 Effect of hydrogen permeation on methane conversion into aromatics and C_2 on Re/HZSM-5 at 858 K and different methane partial pressures

Pressure/ kPa	H_2 separation	Conversion (%)	Selectivity (%)			
			C_2	C_6H_6	C_7H_8	$C_{10}H_8$
50	No	2.8	7.1	60.7	3.6	28.6
	Yes	3.3	9.1	60.6	3.0	27.3
100	No	2.6	6.9	69.2	3.8	19.2
	Yes	4.2	6.4	66.7	4.8	21.4
200	No	2.7	7.4	55.6	3.7	33.3
	Yes	5.8	5.2	51.7	5.2	37.9

Temperature = 858 K; SV = 360 ml h^{-1} g^{-1}; the permeability of H_2 through the membrane is *ca.* 75%.

Notes and references

1 L. Wang, L. Tao, M. Xie, G. Xu, J. Huang and Y. Xu, *Catal. Lett*., 1993, **21**, 35.
2 F. Solymosi, A. Erdohely and A. Szoke, *Catal. Lett*., 1995, **32**, 43.
3 L. Chen, L. Lin, Z. Xu, X. Li and T. Zhang, *J. Catal*., 1995, **157**, 190.
4 D. Wang, J. H. Lunsford and M. P. Rosynek, *J. Catal*., 1997, **169**, 347.
5 S. Liu, Q. Dong, R. Ohnishi and M. Ichikawa, *Chem. Commun*., 1997, 1435.
6 D. Wang, J. H. Lunsford and M. P. Rosynek, *Top. Catal*., 1996, **3**, 289.
7 J. Z. Zhang, M. A. Long and R. F. How, *Catal. Today*, 1999, **44**, 293.
8 R. W. Borry III, Y. H. Kim, A. Huffsmith, J. A. Reimer and E. Iglesia, *J. Phys. Chem. B*, 1999, **103**, 5787.
9 L. Wang, R. Ohnishi and M. Ichikawa, *J. Catal*., 2000, **190**, 276.

CHEMCOMM Communication
www.rsc.org/chemcomm

The first redox controlled hydrogen bonded three-pole switch

Christine Bourgel,[a] Alan S. F. Boyd,[a] Graeme Cooke,*[a] Hugues Augier de Cremiers,[ab] Florence M. A. Duclairoir[a] and Vincent M. Rotello[b]

[a] *Centre for Biomimetic Design and Synthesis, Department of Chemistry, Heriot-Watt University, Riccarton, Edinburgh, UK EH14 4AS. E-mail: G.Cooke@hw.ac.uk*
[b] *Department of Chemistry, University of Massachusetts at Amherst, Amherst, MA 01002, USA*

Received (in Cambridge, UK) 17th July 2001, Accepted 21st August 2001
First published as an Advance Article on the web 19th September 2001

The first example of a redox controlled hydrogen bonded three-pole switch is described, which exploits both electrochemical oxidation and reduction of the host–guest dyad to modulate the intermolecular recognition properties.

Application of the interplay between molecular recognition and electrochemistry to modulate the interactions between host–guest complexes is a burgeoning field within supramolecular chemistry.[1] The electrochemically controlled gain or loss of an electron by a redox active host (or guest) can profoundly influence the charge and/or electronic distribution of the host–guest dyad, leading to major changes in the magnitude and nature of the intermolecular interactions between these units.[2] Recently, the reversibility and convenience of electrochemically controlled supramolecular interactions have been used to produce molecular switches which utilise redox controlled inclusion,[3] hydrogen bonding[4] and charge-transfer (CT)[5] interactions to control the recognition processes between the complementary host–guest moieties. For most of these systems, however, the switching properties are limited to the modulation of the host–guest binding between two distinct states (two-pole switch). Multi-pole switch systems, on the other hand, provide access to new applications within molecular electronics and photonics, due to their enhanced ability to handle and process information at the molecular level.[3,6]

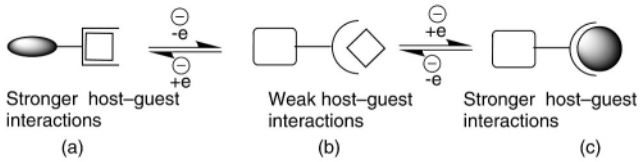

Fig. 1 A redox controlled three-pole switch.

Here, we report the application of dual redox controlled hydrogen bonding interactions between electroactive pyridine host **1** and flavin guest **2**, to produce the first three-pole switch which solely utilises the strength and directionality of hydrogen bonding interactions to control the extent of the intermolecular recognition processes (Fig. 1). In their neutral states [Fig. 1(b)], relatively weak interactions between host **1** and guest **2** are predicted. However, upon electrochemical oxidation of the ferrocene unit of **1** to its ferrocenium state [Fig. 1(a)], an increase in the acidity of the N–H group of the amide moiety of this derivative should result in an increase in the intermolecular hydrogen bond strength between **1** and **2**.[4c] Furthermore, reduction of the flavin moiety of **1**·**2** to its radical anion state [Fig. 1(c)], should give rise to enhanced intermolecular hydrogen bonding interactions due to an increase in the negative charge density of the carbonyl groups of **2**.[7]

The ferrocene host **1** was synthesised by reacting 2-ethylamido-6-aminopyridine with one equivalent of fluorocarbonylferrocene[8] in THF under reflux for two days. Compound **1** was readily purified using column chromatography to afford the host unit in 75% yield.† Flavin **2** was prepared using previously reported procedures.[9]

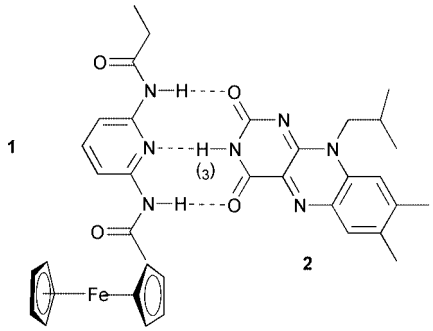

Hydrogen bond formation between **1** and **2** was confirmed by ^{1}H NMR titration in $CDCl_3$. The smooth downfield shift in the resonance of H(3) of **2** upon the addition of ferroreceptor **1** cleanly fits a 1 : 1 binding isotherm, providing an association constant (K_a) of 45 ± 5 M^{-1}.[10] This is considerably lower than the K_a obtained for the 1 : 1 hydrogen bonded complex of **2** and 2,6-diethylamidopyridine (K_a = 537 M^{-1}),[11] presumably due to the bulky ferrocene unit partially masking the hydrogen bonding site of **1**.

With host–guest complexation verified, we next investigated the electrochemically modulated switching properties of this system using cyclic voltammetry (CV).[12] CV studies on compound **1** gave rise to a reversible single-electron oxidation of $E_{1/2}$ = +0.79 V. Addition of an excess of **2** to a solution of **1**, immediately resulted in a −0.034 V shift in the oxidation potential of the ferrocene moiety of receptor **1** (Fig. 2). This negative shift indicates a stabilization (3.28 kJ mol^{-1})[13] of the ferrocenium state of receptor **1**, and hence corresponds to the flavin unit becoming more strongly bound to **1** (**1**$^+$·**2**, K_a = 169 ± 17 M^{-1}).[14] CV studies of flavin **2** show a single, one-electron reduction peak and two separate re-oxidation peaks (Fig. 3).[4f]

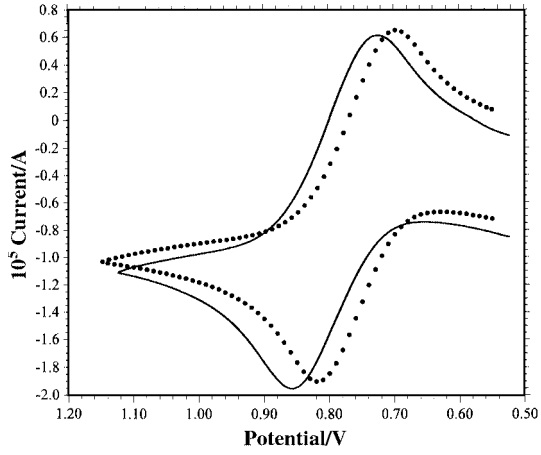

Fig. 2 Cyclic voltammogram of host **1** (——) and in the presence of an excess of **2** (.....).

 DOI: 10.1039/b106342c

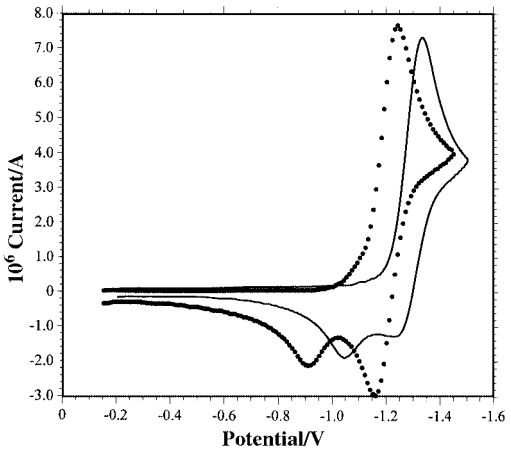

Fig. 3 Cyclic voltammogram of guest **2** (——) and in the presence of an excess of **1** (.....).

Addition of an excess of **1** provides a significant reduction (+0.100 V) in the voltage for both the reduction wave potential and $E_{½}$ for the reversible redox couple, indicating a substantial (9.65 kJ mol^{-1}) stabilization of the radical anion of **2**, which results in a 50-fold increase in the binding strength of the complex (**1**·**2**$^{-\cdot}$, K_a = 2209 ± 221 M^{-1}). In accordance with previously reported data for the hydrogen bonded complex of **2** with 2,6-diethylamidopyridine, the wave corresponding to the re-oxidation of the flavin radical anion is greatly enhanced.[2a] However, the wave due to re-oxidation of the flavohydroquinone anion to the neutral flavin for the **1**·**2** complex is not fully suppressed and is shifted to a more positive potential.

In conclusion, we have produced the first example of a redox controlled hydrogen bonded three-pole switch which exploits the disparate redox properties of the host and guest moieties to modulate their intermolecular hydrogen bonded interactions. Oxidation of the ferrocene moiety results in a four-fold increase in the hydrogen bonding efficiency, whereas reduction of the flavin moiety results in a 50-fold increase in the hydrogen bonding efficiency of **1**·**2**. Structural modification of host **1** is underway (*e.g.* incorporation of moieties capable of increasing the binding efficiency with the reduced flavin *via* donor atom–π interactions) the results of which will be reported in due course.

We gratefully acknowledge support from the EPSRC (F. M. A. D.), The Royal Society, the Royal Society of Chemistry and the National Science Foundation (US) (CHE 9905492, V. M. R.). We thank the EPSRC National Mass Spectrometry Centre for obtaining mass spectra of **1** and **2**.

Notes and references

† *Selected data for* **1**: yield 75%, mp 152–154 °C; Calc. for $C_{19}H_{19}FeN_3O_2$: C, 60.47; H, 5.04; N, 11.14. Found: C, 60.25; H, 5.27; N, 10.80%. ^{1}H NMR (400 MHz, $CDCl_3$): δ 7.92 (d, 1H), 7.86 (d, 1H), 7.70 (s, 1H), 7.67 (t, 1H), 7.52 (s, 1H), 4.72 (t, 2H), 4.39 (t, 2H), 4.20 (s, 5H), 2.37 (q, 2H), 1.20 (t, 3H); MS (EI): *m*/*z* 378 (M + 1).

1 A. E. Kaifer and M. Gómez-Kaifer, *Supramolecular Electrochemistry*, Wiley-VCH, Weinheim, 1999; P. L. Boulas, M. Gomez-Kaifer and L. Echegoyen, *Angew. Chem., Int. Ed.*, 1998, **37**, 216.
2 (*a*) V. M. Rotello and A. Niemz, *Acc. Chem. Res.*, 1999, **32**, 44; (*b*) A. E. Kaifer, *Acc. Chem. Res.*, 1999, **32**, 62.
3 A. Mirzoian and A. E. Kaifer, *Chem. Eur. J.*, 1997, **3**, 1052.
4 (*a*) J. D. Carr, L. Lambert, D. E. Hibbs, M. B. Hursthouse, K. M. A. Malik and J. H. R. Tucker, *Chem. Commun.*, 1997, 649; (*b*) J. D. Carr, S. J. Coles, M. B. Hursthouse, M. E. Light, J. H. R. Tucker and J. Westwood, *Angew. Chem., Int. Ed.*, 2000, **39**, 3296; (*c*) S. R. Collinson, T. Gelbrich, M. B. Hursthouse and J. H. R. Tucker, *Chem. Commun.*, 2001, 555; (*d*) Y. Ge, R. R. Lilienthal and D. K. Smith, *J. Am. Chem. Soc.*, 1996, **118**, 3976; (*e*) Y. Ge, L. Miller, T. Ouimet and D. K. Smith, *J. Org. Chem.*, 2000, **65**, 8831; (*f*) E. Breinlinger, A. Niemz and V. M. Rotello, *J. Am. Chem. Soc.*, 1995, **117**, 5379.
5 W. Devonport, M. A. Blower, M. R. Bryce and L. M. Goldenberg, *J. Org. Chem.*, 1997, **62**, 885.
6 P. R. Ashton, V. Balzani, J. Becher, A. Credi, M. C. T. Fyfe, G. Mattersteig, S. Menzer, M. B. Nielsen, F. M. Raymo, J. F. Stoddart, M. Venturi and D. J. Williams, *J. Am. Chem. Soc.*, 1999, **121**, 3951; A. Goodman, E. Breinlinger and V. M. Rotello, *J. Am. Chem. Soc.*, 2001, **123**, 6214.
7 A. Niemz and V. M. Rotello, *J. Am. Chem. Soc.*, 1997, **119**, 6833.
8 T. H. Gallow, J. Rodrigo, K. Cleary, G. Cooke and V. M. Rotello, *J. Org. Chem.*, 1999, **64**, 3745.
9 A. Niemz, J. Inbriglio and V. M. Rotello, *J. Am. Chem. Soc.*, 1997, **119**, 887.
10 The dimerisation constants (K_{dim}) for host **1** and guest **2** were both found to be 5 M^{-1} in $CDCl_3$.
11 E. Breinlinger, A. Niemz and V. M. Rotello, *J. Am. Chem. Soc.*, 1995, **117**, 5379.
12 All electrochemical experiments were performed using a CH Instruments CH120A electrochemical workstation. The 0.1 M electrolyte solution was prepared from recrystallised Bu_4NPF_6 using spectroscopic grade dichloromethane and purged with nitrogen prior to use. A three-electrode configuration was used with a Pt working electrode, a Ag wire pseudo-reference electrode and a platinum wire counter electrode. The oxidative scans used decamethylferrocene as an internal standard whilst the reductive scans used ferrocene as an internal standard.
13 Calculated from the relationship: $\triangle\triangle G = -nF\triangle E_{½}$, where n is the number of electrons involved in the redox process, F is the Faraday constant (C mol^{-1}) and $\triangle E_{½}$ is the change in the half-wave potential of the redox active host following the addition of the guest.
14 The redox-based enhancement in recognition can be calculated using a thermodynamic cycle which can be expressed mathematically using: K_a(red)/K_a(ox) = $e^{(nF/RT)[E_{1/2}(\text{bound}) - E_{1/2}(\text{unbound})]}$. K_a(red) and K_a(ox) are the association constants in the reduced and oxidized forms, respectively, and $E_{½}$(bound) and $E_{½}$(unbound) are the half-wave redox potentials in the receptor bound and unbound states.

CHEMCOMM Communication
www.rsc.org/chemcomm

The first observation of the $[Cp_3Mn]^-$ anion; structures of hexagonal $[(\eta^2\text{-}Cp)_3MnK\cdot1.5thf]$ and ion-separated $[(\eta^2\text{-}Cp)_3Mn]_2[Mg(thf)_6]\cdot2thf$†

Andrew D. Bond,[a] Richard A. Layfield,[a] Judith A. MacAllister,[a] Mary McPartlin,[b] Jeremy M. Rawson[a] and Dominic S. Wright*[a]

[a] *Chemistry Department, University of Cambridge, Lensfield Road, Cambridge, UK CB2 1EW. E-mail: dsw1000@cus.cam.ac.uk*
[b] *School of Chemistry, University of North London, London, UK N7 8DB*

Received (in Cambridge, UK) 17th July 2001, Accepted 21st August 2001
First published as an Advance Article on the web 18th September 2001

Hexagonal $[(\eta^2\text{-}Cp)_3MnK\cdot1.5thf]$ 1 and ion-separated $[(\eta^2\text{-}Cp)_3Mn]_2[Mg(thf)_6]\cdot2thf$ 2 are obtained from reactions of CpK and Cp_2Mg, respectively, with manganocene, Cp_2Mn; they are the first complexes to be structurally characterised containing the $[Cp_3Mn]^-$ anion.

The greater covalent character of the metal–ligand bonds and the significant involvement of d orbitals in transition metal metallocenes[1] results in some fundamentally different reactivity compared to their main group counterparts.[2] One significant difference is the far greater lability and ionicity of the Cp ligands of main group metallocenes, which are readily displaced by acids and nucleophiles. Nonetheless, although rarely investigated these characteristics have also been found for certain transition metal complexes, such as $[CpCu(PPh_3)]$[3] and $[Cp_2Mn]$.[4,5] The similarity between the ligand reactivity of 17e Cp_2Mn and 14e Cp_2Sn and Cp_2Pb has prompted us recently to investigate the possibility of observing related reactivity at their *metal* centres. We report here, that nucleophilic addition of Cp^- to $[Cp_2Mn]$ gives the first complexes containing the $[Cp_3Mn]^-$ anion, behaviour which is analogous to that of Cp_2Sn and Cp_2Pb.[2]

The complexes $[(\eta^2\text{-}Cp)_3MnK\cdot1.5thf]$ **1** and $[(\eta^2\text{-}Cp)_3Mn]_2[Mg(thf)_6]\cdot2thf$ **2** were prepared by the reactions of $[Cp_2Mn]$ with CpK (1 : 1 equivalents) or $[Cp_2Mg]$ (1 : 2 equivalents), respectively, in thf solvent (Scheme 1).† Spectral characterisation of **1** and **2** was hampered by their paramagnetic nature which made NMR spectroscopic investigations of little value in ascertaining the solution structures. A further complication is the extreme lability of the thf ligands of **1**, which are completely removed by placing the complex under vacuum for even moderately short periods prior to isolation.

Owing to the flaky, laminar nature of crystals of **1** only relatively poor quality X-ray data could be collected (despite repeated attempts).‡ Despite these inherent problems the essential features of the structure were determined unambiguously. The complex consists of $[(\eta^2\text{-}Cp)_3Mn]^-$ anions associated *via* Mn–(μ-Cp)–K interactions into cyclic $[(\eta^2\text{-}Cp)_3MnK]_3$ units, which build into a honeycomb sheet structure (Fig. 1). The extensive static disordering of the K^+ cations and Cp ligands (over two 50 : 50 sites for both; see ESI†) stems from the presence of two crystallographically independent sheets within the structure in which the Cp rings adopt a propeller-like arrangement which is randomly left-handed in half of the sheets and right-handed in the other half. These layers are randomly distributed in the lattice of **1** with an extremely large interlayer spacing between them of *ca.* 9.53 Å. Like graphite, the $[(\eta^2\text{-}Cp)_3MnK]_3$ units of alternate sheets are staggered with respect to each other, with the Mn^{II} cations within a sheet being coincident with the centroid of the $[(\eta^2\text{-}Cp)_3MnK]_3$ units of adjacent layers. The voids between the sheets are occupied by thf molecules {1.5 thf per $[(\eta^2\text{-}Cp)_3MnK]$ monomer unit}. On average, each K^+ cation is solvated by half a thf ligand, with another disordered thf ligand being uncoordinated. The structure of **1** is similar to that of the recently characterised Pb^{II} complex $[(Cp)_2(Cp^{thf})PbNa\cdot0.5thf]$ ($Cp^{thf} = C_5H_4CH_2C_4H_7O$) which also adopts a 'graphite-like' lattice.[6] However, in this case puckered hexanuclear Pb_3Na_3 rings result from the intramolecular coordination of the ligand-bonded ether functionality to the Na^+ cations. The η^5-Cp bonding of three Cp ligands to both of the disordered K^+ sites in **1** [range K–C: 2.968(6)–3.31(2) Å] is similar to that observed previously in the structures of CpK and its Lewis base complexes (*ca.* 2.97–3.13 Å).[7]

The extensive disordering provides a particular complication to the discussion of the metal–ligand bond lengths and metal geometries involved in **1**. However, the significant bonding features of the $[(\eta^2\text{-}Cp)_3Mn]^-$ anion are nonetheless apparent. Most surprisingly, the Mn^{II} centers are clearly coordinated by three η^2-Cp ligands for both of the disordered Cp sites [range

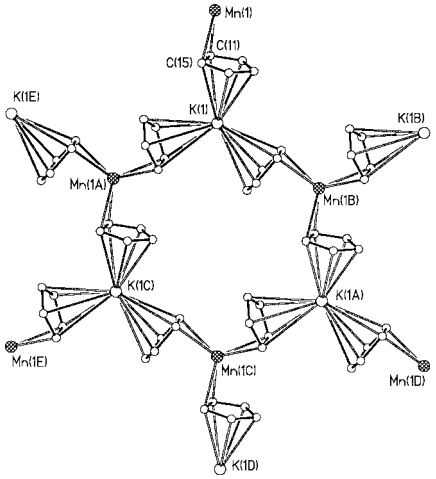

Fig. 1 Sheet structure of **1**, viewed along the *c*-axis. Only one of the sheets is shown {corresponding to anti-clockwise rotation of the $[(\eta^2\text{-}Cp)_3Mn]^-$ anions}. H-atoms and thf ligands have been removed for clarity. Key bond lengths (Å) and angles (°); Mn–C range: 2.36(1)–2.405(4), Mn···η^2-$Cp_{centroid}$(mean) 2.25, K–C 2.96(2)–3.300(4), K···$Cp_{centroid}$(mean) 2.94, K···Mn(mean) 5.26, Mn···Mn 9.09, C–Mn–C(mean) 34.6.

$$Cp_2Mn + CpK \xrightarrow{thf} [(\eta^2\text{–}Cp)_3MnK\cdot1.5thf] \quad \mathbf{1}$$

$$2Cp_2Mn + Cp_2Mg \xrightarrow{thf} [(\eta^2\text{–}Cp)_3Mn]_2[Mg(thf)_6]\cdot2thf \quad \mathbf{2}$$

Scheme 1

† Electronic supplementary information (ESI) available: experimental details and figure of the static disordering arising from superimposition of the two types of sheet of **1**. See http://www.rsc.org/suppdata/cc/b1/b106366a/

 DOI: 10.1039/b106366a

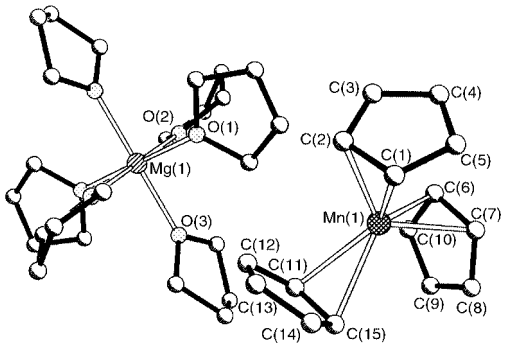

Fig. 2 The ion-separated complex **2**. H-atoms and the lattice-bound thf molecules have been omitted for clarity. Only one of the $[(\eta^2\text{-Cp})_3\text{Mn}]^-$ anions is shown. Key bond lengths (Å) and angles (°): Mn–C range: 2.351(5)–2.392(6) Mn···η^2-$\text{Cp}_{centroid}$(mean) 2.25, Mg–O range: 2.091(3)–2.109(3), C–Mn–C 34.9(2).

Mn–C: 2.36(1)–2.405(4) Å]. This bonding mode is retained in the structure of the ion-separated complex $[(\eta^2\text{-Cp})_3\text{Mn}]_2[\text{Mg(thf)}_6]\cdot 2\text{thf}$ **2** (Fig. 2).‡ Although the three Cp ligands of the $[(\eta^2\text{-Cp})_3\text{Mn}]^-$ anion are crystallographically independent in this case, the Mn–C bond lengths are almost identical to those in **1** [range Mn–C: 2.351(5)–2.392(6) Å]. The outcome of the reaction of $[\text{Cp}_2\text{Mn}]$ with Cp_2Mg is the same as that between Cp_2E (E = Sn, Pb) and Cp_2Mg, producing the ion-separated complexes $[\text{Cp}_3\text{E}]_2[\text{Mg(thf)}_6]\cdot\text{thf}$.[8] However, unlike **2**, ion-separation leads to a change in hapticity from η^5 to η^3 for the group 14 $[\text{Cp}_3\text{E}]^-$ anions, apparently as a consequence of increased p-character in the metal lone pairs.[8]

The only transition metal metallocene anions to be structurally characterised previously have been those derived from d^{10} CpCu^{I}.[9] The $[(\eta^2\text{-Cp})_3\text{Mn}]^-$ anion of **1** and **2** is the first transition metal tris-cyclopentadienide anion[10] and the first containing a paramagnetic metal [(d^5) Mn^{II}]. To our knowledge, the only previous case of η^2-Cp coordination in manganocenes occurs in Cp_2Mn, in which the Mn^{II} centers within the polymer chains are coordinated by three Cp ligands using η^5, η^3 and η^2 bonding modes [C–Mn being 2.44(3) and 2.62(3) Å for the η^2-interactions].[11a] It is interesting that in the previously reported $[\text{Cp}_2\text{Cu}]^-$ and $[\text{Cp}_3\text{Cu}_2]^-$ anions η^2-Cp bonding is also a feature.[9]

Structural investigations of Lewis base adducts of manganocenes indicate that steric factors have a decisive influence on hapticity and ring-slippage.[4a,11] However, there is also some possibility that electronic factors may play a role in the adoption of the η^2-Cp bonding mode in **1** and **2**. Extended Hückel calculations on C_{3v} $[(\eta^5\text{-Cp})_3\text{Ti}]^+$ indicate that only the essentially non-bonding metal d_{z^2} orbital is available for metal electrons.[12] Thus, if a metal has more than 2e these high-energy orbitals must be filled, as would be the case in a 23e $[(\eta^5\text{-Cp})_3\text{Mn}]^-$ anion. The adoption of an η^2-bonding mode therefore avoids an unfavourable electronic situation, by giving the Mn in the $[(\eta^2\text{-Cp})_3\text{Mn}]^-$ anion a 14e count.

Samples of **1** and **2** were examined on a SQUID magnetometer in the temperature range 5–300 K, in an applied field of 700 G.†[13] Both samples show an extremely similar temperature dependence of the magnetic moment. The room-temperature moment of *ca.* 4.8 μ_B is somewhat lower than that expected for an *S* 5/2 paramagnet (5.9 μ_B). On cooling, the effective magnetic moment decreases steadily, reaching a minimum value of 3.7 μ_B at the low-temperature limit of the experiments. The similarity of the behaviour of both complexes strongly suggests that the magnetic properties originate from single-ion effects, rather than intermolecular exchange between Mn^{II} ions. The behaviour of **1** and **2** can be compared to that of Cp_2Mn itself, for which the Mn^{II} centers have been concluded to be antiferromagnetically coupled over a similar temperature range.[11a,14] However, studies of 'magnetically-dilute' Cp_2Mn doped with Cp_2Mg[15] show that the magnetic properties can be explained by zero-field splitting, which is substantially greater than that normally observed for Mn^{II} salts.[15c] Attempts to model the behaviour of **1** and **2** using zero-field splitting alone were unsuccessful.†[13] We therefore conclude that their magnetic behaviour stems from high-/low-spin equilibrium, with a possible component of zero-field splitting. Further detailed magnetic and EPR experiments are planned, to provide a detailed explanation of the electronic structure.

We gratefully acknowledge the EPSRC (A. D. B., R. A. L., J. M. R.) and the Isaac Newton Trust (R. A. L.) and Electron Industries (UK) (R. A. L.) for financial support.

Notes and references

‡ *Crystal data* for **1**: $C_{21}H_{27}KMnO_{1.5}$, M = 397.47, hexagonal, space group $P6_3$, Z = 2, a = b = 9.0860(13), c = 19.164(4) Å, V = 1370.1(4) Å^3, μ(Mo-Kα) = 0.639 mm^{-1}, T = 220(2) K. Of a total of 3700 reflections collected, 1405 were independent (R_{int} = 0.036). The structure was solved by direct methods and refined by full-matrix least squares on F^2. Final $R1$ = 0.088 [$I > 2\sigma(I)$] and $wR2$ = 0.317 (all data). Crystal data on **1** was collected a total of four times at various temperatures. *Crystal data* for **2**: $C_{62}H_{94}MgMn_2O_8$, M = 1101.56, monoclinic, space group $C2/c$, Z = 4, a = 25.0027(9), b = 10.7118(6), c = 24.0194(10) Å, β = 112.560(2)°, V = 5940.7(5) Å^3, μ(Mo-Kα) = 0.487 mm^{-1}, T = 180(2) K. Of a total of 18733 reflections collected, 4500 were independent (R_{int} = 0.074). The structure was solved by direct methods and refined by full-matrix least squares on F^2. Final $R1$ = 0.078 [$I > 2\sigma(I)$] and $wR2$ = 0.231 (all data). Data for **1** and **2** were collected on a Nonius KappaCCD diffractometer.

CCDC reference numbers 164066 and 164067. See http://www.rsc.org/suppdata/cc/b1/b106366a/ for crystallographic data in CIF or other electronic format.

1 J. P. Collman and L. S. Hegedus, *Principles and Applications of Organotransition Metal Chemistry*, University Science Books, Oxford, 1980, ch. 2, pp. 13.

2 P. Jutzi, *Adv. Organomet. Chem.*, 1986, **26**, 217; S. Harder, *Coord. Chem. Rev.*, 1998, **176**, 17; M. A. Beswick, J. S. Palmer and D. S. Wright, *Chem. Soc. Rev.*, 1998, **27**, 225; P. Jutzi, *Chem. Unserer Zeit.*, 1999, **33**, 342; P. Jutzi and N. Burford, *Chem. Rev.*, 1999, **99**, 969.

3 M. A. Beswick, C. Brasse, M. A. Halcrow, P. R. Raithby, C. A. Russell, A. Steiner, R. Snaith and D. S. Wright, *J. Chem. Soc., Dalton Trans.*, 1996, 3793; P. R. Raithby, M.-A. Rennie, C. A. Russell, A. Steiner and D. S. Wright, *Organometallics*, 1996, **15**, 639.

4 (*a*) A. Belforte, F. Calderazzo and P. F. Zanazzi, *J. Chem. Soc., Dalton Trans.*, 1988, 2921; (*b*) M. A. Beswick, M. E. G. Mosquera, J. S. Palmer, P. R. Raithby and D. S. Wright, *New J. Chem.*, 1999, **23**, 1033.

5 For a review of other transition metal Cp complexes: see, K. Jonas, *Angew. Chem.*, 1985, **97**, 292; K. Jonas, *Angew. Chem., Int. Ed. Engl.*, 1985, **24**, 295.

6 N. Feeder, A. D. Hopkins, R. A. Layfield and D. S. Wright, *J. Chem. Soc. Dalton Trans.*, 2000, 2247.

7 V. Jordan, U. Behrens, F. Olbrich and E. Weiss, *J. Organomet. Chem.*, 1996, **517**, 81; R. E. Dinneber, U. Behrens and F. Olbrich, *Organometallics*, 1997, **16**, 3855; S. Neander, F. E. Tio, R. Buschmann, U. Behrens and F. Olbrich, *J. Organomet. Chem.*, 1999, **582**, 58.

8 D. R. Armstrong, M. J. Duer, M. G. Davidson, D. Moncrieff, C. A. Russell, C. Stourton, A. Steiner, D. Stalke and D. S. Wright, *Organometallics*, 1997, **16**, 3340.

9 P. Jutzi, W. Wieland, B. Neumann and H.-G. Stammler, *J. Organomet. Chem.*, 1995, **501**, 369.

10 For examples of *neutral* Cp_3M complexes containing transition metals and lanthanides, see: J. L. Atwood and K. D. Smith, *J. Am. Chem. Soc.*, 1973, **95**, 1488; S. H. Egger, J. Kopf and R. D. Fischer, *Organometallics*, 1986, **5**, 383; M. Adams, U. Behrens and R. D. Fischer, *Acta Crystallogr., Sect. C*, 1991, **47**, 968; W. W. Lukens Jr. and R. A. Andersen, *Organometallics*, 1995, **14**, 3435.

11 (*a*) W. Bünder and E. Weiss, *Z. Naturforsch., Teil B*, 1978, **33**, 1235; (*b*) C. G. Howard, G. S. Girolami, G. Wilkinson, M. Thornton-Pett and M. B. Hursthouse, *J. Am. Chem. Soc.*, 1984, **106**, 2033; (*c*) J. Heck, W. Massa and P. Weinig, *Angew. Chem.*, 1984, **96**, 699; J. Heck, W. Massa and P. Weinig, *Angew. Chem., Int. Ed. Engl.*, 1988, **23**, 722; (*d*) F. Bottomley, P. N. Keizer and P. S. White, *J. Am. Chem. Soc.*, 1988, **110**, 137.

12 J. W. Lauher and R. Hoffmann, *J. Am. Chem. Soc.*, 1976, **98**, 1729.

13 O. Kahn, *Molecular Magnetism*, VCH New York, 1993 and references therein.

14 G. Wilkinson, F. A. Cotton and J. M. Birmingham, *J. Inorg. Nucl. Chem.*, 1956, **2**, 95.

15 (*a*) J. Voitländer and E. Schimitschek, *Z. Electrochem.*, 1957, **61**, 941; (*b*) R. Krieger and J. Voitländer, *Z. Naturforsch., Teil A*, 1972, **27**, 1082; (*c*) M. E. Switzer, R. Wang, M. F. Rettig and A. H. Maki, *J. Am. Chem. Soc.*, 1974, **96**, 7669.

CHEMCOMM Communication
www.rsc.org/chemcomm

Self-assisted tandem Michael-aldol reactions of α,β-unsaturated ketones with aldehydes

Tadashi Kataoka,* Sayaka Kinoshita, Hironori Kinoshita, Masaru Fujita, Tatsunori Iwamura and Shin-ichi Watanabe

Gifu Pharmaceutical University, 6-1 Mitahora-higashi 5-chome, Gifu 502-8585, Japan. E-mail: kataoka@gifu-pu.ac.jp

Received (in Cambridge, UK) 11th July 2001, Accepted 24th August 2001
First published as an Advance Article on the web 10th September 2001

The tandem Michael-aldol reaction of 1-[2-(methylsulfanyl)-phenyl]prop-2-en-1-one (1) or the seleno congener 4 with *p*-nitrobenzaldehyde in the presence of $BF_3{\cdot}Et_2O$ gave the Baylis–Hillman adduct 2 or 5 and onium salt 3 or 6, respectively, and selenochromanone 7 from 4.

The Baylis–Hillman reaction is one of the most popular reactions, and a great number of papers have been recently published on it.[1] This reaction is quite slow, and many changes have been made to it to overcome this drawback.[2] We developed the chalcogenide–$TiCl_4$-mediated reactions of electron-deficient alkenes with aldehydes.[3] The reactions had been deemed to be a chalcogenide version of the Baylis–Hillman reaction because the Baylis–Hillman adducts were given after purification of the products by preparative TLC on silica gel. However, a detailed examination of the reactions revealed that the original products were α-chloromethyl aldols and that dehydrochlorination occurred during purification by the preparative TLC on silica gel.[4] Similar reactions using $TiCl_4$ have been reported by other groups.[5] Very recently, we obtained methyl 3-methylsulfanyl-2-(α-hydroxy-*p*-nitrobenzyl)acrylate from the reaction of methyl propiolate with *p*-nitrobenzaldehyde in the presence of $TiBr_4$–SMe_2 as a minor product.[6] This finding implied that SMe_2 worked as a Lewis base and suggested to us that the intramolecular Michael addition of a sulfanyl group to an enone moiety would proceed more efficiently than the intermolecular one. In other words, the sulfanyl substituent assists the intramolecular Michael addition to form a cyclic sulfonium betaine. Cyclisation of enone sulfides with a Lewis acid has been reported from a different viewpoint.[7] These reports encouraged us to conduct the reactions of 1-[2-(methylsulfanyl)phenyl]prop-2-en-1-one with aldehydes in the presence of $BF_3{\cdot}Et_2O$. In this paper, we would like to describe a new type of tandem Michael-aldol reaction of an enone sulfide with aldehydes using a Lewis acid.†

A chloride ion reacted with an α,β-unsaturated carbonyl compound as a nucleophile in the reaction of the enone with an aldehyde using chalcogenide–$TiCl_4$.[4] In order to avoid this reaction and allow a chalcogenide to react with the enone instead of a chloride ion, we selected a Lewis acid such as metal fluoride or triflate, which releases non-nucleophilic anion, although $BF_3{\cdot}Et_2O$ and triflates of the lanthanide metals had been ineffective for the intermolecularly chalcogenide-promoted tandem Michael-aldol reactions.[3]

Various Lewis acids were examined for the reactions of 1-[2-(methylsulfanyl)phenyl]prop-2-en-1-one (**1**)‡ with *p*-nitrobenzaldehyde (Scheme 1). The reaction mixture was quenched with a saturated aqueous $NaHCO_3$ solution. Results of the reactions are summarised in Table 1. Reactions using $BF_3{\cdot}Et_2O$ were monitored by TLC and stopped when *p*-nitrobenzaldehyde disappeared (entries 1–3). The reaction was accelerated with increase of the amount of $BF_3{\cdot}Et_2O$ and the reaction time was shortened. Prolonged reaction time decreased the yield of **3a** and increased **2a** (entries 1 and 4). Reactions using $BF_3{\cdot}Et_2O$–$LiBF_4$ (1:1) or TiF_4 afforded **2a** only in low yields (entries 5 and 6). Reaction catalyzed $Yb(TfO)_3$ gave **2a**

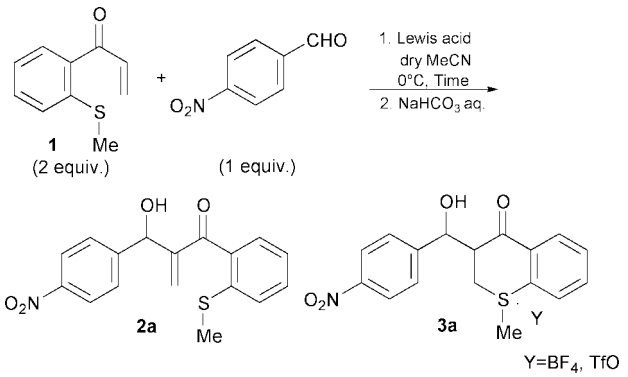

Scheme 1

(21%) and **3a** (42%)§ (entry 7). When 2 equiv. of $BF_3{\cdot}Et_2O$ were used, the highest yields of **2a** (18%) and **3a** (62%)§ were given from the reaction at 0 °C for 1 h (entry 2). The use of lithium perchlorate and aluminium sulfate gave no product, and **1** was recovered without loss.

Other aromatic aldehydes and 3-phenylpropionaldehyde similarly reacted with **1** to give **2** and **3** in low to moderate yields (Scheme 2 and Table 2). Since the reactions of various aldehydes were slower than that of *p*-nitrobenzaldehyde, the reactions were conducted for 2 h and then worked up with aqueous $NaHCO_3$. Seleno derivative **4**‡ reacted with aromatic aldehydes to give α-methylene aldol **5**, aldol selenonium salt **6**§, and 3-(α-hydroxybenzyl)selenochromanone **7**. Demethylation of **6** occurred more easily during the reactions than that of **3** to give **7** as a mixture of diasteroisomers. The *syn*- and *anti*-diastereoisomers were assigned in comparison of the coupling constants of the methine protons [C-CH(OH)-C], *syn*- (0–2.4 Hz) and *anti*-isomer (7.8–8.3 Hz), with those of the cyclohexanone derivative.[8]

^1H NMR spectra of the residues obtained by concentration of the reaction mixtures were measured in order to examine whether α-methylene aldol **2** or **5** was formed *via* the Baylis–Hillman reaction or the β-elimination of **3** or **6** by a work-up with a saturated aqueous $NaHCO_3$ solution. Vinyl proton

Table 1 Lewis acids for reactions of 1-[2-(methylsulfanyl)phenyl]prop-2-en-1-one **1** with *p*-nitrobenzaldehyde.

Entry	Lewis acid (equiv.)	Time	Products (Yield %)
1	$BF_3{\cdot}Et_2O$ (1)	2 h	**2a** (24), **3a** (50)
2	$BF_3{\cdot}Et_2O$ (2)	1 h	**2a** (18), **3a** (62)
3	$BF_3{\cdot}Et_2O$ (3)	45 min	**2a** (36), **3a** (34)
4	$BF_3{\cdot}Et_2O$ (1)	24 h[a]	**2a** (42), **3a** (29)
5	$BF_3{\cdot}Et_2O$–$LiBF_4$ (1:1)	2 h	**2a** (10)
6	TiF_4 (2)	2 h	**2a** (33)
7	$Yb(TfO)_3$ (2)	2 h	**2a** (21), **3a** (42)

[a] Room temperature.

 DOI: 10.1039/b106022h

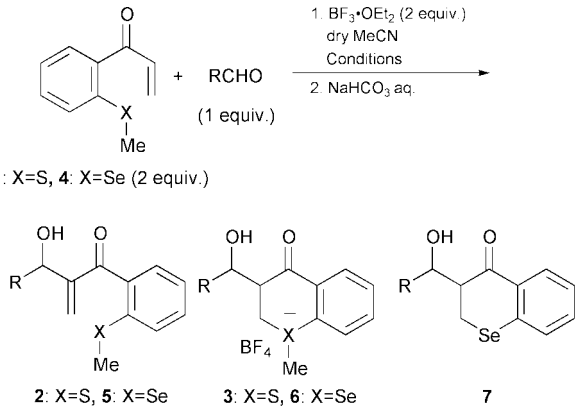

Scheme 2

Table 2 Reactions of 1-[2-(methylchalcogenyl)phenyl]prop-2-en-1-ones **1** and **4** with aldehydes.

Entry	Aldehyde, R	Conditions	Products (Yield %)
1	*p*-ClC_6H_4	0 °C, 2 h	**2b** (24), **3b** (37)
2	*p*-$CF_3C_6H_4$	0 °C, 2 h	**2c** (49), **3c** (17)
3	Ph	0 °C, 2 h then rt, 3 h	**2d** (24), **3d** (37)
4	PhC_2H_4	0 °C, 2 h then rt, 3 h	**2e** (54)
5	*p*-$NO_2C_6H_4$	0 °C, 2 h	**5a** (30), **6a** (45), **7a** (15) (3 : 2)[a]
6	*p*-ClC_6H_4	0 °C, 2 h	**5b** (25), **6b** (25), **7b** (28) (3 : 2)[a]

[a] Diastereoisomer ratio (*syn* : *anti*-isomer).

signals of **2** and **5** were observed in the region of δ 5.80, 6.09 and δ 5.76, 6.06, respectively. This indicates that α-methylene aldol **2** or **5** was formed during the reaction. However, the intensities of the $^+$X-Me signals of **3** and **6** were decreased, and those of the X-Me signals of **2** and **5** were increased after treatment with saturated aqueous $NaHCO_3$ solution. Therefore, some of the onium salts **3** or **6** suffered β-elimination by the work-up with the saturated aqueous $NaHCO_3$ solution to form **2** or **5**, respectively.§

Next, the residue obtained from the reaction of **1** or **4** (2 equiv.) with *p*-nitrobenzaldehyde (1 equiv.) using $BF_3{\cdot}Et_2O$ (2 equiv.) as a Lewis acid was treated with triethylamine (2 equiv.) instead of saturated aqueous $NaHCO_3$ solution in order to obtain α-methylene aldol **2** or **5** (Scheme 3). The reaction of sulfide **1** afforded **2a** in 75% yield, but the reaction of the selenium congener **4** gave **5** (64%) and the demethylated product **7** (10%).

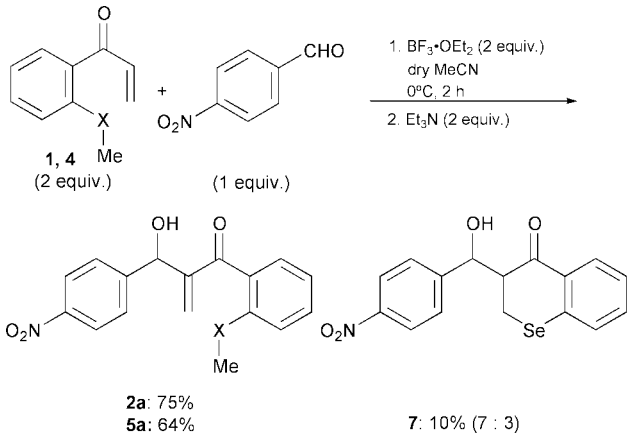

Scheme 3

The reaction conditions presented here were not sufficiently optimised, but this methodology will be the starting point for the development of tandem Michael-aldol reactions as well as the Baylis–Hillman reaction.

This research was partially supported by the Ministry of Education, Science, Sports and Culture, Grant-in-Aid for Scientific Research (C), 12672056.

Notes and references

† A typical example: $BF_3{\cdot}OEt_2$ (126 μl, 1.00 mmol) was added to a stirred solution of *p*-nitrobenzaldehyde (76 mg, 0.50 mmol) and 1-[2-(methylsulfanyl)phenyl]prop-2-en-1-one (**1**) (178 mg, 1.00 mmol) in dry MeCN (1.5 ml) at 0 °C. The mixture was stirred at the same temperature for 2 h, and the reaction was quenched by addition of saturated aqueous $NaHCO_3$ (3 ml). The precipitate of the inorganic material was removed by filtration through Celite and washed with MeCN. The filtrate and the washing were combined, and the solvent was evaporated under reduced pressure. The residue was washed with CH_2Cl_2, and crystals were filtered and recrystallised from MeCN–CH_2Cl_2 to give 3-[(4-nitrophenyl)(hydroxy)methyl]-1-methyl-4-oxo-3,4-dihydro-2*H*-thiochromenium tetrafluoroborate (**3a**), as a white powder of a mixture of diastereoisomers: major isomer: δ_H 3.10 (3H, s, SMe), 3.60 (1H, dd, J = 5 and 15), 3.61 (1H, ddd, J = 3, 5 and 10), 4.02 (1H, dd, J = 10 and 15), 4.36 (1H , d, J = 4, OH), 5.79 (1H, dd, J = 3 and 4, benzylic H), 7.71 (2H, d, J = 9, ArH), 7.89–7.94 (3H, m, ArH), 8.29 (2H, d, J = 9, ArH), 8.38 (2H, dd, J = 2 and 7, ArH). The ^{1}H NMR signals of the minor isomer could not be clearly assigned because of the overlapping absorptions. The washing was concentrated to dryness, and the residue was purified by preparative TLC on silica gel (ethyl acetate–hexane = 1 : 2, v/v) to give 2-[(4-nitrophenyl)(hydroxy)methyl]-1-[2-(methylsulfanyl)phenyl]-prop-2-en-1-one (**2a**) as yellow oil: δ_H 2.40 (3H, s, SCH_3), 3.50 (1H, br s, OH), 5.80 and 6.09 (each 1H, s, olefinic H), 5.91 (1H, s, benzylic H), 7.17 and 7.43 (each 1H, t, J = 8, ArH), 7.27 and 7.34 (each 1H, d, J = 8, ArH), 7.66 and 8.21 (each 2H d, J = 9, ArH); δ_C 17.0 (q), 72.4 (d), 123.8 (d), 124.6 (d), 127.3 (d), 127.4 (d), 129.7 (d), 130.1 (t), 131.7 (d), 136.9 (s), 139.3 (s), 147.5 (s), 149.1 (s), 149.2 (s), 198.2 (s); EIMS *m*/*z* 329 (M^+); Found: C, 61.9; H, 4.9; N, 4.0. $C_{17}H_{15}NO_4S$ requires C, 62.0; H, 4.6; N, 4.3%.

‡ Compounds **1** and **4** were prepared in a similar way as for 1-[2-(ethylsulfanyl)-4,5-dimethoxyphenyl]prop-2-en-1-one in Ref. 7*b*.

§ The onium salts **3** and **6** were obtained as mixtures of stereoisomers based on two chiral carbons and a chalcogenide atom. However, their stereostructures and isomer ratios could not be determined. The stereostructures of onium salts **3** and **6** and their reactivity against a base will be described in the full paper.

1 For reviews: S. E. Drewes and G. H. P. Roos, *Tetrahedron*, 1988, **44**, 4653; D. Basavaiah, P. D. Rao and R. S. Hyma, *Tetrahedron*, 1996, **52**, 8001; E. Ciganek, *Org. React.*, 1997, **51**, 201; P. Langer, *Angew. Chem., Int. Ed.*, 2000, **39**, 3049.

2 E. P. Kunidig, L. H. Xu, P. Romanens and G. Bernardinelli, *Tetrahedron Lett.*, 1993, **34**, 7049; V. K. Aggarwal, A. Mereu, G. J. Tarver and R. McCague, *J. Org. Chem.*, 1998, **63**, 7183; M. Kawamura and S. Kobayashi, *Tetrahedron Lett.*, 1999, **40**, 1539; Y. M. A. Yamada and S. Ikegami, *Tetrahedron Lett.*, 2000, **41**, 2165.

3 T. Kataoka, T. Iwama and S. Tsujiyama, *Chem. Commun.*, 1998, 197; T. Kataoka, T. Iwama, S. Tsujiyama, T. Iwamura and S. Watanabe, *Tetrahedron*, 1998, **54**, 11813.

4 T. Kataoka, H. Kinoshita, T. Iwama, S. Tsujiyama, T. Iwamura, S. Watanabe, O. Muraoka and G. Tanabe, *Tetrahedron*, 2000, **56**, 4725; T. Kataoka, T. Iwama, H. Kinoshita, S. Tsujiyama, Y. Tsurukami, T. Iwamura and S. Watanabe, *Synlett*, 1999, 197; T. Kataoka, T. Iwama, H. Kinoshita, Y. Tsurukami, S. Tsujiyama, M. Fujita, E. Honda, T. Iwamura and S. Watanabe, *J. Organomet. Chem.*, 2000, **611**, 455.

5 S. Uehira, Z. Han, H. Shinokubo and K. Oshima, *Org. Lett.*, 1999, **1**, 1383; G. Li, H.-X. Wei, J. J. Gao and T. D. Caputo, *Tetrahedron Lett.*, 2000, **41**, 1; G. Li, J. Gao, H.-X. Wei and M. Enright, *Org. Lett.*, 2000, **2**, 617; M. Shi and Y.-S. Feng, *J. Org. Chem.*, 2001, **66**, 406.

6 T. Kataoka, S. Kinoshita, H. Kinoshita, T. Iwamura and S. Watanabe, unpublished results.

7 (*a*) V. G. Nenajdenko, M. V. Lebedev and E. S. Balenkova, *Synlett*, 1995, 1133; (*b*) M. V. Lebedev, V. G. Nenajdenko and E. S. Balenkova, *Tetrahedron*, 1998, **54**, 5599.

8 M. Stiles, R. R. Winker, Y. Chang and L. Traynor, *J. Am. Chem. Soc.*, 1964, **86**, 3337.

CHEMCOMM
Communication
www.rsc.org/chemcomm

Peptide conjugation: unexpected ring opening of azacrown ether nucleophiles in the oxazolone-based coupling†

Anatoly M. Belostotskii,* Elisheva Genizi and Alfred Hassner

Chemistry Department, Bar-Ilan University, Ramat-Gan 52900, Israel. E-mail: belostot@mail.biu.ac.il

Received (in Cambridge, UK) 10th July 2001, Accepted 7th August 2001
First published as an Advance Article on the web 10th September 2001

Unexpected cleavage of the macrocyclic ring of secondary azacrown ethers when interacting with the Aib_8 (Aib = α-aminoisobutyric acid) oxazolone indicates the possibility for a new mechanism of peptide racemization due to transformations of the oxazolones formed from the *N*-derivatives of α-amino acids in peptide synthesis.

Peptide–benzocrown ether conjugates have been proposed as metal carriers which are capable of specific membrane penetration.[1] In the framework of developing *a biomembrane active peptide with a C-terminus-attached chelator* we started the synthesis of new peptide conjugates with crown ethers.

As the peptide we chose the octamer of α-aminoisobutyric acid (Aib), Aib_8, since natural and synthetic Aib-enriched peptides (including Aib_8) are capable of strong binding to biomembranes.[2] A preferred approach to preparation of conjugates consists of coupling Aib_8 with derivatives of the desired crown ethers, *i.e.*, of peptide modification in the last synthetic step. We chose the oxazolone-based coupling[3] for the C-terminus modification of this non-racemizing peptide, since other activation of the carboxy group of the C-terminal Aib residues is problematic (see below as well as ref. 4). The oxazolone coupling proceeded smoothly with primary amines but surprisingly led to different products on interaction with secondary amine crown ether nucleophiles.

Basic hydrolysis of octapeptide methyl ester **1a**[4] (NaOH, MeOH–H_2O, 25 °C, 48 h) led to acid **1b**, which was transformed into oxazolone **2** by heating with acetic anhydride (120 °C, 12 h; see Fig. 1). Interaction of oxazolone **2** (as a crude material; NMP, 110 °C, 1–1.5 h) with primary amines **3** and **4c** led to conjugates **5a** and **6a**, respectively, in good yields. Further, Boc-deprotection (TFA, 0 °C, 1 h) afforded peptide trifluoroacetates **5b** and **6b** (isolated by HPLC).[5]

No difficulties were encountered for acylation of azacrown ethers **4a** and **7a** possessing a secondary amino group using different activation methods of the carboxyl group. For instance, derivative **4c** was obtained by triphosgene-assisted coupling[6] of BocGlyOH and **4a** [THF, lutidine, 1 h at 25 °C and then 1 h at 50 °C] followed by acidic deprotection of amide **4b** (see Fig. 2). The PyBOP-provided coupling of **7a** and lithocholic acid **8** (3-fold excess of the amine, DIEA, CH_2Cl_2, 25 °C, 48 h) led to azacrown–steroid conjugate **9** (a steroidal analog of azacrown-based transmembranic carriers).

By contrast, when the coupling of oxazolone **2** with azacrown compounds **4a** and **7b** was carried out under the above conditions, only **10a** and **10b**, respectively, unexpected products of azacrown ring opening, were isolated (as trifluoroacetates)[5] after hydrolysis in TFA (see Fig. 3). No link between the secondary amine **7b** and the sterically hindered carboxyl function of peptide **1b** could be achieved under other conditions employed. For instance, triphosgene-based activation, which has been proposed as an advantageous solution for the often difficult peptide coupling with secondary amines,[6] was unsuccessful, with peptide **1b** being recovered unchanged.

† Electronic supplementary information (ESI) available: spectral data for representative examples of new compounds. See http://www.rsc.org/suppdata/cc/b1/b106106m/

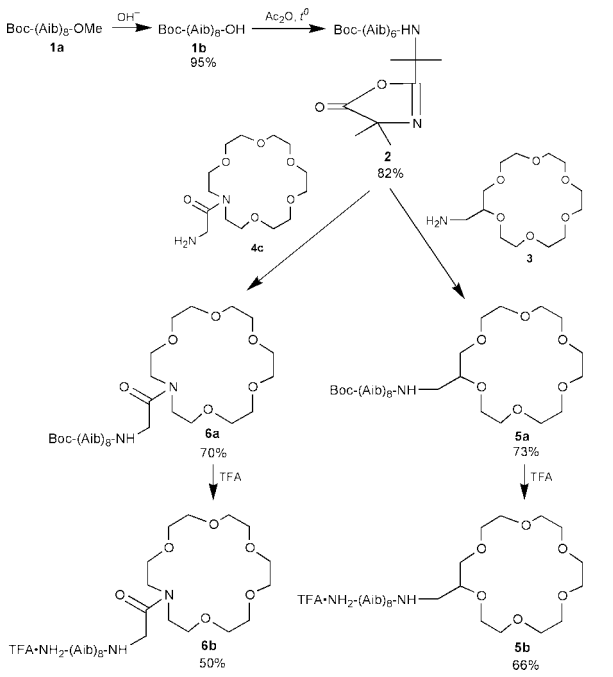

Fig. 1 Synthesis of macrocyclic conjugates **5b** and **6b**.

The drastic difference in the chemical behavior of crown ethers with primary (*e.g.*, **3**) and secondary (*e.g.*, **4a**) amino groups allows us to conclude that different mechanisms are involved in the reaction of these amines with peptide oxazolone **2**. We suggest the scheme in Fig. 3 to account for the azacrown ether ring opening with loss of two carbons.

While formation of conjugates **5a** and **6a** obviously occurs according to the accepted mechanism of nucleophilic cleavage of the peptide oxazolone ring,[7a,b] transformation of intermediate **11** into *O*-alkyl imidonium species **12**[8] under elevated temperatures initiates the azacrown ring opening. The positive charge on the iminium nitrogen atom (stabilized by the highly polar solvent, NMP) facilitates β-elimination of the hydroxy group leading to the cleavage of the macrocyclic ether. It should be noted that in the case of *the primary amine nucleophiles* **3** or **4c**, intermediates of type **12** will be converted in the aprotic

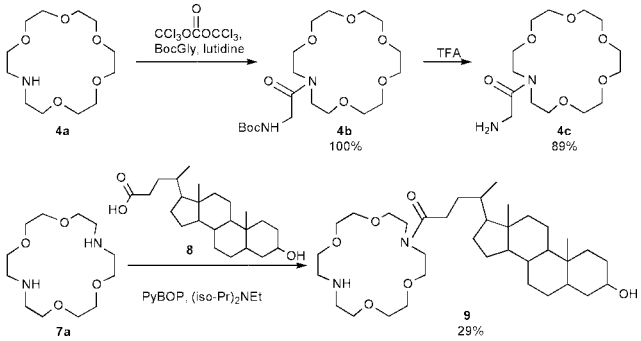

Fig. 2 Synthesis of macrocyclic conjugates **4c** and **9**.

 DOI: 10.1039/b106106m

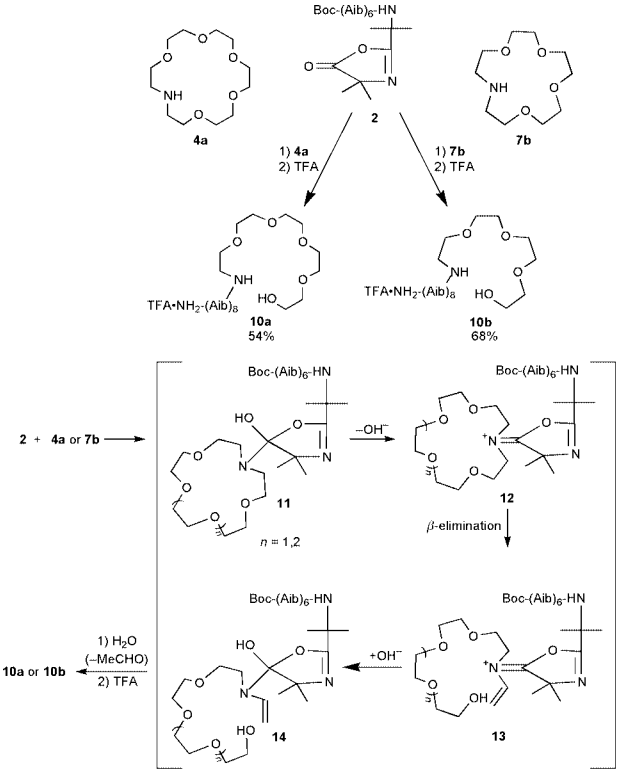

Fig. 3 Azacrown ether ring opening in the reaction of secondary amines **4c** and **7b** with oxazolone **2**.

solvent used into *neutral imidates* (see Fig. 4), which are not capable of β-elimination of alcohols. Imidates **13** afford the corresponding enamines **14** which are hydrolyzed to open chain azacrown compounds **10a** or **10b**.

Oxazolone formation from N-protected amino acids is one of the important factors leading to racemization in peptide synthesis.[7a,9] The observed ring opening indicates a possible *additional mechanism for peptide racemization* through oxazolone derivatives of amino acids (see ref. 7 for the commonly considered mechanisms). If oxazoline intermediates of type **11** are reversibly dehydrated under reaction conditions, the acidity of the 4-H proton is significantly increased due to tautomerization of the imidate structure into the enamine structure (see Fig. 4). Formation of an aromatic oxazole system is the driving force of this bond reorganization.

In order to reveal how reversible the equilibrium between these imine and enamine forms for *N*-Boc derivatives of amino acids is and thus to prove roughly the validity of the proposed racemization mechanism, we estimated the relative stability of the lowest energy conformers for the model tautomers ***I*** and ***E*** using *ab initio* calculations at the MP2/6-31G* level. Conformational space for these tautomers was analyzed using force

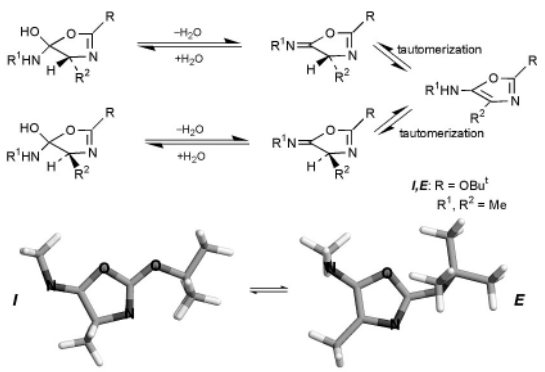

Fig. 4 Intermediate products of reversible transformation of oxazolones which lead to racemization of *N*-acyl of *N*-acyloxy amino acids or peptides. Optimized geometries (MP2/6-31G*) for model imine (***I***) and enamine (***E***) tautomers are shown.

fields Amber, OPLS and MM3 and the Monte-Carlo-based conformational search implemented into the Macromodel 6.0 package. The conformers of ***I*** and ***E*** shown in Fig. 4 were found by these force fields possessing the minimal energy among the conformers of the corresponding tautomer.

Ab initio calculations for the full electron energy (ΔE) of these conformers ***I*** and ***E*** (using also the PCM solvation model, a utility of the Gaussian98 package) demonstrated that imine tautomer ***I*** is more stable than enamine tautomer ***E*** by 6.1 and 5.1 kcal mol^{-1} in the gas phase and in DMSO, respectively. On the other hand, specific intermolecular amine–amide interactions (*e.g.*, H-bond formation) are not included in this solvation model. This high energy H-bonding should stabilize tautomer ***E*** in amidic solvents (*e.g.*, in NMP or DMF). Values of $\Delta H°$ for the H-bond formation are ~5 kcal mol^{-1} in such systems.[9] Taking into account this value and the calculated ΔE values we conclude that tautomers ***I*** and ***E*** should be near in energy in these polar solvents. Therefore, the equilibrium between ***I*** and ***E*** indeed is appreciably reversible (no large energy gap is present for these tautomers). It is known that the racemization in peptide synthesis is promoted by highly polar solvents (NMP, DMF or DMSO).[10] Thus, the above described tautomerization could be involved in the racemization of peptides being prepared in these H-bond-forming solvents.

This research was supported by a grant from the Mallinckrodt Medical B.V., Petten, Holland, and the Israel Ministry of Science and Technology (Grant 1471-1-99).

Notes and references

1 K. Otoda, S. Kimura and Y. Imanishi, *J. Chem. Soc., Perkin Trans. 1*, 1993, 3011.

2 J. W. Taylor and E. T. Kaiser, *Methods Enzym.*, 1987, **154**, 473; K.-P. Voges, G. Jung and W. H. Sawyer, *Biochim. Biophys. Acta*, 1987, **826**, 64.

3 For selected publications for this common synthetic method see (*a*) D. Obrecht, M. Altorfer, C. Lehmann, P. Schönholzer and K. Müller, *J. Org. Chem.*, 1996, **61**, 4080; (*b*) A. Safia, U. Slomczynska and G. R. Marshall, *Lett. Pept. Sci.*, 1995, **1**, 283; (*c*) A. Ewenson, R. Cohen-Suissa, D. Levian-Teitelbaum, Z. Selinger, M. Chorev and C. Gilon, *Int. J. Pept. Protein Res.*, 1988, **31**, 269.

4 Peptide **1a** was synthesized using Boc and Me-ester protections for amino and carboxyl groups, respectively. Cleavage of these protecting groups afforded oligo(Aib) peptides in yields higher than 90%. A successful PyBOP coupling in solution for preparation of Aib-containing peptides (E. Frerot, J. Coste, A. Pantaloni, M.-N. Dufour and P. Jouin, *Tetrahedron*, 1991, **47**, 259;) was used for the stepwise chain elongation up to the $(Aib)_4$ derivative. In order to minimize the number of synthetic steps in our synthesis of Aib_8, the [4 + 4] fragment coupling was examined as an alternative to the known stepwise elongation (see ; D. S. Jones, G. W. Kenner, J. Prenston and R. C. Sheppard, *J. Chem. Soc.*, 1965, 6227;) of the oligo(Aib) chain. Attempts to perform the [4 + 4] coupling using the DCC–HOBt condensation led to preferential formation of the corresponding oxazolone over octapeptide **1a** (~8:1, respectively). Therefore we converted the acid $Boc(Aib)_4OH$ into the oxazolone, which without purification was opened in a nucleophilic reaction with the amine $NH_2(Aib)_4OMe$ (NMP, 110 °C, 2 h), furnishing the desired octapeptide **1a**.

5 See footnote†.

6 E. Falb, T. Yechezkel, Y. Salitra and H. Gilon, *J. Pept. Res.*, 1999, **53**, 507.

7 (*a*) M. Goodman and A. Glazer, in *Peptides, Proceedings of the First American Peptide Symposium*, ed. B. Weinstein and S. Lande, Marcel Dekker, New York, 1970, pp. 267–335 (*b*) J. Ciarkowski, F. M. F. Chen and N. L. Benoiton, *J. Comput. Aided Mol. Des.*, 1991, **5**, 585; (*c*) T. T. Romoff and M. Goodman, *J. Pept. Res.*, 1997, **49**, 281.

8 Structures of type **11** with a tetrahedral carboxylic fragment are accepted intermediates in the stepwise mechanism of aminolysis of esters. (*a*) G. M. Blackburn and W. P. Jencks, *J. Am. Chem. Soc.*, 1968, **90**, 2638; (*b*) A. C. Satterthwait and W. P. Jencks, *J. Am. Chem. Soc.*, 1974, **96**, 7018. Hydrolysis of imidates and aminolysis of esters lead *via* the same intermediate to the same products; (see refs. 8*a*, *b* and *c*); (*c*) A. C. Satterthwait and W. P. Jencks, *J. Am. Chem. Soc.*, 1974, **96**, 7031.

9 J. H. Lady and K. B. Whetsel, *J. Phys. Chem.*, 1967, **71**, 1421.

10 Y. Han, F. Albericio and G. Barany, *J. Org. Chem.*, 1997, **62**, 4307.

CHEMCOMM Communication
www.rsc.org/chemcomm

Chemical modification of schizophyllan by introduction of a cationic charge into the side chain which enhances the thermal stability of schizophyllan–poly(C) complexes†‡

Kazuya Koumoto,[a] Taro Kimura,[a] Masami Mizu,[a] Kazuo Sakurai*[b] and Seiji Shinkai*[b]

[a] *Chemotransfiguration Project, PRESTO, Japan Science and Technology Corporation, Kurume Research Center Building, 2432 Aikawa Kurume, Fukuoka 839-0861, Japan*
[b] *'Organization and Function', PRESTO, Japan Science and Technology Corporation, Kurume Research Center Building, 2432 Aikawa Kurume, Fukuoka 839-0861, Japan. E-mail: seijitcm@mbox.nc.kyushu-u.ac.jp; Fax: +81-942-39-9012; Tel: +81-942-39-9011*

Received (in Cambridge, UK) 26th June 2001, Accepted 24th August 2001
First published as an Advance Article on the web 19th September 2001

Combining oxidation with periodate and reductive amination, the amino group is introduced only in the side chain of schizophyllan and the product can bind to poly(C) with a higher dissociation temperature than that of the unmodified schizophyllan and poly(C) complex.

Schizophyllan (SPG) is a natural polysaccharide produced by the fungus *Schizophyllum commune* and its repeating unit consists of three β(1→3) glucose units and one β(1→6) glucose side chain linked at every third main-chain glucose (see **5** in Scheme 1).[1,2] SPG adopts a triple helix in water and dissociates into a single chain (s-SPG) in dimethyl sulfoxide (DMSO).[3–5] The s-SPG chain can regain the original triple helix by exchanging DMSO for water.[5–7] Recently, we found that when this solvent-exchange process is carried out in the presence of polynucleotides, the resultant triple helix consists of two s-SPG chains and one nucleotide chain.[8,9] Subsequent study reveals that this complexation is characteristic for water-soluble β-1,3-glucans and never observed for other polysaccharides.[10] As far as we know, this is the first clear evidence that a neutral polysaccharide can form a macromolecular complex with polynucleotides. We believe that s-SPG–polynucleotide complexes may provide a new methodology for gene technology, such as gene carriers, affinity separation columns, biosensors, *etc*.[11] Judging from these potential applications, it is advantageous to be able to control the complex stability by chemical modification of SPG. In this paper, we have introduced an amino group into the side chain of SPG by combining periodate oxidation with subsequent reductive amination.

As shown in Scheme 1, oxidation of glucosides by periodate anion (IO_4^-) leads to cleavage of the pyranose ring and converts each cleavage end to a formyl group.[12] The formyl group reacts with 2-aminoethanol and subsequent reduction of the resultant Schiff base produces an amino-appended glucoside (**2c**, **3c**, and **4c**). When this method is applied to SPG, the product is expected to have the chemical structure shown by **6**. Here, *n* is the conversion ratio (or the ratio of cationic monomeric unit), which was estimated to be 2.4 ± 0.3% by nitrogen elemental analysis. Hereinafter, we denote this copolymer as N-s-SPG. Since the ratio of the introduced cationic monomer unit is very low, it is reasonable to consider that the reaction takes place statistically to yield a random copolymer.

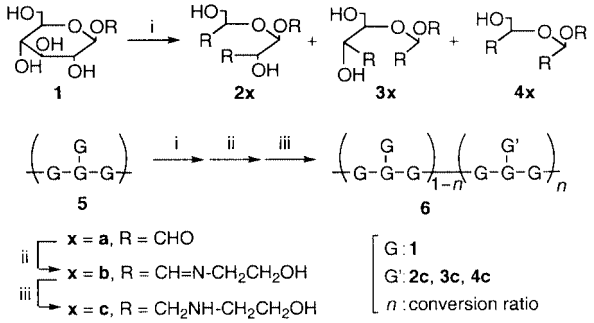

Scheme 1 Schematic illustration for the introduction of an amino group into SPG. *Reagents and conditions*: (i) $NaIO_4$, H_2O, 4 °C, 2 days, (ii) 2-aminoethanol, DMSO, rt, 2 days, (iii) $NaBH_4$, DMSO, rt 1 day.

One of advantages in applying this periodate oxidation method to SPG is that the cleavage reaction takes place only at the side chain and the main chain should be intact during the reaction because the main chain does not have any 1,2-diol groups. Therefore, this method can be extended to other 1,3-glucans such as lentinan and scleroglucan.[11] Although not mentioned in this paper, *n* can be controlled by changing the concentration of the periodate anion. Detailed characterisations and the relationship between *n* and the complex stability will be discussed in the corresponding full paper.

The amino group introduced by the above mentioned method forms an ammonium cation in neutral aqueous solutions. Therefore, when N-s-SPG is mixed with polynucleotides, we expect that an ion-pair can be formed between the phosphate anion of polynucleotide and the cation of N-s-SPG. Once the ion pair is formed, this strong attractive interaction is expected to enhance the complex stability.

Fig. 1 compares the CD spectra between poly(C) itself, a mixture of s-SPG and poly(C) (+s-SPG), and a mixture of N-s-SPG and poly(C) (+N-s-SPG), where [θ] is the molar ellipticity. Neither s-SPG nor N-s-SPG has any absorbance in the wavelengths presented in Fig. 1. Therefore, all CD bands are ascribed to the conformational asymmetry of a poly(C) chain. CD bands in this wavelength region sensitively reflect how the cytosine bases are stacked in the helix.[13]

As shown in Fig. 1, the spectrum of +s-SPG is different from that of poly(C) itself; the 275 nm band increases by 50% and a

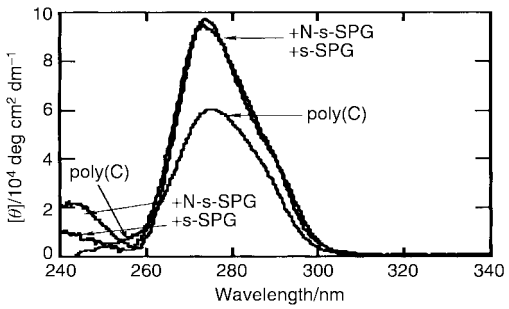

Fig. 1 Comparison of the CD spectra between poly(C), +s-SPG and +N-s-SPG measured at 15 °C in a non-salt solution.

† Electronic supplementary information (ESI) available: experimental details and CD spectra. See http://www.rsc.org/suppdata/cc/b1/b105609n/
‡ This is the 9th paper in the series 'Polysaccharide–polynucleotide complexes'.

 DOI: 10.1039/b105609n

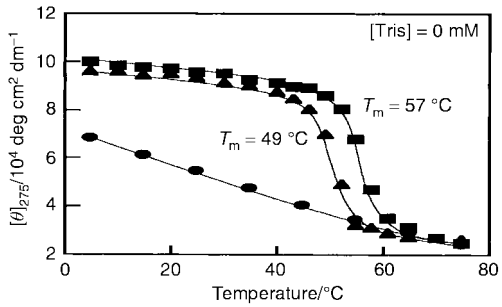

Fig. 2 Comparison of the melting behaviours of the complex between +s-SPG (▲) and +N-s-SPG (■) [Poly(C) (●)].

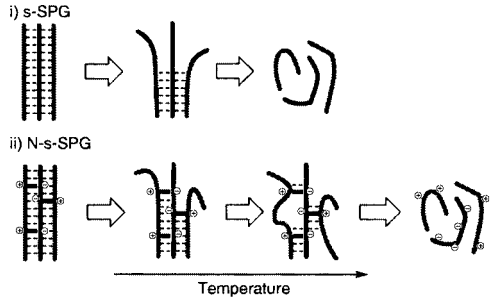

Fig. 4 Schematic illustration of the pinning effect induced by ion-pair formation.

new band arises around 242 nm. According to our previous work,[8,10] these changes can be ascribed to the complex formation between s-SPG and poly(C). The spectrum of +N-s-SPG also has two characteristic bands at 242 and 275 nm, however, the spectrum is slightly different from that of +s-SPG. In particular, the intensity of the 242 nm band of +N-s-SPG is almost twice of that of +s-SPG. Although the origin for the 242 nm band is not clear, this difference should be related to the ion pair formation between the cations in N-s-SPG and the phosphate anions in poly(C). When we measured the CD spectra with increasing Tris concentration, $[\theta]_{242}$ of +s-SPG does not change, whereas $[\theta]_{242}$ of +N-s-SPG merges with that of +s-SPG above 80 mM Tris, where $[\theta]_{242}$ is the molar ellipticity at 242 nm. Since Tris can generate a cationic charge at pH = 8.0, Tris cations presumably can bind to the phosphate anions in poly(C). Therefore, Tris and N-s-SPG cations compete with each other for binding to poly(C) and increasing Tris concentration is favourable for Tris to bind to poly(C).[14] This ion-competition effect can explain why increasing Tris concentration reduces the difference in the CD spectrum between +s-SPG and +N-s-SPG.

Fig. 2 compares the temperature dependence of $[\theta]_{275}$ for poly(C), +s-SPG and +N-s-SPG in a non-salt solution. The melting temperature of the complex (T_m) was determined with a conventional method[15,16] and the resultant values are presented in the figure. The complex of +N-s-SPG dissociates at higher temperature than s-SPG. This feature clearly indicates that the presence of the amino group in s-SPG can stabilise the complex. Fig. 3 plots T_m against Tris concentration for +s-SPG and +N-s-SPG. For +s-SPG, T_m seems to be independent of the Tris concentration, on the other hand, T_m for +N-s-SPG decreases with increasing Tris concentration. This concentration dependence of T_m can be also explained by the ion-competition effect mentioned above. Therefore, we can confirm that the formation of the ion-pair between N-s-SPG and poly(C) enhances the complex stability.

It is interesting that major features of the CD spectrum are common to +N-s-SPG and +s-SPG. This indicates that the poly(C) conformation in the complex is almost same for +s-SPG and +N-s-SPG. The complex of +N-s-SPG melts at 57 °C, whereas that of +s-SPG at 49 °C. This temperature difference of 8 °C approximately corresponds to a difference in enthalpy of 5–10 kcal mol^{-1}. The complex with +N-s-SPG is stabilised compared with +s-SPG in spite of the similarity in their conformation. This phenomenon can be explained by ion-pair formation between the phosphate anion and the ammonium cation. This ion-pair pins the poly(C) chain to the SPG chain to prevent decomplexation. This 'pinning effect' is schematically shown in Fig. 4.

In conclusion, we have successfully introduced an amino group into the side chain of SPG and stabilised the complex. It is undoubted that in the polymer complex the hydrogen-bonding interaction with OH groups and the electrostatic interaction with the amino groups operate synergistically to enhance the complex stability and the latter interaction is selectively reduced by the increase in the Tris concentration. Thus, this result presents a new strategy to control the stability of polynucleotide–polysaccharide complexes.

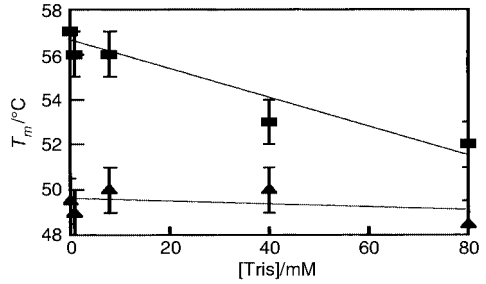

Fig. 3 Tris concentration dependence of T_m for +s-SPG (▲) and N-s-SPG (■).

Notes and references

1 S. Kikumoto, T. Miyajima, S. Yoshizumi, S. Fujimoto and K. Kimura, *J. Agric. Chem. Soc. Jpn*., 1970, **44**, 337.
2 S. Kikumoto, T. Miyajima, K. Kimura, S. Okubo and N. Komatu, *J. Agric. Chem. Soc. Jpn*., 1970, **45**, 162.
3 T. Yanaki, T. Norisuye and H. Fujita, *Macromolecules*, 1980, **13**, 1462.
4 T. Norisuye, T. Yanaki and H. Fujita, *J. Polym. Sci., Polym. Phys. Ed*., 1980, **18**, 547.
5 C. T. Chuah, A. Sarko, Y. Deslandes and R. H. Marchessault, *Macromolecules*, 1983, **16**, 1375.
6 T. M. McIntire and D. A. Brant, *J. Am. Chem. Soc*., 1998, **120**, 6909.
7 B. H. Falch and B. T. Stokke, *Carbohydr. Polym*., 2001, **44**, 113.
8 K. Sakurai and S. Shinkai, *J. Am. Chem. Soc*., 2000, **122**, 4520.
9 K. Sakurai, M. Mizu and S. Shinkai, *Biomacromolecules*, in the press.
10 T. Kimura, K. Koumoto, K. Sakurai and S. Shinkai, *Chem. Lett*., 2000, 1242.
11 K. Sakurai, S. Shinkai, T. Kimura, K. Tabata, K. Koumoto and G. Oliver, filed patent, 2000-, PCT, P0524T.
12 B. T. Hofreiter, I. A. Wolff and C. L. Mehltretter, *J. Am. Chem. Soc*., 1957, **79**, 6457.
13 N. Berova, K. Nakanishi and R. W. Woody, *Circular Dichroism*, Wiley-VCH, New York, 2000.
14 Using inorganic salts such as NaCl and KCl, we found that the salt concentration dependence of the CD spectrum of both +s-SPG and +N-s-SPG, as expected, had a similar effect to that of Tris. However, these inorganic salts stabilise the complex even for the s-SPG system and since this effect takes place more dominantly than the competition effect, we could not see any CD changes due to ion-pair formation.
15 D. Pörschke, *Biopolymers*, 1971, **10**, 1989.
16 U. Schernau and P. L. Privalov, *J. Mol. Biol*., 1978, **122**, 465.

CHEMCOMM Communication
www.rsc.org/chemcomm

Functionalised polyolefin synthesis using [P,O]Ni catalysts

Vernon C. Gibson* and Atanas Tomov

Department of Chemistry, Imperial College of Science, Technology and Medicine, Exhibition Road, South Kensington, London, UK SW7 2AY. E-mail: v.gibson@ic.ac.uk

Received (in Cambridge, UK) 20th July 2001, Accepted 21st August 2001
First published as an Advance Article on the web 19th September 2001

Nickel olefin polymerisation catalysts containing bulky phosphino-enolate ligands are shown to give methyl methacrylate end-functionalised polyolefins.

Industrial processes for the manufacture of most polyolefin materials rely on transition metal catalysts which operate at modest temperatures and pressures and allow the properties of the materials to be tuned to their various applications. The past 20 years or so have seen important advances in the design of 'single-site' molecular catalysts which have given rise to an era of more finely controlled polyolefin materials synthesis.[1] A crucially important industrial and academic objective remains, however, and that is to develop catalysts that will allow the copolymerisation of hydrocarbon monomers such as ethylene and propylene with readily available polar monomers such as methyl methacrylate (MMA), alkylacrylates, and vinyl acetate. At present, commercial processes for the copolymerisation of these monomers rely on high pressure free radical polymerisation technology, and the range of materials accessible *via* this technology is severely restricted. There thus exists a compelling technological requirement for new metal-based catalysts capable of copolymerising hydrocarbon and polar monomers, under low temperature/pressure conditions, to give polyolefins with modified surface properties (adhesion, wettability, *etc*.) or bulk properties, or to act as compatibilisers for polyolefins and functionalised polymers.

To date, late transition metal catalysts have provided the most significant advances in polar comonomer incorporation but the majority only incorporate monomers in which the functionality is remote to the polymerisable vinyl group.[2,3] An important advance was reported by Brookhart and coworkers[4] who showed that α-diimine palladium catalysts are capable of incorporating acrylates into highly branched polyethylene, to give materials that bear resemblance to the copolymers obtained by free radical techniques. More recently nickel catalysts bearing salicylaldimine ligands have been shown to copolymerise ethylene with functionalised norbornenes.[3] These catalysts, however, do not incorporate polar monomers with the polar functionality directly attached to the C–C double bond.†

Recently we described a new family of highly active ethylene polymerisation catalysts **1** and **2** (Scheme 1) based on P–O chelate ligands bearing bulky substituents.[5] Here, we describe the use of this catalyst system to incorporate the readily available polar monomer, methyl methacrylate, into polyolefin materials.

The [P,O]Ni catalysts are readily generated by treatment of $Ni(cod)_2$ with the ligand precursors **1a–c**‡ in the presence of MMA. Interestingly, the catalyst does not form in the absence of an olefin (ethylene or MMA) which is presumed to be required to displace a cod ligand from the nickel centre. The polymerisations were carried out by exposing the nickel catalyst/MMA mixture to a continuous feed of ethylene (1–5 bar) in a glass reactor at temperatures in the range 50–70 °C. At the end of each polymerisation the polymer was precipitated with methanol, filtered, dissolved in 1,2,4-trichlorobenzene at 120 °C and precipitated from tetrahydrofuran. This procedure was repeated twice to remove any traces of poly(MMA). *In situ* generated catalytic mixtures as well as the pre-formed catalysts **2** are found to be equally active in the copolymerisation reaction.

The polymerisation results are collected in Table 1. The activities of the catalysts range from 80 to 418 g $mmol^{-1}$ h^{-1},

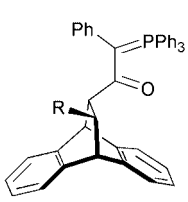

1

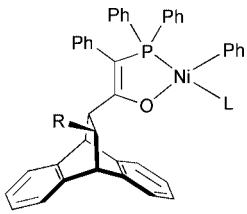

2

1a R = Me
1b R = Ph
1c R = C(O)CH(Ph)$PPh_3^+BAr^F{}_4^-$
2a R = Me, L = PPh_3
2b R = Ph, L = Py
2c R = C(O)CH(Ph)$PPh_3^+BAr^F{}_4^-$, L = PPh_3

Scheme 1 Ligand precursors **1** used in the *in situ* catalyst system **1**/$Ni(COD)_2$/MMA, and the corresponding preformed catalyst precursors **2**. $BAr^F{}_4$ = $[3,5\text{-}(CF_3)_2C_6H_3]_4B$.

Table 1 Ethylene–MMA copolymerisation data[a]

Catalyst[b]	Amount/μmol	C_2H_4/bar	Comonomer/ mmol	Polymer yield/g	Activity[c]/g $mmol^{-1}$ h^{-1}	M_n[d]	M_w/M_n
1a/$Ni(cod)_2$/MMA	65	3	MMA (37)	6.8	418	3600	2.2
1a/$Ni(cod)_2$/MMA	65	5	MMA (74)	3.2	197	3800	2.2
1a/$Ni(cod)_2$/MMA	65	4	MMA (74)	2.4	148	3400	2.0
1a/$Ni(cod)_2$MMA	65	3	MMA (74)	2.1	129	3100	2.1
1a/$Ni(cod)_2$/MMA	65	2	MMA (74)	1.3	80	2600	2.0
2b	65	3	MMA (74)	2.6	160[e]	3800	2.3
1c/$Ni(cod)_2$/MMA	17	1	MMA (19)	0.6	141	3400	2.1
1a/$Ni(cod)_2$/$(MMA)_3$	65	2	$(MMA)_3$[f] (10)	4.7	289	3700	3.1

[a] Polymerisations carried out in Fischer–Porter glass reactors, toluene, 65 °C, reaction time = 15 min. [b] 12 equivalents of $Ni(cod)_2$ employed; this provides an optimal nickel:ylide ratio to disfavour the formation of inactive bis(ylide) species.[2] [c] Based on concentration of ligand precursor. [d] Determined by GPC, uncorrected. [e] Based on concentration of Ni complex **2b**. [f] Methyl methacrylate trimer: $CH_2{=}C(CO_2Me)CH_2C(Me)(CO_2Me)CH_2C(Me)_2CO_2Me$.

 DOI: 10.1039/b106475d

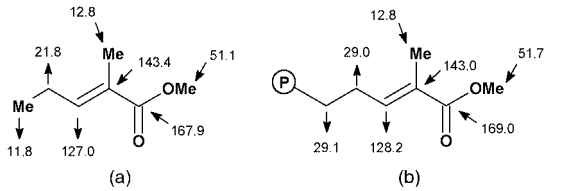

Fig. 1 ^{13}C NMR chemical shifts (δ) for methyl *trans*-2-methylpent-2-enoate (a) and PE–t-MMA (b); solvent $C_2D_2Cl_4$.

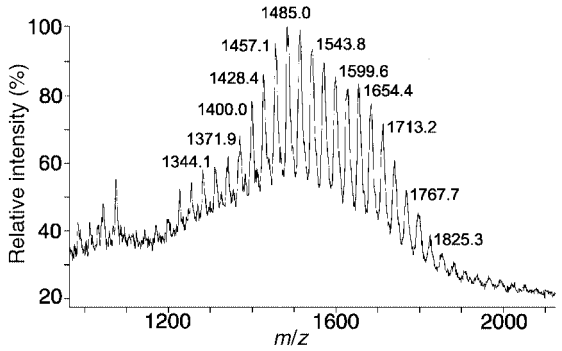

Fig. 2 MALDI-TOF mass spectrum of PE–t-MMA generated using catalyst **1a**. The masses correspond to the potassium adducts [M + K^+]. Repeat unit of all series: 28 Da. Solvent: 1,2,4-trichlorobenzene.

and give a first-order dependence on ethylene concentration, affording number average molecular weights in the range 3000–4000 and with narrow molecular weight distributions.

The isolated polymers were analysed by ^1H, $^{13}C\{^1H\}$ NMR and IR spectroscopies, MALDI-TOF mass spectrometry§ and gel permeation chromatography. In addition to the resonances of linear polyethylene, the $^{13}C\{^1H\}$ NMR spectrum revealed signals consistent with the presence of the methyl methacrylate unit. In particular, resonances at δ 128.2 and 143.0 are attributable to a double bond substituted with an ester functionality, while resonances at δ 169.0 and 51.7 confirm the presence of the methyl ester unit. Comparison of these NMR data with those derived from 2-methylpent-2-enoate (Fig. 1) indicate that the polyethylene chains possesses a methylenoate end-group. The presence of this end-group is confirmed by MALDI-TOF mass spectrometry (Fig. 2) which reveals individual polymer chains [$MeCH_2(CH_2CH_2)_{n-1}CH{=}C(Me)$-$CO_2Me$ (n = 40–60)], each terminated by the methylenoate functionality. In general, MALDI-TOF mass spectrometry would appear to provide a useful direct method of determining whether or not a polar comonomer has been incorporated into the polyolefin, since purely hydrocarbon polyolefins do not generally give good mass spectral data. The presence of the α,β-unsaturated ester functionality can also be observed by IR spectroscopy which affords bands corresponding to the ester group (1720 cm^{-1}) and C=C double bond (1642 cm^{-1}). Methyl methacrylate oligomers can also be incorporated into PE. For example, polymerisation of ethylene in the presence of trimer-MMA affords a PE–t-$(MMA)_3$ block copolymer (Table 1) which is readily identified by NMR and MALDI-TOF mass spectrometry. The presence of the α,β-unsaturated ester groups at the chain ends is consistent with a mechanism involving insertion of MMA or $(MMA)_3$ into the growing polyethylene chain, followed by β-H elimination (Scheme 2) rather than *via* chain transfer to the polar monomer, since the latter, in the

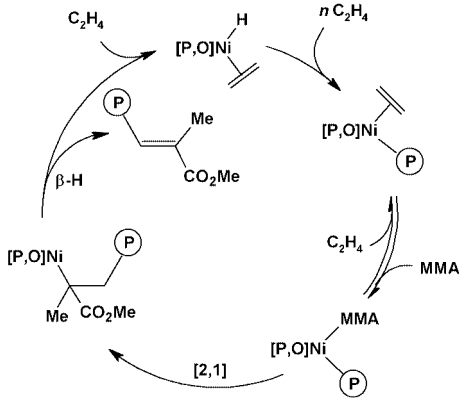

Scheme 2 Proposed mechanism for formation of PE–t-MMA.

absence of chain-walking, would give rise to saturated ester end-groups.

Since this catalyst system has also been shown to be capable of oligomerising propylene with good activities and hex-1-ene with more modest activities,[5] we have also investigated the potential for incorporating MMA into these oligomeric products. Treatment of **1a**/$Ni(cod)_2$ with an equimolar amount of propylene and MMA affords (by GC–MS) the MMA end-functionalised polypropylene oligomers $(C_3H_6)_nMMA$ (n = 1–3) (activity ~12 g $mmol^{-1}$ h^{-1}). In the case of hex-1-ene, a very low activity system (~1 g $mmol^{-1}$ h^{-1}) results in the MMA-functionalised co-dimer and -trimer, $(C_6H_{12})_nMMA$ (n = 1–2).

BP Chemicals Ltd is thanked for financial support. Drs G. Audley and J. Boyle are thanked for GPC and NMR measurements, respectively.

Notes and references

† It should be noted that lanthanide based catalyst systems for the synthesis of ethylene–MMA diblock copolymers have been reported,[6,7] and thiophene end-functionalised polyethylene *via* C–H bond activation[8] has recently been described.

‡ All new compounds gave satisfactory analytical and spectroscopic data.

§ Measured on a Micromass TOFSPEC spectrometer at laser λ_{ex} 337 nm. α-Cyano-4-hydroxycinnamic acid was used as a matrix. It should be noted that MALDI-MS has been shown in certain cases to observe components of lower mass preferentially.[9] This results in M_w being lowered to a greater extent than M_n, consequently affording a lower molecular weight distribution than the true value. The detector response is also known to affect the measured polymer weight distributions.

1 G. J. P. Britovsek, V. C. Gibson and D. F. Wass, *Angew. Chem., Int. Ed.*, 1999, **38**, 429.
2 U. Klabunde and S. D. Ittel, *J. Mol. Catal.*, 1987, **41**, 123.
3 T. R. Younkin, E. F. Conner, J. I. Henderson, S. K. Friedrich, R. H. Grubbs and D. A. Bansleben, *Science*, 2000, **287**, 460.
4 L. K. Johnson, S. Mecking and M. Brookhart, *J. Am. Chem. Soc.*, 1996, **118**, 267.
5 V. C. Gibson, A. Tomov, A. J. P. White and D. J. Williams, *Chem. Commun.*, 2001, 719.
6 H. Yasuda, M. Furo and H. Yamamoto, *Macromolecules*, 1992, **25**, 5115.
7 G. Desurmont, Y. Li, H. Yasuda, T. Mauro, N. Kanehisa and Y. Kai, *Organometallics*, 2000, **19**, 1811.
8 S. N. Ringelberg, A. Meetsma, B. Hessen and J. H. Teuben, *J. Am. Chem. Soc.*, 1999, **121**, 6082.
9 P. M. LLoyd, K. G. Suddaby, J. E. Varney, E. Scrivener, P. J. Derrick and D. M. Haddleton, *Eur. Mass Spectrom.*, 1995, **1**, 293.

CHEMCOMM Communication
www.rsc.org/chemcomm

Palladium-catalysed cross-coupling reactions in supercritical carbon dioxide

Tessa R. Early,[a] Richard S. Gordon,[a] Michael A. Carroll,[a] Andrew B. Holmes,*[a] Richard E. Shute[b] and Ian F. McConvey[c]

[a] *Melville Laboratory for Polymer Synthesis, Department of Chemistry, University of Cambridge, Pembroke Street, Cambridge, UK CB2 3RA. E-mail: abh1@cam.ac.uk; Fax: +44 1223 334866; Tel: +44 1223 334370;*
[b] *AstraZeneca Research and Development, Alderley Park, Macclesfield, Cheshire, UK SK10 4TG*
[c] *AstraZeneca Process Research and Development, Macclesfield, Cheshire, UK SK10 2NA*

Received (in Cambridge, UK) 27th July 2001, Accepted 29th August 2001
First published as an Advance Article on the web 19th September 2001

Heck and Suzuki reactions proceed in good yield in supercritical carbon dioxide in the presence of palladium acetate and tri-*tert*-butylphosphine with both free and polymer-tethered substrates.

The synthesis of organic molecules in the absence of volatile organic solvents remains an important industrial goal and the use of alternative reaction media in synthetic chemistry has attracted widespread attention. Supercritical carbon dioxide ($scCO_2$) has recently attracted much interest as an environmentally benign alternative to many toxic organic solvents.[1–3] It is non-toxic, inexpensive, universally available and affords facile separation from products by simple depressurisation. However, its practical use has been limited by its solvent power. Although $scCO_2$ will dissolve most non-polar compounds of low molecular mass, many catalysts, substrates and reagents are only poorly soluble.

Heck and Suzuki reactions have evolved into one of the most versatile families of reactions, as illustrated in the recent literature.[4,5] Their application in $scCO_2$ media was initially hindered by the poor solubilities of commercially available metal catalysts. In 1998 we[6] and Tumas[7] independently reported the first palladium-catalysed carbon–carbon coupling reactions in $scCO_2$ using fluorinated phosphine ligands to solubilise the palladium complex. To date, although the use of non-fluorinated phosphine ligands has been contemplated, the results have been disappointing, and inferior to the comparable fluorinated system. Rayner[8] reported added advantages in using palladium trifluoroacetate with commercial phosphines and metallocycles in the Heck reaction. Arai and co-workers communicated a Heck reaction in $scCO_2$ using a water soluble catalyst in a biphasic system, in which phase-transfer additives such as ethylene glycol afforded an increased reaction yield.[9] Very recently Bannwarth[10] described the application of perfluoro-tagged triphenylphosphine derivatives in the Stille reaction. Significantly, triphenylphosphine itself was also used as a ligand, with lower overall yields than the fluoro-analogue, but still an improvement over the previously reported work.[7]

Tri-*tert*-butylphosphine [P(*t*-Bu)$_3$] has been shown by Fu to be a highly active catalyst in a variety of palladium-catalysed coupling reactions.[11,12] We now show that the combination of palladium acetate with P(*t*-Bu)$_3$ very effectively catalyses Heck and Suzuki reactions of aryl halides in $scCO_2$. The solubility of triethylphosphine in $scCO_2$ has previously been noted.[13]

We first tested P(*t*-Bu)$_3$ as a ligand in the Heck reaction, a system with which we had previous experience.[6] (Table 1, entries 1a and b). Initial results were promising, and the application of this completely non-fluorous system to the

Table 1 Heck and Suzuki reactions in $scCO_2$ using the Pd(OAc)$_2$–P(*t*-Bu)$_3$ catalytic system[a]

Entry	Substrate 1	Substrate 2	Product	Base	T/°C	Yield[b] (%)
1a		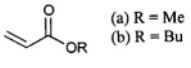 (a) R = Me (b) R = Bu	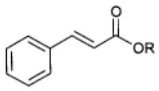	NEt_3	100	77
1b				DIPEA	100	92[c]
2		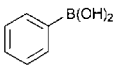	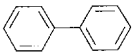	DIPEA	100	68
3a		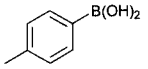	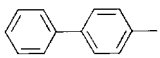	DIPEA	100	73
3b				$Me_2N(CH_2)_6NMe_2$	120	76
3c				Bu_4NOAc	100	69[d]
3d				Et_4NOAc	100	70[d]
4a		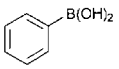	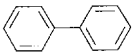	DIPEA	100	54
4b				Cs_2CO_3	100	52
5a	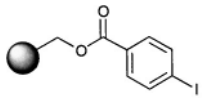	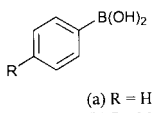 (a) R = H (b) R= Me	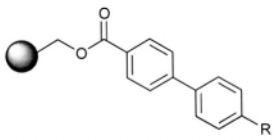	DIPEA	80	67[e]
5b				DIPEA	80	70[e]
6		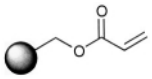	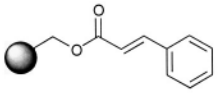	DIPEA	80	98[ce]

[a] All reactions were conducted in $scCO_2$ over a 16 h period with 5 mol% palladium and a two-fold molar ratio of phosphine to palladium acetate unless otherwise stated. [b] Isolated yield by column chromatography. [c] 10 mol% palladium. [d] HPLC yield [e] Isolated yield after base cleavage from resin. DIPEA (Hünig's base) is *N*,*N*-diisopropylethylamine.

 DOI: 10.1039/b106808c

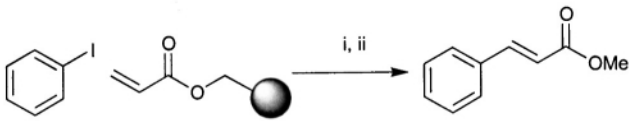

Scheme 1 *Reagents and conditions*: (i) 5 mol% $Pd(OAc)_2$, 10 mol% phosphine **1**, NEt_3, $scCO_2$, 100 °C, 40 h. (ii) NaOMe, MeOH, THF.

Suzuki reaction was also successful (entries 2–4). The yields for these reactions are not yet optimised.†

Both aryl iodides and bromides underwent the Suzuki reaction, although lower yields were obtained with the less reactive bromide coupling partners. A variety of different bases were investigated and shown to be effective in $scCO_2$. Surprisingly these reactions proceeded effectively in the presence of solid tetraalkylammonium acetate salts without addition of any other base. Jeffrey has reported the use of alkylammonium salts for the Heck reaction in conventional solvents.[14] In addition, Bannwarth reported the use of tetra-*n*-butylammonium chloride in a Stille reaction in $scCO_2$.[10] We have found in related cross coupling reactions that the acetate is superior.[15]

Solid phase organic synthesis carried out on a substrate bound to a solid, typically polymeric, support continues to be an area of intense study. The application of solid phase synthesis to palladium-catalysed reactions has been the subject of recent reviews.[16,17] Conducting reactions on a solid support provides an attractive and practical method for clean and efficient synthetic preparations, allowing convenient separation of products from the reaction mixture and forming the basis of combinatorial chemistry. Reactions using polymer supports require the use of a solvent that will swell the polymer and expose reactive sites. The ability of $scCO_2$ to plasticise polymers has been exploited in a number of applications including polymer impregnation, formation of blends and particle formation.[18] We expected therefore that $scCO_2$ would provide a good swelling solvent for polymer supported reagents, allowing access to reactive sites and reducing the amount of excess reagent required to give acceptable coverage.

We now report the successful application of solid supported substrates for palladium catalysed Heck and Suzuki couplings in $scCO_2$. The first pilot reaction employed a catalytic system of palladium acetate with the highly fluorinated phosphine $PhP(CH_2CH_2C_6F_{13})_2$, **1** (Scheme 1).[6] REM resin[19] underwent a Heck reaction with iodobenzene and the modified resin was then cleaved under basic conditions to give (*E*)-methyl cinnamate in 74% yield over the two steps.

After this initial success we then extended the palladium acetate–P(*t*-Bu)$_3$ catalytic system to substrates immobilised on a polymer resin. The Suzuki reaction was applied to a functionalised Merrifield resin and proceeded in good yield, comparable to reactions off resin (Table 1, entries 5a and b). The Heck reaction on REM resin[19] gave a near-quantitative yield (entry 6). These results clearly demonstrate the successful application of the palladium-mediated cross-coupling methodology to a heterogeneous system, and form to our knowledge the first example of the use of polymer supported synthesis in $scCO_2$.

In summary we have shown that the non-fluorinated palladium acetate–P(*t*-Bu)$_3$ catalyst system is highly active in promoting C–C bond forming reactions in $scCO_2$. We have applied this system to the first example of polymer-supported reactions in $scCO_2$.

We thank the EPSRC, AstraZeneca, the Commission of the EU (Brite-Euram Contract BRRT-CT98-5089 'RUCADI') and the Isaac Newton Trust, Cambridge for generous financial support. We thank EPSRC for provision of the Swansea Mass Spectrometry Service.

Notes and references

† Typical procedure for the Suzuki reaction in supercritical carbon dioxide: palladium(II) acetate, (11 mg, 0.05 mmol) and tolylboronic acid (204 mg, 1.5 mmol) were placed in a 10 cm^3 stainless steel cell, which was taken into a nitrogen atmosphere (glove-box) where tri-*tert*-butylphosphine (20 mg, 0.1 mmol) was added, and the cell was sealed, and removed from the glove-box. Iodobenzene (0.204 g, 1 mmol) and *N*,*N*,*N*′,*N*″-tetramethylhexane-1,6-diamine (0.172 g, 1 mmol) were injected through the inlet port. The cell was then connected to the CO_2 line and charged with CO_2 (99.9995%—further purified over an Oxisorb® catalyst) to approximately 880 psi (volume *ca.* 5 cm^3 liquid carbon dioxide). The cell was heated to 100 °C and the pressure was adjusted to 3000 psi by the addition of CO_2. The reagents were maintained at this temperature and pressure for 16 h and the cell was then allowed to cool to room temperature. The contents of the cell were vented into ethyl acetate (100 cm^3), and once atmospheric pressure had been reached the cell was opened and washed out with further ethyl acetate (20 cm^3). The combined organic fractions were concentrated *in vacuo* to give the crude product which was adsorbed onto a flash silica column using CH_2Cl_2 and eluted with hexane to give a white crystalline solid (128 mg, 76%), mp 47–48 °C (lit.[20] 49–50 °C) δ_H (400 MHz; $CDCl_3$) 7.59 (2 H, dd, *o*′-Ph, *J* 7.8, 1.2 Hz), 7.51 (2H, d, *m*-Ar, *J* 8.1 Hz), 7.44 (2 H, dd, *m*′-Ph, *J* 7.8, 7.35 Hz), 7.33 (1 H, td, *p*′-Ph, *J* 7.35, 1.2 Hz), 7.26 (2H, d, *o*-Ar, *J* 8.1 Hz), 2.41 (3 H, s, Ar-CH_3).

1 R. S. Oakes, A. A. Clifford and C. M. Rayner, *J. Chem. Soc., Perkin Trans. 1*, 2001, 917.
2 J. A. Darr and M. Poliakoff, *Chem. Rev.*, 1999, **99**, 495.
3 P. G. Jessop and W. Leitner, *Chemical Synthesis Using Supercritical Fluids*, Wiley-VCH, Weinheim, 1999.
4 I. Beletskaya and A. V. Cheprakov, *Chem. Rev.*, 2000, **100**, 3009.
5 A. Suzuki, *J. Organomet. Chem.*, 1999, **576**, 147.
6 M. A. Carroll and A. B. Holmes, *Chem. Commun.*, 1998, 1395.
7 D. K. Morita, D. R. Pesiri, S. A. David, W. H. Glaze and W. Tumas, *Chem. Commun.*, 1998, 1397.
8 N. Shezad, R. S. Oakes, A. A. Clifford and C. M. Rayner, *Tetrahedron Lett.*, 1999, **40**, 2221.
9 B. M. Bhanage, Y. Ikushima, M. Shirai and M. Arai, *Tetrahedron Lett.*, 1999, **40**, 6247.
10 T. Osswald, S. Schneider, S. Wang and W. Bannwarth, *Tetrahedron Lett.*, 2001, **42**, 2965.
11 A. F. Littke and G. C. Fu, *J. Org. Chem.*, 1999, **64**, 10.
12 A. F. Littke and G. C. Fu, *J. Am. Chem. Soc.*, 2001, **123**, 6989 and references cited therein.
13 I. Bach and D. J. Cole-Hamilton, *Chem. Commun.*, 1998, 1463.
14 T. Jeffrey, *Tetrahedron*, 1996, **30**, 10113.
15 T. R. Early, R. S. Gordon, M. A. Carroll, A. B. Holmes, R. E. Shute and I. F. McConvey, manuscript in preparation.
16 C. L. Kingsbury, S. J. Mehrman and J. M. Takacs, *Curr. Org. Chem.*, 1999, **3**, 497.
17 R. Franzen, *Can. J. Chem.*, 2000, **78**, 957.
18 A. I. Cooper, *J. Mater. Chem.*, 2000, **10**, 207 and references cited therein.
19 J. R. Morphy, Z. Rankovic and D. C. Rees, *Tetrahedron Lett.*, 1996, **37**, 3209.
20 M. S. C. Rao and G. S. K. Rao, *Synthesis*, 1987, 231.

CHEMCOMM Communication
www.rsc.org/chemcomm

A novel route to substituted 4-methylene-4,5-dihydroisoxazoles mediated by hafnium(IV) chloride

Peter J. Dunn,[a] Alison B. Graham,[b] Ronald Grigg,*[b] Paul Higginson,[a] Visuvanthar Sridharan and Mark Thornton-Pett[b]

[a] *Pfizer Global Research & Development (UK), Sandwich, Kent, UK CT13 9NJ*
[b] *Molecular Innovation, Diversity and Automated Synthesis (MIDAS) Centre, School of Chemistry, The University of Leeds, Leeds, UK LS2 9JT. E-mail: R.Grigg@chem.leeds.ac.uk*

Received (in Cambridge, UK) 26th June 2001, Accepted 23rd August 2001
First published as an Advance Article on the web 19th September 2001

Heating alkyl vinyl ketones and *N-tert*-butylarylmethylideneamine *N*-oxides in the presence of $HfCl_4$ results in the formation of 4-methylene-4,5-dihydroisoxazoles in good yield.

We recently reported that hafnium(IV) chloride is an excellent catalyst for the tandem 1,3-azaprotio cyclotransfer–cycloaddition reaction between aldoximes and divinyl ketone, inducing the formation of the *exo*-isomers of substituted 1-aza-8-oxabicyclo[3.2.1]octan-4-ones **3** and reversing the natural regioselectivity of the thermally promoted cascade (Scheme 1).[1] We proposed that the dramatic effect on regioselectivity was due to coordination of the Lewis acid to the carbonyl moiety of the intermediate nitrone enhancing nucleophilicity at the β-carbon and promoting the formation of **3**.

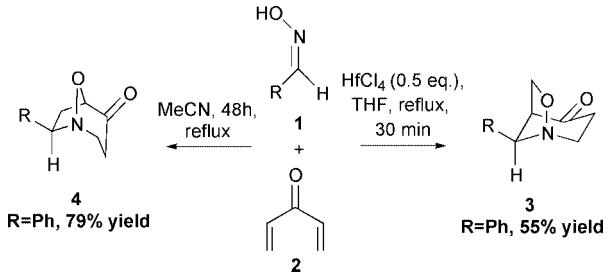

Scheme 1

To study the effect of $HfCl_4$ on a similar intermolecular 1,3-dipolar cycloaddition we reacted *N-tert*-benzylideneamine *N*-oxide **5a** with methyl vinyl ketone **6a**. Under thermal conditions (MeCN, reflux, 48 h) a 4 : 1 mixture of 5-substituted isoxazolidines ***exo*-7** and ***endo*-7** was obtained in 34% combined yield (Scheme 2). When the same substrates were subjected to the $HfCl_4$ catalysed conditions outlined in Scheme 1 only starting material was obtained after the usual reaction time of 30 min. Increasing the reaction time to 8 h did not result in the formation of the expected 4-substituted isoxazolidine **9** but, instead, furnished 4-methylene-4,5-dihydroisoxazole **8a** (80% conversion of nitrone, 51% yield). The structure of **8a** was determined by X-ray crystallography (Fig. 1).† Anhydrous $Sc(OTf)_3$ also induced the formation of **8a** (0.5 eq. $Sc(OTf)_3$, THF, reflux, 8 h) in slightly lower yield (80% nitrone conversion, 48% yield) whereas the addition of $ZnBr_2$ (0.5 eq.) under otherwise identical reaction conditions did not induce the formation of **8a** (^{1}H NMR indicated that the crude reaction mixture was comprised of starting material and traces of the products of a 1,3-dipolar cycloaddition).

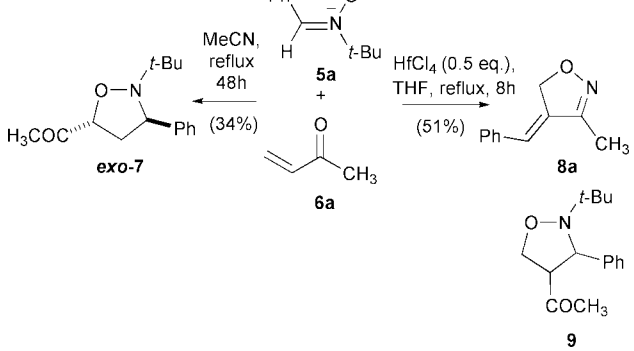

Scheme 2

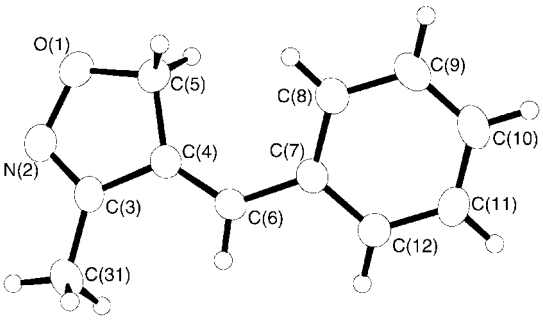

Fig. 1 X-Ray crystal structure of **8a**.†

Further development of this process identified conditions that afford reproducible results (Scheme 3).[2] The methodology encompasses both electron-donating and electron-withdrawing groups on the aromatic ring and variation of the ketone component (**6a–c**) (Table 1). In addition to **8a–h**, which were obtained as single stereoisomers, traces (5%) of the corresponding aromatic aldehydes (from degradation of **5a–f**, *vide infra*) were visible in the ^{1}H NMR spectra of crude products. The stereochemistry of the double bond in compounds **8b–h** was assigned by correlation of the chemical shift and coupling constants of the C=CH and CH_2 moieties in the ^{1}H NMR spectra with those obtained for **8a**.

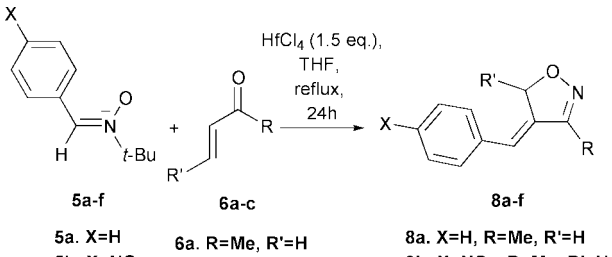

Scheme 3

 DOI: 10.1039/b105561p

Table 1 Hafnium(IV) chloride mediated synthesis of 4-methylene-4,5-dihydroisoxazoles

Nitrone	Vinyl ketone	Product[a]	Yield[b] (%)
5a	**6a**	**8a**	75
5b	**6a**	**8b**	76
5c	**6a**	**8c**	68
5d	**6a**	**8d**	54
5e	**6a**	**8e**	64
5f	**6a**	**8f**	70
5a	**6b**	**8g**	64
5a	**6c**	**8h**	31

[a] In all cases apart from **5a** + **6a**, small amounts (5–10%) of the corresponding aldehydes were detected by ^{1}H NMR. [b] Yield isolated by flash chromatography.

The mechanism of the reaction is a matter of conjecture at present. $HfCl_4$ catalysed degradation of nitrone **5a** may generate benzaldehyde and a hafnium complexed hydroxylamine if traces of water are present in the system. Indeed small amounts of the corresponding aromatic aldehydes are visible in the ^{1}H NMR spectra of the crude products and the amount of these was found to be proportional to the quantity of catalyst and reaction time. The hydroxylamine may react with **6a** to generate nitrone **10**[3] followed by a 6π-electrocyclisation–aldol condensation–dehydration sequence to generate **8a** (Scheme 4). Analogous 6π-electrocyclisation reactions are well known.[4–6]

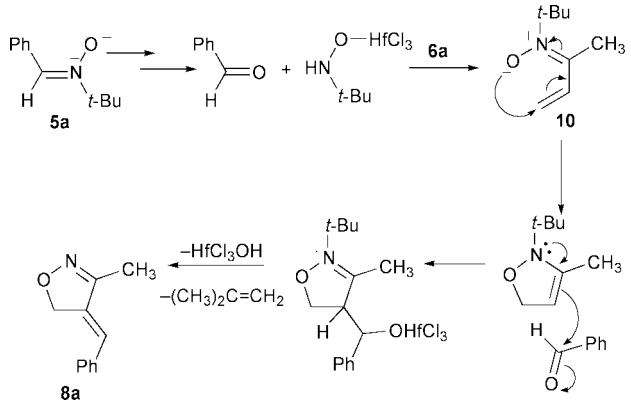

Scheme 4

In summary, we report a novel route to 4-methylene-4,5-dihydroisoxazoles from readily available starting materials.[7] The synthetic value of these systems, and conventional methods to generate them are the subject of a recent review by Zecchi *et al*.[8] Further studies of the mechanism and scope of the reaction are in progress.

We thank Pfizer Global Research & Development (UK), Leeds University and the EPSRC for support.

Notes and references

† *Crystal data*. $C_{11}H_{11}NO$, M = 173.21, orthorhombic, *Pcba*, a = 12.3331(2), b = 7.3853(2), c = 20.0230(9) Å, U = 1823.77(10) Å^3, Z = 8, Mo-Kα radiation, λ = 0.71073 Å, m = 0.081 mm^{-1}, T = 150(2) K, R_1 = 0.0449 for 1319 reflections with $I > 2\sigma(I)$, wR_2 = 0.1063 for all 1787 independent data. CCDC 168614. See http://www.rsc.org/suppdata/cc/b1/b105561p/ for crystallographic data in .cif or other format. Methods and programmes were standard from the SHELX suite.[9]

1 P. J. Dunn, A. B. Graham, R. Grigg and P. Higginson, *Chem. Commun*., 2000, 2035.
2 Typical experimental procedure: methyl vinyl ketone **6a** (0.75 mmol) was added to a solution of nitrone **5a** (0.5 mmol) and $HfCl_4$ (0.75 mmol) in dry THF (20 mL) under a nitrogen atmosphere and the resulting homogeneous solution stirred at reflux for 24 h. The reaction mixture was quenched by the addition of saturated $NaHCO_3$ solution and extracted with dichloromethane. The combined organic extracts were washed with water, dried ($MgSO_4$), filtered and the filtrate concentrated *in vacuo*. The residue was purified by flash chromatography, eluting with 1 : 1 v/v diethyl ether–pentane to afford the product **8a** as a colourless crystalline solid (0.065 g, 75%). Recrystallisation from dichloromethane–pentane afforded the product as colourless needles, mp 107.5–109 °C.
3 When the corresponding oxime of **6a** and benzaldehyde were heated under the reaction conditions ($HfCl_4$ (0.5 eq.), THF, reflux, 8 h) no traces of **8a** were detected and only unreacted material was recovered.
4 R. Grigg, P. Myers, A. Somasunderam and V. Sridharan, *Tetrahedron*, 1992, **48**, 9735.
5 R. Grigg, P. Kennewell, V. Savic and V. Sridharan, *Tetrahedron*, 1992, **48**, 10 423.
6 E. C. Taylor and I. J. Turchi, *Chem. Rev*., 1979, **79**, 181; R. Huisgen, *Angew. Chem., Int. Ed. Engl*., 1980, **19**, 947.
7 *N-tert*-Butylarylmethylideneanine *N*-oxides are readily prepared in high yields by treatment of the corresponding aldehyde with commercially available *N-tert*-butylhydroxylamine hydrochloride (1.5 eq.) and Na_2CO_3 (0.75 eq.) in 1 : 1 THF–H_2O solution and heating at 60 °C for 2 days.
8 G. Broggini, C. La Rosa and G. Zecchi, *Synlett*, 1995, **12**, 1208.
9 G. M. Sheldrick, SHELX97, University of Göttingen, Germany, 1997; G. M. Sheldrick, SHELXTL Manual, Bruker AXS Inc., Madison, WI, USA, 1994 and 1998.

CHEMCOMM Communication
www.rsc.org/chemcomm

Hollow spheres of MCM-41 aluminosilicate with pinholes†

Hong-Ping Lin,*[a] Chung-Yuan Mou,[b] Shang-Bin Liu[a] and Chih-Yuan Tang[c]

[a] *Institute of Atomic and Molecular Sciences Academia Sinica, PO Box 23-166, Taipei, Taiwan 106. E-mail: hplin@gcn.net.tw*
[b] *Department of Chemistry and Center of Condensed Matter, National Taiwan University, Taipei, Taiwan 106*
[c] *Department of Zoology, National Taiwan University, Taipei, Taiwan 106*

Received (in Cambridge, UK) 24th May 2001, Accepted 8th August 2001
First published as an Advance Article on the web 19th September 2001

Hollow spheres of MCM-41 mesoporous aluminosilicates, with two small holes on the shell, have been synthesized from a surfactant–aluminosilicate gel composite.

Hollow spherical ceramic materials of micron size have received a lot of recent attention due to their potential applications in drug-delivery, adsorption, and catalysis.[1–3] The standard approach for generating hollow spheres is to use organic polymer beads as the templates which control the size of the void volume.[4,5] However, large entities such as macromolecules usually cannot penetrate such spheres because of the microporous shell. It would be desirable to leave a macro-hole on the shell surface for transporting macromolecules. Furthermore, a mesoporous shell of the hollow sphere would allow simultaneous embedding of smaller molecules.

In this paper, we report a liquid crystalline/sol–gel approach to the synthesis of vesicular mesoporous aluminosilicates MCM-41. Both the diameters of the hollow spheres and the aluminium content of the materials can be controlled. The vesicular hollow spheres of MCM-41 were reasonably supposed to possess a pair of holes of submicron size on exactly opposite sides.

The hollow spheres of MCM-41 aluminosilicates were prepared according to our previously reported delayed neutralization procedure at 27 °C.[6,7] Typically, the surfactant myristyltrimethylammonium bromide, $CH_3(CH_2)_{13}N(CH_3)_3Br$, ($C_{14}$TMAB), as organic template, and butanol (BuOH), as cosurfactant, were dissolved in sufficient water to form a clear solution. Sodium silicate was added and mixed thoroughly. Then 1.2 M H_2SO_4 (aq) was gradually added to adjust the pH value of the gel solution to *ca*. 9.0. Finally, the gel solution was combined with the required amount of sodium aluminate ($NaAlO_2$). The molar ratios of the resulting gels were 1 C_{14}TMAB : 1.50 SiO_2 : 1.20 NaOH : 0.48 H_2SO_4 : (0.02–0.1) $NaAlO_3$: (1.25–1.85) BuOH : 200 H_2O. The vesicular sphere products were obtained by filtering the solution after hydrothermal treatment at 100 °C for 6 h. After washing with deionised water, drying and calcination at 580 °C in air, hollow spheres of MCM-41 mesoporous aluminosilicate were obtained.

In Fig. 1(A), we see that the aluminosilicate spheres were produced in high yield (~95%) and uniform size (5.0 μm). From some broken spheres (broken by the scraper during the SEM sample preparation process), one can easily distinguish that the micrometer-sized spheres are hollow (Fig. 1(B)). Without the use of sodium aluminate, we previously obtained hollow spheres with a center pillar inside.[7] TEM micrographs (not shown here) of microtomed samples also show the hollow insides of the spheres. Careful checking under higher magnification showed that the surface of every hollow sphere contains a tiny hole of *ca*. 0.1 μm in diameter (Fig. 1(C)). The existence of this tiny hole would allow the large internal void space of the sphere to be more accessible to larger entities such as viruses or macromolecules. An ultra-thin film microtome TEM micrograph of the shell of a hollow sphere is illustrated in Fig. 1(D). This enables the mesostructure of the shell to be examined and clearly shows the hexagonal-arrayed honeycomb mesostructures of MCM-41. This well-aligned structure is in agreement with its XRD pattern, which possesses 3–4 sharp peaks (see ESI†).[8,9]

To understand the direction of the nanochannels on the shell of the hollow sphere, we carefully observed the nanochannels near the tiny hole on the shell under a TEM. Fig. 2(A) clearly shows that the nanochannels of the hollow sphere of the MCM-41 mesoporous aluminosilicates are arranged concentrically around the hole. Taking the hole as the north pole of the sphere, the nanochannels are arranged in the latitudinal direction to form the shell. This is in agreement with our previous observation that nanochannels arrange latitudinally in pillar-within-spheres structures except that this time the center pillar is removed, leaving holes in the shell at the bases of the pillar. The

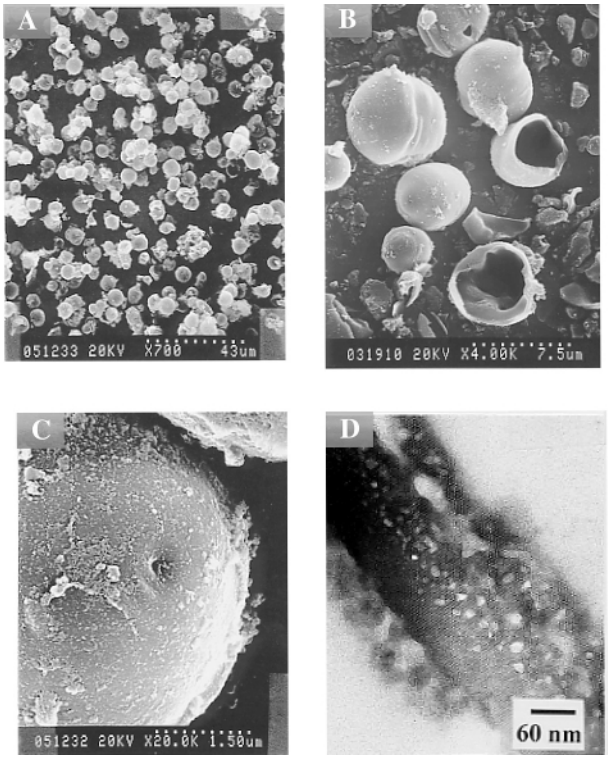

Fig. 1 SEM and TEM micrographs of the mesoporous aluminosilicate (Si/Al = 30) hollow spheres. (A) Low magnification SEM showing the uniform spheres with average diameter of 5 μm. (B) SEM of some broken hollow spheres of MCM-41 mesoporous aluminosilicates. (C) A tiny hole on the shell of the hollow sphere. (D) An ultra-thin section TEM picture displayings the well-ordered nanostructures of the vesicle-shaped aluminosilicate spheres.

† Electronic supplementary information (ESI) available: XRD pattern of a hollow sphere of MCM-41 (Si/Al = 30). See http://www.rsc.org/suppdata/cc/b1/b104600b/

 DOI: 10.1039/b104600b

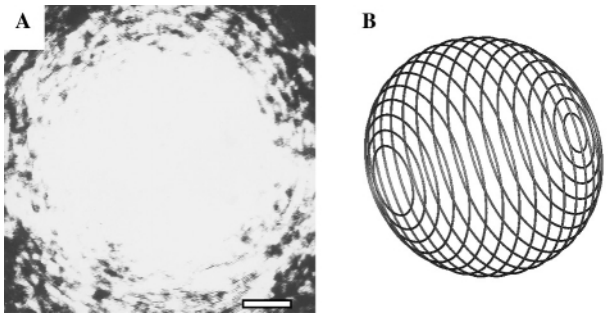

Fig. 2 (A) A HR-TEM micrograph showing nanochannels arranging around the tiny hole. The scale bar in this figure is 110 nm. (B) A schematic diagram of the vesicle-like sphere of aluminosilicates MCM-41.

fact that we can always see only a single hole on the shell leads us to the logical conjecture that every hollow sphere possesses two tiny holes on opposite sides. A schematic diagram of the hollow sphere is shown in Fig. 2(B). Although a direct microscopic observation of both polar holes on a hollow sphere was not obtained, the existence of the tiny holes at both poles can be reasonably explained. The singularity at the pole gives too high an energy penalty to form closed hollow spheres.[10,11] This hollow sphere with two tiny holes at both poles is a novel hierarchical structure that has not previously been identified. Compared with our previous pillar-within-sphere structure,[7] the aluminium component apparently makes the center pillar position of higher energy and the aluminosilicate materials are deposited around the waist to make a thicker shell.

In addition to making hollow spheres with an Si/Al ratio of 30, we can prepare samples with different aluminium contents by simply adding different amounts of sodium aluminate. In the range Si/Al = 15–70, hollow spheres of MCM-41 aluminosilicates with well-aligned mesostructures have been obtained. By examining the ^{27}Al MAS NMR spectra of the uncalcined hollow spheres, we found that only one peak at 54 ppm, referenced to a dilute aqueous solution of $Al(NO_3)_3$, was observed in each sample. This indicates that all the Al atoms are incorporated in the silica framework to form the hollow sphere.[12]

We can also control the size of the hollow spheres. In lyotropic surfactant liquid crystals, the rigidity of the surfactant assembly, such as the membrane, decreases with the amount of cosurfactant alkanol.[13,14] Accordingly, we changed the BuOH/C_{14}TMAB ratio in the reaction mixture. Fig. 3 demonstrates that the diameter of the hollow sphere decreases with an increase of the BuOH/C_{14}TMAB ratio, as we expected. However, the size range can be adjusted only in the range of 2.5 to 7.6 μm using the C_{14}TMAB–BuOH–aluminosilicate–water composition. Outside this range, the morphology will transform into fine particles or tubules-within-tubules structures.[15] We found that

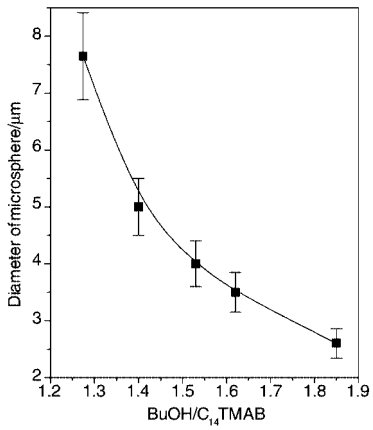

Fig. 3 The diameter of the hollow sphere of MCM-41 aluminosilicates as a function of the BuOH/C_{14}TMAB ratio.

Table 1 The physical properties of the hollow spheres of MCM-41 mesoporous aluminosilicates with different diameters and Si/Al ratio composites

Diameter/ μm	Si/Al	d_{100} value/nm	Pore size[a]/nm	BET surface area/ $m^2\ g^{-1}$	Porosity[b]/ $cm^3\ g^{-1}$
7.5	30	3.25	2.25	960	0.67
5.0	30	3.30	2.30	975	0.65
2.8	30	3.32	2.23	1002	0.62
5.0	60	3.42	2.28	996	0.70
5.0	15	3.25	2.20	952	0.63

[a] The central value of the pore size distribution calculated from the N_2 adsorption isotherm branch using the BJH method. [b] The N_2 adsorption value at $P/P_0 = 0.9$.

the tiny hole size ranges from *ca.* 0.05–0.1 μm and is not apparently dependent on sphere diameter.

Table 1 lists the physical properties of the hollow spheres with various diameters and Al contents. Comparing these data, the surface area, pore size and porosity are not significantly affected by the aluminium content or the diameter. For different Al contents and various sphere diameters, high yields of vesicular hollow spheres of MCM-41 materials with high surface area, uniform pore size and large porosity have been successfully synthesized using a simple self-organization approach.

The discovery of such an intricate hollow spherical topology with two tiny holes at the poles of the sphere will also be interesting to the physics of complex biomineralization processes. It will enrich our ability to build hierarchical complex inorganic–organic composite structures using the bottom-up approach.

This research was financially supported by the China Petroleum Co. and the National Science Council of Taiwan.

Notes and references

1 F. Carusco, *Chem. Eur. J.*, 2000, **6**, 413.
2 D. L. Wilcox, Sr., M. Berg, T. Bernat, D. Kelleman and J. K. Cochran, Jr., *Hollow and Solid Spheres and Microspheres: Science and Technology Associated with their Fabrication and Application*, MRS Proc., Pittsburgh, PA, 1994, vol. 372.
3 H. Huang, E. E. Remsen, T. Kowalewski and K. L. Wooley, *J. Am. Chem. Soc.*, 1999, **121**, 3805.
4 (*a*) Z. Zhong, Y. Yin, B. Gates and Y. Xia, *Adv. Mater.*, 2000, **12**, 206; (*b*) Y. Yin, Y. Lu, B. Gates and Y. Xia, *J. Am. Chem. Soc.*, 2001, **13**, 1146.
5 S. Mecking and R. Thomann, *Adv. Mater.*, 2000, **12**, 593.
6 (*a*) H. P. Lin and C. Y. Mou, *Science*, 1996, **273**, 765; (*b*) H. P. Lin, S. Cheng and C. Y. Mou, *Microporous Mater.*, 1997, **10**, 111.
7 H. P. Lin, Y. R. Cheng and C. Y. Mou, *Chem. Mater.*, 1998, **10**, 3772.
8 C. T. Kresge, M. E. Leonowicz, W. J. Roth, J. C. Vartuli and J. S. Beck, *Nature*, 1992, **359**, 710.
9 D. Zhao, P. Yang, Q. Huo, B. F. Chmelka and G. D. Stucky, *Curr. Opin. Solid State Mater. Sci.*, 1998, **3**, 111.
10 (*a*) P. T. Tanev and T. J. Pinnavaia, *Science*, 1996, **271**, 1267; (*b*) P. T. Tanev, Y. Liang and T. J. Pinnavaia, *J. Am. Chem. Soc.*, 1997, **119**, 861.
11 D. Demus, J. Goodby, G. W. Gray, H. W. Spiess and V. Vill, *Handbook of Liquid Crystals*, Wiley-VCH, Weinheim, New York, 1998, vol. 1.
12 (*a*) M. T. Janicke, C. C. Landry, S. C. Christiansen, S. Birtalan, G. D. Stucky and B. F. Chmelka, *Chem. Mater.*, 1999, **11**, 1342; (*b*) Z. Luan, C. F. Cheng, H. He and J. Klinowski, *J. Phys. Chem.*, 1995, **99**, 10 590.
13 H. P. Lin, Y. R. Cheng, S. B. Liu and C. Y. Mou, *J. Mater. Chem.*, 1999, **9**, 1197.
14 (*a*) H. Hoffmann, C. Thunig, U. Munkert, W. Meyer and W. Richer, *Langmuir*, 1992, **8**, 2629; (*b*) E. Valenzuuela, E. Abiun and E. Lissi, *J. Colloid Interface Sci.*, 1984, **102**, 46.
15 K. M. McGrath, D. M. Dabbs, N. Yao, I. A. Aksay and S. M. Gruner, *Science*, 1997, **277**, 552.

CHEMCOMM Communication
www.rsc.org/chemcomm

Banana-shaped mesogens: observation of a direct transition from the antiferroelectric B_2 to nematic phase†

R. Amaranatha Reddy, B. K. Sadashiva* and Surajit Dhara

Raman Research Institute, C.V. Raman Avenue, Bangalore 560 080, India. E-mail: sadashiv@rri.res.in

Received (in Cambridge, UK) 19th July 2001, Accepted 22nd August 2001
First published as an Advance Article on the web 19th September 2001

The synthesis and characterisation of the first banana-shaped mesogens which exhibit a direct transition from the antiferroelectric B_2 phase to the nematic phase are reported.

During the last couple of years there has been an upsurge in the synthesis and phase transition studies of compounds composed of banana-shaped or bent-core molecules because of the unusual and very interesting mesophases they exhibit. The detection of ferroelectricity in the mesophase of such an achiral compound by Niori *et al.*,[1] which was later determined to be antiferroelectric in the ground state[2–4] by current response measurements, have stimulated further research in this field. Several hundred compounds with a bent molecular shape have been synthesised so far and at least seven different banana (B) phases characterised.[5,6] It has been observed that in many homologous series of compounds only one banana phase exists in one homologue. However, smectic A, smectic C or nematic phases have been obtained either individually or in combination particularly for homologues with short terminal chains. Although the nematic phase has been observed in many series of bent-core molecules,[7–11] there is no example of a compound exhibiting a direct transition from the B_2 phase to nematic. Very recently there was a report of a case in which the B_2 phase and a nematic phase are observed in the same substance and the two are separated by smectic A and smectic C phases.[12] It would be very interesting and useful from an experimental point of view if one could get a direct transition from the antiferroelectric B_2 phase to the nematic phase. We have achieved this objective and report our results in this communication.

The synthesis and characterisation of four compounds composed of banana-shaped molecules, three of which represent the first examples which show a direct transition from the antiferroelectric B_2 to nematic (N) phase transition, is described here. The general method of preparation of the compounds is shown in Scheme 1. As reported[10] by us earlier, 2,7-dihydroxynaphthalene **1** was reacted with 2-fluoro-4-benzyloxybenzoic acid **2** to give the diester **3**. The protective benzyloxy groups were removed using 5% Pd–C as catalyst in an hydrogen atmosphere to yield the diphenol **4**. In the final step (iii) compound **4** was reacted with two equivalents of an appropriate (*E*)-4-*n*-alkoxy-α-methylcinnamic acid to furnish compound **5**.‡ All the compounds were purified by column chromatography (silica gel, 60–120 mesh) and were crystallised several times using suitable solvents.

The liquid-crystalline properties of the compounds were investigated by using optical polarising microscopy and differential scanning calorimetry (DSC). The transition temperatures together with the associated enthalpies are summarised in Table 1. On examination of the samples under a polarising microscope the following are observed. Compound **5**, n = 12, melts into a nematic phase and on cooling the isotropic (I) liquid shows typical schlieren texture. On further cooling, small broken-fan like texture emanates from the nematic phase and the field of view is completely filled with this texture. Fig. 1 shows a typical texture wherein the broken-fans are appearing from the nematic phase and this phase transition is enantiotropic. Compounds **5**, n = 13 and n = 14, are enantiotropic in both nematic and the lower temperature phase while compound **5**, n = 16, is also enantiotropic but without the nematic phase. The N→I transition enthalpy is about 0.4 kJ mol^{-1}. A DSC thermogram obtained for compound **5**, n = 13, is shown in Fig. 2 and all the transitions can be seen clearly.

In order to confirm the nature of the lower temperature phase of these compounds, X-ray investigations were carried out. The X-ray diffraction experiments were conducted using Cu-Kα radiation from a rotating anode generator with a flat graphite crystal monochromator. The diffraction patterns were collected on an image plate (Marresearch). The unoriented sample was contained in a Lindemann capillary and the temperature was controlled to within ±0.1 °C. The diffraction pattern of an unoriented sample of the mesophase of compound **5**, n = 14,

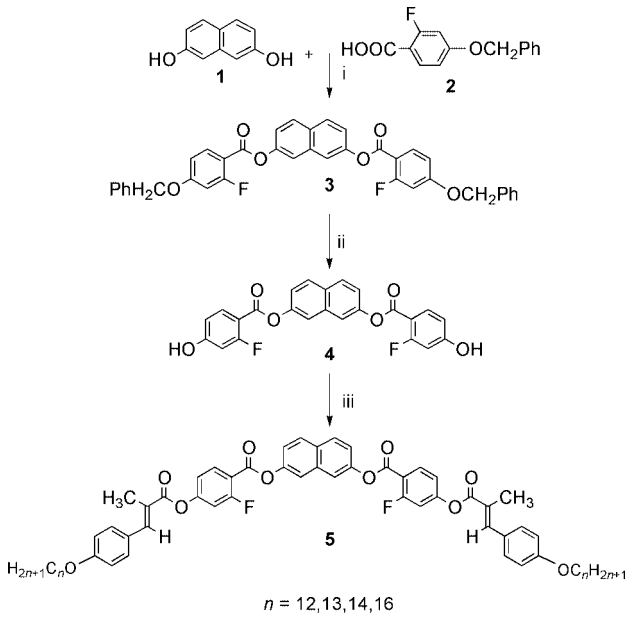

Scheme 1 *Reagents and conditions*: i DCC, cat. DMAP, dry $CHCl_3$, room temp., 12 h, 78%; ii cat. 5% Pd–C, H_2, 1,4-dioxane, 55 °C, 90%; iii (*E*)-4-*n*-alkoxy-α-methylcinnamic acid, DCC, cat. DMAP, dry $CHCl_3$, room temp., 15 h, 65–70%.

Table 1 Transition temperatures and the associated enthalpies (in italics) as determined by DSC

Compound	n	Phase transition temp/°C; enthalpy/kJ mol^{-1}		
5	12	Cr 119.5	[B_2 116.0]	N 127.0 I
		75.56	*13.23*	*0.49*
5	13	Cr 117.5	B_2 120.0	N 125.0 I
		59.28	*13.92*	*0.43*
5	14	Cr 107.0	B_2 123.0	N 124.0 I
		58.6	*14.15*	*0.34*
5	16	Cr 108.0	B_2 128.0 I	
		52.36	*16.84*	

† Electronic supplementary information (ESI) available: Fig. 1 in colour. See http://www.rsc.org/suppdata/cc/b1/b106458b/

 DOI: 10.1039/b106458b

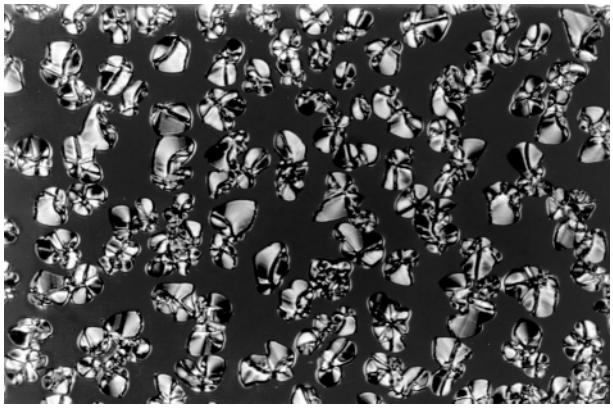

Fig. 1 Photo-micrograph of the B_2 phase appearing on cooling from a homogeneously aligned nematic phase, compound **5**, $n = 13$ (magnification $\times 300$).

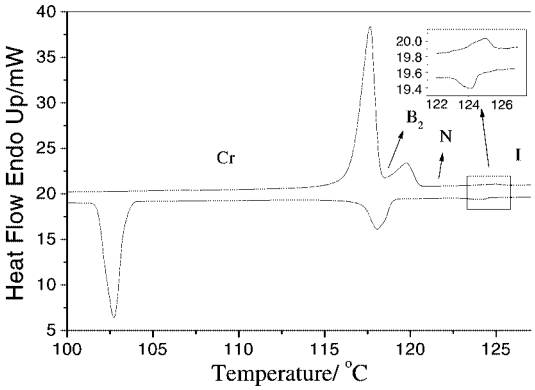

Fig. 2 Differential scanning calorimetric scan of compound **5**, $n = 13$ showing clearly the transition from the B_2 to the nematic phase. The insert shows the amplified N→I transition.

shows a diffuse peak in the wide angle region with $d = 4.6$ Å, indicating liquid-like in-plane order. In addition, three orders of lamellar reflections (in the ratio 1 : 2 : 3) in the small angle region could be clearly seen. From this as well as the textural characteristics we have identified this mesophase to be a B_2 phase.

Finally, the characteristic feature of the B_2 phase, namely the switching current response, was carried out on the mesophase of compound **5**, $n = 14$. An electro-optical switching cell was constructed using two ITO coated glass plates pre-treated with polyimide which enables the sample to align homogeneously. The cell thickness was adjusted to be 6 μm by using appropriate spacers. The sample was filled in the isotropic phase and cooled slowly. A very good alignment of the nematic phase was obtained. On further slow cooling under a low frequency AC triangular voltage, well formed domains of the B_2 phase over the entire field of view were seen. From the visual observations under the polarising microscope, we see colourful circular domains which switch above a threshold voltage. Simultaneously two very sharp current peaks could be seen on the oscilloscope screen for the half period of the triangular voltage (250 V_{pp}). A typical switching current response for this compound is shown in Fig. 3. The current was measured across a 10 kΩ resistance. The apparent 'saturated polarisation' P_s was obtained by measuring the area under the peaks and is about 560 nC cm^{-2}. These observations clearly indicate the antiferroelectric nature of this phase.

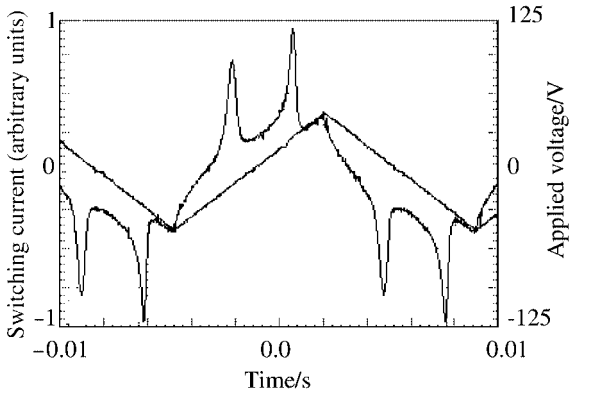

Fig. 3 Switching current response obtained in the B_2 phase of compound **5**, $n = 14$ at 120 °C by applying a triangular voltage (cell thickness: 6 μm, 250 V_{pp}, 29 Hz). (V_{pp} = volt peak-to-peak.)

The presence of this uniaxial nematic phase, as evidenced by numerous $s = \pm 1$ disclinations and fewer $s = \pm\frac{1}{2}$ defects above the B_2 phase helps to align the latter and may contribute to making the measurement of other physical properties of this interesting antiferroelectric phase rather easy.

The authors thank Dr V. A. Raghunathan for help with the X-ray measurements and Mrs K. N. Vasudha for technical support.

Notes and references

‡ The chemical structure of the compounds listed in Table 1 was determined from their spectral data. Typical data obtained for compound **5**, $n = 13$ is given below. γ_{max} (KBr) cm^{-1} 2910, 2850, 1740, 1720, 1605, 1508, 1415, 1250, 1190; δ_H (400 MHz, $CDCl_3$) 8.22 (t, *J* 8.72 Hz, 2H, Ar-H), 7.94 (d, *J* 8.92 Hz, 2H, Ar-H), 7.9 (s, 2H, Ar-CH=C), 7.72 (d, *J* 2.0 Hz, 2H, Ar-H), 7.47 (d, *J* 8.76 Hz, 4H, Ar-H), 7.39 (dd, *J* 2.08 Hz, 2H, Ar-H), 7.13–7.17 (m, 4H, Ar-H), 6.96 (d, *J* 8.68 Hz, 4H, Ar-H),4.01 (t, *J* 6.56 Hz, 4H, 2 × Ar-OCH_2), 2.27 (d, *J* 0.88 Hz, 6H, 2 × Ar-C=C(CH_3)), 1.81 (quin., *J* 6.68 Hz, 4H, 2 × Ar-OCH_2-CH_2), 1.26–1.48 (m, 12H, 6 × CH_2), 0.88 (t, *J* 6.64 Hz, 6H, 2 × CH_3); δ_C (400 MHz, $CDCl_3$) 166.3, 162.1, 161.5, 159.9, 156.4, 149.0, 141.7, 134.3, 133.3, 131.8, 129.7, 129.3, 127.6, 124.2, 121.1, 118.6, 117.8, 115.1, 114.6, 111.4, 111.2, 68.2, 31.9, 29.6, 29.5, 29.3, 29.1, 25.9, 22.6, 14.2, 14.0.

1 T. Niori, T. Sekine, J. Watanabe, T. Furukawa and H. Takezoe, *J. Mater. Chem.*, 1996, **6**, 1231.
2 D. R. Link, G. Natale, R. Shao, J. E. Maclennan, N. A. Korblova and D. M. Walba, *Science*, 1997, **278**, 1924.
3 W. Weissflog, Ch. Lischka, I. Benne, T. Scharf, G. Pelzl, S. Diele and H. Kruth, *Proc. SPIE-Int. Soc. Opt. Eng.*, 1998, **14**, 3319.
4 A. Jakli, S. Rauch, D. Lotzsch and G. Heppke, *Phys. Rev. E: Stat. Phys., Plasmas, Fluids, Relat. Interdiscip. Top.*, 1998, **57**, 6737.
5 G. Pelzl, S. Diele and W. Weissflog, *Adv. Mater.*, 1999, **11**, 707.
6 J. P. Bedel, J. C. Rouillon, J. P. Marcerou, M. Laguerre, H. T. Nguyen and M. F. Achard, *Liq. Cryst.*, 2000, **27**, 1411.
7 D. Shen, S. Diele, G. Pelzl, I. Wirth and C. Tschierske, *J. Mater. Chem.*, 1999, **9**, 661.
8 H. T. Nguyen, J. C. Rouillon, J. P. Marcerou, J. P. Bedel, P. Barois and S. Sarmento, *Mol. Cryst. Liq. Cryst.*, 1999, **328**, 177.
9 J. Matraszek, J. Mieczkowski, J. Szydlowska and E. Gorecka, *Liq. Cryst.*, 2000, **27**, 429.
10 R. Amaranatha Reddy and B. K. Sadashiva, *Liq. Cryst.*, 2000, **27**, 1613.
11 R. Amaranatha Reddy and B. K. Sadashiva, (unpublished results).
12 I. Wirth, S. Diele, A. Eremin, G. Pelzl, S. Grande, L. Kovalenko, N. Pancenko and W. Weissflog, *J. Mater. Chem.*, 2001, **11**, 1642.

CHEMCOMM
Communication
www.rsc.org/chemcomm

Asymmetric synthesis of 2-azido-1-arylethanols from azido aryl ketone–β-cyclodextrin complexes and sodium borohydride in water†

M. Arjun Reddy, N. Bhanumathi and K. Rama Rao*

Organic Chemistry Division-I, Indian Institute of Chemical Technology, Hyderabad-500 007, India. E-mail: ramaraok@iict.ap.nic.in

Received (in Cambridge, UK) 25th July 2001, Accepted 21st August 2001
First published as an Advance Article on the web 10th September 2001

β-Cyclodextrin catalyses for the first time the asymmetric reduction of α-azido aryl ketones to corresponding alcohols of great significance using sodium borohydride in water. The azido group appeared to be the best fit among various groups studied. This asymmetric reduction using water as solvent overcomes many of the drawbacks in the existing methodologies.

Chiral vicinal azidohydrins are of great significance in asymmetric catalysis,[1] chemistry of carbocyclic nucleosides[2,3] and also as precursors for a wide range of pharmaceuticals such as β-blockers and agonists in the treatment of cardiovascular disease, cardiac failure, asthma and glaucoma.[4] However, synthetic methodologies reported until recently consist mainly of either asymmetric ring opening of oxiranes in the presence of chiral organometallic complexes[5] or reduction of prochiral ketones catalysed by oxazaborolidines in presence of $BH_3{\cdot}SMe_2$ *etc*.[6] involving the use of anhydrous organic solvents, moisture sensitive catalysts, expensive and toxic reagents. In view of these limitations, there is still a need for a mild, simple and widely applicable alternative approach to these highly valuable compounds. The best choice would be through supramolecular catalysis involving water as solvent, which is environmentally benign, however, this still remained as a goal.

Though the reduction of some substituted aryl alkyl ketones using sodium borohydride in the presence of cyclodextrin have been reported earlier, the results are not encouraging (optical yields up to 36% ee).[7] However, no attempts have been made so far to involve α-azido aryl ketones in supramolecular catalysis to get the versatile azidoalcohols. In our efforts to develop biomimetic approaches for chemical reactions including asymmetric catalysis using cyclodextrins(CDs),[8] we report herein the first biomimetic approach for the asymmetric synthesis of α-azidoalcohols **2** by reduction of the corresponding ketones **1** as their β-cyclodextrin complexes in water using sodium borohydride (Scheme 1).

Cyclodextrins, which are cyclic oligosaccharides, catalyse reactions by supramolecular catalysis through non-covalent bonding by formation of reversible host–guest complexes as seen in enzymes. Cyclodextrins' chirality can also induce asymmetric reactions but the utility of CDs in asymmetric synthesis is still limited.[8a,e,f, 9,11]

In CD catalysed asymmetric reactions, the following criteria are required to be met for chiral induction: a phenyl ring in the substrate to form the CD inclusion complex and a functional group to interact with CD hydroxy groups to attain rigidity for chiral recognition. Since α-azido aryl ketones **1** conform to these criteria, they have been chosen as substrates for chiral asymmetric reduction. The complexes were formed with β-cyclodextrin since it is the most inexpensive and easily accessible of the cyclodextrins.

The reductions were carried out as follows: β-CD (1 mmol) was dissolved in water (15 ml) and heated up to 60 °C until a clear solution was formed. Then α-azido aryl ketone **1** (1 mmol) dissolved in acetone (1 ml) was added dropwise and allowed to come to room temperature. Later, the reaction mixture was cooled in an ice bath and sodium borohydride (5 mmol) was added slowly, brought to room temperature and stirred for 24 h. It was then quenched with hydrochloric acid (2 M, 10 ml), extracted with ethyl acetate, dried and concentrated under reduced pressure. The crude product was purified by column chromatography on silica gel. The yields obtained were good, ranging from 90–96% and the enantioselectivities observed were also impressive in some cases showing up to 81% ee (Table 1). The ratio of β-CD to the substrate **1** appeared to be

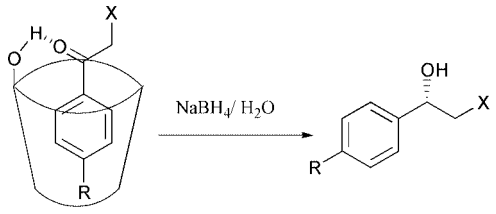

1 **2**

2a R = H, X = N_3 **2i** R = O^{i}Pr, X = N_3
2b R = Cl, X = N_3 **2j** 2-Azido-1-napthylethanol
2c R = Br, X = N_3 **2k** R = H, X = H
2d R = NO_2, X = N_3 **2l** R = CH_3, X = OH
2e R = Me, X = N_3 **2m** R = O^{i}Pr, X = OH
2f R = OH, X = N_3 **2n** R = NO_2, X = OH
2g R = OMe, X = N_3 **2o** R = CH_3, X = OTBDMS
2h R = OEt, X = N_3 **2p** R = O^{i}Pr, X = OTBDMS
2q R = NO_2, X = OTBDMS

Scheme 1

Table 1 Asymmetric synthesis of 2-azido-1-arylethanols

Entry	Product	Ee(%)[a]	Yield (%)[b,c]
1	**2a**	52	92
2	**2b**	10	94
3	**2c**	12	90
4	**2d**	4	89
5	**2e**	80	95
6	**2f**	73	94
7	**2g**	66	96
8	**2h**	53	94
9	**2i**	81	95
10	**2j**	0	90
11	**2k**	15	92
12	**2l**	7	90
13	**2m**	8	89
14	**2n**	0	95
15	**2o**	40	84
16	**2p**	61	80
17	**2q**	11	88

[a] Determined by HPLC analysis with the chiral column 'Diacel Chiralcel OD' (0.46 cm ∅ × 25 cm) using hexane–propan-2-ol (85 : 15) as eluent at a flow rate of 0.5 ml min^{-1} using UV detection (254 nm). [b] Isolated yields. [c] All products were characterised by mass, ^1H, ^{13}C NMR, IR spectroscopy and elemental analysis.

† IICT Communication No. 4769.

 DOI: 10.1039/b106736m

Table 2 Effect of concentration of β-CD on enantioselectivity as shown by **2e**

Entry	Ratio (β-CD–**1**e)	Ee(%)
1	1.5 : 1	80
2	1 : 1	80
3	0.75 : 1	37
4	0.50 : 1	14
5	0.25 : 1	0

optimum at 1 : 1 since a lower ratio of β-CD led to a decrease in ee whereas a higher ratio has not shown any improvement in enantioselectivity (Table 2). The enantiomeric excesses (ee) of the products were determined by chiral HPLC analysis. These compounds have been shown to have *S* configuration by comparison of the sign of rotation with those of the known compounds.[6] An interesting feature of this reaction is that the substrates having electron donating substituents on the aromatic ring have shown higher enantioselectivity compared with the electron withdrawing substituents (Table 1). This may be ascribed to additional stabilization of the transition state of carbonyl–borohydride complex by electron donating substituents which can result in better enantioselectivity. However, this will be complimentary to other factors.

Among the compounds studied, compound **2i** with an isopropoxy group has shown the highest enantioselectivity (81% ee) followed by **2e** (80% ee), **2f** (73% ee), **2g** (66% ee), **2h** (53% ee) and **2a** (52% ee) whereas lower enantioselectivities were observed with the rest of the compounds (0–12% ee). To study the effect of substitution on enantioselectivity, the azido group was replaced by H, OH and OTBDMS with increasing bulkiness. Though increase in bulkiness in this series (**2k–q**) has led to enhancement in enantioselectivity (Table 1) with **2p** showing a maximum of 61% ee, the ketones with azide group (**2a–j**) appeared to fit best in the CD cavity for reduction with sodium borohydride giving an ee up to 81% (Table 1).

The inclusion complex formation was observed from ^{1}H NMR spectra[10] and powder X-ray spectra[11] of the solid CD complexes. Hydrogen bonding of substrates with CD hydroxy groups was seen from IR by a shift of the C=O stretch to lower frequency in CD complexes (in the range of 2–53 cm^{-1}) compared with the uncomplexed substrates. Stronger shifts were observed for the substrate–CD complexes which yielded products with higher ee. Thus, the CD induced asymmetric reductions by supramolecular catalysis may involve various factors such as hydrophobic binding, carbonyl exposure to the CD rim of secondary hydroxy groups, a decrease in the degrees of freedom of the guest molecule possibly through hydrogen bonding, favorable control of geometry in the approach of the substrate to the 'active site' *etc*. A balance of these interactions determines the enantioface selectivity.

These CD mediated water solvent reactions are very useful both from economical and environmental points of view and also for the practical convenience of not having to handle flammable anhydrous organic solvents or toxic and expensive reagents. β-Cyclodextrin, apart from being non-toxic, is also considered as metabolically safe.[12] Thus, the present methodology for the synthesis of chiral 2-azido-1-arylethanols of great significance in asymmetric synthesis and medicinal chemistry involving water as solvent may be considered as simple from the practical point of view with great potential for future applications.

MAR thanks CSIR, New Delhi, India for the award of a fellowship.

Notes and references

1 K. I. Sutawardoyo, M. Emziane, P. Lhoste and D. Sinou, *Tetrahedron*, 1991, **47**, 1437; M. Chini, P. Crotti and F. Macchia, *Tetrahedron Lett*., 1990, **31**, 5641.
2 *The Chemistry of the Azido Group*, ed. S. Patai, Wiley, New York, 1971
3 E. F. V. Scriven and K. Turnbull, *Chem. Rev*., 1988, **88**, 297.
4 E. J. Corey and J. O. Link, *J. Org. Chem*., 1991, **56**, 442.
5 M. Meguro, N. Asao and Y. Yamamoto, *J. Chem. Soc., Chem. Commun*., 1995, 1021; L. E. Martinez, J. L. Leighton, D. H. Carsten and E. N. Jacobsen, *J. Am. Chem. Soc*., 1995, **117**, 5897; H. Lebel and E. N. Jacobsen, *Tetrahedron Lett*., 1999, **40**, 1703.
6 E. J. Corey and C. J. Helal, *Angew. Chem., Int. Ed*., 1998, **37**, 1986; J. S. Yadav, P. T. Reddy and S. Riaz Hashim, *Synlett*, 2000, 1049; B. T. Cho and Y. S. Chun, *J. Org. Chem*., 1998, **63**, 5280.
7 N. Baba, Y. Matsumura and T. Sugimoto, *Tetrahedron Lett*., 1978, **44**, 4281; R. Fornasier, F. Reniero, P. Scrimin and U. Tonellato, *J. Org. Chem*., 1985, **50**, 3209.
8 (*a*) L. R. Reddy, N. Bhanumathi and K. R. Rao, *Chem. Commun*., 2000, 2321; (*b*) L. R. Reddy, M. A. Reddy, N. Bhanumathi and K. R. Rao, *Synlett*, 2000, 339; (*c*) M. A. Reddy, L. R. Reddy, N. B. Hanumathi and K. R. Rao, *New J. Chem*., 2001, **25**, 359; (*d*) M. A. Reddy, L. R. Reddy, N. Bhanumathi and K. R. Rao, *Chem. Lett*., 2001, 246; (*e*) K. R. Rao and H. M. S. Kumar, *Synth. Commun*., 1993, **23**, 1877; (*f*) K. R. Rao and P. B. Sattur, *J. Chem. Soc., Chem. Commun*., 1989, 342.
9 A. W. Czarnik, *J. Org. Chem*., 1984, **49**, 924; V. T. Dsouza and K. B. Lipkowitz, *Chem. Rev*., 1998, **98**, 1741.
10 P. V. Demarco and A. L. Thakkar, *Chem. Commun*., 1970, 2.
11 J. Szejtli and T. Osa, *Comprehensive Supramolecular Chemistry*, Pergamon, UK, 1996, vol. 3, p. 253
12 K. Uekama, F. Hirayama and T. Irie, *Chem. Rev*., 1998, **98**, 2045.

CHEMCOMM Communication
www.rsc.org/chemcomm

Acenaphthenic hopanoids, a novel series of aromatised triterpenoids occurring in crude oil

Teresita Carrillo-Hernández, Philippe Schaeffer and Pierre Albrecht*

Laboratoire de Géochimie Organique, Faculté de Chimie, Université Louis Pasteur, 1 rue Blaise Pascal 67 000. Strasbourg, France. E-mail: albrecht@chimie.u-strasbg.fr; Fax: +33-3 90241764; Tel: +33-3 9024 1696

Received (in Cambridge, UK) 13th June 2001, Accepted 30th August 2001
First published as an Advance Article on the web 10th September 2001

A series of diaromatic 8,14-secohopanoids of microbial origin has been characterized in a petroleum by NMR studies, disclosing novel geochemical transformations.

In the course of our studies dealing with the geochemical characterization of Mexican crude oils, coupled gas chromatography–mass spectrometry (GC-MS) investigation of the 'triaromatic' hydrocarbon fraction separated by thin layer chromatography (SiO_2, hexane as developer) from Lacantún petroleum† revealed the presence of a homologous series of 5 compounds **1a–e** with unknown mass spectra.‡ The lowest homologue **1a** is characterized by a molecular ion at 402 ($C_{30}H_{42}$) and a base peak at *m/z* 195 ($C_{15}H_{15}^+$) which could correspond to an alkylated acenaphthene moiety. In the mass spectra of the higher homologues, the major fragment and the molecular ion are shifted upwards by $n \times 14$ mass units (n = 1–4), indicating that this series extends up to the C_{34} homologue (M_w 458). These mass spectral features, together with the fact that the homologous series ranges from C_{30} to C_{34}, suggest that these new compounds may be related to 8,14-secohopanoids bearing an acenaphthene moiety.[1]

To unambiguously establish the structure of these novel aromatic hydrocarbons, isolation of the predominant C_{30} (**1a**, R = H) and C_{31} (**1b**, R = CH_3) homologues was carried out.§

Following HPLC purification, the structure of compound **1a** was determined by exhaustive 1D and 2D NMR studies including ^1H–^1H COSY, NOESY, direct (HMQC) and long-range (HMBC) ^1H–^{13}C correlation experiments (Table 1). The ^1H spectrum shows the presence of 3 aromatic protons (2 doublets at 7.16 and 7.36 ppm and 1 singlet at 7.32 ppm), 2 benzylic methyl groups (singlets at 2.36 and 2.49 ppm), 3 methyls on quaternary carbons and 1 methyl on a tertiary carbon (doublet at 1.08 ppm). The major part of the carbon framework, including notably the dimethylated acenaphthene moiety was unambiguously established from the ^1H–^{13}C long-range ($^{2,3}J$) connectivities (Fig.1).

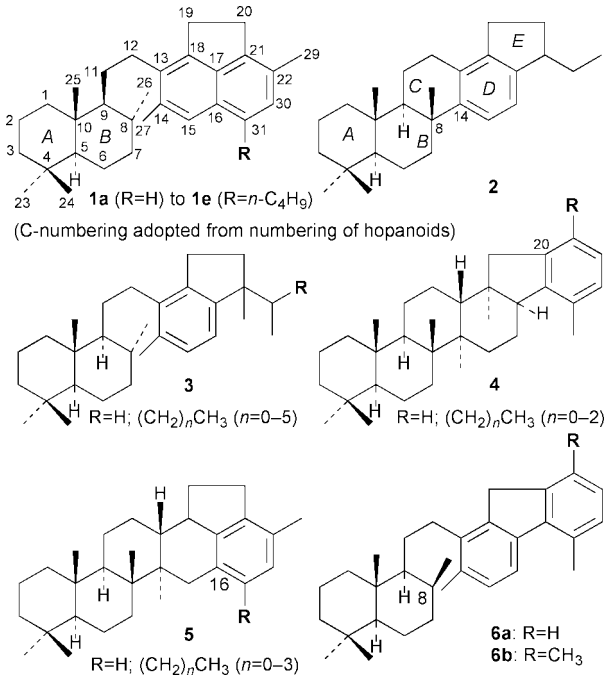

The connection between the bicyclic aliphatic and the aromatic moieties was determined by the presence of a coupling between H-9 and CH_2-11 in the COSY experiment.

Stereochemical information, notably concerning the *trans* junction of rings *A* and *B*, could be obtained from the NOESY experiment (Fig. 1) and is also confirmed by the chemical shifts of the protons and carbon resonances. For example, the shielded ^{13}C signal and deshielded ^1H signal for H-5 is in agreement with an axial orientation. Similarly, the high-field ^{13}C signal ($\delta < 20$ ppm) of CH_3-25 indicates that this methyl at the ring junction is

Table 1 ^1H (500.1 MHz) and ^{13}C (125.8 MHz) NMR data for compound **1a** (Bruker ARX 500; in CD_2Cl_2; δ in ppm relative to $SiMe_4$)

C-atom	$\delta^{13}C$	δ^1H		C-atom	$\delta^{13}C$	δ^1H
1	39.35	1.08 (ax)	1.93 (eq)	16	128.76	
2	19.22	1.47 (eq)	1.62 (ax)	17	138.54	
3	42.58	1.20 (ax)	1.42 (eq)	18	143.23	
4	33.60			19	29.83	3.34
5	55.63	0.92		20	30.09	3.28
6	22.27	1.31 (ax)	1.60 (eq)	21	143.02	
7	37.47	1.06 (ax)	1.77 (eq)	22	127.85	
8	34.85	1.42		23	33.62	0.87 (s)
9	59.36	0.65		24	21.57	0.82 (s)
10	38.98			25	14.38	0.77 (s)
11	29.33	1.21	1.59	26	21.93	1.08 (d, *J* 6.4 Hz)
12	33.94	2.62	2.78	27	20.69	2.49 (s)
13	134.44			29	18.47	2.36 (s)
14	136.09			30	129.57	7.16 (d, *J* 8.2 Hz)
15	123.11	7.32 (s)		31	121.71	7.36 (d, *J* 8.2 Hz)

 DOI: 10.1039/b105198a

axial (presence of γ-*gauche* effects). The equatorial position of CH_3-26 could be established due to the presence of nuclear Overhauser effects between H-8 and CH_3-25, and H-9 and CH_3-26 (Fig. 1).

The ^{1}H NMR spectrum of compound **1b** is almost identical to that of compound **1a**, except for the presence of 1 additional benzylic methyl group superimposed for CH_3-27 at 2.52 ppm and the presence of only 2 aromatic protons. Both protons are uncoupled and resonate at 7.00 (H-30) and 7.39 ppm (H-15), indicating that the methyl group is located at C-31, as expected for a homohopanoid structure.[1]

Aromatisation processes of polycyclic terpenoids are widespread in the sub-surface. Such transformations may be induced by microorganisms at the earliest stages of diagenesis, as demonstrated in the case of higher plant pentacyclic triterpenoids.[2] Alternatively, aromatisation may occur at subsequent stages of dia- and catagenesis *via* abiotic processes, notably driven by thermal stress. Among sedimentary hopanoids, which are molecular fossils of bacteria ubiquitous in geological samples,[1] several aromatic hydrocarbons have been identified. Thus, the presence of functionalities (*e.g.*, double bonds) in intermediates like hop-17(21)-enes or neohop-13(18)-enes may initially trigger aromatisation in ring *D* (*e.g.*, compound **2**) and progress from ring *D* to ring *A*.[3] Aromatisation of ring *D* may also occur in connection with cleavage of the weak C-8(14) bond, yielding monoaromatic 8,14-secohopanes **3**.[4] Aromatisation of hopanoids may also operate at relatively early stages of diagenesis under a different mechanism which involves cyclisation of the hopanoid side-chain at position 20 or 16, leading to the formation of benzohopanes **4** and **5**, respectively.[4,5]

Recently, the aromatic 8,14-secohopanoid **6a** bearing a fluorene moiety has been isolated from the solvent extract of an immature sediment from the Jurassic Kimmeridge Clay Formation and has been characterized by NMR studies.[6] The presence of this compound, which is formed by cleavage of the C-8(14) bond, followed by aromatisation of ring *D* and by cyclization–aromatisation of the hopanoid side chain at C-20, indicates that both aromatisation processes may be operative on the same molecule upon diagenesis or early maturation. In the crude oil from Lacantún, ring *D* monoaromatic 8,14-secohopanoids, **3**, and benzohopanes cyclized at C-20, **4**, occur in relatively high amounts, whereas benzohopanes cyclized at C-16, **5**, are completely absent. Surprisingly, no fluorene hopanoid derivatives such as **6** could be detected, whereas those corresponding to the novel series **1** represent the predominant polyaromatic polycyclic hydrocarbons. It can be proposed that given the relative high maturity reached by Lacantún crude oil, the benzohopanes **5** originally present have been converted into more stable C_{30}–C_{34} hopanoid derivatives belonging to series **1**. This process involves cleavage of the C-8(14) bond and formation of a fused aromatic ring by hydrogen transfer reactions well established to occur in the sub-surface.[7] In contrast, it is likely that compounds **6a**,**b** are not formed by a maturity-driven process, but rather originate from a specific intermediate or precursor.[6] Indeed, these compounds have been characterised in quite immature samples and possess an axial methyl group at C-8, unlike compound **1a** which bears an equatorial methyl at C-8. Furthermore, the C_{32} homologue **6b**, present in trace amounts, represents the highest homologue of this hopanoid fluorene series detected thus far in sediments, whereas benzohopanes **4** usually occur as a series of four homologues (*i.e.*, C_{32}–C_{35}).[4–6] These features seem therefore to indicate that despite some structural similarities, aromatised hopanoids **1** and **6** are formed at different stages of maturity by distinct processes.

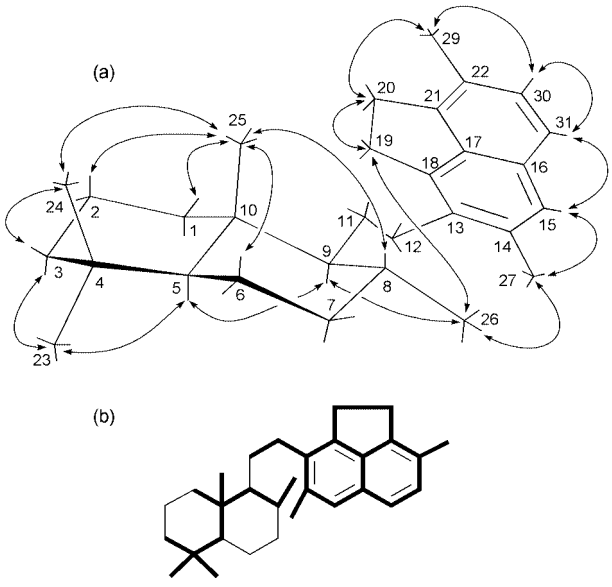

Fig. 1 (a) Spatial representation of **1a** showing the main NOEs observed. (b) In bold: carbon sequence established from the inverse long range ^{1}H–^{13}C (HMBC) correlation experiment.

We thank Drs M. A. Guzmán Vega and J. Connan for providing the crude oil samples from Lacantún, Drs P. Adam and J. M. Trendel for helpful discussions and E. Mastio and Dr R. Graff for their assistance in MS and NMR measurements, respectively. The Instituto Mexicano del Petroleo is acknowledged for financial support (T. C.-H.).

Notes and references

† The crude oil from Lacantún (Southern Chiapas Basin, Mexico) has been generated from Lower Cretaceous source rocks deposited in evaporitic, sabkha-type environments.

‡ *MS data* [Finnigan Mat TSQ 700, EI ,70eV, *m/z* (Rel. Int.)] for **1a**: 402 (M^+, 78%), 209(3), 196(18), 195(100), 180(11), 165(14), 123(3), 69(3); **1b**: 416 (M^+, 100%), 209(98), 194(12), 179(17); **1c**: 430 (M^+, 100%), 415(3), 223(80), 208(8), 193(10), 179(8); **1d**: 444 (M^+, 100%), 415(10), 237(65), 208(12), 193(10); **1e**: 458 (M^+, 100%), 415(11), 251(60), 225(8), 193(8).

§ *Ca.* 30 g of crude oil from Lacantún adsorbed on silica gel, were fractionated by silica gel liquid chromatography with hexane as mobile phase into aromatic hydrocarbon sub-fractions further analysed by GC-MS to detect the fractions containing the novel aromatic hopanoids. Following purification of the latter (260 mg) using reversed phase HPLC (semi-preparative Du Pont 250 × 9.4 mm, Zorbax ODS, 8 μm, 80 Å; CH_3OH–CH_2Cl_2 85 : 15 v/v, 5 ml min^{-1} and then analytical Vydac 250 × 4.6 mm, 201TP, 5 μm, 300 Å; CH_3OH–CH_2Cl_2 85 : 15 v/v, 1 ml min^{-1}), *ca.* 800 μg of **1a** and 1 mg of **1b** were recovered with over 90% purity as determined by GC.

1 G. Ourisson and P. Albrecht, *Acc. Chem. Res.*, 1992, **25**, 398; K. E. Peters and J. M. Moldowan, *The Biomarker Guide*, Prentice Hall, Englewood Cliffs, NJ, USA, 1993

2 F. Lohmann, J. M. Trendel, C. Hetru and P. Albrecht, *J. Labelled Compd. Radiopharm.*, 1990, **28**, 377.

3 A. C. Greiner, C. Spyckerelle and P. Albrecht, *Tetrahedron Lett.*, 1976, **32**, 257.

4 G. Hussler, J. Connan and P. Albrecht, *Org. Geochem.*, 1984, **6**, 39.

5 G. Hussler, P. Albrecht, G. Ourisson, M. Cesario, J. Guilhem and C. Pascard, *Tetrahedron Lett.*, 1984, **25**, 1179; P. Schaeffer, P. Adam, J. M Trendel, P. Albrecht and J. Connan, *Org. Geochem.*, 1995, **23**, 87.

6 J. S. Sinninghe Damsté, S. Schouten, N. H. van Vliet and J. A. J. Geenevasen, *Tetrahedron Lett.*, 1998, **39**, 3021.

7 B. P. Tissot and D. H. Welte, *Petroleum Formation and Occurrence*, 2nd revised and enlarged edition, Springer-Verlag, Berlin, 1984

CHEMCOMM Communication
www.rsc.org/chemcomm

Adsorption and separation of amino acids from aqueous solutions on zeolites

Sven Munsch, Martin Hartmann and Stefan Ernst*

Department of Chemistry, Chemical Technology, University of Kaiserslautern, PO Box 3049, D-67653 Kaiserslautern, Germany. E-mail: sernst@rhrk.uni-kl.de; Fax: +49(0)631-205-4193; Tel: +49(0)631-205-3587

Received (in Cambridge, UK) 18th June 2001, Accepted 21st August 2001
First published as an Advance Article on the web 10th September 2001

The adsorption of various amino acids on zeolites with different structures was studied with regard to dependence of the pH value of the solution and the aluminum content of the zeolite in order to design tailor-made adsorbents for amino acid separations.

Amino acids are used on a large scale as supplements to stock feed and to improve the quality of proteins in food technology. There are several routes for the production of amino acids, *e.g.*, their extraction from natural primary products (*e.g.* feathers), chemical or enzymatic synthesis and microbiological fermentation. All of these methods require the use of separation techniques in order to recover and purify amino acids with similar chemical properties. Beside several chromatographic techniques,[1] organic ion exchange resins are usually used for the recovery of the desired amino acid.[2] A process for the separation of amino acids from aqueous fermentation broths by bringing these solutions into contact with zeolites was claimed recently.[3] Moreover, several zeolites were tested in the separation of leucine and isoleucine from aqueous solutions,[4] but the fundamentals of the decisive interactions between the amino acids and the zeolite framework are still unknown.

To learn more about these interactions, the adsorption of various amino acids has been studied on different zeolites. For this purpose, zeolites ZSM-22, ZSM-5, ZSM-11, MCM-58, Beta and dealuminated Y were synthesized as described in the open literature, calcined at 813 K, subsequently repeatedly ion-exchanged in NH_4NO_3 solution and finally calcined at 723 K to obtain the protonated forms. Characterization of the adsorbents prior to and after the adsorption process was performed by chemical analysis, powder X-ray diffraction and nitrogen sorption at 77 K. The adsorption experiments were conducted in the liquid phase using the batch method at 298 K. In a typical experiment, 0.3 g of the activated zeolite was brought into contact with 5 g of an aqueous solution of the amino acid or a mixture of amino acids. Adsorption equilibrium was reached within 24 h under continuous stirring. The concentrations of the amino acids at the onset of the experiments and after equilibrium were determined by high performance liquid chromatography (HPLC). The extent of adsorption from the liquid-phase is quantified by the specific reduced surface excess $n_{aa}\sigma(n)/m = n^0(x^0_{aa} - x_{aa})/m$, where n^0 is the total number of moles in the original solution and $(x^0_{aa} - x_{aa})$ the change in the molar fraction of the amino acid (aa) in solution due to adsorption on the adsorbent of mass m.[5] The adsorption isotherms were either recorded using solutions buffered at pH 6 or at varying solution pH adjusted by the addition of aqueous HCl or NaOH.

X-Ray powder patterns (not shown), recorded before and after the adsorption of amino acids show no changes, indicating that the zeolite structure remains unaffected during the course of adsorption. Pertinent nitrogen sorption data for zeolite samples before and after the adsorption of phenylalanine reveal that the micropore volume of, *e.g.*, zeolite Beta decreases from 0.28 to 0.09 $cm^3\ g^{-1}$ and for ZSM-5 from 0.17 to 0.08 $cm^3\ g^{-1}$. The significant reduction of the pore volumes due to the adsorption of phenylalanine on the zeolites indicates that the amino acid molecules are located inside the pores.

α-Amino acids are amphoteric compounds, consisting of an amino group, a carboxyl group, a hydrogen atom, and a distinctive side chain R which are bonded to one carbon atom. The ionization state of an amino acid varies with the pH value (*cf.* Scheme 1). Acidic amino acids, such as glutamic acid, additionally contain a second carboxy group in the side chain, and, hence, have a lower isoelectric point pI compared to amino acids with neutral side chains, like phenylalanine. Basic amino acids, such as lysine, contain a second amino group in the side chain, leading to a higher isoelectric point. The influence of the solution pH value on the uptake of an amino acid with an acidic (glutamic acid, pI = 3.24), a neutral (phenylalanine, pI = 5.48) and a basic side chain (lysine, pI = 9.82) on zeolite Beta (n_{Si}/n_{Al} = 25) is depicted in Fig. 1. Glutamic acid is exclusively adsorbed under acidic conditions and the amount adsorbed diminishes for solution pH values exceeding pI = 3.24. This behavior can be explained by electrostatic interactions between the positively charged amino group and the negatively charged lattice of the zeolite. Phenylalanine shows a similar behavior, but the decrease in uptake starts at higher pH since the isoelectric point of phenylalanine is higher (pI = 5.48). Although lysine is positively charged over the whole investigated pH range, its adsorption is particularly favored under strongly basic conditions. Apparently, the additional positively charged ammonium group in the side chain for lower pH results in a reduced uptake of lysine. In order to examine the influence of the nature of the side chain on the adsorption in detail, the adsorption of four amino acids containing different neutral side chains was studied on zeolites Beta and ZSM-5. The hydrophobic properties of these amino acids increase with the number

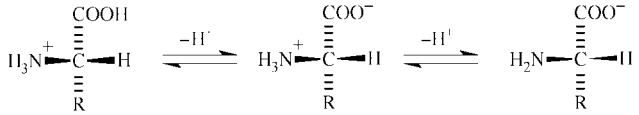

Scheme 1

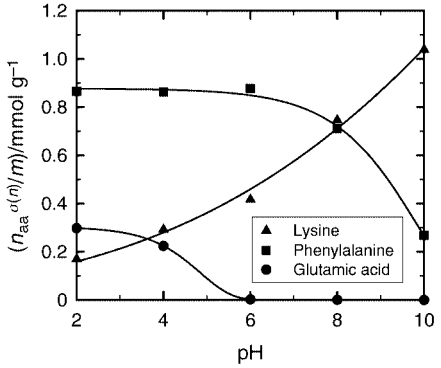

Fig. 1 Influence of the pH on the adsorption of lysine, phenylalanine and glutamic acid on zeolite Beta (n_{Si}/n_{Al} = 25).

 DOI: 10.1039/b105333g

of C-atoms in the side chain, *viz.* in the sequence: alanine (1 C) < valine (3 C) < leucine (4 C) < phenylalanine (7 C). A comparison of the specific reduced surface excesses $n_{aa}{}^{\sigma(n)}/m$ for zeolites Beta and ZSM-5 (Table 1) shows that the loadings achieved for Beta are generally higher than those for ZSM-5, which can be attributed to the different pore volumes (Beta: 0.28 $cm^3\ g^{-1}$, ZSM-5: 0.17 $cm^3\ g^{-1}$). Furthermore, the more hydrophobic amino acids are adsorbed to a considerably higher extent on both zeolites. Therefore, hydrophobic interactions seem to complement the electrostatic interactions of the amino acid with the zeolite. These hydrophobic interactions may either originate from an attraction of the non-polar side chains of the amino acids by siloxane bridges at the zeolite surface or from adsorbate–adsorbate interactions between the hydrophobic side chains of neighboring adsorbate complexes. With respect to the pronounced hydrophobic properties of phenylalanine its adsorption on ZSM-5 is unexpectedly low. The adsorbate–adsorbate interactions between the hydrophobic side chains of neighboring amino acids adsorbed on the zeolite surface are expected to be restricted by the narrow pore system of ZSM-5 and, hence, the bulky phenylalanine molecules interact to a lower extent than in zeolite Beta, which has larger pores. For a closer inspection of the hydrophobic interactions, adsorption isotherms of phenylalanine were recorded on samples of zeolite Beta with different aluminium content from buffered solutions at pH 6 (Fig. 2). The maximum amount adsorbed is nearly the same for all samples, except for the sample with the lowest n_{Si}/n_{Al} ratio of 12 with a slightly lower loading. This can be attributed to an increasing affinity to water due to the high aluminium content. The initial curvature of the corresponding isotherm changes with decreasing aluminium content of the adsorbent. For zeolite Beta with n_{Si}/n_{Al} ratios of 12 and 25, respectively, the isotherms exhibit the common Langmuir-type L-curve, but the shape changes with increasing n_{Si}/n_{Al} ratio to an S-curve. S-curves are characteristic for solutes showing only little attraction to the adsorbent, but possessing stronger intermolecular interactions.[6] At low concentrations, phenylalanine is hardly adsorbed on the surface of the aluminium-free zeolite Beta. This can be rationalized by the absence of aluminium atoms in the zeolite structure, which are the adsorption sites for the amino acids if electrostatic interactions dominate. At higher concentrations, the sudden sharp increase in the amount adsorbed reflects the change in the adsorption conditions: the number of solute molecules is now high enough to form clusters of adsorbed molecules that interact with each other *via* the hydrophobic attractions of their non-polar phenyl-groups and, hence, rapid filling of the zeolite pores with phenylalanine molecules occurs.

Table 1 Adsorption of amino acids with non-polar side chains

Adsorbent	Amino acid	$(n_{aa}{}^{\sigma(n)}/m)^a$/mmol g^{-1}
Beta (n_{Si}/n_{Al} = 25)	Alanine	0.04
	Valine	0.37
	Leucine	0.70
	Phenylalanine	0.84
ZSM-5 (n_{Si}/n_{Al} = 30)	Alanine	0.02
	Valine	0.29
	Leucine	0.40
	Phenylalanine	0.29

[a] Specific reduced surface excess values for equilibrium molar fractions of x_{aa} = 0.001.

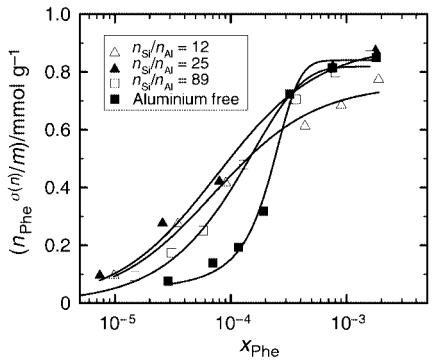

Fig. 2 Effect of the aluminium content of zeolite Beta on the adsorption of phenylalanine at pH 6.

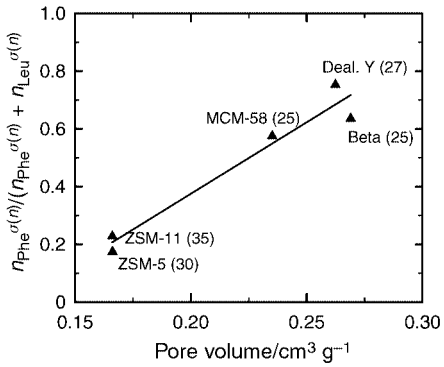

Fig. 3 Separation of leucine and phenylalanine from a mixture of both amino acids in aqueous solution by adsorption on various zeolites.

According to our results, zeolites allow the separation of miscellaneous amino acids from model aqueous solutions. As already demonstrated in Fig. 1 amino acids of different polarity can be separated by adjusting the pH of the solution appropriately. The separation of phenylalanine (Phe) and leucine (Leu) from buffered solutions at pH 6 on various zeolites with n_{Si}/n_{Al} ratios of about 30 is depicted in Fig. 3, where the ratio of phenylalanine adsorbed over the total amount of phenylalanine and leucine adsorbed from the mixture $(n_{Phe}{}^{\sigma(n)}/(n_{Phe}{}^{\sigma(n)} + n_{Leu}{}^{\sigma(n)})]$ is plotted against the pore volumes of the zeolites used as adsorbents. Both amino acids are excluded from the relatively narrow pores of ZSM-22. For ZSM-5, the adsorption of leucine as compared to phenylalanine is clearly favored. Using zeolites with larger pore sizes, the ratio $n_{Phe}{}^{\sigma(n)}/(n_{Phe}{}^{\sigma(n)} + n_{Leu}{}^{\sigma(n)})$ increases and phenylalanine is preferentially adsorbed.

The results obtained for a systematic variation of the side chain of the amino acid, the structure and the aluminium content of the zeolites used as adsorbent and the pH of the solution can be summarized as follows. The adsorption of amino acids seems to be dominated by electrostatic interactions of their positively charged ammonium group with the negatively charged zeolite surface. Moreover, hydrophobic interactions between non-polar side chains of adsorbed amino acid molecules complement the ionic interactions. These two fundamental interactions allow the separation of amino acids from aqueous solutions, as could be demonstrated for a mixture of leucine and phenylalanine.

Financial support by Deutsche Forschungsgemeinschaft and Fonds der Chemischen Industrie is gratefully acknowledged.

Notes and references

1 J. C. Bellot, R. V. Tarantino and J. S. Condoret, *AIChE J.*, 1999, **45**, 329.
2 C. B. Ching and D. M. Ruthven, *Chem. Eng. J.*, 1989, **40**, 1.
3 S. Yonsel, W. Schäfer-Treffenfeldt, A. Kiss, E. Sextl and H. Naujok, *DE Patent* 42 17 203 A1, 1993, assigned to Degussa AG
4 S. Yonsel, G. Richet, W. Schäfer-Treffenfeldt, T. Le Quang, E. Sextl and M. Scholz, *EP* 0 645 371 A1, 1995, assigned to Degussa AG
5 D. H. Everett, *Pure Appl. Chem.*, 1986, **56**, 967.
6 C. H. Giles, T. H. MacEwan, S. N. Nakhwa and D. Smith, *J. Chem. Soc.*, 1960, 3973.

CHEMCOMM Communication
www.rsc.org/chemcomm

Enantioselective crystallization of D,L-amino acids induced by spontaneous asymmetric resolution of D,L-asparagine

Shosuke Kojo* and Kyoko Tanaka

Department of Food Science and Nutrition, Nara Women's University, Nara 630-8506, Japan. E-mail: kojo@cc.nara-wu.ac.jp; Fax: +81 742 20 3459; Tel: +81 742 20 3459

Received (in Cambridge, UK) 27th June 2001, Accepted 30th August 2001
First published as an Advance Article on the web 18th September 2001

Racemic D,L-asparagine induced spontaneous asymmetric resolution of co-existing D,L-phenylalanine or D,L-tryptophan by recrystallization from a homogeneous aqueous solution, and the enantiomeric excess of phenylalanine or tryptophan in the resulting crystals correlated linearly with that of asparagine crystallized with phenylalanine or tryptophan.

Although many efforts have been devoted to the elucidation of why and how L-amino acids were selected in the biosphere,[1–3] it is still difficult to explain the origin of the specificity of L-amino acid, and further to elucidate the relationship in selection among 20 L-amino acids with apparently different structures except the configuration of the α-carbon. Since the famous experiment performed by Pasteur,[4] recrytallization has been tried for asymmetric resolution.[5–7] Among amino acids, D,L-asparagine (D,L-Asn) spontaneously forms crystals of either isomer during recrystallization.[8] In this study, we report that D,L-Asn induces asymmetric resolution of co-existing racemic amino acids during recrystallization. This is the first study that shows the spontaneous induction of enantiomeric excess (ee) of coexisting racemic amino acid by a racemic amino acid (in this case, D,L-Asn), although asymmetric resolution by crystallization using chiral additives and crystal interfaces are well documented.[9,10]

In this study, the ee value was determined by a widely used method utilizing high-performance liquid chromatography (HPLC) equipped with a column {Crownpak CR(+) manufactured by Daicel Chem. Ind. Ltd., Tokyo, Japan} which allowed perfect separation of D- and L-amino acids using perchloric acid solution as an eluent as indicated by the supplier. The determination was made by absorption at 200 nm also indicated by the column supplier. When starting racemic materials {D,L-asparagine, D,L-phenylalanine (D,L-Phe), and D,L-tryptophan (D,L-Trp)} taken as an aliquot just after the first filtration of the recrystallization experiments described below were analyzed, ee of either isomer never exceeded 2.5%. Usually the experimental error in chromatographic analysis is assumed to be 2–3%. Therefore, an ee value of less than 2.5% was defined as racemic.

D,L-Asn monohydrate (2 g) was dissolved in water (10 ml) heated in a boiling water bath. After filtration with a glass filter, the solution was stored in a glass vial with a screw cap, and left at room temperature until a measurable amount of crystals were formed. Crystals weighing from 170 to 652 mg were collected by filtration with a glass filter, dissolved in an appropriate amount of water, and directly applied to HPLC analysis. The ee values of L-Asn were 4.8, 11.2, 11.5, 11.7, 15.5, 26.7, 26.8, 27.1, 64.7, 88.9, and −59.7%, showing that L-rich crystals were obtained 10 times and D-rich crystals were formed once among 11 recrystallizations. These results clearly indicate that crystals formed by recrystallization of D,L-Asn show ee as a whole. To elucidate the mechanism of this resolution, the ee of each crystal taken randomly from recrystallization experiments was measured. Among 35 crystals, 3 crystals gave an ee of either isomer at about 70% and that of 32 crystals was more than 90%. This result indicated that each crystal consisted of almost purely one enantiomer and that the ee of the crystals in total was determined by the weight percent of crystals of the enriched isomer.

D,L-Phe (180 mg) was dissolved in 10 ml of water heated with a boiling water bath. After filtration, recrystallization was similarly performed. Crystals weighing from 17 to 41 mg were collected, and dissolved in water, and applied to HPLC analysis, which showed that the resulting samples from 11 independent recrystallizations were all racemic. D,L-Phe (300 mg) and D,L-Asn monohydrate (2.1 g) were similarly dissolved in 10 ml of water at 100 °C. By similar recrystallization, crystals weighing 62–240 mg were obtained, dissolved in water, and analyzed by HPLC. Thirteen independent experiments were carried out. The ee values of L-Asn (abscissa: *x*-axis) and L-Phe (the ordinate: *y*-axis) for each sample solution were plotted as shown in Fig. 1. The maximal ee values of L-isomer were 22.3 and 41.1% for Phe and Asn, respectively. The maximal ee values of the D-isomer were 35.6 and 89.8% for Phe and Asn, respectively (Fig. 1). These results demonstrate that D,L-Asn causes asymmetric selection of Phe to a significant extent. Furthermore, the ee of Phe correlated almost linearly with that of Asn, and the former was less than the latter (Fig. 1). The content of Phe in these crystals was less than 1% of Asn. The ee of each crystal indicated that the ee of Asn of either isomer was nearly 100% and that of Phe of the corresponding isomer was 60–93%. These results suggested that L-Asn crystallized preferentially involving L-Phe, and *vice versa*, and that asymmetric selection resulted from the relative content of crystals enriched with either Asn isomer.

Trp was examined as the second amino acid. D,L-Trp (133 mg) was dissolved in 10 ml of hot water. After filtration, recrystallization was similarly performed. Crystals weighing from 10 to 43 mg were collected, dissolved in water, and applied to HPLC analysis, which showed that the resulting samples from 11 independent recrystallizations were all racemic as expected. Then, D,L-Trp (125 mg) and D,L-Asn monohydrate (2.5 g) were dissolved in 10 ml of hot water. Similar recrystallization yielded crystals weighing 20–250 mg. After dissolving the crystals in water, HPLC analysis was carried out.

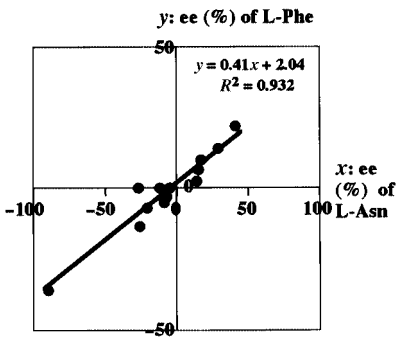

Fig. 1 Plot of ee values of L-phenylalanine and L-asparagine of crystals obtained from recrystallization of D,L-phenylalanine and D,L-asparagine. The ee values of asparagine {Asn: abscissa (*x*-axis)} and phenylalanine {Phe: the ordinate (*y*-axis)} for each sample were plotted as ●.

 DOI: 10.1039/b105663h

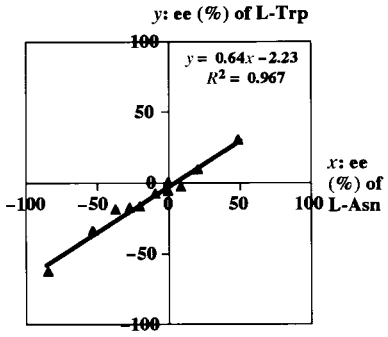

Fig. 2 Plot of ee values of L-tryptophan and L-asparagine of crystals obtained from recrystallization of D,L-tryptophan and D,L-asparagine. The ee values of asparagine {Asn: abscissa (*x*-axis)} and tryptophan {Trp: the ordinate (*y*-axis)} for each sample were plotted as ▲.

Twelve independent experiments were performed. The ee values of L-Asn (the abscissa: *x*-axis) and L-Trp (the ordinate: *y*-axis) for each sample solution were plotted as shown in Fig. 2. The maximal ee values of L-isomer were 30.2 and 48.7% for Trp and Asn, respectively. The maximal ee values of the D-isomer were 62.1 and 83.8% for Trp and Asn, respectively (Fig. 2). These results demonstrate that D,L-Asn also causes asymmetric crystallization of D,L-Trp to a considerable extent. The extent of asymmetric induction in Trp correlated almost linearly with that of Asn, and the ee of the influenced amino acid (Trp) was less than that of the inducer (Asn) (Fig. 2) as in the case of Phe. The content of Trp in these crystals was less than 5% of Asn. Although recrystallization of D,L-Trp with D,L-Asn gave fine powders and a crystal that could be separated with forceps was not obtained, a similar mechanism to the case of Phe was suggested for the optical resolution of Trp.

In conclusion, the present study demonstrates that D,L-Asn can induce a significant enantio-selective crystallization of co-existing amino acids such as Phe and Trp from a homogeneous aqueous solution. Whether the enrichment takes place in L- or D-Asn is accidentally determined. However, once the selection is made, the co-existing amino acid with the same configuration at the α-carbon seems to be preferentially involved in crystals of Asn. This idea may be supported by the observation that the ee of asparagine correlates almost linearly with that of the influenced amino acid (Fig. 1 and 2). These results suggest that the ee of racemic amino acids induced by spontaneous and accidental resolution of co-existing racemic molecules such as D,L-Asn may contribute to the homochirality of L-amino acids in the biosphere.

Notes and references

1 S. Mason, *Chem. Soc. Rev.*, 1988, **17**, 347.
2 M. Avalos, R. Babiano, P. Cintas, J. L. Jimenez and J. C. Palacios, *Chem. Rev.*, 1998, **98**, 2391.
3 G. L. J. A. Rikken and E. Raupach, *Nature*, 2000, **405**, 932.
4 L. Pasteur, *C. R. Acad. Sci. Paris*, 1848, **26**, 535.
5 A. Collet, M.-J. Brienne and J. Jacques, *Chem. Rev.*, 1980, **80**, 215.
6 D. K. Kondepudi, R. J. Kaufman and N. Singh, *Science*, 1990, **250**, 975.
7 R. E. Pincock, R. R. Perkins, A. S. Ma and K. R. Wilson, *Science*, 1971, **174**, 1018.
8 I. Ostromisslensky, *Ber.*, 1908, **41**, 3035.
9 L. Addadi, Z. Berkovitch-Yellin, I. Weissbuch, J. van Mil, L. J. W. Shimon, M. Lahav and L. Leiserowitz, *Angew. Chem., Int. Ed. Engl.*, 1985, **24**, 466.
10 I. Weissbuch, L. Addadi, M. Lahav and L. Leiserowitz, *Science*, 1991, **253**, 637.

CHEMCOMM Communication
www.rsc.org/chemcomm

Sub-ppt detection limits for copper ions with Gly-Gly-His modified electrodes†

Wenrong Yang, David Jaramillo, J. Justin Gooding,* D. Brynn Hibbert, Rui Zhang, Gary D. Willett and Keith J. Fisher

School of Chemistry, The University of New South Wales, Sydney, NSW 2052, Australia. E-mail: justin.gooding@unsw.edu.au

Received (in Cambridge, UK) 25th July 2001, Accepted 30th August 2001
First published as an Advance Article on the web 18th September 2001

An electrochemical metal ion sensor has been developed with a detection limit of less than 0.2 ppt by the covalent attachment of the tripeptide Gly-Gly-His as a recognition element to a 3-mercaptopropionic acid modified gold electrode.

Detecting a number of metal ions at very low concentrations directly in the field is one of the key targets of environmental chemists. Electrochemical sensors have the potential to allow multi-ion analysis in the field because of their small size, low power requirements and the need for little or no sample pretreatment. The majority of research into chemically modified electrodes for the detection of metal ions involves the synthesis and testing of macrocyclic ligands to provide the sensing interface with selectivity for a given metal ion and the ability to pre-concentrate the metal. In nature however, binding metals is achieved with a high degree of selectivity using peptide motifs rather than macrocyclic ligands. Considering the development of biosensors that exploit Nature's methods of selective recognition and the extensive body of literature on the complexation of metal ions with peptides,[1,2] it is surprising how little research has been conducted into the development of solid state metal ion sensors based on peptide ligands.[3] Here we describe an electrode modified with the oligopeptide Gly-Gly-His with an extraordinarily low detection limit in the sub ppt range (pM) for copper ions.

Electrodes modified with Gly-Gly-His were prepared using polycrystalline gold electrodes cleaned as described previously.[4,5] Self-assembly of 3-mercaptopropionic acid (MPA) was achieved by soaking the electrodes in a 1.0 mM MPA solution in ethanol for 12 hours. The carboxylic acid terminated self assembled monolayer (SAM) was activated using a mixture of 15 mM *N*-hydroxysuccinimide (NHS) and 75 mM 1-ethyl-3-(3-dimethylaminopropyl)carbodiimide hydrochloride (EDC) and 2-(*N*-morpholino)ethanesulfonic acid (MES) buffer solution (pH 5.5) for 30 minutes.[6] The resultant succinimide ester monolayers were reacted for 30 minutes in a solution of Gly-Gly-His (50 mg ml^{-1}) in MES buffer to give the modified electrode shown in Fig. 1 where the tripeptide is attached through the amino group of the first glycine and terminates with the carboxylic acid of the histidine.

Copper was accumulated at the Gly-Gly-His modified electrode (GGHME) in an open circuit potential for 10 minutes in a 0.05 M ammonium acetate buffer solution (pH 7.0) containing copper nitrate. Cyclic voltammetry (using a BAS 100B, Bioanalytical System Inc., USA) measured after removal of the electrode from the copper nitrate solution, rinsing and then placing in a copper free ammonia acetate buffer solution showed reversible electrochemistry with a half-wave potential at −55 mV *versus* Ag|AgCl|3.0 M KCl which was attributed to the half cell Au|$Cu(II)_{complex}$, $Cu(I)_{complex}$ as reported previously for cysteine modified electrodes.[7–9] In the absence of accumulated copper no such electrochemistry was observed. Copper free electrodes could be regenerated by elimination of Cu(II) by holding the working electrode at +0.5 V for 30 seconds in 0.1 M $HClO_4$.

That Cu(II) is tightly bound to the GGHME is demonstrated by no diminution of the peak currents with multiple scans, despite the absence of any copper in the test solution. Furthermore, the peak current varies linearly with scan rate, behaviour indicative of the redox active species being strongly bound to the electrode.[10] Hence we propose the copper is bound to the GGHME as shown in Fig. 1 to give the tetragonal coordination preferred by Cu(II). Evidence for the binding of the copper through the nitrogen on the histidine ring, to give coordination by four nitrogen atoms, was obtained from studies of collision-induced dissociation (CID) using electrospray ionization Fourier transform ion cyclotron resonance mass spectroscopy (FT-ICR MS).† In the absence of copper, the negative ion mass spectrum of Gly-Gly-His in pure methanol showed the pseudo-parent ion [Gly-Gly-His − H] at *m*/*z* 268.11 Da and the most prominent fragment ion at *m*/*z* 154.06 Da which arises from the cleavage of histidine to leave [Gly-Gly]. However, in the presence of Cu(II) the cleavage of histidine is prevented by its role in the complexing of copper. The pseudo-parent ion [Gly-Gly-His + Cu^{2+} − 3H] is observed at *m*/*z* 331.02 Da with the most common fragment ion at *m*/*z* 287.03 Da which corresponds to decarboxylation from the histidine; thus confirming in solution that the binding of the copper is through a deprotonated amine of the peptide bond between Gly and His. These results are consistent with mass spectroscopy results reported previously.[11]

Osteryoung square wave voltammetry (OSWV) was employed with a GGHME for detection of low levels of copper in environmental samples. This technique is more sensitive than cyclic voltammetry.[12] Fig. 2a shows OSWV peaks of a GGHME in 0.05 M ammonium acetate buffer solution (pH 7.0) for a series of copper standards adsorbed for ten minutes from solutions with concentrations in the picomolar range, before

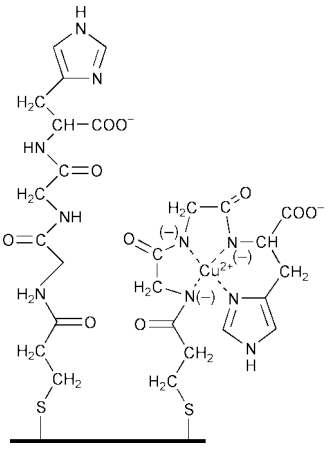

Fig. 1 Schematic of the Gly-Gly-His modified electrode with and without complexed Cu^{2+}.

† Electronic supplementary information (ESI) available: mass spectra and Table S1. See http://www.rsc.org/suppdata/cc/b1/b106730n/

 DOI: 10.1039/b106730n

transfer to the stripping electrolyte. The 3 pM (0.2 ppt) standard could easily be discriminated from the background in which no Cu(II) was added to the buffer (Fig. 2a). The implied detection limit (*i.e.* <3 pM) is several orders of magnitude below that which we have reported previously for cysteine (1.5 ppb)[9] and polyaspartate (0.2 ppb)[13] modified electrodes. The low detection limit and strong binding of copper reflects the well known affinity for Gly-Gly-His, the so called copper binding peptide, for Cu(II).[1,2]

To the best of our knowledge this detection limit is well below any other reported in the literature [50 pM using the subtractive mode of anodic stripping voltammetry[14] (ASV)] and is also well below that observed for most metal ions using anodic stripping voltammetry or catalytic ASV.[15] A fluorimetric method has achieved 125 pM[16] and electrothermal atomic adsorption spectrometry, where the sample was accumulated *via* sorption in a knotted reactor, detected 100 pM.[17]

The calibration curve (Fig. 2b) shows a linear range up to 10 pM with a slope of 2.1 (standard deviation = 0.1) nA pM^{-1}. The standard error in a measurement of concentration made in the middle of the calibration range was 0.33 pM. The electrodes could be regenerated up to 30 times without any apparent change in performance. Four electrodes fabricated on different days with different batches of reagents gave results with RSDs between 10 and 20%, as indicated by the error bars on points in Fig. 2b. The low saturation concentration again reflects the high affinity of the peptide for copper. The selectivity of GGHMEs to copper was tested by measuring the response of the electrode to a number of metals ions commonly found in waste water, shown in Table S1 in the supplementary information. The case of Ni(II) addition of 10 pM of Ni(II) to a solution of 9.8 pM of Cu(II) resulted in a 6.5% decrease in current. Apart from Ni(II) however, none of the other metal ions showed significant interference with the Cu(II) measurement. The interference of Ni(II) is not unexpected considering Ni(II) is also known to form a 4*N* complex with Gly-Gly-His in solution.[2] Analysis of a local tap water was performed by diluting the sample to bring the copper concentration to within the range of the Gly-Gly-His modified electrode. The measured concentration of free Cu(II) in the tap water, when dilutions were accounted for, was 0.27 ppm (standard deviation = 0.03 for 3 samples (*i.e.* $n = 3$)) which agreed well with the total copper concentration measured using inductively coupled plasma optical emission spectroscopy (ICP-OES) of 0.33 ppm.

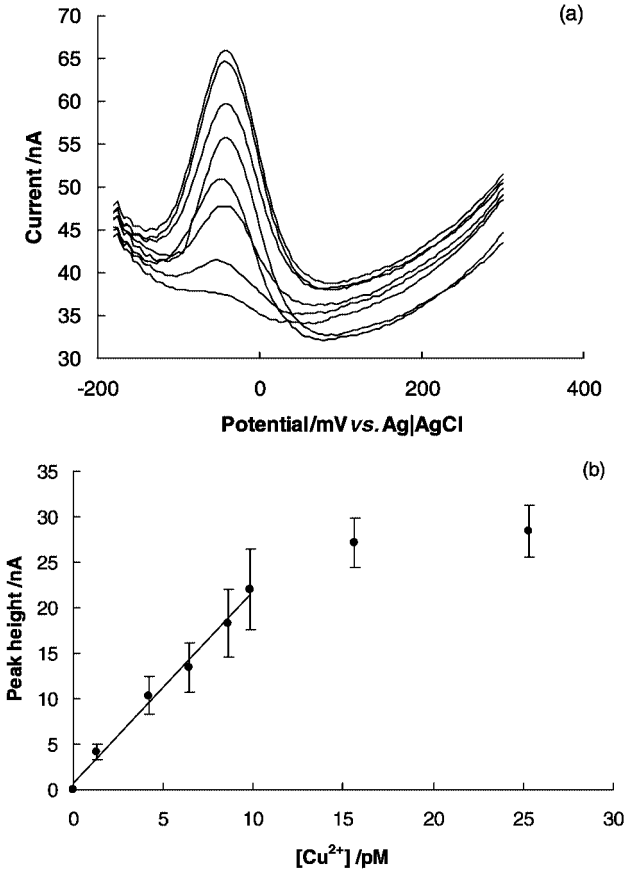

Fig. 2 Response of the Gly-Gly-His modified electrode to complexed Cu(II) (a) Osteryoung square wave voltammetry peaks showing an increase in current with copper concentrations of 0, 1.28, 4.2, 6.4, 8.6, 9.8, 15.6, 25.3 pM and (b) calibration curve derived from the OSWV peaks with error bars as ±1 standard deviation of four electrodes prepared on different days. In all cases Cu(II) was accumulated at the Gly-Gly-His modified electrode in an open circuit over 10 minutes in a 0.05 M ammonium acetate buffer solution (pH 7.0) containing copper nitrate, removed, rinsed and then placed in a copper-free ammonium acetate buffer solution.

These initial results illustrate the potential for peptide-modified electrodes to be used as metal ion sensors with extraordinarily low detection limits. This work is part of our aim to fabricate a multiple metal ion sensor array, based on peptide modified electrodes, where each electrode in the array gives a different response for a given metal ion to produce a characteristic response pattern for different metal ions. Future work involves exploring other peptide modified electrodes for selectivity for other metal ions.

Notes and references

1 H. Sigel and R. B. Martin, *Chem. Rev.*, 1982, **82**, 385.
2 H. Kozlowski, W. Bal, M. Dyba and T. Kowalik-Jankowska, *Coord. Chem. Rev.*, 1999, **184**, 319.
3 J. J. Gooding, D. B. Hibbert and W. Yang, *Sensors*, 2001, **1**, 75.
4 J. J. Gooding, P. Erokhin and D. B. Hibbert, *Biosensors Bioelectronics*, 2000, **15**, 229.
5 Due to the very low concentrations of analyte special care was taken to try to eliminate any copper in solutions or glassware. All solutions were prepared using Milli-Q water and all glassware was soaked in 6 M HNO_3 overnight and rinsed thoroughly in Milli-Q water. All OSWV current measurements were recorded relative to a background containing all species except the copper standard.
6 J. J. Gooding, V. Praig and E. A. H. Hall, *Anal. Chem.*, 1998, **70**, 2396.
7 D. W. M. Arrigan and L. Le Bihan, *Analyst*, 1999, **124**, 1645.
8 A. C. Liu, D. C. Chen, C. C. Lin, H. H. Chou and C. H. Chen, *Anal. Chem.*, 1999, **71**, 1549.
9 W. Yang, J. J. Gooding and D. B. Hibbert, *J. Electroanal. Chem.*, 2001, in the press.
10 E. Laviron, *J. Electroanal. Chem.*, 1979, **101**, 19.
11 P. Hu and J. A. Loo, *J. Am. Chem. Soc.*, 1995, **117**, 11 314.
12 I. Turyan and D. Mandler, *Nature*, 1993, **362**, 703.
13 W. Yang, J. J. Gooding and D. B. Hibbert, *Analyst*, 2001, **126**, 1573.
14 Y. Bonfil, M. Brand and E. Kirowa-Eisner, *Anal. Chim. Acta*, 2000, **424**, 65.
15 M. Z. Czae and J. Wang, *Talanta*, 1999, **50**, 921.
16 K. Watanabe, K. Ohba, A. Iburaim, M. Itagaki and N. Koura, *Bunseki Kagaku*, 1998, **47**, 179.
17 E. Ivanova, K. Benkhedda and F. Adams, *J. Anal. At. Spectrom.*, 1998, **13**, 527.

CHEMCOMM Communication
www.rsc.org/chemcomm

Ab initio structure determination of $BiPb_2VO_6$ from powder diffraction data†

Ivana Radosavljevic Evans,[a] Judith A. K. Howard,[a] Ray L. Withers[b] and John S. O. Evans[a]

[a] *Department of Chemistry, University of Durham, Science Site, Durham, UK DH1 3LE. E-mail: ivana.radosavljevic@durham.ac.uk; john.evans@durham.ac.uk*
[b] *Research School of Chemistry, Australian National University, Canberra, ACT, 0200 Australia*

Received (in Cambridge, UK) 14th June 2001, Accepted 17th August 2001
First published as an Advance Article on the web 12th September 2001

The crystal structure of $BiPb_2VO_6$ has been determined from powder diffraction data using a combination of direct methods and the novel approach of applying simulated annealing methods simultaneously to X-ray and neutron data; $BiPb_2VO_6$ is a polar, noncentrosymmetric, second harmonic generation active material and its crystal structure is one of the more complex to be solved *ab initio* from powder diffraction data.

Bismuth vanadates have been widely studied owing to the interesting properties they exhibit. Materials based on $Bi_4V_2O_{11}$ are good oxide ion conductors.[1] $BiVO_4$ is a ferroelastic and has been patented as a yellow pigment.[2,3] Owing to the Bi(III) lone pair stereoactivity, these materials frequently crystallize in noncentrosymmetric space groups and thus are potential nonlinear optical materials and ferroelectrics. Several vanadates of the BiM_2AO_6 family (M = Ca, Mg, Cd, Cu; A = V, As ,P) have been synthesized and characterized by us and others.[4–9] The different members have related, though subtly different crystal structures and three of them have been shown to be second harmonic generation active. $BiPb_2VO_6$ was first reported in 1995 and its diffraction pattern described[10] as complex and apparently unrelated to other phases of the BiM_2AO_6 family.

Our $BiPb_2VO_6$ samples were prepared by solid state reactions of stoichiometric quantities of Bi_2O_3, PbO and NH_4VO_3 at 720 °C. DSC measurements show that between room temperature and its melting point, $BiPb_2VO_6$ undergoes several phase transformations and displays different behaviour on heating and cooling. Although crystals of this phase can be grown, they exhibit complex intergrowths and twinning, making them unsuitable for structural analysis. This is presumably related to the large number of phase transitions.

In order to solve the structure of this material, we therefore resorted to powder diffraction methods. The first attempt to index[11] the diffraction pattern of the room temperature phase was carried out using laboratory X-ray diffraction data collected on a Siemens D5000 diffractometer. The cell obtained gave a figure of merit of 109 and indexed all but a few weak reflections; it corresponded to the unit cell reported by Mizrahi *et al.*,[10] but with the *c* axis halved. By doubling the *c* cell dimension and applying a simple transformation, we obtained a unit cell with $a = 7.7219(2)$, $b = 5.8443(1)$, $c = 29.0762(7)$ Å and $\beta = 94.278(2)°$. Using this cell and the space group *Pn*, an excellent Pawley fit to the observed X-ray data was achieved. This unit cell was later unambiguously confirmed by electron diffraction[12] which suggested possible space groups *Pn* or *P*2/*n*. The absence of an inversion centre in the structure was confirmed by a positive second harmonic generation test,[13] an observed signal of 2–5 × that of quartz was obtained. This leaves *Pn* as the only possible space group choice.

† Electronic supplementary information (ESI) available: fractional coordinates and valence sums, bond distances and angles and virtual reality image of Fig. 2. See http://www.rsc.org/suppdata/cc/b1/b105242j/

X-Ray diffraction data for structure solution were collected at beam line X7A of the Brookhaven NSLS, using a wavelength of 0.57775 Å, in both flat plate and capillary modes. Structure solution was attempted by direct methods[14] in space group *Pn*, using the flat plate data set. A total of 16 metal sites were found, 12 assigned as Bi/Pb and 4 as V. Owing to minor texture effects in the flat plate data, the metal positions obtained were refined against the capillary synchrotron X-ray data until the best possible fit was achieved. To obtain information on the oxygen positions two approaches were used: ^{51}V solid state NMR and neutron powder diffraction measurements.[15,16] ^{51}V MAS NMR provides valuable information on vanadium coordination. A single peak was observed with an isotropic chemical shift of −496 ppm and a very low chemical shift anisotropy. This is consistent with all V sites existing as regular, isolated VO_4 tetrahedra.[17]

Armed with this information, the X-ray derived metal coordinates were used to calculate a difference Fourier map based on the neutron diffraction data, which are more sensitive to oxygen positions. This revealed a number of difference peaks. Eight peaks could be readily assigned as oxygen atoms tetrahedrally coordinated by four Bi/Pb atoms. Other peaks were observed in the vicinity of vanadium sites suggestive of tetrahedrally coordinated vanadium. In fact, charge balance requires a further 16 oxygens in the asymmetric unit. This, together with the ^{51}V NMR data, provides convincing support for four tetrahedral VO_4 groups.

Introduction of the eight tetrahedrally coordinated oxygen sites and a plausible set of oxygens around vanadium atoms followed by Rietveld refinement led to a model showing reasonable agreement with both X-ray and neutron data sets and agreement factors for neutron data of $wR_p = 6.77\%$ and $R_{Bragg} = 7.26\%$. At this stage of the solution, however, there were still some significant discrepancies between the observed and calculated neutron diffraction data. Since the X-ray scattering is dominated by Bi, Pb and V atoms, whereas neutron data are sensitive to Pb, Bi and O (the coherent cross section of vanadium is only −0.40 fm), we decided to adopt a novel approach of simultaneous simulated annealing of the neutron and X-ray diffraction data in order to complete the structure solution.

Simulated annealing calculations were performed[18,19] in which a structural model was generated by the application of random shifts to the positions and rotations of rigid VO_4 tetrahedra and fractional coordinates of other atoms. These shifts were then scaled according to an arbitrary 'temperature'. Several thousand cycles of full Rietveld refinement followed by perturbation of the structural model were then performed, during which the scaling temperature was varied systematically. In this manner a structural model was found showing excellent agreement with both neutron and X-ray data. From this solution, combined Rietveld refinement of both data sets was performed, in which a total of 128 parameters were varied.[20] The final overall agreement factor was $wR_p = 3.83\%$, while the agreement factors for the individual data sets were wR_p =

 DOI: 10.1039/b105242j

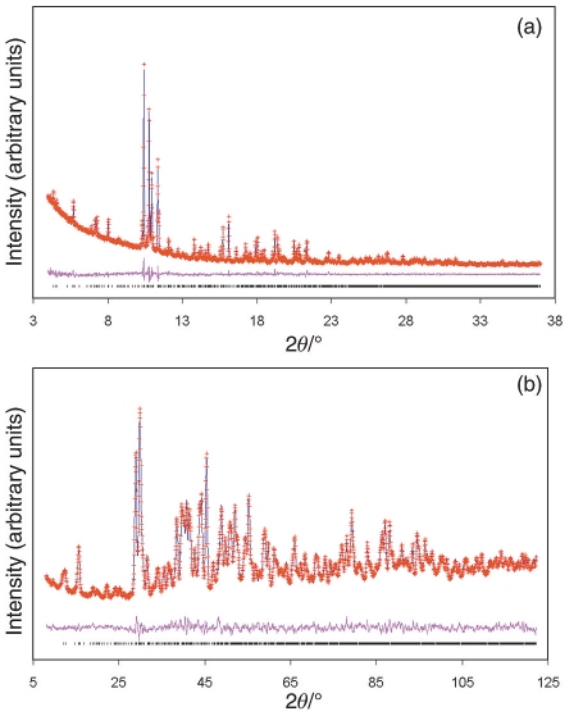

Fig. 1 Final Rietveld plots for (a) X-ray and (b) neutron data.

3.71% and R_{Bragg} = 2.01% for X-ray data [Fig. 1(a)] and wR_p = 3.91% and R_{Bragg} = 3.25% for neutron [Fig. 1(b)].

When rigid VO_4 bodies were allowed to refine freely, the V–O bond lengths refined to values between 1.65 and 1.82 Å and the O–V–O angles to 109 ± 6°, without a significant reduction of the agreement factors. The sensitivity of the data to Bi/Pb occupancies on the various sites of the edge sharing OM_4 tetrahedra was then investigated by perturbing the Bi/Pb distribution several thousand times followed by the full refinement of the model. The data were essentially insensitive to this distribution. By analogy with other BiM_2VO_6 phases we have chosen to assign Bi atoms to the central two positions of the tetrahedral chains of Fig. 2.

Views of the unit cell of $BiPb_2VO_6$ are given in Fig. 2. The structure can be described as containing infinite edge sharing chains of OBi_2Pb_2 tetrahedra similar to those found in fluorite, running parallel to the *b* axis, with isolated VO_4 tetrahedral groups interspersed.

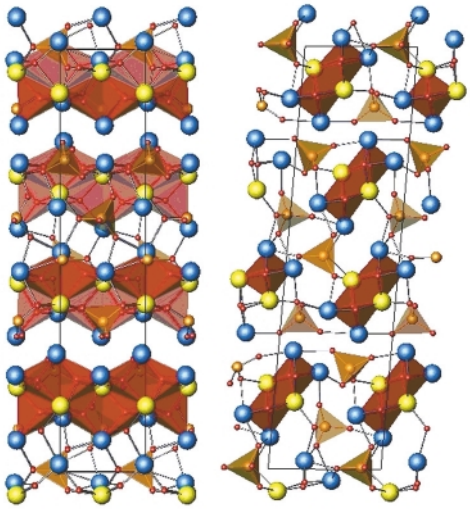

Fig. 2 Views of the $BiPb_2VO_6$ structure down (a) the *a*-axis and (b) the *b*-axis: Bi atoms are depicted in yellow, Pb atoms in blue, V atoms in light brown and O in red; light brown tetrahedra represent VO_4 groups; red tetrahedra represent OBi_2Pb_2 groups which share edges and form chains running parallel to the *b* axis.

Bi and Pb atoms adopt geometrically irregular coordination environments characteristic of lone-pair cations, with coordination numbers between five and seven. Typically, they bond to four oxygen atoms with bond lengths between 2.2 and 2.5 Å and complete their coordination spheres by additional bonds of up to 2.9 Å in length. The VO_4 tetrahedra can be seen to adopt an acentric orientation in accordance with the noncentrosymmetric space group.

More detailed comparison of this structure to other members of the BiM_2AO_6 family and the details of the high temperature structures of $BiPb_2VO_6$ will appear elsewhere.

We wish to acknowledge Dr Pat Woodward of Ohio State University for collecting the synchrotron X-ray diffraction data at Brookhaven National Laboratory, Dr Alan Hewat for the assistance with the neutron diffraction data collection at ILL, Ian King and Dr Franck Fayon of CRMHT-CNRS Orleans for ^{51}V solid state NMR, Dr P. Shiv Halasyamani of The University of Houston for SHG measurements and the EPSRC for a Senior Research Fellowship (J. A. K. H).

Notes and references

1 J. C. Boivin and G. Mairesse, *Chem. Mater.*, 1998, **10**, 2870.
2 A. W. Sleight, H. Y. Chen, A. Ferretti and D. E. Cox, *Mater. Res. Bull.*, 1979, **14**, 1571.
3 L. Balducci and M. Rustioni, *U. S. Pat.*, 4,230,500, 1980.
4 A. Mizrahi, J. P. Wignacour and H. Steinfink, *J. Solid State Chem.*, 1997, **133**, 516.
5 I. Radosavljevic, J. S. O. Evans and A. W. Sleight, *J. Solid State Chem.*, 1998, **137**, 143.
6 I. Radosavljevic, J. S. O. Evans and A. W. Sleight, *J. Solid State Chem.*, 1998, **141**, 149.
7 I. Radosavljevic, J. S. O. Evans and A. W. Sleight, *J. Alloys Compd.*, 1999, **284**, 99.
8 I. Radosavljevic and A. W. Sleight, *J. Solid State Chem.*, 2000, **149**, 143.
9 I. Radosavljevic, J. A. K. Howard and A. W. Sleight, *Int. J. Inorg. Mater.*, 2000, **2**, 543.
10 A. Mizrahi, J. P. Wignacourt, M. Drache and P. Conflant, *J. Mater. Chem.*, 1995, **5**, 901.
11 J. W. Visser, *J. Appl. Crystallogr.*, 1969, **2**, 89.
12 Electron diffraction samples were prepared by crushing and dispersing onto holey-carbon coated molybdenum grids which were subsequently examined in a Philips EM 430 transmission electron microscope.
13 Y. Porter, K. M. Ok, N. S. P. Bhuvanesh and P. Shiv Halasyamani, *Chem. Mater.*, 2001, **13**, 1910.
14 A. Altomare, M. C. Burla, G. Cascarno, C. Giacovazzo, A. Guagliardi, A. G. G. Moliterni and G. Polidori, *J. Appl. Crystallogr.*, 1995, **28**, 842.
15 ^{51}V MAS NMR data were collected at 78.9 MHz on a Bruker DSX-300 spectrometer using a 4 mm outer diameter rotor, and spin rates of 6 and 10 kHz. The pulse width was 1 μs and 4k points were acquired for each transient, with an acquisition time of 0.004 s and a relaxation delay of 10 s. Chemical shifts were referenced relative to neat $VOCl_3$ using V_2O_5 (δ_{iso} = −609 ppm) as a secondary reference.
16 Neutron diffraction data were collected on a 10 g sample on instrument D2B at Institut Laue Langevin, using a Ge (335) monochromator (λ = 1.594 Å) and an array of 64 ^3He detectors spaced at 2.5° intervals.
17 O. B. Lapina, V. M. Mastikhin, V. N. Krasilnikov and K. I. Zamaraev, *Prog. NMR Spectrosc.*, 1992, **24**, 457.
18 Topas v2.0: General Profile and Structure Analysis Software for Powder Diffraction Data, Bruker AXS, Karlsruhe, Germany, 2000.
19 A. A. Coelho, *J. Appl. Crystallogr.*, 2000, **33**, 899.
20 Parameters refined: 1 scale, 1 zero, 7 profile, 7 background terms and 4 cell parameters for neutron data; 1 scale, 1 zero, 7 profile, 8 background terms and 4 cell parameters for synchrotron data; 36 positional parameters and 1 isotropic temperature factor for Bi/Pb atoms, 3 rotations, 3 translations and 1 isotropic temperature factor for rigid VO_4 groups, 24 positional parameters and 1 isotropic temperature factor for tetrahedrally coordinated oxygen atoms; data range 4–37° 2θ for X-rays and 8 to 122.19° for neutrons corresponding to a final *d*-spacing of 0.9104 Å. X-Ray and neutron data were given approximately equal weights in refinement. CCDC reference number 169043. See http://www.rsc.org/suppdata/cc/b1/b105242j/ for crystallographic data in CIF or other electronic format.

CHEMCOMM Communication
www.rsc.org/chemcomm

First synthesis of a highly symmetrical decakis-adduct of fullerene dimer C_{120}

Koichi Fujiwara and Koichi Komatsu*

Institute for Chemical Research, Kyoto University, Uji, Kyoto 611-0011, Japan.
E-mail: komatsu@scl.kyoto-u.ac.jp; Fax: +81 774 38 3178; Tel: +81 774 38 3172

Received (in Cambridge, UK) 25th June 2001, Accepted 29th August 2001
First published as an Advance Article on the web 10th September 2001

The highly symmetrical decakis-cyclopropanated derivative of C_{120} was synthesized using template activation and the structure was determined by X-ray crystallography; the decakis-adduct was converted into the eicosa-carboxylic acid derivative that is water soluble.

Fullerene is considered as a three-dimensional building block, to which multiple organic addends can be introduced. In particular, detailed studies have been conducted concerning the hexakis-adduct of C_{60} with a T_h symmetric octahedral addition pattern.[1–6] For example, regioselective introduction of different addends to these six positions have been reported,[3] giving applications as a core block of dendrimer molecules,[4] an organometallic ligand,[5] or an investigation of organic LEDs using the emisson property of the hexakis-adduct.[6] We have previously reported a highly selective synthesis of the fullerene dimer C_{120} by the solid-state reaction of C_{60} using a high-speed vibration-milling technique.[7,8] Having the two C_{60} cages directly connected, C_{120} can accommodate a larger number of addends. It seems to be a difficult task to precisely control the multi-addition to this very large molecule. However, we succeeded in the synthesis of the decakis-adduct of C_{120} with D_{2h} symmetry by the use of the Bingel cyclopropanation reaction under the template activation with 9,10-dimethylanthracene (DMA).[2] Here we report the synthesis, structure, and properties of this new highly symmetrical decakis-adduct.

The reaction was conducted by addition of excess amounts of diethyl bromomalonate (17 eq.) and 1,8-diazabicyclo[5.4.0]undec-7-ene (DBU) (17 eq.) to a solution of C_{120} and DMA (11 eq.) in *o*-dichlorobenzene (ODCB). After stirring for 3 days, the reaction mixture was roughly separated by flash chromatography over SiO_2 eluted with $CHCl_3$ and washed with diethyl ether to give the D_{2h} symmetric decakis-adduct **1**† as orange crystals in 26% yield (Scheme 1).

In the ^1H NMR spectrum of **1**, four signals (peak intensity 2 : 1 : 1 : 1) corresponding to ethyl groups were observed reflecting the D_{2h} symmetry. In the ^{13}C NMR spectrum, 12 signals were observed in the sp^2 region, which indicated the existence of only two kinds of cyclohexatriene rings on the fullerene cages. In the sp^3 region five signals including a signal for the central cyclobutane ring (71.1 ppm) were observed. The UV-vis spectrum of **1** was similar to that of the T_h symmetric hexakis-cyclopropanated C_{60},[1a] while the extinction coefficients were larger because of the presence of two C_{60} cages. These results clearly support the structure of **1**.

A single crystal of **1** was grown from a $CHCl_3$–chlorobenzene solution (~5 : 1), and its structure was determined by X-ray crystallography‡ as shown in Fig. 1. Four molecules of chlorobenzene were found in the unit cell. With respect to the bond length, the bond alternation between the 6-6 bond (average 1.385 Å) and the 5-6 bond (average 1.424 Å) on the π-system of the C_{60} cages is reduced compared with that of the original C_{120} (6-6 bond, 1.380 Å; 5-6 bond, 1.450 Å).[7a] This is attributed to the presence of the six-membered ring as an isolated π-system (which is somewhat more 'benzene-like') as in the case of T_h symmetric C_{60} hexakis-adducts.[2] The cyclobutane ring connecting the two C_{60} cages lies about an inversion centre and is thus planar; the cyclobutane bond lengths (intra-cage bond length, 1.582(6) Å; inter-cage bond length, 1.579(9) Å) are not significantly different. A similar situation was found in the case of the parent C_{120} (intra-cage bond length, 1.581(7) Å; inter-cage bond length, 1.575(7) Å).[7a]

Just in the same manner as the mother compound C_{120},[7b] the central cyclobutane ring of decakis-adduct **1** in $CHCl_3$ solution slowly underwent cleavage to give C_{60} pentakis-adduct **2** (Scheme 2) with a half-life of 1.5 days under irradiation of room light (*ca.* 100 lux). The same cleavage also took place under thermal conditions: **1** was quantitatively converted to **2** after heating at 200 °C for 0.5 h. This cleavage reaction of decakis-adduct **1** can be regarded as an efficient synthetic method of C_{60} pentakis-adduct **2**, which has only one reactive site left on the C_{60} cage. Thus, **2** is a suitable precursor for the selective synthesis of a hexakis-adduct of C_{60} having different addends. Fullerene **2** was allowed to react with an azomethine ylide,

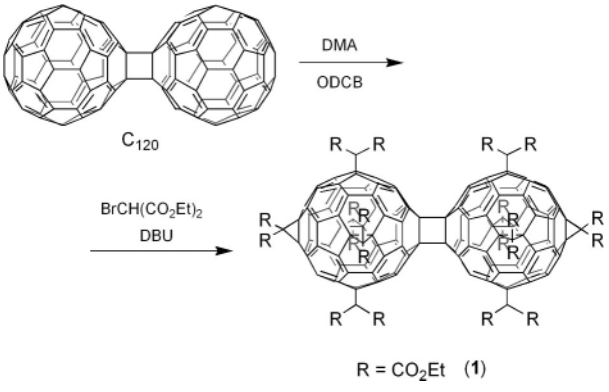

Scheme 1

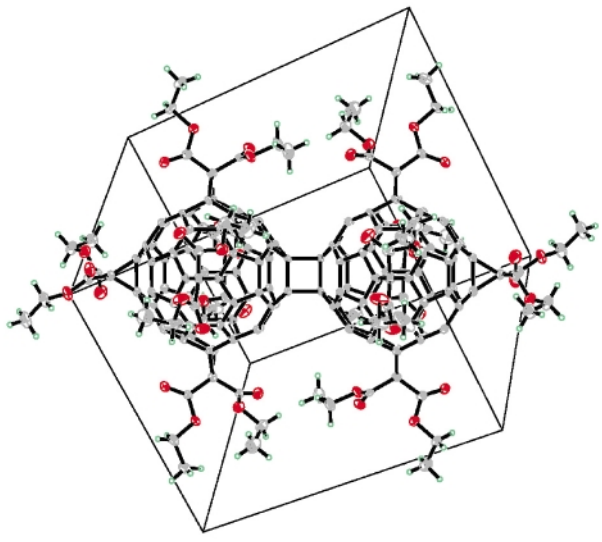

Fig. 1 X-ray crystal structure of **1**. Molecules of chlorobenzene were omitted for clarity.

 DOI: 10.1039/b105191c

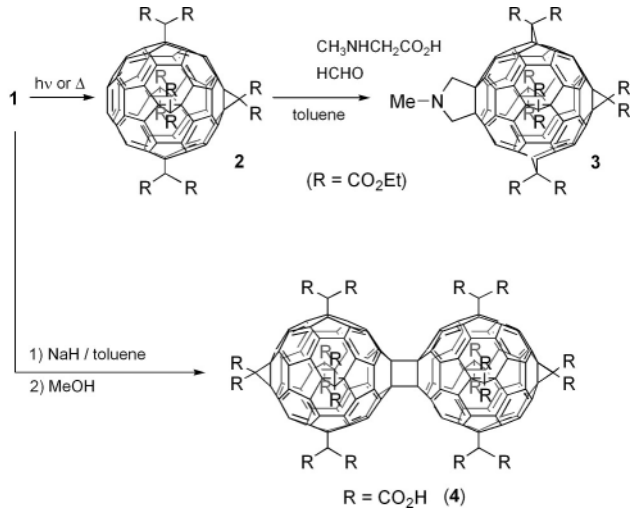

Scheme 2

generated from *N*-methylglycine and formaldehyde,[9] to give a C_{60} hexakis-adduct **3**§ having two kinds of addends in a high yield (82%).

When treated with NaH in toluene and with methanol,[10] the decakis-adduct **1** having 20 ester groups was transformed into the eicosa-carboxylic acid derivative **4**¶ in high yield (91%). In spite of the carbon-rich framework composed of two C_{60} cages, it exhibited considerable solubility in neutral water (16 mg ml^{-1}) to give a yellow–orange solution, owing to the presence of abundant hydrophilic sites.

In summary, the highly symmetrical decakis-adduct of fullerene dimer C_{120} was synthesized by the Bingel reaction with template activation. This adduct is expected to have an applicability as a core block for dendrimeric compounds and also as a precursor to a C_{2v} symmetric pentakis-adduct.

We thank the Ministry of Education, Science, Sports and Culture, Japan, for the Grant-in-Aids for COE Research on Elements Science, No. 12CE2005. K. F. thanks JSPS for a Research Fellowship for Young Scientists.

Notes and references

† ^{1}H NMR (300 MHz, $CDCl_3$) δ 4.34 (q, 8H), 4.38 (q, 16H), 4.32 (q, 8H), 4.21 (q, 8H), 1.37 (t, 12H), 1.34 (t, 24H), 1.32 (t, 12H), 1.22 (t, 12H); ^{13}C NMR (100 MHz, $CDCl_3$) δ 163.65, 163.57, 163.35, 163.08, 148.32, 145.93, 145.70, 145.38, 145.32, 145.24, 145.15, 141.52, 141.07, 140.06, 139.74, 139.39, 71.17, 69.60, 69.21, 68.83, 68.21, 62.75, 62.71, 62.68, 62.29, 45.42, 45.28, 41.04, 14.21, 14.06, 14.06, 14.02; UV-vis (CH_3CN–$CHCl_3$ (19 : 1)) λ_{max} 239 nm (log ε 5.24), 272 (5.13), 280sh (5.12), 320 (5.00), 344sh (4.83), 550sh (3.36).

‡ *Crystal data*: $C_{214}H_{120}Cl_4O_{40}$, M = 3472.90, triclinic space group $P\bar{1}$, a = 14.4234(7), b = 14.5285(7), c = 19.5453(9), α = 105.288(1), β = 100.531(1), γ = 93.227(1) V = 3860.6(3) Å^3, Z = 1, D_{calc} = 1.494 Mg m^{-3} Intensity data were collected at 103 K on a Bruker SMART APEX diffractometer with Mo-Kα radiation and graphite monochromater. The structure was solved by direct methods and refined by full-matrix least-squares on F^2 (SHELXTL). A total of 27583 reflections were measured and 17551 were independent. Final R_1 = 0.0747, wR_2 = 0.2076 ($I > 2\sigma(I)$), and GOF = 0.965 (for all data, R_1 = 0.1230, wR_2 = 0.2370). CCDC 168411. See http://www.rsc.org/suppdata/cc/b1/b105191c/ for crystallographic files in .cif or other electronic format.

§ ^{1}H NMR (300 MHz, $CDCl_3$) δ 4.40–4.23 (m, 20H), 3.70 (s, 4H), 2.63 (s, 3H), 1.40–1.27 (m, 30H); ^{13}C NMR (75 MHz, $CDCl_3$) δ 164.13, 163.92, 163.66, 152.83, 146.21, 145.64 (two overlapped signals), 145.53, 145.11, 143.59 141.77, 141.59, 140.01, 139.55, 139.11, 139.39, 70.01, 69.67, 69.42, 69.19, 68.18, 62.90, 62.79, 62.75, 62.68, 45.34, 44.90, 41.37, 41.23, 14.08, 14.05, 14.01; FAB MS, m/z 1567 (M^+).

¶ ^{13}C NMR (100 MHz, $(CD_3)_2CO$) δ 165.23, 165.71, 165.39, 165.24, 149.29, 146.48, 146.38 (two overlapped signals), 145.76, 145.63, 145.47, 143.07, 142.66, 141.58, 141.10, 141.03, 72.28, 71.18, 70.59, 70.59, 69.69, 48.28, 47.90, 43.77.

1 (*a*) For example: A. Hirsch, I. Lamparth and T. Grösser, *J. Am. Chem. Soc*., 1994, **116**, 9385; (*b*) L. Issacs, R. F. Haldimann and F. Diederich, *Angew. Chem., Int. Ed. Engl*., 1994, **33**, 2339; (*c*) R. F. Haldimann, F.-G. Klärner and F. Diederich, *Chem. Commun*., 1997, 237.

2 I. Lamparth, C. Maichle-Mössmer and A. Hirsch, *Angew. Chem., Int. Ed. Engl*., 1995, **34**, 1607; I. Lamparth, A. Herzog and A. Hirsch, *Tetrahedron*, 1996, **52**, 5065.

3 W. Qian and Y. Rubin, *Angew. Chem., Int. Ed*., 1999, **38**, 2356; W. Qian and Y. Rubin, *J. Am. Chem. Soc*., 2000, **122**, 9564; W. Qian and Y. Rubin, *Angew. Chem., Int. Ed*., 2000, **39**, 3133.

4 X. Camps, H. Schöberger and A. Hirsch, *Chem. Eur. J*., 1997, **3**, 561; X. Camps, E. Dietel, A. Hirsch, S. Pyo, L. Echegoyen, S. Hackbarth and B. Röder, *Chem. Eur. J*., 1999, **5**, 2362; A. Herzog, A. Hirsch and O. Vostrowsky, *Eur. J. Org. Chem*., 2000, 171; M. Brettreich, S. Burghardt, C. Böttcher, T. Bayerl, S. Bayerl and A. Hirsch, *Angew. Chem., Int. Ed*., 2000, **39**, 1845; F. Djojo, E. Ravanelli, O. Vostrowsky and A. Hirsch, *Eur. J. Org. Chem*., 2000, 1051.

5 T. Habicher, J.-F. Nierengarten, V. Gramlich and F. Diederich, *Angew. Chem., Int. Ed*., 1998, **37**, 1916.

6 G. Schick, M. Levitus, L. Kvetko, B. A. Johnson, I. Lamparth, R. Lunkwitz, B. Ma, S. I. Khan, M. A. Garcia-Garibay and Y. Rubin, *J. Am. Chem. Soc*., 1999, **121**, 3246; K. Hutchison, L. Gao, G. Schick, Y. Rubin and F. Wudl, *J. Am. Chem. Soc*., 1999, **121**, 5611.

7 (*a*) G.-W. Wang, K. Komatsu, Y. Murata and M. Shiro, *Nature*, 1997, **387**, 583; (*b*) K. Komatsu, G-W. Wang, Y. Murata, T. Tanaka, K. Fujiwara, K. Yamamoto and M. Saunders, *J. Org. Chem*., 1998, **63**, 9358.

8 For a recent review on C_{60} dimers, see: J. L. Segura and N. Martin, *Chem. Soc. Rev*., 2000, **29**, 13.

9 M. Maggini, G. Scorrano and M. Plato, *J. Am. Chem. Soc*., 1993, **115**, 9798.

10 I. Lamparth and A. Hirsch, *J. Chem. Soc., Chem. Commun*., 1994, 1727.

CHEMCOMM Communication
www.rsc.org/chemcomm

Synthesis and characterisation of $(C_4N_2H_{12})(UO_2)_2(PO_3H)_2\{PO_2(OH)H\}_2$: a three dimensionally connected actinide framework

Michael Doran, Susan M. Walker and Dermot O'Hare*

Inorganic Chemistry Laboratory, University of Oxford, South Parks Road, Oxford, UK OX1 3QR. E-mail: dermot.ohare@chem.ox.ac.uk

Received (in Cambridge, UK) 27th July 2001, Accepted 13th August 2001
First published as an Advance Article on the web 18th September 2001

The material $(C_4N_2H_{12})(UO_2)_2(PO_3H)_2\{PO_2(OH)H\}_2$ (MUPH-1) has been prepared hydrothermally; it is a three dimensional structure consisting of four intersecting elliptical shaped one-dimensional channels, the largest channel has dimensions of 13.1 × 7.2 Å.

In recent years we have been interested in developing the solid state chemistry of uranium. In particular, we have been interested in template-directed hydrothermal syntheses of novel uranium-containing phases. Zeolite-like materials built from MX_7, MX_8, or even MX_9 units, where M is a lanthanide or actinide, would be expected to exhibit unusual structural topologies, connectivity and reactivity. We have previously reported a series of layered uranium(IV) fluorides (UFO-*n*) which were prepared under hydrothermal conditions from UO_2, HF and H_3PO_4 by using $H_2N(CH_2)_nNH_2$ (n = 3, 4 or 6) as the structure directing agents.[1] More recently, we reported $(C_4N_2H_{12})U_2O_4F_6$ MUF-1[2,3] which was the first organically templated microporous actinide material. Here we report the phase pure synthesis and crystal structure of an organically templated actinide phosphite which contains a 3D channel network structure.

$(C_4N_2H_{12})(UO_2)_2(PO_3H)_2\{PO_2(OH)H\}_2$ MUPH-1 was synthesised hydrothermally by combining $UO_2(MeCO_2)_2{\cdot}2H_2O$

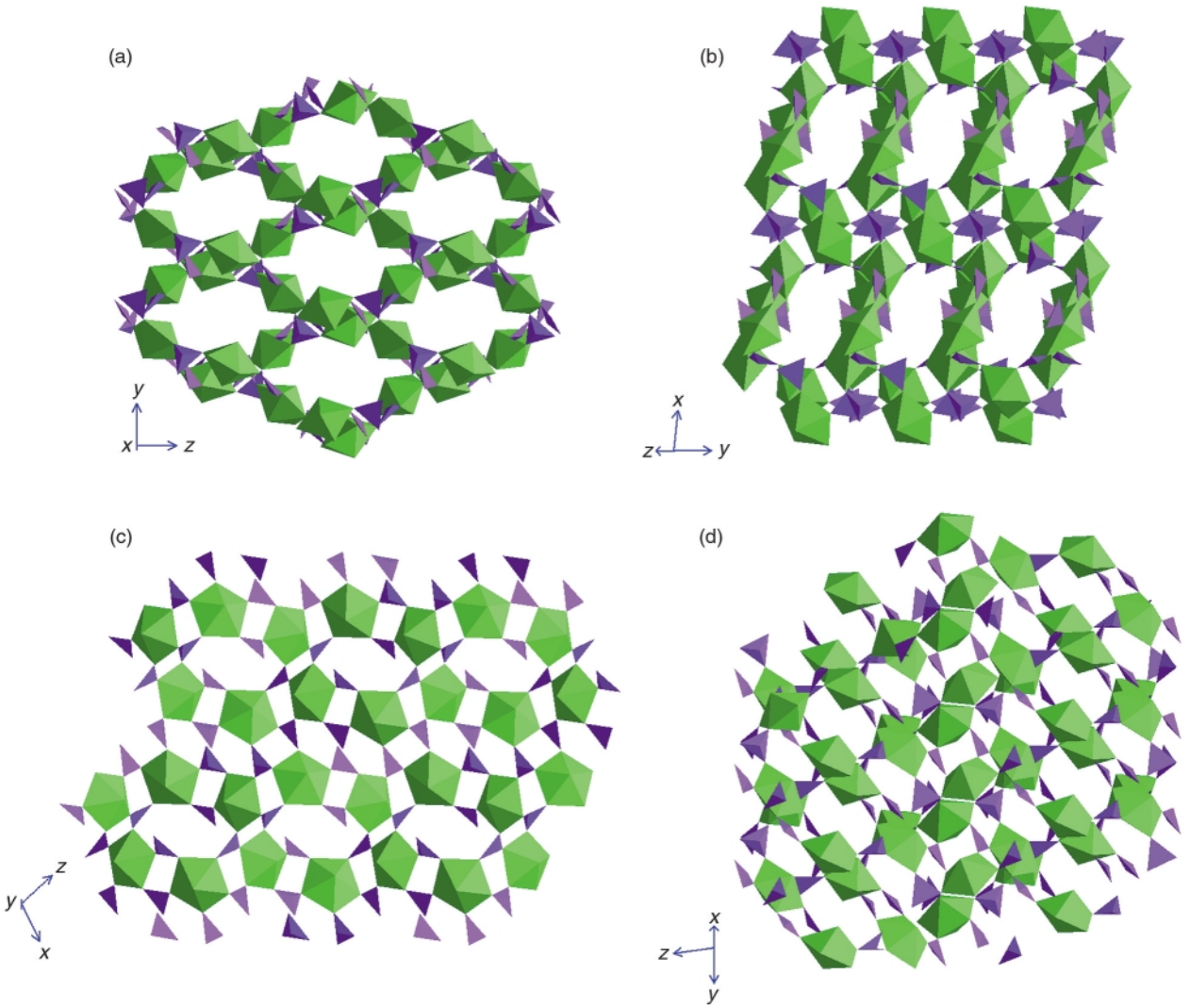

Fig. 1 Views of the structure of MUPH-1 down four crystallographic axes; (a) 100; (b) 011; (c) 010; (d) 110. (Note the piperazine template has been removed for clarity.)

 DOI: 10.1039/b106804k

Table 1 Summary of channel information for MUPH-1

Direction	Shape	Dimensions/Å	Ring size/atoms
100	Elliptical	8.306 × 7.230	12 atoms
011	Elliptical	13.170 × 7.230	12 atoms
010	Elliptical	8.127 × 6.900	8 atoms
110	Elliptical	6.483 × 4.878	8 atoms

(0.406 g, 1.0×10^{-3} mol), H_3PO_3 (Aldrich, 99%) (0.385 g, 4.7×10^{-3} mol), and $C_4N_2H_{10}$ (Aldrich, 95%) (0.043 g, 0.5×10^{-3} mol) in a Teflon-lined, 23 ml stainless steel autoclave. $UO_2(MeCO_2O)_2{\cdot}2H_2O$ was synthesized as previously described.[3] The autoclave was sealed, heated for 1 d at 180 °C, and cooled at 6 °C h^{-1} to room temperature over an additional day. The only product recovered was yellow rods, obtained in 25% yield based on uranium.† The powder X-ray diffraction pattern of this product is in excellent agreement with the pattern generated from the single crystal structure data.‡

MUPH-1 contains two crystallographically unique uranium atoms, both of which adopt seven coordinate, pentagonal bipyramidal geometries. Axially, the uranium atoms are bonded to two oxygen atoms to form uranyl units. The axial U=O bond lengths range between 1.772(10) and 1.780(10) Å, with O=U=O bond angles of 176.2(5) and 176.9(5)°. In the equatorial plane, both uranium atoms are bonded to five oxygen atoms, with U–O bond lengths ranging between 2.321(10) and 2.445(9) Å. The O–U–O bond angles are between 69.4(3) and 75.6(3)°. The uranium polyhedra share all five equatorial vertices with phosphite groups. Bond valence calculations give values of 6.738 and 6.809 for the uranium atoms.[4]

There are four crystallographically distinct phosphorus atoms, each bonded to three oxygen atoms and one hydrogen atom in a truncated tetrahedral environment. Two of the phosphite groups contain three bridging oxygen atoms, while the other two contain two bridging oxygen atoms and one terminal OH group. The bridging P–O bond lengths are between 1.487(13) and 1.533(10) Å whilst the P–OH bond lengths are 1.537(14) and 1.557(11) Å. Bond valence calculations give values between 4.088 and 4.258 for the P–H unit.[5]

The linkages between the polyhedra result in an anionic $[(UO_2)_2(PO_3H)_2\{PO_2(OH)H\}_2]^{2-}$ three dimensional framework, which contains four channels running throughout the structure. These are summarised in Table 1, and shown in Fig. 1. There are two distinct template molecules in MUPH-1, both of which form hydrogen bonds with the inorganic framework. They are found along the 100 channel, stacked in an ABA fashion.

The thermal analysis shows no significant mass loss until between 325 and 400 °C, where 4.5% of the starting mass is lost. This is due to the start of template decomposition. At 400 °C a smoother mass loss of 2% begins, continuing until 725 °C, attributable to further template decomposition and the start of framework breakdown. Between 725 and 850 °C there is a rapid mass loss of 5%, indicating framework breakdown. The final product obtained after heating to 850 °C is UP_2O_7.

The presence of the template is confirmed in the IR spectrum by the N–H stretch at 3024 cm^{-1}, the N–H bend at 1604 cm^{-1} and the C–H bending mode at 1430 cm^{-1}. P–H stretches are observed as sharp peaks at 2426 and 2400 cm^{-1}. P–H bending modes are observed at 1042 and 984 cm^{-1}. A P–O stretch can be seen at 1156 cm^{-1}. The U=O asymmetric and symmetric stretches appear at 950 and 828 cm^{-1} respectively. The MAS ^{31}P solid state NMR spectrum of MUPH-1 exhibits two resonances at 13.4 and 9.2 ppm which is consistent with the crystal chemistry.

We thank the EPSRC for financial support.

Notes and references

† Elemental analysis; found (calc.) for $(C_4N_2H_{12})(UO_2)_2(PO_3H)_2\{PO_2(OH)H\}_2$: C, 5.06 (5.06); N, 2.95 (2.95); H, 2.07 (1.91); P, 12.94 (13.04); U, 50.37 (50.10)%.

‡ *Crystal data* for MUPH-1: $(C_4N_2H_{12})(UO_2)_2(PO_3H)_2\{PO_2(OH)H\}_2$: $C_4H_{18}N_2O_{16}P_4U_2$, M = 950.14, monoclinic, space group $P2_1/n$, a = 13.758(5), b = 8.180(5), c = 18.037(5) Å, β = 106.647(5)°, V = 1944.81(15) $Å^3$, 150 K, Z = 4, D_c = 3.245 g cm^{-3}, μ(Mo-Kα) = 17.042 mm^{-1}, 8286 total (4467 independent) reflections, R = 0.0396 and R_W = 0.1052 for 3315 reflections with $I > 2\sigma(I)$. CCDC reference number 168965. See http://www.rsc.org/suppdata/cc/b1/b106804k/ for crystallographic data in CIF or other electronic format.

1 R. J. Francis, P. S. Halasyamani and D. O'Hare, *Angew. Chem., Int. Ed.*, 1998, **37**, 2214; P. S. Halasyamani, R. J. Francis, J. Bee and D. O'Hare, *J. Am. Chem. Soc.*, 1999, **121**, 1609.

2 P. S. Halasyamani, S. M. Walker and D. O'Hare, *J. Am. Chem. Soc.*, 1999, **121**, 7415.

3 S. M. Walker, P. S. Halasyamani, S. Allen and D. O'Hare, *J. Am. Chem. Soc.*, 1999, **121**, 10 513.

4 P. C. Burns, R. C. Ewing and F. C. Hawthorne, *Can. Miner.*, 1997, **35**, 1551.

5 N. E. Brese and M. O'Keeffe, *Acta Crystallogr., Sect B*, 1991, **47**, 192; I. D. Brown and D. Altematt, *Acta Crystallogr., Sect. B*, 1985, **41**, 244.

CHEMCOMM Communication
www.rsc.org/chemcomm

Direct *in situ* observation of increasing structural dimensionality during the hydrothermal formation of open-framework zinc phosphates

Richard I. Walton,[a] Alexander J. Norquist,[b] S. Neeraj,[c] Srinivasan Natarajan,[c] C. N. R. Rao[c] and Dermot O'Hare*[b]

[a] *School of Chemistry, Stocker Road, University of Exeter, Exeter, UK EX4 4QD*
[b] *Inorganic Chemistry Laboratory, South Parks Road, Oxford, UK OX1 3QR*
E-mail: dermot.ohare@chem.ox.ac.uk
[c] *Chemistry and Physics of Materials Unit, Jawaharla Nehru Centre for Advanced Scientific Research, Jakkur PO, Bangalore, 560 064, India*

Received (in Cambridge, UK) 27th June 2001, Accepted 10th August 2001
First published as an Advance Article on the web 18th September 2001

The first time-resolved *in situ* X-ray diffraction studies of the hydrothermal crystallisation of open-framework zinc phosphates reveal a pathway of sequential crystallisation involving formation of a metastable low dimensional chain phase before the growth of three-dimensional zeolitic architectures.

A great deal of effort is currently focussed on understanding the crystallisation mechanism of microporous solids which can have applications in shape-selective catalysis, separation science, and ion-exchange. It is hoped that an understanding of mechanisms leading to the formation of these zeolite-like solids at the atomic-scale will allow the rational synthesis of new materials.[1,2] The common use of hydrothermal synthesis conditions in the preparation of such open-framework solids requires sealed thick-walled reaction vessels and it is only in recent years that *in situ* probes of hydrothermal crystallisation have been developed to follow reactions under these experimentally-challenging conditions.[3] For example, in a study of the phosphates of gallium using energy-dispersive X-ray diffraction (EDXRD) some of us have observed previously-unknown, transient phases prior to the onset of crystallisation of open-framework phases,[4,5] and Taulelle *et al.* have identified oligomeric 'building blocks' in hydrothermal reaction solutions using NMR spectroscopy.[6] The results of such studies provide a foundation on which to build descriptions of reaction mechanisms.

The first results of an *in situ* EDXRD study of the hydrothermal synthesis of zinc phosphates are described here. This large family of solids has recently been the focus of study by some of us, and an Aufbau principle for the building up of three-dimensional structures from structures of lower dimensionalities proposed.[7] With an aim of gaining further information about crystallisation mechanisms it is crucial to study systems such as these using *in situ* measurements of crystallisation, since it has been established that on arresting a hydrothermal reaction by cooling to room temperature the material recovered is not necessarily representative of the material present under reaction conditions.[4,5] The EDXRD method uses intense synchrotron X-rays which allows the use of a laboratory-sized hydrothermal reaction vessel, mimicking the conditions employed in the synthetic laboratory and permitting rapid data collection (< 1 min) for kinetic studies. An apparatus developed over the past few years by O'Hare and co-workers[8] was used in the current work.†

In the first zinc phosphate system studied we focussed on the reaction between piperazine phosphate ($[C_4N_2H_{12}][HPO_4]\cdot H_2O$, PIP-P) and zinc oxide in dilute hydrochloric acid solution. Fig. 1 shows a stack plot of the time-resolved EDXRD data measured as a reaction mixture of composition ZnO : 1.5 HCl : 1.75 PIP-P : 100 H_2O which was heated to 180 °C in an autoclave at *ca.* 5 °C min^{-1} (detector angle 0.9325°). The use of a three-element energy discriminating detector system[9] allows unambiguous identification of known crystalline phases, owing to the large amount of diffraction data that can be simultaneously recorded.[10] Characteristic Bragg reflections of the phosphate and amine source, PIP-P, are observed only during the first minute before disappearing; presumably this is due to dissolution of this rather soluble species. Remarkably, we observe that characteristic Bragg reflections of a known zinc phosphate, $[C_4N_2H_{12}][Zn(HPO_4)_2(H_2O)]$ (ZnPO–PIP-I),[11] are present in the first spectrum recorded (31 °C), suggesting that this material forms on mixing the chemicals at room temperature. The compound has a 1-D ladder structure (see Table 1 for descriptions of the phases discussed in this paper). After heating to 163 °C new strong Bragg reflections (of a phase not yet identified) are apparent, and these diffraction features, along with those of ZnPO–PIP-I, have constant intensity for 30 min during which time a temperature of 180 °C is reached. Over a period of 10 min, these two phases and the starting material ZnO are replaced by two known zinc phosphates, $[C_4N_2H_{12}][Zn_{3.5}(PO_4)_3(H_2O)]$ (ZnPO–PIP-II)[11,12] and $[C_4N_2H_{12}][Zn_2(HPO_4)_2(H_2PO_4)_2]$ (ZnPO–PIP-III),[11] which are the sole two products after 145 min of heating. ZnPO–PIP-II and ZnPO–PIP-III both have three-dimensional framework structures.

On changing the amount of PIP-P we observed rather different behaviour. For a mixture of composition ZnO : 1.5 HCl : 1 PIP-P : 100 H_2O, held at a constant temperature of 180 °C, the ladder phase ZnPO–PIP-I is present in the first spectrum

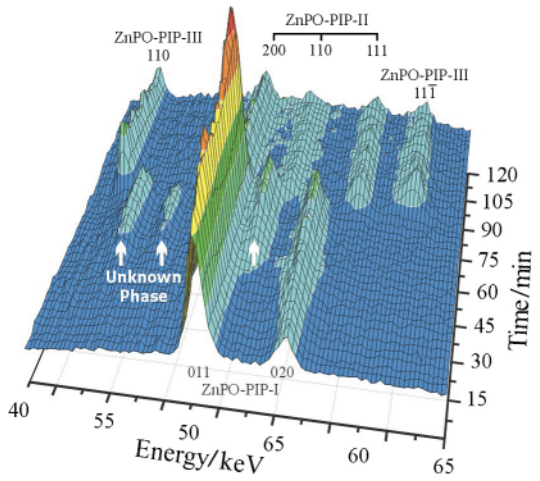

Fig. 1 A stack plot of EDXRD data measured during the sequential crystallisation of zinc phosphates from the reaction mixture ZnO : 1.5 HCl : 1.75 PIP-P : 100 H_2O.

 DOI: 10.1039/b105659j

Table 1 Zinc phosphates observed *in situ* in the ZnO/PIP-P/HCl (aq) system

Compound (dimensionality)	Formula	Miller index, observed *d* (expected)/[c]/Å Lowest EDXRD detector at 0.9325°
ZnPO–PIP-I[a] (1-D)	$[C_4N_2H_{12}][Zn(HPO_4)_2(H_2O)]$	011, 7.77 (7.733) 020, 7.05 (7.012)
ZnPO–PIP-II[a,b] (3-D)	$[C_4N_2H_{12}][Zn_{3.5}(PO_4)_3(H_2O)]$	200, 7.82 (7.813) 110, 7.30 (7.300) 111, 6.74 (6.717)
ZnPO–PIP-III[a] (3-D)	$[C_4N_2H_{12}][Zn_2(HPO_4)_2(H_2PO_4)_2]$	110, 9.285 (9.272) 11$\bar{1}$, 6.37 (6.325)
ZnPO–PIP-IV[a] (3-D)	$[C_4N_2H_{12}][Zn(H_2O)Zn(HPO_4)(PO_4)]_2$	110, 9.35 (9.327) 11$\bar{1}$, 7.73 (7.703) 020, 7.47 (7.444) 111, 6.99 (6.954) 200, 5.96 (5.983)

[a] Ref. 11 [b] Ref. 12. [c] Bottom EDXRD detection.

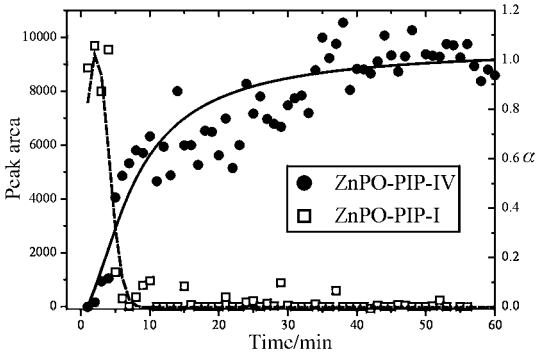

Fig. 2 Integrated peak intensities of ZnPO–PIP-I and ZnPO–PIP-IV during crystallisation from the reaction mixture ZnO : 1.5 HCl : 1 PIP-P : 100 H_2O at 180 °C.

recorded, and almost immediately its Bragg reflections begin to decay. The ladder phase is consequently replaced by a known zinc phosphate with a three-dimensional structure, $[C_4N_2H_{12}][Zn(H_2O)Zn(HPO_4)(PO_4)]$ (ZnPO–PIP-IV).[11] The decay of the precursor phase and growth of the product are not mirrored precisely: integrated peak intensities show that an appreciable amount of ZnPO–PIP-I is consumed before ZnPO–PIP-IV is observed. The decay and growth curves cross at $\alpha \approx 0.3$ of product (α is the extent of reaction; see Fig. 2). This suggests that the transformation of the chain material to the three-dimensional structure is a solution-mediated process involving dissolution of the first phase, rather than a solid-state transformation.

We have presented preliminary results of an *in situ* study of the formation of a large family of open-framework materials. The dissolution of starting materials and sequential crystallisation of a number of open-framework solids was directly observed. In certain cases, crystalline materials with as-yet unknown structures form during the reactions. Given the huge number of zinc phosphate structures that can be formed from reaction mixtures of only slightly differing composition, it is not unexpected to discover new metastable phases. The importance of these crystallisation studies is that for the first time we have observed *under real reaction conditions* the sequential crystallisation of materials with increasing dimensionality. Recently it has been shown that a ladder zinc phosphate, similar to that observed as a transient phase in our *in situ* studies, can be used as a solid precursor to a number of other layered and 3-D phases.[13] Combined with our *in situ* results, such studies of the reactivity of the ZnPO phases provide convincing evidence for the Aufbau principle proposed recently for the building up of 3-D zinc phosphate structures.[7] We are currently extending our *in situ* studies to survey other ZnPO/amine systems in order to understand more fully the nature of the structural transformations taking place.

We thank the EPRSC for funding and provision of beam-time at SRS, Daresbury Laboratory.

Notes and references

† EDXRD experiments were performed on Station 16.4 of the Daresbury Synchrotron Radiation Source ($I \sim 200$ mA, ~ 2 GeV synchrotron). Station 16.4 was illuminated with X-rays in the energy range 5–120 keV from a 6 T superconducting wiggler insertion device. Diffracted X-rays were measured using a three-element germanium solid-state detector; this allowed access to three *d*-spacing ranges, dependant on the angle to which the detector was set. The delay between mixing reagents, sealing in the hydrothermal autoclave and beginning data collection was of the order of 5 min.

1 M. E. Davis, *Stud. Surf. Sci. Catal*., 1995, **97**, 35.
2 R. J. Francis and D. O'Hare, *J. Chem. Soc., Dalton Trans*., 1998, 3133.
3 R. I. Walton and D. O'Hare, *Chem. Commun*., 2000, 2283.
4 R. J. Francis, S. O'Brien, A. M. Fogg, P. S. Halasyamani, D. O'Hare, T. Loiseau and G. Férey, *J. Am. Chem. Soc*., 1999, **121**, 1002.
5 R. I. Walton, T. Loiseau, D. O'Hare and G. Férey, *Chem. Mater*., 1999, 3201.
6 F. Taulelle, M. Haouas, C. Gerardin, C. Estournes, T. Loiseau and G. Férey, *Colloids Surf. A*, 1999, **158**, 299.
7 C. N. R. Rao, S. Natarajan, A. Choudhury, S. Neeraj and A. A. Ayi, *Acc. Chem. Res*., 2001, **34**, 80.
8 J. S. O. Evans, R. J. Francis, D. O'Hare, S. J. Price, S. M. Clarke, J. Flaherty, J. Gordon, A. Nield and C. C. Tang, *Rev. Sci. Instrum*., 1995, **66**, 2442.
9 S. L. Colston, S. D. M. Jacques, P. Barnes, A. C. Jupe and C. Hall, *J. Synchrotron Radiat*., 1998, **5**, 112.
10 G. Muncaster, A. T. Davies, G. Sankar, C. R. A. Catlow, J. M. Thomas, S. L. Colston, P. Barnes, R. I. Walton and D. O'Hare, *Phys. Chem. Chem. Phys*., 2000, **2**, 3523.
11 C. N. R. Rao, S. Natarajan and S. Neeraj, *J. Am. Chem. Soc*., 2000, **122**, 2810.
12 K. O. Kongshaug, H. Fjellvåg and K. P. Lillerud, *J. Mater. Chem*., 1999, **9**, 3119.
13 A. Choudhury, S. Neeraj, S. Natarajan and C. N. R. Rao, *J. Mater. Chem*., 2001, **11**, 1537.

CHEMCOMM Communication
www.rsc.org/chemcomm

3′-Amino-2′,4′-BNA: novel bridged nucleic acids having an N3′→P5′ phosphoramidate linkage

Satoshi Obika,[a] Mayumi Onoda,[a] Koji Morita,[b] Jun-ichi Andoh,[a] Makoto Koizumi[b] and Takeshi Imanishi*[a]

[a] *Graduate School of Pharmaceutical Sciences, Osaka University, 1-6 Yamadaoka, Suita, Osaka 565-0871, Japan. E-mail: imanishi@phs.osaka-u.ac.jp; Fax: (+81) 6-6879-8204; Tel: (+81) 6-6879-8200*

[b] *Exploratory Chemistry Research Laboratories, Sankyo Co., Ltd, 1-2-58 Hiromachi, Shinagawa, Tokyo 140-8710, Japan.*

Received (in Cambridge, UK) 27th June 2001, Accepted 24th August 2001
First published as an Advance Article on the web 18th September 2001

Novel oligonucleotide analogues, containing a 3′-amino-2′,4′-BNA unit, were successfully synthesized, and they showed superior duplex and triplex forming ability as well as BNA itself, along with remarkable enzymatic stability.

Oligonucleotides for practical antisense and/or antigene molecules should fulfil some requirements, such as a high binding affinity for the target ssRNA or dsDNA, high sequence selectivity, and sufficient enzymatic stability. During the past decade, various chemically modified oligonucleotides have been synthesized, and their properties have been investigated;[1–5] however, an ideal antisense or antigene molecule is still lacking. We recently achieved the first synthesis of a novel nucleoside with a fixed *N*-type conformation,[6] 2′-*O*,4′-*C*-methylene bridged nucleic acid (2′,4′-BNA)[7,8] (Fig. 1) and found that 2′,4′-BNA modified oligonucleotides exhibited strong hybridization ability with complementary strands of RNA and DNA.[9,10] Moreover, these 2′,4′-BNA oligonucleotides appeared to possess high affinity for dsDNA forming a stable DNA triplex.[10–15]

On the other hand, Gryaznov *et al*. reported in numerous papers that oligonucleotide analogues with an N3′→P5′ phosphoramidate linkage show superior properties of hybridization to ssDNA, ssRNA and dsDNA, along with high resistance to enzymatic degradation.[16–19]

Therefore, we became interested in a combination of a BNA structure and an N3′→P5′ phosphoramidate linkage.† Here, we report the synthesis, hybridization properties and enzymatic stability of novel oligonucleotide analogues with a 3′-amino-2′,4′-BNA monomer unit (Fig. 1).

The synthesis of 3′-amino-2′,4′-BNA heterodimer building block **1** was accomplished as shown in Scheme 1. After protection of the 5′-hydroxy group in **2**,[20] the 3′-azido group was successfully reduced to give the 3′-amino derivative **3**. Condensation of **3** with a 5′-phosphoramidite **4**[21] was performed according to the reported procedure.[17,21] The obtained heterodimer **5** was converted to the deisred compound **1** by treatment with tetrabutylammonium fluoride and subsequent phosphitylation. The 3′-amino-2′,4′-BNA oligonucleotides **6–8** were prepared using the phosphoramidite **1**.‡

The duplex-forming abilities of the 3′-amino-2′,4′-BNA modified oligonucleotide **6** with complementary ssDNA and ssRNA were elucidated under physiological conditions on the basis of melting temperatures (T_ms) (Table 1). Replacement of a natural 2′-deoxyribonucleotide by a 3′-amino-2′,4′-BNA monomer in the 12-mer oligonucleotide **9** resulted in significant

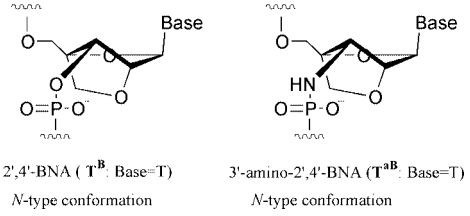

Fig. 1 Structure and conformation of 2′,4′-BNA and 3′-amino-2′,4′-BNA.

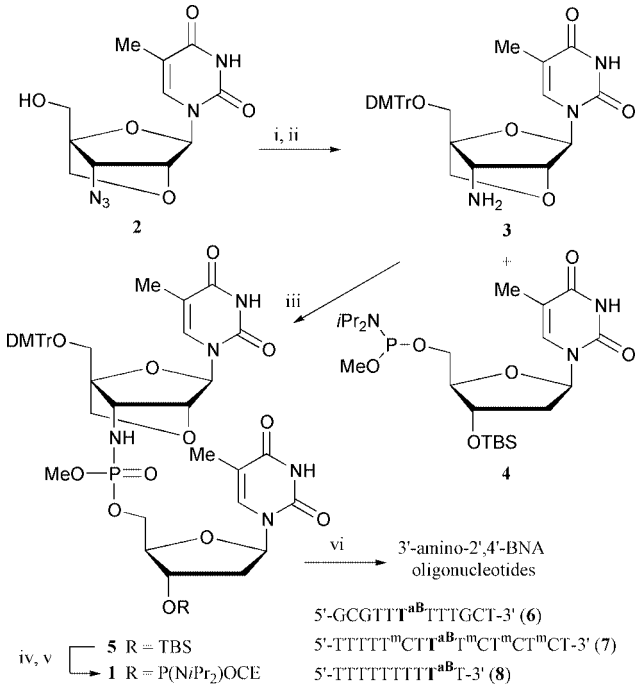

Scheme 1 *Reagents and conditions*: i 4,4′-dimethoxytrityl chloride, DMAP, Py, room temp., 76%; ii Ph_3P, Py, room temp., then NH_4OH aq., room temp., 97%; iii CCl_4, Et_3N, MeCN, room temp., 39%; iv TBAF, THF, room temp., 78%; v 2-cyanoethyl *N*,*N*,*N*′,*N*′-tetraisopropylphosphorodiamidite, diisopropylammonium tetrazolide, MeCN–THF, room temp., 61%; vi DNA synthesizer (AB Expedite™ 8909). CE = 2-cyanoethyl. DMTr = 4,4′-dimethoxytrityl.

Table 1 T_m values for 3′-amino-2′,4′-BNA with complementary DNA and RNA[a]

	T_m (ΔT_m)/°C	
Oligonucleotides	DNA	RNA
5′-GCGTTT**T^aB**TTTGCT-3′ (**6**)	51 (+4)	52 (+7)
5′-GCGTTT**T^B**TTTGCT-3′ (**10**)	53 (+6)	52 (+7)
5′-GCGTTTTTTGCT-3′ (**9**)	47	45

[a] UV melting profiles were measured in 10 mM sodium phosphate buffer (pH 7.2) containing 100 mM NaCl at a scan rate of 0.5 °C min^{-1} at 260 nm. The oligonucleotide concentration used was 4 μM for each strand. The sequence of target DNA or RNA complements is 5′-AGCAAAAAACGC-3′.

 DOI: 10.1039/b105640a

Table 2 T_m values of 3′-amino-2′,4′-BNA with dsDNA[a]

Oligonucleotides	T_m (ΔT_m)/°C	
	+10 mM $MgCl_2$	−$MgCl_2$
5′-TTTTT^{m}CT**T^{aB}**T^{m}CT^{m}CT^{m}CT-3′ (**7**)	55 (+11)	44 (+11)
5′-TTTTT^{m}CT**T^B**T^{m}CT^{m}CT^{m}CT-3′ (**12**)	57 (+13)	44 (+11)
5′-TTTTT^{m}CTTT^{m}CT^{m}CT^{m}CT-3′ (**11**)	44	33

[a] UV melting profiles were measured in 7 mM sodium phosphate buffer (pH 7.0) containing 140 mM KCl without or with additional 10 mM $MgCl_2$. The oligonucleotide concentration used was 1.5 μM for each strand. The sequence of target dsDNA is 5′-GCTAAAAAGAAAGAGAGATCG-3′/3′-CGATTTTTCTTTCTCTCTAGC-5′. ^{m}C means 5-methylcytidine.

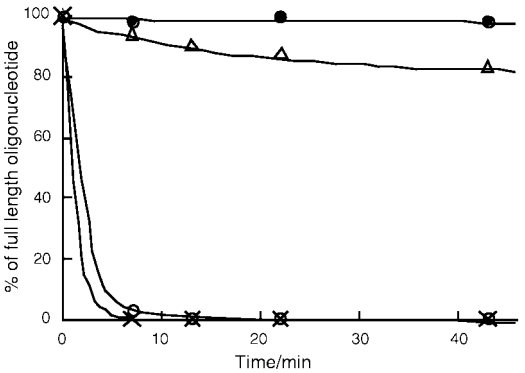

Fig. 2 Enzymatic stability of T_8**T^{aB}**T (**8**) (closed circle), T_{10} (**13**) (cross), T_8**T^B**T (**14**) (open circle) and T_8T_ST (**15**) (triangle). Hydrolysis of the oligonucleotides (10 μg) was carried out at 37 °C in a buffer (320 μl) containing 50 mM Tris–HCl (pH 8.0), 10 mM $MgCl_2$ and SVPDE (0.2 μg). '$_S$' means phosporthioate linkage.

stabilization of the duplexes formed with both complementary DNA and RNA. The increases in T_ms were up to 4 and 7 °C for the duplexes formed with the DNA and RNA strands, respectively. Next, the binding affinity of the oligonucleotide **7** to a homopurine•homopyrimidine dsDNA was also studied and shown to be much higher than that of the natural oligonucleotide **11**. The T_m values of triplex formation for **7** were 55 and 44 °C under neutral conditions with or without 10 mM $MgCl_2$, respectively, which is over 10 °C higher than the corresponding value for **11** as summarized in Table 2.

Thus, the oligonucleotides with one-point modification by 3′-amino-2′,4′-BNA, a combination of the 2′,4′-BNA backbone and N3′→P5′ phosphoramidate linkage, exhibited enhanced hybridizing properties towards complementary ssDNA, ssRNA and dsDNA, compared to the corresponding natural oligonucleotides. These ΔT_m values were almost comparable to those for 2′,4′-BNA singly modified congeners **10** and **12**, and seem to reach the utmost level of hybridization.

The nuclease-resistance of the 3′-amino-2′,4′-BNA modified oligonucleotide **8** was investigated by using snake venom phosphodiesterase (SVPDE), compared with natural and one point modified (2′,4′-BNA or phosphorthioate[22]) oligothymidilate 10-mers **13**, **14** and **15**, respectively. The reaction mixtures were analyzed at several time points by reversed-phase HPLC to monitor the percentage of full length oligonucleotides (Fig. 2). Under the conditions used, the natural T 10-mer control **13** and the 2′,4′-BNA **14** were immediately digested. In both cases, no full length oligomer was detected after 10 min, although the 2′,4′-BNA modification of oligonucleotides was found to be sufficiently resistant to enzymatic hydrolysis in other cases.[10] In contrast, more than 98% of full length 3′-amino-2′,4′-BNA oligonucleotide **8** was unchanged after 40 min, while 83% of **15** was intact after the same time period. It is noteworthy that enzymatic stability of the 3′-amino-2′,4′-BNA **8** was superior to that of the phosphorthioate modified oligonucleotide **15**.[22]

The results presented here clearly demonstrate that the novel nucleic acid analogue, 3′-amino-2′,4′-BNA, was a good candidate for a practical antisense and antigene molecule, due to its potent hybridization ability with DNA and RNA complements and homopurine•homopyrimidine dsDNA, and remarkable enzymatic stability surpassing that of phosphorthioate oligonucleotides. Further investigation of properties of the 3′-amino-2′,4′-BNA is currently under way.

Notes and references

† Recently Wang and Stoisavljevic reported a combination of a phosphoramidate linkage and another type of bicyclic nucleoside, and their modification of oligonucleotides decreased the duplex-forming ability. See ref. 21.

‡ The obtained 3′-amino-2′,4′-BNA oligonucleotides were purified by reversed-phase HPLC, and the compositions were determined by MALDI-TOF-MS. MALDI-TOF-MS data: **6** [M − H]$^-$ 3024.58 (calc. 3024.05); **7** [M − H]$^-$ 4523.32 (calc. 4523.13); **8** [M − H]$^-$ 3615.11 (calc. 3614.47).

1 E. Uhlmann and A. Peyman, *Chem. Rev*., 1990, **90**, 543.
2 S. L. Beaucageand R. P. Iyer, *Tetrahedron*, 1993, **49**, 6123.
3 N. T. Thoung and C. Hélène, *Angew. Chem., Int. Ed. Engl*., 1993, **32**, 666.
4 S. O. Doronina and J.-P. Behr, *Chem. Soc. Rev*., 1997, 63.
5 I. Luyten and P. Herdewijn, *Eur. J. Med. Chem*., 1998, **33**, 515.
6 W. Saenger, *Principles of Nucleic Acid Structure*, Springer-Verlag, New York, 1984, p. 17.
7 S. Obika, D. Nanbu, Y. Hari, K. Morio, Y. In, T. Ishida and T. Imanishi, *Tetrahedron Lett*., 1997, **38**, 8735.
8 We defined BNA as a novel class of nucleic acid analogues containing 2′-*O*,4′-*C*- or 3′-*O*,4′-*C*-methylene bridged structure (*e.g*. 2′,4′-BNA or 3′,4′-BNA). The 2′,4′-BNA was also called 'LNA' by Wengel *et al*. See: S. K. Singh, P. Nielsen, A. A. Koshkin and J. Wengel, *Chem. Commun*., 1998, 455.
9 S. Obika, D. Nanbu, Y. Hari, J. Andoh, K. Morio, T. Doi and T. Imanishi, *Tetrahedron Lett*., 1998, **39**, 5401.
10 T. Imanishi and S. Obika, *J. Syn. Org. Chem., Jpn*., 1999, **57**, 969.
11 S. Obika, Y. Hari, K. Morio and T. Imanishi, *Tetrahedron Lett*., 2000, **41**, 221.
12 S. Obika, Y. Hari, T. Sugimoto, M. Sekiguchi and T. Imanishi, *Tetrahedron Lett*., 2000, **41**, 8923.
13 H. Torigoe, Y. Hari, M. Sekiguchi, S. Obika and T. Imanishi, *J. Biol. Chem*., 2001, **276**, 2354.
14 S. Obika, T. Uneda, T. Sugimoto, D. Nanbu, T. Minami, T. Doi and T. Imanishi, *Bioorg. Med. Chem*., 2001, **9**, 1001.
15 S. Obika, Y. Hari, M. Sekiguchi and T. Imanishi, *Angew. Chem*., 2001, **40**, 2079; S. Obika, Y. Hari, M. Sekiguchi and T. Imanishi, *Angew. Chem., Int. Ed*., 2001, **113**, 2149.
16 S. M. Gryaznov, *Biochim. Biophys. Acta*, 1999, **1489**, 131.
17 J.-K. Chen, R. G. Schultz, D. H. Lloyd and S. M. Gryaznov, *Nucleic Acids Res*., 1995, **23**, 2661.
18 R. G. Schultz and S. M. Gryaznov, *Nucleic Acids Res*., 1996, **24**, 2966.
19 S. M. Gryaznov and H. Winter, *Nucleic Acids Res*., 1998, **26**, 4160.
20 S. Obika, J. Andoh, T. Sugimoto, K. Miyashita and T. Imanishi, *Tetrahedron Lett*., 1999, **40**, 6465.
21 G. Wang and V. Stoisavljevic, *Nucleosides Nucleotides, Nucleic Acids*, 2000, **19**, 1413.
22 The phosphorthioate oligonucleotide used in this study was an S_P-isomer which is known to be more resistant to degradation by SVPDE than an R_P-isomer. See: P. M. J. Burgers, B. K. Sathyanarayana, W. Saenger and F. Eckstein, *Eur. J. Biochem*., 1979, **100**, 585.

CHEMCOMM
Communication
www.rsc.org/chemcomm

Directed assembly of multilayers—the case of Prussian Blue

Roy C. Millward, Claire E. Madden, Ian Sutherland, Roger J. Mortimer, Stephen Fletcher and Frank Marken*

Department of Chemistry, Loughborough University, Loughborough, Leicestershire, UK LE11 3TU
E-mail: F.Marken@lboro.ac.uk

Received (in Cambridge, UK) 23rd July 2001, Accepted 22nd August 2001
First published as an Advance Article on the web 18th September 2001

We introduce the concept of 'directed assembly' of multilayers on surfaces: the overall process involves the exposure of a surface to a series of solutions containing, alternately, adsorbable cations and adsorbable anions, and these are gradually built up into well-defined multilayer structures.

In the present work we describe a new method of assembling multilayers on surfaces. In contrast to the familiar process of *self-assembly*, which is spontaneous and leads to single monolayers, *directed assembly* is driven by the experimenter and leads to extended multilayers. In a proof-of-concept experiment, described below, we show that it is possible to generate multilayers of Prussian Blue and Ruthenium Purple on gold surfaces by exposing them alternately to positively charged ferric cations and negatively charged $Fe(CN)_6^{4-}$ or $Ru(CN)_6^{4-}$ anions. We also show that this process can be controlled with monolayer precision.

Prussian Blue [iron(III) potassium hexacyanoferrate(II)] has the nominal formula $Fe^{III}K[Fe^{II}(CN)_6]\cdot xH_2O$, but commonly contains extensive cation disorder and variable amounts of water. In industry it is employed as a pigment[1] in the formulation of paints and printing inks. It has also found use as a thallium absorbent in medicine, as an electrochromic material, as a catalyst, and as a sequestrant for heavy metals. In the laboratory, its ability to exchange metal ions with ambient solutions makes it an object of continuing curiosity.[2]

For synthetic work, bulk quantities of Prussian Blue can readily be precipitated from aqueous mixtures of Fe^{3+} and $Fe(CN)_6^{4-}$. For solid state electrochemical measurements, however, more complex preparations must be employed, in which electrode surfaces are coated *in situ* by electrochemical reduction of $Fe(CN)_6^{3-}$ to $Fe(CN)_6^{4-}$ in the presence of Fe^{3+}.[3] This leads to thick polycrystalline films. More rarely, films of Prussian Blue have also been prepared by extensive redox cycling of ferrocyanide[4] or by embedding micrometer sized crystals directly into electrode surfaces using powder abrasion.[5]

In our quest to achieve ultra-thin layers of Prussian Blue, our attention was drawn to some recent work in which polymer heterostructures had been successfully deposited on surfaces using alternate adsorption of anions and cations. For example, Stepp and Schlenoff[6] had prepared polyelectrolyte multilayers of poly(butanyl viologen) dibromide and poly(styrene sulfonate) from alternating positive and negative polyion solutions. Mallouk and coworkers had also reported an ionic–covalent strategy for self-assembly of inorganic multilayer films.[7] These works, and others, inspired us to attempt monolayer-by-monolayer deposition of Prussian Blue using a similar approach. Here, we report the successful implementation of this idea.†

Our monolayer-by-monolayer deposition method for Prussian Blue films is as follows. A gold electrode (A = 0.2 cm^2) is immersed in (a) 40 mM Fe^{3+} in aqueous 0.1 M HNO_3 for 60 s, (b) deionized water for 30 s, (c) 40 mM $Fe(CN)_6^{4-}$ in aqueous 0.1 M HNO_3 for 60 s, and finally (d) deionized water for 30 s again. The Fe^{3+} cations adsorbed during the first immersion react with the $Fe(CN)_6^{4-}$ anions adsorbed during the second immersion to form the first monolayer of Prussian Blue. (This is readily confirmed by cyclic voltammetry, as we show later.) This completes the first treatment cycle. Additional monolayers can be added by repeating the treatment cycle. After about fifty cycles, the characteristic colour of Prussian Blue emerges. A cartoon of the deposition process is shown in Fig. 1.

All the Prussian Blue multilayers deposited by the above method exhibit a characteristic voltammetric reduction response at +0.2 V *vs.* Ag/AgCl, which allows them to be quantified. The response is due to the electrochemical reaction [eqn (1)]:

$$Fe^{III}K[Fe^{II}(CN)_6]\cdot xH_2O + K^+ + e^- \rightleftarrows Fe^{II}K_2[Fe^{II}(CN)_6]\cdot(x-n)H_2O + nH_2O \quad (1)$$

and is completely analogous to the reduction of the bulk material. It is noteworthy that the reaction is accompanied by the insertion of K^+ cations into the Prussian Blue framework in order to maintain charge neutrality, and this is accompanied by a change in the hydration state of the crystal lattice.

Cyclic voltammograms for the reduction and re-oxidation of a series of Prussian Blue multilayer deposits are shown in Fig. 2(a). Corresponding numerical data are compiled in Table 1. Immediately after the first treatment cycle, the characteristic voltammetric response for the reduction and re-oxidation of Prussian Blue is detected. As the number of treatments increases, the charge under the reduction peak increases and the peak positions change. The change in peak position during the first six treatments is evidence that the deposited material is not bulk material: each layer deposits on a slightly different substrate until the influence of the underlying substrate becomes negligible.

The charge under the reduction peak increases linearly with the number of treatments, with a slope of *ca.* 26 μC per treatment cycle [see Fig. 2(c)]. This corresponds to an incremental extension of the deposit by 130 μC cm^{-2}, or 2.6 × 10^{-10} mol. Assuming a roughness factor of *ca.* 1.7 (estimated

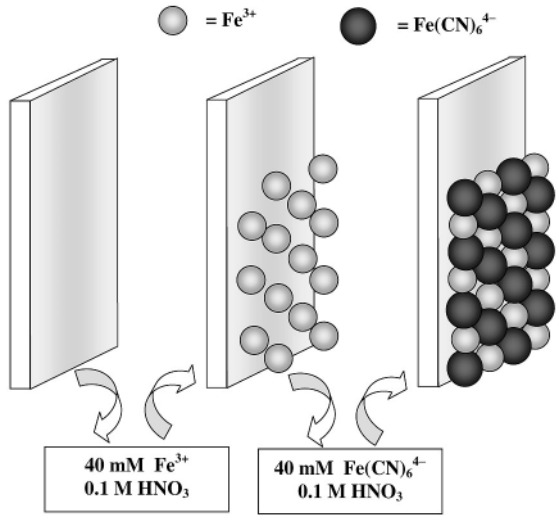

Fig. 1 Cartoon showing the steps involved in the directed assembly of Prussian Blue multilayers.

 DOI: 10.1039/b106616c

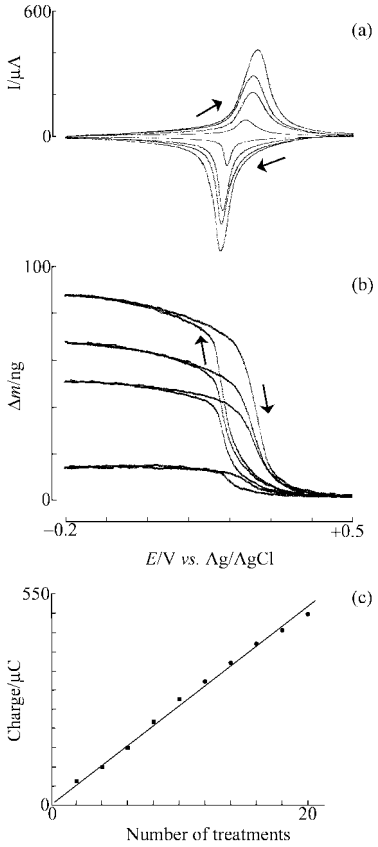

Fig. 2 Cyclic voltammograms (0.5 M KCl, scan rate 0.1 V s^{-1}) for Prussian Blue and Ruthenium Purple formed by layer-by-layer deposition onto a gold plated quartz crystal electrode (area 0.2 cm^2). (a) Cyclic voltammograms for the reduction of Prussian Blue after 4 and 10 treatment cycles and for the reduction of a Prussian Blue/Ruthenium Purple bilayer with 10 treatment cycles of Prussian Blue and with 4 and 10 treatment cycles of Ruthenium Purple. (b) Simultaneous mass changes recorded by quartz crystal microbalance gravimetry. (c) Plot of the charge under the reduction signal *vs.* the number of treatment cycles (Prussian Blue and Ruthenium Purple) with a line indicating 26 μC per treatment cycle.

by SEM), this is as expected for a monolayer quantity of Prussian Blue. The linearity of the plot emphasizes the layer-by-layer nature of the assembly process.

Gravimetric data recorded simultaneously with cyclic voltammetric data provide further insight into the reaction mechanism. By multiplying the total mass change after reduction by Faraday's constant, then dividing by the total charge, the overall mass change per mol of electrons is readily determined (Table 1). This overall mass change per mol of electrons, which stabilizes at *ca.* 17 g mol^{-1}, is clearly inconsistent with the theoretical value for K^+ electroinsertion, 39 g mol^{-1}, but is consistent with the co-expulsion of about 1.2 mol of water for each mol of K^+ inserted.

Table 1 Data obtained from cyclic voltammetry (scan rate 0.1 V s^{-1}) and gravimetry for the reduction of Prussian Blue (treatments 1–10) and Ruthenium Purple (treatments 11–20). Multilayers on a 0.2 cm^2 gold electrode immersed in aqueous 0.5 M KCl

Number of treatments	E_p^{ox}/V	E_p^{red}/V	ΔE_p/ mV	Q_{red}/ μC	Δm/ ng	(ΔmF/ Q_{red})/ g mol^{-1}
Deposition Prussian Blue						
2	0.228	0.199	29	62	4	6.5
4	0.238	0.194	44	99	13	12.9
6	0.246	0.190	56	150	23	15.7
8	0.250	0.184	66	218	36	16.6
10	0.256	0.184	72	272	49	17.9
Deposition of Ruthenium Purple onto Prussian Blue						
10 + 2	0.257	0.184	73	324	58	17.8
10 + 4	0.257	0.181	76	373	66	17.7
10 + 6	0.241	0.168	73	422	72	17.1
10 + 8	0.263	0.179	84	458	78	17.1
10 + 10	0.269	0.177	92	500	86	17.2

Surface analysis by Auger spectroscopy on selected areas of 10 × 10 μm size allowed the elemental composition of the electrode surface to be sampled as a function of the number of treatments. After deposition of 4–6 monolayers of Prussian Blue, strong signals for Fe, K, C, and N were detected in approximately 2 : 1 : 6 : 6 proportions and the signal for Au was considerably diminished. After deposition of 10 monolayers the signal for Au was undetectable, suggesting an even coverage.

Besides creating compositionally uniform structures, the directed assembly technique was also used to create compositionally modulated structures. For example, Ruthenium Purple,[8] $Fe(III)K[Ru(II)(CN)_6]\cdot xH_2O$, has a structure very similar to Prussian Blue (unit cell dimension 1.14 nm)[9] and may also by prepared by directed assembly from solutions of (i) 40 mM Fe^{3+} in aqueous 0.1 M HNO_3 and (ii) 40 mM $Ru(CN)_6^{4-}$ in aqueous 0.1 M HNO_3. Moreover, the reduction of Ruthenium Purple occurs at approximately the same potential as that of Prussian Blue, in accordance with eqn (2):

$$Fe(III)K[Ru(II)(CN)_6]\cdot xH_2O + K^+ + e^- \rightleftarrows Fe(II)K_2[Ru(II)(CN)_6]\cdot(x - n)H_2O + nH_2O \quad (2)$$

Thus, multilayers of Ruthenium Purple could readily be deposited on top of multilayers of Prussian Blue (Fig. 2).

Finally, it should be noted that the voltammetric responses and gravimetric responses shown in Fig. 2 remain sharp even at scan rates above 1 V s^{-1}, and that the charges under the oxidation and reduction peaks are independent of scan rate. This is consistent with very fast insertion of K^+ ions into the multilayers of Prussian Blue, suggesting that the process is field driven rather than diffusion controlled.

In conclusion, we have demonstrated that Prussian Blue multilayers can be formed by *directed assembly* on electrode surfaces. In future, the production of a wide range of compositionally modulated electrode surfaces can be expected, with applications in catalysis, sensors, and electrochromic materials.

F. M. thanks the Royal Society for the award of a University Research Fellowship, and R. C. M. thanks EPSRC for a studentship (grant no. 99305973). We are grateful for help with Auger surface analysis from Ralf Dahm and Gary Critchlow (ISST, Loughborough University).

Notes and references

† Reagents were of analytical grade. Demineralised water was obtained from an Elgastat purification system (Elga, High Wycombe, Bucks). The simultaneous cyclic voltammetry and gravimetry experiments were carried out with a Princeton Applied Research model 173 potentiostat/galvanostat and an Elchema model EQCN-700 electrochemical quartz crystal nanobalance. For mass balance experiments the working electrodes were *AT*-cut 10 MHz gold plated quartz crystals with geometric electrode areas of 0.2 cm^2. All gold electrodes were pretreated by cycling in 0.1 M HNO_3 between 0.0 and 1.0 V *vs.* Ag/AgCl. Auger spectra were recorded on a JEOL 7100 Auger electron spectrometer and quantified based on a $K_4Fe(CN)_6$ reference sample.

1 A. G. Sharpe, *The Chemistry of Cyano Complexes of the Transition Metals*, ed. P. M. Maitlis, F. G. A. Stone and R. West, Academic Press, New York, 1976.
2 For a review, see: K. Itaya, I. Uchida and V. D. Neff, *Acc. Chem. Res.*, 1986, **19**, 162.
3 R. J. Mortimer and D. R. Rosseinsky, *J. Electroanal. Chem.*, 1983, **151**, 133.
4 H. Gomathi and G. P. Rao, *J. Appl. Electrochem.*, 1990, **20**, 454.
5 F. Scholz and B. Meyer, *Electroanal. Chem.*, 1998, **20**, 1.
6 J. Stepp and J. B. Schlenoff, *J. Electrochem. Soc.*, 1997, **144**, L155.
7 R. E. Schaak and T. E. Mallouk, *Chem Mater.*, 2000, **12**, 2513.
8 T. R. I. Cataldi and G. E. Benedetto, *J. Electroanal. Chem.*, 1998, **458**, 149.
9 K. P. Rajan and V. D. Neff, *J. Phys. Chem.*, 1982, **86**, 4361 and references therein.

CHEMCOMM
Communication
www.rsc.org/chemcomm

Reactivity of a metallacyclopentatriene intermediate: metal-to-ligand-to-metal re-migration of a phosphine ligand *versus* a 1,2 hydrogen shift†

Eva Rüba,[a] Kurt Mereiter,[b] Roland Schmid[a] and Karl Kirchner*[a]

[a] *Institute of Inorganic Chemistry, Vienna University of Technology, Getreidemarkt 9, A-1060 Vienna, Austria. E-mail: kkirch@mail.zserv.tuwien.ac.at*

[b] *Institute of Mineralogy, Crystallography, and Structural Chemistry, Getreidemarkt 9, A-1060 Vienna, Austria*

Received (in Cambridge, UK) 5th June 2001, Accepted 17th August 2001
First published as an Advance Article on the web 18th September 2001

The reaction of nona-2,7-diyne, deca-2,8-diyne and hex-1-yne with $[RuCp(PR_3)(MeCN)_2]PF_6$ (R = Cy, Ph, Me) affords, depending on the structure of the alkyne and the substituent of the phosphine ligand, ruthenium metallacyclopentatriene, allyl carbene and/or butadienyl carbene complexes involving either metal-to-ligand-to-metal migration of the phosphine ligand with concomitant C–H activation or a facile 1,2 hydrogen shift.

Transition metal complexes with a vacant coordination site, or bearing weakly coordinating ligands, are known to react with alkynes to form a variety of products such as vinylidene complexes,[1] metallacyclopentadienes,[2] and in some cases metallacyclopentatrienes.[3] We have recently shown[4] that the labile complex $[RuCp(PR_3)(MeCN)_2]PF_6$ [R = Cy (**1a**), Ph (**1b**), Me (**1c**)], which serves as a synthetic equivalent for the 14-electron fragment $[RuCp(PR_3)]^+$, reacts with terminal alkynes to give ruthenium allyl carbene complexes.[5] This conversion is a very complex one involving oxidative coupling of two alkynes and an unusual PR_3 migration. In the course of the reaction, a metallacyclopentatriene complex is a reasonable, though elusive intermediate which is a fascinating entity featuring the cyclic biscarbene structure. Since such species might be important intermediates in various transformations,[6] we set out to modify the reactants with the aim to make such species observable. For this purpose we switched over to using the internal alkynes nona-2,7-diyne and deca-2,8-diyne, the intention being to impede nucleophilic attack at the α carbon of the metallacycle. Along these lines, however, unexpected and novel reactions occurred, which are described herein.

In virtually one case the surmised metallacyclopentatriene intermediate could be isolated, namely when the alkyne was deca-2,8-diyne and the phosphine in **1** was PCy_3. Monitoring the reaction by ^1H, $^{13}C\{^1H\}$, $^{31}P\{^1H\}$ NMR spectroscopy revealed the formation of an intermediate consistent with the cationic metallacyclopentatriene structure $[CpRu\{=C_2(Me)_2C_2(CH_2)_4\}(PCy_3)]^+$ (**2**) (Scheme 1).‡ Thus, the resonances in the $^{13}C\{^1H\}$ NMR spectrum at 325.6 and 170.6 ppm can be associated with the C_α and C_β ring carbons, respectively. The unusual down-field shift of the C_α carbon resonance is in agreement with an unsaturated bis-carbene ligand {*cf.* $RuCp[=C_2(Ph)_2CH_2]Br$, for which the resonances of the C_α and C_β atoms, respectively, are found at 271.1 and 156.0 ppm[3a]}. Finally, the signal at 52.5 ppm is relevant to the methyl carbon atoms. However, this metallacyclopentatriene complex is unstable and transforms directly into the butadienyl carbene complex $[CpRu\{=C(Me)C(CH_2)_4C\text{-}\eta^2\text{-}CH{=}CH_2\}(PCy_3)]PF_6$ **3a** in high yield (for the characterization see below).

The direct step from **2** to **3a** is intriguing in that it involves activation of an α-substituent by an electrophilic carbene (pathway **a**), which is unprecedented for a metallacyclopentatriene. Hitherto, a 1,2 hydrogen shift was known only for electrophilic alkyl carbenes.[7] There is only one other example of a butadienyl carbene as encountered recently in the reaction of an osmacyclopentatriene complex with *tert*-butylamine.[8]

Note that the outcome of the reaction of deca-2,8-diyne with $[RuCp(PR_3)(MeCN)_2]PF_6$ is very sensitive to the substituent of the phosphine ligand. While also with PPh_3 conversion to the butadienyl carbene complex **3b** occurred, although without observing an intermediate, the reaction took another course when PMe_3 was used. In this case, phosphine migration takes place as shown in pathway **b** of Scheme 1, analogously to the reaction of nona-2,7-diyne with $[RuCp(PR_3)(MeCN)_2]PF_6$, independent of the phosphine substituent. Such a phosphine migration results in the formation of the allyl carbene complexes $[CpRu\{=C(Me)\text{-}\eta^3\text{-}C(CH_2)_4CC(Me)PMe_3\}]PF_6$ **4a** and $[CpRu\{=C(Me)\text{-}\eta^3\text{-}C(CH_2)_3CC(Me)PR_3\}]PF_6$ [R = Me (**4b**), Ph (**4c**), Cy (**4d**)] in essentially quantitative yield. This conversion features the same type of reaction that was observed before in the case of terminal alkynes. Products **4** could be readily characterized by their $^{13}C\{^1H\}$ NMR spectra displaying two doublet resonances in the range of 271–252 (J_{CP} 7–4 Hz) and 41–33 ppm (J_{CP} 72–61 Hz) that can be assigned to the carbene carbon atoms and the terminal allyl carbon atoms bearing the phosphine substituent, respectively.

Furthermore, the allyl carbene composition of **4c** proved not to be the most stable one. If a solution of **4c** in acetone-d_6 is kept for several days at room temperature, further rearrangement takes place leading eventually to the butadienyl carbene complex $[CpRu\{=C(Me)C(CH_2)_3C\text{-}\eta^2\text{-}CH{=}CH_2\}(PPh_3)]PF_6$ **3c** in essentially quantitative yield. The ^1H NMR spectroscopic data for **4c** include characteristic resonances centered at 5.42 (dd, H^4, $^3J_{HH}$ 11.4 $^3J_{HH}$ 10.8 Hz), 3.80 (d, H^{5cis}, $^3J_{HH}$ 10.8 Hz) and 1.85 ppm (dd, H^{5trans}, $^3J_{HP}$ 12.0, $^3J_{HH}$ 11.4 Hz) assignable

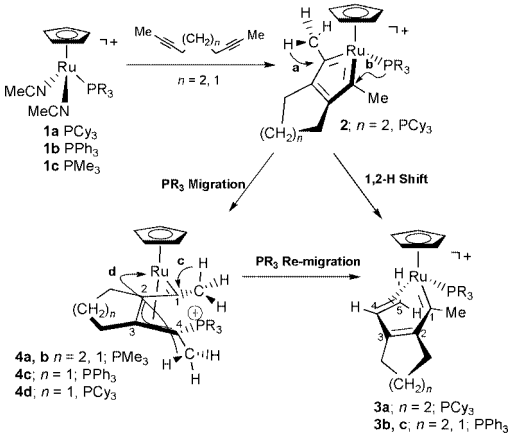

Scheme 1

† Electronic supplementary information (ESI) available: experimental details. See http://www.rsc.org/suppdata/cc/b1/b104927p/

 DOI: 10.1039/b104927p

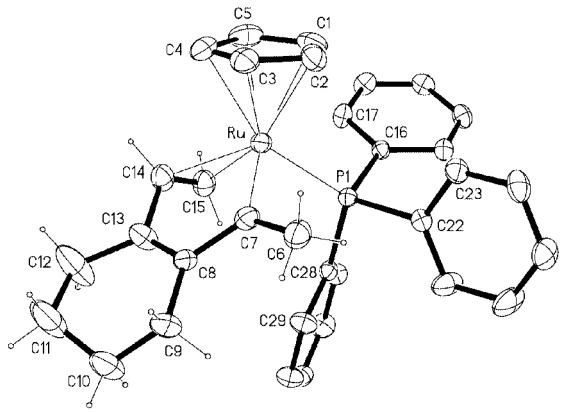

Fig. 1 Structural view of **3b** showing 20% thermal ellipsoids (aromatic H atoms and PF_6^- omitted for clarity). Selected bond lengths (Å) and angles (°): Ru–C(1–5)$_{av}$ 2.245(5), Ru–C(7) 1.934(5), Ru–C(14) 2.212(6), Ru–C(15) 2.265(6), Ru–P(1) 2.358(1), C(7)–C(8) 1.437(7), C(8)–C(13) 1.349(9), C(13)–C(14) 1.471(8), C(14)–C(15) 1.397(8), C(7)–C(8)–C(13) 112.8(4), C(8)–C(13)–C(14) 119.7(5), C(13)–C(14)–C(15) 121.3(6), P(1)–Ru–C(7) 91.8(1).

to the vinyl protons of the coordinated double bond. In the $^{13}C\{^1H\}$ NMR spectrum the characteristic resonance of the carbene carbon occurs as a doublet centered at 330.1 ppm (J_{CP} 15.3 Hz). The uncoordinated and coordinated sp^2 carbon atoms C^2, C^3, C^4 and C^5 of the butadienyl unit exhibit resonances at 199.7, 174.4, 74.4 and 55.1 (d, J_{CP} 5.6 Hz) ppm, respectively. During this conversion, the PPh_3 moiety has re-migrated to the metal center with concomitant C–H bond activation. This may involve either the Me substituent of the carbene carbon atom *via* a 1,2 hydrogen shift (pathway **c**) or the Me group adjacent to the phosphonium moiety (pathway **d**). It is interesting that neither **4a**, **4b** nor **4d** underwent such a rearrangement process.

In addition to a full NMR spectroscopic and analytical characterization of **3a**–**c**,§ the solid state structure of **3b** was determined by single-crystal X-ray diffraction.¶ The solid state structure is depicted in Fig. 1 with important bond distances reported in the legend. Accordingly, **3b** adopts a three legged piano stool conformation with PPh_3 and the two C=C bonds and the carbene carbon atom of the butadienyl moiety as the legs. The most notable feature is the short Ru–C(7) bond distance of 1.934(5) Å, which is in line with a metal–carbon double bond. Furthermore, the butadienyl C–C bonds C(8)–C(13), C(13)–C(14) and C(14)–C(15) show the expected short–long–short pattern (1.349(9), 1.471(8) and 1.397(8) Å, in the same order].

In order to distinguish between the operation of pathways **c** or **d** in Scheme 1, complex **1b** was also reacted with hex-1-yne. The result is depicted in Scheme 2. As expected, the allyl carbene $[CpRu\{=C(Bu^n)(\eta^3\text{-}CHC(Bu^n)CHPPh_3)\}]PF_6$ **4e** was formed in high yield. Owing to the positions of the butyl substituents, however, any rearrangement to the corresponding butadienyl carbene complexes could occur only *via* a 1,2 H shift. Since no such rearrangement was evident, even after a week, it can be concluded that the activation of C–H bonds adjacent to the phosphonium moiety is preferred to a 1,2 H shift. In this context, it is worth mentioning that allyl carbenes can activate alkyl C–H bonds in tertiary phosphine ligands.[5]

In conclusion, we have shown that the reactivity of a cationic metallacyclopentatriene complex varies with the nucleophilicity of the co-ligand and the presence of α-alkyl substituents.

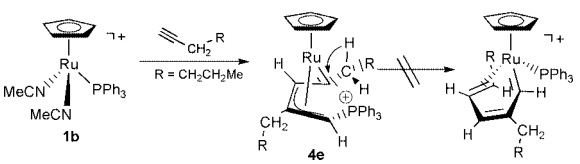

Scheme 2

Ligand migrations give initially allyl carbenes and a 1,2 hydrogen shift gives butadienyl carbenes. Therefore, due to their strong electrophilic character, cationic metallacyclopentatriene complexes are not catalytically active with respect to cyclotrimerizations. Furthermore, the present reluctance with respect of a 1,2 H shift may suggest that allyl carbenes are not electrophilic enough at the carbene carbon. In fact, the carbene carbon of allyl carbenes can be attacked by protons forming η^4-diene complexes.[5]

Financial support by the 'Fonds zur Förderung der wissenschaftlichen Forschung' is gratefully acknowledged (Project No. P14681-CHE).

Notes and references

‡ *Preparation and data* for **2**: to a solution of **1a** (100 mg, 0.148 mmol) in $MeNO_2$ (4 mL) deca-2,8-diyne (28 μl, 0.150 mmol) was added. The colour of the solution changed from yellow to dark violet. After 20 h at room temperature the solvent was removed, the residue was washed with Et_2O (5 mL) and the violet precipitate was filtered off and dried under vacuum. Yield: 75 mg (70%) (Found: C, 54.70; H, 7.19. $C_{33}H_{52}F_6P_2Ru$ requires: C, 54.61; H, 7.22%). ^1H NMR (acetone-d$_6$, 20 °C): δ 5.77 (s, 5H, Cp), 2.51–1.10 (m, 41H, PCy_3, CH_2), 1.69 (s, 6H, CH_3). $^{13}C\{^1H\}$ NMR (acetone-d$_6$, 20 °C): δ 325.6 (d, $^2J_{CP}$ 11.4 Hz, 2C, C^1), 170.6 (2C, C^2), 94.6 (5C, Cp), 52.5 (2C, CH_3), 37.0 (d, $^1J_{CP}$ 22.9 Hz, 3C, Cy^1), 30.3 (br s, 3C, Cy^4), 28.1 (d, $^2J_{CP}$ 10.2 Hz, 6C, Cy$^{2,2'}$), 27.3 (s, 2C, CH_2), 26.4 (br s, 6C, Cy$^{3,3'}$), 22.5 (s, 2C, CH_2).$^{31}P\{^1H\}$ NMR (acetone-d$_6$, 20 °C): δ 48.1 (PCy_3), 142.7 (J_{PF} 707.5 Hz, PF_6^-).

§ *Preparation and data* for **3b**: a solution of **1b** (100 mg, 0.159 mmol) in $MeNO_2$ (3 mL) was treated with deca-2,8-diyne (32 μL, 0.191 mmol) and was stirred at room temperature for 20 h, whereupon the colour of the solution turned from violet to dark orange. The solution was evaporated to dryness, redissolved in CH_2Cl_2 (1 mL) and the product was precipitated with Et_2O (5 mL). The product was filtered, washed twice with Et_2O, and dried *in vacuo*. Yield: 90 mg (80%) (Found: C, 55.98; H, 4.79. $C_{33}H_{34}F_6P_2Ru$ requires: C, 56.01; H, 4.84%). ^1H NMR (CD_2Cl_2, 20 °C): δ 7.71–6.77 (m, 15H, Ph), 5.12 (dd, J_{HH} 11.4 Hz, J_{HH} 10.5 Hz, 1H, H^4), 5.11 (s, 5H, Cp), 3.61 (d, J_{HH} 11.4 Hz, 1H, H^{5a}), 2.76 m, 1H, CH_2), 2.58 (d, J_{PH} 1.3 Hz, 3H, CH_3), 2.47–1.38 [m, 7H, $(CH_2)_4$], 1.59 (ddd, J_{HH} 13.1, J_{HH} 11.4, J_{HH} 1.6 Hz, 1H, H^{5b}). $^{13}C\{^1H\}$ NMR (CD_2Cl_2, 20 °C): δ 338.0 (d, J_{CP} 13.6 Hz, 1C, C^1), 188.2 (1C, C^2), 162.1 (1C, C^3), 134.8–128.5 (18C, Ph), 91.0 (s, 5C, Cp), 78.0 (s, 1C, C^4), 51.9 (d, J_{CP} 6.8 Hz, 1C, C^5), 48.1 (d, J_{CP} 3.4 Hz, CH_3), 36.3 (s, 1C, CH_2), 26.7 (s, 1C, CH_2), 22.1 (2C, CH_2). $^{31}P\{^1H\}$ NMR (CD_2Cl_2, 20 °C): δ 50.5 (PPh_3), −143.7 ($^1J_{PF}$ 710.8 Hz, PF_6).

¶ *Crystal data*: for **3b**: $C_{33}H_{34}F_6P_2Ru$, M = 707.61, monoclinic, space group $P2_1$ (no. 4) a = 9.952(5), b = 15.229(7), c = 10.059(6) Å, β = 92.86(1)°, U = 1523(1) Å^3, T = 297(2) K, Z = 2, μ(Mo-Kα) = 0.679 mm^{-1}, R_1 = 0.045 (all data), wR_2 = 0.102 (all data), no. of reflections 6607, no. of refined parameters 385. CCDC reference number 169027. See http://www.rsc.org/suppdata/cc/b1/b104927p/ for crystallographic data in CIF or other electronic format.

1 M. I. Bruce, *Chem. Rev.*, 1991, **91**, 197; C. Bruneau and P. H. Dixneuf, *Acc. Chem. Res.*, 1999, **32**, 311.

2 C. S. Yi, J. R. Torres-Lubian, N. Liu, A. L. Rheingold and I. A. Guzei, *Organometallics*, 1998, **17**, 1257 and references therein.

3 For metallacyclopentatriene complexes, see: (*a*) M. O. Albers, P. J. A. deWaal, D. C. Liles, D. J. Robinson, E. Singleton and M. B. Wiege, *J. Chem. Soc., Chem. Commun.*, 1986, 1680; (*b*) C. Gemel, A. LaPansée, K. Mauthner, K. Mereiter, R. Schmid and K. Kirchner, *Monatsh. Chem.*, 1997, **128**, 1189; (*c*) L. Pu, T. Hasegawa, S. Parkin and H. Taube, *J. Am. Chem. Soc.*, 1992, **114**, 2712; (*d*) W. Hirpo and M. D. Curtis, *J. Am. Chem. Soc.*, 1988, **110**, 5218; (*e*) J. L. Kerschner, P. E. Fanwick and I. P. Rothwell, *J. Am. Chem. Soc.*, 1988, **110**, 8235; (*f*) B. Hessen, A. Meetsma, F. van Bolhuis, J. H. Teuben, G. Helgesson and S. Jagner, *Organometallics*, 1990, **9**, 1925.

4 E. Rüba, W. Simanko, K. Mauthner, K. M. Soldouzi, C. Slugovc, K. Mereiter, R. Schmid and K. Kirchner, *Organometallics*, 1999, **18**, 3843.

5 K. Mauthner, K. M. Soldouzi, K. Mereiter, R. Schmid and K. Kirchner, *Organometallics*, 1999, **18**, 4681.

6 Y. Yamamoto, H. Kitahara, R. Ogawa, H. Kawaguchi, K. Tatsumi and K. Itoh, *J. Am. Chem. Soc.*, 2000, **122**, 4310.

7 C. Slugovc, K. Mereiter, R. Schmid and K. Kirchner, *Organometallics*, 1998, **17**, 827; D. M. Heinekey and C. E. Radzewich, *Organometallics*, 1998, **17**, 51; T. Bodnar and A. R. Cutler, *J. Organomet. Chem.*, 1981, **213**, 13; E. O. Fischer and W. Held, *J. Organomet. Chem.*, 1976, **112**, 59.

8 L. Pu, T. Hasegawa, S. Parkin and H. Taube, *J. Am. Chem. Soc.*, 1992, **114**, 7609.

CHEMCOMM Communication
www.rsc.org/chemcomm

Dioxygen activation by a neutral β-diketiminato copper(I) ethylene complex†

Xuliang Dai and Timothy H. Warren*

Georgetown University, Department of Chemistry, Box 571227, Washington, D.C. 20057-1227, USA. E-mail: thw@georgetown.edu

Received (in Cambridge, UK) 14th June 2001, Accepted 15th August 2001
First published as an Advance Article on the web 18th September 2001

The synthesis and structure of two thermally stable neutral β-diketiminato copper(I) olefin complexes are presented along with the structure of a Cu(II)$_2$(μ-OH)$_2$ dimer that results from the reaction of the Cu(I) ethylene complex with O_2 *via* the proposed intermediacy of a Cu(III)$_2$(μ-O)$_2$ species.

The diverse biological role copper(I) complexes play motivates a great deal of interest in synthetic nitrogen-ligated systems. For example, the Cu(I)-based ethylene receptor in ETR 1 regulates many facets of plant growth such as fruit ripening, seed germination and even sex determination in some species.[1] Synthetic studies have uncovered that most copper(I)-ethylene complexes are quite labile,[2] with the most robust systems based on very electron-rich neutral donors such as bipyridine[2b] or a recently reported monoanionic iminophosphinamide.[2c] Cu(I) complexes are also responsible for the binding and transport of dioxygen in invertebrates as exemplified by the ubiquitous enzyme hemocyanin whose active site consists of two Cu(I) centers ligated by three histidine residues each.[3] The related enzyme tyrosine is responsible for the selective C–H activation of phenols, ultimately oxidizing them to *ortho*quinones.[4] Whereas much effort has been directed toward a detailed understanding of this biological reactivity,[3] model systems based on bi- and tri-dentate amine donors also offer the synthetic potential for selective C–H bond functionalization.[5] As part of our program to explore the chemistry of electron-rich β-diketiminates of the later first row metals, we report herein our initial results describing a neutral Cu(I) system that both binds olefins and activates dioxygen.[6–8]

Reaction of the thallium β-diketiminate Tl[Me$_2$NN] with CuBr·SMe$_2$ in the presence of either ethylene (1 atm) or styrene (1.2 equiv.) in benzene or toluene provides thermally stable [Me$_2$NN]Cu(alkene) complexes in 60–80% yield as colorless crystals from pentane (Scheme 1) (ESI†). The ^{1}H NMR spectrum of **1** in benzene-d$_6$ shows a significantly upfield shifted resonance (δ 2.91) for bound ethylene. Neither **1** nor **2** is exceptionally labile as exchange with free olefin is slow on the NMR timescale. Reaction of **1** with 1 equiv. styrene at 25 °C in a sealed NMR tube, however, does result in a 1 : 2.3 equilibrium mixture of **1** and **2** after 3 h. Taking the incomplete solubility of ethylene in benzene-d$_6$ into account, styrene complex **2** is actually thermodynamically disfavored over the sterically less hindered ethylene derivative **1** (K = 0.33(2)). Backbonding in **1** and **2** is likely relatively weak as shown by the ethylene $^1J_{CH}$ coupling constant of 158 Hz in **1** and facile rotation about the Cu–styrene bond in **2** ($\Delta G^{\ddagger}$ = 10.7(3) kcal mol^{-1} at 215 K) (ESI†).

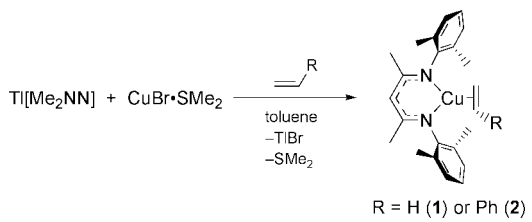

Scheme 1 Synthesis of Cu(I) olefin complexes (ESI†).

The X-ray structures of **1** and **2**‡ (Fig. 1) reveal a coplanar orientation of the olefin with the β-diketiminate backbone which chelates the copper center with bite angles of 98.68(6) and 99.0(1)°, respectively. The ethylene and styrene C–C distances in **1** and **2** (1.365(3) and 1.373(6) Å) are similar to that found in the iminophosphinamide [Bu$^t_2$P(NSiMe$_3$)$_2$-κ^2*N*]Cu(C$_2$H$_4$) (1.362(6) Å)[2c] and [(bipy)Cu(styrene)][ClO$_4$] (1.358(10) Å),[9] slightly elongated as compared to the corresponding free olefins (1.337(1)[10a] and 1.346(2)[10b]). While the above data suggest minimal backbonding from the d^{10} copper(I) center, the observed orientation may be favored on electronic grounds due to an enhanced interaction of the olefin π* orbital with the filled Cu d orbital destabilized by the opposing β-diketiminate N donors.

Treating a diethyl ether solution of ethylene complex **1** with several equivalents of dry dioxygen at room temperature ultimately results in the precipitation of paramagnetic {[Me$_2$NN]Cu(μ-OH)]}$_2$ **3**[6,7] (μ_{eff} = 1.39 μ_B in CDCl$_3$) which is isolated in 80% yield as brown crystals (ESI†). The X-ray structure of **3**‡ (Fig. 2) shows two square planar Cu(II) centers separated by 3.0581(3) Å nearly symmetrically bridged by two hydroxo ligands with Cu–O distances of 1.914(1) and 1.923(1) Å. The hydroxo H-atom was found in the Fourier difference map, corroborated by a sharp, high energy band at 3646 cm^{-1} in the solid state IR spectrum of **3**. We suggest that the reaction proceeds *via* the intermediacy of a Cu(III)$_2$(μ-O)$_2$ dimer[5,11] **4** followed by abstraction of some H-atom donor[5] to provide **3**

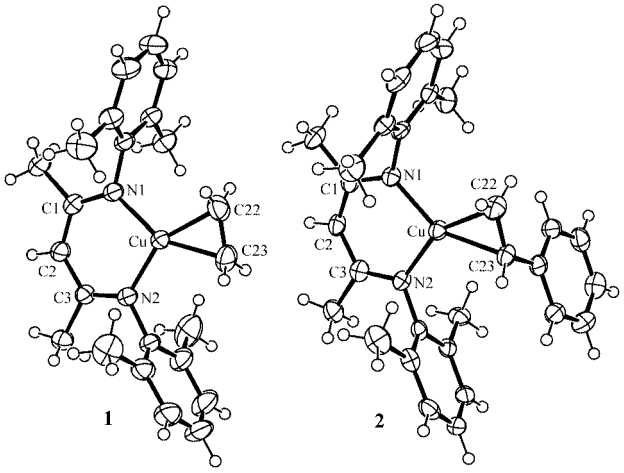

Fig. 1 ORTEP diagrams of the solid state structures of **1** and **2**.‡ Selected bond distances (Å) and angles (°) for **1**·0.5 C$_5$H$_{12}$: Cu–N(1) 1.917(2), Cu–N(2) 1.908(1), Cu–C(22) 1.986(2), Cu–C(23) 1.992(2), C(22)–C(23) 1.365(3), N(1)–Cu–N(2) 98.68(6), C(22)–Cu–C(23) 40.13(9). Selected bond distances (Å) and angles (°) for **2**: Cu–N(1) 1.913(3), Cu–N(2) 1.915(3), Cu–C(22) 1.975(5), Cu–C(23) 2.027(4), C(22)–C(23) 1.373(6), N(1)–Cu–N(2) 99.0(1), C(22)–Cu–C(23) 40.1(2).

† Electronic supplementary information (ESI) available: synthesis of Tl[Me$_2$NN] and **1**–**3** with relevant analytical and spectroscopic details. See http://www.rsc.org/suppdata/cc/b1/b105244f/

 DOI: 10.1039/b105244f

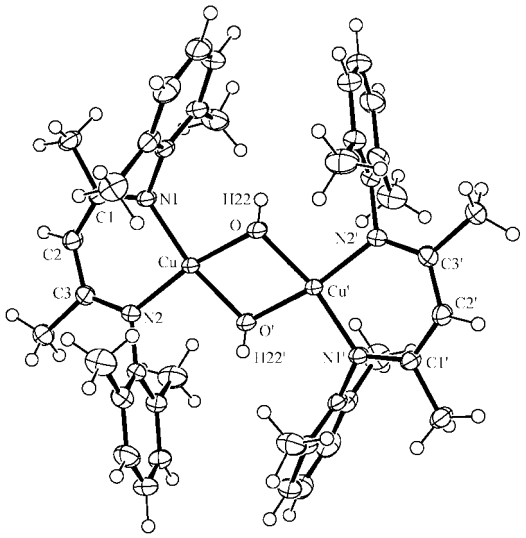

Fig. 2 ORTEP diagram of the solid state structure of **3**.‡ Selected bond distances (Å) and angles (°): Cu–N(1) 1.9446(11), Cu–N(2) 1.9373(11), Cu–O 1.9142(11), Cu–O′ 1.9230(11), Cu–Cu′ 3.0581(3); N(1)–Cu–N(2) 94.83(5), O–Cu–O′ 74.32(5).

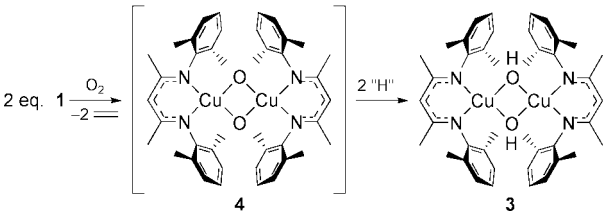

Scheme 2 Proposed formation of **3**.

(Scheme 2). Whereas the source of the hydroxo H-atoms is not yet known, it should be noted that **1** rapidly reacts with H_2O under anaerobic conditions to give the free ligand H[Me_2NN] and an intractable Cu-containing precipitate.

Significantly less thermally stable than the only other reported neutral, iminophosphinamide-based $Cu_2(\mu\text{-}O)_2$ complex which slowly decomposes to an unidentified Cu(II) species,[11a] the enhanced reactivity of proposed μ-oxo dimer **4** has hampered its isolation in pure form. Addition of O_2 to **1** at −78 °C in diethyl ether allows for the isolation of a green microcrystalline material that gradually converts into **3**, even in the solid state. A solution of this freshly isolated green material in CH_2Cl_2 shows an absorption band at 343 nm ($\varepsilon = 2.4 \times 10^4$ M^{-1} cm^{-1}) corresponding to the μ-hydroxo complex **3** as well as two new absorbances at 315 and 420 nm, consistent with characteristic LMCT bands of previously reported $Cu(III)_2(\mu\text{-}O)_2$ complexes.[5,11] Furthermore, oxygenation of **1** with air (THF, 25 °C) results in the initial formation of these bands at 315 and 420 nm followed by their gradual loss in intensity giving rise to the 343 nm band of the μ-hydroxo complex **3** (ESI†).

Low temperature resonance Raman spectroscopy[5,11] in addition to the synthesis of a sterically diverse family of neutral β-diketiminato Cu(I) complexes are underway to uniquely determine the composition of the green intermediate **4** as well as the source of H-atoms that lead to the isolated μ-hydroxo compound **3**. Further protonation studies of the olefin adducts **1** and **2** to yield new cationic β-diimino Cu(I) olefin complexes[6] and their use as cyclopropanation catalysts will also be reported in due course.

We thank the Georgetown University Department of Chemistry for financial support of this work as well as Professor Robert Bachman and Professor K. Travis Holman for assistance with the X-ray structures of **1** and **2**.

Notes and references

‡ Data were collected on a Bruker SMART CCD instrument and the structure solutions were performed using the SHELXTL/PC suite[12a] and XSEED.[12b] Intensities were corrected for Lorentz and polarization effects and an empirical absorption correction was applied to **3** using Blessing's method as incorporated into the program SADABS.[12c]

Crystal data: **1**·0.5 C_5H_{12}: $C_{25.5}H_{35}CuN_2$, M = 433.10, orthorhombic, space group *Aba*2, a = 13.7801(14), b = 23.792(2), c = 14.665(2) Å, V = 4807.9(9) Å^3, Z = 8, one molecule of **1** per asymmetric unit with 0.5 molecule of pentane disordered over two orientations, μ = 0.92 mm^{-1}, 19652 reflections collected at –100 °C, 5807 independent reflections (R_{int} = 0.0303), 5110 reflections observed ($I > 2\sigma(I)$), final agreement factors for 308 parameters and 1 restraint: $R1$ = 0.0288, $wR2$ = 0.0721 (observed reflections) and $R1$ = 0.0363, $wR2$ = 0.0759 (all data), Flack χ = −0.005(11).

2: $C_{29}H_{33}CuN_2$, M = 473.11, orthorhombic, space group *Pbca*, a = 17.4077(14), b = 15.3217(12), c = 18.5088(15) Å, V = 4936.6(7) Å^3, Z = 8, one molecule per asymmetric unit, μ = 0.903 mm^{-1}, 43388 reflections collected at −100 °C, 4355 independent reflections (R_{int} = 0.1818), 2351 reflections observed ($I > 2\sigma(I)$), final agreement factors for 308 parameters: $R1$ = 0.0495, $wR2$ = 0.1075 (observed reflections) and $R1$ = 0.1204, $wR2$ = 0.1240 (all data).

3: $C_{42}H_{52}Cu_2N_4O_2$, M = 771.96, monoclinic, space group *C*2/*c*, a = 23.5194(15), b = 10.6093(7), c = 15.2554(10) Å, β = 93.1880(1)°, V = 3800.7(4) Å^3, Z = 4, one half molecule per asymmetric unit, μ = 1.160 mm^{-1}, 20485 reflections collected at −100 °C, 4581 independent reflections (R_{int} = 0.0189), 4253 reflections observed ($I > 2\sigma(I)$), final agreement factors for 236 parameters: $R1$ = 0.0249, $wR2$ = 0.0686 (observed reflections) and $R1$ = 0.0274, $wR2$ = 0.0701 (all data).

CCDC reference numbers 168944–168946. See http://www.rsc.org/suppdata/cc/b1/b105244f/ for crystallographic data in CIF or other electronic format.

1 F. I. Rodríguez, J. J. Esch, A. E. Hall, B. M. Binder, G. E. Schaller and A. B. Bleecker, *Science*, 1999, **283**, 996; J. R. Ecker, *Science*, 1995, **268**, 667 and references therein.
2 (*a*) J. S. Thompson, R. L. Harlow and J. F. Whitney, *J. Am. Chem. Soc.*, 1983, **105**, 3522; (*b*) M. Munakata, S. Kitagawa, S. Kosome and A. Asahara, *Inorg. Chem.*, 1986, **25**, 2622; (*c*) B. F. Straub, F. Eisenträger and P. Hofmann, *Chem. Commun.*, 1999, 2507.
3 E. I. Solomon, M. J. Baldwin and M. D. Lowery, *Chem. Rev.*, 1992, **92**, 521; K. A. Magnus, H. Ton-That and J. A. Carpenter, *Chem. Rev.*, 1994, **94**, 727; E. I. Solomon, U. M. Sundaram and T. E. Machonkin, *Chem. Rev.*, 1996, **96**, 2563.
4 H. S. Mason, W. L. Fowlks and E. Peterson, *J. Am. Chem. Soc.*, 1955, **77**, 2914.
5 S. Schindler, *Eur. J. Inorg. Chem.*, 2000, 2311; P. L. Holland and W. B. Tolman, *Coord. Chem. Rev.*, 1999, **190–192**, 855; H. V. Obias, Y. Lin, N. N. Murthy, E. Pidcock, E. I. Solomon, M. Ralle, N. J. Blackburn, Y. M. Neuhold, A. D. Zuberbühler and K. D. Karlin, *J. Am. Chem. Soc.*, 1998, **120**, 12960; S. Itoh, M. Taki, H. Nakao, P. L. Holland and W. B. Tolman, *Angew. Chem., Int. Ed.*, 2000, **39**, 398; V. Mahadevan, M. J. Henson, E. I. Solomon and T. D. P. Stack, *J. Am. Chem. Soc.*, 2000, **122**, 10249.
6 Much of this work has been presented in oral form: T. H. Warren, X. Dai, S. Puiu and J. E. McDermott, *Abstracts of Papers, 221st National Meeting of the American Chemical Society*, Washington, DC, April 1–5, 2001, No. INOR 394.
7 Some dioxygen reactivity with two related Cu(I) β-diketiminates as well as the structure of **3** prepared from {[Me_2NN]CuCl}$_2$ and LiOH has been presented: W. B. Tolman, P. L. Holland, B. A. Jazdzewski, A. M. Reynolds, L. L. Bowen, D. J. E. Spencer, D. C. Price, M. Pink and V. G. Young, Jr, *Abstracts of Papers, 221st National Meeting of the American Chemical Society*, Washington, DC, April 1–5, 2001, No. INOR 16.
8 Sterically hindered Cu(II) β-diketiminates are known: P. L. Holland and W. B. Tolman, *J. Am. Chem. Soc.*, 1999, **121**, 7270; P. L. Holland and W. B. Tolman, *J. Am. Chem. Soc.*, 2000, **122**, 6331.
9 H. Masuda, K. Machida, M. Munakata, S. Kitagawa and H. Shimono, *J. Chem. Soc., Dalton Trans.*, 1988, 1907.
10 (*a*) L. S. Bartell, E. A. Roth, C. D. Hollowell, K. Kuchitsu and J. E. Young Jr, *J. Chem. Phys.*, 1965, **42**, 2683; (*b*) J. C. Cochran, K. Hagen, G. Paulen, Q. Shen, S. Tom, M. Traetteberg and C. Wells, *J. Mol. Struct.*, 1997, **413**, 313.
11 (*a*) B. F. Straub, F. Rominger and P. Hofmann, *Chem. Commun.*, 2000, 1611; (*b*) M. J. Henson, P. Mukherjee, D. E. Root, T. D. P. Stack and E. I. Solomon, *J. Am. Chem. Soc.*, 1999, **121**, 10332.
12 (*a*) SHELXTL-PC, Version 5.10; 1998, Bruker-Analytical X-ray Services, Madison, WI; G. M. Sheldrick, SHELX-97, Universität Göttingen, Göttingen, Germany; (*b*) L. Barbour, XSEED, 1999, University of Missouri, Columbia, MO; (*c*) SADABS; G. M. Sheldrick, 1996, based on the method described in R. H. Blessing, *Acta Crystallogr., Sect. A*, 1995, **51**, 33.

CHEMCOMM
Communication
www.rsc.org/chemcomm

Gold nanoparticles containing redox-active supramolecular dendrons that recognize $H_2PO_4^-$

Marie-Christine Daniel,[a] Jaime Ruiz,[a] Sylvain Nlate,[a] Jennifer Palumbo,[a] Jean-Claude Blais[b] and Didier Astruc*[a]

[a] *Groupe de Chimie Supramoléculaire des Métaux de Transition, LCOO, UMR CNRS, 5802, 33405 Talence Cedex, France. E-mail: d.astruc@lcoo.u-bordeaux.fr*
[b] *Laboratoire de Chimie Structurale Organique et Biologique, EP CNRS N° 103, Université Paris VI, 4 Place Jussieu, 75252 Paris, France*

Received (in Cambridge, UK) 27th July 2001, Accepted 16th August 2001
First published as an Advance Article on the web 18th September 2001

Gold nanoparticles have been functionalized with thiol dendrons containing three redox active amidoferrocenyl or silylferrocenyl units; using cyclic voltammetry, these dendronized gold nanoparticles recognize $H_2PO_4^-$

The scope of supramolecular chemistry[1] involves nanoscience including dendrimers[2] and nanoparticles[3] with applications to the field of sensors.[1,4] Beer *et al*. have shown various examples of redox anion recognition by amidoferrocenes bound to endoreceptors,[4] a concept that we have extended to dendrimers[5a] and colloids[5b] as exoreceptors. So far, only a few other reports of molecular recognition by nanoparticles have appeared,[6] althought ferrocenylalkylthiol ligands bonded to surfaces in self-assembled monolayers and colloids have been known for some time.[7] Dendrimer-colloid assemblies have also been successfully designed for the fabrication of a new generation of catalysts and sensors.[3b] We now report the synthesis of dendrons containing silylferrocenyl or amidoferrocenyl termini, their functionalization by thiol ligands, fixation of these dendron-thiol ligands onto gold colloids[8] and recognition of $H_2PO_4^-$ by these thiol-functionalized gold colloids.

Our strategy has consisted of performing ligand exchange reactions between alkylthiol–gold colloids of the Brust type[9] and the thiol dendron, a method that keeps the size of the colloids constant during the ligand exchange reactions, thus retaining their narrow polydispersity.[5b,9] The two syntheses of the triferrocenyl dendron–gold particle assemblies are represented in Scheme 1. Both syntheses represent the first routes to ferrocenyl-containing dendrons, although numerous ferrocenyl- and amidoferrocenyl-containing dendrimers are known.[10–13a] The key to rapid entry into the chemistry of such functionalized dendrons is the direct hydrosilylation of the three allyl groups of the dendron **1**[12] using various silanes[11–13] without any protection of the phenol function (Scheme 1).[14] The two air-sensitive thiol dendrons **8** and **10** were fully characterized by elemental analysis, NMR and the molecular peaks in their MALDI TOF mass spectra. We synthesized gold colloids with 2.1 nm diameter core and approximately 108 ± 5 dodecanethiolate ligands using the method of Brust *et al*.[9] Ligand-exchange reactions between these gold–dodecanethiolate particles and the thiol ligands **8** and **10** were carried out under ambient conditions in CH_2Cl_2 using 2/3 equiv. functional thiol per dodecane thiol

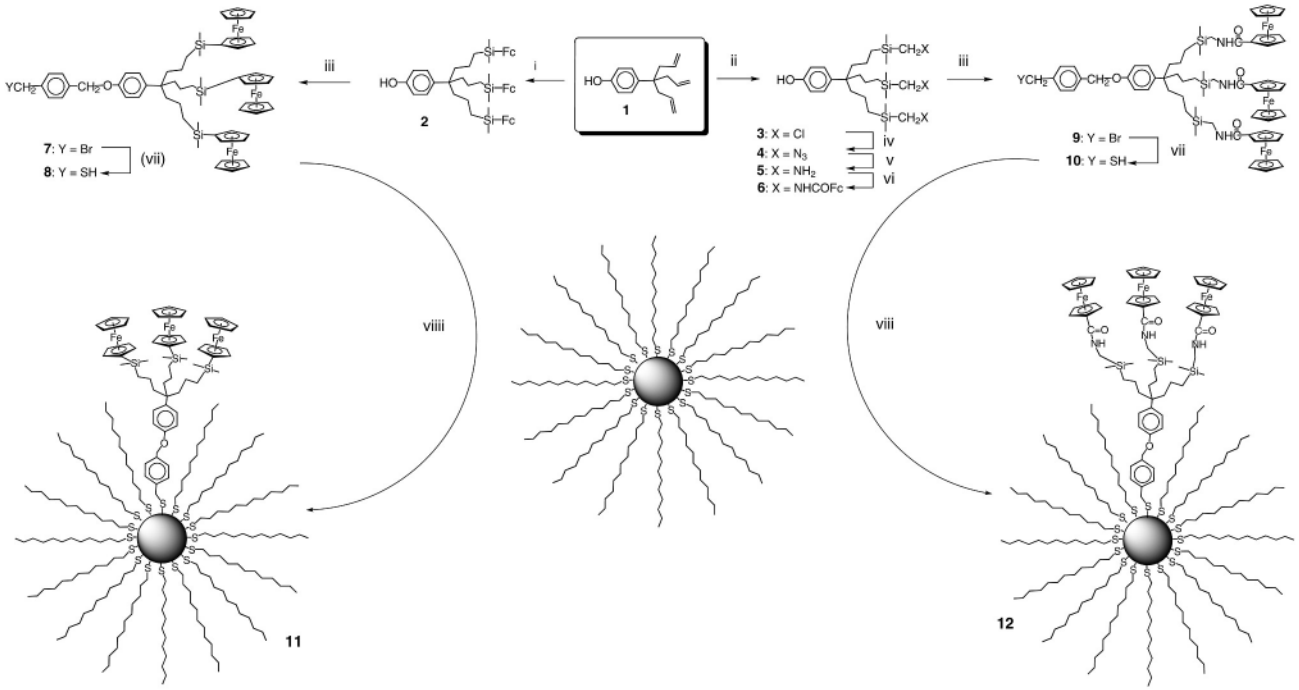

Scheme 1 Syntheses of the dendronized gold colloids. *Reagents and conditions*: i, Karstedt cat., $HSiMe_2Fc$ (Fc = ferrocenyl), Et_2O, reflux, 1 d, 90%; ii, Karstedt cat., $HSiMe_2(CH_2Cl)$, Et_2O, 1 d at room temp., then 1 d at reflux, 85%; iii, 1,1′-dibromo-*p*-xylene, K_2CO_3, MeCN, room temp., 3 d; **7**: 76%; **9**: 70%; iv, NaI, NaN_3, anhydrous DMF, 80 °C, 1 d, 90%; v, PPh_3, H_2O, THF, 80 °C, 1 d, 70%; vi, conc. aq. HCl, then NEt_3, FcCOCl, CH_2Cl_2, 16 h, room temp., 45%; vii, NaSH, THF, 50 °C, 1 d; **8**: 76%, **10**: 90%; viii, thiol dendron (2/3 equiv./equiv. dodecanethiolate ligand), CH_2Cl_2, 3 d, room temp.

 DOI: 10.1039/b106805a

ligand. This led to the dendronized particles **11** and **12**, and the excess of functional ligand was removed by washing **11** and **12** with methanol. The percentage of functional thiolate dendrons introduced as ligands in **11** and **12**, determined by combined HRTEM, ^{1}H NMR spectroscopy and elemental analysis, was 4.8 and 3%, respectively (a little more than five and three dendrons per particle for **11** and **12**, respectively). TEM images confirm that the sizes of the gold cores of the particles remain unchanged after the ligand-substitution reactions.

The cyclovoltammograms of the dendronized colloids **11** and **12** (Pt, CH_2Cl_2, 0.1 M [*n*-Bu_4N][PF_6]) show a chemically (i_a/i_c = 1) and electrochemically ($\Delta E_p \leq 50$ mV) reversible ferrocene/ferrocenium wave.[14] Thus, all the ferrocenyl units appear equivalent in each type of particles, which is due, in particular, to the fact that rotation of the particles is faster than the electrochemical time scale.[15] The separation between the anodic and cathodic peaks is 50 mV for **11**, which almost corresponds to the value expected at 20 °C for a single-electron wave (58 mV). In the case of **12**, however, this peak separation is only 20 mV. This indicates some adsorption, although this phenomenon is not accompanied by an enhanced intensity of the adsorbed species. The $E_{1/2}$ value is 0 V *vs.* $Cp_2Fe^{0/+}$ for **11** and 0.145 V *vs.* $Cp_2Fe^{0/+}$ for **12**.

We then added [*n*-Bu_4N][H_2PO_4] to the electrochemical cell containing **12**, which led to a decrease of the intensity of the amidoferrocene wave of **12** (Fig. 1). The growth of another wave was then observed at a less positive potential until the initial wave had disappeared when the amount of [*n*-Bu_4N][H_2PO_4] added corresponded to 1 equiv. per amidoferrocenyl branch. Thus, the new wave is the signature of a strong amidoferrocenium–$H_2PO_4^-$ interaction. Contrary to the initial wave, it shows the characteristic of slow electron transfer since the ΔE_p value is larger than 60 mV and depends on the scan rate, indicating structural reorganization in the course of the heterogeneous electron transfer.[14] The value of $E_{1/2}$ for each wave does not vary during the titration, the difference remaining equal to 210 ± 10 mV (as for the dendron **8** alone). This corresponds to an apparent association constant K_{app} between the ferrocenium form of **12** and $H_2PO_4^-$ that is 5200 ± 1000 times larger than that between the neutral form of **12** and $H_2PO_4^-$.[16] This shift is very large compared to monomeric amidoferrocenes ($E_{1/2(free)} - E_{1/2(bound)} = 45$ mV) and even to tripodal tris-amidoferrocenes such as PhC{$(CH_2)_3O(CH_2)_3$NHCOFc}$_3$ ($E_{1/2(free)} - E_{1/2(bound)} = 110$ mV), and is about as large as with a nona-amidoferrocene dendrimer.[5a] The known factors involved in the recognition of $H_2PO_4^-$ by amidoferrocenyl-containing receptors are the double hydrogen bonding between this anion and the amido groups, the enhanced electrostatic attraction in the oxidized ferrocenium form and the topographical effect of the receptor.[4]

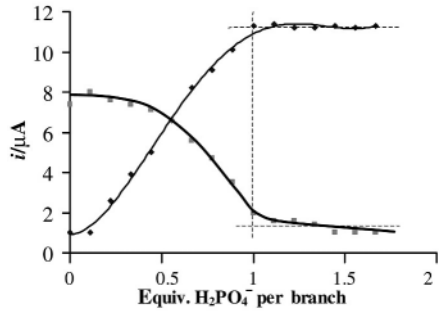

Fig. 1 Titration of **12** (10^{-6} M in CH_2Cl_2) with [*n*-Bu_4N][H_2PO_4] (10^{-2} M in CH_2Cl_2) monitored by CV. Decrease of the intensity of the initial wave at $E_{1/2}$ = 0.145 V *vs.* $FeCp_2^{+/0}$ and increase of the intensity of the new wave at $E_{1/2}$ = –0.065 V *vs.* $FeCp_2^{+/0}$ *vs.* the number of equivalents of [*n*-Bu_4N][H_2PO_4] added per ferrocenyl branch of **12**. [*n*-Bu_4N][PF_6] 0.1 M, 20 °C; internal reference: [Fe(η^5-$C_5Me_5)_2$]; reference electrode: Ag; auxiliary and working electrodes: Pt; scan rate: 0.2 V s^{-1}. A similar response was obtained with **11**.

Interestingly, the silylferrocene-containing colloids **11** also recognize $H_2PO_4^-$. Addition of [*n*-Bu_4N][H_2PO_4] to an electrochemical cell containing **11** provokes the same effect as with **12**, *i.e.* the appearance of a new wave at less positive potential than the original one, while the disappearance of the initial wave is observed for 1 equiv. of anion per silylferrocenyl branch. The difference of potential between the two waves is 110 ± 10 mV, which corresponds to a K_{app} value 85 ± 30 times larger for the ferrocenium form than for the ferrocenyl form. So far, only $H_2PO_4^-$ is recognized, the anions HSO_4^-, Cl^-, Br^- and NO_3^-, for instance, having no significant effect using either **11** or **12**.

It is likely that the supramolecular redox properties of dendronized colloids can be developed for sensoring, catalysis and molecular electronics in the near future.

Notes and references

1 J.-M. Lehn, *Supramolecular Chemistry: Concepts and Perspectives*, VCH, Weinheim, 1995.

2 G. R. Newkome, C. N. Moorefield and F. Vögtle, *Dendritic Molecules: Concepts, Syntheses and Perspectives*, VCH, New York, 1996.

3 (*a*) J. S. Bradley, in *Clusters and Colloïds*, ed. G. Schmid, VCH, Weinheim, 1995, ch. 6 (*b*) R. M. Crooks, M. Zhao, L. Sun, V. Chechik and L. K. Yeung, *Acc. Chem. Res*., 2001, **34**, 181.

4 P. D. Beer, *Adv. Inorg. Chem*., 1992, **39**, 79; P. D. Beer, *Chem. Commun*., 1996, 689; P. D. Beer, *Acc. Chem. Res*., 1998, **31**, 71; P. D. Beer, P. A. Gale and Z. Chen, *Adv. Phys. Org. Chem*., 1998, **31**, 1.

5 (*a*) C. Valério, J.-L. Fillaut, J. Ruiz, J. Guittard, J.-C. Blais and D. Astruc, *J. Am. Chem. Soc*., 1997, **119**, 2588; (*b*) A. Labande and D. Astruc, *Chem. Commun*., 2000, 1007.

6 R. Elghanian, J. J. Storhoff, R. C. Mucic, R. L. Letsinger and C. A. Mirkin, *Science*, 1997, **277**, 1078; S. Sampath and O. Lev, *Adv. Mater*., 1997, **9**, 410; D. Fitzmaurice, S. N. Rao, J. Preece, J. F. Stoddart, S. Wenger and N. Zaccheroni, *Angew. Chem., Int. Ed*., 1999, **38**, 1147; A. Niemz and V. M. Rotello, *Acc. Chem. Res*., 1999, **32**, 44; W. Shenton, D. A. Davis and S. Mann, *Adv. Mater*., 1999, **119**, 11132.

7 K. Weber and S. E. Creager, *Anal. Chem*., 1994, **66**, 3164; K. Weber, L. Hockett and S. E. Creager, *J. Phys. Chem. B*., 1997, **101**, 8286; M. J. Hosteler, S. J. Green, J. J. Stockes and R. W. Murray, *J. Am. Chem. Soc*., 1996, **118**, 4212; T. Horikoshi, M. Itoh, M. Kurihara, K. Kubo and H. Nishihara, *J. Electroanal. Chem*., 1999, **473**, 113; A. C. Templeton, W. P. Wuelfing and R. W. Murray, *Acc. Chem. Res*., 2000, **33**, 27.

8 M.-K. Kim, Y.-M. Jeon, W. S. Jeon, H.-J. Kim, S. G. Hong, C. G. Park and K. Kim, *Chem. Commun*., 2001, 667; R. Wang, J. Yang, Z. Zheng, M. D. Carducci, J. Jiao and S. Searaphin, *Angew. Chem., Int. Ed*., 2001, **40**, 549.

9 M. Brust, M. Walker, D. Bethell, D. J. Schiffrin and R. Whyman, *J. Chem. Soc., Chem. Commun*., 1994, 801; M. Brust, J. Fink, D. Bethell, D. J. Schiffrin and C. Kiely, *J. Chem. Soc., Chem. Commun*., 1995, 1655.

10 A. E. Kaifer and M. Gomez-Kaifer, *Supramolecular Electrochemistry*, Wiley-VCH, Weinheim, 1999, ch. 16, p. 207

11 Review: C. M. Casado, I. Cuadrado, M. Morán, B. Alonso, B. Garcia, B. Gonzales and J. Losada, *Coord. Chem. Rev*., 1999, **185**, 53.

12 (*a*) S. Nlate, J. Ruiz, J.-C. Blais and D. Astruc, *Chem. Eur. J*., 2000, **6**, 2544; (*b*) V. Sartor, L. Djakovitch, J.-L. Fillaut, F. Moulines, F. Neveu, V. Marvaud, J. Guittard, J.-C. Blais and D. Astruc, *J. Am. Chem. Soc*., 1999, **121**, 2929.

13 (*a*) P. Jutzi, C. Batz, B. Neumann and H. G. Stammler, *Angew. Chem., Int. Engl*., 1996, **35**, 2118; (*b*) S. W. Krsda and D. Seyferth, *J. Am. Chem. Soc*., 1998, **120**, 3604.

14 D. Astruc, *Electron-Transfer and Radical Processes in Transition-Metal Chemistry*, VCH, New York, 1995, chapters 2 and 7

15 C. B. Gorman, *Adv. Mater*., 1997, **9**, 1117; C. B. Gorman, *Adv. Mater*., 1998, **10**, 295.

16 S. R. Miller, D. A. Gustowski, Z.-H. Chen, G. W. Gokel, L. Echegoyen and A. E. Kaifer, *Anal. Chem*., 1988, **60**, 2021.

CHEMCOMM Communication
www.rsc.org/chemcomm

Immobilization of chlorophyll derivatives into mesoporous silica and energy transfer between the chromophores in mesopores†

Hiroyasu Furukawa,[a] Tadashi Watanabe[b] and Kazuyuki Kuroda*[a]

[a] *Department of Applied Chemistry, Waseda University, Ohkubo-3, Shinjuku-ku, Tokyo 169-8555, Japan. E-mail: kuroda@mn.waseda.ac.jp*
[b] *Institute of Industrial Science, The University of Tokyo, Komaba-4, Meguro-ku, Tokyo 153-8505, Japan*

Received (in Cambridge, UK) 5th June 2001, Accepted 16th August 2001
First published as an Advance Article on the web 17th September 2001

Chlorophyll derivatives possessing triethoxysilyl groups have been synthesized for the first time and grafted on mesoporous silica to construct an efficient energy transfer system between the chromophores.

In natural photosynthesis, chlorophylls (Chls, Fig. 1) play a key role in converting solar energy to chemical energy. Mimicking the highly efficient energy transfer (ET) systems is a subject to be tackled towards the ultimate goal of establishing solar energy conversion systems.[1] Considerable efforts have been directed toward the preparation of donor–acceptor (D–A) systems immobilized in various media (*e.g.* films,[2] surfactant micelles,[3] and lipid vesicles[4]). On the other hand, we have recently proposed the use of FSM-type mesoporous silica as an adsorbent of Chls,[5–7] because mesoporous silica powders possess high adsorption capacity with well ordered mesopores. However, our previous studies revealed that the surface silanol groups on FSM denatured incorporated chlorophyllous pigments.[5] Although surface modification with diols is an effective approach to suppress denaturation of Chls,[5,7] the plane of chlorin macrocycles should probably lie down on the modified silica surface.[6,7] Moreover, the arrangement between neighboring chromophores in mesopores is difficult to control by simple liquid-phase adsorption,[7] resulting in inefficient ET. In order to control the arrangements of macrocycles which should ideally be located in the center of mesopores, Chl derivatives possessing triethoxysilyl groups (Fig. 1) were therefore synthesized and grafted on mesoporous silica. We used Zn–chlorin and Cu–chlorin as the donor–quencher pair, because the fluorescence of Zn–chlorin should be quenched by Cu–chlorin, a non-fluorescent Chl derivative.[2]

Siliceous FSM was synthesized according to a method reported previously.[5] The X-ray diffraction (XRD) pattern (d_{100} = 4.0 nm) and the BET specific surface area (1000 $m^2\ g^{-1}$) were similar to those reported in ref. 5. A prescribed amount of compound **1**‡ (50–200 nmol of **1a**, **1b**, or a mixture of **1a** and **1b**, see Fig. 1) and 3-aminopropyltriethoxysilane (APTES, 4.3 mmol), a modifier to suppress denaturation of Chls, were dissolved in dry CH_2Cl_2 (2 mL). Then FSM powders (0.1 g), preheated at 150 °C for 3 h under vacuum, were dispersed in the solution of **1** and APTES. The mixtures were stirred at room temperature for 24 h in the dark (*i.e.* under mild conditions) to prevent denaturation of the chlorin macrocycles, centrifuged, washed with acetone, and dried under reduced pressure. The APTES–FSM/**1** compounds (*i.e.* APTES–FSM/**1a**, APTES–FSM/**1b** and APTES–FSM/**1a**–**1b**) were found to be green powders after washing. The mesostructure was retained after silylation according to the XRD patterns of APTES–FSM/**1** which was quite similar to that of pristine FSM (d_{100} = 4.0 nm) (ESI).†

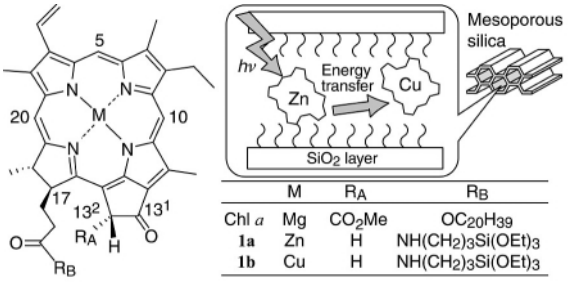

	M	R_A	R_B
Chl *a*	Mg	CO_2Me	$OC_{20}H_{39}$
1a	Zn	H	$NH(CH_2)_3Si(OEt)_3$
1b	Cu	H	$NH(CH_2)_3Si(OEt)_3$

Fig. 1 Molecular structure of chlorophyllous pigments (left) and schematic representation of the ET process in mesopores (right).

† Electronic supplementary information (ESI) available: Figs. S1–3: XRD patterns, ^{29}Si CP/MAS NMR and IR spectra. See http://www.rsc.org/suppdata/cc/b1/b104959n/

The cross polarization (CP) and magic angle spinning (MAS) ^{29}Si NMR spectrum of pristine FSM gives a Q^4 ($Si(OSi)_4$) peak with a relatively small Q^3 ($Si(OSi)_3OH$) band.[8] On the other hand, APTES–FSM gave resonance peaks in the region from −50 to −70 ppm assigned to T^1 (R(OR′)(OR″)*Si*(OSi)), T^2 (R(OR′)*Si*$(OSi)_2$) and T^3 (R*Si*$(OSi)_3$) peaks along with Q^3 and Q^4 peaks (ESI).[9]† A decrease in the number of Si–OH groups after silylation was also indicated by a decrease in the IR absorption in the O–H stretching region (*ca.* 3690 cm^{-1}) (ESI).† These findings confirm that APTES formed Si–O–Si bondings with Si–OH groups on FSM. Oligomerization of APTES in mesopores should be negligible, since silylated FSM powders were washed three times to remove residual silanes. The ^{13}C CP/MAS NMR signals due to CH_2 and CH_3 carbons of unreacted ethoxy groups of APTES appeared at *ca.* 56 and 17 ppm in the spectrum (data not shown).[9] Based on the CHN analysis, the number of grafted aminopropylsilyl groups was roughly estimated to be 1.3 nm^{-2} and the number of reacted ethoxy groups per APTES was calculated to be 1.9 nm^{-2}. The degree of grafting was smaller than that of FSM silylated with APTES by refluxing (1.7 groups nm^{-2}),[8] which is ascribed to the mild reaction conditions.

Because the amounts of **1** introduced were much lower than that of APTES molecules to prevent concentration quenching of ET (see below), there is no spectroscopic evidence whether the compounds **1** formed Si–O–Si bondings with FSM. However, all APTES–FSM/**1** powders were scarcely bleached by repeated washing with acetone. This is in sharp contrast with the observation that Chls incorporated into FSM by simple liquid-phase adsorption were easily desorbed from the mesopores by washing with acetone.[5–7] This finding strongly suggests that the compounds **1** were grafted onto the surface of mesopores as well as APTES–FSM.

Fig. 2(top) and (middle) depict the diffuse reflectance visible absorption spectra of **1a** (M = Zn) and **1b** (M = Cu) grafted on FSM. The Soret and Q_y absorption peaks of **1a** onto FSM were located at 426 and 660 nm, respectively. The spectral shape for APTES–FSM/**1a** is similar to the absorption spectrum of Zn–Chl *a* in methanol.[10] The full width at half maximum of the Q_y band (*ca.* 720 cm^{-1}) was broadened to a lesser extent than that of FSM/Zn–Chl *a* (*ca.* 1100 cm^{-1}),[6] indicating that **1a** was well-dispersed in the mesopores. Compound **1b** showed Soret and Q_y absorption peaks at 413 and 655 nm, respectively. The incorporation of Cu–chlorin was successful, which was in sharp

 DOI: 10.1039/b104959n

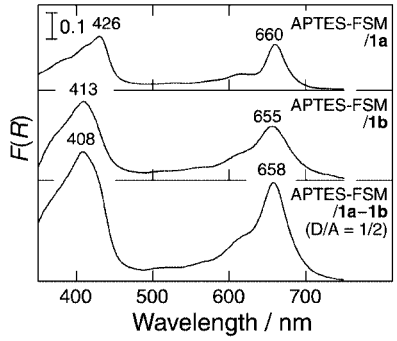

Fig. 2 Diffuse reflectance visible absorption spectra of APTES–FSM/**1** compounds. $F(R)$ refers to the so-called remission function for diffuse reflection measurements; $F(R) = (1 - R)^2/2R$.

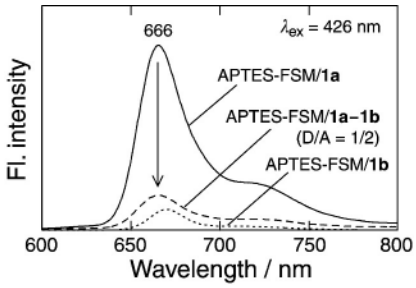

Fig. 3 Fluorescence emission spectra of APTES–FSM/**1** compounds (excited at 426 nm): APTES–FSM/**1a** (M = Zn) (—), APTES–FSM/**1b** (M = Cu) (···), APTES–FSM/**1a**–**1b** (co-adsorption) (– – –).

contrast to the fact that Cu–Chl *a* was scarcely immobilized in APTES–FSM (Furukawa *et al*., unpublished results). In the co-adsorbed state (APTES–FSM/**1a**–**1b**), the absorption band in the Soret region appeared at 408 nm with a small shoulder at 430 nm [Fig. 2(bottom)],[11] which indicates that this absorption spectrum can be roughly interpreted as a summation of those of **1a** and **1b**. This also indicates that the individual chromophores scarcely exhibit any specific interactions in the ground states within the mesopores.

The fluorescence emission spectra of APTES–FSM/**1** powders are illustrated in Fig. 3. Concentration quenching is negligible in all the APTES–FSM/**1** samples since the fluorescence intensity is proportional to the pigment concentration. The amounts of incorporated pigments were also estimated by the difference in the absorption spectra of the supernatant solutions before and after the silylation. The emission peaks of **1a** (M = Zn) and **1b** (M = Cu) on APTES–FSM were located at 666 and 670 nm, respectively. The emission intensity of **1b** was much weaker than that of **1a** in APTES–FSM.[11] The spectral overlap between the donor emission and quencher absorption bands is also relatively large (Figs. 2 and 3). These findings indicate that Förster type donor–acceptor (quencher) ET should occur.[12] In the co-adsorption systems the emission intensity of **1a** (M = Zn) was decreased with an increase in the amount of **1b** (M = Cu). The ET efficiency from **1a** to **1b** was approximately estimated by the considering the decrease in the emission area in the Q_y region in comparison with that of the APTES–FSM/**1a** complex (90% for D/A = 1/2; 50% for D/A = 1/1). In the case of co-adsorption of both Zn–pyroChl *b* and Zn–pyroChl *a* in APTES–FSM, the emission intensity originating from Zn–pyroChl *a* (acceptor) was increased even though there are many NH_2 groups in the mesopores (ET efficiency 75% for D/A = 1/10, Furukawa *et al*., unpublished results). The finding indicates that the NH_2 groups of APTES scarcely act as quenchers in the present system. Based on the pore volume and pore size of APTES–FSM, the critical distance (R_0)[12] between neighboring chromophores is calculated to be *ca*. 12 nm. It is of interest that this efficiency is much higher than the ET efficiency between Chl *b* and Chl *a* in diol modified FSM (70% for D/A = 1/10),[7] though the pigment concentration and R_0 in the mesopores are very similar. Taking into account that fact that highly efficient ET is obtained in this grafted system in comparison to systems obtained by conventional adsorption methods, the planes of chromophores are probably perpendicular to the silica walls in the mesopores. This suggests that the interactions between the chlorin macrocycles and the silica walls are relatively small, and this may be the reason why APTES–FSM/**1a** complexes gave a sharper absorption band in comparison with FSM/Zn–Chl *a*, for which Zn–Chl *a* was incorporated into FSM by liquid-phase adsorption.[6]

We are grateful to Mr T. Shigeno (Waseda Univ.) for his help in NMR measurements. This work was partially supported by a Grant-in-Aid for COE Research, MEXT, Japan. H. F. also acknowledges a Grant-in-Aid for Scientific Research, MEXT, Japan (No. 13750780).

Notes and references

‡ Chl was extracted from spinach tissue and pyrolyzed to suppress denaturation of the chlorin macrocycle.[6] The amidation procedure is as follows: zinc $C13^2$-demethoxycarbonylchlorophyllide *a* (Zn–pyroChlid *a*) was prepared, as described in ref. 13 from Chl *a*. Zn–pyroChlid *a* (60 μmol) was added to a mixture of 3-aminopropyltriethoxysilane (120 μmol), 1-(3-dimethylaminopropyl)-3-ethylcarbodiimide (60 μmol) and dimethylaminopyridinium tosylate (60 μmol) in dry CH_2Cl_2 (10 mL).[14] The mixture was stirred for 12 h under N_2 at room temperature. The crude compound was purified by flash column chromatography over silica gel with acetone and by preparative normal-phase HPLC (column: Senshupak Silica-5251N; eluent: ethyl acetate–hexane–acetone = 6 : 1 : 3). *Characterization data* for zinc $C13^2$-demethoxycarbonylchlorophyllide *a* 3-triethoxysilylpropylamide (**1a**, 60%). Visible (acetone): λ_{max} 656 (relative intensity, 0.66), 609 (0.12), 569 (0.06), 427 (1.00). ^{1}H NMR (400 MHz, $CDCl_3$) δ: 9.42, 9.28, 8.53 (each 1H, s, 10-, 5-, 20-H), 8.03 (1H, dd, J = 12, 18 Hz, 3^1-H), 6.22 (1H, dd, J = 2, 18 Hz, 3^2-*cis*-H), 6.08 (1H, dd, J = 2, 12 Hz, 3^2-*trans*-H), 5.07 (1H, br s, 17^4-NH), 4.16–4.59 (2H + 1H, m, 13^2-CH_2 + 18-H), 3.62–3.86 (1H + 2H, m, 17-H + 17^5-CH_2), 3.70 (2H, q, J = 7 Hz, 8^1-CH_2), 3.62 (6H, q, J = 7 Hz, 17^{10}-$(CH_2)_3$), 3.45, 3.33, 3.24 (each 3H, s, 12^1-, 2^1-, 7^1-CH_3), 1.75–2.30 (each 1H, m, 17-CH_2CH_2), 1.69 (3H, t, J = 7 Hz, 8^2-CH_3), 1.65 (3H, d, J = 7 Hz, 18-CH_3), 1.20–1.28 (each 1H, m, 17^6-CH_2), 1.07 (9H, t, J = 7 Hz, 17^{11}-$(CH_3)_3$), 0.78–0.95 (each 1H, m, 17^7-CH_2). MS (FAB): *m*/*z* 799.3 (M^+, for ^{64}Zn), calc.: 799.3. Copper $C13^2$-demethoxycarbonylchlorophyllide *a* 3-triethoxysilylpropylamide was prepared in the same manner as compound **1a** except for the Cu insertion.[15] *Characterization data* for **1b** (yield = 22%). Visible (acetone): λ_{max} 651 (relative intensity, 0.46), 605 (0.12), 420 (0.94), 410 (1.00). MS (FAB): *m*/*z* 798.4 (M^+, for ^{63}Cu), calc.: 798.3.

1 D. Gust, T. A. Moore and A. L. Moore, *Acc. Chem. Res*., 2001, **34**, 40.
2 A. G. Tweet, W. D. Bellamy and G. L. Gaines, Jr., *J. Chem. Phys*., 1964, **41**, 2068.
3 Z. Jiquan, Z. Jinhquan, X. Jie, Z. Jianping and J. Lijin, *Colloids Surf. B*, 1998, **11**, 9.
4 K. Colbow, *Biochim. Biophys. Acta*, 1973, **314**, 320.
5 S. Murata, H. Hata, T. Kimura, Y. Sugahara and K. Kuroda, *Langmuir*, 2000, **16**, 7106.
6 H. Furukawa, K. Kuroda and T. Watanabe, *Chem. Lett*., 2000, 1256.
7 S. Murata, H. Furukawa and K. Kuroda, *Chem. Mater*., 2001, **13**, 2722.
8 T. Kimura, S. Saeki, Y. Sugahara and K. Kuroda, *Langmuir*, 1999, **15**, 2794.
9 G. S. Caravaja, D. E. Leyden, G. R. Quinting and G. E. Maciel, *Anal. Chem*., 1988, **60**, 1776.
10 H. Furukawa, T. Oba, H. Tamiaki and T. Watanabe, *Bull. Chem. Soc. Jpn*., 2000, **73**, 1341.
11 Taking into account the fact that the absorption maximum in the Soret region of APTES–FSM/**1a**–**1b** was located at a wavelength shorter than that of APTES–FSM/**1a**, the possibility of denaturation (and/or demetalation) of the macrocycle in mesopores cannot be fully excluded. This may be the reason that a weak emission of **1b** was observed (Fig. 3), though Cu–chlorin is normally non-fluorescent.[2] An excitation spectrum of APTES–FSM/**1b** did not resemble that of either pheophytin *a* (free base chlorin) or Zn–Chl *a*, which may also support the possibility of partial pigment denaturation.
12 T. Förster, in *Modern Quantum Chemistry*, ed. O. Sinanoglu, Academic Press, New York, 1965, p. 93.
13 H. Tamiaki, M. Amakawa, Y. Shimono, R. Tanikaga, A. R. Holzwarth and K. Schaffner, *Photochem. Photobiol*., 1996, **63**, 92.
14 L. A. J. Chrisstoffels, A. Adronov and J. M. F. Fréchet, *Angew. Chem., Int. Ed*., 2000, **39**, 2163.
15 M. Fujiwara and M. Tasumi, *J. Phys. Chem*., 1986, **90**, 5646.

CHEMCOMM Communication
www.rsc.org/chemcomm

One-way *EZ*-isomerization of bis(*n*-butylammonium) (*Z,Z*)-muconate under photoirradiation in the crystalline state

Toru Odani,[a] Akikazu Matsumoto,*[a] Kazuki Sada[b] and Mikiji Miyata[b]

[a] *Department of Applied Chemistry, Graduate School of Engineering, Osaka City University and PRESTO, JST, Sugimoto, Sumiyoshi-ku, Osaka 558-8585, Japan. E-mail: matsumoto@a-chem.eng.osaka-cu.ac.jp*

[b] *Graduate School of Engineering, Osaka University, 2-1 Yamadaoka, Suita, Osaka 565-0871, Japan*

Received (in Cambridge, UK) 26th July 2001, Accepted 29th August 2001
First published as an Advance Article on the web 11th September 2001

One-way *EZ*-isomerization of bis(*n*-butylammonium) (*Z,Z*)-muconate [(*Z,Z*)-hexa-2,4-diene-1,6-dioate] to the corresponding (*E,E*)-isomer quantitatively proceeded in the crystalline state under photoirradiation with a high-pressure mercury lamp, being a new type of crystal-to-crystal reaction.

Organic synthesis performed in the solid state is one of the most intriguing fields of chemistry in recent years, because of the specific features of the solid-state reaction including the excellent selectivity of the reaction compared to those in an isotropic medium, the specific molecular alignment in the solid as the product, and the environmental aspect of a solvent-free process.[1] In contrast to cyclization and rearrangement as the unimolecular reaction in the crystalline state, *EZ*-isomerization is difficult due to a drastic and unenviable change in the size and shape of the occupied space by an olefin molecule during the isomerization.[2] During the course of our recent studies of the topochemical polymerization of diene monomers, we have found that some (*Z,Z*)-muconic derivatives provided a geometrical isomer but not a polymer as the photoproduct in a high yield by UV irradiation in the crystalline state.[3] This isomerization is a crystal-to-crystal reaction with an excellent selectivity, being completely different from ordinary photoreactions. Monoolefins and azo compounds generally induce reversible *EZ*-isomerization and the photoproducts are isolated as a mixture of *cis* and *trans* isomers, whose composition is dependent on the wavelength of light used. In the present paper, we describe the unique one-way *EZ*-isomerization of bis(*n*-butylammonium) (*Z,Z*)-muconate [(*Z,Z*)-hexa-2,4-diene-1,6-dioate] (**1**) to the corresponding (*E,E*)-isomer (**2**) as a new type of solid-state topotactic reaction.

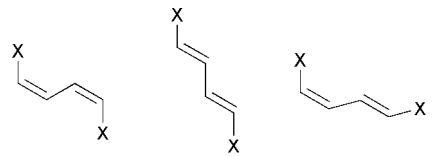

When **1** was irradiated in the crystalline state at room temperature using a high-pressure mercury lamp with a Pyrex filter, the isomerization to **2** proceeded. In this system, no polymer was produced due to the absence of columnar structure appropriate for the topochemical polymerization in the crystals.[3c,d] ^{1}H NMR spectroscopy confirmed that the solid-state photoisomerization is highly stereoselective, *i.e.*, no (*E,Z*)-isomer (**3**) formed during photoirradiation in the crystalline state, in contrast to the photoirradiation in a solution resulting in a mixture of three kinds of isomers, and complementary to the exclusive formation of **3** during thermal isomerization in solution.[4] As summarized in Table 1, the conversion of **1** to **2** achieved 98% for the 10 h irradiation. When **2** was irradiated in the crystalline state under similar conditions, unreacted **2** was recovered. Thus, the isomerization occurs solely one-way from **1** to **2** in the crystalline state, despite similar UV absorption bands of both isomers, *i.e.*, λ = 255 nm and $\varepsilon = 1.77 \times 10^4$ for **1**; λ = 260 nm and $\varepsilon = 2.42 \times 10^4$ for **2**. Similar one-way isomerization was observed for a series of muconic acid derivatives, *e.g.*, *n*-alkyl- and branched alkylammonium salts, alkyl esters, and *N*-alkylamides.

Powder X-ray diffraction has verified that the isomerization occurs *via* a crystal-to-crystal reaction process, and that the diffraction profiles of the crystals after photoirradiation consist of overlapped patterns of the diffraction due to the crystals of **1** and **2** (Fig. 1). This indicates that the crystal domains of each isomer exist simultaneously in the crystals accompanied by crystal phase separation during the photoisomerization. Single crystal structure analysis has disclosed that the crystals of **2** as the photoproduct have a symmetry different from that of the starting crystals of **1** (Fig. 2).† The solid-state photoisomeriza-

Table 1 Photoisomerization of **1** and **2** under irradiation with a high-pressure Hg-lamp in the crystalline state or in solution

			Composition after photoirradiation		
Substrate	Temp./°C	Time/h	**1**	**2**	**3**
1	30	2	79	21	0
		4	44	58	0
		6	30	70	0
		8	5	95	0
		10	2	98	0
2	30	8	0	100	0
1[a]	80	2	60	0	40
1[b]	30	8	24	33	43

[a] Thermal isomerization in D_2O. [b] Photoisomerization in D_2O.

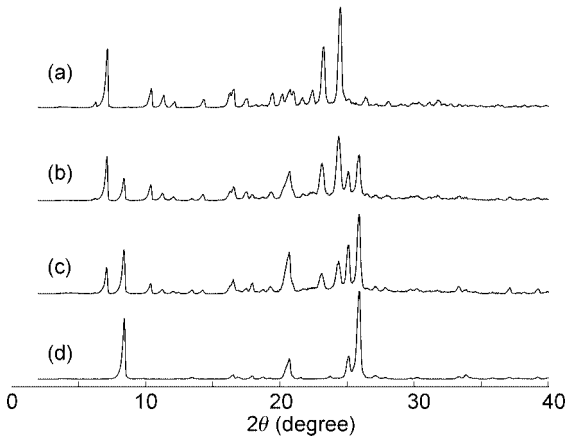

Fig. 1 Powder X-ray diffraction profiles of (a) **1**, (b) after isomerization of **1**, **1**:**2** = 64:36 determined by ^{1}H-NMR, (c) **1**:**2** = 36:64, (d) **2**.

 DOI: 10.1039/b106155k

tion of **1** proceeds *via* a topotactic reaction mechanism.[5] The isomerization from **1** to **2** in the crystalline state requires not only the movement of atoms but also a change in the crystal symmetry and the reconstruction of the hydrogen bond network pattern. In the crystals of these primary ammonium carboxylates, one-dimensional ladder-type hydrogen bonds are observed, consisting of the primary ammonium cations and the carboxylate anions which act as triple hydrogen bond donors and acceptors, respectively.[3c,6] The isomerization of the (*Z,Z*)-diene to the (*E,E*)-diene is associated with the rotation of carbonyl groups and the change in the hydrogen bond structure (Fig. 3). The reconstruction of the hydrogen bond network during the isomerization is accompanied with an inter-ladder reaction, but not intra-ladder. The quantitative transformation of **1** to **2** in the crystalline state suggests that the molecular motion in the crystals occurred cooperatively with the minimum movement of atoms in the crystals *via* a phase transition from the crystal of **1** to that of **2**. It is possible to accelerate the heterogeneous solid-state reaction in a boundary domain between the mutual crystal phases of **1** and **2**.

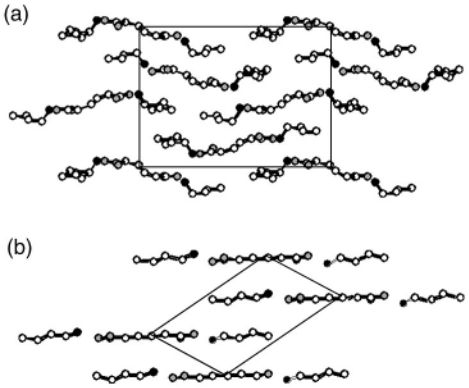

Fig. 2 Crystal structure of (a) **1**, (b) **2** viewed along the crystallographic *a*-axis. Hydrogen atoms are omitted. Hydrogen bond networks run along the crystallographic *a*-axis.

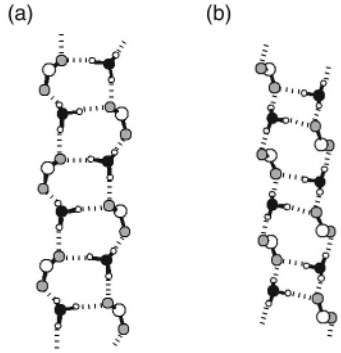

Fig. 3 One-dimensional ladder-type hydrogen bond networks of (a) **1**, (b) **2**.

Topotactic *EZ*-isomerization is advantageous for 1,3-diene derivatives such as muconates, of which both isomers have similar molecular shapes, different from the case of monoolefins. As an exceptional event, unique one-way isomerization of an anthracene-substituted olefin with (*Z*)-configuration has been reported,[7] in which the isomerization to the (*E*)-derivative proceeds during photoirradiation in solution, but the reverse reaction hardly occurs due to the presence of the large aromatic substituent changing in its potential energy surfaces at the excited triplet state. In this work, the excited-state of **1** probably has a conformation similar to that of **2** in the solid state, resulting in a quantitative and one-way isomerization. Further mechanistic studies of the one-way *EZ*-isomerization of the muconic acid derivatives in the crystalline state are now under investigation.

Notes and references

† *Crystallographic data for* **1**: $C_{14}H_{28}N_2O_4$, M_r = 288.39, monoclinic, space group $P2_1/n$, T = 200(1) K, a = 5.7715(4), b = 20.005(1), c = 14.749(1) Å, β = 96.510(4)°, V = 1691.9(2) Å^3, Z = 4, D_c = 1.132 g cm^3, μ(CuKα) = 0.673 mm^{-1}. A total of 10965 reflections was measured, 2864 were unique. 2391 [$I > 1.5\sigma(I)$] were used in the refinement of 199 parameters. R_1 = 0.063, wR_2 = 0.172, GOF = 1.92. A butyl group was disordered. For **2**: $C_7H_{14}NO_2$, M_r = 144.19, triclinic, space group $P\bar{1}$, T = 293(1) K, a = 5.5246(8), b = 7.433(1), c = 10.865 (2) Å, α = 98.88(1), β = 100.86(1), γ = 104.38(1)°, V = 414.8(1) Å^3, Z = 2, D_c = 1.154 g cm^3, μ(MoKα) = 0.084 mm^{-1}. A total of 2103 reflections was measured, 1141 [$I > 1.5\sigma(I)$] were used in the refinement of 105 parameters. R_1 = 0.046, wR_2 = 0.137, GOF = 1.00. CCDC 169916, 169917. See http//www.rsc.org/suppdata/cc/b1/b106155k/ for crystallographic files in .cif format.

1 G. M. J. Schmidt, *Pure Appl. Chem.*, 1971, **27**, 647; *Photochemistry in Organized and Constrained Media*, ed. V. Ramamurthy, VCH, New York, 1991; *Reactivity in Molecular Crystals*, ed. Y. Ohashi, Kodansha-VCH, Tokyo; 1993; F. Toda, *Acc. Chem. Res.*, 1995, **28**, 480; G. R. Desiraju, *Angew. Chem., Int. Ed. Engl.*, 1995, **34**, 2311; F. Toda and K. Tanaka, *Chem. Rev.*, 2000, **100**, 1025.

2 K. Kinbara, Y. Kobayashi and K. Saigo, *J. Chem. Soc., Perkin Trans. 2*, 1998, 1767.

3 (*a*) A. Matsumoto, K. Yokoi, S. Aoki, K. Tashiro, T. Kamae and M. Kobayashi, *Macromolecules*, 1998, **31**, 2129; (*b*) A. Matsumoto, T. Odani and S. Aoki, *Polym. J.*, 1998, **30**, 358; (*c*) A. Matsumoto, T. Odani, M. Chikada, K. Sada and M. Miyata, *J. Am. Chem. Soc.*, 1999, **121**, 11122; (*d*) A. Matsumoto, S. Nagahama and T. Odani, *J. Am. Chem. Soc.*, 2000, **122**, 9109; (*e*) A. Matsumoto, T. Odani, K. Sada, M. Miyata and K. Tashiro, *Nature*, 2000, **405**, 328.

4 J. A. Elvidge, R. P. Linstead, P. Sims and B. A. Orkin, *J. Chem. Soc.*, 1950, 2235.

5 For definition of topochemical and topotactic reactions: H. Nakanishi, M. Hasegawa and Y. Sasada, *J. Polym. Sci., Polym. Phys. Ed.*, 1972, **10**, 1537; J. M. Thomas, *Phil. Trans. R. Soc.*, 1974, **277**, 251; G. Wegner, *Pure Appl. Chem.*, 1977, **47**, 443; M. Thakur, *Encyclopedia of Polymer Science and Engineering*, ed. J. I. Kroschwitz, Wiley, New York, 1989, vol. 15, pp. 362–380.

6 K. Kinbara, Y. Hashimoto, M. Sukegawa, H. Nohira and K. Saigo, *J. Am. Chem. Soc.*, 1996, **118**, 3441.

7 T. Arai, *Organic Molecular Photochemistry*, ed. V. Ramamurthy and K. S. Chanze, Marcel Dekker, New York, 1999, pp. 131–167; T. Arai and K. Tokumaru, *Chem. Rev.*, 1993, **93**, 23 and references therein.

CHEMCOMM
Communication
www.rsc.org/chemcomm

A novel cage organotellurate(IV) macrocyclic host encapsulating a bromide anion guest: $[Li(THF)_4][\{(Pr^iTe)_{12}O_{16}Br_4\{Li(THF)Br\}_4\}Br]\cdot 2THF$

Hélène Citeau, Kristin Kirschbaum, Olaf Conrad and Dean M. Giolando*

Department of Chemistry, University of Toledo, Toledo, OH 43606 USA.
E-mail: Dgiolan@uoft02.utoledo.edu

Received (in Columbia, MO, USA) 5th June 2001, Accepted 2nd August 2001
First published as an Advance Article on the web 19th September 2001

The first structural report of an unprecedented organotellurate(IV) inorganic–organic hybrid macrocyclic host encapsulating a bromide anion guest is described.

In recent years considerable efforts have been directed to gaining an understanding of the fundamental aspects of tellurite glass chemistry because of its potential applications in nonlinear optics and as ionic conductive materials.[1] Tellurites, $(M_2O)_x$-$(TeO_2)_{1-x}$, are glass oxide materials constituted by a network (TeO_2) and a modifier (M_2O, alkali metal oxide). Their remarkable properties arise from the free electron pair in their motif built of TeO_3 or TeO_4 units. In spite of the significant progress in the interpretation of solid state ^{125}Te-NMR spectroscopy data[2] and the structure determination of a few crystalline phases,[3] precise structural data remain elusive due to the amorphous nature of these materials. The development of a 'telluroxane' chemistry of tellurium(IV) as model compounds might be a fruitful approach by analogy to the well-developed chemistry of oligomeric siloxanes, whose importance as molecular precursors and model compounds for zeolitic material is well known.[4] To the best of our knowledge, no comparable oligomeric 'telluroxane' containing exclusively Te–O bonds in their rings has been crystallographically characterized. We present here a novel 'telluroxane' containing a $Te_{12}O_{16}$ ring that can be formally viewed as the condensation product of organotellurium trihydroxides. $[Li(THF)_4][\{(Pr^iTe)_{12}O_{16}Br_4\{Li(THF)Br\}_4\}Br]$ **1** represents the first of a new and potentially rich class of compounds.

Crystals of the title salt† consist of isolated $[Li(THF)_4]^+$ cations, $[\{(Pr^iTe)_{12}O_{16}Br_4\{Li(THF)Br\}_4\}Br]^-$ anions and uncoordinating solvent molecules. The crystals were obtained as colorless air-sensitive trigonal prismatic crystals in a reaction designed initially to prepare a new organotellurium compound, isopropyl hex-1-ynyl telluride,[5] and can be viewed as a partial air oxidation product of a mixture of lithium hex-1-ynyl tellurolate and isopropyl bromide in THF. The structure of this novel tellurium oxide cage compound, with unprecedented molecular macrocyclic character, has been determined by single crystal X-ray diffraction. In the crystalline state, the tellurium oxide framework spherically encapsulates a bromide anion in its cavity. This molecular guest–host entity is stabilized by four Li(THF)Br units and four bromide anions in an outer shell. The capability of entrapping an atomic size guest in its cavity makes it a promising candidate for various applications in chemistry.[6] Moreover, this new example of a self-assembled molecular macrocycle exhibits the remarkably rare[7] property of encapsulating a *negatively* charged ion.

The structure of the skeleton of the anion is shown in Fig. 1. The macrocycle of alternating tellurium and oxygen atoms—constructed of four O–Te–O–Te(μ-O)$_2$Te– monomers attached head-to-tail—folds into a spherical arrangement. With twelve tellurium and sixteen oxygen atoms in a continuous ring the macrocycle is unprecedented for a molecular organotellurate(IV). The closest structural analogs are $[(C_6H_4\text{-}4\text{-}Me)_2Te\{OTe(C_6H_4\text{-}4\text{-}Me)_2\}_2][Te(C_6H_4\text{-}4\text{-}Me)_2OTe(C_6H_4\text{-}4\text{-}Me)_2][CF_3SO_3]_4$ in which Te···O–S–O···Te cation–anion interactions form a 14-membered ring[8] and, the first example of a supramolecular structure of an organotellurium complex, polymeric $[(C_4H_8TeNO_3)_2O]_n$ containing $(NO_3)Te(C_4H_8)$–O–$Te(C_4H_8)(NO_3)$ monomers connected *via* Te···O–N–O···Te secondary semi-bonding interactions.[9]

The arrangement of the Te–O framework around the central bromide anion possesses the point group symmetry D_{2d} and is topologically equivalent to the seams of a tennis ball.[6] The encapsulated bromide anion is located inside a cavity of dimensions 5.0 × 4.1 × 3.2 Å^3, with four long [4.1707(10)–4.2641(10) Å; Te(3), Te(5), Te(9), Te(11)] and eight short [3.5398(9)–3.6625(10) Å; Te(1), Te(2), Te(4), Te(6), Te(7), Te(8), Te(10), Te(12)] Br(9)–Te distances. No bonding interactions are expected for the longer Te···Br distances, which are slightly greater than the sum of van der Waals radii (Te, 2.10 Å; Br, 1.80–2.00 Å).[10] The distance between the central bromide anion and the eight closer tellurium atoms is shorter than the sum of van der Waals radii, but much longer than the sum of the covalent radii (Te, 1.35 Å; Br, 1.14 Å),[10] indicating a stabilizing interaction between guest and host. Similar distances have been ascribed to Te···Br secondary interactions.[11]

The Te–O macrocycle consists of alternating Te(μ-O)$_2$Te and O–Te–O building blocks. In agreement with other Te(μ-O)$_2$Te microcycles[3] the Te(μ-O)$_2$Te rings in **1** possess alternating short [1.916(5)–1.941(5) Å] and long [2.107(5)–2.157(5) Å] bonds between tellurium and oxygen. The shorter ones can be attributed[12] to Te=O bonds, and are slightly shorter than the sum of covalent radii (Te, 1.35 Å; O, 0.73 Å),[10] while the longer ones can be attributed[12] to dative interactions (Te←O). The

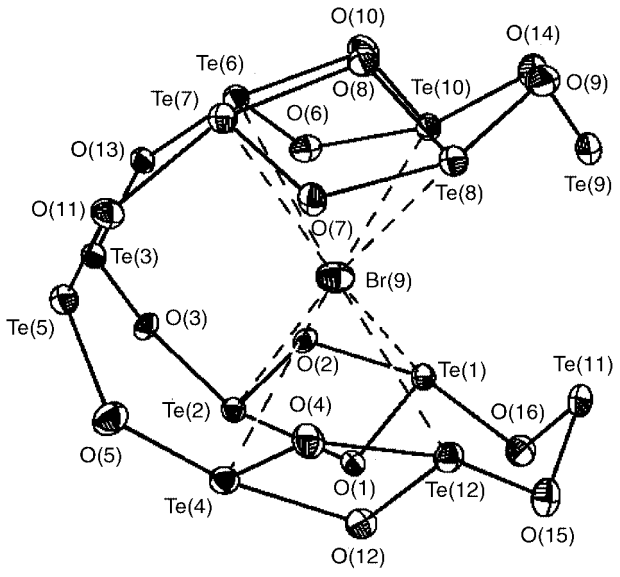

Fig. 1 Labeling scheme of the $Te_{12}O_{16}$ skeleton and the central bromine anion of the anion of **1**. For clarity the Pr^i groups, four Br anions and four Li(THF)Br have been removed.

 DOI: 10.1039/b107147p

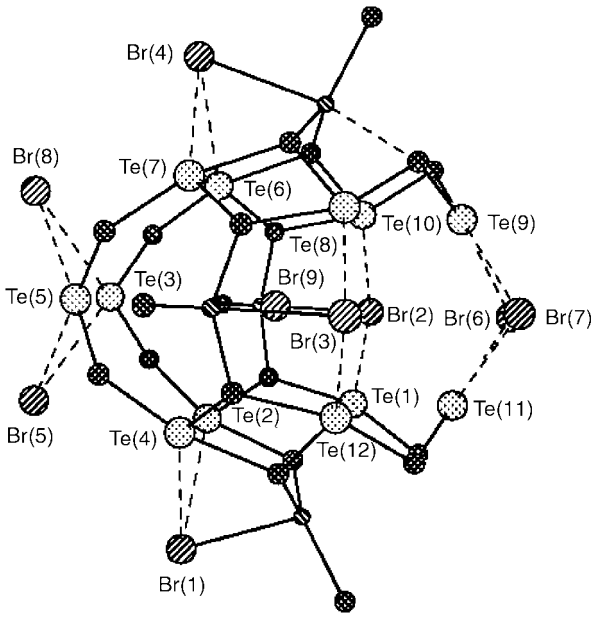

Fig 2 Labeling scheme for the Te and Br atoms of the anion of **1**.

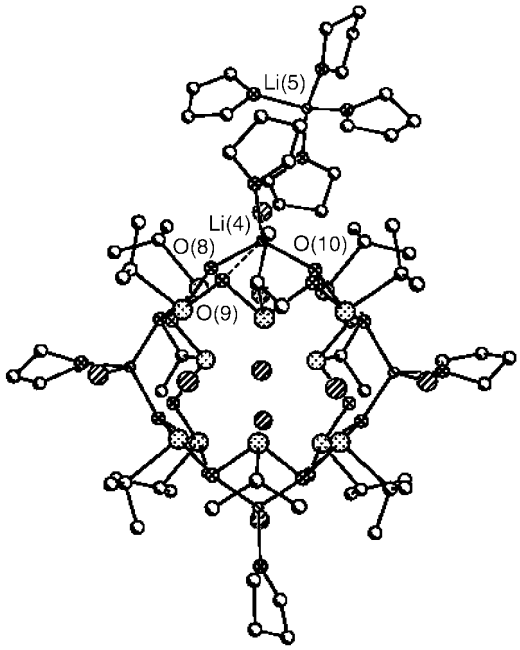

Fig. 3 Drawing showing the $\bar{4}$ symmetry in the title compound.

connection of the four Te(μ-O)$_2$Te rings to the –OTeO– building block occurs by weaker Te–O-interactions [2.091(6)–2.120(5) Å], while the O–Te–O unit itself contains stronger Te–O bonds [1.908(5)–1.924(5) Å]. This sequence of bonding type and the planarity (±0.12 Å) of the Te(μ-O)$_2$Te rings is not uncommon for telluroxides.[12,13]

Stabilization of the spherical $Te_{12}O_{16}$ framework is provided by the nine bromide anions, one inside and eight outside the sphere (Fig. 2). The eight tellurium atoms of the Te(μ-O)$_2$Te microcycle have weak interactions to the central Br(9) and somewhat stronger interactions to the 'outer' bromine atoms [Br(1)–Br(4): Te–Br 3.2444(10)–3.3639(10) Å] of the four Li(THF)Br units in the anion. A stronger set of Te–Br interactions occur between the O–Te–O building blocks and 'outer' bromide anions [Br(5)–Br(8): Te–Br 3.0847(10)–3.1817(11) Å]. Similar Te–Br bridging bonds have been described.[14] Additional stabilization of the $Te_{12}O_{16}$ framework occurs through O–Li–O bridges above the Te(μ-O)$_2$Te microcycles through Li–O [1.914(15)–1.980(15) Å] bonds (Fig. 2). Finally, each tellurium atom bears one Pr^i group with standard Te–C distances [2.132(8)–2.176(8) Å].[15] A [Li(THF)$_4$] cation compensates for the charge of the host–guest assembly in the crystal.

Overall the anion possesses a non-crystallographic $\bar{4}$ symmetry (Fig. 3). A deviation from this point symmetry is most likely caused by packing effects due to the spatial requirements of the [Li(THF)$_4$]$^+$ ion. The proximity of the [Li(THF)$_4$]$^+$ cation to Li(4) causes Li(4) to move toward O(9). As a result one, that attached to Te(9), of the four Pr^i groups on the macrocycle is turned by *ca.* 90°.

Notes and references

† *Systematic name* (from CAS services): tetrabromo[dodecakis(1-methylethyl)octa-μ-oxododecatellurium]octa-μ$_3$-oxotetrakis(tetrahydrofuran)-tetralithium(4+) (*T*-4)-tetrakis(tetrahydrofuran)lithium(1+) bromide compound with tetrahydrofuran (1:1:5:2).

Crystal data: $Te_{12}Br_9O_{26}C_{76}H_{162}Li_5$, M = 3754.97, monoclinic, space group $P2_1$, a = 15.1957(4), b = 27.6216(8), c = 16.0219(3) Å, β = 116.572(1)°, U = 6014.5(3) Å^3, Z = 2, D_c = 2.073 Mg m^{-3}, crystal dimensions 0.30 × 0.38 × 0.18 mm, $F(000)$ = 3516, T = 140(1) K, Mo-Kα radiation, λ = 0.71073 Å. Data collection Bruker CCD. Of the total 43781 independent reflections measured, the final indices for 28382 reflections with $I > 2\sigma(I)$ were $R(F)$ = 0.0422, $wR(F^2)$ = 0.0748 and $R(F)$ = 0.0629, $wR(F^2)$ = 0.0799 for all data. CCDC reference number 168678. See http://www.rsc.org/suppdata/cc/b1/b107147p/ for crystallographic data in CIF or other electronic format.

1 J. S. Aitchison, J. D. Prohaska and E. M. Vogel, *Met. Mater. Processes*, 1996, **8**, 277; J. W. Zwanziger, *Int. Rev. Phys. Chem.*, 1998, **17**, 65; A. Pierre, F. Duboudin, B. Tanguy and J. Portier, *Solid State Ionics*, 1992, **53–56**, 1200.
2 S. Sakida, S. Hayakawa and T. Yoko, *J. Non-Cryst. Solids*, 1999, **243**, 1; S. Sakida, S. Hayakawa and T. Yoko, *J. Non-Cryst. Solids*, 1999, **243**, 13, and references therein.
3 S. L. Tagg, J. C. Huffman and J. W. Zwanziger, *Acta Chem. Scand.*, 1997, **51**, 118, and references therein.
4 R. Murugavel, A. Voigt, M. G. Walawalkar and H. W. Roesky, *Chem. Rev.*, 1996, **96**, 2205.
5 H. A. S. Citeau and D. M. Giolando, *J. Organomet. Chem.*, 2001, **625**, 23.
6 L. R. McGillivray and J. L. Atwood, *Angew. Chem., Int. Ed.*, 1999, **38**, 1019.
7 A. Müller, M. Penk. R. Rohlfing, E. Krickemeyer and J. Döring, *Angew. Chem., Int. Ed. Engl.*, 1990, **29**, 926.
8 K. Kobayashi, N. Deguchi, O. Takahashi, K. Tanaka, E. Horn, O. Kikuchi and N. Furukawa, *Angew. Chem., Int. Ed.*, 1999, **38**, 1638.
9 H. W. Roesky, R. J. Butcher, S. Bajpai and P. C. Srivastava, *Phosphorus Sulfur Silicon Relat. Elem.*, 2000, **161**, 135.
10 J. E. Huheey, *Inorganic Chemistry*, Harper & Row, New York, 3rd edn., 1983, pp. 256–259.
11 N. W. Alcock, *Adv. Inorg. Chem. Radiochem.*, 1972, **15**, 22.
12 G. Schatte, T. Chivers, C. Jaska and N. Sandblom, *Chem. Commun.*, 2000, 1657.
13 W. Levason, *Coord. Chem. Rev.*, 1997, **161**, 33.
14 O. Foss, R. Hermansen, K. Marøy and T. Moberg, *Acta Chem. Scand. Ser. A*, 1987, **41**, 130.
15 W. Levason, S. D. Orchard, G. Reid and V.-A. Tolhurst, *J. Chem. Soc., Dalton Trans.*, 1999, 2071.

CHEMCOMM Communication
www.rsc.org/chemcomm

Formation of stable alkenyl carbenium ions in high yield by adsorption of 1-methylcyclopentene on zeolite Y at low temperature

Shuwu Yang, Junko N. Kondo and Kazunari Domen*

Chemical Resources Laboratory, Tokyo Institute of Technology, 4259 Nagatsuta, Midori-ku, Yokohama 226-8503, Japan. E-mail: kdomen@res.titech.ac.jp

Received (in Cambridge, UK) 19th July 2001, Accepted 20th August 2001
First published as an Advance Article on the web 19th September 2001

The formation of dimerized alkenyl carbenium ions, characterized by an IR band at 1513 cm^{-1} and a UV band at 323 nm, was observed by adsorption of 1-methylcyclopentene on HY and DY zeolites at temperatures as low as 150 K.

The formation of alkenyl carbenium ions on zeolites has attracted much attention in the past decade.[1,2] Using *in-situ* NMR, Haw and his coworkers observed the formation of cyclopentenyl cations on zeolites through propene oligomerization on HY at 293 K,[3] by cracking ethene oligomers on HZSM-5 at 523 K,[4] and by adsorption of some cyclic precursors on HY and HZSM-5.[5] These cations are believed to be the true intermediates in aromatics formation and coke deposition, which are undesirable in some reactions. However, very recently, Haw *et al.*[6] found that cyclopentenyl cations not only play a catalytic role but also act as reactive intermediates in methanol-to-olefin (MTO)/methanol-to-gasoline (MTG) chemistry. The critical and distinct roles of these cations are of great importance, and have motivated us to investigate the initial formation of alkenyl carbenium ions using *in-situ* infrared spectroscopy, a powerful technique that is widely used for studying zeolites. In this work, 1-methylcyclopentene, a cyclic olefin with a tertiary carbon, was selected as a probe molecule.

HY zeolite (Si/Al = 2.8) was pressed into a self-supporting wafer and placed in a quartz IR cell connected to a closed gas-circulation system. The sample was first evacuated and oxidized at 773 K and was then treated with H_2 or D_2 at 673 K, followed by evacuation at room temperature. All IR spectra were recorded on a JASCO 7000 FTIR spectrometer with MCT detector at a resolution of 4 cm^{-1} and 64 scans. Only differential spectra are given, obtained by subtracting the spectra taken at different temperatures before adsorption. UV-vis spectra were collected on a JASCO V-560 UV-vis spectrophotometer, the sample for which was treated in a similar manner as for the IR experiments.

Fig. 1 shows the IR spectra of 1-methylcyclopentene adsorbed on DY zeolite. The spectrum of 1-methylcyclopentene adsorbed on SiO_2 is also given as a reference. A small amount (*ca.* 40 μmol) of 1-methylcyclopentene was introduced to the IR cell at below 150 K, and the sample chamber was immediately evacuated in order to avoid rapid oligomerization and to allow the formation of intermediates to be observed clearly. The IR cell was then gradually warmed under evacuation. On SiO_2 (partially deuterated, Fig. 1(a)), 1-methylcyclopentene is only adsorbed molecularly, *via* hydrogen bonds, as indicated by the two broad bands at 3495 and 2592 cm^{-1} attributable to the shift of the isolated OH and OD bands, respectively. The spectrum of adsorbed 1-methylcyclopentene is identical to that of free 1-methylcyclopentene molecules,[7] and the $\nu_{=C-H}$ and $\nu_{C=C}$ bands appear at 3043 and 1650 cm^{-1}, respectively. With increasing temperature, the adsorbed molecules are simply desorbed from SiO_2 under evacuation. The adsorption of 1-methylcyclopentene on to DY (Fig. 1(b)–(g)), however, induced significant changes. At 150 K, four bands at 3032, 2961, 2931 and 2859 cm^{-1} were identified in the ν_{C-H} region. The band at 3032 cm^{-1} is attributed to olefinic C–H stretching, while the latter three are related to the ν_s and ν_{as} bands of saturated C–H bonds. The $\nu_{C=C}$ band shifts to 1637 cm^{-1}, 13 cm^{-1} lower than that of free molecules,[7] suggesting the formation of a π-BAS (Brønsted acid sites) complex.[8] Meanwhile, a negative band appears at *ca.* 2690 cm^{-1}, confirming the consumption of OD groups. In the low-frequency region (1600–1300 cm^{-1}), a new band appears at 1513 cm^{-1}. With increasing temperature, the bands at 2931, 2859 and 1513 cm^{-1} grow in intensity, and the band at 3032 cm^{-1} due to olefinic C–H stretching has almost disappeared by 245 K. Upon heating to 373 K, the 1513 cm^{-1} band reaches maximum intensity and then disappears with further increases in temperature. At 473 K, only the bands at 2931, 2859, 1465 and 1382 cm^{-1} remain, while a band at 1600 cm^{-1} due to aromatic compounds appears.

The formed species are considered to be alkenyl carbenium ions, as characterized by the band at 1513 cm^{-1}. This band is attributed to the asymmetric stretching vibration of the $[C{=}C{-}C]^+$ unit.[2] Because the positive charge of this unit is delocalized within the three carbon atoms, its vibrational frequency occurs in the region between those of the typical C–C and C=C stretching modes. Buzek *et al.*[9] simulated the IR spectrum of the parent allyl cation and predicted a band at 1558 cm^{-1}, which is in agreement with their experimental data in acidic solutions. This assignment is further supported by our theoretical

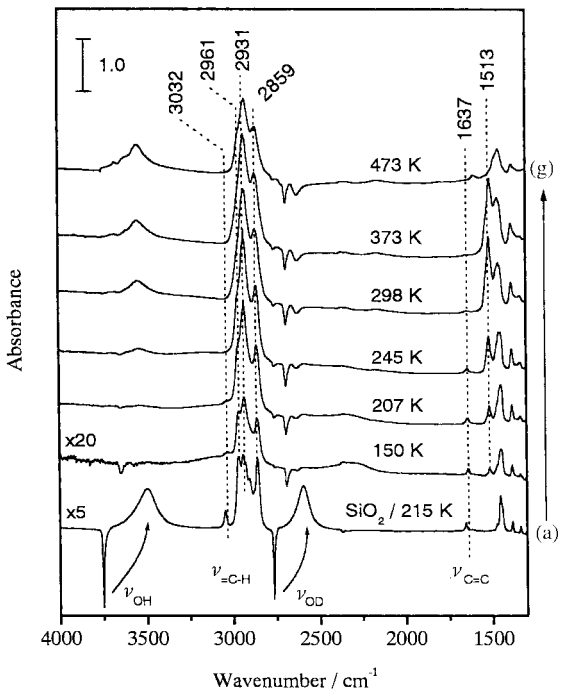

Fig. 1 IR spectra of 1-methylcyclopentene adsorbed on (a) SiO_2 at 215 K; and on DY zeolite at various temperatures: (b) 150 K; (c) 207 K; (d) 245 K; (e) 298 K; (f) 373 K and (g) 473 K. Reverse peaks indicate consumption of OH and OD groups.

 DOI: 10.1039/b106450a

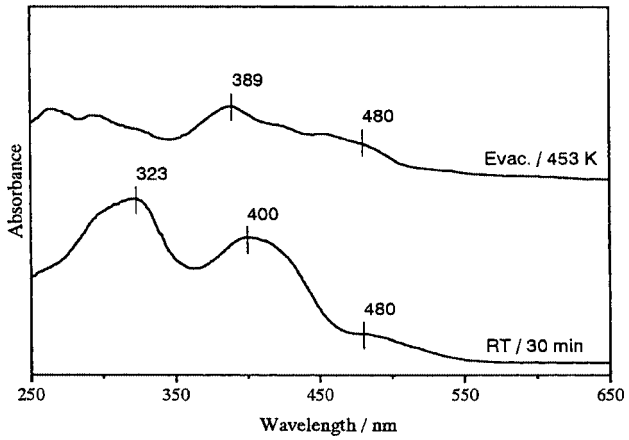

Fig. 2 UV-vis spectra of 1-methylcyclopentene adsorbed on HY at liquid nitrogen temperature and then (a) warmed to RT and maintained for 30 min, and (b) evacuated at 453 K.

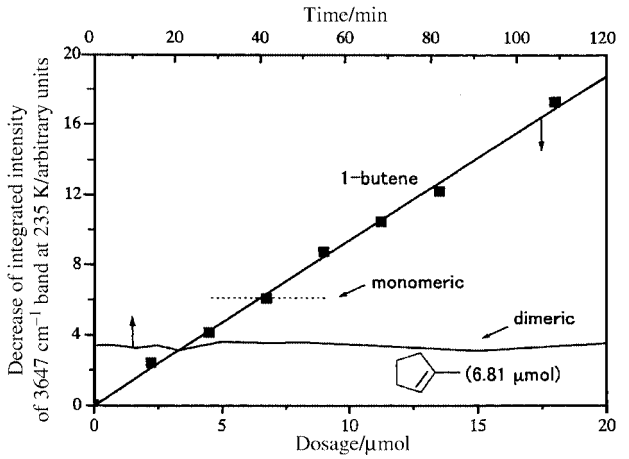

Fig. 3 Calibration of acid sites of HY using 1-butene at 235 K. For comparison, 6.81 μmol 1-methylcyclopentene (0.18 mmol g^{-1} catalyst) was also introduced on HY at 235 K. If monomeric species are formed, the consumption of acid sites should be situated on the dotted line.

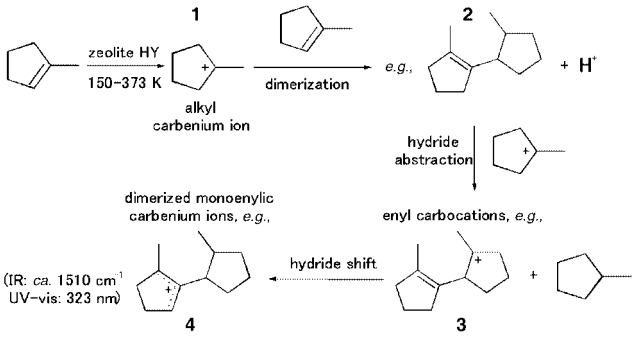

Scheme 1 Possible pathway for the formation of dimerized alkenyl carbenium ions.

calculation of the harmonic IR frequencies of 1-methylcyclopentenyl cations.

UV-vis spectroscopy was also used to confirm the formation of alkenyl carbenium ions, and the results are given in Fig. 2. After 1-methylcyclopentene adsorbed on HY at liquid nitrogen temperature, the sample was warmed to room temperature. Two strong bands appeared at 323 and 400 nm, and a small shoulder could be seen at *ca.* 480 nm. Based on experience with superacid solutions, the bands observed in the ranges 280–330, 360–380 and 430–470 nm have been attributed to π–π* transitions of mono-, di-, and trienylic carbenium ions. Therefore, the three bands observed in our case can be assigned accordingly.[2] The red-shift of the bands is attributed to the formation of branched, *i.e.* alkyl-substituted, carbenium ions. The results clearly show that monoenylic carbenium ions are predominant on the sample, along with a considerable amount of dienylic ones and a small amount of trienylic ones. After evacuation at 453 K, only dienylic and trienylic carbenium ions were left. This is in good agreement with IR results, which show that the 1513 cm^{-1} band disappears at 423 K and above.

To estimate the structure of the species formed on zeolite Y, 1-butene was used to calibrate the acid sites of HY at 235 K. At this temperature, 1-butene is adsorbed only molecularly on the acid sites of HY (forming a 1:1 π-OH complex) without oligomerization.[8] A controlled amount of 1-butene (0.06 mmol g^{-1} catalyst) was then introduced to the IR cell at 235 K. An IR spectrum was taken after 3–5 min of the dosage, and then other doses were given, until saturated adsorption. By measuring the decrease of the integrated intensity of the 3647 cm^{-1} band (stretching vibration of OH groups in supercages), the correlation between the OH band intensity (which represents the amount of acid sites) and the dosage of 1-butene was obtained (Fig. 3). In a separate experiment, 6.81 μmol 1-methylcyclopentene was introduced to the sample, and the weakening of the 3647 cm^{-1} band plotted against adsorption time. If the adsorbed 1-methylcyclopentene species is monomeric, the consumption of acid sites should be the same as for the addition of 6.81 μmol 1-butene, as indicated by the dotted line in Fig. 3. However, only half of the acid sites were consumed, suggesting that the formed species are not monomeric, but dimeric. Of course the formation of trimerized (or even higher) species could not be totally excluded, but their amount should be very small. These results clearly indicate that 1-methylcyclopentene rapidly undergoes oligomerization on zeolite Y even at temperatures as low as 150 K. As a result, dimerized carbenium ions were formed, with a notable absence of monomeric species.

Alkenyl carbenium ions can be formed by hydride transfer between olefin and carbenium ions, or through hydride abstraction from olefins by Lewis acid sites (LAS). Owing to the absence of LAS on our sample, alkyl carbenium ions may act as LAS and abstract hydrogen from olefins or oligomers to form alkenyl carbenium ions. From the integrated intensity of the 1513 cm^{-1} band, it can be deduced that alkenyl carbenium ions have already been formed in high yield at temperatures lower than 298 K. Scheme 1 shows the possible pathway for the formation of dimerized alkenyl carbenium ions. Worth noting is that cation **1** cannot be observed experimentally.

In summary, alkenyl carbenium ions were formed by the adsorption of 1-methylcyclopentene on zeolite Y in high yield at temperatures from 150 to 473 K. The majority of the carbenium ions were present in dimerized form, indicating that the oligomerization of olefins proceeded very rapidly even at temperatures as low as 150 K, and as a result, monomeric forms were not observed.

This work was supported by PEC and Monbusho (C11640600) of Japan. S. Y. thanks JSPS for a fellowship.

Notes and references

1 J. F. Haw, J. B. Nicholas, T. Xu, L. W. Beck and D. B. Ferguson, *Acc. Chem. Res.*, 1996, **29**, 259 and references therein.
2 I. Kirisci, H. Förster, G. Tasi and J. B. Nagy, *Chem. Rev.*, 1999, **99**, 2085 and references therein.
3 J. F. Haw, B. R. Richardson, I. S. Oshiro, N. D. Lazo and A. J. Speed, *J. Am. Chem. Soc.*, 1989, **111**, 2052.
4 F. G. Oliver, F. J. Munson and J. F. Haw, *J. Phys. Chem.*, 1992, **96**, 8106.
5 T. Xu and J. F. Haw, *J. Am. Chem. Soc.*, 1994, **116**, 7753.
6 J. F. Haw, J. B. Nicholas, W. Song, F. Deng, Z. Wang, T. Xu and C. S. Heneghan, *J. Am. Chem. Soc.*, 2000, **122**, 4763.
7 J. R. Durig, A. C. Shing, W. E. Bucy and C. J. Wurrey, *Spectrochim. Acta, Part A*, 1978, **34**, 525.
8 J. N. Kondo, L. Shao, F. Wakabayashi and K. Domen, *J. Phys. Chem. B*, 1997, **101**, 9314.
9 P. Buzek, P. von R. Schleyer, H. Vancik, Z. Mihalic and J. Gauss, *Angew. Chem., Int. Ed. Engl.*, 1994, **33**, 448.

CHEMCOMM Communication
www.rsc.org/chemcomm

Preparation of novel, moisture-stable, Lewis-acidic ionic liquids containing quaternary ammonium salts with functional side chains†

Andrew P. Abbott, Glen Capper, David L. Davies,* Helen L. Munro, Raymond K. Rasheed and Vasuki Tambyrajah

Department of Chemistry, University of Leicester, Leicester, UK LE1 7RH. E-mail: dld3@le.ac.uk

Received (in Cambridge, UK) 17th July 2001, Accepted 29th August 2001
First published as an Advance Article on the web 19th September 2001

A range of novel, moisture-stable, Lewis-acidic ionic liquids has been prepared by mixing appropriate molar ratios of MCl_2 (M = Zn and/or Sn) and quaternary ammonium salts of formula $[Me_3NC_2H_4Y]Cl$ (Y = OH, Cl, OC(O)Me, OC(O)Ph); the influence of substituent Y and metal M on the physical properties of the melts has been investigated.

Ionic liquids, or room temperature molten salts, have attracted increasing interest over recent years, particularly in the area of green chemistry, due to their advantageous properties including negligible vapour pressure and wide liquid range.[1–3] Work has focussed on liquids formed from dialkylimidazolium halides which are readily prepared from 1-methylimidazole and a slight excess of the desired haloalkane.[4] Addition of a suitable molar ratio of aluminium chloride to these salts gives rise to ionic liquids containing complex metal anions which have been used in a number of applications such as electroplating, electrochemical devices and catalysts for organic synthesis.[1,4–6] The main disadvantage of imidazolium-based liquids is their relatively high cost for bulk applications, whilst chloroaluminate ionic liquids have the additional problem of their low tolerance to moisture, necessitating the use of glove box and Schlenk techniques to prepare and investigate their properties. The former problem may be overcome by using cheaper ammonium salts whereas the latter may be solved by replacing aluminium with less reactive metals.

Recently, Freeman and coworkers have characterised ionic liquids formed from $FeCl_2$ or $FeCl_3$ and 1-butyl-3-methylimidazolium chloride.[7] However, other examples of ionic liquids made from metal chlorides other than aluminium are less well characterised and are mainly cited in conference proceedings[8] or in the patent literature.[9,10] Here we report the synthesis and characterisation of new moisture-stable, Lewis-acidic ionic liquids made from metal chlorides and quaternary ammonium salts that are commercially available or simple to synthesise. These offer the potential to tailor the physical properties *e.g.* melting point, viscosity and conductivity, and to tune the Lewis acidity by choosing a different metal or indeed combinations of metals.

To investigate the parameters necessary for a salt to be liquid at or near room temperature we have heated a range of ammonium salts with zinc chloride in a 1:2 molar ratio and the results are shown in Table 1.‡ Using salts of symmetrical cations, H_4NCl and Me_4NCl, no liquid is formed below 200 °C whereas with the longer chain NEt_4Cl the freezing point was *ca.* 90 °C. It has been established in the imidazolium systems that reducing the symmetry of the cation leads to a lower freezing point for the ionic liquid, thus, we have examined cations of the general formula Me_3NR^+. Using Me_3NEt^+ gives a freezing range of 53–55 °C, *i.e.* a reduction of *ca.* 35 or 140 °C compared with Et_4N^+ and Me_4N^+ respectively. However, we have found that functionalised ethyl chains, $Me_3NC_2H_4Y^+$, give even lower freezing points; *e.g.* if Y = OH or Cl, room temperature liquids are observed with freezing points of 23–25 °C. Even when the substituent is significantly larger, *e.g.* Y = OC(O)Me or OC(O)Ph, the salts formed have lower freezing points than for Me_3NEt^+. These results suggest that both lower symmetry and the presence of a functional group reduce the freezing points of the salts formed, though the exact role of the functional substituent is not yet clear. In all cases the liquids formed are viscous and hygroscopic but moisture-stable so can be easily prepared and stored without the need for specialist equipment.

Since choline chloride, $[Me_3NC_2H_4OH]Cl$, gave the lowest freezing point we have characterised this system in more detail. Heating mixtures of choline chloride and zinc chloride in molar ratios between 1:1 and 1:3 gave rise to clear colourless liquids, with the freezing points varying between *ca.* 65 °C (1:1), 25 °C (1:2) and 45 °C (1:3). Unlike analogous aluminium systems,[4,11,12] ratios with a molar excess of choline chloride, *i.e.* basic melts, do not form ambient temperature liquids in these systems. This would imply that complex zinc anions, in which the charge can be delocalised, are necessary in the formation of these ionic liquids. Further characterisation of the 1:2 liquid is described below.

A ^1H NMR spectrum of the neat ionic liquid was recorded and shows resonances at δ 2.97, 3.34 and 3.94 assigned to the methyl groups, N–CH_2 protons, and the CH_2OH protons, respectively, of the choline cation. All signals were broad and poorly resolved, even at 80 °C, due to the viscosity of the melt. The FAB mass spectrum shows the presence of complex zinc chloride ions $[ZnCl_3]^-$, $[Zn_2Cl_5]^-$ and $[Zn_3Cl_7]^-$. Higher clusters are also detectable but occurred at very low intensities. Similar species have been observed in aluminium chloride-based ionic liquids.[13]

The ionic liquid has a conductivity of 36 μS cm^{-1} at 40 °C and this increases exponentially with temperature, due to a decrease in the viscosity and hence an increase in the mobility of the ions in the melt.† The conductivity is similar to that found in alkylpyridinium-based ionic liquids[14] and is sufficient for them to be suitable media for electrochemical applications such

Table 1 Freezing points for the materials formed from heating a quaternary ammonium chloride and MCl_2 (M = Zn, Sn) in a 1:2 molar ratio

	Cation	M	Freezing point/°C
1	NH_4	Zn	>200
2	Me_4N	Zn	>200
3	Et_4N	Zn	90–92
4	Me_3NEt	Zn	53–55
5	$Me_3NCH_2CH_2OH$	Zn	23–25
6	$Me_3NCH_2CH_2Cl$	Zn	23–25
7	$Me_3NCH_2CH_2OC(O)Me$	Zn	30–32
8	$Me_3NCH_2CH_2OC(O)Ph$	Zn	46–48
9	$Me_3NCH_2CH_2OH$	Sn	43–45
10	$Me_3NCH_2CH_2Cl$	Sn	69–71
11	$Me_3NCH_2CH_2OC(O)Me$	Sn	13–15
12	$Me_3NCH_2CH_2OH$	Zn/Sn[a]	21–23

[a] The ratio $[Me_3NCH_2CH_2OH]Cl:ZnCl_2:SnCl_2$ was 1:1:1.

† Electronic supplementary information (ESI) available: plot of conductivity *vs.* temperature for the ionic liquid formed from zinc chloride and choline chloride (2:1). See http://www.rsc.org/suppdata/cc/b1/b106357j/

 DOI: 10.1039/b106357j

as batteries and metal deposition. The liquids provide an electrochemical window of about 2 V positive from the Zn/Zn^{2+} couple. Further details of the conductivity and electrochemical properties are reported elsewhere.[15]

Having established that the cationic component can be varied we have also investigated changing the metal-containing, *i.e.* anionic, component. Heating choline chloride and $SnCl_2$ in a 1:2 molar ratio provides a viscous liquid which has a freezing range of 43–45 °C. The negative ion FAB mass spectrum shows the presence of $[SnCl_3]^-$ and $[Sn_2Cl_5]^-$; however, no higher ions are observed in this case. For the tin-containing melts the liquid formed from $[YC_2H_4NMe_3]Cl$ (Y = OC(O)Me) gave the lowest melting point. Heating choline chloride : $ZnCl_2$: $SnCl_2$ in a 1:1:1 molar ratio gives a liquid with a freezing point of 21–23 °C, *i.e.* similar to the pure zinc-containing melt but significantly lower than the pure tin-containing one. The FAB mass spectrum of this liquid shows the presence of the individual metal-containing ions and the mixed metal ion $[SnZnCl_5]^-$. Mixed metal melts allow the possibility of tuning the catalytic properties of the liquids, as well as opening up possibilities for electrodeposition of metal alloys.

To conclude, we have shown that heating functionalised quaternary ammonium halides $[Me_3NC_2H_4Y]Cl$ and MCl_2 (M = Zn, Sn) gives materials that are conducting, viscous liquids at or around room temperature. The freezing points are dependent upon the symmetry of the cation and upon the nature of the functionalised side chain. The advantages of these new ionic liquids over presently available metal-containing ionic liquids are that they are insensitive to moisture and are much cheaper than imidazolium-based liquids. In addition, their Lewis acidity can be altered by varying the metal chloride(s) used. The use of these liquids as catalysts for the Diels–Alder reaction of acroleins and dienes will be reported elsewhere.

We thank Scionix Ltd., a joint venture company between Whyte Chemicals and the University of Leicester, for financial support.

Notes and references

‡ The general route for the synthesis of the ionic liquids was as follows: quaternary ammonium salt (20 mmol) was mixed with zinc chloride (40 mmol) and heated to *ca.* 150 °C in air with stirring until a clear colourless liquid was obtained. In contrast with the usual $AlCl_3$-based ionic liquids the reaction appears to be endothermic.

Drying the liquids under vacuum at 100 °C overnight has only a small effect on the freezing point, a few degrees, suggesting that immediately after preparation the liquids do not contain much water. The liquids are at least as thermally stable as $AlCl_3$-based liquids, and can be heated to at least 190 °C.

1 T. Welton, *Chem. Rev.*, 1999, **99**, 2071.
2 M. J. Earle and K. R. Seddon, *Pure Appl. Chem.*, 2000, **72**, 1391.
3 P. Wasserscheid and W. Keim, *Angew. Chem., Int. Ed.*, 2000, **39**, 3789.
4 J. S. Wilkes, J. A. Levisky, R. A. Wilson and C. L. Hussey, *Inorg. Chem.*, 1982, **21**, 1263.
5 A. A. Fannin, Jr., L. A. King, J. A. Levisky and J. S. Wilkes, *J. Phys. Chem.*, 1984, **88**, 2609.
6 T. M. Laher and C. L. Hussey, *Inorg. Chem.*, 1983, **22**, 1279.
7 M. S. Sitze, E. R. Schreiter, E. V. Patterson and R. G. Freeman, *Inorg. Chem.*, 2001, **40**, 2298.
8 T. B. Scheffler and M. S. Thompson, *Proc. Electrochem. Soc.*, 1990, **90–17**, (Proc. Int. Symp. Molten Salts, 7th, 1990), 281.
9 N. Koura and N. Takami, *Jpn. Pat.*, 1095469, 1989.
10 F. G. Sherif, L.-J. Shyu, C. P. M. Lacroix and A. G. Auke, *US Pat.*, 5731101, 1998.
11 R. J. Gale, B. P. Gilbert and R. A. Osteryoung, *Inorg. Chem.*, 1978, **17**, 2728.
12 J. S. Wilkes, J. S. Frye and G. F. Reynolds, *Inorg. Chem.*, 1983, **22**, 3870.
13 S. P. Wicelinski, R. J. Gale, K. M. Pamidimukkala and R. A. Laine, *Anal. Chem.*, 1988, **60**, 2228.
14 R. A. Carpio, L. A. King, R. E. Lindstrom, J. C. Nardi and C. L. Hussey, *J. Electrochem. Soc.*, 1979, **126**, 1644.
15 A. P. Abbott and D. L. Davies, *Int. Pat.*, 2000, WO 0056700; A. P. Abbott, G. Capper, D. L. Davies, H. L. Munro, R. K. Rasheed and V. Tambyrajah, in preparation.

CHEMCOMM Communication
www.rsc.org/chemcomm

Supramolecular assemblies formed by new L-lysine derivatives of viologens†

Masahiro Suzuki,*[a] Chad C. Waraksa,[b] Hiroko Nakayama,[c] Kenji Hanabusa,[a] Mutsumi Kimura[c] and Hirofusa Shirai[c]

[a] *Graduate School of Science and Technology, Shinshu University, Ueda, Nagano 386-8567, Japan. E-mail: msuzuki@giptc.shinshu-u.ac.jp; Fax: +81-268-24-7248*
[b] *Department of Chemistry, The Pennsylvania State University, University Park, PA 16802, USA*
[c] *Department of Functional Polymer Science, Faculty of Textile Science and Technology, Shinshu University, Ueda, Nagano 386-8567, Japan*

Received (in Cambridge, UK) 1st August 2001, Accepted 4th September 2001
First published as an Advance Article on the web 19th September 2001

L-Lysine derivatives of viologens form supramolecular assemblies of fibers and ribbons in some aromatic solvents, and the charge separation reaction in these self-assembling systems proceeds with a similar efficiency to the MV^{2+} system.

One of the keywords in supramolecular chemistry, which utilizes relatively weak, noncovalent interactions such as hydrogen bonding, π–π stacking, electrostatic, and van der Waals interactions, is self-assembly.[1] Self-assembly, which is the spontaneous organization of molecules driven by noncovalent interactions or objects into stable aggregates, has been well recognized in biological systems: lipid bilayers, the DNA duplex, and tertiary and quaternary structure of proteins.[2] In chemical synthesis, self-assembly offers considerable advantages over stepwise bond formation in the construction of large supramolecular assemblies. Many reports have appeared on supramolecular assemblies formed from organic compounds, dendrimers, macromolecules, and coordination compounds.[3]

Ordered, self-assembling aggregates of low molecular weight compounds formed through noncovalent interactions such as hydrogen bonding, van der Waals interactions and π–π stacking have been of great interest.[4] These supramolecular assemblies are to some extent similar to macromolecules, as repeating units linked to each other by either noncovalent or covalent bonds (can be both) give a network structure in various solvents, resulting in gelation or a high viscosity. In contrast to the gels obtained from supramolecules, which can be disintegrated by addition of a cosolvent or by heating, the network structures obtained from macromolecules are decomposed only by breaking chemical bonds. Several low molecular mass compounds which form network structures in organic fluids have been reported.[5,6] Recently, L-lysine derivatives have been found to form supramolecular fibrous network structures on the nanometer scale.[7] Here we describe the formation of self-assembling fibers from new L-lysine derivatives of viologens and their photosensitized charge separation using tris(2,2′-bipyridine)ruthenium(II) [$Ru(bpy)_3^{2+}$] as a photosensitizer.

The viologen derivatives (**1**, **2**) were prepared in high yield according to the synthetically simple approach as shown in Scheme 1. The gelation ability of **1** and **2** was evaluated after allowing solutions to stand at rt for 6 h followed by dissociation into organic solvents with heating. Photosensitized charge separation reactions were carried out in methanol–toluene containing 1.0×10^{-5} M $Ru(bpy)_3^{2+}$, 1.0×10^{-3} M viologen, and 0.1 M triethanolamine (TEOA) under an argon atmosphere. Visible light irradiation was performed using a 300 W Xe lamp equipped with a UV cutoff filter ($\lambda > 440$ nm). The rate constants of the elemental reactions were measured by laser flash photolysis.[8]

Both **1** and **2** were completely dissolved with heating in all organic solvents in which the gelation ability was examined. After dissolution of **1** and **2** by heating, they formed gels in aromatic solvents (benzene, toluene, nitrobenzene, chlorobenzene) and reprecipitated in alcohols. In DMF, DMSO, and chloroform, both **1** and **2** have a high solubility and give an isotropic solution. TEM images of samples prepared from these solvents demonstrated that the viologens formed fibrous assemblies in aromatic solvents and alcohols, but not in chloroform; in alcohols, small fibers of **1** and **2** were observed for samples prepared from the dilute solutions (see ESI†). These facts imply that **1** and **2** hardly interact with each other in chloroform and strongly interact in alcohols, which leads to the isotropic solution in chloroform and reprecipitation in the alcohols. As shown in Fig.1, **1** (A) and **2** (B) prepared from toluene create nanometer scale network structures with *ca.* 250–700 nm width for **1** and *ca.* 300–400 nm width for **2** formed by entangling of fine fibers (*ca.* 30–100 nm width) or ribbons (*ca.* 70–200 nm width).[9] It is noteworthy that the viologens form different nanostructures; a fibrous structure for **1** and a ribbon structure for **2**.

To consider the factor of self-assembling behavior, we measured the FTIR spectrum of **1** and **2**. The FTIR spectra in chloroform, in which no self assembly occurs, show the absorption bands at 3440 and 1665 cm^{-1}, characteristic of non-hydrogen bonded N–H and C=O stretching vibrations. In contrast, the FTIR spectra in toluene show almost the same spectra in the solid state and are characterized by a band at 3320 cm^{-1} which is assigned to N–H stretching vibrations of hydrogen bonded amide groups,[10] which indicates that the driving force for the self-assembly is mainly hydrogen bonding. The fine nanofibers and nanoribbons are entangled in a complex way probably through van der Waals interaction between the terminal alkyl groups and the three-dimensional network

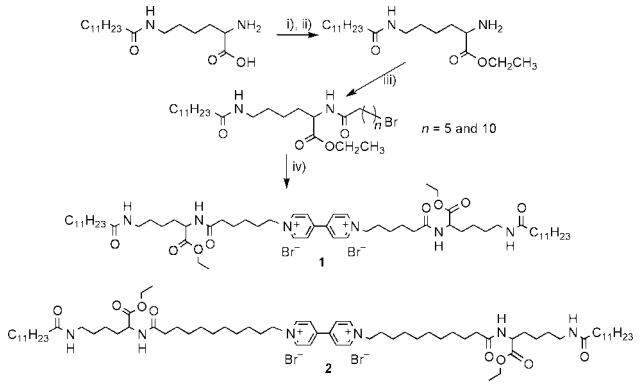

Scheme 1

† Electronic supplementary information (ESI) available: experimental details and Figs. S1 and S2. See http://www.rsc.org/suppdata/cc/b1/b106513k/

 DOI: 10.1039/b106513k

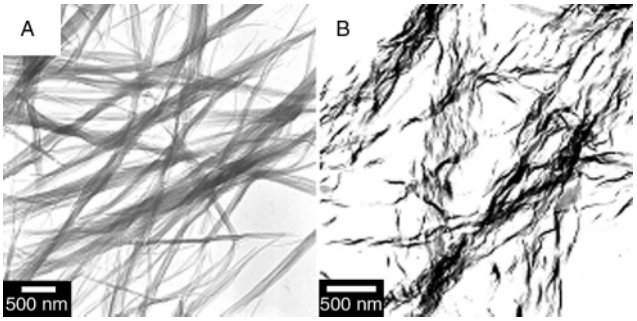

Fig. 1 TEM images of viologens **1** (A) and **2** (B) prepared from toluene solution.

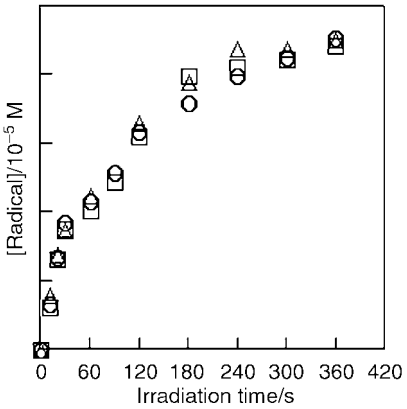

Fig. 2 Viologen radical formation upon visible light irradiation for V1 (○), V2 (□), and MV^{2+} (△) systems.

structure is created, which leads to gelation. Moreover, the shape of the nanostructure is controllable to some extent by the length of alkylene spacer between bipyridine and L-lysine segments.

Next, the photosensitized charge separation reaction was carried out in a mixture of methanol and toluene (1 : 1 v/v).[11] Fig. 2 shows the formation of a viologen radical upon visible light irradiation. Very interestingly, the viologen radical formation in the self-assemblies is the almost the same as in MV^{2+}. In the present systems, the photosensitized charge separation proceeds according to eqns. (1)–(5):

$$\mathrm{Ru(II)} + h\nu \rightarrow {}^*\mathrm{Ru(II)} \quad (1)$$

$${}^*\mathrm{Ru(II)} \xrightarrow{k_0} \mathrm{Ru(II)} + h\nu' + \Delta \quad (2)$$

$${}^*\mathrm{Ru(II)} + \mathrm{V}^{2+} \xrightarrow{k_q} \mathrm{Ru(III)} + \mathrm{V}^{+} \quad (3)$$

$$\mathrm{Ru(III)} + \mathrm{V}^{+} \xrightarrow{k_b} \mathrm{Ru(II)} + \mathrm{V}^{2+} \quad (4)$$

$$\mathrm{Ru(III)} + \mathrm{TEOA} \xrightarrow{k_s} \mathrm{Ru(II)} + \mathrm{TEOAox} \quad (5)$$

where k_0, k_q, k_b, and k_s represent the rate constants for the corresponding reactions. These values are obtained by laser flash photolysis and are listed in Table 1. The rate constants of the quenching reaction (forward reaction), k_q, are almost the same values regardless of the viologens. In contrast, the self-assembling viologens restrict the back electron transfer and accelerate the re-reduction of the Ru(III) to Ru(II) with TEOA. This is probably due to an electrostatic repulsion between the positively charged viologen assembly and the ruthenium(III) complex and a concentration of TEOA in the vicinity of the assemblies.

Table 1 Kinetic parameters obtained from laser flash photolysis

	k_q (M^{-1} s^{-1})[a]	k_b (M^{-1} s^{-1})[b]	k_s (M^{-1} s^{-1})[c]
1	7.0×10^8	1.7×10^{10}	2.7×10^7
2	6.2×10^8	2.3×10^{10}	1.9×10^7
MV^{2+}	6.9×10^8	5.1×10^{10}	1.5×10^7

[a] Stern–Volmer plot (τ_0/τ *vs.* [viologen]) using laser flash photolysis. [b] Rate constants for back electron transfer. [c] The rate constants of re-reduction reaction of Ru(III) with TEOA corresponding to eqn. (5).

In summary, we have found that new L-lysine derivatives of viologens form gels containing nanometre scale organized assemblies in some organic solvents. In particular, the viologens create a network structure by the entangling of nanofibers for viologen **1** and nanoribbons for viologen **2** in some aromatic solvents. In the viologen assembly–$Ru(bpy)_3^{2+}$ systems containing a sacrificial electron donor, the charge separation reaction proceeds with a similar efficiency to MV^{2+}–$Ru(bpy)_3^{2+}$ because of the restriction of the back electron transfer and acceleration of re-reduction of the Ru(III). Furthermore, we find that the nanostructure is controllable by changing the length of the alkylene spacer.

This work was supported by the Division of Chemical Sciences, Office of Basic Energy Sciences, Department of Energy, under contract DE-FG02-93-ER14374 and Grant-in-Aid for COE research (10CE2003) from the Ministry of Education, Culture, Sports, Science, and Technology of Japan.

Notes and references

1 G. M. Whitesides, J. P. Mathias and C. T. Seto, *Science*, 1991, **254**, 1312; J.-M. Lehn, *Science*, 1993, **260**, 1762; J.-M. Lehn, *Supramolecular Chemistry*, VCH, Weinheim, 1995; *Supramolecular Chemistry*, ed. V. Balzani and L. DeCola, Kluwer, Netherlands, 1992.
2 A. Klug, *Angew. Chem., Int. Ed. Engl*., 1983, **22**, 565; E. L. Shakhnovich, V. Abkevich and O. Ptitsyn, *Nature*, 1996, **379**, 96.
3 *Comprehensive Supramolecular Chemistry*, ed. J.-M. Lehn, J. L. Atwood, J. E. D. Davis, D. D. MacNicol and F. Vögtle, Pergamon Press, Oxford, 1996, Vol. 1–11; *Supramolecular Materials and Technologies, Perspective in Supramolecular Chemistry Vol. 4*, ed. D. N. Reinhoudt, Wiley, Chichester, 1999; *Transition Metals in Supramolecular Chemistry, Prespectives in Supramolecular Chemistry Vol. 5*, ed. J.-P. Sauvage, Wiley, Chichester, 1999.
4 D. Philp and J. F. Stoddart, *Angew. Chem., Int. Ed. Engl*., 1996, **35**, 4; P. Terech and R. G. Weiss, *Chem. Rev*., 1997, **97**, 3133; J. H. van Esch and B. L. Feringa, *Angew. Chem., Int. Ed*., 2000, **39**, 2263.
5 Y.-C. Lin, B. Kacher and R. G. Weiss, *J. Am. Chem. Soc*., 1989, **111**, 5542; K. Murata, M. Aoki, T. Suzuki, T. Harada, H. Kawataba, T. Komori, F. Ohseto, K. Ueda and S. Shinkai, *J. Am. Chem. Soc*., 1994, **116**, 6664; T. Shimizu and M. Masuda, *J. Am. Chem. Soc*., 1997, **119**, 2812.
6 R. J. H. Hafkamp, M. C. Feiters and R. J. M. Nolte, *J. Org. Chem*., 1999, **64**, 412; K. Hanabusa, R. Tanaka, M. Suzuki, M. Kimura and H. Shirai, *Adv. Mater*., 1997, **9**, 1095; K. Hanabusa, M. Yamada, M. Kimura and H. Shirai, *Angew. Chem., Int. Ed. Engl*., 1996, **35**, 1949.
7 K. Hanabusa, H. Nakayama, M. Kimura and H. Shirai, *Chem. Lett*., 2000, 1070; K. S. Partridge, D. K. Smith, G. M. Dykes and P. T. McGrail, *Chem. Commun*., 2001, 319; B. Escuder, A. E. Rowan, M. C. Feiters and R. J. M. Nolte, *Tetrahedron Lett*., 2001, **42**, 2751.
8 For experimental details see: G. B. Saupe, T. E. Mallouk, W. Kim and R. H. Schmehl, *J. Phys. Chem. B*, 1997, **101**, 2508.
9 Similar TEM images were observed for samples prepared from other solvents that formed gel.
10 In toluene, a hydrogen bonded C=O stretching vibration could not be detected in the FTIR spectra because the toluene's own spectrum overlaps with viologens around 1650 cm^{-1}.
11 To dissolve $Ru(bpy)_3^{2+}$ and triethanolamine (TEOA), the reaction was carried out in methanol–toluene. The viologens did not gel in methanol–toluene under the reaction conditions, but we obtained the TEM images showing that the viologens formed fibrous nanostructures (but not networks).

CHEMCOMM
Communication
www.rsc.org/chemcomm

First synthesis of porphyrin–phthalocyanine heterodimers with a direct ethynyl linkage

Jonathan M. Sutton[a] **and Ross W. Boyle***[b]

[a] *Department of Biological Sciences, University of Essex, Wivenhoe Park, Colchester, UK CO4 3SQ*
[b] *Department of Chemistry, University of Hull, Cottingham Road, Hull, East Yorkshire, UK HU6 7RX*

Received (in Cambridge, UK) 3rd July 2001, Accepted 8th August 2001
First published as an Advance Article on the web 19th September 2001

The first synthesis of two porphyrin–phthalocyanine heterodimers with a direct triple bond linkage between the macrocycles, designed for the study of photo-induced energy and electron transfer processes, is presented along with preliminary ground state and fluorescence spectroscopic data.

It is well known that metalloporphyrins which are held together in carefully controlled orientations play important roles in photosynthesis and some metalloenzyme catalysed reactions.[1,2] Spectroscopic evidence has suggested that this careful control of spatial orientation allows optimisation of photon or electron transfer processes,[3] and there is now considerable interest in the generation of compounds that can be used to model such processes. A number of covalently linked porphyrin–chlorin[4] and phthalocyanine homo/hetero-dimers[5] have been prepared successfully, as well as a number of porphyrin–phthalocyanine heterodimers.[6–10] Although most of these examples have shown varying degrees of intramolecular energy transfer, they have involved covalent attachment of both macrocycles using ether, phenylethynyl linkages[11–15] or flexible aliphatic chains. As a result, the π electron system of each macrocycle can orient to minimise p–p orbital overlap with the linker, thus inhibiting conjugation of the two systems through these bonds. This effect is well known for *meso*-aryl porphyrins, where the phenyl rings are typically perpendicular to the macrocycle.

We report here the first synthesis and characterisation of a (Zn)porphyrin–(Zn)phthalocyanine heterodimer **1(Zn)**, and also a (H_2)porphyrin–(Zn)phthalocyanine heterodimer **1(H_2)** produced by selective de-metallation of the porphyrin, in which the two macrocycles are directly linked through an ethynyl group. The direct triple bond linkage fully conjugates the two major π systems, irrespective of the torsional angle between the planes of the porphyrin and phthalocyanine. An initial photophysical investigation of these ethynyl linked heterodimers has also been undertaken.

Scheme 1 shows the strategy used to synthesise heterodimers **1(Zn)** and **1(H_2)**. The convergent synthesis involved the preparation of heterodimer precursors **6** and **11**. Hexamethoxydiphenylporphyrin[16] **2** was selectively monoiodinated at one of the available *meso* positions using I_2/trifluoroacetoxybenzene.[17] The crude reaction, containing impurities of starting material and diiodoporphyrin, in addition to monoiodoporphyrin, was purified by flash silica-gel chromatography. The required monoiodoporphyrin **3** was then metallated with zinc acetate. The zinc monoiodoporphyrin **4** was converted into *meso*-(2-(trimethylsilyl)ethynyl) zinc porphyrin **5** by palladium mediated Sonagashiro coupling with TMS-acetylene. Desilylation of **5** using tetrabutylammonium fluoride afforded the *meso*-ethynyl zinc porphyrin **6**. Phthalocyanine **11**, the second macrocycle required for coupling, was synthesised by condensation of 4-(*tert*-butyl)phthalonitrile **7** with 4-nitrophthalonitrile **8** and $Zn(AcO)_2$, to give a statistical mixture composed primarily of tetra(*tert*-butyl)phthalocyanine and mononitrotri(*tert*-butyl)phthalocyanine **9**.[18] The crude reaction mixture was then treated with sodium sulfide to afford a mixture of

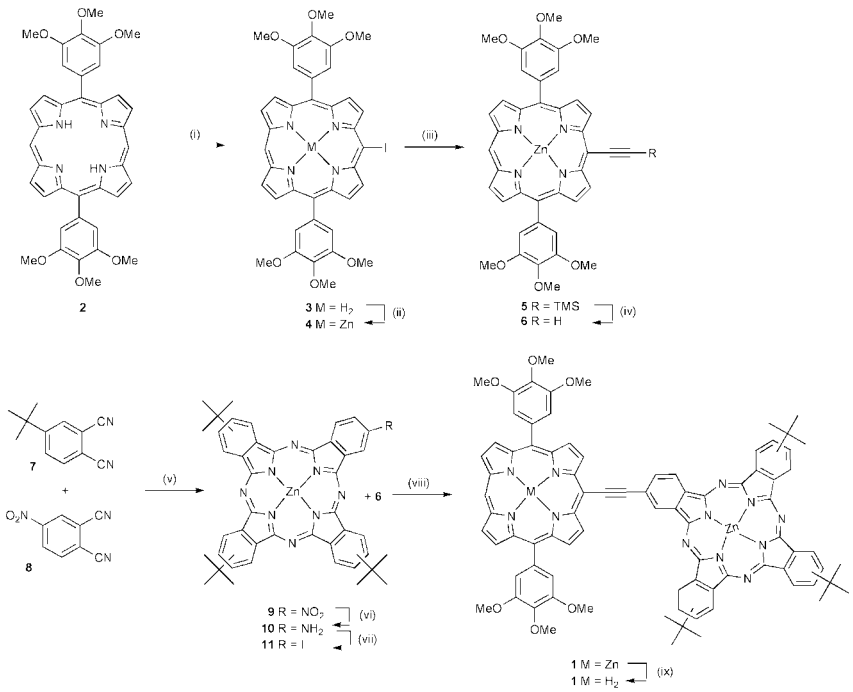

Scheme 1 Conditions: (i) I_2, $PhI(OCOCF_3)_2$, pyridine, 45 min, RT; (ii) $Zn(OAc)_2$, $CHCl_3$ (iii) TMS-acetylene, $[Pd(PPh)_2Cl_2]$, CuI, THF, Et_3N, RT, 16 h; (iv) TBAF, DCM; (v) $Zn(OAc)_2$, fuse 165 °C, 2 h; (vi) $Na_2S{\cdot}9H_2O$, 60 °C, 2 h; (vii) $NaNO_2$(aq), conc. HCl(aq)/glacial acetic acid (1 : 1), acetone, 5 °C, 1 h, then KI(aq); (viii) $Pd_2(dba)_3$, toluene/Et_3N (5 : 1), RT, 3 h (anaerobic conditions); (ix) TFA, DCM, RT, 30 min.

 DOI: 10.1039/b105840c

phthalocyanines containing monoaminotri(*tert*-butyl)phthalocyanine **10**, which was easily separated from the much less polar tetra(*tert*-butyl)phthalocyanine by flash column chromatography.[18] Phthalocyanine **10**, as a mixture of positional isomers, was then converted into a mixture of monoiodotri(*tert*-butyl)phthalocyanine isomers **11** *via* the diazonium salt, using a modified Sandmeyer reaction.[19] A second Sonagashiro palladium mediated coupling between precursors **6** and **11**, under anaerobic conditions, afforded the required heterodimer **1(Zn)** as a mixture of positional isomers in 50% yield. Flash column chromatography of the mixture of heterodimer positional isomers allowed isolation of a greatly enriched sample containing over 75% of the heterodimer **1** as a single positional isomer (the remaining 25% consisting of other positional isomers formed during phthalocyanine condensation). The heterodimer **1(Zn)** could now be characterised by ^{1}H NMR, UV-visible spectroscopy, fluorescence spectroscopy and FAB mass spectrometry.[20] It was then possible to take advantage of the weaker binding of zinc in the central cavity of porphyrins, compared with phthalocyanines, to conduct a facile, and selective, demetallation of the porphyrin component of heterodimer **1(Zn)** using trifluoroacetic acid to give the (H_2)porphyrin–(Zn)phthalocyanine heterodimer **1(H_2)** in quantitative yield.

The UV-visible spectra, in toluene, of heterodimers **1(Zn)** and **1(H_2)** resemble that of an equimolar mixture of porphyrin **6** and phthalocyanine **11**, however a number of differences are apparent (Fig. 1). Firstly, both compound **1(Zn)** and **1(H_2)** show marked bathochromic shifts in their Soret bands of 10 and 13 nm respectively, indicating that effective electronic communication between the two different ring systems occurs. Secondly, the phthalocyanine Q-band in the heterodimer is split as a result of electronic and symmetry effects caused by the porphyrin–ethynyl moiety. Presumably, the closeness of the two ring systems results in a perpendicular, unsymmetrical orientation in solution. Although splitting of the phthalocyanine Q-band has not been reported previously, a broadening of this absorption has been noted in other porphyrin–phthalocyanine dimers[9] and was ascribed to a weak exciton interaction between the two chromophores in the ground state.

An initial examination of the heterodimer **1(Zn)** by fluorescence spectroscopy (Fig. 2) has shown that excitation at the porphyrin Soret band (431 nm) results in an emission spectrum with a major peak between 600–630 nm and a second weaker band at 712 nm. Fig. 2 also shows the effect of solvent polarity on the emission spectrum, where a direct relationship between increasing solvent polarity and the relative intensity of the shorter to longer wavelength emission bands was observed. The solvent dependent behaviour observed here is in accord with spectroscopic data for other porphyrin–phthalocyanine systems[8–10] where it is reported to be indicative of singlet–singlet energy transfer between the porphyrin and phthalocyanine.

Work is currently underway within our laboratory to synthesise a series of metalloporphyrin–(Zn)phthalocyanine heterodimers, by re-metallation of (H_2)porphyrin–(Zn)phthalocyanine **1(H_2)** and to study more closely the influence of the coordinated metal on ground and excited state photochemical processes.

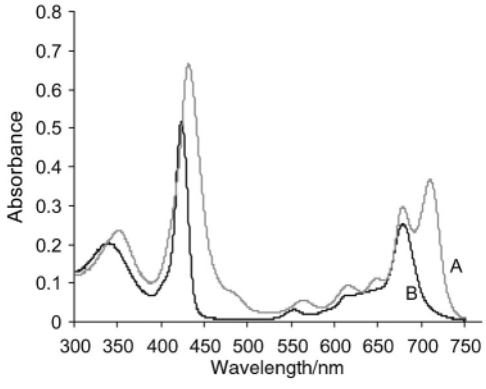

Fig. 1 UV-vis absorption spectra of A: heterodimer **1(Zn)** and B: an equimolar mixture of DPP **6** and PC **11** in toluene.

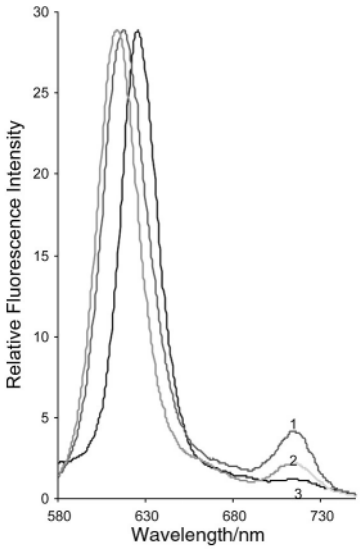

Fig. 2 Fluorescence spectra of heterodimer **1(Zn)** in solvents of different polarity (1–3; toluene/DCM/DMF, respectively).

The authors wish to thank the Wellcome Trust for financial support (052724) and EPSRC Mass Spectrometry Service, Swansea for analyses.

Notes and references

1 J. R. Norris, R. A. Uphans, H. L. Crespi and J. J. Katz, *Proc. Natl. Acad. Sci. USA*, 1971, **68**, 675.
2 V. Fulop, J. W. B. Moir, S. J. Ferguson and J. Hajdu, *Cell*, 1995, **81**, 369.
3 R. L. Brockfeild, H. Ellul, A. Harriman and J. Poter, *J. Chem. Soc., Faraday Trans. 2*, 1986, **82**, 219.
4 W. R. Wasielewski, *Chem. Rev*., 1992, 435.
5 C. C. Leznof, S. M. Marcuccio, S. Greenberg and A. B. P. Lever, *Can. J. Chem*., 1985, **63**, 623.
6 S. Gaspard, C. Giannotti, P. Maillard, C. Schaeffer and T.-H. Tran-Thi, *J. Chem. Soc., Chem. Commun*., 1986, 1239.
7 L. Li, S. Shen, Q. Yu and H. Xu, *J. Chem. Soc., Chem. Commun*., 1991, 619.
8 H.-J. Tian, Q.-F. Zhou, S.-Y. Shen and H.-J. Xu, *J. Photochem. Photobiol., A*, 1993, **72**, 163.
9 H.-J. Tian, Q.-F. Zhou, S.-Y. Shen and H.-J. Xu, *Chin. J. Chem*., 1996, **14**, 412.
10 X.-Y. Li, Q.-F. Zhou, H.-J. Tian and H.-J. Xu, *Chin. J. Chem*., 1998, **16**, 97.
11 R. W. Wagner, T. E. Johnson, F. Li and J. S. Lindsey, *J. Org. Chem*., 1995, **60**, 5266.
12 J. Li and J. S. Lindsey, *J. Org. Chem*., 1999, **64**, 9101.
13 M. A. Miler, R. K. Lammi, S. Prathapan, D. Holten and J. S. Lindsey, *J. Org. Chem*., 2000, **65**, 6634.
14 S. I. Yang, J. Li, H. S. Cho, D. Kim, D. F. Bocian, D. Holten and J. S. Lindsey, *J. Mater. Chem*., 2000, **10**, 283.
15 E. I. Zenkevich, V. N. Knyukshto, A. M. Shugla, V. A. Kuzmitsky, V. I. Gael, E. G. Levenson and A. F. Mironov, *J. Lumin*., 1997, **75**, 229.
16 R. W. Boyle, C. Brückner, J. Posakony, B. R. James and D. Dolphin, *Org. Synth*., 1998, **76**, 287.
17 R. W. Boyle, C. K. Johnson and D. Dolphin, *J. Chem. Soc., Chem. Commun*., 1995, 527.
18 S. V. Kudrevich, H. Ali and J. E. van Lier, *J. Chem. Soc., Perkin Trans. 1*, 1994, 2767.
19 H. Ali and J. E. van Lier, *Tetrahedron Lett*., 1997, **38**, 1157.
20 Selected spectroscopic data for heterodimer **1**: UV-vis (Toluene) λ_{max} (relative intensity) 352 (0.35), 431 (1.0), 562 (0.09), 615 (0.14), 648 (0.17), 679 (0.45), 710 (0.55) nm; ^{1}H NMR (270 MHz, 20% DMSO-d_6 in $CDCl_3$) δ 10.17 (1H, s, 15-meso-H), 10.16 (2H, partly obscured m, 3+7-β-H), 9.70–9.65 (2H, m, PC-Ar), 9.56 (3H, m, PC-Ar), 9.46–9.38 (3H, m, PC-Ar), 9.34 (2H, d, J = 4.5 Hz, 13+17-β-H), 9.27 (2H, m, 2+8-β-H), 9.10 (2H, d, J = 4.5 Hz, 12+18-β-H), 8.83 (1H, m, PC-Ar), 8.33–8.26 (3H, m, PC-Ar), 7.58 (4H, s, 10+20-*o*-Ar), 4.25 (6H, s, 10+20-*p*-OMe), 4.08 (12H, s, 10+20-*m*-OMe), 1.88–1.83 (27H, m, *t*-Bu); FAB-MS *m*/*z* 1474 (M^+, 100%); MALDI-HRMS calc. for $C_{88}H_{78}N_8O_6Zn_2$ (M^+) 1473.4125, found 1473.4105.

CHEMCOMM
Communication
www.rsc.org/chemcomm

Novel organoaluminium (and gallium) carboxylate-bridged ring systems†

Carl Redshaw*[a] and Mark R. J. Elsegood[b]

[a] *Wolfson Materials and Catalysis Centre, School of Chemical Sciences, University of East Anglia, Norwich, UK NR4 7TJ. E-mail: carl.redshaw@uea.ac.uk*
[b] *Chemistry Department, University of Loughborough, Loughborough, Leicestershire, UK LE11 3TU*

Received (in Cambridge, UK) 10th July 2001, Accepted 24th August 2001
First published as an Advance Article on the web 19th September 2001

Treatment of the Schiff-base ligand [3,5-Bu^t_2-2-(OH)$C_6H_2CHNC_6H_4$-2-(CO_2H)] with either Me_3Al, Me_2AlCl or Me_3Ga affords 16-membered macrocyclic tetramers containing both four- and six-coordinate metal centres.

The chemistry of frameworks that permit the binding of two or more multidentate Lewis acid centres is a rapidly emerging area. In particular, organoaluminium chelate complexes are receiving interest not only for their intriguing structural diversity but also for their co-operative effects in organic chemistry.[1] Neutral and more recently cationic organoaluminium species are also known to act as olefin polymerisation catalysts.[2,3] Despite this growing interest, the non-aqueous chemistry of organoaluminium carboxylates is scant.[4] Indeed, structural studies are limited to only a handful of compounds, but do reveal a preference for a bridging, bidentate carboxylate mode. Similarly, the behaviour of a number of bifunctional amine-alcohols towards aluminium trialkyls has revealed a dependence on the nature of both the alkyl and amine groups present.[5] The latter reactions resulting in the formation of mono-, di- or tri-nuclear products. Recent results in our laboratory have focused on reactions of anthranilic acid, 1,2-(H_2N)$C_6H_4CO_2H$.[6] Crystal structure analyses of a number of transition metal complexes have shown its potential to function as a chelating amidobenzoate, imidobenzoate or as a carboxylate group. Extending these studies to Me_3Al led quite unexpectedly to a remarkable macrocyclic deca-ring system {[$Me_2Al(MeAl)(\mu_3$-O)(μ-O)L]}$_3$ (L = quinazoline ring system) arising from insertion of acetonitrile into the generated Al–N bonds.[7] Such insertion reactions also led to novel ring structures by reaction of Me_3Al with 1,1-disubstituted hydrazines.[8] Considering all of this, we were interested in exploring the feasibilty of forming other large aggregates by utilising the coordination properties of these functional groups. To this end, it seemed interesting to ascertain the detailed structural features of the products arising from the interaction of the organoaluminium reagents Me_3Al and Me_2AlCl (as well as the gallium reagent Me_3Ga) with the potentially tridentate Schiff-base ligand **I**. The products from these reactions are remarkable 16-membered macrocyclic tetramers, see Scheme 1. However, despite being recrystallised from acetonitrile none of the products are the result of MeCN insertion into Al–N bonds.

The Schiff-base ligand **I** is formed readily from anthranilic acid and 3,5-di-*tert*-butylsalicylaldehyde in refluxing ethanol. Its molecular structure exhibits both intra- and inter-molecular H-bonding.[9] Addition of 2 molar equivalents of Me_3Al to **I** in toluene results in rapid evolution of methane and formation of a yellow solution. Following work-up, small yellow prisms of **1**, suitable for an X-ray analysis using synchrotron radiation,[10] were grown from acetonitrile in *ca*. 55% yield. The molecular structure of the acetonitrile solvate is shown in Fig. 1, with

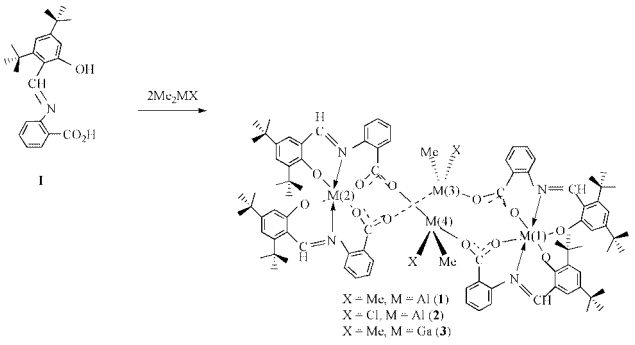

Scheme 1

selected bond lengths given in the caption. The X-ray analysis‡ reveals the product to be a centrosymmetric tetramer. The 16-membered macrocyclic ring is self-filling and comprises four aluminium atoms (two octahedral and two tetrahedral) linked *via* carboxylate groups binding in an *anti*/*syn* fashion. The geometries at the bridging aluminium centres are only slightly distorted from tetrahedral (104–123°). In contrast, the remaining two aluminium centres are octahedral with two tridentate, meridonally coordinated Schiff ligands, binding to aluminium *via* the deprotonated hydroxy oxygen, the imino nitrogen and an oxygen of the carboxylate group (*cis*-oxygens, *trans*-nitrogens). This results in the formation of four six-membered *N,O*-chelate rings per Al centre, each of which adopt a 'boat-like' conformation, the aluminium lying on average about 0.63 Å out of the plane of the other five atoms (which are co-planar to within 0.06 Å). The imino bonds to aluminium are typical [1.986(2)–2.001(3) Å], whilst the C=N bonds (av. 1.31 Å) have clearly retained some double bond character, there being no evidence of significant delocalisation into any of the

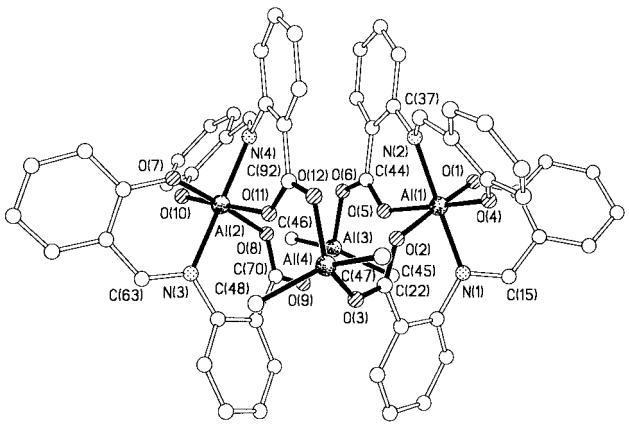

Fig. 1 Molecular structure of **1** with H-atoms, Bu^t groups and MeCN solvent molecules removed for clarity. Selected bond lengths (Å): Al(1)–O(1) 1.833(2), Al(1)–O(2) 1.904(2), Al(1)–O(4) 1.835(2), Al(1)–O(5) 1.885(2), Al(1)–N(1) 1.986(2), Al(1)–N(2) 1.999(2), Al(3)–O(6) 1.826(2), Al(3)–O(9) 1.812(2).

† Electronic supplementary information (ESI) available: full spectroscopic data and elemental analyses for all new compounds. See http://www.rsc.org/suppdata/cc/b1/b106113p/

 DOI: 10.1039/b106113p

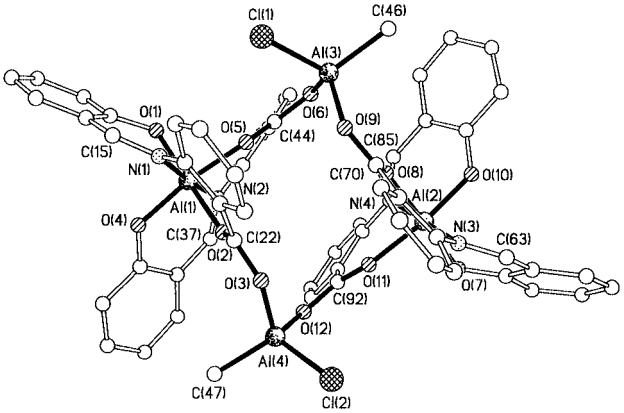

Fig. 2 Molecular structure of **2** with H-atoms, Bu^t groups and MeCN solvent molecules removed for clarity. Selected bond lengths (Å): Al(1)–O(1) 1.826(3), Al(1)–O(2) 1.921(3), Al(1)–O(4) 1.820(3), Al(1)–O(5) 1.915(3), Al(1)–N(1) 2.013(3), Al(1)–N(2) 2.000(3), Al(3)–O(6) 1.802(3), Al(3)–O(9) 1.810(3).

adjoining bonds. The Al–methyl distances [1.940(4)–1.948(4) Å] are typical of others observed in the literature.[11] Despite the apparent inequivalence of the phenyl groups in the structure, the ^{1}H NMR spectrum (ambient temperature, 300 MHz) is relatively simple with only one Al–Me and two *tert*-butyl resonances.

Encouraged by the synthesis of the macrocyclic ring system **1**, we then investigated the reaction of Me_2AlCl with **I**. Addition of Me_2AlCl (2 equivalents) to **I** in toluene, followed by heating to reflux for 12 h, afforded, on work-up, small yellow prisms of **2** suitable for X-ray diffraction in 40% yield. The X-ray analysis‡ reveals the product to be a similar centrosymmetric tetramer (Fig. 2). Again, the 16-membered macrocyclic ring is self-filling and comprises four aluminium atoms (two octahedral and two tetrahedral) linked *via* carboxylate groups binding, as in **1**, in an *anti*/*syn* fashion. The geometries at the bridging aluminium centres are only slightly distorted from tetrahedral (104–106°). The two octahedral aluminium centres are again coordinated by two tridentate, meridonal Schiff ligands, binding to aluminium *via* the deprotonated hydroxy oxygen, the imino nitrogen and an oxygen of the carboxylate group (*cis*-oxygens, *trans*-nitrogens). The resulting four six-membered *N,O*-chelate rings adopt the 'boat-like' conformation seen in **1**, the aluminium lying on average *ca*. 0.61 Å out of the plane of the other five atoms (which are co-planar to within 0.07 Å). The imino bonds to aluminium are typical [2.001(3)–2.012(3) Å], whilst the C=N bonds (av. 1.31 Å) have clearly retained some double bond character, there being no evidence of significant delocalisation into any of the adjoining bonds. The Al–methyl distances [1.939(4) and 1.951(3) Å] are similar to those in **1**; the Al–Cl distances are 2.1169(16) and 2.1015(18) Å. The ^{1}H NMR spectrum of **2** is more complex than that of **1**, doubtless reflecting the increased asymmetry at the bridging Al centres. The ^{27}Al NMR spectra of **1** and **2** consist of two peaks: one in the expected range for six-coordinate aluminium ($\delta \sim 8$) and a second peak which is difficult to interpret ($\delta \sim 120$ (**1**) and 107 (**2**)], but tentatively assigned to the four-coordinate centre. Four- and five-coordinate aluminium centres usually appear at $\delta \sim 150$ and 100, respectively.[12] It is noteworthy that in a related Schiff-base type environment, five-coordinate aluminium is present at $\delta \sim 65$.[13]

The gallium analogue of **1** is readily available in good yield (*ca*. 70%) from the reaction of Me_3Ga (2 equivalents) and **I**. Although compounds **1**–**3** failed to give the expected parent ions in the FAB mass spectra, a number of fragments were consistently observed (see ESI†).

In contrast to the pendant-arm Schiff-base complexes of aluminium reported by Gibson and coworkers (all mono-nuclear),[3d] the present system powerfully illustrates the potential for generating novel macrocyclic ring systems utilising the coordination properties of the carboxylate group. Future studies will focus on further exploiting these coordination properties to access new inorganic ring systems and to examine the catalytic properties thereof.

The Leverhulme Trust (for a Research Fellowship to C. R.) are thanked for financial support. The EPSRC is thanked for the award of beam time at Daresbury. Professor W. Clegg is thanked for the crystallographic facilities at The University of Newcastle, UK. We also thank the EPSRC Mass Spectrometry Service Centre, Swansea.

Notes and references

‡ *Crystal data*: for **1**·MeCN: $C_{92}H_{112}Al_4N_4O_{12}\cdot CH_3CN$, M = 1614.83, monoclinic, space group $P2_1/n$, a = 17.8616(19), b = 27.115(3), c = 19.081(2) Å, β = 95.703(2)°, V = 9195.6(17) Å^3, T = 160 K, Z = 4, μ (silicon 111 monochromated synchrotron radiation, λ = 0.6878 Å) = 0.111 mm^{-1}, 59798 data, 23109 were unique, R_{int} = 0.0939, all unique data used in refinement against F^2 values to give final wR = 0.1792 (on F^2), R = 0.0709 [for 10681 data with $F^2 > 4\sigma(F^2)$].[14] Two-fold disorder modelled with restraints in one Bu^t group.

For **2**·4MeCN: $C_{90}H_{106}Al_4Cl_2N_4O_{12}\cdot 4CH_3CN$, M = 1778.82, monoclinic, space group $P2_1/n$, a = 20.502(2), b = 22.794(3), c = 23.785(2) Å, β = 114.694(2)°, V = 10099(2) Å^3, T = 150 K, Z = 4, μ (Mo-Kα) = 0.159 mm^{-1}, 71603 data, 17785 were unique, R_{int} = 0.0742, wR = 0.1940 (on F^2), R = 0.0627 [for 10465 data with $F^2 > 4\sigma(F^2)$].[14] One of the MeCN solvent molecules is disordered across two sets of positions.

CCDC reference number 167944 and 167945. See http://www.rsc.org/suppdata/cc/b1/b106113p/ for crystallographic data in CIF or other electronic format.

1 V. Sharma, M. Simard and J. D. Wuest, *J. Am. Chem. Soc*., 1992, **114**, 7931; O. Saied, M. Simard and J. D. Wuest, *Organometallics*, 1996, **15**, 2345; T. Ooi, M. Takahashi and K. Maruoka, *J. Am. Chem. Soc*., 1996, **118**, 11 307.
2 H. Martin and H. Bretinger, *Makromol. Chem*., 1992, **193**, 1283.
3 (*a*) M. P. Coles and R. F. Jordan, *J. Am. Chem. Soc*., 1997, **119**, 8125; (*b*) C. E. Radzewich, M. P. Coles and R. F. Jordan, *J. Am. Chem. Soc*., 1998, **120**, 9384; (*c*) M. Bruce, V. C. Gibson, C. Redshaw, G. A. Solan, A. J. P. White and D. J. Williams, *Chem. Commun*., 1998, 2523; (*d*) P. A. Cameron, M. Bruce, V. C. Gibson, C. Redshaw, J. A. Segal, A. J. P. White and D. J. Williams, *Chem. Commun*., 1999, 1883; (*e*) D. A. Robson, L. H. Rees, P. Mountford and M. Schröder, *Chem. Commun*., 2000, 1269; (*f*) P. A. Cameron, V. C. Gibson, C. Redshaw, J. A. Segal, G. A. Solan, A. J. P. White and D. J. Williams, *J. Chem. Soc., Dalton Trans*., 2001, 1472.
4 J. L. Atwood, W. E. Hunter and K. D. Crissinger, *J. Organomet. Chem*., 1977, **127**, 403; M. J. Zaworotko, R. D. Rogers and J. L. Atwood, *Organometallics*, 1982, **1**, 1179; S. G. Bott, A. W. Coleman and J. L. Atwood, *J. Am. Chem. Soc*., 1986, **108**, 1709; Y. Koide and A. R. Barron, *Organometallics*, 1995, **14**, 4026; J. Lewinski, J. Zachara and I. Justyniak, *Organometallics*, 1997, **16**, 3859; J. Lewinski, J. Zachara and I. Justyniak, *Inorg. Chem*., 1998, **37**, 2575.
5 J. Lewinski, J. Zachara and T. Kopec, *Inorg. Chem. Comm*., 1998, **1**, 182 and references therein.
6 V. C. Gibson, C. Redshaw, W. Clegg and M. R. J. Elsegood, *J. Chem. Soc., Dalton Trans*., 1997, 3207; V. C. Gibson, C. Redshaw, W. Clegg and M. R. J. Elsegood, *Inorg. Chem. Comm*., 2001, **4**, 95.
7 V. C. Gibson, C. Redshaw, A. J. P. White and D. J. Williams, *Chem. Commun*., 2001, 79.
8 V. C. Gibson, C. Redshaw, A. J. P. White and D. J. Williams, *Angew. Chem., Int. Ed*., 1999, **38**, 961.
9 R. McCann, C. Redshaw and M. R. J. Elsegood, unpublished results.
10 W. Clegg, M. R. J. Elsegood, S. J. Teat, C. Redshaw and V. C. Gibson, *J. Chem. Soc., Dalton Trans*., 1998, 3037; W. Clegg, *J. Chem. Soc., Dalton Trans*., 2000, 3223.
11 G. H. Robinson, *Coordination Chemistry of Aluminium*, VCH, New York, 1993.
12 D. A. Atwood, J. A. Jegier, S. Liu, D. Rutherford, P. Wei and R. C. Tucker, *Organometallics*, 1999, **18**, 976.
13 P. Wei and D. A. Atwood, *Chem. Commun*., 1997, 1427.
14 Programs used were BRUKER AXS SMART and SAINT for diffractometer control and interpretation, SHELXTL for structure solution, refinement and molecular graphics and local programs.

CHEMCOMM
Communication
www.rsc.org/chemcomm

The first fluorescent sensor for boronic and boric acids with sensitivity at sub-micromolar concentrations—a cautionary tale†

Susumu Arimori, Christopher J. Ward and Tony D. James*

Department of Chemistry, University of Bath, Bath, UK BA2 7AY. E-mail: T.D.James@Bath.ac.uk

Received (in Cambridge, UK) 19th April 2001, Accepted 21st August 2001
First published as an Advance Article on the web 18th September 2001

The first reported fluorescent sensor for boronic and boric acids is actually not a sensor for boronic and boric acids but rather is a sensor for protons; the system is also not the first fluorescent sensor since Alizarin has been used as a fluorescent sensor for boric acids since 1936.

We were very interested to read 'the first fluorescent sensor for boronic and boric acids with sensitivity at sub-micromolar concentrations'. The report[1] described how the interaction between an amine and boronic acid could be used to create a fluorescent sensor for boric and boronic acids. It was proposed that compound **1** formed a stable complex with phenylboronic acid and was fluorescent due to a strong B–N interaction, whereas compound **2** does not interact strongly with phenylboronic acid and remains non-fluorescent due to a weak B–N interaction.†

We have also been interested in the use of such B–N interactions in the development of fluorescent sensors for saccharides.[2] The interaction of a neighbouring amine with boronic acid is strengthened on saccharide binding. The strength of this boronic acid–tertiary amine interaction can be used to signal the binding event. Many successful photoinduced electron transfer (PET) sensors have been developed based on this approach.[3–7]

We were interested in the Wang paper[1] since we believed that molecule **1** would make it possible to develop an independent (of saccharide) scale for boronic acid binding efficiency. We believed that such a scale would help in the development of new saccharide receptors.

We easily repeated the reported syntheses of compounds **1** and **2**, and also prepared compound **3**. Compound **3**, like

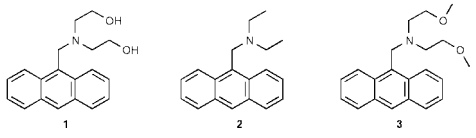

compound **2**, cannot form a cyclic ester with phenylboronic acid but is a closer structural mimic of **1**. With compounds **1**, **2** and **3** we repeated the titration with phenylboronic acid in methanol (Fig. 1). The relative fluorescence intensity of **1**, **2** and **3** increased with added phenylboronic acid. The results we obtained for **1** and **2** are almost identical to the published results.[1] However, we were intrigued by the fluorescence spectra of **1**, **2** and **3** in methanol. The observed fluorescence intensity of **2** in the absence of phenylboronic acid was much higher than the fluorescence intensity of **1** and **3**. Therefore we decided to investigate the fluorescent properties of **1**, **2** and **3** further.

A fluorescence titration of **1** (1.0×10^{-6} mol dm^{-3}) with phenylboronic acid was carried out in pH 8.21 aqueous methanolic buffer solution [52.1 wt% methanol (KCl, 0.01000 mol dm^{-3}; KH_2PO_4, 0.002752 mol dm^{-3}; Na_2HPO_4, 0.002757 mol dm^{-3})].[8] Surprisingly the fluorescence intensity of **1** only increased slightly with added phenylboronic acid. Why was the result for non-buffered methanol and buffered methanolic aqueous solution different?

In order to investigate the above observations we determined the pK_a values of **1**, **2** and **3** in aqueous methanolic solution. The pH titrations of **1**, **2** and **3** (all 1.0×10^{-6} mol dm^{-3}) were carried out in 52.1 wt% methanolic aqueous solution (sodium chloride 0.05 mol dm^{-3}). The pH was controlled using minimum volumes of sodium hydroxide and hydrochloric acid solutions. The fluorescence intensity *vs*. pH curves are shown in Fig. 2, and pK_a values of **1**, **2** and **3** calculated from the relative fluorescence intensity *vs*. pH titration curves[7,9] are given in Table 1. The pK_a values of **1**, **2** and **3** were also determined in

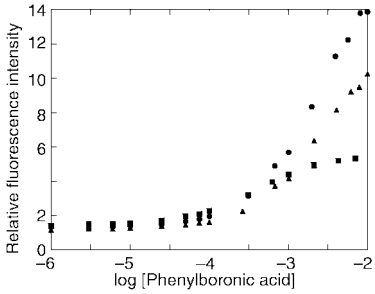

Fig. 1 Relative fluorescence intensity *vs*. log[phenylboronic acid] profile for **1**, **2** and **3** at 25 °C in methanol; [**1**] = [**2**] = [**3**] = 1.0×10^{-6} mol dm^{-3}, [phenylboronic acid] = 0–0.01 mol dm^{-3}: (●) **1**, (■) **2**, (▲) **3**. λ_{ex} = 370 nm, λ_{em} = 417 nm.

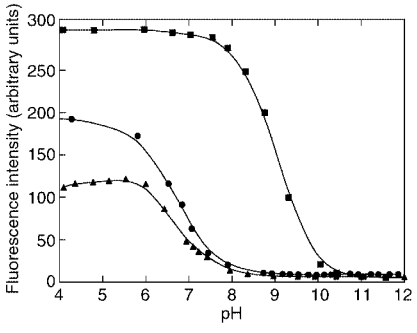

Fig. 2 Fluorescence intensity *vs*. pH profile for **1**, **2** and **3** at 25 °C; [**1**] = [**2**] = [**3**] = 1.0×10^{-6} mol dm^{-3}, 52.1 wt% methanolic aqueous solution in the presence of [NaCl] = 0.05 mol dm^{-3}: (●) **1**, (■) **2**, (▲) **3**. λ_{ex} = 370 nm, λ_{em} = 417 nm.

Table 1 pK_a values of **1**, **2** and **3** with and without phenylboronic acid (PBA)[a]

Compound	pK_a(r^2)	pK_a [PBA (10 mM)] (r^2)
1	6.55 ± 0.03 (1.00)	6.70 ± 0.01 (1.00)
2	9.03 ± 0.01 (1.00)	8.75 ± 0.01 (1.00)
3	6.78 ± 0.03 (0.99)	6.61 ± 0.04 (0.99)

[a] The pH titration was carried out in 52.1 wt% methanolic aqueous solution in the presence of NaCl (0.05 mol dm^{-3}) at 25 °C.

† Electronic supplementary information (ESI) available: PET sensors **1** and **2**, ^{1}H, ^{13}C and ^{11}B NMR data for **1** with and without phenylboronic acid (PBA). See http://www.rsc.org/suppdata/cc/b1/b103533a/

 DOI: 10.1039/b103533a

the presence of phenylboronic acid (0.01 mol dm^{-3}) (Table 1). From Table 1 it can be seen that the pK_a values of **1**, **2** and **3** do not change significantly in the presence of phenylboronic acid. This result indicates that under these conditions **1**, **2** and **3** do not show a significant B–N interaction. From these results it is also evident that **3** (pK_a = 6.78) and not **2** (pK_a = 9.03) should be used as a model for compound **1** (pK_a = 6.55).

The observed lack of a significant B–N interaction was somewhat surprising since Hall *et al.* and ourselves have recently used diethanolamine based polymers to bind with boronic acids.[10,11] However, the loading of diethanolamine based polymers is achieved in THF, which is a non-protic polar solvent.

To confirm these observations we recorded the ^{1}H and ^{13}C NMR spectra of **1** with and without phenylboronic acid, and also the ^{11}B NMR spectra of phenylboronic acid with and without **1** in methanol and chloroform.† The methanol conditions are those employed by Wang *et al.*[1] whereas chloroform is an aprotic solvent that mirrors the conditions used by Hall *et al.* and ourselves for loading boronic acids onto diethanolamine polymers.

^{11}B NMR spectroscopy provides the clearest evidence that no complex is formed in methanol. The boron signal of phenylboronic acid appears at 29.97 ppm and shifts to 30.70 ppm on addition of **1** clearly indicating that the boron remains sp^2 hybridised.[12] In contrast in chloroform the boron signal of phenylboronic acid at 32.27 ppm shifts to 15.90 ppm on addition of **1**, showing that the boron changes hybridisation from sp^2 to sp^3.[12] The ^{13}C NMR spectrum of **1** is also useful since in methanol none of the methylene carbons shift significantly on addition of phenylboronic acid whereas in chloroform the methylene carbon next to the oxygen shifts by 3.03 ppm on addition of phenylboronic acid. The ^{1}H NMR spectrum of **1** is also informative; in methanol none of the methylene protons shift significantly on addition of phenylboronic acid. However, in chloroform the spectrum becomes broad on addition of phenylboronic acid. These NMR measurements indicate that in methanol no complexation with **1** occurs, but in chloroform compound **1** does form a complex with boronic acids.

Wang *et al.*[1] made their conclusions about compound **1** in methanol using model compound **2** and the relative fluorescence intensity. With this research we have shown that compound **3** and not compound **2** should have been used as the model compound. Also, if the data used to produce Fig. 1 is replotted using the raw fluorescence intensity the conclusions drawn about compound **1** are shown to be incorrect. Fig. 3 shows the fluorescence intensity *vs.* log concentration titration curves of **1**, **2** and **3** in methanol with phenylboronic acid. From these curves compound **2** and not compound **1** shows the best response with added phenylboronic acid.

From the experimental pK_a curves (Fig. 2) and the titrations with phenylboronic acid (Fig. 3) an explanation for the observed behaviour of compounds **1**, **2** and **3** is forthcoming. In our experiments we used HPLC grade methanol but took no special precautions to ensure that the solvent was dry. Therefore, it is reasonable to assume that water was present in the methanol. From our observations this water must be sufficiently acidic to partially protonate **2** but not **1** or **3**. This explains why in just methanol, the fluorescence intensity of **1** was much higher than **2** and **3** (Fig. 3). When phenylboronic acid is then added to the methanol solution water molecules present in the methanol coordinate with the boron Lewis acid and become more acidic.[2,13] These more acidic water molecules can now protonate compounds **1** and **3** as well as compound **2**. Because compound **2** is more basic than **1** and **3** it is more sensitive to the addition of phenylboronic acid (Fig. 3). Also, since phenylboronic acid is simply acting as an acid in methanol it is not surprising that the maximum intensities observed in the phenylboronic acid titrations (Fig. 3) mirror the maximum intensities observed in the pH titrations (Fig. 2).

The justification given above explains the observed titration results in methanol and may also explain why in buffered methanolic solution negligible fluorescence changes are observed.

In conclusion, compound **1** in methanol does not act as a fluorescence sensor for boronic and boric acids. The fluorescence increases observed by Wang *et al.*[1] for **1** with added boronic acid are probably due to protonation[14] and not a B–N interaction. If a fluorescence sensor for boronic or boric acid is required the reader is directed to two recent papers where commercial Alizarin Red S has been used.[15,16] In fact Alizarin Red S has been used as a fluorescent sensor for boric acid since 1936.[17]

T. D. J. wishes to acknowledge the Royal Society, the EPSRC, and Beckman-Coulter for support. S. A. wishes to acknowledge Beckman-Coulter for support through the award of a Postdoctoral Research Fellowship. C. J. W. wishes to acknowledge the EPSRC and Avecia Limited for support through the award of a Studentship. We would also like to acknowledge the support of the University of Bath.

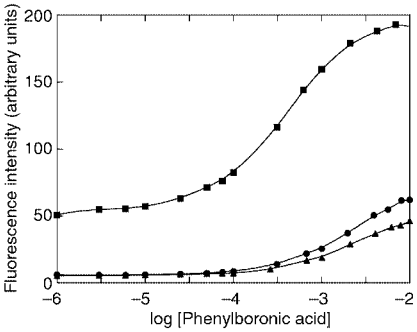

Fig. 3 Fluorescence intensity *vs.* log[phenylboronic acid] profile of **1**, **2** and **3** at 25 °C in methanol; [**1**] = [**2**] = [**3**] = 1.0 × 10^{-6} mol dm^{-3}, [phenylboronic acid] = 0–0.01 mol dm^{-3}: (●) **1**, (■) **2**, (▲) **3**. λ_{ex} = 370 nm, λ_{em} = 417 nm.

Notes and references

1 W. Wang, G. Springsteen, S. Gao and B. Wang, *Chem. Commun*., 2000, 1283.
2 J. H. Hartley, T. D. James and C. J. Ward, *J. Chem. Soc., Perkin Trans. 1*, 2000, 3155.
3 T. D. James, P. Linnane and S. Shinkai, *Chem. Commun*., 1996, 281.
4 T. D. James, K. R. A. S. Sandanayake and S. Shinkai, *J. Chem. Soc., Chem. Commun*., 1994, 477.
5 T. D. James, K. R. A. S. Sandanayake and S. Shinkai, *Angew. Chem., Int. Ed. Engl*., 1996, **35**, 1910.
6 C. R. Cooper and T. D. James, *Chem. Commun*., 1997, 1419.
7 C. R. Cooper and T. D. James, *J. Chem. Soc., Perkin Trans. 1*, 2000, 963.
8 D. D. Perrin and B. Dempsey, *Buffers for pH and Metal Ion Control*, Chapman and Hall, London, 1974, ch. 6.
9 The pK_a values were analysed in KaleidaGraph using non-linear (Levenberg–Marquardt algorithm) curve fitting. The errors reported are the standard errors obtained from the best fit.
10 D. G. Hall, J. Tailor and M. Gravel, *Angew. Chem., Int. Ed*., 1999, **38**, 3064.
11 S. Arimori, J. H. Hartley, M. L. Bell, C. S. Oh and T. D. James, *Tetrahedron Lett*., 2000, **41**, 10291.
12 S. L. Wiskur, J. J. Lavigne, H. Ait-Haddou, V. Lynch, Y. H. Chiu, J. W. Canary and E. V. Anslyn, *Org. Lett*., 2001, **3**, 1311.
13 J. H. Hartley and T. D. James, *Tetrahedron Lett*., 1999, **40**, 2597.
14 A. P. De Silva, H. Q. N. Gunaratne, T. Gunnlaugsson, J. M. Huxley, C. P. McCoy, J. T. Rademacher and T. E. Rice, *Chem. Rev*., 1997, **97**, 1515.
15 A. M. G. Campana, F. A. Barrero and M. R. Ceba, *Analyst (London)*, 1992, **117**, 1189.
16 N. Chimpalee, D. Chimpalee, B. Boonyanitchayakul and D. T. Burns, *Anal. Chim. Acta*, 1993, **182**, 643.
17 L. Szebellady and S. Tomay, *Z. Anal. Chem*., 1936, **107**, 26.

CHEMCOMM
Communication
www.rsc.org/chemcomm

Non-covalent interactions exert extraordinary influence over conformation and properties of a well-known supramolecular building block

Leonard J. Barbour and Jerry L. Atwood*

Department of Chemistry, University of Missouri–Columbia, Columbia, MO 65211, USA
E-mail: atwoodj@missouri.edu

Received (in Cambridge, UK) 13th June 2001, Accepted 18th July 2001
First published as an Advance Article on the web 18th September 2001

At low pH, and in the presence of 4,4′-bipyridine, *p*-sulfonatocalix[4]arene crystallizes in the 1,3-alternate conformation rather than the expected cone conformation and exhibits remarkable stability.

We and others have conducted extensive studies of the solid-state supramolecular complexes of *p*-sulfonatocalix[4]arene **1**.[1]

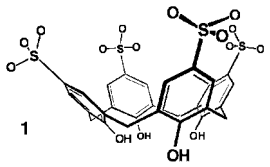

Our primary interest in this compound relates to its amphiphilic nature which is of possible relevance to biological systems. The molecule resembles the shape of a truncated cone and possesses strongly hydrophilic upper and lower rims, while the cavity and outer midsection are strongly hydrophobic. Furthermore, *p*-sulfonatocalix[4]arene is usually terta- or penta-anionic, depending on pH, and highly soluble in aqueous media. To date, this tantalizing blend of properties has yielded several different, but related packing motifs of remarkable complexity. Most commonly, the calixarenes arrange themselves in an up–down fashion to form a bilayer with the hydrophobic midsections of adjacent molecules mutually aligned and engaged in intermolecular π-stacking interactions.

Owing to its truncated cone shape, the bilayers of **1** are necessarily planar and the head and tail groups of the individual molecules constitute hydrophilic surfaces on both sides. The hydrophilic region between adjacent layers is occupied by a complex array of hydrogen bonded water molecules and cations. In the presence of suitably sized aromatic guests, the non-polar portions of the guest molecules usually protrude into the calixarene cavities lining the surface of the bilayer. Recently we were able to show that an up–up arrangement of the cones can be induced, thereby affording curvature to the calixarene 'skin'.[2] This results in the formation of nanometer-scale spheres and tubules with hydrophilic interior and exterior regions. Such studies have relied upon the notion that the cone shape of *p*-sulfonatocalix[4]arene is invariant owing to the rigidity imparted by the cyclic hydrogen bonded array at the lower rim. Indeed, a survey of the Cambridge Crystallographic Database reveals that, of the 102 deposited calixarene structures with at least three hydroxy groups at the lower rim, none deviate from the cone conformation. We now present a crystal structure in which the *p*-sulfonatocalix[4]arene molecule assumes the so-called 1,3-alternate conformation despite all four phenolic hydroxy groups being intact. Furthermore, this conformation markedly affects the solubility properties of the molecule.

As part of our ongoing investigation of the inclusion phenomena of calixarenes, Na_4**1** (0.06 mmol) and 4,4′-bipyridine **2**, (0.48 mmol) were dissolved in a mixture of 2 ml water and 1 ml concentrated HCl. After a period of *ca*. two days, bright yellow crystals appeared and their X-ray structure was determined.† The asymmetric unit consists of one quarter of a calixarene molecule, and one half of a diprotonated 4,4′-bipyridine molecule (1 : 2 molar ratio). As shown in Fig. 1, the calixarene is situated on a position of $\bar{4}$ site symmetry and assumes the completely unanticipated 1,3-alternate conformation.[3] As expected at low pH, **1** possesses a charge of −4 which is counterbalanced by the charge on the bipyridinium cations. To the best of our knowledge, this structure represents the first example of a structure involving *p*-sulfonatocalix[4]arene that is completely devoid of solvent water molecules. A detailed inspection of the intermolecular hydrogen bonded pattern (Table 1) of the structure reveals an intricate network of interactions that provide a high degree of stability to the lattice.

Each *p*-sulfonatocalix[4]arene molecule donates four O–H···O–S and eight C–H···O–S hydrogen bonds to a total of eight neighboring calixarenes. Each sulfonate oxygen atom

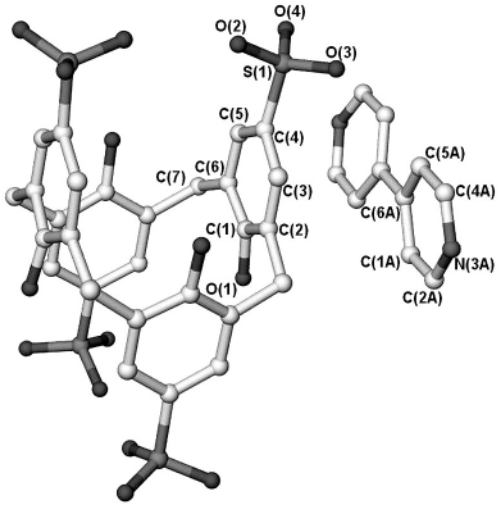

Fig. 1 View of **1** and **2** showing the labeling scheme (only asymmetric unit atoms are labeled) and the 1,3-alternate conformation of the *p*-sulfonatocalix[4]arene molecule. Hydrogen atoms are omitted for clarity.

Table 1 Unique hydrogen bond geometry[a]

No.[b]	D	A	*d*(D···A)	*d*(H···A)	*θ*(D–H···A)
1	O(1)	O(4)^{i}	2.823	1.854	166
2	C(7)	O(4)^{i}	3.290	2.396	150
3	C(7)	O(3)^{ii}	3.500	2.549	161
4	N(3A)	O(2)^{iii}	2.780	1.922	165
5	C(4A)	O(1)^{iv}	3.116	2.313	142
6	C(5A)	O(3)^{v}	3.100	2.370	133

[a] Distances and angles are given in Å and °. D = donor, A = acceptor. Symmetry operations: (i) ½ + *y*, *x* − ½, *z* − ½; (ii) ½ − *x*, ½ − *y*, ½ − *z*; (iii) ½ + *x*, ½ − *y*, ½ − *z*; (iv) ½ + *y*, *x* −½, ½ + *z*; (v) 1 − *x*, −*y*, *z*. [b] See Fig. 2 for bond numbering scheme.

 DOI: 10.1039/b105182m

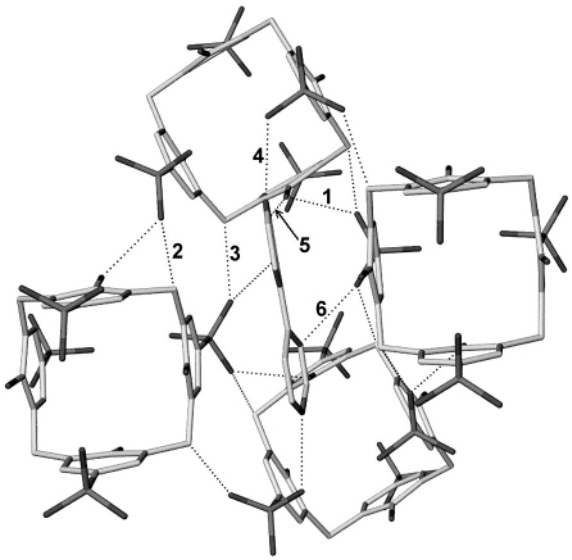

Fig. 2 View showing the hydrogen bonded network. Hydrogen atoms are omitted for clarity (H-bonds are drawn between donor and acceptor atoms). See Table 1 for details of the hydrogen bond geometry.

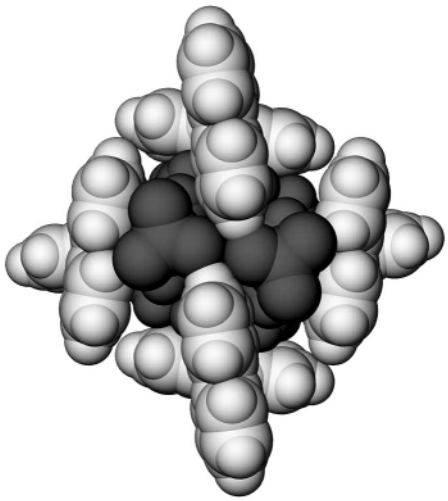

Fig. 3 View along [001] showing the calixarene molecule (dark) surrounded by eight molecules of 4,4′-bipyridine.

O(4) acts as a double receptor of both a strong O–H···O and a moderately strong[4] C–H···O hydrogen bond while each methylene carbon atom C(7) donates its two hydrogen atoms to C–H···O hydrogen bonds to sulfonate oxygen atoms of two separate calixarenes.

The calixarene is surrounded by eight 4,4′-bipyridinium cations. As shown in Fig. 3, four of these are situated about the 4-fold axis while the remaining four protrude into the small clefts beside the sulfonate headgroups. The former interact with the calixarene by means of relatively strong C–H···O hydrogen bonds and face-to-face aromatic π···π interactions (interplanar spacing 3.24 Å) while the latter form strong N–H···O hydrogen bonds to the O(2) atoms of the four symmetry-related sulfonate groups.

A number of additional conformational features of **1** are worthy of mention with regard to the overall stability of the crystal lattice. It is interesting that the sulfonate groups belonging to distal aromatic rings of **1** are aligned such that their O(2) oxygen atoms are separated by a distance of only 2.855 Å. This is well within the van der Waals contact limit and somewhat surprising, considering that the sulfonate groups each carry a negative charge and are thus expected to repel one another strongly.

Furthermore, the phenolic rings deviate significantly from planarity: C(1) and O(1) are at distances of 0.101 and 0.295 Å respectively, from the least-squares plane through C(2)–C(3)–C(4)–C(5)–C(6). The hydroxy groups are pulled away from the $\bar{4}$ axis by the O–H···O hydrogen bond that they donate to a sulfonate oxygen atom of a neighboring calixarene molecule (the methylene carbon atoms C(7) act as hinges to facilitate this motion). However, appropriate angling of the aromatic ring is impeded as the distal sulfonate oxygen atoms O(2) come into close contact with one another as described above. As a result, the aromatic ring is forced to bend outwards near the lower rim.

Finally, since every other known solid-state phase of **1** is highly water-soluble it is noteworthy that the crystals described here are insoluble in water and decompose at *ca*. 344–348 °C. Indeed, it is clear that, in concert, the many intermolecular interactions (*i.e*. O–H···O and C–H···O hydrogen bonds as well as aromatic π···π interactions) impart an extraordinarily high degree of stability to the structure, thereby compensating for the energy involved in disruption of the cone conformation and the strain resulting from close non-interacting O···O contacts and distortion of the calixarene aromatic rings.

We thank the National Science Foundation for support of this work.

Notes and references

† *Crystal data*: $C_{48}H_{40}N_4O_{16}S_4$, M = 1057.08, tetragonal, space group $P\bar{4}2_1c$; $a = b$ = 11.8339(9), c = 14.903(2) Å; V = 2087.0(3) Å^3; Z = 2; D_c = 1.682 g cm^{-3}; $F(000)$ = 1096; λ(Mo-Kα) = 0.71073 Å; T = 173(2) K; crystal dimensions 0.30 × 0.25 × 0.25 mm; reflections collected/unique, 12722/2302 (R_{int} = 0.0379); final R indices [$I > 2\sigma(I)$] $R1$ = 0.0437, $wR2$ = 0.1128; R indices (all data) $R1$ = 0.0480, $wR2$ = 0.1153; absolute structure parameter = 0.06(10); goodness of fit on F^2 = 1.077.

CCDC reference number 165414. See http://www.rsc.org/suppdata/cc/b1/b105182m/ for crystallographic data in CIF or other electronic format.

1 A. W. Coleman, S. G. Bott, S. D. Morley, C. M. Means, K. D. Robinson, H. Zhang and J. L. Atwood, *Angew. Chem., Int. Ed. Engl.*, 1988, **27**, 1361; J. L. Atwood, A. W. Coleman, H. Zhang and S. G. Bott, *J. Inclusion Phenom.*, 1989, **7**, 203; J. L. Atwood, F. Hamada, K. D. Robinson, G. W. Orr and R. L. Vincent, *Nature*, 1991, **349**, 683; S. G. Bott, A. W. Coleman and J. L. Atwood, *J. Am. Chem. Soc.*, 1988, **110**, 610; A. Drljaca, M. J. Hardie, C. L. Raston and L. Spiccia, *Chem. Eur. J.*, 1999, **5**, 2295; A. Drljaca, M. J. Hardie and C. L. Raston, *J. Chem. Soc., Dalton Trans.*, 1999, 3639; A. Drljaca, M. J. Hardie, J. A. Johnson, C. L. Raston and H. R. Webb, *Chem. Commun.*, 1999, 1135; J. L. Atwood, L. J. Barbour, E. S. Dawson, P. C. Junk and J. Kienzle, *Supramol. Chem.*, 1996, **7**, 271; L. J. Barbour, A. K. Damon, G. W. Orr and J. L. Atwood, *Supramol. Chem.*, 1996, **7**, 167; J. L. Atwood, L. J. Barbour, M. J. Hardie, C. L. Raston, M. N. Statton and H. R. Webb, *CrystEngComm.*, 2001, 4; J. L. Atwood, L. J. Barbour, M. J. Hardie, E. Lygris, C. L. Raston and H. R. Webb, *CrystEngComm.*, 2001, 10; P. C. Leverd, P. Berthault, M. Lance and M. Nierlich, *Eur. J. Org. Chem.*, 2000, 133; S. Shinkai, K. Araki, T. Matsuda, N. Nishiyama, H. Ikeda, I. Takasu and M. Iwamoto, *J. Am. Chem. Soc.*, 1990, **112**, 9053; H. Iki, H. Tsuzuki, H. Kijima, I. Hamachi and S. Shinkai, *Supramol. Chem.*, 1995, **4**, 223; M. Selkti, A. W. Coleman, I. Nicolis, N. Douteau-Guevel, F. Villain, A. Tomas and C. de Rango, *Chem. Commun.*, 2000, 161.

2 G. W. Orr, L. J. Barbour and J. L. Atwood, *Science*, 1999, **285**, 1049.

3 C. D. Gutsche, *Calixarenes, Monographs in Supramolecular Chemistry*, ed. J. F. Stoddart, The Royal Society of Chemistry, Cambridge and London, 1989; C. D. Gutsche, *Calixarenes Revisited, Monographs in Supramolecular Chemistry*, ed. J. F. Stoddart, The Royal Society of Chemistry, Cambridge and London, 1998.

4 G. Desiraju, *Acc. Chem. Res.*, 1996, **29**, 441.

CHEMCOMM
Communication
www.rsc.org/chemcomm

A new highly fluorescent probe for monosaccharides based on a donor–acceptor diphenyloxazole

Nicolas DiCesare and Joseph R. Lakowicz*

Center for Fluorescence Spectroscopy, University of Maryland, School of Medicine, 725 W. Lombard St., Baltimore, Maryland 21201, USA. E-mail: cfs@umbi.umd.edu; Fax: +1 410 706-8408

Received (in Covallis, OR, USA) 18th July 2001, Accepted 13th August 2001
First published as an Advance Article on the web 12th September 2001

A diphenyloxazole substituted with a dimethylamino and a boronic acid group showing intramolecular charge transfer in the excited state undergoes large spectral changes in the presence of monosaccharides.

For a decade, the development of synthetic probes for the recognition and analysis of sugar has attracted much attention.[1] Synthetic probes could find useful applications in the food industry as well as in clinical analysis. Detection and monitoring of glucose is particularly important for diabetics.[2] The development of synthetic sensors could be complementary to the present technology of glucose testing by using enzymes.[3] For example, the use of enzymes shows some limitations in the development of implantable sensors for continuous glucose monitoring in blood or in interstitial tissue. Continuous monitoring of glucose blood level is very important for the long term health of the diabetics and synthetic probes could lead to improvements in medical technology such as alarm systems for hypoglycemia and a control device for an insulin pump.

The boronic acids have been known for a few decades for their ability to interact with diols.[4] They have been used for the development of receptor and fluorescent probes for sugars.[1,5–7] The advantages of using boronic acid as chelator group for sugars are the fast and reversible interaction with sugars. In addition, many substituted phenylboronic acids are commercially available allowing the development of a large diversity of synthetic fluorescent probes for sugars with minimal synthetic steps. Different mechanisms have been used to induce spectral change following the interaction of the boronic acid and the sugars. Among these mechanisms, the use of intramolecular charge transfer (ICT) involving the boronic acid is very promising.[6,7] ICT is well known to be very sensitive to small perturbations[8] that can result in spectral shifts, intensity changes and/or lifetime changes. In addition, ICT can be applied to a very large diversity of fluorophores with no limitation of the wavelength range and/or lifetime of the fluorophore.

In an attempt to develop highly effective fluorescent probes for glucose, we synthesized compound **1** (Scheme 1). Compound **1**† is readily synthesized from the reaction between the 2-amino-4′-dimethylaminoacetophenone hydrochloride‡ and 4-(4,4,5,5-tetramethyl-1,3,2-dioxaborolan-2-yl)benzoyl chloride, obtained from the commercially available 4-(4,4,5,5-tetramethyl-1,3,2-dioxaborolan-2-yl)benzoic acid refluxed in $SOCl_2$, following by the dehydratation of the product in $POCl_3$.[9] Donor–acceptor derivatives of diphenyloxazole are well known to show high fluorescence quantum yields, long wavelength emission and to be very sensitive to small variations affecting the ICT properties of the excited state.[9] In this case, the ICT state is between the boronic acid, the electron-withdrawing group, and the *N*,*N*-dimethylamino group, the electron-donating group. As the boronic acid group changes to its anionic form, **2** in Scheme 2, the electron-withdrawing properties of the boron are removed and then the ICT is affected.[6] As the pH increases, we observe a blue shift (results not shown) and a significant increase in the fluorescence intensity. The emission band of the neutral form **1** appears at 557 nm with a ϕ_F value of 0.03, on the other hand, the emission of the anionic form **2** appears at 488 nm with a ϕ_F value of 0.95. These important spectral changes are interpreted by the loss of the ICT property for the anionic form **2**. The intensity change following the pH change is shown in

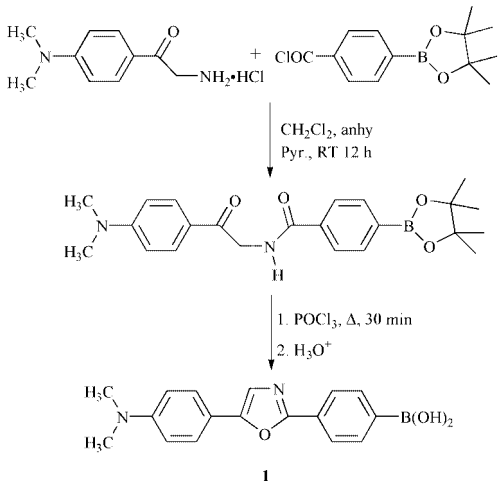

1

Scheme 1 Synthetic route to **1**.

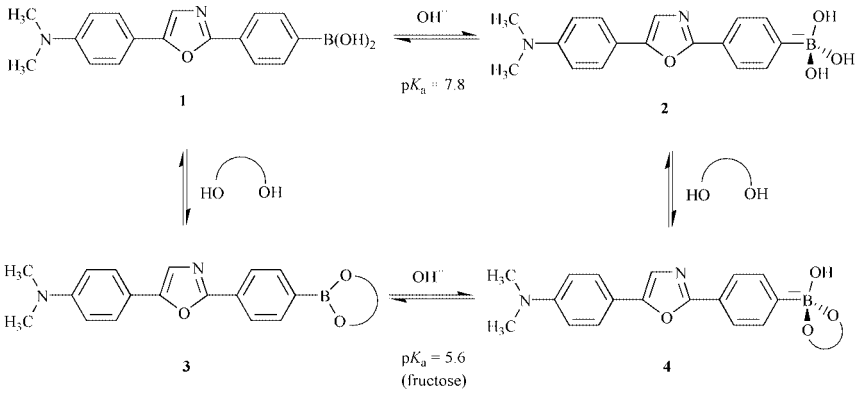

1 **2** **3** **4**

Scheme 2 Equilibrium involving pH and sugars.

 DOI: 10.1039/b106763j

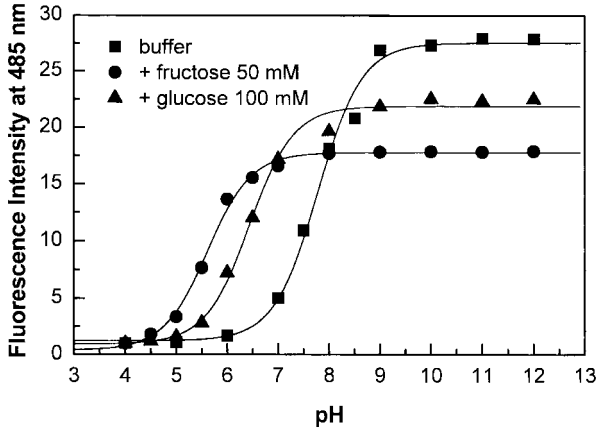

Fig. 1 Titration curves of **1** against the pH in absence and presence of sugars, λ_{ex} = 350 nm.

Fig. 1. Nearly a 30-fold increase in the fluorescence intensity can be observed at 485 nm.

Usually, the effects of sugars are observed since the boronic acid–sugar complex (structure **3** from Scheme 2) has a lower pK_a than the uncomplexed boronic acid. At a selected pH, it is possible to have a predominance of the neutral form (**1**) in absence of sugar and a predominance of the anionic form (**4**) in presence of sugar. This conformational change of the boron group, induced by the presence of sugar, is the origin of the spectral changes observed. Titration curves of **1** in presence of the sugar are displayed in Fig. 1. The observed pK_a of **1** is 7.8 in absence of sugar, pK_as of 5.6 and 6.5 are obtained in presence of fructose and glucose, respectively. Maximum changes between the titration curves with and without sugar are obtained at pH 6.5 and 7.0 for fructose and glucose, respectively. Since the spectral changes induced by sugar are not so different between these two pH values, we performed our measurements at pH 7.0 for all saccharides. It is also interesting to note that large spectral changes could also be observed at a pH higher than 9.0 as seen in Fig. 1. This suggests that probe **1** could also be used for monitoring sugar at high pH.

The effect of fructose on the emission band of **1** is displayed in Fig. 2. As observed for the pH, the presence of the sugar induces a blue shift and an increase in the fluorescence intensity. An isosbestic point is observed at 615 nm showing the equilibrium of the two conformations, the neutral and anionic form of the boronic acid. The same isosbestic point was observed in the pH effects on the emission band. The increase of the emission intensity is about 5-fold in the presence of fructose and about 3-fold in the presence of galactose and glucose. Titration curves of **1** against sugars are displayed in Fig. 3. Dissociation constants (K_D) of **1** were calculated at 1.9 ± 0.1 mM for fructose and 14 ± 1 and 37 ± 3 mM for galactose and glucose, respectively. K_D values are comparable to previous

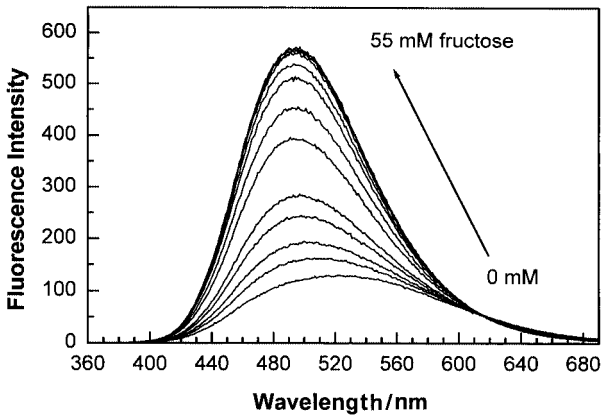

Fig. 2 Effect of fructose on the emission of **1**, measured in phosphate buffer–methanol (2:1 v/v) at pH 7.0, λ_{ex} = 350 nm. Probe concentration: 5 × 10^{-6} M.

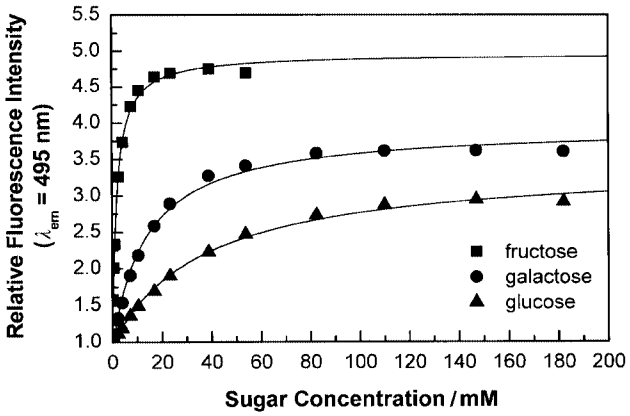

Fig. 3 Titration curves of **1** against sugars, measured in phosphate buffer–methanol (2:1 v/v) at pH 7.0, λ_{ex} = 350 nm. Probe concentration: 5 × 10^{-6} M.

values obtained with donor–acceptor chromophores involving the boronic acid group.[6,7] The higher affinity of the monoboronic acid **1** for fructose in comparison with glucose and the high concentration range of practical usefulness of **1** for glucose would not be suitable for glucose sensing in biological samples and/or in the presence of fructose but could find applications in the food industry and/or in fermentation industry where high concentrations of glucose are used.

In addition to the observed changes in the steady-state emission properties of **1**, we have also observed changes in the fluorescence lifetime of the probes. The neutral structure, **1**, shows a monoexponential fluorescence decay with a lifetime of 1.7 ns while the anionic form **2** possesses a lifetime of 3.7 ns, also monoexponential. At pH 7, the presence of fructose changes the fluorescence lifetime of the probe from 2.8 to 3.6 ns. Fluorescence lifetime changes are useful for sensing and monitoring since they are independent of the total intensity and independent also from the power of the excitation source and the concentration of the probe.[10]

The authors wish to acknowledge the Juvenile Diabetes Foundation, 1-2000-546, and the NIH National Center for Research Resources, RR-08119, for financial support.

Notes and references

† *Selected data* for **1** 5-(4-dimethylaminophenyl)-2-[4-(dihydroxyboranyl)phenyl]oxazole: yellow solid, yield 48%, δ_H(300 MHz; CD_3OD) 2.83 (6 H, s), 6.59 (2H, d), 7.05 (1H, s), 7.40 (2H, d), 7.52 (1H, s), 7.67 (1H, s) and 7.82 (2H, s).

‡ Synthesised from 4′-dimethylaminoacetophenone (TCI America) according to the standard procedure described in the litterature.[11,12]

1 J. H. Hartley, T. D. James and C. J. Ward, *J. Chem. Soc., Perkin Trans. 1*, 2000, 3155.
2 The Diabetes Control and Complications Trial Research Group, *Diabetes*, 1997, **46**, 271.
3 A. Heller, *Annu. Rev. Biomed. Eng*., 1999, **1**, 153.
4 J. P. Lorand and J. O. Edwards, *J. Org. Chem*., 1959, **24**, 769.
5 T. D. James, K. Sandanayake and S. Shinkai, *Angew. Chem., Int. Ed. Engl*., 1996, **35**, 1911.
6 N. DiCesare and J. R. Lakowicz, *J. Phys. Chem*., 2001, **105**, 6834.
7 N. DiCesare and J. R. Lakowicz, *J. Photochem. Photobiol,. A*, 2001, **143**(1), 39
8 B. Valeur, *Topics in Fluorescence Spectroscopy*, ed. J. R. Lakowicz, Plenum Press, New York, 1994, vol. 4, pp. 21–50.
9 Z. Diwu, Y. Lu, C. Zhang, D. H. Klaubert and R. P. Haugland, *Photochem. Photobiol*., 1997, **66**, 424.
10 H. Szmacinski and J. R. Lakowicz, *Topics in Fluorescence Spectroscopy*, ed. J. R. Lakowicz, Plenum Press, New York, 1994, vol. 4, pp. 295–334.
11 Z. Diwu, C. Beachdel and D. H. Klaubert, *Tetrahedron Lett*., 1998, **39**, 4987.
12 C. M. Suter, S. Schalit and R. A. Cutler, *J. Am. Chem.. Soc*., 1953, **75**, 4330.

CHEMCOMM Communication
www.rsc.org/chemcomm

Efficient synthesis of the antigenic phosphoglycans of the *Leishmania* parasite†

Dipali Ruhela and Ram A. Vishwakarma*

Bio-organic Chemistry Lab, National Institute of Immunology, Aruna Asaf Ali Marg, JNU Complex, New Delhi 110067, India. E-mail: ram@nii.res.in; Fax: +91 11 6162125; Tel: +91 11 6174899

Received (in Cambridge, UK) 23rd July 2001, Accepted 21st August 2001
First published as an Advance Article on the web 12th September 2001

Antigenic phosphoglycan repeats of the *Leishmania* parasite can be assembled in a flexible and efficient manner without involving any glycosidation steps, and the chain can be extended either towards the non-reducing (6′-OH) or reducing (1-OH) end suitable for synthesis of lipophosphoglycan, proteophosphoglycan and analogues.

The protozoan parasite *Leishmania* causes visceral and cutaneous leishmaniases and has a remarkable ability to survive and proliferate in extreme environments during its digenetic life cycle in the sandfly vector and the human host. At all life-cycle stages *Leishmania* species assemble an abundance of a unique class of glycoconjugates named phosphoglycans (reviewed in ref. 1). These include the most abundant surface molecule of infectious promastigote stage, the lipophosphoglycan (LPG), and secreted proteophosphoglycan (PPG) of the amastigote stage. There is substantial evidence[1] that the LPG and PPG are antigenic and multifunctional virulence factors essential for infectivity and survival of the parasite. The role of phosphoglycans in parasite virulence is currently a topic of intense debate[2] in parasite biology.

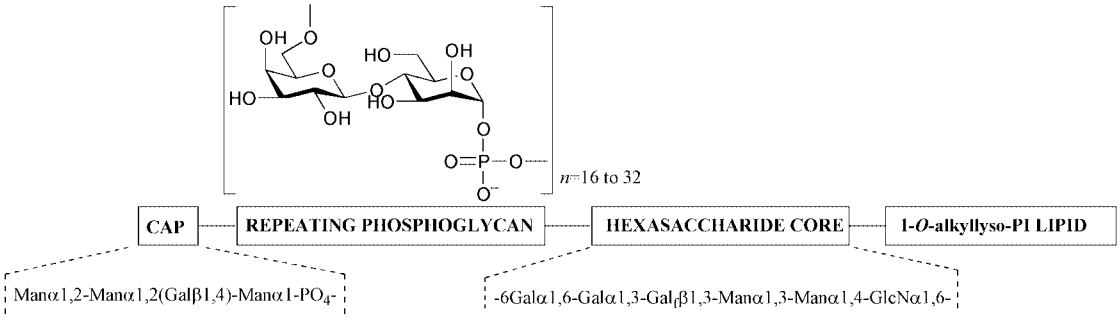

The intriguing structure of the LPG consists of four distinct domains: (i) alkyllysophosphatidylinositol lipid-anchor; (ii) conserved phosphosaccharide core with internal galactofuranose residue; (iii) variable phosphoglycan repeats and (iv) neutral oligosaccharide cap. The unique feature of LPG is the variable phosphoglycan domain made of phosphodisaccharide $[6Gal\textit{p}\text{-}\beta1,4\text{-}Man\textit{p}\text{-}\alpha1\text{-phosphate}]_n$ repeats linked through phosphodiester between the anomeric-OH of mannose of one repeat and the 6-OH of galactose of the adjoining repeat. PPG molecules are made up of the phosphoglycan repeats linked to a peptide anchor.

The biological, biochemical and biophysical experiments to probe the function, biosynthesis and conformation of the *Leishmania* phosphoglycans, and to exploit them in drug and vaccine design, require efficient chemical synthesis. Since the phosphoglycans are labile molecules, due to the presence of anomeric phosphodiester linkages, their synthesis is particularly challenging. The first synthesis of *Leishmania* phosphoglycans was accomplished[3] by the Dundee group from monosaccharide building blocks, using a suitably protected galactose donor and mannose acceptors. This obviously involved multiple protection, deprotection, glycosidation and purification steps even before the phosphoglycan assembly began through the H-phosphonate chemistry.

In our ongoing work on synthesis[4–7] and biosynthesis[8] of *Leishmania* glycoconjugates, an efficient route to construct phosphoglycans was required for the total synthesis of LPG and vaccine design. To circumvent the usual problems associated with glycosidation and to avoid several protection–deprotection steps required in previous synthesis, we used the readily available disaccharide lactose as starting material. Here we report a new efficient synthesis of phosphoglycans, which does not involve any glycosidation steps, and the phosphoglycan chain can be extended either towards the non-reducing (6′-OH) or reducing (1-OH) end in high yielding iterative steps. The important features of our approach include the glycal chemistry mediated gluco→manno transformation and regioselective 6′-protection to convert lactose (Galβ1,4-Glu) into the suitably protected Galβ1,4-Man building block, extension of PG repeats in either direction by selective deprotection at the non-reducing 6′-position or reducing 1-position and α-phosphitylation, followed by iterative PG coupling cycles.

The first intermediate lactal (**1**) was prepared[6,7] from lactose (Scheme 1) in straightforward steps (acetylation, bromination, reductive elimination and deacetylation), and a high yield could be obtained in the reductive elimination step by the application of Zn–Vitamin-B_{12} reagent.[9] The next task was to selectively protect the 6-position of the galactose residue of lactal (**1**) and this was achieved, after a considerable number of experiments, by dibutyltin oxide mediated silylation (Bu_2SnO–MeOH reflux followed by TBSCl) which led exclusively to 6′-*O*-TBS-lactal (**2**). It should be mentioned here that under similar conditions most other protecting groups (benzyl, *p*-methoxybenzyl and allyl) led to C3′-OH protected lactals. The next step involved stereoselective gluco→manno transformation of 6′-*O*-TBS-lactal (**2**) by MCPBA under biphasic conditions which led exclusively to the manno product 6′-*O*-TBS-galactopyranosyl-(1→4)-β-D-mannopyranose (**3**). The acetylation of **3** gave the key intermediate, 1,2,3,6-tetra-*O*-acetyl-4-*O*-(2,3,4,tri-*O*-acetyl-6-*O*-TBS-β-D-galactopyranosyl)-α-D-mannopyranose (**4**), as the major isomer, which served as a central point to both

† Electronic supplementary information (ESI) available: selected data for compounds **7**, **8**, **10** and **11**. See http://www.rsc.org/suppdata/cc/b1/b106634j/

 DOI: 10.1039/b106634j

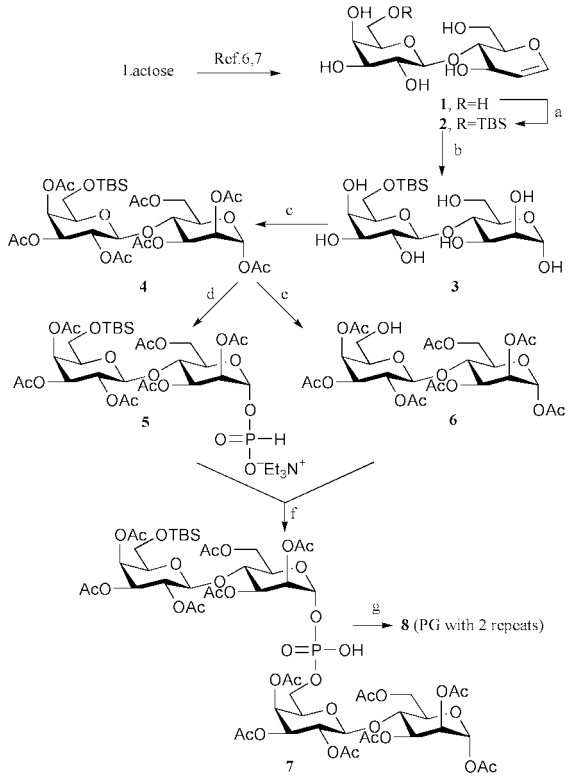

Scheme 1 *Reagents and conditions*: (a) Bu_2SnO, MeOH, reflux, 4 h; *tert*-butyldimethylsilyl chloride (TBSCl) , THF, rt, 48 h, 80%; (b) MCPBA, 0 °C, 4 h, 90%; (c) Ac_2O, Py, rt, 16 h, 99%; (d) Me_2NH, CH_3CN, −20 °C, 3 h, 95% and PCl_3, imidazole, CH_3CN, 0 °C, 2 h, triethylammonium bicarbonate (TEAB), 87%; (e) HF–CH_3CN, 0 °C, 2 h, 85%; (f) **5** and **6**, pivaloyl Cl, Py, rt, 1 h; I_2, 30 min, TEAB work-up, 79%; (g) HF–CH_3CN, 0 °C, 2 h; NaOMe–MeOH, 95%.

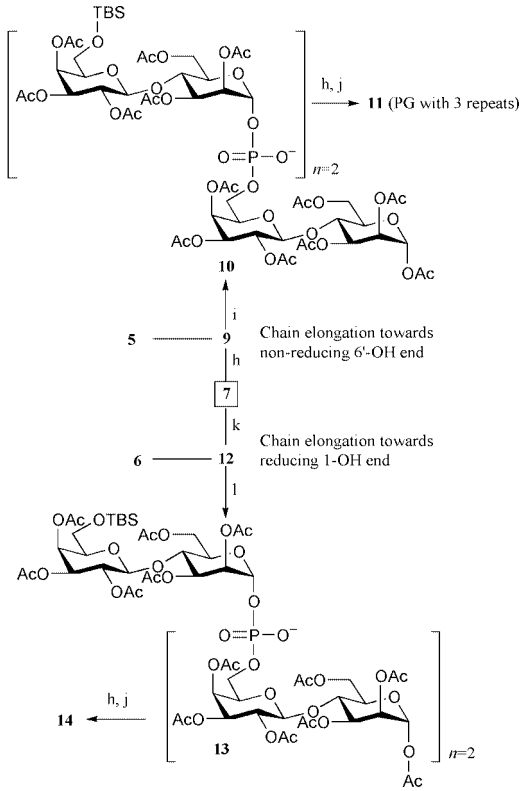

Scheme 2 *Reagents and conditions*: (h) HF–CH_3CN, 0 °C, 2 h, 85%; (i) **5**, pivaloyl Cl, Py, rt 1 h; I_2, 30 min, TEAB work-up, 79%; (j) TEA–MeOH–H_2O, rt, 24 h, 95%; (k) Me_2NH–CH_3CN, −20 °C, 3 h, 95%; PCl_3, imidazole, CH_3CN, 0 °C, 2 h, TEAB, 87%; (l) **6**, pivaloyl Cl, Py, rt, 1 h; I_2, 30 min, TEAB, 79%.

donor and acceptor for iterative assembly of the phosphoglycan repeats. Compound **4** was divided into two parts; the first part was transformed to the PG donor by anomeric deacylation (Me_2NH at −20 °C) followed by phosphitylation (triimidazolylphosphine generated *in-situ* from PCl_3 and imidazole) to provide 2,3,6-tri-*O*-acetyl-4-*O*-[2,3,4-tri-*O*-acetyl-6-*O*-(*tert*-butyldimethylsilyl)-β-D-galactopyranosyl]-α-D-mannopyranosyl H-phosphonate (**5**), isolated as the TEAB salt. The second part of **4** was converted to hepta-acetyl PG-acceptor **6** by removal of the TBS group from the 6-position of the Gal residue. The pivaloyl chloride coupling of PG-H-phosphonate donor **5** with acceptor **6** followed by *in-situ* iodine oxidation afforded fully protected phosphotetrasaccharide **7**; which on full deprotection (HF, NaOMe–MeOH) provided free phosphoglycan **8** (with two PG repeats).

Now the protected phosphotetrasaccharide **7** was well placed (Scheme 2) for further extension of phosphoglycan chain either in the upstream direction (non-reducing 6′-end) or downstream direction (reducing 1-OH end). For upstream extension of the PG domain, the TBS group from the 6′-position of galactose at the non-reducing end of **7** was removed, and the resulting tetrasaccharide **9** was coupled with disaccharide H-phosphonate **5** to provide phosphohexasaccharide **10** in high yield. The global deprotection (HF–CH_3CN and TEA–MeOH–H_2O) led to free phosphoglycan **11** with three PG repeats. For downstream extension of the PG domain, the intermediate **7** was deacetylated (Me_2NH at −20 °C) at the reducing-end anomeric position and converted to H-phosphonate **12** as described above. This was coupled with hepta-*O*-acetyl disaccharide **6** to provide phosphohexasaccharide **13** ready for deprotection or further extension to higher oligomers. The presence of (1→6)-phosphodiester linkages between the PG repeats was confirmed by ^{31}P–^{13}C coupling (doublets, 5 and 7 Hz in ^{13}C NMR) for C-1 and C-2 of the mannose units, and the C-5 and C-6 of the corresponding galactose units; these ^{13}C signals were found to be shifted due to α- and β-phosphorylation effects.

It is obvious from above that the phosphoglycan chain can further be extended to the desired length in either direction, and instead of 2 + 4 (disaccharide + tetrasaccharide) coupling, 4 + 4 coupling can also be carried out for rapid access to desired PGs.

To conclude, a versatile synthesis for rapid assembly of the biologically important *Leishmania* phosphoglycans has been achieved, which does not involve any glycosidation steps and allows the PG chain to grow in either direction. This approach is now being adopted on the solid phase and for the total synthesis of the LPG, which will be communicated shortly.

Authors thank the DST (India) for financial support for this work, and the DBT (India) for core grant to the Institute.

Notes and references

1 S. J. Turco, G. F. Spath and S. M. Beverley, *Trends Parasitol*., 2001, **17**, 223; T. Ilg, *Parasitol. Today*, 2000, **16**, 489.
2 T. Ilg, *EMBO J*., 2000, **19**, 1953; G. F. Spath, L. Epstein, B. Leader, S. M. Singer, H. A. Avila, S. J. Turco and S. M. Beverley, *Proc. Natl. Acad. Sci. USA*, 2000, **97**, 9258.
3 A. V. Nikolaev, T. J. Rutherford, M. A. J. Ferguson and J. S. Brimacombe, *J. Chem. Soc., Perkin Trans 1*, 1995, 1977; A. V. Nikolaev, J. A. Chudek and M. A. J. Ferguson, *Carbohydr. Res*., 1995, **272**, 179; A. P. Higson, Y. E. Tsvetkov, M. A. J. Ferguson and A. V. Nikolaev, *J. Chem. Soc., Perkin Trans 1*, 1998, 2587.
4 P. Sahai and R. A. Vishwakarma, *J. Chem. Soc., Perkin Trans 1*, 1997, 1845.
5 A. K. Tyagi and R. A. Vishwakarma, *Tetrahedron Lett*., 1998, **39**, 6069.
6 M. Upreti and R. A. Vishwakarma, *Tetrahedron Lett*., 1999, **40**, 2619.
7 M. Upreti, D. Ruhela and R. A. Vishwakarma, *Tetrahedron*, 2000, **56**, 6577.
8 P. Sahai, M. Chawla and R. A. Vishwakarma, *J. Chem. Soc., Perkin Trans 1*, 2000, 1283.
9 C. L. Forbes and R. W. Franck, *J. Org. Chem*., 1999, **64**, 1424.

CHEMCOMM
Communication
www.rsc.org/chemcomm

Aminosubstituted *tert*-butylsulfinylferrocenes as a new family of chiral ligands: asymmetric addition of diethylzinc to aldehydes

Julián Priego, Olga García Mancheño, Silvia Cabrera and Juan Carlos Carretero*

Departamento de Química Orgánica, Facultad de Ciencias, Universidad Autónoma de Madrid 28049. Madrid, Spain. E-mail: juancarlos.carretero@uam.es; Fax: 34 91 3973966; Tel: 34 91 3973925

Received (in Cambridge, UK) 5th July 2001, Accepted 3rd September 2001
First published as an Advance Article on the web 12th September 2001

A ready access to a new family of planar chiral ferrocenes, the (R_{Fc},R_S)-2-amino substituted 1-*tert*-butylsulfinylferrocenes, is described; in the case of the sulfonamide series enantioselectivities of up to 96% were obtained in the addition of Et_2Zn to aromatic aldehydes.

During the last two decades the sulfinyl group has been extensively used as a chiral auxiliary in emblematic C–C bond forming reactions, such as Diels–Alder cycloadditions and nucleophile additions,[1] and more recently has started to be applied in transition metal-catalyzed reactions.[2] However, despite the huge interest currently devoted to the development of highly efficient chiral ligands for asymmetric catalysis, usually involving *P*,*P*- *P*,*N*- or *N*,*N*-bidentate metal-coordinating ligands,[3] few examples of chiral ligands based on sulfoxides have been reported,[4] most of them being tested only in asymmetric palladium-catalyzed allylic substitutions. Among the wide structural diversity of chiral frameworks commonly used in asymmetric catalysis, the planar chirality of 1,2-disubstituted ferrocene derivatives has received a great attention.[5] Within this context, we describe herein the synthesis of enantiopure (R_{Fc},R_S)-2-amino substituted *tert*-butylsulfinylferrocenes as a new family of sterically and electronically adjustable chiral ligands and their application to the asymmetric addition of Et_2Zn to aromatic aldehydes.[6]

The synthesis of *tert*-butyl ferrocenyl sulfoxide (**1**) in high optical purity had been previously described by enantioselective oxidation of the corresponding thioether and by sulfinylation of ferrocenyllithium with an enantiopure *tert*-butylsulfinate.[7] Alternatively, we have prepared (*R*)-**1** by direct sulfinylation of ferrocenyllithium (formed *in situ* by deprotonation of ferrocene with *t*-BuLi in THF) with (*R*)-*S*-*tert*-butyl 1,1-dimethylethanethiosulfinate.[8] This one-step procedure is experimentally quite simple (THF, 0 °C), affording ferrocene (*R*)-**1** in 40% yield after flash chromatography (58% of starting ferrocene is recovered). The recrystallization from hexane–ether (1 : 1) yielded (*R*)-**1** in very high optical purity[9] (ee = 99%, HPLC, Daicel Chiralcel OD column).

According to the previously reported cases of highly stereoselective *ortho* C-2 deprotonation of ferrocenyl sulfoxides with strong bases,[7] the treatment of **1** with *n*-BuLi (THF, 0 °C) generated selectively the C-2 lithiated *tert*-butylsulfinylferrocene.[10] This solution was treated with tosyl azide to give the intermediate ferrocenyl azide, followed by *in situ* reduction with $NaBH_4$, which afforded the amino(sulfinyl)ferrocene **2a** (64% yield) in very high optical purity (ee > 98%, HPLC, Chiralpak AS column) (Scheme 1).

In the search of efficient chiral ligands for enantioselective synthesis, the ready access to a wide diversity of substrates with adjustable steric and electronic properties around the metal-coordinating atoms is a crucial point. In this context, having developed a practical two-step procedure for the preparation of enantiopure **2a** in gram quantities from ferrocene, the amino group was readily transformed into a variety of nitrogen

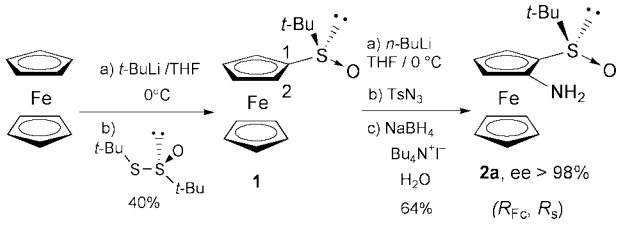

Scheme 1 Synthesis of 2-amino(sulfinyl)ferrocene **2a**.

compounds such as substituted amines (**2b**), amides (**2c–f**) and sulfonamides (**2g–l**) following straightforward reactions of amine derivatization (Scheme 2).

With this family of ligands in hand, we examined their effectiveness as chiral catalysts in one of the most prototypical reactions in chiral ligand screening: the addition of diethylzinc to benzaldehyde.[6] The reactions were performed under typical conditions: 5 mol% of ligand **2**, excess of diethylzinc (200 mol%) in toluene at rt (Table 1). In most cases the complete disappearance of benzaldehyde was observed after 1–4 days, affording in acceptable to good yields the alcohol **3** with enantioselectivities very dependent on the substitution at the nitrogen atom. While a low enantiocontrol occurred using the amine (entries 1 and 2) and amide ligands (entries 3–6), a more interesting outcome was observed in the case of the sulfonamide ligands (entries 7–14), which provided (*R*)-**3** in 42 to 88% ee's. The best ligands were found to be the *p*-tolylsulfonamide **2h** (80% ee, entry 8) and the *p*-methoxyphenylsulfonamide **2i** (82% ee, entry 10). It is worth noting that in both cases the

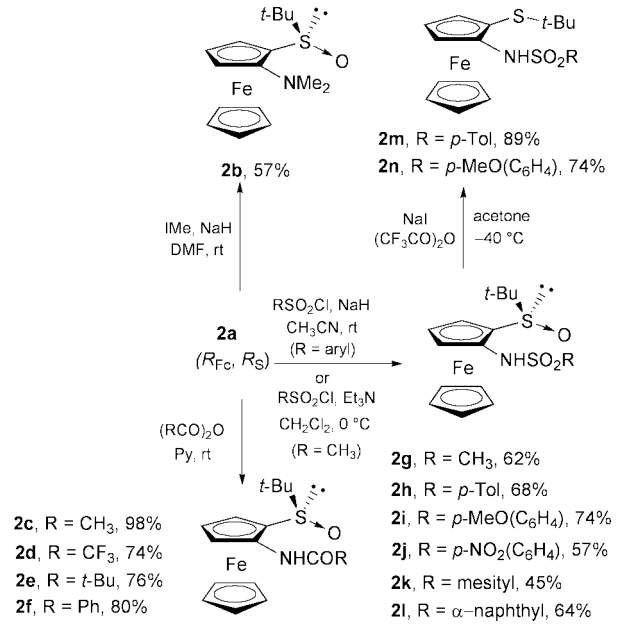

Scheme 2 Synthesis of ligands **2** bearing subtituted amines, amides and sulfonamides.

† Electronic supplementary information (ESI) available: experimental details. See http://www.rsc.org/suppdata/cc/b1/b105962a/

 DOI: 10.1039/b105962a

Table 1 Diethylzinc addition to benzaldehyde catalyzed by the ligands **2**

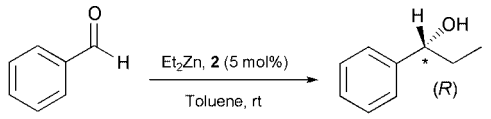

3

Entry[a]	Ligand	3 Ee (%)[b]	3 Conf.	3 Yield (%)[c]
1	**2a**	28	*S*	93
2	**2b**	6	*R*	59
3	**2c**	60	*R*	76
4	**2d**	6	*R*	67[e]
5	**2e**	14	*R*	70
6	**2f**	8	*R*	74
7	**2g**	74	*R*	90
8	**2h**	80	*R*	79
9[d]	**2h**	88	*R*	80[e]
10	**2i**	82	*R*	82
11[d]	**2i**	86	*R*	76[e]
12	**2j**	58	*R*	62[e]
13	**2k**	48	*R*	68
14	**2l**	42	*R*	51
15	**2m**	82	*R*	85
16	**2n**	74	*R*	81

[a] Reaction conditions: Et_2Zn (200 mol%), ligand (5 mol%), toluene, rt, 1–4 days. [b] Determined by HPLC (Daicel Chiralcel OD). [c] In pure alcohol after flash chromatography. [d] Reaction run at −20 °C. [e] Conversion yield.

enantioselectivity of the process was enhanced significantly by performing the reaction at −20 °C instead of rt (entries 9 and 11, 88 and 86% ee, respectively).

In order to clarify whether the enantiocontrol exerted by the chiral ligand was predominantly due to the planar chirality of the ferrocenyl moiety or to the stereogenic sulfur atom, the optimal sulfoxides **2h** and **2i** were reduced to the corresponding thioethers **2m** and **2n** by reaction with NaI–$(CF_3CO)_2O$ in acetone (89 and 74% yields, respectively). Interestingly, the addition of Et_2Zn to benzaldehyde at rt in the presence of both **2m** and **2n** (entries 15 and 16) occurred with an enantioselectivity very similar to that observed for the corresponding sulfoxides **2h** and **2i** (entries 8 and 10), showing that the planar chirality of ferrocene is the main structural factor involved in the asymmetric induction.[11]

Finally, to explore the substrate generality of this enantioselective process, the ligands **2h** and **2i** were tested in the addition of Et_2Zn to differently substituted aromatic aldehydes under the same experimental conditions. As depicted in Table 2, both ligands **2h** and **2i** behaved similarly, affording in all cases the alcohol of (*R*) configuration as the main enantiomer[12] in good chemical yields. With the exception of the case of *p*-nitrobenzaldehyde (entries 1 and 2), moderate to high enantioselectivities were observed with the rest of aldehydes (ee's from 58 to 96%, entries 3–12).

In summary, a novel family of enantiopure ferrocene ligands, the (R_{Fc},R_S)-2-amino substituted 1-*tert*-butylsulfinylferrocenes **2**, has been readily synthesized from ferrocene. Using sulfonamide ligands (especially **2h** and **2i**) moderate to high asymmetric inductions were obtained in the addition of Et_2Zn to aromatic aldehydes. The application of this new type of chiral ferrocene ligand to other asymmetric C–C bond forming reactions is under active investigation.

This work was supported by the Ministerio de Ciencia y Tecnología (project BQU2000-0266). J. P. and O. G. M. also thank the Ministerio de Educación y Cultura for their predoctoral fellowships.

Table 2 Diethylzinc addition to aromatic aldehydes catalyzed by the ligands **2h** and **2i**

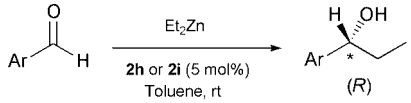

4-9

Entry[a]	Ar	Ligand	Product, (*R*) conf.	Ee (%)[b]	Yield (%)[c]
1	*p*-$NO_2C_6H_4$	**2h**	**4**	28	73[e]
2	*p*-$NO_2C_6H_4$	**2i**	**4**	26	75[e]
3	*p*-$MeOC_6H_4$	**2h**	**5**	66[d]	65[e]
4	*p*-$MeOC_6H_4$	**2i**	**5**	58[d]	61[e]
5	*p*-MeC_6H_4	**2h**	**6**	64[d]	86
6	*p*-MeC_6H_4	**2i**	**6**	66[d]	72
7	*p*-$CO_2MeC_6H_4$	**2h**	**7**	88	71
8	*p*-$CO_2MeC_6H_4$	**2i**	**7**	96	78
9	2-Naphthyl	**2h**	**8**	82	73
10	2-Naphthyl	**2i**	**8**	92	79
11	*m*-FC_6H_4	**2h**	**9**	80	76
12	*m*-FC_6H_4	**2i**	**9**	72	74

[a] Reaction conditions: Et_2Zn (200 mol%), ligand (5 mol%), toluene, rt, 1–4 days. [b] Determined by HPLC (Daicel Chiralpak AD). [c] In pure alcohol after flash chromatography. [d] Determined by HPLC (Daicel Chiralcel OD). [e] Conversion yield.

Notes and references

1 Recent review: J. L. Garcia Ruano and B. Cid de la Plata, *Top. Curr. Chem*., 1999, **204**, 1.

2 Very recent references: K. Hiroi, Y. Suzuki, F. Kato and Y. Kyo, *Tetrahedron: Asymmetry*, 2001, **12**, 37; N. Díaz Buezo, O. García Mancheño and J. C. Carretero, *Org. Lett*., 2000, **2**, 1451; K. Hiroi and A. Yamada, *Tetrahedron: Asymmetry*, 2000, **11**, 1835.

3 *Catalytic Asymmetric Synthesis*, ed. I. Ojima, 2nd edn., VCH, New York, 2000; *Comprehensive Asymmetric Catalysis*, eds. E. N. Jacobsen, A. Pfaltz and H. Yamamoto, Springer, Berlin, 1999.

4 Recent references: K. Hiroi, Y. Suzuki, I. Abe and R. Kawagishi, *Tetrahedron*, 2000, **56**, 4701; D. G. I. Petra, P. C. J. Kamer, A. L. Spek, H. E. Schoemaker and P. W. N. M. van Leeuwen, *J. Org. Chem*., 2000, **65**, 3010; K. Hiroi, Y. Suzuki and R. Kawagishi, *Tetrahedron Lett*., 1999, **40**, 715; K. Hiroi, Y. Suzuki, I. Abe, Y. Hasegawa and K. Suzuki, *Tetrahedron: Asymmetry*, 1998, **9**, 3797; See also: M. C. Carreño, J. L. García Ruano, M. C. Maestro and L. M. Martín Cabrejas, *Tetrahedron: Asymmetry*, 1993, **4**, 727.

5 *Ferrocenes: Homogeneous Catalysis. Organic Synthesis. Material Science*, eds. T. Hayashi and A. Togni, VCH, Weinheim, Germany, 1995. Recent reviews, see: C. J. Richards and A. J. Locke, *Tetrahedron: Asymmetry*, 1998, **9**, 2377; A. Togni, *Angew. Chem., Int. Ed. Engl*., 1996, **35**, 1475.

6 Recent review: L. Pu and H.-B. Yu, *Chem. Rev*., 2001, **101**, 757.

7 N. M. Lagneau, Y. Chen, P. M. Robben, H.-S. Sin, K. Takasu, J.-S. Chen, P. D. Robinson and D. H. Hua, *Tetrahedron*, 1998, **54**, 7301; P. Diter, O. Samuel, S. Taudien and H. B. Kagan, *Tetrahedron: Asymmetry*, 1994, **5**, 549; F. Rebière, O. Riant, L. Ricard and H. B. Kagan, *Angew. Chem., Int. Ed. Engl*., 1993, **32**, 568.

8 D. A. Cogan, G. Liu, K. Kim, B. J. Backes and J. A. Ellman, *J. Am. Chem. Soc*., 1998, **120**, 8011.

9 The sulfinylation of ferrocenyllithium occurred with virtually complete inversion of configuration at sulfur. For instance, from (*R*)-*tert*-butyl 1,1-dimethylethanesulfinate of ee = 80% (*R*)-**1** was obtained with the same optical purity (ee = 80%).

10 This high diastereoselectivity is due to the strong steric preference of the *tert*-butyl group to be in the *anti* orientation with regard to the iron atom, see ref. 7.

11 C. Bolm and K. Muñiz, *Chem. Eur. J*., 2000, **6**, 2309; C. Bolm, K. Muñiz, A. Seger, G. Raabe and K. Günther, *J. Org. Chem*., 1998, **63**, 7860.

12 All obtained alcohols (*R*)-**4**–**9** are dextrorotatory. See, for instance: W.-M. Dai, H.-J. Zhu and X.-J. Hao, *Tetrahedron: Asymmetry*, 2000, **11**, 2315.

CHEMCOMM
Communication
www.rsc.org/chemcomm

Interfacial synthesis of hollow microspheres of mesostructured silica

Christabel E. Fowler, Deepa Khushalani† and Stephen Mann*

School of Chemistry, Univeristy of Bristol, UK BS8 1TS. E-mail: s.mann@bris.ac.uk

Received (in Cambridge, UK) 4th June 2001, Accepted 16th August 2001
First published as an Advance Article on the web 18th September 2001

Hollow microspheres with ordered mesoporous walls are synthesised under ambient conditions by a simple procedure involving dilution and neutralisation of an aqueous tetraethoxysilane/cetyltrimethylammonium bromide reaction mixture.

The size and shape selectivity of porous inorganic structures plays a pivotal role in a wide range of industrial and biological applications involving molecular transport, adsorption, catalysis and separation. The scope of these applications could be significantly increased, for example in the parallel or sequential processing of feedstock, by the use of hierarchically organized architectures that exhibit order and functionality across several length scales. Efforts have therefore been made to invent chemically based routes to the synthesis of inorganic materials with structural and morphological complexity.[1] For example, a variety of multiple templating methodologies involving macro- and microscopic structures such as latex particles,[2] colloidal crystals[3] and bacterial superstructures,[4] in association with preformed nanoparticles or reaction solutions containing supramolecular aggregates, have been investigated. Alternatively, confined reaction environments such as emulsion droplets have been employed to prepare porous hollow spheres and inorganic vesicle-like morphologies that could be useful in controlled storage and release.[5] In particular, multilamellar silica colloids have been synthesised using neutral gemini surfactant vesicles[6] or by spray drying of reaction solutions containing cationic surfactant templates,[7] and semi-hollow microspheres of mesostructured silica prepared using a cosolvent,[8] or oil droplets containing tetraethoxysilane (TEOS) dispersed in aqueous reaction solutions.[9]

We now report the facile synthesis of thermally stable micron-size hollow spherical shells with ordered mesoporous walls, approximately 20 nm or less in thickness. The structures were synthesised at room temperature by hydrolysis and condensation of TEOS in an aqueous solution of cetyltrimethylammonium bromide (CTABr), which was subjected to rapid quenching by dilution followed by pH neutralisation after an induction period.‡ Unlike previous studies, the preparation did not necessitate addition of auxiliary cosurfactants or cosolvents, substrates, stringent conditions and/or specialized equipment, and the products were structurally and morphologically well-defined and stable upon calcination.

Samples of the as-synthesised product were obtained as a cloudy suspension at the air/water interface. Scanning electron microscopy (SEM) studies showed a high yield of micrometre-sized (mean diameter = 0.98 μm, σ = 0.4 μm) spherical structures with a uniform and smooth surface texture [Fig. 1(a)]. The size and shape of the microspheres were unchanged upon heating to 540 °C [Fig. 1(b)]. In general, only a few deformed or cracked structures were observed but when imaged these, as well as samples that had been mechanically fractured, indicated that the silica microspheres were hollow, as shown for example in Fig. 1(b). The shell thickness, which was determined from SEM and transmission electron microscopy (TEM) images of the broken microspheres, was highly uniform and less than 20 nm.

† Current address: School of Physical Sciences, University of Kent at Canterbury, UK CT2 7NR.

TEM studies of the as-synthesised and calcined materials showed hollow shells that occasionally collapsed under the high vacuum. High resolution images of the wall structures showed multiple domains of well-ordered lattice fringes with spacings between 4.2 and 5.8 nm (Fig. 2). The spacings were significantly larger than those reported for MCM-41 silica, and although image artefacts could not be ruled out, the reproducibility in the measurements suggested that the as-synthesised walls consisted of a metastable or swollen silica–surfactant mesophase that was replicated in the form of an ordered mesoporous silica shell upon calcination. In general, the lattice fringes were observed as parallel lines running across the surface of the wall, except at the edges of the projected structures where 'dot' patterns were sometimes observed (Fig. 2). The results were therefore consistent with a wall structure in which the mesoporous channels were predominantly arranged parallel to the shell surface. Pseudo-hexagonal patterns were occasionally observed in the central areas of the projected

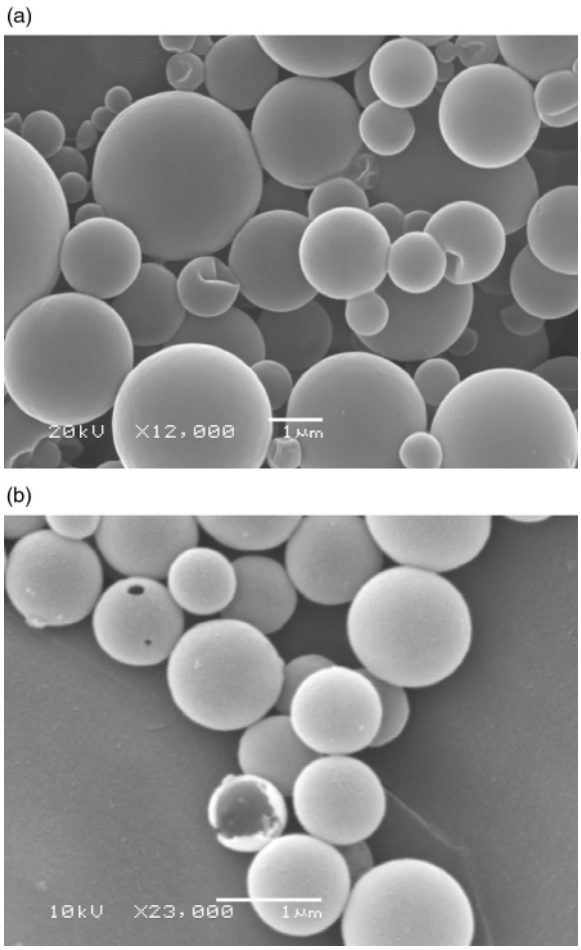

Fig. 1 SEM micrographs showing (a) as-synthesised silica-surfactant hollow mesostructured microspheres; note the partial collapse in the high vaccum of a few of the shells. (b) Hollow microspheres after calcination; a broken shell clearly shows the hollow interior and a thin 20 nm-thick wall. Scale bars, 1 μm.

 DOI: 10.1039/b104879c

images but these were interpreted as fortuitous intersections between different domains rather than regions comprising channels aligned perpendicular to the wall surface.

Small angle X-ray diffraction patterns of the as-synthesised and calcined hollow microspheres showed a single broad reflection centred at approximately 3.7 nm (Cu-Kα, λ = 0.154178 nm). The absence of higher-order reflections was consistent with the limited domain size of the mesostructure imaged by TEM. Surprisingly, thermogravimetric analysis revealed a loss of only *ca*. 2.5 wt% centred at 223 °C that was attributed to removal of surfactant from the shell walls (Fig. 3). This suggests that a significant amount of the micellar template was released *in situ* after formation of the as-synthesised mesophase without loss of the ordered mesostructure. In addition, there was minimal loss attributed to physisorbed water (4 wt% at < 100 °C) or removal of water from the condensation of terminal silanol groups (2 wt% between 400 and 500 °C). Thus, a residual mass of over 90% was obtained after heating at 800 °C for 5 h. This is considerably higher than for bulk mesoporous silica, which for MCM-41 is *ca*. 55 wt%.

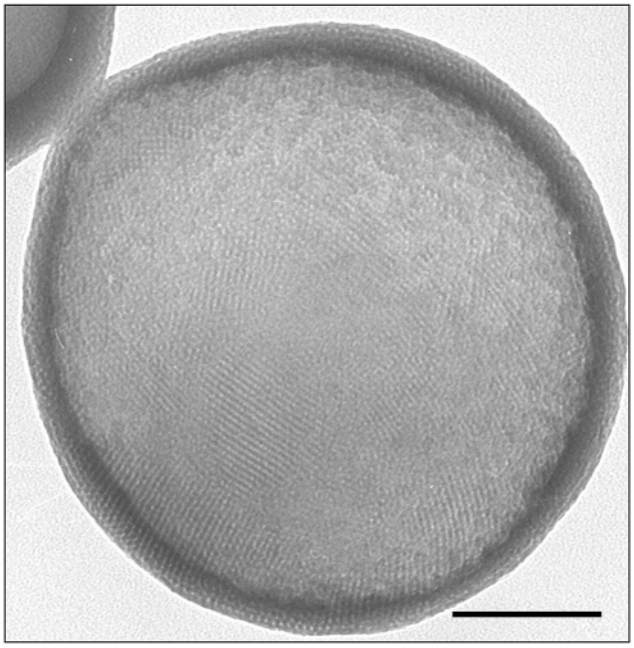

Fig. 2 TEM image of a calcined hollow mesostructured microsphere showing domains of well-ordered lattice fringes with 4.3 nm spacing. Scale bar, 100 nm.

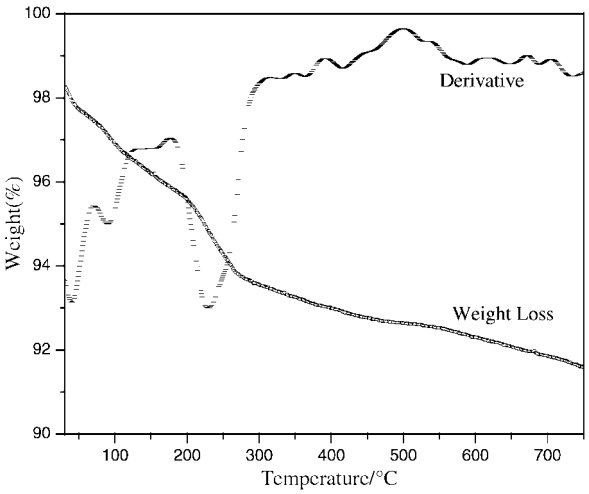

Fig. 3 TGA plot of %wt with increasing temperature and the corresponding derivative curve.

Formation of the mesostructured hollow spheres was sensitive to the stirring conditions, induction time, and time delays between the dilution and neutralisation steps of the synthesis procedure. For the conditions used, TEOS is only partially hydrolysed prior to dilution so droplets of the reactant form in the reaction mixture. These are probably stabilized to some extent by CTABr molecules that partition at the TEOS/water interface. Moreover, as the pH is lowered significantly on dilution and neutralisation, slow hydrolysis and condensation of TEOS at the droplet/water interface is curtailed so that mesostructured spherical shells only 20 nm in thickness are produced. One possibility is that the extremely dilute conditions of the synthesis promote the formation of hemispherical CTABr micelles on the surface of the TEOS droplet,[10] which also promotes the interfacial reactions. However, mesostructured nanoparticles are also formed in the reaction,[11] which indicates that the interfacial synthesis of the hollow microspheres and nucleation of colloidal particles in bulk solution are competitive processes, and explains why the preparation of the mesostructured shells is highly dependent on the reaction conditions.

We would like to thank the University of Bristol and EPSRC for financial support, and Dr C. G. Goeltner for scientific discussions.

Notes and references

‡ Hollow spheres of mesostructured silica were synthesised at room temperature by adding 3.78 g of TEOS to 45 ml of an alkaline solution (0.22 M NaOH) containing 0.049 M CTABr. 40 s after addition of the TEOS, the reaction mixture was poured into an excess of distilled water (300 ml) under slow stirring. The final molar ratio was: 0.12 C_{16}TMABr : 0.5 NaOH : 1.0 SiO_2 : 130 H_2O. When the pH had dropped to *ca*. 10 and the mixture began to appear cloudy (usually 220 s after the dilution step), the reaction was further quenched by the dropwise addition of 2 M HCl. The acid was added with stirring over a period of approximately 1 min until a final pH of 7.0 was attained. The stirring was then stopped and a layer of white product slowly formed at the air/water interface. This layer was recovered after leaving the suspension standing for approximately 2 h. The product was dried overnight under ambient conditions. The solid material was usually calcined by heating to a temperature of 540 °C at a rate of 1 °C min^{-1} although TGA data were recorded up to 800 °C.

1 S. Mann and G. A. Ozin, *Nature*, 1996, **382**, 313; T. J. Barton, L. M. Bull, W. G. Klemperer, D. A. Loy, B. McEnaney, M. Misono, P. A. Monson, G. Pez, G. W. Scherer, J. C. Vartuli and O. M. Yaghi, *Chem. Mater*., 1999, **11**, 2633; S. Mann, *Angew. Chem., Int. Ed*., 2000, **39**, 3392.
2 F. Caruso, *Adv. Mater*., 2001, **13**, 11; K. H. Rhodes, S. A. Davis, F. Caruso, B. J. Zhang and S. Mann, *Chem. Mater*., 2000, **12**, 2832.
3 O. D. Velev and E. W. Kaler, *Adv. Mater*., 2000, **12**, 531; H. Yan, C. F. Blanford, B. T. Holland, M. Parent, W. H. Smyrl and A. Stein, *Adv. Mater*., 1999, **11**, 1003; B. Lebeau, C. E. Fowler, S. Mann, C. Farcet, B. Charleux and C. Sanchez, *J. Mater. Chem*., 2000, **10**, 2105.
4 S. A. Davis, S. L. Burkett, N. H. Mendelson and S. Mann, *Nature*, 1997, **385**, 440; B. J. Zhang, S. A. Davis, N. H. Mendelson and S. Mann, *Chem. Commun*., 2000, 781.
5 J. A. Zasadzinski, E. Kisak and C. Evans, *Curr. Opin. Colloid Interface Sci*., 2001, **6**, 85.
6 S. S. Kim, W. Zhang and T. J. Pinnavaia, *Science*, 1998, **282**, 1302.
7 Y. Lu, H. Fan, A. Stump, T. L. Ward, T. Reiker and C. J. Brinker, *Nature*, 1999, **398**, 223.
8 H.-P. Lin, Y.-R. Cheng and C.-Y. Mou, *Chem. Mater*., 1998, **10**, 3772.
9 S. Schacht, Q. Huo, I. G. Voigt-Martin, G. D. Stucky and F. Schüth, *Science*, 1996, **273**, 768; W.-J. Kim and S.-M. Yang, *Chem. Mater*., 2000, **12**, 3227; P. J. Bruinsma, A. Y. Kim, J. Liu and S. Baskaran, *Chem. Mater*., 1997, **9**, 2507; D. Y. Zhao, P. D. Yang, Q. S. Huo, B. F. Chmelka and G. D. Stucky, *Curr. Opin. Colloid Interface Sci*., 1998, **3**, 111.
10 J. Lang, G. Mascolo, R. Zana and P. I. Luisi, *J. Phys. Chem*., 1990, **94**, 3069.
11 C. E. Fowler, D. Khushalani, B. Lebeau and S. Mann, *Adv. Mater*., 2001, **13**, 649.

CHEMCOMM
Communication
www.rsc.org/chemcomm

An enantio- and stereocontrolled synthesis of (−)-mycestericin E *via cinchona* alkaloid-catalyzed asymmetric Baylis–Hillman reaction†

Yoshiharu Iwabuchi, Mariko Furukawa, Tomoyuki Esumi and Susumi Hatakeyama*

Faculty of Pharmaceutical Sciences, Nagasaki University, Nagasaki 852-8521, Japan. E-mail: susumi@net.nagasaki-u.ac.jp

Received (in Cambridge, UK) 1st August 2001, Accepted 29th August 2001
First published as an Advance Article on the web 18th September 2001

A new enantiocontrolled synthesis of a potent immunosuppressant (−)-mycestericin E has been accomplished by using *cinchona* alkaloid-catalyzed asymmetric Baylis–Hillman reaction of an aldehyde with 1,1,1,3,3,3-hexafluoroisopropyl acrylate and Lewis acid-promoted cyclisation of an epoxytrichloroacetimidate as the key steps.

Recently, we have developed a catalytic asymmetric version of the Baylis–Hillman reaction using an amine catalyst derived from quinidine, which allows us to obtain highly enantiomerically enriched (*R*)-(α-methylene-β-hydroxy)esters.[1] In order to demonstrate the synthetic utility of our methodology, we envisaged its application towards a synthesis of (−)-mycestericin E (**1**), a potent immunosuppressive principle isolated from the culture broth of the fungus *Mycelia sterilia* ATCC 20349.[2] We report herein an enantio- and stereocontrolled synthesis[3] of (−)-mycestericin E (**1**) employing a new strategy which relies on the above-mentioned asymmetric Baylis–Hillman reaction for securing the key chiral framework and Lewis acid-promoted cyclisation of an epoxytrichloroacetimidate[4] for the stereoselective construction of the substituted serine structure with a quaternary centre.

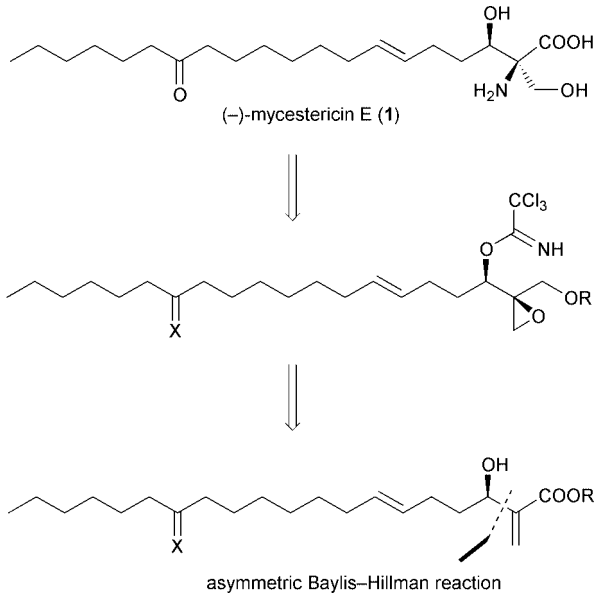

The required long chain aldehyde **6** was prepared from the dithiane **2**[5] in a straightforward manner in 62% overall yield (Scheme 1). Thus, sequential substitution of both terminals of 1,6-diiodohexane with **2** and 5-(*tert*-butyldimethylsilyloxy)-pent-1-yne *via* the lithio-species gave the alkyne **3**. Dethioketalisation with concomitant cleavage of the silyl ether protecting group, followed by ketalisation converted **3** to the dioxolane **5** *via* **4** in good yield. $LiAlH_4$-reduction of **5** in diglyme[6] at 130 °C allowed stereoselective formation of the *E*-olefinic double bond although Birch reduction was unsuccessful in this transformation. Swern oxidation of the reduced product generated the aldehyde **6** quantitatively.

The crucial Baylis–Hillman reaction of **6** thus obtained was investigated using 1,1,1,3,3,3-hexafluoroisopropyl acrylate and the amine catalyst **7** under various conditions according to the procedure we have developed.[1] As a result, we found that our method can be successfully applied to even long chain aldehydes such as **6**. Thus, upon reaction of **6** with 1,1,1,3,3,3-hexafluoroisopropyl acrylate in the presence of the amine catalyst **7** (0.2 equiv.) in DMF–CH_2Cl_2[7] (1 : 1), the (*R*)-ester **8**, $[\alpha]_D^{27}$ +6.9° (*c* 0.72, $CHCl_3$), was produced with excellent enantioselectivity (> 97% ee[8]) in 47% yield together with the dioxanone **9** (14% yield), $[\alpha]_D^{25}$ −2.7° (*c* 1.11, $CHCl_3$), 20% ee (Scheme 1). It is important to note that this reaction could be easily carried out on a multi-gram scale. Interestingly, compared with **8**, the dioxanone **9** again showed the lower optical integrity and the opposite chirality regarding the stereocenter generated in this reaction as we observed previously.[1]

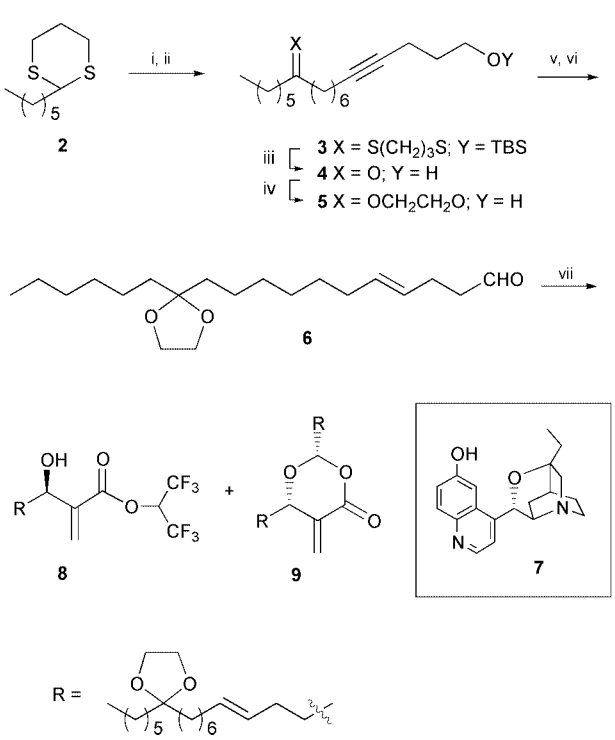

Scheme 1 *Reagents and conditions*: i, *n*-BuLi, THF, −30 °C, then 1,6-diiodohexane, 81%; ii, $LiCC(CH_2)_3OTBS$, THF–HMPA, −20 °C, 87%; iii, MeI, Na_2CO_3, THF–MeCN, sealed tube 70 °C, 91%; iv, ethylene glycol, cat. *p*-TsOH, benzene, 80 °C, 98%; v, $LiAlH_4$, diglyme, 130 °C, 87%; vi, DMSO, $(COCl)_2$, Et_3N, CH_2Cl_2, −78 °C to 0 °C, quant; vii, **7** (0.2 equiv.), 1,1,1,3,3,3-hexafluoroisopropyl acrylate (1.5 equiv.), DMF–CH_2Cl_2 (1 : 1), −55 °C, 24 h, 47% of **8**, 14% of **9**.

† Electronic supplementary information (ESI) available: experimental details. See http://www.rsc.org/suppdata/cc/b1/b106471c/

 DOI: 10.1039/b106471c

With the desired Baylis–Hillman product **8** in hand in almost enantiomerically pure form, we then investigated the construction of the serine structure possessing a quaternary centre. Prior to introduction of the epoxide scaffold, the hexafluoroisopropyl ester of **8** was converted to the methyl ester under methanolytic conditions to give the methyl ester **10**, $[\alpha]_D^{24}$ +9.0° (*c* 1.0, $CHCl_3$), in 95% yield (Scheme 2). Ti(O*i*-Pr)$_4$-mediated epoxidation[8] of **10** was found to proceed with complete diastereoselectivity to furnish the epoxy alcohol **11**, $[\alpha]_D^{17}$ +10.1° (*c* 1.0, $CHCl_3$), in 73% yield. Exposure of **11** to $NaBH_4$ in THF–MeOH allowed chemoselective reduction of the ester functionality to give the diol **12**, $[\alpha]_D^{21}$ +9.7° (*c* 0.95, MeOH), in 79% yield. The primary hydroxy group of **12** was then selectively protected as its *tert*-butyldiphenylsilyl ether to give **13**, $[\alpha]_D^{18}$ −2.6° (*c* 1.0, MeOH), in 95% yield. At this stage stereoselective introduction of a nitrogen atom at the quaternary centre was achieved by taking advantage of Lewis acid-promoted cyclisation of an epoxytrichloroacetimidate which we have previously developed.[4] Thus, the epoxy alcohol **13** was converted to the corresponding trichloroacetimidate **14**, $[\alpha]_D^{22}$ +7.3° (*c* 1.0, $CHCl_3$), in 81% yield by the reaction with trichloroacetonitrile in the presence of DBU. Upon treatment of **14** with 1.0 equiv. of $BF_3{\cdot}OEt_2$[10,11] in CH_2Cl_2 at −23 °C, the cyclisation took place selectively at the quatenary centre of the epoxide with complete inversion of the stereochemistry to produce the oxazolidine **15**, $[\alpha]_D^{23}$ −3.5° (*c* 1.0, $CHCl_3$), in 71% yield along with dihydrooxazine **16** (4% yield). Upon sequential Moffatt oxidation,[12] $NaClO_2$ oxidation,[13,14] and esterification, **15** gave the methyl ester **17**, $[\alpha]_D^{24}$ +26.6° (*c* 1.48, $CHCl_3$), in 55% yield. Treatment of **17** with 47% HF in acetonitrile at 60 °C brought about deprotection of the silyl ether and cyclic ketal protecting groups to give the trichloroacetamide **18** in 87% yield. Finally, saponification of **18**, followed by neutralisation using Amberlite IRC–76 furnished (−)-mycestericin E (**1**). The synthetic substance, mp 183–184 °C, $[\alpha]_D^{27}$ −8.3° (*c* 0.05, MeOH), exhibited spectral properties (^{1}H and ^{13}C NMR, IR, MS) in accord with those reported for natural mycestericin E,[2] mp 184–186 °C, $[\alpha]_D$ −8.6° (*c* 0.06, MeOH).

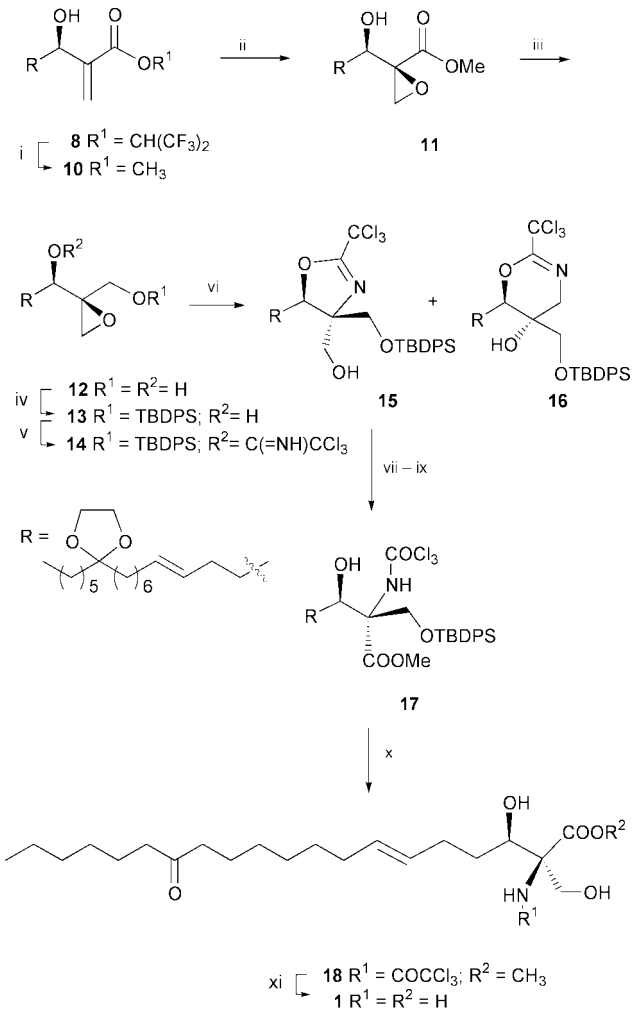

Scheme 2 *Reagents and conditions*: i, cat. NaOMe, MeOH, rt, then Dowex-50 H$^+$ form, 95%; ii, Ti(O*i*-Pr)$_4$, *t*-BuOOH, 4 Å molecular sieves, CH_2Cl_2, −20 °C, 73%; iii, $NaBH_4$, THF–MeOH (1:1), 0 °C, 79%; iv, TBDPSCl, DMAP, Et_3N, CH_2Cl_2, 0 °C, 95%; v, DBU, CCl_3CN, CH_2Cl_2, 0 °C, 81%; vi, $BF_3{\cdot}OEt_2$, CH_2Cl_2, −23 °C , 71% of **15**, 4% of **16**; vii, DMSO, DCC, TFA, pyridine, benzene, 0 °C; viii, $NaClO_2$, NaH_2PO_4, 2-methylbut-2-ene, *t*-BuOH–H_2O (4:1); ix, CH_2N_2, THF, 55% (3 steps); x, 47% HF, MeCN, 60 °C, 87%; xi, 10% NaOH, MeOH, 80 °C, 70%.

In conclusion, we have achieved an asymmetric synthesis of (−)-mycestericin E from the achiral aldehyde **6** in twelve steps in 4.7% overall yield. The present work illustrates a new methodology of general value for the synthesis of various immunosuppressive compounds related to **1**.

This study received financial support from Uehara Memorial Foundation and Japan Society for the Promotion of Science (Grant-in-Aid for Encouragement of Young Scientists).

Notes and references

1 Y. Iwabuchi, M. Nakatani, N. Yokoyama and S. Hatakeyama, *J. Am. Chem. Soc*., 1999, **121**, 10219.
2 S. Sasaki, R. Hashimoto, M. Kikuchi, K. Inoue, T. Ikumoto, R. Hirose, K. Chiba, Y. Hoshino, T. Okamoto and T. Fujita, *J. Antibiot*., 1994, **47**, 420; T. Fujita, N. Hamamichi, M. Kikuchi, T. Matsuzaki, Y. Kitao, K. Inoue, R. Hirose, M. Yoneta, S. Sasaki and K. Chiba, *J. Antibiot*., 1996, **49**, 846.
3 T. Fujita, N. Hamamichi, T. Matsuzaki, Y. Kitao, M. Kikuchi, M. Node and R. Hirose, *Tetrahedron Lett*., 1995, **36**, 8599.
4 S. Hatakeyama, H. Matsumoto, H. Fukuyama, Y. Mukugi and H. Irie, *J. Org. Chem*., 1997, **62**, 2275.
5 D. A. Evans, L. K. Truesdale, K. G. Grimm and S. L. Nesbitt, *J. Am. Chem. Soc*., 1977, **99**, 5009.
6 D. Samain and C. D. Desconis, *Synthesis*, 1978, 388.
7 CH_2Cl_2 was added as co-solvent because the less polar long-chain aldehyde **6** was not dissolved completely in DMF at the reaction temperature. Raising the reaction temperature above −40 °C resulted in decrease of the enantioselectivity although complete dissolution in DMF was obtained.
8 Optical purity was determined by HPLC analysis using a chiral column.
9 M. Bailey, I. E. Markó, D. Ollis and P. R. Rasmussen, *Tetrahedron Lett*., 1990, **31**, 4509; M. Bailey, I. Staton, P. R. Ashton, I. E. Markó and D. Ollis, *Tetrahedron: Asymmetry*, 1991, **2**, 495.
10 D.-G. Liu, B. Wang and G.-Q. Lin, *J. Org. Chem*., 2000, **65**, 9114.
11 Upon treatment of **14** with Et_2AlCl at −20 °C in CH_2Cl_2, a 3.3:1 mixture of **15** and **16** was obtained in 74% yield.
12 T. Nagamatsu, T. Sunazuka, H. Tanaka, S. Omura, P. A. Sprengler and A. B. Smith III, *J. Am. Chem. Soc*., 1996, **118**, 3584.
13 E. Delcanal and F. Montanari, *J. Org. Chem*., 1986, **51**, 567.
14 The oxazolidine ring was hydrolyzed to give the corresponding trichloroacetamide under $NaClO_2$ oxidation conditions.

CHEMCOMM Communication
www.rsc.org/chemcomm

Triblock copolymer assisted synthesis of periodic mesoporous organosilicas (PMOs) with large pores†

Olaf Muth,[a] Carsten Schellbach[a] and Michael Fröba*[b]

[a] *Institute of Inorganic and Applied Chemistry, University of Hamburg, Martin-Luther-King Platz 6, D-20146 Hamburg, Germany*

[b] *Institute of Inorganic and Analytical Chemistry, Justus-Liebig-University Giessen, Heinrich-Buff-Ring 58, D-35392 Giessen, Germany. E-mail: michael.froeba@anorg.chemie.uni-giessen.de*

Received (in Cambridge, UK) 23rd July 2001, Accepted 23rd August 2001
First published as an Advance Article on the web 18th September 2001

Periodic mesoporous organosilicas (PMOs) with unusually large pores and high BET surface areas have been synthesized using triblock PEO–PPO–PEO copolymer P123 as the structure-directing agent and 1,2-bis(trimethoxysilyl)ethane (BTME) as the organically bridged silica source.

In 1999, a new way was found to incorporate organic moieties into M41S silica materials.[1–6] For the first time bridged silsesquioxane[7] precursors, *e.g.* 1,2-bis(trimethoxysilyl)ethane, were used as a silica source in the synthesis of highly ordered hybrid mesoporous materials in order to integrate bridging organic groups directly into the framework of the pore walls instead of grafting these organic species onto the pore wall surface. The obvious advantages of these periodic mesoporous organosilicas (PMOs)[8] over porous sol–gel derived or grafted hybrid materials are that they are highly ordered structures with very uniform pores, have homogeneous distributions of functional groups throughout the whole framework, have high loadings and the absence of any strong pore blocking effects that could be generated by the organic moieties.

Despite the fact that many applications require materials with larger mesopores this approach has so far almost exclusively been restricted to the synthesis of PMOs with rather small pore sizes (diameter < 4 nm).[9–10] A very limited amount of work on large pores has been published to date.[11] We have now extended this method to the application of nonionic poly(alkylene oxide) triblock copolymer surfactants which have already been widely used in the synthesis of large pore M41S pure silica materials.[12–14] By employing the commercially available triblock copolymer P123 ($HO(CH_2CH_2O)_{20}(CH_2(CH_3)CH_2O)_{70}(CH_2CH_2O)_{20}H$) as the surfactant together with BTME (1,2-bis(trimethoxylsilyl)ethane, $(CH_3O)_3Si–CH_2–CH_2–Si(OCH_3)_3$) as the organically bridged silica source we have obtained materials with pores as large as 6.5 nm.

In a typical synthesis 574.8 mg (0.0991 mmol) of P123 were dissolved in 17.31 g (0.961 mol) of water and 3.45 ml (34.5 mmol) of conc. HCl. This solution was stirred at 308 K for 20 min before 800 mg (2.95 mmol) of BTME were added. The overall composition resulted in molar ratios of 0.5 : 0.0168 : 5.85 : 163 for BTME : P123 : HCl : H_2O. Precipitation of a white solid occurred almost immediately. In order to complete hydrolysis of the methoxy groups and to evaporate the methanol evolved the stirring mixture was kept at 308 K for 1 day. To achieve a high degree of condensation the mixture was then transferred into a Teflon-lined autoclave and heated to 358 K for an additional 24 h. After thorough washing with water the precipitate was dried overnight in air to yield a fine white powder. Removal of polymers was accomplished either by extraction in ethanol at room temperature for 10 h or at more elevated temperatures by using a Soxhlet apparatus for 17 h, each with subsequent filtration of the product and drying in air.

† Electronic supplementary information (ESI) available: TG/DTA/MS data. See http://www.rsc.org/suppdata/cc/b1/b106636f/

The powder X-ray diffraction pattern of the as-synthesized product shows one strong reflection at $2\theta = 0.81°$ corresponding to a *d*-value of 10.8 nm (Fig. 1) which is similar to those of pure silica materials synthesized with the same structure-directing agent.[12–14] Both extracted samples reveal almost the same figures and therefore highlight a significant solvothermal stability since the structural order of the product remains unchanged. Even during calcination of the as-synthesized product in a thermogravimetric experiment up to 1073 K under flowing air the mesostructure remains intact to a very high extent whereas a natural shrinkage of the structure of approximately 2.4 nm occurs corresponding to the total loss of the bridging organic moieties from inside the pore walls.

FTIR spectroscopy corroborates the latter result (Fig. 2). While the as-synthesized and the extracted samples clearly show absorption bands assigned to Si–C stretching vibrations (*) at 695 and 768 cm^{-1}, and to C–H deformation vibrations (+) at 1272 and 1412 cm^{-1}, these cannot be observed in the spectra of the calcined sample. Furthermore, absorption bands which could be assigned to the triblock copolymer (#) at 1345, 1376, 1459, 2907 and 2976 cm^{-1} can only be seen in the spectra of the as-synthesized sample indicating that the surfactant is almost completely removed by extraction. In order to elucidate the exact amount of surfactant remaining in the mesostructure, much more sensitive thermoanalytical coupled TG/DTA/MS measurements were carried out.[15] During a continuous heating process, 5 K min^{-1}, all samples showed an endothermic drying step (323–448 K) which was followed by the oxidation of the block copolymer and the bridging organic groups (448–1073 K).

We detected a substantial mass loss of 39.2% in the course of the latter process for the as-synthesized sample whereas mass losses of only 11.8 and 8% were observed for the room temperature and the Soxhlet extracted samples, respectively, Soxhlet extraction being thus the superior method of extraction.

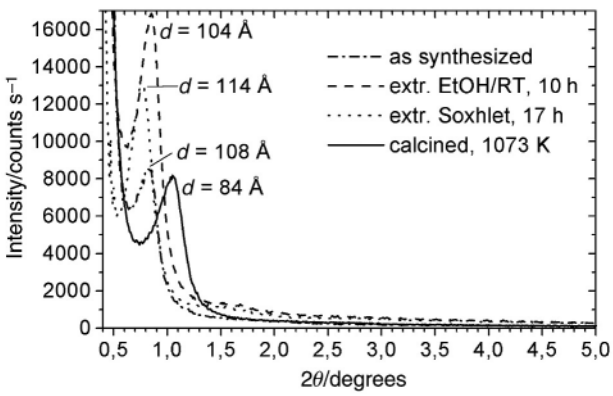

Fig. 1 Powder X-ray diffraction patterns‡ of products synthesized with 1,2-bis(trimethoxysilyl)ethane and triblock copolymer P123: as-synthesized, extracted RT/EtOH/10h, extracted Soxhlet/EtOH/17h, calcined (TG/DTA/MS, 1073 K).

 DOI: 10.1039/b106636f

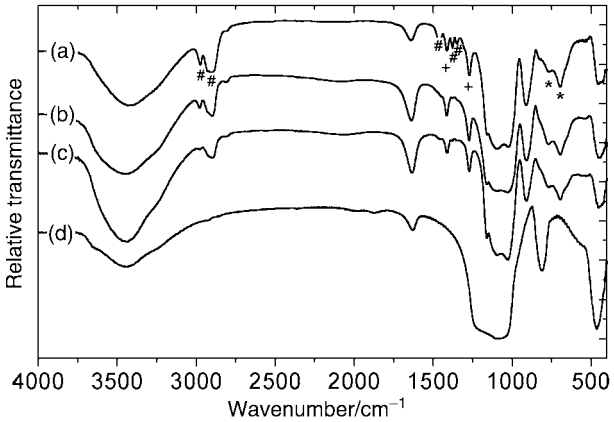

Fig. 2 FTIR spectra§ of products synthesized with 1,2-bis(trimethoxysilyl)-ethane and triblock copolymer P123: (a) as-synthesized, (b) extr. RT/EtOH/10h, (c) extr. Soxhlet/EtOH/17h, (d) calcined (TG/DTA/MS, 1073 K); (#) modes assigned to C–H stretching and deformation vibrations of P123, (+) modes assigned to C–H deformation vibrations of the framework organic groups, (*) modes assigned to Si–C stretching vibrations.

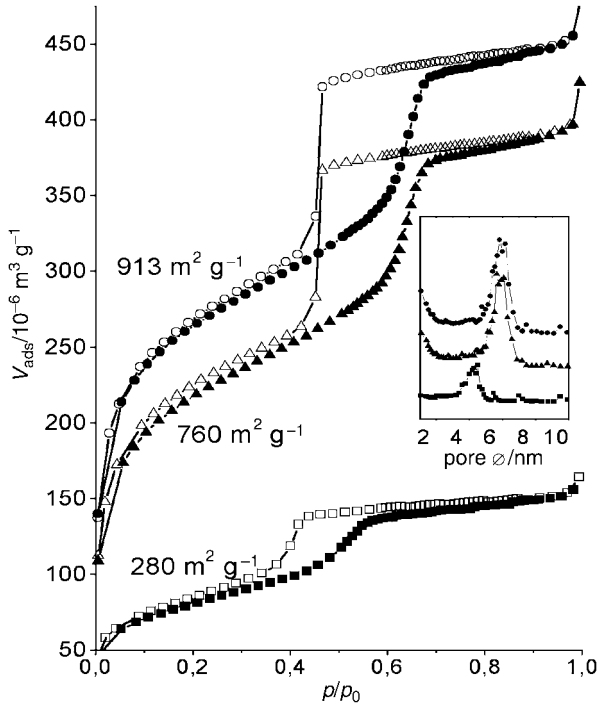

Fig. 3 N_2-physisorption isotherms¶ and BET surface areas of extracted and calcined products synthesized with 1,2-bis(trimethoxysilyl)ethane and triblock copolymer P123: (▲,△) RT/EtOH/10 h, (●,○) Soxhlet/EtOH/17 h, (■,□) calcined (TG/DTA/MS, 1073 K); the inset shows pore size distributions (BJH) calculated from the adsorption branch.

Unfortunately, prolonged extraction experiments always led to a strong reduction in structural order.

N_2-physisorption measurements at 77 K of the extracted samples show typical type IV isotherms of mesoporous materials with large pores where the capillary condensation step is shifted to high relative pressures $>0.6\ p/p_0$ (Fig. 3).

Also typical for these large pore solids is the observed large type I hysteresis. Since the course of the adsorption and desorption branches are not exactly parallel, flask-like pores or interparticle porosity must be considered to be existent in both samples. Again, Soxhlet extraction turns out to be the superior method of surfactant removal because the calculated BET surface area is *ca.* 150 m^2 g^{-1} higher for the Soxhlet extracted material (913 m^2 g^{-1}) than for the room temperature extracted sample (760 m^2 g^{-1}). Pore diameter distributions have been calculated from the adsorption branch using the Barrett–Joyner–Halenda method revealing average pore diameters of 6.5 nm for both extracted samples. A cell constant of 12.4 nm for the Soxhlet extracted sample, which could be derived from the first Bragg reflection of the powder diffraction pattern assuming a two-dimensional hexagonal pore structure, leads to a wall thickness of at least 5.9 nm. This high value is consistent in view of the applied nonionic structuring process which usually favours thick walls.

In conclusion, we have prepared the first PMO materials with pore diameters as large as 6.5 nm and BET surface areas greater than 900 m^2 g^{-1} using the nonionic poly(alkylene oxide) triblock copolymer surfactant P123 and 1,2-bis(trimethoxysilyl)ethane. In addition, we have shown that the structure-directing surfactant can be successfully removed to a very high extent by Soxhlet extraction using ethanol as solvent without loss of the mesostructure or the bridging ethane groups. In order to elucidate further the type of mesostructure, additional TEM, ^{13}C and ^{29}Si MAS-NMR investigations are currently in progress.

This work was supported by the Deutsche Forschungsgemeinschaft (DFG) and the Fonds der Chemischen Industrie (FCI). O. M. is grateful for receiving a postdoctoral scholarship from DFG within the European Graduate School 'Functional Materials'. Furthermore, the authors thank BASF for providing the block copolymer surfactants.

Notes and references

‡ Powder X-ray diffraction patterns were recorded at RT on a Bruker AXS D8 Advance diffractometer using filtered Cu-Kα radiation.
§ FTIR spectra were recorded at RT as KBr pellets with a Perkin-Elmer FT-IR 1720 spectrometer.
¶ N_2-physisorption isotherms were recorded with a Quantachrome Autosorb 1 at 77 K.

1 S. Inagaki, S. Guan, Y. Fukushima, T. Ohsuna and O. Terasaki, *J. Am. Chem. Soc.*, 1999, **121**, 9611.
2 B. J. Melde, B. T. Holland, C. F. Blanford and A. Stein, *Chem. Mater.*, 1999, **11**, 3302.
3 T. Asefa, M. J. MacLachlan, N. Coombs and G. A. Ozin, *Nature*, 1999, **402**, 867.
4 C. Yoshina-Ishii, T. Asefa, N. Coombs, M. J. MacLachlan and G. A. Ozin, *Chem. Commun.*, 1999, 2539.
5 A. Sayari, S. Hamoudi, Y. Yang, I. L. Moudrakovski and J. R. Ripmeester, *Chem. Mater.*, 2000, **12**, 3857.
6 S. Guan, S. Inagaki, T. Ohsuna and O. Terasaki, *J. Am. Chem. Soc.*, 2000, **122**, 5660.
7 R. J. P. Corriu, *Eur. J. Inorg. Chem.*, 2001, 1109.
8 T. Asefa, C. Yoshina-Ishii, M. J. MacLachlan and G. A. Ozin, *J. Mater. Chem.*, 2000, **10**, 1751.
9 T. Asefa, M. J. MacLachlan, H. Grondey, N. Coombs and G. A. Ozin, *Angew. Chem.*, 2000, **112**, 1878.
10 S. Guan, S. Inagaki, T. Ohsuna and O. Terasaki, *Microporous Mesoporous Mater.*, 2001, **44–45**, 165.
11 Y. Lu, H. Fan, N. Doke, D. A. Loy, R. A. Assink, D. A. LaVan and C. J. Brinker, *J. Am. Chem. Soc.*, 2000, **122**, 5258.
12 D. Zhao, J. Feng, Q. Huo, N. Melosh, G. H. Frederickson, B. F. Chmelka and G. D. Stucky, *Science*, 1998, **279**, 548.
13 D. Zhao, Q. Huo, J. Feng, B. F. Chmelka and G. D. Stucky, *J. Am. Chem. Soc.*, 1998, **120**, 6024.
14 C. G. Göltner, S. Henke, M. C. Weißenberger and M. Antonietti, *Angew. Chem.*, 1998, **110**, 633.
15 TG/DTA/MS measurement data can be downloaded from the ESI†.

Typeset and printed by Black Bear Press Limited, Cambridge, England

CHEMCOMM
Feature Article
www.rsc.org/chemcomm

Nanoparticles as structural and functional units in surface-confined architectures

Andrew N. Shipway and Itamar Willner*

Institute of Chemistry, The Hebrew University of Jerusalem, Jerusalem 91904, Israel. E-mail: willnea@vms.huji.ac.il

Received (in Cambridge, UK) 12th June 2001, Accepted 22nd August 2001
First published as an Advance Article on the web 1st October 2001

The nanoscale engineering of functional chemical assemblies has attracted recent research effort to provide dense information storage, miniaturized sensors, efficient energy conversion, light-harvesting, and mechanical motion. Functional nanoparticles exhibiting unique photonic, electronic and catalytic properties provide invaluable building blocks for such nanoengineered architectures. Metal nanoparticle arrays crosslinked by molecular receptor units on electrodes act as selective sensing interfaces with controlled porosity and tunable sensitivity. Photosensitizer/electron-acceptor bridged arrays of Au-nanoparticles on conductive supports act as photoelectrochemically active electrodes. Semiconductor nanoparticle composites on surfaces act as efficient light collecting systems, and nanoengineered semiconductor 'core–shell' nanocrystal assemblies reveal enhanced photoelectrochemical performance due to effective charge separation. Layered metal and semiconductor nanoparticle arrays crosslinked by nucleic acids find applications in the optical, electronic and photoelectrochemical detection of DNA. Metal and semiconductor nanoparticles assembled on DNA templates may be used to generate complex electronic circuitry. Nanoparticles incorporated in hydrogel matrices yield new composite materials with novel magnetic, optical and electronic properties.

Introduction

Increasing interest is directed to miniaturization and the nanoscale engineering of functional chemical assemblies.[1] The development of nanoscale devices will provide dense information storage, ultra-small sensing units, and data processing elements of reduced dimensions. Another important aspect of miniaturization to the nanoscale is the breakdown of macroscopic properties and the emergence of quantum-level phenomena.[2] Metal and semiconductor nanoparticles exhibit unique properties and provide important building blocks for the construction of functional structures.[3] Nanoparticles can be synthesized from a variety of materials with controllable sizes, shapes and morphologies.[4] The electronic properties of nanoparticles, which may be tuned by the particle dimensions, give rise to unique absorbance and emission features.[5] The confined electrons in nanoparticles smaller than the wavelength of light give rise to plasmon excitons.[6] Nanoparticles also offer catalytic properties that differ from the bulk material properties, due to their high surface-area, high edge concentration and unusual electronic properties.[7] This has led to the application of modified nanoparticles in enantioselective catalysis[8] and electrocatalysis on surfaces.[9]

The surface modification of nanoparticles by functional monolayers or polymer 'shells', provides a means to generate composite materials with tunable surface properties (*e.g.* wettability, hydrophobicity, polymerizable units, photosensitive sites or molecular recognition properties).[10] In addition, the surface functionalization of nanoparticles allows their covalent attachment, self-assembly and organization on surfaces.[11] The engineering of nanoparticle surfaces has led to the construction of nanoparticle dimers and trimers,[12,13] controlled aggregates,[14,15] wires[16] ordered monolayers[17] and multilayers.[18] The integration of functional nanoparticles with surfaces has enabled the organization of nanoscale devices[19] including single-electron devices.[20] In this account we focus on the use of modified nanoparticles as structural or functional units in the assembly of composite structures on surfaces. We address the use of the nanoengineered architectures as high surface-area conductive matrices, as optical indicators, and as semiconductor composites for photoelectrochemical functions. We discuss the use of surface-confined architectures for sensoric and photoelectrochemical applications and focus on the tailoring of composite materials with novel electronic properties. We also introduce the conjugation of nucleic acids with nanoparticles for the development of DNA sensors and complex electronic circuits.

Nanoparticle multilayers in sensing applications

The use of metal nanoparticles as conductive elements in electrochemical sensing interfaces has been approached in several different ways. One direction involves the use of gold nanoparticles to contact biocatalysts either by the fabrication of nanoparticle–enzyme conjugates[21] or by the sequential immobilization of the nanoparticles and the biomaterial.[22] The small size of the nanoparticles not only gives a conductive matrix, but also enables them to approach the redox sites of some enzymes closely enough to provide electrical communication between the enzyme redox-center and the electrode, without the need for a diffusional electron mediator. The conductivity of metal nanoparticles also allows their use as gas sensors. Thin films of gold nanoparticles held apart by long chain thiols demonstrate a conductivity that is strongly dependant on gas vapors.[23] The vapors are absorbed by the nanoparticle–thiol matrix, modulating the conductivity of the film (as is also the case in carbon black–polymer composites[24]).

A series of sensors has been developed using Au-nanoparticle multilayers crosslinked by molecular host components. Scheme 1 outlines the general method for the construction of the multilayer Au-nanoparticle structures. First, a conductive glass support is functionalized with a thin film of 3-(aminopropyl)siloxane to yield a positively charged interface. The electrostatic binding of the negatively charged citrate-stabilized Au-nanoparticles (12 ± 1 nm diameter) yields the first layer of Au-nanoparticles.[25] Treatment of the negatively charged interface with the tetracationic cyclophanes cyclobis(paraquat-*p*-phenylene) **1**[26] or cyclobis(paraquat-*p*-biphenylene) **2**,[27] the bipyridinium salts **3** or **4**, or the octacationic Pd(II)-macrocycle **5**,[28] results in the electrostatic association of the molecular host

components. Further interaction of the assembly with the citrate-capped Au-nanoparticles yields the second layer of nanoparticles, and by the alternating treatment of the system with the oligocationic molecular crosslinker and the nanoparticles, an architecture of the desired thickness may be constructed. The crosslinking units need not necessarily be molecules. Analogous results have been obtained using charged polymers,[29] other nanoparticles[30] and even biomaterials.[31] Similarly, covalently linked multilayers can be constructed using gold-binding bisthiol molecules as crosslinkers.[32]

Fig. 1 shows the characterization of 1–5 layers of gold nanoparticles crosslinked by the tetracationic cyclophane cyclobis(paraquat-*p*-phenylene) **1**. The absorbance spectra [Fig. 1(A)] show the characteristic plasmon absorbance of the gold nanoparticles at *ca*. 520 nm,[33] and as more layers are added, an additional absorbance appears at longer wavelengths as a

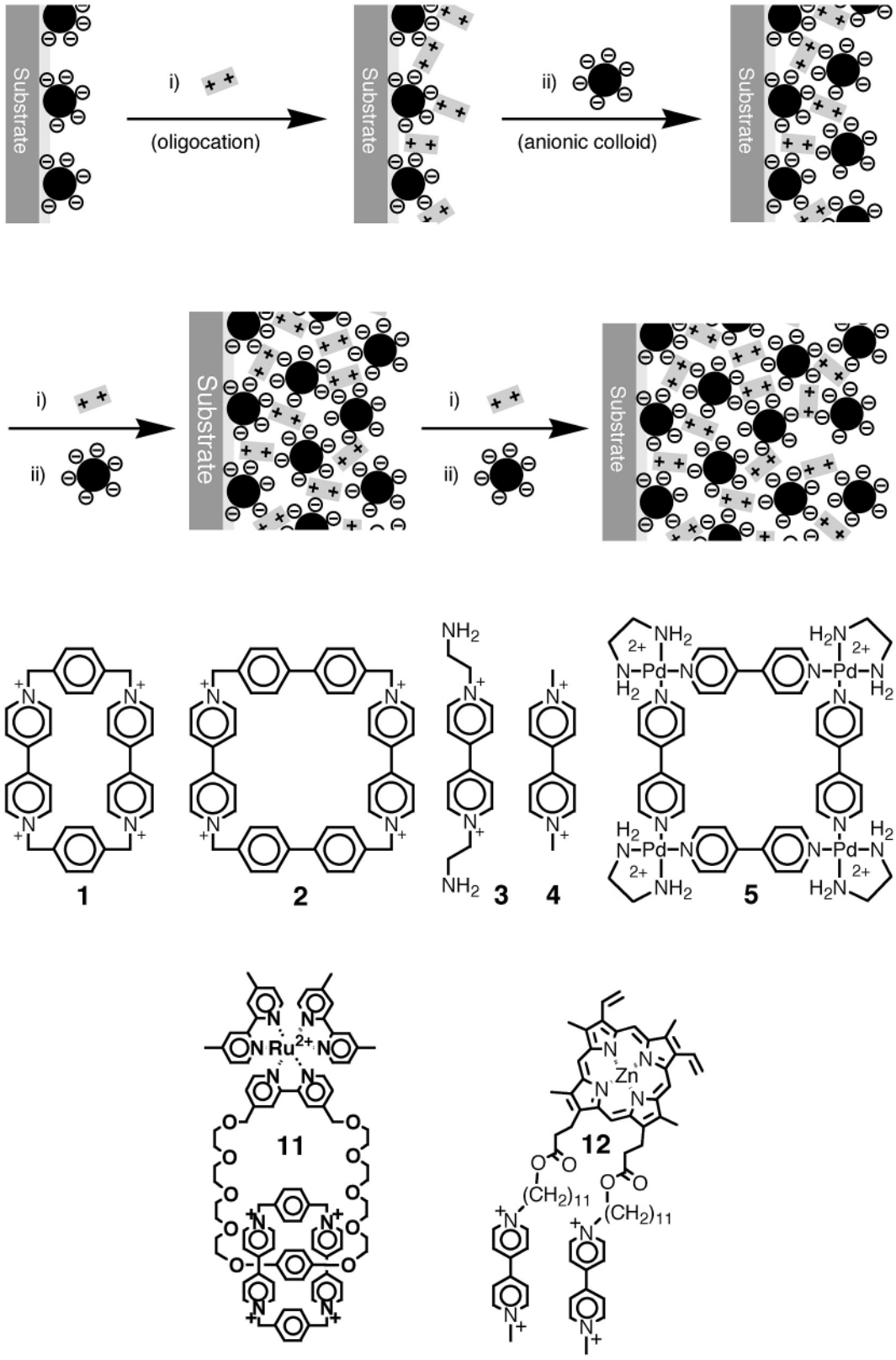

Scheme 1 Method for the construction of oligocation-crosslinked Au-nanoparticle multilayers by electrostatic interactions. The first nanoparticle layer is formed by the interaction of a nanoparticle solution with an amine-functionalized surface.

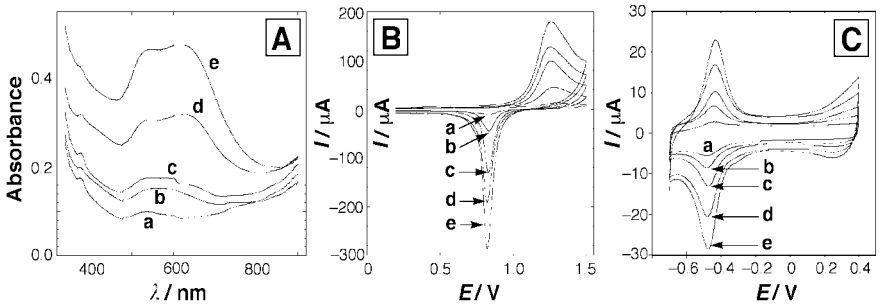

Fig. 1 (A) Absorbance spectra of a glass slide after (a–e) the deposition of 1–5 **1**-crosslinked Au-nanoparticle treatments. (B) Cyclic voltammograms of the Au-surface of **1**-crosslinked assemblies containing (a–e) 1–5 layers of Au-nanoparticles. (C) Cyclic voltammograms of **1** in (a–e) 1–5 layer arrays of **1**-crosslinked Au-nanoparticles.

consequence of interparticle plasmon coupling.[34] Electrochemical analysis of the gold surface [Fig. 1(B)] and the cyclophane crosslinking units [Fig. 1(C)] demonstrate the almost linear buildup of the structure on the conductive support. The fact that the nanoparticles and crosslinker continue to be electrochemically active throughout the crosslinked structure, demonstrates that the array is both porous and conductive. Coulometric assay of the electrical responses of the Au-nanoparticles and the bipyridinium units, indicates that the average surface coverage of the Au-nanoparticles per layer is *ca.* 1×10^{13} particles cm^{-2} and that *ca.* 100 units of **1** are associated with each Au-nanoparticle in the 3D structure.

The crosslinker **1** acts as a π-acceptor and is capable of forming π donor–acceptor complexes.[35] Thus, the association of electroactive π-donor substrates to the π-acceptor receptor sites, together with the 3D conductivity of the nanoparticle architecture, enables electrochemical sensing of the substrates. The cavity of **1** is suited to bind *p*-hydroquinone **6** and other hydroquinone derivatives such as dihydroxyphenylacetic acid **7**, dopamine **8** and adrenaline **9**. All of these substrates can be electrochemically sensed by the **1**-crosslinked Au-nanoparticle architectures assembled on the conductive glass supports.[36] The sensitivity of the functionalized electrodes is controlled by the number of nanoparticle layers in the structures.

Fig. 2(A) shows the electrochemical analysis of *p*-hydroquinone **6** by a 5-layer **1**-crosslinked Au-nanoparticle-functionalized electrode. The sensitivity limit for the sensing of **6** was estimated to be 1 μM. The substrate could not be electrochemically detected in this concentration range by a 5-layer Au-nanoparticle architecture crosslinked by the dicationic *N,N′*-dimethyl-4,4′-bipyridinium unit **3**. These results clearly indicate that the electrochemical sensing of **6** does not originate from the increase in the surface roughness of the electrode, but rather from the concentration of **6** in the receptor sites by supramolecular interactions. Fig. 2(B) exemplifies the electrochemical detection of adrenaline **9** by the **1**-crosslinked Au-nanoparticle array. The electrochemical oxidation of **9** associated with the receptor-sites reveals a broad irreversible wave that leads to a cyclic product that exhibits a reversible-redox response (wave x). The latter wave may act as an indicator for the concentration of adrenaline in the system [Fig. 2(B) inset].

The specificity of sensing by the Au-nanoparticle array is controlled by changing the structure of the crosslinking receptor units.[37] A three-dimensional array of Au-nanoparticles was constructed using the enlarged cyclophane, cyclobis(paraquat-*p*-biphenylene) **2**, Scheme 1. This larger receptor accommodates bishydroxymethylferrocene **10** as a guest. Fig. 3(A) shows the analysis of **10** (1×10^{-6} M) by the **2**-crosslinked Au-nanoparticle electrodes with different numbers of crosslinked Au-nanoparticle layers. As the number of layers increases, the electrical response of **10** is enhanced, demonstrating tunable sensitivity of the nanostructured layered electrode. Fig. 3(B) shows the amperometric responses of the Au-nanoparticle array upon the sensing of different concentrations of **10**. The resulting receptor-crosslinked arrays also reveal selectivity. While **10** is electrochemically sensed by a **2**-crosslinked Au-nanoparticle structure, the receptor **2** is too large to accommodate *p*-hydroquinone **6** in its cavity. Similarly, the **1**-crosslinked Au-nanoparticle assembly is unable to accommodate **10**, but does associate with *p*-hydroquinone, which is electrochemically sensed [Fig. 3(C)]. Selectivity is also observed upon the sensing of *p*-hydroquinone **6** by the Pd(II)-square, **5**-crosslinked Au-nanoparticle structure that is unable to detect the isomer *o*-hydroquinone. The selective sensing of **6** by the oligocationic

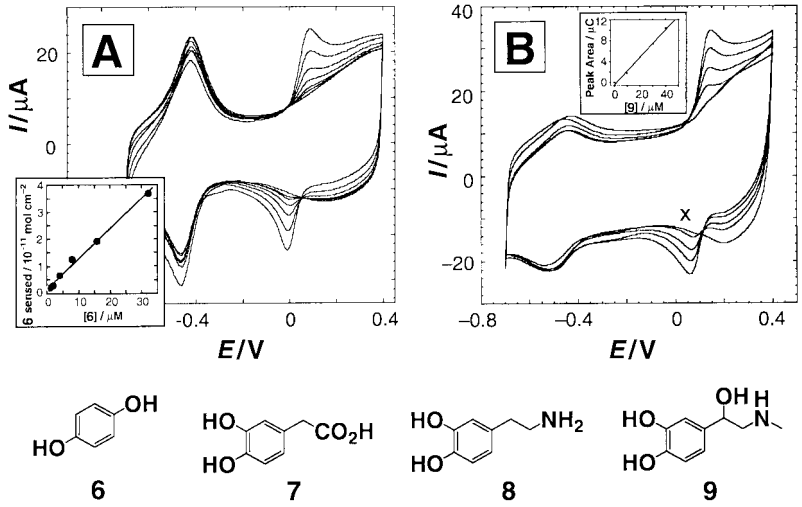

Fig. 2 (A) Cyclic voltammograms for the sensing of hydroquinone **6** (1–30 μM) by a 5-layer **1**-crosslinked Au-nanoparticle array. Inset: calibration curve for the sensing of **6**. (B) The sensing of adrenaline **9** (1–40 μM) by the array. [Wave (x) corresponds to the redox response of an electrocyclized product originating from the oxidized **9**] Inset: calibration curve for the sensing of **9**.

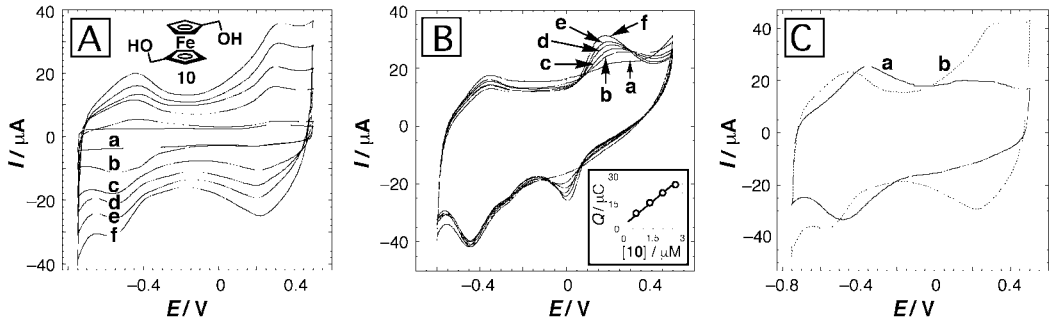

Fig. 3 (A) Cyclic voltammograms for the sensing of **10** (1 μM) with (a–f) 0–5 layers of **2**-crosslinked Au-nanoparticles. (B) The sensing of **10** (a–f = 0.1, 0.2, 0.4, 0.8, 1.5 and 3.0 μM, respectively) by a 5-layer **2**-crosslinked Au-nanoparticle array. (C) Cyclic voltammograms of 5-layer electrodes constructed using cyclophanes **1** (curve a) and **2** (curve b) as crosslinkers in the presence of **10** (1 μM).

macrocycle was attributed to the diagonal association of **6** to the Pd(II)-receptor, that is not possible for the *ortho* isomer.[38]

Receptor-modified Au-nanoparticles were also assembled on the gate interface of an ion-sensitive field-effect-transistor (ISFET).[39] A **1**-functionalized Au-nanoparticle ISFET device was found to effectively detect adrenaline, serotonin and dopamine. Since the ISFET gate-potential is controlled by the charge associated with the interface, the detection of receptor-bound substrates is not limited to electroactive species.

Nanoparticle multilayers in photoelectrochemical applications

The high surface-area, porous and conductive properties of Au-nanoparticle arrays can be exploited for the construction of photoelectrochemically active superstructures. Fig. 4(A) and (B) show absorbance spectra and cyclic voltammograms of a

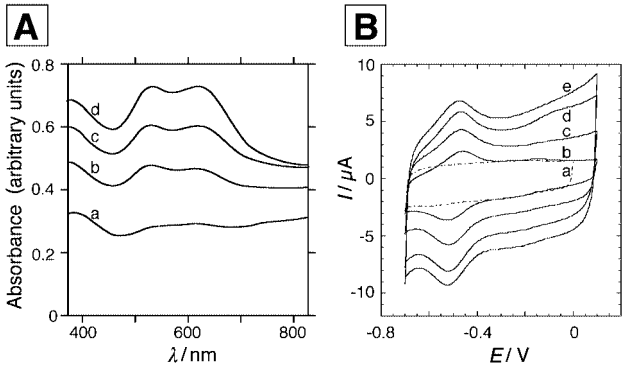

Fig. 4 (A) Absorbance spectra of (a–d) 1–4 layer Au-nanoparticle superstructures crosslinked by the catenane **11**. (B) Cyclic voltammograms of (a) a single nanoparticle layer, and (b–e) 1, 3, 4 and 5-layer **11**-crosslinked Au-nanoparticle arrays.

gold nanoparticle multilayer architecture 'crosslinked' by the hexacationic catenane **11**.[40] This catenane consists of non-covalently bound ruthenium tris(bipyridine) (photosensitizer) and bipyridinium (electron acceptor) groups.[41] The absorbance spectra show similar features to those of other molecule-crosslinked gold nanoparticle arrays, as well as an additional absorbance at 425 nm that is attributed to the ruthenium tris(bipyridinium) chromophore. Coulometric assay of the cyclic voltammograms corresponding to the bipyridinium crosslinking units reveals an almost linear increase in the surface coverage of the crosslinking units upon the build-up of the layers. The derived surface coverage of **11** per layer is 3.6×10^{-12} mol cm^{-2} and it has been estimated that on average *ca.* 45 units of the photosensitizer/acceptor crosslinker are associated with each Au-nanoparticle. Irradiation of the **11**-crosslinked Au-nanoparticle multilayer array results in the photocurrent action spectra shown in Fig. 5(A), which follows the absorbance features of the Ru(II)–tris(bipyridinium) chromophore. The photocurrent increases upon the build-up of the array and is reversibly cycled between 'ON' and 'OFF' states upon switching the light on and off, respectively. Fig. 5(B) shows the dependence of the photocurrent intensity on an applied potential. The photocurrent decreases as the potential is negatively shifted and it is blocked at a potential where the bipyridinium units are reduced to the radical cation. This observation led to the conclusion that the photocurrent originates from the primary electron transfer quenching of the excited Ru(II)–tris(bipyridine) chromophore by the bipyridinium electron acceptor. The reduced acceptor acts as an electron mediator for charge injection into the electrode, Fig. 5(C). Upon the electrochemical reduction of the bipyridinium units, intramolecular electron transfer quenching is inhibited and photocurrent generation is blocked. The nanoengineered electrode operated at a quantum efficiency of 1×10^{-4} in the generation of the photocurrent. A related nanoparticle engineered electrode for photocurrent generation using Zn(II)-protoporphyrin IX–bis(bipyridinium) photosensitizer–electron acceptor (**12**) as a crosslinker has also been developed.[42]

Photoelectrochemical electrodes based on semiconductor nanoparticles offer many advantages in the organization of

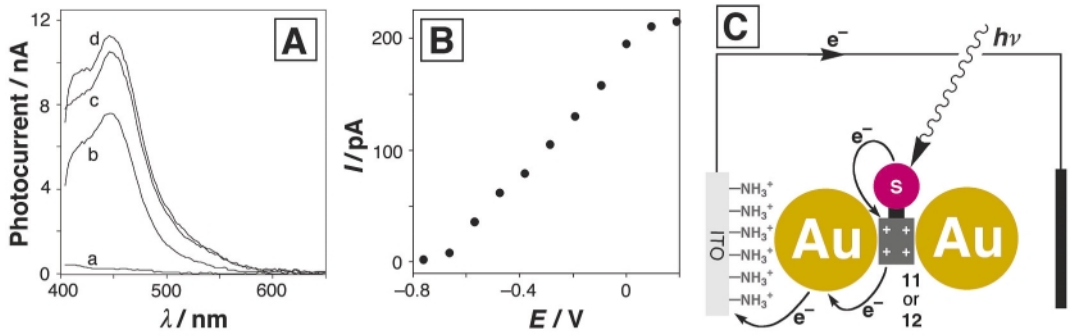

Fig. 5 (A) Photocurrent action spectra (a–d) obtained from 0-, 1-, 3- and 4-layer **11**-crosslinked Au-nanoparticle arrays. (B) Dependance of the photocurrent on the electrode potential. (C) Mechanism for the generation of a photocurrent from a photosensitizer(s)–bipyridinium dyad-crosslinked Au-nanoparticle superstructure.

energy conversion and storage cells. The ability to process, engineer and chemically functionalize semiconductor nanoparticles, enables the control of the properties and functions of the resulting photoelectrochemical cells. The use of nanoparticle-functionalized electrodes for photoelectrochemical applications has been reviewed in depth,[43] and the development and commercialization of solar cells based on photosensitizer/TiO_2 nanoparticle structures[44] represent recent advances in the field. Also, a large number of diverse nanoparticle-based electroluminescent devices have been investigated.[45] The tuning of the band-gap energies and redox properties of the energy levels by controlling the nanoparticle dimensions allows the tailoring of multicomponent systems that reveal new functionalities as a result of interparticle electronic coupling, and interparticle electron or energy transfer.[46] One example of such a system would be a nanoparticle-based 'luminescent collector'.[47] This is a device consisting of a thin sheet of material doped with dyes that absorb ambient light and re-emit it within the material where it is trapped by internal reflection. In order to collect a high proportion of the incident radiation, several chromophores with complementary absorption bands are required. Previous designs have led to problems of finding sets of organic dyes with this complementarity as well as the necessary processing and stability properties,[48] but nanoparticles may offer a feasible alternative.

Interparticle energy transfer between nanoparticles of the same substance but of different sizes exemplifies how multiparticle systems might find applications. It has been shown that both for indium phosphide[49] and cadmium selenide[50] nanoparticles, energy transfer from smaller to larger particles takes place within composite films. Fig. 6 shows absorbance and emission spectra of a 4 : 1 mixture of 2.8 and 3.7 nm-diameter CdSe nanoparticles that were prepared in highly monodisperse samples by selective precipitation. In a dilute solution (curve a), the emissions of both nanoparticles are seen, but in a close-packed film (curve b), energy transfer takes place and emission only from the larger particles is observed.

Extensive recent research effort has been directed towards the assembly of composite nanocrystalline semiconductor films to enhance the activity of photoelectrochemical cells. The coupling of a large bandgap semiconductor with a smaller bandgap semiconductor not only extends the photoresponse of the system to longer wavelengths but also facilitates charge separation. The photogenerated electrons and holes are trapped

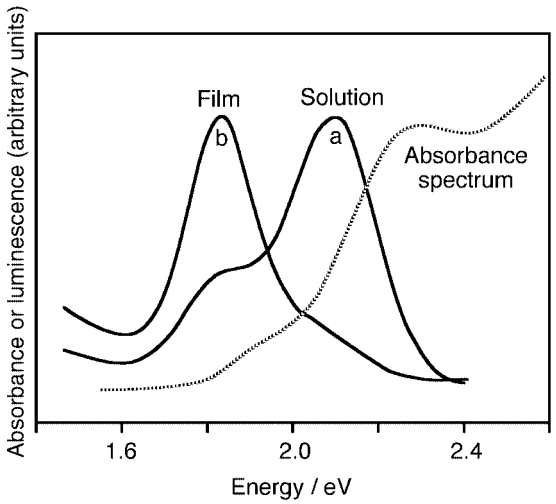

Fig. 6 Absorbance (----) and emission spectra of a 4 : 1 mixture of 2.8 nm and 3.7 nm InP 'quantum dots' (a) in solution, and (b) in a close-packed film.

into different particles, and the interparticle interface acts as a barrier for the recombination of the intermediate redox species. Fig. 7(A) shows the energetics of a SnO_2/CdSe nanocrystalline film assembled on an OTE electrode.[51] This photoelectrochemical electrode was found to operate at an efficiency of 2.25% ($I_{sc} \approx 30$ μA cm^{-2}; V_{oc} = 0.5–0.6 V; ff = 0.47), higher than for nanocrystalline CdS alone. The enhanced photoelectrochemical activity of the composite film is attributed to the charge rectification resulting from interparticle electron transfer. The role of coupled systems in enhancing charge separation has been demonstrated in other systems such as ZnO/CdS[52] and TiO_2/CdS.[53] Photosensitization of nanocrystalline composites results in charge rectification and facilitates the collection of the injected electrons by the electrode. Fig. 7(B) shows a 'core–shell' nanocomposite of TiO_2 coated with Nb_2O_5. Photoejection of electrons from an excited dye [*cis*-di(isothiocyanato)-*N*-bis(4,4′-dicarboxy-2,2-bipyridine)ruthenium(II)] to the Nb_2O_5 conduction-band followed by electron transfer to the TiO_2 conduction band results in the rectification effect. The recombination of the 'core' conduction-band electrons with the oxidized dye are retarded by means of the Nb_2O_5 'shell'.[54] This charge separation improves the photo-

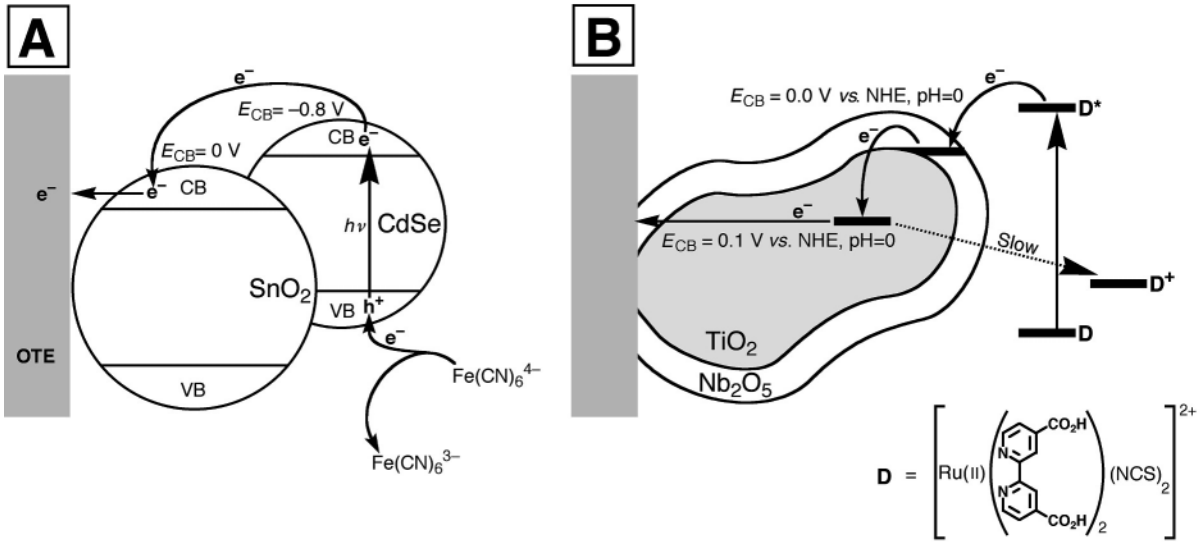

Fig. 7 (A) Suppression of charge recombination in a coupled SnO_2/CdSe system. (B) Charge separation upon photosensitization of a TiO_2/Nb_2O_5 core–shell semiconductor nanocomposite electrode.

electrochemical performance of the cell as compared to the TiO_2/dye system (maximum power of the TiO_2/Nb_2O_5/dye cell is 4.70 mW cm^{-2} as compared to 3.45 mW cm^{-2} for the TiO_2/dye cell). Similar results have been observed for other photosensitized nanocrystalline systems.[55]

DNA-linked nanoparticle superstructures

The study of DNA–nanoparticle conjugates has received special attention in the past few years. DNA is of particular interest since it may be made into complex, highly designed structures.[56] The use of DNA–nucleic acid-complementary binding, along with enzymes that act specifically on DNA (*e.g.* polymerase, ligase, endonuclease for polymerization, lengthening and scission, respectively) make it a useful structural tool. The dimensions and properties of DNA are well known and may be exploited, for instance for the fabrication of conductive wires.[57] In solution, interactions between DNA-functionalized-nanoparticles and DNA-crosslinked nucleic-acid-functionalized nanoparticles have been used for the detection of DNA,[58] and more recently they have allowed the construction of nanoparticle architectures on surfaces.[59] Scheme 2 shows a general method to fabricate a crosslinked multilayer of nanoparticle–DNA composites. First, an appropriate surface (gold or functionalized glass) is reacted with a thiolated oligonucleotide (**13**). This immobilized DNA can hybridize with part of an analyte nucleic acid (**14**) that is complementary with it. The remaining part of the analyte oligonucleotide can then be used to immobilize a nanoparticle that bears an oligonucleotide complementary to it (**15**). The growth may be continued either by reacting with the analyte then a nanoparticle functionalized by **13** [Scheme 2(A)], or by reacting with both at the same time [Scheme 2(B)]. This second layer contains many more nanoparticles since the first immobilized nanoparticles constitute 'branching points'. This 'amplification' allows the microgravimetric sensing of the analyte–DNA at concentrations of 1×10^{-10} M using a quartz-crystal-microbalance as transducer.[59a] If the analyte DNA has a sequence that is not properly complementary to both the surface and the nano-

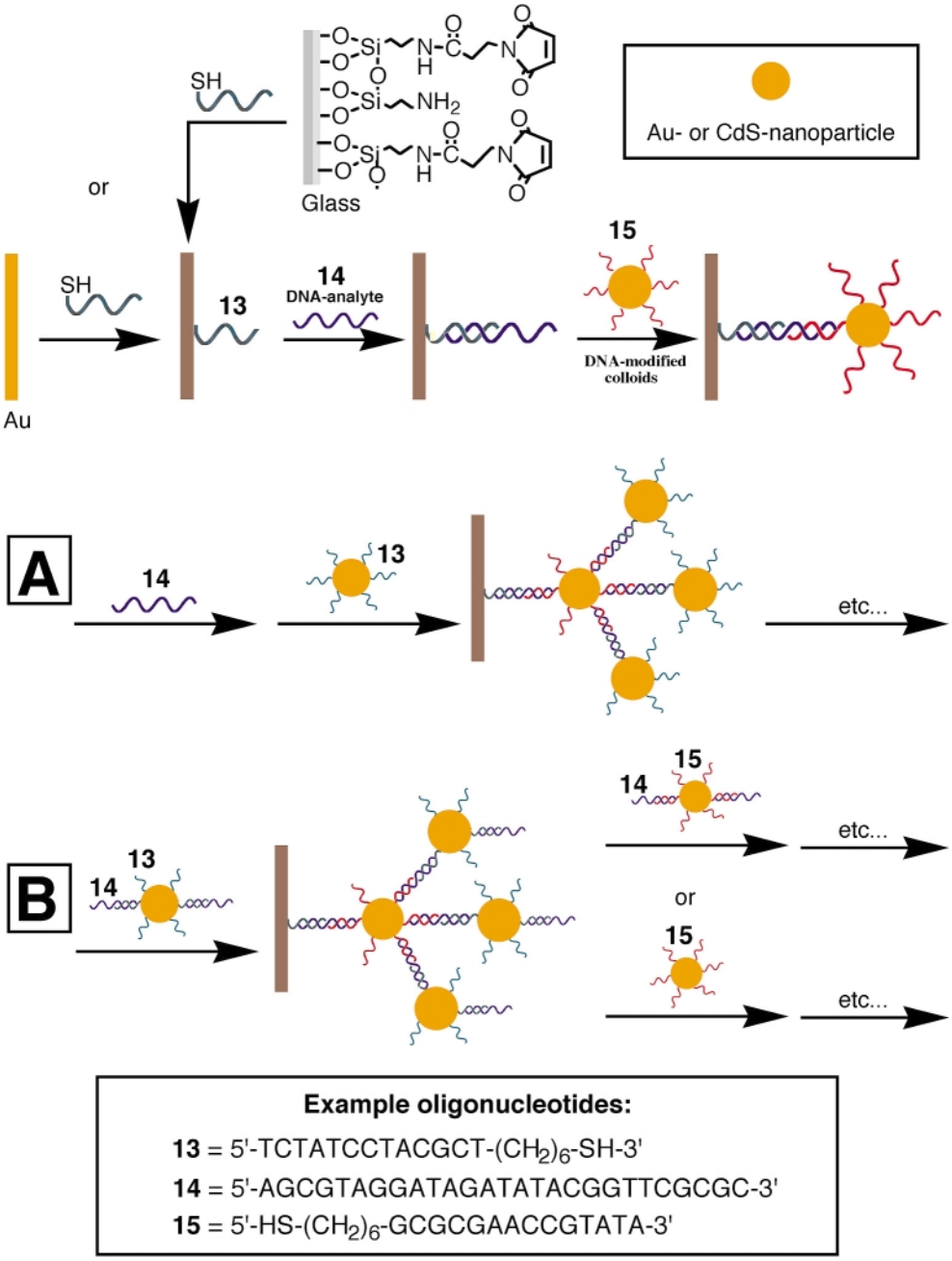

Scheme 2 Method for the construction of DNA-crosslinked metal or semiconductor nanoparticle arrays for the sensing of a DNA analyte, on gold or glass substrates. (A) Continued stepwise growth. (B) Growth with pre-hybridized nanoparticles and analyte.

particle, then the structure is not built up, and no response is measured. Fig. 8 shows results from a similar experiment, where several nanoparticle layers were constructed, and the concentration of the nucleic-acid functionalized nanoparticles and analyte DNA are sufficiently high to generate saturated Au-nanoparticle layers.[59b] Fig. 8(A) shows the absorbance spectra recorded for 1–5 nanoparticle layers. It is seen that non-linear growth only occurs for the first two layers, after which the surface is saturated with nanoparticles and a full layer is added at each step. It is also noteworthy that no additional absorbance above 600 nm appears, which indicates that the nanoparticles are not close enough to develop interparticle coupled plasmons. Finally, as the film becomes thicker, the melt transition for the DNA complex becomes sharper [Fig. 8(B)]. This observation is indicative of the cooperative effect of the nanoparticle network holding the entire assembly together.

Another way to transduce the build-up of these nanoparticle–DNA arrays is to employ functional nanoparticles. The use of cadmium sulfide nanoparticles (CdS) (instead of gold) yields a superstructure with novel fluorescence and photoelectrochemical properties.[60] Absorbance and fluorescence spectra of such a system are shown in Fig. 9(A). Irradiation of the array in the presence of a sacrificial electron donor results in a photocurrent that can also be used as a sensing signal [Fig. 9(B)]. The photocurrent is enhanced as the number of aggregated layers increases. It is also clear that the photocurrent increases non-linearly since the non-particle architecture exhibits a dendritic structure upon aggregation of the layers. Only CdS particles that are in intimate contact with the electrode support are active in the generation of the photocurrent. This was proved by the association of $Ru(NH_3)_6^{3+}$, acting as an electron acceptor, on the DNA strands. The $Ru(NH_3)_6^{3+}$ units trap the conduction-band electrons and mediate their transfer to the electrode, thus enhancing the generated photocurrent.

Hydrogel-entrapped nanoparticle systems

Polymers are extensively used as matrices for processing nanoparticles, and the advances in the assembly of polymer–nanoparticle composites have recently been reviewed.[61] As this review emphasizes the properties and functions of organized nanoparticle architectures, we will specifically discuss the functional features of nanoparticle–hydrogel composites. Hydrogels are highly swollen crosslinked polymers that are generally based on poly(acrylamide) and poly(acrylic acid). Due to the delicate balance of hydrogen bonds that stabilizes the gel's structure, the degree of swelling is highly dependent on factors such as solvent, solutes, pH, temperature and electric fields.[62]

'Ferrogels' are a class of materials that consist of magnetic nanoparticles (or 'ferrofluids') immobilized in hydrogel matrices. Poly(vinyl alcohol)[63] and poly(acrylamide)[64] hydrogels containing 10–12 nm magnetite (Fe_3O_4)[63] or maghemite (γ-Fe_2O_3)[64] particles have been investigated. These magnetic nanoparticles do not aggregate in solution as their mutual attraction is compensated for by repulsion due to surface charges and by loss of alignment of magnetic moments because of Brownian motion. The ferrogels can thus be prepared by a solution-state polymerization in the presence of the particles. Upon exposure to non-uniform magnetic fields, ferrogels deform almost instantaneously, and they return reversibly to their original state when the field is removed. Fig. 10 shows a typical experimental setup. The ferrogel is tethered to a stress-sensitive device from above, and a solenoid is placed below it.

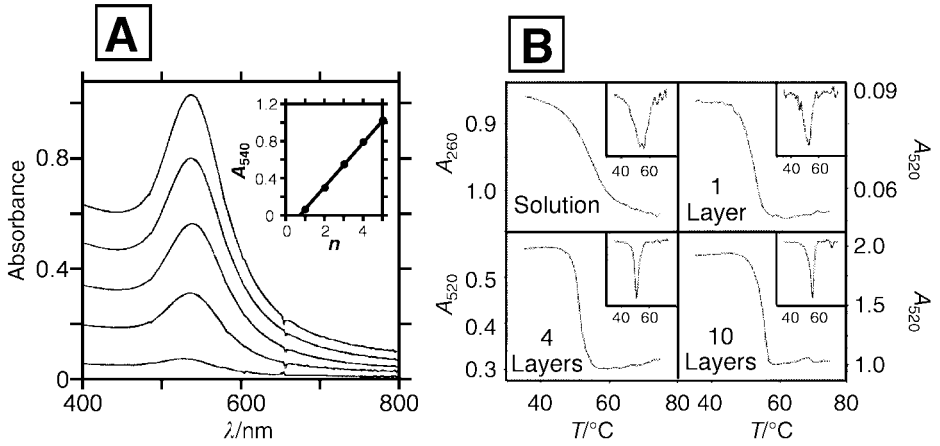

Fig. 8 (A) UV–VIS absorbance spectra of 1–5 Au-nanoparticle layers constructed on glass and linked by DNA (by method A, Scheme 2). Insert: growth of absorbance at 540 nm (A_{540}) with the number of layers (n). (B) Melt transitions of a DNA complex in solution, and the same complex as a nanoparticle linker in architectures of 1, 4 and 10 layers; monitored by absorbance at 260 nm (in solution) or at 520 nm (on surfaces). Insets: first derivatives of the melt curves.

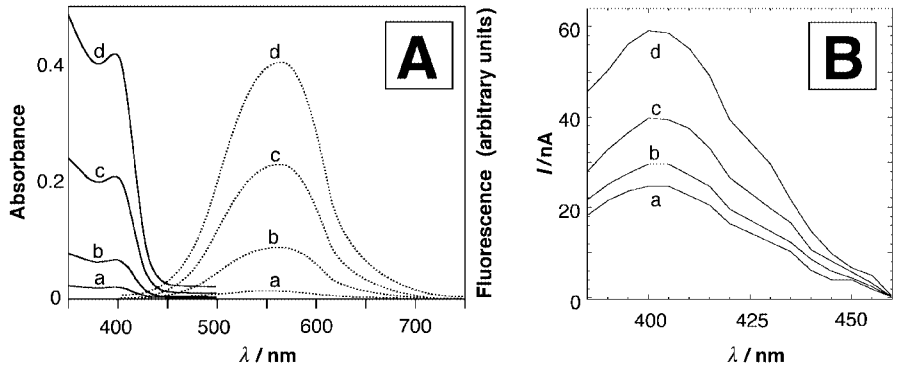

Fig. 9 (A) Absorbance (—) and fluorescence (·····) spectra of (a–d) 1–4 layer 'dendritic-type' DNA/CdS superstructures. (B) Photocurrent spectra of 2-layer (a and c) and 4-layer (b and d) DNA/CdS arrays in the absence (a and b) and presence (c and d) of $Ru(NH_3)_6^{3+}$.

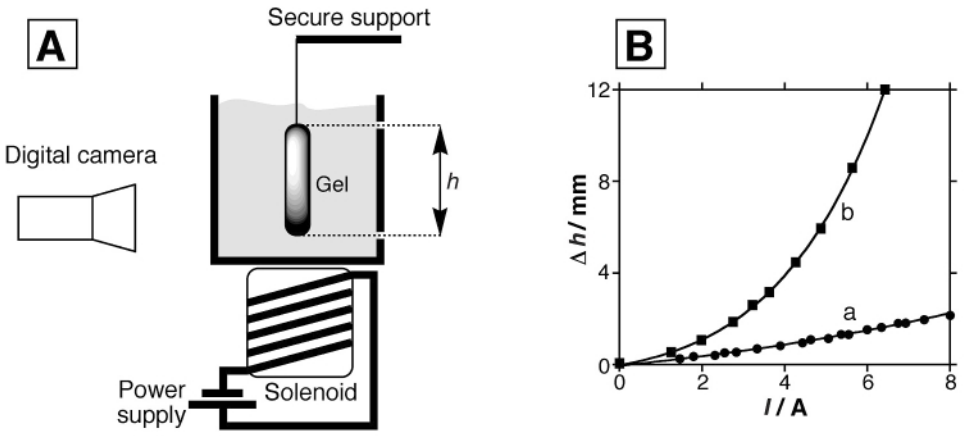

Fig. 10 (A) Experimental setup for the measurement of ferrogel elongation in a non-uniform magnetic field. (B) Elongation of a 120 mm gel as a function of solenoid current for gels containing (a) 2.45 and (b) 4.9 wt% magnetite.

Upon applying a current to the solenoid, the downward force and the elongation of the material can be measured. Fig. 10(B) shows typical curves for the dependence of the elongation of *ca.* 120 mm long gels. Upon applying current to the solenoid, up to a 10% deformation can be achieved. Other magnetic field geometries produce different deformation effects.

Since the swelling and shrinking behavior of hydrogels is extremely sensitive to many environmental factors, it may conceivably be used as a sensing event if a suitable transduction method can be found. Nanoparticles have been shown to provide methodologies for transducing these changes. By one method, crystalline colloid arrays (CCAs) of polystyrene particles (*ca.* 100 nm diameter) inside hydrogel matrices were constructed.[65] The assembly acts as a diffraction grating with a periodicity dependent on the interparticle spacing. It was found that the swelling and shrinking of the gel, brought about by exposure to different solutes or temperatures (depending on the nature of the gel used), causes the entire assembly to deform, thus increasing or decreasing the unit cell size of the crystallized colloid array. This change is easily detected and quantified by examination of the diffraction properties of the assembly. Fig. 11 shows absorbance spectra of a CCA immobilized in a crown ether-containing hydrogel, (**16**). Exposure of the system to Pb^{2+} causes the swelling of the gel as the metal ions are bound to the crown ether. The diffraction properties of the structure follow Bragg's law, and a 0.5% volume change causes a *ca.* 1 nm movement of the diffraction wavelength.

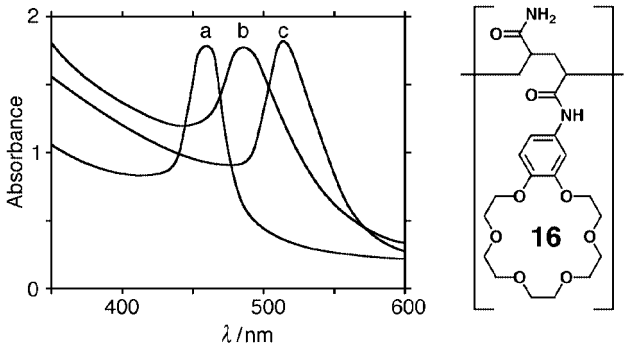

Fig. 11 Absorbance spectra of a polystyrene CCA embedded (7 wt%) in the polymer **16** (*ca.* 1 crown ether unit per 20 monomer units) in the presence of Pb^{2+} at concentrations of (a) 0, (b) 0.4 and (c) 4 ppm. Pb^{2+} can be sensed with a sensitivity limit of *ca.* 20 ppb.

Poly(acrylamide) hydrogels adopt swollen structures in water, but undergo phase transitions to collapsed states upon exposure to less polar solvents such as acetone. Taking advantage of this phenomenon, hydrogels containing a controllable concentration of gold nanoparticles have been synthesized by the route described in Scheme 3.[66] In this procedure, the nanoparticle-free gel is first synthesized on a conductive support by electropolymerization. The nanoparticles are then introduced into the structure by a 'breathing' method. First, the gel is shrunken by immersing it in acetone. This step removes most of the solvent from the gel. The shrunken gel is then immersed in an aqueous nanoparticle solution. The water causes the gel to swell and take the solution into its structure. As it does so, nanoparticles are introduced, where they become stuck by entanglement and the hydrogen bonding network (the gold nanoparticles bear a citrate surface, so have a high hydrogen bonding potential). This 'breathing' mechanism may be repeated several times to gradually increase the nanoparticle content of the gel, and as more nanoparticles are included, the properties of the gel are modified. The electronic properties of the hydrogel are altered upon the incorporation of the Au-nanoparticles. Fig. 12(A) shows Faradaic impedance spectra (in the form of Nyquist plots) of the hydrogel after three 'breathing' cycles. The diameters of the semicircular regions in the plots are indicative of the interfacial electron transfer resistances between the electrode and a solution-solubilized redox probe.[67] As the amount of Au-nanoparticles increases in the hydrogel, the interfacial electron transfer resistance decreases, implying enhanced conductivity of the hydrogel matrix. The electronic properties of the Au-nanoparticle–hydrogel composite are strongly affected upon phase-transition of the polymer matrix. Fig. 12(B) shows chronopotentiometric transients of the polymer matrix in the swollen [curve (a)] and shrunken [curve (b)] states. For comparison, the chronopotentiometric transients of the Au–polymer composite in the swollen [curve (c)] and shrunken [curve (d)] configurations are given. These chronopotentiometric transients indicate the overpotentials required

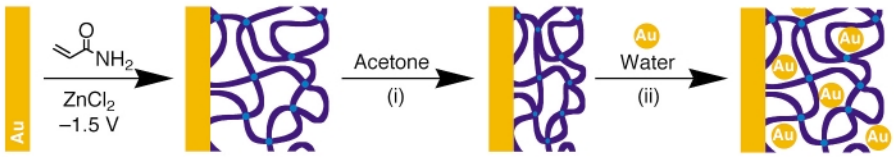

Scheme 3 Method for the assembly of Au-nanoparticle-containing electropolymerized hydrogels by the 'breathing' technique. First the hydrogel is electropolymerized, then the nanoparticles are introduced by (i) shrinking the gel in acetone and (ii) re-swelling the gel in a nanoparticle-containing solution. Steps (i) and (ii) may be repeated to increase the nanoparticle concentration in the gel.

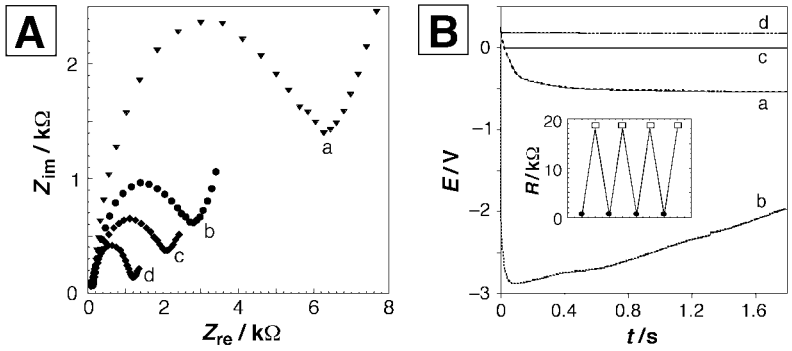

Fig. 12 (A) Faradaic impedance spectra showing the build-up of Au nanoparticles inside a polyacrylamide electrode and the decrease of the interfacial electron transfer resistance: (a) The swollen polyacrylamide gel prior to the introduction of Au-nanoparticles. (b)–(d) The swollen polyacrylamide gel after one, two and three 'breathing' cycles that introduce Au-nanoparticles into the polymer. (B) Chronopotentiometry transients of: (a) the swollen polyacrylamide electrode; (b) the shrunken polyacrylamide gel-electrode; (c) the swollen Au-nanoparticle-containing polyacrylamide electrode; (d) the shrunken Au-nanoparticle-containing polyacrylamide electrode. Inset: reversible switching of the nanoparticle-containing polyacrylamide electrode between swollen (□) and shrunken (●) states.

to retain a constant current in the cell in the presence of a redox label [$Fe(CN)_6^{3-/4-}$], and thus allows the extraction of the values of electrode resistance in the different configurations. The shrunken nanoparticle-free electrode reveals a substantially higher resistance than the swollen configuration (> 300 *vs.* 70 kΩ). On the other hand the shrunken nanoparticle-containing electrode reveals a substantially lower resistance than its swollen state (0.4 *vs.* 20 kΩ, respectively). The low resistance of the shrunken Au-nanoparticle polymer composite is attributed to electrical contact in the nanoparticle network which offers a route for electronic communication between the electrode and the electrolyte solution.

Conclusions and perspectives

The article has addressed means to tailor functional metal and semiconductor nanoparticle arrays for sensoric and electronic uses. The unique conductivity, catalytic, photonic, optical, electronic and photoelectronic properties of metallic and semiconductor nanoparticle systems, originating from the collective interactions in the crosslinked architectures, introduce new perspectives in nanotechnology. The nanostructuring of the assemblies provide high surface-area systems of controllable electronic and optical properties. Crosslinking of nanoparticles with molecular receptors yields conductive arrays with specific recognition features and controllable porosity, and the integration of nanoparticles with polymeric hydrogels paves the way to design signal-triggered materials with novel electronic properties. The conjugation of nanoparticles with nucleic acids establishes a fascinating research area that enables the amplified optical electronic and photoelectrochemical detection of DNA as well as the nanoengineering of predesigned and programmed DNA/nanoparticle circuitry. The application of these methodologies for gene analyses on DNA arrays, and the organization of wired nanoparticle assemblies that include resistance, capacitance and conductivity elements seem to be reachable goals.

We have already discussed some basic nanoparticle-based devices that have found commercial interest such as gas sensors, electrochemical sensors, photovoltaic cells, and luminescence collectors. More advanced applications that use layered nanoparticle composites may need more time to develop, yet they are certainly emerging. For example, nanoparticles may have a large impact in the area of reflective, bistable electronic displays.[68] These displays, known as 'electronic paper', promise to resemble paper in their ease of viewing and portability, without requiring a continuous input of energy to maintain a picture. These technologies are based on variously colored nanoparticles that are aligned inside microcapsules by external electrical fields. Other promising applications of nanoparticles may include displays and memory devices based on electroluminescence matrices[69] or integrated molecule/nanoparticle systems as computing devices.

One important future challenge will involve the organization of addressable nanoparticle architectures of variable composition and functions. Primary efforts in patterning of nanoparticle structures on surfaces have been reported.[70] The rapid advances in developing scanning microscopy 'writing' techniques[71] suggest that the use of 'nanoparticle inks' for nanometer-sized writing is a feasible goal. The progress in the photonic activation of nanometer-sized domains using near-field scanning optical microscopy (NSOM), indicates that the photonic addressability and imaging of nanostructures are viable concepts.

Acknowledgements

Part of the studies are supported by the German–Israel Research Program (DIP). The Max-Planck Award for International Cooperation (I. W.) is acknowledged. A. N. S. gratefully acknowledges a Valazzi Pikovsky fellowship.

Notes and references

1 *Nanosystems, Molecular Machinery, Manufacturing and Computation*, ed. K. E. Drexler, Wiley, New York, 1992; P. Ball, *Nature*, 1993, **362**, 123; P. Ball and L. Garwin, *Nature*, 1992, **355**, 761; *Molecular Electronics*, ed. G. J. Ashwell, Wiley, New York, 1992.
2 A. N. Shipway and I. Willner, *Acc. Chem. Res.*, 2001, **34**, 421; A. N. Shipway, E. Katz and I. Willner, *Struct. Bonding (Berlin)*, 2001, **99**, 237.
3 A. N. Shipway, E. Katz and I. Willner, *Chem. Phys. Chem.*, 2000, **1**, 18.
4 G. Schmid, *Chem. Rev.*, 1992, **92**, 1709; N. Toshima and T. Yonezawa, *New J. Chem.*, 1998, **11**, 1179.
5 H. Weller and A. Eychmüller, *Adv. Photochem.*, 1995, **20**, 165.
6 *Clusters and Colloids*, ed. G. Schmid, VCH, Weinheim, Germany, 1994; P. Mulvaney, *Langmuir*, 1996, **12**, 788; L. E. Brus, *Appl. Phys. A*, 1991, **53**, 465.
7 L. N. Lewis, *Chem. Rev.*, 1993, **93**, 2693; M. Haruta, *Catal. Today*, 1997, **36**, 153.
8 H. Bönnemann and G. A. Braun, *Chem. Eur. J.*, 1997, **3**, 1200.
9 M. M. Maye, Y. Lou and C.-J. Zhong, *Langmuir*, 2000, **16**, 7520.
10 A. C. Templeton, W. P. Wuelfing and R. W. Murray, *Acc. Chem. Res.*, 2000, **33**, 27.
11 A. N. Shipway, M. Lahav and I. Willner, *Adv. Mater.*, 2000, **12**, 993.
12 X. G. Peng, T. E. Wilson, A. P. Alivisatos and P. G. Schultz, *Angew. Chem., Int. Ed. Engl.*, 1997, **36**, 145; L. C. Brousseau, J. P. Novak, S. M. Marikanos and D. L. Feldheim, *Adv. Mater.*, 1999, **11**, 447.
13 A. P. Alivisatos, K. P. Johnsson, X. Peng, T. E. Wilson, C. J. Loweth, M. P. Bruchez Jr. and P. G. Schultz, *Nature*, 1996, **382**, 609.
14 A. N. Shipway, M. Lahav, R. Gabai and I. Willner, *Langmuir*, 2000, **16**, 8789; M. D. Musick, D. J. Peña, S. L. Botsko, T. M. McEvoy, J. N. Richardson and M. J. Natan, *Langmuir*, 1999, **15**, 844.
15 C. Demaille, M. Brust, M. Tsionsky and A. J. Bard, *Anal. Chem.*, 1997, **69**, 2323; A. K. Boal, F. Ilhan, J. E. Derouchey, T. Thurn-Albrecht, T. P.

Russell and V. M. Rotello, *Nature*, 2000, **404**, 746; O. D. Velev, A. M. Lenhoff and E. W. Kaler, *Science*, 2000, **287**, 2240.
16 G. Hornyak, M. Kröll, R. Pugin, T. Sawitowski, G. Schmid, J.-O. Bovin, G. Karsson, H. Hofmeister and S. Hopfe, *Chem. Eur. J*., 1997, **3**, 1951; M. Sano, A. Kamino and S. Shinkai, *Langmuir*, 1999, **15**, 13; S.-W. Chung, G. Markovich and J. R. Heath, *J. Phys. Chem. B*, 1998, **102**, 6685; M. Li, H. Schnablegger and S. Mann, *Nature*, 1999, **402**, 393.
17 C. J. Kiely, J. Fink, J. G. Zheng, M. Brust, D. Bethell and D. J. Schiffrin, *Adv. Mater*., 2000, **12**, 640; L. Motte, F. Billoudet, E. Lacaze, J. Douin and M. P. Pileni, *J. Phys. Chem. B*, 1997, **101**, 138; M. T. Reetz, M. Winter and B. Tesch, *Chem. Commun*., 1997, 147; T. Sato, D. Brown and B. F. G. Johnson, *Chem. Commun*., 1997, 1007; C. B. Murray, C. R. Kagan and M. G. Bawendi, *Science*, 1995, **270**, 1335; G. Schmid, M. Bäumle and N. Beyer, *Angew. Chem., Int. Ed*., 2000, **39**, 181; P. V. Braun, P. Osenar and S. I. Stupp, *Nature*, 1996, **380**, 325; W. Shenton, D. Pum and U. B. Sleytr, *Nature*, 1997, **389**, 585.
18 J. Schmitt, G. Decher, W. J. Dressick, S. L. Brandow, R. E. Geer, R. Shashidhar and J. M. Calvert, *Adv. Mater*., 1997, **9**, 61; D. L. Feldheim, K. C. Grabar, M. J. Natan and T. E. Mallouk, *J. Am. Chem. Soc*., 1996, **118**, 7640; R. Iler, *J. Colloid. Interface Sci*., 1996, **21**, 569.
19 D. I. Gittins, D. Bethell, D. J. Schiffrin and R. J. Nichols, *Nature*, 2000, **408**, 67.
20 S. J. Green, J. J. Stokes, M. J. Hostetler, J. Pietron and R. W. Murray, *J. Phys. Chem. B*, 1997, **101**, 2663; B. Sweryda-Krawiec, T. Cassagneau and J. H. Fendler, *Adv. Mater*., 1999, **11**, 659; R. P. Andres, T. Bein, M. Dorogi, S. Feng, J. I. Henderson, C. P. Kubiak, W. Mahoney, R. G. Osifchin and R. Reifenberger, *Science*, 1996, **272**, 1323; T. Sato, H. Ahmed, D. Brown and B. F. G. Johnson, *J. Appl. Phys*., 1997, **82**, 696; T. Sato and H. Ahmed, *Appl. Phys. Lett*., 1997, **70**, 2759.
21 J. Zhao, R. W. Henkens, J. Stonehuerner, J. P. O'Daly and A. L. Crumbliss, *J. Electroanal. Chem*., 1992, **327**, 109; S. Yabuki and F. Mitzutani, *Electroanalysis*, 1997, **9**, 23.
22 K. R. Brown, A. P. Fox and M. J. Natan, *J. Am. Chem. Soc*., 1996, **118**, 1154.
23 H. Wohltjen and A. W. Snow, *Anal. Chem*., 1998, **70**, 2856.
24 B. L. Doleman, M. C. Lonergan, E. J. Severin, T. P. Vaid and N. S. Lewis, *Anal. Chem*., 1998, **70**, 4177; M. C. Lonergan, E. J. Severin, B. J. Doleman, S. A. Beaber, R. H. Grubbs and N. S. Lewis, *Chem. Mater*., 1996, **8**, 2298; E. J. Severin, B. J. Doleman and N. S. Lewis, *Anal. Chem*., 2000, **72**, 658.
25 A. Doron, E. Katz and I. Willner, *Langmuir*, 1995, **11**, 1313; R. G. Freeman, K. C. Grabar, K. J. Allison, R. M. Bright, J. A. Davis, A. P. Guthrie, M. B. Hommer, M. A. Jackson, P. C. Smith, D. G. Walter and M. J. Natan, *Science*, 1995, **267**, 1629; G. Chumanov, K. Sokolov, B. W. Gregory and T. M. Cotton, *J. Phys. Chem*., 1995, **99**, 9466.
26 A. N. Shipway, M. Lahav, R. Blonder and I. Willner, *Chem. Mater*., 1999, **11**, 13.
27 M. Lahav, A. N. Shipway, I. Willner, M. B. Nielsen and J. Fraser Stoddart, *J. Electroanal. Chem*., 2000, **482**, 217.
28 M. Lahav, R. Gabai, A. N. Shipway and I. Willner, *Chem. Commun*., 1999, 1937.
29 M. Miyake, H. Matsumoto, M. Nishizawa, T. Sakata, H. Mori, S. Kuwabata and H. Yoneyama, *Langmuir*, 1997, **13**, 742; K. Ariga, Y. Lvov, M. Onda, I. Ichinose and T. Kunitake, *Chem. Lett*., 1997, 125; D. L. Feldheim, K. C. Grabar, M. J. Natan and T. E. Mallouk, *J. Am. Chem. Soc*., 1996, **118**, 7640.
30 E. Hao, B. Yang, J. Zhang, X. Zhang, J. Sun and J. Shen, *J. Mater. Chem*., 1998, 1327; R. Iler, *J. Colloid. Interface Sci*., 1996, **21**, 569; A. Kumar, A. B. Mandale and M. Sastry, *Langmuir*, 2000, **16**, 6921.
31 F. Patolsky, T. Gabriel and I. Willner, *J. Electroanal Chem*., 1999, **479**, 69.
32 M. Brust, R. Etchenique, E. J. Calvo and G. J. Gordillo, *Chem. Commun*., 1996, 1949; M. D. Musick, C. D. Keating, M. H. Keefe and M. J. Natan, *Chem. Mater*., 1997, **9**, 1499.
33 S. Norman, T. Andersson, C. G. Granqvist and O. Hunderi, *Phys. Rev. B*, 1978, **18**, 674; R. H. Dormeus, *J. Appl. Phys*., 1996, **37**, 2775.
34 M. Quinten and U. Kreibig, *Surf. Sci*., 1986, **172**, 557; K. C. Grabar, K. J. Allison, B. E. Baker, R. M. Bright, K. R. Brown, R. G. Freeman, A. P. Fox, C. D. Keating, M. D. Musick and M. J. Natan, *Langmuir*, 1996, **12**, 2353.
35 B. Odell, M. V. Reddington, A. M. Z. Slawin, N. Spencer, J. F. Stoddart and D. J. Williams, *Angew. Chem., Int. Ed. Engl*., 1998, **27**, 1547.
36 M. Lahav, A. N. Shipway and I. Willner, *J. Chem. Soc., Perkin Trans. 2*, 1999, 1925.
37 M. Asakawa, P. R. Ashton, S. Menzer, F. M. Raymo, J. F. Stoddart, A. J. P. White and D. J. Williams, *Chem. Eur. J*., 1996, **2**, 877.
38 M. Fujita, J. Yazaki and K. Ogara, *Tetrahedron Lett*., 1991, **32**, 5589.
39 A. B. Kharitonov, A. N. Shipway and I. Willner, *Anal. Chem*., 1999, **71**, 5441.
40 Y. Z. Hu, S. H. Bossmann, D. van Loyen, O. Schwarz and H. Dürr, *Chem. Eur. J*., 1999, **5**, 1267.
41 M. Lahav, V. Heleg-Shabtai, J. Wasserman, E. Katz, I. Willner, H. Dürr, Y.-Z. Hu and S. H. Bossmann, *J. Am. Chem. Soc*., 2000, **122**, 11 480.
42 M. Lahav, T. Gabriel, A. N. Shipway and I. Willner, *J. Am. Chem. Soc*., 1999, **121**, 258.
43 M. Grätzel, Nanocrystalline Electronic Junctions, in *Semiconductor Nanoclusters—Physical, Chemical and Catalytic Aspects*, ed. P. V. Kamat and D. Meisel, Elsevier, Amsterdam, 1997, p. 353; P. V. Kamat, Electron-Transfer Processes in Nanostructured Semiconductor Thin Films, in *Nanoparticles and Nanostructural Films*, ed. J. Fendler, Wiley-VCH, New York, 1998, p. 207.
44 B. O'Regan and M. Grätzel, *Nature*, 1991, **353**, 737; U. Bach, D. Lupo, P. Comte, J. E. Moser, F. Weissortel, J. Salbeck, H. Spreitzer and M. Grätzel, *Nature*, 1998, **395**, 583; S. D. Burnside, V. Shklover, C. Barbé, P. Comte, F. Arendse, K. Brooks and M. Grätzel, *Chem. Mater*., 1998, **10**, 2419; D. Matthews, A. Kay and M. Grätzel, *Aust. J. Chem*., 1994, **47**, 1869; L. Kavan, M. Grätzel, J. Rathousky and A. Zukal, *J. Electrochem. Soc*., 1996, **143**, 394; V. Shklover, M.-K. Nazeeruddin, S. M. Zakeeruddin, C. Barbé, A. Kay, T. Haibach, W. Steurer, R. Hermann, H.-U. Nissen and M. Grätzel, *Chem. Mater*., 1997, **9**, 430.
45 T. Cassagneau, T. E. Mallouk and J. H. Fendler, *J. Am. Chem. Soc*., 1998, **120**, 7848; V. L. Colvin, M. C. Schlamp and A. P. Alivisatos, *Nature*, 1994, **370**, 354; N. D. Kumar, M. P. Joshi, C. S. Friend, P. N. Prasad and R. Burzynski, *Appl. Phys. Lett*., 1997, **71**, 1388; M. Gao, B. Richter and S. Kirstein, *Adv. Mater*., 1997, **9**, 802; S. A. Carter, J. C. Scott and P. J. Brock, *Appl. Phys. Lett*., 1997, **71**, 1145.
46 L. Spanhel, H. Weller and A. Henglein, *J. Am. Chem. Soc*., 1987, **109**, 6632; K. R. Godipas, M. Bohorquez and P. V. Kamat, *J. Phys. Chem*., 1990, **94**, 6435; N. Serpone, E. Borgarello and M. Grätzel, *J. Chem. Soc., Chem. Commun*., 1984, 342; P. Pichat, E. Borgarello, J. Disdier, J.-M. Herrmann, E. Pelizzetti and N. Serpone, *J. Chem. Soc., Faraday Trans. 1*, 1988, **84**, 261; N. Serpone, E. Borgarello and E. Pelizzetti, *J. Electrochem. Soc*., 1988, **135**, 2760; D. Lawless, S. Kapoor and D. Meisel, *J. Phys. Chem. B*, 1995, **99**, 10329.
47 K. Barnham, J. L. Marques and J. Hassard, *Appl. Phys. Lett*., 2000, **76**, 1197.
48 W. H. Weber and J. Lambe, *Appl. Opt*., 1976, **15**, 2299; A. Goetzberger and W. Greubel, *Appl. Phys*, 1977, **14**, 123.
49 O. I. Micic, K. M. Jones, A. Cahill and A. J. Nozic, *J. Phys. Chem. B*, 1998, **102**, 9791.
50 C. R. Kagan, C. B. Murray and M. G. Bawendi, *Phys. Rev. B*, 1999, **54**, 8633.
51 C. Nasr, P. V. Kamat and S. Hotchandani, *J. Electroanal. Chem*., 1997, **420**, 201.
52 S. Hotchandani and P. V. Kamat, *J. Phys. Chem*., 1992, **96**, 6834.
53 R. Vogel, K. Pohl and H. Weller, *Chem. Phys. Lett*., 1990, **174**, 241; S. Hotchandani and P. V. Kamat, *Chem. Phys. Lett*., 1992, **191**, 320.
54 A. Zaban, S. G. Chen, S. Chappel and B. A. Gregg, *Chem. Commun*., 2000, 2231.
55 C. Nasr, S. Hotchandani, W. Y. Kim, R. S. Schmehl and P. V. Kamat, *J. Phys. Chem. B*, 1997, **101**, 7480.
56 N. C. Seeman, *Acc. Chem. Res*., 1997, **30**, 357; C. M. Niemeyer, *Angew. Chem., Int. Ed. Engl*., 1997, **36**, 585.
57 E. Braun, Y. Eichen, U. Sivan and G. Ben-Yoseph, *Nature*, 1998, **391**, 775.
58 R. Elghanian, J. J. Storhoff, R. C. Mucic, R. L. Letsinger and C. A. Mirkin, *Science*, 1997, **277**, 1078; J. J. Storhoff, R. Elghanian, R. C. Mucic, C. A. Mirkin and R. L. Letsinger, *J. Am. Chem. Soc*., 1998, **120**, 1959; C. A. Mirkin, R. L. Letsinger, R. C. Mucic and J. J. Storhoff, *Nature*, 1996, **382**, 607.
59 (*a*) F. Patolsky, K. T. Ranjit, A. Lichtenstein and I. Willner, *Chem. Commun*., 2000, 1025; (*b*) A. T. Taton, R. C. Mucic, C. A. Mirkin and R. L. Letsinger, *J. Am. Chem. Soc*., 2000, **122**, 6305.
60 I. Willner, F. Patolsky and J. Wasserman, *Angew. Chem., Int. Ed*., 2001, **105**, 4205.
61 D. Y. Godovsky, *Adv. Polym. Sci*., 2000, **153**, 163.
62 T. Tanaka, I. Nishio, S.-T. Sun and S. Uneo-Nishio, *Science*, 1982, **218**, 467; T. Oya, T. Enoki, A. Y. Grosberg, S. Masamune, T. Sakiyama, Y. Takeoka, K. Tanaka, G. Wang, Y. Yilmaz, M. S. Feld, R. Dasari and T. Tanaka, *Science*, 1999, **286**, 1543; T. G. Park and A. S. Hoffman, *J. Appl. Polym. Sci*., 1992, **46**, 659; J. H. Holtz, J. S. W. Holtz, C. H. Munro and S. A. Asher, *Anal. Chem*., 1998, **70**, 780.
63 M. Zrínyi, L. Barsi and A. Büki, *J. Chem. Phys*., 1996, **104**, 8750; M. Zrínyi, L. Barsi, D. Szabó and H.-G. Kilian, *J. Chem. Phys*., 1997, **106**, 5685.
64 C. R. Mayer, V. Cabuil, T. Lalot and R. Thouvenot, *Angew. Chem., Int. Ed*., 1999, **38**, 3672.
65 J. M. Weissman, H. B. Sunkara, A. S. Tse and S. A. Asher, *Science*, 1996, **274**, 959; J. H. Holtz and S. A. Asher, *Nature*, 1997, **389**, 829.
66 V. Pardo-Yissar, R. Gabai, T. Bourenko, A. N. Shipway and I. Willner, *Adv. Mater*., 2001, **13**, 1320.

67 A. J. Bard and L. R. Faulkner, *Electrochemical Methods: Fundamentals and Applications*, Wiley, New York, 1980.
68 B. Comiskey, J. D. Albert, H. Yoshizawa and J. Jacobson, *Nature*, 1998, **394**, 253; R. Dagani, *Chem. Eng. News*, 2001, Jan 15, 40.
69 V. L. Colvin, M. C. Schlamp and A. P. Alivisatos, *Nature*, 1994, **370**, 354; B. O. Dabbousi, M. G. Bawendi, O. Onitsuka and M. F. Rubner, *Appl. Phys. Lett*., 1995, **66**, 1316.
70 J. Liu, L. Zhang, P. Mao, D. Chen, N. Gu, J. Ren, Y. Wu and Z. Lu, *Chem. Lett*., 1997, 1147; J.-F. Liu, L.-G. Zhang, J.-Y. Ren, Y.-P. Wu, Z.-H. Lu, P.-S. Mao and D.-Y. Chen, *Thin Solid Films*, 1998, **327**–**329**, 176; T. Vossmeyer, E. DeIonno and J. R. Heath, *Angew. Chem., Int. Ed. Engl*., 1997, **36**, 1080; W. J. Dressick, C. S. Dulcey, S. L. Brandow, H. Witschi and P. F. Neeley, *J. Vac. Sci. Technol. A*, 1999, **17**, 1432; S. L. Brandow, M.-S. Chen, R. Aggarwal, C. S. Dulcey, J. M. Calvert and W. J. Dressick, *Langmuir*, 1999, **15**, 5429; P. C. Hidber, W. Helbig, E. Kim and G. M. Whitesides, *Langmuir*, 1996, **12**, 1375; J. L. Coffer, S. R. Bigham, R. F. Pinizzotto and H. Yang, *Nanotechnology*, 1992, **3**, 69.
71 F. P. Zamborini and R. M. Crooks, *J. Am. Chem. Soc*., 1998, **120**, 9700; R. D. Piner, J. Zhu, F. Xu, S. H. Hong and C. A. Mirkin, *Science*, 1999, **283**, 661; R. Resch, C. Baur, A. Bugacov, B. E. Koel, A. Madhukar, A. A. G. Requicha and P. Will, *Langmuir*, 1998, **14**, 6613; S. L. Brandow, W. J. Dressick, C. S. Dulcey, T. S. Koloski, L. M. Shirey, J. Schmidt and J. M. Calvert, *J. Vac. Sci. Technol. B*, 1997, **15**, 1818; A. Doron, E. Joselevich, A. Schlittner and I. Willner, *Thin Solid Films*, 1999, **340**, 183; M. T. Reetz and M. Winter, *J. Am. Chem. Soc*., 1997, **119**, 4539.

CHEMCOMM Communication
www.rsc.org/chemcomm

Effect of phthalates on the stability and performance of $AgBF_4$–PVP membranes for olefin/paraffin separation

Binoy Jose,[ab] Jae Hee Ryu,[b] Byung Gwon Lee,[a] Hyunjoo Lee,[a] Yong Soo Kang[b] and Hoon Sik Kim*[a]

[a] *CFC Alternatives Research Center, Korea Institute of Science and Technology, 39-1, Hawolgokdong, Seongbukgu, Seoul 136-791, Korea*
[b] *Center for Facilitated Transport Membrane, Korea Institute of Science and Technology, 39-1, Hawolgokdong, Seongbukgu, Seoul 136-791, Korea. E-mail: khs@kist.re.kr*

Received (in Cambridge, UK) 27th June 2001, Accepted 22nd August 2001
First published as an Advance Article on the web 17th September 2001

The presence of a phthalate in dry polymer membranes consisting of polyvinylpyrrolidone (PVP) and $AgBF_4$, $AgBF_4$–PVP, provides long-term stability and better performance for the separation of propylene/propane gas mixtures.

Olefin/paraffin separation by facilitated transport polymer membranes consisting of silver salts and polymers has attracted much interest because of its advantages of low energy consumption, compact apparatus and simple operation.[1,2] However, polymer membranes containing silver salts exhibit some disadvantages that prevent the commercialization of this separation process.[3] One major drawback observed in the membranes is the gradual decrease in membrane performance with time, possibly due to the reduction of silver ions to silver particles.

To our knowledge, however, no report has been published on the long-term stability of polymer membranes containing silver salts. It is well known that the ionic mobility and conductivity of lithium ions in PEO-based lithium polymer electrolytes can be significantly increased by the incorporation of a plasticizer such as dibutyl or dioctyl phthalate.[4] The dissociation of lithium salts into ions seems to be more facilitated by the strong interaction between the ester groups of phthalates and lithium ions. Furthermore, each dissociated lithium ion can be further stabilized by forming a chelating bond to two adjacent ester groups. In this context, we have employed phthalates as stabilizers for silver ions in dry polymer membranes containing silver salts for olefin/paraffin separation.

We report here that plasticizers such as dialkyl and diaryl phthalates are highly effective for stabilizing silver ions, thereby improving the performance of a dry polymer membrane consisting of $AgBF_4$ and polyvinylpyrrolidone (PVP), $AgBF_4$–PVP. Of the several polymer membranes containing silver salts, $AgBF_4$–PVP membranes are chosen for our study because PVP is often used for reducing silver salts to silver nanoparticles.[5,6]

$AgBF_4$–PVP membranes were prepared by dissolving $AgBF_4$ in methanol solution containing 20 wt% of PVP or 20 wt% of PVP and a phthalate. The molar ratio of $AgBF_4$:PVP and the weight ratio of phthalate:PVP were fixed at 1 and 0.02, respectively. The resulting solution was coated onto a polysulfone microporous membrane support (SEAHAN Industries Inc., Seoul, Korea) using an RK Control Coater. The solvent was evaporated in a light-protected convection oven at 25 °C under a stream of nitrogen, and then the membrane was dried completely in a vacuum oven for 24 h at room temperature. The thickness of the top polymer electrolyte layer was *ca.* 1 μm. Permeation tests were performed in a stainless steel separation module as described elsewhere.[7] The flow rates of the mixed gas and sweep gas (helium) were controlled using mass flow controllers and the gas flow rates represented by permeance were determined using a soap-bubble flowmeter. The mixed gas (50:50 vol% of a propylene/propane mixture) separation properties of the membranes were evaluated using gas chromatography (Gow-Mac) equipped with a TCD and a unibead 2S 60/80 packed column. The separation of propylene/propane mixtures was conducted to evaluate the effect of plasticizers on the performance of the $AgBF_4$–PVP membranes. As shown in Figs. 1 and 2, the selectivity of propylene over propane and permeance for the $AgBF_4$–PVP membrane without a phthalate decreases with time.

On the other hand, the incorporation of a plasticizer, such as dibutyl phthalate (DBP), dioctyl phthalate (DOP) and diphenyl phthalate (DPP), significantly improves the performance of the $AgBF_4$–PVP membranes. The selectivity and permeance for the membranes containing phthalates remain nearly constant throughout the experiments for up to 100 h. Furthermore, the

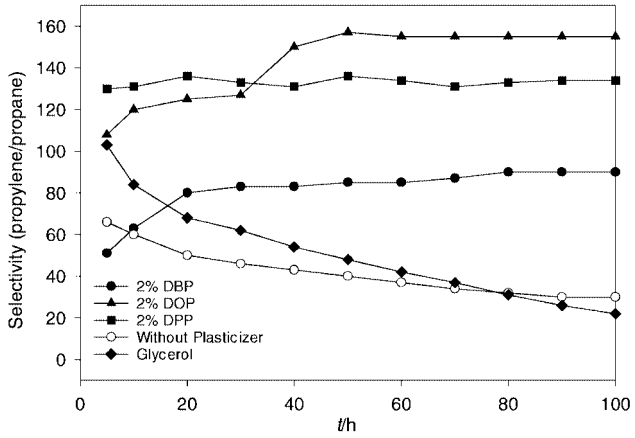

Fig. 1 Selectivity of propylene/propane with time for $AgBF_4$–PVP membranes with or without a plasticizer.

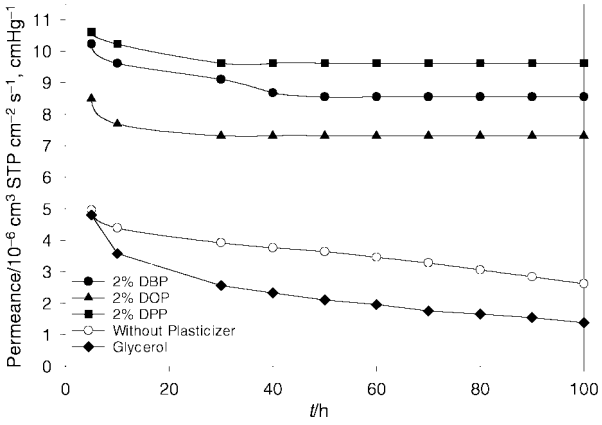

Fig. 2 Mixed gas permeance with time for $AgBF_4$–PVP membranes with or without a plasticizer.

 DOI: 10.1039/b105656p

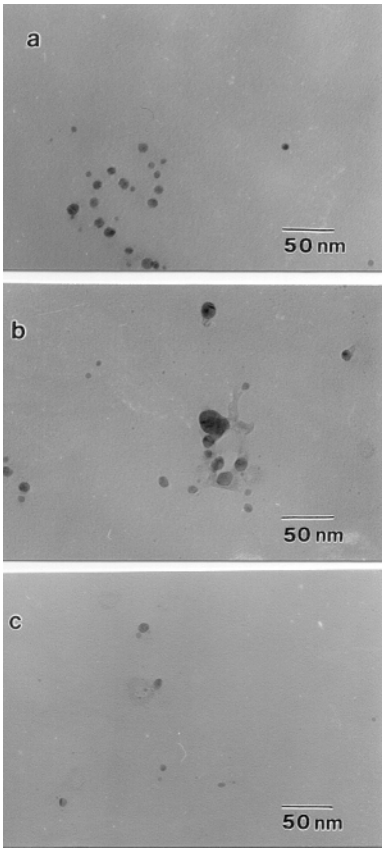

Fig. 3 Electron micrographs of $AgBF_4$–PVP membranes with or without a plasticizer: (a) $AgBF_4$–PVP membrane just after preparation, (b) $AgBF_4$–PVP membrane after one week of preparation, (c) $AgBF_4$–PVP membrane containing 2 wt% dioctyl phthalate after one week of preparation.

selectivity and permeance measured at 100 h are much higher for the membranes containing phthalates in comparison with those of the membranes without phthalates. From these results, it is likely that phthalates in $AgBF_4$–PVP membranes are playing an important role in preventing the reduction of silver ions as well as in increasing the mobility of the silver ions, thereby facilitating the propylene transport.

The effect of plasticizers on the reduction of silver ions in the $AgBF_4$–PVP membrane was investigated using TEM analysis. The TEM micrograph of the $AgBF_4$–PVP membrane without a phthalate taken just after preparation shows the presence of a small number of particles of approximately 5 nm in size (Fig. 3a). The TEM micrograph of the same membrane after one week shows an increase in the number of particles and in particle size (Fig. 3b). However, as shown in Fig. 3c, the TEM micrograph of a membrane containing 2 wt% dioctyl phthalate taken after one week of preparation shows a much smaller number of silver nanoparticles, indicating that dioctyl phthalate is playing an important role in preventing the reduction of silver ions in the $AgBF_4$–PVP membranes. This stabilization of silver ions in the $AgBF_4$–PVP membrane can be explained by the strong interaction of silver ions with the two carbonyl groups of the phthalate, as shown in Scheme 1. FTIR study shows that the carbonyl stretching frequency of the free DOP at 1729 cm^{-1} shifts to a much lower frequency, by about 46 cm^{-1}, upon

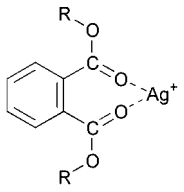

R = butyl, 2-ethylhexyl or phenyl

Scheme 1

interaction with $AgBF_4$, indicating the strong interaction between the carbonyl groups of DOP and silver ions.[1]

To compare the effects of phthalates and non-phthalate plasticizers, we have carried out a separation experiment using 2 wt% glycerol which is a weakly coordinating plasticizer to silver ions. Completely non-coordinating plasticizers like chlorinated paraffins were not tested due to their extremely low solubility in lower alcohols and water. As shown in Figs. 1 and 2, the membrane containing 2 wt% glycerol showed a selectivity of 103 for propylene over propane with a permeance of 4.8×10^{-6} cm^3(STP) cm^{-2} s^{-1} $cmHg^{-1}$ initially. However, the selectivity and permeance rapidly decrease as in the case without a plasticizer. Furthermore, the color of the membrane containing glycerol becomes dark brown within a day, indicating the rapid formation of silver particles. On the other hand, no color change was observed after one week for the membrane containing phthalate. These results suggest that enhanced performance of the membranes can be achieved only in the presence of a plasticizer which can strongly interact with silver ions.

In summary, the $AgBF_4$–PVP membranes show high initial selectivity for propylene/propane separation, but the selectivity was found to continuously decrease with time, most possibly due to the reduction of silver ions to silver nanoparticles. The TEM results support this argument. The addition of small amounts of plasticizer such as dibutyl phthalate, dioctyl phthalate or diphenyl phthalate significantly increase the membrane stability with an unexpected increase in the selectivity and permeance. TEM analysis shows that the formation of silver nanoparticles can be significantly retarded by the presence of small amounts of plasticizer in the membrane.

The authors acknowledge the financial support from the Ministry of Science and Technology of Korea through the Creative Research Initiatives program.

Notes and references

1 H. S. Kim, J. H. Ryu, H. Kim, B. S. Ahn and Y. S. Kang, *Chem. Commun*., 2000, 1261; J. H. Ryu, H. Lee, Y. J. Kim, Y. S. Kang and H. S. Kim, *Chem. Eur. J*., 2001, **7**, 1525.
2 Y. S. Yoon, J. Won and Y. S. Kang, *Macromolecules*, 2000, **33**, 3185; S. U. Hong, J. Won and Y. S. Kang, *Adv. Mater*., 2000, **12**, 968.
3 R. B. Eldridge, *Ind. Eng. Chem. Res*., 1993, **32**, 2208; I. Pinnau and L. G. Toy, *J. Membr. Sci*., 2001, **184**, 39.
4 M. S. Michael, M. M. E. Jacob, S. R. S. Prabaharan and S. Radhakrishna, *Solid State Ionics*, 1997, **98**, 167; A. M. Sukeshini, A. R. Kulkarni and A. Sharma, *Solid State Ionics*, 1998, **113**, 179.
5 Y. Shiraishi and N. Toshima, *J. Mol. Catal. A: Chem*., 1999, **141**, 187; S. Kapoor, *Langmuir*, 1998, **14**, 1021.
6 Compounds containing an amide group in the molecule are known as reducing agents for silver salts. For example, see: I. Pastoriza-Santos and L. M. Liz-Marzan, *Langmuir*, 1999, **15**, 948.
7 S. Bai, S. Sridhar and A. A. Khan, *J. Membr. Sci*., 1998, **147**, 131.

CHEMCOMM Communication
www.rsc.org/chemcomm

A high coking-resistance catalyst for methane aromatization

Yuan Lu,[a] Ding Ma,[b] Zhusheng Xu,[a] Zhijian Tian,[a] Xinhe Bao*[b] and Liwu Lin*[b]

[a] *Laboratory of Natural Gas Utilization and Applied Catalysis, Dalian Institute of Chemical Physics, The Chinese Academy of Sciences, 457 Zhongshan Road, Dalian 116023. P. R. China. E-mail: linliwu@mail.dlptt.ln.cn*

[b] *State Key Laboratory of Catalysis, Dalian Institute of Chemical Physics, The Chinese Academy of Sciences, 457 Zhongshan Road, Dalian 116023, P. R. China. E-mail: xhbao@dicp.ac.cn*

Received (in Cambridge, UK) 3rd July 2001, Accepted 30th August 2001
First published as an Advance Article on the web 27th September 2001

Steaming-dealuminated HZSM-5-supported molybdenum catalysts have been found to be high coking-resistance catalysts for methane aromatization reactions; compared with conventional catalysts, they give a much higher selectivity towards aromatics.

The scission of a C–H bond is the first step for a hydrocarbon transformation reaction. The main reason for the relatively low conversion obtained upon oxidation, functionalization and dehydro-aromatization activation of these hydrocarbons is the high activation energy for C–H bond scission, which requires high reaction temperatures.[1–3] At the high temperature used for aromatization of alkanes on zeolite catalysts, how to suppress coke formation during the reaction remains a big problem. This is especially the case when methane is activated and transformed to aromatics over bifunctional Mo/HZSM-5 catalysts under non-oxidative conditions.[4–12] At 973 K, *ca.* 20–40% of the methane converted is deposited on the catalyst surface as coke species,[6,9,11] lowering the selectivity to desired products as well as masking the active center for the catalytic reaction. The latter process decreases catalytic activity *vs.* time on-stream and eventually leads to the complete deactivation of the catalyst. On considering this, great attention has been paid to the suppression of coke formation in this reaction. Successful examples arise from adding a small amount of CO, CO_2 or O_2 into the reactant, which efficiently suppresses the carbonaceous deposits on the catalyst surface.[8,12] Consequently, it results in much lower coke selectivity and thus a greater durability of Mo/HZSM-5 catalysts. However, using an oxidative co-feed material increases the complicacy of the reaction requirements and at the same time enhances the cost of the potential of putting this reaction into industrial use. Here, we report an alternative but easy handling method (without the addition of oxidative gases) to suppress coke formation by pre-dealumination of the parent HZSM-5 zeolite using a steaming-treatment. Significant improvement has been realized from this method, *i.e.* in a proper-dealuminated ZSM-5-supported Mo catalyst the benzene yield increases by 32% while the selectivity to coke formation drops dramatically from *ca.* 20 to 8% when compared with the conventional Mo/HZSM-5 catalyst.

HZSM-5 with Si/Al mole ratio of 25 [denoted as HZSM-5(P), supplied by Nankai University] was used as the parent zeolite. The dealumination of the parent zeolite was realized by a steaming method, resulting in a series of dealuminated samples [HZSM-5(ST*n*), *n* = 1–3]. The steam treatment conditions (temperature/K, partial pressure of steam/kPa, time/h) of HZSM-5(ST1), HZSM-5(ST2) and HZSM-5(ST3) were (773, 38, 6), (823, 38, 6) and (823, 70, 6), respectively. With *n* varying from 1 to 3, the severity of dealumination increases. After the steam treatment, the samples were washed by 0.5 M HCl solution at room temperature in order to remove the additional extra-framework aluminium species which are expelled from the zeolite lattice during steaming. The parent HZSM-5 was treated with 0.5 M HCl prior to Mo loading and was denoted as HZSM-5(HCl) for the blank experiment. No obvious dealumination of HZSM-5(HCl) was detected compared with HZSM-5(P). Mo-containing catalysts (Mo wt% = 4%) were prepared by incipient wetness impregnation of HZSM-5(P), HZSM-5(HCl) and HZSM-5(ST*n*) (*n* = 1, 2, 3) with an aqueous solution of ammonium heptamolybdate ($(NH_4)_6Mo_7O_{24}{\cdot}H_2O$). Methane aromatization reactions were carried out in a continuous flow reactor system equipped with a quartz tube (10 mm id) packed with 1.5 ml of catalyst pellets of 40–60 mesh. A feed gas mixture of 97.5% CH_4 with 2.5% Ar was purified and then introduced into the reactor at a flow rate of 1500 ml g^{-1} h^{-1} (GHSV = 600 h^{-1}). The reaction was conducted at 973 and 1023 K under a total pressure of 1 atm. The tail gas out of the reactor was detected on-line by a six-way valve connected with two sets of gas chromatographs. The conversion of methane and selectivity to products were calculated by a method similar to that reported by Liu *et al.*[8] Details can be found from our previous publication.[11] TPO (temperature programmed oxidation) experiments of coked catalysts (after 8 h time on-stream, 1 atm, GHSV = 600 h^{-}) were performed with a 20% O_2/He mixture (20 ml min^{-1}, after dehydration) as the oxidant at a heating rate of 10 K min^{-1}. The concentrations of CO_2 in the discharged gas were monitored by gas chromatography.

Fig. 1 shows the methane conversion, benzene yield and the distribution of various products of Mo/HZSM-5 and Mo/HZSM-5(ST*n*) after 360 min time on-stream at 973 K and 1 atm. While methane conversion of heavily dealuminted catalyst Mo/HZSM-5(ST3) dropped sharply to less than 6% due to a loss in lattice cystallinity (*ca.* 60% of that of the parent, XRD pattern not shown here), it is clear that C_{CH_4} remained stable (*ca.* 9.5%) for the Mo/HZSM-5(P), Mo/HZSM-5(ST1) and Mo/HZSM-5(ST2) catalysts [Fig. 1(a)]. On the other hand, a dramatic increase in benzene yield is observed after steaming-treatment. Compared with Mo/HZSM-5(P), the benzene yield of the dealuminated catalysts gradually reaches a plateau at Mo/HZSM-5(ST2), raised by about 1/3, *i.e.* from 4.8 to 6.4%. With methane conversion being similar, an increase in benzene yield means that the product distribution of this reaction is changed. It is interesting to note that the enhancement of benzene selectivity after dealumination treatment arises from the strong suppression of coke formation [the selectivity towards toluene and naphthalene remains also intact, see Fig. 1(b)]. For the parent and HZSM-5-supported molybdenum catalysts dealuminated to different extents, the coke selectivity bottomed out at Mo/HZSM-5(ST2) [for Mo/HZSM-5(P) it is 20.3%, whereas that of Mo/HZSM-5(ST2) is 8.2%], in line with maximum benzene selectivity. Parallel, improved catalytic behavior is obtained as for the reaction conducted at 1023 K (Table 1), where the yield of aromatics from the dealumintated catalyst after 420 min time on-stream is about 32% higher than that of parent Mo/HZSM-5(P) (8.7% *cf.* 6.6%). To rule out the possible role of HCl treatment, Mo/HZSM-5(HCl) was tested in the methane aromatization reaction (Table 1). It is obvious from Table 1 that washing that catalyst with 0.5 M HCl solution at RT does not alter its catalytic performance significantly. Hence, it is concluded that suitable dealumination of the zeolite will benefit aromatics formation and coke suppression and, as a con-

 DOI: 10.1039/b105853n

Table 1 Catalytic performance of 4wt% Mo/HZSM-5(P), 4wt% Mo/HZSM-5(HCl) and 4wt% Mo/HZSM-5(ST2) catalysts

Catalyst	CH_4 conversion (%)	Selectivity (%)						Yield of aromatics (%)
		Benzene	Toluene	Naphthalene	$C_2^=$	C_2^0	Coke	
4wt% Mo/HZSM-5(P)	11.9	46.1	2.7	6.3	4.7	1.1	37.9	6.6
4wt% Mo/HZSM-5(HCl)	11.7	48.6	2.2	7.0	4.3	1.6	35.2	6.8
4wt% Mo/HZSM-5(ST2)	10.9	63.5	3.1	8.3	4.9	1.4	18.9	8.7

Time on-stream 420 min; reaction temperature 1023 K; reaction pressure 1atm; GHSV 600 h^{-1}.

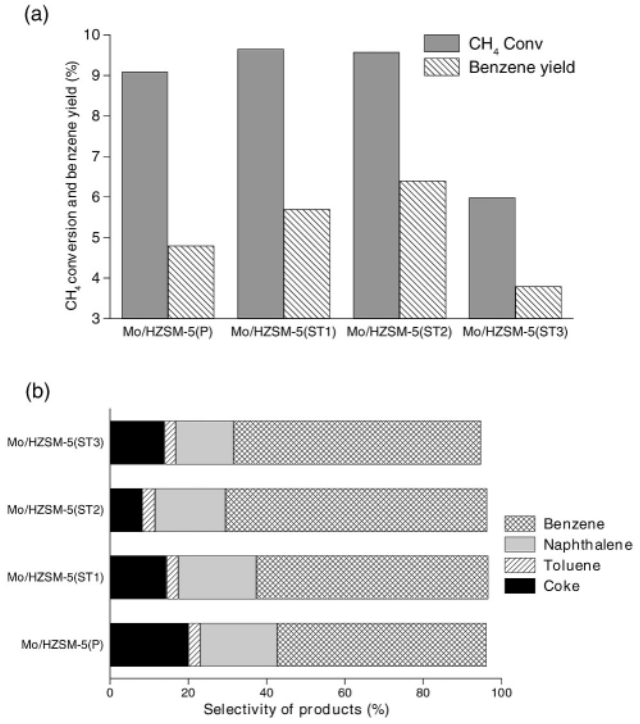

Fig. 1 Methane conversion, benzene yield (a) and product distribution (b) of Mo/HZSM-5(P) and Mo/HZSM-5(ST*n*) (*n* = 1–3) catalysts after 360 min time on-stream of methane aromatization reaction (973 K; 1 atm; GHSV = 600 h^{-1}).

sequence, will benefit the stability of the catalyst. These facts indicate that, different from previous suggestions, only a relatively small amount of Bronsted sites (aluminium connected with the zeolite framework) is necessary for Mo/HZSM-5 to be an efficient and effective methane aromatization catalyst. Superfluous framework aluminium (which is associated with bridging hydroxy) will benefit the formation of carbonaceous deposits, which may initialize and grow in the sites and then ultimately lead to channel blockage and destruction of the catalyst.[13,14] It is precisely the removal of excess framework aluminium (from these dealuminated catalysts) that inhibits the formation of harmful coke and therefore increases the benzene yield and durability of catalysts.

To further endorse these conclusions, TPO experiments of coked Mo/HZSM-5(P) and Mo/HZSM-5(ST2) catalysts were conducted and the results are displayed in Fig. 2. It is obvious that the TPO profiles of deactivated Mo/HZSM-5(P) (after 8 h reaction at 973 and 1023 K) are of double-peak structure, with the low temperature oxidation peak attributed to carbon associated with molybdenum, and the high temperature peak to the carbonaceous deposits on the zeolite Bronsted acid sites.[8,9] After pre-dealumination treatment [TPO profiles of coked Mo/HZSM-5(ST2)], the amount of coke on the catalysts decreased remarkably. In fact, only a peak which is the low temperature peak of TPO of coked Mo/HZSM-5(P) could be monitored, in conjunction with an indistinct tail in the high temperature region. This observation supports our conclusion that dealumination successfully removed the excess framework aluminum (Bronsted sites), which is the main drawback of this reaction, *i.e.* acid-associated carbonaceous depositions in the methane aromatization reaction.

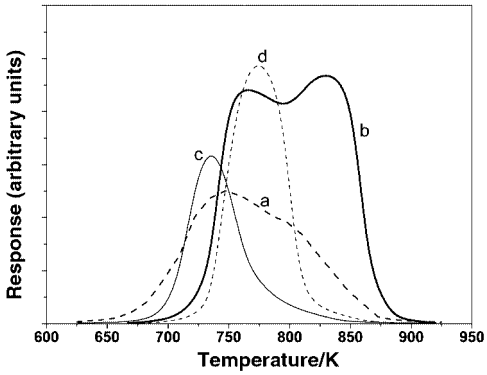

Fig. 2 TPO profiles of (a) Mo/HZSM-5(P) after reaction at 973 K for 8 h; (b) Mo/HZSM-5(P) after reaction at 1023 K for 8 h; (c) Mo/HZSM-5(ST2) after reaction at 973 K for 8 h; (d) Mo/HZSM-5(STZ) after reaction at 1023 K for 8 h. All methane aromatization reactions were conducted at 1 atm, GHSV = 600 h^{-1}.

In summary, an easy way (without addition of any oxidative gases in reactant) for modification of catalyst has been presented here that effectively suppresses coke formation in methane aromatization reactions. It gives a much higher benzene yield and a longer durability as compared with conventional Mo/HZSM-5 catalysts.

This work was sponsored by the National Natural Science Foundation under grant no. 29573137.

Notes and references

1 L. Guczi, R. A. Van Santen and K. V. Sarma, *Catal. Rev.-Sci. Eng*., 1996, **38**, 249.
2 P. Meriaudeau and C. Naccache, *Catal. Rev.-Sci. Eng*., 1997, **39**, 5.
3 F. Cavani, F. Trifiro, G. Fiordano and K. J. Waghmare, *Appl. Catal., A: General*, 1993, **94**, 131.
4 L. Wang, L. Tao, M. Xie, G. Xu, J. Huang and Y. Xu, *Catal. Lett*., 1993, **21**, 35.
5 L. Chen, L. Lin, Z. Xu, X. Li and T. Zhang, *J. Catal*., 1995, **157**, 190.
6 D. Wang, J. H. Lunsford and M. P. Rosynek, *J. Catal*., 1997, **169**, 347.
7 F. Solymosi, J. Cserenyi, A. Szoke, T. Bansagi and A. Oszko, *J. Catal*., 1997, **165**, 150.
8 S. Liu, Q. Don, R. Ohnishi and M. Ichikawa, *Chem. Commum*., 1999, 1455; R. Ohnishi, S. Liu, Q. Dong, L. Wang and M. Ichikawa, *J. Catal*., 1999, **182**, 92.
9 D. Ma, W. Zhang, Y. Shu, Y. Xu and X. Bao, *Catal. Lett*., 2000, **66**, 155.
10 R. W. Borry, Y. H. Kim, A. Huffsmith, A. Reimer and I. Iglesia, *J. Phys. Chem. B*, 1999, **103**, 5787.
11 Y. Lu, Z. Xu, Z. Tian, T. Zhang and L. Lin, *Catal. Lett*., 1999, **62**, 215.
12 S. Yuan, J. Li, Z. Hao, Z. Feng, Q. Xin, P. Ying and C. Li, *Catal. Lett*., 1999, **63**, 73.
13 S. M. Campbell, D. M. Bibby, J. M. Coddington and R. F. Howe, *J. Catal*., 1996, **161**, 350.
14 W. Zhang and P. G. Smirniotis, *Appl. Catal., A: General*, 1998, **168**, 113; W. Zhang and P. G. Smirniotis, *Catal. Lett*., 1999, **60**, 223.

CHEMCOMM Communication
www.rsc.org/chemcomm

Sequence fidelity of a template-directed PNA-ligation reaction†

Amos Mattes and Oliver Seitz*

Max-Planck-Institut für Molekulare Physiologie, Otto-Hahn-Str. 11, D-44227 Dortmund, Germany and Institut für Organische Chemie, Universität Dortmund, Germany.
E-mail: oliver.seitz@mpi-dortmund.mpg.de; Fax: 0049 231 1332499; Tel: 0049 231 1332424

Received (in Cambridge, UK) 10th July 2001, Accepted 29th August 2001
First published as an Advance Article on the web 14th September 2001

The ligation method and an appended duplex-stabilizing dye affect both yield and sequence selectivity of a template-controlled PNA-ligation. The highest selectivity was obtained with a peptide condensation that formed an abasic site.

In key biological processes like replication, transcription and translation nucleic acids serve as templates that organize nucleic acid substrates such that ligation reactions are facilitated.[1] A great deal of research has been devoted to the construction of chemical models that can help to unravel the molecular basis of evolution.[2] Ligation reactions that proceed under the control of a DNA-like template are useful examples and illustrate how chemical reactivities can be controlled by Watson–Crick base-pairing. It is commonly accepted that the fidelity of a DNA-controlled ligation reaction, a critical issue for chemical evolution and gene diagnostics, is dependent on the selectivity of nucleic acid hybridisation. The results that will be presented in the following support the notion that it is not only the template binding that accounts for ligation selectivity but also the ligation method itself.

Several oligonucleotide modifications were developed with the aim of enhancing the affinity and the selectivity of their binding to complementary DNA and RNA.[3] Only a few artificial base-pairing systems were used in template-directed ligations.[4] None of these studies addressed the issue of ligation fidelity as far as single base mutations are concerned. We examined the ligation fidelity of one of the most successful DNA-analogues, the peptide nucleic acids (PNA).[5]

Orgel and co-workers have shown that a template-controlled ligation of PNA is possible when a peptide coupling is carried out by using a water-soluble carbodiimide in an imidazole buffer.[4b] Therefore the carbodiimide-mediated condensation of PNA-fragments **1a** and **2a** was investigated. Fig. 1A shows the kinetic monitoring of product formation. In the absence of a template the ligation reaction of the PNA-fragments was inefficient and leveled off at 6% after 24 h. In the presence of the complementary PNA-template **3a** the yield of the ligation reaction was increased but to a moderate extent. Astonishingly, the use of PNA-template **3b**, which contained a single base mismatch, led to the formation of **4a** in an even higher yield.

To enhance the ligation selectivity we envisioned incorporating an abasic site. We speculated that the introduction of an abasic site would disrupt the cooperativity of base stacking and would therefore render the ligation system less tolerant in accommodating further disturbances such as a mismatch.[6] The abasic site was integrated by replacing a central PNA-monomer such that an isosteric dipeptide would be formed upon ligation of two PNA-amino acid conjugates. Two ligation methods were compared.

According to the protocol of native chemical ligation (NCL),[7] the PNA–glycine thioester **1b** was allowed to react with the PNA-conjugate **2b** bearing an *N*-terminal cysteine residue (Fig. 1B). In the event of the ligation, conjugation proceeded smoothly reaching ligation yields of 77% after 150 min. However, ligation product **4b** was formed in high yield independently of the presence of the matched or mismatched template. In contrast, a substantial template effect was obtained by employing a carbodiimide-mediated ligation of the PNA–glycine conjugates **1c** and **2c** shown in Fig. 1C. In the absence of a template the formation of the ligation product **4c** was a slow process. The addition of the perfectly complementary template **3a** enhanced the ligation efficiency by a factor of 5 and led to the formation of **4c** in 37% yield. Importantly, this ligation displayed a remarkable sequence selectivity. The single mismatch template **3b** was ineffective in accelerating the formation of PNA–dipeptide hybrid **4c** and the kinetic profile was virtually indistinguishable from the non-templated reaction.

† PNA = peptide nucleic acid.[12]

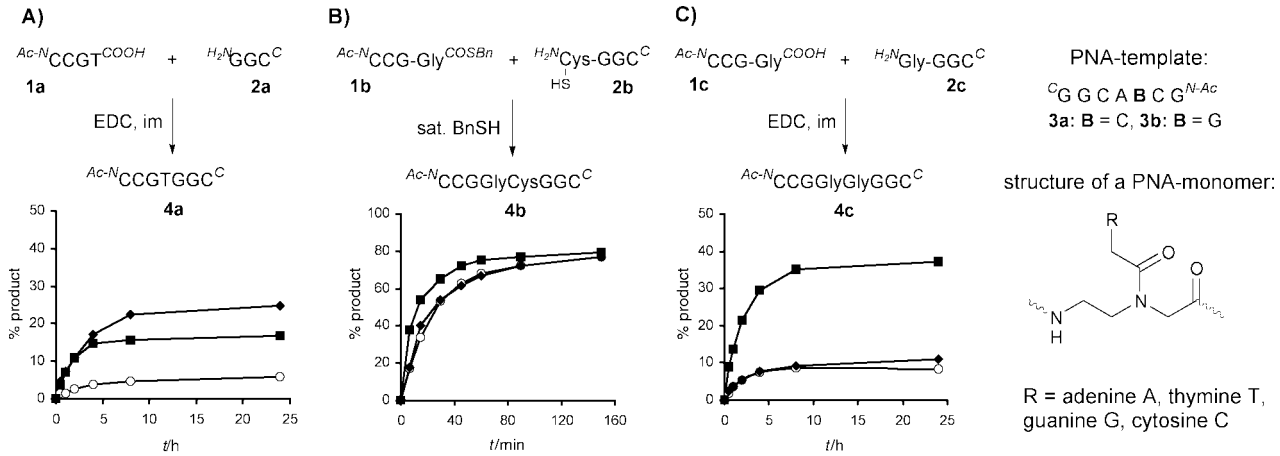

Fig. 1 Time course of the template-controlled ligation of PNA-fragments **1** and **2** in the presence of match-template **3a** (■), mismatch-template **3b** (◆) and in the absence of template (○). A) PNA fragment ligation. B) Native chemical ligation forming an abasic site. C) Carbodiimide-mediated ligation forming an abasic site. Concentration of probes and templates: 160 μM; T = 25 °C; EDC = 1-ethyl-3-(3′-dimethylaminopropyl)carbodiimide hydrochloride; im = imidazole. Yields were determined by subjecting aliquots to HPLC-analysis. Data points were averaged over 3 independent experiments.

 DOI: 10.1039/b106109g

In order to facilitate the detection of the ligation products we attached a fluorescence marker. Acridine was preferred since Göbel and co-workers reported that the use of this duplex-stabilizing dye increased the yield of a template-directed oligomerisation reaction.[8] The acridine-labelled PNAs **2d** and **2e** (Fig. 2) were examined in the template-controlled ligation reactions. As shown in Fig. 2A, in the case of the carbodiimide-mediated reaction with **2d**, an increase of the reaction yield was observable. However, this effect impaired the template selectivity. The ligation of the conjugates **1c** and **2d** performed on the matched template **3a** and the mismatched template **3b** with different efficiency, but the discrimination power did not reach the level of the system in Fig. 1C. The incorporation of acridine resulted in a significant template effect when NCL was employed (Fig. 2B). Interestingly, rather than enhancing the templated ligation the presence of the acridine reduced the yield of the ligation performed in absence of a template. A selectivity to different template sequences was not detectable.

The template-directed PNA ligation system showed a remarkable sensitivity towards the different reaction conditions. It is important to note that due to the short oligomer length fragments **1** and **2** are in a rapid dynamic equilibrium between template-bound and unbound species. Taking into account the low stability of duplex structures involving only two base pairs, it was expected that a template-directed ligation at the mismatched template **3b** was unlikely to occur. However, the mismatched template **3b** was more effective in accelerating the ligation of **1a** and **2a** than the perfectly complementary template **3a**. One way of interpreting this result is that ligation reactions require some flexibility. Additional flexibility was introduced by the incorporation of an abasic site. Indeed, it was the abasic site forming ligation of **1c** with **2c** that showed the highest ligation fidelity (Fig 1C). Support for this idea comes from the pioneering work of Shabarova and the work of others, in which it has been shown that DNA-directed reactions perform well when a distorted nucleic acid duplex is produced.[9] On the contrary, the best performing oligonucleotide ligation to date produces a phosphothioate linkage, which closely resembles the phosphodiester structure as found in DNA.[10] It is therefore conceivable that additional effects influence yield and selectivity of the PNA-ligation. For example, any ligation that proceeds *via* a product-like transition state should be affected by the stability of the evolving duplex. The introduction of the abasic site is expected to disrupt the cooperativity of the "unselective" base-stacking thereby increasing the contribution of the selective Watson–Crick hydrogen-binding. It appears plausible that an unselective hybridisation or an unselective ligation process can be rendered selective when an abasic site is involved.

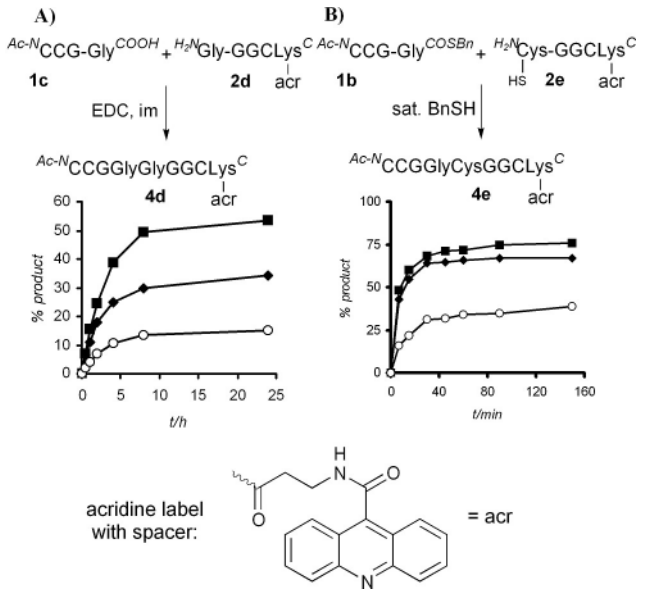

Fig. 2 A) Carbodiimide-mediated ligation of dye-labelled PNA–glycine conjugate **2d**. B) Native chemical ligation of dye-labelled PNA-cysteine conjugate **2e**. Reaction conditions: see Fig. 1.

The ligation method also plays an important role. The insensitivity of NCL to the presence of template was surprising (Fig. 1B). Ghadiri and co-workers were successful in using this ligation reaction for achieving a template-controlled self-replication of a hydrophobic coiled-coil peptide.[11] It can be speculated that nucleic acid-directed reactions that are under control of directed hydrogen bonding show an increased sensitivity to geometric constraints as compared to reactions that are controlled by hydrophobic interactions. In this context, it is a noticable observation that melting experiments with a **3a**–**4b**-mixture failed to show a sigmoidal melting curve, which suggests that binding of the template **3a** to the ligation product **4b** does not suceed.

The examination of the PNA system also provided evidence that the introduction of duplex-stabilising dyes like acridine can increase the overall ligation yield. This is in agreement with previous reports which described a substantial enhancement of oligomerisation yields on acridine-labelled hairpin templates.[8] However, the results shown in Figs 2A and 2B demonstrate that an increase of ligation yield can lead to reduced fidelity of the ligation reaction. It hence seems likely that the acridine-intercalator induced an unspecific association which stabilised both matched and single-mismatched complexes. This indicates that duplex-stabilising dyes should be used with caution when the selectivity of a ligation process is under scrutiny.

In conclusion we have shown that a careful analysis is required before employing PNA-based ligations. The abasic site ligation of PNA-glycine conjugates (Fig. 1C) displays the desired sequence selectivity and DNA-targeting applications will be reported in due course.

This work was supported by the DFG and the Fonds der chemischen Industrie. A. M. is grateful for a Kekulé-fellowship. O. S. is grateful for Liebig- and DFG-fellowships.

Notes and references

1 Reviews on template-controlled reactions of non-nucleic acid substrates: J. K. M. Sanders, *Pure Appl. Chem.*, 2000, **72**, 2265; A. Robertson, A. Sinclair and D. Philp, *Chem. Soc. Rev.*, 2000, **29**, 141.
2 L. Orgel, *Nature*, 1992, **358**, 203; B. Bag and G. v. Kiedrowski, *Pure Appl. Chem.*, 1996, **68**, 2145.
3 P. K. Ghosh, P. Kumar and K. C. Gupta, *J. Indian Chem. Soc.*, 2000, **77**, 109; E. Uhlmann and A. Peyman, *Chem. Rev.*, 1990, **90**, 543.
4 (*a*) M. Bolli, R. Micura, S. Pitsch and A. Eschenmoser, *Chem. Biol.*, 1997, **4**, 309; (*b*) C. Böhler, P. Nielsen and L. Orgel, *Nature*, 1995, **376**, 578; (*c*) I. Kozlov, M. Zielinski, B. Allart, L. Kerremans, A. Aerschot, R. Busson, P. Herdewijn and L. Orgel, *Chem. Eur. J.*, 2000, **6**, 151.
5 P. Nielsen, M. Egholm, R. Berg and O. Buchardt, *Science*, 1991, **254**, 1497.
6 Abasic sites confer a dramatic destabilisation: C. Gelfand, G. Plum, A. Grollman, F. Johnson and K. Breslauer, *Biochemistry*, 1998, **37**, 7321.
7 P. E. Dawson, T. Muir, I. Clark-Lewis and S. B. Kent, *Science*, 1994, **266**, 776.
8 M. Kurz, K. Göbel, C. Hartel and M. Göbel, *Angew. Chem.*, 1997, **109**, 873.
9 N. Dolinnaya, N. Sokolova, O. Gryaznova and Z. Shabarova, *Nucleic Acids Res.*, 1988, **16**, 3721; R. Letsinger, T. Wu and R. Elghanian, *Nucleosides Nucleotides*, 1997, **16**, 643; D. Albagli, R. Atta, P. Cheng, B. Huan and M. Wood, *J. Am. Chem. Soc.*, 1999, **121**, 6954; Z. J. Gartner and D. R. Liu, *J. Am. Chem. Soc.*, 2001, **123**, 6961.
10 Y. Xu and E. Kool, *Nucleic Acids Res.*, 1999, **27**, 875.
11 D. Lee, J. Granja, J. Martinez, K. Severin and R. Ghadiri, *Nature*, 1996, **382**, 525.
12 P. Nielsen, *Curr. Opin. Biotechnol.*, 2001, **12**, 16.

CHEMCOMM
Communication
www.rsc.org/chemcomm

(η^5-Cyclopentadienyl)(κ^3-hydrotris(pyrazolyl)borate)cobalt(II)—the first high-spin cobalt organometallic complex†

Tim J. Brunker, Stephen Barlow and Dermot O'Hare*

Inorganic Chemistry Laboratory, University of Oxford, South Parks Road, Oxford, UK OX1 3QR

Received (in Cambridge, UK) 27th June 2001, Accepted 16th August 2001
First published as an Advance Article on the web 27th September 2001

(η^5-Cyclopentadienyl)(κ^3-hydrotris(pyrazolyl)borate)-cobalt(II) has been synthesised; magnetic and crystallographic data indicate this to be the first example of a high-spin cobalt organometallic complex whilst its pentamethylcyclopentadienyl analogue is found to have a low-spin electronic configuration.

The vast majority of transition metal cyclopentadienyl (Cp) complexes adopt low-spin ground state electronic configurations. When a molecule has a d-electron count such that the high-spin state would require occupancy of an antibonding level (in an axially symmetric system the d-orbitals of π symmetry with respect to the M-centroid axis) in preference to a vacant bonding or non-bonding level (d-orbitals of δ or σ symmetry) the low-spin state is almost invariably observed. A few exceptions that exhibit high-spin behaviour (over all temperatures studied) exist in the first-row transition metal series and include 1,1′-bis(trimethylsilyl)manganocene, bis(1,3-diisopropylindenyl)chromium and the (ferromagnetically coupled) 1,2,3,4-tetra- and 1,2,3,4,5-pentaisopropylcyclopentadienyliron(II) bromide dimers. To date no example of high-spin behaviour has been found for an element from Group 9.[1] We have been interested in synthesising mixed-sandwich compounds containing a Cp and a hydrotris(pyrazolyl)borate (Tp) ligand. In the course of our studies we have isolated CoCpTp, the first example of an organometallic cobalt complex which adopts a maximum spin configuration in preference to a potential low-spin alternative.

Reaction of $CoCp(CO)I_2$[2] with KTp gave $[CoCpTp]^+I^-$, $[\mathbf{1}]^+I^-$ as a dark purple solid (Scheme 1).[3] Reduction of $[\mathbf{1}]^+I^-$ yielded CoCpTp, **1**, as a green-yellow crystalline solid. The pentamethylcyclopentadienyl (Cp*) analogue, CoCp*Tp, **2**, was directly obtained as a red-brown solid from $[CoCp^*Cl]_2$[4] and was oxidised to $[CoCp^*Tp]^+[PF_6]^-$, $[\mathbf{2}]^+[PF_6]^-$, by reaction with $[FeCp_2]^+[PF_6]^-$.

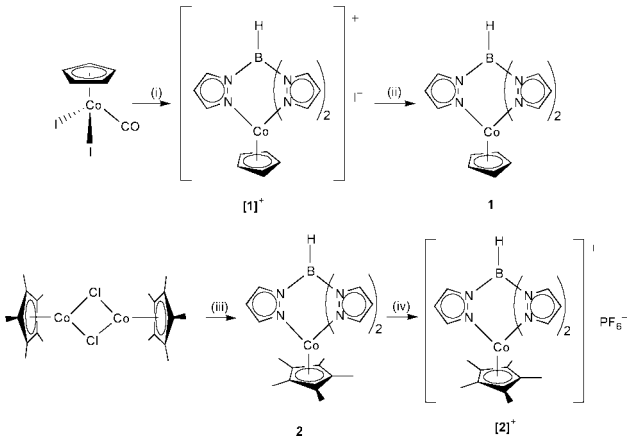

Scheme 1 *Reagents and conditions*: (i) KTp, thf, 98%; (ii) $CoCp_2$, thf, 83%; (iii) KTp, thf, 43%; (iv) $[FeCp_2]^+[PF_6]^-$, MeCN, 72%.

† Electronic supplementary information (ESI) available: full characterisation data for all compounds. See http://www.rsc.org/suppdata/cc/b1/b105661c/

Both **1** and **2** were characterised by elemental analysis, and mass spectrometry (EI). Infra-red spectroscopy revealed characteristic ν_{B-H} at 2494 and 2448 cm^{-1} respectively.† Surprisingly **1**, in contrast to $CoCp_2$ and $CoCp^*_2$, is essentially air-stable in the solid-state and solutions only decompose slowly when exposed to air, whereas **2** is very air-sensitive in solution but less so in the solid-state. Despite being paramagnetic, **1** has a well-defined ^1H NMR spectrum whereas that of **2** is very broad.

SQUID magnetometry measurements were performed on powdered samples of both **1** and **2**. **1** gave a moment of 5.84 μ_B (± 0.1 μ_B) at 300 K which can be accounted for by a high-spin electronic configuration, *i.e.* three unpaired electrons. The large deviation from the spin-only value for $S = 3/2$ (3.87 μ_B) is due to a large spin–orbit contribution to the moment and is only slightly larger than the typical values observed for high-spin Co(II) complexes (4.77–5.40 μ_B).[5] **1** shows non-Curie–Weiss behaviour between 5 and 300 K, see Fig. 1. In contrast, **2** is in the low-spin state over the entire temperature range, and obeys the Curie–Weiss law in the range 40–300 K ($C = 0.51$ emu K mol^{-1}, $\theta = -15.46$ K). It has a moment of 1.95 μ_B at 300 K (spin–only value for $S = 1/2$ is 1.73 μ_B) falling to 1.20 μ_B at 5 K, presumably as a result of intermolecular antiferromagnetic interactions.

Electronic spectra of **1** and **2** in thf are shown in Fig. 2. Three spin-allowed d–d transitions are expected for a high-spin octahedral d^7 ion corresponding to the transitions $^4T_{1g}(F) \rightarrow {}^4T_{2g}$, $^4T_{1g}(F) \rightarrow {}^4T_{1g}(P)$ and $^4T_{1g}(F) \rightarrow {}^4A_{2g}$. For **1**, we observe 3 bands in the near IR/visible whose energies correlate well with reported high-spin octahedral Co(II) spectral data (10800, 20800, 24400 cm^{-1}), but whose relative intensities are increased as a consequence of the symmetry lowering in **2** from O_h.[5] In the spectrum of **2**, the d–d transitions are only poorly resolved and assignment is difficult. The spectrum is similar to that of cobaltocene where transitions to excited doublet states of similar energy overlap and are also poorly resolved.[6]

An ESR (X-band) spectrum of **2** was obtained in a frozen toluene solution at 15 K and a rhombic g tensor was observed with hyperfine coupling on all 3 components to ^{59}Co ($I = 7/2$). The spectrum is similar to those observed for cobaltocenes[7,8] and monomeric CoCp*X (X = Cl, NH_2, OEt) and CoCp*XL (X = Cl, L = PMe_3 and py) species,[4] confirming a low-spin $^2\Pi$ ground state. In comparison **1** was silent at room temperature

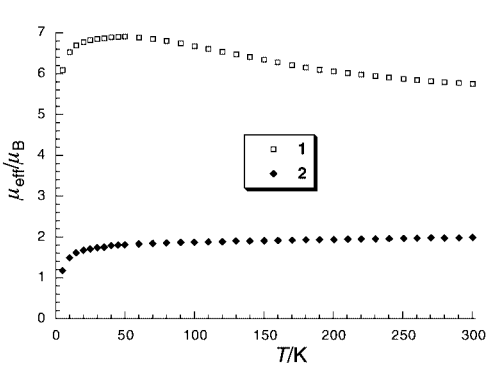

Fig. 1 Plot of μ_{eff} (μ_B) against T (K) for **1** and **2**.

 DOI: 10.1039/b105661c

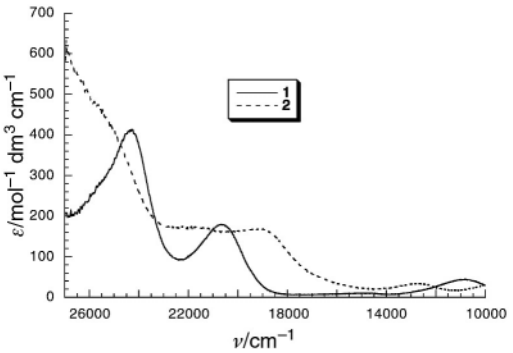

Fig. 2 Electronic spectra of **1** and **2** in thf solution.

and below 20 K in toluene solution, indicating a very different ground state electronic configuration to that of **2**.

Spectral and magnetic data support a greater ligand-field splitting in **2** as compared to **1** resulting in different electronic ground states, a phenomenon also observed in manganocenes but never before for Co.[9] The stronger electron-donating ability of Cp* in comparison to Cp has been demonstrated to lead to an increased ligand-field splitting in the decamethylmetallocenes compared to unsubstituted metallocenes,[7] and we can rationalise the difference between **1** and **2** in these terms.

Single crystals of **1** were grown by slow-cooling of a saturated pentane solution to −35 °C; the molecular structure is shown in Fig. 3.‡ Comparison of the Co–C bond lengths (average 2.290(2) Å) and the Co–Cp(centroid) distance (1.97 Å) with a range of previously reported Co(II)Cp compounds incorporating various ancillary ligands (see Table 1) indicates that these parameters lie well outside the limits previously observed for low-spin complexes. This increase is clearly consistent with the high-spin electronic configuration indicated by the other data: double occupation of the antibonding π level (assuming the symmetry can be well approximated as $C_{\infty v}$) necessary for a high-spin d^7 configuration, $[\delta^4\sigma^1\pi^2]$ or $[\sigma^2\delta^3\pi^2]$, will lead to a weakening of the Co–Cp bonds compared to the low-spin state where this is only singly occupied $[\delta^4\sigma^2\pi^1]$. The Co–N bond lengths (av. 2.091(2) Å) are slightly shorter (significant at the 3σ level) than those in $CoTp_2$ (av. 2.129(7) Å),[10] which has a high-spin configuration.[11]

The air-stable 18 electron species $[\mathbf{1}]^+I^-$ and $[\mathbf{2}]^+[PF_6]^-$ are diamagnetic and were characterised by ^1H, ^{13}C and ^{11}B NMR spectroscopy, showing resonances consistent with axially symmetric species.† IR spectroscopy revealed ν_{B-H} typical for κ^3-Tp ligands of 2501 and 2505 cm^{-1} respectively. The redox couple $[\mathbf{1}]^+/\mathbf{1}$ was measured at −590 mV *versus* ferrocenium/ferrocene in CH_2Cl_2 and the $[\mathbf{2}]^+/\mathbf{2}$ couple at −890 mV. **2** is more readily oxidised than **1** despite the high-spin ground state

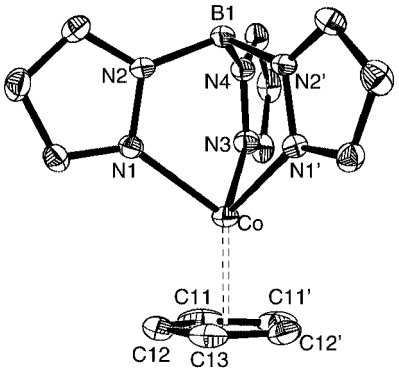

Fig. 3 Molecular structure of **1** with thermal ellipsoids at 50% probability (hydrogen atoms have been omitted for clarity). Primed atoms are generated by symmetry. Selected interatomic distances (Å): Co–N1 2.103(1), Co–N3 2.069(2), Co–C11 2.305(2), Co–C12 2.286(2), Co–C13 2.268(3).

Table 1 Summary of structural parameters for selected CpCo(II) complexes

Compound	Co–C (average)/Å	Co–Cp (centroid)/Å	Ref.
$CoCp_2$	2.096(8)	1.70	14
$Co(C_5(i\text{-}Pr)_3H_2)_2$	2.122(7)	1.75	15
CoCp*(acac)	2.089(5)	1.70	16
$[Co(C_5(i\text{-}Pr)_4H)Cl]_2$	2.061(4)	1.68	17
CoCp*(py)Cl	2.076(2)	1.70	18
CoCpTp	2.290(2)	1.97	This work

acac = acetylacetonate, py = pyridine.

of **1**. Both compounds are less readily oxidised than $CoCp_2$[12] and are more readily oxidised than $CoTp_2$.[13]

We have succeeded in isolating a hitherto unseen high-spin state for a Co organometallic compound by synthesis of a mixed-sandwich complex with Cp and the weak-field Tp ligand. Investigations utilising other metals from across the first transition series also illustrate a tendency towards high-spin configurations in such complexes and will be reported in future.

We thank the EPSRC for a studentship (T. J. B.) and A. R. Cowley and T. Hascall for crystallographic assistance.

Notes and references

‡ *Crystal data*: For **1**, $C_{14}H_{15}BCoN_6$, M = 337.06, orthorhombic, a = 8.1066(3), b = 10.3543(3), c = 17.9336(6) Å, V = 1505.31(9) Å^3, T = 150(2) K, space group $Pcmn$, Z = 4, μ = 1.144 mm^{-1}, 3120 total reflections, 1791 unique (R(int) = 0.0203), R = 0.031, wR = 0.0689 for $I > 2\sigma(I)$.

CCDC reference number 168886. See http://www.rsc.org/suppdata/cc/b1/b105661c/ for crystallographic data in CIF or other electronic format.

1 H. Sitzmann, *Coord. Chem. Rev.*, 2001, **214**, 287 and references therein.
2 R. B. King, *Inorg. Chem.*, 1966, **5**, 82.
3 The syntheses of $[\mathbf{1}]^+$ and $[\mathbf{2}]^+$ have previously been claimed but no characterising data was reported. An attempt to reduce $[\mathbf{1}]^+$ to **1** was reported to be unsuccessful. See D. J. O'Sullivan and F. J. Lalor, *J. Organomet. Chem.*, 1973, **57**, C58.
4 U. Koelle, B. Fuss, M. Belting and E. Raabe, *Organometallics*, 1986, **5**, 980.
5 L. Banci, A. Bencini, C. Benelli, D. Gatteschi and C. Zanchini, *Struct. Bonding (Berlin)*, 1982, **52**, 37.
6 J. Weber, A. Goursot, E. Penigault, J. H. Ammeter and J. Bachmann, *J. Am. Chem. Soc.*, 1982, **104**, 1491.
7 J. L. Robbins, N. Edelstein, D. Spencer and J. C. Smart, *J. Am. Chem. Soc.*, 1982, **104**, 1882.
8 M. P. Castellani, S. J. Geib, A. L. Rheingold and W. C. Trogler, *Organometallics*, 1987, **6**, 1703.
9 J. L. Robbins, N. M. Edelstein, S. R. Cooper and J. C. Smart, *J. Am. Chem. Soc.*, 1979, **101**, 3853.
10 M. R. Churchill, K. Gold and C. E. Maw, *Inorg. Chem.*, 1970, **9**, 1597.
11 C. Hannay, M.-J. Hubin-Franskin, F. Grandjean, V. Brois, J.-P. Itie, A. Polian, S. Trofimenko and G. J. Long, *Inorg. Chem.*, 1997, **36**, 5580.
12 We have measured the $CoCp_2^+/CoCp_2$ couple at −1320 mV and the CoCp*Cp$^+$/CoCp*Cp couple at −1625 mV *vs.* ferrocenium/ferrocene in CH_2Cl_2.
13 C. Janiak, T. G. Scharmann, J. C. Green, R. P. G. Parkin, M. J. Kolm, E. Riedel, W. Mickler, J. Elguero, R. M. Claramunt and D. Sanz, *Chem. Eur. J.*, 1996, **2**, 992.
14 W. Bunder and E. Weiss, *J. Organomet. Chem.*, 1975, **92**, 65.
15 D. J. Burkey, M. L. Hays, R. E. Duderstadt and T. P. Hanusa, *Organometallics*, 1997, **16**, 1465.
16 M. E. Smith and R. A. Andersen, *J. Am. Chem. Soc.*, 1996, **118**, 11119.
17 F. Baumann, E. Dormann, Y. Ehleiter, W. Kaim, J. Karcher, M. Kelemen, R. Krammer, D. Saurenz, D. Stalke, C. Wachter, G. Wolmershauser and H. Sitzmann, *J. Organomet. Chem.*, 1999, **587**, 267.
18 E. Raabe and U. Koelle, *J. Organomet. Chem.*, 1985, **279**, C29.

CHEMCOMM Communication
www.rsc.org/chemcomm

Diastereoselectivity controlled by electrostatic repulsion between the negative charge on a trifluoromethyl group and that on aromatic rings†

Toshimasa Katagiri, Sachiko Yamaji, Michiharu Handa, Minoru Irie and Kenji Uneyama*

Department of Applied Chemistry, Faculty of Engineering, Okayama University, Tsushimanaka 3-1-1, Okayama 700-8530, Japan. E-mail: tkata@cc.okayama-u.ac.jp

Received (in Cambridge, UK) 26th June 2001, Accepted 29th August 2001
First published as an Advance Article on the web 27th September 2001

Intramolecular electrostatic repulsions between the local negative charge on a trifluoromethyl group and that on the *ortho* position of an aryl moiety of a nucleophile was found to be a controlling factor of the diastereoselectivity in a cyclopropanation reaction, in which the electrostatic repulsion was evaluated quantitatively.

Non-covalent interactions are not only the basis of the functional properties of molecules[1] but are also fundamental to the explanation and prediction of relationships between chemical structure and reactivity. In the field of organic chemistry, the exchange repulsion, or the so-called steric repulsion, has been paid much attention among so many repulsive forces. Thus have been predicted and explained the stereoselectivities of reactions using the CPK model, a substitute for the Van der Waals surface.[2] On this basis, fluorinated groups have sometimes been considered to resemble their parent non-fluorinated groups in their steric size, which is consistent with the so-called mimic effect of fluorinated bioactive compounds.[3]

In spite of the situation, the 'size' of the trifluoromethyl group (CF_3) is still of controversy.[3,4] The steric effect of CF_3, especially in nucleophilic reactions, has also been suggested to be comparable to that of isopropyl or *tert*-butyl groups.[5] This unexpected large steric effect of CF_3 has been attributed to a possible participation of electrostatic repulsions although quantitative confirmation or proof is still lacking. The primary aim of this report is to propose the electrostatic interaction of CF_3; the secondary aim is to develop a method for the quantitative estimation of the electrostatic interaction around CF_3.

Very recently, we have developed a nucleophilic cyclization of 1-aryl-1-cyano-3-(*p*-toluenesulfonyloxy)-4,4,4-trifluorobutanes to produce cyclopropanes *via* cyano-stabilized carbanions (Scheme 1),[6] in which a stereochemical inversion on the carbon bearing the trifluoromethyl and hydroxy groups was observed.†

Detailed results of the present study on the diastereoselectivity of the cyclopropane products having various aryl moieties are summarized in Table 1. Except for Ar = C_6F_5, the major isomers were *cis* in which the CF_3 and aryl groups were *anti*. The results shown in Table 1 demonstrate that the orders of these de values are dependent upon the substituents on the aromatic rings. However, this order of de values cannot be explained in terms of electronic effects of substituents or by conventional bulkiness. For instance, the de for *p*-MeO-C_6H_4 (entry 3) is lower than that of C_6H_5 (entry 1), and the de for naphthyl (entry 2) is much lower than that of *p*-MeO-C_6H_4 (entry 3). Moreover, the compound having C_6F_5 as the aryl moiety gave the opposite diastereomer (*trans*) as a major product to those of other substituents, and whose structure was confirmed by X-ray crystallographic analysis.[7]‡ This result implies that the C_6F_5 moiety is 'less bulky' than CN or CF_3.

† Electronic supplementary information (ESI) available: general experimental methods and typical reaction procedure. See http://www.rsc.org/suppdata/cc/b1/b105602f/

The CF_3 attached with some alkyl moiety should have a negative charge due to the strong electron withdrawing effect of the group. Here, the aryl moiety of the intermediate is π-conjugated to the anion center; thus, the moiety should also be negatively charged. Therefore, the CF_3 should make a repulsive interaction toward the negatively charged aromatic ring. The diastereoselection will therefore be controlled by the energetic difference between the two conformations of the intermediates, A and B, in Scheme 1. Conformation A has a structure in which CF_3 and the aryl group are *anti*, to give the *cis* product as the major product except for when Ar = C_6F_5. Meanwhile, conformation B should have a repulsive electrostatic interaction of the negative charge on CF_3 with that of the aryl group, which makes this structure rather unstable. It is noteworthy that the local minimum structure of this *syn* intermediate, which was estimated by geometry optimization by PM3, has no direct contact of the Van der Waals surfaces of CF_3 and aryl moieties.

This *syn* structure suggests that the fluorine atoms on CF_3 should have the largest overlapping of their reflection on the *ortho* carbon of an aryl moiety (γ from the carbanion center). Thus, we estimate the effective negative charges on these positions of the anion moiety (A in Scheme 1) by the Mulliken method of PM3 level MO calculations. The sum of the electrostatic charges on these two *ortho* carbons, an estimated effective charge (*q*), is also summarized in Table 1, and the free

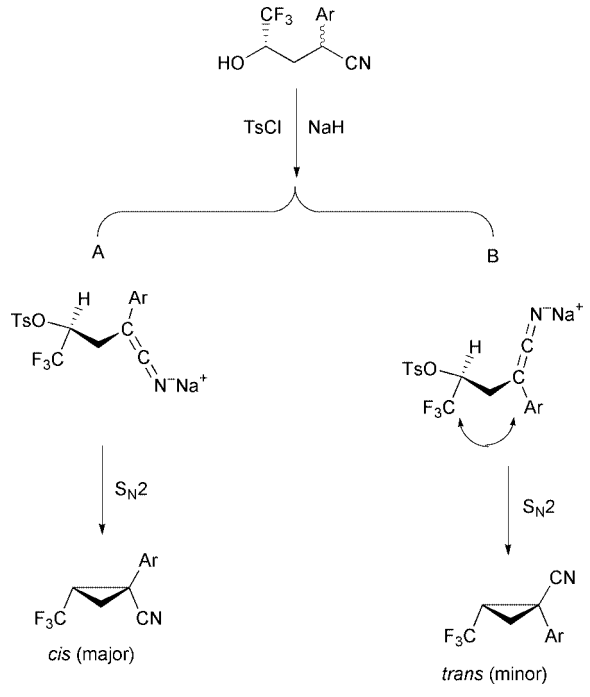

Scheme 1

 DOI: 10.1039/b105602f

Table 1 Diastereoselectivity depending on the substituents with the sum of charges on *ortho* carbons

Entry	Aryl moiety[a]	de (%)	ln (major/minor)	q
1		80.7 ± 3.5	2.24 ± 0.20	−0.36
2	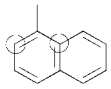	46.6 ± 8.7	1.01 ± 0.23	−0.22
3	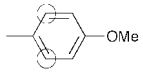	63.0 ± 2.4	1.48 ± 0.08	−0.29
4	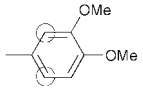	83.5 ± 1.3	2.41 ± 0.09	−0.37
5	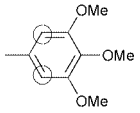	89.6 ± 1.1	2.90 ± 0.11	−0.49
6	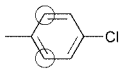	65.8 ± 4.3	1.58 ± 0.16	−0.34
7	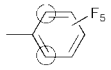	−77.0 ± 3.2[b]	−2.04 ± 0.15[b]	−0.04
8	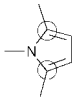	>98[c]	>4.60[c]	−0.62

[a] The circles indicate the *ortho* positions for estimation of q values. [b] The major diastereomer was found to be *trans*, see text and ref. 6. [c] Only one diastereomer was found.

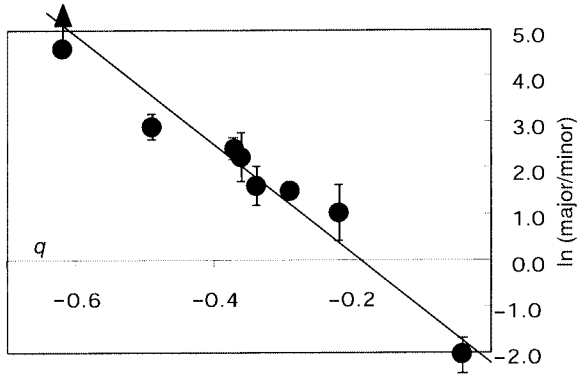

Fig. 1 Relationship between discrimination energy and the sum of charges on *ortho* positions.

energy relationship of q to the logarithm of the ratio of the two diastereomers is illustrated in Fig. 1.[8]

The correlation coefficient of this relationship shown in Fig. 1 is 0.965, that is, the relation is 'satisfactorily' linear. This linear relationship is consistent with our working hypothesis that the diastereoselectivity of the reaction is controlled by electrostatic repulsion between CF_3 and the aryl moiety.[6] Here, the destabilizing energy by the electrostatic repulsion should be $-qq'/4\pi\varepsilon_0 r$, where q is the effective negative charge on the aryl moiety, q' is that of CF_3, and r is the distance between the negative charges. In the case of C_6H_5 as the Ar group, the equation estimates a repulsion energy between CF_3 and Ar to be 2.8 kcal mol^{-1}, and that between CF_3 and CN to be 1.6 kcal mol^{-1}; thus, the energetic difference between conformers A and B in Scheme 1 is estimated to be 1.2 kcal mol^{-1}, which is very close to the known value for 80% de, 1.3 kcal mol^{-1}.[9] It is also of note that the anionized C_6F_5 group has a relatively small electrostatic repulsion toward CF_3, which is consistent with a known inverse quadrupole of hexafluorobenzene.[10] The q value for C_6F_5 was estimated to be −0.04 e, thus the repulsion energy of CF_3 to C_6F_5 is estimated to be only 0.3 kcal mol^{-1}, which is apparently smaller than that of CF_3 to CN (1.6 kcal mol^{-1}). Therefore, the diastereoselectivity of the product where Ar = C_6F_5 is inverted compared with the other cases.

In conclusion, we have clarified that CF_3 should be considered to be a negatively charged moiety, and its interaction can be estimated by the Coulomb equation. Such an electrostatic repulsion, a longer distance interaction than the Van der Waals repulsion, should be utilizable for discrimination between functional groups and/or moieties having similar sizes with different charges.[11] Further utilization of this function for CF_3 as a chiral auxiliary and chiral ligand are now in progress in our laboratory.

We thank the SC-NMR Laboratory of Okayama University for ^{19}F and ^{1}H NMR analyses, and the Venture Business Laboratory of Graduate School, Okayama University, for X-ray crystallographic analysis. We are grateful for financial support for this work from Monbusho (Grant-in-Aid for Scientific Research on Priority Areas, No.706 Dynamic Control of Stereochemistry, and No. 12650854), and by The Shorai Foundation for Science and Technology.

Notes and references

‡ *Crystal data* for 2-trifluoromethyl-1-(2,3,4,5,6-pentafluorophenyl)cyclopropyl cyanide (major product, entry 7 in Table 1): $C_{11}H_3F_8N$; M = 301.14, rhombohedral, space group $R\bar{3}$; a = 10.6401(4) Å, α = 111.8530(4)°, V = 835.60(6) Å^3, Z = 3, D_c = 1.795 g cm^{-3}; μ = 2.01 cm^{-1} for Mo Kα radiation (λ = 0.7107 Å). The structure was solved by direct methods (SHELXS86), and refined by a full-matrix least squares method. Final R was 0.032 and R_w was 0.031 for 1236 reflections with $I_0 > 0.80\sigma(I_0)$. Reflection/parameter ratio was 6.31, goodness of fit indicator was 1.41. Max shift/error in final cycle was 0.00. CCDC reference number 169307. See http://www.rsc.org/suppdata/cc/b1/b105602f/ for crystallographic data in CIF or other electronic format.

1 N. Israelachivili, *Intermolecular and Surface Forces, 2nd edn*, Academic Press, London, 1985.
2 A. Bondi, *J. Phys. Chem.*, 1964, **68**, 441.
3 M. Schlosser and D. Michel, *Tetrahedron*, 1996, **52**, 99.
4 T. Katagiri, *Enantiocontrolled Synthesis of Fluoro-Organic Compounds: Stereochemical Challenges and Biomedicinal Targets*, ed. V. A. Soloshonok, Wiley, Chichester, 1999, p. 161; T. Katagiri and K. Uneyama, *J. Fluorine Chem.*, 2000, **105**, 285.
5 T. Nagai, G. Nishioka, M. Koyama, A. Ando, T. Miki and I. Kumadaki, *J. Fluorine Chem.*, 1992, **57**, 29.
6 (*a*) T. Katagiri, M. Irie and K. Uneyama, *Tetrahedron: Asymmetry*, 1999, **10**, 2583; (*b*) T. Katagiri, M. Irie and K. Uneyama, *Org. Lett.*, 2000, **2**, 2423.
7 For crystallographic analysis of the major product of entry 1, see ref. 6*a*; that of entries 4 and 8, see ref. 6*b*.
8 In the case of the compound with the 2,5-dimethylpyrrolyl group, only one diastereomer was detected by ^{19}F NMR and GC analysis in five repeated experiments. Thus, we concluded that the diastereoselectivity would be >98% de, based on the limitations of these analyzing methods.
9 J. Seyden-Penne, *Chiral Auxiliaries and Ligands in Asymmetric Synthesis*, John Wiley & Sons, New York, 1995, p. 4.
10 For a recent review see: C. A. Hunter, K. R. Lawson, J. Perkins and C. J. Urch, *J. Chem. Soc., Perkin Trans. 2*, 2001, 651.
11 G. D. Purvis III, *J. Comput.-Aided Mol. Des.*, 1991, **5**, 55.

CHEMCOMM
Communication
www.rsc.org/chemcomm

Solid state coordination chemistry: construction of 2D networks and 3D frameworks from phosphomolybdate clusters and binuclear Cu(II) complexes. The syntheses and structures of $[\{Cu_2(tpypyz)(H_2O)_2\}(Mo_5O_{15})(HOPO_3)_2]\cdot nH_2O$ [n = 2, 3; tpypyz = tetra(2-pyridyl)pyrazine]†

Eric Burkholder and Jon Zubieta*

Department of Chemistry, Syracuse University, Syracuse, NY 13200, USA. E-mail: jazubiet@syr.edu

Received (in Cambridge, UK) 26th June 2001, Accepted 29th August 2001
First published as an Advance Article on the web 27th September 2001

The hydrothermal reaction of MoO_3, $Cu(C_2H_3O_2)_2\cdot H_2O$, tpypyz, H_3PO_4 and H_2O yields a 2D material, $[\{Cu_2(tpypyz)(H_2O)_2\}(Mo_5O_{15})(HOPO_3)_2]\cdot 2H_2O$ (1·2H$_2$O), constructed from $\{Mo_5O_{15}(HOPO_3)_2\}^{4-}$ clusters linked through $\{Cu_2(tpypyz)(H_2O)_2\}^{2+}$ components; in contrast, use of Cu_2O in the synthesis in place of $Cu(C_2H_3O_2)_2\cdot H_2O$ yields a 3D material $[\{Cu_2(tpypyz)(H_2O)_2\}(Mo_5O_{15})(HOPO_3)_2]\cdot 3H_2O$ (2·3H$_2$O), constructed from the same building blocks as 1·2H$_2$O.

Inorganic oxides are ubiquitous materials exhibiting a vast compositional range and significant structural versatility,[1] characteristics which endow these phases with useful physical properties which can be exploited in applications ranging from heavy construction to microelectronics.[2,3] The design of new materials is driven by synthesis, and several strategies for the construction of specific oxide architectures have been described. One approach relies upon the profound influences of organic components on oxide structrures,[4] as manifested in zeolites,[5] mesoporous materials of the MCM-41 class,[6] and oxometal phosphates with entrained organic cations.[7] Another approach employs well-defined oxometalate clusters as molecular building blocks in the self-assembly of ordered oxide structures.[8–12] We recently demonstrated the confluence of these strategies in the design of the 2D network $[\{Cu_2(tpypyz)(H_2O)_2\}(Mo_5O_{15})(O_3PCH_2CH_2PO_3)]$, in which molybdate clusters are linked in one-dimension through organic tethers and crosslinked by binuclear Cu(II) complexes into a 2D network.[13] A prominent feature of the structural chemistry of this and related materials is the requirement of the secondary metal complex, such as Cu(II) organoimine, for the isolation of the product. This observation suggests that the well-known phosphomolybdate cluster $\{Mo_5O_{15}(HOPO_3)_2\}^{4-}$ could serve as one molecular building block, with an appropriate binuclear secondary metal–ligand complex acting as a linker in the construction of the extended structure. This expectation was realized in the reaction of $\{Mo_5O_{15}(HOPO_3)_2\}^{4-}$ with copper and a binucleating ligand to produce crystalline solid state oxides. However, minor variations in reaction conditions unexpectedly resulted in significant structural changes, as manifested in the 2D network material $[\{Cu_2(tpypyz)(H_2O)_2\}(Mo_5O_{15})(HOPO_3)_2]\cdot 2H_2O$ (1·2H$_2$O) and the 3D framework $[\{Cu_2(tpypyz)(H_2O)_2\}(Mo_5O_{15})(HOPO_3)_2]\cdot 3H_2O$ (2·H$_2$O).

The hydrothermal reaction of MoO_3, $Cu(C_2H_3O_2)_2\cdot H_2O$, tpypyz (tetrapyridylpyrazine), H_3PO_4 and H_2O in the mole ratio 5.80 : 2.14 : 1.00 : 4.85 : 2740 at 150 °C for 48 h yields dark green crystals of 1·2H$_2$O in 40% yield as a monophasic product.‡ In contrast, the reaction of MoO_3, Cu_2O, tpypyz, H_3PO_4, and H_2O in the mole ratio 5.89 : 1.20 : 1.00 : 7.00 : 2670 at 150 °C for 48 h yielded green crystals of 2·3H$_2$O in 35% yield. The Cu(I) starting material is required for the isolation of **2**, as is the increased ratio of MoO_3 to copper precursor since part of the molybdate is employed in the oxidation of the Cu(I) to Cu(II). The IR spectra of **1** and **2** are characterized by a series of seven median intensity bands in the 1000–1560 cm^{-1} region associated with the tpypyz ligand and two strong bands at *ca.* 921 and 897 cm^{-1} assigned to ν(Mo=O). A prominent feature at 785 cm^{-1} may be attributed to ν(Mo–O–M).

As shown in Fig. 1, the structure of 1·2H$_2$O§ consists of 2D sheets, constructed from $\{Mo_5O_{15}(HOPO_3)_2\}^{4-}$ clusters[14] linked through $\{Cu_2(tpypyz)(H_2O)_2\}^{2+}$ subunits. Each binuclear copper component links three phosphomolybdate clusters, while each cluster is in turn bonded to three binuclear copper subunits, which bridge to six neighboring clusters of the network. The periphery of a phosphomolybdate cluster is decorated by four corner-sharing copper(II) octahedra.

The phosphomolybdate cluster $\{(Mo_5O_{15})(HOPO_3)\}^{4-}$ consists of a ring of edge- and corner-sharing $\{MoO_6\}$ octahedra capped on both poles by phosphate tetrahedra sharing three vertices with the ring molybdenum centers. The pendant oxygen atom of each phosphorus tetrahedron is protonated, as indicated by charge balance considerations and confirmed by valence sum calculations. The copper coordination of the $\{Cu_2(tpypyz)(H_2O)_2\}^{4+}$ subunit is defined by two bridging oxo-groups from the phosphomolybdate clusters, three nitrogen donors from the chelating and bridging tpypyz ligands and an aqua ligand. The geometry is the common '4 + 2' variant with normal distances in the equatorial plane [Cu–O, 1.932(3) Å; 3 × N, 1.969(3) Å (ave)] and long axial distances [Cu–O(oxo), 2.409 (3)Å; Cu–O(aqua), 2.665(5) Å]. The metal-oxide substructure $\{Cu_2Mo_5O_{15}(HOPO_3)_2\}$ is 2D with intralamellar cavities occupied

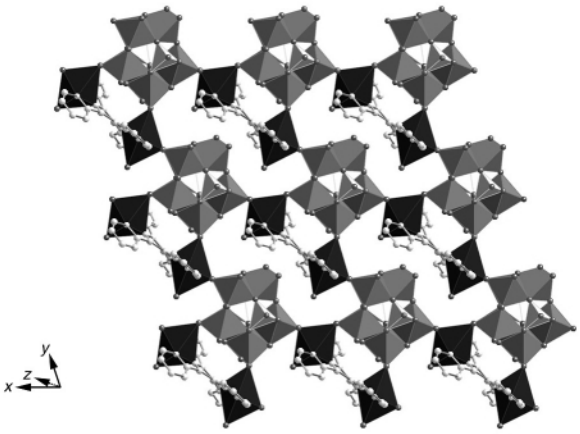

Fig. 1 Polyhedral view of the network structure of 1·2H$_2$O parallel to the crystallographic *c* axis. For colour version see ESI.†

† Electronic supplementary information (ESI) available: colour polyhedral representations of the structures 1·2H$_2$O and 2·3H$_2$O. See http://www.rsc.org/suppdata/cc/b1/b105563c/

 DOI: 10.1039/b105563c

by the organic component and the water molecules of crystallization.

It is now well-documented that variations in hydrothermal reaction conditions can afford quite different products. In this case, substitution of Cu_2O for $Cu(C_2H_3O_2)_2{\cdot}H_2O$ results in the isolation of $[\{Cu_2(tpypyz)(H_2O)_2\}(Mo_5O_{15})(HOPO_3)_2]{\cdot}3H_2O$§ (**2**·3$H_2O$), a material constructed from the same building blocks as **1**, in the same ratios, but with a dramatically different structure. As shown in Fig. 2(a), the structure of **2** is a 3D framework constructed from phosphomolybdate clusters and Cu(II)–tpypyz binuclear subunits. As illustrated in Fig. 2(b), the building blocks connect to form 1D $\{Cu_2Mo_5O_{15}(HOPO_3)_2\}$ chains, in contrast to the $\{Cu_2Mo_5O_{15}(HOPO_3)_2\}$ sheets formed in **1**. The Cu sites of a given chain link through the tpypyz bridges to Cu sites on four adjacent chains to provide the 3D connectivity.

The structural differences between **1** and **2** are reflected in their thermal behavior. Thus, the thermogravimetric curve for **1** exhibits a weight loss of *ca*. 2.5% between 110 and 125 °C, corresponding to the loss of two molecules of water of crystallization. In contrast, the dehydration process for **3** occurs at 170–190 °C (3.2% weight loss; 3.6% theoretical for three water molecules of crystallization). The mechanism of dehydration is dependent upon topological and energetic considerations.[15] Consequently, a lower dehydration energy is associated with accessibility of water molecules to crystal void volume such as channels or interlamellar regions. The more open layered structure of **1**, in contrast to the more dense 3D framework of **2**, is consistent with the dehydration curves. A second dehydration step, corresponding to the loss of the aqua ligands associated with the Cu(II) sites occurs at 225–240 °C for **1** and at 250–280 °C for **2**. Both **1** and **2** exhibit ligand loss in steps at 350–450 °C to give a mixture of P_2O_5 and MoO_3 as the final residues.

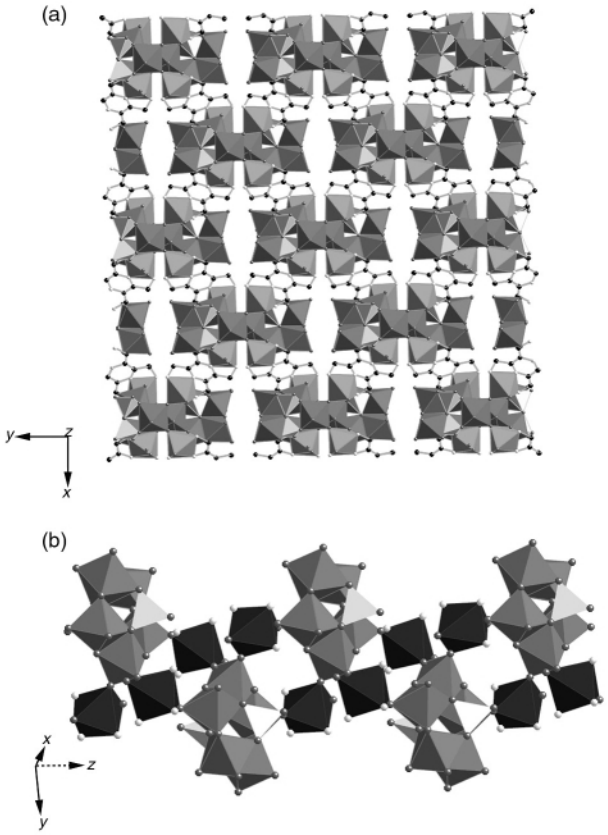

Fig. 2 (a) Polyhedral representation of the 3D structure of **2**·3H_2O viewed parallel to the *c* axis. (b) View of the 1D chain $\{Cu_2Mo_5O_{15}(HOPO_3)_2\}$ substructure of **2**. For colour versions see ESI.†

The structures of this study demonstrate that a building block approach to solid oxide materials based on molecular cluster precursors is practical.[16] However, the strategy relies on the judicious choices of a secondary metal and ligand subunits, such that the final structure reveals a synergism between the basicity of surface oxo-groups on the cluster, the coordination preferences of the secondary metal and the ligand geometry and denticity. Furthermore, the inherent versatility of metal coordination modes produces a certain unpredictability in the linkages between building blocks as manifested in this instance in the contrasting dimensionalities of the structures of **1** and **2**. While the information required for the self-assembly of the extended hybrid structures is present at the molecular level in the component building blocks, this provides only a broad blueprint for design, while further elaboration relies upon empirical observation of novel architectures derived from manipulation of reaction conditions and selection of component substructures.

This work was supported by a grant from the National Science Foundation (CHE9987471).

Notes and references

‡ The product purity was checked by powder X-ray diffraction.

§ *Crystal data* for $C_{24}H_{26}Cu_2Mo_5N_6O_{27}P_2$ (**1**·2H_2O): M = 1499.23, triclinic, space group $P\bar{1}$, a = 11.0736(5), b = 11.0775(5), c = 17.7972(8) Å, α = 85.178(1), β = 79.964(1), γ = 68.271(1)° V = 1995.5(2) Å^3, Z = 2, D_c = 2.494 g cm^{-3}, T = 90 K; structure solution and refinement based on 5720 reflections converged at R_1 = 0.0310 and wR_2 = 0.0687.

For $C_{24}H_{28}Cu_2Mo_5N_6O_{28}P_2$ (**2**·3H_2O): M = 1517.24, monoclinic, space group $C2/c$, a = 18.3609(1), b = 16.0705(1), c = 13.4127(9) Å, β = 102.6690(1)°, V = 3861.3(4) Å^3, Z = 4, D_c = 2.610 g cm^{-3}, T = 90(2) K; structure solution and refinement based on 2789 reflections converged at R_1 = 0.0475 and wR_2 = 0.0981.

CCDC reference numbers 167763 and 167764. See http://www.rsc.org/suppdata/cc/b1/b105563c/ for crystallographic data in CIF or other electronic format.

1 A. F. Wells, *Structural Inorganic Chemistry*, 4th edn., Oxford University Press, Oxford, 1975.
2 A. K. Cheetham, *Science*, 1994, **264**, 794.
3 W. Buchner, R. Schiebs, G. Winter and K. H. Buchel, *Industrial Inorganic Chemistry*, VCH, New York, 1989; *Modern Oxide Materials*, ed. B. Cockayne and D. W. Jones, Academic Press, New York, 1972.
4 S. I. Stupp and P. V. Braun, *Science*, 1997, **277**, 1242 and references therein.
5 M. L. Occelli and H. C. Robson, *Zeolite Synthesis*, American Chemical Society, Washington, DC, 1989.
6 C. T. Kresge, M. E. Leonowicz, W. J. Roth, J. C. Vartuli and J. S. Beck, *Nature*, 1997, **359**, 710.
7 R. C. Haushalter and L. A. Mundi, *Chem. Mater*., 1992, **4**, 31; M. I. Khan, L. M. Meyer, R. C. Haushalter, C. L. Schwietzer, J. Zubieta and J. L. Dye, *Chem. Mater*., 1996, **8**, 43.
8 P. J. Hagrman, D. Hagrman and J. Zubieta, *Angew. Chem., Int. Ed*., 1999, **38**, 2638.
9 A. Müller, E. Krickemeyer, S. K. Das, P. Kögerler, S. Sarkar, H. Bögge, M. Schmidtmann and S. Sarkar, *Angew. Chem., Int. Ed*., 2000, **39**, 1612.
10 M. I. Khan, *J. Solid State Chem*., 2000, **152**, 105.
11 M. Sadakane, M. H. Dickman and M. T. Pope, *Angew. Chem., Int. Ed*., 2000, **39**, 2914.
12 D. Hagrman, P. J. Hagrman and M. Zubieta, *Angew. Chem., Int. Ed*., 1999, **38**, 3165; D. Hagrman, P. Hagrman and J. Zubieta, *Inorg. Chim. Acta*, 2000, **300**–**302**, 212.
13 R. C. Finn and J. Zubieta, *Inorg. Chem*., 2001, **40**, 2466.
14 B. Hedman, *Acta Chem. Scand*., 1977, **27**, 3335.
15 S. Petit and G. Coquerel, *Chem. Mater*., 1996, **8**, 2247.
16 For a more general application of the building block approach, see also: M. J. Zaworotko, *Angew. Chem., Int. Ed*., 2000, **39**, 3052; G. Ferey, *J. Solid State Chem*., 2000, **152**, 37.

CHEMCOMM
Communication
www.rsc.org/chemcomm

Extreme (10^9) acidification of adenine-NH_2 in an open platinated nucleobase quartet. A pH switch with potential as a biological acid/base catalyst†

Marc S. Lüth, Michael Willermann and Bernhard Lippert*

Fachbereich Chemie, Universität Dortmund, 44221 Dortmund, Germany.
E-mail: lippert@pop.uni-dortmund.de

Received (in Cambridge, UK) 20th June 2001, Accepted 23rd August 2001
First published as an Advance Article on the web 18th September 2001

The combination of electronic effects (Pt^{II} binding to N^7 and N^1) and a favourable conformation permitting efficient stabilization of the anion brings about a 10^9 fold increase in the exocyclic amino group acidity of 9-ethyladenine.

The heterocyclic nucleobases generally do not have groups with pK_a values corresponding to the physiological pH, unless present in a particular environment or chemically altered.[1] For example, the 'i motif' of hemiprotonated cytosine bases[2] is stable up to neutral pH despite the pK_a of protonated cytosine being between 4 and 5, and methylation of guanine-N^7 increases the acidity of the N1 proton by about 2.5 log units, thus bringing it down to 7.[3] Similarly, metal coordination to guanine-N^7 shifts the pK_a to *ca*. 8.[4] There is an increasing awareness that unusual pK_a shifts of nucleobase groups leading to pK_a values close to physiological pH might be the clue to an understanding of catalysis involving nucleic acids.[5–9] Scenarios include either general acid–base catalysis[5–8] or structural changes of the catalytic site due to formation of non-canonical base pairs.[9] Probably the most exciting recent example is RNA being the catalyst in the ribosomal peptidyl transferase center,[10] with a highly preserved adenine residue acting as a reversible proton acceptor and donor. The pK_a of this adenine is unusual in that it is 7.6 ± 0.2.[5]

In the course of our studies on metal-modified nucleobase quartets[11] we have now come across an example of an extreme acidification (10^9) of the 6-amino group of adenine in a complex consisting of two 9-ethyladenine (eade, A) and two 1-methyluracilate (mura, U) model nucleobases and three *trans*-a$_2$Pt^{II} entities (a = NH_3 or $MeNH_2$). *trans*,*trans*,*trans*-{$(NH_3)_2$Pt(N^7-eade-N^1)$_2$[$(MeNH_2)_2$Pt(mura-N^3)]$_2$} {**1**}$(ClO_4)_4$·4H_2O‡ crystallizes in a characteristic Z-shape with the four bases being nearly coplanar (Fig. 1).§ As in related compounds,[11] Pt–N^1 and Pt–N^7 vectors are approximately perpendicular to each other [91.8(4)°]. The ^{1}H NMR solution spectra (1D; ^{1}H–^{1}H-NOESY) in D_2O are consistent with the existence of different rotameric forms in this medium (at ambient temperature). The assignment of the resonances is realized by evaluating the ^{1}H–^{1}H-NOESY spectrum, because the A-H8 (9.31 ppm) and A-CH_2 (4.52 ppm) protons generate an intense cross-peak. Hence, the two signals at 9.35 and 9.32 ppm, which are two singlets with relative intensities of 1 : 1, can be attributed to the A-H2 protons.‡ The fact that this resonance is split suggests that the externally bonded mura ligands undergo hindered rotation about the U-N^3–Pt(1)–N^1-A bonds.[12] The corresponding A-H8 signal shows no doubling. Therefore, a rotation with a different activation energy about the central A-N^7–Pt(2)–N^7-A bonds is assumed, with the repulsive interaction of the two exocyclic A-NH_2 groups favouring the Z-form, as found in the solid state (*cf*. Fig. 1).

pD-dependent ^{1}H NMR spectra (2 < pD < 14) reveal two deprotonation steps occurring with pK_{a1} = 7.94 ± 0.31 and pK_{a2} = 11.66 ± 0.30 (3σ) (calculated for H_2O¶), which are assigned to two successive single deprotonation steps of NH_2 groups of the two adenine bases. Furthermore, the difference between the two acidity constants amounts to ΔpK_a = (11.66 ± 0.30) − (7.94 ± 0.31) = 3.72 ± 0.43. Comparison with literature data show that the amino group acidity (pK_a ≅ 16.7 in the free base[13]) increases upon Pt^{II} coordination to N^7 or N^1 by 2–3 log units and even more so if both positions are simultaneously platinated (pK_a ≅ 10.8–12.6[11,14]). The unusually low pK_{a1} of 7.94 (and the large difference between the two pK_a values) can only be rationalized if in addition to the polarizing effect of the two metal ions a fundamental conformational change is taken into account. We propose that the transition of the Z-shaped cation to a U-shaped one takes place, which stabilizes the first deprotonated species {**1**–H^+}$^{3+}$ (Fig. 2). On the basis of structural models as well as X-ray data of fragments of the title compound[15] it is obvious that (i) the four bases in the U-shape *can* adopt a perfectly planar arrangement, and (ii) the exocyclic amino groups of the *head–head* arranged adenine bases are 3 Å or less apart. In fact, any reduction of the N^7–Pt–N^7 angle from 180° further reduces this separation. This short distance permits an efficient stabilization of the NH^- group by the NH_2 group of the second adenine through intramolecular H bond formation (*cf*. Fig. 2, bottom). The situation is reminiscent of that occurring in the $N_2H_5^-$ ligand of the dinuclear Pt^{IV} complex $[(NH_3)_3Pt(NH_2)_2(N_2H_5)Pt(NH_3)_3]^{5+}$.[16] Our conclusion concerning the conformational change during the first deprotonation of the title compound is in agreement with observations for linkage isomers, *viz*. complexes containing a central N^1–Pt–N^1 bond and additional Pt^{II} entities at the N^7 positions.[11,17] There, mainly the electronic effects of the two metal ions are operative, hence pK_a values are higher and close to the normal range (10–11). As the pH is raised further, the cation is expected to adopt again the Z-shape to avoid the mutual repulsion of the two amide groups. Consequently, pK_{a2} is in the expected range

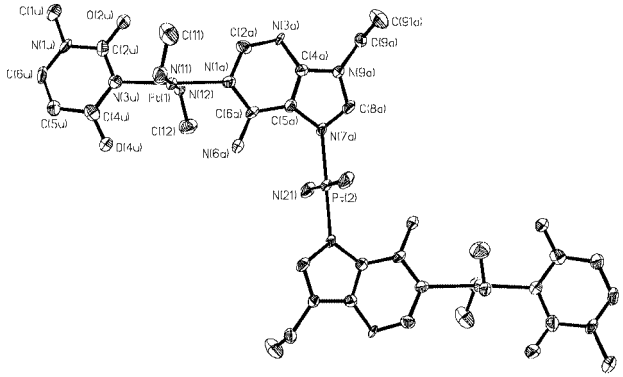

Fig. 1 X-Ray structure of the cation of {**1**}$(ClO_4)_4$·4H_2O. Selected bond distances (Å) and angles (°) are: Pt(1)–N(3u) 2.026(8), Pt(1)–N(1a) 2.055(8), Pt(2)–N(7a) 2.014(7), Pt(2)–N(21) 2.041(7); N(3u)–Pt(1)–N(1a) 175.8(3), N(3u)–Pt(1)–N(12) 87.5(3), N(7a)^a–Pt(2)–N(7a) 180.0, with the symmetry code: ^{a} $-x$, $-y$, $-z$ + 1.

† Electronic supplementary information (ESI) available: table of the determined values of the different evaluated protons and Figures of the fits under discussion. See http://www.rsc.org/suppdata/cc/b1/b105395g/

 DOI: 10.1039/b105395g

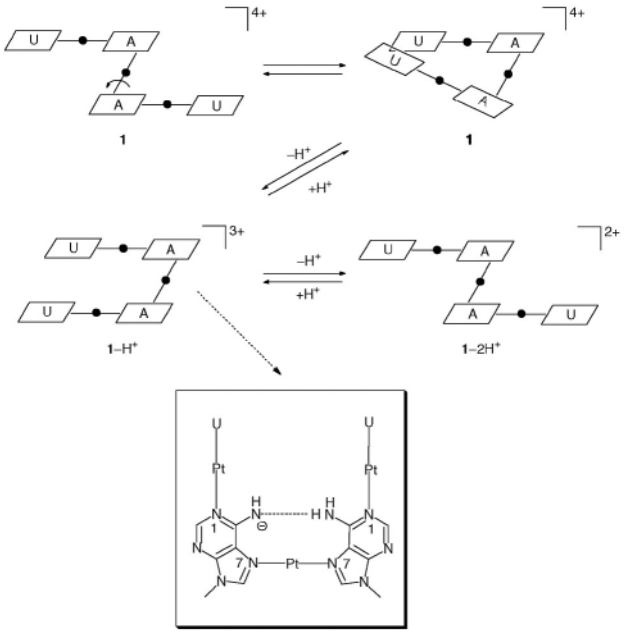

Fig. 2 Schematic presentation of the conformational pH switch.

(11.66). In the pD range corresponding to pK_{a1}, the A-H2 resonance is split into a multiplet, indicating again a hindered rotation of the terminal coordinated mura ligands in the U-form of the cation, which leads to different conformations. There is no indication of any (fast) Pt migration from either N^1 or N^7 to N^6 as observed by Arpalahti and coworkers upon heating.[18]

The compound described here behaves as a pH switch,[19] and hence changes its conformation from Z to U upon removal of a single proton and again from U to Z if a second proton is removed. *Vice versa*, the mutual orientation of the two adenine nucleobases and the close distance of the exocyclic amino groups make the compound a system with the potential of acting as an acid and a base in a reversible manner at physiological pH. The only requirement to achieve such a function would be to have the system confined in space to a situation in which the cation adopts a structure halfway between the two extremes (*cf.* Fig. 2, top). Slight mechanical oscillations of the two halves could then eject a proton or pick one up from the environment.

There is a second feature of interest to cationic {**1**–H$^+$}$^{3+}$ in its U-shape, which refers to its possible interaction with (anionic) telomere sequences of DNA. The enzyme telomerase is a key player in the development of cancer and has been found to be inhibited by conjugated π-systems capable of stabilizing guanine quartet structures of the telomeres.[20]

This work was supported by the DFG and FCI.

Notes and references

‡ *Experimental procedure*: *trans*-$(MeNH_2)_2Pt(mura\text{-}N^3)Cl$ (220 mg, 0.54 mmol)[21] was suspended in a weakly acidic (HNO_3, pH 4.5) aqueous solution (40 mL) of *trans*-$[(NH_3)_2Pt(eade\text{-}N^7)_2](NO_3)_2{\cdot}3H_2O$ (200 mg, 0.27 mmol).[17] A solution of $AgNO_3$ (91 mg, 0.53 mmol) in H_2O (10 mL) was added dropwise over a period of 6 h with daylight excluded and stirred for 6 d at 40 °C. After the mixture was cooled to 4 °C, AgCl was removed by filtration. The colourless filtrate was concentrated to a 20 mL volume (N_2-stream) and an excess of $NaClO_4$ was added. After 2 d, pure {**1**}$(ClO_4)_4{\cdot}1.5H_2O$ precipitated as long needles. These were filtered off and dried in air (150 mg, 32%). ^{1}H NMR (D_2O, 0.02 mol L^{-1}, 200.13 MHz, TSP, ambient temperature, pD = 5.7): δ 9.35, 9.32 (s, A-H2 with relative intensities of 1 : 1), 9.31 (s, A-H8), 7.45 (d, U-H6, ^3J 8 Hz), 5.81 (d, U-H5, ^3J 8 Hz), 4.52 (q, A-CH_2, ^3J 8 Hz), 3.46, 3.45 (s, U-CH_3 with relative intensities of 1 : 1), 1.62 (t, A-CH_3, ^3J 8 Hz); ^{195}Pt NMR (D_2O, 0.02 mol L^{-1}, 42.95 MHz, Na_2PtCl_6, ambient temperature, pD = 5.7, with relative intensities of 1:2): δ −2466 (A-N^7–Pt–N^7-A), −2594 (U-N^3–Pt–N^1-A); Anal. calc. for $C_{28}H_{57}N_{20}O_{21.5}Pt_3Cl_4$ (M = 1744.9 g mol^{-1}): C 19.3, H 3.3, N 16.1. Found: C 19.1, H 3.1, N 15.9%. Recrystallization of {**1**}$(ClO_4)_4{\cdot}1.5H_2O$ from D_2O gave suitable crystals for X-ray structure analysis and showed the presence of four water molecules per quartet in contrast to elemental analysis.

§ *Crystal data*: asymmetric unit: $C_{14}H_{31}N_{10}O_{12}Cl_2Pt_{1.5}$, M = 895.02, monoclinic, space group $P2_1/n$, a = 8.364(2), b = 26.394(5), c = 12.751(3) Å, β = 106.58(3)°, U = 2697.9(10) Å^3, T = 154(2) K, Z = 4, μ(Mo-Kα) = 8.054 mm^{-1}, Enraf-Nonius-Kappa CCD[22] with graphite monochromator, ω-scans, 5574 independent reflections, R_{int} = 0.1234; structure was solved by standard Patterson methods[22] and refined by full-matrix, least sqares on F^2 using SHELXL-93.[22] Refinement of 367 parameters converged at final R_1 = 0.0511 and wR_2 = 0.1191 for 3932 reflections with $I = 2\sigma(I)$ and R_1 = 0.0768 and wR_2 = 0.1676 for all data (5560 reflections), min. and max. features in difference Fourier map: 3.934 and −3.375 e Å^{-3}. CCDC reference number 165198. See http://www.rsc.org/suppdata/cc/b1/b105395g/ for crystallographic data in CIF or other electronic format.

¶ *Determination of the acidity constants*: the pK_a values of the nucleobase quartet {**1**}$(ClO_4)_4{\cdot}1.5H_2O$ were determined using pH-dependent ^{1}H NMR measurements in D_2O (20 °C; I = 0.1 mol L^{-1}, $NaNO_3$). Changes in chemical shifts of all non-exchangeable protons of the complex due to the change in pD were evaluated with a nonlinear least squares fit after Newton–Gauss.[23] The obtained acidity constants were then transformed to the values valid for water according to the literature.[24]

1 W. Saenger, *Principles of Nucleic Acid Structure*, Springer, New York, 1984.
2 K. Gehring, J.-L. Leroy and M. Guéron, *Nature*, 1993, **363**, 561.
3 W. Pfleiderer, *Liebigs Ann. Chem.*, 1961, **646**, 167.
4 B. Song, J. Zhao, R. Griesser, C. Meiser, H. Sigel and B. Lippert, *Chem. Eur. J.*, 1999, **5**, 2374 and references cited therein.
5 G. W. Muth, L. Ortoleva-Donnelly and S. A. Strobel, *Science*, 2000, **289**, 947.
6 A. C. Drohat and J. T. Stivers, *J. Am. Chem. Soc.*, 2000, **122**, 1840.
7 A. T. Perrotta, I.-H. Shih and M. D. Been, *Science*, 1999, **286**, 123.
8 G. J. Narlikar and D. Herschlag, *Ann. Rev. Biochem.*, 1997, **66**, 19.
9 P. Legault and A. Pardi, *J. Am. Chem. Soc.*, 1997, **119**, 6621.
10 P. Nissen, J. Hansen, N. Ban, P. B. Moore and T. A. Steitz, *Science*, 2000, **289**, 920.
11 See, *e.g.*: M. S. Lüth, E. Freisinger, F. Glahé and B. Lippert, *Inorg. Chem.*, 1998, **37**, 5044; R. K. O. Sigel, S. M. Thompson, E. Freisinger, F. Glahé and B. Lippert, *Chem. Eur. J.*, 2001, **7**, 1968; M. S. Lüth, E. Freisinger and B. Lippert, *Chem. Eur. J.*, 2001, **7**, 2104 and references cited therein.
12 O. Krizanovic, M. Sabat, R. Beyerle-Pfnür and B. Lippert, *J. Am. Chem. Soc.*, 1993, **115**, 5538; S. Metzger, A. Erxleben and B. Lippert, *J. Biol. Inorg. Chem.*, 1997, **2**, 256.
13 R. Stewart and M. G. Harris, *Can. J. Chem.*, 1977, **55**, 3807.
14 K. Inagaki, M. Kuwayama and Y. Kidani, *J. Inorg. Biochem.*, 1982, **16**, 59; J. H. J. den Hartog, H. van den Elst and J. Reedijk, *J. Inorg. Biochem.*, 1984, **21**, 83.
15 M. S. Lüth, E. Freisinger, F. Glahé, J. Müller and B. Lippert, *Inorg. Chem.*, 1998, **37**, 3195.
16 L. Heck, M. Ardon, A. Bino and J. Zapp, *J. Am. Chem. Soc.*, 1988, **110**, 2691.
17 M. S. Lüth, E. Freisinger, M. Drumm, G. Kampf, H. Sigel and B. Lippert, unpublished results.
18 J. Viljanen, K. D. Klika, R. Sillanpää and J. Arpalahti, *Inorg. Chem.*, 1999, **38**, 4924; J. Arpalahti and K. D. Klika, *Eur. J. Inorg. Chem.*, 1999, 1199.
19 J. Müller, F. Glahé, E. Freisinger and B. Lippert, *Inorg. Chem.*, 1999, **38**, 3160.
20 R. T. Wheelhouse, D. Sun, H. Han, F. X. Han and L. H. Hurley, *J. Am. Chem. Soc.*, 1998, **120**, 3261; H. Han, C. L. Cliff and L. H. Hurley, *Biochemistry*, 1999, **38**, 6981.
21 R. K. O. Sigel, S. M. Thompson, E. Freisinger and B. Lippert, *Chem. Commun.*, 1999, 19.
22 Nonius BV, Kappa CCD package, Röntgenweg 1, PO Box 811, 811, 2600 AV Delft, Netherlands; Z. Otwinowsky and W. Minor, *Processing of X-Ray Diffraction Data Collected in Oscillation Mode, Methods in Enzymology*, ed C. W. Carter, Jr. and R. M. Sweet, Academic Press, New York, 1996, vol. 276, p. 307; G. M. Sheldrick, *Acta Crystallogr., Sect. A*, 1990, **46**, 467; G. M. Sheldrick, *SHELXL-93, Program for Crystal Structure Refinement*, University of Göttingen, Germany, 1993.
23 R. K. O. Sigel, E. Freisinger and B. Lippert, *J. Biol. Inorg. Chem.*, 2000, **5**, 287; R. K. O. Sigel and B. Lippert, *Chem. Commun.*, 1999, 2167; R. Tribolet and H. Sigel, *Eur. J. Biochem.*, 1987, **163**, 353.
24 R. B. Martin, *Science*, 1963, **139**, 1198.

CHEMCOMM Communication
www.rsc.org/chemcomm

A one step process for grafting organic pendants on alumina *via* the reaction of alumina and phosphonate under microwave irradiation

Didier Villemin,*[a] Bernard Moreau,[a] Fabrice Siméon,[a] Géraldine Maheut,[a] Christian Fernandez,[b] Valérie Montouillout,[b] Vincent Caignaert[c] and Paul-Alain Jaffrès[a]

[a] *Laboratoire de Chimie Moléculaire et Thioorganique, UMR CNRS 6507, Ecole Nationale Supérieure d'Ingénieur de Caen, Université de Caen, ISMRA, 6 Bd du Maréchal Juin, F-14050 Caen, France. E-mail: didier.villemin@ismra.fr*

[b] *Laboratoire de Catalyse et Spectroscopie, UMR CNRS 6506, Ecole Nationale Supérieure d'Ingénieur de Caen, Université de Caen, ISMRA, 6 Bd du Maréchal Juin, F-14050 Caen, France*

[c] *Laboratoire de Cristallographie et Science des Matériaux, UMR CNRS 6508, Ecole Nationale Supérieure d'Ingénieur de Caen, Université de Caen, ISMRA, 6 Bd du Maréchal Juin, F-14050 Caen, France*

Received (in Cambridge, UK) 14th June 2001, Accepted 31st July 2001
First published as an Advance Article on the web 2nd October 2001

Phosphonate esters react with γ-alumina under microwave (MW) irradiation; this reaction is a simple preparative method to graft organic pendant groups onto the surface of alumina; the efficiency of the grafting was readily checked by solid-state NMR techniques (^{31}P and ^{27}Al).

The grafting of organic moieties onto the surface of inorganic compounds is an important process widely used in numerous applications. These include, heterogenisation of homogeneous catalysts,[1] elaboration of solid phases for chromatography, organic synthesis on solid phases and the modification of the surface properties of solids. For silica, the use of siloxy groups for grafting silica is very common while for other oxides such as alumina there is no satisfactory method for grafting organic pendant groups. Alumina provides excellent properties as a support. These include ease of diffusion of reactant in the pore structure and a large available specific surface, leading to its high popularity as a support for both heterogeneous catalysis[2] and chromatography.

Phosphonyl groups are known to form very stable networks in aluminium phosphate and in ALPOs. Thus we speculated that phosphonate could be grafted onto alumina with strong bonding.[3]

Although several reactions of phosphoric or phosphonic derivatives with alumina have already been reported in the literature (studies of surface modification of oxidised aluminium[4] or surface modification of aluminosilicate[5]), the use of such reactions for grafting of functionalised organic groups has not, to our knowledge, been previously studied.

After many trials with phosphonic acid and phosphonate esters under classical heating and under microwave activation, we found that the best procedure was the reaction of a phosphonate with alumina under MW irradiation (Scheme 1 and Table 1).

The grafting of the organic chain was followed by elemental analysis (%C) of the obtained material. Although a phosphonic acid can be used to give the same type of material, phosphonate esters produced better yields in grafting than phosphonic acid (R^2 = $PhCH_2$, R^1 = OH, %C = 4.63 *cf.* entry 3 in Table 1, %C = 6.08). One reason may be that phosphonates are more easily dispersed.[6] Whatever the reason, the higher loadings were obtained by MW activation and by the use of phosphonate esters without solvent. Classical heating conditions under the same conditions (130 °C) produced inferior results when compared to MW irradiation. Although alumina is a thermal insulator it is transparent to microwaves, and therefore it is easy to activate polar molecules such as phosphonates using MWs in the presence of alumina.[7] The molecular mobility of small polar molecules (water, alcohols) is increased by MW irradiation and they desorb rapidly, hence microwave activation is well adapted for the hydrolysis–condensation reaction (Scheme 1). During the anchoring process with phosphonate, the phosphonate function was dealkylated and some monodealkylated phosphonates were recovered by washing with methanol. This dealkylation process was previously reported by Weinberg *et al.*[8] who described *via* a spectroscopic study, the adsorption of gaseous dimethylmethylphosphonate onto alumina. More recently in a spectroscopic study of the reaction of war gas on alumina, Wagner *et al.*[9] observed similar results.

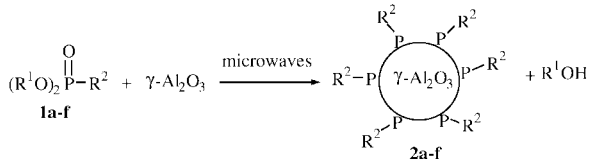

Scheme 1 Reaction of phosphonate esters with γ-alumina under microwave irradiation.

A readily available commercial γ-alumina with a specific surface area of 132 $m^2\ g^{-1}$ was used. In a typical preparation, 3 g of γ-Al_2O_3 (Merck, BET = 132 $m^2\ g^{-1}$; 30 mmol) and diethylcyanoethylphosphonate **1a** (1.06 g; 6 mmol) were mixed and irradiated (15 × 4 min) by microwaves at 150 W (focused irradiation 2450 MHz; Prolabo Synthewave 402). The highest temperature observed was 198 °C. After cooling to room temperature the crude product was washed with dichloromethane (3 × 20 ml) and 150 mg of starting compound **1a** was recovered. Further washing with methanol up to a constant weight (3 × 20 ml) led to the recovery of 60 mg of monodealkylated ethylcyanomethylphosphonate in the filtrate. Further washing of compounds **2** with water at room temperature did not lead to any removal of loading groups of the grafted phosphonate. The specific surface areas of compounds **2** are

Table 1 Reaction of phosphonate esters with γ-alumina under microwave irradiation

Entry	Reactant	R^1	R^2	Al_2O_3/**1** ratio	%C in **2**	mmol $PR^2\ g^{-1}$
1	**1a**	Et	$-CH_2CN$	5	4.58	2
2	**1b**	Me	Me	10	0.59	0.5
3	**1c**	Et	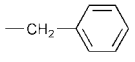	5	6.08	0.9
4	**1d**	Et	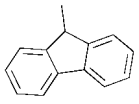	10	4.97	0.3
5	**1e**	Et	$-CH_2(CH_2)_3$	10	3.00	0.6
6	**1f**	Et	$-CH_2C(O)OEt$	5	5.54	1.2

 DOI: 10.1039/b105240n

slightly decreased (104–130 $m^2\ g^{-1}$) compared to the starting γ-Al_2O_3 (132 $m^2\ g^{-1}$).

Upon drying at 200 °C for 24 h the products *e.g.* **2a** (3.50 g; %C = 4.58) were obtained and were found to be amorphous by powder X-ray diffraction. The FTIR spectrum of **2a** exhibits a sharp peak at 2254 cm^{-1} arising from the stretching mode of the nitrile group. Another important modification observed by IR (compared to the parent γ-Al_2O_3) relates to the P–O and P=O stretching bands that are located at 1042, 1114 and 1198 cm^{-1}. ^{31}P MAS NMR indicates an intense peak at 3.6 ppm (Fig. 1, ^{31}P MAS) and a wide background signal which is presumably the result of a chemical shift distribution of small peaks.

The ^{27}Al MAS NMR spectrum of **2a** (Fig. 1) shows three signals. The two main resonances are broad, with an isotropic chemical shift in the range 70–80 ppm and 10–20 ppm, arising from four- and six-fold aluminium, respectively, of γ-Al_2O_3.[10] Their asymmetric line-shape is characteristic of an amorphous material in which aluminium sites present a distribution of quadrupolar interactions.[11] Interestingly a third weaker resonance, not present in the starting γ-Al_2O_3 (not shown) is observed at −15 ppm. Its isotropic chemical shift corresponds to an octahedral aluminium site and is close to the chemical shift observed for bulk aluminophosphonate materials.[12]

DTA analysis of material **2a** shows an endothermic transition around 100 °C and a broad exothermic transition ranging from 269 to 395 °C. According to TGA a first weight loss arising from residual water is observed around 100 °C and further stepwise mass losses starting at 250 °C are observed at 280, 344 and 407 °C. The total mass loss above 250 °C represents 7.7% of the total weight.

In order to investigate the bonding mode between phosphonic acids and γ-Al_2O_3, the bonding of phosphorus with aluminium nuclei has been determined *via* a ^{27}Al–^{31}P HETCOR experiment.[13] This experiment reveals the presence of magnetization transfer and hence the spatial proximity of phosphorus and aluminium. The spectrum (Fig. 1) consists of a single cross-peak centred at −15 ppm for ^{27}Al and 3.7 ppm for ^{31}P. The ^{31}P projection corresponds closely to the one-dimensional ^{31}P MAS NMR spectra, with both a 'weak' and wide component. By contrast the ^{27}Al HETCOR projection shows only the additional resonance at −15 ppm caused by phosphorus impregnation. Unlike the two γ-Al_2O_3 signals, this resonance can be simulated with a Lorentzian line shape, indicating a more symmetric environment. This experiment suggests that the weak ^{27}Al signal at −15 ppm can be attributed to aluminium surrounded by phosphorus, and that all the phosphorus nuclei are close to aluminium nuclei. The distance between the aluminium and phosphorus atoms was estimated by a ^{27}Al–{^{31}P} REDOR experiment.[14] In this experiment, a ^{27}Al rotor synchronised Hahn-echo spectrum (S_0) was compared to the ^{27}Al REDOR spectrum (S_f), in which the heteronuclear dipolar coupling is reintroduced by application of radiofrequency pulses on ^{31}P. The difference $\Delta S = S_0 - S_f$ gives the spectrum of aluminium close to phosphorus. As expected, the difference spectrum consists of a single resonance at −15 ppm, confirming its attribution to aluminium surrounded by phosphorus nuclei.

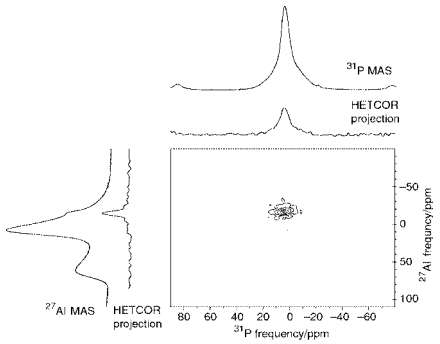

Fig. 1 ^{27}Al–^{31}P HETCOR spectrum of compound **2a** (MAS speed 14.3 kHz, CP contact time 5 ms). ^{27}Al and ^{31}P resonances are shown along the vertical and horizontal axes and are compared to the MAS spectra.

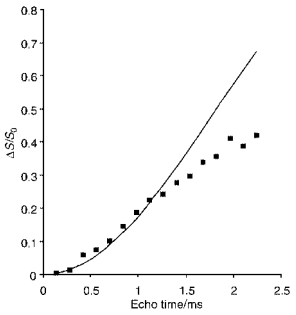

Fig. 2 REDOR fraction $\Delta S/S_0$ of the −15 ppm ^{27}Al resonance *vs.* the total echo time (MAS 14.3 kHz). The squares indicate the measured data while the solid line is the simulated curve for $D = 420$ Hz and $r = 3.12$ Å.

Fig. 2 shows the relative intensity of the REDOR fraction, $\Delta S/S_0$, as a function of echo time for the −15 ppm ^{27}Al signal. For relatively short echo times, the difference intensity increases as the dipolar coupling increases.

The dipolar coupling constant was obtained by fitting the experimental data (Fig. 2; the theoretical curve was calculated assuming that each aluminium can only be connected to one phosphorus[15]). From this fit, the dipolar coupling constant was estimated to be 420 ± 30 Hz which corresponds to a ^{31}P–^{27}Al distance of 3.12 ± 0.08 Å. This distance is consistent with an Al–O–P arrangement for which the P–Al distance is in the range of 3.10–3.22 Å as reported in the literature.[16] From the MAS NMR study, it can be stated that the global structure of aluminis not deteriorated by the grafting reaction. Indeed, the characteristic peaks around 15 and 75 ppm observed by ^{27}Al MAS NMR, corresponding to six and four-fold aluminium, respectively, are still present in the resulting materials.

In conclusion, a general preparative method for coating γ-Al_2O_3 with organic groups based on the reaction of phosphonate and γ-Al_2O_3 is proposed.

C. F. and V. M. are grateful to the CNRS, FEDER and Région Basse-Normandie for funding. Thanks go to the 'Région Basse et Haute-Normandie' (Punch) for their financial support.

Notes and references

1 E. F. Vansant, P. Van der Voort and K. C. Vrancken, *Characterization and chemical modification of silica surface*, in *Studies in Surface Science and Catalysis*, Elsevier, Amsterdam, 1993, vol. 93; *Chiral catalyst immobilisation and recycling*, ed. D. E. De Vos, I. F. J. Vankelecom and P. A. Jacobs, Wiley-VCH, New York, 2001.
2 *Solid supports and catalysts in organic synthesis*, ed. K. Smith, Ellis Horwood and Prentice Hall, Chichester, 1992.
3 D. Villemin, enveloppe Soleau No. 89644 300697 (1st July 1997), Institut National de la Propriété Industrielle, Paris.
4 R. Coast, M. Pikus, P. N. Henriksen and G. A. Nitowski, *J. Adhes. Sci. Technol.*, 1996, **10**, 101; K. Tsujii, T. Yamamoto, T. Onda and S. Shibuich, *Angew. Chem., Int. Ed. Engl.*, 1997, **36**, 1011; C. Yee, G. Kataby, A. Ulman, T. Prozoroc, H. White, A. King, M. Rafailovich, J. Sokolov and A. Gedanken, *Langmuir*, 1999, **15**, 7111.
5 J. L. Guimaraes, P. Peralta-Zamora and F. Wypych, *J. Colloid Interface Sci.*, 1998, **206**, 281.
6 Phosphonate esters are usually oils or low melting point solids.
7 A. Ben Alloum, B. Labiad and D. Villemin, *J. Chem. Soc., Chem. Commun.*, 1989, 386.
8 M. K. Templeton and W. H. Weinberg, *J. Am. Chem. Soc.*, 1985, **107**, 97.
9 G. W. Wagner, L. R. Procell, R. J. O'Connor, S. Munavalli, C. L. Carnes, P. N. Kapoor and K. J. Klabunde, *J. Am. Chem. Soc.*, 2001, **123**, 1636.
10 E. R. H. Van Eck, A. P. M. Kentgens, H. Kraus and R. Prins, *J. Phys. Chem.*, 1995, **99**, 16 080.
11 G. Engelhardt and D. Michel, *High Resolution Solid State NMR of silicates and zeolites*, Wiley, New York, 1987.
12 J. E. Haky, J. B. Brady, N. Dando and D. Weaver, *Mater. Res. Bull.*, 1997, **32**, 297.
13 A. A. Maudsley and R. R. Ernst, *Chem. Phys. Lett.*, 1977, **50**, 368.
14 T. Gullion and J. Schaefer, *J. Magn. Res.*, 1989, **81**, 196.
15 Y. Pan, T. Gullion and J. Schaefer, *J. Magn. Res.*, 1990, **90**, 330.
16 E. R. H. Van Eck and W. S. Veeman, *Solid State NMR*, 1992, **1**, 1; H. G. Harvey, S. J. Teat and M. P. Attfield, *J. Mater. Chem.*, 2000, **10**, 2632.

CHEMCOMM Communication
www.rsc.org/chemcomm

Steric acceleration of an uncatalysed ene reaction at room temperature

Nandeo Choony,[a] Peter G. Sammes,*[a] Graham Smith[a] and Robert W. Ward[b]

[a] *Department of Chemistry, School of Physics and Chemistry, UniS, Guildford, Surrey, UK GU2 7XH. E-mail: p.sammes@surrey.ac.uk*
[b] *GlaxoSmithKline Pharmaceuticals, New Frontiers Science Park, Third Avenue, Harlow, Essex, UK CM19 5AW*

Received (in Cambridge, UK) 24th July 2001, Accepted 7th September 2001
First published as an Advance Article on the web 27th September 2001

The bulky trityl steric buttress is used to effect an intramolecular, uncatalysed ene reaction that operates at room temperature, whilst smaller buttresses require heat.

The ene[1] reaction and its intramolecular counterpart[2] are synthetically useful processes that have been exploited in a wide range of chemistry. Normally the ene reaction requires the use of heat at temperatures greater than 140 °C to proceed and, for systems where the enophile is not activated by an electron withdrawing group, *much* higher temperatures are often required.[3] For systems with electron deficient enophiles, the process may be catalysed with Lewis acids, whereby the reaction has been observed to proceed at ambient temperatures[4] but such catalysis is not generally effective for non-activated enophiles.

The stereochemistry of the intramolecular ene process[2] has also been examined and, under vigorous thermal conditions, stereocontrol is often lost. Thus, heating the simple *N*-trifluoroacetyl-*N*-allyl-*N*-dimethylallylamide compound **1** at 220 °C for 30 min effects an intramolecular ene reaction and converts it into the mixture of *cis* and *trans*-pyrrolidines **2** and **3**.[5] The latter compounds are of interest as members of the kainic acid family of neuroactive agents,[6] the kainic acid series having the *cis*-stereochemistry **2** and the *allo* series the *trans*-stereochemistry **3**.[7] Thus any means of controlling the stereochemistry of the intramolecular ene process would be of synthetic value.

As part of our interest in the use of steric buttressing as an aid to reactions,[8] herein we describe examples of use of a steric buttress that assists ene reactions to occur under uncatalysed and low temperature conditions.

Upon heating in xylene, under argon at 140 °C, for 100 h, the trityl-protected *N*-allyl-*N*-dimethylallylamine **4**, prepared by standard methods,† smoothly produced the ene product **6** in almost quantitative yield (Scheme 1). Only one isomer could be detected by ^{1}H NMR spectroscopy (>95%), assigned from ^{1}H NOE experiments, as the *cis*-isomer. The *cis*-isomer is known to be the preferred stereoisomer in analogous carbocyclic ene reactions.[2] That a buttressing effect is operating was supported by the observation that no sign of any cyclisation product was obtained upon heating the parent amine **5** under the same conditions. The ease of the buttressed cyclisation, compared with the harsh conditions normally reported for unactivated ene reactions,[3] led us to seek other examples of the sterically assisted ene process.

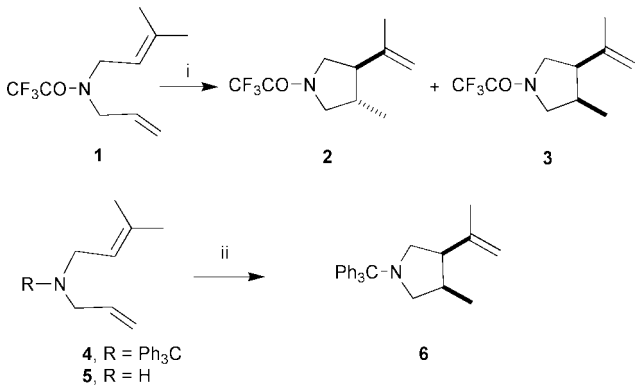

Scheme 1 i, 220 °C, 30 min; ii, 140 °C, 4 days.

In earlier work we had shown that, on heating, the trityl protected *N*-allylfurfurylamine **7** undergoes an intramolecular Diels–Alder cycloaddition to the corresponding cycloadduct **8** in almost quantitative yield. At rt a competing intermolecular cycloaddition, with dimethyl butynedioate, is possible to give the cycloadduct **9** but, on heating, this loses the acetylenic ester by a retro-cycloaddition reaction and again forms the thermodynamically favoured cycloadduct **8** (Scheme 2).

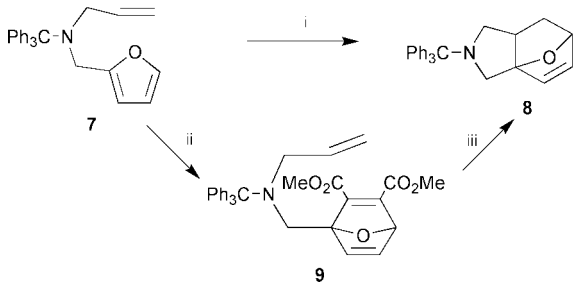

Scheme 2 i, 120 °C, 24 h; ii, $MeO_2C–C\equiv C–CO_2Me$, rt; iii, 120 °C.

The intramolecular process, *e.g.* **7** to **8**, is sensitive to substituents on the allyl group and the dimethylallyl derivative **10**, only undergoes partial cycloaddition to **11** on heating, to form an 80:20 equilibrium ratio of the cyclised to uncyclised components at 140 °C. A similar competing, intermolecular cycloaddition was attempted with **10** as a parallel reaction to that performed on the unsubstituted allyl compound **7**.

When the tritylated amine **10** was allowed to react with dimethyl butynedioate at rt over 5 d, a new product formed in high yield. However, the compound was *not* the expected Diels–Alder product **12** but, instead, the ene product **13**, isolated as a crystalline solid, mp 164–166 °C (Scheme 3). In its ^{1}H NMR spectrum **13** showed loss of the isopropylidene group and the furan ring protons and formation of the isopropenyl group. The ring protons, H_a to H_d, showed as a tightly coupled ABXY system. NOE experiments indicated the geometry shown, resulting from an approach, *via* the transition state **12a**, from the least hindered, *exo*-face of the oxabicycloheptadiene system. It should be noted that this ene reaction involves a type 1 process

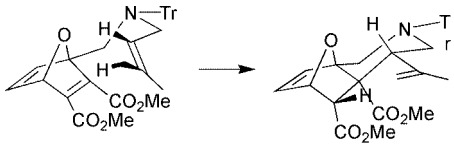

 DOI: 10.1039/b106669m

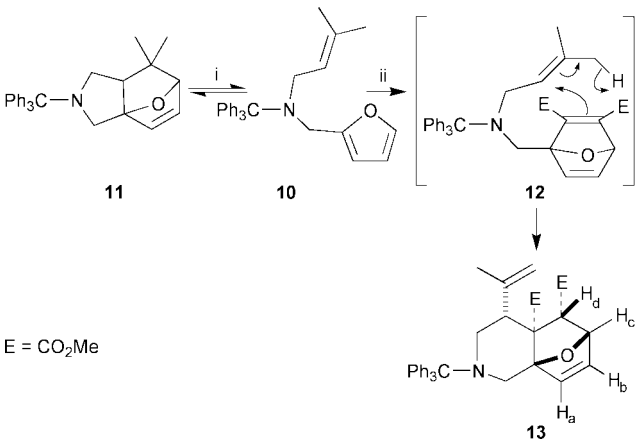

Scheme 3 i, 140 °C, xylene; ii, $MeO_2C–C\equiv C–CO_2Me$, rt.

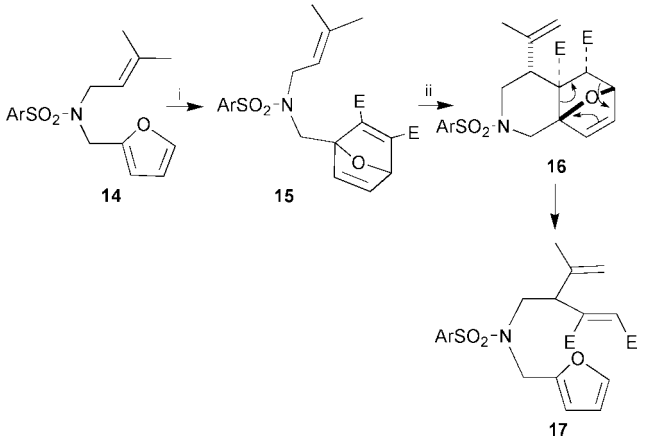

Scheme 4 i, $MeO_2C–C\equiv C–CO_2Me$, rt, 7 days; ii, heat, 70 °C, 3 days.

of a 1,7-diene system, that normally proceed in only modest yields at very high temperatures.[2,9]

The striking buttressing effect of the trityl group was further illustrated by repeating the reaction using the 'smaller' buttress, the 4-toluenesulfonamide **14**.[10] In this case the dimethyl butynedioate adduct **15** could be isolated but showed no sign of ene products after leaving at rt for several weeks. However, on heating to 70 °C, compound **15** slowly reacted further, an ene reaction being observed, as indicated by the appearance of the compound **16** as a transient intermediate but which was unstable to the reaction conditions and underwent a subsequent retro-Diels–Alder reaction to form the furfuryl derivative **17** (Scheme 4). That this sequence of ene reaction followed by the retro-Diels–Alder process occurred, rather than an initial retro-Diels–Alder reaction, followed by an intermolecular ene process was supported by the absence of any of the starting material **14** either as a reaction product or as a transient intermediate. In contrast to the behaviour of the tosylated intermediate **16**, heating the *N*-tritylated ene product **13** at 70 °C gave no indication of the competing retro-Diels–Alder reaction, none of the open form corresponding to **17** being formed. Thus, not only does the trityl buttress assist in lowering the activation energy for the ene process but it also helps prevent the subsequent retro-Diels–Alder process from occurring. Presumably the open form (*cf.* **17**) would occupy more conformational space than is available in the presence of the sterically demanding trityl group, hence leaving the equilibrium firmly in favour of the closed form **13**.

We thank GlaxoSmithKline Pharmaceutical Research and the EPSRC for a research studentship (to G. S.)

Notes and references

† Satisfactory microanalytical and spectroscopic data were recorded for all new compounds described in this communication.

1 H. M. R. Hoffmann, *Angew. Chem., Int. Ed. Engl.*, 1969, **8**, 556.
2 W. Oppolzer and V. Snieckus, *Angew. Chem., Int. Ed. Engl.*, 1978, **17**, 476.
3 W. D. Huntsman, V. C. Solomon and D. Eros, *J. Am. Chem. Soc.*, 1958, **80**, 5455.
4 B. B. Snider, *Acc. Chem. Res.*, 1980, **13**, 426.
5 P. D. Kennewell, S. S. Matharu, J. B. Taylor and P. G. Sammes, *J. Chem. Soc., Perkin Trans. 1*, 1980, 2542.
6 H. Shinozaki and S. Konishi, *Brain Res.*, 170, **24**, 368; G. A. R. Johnston, D. R. Curtis, J. Davies and R. M. McCulloch, *Nature*, 1974, **248**, 804.
7 M. V. Chevliakov and J. Montgomery, *J. Am. Chem. Soc.*, 1999, **121**, 11 139.
8 P. G. Sammes and D. J. Weller, *Synthesis*, 1995, 1205.
9 W. D. Huntsman, P. C. Lang, N. L. Madison and D. A. Ulrick, *J. Org. Chem.*, 1962, **27**, 1983.
10 N. Choony, A. Dadabhoy and P. G. Sammes, *J. Chem. Soc., Perkin Trans. 1*, 1998, 2017.

CHEMCOMM Communication
www.rsc.org/chemcomm

The first Ru(II)-catalysed asymmetric hydrogen transfer reduction of aromatic ketones in aqueous media

Hae Yoon Rhyoo, Hee-Jung Park and Young Keun Chung*

School of Chemistry and Center for Molecular Catalysis, Seoul National University, Seoul 151-747, Korea. E-mail: ykchung@plaza.snu.ac.kr; Fax: 82-2-889-1568; Tel: +82-2-880-6662(Office)/880-6815(Lab.)

Received (in Cambridge, UK) 4th July 2001, Accepted 5th September 2001
First published as an Advance Article on the web 27th September 2001

The first water-soluble asymmetric hydrogen-transfer ruthenium(II) catalyst system consisting of [Ru(*p*-cymene)Cl_2]$_2$, (*S*)-proline amide, and sodium formate, which gives high conversion rates with high ee values up to 95.3% and is reusable, has been developed.

Extensive research on new and effective catalytic asymmetric reactions has been continuing to find more efficient methods for the preparation of optically active compounds.[1] While several excellent chiral catalysts have been developed, most of them have to be used in strictly anhydrous organic solvents. As a consequence of the increasing demand for efficient and environmental friendly methods, heterogenization of homogeneous catalysts by immobilizing them with the aid of liquid or solid supports is now of great interest.[2] While there have been many trials to immobilize homogeneous catalysts on solid supports, successful examples are still rare.[3] The use of homogeneous catalysts in aqueous solution and on liquid supports is more feasible and can offer a great opportunity for green chemistry.[4]

Catalytic asymmetric transfer hydrogenation of ketones has recently emerged as a viable means of synthesizing chiral alcohols.[5] Due to its operational simplicity, the easy availability of reductants, and the high enantioselectivities, the catalytic enantioselective reduction of ketones has been extensively studied during the last decade. In particular, a ruthenium catalyst bearing a chiral ligand such as mono *N*-tosylated diphenylethylenediamine (DPEN-Ts, Noyori's ligand) has been well studied.[6] In the hope of finding efficient and environmental friendly methods, we focused our efforts on finding a water-soluble catalyst system. During the course of our study on the use of amino amide as a chiral ligand,[7] we found that a combination of (*S*)-proline amide and [Ru(*p*-cymene)Cl_2]$_2$ was quite soluble in water. Recently, Williams *et al.*[8] reported the synthesis of water-soluble aminosulfonamide ligands and their applications in the Ru(II)-catalyzed enantioselective transfer hydrogenation of aromatic ketones. However, they used water as an additive to stabilize the catalyst. In this paper, we report the first water-soluble Ru(II)-catalyst system that can catalyze an asymmetric hydrogen-transfer reduction of aromatic ketones in aqueous solution. In addition to the high conversion rates and enantioselectivities, the catalytic system can be recycled at least six times withou loss of performance.

(*S*)-Proline amides **1**, **2**, and **3** (Chart 1) were synthesized according to the published methods.[9] Structure **1** was modified by the addition of a hydroxy group, as in **2**, to increase water solubility. Likewise, a fluoride group was introduced to increase polarity and to test its electronic effect. Combination of the ligand with [Ru(*p*-cymene)Cl_2]$_2$ and a hydrogen source was examined for the asymmetric hydrogen-transfer reduction of ketones. Because the organic substrates have no noticeable solubilities in aqueous solution, they form an aqueous biphasic system and the reaction occurs at the interface.

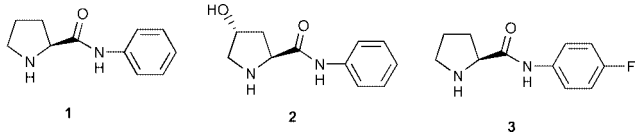

Chart 1 Proline aromatic amide derivatives.

We screened several hydrogen sources and found that HCOONa[10] was the best for the catalytic system. Ketones **4**, **5**, **6**, and **7** (Chart 2) were reduced to give *sec*-alcohols (Table 1).† The absolute configuration of the product was *R* as in the homogeneous reaction. For **4**, the conversion yields were quite high and enantioselectivities up to 95.3% were obtained. The best results were obtained for **4b**. In our previous study regarding the catalytic reaction in organic solvent such as dichloromethane using HCOOH–Et_3N (5:2) as a hydride source,[7] **1** and **3** had been used as the chiral ligands. In that case,

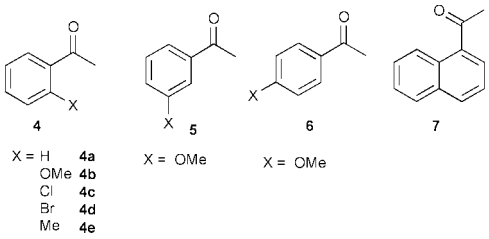

Chart 2 Prochiral aromatic ketones.

Table 1 Asymmetric hydrogen-transfer reduction of prochiral aromatic ketones[a]

Entry	Ligand	Substrate	Conv. (%)	E.e. (%)
1	**1**	**4a**	99.4	61
2	**2**	**4a**	99.5	46.1
3	**3**	**4a**	99.3	61.1
4	**1**	**4b**	99.1	94.7
5	**2**	**4b**	99.1	89.6
6	**3**	**4b**	99.6	95.3
7[b]	**1**	**4c**	100	91.6
8[b]	**2**	**4c**	60	86
9[b]	**3**	**4c**	99.7	91.6
10[b]	**1**	**4d**	100	92.3
11[b]	**2**	**4d**	100	91
12[b]	**3**	**4d**	100	91.3
13	**1**	**4e**	99.7	91.6
14	**2**	**4e**	30	83.8
15	**3**	**4e**	97.5	91.4
16	**2**	**5**	86	40.2
17	**3**	**5**	96	54.2
18	**1**	**6**	99.1	58.3
19	**3**	**6**	85	57.3
20	**3**	**7**	100	89.4[c]

[a] All were reacted for 4 h at 30 °C. [b] The configuration *R* was determined by the optical rotation and the retention time of chiral GC using a Chrompak Chirasil DEX CB 25 m × 0.32 μm column. [c] The conversion of **4c**, **4d** and **7** were determined by GC using a Ultra 2 50 m × 0.32 μm. E.e. was determined by HPLC using Daicel OD column.

 DOI: 10.1039/b106130p

high conversion yields (96–100%) were obtained for **4b** and **4c** and the highest enantioselectivity, up to 98.8%, was obtained for **4d**. When the substrate was **4b**, the conversion yields (>99%) and enantioselectivities (95.3%) in an aqueous solution were quite comparable to those in the homogeneous solution (96–100% and 94.6–94.8% ee, respectively). To compare the enantioselectivity dependency upon the position of the methoxy substituent, the *m*- and *p*-methoxy substituted compounds **5** and **6** were tested. For **5** and **6**, the conversion yields were quite high but the enantioselectivities were moderate. Thus, the *meta*- and *para*-substitutions were less effective than the *ortho*-substitution. Transfer hydrogenation of **7** with ligand **3** gave (*R*)-1-naphthylethanol in a quantitative yield with 89.4% ee.

Recovery and reusability of the catalytic system were tested by carrying out consecutive cycles for **4b** with ligand **3** (Table 2), with the same catalyst in aqueous solution, carefully separated from the organic phase at the end of each run. Substrate **4b** was chosen because it was used for the synthesis of medicinal intermediates.[11] After each catalytic reaction, 1 equiv. formic acid was added to regenerate sodium formate. The conversion yields and enantioselectivities were quite high even on the 6th run. The relative invariance of the conversion yields and enantioselectivities means that the catalyst system is quite stable and the environment around the reaction center is intact during the catalysis. The catalytic system can be recycled at least six times with little loss of perfomance and without producing waste water.

Table 2 Recycle test[a]

Recycle no.	Additive	Time/h	Conv. (%)	Ee (%)
0		4	99.6	95.3
1	HCOOH	5	99.3	95.3
2	HCOOH	6	99.8	95.3
3	HCOOH	6.5	99.8	95.1
4	HCOOH	7	99.7	94.6
5	HCOOH	7	99.3	94.2

[a] Reaction conditions: ligand **3**, substrate **4b**, at 30 °C.

In summary, we have demonstrated that the combination of (*S*)-proline amide and $[Ru(p\text{-cymene})Cl_2]_2$ could be used as an asymmetric hydrogen transfer catalyst for aryl ketones in an aqueous solution. To the best of our knowledge, this is the first example of the Ru(II)-catalyzed asymmetric hydrogen-transfer reduction of aromatic ketones in an aqueous solution. The catalytic system shows a catalyst performance comparable with that in homogeneous solution. The amino amide can readily be fine-tuned by changing the functional group on the amide or by incorporating different amino acids. Other asymmetric reactions with amino amides are being carried out and progress will be reported in due course.

This work was supported by grant No. 2000-2-12200-001-1 from the Basic Research Program of the Korea Science and Engineering Foundation (KOSEF) and (1999-1-122-001-5) and the KOSEF through the Center for Molecular Catalysis. H.-J. P. thanks the Ministry of Education for the Brain Korea 21 Fellowship.

Notes and references

† In a typical catalysis experiment: (*S*)-proline amide (0.1 mmol) and (*p*-cymene)ruthenium(II) chloride dimer (0.05 mmol) in 4 ml of water was stirred for 1 h at 30 °C. After addition of sodium formate (10 mmol), substrate (1 mmol) was added. After the solution was stirred for the predetermined time, *n*-hexane (4 ml) was added to the solution. The resulting solution was stirred for 10 min. Taking some of the hexane solution followed by GC analysis using Ultra 2 50 m × 0.32 μm and CP Chirasil DEX CB 25 m × 0.32 μm columns gave the results.

1 I. Ojima, *Catalytic Asymmetric Synthesis*, 2nd edn., Wiley-VCH, New York, 2000; *Comprehensive Asymmetric Catalysis*, ed. B. Jacobsen, A. Pfaltz and H. Yamamoto, Springer, Heidelberg, 1999; R. Noyori, *Asymmetric Catalysis in Organic Synthesis*, John Wiley & Sons, New York, 1994.

2 A. Choplin and F. Quignard, *Coord. Chem. Rev*., 1998, **178–180**, 1679; S. J. Shuttleworth, S. M. Allin, R. D. Wilson and D. Nasturica, *Synthesis*, 2000, 1035; F. Lindner, T. Schneller, F. Auer and H. A. Mayer, *Angew. Chem., Int. Ed*., 1999, **38**, 2154; S. E. Sen, S. M. Smith and K. A. Sullivan, *Tetrahedron*, 1999, **55**, 12 657; M. Hartmann and L. Kevan, *Chem. Rev*., 1999, **99**, 635; B. Cornils, *J. Mol. Catal. A: Chem*., 1999, **143**, 1; B. E. Hanson, *J. Mol. Catal. A: Chem*., 1999, **185–186**, 795; K. V. Katti, H. Gali, C. J. Smith and D. E. Berning, *Acc. Chem. Res*., 1999, **32**, 9.

3 T. Bein, *Curr. Opin. Solid State Mater. Sci*., 1999, **4**, 85.

4 Reviews: I. T. Horváth and F. Joó, in *Aqueous Organometallic Chemistry and Catalysis*, Kluwer Academic Publishers, Dordrecht, 1995, p. 317, and references therein; D. M. Roundhill, *Adv. Organomet. Chem*., 1995, **38**, 155; B. Cornils and W. A. Herrmann, in *Aqueous-Phase Organometallic Catalysis*, Wiley-VCH, Weinheim, 1998, p. 615, and references therein; W. A. Herrmann and C. W. Kohlpaintner, *Angew. Chem., Int. Ed. Engl*., 1993, **32**, 1524; C.-J. Li and T.-H. Chan, in *Organic Reactions in Aqueous Media*, John Wiley & Sons, New York, 1997, p. 199, and references therein.

5 For a recent review, see: M. J. Palmer and M. Wills, *Tetrahedron: Asymmetry*, 1999, **10**, 2045.

6 S. Hashiguchi, A. Fujii, J. Takehahra, T. Ikariya and R. Noyori, *J. Am. Chem. Soc*., 1995, **117**, 7562; A. Fujii, S. Hashiguchi, N. Uematsu, T. Ikariya and R. Noyori, *J. Am. Chem. Soc*., 1996, **118**, 2521; K.-J. Haack, S. Hashiguchi, A. Fujii, T. Ikariya and R. Noyori, *Angew. Chem., Int. Ed. Engl*., 1997, **36**, 285; K. Matsummura, S. Hashiguchi, T. Ikariya and R. Noyori, *J. Am. Chem. Soc*., 1997, **119**, 8738; K. Murata, K. Okano, M. Miyagi, H. Iwane, R. Noyori and T. Ikariya, *Org. Lett*., 1999, **1**, 1119; R. Noyori and S. Hashiguchi, *Acc. Chem. Res*., 1997, **30**, 97; M. Yamakawa, H. Ito and R. Noyori, *J. Am. Chem. Soc*., 2000, **122**, 1466; J. Takehara, S. Hashiguchi, A. Fujii, I. Shin-ichi, T. Ikariya and R. Noyori, *J. Chem. Soc., Chem. Commun*., 1996, 233.

7 H. Rhyoo, Y. A. Yoon, H. J. Park and Y. K. Chung, *Tetrahedron Lett*., 2001, **42**, 5045.

8 C. Bubert, J. Blacker, S. M. Brown, J. Crosby, S. Fitzjohn, J. P. Muxworthy, T. Thorpe and J. M. J. Williams, *Tetrahedron Lett*., 2001, **42**, 4037.

9 A. Corma, M. Iglesias, C. del Pino and F. Sanchez, *J. Organomet. Chem*., 1992, **431**, 233; K. Suzuki, A. Ikegawa and T. Mukaiyama, *Bull. Chem. Soc. Jpn*., 1982, **55**, 3277.

10 J. M. Brown, H. Btunner, W. Leitner and M. Rose, *Tetrahedron: Asymmetry*, 1991, **2**, 331; S. Ogo, N. Makihara and Y. Watanabe, *Organometallics*, 1999, **18**, 5470; K. Nomura, *J. Mol. Catal. A: Chem*., 1998, **130**, 1.

11 T. S. Kaufman, *Tetrahedron Lett*., 1996, **37**, 5329.

CHEMCOMM Communication
www.rsc.org/chemcomm

Organocatalytic chain scission of poly(lactides): a general route to controlled molecular weight, functionality and macromolecular architecture

Frederik Nederberg, Eric F. Connor, Thierry Glausser and James L. Hedrick*

IBM Almaden Research Center and Center for Polymeric Interfaces and Macromolecular Assemblies, 650 Harry Road, San Jose, CA 95120, USA. E-mail: hedrick@almaden.ibm.com; Fax: 1-408-927-3310; Tel: 1-408-927-1632

Received (in Cambridge, UK) 6th July 2001, Accepted 3rd September 2001
First published as an Advance Article on the web 20th September 2001

A facile, single-step transesterification approach to poly(lactides) with controlled molecular weights and end-group functionality, as well as block and star-shaped architectures is described using nucleophilic amine catalysts.

Tailor made bioresorbable polymers, particularly poly(lactide), are needed for a wide variety of biomedical applications and for controlled drug delivery media.[1] For many of these applications, molecular weight modification is accomplished by controlled chain-growth polymerization, *via* ring opening of the cyclic diester in the presence of a suitable organometallic promoter.[2–4] Another recognized procedure for the preparation of defined telechelic polymers involves the depolymerization of a high molecular weight polymer *via* metal catalysis *e.g.* the chain-end functionalization of poly(butadiene) by olefin metathesis.[5,6] Gross *et al.*[7,8] demonstated the versatility of lipase catalyzed transesterification and transacylation chain scission as a route to low molecular weight poly(ε-caprolactone) and block copolymers. In this communication, a new methodology of poly(lactide) (PLA) depolymerization is introduced as a general route to controlled molecular weight, end-group functionality and complex macromolecular architectures in a single step procedure using nucleophilic catalysts (Scheme 1). Nucleophilic catalysts (*i.e.*, tertiary amines, pyridines, imidazoles and tertiary phosphines)[9–12] have been shown to accelerate a wide variety of processes including the 'living' ROP of lactide, initiated from primary alcohols, in the presence of either 4-(dimethylamino)pyridine (DMAP) or 4-pyrrolidinopyridine (PPY).[13] The 'living' character is a manifestation of the rapid initiation and the weakly nucleophilic propagating species (secondary alcohol) that is active only to the cyclic diester monomer, precluding undesirable transesterification reactions. The new depolymerization strategy is based on a single transesterification reaction that should occur between a primary alcohol and poly(lactide), in the presence of DMAP to selectively cleave the PLA chain and produce an α-chain-end bearing the ester of the alcohol and a ω-chain-end having a secondary hydroxy, which is dormant to subsequent reactions (Scheme 1).

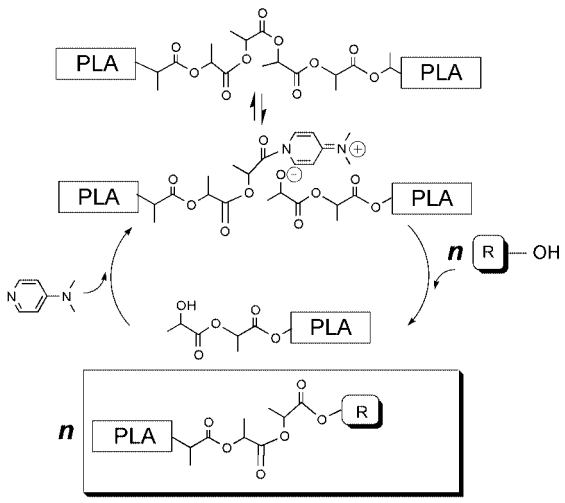

Scheme 1 Depolymerisation cycle.

Model reactions were performed to demonstrate the selectivity of the DMAP catalyzed transesterification of primary alcohols with poly(lactide). Excess of either benzyl alcohol or α-methylbenzyl alcohol were reacted with lactide in the presence of DMAP in CH_2Cl_2 at 38 °C (Scheme 2). The lactide was ring-opened by the benzyl alcohol with the formation of the benzyl ester. However, quantitative transesterification of the diester ring-opened product, by the excess benzyl alcohol afforded the monoester, **1**.[14] Conversely, the α-methylbenzyl alcohol ring-opened lactide produced quantitatively the diester product with no evidence of adverse side reactions, **2**.[15] This data clearly demonstrates the susceptability of lactic acid derivatives towards selective transesterification with primary alcohols and confirms that secondary alcohols are dormant towards transesterification with the ring-opened products.

The feasibility of the organocatalytic chain scission of poly(lactide) was demonstrated with several modest molecular weight polymers, to discern the end-groups and molecular weight, including; poly(D,L-lactide) having an average DP of 120 and a polydispersity of 1.14 (**3**) and a poly(L-lactide) having an average DP of 88 and a polydispersity index of 1.06, **4**. In addition, two commercially available high molecular weight poly(L-lactides) (Mn 50 000 g mol^{-1}, M_w/M_n = 1.60, **5**, and M_n 100 000, M_w/M_n = 1.61, **6**) were also used to demonstrate the generality of the procedures. Various compositions of benzyl alcohol together with 2.5 equivalents of either PPY or DMAP were allowed to react in solution (36 °C, CH_2Cl_2) with **3**.[16] The size exclusion chromatography (SEC) data (Fig. 1) clearly shows a systematic decrease in the hydrodynamic volume with benzyl alcohol content. Consistent with the SEC results, predictable molecular weights, determined from end-group analysis (^{1}H-NMR), were obtained from the alcohol to polymer ratio, further demonstrating the versatility of the transesterification approach (**7–9**, Table 1). The ^{1}H-NMR spectra clearly show the presence of the benzyl ester α-chain end and the ω-hydroxy chain-end.[13] The reactions were performed in either solution

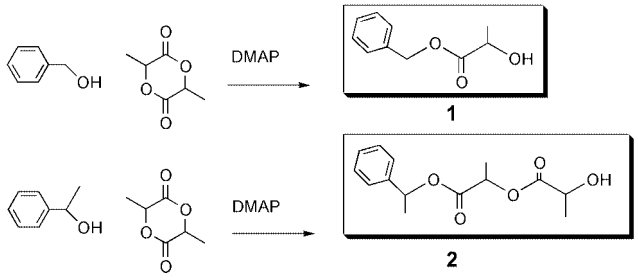

Scheme 2 Model compounds.

 DOI: 10.1039/b106125a

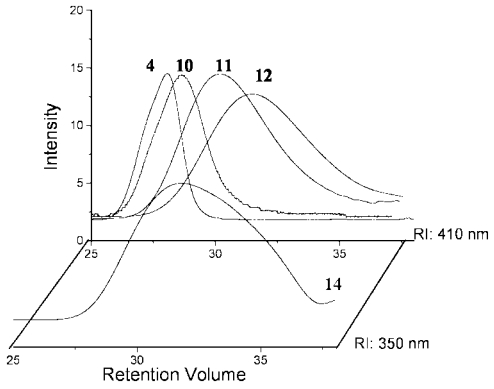

Fig. 1 SEC chromatography.

(36 °C, CH_2Cl_2) or bulk (135 or 185 °C for the D,L- or L-lactide, respectively) in the presence of either PPY or DMAP. The low temperature solution reactions took between 2 and 4 days and were particularly sluggish in the case of DMAP, whereas the bulk reactions took only 15–30 min., irrespective of the catalysts. Notably, these procedures are general and applicable towards high molecular weight commercial poly(lactides) (samples **13**–**14**, Table 1). Pyrenebutanol was used as the nucleophile and the reaction was followed by SEC using a diode array UV detector, **11**, Fig. 1. This data clearly shows that the pyrene is statistically distributed throughout the sample, confirming the utility of the procedure as a general route to functional poly(lactides). The use of α-methylbenzyl alcohol as the nucleophile in the transesterification with poly(lactide) did not result in a molecular weight or end-group change.

The organocatalytic transesterification of poly(lactide) to novel macromolecular architectures and block copolymers is demonstrated by the use of pentaerythritol and monohydroxy functional poly(ethylene oxide) (PEO) oligomers that produced either star-shaped (**15**–**17**) or block polymers (**18**–**21**), respectively. The reactions were performed in bulk and, at these temperatures, the homogeneous mixtures allowed effective transesterification for both of the high molecular weight poly(lactide) samples investigated. In each case, the ^{1}H-NMR spectra clearly show the resonances associated with the transesterification alcohol as well as the resonances associated with the hydroxy chain end, allowing molecular weight determination. In each case, the molecular weight of the polylactide was comparable to the alcohol-to-polymer ratio and the polydispersities were monomodal with no evidence of either of the homopolymers. These combined data clearly demonstrate the versitility of the organic catalyzed chain scission approach to functional poly(lactide) block copolymers and architectures in a single-step one-pot aproach.

Table 1 Depolymerization of polylactide: reactivity of assorted alcohols

Entry	PLA	Alcohol	Target DP	Exptl DP[e]	PDI[f]
7	**3**	$PhCH_2OH$[a,c]	56	56	1.15
8	**3**	$PhCH_2OH$[a,c]	28	28	1.28
9	**3**	$PhCH_2OH$[a,c]	18	16	1.38
10	**3**	$PhCH_2OH$[a,c]	18	17	1.31
11	**3**	Pyrenebutanol[b,c]	18	13	1.28
12	**4**	Pyrenebutanol[a,d]	22	18	1.30
13	**5**	$PhCH_2OH$[a,d]	110	95	1.25
14	**5**	$PhCH_2OH$[a,d]	18	10	1.35
15	**5**	Pentaerythritol[a,d]	50	48	1.65
16	**5**	Pentaerythritol[a,d]	25	16	1.26
17	**5**	Pentaerythritol[a,d]	10	6	1.21
18	**5**	PEO[a,d,g]	100	78	1.55
19	**5**	PEO[a,d,g]	40	31	1.61
20	**6**	PEO[a,d,g]	180	160	1.67
21	**6**	PEO[a,d,g]	58	55	1.60

[a] PPY. [b] DMAP. [c] CH_2Cl_2, 38 °C. [d] Bulk, 135 °C. [e] DP = degree of polymerization, experimentally measured by end group analysis from ^{1}H NMR spectroscopy. [f] PDI = polydispersity index, experimentally measured by gel permeation chromatography. [g] M_w = 2000 g mol^{-1}, monohydroxy terminated.

Notes and references

1 R. Langer, *Acc. Chem. Res*., 2000, **33**, 94.
2 D. Mecerreyes, Ph. Dubois and R. Jerome, *Adv. Polym. Sci*., 1999, **147**, 1.
3 A. Lofgren, A.-C. Albertsson, Ph. Dubois and R. Jerome, *J. Macromol. Sci., Rev. Macromol. Chem. Phys*., 1995, **C35**, 279.
4 T. M. Ovitt and G. W. Coates, *J. Am. Chem. Soc*., 1999, **121**, 4072.
5 M. A. Hillmyer, S. T. Nguyen and R. H. Grubbs, *Macromolecules*, 1997, **30**, 718.
6 C. W. Bielawsli, O. A. Scherman and R. H. Grubbs, *Polymer*, 2001, **42**, 4939.
7 A. Kumar and R. A. Gross, *J. Am. Chem. Soc*., 2000, **122**, 11767.
8 A. Kumar and R. A. Gross, *Polym. Prepr*., 2000, **41**, 1863.
9 G. C. Fu, *Acc. Chem. Res*, 2000, **33**, 412.
10 E. Vedejs and S. T. Diver, *J. Am. Chem. Soc*., 1993, **115**, 3358.
11 W. Steglich and G. Hofle, *Tetrahedron Lett*., 1970, 4727.
12 T. Sammakia and T. B. Hurley, *J. Org. Chem*., 2000, **65**, 974.
13 F. Nederberg, E. F. Connor, M. Moller, T. Glauser and J. L. Hedrick, *Angew. Chem., Int. Ed*., 2000, **40**, 2712.
14 In a glove box, DL-lactide (1.0 g, 6.94 mmol) and DMAP (1 eq. to the DL-lactide, 0.848 g, 6.94 mmol) was added to a round bottom flask. An excess of benzyl alcohol (10 eq. to the DL-lactide, (7.18 ml, 0.069 mmol) was charged together with CH_2Cl_2 and the reaction flask was slowly heated to 35 °C (5 h). The product was isolated by flash chromatography (90% dichloromethane–10% ethyl acetate). ^{1}H-NMR (acetone-d_6) δ = 1.34 (d, 3H, -CH_3), 2.05 (s, H, -OH), 4.30 (q, H, -CH-), 5.16 (s, 2H, -CH_2-), 7.40–7.30 (m, 5H, C_6H_5-). ^{13}C-NMR (acetone-d_6) δ = 175.4, 137.3, 129.3, 128.9, 128.8, 67.6, 66.8, 20.8.
15 In a glove box, the DL-lactide monomer (1.0 g, 6.94 mmol) and the DMAP (1 eq. to the DL-lactide, 0.848 g, 6.94 mmol) were added into a round bottom flask. An excess of α-methylbenzyl alcohol (10 eq. to the DL-lactide, 8.36 ml, 0.069 mmol) was added under nitrogen and the reaction flask was slowly heated to 35 °C. The reaction was followed by TLC and ^{1}H-NMR. After completion the reaction mixture was separated by flash chromatography (80% hexanes–20% ethyl acetate). ^{1}H-NMR (acetone-d_6) δ = 1.34 (d, 3H, -CH_3), 1.44 (d, 3H, -CH_3), 1.54 (d, 3H, -CH_3), 4.30 (q, H, -CH-), 5.10 (q, H, -CH-), 5.87 (q, H, -CH), 7.30–7.40 (m, 5H, C_6H_5-). ^{13}C-NMR (acetone-d_6) δ = 175.1, 170.3, 142.3, 129.3, 128.7, 126.7, 73.9, 69.7, 67.2, 22.4, 20.8, 17.1.
16 In a glove box, poly(D,L-lactide) (1.00 g, 0.0009 mol), DMAP (0.082 g, 0.00072 mol) and benzyl alcohol (0.039 g, 0.00036 mol) were charged into a round bottom flask and sealed with a septum. The transesterification reaction was allowed to proceed either in solution (CH_2Cl_2 5 ml, 38 °C, 3–4 days) or in bulk (135 °C, 30 min.). ^{1}H-NMR (acetone-d_6) δ = 1.46–1.56 (d, poly -CH_3), 4.15–4.29 (q, H, -CH_2-), 5.05–5.28 (q, poly -CH_2-), 7.3–7.4, (5H, C_6H_5).

CHEMCOMM Communication
www.rsc.org/chemcomm

Stereoselective preparation of highly functionalized (*Z*)-3-magnesiated enoates by an iodine–magnesium exchange reaction

Ioannis Sapountzis, Wolfgang Dohle and Paul Knochel*

Department Chemie, Ludwig-Maximilians-Universität München, Butenandstr. 5-13, Haus F, D-81377 München, Germany. E-mail: Paul.Knochel@cup.uni-muenchen.de; Fax: +49-089-2180-7680; Tel: +49-089-2180-7681

Received (in Cambridge, UK) 12th July 2001, Accepted 5th September 2001
First published as an Advance Article on the web 27th September 2001

3-Iodoenoates are converted into the corresponding alkenylmagnesium species with complete retention of configuration of the double bond; both direct reaction and copper(I)-mediated reactions with various electrophiles provide polyfunctional enoates.

Functionalized organometallics are key intermediates for the synthesis of complex polyfunctional molecules.[1] Although organozinc reagents have been proven to tolerate many functional groups, their low reactivity precludes their reaction with some electrophiles.[1] Recently, we have shown that the iodine–magnesium exchange reaction allows the preparation of highly functionalized aryl and heteroaryl magnesium reagents[2,3] and this methodology has also been used to access alkenylmagnesium compounds.[4] Since the stereoselective preparation of stereochemically well defined *E*- or *Z*-alkenylmagnesium compounds is not possible by the direct insertion of magnesium into *E*- or *Z*-alkenyl halides, the iodine–magnesium exchange reaction may be a unique way of preparing stereochemically pure *E*- or *Z*-alkenylmagnesium derivatives.[5] Especially useful for synthetic applications are organometallic reagents bearing functional groups in close proximity to the carbon–magnesium bond in an arrangement which provides an umpolung of the standard reactivity.[6] This led us to investigate the stereoselective preparation of 3-magnesiated enoates[7] of type **1** displaying a d^3-reactivity.[6] The required 3-iodoenoates of type **2** are readily available by literature procedures.[8] Thus, the reaction of (*Z*)-ethyl 3-iodocrotonate (**2a**) with isopropylmagnesium bromide in THF at −20 °C for 2 h leads to the desired (*Z*)-ethyl 3-magnesiated crotonate (**1a**). After quenching with an electrophile, products of type **3** are obtained in good yields (Scheme 1, Table 1). (*Z*)-Ethyl 3-iodocinnamate (**2b**) behaves in a similar fashion; the I/Mg-exchange reaction is complete within 0.5 h as indicated by GC analysis of iodolized and hydrolyzed reaction aliquots. Transmetalation of **1a** or **1b** with the THF-soluble copper salt CuCN·2LiCl[9] provides a functionalized copper reagent with complete retention of the double

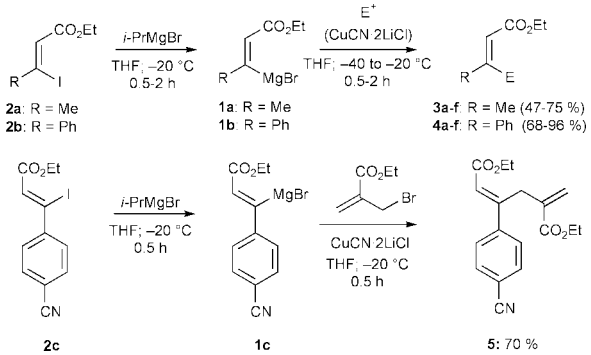

Scheme 1

Table 1 Stereoselective preparation of 3-substituted crotonates and cinnamates of type **3** and **4** obtained by the reaction of the 3-magnesiated crotonates **1a** and 3-magnesiated cinnamates **2b** with various electrophiles

Entry	Grignard reagent	Electrophile	Product of type **3** or **4**	Yield (%)[a]
1	**1a**		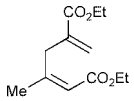 **3a**	69[b]
2	**1a**	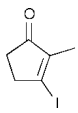	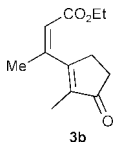 **3b**	69[b]
3	**1a**	Me_3SnCl	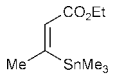 **3c**	72
4	**1a**	PhCHO	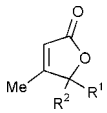 **3d**: R^1 = H; R^2 = Ph	75
5	**1a**	*c*-HexCHO	**3e**: R^1 = H; R^2 = *c*-Hex	73
6	**1a**	$PhCOCH_3$	**3f**: R^1 = Me; R^2 = Ph	47
7	**1b**		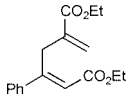 **4a**	92[b]
8	**1b**	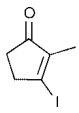	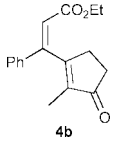 **4b**	90[b]
9	**1b**	TosCN	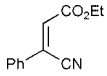 **4c**	75
10	**1b**	PhCOCl	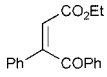 **4d**	96[b]
11	**1b**	PhCHO	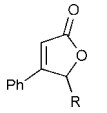 **4e**: R = Ph	72
12	**1b**	*c*-HexCHO	**4f**: R = *c*-Hex	68

[a] Yield of analytically pure products. [b] A transmetalation to a copper reagent with CuCN·LiCl (1 equiv.) was performed prior to the addition of the electrophile.

 DOI: 10.1039/b106195j

bond configuration. Reaction of the cuprate derived from **1a** with ethyl (2-bromomethyl)acrylate[10] provides the (*Z*)-unsaturated diester **3a** in 69% yield (>99% *Z*). Similarly, 3-magnesiated cinnamate **1b** furnishes after transmetalation with copper *E*-**4a** (92% yield; >99% *E*), thus showing in both cases complete retention of configuration of the double bond (entries 1 and 7 of Table 1).[11] Additionally we have prepared iodide **2a** as a 2:7 *E*/*Z* mixture.[12] We observed that both isomers undergo the I/Mg-exchange. However, iodolysis experiments indicate that the *E*-isomer of **1a** is less stable (30 min at −60 °C) which can be explained by the absence of chelation for this Grignard species. Due to the difficulty of preparing pure *E*-**2a** no additional experiments have been performed so far. The fact that the *E*-isomer of **2a** undergoes the I/Mg-exchange under similar conditions as the corresponding *Z*-isomer seems to indicate that chelation is not essential. The reaction of the copper derivatives of **1a**,**b** with 3-iodo-2-methylcyclopent-2-enone (−20 °C, 2 h) furnishes the dienic ketoesters **3b** and **4b** in 69% and 92% yield respectively (>99% *Z* for **3b** and >99% *E* for **4b**; entries 2 and 8). Reactive electrophiles like Me_3SnCl and tosyl cyanide react directly with the functionalized alkenylmagnesium reagents **1a**,**b** providing the *Z*-organotin derivative **3c** (72% yield; >99% *Z*) and the *Z*-1,2-cyanoester **4c** (92% yield; >99% *Z*); entries 3 and 9. After transmetalation to the copper derivative, **1b** reacts with PhCOCl to give the unsaturated 1,4-ketoester **4d** (96% yield; >99% *Z*). The unsaturated Grignard reagent **1a**,**b** adds directly to aldehydes and ketones, furnishing the corresponding lactones in 47–75% yield (entries 4–6 and 11–12). Finally, an additional cyano group is also well tolerated. Thus, ethyl 3-iodo-*p*-cyanocinnamate **2c** can be converted into the corresponding magnesium derivative (**1c**) under our standard conditions (*i*-PrMgBr (1 equiv); THF; −20 °C; 0.5 h) in high yield. After transmetalation with CuCN·2LiCl and reaction with ethyl (2-bromomethyl)-acrylate, the expected allylation product **5** is obtained (>99% *E*; 70% yield; Scheme 1).

In summary, we have demonstrated that new 3-magnesiated enoates can be prepared with high stereoselectivity (>99%) starting from isomerically pure *Z*-3-iodoenoates. These functionalized alkenylmagnesium reagents react with a range of electrophiles either directly or after transmetalation to the corresponding alkenylcopper species.[13] Extension of this method to other polyfunctional iodoalkenes and related organic halides is currently underway in our laboratories.

We thank Aventis Pharma and the Deutsche Forschungsgemeinschaft (Leibniz program) for financial support. We also thank BASF AG (Ludwigshafen), Chemetall GmbH (Frankfurt) and Degussa AG (Hanau) for generous gifts of chemicals.

Notes and references

1 A. Boudier, L. O. Bromm, M. Lotz and P. Knochel, *Angew. Chem., Int. Ed.*, 2000, **39**, 4415.

2 M. Rottländer, L. Boymond, L. Bérillon, A. Leprêtre, G. Varchi, S. Avolio, H. Laaziri, G. Quéguiner, A. Ricci, G. Cahiez and P. Knochel, *Chem. Eur. J.*, 2000, **6**, 767; L. Boymond, M. Rottländer, G. Cahiez and P. Knochel, *Angew. Chem., Int. Ed.*, 1998, **37**, 1701; L. Bérillon, A. Leprêtre, A. Turck, N. Plé, G. Quéguiner, G. Cahiez and P. Knochel, *Synlett*, 1998, 1359; G. Varchi, A. E. Jensen, W. Dohle, A. Ricci, G. Cahiez and P. Knochel, *Synlett*, 2001, 477.

3 F. Trécourt, G. Breton, V. Bonnet, F. Mongin, F. Marsais and G. Quéguiner, *Tetrahedron Lett.*, 1999, **40**, 4339; K. Kitagawa, A. Inoue, H. Shinokubo and K. Oshima, *Angew. Chem., Int. Ed.*, 2000, **39**, 2481; P. M. Herrinton, C. E. Owen and J. R. Gage, *Org. Process Res. Dev.*, 2001, **5**, 80.

4 (*a*) M. Rottländer, L. Boymond, G. Cahiez and P. Knochel, *J. Org. Chem.*, 1999, **64**, 1080; (*b*) J. Thibonnet and P. Knochel, *Tetrahedron Lett.*, 2000, **41**, 3319.

5 The direct insertion of magnesium into alkenyl halides is not stereoselective. For example, the reaction of (*Z*)-1-bromooctene with magnesium in THF produces a 15:85 *E*:*Z* mixture of 1-octenylmagnesium bromide. The same behaviour is observed for the insertion of zinc dust into alkenyl iodides. In both cases, a radical mechanism operates. T. N. Majid and P. Knochel, *Tetrahedron Lett.*, 1990, **31**, 4413.

6 D. Seebach, *Angew. Chem.*, 1979, **91**, 259.

7 T. Takahashi, C. Xi, Y. Ura and K. Nakajima, *J. Am. Chem. Soc.*, 2000, **122**, 3228.

8 E. Piers, T. Wong, P. D. Coish and C. Rogers, *Can. J. Chem.*, 1994, **72**, 1816.

9 P. Knochel, M. C. P. Yeh, S. C. Berk and J. Talbert, *J. Org. Chem.*, 1988, **53**, 2390.

10 J. Villieras and M. Rambaud, *Synthesis*, 1982, 924.

11 The corresponding 3-zincated enoates obtained by the insertion of zinc to the precursor 3-iodoenoates are obtained as *E*:*Z* mixtures; see P. Knochel and C. Janakiram Rao, *Tetrahedron*, 1993, **49**, 29. Compare also with ref. 4*a*.

12 W. J. Le Noble, *J. Am. Chem. Soc.*, 1961, **83**, 3897.

13 Typical procedure: preparation of 5-cyclohexyl-4-methylfuran-2(5*H*)-one: a dry and argon flushed 25 mL flask, equipped with a magnetic stirrer and a septum, was charged with **2a** (480 mg, 2 mmol). Dry THF was added and the mixture cooled to −20 °C. *i*-PrMgBr (3.7 mL, 0.54 M in THF, 2 mmol) was added dropwise. The exchange was complete after 2 h (checked by GC analysis of reaction aliquots) and the magnesiated crotonate **1a** was added *via* cannula to a solution of cyclohexanecarboxaldehyde (168 mg, 1.5 mmol) in THF (1.5 mL) cooled to −40 °C. After 30 min stirring at −40 °C the reaction was quenched with saturated NH_4Cl solution (2 mL) and poured into water (50 mL). The aqueous phase was extracted with diethyl ether (2 × 60 mL). The organic fractions were washed with brine (40 mL) then dried over $MgSO_4$ and concentrated *in vacuo*. The crude product was purified by flash chromatography (pentane–EtOAc 4:1) yielding the lactone **3e** as a pale colourless oil (200 mg, 73%).

CHEMCOMM
Communication
www.rsc.org/chemcomm

Solvation of 1-butyl-3-methylimidazolium hexafluorophosphate in aqueous ethanol–a green solution for dissolving 'hydrophobic' ionic liquids

Richard P. Swatloski, Ann E. Visser, W. Matthew Reichert, Grant A. Broker, Lindsy M. Farina, John D. Holbrey and Robin D. Rogers*

Department of Chemistry and Center for Green Manufacturing, The University of Alabama, Tuscaloosa, AL 35487, USA. E-mail: rdrogers@bama.ua.edu

Received (in Columbia, MO, USA) 1st July 2001, Accepted 28th August 2001
First published as an Advance Article on the web 27th September 2001

The relatively hydrophobic ionic liquid 1-butyl-3-methylimidazolium hexafluorophosphate has been found to be totally miscible with aqueous ethanol between 0.5 and 0.9 mol fraction ethanol, whereas the ionic liquid is only partially miscible with either pure water or absolute ethanol; the ability to dissolve 1-butyl-3-methylimidazolium hexafluorophosphate in a 'green' aqueous solvent system has important implications for cleaning, purification, and separations using ionic liquids.

Current interest in ionic liquids[1,2] (IL) stems primarily from the heightened awareness of the potential applications for IL in Green Chemistry[3] and the associated emphasis on clean manufacturing processes. We have investigated IL as clean, environmentally benign solvents as replacements for VOCs in liquid/liquid separations and extraction processes.[4–9] From the 'green' perspective, an issue of primary importance is the separation and recovery of products from reaction systems, as well as the potential to recycle and reuse the reaction/separations media without generating secondary waste. There is concern about how to address issues such as cleaning and removal of *non-volatile* IL from surfaces or from solid products without using VOCs. For example, the commonly used 'hydrophobic' IL 1-butyl-3-methylimidazolium hexafluorophosphate, [C_4mim][PF_6],† is readily soluble in many common organic solvents but is relatively insoluble in most green solvents including water and sc-CO_2. Here, we demonstrate that [C_4mim][PF_6] can be solubilized in a green aqueous solvent system–ethanol/water.

In a traditional liquid/liquid separation processes, the principle of 'like dissolves like' forms the basis for the partitioning of solutes between the two phases; the less water-soluble the solute, the higher its affinity for the hydrophobic extracting phase. The partitioning of organic solutes in IL/water systems shows a correlation with the octan-1-ol/water partition coefficient.[6] This is consistent with solvatochromatic studies[10,11] which appear to show that IL have solvent characteristics similar to moderately polar organic molecules, but with some important and inherent differences.[12] The solvent parameters determined for IL can vary significantly depending on the experimental probe used, and depend upon the contributions from specific interactions between IL and solutes. Volume and hydrogen-bond acceptor terms appear to be most important to the overall solvating environment. In light of this, it is important to note that PF_6^- is a poor hydrogen-bond acceptor and consequently ethanol and water should not partition in significant concentrations to [C_4mim][PF_6].

Dullius *et al.*[13] have shown that tetrafluoroborate-containing IL display miscibility curves with water typical of a partially miscible two-component system with an upper thermal critical point and, at lower temperatures, the formation of a two-phase system containing IL-rich and aqueous-rich layers. Work by Friberg *et al.*[14] has highlighted the complexity of the co-miscibility/solvation profile in [C_4mim][PF_6]/water/nonionic surfactant systems and also noted that the IL exhibited only partial miscibility with hydrated ethanol.

During partitioning studies, we were intrigued by the variation in miscibility of IL with molecular solvents we had observed from simple bench tests, and in particular, the observation that [C_4mim][PF_6] was totally miscible with 80% aqueous ethanol and yet formed biphasic mixtures with both pure water *and* pure ethanol. This prompted a more detailed investigation of the phase behavior.

The ternary phase diagram for [C_4mim][PF_6] in contact with ethanol and water was determined by cloud-point titration[15] at 25 °C and is shown in Fig. 1. [C_4mim][PF_6] is partially miscible with both pure water and with pure ethanol. Regions of biphasic coexistence extend along the [C_4mim][PF_6]/H_2O and [C_4mim][PF_6]/ethanol axes, respectively. The solubility limit of absolute ethanol in the IL was determined to be 10.1 wt% and the solubility of water was 1.2 wt%. The water content of saturated [C_4mim][PF_6] has been reported in the literature ranging from 1.2 to 2.3 wt%,[7,16,17] corresponding to a mol fraction between 0.16 to 0.27. The region of complete miscibility of the three components, water, ethanol, and [C_4mim][PF_6], is shown between the two binodal curves and extends from the EtOH/H_2O axis.

To further our characterization of the ethanol/water solubility in [C_4mim][PF_6], the distribution of ethanol and water to the IL was determined (Fig. 2). Samples containing 2 mL of IL were contacted with an equal volume of aqueous ethanol solution labeled with a ^{14}C-ethanol tracer.[12] The distribution of ethanol was determined from the radiotracer partitioning, and the water content of the IL phase was measured by Karl Fischer titration.[12] In the biphasic regions, the distribution of ethanol is

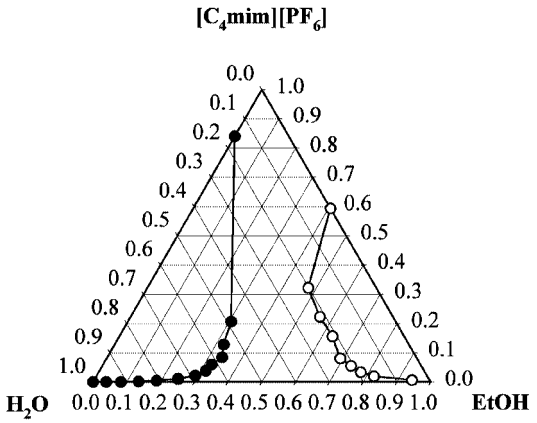

Fig. 1 Triangular phase diagram for ternary compositions of [C_4mim][PF_6], ethanol, and water determined at 25 °C and plotted as mol fraction. The region to the left of the binodal line, -●- is biphasic with water- and [C_4mim][PF_6]-rich phases; the region to the right of the line -○- is biphasic comprising ethanol- and [C_4mim][PF_6]-rich phases. In the central region, the three components are totally miscible and form a single monophasic solution.

 DOI: 10.1039/b106601n

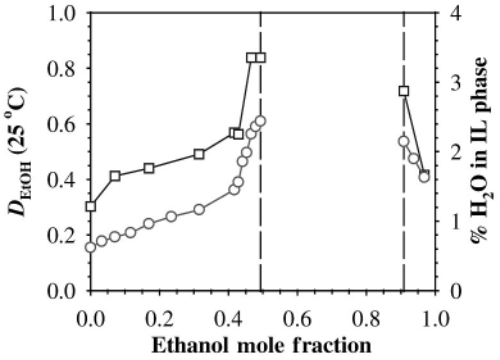

Fig. 2 The distribution ratios at 25 °C of ethanol (D_{EtOH} = ○) and water content of the IL phase (□) in 1 : 1 volume mixtures of [C_4mim][PF_6] and aqueous ethanol as a function of initial mol fraction of ethanol in the aqueous phase prior to contact with the IL phase. The monophasic region is bounded by the vertical dashed lines.

less than 1, which indicates the tendency for ethanol to remain in the aqueous phase. For the two-component [C_4mim][PF_6]/water system, the distribution ratio for the ethanol tracer between the IL and water is only 0.16. Successive increases in the mol fraction of ethanol cause an increase in ethanol distribution ratios up to a maximum of 0.61 at 0.5 mol fraction of ethanol in water. In the range 0.4–0.5 mol fraction, the distribution of ethanol to [C_4mim][PF_6] and the water content of the IL increases dramatically, and for 0.5–0.9 mol fraction the system is monophasic, shown by the vertical lines in Fig. 2. Above 0.9 mol fraction, a biphasic mixture is once again obtained.

The solubility of both ethanol and water in the IL phase increases in the presence of the other component, leading to the large homogeneous region in the phase diagram. The D_{EtOH} and water content data shown in Fig. 2 indicate that ethanol and water are dissolved together in the IL. Both the D_{EtOH} and water content increase linearly with X_{EtOH} from 0 to 0.40, where a sharp rise in both is maintained until the miscibility region. At X_{EtOH} = 0.90 a biphasic region is again observed and D_{EtOH} and water content decrease with the addition of ethanol.

The liquid structure and association in ethanol/water compositions has been the subject of extensive study;[18] when X_{EtOH} < 0.2, ethanol molecules cluster with the ethyl chains forming a hydrophobic core surrounded by water molecules. At 0.2 < X_{EtOH} < 0.8, a sandwich-type cluster containing extended chains of hydrogen-bonded ethanol and water occurs. The interactions that could occur between the water/ethanol clusters and the IL to lead to the total miscibility region is not yet clear. Free-volume cavities, or void space within the IL matrix[17] may allow ethanol and water to be dissolved together, whilst maintaining the bulk ethanol/water hydrogen-bonding structure with only weak interactions between the alkyl-groups of the IL and the hydrophobic ethyl-substituents of the water/ethanol chains.

A comparison of the vapor phase compositions above the [C_4mim][PF_6]/water/ethanol mixtures with ethanol/water mixtures only was made using SPME/GC. No discernable differences in the ethanol/water composition of the gas vapor phase was observed. This adds to our supposition that ethanol/water compositions mix with the IL whilst maintaining the bulk ethanol/water hydrogen-bonded structure.

The observation that [C_4mim][PF_6], regarded as a hydrophobic IL, can be dissolved in a 'green' aqueous solvent system has important implications for purification and separations from IL. As shown here, the addition of a solute or combination of solutes dramatically affects the solution behavior of IL, highlighting the need to fully understand these systems and instances in which their solution chemistry may vary from that of traditional organic solvents. At a practical level, these results show a method by which [C_4mim][PF_6] can be dissolved and cleaned from, for example, a reaction vessel or a solid product without using volatile chlorinated organic solvents. The IL can be recovered by distilling the water/ethanol azeotrope or by changing the solution composition to form a biphasic system.

This research was supported by the US Environmental Protection Agency's STAR program (grant number R-82825701-0). Additional support was provided to the Center for Green Manufacturing from the National Science Foundation Grant EPS-9977239 and the PG Research Foundation. The authors appreciate the chemicals supplied by Ozark Fluorine Specialties.

Notes and references

† The synthesis of 1-butyl-3-methylimidazolium hexafluorophosphate from [C_4mim]Cl and HPF_6 (Ozark Fluorine Specialties) and the procedures used for the standard radiochemical assay utilized are described in ref. 12. The radiochemical assay of equal volumes of the two separated phases allows calculation of the distribution ratios directly from the activity of the two phases. ^{14}C-labeled ethanol was obtained from Sigma (St. Louis, MO). All aqueous solutions were prepared with deionized water that was purified with a Barnsted deionization system (Dubuque, IA) and polished to 18.3 MΩ cm. The water content of each ionic liquid or its mixtures was determined by Karl Fischer titration (Aquastar Karl Fischer titrator, EM Science, Gibbstown, NJ) with Composite 5 solution as the titrant in anhydrous methanol. The ternary composition diagram was determined by direct observation using the cloud-point titration method described in ref. 15.

1 R. D. Rogers, *Green Chem*., 2000, **2**, G94; W. Keim and P. Wasserscheid, *Angew. Chem., Int. Ed*., 2000, **39**, 3772; J. D. Holbrey and K. R. Seddon, *Clean Prod. Process*., 1999, **1**, 233; T. Welton, *Chem. Rev*., 1999, **99**, 2071.
2 D. Adam, *Nature*, 2000, **407**, 938; M. Freemantle, *Chem. Eng. News*, 2000, **78** (May 15), 37.
3 P. T. Anastas and J. C. Warner, *Green Chemistry: Theory and Practice*, Oxford University Press, New York, 1998.
4 A. E. Visser, R. P. Swatloski and R. D. Rogers, *Green Chem*., 2000, **1**, 1.
5 A. E. Visser, R. P. Swatloski, W. M. Reichert, R. Mayton, S. Sheff, A. Wierzbicki, J. H. Davis Jr. and R. D. Rogers, *Chem. Commun*., 2001, 135.
6 J. G. Huddleston, H. D. Willauer, R. P. Swatloski, A. E. Visser and R. D. Rogers, *Chem. Commun*., 1998, 1765.
7 A. E. Visser, R. P. Swatloski, W. M. Reichert, S. T. Griffin and R. D. Rogers, *Ind. Eng. Chem. Res*., 2000, **39**, 3596.
8 A. E. Visser, W. M. Reichert, R. P. Swatloski, H. D. Willauer and R. D. Rogers, *Physical Properties of Room Temperature Ionic Liquids as Alternative Solvent Media for Liquid/Liquid Separations*, in *Green Industrial Applications of Ionic Liquids*, ed. R. D. Rogers and K. R. Seddon, ACS, San Diego, CA, 2001, in press.
9 A. E. Visser, R. P. Swatloski, S. T. Griffin, D. H. Hartman and R. D. Rogers, *Sep. Sci. Technol*., 2001, **36**, 785.
10 M. J. Muldoon, C. M. Gordon and I. R. Dunkin, *J. Chem. Soc., Perkin Trans. 2*, 2001, 433; A. J. Carmichael and K. R. Seddon, *J. Phys. Org. Chem*., 2000, **13**, 591; S. N. V. K. Aki, J. F. Brennecke and A. Samanta, *Chem. Commun*., 2001, 413.
11 J. G. Huddleston, A. E. Visser, G. A. Broker, W. M. Reichert, H. D. Willauer and R. D. Rogers, *Green Chem*., 2001, in preparation.
12 J. G. Huddleston, A. E. Visser, W. M. Reichert, H. D. Willauer, G. A. Broker and R. D. Rogers, *Green Chem*., 2001, **3**, 156.
13 J. E. L. Dullius, P. A. Z. Suarez, S. Einloft, R. F. de Souza and J. Dupont, *Organometallics*, 1998, **17**, 815.
14 S. E. Friberg, Q. Yin, F. Pavel, R. A. Mackay, J. D. Holbrey, K. R. Seddon and P. A. Aikens, *J. Dispersion Sci. Technol*., 2000, **21**, 185.
15 R. E. Treybil, *Liquid Extraction*, McGraw Hill, New York, 2nd edn., 1963.
16 K. R. Seddon, A. Stark and M. J. Torres, *Pure Appl. Chem*., 2000, **72**, 2275.
17 L. A. Blanchard, Z. Gu and J. F. Brennecke, *J. Phys. Chem. B*, 2001, **105**, 2437.
18 F. Francks and D. J. G. Ives, *Quart. Rev*., 1966, **20**, 1; V. Gomiz, F. Ruiz, N. Boluda and M. D. Saquete, *Ind. Eng. Chem. Res*., 1998, **37**, 599; A. Sacco, F. M. De Cillis and M. Holz, *J. Chem. Soc., Faraday Trans*., 1998, **94**, 2089; F. Ruiz, V. Gomiz and R. F. Bottella, *Ind. Eng. Chem. Res*., 1987, **26**, 696; J. J. Malinowski and A. J. Daugulis, *AIChE J*., 1994, **40**, 1459.

CHEMCOMM Communication
www.rsc.org/chemcomm

Agostic deformations based on electron delocalization in the alkyllithium-complex [{2-$(Me_3Si)_2CLiC_5H_4N$}$_2$]†

Wolfgang Scherer,*[a] Peter Sirsch,[a] Manja Grosche,[a] Michael Spiegler,[a] Sax A. Mason[b] and Michael G. Gardiner*[c]

[a] *Anorganisch-chemisches Institut der Technischen Universität München, Lichtenbergstraße 4, D-85747 Garching bei München, Germany. E-mail: wolfgang.scherer@ch.tum.de*
[b] *Institut Laue-Langevin, BP156, 38042 Grenoble Cedex 9, France*
[c] *School of Chemistry, University of Tasmania, GPO Box 252-75, Hobart TMS 7001, Australia*

Received (in Cambridge, UK) 21st June 2001, Accepted 24th August 2001
First published as an Advance Article on the web 1st October 2001

Topological analysis of experimental and theoretical charge densities in the title complex [{2-$(Me_3Si)_2CLiC_5H_4N$}$_2$] 1 reveals the nature of the agostic deformation postulated for this complex: delocalization of the Li–C bonding electrons over the entire agostic alkyl group controls the formation of an acute Li–C–Si angle and thus a sufficient electronic saturation of the electron deficient lithium atom *via* secondary interactions.

Alkyllithium complexes are of fundamental interest in organic synthesis and as anion transfer reagents in organometallic synthesis. Their crystal structures display a remarkable range of bonding modes which have been compiled and rationalized in several surveys of this field.[1] In the title compound[2] featuring a formal lithium coordination number of only 2, 'secondary interactions', which compensate for the electron deficiency of the metal centre, should be of great importance in understanding not just the structure adopted by the complex, but also the reactivity of the species. Despite this, little is known about the details of such interactions which compensate for the electron deficiencies of the metal centres in their reduced coordination state, and include (i) close Li···Li contacts[3] and (ii) close 'agostic' type Li···H–C interactions—as evident in the title compound.[2] The importance of these Li···H–C agostic interactions was highlighted in early calculations on the trimeric lithium amide complex [{Li[μ-$N(CH_2Ph)_2$]}$_3$][4a] which concluded that Li···H–C interactions might account for 40% of the valence shell electron density for the lithium atom. Furthermore, agostic interactions[4b] are of particular interest in organotransition-metal chemistry in view of their potential relevance to important processes like C–H activation in catalytic reactions. Reliable ways of pinning down these interactions are still at a premium, notwithstanding the numerous examples reported on the basis of structural or spectroscopic measurements or of theoretical studies.

In a recent charge density study on an agostic compound we demonstrated that *topological analysis of experimental charge densities* can be used to identify β-agostic interactions in $EtTiCl_3$(dmpe) by locating the Ti···H bond critical point.[5] In this combined neutron and X-ray charge density study, however, we show that Li···H secondary interactions only play a minor role in compensating for the electron deficiency of the metal center. Fig. 1 shows the relevant molecular agostic fragment in **1** based on a precise neutron diffraction study at 20 K. This displays an acute Li–C1–Si2 angle of 88.8(2)°, leading to short Li···Si2, Li···C7 and Li···H7c contacts of 2.850(5), 2.658(5) and 2.320(6) Å, respectively. In addition, the presence of two further short intermolecular Li···H contacts [Li···H3b* = 2.329(5) and Li···H3c* = 2.245(5) Å] and a rather short Li···C3* contact of 2.496(4) Å were confirmed by the neutron diffraction study. All the Li···H contacts are remarkably short (*ca*. 0.7 Å less than the sum of the van der Waals radii; *cf*. the Li···H distance of 2.043(1) Å in crystalline lithium hydride).[6] Thus, they might be interpreted as agostic Li···H interactions. However, no significant C–H activation is evident from the neutron diffraction data [C7–H7a = 1.089(4), C7–H7b = 1.086(4), C7–H7c = 1.087(4) Å; C3–H3b = 1.085(3), C3–H3c = 1.097(4) Å]. We have therefore performed a combined X-ray and neutron charge density study[7,8] to explore for the first time the nature of Li···H–C agostic interactions on the basis of an experimental topological analysis of the electron density $\rho(\boldsymbol{r})$ of **1** using the 'Atoms in Molecules' (AIM) approach of Bader.[9,10]

DFT calculations at the B3LYP/6-311G(3d,3p) level of theory[11] on several monomeric model systems such as the donor-free species $LiCMe_2SiMe_3$ **1a** show alkyl coordination geometries (Li–C_α–Si = 85.3°, Li···H_γ = 2.11–2.29 Å) rather similar to that of the agostic alkyl backbone Li–C1–Si2–C7–H7c (Li–C_α–Si_β–C_γ–H_γ) in **1**. The agostic deformations in **1** clearly do not originate from any of the following: (i) the coordination of the σ-donor ligand, despite the short Li–N distance of 1.9508 Å; (ii) π-electron delocalization involving the aromatic pyridine ring; (iii) secondary interactions such as Li···Li contacts or intermolecular Li···H contacts; or (iv) other crystal-packing effects. Thus, **1** seems an ideal experimental benchmark system to study the nature of Li···H–C bonding, since we can focus our discussion solely on the bonding situation of the agostic backbone Li–C_α–Si_β–C_γ–H_γ of **1** (Fig. 1). Indeed, the topology of $\rho(\boldsymbol{r})$ of this fragment reveals the

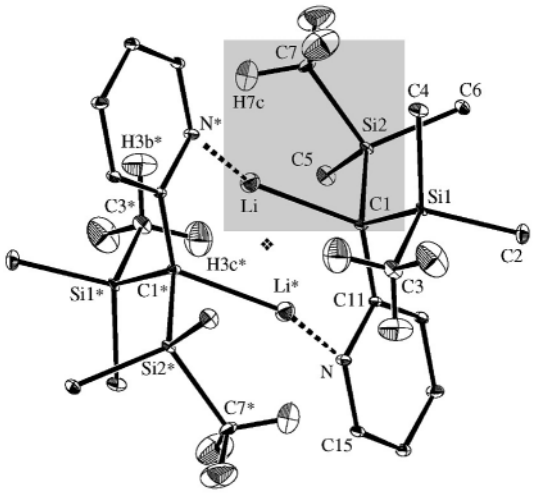

Fig. 1 Molecular structure of [{2-$(Me_3Si)_2CLiC_5H_4N$}$_2$] **1** at the 50% probability level and 20 K. Only relevant hydrogen atoms are shown. Atoms labeled with or without * are related by a crystallographic inversion centre at the midpoint of the Li–Li* vector. The location of the agostic alkyl group is indicated by a shaded area.

† Electronic supplementary information (ESI) available: experimental and theoretical details of multipole refinements and model systems. See http://www.rsc.org/suppdata/cc/b1/b105452j/

 DOI: 10.1039/b105452j

unusual electronic nature of the alkyl ligand. We first note the absence of a Li···H_γ bond critical point (bond CP)[9] in the experimental or theoretical $\rho(\boldsymbol{r})$ maps, indicating a lack of any significant agostic interaction. This accords with the absence of any significant C_γ–H_γ bond activation revealed by the low temperature neutron diffraction study. At this stage, the origin of the deformation of the alkyl group remains unclear.

However, analysis of the geometry of the Li–C_α–Si_β–C_γ–H_γ backbone gives some guidelines by revealing two significantly different C–Si bonds: C_α–Si_β and C_γ–Si_β [C1–Si2 = 1.8592(4) and Si2–C7 = 1.8947(7) Å, respectively]. While C_γ–Si_β seems to be slightly enlarged compared with standard single C–Si bonds such as Si2–C5(6) or Si1–C2(4) [Si–C = 1.8781(7)–1.8888(6) Å], the C_α–Si_β bond length is clearly shortened. Furthermore, the discrepancy in Si–C bond lengths is accompanied by significant differences in the nature of the C_α–Si and C_γ–Si bonding as shown by the combined charge density study: the value of $\rho(\boldsymbol{r})$ at the bond CP, $\rho(\boldsymbol{r}_c)$, for the C_α–Si_β bond [$\rho(\boldsymbol{r}_c)$ = 0.86(2) e Å^{-3}] is clearly larger than that for the corresponding C_γ–Si_β bond [0.72(2) e Å^{-3}], hinting at an increased bond order in the C_α–Si *vs.* the C_γ–Si bond. This conclusion is supported by a pronounced bond ellipticity ε of 0.13 at the C_α–Si_β bond CP (see ref. 9 and Fig. 2 for a definition of ε). Tracing the bond ellipticity between C_α and Si along the bond path[9] reveals the unusual nature of this bond in comparison with the ellipticity profiles of the theoretical benchmark systems for a C–Si single (CH_3–SiH_3) and a C=Si double bond (CH_2=SiH_2) (Fig. 2).

We further note that the Li–C_α (Li–C1) bond in **1** is significantly longer than the corresponding distance in the theoretical reference molecule LiMe:[12] Li–C_α = 2.2049 *vs.* 1.966 Å; and that the topological features of $\rho(\boldsymbol{r})$ in the two compounds indicate that the Li–C bond in the former is weaker [$\rho(\boldsymbol{r}_c)$ = 0.150(2) *vs.* 0.30 e Å^{-3}], and has a pronounced bond ellipticity (ε = 0.12 *vs.* 0.0). This suggests that the unusual double bond character of the C_α–Si_β bond might be associated with a delocalization of the Li–C bonding electrons into the C_α–Si_β bonding region, as revealed by the relief map of the negative Laplacian,[9] $-\nabla^2\rho(\boldsymbol{r})$, in the Li,$C_\alpha$,$Si_\beta$-plane (Fig. 3). This effect might be related to negative (anionic) hyperconjugation.

In conclusion, we have demonstrated by a combined neutron and X-ray charge density study on the lithium–alkyl system **1** that secondary, agostic Li···H interactions are not necessarily paralleled by significant C–H activation. Despite our findings, C–H activation probably plays an important role in lithium organic chemistry and is certainly significant in the characteristic reactivity of lithium in salient reactions such as β-H-elimination or even metallation. Furthermore, our results clearly indicate that Li···H contacts in **1** are not responsible for the unusual alkyl deformation. These deformations seem more likely to be a result of electron delocalization of the Li–C_α bonding electrons over the entire (agostic) alkyl group, leading to a reduced Li–C_α–Si_β angle, a pronounced C_α–Si_β double bond character, short Li···Si_β, Li···C_γ and Li···H_γ distances, and thus allowing a more efficient charge transfer between the electron deficient metal center and the agostic C_α–Si_β–C_γ–H_γ backbone.

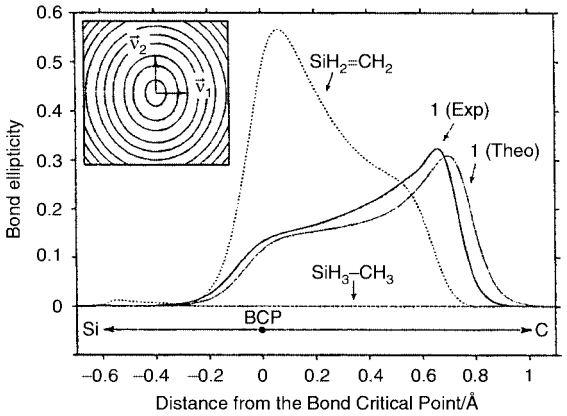

Fig. 2 Bond ellipticity[9] along the C1–Si2 bond path of **1**. The definition of the bond ellipticity is illustrated by the $\rho(\boldsymbol{r})$ contour map in the left corner showing the charge density in the plane perpendicular to the bond path at the C–Si bond CP of SiH_2=CH_2. ε is thus a measure of the non-spherical charge distribution of $\rho(\boldsymbol{r})$: $\varepsilon = \lambda_1/\lambda_2 - 1$. λ_i are eigenvalues of the corresponding eigenvectors $\vec{v}_1$ and $\vec{v}_2$ of the Hessian matrix of $\rho(\boldsymbol{r})$.

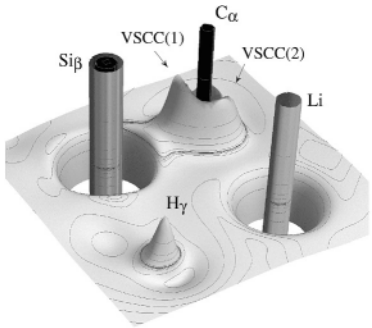

Fig. 3 Relief map of the negative Laplacian, $-\nabla^2\rho(\boldsymbol{r})$, showing the close-to-merging situation of the two valence shell charge concentrations VSCC(1) and VSCC(2) in the Li,C_α,Si_β-plane. Normally, the VSCCs on sp^3-hybridized carbon atoms are clearly separated. This effect might indicate a delocalization of the Li–C bonding electrons into the C_α–Si_β bonding region.

Notes and references

1 See, for example: R. E. Mulvey, *Chem. Soc. Rev.*, 1998, **27**, 339.
2 I. Papasergio, C. L. Raston and A. H. White, *J. Chem. Soc., Chem. Commun.*, 1983, 1419.
3 D. Barr, W. Clegg, S. M. Hodgson, R. E. Mulvey, D. Reed, R. Snaith and D. S. Wright, *J. Chem. Soc., Chem. Commun.*, 1988, 367.
4 (*a*) D. R. Armstrong, R. E. Mulvey, G. T. Walker, D. Barr, R. Snaith, W. Clegg and D. Reed, *J. Chem. Soc., Dalton Trans.*, 1988, 617; (*b*) M. Brookhart, M. L. H. Green and L.-L. Wong, *Prog. Inorg. Chem.*, 1988, **36**, 1.
5 W. Scherer, W. Hieringer, M. Spiegler, P. Sirsch, G. S. McGrady, A. J. Downs, A. Haaland and B. Pedersen, *Chem. Commun.*, 1998, 2471.
6 E. Zintl and A. Harder, *Z. Phys. Chem. Abt. B*, 1935, **28**, 478.
7 (*a*) E. Clementi and D. L. Raimondi, *J. Chem. Phys.*, 1963, **38**, 2686; (*b*) N. K. Hansen and P. Coppens, *Acta Crystallogr., Sect. A*, 1978, **34**, 909; (*c*) T. Koritsánszky, S. Howard, T. Richter, Z. W. Su, P. R. Mallinson and N. K. Hansen, *XD - A Computer Program Package for Multipole Refinement and Analysis of Electron Densities from Diffraction Data*, Free University of Berlin, Germany, 1995.
8 Data for **1**: M_r = 486.85, yellow prisms; monoclinic, space group $P2_1/n$, a = 11.7233(2), b = 9.8814(2), c = 12.7702(2) Å, β = 93.481(1)°, V = 1476.60(5) Å^3; T = 115(1) K; Z = 2, $F(000)$ = 528, D_c = 1.095 g cm^{-3}, μ = 2.2 cm^{-1}. 80348 Bragg reflections were collected on a Nonius kappa-CCD system with a rotating anode generator (Nonius FR591; Mo-Kα, λ = 0.71073 Å); 15534 independent reflections; R_{int} = 0.034. The data set was corrected for beam inhomogeneity and absorption effects: 97.5% completeness in the data range $\sin\theta/\lambda_{max}$ = 1.09 Å^{-1}. The deformation density was described by a multipole model in terms of spherical harmonics multiplied by Slater-type radial functions with energy-optimised exponents (see ref. 7 and ESI†). During refinement the Li and H atom positions and their anisotropic thermal parameters (after scaling) were fixed at the values obtained by another neutron diffraction study at 100 K (see ESI†). The refinement of 301 parameters against 8905 observed reflections [$F > 3\sigma(F)$; $\sin\theta/\lambda_{max,final}$ = 1.0 Å^{-1}] converged to R_1 = 0.025, wR_2 = 0.0314, GOF = 1.06, and a featureless residual $\rho(\boldsymbol{r})$. CCDC reference numbers 169890 and 169891. See http://www.rsc.org/suppdata/cc/b1/b105452j/ for crystallographic data in CIF or other electronic format.
9 R. F. W. Bader, *Atoms in Molecules—A Quantum Theory*, Clarendon Press, Oxford, 1990.
10 F. W. Biegler-König, R. F. W. Bader and T. Tang, *J. Comput. Chem.*, 1982, **3**, 317.
11 All calculations were performed at the B3LYP/6-311G(3d,3p) level of theory, except **1** [B3LYP/6-311G(3d,3p)//B3LYP/6-31G(d)] using Gaussian 98. The topology of $\rho(\boldsymbol{r})_{calc}$ was analyzed using the AIM software package (ref. 10).
12 Exp. value: 1.959 Å; see D. B. Grotjahn, T. C. Pesch, J. Xin and L. M. Ziurys, *J. Am. Chem. Soc.*, 1997, **119**, 12368.

CHEMCOMM
Communication
www.rsc.org/chemcomm

Discotic mesogens with potential electron carrier properties

Gaël Kestemont,[a] Véronique de Halleux,[a] Matthias Lehmann,*[a] Dimitri A. Ivanov,[b] Mark Watson[c] and Yves Henri Geerts*[a]

[a] *Laboratoire de Chimie des Polymères, CP 206/1, Université Libre de Bruxelles, Boulevard du Triomphe 1050. Bruxelles, Belgium. E-mail: ygeerts@ulb.ac.be*
[b] *Laboratoire de Physique des Polymères, CP 223, Université Libre de Bruxelles, Boulevard du Triomphe 1050. Bruxelles, Belgium*
[c] *Max-Planck-Institute für Polymerforschung, Ackermannweg 10 55128. Mainz, Germany*

Received (in Cambridge, UK) 10th August 2001, Accepted 29th August 2001
First published as an Advance Article on the web 19th September 2001

A new family of discotic liquid crystals, potentially electron carriers, has been synthesised, some members of which exhibit a particularly rich thermotropic behaviour.

The discovery that 2,3,6,7,10,11-hexakis(hexylthio)triphenylene (HHTT), in a highly ordered helical (H) mesophase,[1] exhibits a charge carrier mobility (μ) on the order of $\mu = 0.1$ cm^2 V^{-1} s^{-1}, has created wide scientific and technological interests in discotic liquid crystals[2a] as potential candidates for optoelectronic applications.[2b] Since then, the charge carrier mobilities of several mesogens based on hexabenzocoronene, triphenylene, and phthalocyanine aromatic cores have been studied.[3] Values of μ as high as 0.5 cm^2 V^{-1} s^{-1} have been reported for the columnar mesophase of hexabenzocoronene derivatives.[4] Such mobility approaches the corresponding value for the intersheet mobility in graphite (3 cm^2 V^{-1} s^{-1}) and matches those of single crystals of aromatic compounds.[4] However, most of the discotic mesogens reported so far are better hole carriers than electron carriers.[3a] Only a few examples of electron carrier discotic mesogens exist to date[5,6] creating, therefore, the need for new materials.

In this communication, we report the synthesis and preliminary mesophase characterisation of a new type of discotic mesogen **4a–d**. The presence of six nitrogen atoms in the aromatic core is anticipated to significantly increase the first reduction potential facilitating electron injection and high electron mobility.[7]

The synthetic route is short and efficient (Scheme 1). The first step consists of the condensation of hexaoxocyclohexane octahydrate (**1**) with 4,5-dichlorobenzene-1,2-diamine (**2**) to afford the 2,3,8,9,14,15-hexachlorodiquinoxalino[2,3-*a*:2′,3′-*c*]phenazine **3** in 94% yield.[8] The second step is the nucleophilic aromatic substitution of **3** by alkyl thiolates.† The yield of hexakis(alkylthio)diquinoxalino[2,3-*a*:2′,3′-*c*]phenazines **4a–d** ranges between 29 and 67% depending on the ease of purification. Compounds **4b**,**c,** exhibiting a crystalline phase at room temperature, are easily purified by recrystallization whereas mesogens **4a** and **4d** having an X phase at room temperature necessitate several recrystallizations and chromatographic separations. The solubility of **4a–d** is good in common organic solvents such as $CHCl_3$ and THF. The structure and purity of **4a–d** were confirmed by ^{1}H- and ^{13}C NMR spectroscopy, mass spectrometry, and UV-visible absorption spectroscopy. In deuterated chloroform, the ^{1}H-NMR chemical shift of the aromatic protons moves to higher field on increasing the concentration, ranging from 8.26 ppm at 1.3×10^{-3} M to 8.11 ppm at 2.85×10^{-2} M.

The thermotropic behaviour of **4a–d**, as studied by differential scanning calorimetry (DSC), is strongly dependent on thioalkyl chain length (Table 1). Particularly unexpected is the number of mesophases observed upon heating for **4b** and **4c** (three and five, respectively) whereas **4a** and **4d** exhibit only two mesophases from room temperature to decomposition around 250 °C. This rich thermotropic behaviour and dependence on flexible chain length of **4a–d** is reminiscent of some LC derivatives of truxene and thiatruxene.[2b] Interestingly enough, they all have in common the same molecular shape of the aromatic core, *i.e.* a three-arm star shape rather than a disk-like shape. No clearing temperature, below decomposition, was observed for any of the four mesogens.

The types of the mesophases have been tentatively assigned based on the observations made by polarised optical microscopy and X-ray diffraction.‡ Characteristically, besides crystalline phases (Cr), LC mesophases and non-specified phases (X) were observed. Phases X are not solid, rather waxy and show birefingence. Powder diffraction patterns from these phases

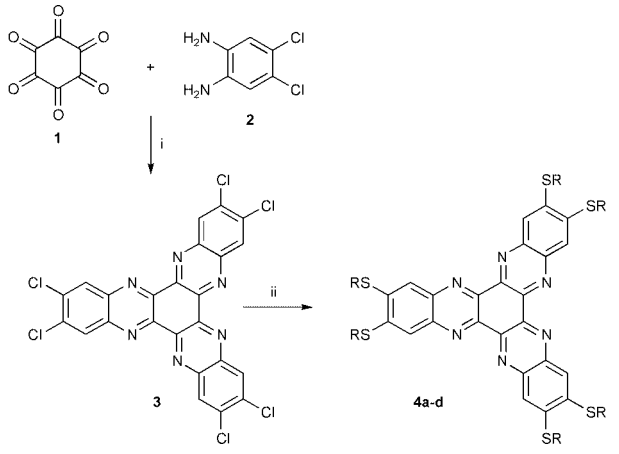

Scheme 1 Synthetic route to mesogens **4a–d**; **a**: R = C_6H_{13}, **b**: R = C_8H_{17}, **c**: R = $C_{10}H_{21}$, **d**: R = $C_{12}H_{25}$. i) Six-fold excess of 4,5-dichlorobenzene-1,2-diamine (**2**), acetic acid, reflux, 2 h, ii) ten-fold excess of $C_nH_{2n+1}SH$, K_2CO_3, DMF, 85 °C, 5 d.

Table 1 Tentative mesophase assignment,[a] transition temperatures, °C (onset),[b] and transition enthalpies (kJ mol^{-1}) of discotic mesogens **4a–d**

4a	X $\xrightarrow{206\ (26.4)}$ LC $\longrightarrow$ decomp.[c]
	X $\xleftarrow{196\ (-26.5)}$ LC
4b	Cr $\xrightarrow{77\ (5.6)}$ X_1 $\xrightarrow{142\ (14.0)}$ X_2 $\xrightarrow{178\ (13.5)}$ LC $\longrightarrow$ decomp.[c]
	Cr $\xleftarrow{43\ (-7.6)}$ X $\xleftarrow{174\ (-12.5)}$ LC
4c	Cr_1 $\xrightarrow{26\ (4.5)}$ Cr_2 $\xrightarrow{40\ (18.4)}$ X_1 $\xrightarrow{50\ (-24.1)}$ X_2 $\xrightarrow{116\ (30.6)}$ LC_1 $\xrightarrow{134\ (1.6)}$ LC_2 $\xrightarrow{180\ (0.4)}$ LC_3 $\longrightarrow$ decomp.[c]
	Cr $\xleftarrow{17\ (-28.1)}$ X $\xleftarrow{95\ (-3.7)}$ LC_1 $\xleftarrow{128\ (-1.8)}$ LC_2 $\xleftarrow{181\ (0.3)}$ LC_3
4d	X $\xrightarrow{99\ (31.7)}$ LC $\longrightarrow$ decomp.[c]
	X $\xleftarrow{79\ (-32.4)}$ LC

[a] Based on optical microscopy and X-ray diffraction investigations. [b] Measured by DSC at heating and cooling rate of 10° min^{-1}. The data from second heating scan and first cooling scan are given and were found to be fully reproducible. [c] Decomposition occurs around 250 °C.

 DOI: 10.1039/b107135c

exhibit less order than for the solid crystalline phases but a 3-dimensional correlation of molecules is maintained, which is manifested by maxima superimposed on the halo of the isotropic alkyl side chains. We propose phases X to be mesophases of higher, three dimensional order. The presence of highly ordered mesophases for compounds **4a–d** is particular important in view of charge transport properties since well-ordered plastic crystals (PC) or helical columnar phase (H) are known to exhibit higher charge carrier mobilities than less-ordered LC mesophases.[1,6,9] LC phases show birefringence and a significant fluidity. The textures are rather unspecific for **4b–d**, whereas **4a** displays a fan-like texture with large domains, spontaneously forming above the Cr–LC transition, which can be frequently found for columnar phases. Interestingly, the X-ray investigation of the mesophases reveals rather unconventional supramolecular arrangements. Beside halos with maxima at 0.45 nm for the average distance of isotropic alkyl chains and shoulders at 0.37–0.40 nm assigned to average intracolumnar distances separating aromatic cores, several maxima are observed at small angles which can not be unambiguously indexed for all observed mesophases. Fig. 1 depicts the X-ray pattern of **4c** at 170 °C, for which we could obtain the clearest assignment of the diffraction pattern. Three dominant diffraction peaks are found which can be attributed to an oblique unit cell with the parameters a = 2.24 nm , b = 2.13 nm and β = 83.5°. The calculated data is in agreement with the observed distances. The unit cell is significantly smaller than the diameter of **4c**, which is 1.30 nm for the core including the sulfur atoms and between 3.4 and 4.2 nm depending on the orientation of the alkyl chains in the all-*trans* conformation. Thus, like in hexakis(alkylthio)triphenylenes, this implies a large degree of penetration of the alkyl chains in the aliphatic region of the neighbouring column.[11] Similar data, but with lower intensity, was obtained for **4d**, however, for **4a** and **4b** the X-ray patterns remain complex for the fluid phase at high temperature. The precise supramolecular order of these molecules is under investigation. 2D X-ray data of oriented samples and solid state NMR is in progress and will be published in detail elsewhere.

Compounds **4a–d** strongly absorb in the visible range. In toluene solution, the absorption maxima at the longest wavelength (λ_{max}) of **4a–d** are identical, located at 470 nm with an absorption coefficient (ε) of 105000 M^{-1} cm^{-1}. These compounds emit weakly in dilute solution, when excited either at 254 or 366 nm. In the solid state, absorption peaks are broadened and bathochromically shifted. This shift decreases for longer thioalkyl chains, *i.e.* λ_{max} = 503, 496, 494, and 491 nm for **4a–d**, respectively.

In conclusion, a new type of discotic mesogen, potentially electron carriers, is reported. These compounds have one or several mesophases at low temperature and one or more LC mesophases at high temperature. Future work involves: the investigation of charge carrier mobility, the synthesis of new members of the same family with lower clearing temperatures, and detailed X-ray investigations.

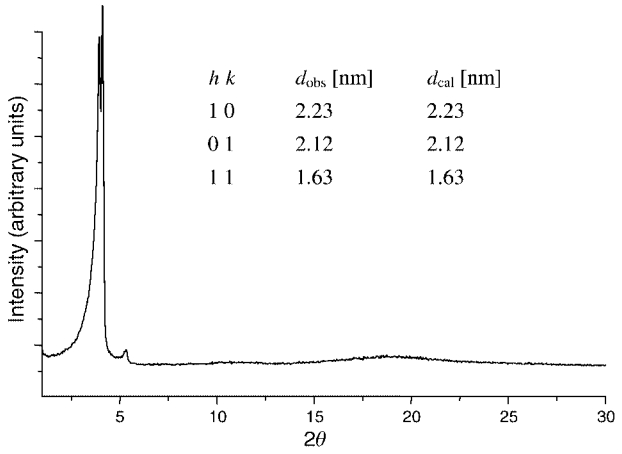

Fig. 1 X-Ray diffraction pattern of **4c** measured at 170 °C using Cu-Kα radiation. d values are calculated for an oblique unit cell with a = 2.24 nm, b = 2.13 nm, β = 83.5°.

This work was financially supported by the Belgian National Science Foundation (FNRS FRFC-n° 2.4560.00), by the Université Libre de Bruxelles, by the Banque National de Belgique, by the Communauté Française de Belgique (ARC n° 00/05-257), and by the European Union (DISCEL G5RD-CT-2000-00321). G. K. and V. d. H. acknowledge the FRIA for a fellowship. Paul A. Heiney from the University of Pennsylvania is also acknowledged for fruitful discussions.

Notes and references

† The synthesis and characterisation of 2,3,8,9,14,15-hexakis(octylthio)-diquinoxalino[2.3-*a*:2′,3′-*c*]phenazine (**4b**) is given as a representative example. An excess of octane-1-thiol (0.95 ml, 5.47 mmol) and potassium carbonate (2.53 g, 18.32 mmol) are added to a solution of 2,3,8,9,14,15-hexachlorodiquinoxalino[2,3-*a*:2′,3′-*c*]phenazine **3** (304 mg, 0.51 mmol) in 100 ml *N*,*N*-dimethylformamide. This solution is heated at 85 °C and stirred for 5 days. The reaction mixture is then poured into a large volume of water and neutralised with hydrochloric acid. The yellow precipitate is filtrated and washed with copious amounts of water. Two recrystallisations in ethanol with toluene afforded the title compound as a yellow powder in 67% yield. ^{1}H-NMR (250 MHz, $CDCl_3$, 30 °C, 2.85 10^{-2} M): δ = 8.11 (s, 6H, arom.), 3.17 (t, 12H, aliph.), 1.83 (m, 12H, aliph.), 1.54 (m, 12H, aliph.), 1.31 (m, 48H, aliph.), 0.89 (t, 18H, aliph.). ^{13}C-NMR (63 MHz, $CDCl_3$, 30 °C): δ = 144.20 (arom.), 142.39 (arom.), 141.37 (arom.), 123.19 (arom.), 31.81 (aliph.), 29.26 (aliph.), 29.17 (aliph.), 28.11 (aliph.), 22.63 (aliph.), 14.06 (aliph.). FD-MS: $C_{72}H_{108}N_6S_6$, calculated 1250.6, found 1249.8. UV-vis: λ_{max} = 470 nm, ε = 105 000 M^{-1} cm^{-1}.

‡ X-Ray diffraction investigations were carried out using a Siemens D 500 Kristalloflex with a graphite-monochromatized Cu-Kα X-ray beam. This one was emitted from a Rotating Rigaku RV-300 anode. The temperature of the sample on a copper sample holder was monitored with a bimetal sensor, previously calibrated by reference measurements.

1 (*a*) D. Adam, P. Schumacher, J. Simmerer, L. Haussling, K. Siemensmeyer, K. H. Etzbach, H. Ringsdorf and D. Haarer, *Nature*, 1994, **371**, 141; (*b*) E. Fontes, P. A. Heiney and W. H. de Jeu, *Phys. Rev. Lett.*, 1998, **61**, 1202.

2 (*a*) For a comprehensive review of discotic structures see: A. N. Cammidge and R. J. Bushby, '*Synthesis and strucutual features*' , in *Handbook of Liquid Crystals*, Vol. 2B, eds. D. Demus, J. W. Goodby, G. W. Gray, H.-W. Spiess and V. Vill, Wiley VCH, Weinheim, 1998. For a general discussion of applications of discotic LC see: (*b*) N. Boden and B. Movaghar, '*Applicable Properties of Columnar Discotic Liquid Crystals*', in *Handbook of Liquid Crystals*, Vol. 2B, eds. D. Demus, J. W. Goodby, G. W. Gray, H.-W. Spiess and V. Vill, Wiley VCH, Weinheim, 1998.

3 (*a*) H. Eichhorn, *J. Porphyrins Phthalocyanines*, 2000, **4**, 88; (*b*) A. van de Craats and J. M. Warman, *Adv. Mater.*, 2001, **13**, 130.

4 A. van de Craats, J. M. Warman, K. Müllen, Y. Geerts and J. D. Brand, *Adv. Mater.*, 1998, **10**, 36; A. van de Craats, J. M. Warman, A. Fechtenkötter, J. D. Brand, M. A. Harbison and K. Müllen, *Adv. Mater.*, 1999, **11**, 1469.

5 N. Boden, R. C. Borner, R. J. Bushby and J. Clements, *J. Am. Chem. Soc.*, 1994, **116**, 10807; Corien W. Struijk, Alexander B. Sieval, Jarno E. J. Dakhorst, Marinus van Kijk, Peter Kimkes, Rob B. M. Koehorst, Harry Donker, Tjeerd J. Schaafsma, Stephen J. Picken, Anick M. van de Craats, John M. Warman, Han Zuilhof and Ernst J. R. Sudhölter, *J. Am. Chem. Soc.*, 2000, **122**, 11057.

6 A. van de Craats, Ph.D. Dissertation, Delft University of Technology, June 2000.

7 F. Uckert, Y.-H. Tak, D. Müllen and H. Bässler, *Adv. Mater.*, 2000, **12**, 905.

8 S. Skujins and G. A. Webb, *Tetrahedron*, 1969, **25**, 3935.

9 J. Simmerer, B. Glüsen, W. Paulus, A. Kettner, P. Schumacher, D. Adam, K.-H. Etzbach, K. Siemensmeyer, J. J. Wendorff, H. Ringsdorf and D. Haarer, *Adv. Mater.*, 1996, **8**, 815.

10 S. Chandrasekhar, '*Columnar, Discotic Nematic and Lamellar Liquid Crystals: Their Structures and Physical Properties*', in *Handbook of Liquid Crystals*, Vol. 2B, eds. D. Demus, J. W. Goodby, G. W. Gray, H.-W. Spiess and V. Vill, Wiley VCH, Weinheim, 1998.

11 (*a*) E. F. Gramsbergen, H. J. Hoving, W. H. de Jeu, K. Praefck and B. Kohne, *Liq. Cryst.*, 1986, **1**, 397; (*b*) P. A. Heiney, E. Fontes, W. H. de Jeu, A. Riera, P. Carroll and A. B. Smith, *J. Phys. (Paris)*, 1989, **50**, 461.

CHEMCOMM Communication
www.rsc.org/chemcomm

Directed and undirected asymmetric dihydroxylation reactions: application in the synthesis of a *C*-linked analogue of allolactose

Robert Hodgson,[a] Tajir Mahid[b] and Adam Nelson*[a]

[a] *School of Chemistry, University of Leeds, Leeds, UK LS2 9JT. E-mail: adamn@chem.leeds.ac.uk*
[b] *Aventis Pharma US, Route 202–206, Bridgewater, New Jersey 08807, USA*

Received (in Cambridge, UK) 24th August 2001, Accepted 5th September 2001
First published as an Advance Article on the web 1st October 2001

The complex OsO_4·(*S*,*S*)-1,2-diphenyl-*N*,*N*′-bis(2,4,6-trimethylbenzyl)ethane-1,2-diamine is an effective reagent for the desymmetrisation of *meso*-1,2-bis(3,6-dihydro-2*H*-pyran-2-yl)ethanes by asymmetric dihydroxylation; this process, whose sense of diastereoselectivity depends on substitution and stereochemistry, has been exploited in the synthesis of a *C*-linked analogue of allolactose.

Previously, we have described methods for the synthesis of some stereoisomeric *C*-linked disaccharide mimetics.[1] A key feature of our approach was that diastereomeric mimetics could be prepared by minor variation of a general reaction sequence. For example, complementary undirected[2] and directed[3] dihydroxylation reactions were exploited in the two-directional elaboration of diols (such as C_2-symmetric **1**) to give products of general stucture **2** with 1,4-syn stereochemistry. In order to

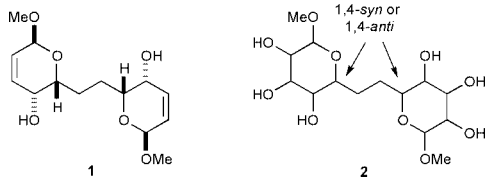

synthesise the mimetics with the opposite 1,4-stereochemical relationship, an efficient method for the desymmetrisation[4] of the *meso* difuryl diol[1] **3** or one of its derivatives would be required.

Oxidative ring expansion of the furan rings of the diol **3** using $VO(acac)_2$–^{t}BuOOH, and acetalisation, gave the dipyranone **4** as a 75 : 25 mixture of *meso* and unsymmetrical anomers, from which the required *meso* diastereoisomer was crystallised in 52% yield (Scheme 1). Reduction of **4** under Luche's conditions gave the diol **5** in > 98% yield, which was converted into the *p*-methoxybenzoyl diester **6**. The diastereoisomeric diol **8** was synthesised by hydrolysis of the diacetate **7** obtained by inversion of the dimesylate derived from **5**.

Treatment of **6** with OsO_4·**10** at −20 °C lead to complete consumption of the starting material and gave the desymmetrised diol **9**† as a single diastereoisomer in 84% yield with 60% ee (Scheme 2). Dihydroxylation occurred *anti*[2] to the pseudo-equatorial allylic *p*-methoxybenzoyloxy group. Previously, prochiral cyclic dienes have been desymmetrised using AD-mix β, with dihydroxylation occurring on the outside of their bicyclic structure.[6] This natural diastereoselectivity could be reversed by delivery of OsO_4·**10** to the double bond: dihydroxylation of **8** was highly *syn* selective, and gave, after peracetylation, the tetraacetate **11** with 93% ee (87% yield based on recovered starting material). We believe that diastereoselectivity stems from hydrogen bonding of the reagent to the pseudoaxial hydroxy group,[3] and that this reaction is the first example of a directed asymmetric dihydroxylation.

As a prelude to the diastereoselective functionalisation of the remaining double bond of **9**, we studied the functionalisation of the allylic *p*-methoxybenzoate **15** using iodine and silver benzoate in dry carbon tetrachloride (Scheme 3).[7] In view of the

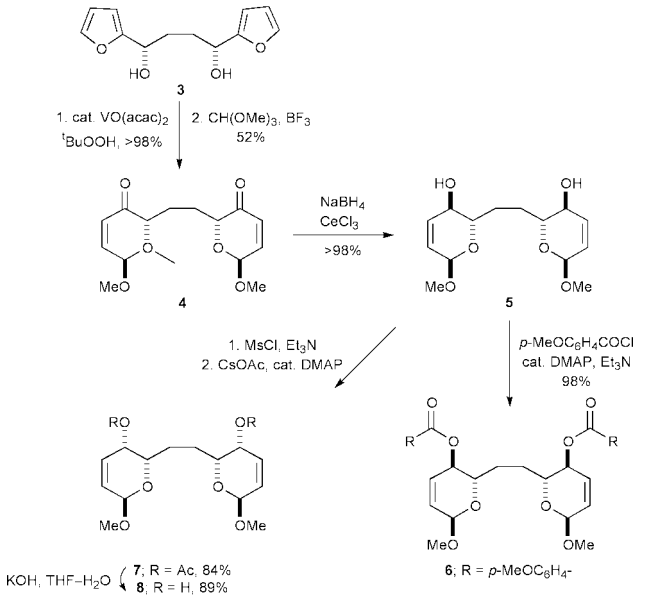

Scheme 1

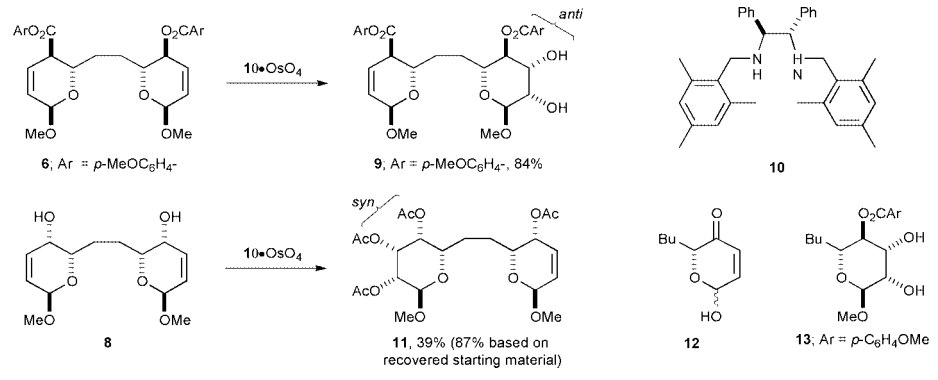

Scheme 2

 DOI: 10.1039/b107643d

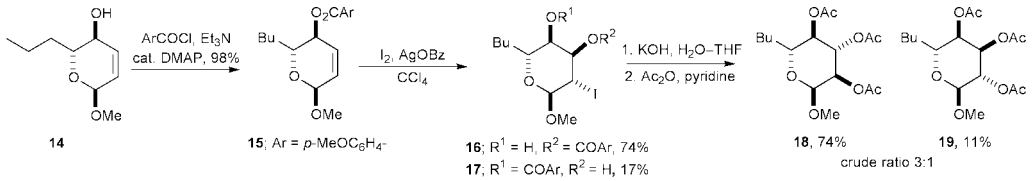

Scheme 3

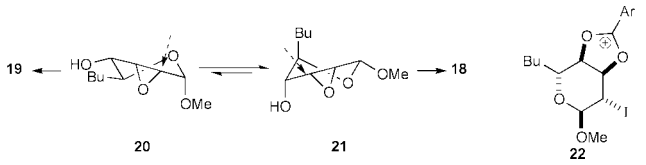

Scheme 4

rigorously dry reaction conditions of these reactions, the *syn* stereospecificity of this process (**15** → **16**, **17**) and the absence of benzoate from the products are remarkable. Presumably, participation[8] of the *p*-methoxybenzoyloxy group gave the dioxonium ion **22** which was stable to the reaction conditions; subsequent hydrolysis of this intermediate, presumably on aqueous work-up, gave the observed *syn* hydroxy *p*-methoxybenzoates **16** and **17**. In general, *syn* hydroxyesters are only obtained when Prévost reactions are conducted in the presence of water because, under these conditions, the intermediate dioxonium is hydrolysed *in situ*.[9]

Treatment of the iodoesters **16**–**17** (4:1 mixture of regioisomers) with potassium hydroxide in water–THF, followed by peracetylation, gave a 3:1 diastereomeric mixture of the triacetates **18** and **19**. Presumably, **16** and **17** were converted into the same epoxide which was opened by hydroxide ion.‡ *trans*-Diaxial opening[11] of the major conformer (**20** → **19**, Scheme 4) requires opening at the site which is β to the two oxygens of the acetal;[12] consequently, reaction *via* the conformer **21** (→ **18**)—that is, away from the two β oxygens[12]—is competitive with, and in fact dominates over, this process.

In a similar vein, treatment of the desymmetrised compound **23** with iodine and silver benzoate in dry carbon tetrachloride, followed by treatment with aqueous potassium hydroxide solution, gave the *C*-linked disaccharide mimetic *ent*-**25** (Scheme 5); peracetylation gave the hexaacetate **24** in 64% yield over 3 steps. The *C*-linked allolactose mimetic **25**, in which C-6 of the galactose ring has been replaced by a methoxy group, could clearly have been prepared by the same synthetic methods using the enantiomeric diamine ligand in the key desymmetrisation step. It has been suggested that stable analogues of allolactose, the intracellular inducer of the lactose (*lac*) operon, may also exert negative control over gene expression.[13]

Our synthesis of the *C*-linked disaccharide mimetic *ent*-**25** is unusual in that neither ring derives directly from a sugar, though Vogel has reported the use of a non-carbohydrate based template to introduce one of the sugar rings to some *C*-linked disaccharides.[14] Key steps in our synthesis include the desymmetrisation of a highly functionalised *meso* di-DHP using an asymmetric dihydroxylation reaction, and the use of a *p*-methoxybenzoate ester to control the stereospecificity of a Prévost reaction.

We thank EPSRC and Aventis for providing funds under the CASE scheme for new appointees, the Royal Society for a grant and Pfizer and AstraZeneca for strategic research funding.

Notes and references

† The absolute configuration of **9** was deduced by comparing the 500 MHz ^{1}H NMR spectra of its (*R*)- and (*S*)-Mosher diesters with those of the diol **13**, which was derived from the pyranone[5] (2*R*)-**12**.

‡ For the hydrolysis of similar epoxides, see ref. 10.

1 M. Harding and A. Nelson, *Chem. Commun*., 2001, 695.
2 J. K. Cha, W. J. Christ and Y. Kishi, *Tetrahedron*, 1984, **40**, 2247.
3 T. J. Donohoe, P. R. Moore, M. J. Waring and N. J. Newcombe, *Tetrahedron Lett*., 1997, **38**, 5027.
4 M. C. Willis, *J. Chem. Soc., Perkin Trans. 1*, 1999, 1765.
5 T. Kametani, M. Tsubuki, Y. Tatsuzaki and T. Honda, *J. Chem. Soc., Perkin Trans. 1*, 1990, 639.
6 S. Takano, T. Yoshimitsu and K. Ogasawara, *J. Org. Chem*., 1994, **59**, 54.
7 C. Prévost, *C. R. Hebd. Seances Acad. Sci*., 1933, **196**, 1129; C. Prévost, *C. R. Hebd. Seances Acad. Sci*., 1933, **197**, 1661.
8 See: A. H. Haines, A. S. H. King, J. R. Knight and V.-A. Nguyen, *Tetrahedron Lett*., 1998, **39**, 4393.
9 R. B. Woodward and F. V. Brutcher, Jr., *J. Am. Chem. Soc*., 1958, **80**, 209.
10 K. Takeo, M. Nakagen and Y. Teramoto, *Carbohydr. Res*., 1990, **201**, 261.
11 J. C. Leffingwell and E. E. Rayals, *Tetrahedron Lett*., 1965, 3829.
12 C. H. Behrens and K. B. Sharpless, *J. Org. Chem*., 1985, **50**, 5696.
13 W. R. Kobertz, C. R. Bertozzi and M. D. Bednarski, *J. Org. Chem*., 1996, **61**, 1894; A. Dondoni, H. M. Zuurmond and A. Boscarato, *J. Org. Chem*., 1997, **62**, 8114.
14 R. Ferritto and P. Vogel, *Tetrahedron: Asymmetry*, 1994, **5**, 2077; R. M. Bimwala and P. Vogel, *J. Org. Chem*., 1992, **57**, 2076.

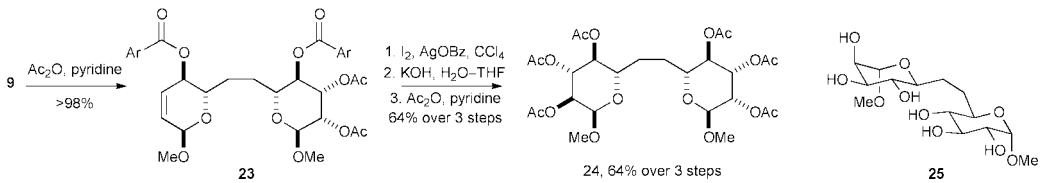

Scheme 5

CHEMCOMM Communication
www.rsc.org/chemcomm

The regioselective aminohydroxylation of allylic carbamates

Timothy J. Donohoe,*†[a] Peter D. Johnson,[a] Madeleine Helliwell‡[a] and Martine Keenan[b]

[a] *Department of Chemistry, The University of Manchester, Oxford Road, Manchester, UK M13 9PL. E-mail: t.j.donohoe@man.ac.uk*
[b] *Lilly Research Centre, Erl Wood Manor, Sunninghill Road, Windlehsam, Surrey, UK GU20 6PH*

Received (in Cambridge, UK) 10th August 2001, Accepted 5th September 2001
First published as an Advance Article on the web 1st October 2001

The synthesis and aminohydroxylation of a series of acyclic allylic carbamates is described: the formation of a putative O=Os=NR linkage between the transition metal and substrate is proposed to account for the high levels of regioselectivity that were observed; proof of the structure of one of the aminohydroxylation products was obtained through X-ray crystallography.

The aminohydroxylation reaction has emerged as a particularly powerful method for the oxidation of alkenes, introducing both oxygen and nitrogen in a stereospecific manner.[1] The asymmetric variant of this reaction, as pioneered by Sharpless,[2] is adept at transforming alkenes into amino alcohols with high levels of enantioselectivity. However, control of the regiochemistry of oxidation can be difficult with mixtures frequently being formed. Our interest in this reaction derives from our work on the regio- and stereoselective dihydroxylation of allylic alcohols[3] and we sought to control the aminohydroxylation of these substrates. Early work on the asymmetric aminohydroxylation (AA) reaction of allyl alcohol by Landais and coworkers[4] suggested that these substrates might show high levels of regiocontrol. However, our own work,[5] and a further study by Landais,[6] has shown that substituted allylic alcohols are not oxidised with any appreciable regioselectivity. Janda and coworkers recently modified allylic alcohol substrates and developed a range of protecting groups that bias the AA reaction (Scheme 1):[7] these allow the formation of individual regioisomers with high selectivity when the alkene is monosubstituted and with moderate selectivity when the allylic alcohol becomes more heavily substituted.

We sought to control the regioselectivity of oxidation in a different way, by formation of a carbamate derivative of allylic alcohols (Fig. 1). When subjected to the aminohydroxylation regime, the carbamate group will be chlorinated and deprotonated to form a nitrene equivalent that acts as both the oxidant and nitrogen source for the aminohydroxylation reaction. Of course, as the putative RN=Os=O fragment is contained within the allylic alcohol, we should expect high control of regioselectivity in the ensuing oxidation event.

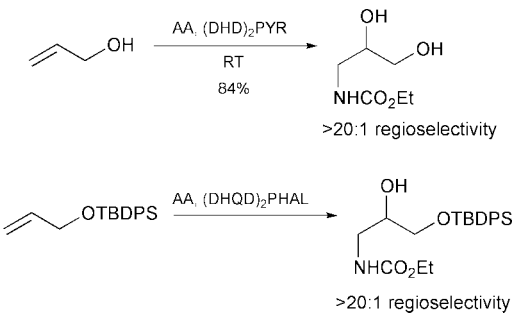

Scheme 1

† Present address, Dyson Perrins Laboratory, South Parks Road, Oxford, UK OX1 3QY.
‡ Author to whom correspondence regarding the X-ray crystal stucture should be addressed.

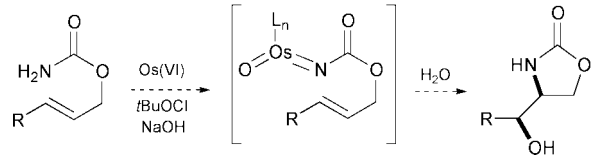

Fig. 1

The following sequence was used to prepare allylic carbamates from the corresponding alcohol (Scheme 2) and, generally, the reaction was convenient and high yielding.

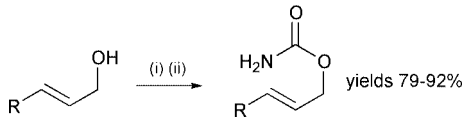

Scheme 2 *Reagents and conditions*: Cl_3CNCO; ii, K_2CO_3.

Preliminary studies concentrated on the oxidation of **1** under a range of conditions, mostly those developed by Sharpless (Scheme 3).§ Pleasingly, the reaction worked as planned, giving decent yields of hydroxyoxazolidinone **2**¶ from the allylic carbamate. Unfortunately, reaction with Sharpless' ligand $(DHQ)_2PHAL$ gave material that was racemic; this is surprising as the reactions were clearly faster in the presence of this amine ligand than without it. Other amine additives had mixed effects: quinuclidine was not shown to be efficient in promoting the reaction, whereas Hunig's base[6] gave good yields in a process that was still faster than that without any ligand at all. The reisolation of starting material was difficult to avoid and attempts to push the reaction to completion by increasing the amount of *t*BuOCl and NaOH in the mixture simply gave a more complex array of products.

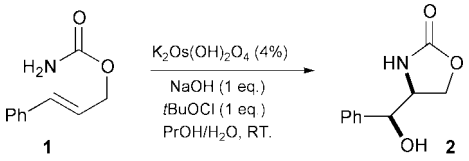

Ligand (5%)	Yield of **2** (%)	Recovered **1** (%)
$(DHQ)_2PHAL$	62	12
Quinuclidine	26	0
iPr_2NEt	59	23
None	42	23

Scheme 3

Buoyed by these encouraging results, we prepared a range of allylic carbamates and subjected them to cyclisation with catalytic potassium osmate and iPr_2NEt (Scheme 4). The reaction is clearly regioselective and stereospecific as shown by the selective formation of **2** and **4** from **1** and **3**, and of **6** and **8** from **5** and **7** respectively.

Most of the compounds shown in Scheme 4 have been reported previously in the literature[8] and we were able to

 DOI: 10.1039/b107253f

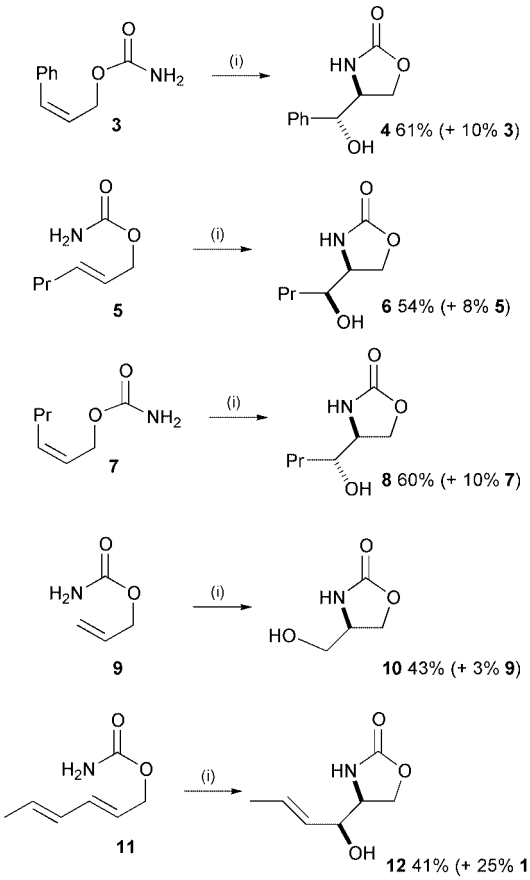

Scheme 4 *Reagents and conditions*: i, $K_2Os(OH)_2O_4$ (4%), NaOH (1 eq.), *t*BuOCl (1 eq.), *i*Pr_2NEt (5%), PrOH/H_2O, RT.

correlate the products from the aminohydroxylation reaction with that data. While compound **12** is novel, hydrogenation over palladium on carbon formed compound **6** in good yield (86%), thus allowing us to confirm the identity of **12**. In addition, we managed to obtain an X-ray crystallography analysis of **2** thus verifying its structure (Fig. 2).

The stereospecific (and suprafacial) nature of the addition leads us to postulate a mechanism based around that described in Fig. 1. A series of control experiments whereby **1**, **3**, **5**, **7**, **9** and **11** were subjected to all of the ingredients shown in Scheme 4, bar potassium osmate, gave no oxazolidinone products at all, thus ruling out a more conventional type of cyclisation reaction *via* an epi-ion.

Certainly, the success of these reactions depends on the presence of osmium which supports the *in situ* formation of a O=Os=NR fragment. The lack of enantioselectivity with Sharpless' catalysts is disappointing and could be due to a number of factors such as a lack of involvement of the ligand during the stereoselectivity determining step, disruption of the binding pocket by the carbamate tether or slow hydrolysis of the osmate ester thus promoting reaction *via* the (non-selective) second cycle.

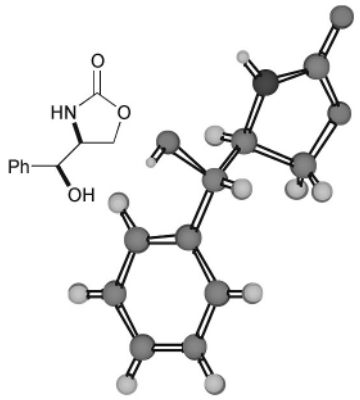

Fig. 2 X-ray structure of **2**.

To conclude, we have developed a completely regioselective regime for the hydroxyamination reaction of allylic carbamates. The reaction is stereospecific and proceeds with only catalytic amounts of transition metal. One might expect that the aminohydroxylation of chiral cyclic and acyclic allylcarbamates under these conditions should lead to diastereoselectivity as well as regioselectivity: this aspect of the work is currently under active investigation.

We are grateful to the EPSRC and Lilly for financial support of this project. AstraZeneca, GlaxoSmithKline and Pfizer are thanked for unrestricted financial support.

Notes and references

§ *Representative experimental procedure*: A fresh, aqueous solution (15 mL) of NaOH (45 mg, 1.1 mmol) was prepared. 14 mL of this was added in one portion to a magnetically stirred solution of *trans*-cinnamyl carbamate **1** (200 mg, 1.13 mmol) in *n*PrOH (12 mL). The solution was allowed to stir for 5 min, then *tert*-butyl hypochlorite (129 μL, 1.13 mmol) was added. The mixture was again allowed to stir for 5 min. To this was then added a solution of $(DHQ)_2PHAL$ (44 mg, 5 mol%) in *n*PrOH (13 mL) in one portion. The mixture was allowed to stir for a further 5 min before the final addition of a solution of potassium osmate (21 mg, 4 mol%) in the NaOH solution made previously (1 mL). The reaction was followed by TLC until the solution turned black, which denoted the end of turnover (12 h). The reaction was quenched by the addition of Na_2SO_3 (500 mg), and allowed to stir for 30 min. The mixture was extracted with EtOAc (1 × 25 mL), and the organic layer washed with brine (25 mL). The organic layer was then collected and concentrated under reduced pressure. Column chromatography (3 : 2 EtOAc–petroleum ether 40–60) of the crude product yielded the oxazolidinone **2** (135 mg, 62%) as a colourless crystalline solid. R_f: 0.44 (EtOAc); mp 142–143 °C; IR ($CHCl_3$): 3366 (br, OH), 3230 (NH), 3054, 1730 (CO); ^{1}H NMR (500 MHz, $CDCl_3$): 7.32–7.44 (5H, m, PhH), 5.54 (1H, br s, NH), 4.63 (1H, dd, *J* 7.5, 3.5, PhCH), 4.23 (1H, t, *J* 9, C*H*H′), 4,12 (1H, dd, *J* 9, 5.5, CH*H*′), 4.05 (1H, m, CHNH), 2.48 (1H, d, *J* 3.5, OH); ^{13}C NMR: 159, 139, 129, 126, 76, 66, 58; MS 194 ($M + H^+$), 211 ($M + NH_4^+$); HRMS calculated ($M + H^+$) 194.0817, found 194.0816

¶ *Crystal data*: **2**, $C_{10}H_{11}NO_3$: M = 193.20, monoclinic, a = 7.551(4), b = 23.367(3), c = 5.612(5) Å, β = 111.25(6)°, V = 922.7(9) Å^3, T = 293 K, space group $P2_1/n$ (no. 14), Z = 4, μ(Mo-Kα) = 0.104 mm^{-1}, 1520 independent reflections, final $\omega R(F^2)$ = 0.1121 (all data) and $R(F)$ = 0.0390 using 1303 reflections with $I > 2\sigma(I)$. The structure was solved by direct methods. H atoms bonded to C were included in calculated positions, and those bonded to N and O were found by difference Fourier methods and refined isotropically. The non-H atoms were refined anisotropically. Refinement was carried out on F^2 using full matrix least squares. CCDC 169247. See http://www.rsc.org/suppdata/cc/b1/b107253f/ for crystallographic files in .cif or other electronic format.

1 For representative references see: G. Li, H. H. Angert and K. B. Sharpless, *Angew. Chem., Int. Ed. Engl.*, 1996, **35**, 2813; M. Brunko, G. Schlingloff and K. B. Sharpless, *Angew. Chem., Int. Ed. Engl.*, 1997, **36**, 1483; A. E Rubin and K. B. Sharpless, *Angew. Chem., Int. Ed. Engl.*, 1997, **36**, 2637.

2 For a review see: H. C. Kolb and K. B. Sharpless, in *Transition Metals For Organic Synthesis*, ed. M. Beller and C. Bolm, Vol. 2, Wiley, 1998, pp. 243; O. Reiser, *Angew. Chem., Int. Ed. Engl.*, 1996, **35**, 1309.

3 T. J. Donohoe, P. R. Moore, M. J. Waring and N. J. Newcombe, *Tetrahedron Lett.*, 1997, **38**, 5027.

4 R. Angelaud, Y. Landais and K. Schenk, *Tetrahedron Lett.*, 1997, **38**, 1407.

5 T. J. Donohoe and P. D. Johnson, *unpublished work*.

6 R. Angelaud, O. Babot, T. Charvat and Y. Landais, *J. Org. Chem.*, 1999, **64**, 9613.

7 H. Han, C.-W. Cho and K. D. Janda, *Chem. Eur. J.*, 1999, **5**, 1565.

8 Literature references to the following compounds: **4**, S. Knapp, P. J. Kukkola, S. Sharma, T. G. Mirali Dhar and A. B. J. Naughton, *J. Org. Chem.*, 1990, **55**, 5700; **8**, S. C. Bergmeir and D. M. Stanchina, *J. Org. Chem.*, 1997, **62**, 4449; **10**, M. P. Sibi, D. Rutherford and R. Sharma, *J. Chem. Soc., Perkin Trans. 1*, 1994, 1675. The literature does not contain data for **6** and the identity of this compound was proven when it was oxidised to the corresponding ketone under Jones' conditions; subsequent oxidation of the (known) diastereoisomer **8** gave the same ketone.

CHEMCOMM
Communication
www.rsc.org/chemcomm

The synthesis and solid state structure of (8*S*)-8-benzyl-8,9-dihydro-7*H*-tetrazolo[1,5-*d*][1,4]diazepin-6-one

Barnaby C. H. May* and Andrew D. Abell*

Department of Chemistry, University of Canterbury, Private Bag 4800, Christchurch, New Zealand. E-mail: a.abell@chem.canterbury.ac.nz

Department of Cellular and Molecular Pharmacology, University of California San Francisco, San Francisco, California 94143-0450, USA. E-mail: alchemi@itsa.ucsf.edu

Received (in Cambridge, UK) 11th July 2001, Accepted 3rd September 2001
First published as an Advance Article on the web 19th September 2001

An unusual tetrazolodiazepin-6-one was prepared and shown, by X-ray crystallography, to adopt an essentially planar conformation about the tetrazole ring with geometry that closely approximates a *cis*-amide bond.

The process of transforming the topology of a bioactive molecule onto a different molecular scaffold is an important method for generating new classes of bioactive molecules. This procedure can provide important biological probes and potential therapeutics with improved potency, stability and other characteristics relative to their parent. The diazepine ring system has been used extensively in this respect; for example, benzodiazepines have found wide-spread medicinal applications and a number of diazepine-based systems have been used to construct peptidomimetic scaffolds that possess well-defined geometries, such as those found in β-turns.[1] Another important peptidomimetic scaffold is the 1,5-disubstituted tetrazole ring that has been identified as an effective *cis*-amide bond mimic.[2] The incorporation of this moiety into peptides gives *cis*-restricted peptidomimetics that have found use as protease inhibitors,[3] and biological probes.[4] In this paper we present the synthesis and X-ray structure of (8*S*)-8-benzyl-8,9-dihydro-7*H*-tetrazolo[1,5-*d*][1,4]diazepin-6-one, **1**. This compound was isolated and characterized as part of our continuing program to develop non-hydrolysable tetrazole-based *cis*-amide bond isosteres and to investigate their applications.[3,5,6] This compound is important in that it represents a combination of the two aforementioned scaffolds into one, new class of dipeptidomimetic.

Compound **1** was isolated from an attempted coupling of *N*-Boc-protected dipeptide mimic **2**,[6] with the benzyl ester hydrobromide **3**,[6] under standard EDCI mediated peptide coupling conditions (Scheme 1). The desired tetrapeptide, **4**, was not observed in the crude reaction product by ^{1}H NMR or mass spectrometry.† Purification of the crude mixture by flash column chromatography gave the cyclic tetrazole-based dipeptide mimic, **1**, in 93% yield,‡ which was recrystallised from methanol.

A few related nitrogen-containing five-membered rings fused to the diazepine scaffold are known and these have been shown to possess interesting pharmacological properties.[7,8] However, our structure is unique in that its diazepinone scaffold contains a homophenylalanine–glycine based cyclic dipeptide in which one of its *cis*-amide bonds is constrained within a tetrazole-based amide surrogate. The tetrazole moiety forces the system to adopt a '*cis*-like' geometry at the homophenylalanine–[CN_4]–glycine junction that is necessitated by the cyclic architecture of the diazepinone scaffold.

The structure of **1** was confirmed by an X-ray structure determination at 173(2) K and was satisfactorily refined (Fig. 1).§ The structural data from **1** provides information for the design of *cis*-constrained tetrazole-based peptidomimetics, and also diazepine-based dipeptidomimetic scaffolds. Very few solid state structures of tetrazole-based peptidomimetics have been reported.[9] Consequently, this class of peptidomimetic

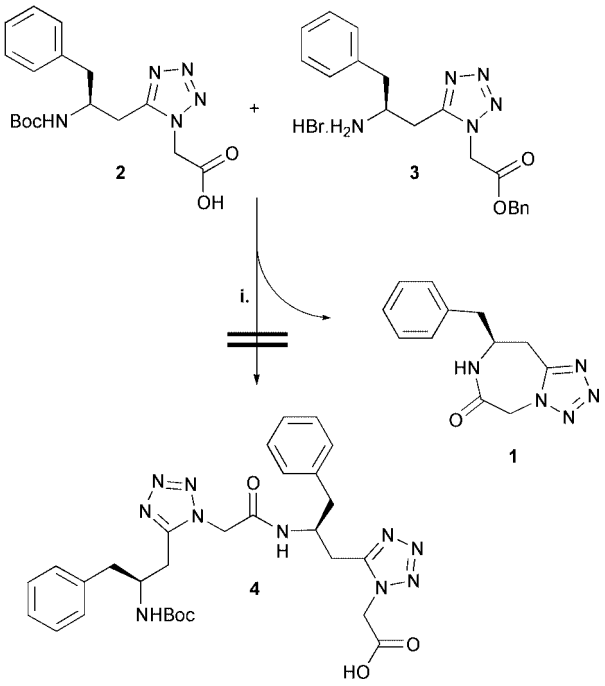

Scheme 1 Synthesis of (8*S*)-8-benzyl-8,9-dihydro-7*H*-tetrazolo[1,5-*d*]-[1,4]diazepin-6-one. *Reagents and conditions*: i) EDCI [1-(3-dimethylaminopropyl)-3-ethylcarbodiimide hydrochloride], HOBt (1-hydroxybenzotriazole hydrate), DIPEA (*N*,*N*-diisopropylethylamine), rt, 18 h.

remains relatively uncharacterized with regards to its geometry. Such information is required if these compounds are to be fully exploited as conformationally restricted peptidomimetics.

The structural data obtained for **1** compares well with other reported 1,5-disubstituted tetrazole groups.[10] The tetrazole ring of **1** was found to be essentially planar with the torsion angles N2–C5–N5–N4, C5–N5–N4–N3, N5–N4–N3–N2, N4–N3–N2–C5, and N3–N2–C5–N5 being −0.55(15), 0.17(16)°, 0.27(16), −0.62(15) and 0.74(15)°, respectively and the ring atoms show a mean deviation from the plane of 0.003 Å. The

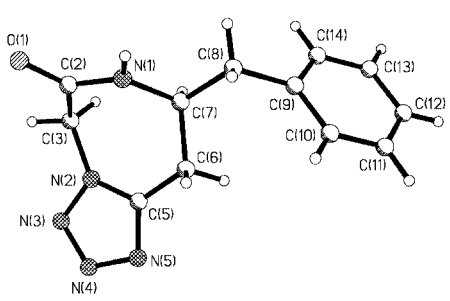

Fig. 1 Molecular structure of (8*S*)-8-benzyl-8,9-dihydro-7*H*-tetrazolo-[1,5-*d*][1,4]diazepin-6-one, **1**.

 DOI: 10.1039/b106175p

N3–N4 bond [1.2887(18) Å] possesses the most double bond character of the heterocyclic bonds. The N2–N3 and N4–N5 bonds are the longest being 1.3537(16) and 1.3650(18) Å, respectively. The N5–N4–N3 endocyclic bond angle, 111.37(11)°, is wider than the C5–N5–N4 and N4–N3–N2 bond angles, 105.79(12) and 105.56 (12)°. The dipeptide mimic is folded at the homophenylalanine–[CN_4]–glycine sequence with the torsion angles, C5–C6–C7–N1, N2–C5–C6–C7, C6–C5–N2–C3, and C2–C3–N2–C5, being 59.53(16), −9.2(2), 3.3(2), and −48.92(19)° respectively. The diazepinone ring is puckered with a mean deviation from the plane of 0.317 Å, while the phenylalanine ring adopts a flagpole orientation over the diazepin-6-one scaffold.

The tetrazole-based *cis*-amide bond mimic is known to compare well with the geometric properties of a generic *cis*-amide bond obtained from statistical analysis of published X-ray diffraction structures.[11] However, the solid state structure of **1** provides an excellent opportunity for a direct comparison of the tetrazole-based amide bond surrogate and the *cis*-amide bond, as **1** contains both these structural motifs within the constrained diazepinone ring. The geometric properties of the tetrazole-based surrogate of **1** and the *cis*-amide bond of **1** compare favourably. The N2–C5 bond [1.3455(18) Å] of the tetrazole is slightly shorter than the amide bond, N1–C2 [1.3508(19) Å]. The separation between carbon centres adjacent to the tetrazole ring [C3···C6] and the corresponding distance between α-carbons adjacent to the amide bond [C7···C3] are similar, being 3.229 and 2.911 Å, respectively. The small variation between these distances is a consequence of the increased steric bulk of the tetrazole moiety. Hence, the bond angles C6–C5–N2 [127.19(13)°] and C3–N2–C5 [131.98(12)°] of **1** are greater than the corresponding bond angles of the *cis*-amide bond, C7–N1–C2 [127.05(12)°] and N1–C2–C3 [115.81(12)°]. The $\bar{\omega}$ torsion angle at the homophenylalanine–[CN_4]–glycine junction, [C6–C5–N2–C3], is forced to adopt a planar *cis*-conformation by the fused tetrazole ring, where $\bar{\omega}$ = 3.3(2)°. Similarly, the torsion angle about the *cis*-amide bond of **1**, [C7–N1–C2–C3], is essentially planar, where $\bar{\omega}$ = 3.11(19)°.

In this paper we have presented the synthesis and solid state structure of a new class of peptidomimetic diazepinone molecular scaffold. This architecture should be amenable to attaching a wide range of amino acid R groups and thus the presentation of a diverse range of topologies.

The work was supported by a Royal Society of New Zealand Marsden grant. We are indebted to Peter Steel and Chris Fitchett for their assistance in solving the structure presented in this paper.

Notes and references

† We have recently been concerned with investigating the secondary structure of peptidomimetics that contain multiple constrained *cis*-amide bonds. To this end we targeted tetrapeptide mimic, **4**, that contains two tetrazole based *cis*-amide bond mimics.

‡ Calculated yield of **1** was based on starting benzyl ester, **3**.

§ *Crystallographic data* for **1**: $C_{12}H_{13}N_5O$, M 243.27, mp 198–200 °C, crystal dimensions 0.63 × 0.24 × 0.21 mm, orthorhombic, a = 6.374 (2), b = 8.621 (3), c = 20.890 (7) Å, γ90 (2)°, V = 1147.8 (7) Å^3, spacegroup $P2_12_12_1$, Z = 4, $F(000)$ = 512, D_{calc} = 1.408 mg m^{-3}, absorption coefficient 0.096 mm^{-1}, θ range for data collection 2.56 to 26.42, index ranges $-4 \leq h$ 7, $10 \leq k \leq 10$, $-26 \leq l \leq 25$, data/restraints/parameters 2338/0/163, goodness of fit on F^2 was 1.063, final R indices [$I > 2\sigma(I)$] R_1 = 0.0323, wR_2 = 0.0827, R indices (all data) R_1 = 0.0374, wR_2 = 0.0853, largest difference peak and hole 0.148 and −0.191 e Å^{-3}. A full sphere of data was collected at 163(2) K. Of the 14344 reflections obtained, 2338 were unique (R_{int} = 0.0271) and were used in the full-matrix least-squares refinement. CCDC 162685. See http://www.rsc.org/suppdata/cc/b1/b106175p/ for crystallographic data in .cif or other format.

1 *For example*: A. Nouvet, F. Lamaty and R. Lazaro, *Tetrahedron Lett*., 1998, **39**, 2099; I. S. Weitz, M. Pellegrini, M. Royo, D. F. Mierke and M. Chorev, *Lett. Pept. Sci*., 1998, **5**, 83.

2 J. Zabrocki, G. D. Smith, J. B. Dunbar, H. Iijima and G. R. Marshall, *J. Am. Chem. Soc*., 1988, **110**, 5875.

3 *For example*: A. D. Abell and G. J. Foulds, *J. Chem. Soc., Perkin Trans. 1*, 1997, 2475.

4 *For example*: D. D. Beuson, J. Zabrocki, U. Slomczynska, R. D. Head, J. L.-F. Kao and G. R. Marshall, *Biopolymers*, 1995, **36**, 181; L. W. Boteju, T. Zalewska, H. I. Yamamura and V. J. Hruby, *Bioorg. Med. Chem. Lett*., 1993, **3**, 2011; A. Garofalo, C. Tarnus, J.-M. Remy, R. Leppik, F. Piriou, B. Harris and J. T. Pelton, in *Peptides: Chemistry and Biology; Proceedings of the 11th American Peptide Symposium*., ed. J. E. Rivier and G. R. Marshall, ESCOM, Leidon, 1990, 833.

5 G. J. Foulds, *Biologically Active Peptide Analogues*, PhD thesis, University of Canterbury, 1996.

6 B. C. H. May, *Conformationally Restricted Peptidomimetics*, PhD thesis, University of Canterbury, 2000B. C. H. May and A. D. Abell, *Tetrahedron Lett*., 2001, **42**, 5641.

7 N. P. Peet and S. J. Sunder, *J. Heterocycl. Chem*., 1977, **14**, 561; C. J. Shishoo, M. B. Devani, G. V. Ullas, S. Ananthan and V. S. J. Bhadti, *J. Heterocycl. Chem*., 1988, **25**, 615.

8 Y. Ohba, I. Matsukura, Y. Fukazawa and T. Nishiwaki, *Heterocycles*, 1985, **23**, 287.

9 G. Valle, M. Crisma, K.-L. Yu, C. Toniolo, R. K. Misha and R. L. Johnson, *Collect. Czech. Chem. Commun*., 1988, **53**, 2863; G. D. Smith, J. Zabrocki, T. A. Flak and G. R. Marshall, *Int. J. Pept. Protein Res*., 1991, **37**, 191; J. Zabrocki, G. D. Smith, J. B. Dunbar, H. Iijima and G. R. Marsahll, *J. Am. Chem. Soc*., 1988, **110**, 5875.

10 Z. Dauter, S. A. Chawdhuri and M. A. Hamid, *Cryst. Struct. Commun*., 1982, **11**, 999.

11 B. Liberek and R. Kasprzykowska, *Int. J. Pept. Protein Res*., 1987, **30**, 522.

CHEMCOMM Communication
www.rsc.org/chemcomm

Synthesis and properties of *fac*-Re(dmbpy)(CO)$_3$CHO (dmbpy = 4,4′-dimethyl-2,2′-bipyridine), a possible intermediate in reductions of CO_2 catalyzed by *fac*-Re(dmbpy)(CO)$_3$Cl

Dorothy H. Gibson* and Haiyang He

Department of Chemistry and Center for Chemical Catalysis, University of Louisville, Louisville, KY 40292, USA. E-mail: dorothy.gibson@louisville.edu

Received (in West Lafayette, IN, USA) 11th July 2001, Accepted 31st August 2001
First published as an Advance Article on the web 1st October 2001

Synthesis of *fac*-Re(dmbpy)(CO)$_3$CHO 2 and its reactions with CO_2 in DMF and DMSO have been conducted; 2 transfers hydride to CO_2 to give Re(dmbpy)(CO)$_4^+$ OCHO$^-$ 5 which is rapidly transformed to *fac*-Re(dmbpy)(CO)$_3$(OCHO) 3 in DMF, thus supporting the viability of 2 in photocatalytic reactions of *fac*-Re(dmbpy)(CO)$_3$Cl with CO_2.

Photo- and electrochemical reductions of carbon dioxide catalyzed by *fac*-Re(N–N)(CO)$_3$Cl (N–N = 4,4′-dimethyl-2,2′-bipyridine) lead to carbon monoxide and *fac*-Re(N–N)(CO)$_3$(OCHO).[1] Scheme 1 shows a previously proposed photocatalytic cycle leading to CO.[1b] Proton-promoted dehydroxylation of *fac*-Re(N–N)(CO)$_3$CO$_2$H **1** would yield Re(N–N)(CO)$_4^+$ which was thought to react with chloride ion, with CO loss, to regenerate the starting rhenium complex; the photocatalytic reactions were typically conducted for *ca.* 4 h in DMF solution. The formate complex could result from intermediate metallocarboxylic acid **1** after decarboxylation to *fac*-Re(N–N)(CO)$_3$H followed by CO_2 insertion into the metal hydride bond.[2] Also, the formate could result from protonation of Re(N–N)(CO)$_3^-$ (**c** in Scheme 1) followed by rapid CO_2 insertion. Thus, competition between CO_2 and H^+ for the anion could determine the CO : formate ratio. We recently prepared the metalloacid **1**, and studied its thermolysis reactions.[3] However, reactions of **1** do not provide the formate complex even when conducted in the presence of added CO_2.

The possible intermediacy of a formyl complex as a precursor to the formate in photochemical reactions of CO_2 with *fac*-Re(bpy)(CO)$_3$H was suggested by Sullivan and Meyer.[2] Also, the possibility of formyl intermediates in photocatalytic reactions of *fac*-Re(N–N)(CO)$_3$Cl with CO_2 has been suggested by us[3,4] and others[5] because of the reaction conditions used. Triethanolamine (TEOA) was used as a sacrificial electron donor in the photocatalytic reactions.[1a,b] The decomposition of the resulting TEOA cation radical occurs through H-atom transfer from a second TEOA (yielding TEOAH$^+$ and providing a proton source in the reactions) and concurrent formation of one or more carbon-centered radicals;[6] the carbon-centered radicals are subject to further transformations.[7] Since Re(N–N)(CO)$_4^+$ is a likely reaction intermediate, as discussed above, its one-electron reduction to the acyl radical [Re(N–N)(CO)$_3$(C=O)]$^\cdot$ is possible,[8] and hydrogen atom abstraction[8,9] by this radical (from a carbon-centred TEOA radical) could yield *fac*-Re(N–N)(CO)$_3$CHO. As with other formyl complexes,[10] these could be expected to decarbonylate to *fac*-Re(N–N)(CO)$_3$H; the hydrides are known to insert CO_2 and provide formates.[2,3a] This side reaction leading to the formyl complex from Re(N–N)(CO)$_4^+$ would explain why excess Cl$^-$ is effective in suppressing formate since Cl$^-$ should speed the conversion to **a** (Scheme 1) and diminish the availability of Re(N–N)(CO)$_4^+$ for the side reaction.

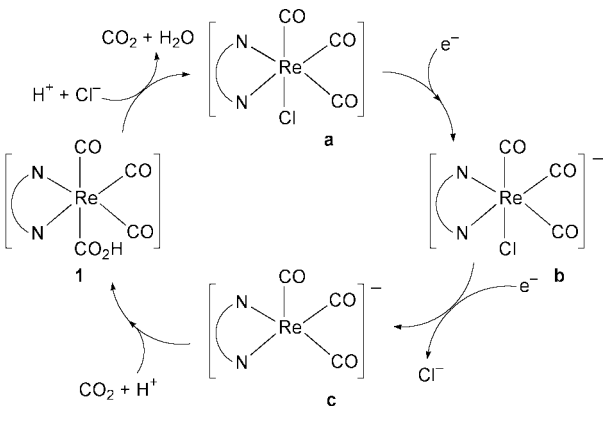

Scheme 1

We have now prepared and characterized *fac*-Re(dmbpy)(CO)$_3$CHO **2**,† and studied its reactions with CO_2 and with metalloacid **1**. Reaction of **2** with CO_2 in DMF-d$_7$ leads, primarily, to Re(dmbpy)(CO)$_3$OCHO[2,3a] (**3**; 76% yield after 1 h, 85% yield after 4.5 h at room temperature) together with the bicarbonato complex *fac*-Re(dmbpy)(CO)$_3$OCO$_2$H[3b] (**4**; 10% yield at either time). However, in monitoring the reaction solution (0.013 M in **2** and 0.17 M in CO_2[11] with ferrocene as an internal standard) at 25 °C by ^{1}H NMR spectra during the early stages of the reaction, we observed that the initial products were Re(dmbpy)(CO)$_4^+$ OCHO$^-$ **5**,‡ acid **1** and the CO_2-bridged compound *fac*,*fac*-Re(dmbpy)(CO)$_3$(CO$_2$)Re(dmbpy)(CO)$_3$ **6**.[3a] Over time, **1** and **6** are converted to **4** in the presence of CO_2 and the small amount of water in the solvent.[3b] After 20 min, **5** and **3** were present in approximately equal amounts; after 1 h, the ionic formate **5** had mostly converted (10% remaining) to the covalent formate **3**. In a second reaction, beginning at −10 °C and then warming to +10 °C and finally to 25 °C during 2 h, the yield of **5** reached *ca.* 40% (at +10 °C) before **3** began to appear. After warming to 25 °C, however, the transformation of **5** to **3** was enhanced (45% yield of **3** after 30 min). Reaction of **2** with CO_2 was also conducted in DMSO-d$_6$ (0.005 M in **2**, 0.115 M in CO_2[11]) at 25 °C for comparison. After 1.5 h, the yield of ionic formate **5** had reached 60% and **2** had been mostly consumed (< 5%); at this time no **3** had yet been formed. Also formed were **4** (10%), **6** (5%) and **1** (15%). After 24 h, the yield of **5** had dropped only to 50% as **3** was generated. Thus, the rate of conversion of **5** to **3** is highly solvent dependent.

Parts of Scheme 1 are certainly viable: we have prepared *fac*-Re(dmbpy)(CO)$_4^+$ Cl$^-$ **7**§ and observed that it slowly converts to *fac*-Re(dmbpy)(CO)$_3$Cl **8** at room temperature (38% after 5.5 h) in DMF-d$_7$. However, irradiation (450 W mercury arc lamp through a Pyrex cooling jacket) of **7** in DMF-d$_7$ showed that 84% of it was converted to **8** after 2.5 h, thus the conversion should have been complete within the time of the catalytic experiments. Ziessel[1a] found that it was necessary to increase [Cl$^-$] in order to suppress formate. While increased [Cl$^-$] could certainly increase the rate of conversion of **7** to **8**, it should have little impact on protonation of anion **c** (Scheme 1). In the manner of other metallocarboxylic acids,[12] **1**, in DMF-d$_7$, is

 DOI: 10.1039/b106270k

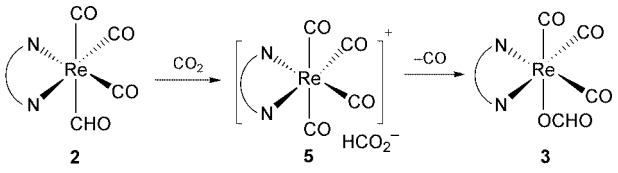

N–N = dmbpy = 4,4'-dimethyl-2,2'-bipyridine

Scheme 2

rapidly dehydroxylated by concentrated HCl, yielding **7** (88%) and **8** (12%) upon mixing. Efforts to prepare an authentic sample of formate **5** in the manner of **7** have failed because the excess formic acid necessary to bring the reaction to completion ensures that the formate anion is converted to the formic acid solvate.[13]

Since ruthenium formyl complexes with polypyridine ligands are reactive toward the corresponding metallocarboxylic acids[14] and **1** was expected to be a product in the photocatalytic reactions involving **8**, we have also probed the reactivity of **2** toward **1**. In DMF-d_7 (0.013 M in both **2** and **1**) after 1 h, the major product (83%) is the same intermediate species that was generated from **1** alone in this solvent; the intermediate is eventually transformed to the CO_2-bridged complex, **6**.[3b]

We found no evidence for rhenium hydrides in decompositions of **2** conducted in the presence of CO_2; the formyl complex reacts directly with CO_2 to produce **5** as shown in Scheme 2. Direct transfers of hydride from formyl complexes to carbon electrophiles are well known,[10a,c] although the electrophiles are usually stronger than CO_2. However, hydride transfer has been suggested in reactions of $Ru(bpy)_2(CO)(CHO)^+ PF_6^-$ with CO_2 although the product was not characterized.[15] The reactions of formyl complex **2** with CO_2 and the subsequent rapid conversion of **5** to **3** support the suggestion that **2** could be a viable reaction intermediate in the catalytic reactions.

This work has been supported by the United States Department of Energy, Division of Chemical Sciences, Office of Science.

Notes and references

† *Preparation of* **2**: to a solution of $Re(CO)_4(dmbpy)(OTf)$ (0.25 g, 0.40 mmol) in MeCN (16 mL) and H_2O (4 mL) at −5 °C was added Et_4NBH_4 (0.064 g, 0.44 mmol). The mixture was stirred for 2 min and allowed to stand for an additional 5 min. A yellow precipitate formed and was collected, washed with water (30 mL) and MeCN (15 mL) and then dried (0.16 g, 83%), mp 162 °C (decomp.). Anal. calc. for $C_{16}H_{13}N_2O_4Re$: C, 39.75; H, 2.71. Found: C, 39.41; H, 2.82%. IR ν_{CO} (KCl, DRIFTS)/cm^{-1}: 2005 (s), 1907 (s), 1882 (vs), 1554 (m). ^{1}H NMR (DMF-d_7, 25 °C): δ 14.69 (1H, s), 8.88 (2H, d, *J* 5.5 Hz), 8.75 (2H, s), 7.57 (2H, d, *J* 5.5 Hz), 2.60 (6H, s). ^{1}H NMR (DMSO-d_6, 25 °C): δ 14.49 (1H, s), 8.76 (2H, d, *J* 5.5 Hz), 8.65 (2H, s), 7.49 (2H, d, *J* 5.5 Hz), 2.54 (6H, s). **Note**: the formyl proton has a long relaxation time. In order to obtain accurate integrations of this proton relative to the dmbpy protons it was necessary to use a pulse delay of 25 s.

‡ ^{1}H NMR spectral properties of **5** in DMF-d_7: δ 9.09 (d), 8.86 (s), 8.58 (s, OCHO), 7.79 (d) and 2.65 (s).

§ *Preparation of* **7**: $Re(dmbpy)(CO)_3CO_2Me$[3a] (0.40 g) and CH_2Cl_2 (15 mL) were stirred in a 100 mL flask under N_2 at −5 °C and then HCl (gas) was bubbled through the yellow suspension for 30 s to provide a pale yellow solution. The solution was stirred for 5 min, then purged with N_2 at −5 °C; ether (50 mL) was then added to precipitate the product (0.41 g, 100% yield), mp 92 °C (decomp.). Anal. calc. for $C_{16}H_{12}ClN_2O_4Re + 2.5H_2O$: C, 34.10; H, 3.02. Found: C, 33.79: H, 2.71%. IR ν_{CO} (KCl, DRIFTS)/cm^{-1}: 2109 (s), 1994 (vs), 1966 (s), 1934 (s). ^{1}H NMR (CD_2Cl_2): δ 9.32 (2H, s), 8.75 (2H, d), 7.53 (2H, d), 2.75 (6H, s). ^{1}H NMR (DMF-d^7): δ 9.08 (2H, d), 8.99 (2H, s), 7.79 (2H, d), 2.66 (6H, s). ^{13}C NMR (CD_2Cl_2): δ 187.96, 183.30, 156.46, 155.70, 153.50, 129.87, 127.50, 21.83.

1 (*a*) J. Hawecker, J.-M. Lehn and R. Ziessel, *Helv. Chim. Acta*, 1986, **69**, 1990; (*b*) R. Ziessel, in *Catalysis by Metal Complexes: Photosensitization and Photocatalysis Using Inorganic and Organometallic Compounds*, ed. K. Kalayanasundaram and M. Gräetzel, Kluwer Academic Publishers, Dordrecht, Netherlands, 1993, p. 217; (*c*) F. R. Keene and B. P. Sullivan, in *Electrochemical and Electrocatalytic Reactions of Carbon Dioxide*, ed. B. P. Sullivan, K. Krist and H. E. Guard, Elsevier, Amsterdam, 1993, ch. 5.

2 B. P. Sullivan and T. J. Meyer, *Organometallics*, 1986, **5**, 1500.

3 (*a*) D. H. Gibson and X. Yin, *J. Am. Chem. Soc*., 1998, **120**, 11 200; (*b*) D. H. Gibson and X. Yin, *Chem. Commun*., 1999, 1411.

4 D. H. Gibson, B. A. Sleadd, M. S. Mashuta and J. F. Richardson, *Organometallics*, 1997, **16**, 4421.

5 T. Scheiring, A. Klein and W. Kaim, *J. Chem. Soc., Perkin Trans. 2*, 1997, 2569.

6 S.-F. Chan, M. Chou, C. Creutz, T. Matsubara and N. Sutin, *J. Am. Chem. Soc*., 1981, **103**, 369; N. Sutin, C. Creutz and E. Fujita, *Comments Inorg. Chem*., 1997, **19**, 67.

7 H. A. Schwarz, *J. Phys. Chem*., 1982, **86**, 3431.

8 B. A. Narayanan and J. K. Kochi, *Organometallics*, 1986, **5**, 926; B. B. Wayland, A. E. Sherry and V. L Coffin, in *Homogeneous Transition Metal Catalyzed Reactions*, ed. W. R. Moser and D. W. Slocum, Adv. Chem. Ser., No. 230, American Chemical Society, Washington, DC, 1992, ch. 17.

9 D. Astruc, *Electron Transfer and Radical Processes in Transition Metal Chemistry*, VCH Publishers, New York, 1995, ch. 5 and 6 and references therein.

10 (*a*) J. A. Gladysz, *Adv. Organomet. Chem*., 1982, **20**, 1; (*b*) D. H. Gibson, K. Owens, S. K. Mandal, J. O. Franco and W. E. Sattich, *Organometallics*, 1989, **8**, 498; (*c*) H. Konno, K. Sakamoto and O. Ishitani, *Angew. Chem., Int. Ed*., 2000, **39**, 4061.

11 H. L. Clever, in *Carbon Dioxide in Non-aqueous Solvents at Pressures Less than 200 KPA*, Solubility Data Series, vol. 50, ed. P. G. T. Fogg, Pergamon Press, Oxford, 1992, p. 343 for DMF, p. 382 for DMSO.

12 M. A. Bennett, *J. Mol. Catal*., 1987, **41**, 1.

13 See: H. Basch and W. J. Stevens, *J. Am. Chem. Soc*., 1991, **113**, 95 and references therein.

14 D. H. Gibson, Y. Ding, B. A. Sleadd, J. O. Franco, J. F. Richardson and M. S. Mashuta, *J. Am. Chem. Soc*., 1996, **118**, 11 984; D. H. Gibson, Y. Ding, J. G. Andino, M. S. Mashuta and J. F. Richardson, *Organometallics*, 1998, **17**, 5178.

15 K. Toyohara, H. Nagao, T. Muzukawa and K. Tanaka, *Inorg. Chem*., 1995, **34**, 5399.

CHEMCOMM Communication
www.rsc.org/chemcomm

A new practical ketone synthesis directly from carboxylic acids: first application of coupling reagents in palladium catalysis

Lukas J. Gooßen* and Keya Ghosh

Max-Planck-Institut für Kohlenforschung, Kaiser-Wilhelm-Platz 1, D-45470 Mülheim an der Ruhr, Germany. E-mail: goossen@mpi-muelheim.mpg.de; Fax: +49-208-306-2985; Tel: 49-208-306-2392

Received (in Cambridge, UK) 26th July 2001, Accepted 5th September 2001
First published as an Advance Article on the web 1st October 2001

A new palladium-catalyzed cross-coupling reaction between arylboronic acids and carboxylic acids, activated *in situ* for the oxidative addition to a tricyclohexylphosphine palladium(0) catalyst by treatment with di(*N*-succinimidyl) carbonate (DSC) is disclosed, which allows the high-yielding synthesis of various functionalized arylketones under mild conditions.

The reaction of carboxylic acid derivatives, for example nitriles, Weinreb-amides, anhydrides, or acid chlorides with carbon nucleophiles to the corresponding ketones is an important C–C bond-forming reaction that is commonly used in organic synthesis.[1] Various procedures have been developed to optimize the yield of the ketones and avoid the formation of the tertiary alcohols.[2] Highly reactive acid chlorides can be alkylated with a number of mild carbon nucleophiles, for example organotin, -zinc and -copper compounds or boronic acids.[3,4] Furthermore, ketone synthesis from thioesters[5] has been reported. However, only a few protocols have been disclosed for the highly desirable direct conversion of the plethora of carboxylic acids into ketones and all of these require aggressive lithium, magnesium, or aluminum reagents intolerant of most functional groups.[6] Recently, we reported a novel palladium catalyzed synthesis of arylketones directly from carboxylic acids and boronic acids using pivalic anhydride as an activating agent.[7] This transformation gives good yields for many substrates, however, the reactivity of the pivalic anhydride against basic groups and the inconvenience of the separation of the products from the pivalic acid are still disadvantageous. A milder and more practical ketone synthesis from carboxylic acids and readily available boronic acids,[8] which works under neutral conditions in the presence of many functional groups would be of great value especially for applications in combinatorial chemistry.

The utilization of mild coupling reagents such as DCC–HOBt, CDI (1,1′-carbonyldiimidazole) or DSC for the activation of the carboxylic acids could be the key to a much-improved process (Scheme 1). These compounds are known to cleanly convert carboxylic acids into stable intermediates, which are just reactive enough to ensure smooth conversion to the corresponding amides.[9] Due to their easy handling, their reliability and selectivity combined with an excellent tolerance of functional groups, coupling reagents have become indispensable for most applications in peptide synthesis.

In principle, a catalytic cycle for the palladium-catalyzed reaction of carboxylic acids with boronic acids consisting of the oxidative addition of an activated acid derivative producing an acyl palladium complex, followed by transmetallation of a boronic acid, and reductive elimination of the ketone appeared to be feasible.[10] However, to the best of our knowledge there is no literature precedent for the use of coupling reagents in transition-metal catalysis.[11]

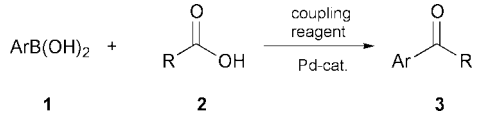

Scheme 1 Cross-coupling of boronic acids and carboxylic acids.

Due to the high stability and easy handling, we chose phenylboronic acid (**1a**) and *N*-benzoyloxysuccinimide (**4**) as our model substrates and screened various palladium catalysts for activity in the desired conversion (Scheme 2). The catalysts were prepared *in situ* from Pd(II) precursors and two equivalents of different phosphines. Some results are summarized in Table 1.

Whereas no reaction was observed for triarylphosphines, with electron-rich trialkylphosphines moderate yields were obtained (Entries 1–6). This may indicate that the oxidative addition of the *N*-benzoyloxysuccinimide is the rate-determining step which should be facilitated by increasing the electron density on the palladium. Sterically demanding tricyclohexylphosphine gave best results while tri-*tert*-butylphosphine complexes were not stable under the reaction conditions and precipitation of palladium(0) was observed.

THF proved to be the most effective solvent (Entries 6–8). The stability of the catalytic system was significantly enhanced when a mild base was added (Entries 9–13). Best results were obtained with Na_2CO_3 while the presence of soluble bases appeared to inhibit the reaction. We also investigated the

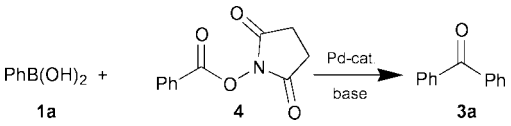

Scheme 2 Cross coupling of *N*-benzoyloxysuccinimide.

Table 1 Effects of the reaction conditions on the yield[a]

	Ligand	Pd-source	Solvent	Base	Product (%)[b]
1	PPh_3	$Pd(OAc)_2$	THF	—	< 2
2	DPPF	$Pd(OAc)_2$	THF	—	< 2
3	P(*o*-Tol)$_3$	$Pd(OAc)_2$	THF	—	< 2
4	P(*t*Bu)$_3$	$Pd(OAc)_2$	THF	—	< 2
5	P(*n*Bu)$_3$	$Pd(OAc)_2$	THF	—	19
6	PCy_3	$Pd(OAc)_2$	THF	—	33
7	PCy_3	$Pd(OAc)_2$	DMF	—	6
8	PCy_3	$Pd(OAc)_2$	Toluene	—	12
9	PCy_3	$Pd(OAc)_2$	THF	K_2CO_3	48
10	PCy_3	$Pd(OAc)_2$	THF	Cs_2CO_3	< 2
11	PCy_3	$Pd(OAc)_2$	THF	KF	40
12	PCy_3	$Pd(OAc)_2$	THF	NEt_3	41
13[c]	PCy_3	$Pd(OAc)_2$	THF	Na_2CO_3	64,[e] 76, 98[f]
14[d]	PCy_3	$Pd(OAc)_2$	THF	Na_2CO_3	74
15	PCy_3	$Pd(OAc)_2$	THF	Na_2CO_3	48
16	PCy_3	dba_3Pd_2	THF	Na_2CO_3	5,[e] 36, 45[f]
17	PCy_3	$Pd(NO_3)_2$	THF	Na_2CO_3	70,[e] 92, 97[f]
18	PCy_3	$PdCl_2$	THF	Na_2CO_3	15,[e] 25, 26[f]
19	PCy_3	$Pd(acac)_2$	THF	Na_2CO_3	2,[e] 80, 98[f]
20	PCy_3	$Pd(F_6\text{-acac})_2$	THF	Na_2CO_3	67,[e] 81, 97[f]

[a] Conditions: 1 mmol *N*-benzoyloxysuccinimide, 1.2 mmol phenylboronic acid, 3 mol% Pd, 7 mol% ligand, 2 mmol base, 60 °C, 14 h. [b] Yields determined by GC. [c] 1 mmol water added. [d] 10 mmol water added. [e] 3 h; [f] 36 h.

 DOI: 10.1039/b106779f

influence of the counter ion on the palladium pre-catalyst and observed faster reactions with weakly coordinating counter-ions such as NO_3^- or F_6-acac than with stronger coordinating Cl^- (Entries 16–20).[10] Under the reaction conditions, the boronic acids act as the reducing agents for the palladium so that biaryls are formed in small quantities. With dba_3Pd_2 as a pre-catalyst, lower yields were observed, which may be due to an insufficient dissociation of the dba from Pd(0). The presence of small quantities of water has little effect on the reaction outcome so that it is not necessary to dry the reagents or solvents, however, the presence of a large excess of water was found to lower the yields (Entries 13–15).

We then set out to combine the activation of the carboxylic acid with di(*N*-succinimidyl) carbonate and the transformation to the ketone into a convenient one-pot procedure (Scheme 3).† Since the activation of the acid was found to proceed smoothly within a few minutes in THF in the presence of Na_2CO_3, this was easily accomplished: in a typical procedure, all reagents except the boronic acid are dissolved in THF and the mixture is stirred until the CO_2 evolution has ceased. Then, the boronic acid is added and the reaction is heated until complete conversion. Under these conditions F_6-acac gave best results, and it is beneficial to add a slight excess of the phosphine to make up for losses during the first reaction step. The water-soluble by-products *N*-hydroxysuccinimide and boric acid are easily removed by a single water wash.

In order to test the generality of this protocol, we applied it to a variety of different substrates. Table 2 shows the broad scope of the new transformation. Both electron-rich and electron-poor alkyl, aryl and even heteroaryl carboxylic acids work equally well, many functional groups such as keto, cyano, ester, nitro, amido and even hydroxy groups are tolerated, and no side products arising from enolisation of the keto groups were observed in significant quantities.

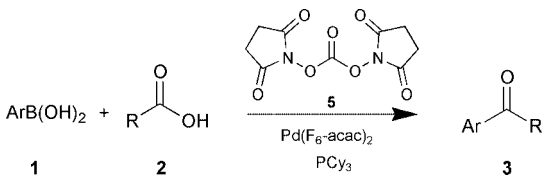

Scheme 3 One-pot synthesis of arylketones from carboxylic acids.

Table 2 Pd-catalyzed synthesis of arylketones[a]

Comp.	Ar	R	Yield (%)[b]
3a	Phenyl	Phenyl	90
3b	Phenyl	2-Phenylethyl	95
3c	*o*-Tolyl	2-Phenylethyl	90
3d	1-Naphthyl	2-Phenylethyl	90
3e	*p*-Methoxyphenyl	2-Phenylethyl	91
3f	*p*-Acetylphenyl	2-Phenylethyl	56
3g	3-Thienyl	2-Phenylethyl	88
3h	2-Furyl	2-Phenylethyl	55
3i	Phenyl	2-Methoxycarbonylethyl	51
3k	Phenyl	*m*-Acetoxyphenyl	42
3l	Phenyl	4-Pyridyl	42
3m	Phenyl	*p*-Methoxycarbonylphenyl	53
3n	Phenyl	3-Thienyl	49
3o	Phenyl	3-Furyl	48
3p	Phenyl	*p*-Acetylphenyl	88
3q	Phenyl	Cyclohexyl	81
3r	Phenyl	*p*-Nitrophenyl	37
3s	Phenyl	*p*-Methoxyphenyl	68
3t	Phenyl	*p*-Cyanophenyl	95
3u	Phenyl	*p*-Trifluoromethylphenyl	89
3v	Phenyl	*p*-Acetamidophenyl	86
3w	Phenyl	*m*-Cyanophenyl	90
3x	Phenyl	HO-$C_{11}H_{22}$	78

[a] Conditions: 1 mmol carboxylic acid, 1.2 mmol boronic acid, 1.3 mmol DSC, 3 mol% $Pd(F_6\text{-acac})_2$, 9 mol% PCy_3, 2 mmol Na_2CO_3, 60 °C, 20 h. [b] Isolated yields.

In summary, the introduction of easy-to-handle coupling reagents as activating agents for acids in transition-metal catalysis led to the discovery of a convenient new ketone synthesis from carboxylic acids and boronic acids. Further applications of this new concept, for example, in the reduction of carboxylic acids to aldehydes or the Heck reaction of benzoic acid derivatives are under current investigation.

We thank M. Rössig and L. Winkel for technical assistance and Professor Dr M. T. Reetz for generous support and constant encouragement.

Notes and references

† *Synthesis of 2-(4′-methoxyphenyl) ethylphenyl ketone* (**3e**): a 100 mL flask was charged with palladium hexafluoroacetylacetonate (156 mg, 0.30 mmol), tricyclohexylphosphine (252 mg, 0.90 mmol), 3-phenylpropionic acid (**2e**) (1.50 g, 10.0 mmol), Na_2CO_3 (2.08 g, 20.0 mmol), and di(*N*-succinimidyl) carbonate (3.33 g, 13.0 mmol). The reaction vessel was purged with argon and degassed THF (30 mL) was added. The yellow mixture was stirred at 60 °C for a few minutes until the gas evolution had ceased. Then, the solution was cooled down to RT, a solution of 4-methoxyphenylboronic acid (**1a**) (1.82 g, 12.0 mmol) in THF (30 mL) was added and the purple reaction mixture was stirred at 60 °C overnight. The reaction slurry was then poured into water (300 mL) and extracted 3 times with 100 mL portions of ethyl acetate. The combined organic layers were dried over $MgSO_4$, filtered, and the volatiles were removed *in vacuo*. The residue was adsorbed on a plug of Al_2O_3. Nonpolar impurities such as the phosphine or the biaryl were removed by elution with hexane. The product (2.19 g, 91%) was then eluted with 20% ethyl acetate in hexane. ^{1}H NMR (300 MHz, $CDCl_3$, 25 °C, TMS): δ = 7.93 (d, ^3J (H,H) = 9 Hz, 2H), 7.23–7.19 (m, 5H), 6.92 (d, ^3J (H,H) = 9 Hz, 2H), 3.85 (s, 3H), 3.24 (t, ^3J (H,H) = 7 Hz, 2H), 3.06 (t, ^3J (H,H) = 7 Hz, 2H) ppm; ^{13}C NMR (75 MHz, $CDCl_3$, 25 °C, TMS): δ = 197.8, 163.5, 141.5, 130.3, 130.0, 128.5, 128.4, 126.1, 113.7, 55.5, 40.1, 30.3 ppm; MS (70 eV): *m*/*z* (%): 240 (33) [M$^+$], 135 (100), 121 (2), 107 (6), 92 (8), 77 (13); HRMS: calcd. for $C_{16}H_{16}O_2$ [M$^+$]: 240.115029; found: 240.115132; anal. calcd. for $C_{16}H_{16}O_2$ (240.30): C, 79.97; H, 6.71; N, 0.0; found: C, 80.12; H, 6.78; N, 0.0. The reactions in Table 1 and Table 2 were performed on a 1 mmol scale using 50 mg tetradecane as an internal GC standard. The products were isolated by column chromatography (Al_2O_3 hexane–ethyl acetate 10:1) and characterized by means of ^{1}H and ^{13}C NMR as well as by GC-MS and HRMS.

1 (*a*) J. March, *Advanced Organic Chemistry*, Wiley, New York, 3rd Edition, 1985, 433–435, 824–827; (*b*) R. C. Larock, *Comprehensive Organic Transformations*, VCH, New York, 1989, 685–702; (*c*) D. A. Shirley, *Organic Reactions*, Wiley, New York, 1954, Vol. 8, 28–58; (*d*) B. T. O'Neill, in *Comprehensive Organic Synthesis*, ed. B. Trost and I. Fleming, Pergamon, Oxford, 1991, Vol. 1, 397–458.

2 (*a*) G. M. Rubottom and C. Kim, *J. Org. Chem*., 1983, **48**, 1550; (*b*) Y. Ahn and T. Cohen, *Tetrahedron Lett*., 1994, **35**, 203; (*c*) T. Fujisawa, S. Iida, H. Uehara and T. Sato, *Chem. Lett*., 1983, 1267.

3 (*a*) R. K. Dieter, *Tetrahedron*, 1999, **55**, 4177; (*b*) M. P. Sibi, *Org. Prep. Proced. Int*., 1993, **25**, 15; (*c*) V. Farina, V. Krishnamurthy and W. Scott, in *Organic Reactions*, Wiley, New York, 1997, Vol 50, 1–652.

4 (*a*) M. Haddach and J. R. McCarthy, *Tetrahedron Lett*., 1999, **40**, 3109; (*b*) N. A. Bumagin and D. N. Korolev, *Tetrahedron Lett*., 1999, **40**, 3057.

5 (*a*) L. Liebeskind and J. Srogl, *J. Am. Chem. Soc*., 2000, **122**, 11 260; (*b*) P. Zurer, *Chem. Eng. News*, 2000, **78**, 26.

6 (*a*) M. J. Jorgenson, *Organic Reactions*, Wiley, New York, 1970, Vol. 18, 1–97; (*b*) C. R. Iwanow, *Hebd. Seances Acad. Sci*., 1928, **186**, 442; (*c*) A. Meisters and T. Mole, *Aust. J. Chem*., 1974, **27**, 1665.

7 L. J. Gooßen and K. Ghosh, *Angew. Chem*., 2001, **113**, 3566.

8 (*a*) T. Ishiyama, M. Murata and N. Miyaura, *J. Org. Chem*., 1995, **60**, 7508; (*b*) M. Murata, T. Oyama, S. Watanabe and Y. Masuda, *J. Org. Chem*., 1997, **62**, 6458; (*c*) M. Murata, T. Oyama, S. Watanabe and Y. Masuda, *J. Org. Chem*., 2000, **65**, 164.

9 M. Bodanszky and A. Bodanszky, *The Practice of Peptide Synthesis*, ed. K. Hafner, J.-M. Lehn, C. W. Rees, P.v.R. Schleyer, B. M. Trost, R. Zahradnik, Springer, Berlin, 1984.

10 C. Amatore and A. Jutand, *Acc. Chem. Res*., 2000, **33**, 314.

11 Reactions of acylmidazolides with Grignard reagents have however been reported, some of them being enhanced by addition of Cu(I): (*a*) H. A. Staab, *Angew. Chem., Int. Ed. Engl*., 1962, **1**, 351; (*b*) B. F. Bonini, M. Comes-Franchini, M. Fochi, G. Mozzanti, A. Ricci and G. Varchi, *Synlett*, 1998, **9**, 1013.

CHEMCOMM Communication
www.rsc.org/chemcomm

S_3O, a new sulfur oxide identified in the gas phase

Fulvio Cacace,[a] Giulia de Petris,*[a] Marzio Rosi[b] and Anna Troiani[a]

[a] *Dipartimento di Studi di Chimica e Tecnologia delle Sostanze Biologicamente Attive dell'Università 'La Sapienza', P. le Aldo Moro 5 00185, Roma, Italy. E-mail: giulia.depetris@uniroma1.it*
[b] *Dipartimento di Ingegneria Civile ed Ambientale, Sezione Tecnologie Chimiche e Materiali per l'Ingegneria, Università di Perugia, Via Duranti 06131, Perugia, Italy*

Received (in Cambridge, UK) 16th May 2001, Accepted 7th September 2001
First published as an Advance Article on the web 21st September 2001

S_3O, a novel, linear sulfur oxide has been detected in the gas phase by means of neutralization reionization mass spectrometry; the upper limit of stability of acyclic forms of S_nO oxides has been set by theoretical calculations.

Disulfur monoxide, S_2O, and homocyclic sulfur oxides, S_nO (n = 5–10), are well known non-polymeric, sulfur-containing species formed by oxidation of cyclosulfurs S_n, and are relevant to combustion processes.[1,2] They have been detected in both the solid-state and in solution, apart from S_2O which has also been observed in the gas phase. We now report the first experimental detection of S_3O oxide, potentially significant in combustion processes but also in sulfur-rich extraterrestrial atmospheres such as that of Venus, where S_2, S_3 and higher S_n oligomers are present mainly in the sub-cloud region. Polysulfur species, that partially reach the upper region, include S_3, also denoted 'thiozone', whose role in the Venusian atmosphere can be thought of as that of ozone in the Earth's upper atmosphere.[3] As an example, the result obtained may suggest an additional way of depletion of S_3 (so far traced to photodissociation), *i.e.* the oxidation to S_3O, likely occurring from O_2 and SO_3, produced by photolysis at the cloud tops.

In this work, detection of S_3O oxide, as an isolated gaseous molecule, was accomplished by the neutralization reionization (NR) mass spectrometric technique[4] from the S_3O^+ ion, obtained by SO^+ chemical ionization (CI) of carbonyl sulfide, in the high-pressure source (0.1–0.2 Torr) of a ZABSpec-oa TOF mass spectrometer. The S_3O^+ ion and the S_3O oxide were characterized by mass spectrometric techniques and theoretical calculations.

The S_3O^+ ion was generated according to the general reaction

$$S_{n-1}O^+ + COS \longrightarrow S_nO^+ + CO$$

recently described as an oligomerization process, where each S_nO^+ ion formed further reacts with COS giving $S_{n+1}O^+$.[5]

However, in the specific case of interest, detection and structural characterization of S_3O^+ is hindered by the superimposition of the isobaric species formed in the CI of the most commonly used precursors of the SO^+ reagent. As an example, in the SO_2/CI of COS,

$$SO^+ \xrightarrow{+COS,\ -CO} S_2O^+ \xrightarrow{+COS,\ -CO} S_3O^+ \quad (1)$$

$$SO^+ \xrightarrow{+SO_2} S_2O_3^+ \quad (2)$$

the isobaric $S_2O_3^+$ ion is formed by the very efficient reaction (2).[5,6] To circumvent the problem we exploited instead the reaction occurring in the O_3/CI of COS

$$O_3^+ + COS \longrightarrow SO^+ + O_2 + CO \quad (3)$$

which proved an effective route to SO^+ in the absence of SO_2.[5] This rules out reaction (2) and allows the S_3O^+ ion from reaction (1) to be mass selected and structurally assayed by collisionally activated dissociation (CAD) mass spectrometry. The CAD spectra of the $^{32}S_3O^+$, $^{34}S^{32}S_2O^+$ and $^{32}S^{34}S_2O^+$ isotopomers were recorded, as well as the MS^3 (multi-stage mass spectrometry) spectra of several significant daughter ions, which confirmed the elemental composition of the S_3O^+ precursor ion. As an example, the CAD spectrum of $^{32}S_3O^+$ has been reported in Fig.1(a). S_3O^+ was then mass selected and neutralized by electron exchange with Xe in a first collision cell located along the flying path. After deflection of any surviving ions by a high-voltage electrode, the neutral beam was reionized in a second cell by collision with O_2. The NR spectra of $^{32}S_3O^+$ and $^{34}S^{32}S_2O^+$ ions were recorded, showing significant 'recovery' peaks of m/z 112 and 114, respectively, and pointing to the existence of neutral S_3O as an isolated species in the gas phase, with a lifetime in excess of 1 μs. As an example, the NR spectrum of $^{32}S_3O^+$ is shown in Fig.1(b). The identity of the S_3O^+ ion from the reionization process was ascertained by its CAD-TOF mass spectrum, which was compared with that of the S_3O^+ ion from the source.

The optimized geometries of the minima identified on the potential energy surfaces of S_3O^+, computed using the hybrid B3LYP function[7,8] are shown in Fig. 2. Single point energy calculations at the optimized geometries were performed using the coupled-cluster single and double excitation method, with a perturbational estimate of the triple excitations [CCSD(T)] approach,[9] using the 6-311+G(3df) basis set,[10] which includes a set of diffuse functions and three d and one f polarization functions, both on oxygen and on sulfur. All the species display a terminal oxygen atom, the most stable being the $^2A''$ planar structure **1**, as illustrated by the total and relative energies reported in Table 1.[11] All structures are probably accessible to the formation process; nevertheless, in the absence of appreciable barriers to the isomerization typical of conformer relaxation,

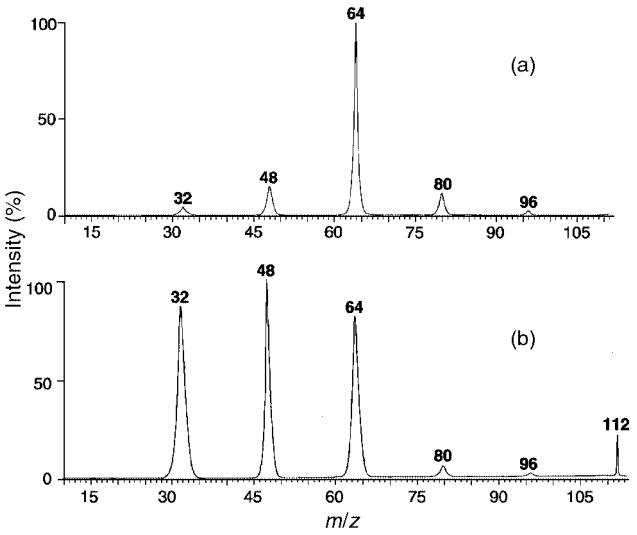

Fig. 1 (a) CAD spectrum of $^{32}S_3O^+$, He collision gas. The out-of-scale m/z 112 parent ion is not shown. (b) NR spectrum of $^{32}S_3O^+$, neutralizing gas Xe, reionizing gas O_2, 80% transmittance.

 DOI: 10.1039/b104329n

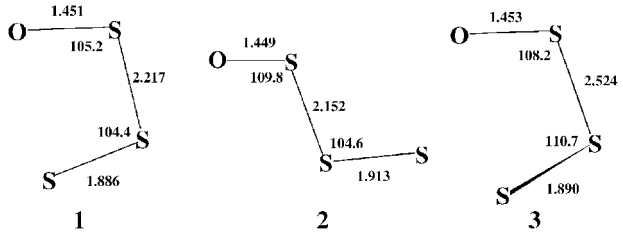

Fig. 2 Optimized geometries of the localized minima on the potential energy surface of the S_3O^+ system, computed at the B3LYP/6-311+G(3df) level. Only the main geometrical parameters are shown. Bond lengths in Å, angles in °.

Table 1 Total energies, relative enthalpies and relative free energies at 298 K of the $S_3O^{+/0}$ systems computed using the 6-311+G(3df) basis set. Total energies in Hartrees, relative energies in kcal mol^{-1}

Species	Symmetry	Relative enthalpy (B3LYP)	CCSD(T)	Relative free energy (B3LYP)	CCSD(T)
1	$^2A''$	0	0	0	0
2	$^2A''$	1.6	2.2	1.8	2.4
3	^4A	7.9	10.1	6.0	8.2
A	$^1A'$	0	0	0	0
B	^3A	7.3	12.8	5.4	11.0
C	$^3A'$	7.3	12.4	5.1	10.2
D	$^1A'$	3.8	4.3	3.6	4.1

structures **1** and **2** are expected to be the most representative of the population sampled, the quartet state being considerably less stable.

Fig. 3 shows the structures of the minima identified on the potential energy surfaces of S_3O. The most stable species are the $^1A'$ planar structures **A** and **D**, the triplet states **B** and **C** being less stable by some 10 kcal mol^{-1} (Table 1). Inspection of Figs. 2 and 3 shows that the geometrical correlation between the most stable charged and neutral species makes conceivable the formation of the latter ones by a vertical neutralization process. From a more general standpoint, the results have some bearing

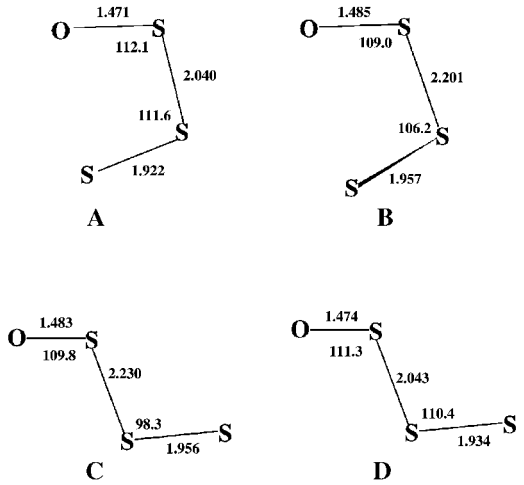

Fig. 3 Optimized geometries of the localized minima on the potential energy surface of the S_3O system, computed at the B3LYP/6-311+G(3df) level. Only the main geometrical parameters are shown. Bond lengths in Å, angles in °.

on the question concerning the relative stability of cyclic *vs.* acyclic S_nO oxides. It is well known that S_2O is an acyclic, angular molecule with a terminal O atom. As for S_3O, the only minima theoretically localized are also characterized by an acyclic structure, with a terminal O atom. Extension of the analysis to S_4O[12] shows that at the B3LYP/CCSD(T) level of theory the $\Delta H^{\ominus}$ values of the most stable acyclic isomer and the cyclic one are very close, falling within 1 kcal mol^{-1}. In summary, it appears that, among the S_nO oxides, S_3O sets the upper *n* limit of the range where acyclic species are significantly more stable.

Financial support from Ministero dell'Università e della Ricerca Scientifica e Tecnologica (MURST), from Consiglio Nazionale delle Ricerche (CNR) and from the Rome University 'La Sapienza' is gratefully acknowledged. The authors thank A. Di Marzio for its helpful assistance.

Notes and references

1 P. W. Schenk, *Z. Anorg. Allg. Chem.*, 1933, **211**, 150; D. J. Meschi and R. J. Meyers, *J. Am. Chem. Soc.*, 1956, **78**, 6220; J. Lindenmayer, H. D. Rudolph and H. Jones, *J. Mol. Spectrosc.*, 1986, **119**, 56; D. J. Clouthier and M. L. Rutherford, *Chem. Phys.*, 1988, **127**, 189; W. Genz and P. W. Schenk, *Z. Anorg. Allg. Chem.*, 1970, **379**, 300; E. Fluck, *Chem.-Ztg.*, 1980, **104**, 206.

2 R. Steudel and T. Sandow, *Angew. Chem., Int. Ed. Engl.*, 1976, **15**, 772; R. Steudel and M. Rebsch, *Z. Anorg. Allg. Chem.*, 1975, **413**, 252; R. Steudel, T. Sandow and J. Steidel, *Z. Naturforsch., B: Anorg. Chem. Org. Chem.*, 1985, **40**, 594.

3 R. P. Wayne, *Chemistry of Atmospheres*, Clarendon Press, Oxford, 2nd edn., 1996, p. 331.

4 J. K. Terlouw and H. Schwarz, *Angew. Chem., Int. Ed. Engl.*, 1987, **26**, 805.

5 F. Cacace, G. de Petris, M. Rosi and A. Troiani, *J. Phys. Chem.*, 2001, **105**, 1144.

6 F. Cacace, R. Cipollini, G. de Petris, M. Rosi and A. Troiani, *J. Am. Chem. Soc.*, 2001, **123**, 478.

7 A. D. Becke, *J. Phys. Chem.*, 1993, **98**, 5648; P. J. Stevens, F. J. Devlin, C. F. Chablowski and M. J. Frisch, *J. Phys. Chem.*, 1994, **98**, 11 623.

8 B. Mannfors, J. T. Koskinen, L.-O. Pietilä and L. Ahjopalo, *J. Mol. Struct. (THEOCHEM)*, 1997, **39**, 393; C. W. Bauschlicher, A. Ricca, H. Partridge and S. R. Langhoff, in *Recent Advances in Density Functional Theory*, ed. D. P. Chong, World Scientific Publishing Co., Singapore, 1997, Part II.

9 R.J. Bartlett, *Annu. Rev. Phys. Chem.*, 1981, **32**, 359; J. Olsen, P. Jorgensen, H. Koch, A. Balkova and R. J. Bartlett, *J. Chem. Phys.*, 1996, **104**, 8007; K. Raghavachari, G. W. Trucks, J. A. Pople and M. Head-Gordon, *Chem. Phys. Lett.*, 1989, **157**, 479.

10 R. Krishnam, J. S Binkley, R. Seeger and J. A. Pople, *J. Chem. Phys.*, 1980, **72**, 650; A. D. McLean and G. S. Chandler, *J. Chem. Phys.*, 1980, **72**, 5639; T. Clark, J. Chandrasekhar, G. W. Spitznagel and P. v. R. Schleyer, *J. Comput. Chem.*, 1983, **4**, 294; M. J. Frisch, J. A. Pople and J. S. Binkley, *J. Chem. Phys.*, 1984, **80**, 3265.

11 All calculations were performed using Gausssian 98: M. J. Frisch, G. W. Trucks, H. B. Schlegel, G. E. Scuseria, M. A. Robb, J. R. Cheeseman, V. G. Zakrewski, J. A. Montgomery, R. E. Stratmann, J. C. Burant, S. Dapprich, J. M. Millam, A. D. Daniels, K. N. Kudin, M. C. Strain, O. Farkas, J. Tomasi, V. Barone, M. Cossi, R. Cammi, B. Mennucci, C. Pomelli, C. Adamo, S. Clifford, J. Ochterski, G. A. Petersson, P. Y. Ayala, Q. Cui, K. Morokuma, D. K. Malick, A. D. Rabuck, K. Raghavachari, K. X. Foresman, J. Cioslowski, J. V. Ortiz, A. G. Baboul, B. B. Stefanov, G. Liu, A. Liashenko, P. Piskorz, I. Komaromi, R. Gomperts, R. L. Martin, D. J. Fox, T. Keith, M. A. Al-Laham, C. Y. Peng, A. Nanayakkara, C. Gonzalez, M. Challacombe, P. M. W. Gill, B. Johnson, W. Chen, M. W. Wong, J. L. Andres, M. Head-Gordon, E. S. Repogle and J. A. Pople, *Gaussian 98, Revision A.7*, Gaussian, Inc., Pittsburgh PA, 1998.

12 M. Rosi, unpublished results.

CHEMCOMM Communication
www.rsc.org/chemcomm

Interaction-induced enhancement in the activity and selectivity of a titania-supported ammonium salt of a 12-molybdophosphoric acid catalyst during ammoxidation of 2-methylpyrazine†

K. Narasimha Rao, Rajesh Gopinath, M. Santhosh Kumar, I. Suryanarayana and P. S. Sai Prasad*

Catalysis & Physical Chemistry Division, Indian Institute of Chemical Technology, Hyderabad - 500 007, India. E-mail: saiprasad@iict.ap.nic.in

Received (in Cambridge, UK) 9th July 2001, Accepted 4th September 2001
First published as an Advance Article on the web 1st October 2001

A titania-supported ammonium salt of 12-molybdophosphoric acid has been synthesized, and the salt–support interaction, which enhanced the reaction rate, has been correlated with the activity of the catalyst in the ammoxidation of 2-methylpyrazine.

12-Molybdophosphoric acid (MPA) is an effective catalyst[1] for acid catalysed and redox reactions. The ammonium salt of MPA (AMPA), which exhibits better thermal stability than MPA, is also reported as a good catalyst for several reactions.[2] However, studies on the effect of impregnation of AMPA on supports are scarce. The influence of the salt–support interaction upon the activity and selectivity of the catalyst has also not yet been reported. Ammoxidation of 2-methylpyrazine (MP) to 2-cyanopyrazine (CP) is a crucial step in the production of pyrazinamide, an important anti-tubercular drug,[3] for which MPA is an effective low temperature catalyst. Recently, it has been reported[4] that higher CP selectivity may be achieved using AMPA as a catalyst rather than MPA. Hence, it is important to study the influence of support on the activity and selectivity of AMPA. It is also interesting to elucidate the effect of loading, reflected by the extent of interaction, on the performance of the catalysts.

In the present investigation we report, for the first time, the synthesis of titania supported AMPA catalysts.‡ Catalysts with varying AMPA loading have been prepared and characterized by nitrogen adsorption, X-ray diffraction (XRD), Fourier transform infrared (FTIR) spectroscopy and ^{31}P MAS NMR techniques. We have observed higher activity and selectivity on the supported catalysts than on the bulk AMPA, for the ammoxidation of MP. A good correlation is observed between the extent of interaction and the activity of the catalyst, which helps optimize the loading on the support.

A gradual decrease in the BET surface area of the catalyst with an increase in AMPA loading (Table 1) implies its uniform impregnation since titania favours interaction with the active phase.[5] The XRD patterns of 5, 10 and 15 wt% loaded catalysts show no indication of the crystallinity of the salt. This observation is in conformity with the results reported by Roy *et al*. and Pizzio *et al*.[6] The amorphous nature can be explained as follows. The hydroxy groups on the titania surface acquire a positive charge due to protonation in the acidic solution, and bind the complex Keggin ion $[PMo_{12}O_{40}]^{3-}$ by electrostatic attraction,[7] leading to interaction of AMPA with the surface. Catalysts with 20 and 25 wt% loading clearly reveal the formation of the crystalline ammonium salt, $(NH_4)_3PO_4(MoO_3)_{12}\cdot 4H_2O$ (ASTM File No. 9-412) in their diffraction patterns, indicating the completion of the interaction at 15 wt% loading.

FTIR spectra of the titania-supported AMPA catalysts with different loadings are presented in Fig. 1. The spectra show intense bands at 672 and 528 cm^{-1} due to the titania support, in addition to bands with medium intensity at 1060 and 960 cm^{-1} due to the AMPA with the characteristic Keggin structure. Literature reveals[8] that AMPA exhibits IR bands at 1410, 1065, 960, 873 and 786 cm^{-1} assigned to stretching vibrations of the NH_4^+ ion, (P–O_d), (Mo–O_t), (Mo–O_b–Mo) and (Mo–O_c–Mo)

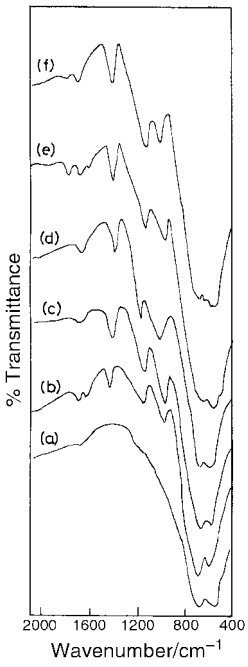

Fig. 1 FTIR spectra of the AMPA-loaded titania catalysts. Titania support (a), catalysts loaded with 5 wt% AMPA (b), 10 wt% AMPA (c), 15 wt% AMPA (d), 20 wt% AMPA (e) and 25 wt% AMPA (f).

† IICT Communication No. 4793.

Table 1 Surface area of the catalysts and selectivity to cyanopyrazine during the ammoxidation of 2-methylpyrazine

	Titania support	Bulk AMPA catalyst	Titania supported AMPA catalysts				
			AMPA-5[a]	AMPA-10[a]	AMPA-15[a]	AMPA-20[a]	AMPA-25[a]
BET surface area/m^2 g^{-1}	55	10	8.6	5.4	3.2	1.4	0.8
Selectivity to CP at 360 °C (%)	40	78	83	86	91	92.5	94
Selectivity to CP at 380 °C (%)	33	75	79	81	90	90	93

[a] Numbers indicate wt% loading of AMPA on the support.

 DOI: 10.1039/b106055b

respectively. As reported by Damyanova and Fierro,[9] titania-supported MPA exhibits strong framework vibration bands of titania below 900 cm^{-1}, overshadowing the bands at 873 and 787 cm^{-1} and making interpretation of the bands based on the Mo–O bond difficult. In the present study it has been observed that the amount of AMPA loading has a marked effect on the characteristic P–O_d band at 1060 cm^{-1}. Characterization of this band by standard half-band width analysis[10] reveals some interesting observations. The half-band widths of catalysts with 5, 10 and 15 wt% loading gradually increase with values equal to 112, 160 and 176 cm^{-1}, respectively. This phenomenon indicates that the P=O bond becomes progressively weaker due to interaction of the salt with the support. As the loading increases the magnitude of the half-band width attains a constant value (180 cm^{-1}) revealing that the P=O group has attained saturation. The FTIR results are in full agreement with those of the XRD data.

^{31}P MAS NMR spectra of the 5, 10 and 15 wt% AMPA catalysts exhibit singlets at −6.300, −6.534 and −7.605 ppm, respectively. The 20 and 25 wt% samples show peaks at −10.7 ppm. Vazquez *et al*.,[7] in their studies on supported MPA, have observed a MAS NMR broad band at −7.49 ppm in the case of a carbon support and at −10.76 ppm in the case of an alumina support. This observation is in close corroboration with our results where the protonated titania is initially acidic and exhibits an NMR peak in the range −6.3 to −7.6 ppm. Once the interaction of the salt species with the acid centers is complete the NMR signal shifts to −10.7 ppm.

The variation in the activity of the catalysts (expressed as percentage conversion of MP) with the salt loading, evaluated at two reaction temperatures, is shown in Fig. 2 (MP conversion values on the bulk AMPA are 5 and 23% at 360 and 380 °C, respectively). The conversion percentage increases up to a loading of 15 wt% and remains almost constant from then on. Values of the half-width of the 1060 cm^{-1} band also display a similar trend. Hence, it appears that the extent of interaction of the salt with the support reaches a maximum at *ca*. 15 wt% loading of AMPA. Further increase in loading (where crystallization of the salt is observed) does not increase the conversion. This observation may be valuable in the characterization of supported heteropolyacids and their salts in determining the maximum extent of loading where the activity is also the maximum.

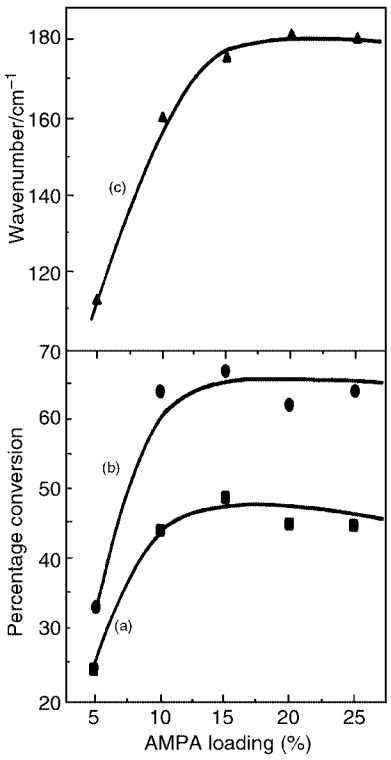

Fig. 2 Variation of conversion and the half-width of the 1060 cm^{-1} band with AMPA loading. (a) MP conversion at 360 °C; (b) MP conversion at 380 °C; and (c) half-bandwidth values.

The significance of impregnation of the salt on the support is also manifested in obtaining enhanced selectivity. Whereas high selectivity to pyrazine is observed on a titania support, impregnation of the support with 5 wt% salt completely reverses the trend by offering high selectivity to CP. This indicates that the acid centers on titania, on which pyrazine formation is more facile, are progressively covered by the salt, simultaneously exposing more active sites of AMPA. An interesting question to be answered at this juncture is how the 20 and 25 wt% catalysts, after attaining crystallinity (expected to behave like bulk AMPA), show continuous increase in selectivity. It may be expected that diffusional limitations may be responsible for lower activity and reduced selectivity in the bulk catalysts, as expressed by Forni[11] Impregnation of the active component on a suitable support, like titania, with higher loading eliminating narrow pores, appears to minimize the diffusional resistance, thus increasing the selectivity.

It may be concluded that the salt–support interaction in titania-supported AMPA offers higher activity and selectivity in the ammoxidation of MP than that of the bulk catalyst. The FTIR half-band width analysis could be a useful method in characterizing the extent of interaction and correlating it with the performance of the catalyst.

The authors are grateful to Dr K. V. Raghavan, Director, IICT, for permitting publication of the results. K. N. R. thanks CSIR, India, for the award of a Senior Research Fellowship.

Notes and references

‡ The bulk AMPA was prepared by dissolving, in a minimum amount of water, ammonium heptamolybdate (S.D. Fine Chemicals, India, AR grade) and diammonium hydrogen orthophosphate (Loba Chemie, India, AR grade) in the stoichiometric ratio, maintaining the pH at 2, followed by reflux at 100 °C for 6 h. The supported catalysts were prepared by impregnating TiO_2 (Ti Oxide, UK) with known amounts of the above salt solution, followed by drying at 120 °C. All the samples were calcined at 400 °C for 4 h in presence of air.

The BET surface area of the catalyst was determined by nitrogen adsorption, at liquid nitrogen temperature, on a conventional all-glass high vacuum apparatus. XRD patterns of the catalysts were obtained on a Siemens D-5000 diffractometer using Cu-Kα radiation. FTIR spectra were recorded on a Biorad-175 C (USA) spectrometer using the KBr disc method. ^{31}P MAS NMR spectra of solids were recorded in a 300 MHz Bruker ASX-300 spectrometer. A 4.5 μs pulse (90°) was used with repetition time of 5 s between pulses in order to avoid saturation effects. The spinning rate was 5 kHz. All measurements were carried out at room temperature using 85% H_3PO_4 as standard reference. Ammoxidation of MP was carried out at atmospheric pressure in a glass reactor taking 5 g of the catalyst (crushed to 18/25 BSS sieve) and passing a reactant mixture containing MP, ammonia, air and water at a molar ratio of 1:13:7:38, respectively, in the temperature range 360–400 °C. Steady-state product composition was analyzed by gas chromatography.

1 N. Mizuno and M. Misono, *Chem. Rev*., 1998, **98**, 199.
2 C. Marchal-Roach, N. Loronze, N. Guillou, A. Teze and G. Herve, *Appl. Catal., A*, 2000, **199**, 33; C. Marchal-Roach, N. Loronze, N. Guillou, A. Teze and G. Herve, *J. Catal*., 2000, **190**, 173.
3 V. M. Bondareva, T. V. Andrushkevich, L. G. Detusheva and G. S. Litvak, *Catal. Lett*., 1996, **42**, 113; L. Forni, *Appl. Catal*., 1986, **20**, 219.
4 K. Narasimha Rao, R. Gopinath and P. S. Sai Prasad, *Green Chem*., 2001, **3**, 20; K. Narasimha Rao, R. Gopinath, A. Hussain, N. Lingaiah and P. S. Sai Prasad, *Catal. Lett*., 2000, **68**, 223.
5 M. L. Cubeiro, S. Damyanova and J. L. G. Fierro, *Catal. Lett*., 1997, **49**, 223; S. Damyanova, M. L. Cubeiro and J. L. G. Fierro, *J. Mol. Catal. A: Chem*., 1999, **142**, 85.
6 M. Roy, M. G. Bonneu, H. Ponceblanc and J. C. Volta, *Catal. Lett*., 1996, **42**, 93; L. R. Pizzio, C. V. Caceres and M. N. Blanco, *Appl. Catal., A*, 1998, **167**, 283.
7 P. G. Vazquez, M. N. Blanco and C. V. Caceres, *Catal. Lett*., 1999, **60**, 205.
8 S. Albonetti, F. Cavani, F. Trifiro, M. Gazzano, M. Koutyrev, F. C. Aissi, A. Aboukais and M. Guelton, *J. Catal*., 1994, **146**, 491.
9 S. Damyanova and J. L. G. Fierro, *Appl. Catal., A*, 1996, **144**, 59.
10 G. H. Little, *Infrared spectra of adsorbed species*, Academic Press, 1996, p. 383.
11 L. Forni, *Appl. Catal*., 1988, **37**, 305.

CHEMCOMM Communication
www.rsc.org/chemcomm

A silver-containing halogen-free inorganic photochromic glass

Sihai Chen, Tomoko Akai, Kohei Kadono and Tetsuo Yazawa*

Ecoglass Research Group, Division for Green Life Technology, National Institute of Advanced Industrial Science and Technology, AIST Kansai, Midorigaoka 1-8-31, Ikeda, Osaka 563-8577, Japan. E-mail: te-yazawa@aist.go.jp

Received (in Cambridge, UK) 11th July 2001, Accepted 3rd September 2001
First published as an Advance Article on the web 1st October 2001

A halogen-free inorganic photochromic soda-lime silicate glass containing silver ions has been developed; reversible change between colorless and yellow color in this glass is achieved through combined 193 nm excimer laser irradiation and heat treatment.

Photochromic glasses refer to the glasses that change color reversibly when exposed to actinic radiation. The word *reversibly* does not exclude examples having immeasureably slow reverse rates, but does exclude those in which the state resulting from photolysis is thermodynamically more stable than the initial states.[1] These glasses have a wide range of applications such as ophthalmic lenses, architectural or automotive glazing, information storage and display devices.[2] Until now, the most extensively studied and widely commercialized glasses are those which contain silver halide crystallites, and which were first reported in 1965 by Armistead and Stookey.[3] Although the silver ions can be sometimes replaced by other ions such as copper,[4] the halogen ions are normally irreplaceable since they act as the reducing agent during photolysis to render the electrons for silver particle formation.

In response to the increased demand for green life technology in the color glass industry, a plan to make recyclable colored glass is proposed,[5] where the color of the glass is required to be generated or erased using simple physical treatment such as photo-irradiation or heat annealing. An important point in this plan is that environment-unfriendly materials such as halogens should not be included in the glass. The normal photosensitive glasses[6] that contain silver ions and optical (such as cerium) or thermal (such as tin or antimony) sensitizers seem to comply with this requirement, but the yellow color formed cannot be erased unless melting of the glass is carried out.

In this communication, we report a successful preparation of a halogen-free photochromic glass. Different from the previously reported ones, the glass contains only silver ions, without any other sensitizers. The transparent, colorless glass gives a yellow color after treatment with 193 nm excimer laser irradiation and heat annealing at 400 °C; however this color can also be erased through heating at 500 °C.

The raw materials used are SiO_2, Na_2CO_3, $Al(OH)_3$, $CaCO_3$ and $AgNO_3$ (all analytical grade). The soda-lime silicate glass with composition of 75% SiO_2, 17% Na_2O, 3% Al_2O_3 and 5% CaO containing 0.02% Ag was prepared by melting the mixture of the above raw materials in a platinum crucible at 1450 °C for 4 h under an air atmosphere. Absorption and fluorescence measurements were conducted using a Hitachi U-4000 UV-VIS-NIR and an F-4500 fluorescence spectrophotometer, respectively. The 193 nm excimer laser applied was a Lambda Physik COMPex 102 ArF laser with pulse duration of 25 ns. The frequency of pulse irradiation was fixed at 10 Hz. The average intensity of the laser beam was measured with a Vector H 410 (Scientech) power meter.

The glass changed immediately from colorless to slightly black after exposure to the laser irradiation. As shown in Fig. 1, curve (a), several absorption bands can be clearly identified at 620, 460, 233 and 333 nm. The former three peaks are caused by the formed defects in the glass matrix. They can be assigned to non-bridging oxygen hole centers (HC_1 for 460 nm and HC_2 for 620 nm), and E′ centers (for 233 nm).[7] The 333 nm peak is caused by the formation of silver atoms.[8] Since the glass does not contain any other reducing agents, it is evident that the silver atoms are formed through electrons trapped by silver ions, resulting in the generation of large amounts of hole centers.

$$\text{Glass} \xrightarrow{\text{Laser}} h^+ + e^- \quad (1)$$

$$Ag^+ + e^- \rightarrow Ag^0 \quad (2)$$

After heating at 400 °C for 15 min [Fig. 1, curve (b)], the characteristic surface plasmon absorption band of silver particles at 406 nm appeared indicating the formation of silver particles.

$$nAg^0 \rightarrow Ag_n \quad (3)$$

More information about the fate of silver ions in the glass was traced from the fluorescence spectra, where a 335 nm fluorescence emission was assigned to the free Ag^+ ions in the soda-lime glass.[9] As shown in Fig. 2, curve (a), excimer laser irradiation resulted in *ca.* 85% decrease in the fluorescence intensity, which corresponds to a decrease in free silver ion concentration as a result of silver atom formation. Heating at 400 °C leads to *ca.* 80% recovery of silver ion concentration [Fig. 2, curve (b)], implying that large amounts of reduced silver atoms should have lost electrons to form ions again.

$$Ag^0 \rightarrow Ag^+ + e^- \quad (4)$$

It can be seen that treatment at 400 °C gives two results: one is the aggregation of silver atoms to form particles, the other is the direct dissolution of silver atoms to form silver ions.

The most interesting feature is that further heating at 500 °C for 15 min results in the disappearance of the yellow color [Fig. 1, curve (c)}, *i.e.* the silver particles, once formed, dissolved again.

$$Ag_n \rightarrow nAg^+ + ne^- \quad (5)$$

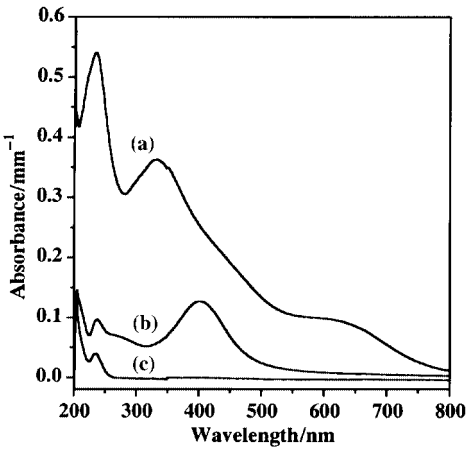

Fig. 1 Absorption spectra of the soda-lime glass containing 0.02 wt% Ag, (a) after 30 min of 193 nm excimer laser irradiation at an intensity of 100 mW cm^{-2}, and then (b) after heat annealing at 400 °C for 15 min; (c) further heat annealing at 500 °C for 15 min. The absorption spectra are referenced with an untreated sample.

 DOI: 10.1039/b106179h

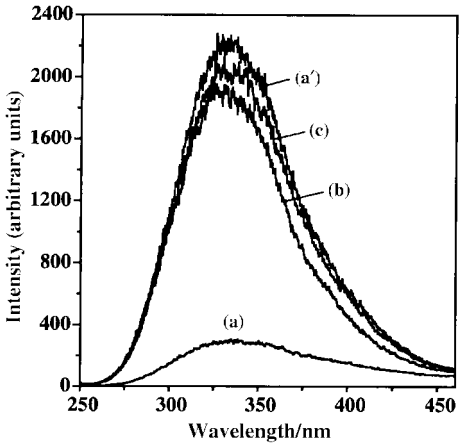

Fig. 2 The corresponding fluorescence spectra during the treatment of the glass as shown in Fig. 1. The excitation wavelength is 240 nm; (a′) represents the spectrum before treatment; (a), (b) and (c) are as detailed in Fig. 1.

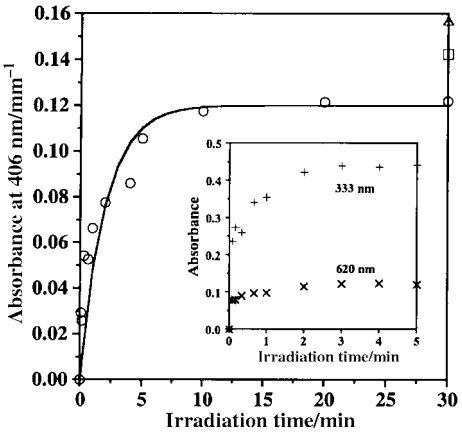

Fig. 3 The effect of laser irradiation time (*i.e.* the amount of laser irradiation pulse) on the 406 nm absorbance obtained after heat annealing at 400 °C for 15 min. The irradiation intensity is 100 mW cm^{-2}. The solid line shows a fitting of the experimental data with $y = 0.12 \times (1 - e^{-x/2})$. The inset is the change of the 333 and 620 nm absorbances after irradiation at different times. The symbols □ and △ show the 406 nm absorbance obtained at irradiation intensities of 200 and 400 mW cm^{-2} for 30 min, respectively.

This is also indicated by the further increase in silver ion concentration shown by the fluorescence spectrum [Fig. 2, curve (c)].

The reason for the silver particle dissolution may be the same as the silver atom dissolution during 400 °C treatment. Since no other oxidants are present in the glass, the hole centers produced by the excimer irradiation may be considered as the oxidant to oxidize the silver particles. As shown in Fig. 1, the band of the hole centers at 620 or 460 nm in the glass continuously decreases and finally disappears after heat treatment at 400 and 500 °C.

The silver particle formation is related to the defects formed within the glass, which is dependent upon the duration of the irradiation pulse, as well as on the laser intensity. As shown in Fig. 3, at an average intensity of 100 mW cm^{-2}, after treatment at 400 °C the formed amounts of silver particles, as indicated by the 406 nm absorbance, level off after 5–10 min of irradiation. This is explainable since the amount of HC_1 centers (at 620 nm) formed, as well as that of silver atoms (at 333 nm) reaches a maximum within 5 min of irradiation (Fig. 3 inset). Increasing the laser intensity to 200 and 400 mW cm^{-2} can stimulate the formation of silver particles, and this was shown by the increased 406 nm absorbance (□ and △ symbols in Fig. 3).

Information about the size of the silver particles formed was obtained by studying the absorption curve of the silver plasmon band, where the width of the band is related to the particle size.[10] It was found that the plasmon band can be fitted with a Lorentz function in the present experiments and that the band widths are in the range of 100–130 nm. Estimated with Mie theory corrected by the 'mean free path' effect,[10] the particle size is estimated at < 2 nm.

The experiments shown in Fig. 1 were also found to be repeatable, *i.e.* the color of the glass can be switched from colorless to yellow, and then to colorless again for many cycles. Since the defects induced by the laser irradiation finally disappeared after high temperature annealing, severe fatigue of the base glass itself was not found in the present system. This property makes this glass very attractive, not only for glass recycling, but also as an advanced material used for erasable high density information storage.

The authors thank New Energy and the Industrial Technology Development Organization of Japan (NEDO) for financial support.

Notes and references

1 R. J. Araujo and N. F. Borelli, in *Optical Properties of Glass*, ed. D. R. Uhlmann and N. J. Kreidl, The American Ceramic Society, Inc., Westerville, OH, 1991, p. 125.
2 R. J. Araujo, in *Photochromism*, ed. G. H. Brown, John Wiley & Sons, Inc., New York, 1971, p. 667.
3 W. H. Armistead and S. D. Stookey, *US Pat.* 3 208 860, 1965.
4 R. Fachet, M. Muller and H. Burger, *Glastech. Ber. Glass Sci. Technol.*, 2000, **73**, 239; S. L. Kraevskii, V. F. Solinov and A. M. Zyabnev, *Glass Phys. Chem.*, 1999, **25**, 151.
5 T. Yazawa, *Osaka Natl. Res. Inst. News*, 2000, **44**, 4.
6 S. D. Stookey, *Ind. Eng. Chem.*, 1949, **41**, 856.
7 E. J. Friebele, in *Optical Properties of Glass*, ed. D. R. Uhlmann and N. J. Kreidl, The American Ceramic Society, Inc., Westerville, OH, 1991, p. 205; M. Mofz, C. Reich, R. Stosser, J. Bartoll and E. Janata, *Glastech. Ber. Glass Sci. Technol.*, 1999, **72**, 76.
8 P. Mulvaney and A. Henglein, *J. Phys. Chem.*, 1990, **94**, 4182.
9 E. Borsella, F. Gonella, P. Mazzoldi, A. Quaranta, G. Battaglin and R. Polloni, *Chem. Phys. Lett.*, 1998, **284**, 429.
10 U. Keribig and C. v. Fragstein, *Z. Phys.*, 1969, **224**, 307.

CHEMCOMM Communication
www.rsc.org/chemcomm

New fluorescent probes for the detection of mixed sodium and potassium metal ions

Xiaohe Xu, Hao Xu and Hai-Feng Ji*

Department of Chemistry and Institute for Micromanufacturing, Louisiana Tech University, Ruston, LA 71272, USA. E-mail: hji@chem.latech.edu; Fax: 01-318-257-3823

Received (in Cambridge, UK) 23rd July 2001, Accepted 3rd September 2001
First published as an Advance Article on the web 24th September 2001

A new fluorescent probe 2 is developed that is capable of measuring the concentration of a mixture of sodium and potassium ions in the solution. This probe contains a fluorophore that is utilized in two ways depending on the pH of the solution.

A large family of the fluorescent chemical sensors is based on photo-induced electron transfer quenching (PET) of the fluorophore by the receptor.[1–4] Most of the current PET fluorescent probes are designed for only one species. A multicolor labeling experiment entails the deliberate introduction of two or more probes to monitor simultaneously different species. This technique has major applications in flow cytometry, DNA sequencing, *in situ* hybridization, *etc*. However, only a few such two or multicolor systems have been studied because of the strict prerequisites of this technique, including absorption at a coincident excitation wavelength and well-separated emission spectra of two or more fluorophores,[5] no energy transfer between two fluorophores, no transient excited-state collisional quenching, and no excited state dimer, *etc*. These prerequisites increase the barrier in the development of multicolor sensors.

Recently,[6] we designed and synthesized one novel fluorescent probe **1**. Our results have shown that this molecule can be used to detect caesium ions in acid conditions, but potassium ions in basic solutions. Based on the same design, we synthesized another probe **2**. Logically, **2** would be a potassium sensor in basic solution and a sodium sensor in acidic solution. In this paper, we report the fluorescence-sensing behavior of probe **2**. Furthermore, the unique fluorescence behaviors of **1** and **2** suggest that another approach for a mixture of dual component sensing is feasible. We also report here that probe **2** could be a potential sensor for a mixture of sodium *and* potassium ions.

In molecule **2**, two receptors are connected with the anthracene. One receptor is benzo-15-crown-5, which is a good host for sodium ions.[7] Another is aza-18-crown-6, which is the right size for K^+ complexation.[8]

Under basic conditions, the PET fluorophore–receptor pair is anthracene and aza-crown-6 ether (ring **I**). The lone-pair electrons on nitrogen in ring **I** quench the fluorescence of anthracene. Addition of K^+ in the solution causes an enhancement in the fluorophore's emission due to the formation of the K^+–**2** complex as shown in Fig. 1. The complexations of ring **I** with other alkali metal ions are weaker than ring **I** with K^+ and only cause weak fluorescence enhancement of **2**. Meanwhile, since the crown ring **II** has no contribution to the PET process, the complexation of alkali metals by the crown ring **II** under basic conditions has no effect on the fluorophore's emission.

In an acidic environment, where the nitrogen atom of aza-crown ring **I** of **2** is protonated (hereafter referred as **2-H**$^+$), the PET fluorophore–receptor pair is switched to anthrylmethylammonium and benzo group in benzo-15-crown-5. The low fluorescence quantum yield of **2-H**$^+$ is similar to that of **2** in basic solution. The diminished emission intensity of anthrylmethylammonium is due to PET quenching of the fluorophore by the dialkoxybenzene moiety of crown ring **II**. The driving force, ΔG, is calculated to be -0.1 eV.[9] Addition of Na^+ to the solution results in an enhancement of fluorescence intensity of **2-H**$^+$ because the complexation between Na^+ and benzo-15-crown-5 (ring **II**) inhibits the PET process from benzo to anthrylmethylammonium. The complexation constants of ring

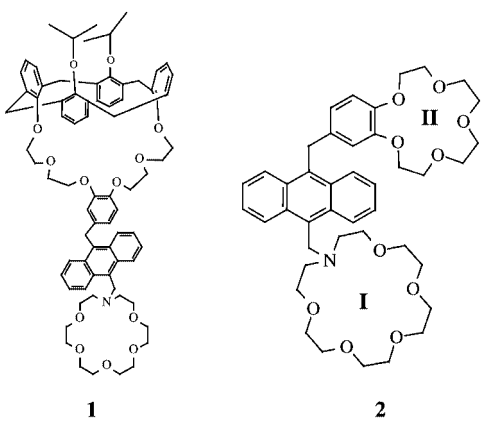

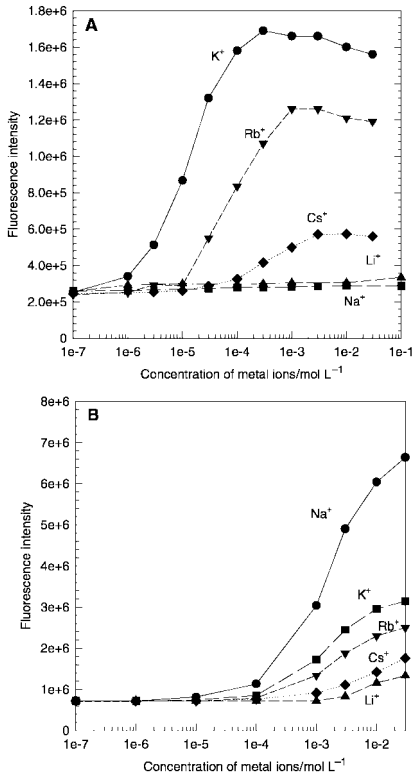

Fig. 1 (A) Changes in the fluorescence intensity (λ_{em} = 426 nm) of **2** (1×10^{-6} M) in basic methanol (morpholine, 1×10^{-2} M as proton scavenger) as a function of concentration of various alkali metal ions. (B) Change in the emission intensity (λ_{em} = 425nm) of **2-H**$^+$ (1×10^{-6} M) in acidic methanol (1×10^{-2} M HCl) as a function of concentrations of various alkali metal ions. Excitation at the isosbestic point for both **2** and **2-H**$^+$ is at 376 nm.

 DOI: 10.1039/b106632n

Table 1 The maximum fluorescence quantum yield (Φ) and complexation constants, K, for the complexation of various alkali metal ions by **2** and **2-H**$^+$ (1×10^{-6} mol L^{-1}) in CH_3OH. λ_{ex} = 376 nm at the isosbestic point for both **2** and **2-H**$^+$. The quantum yields were determined relative to 9,10-diphenylanthracene in MeOH, $\Phi_f = 0.94$[6]

	Metal ion M^+ Free	Li^+	Na^+	K^+	Rb^+	Cs^+
Φ_{em} of **2**	0.048	0.060	0.053	0.39	0.31	0.12
K of aza-crown in **2** with ions	—	10	7.4×10^2	6.30×10^4	1.26×10^4	2.82×10^3
Φ_{em} of **2-H**$^+$	0.060	0.098	0.55	0.26	0.22	0.15
K of **2-H**$^+$	—	65	6.2×10^2	6.0×10^2	3.9×10^2	1.5×10^2

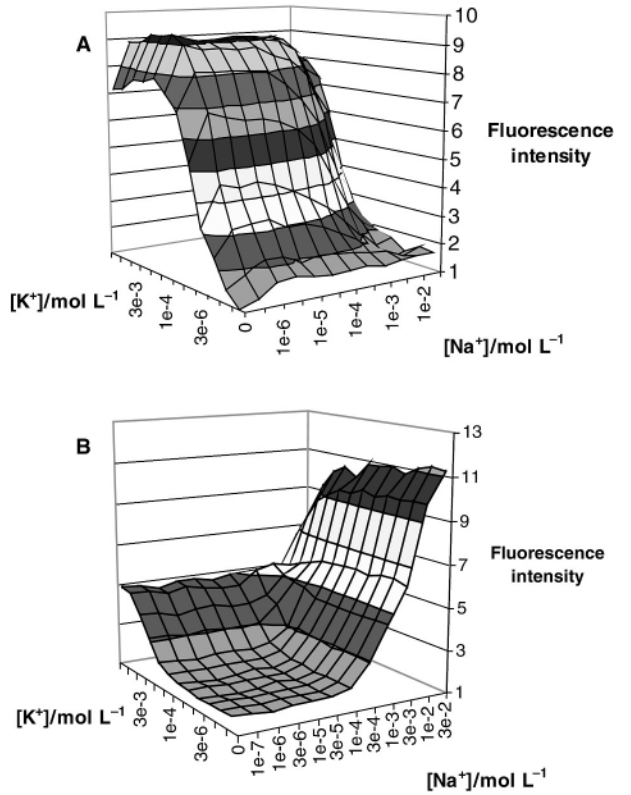

Fig. 2 (A) Changes in the fluorescence intensity (λ_{em} = 426 nm) of **2** (1×10^{-6} M) in basic methanol (morpholine, 1×10^{-2} M as proton scavenger) as a function of different concentrations of K^+ and Na^+. (B) Change in the emission intensity (λ_{em} = 425 nm) of **2-H**$^+$ (1×10^{-6} M) in acidic methanol (1×10^{-2} M HCl) as a function of different concentrations of K^+ and Na^+. Excitation at the isosbestic point for both **2** and **2-H**$^+$ is at 376 nm.

II with other alkali metal ions, except K^+, are weaker than those with Na^+, which results in weaker fluorescence enhancement of **2-H**$^+$. Though the complexation constant of ring **II** with K^+ (6.0×10^2 L mol^{-1}) is similar to the ring **II** with Na^+ (6.2×10^2 L mol^{-1}), which is consistent with those of other benzo-15-crown-5 derivatives with Na^+ and K^+ in methanol,[10–12] the fluorescence enhancement of **2** upon addition of K^+ is weaker than addition of Na^+. This is probably due to the metal ion size effect and will be explained in a full paper. Since nitrogen in ring **I** is protonated, no metal ions can be complexed into ring **I** because of electrostatic repulsion.

In probe **2**, fluorophore **I** (anthracene) and fluorophore **II** (anthrylmethylammonium) are switched by H^+, and **2** could be used to detect Na^+ at low pH, and to detect the K^+ by raising the pH of the solution. The maximum fluorescence quantum yields and the complexation constants of various metal ions with **2** under different conditions are listed in Table 1.

Further study of the fluorescence sensing behavior of **2** is conducted in a mixture of various concentrations of Na^+ and K^+ in two pH conditions (one acidic and the other basic), which is shown as a three-dimensional map in Fig. 2. In basic solution, the fluorescence enhancement region of **2** occurs when $[K^+]$ = 1×10^{-6} M to 1×10^{-4} M in the absence or presence of low concentration of Na^+ as shown in Fig. 2A. However, although the complexation constant of **2** with Na^+ is low, high concentration of Na^+ would affect the complexation of K^+ with **2**. In consequence, the fluorescence enhancement of **2** occurs at higher concentration of K^+ in the presence of high concentration of Na^+. For instance, when $[Na^+] = 3 \times 10^{-2}$ M, the fluorescence enhancement of **2** begins at $[K^+] = 1 \times 10^{-4}$ M and is completed at $[K^+] = 1 \times 10^{-2}$ M. In acidic solution as shown in Fig. 2B, the fluorescence enhancement of **2-H**$^+$ begins at $[Na^+] = 1 \times 10^{-4}$ M and is completed at $[Na^+] = 3 \times 10^{-2}$ M in the absence of K^+. In the presence of high K^+ concentrations, such as 3×10^{-3} M of K^+, the fluorescence enhancement of **2-H**$^+$ begins at $[Na^+] = 3 \times 10^{-4}$ M, which is slightly higher than that in the absence of K^+. It is also noticed that at fixed $[Na^+]$, especially at low $[Na^+]$, the fluorescence of **2-H**$^+$ increases upon addition of $[K^+]$ because K^+ could also complex with **2-H**$^+$ and cause a relatively weaker fluorescence enhancement of **2-H**$^+$ than Na^+ does.

These results suggest that probe **2** could be a potential fluorescent sensor to measure a mixture of Na^+ and K^+ in solution, the fluorescence intensity of **2** in a solution containing a Na^+–K^+ mixture is significantly different from only one metal ion species in the solution. By computer analysis of the data collected in both acidic and basic solutions, the concentrations of both K^+ and Na^+ in the solution may be determined simultaneously.

Currently, we are seeking the design of a similar system with two fluorophores switched by other factors, such as temperature, hydrogen bonds, or other supramolecular interactions.

The authors thank the Louisiana Board of Regents through the Board of Regents Support Fund under contract number LEQSF(2001-04)-RD-A-16 for financial support.

Notes and references

1 A. P. de Silva, H. Q. N. Gunaratne, T. Gunnlaugsson, A. J. M. Huxley, C. P. McCoy, J. T. Rademacher and T. E. Rice, *Chem. Rev.*, 1997, **97**, 1515.
2 R. A. Bissell, A. P. de Silva, H. Q. N. Gunaratne, P. L. Lynch, G. E. M. Maguire, C. P. McCoy and K. R. A. S. Sandanayake, *Top. Curr. Chem.*, 1993, **168**, 223.
3 A. W. Czarnik, *Acc. Chem. Res.*, 1994, **27**, 302.
4 J.-P. Desvergne, F. Fages, H. Bouas-Laurent and P. Marsau, *Pure. Appl. Chem.*, 1992, **64**, 1231.
5 M. L. Metzker, J. Lu and R. A. Gibbs, *Science*, 1996, **271**, 1420.
6 H.-F. Ji, R. Dabestani and G. Brown, *J. Am. Chem. Soc.*, 2000, **122**, 9306.
7 A. P. de Silva and K. R. A. S. Sandanayake, *J. Chem. Soc., Chem. Commun*, 1989, 1183.
8 H.-F. Ji, R. Dabestani, G. M. Brown and R. L. Hettich, *Photochem. Photobiol.*, 1999, **69**, 513.
9 A. P. de Silva, I. M. Dixon, H. Q. N. Gunaratne, T. Gunnlaugsson, P. R. S. Maxwell and T. E. Rice, *J. Am. Chem. Soc.*, 1999, **121**, 1393.
10 D. G. Parsons, M. R. Truter and J. N. Wingfield, *Inorg. Chim. Acta*, 1980, **47**, 81.
11 D. E. Fenton, D. Parkin and R. F. Newton, *J. Chem. Soc., Perkin Trans. 1*, 1981, 449.
12 A. P. de Silva, H. Q. N. Gunaratne and C. P. McCoy, *J. Am. Chem. Soc.*, 1997, **119**, 7891.

CHEMCOMM
Communication
www.rsc.org/chemcomm

Monomeric uni-ligated aluminates

Melanie J. Harvey, Mary Proffitt, Pingrong Wei and David A. Atwood*

Department of Chemistry, University of Kentucky, Lexington, KY 40506-0055, USA.
E-mail: datwood@pop.uky.edu

Received (in Cambridge, UK) 26th July 2001, Accepted 5th September 2001
First published as an Advance Article on the web 1st October 2001

The tetradentate ligand, common name Salban(Bu^t)H_4 (*N*,*N*′-bis(2-hydroxy-3,5-di-*tert*-butylbenzyl)-1,4-diaminobutane) combines with appropriate amounts of $LiAlH_4$ to produce the unique monomeric, uni-ligated aluminate [Salban(Bu^t)Al]Li(thf)$_2$ (1) and the bimetallic derivative Salban(Bu^t){AlH_2Li(thf)$_2$}$_2$ (2).

Group 13 anions have become increasingly important in recent years as reducing agents,[1] cocatalysts or counter ions for polymerization reactions[2] and in ionic liquids.[3] In their most commonly reported form, aluminates are composed of a combination of four singly-charged ligands, $[AlR_4]^-$. By comparison, there is relatively little literature focusing on chelated aluminium anions. Less frequently, they have been formed from bidentate ligands, and have the form $[L_2Al]^-$ (where L = diamine[4] or diol,[5] for example). Rarer still are those supported by a single ligand. Of this sort, only anions supported by Salan-type ligands have been reported.[6]

The Salan ligands are ideal candidates for supporting Group 13 anions since they can be deprotonated in four places to form, potentially, tetra-anions. Additionally, the hydrocarbon 'backbone' can easily be altered to allow for the synthesis of complexes with a wide variety of structures.[6,7] Two dimeric aluminates have previously been formed from Salan ligands with two- or three-carbon backbones: [SalanAl{Li(thf)$_2$}$_2$ [where Salan = Salpan (*N*,*N*′-bis(2-hydroxybenzyl)-1,4-diaminopropane)], and Salomphan (*N*,*N*′-bis(2-hydroxybenzyl)-*o*-diamino(4,5-dimethyl)phenyl).[6] In the present work we describe the first uni-ligated *monomeric* aluminate, as well as an unusual bimetallic AlH_2 derivative. These compounds have been made accessible by the use of a bulky Salan ligand with four carbons in its backbone, Salban(Bu^t)H_4 (*N*,*N*′-bis(2-hydroxy-3,5-di-*tert*-butylbenzyl)-1,4-diaminobutane).

The reaction of $LiAlH_4$ with a secondary amine was first reported in 1988.[8] Later, the intermediates in these reactions were isolated using $HN(SiMe_3)_2$.[9] More recently, several possible intermediates in the reactions of primary amines with $LiAlH_4$ have been reported.[10] We report here reactions of $LiAlH_4$ with the Salban(Bu^t)H_4 ligand. The Salban(Bu^t)H_4 ligand reacts with two moles of $LiAlH_4$ to form a mixture of two compounds, [Salban(Bu^t)Al]Li(thf)$_2$ **1** and Salban(Bu^t){AlH_2-Li(thf)$_2$}$_2$ **2**.† The ratio of reactants can be selected to favor one product exclusively over the other: **1** is isolated as a pure product from the reaction of an equimolar ratio of the two reactants, and **2** can be obtained by using four equivalents of $LiAlH_4$ (Scheme 1).

The $(CH_2)_4$ linkage in the backbone of Salban(Bu^t) is of sufficient flexibility to allow the ligand to coordinate just one metal. The structure of **1** (Fig. 1)[11] demonstrates the distorted tetrahedral geometry that results for the aluminum atom when this occurs. The angles range from 122.59(10)° (for O2–Al1–N1) to 91.48(8)° (for O2–Al1–O1). The Al–N and Al–O are suprisingly similar [Al1–N1, 1.801(2); Al1–N2, 1.785(2); Al1–O1, 1.7997(18); Al1–O2, 1.7944(17)], and short, for this type of complex. By comparison, these distances for [SalpanAl{Li(thf)$_2$}]$_2$ are 1.8–2.0 Å.[6] In fact, values of Al–O ≈ 1.7 Å are close to those ascribed to π-bonded systems such as dialkyl aluminium aryloxides[12] and Al–N distances ≈ 1.8 Å for monomeric aluminium amides with some π-bonding.[13] It is remarkable that compound **1**, which does not fulfill the usual criteria for π-bonded systems, should demonstrate such short, and uniform, bonds. However, alumoxanes such as [(Me_2AlO-Li)$_4$·7thf)] also demonstrate relatively short distances (Al–O 1.769 Å).[14] The lithium atom is coordinated to both oxygens of the Salban(Bu^t) ligand [Li1–O1, 1.963(5) Å; Li1–O2, 2.023(5) Å] and to two terminal thf molecules [Li1–O3, 1.958(5) Å; Li1–O4, 1.917(5) Å].

The crystal structure of **2** reveals the bimetallic nature of the compound (Fig. 2).[11] The aluminium atoms are five-coordinate and have a trigonal-bipyramidal geometry. The axial sites are occupied by oxygen and nitrogen atoms [O1–Al1–N1′, 167.30(11)°]. These nitrogens form longer bonds to aluminium [Al1–N1′ 2.113(3) Å] than the equatorial nitrogens [Al1–N1 1.938(3) Å]. Despite the charge on aluminium, the Al–O and Al–N distances are comparable to those demonstrated in the neutral Salan derivatives [SalanAlR(AlR$_2$)$_2$].[7] A similarity in these distances for related charged (cationic or anionic) and neutral derivatives is common. The other equatorial sites are filled by hydrogens, which were located in the structure determination. The Li–O distances for **2** are comparable to those demonstrated in **1** and do not reflect any steric interaction between the ligand Bu^t groups and the Li(thf)$_2$ unit. The Li1–H1 distance of 1.8929 Å is within the range observed for similar compounds (1.83–2.00 Å).[9,10]

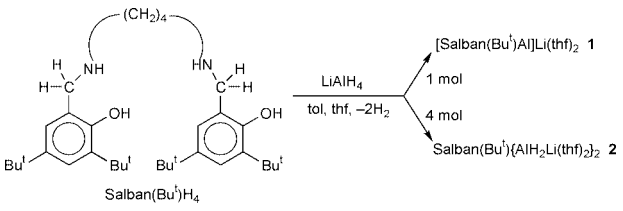

Scheme 1 View of the SalbanH_4 ligand and the preparation of compounds **1** and **2**.

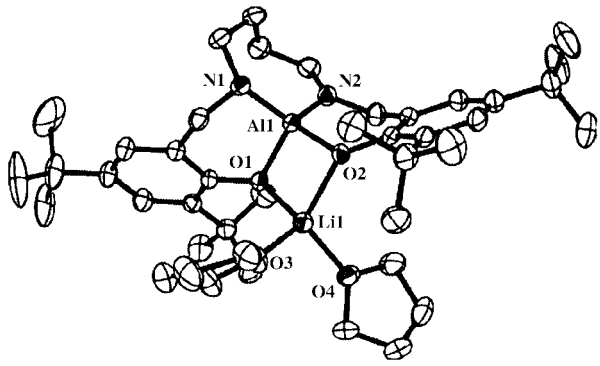

Fig. 1 Molecular structure and atom numbering scheme for **1** with selected bond distances (Å) and angles (°): Al1–N1 1.801(2), Al1–N2 1.785(2), Al1–O1 1.7997(18), Al1–O2 1.7944(17), Li1–O1 1.963(5), Li1–O2 2.023(5), Li1–O3 1.958(5), Li1–O4 1.917(5); N2–Al1–O2 101.29(9), N2–Al1–N1 118.30(11), O2–Al1–N1 122.59(10), N2–Al1–O1 120.36(10), O2–Al1–O1 91.48(8), N1–Al1–O1 101.00(9), Al1–O1–Li1 94.58(15), Al1–O2–Li1 92.73(15).

 DOI: 10.1039/b106772a

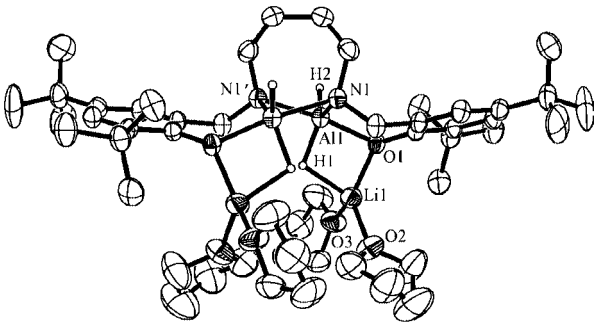

Fig. 2 Molecular structure and atom numbering scheme for **2** with selected bond distances (Å) and angles (°): Al1–H1 1.5718, Al1–H2 1.5175, Al1–O1 1.927(2), Al1–N1 1.938(3), Al1–N1′ 2.113(3), Al1–Li1 2.739(7), Li1–O1 1.887(7), Li1–O2 1.909(14), Li1–O3 1.958(18), Li1–H1 1.8929; O1–Al1–N1 93.21(11), O1–Al1–N1′ 167.30(11), N1–Al1–N1′ 79.88(13), O1–Al1–H1 85.3, N1–Al1–H1 114.4, N1′–Al1–H1 87.9, O1–Al1–H2 97.5, N1–Al–H2 123.5, N1′–Al1–H2 95.2.

In the ^{1}H NMR spectrum of **2**, one of the two Al–H resonances appears at δ 0.29 while the second is either broadened or coincident with other resonances, probably in the range 3–5 ppm, where the Al–H groups of other compounds appear ([H_2Al(pmdta)]$^+$ (pmdta = pentamethyldiethylenetriamine) = 3.09 ppm (br),[15] H_3Al–NMe_3 = 4.0 ppm[16] and [H_2AlOBu^t]$_2$ = 4.43 ppm (br)[17]. The NCH_2 groups show AB coupling consistent with diastereotopic, non-fluxional behavior in solution. In contrast, compound **1** demonstrates only one resonance for this group. Additionally, the ^{7}Li NMR spectrum of compound **2** shows two resonances in C_6D_6. However, in THF-d_8, the ^{7}Li NMR spectrum shows only one resonance which does not broaden significantly, even at −85 °C. Attempts were made to resolve ^1J(Li, H) coupling in **2** in a ^{7}Li NMR experiment similar to that reported by Heine and Stalke;[9] however, in **2** we could not observe the coupling at any temperature between 25 and −85 °C in either toluene-d_8 or THF-d_8. Our observations of the single ^{7}Li NMR resonance in THF-d_8, combined with the absence of ^1J(Li, H) coupling, suggest that the bonding of the lithium atoms in this compound are highly ionic in character.

Attempts to make boron and gallium complexes analogous to compound **1** have not been successful using the corresponding reagents $NaBH_4$ and $LiGaH_4$. In the case of $NaBH_4$ no reaction occurred after overnight reflux, and $LiGaH_4$ decomposed (depositing gallium metal) before it could react with Salban(Bu^t)H_4. We are currently exploring the utility of the chelated anion **1** as a cocatalyst in olefin polymerization and are working towards the synthesis of analogous complexes of boron and gallium using alternative routes.

Acknowledgement is made to the National Science Foundation (NSF) (Grant 9816155) for support. M. J. H. would like to thank the University of Kentucky for a Post-doctoral Fellowship for Women. NMR instruments used in this research were obtained with funds from the CRIF program of the NSF (CHE 997841) and the Research Challenge Trust Fund of the University of Kentucky. M. P. was supported by the NSF Research Experiences for Undergraduates Program. The authors also wish to thank Dr Sean Parkin for crystallographic advice.

Notes and references

† *Preparation of* Salban(Bu^t)[AlLi(thf)$_2$] **1**: Salban(Bu^t)H_4 (1.00 g, 1.91 mmol) and $LiAlH_4$ (0.07 g, 1.91 mmol) were placed in a dry flask under nitrogen. Dry toluene (50 mL) was added at 25 °C and the solution stirred for 15 min. Dry tetrahydrofuran (20 mL) was added and the exothermic reaction was refluxed for 10 h. After filtration and removal of the volatile components under vacuum the residue was recrystallized from n-hexane–toluene (10 : 1) to afford **1** as pale yellow crystals (0.30 g, 23%), mp 235–239 °C. ^{1}H NMR (270 MHz, THF-d_8, TMS): δ 1.22 (s, 18H, CCH_3), 1.34 (s, 18H, CCH_3), 1.47 (m, 4H, CH_2CH_2), 1.71 (m, 8H, THF), 2.58–2.65 (m, 4H, NCH_2CH_2), 3.57 (m, 8H, THF), 3.88 (s, 4H, NCH_2), 6.81 (m, 2H, Ph*H*), 7.16 (m, 2H, Ph*H*); IR (KBr)/cm^{-1}: 2970 (s), 2864 (s), 1620 (m), 1479 (s), 1446 (s), 1361 (m), 1305 (s), 1276 (s), 1240 (s), 1203 (m), 1170 (m), 1132 (w), 1049 (s), 918 (w), 868 (s), 765 (m), 646 (w), 586 (w), 497 (w), 414 (w). Anal. Calc. for $C_{42}H_{68}N_2O_4AlLi$: C, 72.15; H, 9.81; N, 4.01. Found: C, 72.35; H, 9.97; N, 4.50%.

Preparation of Salban(Bu^t)[AlH_2Li(thf)$_2$]$_2$ **2**: Salban(Bu^t)H_4 (1.00 g, 1.91 mmol) and $LiAlH_4$ (0.29 g, 7.66 mmol) were placed in a dry flask under nitrogen. Dry toluene (50 mL) was added at 25 °C and the solution stirred for 15 min. Dry tetrahydrofuran (20 mL) was added and the exothermic reaction was refluxed for 10 h. After filtration and concentration, colorless crystals were grown at −30 °C [0.95 g, 59%, based on Salban(Bu^t)H_4], mp > 260 °C. ^{1}H NMR (270 MHz, C_6D_6, TMS): δ 0.29 (s, 4H, AlH), 1.23 (s, 18H, CCH_3), 1.41 (s, 18H, CCH_3), 1.58 (t, 2H, CH_2CH_2), 1.73 (m, 16H, THF), 1.89 (t, 2H, CH_2CH_2), 2.82 (t, 2H, NCH_2CH_2), 3.37 (m, 16H, THF), 3.45 (t, 2H, NCH_2CH_2), 3.82 (d, 2H, NCH_2), 4.82 (d, 2H, NCH_2), 7.21 (d, 2H, Ph*H*), 7.46 (d, 2H, Ph*H*); ^{7}Li NMR (C_6D_6, 24 °C): δ −1.90 and –2.55; ^{7}Li NMR (THF-d_8, 24 °C): δ 0.84. IR (KBr)/cm^{-1}: 2949 (s), 2868 (m), 1622 (m), 1479 (s), 1442 (s), 1359 (w), 1303 (m), 1236 (m), 1167 (m), 1122 (m), 1045 (m), 875 (m), 841 (m), 744 (m), 603 (w), 549 (w), 449 (w). Anal. Calc. for $C_{50}H_{88}N_2O_6Al_2Li_2$: C, 68.16; H, 10.07; N, 3.18. Found: C, 67.75; H, 9.64; N, 3.29%.

1 A. R. Barron and G. Wilkinson, *Polyhedron*, 1986, **5**, 1897; B. M. Bulychev, *Polyhedron*, 1990, **9**, 387; *Comprehensive Organic Synthesis*, ed. B. M. Trost and I. Fleming, Pergamon Press, Oxford, 1991, ch. 8; N. M. Yoon, *Pure Appl. Chem*., 1996, **68**, 843.
2 H. Kobayashi, *J. Fluorine Chem*., 2000, **105**, 201; L. Li, C. L. Stern and T. J. Marks, *Organometallics*, 2000, **19**, 3332; L. Li and T. J. Marks, *Organometallics*, 1998, **17**, 3996; Y.-X. Chen, M. V. Metz, L. Li, C. L. Stern and T. J. Marks, *J. Am. Chem. Soc*., 1998, **120**, 6287; Y.-X. Chen, C. L. Stern and T. J. Marks, *J. Am. Chem. Soc*., 1997, **119**, 2582.
3 P. Wasserscheid and W. Keim, *Angew. Chem., Int. Ed*., 2000, **39**, 3772; D. Bradley, P. Dyson and T. Welton, *Chem. Rev*., 2000, **9**, 18; H. Olivier, *J. Mol. Catal. A: Chem*., 1999, **146**, 285.
4 M. G. Gardiner, C. L. Raston, B. W. Skelton and A. H. White, *Inorg. Chem*., 1997, **36**, 2795.
5 T. Arai, Y. M. A. Yamada, N. Yamamoto, H. Sasai and M. Shibasaki, *Chem. Eur. J*., 1996, **2**, 1368.
6 D. A. Atwood and D. Rutherford, *Inorg. Chem*., 1995, **34**, 4008.
7 D. A. Atwood and D. Rutherford, *Comments Inorg. Chem*., 1996, **19**, 25; D. A. Atwood, *Coord. Chem. Rev*., 1998, **176**, 407.
8 St. Böck, H. Nöth and P. Rahm, *Z. Naturforsch., Teil B*, 1988, **43**, 53.
9 A. Heine and D. Stalke, *Angew. Chem., Int. Ed. Engl*., 1992, **31**, 854.
10 M. L. Montero, H. Wessel, H. W. Roesky, M. Teichert and I. Usón, *Angew. Chem., Int. Ed. Engl*., 1997, **36**, 629.
11 *Crystal data* for compound **1**, $C_{42}H_{68}N_2O_4AlLi$, M = 698.94, monoclinic, space group $P2_1/c$, a = 12.001(2), b = 19.624(4), c = 18.618(4) Å, β = 93.61(3)°, V = 4376.0(15) Å^3, T = 298(2) K, Z = 4, μ = 0.085 mm^{-1}, 20 060 reflections measured, 7534 unique, R_1 = 6.96% [$I > 2(\sigma)I$] and R_{all} = 10.19%; for compound **2**: $C_{50}H_{88}N_2O_6Al_2Li_2$ (note: **2** crystallizes with a disordered solvent molecule in the lattice which is probably a thf molecule with partial occupancy), M = 881.10, monoclinic, space group $C2/c$, a = 14.915(3), b = 16.742(3), c = 25.631(5) Å, β = 99.52(3)°, V = 6312(2) Å^3, T = 298(2) K, Z = 4, μ = 0.09 mm^{-1}, 11 804 reflections collected, 4075 unique, R_1 = 7.08% [$I > 2(\sigma)I$], R_{all} = 10.02%. CCDC reference numbers 168120 and 168121. See http://www.rsc.org/suppdata/cc/b1/b106772a/ for crystallographic files in CIF or other electronic format.
12 M. D. Healy, M. B. Power and A. R. Barron, *Coord. Chem. Rev*., 1994, **130**, 63.
13 M. A. Petrie, K. Ruhlandt-Senge and P. P. Power, *Inorg. Chem*., 1993, **32**, 1135; K. M. Waggoner, K. Ruhlandt-Senge, R. J. Wehmschulte, X. He, M. M. Olmstead and P. P. Power, *Inorg. Chem*., 1993, **32**, 2557; P. J. Brothers, R. J. Wehmschulte, M. M. Olmstead, K. Ruhlandt-Senge, S. R. Parkin and P. P. Power, *Organometallics*, 1994, **13**, 2792.
14 J. Storre, C. Schnitter, H. W. Roesky, H.-G. Schmidt, M. Noltemeyer, R. Fleischer and D. Stalke, *J. Am. Chem. Soc*., 1997, **119**, 7505.
15 J. L. Atwood, K. D. Robinson, C. Jones and C. L. Raston, *J. Chem. Soc., Chem. Commun*., 1991, 1697.
16 R. A. Kovar and J. O. Callaway, *Inorg. Synth*., 1976, **17**, 36.
17 M. Veith, S. Faber, H. Wolfganger and V. Huch, *Chem. Ber*., 1996, **129**, 381.

CHEMCOMM
Communication
www.rsc.org/chemcomm

The first isolable pentacoordinate 1,2λ⁵-azaphosphetine: synthesis, X-ray crystallographic analysis, and dynamic behaviour

Naokazu Kano, Azusa Kikuchi and Takayuki Kawashima*

Department of Chemistry, Graduate School of Science, The University of Tokyo, 7-3-1 Hongo, Bunkyo-ku, Tokyo 113-0033, Japan. E-mail: takayuki@chem.s.u-tokyo.ac.jp; Fax: +81 3 5800 6899; Tel: +81 3 5841 4338

Received (in Cambridge, UK) 20th July 2001, Accepted 13th September 2001
First published as an Advance Article on the web 1st October 2001

Cycloaddition reaction of an iminophosphorane bearing the Martin ligand with an alkyne gave the first stable 1,2λ⁵-azaphosphetine, whose structure was determined by X-ray crystallographic analysis, and variable temperature NMR spectroscopy revealed the existence of equilibrium with the corresponding α-iminoalkylidenephosphorane.

There has been much interest in the chemistry of four-membered heterocyclic compounds containing a pentacoordinate phosphorus atom in view of their unique structures and reactivities.[1] For example, 1,2λ⁵-oxaphosphetanes have been intensely studied as the intermediates of Wittig reactions.[2] Such heterocycles bearing a C=C double bond in the ring would have a much more strained structure than the corresponding saturated ring compounds because of shortening of the bond length. They are expected to show interesting properties due to ring strain such as rearrangement to the corresponding conjugate phosphorus ylide accompanying bond dissociation between phosphorus and the adjacent heteroatom.[3] To the best of our knowledge, however, there have been only a few examples of such unsaturated ring compounds, *i.e.* 1σ⁴,2σ⁵-diphosphete, 1,2λ⁵-thiaphosphetene, and 1,2λ⁵-oxaphosphetene.[4–6] Furthermore, only one example of crystallographic analysis has been reported to date in spite of their potentially interesting structures.[4] On the other hand, the nitrogen analogue of a phosphonium ylide, *i.e.* an iminophosphorane, is expected to be a useful building block for nitrogen-containing four-membered heterocycles.[7] The reaction of an iminophosphorane with a reactive alkyne has been intensely studied because it is a convenient synthetic method for the corresponding α-iminoalkylidenephosphorane presumably *via* a [2 + 2]-cycloadduct of the two molecules although the intermediate has neither been observed nor been isolated yet.[8] We report here the synthesis and crystal structure of the first stable 1,2λ⁵-azaphosphetine derived from the corresponding iminophosphorane bearing the Martin ligand as well as a bulky 2,4,6-triisopropylphenyl (denoted as Tip hereafter) group.[9,10]

Reaction of iminophosphorane **1** which was prepared *in situ* from PCl_3, with alkyne **2** (1.2 eq.) in toluene-d_8 at 50 °C gave the corresponding cycloadduct **3** (27%) as colourless crystal (Scheme 1).[11]† Pentacoordinate 1,2λ⁵-azaphosphetine **3** was also obtained (5%) by thermal reaction of 1,3λ⁵,2-oxazaphosphetidine **4** with alkyne **2** (2.7 eq.) in toluene-d_8 at 140 °C, together with cyclic phosphinate **5**, ketone **6**, and imine **7**.[12] In the latter reaction, iminophosphorane **1** should be generated *in situ* together with formation of phosphinate **5** and imine **7** as indicated in the thermolysis of **4**.[11,12]

The molecular structure of **3** was determined by X-ray crystallographic analysis as shown in Fig. 1.‡ The 1,2λ⁵-azaphosphetine ring is almost planar, judging from the sum of the interior angles of the ring (359.6(8)°) and the small torsion angle of P(1)–C(1)–C(2)–N(1) (6.6(3)°). The P(1)–N(1) bond length (2.170(3) Å) is much greater than that of the trivalent 1,2-azaphosphetine, (1.824(6) Å), and that of the corresponding saturated compound, 1,2λ⁵-azaphosphetidine, (1.789(5) Å), but it is shorter than the sum of the van der Waals radii (3.40 Å),

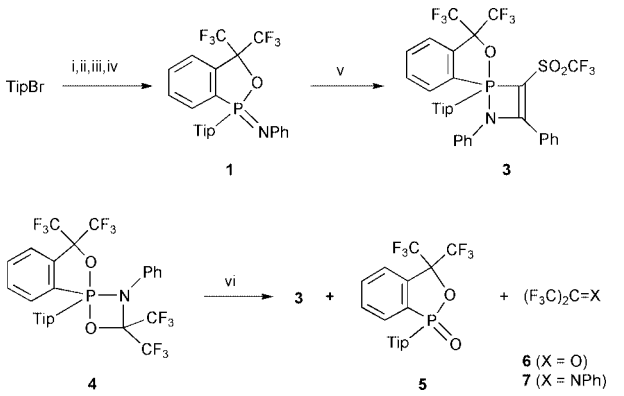

Scheme 1 i. *n*-BuLi (1.9 eq.), Et_2O, 0 °C, 3 h; ii. PCl_3 (2.5 eq.), Et_2O, −70 °C to rt, 13 h; iii. 2-(LiOC$(CF_3)_2$)C_6H_4Li (0.5 eq.), THF–hexane, −78 °C, 30 min; iv. PhN_3 (0.9 eq.), THF, −78 °C, 12 h; v. PhC≡CSO_2CF_3 **2**, (1.2 eq.), toluene-d_8, 50 °C, 27 h, (27%); vi. PhC≡CSO_2CF_3 **2**, (2.7 eq.), toluene-d_8, 140 °C, 25 h (5%).

indicating a characteristic feature of the apical bond.[10b,13] The pentacoordinate phosphorus atom shows a distorted trigonal bipyramidal (TBP) structure with a nitrogen and an oxygen

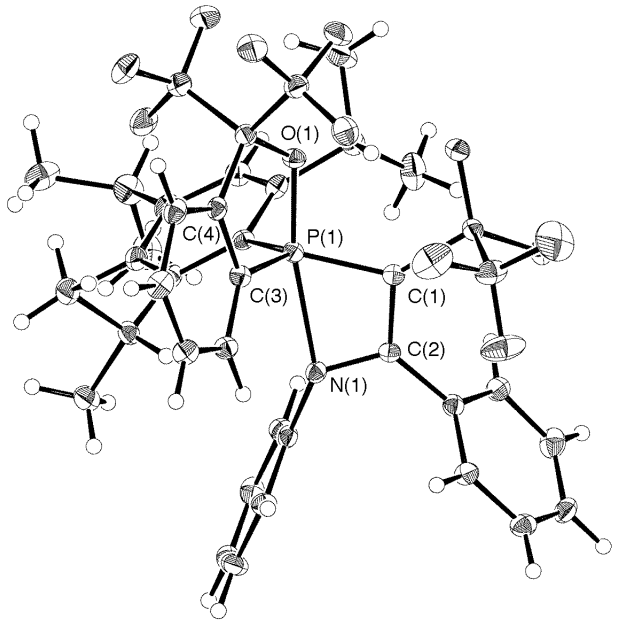

Fig. 1 ORTEP drawing of **23**·$\frac{3}{2}C_6H_6$ with thermal ellipsoid plot (30% probability for all non-hydrogen atoms). One of the enantiomers of **3** and a solvent molecule are omitted for clarity. Selected bond lengths (Å), bond angles (deg), and torsion angle (deg): P(1)–N(1), 2.170(3); P(1)–O(1), 1.676(2); P(1)–C(1), 1.773(3); C(1)–C(2), 1.415(4); C(2)–N(1), 1.314(4); O(1)–P(1)–N(1), 168.95(11); C(1)–P(1)–N(1), 66.79(13); P(1)–C(1)–C(2), 99.9(2); C(1)–C(2)–N(1), 107.1(3); P(1)–N(1)–C(2), 85.8(2); C(2)–N(1), 6.6(3).

 DOI: 10.1039/b106501g

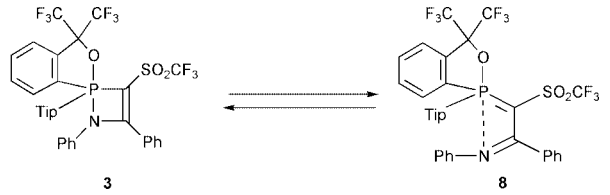

Scheme 2

atom at the apical positions and three carbon atoms at the equatorial positions. The deviation from the ideal TBP structure is exemplified by the position of the phosphorus atom slightly above the equatorial plane by 0.204 Å and the bond angle between apical bonds (168.95(11)°). The pentacoordination characters, %TBP_a and %TBP_e were determined as 66% and 88%, respectively.[14] The deviation from ideal TBP structure seems to emerge from a steric repulsion between the N–Ph group and substituents on the phosphorus atom.

In the ^{1}H NMR spectrum of **3**, the *ortho* proton of the Martin ligand resonated at low field (δ_H 9.06 in $CDCl_3$), which is a typical feature of compounds with a TBP structure bearing a polar apical bond.[15] On the other hand, the chemical shift of **3** (δ_P 25.6 in the $CDCl_3$) in the ^{31}P NMR spectrum was at a low field for a phosphorane structure.[16] The low field shift compared to that of 1,2λ^5-azaphosphetidine indicates the contribution of the phosphorus ylide.[13] In the variable temperature ^{31}P NMR spectra of **3** in toluene-d_8, the signal shifted to the higher field almost linearly with decrease in the temperature from +90 °C (δ_P 26.9) to −90 °C (δ_P 15.6). The chemical shift of **3** in the more polar solvent, CD_3CN, also showed similar temperature dependence between +70 °C (δ_P 23.1) and −40 °C (δ_P 16.6). These results definitely show the equilibrium between **3** and **8** (Scheme 2). The higher the temperature, the more the equilibrium inclines to **8**. Compound **3** serves as a model for sequential structural change between TBP geometry of a 1,2λ^5-azaphosphetine and tetrahedral geometry of the corresponding conjugate α-iminoalkylidenephosphorane along with P–N bond formation–dissociation.

While spectroscopic studies revealed the existence of an equilibrium with the conjugate phosphorus ylide, no evidence of such an equilibrium was obtained by the following reactions. 1,2λ^5-Azaphosphetine **3** was thermally stable, and it did not decompose after heating in toluene-d_8 at 180 °C for three days. Heating of a toluene-d_8 solution of **3** with benzaldehyde at 80 °C or phenyl isocyanate at 140 °C resulted in no reaction instead of giving the corresponding Wittig-reaction products.[17]

In summary, we achieved the isolation and X-ray crystallographic analysis of the first example of a 1,2λ^5-azaphosphetine, which has been assumed to be an intermediate of the reaction of an iminophosphorane and an alkyne giving the α-iminoalkylidenephosphorane.

We thank Central Glass and Tosoh Finechem Corporation for the gifts of organofluorine compounds and alkyllithiums, respectively.

Notes and references

† *Spectral and analytical data of* **3**: colourless crystals; mp 225.6–226.9 °C (dec.); ^{1}H NMR (500 MHz, $CDCl_3$) δ_H −0.10 (br s, 3H), −0.05 (br s, 3H), 1.16 (dd, $^3J_{HH}$ = 6.85, $^3J_{HH}$ = 6.90 Hz, 6H), 1.43 (br s, 3H), 1.63 (br s, 3H), 2.79 (septet, $^2J_{HH}$ = 6.90 Hz, 1H), 2.99 (br s, 1H), 4.96 (br s, 1H), 7.04–7.15 (m, 3H), 7.29 (br s, 3H), 7.78 (br s, 1H), 7.86 (t, $^3J_{HH}$ = 7.70 Hz, 1H), 7.91 (t, $^3J_{HH}$ = 7.70 Hz, 1H), 9.06 (dd, $^3J_{HH}$ = 7.85, $^3J_{PH}$ = 11.7 Hz, 1H); ^{13}C{^{1}H} NMR (126 MHz, $CDCl_3$) δ_C 22.0 (s), 23.4 (s), 23.6 (s), 23.9 (s), 24.1 (s), 26.1 (s), 30.9 (s), 31.5 (s), 34.0 (s), 80.1 (d, $^1J_{CP}$ = 144 Hz), 85.2 (sepet, $^2J_{CF}$ = 289 Hz), 120.5 (q, $^1J_{CF}$ = 329 Hz), 121.8 (q, $^1J_{CF}$ = 290 Hz), 122.0 (s), 124.4 (d, $^3J_{CP}$ = 33.6 Hz), 125.4 (s, 2C), 125.6 (s), 125.9 (d, $^1J_{CP}$ = 140 Hz), 126.5 (s), 127.0 (s, 3C), 128.6 (s, 2C), 130.0 (s, 3C), 131.1 (d, $^3J_{CP}$ = 11.7 Hz), 132.0 (d, $^3J_{CP}$ = 12.9 Hz), 132.9 (d, $^2J_{CP}$ = 10.6 Hz), 133.0 (d, $^1J_{CP}$ = 113 Hz), 134.5 (d, $^4J_{CP}$ = 2.5 Hz), 137.8 (d, $^2J_{CP}$ = 18.9 Hz), 145.7 (s), 150.5 (d), 152.5 (d, $^2J_{CP}$ = 27.1 Hz), 178.1 (d, $^2J_{CP}$ = 10.3 Hz); ^{31}P NMR (109 MHz, $CDCl_3$) δ_P 25.6 (s); Anal. Calcd. for $C_{39}H_{37}F_9NO_3PS$: C, 58.42; H, 4.65; N, 1.75. Found: C, 57.91; H, 4.64; N, 1.40%.

‡ *Crystal data* for **23**·$\frac{3}{2}C_6H_6$. $C_{87}H_{83}F_{18}N_2O_6P_2S_2$, M = 1720.66, triclinic, space group $P\bar{1}$, a = 12.246(2), b = 16.830(2), c = 20.7758(11) Å, α = 79.555(3), β = 85.597(3), γ = 86.0042(10)°, V = 4191.6(7) Å^3, Z = 2, T = 150 K, D_c = 1.363 g cm^{-3}, μ = 1.95 cm^{-1}. The intensity data were collected on a Rigaku Mercury CCD. 37809 reflections collected, 17840 unique (R_{int} = 0.039). Refinement based on 9247 observed reflections ($I > 3.00\sigma(I)$) and 1137 variable parameters converged to R = 0.041, R_w = 0.043. CCDC reference number 166846. See http://www.rsc.org/suppdata/cc/b1/b106501g/ for a crystallographic files in .cif or other format.

1 K. Dimroth, in *Comprehensive Heterocyclic Chemistry*, ed. A. R. Katritzky and C. W. Rees, Pergamon, Oxford, 1984, vol. 1, ch. 17, p 493; T. Kawashima and R. Okazaki, in *Comprehensive Heterocyclic Chemistry II*, ed. A. R. Katritzky, C. W. Rees and E. F. V. Scriven, Pergamon, Oxford, 1996, vol. 1, ch. 27, p. 833.

2 For recent reviews, see: B. E. Maryanoff and A. B. Reitz, *Chem. Rev.*, 1989, **89**, 863; E. Vedejs and C. F. Marth, in *Phosphorus-31 NMR Spectral Properties in Compound Characterization and Structural Analysis*, ed. L. D. Quin and J. G. Verkade, VCH, New York, 1994, ch. 23, p. 297.

3 G. Keglevich, A. G. Vaskó, A. Dobó, K. Ludányi and L. Tõke, *J. Chem. Soc., Perkin Trans. 1*, 2001, 1062; G. Keglevich, T. Körtvélyesi, H. Forintos, A. Tamás, K. Ludányi, V. Izvekov and L. Tõke, *Tetrahedron Lett.*, 2001, **42**, 4417; G. Keglevich, H. Forintos, H. Szelke, T. Körtvelyesi, L. Kollár and L. Tõke, *Phosphorus, Sulfur Silicon Relat. Elem.*, in press.

4 M. Sanchez, R. Réau, H. Gornitzka, F. Dahan, M. Regitz and G. Bertrand, *J. Am. Chem. Soc.*, 1997, **119**, 9720.

5 T. Kawashima, T. Iijima, H. Kikuchi and R. Okazaki, *Phosphorus, Sulfur Silicon Relat. Elem.*, 1999, **144–146**, 149.

6 G. Keglevich, H. Forintos, A. Szöllõsy and L. Tõke, *Chem. Commun.*, 1999, 1423; G. Keglevich, H. Forintos, A. Szöllõsy and L. Tõke, *Tetrahedron*, 2000, 4823.

7 Yu. G. Gololobov, I. N. Zhmurova and L. F. Kasukhin, *Tetrahedron*, 1981, **37**, 437; Yu. G. Gololobov and L. F. Kasukhin, *Tetrahedron*, 1992, **48**, 1353.

8 J. Bellan, M. Sanchez, M.-R. Marre and A. M. Bertrand, *Bull. Soc. Chim. Fr.*, 1985, 491; J. Barluenga, F. López and F. Palacios, *J. Chem. Soc., Chem. Commun.*, 1985, 1681; J. Barluenga, F. Lopez and F. Palacios, *J. Chem. Soc., Perkin Trans. 1*, 1989, 2273; E. Anders and F. Markus, *Chem. Ber.*, 1989, **122**, 119; F. Palacios, A. M. Ochoa de Retana and J. Pagalday, *Tetrahedron*, 1999, 14451; T. Uchiyama, T. Fujimoto, A. Kakehi and I. Yamamoto, *J. Chem. Soc., Perkin Trans. 1*, 1999, 1577.

9 A bidentate ligand, –$C_6H_4C(CF_3)_2O$–, developed by Martin for stabilizing hypervalent species, see: E. F. Perozzi, R. S. Michalak, G. D. Figuly, W. H. Stevenson III, D. B. Dess, M. R. Ross and J. C. Martin, *J. Org. Chem.*, 1981, **46**, 1049.

10 For tricoordinate and tetracoordinate 1,2-azaphosphetines, see: (*a*) K. Bieger, J. Tejeda, R. Réau, F. Dahan and G. Bertrand, *J. Am. Chem. Soc.*, 1994, **116**, 8087; (*b*) D. Lentz, M. Anibarro, D. Preugschat and G. Bertrand, *J. Fluorine Chem.*, 1998, **89**, 73.

11 N. Kano, J.-H. Xing, A. Kikuchi and T. Kawashima, *Heteroat. Chem.*, 2001, **12**, 282.

12 N. Kano, X. J. Hua, S. Kawa and T. Kawashima, *Tetrahedron Lett.*, 2000, **41**, 5237.

13 T. Kawashima, T. Soda and R. Okazaki, *Angew. Chem., Int. Ed. Engl.*, 1996, **35**, 1096.

14 The pentacoordination characters, %TBP_a and %TBP_e, are used as indicators of the structure about the central element in terms of the percentage TBP geometry along a tetrahedron→TBP reaction coordinate based on the apical–element–equatorial bond angles and equatorial-element-equatorial bond angles, respectively, see: K. Tamao, T. Hayashi, Y. Ito and M. Shiro, *Organometallics*, 1992, **11**, 2099. According to the private discussion with K. Tamao, the equation of the definition of %TBP_e should be replaced by eqn. (1)

$$\%TBP_e = \left\{\frac{1}{3}\left(\sum_{n=1}^{3}\varphi_n\right) - 109.5\right\} \Big/ (120 - 109.5) \times 100 \qquad (1)$$

where φ_n is the angle L_{eq}–E–L_{eq}. E and L_{eq} in this case are P1 and C(x) (x = 1, 3 and 4) atoms, respectively.

15 I. Granoth and J. C. Martin, *J. Am. Chem. Soc.*, 1979, **101**, 4618.

16 T. Kawashima, K. Kato and R. Okazaki, *J. Am. Chem. Soc.*, 1992, **114**, 4008; T. Kawashima, K. Kato and R. Okazaki, *Angew. Chem., Int. Ed. Engl.*, 1993, **32**, 869.

17 T. Saito, M. Nakane, T. Miyazaki and S. Motoki, *J. Chem. Soc., Perkin Trans. 1*, 1989, 2140.

CHEMCOMM Communication
www.rsc.org/chemcomm

Enhanced acid stability of a reduced nicotinamide adenine dinucleotide (NADH) analogue

Philip L. Hentall, Nadine Flowers and Timothy D. H. Bugg*

Department of Chemistry, University of Warwick, Coventry, UK CV4 7AL.
E-mail: mssgv@warwick.ac.uk; Fax: 02476-524112; Tel: 02476-573018

Received (in Cambridge, UK) 23rd August 2001, Accepted 12th September 2001
First published as an Advance Article on the web 3rd October 2001

A methyl substituent at C-5 of the nicotinamide ring is found to confer increased acid stability in a reduced nicotinamide model (5–20 fold) and in a reduced dinucleotide coenzyme (2–3 fold), while retaining reactivity towards hydride transfer.

Nicotinamide adenine dinucleotide is a redox coenzyme used by a large family of dehydrogenase enzymes, operating *via* a hydride transfer mechanism.[1] Dehydrogenase enzymes have found applications as catalysts for biotransformations,[2] and also as analytical biosensors.[3] Although methods for re-cycling of NADH have been developed for large scale biotransformations,[4] one major limitation of NADH and NADPH for biotechnological applications is their instability in aqueous solution. Under neutral and acidic conditions, NADH decomposes *via* general acid-catalysed protonation at C-5 ($t_{1/2}$ 2–24 h), and nucleophilic attack upon the resulting imine, as shown in Scheme 1.[5]

Model studies have shown that dihydronicotinamide analogues in which the 5,6-double bond is fused to a benzene ring,[6] or to a heterocyclic ring,[7] possess increased stability towards acid-catalysed decomposition, but the effects of such modifications in a dinucleotide coenzyme analogue have not been reported. As part of a study of bio-electrochemical applications of engineered dehydrogenase enzymes, we required a dinucleotide analogue of NADH that showed enhanced stability in aqueous solution, but which might also be accepted into dehydrogenase active sites. We describe here a simple modification to the nicotinamide skeleton, which confers increased acid stability in a nicotinamide model, and in a dinucleotide coenzyme.

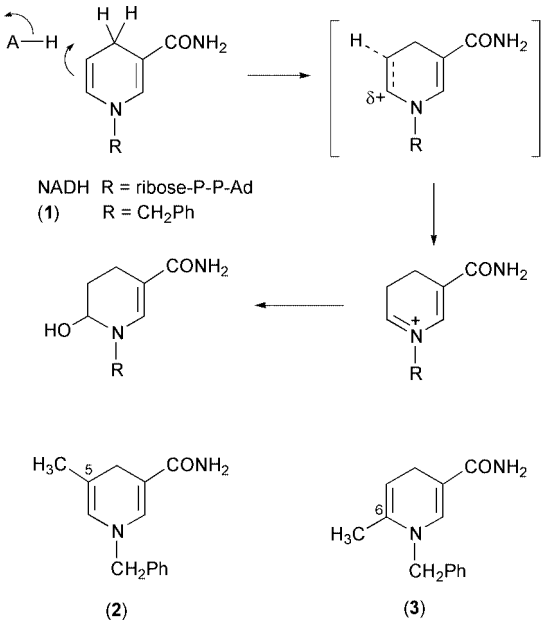

Scheme 1 Mechanism for acid-catalysed decomposition of dihydronicotinamide cofactors (ref. 5).

In order to disfavour the protonation of the 5,6-double bond of reduced nicotinamide, we investigated the effect of substituting the C-5 or C-6 position with a methyl substituent. 5-Methylnicotinamide, prepared as described by Kyba *et al.*,[8] and 6-methylnicotinamide were converted to their respective *N*-benzyl derivatives, and reduced to the corresponding *N*-benzyldihydronicotinamides (**2**) and (**3**) by treatment with sodium dithionite.[9] Their stability in aqueous buffers was then compared with *N*-benzyldihydronicotinamide (BNAH, **1**). The decomposition of 0.2 mM solutions of each compound was monitored at the respective λ_{max} as described in Table 1.

In each case the rate of decomposition was found to increase with decreasing pH, indicating an acid-catalysed process. Higher rates of decomposition were found in phosphate buffer, which is known to accelerate the decomposition of NADH.[5] In each case the presence of a 5-methyl substituent led to a 5–20 fold decreased rate of decomposition, whereas the presence of a 6-methyl substituent led to a 30–70 fold increased rate of decomposition. The instability of the 6-methyl analogue (**3**) can be rationalised by the electron-donating effect of the methyl substituent upon C-6 of the nicotinamide ring, where a partial positive charge would accumulate in the transition state for protonation at C-5 (see Scheme 1). Therefore, the stabilising effect of the 5-methyl group must be due primarily to steric hindrance of attack at C-5, rather than electronic effects.

The reactivity of dihydronicotinamides (**1**)–(**3**) towards hydride transfer was assessed by reaction of 10 mM solutions in dry acetonitrile with 10 equiv. *p*-trifluorobenzaldehyde and 1 equiv. $Mg(ClO_4)_2$ at 25 °C, monitoring the disappearance of reduced nicotinamide by reverse phase HPLC *vs.* time. The half-life for reaction of BNAH (**1**) was 6 h, whereas half-lives of 1.5 h and 3.5 h were measured for (**2**) and (**3**) respectively. Therefore, no loss of chemical reactivity is observed upon addition of a methyl substituent to the 5- or 6-positions; in fact the substituted analogues are somewhat more reactive.

The same modification was then introduced into a dinucleotide analogue of NADH (see Scheme 2), using the enzyme NAD^+ glycohydrolase to catalyse the exchange of nicotinamide with an unnatural substituted nicotinamide.[10] Incubation of 0.2 g 5-methylnicotinamide with 1 unit porcine brain NAD^+ glycohydrolase and 0.2 g NAD^+ in 100 mM potassium phosphate buffer pH 7.5 for 16 h at 37 °C gave a reaction mixture containing 5:1 5-methyl-NAD^+:NAD^+. The two dinucleotides were separated by reverse phase HPLC,† and the 5-methyl NAD^+ purified preparatively. Reduction of 5-methyl NAD^+ to 5-methyl-NADH (**4**) was achieved by treatment with sodium dithionite, followed by ethanol precipitation.

The decomposition of 0.1 mM 5-methyl-NADH (**4**) was assessed in 50 mM MES buffer pH 5.5–6.5 and 50 mM potassium phosphate buffer pH 6.0–7.0, and was compared with NADH under the same conditions (see Table 1). Dinucleotides NADH and (**4**) were in general more stable than the *N*-benzylnicotinamide analogues (**1**)–(**3**), perhaps due to the folded conformation adopted by the dinucleotide in water,[11] which would offer some protection of the 5,6-double bond. Rates of

 DOI: 10.1039/b107634p

Table 1 Half-lives for stability of reduced nicotinamides (**1**)–(**3**) and reduced dinucleotide coenzymes NADH and 5-methyl-NADH (**4**). Assays were carried out in 50 mM ammonium acetate buffer pH 5.0, 50 mM MES buffer pH 5.5–6.5, or 50 mM potassium phosphate buffer pH 6.0–7.0, at 25 °C, at a final concentration of 0.1–0.2 mM dihydronicotinamide. Decomposition was monitored at the appropriate λ_{max} (**1**, 355 nm; **2**, 360 nm; **3**, 350 nm; NADH, 340 nm; **4**, 345 nm), and first order half-life determined from a plot of lnA *vs.* time

		Half-life/min			Ratio $t_{1/2}/t_{1/2}$(**1**)		Half-life/h		Ratio
Buffer	pH	BNAH (**1**)	5-methyl (**2**)	6-methyl (**3**)	5-methyl (**2**)	6-methyl (**3**)	NADH	5-methyl (**4**)	$t_{1/2}/t_{1/2}$(NADH)
Acetate	5.0	6.1	134	0.11	21.9	0.018	2.0	5.7	2.8
MES	5.5	66	490	2.0	7.4	0.030	18.2	51.2	2.8
MES	6.0	89	820	2.9	9.2	0.033	40.4	106	2.6
MES	6.5	220	1570	5.9	7.1	0.027	86.2	191	2.2
KP_i	6.0	30.5	153	0.44	5.0	0.015	16.2	50.0	3.1
KP_i	6.5	39.3	483	0.52	12.3	0.013	31.1	68.4	2.2
KP_i	7.0	63.0	1010	0.81	16.0	0.013	48.8	145	3.0

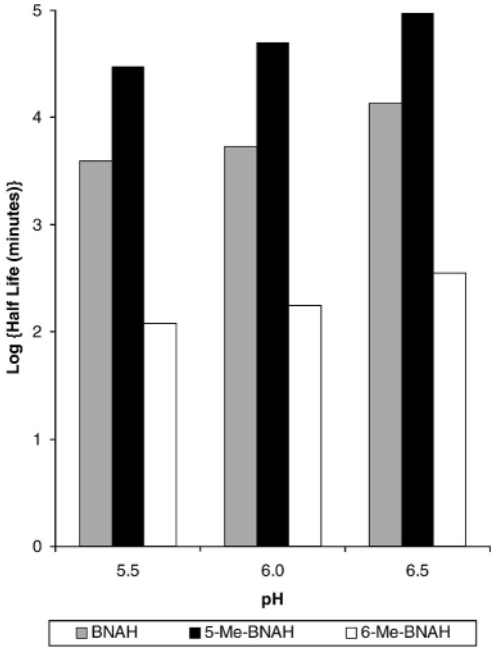

Fig. 1 Half-lives for first-order decomposition of dihydronicotinamides BNAH (**1**), 5-methyl-BNAH (**2**), and 6-methyl-BNAH (**3**) in 50 mM MES buffer pH 5.5, 6.0, and 6.0 at 25 °C.

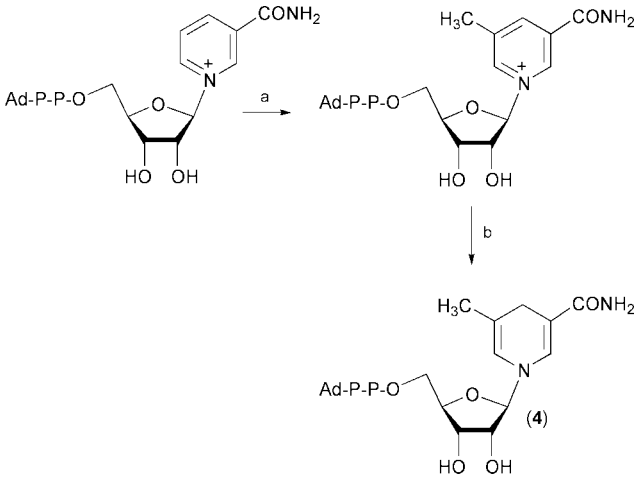

Scheme 2 Preparation of 5-methyl-NADH (**4**): a. 5-methylnicotinamide (5 equiv.), Porine brain NAD^+ glycohydrolase (1 units), 100 mM potassium phosphate pH 7.5; b. sodium dithionite (1.5 equiv.), sodium bicarbonate (1.5 equiv.), H_2O.

decomposition were again higher in more acidic buffer, consistent with an acid-catalysed decomposition mechanism. 5-Methyl-NADH (**4**) showed 2–3-fold increased stability, relative to NADH, in 50 mM MES buffer pH 5.5–6.5 and in 50 mM potassium phosphate buffer pH 6.0–7.0 (see Table 1). Thus, the stabilising effect of the 5-methyl substituent is also observed in the dinucleotide series, but is less marked than in the *N*-benzylnicotinamide series.

5-Methyl-NADH (**4**) was found to support the turnover of pyruvate by rabbit muscle L-lactate dehydrogenase, but at reduced catalytic efficiency (k_{cat} 0.0028 s^{-1}; K_M 55 μM; k_{cat}/K_M 50 M^{-1} s^{-1}) compared with NADH (k_{cat} 14 s^{-1}; K_M 7.0 μM; k_{cat}/K_M 2.0 × 10^6 M^{-1} s^{-1}), implying that the native enzyme is selective for the bound cofactor. Nevertheless, it is realistic to suggest that protein engineering could be used to design dehydrogenase enzymes capable of more efficient turnover of modified cofactors.

In summary, the introduction of a methyl group into the 5-position of the nicotinamide ring is shown to confer enhanced stability in aqueous buffers, due to the shielding of the 5,6-double bond from protonation. The same effect has been demonstrated in a dinucleotide coenzyme, which, although smaller in magnitude than in a nicotinamide model, demonstrates the feasibility of designing redox coenzymes of improved stability, which could be of considerable utility for biotechnological applications.

The authors thank the Office of Naval Research (Grant N00014-98-1-0898) for financial support, Dr H. Bright (ONR) and Dr A. Ellington (University of Texas at Austin) for helpful discussions, and Christopher Beadle (University of Southampton) for preliminary work.

Notes and references

† HPLC retention times 11.2 min for 5-methyl-NAD^+, 9.9 min for NAD^+ on Phenomenex ODS C_{18} reverse phase column, eluted from H_2O–0.1% CF_3COOH to 15% MeCN–0.1% CF_3COOH over 18 min at flow rate 0.8 ml min^{-1}.

1 T. D. H. Bugg, *An Introduction to Enzyme and Coenzyme Chemistry*, Blackwells Science, Oxford, 1997, pp. 108–113.
2 C. H. Wong and G. M. Whitesides, *Enzymes in Synthetic Organic Chemistry*, 1994, Pergamon Press, Oxford, pp. 131–194.
3 P. C. Pandey, S. Upadhyay, B. C. Upadhyay and H. C. Pathak, *Anal. Biochem.*, 1998, **260**, 195; A. K. Williams and J. T. Hupp, *J. Am. Chem. Soc.*, 1998, **120**, 4366; P. Jaraba, L. Agui, P. Yanez-Sedeno and J. M. Pingarron, *Electrochimica Acta*, 1998, **43**, 3555; R. J. Olson-Cosford and W. G. Kuhr, *Anal. Chem.*, 1996, **68**, 2164; M. Stredansky, A. Pizzariello, S. Stredanska and S. Miertus, *Anal. Commun.*, 1999, **36**, 57.
4 Z. Shaked and G. M. Whitesides, *J. Am. Chem. Soc.*, 1980, **102**, 7104.
5 N. J. Oppenheimer and N. O. Kaplan, *Biochemistry*, 1974, **13**, 4675; C. H. Wong and G. M. Whitesides, *J. Am. Chem. Soc.*, 1981, **103**, 4890.
6 S. Shinkai, H. Hamada, Y. Kusano and O. Manabe, *J. Chem. Soc., Perkin Trans. 2*, 1979, 699.
7 J. Cazin, G. Dupas, J. Bourgignon and G. Queguiner, *Tetrahedron Lett.*, 1986, **27**, 2375.
8 E. P. Kyba, S. T. Liu, K. Chuckalingam and B. R. Reddy, *J. Org. Chem.*, 1988, **53**, 3513.
9 J. D. Bossaerts, R. A. Dommisse, F. C. Alderweireldt and P. Geerlings, *J. Chem. Res. (M)*, 1987, 2355.
10 B. M. Anderson, C. J. Ciotti and N. O. Kaplan, *J. Biol. Chem.*, 1959, **234**, 1228; J. P. Samama, A. D. Wrixon and J. F. Biellmann, *Eur. J. Biochem.*, 1981, **118**, 479.
11 N. J. Oppenheimer, L. J. Arnold and N. O. Kaplan, *Proc. Natl. Acad. Sci. USA*, 1971, **68**, 3200.

CHEMCOMM
Communication
www.rsc.org/chemcomm

Porous clay heterostructures with enhanced acidity obtained from acid-activated clays

Mark Pichowicz and Robert Mokaya*

School of Chemistry, University of Nottingham, University Park, Nottingham, UK NG7 2RD. E-mail: r.mokaya@nottingham.ac.uk

Received (in Cambridge, UK) 24th July 2001, Accepted 5th September 2001
First published as an Advance Article on the web 1st October 2001

Porous clay heterostructures (PCHs) with enhanced acidity may be prepared from suitably acid-activated montmorillonite clays; the higher acidity arises from Brønsted acid sites generated by acid treatment of the clay prior to its use as a host for PCH formation.

Over the past decade, extensive research has been undertaken in the synthesis of porous inorganic materials, which may be used as heterogeneous catalysts, adsorbents or as hosts for composite materials. Examples are the synthesis of pillared clays and mesoporous molecular sieves.[1–3] A recent class of clay based high surface area, porous materials are porous clay heterostructures (PCHs).[4] In the synthesis of a PCH, the clay is firstly opened up by the introduction of an ionic surfactant (*via* a cation exchange reaction) thus allowing easier access to the interlayer region.[4] Neutral amine co-surfactant molecules are then intercalated along with silica species, which leads to self-assembly of the silica into a porous network within the interlayer region. This gives an interlayer silica structure similar to that of MCM-41 molecular sieves.[4,5] The synthesis of PCHs was first reported using a fluorohectorite clay with a high cation exchange capacity (CEC).[4,6,7] A host clay with a high CEC was considered essential for the formation of PCHs.[4,6,7] However, more recently PCHs have been successfully synthesised from saponites and montmorillonites.[8,9] PCHs have been shown to act as solid acid catalysts;[6] their acidity arises from the clay and also from protons which are released during the silica polymerisation reaction to balance the layer charge of the clay. The acidity of PCHs may be improved *via* post-synthesis grafting of Al[9] or by using saponite clays with a high (tetrahedrally coordinated) Al content.[8] Here we explore the possibility of enhancing the acidity of PCHs by using acid-activated clays as hosts for the formation of porous acid-activated clay heterostructures (PAACHs). Since most of the (Brønsted) acid sites on PCHs are associated with the layers of the clay, we have attempted to enhance the acidity of the host matrix by acid treatment prior to PCH formation.

It is known that the number of matrix protons (on clay sheets), not associated with the interlayer cation, may be increased by acid treatment.[10,11] We have previously synthesised pillared acid-activated clays (PAACs) derived from an acid treated clay matrix and shown that due to the acidic nature of the host matrix, PAACs exhibit significantly different characteristics compared to conventional pillared clays and that they are superior (to conventional pillared clays) in terms of their acidity and catalytic activity for acid catalysed reactions.[12,13] We show here that high surface area PCH materials with enhanced acidity may be prepared from suitably acid-activated clays. The lower CEC of the acid-activated clay does not seem to affect the formation of a porous clay heterostructure.

The starting raw clay used was a Peruvian montmorillonite with a CEC of 91 meq (100 g)$^{-1}$, a basal (001) spacing of 15.4 Å and an anhydrous structural (layer) formula: $[Si_{7.86}Al_{0.14}]$-$[Al_{2.84}Fe_{0.30}Mg_{0.86}]O_{20}(OH)_4$. The raw clay was acid treated as previously described[11–13] to yield an acid-activated clay with a CEC of 71 meq (100 g)$^{-1}$ and a basal spacing of 15.5 Å. We were careful to ensure that the level of acid treatment was such that the acid-activated clay retained a layered structure and a substantial CEC. PCHs were prepared as follows: the clay (raw or acid-activated) was suspended in water (100 cm^3 per g clay) to which 0.5 M cetyltrimethylammonium bromide (CTAB) was added in a two fold excess of the clay CEC. The clay/CTAB suspension was stirred for 24 hours at 50 °C following which the clay was recovered by filtration and washed with deionised water to remove excess CTAB (*i.e.* until pH 7 was reached) and air dried overnight. The CTAB intercalated clay (Q^+-clay) was then stirred in neutral primary amine (octylamine or decylamine) at room temperature for 20 minutes following which tetraethylorthosilicate (TEOS) was added and the resulting suspension stirred for a further 3 hours. The final synthesis gel mixture had the molar ratio: Q^+-clay : amine : TEOS of 1 : 2 : 12. The precursor PCH was then recovered by filtration, air dried overnight and calcined at 650 °C for 5 hours. The final samples were designated PCH (from raw clay) or PAACH (from acid-activated clay) followed by C8 or C10 in parentheses to denote the use of octylamine or decylamine, *e.g.* PAACH(C8) is derived from acid activated clay using octylamine.

The CTAB solvated Q^+-clays from both the raw and acid-activated clays had basal spacings of *ca.* 22 Å; an increase in interlayer spacing of 6.5 Å. On intercalation of TEOS the basal spacings increased further to between 35–40 Å and then decreased slightly on calcination. Fig. 1 shows a representative powder XRD pattern obtained for calcined PAACH(C8). It is clear that the interlayer space is greatly expanded and that the layered structure of the clay is retained as indicated by the presence of higher order peaks. It is worth noting that, in the present case, the basal peak for PAACH samples (see Fig. 1) was much more clearly defined compared to that of PCH samples. We however also note that, during calcination, the removal of the organic matter was far quicker for PAACHs samples than for PCH samples. The PCH samples required calcination for 16 hours (at 650 °C) to totally remove the organic matter and obtain an off-white sample while a heating time of 5 hours was sufficient for PAACHs. This may suggest that PAACHs are more reactive (acidic) and therefore more readily catalyse the decomposition and removal of organic

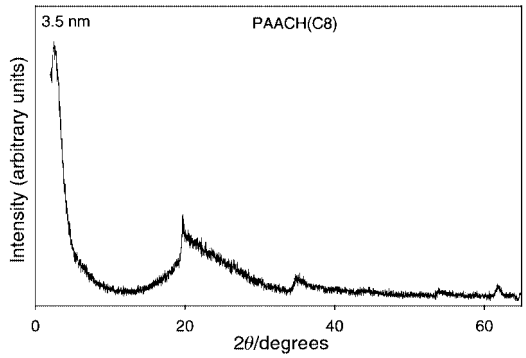

Fig. 1 A representative powder XRD pattern of a porous clay heterostructure (PAACH(C8)) derived from an acid-activated montmorillonite clay.

 DOI: 10.1039/b106660a

matter. Another possibility is that the more flexible acid-activated layers of the precursor PAACH allow easier removal (diffusion) of the organic matter; the assumption here is that acid activation disrupts the rigidity of the clay layers by removing some metal ions resulting in layers that are more structurally flexible. The manner and ease with which the organic matter is removed during calcination may therefore contribute to structural differences between PCH and PAACH that are reflected in the intensity of their basal peaks. We however note that calcining the precursor PAACH for 16 instead of 5 hours did not alter the properties of the final PAACH.

Table 1 shows the textural data obtained for PCHs and PAACHs. The PCH samples have surface area of *ca*. 800 m^2 g^{-1} while the acid-activated clay derived samples have higher surface area of 915 m^2 g^{-1} for PAACH(C8) and 951 m^2 g^{-1} for PAACH(C10). All the samples however have comparable pore volumes. The surface areas of the present materials are generally higher than that of fluorohectorite-PCH[6] but comparable to those of saponite and montmorillonite derived PCHs.[8,9] The pore volumes observed here (0.71 to 0.82 cm^3 g^{-1}) are similar to those of montmorillonite and saponite derived PCHs prepared by Ahenach *et al*.[9] but higher than that of saponite-PCH reported by Polverejan *et al*.[8] This is not unexpected since the synthesis method used here was similar to that of Ahenach *et al*.[9] The chain length of the neutral amine used has no influence on the surface area. However, using a longer chain amine (decylamine, C10) results in a slightly higher pore volume. The N_2 sorption isotherms obtained here for the PCH and PAACH materials are shown in Fig. 2. The isotherms are similar to those previously reported for PCHs.[8,9] A gradual increase in N_2 adsorption at low to medium partial pressures suggests that the materials possess supermicropores and small mesopores. The hysteresis loops are characteristic of cylindrical pores which are open at both ends, or of spaces between parallel plates, which is consistent with the structure of PCHs.[4] It is worth noting that the isotherms in Fig. 2 are significantly different from those exhibited by so-called silica bonded montmorillonite, SBM.[14]

The textural properties discussed above clearly illustrate that PCHs can be obtained using acid-activated clays as hosts. The acid contents of the present PCHs and PAACHs are given in Table 1. The acid content was determined using thermally programmed desorption of cyclohexylamine (CHA) as previously described.[15,16] Prior to thermogravimetric analysis, the base-containing samples were heated at 80 °C for 2 hours. The weight loss due to amine desorption from acid sites between 200 and 420 °C was used to quantify the acidity in mmol of CHA, assuming that each base molecule interacts with one Brønsted acid site. The total acid content (desorption between 200 and 420 °C) of PAACH is at least 30% higher than that of PCH. Furthermore the number of medium to strong acid sites (desorption between 300 and 420 °C) for PAACH is almost twice that of PCH. This suggests that the higher acidity in PAACHs is mainly due to an increase in the number of medium to strong acid sites. This is expected to have positive implications for the use of PAACHs as solid acid catalysts. We propose that the higher/stronger acid content of PAACHs is a consequence of the enhanced acidity on the clay sheets (after acid treatment) used for PAACH formation. It is also possible that some loose Al, present in the host acid-activated clay, is incorporated into the interlayer silica network. We are currently investigating the effect of using aluminosilicate rather than silica sources for PCH formation and anticipate that even higher acidity can be obtained if acid-activated saponites are used as hosts or by combining an acid activated host matrix (saponite or montmorillonite) with an aluminosilicate interlayer structure. The findings reported here open new opportunities for the preparation of acidic PCHs where the acidity can be optimised by varying the nature of the host clay and/or the type of interlayer network.

Table 1 Textural properties and acidity of porous clay heterostructures derived from raw montmorillonite (PCH) and acid-activated montmorillonite (PAACH) clays

Sample	Surface area/m^2 g^{-1}	Pore volume/cm^3 g^{-1}	Acidity[a]/mmol CHA g^{-1}
PCH(C8)	795	0.75	0.54 (0.14)
PCH(C10)	782	0.82	0.56 (0.15)
PAACH(C8)	915	0.71	0.71 (0.25)
PAACH(C10)	951	0.78	0.74 (0.27)

[a] Total acid content obtained from weight loss between 200 and 420 °C. Values in parentheses are the amounts of medium to strong acid sites obtained from weight loss between 300 and 420 °C.

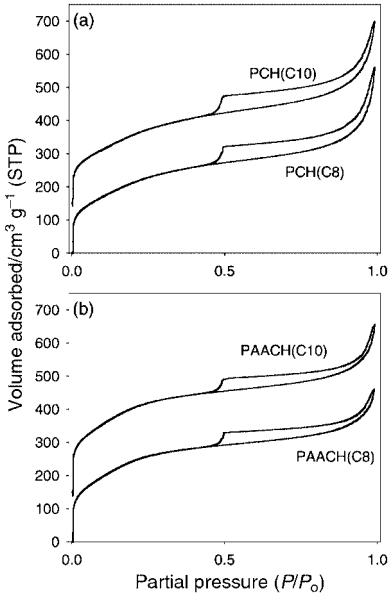

Fig. 2 Nitrogen sorption isotherms of porous clay heterostructures: (a) PCH, derived from a raw montmorillonite clay and (b) PAACH, derived from an acid-activated montmorillonite clay. C8 and C10 denote the use of octylamine or decylamine respectively as co-surfactant. For clarity, the isotherms of PCH(10) and PAACH(10) are offset (*y* axis) by 150.

R. M. is grateful to the EPSRC for an Advanced Fellowship. We are also grateful to S. Sajidu (University of Cambridge) for some of the acidity measurements.

Notes and references

1 A. Gil, L. M. Gandia and M. A. Vicente, *Catal. Rev. Sci. Eng*., 2000, **42**, 145.
2 J. Y. Ying, C. P. Mehnert and M. S. Wong, *Angew. Chem., Int. Ed*., 1999, **38**, 56.
3 G. Øye, J. Sjöblom and M. Stöcker, *Adv. Colloid. Interface Sci*., 2001, **89–90**, 439.
4 A. Barodawalla, A. Galarneau and T. J. Pinnavaia, *Nature*, 1995, **374**, 529.
5 C. T. Kresge, M. E. Leonowicz, W. J. Roth, J. C. Vartuli and J. S. Beck, *Nature*, 1992, **359**, 710.
6 A. Galarneau, A. Barodawalla and T. J. Pinnavaia, *Chem. Commun*., 1997, 1661.
7 L. Mercier and T. J. Pinnavaia, *Microporous Mesoporous Mater*., 1998, **20**, 101.
8 M. Polverejan, T. R. Pauly and T. J. Pinnavaia, *Chem. Mater*., 2000, **12**, 2698.
9 J. Ahenach, P. Cool and E. F. Vansant, *Phys. Chem. Chem. Phys*., 2000, **2**, 5750.
10 R. Mokaya and W. Jones, in *ION-EX 93, Proceedings of conference on Ion Exchange Materials*, ed. A. Dyer, M. J. Hudson and P. A. Williams, Special Publication 122, Royal Society of Chemistry, Cambridge, 1993, p. 243.
11 R. Mokaya, W. Jones, M. E. Davies and M. E. Whittle, *J. Solid State Chem*., 1994, **111**, 157.
12 R. Mokaya and W. Jones, *J. Chem. Soc., Chem. Commun*., 1994, 929.
13 R. Mokaya and W. Jones, *J. Catal*., 1995, **153**, 76.
14 S. Kawi and Y. Z. Yao, *Microporous Mesoporous Mater*., 1999, **28**, 25.
15 C. Breen, *Clay Miner*., 1991, **26**, 487.
16 R. Mokaya, W. Jones, S. Moreno and G. Poncelet, *Catal. Lett*., 1997, **49**, 87.

CHEMCOMM Communication
www.rsc.org/chemcomm

Alkane oxidation by a carboxylate-bridged dimanganese(III) complex

Gonzalo Blay,[a] Isabel Fernández,[a] Tomás Giménez,[a] José R. Pedro,*[a] Rafael Ruiz,[a] Emilio Pardo,[b] Francesc Lloret[b] and M. Carmen Muñoz[c]

[a] *Departament de Química Orgànica, Facultat de Química, Universitat de València, 46100 Burjassot, València, Spain. E-mail: jose.r.pedro@uv.es*
[b] *Departament de Química Inorgànica, Facultat de Química, Universitat de València, 46100 Burjassot, València, Spain*
[c] *Departamento de Física Aplicada, Universidad Politécnica de València, 46071 València, Spain*

Received (in Cambridge, UK) 12th June 2001, Accepted 6th September 2001
First published as an Advance Article on the web 1st October 2001

A new manganese(III) oxamato dimer possesing an unprecedented $Mn_2(\mu\text{-}O_2CR)(\mu\text{-}OH_2\cdots O_2CR)$ core has been synthesised, structurally and magnetically characterised, and used as a catalyst for the oxidation of alkanes to alcohols and ketones by Bu^tO_2H and O_2 in CH_2Cl_2 at rt.

The past two decades have seen a considerable interest in manganese redox enzymes, particularly those containing carboxylate-bridged dinuclear active sites.[1] Among them, the less well understood but functionally important is manganese ribonucleotide reductase (MnRR), which catalyses the dioxygen-dependent reduction of ribonucleotides to deoxyribonucleotides in certain groups of bacteria.[2] This key reaction for the synthesis of DNA initiates, however, with hydrogen atom abstraction from the furanose ring of the ribonucleotide substrate by a tyrosyl protein radical generated during the process of O_2 activation by the dimanganese center.[2c] Although no crystallographic data are yet available for the native manganese enzyme, a manganese-substituted inactive form of the more extensively studied iron ribonucleotide reductase (FeRR) has been isolated and structurally characterised.[3] In this case, two Mn^{II} ions are doubly-bridged by two bidentate carboxylates of glutamato protein residues at a separation of 3.6 Å.[3b] That being so, studies concerning the reactivity of manganese model complexes bearing some structural features similar to those proposed for the different forms of the enzyme can help to understand the mechanism of conversion of ribonucleotides by MnRR.[4] Here we report on the synthesis and general physical characterisation,† crystal and molecular structure,‡ and magnetic properties of the manganese(III) dimer complex $(Ph_4P)_2[Mn_2(opba)_2(H_2O)_3]\cdot 3H_2O\cdot MeCN$ **1**, where opba is *o*-phenylenebis(oxamato). We also report a preliminary investigation of the catalytic activity of **1** towards the oxidation of hydrocarbons with alkyl hydroperoxides in the presence of dioxygen under mild conditions.

The structure of **1** consists of non-centrosymmetric dinuclear manganese(III) complex anions, $[Mn_2(opba)_2(H_2O)_3]^{2-}$ (Fig. 1), tetraphenylphosphonium cations and both water and acetonitrile solvent molecules. The coordination environment about each Jahn–Teller-elongated octahedral manganese atom is formed by two amide nitrogen and two carboxylate oxygen atoms of the tetradentate opba ligand defining the equatorial plane and with the two labile axial positions being occupied by water and/or carboxylate oxygen atoms. In fact, within the dinuclear unit, a carboxylate group from one planar [Mn(opba)] moiety is axially bound to the manganese atom from the other moiety (*syn–anti* bidentate bridging mode),[5] while a free carboxylate oxygen atom from the latter [Mn(opba)] fragment is hydrogen-bonded to an axial, manganese-bound water molecule of the former fragment [O(8)···O(14) separation of 2.702(9) Å]. This leads to an overall asymmetric doubly-bridged dimanganese(III) core which is reminiscent of the structure of the diiron(III) form of FeRR, but without the oxo bridge present therein.[3a] The Mn(1)···Mn(2) intramolecular separation through this unique nine-membered metallacyclic ring, $Mn^{III}_2(\mu\text{-}O_2CR)(\mu\text{-}OH_2\cdots O_2CR)$, in **1** is 5.693(3) Å. This is *ca.* 2.5 Å longer than the corresponding distance in the related triply-bridged $Mn^{III}_2(\mu\text{-}O)(\mu\text{-}O_2CR)_2$ species, which have been proposed as suitable structural models of the dimanganese(III) form of MnRR.[6]

The magnetic behaviour of **1** is typical of an antiferromagnetically-coupled dimanganese(III) pair. At room temperature, the product $\chi_M T$ (χ_M being the molar magnetic susceptibility per dinuclear unit and T the temperature) is equal to 6.0 $cm^3\ mol^{-1}$ K (6.9 μ_B), a value which is consistent with two Mn^{III} ($S = 2$) ions. Upon cooling, $\chi_M T$ continuously decreases from room temperature to 0.8 $cm^3\ mol^{-1}$ K (2.5 μ_B) at 2.0 K, whereas χ_M exhibits a characteristic maximum around 6.0 K, which unambiguously indicates a diamagnetic ground singlet ($S = 0$) pair spin state. The least-squares fitting of the magnetic susceptibility data gives $g = 2.00$ and $J = -2.0\ cm^{-1}$ (where $H = -JS_1\cdot S_2$; $S_1 = S_2 = 2$). The value of the exchange coupling parameter for **1** compares well with that found for other weakly coupled di(μ-carboxylato)dimanganese(II) complexes (J values of -1.4 and $-1.9\ cm^{-1}$).[7] On the other hand, this certainly weak, although non-negligible, antiferromagnetic coupling through the carboxylate bridge found in **1** emphasises the relative importance of the exchange pathways involving the bridging carboxylate groups for the analysis of the variations in the sign and the magnitude of the exchange coupling in (μ-oxo)di(μ-carboxylato)dimanganese(III) complexes (J values ranging from +18.0 to $-8.2\ cm^{-1}$).[6b]

The oxidation catalytic activity of **1** has been examined in a non-coordinating solvent like methylene chloride and at room temperature using *tert*-butyl hydroperoxide as oxidant under aerobic conditions. The results for some representative alkanes

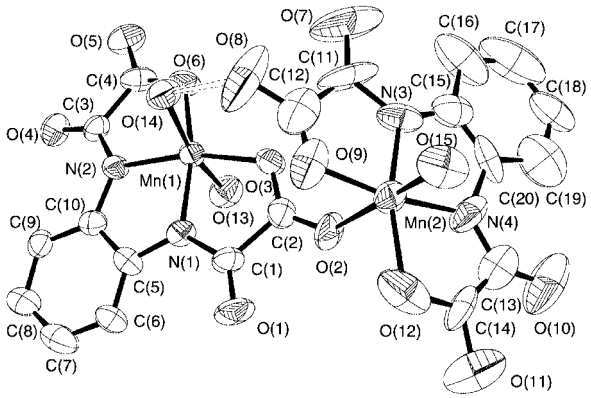

Fig. 1 Perspective view of the anionic dinuclear unit of **1** with the atom-numbering scheme (thermal ellipsoids are at the 50% probability level and hydrogen atoms have been omitted for clarity). Selected bond distances (Å) with standard deviations in parentheses: Mn(1)–N(1) 1.919(5), Mn(1)–N(2) 1.914(5), Mn(1)-O(3) 1.968(4), Mn(1)–O(6) 1.935(5), Mn(1)–O(13) 2.318(6), Mn(1)–O(14) 2.323(5), Mn(2)–N(3) 1.883(6), Mn(2)–N(4) 1.920(8), Mn(2)–O(9) 1.911(7), Mn(2)–O(12) 2.019(7), Mn(2)–O(15) 2.272(6), Mn(2)–O(2) 2.321(5).

 DOI: 10.1039/b105132f

Table 1 Results for the oxidation of alkanes and alkyl arenes catalysed by **1**[a,b]

Entry	Substrate	Product	Yield (%)[c]
1	Cyclohexane	Cyclohexanol	1.9 (3.5)[d]
		Cyclohexanone	2.2 (5.4)[d]
2	Adamantane	1-Adamantanol	8.0
		2-Adamantanol/one	1.0
3	Toluene	Benzaldehyde	3.1
		Benzoic acid	1.3
4	Ethylbenzene	1-Phenylethanol	4.2
		Acetophenone	16.9
5	Diphenylmethane	Benzhydrol	5.2
		Benzophenone	37.3

[a] Reactions were carried out at room temperature by adding a solution of the substrate (0.10 mmol) in CH_2Cl_2 (0.2 mL) to a stirred mixture of the metal catalyst (5.0×10^{-3} mmol) and Bu^tO_2H (0.30 mmol) in CH_2Cl_2 (0.2 mL) under an O_2 atmosphere for a period of 24 h. [b] In the absence of catalyst no oxidation was observed. [c] Yields refer to GLC determination based on the starting substrate. [d] With a reaction time of 72 h.

and alkyl arenes are summarised in Table 1. Complex **1** catalysed the oxidation of cyclohexane to the corresponding alcohol and ketone, cyclohexanol and cyclohexanone, respectively, with varying yields depending on the reaction time (entry 1). Interestingly, the cyclohexanol : cyclohexanone ratio dropped from 0.9 to 0.6 with longer reaction times, suggesting that secondary alcohols are further oxidised to ketones under the experimental conditions. It is also noteworthy that for our catalytic system the tertiary to secondary C–H bond relative reactivities (k_{tert}/k_{sec}; on a per bond basis) for the oxidation of adamantane was as high as 24 (entry 2). On the other hand, alkyl arenes such as toluene, ethylbenzene or diphenylmethane were oxidised selectively at the benzylic position to give the corresponding benzylic oxygenation products, and no traces of the corresponding aromatic ring hydroxylation products were detected by GLC analysis in any case. As expected, the oxidation of toluene gave some minor amounts of benzoic acid together with the main product benzaldehyde, whereas no benzyl alcohol was observed among the oxygenation products (entry 3). The oxidation of ethylbenzene and diphenylmethane afforded mixtures of the corresponding alcohol and ketone exclusively (entries 4 and 5, respectively). The total yields of benzylic oxygenation products followed the trend toluene < ethylbenzene < diphenylmethane (entries 3–5). Indeed, the oxidation efficiency along this series of alkyl arenes $PhCH_2R$ (R = H, Me, Ph) correlates directly with the C–H bond strength, thus suggesting that C–H bond cleavage is the rate-determining step of the catalytic cycle. Further kinetic studies are in progress to determine the detailed mechanism and the exact chemical nature of the active oxidant in these biomimetic oxidations.

This work was supported by the Dirección General de Enseñanza Superior e Investigación Científica (Spain) through projects PB97-1411 and PB97-1397. R. R. thanks the Ministerio de Ciencia y Tecnología (Spain) for a grant. We are specially thankful to Pedro Palanca for the assistance with the GLC measurements.

Notes and references

† *Synthesis and selected data*: to a solution of the diethyl ester derivative of the ligand (1.54 g, 5.0 mmol) in methanol (50 mL) was added a 25% methanol solution of Me_4NOH (8.0 mL, 20.0 mmol). Solid $Mn(MeCO_2)_3 \cdot 2H_2O$ (1.35 g, 5.0 mmol) was then added in small portions under stirring, and the resulting reaction mixture was further stirred for 15 min at room temperature. A brick-red microcrystalline solid formed abundantly which was collected by filtration and dried under vacuum. The filtered deep brown solution was reduced to a final volume of 25 mL in a rotatory evaporator. Upon standing at 4 °C in a refrigerator, a second crop of crystals separated from the concentrated solution which was also collected and dried (60%). Anal. Calc. for $C_{14}H_{16}MnN_3O_6 \cdot 2H_2O$: C 40.67, H 10.17, N 4.84. Found: C 41.05, H 9.91, N 5.12%. $(Me_4N)[Mn(opba)] \cdot 2H_2O$ (0.83 g, 2.0 mmol) was dissolved in water (50 mL) and the reaction mixture was filtered on paper to eliminate a small amount of solid particles. A solution of Ph_4PCl (0.75 g, 2.0 mmol) in acetonitrile (25 mL) was then added to the filtered deep brown aqueous solution. Well-shaped, brick-red elongated prisms of **1** suitable for X-ray diffraction were deposited after a few hours of slow evaporation at room temperature. They were filtered off and air-dried (90%). ν(KBr)/cm^{-1} 3422s (O–H) from H_2O, 2254w (C≡N) from MeCN, 1669vs and 1645vs (C=O), 1381s and 1280s (C–O) from opba. UV–Vis (MeCN) λ_{max}/nm: 210 (ε/L mol^{-1} cm^{-1} 1.4×10^5), 225 (sh), 260 (4.0×10^4), 275 (sh), 340 (9.4×10^3) and 410 (sh).

‡ *Crystal data for* $C_{70}H_{63}Mn_2N_5O_{18}P_2$: M = 1434.1, triclinic, space group $P\bar{1}$, a = 13.099(3), b = 15.446(3), c = 17.687(4) Å, α = 73.04(3), β = 79.94(3), γ = 80.84(3)°, U = 3348(1) Å^3, T = 293 K, Z = 2, μ(MoKα) = 0.50 mm^{-1}, 11 665 reflections measured, 7556 assumed as observed with $I \geq 2\sigma(I)$. Hydrogen atoms were located from a difference synthesis and refined with an overall isotropic thermal parameter. Refinement on F^2 of 875 variables with anisotropic thermal parameters for all non-hydrogen atoms gave R = 0.092 and wR = 0.251 with S = 0.94 (observed data).

CCDC reference number 166256. See http://www.rsc.org/suppdata/cc/b1/b105132f/ for crystallographic data in CIF or other electronic format.

1 N. A. Law, M. T. Caudle and V. L. Pecoraro, *Adv. Inorg. Chem.*, 1998, **46**, 305.
2 (*a*) G. S. Schimpff-Weiland, H. Follmann and G. Auling, *Biochem. Byophys. Res. Commun.*, 1981, **102**, 1276; (*b*) A. Willing, H. Follmann and G. Auling, *Eur. J. Biochem.*, 1988, **178**, 603; (*c*) U. Griepenburg, G. Lassmann and G. Auling, *Free Radical Res.*, 1996, **26**, 473.
3 (*a*) P. Nordlund, B. M. Sjöberg and H. Eklund, *Nature*, 1990, **345**, 593; (*b*) M. Atta, P. Nordlund, A. Aberg, H. Eklund and M. Fontecave, *J. Biol. Chem.*, 1992, **267**, 20682; (*c*) P. J. Riggs-Gelasco, L. Shu, S. Chen, D. Burdi, B. H. Huynh, L. Que, Jr. and J. Stubbe, *J. Am. Chem. Soc.*, 1998, **120**, 849.
4 R. Hage, *Recl. Trav. Chim. Pays-Bas*, 1996, **115**, 385; M. T. Caudle, P. Riggs-Gelasco, A. K. Gelasco, J. E. Penner-Hahn and V. L. Pecoraro, *Inorg. Chem.*, 1996, **35**, 3577; K. Wang and J. M. Mayer, *J. Am. Chem. Soc.*, 1997, **119**, 1470; R. Ruiz, A. Aukauloo, Y. Journaux, I. Fernández, J. R. Pedro, A. L. Roselló, B. Cervera, I. Castro and M. C. Muñoz, *Chem. Commun.*, 1998, 989; G. B. Shul'pin, G. Süss-Fink and L. S. Shul'pina, *J. Mol. Catal. A*, 2001, **170**, 17 and references cited therein.
5 R. L. Rardin, W. B. Tolman and S. J. Lippard, *New J. Chem.*, 1991, **15**, 417.
6 (*a*) K. Wieghardt, U. Bossek, B. Nuber, J. Weiss, J. Bonvoisin, M. Corbella, S. E. Vitols and J. J. Girerd, *J. Am. Chem. Soc.*, 1988, **110**, 7398; (*b*) J. B. Vincent, H. L. Tsai, A. G. Blackman, S. Wang, P. D. W. Boyd, K. Folting, J. C. Huffman, E. B. Lobkovsky, D. N. Hendrickson and G. Christou, *J. Am. Chem. Soc.*, 1993, **115**, 12 353; (*c*) T. Tanase and S. J. Lippard, *Inorg. Chem.*, 1995, **34**, 4682; (*d*) R. Ruiz, C. Sangregorio, A. Caneschi, P. Rossi, A. B. Gaspar, J. A. Real and M. C. Muñoz, *Inorg. Chem. Commun.*, 2000, **3**, 361.
7 H. Oshio, E. Ino, I. Mogi and T. Ito, *Inorg. Chem.*, 1993, **32**, 5697; J. Cano, G. De Munno, J. L. Sanz, R. Ruiz, F. Lloret, J. Faus and M. Julve, *J. Chem. Soc., Dalton Trans.*, 1994, 3465.

CHEMCOMM
Communication
www.rsc.org/chemcomm

Triprotic 2,4,6-tris(organoamino)-1,3,5-triazenes as precursors to multi-site triazenate ligands

Frederic Rivals and Alexander Steiner*

Department of Chemistry, University of Liverpool, Crown Street, Liverpool, UK L69 7ZD. E-mail: A.Steiner@liv.ac.uk

Received (in Cambridge, UK) 20th June 2001, Accepted 6th September 2001
First published as an Advance Article on the web 1st October 2001

2,4,6-Tris(2-fluoroanilino)-1,3,5-triazene successively undergoes one-, two- and three-fold deprotonation in the presence of Bu^{n}Li; the dilithiated triazenate exists as the dimeric complex (thf)$_6$Li$_4$[(RN)$_2$(RNH)C$_3$N$_3$]$_2$ in the solid state (R = 2-F-C$_6$H$_4$) featuring bidentate N$_{endo}$–C–N$_{exo}$ chelation sites.

The resemblance of monoanionic amidinates $[RC(NR)_2]^-$ [1] and bis-imino phosphinates $[R_2P(NR)_2]^-$ [2] in reaction and coordination behaviour corroborate the diagonal relationship between carbon and phosphorus. Both are sterically demanding, electron-rich bidentate chelates, which can be obtained from the protic precursor [RC(NR)(NHR)] and [R$_2$P(NR)(NHR)], respectively. Recently, we have shown that hexakis(organoamino)cyclotriphosphazenes $(RNH)_6P_3N_3$ act as multiprotic acids in the presence of strong bases yielding trianionic $[(RNH)_3(RN)_3P_3N_3]^{3-}$ and hexaanionic phosphazenates $[(RN)_6P_3N_3]^{6-}$.[3] Considering the diagonal C–P relationship, analogous triprotic 2,4,6-tris(organoamino)-1,3,5-triazenes **1**H$_3$ are expected to be metallated correspondingly to give anionic triazenates (Scheme 1), which promise interesting coordination modes, due to the potential three-fold symmetry of the anticipated multi-site ligands.

Here, we present initial lithiation studies of 2,4,6-tris(2-fluoroanilino)-1,3,5-triazene (**1**H$_3$), which was generated by the reaction of cyanuric chloride with an excess of 2-fluoroaniline. We monitored the reaction of **1**H$_3$ with Bu^{n}Li in THF using ^{1}H and ^{13}C NMR spectroscopy (Fig. 1). Upon addition of Bu^{n}Li the NH signal gradually shifts up-field and decreases in intensity until it vanishes once three equivalents of Bu^{n}Li have been added. The ^{13}C NMR shift of C(1) moves down-field from 127 in **1**H$_3$ to 144 ppm in Li$_3$**1**, and that of C(6) up-field from 124 (**1**H$_3$) to 115 ppm (Li$_3$**1**) (see Fig. 1 for numbering scheme). The signal of the ^{13}C nuclei of the central triazene ring shifts only slightly from 165 (**1**H$_3$) to 169 ppm (Li$_3$**1**). Throughout lithiation the ^{19}F NMR consists of a single peak, which also shifts only marginally from 130 to 132 ppm. Both ^{1}H and ^{13}C NMR of partially deprotonated species display only one set of signals for both 2-fluoroanilino and triazene moieties, indicating rapid proton transfer at room temperature. However, two sets of signals with an intensity ratio of 2:1 appear in the ^{13}C NMR spectrum of a THF solution containing the dilithiated species Li$_2$**1**H, which was recorded at −80 °C. The chemical shifts of the set of lower intensity are similar to the spectrum of **1**H$_3$ and can be attributed to the non-deprotonated anilino substituent, wheras those of the set of higher intensity, which resemble the pattern observed in the spectrum of Li$_3$**1**, are caused by the two deprotonated substituents. At −80 °C the ^{13}C nuclei of the triazene ring also give two resonances (at 164 and 169 ppm).

Single crystals were obtained from the reaction of **1**H$_3$ with two equivalents of Bu^{n}Li in THF. X-Ray structure determination revealed that two-fold deprotonation had occurred and the resulting Li$_2$**1**H exists as the centrosymmetric dimer (thf)$_6$Li$_4$(**1**H)$_2$ **2** in the solid state (Fig. 2).† Both ligands in **2** are linked by the two centrally arranged lithium ions (Li1, Li1a) forming an eight-membered [Li–N$_{exo}$–C–N$_{endo}$–]$_2$ ring core. In addition, Li1 and Li1a undergo weak cross-ring interactions to N$_{exo}$-sites and each is coordinated to an F-aryl atom and a thf molecule resulting in distorted trigonal bipyramidal coordination geometries. The other two lithium ions (Li2, Li2a) are accommodated in neighbouring N$_{exo}$–C–N$_{endo}$ chelates and are additionally coordinated to two thf molecules giving tetrahedral metal surroundings. **2** combines coordination modes of monomeric and dimeric lithium complexes of ligands featuring bidentate N–E–N chelates [E = (R)C,[4] (R$_2$)P,[5] (R)S[6]]. Li2

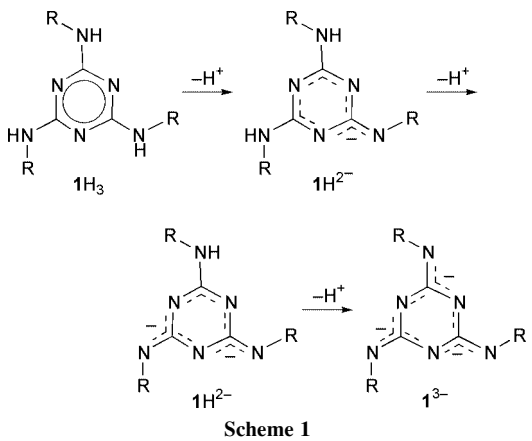

Scheme 1

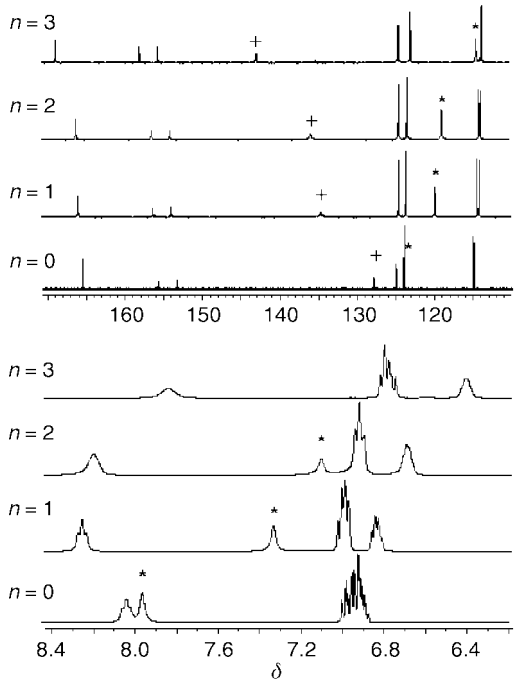

Fig. 1 ^{13}C NMR (top) and ^{1}H NMR (bottom) spectra of stepwise reaction of **1**H$_3$ with *n* equivalents of Bu^{n}Li in thf at 20 °C. In ^{13}C NMR '+' refers to the C(1) (= C–N) and '*' to the C(6) position of 2-fluoroaniline substitutents; in ^{1}H NMR '*' refers to the NH signal.

 DOI: 10.1039/b105435j

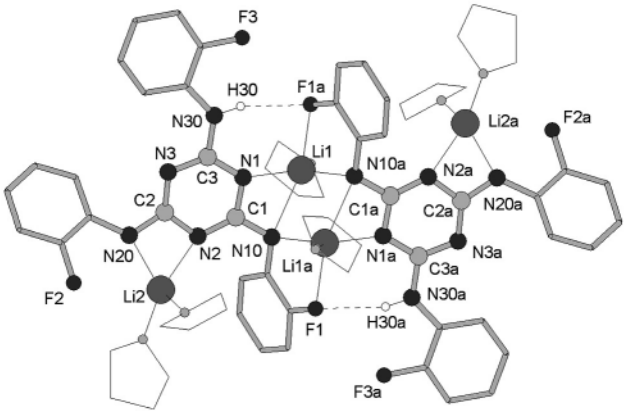

Fig. 2 X-Ray structure of **2**. Selected bond lenghts (Å) and angles (°): N1–C1 1.339(9), N1–C3 1.351(9), N2–C1 1.343(9), N2–C2 1.359(9), N3–C3 1.336(9), N3–C2 1.341(9), C1–N10 1.353(9), C2–N20 1.334(9), C3–N30 1.374(10), Li1–N1 2.03(2), Li1–N10 2.32(2), Li1–N10a 2.07(2), Li1–F1a 2.15(2), Li2–N2 2.11(2), Li2–N20 1.99(2), Li2···F2 3.072(15); C1–N1–C3 113.1(7), C1–N2–C2 115.7(7), C2–N3–C3 114.3(7), N1–C1–N2 125.5(8), N2–C2–N3 124.0(8), N3–C3–N1 127.3(7), N1–C1–N10 111.6(8), N2–C2–N20 110.5(7), N3–C3–N30 118.5(8).

corresponds to the 'monomeric' mode, where the lithium ion is chelated by a single N–E–N unit, and Li1 to the often encountered N–E–N dimer mode, where two ligands encapsulate two lithium ions in both mono- and bi-dentate fashion. A similar motif is observed in the polymeric trilithium salt of trithiocyanuric acid.[7]

In contrast to phosphazenates, where the metallation causes a marked impact on the structural parameters of the central P_3N_9 core, bonding parameters within the central C_3N_6 ligand core of **2** are not very much affected upon metallation. The C–N_{exo} bond involving the non-metallated anilino group is only marginally longer [C3–N30 1.374(10) Å] than those of the deprotonated substituents [C1–N10 1.353(9), C2–N20 1.334(9) Å], which are of similar lengths as C–N_{endo} bonds ranging from 1.336(9) to 1.359(9) Å. Accordingly, in neutral 2,4,6-tris-(amino)-1,3,5-triazenes C–N_{exo} bonds are on average only 0.02 Å longer than C–N_{endo} bonds.[8]

1H_3 is deprotonated without undergoing side reactions. The lithiation is reversible as **1**H_3 is recovered after protolysis of Li_3**1**. On the other hand, 1,3,5-triazene and 2,4,6-tris(organo)-1,3,5-triazenes are prone to nucleophilic attack by organolithium reagents at C_{endo} positions, which leads to either nucleophilic addition, substitution or ring cleavage.[9] F(aryl) functions in **2**, initially introduced to act as ^{19}F NMR spectator sites, are inert on lithiation. The absence of line broadening of ^{19}F signals indicates that there are no considerable ^{7}Li–^{19}F interactions in solution.

The electron deficiency of the central C_3N_3 ring in **1**$^{3-}$ is compensated for by the π-donating character of exocylic N centres, which allow delocalisation of negative charge across the entire C_3N_6 core. In contrast to the non-aromatic tri- and hexa-anionic triphosphazenates, triazenates H**1**$^{2-}$ and **1**$^{3-}$ feature an aromatic ligand core. This enables electronic interaction between accommodated metal centres across the aromatic ligand system. In addition, the D_{3h} symmetry of the C_3N_6 ligand core and the straightforward introduction of organo amino groups with various functionalities promise the generation of metal complexes with interesting properties.

This work was supported by the EPSRC and the Royal Society.

Notes and references

† *Crystal data* for **2**·C_4H_8O·C_6H_{14} were collected on a Stoe-IPDS at 200 K using Mo-Kα radiation (λ = 0.71073 Å). Full-matrix, least squares refinements on F^2 using all data.[10] $C_{66}H_{74}F_6Li_4N_{12}O_6$·$C_4H_8O$·$C_6H_{14}$, M = 1431.41, triclinic, space group $P\bar{1}$, a = 10.121(6), b = 14.415(3), c = 15.282(3) Å, α = 68.66(3), β = 72.98(5), γ = 79.06(5)°, U = 1977.0(13) Å^3, Z = 1, μ(MoKα) = 0.087 mm^{-1}, $R1$ [$I > 2\sigma(I)$] = 0.095, $wR2$ (all 3514 data) = 0.231. **2** crystallises with one molecule of thf and one molecule of hexane as lattice solvent per formula unit. Both coordinated and non-coordinated thf molecules as well as the hexane molecule are disordered and were split in the refinement on two positions using similar distance and similar U restraints. All non-hydrogen atoms were refined anisotropically with the exception of disordered atoms which were treated isotropically. **2** forms thin and highly fragile plates, which are prone to solvent loss in the absence of the mother-liquor, and give a rather weak diffraction pattern of low resolution ($2\theta_{max}$ = 40°).

CCDC reference number 166359. See http://www.rsc.org/suppdata/cc/b1/b105435j/ for crystallographic data in CIF or other electronic format.

1 F. T. Edelmann, *Coord. Chem. Rev.*, 1994, **137**, 403; J. Barker and M. Kilner, *Coord. Chem. Rev.*, 1994, **133**, 219.
2 M. Witt and H. W. Roesky, *Chem. Rev.*, 1994, **94**, 1163.
3 A. Steiner and D. S. Wright, *Angew. Chem., Int. Ed. Engl.*, 1996, **35**, 636; G. T. Lawson, C. Jacob and A. Steiner, *Eur. J. Inorg. Chem.*, 1999, 1881; G. T. Lawson, F. Rivals, M. Tascher, C. Jacob, J. F. Bickley and A. Steiner, *Chem. Commun.*, 2000, 341.
4 D. Stalke, M. Wedler and F. T. Edelmann, *J. Organomet. Chem.*, 1992, **431**, C1; J. Barker, D. Barr, N. D. R. Barnett, W. Clegg, I. Cragg-Hine, M. G. Davidson, R. P. Davies, S. M. Hodgson, J. A. K. Howard, M. Kilner, C. W. Lehmann, I. Lopez-Solera, R. E. Mulvey, P. R. Raithby and R. Snaith, *J. Chem. Soc., Dalton Trans.*, 1997, 951.
5 A. Steiner and D. Stalke, *Inorg. Chem.*, 1993, **32**, 1977; R. Fleischer and D. Stalke, *Inorg. Chem.*, 1997, **36**, 2413; S. Wingerter, M. Pfeiffer, A. Murso, C. Lustig, T. Stey, V. Chandrasekhar and D. Stalke, *J. Am. Chem. Soc.*, 2001, **123**, 1381.
6 F. Pauer and D. Stalke, *J. Organomet. Chem.*, 1991, **418**, 127; S. Freitag, W. Kolodziejski, F. Pauer and D. Stalke, *J. Chem. Soc., Dalton Trans.*, 1993, 3779.
7 D. R. Armstrong, J. E. Davies, N. Feeder, E. Lamb, J. J. Longridge, J. M. Rawson, R. Snaith and A. E. H. Wheatley, *J. Mol. Model.*, 2000, **6**, 234.
8 A. R. Katritzky, I. Ghiviriga, P. J. Steel and D. C. Oniciu, *J. Chem. Soc., Perkin Trans. 2*, 443, 1996.
9 W. M. Boesveld, P. B. Hitchcock and M. F. Lappert, *J. Chem. Soc., Dalton Trans.*, 1999, 4041; D. R. Armstrong, K. W. Henderson, M. MacGregor, R. E. Mulvey, M. J. Ross, W. Clegg and P. A. O'Neil, *J. Organomet. Chem.*, 1995, **486**, 79.
10 G. M. Sheldrick, SHELX97, X-ray structure determination program, Universität Göttingen, Germany, 1997.

CHEMCOMM Communication
www.rsc.org/chemcomm

First molecular switch encapsulated within the cavities of a zeolite. A dramatic lifetime increase of the charge-separated state

Mercedes Álvaro,[a] Michelle N. Chretien,[b] Belén Ferrer,[a] Vicente Fornés,[a] Hermenegildo García*[a] and J. C. Scaiano*[b]

[a] *Instituto de Tecnología Química CSIC-UPV and Departamento de Química UPV, Avda de los Naranjos s/n 46022. Valencia, Spain. E-mail: hgarcia@qim.upv.es*
[b] *Department of Chemistry, University of Ottawa, 10 Marie Curie, Ottawa, Canada K1G 6N5*

Received (in Cambridge, UK) 14th May 2001, Accepted 7th September 2001
First published as an Advance Article on the web 24th September 2001

A [2]-catenane consisting of a bipyridinium cyclophane and a dioxybenzene macrocyclic polyether has been encapsulated within the supercages of zeolite Y by ship-in-a-bottle synthesis; laser flash photolysis reveals that the charge-separated species decays in hundreds of microseconds in contrast to the few picoseconds previously reported for the same transient in acetonitrile.

The action of many photoresponsive switches and supramolecular machines is based on the occurrence of an intramolecular electron transfer triggered by light.[1] However, one of the major problems thwarting the operation of these supramolecular devices is a fast deactivation pathway of the charge-separated transient species consisting of reverse electron transfer leading back to the ground state.[2] This energy-wasting process is generally very efficient and limits the lifetime of the photogenerated transient to the subnanosecond time scale. Generally, the 'action' of the supramolecular machine is expected to consist of the movement of a shuttle from one station to a second in the supramolecular assembly during the lifetime of the charge-separated state. This co-conformational movement requires a sufficiently long transient lifetime and is related to a retardation of the back electron transfer (BET) to the microsecond time scale.

In a different context, it has been reported that incorporation of a charge-transfer (CT) complex within the internal voids of zeolites may increase the lifetime of the photoinduced radical ion pair by over six orders of magnitude.[3] As a part of our ongoing research focussed on the encapsulation of photoresponsive rotaxanes and catenanes within the rigid internal voids of zeolites, we report here the ship-in-a-bottle synthesis of [2]-catenane $\mathbf{3}^{4+}$ encapsulated within the supercages of zeolite Y ($\mathbf{3}^{4+}$@Y). We provide laser flash photolysis evidence showing that the transient of [2]-catenane $\mathbf{3}^{4+}$ within zeolite Y is much longer lived (hundreds of μs) than that observed for the same switch in MeCN (tens of ps).[4] Our report is the first to show the benefits of immobilization of a molecular switch within the rigid matrix of a zeolite.

Based on the reported single-crystal X-ray diffraction,[5] the dimensions of the [2]-catenane $\mathbf{3}^{4+}$, comprised of the viologen cyclophane as the electron-acceptor unit and the macrocyclic hydroquinone polyether as the electron-donor unit, are too large (11.7 × 10.3 × 7.0 Å) to allow its free diffusion from the exterior to the interior cages of the zeolite Y (openings 7.4 Å in diameter). It is, however, sufficiently small for accommodation within the spherical supercages (13 Å). In contrast, the smaller dimension of the macrocyclic polyether (10.6 × 4.7 Å) should allow its free diffusion through the zeolite Y micropores. A suitable strategy to prepare $\mathbf{3}^{4+}$@Y is a ship-in-a-bottle synthesis[6] consisting of constructing the big catenane within the cage by reacting smaller precursors that diffuse through the pore openings.

We have adapted the reported synthesis of catenane $\mathbf{3}^{4+}$ in solution[5] to obtain it by a ship-in-a-bottle methodology (Scheme 1).† In the first step, the open precursor $\mathbf{1}^{2+}$ is ion-exchanged inside zeolite NaY ($\mathbf{1}^{2+}$@Y), by stirring an aqueous solution of preformed $\mathbf{1}(PF_6)_2$ in the presence of the zeolite. Zeolites are microporous solids that are well suited to adsorb positively charged organic species. Subsequent formation of the [2]-catenane $\mathbf{3}^{4+}$ encapsulated within the cages of Y zeolite was accomplished by treating $\mathbf{1}^{2+}$@Y first with the macrocyclic polyether (CT complex formation), and then with 1,4-bis-(bromomethyl)benzene (closure of the cyclophane macro-ring). Formation of $\mathbf{3}^{4+}$@Y was assessed by comparing the spectra of the solid sample with those of its precursor $\mathbf{1}^{2+}$@Y and the corresponding viologen macro-ring $\mathbf{2}^{4+}$@Y.

The UV–vis absorption spectra of the cyclophane $\mathbf{2}^{4+}$ and the [2]-catenane $\mathbf{3}^{4+}$ inside zeolite Y are similar to the reported absorption spectra of these compounds in MeCN.[5] Fig. 1 shows the diffuse reflectance UV–vis absorption spectra of the samples $\mathbf{2}^{4+}$@Y and $\mathbf{3}^{4+}$@Y. A weak band with its onset at 800 nm, whose absorption increases linearly as the wavelength decreases, is observed in the spectrum of $\mathbf{3}^{4+}$@Y but is absent in the spectrum of the cyclophane $\mathbf{2}^{4+}$@Y. This absorption band is known to arise from the interaction between the electron-rich crown ether moiety and the electron-poor tetracationic cyclophane. The presence of this broad, structureless band has been taken as the simplest criterion to establish the formation of this type of complex.[5,7,8]

IR spectroscopy provides useful information since it allows differentiation between pyridine and pyridinium rings.[9] Considering the difference between $\mathbf{1}^{2+}$ and $\mathbf{2}^{4+}$ or $\mathbf{3}^{4+}$, the presence or absence of neutral pyridine rings can be used as a criterion to establish the success of the formation of catenane $\mathbf{3}^{4+}$. To follow the cyclization step shown in Scheme 1 without interference from the polyether macrocycle, FT-IR spectra of $\mathbf{1}^{2+}$@Y were

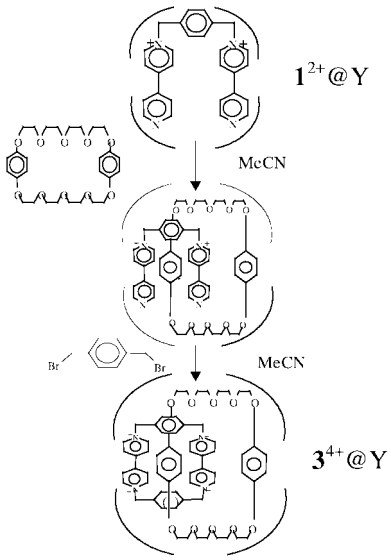

Scheme 1

 DOI: 10.1039/b104206h

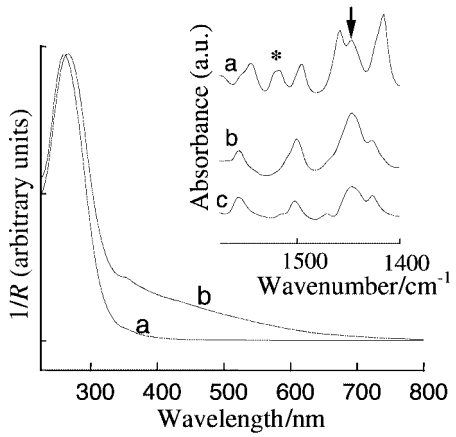

Fig. 1 Diffuse reflectance UV–vis spectra (plotted as the inverse of *R*) of $\mathbf{2}^{4+}$@Y (a) and $\mathbf{3}^{4+}$@Y (b). The inset shows part of the IR spectra of $\mathbf{1}^{2+}$@Y (a), $\mathbf{2}^{4+}$@Y (b) recorded at room temperature after outgassing at 200 °C for 1 h at 10^{-2} Pa, and that of $\mathbf{2}^{4+}(PF_6)_4$ (c) in a KBr disk. The three spectra exhibit the band corresponding to the *N*-alkylpyridinium ring (↓), but only the uncyclised $\mathbf{1}^{2+}$ has the band characteristic of the free pyridine ring (*).

compared with those for $\mathbf{2}^{4+}$@Y and for an authentic specimen of $\mathbf{2}^{4+}(PF_6)_4$ prepared as reported. Fig. 1 inset shows the corresponding FT-IR spectra.

In the context of the characterization of acidity in zeolites, it has been reported that pyridine and pyridinium ions can be safely distinguished by the presence of 1560 and 1450 cm^{-1} bands, respectively.[9] Accordingly, the IR spectrum of the viologen cyclophane shows only vibration bands corresponding to *N*-alkylpyridinium and is different from that of $\mathbf{1}^{2+}$@Y which contains bands corresponding to both *N*-alkylpyridinium and free pyridine. Similarly, the aromatic region of the IR spectrum of $\mathbf{2}^{4+}$@Y viologen macro-ring can be taken as a fingerprint, and is very similar to that recorded for the $\mathbf{2}^{4+}(PF_6)_4$ salt in the form of a KBr disk. This good match was also considered to be a good means of assessing the success of the cyclization of the bipyridinium macro-ring inside the zeolite Y supercages, providing solid evidence in support of the formation of $\mathbf{2}^{4+}$@Y and $\mathbf{3}^{4+}$@Y.

Diffuse reflectance-laser flash photolysis of $\mathbf{3}^{4+}$@Y was carried out exciting at 532, 355 or 308 nm. According to the reported work on laser flash photolysis of arene–methylviologen complexes,[3,10] it was anticipated that 532 nm would selectively excite the CT complex band. However, in our case the low extinction coefficient of $\mathbf{3}^{4+}$ at 532 nm (see Fig. 1) prevented us from obtaining any detectable transient signal upon excitation at 532 nm. Thus, we recorded the spectrum at both 355 and 308 nm. The same transient spectrum was obtained in both cases. These wavelengths, however, do not provide selective excitation of the CT complex of catenane $\mathbf{3}^{4+}$; excitation of the uncomplexed bipyridinium or hydroquinone moieties also occurs. To distinguish the contribution of the CT complex in $\mathbf{3}^{4+}$, the transient spectrum of $\mathbf{3}^{4+}$@Y was compared with that recorded for $\mathbf{2}^{4+}$@Y as a control (Fig. 2). Both spectra show similar features corresponding to bipyridinium radical cations.[11,12] However, closer inspection reveals that the absorption in the 600–750 nm region for $\mathbf{3}^{4+}$ is significantly more intense than for $\mathbf{2}^{4+}$. In addition, the decays monitored at 390 and 750 nm for $\mathbf{3}^{4+}$ are significantly different (see Fig. 2 inset), firmly proving that at least two different species are involved. This second transient would correspond to the charge-separated state of the CT complex of $\mathbf{3}^{4+}$. As expected for a single transient, the decays for $\mathbf{2}^{4+}$ monitored at 390 or 750 nm coincide.

Importantly, as Fig. 2 shows, the lifetime of the photogenerated charge-separated state of the $\mathbf{3}^{4+}$ CT complex is

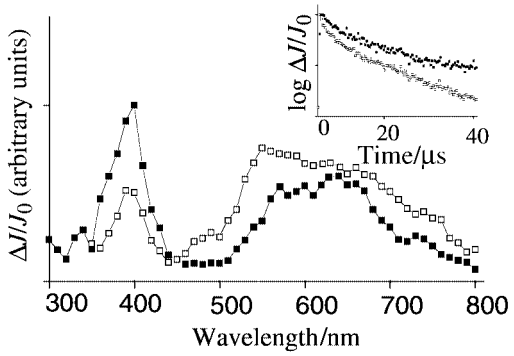

Fig. 2 Time-resolved diffuse reflectance UV–vis spectra of $\mathbf{3}^{4+}$@Y recorded 15 μs after 308 nm excitation (□), and $\mathbf{2}^{4+}$@Y recorded 2 μs after 266 nm excitation (■). The inset shows the decays of $\mathbf{3}^{4+}$@Y monitored at 705 (□) and 450 nm (■).

hundreds of μs. This contrasts sharply with previous laser flash photolysis studies of [2]-catenane $\mathbf{3}^{4+}$ in MeCN where the lifetime was tens of ps.[4] Therefore, incorporation of catenane $\mathbf{3}^{4+}$ into zeolite Y increases the lifetime of the charge-separated transient species by six orders of magnitude. This dramatic effect of incorporation of $\mathbf{3}^{4+}$ on the lifetime of the photogenerated radical ion pair can been explained by the stabilization due to the intense electrostatic fields experienced inside the zeolite pores. Since co-conformational movements are predicted to take place on the μs time scale,[2] the present finding that the charge-separated state of catenane $\mathbf{3}^{4+}$ exists for hundreds of μs when encapsulated in zeolite Y could open the possibility of observing the cyclic action of molecular-level machines.

Financial support by the Spanish CICYT (HG, MAT 2000, 1768-002-01) and the Canadian NSERC (JCS) are gratefully acknowledged. B. F. thanks the Spanish Ministry of Education for a scholarship.

Notes and references

† [2]-Catenane incorporated inside zeolite Y ($\mathbf{3}^{4+}$@Y) was prepared by adding a solution of the macrocyclic polyether (0.0426 g, 0.08 mmol) in dry MeCN (5 ml) to the partially-exchanged $\mathbf{1}^{2+}$@Y (0.5 g) ($\mathbf{1}^{2+}$ content 0.026 g, 0.03 mmol) previously dehydrated at 200 °C under 0.10 Torr for 2 h. The suspension was stirred at room temperature under Ar. Then, a solution of 1,4-bis(bromomethyl)benzene (0.0083 g, 0.03 mmol) in dry MeCN (5 ml) was added and the suspension was stirred at room temperature under Ar for 5 d, and then at reflux temperature for 24 h. The resulting solid was filtered off and submitted to exhaustive solid–liquid extraction using MeCN as the solvent.

1 V. Balzani, A. Credi, F. Raymo and J. Stoddart, *Angew. Chem., Int. Ed.*, 2000, **39**, 3348.
2 P. Asthon, R. Ballardini, V. Balzani, A. Credi, K. Dress, E. Ishow, C. Kleverlaan, O. Kocian, J. Preece, N. Spencer, J. Stoddart, M. Venturi and S. Wenger, *Chem. Eur. J.*, 2000, **6**, 3558.
3 S. Sankararaman, K. B. Yoon, T. Yabe and J. K. Kochi, *J. Am. Chem. Soc.*, 1991, **113**, 1419.
4 A. C. Benniston and A. Harriman, *NATO ASI Ser., Ser. C, Phys. Supramol. Chem.*, 1996, **485**, 179.
5 P. L. Anelli, P. R. Ashton, R. Ballardini, V. Balzani, M. Delgado, M. T. Gandolfi, T. T. Goodnow, A. E. Kaifer, D. Philp, M. Pietraszkiewicz, L. Prodi, M. V. Reddington, A. M. Z. Slawin, N. Spencer, J. F. Stoddart, C. Vicent and D. J. Williams, *J. Am. Chem. Soc.*, 1992, **114**, 193.
6 J. C. Scaiano and H. García, *Acc. Chem. Res.*, 1999, **32**, 783.
7 K. B. Yoon, T. J. Huh, D. R. Corbin and J. K. Kochi, *J. Phys. Chem.*, 1993, **97**, 6492.
8 S. Hashimoto, *Tetrahedron*, 2000, **56**, 6957.
9 A. Corma, *Chem. Rev.*, 1995, **95**, 559.
10 K. B. Yoon, *Chem. Rev.*, 1993, **93**, 321.
11 K. B. Yoon, S. M. Hubig and J. K. Kochi, *J. Phys. Chem.*, 1994, **98**, 3865.
12 M. Alvaro, H. García, S. García, F. Marquez and J. C. Scaiano, *J. Phys. Chem.*, 1997, **101**, 3043.

CHEMCOMM Communication
www.rsc.org/chemcomm

The significance of proton migration during hole hopping through DNA

Bernd Giese* and Stephan Wessely

Department of Chemistry, University of Basel, St. Johanns Ring 19, CH-4056 Basel, Switzerland. E-mail: bernd.giese@unibas.ch; Fax: 0041-61-267-1105; Tel: 0041-61-267-1106

Received (in Cambridge, UK) 9th July 2001, Accepted 22nd August 2001
First published as an Advance Article on the web 1st October 2001

Hole transfer through DNA is coupled with proton transfer processes.

The controversial long distance hole transfer through DNA was debated over the course of the last decade.[1] Today, a consensus exists that this process occurs as a multistep hopping reaction[2] with guanines (G), the DNA bases of lowest ionisation potentials, as possible carriers of the positive charge.[3,4] Since Steenken has measured a pK_a value of 3.9 for the guanine radical cation ($G^{\cdot+}$),[5] one would expect that $G^{\cdot+}$ loses the positive charge by proton transfer to the surrounding water in poorly paired (mismatched) strands. This should retard or even stop hole transfer through DNA. Recently, we have observed such a decrease of the charge transfer efficiency in experiments with double strands **1a**,**b** (Fig. 1).[6]

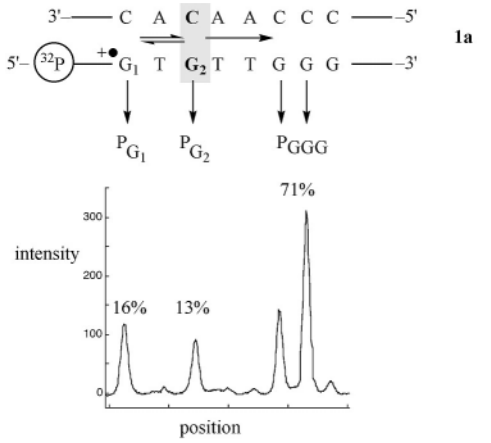

Fig. 1 Histograms of denaturing polyacrylamide gels, obtained by subtraction of control experiments (irradiation of unmodified strands) from irradiation experiments with the modified strands, which contain a 4′-pivaloylthymidine next to G_1 in the complementary strand. The histograms show the yields of products P_{G_1}, P_{G_2}, and P_{GGG} at the different positions of the radiolabelled strand. These products are formed by water trapping of the guanine radical cations and subsequent site selective strand cleavage of the radiolabelled strands.

The positive charge was injected into G_1 of strands **1a**,**b** by photolysis of a 4′-pivaloylated thymidine, situated next to G_1 in the complementary strand.[7] The hole migrates *via* G_2 through DNA until it reaches the GGG sequence, a thermodynamic sink for the positive charge.[8] The charge could be detected by nucleophilic water trapping of $G^{\cdot+}$, which led to strand cleavage products P_{G_1}, P_{G_2} and P_{GGG} after piperidine treatment (Fig. 1).[3,6] In the paired double strand **1a** the P_{GGG} yield was 71%. Thus, most of the charge migrated from G_1 to the GGG sequence in strand **1a** where the acidic proton is held within the G–C base pair by a hydrogen bridge (**2a** ⇌ **2b**). However, the P_{GGG} yield dropped from 71 to 12% in the mismatched strand **1b** having an abasic site (H) opposite G_2.[9] We explained this effect by a proton transfer from the non-paired $G_2^{\cdot+}$ in strand **1b** to the surrounding water (**3** → **4**), which slows down or even stops the charge transfer (Scheme 1).

If this interpretation is correct, methylguanosine **5** (G_{Me} in **1c**) should not stop the hole transfer through DNA because the acidic hydrogen atom is exchanged by a methyl group.[10] We therefore synthesized double strand **1c** where the abasic site is opposite to G_{Me}. Charge injection into G_1 led to the results shown in Fig. 2. Compared to the inefficient charge transfer in strand **1b**, where an abasic site opposite to G_2 reduced the P_{GGG} yield from 71 to 12%, with methyl guanosine **5** (G_{Me}) opposite the abasic site in **1c** the P_{GGG} yield increased again to 53%. This experiment strongly supports the explanation that mismatches in G–C base pairs interrupt the hole transfer through DNA by a proton shift from the mismatched $G^{\cdot+}$ to the surrounding water (**3** → **4**).

In contrast to the decrease of the hole transfer efficiency through DNA by deprotonation of $G^{\cdot+}$ (**3** → **4**), a proton shift within the oxidized hydrogen-bridged G–C base pair could increase the hole transfer rate, because the proton shift

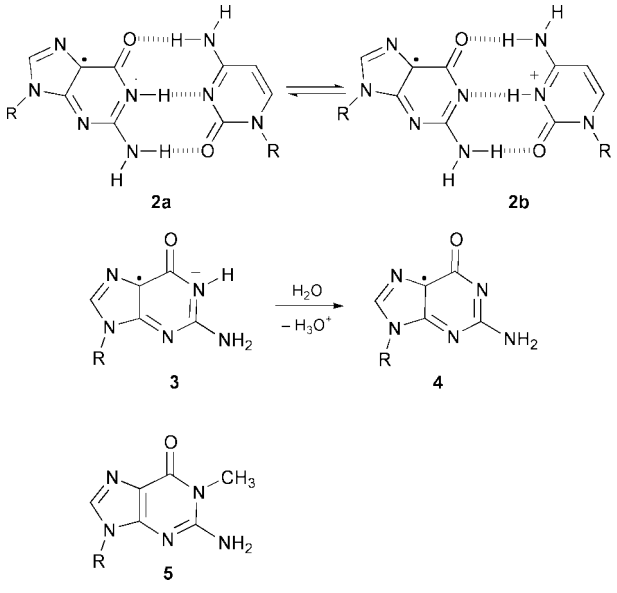

Scheme 1

 DOI: 10.1039/b106059g

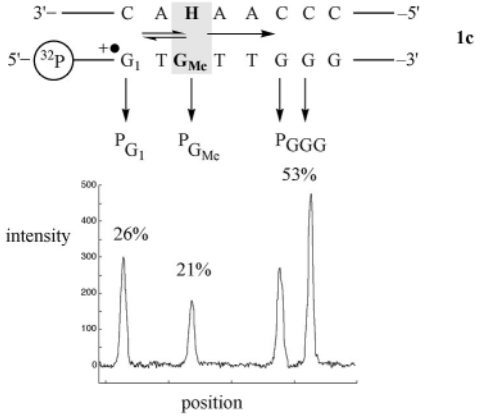

Fig. 2 Histogram of denaturing polyacrylamide gels, obtained by subtraction of control experiments (irradiation of unmodified strands) from irradiation experiments with the modified strand, which contained a 4′-pivaloylthymidine next to G_1 on the complementary strand. The histogram shows the yields of products P_{G_1}, P_{GMe}, and P_{GGG} at the different positions of the radiolabelled strand. These products are formed by water trapping of the guanine radical cations and subsequent site selective strand cleavage of the radiolabelled strands.

(**2a** ⇌ **2b**) stabilizes the positive charge.[5,11] The prerequisite for a rate increase is that hole and proton transfer reactions are coupled with each other. Recently, Thorp proved this process by a kinetic deuterium isotope effect of the hole injection step into G.[12] We have now demonstrated that a deuterium isotope effect also exists during hole transfer reactions between guanines. The effect was measured using double strand **6** where the hole migrates from G to the GGG sequence and its relative rate was determined by the yield ratio P_{GGG}–P_G.[13]

The results are presented in Fig. 3. As observed previously,[13] in H_2O the P_{GGG}–P_G ratio is 9.0 ± 1.0 for double strand **6**. This ratio decreases to 3.0 ± 1.0 in D_2O where all acidic protons are replaced by deuterons. A decrease of the charge transfer efficiency by a factor of 3 in D_2O can be explained by a slower deuteron shift from G·+ to C compared to the corresponding proton shift (**2a** ⇌ **2b**). But this kinetic deuterium isotope effect

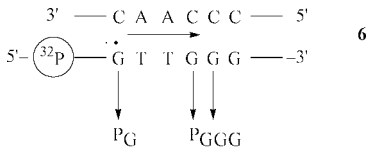

H_2O: $P_{GGG}/P_G = 9.0 = 1.0$

D_2O: $P_{GGG}/P_G = 3.0 = 1.0$

Fig. 3 Product ratios P_{GGG}–P_G resulting from water trapping of the guanine radical cations and subsequent site selective strand cleavage of the radiolabelled strand. The experiments were carried out in H_2O and D_2O, respectively.

influences the rate of the hole transfer only if both processes are coupled. Thus, in charge transfer reactions through DNA the hole hopping processes between guanines are coupled with proton transfer reactions.[14,15]

Generous financial support by the Swiss National Science Foundation and the Volkswagen Foundation is gratefully acknowledged.

Notes and references

1 E. K. Wilson, *Chem. Eng. News*, 1999, **77**(34), 43; M. Ratner, *Nature*, 1999, **397**, 480; M. W. Grinstaff, *Angew. Chem., Int. Ed.*, 1999, **38**, 3629.
2 G. B. Schuster, *Acc. Chem. Res.*, 2000, **33**, 253; B. Giese, *Acc. Chem. Res.*, 2000, **33**, 631; F. D. Lewis, R. L. Letsinger and M. R. Wasielewski, *Acc. Chem. Res.*, 2001, **34**, 159; C. Wan, T. Fiebig, O. Schiemann, J. K. Barton and A. H. Zewail, *Proc. Natl. Acad. Sci. USA*, 2000, **97**, 14052; J. Jortner, M. Bixon, T. Langenbacher and M. E. Michel-Beyerle, *Proc. Natl. Acad. Sci. USA*, 1998, **95**, 12759; Y. A. Berlin, A. L. Burin and M. A. Ratner, *J. Am. Chem. Soc.*, 2001, **123**, 260.
3 E. Meggers, M. E. Michel-Beyerle and B. Giese, *J. Am. Chem. Soc.*, 1998, **120**, 12950.
4 In long A–T sequences adenine also becomes the carrier of the positive charge. See: B. Giese and M. Spichty, *ChemPhysChem.*, 2000, **1**, 195; B. Giese, J. Amaudrut, A.-K. Köhler, M. Spormann and S. Wessely, *Nature*, 2001, **412**, 318.
5 S. Steenken, *Free Rad. Res. Commun.*, 1992, **16**, 349; S. Steenken, *Biol. Chem.*, 1997, **378**, 1293.
6 B. Giese and S. Wessely, *Angew. Chem., Int. Ed.*, 2000, **39**, 3490.
7 The strands and the methods are described in ref. 3 and 6.
8 H. Sugiyama and I. Saito, *J. Am. Chem. Soc.*, 1996, **118**, 7073; F. Prat, K. N. Houk and C. S. Foote, *J. Am. Chem. Soc.*, 1998, **120**, 845.
9 In the abasic monomer H, a hydrogen atom replaces the nucleobase.
10 The radical cation of methylguanine **5** can only deprotonate from the exocyclic N^2. The pK_a for this process is almost one unit higher (pK_a = 4.7) than for guanosine radical cation **3**: L. P. Candeias and S. Steenken, *J. Am. Chem. Soc.*, 1998, **111**, 1094. Our experiments were performed at pH = 5.0.
11 M. Huter and T. Clark, *J. Am. Chem. Soc.*, 1996, **118**, 7574; K. Kawai, Y. Wata, N. Ichinose and T. Majima, *Angew. Chem., Int. Ed.*, 2000, **39**, 4327.
12 S. C. Weatherly, I. V. Yang and H. H. Thorp, *J. Am. Chem. Soc.*, 2001, **123**, 1236.
13 The strands and the reaction conditions are described in: B. Giese, S. Wessely, M. Spormann, U. Lindemann, E. Meggers and M. E. Michel-Beyerle, *Angew. Chem., Int. Ed.*, 1999, **38**, 996. The addition of water to G·+, which leads to P_G, competes with the hole transfer from G to GGG in double strand **6**. A kinetic isotope effect in the water addition reaction should decrease its rate in D_2O and will therefore increase the P_{GGG}–P_G ratio. The observed decrease of the P_{GGG}–P_G ratio in D_2O (Fig. 3) is therefore a lower limit for the kinetic isotope effect of the hole transfer process.
14 Proton shifts from G to C also influence the electron transfer in radical anions of G–C base pairs: A. Messer, K. Carpenter, K. Forzley, J. Buchanan, S. Yang, Y. Razskazovskii, Z. Cai and M. D. Sevilla, *J. Phys. Chem. B*, 2000, **104**, 1128.
15 For a general discussion on proton coupled electron transfer, see: A. Kohen and J. P. Klinman, *Acc. Chem. Res.*, 1998, **31**, 397; S. Hammes-Schiffer, *Acc. Chem. Res.*, 2001, **34**, 273.

CHEMCOMM Communication
www.rsc.org/chemcomm

Synthesis and reactivity of an efficient 1,2-dehydrocarborane precursor, phenyl[*o*-(trimethylsilyl)carboranyl]iodonium acetate

Joonsang Jeon,[a] Tsugio Kitamura,[b] Byung-Woo Yoo,[a] Sang Ook Kang*[a] and Jaejung Ko*[a]

[a] *Department of Chemistry, Korea University, Chochiwon, Chungnam 339-700, Korea. E-mail: jko@tiger.korea.ac.kr*
[b] *Department of Chemistry and Biochemistry, Graduate School of Engineering, Kyushu University, Hakozaki, Fukuoka 812-8581, Japan*

Received (in Cambridge, UK) 15th August 2001, Accepted 7th September 2001
First published as an Advance Article on the web 25th September 2001

The reaction of [*o*-(trimethylsilyl)carboranyl]lithium with $IPh(OAc)_2$ in diethyl ether affords an efficient 1,2-dehydro-*o*-carborane precursor 4: the facile 2 + 4 cycloaddition of 4 with dienes in the presence of the desilylating agent is reported.

Although benzyne **1** has been widely used in organic synthesis, mechanistic studies, and synthesis of functional materials,[1–3] the chemistry of 1,2-dehydro-*o*-carborane **2**, the carborane version of benzyne, has sporadically appeared. Recently, Jones and coworkers[4–11] have described its reactions with a variety of dienes, alkynes and alkenes. In order to generate **2**, they used the bromo anion **3** as an 1,2-dehydro-*o*-carborane precursor, which is stable at 0 °C. However, the yields in their reactions are too low. To make a plausible advance into consideration in this area, methodology is desired for 1,2-dehydro-*o*-carborane precursors to generate **2** with high efficiency and under mild conditions. Recently, we found that phenyl[*o*-(trimethylsilyl)carboranyl]iodonium acetate **4** has proved to be such an example since this precursor is readily prepared from available chemicals and is stable enough to be handled without any special precaution. We now describe (i) the isolation of an excellent 1,2-dehydro-*o*-carborane precursor **4** and (ii) the efficient reactions of **4** with dienes under mild condition.

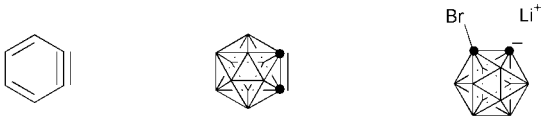

1 **2** **3**

Addition of 1 equiv. of [*o*-(trimethylsilyl)carboranyl]lithium, prepared from *o*-(trimethylsilyl)carborane and 1 equiv. of *n*-BuLi, to $IPh(OAc)_2$ in diethyl ether gave phenyl[*o*-(trimethylsilyl)carboranyl]iodonium acetate **4** as a spectroscopically pure, colorless powder relatively sensitive to air in 46% yield [eqn. (1)].†

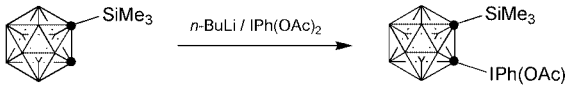

(1)

4

The ^1H and ^{13}C NMR spectra for **4** support the proposed structure.

The intermediate **4** was found to be an efficient precursor for the generation of 1,2-dehydro-*o*-carborane under mild conditions. The reaction of **4** with anthracene (1.2 equiv.) in the presence of CsF (2.4 equiv.) in diethyl ether at room temperature for 24 h afforded the carborane adduct **5** in 48% yield [eqn. (2)].‡

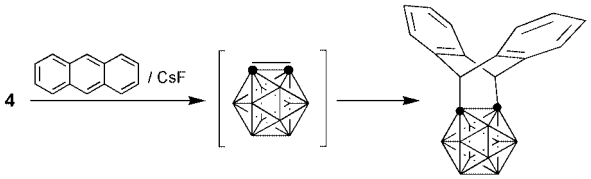

(2)

5

When KF was used as the desilylating agent with 18-crown-6, the adduct **5** was also obtained in 40% yield.[12] All the spectral data of **5** were consistent with the proposed formulation. A key feature in the ^1H NMR spectrum of **5** includes a singlet at δ 4.74 assigned to the bridgehead hydrogens. A high-field resonance at δ 51.17 in the ^{13}C NMR provides evidence for bridgehead carbon atoms. The structure of **5** was unambiguously established by a single-crystal X-ray analysis (Fig. 1).§ The central six-membered ring (C3, C4, C5, C10, C11 and C16) is puckered. The dihedral angle between C1–C2–C3–C4 and C3–C4–C11–C16 is 58.4(3)°, and that between C1–C2–C3–C4 and C3–C4–C5–C10 is 58.6(3)°.

The reaction of **4** with 3 equiv. of norborna-2,5-diene under the same reaction conditions takes place and affords three isomers (**7**, **8**, and **9**) in 62% yield [eqn. (3)].

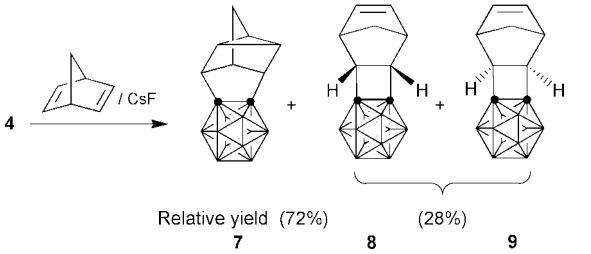

(3)

7 **8** **9**

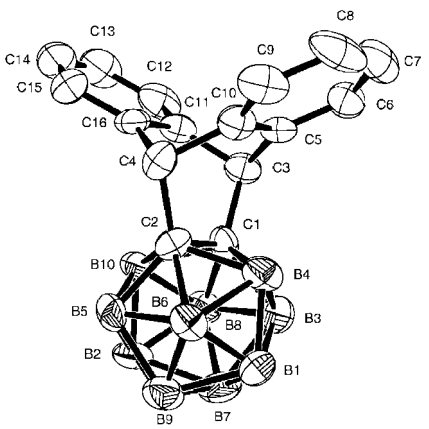

Fig. 1 Molecular structure of **5** showing the atom numbering scheme. Selected distances (Å) and angles (°): C(1)–C(2) 1.6072, C(1)–C(3) 1.5639, C(2)–C(4) 1.593(10), C(3)–C(5) 1.518(8); C(1)–C(3)–C(5) 108.6(3), C(5)–C(3)–C(11) 103.5(5), C(3)–C(1)–C(2) 109.6.

 DOI: 10.1039/b107343e

We were not able to separate **8** and **9** as also found in Jones' work.[6] Three resonances (δ 3.10, 2.80 and 1.57) and two doublets (δ 1.42 and 1.40) in the ^{1}H NMR spectrum of **7** are assigned to the methine proton and methylene proton, respectively. Five ^{13}C NMR resonances (δ 56.52, 49.83, 32.24, 25.04 and 24.58) provide evidence for the adduct **7**. The structure of **7** has been determined by X-ray crystallography (Fig. 2).§ The formation of **7–9** may involve 2 + 4 and 2 + 2 cycloaddition.

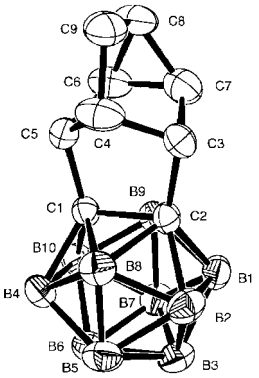

Fig. 2 Molecular structure of **7** showing the atom numbering scheme. Selected distances (Å) and angles (°): C(1)–C(2) 1.618(2), C(5)–C(6) 1.516(3), C(6)–C(7) 1.478(4), C(3)–C(7) 1.493(3); C(3)–C(4)–C(5) 92.80(15), C(4)–C(9)–C(8) 98.89(17), C(6)–C(8)–C(7) 58.40(16).

Other dienes such as naphthalene, 2,5-dimethylfuran and thiophene worked well as trapping agents for 1,2-dehydro-*o*-carborane. The results are summarized in Table 1. When the results obtained here are compared with the reported data available in the literature, much improved results are obtained by using the hypervalent iodine-1,2-dehydro-*o*-carborane precursor.

In summary, we have isolated an efficient 1,2-dehydro-*o*-carborane precursor, phenyl[*o*-(trimethylsilyl)carboranyl]iodonium acetate **4**, which readily reacts with dienes such as anthracene, naphthalene, norborna-2,5-diene, 2,5-dimethylfuran and thiophene, efficiently generating 1,2-dehydro-*o*-carborane adducts in good yield. This potential has been further exploited in a series of novel chemical transformations with this system.

We are grateful to BK21(2001) for generous financial support.

Notes and references

† *Experimental procedure* for **4**: to a stirred diethyl ether solution (15 mL) of *o*-(trimethylsilyl)carborane was added *n*-BuLi (1.43 mL of 1.6 M solution of hexane, 2.3 mmol) at 0 °C. The temperature was warmed to room temperature and stirring continued for 6 h at that temperature. The solution was slowly added to a diethyl ether solution of $IPh(OAc)_2$ (0.74 g, 2.3 mmol) at −78 °C and warmed to room temperature. The solution was stirred for 6 h. The solvent was removed *in vacuo* and washed with hexane (5 mL × 3). The residue was extracted with methylene chloride to afford **4** in 46% yield. ^{1}H NMR (CD_2Cl_2): δ 8.06–7.36 (m, 5H, aromatic proton), 1.96 (s, 3H, $COCH_3$), 0.20 (s, 9H, $SiCH_3$). ^{13}C{^{1}H} NMR (CD_2Cl_2): δ 176.43 (CO), 134.97, 133.43, 132.20, 131.53, 130.22, 121.27 (Ph), 20.47 ($COCH_3$), −0.97 ($SiCH_3$).

‡ *Experimental procedure* for **5**: anthracene (0.49 g, 2.75 mmol) and CsF (0.87 g, 5.75 mmol) were added to a stirred diethyl ether (20 mL) solution of **4** (1.31 g, 2.75 mmol) at room temperature. After stirring for 24 h, the mixture was filtered. The solvent was removed *in vacuo* and extracted with hexane. The solution was chromatographed using hexane as eluent. Recrystallization from hexane at −15 °C afforded **5** in 48% yield. mp 248 °C. ^{1}H NMR ($CDCl_3$): δ 7.24–7.00 (m, 8H, aromatic proton), 4.74 (s, 2H, CH). ^{13}C{^{1}H} NMR ($CDCl_3$): δ 144.12, 127.62, 124.28, 51.17. MS: *m*/*z* 320 [M$^+$].

§ *Crystal data* for **5**: $C_{16}H_{20}B_{10}$, M = 320.42, orthorhombic, space group $Pca2_1$, a = 8.742(2), b = 15.710(3), c = 13.300(2) Å, V = 1826.6(5) Å^3, Z = 4, D_c = 1.165 g cm^{-3}, μ(Mo-Kα) = 0.058 mm^{-1}, 880 reflections observed [$I > 2\sigma(I)$], 227 parameters, largest difference peak 0.285 e Å^{-3}, final R and R_w were 0.0842 and 0.1912, goodness of fit on F^2 = 1.044. For **7**: $C_9H_{18}B_{10}$, M = 234.33, monoclinic, space group $P2_1/c$, a = 7.6927(8), b = 13.5948(14), c = 12.9203(14) Å, β = 100.354(2)°, V = 1329.2(2) Å^3, Z = 4, D_c = 1.171 g cm^{-3}, μ(Mo-Kα) = 0.054 mm^{-1}, 3195 reflections observed [$I > 2\sigma(I)$], 172 parameters, largest difference peak 0.571 e Å^{-3}, final R and R_w were 0.0665 and 0.1804, goodness of fit on F^2 = 1.047. CCDC reference numbers 170498 and 170499. See http://www.rsc.org/suppdata/cc/b1/b107343e/ for crystallographic data in CIF or other electronic format.

Table 1 Trapping reaction of 1,2-dehydro-*o*-carborane derived from iodonium acetate **4**

Substrate	Product	Yield(%) This work[a]	Yield(%) Reported
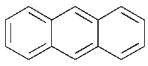	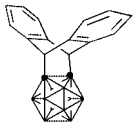	48	19[b]
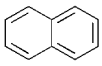	**5** 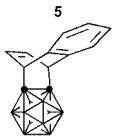	33	15[c]
	**6** 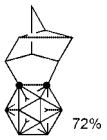 72%	62	19[d]
	7 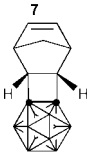 **9** 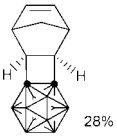 28%		
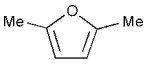	**8** 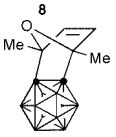	46	25[d]
	**10**  **11**	38	19[e]

[a] Isolated yield. [b] Ref. 4. [c] Ref. 11. [d] Ref. 6. [e] Ref. 10.

1 H. Hart, in *The Chemistry of Triple-Bonded Functional Groups*, Supplement C2, ed. S. Patai, Wiley, Chichester, 1994, ch. 18
2 R. W. Hoffmann, *Dehydrobenzene and Cycloalkynes*, Academic Press, New York, 1967
3 T. L. Gilchrist, in *The Chemistry of Functional Groups*, Supplement C, ed. S. Patai and Z. Rappoport, Wiley, Chichester, 1983, ch. 11
4 H. L. Gingrich, T. Ghosh, Q. Huang and M. Jones, Jr., *J. Am. Chem. Soc*., 1990, **112**, 4082.
5 Q. Huang, H. L. Gingrich and M. Jones, Jr., *Inorg. Chem*., 1991, **30**, 3254.
6 T. Ghosh, H. L. Gingrich, C. K. Kam, E. C. Mobraaten and M. Jones, Jr., *J. Am. Chem. Soc*., 1991, **113**, 1313.
7 H. L. Gingrich, Q. Huang, A. L. Morales and M. Jones, Jr., *J. Org. Chem*., 1992, **57**, 3803.
8 R. T. Cunningham, N. Bian and M. Jones, Jr., *Inorg. Chem*., 1994, **33**, 4811.
9 D. M. Ho, R. J. Cunningham, J. A. Brewer, N. Bian and M. Jones, Jr., *Inorg. Chem*., 1995, **34**, 5274.
10 L. Barnett-Thamattoor, G. Zheng, D. M. Ho, M. Jones, Jr. and J. E. Jackson, *Inorg. Chem*., 1996, **35**, 7311.
11 J. H. Atkins, D. M. Ho and M. Jones, Jr., *Tetrahedron Lett*., 1996, **37**, 7217.
12 For a fluoride ion-induced desilylation, see: T. Kitamura, M. Yamane, K. Inoue, M. Todaka, N. Fukatsu, Z. Meng and Y. Fujiwara, *J. Am. Chem. Soc*., 1999, **121**, 11674; N. A. Atanes, S. Escudero, D. Perez, E. Guitia and L. Castedo, *Tetrahedron Lett*., 1998, **39**, 3039; R. F. Cunico and E. M. Dexheimer, *J. Am. Chem. Soc*., 1972, **94**, 2868.

CHEMCOMM Communication
www.rsc.org/chemcomm

Evidence of ^{29}Si NMR paramagnetic shifts in rare-earth zeolite LSX

Jacques Plévert,*[a] Tatsuya Okubo,[b] Yuji Wada,[c] Michael O'Keeffe[a] and Takashi Tatsumi[d]

[a] *Department of Chemistry and Biochemistry, Arizona State University, Tempe, AZ 85287-1604, USA. E-mail: JPlevert@asu.edu*
[b] *Department of chemical System Engineering, The University of Tokyo, Tokyo 113-8656, Japan*
[c] *Material and Life Science, Osaka University, Suita 565-0871, Japan*
[d] *Division of Materials Science and Chemical Engineering, Yokohama National University, Yokohama 240-8501, Japan*

Received (in Cambridge, UK) 3rd July 2001, Accepted 12th September 2001
First published as an Advance Article on the web 2nd October 2001

Paramagnetic shifts have been observed for the first time in rare-earth zeolites; the ^{29}Si MAS NMR spectra of rare-earth ion-exchanged low silica X show a large range of isotropic chemical shifts that can be attributed to Fermi contact interactions with the lanthanide electronic moments.

Many zeolites of importance are solids exchanged with paramagnetic cations such as lanthanides. In the faujasite group, rare-earth zeolite Y is of high interest due to its performance as an octane-enhancing catalyst,[1] and rare-earth zeolite X is a promising material for laser applications due to the strong luminescent properties of the lanthanide complex immobilized within its cages.[2]

The effects of magnetic impurities on the ^{29}Si NMR spectra of alumino-silicates are well known. They decrease the spin–lattice relaxation, substantially broaden the resonance line as a function of the concentration of impurities,[3] and enhance the spinning-sideband patterns.[4] High concentrations of paramagnetic species in zeolites make the acquisition of NMR spectra difficult and, in general, the signal of nuclei in the neighbourhood of paramagnetic centers is not detected.[5] The use of NMR spectroscopy is relatively limited; at best, the proportion of nuclei close to paramagnetic centers can be estimated based on the intensity loss compared with diamagnetic samples.[6] In this work we show that ^{29}Si paramagnetic shifts can be observed in the NMR spectra of rare-earth zeolites, which provide information on the interaction between the paramagnetic species and the silicon atoms.

Fully exchanged rare-earth zeolites LSX are prepared by ion exchange in aqueous solution. A key parameter controlling the location of the lanthanide in the structure is the degree of hydration of the cation. The large diameter of the hydration sphere of the lanthanide cations prevents their access to the sodalite cages.† By heating the solution, the trivalent cations are partly dehydrated and are found essentially in only one site. They occupy sites on top of the six-ring windows of the sodalite cages (sites II), within the supercages of the zeolite.[7,8]

The ^{29}Si MAS NMR spectrum of LaLSX‡ exhibits a single resonance line at −83 ppm§ [Fig. 1(a)], corresponding to silicon atoms in a single environment Si(4Al). The ^{29}Si chemical shift of Si(4Al) sites does not exceed a range of 20 ppm, and varies from *ca.* −75 to −95 ppm, depending on the environment geometry.[9] The spectra of fully exchanged paramagnetic zeolites NdLSX [Fig. 1(b)] and EuLSX [Fig. 1(c)] show dramatic changes. The overall signal is very broad and exceeds 60 kHz in width, but the individual spinning sidebands are sharp. The relaxation times are very short and they are estimated to be *ca.* 0.2 s for NdLSX. The isotropic chemical shifts spread over an unusually large range, varying from *ca.* +6 to −146 ppm for our samples.

The appearance of widely spread resonance lines can be attributed to the interaction between the electronic moment of the rare-earth cations, siting on top of the six-ring windows of the sodalite cages, and the silicon nucleus. Lanthanide complexes are largely used as shift reagents in solution NMR,[10,11] where large shifts induced by the paramagnetic centers to close nuclei allow enhancement of the spectral resolution. However, only few examples in solid state NMR have been reported.[12–15]

Paramagnetic signals are difficult to detect due to the substantial broadening of the resonance lines. They can go almost unnoticed under the typical acquisition conditions for zeolites that require long recycle times, limiting the numbers of scans. Large numbers of scans are needed to get a good signal/noise ratio, but the significant decrease of the spin–lattice relaxation time enables data acquisition within reasonable times.

The overall width of the resonance line is dominated by the anisotropic part of the dipolar interaction between electronic and nuclear spins, and is proportional to the square of the magnetic moment μ of the rare-earth cations.[16,17] We observed experimentally, with a series of rare-earth LSX, that the overall width is relatively well correlated with μ^2 (Table 1).

The interaction between the unpaired electron and a given nucleus consists of two contributions: (i) the Fermi contact shift, which arises from the electron–nucleus hyperfine interaction

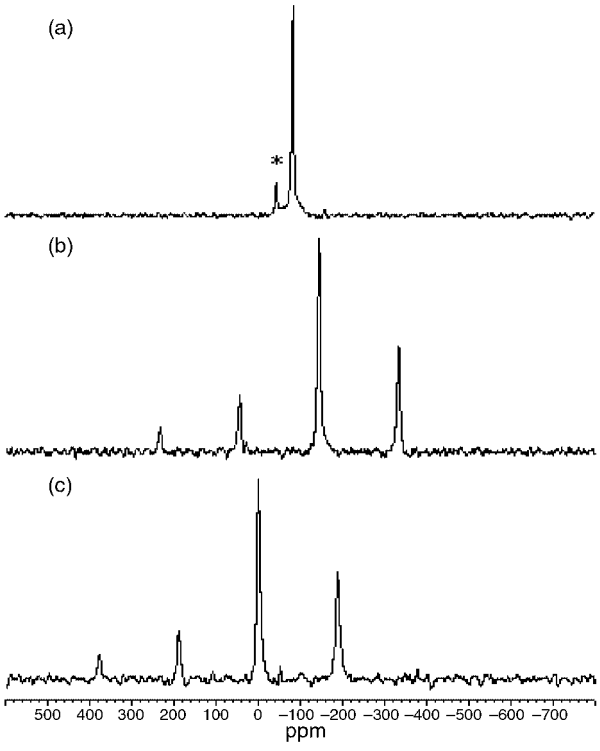

Fig. 1 ^{29}Si MAS NMR spectra of rare-earth LSX at spinning rate of 15 kHz, (a) LaLSX, (*) is the rotor contribution, (b) NdLSX and (c) EuLSX show a single line with a pattern of spinning sidebands. The pulse delay is 10 s for LaLSX and 0.1–0.8 s for the paramagnetic zeolites.

 DOI: 10.1039/b105881a

Table 1 ^{29}Si isotropic chemical shifts of some rare-earth LSX

Ion	$4f^n$	$<S_z>^a$	δ^{iso}/ppm	μ/μ_B
La^{3+}	$4f^0$	0.0	−83	0.0
Ce^{3+}	$4f^1$	0.98	−106	2.3
Pr^{3+}	$4f^2$	2.97	−142	3.4
Nd^{3+}	$4f^3$	4.49	−146	3.5
Sm^{3+}	$4f^5$	−0.063	−81	1.6
Eu^{3+}	$4f^6$	−10.7	+6	3.4

^{a} $<S_z>$ calculated according to Golding and Halton.[19]

and (ii) the pseudo-contact shift resulting from through-space dipolar interaction. The Fermi contact is proportional to $<S_z>$, the average value of the rare-earth spin over the spin levels, assuming that the hyperfine coupling constant A_{hf} does not vary across the rare-earth zeolite series, which seems reasonable as the ionic radius of the lanthanide cation remains relatively constant. The contact shift is expressed as $\Delta H = A_{hf}<S_z>\hbar\gamma_n$, where $\hbar$ is the reduced Planck's constant and γ_n the nuclear gyromagnetic factor of the observed nucleus.[18]

Fig. 2 shows a plot of $<S_z>$, calculated by Golding and Halton,[19] as a function of the experimental shift of a series of rare-earth zeolites LSX (Table 1). The variation is linear with a relatively good correlation, which suggests that the contact interaction is the predominant contribution to the paramagnetic shift. It is a through-bond mechanism despite the absence of a *direct* bond between the trivalent cation and the silicon atom. Other lanthanide systems show similar results.[13–15] The good correlation obtained in Fig. 2 confirms that the hyperfine coupling constant A_{hf} does not vary in rare-earth LSX, suggesting that the geometry of the cation site remains the same across the first half of the lanthanide series studied here.

The sign of $<S_z>$ changes once in the lanthanide series at Eu^{3+} and explains the downfield shift observed for this cation. On the other hand, a pseudo-contact shift should show an alternation of sign not observed experimentally.[20] It is interesting to note a correlation factor better than 0.997 between the ^{29}Si isotropic shifts of rare-earth LSX and the ^{119}Sn isotropic shifts in rare-earth stannates reported by Grey *et al.*[14] The deviations from the strict linear dependence of the chemical shift on $<S_z>$ due to Fermi contact, probably have the same origin in both solids.

We have demonstrated in this work that ^{29}Si NMR spectra of zeolites containing high concentrations of paramagnetic cations can be obtained. We observed paramagnetic shifts and found that the predominant contribution to the shift is the Fermi contact interaction. The shifting ability of lanthanide to close silicon atoms allows the discrimination between silicon sites in partly exchanged zeolites. Applications of rare-earth cations acting as paramagnetic shift agent in zeolites will be published later.

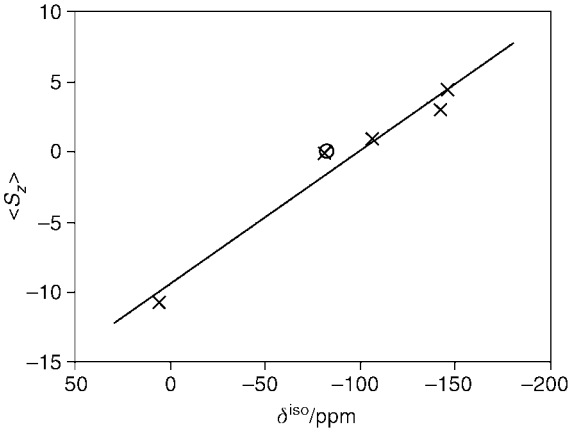

Fig. 2 Variation of $<S_z>$[19] as a function of the ^{29}Si chemical shift of paramagnetic rare-earth LSX (×) and LaLSX (○).

We thank Dr N. Mizuno and Ms S. Uchida for help in the NMR acquisitions at the University of Tokyo and Dr M. D. Williams for the NMR acquisitions performed at Arizona State University. Work at A. S. U. is supported by the U. S. National Science Foundation, Grant DMR 9804817. The NMR equipment was purchased under NSF Grant CHE 9808678.

Notes and references

† The structure of zeolite LSX (Low Silica X), the end-member of the faujasite group, with ratio Si/Al = 1, is composed of strictly alternating SiO_4 and AlO_4 tetrahedra. Faujasite consists of sodalite cages linked together through six-membered rings by oxygen atoms, forming small hexagonal prism cages. The sodalite cages are packed in a diamond-like arrangement forming large cavities with 12-ring openings, the supercages.

‡ Fully-exchanged rare-earth zeolite LSX were prepared by ion-exchanges of (Na,K)LSX (Tosoh Co. Ltd) in an aqueous solution of 0.1 M lanthanide chloride at 373 K for 24 h. Elemental analysis revealed only traces of alkali metal in the final samples.

§ ^{29}Si MAS NMR spectra were recorded at 79.5 MHz. The samples were packed in a 4-mm silicon nitride rotor and spun at 15 kHz. Acquisition parameters were π/4 pulse width, 10 s pulse delay and 2500 scans for diamagnetic samples and π/4 pulse width, 0.1–0.8 s pulse delay and a number of scans around 10000 for paramagnetic samples. Chemical shifts are reported relative to tetramethylsilane with an uncertainty of 2 ppm. Background correction was applied to remove rolling baseline when necessary.

1 F. N. Guerzoni and J. Abbot, *Appl. Catal. A*, 1995, **127**, 41.
2 Y. Wada, T. Okubo, M. Ryo, T. Nakazawa, Y. Hasegawa and S. Yanagida, *J. Am. Chem. Soc.*, 2000, **122**, 8583.
3 T. Watanabe, H. Shimizu, A. Masuda and H. Saito, *Chem. Lett.*, 1983, 1293.
4 E. Oldfield, R. A. Kinsey, K. A. Smith, J. A. Nichols and R. J. Kirkpatrick, *J. Magn. Reson.*, 1983, **51**, 325.
5 J. G. Nery, M. V. Giotto, Y. P. Mascarenhas, D. Cardoso, F. M. Z. Zotin and E. F. Sousa-Aguiar, *Microporous Mesoporous Mater.*, 2000, **41**, 281.
6 A. Labouriau, K. C. Ott, J. Rau and W. L. Earl, *J. Phys. Chem. B*, 2000, **104**, 5890.
7 D. H. Olson, G. T. Kokotailo and J. P. Charnell, *J. Colloid Interface Sci.*, 1968, **28**, 305.
8 H. S. Park and K. Seff, *J. Phys. Chem. B*, 2000, **104**, 2224.
9 M. T. Teller and G. Wong, *J. Chem. Soc., Chem. Commun.*, 1988, 1103.
10 W. DeW. Horrocks, *NMR of Paramagnetic Molecules*, ed. G. N. La Mar, W. DeW. Horrocks and R. H. Holm, Academic Press, New York, 1973, ch. 12.
11 J. A. Peters, J. Huskens and D. J. Raber, *Prog. Nucl. Magn. Reson. Spectrosc.*, 1996, **28**, 283.
12 V. P. Chacko, S. Ganapathy and R. G. Bryant, *J. Am. Chem. Soc.*, 1983, **105**, 5491.
13 M. Bose, M. Bhattacharya and S. Ganguli, *Phys. Rev. B*, 1979, **19**, 72.
14 C. P. Grey, C. M. Dobson, A. K. Cheetham and R. J. B. Jakeman, *J. Am. Chem. Soc.*, 1989, **111**, 505.
15 S. Yang, J. Shore and E. Oldfield, *J. Magn. Reson.*, 1992, **99**, 408.
16 A. Sobel, *J. Phys. Chem. Solids*, 1967, **28**, 185.
17 A. Nayeem and J. P. Yesinowski, *J. Chem. Phys.*, 1988, **89**, 4600.
18 J. P. Jesson, *NMR of Paramagnetic Molecules*, ed. G. N. La Mar, W. DeW. Horrocks and R. H. Holm, Academic Press, New-York, 1973, ch. 1.
19 R. M. Golding and M. P. Halton, *Aust. J. Chem.*, 1972, **25**, 2577.
20 R. Bleaney, *J. Magn. Reson.*, 1972, **8**, 91.

CHEMCOMM
Communication
www.rsc.org/chemcomm

Universal hybridization using LNA (locked nucleic acid) containing a novel pyrene LNA nucleotide monomer

B. Ravindra Babu and Jesper Wengel*

Department of Chemistry, University of Southern Denmark, DK-5230 Odense M, Denmark. E-mail: jwe@chem.sdu.dk

Received (in Cambridge, UK) 9th July 2001, Accepted 21st August 2001
First published as an Advance Article on the web 2nd October 2001

A novel pyrene LNA nucleotide monomer is shown to mediate universal hybridization when incorporated into a DNA strand or a 2′-OMe-RNA/LNA chimeric strand. For the latter, high-affinity universal hybridization without compromising the base-pairing selectivity of bases neighbouring the universal pyrene LNA nucleotide monomer is documented.

Currently, there is much focus on the development of chemically modified nucleotide monomers for universal hybridization, *i.e.* so-called universal bases able to bind isoenergically with each of the natural bases.[1] The main applications of these universal bases are as primers for degenerate PCR reactions or as hybridization probes. Promising universal bases with a 2-deoxy-β-D-ribofuranosyl moiety have been reported, *e.g.* 3-nitropyrrole,[2] 5-nitroindole,[3] pyrene,[4] isocarbostyril[5] and 8-aza-7-deazaadenine[6] derivatives. While incorporation of one of these monomers into a DNA strand induces little variation in the melting temperature (T_m value) when placed opposite the four natural DNA bases (ΔT_m ~1–3 °C), decreases in the T_m value of between 4 to 10 °C per universal nucleotide monomer incorporated compared to the corresponding fully complementary reference DNA–DNA duplex are typical.[1–7] Therefore, improved binding affinity beside applicability in PCR-based applications have been considered desirable properties of an ideal universal base.[1,5]

Stimulated by the work of Kool and collaborators on hybridization using non-polar aromatic moieties as replacements of the natural bases,[4,8] we became interested in studying LNA (locked nucleic acid)[9–12] derivatives containing non-polar aromatic moieties.† The hybridization properties of LNA are characterised by very high binding affinity and strong Watson–Crick discrimination[9–12] both as fully modified LNA and as mix-meric LNA also containing, *e.g.* DNA,[9–12] RNA[13] or 2′-OMe-RNA monomers.[14] Matray and Kool showed that the pyrene nucleoside analogue **Py** (Fig. 1) when incorporated into a DNA strand paired in a universal way with the four natural bases with moderately decreased thermal affinity (−4.5 to −6.8 °C). This behaviour was explained by intercalation of the pyrene moiety within the helix.[4] As both synthetic work[15] and NMR studies[16] have indicated the importance of the nucleobases for structural organisation and thus the remarkable binding affinity of LNA, we decided to synthesise LNA containing the derivatives **Ph^L** and **Py^L** (Fig. 1, Table 1),[17] both based on the 2′-*O*,4′-*C*-methylene-β-D-ribofuranosyl moiety known to adopt a locked C3′-*endo* RNA-like furanose conformation.[9–11]

Initially, the hybridization of the oligonucleotides **ON1**–**ON6** (Table 1) towards four 9-mer DNA targets with the central base being each of four natural bases was studied by thermal denaturation experiments.‡ Compared to the DNA reference **ON1**,[10] introduction of one abasic LNA monomer **Ab^L** (**ON2**) has earlier been reported to prevent the formation of a stable duplex above 0 °C (only evaluated with adenine as the opposite base).[15] With the phenyl monomer **Ph^L** (**ON3**), thermal denaturation with T_m values in the range of 5–12 °C was observed. Thus, compared to **Ab^L**, the phenyl moiety stabilises the duplexes, but universal hybridization is not achieved—a preference for an adenine complement being observed instead. In addition, significant destabilisation compared to the **ON1**–DNA reference was observed.

The pyrene LNA nucleotide **Py^L** (**ON4**) displays more encouraging properties. Firstly, the binding affinity towards all four complements is increased compared to **ON3** (containing **Ph^L**). Secondly, universal hybridization is induced as shown by the four T_m values all being within the range 17–19 °C. With

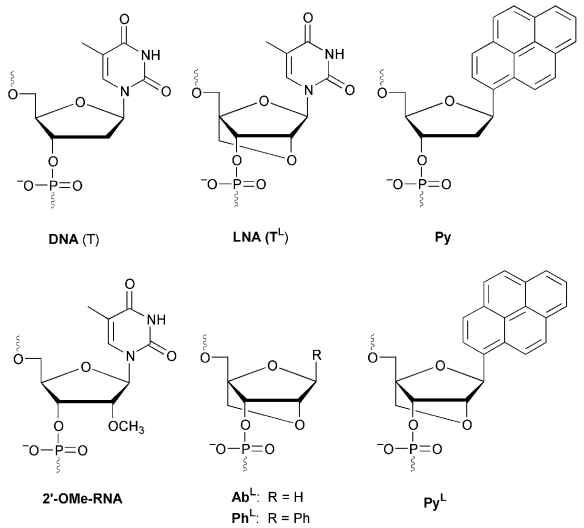

Fig. 1 Structures of selected nucleotide monomers: DNA (T), LNA (**T^L**), pyrenyl DNA (**Py**), 2′-OMe-RNA [2′-OMe(T)], abasic LNA (**Ab^L**), phenyl LNA (**Ph^L**), and pyrenyl LNA (**Py^L**). The short notations shown are used in Tables 1 and 2. For DNA, LNA and 2′-OMe-RNA, the thymine monomers are shown as examples.

Table 1 Thermal denaturation experiments (T_m/°C values shown) for **ON1**–**ON6** towards DNA complements 3′-d(CACT**Y**TACG) with each of the four natural bases in the central position[a]

		Y			
		A	C	G	T
ON1	5′-d(GTGATATGC)[10]	28	11	12	19
ON2	5′-d(GTGA**Ab^L**ATGC)[15]	< 3	nd	nd	nd
ON3	5′-d(GTGA**Ph^L**ATGC)	12	5	6	7
ON4	5′-d(GTGA**Py^L**ATGC)	18	17	18	19
ON5	2′-OMe(GTGATATGC)	35	14	19	21
ON6	2′-OMe(G**T^L**GA**Py^L**A**T^L**GC)	39	38	37	40

[a] Melting temperatures (T_m/°C values) measured as the maximum of the first derivative of the melting curve (A_{260} *vs.* temperature) recorded in medium salt buffer (10 mM sodium phosphate, 100 mM sodium chloride, 0.1 mM EDTA, pH 7.0) using 1.5 μM concentrations of the two strands; A = adenine monomer, C = cytosine monomer, G = guanine monomer, T = thymine monomer; See Fig. 1 for structures of **T^L**, **Ab^L**, **Ph^L** and **Py^L**; DNA sequences are shown as d(sequence) and 2′-OMe-RNA sequences as 2′-OMe(sequence); 'nd' denotes 'not determined'.

 DOI: 10.1039/b106065c

respect to universal hybridization, **Py^L** thus parallels the pyrene DNA derivative **Py**,[4] but the decrease in thermal stability compared to the **ON1**–DNA reference is more pronounced for **Py^L** (~10 °C) than reported for **Py** (~5 °C in a 12-mer polypyrimidine DNA sequence[4]). It therefore appears that stacking (or intercalation) by the pyrene moiety is not favoured by the conformational restriction of the furanose ring of **Py^L**, although a comparison of the thermal stabilities of **ON2**, **ON3** and **ON4** strongly indicates interaction of the pyrene moiety within the helix.

The effect of **Py^L** could be different in an RNA-like strand, and we therefore synthesised **ON5** and **ON6**, the former being composed entirely of 2′-OMe-RNA monomers and the latter of six 2′-OMe-RNA monomers, two LNA thymine monomers **T^L**, and one central LNA pyrene monomer **Py^L**. A sequence corresponding to **ON6** but with three **T^L** monomers has earlier been shown to form a duplex with complementary DNA of very high thermal stability.[14] **ON6** is therefore suitable for evaluation of the effect of introducing high-affinity monomers around a universal base. As seen in Table 1, the 2′-OMe-RNA reference **ON5** binds to the DNA complement with slightly increased thermal stability and conserved Watson–Crick discrimination (compared to the DNA reference **ON1**). Indeed, the 2′-OMe-RNA/LNA chimera **ON6** displays universal hybridization behaviour as revealed from the four T_m values (37, 38, 39 and 40 °C). All four T_m values obtained for **ON6** are higher than the T_m values obtained for the two fully complementary reference duplexes **ON1**–DNA (T_m = 28 °C) and **ON5**–DNA (T_m = 35 °C). These data demonstrate that the pyrene LNA monomer **Py^L** displays universal hybridization behaviour both in a DNA context (**ON4**) and in an RNA-like context (**ON6**), and that the problem of decreased affinity of universal hybridization probes can be solved by the introduction of high-affinity monomers, *e.g.* 2′-OMe-RNA and/or LNA monomers.

Very recently, the effect of the universal 3-nitropyrrole DNA nucleotide on the base-pairing selectivity of neighbouring natural bases was for the first time systematically studied.[7] Reduced discriminatory ability was demonstrated in some cases suggesting caution when using this universal base in hybridization probes.[7] We therefore performed a systematic thermal denaturation study with **ON6** (Table 2). For each of the four DNA complements (monomer **Y** = A, C, G or T) used in the study shown in Table 1, **ON6**, containing a central pyrene LNA monomer **Py^L**, was hybridised with all four base combinations in the neighbouring position towards 3′-end of **ON6** (monomer **Z** = A, C, G or T, monomer **X** = T) and the same towards the 5′-end of **ON6** (monomer **X** = A, C, G or T, monomer **Z** = T). In all eight subsets of four data points, satisfactory to excellent Watson–Crick discrimination was observed between the match and the three mismatches (ΔT_m values in the range 5–25 °C).

Table 2 Thermal denaturation experiments (T_m/°C values shown) to evaluate the base-pairing selectivity of the bases neighbouring the universal pyrene LNA monomer **Py^L** in the 2′-OMe-RNA/LNA chimera **ON6**. In the target strand [3′-d(CAC**XYZ**ACG)], the central three bases **XYZ** are varied among each of the four natural bases[a]

XYZ	T_m/°C	XYZ	T_m/°C	XYZ	T_m/°C	XYZ	T_m/°C
TAA	26	TCA	22	TGA	22	TTA	29
TAC	26	TCC	29	TGC	26	TTG	31
TAG	24	TCG	24	TGG	30	TTC	32
TAT	*39*	TCT	*38*	TGT	*37*	TTT	*40*
AAT	18	ACT	27	AGT	22	ATT	28
CAT	30	CCT	31	CGT	27	CTT	35
GAT	14	GCT	28	GGT	16	GTT	27
TAT	*39*	TCT	*38*	TGT	*37*	TTT	*40*

[a] See caption below Table 1 for abbreviations and conditions used; the data for matched neighbouring bases (**X** = **Z** = T) are shown in italic.

The results reported herein have several implications for the design of probes for universal hybridization. Firstly, universal hybridization is possible with a conformationally restricted monomer as demonstrated for the pyrene LNA monomer. Secondly, universal hybridization behaviour is feasible in an RNA context. Thirdly, the binding affinity of probes for universal hybridization can be increased by the introduction of high-affinity monomers without compromising the base-pairing selectivity of bases neighbouring the universal base.§

We thank The Danish Research Agency and Exiqon A/S for financial support, Ms Britta M. Dahl for oligonucleotide synthesis, and Dr Carl E. Olsen for MALDI-MS analyses.

Notes and references

† We have defined LNA as an oligonucleotide containing one or more conformationally locked 2′-*O*,4′-*C*-methylene-β-D-ribofuranosyl nucleotide monomer(s).[9]

‡ MALDI-MS ([M − H]$^-$; found/calcd.: **ON3** 2731/2733; **ON4** 2857/2857; **ON6** 3094/3093). The purity of **ON3**, **ON4** and **ON6** was verified as >80% by capillary gel electrophoretic analysis.

§ We are currently evaluating chimeric oligonucleotides containing pyrene and other known universal bases attached to various backbones (*e.g.* LNA-type monomers, ribofuranose monomers or deoxyribose monomers in 2′-OMe-RNA–LNA oligos). One purpose of these further experiments is to evaluate the possibility of obtaining similar results as for the 2′-OMe-RNA/LNA oligo **ON6** at a lower cost, *e.g.* by substituting **Py^L** with a pyrenyl-2′-OMe-ribonucleotide monomer.

1 D. Loakes, *Nucleic Acids Res.*, 2001, **29**, 2437 and references therein.
2 R. Nichols, P. C. Andrews, P. Zhang and D. E. Bergstrom, *Nature*, 1994, **369**, 492.
3 D. Loakes and D. M. Brown, *Nucleic Acids Res.*, 1994, **22**, 4039.
4 T. J. Matray and E. T. Kool, *J. Am. Chem. Soc.*, 1998, **120**, 6191.
5 M. Berger, Y. Wu, A. K. Ogawa, D. L. McMinn, P. G. Schultz and F. E. Romesberg, *Nucleic Acids Res.*, 2000, **28**, 2911.
6 F. Seela and H. Debelak, *Nucleic Acids Res.*, 2000, **28**, 3224.
7 J. S. Oliver, K. A. Parker and J. W. Suggs, *Org. Lett.*, 2001, **3**, 1977.
8 E. T. Kool, J. C. Morales and K. M. Guckian, *Angew. Chem. Int. Ed.*, 2000, **39**, 990 and references herein.
9 S. K. Singh, P. Nielsen, A. A. Koshkin and J. Wengel, *Chem. Commun.*, 1998, 455.
10 A. A. Koshkin, S. K. Singh, P. Nielsen, V. K. Rajwanshi, R. Kumar, M. Meldgaard, C. E. Olsen and J. Wengel, *Tetrahedron*, 1998, **54**, 3607.
11 S. Obika, D. Nanbu, Y. Hari, J. Andoh, K. Morio, T. Doi and T. Imanishi, *Tetrahedron Lett.*, 1998, **39**, 5401.
12 J. Wengel, A. Koshkin, S. K. Singh, P. Nielsen, M. Meldgaard, V. K. Rajwanshi, R. Kumar, J. Skouv, C. B. Nielsen, J. P. Jacobsen, N. Jacobsen and C. E. Olsen, *Nucleosides Nucleotides*, 1999, **18**, 1365.
13 S. K. Singh and J. Wengel, *Chem. Commun.*, 1998, 1247.
14 J. Wengel, M. Petersen, K. E. Nielsen, G. A. Jensen, A. E. Håkansson, R. Kumar, M. D. Sørensen, V. K. Rajwanshi, T. Bryld and J. P. Jacobsen, *Nucleosides, Nucleotides Nucleic Acids*, 2001, **20**, 389.
15 L. Kværnø and J. Wengel, *Chem. Commun.*, 1999, 657.
16 K. E. Nielsen, S. K. Singh, J. Wengel and J. P. Jacobsen, *Bioconjugate Chem.*, 2000, **11**, 228.
17 The synthesis of *C*-nucleosides corresponding to **Ph^L** and **Py^L**, as well as their oligomerization will be described elsewhere; B. R. Babu, A. K. Prasad and J. Wengel, manuscript in preparation.

CHEMCOMM Communication
www.rsc.org/chemcomm

Characterization of an oxaluric acid derivative as a guanine oxidation product

Christel Seguy, Geneviève Pratviel* and Bernard Meunier*

Laboratoire de Chimie de Coordination du CNRS, 205 route de Narbonne, 31077 Toulouse cedex 4, France

Received (in Cambridge, UK) 26th July 2001, Accepted 13th September 2001
First published as an Advance Article on the web 2nd October 2001

The oxidation of guanine in the dinucleoside monophosphate d(GpT) by an oxo-metalloporphyrin generates a linear oxaluric acid† derivative after heating at 65 °C for 30 min and at neutral pH.

Guanine is the most easily oxidizable nucleobase of DNA by electron abstraction since it has the lowest ionization potential.[1] The 8-oxo-7,8-dihydroguanine (8-oxo-G) derivative was reported to be one of the products of guanine oxidation by one-electron transfer.[2,3] However many other oxidation products were described including an imidazolone derivative,[4–7] a dehydroguanidinohydantoin[8,9] and a dihydroxylated derivative of guanine at C5 and C8.[8,10] These products are not highly stable under physiological conditions. Imidazolone is transformed into an oxazolone derivative[11] upon hydrolysis. The half-life of imidazolone in water at 37 °C is 2.5 h.[12] The structures of imidazolone and oxazolone derivatives are well documented.[12] The dehydroguanidinohydantoin compound was recently analyzed by NMR after stabilization by reduction into the corresponding guanidinohydantoin.[9] The half-life of dehydroguanidinohydantoin in water is 5 h at 37 °C[13] or 8 h at 0 °C.[9] The hydrolysis product of dehydroguanidinohydantoin is proposed to be an oxaluric acid derivative arising from the hydrolysis of a postulated parabanic acid intermediate (Scheme 1). Considering the short half-life of dehydroguanidinohydantoin, its hydrolysis product may be important *in vivo* as a guanine lesion. In order to determine the exact structure of this compound, we report here the ^{1}H NMR analysis of the oxaluric acid derivative, **d(OxapT)** (see Scheme 1), obtained from the two-electron oxidation of guanine in a dinucleoside monophosphate **d(GpT)**.

This oxaluric acid derivative was initially described in the literature as the oxidation product of 8-oxo-G but not in the oxidation of guanine itself. Oxidation products of 8-oxo-G were more studied than those of guanine oxidation. This is due to the easier oxidation of 8-oxo-G compared to that of guanine by available reagents.[13–17] When the guanine oxidation products arise from an intermediate oxidation at C8, they are identical to the products generated in the oxidation of 8-oxo-G. In the oxidation of 8-oxo-G by peroxynitrite, a nitration product of the dehydroguanidinohydantoin derivative was formed and its hydrolysis product, an oxaluric acid derivative, was analyzed by NMR.[17] This oxaluric acid derivative, was analyzed after incubation of the nitrodehydroguanidinohydantoin derivative for 2 days at ambient temperature. The oxidation of 8-oxo-G by singlet oxygen also gave a dehydroguanidinohydantoin derivative that was transformed into an oxaluric acid lesion.[13] The latter was analyzed by electrospray MS/MS after incubation of the reaction medium for 2 or 9 h at 37 °C. The structure of the oxaluric acid derivative obtained in this work from the oxidation of guanine was compatible with the two previously proposed structures from 8-oxo-G oxidation.[13,17]

The oxidation of guanine was performed by a cationic manganese porphyrin, Mn–TMPyP,[18] activated by $KHSO_5$, an oxygen atom donor. Oxo-Mn(v)–TMPyP is able to mediate a two-electron oxidation of guanine.[7–9] The high yield in guanine oxidation allowed us to isolate the products of guanine oxidation and to analyse them by NMR on the simplified DNA model, a dinucleoside monophosphate **d(GpT)**. The oxidation of guanine on this substrate led to two products, an imidazolone and a dehydroguanidinohydantoin derivative, referred to as **d(G+4pT)** since it corresponds to an increase of 4 amu compared to **d(GpT)**.[9]

In order to obtain the NMR data of the oxaluric acid derived from **d(G+4pT)**, the oxidation reaction of **d(GpT)** was carried out on a semi-preparative scale. The starting dinucleoside monophosphate **d(GpT)** (3 mM, 3.4 mg) was incubated with Mn–TMPyP (16 μM) and $KHSO_5$ (3.5 mM) in 80 mM TEAA, triethylammonium acetate buffer pH 6.5, at 0 °C for 10 min (final concentrations are indicated, total reaction volume = 2 mL). The reaction was stopped by the addition of HEPES buffer pH 8 (35 mM) and the products were separated by semi-preparative HPLC. This individual reaction was repeated 10 times to obtain enough material. The isolation of the oxidation

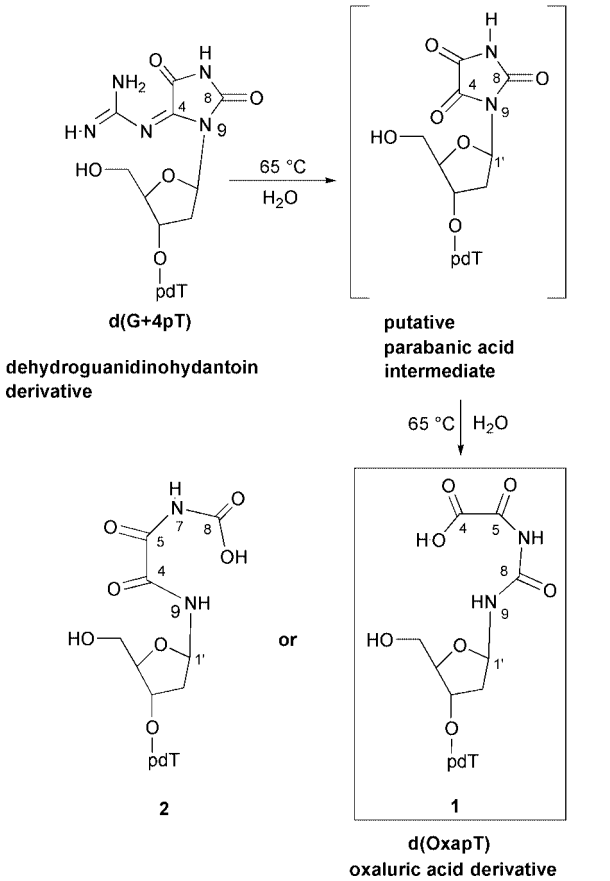

Scheme 1 Oxidation of **d(GpT)** by Mn–TMPyP–$KHSO_5$ leads to a dehydroguanidinohydantoin derivative, **d(G+4pT)**, that undergoes hydrolysis upon heating. The resulting product is an oxaluric acid derivative, **d(OxapT)**, corresponding to the highlighted structure **1** (the numbering of atoms being that of the initial guanine).

 DOI: 10.1039/b106799k

Table 1 ^{1}H NMR data [δ (ppm)] for **d(OxapT)** in DMSO-d_6

	Deoxyribose							Oxa			Thymine		
	H1′	H2′ H2″	H3′	H4′	H5′ H5″	3′-OH	5′-OH	COOH	NH	NH	CH_3	H6	NH
Oxa	5.62 (q)	1.91–2.14 (m)	4.51 (m)	3.79–3.85 (m)	3.39–under DMSO (m)		5.35–5.38	9.4 (br s)	9.61 (s)	8.59 (d) $^3J_{HH}$ = 9.4 Hz			
T	6.21 (t)	1.91–2.14 (m)	4.28 (m)	3.79–3.85 (m)	3.39–under DMSO (m)	5.35–5.38					1.82 (s)	7.82 (s)	11.24 (s)

product of **d(GpT)** was done by collecting the products eluted from a reverse phase semi-preparative column (nucleosil C18, 10 μm, 250 × 6.2 mm from Interchrom, France) eluted in a gradient mode at 2 mL min^{-1}. The gradient was from 1 to 20% of CH_3CN for 1 h by combination of the two eluents, solvent A = 10 mM TEAA pH 6.5, solvent B = solvent A containing 20% CH_3CN (detection was at 260 nm). The reaction volume (2 mL) was injected directly. The collected **d(G+4pT)** fractions were pooled together and lyophilized to reduce the collected volume. The pooled fractions were then heated at 65 °C for 30 min (reaction volume = 1 mL). The hydrolysis of **d(G+4pT)** was complete under these conditions. The oxaluric acid derivative **d(OxapT)** was purified again by semi-preparative HPLC for desalting. The dried sample was dissolved in 0.5 mL of NMR solvent (DMSO-d_6). The NMR data are listed in Table 1.[19] The NH protons of the oxaluric acid moiety were at 8.59 and 9.61 ppm. The signal at 8.59 ppm was coupled to the H1' proton of the sugar moiety with a coupling constant of 9.4 Hz. The coupling between NH of the oxaluric acid moiety and H1′ from the sugar was confirmed by a 1D-TOCSY experiment (not shown).[20] These NMR data are in favor of a linear structure for the oxaluric acid derivative without having the possibility of discriminating between the two possible linear structures derived from the hydrolysis of **d(G+4pT)** to **d(OxapT)** **1** or **2** (see Scheme 1). Structures **1** and **2** correspond to the cleavage of the former C4–N9 and C8–N9 bonds of the guanine oxidation product, respectively (the numbering of atoms being that of the initial guanine). However our previous electrospray MS/MS data on **d(OxapT)**[9] are in favor of structure **1**. Structure **2** can be discarded. The fragmentation of oxaluric acid derivative (m/z = 551.0 with z = 1) during negative electrospray mass analyses gave signals at m/z = 479.1, 436.1 and 321.0 corresponding to structure **1**. The 479.1 signal corresponds to a –NH–CO–NH_2 residue attached to the sugar C1′ carbon (cleavage of the N7–C5 bond). The 436.1 signal was attributed to an amino-sugar derivative (cleavage of the N9–C8 bond) and the 321.0, to 2′-deoxythymidine 5′-monophosphate. Depending on the electrospray conditions, the loss of CO_2 due to the decarboxylation of the last carboxylic function can also be observed (cleavage of C4–C5 bond).[8] A signal at m/z = 492 was not observed. It would have corresponded to a –NH–CO–CHO residue attached to the sugar C1′ carbon (cleavage of the N7–C5 bond of structure **2**).

In conclusion the oxidative lesion of guanine, dehydroguanidinohydantoin **d(G+4pT)**, was isolated from the oxidation of **d(GpT)** by Mn–TMPyP–$KHSO_5$. It was transformed into a linear oxaluric acid derivative **d(OxapT)** upon heating at 65 °C for 30 min and at neutral pH. The linear structure of this oxaluric acid lesion is **1**, as depicted in Scheme 1, resulting from the hydrolysis of the C4–N9 bond.

The authors are indebted to Yannick Coppel for recording the NMR data, to Igor Dubey for the synthesis of **d(GpT)** and to Professor Jean Bernadou for fruitful discussions.

Notes and references

† The IUPAC name for oxaluric acid is carbamoyloxamic acid.

1 S. Steenken and S. V. Jovanovic, *J. Am. Chem. Soc*., 1997, **119**, 617.
2 H. Kasai, Z. Yamaizumi, M. Berger and J. Cadet, *J. Am. Chem. Soc*., 1992, **114**, 9692.
3 P. M. Cullis, M. E. Malone and L. A. Merson-Davies, *J. Am. Chem. Soc*., 1996, **118**, 2775.
4 Imidazolone corresponds to 2-amino-5-[(2-deoxy-β-D-*erythro*-pentofuranosyl)amino]-4*H*-imidazol-4-one.
5 D. Gasparutto, J.-L. Ravanat, O. Gérot and J. Cadet, *J. Am. Chem. Soc*., 1998, **120**, 10 283.
6 K. Kino, I. Saito and H. Sugiyama, *J. Am. Chem. Soc*., 1998, **120**, 7373.
7 C. Vialas, G. Pratviel, C. Claparols and B. Meunier, *J. Am. Chem. Soc*., 1998, **120**, 11 548.
8 C. Vialas, C. Claparols, G. Pratviel and B. Meunier, *J. Am. Chem. Soc*., 2000, **122**, 2157.
9 A. Chworos, Y. Coppel, I. Dubey, G. Pratviel and B. Meunier, *J. Am. Chem. Soc*., 2001, **123**, 5867.
10 A. Lapi, G. Pratviel and B. Meunier, *Met.-Based Drugs*, 2001, **8**, 47.
11 Oxazolone corresponds to 2,2-diamino-4-[(2-deoxy-β-D-*erythro*-pentofuranosyl)amino]-2,5-dihydrooxazol-5-one.
12 S. Raoul, M. Berger, G. W. Buchko, P. C. Joshi, B. Morin, M. Weinfeld and J. Cadet, *J. Chem. Soc., Perkin Trans. 2*, 1996, **2**, 371.
13 V. Duarte, D. Gasparutto, L. F. Yamaguchi, J.-L. Ravanat, G. R. Martinez, M. H. G. Medeiros, P. Di Mascio and J. Cadet, *J. Am. Chem. Soc*., 2000, **122**, 12 622.
14 W. Luo, J. G. Muller, E. M. Rachlin and C. J. Burrows, *Org. Lett*., 2000, **2**, 613.
15 W. Luo, J. G. Muller, E. M. Rachlin and C. J. Burrows, *Chem. Res. Toxicol*., 2001, 927.
16 J. C. Niles, S. Burney, S. P. Singh, J. S. Wishnok and S. R. Tannenbaum, *Proc. Natl. Acad. Sci. USA*, 1999, **96**, 11 729.
17 J. C. Niles, J. S. Wishnok and S. R. Tannenbaum, *Chem. Res. Toxicol*., 2000, **13**, 390.
18 Mn–TMPyP stands for manganese(III)-bis-aqua-*meso*-tetrakis(4-*N*-methylpyridinium-4-yl)porphyrin.
19 ^{1}H NMR spectrum was recorded on a Bruker AMX400 spectrometer. The chemical shifts are relative to TMS using the solvent shift as a secondary standard.
20 The 1D-TOCSY was performed with T_m = 30 ms.

CHEMCOMM
Communication
www.rsc.org/chemcomm

Single crystal particles of a mesoporous mixed transition metal oxide with a wormhole structure†

Byongjin Lee,[a] Daling Lu,[b] Junko N. Kondo[a] and Kazunari Domen*[ab]

[a] *Chemical Resources Laboratory, Tokyo Institute of Technology, 4529 Nagatsuta-cho, Midori-ku, Yokohama 226-8503, Japan. E-mail: kdomen@res.titech.ac.jp*
[b] *Core Research for Evolutional Science and Technology, Japan Science and Technology, 2-1-13 Higashiueno, Taito-ku, Tokyo 110-0015, Japan*

Received (in Cambridge, UK) 22nd May 2001, Accepted 13th September 2001
First published as an Advance Article on the web 2nd October 2001

A new type of mesoporous mixed transition metal oxide of Nb and Ta (NbTa-TIT-1) has been prepared through a two-step calcination, which consists of single crystal particles with wormhole mesoporous structure.

Recently, various types of mesoporous materials have been extensively synthesized. However, the walls of all the synthesized mesoporous materials are amorphous. Mesoporous materials possessing crystallized wall structure would show mechanical, thermal and hydrothermal stability, and are expected to have applications other than catalysis[1] such as for semiconductors,[2] optical devices[2] and fuel cells,[3,4] *etc*. Moreover, electronic transfer throughout the crystallized framework could enable wide application in nanotechnology.

Neutral templating routes for syntheses of inorganic mesoporous materials have introduced thick wall structures to silica with wormhole-like,[5–8] lamellar,[9,10] cubic[10] or hexagonal[10,11] mesostructures. Successful applications of these methods to other mesoporous metal oxides have shown the great utility of the synthetic procedure.[12,13] Following a typical neutral block copolymer templating route in ref. 12, we have attempted to produce various mixed metal oxides with mesoporous structure. Our efforts have been focused especially on the formation of mesopores among crystallized wall structures. Initially, we prepared niobium–tantalum mixed oxide, which has a stable oxidation state. Almost identical atomic and ionic radii might lead to full solid solubility and mixing, and are expected to promote stable crystallization.[14] In this communication, we report on the synthesis of a crystallized niobium–tantalum (1 : 1) mixed oxide with mesoporous structure.

In the synthetic route, neutral block copolymer was employed as a template for the mesoporous structure. 0.005 mol of $TaCl_5$ and $NbCl_5$ were added to 1 g of poly(alkylene oxide) block copolymer $HO(CH_2CH_2O)_{20}(CH_2CH(CH_3)O)_{70}(CH_2CH_2O)_{20}H$ (Pluronic P-123, BASF) dissolved in 10 g of ethanol. After vigorous stirring for 30 min, the resulting sol solution was aged at 40 °C in air for 7 days. Crystallized mesoporous material was obtained by a two-step calcination. First, the template was completely removed by calcination at 400 °C for 20 h to form the precursor, and in the second step the sample was calcined at 650 °C for 1 h to yield the final product. X-Ray diffraction (XRD) patterns for the two-step calcined sample confirmed crystallization of the wall structure. All the peaks can be assigned to the orthorhombic-like structure of a $(Nb,Ta)_2O_5$ mixed oxide.

To study the details of the crystallized sample, observations by transmission electron microscopy (TEM) were carried out. Fig. 1(a) presents the TEM image of a particle (*ca*. 500 nm) and its electron diffraction (ED) pattern (inset) which is typical with respect to particle size and lattice structure of the product calcined at 650 °C. The crystallinity of the sample was determined by TEM observation of diffraction patterns of 50 particles sized from 100 to 1000 nm. From the observation, we confirmed >90% of the particles were totally crystallized. Three-dimensional open pores and the wormhole-like mesoporosity are identified. The mean pore diameter is roughly estimated as 10 nm and the wall thickness is >5 nm. Fig. 1(b) shows the lattice image obtained at the edge of the particle. It demonstrates clearly the crystallized lattice of the wall around a pore. Analysis of the particle by ED and high resolution TEM observation demonstrate that this particle is a single crystal. We collected ED patterns from 10 local regions of the particle in 250-nm range and confirmed the identical patterns. (Detailed analysis will be reported elsewhere.) The regular spot patterns of the whole region and each local area indicate that the whole

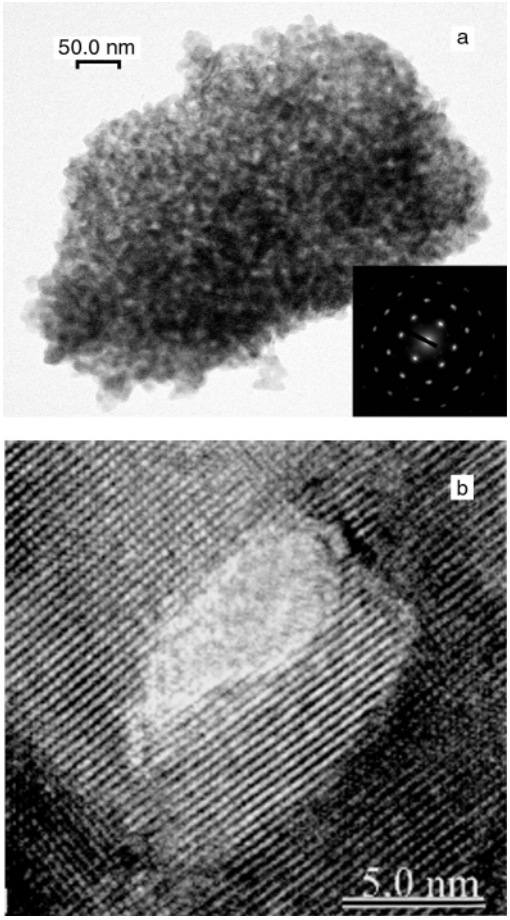

Fig. 1 TEM image and electron diffraction pattern of the sample calcined at 650 °C for 1 h (a) and the high resolution TEM image of a mesopore and wall structure (b). The images were recorded with a 200 kV JEOL JEM2010F system.

† Electronic supplementary information (ESI) available: Fig. S1: XRD patterns; Table S1: comparison of XRD data of niobium, tantalum oxides and NbTa-TIT-1; Table S2: typical EDX results of NbTa-TIT-1. See http://www.rsc.org/suppdata/cc/b1/b104516b/

 DOI: 10.1039/b104516b

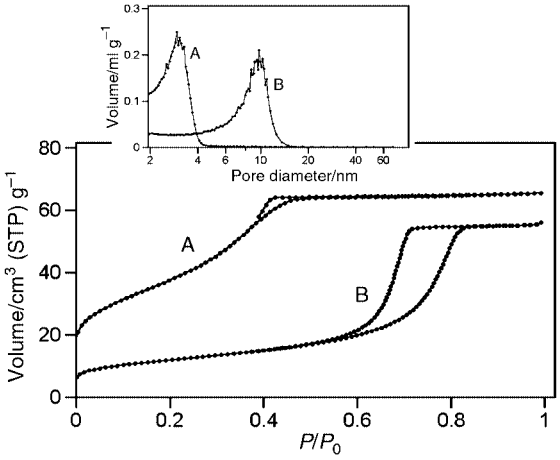

Fig. 2 Nitrogen gas adsorption–desorption isotherm and pore-size distribution (inset) of the sample calcined at 400 °C for 20 h (curve A) and that calcined at 650 °C for 1 h in the second-step (curve B). Data was collected with a Coulter Omnisorp 100CX system.

particle is crystallized in the same direction. We also carefully observed several successive lattice images of a 100 nm-region and the whole particle was confirmed to have exactly the same periodic atomic arrays. It is, therefore, concluded that this particle is a single crystal with wormhole-like mesoporous structure. From these results we conclude that the mesoporosity does not arise from the agglomeration or aggregation of smaller crystallites. Although the typical particle size of the sample after the second-step calcination was in the sub-μm range, there were particles over μm-size. They were confirmed to consist of several single crystal domains of sub-μm size. Energy dispersive X-ray (EDX) analysis on various regions (several hundreds nm in diameter for each region) in a whole particle indicated that Nb and Ta atoms were homogeneously mixed in each region, *i.e.* the particle is confirmed to be $(Nb,Ta)_2O_5$ mixed oxide.

The mesoporosity of the sample after the second-step calcination was testified by the N_2 adsorption–desorption isotherm and Barrett–Joyner–Halenda (BJH) pore size distribution analysis in the adsorption branch of the isotherm (curve B) as shown in Fig. 2. The results are also compared with the sample before the second-step calcination (curve A). Both samples indicate type IV isotherms, which are attributed to typical mesoporous structure.[15] The hysteresis loop in the isotherm curve of the crystallized sample (curve B) indicates a network pore system, *i.e.* mesopores run through the particles with a wormhole trace and form three-dimensionally complex pore media. The maximum of the pore size distribution of the sample calcined at 650 °C for 1 h of *ca.* 10 nm (Fig. 2, inset, curve B) agrees well with the TEM result. It should be noted that pore diameter expansion due to the crystallization is observed; the pore diameter of 4 nm before calcination at 650 °C (Fig. 2, inset, curve A) disappeared, while a new peak at around 10 nm appeared after the second-step calcination (Fig. 2, inset, curve B). The Brunaer–Emmett–Teller (BET) surface area decreased from 140 to 48 $m^2\ g^{-1}$ after the second-step calcination. The considerably high surface area for the crystallized oxide is a result of the mesoporous structure.

Results from TEM observation and N_2 adsorption isotherms clearly confirm the formation of single crystal particles of $(Nb,Ta)_2O_5$ with wormhole mesoporous structure. We denote this new type of single crystal particles of oxides with mesopores as M-TIT (M denotes a metal in metal oxide) type material, and we classify an M-TIT with wormhole-like mesoporous structure as M-TIT-1. The present sample is thus represented as NbTa-TIT-1. In the cases of pure Nb_2O_5 and Ta_2O_5, the wormhole-like mesoporous materials were obtained after the first-step calcination at 400 °C. However, crystallization in the second-step calcination led to the destruction of the mesoporous structure. Therefore, the mixing of two components is preferable for the preparation of M-TIT-1 materials in addition to the stepwise calcination.

The NbTa-TIT-1 showed mechanical and hydrothermal stability: no structure and surface area changes were confirmed by N_2 adsorption isotherms even after mechanical pressing at 500 kgf cm^{-2} for 17 h and after hydrothermal treatment at 200 °C and at 20 atm for 24 h.

It is reasonably expected that for other combination of metals, TIT-type materials may be formed. In preliminary results, ZrNb-TIT-1, ZnNb-TIT-1 and MgTa-TIT-1 have been prepared by the two-step calcination method. Indeed, we believe that the hexagonal-arrayed TIT series also can be prepared. Further investigation for wide variety of components is now in progress.

Notes and references

1 Y. Yue and Z. Gao, *Chem. Commun*., 2000, 1755.
2 L. W. Miller, M. I. Tejedor, B. P. Nelson and M. A. Anderson, *J. Phys. Chem. B*, 1999, **103**, 8490.
3 M. Mamak, N. Coombs and G. Ozin, *Adv. Mater*., 2000, **12**, 198.
4 F. Chen, Z. Shi and M. Liu, *Chem. Commun*., 2000, 2095.
5 P. T. Tanev and T. J. Pinnavaia, *Science*, 1995, **267**, 865.
6 S. A. Bagshaw, E. Prouzet and T. J. Pinnavaia, *Science*, 1995, **269**, 1242.
7 E. Prouzet and T. J. Pinnavaia, *Angew. Chem., Int. Ed. Engl*., 1997, **36**, 516.
8 E. Prouzet, F. Cot, G. Nabias, A. Larbot, P. Kooyman and T. J. Pinnavaia, *Chem. Mater*., 1999, **11**, 1498.
9 P. T. Tanev, Y. Liang and T. J. Pinnavaia, *J. Am. Chem. Soc*., 1997, **119**, 8616.
10 D. Zhao, Q. Huo, J. Feng, B. F. Chmelka and G. D. Stucky, *J. Am. Chem. Soc*., 1998, **120**, 6024.
11 D. Zhao, J. Feng, Q. Huo, N. Melosh, G. H. Fredrickson, B. F. Chmelka and G. D. Stucky, *Science*, 1998, **279**, 548.
12 P. Yang, D. Zhao, D. I. Margolese, B. F. Chemlka and G. D. Stucky, *Nature*, 1998, **396**, 152.
13 P. Yang, D. Zhao, D. I. Margolese, B. F. Chmelka and G. D. Stucky, *Chem. Mater*., 1999, **11**, 2813.
14 D. Lupton, F. Aldinger and K. Schulze, in *Proceedings of the International Symposium, Niobium '81*, San Francisco, CA, November 8–11, 1981.
15 S. Lowell and J. E. Shields, *Adsorption by Powders and Porous Solids. Principles, Methodology and Applications*, Academic Press, San Diego, 1999, ch. 7.

CHEMCOMM Communication
www.rsc.org/chemcomm

Living polymerization and block copolymerization of α-olefins by an amine bis(phenolate) titanium catalyst†

Edit Y. Tshuva,[a] Israel Goldberg,[a] Moshe Kol*[a] and Zeev Goldschmidt*[b]

[a] *School of Chemistry, Raymond and Beverly Sackler Faculty of Exact Sciences, Tel Aviv University, Tel Aviv 69978, Israel. E-mail: moshekol@post.tau.ac.il*
[b] *Department of Chemistry, Bar-Ilan University, Ramat-Gan, 52900, Israel. E-mail: goldz@mail.biu.ac.il*

Received (in Cambridge, UK) 21st June 2001, Accepted 3rd September 2001
First published as an Advance Article on the web 2nd October 2001

An amine bis(phenolate) dibenzyl titanium complex having a methoxy donor on a side arm leads, upon activation with tris(pentafluorophenyl)borane, to unique living properties in α-olefin polymerization: exceptionally high molecular weight poly(1-hexene) is obtained in a living fashion at room temperature, living polymerization of 1-hexene is obtained above room temperature, and block copolymerization of 1-hexene and 1-octene at room temperature is described as well.

The quest for new α-olefin polymerization catalysts has involved many research groups for half a century. A recent addition to the arsenal of polymerization possibilities is the ability to produce polymers having narrow molecular weight distributions, and living polymerization processes. The vast majority of living processes are possible only below room temperature,[1] and the molecular weights of the polymers obtained in living processes are usually not very high. These systems are rarely utilized for block copolymerization of different monomers,[1c–e] since complete consumption of the monomer in a living fashion, followed by resumption of the polymerization process upon addition of the second monomer is difficult to achieve. Thus, all block copolymerization processes of α-olefins known to date are conducted below room temperature.

Recently, various Cp-free group IV metal complexes have been introduced as polymerization catalysts.[2] The most widely studied ligands are of the diamido type,[3] and one such system was the first to lead to living polymerization of α-olefins at room temperature.[1a] On the other hand, living polymerization involving alkoxo-type ligands[4] is quite rare.[1b,c] In this communication we introduce an amine bis(phenolate) titanium complex which, upon activation with tris(pentafluorophenyl)borane, leads to a polymerization process having unique living manifestations.

We recently introduced the amine bis(phenolate) group IV metal complexes and their application in α-olefin polymerization.[5–9] We revealed a unique effect of an extra donor arm in a titanium based catalyst on the complex reactivity and the termination/propagation rate ratio:[6] an [ONNO]-type complex was found to lead to living polymerization of 1-hexene, whereas an [ONO]-type complex led only to oligomerization of that monomer.

In our search for modified living catalysts of this family, we turned to a ligand having a side oxygen donor (Scheme 1).[9] We were interested in evaluating the effect of such a side donor, expected to bind strongly to the metal, on the living nature of a potential polymerization process. Furthermore, we wanted to explore the limits of the living process, in terms of polymerization time, molecular weight obtained, percentage of conversion and reaction temperature.

1 reacted cleanly with 1 mol equiv. of titanium tetra(isopropoxide) yielding the bis(isopropoxide) complex quantitatively. This complex was further reacted with 2 mol equiv. of chlorotrimethylsilane followed by reaction of the product with 2 mol equiv. of benzyl magnesium chloride, yielding the dibenzyl titanium complex **1a** in an overall yield of 95% (Scheme 1).

The ^{1}H NMR data are consistent with the formation of a C_s-symmetrical complex having two equivalent phenolate rings bound to the metal in a *trans* configuration, and two different benzyl groups bound in a *cis* configuration. The X-ray structure of **1a** (Fig. S1, ESI†) supported this notion, and indicated binding of the methoxy group to the titanium atom.‡

Upon activation with $B(C_6F_5)_3$, **1a** was found to be reactive in the polymerization of neat 1-hexene, exhibiting a reactivity of 20-35 g $mmol_{cat}^{-1}$ h^{-1}.§ The polymerization process induced by **1a** was found to be living for an exceptionally long time: as long as 31 hours, as expressed in the linearity of the molecular weight dependence on time (Fig. 1).[1a,e]

This system represents a rare example of living polymerization of α-olefins at room temperature.[1] Moreover, the long period at which the system remains living gives rise to a polymer having an exceptionally high molecular weight of M_w = 445 000 with a PDI of 1.12.

As this catalyst led to such a well-behaved polymerization at room temperature, it was interesting to find the temperature at which it lost its living nature. Increasing the reaction temperature to 40 °C in chlorobenzene resulted in a living process. The polymer obtained after 1 hour had a molecular weight of M_w = 16 000 with a PDI value of 1.14. Thus, this system gives rise to a rare living polymerization of α-olefins above room temperature. At 55 °C the PDI obtained was found to be 1.25 (M_w = 18 000 after one hour), and further broadening of the PDI to 1.30 (M_w = 22 000 after one hour) was obtained upon a temperature increase to 65 °C.

The most important application of living polymerization is in block copolymerization.[10] 16 μmol of **1a** were dissolved in 2.50 g of chlorobenzene, and 110 mol equiv. of 1-hexene were added. Activation with approximately 1 mol equiv. of $B(C_6F_5)_3$ dissolved in 2.50 g of chlorobenzene resulted in a living process characterized by a narrow PDI of 1.2. After 3.5 hours, complete consumption of the monomer was observed, and a polymer having a molecular weight of M_n = 9000 was obtained, supporting the polymerization of the 1-hexene employed in a living fashion (expected M_w = 9400). To further ascertain the complete consumption of the first monomer, the second monomer (1-octene) was added only after a 1.5 hours delay period (Fig. 2), resulting in resumption of the polymerization process. Stopping the polymerization after an additional 3 hours

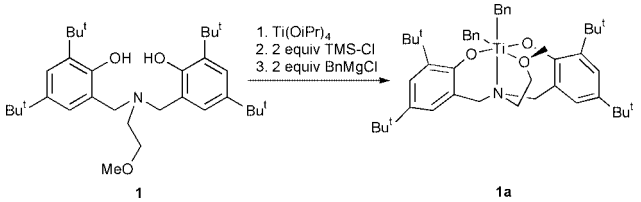

1 **1a**

Scheme 1

† Electronic supplementary information (ESI) available: Fig. S1: molecular structure of **1a**. Preparation and characterization data for **1a**. Crystallographic data for **1a**. See http://www.rsc.org/suppdata/cc/b1/b105492a/

 DOI: 10.1039/b105492a

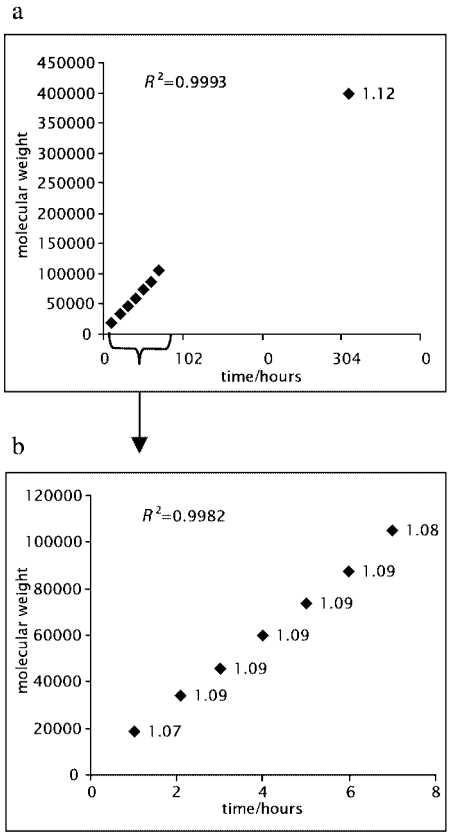

Fig. 1 Dependence of the number average molecular weight (M_n) on time (hours) using 20 mg of **1a** and 1.1 mol equiv. of $B(C_6F_5)_3$ in 30 mL of neat 1-hexene at RT and PDI values. (a) 31 hours of reaction, (b) first 7 hours of reaction.

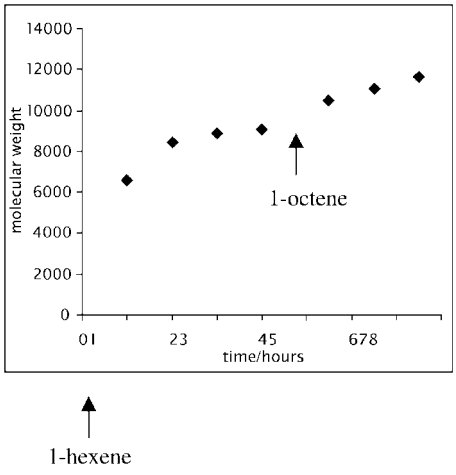

Fig. 2 Dependence of the number average molecular weight (M_n) on time (hours) in the block copolymerization of 1-hexene and 1-octene using **1a**.

yielded poly(1-hexene-block-1-octene) having M_n = 11 600 and PDI of 1.2. A ^{13}C NMR spectrum of the resulting polymer supported its assignment as an atactic copolymer of 1-hexene and 1-octene. This is a rare example of block copolymerization of α-olefins conducted at room temperature.

In summary, we present a catalytic system for polymerization of α-olefins that exhibits several unique living properties. When conducted at room temperature, the polymerization of neat 1-hexene is practically 'immortal'. Even when the reaction is allowed to stand for days, the only cause of loss of 'life' is the increased viscosity of the polymerization mixture. Thus, very high molecular weights may be obtained with extremely narrow PDI values. A solution of the monomer in chlorobenzene (diluted to enable its complete consumption) was employed for block copolymerization of α-olefins to give a di-block of homopolymers, at room temperature. We are currently studying related systems and the polymerization mechanism by which they operate.

This research was supported by the Israel Ministry of Science, Culture and Sports, and was also supported in part by the Israel Science Foundation founded by the Israel Academy of Sciences and Humanities. We thank Sima Alfi (BIU) for technical assistance.

Notes and references

‡ CCDC reference number 166843. See http://www.rsc.org/suppdata/cc/b1/b105492a/ for crystallographic data in CIF or other electronic format.

§ In a typical polymerization of neat 1-hexene, 14 mg of **1a** (19 μmol) were added to 10.0 mL of neat 1-hexene and activated with 1 equiv. of $B(C_6F_5)_3$ at room temperature. The reaction was followed by taking 0.50 mL aliquots, weighing out the non-volatile residue, and analyzing it by GPC relative to polystyrene standards. This analysis indicated a linear consumption of the monomer and linear rise in molecular weight. A sample taken after 150 min showed a reactivity of 23.5 g $mmol_{cat}^{-1}$ h^{-1}, consistent with a TOF of 280 h^{-1}, giving an expected molecular weight of 58 800. The GPC analysis gave M_w = 55 600, M_n = 50 200, and PDI = 1.11. In a typical polymerization of dilute 1-hexene, 31 mg of **1a** (42 μmol) and 27 mg of $B(C_6F_5)_3$ were added to 502 mg of 1-hexene in 5.00 g of chlorobenzene at room temperature. A sample taken after 160 min indicated that all the monomer had been consumed. The expected molecular weight is 12 000. The GPC analysis gave M_w = 11700, M_n = 10 200 and PDI = 1.15. Occasionally, the weight of the obtained polymer was found to be lower than expected, probably due to incomplete catalyst activation, however, the TOFs were consistent with the values specified above.

1 For living polymerization at room temperature, see: (*a*) J. D. Scollard and D. H. McConville, *J. Am. Chem. Soc*., 1996, **118**, 10008; (*b*) E. Y. Tshuva, I. Goldberg and M. Kol, *J. Am. Chem. Soc*., 2000, **122**, 10706; (*c*) J. Tian, P. D. Hustad and G. W. Coates, *J. Am. Chem. Soc*., 2001, **123**, 5134. For living polymerization below room temperature, see: (*d*) K. C. Jayaratne, R. J. Keaton, D. A. Henningsen and L. R. Sita, *J. Am. Chem. Soc*., 2000, **122**, 10490; (*e*) C. M. Killan, D. J. Tempel, L. K. Johnson and M. Brookhart, *J. Am. Chem. Soc*., 1996, **118**, 11664; (*f*) K. C. Jayaratne and L. R. Sita, *J. Am. Chem. Soc*., 2000, **122**, 958; (*g*) R. Baumann, W. M. Davis and R. R. Schrock, *J. Am. Chem. Soc*., 1997, **119**, 3830; (*h*) Y.-M. Jeon, S. J. Park, J. Heo and K. Kim, *Organometallics*, 1998, **17**, 3161; (*i*) Y. Doi, S. Suzuki and K. Soga, *Macromolecules*, 1986, **19**, 2896; (*j*) H. Hagihara, T. Shiono and T. Ikeda, *Macromolecules*, 1998, **31**, 3184; (*k*) K. Mashima, S. Fujikawa and A. Nakamura, *J. Am. Chem. Soc*., 1993, **115**, 10990; (*l*) Y. Doi, S. Ueki and T. Keii, *Macromolecules*, 1979, **12**, 814; (*m*) Y. Fukui, M. Murata and K. Soga, *Macromol. Rapid. Commun*., 1999, **20**, 637.

2 G. J. P. Britovsek, V. C. Gibson and D. F. Wass, *Angew. Chem., Int. Ed.*, 1999, **38**, 428.

3 For recent reviews of amido ligands, see: (*a*) L. H. Gade, *Chem. Commun*., 2000, 173; (*b*) R. Kempe, *Angew. Chem., Int. Ed*., 2000, **39**, 468.

4 (*a*) A. van der Linden, C. J. Schaverien, N. Neijboom, C. Ganter and A. G. Orpen, *J. Am. Chem. Soc*., 1995, **117**, 3008; (*b*) E. B. Tjaden, D. C. Swenson, R. F. Jordan and J. L. Petersen, *Organometallics*, 1995, **14**, 371; (*c*) L. Matilainen, M. Klinga and M. Leskala, *J. Chem. Soc., Dalton Trans*., 1996, 219; (*d*) P. Shao, R. L. A. Gendron, D. J. Berg and G. W. Bushnell, *Organometallics*, 2000, **19**, 509; (*e*) S. Fokken, T. P. Spaniol, J. Okuda, F. G. Sernetz and R. Mulhaupt, *Organometallics*, 1997, **16**, 4240; (*f*) X. Bei, D. C. Swenson and R. F. Jordan, *Organometallics*, 1997, **16**, 3282; (*g*) M. G. Thorn, Z. C. Etheridge, P. E. Fanwick and I. P. Rothwell, *Organometallics*, 1998, **17**, 3636.

5 E. Y. Tshuva, M. Versano, I. Goldberg, M. Kol, H. Weitman and Z. Goldschmidt, *Inorg. Chem. Commun*., 1999, **2**, 371.

6 E. Y. Tshuva, I. Goldberg, M. Kol and Z. Goldschmidt, *Inorg. Chem. Commun*., 2000, **3**, 610.

7 E. Y. Tshuva, I. Goldberg, M. Kol, H. Weitman and Z. Goldschmidt, *Chem. Commun*., 2000, 379.

8 E. Y. Tshuva, I. Goldberg, M. Kol and Z. Goldschmidt, *Organometallics*, 2001, **20**, 3017.

9 E. Y. Tshuva, I. Goldberg, M. Kol and Z. Goldschmidt, submitted.

10 M. Hillmyer, *Curr. Opin. Solid State Mater. Sci*., 1999, **4**, 559.

11 (*a*) SIR-92: A. Altomare, M. C. Burla, M. Camalli, M. Cascarano, C. Giacovazzo, A. Guagliardi and G. Polidori, *J. Appl. Crystallogr*., 1994, **27**, 435; (*b*) P. T. Beurskens, G. Beurskens, W. P. Bosman, R. de Gelder, S. Garcia-Granda, R. O. Gould, R. Israel and J. M. M. Smits, *DIRDIF-96, Crystallographic Laboratory*, University of Nijmegen, The Netherlands, 1996.

12 G. M. Sheldrick, SHELXL-97, Program for the refinement of crystal structures from diffraction data, University of Göttingen, Germany, 1997.

CHEMCOMM
Communication
www.rsc.org/chemcomm

Simultaneous combination of *in situ*-EPR/UV–VIS/on line GC: a novel setup for investigating transition metal oxide catalysts under working conditions

Angelika Brückner

Institut für Angewandte Chemie Berlin-Adlershof e. V. Richard-Willstätter-Str.12, D-12489 Berlin, Germany. E-mail: ab@aca-berlin.de

Received (in Cambridge, UK) 3rd August 2001, Accepted 12th September 2001
First published as an Advance Article on the web 2nd October 2001

***In situ*-EPR, *in situ*-UV–VIS spectroscopy and on line-GC have been for the first time simultaneously combined to follow the behaviour of lanthanum-doped CrO_x/ZrO_2 and CrO_x/Al_2O_3 catalysts during the dehydrogenation of propane to propene.**

Understanding the role of active sites in solid catalysts under working conditions is a major research goal in heterogeneous catalysis and a number of spectroscopic techniques have been adapted in recent years to study solid catalysts during reaction,[1] among them UV–VIS diffuse reflectance[2,3] and EPR spectroscopy.[4,5] These techniques provide complementary information on the structure and valence state of transition metal ions (TMI) during reaction. For example, Cr^{6+} species are not visible by EPR but do give rise to intense charge-transfer (CT) transitions in the UV–VIS spectrum while EPR is able to distinguish between Cr^{5+} and Cr^{3+} sites of different structure.[2,6] A similar situation arises, *e.g.* for different valence states in vanadia-based catalysts.[7]

In this work, both techniques have been for the first time coupled to each other and to on line-GC to widen the variety of TMI that can be simultaneously monitored under reaction conditions. Moreover, this set-up ensures identical reaction conditions for both spectroscopic techniques that are almost equal to those usually applied in catalytic tests since a fixed-bed flow reactor of similar dimensions is used. Thus, limitations in the comparability of spectroscopic results are eliminated that otherwise might arise from variations of the reaction conditions when different *in situ*-cells are used for separate EPR and UV–VIS measurements.

Combined *in situ*-EPR/UV–VIS measurements were performed using a home-made flow reactor[4,5] which was implemented in the rectangular cavity of a c.w. spectrometer ELEXSYS 500-10/12 (Bruker) operating in X-band. Details of the flow reactor are described elsewhere.[4] Simultaneous UV–VIS reflectance spectra were recorded by a fibre optics AVS-PC-2000 plug-in spectrometer (Avantes) equipped with a CCD array detector responsive from 200 to 1100 nm. The two channels of the spectrometer (master: 200–500 nm; slave: 500–1100 nm) as well as a DH-2000 deuterium-halogen light source were connected to a cylindrical quartz sensor (Optran WF, length 200 mm, diameter 1.5 mm) by fibre optic cables (length 2 m) consisting of a core of pure silica (diameter 0.4 mm) coated with polyimide. The sensor fits into the reactor through a Teflon sealing disk which is fixed by a screwing at the top end of the reaction tube. The tip of the sensor is a plane polished surface and is placed within the catalyst bed. The feed-through of the thermocouple at the bottom end of the reaction tube is realized in the same way. For on line product analysis, the reactor outlet was connected to a GC 17AAF capillary gas chromatograph (Shimadzu) equipped with a 30 m × 0.32 mm Silicaplot column (Chrompack) and a FID. The main features of the arrangement are schematically displayed in the graphic contents entry.

This setup has been used to study the dehydrogenation of propane to propene over two CrO_x catalysts: (a) $Cr/La,Al_2O_3$ prepared by thermal decomposition of ammonium dawsonite, $NH_4Al(OH)_2CO_3$, doped with 10 wt% Cr and 3.9 wt% La and (b) $Cr//La,ZrO_2$ prepared by impregnating a commercial 7 wt% La_2O_3/ZrO_2 support (MEL-CAT XZ0681/01, MEL Chemicals) with an aqueous $(NH_4)_2CrO_4$ solution to result in a Cr loading of 0.5 wt% followed by calcination at 873 K.[6] Doping by La was used since La is known to stabilize the Cr species on the surface.[8] The BET surface areas were 345 $m^2\,g^{-1}$ ($Cr/La,Al_2O_3$) and 104 $m^2\,g^{-1}$ ($Cr//La,ZrO_2$). In each run, 125 mg catalyst particles (250–355 μm) were treated in a flow of 23% C_3H_8/N_2 (W/F = 16.2 g h mol^{-1}).

The as-synthesized catalysts contain mainly hexavalent chromate species evidenced by intense CT bands around 370 nm in the UV–VIS spectra [Fig. 1(a) and 2(a)][9] besides traces of Cr^{5+} species that give rise to the very narrow singlet at $g' \approx 1.97$ in the EPR spectra [Fig. 1(b) and 2(b)]. The as-synthesized sample $Cr/La,Al_2O_3$ contains also a certain amount of Cr^{3+} reflected by a broad d–d transition band around 630 nm [Fig. 1(a)].[9] Upon heating under feed, the CT bands of chromate

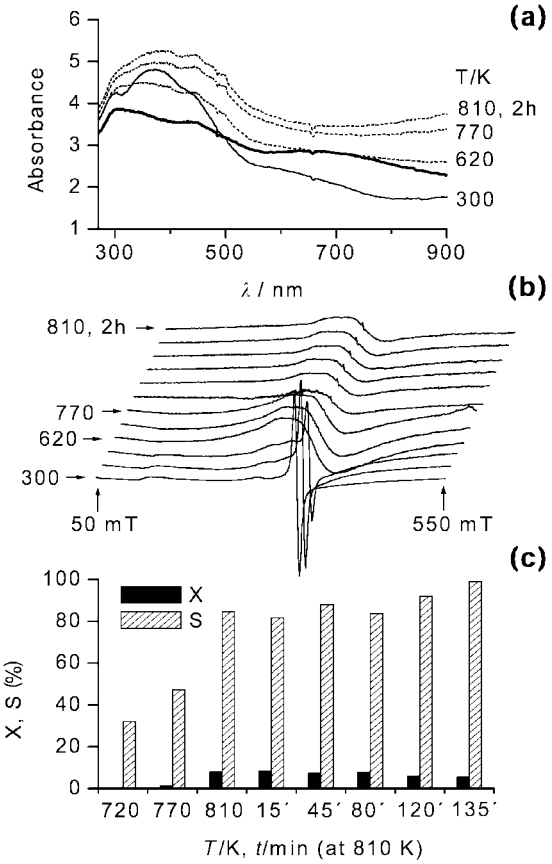

Fig. 1 UV–VIS (a) and EPR (b) spectra alongside propane conversion and propene selectivity results during heating of the $Cr/La,Al_2O_3$ catalyst in a flow of 23% C_2H_8/N_2. For comparison the UV–VIS spectrum at 810 K in H_2 flow is also shown (thick line).

 DOI: 10.1039/b107005c

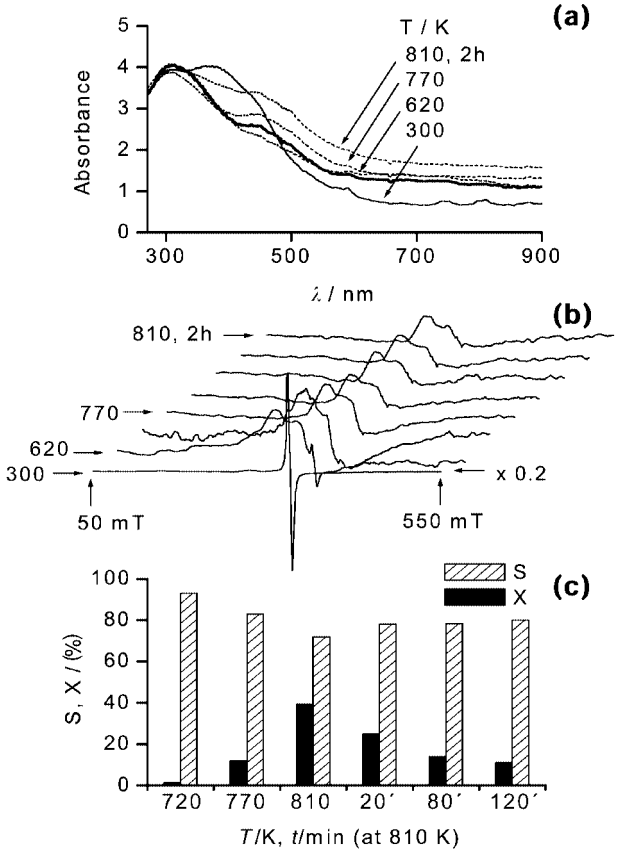

Fig. 2 UV–VIS (a) and EPR (b) spectra alongside propane conversion and propene selectivity results during heating of the $Cr/La,ZrO_2$ catalyst in a flow of 23% C_2H_8/N_2. For comparison the UV–VIS spectrum at 810 K in H_2 flow is also shown (thick line).

around 370 nm vanish and d–d bands of Cr^{3+} appear in the UV–VIS spectra [Fig. 1(a) and 2(a)]. Simultaneously, the narrow EPR singlets of Cr^{5+} disappear and a broad singlet at $g' \approx 2$ arises from weakly interacting Cr^{3+} species [Fig. 1(b) and 2(b)]. By comparing these results with the catalytic data [Fig. 1(c) and 2(c)] it is clearly evident that the reduction of Cr^{6+} and Cr^{5+} to Cr^{3+} occurs already at temperatures well below the onset of the dehydrogenation reaction. This information cannot be derived post mortem from measurements of quenched catalysts and shows that Cr sites in oxidation states higher than +3 do not exist under reaction conditions. With increasing time on stream at 810 K the propane conversion over the $Cr/La,ZrO_2$ catalyst drops markedly [Fig. 2(c)]. This is due to the partial coverage of active Cr^{3+} sites by coke deposits.[6] As a consequence, the EPR singlet of Cr^{3+} loses intensity since magnetic interaction with paramagnetic coke species may cause line broadening. In the UV–VIS spectra, deactivation leads to a gradual increase of absorbance in the visible range of the spectrum with a maximum around 470 nm arising from higher condensed carbon species such as polyaromatics and condensed rings.[10]

In comparison to sample $Cr/La,ZrO_2$, the $Cr/La,Al_2O_3$ catalyst is, despite a higher BET surface area and Cr content, less active but more stable against deactivation [Fig. 1(c)]. As for $Cr/La,ZrO_2$, carbon deposits are also formed with increasing time on stream. However, the maximum of absorbance is shifted to lower wavelength around 360 nm being characteristic of less condensed rather linear polyenylic species[10] which might be less deactivating [Fig. 1(a)]. Unfortunately, the d–d bands of Cr^{3+} ions and bands of the different carbonaceous deposites fall partially in the same wavelength range. However, the contribution of the carbon deposits to the overall absorbance is readily evident by comparing the UV–VIS spectra at 810 K in H_2 flow [thick line in Fig. 1(a) and 2(a)] reflecting only bands of reduced Cr species with those in propane/N_2 flow. The latter show higher absorbance even at 620 K when propane conversion is still below the detection limit. This suggests that carbon deposits start to form quite early but probably need to exceed a certain polymerization degree to become deactivating. Again, this is a result that cannot be obtained from *ex situ*-measurements of deactivated catalysts. The lower activity of the $Cr/La,Al_2O_3$ catalyst is most probably due to the fact that most of the Cr ions are incorporated in Al lattice positions of the catalyst bulk and, thus, not accessible by reactants. This is also supported by XPS measurements that reveal a markedly lower Cr concentration on the surface than in the bulk already for the as-synthesized catalyst which is expected to decrease even more upon reduction during time on stream. This behaviour is well known for Cr/Al_2O_3 catalysts.[9] In contrast to $Cr/La,ZrO_2$ catalysts[8] this obviously can not markedly be prevented by doping with La.

The obtained results demonstrate that the simultaneous coupling of *in situ*-EPR/UV–VIS/on-line-GC is a powerful new tool to follow the reaction-dependent interconversion of different Cr oxidation states and the deactivation behaviour of CrO_x catalysts.

Dr I. Pitsch and Dr D. L. Hoang are thanked for providing the catalyst samples as are the German Federal Ministry of Education and Research for financial support (grant no. 03C0280).

Notes and references

1 *Catalyst Characterization under Reaction Conditions*, ed. G. A. Somorjai and J. M. Thomas, *Top. Catal.*, 1999, **8** (1/2).
2 B. M. Weckhuysen, A. A. Verberckmoes, J. Debaere, K. Ooms, I. Langhans and R. A. Schoonheydt, *J. Mol. Catal. A: Chemical*, 2000, **151**, 115.
3 X. Gao, M. A. Bãnares and I. E. Wachs, *J. Catal.*, 1999, **188**, 325.
4 A. Brückner, B. Kubias and B. Lücke, *Catal. Today*, 1996, **32**, 215.
5 H. G. Karge, J.-P. Lange, A. Gutsze and M. Laniecki, *J. Catal.*, 1988, **114**, 144.
6 A. Brückner, J. Radnik, D.-L. Hoang and H. Lieske, *Catal. Lett.*, 1999, **60**, 183.
7 P. Rybarczyk, H. Berndt, J. Radnik, M.-M. Pohl, O. Buyevskaya, M. Baerns and A. Brückner, *J. Catal.*, 2001, **202**, 45.
8 A. Trunschke, D. L. Hoang, J. Radnik and H. Lieske, *J. Catal.*, 2000, **191**, 456.
9 B. M. Weckhuysen, L. M. De Ridder and R. A. Schoonheydt, *J. Phys. Chem.*, 1993, **97**, 4756.
10 H. G. Karge, M. Laniecki, M. Ziolek, G. Onyestyak, A. Kiss, P. Kleinschmit and M. Siray, in *Zeolites: Facts, Figures, Future*, ed. P. A. Jacobs and R. A. van Santen, Elsevier, Amsterdam, 1989, p. 1327.

CHEMCOMM Communication
www.rsc.org/chemcomm

Ion-exchange as a mode of cation transfer into room-temperature ionic liquids containing crown ethers: implications for the 'greenness' of ionic liquids as diluents in liquid–liquid extraction

Mark L. Dietz* and Julie A. Dzielawa

Chemistry Division, Argonne National Laboratory, 9700 S. Cass Avenue, Argonne, IL 60439, USA. E-mail: mdietz@anl.gov; Fax: +1-630-252-7501; Tel: +1-630-252-3647

Received (in Cambridge, UK) 17th May 2001, Accepted 5th September 2001
First published as an Advance Article on the web 2nd October 2001

The transfer of strontium ion from acidic nitrate media into a series of 1-alkyl-3-methylimidazolium-based room-temperature ionic liquids containing dicyclohexano-18-crown-6 is shown to proceed *via* cation-exchange, in contrast to conventional solvents such as alkan-1-ols, in which extraction of a strontium nitrato-crown ether complex is observed.

Room-temperature ionic liquids (RTILs) have recently garnered increasing attention as environmentally benign alternatives to conventional organic solvents in a variety of synthetic,[1] catalytic,[2] and electrochemical[3] applications, a result of their unique physical and chemical properties and the relative ease with which these properties can be fine-tuned by altering the cationic or anionic moieties comprising the RTIL.[4] Very recent efforts by several investigators have focused on the application of ionic liquids in separations,[5–9] in particular, on the utility of these materials as replacements for the organic diluents employed in traditional liquid–liquid separations of organic solutes[5,6] or metal ions,[7–9] generally with encouraging results. Dai *et al*.,[7] for example, have demonstrated that highly efficient extraction of strontium ion from water ($D_{Sr} > 10^4$) can be achieved when dicyclohexano-18-crown-6 (DCH18C6) is combined with various water-immiscible 3-methylimidazolium-based RTILs, and thus, that ionic liquids offer considerable potential as diluents in metal ion separations. Full realization of this potential, however, requires a greater understanding of the metal ion partitioning process in these systems than is now available. To this end, we have examined the extraction of strontium ion from acidic nitrate media by DCH18C6 (a mixture of the A and B isomers) dissolved in a series of 1-alkyl-3-methylimidazolium (alkyl = ethyl, *n*-butyl, *n*-pentyl, *n*-hexyl, or *n*-octyl) bis[(trifluoromethyl)sulfonyl]-amides (abbreviated as C_n mim$^+$ Tf_2N^-, with n = 2, 4, 5, 6, or 8).† Comparison of the results to those obtained using a series of *n*-alkanols as diluents is shown to provide insight into the process of metal ion extraction by crown ethers in the RTILs.

Measurements of the dependency on crown ether concentration of the distribution ratio, D_{Sr} (defined as $[Sr]_{org}/[Sr]$, where the subscript 'org' and the absence of a subscript designate organic and aqueous phase species, respectively), for strontium extraction from nitric acid solution into the five RTILs yield lines of unit slope, consistent with the partitioning of a 1:1 strontium–crown ether complex ($Sr{\cdot}CE^{2+}$). The linearity of these dependencies contrasts with the non-linear dependencies observed for DCH18C6 in *n*-alkanols,[11] indicating that unlike extraction into the more conventional solvents,[11,12] the equilibrium aqueous phase concentration of the strontium–crown ether complex is not high in the RTIL systems under the experimental conditions.

As is well known, the extraction of a metal ion from an aqueous solution into an organic solvent requires that electroneutrality be maintained.[13] In conventional solvent systems involving the use of a neutral extractant, such as in the extraction of metal ions into an *n*-alkanol by a crown ether, this is achieved by aqueous phase anion coextraction. In the extraction of Sr^{2+} from nitric acid into octan-1-ol by DCH18C6,[11] for example, the 1:1 strontium–crown ether complex is accompanied by two nitrate ions:

$$Sr{\cdot}CE^{2+} + 2\ NO_3^- \rightleftharpoons Sr(NO_3)_2{\cdot}CE_{org} \quad (1)$$

For this process, the following equilibrium expression can be written:[11]

$$K'_{ex,Sr} = D_{Sr}\,[NO_3^-]^{-2}\,[CE]_{org}^{-1} \quad (2)$$

where $K'_{ex,Sr}$ is the conditional extraction constant and CE represents the crown ether. Not unexpectedly, the nitric acid dependency of D_{Sr} for DCH18C6 in such systems is characterized by increasing strontium partitioning with increasing nitrate (*i.e*. nitric acid) concentration. For example, D_{Sr} rises from 0.0025 at 0.010 M HNO_3 to 4.2 at 3.0 M acid for a 0.50 M solution of DCH18C6 in octan-1-ol. In contrast, the nitric acid dependency of D_{Sr} in the $C_n$mim$^+$ systems exhibits a significant decline in strontium partitioning as the acidity is increased. For a 0.1 M solution of DCH18C6 in C_2mim$^+Tf_2N^-$, for example, D_{Sr} falls from 468 at 0.010 M HNO_3 to 18 at 3.0 M acid. Such a result, while consistent with previously reported results in related $C_n$mim$^+PF_6^-$ systems,[9] is clearly inconsistent with the extraction of a strontium nitrato–crown complex [eqn. (1)]. (It is important to note here that repeated contact of the ionic liquids with an excess of an aqueous phase containing a high concentration of nitric acid results in the gradual disappearance of the organic phase, an apparent result of the replacement of Tf_2N^- by nitrate.)

A further indication that the observed strontium partitioning into the RTILs does not involve nitrate ion coextraction is found in the acid dependencies of D_{Sr} for DCH18C6 in C_2mim$^+Tf_2N^-$ using HCl or H_2SO_4 solutions as the aqueous phase, both of which differ little from that observed with HNO_3. Prior studies of the effect of anion on the extraction of metal ions by neutral extractants into various organic solvents have demonstrated that the need to dehydrate the anion upon phase transfer and the significant differences in the hydration energy between anions (*e.g*. $\Delta G_{hydration}$ = 293 and 318 kJ mol^{-1} for nitrate and chloride, respectively[14]) typically give rise to substantial differences in the extraction of, for example, metal nitrates and chlorides.[11] Although these differences diminish when the organic solvent is capable of dissolving high concentrations of water (thereby facilitating transfer of a hydrated anion) they remain significant. In fact, a factor of 73 difference in strontium extraction into octan-1-ol by DCH18C6 from HCl and HNO_3 has been observed, despite the presence of more than 2 M water in the solvent.[11] The absence of an appreciable anion effect in the extraction of strontium into C_2mim$^+Tf_2N^-$, particularly given the fact that the solvent, like other related RTILs[7] dissolves only a modest amount ($\leqslant$2% w/w) of water, thus strongly suggests that strontium partitioning in the $C_n$mim$^+$ systems does not involve nitrate ion coextraction.

When an ionic liquid, rather than a conventional organic solvent, is employed as a diluent for metal ion extraction by a neutral extractant, there are two other means by which

 DOI: 10.1039/b104349h

electroneutrality could conceivably be maintained. First, the anionic component of the RTIL, here the bis[(trifluoromethyl)sulfonyl]amide anion, arising in the aqueous phase from solubilization of the RTIL, could serve as the counterion:

$$Sr^{2+} + 2\ Tf_2N^- + CE_{org} \rightleftharpoons Sr(Tf_2N)_2{\cdot}CE_{org} \quad (3)$$

In the alternative, strontium partitioning could involve not extraction, but rather exchange of the strontium–crown ether complex, $Sr{\cdot}CE^{2+}$, for the cationic constituent of the ionic liquid, here $C_n mim^+$:

$$Sr{\cdot}CE^{2+} + 2\ C_n mim^+_{org} \rightleftharpoons Sr{\cdot}CE^{2+}_{org} + 2\ C_n mim^+ \quad (4)$$

for which the following equilibrium expression can be written:

$$K'_{ix,Sr} = [Sr{\cdot}CE^{2+}]_{org}\,[C_n mim^+]^2\,[Sr{\cdot}CE^{2+}]^{-1}\,[C_n mim^+]_{org}^{-2} \quad (5)$$

where $K'_{ix,Sr}$ is the conditional exchange constant. Obviously, in this case, no anion coextraction is required to maintain electroneutrality.

If extraction of a complex incorporating Tf_2N^- counterions is indeed occurring, conditions that increase the aqueous concentration of the anion would be expected to yield the highest distribution ratios. This is not the case, however. That is, although increasing nitric acid concentration is accompanied by greater aqueous solubility of the RTILs, higher acidity is also accompanied (as already noted) by decreasing D_{Sr} values. This result, together with the apparent absence of nitrate ion coextraction and the poor strontium extraction observed in the absence of the crown ether, strongly suggests that strontium partitioning in these systems involves the process depicted in [eqn. (4)].

Additional support for this conclusion is found in Fig. 1A, which depicts the relationship between the conditional partition constant for strontium and the number of carbon atoms in the alkyl group of the 1-alkyl-3-methylimidazolium cation. If we assume, as implied by eqn. (4), that differences in the extent of strontium partitioning into the various RTILs arise from differences in the free energy of transfer of the various $C_n mim^+$ cations from the organic to the aqueous phase, then previously reported values of ΔG associated with the transfer of a methylene unit from water to a water–hydrocarbon interface (-3.0 to -3.5 kJ mol^{-1})[15] or from water into a bulk hydrocarbon (-3.7 kJ mol^{-1})[16] imply that a plot of log $K'_{ix,Sr}$ *vs.* n should yield a line whose slope lies in the range -0.53 to -0.66, consistent with the observed slope of Fig. 1A (-0.64). Not unexpectedly, the analogous plot of log $K'_{ex,Sr}$ [as per eqn. (2)] *vs.* n for a series of alkan-1-ols [Fig. 1(B)] does not yield such a line, providing yet another indication that the process involved in strontium partitioning in the RTIL systems differs from that observed for conventional organic diluents.

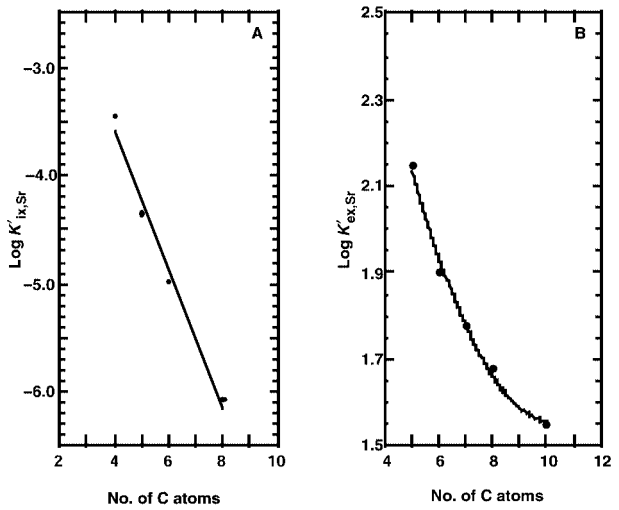

Fig. 1 Dependence of the conditional partition constants for strontium in DCH18C6–$C_n mim^+$ Tf_2pN^- (panel A; 0.1 M HNO_3) or alkan-1-ol (panel B; 1.0 M HNO_3) systems on the alkyl chain length of the solvent. (The solid line in panel A represents the line of best fit, while that in panel B is intended only as a guide to the eye.)

That ion-exchange may constitute the predominant mode by which a cation is transferred into an RTIL in the presence of a neutral extractant would seem to have significant implications for the 'greenness' of these solvents in the area of liquid–liquid extraction. That is, eqn. (4) indicates that increasing metal ion extraction will be accompanied by increasing solubilization of the RTIL in the aqueous phase, as the $M{\cdot}CE^{2+}$ complex is exchanged for $C_n mim^+$. Indeed, while the water solubility of $C_5mim^+Tf_2N^-$, for example, is only 0.03 M, this solubility is increased by 0.066, 0.082, and 0.093 M upon extraction of 0.030, 0.040 and 0.05 M $Sr(NO_3)_2$, respectively, into a 0.10 M solution of DCH18C6 in it, a result consistent with the 2:1 $C_n mim^+$:$Sr{\cdot}CE^{2+}$ stoichiometry depicted in eqn. (4). Thus, although RTILs clearly offer advantages in terms of enhanced extraction efficiency and reduced volatility *vs.* conventional organic solvents, these advantages may be diminished by aqueous phase solubility losses when they are employed as diluents in certain metal ion extraction applications. Work to further delineate the benefits and limitations of RTILs as separation media is now underway in this laboratory.

This work was performed under the auspisces of the Office of Basic Energy Sciences, Division of Chemical Sciences, United States Department of Energy, under contract No. W-31-109-ENG-38.

Notes and references

† The ionic liquids were prepared according to published methods.[10] The aqueous phase solubility of the RTILs was quantified by UV-visible spectrophotometry.[8] As anticipated, their water solubility decreased markedly (from 0.187 to 0.013 M) as the alkyl chain length increased from C_2 to C_8. The solubility of water in the RTILs was determined *via* Karl Fischer titration, and was found to decrease (from 1.84 to 0.80 M) over the range of chain lengths examined. That the RTILs are stable to contact with nitric acid was verified by examination of ^{1}H-NMR spectra acquired following 24 h contact of the ionic liquid with 3 times its volume of 8 M HNO_3. All strontium distribution ratios were determined radiometrically using a commercial Sr-85 radiotracer, assayed *via* gamma spectroscopy using standard procedures. The choice of Tf_2N^- anion was prompted by satisfactory results obtained with it in prior studies of cation extraction from water.[7]

1 C. J. Adams, M. J. Earle and K. R. Seddon, *Chem. Commun.*, 1999, 1043.
2 N. Karodia, S. Guise, C. Newlands and J. Andersen, *Chem. Commun.*, 1998, 2341.
3 J. Fuller, R. T. Carlin and R. A. Osteryoung, *J. Electrochem. Soc.*, 1997, **144**, 3881.
4 K. R. Seddon, *J. Chem. Tech. Biotechnol.*, 1997, **68**, 351.
5 L. A. Blanchard and J. F. Brennecke, *Ind. Eng. Chem. Res.*, 2001, **40**, 287.
6 J. G. Huddleston, H. D. Willauer, R. P. Swatloski, A. E. Visser and R. D. Rogers, *Chem. Commun.*, 1998, 1765.
7 S. Dai, Y. H. Ju and C. E. Barnes, *J. Chem. Soc., Dalton Trans.*, 1999, 1201.
8 A. E. Visser, R. P. Swatloski, W. M. Reichert, S. T. Griffin and R. D. Rogers, *Ind. Eng. Chem. Res.*, 2000, **39**, 3596.
9 A. E. Visser, R. P. Swatloski, W. M. Reichert, R. Mayton, S. Sheff, A. Weirzbicki, J. H. Davis, Jr. and R. D. Rogers, *Chem. Commun.*, 2001, 135.
10 P. Bonhôte, A.-P. Dias, N. Papageorgiou, K. Kalyanasundaram and M. Grätzel, *Inorg. Chem.*, 1996, **35**, 1168.
11 E. P. Horwitz, M. L. Dietz and D. E. Fisher, *Solvent Extr. Ion Exch.*, 1990, **8**, 199.
12 M. L. Dietz, A. H. Bond, M. Clapper and J. W. Finch, *Radiochim. Acta*, 1999, **85**, 119.
13 M. L. Dietz, A. H. Bond, B. P. Hay, R. Chiarizia, V. J. Huber and A. W. Herlinger, *Chem. Commun.*, 1999, 1177.
14 R. M. Izatt, R. L. Bruening, G. A. Clark, J. D. Lamb and J. J. Christensen, *J. Membr. Sci.*, 1986, **28**, 77.
15 M. J. Rosen, *Surfactants and Interfacial Phenomena*, John Wiley, New York, 2nd edn., 1989.
16 F. MacRitchie, *Chemistry at Interfaces*, Academic Press, San Diego, 1990.

CHEMCOMM Communication
www.rsc.org/chemcomm

Mimicking oxide surfaces: different types of defects and ligand coordination at well defined positions of a molybdenum oxide based nanocluster†

Achim Müller,* Rabindranath Maiti, Marc Schmidtmann, Hartmut Bögge, Samar K. Das and Wenjian Zhang

Fakultät für Chemie der Universität, D-33501, Bielefeld, Germany. E-mail: a.mueller@uni-bielefeld.de

Received (in Cambridge, UK) 10th July 2001, Accepted 17th August 2001
First published as an Advance Article on the web 18th September 2001

The mixed valence cluster anion of the compound $(NH_4)_{32}[Mo^{VI}_{110}Mo^{V}_{28}O_{416}H_6(H_2O)_{58}(CH_3CO_2)_6]\cdot xH_2O$ 1 ($x \sim 250$), synthesized under one-pot conditions, contains well-defined different types of defects—missing groups compared to the complete parent $\{Mo_{154}\}$ type cluster with full D_{7d} symmetry—and acetate ligand coordination; this proves that the giant-wheel type anion can be considered as an object with a variety of nanoscale structural features ("nanostructured landscape") allowing reactions at a variety of well defined centers.

It is still a challenge to understand details of the interaction mechanisms of substrates with the surfaces of heterogeneous catalysts,[1,2] as for instance in the case of transition metal oxides which play an important role in industrial processes, *e.g.* in selective oxidations.[3] Of particular interest is MoO_3, which shows an enormous versatility of catalytical properties.[3a] A tremendous step to this end would be to consider the well defined discrete giant metal–oxide based cluster species, *i.e.*, nanoreactors (which show the same or a similar structure including defects on their large surfaces), as relevant catalytically active bulk materials, the surface of which is difficult to investigate. Remarkably, very little is known as yet about the influence of such defects present on the surface of an oxide, and their role in determining the catalytic properties.[3b] Here we report on the synthesis of $(NH_4)_{32}[Mo^{VI}_{110}Mo^{V}_{28}O_{416}H_6(H_2O)_{58}(CH_3CO_2)_6]\cdot xH_2O$ **1** ($x \sim 250$) which shows different types of well defined defects, substrate interactions/activation, and even other important structural features such as $Mo^{VI/V}$ type redox as well as acid sites, important for the catalytic action of molybdenum–oxide based catalysts. In particular the pentagonal bipyramidal MoO_7 polyhedra seem to be of interest for understanding selective oxidations.[3c]

When an aqueous solution of ammonium heptamolybdate is reduced with hydrazinium sulfate in the presence of a high acetic acid concentration, blue crystals of **1** precipitate within three weeks.‡ Compound **1** was characterized by elemental analysis, thermogravimetric analysis (to determine the crystal water content), cerimetric titrations [for the determination of the (formal) number of Mo^V centers], spectroscopic methods (IR, resonance Raman, VIS–NIR)§ and single crystal X-ray structure analysis, including bond valence sum (BVS) calculations (to determine the number and positions of H_2O and OH groups as well as the formal number of Mo^V centers).¶ The relatively low solubility of **1** in water is due to the abundance of acetate ligands and ammonium cations.

The crystal structure of **1** shows in the lattice the presence of a derivative of the "classical" tetradecameric type of molybdenum–oxide based anionic giant wheel, formulated with its characteristic building blocks as $[\{Mo_2\}_{14}\{Mo_8\}_{14}\{Mo_1\}_{14}]^{14-}$ = $[\{(O)_2{=}Mo^{VI}(H_2O)(\mu\text{-}O)(H_2O)Mo^{VI}{=}(O)_2\}^{2+}_{14}\{Mo^{VI/V}_8O_{26}(\mu_3\text{-}O)_2H(H_2O)_3Mo^{VI/V}\}^{3-}_{14}]^{14-} \equiv [Mo^{VI}_{126}Mo^{V}_{28}O_{462}H_{14}(H_2O)_{70}]^{14-}$ **2a**.[4] In **1a** (Fig. 1) there

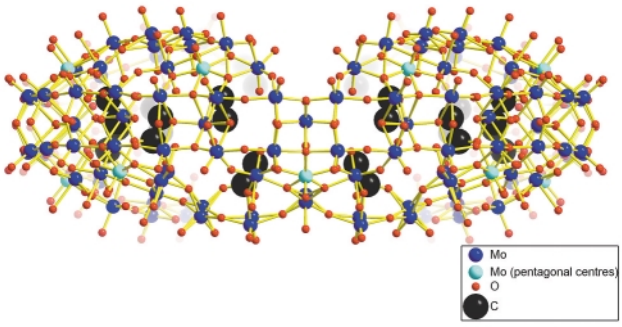

Fig. 1 Side view of the structure of **1a** in crystals of **1** in ball and stick representation with enlarged C atoms of the acetate ligands.

are six $\{Mo_2\}$ units missing while two bidentate acetate ligands are coordinated to other abundant $\{Mo_2\}$ units thereby replacing four H_2O ligands with the formation of $\{Mo_2Ac\}$* units. In addition, four $\{Mo_1\}$ units are—compared to **2a**—"released". Describing the "release" of these $\{Mo_1\}$ units is somewhat difficult (see Fig. 2): formally, 4 $\{\{MoO_2\}^{2+} + H_2O + H^+\}$ collectives of **2a** are removed and 4 $\{CH_3CO_2^- + 3H^+\}$ added, thus leading to the schematic description of **1a** as $[\{Mo_2\}_6\{Mo_2Ac\}^*_2\{Mo_8\}_{10}\{Mo_8Ac\}^*_4\{Mo_1\}_{10}]^{32-}$ or to the formula $(NH_4)_{32}[Mo^{VI}_{110}Mo^{V}_{28}O_{416}H_6(H_2O)_{58}(CH_3CO_2)_6]\cdot xH_2O$ ($x \sim 250$) for the resulting compound **1**, as stated

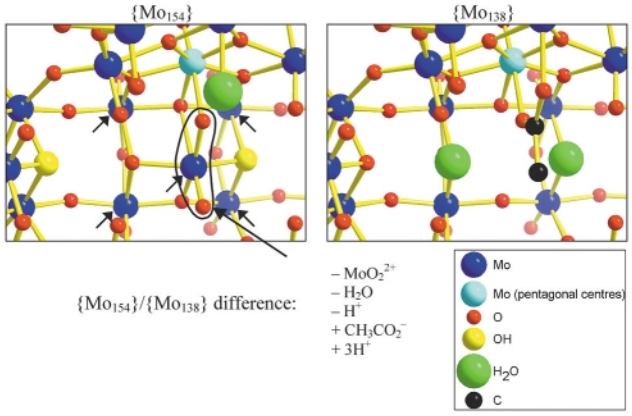

Fig. 2 Schematic representation (view from the inside of the rings) of the structural change from **2a** to **1a** at one representative $\{Mo_5O_6\}$ type compartment built up by four $\{Mo_8\}$ and one $\{Mo_1\}$ type atoms: formally, one MoO_2^{2+} group, *i.e.* the $\{Mo_1\}$ type atom with the terminal oxygen atom bonded to it and the μ-O atom bridging the Mo atom and the pentagonal Mo center of the $\{Mo_8\}$ group, is removed from **2a**. The vacant position due to the loss of μ-O at the pentagonally coordinated Mo atom is filled by an O atom of an acetate ligand while the other O atom of the carboxylate group substitutes a H_2O ligand of a neighbouring Mo center. The two μ_3-O type atoms (one of which is protonated in **2a**) of the complete $\{Mo_5O_6\}$ compartment of **2a** situated on the equator are doubly protonated in **1a**. Consequently, a protonation at the μ_3-O type atom of a neighbouring intact compartment is not possible due to space limitations.

† Dedicated to Prof. J. Strähle on the occasion of his 65th birthday.

 DOI: 10.1039/b106092a

in the abstract ({Mo_8Ac}* = {$Mo^{VI/V}{}_8O_{24}(\mu\text{-}H_2O)_2(H_2O)_2(CH_3CO_2)$}$^{3-}$; for the differing number of H atoms in {Mo_8} units see Fig. 1).

These novel {Mo_1} type defects have been generated now for the first time and could in principle be formed in the following way: **1a** is initially formed while the acetate ligands, after coordination to the {Mo_8} units (comparable to the situation of pentagonal units of the ball/basket type species[5]), subsequently expel the {Mo_1} units in order to overcome the steric strain imposed on the specific sites. Due to the loss of four {Mo_1} type centers from the cubane {Mo_5O_6} compartment, present in **1a** and for instance in $[Mo^{VI}{}_{114}Mo^{V}{}_{28}O_{432}H_{14}(H_2O)_{58}]^{26-}$ **3a**[6] as well as in all other ring type species, eight of the related 28 (μ_3-O) type atoms abundant in **2a** become doubly protonated (by reason of their *trans* positions to terminal O atoms and the removal of the {Mo_1} type atoms, corresponding to Fig. 2). This causes the absence of protonations at neighbouring {Mo_5O_6} compartments like in the parent **2a**, since the space which would be required is already occupied by the hydrogen atoms of the "new" μ-H_2O ligands (Fig. 2).

The maximum possible number of {Mo_2} type defects is six, as observed also in **3a**,[6] because more than three defects in one half of the ring would cause at least one {Mo_8} unit not to link to an {Mo_2} unit, a situation which would result in the collapse of the ring skeleton. For this type of defect generation, a relatively high pH value as in the case of lacunary Keggin ions is obligatory.[7] On the other hand, aging also favours their formation.

A significant aspect of our work is that we are able to study a variety of reactions at well defined sites of the same structurally characterized nanoobjects[4,8–10] including the deliberate generation of different types of defects.

Notes and references

‡ *Synthesis* of **1**: To a solution of $(NH_4)_6Mo_7O_{24}{\cdot}4H_2O$ (2.0 g, 1.62 mmol) in 75 mL of water, acetic acid (9.0 mL, 100%) and hydrazinium sulfate (0.05 g, 0.38 mmol) were added. After stirring the mixture (pH = 3.5) in a closed flask for 75 min, the resulting blue solution was kept undisturbed at room temperature for 3 weeks. The precipitated blue crystals were filtered off, washed quickly with a small amount of cold water and sucked dry. Yield: 0.66 g (30% based on Mo).

§ *Selected data* for **1**: VIS–NIR (in H_2O) [λ_{max}/nm (ε/dm^3 mol^{-1} cm^{-1})]: 744 (1.75×10^5), 1090 (1.3×10^5). IR (KBr pellet, ν/cm^{-1}): 1616m {$\delta(H_2O)$}, 1400s {$\delta(NH_4^+)$}, 959s/906m {ν(Mo=O)}, 799m, 748m, 634s, 558vs. Resonance-Raman (H_2O, λ_e = 1064 nm, ν/cm^{-1}): 798vs, 531s, 465s, 322s, 215s. Anal. Calc. for $C_{12}H_{768}Mo_{138}N_{32}O_{736}$ (M 26382.30) C, 0.55; N, 1.70; Mo^V, 10.18 (non-coordinated) crystal water 17.07%. Found: C, 0.47; N, 1.6; Mo^V, 10.3; non-coordinated crystal water ~19% (thermogravimetry).

¶ *Crystal data* for **1**: $C_{12}H_{768}Mo_{138}N_{32}O_{736}$, M = 26382.30 g mol^{-1}, monoclinic, space group $C2/m$, a = 42.0716(14), b = 40.2653(14), c = 26.0734(9) Å, β = 112.019(1)°, V = 40947(2) Å^3, Z = 2, D_c = 2.140 g cm^{-3}, μ = 2.145 mm^{-1}, $F(000)$ = 25496, crystal size = 0.15 × 0.15 × 0.10 mm. Crystals of **1** were removed from the mother-liquor and immediately cooled to 183(2) K on a Bruker AXS SMART diffractometer (three circle goniometer with 1K CCD detector, Mo-Kα radiation, graphite monochromator; hemisphere data collection in ω at 0.3° scan at a detector distance of 5.0 cm). A total of 94 714 reflections ($0.73 < \theta < 25.01°$) were collected of which 36 348 unique reflections (R_{int} = 0.0445) were used. An empirical absorption correction using equivalent reflections was performed with the program SADABS. The structure was solved with the program SHELXS-97 and refined using SHELXL-93 to R = 0.0551 for 24 378 reflections with $I > 2\sigma(I)$, R = 0.1000 for all data; max./min. residual electron density 2.160 and −1.503 e Å^{-3}. (SHELXS/L, SADABS from G.M. Sheldrick, University of Göttingen 1997, 1993; structure graphics with DIAMOND 2.1 from K. Brandenburg, Crystal Impact GbR, 1999.) Whereas the {Mo_2} type defects show no disorder, this is the case for the {Mo_1} type units. CCDC reference number 166020. See http://www.rsc.org/suppdata/cc/b1/b106092a/ for crystallographic data in CIF or other electronic format.

1 (*a*) I. M. Campbell, *Catalysis of Surfaces*, Chapman and Hall, London, 1988; (*b*) J. M. Thomas and W. T. Thomas, *Principles and Practice of Heterogeneous Catalysis*, VCH, Weinheim, 1997.

2 (*a*) For some related aspects see H. H. Kung, *Transition Metal Oxides: Surface Chemistry and Catalysis*, Elsevier, Amsterdam, 1989 (*b*) J. M. Thomas and R. Raja, *Chem. Commun*., 2001, 675.

3 (*a*) J. Haber and E. Lalik, *Catal. Today*, 1997, **C33**, 119; (*b*) J. Haber, Molecular mechanism of heterogeneous oxidation—Organic and solid state chemists' views, in *Studies in Surface Science and Catalysis*, ed. B. Delmon and J. T. Yates, Elsevier, Amsterdam, 1997, vol. 110, p. 1 (*c*) G. Mesh, C. Linsmeyer, R. Gottschall, M. Dieterle, J. Find, D. Herein, J. Jäger, Y. Uchida and R. Schlögl, *J. Mol. Catal. A: Chem*., 2000, **162**, 463.

4 A. Müller, P. Kögerler and C. Kuhlmann, *Chem. Commun*., 1999, 1347; A. Müller and C. Serain, *Acc. Chem. Res*., 2000, **33**, 2.

5 A. Müller, P. Kögerler and H. Bögge, *Struct. Bonding (Berlin)*, 2000, **96**, 203.

6 A. Müller, C. Beugholt, M. Koop, S. K. Das, M. Schmidtmann and H. Bögge, *Z. Anorg. Allg. Chem*., 1999, **625**, 1960.

7 M. T. Pope and A. Müller, *Angew. Chem., Int. Ed. Engl*., 1991, **30**, 34.

8 A. Müller, M. Koop, H. Bögge, M. Schmidtmann and C. Beugholt, *Chem. Commun*, 1998, 1501.

9 A. Bielanski, A. Malecka-Lubanska, J. Pozniczek, A. Müller, E. Krickemeyer and E. Diemann, *Bull. Pol. Acad. Sci. Chem*., 2001, **49**, 85.

10 A. Müller, S. K. Das, C. Kuhlmann, H. Bögge, M. Schmidtmann, E. Diemann, E. Krickemeyer, J. Hormes, H. Modrow and M. Schindler, *Chem. Commun*., 2001, 655.

CHEMCOMM
Communication
www.rsc.org/chemcomm

Tunable clathrates

Mino R. Caira, Tanya le Roex and Luigi R. Nassimbeni*

Department of Chemistry, University of Cape Town, Rondebosch 7701, South Africa.
E-mail: xrayluig@science.uct.ac.za

Received (in Cambridge, UK) 10th July 2001, Accepted 29th August 2001
First published as an Advance Article on the web 1st October 2001

Investigation of the selectivity of a diol organic host for mixtures of DMF and DMSO, showed the formation of five inclusion compounds in which the stoichiometry varies in discrete steps and is determined by the composition of the liquid guest mixture; the structures of these compounds are described.

Molecular recognition is fundamental to supramolecular chemistry, and the formation and stability of a particular inclusion compound depends on the strengths and direction of the intermolecular forces which impinge on a particular host–guest system.[1–5] This can be exploited to carry out selective enclathration, whereby a given host molecule is exposed to a mixture of possible guests, and preferentially forms an inclusion compound with only one guest, thus enacting a perfect separation. In practice, this is seldom achieved in a single cycle, particularly when we seek to separate close isomers, where the differences between guests may be subtle.

The results of competition experiments whereby inclusion compounds are grown from solutions of pairs of guests A and B of known compositions, usually give rise to selectivity curves shown in Fig. 1.

X_B is the mole fraction of guest B in the liquid mixture and Z_B that of guest B which has been enclathrated in the host–guest crystal. Curve a results from a host displaying no selectivity,[6] curve b occurs when guest B is strongly selected over A for the whole concentration range[7] and curve c occurs when the selectivity is concentration dependent.[8] In this work, however, we present results of a host–guest system which behaves in a totally different manner.

When the host *trans*-9,10-dihydroxy-9,10-bis(*p*-*tert*-butylphenyl)-9,10-dihydroanthracene = H, is exposed to mixtures of dimethylformamide, A, and dimethyl sulfoxide, B, it forms a series of inclusion compounds of the type H·nA·(4 − *n*)B, such that *n* varies integrally from 0 to 4. The results of the competition experiments are given in Fig. 2, which shows that the stoichiometry of the inclusion compounds varies in discrete steps, and gives rise to five distinct compounds: H·4A, H·3A·B, H·2A·2B, H·A·3B and H·4B. The stoichiometry can be controlled by changing the composition of the liquid guest mixture.

Thermal gravimetry, TG, and differential scanning calorimetry, DSC were employed to analyse the stoichiometries and thermal stabilities of all five inclusion compounds.[9,10] The compound H·A·3B was difficult to isolate, because when the guest liquid mixture is in the mole fraction range X_B 0.5–1.0, the host shows a strong propensity for the formation of H·2A·2B.

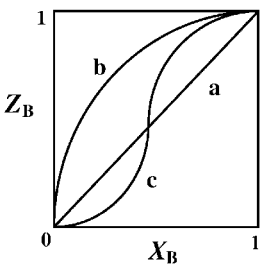

Fig. 1 Typical selectivity curves obtained from competition experiments.

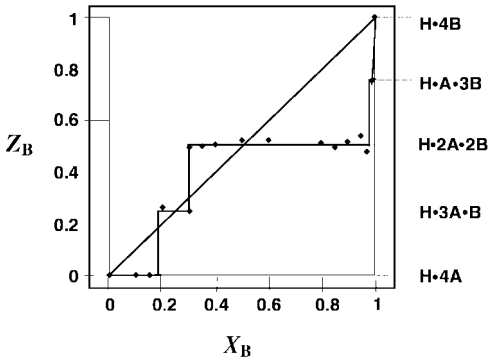

Fig. 2 Results of the competition experiments.

We therefore prepared the H·A·3B compound by using an initial guest mixture with a mole fraction X_B of 0.99.

We have elucidated the structures of all five compounds by single crystal X-ray diffraction methods at low temperatures.† The five structures are all triclinic, with similar cell dimensions and all crystallise in the space group $P\bar{1}$. A typical example, that of the H·2A·2B structure, is displayed in Fig. 3. This shows that the host molecule is located at the origin on a centre of inversion. The two DMSO molecules are hydrogen bonded to the host and the two DMF molecules are disordered and located close to a centre of inversion at Wyckoff position g.

The TG and DSC curves for H·2A·2B are given in Fig. 4. This shows that the compound desolvates in two distinct steps, the first corresponding to the loss of two DMF molecules, followed by the loss of two DMSO guest molecules. The DSC displays the concomitant A and B endotherms, while peak C is due to the melting of the host. Similar curves were obtained for the other four compounds, and allowed us to establish the stoichiometry unambiguously in each case.

The compounds are isostructural with respect to the location of the host atoms. The changes which occur in the positions of the guest molecules are summarised in Fig. 5a to 5e. In all cases

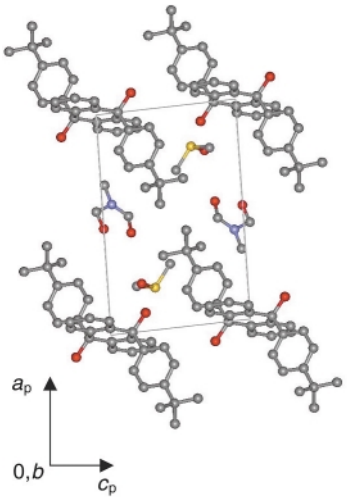

Fig. 3 Projection of the H·2A·2B structure along [010].

 DOI: 10.1039/b106080p

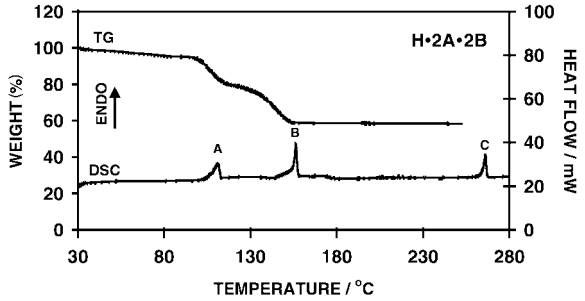

Fig. 4 TG and DSG curves for H·2A·2B.

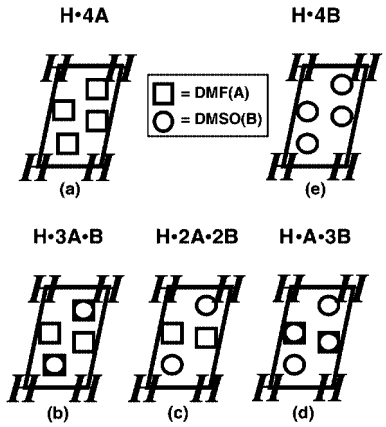

Fig. 5 Schematic diagram summarising the differences beteen the five structures.

only two guests are hydrogen bonded to the host. For the H·3A·B structure, symmetry requires the DMSO guest, B, and at least one DMF molecule to be located at two sites, each with site occupancies of 0.5. The difference electron density map showed that these guests shared the same general location. The same situation is obtained for the compound H·A·3B.

The occurrence of a host–guest system in which the ratio of mixed guests can be controlled, has implications for crystal engineering.[11,12] Thus the physical and chemical properties of such compounds can be governed, and this has significance in such fields as chemical sensors, optical and electronic properties of organic crystals as well as their thermal stabilities and kinetics of desolvation.

We are currently investigating the possibility of incorporating a variety of other guests, including chiral molecules, in clathrates formed by this host, and investigating their thermodynamic and kinetic properties.

Notes and references

† CCDC 168239–168243. See http://www.rsc.org/suppdata/cc/b1/b105080p/ for crystallograhic data in .cif or other format.

Crystal data for H·4A: $C_{34}H_{36}O_2·4(C_3H_7NO)$, M = 769.01, triclinic, $P\bar{1}$, a = 8.9414(3), b = 9.0806(4), c = 14.935(1) Å, α = 91.307(2), β = 105.523(2), γ = 110.189(3)°, U = 1087.67(9) Å^3, Z = 1, T = 173 K, μ = 0.077 mm^{-1}, 7032 reflections measured, 4823 unique (R_{int} = 0.0163), final R index [$I > 2\sigma(I)$]: R_1 = 0.0554.

Crystal data for H·3A·B: $C_{34}H_{36}O_2·3(C_3H_7NO)·(C_2H_6OS)$, M = 774.08, triclinic, $P\bar{1}$, a = 9.0806(3), b = 9.0909(3), c = 14.6632(7) Å, α = 72.294(1), β = 87.660(1), γ = 70.299(2)°, U = 1083.05(8) Å^3, Z = 1, T = 173 K, μ = 0.124 mm^{-1}, 6646 reflections measured, 4955 unique (R_{int} = 0.0190), final R index [$I > 2\sigma(I)$]: R_1 = 0.1410 (guest molecules disordered).

Crystal data for H·2A·2B: $C_{34}H_{36}O_2·2(C_3H_7NO)·2(C_2H_6OS)$, M = 779.12, triclinic, $P\bar{1}$, a = 9.1425(3), b = 9.173(3), c = 14.273(1) Å, α = 71.356(1), β = 81.229(1), γ = 69.938(1)°, U = 1064.13(9) Å^3, Z = 1, T = 173K, μ = 0.173 mm^{-1}, 5770 reflections measured, 4625 unique (R_{int} = 0.0145), final R index [$I > 2\sigma(I)$]: R_1 = 0.0967.

Crystal data for H·A·3B: $C_{34}H_{36}O_2·(C_3H_7NO)·3(C_2H_6OS)$, M = 784.15, triclinic, $P\bar{1}$, a = 9.046(2), b = 9.1291(2), c = 14.409(1) Å, α = 72.559(1), β = 80.132(1), γ = 71.486(2)°, U = 1072.64(8) Å^3, Z = 1, T = 173 K, μ = 0.218 mm^{-1}, 5828 reflections measured, 3710 unique (R_{int} = 0.0163), final R index [$I > 2\sigma(I)$]: R_1 = 0.0931.

Crystal data for H·4B: $C_{34}H_{36}O_2·4(C_2H_6OS)$, M = 789.19, triclinic, $P\bar{1}$, a = 9.0330(4), b = 9.1302(5), c = 14.404(1) Å, α = 72.870(3), β = 80.072(3), γ = 71.659(3)°, U = 1073.4(4) Å^3, Z = 1, T = 173 K, μ = 0.265 mm^{-1}, 5632 reflections measured, 3823 unique (R_{int} = 0.0262), final R index [$I > 2\sigma(I)$]: R_1 = 0.1283 (guest molecules disordered).

1 J. W. Steed and J. L. Atwood, *Supramolecular Chemistry*, Wiley, Chichester, 2000.
2 E. Dicera, *Chem. Rev.*, 1998, **98**, 1563.
3 C. A. Hunter, *Chem. Soc. Rev.*, 1994, **23**, 101.
4 P. Wallimann, T. Marti, A. Fürer and F. Diederich, *Chem. Rev.*, 1997, **97**, 1567.
5 D. M. Rudkevich and J. Rebek, Jr., *Eur. J. Org. Chem.*, 1999, 1991.
6 M. R. Caira, A. Horne, L. R. Nassimbeni and F. Toda, *J. Mater. Chem.*, 1997, **7**, 2145.
7 M. R. Caira, L. R. Nassimbeni, D. Vujovic, E. Weber and A. Wierig, *Struct. Chem.*, 1999, **10**, 205.
8 J. Bacsa, M. R. Caira, A. Jacobs, L. R. Nassimbeni and F. Toda, *Cryst. Eng.*, 2000, **3**, 251.
9 A. Sopkova, P. Mondik and M. Rehakova, *J. Therm. Anal.*, 1996, **47**, 365.
10 H. K. Cammenga and M. Epple, *Angew. Chem., Int. Ed. Engl.*, 1995, **34**, 1171.
11 G. R. Desiraju, *Crystal Engineering*, Elsevier, Amsterdam, 1989.
12 W. Jones, *Organic Molecular Solids*, ch. 6, CRC Press, New York, 1997.

CHEMCOMM Communication
www.rsc.org/chemcomm

Shape-selective photocatalytic transformation of phenols in an aqueous medium

Paola Calza,[a] Costanza Pazé,[b] Ezio Pelizzetti*[a] and Adriano Zecchina[b]

[a] *Dipartimento di Chimica Analitica, Università di Torino, Via P. Giuria 5/7, Torino, Italy I-10125. E-mail: pelizzet@ch.unito.it; Fax: +39011 6707615; Tel: +39011 6707630*

[b] *Dipartimento di Chimica Inorganica, Chimica Fisica e Chimica dei Materiali, Università di Torino, Via P. Giuria 5/7, Torino, Italy I-10125*

Received (in Cambridge, UK) 19th July 2001, Accepted 11th September 2001
First published as an Advance Article on the web 24th September 2001

A zeolitic material containing Ti chains activated by light allows a shape-selective transformation of organic compounds; the molecules that can enter into the zeolitic cavities are protected from the light-induced processes, while the other are degraded.

It is well known that light activated processes on TiO_2 have applications in several fields such as the removal of water pollutants[1] and organic synthesis.[2,3] When dealing with pollution problems, the complete degradation of the polluting organic molecules is of course the goal. The photoactivity of TiO_2 is generally not selective, leading to the complete decomposition of the organic compounds. However, it is intriguing to test the feasibility of selective phototransformation of organic species in an aqueous medium. For this purpose, materials that show shape selectivity properties, such as zeolites, could be used. Among them, ETS-10 (Engelhard Titanosilicate Structure 10)[4] is particularly interesting for photocatalytic applications. In fact, it has two main features: i) it is a semiconductor containing photo-excitable titanium moieties, and ii) its structure is characterized by a three-dimensional set of channels with a free entrance of about 0.8 × 0.5 nm, ref. 5 (Fig. 1). The UV-VIS spectrum of ETS-10 shows two absorption bands at 282 and 214 nm, which have been assigned to ligand-to-metal charge transfer (LMCT) transitions, involving two kinds of oxygen ligands: those which bridge Ti atoms along straight Ti–O–Ti chains (282 nm), and those in the Si–O–Ti groups (214 nm).[6] The band gap of the –Ti–O–Ti– quantum wire is 4.03 eV[7] and is slightly higher than that of TiO_2.[8] A higher energy is then necessary to obtain the production of the active carriers (electrons and holes) and for this reason, in the experiments reported below a 310 nm cut-off filter has been adopted. The irradiation of the single species were carried out on 5 ml of aqueous suspension containing 1×10^{-4} M organic compound and 1 g L^{-1} of catalyst, using a 1500 W Xenon lamp (Solarbox, CO.FO. MEGRA, Milan, Italy) simulating AM1 solar light and equipped with a 310 nm cut-off filter. The irradiance spectrum and the cells have been described elsewhere.[9] The photonic flux entering into the cell is 7.9×10^{-6} einstein min^{-1}. The content of the cell was filtered through a 0.45 μm cellulose acetate filter (Millipore HA) and analyzed by the appropriate analytical technique.

To test the selective photoactivity of ETS-10, molecules of different steric hindrance were investigated: phenol (P), 1,3,5-trihydroxybenzene (3HP) and 2,3-dihydroxynaphthalene (2HPP) have been chosen. A comparison of the relative dimensions of the molecules and of the zeolitic cavities is shown in Fig. 1, while an analysis of the degradation rate ratios is reported in Table 1. In the same Table the results obtained with TiO_2 P25 as photocatalyst are reported for comparison. The contribution of direct photolysis is negligible (see Table 1).

An interesting correlation between the size of the molecule and its photodegradability is shown. This is particularly evident comparing P and 2HPP degradation, 2HPP being degraded on ETS-10 with a rate which is 56 times higher than P, and with a degradation efficiency of the same order as TiO_2. These results provide, for the first time, evidence of the feasibility of selective photocatalytic degradation in aqueous medium. A study of the intermediates of the degradation of phenol shows that they are the same catechol and quinol on TiO_2 and ETS-10. In the case of 3HP and 2HPP, even if the intermediates have not been identified, they show the same chromatographic pattern both on

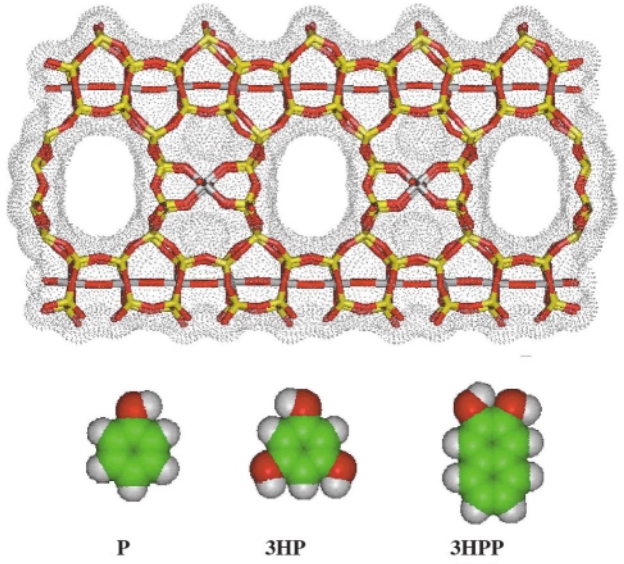

Fig. 1 Structure of zeolite ETS-10 and of the degraded molecules: phenol (P), 1,3,5-trihydroxybenzene (3HP) and 2,3-dihydroxynaphthalene (2HPP). The pointed surface in the zeolite structure evidences the accessible spaces as determined by the Connolly algorithm.[14]

Table 1 Degradation rate of hydroxyaromatic compounds on TiO_2 and on zeolite ETS-10. From these experimental data, the process efficiency (rate of degradation/photonic flux incoming into the cell) can be easily calculated;[10] in the case of dihydroxynaphthalene on ETS-10, a process efficiency of 2.8% is obtained. In parentheses are reported the degradation rate ratios (r_x/r_P) obtained comparing the values obtained in each set of experiments with that obtained for P. H-ETS-10 in the acid form was kindly supplied by the Engelhard Corporation (Iselin, NJ, USA); its external surface area is 21 m^2 g^{-1} (T-plot volumetric measurements with N_2 made with a Micromeritics apparatus). TiO_2 was a commercial Degussa P25 sample (surface area: about 50 m^2 g^{-1})

Rate/10^5 M min^{-1}	TiO_2	ETS-10	Direct photolysis
P	2.77 (1)	0.08 (1)	—
3HP	5.74 (2.07)	0.38 (4.75)	—
2HPP	7.90 (2.85)	4.46 (55.7)	0.21

 DOI: 10.1039/b106445m

TiO_2 and ETS-10. These results indicate that the degradation mechanism is similar and suggests that, like on TiO_2, the catalytic active sites of ETS-10 are titanols linked on external surfaces where the –Ti–O–Ti–O–Ti– chains are emerging and the TiO bonds are consequently broken. The bulk Ti atoms of ETS-10 cannot be considered as playing a role in the degradation for two reasons: i) imperfect structures are not directly exposed on the channels walls (see Fig. 1); ii) it has been shown[11,12] that when degradation takes place at centers located in restricted places (like titanols in defects located in zeolitic channels), the intermediate degradation products are able to back react with active species, favoring recombination. It is also to be noted that in the photocatalytic process there is no relation between the absorption on the surface and the rate of disappearance, as shown in the case of phenol (not adsorbed) and catechol (adsorbed).[13]

In view of these results and of the fact that the catalytic centers are located on the surface, it can be concluded that the zeolitic internal cavities offer a protective environment against degradation to those species which, for their small size, easily diffuse inside. This shielding effect against photodegradation is particularly marked for P, which was the smallest molecule investigated, and not present for 2HPP, which is the only studied species whose size surely does not fit the channel size and so it is the most degraded molecule. The ability to diffuse inside the cavities is then the main factor determining the shape selective degradation.

Finally, a further confirmation of the presence of catalytic sites on the external surface is given by the fact that the degradation rate of 2HPP on TiO_2 and on ETS-10, which have similar external surface area, is of the same order of magnitude.

Future developments also have to consider the influence of competitive diffusion of the molecules; this probably explains the small differences that can be observed in the rate constant values, compared to the values obtained in the degradation of the single molecules.

Notes and references

1 R. W. Matthews, *J. Phys. Chem.*, 1987, **91**, 3328.
2 M. A. Fox, *Acc.Chem.Res.*, 1983, **16**, 314.
3 M. A. Fox, C. C. Chen, K. Park and N. J. Younathan, *ACS Symp. Ser.*, 1985, **278**, 69.
4 S. M. Kuznicki, *US Pat.*, 4 853 202, 1989.
5 M. W. Anderson, O. Teresaki, T. Ohsuna, A. Philippou, S. P. MacKay, A. Ferreira, J. Rocha and S. Lidin, *Nature*, 1994, **367**, 347.
6 E. Borello, C. Lamberti, S. Bordiga, A. Zecchina and C. O. Areán, *Appl. Phys. Lett.*, 1997, **71**(16), 2319.
7 C. Lamberti, *Microporous Mesoporous Mater.*, 1999, **30**, 155.
8 E. Pelizzetti and C. Minero, *Comments Inorg. Chem.*, 1994, **15**, 297.
9 C. Minero, E. Pelizzetti, S. Malato and J. Blanco, *Chemosphere*, 1993, **26**, 2103.
10 N. Serpone, G. Sauvé, R. Koch, H. Tahiri, P. Pichat, P. Piccinini, E. Pelizzetti and H. Hidaka, *J. Photochem. Photobiol., A: Chem.*, 1996, **94**, 191.
11 C. Minero, *Catal. Today*, 1999, **54**, 205.
12 J. Cunningham, G. Al-Sayyed, P. Sedlak and J. Caffrey, *Catal. Today*, 1999, **53**(16), 145.
13 C. Minero, G. Mariella, V. Maurino and E. Pelizzetti, *Langmuir*, 2000, **16**, 2632.
14 M. L. Conolly, *Science*, 1983, **221**, 709.

CHEMCOMM Communication
www.rsc.org/chemcomm

Site effects in controlling the chemical reactivity in crystals: solid-state photochromism of *N*-(*n*-propyl)nitrospiropyrane†

Oded Godsi,*[a] Uri Peskin,*[ab] Moshe Kapon,[a] Ezra Natan[a] and Yoav Eichen*[ac]

[a] *Department of Chemistry, Technion–Israel Institute of Technology, Technion City, 32000 Haifa, Israel. E-mail: chryoav@tx.technion.ac.il; Fax: 972-4-8233735; Tel: 972-4-8293708*
[b] *Lise Mitner Center for Computational Quantum Chemistry, Technion–Israel Institute of Technology, Technion City, 32000 Haifa, Israel*
[c] *Solid State Institute, Technion–Israel Institute of Technology, Technion City, 32000 Haifa, Israel*

Received (in Cambridge, UK) 6th March 2001, Accepted 7th September 2001
First published as an Advance Article on the web 2nd October 2001

The dynamics of decay of the photoproducts of the two non equivalent molecules of *N*-(*n*-propyl) nitrospiropyrane‡ in the crystalline state is significantly different due to the effect of the specific site where each of the molecules is located in the crystal latice.

Reversible molecular transformations have been studied extensively through the years due to their fundamental importance in many chemical and biological processes and their relevance to artificial sensing.[1] Amongst the most frequently addressed optical switch systems are spiropyranes.[2] Reversible photoinduced and thermally activated ring transformations of spiropyrane systems have been studied in great detail in different solutions, including solid solutions.[3] The utilization of spiropyrane derivatives as molecular optical switches for different applications such as LC switching,[4] optical recording,[5] sensing,[6] and other optoelectronic devices[7] was also reported. Curiously, the photoactivity of spiropyranes in the crystalline state was reported only recently.[8]

The study of chemical processes in well-defined media, such as crystals, provides direct evidence for the effect of the molecular environment on the chemical reactivity. In most chemical transformations, the molecular environment in which the reaction is performed plays an important role by influencing the reaction path. Such site effects are the source of the ultimate chemical selectivity of enzymes and other biological systems. In the biological realm, a tailor-made restrictive anisotropic environment results in the selection of one specific reaction path, leading to a specific target molecule. Similar site effects are found for numerous reactions that take place in crystalline systems.[9] In many of those systems, a slight variation in the environment of the reactants results in a significant change in reactivity or in the mechanism path selection.[10] The establishment of quantitative correlations between the molecular and supramolecular structure and respective changes in properties is a long-standing goal in solid state chemistry and photochemistry. Such studies are essential for better understanding and mastering reactions in restrictive anisotropic environments.

Here we report on the photochromism of 1′-(*n*-propyl)-3′,3′-dimethyl-6-nitrospiro[2*H*-[1]benzopyran-2,2′-indoline], **1a**, in the crystalline state and on the effect of the crystal site on the chemical reactivity of the open merocyanine species.

Crystals of **1** develop a red–purple color (λ_{max} = 600 nm) upon exposure to near UV light (λ = 360 nm). The formation of the new optical band is correlated to the appearance of several new IR peaks between 1000 and 1600 cm^{-1} while the intensity of the IR bands at 1338, 1276 and 1172 cm^{-1}, decreases. These

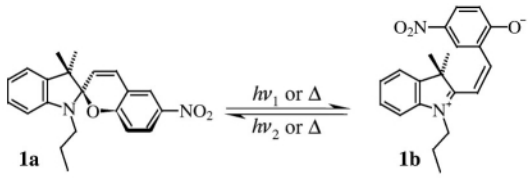

changes in the IR and visible spectra are indicative of the formation of the merocyanine species, **1b**.[11] Based on the IR spectra we estimate that at a photostationary state the ratio between the open and the closed forms is at least 1:3.

In the dark, both the visible and IR bands decay homogeneously, an indication of a back, thermally activated, **1b** → **1a** ring closure process. The decay of the IR bands is associated with a decay of the band at λ = 600 nm. Fig. 1A depicts the absorbance of a crystalline sample at λ = 600 nm and T = 304 ± 0.1 K as a function of the time after irradiation.§ Interestingly, in contrast to most chemically active systems in crystals (but note ref. 1*a*, 9) the decay curves of the band at λ = 600 nm can be fitted only to a biexponential decay curve, indicating the presence of two independent decaying merocyanine species.¶ For example, at 304.5 K, the lifetimes of the two merocyanine species are 3095 ± 25 and 19040 ± 60 s. At 315 K the lifetimes of these two species are shortened to 875 ± 14 and 5910 ± 150 s

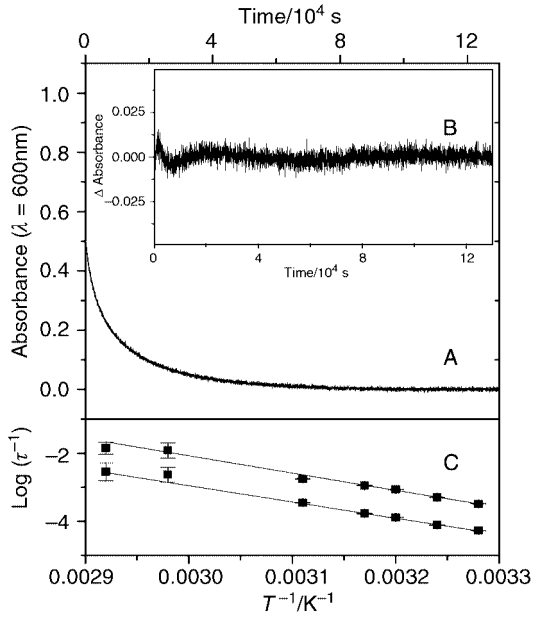

Fig. 1 (A) The absorbance of an irradiated crystalline sample of **1** as a function of the time after irradiation, λ = 600 nm; T = 304 ± 0.1 K. (B) The difference between the experimental signal depicted in A and a best-fitted biexponential curve. (C) Arrhenius plots for the two different sets of rate constants composing the biexponential decay curves.

† Electronic supplementary information (ESI) available: time decay of merocyanine absorption; overlay plot of molecules $\mathbf{1}_{(A)}$ and $\mathbf{1}_{(B)}$; plot of the ratio between the effective volume of the two sites as a function of the radius of the rigid sphere in the Monte Carlo calculation. See http://www.rsc.org/suppdata/cc/b1/b102121b/

 DOI: 10.1039/b102121b

respectively. The two sets of lifetimes extracted from the biexponential decay curves at different temperatures form two linear Arrhenius plots, Fig. 1C, attributed to the two different coexisting merocyanine species that are photogenerated simultaneously in the crystal. These two different merocyanine species are characterized by somewhat different activation energies and pre-exponential factors: $E_{a(1)} = 23.4 \pm 0.8$ kcal mol^{-1} and $E_{a(2)} = 21.9 \pm 0.9$ kcal mol^{-1}, $A_{(1)} = 13.2 \pm 0.6$ and $A_{(2)} = 11.3 \pm 0.8$ for the short-lived and long-lived species respectively. The origin of the two different photogenerated merocyanine species is revealed from the crystal structure. Crystals of **1** contain two nonequivalent spiropyrane molecules, $\mathbf{1}_{(A)}$ and $\mathbf{1}_{(B)}$, in the asymmetric unit, Fig. 2. The two nonequivalent molecules of **1** are almost identical with respect to their internal coordinates when considered as rigid bodies and the overlap between them is maximized. The minimal distance, D, between the overlapping molecules is $D = 0.137$ Å, where $D = \{[\Sigma(x_i^{(1)} - x_i^{(2)})^2]/(3N)\}^{\frac{1}{2}}$, (see supplementary material for an overlay plot of $\mathbf{1}_{(A)}$ and $\mathbf{1}_{(B)}$). The main differences between the two molecules are expressed in the nature of the sites the molecules occupy in the crystal. In the absence of a unique definition of the exact volume the molecule occupies in the crystal, we defined it using the following scheme. The molecular environment was represented by spheres having the Van der Waals radii of the atoms. A dynamical rigid sphere was placed in the void which was created by removing the reacting molecule and the diffusion equation was solved for this sphere within the rigid cage using *Monte Carlo* integration. The space that was sampled by the sphere in the infinite time-limit provides a practical definition of the volume and shape of the site hosting the molecule. The results were insensitive to the choice of the rigid sphere radius (r_s) in the range $1.6 < r_s < 2.5$ Å. The two sites are found to have roughly the same volume, Fig. 3, nevertheless, the shapes of the cavities that host each of the two molecules are remarkably different. The *n*-propyl moiety of $\mathbf{1}_{(A)}$ is interlocked between two *n*-propyl groups of neighboring molecules. In contrast, the *n*-propyl group of $\mathbf{1}_{(B)}$ is loosely bound to its environment but its nitroindoline skeleton is more tightly packed in its environment compared to $\mathbf{1}_{(A)}$. The difference in the shape of the cavities and nature of nearest neighbors seem to impose different restrictions on the degree of relaxation of the photoproduct of the reacting molecule within the reaction site. Based on this analysis we conclude that two almost equivalent molecules of **1**, that occupy two non-equivalent sites in the crystal lattice are photoactive and that they yield two structurally different merocyanine species. These two merocyanine moieties relax into two different sites in the crystal lattice and therefore exhibit different thermal reactivity for the back cyclization process.

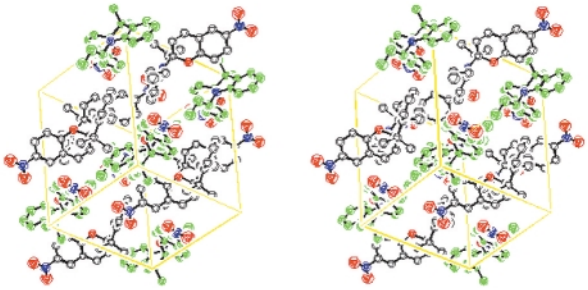

Fig. 2 A stereoscopic view of the unit cell of **1** containing two nonequivalent spiropyrane molecules $\mathbf{1}_{(A)}$ (black) and $\mathbf{1}_{(B)}$ (green).

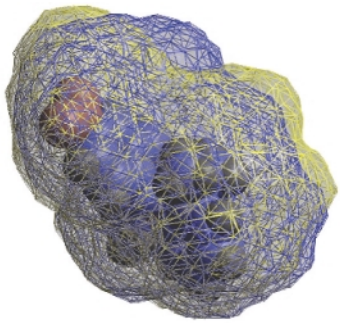

Fig. 3 The superposition of the two cavities hosting the molecules $\mathbf{1}_{(1)}$ (blue) and $\mathbf{1}_{(2)}$ (yellow). The effective volumes, defined by the diffusion of a rigid sphere of radius 1.8 Å, are $V(1) = 912$ and $V(2) = 1051$ Å^3, respectively.

This research was supported by the US–Israel Binational Science Foundation (BSF) and the Foundation for Promotion of Research at the Technion.

Notes and references

‡ 1′-(*n*-Propyl)-3′,3′-dimethyl-6-nitrospiro[2*H*-[1]benzopyran-2,2′-indoline], **1**, was prepared according to a modification of a literature procedure.[12] Crystal data for **1**: $C_{21}H_{22}N_2O_3$, $M_r = 350.41$, triclinic, space group $P\bar{1}$, $a = 12.1910(5)$, $b = 12.4340(5)$, $c = 12.9160(4)$ Å, $\alpha = 101.743(2)$, $\beta = 104.914(2)$, $\gamma = 90.647(2)°$, $V = 1848.09(12)$ Å^3, $Z = 4$, $\rho_{calc} = 1.259$ g cm^{-3}. Data for a crystal of dimensions of $0.3 \times 0.25 \times 0.3$ mm were collected at 293(2) K on a Kappa CCD diffractometer using MoKα radiation ($\lambda = 0.7107$ Å). Data collection was performed using ω and φ scans. Data processing was performed using SHELXL-97 and SHELXS-97. $R_1 = 0.043$ for 3935 independent reflections with $I > 2\sigma(I)$. CCDC 147145. See http://www.rsc.org/suppdata/cc/b1/b10212b/ for crystallographic data in .cif or other format. Transient optical absorption spectra were recorded on a computer controlled home-made optical spectrometer equipped with a high pressure mercury lamp for excitation, a tungsten lamp and a monochromator (Acton Research 150I) as the probe light. The sample was placed in a temperature-controlled (Lake Shore 330, Cryotronics), liquid nitrogen-cooled optical cryostat (Oxford, DN1704).

§ All the kinetics measuements were performed in high dilution, where about 0.005% of the molecules in the crystal were photoexcited.

¶ Attempts to fit the data using three or more exponents failed to yield more than two different decay rates.

1 (*a*) *Photochromism: Molecules and Systems, Studies in Organic Chemistry*, Vol. 40; ed. H. Durr and H. Bouas-Laurant, Elsevier, Amsterdam, 1990 and references therein; (*b*) S. H. Kawai, L. S. Gilat and J. M. Lehn, *Eur. J. Org. Chem.*, 1999, 2359; (*c*) L. Fabrizzi, M. Licchelli and P. Pallavicini, *Acc. Chem. Res.*, 1999, **32**, 846; (*d*) J. M. Lehn, *Angew. Chem., Int. Ed. Engl.*, 1988, **27**, 89; (*e*) J. M. Lehn, *Angew. Chem., Int., Ed. Engl.*, 1990, **29**, 1304; (*f*) J. M. Lehn, *Supramolecular Chemistry Concepts and Perspectives*, VCH, Weinheim, 1995; (*g*) E. Katz, B. Willner and I. Willner, *Biosensors and Bioelectronics*, 1997, **12**, 703; (*h*) I. Willner, *Acc. Chem. Res.*, 1997, **30**, 347; (*i*) I. Willner and B. Willner, *Adv. Mater.*, 1997, **9**, 351; (*j*) J. La Clair, *Angew. Chem., Int. Ed.*, 1999, **38**, 3045.

2 G. Berkovic, V. Krongauz and V. Weiss, *Chem. Rev.*, 2000, **100**, 1741; K. Sasaki and T. Nagamura, *J. Appl. Phys.*, 1998, **83**, 2894.

3 P. Uznanski and A. Wojda, *Eur. Polym. J.*, 1990, **26**, 141.

4 F. Shvartsman and V. Krongauz, *Nature*, 1984, **309**, 608; P. Cabrera, F. Shvartsman, O. Veinberg and V. Krongauz, *Science*, 1984, **226**, 341; T. Sasaki and T. Ikeda, *J. Phys. Chem.*, 1995, **99**, 13013.

5 A. Y. Bobrovsky, N. I. Boiko and V. P. Shibaev, *Adv. Mater.*, 1999, **11**, 1025; R. A. Lessard and G. Manivannan, *Proc. SPIE-Int. Soc. Opt. Eng.*, 1998, **3347**, 11.

6 J. D. Winkler, C. M. Bowen and V. Michelet, *J. Am. Chem. Soc.*, 1998, **120**, 3237.

7 A. Doron, E. Katz, G. Tao and I. Willner, *Langmuir*, 1997, **13**, 1783.

8 S. Benard and P. Yu, *Adv. Mater.*, 2000, **12**, 48.

9 Y. Eichen, M. Botoshansky, U. Peskin, M. Scherl, D. Haarer and S. Khatib, *J. Am. Chem. Soc.*, 1997, **119**, 7167; A. Schmidt, S. Kababaya, M. Appel, S. Khatib, M. Botoshansky and Y. Eichen, *J. Am. Chem. Soc.*, 1999, **121**, 11291; Y. Eichen, J.-M. Lehn, M. Scherl, D. Haarer, J. Fischer, A. DeCian, A. Corval and H. P. Trommsdorff, *Angew. Chem., Int. Ed. Engl.*, 1995, **34**, 2530; M. Scherl, D. Haarer, J. Fischer, A. DeCian, J.-M. Lehn and Y. Eichen, *J. Phys. Chem.*, 1996, **100**, 16175; S. Khatib, M. Botoshansky and Y. Eichen, *Acta Crystallogr., Sect. B*, 1997, **53**, 306; T. Nunes, Y. Eichen, M. Bastos, H. D. Burrows and H. P. Trommsdorff, *J. Phys., Appl. Phys.*, 1999, **32**, 2108; S. Khatib, S. Tal, O. Godsi, U. Peskin and Y. Eichen, *Tetrahedron*, 2000, **56**, 6753.

10 A. E. Keating, S. H. Shin, K. N. Houk and M. A. Garcia-Garibay, *J. Am. Chem. Soc.*, 1997, **119**, 1474; H. E. Zimmerman, P. Sebek and Z. Zhu, *J. Am. Chem. Soc.*, 1998, **120**, 8549.

11 E. Davin, M. Guiliano, H. Reymond, G. Mille and B. Kister, *J. Anal. Chim. Acta*, 1983, **148**, 271.

12 K. G. Dzhaparidze, D. P. Maisuradze, G. G. Gachechiladze and E. S. Gomelauri, *Khim. Geterotsikl. Soedin.*, 1971, **7**, 775.

CHEMCOMM Communication
www.rsc.org/chemcomm

A polymeric sodium complex of 3,6-bis(2-pyridyl)-1,2,4,5-tetrazine

Edwin C. Constable,* Catherine E. Housecroft, Benson M. Kariuki, Natalie Kelly and Christopher B. Smith

School of Chemical Sciences, University of Birmingham, Edgbaston, Birmingham, UK B15 2TT. E-mail: e.c.constable@bham.ac.uk

Received (in Cambridge, UK) 25th July 2001, Accepted 7th September 2001
First published as an Advance Article on the web 27th September 2001

The ligand 3,6-bis(2-pyridyl)-1,2,4,5-tetrazine forms a 1:1 complex with Na[BPh_4], which has been structurally characterised as a one-dimensional polymeric system with an unusual coordination geometry about the sodium.

Polytopic ligands incorporating multiple oligopyridine metal-binding domains are important components in the development of metallosupramolecular chemistry.[1] A key early observation was the spontaneous self-assembly of a 2 × 2 grid from the reaction of a copper(I) salt with 3,6-bis(2-pyridyl)pyridazine **I**.[2] We have recently commenced a systematic study of compounds related to **I**, including 3,6-bis(2-pyridyl)-1,2,4,5-tetrazine **II** which has been shown to have a rich supramolecular chemistry.[3] In this paper, we report the unexpected formation of a sodium complex of **II**.

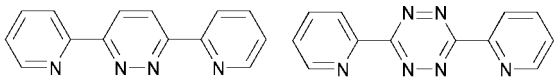

I II

In the course of our studies with **II** we noted that the purple ligand **II** gave rise to a series of variously hued pink species in addition to the expected metal complexes. These pink species, which we initially believed to be salts of **II** gave differing but repeatable ^{1}H NMR spectra. In some cases, the ^{1}H NMR spectra differed significantly from that of **II** and the compounds were characterised as protonated derivatives of **II**. In other cases, the ^{1}H NMR spectra were essentially identical to **II**. When the purple complex $[Ag_2(\mathbf{II})_2][CF_3SO_3]_2$[4] was treated with an excess of Na[BPh_4] a pink solution was obtained which eventually deposited red crystals. The same red crystalline compound was obtained directly from the reaction of **II** with Na[BPh_4] in nitromethane† No change occurred in the UV–VIS spectrum of a nitromethane solution of **II** upon the addition of three equivalents of Na[BPh_4].

In the ^{1}H NMR spectrum of the red solid, the ligand resonances are essentially identical to those of **II** in CD_3COCD_3 or CD_3SOCD_3, although the signals due to H^3 and H^6 were slightly broadened and shifted downfield by ≈ 5 Hz (300 MHz). Elemental analysis was consistent with a formulation {Na(**II**)(BPh_4)} and the FAB MS exhibited peaks at *m*/*z* 495 and 601 assigned to $\{Na(\mathbf{II})_2\}^+$ and $\{Na_2(\mathbf{II})(BPh_4)\}^+$, respectively. Somewhat surprisingly, in view of the ^{1}H NMR data, ESMS studies in MeCN exhibited the peaks at *m*/*z* 495 and 601 together with one at *m*/*z* 300 assigned to $\{Na(\mathbf{II})(MeCN)\}^+$. These data strongly suggest that the red compound is a sodium complex of **II**. Although alkali metal complexes of oligopyridines have been reported over a number of years,[5] structural data establishing the coordination mode are sparse.[6]

The solid state structure of $[\{Na(\mathbf{II})(BPh_4)\}_n]$ is presented in Fig. 1.‡ Each **II** ligand is in a transoid arrangement and presents a didentate N_2 donor set to each of two sodium ions. Although each of the aromatic rings is planar, **II** is riffled with the terminal pyridine rings making dihedral angles of 13–17° with the central tetrazine ring. As far as conventional donor atoms are concerned, each sodium is in a four-coordinate environment comprising two **II** ligands with unremarkable[6] Na–N distances in the range 2.465(2)–2.533(1) and a bite angle of 65.93(4)°. The result is a polymeric structure with chains of {Na(**II**)} units. However, before discussing the nature of the polymer, there is a feature of the coordination environment about the sodium which deserves comment.

Examination of the coordination geometry about the sodium reveals bond angles which imply that the two 'bipy' domains coordinated to each metal are best described in terms of an octahedral *cis*-$\{Na(bipy)_2X_2\}$ structure [N(3)–Na(1)–N(3B) 88.18°, N(2)–Na(1)–N(2B) 174.03°]. The sodium and boron atoms lie on two-fold axes and the tetraphenylborate ion is located in the lattice such that the ring containing C(7) is π-stacked with the tetrazine ring containing N(1) [and of course the same interaction between the symmetry related rings containing C(7B) and N(1B)]. The simplest explanation for the coordination geometry of the sodium is that the remaining two sites of the octahedron are voids filled by the two π-stacked phenyl rings. However, the stacking results in close contacts between the sodium and the two phenyl rings [Na(1)–C(12) 2.8332(18) Å, Na(1)–H(12) 2.6745 Å].

The bridging ligand **II** results in the formation of a one-dimensional polymer which is decorated by the tetraphenylborate counter ions which are locked in at each metal centre (Fig. 2). The polymeric units are then assembled in sheets with no short contacts between adjacent layers. Within each layer, the phenyl rings of the tetraphenylborates are locked into the notches between BPh_4 units of the adjacent chain, although there are no short contacts or additional stacking interactions. The ^{1}H NMR data indicate that this interaction is primarily a solid state phenomenon and no evidence for direct interaction of the tetraphenylborate with the metal centre in solution has been obtained.

We are currently investigating the coordination behaviour of **II** with other sodium salts and with other group 1 metals and

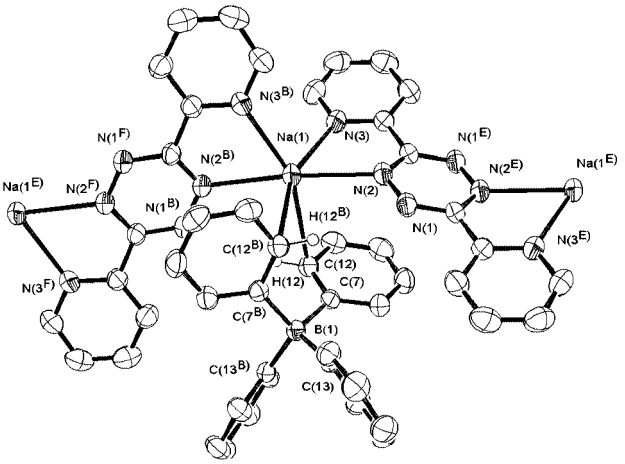

Fig. 1 The coordination geometry about sodium in the complex $[\{Na(\mathbf{II})(BPh_4)\}_n]$ as found from the solid state X-ray structure. With the exception of H(12), hydrogen atoms have been omitted and carbon atoms have only been labelled where necessary to identify phenyl rings or at sites of chemical interest.

 DOI: 10.1039/b106728c

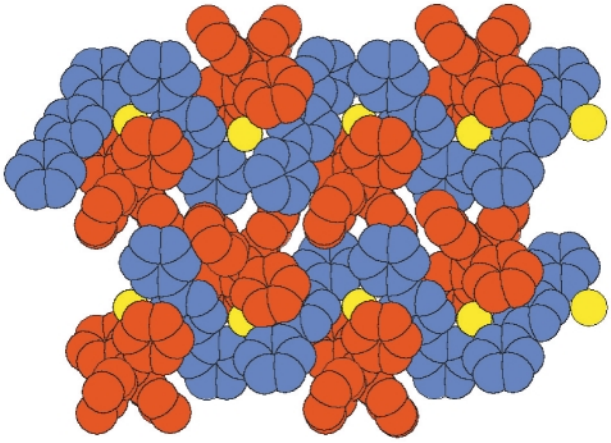

Fig. 2 A view of the part of the polymeric chain formed by the **II** ligands (blue) and sodium ions (yellow) showing how the tetraphenylborate anions (red) are located about the metal and the interactions which construct a sheet structure from adjacent one-dimensional polymeric chains.

have recently shown that **II** forms stable complexes with $LiClO_4$ which exhibit a different one-dimensional polymeric structure.[7]

We gratefully acknowledge financial support from the University of Birmingham and the EPSRC.

Notes and references

† Sodium tetraphenylborate (30.1 mg, 0.88 mmol) was added to a solution of **II** (20.8 mg, 0.88 mmol) in nitromethane (10 cm^3), and the solution stirred at room temperature for 10 min. After standing the solution in the refrigerator overnight, red block-like crystals which were suitable for X-ray structural analysis deposited from the reaction mixture. Yield 24.1 mg, 47%. Found: C, 74.71; H, 4.94; N, 14.35. $C_{36}H_{28}BN_6Na$ requires C, 74.75; H, 4.88; N, 14.53%.

‡ *Crystal data*: $C_{36}H_{28}BN_6Na$, M = 578.44, monoclinic, space group $C2/c$, a = 17.2064(4), b = 12.4777(3), c = 15.3058(3) Å, β = 115.529(1)°, V = 2965.27(11) $Å^3$, Z = 4, μ(Mo-Kα) = 0.738 mm^{-1}, 5413 reflections measured, 2639 unique which were used in all calculations. Final $R1$ = 0.0551 and wR_2 = 0.1432 (all data). Data were measured at 296 K on a Bruker SMART CCD 6000 diffractometer [λ(Mo-Kα) = 1.5418 Å], graphite monochromator, 1722 frames were recorded in 0.4° steps, each for 30 s, crystal-detector distance 40 mm, collimator 0.5 mm. Data reduction by SAINTPLUS, structure solution and refinement by SHELXTL. Hydrogen atom positions calculated and subsequently riding. CCDC reference number 168478. See http://www.rsc.org/suppdata/cc/b1/b106728c/ for crystallographic data in CIF or other electronic format.

1 *Perspectives in Supramolecular Chemistry Volume 5, Transition Metals in Supramolecular Chemistry*, ed. J.-P. Sauvage, Wiley, Chichester, 1999, and references therein.
2 M.-T. Youinou, N. Rahmouni, J. Fischer and J. A. Osborn, *Angew. Chem., Int. Ed. Engl.*, 1992, **6**, 733.
3 X.-H. Bu, H. Moroshita, K. Tanaka, K. Biradha, S. Furusho and M. Shionoya, *Chem. Commun.*, 2000, 971; C. S. Campos-Fernandez, R. Clerac, J. M. Koomen, D. H. Russell and K. R. Dunbar, *J. Am. Chem. Soc.*, 2001, **123**, 773; C. S. Campos-Fernandez, R. Clerac and K. R. Dunbar, *Angew. Chem., Int. Ed.*, 1999, **38**, 3477.
4 E. C. Constable, C. E. Housecroft, B. Kariuki, N. Kelly and C. Smith, unpublished results.
5 E. C. Constable, *Adv. Inorg. Chem. Radiochem.*, 1986, **30**, 69.
6 A. Caron, J. Guilheim, C. Riche, C. Pascard, B. Alpha, J.-M. Lehn and J.-C. Rodriguez-Ubis, *Helv. Chim. Acta*, 1985, **68**, 1577; H. Bock, J.-M. Lehn, S. Holl, V. Krenzel and J. Pauls, *Angew. Chem., Int. Ed.*, 1999, **38**, 952; C. Qian, B. Wang, Y. Xin and Y. Lin, *J. Chem. Soc., Dalton Trans.*, 1994, 2109; C. Papadimitriou, P. Veltsistas, J. Marek, J. Novosad, A. M. Z. Slawin and J. D. Woollins, *Inorg. Chem. Commun.*, 1998, **1**, 418; C. D. Hall, T.-K.-U. Truong, J. H. R. Tucker and J. W. Steed, *Chem. Commun.*, 1997, 2195; L. Echegoyen, A. DeCian, J. Fischer and J.-M. Lehn, *Angew. Chem., Int. Ed. Engl.*, 1991, **30**, 838; M. Veith, J. Bohnlein and V. Huch, *Chem. Ber.*, 1989, **122**, 841.
7 E. C. Constable, C. E. Housecroft, B. Kariuk and C. Smith, unpublished results.

CHEMCOMM
Communication
www.rsc.org/chemcomm

Structural characterisation of the H-bonded $[Mn^{II}(OH_2)_2\cdots(OCH_3)_2Mn^{III}]$ motif: A model for resting state hydroxylic solvent coordination in M(II)–M(III) enzymes

Astrid Boisen,[a] Alan Hazell[b] and Christine J. McKenzie*[a]

[a] *Department of Chemistry, University of Southern Denmark, Campus, 5230 Odense M, Denmark. E-mail: chk@chem.sdu.dk*

[b] *Department of Chemistry, Aarhus University, 8000 Århus C, Denmark*

Received (in Cambridge, UK) 15th August 2001, Accepted 14th September 2001
First published as an Advance Article on the web 2nd October 2001

A mixed-valence dimanganese complex with two water ligands bound to the Mn(II) ion and two methoxide ligands bound to the Mn(III) ion in a H-bonded arrangement has been structurally characterised and models possible resting state water/hydroxide coordination in purple acid phosphatases.

The majority of proposals for the mechanisms of metal-containing enzymes and catalysts involve reactive intermediates incorporating labile ligands which can be substituted by substrate. For metalloenzymes labile ligands are commonly water while water-derived ligands, H_2O, OH^-, $OH^{\cdot}$, O^{2-}, are also reactants in hydrolysis and oxidation reactions. Of the limiting forms of water-derived ligands, it is the *terminal* hydroxides and oxides that are rarely structurally characterised with biologically important metal ions, presumably due to their high reactivity. Despite this, terminal (hydr)oxides of iron and manganese have been designated significant biological roles.

The present report concerns the structural characterisation of a unique mixed-valence complex containing two H-bonded methoxo–water dimetal 'bridging groups', μ-($HOHOCH_3$). This moiety is homologous to the μ-(H_3O_2) group which was, in fact, our original target. Only a handful of complexes with a μ-(H_3O_2) group have been crystallographically characterised. These are exclusively homovalent. Notably the first examples were obtained using the robust metal ions, dichromium(III),[1,2] diiridium(III)[3] and dicobalt(III).[4] More recently labile diiron(III) complexes[5,6] have been characterised. In contrast to the solid state, μ-(H_3O_2) moieties are almost certainly important in the aqueous chemistry of labile dinuclear systems. The μ-(H_3O_2) group is a likely intermediate in the formation of μ-OH bridged dimers and polymers from metal aqua ions *via* 'olation' reactions,[1] and for dimetallic complexes and enzymes known to promote/catalyse hydrolysis reactions.[5,7,8]

Reaction of bpbpH† with manganese perchlorate in dry methanol leads to formation of the dark green compound $[Mn_2(bpbp)(CH_3O)_2(H_2O)_2](ClO_4)_2$.[9] The X-ray crystal structure shows the two aqua and two methoxide ligands in the H-bonded $[Mn^{II}(OH_2)_2\cdots(OCH_3)_2Mn^{III}]$ motif, Fig. 1.[10] The Mn(II) and Mn(III) atoms are linked asymmetrically by the phenolate oxygen atom of $bpbp^-$. Shorter metal–ligand bond distances, and an axial Jahn–Teller distortion along the O(1)–Mn(2)–N(41) axis, identify the Mn(III) atom as that bound by the two methoxide ligands. The location of hydrogen atoms in difference maps supports assignment of two methoxide and two aqua ligands rather than two methanol and two hydroxide ligands or an intermediate symmetrically H-bonded arrangement. The terminal ligands are H-bonded with O_{aq}–H 0.97 Å, H···O_{meth} 1.80 Å, O···O 2.691(5) Å and O–H···O 152° for O(2) and O_{aq}–H 0.96 Å, H···O_{meth} 1.65 Å, O···O 2.563(4) Å and H···O 158° for O(3). To our knowledge $[Mn_2(bpbp)(CH_3O)_2(H_2O)_2](ClO_4)_2$ incorporates the first example of an *unsymmetrical* μ-(ROHOR) group in two senses: (i) the complex is mixed-valent, and (ii) the terminal ligands are derived from two different hydroxylic solvents. Despite considerable effort we were not successful in isolating a homologous di-μ-(H_3O_2) bridged complex from reactions without methanol, or by exchange of methoxide for hydroxide by reaction of $[Mn_2(bpbp)(CH_3O)_2(H_2O)_2](ClO_4)_2$ with water.

The cyclic voltammogram of $[Mn_2(bpbp)(CH_3O)_2(H_2O)_2](ClO_4)_2$ attests to its lability in solution: no distinct electrochemical response was observed in CVs recorded under identical conditions to those recorded for the related bis-acetate-bridged Mn^{II}–Mn^{III} complex, $[Mn_2(bpbp)(CH_3CO_2)_2](ClO_4)_2$ which we prepared for comparative purposes: $[Mn_2(bpbp)(CH_3CO_2)_2](ClO_4)_2$[12] shows a reversible wave for the Mn^{II}–Mn^{II}/Mn^{II}–Mn^{III} couple and a quasi-reversible wave for the Mn^{II}–Mn^{III}/Mn^{III}–Mn^{III} couple reflecting the structural stability of this compound in solution compared to $[Mn_2(bpbp)(CH_3O)_2(H_2O)_2](ClO_4)_2$.

X-Band EPR spectra of $[Mn_2(bpbp)(CH_3O)_2(H_2O)_2](ClO_4)_2$ as a powder or acetone glass at 102 K (Fig. 2) display multiple, broad lines in the range 0–6000 G with the strongest resonances occurring in the 3500 G region. The spectrum of the neat powder, at 295 K, though less well resolved, is generally similar to that of the acetone glass, suggesting that either the complex retains its integrity in acetone solution or that coordinated solvent exchange has little effect on the electronic structure. Assignment of the signals has not been attempted since they result from a complicated combination of exchange, dipolar and zero-field splitting effects. The multiple hyperfine lines originating from the $S = ½$ coupled ground state are resolved at $g \sim 2$, as noted by Hendrickson and coworkers[12] for a bis-acetate-bridged Mn(II)-Mn(III) compound $[Mn_2(bcmp)(CH_3CO_2)_2](ClO_4)_2\cdot CH_2Cl_2$.†

ESI mass spectra of $[Mn_2(bpbp)(CH_3O)_2(H_2O)_2](ClO_4)_2$ give no indication of the structure of the cation. The $[Mn_2(bpbp)(CH_3O)_2(H_2O)_2]^{2+}$ ion was not observed. A mixture

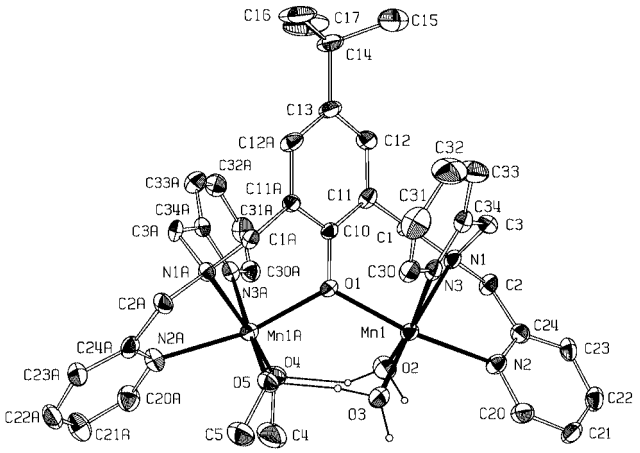

Fig. 1 Structure of the cation in $[Mn_2(bpbp)(CH_3O)_2(H_2O)_2](ClO_4)_2$. Selected bond lengths (Å): Mn^{III}–OCH_3 1.849(3), 1.900(4), Mn^{II}–OH_2 2.132(3), 2.176(3), Mn^{II}–$O_{phenoxide}$ 2.143(3), Mn^{III}–$O_{phenoxide}$ 2.155(3) Å, Mn···Mn, 3.776(1) Å.

 DOI: 10.1039/b107398m

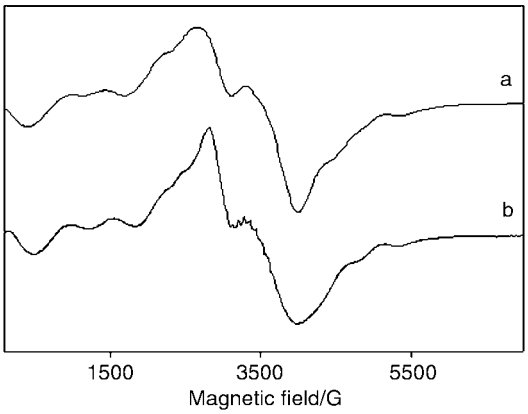

Fig. 2 The EPR spectrum of $[Mn_2(bpbp)(H_2O)_2(CH_3O)_2](ClO_4)_2$ **2**: (a) neat powder, 295 K; (b) frozen glass acetone solution, 102 K.

of solvent-dependent ions with the Mn(III)–Mn(II) $[Mn_2(bpbp)]^{4+}$ core were observed in all solvents tried (CH_3OH, CH_3CN, H_2O) reflecting the lability of the auxilary ligands. The major ion in all spectra was at *m*/*z* 348.7 which can be assigned to an oxide, $[Mn_2(bpbp)(O)]^{2+}$. The following MS/MS experiment indicates that this oxide ion is not present in solution: $[Mn_2(bpbp)(O)]^{2+}$ is produced easily by collision activated dissociation (CAD) of the $[Mn_2(bpbp)(RO)_2]^{2+}$ ions, R = H (*m*/*z* 357.8) or CH_3 (*m*/*z* 371.7), which are obtained from water or methanol solutions respectively when these are sprayed using very mild source conditions. Thus, the loss of a mass equivalent of water or dimethyl ether from the $[Mn_2(bpbp)(RO)_2]^{2+}$ (R = H, CH_3) ions to give the dominant $[Mn_2(bpbp)(O)]^{2+}$ ions is a facile fragmentation pathway. We have previously noted the facile gas phase formation of metal oxides from metal carbonates,[13] and the present case is another example which should serve as a warning to the assignment of 'novel metal–oxide' species on the basis of ESI MS alone.

The arrangement of the auxiliary solvent-derived ligands as two μ-($HOHOCH_3$) groups in, $[Mn_2(bpbp)(CH_3O)_2(H_2O)_2](ClO_4)_2$ can be regarded as a pertinant structural motif for coordinated solvent interactions at the active sites of dimetallic proteins, particularly those containing a mixed valence site, *e.g.* the purple acid phosphatases (PAPs). Like $[Mn_2(bpbp)(CH_3O)_2(H_2O)_2](ClO_4)_2$ the PAPs contain one trivalent metal ion [Fe(III)] and one divalent metal ion [Fe(II) or Zn(II)].[14] The mechanistically important nucleophilic hydroxide has been proposed to be metal coordinated; whether or not it is terminal or bridging is uncertain. $[Mn_2(bpbp)(CH_3O)_2(H_2O)_2](ClO_4)_2$ with its trivalent and divalent metal ion at a distance of 3.77 Å shows a way in which a M(III)-bound hydroxide (by analogy to methoxide) ion could be stabilised by H-bonding to a water molecule bound to the adjacent M(II) to give the μ-(H_3O_2) group and thus support the notion of a terminally bound hydroxide as the nucleophile and terminal water as a substitutionally labile ligand on the adjacent metal ion in PAPs. Although $[Mn_2(bpbp)(CH_3O)_2(H_2O)_2](ClO_4)_2$ is a plausible structural model for resting state PAP, we have no indications that it might be a useful functional model from our investigations of reactivity in promotion/catalysis of PAP-like hydrolysis reactions using phosphate ester, alkyl ester and nitrile substrates in solutions containing water. This contrasts to a structurally characterised diiron system with a μ-(H_3O_2) bridge which was shown to promote hydrolysis of acetonitrile and triphenylphosphate.[5]

Finally, the formation of $[Mn_2(bpbp)(CH_3O)_2(H_2O)_2](ClO_4)_2$ formally requires a one-electron oxidation of one manganese ion. The reaction occurs only in the presence of oxygen. Such spontaneous air oxidations are normal, however they are often not elucidated mechanistically. Preliminary results suggest that a background oxidation of the methanol solvent (and presumably concomitant reduction of dioxygen) has occured during the reaction. Repitition of the work using cyclohexanol to replace methanol in the reaction mixture showed a background formation of cyclohexanol. This air alcohol oxidation to aldehydes is slow but catalytic.[15]

In summary, the μ-($HOHOCH_3$) group in $[Mn_2(bpbp)(CH_3O)_2(H_2O)_2](ClO_4)_2$ is a plausible structural model for water/hydroxide coordination and interactions in the resting state of PAPs which, like the complex here, contain a trivalent and divalent metal ion. Preliminary work indicates that the labile $[Mn_2(bpbp)(solv)_x]^{3+}$ (solv = water and alcohols), activates oxygen to form an oxidant capable of oxidising alcohols. Future investigations will centre around the selectivity, extent and efficiency of the $[Mn_2(bpbp)(solv)_x]^{3+/4+}/O_2$ system, as an oxidation catalyst.

Support from the Danish Natural Science Council (C. J. M.) is gratefully acknowledged. Professor Keith S. Murray (Monash University) is thanked for helpful discussions. At the University of Southern Denmark we are grateful to Dr Kenneth Bendix Jensen for recording the ESI mass spectra and Jens Zacho Pedersen for recording EPR spectra.

Notes and references

† bpbpH = 2,6-bis{[*N*,*N*′-bis(2-picolyl)amino]methyl}-4-*tert*-butylphenol; bcmpH = 2,6-bis[bis(1,4,7-triazacyclonon-1-ylmethyl)aminomethyl]-4-methylphenol; bpmpH = 2,6-bis[bis(2-pyridylmethyl)aminomethyl]-4-methylphenol.

1 M. Arden and A. Bino, *J. Am. Chem. Soc*., 1983, **105**, 7747; M. Ardon and A. Bino, *Inorg. Chem*., 1985, **24**, 1343; M. Arden, A. Bino and K. Mickelsen, *J. Am. Chem. Soc*., 1987, **109**, 1986.
2 P. Andersen, A. Døssing and S. Larsen, *Acta Chem. Scand*., 1990, **44**, 455.
3 F. Galsbøl, S. Larsen, B. Rasmussen and J. Springborg, *Inorg. Chem*., 1986, **25**, 290.
4 J. S. Seo, N.-D. Sung, R. C. Hynes and J. Chin, *Inorg. Chem*., 1996, **35**, 7472.
5 A. Hazell, K. B. Jensen, C. J. McKenzie and H. Toftlund, *Inorg. Chem*., 1993, **33**, 3127.
6 E. C. Wilkinson, Y. Dong, Yanhong and L. Que, Jr., *J. Am. Chem. Soc*., 1994, **116**, 8394; S. Poussereau, G. Blondin, G. Chottard, J. Guilhem, L. Tchertanov, E. Riviere and J.-J. Girerd, *Eur. J. Inorg. Chem*., 2001, **4**, 1057.
7 D. E. Wilcox, *Chem. Rev*., 1996, **96**, 2435,
8 S. H. Gellman, R. Petter and R. Breslow, *J. Am. Chem. Soc*., 1986, **108**, 2388; W. H. Chapman, Jr. and R. Breslow, *J. Am. Chem. Soc*., 1995, **117**, 5462; M. Yashiro, A. Ishikubo and M. Komiyama, *J. Chem. Soc., Chem. Commun*., 1995, 1973; P. Hendry and A. M. Sargeson, *Prog. Inorg. Chem*., 1990, **38**, 201; C. J. McKenzie and R. Robson, *J. Chem. Soc., Chem. Commun*., 1988, 112.
9 Anal. Calc. for $C_{38}H_{49}Cl_2Mn_2N_6O_{13}$: C, 46.64; H, 5.05; N, 8.59; Cl, 7.25. Found: C, 45.79; H, 5.10; N, 8.68; Cl, 7.36%.
10 Dark green crystals of $[Mn_2(bpbp)(CH_3O)_2(H_2O)_2](ClO_4)_2$ are orthorhombic, space group *Pna*2$_1$, *Z* = 4, *a* = 22.331(1), *b* = 18.351(1), *c* = 10.922(1) Å. CCDC reference number 160800. See http://www.rsc.org/suppdata/cc/b1/b107398m/ for crystallographic data in CIF or other electronic format.
11 $E_{½}$ for $[Mn_2(bpbp)(CH_3CO_2)_2](ClO_4)_2$: Mn^{II}–Mn^{II}/Mn^{II}–Mn^{III}, 70 mV, reversible; Mn^{II}–Mn^{III}/Mn^{III}–Mn^{III}, 630 mV, quasireversible. Acetonitrile solution with Bu_4NPF_6 electrolyte *vs.* Fc/Fc$^+$.
12 H. Diril, H.-R. Chang, M. J. Nilges, X. Zhang, S. K. Larsen, J. A. Potenza, H. J. Schugar, S. S. Isied and D. N. Hendrickson, *J. Am. Chem. Soc*., 1989, **111**, 5102.
13 P. Dalgaard and C. J. McKenzie, *Int. J. Mass Spectrom*., 1999, **34**, 1033.
14 T. Klabunde, N. Sträter, R. Frölich, H. Witzel and B. Krebs, *J. Mol. Biol*., 1996, **259**, 737.
15 A 0.2 mM solution of dinuclear complex formed *in situ* from $Mn(ClO_4)_2·6H_2O$–bpbpH–Et_3N (2 : 1 : 1), dissolved in 9 ml acetonitrile and 1 ml cyclohexanol was kept under 1 atm O_2. The cyclohexanol is oxidized with 99% selectivity to cyclohexanone with a turnover number (TON) of *ca*. 30 in 24 h (GC analysis). This result provides circumstantial evidence for an undetected oxidation of methanol to formaldehyde in the synthesis of $[Mn_2(bpbp)(CH_3O)_2(H_2O)_2](ClO_4)_2$.

CHEMCOMM Communication
www.rsc.org/chemcomm

The first structurally characterised homoleptic organovanadium(III) compound†

Pablo J. Alonso, Juan Forniés,* M. Angeles García-Monforte, Antonio Martín and Babil Menjón

Instituto de Ciencia de Materiales de Aragón, Facultad de Ciencias, Universidad de Zaragoza–C.S.I.C., Pza. S. Francisco s/n, E-50009 Zaragoza, Spain. E-mail: forniesj@posta.unizar.es

Received (in Cambridge, UK) 17th July 2001, Accepted 4th September 2001
First published as an Advance Article on the web 3rd October 2001

The homoleptic, tetrahedral, paramagnetic d^2 species $[NBu_4][V^{III}(C_6Cl_5)_4]$ 1 has been obtained and characterised by analytical, spectroscopic and X-ray diffraction methods.

The organometallic chemistry of vanadium is chiefly dominated by species containing carbonyl and cyclopentadienyl ligands.[1] In contrast, simple, homoleptic σ-organovanadium compounds unsupported by cyclopentadienyl or other donor ligands are still rare. The chemistry of these derivatives has, however, received renewed attention especially because some organovanadium(II) or -(III) species appear as active intermediates in chemical fixation processes of molecular nitrogen.[2] It is thus thought that the formation of $[(VR_3)_2(\mu\text{-}N_2)]$ is likely to occur *via* the homoleptic intermediates VR_3 [R = $C_6H_2Me_3$-2,4,6 (mes)[3] or CH_2Bu^t[4]]. To the best of our knowledge, the only homoleptic organovanadium(III) compounds that have been isolated to date are: anionic $[VR_4]^-$ [R = mes[5] or $C_6H_3(OMe)_2$-2,6[6]] and neutral $[VR_3]$ [R = mes,[3] $C(CN)_3$[7] or $CH(SiMe_3)_2$[8]]. However, unequivocal structural information is not available for any of them. We now report the synthesis and structural characterisation of $[NBu_4][V(C_6Cl_5)_4]$ **1**, a remarkably stable homoleptic organovanadium(III) compound.

The reaction of $[VCl_3(thf)_3]$[9] with LiC_6Cl_5[10] in a 1:8 molar ratio followed by the appropriate treatment‡ allows the isolation of $[NBu_4][V(C_6Cl_5)_4]$ **1** as a deep green solid. Once isolated, complex **1** is air- and moisture-stable in the solid state. This behaviour is in contrast with the reported observation of the ease with which the related compound $[Li(thf)_4][V(mes)_4]$ is air-oxidised to give neutral $[V(mes)_4]$.[12] Complex **1** behaves as a 1:1 electrolyte in dilute acetone solution (3.1×10^{-1} mol dm^{-3}).[13]

The solid-state structure of **1** has been established by single-crystal X-ray diffraction analysis.§ The structure of the anion $[V(C_6Cl_5)_4]^-$ is depicted in Fig. 1. It can be seen that all four σ V–C bonds are virtually identical, while the C–V–C angles take values between 98.1(2) and 117.6(2)°. Hence, the local geometry around the vanadium centre can be described as slightly distorted tetrahedral (*cf.* ideal C–V–C angle: 109.5°). The V–C distances in **1** [ranging from 214.2(5) to 215.8(5) pm] are similar to those found in other heteroleptic σ-arylvanadium(III) compounds, such as $[V\{C_6H_2(CF_3)\text{-}2,4,6\}_2Cl(thf)]$ [V–C 214.5(4) and 215.9(4) pm],[15] $[PF(NEt_2)_3][V(mes)_3F]$ [V–C 210.7(4)–213.2(4) pm][16] and $[V(mes)_3(thf)]$ [V–C 209.5(6)–211.7(7) pm].[17] The V–C_{ipso}–C_{ortho} angles within each pentachlorophenyl ring are dissimilar with values amounting to *ca.* 115 and *ca.* 130°, respectively. The swing of the aryl rings also implies the existence of two sets of *ortho*-Cl–V distances each approaching 310 and 366 pm, respectively. These structural features have been previously used as criteria which help to determine the existence of *ortho*-Cl···M interactions in other pentachlorophenyl metal derivatives.[18] Bearing in mind these criteria we suggest the non-existence of additional *ortho*-Cl···V interactions in **1** since: (i) the swing of the C_6Cl_5 rings is only moderate; (ii) the *ortho*-Cl–V distances are too long to be considered as the result of a bonding interaction; and (iii) the central core is well described as a slightly distorted tetrahedron with no evidence for the need of a higher coordination polyhedron.

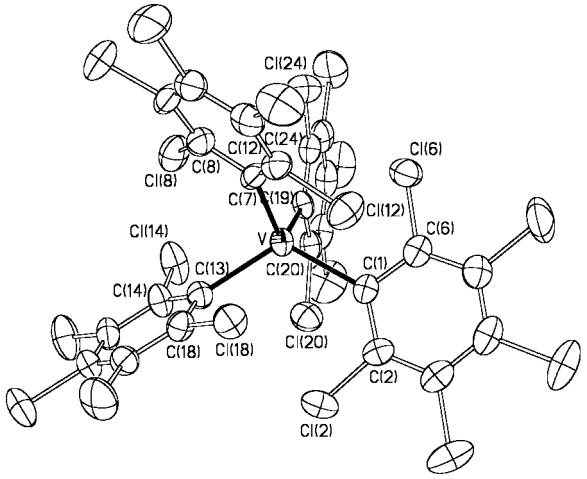

Fig. 1 Thermal ellipsoid diagram of the anion of **1**. Selected distances (pm) and angles (°): V–C(1) 214.4(5), V–C(7) 215.8(6), V–C(13) 215.2(5), V–C(19) 214.2(5), V–Cl(2) 364.6(2), V–Cl(6) 311.6(2), V–Cl(8) 311.5(2), V–Cl(12) 366.3(2), V–Cl(14) 366.3(2), V–Cl(18) 313.6(2), V–Cl(20) 304.9(2), V–Cl(24) 368.3(2); C(1)–V–C(7) 112.1(2), C(1)–V–C(13) 117.6(2), C(1)–V–C(19) 101.2(2), C(7)–V–C(13) 98.1(2), C(7)–V–C(19) 116.1(2), C(13)–V–C(19) 112.6(2).

Complex **1** has also been studied by EPR spectroscopy both in the X- and Q-bands.¶ Frozen solutions of **1** in THF/CH_2Cl_2 mixtures gave poor-quality spectra with very low signal-to-noise ratios. However, the X-band EPR spectrum of a powder sample of **1** shows four clearly defined features at room temperature, located at *ca.* 120, 280, 670 and 840 mT (Fig. 2). At lower temperatures, the two outer signals shift downfield, whereas the central ones remain almost unchanged.

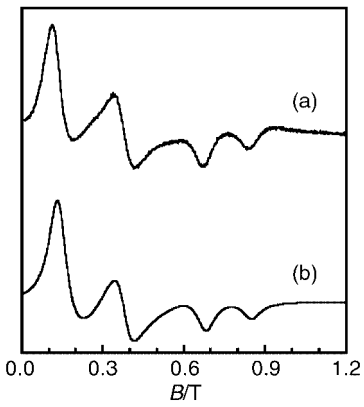

Fig. 2 X-band EPR spectrum of a powder sample of **1** at room temperature (microwave frequency 9.545 GHz): experimental (a) and calculated (b).

† Dedicated to Professor Dr Rafael Usón on the occasion of his 75th birthday.

 DOI: 10.1039/b106364m

Vanadium(III) is a non-Kramers paramagnetic system (d^2), which is usually 'EPR silent' unless located in a high-symmetry site such as cubic, octahedral or tetrahedral. When located in a tetrahedral site, the ^3F ground term in the free V(III) ion splits into two triplets ($^3T_1$ and $^3T_2$) and one singlet ($^3A_2$), the latter being the lowest energy level. Since the V(III) centre in **1** is in a nearly tetrahedral environment, the ground state orbital wave function is expected to be close to a $^3A_2$ orbital with an isotropic g-factor and the spin-Hamiltonian given in eqn. (1).‖

$$H = g\mu_B \vec{B}\cdot\vec{S} + D\left[S_Z^2 - \tfrac{1}{3}S(S+1)\right] + E(S_X^2 - S_Y^2) \qquad (1)$$

The analysis of the EPR spectrum of **1** using eqn. (1) gives a satisfactory agreement between the calculated [Fig. 2(b)] and experimental [Fig. 2(a)] spectra with the following values of the spin-Hamiltonian parameters: g = 1.98(1), D = 13.59(5) GHz and η = 0.16(1). It is interesting to note that these values also allow the reproduction of the Q-band spectrum.

In contrast to the profusion of EPR reports involving V(IV) species (d^1), there are very few EPR data available for V(III). These data have been obtained on samples of V(III) doped into ionic lattices (*e.g.* CaF_2:V, g = 1.933[19] and CdF_2:V, g = 1.937[20]) and into semiconductors (g = 1.92–1.99).[21] Recently, a detailed EPR study on samples of V(III) doped into $CsGa(SO_4)_2\cdot 12H_2O$ has been reported using high-field, multi-frequency techniques. The spectra thus obtained for the $[V(H_2O)_6]^{3+}$ cation have been analysed with an axial spin-Hamiltonian with $g_\parallel$ = 1.955, $g_\perp$ = 1.869 and D = 143 GHz.[22]

The moderate departure of the g value obtained for **1** from the free electron value can be attributed to some degree of delocalisation of the unpaired electrons over the aryl ligands in the $[V(C_6Cl_5)_4]^-$ anion. This assumption, however, cannot yet be confirmed, since the hyperfine structure expected to appear in **1** (^{51}V, I = 7/2, 100% natural abundance) is unresolved due to the broadness of the features in the EPR spectrum.

The remarkable stability of **1** has allowed the first structural characterisation of a homoleptic organovanadium(III) derivative to be obtained. Moreover, this is, to the best of our knowledge, the first V(III) compound which has a defined EPR spectrum and in which the vanadium centre is not a doping but rather a constituent element of the sample. On the other hand, the inertness of **1** could well act as a drawback for its chemical reactivity which is currently under study.

We thank Professor P. H. Rieger (Brown University, Providence) for helpful EPR discussions and suggestions. We also thank the Dirección General de Enseñanza Superior (Projects PB98-1595-C02-01 and PB98-1593) for financial support and the Gobierno de Aragón for a grant to M. A. G.-M.

Notes and references

‡ *Experimental procedure*: to a solution of LiC_6Cl_5 (*ca.* 55 mmol) in Et_2O (60 cm^3) at −78 °C was added $[VCl_3(thf)_3]$ (2.54 g, 6.80 mmol). The suspension was allowed to warm up to room temperature and, after 15 h of stirring, the by then deep green solid was filtered, washed with Et_2O (3 × 5 cm^3) and extracted in CH_2Cl_2 (50 cm^3). The extract was evaporated to dryness and the resulting residue was redissolved in Pr^iOH (80 cm^3) and filtered. The addition of NBu_4Br (4.4 g, 13.6 mmol) to the filtrate caused the precipitation of a first fraction of **1** as a deep green solid. By standing the mother liquor at −30 °C overnight, a second crop of **1** was obtained (45% overall yield). Anal. found for $C_{40}H_{36}Cl_{20}NV$: C 37.28, H 2.80, N 0.65. Calc.: C 37.22, H 2.80, N 1.08%. IR(KBr)/cm^{-1}: 1482m, 1458w, 1379w, 1321s, 1312s, 1283vs, 1224m, 1145w, 1063s, 1025w, 883w (NBu_4^+), 828s (C_6Cl_5: X-sensitive vibr.),[11] 740w (NBu_4^+), 669s and 346w. FAB-MS: *m*/*z* 1039 $[V(C_6Cl_5)_4]^-$, 827 $[V(C_6Cl_5)_3Cl]^-$, 792 $[V(C_6Cl_5)_3]^-$, 615 $[V(C_6Cl_5)_2Cl_2]^-$ and 545 $[V(C_6Cl_5)_2]^-$. Λ_M(acetone) = 108.1 S cm^2 mol^{-1}.

§ *Crystal data* for **1**: $C_{40}H_{36}Cl_{20}NV$, M = 1290.64, orthorhombic, space group *Pbca* (no. 61), a = 1938.00(10), b = 2125.86(13), c = 2590.52(14) pm, U = 10.6727(10) nm^3, T = 293(2) K, graphite-monochromated Mo-Kα radiation, λ = 71.073 pm, Z = 8, D_c = 1.606 g cm^{-3}, $F(000)$ = 5168, measured absorption correction based on ψ scans, Enraf-Nonius CAD4 diffractometer, 9361 intensity data collected, 9358 unique (R_{int} = 0.0031) which were used in all calculations. The structure was solved by Patterson and Fourier methods and refined anisotropically by full-matrix, least squares on F^2 (program SHELXL 93; ref 14) to final values of R_1 = 0.0589 [for 5228 data with $I > 2\sigma(I)$] and wR_2 = 0.1398 (all data) for 559 parameters.

CCDC reference number 167901. See http://www.rsc.org/suppdata/cc/b1/b106364m/ for crystallographic data in CIF or other electronic format.

¶ EPR spectra were measured using a Bruker ESP388E spectrometer equipped with an ERV411T variable temperature device. The microwave frequency was determined with a Hewlett/Packard HP5350B frequency counter and the magnetic field strength was measured with a Bruker ER035M gaussmeter.

‖ S = 1, μ_B is the Bohr magneton, (X, Y, Z) are the principal axes of the second rank tensor describing the zero-field splitting (ZFS) effects due to the admixture of the triplet orbitals to the ground state singlet. This mixture is a consequence of both the spin-orbit and the non-cubic crystal field contributions and is usually described by the D and E parameters, being $0 \leqslant \eta = E/D \leqslant 1/3$.

1 N. G. Connelly, in *Comprehensive Organometallic Chemistry*, ed. G. Wilkinson, F. G. A. Stone and E. W. Abel, Pergamon Press, Oxford, 1982, vol. 3, ch. 24, pp. 647–704; P. Berno, S. Gambarotta and D. Richeson, in *Comprehensive Organometallic Chemistry II*, ed. E. W. Abel, F. G. A. Stone and G. Wilkinson, Elsevier Science Ltd., Oxford, 1995, vol. 5, ch. 1, pp. 1–55.
2 G. J. Leigh and J. S. de Souza, *Coord. Chem. Rev*., 1996, **154**, 71.
3 R. Ferguson, E. Solari, C. Floriani, D. Osella, M. Ravera, N. Re, A. Chiesi-Villa and C. Rizzoli, *J. Am. Chem. Soc*., 1997, **119**, 10 104.
4 J.-K. F. Buijink, A. Meetsma and J. H. Teuben, *Organometallics*, 1993, **12**, 2004.
5 W. Seidel and G. Kreisel, *Z. Anorg. Allg. Chem*., 1976, **426**, 150.
6 W. Seidel, P. Scholz and G. Kreisel, *Z. Anorg. Allg. Chem*., 1979, **458**, 263.
7 H. Koehler, P. Laub and A. Frischkorn, *J. Less-Common Met*., 1971, **23**, 171.
8 G. K. Barker, M. F. Lappert and J. A. K. Howard, *J. Chem. Soc., Dalton Trans*., 1978, 734.
9 B. Heyn, B. Hipler, G. Kreisel, H. Schreer and D. Walther, *Anorganische Synthesechemie*, Springer-Verlag, Berlin, 1990, 2nd edn., pp. 18, 19.
10 M. D. Rausch, F. E. Tibbets and H. B. Gordon, *J. Organomet. Chem*., 1966, **5**, 493.
11 R. Usón and J. Forniés, *Adv. Organomet. Chem*., 1988, **28**, 219; E. Maslowsky, Jr., *Vibrational Spectra of Organometallic Compounds*, John Wiley & Sons, New York, 1977, pp. 437–442.
12 W. Seidel and G. Kreisel, *Z. Chem*., 1976, **16**, 115.
13 W. J. Geary, *Coord. Chem. Rev*., 1971, **7**, 81.
14 G. M. Sheldrick, SHELXL 93, Program for the Refinement of Crystal Structures from Diffraction Data, University of Göttingen, Göttingen, Germany, 1993.
15 V. C. Gibson, C. Redshaw, L. J. Sequeira, K. B. Dillon, W. Clegg and M. R. J. Elsegood, *Chem. Commun*., 1996, 2151.
16 M. R. Kopp and B. Neumüller, *Z. Anorg. Allg. Chem*., 1999, **625**, 363.
17 M. Vivanco, J. Ruiz, C. Floriani, A. Chiesi-Villa and C. Rizzoli, *Organometallics*, 1993, **12**, 1794.
18 J. Forniés, B. Menjón, R. Mª Sanz-Carrillo, M. Tomás, N. G. Connelly, J. G. Crossley and A. G. Orpen, *J. Am. Chem. Soc*., 1995, **117**, 4295; M. P. García, M. V. Jiménez, A. Cuesta, C. Siurana, L. A. Oro, F. J. Lahoz, J. A. López, M. P. Catalán, A. Tiripicchio and M. Lanfranchi, *Organometallics*, 1997, **16**, 1026.
19 M. M. Zaripov, V. S. Kropotov, L. P. Livanova and V. A. Stepanov, *Sov. Phys. Solid State*, 1968, **9**, 2346.
20 M. M. Zaripov, V. S. Kropotov, L. P. Livanova and V. A. Stepanov, *Sov. Phys. Solid State*, 1968, **10**, 262.
21 R. N. Schwartz, M. Ziari and S. Trivedi, *Phys. Rev. B*, 1994, **49**, 5274 and references cited therein.
22 P. L. W. Tregenna-Piggott, H. Weihe, J. Bendix, A.-L. Barra and H.-U. Güdel, *Inorg. Chem*., 1999, **38**, 5928.

CHEMCOMM Communication
www.rsc.org/chemcomm

Biaxial smectic A liquid crystal in a pure compound

B. K. Sadashiva,* R. Amaranatha Reddy, R. Pratibha and N. V. Madhusudana

Raman Research Institute, C.V. Raman Avenue, Bangalore 560 080, India. E-mail: sadashiv@rri.res.in

Received (in Cambridge, UK) 10th July 2001, Accepted 31st August 2001
First published as an Advance Article on the web 26th September 2001

The synthesis and characterisation is reported of a low molecular weight organic compound to exhibit the biaxial smectic A (SmA_b) phase, which shows a transition from the partial bilayer uniaxial SmA_d phase to the SmA_{db} phase as the temperature is lowered.

The discovery of liquid crystalline phases in compounds with bent-core (BC) or banana-shaped molecules[1] has led to a very intense research activity in the field.[2] In the past couple of years several new compounds having this molecular architecture have been reported[3–8] in an effort to find the relationship between the molecular structure and the mesomorphic properties associated with it. At least five different B-(banana) types of liquid crystal have been clearly identified in pure compounds, though recently some new variants have been found.[8] The most fluid of the B-type of liquid crystals, which is also electrically switchable is the B_2 phase in which the bent-cores pack along a common axis to give rise to an electric polarisation of the layer. The molecular plane tilts with respect to the layer-normal to produce a *chiral* layer, though the molecules themselves are usually achiral.[9] In an earlier study, we found that binary mixtures of a compound exhibiting the B_2 phase with one made of rod-like molecules exhibiting the bilayer smectic A_2 phase showed a very interesting phase diagram.[10,11] If the concentration of the rods is between 4 and 13 mol% the mixtures exhibit a biaxial smectic A_2 (SmA_{2b}) phase in which the BC molecules undergo an orientational transition as the temperature is lowered from the uniaxial SmA_2 phase. The other known systems exhibiting the SmA_b phase were found (i) in a binary mixture of polymeric and monomeric species,[12] (ii) in an oxadiazole derivative[13] at high temperatures (above 235 °C), and (iii) in a binary mixture involving a metallomesogen.[14]

It is of obvious interest to find the biaxial SmA_b phase in a low molecular weight pure compound at a relatively low temperature. Compounds whose molecules have a strong biaxiality of shape are necessary for this purpose and the best systems appear to be those made of BC molecules. Indeed, several compounds with BC molecules are known to exhibit the smectic A (SmA) phase but NMR studies have shown that in such molecules the angle between the two arms of the bent-core is about 160°, which means that the deviation from a rod-like structure (in which this angle would be 180°) is quite small.[2] On the other hand, if the molecules have highly bent cores the compounds are known to exhibit only the B-type of liquid crystal.

Here, we report the synthesis of a compound made of BC molecules with a new architecture. The unsymmetrical molecule has an alkoxy chain attached to only one of the arms of the bent-core, while the other arm ends with the highly polar cyano group. The synthetic pathway used to obtain this compound is shown in Scheme 1.‡ Our studies show that the compound exhibits a partial bilayer smectic A_d phase in which the bent-cores of two neighbouring molecules overlap in an antiparallel orientation, as in the case of highly polar rod-like molecules.[15,16] Indeed, this is the first example of a single-component, low molecular weight compound to exhibit the biaxial smectic A to uniaxial smectic A transition.

† Electronic supplementary information (ESI) available: spectroscopic data for **1**. See http://www.rsc.org/suppdata/cc/b1/b106084h/

The liquid crystalline properties were investigated by differential scanning calorimetry (DSC, Pyris 1D, 5 °C min^{-1}) and polarised optical microscopy (Leitz Laborlux 12 POL). Observation using a polarising microscope of a sample taken from between the untreated slide and coverslip shows the following sequence of textures as the temperature is lowered. The dark field of view, corresponding to the isotropic phase, goes over at a transition point to an SmA texture in which most of the sample has a homeotropic alignment, but some parts clearly show focal-conic domains. As the temperature is lowered further, there is another phase transition in which the homeotropic regions exhibit a schlieren texture (Fig. 1), with both two-brush and four-brush defects. Strong fluctuations in intensity are seen as in the SmA_{2b} phase.[10] The presence of two-brush defects indicates that the low temperature phase has one of the following structures: (i) a biaxial smectic A phase in which the two orthogonal directors in the plane of smectic layers are also *apolar* in nature; (ii) a packing of the BC molecules of compound **1** such that each layer is polarised, but with a mutually antiferroelectric arrangement in neighbouring layers (the two-brush defects in such a case are dispirations, which are combinations of half strength disclinations which are defect patterns in the in-plane director, and screw dislocations;[17] this structure can also be described as a biaxial SmA); and (iii) another possibility would be for the molecules to tilt with an anticlinic arrangement in successive layers, in which

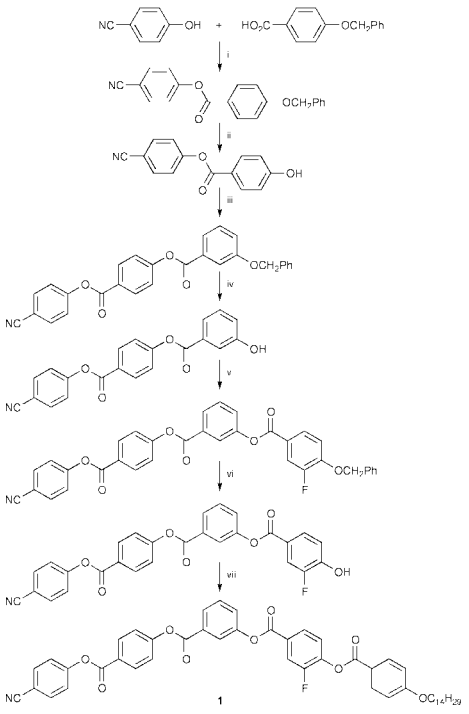

Scheme 1 *Reagents and conditions*: i, DCC, cat. DMAP, dry $CHCl_3$, rt, 15 h, 81%; ii, cat. 5%Pd–C, H_2, 1,4-dioxane, 55 °C, 75%; iii, 3-benzyloxybenzoic acid, DCC, cat. DMAP, dry $CHCl_3$, rt, 15 h, 72%; iv, cat. 5% Pd–C, H_2, 1,4-dioxane, 55 °C, 73%; v, 3-fluoro-4-benzyloxybenzoic acid, DCC, cat. DMAP, dry $CHCl_3$, rt, 20 h, 68%; vi, cat. 5% Pd-C, H_2, 1,4-dioxane, 55 °C, 80%; vii, 4-*n*-tetradecyloxybenzoic acid, DCC, cat. DMAP, dry $CHCl_3$ rt, 20 h, 61%.

 DOI: 10.1039/b106084h

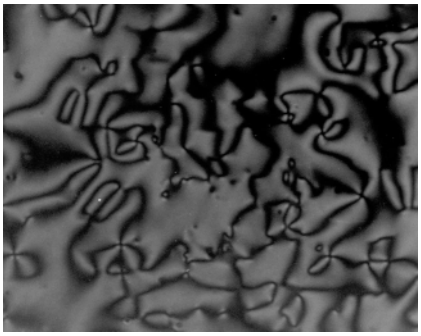

Fig. 1 Photograph of the schlieren texture of a homeotropic sample of the biaxial smectic liquid crystal of compound **1**. Note several half strength disclinations with two dark brushes which indicate an apolar in-layer director field (crossed polars, ×250).

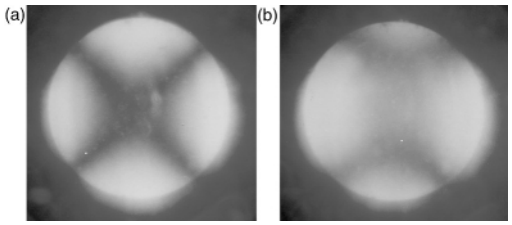

Fig. 2 Photographs of the conoscopic patterns from a homeotropically aligned sample of (a) the uniaxial smectic A_d phase at 128 °C, and (b) the biaxial smectic A_{db} phase at 124 °C.

case again dispirations can produce two-brush defects. We rule out the last possibility in view of the X-ray results to be described later.

DSC of compound **1** shows the following sequence of transitions. The numbers above the arrows are transition temperatures in °C and the numbers in parentheses are

$$\text{Iso} \underset{(4.77)}{\overset{130}{\longleftrightarrow}} \text{SmA} \underset{(0.04)}{\overset{126.2}{\longleftrightarrow}} \text{SmA}_b \underset{(85.46)}{\overset{120.5}{\longleftrightarrow}} \text{Cr} \qquad (1)$$

enthalpies in kJ mol^{-1}. In order to confirm the biaxiality of the low temperature phase, samples contained in a cell and well aligned using a lateral electric field are employed. The thickness of the sample is 37.3 μm which is controlled using appropriate spacers and measured using an interference technique before filling the sample. As the temperature of the cell is lowered below the SmA to SmA_b transition point (T_{bu}) again the schlieren texture is seen. The application of an electric voltage of *ca.* 200 V at 10 kHz between the two ITO regions aligns the sample uniformly in the gap. Conoscopic observations between crossed polarisers, which are set at 45° to the direction of the electric field, clearly show that the uniaxial cross in the SmA phase splits to give a biaxial pattern below the relevant transition temperature (Fig. 2). As the temperature is lowered, the separation between the hyperbolic isogyres [the two dark arcs seen in Fig. 2(b)] continuously increases.

X-Ray scattering studies have been carried out by taking the sample in a Lindemann capillary tube which is slowly cooled to the desired temperature under a magnetic field of strength *ca.* 2 kG applied perpendicular to the axis of the tube. The alignment is only partial as the isotropic to SmA transition has a strong first-order character. X-Rays of $\lambda = 1.54$ Å from a rotating anode generator are used to study the scattered pattern collected using a 2D image plate. In the small angle region, a sharp reflection corresponding to the smectic layer spacing can be clearly seen (Fig. 3). As usual, the second-order reflection is very weak. The wide angle scattering corresponds to a liquid-like pattern. The measured layer spacing is equal to *ca.* 54 Å which does not vary with temperature as the sample is cooled from the SmA to the lowest temperature to which the SmA_b phase can be supercooled. This, in conjunction with the observation of two-brush defects described earlier, clearly indicates that the lower temperature phase with layer birefringence is not a tilted SmC phase. The layer spacing $d = 54$ Å is significantly larger than the calculated molecular length $l \approx 49$ Å in its most extended form with an all-*trans* configuration of the alkoxy chain. This clearly implies a partial bilayer structure of the smectic layers in both SmA and SmA_b phases, which we have to designate as SmA_d and SmA_{db} respectively.

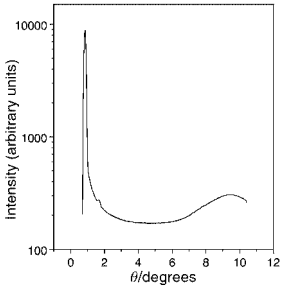

Fig. 3 Intensity profile of the X-ray diffraction pattern in the SmA_{db} phase of compound **1** at 123 °C as a function of the Bragg angle, θ. The sharp reflection corresponds to a layer spacing of 54 Å. A very weak second order reflection can also be seen. The diffuse maximum corresponds to 4.6 Å, which is a typical intermolecular separation in the liquid layers.

Thus, we believe that the occurrence of both the uniaxial and biaxial smectic A phases in compound **1** is mainly a consequence of the partial bilayer structure in which there is a dense region of biaxial aromatic cores and relatively sparsely populated aliphatic regions, which allow for considerable orientational freedom of the chains. The arrangement of the BC molecules in the SmA_{db} phase in the pure compound **1** is hence quite different from that proposed for the SmA_{2b} phase occurring in binary mixtures of rod-like and bent-core molecules. In the latter the BC molecules orient with their arrow axes along the layer-normal, whereas in the SmA_{db} phase the arrows lie in the layer-plane.

The authors wish to thank Dr V. A. Raghunathan for help in the X-ray experiments and Mr P. N. Ramachandran and Ms K. N. Vasudha for technical support.

Notes and references

‡ Compound **1** was synthesised according to a procedure which will be described in a publication under preparation. The intermediate compounds have spectral data consistent with their molecular structure.

1 T. Niori, T. Sekine, J. Watanabe, T. Furukawa and H. Takezoe, *J. Mater. Chem.*, 1996, **6**, 1231.
2 G. Pelzl, S. Diele and W. Weissflog, *Adv. Mater.*, 1999, **11**, 707.
3 B. K. Sadashiva, *Pramana*, 1999, **53**, 213.
4 W. Weissflog, L. Kovalenko, I. Wirth, S. Diele, G. Pelzl, H. Schmalfuss and H. Kresse, *Liq. Cryst.*, 2000, **27**, 677.
5 D. Shen, A. Pegenau, S. Diele, I. Wirth and C. Tschierske, *J. Am. Chem. Soc.*, 2000, **122**, 1593.
6 B. K. Sadashiva, V. A. Raghunathan and R. Pratibha, *Ferroelectrics*, 2000, **243**, 249.
7 R. Amaranatha Reddy and B. K. Sadashiva, *Liq. Cryst.*, 2000, **27**, 1613.
8 J. P. Bedel, J. C. Rouillon, J. P. Marcerou, M. Laguerre, H. T. Nguyen and M. F. Achard, *Liq. Cryst.*, 2000, **27**, 1411.
9 D. R. Link, G. Natale, R. Shao, J. E. Maclennan, N. A. Korblova and D. M. Walba, *Science*, 1997, **278**, 1924.
10 R. Pratibha, N. V. Madhusudana and B. K. Sadashiva, *Science*, 2000, **288**, 2184.
11 R. Pratibha, N. V. Madhusudana and B. K. Sadashiva, *Mol. Cryst. Liq. Cryst.*, in press
12 H. F. Leube and H. Finkelmann, *Makromol. Chem.*, 1991, **192**, 1317.
13 K. J. K. Semmler, T. J. Dingemans and E. T. Samulski, *Liq. Cryst.*, 1998, **24**, 799.
14 T. Hegmann, J. Kain, S. Diele, G. Pelzl and C. Tschierske, *Angew. Chem., Int. Ed.*, 2001, **40**, 887.
15 N. V. Madhusudana and S. Chandrasekhar, *Pramana Suppl.*, 1975, **1**, 57.
16 A. J. Leadbetter, J. C. Prost, J. P. Gaughan, G. W. Gray and A. Mosley, *J. Phys.*, 1979, **40**, 375.
17 Y. Takanishi, H. Takezoe, A. Fukuda and J. Watanabe, *Phys. Rev.*, 1992, **45**, 7684.

CHEMCOMM Communication
www.rsc.org/chemcomm

Photosensitization of nanocrystalline TiO_2 films by pomegranate pigments with unusually high efficiency in aqueous medium

Qing Dai and Joseph Rabani*

Department of Physical Chemistry and the Farkas Center, The Hebrew University of Jerusalem, Jerusalem 91904, Israel. E-mail: rabani@vms.huji.ac.il

Received (in Cambridge, UK) 12th July 2001, Accepted 13th September 2001
First published as an Advance Article on the web 2nd October 2001

An aqueous system based on a TiO_2 layer photosensitized by natural pigment(s) from pomegranate, shows relatively high stability under illumination with a quantum yield of 0.74 and a photovoltage of 0.46 V.

Sensitization of wide band gap semiconductor electrodes by dyes absorbing visible light has been a topic of continuing interest since its introduction by Gerischer in 1972.[1] While early versions of dye-sensitized photoelectrochemical cells were inefficient, Graetzel and coworkers,[2] followed by many others (see for example refs. 3–7 and references cited therein) succeeded in achieving relatively high photon-to-current conversion efficiencies. The Graetzel cell is based on a dye adsorbed to a porous TiO_2 layer. Upon light absorption, electron injection from the excited dye to the conduction band of the semiconductor may occur on an ultrafast time scale. In a typical Graetzel cell, I^-/I_3^- ions in organic solvents serve as charge carriers. Aqueous solutions of the charge carriers have been employed only rarely,[8–11] and with one exception (showing, however, low yield)[12] were abandoned after 1990 because of low photocurrent, photovoltage or stability. However, equilibration of the TiO_2 layers with photosensitizers has often been carried out using aqueous solutions, with reasonably good results. Several natural pigments have been used as photosensitizers in organic environments,[13,14] showing ultrafast electron injection from anthocyanin dyes to TiO_2 nanocrystallite electrodes. Most of this work did not report the efficiency.

The present work shows unusual high yields in an aqueous system. The active pigment was adsorbed from seed coats of the pomegranate fruit, which is a rich source of anthocyanins.[15] The present results indicate good stability (tested for several days) besides unusually high photocurrent yields. These features were unexpected for such a simple system in an aqueous environment.

The seed coats of the pomegranate fruit were processed and separated from the solid residue by filtration. The resulting liquid was kept frozen until used. Transparent TiO_2 layers (3.3 μm thickness) were prepared on ITO surfaces using TiO_2 nanocrystallites dispersed in water at pH 1.8 by successive spin coatings followed by heating at 450 °C. The TiO_2 colloid (5 nm diameter) was prepared by hydrolysis of titanium isopropoxide. The ITO/TiO_2/dye working electrode was separated from the ITO/Pt counter electrode by a thin Teflon spacer. Iodide and iodine in water solution added at the bottom filled the space between the two plates as a consequence of capillary forces.

The ITO/TiO_2 electrode was equilibrated with the pomegranate liquid (natural pH 2.8) to which acid (HCl) or alkali (NaOH) had been added to adjust the pH in the range 1.0–5.6 by shaking for 12–24 h, inducing a violet coloration of the film. Note that low photocurrent yields were observed when the electrodes were initially equilibrated with the natural pomegranate liquid at the natural pH and subsequently washed or shaken with acidic water. This observation is apparently related to the buffer capacity of the TiO_2/H^+/dye system, which seems to have been ignored in previous works.

The natural red dye is likely to be a mixture of several pigments. The spectrum in the TiO_2 layer in the range 500–700 nm resembles that of cyanidin 3-O-β-glucoside and cyanidin 3,5-O-β-diglucoside, which are among the six pigments identified in pomegranates. Deviations below 500 nm, increasing towards the UV, indicate the presence of additional absorbing materials in the natural dye mixture. Fig. 1 shows the chemical structure of the cyanidin-3-glucoside pigment.

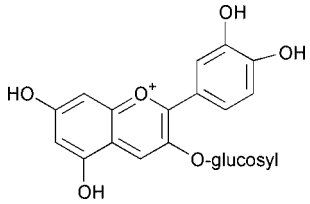

Fig. 1 Chemical formula of cyanidin-3-glucoside.

The optical absorption spectrum of the pomegranate pigments adsorbed to TiO_2 shows a peak at 560 nm, *i.e.* 40–50 nm red shifted compared to the absorption in aqueous solution. This indicates that chemical binding takes place, apparently through the hydroxy groups (Scheme 1). The formation of a very strong complex[14] takes place despite of the predominantly cationic form of TiO_2 at acid pH.

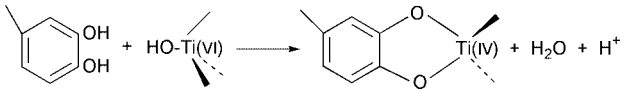

Scheme 1 Adsorption of aromatic dihydroxy compounds to TiO_2.

Typical short circuit photocurrents and open circuit photovoltages observed upon illumination with the entire visible range of a halogen lamp are presented in Table 1. The photocurrents were normalized to the light absorption and show the relative photon to current efficiencies. Table 1 shows that the aqueous Na^+ counter ion is the most effective in photocurrent generation, and the results in aqueous solutions are comparable to results in ethanol.

The spectrum of the photocurrent follows fairly closely the absorption spectrum of the dye. The effect of pH is remarkable: using 2.5 M NaI and 0.1 M I_2 in water as charge carriers, the quantum yield of the photocurrent increases from *ca.* 0.03 at pH 5.5 to 0.74 at pH 1. At the same time, the photovoltage changes only little, remaining between 0.4 and 0.46 V through the entire tested pH range. This observation is unusual, because so far it is believed that aqueous solutions much more strongly lower the

Table 1 Photocurrents and photovoltages for various iodides and solvents[a]

Counter ion	Li^+ (H_2O)	K^+ (H_2O)	Na^+ (H_2O)	Na^+ (ethanol)	$Bu^t_4N^+$ (ethanol)
Photocurrent/mA	0.45	1.2	2.2	2.1	0.78
Photovoltage/V	0.30	0.33	0.44	0.41	0.48

[a] TiO_2 layers are equilibrated with natural pomegranate liquid at the natural pH (2.8) for 24 h. Peak absorbance in the layers was 0.4. All systems contain 1 M iodide and 0.1 M iodine. Illumination carried out at 400–700 nm.

 DOI: 10.1039/b106197f

photovoltage, reduce the photocurrent and in many, if not most cases, destabilize the dye–TiO_2 binding. Stability tests of the present system showed no measurable decrease of photocurrent after 24 h illumination, corresponding to an estimated turnover number of $>10^5$. Washing the layer with water at the appropriate pH does not reduce the photocurrent magnitude or its stability. These results rule out the possibility that impurities act as a source of energy for the operation of the photoelectrochemical cell, since washing of the layers leaves only the adsorbed components in the layer, the concentration limit of which is of the order of the adsorbed pigments. Even if oxidation of photosensitizer molecules or impurities may take place in the absence of iodide, the high iodide concentrations suppress these reactions.

Another very interesting effect is the TiO_2 particle size used to prepare the layer: When nanocrystallites of diameter 18 nm are used instead of the usual 5 nm, the photocurrent decreases considerably. This is in contrast to the behavior of the popular $Ru(dcbpy)_2(SCN)_2$ (dcbipy = dicarboxybipyridine) (ethanol used as charge carrier solvent), which under similar conditions shows 50% increase of photocurrent. Apparently, the small pores in the 5 nm diameter layer serve as a filter, preventing or minimizing adsorption of undesired molecules, which reduce the photocurrent by competition for photons. Another observation of considerable interest is the decrease of photocurrent yield in the absence of bound glucose (see Fig. 1). The role of the glucose is not clear, although control experiments show that regeneration of the photosensitizer from its oxidized state is carried out predominantly, if not solely, by the iodide ions.

In conclusion, the combination of high photocurrent yield, reasonably high photovoltage and apparently good stability of the very simple dye sensitized TiO_2 system operating under aqueous conditions opens interesting perspectives in the field of solar energy conversion. Further work is in progress on the natural pigment mixture as well as on the isolated pigments, in order to better understand the chemistry, which provides the photoelectrochemical cell its unique features.

This work was supported by the Ministry of National infrastructure, and by the Belfer and Berman Foundations, Israel.

Notes and references

1 H. Gerischer, *Photochem. Photobiol.*, 1972, **16**, 243.
2 J. E. Moser, P. Bonhoete and M. Graetzel, *Chem. Rev.*, 2001, in press.
3 R. Argazzi, C. A. Bignozzi, G. M. Hasselmann and G. J. Meyer, *Inorg. Chem.*, 1998, **37**, 4533.
4 A. Solbrand, A. Henningsson, S. Sodergren, H. Lindstrom, A. Hagfeldt and S.-E. Lindquist, *J. Phys. Chem. B*, 1999, **103**, 1078.
5 S. Ferrere, A. Zaban and B. A. Gregg, *J. Phys. Chem. B*, 1997, **101**, 4490.
6 T. Yoshida, K. Terada, D. Schlettwein, O. T. T. Sugiura and H. Minoura, *Adv. Mater.*, 2000, **12**, 1214.
7 K. Sayama, K. Hara, N. Mori, M. Satsuki, S. Suga, S. Tsukagoshi, Y. Abe, H. Sugihara and H. Arakawa, *Chem. Commun.*, 2000, 1173.
8 J. Desilvestro, M. Graetzel, L. Kavan and J. Moser, *J. Am. Chem. Soc.*, 1985, **107**, 2988.
9 P. Liska, N. Vlachopoulos, M. K. Nazeeruddin, P. Comte and M. Graetzel, *J. Am. Chem. Soc.*, 1988, **110**, 3686.
10 B. O'Regan, J. Moser, M. Anderson and M. Graetzel, *J. Phys. Chem.*, 1990, **94**, 8720.
11 N. Vlachopoulos, P. Liska, J. Augustynski and M. Graetzel, *J. Am. Chem. Soc.*, 1988, **110**, 1216.
12 S. Taira, T. Miki and H. Yanagi, *Appl. Surf. Sci.*, 1999, **143**, 23.
13 K. Tennakone, G. R. R. A. Kumara, I. R. M. Kottegoda, V. P. S. Perera and P. S. R. S. Weerasundara, *J. Photochem. Photobiol. A: Chem.*, 1998, **117**, 137.
14 N. J. Cherepy, G. P. Smestad, M. Graetzel and J. Z. Zhang, *J. Phys. Chem. B*, 1997, **101**, 9342.
15 M. Gil, I. C. Garcia-Viguera, F. Artes and F. A. Tomas-Barberan, *J. Sci. Food Agric.*, 1995, **68**, 77.

CHEMCOMM
Communication
www.rsc.org/chemcomm

New binucleating ligands to support dizirconium organometallics

John R. Hagadorn

Department of Chemistry and Biochemistry, University of Colorado, Boulder, CO 80309-0215, USA. E-mail: hagadorn@stripe.colorado.edu

Received (in West Lafayette, IN, USA) 2nd August 2001, Accepted 1st September 2001
First published as an Advance Article on the web 2nd October 2001

A new class of bis(amidinato) ligands, which feature dibenzofuran or 9,9-dimethylxanthene spacers, are used to prepare structurally characterized dizirconium complexes.

The development of single-site catalysts for selective bond forming and cleaving processes is a major topic in organometallic chemistry. Toward this goal, much effort has gone into controlling chemical reactivity through the modification of supporting ligands.[1] This approach has been highly successful for the preparation of new mononuclear catalysts; however, equivalent advances have not been made for bimetallic complexes. The use of well-defined bimetallics as catalysts, however, is highly desirable because multiple metals acting cooperatively can activate substrates and perform reactions that fail to occur in mononuclear systems.[2,3] Thus, we have begun to develop new binucleating ligands which will allow us to explore the reactivity of binuclear organometallic complexes. Here we report two new bis(amidinato)[4] ligands and their structurally characterized Zr derivatives.

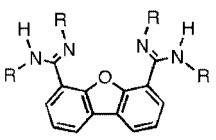

$(Pr^i_4DBF)H_2$

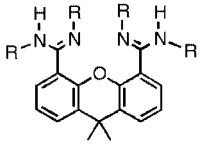

$(Pr^i_4Xan)H_2$

The bis(amidine) ligands $(Pr^i_4DBF)H_2$† and $(Pr^i_4Xan)H_2$ were prepared by the reaction of diisopropylcarbodiimide with doubly deprotonated dibenzofuran or 9,9-dimethylxanthene.[5] The ligands are highly soluble in hydrocarbon solvents, but they can be readily isolated as colorless crystals from warm acetonitrile solutions in moderate yield. Combustion analysis and ^1H NMR spectroscopy confirmed their formulations. IR absorption spectroscopy of $(Pr^i_4Xan)H_2$ (Nujol) revealed characteristic absorptions at ν_{NH} 3440 and ν_{CN} 1639 cm^{-1}. Related parameters for $(Pr^i_4DBF)H_2$ were observed at 3434, 3427, 3402 and 1633 cm^{-1}.

Entry into transition metal derivatives was accomplished by reaction of $(Pr^i_4DBF)H_2$ with 2 equivalents of $Zr(CH_2Ph)_4$ in toluene solution [eqn. (1)]. Removal of the volatiles under

$$(Pr^i_4DBF)H_2 + 2Zr(CH_2Ph)_4 \rightarrow (Pr^i_4DBF)Zr_2(CH_2Ph)_6 + 2PhCH_3 \quad (1)$$

reduced pressure afforded yellow $(Pr^i_4DBF)Zr_2(CH_2Ph)_6$ in quantitative yield. ^1H and ^{13}C NMR spectroscopy (C_6D_6) reveal a symmetrical ligand environment and equivalent benzyl ligands, consistent with fast fluxional behavior in solution. Crystallization of the product, however, was slow, and crystals suitable for X-ray diffraction‡ studies were obtained only after storing Et_2O solutions at −40 °C for two weeks. The solid-state structure (Fig. 1) confirmed the formulation of the dizirconium complex. Geometry at each Zr center resembles that of the guanidinate derivative $\{CyNC[N(SiMe_3)_2]NCy\}Zr(CH_2Ph)_3$, which was recently reported by Richeson and coworkers.[6] The η^2-benzyl ligands feature Zr–CH_2–C_{ipso} angles of 90.9(2) and 88.1(2)° with Zr–C_{ipso} distances of 2.721(3) and 2.682(3) Å, values which are similar to other reported Zr(η^2-benzyl) compounds.[7] The intermetal distance of 8.574(1) Å is significantly longer than the value predicted from simple MM2 calculations (7.3 Å). Interestingly, this is due to the presence of a cocrystallized Et_2O that is located between the two Zr atoms yet is not coordinated to either metal. The Zr–ether distances are short (Zr1–C69, 4.46 Å; Zr2–C69, 4.27 Å), with the H atoms bound to C69 approaching to within 3.5 Å of Zr2. This presents the intriguing possibility of using the intermetal gap as a docking site for incoming substrates that could subsequently react with metal-bound ligands.

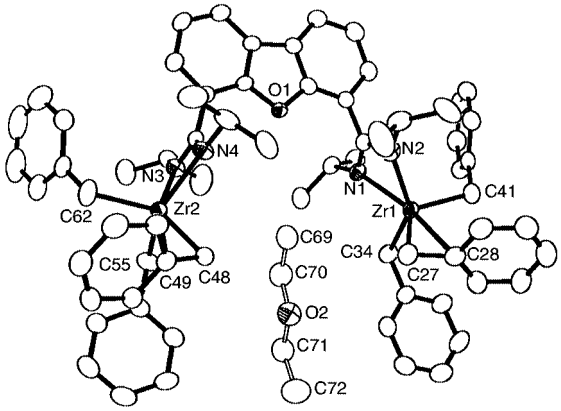

Fig. 1 Molecular structure of $(Pr^i_4DBF)Zr_2(CH_2Ph)_6 \cdot 1.5Et_2O$ drawn with 50% thermal ellipsoids. Half occupancy ether is omitted. Selected distances (Å) and angles (°): Zr1–N_{av} 2.25, Zr1–C_{av} (excl. C28) 2.27, Zr1–C28 2.721(3), Zr1–C69 4.467(4), Zr2–N_{av} 2.25, Zr2–C_{av} (excl. C49) 2.28, Zr2–C49 2.682(3), Zr2–C69 4.273(4), C48–C69, 3.756(6), Zr1–Zr2 8.574(1); Zr1–C27–C28 90.9(2), Zr2–C48–C49 88.1(2).

The related xanthene-bridged dizirconium complex $(Pr^i_4Xan)Zr_2(CH_2Ph)_6$ was prepared following the methodology similar to that used for $(Pr^i_4DBF)Zr_2(CH_2Ph)_6$ (Scheme 1). The product was isolated as yellow microcrystals from toluene–hexamethyldisiloxane mixtures in high yield. ^1H NMR spectra (C_6D_6) reveal a fluxional ligand environment. Crystals suitable for X-ray diffraction studies were grown from Et_2O at −40 °C. Metrical parameters (Fig. 2) are very similar to those of $(Pr^i_4DBF)Zr_2(CH_2Ph)_6$; however, the xanthene-bridge closes the gap between the two $Zr(CH_2Ph)_3$ moieties. Consequently, there is not a solvent molecule present between them, and the intermetal distance is reduced by over 2 Å [Zr1–Zr2 6.489(1) Å].

Reaction of a single equivalent $Zr(CH_2Ph)_4$ with $(Pr^i_4Xan)H_2$ (Scheme 1) yielded an orange solution. After stirring overnight and removal of the volatiles, the residue was extracted into warm Et_2O. Cooling to −40 °C gave orange crystals in good yield. Combustion analysis of the product indicated the

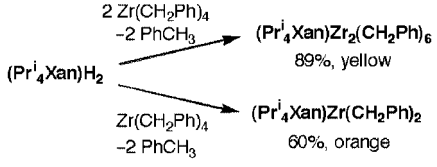

Scheme 1

 DOI: 10.1039/b106972a

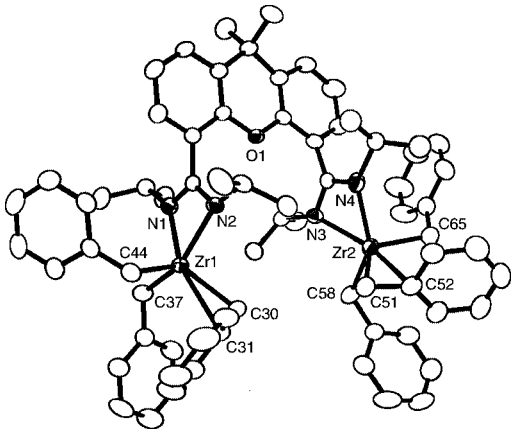

Fig. 2 Molecular structure of $(Pr^i_4Xan)Zr_2(CH_2Ph)_6{\cdot}Et_2O$ drawn with 50% thermal ellipsoids. Cocrystallized ether is omitted. Selected distances (Å) and angles (°): Zr1–N_{av} 2.24, Zr1–C_{av} (excl. C31) 2.28, Zr1–C31 2.627(3), Zr2–N_{av} 2.24, Zr2–C_{av} (excl. C52) 2.28, Zr2–C52 2.678(4), Zr1–Zr2 6.489(1); Zr1–C30–C31 86.2(2), Zr2–C51–C52 89.8(2).

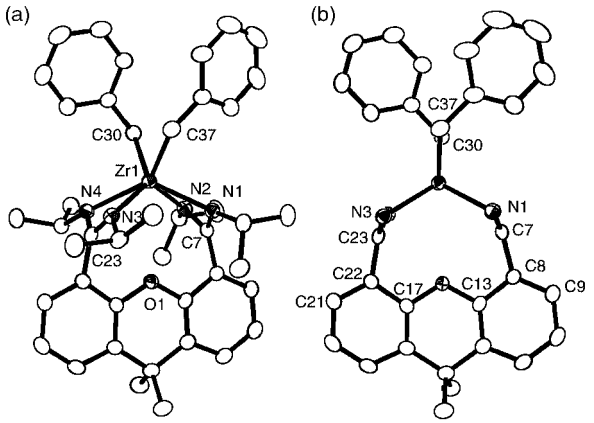

Fig. 3 Views of the molecular structure of $(Pr^i_4Xan)Zr(CH_2Ph)_2$ drawn with 50% thermal ellipsoids. Pr^i groups omitted in (b) for clarity. Selected distances (Å) and angles (°): Zr1–N1 2.269(2), Zr1–N2 2.247(2), Zr1–N3 2.288(2), Zr1–N4 2.308(2), Zr1–C30 2.280(2), Zr1–C37 2.284(2); C30–Zr1–C37 88.87(8).

empirical formula $[(Pr^i_4Xan)Zr(CH_2Ph)_2]_n$. ^{1}H NMR spectra ($C_6D_6$) were also consistent with this formulation and featured a single set of resonances for the benzyl ligands. Single crystal X-ray diffraction studies revealed the product to be mononuclear, with a single Zr atom bridging the two amidinates of the (Pr^i_4Xan) ligand (Fig. 3). Geometry at the Zr center closely resembles that observed for Group 4 dialkyl derivatives of N_4-macrocycles.[8] Interestingly, there appears to be significant ring strain as a result of this binding mode. As shown in Fig. 3(b), the amidinates are bent towards Zr giving angles of 114.1(2) and 115.2(2)° for C7–C8–C13 and C23–C21–C17, respectively. Additionally, the Zr atom is coordinated *ca.* 1.2 Å out of each NCN amidinate plane, and the Zr–N bond lengths suggest stronger coordination to one of the amidinates. Asymmetric binding, however, is not observed by ^{1}H NMR spectroscopy (in C_6D_6), and it is unclear whether this is due to fluxionality or a lack of asymmetry.

We thank Professor Clark R. Landis for helpful discussions and the University of Colorado for funding.

Notes and references

† All compounds analyzed satisfactorily. *Selected data* for $(Pr^i_4DBF)H_2$: ^{1}H NMR (d_6-acetone): δ 8.12 (d, *J* 7.7 Hz, 2H), 7.42 (t, *J* 7.5 Hz, 2H), 7.33 (d, *J* 7.3 Hz, 2H), 4.20 (br, 2H), 3.10 (br, 2H), 2.86 (br, 2H), 1.22 (br, 12H), 0.98 (br, 12H). For $(Pr^i_4Xan)H_2$: ^{1}H NMR (d_6-acetone): δ 7.53 (d, *J* 7.7 Hz, 2H), 7.11 (t, *J* 7.5 Hz, 2H), 6.94 (d, *J* 7.1 Hz, 2H), 4.13 (br, 2H), 2.85 (m, br, 4H), 1.63 (s, 6H), 1.36–0.80 (br, 24H). For $(Pr^i_4DBF)Zr_2Bn_6$: ^{1}H NMR (C_6D_6): δ 7.52 (dd, *J* 1.2, 7.5 Hz, 2H), 7.25 (t, *J* 7.6 Hz, 12H), 7.11 (t, *J* 7.5 Hz, 2H), 7.06–7.00 (m, 20H), 3.27 (sept, *J* 6.5 Hz, 4H), 2.53 (s, 12H), 1.08 (d, *J* 6.5 Hz, 12H), 0.93 (d, *J* 6.5 Hz, 12H). ^{13}C{^{1}H} NMR (C_6D_6): δ 175.9, 152.1, 143.8, 129.9, 128.5, 128.3, 126.8, 124.7, 123.7, 123.2, 121.8, 116.6, 77.2, 50.9, 25.3, 24.2. For $(Pr^i_4Xan)Zr_2Bn_6$: ^{1}H NMR (C_6D_6): δ 7.18 (t, *J* 7.7 Hz, 12H), 7.04 (dd, *J* 1.6, 7.8 Hz, 2H), 7.00 (d, *J* 7.3 Hz, 12H), 6.97 (t, *J* 7.4 Hz, 6H), 6.92 (t, 7.5 Hz, 2H), 6.71 (dd, *J* 1.6, 7.3 Hz, 2H), 3.36 (sept, *J* 6.6 Hz, 4H), 2.65 (s, 12H), 1.35 (s, 6H), 1.31 (d, *J* 6.5 Hz, 12H), 0.91 (d, *J* 6.7 Hz, 12H); ^{13}C{^{1}H} NMR (C_6D_6): δ 177.1, 146.2, 144.3, 130.2, 129.7, 128.6, 128.3, 128.1, 127.9, 127.5, 123.7, 123.0, 120.5, 78.2, 51.0, 34.2, 33.4, 26.4, 24.2. For $(Pr^i_4Xan)ZrBn_2$: ^{1}H NMR (C_6D_6): δ 7.61 (d, *J* 7.6 Hz, 4H), 7.42 (t, *J* 7.6 Hz, 4H), 7.08 (t, *J* 7.3 Hz, 2H), 7.05 (dd, *J* 1.4 Hz, 7.3 Hz, 2H), 6.93 (dd, *J* 1.4, 7.9 Hz, 2H), 6.74 (t, *J* 7.6 Hz, 2H), 3.54 (sept, *J* 6.5 Hz, 4H), 2.92 (s, 4H), 1.27 (s, 6H), 1.12 (d, *J* 6.5 Hz, 12H), 0.84 (d, *J* 6.3 Hz, 12H); ^{13}C{^{1}H} NMR (C_6D_6): δ 165.2, 148.5, 144.5, 129.1, 128.5, 128.3, 127.9, 126.7, 126.5, 125.1, 123.0, 121.6, 75.2, 50.8, 34.2, 32.5, 25.6, 25.1.

‡ *Crystal data* for $(Pr^i_4DBF)Zr_2(CH_2Ph)_6{\cdot}1.5Et_2O$: $C_{74}H_{91}N_4O_{2.5}Zr_2$, *M* = 1258.95, triclinic, space group $P\bar{1}$ (no. 2), *a* = 11.392(2), *b* = 18.274(4), *c* = 18.717(4) Å, α = 109.66(3), β = 102.65(3), γ = 105.50(3)°, *V* = 3324.7(12) Å^3, *Z* = 2, μ = 0.34 mm^{-1}, *T* = −138 °C, 20 243 independent reflections, R_{int} = 0.0482, 11 705 observations, 783 parameters, R_1 = 0.0603, wR_2 = 0.1571, GOF = 0.973. For $(Pr^i_4Xan)Zr_2(CH_2Ph)_6{\cdot}Et_2O$: $C_{75}H_{92}N_4O_2Zr_2$, *M* = 1263.97, monoclinic, space group $P2_1/n$ (no. 14), *a* = 17.940(4), *b* = 18.075(4), *c* = 21.577(4) Å, β = 105.70(3)°, *V* = 6736(2) Å^3, *Z* = 4, μ = 0.36 mm^{-1}, *T* = −138 °C, 21 557 independent reflections, R_{int} = 0.1058, 10 074 observations, 752 parameters, R_1 = 0.0637, wR_2 = 0.1561, GOF = 0.929. For $(Pr^i_4Xan)Zr(CH_2Ph)_2$: $C_{43}H_{54}N_4OZr$, *M* = 734.12, monoclinic, space group $P2_1/c$ (no. 14), *a* = 10.887(2), *b* = 16.325(3), *c* = 21.427(4) Å, β = 96.47(3)°, *V* = 3784.1(13) Å^3, *Z* = 2, μ = 0.33 mm^{-1}, *T* = −138 °C, 12 039 independent reflections, R_{int} = 0.0554, 8425 observations, 452 parameters, R_1 = 0.0455, wR_2 = 0.1176, GOF = 1.008. Refinements were performed (SHELXTL-Plus V5.0) on F^2.

CCDC reference numbers 170218–170220. See http://www.rsc.org/suppdata/cc/b1/b106972a/ for crystallographic data in CIF or other electronic format.

1 For selected reviews, see: F. Fache, E. Schulz, M. L. Tommasino and M. Lemaire, *Chem. Rev.*, 2000, **100**, 2159; A. Togni and L. M. Vananzi, *Angew. Chem., Int. Ed. Engl.*, 1994, **33**, 497; M. J. Bartos, S. W. Gordon-Wylie, B. G. Fox, L. J. Wright, S. T. Weintraub, K. E. Kauffmann, E. Münck, K. L. Kostka, E. S. Uffelman, C. E. F. Rickard, K. R. Noon and T. J. Collins, *Coord. Chem. Rev.*, 1998, **174**, 361; G. J. P. Britovsek, V. C. Gibson and D. F. Wass, *Angew. Chem., Int. Ed.*, 1999, **38**, 428.

2 For metalloenzymes, see: F. A. Cotton and G. Wilkinson, *Advanced Inorganic Chemistry*, Wiley Interscience, New York, 1988, 5th edn., ch. 30.

3 For selected synthetic examples and reviews, see: G. J. Rowlands, *Tetrahedron*, 2001, **57**, 1865; N. Wheatley and P. Kalck, *Chem. Rev.*, 1999, **99**, 3379; *Catalysis by Di- and Polynuclear Metal Cluster Complexes*, ed. R. D. Adams and F. A. Cotton, Wiley-VCH, Inc., New York, 1998; R. G. Konsler, J. Karl and E. N. Jacobsen, *J. Am. Chem. Soc.*, 1998, **120**, 10 780; T. Ooi, M. Takahashi and K. Maruoka, *Angew. Chem., Int. Ed.*, 1998, **37**, 835; J. D. Wuest, *Acc. Chem. Res.*, 1999, **32**, 81; A. Cottone III and M. J. Scott, *Organometallics*, 2000, **19**, 5254; M. E. Broussard, B. Juma, S. G. Train, W.-J. Peng, S. A. Laneman and G. G. Stanley, *Science*, 1993, **260**, 1784.

4 For other binucleating amidinates, see: J. R. Babcock, C. Incarvito, A. L. Rheingold, J. C. Fettinger and L. R. Sita, *Organometallics*, 1999, **18**, 5729; S. Appel, F. Weller and K. Dehnicke, *Z. Anorg. Allg. Chem.*, 1990, **583**, 7; C. Chen, L. H. Rees, A. R. Cowley and M. L. H. Green, *J. Chem. Soc., Dalton Trans.*, 2001, 1761; M. Ruben, D. Walther, R. Knake, H. Görls and R. Beckert, *Eur. J. Inorg. Chem.*, 2000, **5**, 1055.

5 For related bis(phosphine) and bis(porphyrin) ligands, see: C. J. Chang, Y. Q. Deng, A. F. Heyduk, C. K. Chang and D. G. Nocera, *Inorg. Chem.*, 2000, **39**, 959; M. W. Haenel, D. Jakubik, E. Rothenberger and G. Schroth, *Chem. Ber.*, 1991, **124**, 1705.

6 D. Wood, G. P. A. Yap and D. S. Richeson, *Inorg. Chem.*, 1999, **38**, 5788.

7 B. Qian, W. J. Scanlon, M. R. Smith and D. H. Morty, *Organometallics*, 1999, **18**, 1693; R. F. Jordan, R. E. Lapointe, C. S. Bajgur, S. F. Echols and R. Willett, *J. Am. Chem. Soc.*, 1987, **109**, 4111; S. L. Latesky, A. K. McMullen, G. P. Niccolai, I. P. Rothwell and J. C. Huffman, *Organometallics*, 1985, **4**, 902.

8 D. G. Black, D. C. Swenson, R. F. Jordan and R. D. Rogers, *Organometallics*, 1995, **14**, 3539; M. J. Scott and S. J. Lippard, *Inorg. Chim. Acta*, 1997, **263**, 287; H. Brand and J. Arnold, *Coord. Chem. Rev.*, 1995, **140**, 137; L. Giannini, E. Solari, S. De Angelis, T. R. Ward, C. Floriani, A. Chiesi-Villa and C. Rizzoli, *J. Am. Chem. Soc.*, 1995, **117**, 5801.

CHEMCOMM Communication
www.rsc.org/chemcomm

A new pathway in the reaction of disilene with carbonyl compounds: an 'ene' reaction instead of cycloaddition

Vladimir Ya. Lee, Masaaki Ichinohe and Akira Sekiguchi*

Department of Chemistry, University of Tsukuba, Tsukuba, Ibaraki, 308-8571, Japan. E-mail: sekiguch@staff.chem.tsukuba.ac.jp

Received (in Cambridge, UK) 26th July 2001, Accepted 7th September 2001
First published as an Advance Article on the web 2nd October 2001

The 3*H*-disilagermirene, $(^tBu_2MeSi)_4GeSi_2$, reacts with α-hydrogen containing carbonyl compounds (acetophenone, butane-2,3-dione) by an 'ene'-reaction pathway followed by isomerization or insertion reactions, representing a new mode in the reaction of disilenes with carbonyl compounds.

The stable dimetallenes containing M=M double bonds (M = heavier Group 14 elements) have now become common, easily accessible and a rather important class of organometallic compounds of Group 14 elements.[1] The reactivity of such dimetallenes has been widely studied, including a variety of addition and cycloaddition reactions. Thus, it is well established that disilenes with a Si=Si double bond react with carbonyl compounds, such as benzaldehyde, acetone, acetophenone and dibenzyl, by [2 + 2] or [4 + 2] cycloaddition reaction modes.[2] In contrast, the reaction of carbonyl compounds having α-hydrogen atoms with compounds containing polar bonds, such as Si=C or Ge=P, proceeded as an 'ene' reaction resulting in the formation of enol ether products.[1,2] Quite recently, we prepared 3*H*- and 1*H*-disilagermirenes; that is, three-membered ring compounds with endocyclic metal–metal double bonds.[3] We have found that such compounds exhibit a high reactivity of both the double bond and the strained three-membered ring skeleton.[4–6] In this paper, we report the reactions of a 3*H*-disilagermirene with carbonyl compounds containing α-hydrogen atoms. They unexpectedly produce enol ether type products, which subsequently undergo further interesting isomerization and insertion reactions.

The reaction of 3*H*-disilagermirene **1** with a slight excess of acetophenone in C_6D_6 at room temperature was complete in two hours to form quantitatively a single product. It was identified by NMR spectroscopy data as *cis*-1,2,3,3-tetrakis(di-*tert*-butyl(methyl)silyl)-1-(1-phenylvinyloxy)disilagermirane **2** (Scheme 1). The formation of this compound can be considered the result of nucleophilic attack of the carbonyl oxygen atom on the sp^2-Si atom through either a zwitterionic intermediate or six-centered transition state. This resulted in the formation of the product of a formal 1,2-addition of 1-phenylvinyl alcohol to a Si=Si double bond of **1**. The enol ether **2** was not stable at room temperature and spontaneously isomerized to the thermodynamically more stable *trans*-isomer **3**. After one day the ratio of *cis*- and *trans*-isomers of **2** and **3** was 1 : 1, whereas after two days **2** was completely isomerized to **3**. The driving force for such isomerization is most likely to be the decrease of the steric hindrance on going from the *cis*- to the *trans*-isomer.[7]

The *trans*-isomer **3** was isolated quantitatively as pale-yellow crystals by recrystallization from hexane. Its structure was determined by all spectral data† and finally confirmed by X-ray analysis.‡ From the crystal structure, the three-membered ring skeleton with a *trans*-arrangement of H- and H_2C=C(Ph)O-substituents can be clearly seen. The bond lengths lie in the normal range and the Si–Si bond length of the three-membered skeleton is 2.3383(6) Å, which is very similar to those of disilagermirane derivatives that we have previously reported (2.342(2)[5] and 2.3269(6) Å[6]). The formation in the first step of the *cis*-isomer **2** agrees with the previously established mechanism for the reaction of disilenes with alcohols, which proceeds as *syn*-addition.[8]

The reaction of 3*H*-disilagermirene **1** with an excess of the dicarbonyl compound butane-2,3-dione also occurred smoothly and cleanly in C_6D_6 at room temperature to produce quantitatively a single product in 30 minutes. Its structure was established by spectral data§ and X-ray crystallography¶ to be 1,2,3,3-tetrakis(di-*tert*-butyl(methyl)silyl)-4-methyl-5-methylene-6,7-dioxa-1,2-disila-3-germabicyclo[2.2.1]heptane **4** (Scheme 2).

X-Ray analysis of **4** showed a bicyclic structure with the norbornane-type skeleton (Fig. 1). Compound **4** has two oxygen atoms incorporated in the rings, one of which occupies the bridging 7-position. Formation of the norbornane **4** can be rationalized as the following reaction sequence. In the first step, nucleophilic attack of the carbonyl oxygen lone pair on the doubly-bonded Si atom results in the formation of the *cis*-adduct–enol ether **5**. The primarily formed **5** may isomerize to a thermodynamically more favorable **6**, due to the lower steric repulsions of the bulky silyl substituents in the *trans*-isomer. In the last step, the second carbonyl group in **6** undergoes an intramolecular insertion into the endocyclic Si–Ge bond of the three-membered ring to form the final norbornane **4**. The proposed mechanism satisfactorily explains the structure of compound **4**, in which the H atom on the Si atom is directed towards the bridge; that is, it occupies the *exo*-position. Such an arrangement of the H atom in **4** can be obtained from the *trans*-isomer **6** only by geometrical reasons, and the last compound can be imagined as the result of isomerization of the initially formed *cis*-isomer **5**.

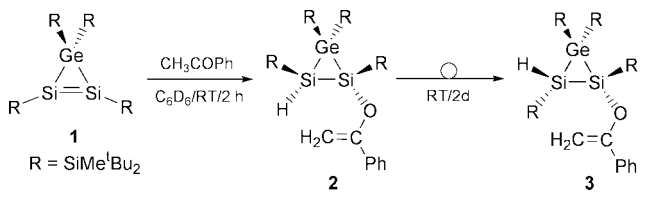

Scheme 1

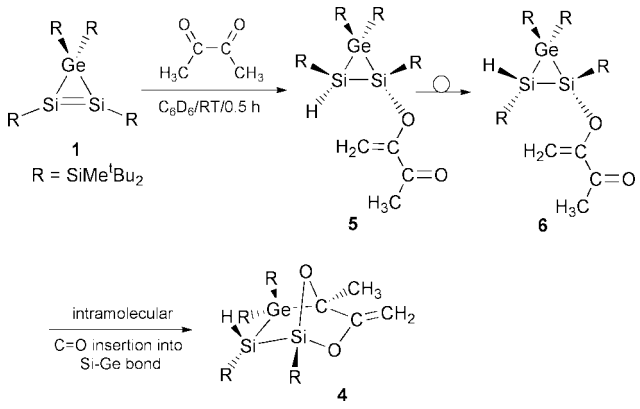

Scheme 2

 DOI: 10.1039/b106801f

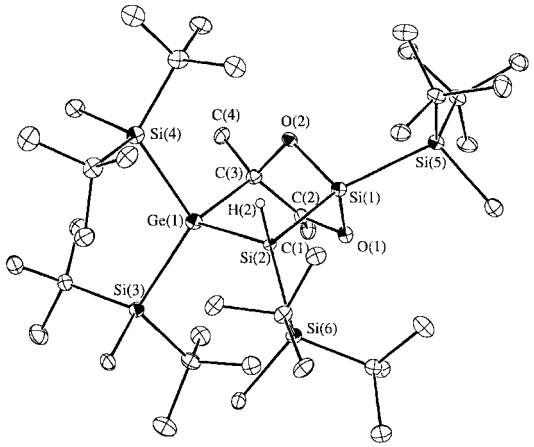

Fig. 1 Structure of **4** (hydrogen atoms are omitted for clarity). Selected bond distances [Å] are: Ge(1)–Si(2) 2.460(1), Si(1)–Si(2) 2.369(1), Ge(1)–C(3) 2.086(5), Si(1)–O(1) 1.701(4), O(1)–C(2) 1.394(6), C(2)–C(3) 1.503(7), Si(1)–O(2) 1.685(3), C(3)–O(2) 1.459(6). Selected bond angles [°] are: C(3)–Ge(1)–Si(2) 95.0(1), Ge(1)–Si(2)–Si(1) 86.1(0), C(3)–C(2)–O(1) 110.6(4), Si(1)–O(1)–C(2) 108.1(3), Si(1)–O(2)–C(3) 104.9(3).

Both reactions of 3*H*-disilagermirene **1** with acetophenone and butane-2,3-dione represent the first examples of an 'ene'-type reaction of disilenes with carbonyl compounds, which were previously commonly recognized to react only by cycloaddition pathways to form cyclic compounds.[2,9] The *cis*–*trans* isomerization of the enol ether was also previously unknown, as well as the combination of 1,2-addition and insertion pathways in one reaction.

This work was supported by a Grant-in-Aid for Scientific Research (Nos. 12042213, 13440185, 13029015) from the Ministry of Education, Science and Culture of Japan, and TARA (Tsukuba Advanced Research Alliance) fund.

Notes and references

† *Spectral data* for **3**: mp 179–181 °C; δ_H (300 MHz, C_6D_6) 0.23 (s, 3H, Me), 0.39 (s, 3H, Me), 0.41 (s, 3H, Me), 0.47 (s, 3H, Me), 1.22 (s, 9H, ^{t}Bu), 1.23 (s, 9H, ^{t}Bu), 1.26 (s, 9H, ^{t}Bu), 1.28 (s, 9H, ^{t}Bu), 1.29 (s, 9H, ^{t}Bu), 1.30 (s, 9H, ^{t}Bu), 1.31 (s, 18H, 2^{t}Bu), 3.01 (s, 1H, Si-H), 5.07 (d, J = 1.6 Hz, 1H, C=CH_2), 5.14 (d, J = 1.6 Hz, 1H, C=CH_2), 7.07 (d, J = 7.2 Hz, 1H, ArH), 7.19 (t, J = 7.2 Hz, 2H, ArH), 7.69 (d, J = 7.2 Hz, 2H, ArH); δ_C (75.5 MHz, C_6D_6) −4.24, −4.21, −0.2, 0.1, 22.3 (2C), 22.5 (2C), 22.7, 23.1, 23.5, 25.0, 30.4, 30.5, 30.6, 30.7, 31.1, 31.3, 31.5, 32.0, 94.1 (C=CH_2), 126.8, 128.3, 128.6, 138.5, 159.3 (*C*=CH_2); δ_{Si} (59.6 MHz, C_6D_6) −142.2, −17.6, 17.2, 23.0, 28.8, 32.4; Anal. Calcd for $C_{44}H_{92}OSi_6$: C, 60.17; H, 10.56. Found: C, 60.50; H, 10.45%.

‡ *Crystal data* for **3**: $C_{44}H_{92}GeOSi_6$, M = 878.31, monoclinic, a = 11.0980(2), b = 20.9340(5), c = 22.8640(6) Å, β = 96.8960(10) °, V = 5273.5(2) Å^3, T = 120 K, space group = $P2_1/c$, Z = 4, ρ_{calcd} = 1.106 g cm^{-3}. The final R factor was 0.0348 (Rw = 0.0953 for all data) for 10698 reflections with $I > 2\sigma(I)$. GOF = 1.028. CCDC 170581.

§ *Spectral data* for **4**: mp 132–134 °C; δ_H (300 MHz, C_6D_6) 0.40 (s, 3H, Me), 0.45 (s, 3H, Me), 0.53 (s, 3H, Me), 0.55 (s, 3H, Me), 1.19 (s, 9H, ^{t}Bu), 1.20 (s, 9H, ^{t}Bu), 1.218 (s, 18H, 2^{t}Bu), 1.222 (s, 9H, ^{t}Bu), 1.24 (s, 9H, ^{t}Bu), 1.28 (s, 18H, 2^{t}Bu), 2.20 (s, 3H, C-Me), 3.46 (s, 1H, Si-H), 4.13 (d, J = 1.1 Hz, 1H, C=CH_2), 4.39 (d, J = 1.1 Hz, 1H, C=CH_2); δ_c (75.5 MHz, C_6D_6) −6.2, −2.8, −1.2, −0.3, 21.6, 21.9, 22.2, 22.4, 22.6, 24.1, 24.4, 24.5, 28.9, 29.4, 29.7, 30.0, 30.8, 31.5, 32.1, 32.16, 32.21, 83.7 (*C*-O), 85.7 (C=CH_2), 168.1 (*C*=CH_2); δ_{Si} (59.6 MHz), C_6D_6) −90.2, 5.4, 19.9, 26.7, 27.3, 41.8.

¶ *Crystal data* for **4**: $C_{40}H_{90}GeO_2Si_6$, M = 844.25, triclinic, a = 12.431(1), b = 12.879(1), c = 16.286(1) Å, α = 81.534(6), β = 84.167(5), γ = 86.007 (6)°, V = 2561.6(4) Å^3, T = 120 K, space group = $P\bar{1}$, Z = 2, ρ_{calcd} = 1.095 g cm^{-3}. The final R factor was 0.0784 (Rw = 0.2356 for all data) for 7486 reflections with $I > 2\sigma(I)$. GOF = 1.038. Diffraction data were collected on a Mac Science DIP2030K Image Plate Diffractometer employing graphite-monochromatized Mo-Kα radiation (λ = 0.71070 Å). The structure was solved by the direct method and refined by the full-matrix least-squares method using SHELXL-97 program. CCDC 160777.

1 Recent reviews on metallenes and dimetallenes of Group 14 elements: M. Weidenbruch, *Eur. J. Inorg. Chem.*, 1999, 373; P. P. Power, *Chem. Rev.*, 1999, **99**, 3463; J. Escudié and H. Ranaivonjatovo, *Adv. Organomet. Chem.*, 1999, **44**, 113.
2 M. J. Fink, D. J. DeYoung, R. West and J. Michl, *J. Am. Chem. Soc.*, 1983, **105**, 1070; R. West, *Angew. Chem., Int. Ed. Engl.*, 1987, **26**, 1201; G. Raabe and J. Michl, *The Chemistry of Organic Silicon Compounds*, S. Patai and Z. Rappoport, Eds., Wiley, Chichester, 1989, Part 2, ch. 17.
3 V. Ya. Lee, M. Ichinohe, A. Sekiguchi, N. Takagi and S. Nagase, *J. Am. Chem. Soc.*, 2000, **122**, 9034.
4 V. Ya. Lee, M. Ichinohe and A. Sekiguchi, *J. Am. Chem. Soc.*, 2000, **122**, 12604.
5 V. Ya. Lee, T. Matsuno, M. Ichinohe and A. Sekiguchi, *Heteroatom. Chem.*, 2001, **12**, 223.
6 V. Ya. Lee, M. Ichinohe and A. Sekiguchi, *Chem. Lett.*, 2001, 728.
7 The mechanism of such isomerization may involve the nucleophilic assistance of an excess of carbonyl compound, due to the attack of carbonyl oxygen atom on the back side of the silicon atom bearing oxygen substituent, which results in the formation of a *trans*-isomer.
8 A. Sekiguchi, I. Maruki and H. Sakurai, *J. Am. Chem. Soc.*, 1993, **115**, 11460.
9 An example of [2 + 2] cycloaddition reaction of Si=Si and C=O double bonds to form the corresponding disilaoxetane followed by its isomerization to the corresponding disilyl enol ether under photochemical conditions has previously been reported: A. Schäfer and M. Weidenbruch, *J. Organomet. Chem.*, 1985, **282**, 305.

CHEMCOMM Communication
www.rsc.org/chemcomm

Characterization of germanium site distribution in zeolite ITQ-7 by photoluminescence

Avelino Corma,* María J. Díaz–Cabañas, Hermenegildo García,* and Emilio Palomares

Instituto Tecnología Química CSIC–UPV, Av. Naranjos s/n, Universidad Politécnica Valencia, 46022-Valencia, Spain. E-mail: hgarcia@qim.upv.es

Received (in Cambridge, UK) 4th April 2001, Accepted 10th August 2001
First published as an Advance Article on the web 2nd October 2001

Zeolite ITQ-7 containing germanium emits luminescence upon excitation at the wavelength of the absorption maxima; control experiments with amorphous GeO_2 and all-silica zeolites indicate that the emission is attributable to Ge atoms occupying framework positions; the emission decays on the nanosecond time scale and it fits to variable proportions of three exponential kinetics, this being compatible with the presence of three families of Ge atoms in the solid.

Zeolites in which a fraction of the framework silicon atoms are isomorphically replaced by a heteroatom, particularly by transition metals, are important heterogeneous solid catalysts. For instance, a case of special industrial relevance is titanosilicates.[1,2] Given that the heteroatom content in these crystalline metallosilicates is usually very low (< 1 wt%), there has been a considerable interest in developing experimental techniques to determine the metal atom distribution among families depending on their framework *versus* non-framework location, coordination sphere or crystallographic positions. This information is highly valuable to rationalise the activity of these solids and to find a correlation between optimum catalytic activity and the structure of the active sites.

In the context of the characterization of heteroatom distribution in crystalline silicates, pioneering reports showing that photoluminescence spectroscopy can be applied to determine the different coordination spheres of Ti atoms in titanosilicates have constituted a significant contribution.[3,4] Photoluminescence is a non-destructive routine spectroscopic technique widely available in common photochemical laboratories whose distinctive feature is high sensitivity. This contrasts with XANES and EXAFS techniques that require very sophisticated facilities.

Germanium-containing zeolites as well as microporous germanates are interesting materials. By introducing Ge into a zeolite framework one can not only change the basicity of the support[5] or influence the redox properties of the next nearest neighbour framework transition metal,[6] but the introduction of Ge can also accelerate the growth of some existing zeolites as well as the nucleation of new ones.

Unfortunately, Ge characterization in zeolites has been elusive to most of the current techniques, such as NMR and IR. Only EXAFS-XANES has been used to ascertain framework incorporation and to discuss the nature of the next nearest neighbours. There is no doubt that it would be very useful to have a more easily available technique that can give information on the following issues: is Ge incorporated in the zeolite framework? Is there a uniform (statistical) distribution of Ge in the framework? If the answer to the latter is no, the question then will be: what is the proportion of Ge among the different T positions? Herein, we present for the first time evidence that Ge-containing zeolites emit photoluminescence. The evidence that will be presented in this work shows that only the framework Ge originates photoluminescence, extra-framework GeO_2 species giving no signal under the same conditions of low-power excitation. By comparing the kinetic analysis of the emission decay with information from ^{29}Si NMR we have proposed a Ge atom distribution among different sites. The reference zeolite Ge/ITQ-7 was prepared following reported procedures.[7,8] The composition of the resulting Ge/ITQ-7 sample was 57.6 SiO_2:6.4 GeO_2[$4C_{14}H_{26}NF$], the surface area and micropore volume being equal to 660 $m^2\ g^{-1}$ and 0.24 $cm^3\ g^{-1}$, respectively.

The Ge/ITQ-7 sample exhibited room temperature emission (λ_{em} 515 nm) upon excitation at wavelengths between 220 and 300 nm. The emission and excitation spectra are shown in Fig. 1.

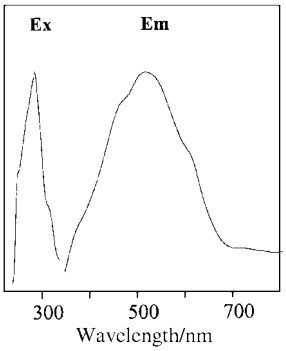

Fig. 1 Excitation (Ex, λ_{em} 515 nm) and emission (Em, λ_{ex} 290 nm) spectra of Ge/ITQ-7 after N_2 purging.

Control measurements with all-silica ITQ-7, as well as amorphous GeO_2 showed no emission, and consequently we can conclude that the emission from the Ge-containing zeolite arises from Ge atoms occupying tetrahedral framework positions. We have ascertained this by observing that other related Ge-zeolites in which Ge is known to occupy framework positions (such as ocatadecasil germanates) also exhibit photoluminescence. We propose that the emission observed arises in tetrahedral Ge atoms from the singlet ligand-to-metal charge transfer state as shown in Scheme 1. This proposal is analogous to the emission mechanism of vanadium supported on inorganic oxides and Ti emission in titanosilicates.[9]

The emission decay of Ge/ITQ-7 depends significantly on the wavelength being monitored and takes place on the nanosecond time scale (Fig. 2). The photoluminescence decay monitored at the emission maximum wavelength was clearly not mono-exponential. The variation of the temporal decay depending on the emission wavelength and the non-monoexponential kinetics can be taken as evidence for a distribution of Ge atoms among different sites. A reasonably good fit (χ^2 = 1.1) could be obtained using a three exponential function. From this theoretical fitting the lifetimes and relative contributions measured at 515 nm were 1.2 ns (24%), 5.3 ns (35%) and 12.2 ns (41%).

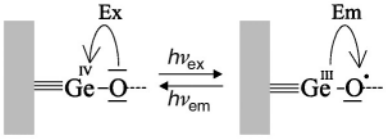

Scheme 1 Proposed mechanism for the observed ≡Ge–O photoluminescence.

 DOI: 10.1039/b103034p

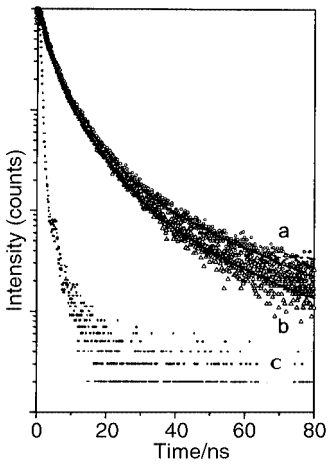

Fig. 2 Emission decays monitored at 515 (a) or 550 (b) nm upon excitation at 290 nm for Ge/ITQ-7 after N_2 purging. The lamp pulse (c) is also given to show the instrumental response. The continuous lines correspond to the fitting from which kinetic data has been obtained and they give a visual indication of the quality of the data.

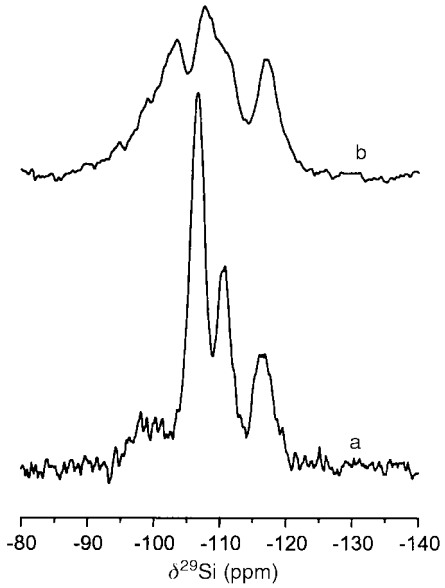

Fig. 3 MAS ^{29}Si NMR spectra of all-silica ITQ-7 (a) and Ge/ITQ-7 (b). Note that the area of the signal at −117 ppm remains unchanged, while the intensity of the peak at −107 ppm is much reduced. A new signal at −100 ppm corresponding to Ge–O–Si appears in spectrum (b).

Therefore, according to kinetic analysis and assuming identical emission efficiency for all the lumophores, the novel Ge/ITQ-7 sample should contain three different Ge sites, whose relative populations measured at 515 nm are 24:35:41. Some other non-emissive Ge atoms such as amorphous germanium oxides may also be present in the solid. Unfortunately, although photoluminescence spectroscopy is a very sensitive technique that is useful for lumophore distribution analysis, it does not give structural information on the species responsible for the emission. Herein we have addressed the structural characterization by comparing the relative intensities of the signals corresponding to the different Si nuclei in the ^{29}Si NMR spectra of the germanosilicate with that for analogous all-silica zeolites (Fig. 3). This gives indirect information on the location of the Ge atoms in the germanosilicate. As it can be seen, the intensity of the band at −117 ppm remains unchanged upon the incorporation of Ge, but there is a significant decrease in the area of the band at −107 ppm. At the same time, a new signal appears at −100 ppm corresponding to Si atoms having Ge in the coordination sphere. It is known that the signal at −117 ppm corresponds to framework atoms occupying positions in the double four member ring (4MR) units. This clearly indicates that incorporation of Ge atoms into the framework occurs preferentially in the 4MR units. In these units there is, however, the same proportion of two different crystallographic sites (T_1 and T_4). The third population observed by photoluminescence characterized by a shorter lifetime would correspond to those Ge atoms located either at T_1 or T_4 (same probability) but having a second Ge in the same 4MR unit. According to the Si/Ge ratio in a unit cell there are 6.4 Ge atoms and four 4MR units.

Alternatively, it could also be possible that the prepared material still containing its template could be somewhat distorted due to the presence of quaternary ammonium ions. Then, the third Ge atom population could arise from this lack of complete symmetry of the as-synthesized ITQ-7. Calcination was not carried out in order to minimise the presence of extra-framework Ge atoms.

In conclusion we have observed for the first time photoluminescence in Ge-containing zeolites. Controls indicate that photoluminescence originates from framework Ge atoms. Therefore, this technique is applicable for the routine determination of Ge distribution in crystalline germanosilicates. Comparison of indirect ^{29}Si NMR spectroscopy data is also in accord with framework Ge incorporation, preferentially in two equally probable crystallographic positions in the 4MR units. Although the assignment is tentative, we propose that the three different populations of Ge atoms observed by photoluminescence correspond to Ge atoms ocuppying these two crystallographic positions together with a third population corresponding to those 4MR units that contain two Ge atoms. Since it can be anticipated that germanosilicates can be applied to the synthesis of novel zeolite-containing heteroatoms, the present study is relevant to provide a routine tool to assess Ge distributions.

Financial support by the Spanish DGES (HG project MAT2000 1768-C02-01) is gratefully acknowledged.

Notes and references

1 M. P. Tamaraso and B. Notari, *US Pat*., 4 410 501, 1983.
2 G. Bellussi, A. Carati, M. G. Clerici, A. Esposito, R. Millini and F. Buonomo, *Belg. Pat*., 1,001,038, 1989.
3 L. Marchese, T. Maschmeyer, E. Gianotti, S. Coluccia and J. M. Thomas, *J. Phys. Chem. B*, 1997, **101**, 8836.
4 C. Lamberti, S. Bordiga, D. Arduino, A. Zecchina, F. Geoblado, G. Spani, F. Genoni, G. Petrini, F. Villain and G. Vlaic, *J. Phys. Chem. B*, 1998, **102**, 6382.
5 C. M. Zicovich-Wilson and A. Corma, *J. Phys. Chem. B*, 2000, **104**, 4134.
6 J. M. Thomas, G. N. Greaves, G. Sankar, P. A. Wright, A. J. Chen and L. Marchese, *Angew. Chem., Int. Ed. Engl*., 1994, **33**, 1871.
7 A. Corma, M. J. Díaz-Cabañas and V. Fornés, *Angew. Chem., Int. Ed. Engl*., 2000, **39**, 2346.
8 A. Corma, M. J. Díaz-Cabañas, M. E. Domine and F. Rey, *Chem. Commun*., 2000, 1725.
9 M. Anpo and H. Yamashita, in *Surface Photochemistry*, ed. M. Anpo, John Wiley and Sons, Chichester, 1996, p. 117.

CHEMCOMM Communication
www.rsc.org/chemcomm

A bis-bidentate dioxolene ligand induces thermal hysteresis in valence tautomerism interconversion processes

Scot H. Bodnar,[a] Andrea Caneschi,[b] Andrea Dei,*[b] David A. Shultz*[a] and Lorenzo Sorace[b]

[a] *Department of Chemistry, North Carolina State University, Raleigh, North Carolina, USA. E-mail: shultz@chemdept.chem.ncsu.edu*
[b] *Dipartimento di Chimica, Università di Firenze, Via Maragliano 75, 50144 Firenze, Italy. E-mail: adei@chim1.unifi.it*

Received (in Cambridge, UK) 12th July 2001, Accepted 11th September 2001
First published as an Advance Article on the web 2nd October 2001

The use of a bis-bidentate ligand in a solid cobalt dioxolene complex affords the necessary cooperative properties that lead to thermal hysteresis in a valence tautomeric interconversion equilibrium.

Among the molecular systems that undergo valence tautomerism, cobalt–dioxolene complexes are the most attractive from a magnetic point of view. For all of the examples reported to date the tautomeric interconversion involves an intramolecular electron transfer between a six-coordinate diamagnetic cobalt(III) metal ion and a coordinated catecholate ligand yielding a cobalt(II)–semiquinone species, the metal ion being in the high-spin electronic configuration.[1–9] It is well established that the transition between the two forms can be induced by temperature and pressure changes as well as by optical irradiation. However, to date the potential application of these systems has been limited by the paucity of materials exhibiting thermal hysteresis, a necessary prerequisite for obtaining memory effects. A small hysteresis width (5 K) was found to be associated to the tautomeric interconversion showed by the Co^{III}(phen)(DBSQ)(DBCat)·$C_6H_5CH_3$ complex,[3] whereas a rather large effect was detected for Co^{III}(3,6-DBCat)(3,6-DBSQ)(py_2O) and Co^{II}(3,6-DBSQ)$_2$(py_2O) valence tautomeric pair (DBCat and DBSQ are semiquinonate and catecholate species derived from 5,5′-di-*tert*-benzylquinone).[9] In the latter system the observed behaviour has been attributed to the planar/folded change in conformation due to the steric requirements of the ancillary diazine ligand. In this sense the observed magnetic behaviour of this molecular system must be considered as a very interesting exception, but, because of its pure molecular origin, it cannot provide the basis for the development of a class of magnetic materials. The attractiveness of a class of compounds exhibiting molecular bistability is due to the fact that their properties can be tuned by means of molecular chemistry techniques. Since the fundamental origin of valence tautomerism is molecular and the cobalt(III)–catecholate and cobalt(II)–semiquinone species involved in the interconversion have different molecular volumes, a thermal hysteresis and then a memory effect must be associated with the existence of a strong cooperativity between the cobalt centers. Following this elementary paradigm, we thought that efforts of the research must be focused towards the design of molecular assemblies with mutually interacting metal centers undergoing valence tautomerism.

Bearing this in mind, we have synthesized a 1,10–phenanthroline–cobalt adduct (Scheme 1) of the dioxolene ligand 3,5-bis(3′,4′-dihydroxy-5′-*tert*-butylphenyl)-1-*tert*-butylbenzene (L)[10] which according to its geometry may act as bis-bidentate ligand towards two different metal ions. Once coordinated this ligand may give by one-electron oxidation the trinegative radical anion we indicate as Sq–Cat, which, although not physically characterized, can be expected to behave as a class II mixed valence radical ligand. A further one-electron oxidation has been shown to yield the diradical Sq–Sq species, which according to its topological properties, is characterized

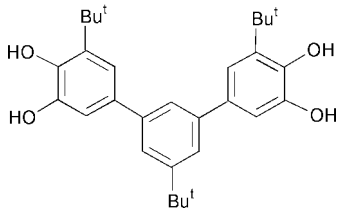

Scheme 1

by a triplet electronic ground state. We have recently shown how the topology of this ligand may enforce the achievement of high multiplicity ground-states when the Sq–Sq is coordinated to two paramagnetic metal ions.[11]

The reaction of cobalt(II) chloride, 1,10 phenanthroline and L in 1:1:1 ratio in ethanol–dichloromethane (1:2 v/v) in the presence of a stoichiometric amount of triethylamine (4:1) affords a black–green powder (30% yield) of analytical formula Co(phen)L·0.5CH_2Cl_2 **1**. Compound **1** is insoluble in common organic solvents. It is reasonable to believe that this compound contains six-coordinated cobalt ions like all Co(N–N)(diox)$_2$ (N–N = diazine ligand, diox = catecholate or semiquinone) species previously described.[1,2] The main difference between this compound and previous ones is the fact that each dioxolene ligand is paramagnetic and coordinated to two different cobalt ions, thus giving rise to a polymeric structure.

The temperature dependent magnetic behavior of compound **1** is shown in Fig. 1.†

The observed magnetic behaviour is consistent with the presence of a cobalt(III)–catecholato–semiquinonato dominant species at low temperature undergoing a thermally induced valence tautomeric transition to a high spin cobalt(II)–bis(semiquinonato) species according to equilibrium (1). At 310 K, the highest temperature value we measured, it can be estimated from the χT value that each tautomer is present in equal concentration: indeed, the expected χT value for a Co^{II} center and two SQ units would be *ca.* 3.3 emu K mol^{-1}.[12] Using the

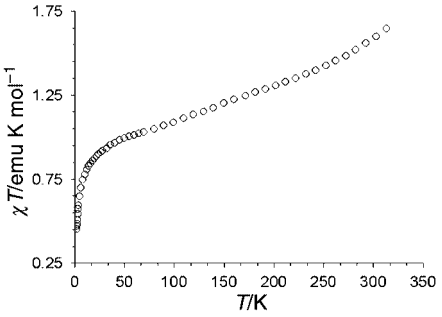

Fig. 1 χT values *vs.* T for compound **1** reported for a single Co center; it is evident that the gradual transition is due to a valence tautomeric process [eqn. (1)] occurring above 50 K.

$$[(Co^{III}/2)SQ–Cat(Co^{III}/2)]_n \rightarrow [(Co^{II}/2)SQ–SQ(Co^{II}/2)]_n \quad (1)$$

 DOI: 10.1039/b106192p

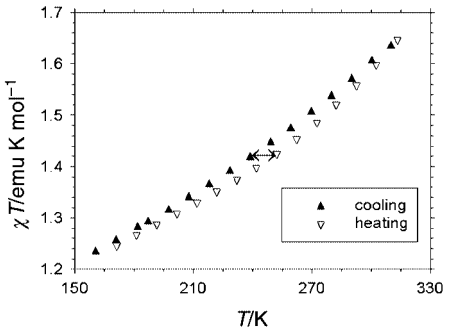

Fig. 2 Difference in the measured χT when heating (▽) and cooling (▲) the sample, respectively. The arrow evidences the maximum width of thermal hysteresis, *ca*. 12 K at 250 K.

nomenclature currently used for spin-crossover systems, the transition can be classified as gradual, but, more importantly, a thermal hysteresis width of *ca*. 12 K is observed (see Fig. 2), though the optimum conditions for observing this phenomenon, *i.e*. the full conversion to hs-cobalt(II), are not reached.

This result was obtained in three independent measurements repeated on the same sample, using 30 min for each point to ensure sample thermal equilibration. These experimental data, therefore, suggest the existence of a strong cooperativity between the magnetic centers.

A comprehensive analysis of magnetic data is not straightforward owing to the high complexity of the different magnetic interactions occurring in the present system and the orbital degeneracy of octahedral Co(II). Moreover the χT value characterizing the cobalt(II)–bis(semiquinonato) species is unknown.

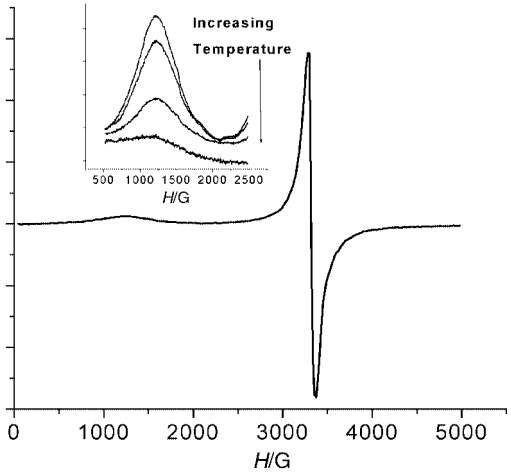

Fig. 3 EPR spectrum of **1** at 4 K. The inset shows the temperature evolution of the low-field transition at 4, 10, 20 and 40 K, respectively.

Furthermore the powder EPR spectrum (see Fig. 3) at 4 K shows a broad transition at 1530 G ($g = 4.3$) and a sharper one at 3300 G ($g = 2$). The transition at $g = 2$ can be assigned to a $Co^{III}SQ$ species and is detected also at room temperature, whereas the transition at $g = 4.3$ seems to be due to the presence of $Co^{II}SQ$ or $Co^{II}(SQ)_2$. This assignment is supported by the fact that these absorptions disappear as the temperature is increased to 40 K (Fig. 3, inset), which is a typical behavior for Co^{II} species. Detection of the $g = 2$ signal at room temperature is of significance since under fast interconversion between the cobalt(III) and cobalt(II) centers, this transition should not be detected on the EPR time scale.

The most important finding of the present experimental results is the strong cooperativity shown by compound **1**, a property that we were looking for in designing this peculiar molecular system. We feel that the observed properties can be easily manipulated by changing the dioxolene substituents, the diazine acceptors as well the crystallization solvent, in agreement with the suggestions of previous work concerning more simple molecular $Co(NN)(diox)_2$ complexes.

Financial support of the EC through the projects ERB 4061 Pl 97-0197 and HPRN-CT-1999-00012, and of the Italian MURST and CNR is gratefully acknowledged. D. A. S. thanks the NSF for financial support.

Notes and references

† The magnetic susceptibility of polycrystalline powder samples of **1** was measured between 2 and 310 K at an applied magnetic field of 0.1 or 1 T using a Cryogenic S600 SQUID magnetometer. Data were corrected for the magnetism of the sample holder that was determined separately in the same temperature range and field, and the underlying diamagnetism of the samples was estimated from Pascal's constants. EPR spectra were recorded at X-band frequency (9.23 GHz) on a Varian ESR9 spectrometer equipped with a continuous flow ^{4}He cryostat.

1 C. G. Pierpont and C. W. Lange, *Prog. Coord. Chem*., 1993, **41**, 381.
2 P. Gütlich and A. Dei, *Angew. Chem., Int. Ed. Engl*., 1997, **36**, 2734.
3 D. M. Adams, A. Dei, A. L. Rheingold and D. N. Hendrickson, *J. Am. Chem. Soc*., 1993, **115**, 8221.
4 G. A. Abakumov, V. K. Cherkasov, M. P. Bubnov, O. G. Ellert, Z. B. Dobrokhotova, L. N. Zakharov and Y. T. Struchovkov, *Dokl. Akad. Nauk*., 1993, **328**, 12.
5 O. S. Jung and C. G. Pierpont, *Inorg. Chem*., 1994, **33**, 2227.
6 O. S. Jung and C. G. Pierpont , *J. Am. Chem. Soc*., 1994, **116**, 1127.
7 D. M. Adams and D. N. Hendrickson, *J. Am. Chem. Soc*., 1996, **118**, 11 515.
8 C. Roux, D. M. Adams, J. P. Itiè, A. Polian, D. N. Hendrickson and M. Verdaguer, *Inorg. Chem*., 1996, **35**, 2846.
9 O. S. Jung, D. H. Jo, Y. A. Lee, B. J. Conklin and C. G. Pierpont, *Inorg. Chem*., 1997, **36**, 19.
10 D. A. Shultz, A. K. Boal, D. J. Driscoll, J. R. Kitchin and G. N. Tew, *J. Org. Chem*., 1995, **60**, 3578.
11 A. Caneschi, A. Dei, H. Lee, D. A. Shultz and L. Sorace, *Inorg. Chem*., 2001, **40**, 408.
12 A. Caneschi, A. Dei, D. Gatteschi and V. Tangoulis, *Inorg. Chem*., in press.

CHEMCOMM
Communication
www.rsc.org/chemcomm

A homoleptic phosphine adduct of Tl(I)†

Ian R. Shapiro, David M. Jenkins, J. Christopher Thomas, Michael W. Day and Jonas C. Peters*

Division of Chemistry and Chemical Engineering, California Institute of Technology, Pasadena, CA 91125, USA. E-mail: jpeters@caltech.edu

Received (in Cambridge, UK) 21st May 2001, Accepted 22nd August 2001
First published as an Advance Article on the web 27th September 2001

A homoleptic phosphine adduct of thallium(I) supported by a tris(phosphino)borate ligand has been isolated and structurally characterized.

Although hard donor ligands are known to stabilize simple molecular complexes of thallium-(I) and -(III),[1] well-defined examples of thallium supported by correspondingly soft donor ligands are relatively rare.[2] Regarding phosphine donors specifically, only two phosphine adducts have been structurally characterized: both of thallium(III);[3] to our knowledge, there are no well-characterized phosphine adducts for thallium(I). By comparison, there are numerous structurally characterized examples of thallium(I) supported by hard N-donor ligands including the tripodal ligands Tp (Tp = tris(pyrazolyl)borate) and Me_3-TACN (TACN = triazacyclononane).[4,5]

Our group is developing transition metal chemistry utilizing anionic tris- and bis-(phosphino)borate ligands.[6] We have set out to prepare a thallium adduct of the tris(phosphino)borate ligand, [$PhBP_3$] ($PhBP_3$ = $PhB(CH_2PPh_2)_3$),[7] for two reasons. We were surprised by the dearth of well-defined phosphine complexes of thallium and hoped that the anionic [$PhBP_3$] ligand might support and stabilize a thallium(I) species. Additionally, the previously reported lithium salt of this ligand, [Li(tmeda)][$PhBP_3$] (tmeda = tetramethylethylenediamine), is not a reagent of general synthetic utility for clean delivery of the [$PhBP_3$] ligand to transition metals. A versatile thallium reagent of this ligand therefore seems highly desirable. Herein we report the isolation and structural characterization of a homoleptic phosphine adduct of thallium(I) stabilized by the [$PhBP_3$] ligand.

It was convenient to prepare the target complex, [$PhBP_3$]Tl, **1**, by transmetallation of lithium for thallium upon addition of $TlPF_6$ to a methanolic solution of [Li(tmeda)][$PhBP_3$] (Scheme 1).‡ The reaction occurred rapidly and cleanly at ambient temperature as indicated by ^{31}P NMR spectroscopy. Following work-up, the light yellow product was isolated in reasonable yield (65%). It is worth noting that the entire reaction sequence can be executed in air without decomposition. Furthermore, the thallium salt itself is stable to moisture and oxygen for an extended period, both in solution and in the solid state.

Examination of the ^{31}P NMR spectrum of **1** (C_6D_6) showed two resonances (1 : 1 ratio) separated by more than 40 ppm, each resonance bearing a resolvable shoulder (ESI†). This spectrum represents two separate doublets from a very strong $^1J_{TlP}$ coupling interaction (5214, 5168 Hz) for each of the naturally occurring spin ½ thallium isotopes {^{205}Tl (70.5%), ^{203}Tl (29.5%), respectively}. Notably, these coupling values are significantly larger than those reported for phosphine complexes of thallium(III) (approximately 1500 Hz).[3]

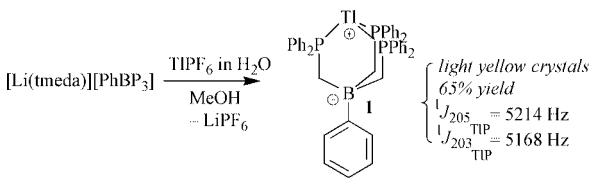

Scheme 1

In order to corroborate the NMR assignment, consistent with a structure resulting from symmetric, tridentate binding of the [$PhBP_3$] ligand to the thallium cation, we sought independent structural confirmation. Slow evaporation of a benzene solution of **1** afforded crystals suitable for an X-ray diffraction study. A structural representation of complex **1** is shown in Fig. 1 (top view, 50% ellipsoids).[8] The structure confirms our assignment of **1** as a homoleptic phosphine adduct of thallium. The anionic [$PhBP_3$] ligand coordinates the thallium cation in the expected tridentate conformation (top view). The large ionic radius of the thallium(I) ion forces it to sit well above the basal plane (2.074 Å) defined by its three phosphine donor atoms. This structural feature affords a significant separation between the thallium ion and the molecule's anionic borate counter-anion (Tl1–B distance = 4.253 Å). It is interesting to compare the intramolecular Tl–B distance found in a host of structurally characterized thallium(I) adducts of variously substituted Tp ligands. The Tl–B distance is much longer in **1** than in all related Tp adducts of thallium(I) (range = 3.46–3.90 Å), and is approximately 0.6 Å longer than the mean distance (3.65 Å) for the related Tp systems.[4] The pronounced Tl–B distance in **1**, in conjunction with the absence of simple resonance contributors

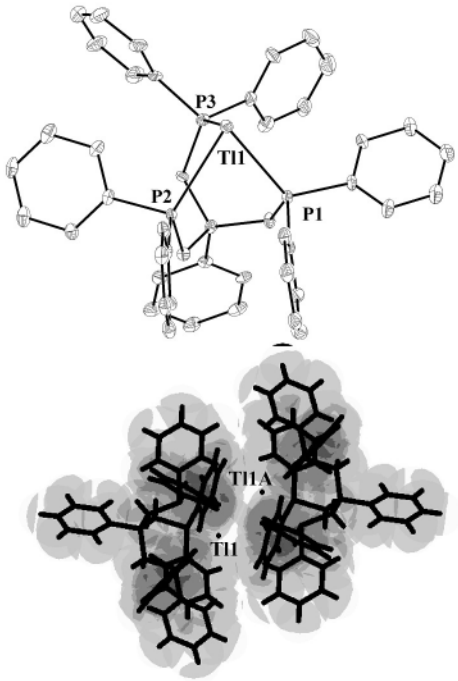

Fig. 1 Displacement ellipsoid (50%) representation of Tl[$PhBP_3$], **1**. Hydrogen atoms have been omitted for clarity. Selected interatomic distances (Å) and angles (°): Tl1–P1 2.878, Tl1–P2 2.953, Tl1–P3 2.932, Tl1–B 4.254; P1–Tl1–P2 70.82, P1–Tl1–P3 76.78, P2–Tl1–P3 77.46. The bottom view shows a transparent space-filling model of **1** depicted as a dimer [Tl1–Tl1A = 3.5652(2) Å]. The [$PhBP_3$] ligands are highlighted as bold stick figures and the positions of the Tl nuclei are labelled.

† Electronic supplementary information (ESI) available: ^{31}P and ^{205}Tl NMR spectra of [$PhBP_3$]Tl in C_6D_6. See http://www.rsc.org/suppdata/cc/b1/b104447h/

 DOI: 10.1039/b104447h

that delocalize the anionic charge from the borate counter-anion to the Tl center, suggests that **1** may be represented as a simple zwitterion (Scheme 1). Although equivalent phosphorus nuclei are observed by ^{31}P NMR spectroscopy, the three phosphine donors are not symmetrically bound in the solid state. The Tl1–P3 distance, 2.880 Å, is appreciably shorter than the Tl1–P1 and Tl1–P2 distances (2.953 and 2.934 Å, respectively).

The bottom view of Fig. 1 shows a transparent space-filling model of **1** and its neighboring thallium adduct. The asymmetric unit of **1** contains a single thallium complex that is related to the neighboring thallium atom, Tl1A, by a center of symmetry. The distance between these thallium atoms is 3.5652(2) Å, which is considerably longer than twice the covalent radius (1.64 Å) of thallium, and is consistent with a thallium–thallium dimer resulting from weak interactions. This dimeric structure does not exist in solution. Direct evidence for assigning **1** as a monomer in solution is as follows: the ^{31}P NMR spectrum of **1** shows only $^{1}J_{\mathrm{TlP}}$ coupling. We would expect to observe a weaker $^{2}J_{\mathrm{TlP}}$ coupling to the neighboring Tl nucleus if the dimeric structure exists in solution. To buttress this argument, the ^{205}Tl NMR spectrum of **1** was obtained in C_6D_6:[9] a single resonance (2809 ppm) split into a quartet by the three equivalent phosphine donors was observed (ESI†). There was no evidence for $^{1}J_{(205)\mathrm{Tl}(203)\mathrm{Tl}}$ coupling, ruling out Tl–Tl interactions in benzene solution. Finally, **1** was analyzed by electrospray mass spectroscopy (ESI/MS). The parent ion observed in positive mode (891) was consistent with the protonated monomeric form of **1**. Thus, our data imply a monomeric formulation of **1** in solution,[10] consistent with its readiness to undergo thallium loss by transmetallation chemistry (*vide infra*).

Regarding other soft, tripodal donor ligands supporting thallium(I), a good comparison to complex **1** comes from Riordan and coworkers, who recently reported a thallium(I) adduct of their second generation, anionic tris(thioether)borate ligand, [PhTt$^{t\text{-Bu}}$].[11] Notably, [PhTt$^{t\text{-Bu}}$] does not enforce a simple, 1 : 1 complex between thallium(I) and the tris(thioether) ligand in the solid state. This is despite the fact that the Tl[PhTt$^{t\text{-Bu}}$] reagent enables access to monomeric, pseudo-tetrahedral geometries for simple divalent nickel and cobalt chlorides.

To highlight the synthetic utility of the thallium reagent **1**, we examined its reactivity with CoI_2. The previously prepared Li(tmeda) adduct of [$PhBP_3$], in addition to its related ammonium salt [$^{n}Bu_4N$][$PhBP_3$], afforded ill-defined mixtures of paramagnetic products on attempted metathesis with CoI_2 in benzene and other solvents.[6] By contrast, the softer and presumably less-reducing thallium reagent **1** reacted cleanly with CoI_2 in benzene to afford the bright green, low spin cobalt iodide complex [$PhBP_3$]CoI, **2**, in good yield (91%).§ Complex **2** was structurally characterized and adopts the expected pseudo-tetrahedral geometry in the solid state (Scheme 2).[8]

In summary, we have isolated and structurally characterized a rare example of a simple phosphine adduct of thallium(I). It has been found that complex **1** displays a signature $^{1}J_{\mathrm{TlP}}$ coupling constant of 5214 Hz. In addition to exposing new possibilities for thallium coordination chemistry within a phosphine donor sphere, complex **1** promises to be an important reagent for delivering the relatively unexplored [$PhBP_3$] ligand to transition metals.

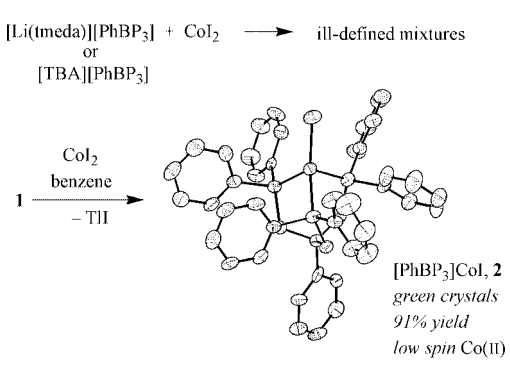

Scheme 2

We thank the Dreyfus Foundation, Caltech, and the NSF for financial support of this work.

Notes and references

‡ *Synthesis* of [$PhBP_3$]Tl, **1**: solid [Li(tmeda)][$PhBP_3$] (7.1 g, 8.6 mmol), generated as previously described,[7] was suspended in methanol (60 mL). To this stirring suspension was added an aqueous solution (30 mL) of $TlPF_6$ (3.00 g, 8.6 mmol) over a period of 5 min. A cloudy white suspension resulted which was stirred for an additional 5 min, followed by extraction with dichloromethane (2 × 150 mL). Drying the organic extract *in vacuo* afforded a light yellow powder that was subsequently washed with hexanes and Et_2O (40 mL each). The remaining powder was extracted into benzene, stirred over $MgSO_4$, and dried thoroughly *in vacuo* to afford the thallium adduct **1** as a fine yellow powder (5.00 g, 65%). ^{1}H NMR (C_6D_6, 300 MHz, 25 °C): δ 8.13 (d, J = 6.6 Hz, 2H), 7.67 (m, J = 7.5 Hz, 2H), 7.42 (tt, J = 6.6, 1.2 Hz, 1H), 7.18–7.11 (m, 12H), 6.80–6.77 (m, 18H), 1.96 (br m, 6H). ^{31}P NMR (C_6D_6, 121.4 MHz, 25 °C): δ 21.6 [d, $^{1}J_{\mathrm{TlP}}$ = 5214 Hz for ^{205}Tl (70.5% abundance), $^{1}J_{\mathrm{TlP}}$ = 5168 Hz for ^{203}Tl (29.5% abundance)]. ^{205}Tl NMR (C_6D_6, 231.31 MHz, 25 °C): δ 2810 (q, $^{1}J_{\mathrm{TlP}}$ = 5204 ± 116 Hz). ^{13}C NMR (C_6D_6, 125.7 MHz, 25 °C): δ 139.8, 132.5, 128.8–129.1 (overlapping resonances), 124.6, 17.0 (br). ^{11}B NMR (C_6D_6, 128.3 MHz, 25 °C): δ −10.96. Anal. Calc. for $C_{47}H_{48}BP_3Tl$: C, 60.73; H, 4.64. Found: C, 61.75; H, 4.76%.

§ *Synthesis* of [$PhBP_3$]CoI, **2**: a benzene solution (50 mL) of the thallium reagent **1** (0.356 g, 0.40 mmol) was added to a stirring suspension of CoI_2 (0.250 g, 0.80 mmol) in benzene (20 mL). After stirring at ambient temperature for 24 h, the resulting green solution was filtered through Celite, concentrated *in vacuo* (50%) and filtered through Celite once again. Vapor diffusion of petroleum ether into the resulting green filtrate afforded a good yield of the desired crystalline product (0.317 g, 91.1% yield). ^{1}H NMR (C_6D_6, 300 MHz, 25 °C): δ 22.2 (br s), 15.8 (s), 10.8 (s), 7.7 (s), 7.5 (s), 4.3 (br s), 2.2 (s), −8.5 (s). IR (ν/cm^{-1}): 1433 (s), 1091 (b), 739 (s). μ_{eff} = 2.60 μ_{B} (SQUID). UV–vis (C_6H_6): 638 nm (ε = 1112), 738 nm (ε = 627). Anal. Calc. for $C_{45}H_{41}BCoIP_3$: C, 62.03; H, 4.74. Found: C, 61.76; H, 4.75%.

1 A. J. Canty, K. Mills, B. W. Skeleton and A. H. White, *J. Chem. Soc., Dalton Trans.*, 1986, 939; K. Henrick, R. W. Matthews and P. A. Tasker, *Inorg. Chem.*, 1977, **16**, 3293.

2 A. J. Blake, J. A. Greig and M. Schröder, *J. Chem. Soc., Dalton Trans.*, 1991, 529; J. A. Blake, G. Reid and M. Schröder, *J. Chem. Soc., Dalton Trans.*, 1992, 2987.

3 G. Muller and J. Lachmann, *Z. Naturforsch., Teil B*, 1993, **48**, 1544; R. A. Baldwin, R. L. Wells and P. S. White, *Main Group Chem.*, 1986, **2**, 67.

4 For recent references, see: P. Ghosh, D. G. Churchill, M. Rubeinshtein and G. Parkin, *New J. Chem.*, 1999, **23**, 961; C. Janiak, L. Braun and F. Girgsdies, *J. Chem. Soc., Dalton Trans.*, 1999, 3133; A. L. Rheingold, B. S. Haggerty, L. M. Liable-Sands and S. Trofimenko, *Inorg. Chem.*, 1999, **38**, 6306.

5 K. Wieghardt, M. Kleine-Boymann, B. Nuber and J. Weiss, *Inorg. Chem.*, 1986, **25**, 1309.

6 J. C. Thomas and J. C. Peters, *J. Am. Chem. Soc.*, 2001, **123**, 5100; J. C. Peters and J. C. Thomas, *Inorg. Synth.*, 2001, submitted; D. Jenkins, M. J. Allen and J. C. Peters, 2001, manuscript in preparation.

7 J. C. Peters, T. D. Feldman and T. D. Tilley, *J. Am. Chem. Soc.*, 1999, **121**, 9871; see also: A. A. Barney, A. F. Heyduk and D. G. Nocera, *Chem. Commun.*, 1999, 2379.

8 *Crystal data* for **1**: $C_{45}H_{41}BP_3Tl$, M = 889.87, pale yellow rhombohedral plate, T = 98 K, monoclinic, space group $P2_1/n$, a = 13.7449(7), b = 13.5812(7), c = 20.5487(10) Å, β = 94.536(1)°, V = 3823.9(3) Å^3, Z = 4, R_1 = 0.0221 [$I > 2\sigma(I)$], GOF = 1.308. For **2**: ($C_{45}H_{41}BCoIP_3$), M = 910.38, dark green blade, T = 98 K, monoclinic, space group $P2_1/c$, a = 22.5443(17), b = 12.7044(9), c = 29.526(2) Å, β = 90.230(2)°, V = 8456.6(11) Å^3, Z = 8, R_1 = 0.0476 [$I > 2\sigma(I)$], GOF = 1.137. CCDC reference numbers 160107 and 162229. See http://www.rsc.org/suppdata/cc/b1/b104447h/ for crystallographic data in CIF or other electronic format.

9 Dr Todd Alam from Sandia National Laboratory is acknowledged for obtaining the ^{205}Tl NMR spectrum of **1**.

10 Attempts to obtain a solution molecular weight estimate for **1** by the Signer method have thus far been inconclusive due its tendency to precipitate from solution on prolonged standing.

11 P. J. Schebler, C. G. Riordan, I. A. Guzei and A. L. Rheingold, *Inorg. Chem.*, 1998, **37**, 4754.

CHEMCOMM
Communication
www.rsc.org/chemcomm

Revision of the absolute configuration of the tricyclic sesquiterpene (+)-kelsoene by chemical correlation and enantiospecific total synthesis of its enantiomer

Sonja Fietz-Razavian,[a] Stefan Schulz,*[a] Ina Dix[a] and Peter G. Jones[b]

[a] *Institut für Organische Chemie, Technische Universität Braunschweig, Hagenring 30, D-38108, Braunschweig, Germany. E-mail: stefan.schulz@tu-bs.de; Fax: +49 531 391 5272; Tel: +49 531 391 7353*

[b] *Institut für Anorganische Chemie, Technische Universität Braunschweig, Hagenring 30, D-38108 Braunschweig, Germany*

Received (in Cambridge, UK) 8th March 2001, Accepted 4th September 2001
First published as an Advance Article on the web 2nd October 2001

The absolute configuration of the recently identified sesquiterpene (+)-kelsoene was revised by chemical correlation with (*R*)-(+)-pulegone; the correct structure is (1*R*,2*S*,5*R*,6*R*,7*R*,8*S*)-2,8-dimethyl-6-(1-methylethenyl)tricyclo[5.3.0.0^{2,5}]decane.

Recently the sesquiterpene hydrocarbon (+)-kelsoene (**1**, also called tritomarene) was isolated from the marine sponge *Cymbastela hooperi*[1] as well as from the liverworts *Ptychanthus straitus*,[2] *Calypogeia muelleriana*,[3] and *Tritomaria quinquedentata*.[4] The relative configuration was elucidated during these studies; **1** contains a rare *cis,anti,cis* 4-5-5 carbotricyclic ring system, previously only found in the tetraterpene poduran[5] and the sesquiterpenoid sulcatine G.[6] The analysis of NMR data obtained from two dihydroisoxazoles formed after addition of (a*S*)-2′-methoxy-1,1′-binaphthalene-2-carbohydroximoyl chloride (MBCC) to the double bond of **1** according to the method of Fukui *et al*.[7] led to the conclusion that (+)-**1** possesses a (1*S*,2*R*,5*S*,6*S*,7*S*,8*R*)-2,8-dimethyl-6-(1-methylethenyl)tricyclo[5.3.0.0^{2,5}]decane structure.[8] In the present study we will show by chemical correlation with the ketone **3** and further with (*R*)-(+)-pulegone (**4**) that this assignment is incorrect. We will also present the first synthesis of enantiomerically pure **1**, which has previously only been synthesized in racemic form.[9]

Natural **1** can be isomerized by a short treatment with toluene-*p*-sulfonic acid into the more stable isomer **2**, which in turn is cleaved by ozonolysis to the tricyclic ketone **3**. Under the reaction conditions no excessive degradation of **3** or **1** or formation of byproducts occurs. The ketone **3** was the target of a short enantiospecific synthesis, because we reasoned that its racemate may be well suited to separation by GC on chiral phases due to its rigidity. It would also be formed by degradation of other terpenes exhibiting the same ring system, such as *e.g*. the tetraterpene poduran recently identified by us,[5] thus allowing its use for the determination of the absolute configuration of several natural products.

The ketone **3** was synthesized starting from (*R*)-(+)-pulegone (**4**), which was transformed by bromination and Favorskii-rearrangement into a mixture of *cis*- and *trans*-pulegonic acids (**5**),[10] separable by column chromatography. Isomerization of the double bond into the terminal position was achieved by lactonization of pure *cis*-**5** to **6**, followed by elimination with a bulky base, as has been described for *anti*-**5**.[10,11] The double bond of the resulting acid **7** was now internally acylated *via* the acid chloride to form the ketone **8**, which was photochemically transformed by a [2 + 2]-cycloaddition with ethylene into the desired ketone (1*S*,2*R*,5*R*,7*R*,8*R*)-2,8-dimethyltricyclo-[5.3.0.0^{2,5}]decan-6-one (*ent*-**3**). The ethylene attack occurs from the less hindered side. In an identical manner, *rac*-**3** was synthesized starting from *rac*-**4**. To exclude the unlikely possibility of inversion of the stereogenic centers in the course of our synthesis, *ent*-**3** was reduced with $LiAlH_4$. Preferential attack of the hydride from the less hindered side and reaction of the alcohol with tosyl chloride resulted in formation of the

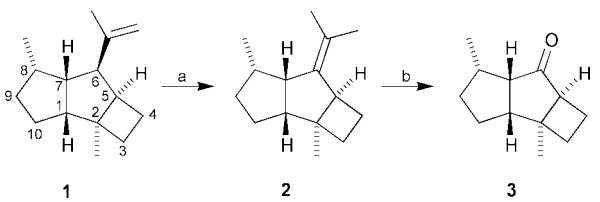

Scheme 1 *Reagents and conditions*: (a) p-TSA, 15 min, CH_2Cl_2, Δ; (b) O_3, CH_2Cl_2, −78 °C, then Me_2S.

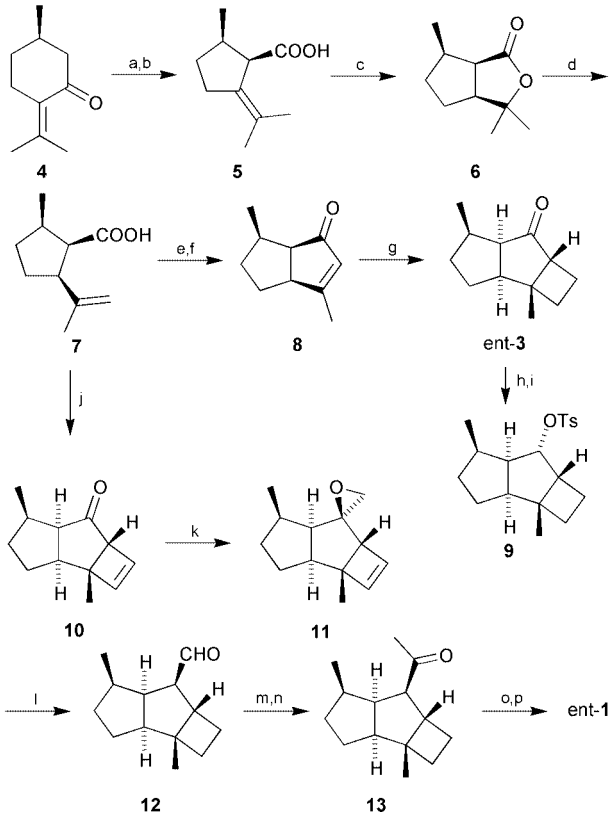

Scheme 2 *Reagents and conditions*: (a) Br_2, Et_2O, 0 °C; (b) 25% aq. KOH, Δ, column separation; (c) aq. HCl, MeOH, Δ; (d) *t*-BuOK, DMF, 140 °C; (e) $(COCl)_2$, CH_2Cl_2; (f) $AlCl_3$, CH_2Cl_2; (g) $CH_2{=}CH_2$, hν, CH_2Cl_2, 0 °C; (h) $LiAlH_4$, Et_2O; (i) *p*-TsCl, py; (j) see[9,13]; (k) Me_3SOI, DMSO; (l) H_2, Pd/C, Et_2O; (m) MeLi, THF, −78 °C; (n) PDC, CH_2Cl_2; (o) NaOMe, MeOH, Δ; (p) Cp_2TiMe_2, THF, Δ.

 DOI: 10.1039/b101579f

tosylate **9**. An X-ray analysis of **9**† allowed the determination of its absolute configuration.[12] This tosylate could be thus identified as (1*S*,2*R*,5*R*,6*S*,7*R*,8*R*)-2,8-dimethyltricyclo-[5.3.0.0^{2,5}]dec-6-yl tosylate, exhibiting the expected absolute configuration.

Being confident on the absolute configuration of *ent*-**3**, we were now able to perform GC analyses. The absolute configuration of natural (+)-**1** can be deduced by analysis of its degradation product **3**, because its relative configuration has been elucidated during its isolation.[1] Separation of *rac*-**3** was achieved on a chiral Hydrodex-6-TBDMS stationary phase.‡ The (−)-enantiomer of **3** eluted first, as did the degradation product of synthetic (−)-kelsoene. The ketone **3** derived from natural (+)-kelsoene eluted as second peak. In addition, the synthetic (−)-**1** prepared by us showed the expected sign of optical rotation of $[\alpha]_D^{20} = -78.3$. These data unequivocally prove that natural (+)-kelsoene has the opposite configuration as previously reported and possesses a (1*R*,2*S*,5*R*,6*R*,7*R*,8*S*)-2,8-dimethyl-6-(1-methylethenyl)tricyclo[5.3.0.0^{2,5}]decane structure.

We proceeded with the synthesis of enantiomerically pure (−)-**1** to further underline the consistency of our data set. In their synthesis of *rac*-**1**, Mehta and Srinivas showed that ketone **3** is strongly hindered and not readily attacked by nucleophiles. We therefore chose their strategy to reduce steric hindrance: The bicyclic ketone **8** was transformed into the cyclobutene derivative **10** as described.[9,13] The side chain was then elaborated in a new way. Even after reduction of the steric hindrance, only small nucleophiles can be used to attack the carbonyl carbon atom. Nevertheless, epoxidation with trimethylsulfoxonium iodide was feasible with satisfactory yield. The epoxide **11** was then hydrogenated and rearranged in one step to form the aldehyde **12**. Addition of methyllithium followed by oxidation with PDC afforded the ketone **13** in a 80 : 20 dr in favor of the unwanted diastereomer. Obviously the less hindered hydrogen moves more readily in the epoxide–aldehyde rearrangement of **12**. Nevertheless, simple treatment with base epimerized this center to the thermodynamically more favored arrangement, which is also found in the natural product. Kelsoene was then formed by final methenylation with Me_2TiCp_2,[14] because Wittig olefination, despite reported by Mehta and Srinivas,[13] did not proceed with satisfactory yields. Thus enantiomerically pure (−)-**1** has been synthesized, confirming our previous assignments.§,¶

We thank Professor Nabeta and Professor G. König for kindly providing us with samples of (+)-kelsoene. We also thank the Deutsche Forschungsgemeinschaft and the Fonds der chemischen Industrie for financial support.

Note added in proof. Similar results were obtained recently by G. Mehta and K. Srinivas, *Tetrahedron Lett*., 2001, **42**, 2855, using a different synthetic strategy.

Notes and references

† *Crystal data* for **9**: orthorhombic, space group $P2_12_12_1$, $a = 9.1578(8)$, $b = 11.7038(10)$, $c = 16.1527(14)$ Å, $U = 1731.3$ Å^3, $Z = 4$, $T = -130$ °C. *Data collection*: a crystal *ca*. 0.4 × 0.16 × 0.09 mm was used to record 26944 intensities on a Bruker SMART 1000 CCD diffractometer (Mo-Kα radiation, $2\theta_{max}$ 57°). *Structure refinement*: the structure was refined anisotropically on F^2 (program *SHELXL*-97, G. M. Sheldrick, University of Göttingen) to *wR*2 0.083, *R*1 0.032 for 211 parameters and 4388 unique reflections. The hydrogens were refined using a riding model or rigid methyl groups. The Flack parameter refined to −0.07(5). CCDC 171200. See http://www.rsc.org/suppdata/cc/b1/b101579f/ for crystallographic files in .cif or other electronic format.

‡ Separations were performed on a 15 m Hydrodex-6-TBDMS capillary column (Macherey & Nagel), id 0.25 mm, programmed from 60 to 180 with 5 min after a 2 min isothermal period with H_2 as the carrier gas (45 psi).

§ The ^{1}H NMR, ^{13}C NMR, and MS data are identical to those reported in the literature.[1] $[\alpha]_D^{25} = -78.3$ ($c = 0.31$, $CHCl_3$). Literature data for (+)-**1**: $[\alpha]_D^{25} = +78.1$ ($c = 1.98$, $CHCl_3$).[1]

¶ We also tried to find out why the NMR study by Nabeta *et al*.[8] furnished the opposite result. In their work Nabeta *et al*. presented a preferred conformation for one of the two formed kelsoene-MBCC adducts. Unfortunately, they did not explain how they obtained this conformation. These adducts contain a single bond between the heterocyclic ring and the cyclic core of **1**, while in the original paper introducing this method[7] all examples contain a dihydroisoxazole ring directly linked to the parent cyclic hydrocarbon, thus reducing the inherent flexibility. Finally, only one of two formed diastereomers was investigated by NMR and no comparison with the respective (a*R*)-MBCC was performed, as should be done in Mosher-like methods. In essence, their determination of the absolute configuration relies on several NOE signals observed, while in the present study a sound chemical correlation is performed. It should be noted that recently a very informative critique of the Mosher method has been published, which also applies to related methods.[15]

1 G. M. König and A. D. Wright, *J. Org. Chem*., 1997, **62**, 3837.
2 K. Nabeta, K. Yamamoto, M. Hashimoto, H. Koshino, K. Funatsuki and K. Katoh, *Chem. Commun*., 1998, 1485.
3 U. Warmers, K. Wihstutz, N. Bülow, C. Fricke and W. A. König, *Phytochemistry*, 1998, **48**, 1723.
4 U. Warmers and W. A. König, *Phytochemistry*, 1999, **52**, 1519.
5 S. Schulz, C. Messer and K. Dettner, *Tetrahedron Lett*., 1997, **53**, 2077.
6 A. Arnone, G. Nasini and O. V. de Pava, *J. Chem. Soc., Perkin Trans. 1*, 1993, 2723.
7 H. Fukui, Y. Fukushi and S. Tahara, *Tetrahedron Lett*., 1999, **40**, 325.
8 K. Nabeta, M. Yamamoto, H. Koshino, H. Fukui, Y. Fukushi and S. Tahara, *Biosci., Biotechnol., Biochem*., 1999, **63**, 1772.
9 G. Mehta and K. Srinivas, *Tetrahedron Lett*., 1999, **40**, 4877.
10 J. Wolinsky, H. Wolf and T. Gibson, *J. Org. Chem*., 1963, **28**, 274.
11 J. Wolinsky and E. J. Eustache, *J. Org. Chem*., 1972, **37**, 3376.
12 P. Jones, I. Dix, S. Fietz-Razavian and S. Schulz, unpublished results.
13 G. Mehta and K. Srinivas, *Synlett*, 1999, **5**, 555.
14 N. A. Petasis and E. I. Bzowej, *J. Am. Chem. Soc*., 1990, **112**, 6392.
15 J. M. Seco, E. Quiñoá and R. Riguera, *Tetrahedron: Asymmetry*, 2000, **11**, 2781.

CHEMCOMM
Communication
www.rsc.org/chemcomm

Biosynthesis of the vancomycin group of antibiotics: characterisation of a type III polyketide synthase in the pathway to (*S*)-3,5-dihydroxyphenylglycine†

Tsung-Lin Li, Oliver W. Choroba, Hui Hong, Dudley H. Williams and Jonathan B. Spencer*

Cambridge Centre for Molecular Recognition, Department of Chemistry, Cambridge University, Lensfield Road, Cambridge, UK CB2 1EW. E-mail: jbs20@cam.ac.uk; Fax: 44 1223 336362; Tel: 44 1223 331696

Received (in Cambridge, UK) 23rd July 2001, Accepted 30th August 2001
First published as an Advance Article on the web 2nd October 2001

3,5-dihydroxyphenylacetate, a precursor for the non-proteinogenic amino acid 3,5-dihydroxyphenylglycine occurring in glycopeptide antibiotics, is determined to be catalysed by a type III polyketide synthase using malonyl-CoA as a starter unit.

Vancomycin **1** (Fig. 1) is currently the antibiotic of last resort against methicillin-resistant *Staphylococcus aureus* (MRSA).[1] We are investigating the biosynthetic pathway of chloroeremomycin **2**, another important member of this family of glycopeptide antibiotics.

A number of unusual amino acids, such as (*S*)-4-hydroxyphenylglycine (4-HPG) and (*S*)-3,5-dihydroxyphenylglycine (3,5-DHPG) are found in glycopeptide antibiotics. Recently the pathway to 4-HPG from tyrosine has been elucidated[2–4] and the pivotal enzyme, 4-hydroxymandelic acid‡ synthase determined to be a novel dioxygenase.[2] In this paper we report the identification of the protein coded for by *orf*27 from the chloroeremomycin gene cluster, now named 3,5-dihydroxyphenylacetate synthase (DhpaS), as the first enzyme involved in the pathway to 3,5-DHPG. DhpaS catalyses the formation of 3,5-dihydroxyphenylacetate (3,5-DHPA) from four malonyl-CoA units and is only the second type III polyketide synthase fully characterised in bacteria.

Previous feeding studies using vancomycin-producing organisms and labeled acetate showed that the carbon skeleton of 3,5-DHPG was of polyketide origin.[5] Recently we have shown the involvement of 3,5-DHPA in the pathway to this amino acid by feeding experiments using the chloroeremomycin-producing strain *Amycolatopsis orientalis*. NMR studies showed that ^{13}C-labeled 3,5-DHPA was incorporated into the 3,5-DHPG moiety of the isolated antibiotic.[6] Homology searches of the open reading frames (*orfs*) from the biosynthetic gene cluster of chloroeremomycin[7] revealed that *orf*27 had homology (37% similarity, 28% identity) to a group of plant chalcone synthases which provide precursors for flavonoids.[8] This family of small discrete enzymes have been called type III polyketide synthases. They differ from other polyketide synthases by not possessing a phosphopantetheine prothetic group. Chalcone synthases typically use aromatic coenzyme A esters, such as coumaryl-CoA, as starter units and malonyl-CoA as the chain extender unit. Based on these findings we felt that ORF27 might catalyse the formation of 3,5-DHPA **4** from an acetyl-CoA starter unit and three malonyl-CoA extender units. Hydroxylation at the benzylic position of **4** would lead to 3,5-dihydroxymandelic acid **5**, oxidation to 3,5-dihydroxyphenylglyoxylic acid **6** and subsequent transamination should then furnish 3,5-dihydroxyphenylglycine **7** (Scheme 1).

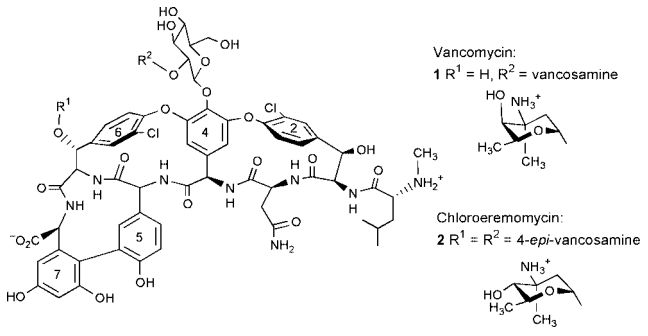

Fig. 1 Structures of vancomycin and chloroeremomycin.

To test this hypothesis *orf*27 from the chloroeremomycin gene cluster was amplified by polymerase chain reaction using the cosmid pCZA361. Ligation into pET28 (Novagen) and transformation into *E. coli* BL21(DE3) yielded the *N*-terminal His_6-tagged protein which was purified using Ni^{2+}-NTA agarose. Electrospray mass spectrometry of the purified protein confirmed the right molecular weight for the protein without a phosphopantheine arm, therefore being consistent with a type III polyketide synthase. The enzyme was incubated in Hepes buffer (50 mM, pH 7.2) containing DTT (1,4-sulfanylbutane-2,3-diol,1.0 mM), acetyl-CoA (3.3 mM) and malonyl-CoA (10 mM) for 2 h. The enzymic mixture was acidified and extracted with ethyl acetate, silylated and analyzed by GC-CI-MS (NH_3 as reaction gas). The GC trace revealed a new peak when compared to a control reaction (Fig. 2). This compound was identified as the tris(trimethylsilyl) derivative of 3,5-dihydroxyphenylacetate by comparison with an authentic sample (identical retention time and fragmentation pattern) (Fig. 3). This proves that ORF27 is a type III polyketide synthase that catalyses the first step in the pathway to 3,5-DHPG.

The mechanism in which the polyketide chain cyclises to form 3,5-DHPA is interesting since it predicts that, if acetyl-CoA is the starter unit, an anion must be formed from a methyl ketone **8** (Scheme 2, A). In the vast majority of polyketides the folding pattern arises from an anion generated at a more acidic methylene position. It has recently been reported that malonyl-CoA serves as the starter unit for the formation of the polyketide 1,3,6,8-tetrahydroxynaphthalene.[9] If malonyl-CoA was used as the starter unit for 3,5-DHPA then the anion of the methyl ketone could be generated by decarboxylation of **9**,[10] which would be energetically more favorable than deprotonation of the

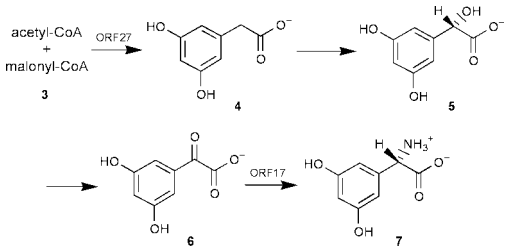

Scheme 1 Proposed pathway for 3,5-dihydroxyphenylglycine formation.

† Electronic supplementary information (ESI) available: electrospray mass spectrum of DhpaS. See http://www.rsc.org/suppdata/cc/b1/b106638b/

 DOI: 10.1039/b106638b

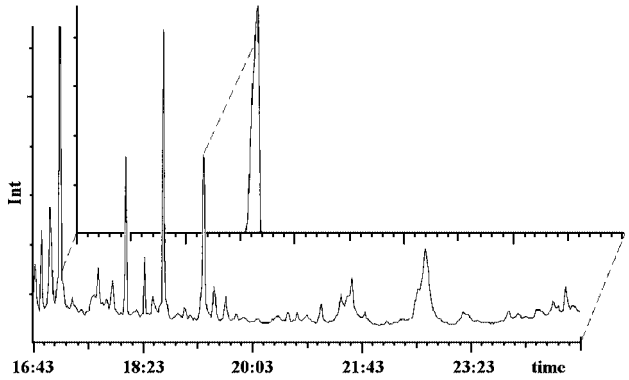

Fig. 2 GC trace on an enzymic reaction of malonyl-CoA in the presence of ORF27 (standard of 1-[^{13}C]-3,5-DHPA in the background).

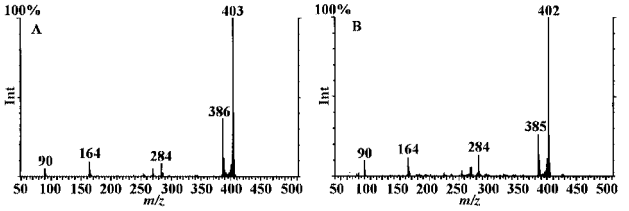

Fig. 3 (A) CI-MS spectrum of [1-^{13}C]-3,5-DHPA standard silylated (note that the standard has one ^{13}C atom and therefore gives a molecular ion one mass higher than the enzymic sample). (B) CI-MS spectrum of the peak at 19.2 minutes from the enzymic reaction (Fig. 2).

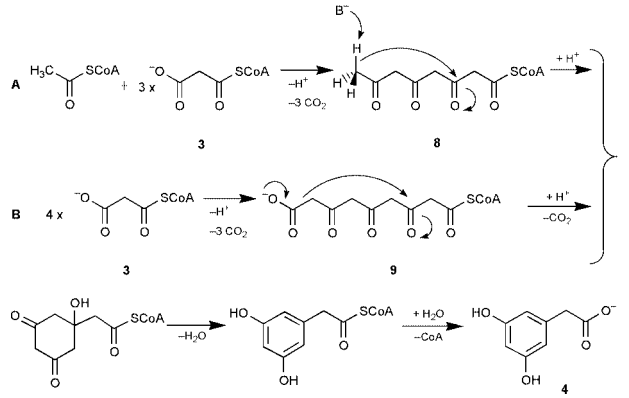

Scheme 2 Formation of 3,5-dihydroxyphenylacetic acid using either acetyl-CoA and malonyl-CoA (A) or malonyl-CoA only (B).

methyl ketone (Scheme 2, B). To determine the origin of the starter unit and investigate these two possible reaction mechanisms, labeled malonyl-CoA (formed *in situ* by transfer of CoA from acetoacetyl-CoA to [1,2,3-$^{13}C_3$]malonic acid using succinyl-CoA transferase[11]) was incubated with DhpaS in the presence of unlabeled acetyl-CoA (Scheme 3). The mass spectrum of the isolated 3,5-DHPA gives only an $[M + 8]^+$ peak, clearly showing that all the carbon atoms come from malonyl-CoA (Fig. 4).

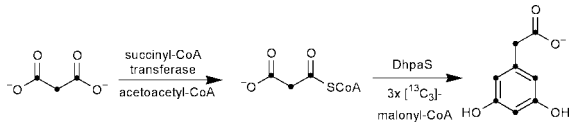

Scheme 3 *In situ* formation of [1,2,3-$^{13}C_3$]malonyl-CoA and its utilisation by DhpaS to form labeled 3,5-DHPA (^{13}C represented as •).

The family of chalcone synthases are relatively small proteins that appear to have only one active site.[12] This is in contrast to type I polyketide synthases which are typically very large multifunctional proteins with a separate active site for each

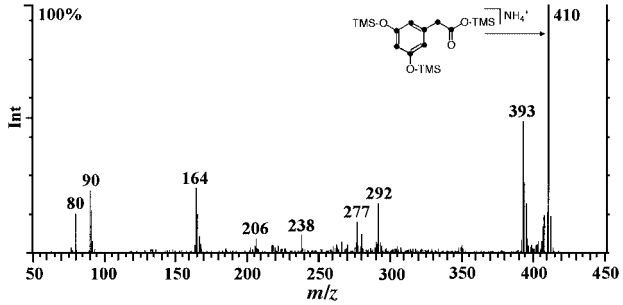

Fig. 4 Mass spectrum of labeled 3,5-DHPA formed by enzymic reaction of dihydroxyphenylacetate synthase with [1,2,3-$^{13}C_3$]malonyl-CoA in the presence of unlabeled acetyl-CoA.

reaction that they catalyse. It is therefore tempting to propose that the cyclisation to form 3,5-DHPA might be catalyzed by the same amino acids that carry out the Claisen condensation of malonyl-CoA with the growing polyketone chain since the two reactions are very similar.

In summary, we have shown that ORF27 from the chloroeremomycin gene cluster is an unusual type III polyketide synthase catalyzing the formation of 3,5-dihydroxyphenylacetic acid. Labeling experiments prove that malonyl-CoA acts not only as the chain-extender unit but also as the starter unit. This leads us to propose that cyclisation to form 3,5-dihydroxyphenylacetic acid is initiated by decarboxylation of the polyketone chain **9**.[13] This study determines that the biosynthesis of 3,5-dihydroxyphenylglycine begins with the formation of 3,5-dihydroxyphenylacetic acid or its CoA-ester, and therefore affords a new insight into how the biosynthesis of these important antibiotics occurs.

We thank the Royal Society for a Research Fellowship (J. B. S.), the Ministry of Education, Taiwan, for a Research Fellowship (T.-L. L.), the European Union for a TMR Marie-Curie Research Fellowship (O. W. C.), St. John's College, Cambridge for a Junior Research Fellowship (O. W. C.), and the BBSRC for financial support.

Notes and references

‡ The IUPAC name for mandelic acid is phenylhydroxyacetic acid.

1 M. Foldes, R. Monro, T. C. Sorell, S. Shankar and M. Toohey, *J. Antimicrob. Chemother.*, 1983, **11**, 21.
2 O. W. Choroba, D. H. Williams and J. B. Spencer, *J. Am. Chem. Soc.*, 2000, **122**, 5389.
3 T.-L. Li, O. W. Choroba, E. H. Charles, A. M. Sandercock, D. H. Williams and J. B. Spencer, *Chem. Commun.*, 2001, **1**, 752.
4 B. K. Hubbard, M. G. Thomas and C. T. Walsh, *Chem. Biol.*, 2000, **7**, 931.
5 S. J. Hammond, M. P. Williamson, D. H. Williams, L. D. Boeck and G. G. Marconi, *J. Chem. Soc., Chem. Commun.*, 1982, 344.
6 A. M. Sandercock, E. H. Charles, W. Scaife, P. N. Kirkpatrick, S. W. O'Brien, E. A. Papageorgiou, J. B. Spencer and D. H. Williams, *Chem. Commun.*, 2001, 1252.
7 A. M. A. van Wageningen, P. N. Kirkpatrick, D. H. Williams, B. R. Harris, J. K. Kershaw, N. J. Lennard, M. Jones, S. J. M. Jones and P. J. Solenberg, *Chem. Biol.*, 1998, **5**, 155.
8 J. Schroder, *Nature Struct. Biol.*, 1999, **6**, 714.
9 N. Funa, Y. Ohnishi, I. Fujii, M. Shibuya, Y. Ebizuka and S. Horinouchi, *Nature*, 1999, **400**, 897.
10 Alternatively, decarboxylation could occur after cyclisation which would also be a more attractive pathway than using acetyl-CoA as the starter unit.
11 P. M. Jordan, J. B. Spencer and D. L. Corina, *J. Chem. Soc., Chem. Commun.*, 1986, 911.
12 J.-L. Ferrer, J. M. Jez, M. E. Bowman, R. A. Dixon and J. P. Noel, *Nature Struct. Biol.*, 1999, **6**, 775.
13 The labeling experiments would also be consistent with the first malonyl unit loaded onto the enzyme being decarboxylated to give an acetyl starter unit. However, this reaction pathway seems unlikely since acetyl-CoA is not accepted at all by the enzyme.

Typeset and printed by Black Bear Press Limited, Cambridge, England

CHEMCOMM
Feature Article
www.rsc.org/chemcomm

Recent advances in solventless organic reactions: towards benign synthesis with remarkable versatility

Gareth W. V. Cave,[a] Colin L. Raston*[b] and Janet L. Scott[a]

[a] *Centre for Green Chemistry, School of Chemistry, Monash University, Clayton, Melbourne, Victoria 3800, Australia*
[b] *School of Chemistry, University of Leeds, Leeds, UK LS2 9JT. E-mail: c.l.raston@chem.leeds.ac.uk*

Received (in Cambridge, UK) 24th July 2001, Accepted 18th September 2001
First published as an Advance Article on the web 17th October 2001

A paradigm shift away from using solvents in organic synthesis as solventless reactions can lead to improved outcomes, and more benign synthetic procedures, in for example aldol condensation reactions, sequential aldol and Michael addition reactions *en route* to Kröhnke type pyridines, reactions leading to 3-carboxycoumarins, benzylidenes, 4-aryl-1,4-dihydropyridines and 2-aryl-1,2,3,4-tetrahydroquinazolines, and oligomerisation reactions for the synthesis of cavitands; kinetic considerations for the reaction of two solids can only be explained if a eutectic melt is formed during the reaction.

Dr Gareth Cave is a postdoctoral Research Fellow at the Centre for Green Chemistry, Monash University. Before moving to Australia he completed a PhD under the supervision of Dr Johnathan Rourke at the University of Warwick (1999), investigating the cyclometallation properties of platinum and palladium metals, whereupon he started postdoctoral studies at Monash University under the direction of Professor Colin Raston (2000). Research interests cover aspects of cyclometallation, metallomesogens, supramolecular and Green Chemistry.

Professor Colin Raston holds the Chair of Inorganic Chemistry, School of Chemistry, University of Leeds. He completed a PhD under the guidance of Professor Allan White, and after postdoctoral studies with Professor Michael Lappert at the University of Sussex, he was appointed Lecturer at the University of Western Australia (1981) then to Chairs of Chemistry at Griffith University (1988), being awarded a DSc there in 1993, and Monash University (1995), as an ARC Senior Research Fellow and ARC Special Investigator followed by the move to the University of Leeds early 2001. Research interests cover aspects of main group, supramolecular and Green Chemistry, having helped to establish the Centre for Green Chemistry at Monash University.

Dr Janet Scott is a lecturer and a Deputy Director of the Centre for Green Chemistry, Monash University. She completed a PhD under the supervision of Professors Luigi Nassimbeni and Mino Caira at the University of Cape Town where she also held the position of Lecturer until 1995. She was appointed Research and Development Manager at Fine Chemicals Corporation Pty. (Ltd) for the period 1996–1998 whereafter she moved to Australia and the Centre for Green Chemistry at Monash University, Melbourne, Australia. Her research interests centre around Green Chemistry and include the use and understanding of solvent-free reactions with the goal of attaining greater reaction control.

Introduction

Sustainability is increasingly an important issue in the wider context dealing with population, health, the environment, energy, technology, renewable resources, and, in the sciences, as an integral part of the rapidly emerging field called Green Chemistry.[1,2] This is a multidisciplinary field, requiring integrated study in the chemical, biological and physical sciences as well as many aspects of engineering. Even nanotechnology is important in Green Chemistry, providing a way of dematerialising society while providing the benefits of technology.[3] The twelve principles of Green Chemistry, as defined by Anastas and Warner,[1] and generally accepted internationally, cover complex issues including waste minimisation, reduction in energy usage, and the use of renewable resources rather than depleting natural resources such as oil, coal and gas. Biocatalysis is an important area of Green Chemistry providing a means of converting biomass, a renewable resource, into commodity chemicals.[1–3] In the chemical sciences there is a need to develop benign synthetic pathways which, in addition to being high yielding (historically the most important measure of the success of a reaction), are simple and exhibit high atom efficiency, hence a reduced number of steps and no waste, are safe, and are environmentally acceptable.[2] Another measure of the 'greenness' of a reaction is the *E* factor (= waste (kg)/1 kg product),[4] which, for pharmaceuticals, is typically >100. The emergence of Green Chemistry has resulted in a paradigm shift in the way chemists develop processes and products, and requires the development of a Green Chemistry toolbox.

Removing organic solvents in chemical synthesis is important in the drive towards benign chemical technologies. Organic solvents are high on the list of toxic or otherwise damaging compounds because of the large volumes used in industry, and difficulties in containing volatile compounds. Replacement reaction media include ionic liquids[5–7] (which have extremely low vapour pressure and can be recycled), liquid and supercritical CO_2,[8] water (often at high temperature under microwave irradiation),[1,9,10] and polyethylene and polypropylene glycol[11] (Fig. 1). Another alternative is not to use a reaction medium, the so called solventless reactions, which is the main focus of this article.[7,11–20] The choice of solventless or specific non-organic solvent reaction medium will depend on several issues, including selectivity, stereochemistry, yield, waste, viscosity, ease of recycling, energy usage, ease of isolation of product(s), competing reactions, and heat of reaction. In using a reaction medium, there are many choices within each system, for example using ionic liquids with the appropriate hydrophobic–hydrophilic balance, and varying the density of liquid and supercritical CO_2, which can affect the stereochemical outcome of addition reactions.[8]

Advantages in using solventless reactions, particularly those described herein, relative to using organic or other reaction

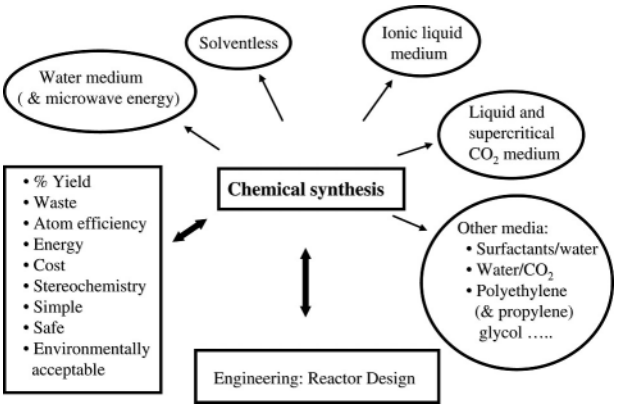

Fig. 1 Non-organic solvent reaction medium linking into reactor design.

media include: (i) there is no reaction medium to collect, purify and recycle, (ii) the compounds formed are often sufficiently pure to circumvent extensive purification using chromatography, and indeed in some cases the need for recrystallisation, (iii) sequential solventless reactions are possible in high yielding systems, (iv) the reactions can be rapid, often reaching substantial completion in several minutes compared to hours in organic solvents, (v) there is often no need for specialised equipment (see below), (vi) energy usage can be much lower, (vii) the need for pre-formed salts and metal–metalloid complexes may often be dispensed with, (viii) functional group protection–deprotection can be avoided, (ix) lower capital outlay for equipment in setting up industrial processes, and (x) considerable batch size reduction and processing cost savings are achievable such that such solvent-free protocols are not only more environmentally benign but are also more economically feasible. This is one of the original considerations in bringing Green Chemistry to the fore.[1]

There are some disadvantages in solventless reactions but these are solvable using developments in engineering reactor technology[21] (Fig. 1). Objections to the use of solventless reaction conditions include the formation of hot spots and the possibility of runaway reactions. Instead of operating in the old paradigm, notably the use of a reaction medium or solvent as a heat sink or heat transfer agent, consideration could be given to applying developments in reactor design either for continuous flow or batch systems. Our recent paper on the solventless aldol condensation reaction,[15] attracted attention in *Chem. Brit.* (June 2000, p. 18) with a subsequent letter to the editor drawing attention to the potential for run away reactions (January 2001, p. 14). Clearly measurement of heat of reaction in solventless systems is important as is effective heat dissipation. If highly exothermic reactions are identified which are otherwise suited to solventless conditions the problem could be addressed through advanced reactor design. Another objection can be difficulties in handling solid or highly viscous material. Again this can be overcome by advances in engineering and innovative reactor design. Solventless reactions may be more appropriate for small volume commodity chemicals rather than high throughput although it is possible to envisage extrusion type continuous reactors. Though the concept of grinding (including ultra high energy grinding) to promote chemical reactions has been known for some time, there have been few reports of applications of high intensity grinding in organic synthesis.[22–24]

Historically organic synthesis was carried out in organic solvents even in the absence of apparent reasons to do so (other than heat transfer considerations). In moving towards sustainable technologies the issue now becomes either carrying out solventless reactions, or using alternative reaction media, or (for a multi-step synthesis) a combination of these. In covering recent advances in solventless reactions, we will compare (where information is available) reactions in organic solvents and in other media. We initially entered Green Chemistry as a challenge to establish solventless procedures for reactions which traditionally play a pivotal role in organic synthesis. We also targeted solventless reactions, and reactions in ionic liquids, for preparing building molecules which feature extensively in supramolecular chemistry leading to advances in materials chemistry and nano-technology. This is based on the premise that any developments in supramolecular chemistry are more likely to have downstream applications if the building molecules are readily available using benign synthetic protocols. Specific reactions studied include solventless aldol reactions,[15] sequential aldol and Michael addition reactions as a route to symmetrical and unsymmetrical 1,5-diketones leading to Kröhnke type pyridines,[17–19] synthesis of 3-carboxycoumarins (and a comparison with using an aqueous slurry),[16] oligomerisation reactions affording cavitands, notably cyclotriveratrylene and related compounds (and a comparison with an ionic liquid reaction medium),[7] calix[4]resorcinarenes,[11] and 4-substituted-1,4-dihydropyridine compounds such as the commonly used cardiovascular drug Felodipine.[25] All these reactions have a common theme of dehydration, and most exhibit high atom efficiency. We note that Kröhnke type pyridines and cavitands have 'high technology' applications, for example in devices, materials chemistry, and liquid crystals, and ultimately in developing sustainable technologies, Fig. 2, but this is not

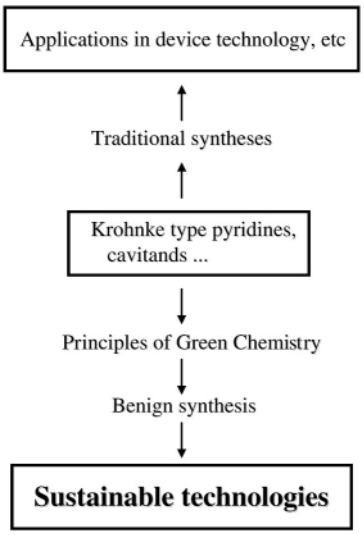

Fig. 2 Relationship between compounds with materials applications and sustainable technologies.

matched by their syntheses. We have also studied the kinetics of these solventless reactions, to help understand the chemistry at the molecular level which is important in developing tools for Green Chemistry.

Chemoselective, aldol condensation reactions

The aldol reaction, the formation of a β-hydroxycarbonyl compound from two carbonyl compounds with at least one being enolisable, which on dehydration becomes an α,β-unsaturated carbonyl compound, can be carried out by simply grinding together solid (or liquid) aldehydes and ketones in the presence of solid NaOH followed by washing with a dilute aqueous acid solution, Scheme 1.[15] No preformed enolates are used, no heating or cooling is required, no organic solvent is utilised in the reaction (unless product recrystallisation is required), and the only waste produced is a small amount of acidic aqueous waste. Single crossed aldol condensation products are produced in high yield even in reactions where a mixture of products is possible. Solvent free aldol condensation reactions of benzaldehyde and acetophenone derivatives have been reported by Toda *et al.*,[26] although in all cases the

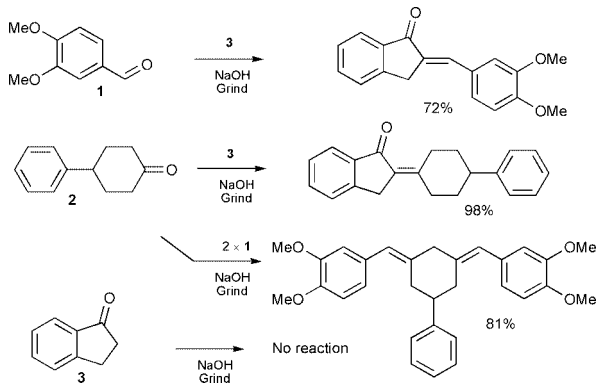

Scheme 1

aldehydes are devoid of α-hydrogen atoms, thereby ensuring that only a single aldol condensation product is possible.

Interestingly, the first reports of aldol reactions utilised underivatised ketones and aldehydes with simple acid[27] or base[28] catalysis. The trend has been towards reactions using pre-formed enolates, which serve both to increase the driving force of the reaction and to ensure that the desired chemoselectivity is achieved. Numerous elegant procedures have been developed to this end[29] but they frequently require the use of reagents which are themselves somewhat noxious and result in the generation of significant quantities of waste containing metal salts such as Li^+ salts. Some routes use enol esters or silyl enol ethers but these are poor performers with regard to atom efficiency and often require the use of potentially polluting solvents and low temperatures.

In highlighting the solventless approach, the solids veratraldehyde, **1**, 4-phenylcyclohexanone, **2**, and indan-1-one, **3**, are reacted in various combinations affording aldol condensation products, with a high degree of conversion and a single major product, Scheme 1.[15] In the case of **1** and **3** a single condensation product is obtained as expected, since the aldehyde bears no α-hydrogen atoms and cannot therefore act as a carbon nucleophile. Compounds **1** and **2** may yield two products (a mono- and bis-adduct). The combination of **2** and **3** is less straightforward and a number of possible products may be envisioned including crossed aldol products with either ketone acting as a nucleophile, self condensation products of the ketones and a mixture of these two. Under solventless conditions, only one crossed aldol product is isolated. In stark contrast, for the reaction of compounds **2** and **3** in solution, without the use of a pre-formed enolate, a complex mixture of products results.[30] Attempted self-condensation of **3** under solventless conditions fails to give the condensation product.

Where reaction occurs, a eutectic mixture, with melting point lower than the ambient temperature, results and the reaction mixture is in fact a *mutual solution* of the carbonyl compounds reacting together to yield a solid product which separates from this solution as the reaction proceeds.[20] This observation may provide insight into the remarkable selectivity of the ketone–ketone reaction involving **2** and **3** under these conditions, with the product arising from attack by a carbanion formed by indan-1-one on the electrophilic carbonyl carbon of 4-phenylcyclohexanone followed by spontaneous dehydration and sequestration of the product as a separate solid phase.

If dehydration occurs immediately and is *irreversible under the conditions of the reaction* the product is trapped and no equilibration occurs. The solid product appears to be insoluble in the reaction mixture and is effectively removed by this change in phase driving the reaction rapidly to completion. Stabilisation of the indanon-1-one carbanion intermediate leads to higher acidity of the α-hydrogen atoms and, as no equilibration is possible (as the product is removed from the 'reaction solution'), no products due to attack of 4-phenylcyclohexanone carbanions are noted.

Adopting the principles of Green Chemistry for the aldol condensation reaction, has resulted in establishing a new benchmark for minimising waste in these reactions while allowing for a greater degree of chemoselectivity than in solution. These are distinct advantages over the classical reactions in organic solvent. Moreover, intermediates formed by grinding together two solids and the base catalyst may be stored for months without impact on product quality, and this issue alone may be attractive in industrial applications of the solventless aldol reaction.

3-Carboxycoumarins

These compounds, **7**, can be readily prepared from 2-hydroxybenzaldehydes, **4**, and Meldrum's acid, **5**, by a room temperature reaction involving two solids or a solid and a liquid with a catalytic amount of ammonium acetate, Scheme 2.[16] The

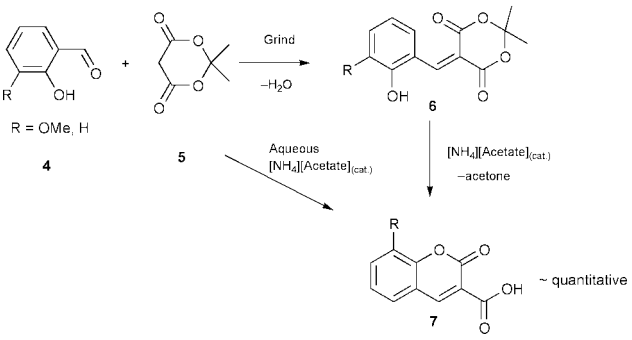

Scheme 2

yields of **7** are quantitative, with no heating, and no use of organic solvent, with purification achieved by an aqueous wash. Alternatively the reactions can be carried out as slurries in aqueous solutions of ammonium acetate, despite the extremely low solubility of Meldrum's acid, **5**. As for the solventless reaction, the ammonium acetate solution can be reused without affecting product quality. The Knoevenagel reaction product (the benzylidene intermediate, **6**) can be isolated from a reaction mixture devoid of catalyst and further reacted, in the presence of the catalyst, either as a solid or in aqueous slurry to effect ring closure to the coumarin. Remarkably, the reaction of **4** and **5** to produce **7** proceeds *more* rapidly when carried out under aqueous slurry conditions. It is generally accepted that the 1,2-elimination in the Knoevenagel reaction is inhibited in protic solvents[31] and this provides a clue to an increase in the rate of the reactions in aqueous slurries. If the 1,2-elimination is inhibited and hydrolysis of Meldrum's acid and ring closure proceeds once the β-hydroxydiketone is formed, *i.e.* before or concomitantly with 1,2-elimination of water, then the longer lived the flexible β-hydroxydiketone, the more favourable are the conditions for coumarin formation and the more rapid the reaction.[16]

3-Carboxycoumarins represent an important class of biologically active compounds, and their synthesis is now more convenient, clean and efficient. There is no need for the use of polar aprotic solvents such as DMF or solvents in general, no heating is required, and minimal waste is generated.[16] The procedure becomes almost facile in its simplicity and equipment use is limited to vessels for stirring and suitable filtration devices. The Knoevenagel reaction of active methylene compounds with 2-hydroxybenzaldehdes has been extensively used in the first step in the synthesis of 3-carboxycoumarins. Knoevenagel himself described the solution phase condensation of 2-hydroxybenzaldehydes with malonic acid more than 100 years ago.[32] Numerous routes to 3-substituted coumarins have been published, including the use of noxious compounds such as $POCl_3$,[33] bases such as piperidine,[34] solvents such as DMF,[35] and, recently, a low-yielding 'solid phase' synthesis, utilising

ethyl malonate tethered to a Wang resin and suspended in pyridine.[36] A more benign method is a one pot microwave mediated synthesis which entails the use of a solid catalyst,[37] but this is not solvent free, unlike in our methods, Scheme 2, requiring removal of the product from the catalyst using a solvent, followed by extensive use of solvent for chromatographic purification.[37]

Synthesis of Kröhnke type pyridines

Despite the continual research and applications surrounding Kröhnke type pyridines and related compounds, the methodologies used to synthesise these compounds have changed little since a review article by Kröhnke in 1976,[38] which involves volatile organic solvents and displays only moderate to low yields with low atom efficiency. In applying the principles of Green Chemistry a new and indeed more versatile protocol has been established.[17–19] The aldol condensation of an enolisable ketone and a benzaldehyde followed by Michael addition of the enone, **8**, with a second enolisable ketone, both steps under solvent free conditions involving grinding with solid NaOH, leads to the quantitative formation of a 1,5-diketone, **9**, either symmetrical or unsymmetrical with respect to the aromatic rings, depending on the ratio of reactants and order of addition.[17–19] A Kröhnke type pyridine, either a terpyridyl **10**, or a bipyridyl or pyridine **11**, is then readily formed in high yield *via* a double condensation in the presence of ammonium acetate in acetic acid. Some of the types of compounds prepared using this new approach are shown in Scheme 3. Overall, this

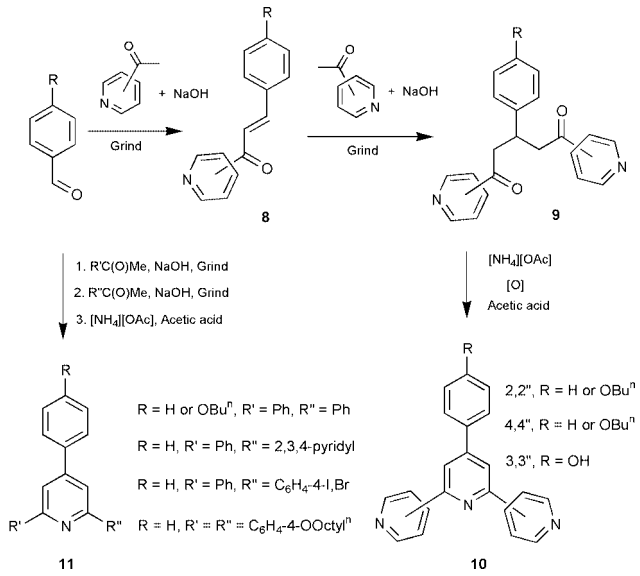

Scheme 3

solventless approach coupled with the ring closure in acetic acid allows access to a diverse range of oligopyridyls, including bipyridyls and terpyridyls (symmetrical and unsymetrical) which in many cases are not accessible using traditional methods, or are accessible only in low yields. Thus the Green Chemistry approach not only reduces the use of organic solvents and minimises other waste,[1] it allows access to new classes of compounds and associated applications. It is noteworthy that the new method is simple, occurs under mild conditions (improved energy usage), and has inherently lower costs.[18] In keeping with our 'green' approach we have also synthesised all non-commercially available starting alkoxybenzaldehydes and alkoxyacetophenones for **10** and **11** using recyclable polypropylene glycol as a low vapour pressure reaction medium.[11]

It is noteworthy that Kröhnke type pyridines and other substituted pyridines, including the related terpyridines, with their π-stacking ability, directional H-bonding and coordination properties, are prominent building blocks in both organic and inorganic supramolecular chemistry.[19,39–41] They also have luminescence properties,[42] with applications in liquid crystals,[43] photosensitisers,[44] and biochemical DNA binding reaction mechanisms.[45] Studies into the possible medical applications of substituted terpyridines have shown promising results, attributed to their ability to form complexes with metals, although the toxicity of previously synthesised materials has hampered clinical trials.[46] The significance of being able to synthesise such substituted terpyridines for use in pharmacological testing alone is reflected in the increasing number of associated international patents in recent years.[47]

The solventless reactions, Scheme 3, occur for combinations of liquids, liquids and solids, and solids. In a typical experiment, benzaldhyde and acetophenone are both colourless liquids at room temperature and upon addition of the NaOH the liquids immediately turn yellow indicating the formation of the enolate. By aggregating the reaction mixture in a mortar and pestle, the viscosity rapidly increases to form a tacky solid after *ca.* 5 min of constant mixing, which hardens after *ca.* 30 minutes as the solid aldol product, **8**. During the reaction between two solids the reaction mixture undergoes a phase transition into a eutectic melt. Grinding the solid starting materials in the absence of base, this eutectic phase can be reproduced, however, there is no observed conversion to the aldol product.

A conventional Kröhnke synthesis proceeds by treating an unsaturated ketone with the pyridinium salt formed by reacting halogenated-methyl ketone with pyridine, Scheme 4, to produce

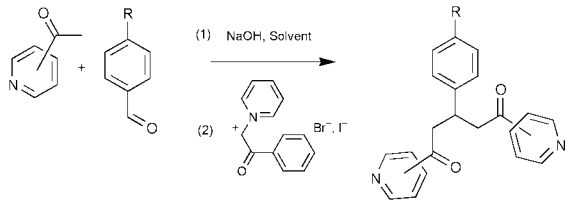

Scheme 4

the Michael addition product **9**. Although this step is reported to be high yielding, the byproducts of the reaction generate significant waste and the reagents are expensive (see below). The direct reaction of the enone with an enolisable aryl methyl ketone in a basic solution proceeds to the 1,5-diketone,[48] thus eliminating the preliminary pyridinium salt formation. In the case of unsymmetrical compounds, there is no need to isolate the intermediate enone which is essentially formed quantitatively, thereby eliminating an intermediate purification step, and without the need to add more NaOH.

When the solvent based methods were adopted in an attempt to prepare **10**, 4,4″, R = *O*-alkyl, only the cyclohexyl product

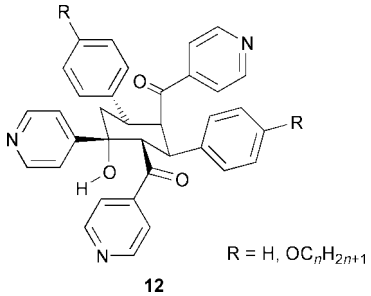

12

12 could be isolated from the complex reaction mixture which was devoid of target molecules. A recent paper describes the synthesis of **10**, 4,4″, R = H, under somewhat harsh conditions with a moderate 6% overall yield,[49] compared with 84% using the solventless approach.[17–19]

After the final ring closure reaction in acetic acid, addition of water results in precipitation of the product which can be collected and washed with ethanol. Although this stage of the

synthesis requires the use of a solvent, it should be noted that the low vapor-pressure of the acetic acid allows the use of an air condenser during the reflux, following the workup process the acetic acid can be efficiently regenerated and used as a batch process. The chosen solvent is also a naturally renewable source in alignment with the principals of Green Chemistry. Typically the traditional methods to prepare Kröhnke type pyridines generates as much as 29 times more solid waste than the 'greener' route to the same compound.[50] Moreover, even for a compound available in modest yield using traditional methods,[50] the 'greener' route is estimated to be 600% more cost effective, not taking into account the cost of energy usage and waste disposal, which is rapidly escalating. Then there is the new chemistry which is accessible, for example the synthesis of the complex molecules **13** and **14**.[50]

By utilising the above techniques, we have synthesised several novel building blocks, including **13** and **14**,[50] which have potential as supramolecular synthons, polymeric monomers, coordination ligands, mono- and di-cyclometallation ligands, and as molecules with pharmacological properties. The added halogen functionality on the terminal carbon of the alkyl chains in compounds also allows for great scope. As an example of the utility of the new pyridines now available in supramolecular chemistry, compound **10**, 4,4″, R = *O*-Octyl^n, forms hetero-multi-component molecular capsules with *C*-methylcalix[4]resorcinarene, Scheme 5.[19] The calix[4]resorcinarene is also readily prepared in high yield as the cavitand C_{4v} isomer under solvent free conditions[19] which dispenses with the need for using large volumes of acid and solvent (see below).[51] Overall, supramolecular chemistry is part of the drive towards sustainable technologies in nano-chemistry and beyond. Molecular capsules in general find applications in clean chemical synthesis,[52] drug delivery, materials and separation sciences,[53] and they are structurally related to components in biological systems such as those in viruses.[54]

The molecular capsules contain microenvironments of solvent, either four toluene molecules, or if a trace of diethyl ether is present, two diethyl ether molecules and two toluene molecules, which has implications in separation technology. Both capsules have been structurally authenticated, with the structure of the latter shown in Fig. 3, and are held together by

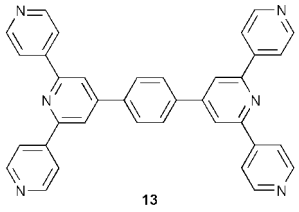

13

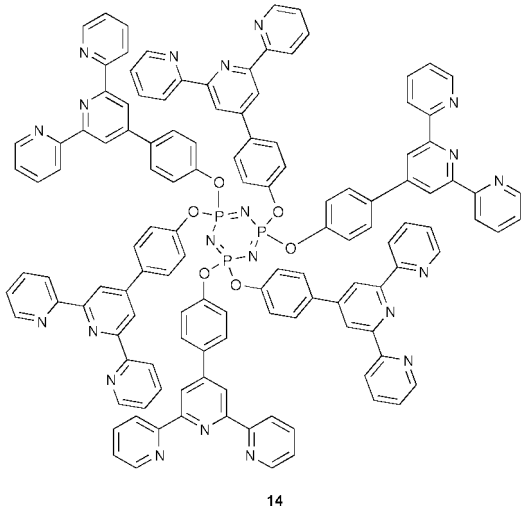

14

a total of 8 N···HO hydrogen bonds, and π-stacking associated with pairs of terpyridines.

Cavitands: calix[4]resorcinarenes, cyclotriveratrylene (CTV) and related molecules

The synthesis of *calix[4]resorcinarenes* was first reported in the late 19th century by Baeyer[55] and in spite of the increased interest in such compounds the synthetic methodology used has changed little. This typically involves heating resorcinol and the appropriate aldehyde to reflux for hours to days in a mixture of mineral acid and alcohol (usually a 2 : 2 : 1 ratio of ethanol, water

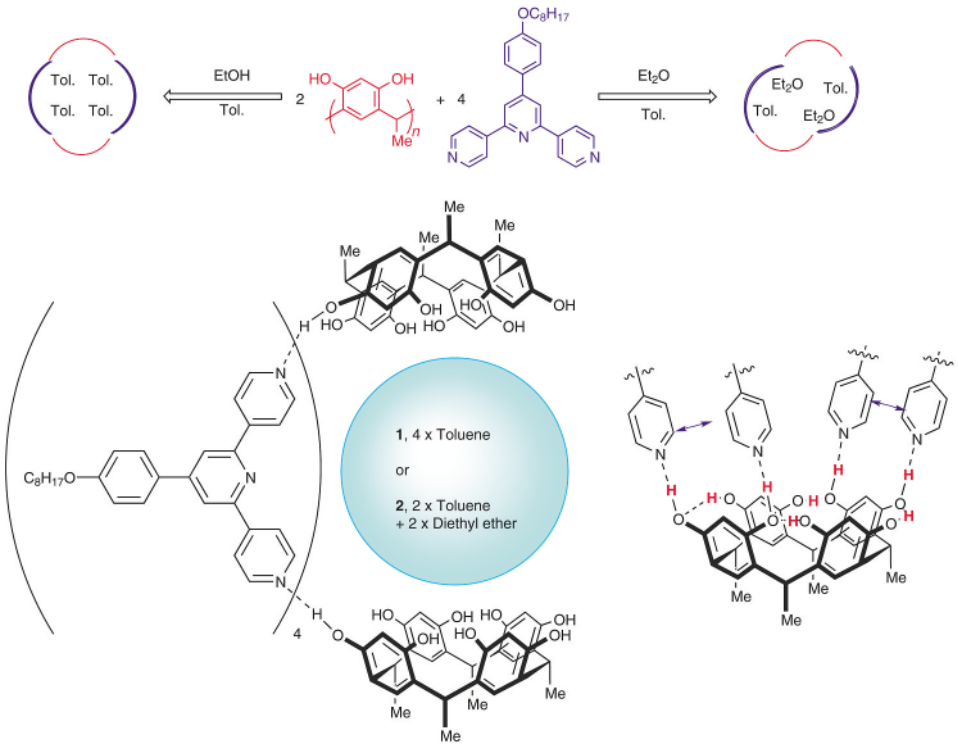

Scheme 5

and concentrated HCl).[56] In applying the principles of Green Chemistry *C*-aryl and *C*-methylcalix[4]resorcinarenes are now accessible in substantially higher yields and high purity by the direct reaction of resorcinol and aldehyde in the presence of a catalytic amount of solid acid, tolyl-*p*-sulfonic acid, at ambient temperature, under solvent-free conditions with grinding for a few minutes, Scheme 6.[11,19] This represents a significant improvement on the traditional solution phase methodology with respect to energy usage, solvent wastes and associated hazards, reaction time and yield. In addition, and again applying the principles of Green Chemistry, the relevant benzaldehyde derivatives are prepared in polypropylene glycol, which is readily recycled. Calix[4]resorcinarenes find applications as supramolecular tectons[19,57] and host molecules,[58] as components in liquid crystals,[59] photoresists,[60] selective membranes,[61] surface reforming agents,[62] HPLC stationary phases,[63] as ion channel mimics[64] and metal ion extraction agents.[65]

As noted previously,[7,20] the reaction mixtures are viscous liquids or pastes even where all reagents are solids; the melt formed on mixing the reagents stiffens within minutes to yield a sticky solid that hardens further on standing. This material is mainly the product **14** and purification involves washing with water to effect removal of the catalyst, followed by recrystallisation from hot methanol where required.

Calix[4]resorcinarenes commonly occur in two isomeric forms, namely the *rccc* or C_{4v} and the *rctt* or C_{2h} isomers.[66] For *C*-methyl- and *C*-C_6H_4-4-*O*-Octyl^n–calix[4]resorcinarenes the C_{4v} isomer results, whereas for *C*-C_6H_4-2-OH–calix[4]resorcinarene the C_{2h} isomer predominates and, for *C*-C_6H_4-4-O$(CH_2)_4$Br–calix[4]resorcinarene, a mixture of the two isomers is obtained (Scheme 6). The predominance of the C_{2h} isomer contrasts with molecular modelling calculations,[11] which indicate that the C_{4v} isomer in the crown conformer is favoured over the C_{2h} isomer in the chair conformer (in the absence of solvent effects) by 6.3 and 14.4 kcal mol^{-1} for *C*-C_6H_4-4-*O*-Octyl^n–calix[4]resorcinarenes and *C*-C_6H_4-4-O$(CH_2)_4$Br–calix[4]resorcinarene respectively. Altering the reaction time does not lead to an increase in the formation of the C_{4v} isomer.

CTV and related molecules, **16**, are versatile supramolecular host molecules, recently gaining prominence in forming complexes with large globular molecules such as fullerenes and

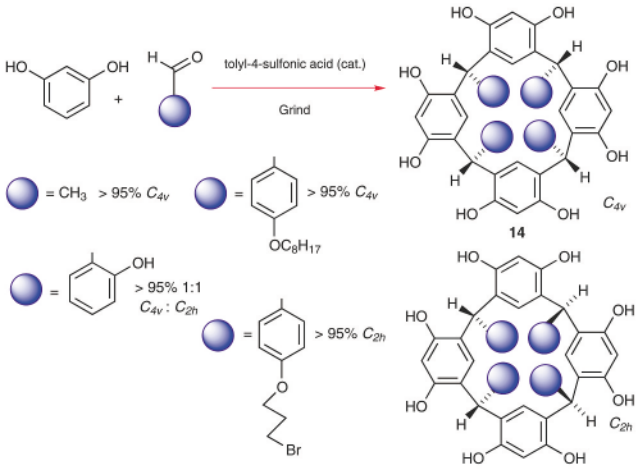

Scheme 6

carboranes,[67,68] yet the synthesis of these host molecules has changed little since their discovery earlier last century.[69] CTV is formed by the harsh acid catalysed condensation of veratryl alcohol **15**, or veratrole and formaldehyde. In focusing on more benign syntheses, two new methods have been developed, solventless and the use of an ionic liquid as a reaction medium, both providing reasonable yields yet being low waste generating, Scheme 7.[7] The solvent free method is particularly well suited to the analogues of CTV derived from the corresponding benzyl alcohol which are sensitive to strongly acidic conditions, while condensation in the ionic liquid N_{6444} Amide facilitates the condensation of liquid or molten benzyl alcohol monomers to the cyclic trimers. While the yields from the solventless reactions carried out at room temperature are modest, 41–59%, these are readily improved by the use of elevated temperatures.[70] The trimer is more easily isolated than in traditional syntheses, and only a catalytic amount of acid is required, the volume of solvent used is hugely reduced and is only associated with product purification. Phosphoric acid proved the best catalyst as solid tolyl-*p*-sulfonic acid results in the formation of solid product shells around the catalyst, effectively rendering the catalyst inactive.[7] Organic solvents used in product isolation are not heated above ambient temperature, thus reducing the difficulties associated with containment of vapours.

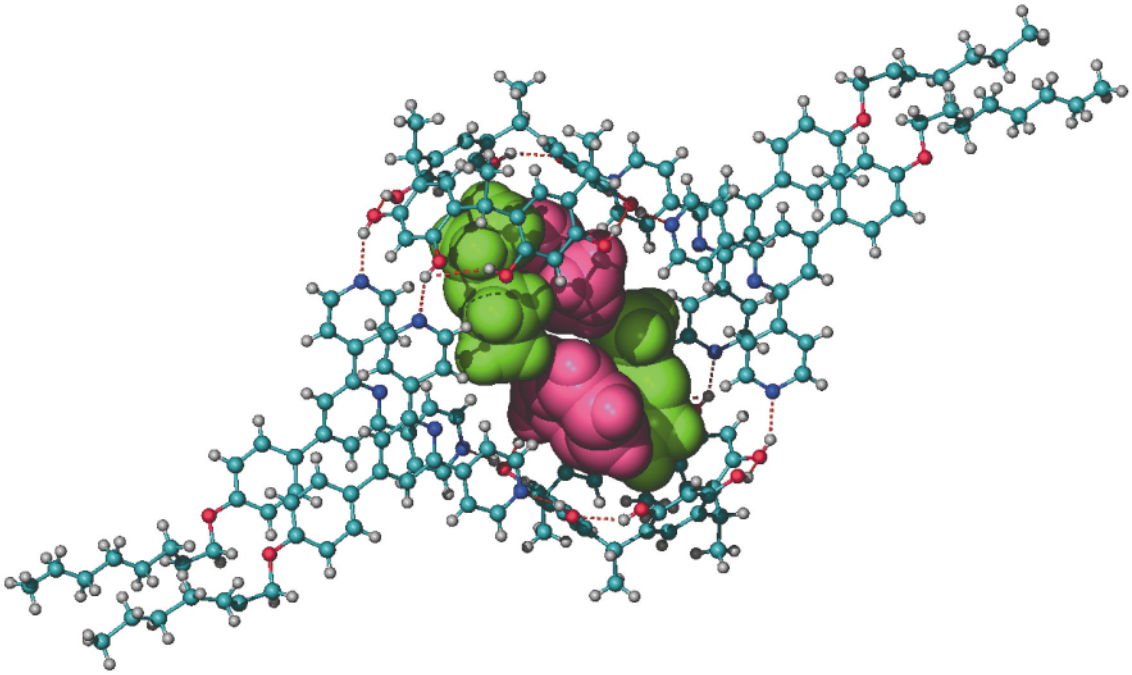

Fig. 3 Structure of [{$(OEt_2)_2$(toluene)$_2$}⊂(*C*-Methylcalix[4]resorcinarane)$_2$ (**10**, 4,4″, R = –*O*-Octyl^n)$_4$].

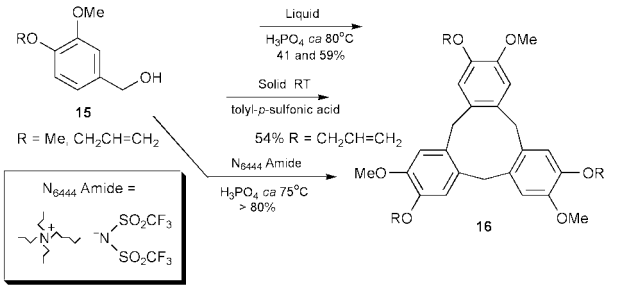

Scheme 7

In the case of the ionic liquid method, the reaction of **15** with a catalytic amount of phosphoric acid affords the trimer in very high yield, >82%, and the non-volatility of the ionic liquid provides unique recycling possibilities. Indeed it can be recycled five times before product quality is compromised and the scheme for recycling the ionic liquid is shown in Fig. 4. The

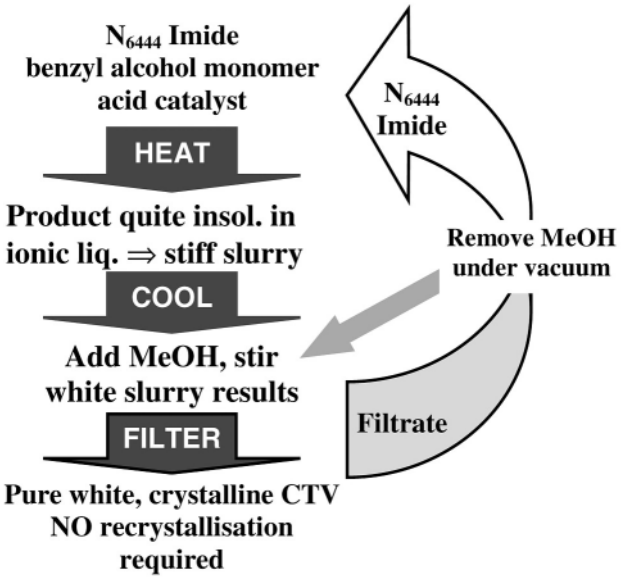

Fig. 4 Procedure for recycling of ionic liquid N_{6444} Amide in the synthesis of CTV. This anion is also commonly described in the materials and electrochemistry literature as the bis(trifluoromethylsulfonyl)*imide* ion, hence the abbreviation N_{xyyy}*Imide*.

methanol used in the scheme can be removed by distillation and recycled. The high yielding reaction occurs in an ionic liquid which is strongly hydrophobic and with the negative charge on the anion diffuse and partially protected.[7] The low equilibrium concentration of water in the reaction mixture assists in driving the reaction to high yield, the excess water being continuously lost as vapour. The properties of the ionic liquid which favour the trimerisation reaction underscores the need to develop a wide range of ionic liquids of varying properties, and this is an important part of the rapidly expanding research in ionic liquids.[5–7]

Therapeutic agents

4-Aryl-1,4-dihydropyridines such as **21** are potent calcium channels agonists and antagonists and are extensively used in the treatment of cardiovascular disease (CVD),[71] which is one of the leading causes of death the world over (for example, 41.4% of deaths in the USA in 1996 were a result of CVD).[72] Following the two step regime illustrated in Scheme 8 (and similar to most industrially used synthetic routes to such unsymmetrically substituted dihydropyridine derivatives), but using solventless reaction conditions, leads to a vast improvement in extent of conversion and isolated yield while delivering significantly shortened reaction times, batch sizes that are defined only by the quantity of drug to be produced and

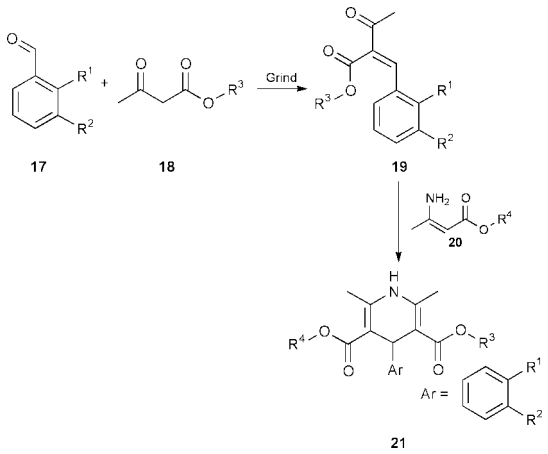

Scheme 8

concomitant improvements in energy utilisation.[73] Volatile organic compound (VOC) use is restricted to product recrystallisation, in turn facilitated by the high degree of conversion achieved which results in low quantities of residual starting materials or impurities.

The simplicity and efficacy of the solventless methodology may again be contrasted with the various strategies that have been employed to maximise conversion and minimise reaction time in traditional solvent-phase syntheses. These include azeotropic removal of water,[76–76] catalyst optimisation,[74,77] and selective deesterification of diesters using acid catalysts.[78] Reaction times are of the order of 2 to 40 hours and overall yields for the two step synthesis are significantly lower than quantitative (30 to 65%). Extractive workups[79] and the need to separate symmetrical diester byproducts from the desired product[74] serve to increase the usage of volatile organic compounds and decrease efficiency with respect to yield and number of process steps.

These reactions proceed at ambient temperature but, in common with the solution phase methods, more rapid conversion is achieved at elevated temperatures. To gain further understanding of these reactions, we have studied the rate of formation of the products **19** and **21** and find that it is possible to optimise reaction conditions with respect to maximum rate of conversion *vs*. energy use.[73]

Remarkable improvements in yield, energy use and waste minimisation are also achieved in the synthesis of 1,2,3,4-tetrahydroquinazolines **22** and the related fully aromatised quinazolines **23** (Scheme 9).[80] These compounds are biologically

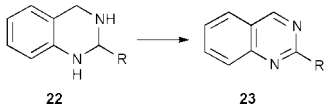

Scheme 9

active[81] and derivatives are of interest as dihydrofolate reductase inhibitors,[82] antitubercular[83] and antibacterial agents.[84]

Mechanistic considerations

That many of the solventless reactions discussed above involve the reaction of macroscopic solid organic particles, yet proceed *via* a liquid or melt phase is intriguing and has formed the basis of a detailed study of several organic reactions.[20] Some of these reactions have been reported to proceed 'in the solid phase' but clearly involve the formation of a liquid phase. Catalytic transformations, including aldol condensations and oligomerisation of benzylic compounds to form cavitands, proceed *via* a liquid phase, as do many non-catalytic reactions including Baeyer–Villiger oxidations, oxidative coupling of naphthols using iron chloride, condensation of amines and aldehydes to

form azomethines, homo-etherification of benzylic alcohols using tolyl-*p*-sulfonic acid, and nuclear aromatic bromination with NBS.[20] This liquefaction implies the existence of a eutectic mixture with T_{fusion} below ambient temperature (although both reagents have higher than ambient melting points). In cases where heating is required, it is again clear that a phase change (from solid to liquid) occurs, explaining the observed reaction kinetics. We have previously examined a number of experimental examples,[20] and these along with the examples described above provide the basis for a description of such reactive systems involving intervention of a liquid phase resulting from the occurrence of a eutectic (or peritectic) melt phase. When considering reactions between solids it is important to distinguish between **solid phase synthesis** (the reaction of molecules from a fluid phase with a solid substrate as in the polymer-supported peptide syntheses); **solvent-free synthesis** (any system in which neat reagents react together, in the absence of a solvent); and **solid-state synthesis** or **solid-solid reactions**, in which two macroscopic solids interact *directly* and form a third, solid product *without intervention of a liquid or vapour phase*. A cartoon of these three processes is shown in Fig. 5. Numerous reactions such as those resulting in

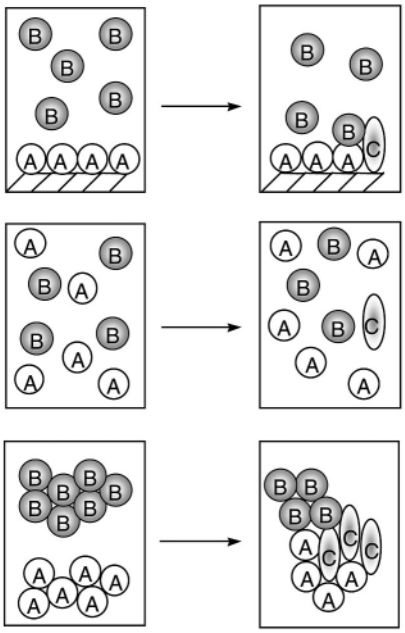

Fig. 5 Cartoon of solid phase reaction (top), solvent-free reaction (middle), and solid-state reaction (bottom).

the formation of a complex such as a charge-transfer or molecular complex,[85] reactions in a single crystalline phase such as photochemically induced solid-state transformations,[86] or the reaction of two components that crystallise together to form a discrete stoichiometric co-crystal (or inclusion compound), may be considered to occur in the solid phase.[87] However, it may be demonstrated that many reactions between discrete solid particles are actually reactions in a liquid melt phase.[20]

In the aldol condensation, observation of the phase resulting on grinding together the solid aldehydes or ketones *without* addition of the base catalyst, reveals that in some cases a liquid melt forms while in others the solid reagents occur as mechanically mixed, discrete crystalline phases (as verified by powder X-ray diffraction studies). More importantly, upon addition of the solid base catalyst, reaction is *only* observed in those systems that exhibit a phase change to a melt.[15] Thus, *the existence of a liquid phase is a prerequisite for reaction in these systems!* In systems such as these, which require addition of an acid or base catalyst, it is possible to construct the phase diagram for the two component reagent mixture. Measurement of thaw and liquidus points for the system indan-1-one **2** and 4-phenylcyclohexanone **3** yields Fig. 6. The eutectic temperature of 19 °C is below the ambient temperature of the reaction experiments. However, it is interesting to note that at a 1 : 1 mole ratio of **1** : **2** the liquidus temperature is above ambient *T*, implying that some unmelted solid **2** would be present. This is not observed in the bulk samples and may indicate the tendency of the system to supercool.[88] In addition, this implies that some heat is released on grinding of the two components which leads to complete melting of the mixture. Such heat may be generated by the occurrence of 'hot spots'[89] during initial grinding of the solids and this phenomenon should be carefully considered when high intensity grinding techniques, such as ball milling, are employed (even in cases where temperature-controlled apparatus is used).

Similar melt behaviour is noted in a number of reactions and, for example, trimerisation of benzylic alcohols, achieved by grinding 4-allyloxy-3-methoxybenzylalcohol with one equivalent of tolyl-*p*-sulfonic acid, yields a viscous melt that solidifies over a period of days yielding **16**, R = allyl (Scheme 7), which separates as a microcrystalline solid. Once again, this solvent-free reaction is not a solid–solid reaction in spite of the relatively high melting points (86 °C and 103–105 °C, respectively) of both reagents. One mole of water is produced for each mole of benzyl alcohol condensed, but this does not account for the apparent liquefaction of the reaction mixture. Although the viscosity of the monomer–acid mixture is lowest directly after the grinding of the two components, TLC analysis reveals < 5% product at this point. Thus, the water present is derived chiefly from the monohydrate catalyst and would be insufficient to achieve dissolution of the very sparingly soluble benzyl alcohol monomer.

Highly efficient solventless transformations of benzaldehyde and aniline derivatives have been reported previously,[90] and the reaction between *o*-vanillin **24** and *p*-toluidine **25** to yield the azomethine product **26** (Scheme 10), provides a striking example of a melt phase on mixing of the solid reagents.

Mixing of the finely powdered reagents (without grinding) immediately yields a bright orange fluid that has a low viscocity and may be drawn into a pasteur pipette as illustrated in Fig. 7. This liquid rapidly solidifies yielding a bright orange crystalline solid that is slightly wetted (presumably by the water produced in the condensation reaction). As with many solventless reactions, reaction is rapid and conversion virtually quantitative. Aside from drying, no further purification is required.

Clearly many of the so-called 'solid–solid' reactions are not reactions in the solid-state. Solid–solid reactions occurring between two discrete crystalline solids, without intervention of

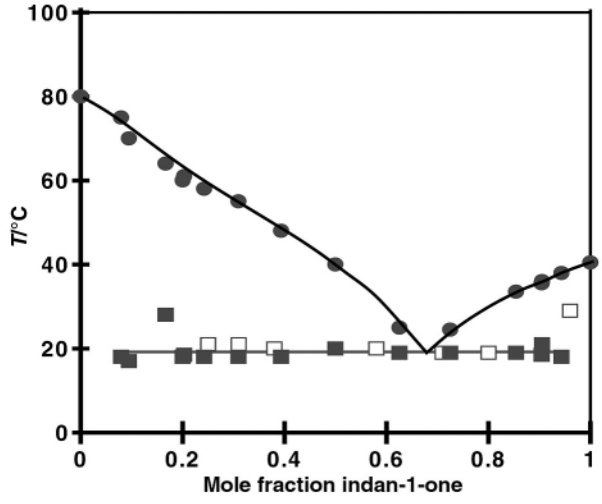

Fig. 6 Phase diagram of indan-1-one **1** and 4-phenylcyclohexanone **2** at constant (ambient) pressure. Filled circles represent liquidus temperatures, filled squares, thaw points, and open squares the onset temperature of the first endotherm measured by DSC analysis.

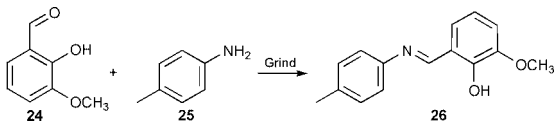

Scheme 10

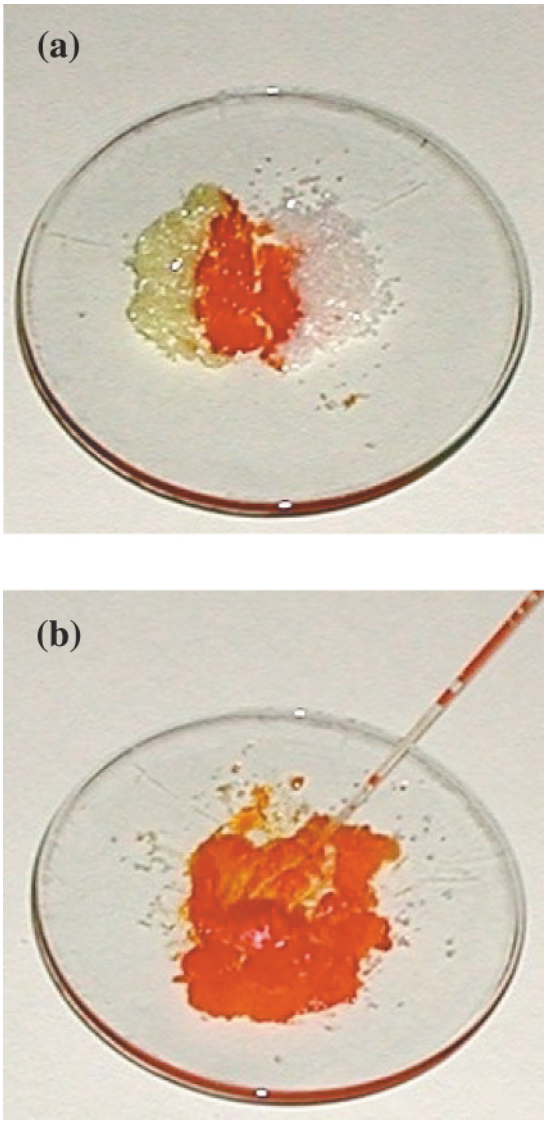

Fig. 7 Photographs of liquid phase formed upon mixing of *o*-vanillin and *p*-toluidine. (a) Pale yellow crystalline *o*-vanillin (left) and white crystalline *p*-toluidine (right) form an orange liquid phase upon contact. (b) The orange liquid phase is fluid enough to be drawn into a Pasteur pipette and solidifies rapidly to form the orange crystalline solid azomethine product.

a mobile phase (which allows a large number of productive molecular collisions) would be expected to exhibit diffusion-controlled kinetics.[91] Thus, the rapid rates noted do not support the theory of two solids reacting together without intervention of a new (liquid) phase that enables higher substrate mobility.[20]

A description of the behaviour noted is described: upon mixing of the reagents, a melt of mutually miscible A and B exists, so that these may be considered to be *mutually soluble*. In the reaction A + B ⇒ C, the overall phase equilibria may be represented by a triangular prism as shown in Fig. 8a. In this prism each rectangular face represents one binary diagram (AB, AC *etc*.).[92] Since the reactions are not thermally isolated these approximate systems at constant *T*, and the chemical and phase composition may be represented by triangular cross sections of the prism such as the central triangle in Fig. 8(b) which represent a cross-section at *T*1. This figure illustrates the situation where the temperature is above that of the binary eutectic formed by A and B (and above the binary eutectics formed by A and C, B and C and the ternary eutectic formed by A, B and C). Thus as A and B react in 1 : 1 stoichiometry to form product C the composition changes along the line qC. The liquid phase, initially composed of 1 : 1 A : B, becomes enriched in C until the liquidus line is crossed and C begins to crystallise out of the melt. At complete conversion the only phase present will be a solid, crystalline C. As the quantities of A and B, relative to each other, remain constant throughout the reaction, a vertical section of the triangular prism such as Fig. 8c can be used to depict the phase equilibria occurring. Each face of the prism is in fact a two component diagram such as that appended to the base of the triangular cross section in Fig. 8b. It may be illustrated that a number of reactive systems exhibit 2 component phase diagrams AC and BC such as those represented as dotted rectangles appended to the sides of the triangle (Fig. 8b).

Overall, these reactions should therefore be classified together with classical liquid–liquid and liquid–solid systems that react in the absence of an added solvent such as many of the solid–liquid or liquid–liquid systems presented above.

Future trends

The remarkable versatility and success of using solventless reactions to prepare several classes of compounds demonstrates that this methodology has an important place in the toolbox arsenal for Green Chemistry. In accepting the enormous challenge of Green Chemistry in the march towards sustainability, new chemistry can emerge as well as access to compounds not possible using traditional methods, and on this

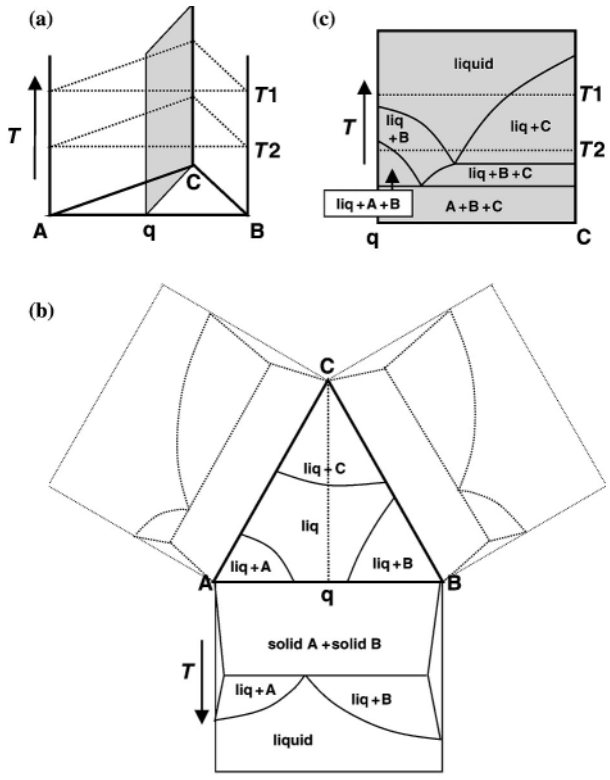

Fig. 8 (a) Triangular prism basis for a 3 component phase diagram at constant *P* (vertical axis represents increasing *T*). Consideration of cross sections such as *T*1 and *T*2 allow analysis of the phases occurring at various component concentrations at a specific, constant temperature. (b) Represents a cross section of this prism at a particular temperature (central triangle) greater than the AB, BC, AC or ABC eutectic temperature (note liquid phase at *C* = 0). (c) Diagram representing constant A and B composition of 1 : 1 mole ratio with increasing *T*. Moving along the dotted lines marked *T*1 and *T*2 indicates the phase changes occurring as *C* increases.

issue alone, the results challenge the classical approach of using volatile organic solvents in synthesis. Green Chemistry is an area of chemistry where applied and fundamental research collapses with a common thread of sustainability. It also challenges the description of certain classes of reactions between organic solids as being solid state reactions. Applying the principles of Green Chemistry has led us into developing new building blocks for supramolecular chemistry, and establishing protocol for organic synthesis. In this context then the question is: 'why wouldn't you want to embark on research in Green Chemistry?'

Acknowledgments

The authors wish to acknowledge the contribution from co-workers at Monash University and the University of Leeds, financial support from these universities and from the Australian Research Council.

Notes and references

1 P. T. Anastas and J. C. Warner, *Green Chemistry: Theory and Practice*, Oxford Science Publications, New York, 1998; P. Anastas and T. Williamson, *Green Chemistry, Frontiers in Benign Chemical Synthesis and Processes*, Oxford Science Publications, New York, 1998.
2 *Green Chemistry: Challenges and Opportunities*, J. H. Clark, *Green Chem*., 1999, **1**, 1; *The Greening of Chemistry*, J. H. Clark, *Chem. Brit*., 1998, October, 43.
3 P. T. Anastas, *Green Chemistry: Sustainable Products and Processes Conference*, University of Wales, Swansea, UK, 2001.
4 R. G. Sheldon, *Chem. Ind*., 1992, 903.
5 *E.g*. J. D. Holbrey and K. R. Seddon, *J. Chem. Soc., Dalton Trans*., 1999, 2133; T. Welton, *Chem. Rev*., 1999, **99**, 2701.
6 D. MacFarlane, P. Meakin, J. Sun, N. Amini and M. Forsyth, *J. Phys. Chem. B*, 1999, **103**, 4164.
7 J. L. Scott, D. R. MacFarlane, C. L. Raston and M. Teoh, *Green Chem*., 2000, **2**, 123.
8 *E.g*. R. S. Oakes, T. J. Heppenstall, N. Shezad, A. A. Clifford and C. M. Rayner, *Chem. Commun*., 1999, 1459; N. Shezad, A. A. Cliffor and C. M. Rayner, *Tetrahedron Lett*., 2001, **42**, 323; J. A. Darr and M. Poliakoff, *Chem. Rev*., 1999, **99**, 495.
9 C. R. Strauss, *Aust. J. Chem*., 1999, **52**, 83, and references therein.
10 C. Li and T. Chen, *Organic Reactions in Aqueous Media*, Wiley Interscience, New York, 1997; C.-H. Li and W.-C. Zhang, *J. Am. Chem. Soc*., 1998, **120**, 9102.
11 B. A. Roberts, G. W. V. Cave, C. L. Raston and J. L. Scott, *Green Chem*., in press.
12 For reviews see F. Toda, *Acc. Chem. Res*., 1995, **28**, 480; F. Toda, *Synlett*, 1993, 303.
13 R. P. Rastogi, N. B. Singh and R. P. Singh, *J. Solid State Chem*., 1977, **20**, 191.
14 F. Toda and K. Tanaka, *Chem. Rev*., 2000, **100**, 1025.
15 C. L. Raston and J. L. Scott, *Green Chem*., 2000, **2**, 49.
16 J. L. Scott and C. L. Raston, *Green Chem*., 2000, **2**, 245.
17 G. W. V. Cave and C. L. Raston, *Chem. Commun*., 2000, 2199.
18 G. W. V. Cave and C L. Raston, *J. Chem. Soc., Perkin Trans. 1*, submitted.
19 G. W. V. Cave, M. J. Hardie, B. A. Roberts and C. L. Raston, *Eur. J. Org. Chem*., 2001, 3227.
20 G. Rothenberg, A. P. Downie, C. L. Raston and J. L. Scott, *J. Am. Chem. Soc*., 2001, **123**, 8701.
21 For example: B. Dunk and R. Jachuck, *Green Chem*., 2000, **2**, G13.
22 J. L. Atwood, M. J. Hardie, C. L. Raston and C. A. Sandoval, *Org. Lett*., 1999, **1**, 1523.
23 T. H. Grindstaff, *US Patent*, US5,153,324, 1992.
24 K. Komatsu, K. Fujiwara, T. Tanaka and Y. Murata, *Carbon*, 2000, **38**, 1529; K. Komatsu, G.-W. Wang, Y. Murata, T. Tanaka, K. Fujiwara, K. Yamamoto and M. Saunders, *J. Org. Chem*., 1998, **63**, 9358.
25 W. H. Correa and J. L. Scott, *Green Chem*., 2001, in press.
26 F. Toda, K. Tanaka and K. Hamai, *J. Chem. Soc., Perkin Trans. 1*, 1990, 3207.
27 R. Kane, *Ann. Phys. Chem., Ser. 2*, 1838, **44**, 474; *J. Prakt, Chem*., 1838, **15**, 129; A. Wurtz, *Bull. Soc. Chim. Fr., Part 2*, 1872, **17**, 436; *Ber. Dtsch. Chem. Ges*., 1872, **5**, 326; *Hebd. Seances. Acad. Sc*., 1872, **74**, 1361.
28 J. G. Schmidt, *Ber. Dtsch. Chem. Ges*., 1880, **13**, 2342; 1881, **14**, 1459.
29 C. H. Heathcock, ch 1.6; B. Moon, S. F. Williams and S. Masamune, ch. 1.7; M. W. Rathe and P. Weipert, ch. 1.8; I. Paterson, ch. 1.9, *Comprehensive Organic Synthesis—Selectivity, Strategy and Efficiency in Modern Organic Chemistry*, ed. B. M. Trost, and I. Fleming, Pergamon Press, Oxford and New York, vol. 2, 1991.
30 S. Wattanasin and W. S. Murphy, *Synthesis*, 1980, 647.
31 L. F. Tietze and U. Beifuss, *Comprehensive Organic Synthesis—Selectivity, Strategy and Efficiency in Modern Organic Chemistry*, ed. B. M. Trost, Pergamon Press, Oxford and New York, 1991, vol. 2, p. 341.
32 E. Knoevenagel, *Chem. Ber*., 1898, **31**, 2585.
33 C. P. Phadke, S. L. Kelkar and M. S. Wadia, *Synth. Commun*., 1984, **14**, 407; A. K. Awasthi and R. S. Tewari, *Synthesis*, 1986, 1061.
34 L. Bonsignore, F. Cottiglia, S. M Lavagna, G. Loy and D. Secci, *Heterocycles*, 1999, **50**, 469.
35 V. Armstrong, O. Sotto, J. A. Valderrama and R. Tapia, *Synth. Commun*., 1988, **8**, 717.
36 B. T. Watson and G. E. Christiansen, *Tetrahedron Lett*., 1998, **39**, 6087.
37 B. P. Bandgar, L. S. Uppalla and D. S. Kurule, *Green Chem*., 1999, **1**, 243.
38 F. Kröhnke, *Synthesis*, 1976, 1.
39 E. C. Constable, C. E. Housecroft, M. Neuburger, D. Phillips, P. R. Raithby, E. Schofield, E. Sparr, D. A. Tocher, M. Zehnder and Y. Zimmermann, *J. Chem. Soc., Dalton Trans*., 2000, 2219.
40 R. K. R. Jetti, A. Nagia, F. Xue and T. C. W. Mak, *Chem. Commun*., 2001, 919.
41 Z. C. Watson, N. Bampos and J. K. M. Sanders, *New J. Chem*., 1998, 1135.
42 R. Büchner, C. T. Cunningham, J. S. Field, R. J. Haines, D. R. McMillin and G. C. Summerton, *J. Chem. Soc., Dalton Trans*., 1999, 711.
43 F. Neve, S. Campagna and A. Crispini, *Inorg. Chem*., 1997, **36**, 6150.
44 C. R. Rice, M. D. Ward, M. K. Nazeeruddin and M. Gräzel, *New J. Chem*., 2000, **24**, 651.
45 H.-Q. Liu, T.-C. Cheung, S.-M. Peng and C.-M. Che, *Chem. Commun*., 1995, 1787.
46 N. Kalyanam, M. A. Likhate and S. G. Manjunatha, *Indian J. Chem*., 1992, **31B**, 555.
47 *E.g*. G. Lowe, Int. Publication number WO 00/50431, (31/08/2000).
48 E. C. Constable, C. E. Housecroft, M. Neuburger, A. G. Schneider, B. Springler and M. Zehnder, *Inorg. Chim. Acta*, 2000, **300–302**, 49.
49 H. L. Anderson, S. Anderson and J. K. M. Sanders, *J. Chem. Soc. Perkin Trans. 1*, 1995, 2231.
50 G. W. V. Cave and C. L. Raston, unpublished results.
51 L. M. Tunstad, J. A. Tucker, E. Dalcanale, J. Weiser, J. A. Bryant, J. C. Sherman, R. C. Helgeson, C. B. Knobler and D. J. Cram., *J. Org. Chem*., 1989, **54**, 1305.
52 H. Ito, T. Kusukawa and M. Fujita, *Chem. Lett*., 2000, 598; M. Yoshizawa, T. Kusukawa, M. Fujita and K. Yamaguchi, *J. Am. Chem. Soc*., 2000, **122**, 6311.
53 *E.g*. L. R. MacGillivray and J. L. Atwood, *Angew. Chem*., 1999, **111**, 1080; *Angew. Chem., Int. Ed. Engl*., 1999, **38**, 1018.
54 L. R. MacGillivray and J. L. Atwood, *Nature*, 1997, **389**, 469; T. Douglas and M. Young, *Nature*, 1998, **393**, 152.
55 A. Baeyer, *Ber. Disch. Chem. Ges*., 1872, **5**, 25; A. Baeyer, *ibid*., 1872, **5**, 280.
56 T. Haino, D. M. Rudkevich, A. Shivanyuk, K. Rissanen and J. Rebek, Jr, *Chem. Eur. J*., 2000, **6**, 3797.
57 L. R. MacGillivray and J. L. Atwood, *J. Solid State Chem*., 2000, **152**, 199; L. R. MacGillivray, P. R. Diamente, J. L. Reid and J. A. Ripmeester, *Chem. Commun*., 2000, 359; R. G. Harrison, N. K. Dalley and A. Y. Nazarenko, *Chem. Commun*., 2000, 1387.
58 G. M. Martinez, C. R. Teran, O. A. Tlapanco, A. Toscano and R. Cruz-Almanza, *Fullerene Sci. Technol*., 2000, **8**, 475; F. C. Tucci, A. R. Renslo, D. M. Rudkevich and J. Rebek, *Angew. Chem., Int. Ed*., 2000, **39**, 1076.
59 K. Yonetake, T. Nakayama and M. Ueda, *J. Mater. Chem*., 2001, **11**, 761.
60 H. Ito, T. Nakayama and M. Ueda, *United States Patent*, US 6093517, 2000; O. Haba, K. Haga, M. Ueda, O. Morikawa and H. Konishi, *Chem. Mater*., 1999, **11**, 427; T. Nakayama, D. Takhashi, K. Takeshi and M. Ueda, *J. Photopolym. Sci. Technol*., 1999, **12**, 347.
61 N. Tbeur, T. Rhlalou, M. Hlaibi, D. Langevin, M. Metayer and J.-F. Verchere, *Carbohydr. Res*., 2000, **329**, 409; O. Pietraszkiewicz, M. Kozbial and M. Pietraszkiewicz, *Pol. J. Chem*., 1998, **72**, 886.
62 K. Ichimura, E. Kurita and M. Ueda, *European Patent*, EP 671220, 1995.
63 O. Pietraszkiewicz and M. Pietraszkiewicz, *J. Inclusion Phenom. Macrocyclic Chem*., 1999, **35**, 261.
64 N. Yoshino, A. Satake and Y. Kobuke, *Angew. Chem., Int. Ed*., 2001, **40**, 457.
65 E. Gaunert, H. Barnier, L. Nicod, A. Favre-Reguillon, J. Foos, A. Guy, C. Bardot and M. Lemaire, *Sep. Sci. Technol*., 1997, **32**, 2309; L. S.

Kuznetsova, A. R. Mustafina, A. Y. Ziganshina and E. K. Kazakova, *J. Inclusion. Phenom. Macrocyclic Chem*., 2001, **37**, 65.
66 F. Weinelt and H.-J. Schneider, *J. Org. Chem*., 1991, **56**, 5527.
67 J. L. Atwood, M. J. Barnes, R. S. Burkhaller, P. C. Junk, J. W. Steed and C. L. Raston, *J. Am. Chem. Soc*., 1994, **116**, 10346; J. L. Atwood, M. Barnes, M. G. Gardiner and C. L. Raston, *J. Chem. Soc., Chem. Commun*., 1996, 1449.
68 R. J. Blanch, M. Williams, G. D. Fallon, M. G. Gardiner, R. Kaddour and C. L. Raston, *Angew. Chem., Int. Ed. Engl*., 1997, **36**, (5), 504; M. J. Hardie and C. L. Raston, *J. Chem. Soc., Chem. Commun*., 1999, 1153; M. J. Hardie, P. D. Godfrey and C. L. Raston, *Chem. Eur. J*., 1999, **5**, (6), 1828.
69 G. M. Robinson, *J. Am. Chem. Soc*., 1915, **102**, 266.
70 J. L. Scott and G. Annat, unpublished results.
71 J. G. Gerber and A. S. Nies, in *Gilman and Goodman's the Pharmacological Basis of Therapeutics*, 8th edn., ed. A. G. Gilman., T. W. Rall, A. S. Nies and P. Taylor, Pergamon Press, New York, 1990, p. 784–813.
72 G. B. Zavoico, *Drug and Market Development Newsletter*, 2000, http://www.pharmalicensing.com/features/disp/961691288_39523e988df12
73 W. H. Correa and J. L. Scott, *Green Chem*., 2001, in press.
74 R. Desai, D. A. Aguilar and M. Aslam, *World Patent* No. 9724326, 1997.
75 P. Naab, W. Lange, W. Teller, *United States Patent* No. 4904789, 1990.
76 S. Hiroaki and H. Shizuo, *European Patent* No. 0371492, 1990.
77 J. Auerbach, *United States Patent* No. 5310917, 1994.
78 A. Kakuiri and H. Ikawa, *Japanese Patent* No. 07196612, 1995.
79 A. Gustavsson, A. Kallstrom and S. Palmer, *World Patent* No. 9725313, 1997; D. Pieraccioli, *Europen Patent* No. 0370974, 1990.
80 P. Radnidge, W. H. Correa, S. Papadopolous and J. L. Scott, unpublished results.
81 L. N Yakhontov, S. S. Liberman, G. P. Zhikhareva and K. K. Kuz'mina, *Khim.-Farm. Zh*., 1977, **11**, 14.
82 H. Lau, J. T. Ferlan, V. H. Brophy, A. Rosowsky and C. H. Sibley, *Antimicrob. Agents Chemother*., 2001, **45**, 187; A. H. Calvert, T. R. Jones, P. J. Dady, B. Grzelakowska-Sztabert, R. Paine and G. A. Taylor, *Eur. J. Cancer*, 1980, **16**, 713; A. H. Calvert, T. R. Jones, P. J. Dady, B. Grzelakowska-Sztabert, R. M. Paine, G. A. Taylor and K. R. Harrap, *Eur. J. Cancer*, 1980, **16**, 71; J. B. Hynes, J. M. Buck, L. D'Souza and J. H. Freisheim, *J. Med. Chem*., 1975, **18**, 1191.
83 P. Desai, B. Naik, C. M. Desai and D. Patel, *Asian J. Chem*., 1998, **10**, 615.
84 D. M. Purohit and V. H. Shah, *Indian J. Heterocycl. Chem*., 1999, **8**, 213.
85 R. P. Rastogi, N. B. Singh and R. P. Singh, *J. Solid State Chem*., 1977, **20**, 191; R. P. Rastogi, N. B. Singh and R. P. Singh, *Indian J. Chem., Sect. A*, 1977, **15A**, 941; R. P. Rastogi, N. B. Singh and R. P. Singh, *Indian J. Chem., Sect. B*, 1995, **34B**, 764.
86 A. R. West, *Solid State Chemistry and it's Applications*, Wiley, Chichester, 1987, pp. 666. See also K. Tanaka, F. Toda, E. Mochizuki, N. Yasui, Y. Kai, I. Miyahara and K. Hirotsu, *Angew. Chem., Int. Ed*., 1999, **38**, 3523. This reactivity in the solid phase pertains chiefly to photochemical processes (*e.g*. dimerisations, polymerisations) but also for some thermochemical rearrangements and isomerisations, and should not be confused with the subject of the present study. For examples see M. D. Cohen, in *Reactivity of Solids*, ed. J. S. Anderson, M. W. Roberts and F. S. Stone, Chapman and Hall, London, 1972, pp. 456; G. Alder, *Organic Solid State Chemistry*, Gordon and Breach, New York, NY, 1969. For X-ray diffraction studies of such solid-state photochemical transformations see J. Z. Gougoutas, *Pure Appl. Chem*., 1971, **27**, 305.
87 R. Popovitz-Biro, C. P. Tang, H. C. Chang, M. Lahav and L. Leiserowitz, *J. Am. Chem. Soc*., 1985, **107**, 4043; Y. Weisenger-Lewin, M. Vaida, R. Popovitz-Biro, H. C. Chang, F. Mannig, F. Frolow, M. Lahav and L. Leiserowitz, *Tetrahedron*, 1987, **43**, 1449; M. C. Etter, G. M. Frankenbach and J. Bernstein, *Tetrahedron Lett*., 1989, **30**, 3617.
88 J. Sangster, *J. Phys. Chem. Ref. Data*, 1997, **26**, 351.
89 F. P. Bowden and A. D. Yoffe, *Fast Reactions in Solids*, Butterworths Scientific Publications, London, 1958, pp. 57.
90 J. Schmeyers, F. Toda, J. Boy and G. Kaupp, *J. Chem. Soc., Perkin Trans. 2*, 1998, 989.
91 R. P. Rastogi, A. K. Singh and C. S. Shukla, *J. Solid State Chem*., 1982, **42**, 136.
92 G. Masing, *Ternary Systems; introduction to the theory of three component systems*, Dover Publications Inc., NY, 1944, pp 9–31.

CHEMCOMM
Communication
www.rsc.org/chemcomm

Sustainable metal nano-contacts showing quantized conductance prepared at a gap of thin metal wires in solution

Jingze Li,[a] Yusuke Yamada,[a] Kei Murakoshi*[ab] and Yoshihirop Nakato[a]

[a] *Department of Chemistry, Graduate School of Engineering Science, Osaka University, Toyonaka, Osaka 560-8531, Japan. E-mail: kei@chem.es.osaka-u.ac.jp*
[b] *Precursory Research for Embryonic Science and Technology (PRESTO), Japan Science and Technology Corporation, Toyonaka, Osaka 560-8531, Japan*

Received (in Cambridge, UK) 31st July 2001, Accepted 17th September 2001
First published as an Advance Article on the web 1st October 2001

Sustainable silver and copper nano-contacts showing quantized conductance are prepared at a gap between two thin gold wires in solution.

Facile preparation of metal nano-structures, such as nano-wires and nano-gaps, has become an important subject in recent nano-technologies. The techniques enable us to evaluate various characteristics of nano-structures, such as quantized conductance, single-electron charging, and specific conductivity of a single organic molecule, which are useful for the fabrication of novel devices such as quantum devices.[1] Of various possibilities to fabricate nano-structures on solid surfaces, chemical techniques are of much interest because they give stable and self-ordered structures by low-cost processes.[2–4] Especially, an electrochemical method is one of the most promising techniques[4] since the control of the electrode potential leads to precise control of atomic processes on solid surfaces.[5]

Recently interesting examples have been reported[6–11] on the fabrication of nano-junctions *via* electrochemical processes and on the observation of the conductance quantization. The nano-junctions are prepared either at a gap between the tip and the substrate of a scanning tunneling microscope (STM)[6–8] or a gap between two micro-electrodes prepared by photolithography.[9,11] Another interesting method is to use the electrochemical dissolution and deposition of a thin metal wire in solution. This method is one the simplest and very useful if sustainable nano-contacts can be prepared reproducibly. At present, only one example is reported[10] for a Cu wire though the detailed preparation method is not reported.

In this paper, we report the successful observation of the quantized conductance in sustainable Cu nano-contacts, prepared by the electrochemical dissolution and deposition of Cu wires. We also report that the method is extended to the preparation of nano-contacts of various other metals such as Ag by use of the electrochemical deposition and dissolution of the metals at a stable gap such as an Au gap. This gives an interesting way to prepare nano-contacts of a variety of metals, for the fabrication of nano-contacts in solution are now only limited to Cu[7–10,12] and Au.[6,11]

The metal nano-contacts were prepared as follows. A Cu or Au wire (30 μm in diameter, 99.95% purity) was attached to a glass plate with adhesive insulating tapes, with a region of a few hundred μm in width being left as a gap, at which the metal wire could be in contact with an electrolyte solution. The electrochemical dissolution of the metal wire at the gap resulted in the formation of a thin metal wire with a diameter of a few μm (Fig. 1). Further dissolution led to the disconnection of the wire, which was easily detected by simultaneous measurement of its conductance. The nano-contact was formed just before the wire was disconnected. The formation of Ag nano-contacts was performed by the controlled deposition and dissolution of Ag at the gap of an Au wire.

A potentiostat (Toho Technical Research, 2001) and a programmed function generator (Toho Technical Research, FG-02) were used to control the potential of the thin metal wire with respect to the Ag/AgCl reference electrode. The current flowing through the thin metal wire under a constant bias (18.8 mV) was measured in the course of its electrochemical dissolution and deposition with an electrometer (Keithley 6517A), to obtain the conductance.

Fig. 1 shows an example of a thin Cu wire with a diameter of a few μm, prepared by the electrochemical dissolution of a Cu wire (d = 30 μm) for 3 min in 0.1 M H_2SO_4 + 1 mM $CuSO_4$ (M = mol dm^{-3}) at 0.3 V *vs.* Ag/AgCl, which is *ca.* 0.17 V more positive than the equilibrium potential for Cu dissolution (0.13 V). By this method, a long sustainable thin metal wire of approximately 100–300 μm in length was successfully prepared.

After the preparation of the thin Cu wire, the potential was changed from 0.3 to 0.2 V to cause further slow dissolution. The current flowing through the thin metal wire decreased with time and finally became zero, indicating that the wire was broken. Just before the wire was broken, the current showed stepwise changes, as shown in Fig. 2(a). The conductance of the Cu wire, calculated form the current and the bias voltage, is also shown on the right axis of the figure in units of quantized conductance ($G_0 = 2e^2/h$). A unit conductance of 1 G_0 is clearly observed for a long time of about 8 s. It is likely that the half unit conductance, 1/2 G_0, is also observed. Repeated experiments have shown that the conductance of 1 G_0 continues for 10 to 100 s. The observation of the unit quantized conductance indicates the formation of a Cu nano-wire consisting of a few Cu atoms. Essentially the same behavior was reported in Cu nano-contacts prepared at a gap of Cu wires[10] and a junction of electrochemical STM.[7,8]

We also succeeded in preparing sustainable Cu and Ag nano-contacts at a gap between two thin Au wires. The dissolution of an Au wire (d = 30 μm) proceeded in 0.5 M KCl when the potential was kept at 0.8 V or more positive,[13] leading to the

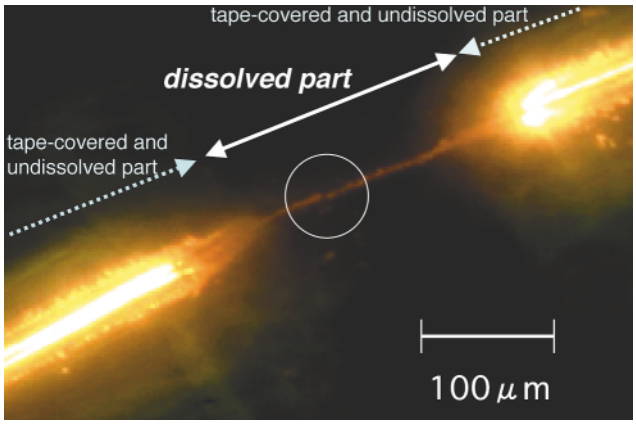

Fig. 1 Optical microscopic image of a thin Cu wire (d = 1–2 μm) prepared by electrochemical dissolution of a thick Cu wire (d = 30 μm) at 0.3 V *vs.* Ag/AgCl. The circle shows the broken part of the thin Cu wire, caused by further slow dissolution at 0.2 V.

 DOI: 10.1039/b106961f

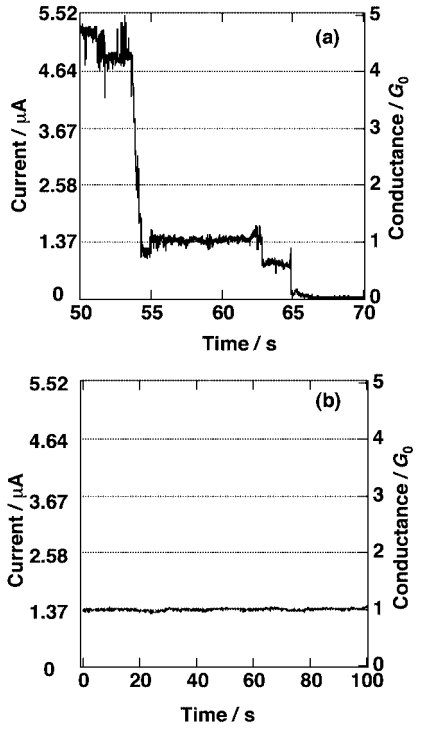

Fig. 2 Time courses of the conductance during the electrochemical dissolution of (a) a Cu wire and (b) Cu deposited at a gap of Au wires. The potential for the Cu dissolution was 0.03 V *vs.* Ag/AgCl; electrolyte: 1 mM $CuSO_4$ + 0.1 M H_2SO_4.

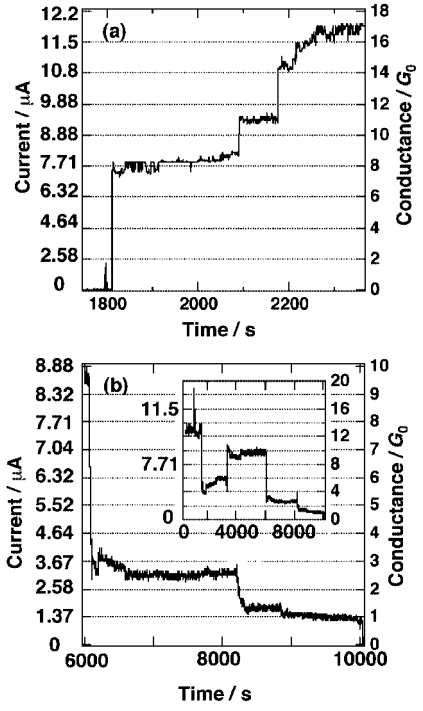

Fig. 3 Time courses of the conductance (a) during the electrochemical deposition of Ag at a gap of Au wires at −0.1 V, and (b) during the electrochemical dissolution of the deposited Ag at 0.3 V; electrolyte: 1 mM $AgNO_3$ + 0.05 M H_2SO_4

formation of a thin Au wire and finally disconnection. After the formation of a gap in a thin Au wire, Cu was deposited on it at 0.3 V in 0.1 M H_2SO_4 + 1 mM $CuSO_4$. Several repeated Cu deposition and dissolution cycles led to the formation of Cu nano-contacts showing unit quantized conductance lasting for 100 s or more [Fig. 2(b)]. The result indicates that a gap between two thin Au wires can be used effectively for the fabrication of sustainable nano-contacts of other metals.

Fig. 3 shows results of similar experiments for the deposition and dissolution of Ag at a gap of thin Au wires. Ag was deposited on Au when the potential of Au was kept at −0.3 V in 0.05 M H_2SO_4 + 1 mM $AgNO_3$, which is about 0.7 V more negative than the equilibrium potential for Ag dissolution (0.4 V). The deposited Ag was dissolved at 0.44 V. The stepwise changes of the conductance were observed both for the deposition of Ag [Fig. 3(a)] and the dissolution of it [Fig. 3(b)]. In the latter case, unit conductance, G_0, was observed for a long time of more than a 1000 s. The results again clearly show the formation of sustainable metal nano-contacts showing quantized conductance, indicating the effectiveness of the present method.

It may be noted in Fig. 3 that the conductance at several current plateaus show conductances different from integral multiples of the unit conductance (G_0). Similar behavior is also observed for Cu nano-contacts [Fig. 2(a)]. Such deviations are often observed in electrochemical systems, as reported by other workers,[6,12] The formation of certain characteristic configurations of metal atoms[14] in electrolyte solutions may be responsible for the deviations, since it is plausible that the structure of the metal nano-contacts depends on the nature of the solvent and electrolyte ions used.

In conclusion, sustainable metal nano-contacts showing conductance quantization have been successfully prepared by electrodeposition and dissolution of Cu and Ag metals at a gap of Au wires. Especially, the Ag nano-contacts, which were prepared for the first time in the present work, showed unit quantized conductance for more than 1000 s. The technique may be applied easily to various metals and other materials, whose structures can be controlled by electrochemical process, to investigate detailed properties of nano-contacts in solution.

This work was partially supported by a Grant-in-Aid for Scientific Research from the Ministry of Education, Culture, Sports, Science and Technology, Japan.

Notes and references

1 G. Timp, in *Nanotechnology*, ed. G. Timp, Springer-Verlag, New York, 1999.
2 K. Murakoshi and Y. Nakato, *Adv. Mater.*, 2000, **12**, 791.
3 A. Tsujiko, T. Kisumi, Y. Magari, K. Murakoshi and Y. Nakato, *J. Phys. Chem. B*, 2000, **104**, 4873.
4 A. Imanishi, K. Morisawa and Y. Nakato, *Electrochem. Solid-State Lett.*, 2001, **4**, C69.
5 K. Itaya, *Prog. Surf. Sci.*, 1998, 121.
6 C. Shu, C. Z. Li, H. X. He, A. Bogozi, J. S. Bunch and N. J. Tao, *Phys. Rev. Lett.*, 2000, **84**, 5196.
7 C. Z. Li and N. J. Tao, *Appl. Phys. Lett.*, 1998, **72**, 894.
8 C. Z. Li, H. Sha and N. J. Tao, *Phys. Rev. B*, 1998, **58**, 6775.
9 C. Z. Li, H. X. He, A. Bogozi, J. S. Bunch and N. J. Tao, *Appl. Phys. Lett.*, 2000, **76**, 1333.
10 C. Z. Li, A. Bogozi, W. Huang and N. J. Tao, *Nanotechnology*, 1999, **10**, 221.
11 A. F. Morpurgo, C. Marcus and D. B. Robinson, *Appl. Phys. Lett.*, 1999, **74**, 2084.
12 A. Bogozi, O. Lam, H. He, C. Li, N. J. Tao, L. A. Nagahara and I. Amlani and R. Tsui, *J. Am. Chem. Soc.*, 2001, **123**, 4585.
13 K. Murakoshi, T. Kitamura and Y. Nakato, *Jpn. J. Appl. Phys.*, 2001, **40**, 1918.
14 B. Loudoph, M. H. Devoret, D. Esteve, C. Urbina and J. M. v. Ruitenbeek, *Phys. Rev. Lett.*, 1999, **82**, 1530.

CHEMCOMM Communication
www.rsc.org/chemcomm

Heptanuclear hydroxo-bridged copper cluster of the dicubane-like type: structural and magnetic characterisations of $[Cu_7(OH)_6Cl_2(pn)_6(H_2O)_2](C(CN)_3)_4Cl_2$ (pn = 1,3-diaminopropane)†

Smaïl Triki,*[a] Franck Thétiot,[a] Jean Sala Pala,[a] Stéphane Golhen,[b] Juan M. Clemente-Juan,[c] Carlos J. Gómez-García[c] and Eugenio Coronado[c]

[a] *UMR CNRS 6521, Univ. de Bretagne Occidentale, BP 809, 29285 Brest Cedex, France. E-mail: smail.triki@univ-brest.fr*
[b] *UMR CNRS 6511, Univ. de Rennes 1, 35042 Rennes Cedex, France*
[c] *Instituto de Ciencia Molecular, Univ. de Valencia, Dr. Moliner 50, 46100 Burjasot, Spain*

Received (in Cambridge, UK) 14th June 2001, Accepted 12th September 2001
First published as an Advance Article on the web 5th October 2001

A new polynuclear copper(II) complex $[Cu_7(OH)_6Cl_2(pn)_6(H_2O)_2](C(CN)_3)_4Cl_2$ with hydroxo-bridging ligands has been prepared; the centrosymmetric cluster cation can be described as two Cu_4O_3Cl distorted cubane units sharing one copper cation.

Various multinuclear copper(II) complexes have been reported in the last decade with a great number of simple and sophisticated bridging ligands;[1–5] however, some nuclearities remain comparatively scarce. In the case of tetranuclear complexes with Cu_4O_4 cubane-like clusters some examples have been thoroughly described,[2] but to date little is known about clusters involving more than four metal centres.[3,4] Concerning the heptanuclear copper(II) clusters, as far as we are aware, only one example of the dicubane-like type has been described.[5] Here we report the structure and preliminary magnetic studies of a novel vertex sharing dicubane-like heptanuclear copper(II) cluster $[Cu_7(OH)_6Cl_2(pn)_6(H_2O)_2](tcm)_4Cl_2$ (**1**) [pn = 1,3-diaminopropane; $tcm^- = C(CN)_3^-$ = tricyanomethanide] with chloro- and hydroxo-bridging ligands.

1.00 mL (12 mmol) of 1,3-diaminopropane (pn) was slowly added to a warm aqueous solution of $CuCl_2{\cdot}2H_2O$ (12 mmol) and then an aqueous solution of sodium hydroxide (12 mmol) was added. To the resulting clear solution were immediately and consecutively added concentrated aqueous solutions of $CuCl_2{\cdot}2H_2O$ (2 mmol) and potassium tricyanomethanide (8 mmol). Slow evaporation gave prismatic blue crystals of $[Cu_7(OH)_6Cl_2(pn)_6(H_2O)_2](tcm)_4Cl_2$ (yield 1.28 g, 42%) suitable for crystallography.‡ The structure of **1** is unique and consists of a centrosymmetric hydroxo-bridged heptanuclear copper(II) cation (Fig. 1) which can be described as two Cu_4O_3Cl distorted cubanes which share one copper cation (Cu1) (Fig. 1 and 2). The four crystallographically independent Cu(II) centres differ markedly in their co-ordination geometry. The central atom (Cu1) presents a strongly elongated octahedral coordination which involves a CuO_4 equatorial plane with essentially equivalent Cu–O bonds [see Fig. 2(a)] and two semi-coordinated Cl anions in axial positions (Cu···Cl = 3.029(2) Å). The Cu2 and Cu3 cations have distorted square pyramidal CuO_2N_2Cl environments. In both cases, the basal planes are occupied by two hydroxo bridging ligands (O1 and O3 for Cu2; O2 and O3 for Cu3) and two nitrogen atoms of the chelating pn ligand (Cu–O range 1.977–2.016 Å and Cu–N range 1.975–2.021 Å). Both pyramids share a strongly elongated axial position filled by the bridging Cl1 atom (Cu2–Cl1 = 2.654(2) Å and Cu3–Cl1 = 2.679(2) Å) (Fig. 1). The co-ordination

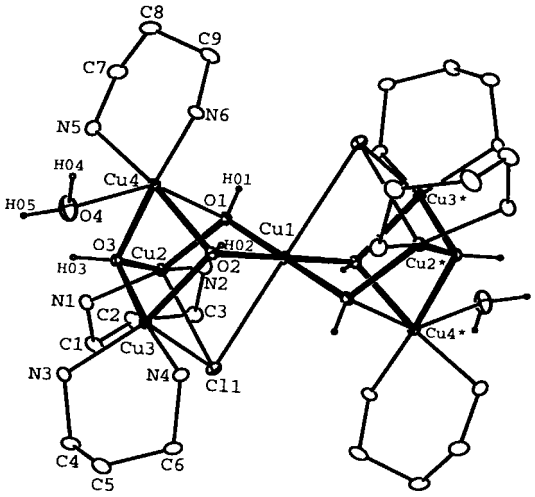

Fig. 1 ORTEP of the heptanuclear cation in **1** showing atomic labelling scheme (30% probability ellipsoids). Shortest Cu···Cu distances (Å) and selected bond angles (°): Cu1–Cu2 3.3796(5), Cu1–Cu3 3.3719(5), Cu1–Cu4 3.1873(5), Cu2–Cu3 3.2829(8), Cu2–Cu4 3.1607(8), Cu3–Cu4 2.9610(8); O1–Cu1–O2 83.9(1), O1–Cu2–O3 84.5(1), O2–Cu3–O3 80.1(1), O1–Cu4–O2 72.0(1), O1–Cu4–O3 73.7(1), O2–Cu4–O3 79.5(1). Code of equivalent positions: (*) ½ − *x*, ½ − *y*, 1 − *z*.

† Electronic supplementary information (ESI) available: detailed synthesis and X-ray crystallography of **1**. See http://www.rsc.org/suppdata/cc/b1/b105231b/

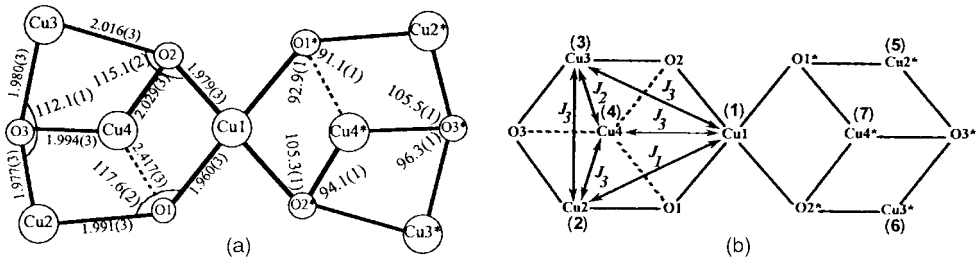

Fig. 2 (a) Schematic projection of the copper cluster including pertinent bond lengths and bond angles; (b) schematic representation of the magnetic coupling model in **1**. Code of equivalent positions: (*) ½ − *x*, ½ − *y*, 1 − *z*.

 DOI: 10.1039/b105231b

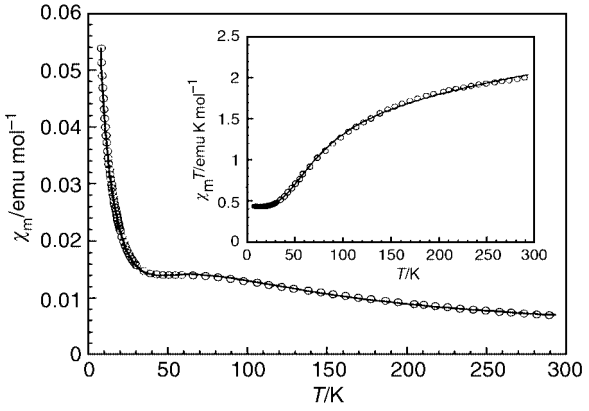

Fig. 3 Plots of molar susceptibility χ_m *vs.* T (the inset shows the $\chi_m T$ product *vs.* T) for **1** measured in a field of 1 T. The solid line was calculated using the magnetic coupling model (see text).

polyhedron of the Cu4 cation can be described as a $Cu(N_2O_2)(O_2)$ pseudo-octahedron generated by a CuN_2O_2 plane arising from two nitrogen atoms of the chelating pn ligand and the two μ_3-hydroxo ligands (O2 and O3), and two axial positions filled by the O1 hydroxo ligand and a water molecule (O4) (Cu···O4 = 2.524(4) Å). Note that the O1 hydroxo ligand may be viewed as a μ_2-bridging group since it involves two short and one long Cu–O distances as clearly shown on Fig. 2(a). Further examination of the structure shows that the tcm units, which usually act as μ_2- or μ_3-bridging ligands, are here uncoordinated; however, there are significant hydrogen bonds formed between their nitrogen atoms and the hydroxo-bridging ligands [N7(tcm)···O2 = 2.826(6) Å, O1–H···N7 = 167.3(3)° and N8(tcm)···O1 = 2.961(6) Å, O1–H···N7 = 160.6(2)°]. Such intermolecular hydrogen bonds may contribute to the stabilisation of the cluster conformation.

Magnetic susceptibility data for **1** were collected in the temperature range 2–300 K, the χ_m and $\chi_m T$ product *vs.* T plots are depicted in Fig. 3. From room temperature down to 25 K the $\chi_m T$ product decreases continuously and then reaches a plateau close to 0.43 emu K mol^{-1}, which corresponds to an $S = 1/2$ ground state. This behaviour is indicative of an overall antiferromagnetic coupling between the Cu(II) centres; this is in agreement with the strongly reduced magnetic moment at room temperature ($\chi_m T$ = 2.01 emu K mol^{-1}). Taking into account the cluster topology and connectivity (Fig. 2), it is possible to distinguish up to six different exchange pathways. However, in order to avoid an overparameterization and in view of the Cu–O–Cu angles and connectivity of the OH bridges (μ_2-OH or μ_3-OH), these six exchange pathways have been grouped into three averaged different exchange parameters. The magnetic data have been analysed with the following spin Hamiltonian:

$$\hat{H} = -2J_1(\hat{S}_1\hat{S}_2 + \hat{S}_1\hat{S}_5) - 2J_2(\hat{S}_3\hat{S}_4 + \hat{S}_6\hat{S}_7) - 2J_3(\hat{S}_1\hat{S}_3 + \hat{S}_1\hat{S}_4 + \hat{S}_2\hat{S}_3 + \hat{S}_2\hat{S}_4 + \hat{S}_1\hat{S}_6 + \hat{S}_1\hat{S}_7 + \hat{S}_5\hat{S}_6 + \hat{S}_5\hat{S}_7)$$

Calculations have been performed with the magnetism package MAGPACK.[6] The best fit obtained from a least-squares analysis of the $\chi_m T$ is $J_1 = -188.4$ cm^{-1}, $J_2 = -52.6$ cm^{-1}, $J_3 = -10.8$ cm^{-1} and $g = 2.15$ ($R = \Sigma [((\chi_m T)_{obs}^2 - (\chi_m T)_{calc}^2)/(\chi_m T)_{obs}^2] = 7.8 \times 10^{-3}$). Attempts to fit with only one or two averaged exchange parameters failed. As expected from the structural parameters depicted in Fig. 2(a) (Cu–O distances and Cu–O–Cu angles), the results show the presence of two weak antiferromagnetic interactions (J_2 and J_3) associated to the interactions by μ_3-OH as have been observed in previous cubane-type systems[2,3] and a strong one (J_1) corresponding to the exchange interaction between the two Cu connected by O1 that has a main component of μ_2-OH and a large Cu–O–Cu angle (117.6°).

This work was supported by CNRS (Centre National de la Recherche Scientifique, UMR 6521), the University of Brest (SUCRI 2E). F. T. thanks the 'Ministère de l'Education Nationale, de la Recherche et de la Technologie' for a postgraduate grant.

Notes and references

‡ Anal. Calc. for $C_{34}H_{70}Cl_4Cu_7N_{24}O_8$: C, 26.7; H, 4.6; Cl, 9.3; Cu, 29.1; N, 22.0. Found: C, 26.9; H, 4.6; Cl, 9.2; Cu, 29.2; N, 21.9%. IR data: ν/cm^{-1}: 3293m, 3247m, 2175s, 2168s, 1588m, 1195m, 1037w, 1023w, 900m, 561m, 494m.

Crystal data for **1**. $C_{34}H_{70}N_{24}O_8Cl_4Cu_7$, M = 1529.68, monoclinic, space group $C2/c$ (no. 15), a = 24.8994(3), b = 11.9801(2), c = 21.4298(3) Å, β = 112.14(6)°, U = 5920(2) Å^3, Z = 4, D_c = 1.72 g cm^{-3}, μ(Mo-Kα) = 2.72 mm^{-1}, T = 288 K, final R = 0.044, wR = 0.065 for 3924 observed reflections [$I > 4\sigma(I)$] and 351 variables.

CCDC reference number 165568. See http://www.rsc.org/suppdata/cc/b1/b105231b/ for crystallographic data in CIF or other electronic format.

1 G. Kolks, S. J. Lippard, J. V. Waszczak and H. R. Lilienthal, *J. Am. Chem. Soc.*, 1982, **104**, 717; S. Teipel, K. Griesar, W. Haase and B. Krebs, *Inorg. Chem.*, 1994, **33**, 456; S. S. Tandon, L. K. Thompson and D. O. Miller, *J. Chem. Soc., Chem. Commun.*, 1995, 1907; V. Tangoulis, C. P. Raptopoulou, S. Paschalidou, A. E. Tsohos, E. G. Bakalbassis, A. Terzis and S. P. Perleps, *Inorg. Chem.*, 1997, **36**, 5270.

2 J. W. Hall, W. E. Estes, E. D. Estes, R. P. Scaringe and W. E. Hatfield, *Inorg. Chem.*, 1977, **16**, 1572; L. Walz, H. Paulus, W. Haase, H. Langhof and F. Nepveu, *J. Chem. Soc., Dalton Trans.*, 1983, 657; J. Sletten, A. Sørensen, M. Julve and Y. Journaux, *Inorg. Chem.*, 1990, **29**, 5054; L. P. Wu, T. Kuroda-Sowa, M. Maekawa, Y. Suenaga and M. Munakata, *J. Chem. Soc., Dalton Trans.*, 1996, 2179; X. S. Tan, Y. Fujii, R. Nukada, M. Mikuriya and Y. Nakano, *J. Chem. Soc., Dalton Trans.*, 1999, 2415.

3 H. Muhonen, W. E. Hatfield and J. H. Helms, *Inorg. Chem.*, 1986, **25**, 800; V. Tangoulis, S. Paschalidou, E. G. Bakalbassis, S. P. Perlepes, C. P. Raptopoulou and A. Terzis, *Chem. Commun.*, 1996, 1297.

4 V. Tangoulis, C. P. Raptopoulou, S. Paschalidou, E. G. Bakalbassis, S. P. Perleps and A. Terzis, *Angew. Chem., Int. Ed. Engl.*, 1997, **36**, 1083.

5 J. A. Real, G. D. Munno, R. Chiappetta, M. Julve, F. Lloret, Y. Journaux, J.-C. Colin and G. Blondin, *Angew. Chem., Int. Ed. Engl.*, 1994, **33**, 1184.

6 J. J. Borrás-Almenar, J. M. Clemente-Juan, E. Coronado and B. Tsukerblat, *Inorg. Chem.*, 1999, **38**, 6081; J. J. Borrás-Almenar, J. M. Clemente-Juan, E. Coronado and B. Tsukerblat, *J. Comput. Chem.*, 2001, **22**, 985.

CHEMCOMM Communication
www.rsc.org/chemcomm

High regioselectivity in propylene hydroformylation using rhodium-bisphosphite catalysts is due to properties of the *SRS* diastereomer

John R. Briggs and Gregory T. Whiteker*

Corporate R&D, The Dow Chemical Company, 3200 Kanawha Turnpike, South Charleston, WV 25303, USA. E-mail: whitekgt2@dow.com

Received (in Cambridge, UK) 26th June 2001, Accepted 14th September 2001
First published as an Advance Article on the web 18th October 2001

The large cone angle and bite angle of the *SRS* ligand diastereomer in biphenol-based Rh-bisphosphite catalysts lead to high linear regioselectivity in the hydroformylation of propylene.

Rhodium-catalyzed hydroformylation of α-olefins is widely used for the industrial synthesis of alcohols and carboxylic acid derivatives.[1] Biphenol-based bisphosphite ligands, such as **1**,

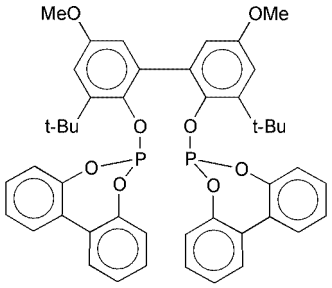

1

offer increased reaction rates and dramatic improvements in linear/branched regioselectivity (l/b) and chemoselectivity over conventional phosphine ligands in rhodium-catalyzed hydroformylation.[2] Unfortunately, a comprehensive mechanistic explanation of the factors that control hydroformylation regioselectivity has remained elusive. Several ligand structural features have been identified to be important in determining regiochemistry in hydroformylation, including steric bulk,[3] electrophilicity,[4] and, in bidentate ligands, bite angle.[5] In this communication we show that in this class of bisphosphite ligands, diastereomeric configuration can also have a profound effect on catalytic hydroformylation regiochemistry and activity.

Rhodium-catalyzed hydroformylation of α-olefins using **1** produces linear aldehydes with high regioselectivities while tolerating a wide variety of functional groups.[6] Structurally related optically-active bisphosphites have been developed which result in high regio- and enantioselectivities for asymmetric hydroformylation.[7] Due to the presence of three axial elements of chirality, bisphosphite **1** can potentially adopt three diastereomeric forms. The notation for these diastereomers (*RRR, SRR, SRS*) uses the middle descriptor for the central bridging biphenoxide moiety. Interconversion of these diastereomers can occur by rotations about the biaryl axes. Previous NMR studies have demonstrated facile epimerization of the cyclic dibenzo[*d*,*f*][1,3,2]dioxaphosphepin moiety in related bisphosphites.[8] This rotational process can interconvert all three possible diastereomers (*RRR, SRR, SRS*).

Rotation about the central *tert*-butyl substituted biphenyl axis could also interconvert *RRR* and *RSR* diastereomers, however, chiral HPLC studies reveal this process is slow. Analytical chiral stationary phase HPLC (Chiralcel OD, 99 : 1 hexane–propan-2-ol) separated **1** into two fractions (1 : 1 ratio) which exhibited identical UV spectra. When the column eluent was monitored using a polarimetric detector, the first peak exhibited a negative optical rotation; the second peak had a positive optical rotation. These enantiomers were physically separated by preparative chiral HPLC and then re-analyzed. Slow racemization of these enantiomers occurred ($t_{\frac{1}{2}}$ = 53 min) at 34 °C by rotation about the central bridging biaryl bond. Interconversion of diastereomers of **1**, therefore, most often occurs *via* dibenzo[*d*,*f*][1,3,2]dioxaphosphepin epimerization with a rate faster than the rate of hydroformylation.

Given the possibility that diastereomeric forms of **1** could contribute to the observed catalytic behavior, we sought to study the effect of isolated configurationally-stable bisphosphite diastereomers in propylene hydroformylation. Bisphosphite **2** was selected for study due to the presence of 6,6′-methyl substituents which prevent biaryl rotation. In addition, bisphosphite **2** contains 3,3′-*tert*-butyl substituents, which are necessary for high hydroformylation regioselectivity using ligands such as **1**. The synthesis of two of the three possible diastereomeric bisphosphites, **2**, is depicted in Scheme 1. Acid-catalyzed alkylation of enantiomerically-pure[9] (*R*)-**3** led to (*R*)-**4**. Synthesis of (*RRR*)-**2** and (*SRS*)-**2** as pure enantiomers was performed by reaction of (*R*)-**4** with the phosphorochloridite prepared by reaction of PCl_3 with the requisite enantiomer of **3**.

Rhodium-catalyzed propylene hydroformylation† was performed using (*RRR*)-**2** and (*SRS*)-**2** to investigate the effects of relative ligand stereochemistry. Hydroformylation using Rh–(*SRS*)-**2** resulted in a high regioselectivity (l/b = 46) with an

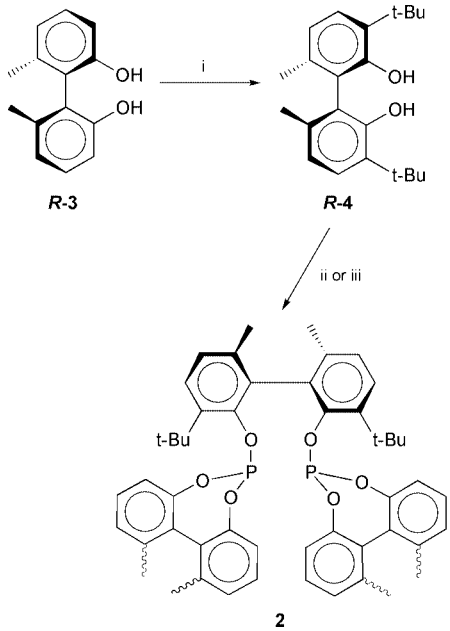

2

Scheme 1 *Reagents and conditions*: (i) isobutylene, nitrobenzene, triflic acid (5 mol%); (ii) for (*RRR*)-**2**: *R*-6,6′-dimethylbiphenylphosphochloridite (2 equiv.), NEt_3, THF; (iii) for (*SRS*)-**2**: *S*-6,6′- dimethylbiphenylphosphochloridite (2 equiv.), nBuLi, THF.

 DOI: 10.1039/b105391b

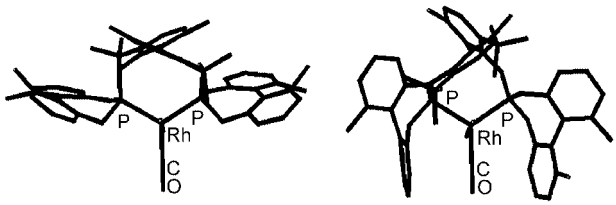

Fig. 1 Molecular mechanics structures of [(*RRR*)-**2**]Rh(CO)$_2$H (left) and [(*SRS*)-**2**]Rh(CO)$_2$H (right). Hydrogen atoms are omitted for clarity.

average rate of 513 turnovers h^{-1} over the course of 6 h. Under identical conditions, Rh–(*RRR*)-**2** gave a much lower rate (110 turnovers h^{-1}) and regioselectivity (l/b = 4) than the *SRS* diastereomer. Bisphosphite **1** exhibited a rate (434 turnovers h^{-1}) and regioselectivity (l/b = 53)[2] which was very similar to that observed with (*SRS*)-**2**. These results demonstrate that rhodium complexes of the *RRR* and *SRS* diastereomers of ligand **2** lead to inherently different regioselectivities and rates for propylene hydroformylation. The similarity between the catalytic performance of (*SRS*)-**2** and **1** suggests that during catalysis, **1** exists predominantly in the *SRS* configuration. Similar differences between bisphosphite diastereomers have been reported by van Leeuwen for asymmetric styrene hydroformylation, where the branched isomer predominates.[10] Reetz has recently reported that asymmetric alkene hydrogenation with biphenyl-based bisphosphite ligands displays an analogous difference between ligand diastereomers.[11] Our results obtained using diastereomeric structures of **2** indicate that achiral transformations mediated by bisphosphites are likewise effected by ligand structure.

Molecular mechanics calculations‡ of [(*SRS*)-**2**]Rh(CO)$_2$H and [(*RRR*)-**2**]Rh(CO)$_2$H were performed to identify the factors which could lead to their dramatically different hydroformylation behavior. The strain energies calculated for these two diastereomeric complexes were essentially identical (within 2 kcal mol^{-1}). The natural bite angle[12] for the *SRS* diastereomer was calculated to be 117°, whereas the *RRR* diastereomer was calculated to have a natural bite angle of 111°. Consistent with previous correlations[5] between hydroformylation regioselectivity and chelate natural bite angle, the more regioselective *SRS* diastereomer of **2** exhibits a larger natural bite angle than the less regioselective *RRR* diastereomer. In addition to differences in natural bite angle, these calculations also revealed a significant difference in cone angle between these two diastereomeric catalysts (Fig. 1). The cone angles at each phosphorus atom in (*RRR*)-**2** and (*SRS*)-**2** were calculated to be 104° and 157°, respectively. The *RRR* (low l/b) catalyst adopts an open geometry around the equatorial CO ligand, which should result in minimal energy differences between linear and branched alkyl or acyl intermediates. The *SRS* diastereomer, which dominates hydroformylation catalysis, is calculated to form a more crowded complex in which the two dibenzo[*d*,*f*]-[1,3,2]dioxaphosphepin moieties flank the equatorial CO ligand. This arrangement should result in large energy differences between linear and branched alkyl or acyl intermediates and could account for the high regioselectivity for linear aldehyde observed with ligands such as **1**.

Previous observations of increased hydroformylation regioselectivity with increased natural bite angle have been complicated by the relationship between cone angle and bite angle for chelating ligands.[5,12] Since large bite angle diphosphines and bisphosphites typically have larger cone angles than their smaller bite angle analogs, the inherent effect of the natural bite angle on hydroformylation regioselectivity is unclear. Recent calculations by Bo and van Leeuwen suggest that steric effects play the dominant role in determining hydroformylation regioselectivity.[13] Although the natural bite angles of (*RRR*)-**2** and (*SRS*)-**2** correlate with their hydroformylation regioselectivity, the very large difference in cone angles for these two diastereomers suggests that the high hydroformylation regioselectivity of (*SRS*)-**2** is predominantly due to an increase in steric influence of the bisphosphite ligand.

Notes and references

† Propylene hydroformylation experiments were performed in tetraglyme solution in a stirred autoclave at constant pressure (148 ppm Rh (1.4 mM), L:Rh(CO)$_2$(acac) = 2.0, 82 °C, 85 psi propylene, 45 psi 1:1 H$_2$–CO).

‡ Molecular mechanics calculations were performed using the augmented MM3 force field implemented in the CAChe software package. Natural bite angles were calculated by using a P–Rh–P bending force constant of 0 kcal mol^{-1} deg^{-2}. The authors are indebted to the reviewers for insight regarding these calculations.

1 *Rhodium Catalyzed Hydroformylation (Catalysis by Metal Complexes, Vol. 22)*, ed. P. W. N. M. van Leeuwen and C. Claver, Kluwer Academic Press, Dordrecht, 2000.
2 E. Billig, A. G. Abatjoglou and D. R. Bryant, *US Pat*., 4,769,498, 1988.
3 P. W. N. M. van Leeuwen and C. F. Roobeek, *J. Organomet. Chem*., 1983, **258**, 343.
4 W. R. Moser, C. J. Papite, D. A. Brannon, R. A. Duwell and S. J. Weininger, *J. Mol. Catal. A: Chem*, 1987, **41**, 271; J. D. Unruh and J. R. Christenson, *J. Mol. Catal. A: Chem*, 1982, **14**, 19.
5 C. P. Casey, G. T. Whiteker, M. G. Melville, L. M. Petrovich, J. A. Gavney and D. R. Powell, *J. Am. Chem. Soc*., 1992, **114**, 5535; M. Kranenburg, Y. E. M. van der Burgt, P. C. J. Kamer and P. W. N. M. van Leeuwen, *Organometallics*, 1995, **14**, 3081.
6 G. D. Cuny and S. L. Buchwald, *J. Am. Chem. Soc*., 1993, **115**, 2066.
7 J. E. Babin and G. T. Whiteker, *US Pat*. 5,360,938, 1994; G. J. H. Buisman, P. C. J. Kamer and P. W. M. N. van Leeuwen, *Tetrahedron: Asymmetry*, 1993, **4**, 1625.
8 G. T. Whiteker, A. M. Harrison and A. G. Abatjoglou, *J. Chem. Soc., Chem. Commun*., 1995, 1805.
9 S. Kanoh, N. Tamura, M. Matoi and H. Suda, *Bull. Chem. Soc. Jpn*., 1987, **60**, 2307.
10 G. J. H. Buisman, L. A. van der Veen, A. Klootwijk, W. G. J. de Lange, P. C. J. Kamer, P. W. N. M. van Leeuwen and D. Vogt, *Organometallics*, 1997, **16**, 2929.
11 M. Reetz and T. Neugebauer, *Angew. Chem., Int. Ed. Engl*., 1999, **38**, 179.
12 C. P. Casey and G. T. Whiteker, *Isr. J. Chem*., 1990, **30**, 299.
13 J. J. Carbo, F. Maseras, C. Bo and P. W. N. M. van Leeuwen, *J. Am. Chem. Soc*., 2001, **123**, 7630.

CHEMCOMM
Communication
www.rsc.org/chemcomm

An unusual hexanickel cage complex with μ- and μ_3-chloro bridges and an interstitial μ_6-chloride

Jens C. Röder, Franc Meyer* and Hans Pritzkow

Anorganisch-Chemisches Institut, Universität Heidelberg, D-69120 Heidelberg, Germany. E-mail: franc.meyer@urz.uni-heidelberg.de

Received (in Cambridge, UK) 13th July 2001, Accepted 14th September 2001
First published as an Advance Article on the web 5th October 2001

A pyrazolate-based dinucleating ligand of the bis(α-diimine) type forms an unusual hexanuclear nickel(II) cage complex incorporating an interstitial μ_6-Cl atom.

Since Brookhart and coworkers[1] introduced nickel and palladium complexes of α-diimine ligands with bulky aryl substituents as efficient pre-catalysts for olefin polymerisation,[1] these systems and various derivatives thereof have been studied extensively.[2] Most of the catalytic chemistry of such type **A** compounds is based on the presence of two active coordination sites at the single metal centre, which suggests to devise novel bimetallic type **B** complexes where two adjacent metal ions

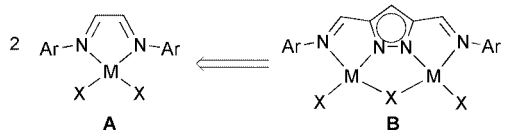

might work in concert. The basic concept, *i.e*. the use of a pyrazolate bridge to (in a formal sense) link two N-based ligand compartments in a preorganized dinucleating scaffold, has been outlined previously and has proven to be successful for the investigation of bimetallic versions of N-donor-functionalized cyclopentadienyl compounds[3] as well as bimetallic versions of classical Werner-type coordination compounds.[4,5]

A synthetic route to a multidentate pyrazolate ligand HL that bears bulky 2,6-diisopropylphenyl substituents at the imine-N atoms and that appears suitable for the preparation of type **B**

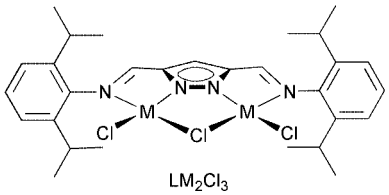

systems has been described recently.[6] Here we report the first transition metal complexes of HL. While HL forms the sought-after LM_2Cl_3 coordination compounds for M = Pd,[7] its coordination chemistry with $NiCl_2$ was found to give rise to oligonuclear species of quite unusual topology.

Treatment of HL with 1 equivalent of KO^{t}Bu and 2 equivalents of [$NiCl_2$(dme)] afforded a green complex **1** that could be crystallised from CH_2Cl_2–light petroleum (bp 40–60 °C) solution. Its analytical data† were in accord with the anticipated composition LNi_2Cl_3, but UV–VIS spectra suggested an *OC*-6 rather than a *SP*-4 coordination of the nickel(II) ions, and FAB-MS spectra were indicative of the presence of species of higher nuclearity (Fig. 1).

The molecular structure of **1** was elucidated by X-ray crystallography‡ and is shown in Fig. 2. In **1**, three bimetallic LNi_2Cl_3 building blocks have assembled *via* Cl-bridges to form a hexanuclear array with all metal ions in distorted octahedral coordination spheres. The central Ni_6Cl_9 core consists of two roughly planar Ni_3Cl_3 ring systems that are each capped by a μ_3-Cl atom. These two Ni_3Cl_3 planes are almost parallel and are held together by the three pyrazolate clips, thus forming a cage-like structure which accommodates a single Cl atom in its

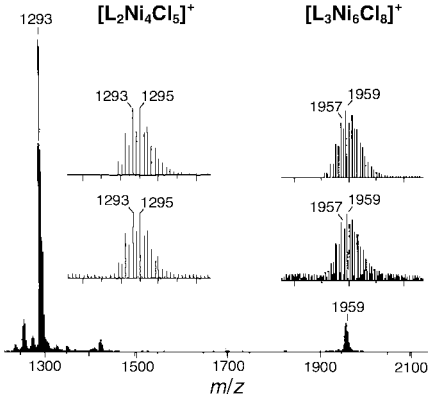

Fig. 1 FAB-MS spectrum of **1**; the inset shows the experimental (lower) and theoretical (upper) isotopic distribution for the tetranuclear $[L_2Ni_4Cl_5]^+$ and the hexanuclear $[L_3Ni_6Cl_8]^+$.

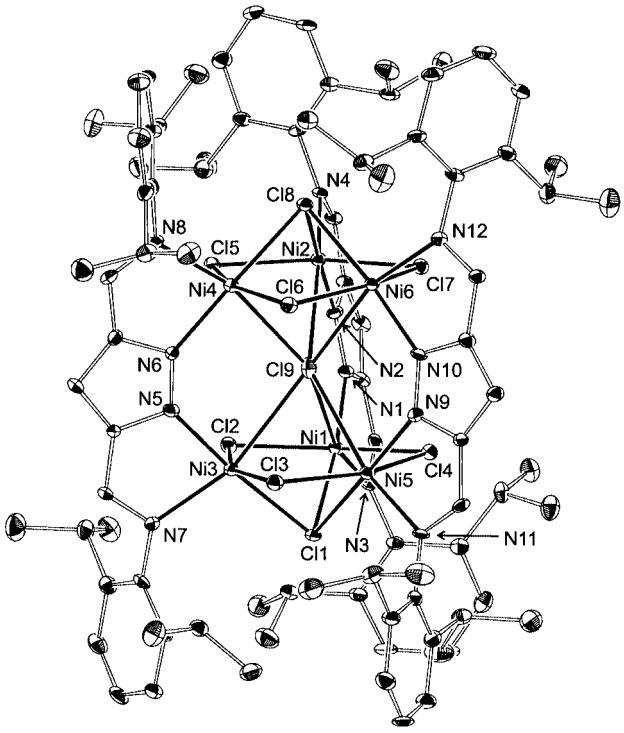

Fig. 2 Molecular structure of **1**. For clarity all hydrogen atoms have been omitted. Selected atom distances (Å): Ni–(μ-Cl) 2.360(3)–2.466(3), Ni-(μ_3-Cl) 2.402(3)–2.466(3), Ni–$N_{pyzazole}$ 1.965(7)–1.980(6), Ni-N_{imine} 2.102(7)–2.120(7), Ni1–Cl9 2.835(3), Ni3–Cl9 2.805(3), Ni5–Cl9 2.796(3), Ni2–Cl9 2.775(3), Ni4–Cl9 2.710(3), Ni6–Cl9 2.724(3), Ni···Ni within the Ni_3Cl_3 rings: 3.136(2)–3.195(3), Ni···Ni bridged by pyrazolate: 4.167(2)–4.216(2).

 DOI: 10.1039/b106258c

centre. That interstitial μ_6-Cl atom is bound to all six nickel ions in an almost trigonal prismatic fashion (trigonal twist ~ 10°). The bulky aryl substituents provide a hydrophobic shell encapsulating the central core structure.

Compared to the ubiquitous occurrence of terminal Cl and μ-Cl ligands and the frequently observed μ_3-Cl coordination, higher coordination numbers for halide ligands in discrete molecules are much less common.[8] To the best of our knowledge, μ_6-Cl atoms bound to six metal ions are very rare in molecular compounds,[9–11] and structurally characterised examples are mainly restricted to a few siloxane clusters.[11] In the latter compounds, however, the central Cl atoms are generally found in a hexagonal-planar surrounding of metal ions and feature significantly longer (and differing) metal–Cl bonds,[11] while in **1** all Ni–Cl9 distances are found in the narrow range 2.724(3)–2.835(3) Å. The structure of **1** allows for a direct comparison of these values for the μ_6-Cl with the Ni–Cl bond lengths for the μ- and μ_3-Cl bridges [*d*(Cl–Ni) = 2.360(3)–2.446(3) and 2.402(3)–2.466(3) Å, respectively], which follows the expected trend. Trigonal prismatic coordination of a Cl equidistant from six metal ions has also been reported for a hexanuclear neodymium isopropoxide complex.[9]

In the presence of donor solvents, the hexanuclear entity of **1** is degraded to complexes of lower nuclearity. From a $CHCl_3$ solution of **1** containing small amounts of EtOH, the tetranickel(II) compound $[LNi_2Cl_3(EtOH)_2]_2$ **2** was obtained in crystalline form. Its molecular structure is depicted in Fig. 3.

In **2**, two LNi_2Cl_3 building blocks are linked *via* μ- and μ_3-Cl bridges to form a stair-like dimeric aggregate (distance between the two parallel pyrazolate planes 2.034 Å), with the remaining coordination site at each metal ion now being blocked by an EtOH solvent molecules. The *OC*-6 coordination spheres of both Ni1 and Ni2 are somewhat distorted, and in particular a hydrogen bond between Cl1 and O2 causes these ligands to bend towards each other [*d*(O2···Cl1) = 3.512(2) Å]. A further H-bonding interaction is detected between the ethanol O1 atom and the π system of the opposite aryl ring [distance between O1 and the centre of the ring (C18–C23): 3.487 Å].

Formation of the unusual cage-like hexanickel array observed in **1** is not restricted to the presence of a templating μ_6-Cl atom: structures analogous to those of **1** and **2** have been obtained from the reaction of HL with $NiBr_2$(dme), where in the case of the bromo derivative of **1** the expanded Ni_3Br_3 belts give rise to an enlarged cavity suited to accommodate the larger Br atom.[6]

We thank Professor Dr G. Huttner for his generous support. Funding by the Deutsche Forschungsgemeinschaft (SFB 247, Heisenbergstipendium for F. M.) and by the Fonds der Chemischen Industrie is gratefully acknowledged.

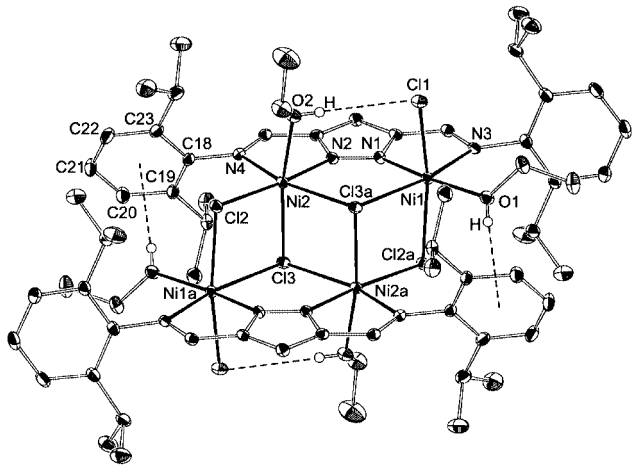

Fig. 3 Molecular structure of **2** (30% probability ellipsoids). For clarity most of the H atoms have been omitted. Selected atom distances (Å) and bond angles (°): Ni1–N1 1.963(2), Ni1–O1 2.033(2), Ni1–N3 2.243(2), Ni1–Cl(1) 2.377(1), Ni1–Cl2a 2.436(1), Ni1–Cl3a 2.641(1), Ni2–N2 2.002(2), Ni2–O2 2.110(2), Ni2–N4 2.182(2), Ni2–Cl2 2.359(1), Ni2–Cl3 2.360(1), Ni2–Cl3a 2.655(1), Ni1···Ni2 4.023(1), Ni1···Ni2a 3.670(1), Ni1···Ni1a 6.792(1), Ni2···Ni2a 3.629(1), Cl1···O2 3.512(2); Cl1–Ni1–Cl2a 164.89(2), O2–Ni2–Cl3 167.73(6).

Notes and references

† $(LNi_2Cl_3)_3$ **1**: elemental analysis: calc. for $C_{87}H_{111}Cl_9N_{12}Ni_6$ (found): C, 52.34 (51.52); H, 5.60 (5.77); N, 8.42 (8.14); Cl, 15.98 (16.06%); selected IR bands: ν_{max}/cm^{-1} (KBr) 3389vs, 2956vs, 2918vs, 2861s, 1593vs, 1577vs, 1455s, 1379m, 1356s, 1129m, 906s, 800s; UV–VIS absorptions: λ/nm (ε/M^{-1} cm^{-1} per Ni^{II}): 440(sh), 741(25), 1283(27).

‡ *Crystal data* for **1**·5CH_2Cl_2: $C_{87}H_{111}Cl_9N_{12}Ni_6$·5$CH_2Cl_2$, M = 2420.8, monoclinic, space group $P2_1/n$, a = 14.699(10), b = 34.114(15), c = 22.346(17) Å, β = 107.01(4)°, V = 10715(12) Å^3, Z = 4, D_c = 1.501 g cm^{-3}, μ(Mo-Kα) = 1.56 mm^{-1}, 18308 unique reflections measured (R_{int} = 0.080), 12524 observed [$I > 2\sigma(I)$], 1192 parameters, largest diff. peak 3.1 e Å^{-3}, final $R1[I > 2\sigma(I)]$ = 0.080, $wR2$ = 0.254, goodness of fit on F^2 = 1.038.

For **2**·4$CHCl_3$: $C_{66}H_{98}Cl_6N_8Ni_4O_4$·4$CHCl_3$, M = 1992.5, triclinic, space group $P\bar{1}$, a = 11.5542(2), b = 13.6937(2), c = 16.0974(3) Å, α = 97.368(1), β = 110.249(1), γ = 102.478(1)°, V = 2275.1(1) Å^3, Z = 1, D_c = 1.454 g cm^{-3}, μ(Mo-Kα) = 1.391 mm^{-1}, 11068 unique reflections measured (R_{int} = 0.033), 8851 observed [$I > 2\sigma(I)$], 656 parameters, largest diff. peak 0.67 e Å^{-3}, final $R1[I > 2\sigma(I)]$ = 0.038, $wR2$ = 0.106, goodness of fit on F^2 = 1.056. CCDC reference numbers 171005 and 171006. See http://www.rsc.org/suppdata/cc/b1/b106258c/ for crystallographic data in CIF or other electronic format.

1 L. K. Johnson, C. M. Killian and M. Brookhart, *J. Am. Chem. Soc.*, 1995, **117**, 6414; L. K. Johnson, S. Mecking and M. Brookhart, *J. Am. Chem. Soc.*, 1996, **118**, 267.

2 See for example: M. Svoboda and H. tom Dieck, *J. Organomet. Chem.*, 1980, **191**, 321; G. van Koten and K. Vrieze, *Adv. Organomet. Chem.*, 1982, **21**, 151; T. Schleis, T. P. Spaniol, J. Okuda, J. Heinemann and R. Mülhaupt, *J. Organomet. Chem.*, 1998, **569**, 159; S. A. Svejda and M. Brookhart, *Organometallics*, 1999, **18**, 65; T. V. Laine, M. Klinga and M. Leskelä, *Eur. J. Inorg. Chem.*, 1999, 959; A. Köppl and H. G. Alt, *J. Mol. Catal. A*, 2000, **154**, 45; S. Mecking, *Coord. Chem. Rev.*, 2000, **203**, 325.

3 J. C. Röder, F. Meyer and H. Pritzkow, *Organometallics*, 2001, **20**, 811; J. C. Röder, F. Meyer, R. F. Winter, I. Hyla-Kryspin and E. Kaifer, *Chem.-Eur. J.*, in press.

4 F. Meyer, S. Beyreuther, K. Heinze and L. Zsolnai, *Chem. Ber./Recueil*, 1997, **130**, 605; F. Meyer and P. Rutsch, *Chem. Commun.*, 1998, 1037; F. Meyer, E. Kaifer, P. Kircher, K. Heinze and H. Pritzkow, *Chem.-Eur. J.*, 1999, **5**, 1617.

5 Examples of complexes of dinucleating azolato-based N_4 ligands: F. S. Keij, R. A. G. de Graaff, J. G. Haasnoot and J. Reedijk, *J. Chem. Soc., Dalton Trans.*, 1984, 2093; P. J. van Koningsbruggen, D. Gatteschi, R. A. G. de Graaff, J. G. Haasnoot, J. Reedijk and C. Zanchini, *Inorg. Chem.*, 1995, **34**, 5175.

6 J. C. Röder, F. Meyer, M. Konrad, S. Sandhöfner, E. Kaifer and H. Pritzkow, *Eur. J. Org. Chem.*, in press.

7 J. C. Röder, F. Meyer, E. Kaifer and H. Pritzkow, unpublished work.

8 A. J. Edwards, *Halogens as Ligands* in *Comprehensive Coordination Chemistry*, Pergamon, Oxford, 1987, vol. 2, pp. 675–688; P. J. M. W. L. Birker and H. C. Freeman, *J. Am. Chem. Soc.*, 1977, **99**, 6890; P. J. M. W. L. Birker, *Inorg. Chem.*, 1979, **18**, 3502; C. Bartolomé, R. de Blas, P. Espinet, J. M. Martin-Álvarez and F. Villafañe, *Angew. Chem., Int. Ed.*, 2001, **40**, 2521.

9 R. A. Andersen, D. H. Templeton and A. Zalkin, *Inorg. Chem.,* 1978, **17**, 1962.

10 J. Eisenmann, D. Fenske and F. Hezel, *Z. Anorg. Allg. Chem.*, 1998, **624**, 1095.

11 G. Gavioli, R. Battistuzzi, P. Santi, C. Zucchi, G. Palyi, R. Ugo, A. Vizi-Orosz, O. I. Shchegolikhina, Y. A. Pozdniakova, S. V. Lindemann and A. A. Zhdanov, *J. Organomet. Chem.*, 1995, **485**, 257; A. Cornia, A. C. Fabretti, D. Gatteschi, G. Palyi, E. Rentschler, O. I. Shchegolikhina and A. A. Zhdanov, *Inorg. Chem.*, 1995, **34**, 5383; A. Cornia, A. C. Fabretti, G. Gavioli, C. Zucchi, M. Pizzotti, A. Vizi-Orosz, O. I. Shchegolikhina, Y. A. Pozdniakova and G. Palyi, *J. Cluster Sci.*, 1998, **9**, 295; C. Zucchi, M. Mattioli, A. Cornia, A. C. Fabretti, G. Gavioli, M. Pizzotti, R. Ugo, Y. A. Pozdniakova, O. I. Shchegolikhina, A. A. Zhdanov and G. Palyi, *Inorg. Chim. Acta*, 1998, **280**, 282.

CHEMCOMM Communication
www.rsc.org/chemcomm

Sulfonic acid functionalized mesoporous MCM-41 silica as a convenient catalyst for Bisphenol-A synthesis

Debasish Das,[a] Jyh-Fu Lee[b] and Soofin Cheng*[a]

[a] *Department of Chemistry, National Taiwan University, Taipei 106, Taiwan. E-mail: chem1031@ccms.ntu.edu.tw*
[b] *Research Division, Synchrotron Radiation Research Center, Hsinchu 300, Taiwan*

Received (in Cambridge, UK) 7th August 2001, Accepted 18th September 2001
First published as an Advance Article on the web 5th October 2001

Sulfonic acid groups anchored to the surface of mesoporous MCM-41 silica have been identified with S K-edge XANES spectra and the material is an efficient catalyst for the liquid phase condensation of phenol with acetone to form Bisphenol-A with high selectivity.

We report here that sulfonic acid functionalized mesoporous MCM-41 silica can be an efficient catalyst for the condensation of phenol and acetone at relatively low temperature to synthesize Bisphenol-A with a very high selectivity. Bisphenol-A is an important raw material for polymer and resin production, and it is produced industrially using ion-exchange resins such as Amberlyst.[1] However, thermal stability and fouling of the resins are major problems for these catalysts and the search for thermally stable and regenerable solid acid catalysts are continuing.

Zeolites have been increasingly used in the synthesis of fine chemicals due to their high surface area and confined domains.[2] However, the suitability of zeolites for the conversion of larger substrates has been severely limited by the available dimensions of their pores, which are in the micropore region with pore mouth diameter usually less than 1 nm.[3] For reactions to occur within the pores, the reaction substrates and products must be allowed to diffuse smoothly through the zeolite pores. The discovery of surfactant–templated mesoporous silica materials such as MCM-41 (hexagonal *P6m* symmetry) and MCM-48 (cubic *Ia3d* symmetry) with controlled pore diameters (2–10 nm) and topologies has extended the suitability of these materials for the conversion of larger substrates.[4] They are very promising for the application as catalysts and/or catalyst supports and are likely to offer potential improvements in reaction selectivity in the conversion of larger substrate molecules in their well-defined channels with narrow pore size distributions. However, in spite of these favorable pore dimensions, the acidity of Al-substituted mesoporous materials such as Al-MCM-41, is much weaker than that of microporous zeolites.[5] To overcome this drawback, the synthesis of inorganic–organic hybrid mesoporous materials with alkylsulfonic acid groups has been reported recently.[6–9] These hybrid materials can be synthesized either by direct one-step synthesis or *via* secondary silylation. Thus, MCM-SO_3H prepared by direct synthesis and secondary silyation is reported to be highly efficient in the synthesis of bisfurylalkanes[6] and also in the esterification of glycerol with fatty acids.[7,9] However, as the organic functional groups may be damaged or destroyed during the template removal process, the secondary silylation technique seems to offer a better alternative for preparing mesoporous acid catalysts.

Pure silica MCM-41 was synthesized according to the method described earlier.[10] Surface functionalization with sulfonic acid groups was carried out according to the method described in the literature.[7,8] Typically, 3.0 g of the freshly calcined MCM-41 sample was evacuated at 150 °C and then an excess of 3-mercaptopropyltrimethoxysilane (MPTS) in dry toluene was introduced. The mixture was refluxed for 6 h and the solid was filtered off, washed with dry toluene and air-dried. The –SH groups were converted into $–SO_3H$ groups by mild oxidation with H_2O_2 (stirring for 24 h at 60 °C with excess oxidant). The solid was filtered off, washed with water and ethanol, followed by acidification with 0.1 M H_2SO_4 followed by thorough washing with water to remove all traces of liquid acid. The solid material was finally dried at 60 °C overnight.

Sulfur loading of the solid material was determined by elemental analysis (Heraeus) and was typically in the range 0.9–1.8 meq. g^{-1} of solid. Thermogravimetric analysis (Du Pont 950) shows the material to be more hydrophobic than MCM-41. While calcined pure silica MCM-41 shows *ca.* 5% weight loss in the range 30–100 due to water removal, sulfonic acid functionalized MCM-41 (denoted MCM-SO_3H) showed only $<1\%$ weight loss in this region. Loss of sulfonic acid groups starts at *ca.* 200 °C and is completed by 325 °C. The specific surface area and pore volume of the pure silica MCM-41 material was reduced from 1035 $m^2\ g^{-1}$ and 0.85 $cm^3\ g^{-1}$, respectively, to 690 $m^2\ g^{-1}$ and 0.42 $cm^3\ g^{-1}$ after anchoring the sulfonic acid groups. Although the pore size distribution curve (Fig. 1) becomes somewhat broad after sulfonic acid group introduction and the peak maximum shifts from 27 Å (pure MCM-41) to 22 Å, the pore size distribution still remains very narrow with major fractions of pores lying within the 7 Å region. These results indicate that anchoring sulfonic groups to the channels of MCM-41 reduced the pore diameter and volume of MCM-41 but did not damage the mesoporous structure. This was also affirmed by the retention of sharp diffraction peaks in the corresponding XRD pattern.

To obtain good catalytic activity it is imperative that the thiol groups can be effectively oxidized to active sulfonic acid groups. To monitor this process, the oxidation states of sulfur were examined by studying the S K-edge XANES spectra of the sample before and after oxidation. The XANES experiments were performed at Beam line 15B at the Synchrotron Radiation Research Center facility at Hsinchu, Taiwan. Standard operating conditions were 1.5 GeV and 200 mA beam current and the

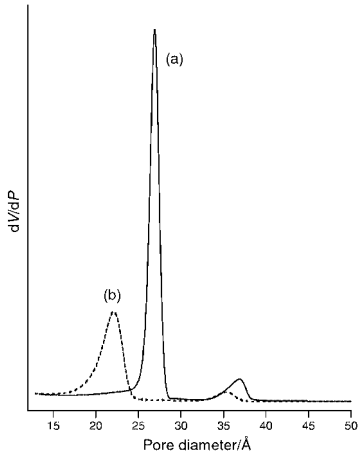

Fig. 1 Pore size distribution of (a) calcined pure silica MCM-41 and (b) MCM-41 functionalized with sulfonic acid groups.

 DOI: 10.1039/b107155f

photon energies were calibrated using the L-edge of pure Mo foil. Fig. 2 shows the S K-edge XANES spectra of the thiol functionalized samples before and after H_2O_2 oxidation. It has been reported that both the energy position (E_k) and intensity of the S s→p transition peak (white-line) are sensitively related to the oxidation state of the S atom.[11] Studies with model compounds showed an increase of E_k and amplitude of the white-line with increasing formal oxidation states of S. Thus, for unoxidized sample containing thiol groups the white-line appears at 2472 eV corresponding to sulfur in the reduced state. After H_2O_2 oxidation the white-line shifts to higher energy (2481 eV) which corresponds to sulfonic acid with S in the +5 state.[11,12] It can be seen from Fig. 2 that most of the anchored thiol groups have been oxidized to sulfonic acid groups under the above oxidation conditions.

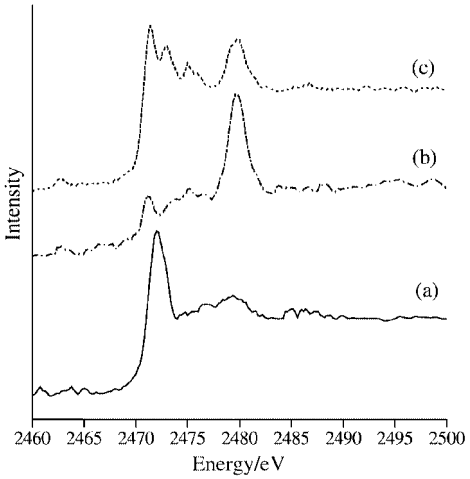

Fig. 2 S K-edge XANES spectra of thiol functionalized MCM-41 materials (a) before oxidation, (b) after oxidation and (c) sample with incomplete oxidation of thiol groups.

Condensation of phenol and acetone to Bisphenol-A (Scheme 1) was carried out at temperatures of 70–125 °C with the sulfonic acid functionalized MCM-41 silicas. Several other acidic zeolites such as H-ZSM-5, H-Y and H-beta have also been used for comparison. The products were analyzed and identified using a Chrompak 9000 gas chromatograph and HP 6890 GC-MS, and the results are given in Table 1. No conversion of phenol was observed in the absence of catalyst. While acidic zeolites like H-ZSM-5, H-Y and H-beta showed negligible activity at 70 °C, MCM-SO_3H showed 30% phenol conversion (*cf.* 40% maximum theoretical conversion at a phenol : acetone molar ratio of 5 : 1) with >90% selectivity towards *p,p′*-Bisphenol-A; the other product was *o,p′*-Bisphenol-A. The conversion was found to increase with the reaction temperature, but the selectivity remained almost unchanged up to 120 °C. Chroman and trisphenols were not detected at temperature below 125 °C, but small amounts (<1%) of these byproducts were detected at or above 125 °C. Recently, the synthesis of Bisphenol-A over heteropolyacid encapsulated MCM-41 has been reported.[13] However, 12-tungstophosphoric acid encapsulated MCM-41 was found to be catalytically active only at temperatures above 120 °C. Due to this high reaction temperature, several by-products such as alkylated phenols and chroman derivatives were formed, and

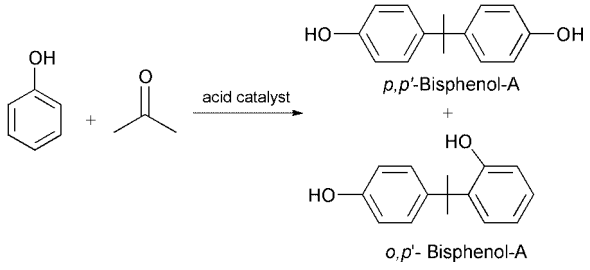

Scheme 1

Table 1 Synthesis of Bisphenol-A with sulfonic acid functionalized MCM-41 silicas[a]

Entry	Catalyst	Phenol conversion (%)	Selectivity[b] (%)
1	—	0	—
2	H-beta[c]	5	55
3	HY[d]	7	—
4	HZSM-5[e]	<5	10
5	MCM-SO_3H	30	92
6	MCM-SO_3H[f]	17	90

[a] *Reagents and conditions*: Phenol 4.7 g, acetone 0.58 g, (molar ratio = 5 : 1), catalyst 50 mg, 70 °C, 24 h. [b] Selectivity to *p,p′*-Bisphenol-A. [c] Si/Al = 50. [d] Si/Al = 10.6. [e] Si/Al = 80. [f] Incomplete oxidation (from XANES).

the selectivity to Bisphenol-A was much lower than that obtained with MCM-SO_3H. Furthermore, leaching of sulfur during the catalytic reaction was found to be negligible with MCM-SO_3H. Elemental analysis of the catalyst before reaction indicated *ca.* 3.4% sulfur and 5.6% carbon content. After reaction at 70 °C, these values were 3.2% S and 9.5% C. The slight decrease in sulfur content is mainly due to the increase in weight from adsorption of organic species. On the other hand, it is noted that optimization of the oxidation process in the preparation of MCM-SO_3H is essential to achieve high catalytic activity. For samples with similar sulfur loadings but with incompletely oxidized thiol groups (dotted line in Fig 2) the activity was found to be much lower (see Table 1). XANES spectra of the samples with incompletely oxidized sulfur species showed a number of peaks around 2472 eV, suggesting the presence of lower valent sulfur species such as sulfides and disulfides.[11,12] It has also been observed that at higher sulfur loadings (>1.5 meq. g^{-1} solid) part of the sulfur remains in the reduced form even after prolonged oxidation, probably due to formation of sulfides and disulfides.

In conclusion, sulfonic acid anchored MCM-41 has been found to be very effective in the synthesis of *p,p′*-Bisphenol-A with very high selectivity at relatively low reaction temperatures. S K-edge XANES studies can be used as a convenient tool for easy monitoring of the oxidation state of sulfur in the samples.

Financial support was provided by the Chinese Petroleum Corporation and the Ministry of Education, Taiwan.

Notes and references

1 G. D. Yadov and N. Kirthivasan, *Appl. Catal.*, 1997, **154**, 29.
2 M. E. Davis, *Microporous Mesoporous Mater.*, 1998, **21**, 173; R. A. Sheldon, J. A. Elings, S. K. Lee, H. E. B. Lempers and R. S. Downing, *J. Mol. Catal. A*, 1998, **134**, 129; S. Feast and J. A. Lercher, *Stud. Surf. Sci. Catal.*, 1996, **102**, 363.
3 M. E. Davis, *Acc. Chem. Res.*, 1993, **26**, 111.
4 J. S. Beck, J. C. Vartuli, W. J. Roth, M. E. Leonowicz, C. T. Kresge, K. D. Schmitt, C. T. Chu, D. H. Olson, E. W. Sheppard, S. B. McCullen, J. B. Higgins and J. L. Schlenker, *J. Am. Chem. Soc.*, 1992, **114**, 10834; P. T. Tanev and T. J. Pinnavaia, *Science*, 1995, **267**, 865; X. S. Zhao, G. Q. Lu and G. J. Miller, *Ind. Eng. Chem. Res.*, 1996, **35**, 2075.
5 A. Corma, V. Fornes, M. T. Navarro and J. Perez-Pariente, *J. Catal.*, 1994, **148**, 569.
6 W. Van Rhijn, D. De Vos, W. Bossert, J. Bullen, B. Wouters, P. Grobet and P. Jacobs, *Stud. Surf. Sci. Catal.*, 1998, **117**, 183; W. M. Van Rhijn, D. E. B. F. Sels, W. D. Bossert and P. A. Jacobs, *Chem. Commun.*, 1998, 317.
7 W. D. Bossert, D. E. De vos, W. M. Van Rhijn, J. Bullen, P. J. Grobet and P. A. Jacobs, *J. Catal.*, 1999, **182**, 156.
8 M. H. Lim, C. F. Blanford and A. Stein, *Chem. Mater.*, 1998, **10**, 467.
9 I. Diaz, F. Mohino, J. Perez-Pariente and E. Sastre, *Appl. Catal. A*, 2001, **205**, 19.
10 D. Das, C-M. Tsai and S. Cheng, *Chem. Commun.*, 1999, 473.
11 G. Sarret, J. Connan, M. Kasrai, G. M. Bancroft, A. Charrie-Duhaut, S. Lemoine, P. Adam, P. Albrecht and L. Eybert-Berard, *Geochim. Cosmochim. Acta.*, 1999, **63**, 3767.
12 K. Xia, F. Weesner, W. F. Bleam, P. R. Bloom, U. L. Skyllberg and P. A. Helmke, *Soil Sci. Soc. Am. J.*, 1998, **62**, 1240.
13 K. Nowinska and W. Kaleta, *Appl. Catal. A*, 2001, **203**, 91.

CHEMCOMM Communication
www.rsc.org/chemcomm

Oxy-function promoted hydroboration of conjugated dienes with controlled allylic borane rearrangement

Takashi Sugimura,* Futoshi Nishida, Takahiro Tei, Akiko Morisawa, Akira Tai and Tadashi Okuyama

Faculty of Science, Himeji Institute of Technology, Kohto, Kamigori, Ako-gun, Hyogo 678-1297, Japan. E-mail: sugimura@sci.himeji-tech.ac.jp; Fax: +81-791-58-0115; Tel: +81-791-58-0168

Received (in Cambridge, UK) 31st July 2001, Accepted 13th September 2001
First published as an Advance Article on the web 1st October 2001

Hydroboration of conjugated dienes is promoted by the hydroxy and methoxy groups, which also control the rearrangement of the initially produced allylic boranes.

The hydroboration–oxidation process has been established as a useful synthetic tool for conversion of an olefinic function to a hydroxy group with control of the regio- and stereochemistries.[1] The reaction can also be applied to conjugated diene systems but the factors governing the reaction selectivities are more complicated.[2] Synthetic use of hydroboration with conjugated diene substrates requires not only control of these factors but also a solution to overcome the poorer reactivity of the diene unit, especially those likely to give a mono-hydroboration product. Hence, only limited examples of such reactions have been reported.[3] The expected difficulties are in controlling: 1) regioselectivity of the initial addition, 2) allylic borane rearrangement of the adduct, and 3) the second addition through cyclic hydroboration and through hydroboration with an external borane.

In contrast to hydrosilylation,[4] hydroboration is known not to be directed by a hydroxy group. Borane reagents readily react with the hydroxy group before the addition to the olefinic unit, and the produced borate acts only as a steric fence for the second borane reagent. Thus, more than two equivalents of a borane reagent have been employed.[5] However, during the study of asymmetric synthesis of polypropionate units through chiral cyclic dienes, we found that the hydroxy group in **3b** promotes mono-hydroboration and the reaction completed only with one equivalent of $ThexBH_2$. Strict control of rearrangement of the initially produced allylic boranes is also caused by the oxy-functions.

Optically active cyclic dienes **3a**–**e** (Scheme 1) were prepared under strict stereocontrol by the rhodium-catalyzed reaction of stereochemically pure **1**.[6,7]

Hydroboration of an unfunctionalized substrate **3a** (X = H) with $ThexBH_2$ (2 eq.) in THF at room temperature was slow, and 48 h was required to complete the reaction. After the usual workup (30% H_2O_2 with 1 M NaOH for 5 h), two diols **4** and **5** were obtained in a 2 : 1 ratio (66.3%, Scheme 2).[8] The reaction with a smaller amount of $ThexBH_2$ (1 eq.) or a shorter reaction time (5 h) did not give any mono-hydroboration product but only the two diols **4** and **5** at the same ratio in low conversion of the reactant. Bis-substituted boranes like diisoamylborane and 9-BBN did not cause the hydroboration of **3a**, but most of **3a** was recovered after the oxidative workup.

The result with **3a** is just an additional example of a less active diene substrate for the hydroboration indicating the difficulty in interruption of the second hydroboration. In contrast, the hydroboration of a hydroxylated substrate **3b** (X = OH) occurred smoothly at room temperature with $ThexBH_2$, and was completed within 2–4 h. The product after workup was mono-hydroborated product **6** as a single isomer (>99% selectivity), and no bis-hydroboration was observed even with excess $ThexBH_2$ for a longer reaction time. Unexpectedly, the substrate **3b** was consumed even with one equivalent of $ThexBH_2$, and **6** was isolated in 86.1% yield after workup.

Since the reaction of **3b** with $ThexBH_2$ should start with quick reaction at the hydroxy group to give **A** in Scheme 3,[5] further reaction at the olefinic bond was expected to be sluggish with one equivalent of $ThexBH_2$. However, a small amount of $ThexBH_2$ can remain. Considering the low reactivity of **3a**, the oxy-function in **A** should play a role in promoting the addition of $ThexBH_2$ at the 10,11-bond from the same face of the hydroxy group. Facile allylic rearrangement in the adduct **B** results in a stable cyclic borate **D** with regeneration of $ThexBH_2$. Thus, a disproportionation of the borate species may facilitate this process.

Promotion of the hydroboration by the oxy-function in **A** was mimicked with O-protected substrates **3c**–**e** (X = OR). The

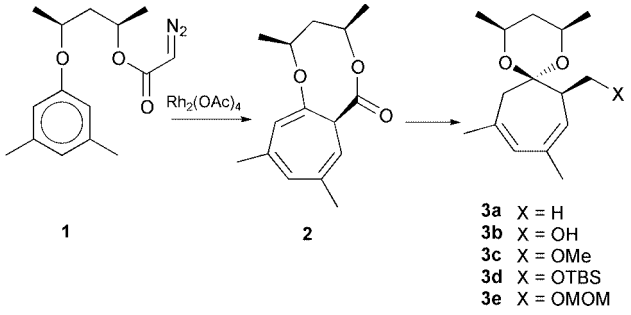

Scheme 1 Synthesis of chiral dienes.

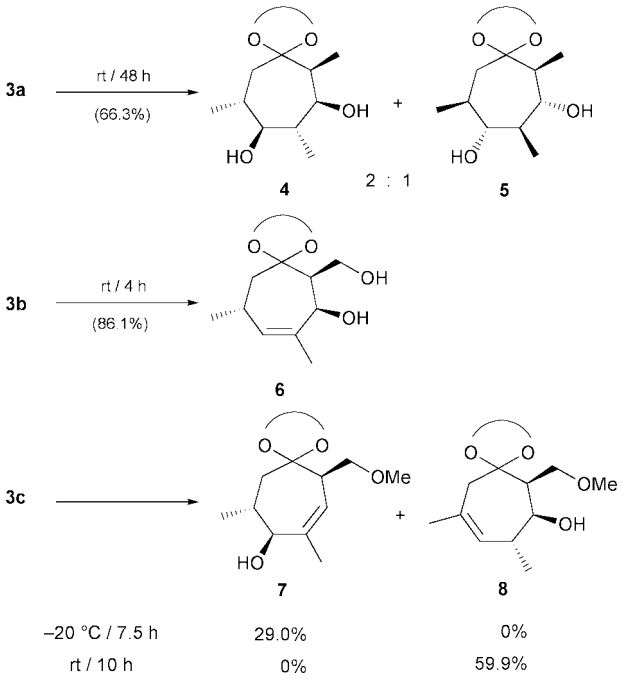

Scheme 2 Hydroboration of **3** with $ThexBH_2$ in THF followed by the oxidation with NaOH–H_2O_2 (O–O = *meso*-pentane-2,4-diol moiety).

 DOI: 10.1039/b106850d

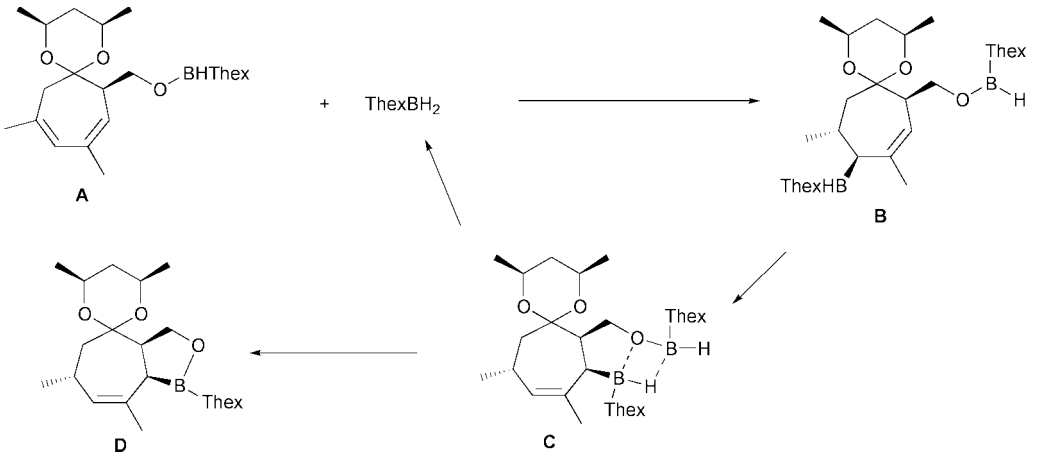

Scheme 3 Plausible mechanism of the hydroboration of **3b** with $ThexBH_2$.

reaction of **3d** or **3e** with excess $ThexBH_2$ at room temperature did not give any hydroboration product but resulted in the substrate recovery after the oxidative workup. In contrast, the reaction of **3c** (X = OMe) with one equivalent of $ThexBH_2$ proceeded even at −20 °C (7.5 h) to give **7** as a sole product in 29.0% yield together with a recovery of **3c** in 50.1%. Thus, the oxy-function having proper bulkiness and coordination ability was found to promote the hydroboration of the diene. It was also confirmed that the initial site of addition is at the 10,11-bond when the reaction is promoted by the oxy-functions. Elevation of the hydroboration temperature of this reaction increases the reaction conversion accompanied by rearrangement of **7**, which resulted in production of another regioisomer, **8**. The reaction at room temperature for 10 h afforded **8** as a single isomer in 59.9% yield after workup.

The results with **3c** indicate that the borane adduct at the 10,11-bond is fragile at room temperature. Although the observed rearrangement in **3c** is possible through cyclohydroboration (in giving a 4-membered carboborane) and retro-hydroboration, a process consisting of retro-hydroboration of the kinetic adduct and then re-hydroboration to give a thermodynamically stable adduct is more likely. When the adduct was treated with cyclohexene at −20 °C followed by warming up to room temperature, **8** was not obtained and the conversion of **3c** to **7** was reduced. Since the second olefin addition to a $ThexBH_2$ adduct is known to be slower than the first addition,[9] cyclohexene should have trapped the regenerated free $ThexBH_2$.

In this communication, we have demonstrated that the hydroxy and methoxy groups promote the hydroboration of the diene, and fully control the rearrangement of the initial adduct in a different manner. The role of the oxy-functions in the promotion of the hydroboration is suggested to be due to interruption of the retro-hydroboration. Details of the further reactions of the obtained products aiming at asymmetric synthesis of polypropionate units are in progress.

Notes and references

1 H. C. Brown, *Boranes in Organic Chemistry*, Cornell University Press, Ithaca, 1972; A. Pelter, K. Smith and H. C. Brown, *Borane Reagents*, Academic Press, London, 1988; K. Smith and A. Pelter, in *Comprehensive Organic Synthesis*, ed. B. M. Trost, Pergamon, Oxford, 1991, vol. 8, pp. 703–731; M. Zaidlewicz, in *Stereoselective Synthesis*, Thieme, Stuttgart, 1996, vol. E21, pp. 4519–4530.

2 G. Zweifel, K. Nagase and H. C. Brown, *J. Am. Chem. Soc*., 1962, **84**, 183 and 190; G. Zweifel and H. C. Brown, *J. Am. Chem. Soc*., 1063, **85**, 2066; H. C. Brown and E. Negishi, *Pure. Appl. Chem*., 1972, **29**, 527; H. C. Brown and E. Negishi, *Tetrahedron*, 1977, **33**, 2331; H. C. Brown, R. Liotta and G. W. Kramer, *J. Org. Chem*., 1978, **43**, 1058; H. C. Brown and K. S. Bhat, *J. Org. Chem*., 1986, **51**, 445; H. C. Brown, K. S. Bhat and P. K. Jadhav, *J. Chem. Soc., Perkin Trans. 1*, 1991, 2633.

3 J. J. Partridge, N. K. Chadha and M. R. Uskokovic, *J. Am. Chem. Soc*., 1973, **95**, 7171; A. Ruttimann and H. Mayer, *Helv. Chim. Acta*., 1980, **63**, 1456; U. D. Dhokte, P. M. Pathare, V. K. Mahindroo and H. C. Brown, *J. Org. Chem*., 1998, **63**, 8276.

4 K. Tamao, T. Nakajima, R. Sumiya, H. Arai, N. Higuchi and Y. Ito, *J. Am. Chem. Soc*., 1986, **108**, 6090; K. Tamao, Y. Nakagawa, H. Arai, N. Higuchi and Y. Ito, *J. Am. Chem. Soc*., 1988, **110**, 3712.

5 G. Schmid, T. Fukuyama, K. Akasaka and Y. Kishi, *J. Am. Chem. Soc*., 1979, **101**, 259; W. C. Still and J. C. Barrish, *J. Am. Chem. Soc*., 1983, **105**, 2487; C. H. Heathcock, E. T. Jarvi and T. Rosen, *Tetrahedron Lett*., 1984, **25**, 243; K. N. Houk, N. G. Rondan, Y. Wu, J. T. Metz and M. N. Paddon-Row, *Tetrahedron*, 1984, **40**, 2257; D. H. Birtwistle, J. M. Brown and M. W. Foxton, *Tetrahedron Lett*., 1986, **27**, 4367; T. W. Bell, J. R. Vargas and G. A. Crispino, *J. Org. Chem*., 1989, **54**, 1978.

6 T. Sugimura, S. Nagano and A. Tai, *Chem. Lett*., 1998, 45; T. Sugimura, H. Kohno, S. Nagano, F. Nishida and A. Tai, *Chem. Lett*., 1999, 1143.

7 Stereochemically pure **1** was prepared in three steps by the reported method (see ref. 4, 64%). Treatment of **1** with $Rh_2(OAc)_4$ at room temperature resulted in predominant formation of **2** (97.1%, >99.6% diastereomeric excess). Lithium aluminium hydride reduction of **2** (94.5%) followed by isomerization with pyridinium tosylate proceeded regio- and stereo-specifically to give **3b** as the sole product (91.9%). Stereochemistry of **3b** at the acetal position was determined by NOE. The enantiomeric purity of **3b** at the 7-position was confirmed to be over 99.6%. Treatment of **3b** with methyl iodide and sodium hydride gave **3c** (93.3%), and tosylation of **3b** followed by lithium aluminium hydride reduction gave **3a** (66.5% for two steps).

8 Structures of all new compounds were fully characterized. Stereochemical assignments were based on the NOE experiments of ^1H NMR and chemical correlations.

9 G. Zweifel and H. C. Brown, *J. Am. Chem. Soc*., 1963, **85**, 2066.

CHEMCOMM Communication
www.rsc.org/chemcomm

Spontaneous polymerisation on amphibole asbestos: relevance to asbestos removal

Ivana Fenoglio, Maura Tomatis and Bice Fubini*

Dipartimento di Chimica Inorganica, Chimica Fisica e Chimica dei Materiali and Interdepartmental Center 'G. Scansetti' for Studies on Asbestos and other Toxic Particulates, Università di Torino, Via P. Giuria 7, Torino, Italy. E-mail: fubini@ch.unito.it

Received (in Cambridge, UK) 23rd July 2001, Accepted 14th September 2001
First published as an Advance Article on the web 1st October 2001

Taking advantage of the spontaneous polymerisation of eugenol to lignin-like species catalysed by the surface of crocidolite fibres, a procedure is proposed, possibly useful in asbestos removal and disposal, where the polymer avoids the release of airborne fibres and also scavenges ROS (reactive oxygen species).

Pioneering studies on the formation of protobiopolymers following Bernal's hypothesis[1a] on the origin of life have focused attention on the polymerisation of eugenol to lignin-like polymers,[1b] because lignin is, after cellulose, the most abundant organic material on Earth. Silica and silicates, the major constituents of the Earth's crust, have been proposed as materials exhibiting appropriate surface sites for catalysed polymerisation.[2] Various silicates have indeed been found to catalyse the polymerisation of eugenol in the presence of hydrogen peroxide. The reaction appears to be promoted by hydroxyl radicals released from the Fenton-like decomposition of hydrogen peroxide.[2a]

We have revisited this reaction from a different viewpoint and investigated whether it could take place not only on serpentine asbestos (chrysotile) but also on the amphibole asbestos crocidolite (fibrous riebeckite), considered to be the most dangerous form of asbestos.[3] The reaction was carried out by adding a solution of hydrogen peroxide to a suspension of crocidolite in an aqueous solution of eugenol. After the reaction, crocidolite fibres appear to be completely included in a polymer matrix and the resulting product is a bulk solid material. Fig. 1 compares the SEM (scanning electronic microscope) images of the product obtained with crocidolite with the original fibre. No free fibres are present at the surface of the product which appears smooth and polished. Only at higher magnification are the individual fibres trapped within the polymeric matrix detectable. No modifications in the polymer were detectable several months after the polymerisation had occurred.

It is generally accepted that free radical generation upon fibre/cell contact is one of the steps yielding the pathogenic response to inhaled fibres.[4–6] Crocidolite is highly reactive in releasing free radicals.[4,5,7,8] Two radical-generating mechanisms are usually investigated in cell-free systems[4,5,8,9] (Scheme 1): (i) the release of $OH^{\cdot}$ radicals in the presence of hydrogen peroxide, mimicking contact with lysosomal fluids, following phagocytosis by alveolar macrophages and recruited polymorphonucleated cells (PMN); (ii) the release of $CO_2^{\cdot -}$ radicals from the formate ion, used as target molecule for homolytic cleavage of a carbon–hydrogen bond, which occurs with several endogenous molecules such as peptides, proteins and lipids. The free radical release from aqueous buffered suspensions of crocidolite was measured before and after the treatment by means of the classical spin trapping technique.[5] Fig. 2 shows the EPR (electronic paramagnetic resonance) spectra of the radical adducts obtained from suspensions of, respectively, crocidolite and crocidolite treated with eugenol in a buffered solution (pH 7.4) of (a) hydrogen peroxide and (b)

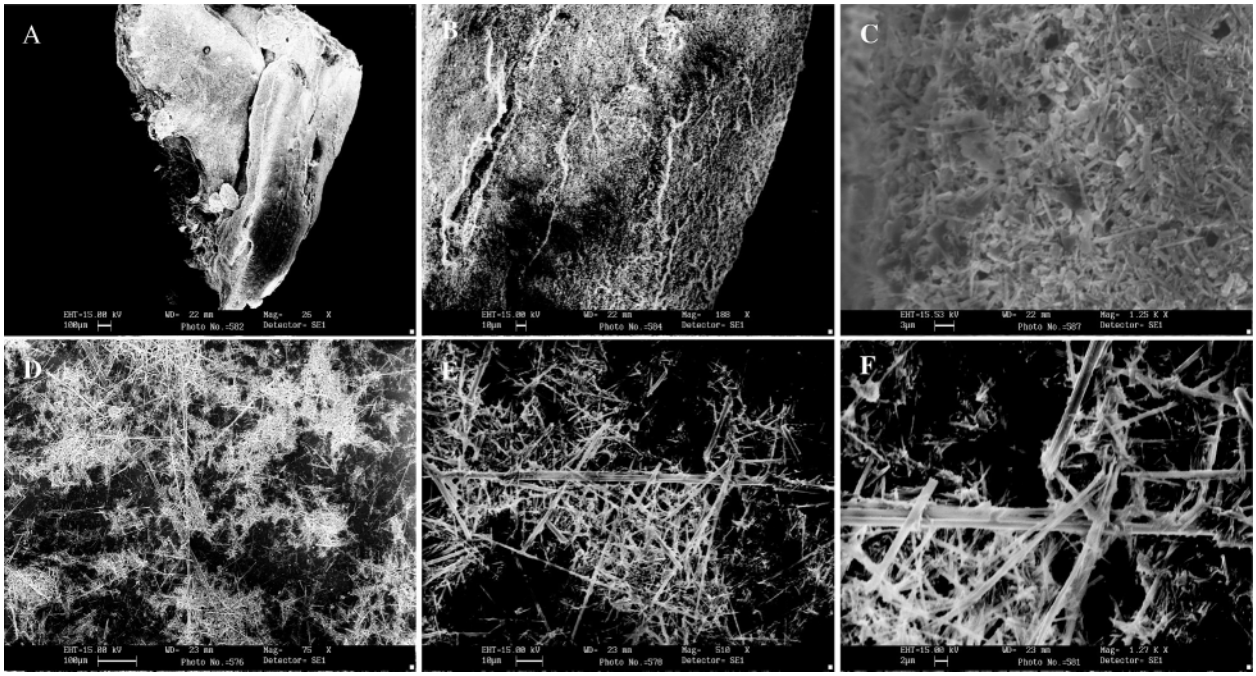

Fig. 1 SEM images at increasing magnitude of a fragment of crocidolite following surface polymerisation of eugenol (A, B, C), compared with original crocidolite fibres (D, E, F) at the same magnification. When treated with eugenol, crocidolite appears a solid, non-fibrous material. A very high magnification is required to detect the single fibres trapped into the polymeric matrix.

 DOI: 10.1039/b106541f

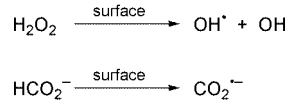

Scheme 1 Hydroxyl radical release and homolytic cleavage of carbon–hydrogen bond mediated by asbestos fibers.

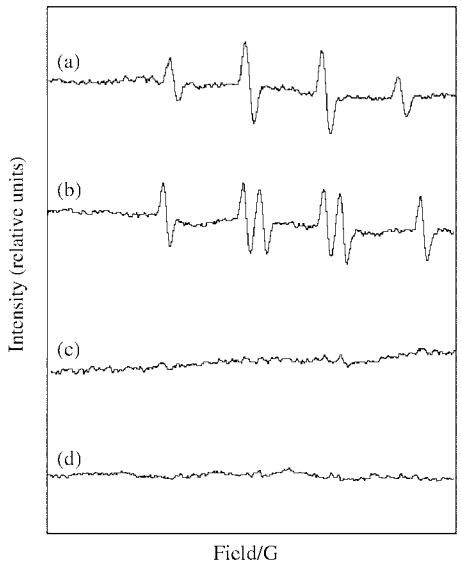

Fig. 2 Free radical release from crocidolite fibres (signals a, b) and of eugenol-treated crocidolite (signals c, d): in the presence of hydrogen peroxide (signals a, c) or sodium formate (signals b, d) the EPR spectra of the supernatant from an aqueous suspension of fibres (pH 7.4, phosphate buffer) recorded after 60 min show, with crocidolite, the typical signals of the [DMPO–OH] and [DMPO–CO_2]$^{\bullet-}$ adducts, respectively. Crocidolite fibres contacted with eugenol lose their radical release potential.

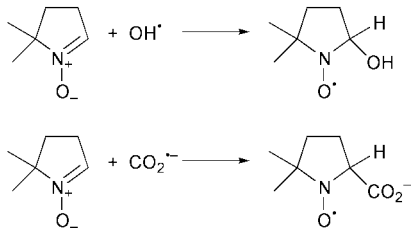

Scheme 2 Reaction of hydroxyl radical and carboxylate radical with the spin trap DMPO.

sodium formate in the presence of the spin trap 5-5′-dimethyl-1-pyrroline-*N*-oxide (DMPO) (Scheme 2). The amount of radical released is proportional to the intensity of the signals of the [DMPO–OH]$^{\bullet}$ and [DMPO–CO_2]$^{\bullet-}$ adducts, respectively. No radical release was observed from the crocidolite treated with eugenol. The activity was partially restored only after heavy grinding, which exposed fresh surfaces of fibres to the air. The inactivation may be partially ascribed to the dramatic decrement of the exposed surface but is also due to a scavenging effect of the lignin-like polymer. Lignin is, in fact, considered responsible for the antimutagenic/anticarcinogenic effect of dietary fibre. The protective effect is attributed to the scavenging property towards free radicals.[10] There is evidence that the inactivation is not due to the reaction of the surface with hydrogen peroxide: the active sites present on the surface of the crocidolite fibres are catalytic sites not consumed during the reaction with hydrogen peroxide.[8,11]

The reaction described, once set up for practical application, may be proposed as an intermediate step to be taken in the procedure of asbestos removal, which is still a controversial issue.[3,12,13] This could avoid the formation of airborne fibres, transforming a fibrous particulate material into a bulk solid for disposal. Note that if the polymerisation solution is maintained over the surface of the material during removal, any accidentally detached fibres will act as a catalyst for the reaction and will consequently be covered by the lignin-like polymer. The observed inactivation of radical release by the action of the lignin-like polymer makes this reaction advantageous with respect to other methods.[14,15] It can thus be regarded as a new approach to the problem of disposal employing a one-pot reaction under mild conditions, as a continuous surface-inactivating process takes place along with asbestos removal.

This study was supported by the Regione Piemonte, Italy.

Notes and references

1 (*a*) J. D. Bernal, *The Physical Basis of Life*, Routledge & Kegan Paul, London, 1951; (*b*) S. M. Siegel, *Proc. Nat. Acad. Sci*., 1957, **43**, 811.
2 (*a*) S. M. Siegel, *J. Am. Chem. Soc*., 1957, **79**, 1628; (*b*) V. A. Basiuk, T. Y. Gromovoy and E. G. Khil'chevskaya, *Origin Life Evol. Biosphere*, 1995, **25**, 375.
3 B. T. Mossman, J. Bignon, M. Corn, A. Seaton and J. B. L. Gee, *Science*, 1990, **247**, 294.
4 D. W. Kamp, P. Graceffa, W. A. Pryor and S. A. Weitzman, *Free Radical Biol. Med*., 1992, **12**, 293; D. W. Kamp and S. A. Weitzman, *Thorax*, 1999, **54**, 638.
5 J. A. Hardy and A. E. Aust, *Chem. Rev*., 1995, **95**, 97.
6 B. Fubini and C. Otero-Aréan, *Chem. Soc. Rev*., 1999, **28**, 373.
7 S. A. Weitzman and P. Graceffa, *Arch. Biochem. Biophys*., 1984, **228**, 373.
8 B. Fubini, L. Mollo and E. Giamello, *Free Radical Res*., 1995, **23**, 593.
9 M. Gulumian and J. A. van Wyk, *Chem.-Biol. Interact*., 1987, **62**, 89; R. Zalma, J. Guignard, H. Pezerat and M. C. Jaurand, *Effect of Mineral Dusts on Cells*, NATO ASI Series, Springer-Verlag, Berlin, 1989
10 F. J. Lu, L. H. Chu and R. J. Gau, *Nutr. Cancer*, 1998, **30**, 31; L. Ebringen, L. Krizkova, J. Polony, J. Dobias and N. Lahitova, *Anticancer Res*., 1999, **19**, 569.
11 I. Fenoglio, L. Prandi, M. Tomatis and B. Fubini, *Redox Rep*., 2000, in press.
12 G. Ryan, R. M. Buchan, T. J. Keefe and C. S. McCammon, *Appl. Occup. Environ. Hyg*., 1996, **11**, 1417.
13 J. D. Burdett, S. A. Jaffrey and A. P. Rood, *Non Occupational Exposure to Mineral Fibres*, IARC, Lyon, France, 1989
14 T. Inaba, M. Nagano and M. Endo, *Electr. Eng. Jpn*., 1999, **126**, 73; T. Inaba and T. Iwao, *IEEE Trans. Dielec. Electr. Insul*., 2000, **7**, 684.
15 A. F. Gualtieri, *J. Appl. Polym. Sci*., 2000, **75**, 713.

CHEMCOMM Communication
www.rsc.org/chemcomm

Carbon nanotube template promoted growth of NbS_2 nanotubes/nanorods†

Yan Qiu Zhu, Wen Kuang Hsu, Harold W. Kroto and David R. M. Walton*

Fullerene Science Centre, School of CPES, University of Sussex, Brighton, UK BN1 9QJ. E-mail: d.walton@sussex.ac.uk

Received (in Cambridge, UK) 18th July 2001, Accepted 11th September 2001
First published as an Advance Article on the web 5th October 2001

NbS_2 nanotubes/rods have been generated successfully employing carbon nanotube template promoted growth; high resolution transmission electron microscopy, coupled with EDX analysis, confirm the template effect and existence of NbS_2 tube structures.

Inorganic nanotubes/nanoparticles, first reported by Tenne *et al.*,[1] have engendered intense scientific interest because of their promising electronic and mechanical properties. For example, WS_2 nanotubes have been used as scanning probe microscope tips,[2,3] and MoS_2 nanoparticle-based lubricants display excellent wear-resistance.[4] Syntheses of these materials include chemical transport,[5] gas–solid reactions[6] and *in situ* heating,[7] leading to pure MS_2 nanoparticles, short and long tubes, bundles and even microtubes. The family of inorganic nanostructures has been widened in various ways, *e.g.* by creating so-called inorganic–organic dual phase nanostructures (mixing MX_2 layers with C layers);[8,9] intercalating noble metals (Au and Ag) within the tube walls;[10,11] Ti and Nb doped MX_2 composite nanotubes.[12,13] Recently, significant developments in the generation of single-layered MX_2 tubes have been reported,[14,15] years after single-walled carbon nanotubes were first described.[16] Single layered MoS_2 nanotubes have been formed successfully using chemical transport[14] and WS_2 nanotubes have been the subject of template generation.[15,16] However, it is noteworthy that after several years of effort, NbS_2 nanotubes, a layered material possessing interesting electronic properties (*e.g.* superconducting), have only just been prepared.[17] Unfortunately, this communication contained no high resolution TEM images, so that detailed tube structures need to be determined. We now describe the successful generation of NbS_2 nanotubes/nanorods *via* a carbon nanotube template process.

A 20 mg sample of $NbCl_4$ (Aldrich Co) was added to a suspension of carbon nanotubes (20 mg, produced by the arc-discharge process), in CCl_4 (30 cm^3), and the mixture was subjected to ultrasound treatment for 30 min. It was set aside for 72 h at room temperature, then heated at 80 °C to remove the CCl_4, leaving a black powder consisting of $NbCl_4$-coated nanotubes. The nanotubes were transferred to a quartz boat placed in a quartz tube inside an electrical resistance furnace. The sample was heated at *ca.* 500 °C for 30 min in air, then at *ca.* 1100 °C in an Ar atomsphere. This temperature was maintained for a further 30 min, whilst H_2S was passed through the tube. After cooling to room temperature, the nanotube sample was examined using a CM-200 high resolution transmission microscope, with energy dispersive X-ray analysis equipment attached (EDX, element $\geq$ B).

TEM observations revealed that a proportion of the carbon nanotube surfaces were modified during the preheating process (500 °C in air). Notably, some of the tube bodies were discontinuously sheathed with crystalline structures [Fig. S1(a), ESI†]. Under these conditions, the layered structure and the hollow cores of the carbon nanotubes were difficult to recognise because of a lack of carbon contrast due to the wrapped oxide crystals. However, using focus/defocus techniques, we were able to observe the carbon layer fringes (*ca.* 0.34 nm separation) and the hollow core at the centre of the tube [Fig. S1(b) arrowed, ESI†]. The outer crystalline shell of this tube, containing Nb and O (as well as C, which presumably arises from the central carbon nanotube) according to our EDX ananlysis, was NbO_x. The lattice separation of the oxide is *ca.* 0.36–0.37 nm, *i.e.* close to that of NbO_2.

After the passage of H_2S, HRTEM analysis showed that NbS_2 nanotubes/rods (*ca.* 5–10%) were present in the specimen, together with micro-polygonal particles. The diameter of the nanotubes varies from 50 to 200 nm, and their lengths are up to a few microns. The nanotube layers are separated by *ca.* 0.60 nm [Fig. 1(a)], corresponding to layered hexagonal NbS_2 structures (a = 3.31 Å, c = 11.89 Å).[18] The inner carbon nanotube layer separation is *ca.* 0.34 nm, *i.e.* identical to the separation in the starting materials. It is apparent that the carbon template has been sheathed incompletely with NbS_2 layers, and

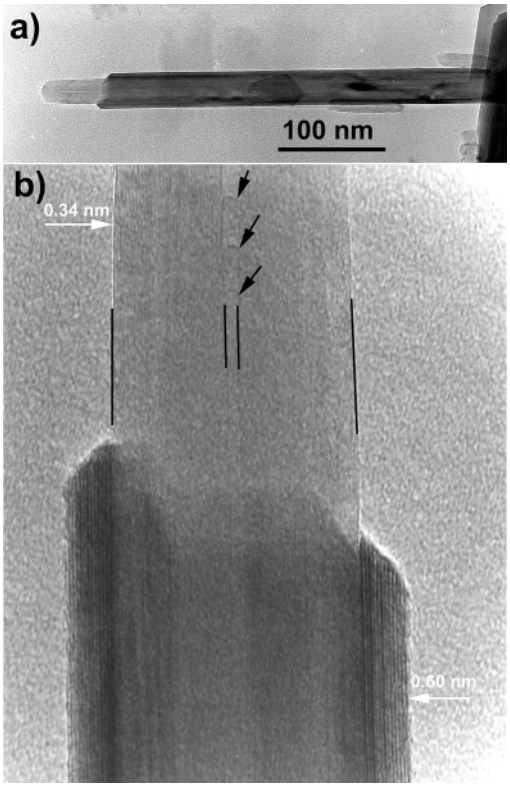

Fig. 1 HRTEM images: (a) a long open-tipped NbS_2 nanotube grown on a close-tipped carbon nanotube template; (b) the outer NbS_2 layer distance is 0.6 nm, the inner carbon layer separation 0.34 nm. The tube wall and the hollow core of the carbon template are marked by the vertical lines. Several closed inner layers of the carbon nanotube are arrowed.

† Electronic supplementary information (ESI) available: HRTEM images of a carbon nanotube wrapped in Nb oxide (a), of the inner carbon layers (b) and of an NbS_2 nanorod with NbO_x residue at the tip (c); (d) EDX profile of an isolated NbS_2 nanotube. See http://www.rsc.org/suppdata/cc/b1/b106388j/

 DOI: 10.1039/b106388j

the open-ended growth of the NbS_2 nanotube is visible [Fig. 1(b)]. In some cases, it was difficult to determine whether or not the layered nanorods had circular cross-sections [Fig. S1(c), ESI†]. The interlayer separation of this rod is *ca*. 0.60 nm, the same value as found for the tubes. At the rod tip, traces of the NbO_x lattice (indicated by the *ca*. 0.37 nm layer distance) are clearly visible [Fig. S1(c) arrowed, ESI†]. The oxide appears to be attached to the larger NbS_2 layers [Fig. S1(c) insert, ESI†] and indicates incomplete oxide-to-sulfide conversion.[19] Large polygonal particles, *ca*. 5 μm diameter, are often observed and appear to possess a layer construction at their edges, akin to the tube layers. EDX analysis revealed that most of the tubes/rods contain Nb, S and C only [Fig. S1(d), ESI†]; the Nb : S ratio is *ca*. 1 : 2. The nanoparticles in which less carbon was detected have the same Nb : S ratio, indicating that they may not be attached to any carbon nanotube templates. These experiments show that NbS_2 nanotubes and nanorods had been successfully generated. The carbon nanotubes located in the middle of the NbO_2 and NbS_2 shells [Fig. S1(b), ESI† and Fig. 1] provide direct evidence for the template effect during NbS_2 formation.

Various phases have been reported in the Nb–S system,[18] however in order to form a tube by rolling up these layers, NbS_2 needs to adopt hexagonal structures, as do WS_2 and MoS_2 nanotubes. This is shown by their 0.60 nm layer separation (Fig. 1), which is *ca*. 0.5 *c*. Prior to the report of Nath *et al*. the existing approaches to MS_2 nanotubes, *e.g*. chemical transport,[5] gas–solid reactions[6] and *in situ* heating,[7] proved to be inapplicable to NbS_2 tubes. Carbon nanotubes have often been used as templates to fabricate novel nanostructures, the most successful examples being the generation of ceramic nanorods (SiC, Si_3N_4, GaN)[20,21] and single-layered inorganic nanotubes (WS_2).[15] Taking advantage of these carbon templates, we have endeavoured to produce inorganic nanotubes by an alternative method. Furthermore, another advantage of this process is that the remaining carbon nanotube templates in the centre, together with the NbS_2 shells, form a kind of composite which may be used as a nanocable (*e.g*. metallic–metallic or a semiconducting–metallic cable).

Upon passage of H_2S at *ca*. 1100 °C over the oxidised sample, oxide-to-sulfide conversion occurs, resulting in sulfide wrapping of the template, as observed for MS_2 species formed in various processes. Further EDX analysis revealed that the Nb:S ratio is close to 1 : 2. Taking account of the 0.60 nm layer separations, we believe that our product consists of NbS_2 nanotubes/nanorods. It is noteworthy that the oxide might be unevenly and discontinuously deposited on the template surfaces [Fig. S1(a), ESI†], however after the passage of H_2S, we rarely found any uneven NbS_2 tubes (Fig. 1). This result could have arisen from the structural rearrangement occurring during lattice replacement of oxide by sulfide, *i.e*. from monoclinic NbO_2 (or other oxides) to hexagonal NbS_2. However, this conversion appears to be different from the route involved in most MoS_2 or WS_2 conversions, in which transformation proceeds from the outer shell inwards, as established by Tenne and coworkers.[19] The incompletely converted oxide residue at the tip [Fig. S1(c), particularly the insert, ESI†] provides direct evidence for this conjecture. We suggest that the oxide residue may again arise as a result of lattice rearrangement during the conversion, which may take place at one or more points (nuclei sites) and subsequent passage along the template. Meanwhile, the temperature (1100 °C) could also contribute to the smooth tube surfaces. As a result, relatively straight uniform NbS_2 nanotubes/nanorods were produced. This growth is similar to that associated with the continuous growth of WS_2 and MoS_2 nanotubes by *in situ* heating, which sometimes leaves an open growing end.[7] The main process may be represented by eqns. (1) and (2)

$$2NbCl_5 + 2O_2 \rightarrow 2NbO_2 + 5Cl_2 \quad (1)$$

$$NbO_2 + 2H_2S \rightarrow NbS_2 + 2H_2O \quad (2)$$

We thank the Leverhulme Trust, the JFCC and the Royal Society for financial support. We are grateful to J. Thorpe and D. Randall (Sussex) for assistance with TEM and SEM facilities.

Notes and references

1 R. Tenne, L. Margulis, M. Genut and G. Hodes, *Nature*, 1992, **360**, 444.
2 M. Homyonfer, B. Alperson, Y. Rosenberg, L. Sapir, S. R. Cohen, G. Hodes and R. Tenne, *J. Am. Chem. Soc*., 1997, **119**, 2693.
3 A. Rothschild, S. R. Cohen and R. Tenne, *Appl. Phys. Lett*., 1999, **75**, 4025.
4 L. Rapoport, Y. Bilik, Y. Feldman, M. Homyonfer, S. R. Cohen and R. Tenne, *Nature*, 1999, **387**, 791.
5 M. Remskar, Z. Skraba, M. Regula, C. Ballif, R. Sanjines and F. Levy, *Adv. Mater*., 1998, **10**, 246.
6 A. Rothschild, G. L. Frey, M. Homyonfer, R. Tenne and M. Rappapport, *Mater. Res. Innov*., 1998, **3**, 145.
7 Y. Q. Zhu, W. K. Hsu, N. Grobert, B. H. Chang, M. Terrones, H. Terrones, H. W. Kroto, D. R. M. Walton and B. Q. Wei, *Chem. Mater*., 2000, **12**, 1190.
8 W. K. Hsu, Y. Q. Zhu, C. B. Boothroyd, I. Kinloch, S. Trasobares, H. Terrones, N. Grobert, M. Terrones, R. Escudero, G. Z. Chen, C. Colliex, A. H. Windle, D. J. Fray, H. W. Kroto and D. R. M. Walton, *Chem. Mater*, 2000, **12**, 3541.
9 W. K. Hsu, Y. Q. Zhu, H. W. Kroto, D. R. M. Walton, R. Kamalakaran and M. Terrones, *Appl. Phys. Lett*., 2000, **77**, 4130.
10 M. Remskar, Z. Skraba, C. Ballif, R. Sanjines and F. Levy, *Surf. Rev. Lett*., 1999, **6**, 1283.
11 M. Remskar, Z. Skraba, P. Stadelmann and F. Levy, *Adv. Mater*., 2000, **12**, 814.
12 W. K. Hsu, Y. Q. Zhu, N. Yao, S. Firth, R. J. H. Clark, H. W. Kroto and D. R. M. Walton, *Adv. Funct. Mater*., 2001, **1**, 69.
13 Y. Q. Zhu, W. K. Hsu, M. Terrones, S. Firth, N. Grobert, R. J. H. Clark, H. W. Kroto and D. R. M. Walton, *Chem. Commun*., 2001, 121.
14 M. Remskar, A. Mrzel, Z. Skraba, A. Jesih, M. Ceh, J. Demsar, P. Stadelmann, F. Levy and D. Mihailovic, *Science*, 2001, **292**, 479.
15 R. L. D. Whitby, W. K. Hsu, C. B. Boothroyd, P. K. Fearon, H. W. Kroto and D. R. M. Walton, *Chem. Phys. Chem*., in press.
16 S. Iijima and T. Ichihashi, *Nature*, 1993, **363**, 603.
17 M. Nath and C. N. R. Rao, *J. Am. Chem. Soc*., 2001, **123**, 4841.
18 F. Jellinek, G. Brauer and H. Muller, *Nature*, 1960, **185**, 376.
19 Y. Feldman, G. L. Frey, M. Homyonfer, V. Lyakhovitskaya, L. Margulis, H. Cohen, G. Hodes, J. L. Hutchison and R. Tenne, *J. Am. Chem. Soc*., 1996, **118**, 5362.
20 H. J. Dai, E. W. Wong, Y. Z. Lu, S. S. Fan and C. M. Lieber, *Nature*, 1995, **375**, 769.
21 W. Q. Han, S. S. Fan, Q. Q. Li and Y. D. Hu, *Science*, 1997, **277**, 1287.

CHEMCOMM
Communication
www.rsc.org/chemcomm

Observation of a P/M interconversion of a gold–phosphine helicate *via* ^{31}P NMR

Walter Schuh, Holger Kopacka, Klaus Wurst and Paul Peringer*

Institut für Allgemeine, Anorganische und Theoretische Chemie, Universität Innsbruck, Innrain 52a, A-6020 Innsbruck, Austria. E-mail: paul.peringer@uibk.ac.at

Received (in Cambridge, UK) 9th July 2001, Accepted 5th September 2001
First published as an Advance Article on the web 5th October 2001

Ligands containing P–CH_2–CH_2–P elements have been shown to form double-stranded helicates whose axis consists of gold atoms with Au···Au contacts; the interconversion of the P and M forms of the helicate $[Au_3(\mu\text{-}pp_2)_2](OTf)_3$ (pp_2 = $PhP(CH_2CH_2PPh_2)_2$) is monitored *via* ^{31}P NMR.

The occurrence of helical motifs is of great current interest. Helical co-ordination complexes have attracted attention in view of the development and understanding of self processes.[1] We report in this paper that ligands containing P–CH_2–CH_2–P elements form double-stranded helicates whose axis consists of gold atoms with Au···Au contacts. The interconversion of the P and M helicates may be observed *via* ^{31}P NMR in solutions of the tricationic helicate $[Au_3(\mu\text{-}pp_2)_2]^{3+}$.

Whilst gold complexes of the tridentate dppm analogue Ph_2P–CH_2–PPh–CH_2–PPh_2 (dmmp) in the molar ratio of 3:2 are well known,[2] no complexes of Ph_2P–CH_2–CH_2–PPh–CH_2–CH_2–PPh_2 (pp_2) in this stoichiometry appear to be reported. Reaction of $Au(SMe_2)Cl$ with pp_2 and TlOTf in the molar ratio of 3:2:3 in MeOH results in the formation of $[Au_3(\mu\text{-}pp_2)_2](OTf)_3$, **1**, which was isolated as colourless crystals which exhibit a violet glimmer in daylight.†

The structure of **1** (Fig. 1) shows two ligand strands wrapped as a double helix around three essentially linear gold atoms. Crystals of **1** are a racemic compound: the asymmetric unit contains one helicate. The symmetry operations of the centrosymmetric space group $P2_1/c$ additionally provide one identical and two inverted helicates corresponding to a P:M ratio of 1:1 as usually observed when achiral ligands are employed. The Au–Au distances are less than 300 pm as a result of 1,6-transannular Au–Au d^{10}–d^{10} interactions in the 10-membered $(Au–P–CC–P)_2$ rings. Each gold atom is co-ordinated by two P atoms in a nearly linear geometry. It is interesting to note that the related compound $[Au_3(\mu\text{-}pp_2)I_3]$ as well as the Au(III) complex $[Au(C_6F_5)_3]_3(pp_2)$, both with the ligand:Au ratio of 1:3, do not show any helical suprastructures.[5]

The ^{31}P NMR pattern of **1** in MeOH at 333 K consists of an $[A_2X]_2$ pattern; at 213 K an $[AMX]_2$ spin system is observed in keeping with a *C*2 symmetry of the complex cation.[6] The coalescence temperature is 260 K, corresponding to a $\Delta G^{\ddagger}$ of 46 kJ.

In order to rationalise the ^{31}P NMR results with respect to the quasi-*C*2 symmetry in the crystal structure there must exist an intramolecular mechanism in solution which interconverts the terminal phosphorus atoms of the pp_2 ligand P1/P6 and P3/P4 (labelling as in Fig. 1). This is attributed to a molecular torsion pendulum motion, which converts the right-handed into the left-handed enantiomer, and *vice versa*, and thus generates an intramolecular mirror plane perpendicular to the *C*2 axis provided for rapid exchange on the ^{31}P NMR time-scale. A related dynamic process has been described for the 10-membered inorganic mesocycle $[Hg\{Fe[Si(OMe)_3](CO)_3(\mu\text{-}dppm)_2\}Cu](PF_6)$ by Braunstein and coworkers.[7]

The related dication $[Au_2(\mu\text{-}dppe)_2]^{2+}$ has been previously reported but was not structurally characterised.[8] $[Au_2(\mu\text{-}dppe)_2](OTf)_2$, **2**, was obtained analogously to **1**. The solid state structure of **2**† (Fig. 2) is related to that of **1**: the dppe ligands form a double helix whose axis passes through the two gold atoms connected by a 1,6-transannular Au–Au d^{10}–d^{10} interaction in a 10-membered $Au_2(\mu\text{-}dppe)_2$ ring [Au1–Au2, 295.94(10) pm], and the unit cell contains one left- and one right-handed isomer. Although the phosphorus atoms of the dppe ligands are inequivalent in the solid state (see Fig. 2), their

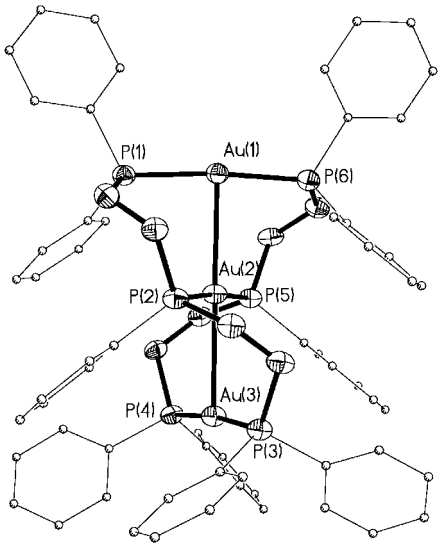

Fig. 1 Structure of the complex cation of **1**. Selected distances (pm) and angles (°): Au(1)–Au(2) 294.86(4), Au(2)–Au(3) 299.15(4); P(1)–Au(1)–Au(2)–P(2) 54.57(6), P(2)–Au(2)–Au(3)–P(3) 50.66(7).

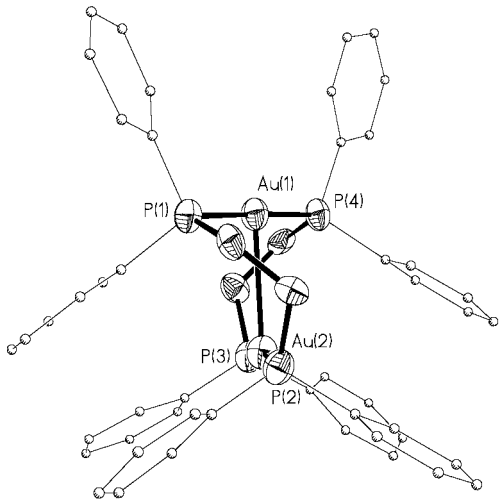

Fig. 2 Structure of the complex cation of **2**. Selected distances (pm) and angles (°): Au(1)–Au(2) 295.94(10); P(1)–Au(1)–Au(2)–P(2): 43.8(2).

 DOI: 10.1039/b106058a

exchange is fast on the ^{31}P NMR time-scale in MeOH down to the temperature limit of the solvent.

Notes and references

† *Crystal data* for **1**: $C_{71}H_{66}Au_3F_9O_9P_6S_3{\cdot}3MeOH{\cdot}2H_2O$, M = 2239.30, monoclinic, space group $P2_1/c$ (no. 14), a = 1687.43(3), b = 1484.24(3), c = 3403.69(4) pm, β = 104.007(1)°, V = 8.2712(2) nm^3, T = 223(2) K, Z = 4, Mo-Kα radiation (λ = 71.073 pm), 36 441 reflections collected, 11 248 independent reflections (R_{int} 0.0497), reflections with $I > 2\sigma(I)$ 9576, $R1$ [$I > 2\sigma(I)$] = 0.0363, $wR2$ (all data) = 0.0932, goodness-of-fit 1.025.

For **2**: $C_{54}H_{48}Au_2F_6O_6P_4S_2{\cdot}2MeOH$, M = 1552.94, monoclinic, space group $P\bar{1}$ (no. 2), a = 1467.2(2), b = 1488.0(1), c = 1637.9(2) pm, α = 91.912(6), β = 111.136(5), γ = 115.533(5)°, V = 2.9329(6) nm^3, T = 223(2) K, Z = 2, Mo-Kα radiation (λ = 71.073 pm), 9977 reflections collected, 5441 independent reflections (R_{int} 0.0508), reflections with $I > 2\sigma(I)$ 3829, $R1$ [$I > 2\sigma(I)$] = 0.0486, $wR2$ (all data) = 0.1207, goodness-of-fit 1.043.

The structures were solved by direct methods (SHELXS-86),[3] and refined by full-matrix, least squares methods on F^2 (SHELXL-93).[4]

CCDC reference numbers 171151 and 171152. See http://www.rsc.org/suppdata/cc/b1/b106058a/ for crystallographic data in CIF or other electronic format.

1 J. M. Lehn, *Supramolecular Chemistry*, VCH, Weinheim, 1995.

2 H. Xiao, Y.-X. Wenig, W.-T. Wong, T. C. W. Mac and C. M. Che, *J. Chem. Soc., Dalton Trans*., 1997, 221; M. Bardají, A. Laguna, V. M. Orera and M. D. Villacampa, *Inorg. Chem*., 1998, **37**, 5125; T. Tanase, K. Masuda, J. Matsuo, M. Hamaguchi, R. A. Begum and S. Yano, *Inorg. Chim. Acta*, 2000, **299**, 91 and references cited therein.

3 G. M. Sheldrick, SHELXS-86: program for crystal structure solution, Universität Göttingen, Germany, 1986.

4 G. M. Sheldrick, SHELXL-93: program for refinement of crystal structures, Universität Göttingen, Germany, 1993.

5 B. C. Tzeng, J. Zank, A. Schier and H. Schmidbaur, *Z. Naturforsch., B: Chem. Sci*., 1999, **54**, 825; M. Bardají, A. Laguna, J. Vincente and P. G. Jones, *Inorg. Chem*., 2001, **40**, 2675.

6 ^{31}P NMR (MeOH, 333 K): δ 38.2 (terminal P atoms), 31.2 (central P atoms), $J^{31}P_{central}{}^{31}P_{terminal}$ 25; (213 K): δ 43.1, 31.7 (terminal P atoms, m), 33.2 (central P atom, m). According to ^{31}P NMR spectroscopy, solutions of **1** contain a second species (*ca*. 10%) which is tentatively assigned to the *syn* orientation of the phenyl groups attached to the central phosphorus atoms of the pp_2 ligands. All crystals examined exhibit an *anti* orientation (see Fig. 1) and hence the *syn* isomer was either overlooked in the solid state or is formed fast on the preparative time-scale upon dissolving **1**.

7 M. Bénard, U. Bodensieck, P. Braunstein, M. Knorr, M. Strampfer and C. Strohmann, *Angew. Chem., Int. Ed. Engl*., 1997, **36**, 2758.

8 J. Yau and D. M. P. Mingos, *J. Chem. Soc., Dalton Trans*., 1997, 1103; S. Al-Baker, W. E. Hill and C. A. McAuliffe, *J. Chem. Soc., Dalton Trans*., 1985, 2655.

CHEMCOMM
Communication
www.rsc.org/chemcomm

Blue emission from cysteine ester passivated cadmium sulfide nanoclusters

Sameer Sapra,[a] J. Nanda,[a] D. D. Sarma,*[a] F. Abed El-Al[b] and G. Hodes[b]

[a] *Solid State and Structural Chemistry Unit, Indian Institute of Science, Bangalore-560 012, India. E-mail: sarma@sscu.iisc.ernet.in*
[b] *Department of Materials and Interfaces, The Weizmann Institute of Science, Rehovot 76100, Israel*

Received (in Cambridge, UK) 20th July 2001, Accepted 18th September 2001
First published as an Advance Article on the web 5th October 2001

A one-pot synthesis is reported of water-soluble cadmium sulfide nanoclusters capped with cysteine ester, with an average size of 2.0 nm and fluorescing in the blue region, establishing the possibility of using these as fluorescent biological probes.

Nanoclusters of II–VI semiconductors have been extensively studied during the past two decades.[1] On reducing the size of bulk semiconducting materials below their Bohr exciton diameter,[2] the band gap can be varied continuously from the bulk value to a relatively large one, thus allowing one to tune the electronic properties.[3] These nanoclusters are typically of the order of or smaller than characteristic sizes of various features in biological molecules and therefore have potential applications as biological sensors.[4] With this application in mind, we have synthesized CdS nanoclusters passivated with cysteine ester. Our study establishes the feasibility to cap the CdS nanoclusters with biological molecules such as peptides having the cysteine amino acid, for possible use as a fluorescent probe.[5] Also, cysteine ester passivates the surface states of the nanoclusters more effectively compared to other thiols and shifts the mid-gap, surface-state dominated fluorescence closer to the band edge. For example, the PL spectra from CdS nanoclusters capped with thioglycerol always peaks at 530 ± 20 nm, although the cluster size is varied from 2.0 to 4.5 nm, thereby tuning the bandgap from 3.8 eV (≈ 325 nm) to 2.5 eV (≈ 500 nm).[6] The cysteine ester therefore acts as both a more effective capping agent, resulting in a blue emission (≈ 470 nm), as well as a biologically active end-group for targeting specific cell sites.

We have prepared cysteine ester passivated CdS nanoclusters by a one-pot solution phase technique. 1.066 g (4.0 mmol) $Cd(OAc)_2{\cdot}2H_2O$ was dissolved in 40 ml dimethylformamide (DMF) along with 0.858 g (5.0 mmol) L-cysteine methyl ester hydrochloride. 0.480 g (2.0 mmol) $Na_2S{\cdot}9H_2O$ was dissolved in 10 ml double-distilled water and added to the DMF solution dropwise under an argon atmosphere. The solution was then heated at 60 °C for 12 h. A light yellow powder of CdS nanoclusters capped with cysteine ester was precipitated with acetone after rotavaporizing the solution. The powder was dried *in vacuo* for 5 h, yielding water soluble CdS nanoclusters.

Fig. 1(a) shows a high-resolution transmission electron micrograph (HRTEM) of a CdS nanocluster. The particles are spherical in shape and the lattice fringes can be clearly observed. In order to estimate the particle size distribution, the nanoclusters were dispersed on the TEM sample holder grid and a lower resolution transmission electron micrograph, as shown in Fig. 1(b), recorded. The histogram of cluster size obtained from Fig. 1(b) is shown in Fig. 1(c), indicating an average particle diameter, d_{av}, of 2.0 nm with a standard deviation of 0.19 nm.

The powder X-ray diffraction pattern is shown in Fig. 2. The peak at $2\theta = 5.1°$ arises from the close packing of the individual clusters, defining a characteristic separation equal to the average diameter of the clusters; we estimate the d_{av} from this to be 1.7 nm, in reasonable agreement with the TEM result. The width of the diffraction peak at 27.6° is determined by the particle size *via* the Debye–Scherrer formula. We have performed a Debye–Scherrer broadening[7] on the bulk CdS XRD pattern. The bulk XRD pattern[8] and the broadened pattern are also shown in the Figure with the extent of broadening corresponding to a cluster size of 1.5 nm. The slight underestimation of particle size in this case may be due to defects present in the nanoclusters.[9,10]

The UV–VIS absorption spectra of an aqueous solution of the nanoclusters, shown by the solid curve in Fig. 3, exhibits a fairly sharp excitonic peak at 303 nm (4.1 eV), with the bandgap ≈ 3.6 eV estimated from the absorption onset. To correlate the size with the absorption threshold of the nanoclusters, we have developed a method using a realistic sp^3d^5 orbital basis[11] instead of the previously used sp^3s^* basis[12] within the tight-

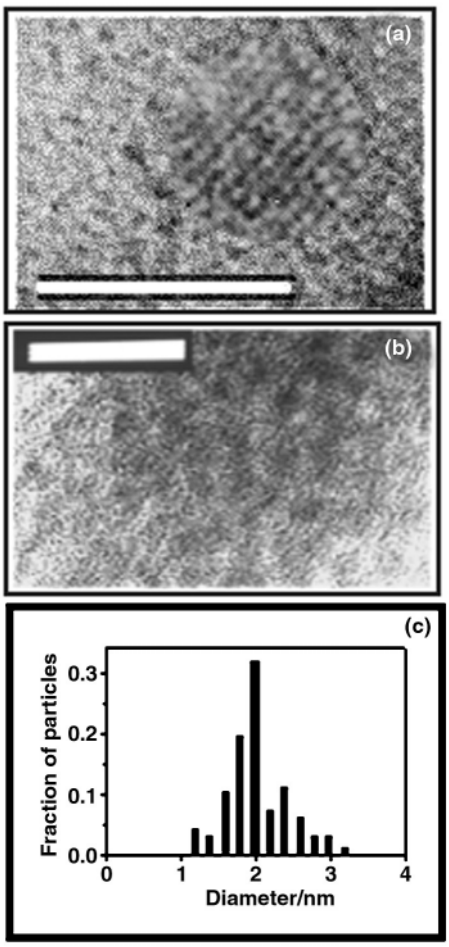

Fig. 1 (a) HRTEM of a cysteine-ester passivated CdS nanocluster showing the lattice fringes. The length of the bar is 2.5 nm. (b) TEM showing the CdS nanoclusters. The length of the bar is 20 nm. (c) Histogram for the cluster size, obtained from TEM.

 DOI: 10.1039/b106420g

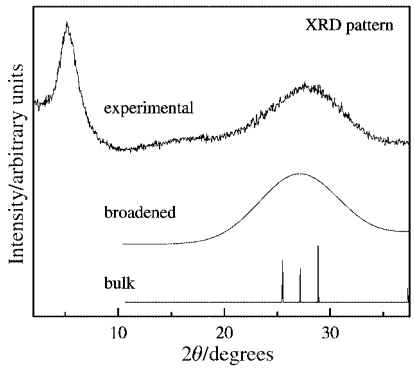

Fig. 2 XRD pattern of CdS nanoclusters. Shown below are the simulated XRD pattern for 1.5 nm clusters and the experimental bulk CdS XRD pattern.

binding model. According to our calculations, the size of CdS nanoclusters corresponding to the absorption onset shown in Fig. 3 is 1.8 nm. This is in good agreement with the size determined from TEM and XRD. The fluorescence excitation and emission spectra are also shown in Fig. 3. The particles emit strongly in the blue region of the visible spectrum (470 nm) upon illumination by UV radiation, establishing a substantial blue shift in emission compared to normally produced CdS nanoclusters with most other organic passivating agents such as

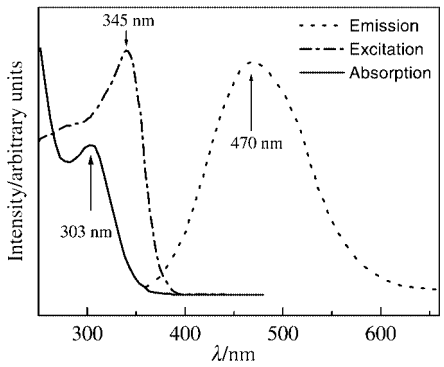

Fig. 3 UV–VIS and fluorescence spectra recorded from an aqueous solution of CdS nanoclusters.

thiols, thereby confirming cysteine as a more effective capping agent compared to thiols. FTIR results from the sample (not shown here) show that all the absorption bands of the cysteine shifted towards lower wavenumbers compared to the spectra for the pure ester, thereby indicating that the ester is bound to the heavy nanoclusters.

In conclusion, we have synthesized CdS nanoclusters passivated by cysteine-ester, suggesting the possible use as biological probes. This passivation quenches the deep trapped surface states and causes the nanoclusters to emit in the blue region, which otherwise emit yellow–orange radiation. The sizes determined from various methods are in good agreement.

We thank Mr J. Basu and Professor V. Jayaram for help with the TEM work and useful discussions. This work is supported by the Department of Science and Technology, Government of India, under the Indo–Israeli program of cooperation.

Notes and references

1 A. P. Alivisatos, *J. Phys. Chem.*, 1996, **100**, 13 226; A. D. Yoffe, *Adv. Phys.*, 2001, **50**, 1.
2 L. E. Brus, *J. Chem. Phys.*, 1984, **80**, 4403.
3 H. Weller, *Angew. Chem., Int. Ed.*, 1998, **37**, 1658; D. L. Klein, R. Roth, A. K. L. Lim, A. P. Alivisatos and P. L. McEuen, *Nature*, 1997, **389**, 699; J. Nanda, K. S. Narayan, B. A. Kuruvilla, G. L. Murthy and D. D. Sarma, *Appl. Phys. Lett.*, 1998, **72**, 1335.
4 W. C. W. Chan and S. Nie, *Science*, 1998, **281**, 2016; M. Bruchez, Jr., M. Moronne, P. Gin, S. Weiss and A. P. Alivisatos, *Science*, 1998, **281**, 2013.
5 C. T. Dameron, R. N. Reese, R. K. Mehra, A. R. Kortan, P. J. Carroll, M. L. Steigerwald, L. E. Brus and D. R. Winge, *Nature*, 1989, **338**, 596; W. Bae and R. K. Mehra, *J. Inorg. Biochem.*, 1998, **70**, 125; N. N. Mamedova, N. A. Kotov, A. L. Rogach and J. Studer, *Nano Lett.*, 2001, **1**, 281.
6 J. Nanda, Ph.D. Thesis, Indian Institute of Science, Bangalore, 2000.
7 A. Guinier, *X-Ray Diffraction*, Freeman, San Francisco, CA, 1963.
8 At such small sizes, the nanoclusters are generally a mixture of the two phases wurtzite and zinc blende. For these nanoclusters broadening on either phase gives the same results.
9 W. Vogel, J. Urban, M. Kundu and S. K. Kulkarni, *Langmuir*, 1997, **13**, 827.
10 J. Nanda, S. Sapra, D. D. Sarma, N. Chandrasekharan and G. Hodes, *Chem. Mater.*, 2000, **12**, 1018.
11 S. Sapra and D. D. Sarma, *Proc. 3rd Japan–Korea Joint Workshop on First-Principles Electronic Structure Calculations*, Tsukuba, Oct.–Nov. 2000, p. 105.
12 P. E. Lippens and M. Lannoo, *Phys. Rev. B*, 1989, **39**, 10 935.

CHEMCOMM Communication
www.rsc.org/chemcomm

Sn-MCM-41—a heterogeneous selective catalyst for the Baeyer–Villiger oxidation with hydrogen peroxide†

Avelino Corma,*[a] María Teresa Navarro,[a] Laszlo Nemeth[b] and Michael Renz[a]

[a] *Instituto de Tecnología Química, UPV-CSIC, Avda. de los Naranjos s/n, 46022 Valencia, Spain. E-mail: acorma@itq.upv.es*
[b] *UOP Research Center, 50 East Algonquin Road, Des Plaines, IL 60017-5016, USA*

Received (in Cambridge, UK) 4th July 2001, Accepted 13th September 2001
First published as an Advance Article on the web 5th October 2001

A new heterogeneous catalyst, Sn-MCM-41, is described for the Baeyer–Villiger reaction with hydrogen peroxide which selectively activates the carbonyl function for the nucleophilic attack by the oxidant, with high chemoselectivities when double bonds are present in the molecule.

The Baeyer–Villiger (BV) reaction is one of the most important transformations in synthetic organic chemistry. Its mechanism involves a nucleophilic attack on the carbonyl group by the oxidant followed by a concerted rearrangement with retention of the configuration at the migrating carbon atom [eqn. (1)].[1]

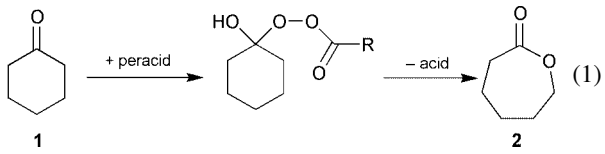

(1)

1 **2**

Up to the present, the only suitable oxidants for the BV reaction were the peracids which involve not only safety problems but also a bad atom economy and therefore cause waste material.[2] For economic and environmental reasons a big effort has been made to develop a catalytical method, preferentially a heterogeneous one. Recently, the catalytic action of redox molecular sieves, namely Mn-AlPO-36 and Co-AlPO-36, on the oxidation of ketones to lactones has been reported.[3] However, the reaction is carried out by peracids prepared *in-situ* from sacrificial benzaldehyde and oxygen. To overcome the waste problem, the peracid oxidant should be replaced by hydrogen peroxide activated by a suitable catalyst. Soluble Pt complexes have shown a good activity and turnover numbers (TON, catalytic cycles per metal centre) close to 50 with good selectivities towards the lactones.[4] The anchoring of these complexes onto a polymer has been attempted, but the loss of catalytic activity with respect to the homogeneous system observed introduced a serious limitation for a potential commercial application.[5] TS-1 zeolite has been used in the presence of H_2O_2 as catalyst for the BV reaction, but the selectivity to the desired product was lower than 65% due to the formation of α-hydroxy ketones and other undesired products.[6] These catalysts were designed to activate H_2O_2 by co-ordination with the metal, forming the corresponding metal peroxide that was the oxidising agent. Unfortunately, the metal peroxide formed also oxidises other functions such as alcohol or olefinic groups that may be present in the reactant molecule, and thus strongly limits the chemoselectivity of these catalysts.

We have developed a solid catalyst for the BV reaction which allows the reaction the reaction to work with H_2O_2 and is highly selective. We started from the concept that, for making a good BV solid catalyst, the catalytic sites should selectively activate the ketone instead of the H_2O_2. In this way, we could increase the positive charge on the carbon atom of the carbonyl group and facilitate the nucleophilic attack on this group by H_2O_2. Thus, Sn-MCM-41 samples with 1, 2 and 9 wt% of Sn, calculated from SnO_2, were synthesised in the following way.

An aqueous solution of hexadecyltrimethylammonium hydroxide/bromide (C_{16}TAOH/Br) was mixed with a tetramethylammonium hydroxide solution (25%, Aldrich) and an aqueous solution of $SnCl_4 \cdot 5H_2O$ (98%, Aldrich). After homogenisation, the silica (Aerosil, Degussa) was added under continuous stirring. The final composition was the following: 1 SiO_2:(0.16 − 4x) C_{16}TABr:4x C_{16}TAOH:0.26 TMAOH:x $SnCl_4$:24.3 H_2O, where x was varied between 0.04 and 0.01. C_{16}TABr was partially exchanged in order to compensate for the OH^- depletion produced by the incorporation of $SnCl_4$ into the synthesis gel. The homogeneous gel was sealed in Teflon-lined stainless steel autoclaves and heated at 135 °C under static conditions for 24 h. The resulting solid product was recovered by filtration, washed with water and dried at 60 °C for 24 h. The occluded organic was removed by heating the solid at 540 °C for 1 h in a flow of N_2, followed by 6 h in air. The solid obtained presents a typical XRD pattern of MCM-41 structure.†

For the catalytic activity tests *ca.* 1.2 mmol cyclohexanone (**1**) and *ca.* 1.5 mmol of H_2O_2 (35 wt%) were dissolved in 3.00 g of methyl *tert*-butyl ether (MTBE) and were stirred and heated to 56 °C with 50 mg of the catalyst for 6 h. The reaction was followed by GC analysis and the ε-caprolactone (**2**) product was identified by GC-MS analysis and by comparison with the authentic sample. With the Sn-MCM-41 catalyst with 1% SnO_2 a conversion of 15% was observed which corresponded to a turnover number (TON) of 55 (Table 1, entry 1), while the selectivity towards the lactone was 96%. This result was a big improvement compared to the selectivities obtained with the TS-1/H_2O_2 oxidation system (Table 1, entry 5). Conversion was increased by increasing the amount of Sn, and the high selectivity to the lactone was maintained (Table 1, entries 2 and 3). However, the TON was lower when the Sn content was increased, indicating that not all the Sn introduced was active. It must be noted that SnO_2 impregnated on silica gave no activity for the BV reaction (Table 1, entry 4). In order to discuss the nature of the active sites, a Sn-MCM-41 sample was prepared using the ^{119}Sn isotope (2% SnO_2), which can be detected by

Table 1 Baeyer–Villiger oxidation of cyclohexanone (**1**) by hydrogen peroxide catalysed by Sn-MCM-41 with different Sn contents

Entry	Catalyst	Conversion (%)	TON[a]	TOF[b]	Lactone selectivity (%)
1	Sn-MCM-41 (1% SnO_2)	15	55	23	96
2	Sn-MCM-41 (2% SnO_2)	22	40	13	94
3	Sn-MCM-41 (9% SnO_2)	36	12	7	97
4	SiO_2–SnO_2[c]	0	0		
5	$SnCl_4$[c]	3	5		
6	TS-1[d]	31	21		20

[a] Turnover number; catalytic cycles per metal centre. [b] Turnover frequency; TON per hour; calculated on the conversion after 1 h of reaction time. [c] The Sn content corresponded to that of the catalyst with 2 wt% of SnO_2. [d] Data from ref. 6.

† Electronic supplementary information (ESI) available: XRD pattern of as-prepared Sn-MCM-41. See http://www.rsc.org/suppdata/cc/b1/b105927k/

 DOI: 10.1039/b105927k

Table 2 Baeyer–Villiger oxidation of adamantanone (**3**) by hydrogen peroxide catalysed by Sn-MCM-41

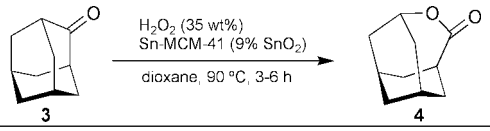

3 4

Entry	Time/h	**3**/mg	Ratio Sn/**3** (mol/mol)	Conv. (%)	TON[a]	TOF[a]	Selectivity (%)
1	6	150	0.03	>98	32	24	>98
2	6	150	0.03	72[b]	24	48[c]	>98

[a] See Table 1. [b] The catalyst was removed by filtration after 30 min. The conversion after 30 min was already 72% and did not change during the rest of the reaction time. [c] TOF calculated on the first 0.5 h.

MAS NMR. Indeed, by this analytical method it could be confirmed that the Sn sites of Sn-MCM-41 were different to those of SnO_2.

The large pore diameter of MCM-41 should allow the oxidation of sterically more demanding reactants. To study this, adamantanone (**3**) was reacted in the following way: 1 mmol of adamantanone and 1.5 mmol of H_2O_2 (35%) were dissolved in 3.00 g of dioxane, and 50 mg of Sn-MCM-41 (9% SnO_2) catalyst were added and stirred at 90 °C. After 6 h no substrate could be detected and the corresponding lactone **4** was the only product, with a selectivity to H_2O_2 of >90% (Table 2, entry 1). In order to check the possible contribution of the homogeneous reaction, another experiment was carried out in which the catalyst was separated by filtration after 30 minutes reaction time and 70% conversion. The solution was further heated for 5.5 h and the conversion did not proceed further, confirming that the active species was the metal incorporated into the framework and not any leached species in solution. Furthermore, it was shown that a homogeneous Sn species has an activity almost one order of magnitude lower than the Sn incorporated into the MCM-41 framework (*cf.* Table 1, entries 2 and 5).

With respect to catalyst life, we have observed that some deactivation occurs during the reaction when the same catalyst is recycled three times. The decrease in the catalyst activity is especially pronounced after the first recycle for which the TON decreased from 42 to 17 after 3 h. However, further recycling did not show any notable decrease in activity (16 and 16 TON for cycles 3 and 4, respectively). In order to check if the deactivation during the first recycling was due to leaching and/or to the adsorption of some product, the catalyst after the first recycling was filtered at the reaction temperature (90 °C) and then air calcined at 540 °C for 6 h. The calcined catalyst was again used in the reaction, and a TON of 35 was observed. This indicated that the decrease in activity observed in the first cycle cannot be attributed mostly to leaching of some of the less stable Sn, but it is mainly due to catalyst poisoning by organic deposits.

A very interesting result was observed when an unsaturated ketone was employed as substrate, *e.g.* dihydrocarvone (**5**). With the traditional oxidant for the BV oxidation, the peracids, the main product was the epoxyketone **7** in the case of a deficit of oxidant (Table 3, entry 1). When an excess of the oxidant was used, both types of oxidation, *i.e.* BV oxidation and epoxidation, occurred and consequently the epoxylactone **8** was obtained. When Sn-MCM-41 (9% SnO_2) was used as catalyst and H_2O_2 (35 wt%) as oxidant, the lactone **6** was the main product, although the selectivity was lower than with Sn-Beta zeolite[7] (Table 3, entry 3). This showed that with the Sn-MCM-41 catalyst unsaturated lactones can be obtained while, with the classic peracid or other reported catalysts, the unsaturated lactones cannot be synthesised because the epoxidation reaction competes very effectively (see ref. 8 and Table 3).

The reason for this extraordinary selectivity probably has its origin in the type of catalysis. If the catalyst can activate the peroxide, epoxidation will also be observed. This was the case

Table 3 Selectivities in the oxidation of dihydrocarvone (**5**) with different oxidants.

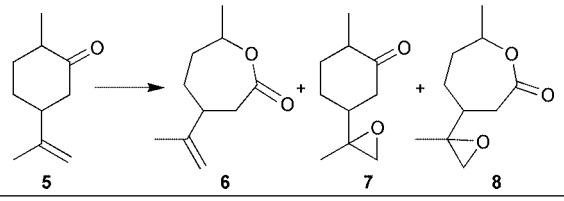

5 6 7 8

Oxidant	Equiv.	Conv. (%)	Product distribution (%) **6**	**7**	**8**	Other[a]
mCPBA	0.88	85	11	71	18	0
mCPBA	1.65	100	4	11	82	3
Sn-MCM-41/H_2O_2	2.05	22	68	18	0	14

[a] Others products include: other oxidation products, *e.g.* the α-hydroxyketone or hydrolysis products.

for $MeReO_3$ which catalysed BV oxidation[9] as well as epoxidation.[10] So, it was more probable that the Sn-MCM-41 interacted with the ketone by activating the carbonyl group for the nucleophilic attack by hydrogen peroxide. This was tested by carrying out *in-situ* IR experiments in which cyclohexanone was adsorbed on Sn-MCM-41. The results showed that, indeed, a shift of the carbonyl band towards lower wavenumbers occurred (48 cm^{-1}), and the ketone remained co-ordinated even at 100 °C. With an all-silicon MCM-41 sample this shift in the carbonyl signal was not observed.

In summary, Sn-MCM-41 opens up a new class of catalysts for the BV reaction with hydrogen peroxide. High turnover numbers with good selectivities to lactones are observed and, furthermore, the catalysts show a reasonable chemoselectivity when olefinic groups are present in the reaction.

The authors thank the CICYT (MAT2000-1392) and UOP for financial support. M. T. N. thanks the 'Fundación Ana y José Royo' for a postdoctoral grant.

Notes and references

1 M. Renz and B. Meunier, *Eur. J. Org. Chem.*, 1999, 737.
2 B. M. Trost, *Science*, 1991, **254**, 1471.
3 R. Raja, J. M. Thomas and G. Sankar, *Chem. Commun.*, 1999, 525.
4 G. Strukul, *Angew. Chem., Int. Ed.*, 1998, **37**, 1198.
5 C. Palazzi, F. Pinna and G. Strukul, *J. Mol. Catal. A: Chem.*, 2000, **151**, 245.
6 A. Bhaumik, P. Kumar and R. Kumar, *Catal. Lett.*, 1996, **40**, 47.
7 A. Corma, L. T. Nemeth, M. Renz and S. Valencia, *Nature*, 2001, **412**, 423.
8 (*a*) M. D. T. Frisone, F. Pinna and G. Strukul, *Organometallics*, 1993, **12**, 148; (*b*) G. R. Krow, *Org. React.*, 1993, **43**, 251.
9 W. A. Herrmann, R. W. Fischer and J. D. G. Correia, *J. Mol. Catal.*, 1994, **94**, 213.
10 W. A. Herrmann, *J. Organomet. Chem.*, 1995, **500**, 149.

CHEMCOMM Communication
www.rsc.org/chemcomm

Anion directed assembly of a dinuclear double helicate†

Jennifer Keegan,[a] Paul E. Kruger,*[b] Mark Nieuwenhuyzen,[c] John O'Brien[b] and Noreen Martin*[a]

[a] *Department of Chemistry, Royal College of Surgeons, Dublin 2, Ireland. E-mail: nmartin@rcsi.ie*
[b] *Department of Chemistry, Trinity College, Dublin 2, Ireland. E-mail: paul.kruger@tcd.ie*
[c] *School of Chemistry, The Queen's University of Belfast, Belfast, UK, BT9 5AG. E-mail: woody.m@qub.ac.uk*

Received (in Cambridge, UK) 1st August 2001, Accepted 18th September 2001
First published as an Advance Article on the web 5th October 2001

The synthesis and structural characterisation of the diamino-bis-pyridine ligand L^2 and its diammonium-bis-pyridinium salt $[(H_4L^2Cl)_2]\cdot 6Cl\cdot H_2O$ 1, are reported; X-ray diffraction studies reveal that chloride coordination causes the latter to adopt a double-helicate structure in the solid-state.

In recent years coordination chemists have developed several strategies to predict the outcome of self-assembly processes and have used this information to exert influence over the subsequent architectures adopted during these processes.[1] Much of the current literature has concentrated on metal-assisted, self-assembly processes where ligands are tailored for the recognition of the intrinsic stereochemical properties of a particular metal ion. Fine tuning of ligand properties such as donor density, type and number as well as the spacer group separating coordination sites has led to a plethora of resultant structural motifs such as grids,[2] boxes,[3] cylinders,[4] helicates[5] and molecular polyhedra.[6] In contrast, there have been relatively few reports detailing 'metal-free' anion directed self-assembly processes, despite there being considerable current interest in the development of molecular and supramolecular systems which have the ability to bind negatively charged ions.[7,8] The motivation behind such studies is the recognition that anions enjoy an important role in biology, medicine and the environment.[8] Typically, these systems utilise hydrogen bonding and electrostatic interactions to bind anions, and many varieties exist based on chemical archetypes including amides, ureas, pyrroles, ammonium macrocycles, guanidinium and pyridinium moieties.[7,8] However, we are aware of only one such report detailing the formation of a helical structure as a result of an anion directed self-assembly process. de Mendoza and coworkers synthesised a tetraguanidinium strand that self-assembled around sulfate ions to form a double helix, as evidenced by ROESY NMR spectroscopy.[9] Herein, we report the synthesis and structural characterisation of the diamino-bis-pyridine ligand L^2 and the dinuclear double helicate of its diammonium-bis-pyridinium salt $[(H_4L^2Cl)_2]\cdot 6Cl\cdot H_2O$ **1**. To the best of our knowledge, this is the first structurally characterised example of an anion directed assembly of a helicate.

L^2 was prepared from its bis-imine progenitor,[10] L^1, by standard borohydride reduction and isolated in 65% yield as a white crystalline product of suitable quality for a diffraction study.‡§ The atomic numbering scheme and atom connectivity are shown in Fig. 1. There is a clear twist evident on traversing the molecule from N(1), through the central phenyl rings, to N(29). The two pyridyl moieties are inclined at an angle of 81° to one another and the phenyl groups are rotated by 99° with respect to each other. The nitrogen atoms N(1) and N(29) make close contacts with H(7a) and H(23a') (symmetry code: $-1+x$, $1+y$, z), respectively, forming C–H···N hydrogen bonded chains. The chains are further linked into a 3D hydrogen bonded network *via* edge-to-face N–H···π [N(22)–H(22)–centre-of-ring, 2.77] and combined N–H···π, C–H···π interactions (3.14 and 2.80 Å to centre-of-ring, respectively). Interestingly, there are no face-to-face π···π interactions between the molecules.

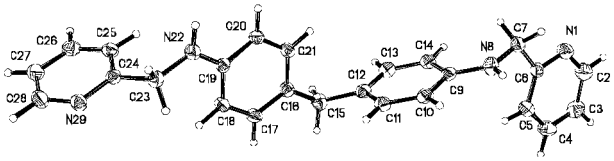

Fig. 1 Molecular structure and atomic numbering scheme of L^2.

Addition of dilute hydrochloric acid to a methanolic solution of L^2 induced the precipitation of a pale yellow solid in quantitative yield. Recrystallization afforded single crystals of **1** suitable for a diffraction study.‡§ The atomic numbering scheme and atom connectivity are shown in Fig. 2. The asymmetric unit contains two independent cations located about twofold axes. Two of the Cl^- anions are also located on two-fold axes. The structure consists of two ligand strands that wrap around two chloride anions in a double helical arrangement with a major and minor groove, both enantiomers of which are present. The chloride ions are coordinated by two pyridinium moieties, with further weaker interactions from the methylene and aromatic CH residues being evident. There is no interaction between the coordinated chloride ions and the ammonium moieties N(8). Coordination is such that the anions reside within a cleft formed by the two ligand strands giving an intramolecular $Cl^-\cdots Cl^-$ separation of 13.17 Å, (Fig. 3). Interestingly, there are no intrahelicate cross-strand π···π interactions (closest contact > 4.5 Å). There are, however, extensive inter-helicate intermolecular π···π interactions (3.4–3.9 Å) between the phenyl rings [C(9)–C(14)] and the pyridyl rings [N(1)–C(6)] of neighbouring helicates in contrast to L^2. The lattice anions are involved in extensive hydrogen bonding with the ammonium moieties [N(8)] and this results in the formation of a 3D network supported by a combination of these hydrogen

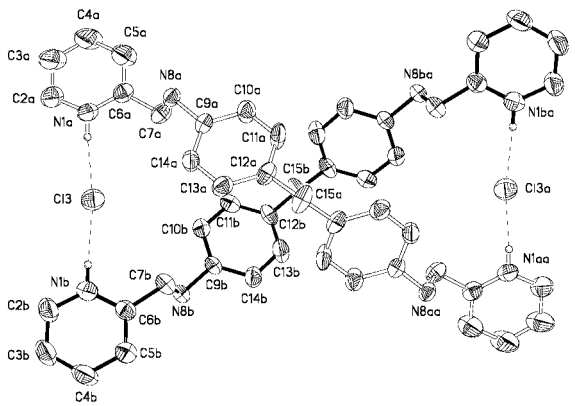

Fig. 2 Molecular structure and atomic numbering scheme in **1**. Thermal ellipsoids at 50% probability level. Hydrogen atoms, lattice anions and water solvent omitted for clarity. Selected bond lengths (Å) and angles (°) for **1**: N(1a)–Cl(3) 3.039(3), N(1b)–Cl(3) 3.031(3), H(1a)–Cl(3) 2.16, H(1b)–Cl(3) 2.16; N(1a)–H(1a)–Cl(3) 175, N(1b)–H(1b)–Cl(3) 172.

† Electronic supplementary information (ESI) available: Fig. S1: stereo-views showing the packing of **1** in the solid state. Fig. S2: partial ^1H NMR spectra of L^2 and **1** and their assignment. See http://www.rsc.org/suppdata/cc/b1/b106981k/

 DOI: 10.1039/b106981k

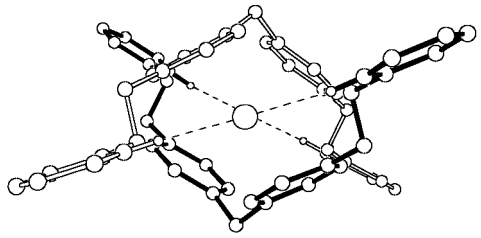

Fig. 3 The helical arrangement in **1** viewed down the Cl···Cl vector. Hydrogen atoms, lattice anions and water solvent omitted for clarity.

bonds and the π···π interactions. This is further enhanced by hydrogen bonding between Cl(4) and the lattice water molecule O(1w).

It is instructive here to compare and contrast the structures of L^2 and **1** with the metal helicate complexes of the bis-imine ligand L^1.[10] From the structure of L^2 it is evident that nothing inherent within it pre-organises it to form a helical motif in the absence of a suitable template. The rigid nature of the central diphenylmethane spacer does, however, predispose L^2 to coordinate to two (or more) guests. This is probably the key feature of L^2 that leads to the formation of the helicate, as it has been shown that highly flexible, sterically unencumbered polyammonium hosts do not generate this topology upon guest binding.[11] The formation of **1** is also due to the template effect of the chloride anion following protonation of L^2. Once coordinated, the anion resides within a shielded pocket at the head of the helicate. It is coordinated in pincer fashion by the two pyridinium moieties *via* charge assisted hydrogen bonds, and further stabilised by weaker interactions with methylene and aromatic hydrogen atoms from deeper within the pocket. Despite the inherent flexibility in the system, there are no intramolecular interactions between the ligand strands. Previously, it has been proposed that contacts of this type help promote and stabilise the formation of related metallo-helicates, $[M_2L^1{}_3]$, and are responsible for the resultant helicate micro-architecture.[10b–e] The lack of any cross-strand contacts here may potentially arise from the relatively larger ionic radius of the chloride anion {*cf.* M(II) cations}, but we suspect that the lack of a preferred coordination geometry for chloride more than adequately offsets this size difference. This adds weight to our contention that metal coordination, and not intra-helicate π···π interaction, is a primary driving force for helicate formation and the resultant solid-state structures in $[M_2L^1{}_3]$ compounds.[10af] The coordination of L^1 to a metal centre applies strain to the ligand, whereas the hydrogen-bonded nature of **1** allows the ligand, L^2, to adopt an unstrained conformation, notably with no intra-strand interactions. We would therefore expect protonated salts of L^1 and related ligands to coordinate anions in a similar fashion and are currently investigating these systems. ^{1}H NMR and potentiometric titration experiments are also underway to determine the stability constants of **1** and analogous systems in solution.

In conclusion, we report here the synthesis and structural characterisation of a new diamino-bis-pyridine ligand L^2 and demonstrated that it, on addition of HCl, generates a novel dinuclear double helicate. We believe this to be the first structurally characterised example of the anion directed assembly of such a motif.

Enterprise Ireland is thanked for financial support by way of a Ph.D. studentship to J. K. Mr Robert Doyle (TCD) is thanked for assistance with the ESMS.

Notes and references

‡ *Selected data* for L^2 MS (ESI): *m*/*z* 381 $[L^2]^+$. Found: C, 78.65; H, 6.37; N, 14.73. $C_{25}H_{24}N_4$ requires C, 78.94; H, 6.31; N, 14.64%. δ_H (400 MHz; d_6-DMSO) 8.51 (2H, d, Py), 7.71 (2H, dt, Py), 7.32 (2H, d, Py), 7.23 (2H, t, Py), 6.85 (4H, d, Ar), 6.48 (4H, d, Ar), 6.10 (t, NH), 4.31 (4H, d, CH_2 spacer), 3.59 (2H, s, CH_2 bridge).

For **1**: found: C, 55.90; H, 5.70; N, 10.38. $C_{50}H_{56}N_8Cl_8O$ requires C, 56.14; H, 5.24; N, 10.66%. δ_H (400 MHz; d_6-DMSO) 8.79 (2H, d, Py), 8.46 (2H, dt, Py), 7.97 (2H, Py), 7.87 (2H, t, Py), 6.94 (4H, Ar), 6.63 (4H, d, Ar), 4.71 (4H, s, CH_2, spacer), 3.62 (2H, s, CH_2, bridge).

§ *Crystal data*: for L^2: $C_{25}H_{24}N_4$, M = 380.48, monoclinic, space group $P2_1/c$, a = 11.5546(8), b = 8.1809(5), c = 21.5214(14) Å, β = 97.881(1)°, U = 2015.1(2) Å^3, Z = 4, μ = 0.076 mm^{-1}, R_{int} = 0.0604. A total of 22756 reflections were measured for the angle range $4 < 2\theta < 58$ and 4724 independent reflections were used in the refinement. The final parameters were $wR2$ = 0.1275 and $R1$ = 0.0462 [$I > 2\sigma(I)$].

For **1**: $C_{25}H_{28}N_4Cl_4O_{0.5}$ M = 534.31, orthorhombic, space group *Pnna*, a = 17.656(4), b = 24.275 (6), c = 12.263(3) Å, U = 5256(2) Å^3, Z = 8, μ = 0.474 mm^{-1}, R_{int} = 0.1325 A total of 48268 reflections were measured for the angle range $4 < 2\theta < 50$ and 4638 independent reflections were used in the refinement. The final parameters were $wR2$ = 0.1878 and $R1$ = 0.0662 [$I > 2\sigma(I)$]. A check for higher symmetry using PLATON[12] suggested the space group should be *Pban*. Refinement of the structure in this cell gave a fit which was 0.5% worse. Furthermore, the atomic displacement parameters of the pyridinium ring indicated it was disordered. This is not true for the original assignment and thus we discounted this alternative cell.

Data were collected on a Bruker SMART diffractometer using the SAINT-NT[13] software with phi/omega scans. A crystal was mounted on to the diffractometer at low temperature under dinitrogen at *ca.* 120 K. The structures were solved using direct methods and refined with the SHELXTL program package.[13]

CCDC reference numbers 169237 and 169238. See http://www.rsc.org/suppdata/cc/b1/b106981k/ for crystallographic data in CIF or other electronic format.

1 J.-M. Lehn, *Supramolecular Chemistry, Concepts and Perspectives*, VCH, Weinheim, 1995; *Comprehensive Supramolecular Chemistry*, ed. J. L. Atwood, J. E. D. Davies, D. D. MacNicol, F. Vögtle and J.-M. Lehn, Pergamon, Oxford, 1996, vol. 9, p. 165; G. F. Swiegers and T. J. Malefetse, *Chem. Rev*., 2000, **100**, 3483.

2 E. Breuning, M. Ruben, J.-M. Lehn, F. Renz, Y. Garcia, V. Ksenofontov, P. Gütlich, E. Wegelius and K. Rissanen, *Angew. Chem., Int. Ed*., 2000, **39**, 2504; L. A. Zhao, Z. Q. Xu, L. K. Thompson, S. L. Heath, D. O Miller and M. Ohba, *Angew. Chem., Int. Ed*., 2000, **39**, 3114.

3 X. H. Bu, H. Morishita, K. Tanaka, K. Biradha, S. Furusho and M. Shionoya, *Chem. Commun*., 2000, 971; M. Fujita, K. Ume-moto, M. Yoshizawa, N. Fujita, T. Kusukawa and K. Biradha, *Chem. Commun*., 2001, 509.

4 D. W. Johnson, J. D. Xu, R. W. Saalfrank and K. N. Raymond, *Angew. Chem., Int. Ed*., 1999, **38**, 2882.

5 O. Mamula and A. von Zelewsky, *J. Chem. Soc., Dalton Trans*., 2000, 219; O. Mamula, A. von Zelewsky, T. Bark and G. Bernardinelli, *Angew. Chem., Int. Ed*., 1999, **38**, 2945; C. Piguet, G. Bernardinelli and G. Hopfgartner, *Chem. Rev*., 1997, **97**, 2005; M. Albrecht, *Chem. Eur. J*., 2000, **6**, 3485.

6 B. J. Holliday and C. A. Mirkin, *Angew. Chem. Int. Ed*., 2001, **40**, 2022; M. Fujita, *Struct. Bonding* (*Berlin*), 2000, **96**, 177; P. J. Stang and B. Olenyuk, *Acc. Chem. Res*., 1997, **30**, 502.

7 *Supramolecular Chemistry of Anions*, ed. A. Bianchi, K. Bowman-James and E. Garcia-Espana, Wiley–VCH, New York, 1997; F. P. Schmidtchen and M. Berger, *Chem. Rev*., 1997, **97**, 1609; B. Dietrich, *Pure Appl. Chem*., 1993, **65**, 1457.

8 P. A. Gale, *Coord. Chem. Rev*., 2001, **213**, 79; P. D. Beer and P. A. Gale, *Angew. Chem., Int. Ed*., 2001, **40**, 486; P. E. Kruger, P. R. Mackie and M. Nieuwenhuyzen, *J. Chem. Soc., Perkin Trans. 2*, 2001, 1079; B. M. Maubert, J. Nelson, V. McKee, R. M. Town and I. Pal, *J. Chem. Soc., Dalton Trans*., 2001, 1395.

9 J. Sanchez-Queseda, C. Seel, P. Prados and J. de Mendoza, *J. Am. Chem. Soc*., 1996, **118**, 277.

10 (*a*) P. E. Kruger, N. Martin and M. Nieuwenhuyzen, *J. Chem. Soc., Dalton Trans*., 2001, 1966; (*b*) M. J. Hannon, C. L. Painting and W. Errington, *Chem. Commun*., 1997, 307; (*c*) M. J. Hannon, C. L. Painting, A. Jackson, J. Hamblin and W. Errington, *Chem. Commun*., 1997, 1807; (*d*) M. J. Hannon, C. L. Painting and N. W. Alcock, *Chem. Commun*., 1999, 2023; (*e*) N. Yoshida, K. Ichikawa and M. Shiro, *J. Chem. Soc., Perkin Trans. 2*, 2000, 17; (*f*) P. E. Kruger, N. Martin and M. Nieuwenhuyzen, unpublished work.

11 C. A. Iliodis, K. S. B. Hancock, D. G. Georganopolou and J. W. Steed, *New. J. Chem*., 2000, **24**, 787.

12 A. L. Spek, PLATON—A Multipurpose Crystallographic Tool, Utrecht University, The Netherlands, 2000.

13 SAINT-NT, program for data collection and data reduction, Bruker-AXS, Madison, WI, 1998; G. M. Sheldrick, SHELXTL Version 5.0, A System for Structure Solution and Refinement, Bruker-AXS, Madison, WI, 1998.

CHEMCOMM Communication
www.rsc.org/chemcomm

Conversion of pyrrole to pyrrole-2-carboxylate by cells of *Bacillus megaterium* in supercritical CO_2

Tomoko Matsuda,*[a] Yoichi Ohashi,[a] Tadao Harada,[a] Reiko Yanagihara,[b] Toru Nagasawa[b] and Kaoru Nakamura[c]

[a] *Department of Materials Chemistry, Faculty of Science and Technology, Ryukoku University, Otsu, Shiga 520-2194, Japan*
[b] *Department of Biomolecular Science, Gifu University, 1-1 Yanagido, Gifu 501-1193, Japan*
[c] *Institute for Chemical Research, Kyoto University, Uji, Kyoto 611-0011, Japan*

Received (in Cambridge, UK) 12th June 2001, Accepted 17th September 2001
First published as an Advance Article on the web 3rd October 2001

Pyrrole was converted to pyrrole-2-carboxylate in supercritical CO_2 using cells of *Bacillus megaterium* PYR 2910, and the yield of the carboxylation reaction in supercritical CO_2 was 12 times higher than that under atmospheric pressure.

The development of CO_2 fixation reactions on organic molecules is one of the challenges in synthetic chemistry. An increasing number of chemical CO_2 fixation reactions[1] have been reported, especially using supercritical CO_2 (CO_2 above its critical temperature (31.0 °C) and pressure (7.38 MPa, 72.8 atm)), such as the synthesis of urethane,[1b] dimethyl carbonate,[1c] styrene carbonate[1d] methyl ethanoate.[1e] On the other hand, biocatalysis is now one of the most powerful and indispensable tools for organic synthesis due to its environmentally friendliness and excellent enantio-, regio- and chemo-selectivities.[2] Some enzymatic CO_2 fixation reactions have also been reported including the central CO_2 fixation reaction in photosynthetic organisms catalyzed by ribulose-1,5-diphosphate carboxylases,[3] the reduction of CO_2 to formic acid or methanol by dehydrogenases,[4] the reductive CO_2 fixation on 2-oxoglutarate and pyruvate by isocitrate[5] or malate[6] dehydrogenases, and the CO_2 fixation on pyrrole and phenolic compounds (phenol and catechol) by decarboxylases from *B. megaterium*[7] or *Clostridium hydroxybenzoicum*,[8] respectively.

Although enzymes in nature catalyze reactions in aqueous media, their use in supercritical CO_2 has been attracting increasing attention due to its gas-like low viscosities and high diffusivities and its liquid-like solubilizing power,[9] and mostly hydrolytic enzymes, with the exception of the cholesterol oxidases[10] and the alcohol dehydrogenase,[11] have been used in supercritical fluids to improve their functions, *i.e.*, faster reaction rates.[12] Here we report that cells of *Bacillus megaterium* PYR2910 catalyzes the reverse reaction, CO_2 fixation, in supercritical CO_2 for the first time. As shown in Scheme 1, CO_2 was fixed on pyrrole to produce pyrrole-2-carboxylate at 10 MPa and 40 °C. The yield of the reaction in supercritical CO_2 was much higher than that at atmospheric pressure.

The cells of *Bacillus megaterium* PYR2910[7] were employed for the CO_2 fixation reaction. The reaction was conducted by adding CO_2 to 10 MPa to the mixture of pyrrole, the cells, $KHCO_3$, and NH_4OAc in potassium phosphate buffer. For the reaction at atmospheric pressure (0.1 MPa), the evolved CO_2 was released to keep the pressure atmospheric. The yields of the reaction at 40 °C are listed in Table 1. The yield is much higher for the reaction in supercritical CO_2 than at atmospheric pressure (Table 1, Entries 1–4). It was also confirmed by the control experiment without the cells that the non-biocatalytic carboxylation of pyrrole did not proceed (Table 1, Entry 5).[13] Therefore, the cell is surely catalyzing the CO_2 fixation reaction more effectively in supercritical CO_2 than at atmospheric pressure.

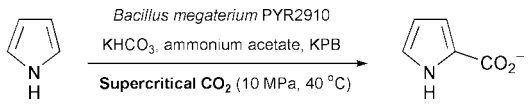

Scheme 1

The time courses of the reaction at 10 MPa and at atmospheric pressure in Fig. 1 also have a higher yield for the supercritical reaction than that of the atmospheric reaction. The reaction reached an equilibrium position within a few hours and did not proceed further. As listed in Table 1, the doubling of the quantity of cells (Entry 6) as well as the change in the initial pH value from 5.5 to 7.0 to prevent a pH decrease caused by CO_2 (Entry 7) did not have any significant effect on the equilibrium position.

The effect of pressure on the carboxylation of pyrrole was also investigated, and the result is shown in Fig. 2. The maximum yield was between 4 and 7 MPa; the yield at just above its critical pressure (7.6 MPa) is about 12 times that at atmospheric pressure (0.1 MPa). Similar pressure dependencies of the yield on pressure were also observed using an increased quantity of the cells, shorter reaction times, and different temperatures (data not shown). At present, it is not clear why the increased concentration of CO_2 in the range greater than the

Table 1 Conversion of pyrrole to pyrrole-2-carboxylate in supercritical CO_2 at 40 °C

Entry	Pressure/MPa	Cells/mL[a]	pH	Time/h	Yield (%)[b]
1	0.1 (Atmospheric)	0.5	5.5	1	7
2	0.1 (Atmospheric)	0.5	5.5	3	6
3	10 (Supercritical)	0.5	5.5	1	54
4	10 (Supercritical)	0.5	5.5	3	55
5	10 (Supercritical)	0.0	5.5	3	0
6	10 (Supercritical)	1.0	5.5	3	59
7	10 (Supercritical)	0.5	7.0	1	59

[a] OD_{610} = 32; decarboxylation activity for pyrrole-2-carboxylate = 0.024 mmol min $^{-1}$ml^{-1}. [b] Based on the starting amount of pyrrole determined by HPLC analysis.

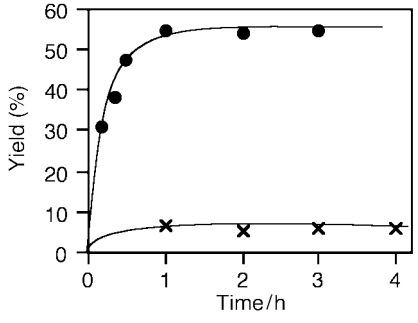

Fig. 1 Time course of conversion of pyrrole to pyrrole-2-carboxylate [●: 10 MPa (supercritical), × 0.1 MPa (atmospheric)].

 DOI: 10.1039/b105137g

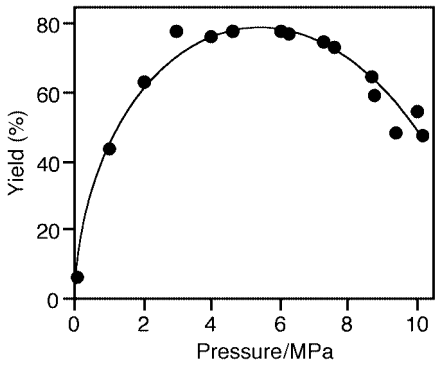

Fig. 2 Effect of pressure on conversion of pyrrole to pyrrole-2-carboxylate by the cells.

critical pressure did not favorably shift the carboxylation equilibrium.

In a typical experiment, *B. megaterium* PYR2910 was grown as previously described.[7b] To a stainless steel pressure-resistant vessel containing a magnetic stirrer bar as previously described,[11] pyrrole (0.40 M, 0.50 mL), potassium phosphate buffer (pH 5.5, 0.40 M, 0.50 mL), ammonium acetate (0.56 M, 0.50 mL), the cells (OD_{610} = 32, 0.50 mL) and $KHCO_3$ (0.60 g) were added. The vessel was then warmed to 40 °C, and CO_2 preheated to 40 °C was introduced to a final pressure of 10 MPa. The mixture was stirred at 40 °C for 3 h, and the CO_2 was liquefied at −10 °C and then the gas pressure was released. The chemical yield was measured by HPLC analysis as previously described.[7b]

In conclusion, cells of *B. megaterium* catalyzed the conversion of pyrrole to pyrrole-2-carboxylate in supercritical CO_2 at 40 °C with pressures up to 10 MPa, and a higher yield was obtained under supercritical conditions than at atmospheric pressure. This finding will play a significant role both in investigating enzyme species suitable for the biocatalysis in supercritical CO_2 and in developing synthetic methods utilizing CO_2.

This work was supported by a Grant-in-Aid from the Taisho Pharmaceutical Co. Award in Synthetic Organic Chemistry, Japan, the Sasakawa Scientific Research Grant from the Japan Science Society, a Grant-in-Aid for Encouragement of Young Scientists (No. 12740400) and a Grant-in-Aid for Scientific Research (C) (No. 11640602) from the Ministry of Education, Science, Sports and Culture of Japan.

Notes and references

1 (*a*) P. G. Jessop, T. Ikariya and R. Noyori, *Chem. Rev*., 1999, **99**, 475; (*b*) M. Yoshida, N. Hara and S. Okuyama, *Chem. Commun*., 2000, 151; (*c*) T. Sakakura, J.-C. Choi, Y. Saito, T. Masuda, T. Sako and T. Oriyama, *J. Org. Chem*., 1999, **64**, 4506; (*d*) H. Kawanami and Y. Ikushima, *Chem. Commun*., 2000, 2089; (*e*) R. J. Sowden, M. F. Sellin, N. D. Blasio and D. J. Cole-Hamilton, *Chem. Commun*., 1999, 2511; (*f*) T. Mizuno, N. Okamoto, T. Ito and T. Miyata, *Tetrahedron Lett*., 2000, **41**, 1051; (*g*) M. Kunert, M. Brauer, O. Klobes, H. Gorls and E. Dinjus, *Eur. J. Inorg. Chem*., 2000, 1803; (*h*) Y. Wada, T. Kitamura and S. Yanagida, *Res. Chem. Intermed*., 2000, **26**, 153; (*i*) M. Tokuda, T. Kabuki, Y. Kato and H. Suginome, *Tetrahedron Lett*., 1995, **36**, 3345.

2 B. Zwanenburg, M. Mikolajczyk and P. Kielbasinski, *Enzymes in Action*, Kluwer Academic Publishers, Dordrecht, 2000; W.-D. Fessner, *Biocatalysis, From Discovery to Application*, Springer-Verlag, Berlin, 2000; K. Faber, *Biotransformations*, Springer-Verlag, Berlin, 2000; S. M. Roberts, *J. Chem. Soc., Perkin Trans. 1*, 2000, 611; S. M. Roberts, *J. Chem. Soc., Perkin Trans. 1*, 1999, 1; S. M. Roberts, *J. Chem. Soc., Perkin Trans. 1*, 1998, 157.

3 F. C. Hartman and M. R. Harpel, *Annu. Rev. Biochem*., 1994, **63**, 197.

4 B. A. Parkinson and P. F. Weaver, *Nature*, 1984, **309**, 148; M. Kodaka and Y. Kubota, *J. Chem. Soc., Perkin Trans. 2*, 1999, 891; R. Obert and B. C. Dave, *J. Am. Chem. Soc*., 1999, **121**, 12192; S. Kuwabata, R. Tsuda, K. Nishida and H. Yoneyama, *Chem. Lett*., 1993, 1631; S. Kuwabata, R. Tsuda and H. Yoneyama, *J. Am. Chem. Soc*., 1994, **116**, 5437.

5 K. Sugimura, S. Kuwabata and H. Yoneyama, *J. Am. Chem. Soc*., 1989, **111**, 2361.

6 K. Sugimura, S. Kuwabata and H. Yoneyama, *J. Electroanal. Chem*., 1990, **299**, 241.

7 (*a*) M. Wieser, T. Yoshida and T. Nagasawa, *Tetrahedron Lett*., 1998, **39**, 4309; (*b*) M. Wieser, N. Fujii, T. Yoshida and T. Nagasawa, *Eur. J. Biochem*., 1998, **257**, 495; (*c*) T. Yoshida and T. Nagasawa, *J. Biosci. Bioeng*., 2000, **89**, 111; (*d*) M. Wieser, T. Yoshida and T. Nagasawa, *J. Mol. Catal. B: Enzymatic*, 2001, **11**, 179.

8 Z. He and J. Wiegel, *Eur. J. Biochem*., 1995, **229**, 77; Z. He and J. Wiegel, *J. Bacteriol*., 1996, **178**, 3539.

9 A. J. Mesiano, E. J. Beckman and A. J. Russell, *Chem. Rev*., 1999, **99**, 623; Y. Ikushima, *Adv. Colloid Interface Sci*., 1997, **71–72**, 259; E. Cernia and C. Palocci, in *Methods in Enzymology*, ed. J. N. Abelson and M. I. Simon, Academic Press, San Diego, 1997, vol. 286, p. 495; A. M. Klibanov, *Nature*, 2001, **409**, 241; S. V. Kamat, E. J. Beckman and A. J. Russell, *J. Am. Chem. Soc*., 1993, **115**, 8845; O. Aaltonen and M. Rantakylä, *Chemtech*, 1991, 240; S.-H. Yoon, H. Nakaya, O. Ito, O. Miyawaki, K.-H. Park and K. Nakamura, *Biosci. Biotechnol. Biochem*., 1998, **62**, 170.

10 T. W. Randolph, D. S. Clark, H. W. Blanch and J. M. Prausnitz, *Science*, 1988, **239**, 387; T. W. Randolph, H. W. Blanch and J. M. Prausnitz, *AIChE J*., 1988, **34**, 1354.

11 T. Matsuda, T. Harada and K. Nakamura, *Chem. Commun*., 2000, 1367.

12 T. Mori and Y. Okahata, *Chem. Commun*., 1998, 2215; T. Mori, A. Kobayashi and Y. Okahata, *Chem. Lett*., 1998, 921.

13 Control reaction using inactivated cells of *B. Megaterium* [inactivation conditions: 90 °C, 2 h, reaction conditions: 10 MPa, 40 °C, 3 h, cells: 1.0 mL (OD_{610} = 32)] afforded no carboxylation product, which indicates that a biocatalyst is at work and that the carboxylation is not an unexpected process promoted by non-enzymic constituents of the cell.

CHEMCOMM Communication
www.rsc.org/chemcomm

IR detection of NO_2 using p^+ porous silicon as a high sensitivity sensor

F. Geobaldo,[a] B. Onida,[a] P. Rivolo,[a] S. Borini,[bc] L. Boarino,[b] A. Rossi,[bc] G. Amato[b] and E. Garrone*[a]

[a] *Dipartimento di Scienza dei Materiali e Ingegneria Chimica, Politecnico di Torino, Corso Duca degli Abruzzi 24 10129. Torino, Italy. E-mail: garrone@athena.polito.it*
[b] *ThinFilmLab, Istituto Elettrotecnico Nazionale Galileo Ferraris, Strada delle Cacce 91 10135. Torino, Italy*
[c] *INFM, Politecnico di Torino, Corso Duca degli Abruzzi 24 10129. Torino, Italy*

Received (in Cambridge, UK) 12th July 2001, Accepted 31st August 2001
First published as an Advance Article on the web 3rd October 2001

Mesoporous silicon doped with 3.0×10^{19} B atoms cm^{-3} (p^+-type) is an insulating material which dramatically increases its electrical conductivity when exposed to traces of gaseous NO_2; nitrogen dioxide chemisorption at the surface generates carriers, the population of which is readily evaluated through the intensity of IR absorption.

Porous silicon (PS) is obtained through the electrochemical etching of semiconducting phosphorus- (n-type) or boron- (p-type) doped crystalline silicon.[1–3] When the etching is performed on silicon with an impurity level of around 1×10^{19} B cm^{-3} (p^+ type), a mesoporous system with a dendritic structure (see graphical abstract) is obtained, with a surface area ranging from 200 to 600 m^2 cm^{-3} (N_2 BET). Although the etching process is believed to remove selectively only silicon atoms,[4] it causes the depletion of carriers present in the pristine material: PS nearly behaves like an insulator and is consequently practically transparent to mid-IR radiation.

Curve **a** in Fig. 1 reports the spectrum, taken under vacuum, of a self-supporting membrane of PS (40 μm thick, 60% porosity). Peaks are seen around 2100 cm^{-1} and below 1000 cm^{-1}, where fall the vibrational modes of hydride-terminated silicon species,[5–7] SiH_x (or Si_yH_x) formed during the electrochemical etching, and those related to oxidised species.

The smooth increase of the background absorption below 2000 cm^{-1} (broken curve) is due to residual free carriers and is therefore described by the Drude equation,[8] according to which the absorption coefficient is proportional to both the square of the wavelength and to the concentration of carriers. Fitting the Drude equation to the background of curve **a** yields[9] *ca.* 3×10^{17} cm^{-3} free carriers, *i.e.* about 99% of the boron atoms no longer act as electron traps. Curve **a** also shows interference fringes, due to multiple reflections of the IR beam at the rather regular boundaries of the sample.

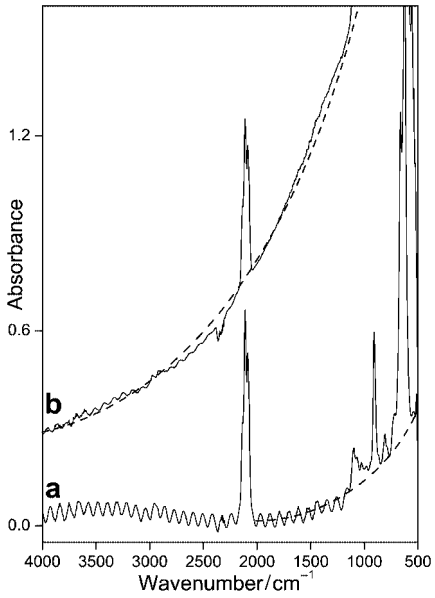

Fig. 1 IR spectra of p^+-type PS *in vacuo* (curve **a**) and under 1 mbar of pure NO_2 (curve **b**). Broken curves are simulations of the background according to the Drude law (see text).

With p^+-type PS (and only in this case), the electrical conductivity has been found[10] to increase when the voids are filled by polar liquids with high dielectric constant. On the other hand, still with p^+-type PS, it has recently been observed, through dc electrical measurements,[11] that the original semiconducting character may be partially restored through the contact of gaseous NO_2 already at very low (sub-ppm) concentrations.

We used FTIR *in situ* spectroscopy to investigate the interaction of gaseous species on the PS surface in the mid-IR region. Whereas extensive studies[5–7] have been performed on H_2 and O_2 environments in PS, no FTIR study of the interaction of other gases with the PS surface is available. A sample of p^+-PS was exposed to a few mbar of different pure gases: NO_2, CO, NH_3, NO, O_2 and acetone. While no response to the latter five species is seen, an impressive response to NO_2 develops in a few seconds. Curve **b** in Fig. 1 shows that, after the admission of gaseous NO_2, an absorption appears, monotonically increasing from about 4000 cm^{-1}. This spectral profile is again described by the Drude law: as a consequence of the interaction with NO_2, a higher concentration of carrier is observed (around 3×10^{18} holes cm^{-3}). Because of the increased absorption, interference fringes are drastically decreased.

The intensity of the IR absorption (*i.e.* the concentration of carriers) depends upon pNO_2. Fig. 2 reports the intensity measured at three arbitrarily chosen frequencies (1300, 1900 and 2500 cm^{-1}) plotted against the equilibrium pNO_2: a saturation effect is seen for comparatively low pressures, irrespective of the wavelength chosen. This suggests that the behaviour of PS in the presence of NO_2 is due to an entirely different mechanism with respect to dielectric or polarization effects invoked as explanation of the conductivity induced by polar substances condensed in the pores.[10] A chemically guided process, *i.e.* a chemisorption phenomenon, is likely to be the reason for the generation of free carriers. Attempts to evaluate volumetrically the amount of adsorbed molecules showed that this is rather small, at the most a fraction of the boron atoms present in the system. This is probably also the reason why no signal due to chemisorbed molecules is seen in curve **b** of Fig. 1.

The chemical nature of the interaction between PS and NO_2 is supported by the fact that NO_2 has the highest electron affinity[12] among the gases studied by us. This high value (2.273 eV) is probably the key factor in determining the unique selectivity shown by PS. A species roughly describable as NO_2^- may be formed by the trapping of an electron at the surface, whereas such a process is far less likely for NO and O_2, with a much smaller electron affinity[13,14] (0.45 and 0.026 eV,

 DOI: 10.1039/b106188g

respectively), and is impossible for the other molecules which do not accept electrons easily.

As it concerns the evolution of the spectra with time, two different behaviours have been observed, depending upon the NO_2 partial pressure. With pNO_2 less than 1 mbar, the intensity grows rapidly and remains constant; with higher partial pressures, the absorption reaches a maximum and than decreases slowly, the rate of decrease strongly depending upon the NO_2 pressure. Such an effect, probably due to successive reactions involving nitrogen dioxide, does not interfere, however, with the possible use of PS as an NO_2 sensor, which is of interest in the pressure region to which Fig. 2 refers.

The effect of NO_2 at low pressures is completely reversible within a few seconds, and the interaction can be repeated on the same sample several times. In contrast, with higher NO_2 pressures, the decrease of intensity of the IR absorption is accompanied by a slight oxidation of the PS sample, as shown by the increase of the absorption bands due to the stretching vibrations of oxidised species (Si–O–Si, O_3SiH and O_2SiH_2).[6] This process is irreversible and causes a decrease in the response to NO_2 in successive experiments. Uptake of oxygen by PS is mainly a surface process, at least in the initial stages, leading to the formation of a surface oxidised layer that prevents the chemisorption process. This is further evidence that the generation of free carriers in PS involves adsorption of NO_2 at the surface.

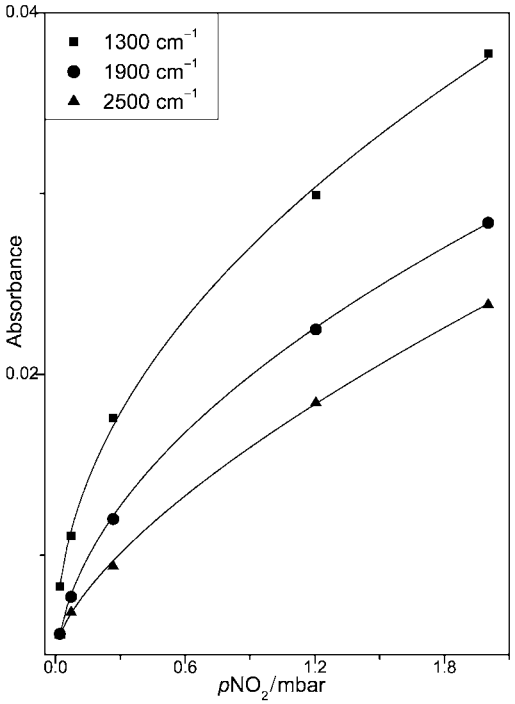

Fig. 2 Absorption normalised to unit thickness (1 μm) at three different wavenumbers against NO_2 equilibrium pressure.

For the sake of completeness, the same experiments were run on a lightly B-doped PS and on n-type PS, and no effect on the background spectrum was seen.

In conclusion, the experimental evidence reported shows that a real chemisorption process takes place at the surface of PS. Also, it suggests that PS may probably be used as a very sensitive NO_2 sensor working at room temperature. At variance with what is observed for oxide-based NO_2 sensors, PS shows a unique selectivity to NO_2 and does not sense other nitrogen compounds such as NO. We have evidence that other atmospheric components like H_2O and CO_2 do not interfere with NO_2: future work will deal with ozone, a molecule strictly similar to NO_2, and therefore a possible source of interference. The detection of the sensing effect is possible on the basis of IR measurements (Fig. 2): taking into account the availability of IR LEDs, the results reported may open a new possibility in the applications of PS as a chemical sensor towards a hazardous pollutant like NO_2, especially when present in trace amounts.

Notes and references

1 M. J. Sailor and E. J. Lee, *Adv. Mater.*, 1997, **9**, 783.
2 R. L. Smith and S. D. Collins, *J. Appl. Phys.*, 1992, **71**, R1.
3 A. Halimaoui, in *Properties of Porous Silicon*, EMIS data review series, ed. L. T. Canham, INSPEC, London, 1997, pp. 12–22.
4 G. Polisski, D. Kovalev, G. Dollinger, T. Sulima and F. Koch, *Physica B*, 1999, **273**, 951.
5 Y. Ogata, H. Niki, T. Sakka and M. Iwasaki, *J. Electrochem. Soc.*, 1995, **142**, 195.
6 Y. Ogata, H. Niki, T. Sakka and M. Iwasaki, *J. Electrochem. Soc.*, 1995, **142**, 1595.
7 T. Tsuboi, T. Sakka and Y. H. Ogata, *Phys. Rev. Sect. B*, 1998, **58**, 13 863.
8 S. Perkowitz, *Optical Characterization of Semiconductors*, Academic Press, Cambridge, UK, 1993, p. 399.
9 M.Theiss, SCOUT_98, Hard- and Software for Optical Spectroscopy, Dr. Bernard Klein Str. 110, D-52078 Aachen, Germany.
10 V. Yu. Timoshenko, V. Lysenko, Th. Dittrich and F. Koch, *Phys. Status Solidi A*, 2000, **182**, 163.
11 L. Boarino, M. Rocchia, C. Baratto, A. M. Rossi, E. Garrone, S. Borini, F. Geobaldo, E. Comini, G. Faglia, G. Sberveglieri and G. Amato, *Phys. Status Solidi A*, 2000, **182**, 465.
12 K. M. Ervin, J. Ho and W. C. Lineberger, *J. Phys. Chem.*, 1988, **92**, 5405.
13 M. J. Travers, D. C. Cowles and G. B. Ellison, *Chem. Phys. Lett.*, 1989, **164**, 449.
14 R. J. Celotta, R. A. Bennett, J. L. Hall, M. W. Siegel and J. Levine, *Phys. Rev. Sect. A*, 1972, **6**, 631.

CHEMCOMM Communication
www.rsc.org/chemcomm

Formation and reactivity of a cobalt(II) hydroperoxide intermediate

Sunita Thyagarajan, Christopher D. Incarvito, Arnold L. Rheingold and Klaus H. Theopold*

Department of Chemistry and Biochemistry, Center for Catalytic Science and Technology, University of Delaware, Newark, DE 19716, USA. E-mail: theopold@udel.edu

Received (in Cambridge, UK) 9th August 2001, Accepted 14th September 2001
First published as an Advance Article on the web 11th October 2001

Reaction of Tp$^{t\text{-Bu,Me}}$Co–H with O_2 proceeds *via* a spectroscopically observable hydroperoxide whose reactivity in solution and in the solid state differ dramatically.

Metal hydroperoxides (M–OOH) are reactive intermediates in metal mediated reactions of hydrogen peroxide and dioxygen. Due to their lability, there are few instances in which such species can be observed spectroscopically,[1] much less characterized structurally.[2] Migratory insertion reactions of O_2 into metal–carbon bonds are rare and mechanistically diverse;[3] their extension to metal hydrides is of interest.[4]

Exposure of a C_6D_6 solution of Tp$^{t\text{-Bu,Me}}$Co-H[5] to an excess of O_2 gas at room temperature caused a rapid reaction that yielded only the known complexes Tp$^{t\text{-Bu,Me}}$Co(O_2) and Tp$^{t\text{-Bu,Me}}$Co–OH in approximately equal amounts (see Scheme 1).[6] In contrast, exposure of solid Tp$^{t\text{-Bu,Me}}$Co–H to oxygen gas (1 atm) produced a new cobalt complex (**1**), along with minor amounts of Tp$^{t\text{-Bu,Me}}$Co–OH.

1 could be separated from the hydroxide by differential solubility and recrystallization from ether yielded purple crystals of **1** in 70% yield. The ^{1}H NMR spectrum of **1** indicated a loss of the threefold symmetry of the Tp$^{t\text{-Bu,Me}}$ ligand. Structural characterization of **1** by X-ray diffraction revealed that one of the hydrogen atoms of a *tert*-butyl group had been replaced with an oxygen atom that was also bonded to cobalt, thus forming a cobalt(II) alkoxide featuring a six-membered ring. The structure determination was unfortunately marred by multiple disorder; however, it allowed the unambiguous assignment of the connectivity of **1**. Addition of one equivalent of 3-*tert*-butyl-5-methylpyrazole to **1** yielded **2**, the structure of which is shown in Fig. 1.[7] Five-coordinate **2** adopts trigonal bipyramidal geometry, with the nitrogen atoms of the free pyrazole (N31) and the functionalized pyrazole (N21) occupying axial positions and those of the remaining two pyrazoles (N1, N11) and the alkoxide oxygen (O1) taking up the equatorial positions.

Carrying out the oxygenation of Tp$^{t\text{-Bu,Me}}$Co–H in toluene at low temperature (−78 °C) revealed a color change from bright blue to purple (reminiscent of the color of Tp$^{t\text{-Bu,Me}}$Co–OH), followed by another change to a grayish green upon warming to room temperature. ^{1}H NMR monitoring of this reaction at −78 °C showed that the resonances of Tp$^{t\text{-Bu,Me}}$Co–H were slowly replaced by a new set of resonances consistent with a three-fold symmetric Co(II) species of the type Tp$^{t\text{-Bu,Me}}$Co–X.[8] Upon warming the solution to room temperature, these resonances disappeared, while those of Tp$^{t\text{-Bu,Me}}$Co(O_2) and Tp$^{t\text{-Bu,Me}}$Co–OH appeared. Further characterization of the intermediate was obtained using *in-situ* IR spectroscopy. When a toluene solution of the hydride at −61 °C was exposed to dioxygen, the Co–H stretch at 1671 cm^{-1} gradually disappeared and was replaced by a broad peak at 3347 cm^{-1}; the latter disappeared upon warming to room temperature. We note that the IR spectrum of a solution of *tert*-butyl hydroperoxide exhibits its broad O–H stretch at 3304 cm^{-1}. Repetition of the same experiment with Tp$^{t\text{-Bu,Me}}$Co–D showed a replacement of ν_{Co-D} (at 1208 cm^{-1}) with a new resonance at 2486 cm^{-1}. Unfortunately, neither experiment revealed the expected ν_{O-O} (*ca.* 800–900 cm^{-1}), which is likely obscured by the many strong bands attributable to the Tp ligand. All these observations are most consistent with the formation and subsequent decomposition of the Co(II) hydroperoxide Tp$^{t\text{-Bu,Me}}$Co–OOH.

A mechanistic proposal for the formation of Tp$^{t\text{-Bu,Me}}$Co–OOH and its different thermal decompositions is shown in

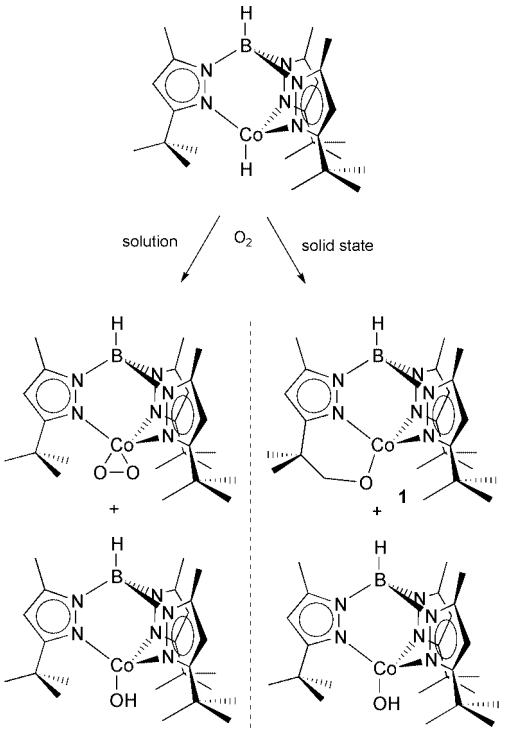

Scheme 1

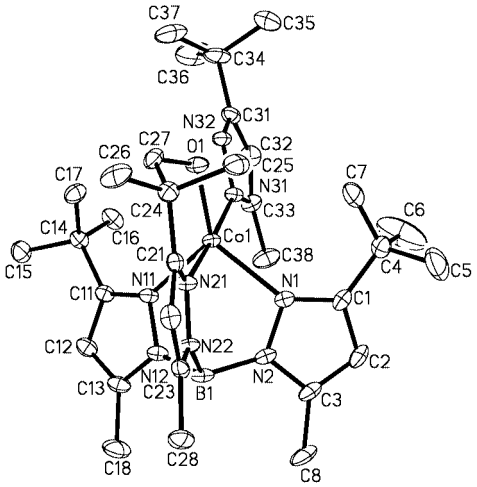

Fig. 1 The molecular structure of **2**. Selected interatomic distances (Å) and angles (°): Co1–O1, 1.929(3); Co1–N1, 2.126(4); Co1–N11, 2.133(3); Co1–N21, 2.126(4); Co1–N31, 2.074(3); N21–Co1–N31, 174.83(12); O1–Co1–N1, 133.66(13); O1–Co1–N11, 126.98(14); N1–Co1–N11, 99.45(13).

 DOI: 10.1039/b107080k

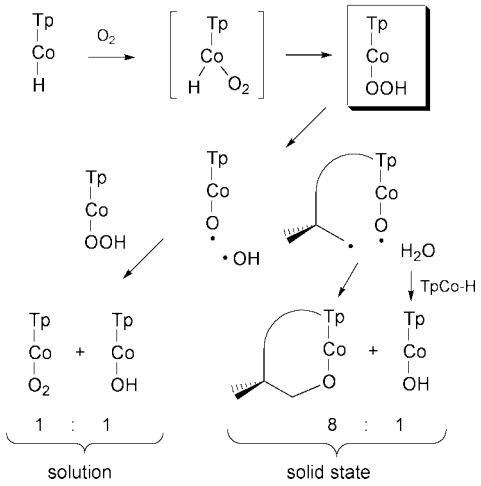

Scheme 2

Scheme 2. The commonly discussed mechanisms for reactions of metal hydrides with O_2 seem not germane here. Thus, a radical chain reaction is ruled out by the observation that Tp$^{t\text{-Bu,Me}}$Co(O_2) does not react with Tp$^{t\text{-Bu,Me}}$Co–H. An alternative deprotonation/O_2-coordination/protonation sequence is unlikely in light of the extremely low expected acidity of the hydride precursor, the conjugate base of which—*i.e.* [Tp$^{t\text{-Bu,Me}}$Co]$^-$—is highly destabilized. We favor a migratory insertion of coordinated O_2 into the Co–H bond. Such a process finds a parallel, if not exact precedent, in the reaction of Tp$^{t\text{-Bu,Me}}$Cr–Ph with O_2.[3g] Hydrogen atom abstraction by O_2, followed by binding of the resulting HO_2, is another possible pathway given the comparable strengths of the Co–H bond of Tp$^{t\text{-Bu,Me}}$Co–H ($D_{Co–H} \approx 60$ kcal mol^{-1}) and the O–H bond of the HO_2 radical ($D_{O–H} = 49$ kcal mol^{-1}).[9]

The O–O bond of peroxides is weak, and cobalt alkylperoxides have been implied to suffer homolysis of this linkage.[10] Homolytic cleavage of the O–O bond of the common intermediate Tp$^{t\text{-Bu,Me}}$Co–OOH would generate a terminal cobalt oxo species (Tp$^{t\text{-Bu,Me}}$Co=O $\leftrightarrow$ Tp$^{t\text{-Bu,Me}}$Co–O$^{\cdot}$) as well as hydroxyl radical. At this point the mechanistic pathways may diverge. In solution the fragments are free to move about and encounter other molecules; the cobalt oxo species may show selectivity and abstract weakly bonded hydrogen from Tp$^{t\text{-Bu,Me}}$Co–OOH in a bimolecular reaction yielding Tp$^{t\text{-Bu,Me}}$Co(O_2) and Tp$^{t\text{-Bu,Me}}$Co–OH in equal amounts. In contrast, in the solid the movements of both fragments are restricted. The hydroxyl radical may abstract a hydrogen atom from the nearest methyl group. The resulting primary radical then combines with the Co–O$^{\cdot}$ moiety to form **1**. The small amount of Tp$^{t\text{-Bu,Me}}$Co–OH produced probably results from diffusion of the reaction product water to unreacted Tp$^{t\text{-Bu,Me}}$Co–H.

In conclusion, our observations show that the reaction of a cobalt(II) hydride with O_2 proceeds *via* the formation of a reactive hydroperoxide intermediate; we propose that the latter is formed by a migratory insertion of bound O_2 into the metal–hydrogen bond. The subsequent transformations of Tp$^{t\text{-Bu,Me}}$Co–OOH are consistent with the formation of a terminal cobalt oxo complex. They also provide another example of different reactivity in solution *versus* the solid state. We have previously made good use of this phenomenon,[11] and it may prove of general utility in synthetic chemistry and mechanistic investigations.

This research was supported by a grant from the United States Department of Energy (ER14273).

Notes and references

1 (*a*) J. H. Bayston and M. E. Winfield, *J. Catal.*, 1964, **3**, 123; (*b*) L. E. Johnston and J. H. Page, *Can. J. Chem.*, 1969; **47**, 4241; (*c*) R. A. Michelin, R. Ros and G. Strukul, *Inorg. Chim. Acta*, 1979, **37**, L491; (*d*) M. T. Atlay, M. Preece, G. Strukul and B. R. James, *J. Chem. Soc., Chem. Commun.*, 1982, **7**, 406; (*e*) G. Strukul, R. Ros and R. A. Michelin, *Inorg. Chem.*, 1982, **21**, 495; (*f*) H. Suzuki, S. Matsuura, Y. Morooka and T. Ikawa, *Chem. Lett.*, 1982, 1011; (*g*) M. T. Atlay, M. Preece, G. Strukul and B. R. James, *Can. J. Chem.*, 1983, **61**, 1332; (*h*) H. Suzuki, S. Matsuura, Y. Moro-oka and T. Ikawa, *J. Organomet. Chem.*, 1985, **286**, 247; (*i*) K. D. Karlin, P. Gosh, R. W. Cruswe, A. Farooq, Y. Gultneh, R. R. Jacobson, N. J. Blackburn, R. W. Strange and J. Zubieta, *J. Am. Chem. Soc.*, 1988, **110**, 6769; (*j*) M. Mahroof-Tahir, N. N. Murthy, K. D. Karlin, N. J. Blackburn, S. N. Shaikh and J. Zubieta, *Inorg. Chem.*, 1992, **31**, 3001; (*k*) M. Lubben, A. Meetsma, E. C. Wilkinson, B. Feringa and J. L. Que, *Angew. Chem., Int. Ed.*, 1995, **34**, 1512; (*l*) M. E. de Vries, R. M. La Crois, G. Roelfes, H. Kooijman, A. L. Spek, R. Hage and B. L. Feringa, *Chem. Commun.*, 1997, 1549; (*m*) B. Miller, J. Altman and W. Beck, *Inorg. Chim. Acta*, 1997, **246**, 101; (*n*) D. E. Root, M. Mahroof-Tahir, K. D. Karlin and E. I. Solomon, *Inorg. Chem.*, 1998, **37**, 4838; (*o*) M. Akita, T. Miyaji, S. Hikichi and Y. Moro-oka, *Chem. Commun.*, 1998, 1005; (*p*) H. Ohtsu, S. Itoh, S. Nagatomo, T. Kitagawa, S. Ogo, Y. Watanabe and S. Fukuzumi, *Chem. Commun.*, 2000, 1051.

2 (*a*) U. Thewalt and R. Marsh, *J. Chem. Soc. A*, 1967, **89**, 6364; (*b*) D. Carmona, M. P. Lamata, J. Ferrer, J. Modrego, M. Perales, F. J. Lahoz, R. Atencio and L. A. Oro, *J. Chem. Soc., Chem. Commun.*, 1994, 575; (*c*) A. Wada, M. Harata, K. Hasegawa, K. Jitsukawa, H. Masuda, M. Mukai, T. Kitagawa and H. Einaga, *Angew. Chem., Int. Ed.*, 1998, **37**, 798; (*d*) M. Akita, T. Miyaji, S. Hikichi and Y. Moro-oka, *Chem. Lett.*, 1999, 813; (*e*) Y. Takahashi, M. Hashimoto, S. Hikichi, M. Akita and Y. Moro-oka, *Chem. Commun.*, 1999, 3074; (*f*) D. D. Wick and K. I Goldberg, *J. Am. Chem. Soc.*, 1999, **121**, 11900.

3 (*a*) T. P. Blackburn, J. A. Labinger and J. Schwartz, *Tetrahedron Lett.*, 1975, 3041; (*b*) D. A. Ryan and J. A. Espenson, *J. Am. Chem. Soc.*, 1979, **101**, 2488; (*c*) T. V. Lubben and P. T. Wolczanski, *J. Am. Chem. Soc.*, 1987, **109**, 424; (*d*) A. Van Asselt, M. S. Trimmer, L. M. Henling and J. E. Bercaw, *J. Am. Chem. Soc.*, 1988, **110**, 8254; (*e*) R. Han and G. Parkin, *J. Am. Chem. Soc.*, 1990, **112**, 3662; (*f*) R. Han and G. Parkin, *Polyhedron*, 1990, **9**, 2655; (*g*) A. Hess, M. R. Hörz, L. M. Liable-Sands, D. C. Lindner, A. L. Rheingold and K. H. Theopold, *Angew. Chem., Int. Ed.*, 1999, **38**, 166.

4 (*a*) J. F. Endicott, C. L. Wong, T. Inoue and P. Natarajan, *Inorg. Chem.*, 1979, **18**, 450; (*b*) T. T. Wenzel, in *Dioxygen Activation and Homogeneous Catalytic Oxidation*, ed. L. I. Simandi, Elsevier Science Publishing Co. Inc., New York, 1991, p. 545; (*c*) A. Bakac, *J. Am. Chem. Soc.*, 1997, **119**, 10 726; (*d*) A. Bakac, *J. Photochem. Photobiol. A-Chem.*, 2000, **132**, 87.

5 J. D. Jewson, L. M. Liable-Sands, G. P. A. Yap, A. L. Rheingold and K. H. Theopold, *Organometallics*, 1999, **18**, 300.

6 J. W. Egan, Jr., B. S. Haggerty, A. L. Rheingold, S. C. Sendlinger and K. H. Theopold, *J. Am. Chem. Soc.*, 1990, **112**, 2445.

7 **2**: $C_{32}H_{53}BCoN_8O$, $M = 635.56$, monoclinic, $P2_1/c$, $a = 19.9942(2)$, $b = 9.8211(2)$, $c = 18.7466(2)$ Å, $\beta = 109.131(9)°$, $V = 3477.87(9)$ Å^3, $T = 203(2)$ K, $Z = 4$, $\mu = 0.53$ mm^{-1}, $R = 6.83\%$, GOF = 1.698. CCDC reference number 170801. See http://www.rsc.org/suppdata/cc/b1/b107080k/ for crystallographic data in CIF or other electronic format.

8 ^{1}H NMR (toluene-d_8, 195 K): δ 96.2 (3H), 26.5 (9H), 0.3 (27H); compare to Tp$^{t\text{-Bu,Me}}$Co–H: δ 90.6 (3H), 26.9 (9H), −5.5 (27H) and Tp$^{t\text{-Bu,Me}}$Co–OH: δ 100.3 (3H), 15.8 (9H), 0.3 (27H); $\nu_{O\text{-}H} = 3664$ cm^{-1}.

9 D. M. Golden, V. M. Bierbaum and C. J. Howard, *J. Phys. Chem.*, 1990; **94**, 5413.

10 (*a*) S. Hikichi, H. Komatsuzaki, M. Akita and Y. Moro-Oka, *J. Am. Chem. Soc.*, 1998, **120**, 4699; (*b*) F. A. Chavez and P. K. Mascharak, *Acc. Chem. Res.*, 2000, **33**, 539.

11 O. M. Reinaud and K. H. Theopold, *J. Am. Chem. Soc.*, 1994, **116**, 6979.

CHEMCOMM Communication
www.rsc.org/chemcomm

Placement of cations in NaX faujasite-type zeolite using (*N,V,T*) Monte Carlo simulations

Caroline Mellot-Draznieks,*[a] Severine Buttefey,[b] Anne Boutin[b] and Alain H. Fuchs[b]

[a] *Institut Lavoisier, UMR CNRS 8637, Université de Versailles Saint-Quentin, 45 avenue des Etats-Unis, Versailles Cedex, 78035 France. E-mail: mellot@chimie.uvsq.fr*
[b] *Laboratoire de Chimie Physique, UMR 8000 CNRS, Université Paris-Sud, 91405 Orsay, France*

Received (in Cambridge, UK) 27th April 2001, Accepted 7th September 2001
First published as an Advance Article on the web 11th October 2001

The cation distribution in dehydrated NaX was predicted using appropriate interatomic potentials and (*N,V,T*) simulations, considering the cations as 'guest' particles and the framework as a 'host'; the simulations not only yield the expected different types of sites, but also highlight the cooperative placement of supercage cations which results essentially from electrostatic interactions between the cations.

The dehydrated forms of X faujasite-type zeolites have attracted much attention in the last five years, largely owing to their industrial use for gas adsorption and separation. Adsorption properties are closely related to the location of extraframework cations and to their accessibility to adsorbed molecules. The precise location of cations in channels and cages is an important prerequisite for understanding the adsorption properties of the zeolite of interest. However, the precise location of supercage cations in monovalent zeolites by conventional diffraction techniques is rendered especially difficult because of partial occupancies affecting low symmetry sites. Typically, since the initial diffraction work by Mortier,[1] there have been a significant number of studies dedicated to the reinvestigation of the location of cations in monovalent X zeolites like NaX or LiX, ranging from conventional powder or single crystal diffraction refinements[2–8] to NMR studies[5,9–12] and computational approaches.[3,13,14]

The cation distribution in NaX is usually described as follows: 32 Na^+ ions are in sites I′ within the sodalite cages facing the six-rings of hexagonal prisms (partial occupancy of site I inside the hexagonal prims may occur); 32 Na^+ ions are in sites II facing the six-rings of sodalite cages towards the supercages; the extra cations are distributed in the supercages near the 12-ring or 4-ring windows over a variety of sites referred to as III or III′ depending on their framework environment (Fig. 1). While the location of Na ions in sites I′ and II is well established, the location of the remaining Na ions in the supercages has been the subject of much controversy.

In recent years, atomistic simulations have been recognized to be an interesting alternative for yielding valuable insights into the structure and energetics of zeolites.[15] Typically, energy minimizations have been successfully applied to the siting of cations in various zeolites: Li-ABW and 4A,[16] ETS-10,[17] NaX[3,14] or Na-clinoptilolite.[18]

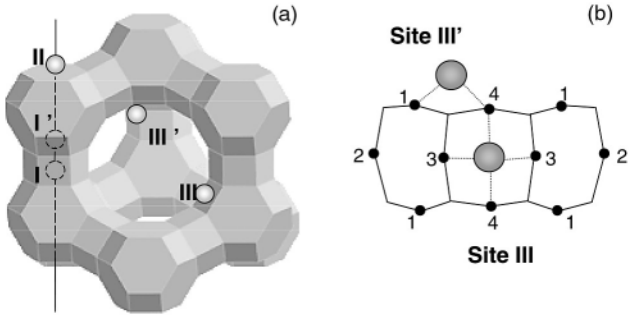

Fig. 1 (a) Schematic representation of the faujasite-type X zeolite with extra-framework cation positions. **(b)** Sites III and III′ differ in their placement relative to the four-ring windows of the supercages.

Here we predict the equilibrium distribution of Na ions in the NaX ($Na_{86}Al_{86}Si_{106}O_{384}$) zeolite using Monte Carlo simulations in the (*N,V,T*) ensemble, considering the cations as 'guest' particles and the rest of the structure as the 'host'. We believe this stochastic simulation method should be the most appropriate one to tackle this problem, especially since an important amount of Na ions are known to be statistically disordered.

The sensitivity of the equilibrium cation distribution to the framework model was explored through the use of two distinct rigid framework models. In the first one (Model 1), the host structure consisted of an incomplete and negatively charged unit-cell [$(Si/Al)_{192}O_{384}$] considering an *average* T(Si/Al) framework atom. The cation/framework interactions were modeled using a dispersion–repulsion term acting between cations and oxygen atoms only, together with a coulombic term using partial charges on all atoms (T, +1.24, Na, +1; O, −0.84396).[19] In the second model (Model 2), Si and Al were explicitly distinguished, adding explicit repulsive–dispersive interactions for Si and Al with Na ions as encapsulated in the cvff_aug forcefield.[20] In this latter case, the [$Si_{106}Al_{86}O_{384}$] host model was obtained by substituting ten randomly chosen Al atoms with Si atoms from a framework model with a strict alternation of AlO_4 and SiO_4 tetrahedra (Si : Al = 1). Following our previous computational work on NaX,[3] the following partial charges were used: Si, +2.4; Al, +1.4; Na, +1, O, −1.2. While constructed starting from the original cubic form, both incomplete zeolite models were converted into *P*1 in order to perform the simulations. Finally, (*N,V,T*) simulations were performed at 298 K using both host models over one unit-cell with periodic boundary conditions. Random translational displacements of cations (maximum of 0.3 Å) were adjusted so as to obtain an acceptance rate of 50%. A standard MC simulated annealing procedure had to be used to accelerate convergence to the most stable configuration. Equilibrium was typically reached after 10^5 moves. A further 10^6 production steps were performed to average quantities. More details are given in ref. 19.

Monte Carlo (MC) simulations using Model 1 lead to an average cation distribution in NaX where sites I′ and II are fully occupied as expected from diffraction data, with average atomic coordinates very close to the experimental ones (Fig. 2(a) and (b)). The 22 extra cations are found mainly in sites III with a small proportion in sites III′ (Fig. 2(c)), a result that contrasts with the experimental predominance of sites III′.[2,3,6,7] Neither do we obtain the secondary sites III′, recently reported as sites III′ and III″ by Seff *et al*. for example, facing AlO_4 and SiO_4 tetrahedra respectively.[6] A small 1 Å deviation is obtained between the simulated site III and its reported experimental position,[8] while the simulated sites III′ correspond quite well to the experimental ones. Both types of sites yield average simulated Na–O distances to the closest oxygens of 2.37 and

 DOI: 10.1039/b103808g

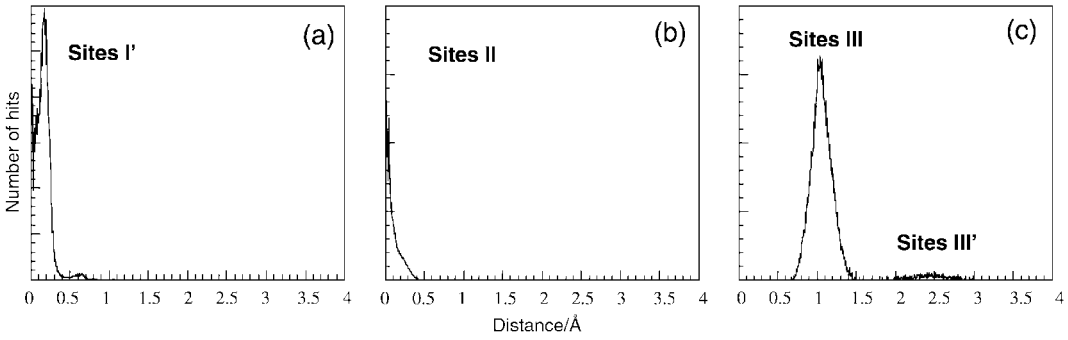

Fig. 2 Predicted cation distribution in NaX using Model 1. The computed distance distributions are indicated by reference to the observed crystallographic positions in sodium-exchanged faujasites.[8,21]

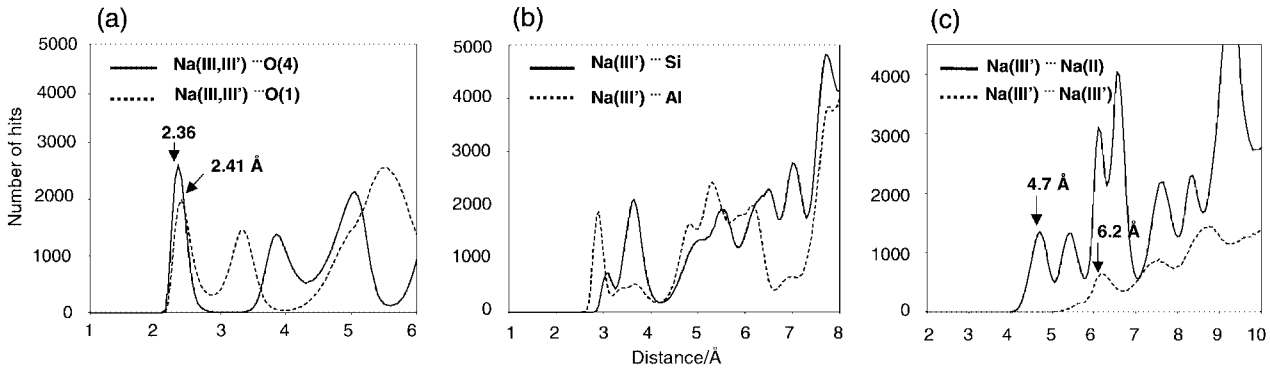

Fig. 3 Predicted cation distribution in NaX using Model 2. Selected pair distribution functions for the extra Na cations of the supercage in sites III′ (a) with framework oxygens O(1) and O(4); (b) with Si and Al framework atoms; (c) with Na ions in sites II and III′.

2.26 Å for Na ions in sites III and III′ respectively. Indeed, it turns out that the structural features of the cation distribution in the NaX zeolite are correctly predicted by the MC simulations using a crude model for the framework itself and cation/framework interactions; however, these simulations failed to predict the correct location of supercage Na ions. We concluded that such a detailed and correct description of Na ion distribution probably cannot be obtained as long as Al and Si atoms cannot be distinguished in the faujasite framework model.

Simulations were then performed with Model 2, which explicitly distinguishes Al and Si atoms in terms of coulombic and short-range interactions. Prior to the simulations, 32 Na ions were placed in sites I and 32 Na ions in sites II, so that insertions were performed on the remaining 22 Na ions exclusively. The simulated pair distribution functions reveal that all Na ions are located in sites III′, with Na···O(1) and Na···O(4) distances typical of sites III′ (Fig. 3(a)), in excellent agreement with the most recent crystal structures of NaX.[3,6] No cation was detected in sites III. Another key feature of the simulations is that they successfully predict the location of Na ions in sites III′ facing both AlO_4 tetrahedra and SiO_4 tetrahedra: Na···Si and Na···Al pair distribution functions (Fig. 3(b)) are in excellent agreement with the two types of sites III′/III″ recently evidenced in ref. 6. Also, different Al distributions were tested as starting points for our MC calculations; it shows that the location of the additional Na cations always follows the above features, assessing the influence of the specific Al distributions chosen.

Interestingly, MC simulations with both models show that the placement of supercage cations is driven by electrostatic repulsion with Na ions in sites II together with electrostatic repulsion among sites III′ themselves. Typically, Model 2 yields first II···III′ neighbours at 4.7 Å and first III′···III′ neighbours at 6.2 Å (Fig. 3(c)). Such features, difficult to pinpoint when using diffraction techniques, tend to show that the placement of cations in zeolites is to be regarded as a cooperative process rather than the occupancy of sites with specific energies, resulting from both short-range interactions with the framework and cation–cation repulsive interactions.

Notes and references

1 W. J. Mortier, *Compilation of Extra-framework Sites in Zeolites*, Butterworth Scientific Ltd., Guildford, UK, 1982.
2 D. H. Olson, *Zeolites*, 1995, **15**, 439.
3 G. Vitale, C. F. Mellot, L. M. Bull and A. K. Cheetham, *J. Phys. Chem.*, 1997, **101**, 4559.
4 J. Plevert, F. DiRenzo, F. Fajula and G. Chiari, *J. Phys. Chem.*, 1997, **101**, 10340.
5 M. Feuerstein and R. F. Lobo, *Chem. Mater.*, 1998, **10**, 2197.
6 L. Zhu and K. Seff, *J. Phys. Chem.*, 1999, **103**, 9512.
7 F. Porcher, M. Souhassou, Y. Dusausoy and C. Lecomte, *Eur. J. Miner.*, 1999, **11**, 333.
8 C. F. Mellot, *PhD Thesis*, Université Pierre et Marie Curie, 1993.
9 M. Feuerstein, M. Hunger, G. Engelhardt and J. P. Amoureux, *Solid State Nucl. Magn. Reson.*, 1996, **7**, 95.
10 J. Plevert, L. C. DeMenorval, F. DiRenzo and F. Fajula, *J. Phys. Chem. B*, 1998, **102**, 3412.
11 M. Feuerstein and R. F. Lobo, *Chem. Commun.*, 1998, 1647.
12 K. H. Lim and C. P. Grey, *J. Am. Chem. Soc.*, 2000, **122**, 9768.
13 C. F. Mellot and A. K. Cheetham, *C. R. Acad. Sci., Sér. IIc: Chim.*, 1998, 737.
14 E. Jaramillo and S. M. Auerbach, *J. Phys. Chem. B*, 1999, **103**, 9589.
15 *Computer Modelling in Inorganic Crystallography*, ed. C. R. A. Catlow, Academic Press, London, 1997.
16 J. M. Newsam, C. M. Freeman, A. M. Gorman and B. Vessal, *Chem. Commun.*, 1996, 1945.
17 M. E. Grillo and J. Carrazza, *J. Phys. Chem.*, 1996, **100**, 12261.
18 A. R. Ruiz-Salvador, D. W. Lewis, J. Rubayo-Soneira and G. Rodriguez-Fuentes, *J. Phys. Chem. B*, 1998, **102**, 8417.
19 S. Buttefey, A. Boutin, C. Mellot-Draznieks and A. H. Fuchs, *J. Phys. Chem.*, submitted; S. Buttefey, A. Boutin and A. H. Fuchs, *Mol. Simul.*, submitted;
20 Catalysis 4.0 Software Suite and Discover, Version 3.2; MSI: San Diego, CA.
21 A. N. Fitch, H. Jobic and A. J. Renouprez, *J. Phys. Chem.*, 1986, **90**, 1311.

CHEMCOMM
Communication
www.rsc.org/chemcomm

Synthesis and oxygenation of selenophosphate dendrimers†

Grzegorz M. Salamończyk,* Maciej Kuźnikowski and Elżbieta Poniatowska

Centre of Molecular and Macromolecular Studies, The Polish Academy of Sciences, Sienkiewicza 112, 90-363 Łódź, Poland. E-mail: gmsalamo@bilbo.cbmm.lodz.pl; Fax: +48 (42) 684-7126; Tel: +48 (42) 681-8952

Received (in Cambridge, UK) 27th July 2001, Accepted 11th September 2001
First published as an Advance Article on the web 2nd October 2001

The backbone of a selenophosphate-based dendrimer of generation 3 having three and four carbon chains is flexible enough to allow its chemical modification by means of partial or complete oxygenation with bulky peroxide.

Dendrimers constitute a relatively young, yet rapidly evolving field of chemistry. A diverse array of dendrimers have been synthesised and applied in different research areas.[1] Modification and introduction of functional groups to a dendrimer are of great present interest. However, most of these transformations rely on the formation of a bond to the surface.[2] Site directed alterations of the interior of a dendrimer appears to be a much more difficult task.[3]

We turn our attention to preparing the first dendrimers based on selenium,[4] which has been increasingly recognised as an essential element in biology and medicine.[5]

Recently, we have disclosed an expedient synthesis of thiophosphate-based dendrimers[6] involving phosphoroamidite chemistry.[7] In this paper, we report on 1) a divergent synthesis of new phosphorus- and selenium-containing dendrimers applying our developed methodology; 2) an unprecedented oxygenation of branching units of selenophosphate dendrimers to the corresponding phosphate functions, which provided another new type of dendrimer. Starting materials, the core compound, tris(3-hydroxypropyl) selenophosphate (**1**) and phosphitylating agent, bis(4-acetoxybutoxy)-*N*,*N*-diethylaminophosphine (**2**) were prepared[8] in high yield from corresponding alkanediol monoacetates[9] and cheap chemicals, in analogous manner to that described previously.[6] The key dendrimer growth step is based on acid mediated alcoholysis of phosphoroamidite.[7] For instance, Se═P[O(CH$_2$)$_3$OH]$_3$ (**1**) reacts smoothly with 3.4 equiv. of Et$_2$NP[O(CH$_2$)$_4$OAc]$_2$ (**2**) in the presence of an excess of tetrazole to furnish trisphosphite intermediate Se═P{O-(CH$_2$)$_3$OP[O(CH$_2$)$_4$ OAc]$_2$}$_3$ and the diethylammonium salt of tetrazole. Addition of pyridine[10] and black selenium to the above reaction mixture afforded first generation dendrimer **3P$_4$Se$_4$**, as shown in Scheme 1. The product, purified on the short pad of silica gel was isolated in 94% yield.

Cleavage of terminal acetates in **3P$_4$Se$_4$** using K_2CO_3 in methanol provided polyalcohol **4P$_4$Se$_4$** in quantitative yield. Reiteration of growth and deprotection reactions afforded the 2nd (**3P$_{10}$Se$_{10}$**, **4P$_{10}$Se$_{10}$**, 98% yield), 3rd (**3P$_{22}$Se$_{22}$**, **4P$_{22}$Se$_{22}$**, 70%) and 4th (**3P$_{46}$Se$_{46}$**, **4P$_{46}$Se$_{46}$**, 52%) generation dendrimers. All compounds are stable, colourless oils whose viscosity increases with increase of molecular weight.

The obtained dendrimers were characterised by ^{1}H NMR, ^{13}C NMR, ^{31}P NMR, ^{77}Se NMR, FT-IR and MALDI TOF mass spectrometry. Especially, the ^{31}P NMR proved to be useful. For example, the ^{31}P{^{1}H}NMR spectrum of the somewhat large 4th generation dendrimer **3P$_{46}$Se$_{46}$** (theoretical molecular weight 15275) showed five distinct resonance lines with accurate integration: δ = 73.99(1P, core), 73.72(3P), 73.57(6P), 73.54(12P), 73.41(24P) ppm. All signals displayed satellite side bands with the splitting of 931 Hz due to ^{31}P–^{77}Se coupling.

The chemical behaviour of selenophosphate dendrimers was found to be rather intriguing. Oxidation of thio- and selenophosphates with hydrogen peroxide[11] and its bis-silyl[12] derivative to their corresponding oxo compounds is documented and presumably proceeds *via* an addition–elimination mechanism with formation of pentacovalent phosphorus intermediates.[11]

Treatment of the 3rd generation dendrimer **3P$_{22}$Se$_{22}$** (^{31}P{^{1}H}NMR and MALDI TOF MS spectra, Fig. 1A and 1D) with *tert*-butylperoxytrimethylsilane[13] (7.7 equiv., CH_2Cl_2, rt, 2 h) resulted in regioselective oxygenation of phosphorus atoms at peripheral branching and extrusion of red selenium, which precipitated from the reaction medium.

The ^{31}P{^{1}H}NMR spectrum (Fig. 1B) shows the decline of the resonance line corresponding to P═Se (δ = 72.7 ppm) at the 3rd sphere to about half of its original height along with the appearance of new lines (P═O, δ = −0.4, −0.5 ppm). It gives the evidence that on average 6 out of 12 phosphorus atoms at third branching were oxygenated. Two resonance lines (P═O range) prompt dissymmetrisation of the macromolecule and/or existence of dendrimeric regioisomers. Addition of the next amount of peroxide (7.7 equiv., 16 h) shifts the degree of oxygenation to about 70%. At this stage more definitive information came from MALDI spectral analysis (Fig. 1E). All peaks differ in mass exactly 63 amu due to replacement of selenium (79) by oxygen (16). Major products (central peak) contain 4 P═Se and 18 P═O functions suggesting that most of the selenium left is located in the core and at first generation. Apparently no degradation of dendrimer framework has occurred. Consecutive addition of organic peroxide (7.7 equiv., 2 h) to the above mixture led to 96% of oxygenation (calculated from the integral of ^{31}P signals) with at least two compounds detected by the ^{31}P{^{1}H}NMR (spectrum not shown). The total conversion of hydrophobic dendrimer **3P$_{22}$Se$_{22}$** into water-soluble phosphate **3P$_{22}$O** took place in three days (Scheme 2).

Isolation of novel phosphate dendrimer **3P$_{22}$O** required only removal of insoluble selenium and evaporation of all the volatiles. Its ^{31}P{^{1}H}NMR spectrum (Fig. 1C) shows the coincidence of chemical shifts of the signals from all the phosphorus atoms present in the molecule.[6] The MALDI TOF

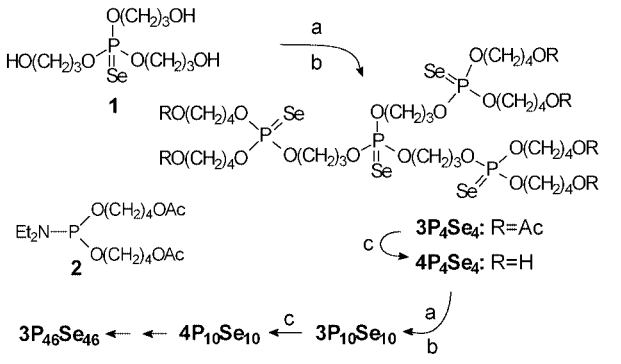

Scheme 1 The synthesis of selenophosphate dendrimers up to generation 4. (a) **2**, tetrazole, dichloromethane; (b) selenium, pyridine; (c) K_2CO_3, methanol, water.

† Electronic supplementary information (ESI) available: experimental procedures and full characterization of new compounds. See http://www.rsc.org/suppdata/cc/b1/b106849k/

 DOI: 10.1039/b106849k

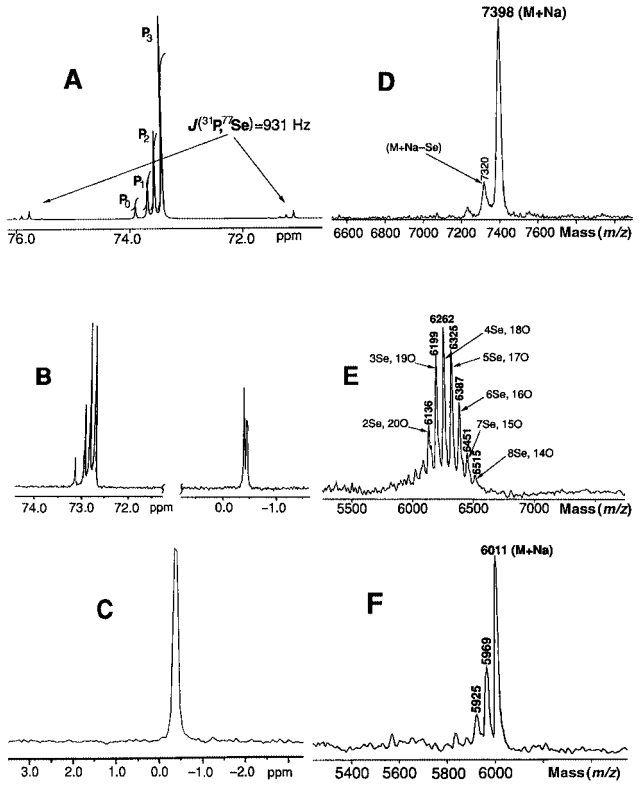

Fig. 1 $^{31}P\{^{1}H\}$NMR spectra of $\mathbf{3P_{22}Se_{22}}$ (A), at 30% conversion of $\mathbf{3P_{22}Se_{22}}$ into $\mathbf{3P_{22}O}$ (B) and $\mathbf{3P_{22}O}$ (C); MALDI TOF MS spectra of $\mathbf{3P_{22}Se_{22}}$ (D), at 70% conversion of $\mathbf{3P_{22}Se_{22}}$ into $\mathbf{3P_{22}O}$ (E) (number of oxygen atoms refers to phosphoryl oxygen) and $\mathbf{3P_{22}O}$ (F).

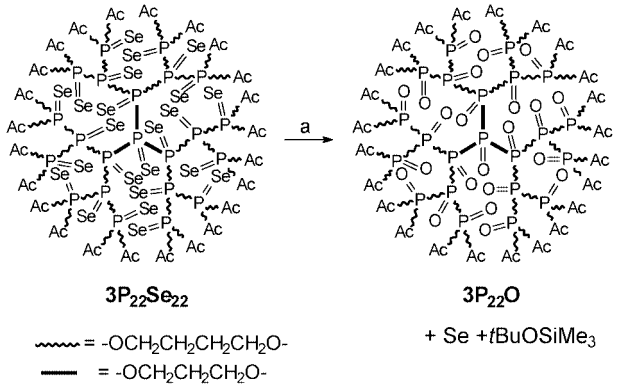

Scheme 2 The oxygenation of 3rd generation dendrimer $\mathbf{3P_{22}Se_{22}}$. (a) *t*BuOOSiMe$_3$, dichloromethane, 75 h.

MS (Fig. 1F) unambiguously confirms complete oxygenation of $\mathbf{3P_{22}Se_{22}}$ without any damage to the dendrimer backbone. Two minor peaks, which are *ca*. 43 and 86 amu in mass lower than the major one (M + Na), presumably arose due to insignificant cleavage (3% calcd. from ^{1}H NMR) of one and two peripheral acetates during the long reaction period. Interestingly, the entire dendritic structure was sufficiently flexible to allow bulky peroxide to penetrate the depth of the macromolecule. Moreover, during the reaction time, all branching units and the core must have changed their geometry from tetrahedral to trigonal bipyramidal and back to tetrahedral. It is also noteworthy to point out that the corresponding thiophosphate[6] dendrimer did not undergo oxygenation in these mild conditions.

In conclusion, we have synthesised highly pure, novel selenophosphate dendrimers *via* simple one-pot phosphitylation and selenium addition reactions. These compounds are not only the first selenium-based dendrimers, but also seem to be the largest synthetic selenium derivatives ever reported having molecular weight comparable with selenoproteins.[14] In addition, the selenophosphate dendrimer served as a macromolecular substrate for partial or complete oxygenation. The oxygenation reaction proceeded cleanly. Initially, peroxide reagent oxidised peripheral branching, then it was capable to penetrate deeper into the cascade structure. The dendrimer was even adaptable enough to make possible the modification in the core.

This study was supported by the Committee for Scientific Research, Grant No 3T09A 040 19. The authors are grateful to Professor Dr A. Skowrońska for her encouragement to work with dendrimers.

Notes and references

1 Reviews: (*a*) F. Zeng and S. C. Zimmerman, *Chem. Rev.*, 1997, **97**, 1681; (*b*) J. P. Majoral and A. M. Caminade, *Chem. Rev.*, 1999, **99**, 845; (*c*) A. W. Bosman, H. M. Janssen and E. W. Meijer, *Chem. Rev.*, 1999, **99**, 1665; (*d*) G. R. Newkome, E. He and C. N. Moorefield, *Chem. Rev.*, 1999, **99**, 1689; (*e*) A. Adronow and J. M. J. Fréchet, *Chem. Commun.*, 2000, 1701; (*f*) M. Fisher and F. Vögtle, *Angew. Chem., Int. Ed.*, 1999, **38**, 884; (*g*) G. R. Newkome, C. N. Moorefield and F. Vögtle, *Dendritic Molecules: Concepts, Syntheses, Perspectives*, VCH, Weinheim, 1996; (*h*) D. A. Tomalia, *Sci. Am.*, 1995, **272**, 62.

2 (*a*) See for example: C. O. Noble IV and R. L. McCarley, *J. Am. Chem. Soc.*, 2000, **122**, 6518; (*b*) E. Aloso and D. Astruc, *J. Am. Chem. Soc.*, 2000, **122**, 3222; (*c*) A. Archut, G. C. Azzellini, V. Balzani, L. De Cola and F. Vögtle, *J. Am. Chem. Soc.*, 1998, **120**, 12187; (*d*) J. F. G. A. Jansen and E. W. Meijer, *J. Am. Chem. Soc.*, 1995, **117**, 4417; (*e*) H. Stephan, H. Spies, B. Johannsen, L. Klein and F. Vögtle, *Org. Lett.*, 2000, **2**, 1285; (*f*) J. W. Lee, Y. H. Ko, S-H. Park, K. Yamaguchi and K. Kim, *Angew. Chem., Int. Ed.*, 2001, **40**, 746.

3 (*a*) C. Galliot, C. Larré, A. M. Caminade and J. P. Majoral, *Science*, 1997, **277**, 1981; (*b*) C. Larré, B. Donnadieu, A. M. Caminade and J. P. Majoral, *J. Am. Chem. Soc.*, 1998, **120**, 4029; (*c*) C. Larré, D. Bressolles, C. Turrin, B. Donnadieu, A. M. Caminade and J. P. Majoral, *J. Am. Chem. Soc.*, 1998, **120**, 13070; (*d*) L. J. Twyman, *Tetrahedron Lett.*, 2000, **41**, 6875.

4 (*a*) Introduction of selenium to the core and surface of dendrimers only has been reported: Y. Takaguchi, S. Suzuki, T. Mori, J. Motoyoshiya and H. Aoyama, *Bull. Chem. Soc. Jpn.*, 2000, **73**, 1857; C. Francavilla, M. D. Drake, F. V. Bright and M. R. Detty, *J. Am. Chem. Soc.*, 2001, **123**, 57.

5 J. Kohrle, R. Brigelius-Flohe, A. Bock, R. Gartner, O. Meyer and L. Flohe, *Biol. Chem.*, 2000, **381**, 849.

6 G. M. Salamończyk, M. Kuźnikowski and A. Skowrońska, *Tetrahedron Lett.*, 2000, **41**, 1643.

7 (*a*) M. D. Matteucci and M. H. Caruthers, *J. Am. Chem. Soc.*, 1981, **103**, 3185; (*b*) L. J. McBride and M. H. Caruthers, *Tetrahedron Lett.*, 1983, **24**, 245; (*c*) S. L. Beaucage, *Tetrahedron Lett.*, 1984, **25**, 375.

8 See ESI.

9 T. Nishigushi and H. Taya, *J. Am. Chem. Soc.*, 1989, **111**, 9102.

10 Without pyridine, substantial degradation of dendrimer was observed.

11 (*a*) W. J. Stec, A. Okruszek and J. Michalski, *J. Org. Chem.*, 1976, **41**, 233; (*b*) N. J. De′ath, K. Ellis, D. J. H. Smith and S. Trippett, *J. Chem. Soc., Chem. Commun.*, 1971, 714.

12 L. Wozniak, J. Kowalski and J. Chojnowski, *Tetrahedron Lett.*, 1985, **26**, 4965.

13 (*a*) E. Buncel and A. G. Davies, *J. Chem. Soc.*, 1958, 1550; Y. L. Fan and R. G. Shaw, *J. Org. Chem.*, 1973, **38**, 2410.

14 (*a*) Q. P. Gu, M. A. Beilstein, E. Barofsky, W. Ream and P. D. Whanger, *Arch. Biochem. Biophys.*, 1999, **361**, 25; (*b*) Q. Liu, E. Lauridsen and J. Clausen, *Biol. Trace Elem. Res.*, 1998, **61**, 237; (*c*) G. V. Kryukov and V. N. Gladyshev, *Genes Cells*, 2000, **5**, 1049.

CHEMCOMM Communication
www.rsc.org/chemcomm

Structural transformations in zopiclone

Norman Shankland,*[a] William I. F. David,[b] Kenneth Shankland,[b] Alan R. Kennedy,[c] Christopher S. Frampton[d] and Alastair J. Florence[a]

[a] *Department of Pharmaceutical Sciences, University of Strathclyde, Glasgow, UK G4 0NR. E-mail: n.shankland@strath.ac.uk; Fax: +44 141 552 6443; Tel: +44 141 548 2969*
[b] *ISIS Facility, Rutherford Appleton Laboratory, Chilton, Didcot, Oxon., UK OX11 0QX*
[c] *Department of Pure and Applied Chemistry, University of Strathclyde, Glasgow, UK G1 1XL*
[d] *Roche Discovery Welwyn, Welwyn Garden City, Herts., UK AL7 3AY*

Received (in Cambridge, UK) 8th August 2001, Accepted 4th September 2001
First published as an Advance Article on the web 11th October 2001

A monoclinic centrosymmetric form of zopiclone dihydrate undergoes a sequential, two-step transformation in the solid-state upon heating which results in separation of the enantiomers into a racemic conglomerate or racemic twins.

Racemic zopiclone (a cyclopyrrolone hypnotic drug marketed as Zimovane® tablets) crystallises in two centrosymmetric forms: monoclinic dihydrate (**I**) and monoclinic anhydrous (**II**). Zopiclone is also known to form a non-centrosymmetric orthorhombic anhydrous structure[1] (**III**) (Fig. 1). This communication describes the structural basis for the reversible transformation **I**↔**II**, and provides evidence for an irreversible solid-state chiral separation in which the racemic crystal structure **II** loses its centre of symmetry during a transformation to form **III**.†

The crystal structures of all three forms were determined directly from data collected on BM16 at the ESRF (Table 1, Fig. 1), using the simulated annealing procedure described previously[4] which is now implemented in the DASH computer program.[5] In each case, repeat DASH runs converged to substantially the same crystal structure, and the ratio $\chi^2_{\text{Rietveld}}/\chi^2_{\text{Pawley}}$ (Table 1) was sufficiently small to confirm that the solution was correct.‡ As the form **II** structure was previously unknown, and is therefore the principal focus of our attention, the correctness of this solution merits careful consideration. The potential accuracy of structures solved using the global optimisation procedure implemented in DASH has already been demonstrated[4] and, reassuringly, the DASH solutions for forms **I** and **III** are essentially superimposable on the corresponding single-crystal structures.[6] This close agreement arises from the ability of the simulated annealing algorithm to 'fine-tune' both the internal and external degrees of freedom of the zopiclone molecule (and the positions of both water molecules in the case of form **I**), effectively implementing a rigid body Rietveld refinement of the structure. Although the absolute magnitudes of χ^2 for form **II** are high (*cf.* forms **I** and **III**, Table 1), it is the ratio $\chi^2_{\text{Rietveld}}/\chi^2_{\text{Pawley}}$ which is important and this is satisfactory in each case.

Our confidence in the form **II** solution is further increased by the following observations: (i) no unfavourable contacts are observed within the crystal structure; (ii) the molecular conformation and crystal packing in form **II** relate to form **I** in a way which is both obvious and physicochemically sensible in the context of the transformation. In fact, the high χ^2 values for the form **II** pattern are attributable to a degree of anisotropic line broadening, plus the presence of trace amounts of forms **I** and **III** in the form **II** sample, arising as a consequence of producing the form **II** sample *in situ*.

Examination of the crystal structures of forms **I** and **II** reveals many striking similarities. The molecular conformations of the zopiclone molecules are essentially identical (Fig. 2). Moreover, the basic packing motif is the same in forms **I** and **II** (Fig. 3). In both structures, the zopiclone molecules arrange themselves in bilayer sheets and these sheets remain essentially

Table 1 Refined unit cells, extracted intensity information and final χ^{2a}

	Zopiclone form		
	I	**II**	**III**
Space group	$P2_1/c$	$P2_1/c$	$P2_12_12_1$
a/Å	16.4834(1)	15.2023(4)	5.5813(1)
b/Å	7.1465(1)	7.1510(1)	8.8467(1)
c/Å	17.4026(1)	17.6577(3)	35.6588(3)
β/°	109.8065(4)	111.213(1)	—
V/Å^3	1928.7	1789.5	1760.7
T/K	298	325	298
Data range/°2θ (BM16, λ = 0.8 Å)	1.0–23.0	1.0–17.8	1.0–-22.0
t_d/min	60	200	42
Resolution/Å	2.0	2.6	2.1
$N_{\text{reflections}}$	254	109	143
$N_{\text{parameters}}$	17	11	11
N_{tps}/s^{-1}	3100	5500	4000
t_s/min	27	24	5
χ^2_{Pawley}	5.1	28.2	2.0
χ^2_{Rietveld}	31.5	107.0	7.2

[a] t_d = data collection time over specified range; resolution = maximum spatial resolution of data; $N_{\text{reflections}}$ = number of reflections in data range shown; χ^2_{Pawley} = chi-squared for Pawley-type fit[3] to data range shown; χ^2_{Rietveld} = chi-squared for DASH Rietveld-type fit to data range shown, varying only scale factor; $N_{\text{parameters}}$ = number of parameters optimised during DASH structure solution; N_{tps} = number of trial structures evaluated by DASH per second (800 MHz PIII PC); t_s = time to solution.

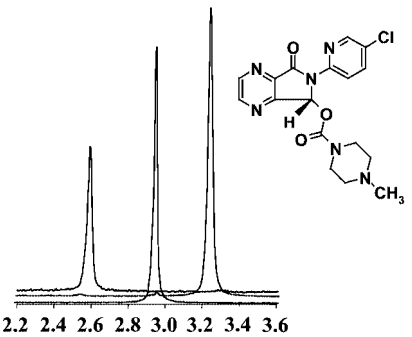

Fig. 1 Capillary X-ray powder diffraction (XRPD) patterns in the range 2.2–3.6° 2θ (λ = 0.8 Å) for the three forms of zopiclone. The data were collected on BM16 of the European Synchrotron Radiation Facility (ESRF).[2] Form **II** was produced *in situ* from the starting sample (form **I**, crystallised from toluene) by breaking the sealed end of the capillary and exposing the sample to a warm N_2 stream. The transformation was monitored *via* the growth on heating of the diagnostic (100) reflection at *ca.* 3.23°, which occurs at the expense of the dihydrate (100) reflection at *ca.* 2.96°. Further heating transformed **II** → **III**, as evidenced by the appearance of the form **III** (002) reflection at *ca.* 2.57°.

 DOI: 10.1039/b107075d

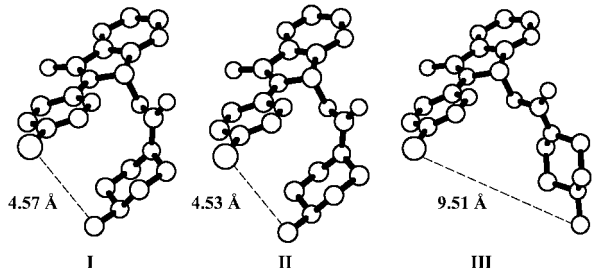

Fig. 2 The conformation of zopiclone in the crystal structures of forms **I**, **II** and **III** as determined directly from the XRPD data. The molecular conformations in forms **I** and **II** are virtually superimposable, as exemplified by the fact that the highlighted distances are approximately equal. The conformation in form **III** is significantly different.

unchanged in the dehydration process as the water molecules are cooperatively removed from the crystal structure. The process is facile and thus energetically straightforward since the principal structural change during dehydration is the slipping of each bilayer sheet by 6.61 Å along the *c* axis and 1.48 Å along the *a* axis, both relative to the form **I** unit cell.

This close structural similarity also accounts for the ease with which hygroscopic form **II** reverts to form **I** on exposure to high relative humidity at rt. The thermodynamic gain in transforming **II**→**I** is associated with the formation of $1 \times O_w$–H···N_{zop}, $1 \times O_w$–H···O_{zop} and $2 \times O_w$–H···O_w hydrogen bonds.

The exothermic transformation of form **II**→**III** at elevated temperature constitutes a spontaneous resolution of enantiomers in the solid state and is accompanied by a significant change in molecular conformation (Fig. 2). The transformation is not reversed on cooling and, unlike form **II**, form **III** is stable to high humidity. Whilst spontaneous resolution is well documented for compounds crystallising from solution or from the molten state, it is less well known (but not unknown[7]) for such a transformation to occur in the solid state. There is no doubt that the (*R*) and (*S*) enantiomers separate during the transformation, since the form **III** unit cell volume can only accommodate four zopiclone molecules and the chiral space group $P2_12_12_1$ can accommodate only one enantiomer or the other.§ What the XRPD experiment cannot tell us is whether this solid-state separation results in the formation of racemic twins or a racemic conglomerate—either possibility is consistent with the diffraction data. However, the sharpness of the powder diffraction lines indicates domain sizes in excess of 1000 Å.

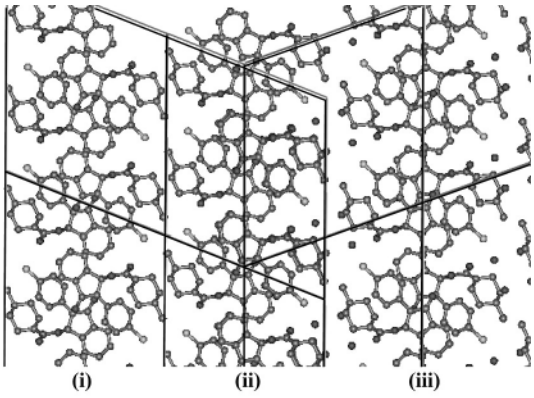

Fig. 3 Four unit cells of form **II** (left), plus four unit cells of form **I** (right), viewed down the common *b*-axis. The two structures are shown overlaid on their common packing motif to emphasise the high degree of correspondence. Viewing left-to-right: (i) the first bilayer of zopiclone molecules in form **II**; (ii) the second bilayer of form **II** overlaid by the first bilayer of form **I**. It is almost impossible to distinguish the individual bilayers in this region—the r.m.s. deviation between corresponding atoms is small (*ca*. 0.2 Å, with structures positioned on a single common atom and no least-squares fitting employed); (iii) the next bilayer of form **I**, showing the dihydrate O-atoms sandwiched between the bilayer sheets. When water is driven off, the bilayers close-pack to reduce the unoccupied volume.

Strong additional evidence to support the favourability of enantiomer separation comes from the fact that we have observed spontaneous resolution upon crystallising zopiclone from a racemic solution of the compound in ethyl acetate. The refined Flack (absolute structure) parameter[8] for a single crystal of (*R*)-zopiclone[6] (−0.04(6)) and a single crystal of (*S*)-zopiclone[6] (−0.04(6)) produced in this way was sufficient to confirm unambiguously that separation to a racemic conglomerate had indeed occurred.

We conclude that racemic zopiclone can crystallise from solution either as enantiomerically pure crystals (a racemic conglomerate formed *via* spontaneous resolution) or in the form of a centrosymmetric racemic dihydrate. Heating the latter produces a centrosymmetric racemic anhydrous structure, which undergoes chiral separation upon further heating. The analysis presented here helps to explain the significant batch-to-batch variation in physical form reported for commercial samples of zopiclone.[9] Central to detailing the transformations at molecular level was our requirement to produce a sharply diffracting sample of form **II** and then solve its crystal structure. In this regard the combination of the high instrumental resolution and count rate offered by BM16, plus the efficient global optimisation method, was ideally suited to the experiment.

We thank Paul J. Harrison for providing the stimulus to study zopiclone; Hendra for technical services; Olivier Masson for setting up BM16; the EPSRC X-ray crystallography service at the University of Southampton for absolute structure determinations and Francisco Ros for helpful comments.

Notes and references

† The solid-state transformation of form **I**→**II** was identified initially by DSC/TGA as an endothermic weight loss from rt to *ca*. 75 °C. The subsequent transformation **II**→**III** was apparent as an exotherm (*ca*. −2.4 kJ mol^{-1}) with onset *ca*. 112 °C and no corresponding weight loss. The transformations were confirmed by multi-temperature laboratory XRPD, and the reversibility **I**↔**II** was apparent in XRPD data collected at 0 and 94% relative humidities.

‡ The form **I** and form **III** solutions are redeterminations of known structures: (i) form **I** single-crystal (determined as part of this work), a = 16.374(4), b = 7.030(3) , c = 17.185(2) Å, β = 108.62(1)° at T = 123 K;[6] (ii) form **III** single-crystal, a = 5.567(3), b = 8.852(2), c = 35.677(17) Å at T = 295 K.[1] Single-crystals of form **II** could not be obtained and therefore the structure of form **II** had to be determined directly from the polycrystalline powder.

§ The possibility that form **III** is a non-centrosymmetric racemate was eliminated on the grounds that the XRPD data are entirely consistent with two single-crystal absolute configuration determinations[6] which unambiguously identify one molecule in the asymmetric unit.

1 V. Bertolasi, V. Ferretti, G. Gilli and P. A. Borea, *J. Chem. Soc., Perkin Trans. 2*, 1990, 283.
2 A. N. Fitch, *Nuc. Instr. Methods Phys. Res. B*., 1995, **97**, 63.
3 G. S. Pawley, *J. Appl. Cryst*., 1981, **14**, 357.
4 W. I. F. David, K. Shankland and N. Shankland, *Chem. Commun*., 1998, 931.
5 W. I. F. David, K. Shankland, J. Cole, S. Maginn, W. D. S. Motherwell and R. Taylor, *DASH User Manual*, Cambridge Crystallographic Data Centre, Cambridge, UK, 2001.
6 CCDC 171568–171571. See http://www.rsc.org/suppdata/cc/b1/b107075d/ for electronic files in .cif or other electronic format.
7 F. Ros and M. T. Molina, *Eur. J. Org. Chem*., 1999, 3179.
8 H. D. Flack, *Acta Cryst*., 1983, **A39**, 876.
9 R. J. Terblanche, W. Liebenberg, M. M. de Villiers and A. P. Lötter, *Drug Dev. Ind. Pharm*., 2000, **26**, 531.

CHEMCOMM
Communication
www.rsc.org/chemcomm

Pentaporphyrin with flexible, chiral nucleosidic linkers: unexpected duality of the physico-chemical properties of its core†

Nathalie Solladié,* Maurice Gross,* Jean-Paul Gisselbrecht and Chloé Sooambar

Laboratoire d'Electrochimie et de Chimie Physique du Corps Solide, Université Louis Pasteur et CNRS, 4 rue Blaise Pascal, 67000 Strasbourg, France. E-mail: nsolladie@chimie.u-strasbg.fr, gross@chimie.u-strasbg.fr

Received (in Cambridge, UK) 17th July 2001, Accepted 29th August 2001
First published as an Advance Article on the web 11th October 2001

A new star-like pentaporphyrin, bearing nucleosidic linkers, has been synthesized, and the unexpected duality of the physico-chemical properties of its core is reported; beside the quenching of the fluorescence of the peripheral porphyrins by the central chromophore, this pentaporphyrin exhibits an unexpected shielding of the redox capabilities of its central core.

In photosynthetic systems the absorption of a photon by the light harvesting antennas is followed with minimal loss by the extremely fast migration of the excited state among the pool of chlorophylls until the reaction center is reached in the cell membrane.[1]

With the aim of mimicking these antenna complexes, multiporphyrinic dendrimers are attracting growing interest.[2] Increasing the number of chromophores around one single energy acceptor enhances the probability of capturing a photon and thus transfering energy towards the central chromophore.

We now report the synthesis of the tetranucleosidic pentaporphyrin **1**, and the interesting duality of the physico-chemical properties of its core chromophore (Fig. 1). This multichromophore device is built on a free-base porphyrin surrounded by four peripheral Zn(II) porphyrins. Beside the expected— and actually observed—antenna effect, this pentaporphyrin **1** also exhibits the characteristics which prevent electron transfers with the central porphyrin, an unexpected feature in a molecule whose arborescent shape resembles a first generation dendrimer.

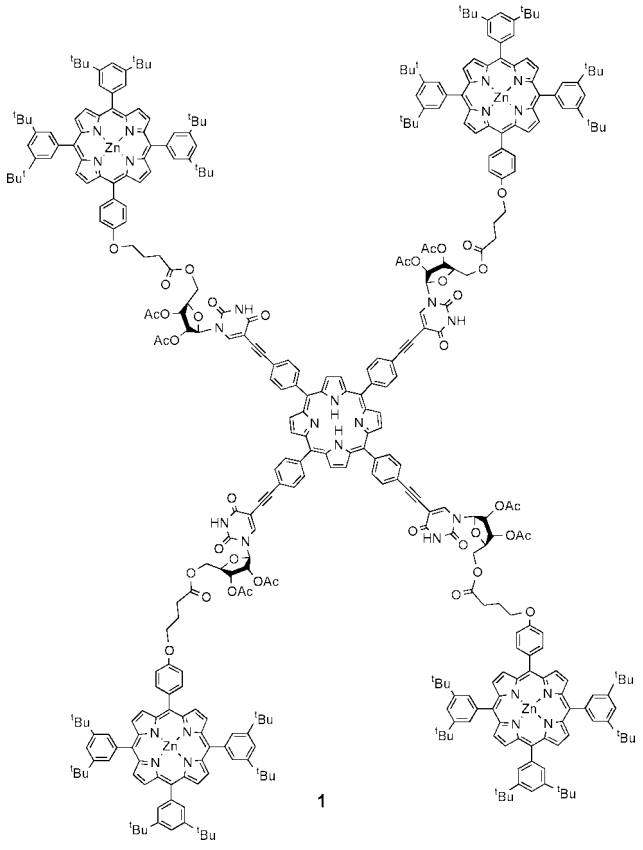

Fig. 1 Tetranucleosidic pentaporphyrin **1**.

The synthetic strategy for obtaining **1** is based on the functionalization of the nucleosidic linker **2** at the O-5′ and C-5 positions. Compound **2** was prepared in five steps from the commercially available uridine.[3] The nucleoside–porphyrin conjugate **4**[4] was then obtained in 64% yield by esterification of the carboxylic acid function of the A_3B type Zn(II) porphyrin derivative **3** with the alcohol **2** (Scheme 1).[5] Preparation of pentaporphyrin **1** was achieved by construction of the central porphyrin under the conditions developed by Lindsey for the synthesis of sterically hindered porphyrins (Scheme 1).[6] Compound **1** was isolated with 35% yield after tedious purification by successive column chromatography on silica gel, followed by gel permeation chromatography (GPC) to remove some low molecular weight impurities which couldn't be removed by classical chromatography. The purity of pentaporphyrin **1** was then certified by analytical GPC. ^{1}H-NMR spectroscopy experiments were carried out at room temperature and under heating, but only ill resolved spectra were obtained. A fine structure emerged in the ^{1}H NMR spectrum recorded at 400 K, but it was not resolved enough to allow clear interpretation of the spectrum. This result suggests that compound **1** exists as a mixture of conformers. The

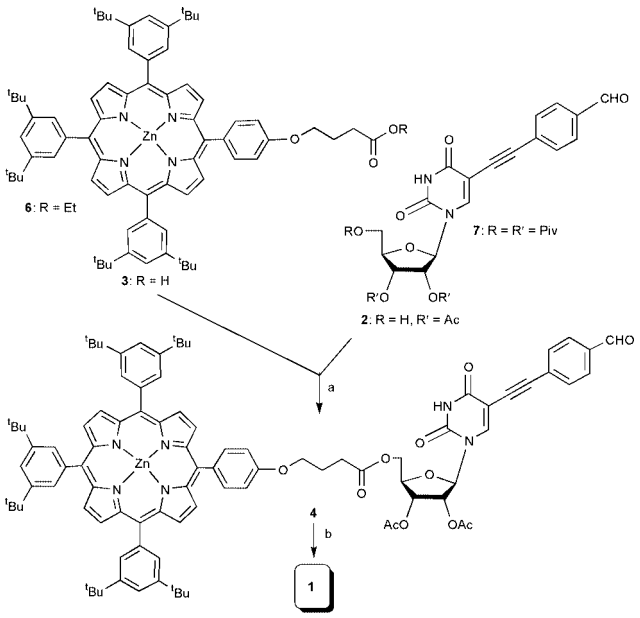

Scheme 1 (a) DCC (1.4 eq.), DMAP (1.2 eq.), CH_2Cl_2, rt, 4 h, 64%; (b) Pyrrole (10^{-2} M), $BF_3{\cdot}OEt_2$ cat., $CHCl_3$, rt, 48 h, then *p*-chloranil (3 eq.), reflux, 2 h, 35%.

† Electronic supplementary information (ESI) available: spectroscopic data for **4** and **1**. See http://www.rsc.org/suppdata/cc/b1/b106337p/

 DOI: 10.1039/b106337p

pentaporphyrin **1** was finally identified by FAB mass spectrometry (6411.6, $[M]^+$, calcd: 6411.3).

The UV-visible absorption spectrum of **1** is essentially the addition of the spectra characterizing the individual free-base and Zn(II) porphyrin components. The Soret band is however slightly broadened (from 13 to 15 nm) if compared with the distinct constituents.

Fluorescence measurements were carried out in CH_2Cl_2 on pentaporphyrin **1** (605, 653, 718 nm; relative intensities 3/11/12 respectively) and on the precursors **5** (653, 719 nm; relative intensities 10/2 respectively) and **6** (599, 649 nm; relative intensities 3/2 respectively). Upon excitation at 420 nm, the fluorescence spectrum of **1** is dominated by emission of the core free-base porphyrin. The emission of the four peripheral Zn(II) porphyrins is partially quenched: only a weak band is observed at 605 nm. The assumption of an energy transfer from the peripheral porphyrins to the free-base core was corroborated by the excitation spectrum of pentaporphyrin **1**, which matches the absorption of the multicomponent system fairly well.

The redox properties of **1** were ascertained by steady state and cyclic voltammetry experiments, carried out on a glassy carbon electrode in CH_2Cl_2 + 0.1 M *n*-Bu_4NPF_6. Cyclic voltammetry exhibited, for each of the precursors **5** and **6**, two reversible one-electron reductions as well as two reversible one-electron oxidations, as expected for porphyrins (Table 1).[7] Pentaporphyrin **1** gave a well resolved cyclic voltammogram, where only two oxidation and two reduction steps can be observed. The peak characteristics (ΔEp = 60 mV and peak current corresponding to a four-electron transfer) are in agreement with electron transfers on four independent redox centers. The comparison of the redox characteristics of **1** with the redox patterns of the reference compounds **5** and **6** suggests that the four distinct electron transfers occur on the Zn(II) porphyrin moieties. The potential difference between the first oxidation and the first reduction steps in **1** and in the synthons **5** and **6** indicates that the HOMO–LUMO energy gap in the Zn(II) porphyrins increases from **6** to **1**, thus indicating that the net effect of bonding **5** to **6** in the pentaporphyrin **1** is tantamount to a slightly electron-donating effect on **6**. This is consistent with the measured shifts of the potentials from **6** to **1**: 50 mV for the first oxidation and −120 mV for the first reduction (Table 1). It is worth noting that, unexpectedly, the voltammogram of pentaporphyrin **1** does not reveal any reduction or oxidation step which could correspond to the free-base core, whose potentials (Table 1) are expected to be very different to those of the zinc porphyrin. Such observations are known for bulky dendritic molecules, but is unprecedented in a molecule similar to a first generation dendrimer.[8] A tentative explanation may be found in the flexible nucleosidic linkers. Indeed, these linkers are flexible enough to allow the four arms in **1** to fold up—or collapse—on its core. Such a constriction could induce a shielding effect on the central free-base porphyrin in **1**, as it creates, both physically and in terms of spatial dielectric characteristics inside **1**, very unfavorable conditions which could slow down any electron exchange between the electrode surface and the central free-base porphyrin. The signals would thus be broadened and ultimately become undetectable on the voltammogram. Similar situations have been observed up to now with bulky dendrimers only.[8b–8d] The ^{1}H-NMR results obtained on pentaporphyrin **1**, which did not produce any well resolved spectra, also find a reasonable explanation in such a shrivelled conformation of the pentaporphyrin **1**. Recent studies consistently support this interpretation.[8f,8i] They make clear that, in a flexible molecule such as pentaporphyrin **1**, it may reasonably be expected that the important decrease in the electron transfer rate on the porphyrin core, *i.e.* the restricted accessibility to this core, is ascribable to conformational effects rather than solely to steric factors. Hence, the central free-base porphyrin behaves here as an encapsulated electroactive molecule, which is masked for electron transfer in the present experimental conditions.

Table 1 Redox potential of the studied species (**5**, **6** and **1**; **5** is the reference free-base porphyrin synthesized by condensation of **7** with pyrrole) observed in CH_2Cl_2 + 0.1 M *n*-Bu_4NPF_6 on a glassy carbon working electrode

	Reduction[a] *E*/(V *vs.* Fc^+/Fc)		Oxidation[a] *E*/(V *vs.* Fc^+/Fc)		
Species	Red_2	Red_1	Ox_1	Ox_2	$Ox_1 - Red_1$/V
5	−1.96 (1 e$^-$)	−1.58 (1 e$^-$)	+0.61 (1 e$^-$)	+0.89 (1 e$^-$)	2.19
6	−2.18 (1 e$^-$)	−1.76 (1 e$^-$)	+0.35 (1 e$^-$)	+6.0 (1 e$^-$)	2.11
1	−2.24 (4 e$^-$)	−1.88 (4 e$^-$)	+0.30 (4 e$^-$)	+0.64 (4 e$^-$)	2.18

[a] All potentials are given *versus* ferrocene used as internal standard. Reversible electron transfer: $E° = (Epc + Epa)/2$.

Since the insertion of any energy transfer relay between the core and the periphery would seriously decrease the rate of energy transfer and favour a loss of energy, the elaboration of a new family of arborescent molecules by directly attaching more than four peripheral porphyrins to the free-base core is currently under way. It is expected that such an arborescence will significantly enhance the antenna effect while retaining a shielded electroactive core. Beside the covalent approach mentioned above, the possibility of taking advantage of the nucleosidic linkers is also being explored. Indeed, it seems likely that our pentaporphyrin **1** could self-assemble with properly chosen complementary porphyrinic synthons to generate, through hydrogen bonds, more sophisticated architectures. Furthermore, the chiral nucleosidic linkers may play a key role in inducing enantioselective energy transfers.

This work was supported by the C.N.R.S. C. Sooambar thanks the Région Guyane for a fellowship.

Notes and references

1 J. Barber and B. Andersson, *Nature*, 1994, **370**, 31; W. Kühlbrandt, *Nature*, 1995, **374**, 497; T. Pullerits and V. Sundström, *Acc. Chem. Res.*, 1996, **29**, 381.

2 S. Prathapan, T. E. Johnson and J. S. Lindsey, *J. Am. Chem. Soc.*, 1993, **115**, 7519; C. Ching Mak, N. Bampos and J. K. M. Sanders, *Angew. Chem., Int. Ed. Engl.*, 1998, **37**, 3020; L. Ruhlmann, S. Lobstein, M. Gross and A. Giraudeau, *J. Org. Chem.*, 1999, **64**, 1352; M. Ravikanth, *Tetrahedron Lett.*, 2000, **41**, 3709; R. A. Haycock, A. Yartsev, U. Michelsen, V. Sundström and C. A. Hunter, *Angew. Chem., Int. Ed. Engl.*, 2000, **39**, 3616.

3 W.-W. Sy, *Synth. Commun.*, 1990, **20**(21), 3391; C. Cai and A. Vasella, *Helv. Chim. Acta*, 1995, **78**, 2053; N. Solladié and M. Gross, *Tetrahedron Lett.*, 1999, **40**, 3359.

4 For examples of nucleotide–porphyrin conjugates, see: J. L. Sessler, B. Wang and A. Harriman, *J. Am. Chem. Soc.*, 1993, **115**, 10418; N. Solladié and M. Gross, *Tetrahedron Lett.*, 1999, **40**, 3359; S. Masiero, G. Gottarelli and S. Pieraccini, *Chem. Commun.*, 2000, 1995.

5 N. Solladié, A. Hamel and M. Gross, *Tetrahedron Lett.*, 2000, **41**, 6075.

6 J. S. Lindsey, I. C. Schreiman, H. C. Hsu, P. C. Kearney and A. M. Marguerettaz, *J. Org. Chem.*, 1987, **52**, 827; J. S. Lindsey and R. W. Wagner, *J. Org. Chem.*, 1989, **54**, 828.

7 K. M. Kadish, G. Royal, E. Van Caemelbecke and L. Gueletti, in *The Porphyrin Handbook, Vol. 9*, Eds. K. M. Kadish, K. M. Smith and R. Guilard, Academic Press, San Diego, 2000, p. 1–220.

8 (*a*) C. B. Gorman, *Adv. Mater.*, 1997, **9**, 1117; (*b*) P. J. Dandliker, F. Diederich, M. Gross, C. B. Knobler, A. Louati and E. M. Sanford, *Angew. Chem., Int. Ed. Engl.*, 1994, **33**, 1739; (*c*) P. J. Dandliker, F. Diederich, A. Zingg, J.-P. Gisselbrecht, M. Gross, A. Louati and E. Sanford, *Helv. Chim. Acta*, 1997, **80**, 1773; (*d*) P. Weyermann, J.-P. Gisselbrecht, C. Boudon, F. Diederich and M. Gross, *Angew. Chem., Int. Ed.*, 1999, **38**, 3215; (*e*) N. Armaroli, C. Boudon, D. Felder, J.-P. Gisselbrecht, M. Gross, G. Marconi, J.-F. Nicoud, J.-F. Nierengarten and V. Vicinelli, *Angew. Chem., Int. Ed.*, 1999, **38**, 3730; (*f*) C. B. Gorman, J. C. Smith, M. W. Hager, B. L. Parkhurst, H. Sierzputowska-Gracz and C. A. Haney, *J. Am. Chem. Soc.*, 1999, **121**, 9958; (*g*) C. M. Cardona, S. Mendoza and A. E. Kaifer, *Chem. Soc. Rev.*, 2000, **29**, 37; (*h*) S. Hecht and J. M. J. Fréchet, *Angew. Chem., Int. Ed.*, 2001, **40**, 74; (*i*) C. B. Gorman and J. C. Smith, *Acc. Chem. Res.*, 2001, **34**, 60.

CHEMCOMM
Communication
www.rsc.org/chemcomm

Synthesis and crystal structure determination of tetramethylammonium auride

Pascal D. C. Dietzel and Martin Jansen*

Max-Planck-Institut für Festkörperforschung, Heisenbergstr. 1, D-70569 Stuttgart.
E-mail: martin@jansen.mpi-stuttgart.mpg.de

Received (in Cambridge, UK) 27th June 2001, Accepted 24th September 2001
First published as an Advance Article on the web 11th October 2001

Tetramethylammonium auride, the first compound of negatively charged gold with a non-metal cation, has been synthesised by cation exchange in liquid ammonia; it is isostructural to the corresponding bromide which further illustrates the similarities between the halogens and gold.

Gold is unique among the transition metals in its ability to form isolable non-metallic compounds that contain a monoatomic anion. The binary alkali metal aurides RbAu and CsAu have been known for about half a century,[1] but the ternary auride oxides M_3AuO (M = K, Rb, Cs) and the aurideaurates $Rb_5Au_3O_2$, and $M_7Au_5O_2$ (M = Rb, Cs)[2] have only recently been discovered.

To establish that gold in these compounds does indeed carry a negative charge numerous experiments have been undertaken. CsAu crystallises in the CsCl-structure,[1] a typical structure to be adopted by an ionic substance, and it is a semiconductor with a band gap of 2.6(2) eV.[3] CsAu liquifies at 590 °C to give a melt that exhibits ionic conductivity.[4] In addition, an ESCA study on RbAu and CsAu,[5] reveals the high value for the binding energy of the CsAu molecule,[6] and UV-photoemission experiments[7] on solid CsAu support the ionic interpretation. The anionic character of the gold in RbAu and CsAu has also been studied by ^{197}Au Mössbauer spectroscopy.[8] The ternary phases M_3AuO have been investigated by X-ray absorption spectroscopy.[9]

Furthermore, the auride ion is the only monoatomic metal anion proposed to exist in liquid ammonia.[10] Recently, it was found that the golden-brown CsAu dissolves in liquid ammonia forming colourless to pale yellow solutions, from which a characteristically blue ammoniate can be isolated.[11] The only other known reaction is the formation of the cryptated alkali metal aurides.[8] The solubility of caesium auride in liquid ammonia has prompted us to try to apply a method originally developed for the synthesis of novel ionic ozonides and superoxides to the chemistry of the auride ion.[12]

Using a macroreticular ion exchange resin with a high affinity towards caesium ions in liquid ammonia, we have managed to exchange caesium for tetramethylammonium, and have obtained tetramethylammonium auride **1** as transparent crystals.† Tetramethylammonium was chosen as the cation for this experiment, because being a derivative of the ammonium ion it behaves chemically much like an alkali metal. However, it is less reactive than the ammonium ion, since it does not contain any acidic hydrogen atoms. In addition, the positive charge is stabilised by the presence of the methyl groups.

Recently, it has been shown that **1** can also be obtained impure in a mixture with caesium chloride by a metathesis reaction of tetramethylammonium chloride and caesium auride in liquid ammonia.[13] The auride **1** has to be handled very carefully. It spontaneously ignites on contact with air and is very sensitive to pressure. It slowly decomposes at room temperature. Several powder X-ray patterns taken of the same sample sealed in a capillary show that already overnight the gold 111 reflection grows considerably in intensity, and after two weeks the sample consists solely of gold and decomposition products. Compound **1** can be stored for months without noticeable decomposition at −55 °C.

The crystal structure determination‡ shows that in **1** each gold atom is surrounded by eight tetramethylammonium ions and *vice versa* (Fig. 1). The geometrical features of the tetramethylammonium ion are as expected, with C–N bond lengths of 1.481(6) Å and C–N–C angles of 109.1(5)° and 109.6(2)°. There are four short Au···H contacts of 2.92(10) Å, eight longer ones of 3.30(4) Å and another eight of 3.35(6) Å length. The closest Au···C distances are 4 × 3.663(1) Å and 4 × 3.849(1) Å. The closest Au···Au distances are 2 × 5.433(3) Å and 4 × 5.568(1) Å. The nitrogen atoms form a lattice that is almost perfectly cubic. Thus, the structure can be derived from a caesium chloride type structure by displacing the anion from the center of the parallelepiped formed by the nitrogen atoms, as has been observed previously for other tetramethylammonium salts.[14,15] The displacement is due to four methyl groups pointing towards the auride ion from one direction, thus pushing it out of the center of the cuboid. In effect, this is the same structure as found for tetramethylammonium bromide.[15]

Taking the shortest Au···H contact in **1** and subtracting the van der Waals radius of 1 Å for the hydrogen atom, we can estimate the radius of the auride ion to be 1.9 Å, which is very similar to the bromide ion. These relatively short Au···H contacts also might be interpreted as weak hydrogen bonds between the auride ion and the tetramethylammonium ion, especially in light of the fact that hydrogen bonds have been detected in tetramethylammonium bromide,[16] in which the shortest Br···H distances are of a comparable length. The coordination of the auride and bromide ion by hydrogen in the two structures is identical and shown in Fig. 2.

Our findings correspond very well with earlier observations that the auride anion behaves crystallographically like a halide ion. Not only do RbAu and CsAu crystallise in the CsCl-structure, but CsBr and CsAu are also completely miscible in the liquid and solid state.[17] The analogy between the auride, and especially the bromide, is further supported by comparison of

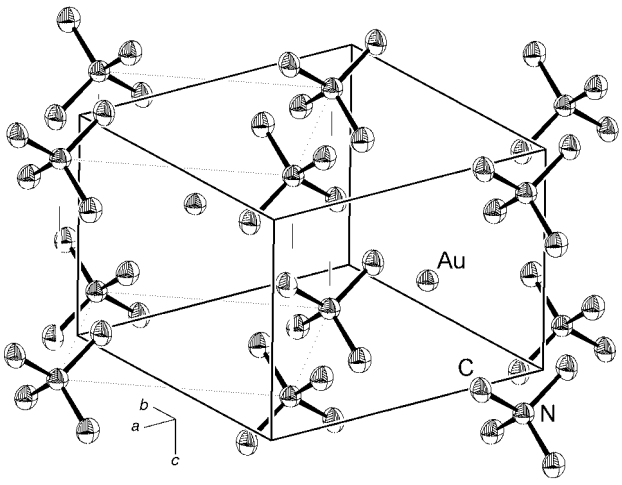

Fig. 1 Crystal structure of tetramethylammonium auride **1** (70% thermal ellipsoids, hydrogen atoms omitted). The caesium chloride type sub-cell is indicated by thin lines.

 DOI: 10.1039/b105648b

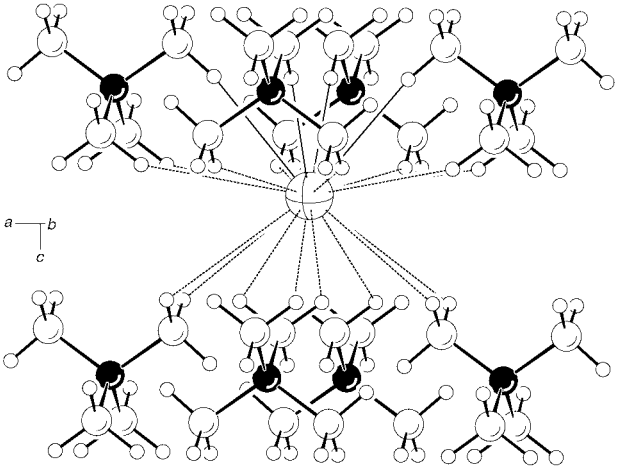

Fig. 2 Close C–H···Au contacts in **1** (thin solid lines: < 3 Å, dashed lines: 3–3.5 Å).

the crystal structures of the ternary auride oxides M_3AuO and the corresponding bromides and iodides.[18]

The presence of the auride ion in **1** is also confirmed by ^{197}Au Mössbauer spectroscopy.[19] The isomer shift of 6.33(2) mm s^{-1} relative to the source lies well within the range usually found for gold(−I) ions. The resonance signal displays no quadrupole splitting. Apparently, it is unaffected by the reduced symmetry of the auride site in comparison to the cubic environment in the CsCl-type structure.

The colourlessness of **1** seems to imply that the charge separation between the cation and the auride is very large in the sense that gold should have a filled $5d^{10}6s^2$ electron configuration. However, the isomer shift is not quite as large as that found for caesium auride [7.09(6) mm s^{-1}].[8] The C–H···Au hydrogen bonds discussed above would result in a reduction of charge at the gold atom, but it seems unlikely that such a very weak interaction would show this large an effect. The Mössbauer isomer shift is sensitive to the electronic density at the nucleus. It has been estimated that the addition of one 6s electron leads to an isomer shift of +8 mm s^{-1}. The removal of one gold 5d electron would lead to a shift of at least +1 mm s^{-1}, because a lower 5d-electron density decreases the shielding of the 5s and 6s levels, in turn increasing their density at the nucleus.[8] If back-donation of 5d electron density from the gold to empty orbitals on the alkali metal occured to some extent, then the measured isomer shift for CsAu would be expected to be larger than the isomer shift of the 'free' auride ion in compound **1**. It would also explain the observation that encapsulation of the alkali metal by a cryptand, which increases the distance between cation and anion and reduces the cation–anion interaction, leads to a decrease in isomer shift. In fact, the isomer shift values of M(2,2,2-crypt)Au (M = K, Rb, Cs) of 6.29(5), 6.08(4) and 6.08(5) mm s^{-1}, lie very close to our value.[8]

The authors wish to thank Dr Oliver Oeckler for the data collection and Sanela Kevrić for assistance with the preparative work.

Notes and references

† All operations were carried out under inert conditions either *in vacuo* or in a dry argon atmosphere.

The acidic form of the ion exchange resin (type Amberlyst 15) was charged with tetramethylammonium by reaction with a solution of tetramethylammonium hydroxide in methanol over five days. It was washed several times with methanol and thoroughly dried at 105 °C *in vacuo*.

In a typical experiment 1.5 g of ion exchange resin and 200 mg of CsAu were put into one leg of an H-shaped reaction apparatus. The connection between the legs was fitted with a glass sieve to allow filtration. Ammonia was stored over potassium at −78 °C and condensed into the reaction vessel. The colourless solution was left to stand for 4 h and then filtered to separate it from the ion exchange resin. Upon slow removal of the ammonia at −60 °C transparent crystals started to precipitate. The yield is typically < 60 mg (37%), but more of the colourless crystalline substance can be seen surrounding the ion exchange pellets.

‡ The crystals were immersed in perfluorinated polyether, selected under a microscope and picked up with a nylon loop attached to the goniometer head, transferred in liquid nitrogen to the diffractometer and mounted on the diffractometer in a cooling stream.

Crystal data for **1**: $C_4H_{12}NAu$, M_r = 271.11, tetragonal, space group $P4/nmm$, a = 7.599(3), c = 5.433(3) Å, V = 313.7(2) Å^3, Z = 2, D_c = 2.87 g cm^{-3}, T = 93 K, 7722 reflections measured belonging to two twin domains, 296 unique reflexes, μ(Ag-Kα) = 12.717 mm^{-1}, absorption correction by multi-scan, $R1$ = 0.0436 [$I > 2\sigma(I)$], $wR2$ = 0.1215 (all data), goodness-of-fit 1.102. Data were collected on a Stoe-IPDS area detector diffractometer. The SHELX-97 suite of programs for crystal structure analysis was used for solution and refinement of the structure.[20]

CCDC reference number 170528. See http://www.rsc.org/suppdata/cc/b1/b105648b/ for crystallographic data in CIF or other electronic format.

1 A. Sommer, *Nature*, 1943, **152**, 215; W. E. Spicer, A. H. Sommer and J. G. White, *Phys. Rev.*, 1959, **115**, 57.
2 C. Feldmann and M. Jansen, *Angew. Chem.*, 1993, **105**, 1107; *Angew. Chem., Int. Ed.*, 1993, **32**, 1049; C. Feldmann and M. Jansen, *Z. Anorg. Allg. Chem.*, 1995, **621**, 201; A.-V. Mudring and M. Jansen, *Angew. Chem.*, 2000, **112**, 3194; A.-V. Mudring and M. Jansen, *Angew. Chem., Int. Ed.*, 2000, **39**, 3066; A.-V. Mudring, J. Nuss, U. Wedig and M. Jansen, *J. Solid State Chem.*, 2000, **155**, 29.
3 W. E. Spicer, *Phys. Rev.*, 1962, **125**, 1297.
4 H. Hoshino, R. W. Schmutzler and F. Hensel, *Phys. Lett. A*, 1975, **51**, 7; K. D. Krüger and R. W. Schmutzler, *Ber. Bunsen-Ges. Phys. Chem.*, 1976, **80**, 816.
5 J. Knecht, R. Fischer, H. Overhof and F. Hensel, *J. Chem. Soc., Chem. Commun.*, 1976, 905.
6 B. Busse and K. G. Weil, *Angew. Chem.*, 1979, **91**, 664; B. Busse and K. G. Weil, *Angew. Chem., Int. Ed. Engl.*, 1979, **18**, 629.
7 H. Overhof, R. Fischer, M. Vulli and F. Hensel, *Ber. Bunsen-Ges. Phys.*, 1976, **80**, 871.
8 G. K. Wertheim, R. L. Cohen, G. Crecelius, K. W. West and J. H. Wernick, *Phys. Rev. B*, 1979, **20**, 860; R. J. Batchelor, T. Birchall and R. C. Burns, *Inorg. Chem.*, 1986, **25**, 2009.
9 A. Pantelouris, G. Küper, J. Hormes, C. Feldmann and M. Jansen, *J. Am. Chem. Soc.*, 1995, **117**, 11 749.
10 W. J. Peer and J. J. Lagowski, *J. Am. Chem. Soc.*, 1978, **100**, 6260; T. H. Teherani, W. J. Peer, J. J. Lagowski and A. J. Bard, *J. Am. Chem. Soc.*, 1978, **100**, 7768.
11 A.-V. Mudring, M. Jansen, J. Daniels, S. Krämer, M. Mehring, J. P. Ramalho, A. H. Romero and M. Parrinello, *Angew. Chem.*, in press.
12 N. Korber and M. Jansen, *Chem. Ber.*, 1992, **125**, 1383; H. Seyeda and M. Jansen, *J. Chem. Soc., Dalton Trans.*, 1998, 875.
13 A.-V. Mudring, *Ein Beitrag zur Chemie des Goldes, Darstellung, Struktur und Eigenschaften von Auriden, Auraten und Auridauraten* Wissenschaft und Technik Verlag, Berlin, 2001.
14 J. D. McCullough, *Acta Crystallogr.*, 1964, **17**, 1067; Y. Wang, L. D. Calvert and S. K. Brownstein, *Acta Crystallogr., Sect. B*, 1980, **36**, 1523.
15 D. J. Evans and D. L. Hughes, *Acta Crystallogr., Sect. C*, 1990, **46**, 1452.
16 K. M. Harmon, I. Gennick and S. L. Madeira, *J. Phys. Chem.*, 1974, **78**, 2585.
17 R. Wormuth and R. W. Schmutzler, *Thermochim. Acta*, 1990, **160**, 97; R. Erdmann, R. Wormuth and R. W. Schmutzler, *Mater. Sci. Forum*, 1991, **73**, 45.
18 C. Feldmann and M. Jansen, *Z. Anorg. Allg. Chem.*, 1995, **621**, 1907.
19 F. E. Wagner, P. D. C. Dietzel and M. Jansen, unpublished results.
20 G. M. Sheldrick, SHELX-97, University of Göttingen, Göttingen, Germany, 1997.

CHEMCOMM Communication
www.rsc.org/chemcomm

Multi-component assembly of the bicyclic core associated with the tRNA synthetase inhibitors SB-203207 and SB-203208. Application to the synthesis of biologically active analogues†

Martin G. Banwell,*[a] Curtis F. Crasto,[a] Christopher J. Easton,*[a] Tomislav Karoli,[a] Darren R. March,[a] Michael R. Nairn,[a] Peter J. O'Hanlon,[b] Mark D. Oldham,[a] Anthony C. Willis[a] and Weimin Yue[a]

[a] *Research School of Chemistry, Institute of Advanced Studies, The Australian National University, Canberra, ACT 0200, Australia. E-mail: mgb@rsc.anu.edu.au*
[b] *GlaxoSmithKline, New Frontiers Science Park, Harlow, UK CM19 5AW*

Received (in Cambridge, UK) 4th June 2001, Accepted 21st June 2001
First published as an Advance Article on the web 11th October 2001

The ketone (±)-5, which embodies the bicyclic core associated with the title tRNA synthetase inhibitors 1 and 2, has been prepared *via* a three-component coupling reaction involving 2-(hydroxymethyl)cyclopent-2-enone (15), methylamine (6) and propiolamide (10); straightforward elaboration of the readily derived acetates (−)-21 and (+)-21 has provided the biologically active analogues 23 and 24, respectively, of the title compounds.

The emergence of 'superbugs' such as vancomycin-resistant *Staphylococcus aureus* has prompted extensive efforts to identify new anti-infective agents.[1] High throughput screening regimes have led to the discovery of a number of novel leads including SB-203207 (**1**) and SB-203208 (**2**) which are potent inhibitors of both bacterial and mammalian isoleucyl tRNA synthetases.[2] The structurally related natural product altemicidin (**3**),[3] a novel acaricidal and anti-tumour agent, has been the subject of an elegant total synthesis.[4] However, the methods[4,5] currently available for construction of the hexahydroazaindene core associated with such compounds are unlikely to be practical in providing a broad range of analogues of **1** and **2** for testing as anti-infective agents. On this basis we now describe a multi-component and potentially highly flexible method for construction of the azabicyclic ketones (±)-**4** and (±)-**5** as well as conversion of the latter into biologically active analogues of the title compounds.

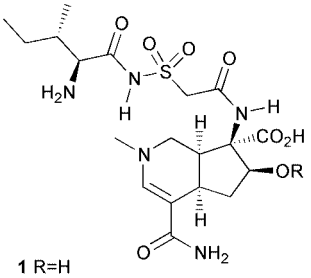

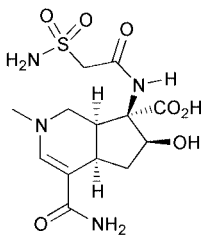

In our initial approach to (±)-**4** and (±)-**5** we envisaged that these might be constructed in a one-pot process from methylamine (**6**), formaldehyde (**7**), cyclopent-2-enone (**8**) and the appropriate propiolic acid derivative **9** or **10** (Fig. 1). In particular, it seemed possible that in the presence of a suitable catalyst the Schiff-base (imine) derived from condensation of **6** and **7** could participate in an 'aza-Baylis–Hillman' reaction[6] with **8** to give *N*-methyl-2-(aminomethyl)cyclopent-2-enone

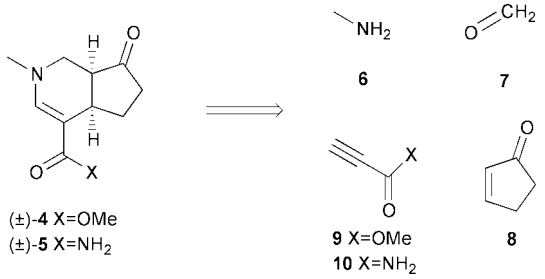

Fig. 1

which would then react, through nitrogen in a hetero-Michael-addition reaction, with **9** or **10**. The enamine–cyclopentenone conjugate thus formed might then be expected to undergo an intra-molecular Michael-addition reaction,[7] thereby providing the target ketones (±)-**4** and (±)-**5**. In the event, mixing the four components **6**–**9** with DABCO, a proven catalyst for the Baylis–Hillman reaction, in water at room temperature (**CAUTION**—highly exothermic!) resulted in a complex mixture of products from which the 1,5-diazacycloocta-2,6-diene **13** could be isolated and the structure of which follows from spectroscopic analysis. Clearly, **6**, **7** and **9** but not **8** have been incorporated into this product and further studies revealed that simply mixing the former compounds in water (Scheme 1) provided diene **13** in 45% yield. Presumably, a key intermediate in this conversion

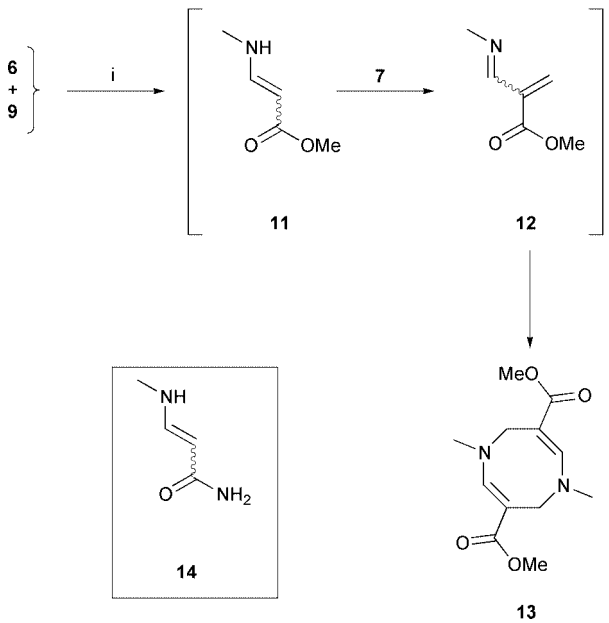

Scheme 1 *Conditions*: (i) H_2O, DABCO (cat.), *ca.* 18 °C, 16 h.

† Electronic supplementary information (ESI) available: spectral data for **5**, crystal data for (±)-**21** (CCDC 165269), HPLC for (+)- and (−)-**21**. See http://www.rsc.org/suppdata/cc/b1/b104890m/

 DOI: 10.1039/b104890m

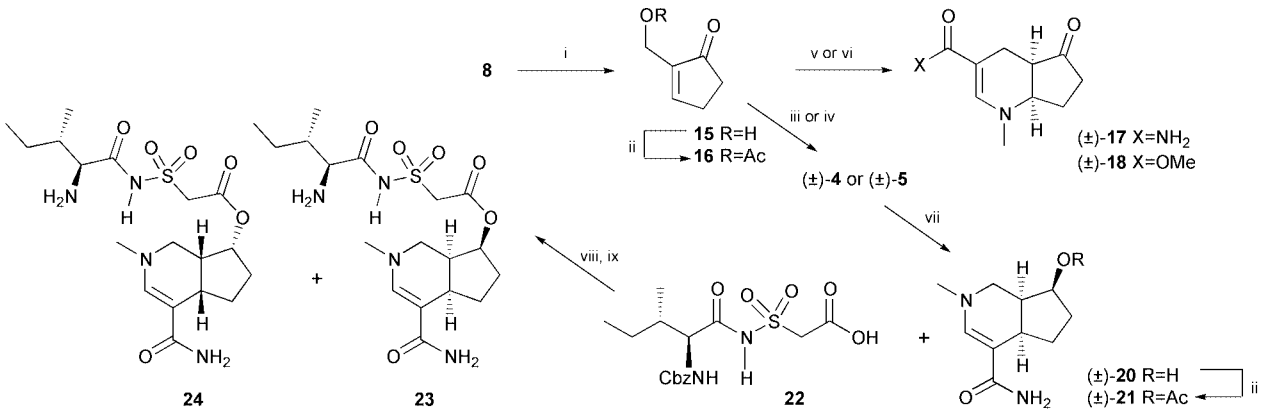

Scheme 2 *Reagents and conditions*: (i) DABCO (*ca*. 0.25 mol% wrt **8**), aq. HCHO (1.5 mole equiv.), THF, 18 °C, 23 h; (ii) Ac_2O (2 mole equiv.), Et_3N (1.65 mole equiv.), DMAP (cat.), CH_2Cl_2; (iii) **6** (1.5 mole equiv.), **9** (1.5 mole equiv.), DABCO (1.25 mole equiv.), H_2O, 18 °C, 5–7 days; (iv) **14** (1.6 mole equiv.), DABCO (1 mole equiv.), EtOH, 18 °C, 15 h; (v) **14** (1.7 mole equiv.), EtOH, 18 °C, 15 h; (vi) **11** (1 mole equiv.), $Pd(PPh_3)_4$ (10 mol%), THF, 18 °C, 10–14 days; (vii) L-Selectride® (1.0 mole equiv. of a 1 M solution in THF), THF, −17 °C, 0.5 h; (viii) **22** (2 mole equiv,), Et_3N (2 mole equiv.), ClCOCOCl (2 mole equiv.), 0 °C, 0.5 h then (+)- or (−)- **20**, Et_3N (1 mole equiv.), DMAP (cat.), DMF, 0 to 18 °C, 1.5 h; (ix) H_2 (1 atm), 10% Pd on C (cat.), MeOH, 18 °C, 4 h.

is the enamine **11**[8,9] (resulting from Michael addition of methylamine to methyl propiolate) which condenses with **7** to give the 1-aza-3-methoxycarbonylbuta-1,3-diene **12** that, in turn, undergoes cyclodimerisation to the observed product. An analogous sequence starting with amide **10**, and which would have been presumed to involve intermediate **14**,[8] failed to deliver the bis(carboxamide) analogue of compound **13**.

The above-mentioned and ready condensation of **7** with **11**, rather than its participation in an initial Baylis–Hillman reaction with **8**, clearly thwarted attempts to implement the proposed four-component coupling approach to targets (±)-**4** and (±)-**5**. To circumvent such problems, **7** and **8** were subject to a dedicated Baylis–Hillman reaction then an aqueous solution of the resulting 2-(hydroxymethyl)cyclopent-2-enone (**15**)[10] (Scheme 2) was treated with **6** and **9** in the presence of stoichiometric amounts of DABCO. In this manner the unstable ketone (±)-**4** was eventually obtained (*ca*. 20% after *ca*. 5 days). An analogous reaction using propiolamide **10** afforded the more stable congener (±)-**5** (*ca*. 20%). A superior method (40% yield after *ca*. 15 h) for producing (±)-**5** involved treating an ethanolic solution of the acetate **16**, derived from alcohol **15**, with **14**[8] (resulting from Michael addition of methylamine to propiolamide) in the presence of DABCO. Surprisingly, the same reaction when carried out in the absence of DABCO afforded the isomeric hexahydroazaindene (±)-**17** (40%) as the major product of reaction. Similarly, when a THF solution of **16** was treated with **11** in the presence of $(Ph_3P)_4Pd$ the structurally related ester (±)-**18** (*ca*. 20%) was obtained.

Diastereofacially selective reduction of ketone (±)-**5** with L-Selectride® yielded the alcohol (±)-**20** (96%), the readily available acetate derivative, (±)-**21** (63%), of which proved suitable for single-crystal X-ray analysis. Alcohol (±)-**20** was readily coupled with the acid chloride derived from **22** and the resulting diastereomeric mixture of esters was subjected to hydrogenolytic deprotection to produce an inseparable and *ca*. 1 : 1 mixture of **23** and **24**. In an effort to obtain diastereomerically pure samples of these materials several methods for preparing the monochiral forms of ketone **5** were examined but none of the several chiral catalysts that have been used to effect asymmetric Baylis–Hillman reactions[11] proved effective in promoting the enantioselective coupling of **14** and **15**. While various chiral ester derivatives of **15** participated in reaction with **14** to produce ketone **5** in acceptable chemical yield, the observed diastereomeric excesses were disappointing (< 17%). As a consequence, the racemic acetate (±)-**21** was resolved using chiral HPLC techniques (see ESI†). Coupling of each of the enantiopure alcohols with the acid chloride derivative of **22** gave, after hydrogenolytic deprotection, the target molecules **23** [from (−)-**21**] and **24** [from (+)-**21**]. Independent testing of **23** and **24** as inhibitors of *S. aureus*-derived IRS[12] revealed that the former compound shows an IC_{50} of 3.7 μM while the analogous value for the 'unnatural' diastereoisomer **24** is 12.4 μM. Interestingly, this difference in activity is even more pronounced with *S. aureus*-derived LRS (0.42 μM *vs*. no inhibition at 100 μM), *S. aureus*-derived VRS (6.35 μM *vs*. no inhibition at 100 μM) and rat liver IRS (0.57 μM *vs*. 13.5 μM).

We thank GlaxoSmithKline (Australia) Pty Ltd for financial support and Dr Brian Metcalf (formerly of SmithKline Beecham US) for his encouragement and advice. Lucy M. Mensah (GSK, Harlow) is thanked for carrying out the reported enzyme inhibition assays.

Notes and references

1 T. F. Gale, J. Görlitzer, S. W. O'Brien and D. H. Williams, *J. Chem. Soc., Perkin Trans. 1*, 1999, 2267. For an up-to-date overview of antibiotic resistance see: C. M. Henry, *Chem. Eng. News*, 2000, **78**, 41.

2 A. L. Stefanska, R. Cassels, S. J. Ready and S. R. Warr, *J. Antibiot*., 2000, **53**, 357; C. S. V. Houge-Frydrych, M. L. Gilpin, P. W. Skett and J. W. Tyler, *J. Antibiot*., 2000, **53**, 364. For the production and biological evaluation of semi-synthetic analogues of **1** and **2** see: M. G. Banwell, C. F. Crasto, C. J. Easton, A. K. Forrest, T. Karoli, D. R. March, L. Mensah, M. R. Nairn, P. J. O'Hanlon, M. D. Oldham and W. Yue, *Biorg. Med. Chem. Lett*., 2000, **10**, 2263.

3 A. Takahashi, H. Naganawa, D. Ikeda and Y. Okami, *Tetrahedron*, 1991, **47**, 3621 and references cited therein.

4 A. S. Kende, *Pure Appl. Chem*., 1997, **69**, 407 and references cited therein.

5 T. Sano, Y. Horiguchi, K. Imafuku and Y. Tsuda, *Chem. Pharm. Bull*., 1990, **38**, 366; E. W. Baxter, D. Labaree, S. Chao and P. S. Mariano, *J. Org. Chem*., 1989, **54**, 2893.

6 A. Kamimura, Y. Gunjigake, H. Mitsudera and S. Yokoyama, *Tetrahedron Lett*., 1998, **39**, 7323 and references cited therein.

7 For examples of related cyclisations see: Y. Özlü, D. E. Cladingboel and P. J. Parsons, *Tetrahedron*, 1994, **50**, 2183.

8 Yu. I. El'natanov and R. G. Kostyanovskii, *Izv. Akad. Nauk SSSR, Ser. Khim*., 1988, 382 (*Chem. Abtsr*., 1989, **110**, 23303).

9 N. L. Zaichenko, I. I. Chervin, V. N. Voznesenskii, Yu. I. El'natanov and R. G. Kostyanovskii, *Izv. Akad. Nauk SSSR, Ser. Khim*., 1988, 779 (*Chem. Abtsr*., 1989, **110**, 22952).

10 A. B. Smith III, S. J. Branca, M. A. Guaciaro, P. M. Wovkulich and A. Korn, *Org. Synth*., 1983, **61**, 65.

11 Y. Iwabuchi, M. Nakatani, N. Yokoyama and S. Hatakeyama, *J. Am. Chem. Soc*., 1999, **121**, 10219 and references cited therein.

12 A. J. Pope, M. McVey, K. Fantom and K. J. Moore, *J. Biol. Chem*., 1998, **273**, 31702 and references cited therein.

CHEMCOMM Communication
www.rsc.org/chemcomm

Colloidal cobalt nanoparticles: a highly active and reusable Pauson–Khand catalyst†

Sang-Wook Kim,[a] Seung Uk Son,[b] Su Seong Lee,[a] Taeghwan Hyeon*[a] and Young Keun Chung*[b]

[a] *School of Chemical Engineering and Institute of Chemical Processes, Seoul National University, Seoul 151-742, Korea. E-mail: thyeon@plaza.snu.ac.kr*

[b] *School of Chemistry and Center for Molecular Catalysis, Seoul National University, Seoul 151-742, Korea. E-mail: ykchung@plaza.snu.ac.kr*

Received (in Cambridge, UK) 21st August 2001, Accepted 18th September 2001
First published as an Advance Article on the web 11th October 2001

A new Pauson–Khand catalyst based on colloidal cobalt nanoparticles has been developed; the catalyst is highly effective for many intra- and inter-molecular Pauson–Khand reactions and can be recycled and reused many times without losing catalytic activity.

The development of uniform nanometer size particles has been intensively pursued because of their technological and fundamental scientific interest.[1] They have a characteristic high surface-to-volume ratio, and consequently a large fraction of the metal atoms are at the surface and hence are available for catalysis.[2] Many colloidal transition metal nanoparticles, especially noble metals, have been applied as catalysts for the hydrogenation of olefins,[3] for carbon–carbon coupling reactions and for other reactions.[4] However, colloidal nanoparticles of first-row transition metals have seldom been applied as catalysts. Here we present the application of colloidal cobalt nanoparticles for catalytic Pauson–Khand reactions.

Pauson–Khand (P–K) reactions, the cycloaddition of alkynes with alkenes and carbon monoxide to cyclopentenones, have been recognized as one of the most important methodologies in the synthesis of cyclopentenone derivatives.[5] Several research groups, including ourselves, have developed the catalytic version of P–K reactions.[6] Various catalysts applied in P–K reactions include the most popular dicobalt octacarbonyl and several other carbonyl-ligand containing organometallic compounds. Very recently, we demonstrated the first heterogeneous catalytic P–K reactions using metallic cobalt supported on either mesoporous silica or charcoal.[7] Even though these heterogeneous metallic cobalt catalysts exhibit good performance for many intramolecular and intermolecular P–K reactions, they require extreme reaction conditions of CO pressures > 20 atm and temperatures > 120 °C. For diverse applications of P–K reactions, the development of recyclable heterogeneous catalysts able to work in much milder conditions is desirable.

Several synthetic methods have been applied in the fabrication of colloidal cobalt nanoparticles, including the thermal and sonochemical decomposition of organometallic compounds,[8] and the reduction of metal salts.[9] In this report, we have applied a recently developed synthetic method to fabricate cobalt nanoparticles. This method comprises the formation of seed particles at low temperature and further aging at high temperature. For the synthesis of cobalt nanoparticles, $Co_2(CO)_8$ (2.04 g, 6 mmol), oleic acid (1.68 g, 6 mmol), trioctylphosphine (0.6 mL) and dioctyl ether (20 mL) were mixed with stirring at room temperature. The mixture was heated slowly to reflux and the refluxing was maintained for 30 min, after which the reaction mixture was allowed to cool to room temperature. A black precipitate was obtained by adding 50 mL of ethanol followed by washing with 20 ml of acetone and drying *in vacuo*. A transmission electron microscopic (TEM) image (see ESI†) confirmed that the particles are well separated and that they are nearly monodisperse, having a mean diameter of 8 nm.

The intramolecular P–K reaction of an enyne was investigated as a test reaction [eqn. (1)]. Table 1 summarizes the results of this reaction under various reaction conditions.

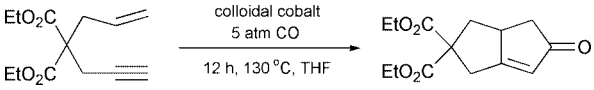

(1)

Entry 1 shows that colloidal cobalt is very active with an isolated yield of product of 97% at 130 °C and a CO pressure of 5 atm. The colloidal cobalt catalyst is more active than heterogeneous catalysts based on metallic cobalt supported on mesoporous silica or charcoal.[7] Using these heterogeneous catalysts, a CO pressure of > 20 atm was required to achieve a yield of > 95% under otherwise identical reaction conditions. To check the recyclability, the catalyst was separated and reused several times (entries 2–5). The results shown in Table 1 confirm that the catalyst maintained its high activity even after five cycles of recycling and reuse. A TEM image of the catalyst after running four reaction cycles showed that the particle size of the cobalt nanoparticles was unchanged and confirmed that no particle agglomeration was observed (ESI†). However, when either the reaction temperature was decreased to 110 °C or the CO pressure was lowered to 3 atm, the catalytic activity was found to decrease significantly (entries 6–9). Thus, to preserve a high catalytic activity, the reaction temperature and CO pressure have to be maintained at a minimum of 130 °C and 5 atm of CO. Nevertheless, the colloidal cobalt catalyst still sustained a degree of activity at 3 atm of CO pressure and 130 °C, with 45% yield of product being obtained.

Table 1 Intramolecular Pauson–Khand reactions under various conditions[a]

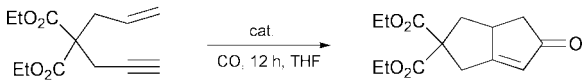

Entry	Catalyst	*T*/°C	Pressure/atm	Yield[b] (%)
1	Colloidal cobalt	130	5	97
2	Recovered from #1	130	5	94[c]
3	Recovered from #2	130	5	94[c]
4	Recovered from #3	130	5	94[c]
5	Recovered from #4	130	5	95[c]
6	Colloidal cobalt	120	5	89
7	Colloidal cobalt	110	5	26
8	Colloidal cobalt	130	3	45
9	Colloidal cobalt	130	1	0

[a] Reaction conditions: colloidal cobalt (25 mg, 45 wt% cobalt), allylpropargyl diethylmalonate (0.42 mmol), THF, 12 h. [b] Isolated yield. [c] Yield obtained from GC.

† Electronic supplementary information (ESI) available: experimental details for the catalytic Pauson–Khand reaction. Transmission electron micrographs of colloidal cobalt nanoparticles before and after reaction. See http://www.rsc.org/suppdata/cc/b1/b107577m/

 DOI: 10.1039/b107577m

Table 2 Pauson–Khand reactions with various substrates[a]

Entry	Substrate	Product	Yield[b](%)
1	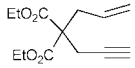	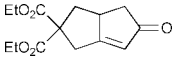	97
2	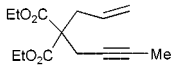	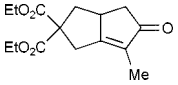	97
3[c]	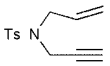	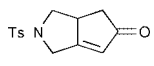	90
4[c]	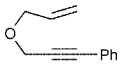	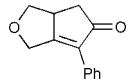	85
5	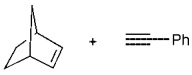	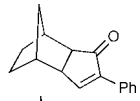	94
6	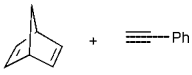	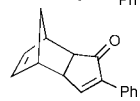	97
7	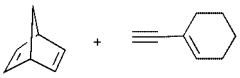	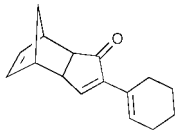	93

[a] Reaction conditions: colloidal cobalt nanoparticles (25 mg, 45 wt% cobalt), substrate (0.42 mmol), CO (5 atm), THF, 130 °C, 12 h. [b] Isolated yield. [c] 10 atm CO applied.

To demonstrate the versatility of the colloidal cobalt catalyst, we applied various substrates for catalytic P–K reactions and the results are shown in Table 2. While the general intramolecular P–K reactions proceeded smoothly at 5 atm (entries 1 and 2), heteroatom-bridged enynes (entries 3 and 4), which contain either an oxa or aza functional group, required a higher CO pressure of 10 atm. The catalyst was also tested for intermolecular cycloaddition reactions (entries 5–7). Overall the colloidal cobalt catalyst is very active for these reactions. The reaction of norbornene or norbornadiene and phenylacetylene (entries 5, 6) proceeded well. The reaction between norbornadiene and alkyl-substituted acetylene also gave a good yield (entry 7).

In conclusion, we present the development of a new Pauson–Khand catalyst using colloidal cobalt nanoparticles. The catalyst is more active than heterogeneous cobalt catalysts supported on either mesoporous silica or charcoal. It can be reused several times without particle agglomeration or loss of activity. The catalyst systems are effective for many intra- and inter-molecular Pauson–Khand reactions.

Notes and references

1 *Clusters and Colloids*, ed. G. Schmid, VCH, New York, 1994; A. P. Alivisatos, *Science*, 1996, **271**, 933; S.-J. Park, S. Kim, S. Lee, Z. G. Khim, K. Char and T. Hyeon, *J. Am. Chem. Soc*., 2000, **122**, 8581.

2 J. D. Aikin III and R. G. Finke, *J. Mol. Catal. A: Chem*., 1999, **145**, 1; B. F. G. Johnson, *Coord. Chem. Rev*., 1999, **190–192**, 1269.

3 V. Chechik and R. M. Crooks, *J. Am. Chem. Soc*., 2000, **122**, 1243; P. Lu, T. Teranishi, K. Asakura, M. Miyake and N. Toshima, *J. Phys. Chem. B*, 1999, **103**, 9673; J. D. Aikin III and R. G. Finke, *Chem. Mater*., 1999, **11**, 1035.

4 M. Beller, H. Fischer, K. Kühlein, C.-P. Reisinger and W. A. Herrmann, *J. Organomet. Chem*., 1996, **520**, 257; M. T. Reetz and G. Lohmer, *Chem. Commun*., 1996, 1921; M. T. Reetz and E. Westermann, *Angew. Chem., Int. Ed*., 2000, **39**, 165.

5 For recent reviews: Y. K. Chung, *Coord. Chem. Rev*., 1999, **188**, 297; O. Geis and H. –G. Schmalz, *Angew. Chem., Int. Ed*., 1998, **37**, 911.

6 N. Jeong, S. H. Hwang, B. Y. Lee and Y. K. Chung, *J. Am. Chem. Soc*., 1994, **116**, 3159; V. Rautenstrauch, P. Megard, J. Conesa and W. Kuster, *Angew. Chem., Int. Ed. Engl*., 1990, **29**, 1413; B. L. Pagenkopf and T. Livinghouse, *J. Am. Chem. Soc*., 1996, **118**, 2285.

7 S.-W. Kim, S. U. Son, S.-I. Lee, T. Hyeon and Y. K. Chung, *J. Am. Chem. Soc*., 2000, **122**, 1550; S. U. Son, S. I. Lee and Y. K. Chung, *Angew. Chem., Int. Eng. Ed*., 2000, **39**, 4158.

8 K. S. Suslick, M. Fang and T. Hyeon, *J. Am. Chem. Soc*., 1996, **118**, 11960; V. F. Puntes, K. M. Krishnan and A. P. Alivisatos, *Science*, 2001, **291**, 2115.

9 S. Sun and C. B. Murray, *J. Appl. Phys*., 1999, **85**, 4325; V. Russier, C. Petit, J. Legrand and M. P. Pileni, *Phys. Rev. B*, 2000, **62**, 3910.

CHEMCOMM Communication
www.rsc.org/chemcomm

Differentiation of mobile and immobile pesticides on anionic clays by ^{1}H HR MAS NMR spectroscopy

Bruno Combourieu,[a] Jérôme Inacio,[b] Anne-Marie Delort*[a] and Claude Forano[b]

[a] *Laboratoire de Synthèse et Etude des Systèmes à Intérêt Biologique, Université Blaise Pascal, CNRS UMR 6504, France. E-mail: amdelort@chimtp.univ-bpclermont.fr*

[b] *Laboratoire des Matériaux Inorganiques, Université Blaise Pascal, CNRS UMR 6002, 24 Avenue des Landais, 63177 Aubière Cedex, France*

Received (in Cambridge, UK) 2nd August 2001, Accepted 18th September 2001
First published as an Advance Article on the web 11th October 2001

Adsorbed *vs.* intercalated MCPA (4-chloro-2-methylphenoxyacetic acid) in highly hydrated clays taken as a soil model were clearly distinguished by ^{1}H HR MAS NMR; adsorbed herbicide gave sharp signals indicating high mobility while intercalated herbicide gave very wide unresolved spectra due to its strong interaction with the solid matrix.

Adsorption is one of the key processes affecting the ultimate fate of pesticides, or other xenobiotics, in the environment as it controls transport, mobility and degradability in soils and ground water. The adsorption–desorption mechanisms at the interface between organic and inorganic soil colloids influence movement of pesticides, and thus their availability for plant or microbial uptake, or their transformation by abiotic or biotic agents. However, the study of the biodegradation and fate of organic pollutants in soils suffers of a lack of analytical methods to follow *in situ* the biotransformation process. Direct analyses of dry parts of soils have been reported using solid-state cross-polarization magic angle spinning (CP-MAS) NMR spectroscopy. For example, ^{13}C CP-MAS NMR was used to characterize ^{13}C-atrazine (entirely labelled) residues and to follow the binding reactivity of organic matter after addition of fresh and decomposed straw.[1] These experiments, performed on dry samples, do not give the real fingerprint of an environmental material, which is usually highly hydrated with mobile pollutant at its surface. Particularly, solid-state NMR, albeit very efficient to provide structural information, cannot allow quantification of the 'bioavailability' of the pollutant. This could be elucidated by using liquid state high-resolution (HR) MAS NMR on hydrated samples. Indeed, HR MAS allows the characterization by NMR of inhomogeneous compounds with liquid-like dynamics.[2] In such systems with restricted or anisotropic motions, the effects of dipolar coupling, CSA and inhomogeneous susceptibility on resonance line widths are not averaged to zero in static experiments but are dramatically decreased by MAS. In environmental chemistry, only one example using ^{13}C MAS NMR has been described.[3] However, this approach is limited because it requires labelled xenobiotics, which are expensive and difficult to synthesize. By contrast ^{1}H NMR can be applied to any class of xenobiotic, as shown by recent studies carried out on liquid incubation media.[4] ^{1}H HR MAS NMR spectroscopy is increasingly used to study intact suspension cells or tissue metabolite composition.[5] It is also emerging as a new tool to quantitatively monitor solid phase organic reactions in combinatorial chemistry and thus to analyse resin-bound structures without any sample preparation.[6]

The purpose of the present study is to develop a method to characterize the interactions between organic pollutants and a model of soil, allowing direct analyses of contaminated soils, without any sample preparation. In this paper, we present the differentiation by ^{1}H HR MAS NMR of mobile 4-chloro-2-methylphenoxyacetate (MCPA), adsorbed at the surface of a well defined synthetic hydrotalcite used as a soil model and immobile MCPA intercalated in this bidimensional host structure [Fig. 1(a)].

Layered double hydroxides (LDH) are natural minerals, considered as the anti-type of 2:1 smectites and regarded as anionic clays. They are lamellar compounds, built by a stacking of positive $[M^{2+}_{1-x}M^{3+}_{x}(OH)_2]^{x+}$ layers, separated by inter-

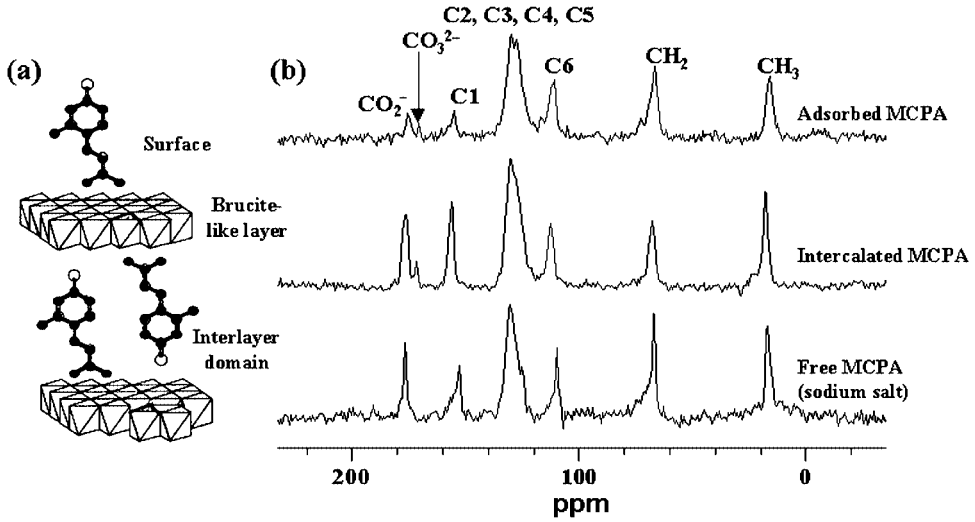

Fig. 1 (a) Structural model of the interaction of MCPA with HTLCs. (b) ^{13}C CP MAS ($\omega_r/2\pi$ = 10 kHz) spectra of adsorbed and intercalated MCPA clay, and free MCPA recorded at 75.46 MHz (recycle delay : 3 s; contact time : 1 ms; 2000 scans). The arrow indicates the presence of carbonates trapped in exchanged clays during the storage and the preparation of the samples.

 DOI: 10.1039/b106964k

layer domains containing hydrated anions $[X^{m-}_{x/m}\cdot nH_2O]$.[7] Synthetic minerals are simple to prepare with tunable M^{2+} and M^{3+} composition, layer charge density ($0.20 \leqslant x \leqslant 0.33$) and intercalated anion X^{m-}.[8] Their high anion exchange capacities make them interesting materials for the elimination of ecologically undesirable organic anions such as pesticides[9] from contaminated water or waste. Sorption studies recently demonstrated that pesticides of the chlorophenoxy carboxylate family (2.4D, MCPA, 2.4.5T) display very strong affinities to LDHs.

Adsorbed and intercalated MCPA on $Mg_{3.1}Al(OH)_{8.2}Cl\cdot nH_2O$ [Mg_3AlCl] were prepared as previously described.[10] The adsorption proceeds in two steps as shown on the adsorption isotherm (10 mg of solid, 50 ml of MCPA aqueous solution, 25 °C, 24 h equilibrium time).[10] The isotherm is clearly a mixture of S-type at low C_e equilibrium concentration (< 1.5 mmol l^{-1}) and L-type.[11] The change from S- to L-type within the same isotherm is likely to be due to changes from external to interlayer adsorption. The sorption data, at low C_e, were analysed according to the Freundlich equation: $Q = K_f C_e^{1/n}$ where $K_f = 0.666$ mmol g^{-1} and $n = 0.671$ are constants that give estimation of the adsorption capacity and intensity, respectively. The maximum of adsorption is reached for $C_e = 0.50$ mmol l^{-1}, *i.e.* 15% of the total exchange capacity at a specific surface area of the solid = 44 m^2 g^{-1}. Over this C_e value, intercalation proceeds *via* an increase of the basal spacing from 0.794 nm for [Mg_3AlCl] to 2.21 nm for [Mg_3Al(MCPA)] as shown by powder X-ray diffraction.

This high basal spacing results from the formation of intertwined double-layers of MCPA in the interlayer spaces, as reported by Prevot *et al.*,[12] with the anions hydrogen bonded to the hydroxylated surfaces in a perpendicular orientation [Fig. 1(a)].

Solid state ^{1}H MAS ($\omega_r/2\pi$ = 12 kHz) experiments carried out on both adsorbed and intercalated MCPA clays show very broad signals and do not allow the differentiation of both populations of MCPA (not shown). ^{13}C CP MAS spectra [Fig 1(b)] clearly show the presence of adsorbed and intercalated MCPA in the clay samples. The different carbons of the MCPA molecule were easily identified and their NMR signals were not shifted compared to free MCPA. A slight difference of relative CO_2^- and C1 signal intensities for the two populations (adsorbed and intercalated) was due to a lower efficiency of the CP technique at the surface. The better resolution of the intercalated MCPA spectrum can be explained by the higher structural order of this solid phase. To assess the mobility of adsorbed *vs.* intercalated MCPA in anionic clays, the samples (40 mg) were swollen with D_2O (80 μL). The sample volume was restricted to about 50 μL in the center of the rotor to increase the r.f. field homogeneity. The ^{1}H HR MAS NMR spectra were acquired at 300.13 MHz with a double bearing 4 mm MAS probehead using a single pulse experiment ($t_{90°}$ = 6.2 μs) with presaturation during relaxation for water resonance suppression. The samples were spun in a speed range of 1.33 to 1.80 kHz, sufficient for high resolution. Chemical shifts are reported in ppm relative to TSP-d_4 as external standard. The number of transients was typically 256 to achieve good signal to noise ratio.

Fig. 2(a) displays the ^{1}H spectrum of the adsorbed MCPA (0.49 mmol g^{-1}) clay hydrated with D_2O. All protons of MCPA are visible and chemical shifts are identical to those of the solution state NMR spectrum, thus indicating an efficient tumbling of the molecules at the surface. These sharp signals are

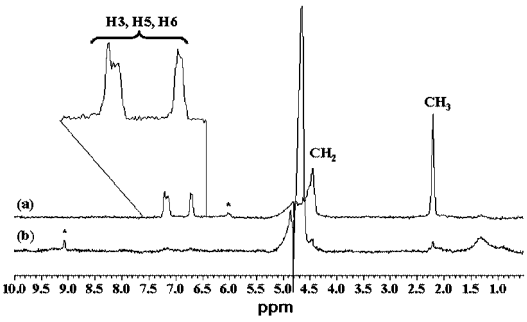

Fig. 2 ^{1}H HR MAS spectra of (a) adsorbed and (b) intercalated MCPA clay. The asterisk in spectra indicates spinning sidebands.

characteristic of weakly bounded compounds. The spectrum of the MCPA intercalated (> 4 mmol g^{-1}) compounds [Fig. 2(b)], recorded under the same conditions, displays only residual signals. In this sample the MCPA anions are tightly packed either inside the structure or at the surface because of a high packing of organic molecules which are not observed by HR MAS. These small signals could be explained by the release of a minor fraction of MCPA due to a slight hydrolysis of the matrix. This is confirmed by the presence of two broad peaks at 0.85 and 1.25 ppm, identified as protons of metallic hydroxides under colloidal form.

This communication demonstrates the potential of the ^{1}H HR MAS technique to study *in situ* interactions at the solid–aqueous interface of a solid matrix. By using a well-characterized model of soil it was possible to distinguish unambiguously the mobile and immobile pesticide. Therefore the ^{1}H HR MAS technique is a promising approach to quantitatively evaluate the bioavailable (mobile) fraction of a xenobiotic in such a solid matrix as it will be the only one giving rise to sharp ^{1}H NMR signals; any pesticide fraction strongly interacting with the soil model will not be detected. Although the detection limit of xenobiotic concentration can be evaluated to 50 μM, the environmental interactions in a whole soil will also be observable by this technique since all the powerful and sensitive solution-state experiments can be used.

We thank the CNRS (PEVS) for financial support.

Notes and references

1 P. Benoit and C. M. Preston, *Eur. J. Soil Sci.*, 2000, **51**, 43.
2 M. Piotto, M. Bourdonneau, J. Furrer, A. Bianco, J. Raya and K. Elbayed, *J. Magn. Reson.*, 2001, **149**, 114.
3 G. W. Wagner and B. K. MacIver, *Langmuir*, 1998, **14**, 6930.
4 A. M. Delort and B. Combourieu, *NMR in Microbiology: Theory and applications; microbial degradation of xenobiotics*, ed. J. C. Portais and J. N. Barbotin, Horizon Scientific, UK, 2000, p. 411.
5 S. Garrod, E. Humpher, S. C. Connor, J. C. Connelly, M. Spraul, J. K. Nicholson and E. Holmes, *Magn. Reson. Med.*, 2001, **45**, 781.
6 R. Warrass and G. Lippens, *J. Org. Chem.*, 2000, **65**, 2946.
7 R. Allman, *Acta Crystallogr., Sect. B*, 1968, **B24**, 972.
8 A. Vaccari, *Appl. Clay Sci.*, 1999 **14**, 161.
9 M. V. Villa, M. J. Sanchez-Martin and M. Sanchez-Camazano, *J. Environ. Sci. Health B*, 1999, **34**, 509.
10 J. Inacio, C. Taviot-Guého, C. Forano and J. P. Besse, *Appl. Clay Sci.*, 2001, **18**, 255.
11 C. H. Giles, T. H. Mac Ewan, S. N. Nakhwa and P. Smith, *J. Chem. Soc.*, 1960, 3973.
12 V. Prevot, C. Forano and J. P. Besse, *Appl. Clay Sci.*, 2001, **18**, 3.

CHEMCOMM Communication
www.rsc.org/chemcomm

Permeability of micelles in surfactant-containing MCM-41 silica as monitored by embedded dye molecules

B. Onida,[a] B. Bonelli,[a] L. Flora,[a] F. Geobaldo,[a] C. Otero Arean[b] and E. Garrone*[a]

[a] *Dipartimento di Scienza dei Materiali e Ingegneria Chimica, Corso Duca degli Abruzzi, 24, 10129 Torino, Italy. E-mail: garrone@athena.polito.it*
[b] *Departamento de Química, Universidad de las Islas Baleares, 07071 Palma de Mallorca, Spain*

Received (in Cambridge, UK) 14th June 2001, Accepted 24th September 2001
First published as an Advance Article on the web 11th October 2001

Mesoporous (MCM-41 type) silica containing surfactant-embedded Congo Red has been prepared and tested against gas phase HCl and ammonia, as well as solutions of ionic species; it is shown that the hybrid (organic–inorganic) material is permeable to both gases and ionic species, and can act as a pH indicator and as a selective chelating agent.

Since their discovery in 1992, ordered mesoporous silicas, prepared by using surfactant molecules, have been much studied. Most work has concerned materials freed from surfactant either by calcination or extraction, those materials being suitable for catalysis, adsorption and inclusion of functional species.[1] The hybrid surfactant–silica systems have been investigated much less, and regarded usually as merely the precursors to active materials. Hybrid MCM-41 systems have been prepared with included paramagnetic molecules,[2] the motional freedom of which was measured by means of EPR spectroscopy. Some authors solubilised dyes in the surfactant solution in order to study formation of micelles and the growth of ordered mesoporous silica films by means of fluorescence.[3,4] Incorporation of dye-molecules in the micellar phase of surfactant–silica mesophases has also been achieved,[5] as dye-modified ordered mesoporous silica and zeolites may find applications in optical, optoelectronic and electrochromic devices, and in chemical sensors.[6–8]

Details on the nature of organic mesophases is lacking. Jaroniec and Antochshuck[9] have shown that the surfactant–MCM-41 hybrid material is somehow permeable to Me_3SiCl, which can diffuse and be grafted on the internal silica surface, causing some surfactant displacement. Here, we report data on the permeability of MCM-41 hybrid systems to acidic/basic gases or to solutions, obtained by means of common pH indicators embedded in the micelle. Congo Red (hereafter CR, Scheme 1) was used: nearly identical results obtained with Curcumin are not reported.

Both dye-free (MCM-41) and dye-containing (CR-MCM-41) samples were prepared following ref. 10 using tetraethylorthosilicate (TEOS, Aldrich), distilled water, hexadecyltrimethylammonium bromide (CTAB, Aldrich), Congo Red (Merck) and NaOH (Carlo Erba). 2.0 g of CTAB was added at room temperature to a basic solution (0.96 g of NaOH in 475 ml of water) under stirring. When the solution became homogenous, CR was then added. 10 ml of TEOS was added, giving rise to a coloured slurry. After 3 h the product was filtered off, washed first with distilled water and then with ethanol, and dried at 40 °C. The composition of the synthesis mixture was 1 TEOS:0.125 CTABr:0.400 NaOH:0.01 dye:525 H_2O. Samples were stored before use in a P_2O_5 desiccator. IR spectra showed the presence of negligible amounts of residual water.

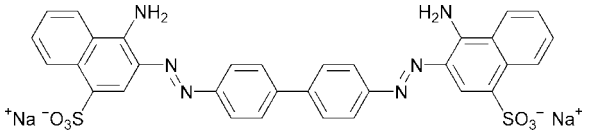

Scheme 1 The Congo Red molecule.

No leaching of dye occurred when washing with either ethanol or water; the CR-containing sample was bright red. For comparison, two surfactant-free CR/SiO_2 systems were prepared, one by precipitating SiO_2 from a basic solution of TEOS in the presence of CR, and the other by impregnation of MCM-41 (after calcination in flowing air at 773 K) with a CR solution. It was found that in the surfactant-free sample washing with water brought about dye leaching. Surfactant micelles are effective in retaining the dye in the material. Indeed, ionic dyes, such as CR, can be removed from aqueous solution by ionic surfactants, which collect the dye in the froth, and have themselves a tendency to form micelles.[11]

Fig. 1 shows the XRD patterns of MCM-41 and CR-MCM-41 with high amount of dye (Si/CR = 25). In both cases, the hexagonal phase is present. A smaller d_{100} is observed for the latter: the increase in size of the hexagonal cell (from 444 to 464 pm) indicates that the dye embedded in the micelles causes some swelling. Sulfonate groups in CR probably interact with the cationic heads of surfactant molecules, which in turn interact with the negatively charged silica wall:[12] the sulfonic groups of CR are thus probably located at the surfactant–silica interface, whereas the rest of the molecule, *i.e.* aromatic rings, amino and azo groups, is embedded in the micelle.

Accessibility of the dye molecules to gases was investigated by exposing the powder to vapours of HCl and NH_3. Fig. 2 shows the diffuse-reflectance UV–VIS spectra of CR-MCM-41 before (curve 1) and after exposure to gases (curves 2–4). In curve 1, the band at 500 nm is due to the π–π* transition of the azo group,[13] which is rather sensitive to protonation. The shoulder at 530 nm could be due to some amount of ordered dye aggregates, in a head-to-tail stacking arrangement.[14]

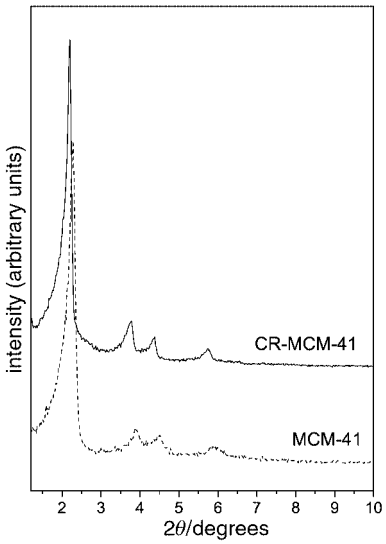

Fig. 1 XRD patterns of dye-free (MCM-41) and CR-containing (CR-MCM-41) surfactant–silica hybrid MCM-41 materials.

 DOI: 10.1039/b105261f

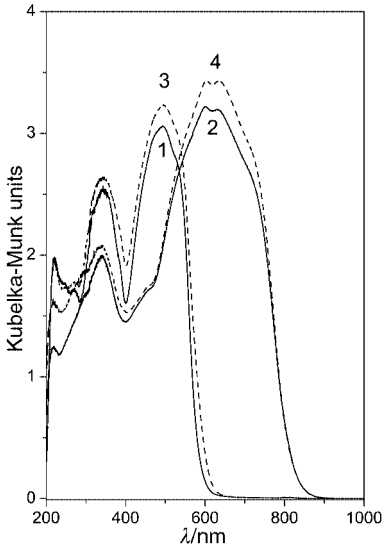

Fig. 2 Electronic diffuse reflectance spectra of CR-MCM-41 as-synthesized (curve 1), exposed to HCl (curve 2), exposed to NH_3 after HCl (curve 3) and re-exposed to HCl (curve 4).

Exposure to HCl causes a colour change from red to blue, the colour of the acidic form of CR (the same is observed with pure CR): accordingly, the π–π* transition of the azo group shifts to higher wavelength because of protonation (curve 2). Exposure to ammonia restores immediately the spectrum of the as-synthesised CR-MCM-41 (curve 3), since deprotonation of Congo Red occurs with formation of ammonium ions, the presence of which is revealed by IR spectroscopy. Subsequent exposure to HCl restores spectrum 2 (curve 4). The IR spectrum of CR-MCM-41 shows parallel changes after exposure to HCl and NH_3. More than 10 protonation–deprotonation cycles were observed, *i.e.* the probable formation of ammonium chloride within the solid does not prevent the permeation to gases.

The permeability of the hybrid material to species in solution has been investigated as follows. In a first experiment, CR-MCM-41 was contacted with an acidic solution at pH < 1, to assess whether the dye molecules were reachable by H_3O^+ species and able to display their pH-sensing properties. A change in colour from red to blue was observed immediately, indicating that protonation of CR occurs and that the azo group is accessible to H_3O^+ ions from aqueous solution. When the acidic solution was diluted, the sample colour changed back to red, indicating a reversible protonation of embedded CR. The pH at which colour change takes place is lower than with CR in aqueous solution: the same was observed for the dye in CTAB-containing aqueous solutions. This lower pH value may be accounted for considering a partition of H_3O^+ species between the hydrophilic phase (water) and the hydrophobic phase (micelles), causing a lower H_3O^+ concentration in the micelles than in aqueous solution. In order to observe the colour change of the micelle-embedded indicator, a higher H_3O^+ concentration in the aqueous phase is required with respect to the value observed for CR aqueous solution.

As CR may act as a sensitive photometric reagent toward metal ions,[15] such as Cu^{2+} (chelation involves both azo and amino groups, causing a red shift of the π–π* transition), in a second experiment CR-MCM-41 was stirred in a $CuSO_4$ solution for 12 h, then filtered off and washed. Two solvents have been considered, *i.e.* water and ethanol (95 wt%).

After contact with an aqueous Cu^{2+} solution no change occurred in the UV–VIS spectrum of the material. However, after contact with ethanol solution, a new absorption appears at *ca.* 630 nm, ascribed to π–π* transition of molecules complexing Cu^{2+} ions, in agreement with what is observed for other metal ions complexed by CR linked to a polymeric matrix.[15] Ethanol-solvated Cu^{2+} ions most probably have a higher hydrophobicity, *i.e.* a larger affinity for the micellar phase, than aquo-ions, so that the former diffuse inside the dye-containing mesophases more easily than the latter.

In conclusion, the surfactant–silica hybrid material is permeable to both gases, even strongly polar such as HCl, and ionic species. The micelle-embedded CR is readily accessible to such species and still acts as a pH sensor, in that reversible protonation–deprotonation occurs at the azo group. The embedded molecules can still act as a chelating agent through the azo and the amino groups towards Cu^{2+} ions.

We thank Professor M. Lucco Borlera (Politechnic of Turin) and Professor G. Viscardi (University of Turin) for fruitful discussions.

Notes and references

1 C. T. Kresge, M. E. Leonowicz, W. J. Roth, J. C. Vartuli and J. S. Beck, *Nature (London)*, 1992, **359**, 710.
2 A. Galarneau, F. Di Renzo, F. Fajula, L. Mollo, B. Fubini and M. F. Ottaviani, *J. Colloid Interface Sci*., 1998, **201**, 105.
3 M. Ferrer and P. Lianos, *Langmuir*, 1996, **12**, 5620.
4 Y. Lu, R. Ganguli, C. A. Drewien, M. T. Anderson, C. J. Brinker, W. Gong, Y. Guo, H. Soyez, B. Dunn, M. H. Huang and J. I. Zink, *Nature*, 1997, **389**, 364.
5 H. S. Zhou, H. Sasabe and I. Honna, *J. Mater. Chem*., 1998, **8**, 515.
6 K. Moller and T. Bein, *Chem. Mater*., 1998, **10**, 2950
7 C. E. Fowler, B. Lebeau and S. Mann, *Chem. Commun*., 1998, 1825.
8 S. Wohlrab, R. Hoppe, G. Schulz-Ekloff and D. Wöhrle, *Zeolites*, 1992, **12**, 862.
9 M. Jaroneic and V. Antochshuck, *Chem. Mater*., 2000, **12**, 21 196.
10 Q. Cai, W. Y. Lin, F. S. Xiao, W. Q. Pang, X. H. Chen and B. S. Zou, *Microporous Mesoporous Mater*., 1999, **32**, 1.
11 F. Sebba, *Nature*, 1960, **184**, 1062.
12 G. D. Stucky, D. Zhao, P. Yang, W. Lukens, N. Melosh and B. F. Chmelka, *Stud. Surf. Sci. Catal*., 1998, **117**, 1.
13 R. A. Edwards and R. W. Woody, *J. Phys. Chem*., 1983, **87**, 1329..
14 T. M. Cooper and M. O. Stone, *Langmuir*, 1988, **14**, 6662.
15 T. S. Lee, C. Yang, *Polym. Bull*., 1999, **42**, 655.

CHEMCOMM Communication
www.rsc.org/chemcomm

Efficient and selective catalytic oxidative cleavage of α-hydroxy ketones using vanadium-based HPA and dioxygen

Leïla El Aakel,[ab] Franck Launay,*[a] Ahmed Atlamsani[b] and Jean-Marie Brégeault[a]

[a] *Laboratoire des Systèmes Interfaciaux à l'Echelle Nanométrique, Université Pierre et Marie Curie, unité CNRS 2312, case 196, 4 place Jussieu, 75252 Paris cedex 05, France. E-mail: flaunay@ccr.jussieu.fr; Fax: 33 (0)1 44 27 55 36*

[b] *Laboratoire de Chimie Physique Appliquée, Département de Chimie, Faculté des Sciences, Université Abdelmalek-Essaadi, BP2121, 93000 Tétouan, Morocco*

Received (in Cambridge, UK) 2nd August 2001, Accepted 18th August 2001
First published as an Advance Article on the web 5th October 2001

The combination of $H_{3+n}[PMo_{12-n}V_nO_{40}]$·aq (HPA-*n*, *n* = 3) and dioxygen provides a clean and regioselective reagent for the homolytic cleavage of various representative α-hydroxy ketones (primary to tertiary) and turns out to be as efficient for the catalytic ring opening of chiral natural products.

Keggin type mixed-addenda heteropolyanions such as $[PMo_{12-n}V_nO_{40}]^{(3+n)-}$, denoted HPA-*n* (*n* = 1, 2, 3, *etc.*), have found many applications in catalysis.[1] Recently, their variable redox and acid–base properties have been used for the catalytic cleavage of different cycloalkanones by dioxygen.[2,3] Carboxylic acids, including adipic acid were obtained with high yields and selectivities. Early mechanistic studies showed clearly that the α-ketol (α-hydroxy ketone) is not a major intermediate during cyclohexanone oxidation. In fact, 2-hydroxycyclohexanone is converted to adipic acid with a better yield.

The oxidative cleavage of carbon–carbon bonds in α-ketols is widely used in organic synthesis. In many synthetic schemes, including that of Taxol®, ring opening strategies are based on prior formation of α-hydroxy ketones.[4] Most of the published procedures use stoichiometric reagents.[5] Efforts have been made to find dioxygen-based catalytic pathways running either with Bi(0)/Bi(III) salts or moisture-sensitive dichloro(ethoxy)-oxy vanadium complexes.[6] In this communication, we report on the synthetic utility of the reaction catalysed by robust oxidation-resistant compounds like vanadium-based HPA and present a general route for the selective homolytic carbon–carbon bond cleavage of α-hydroxy ketones.

Using 2-hydroxycyclohexanone (**1a**) and $H_6[PV_3Mo_9O_{40}]$·aq as the catalyst precursor, the reaction was carried out either in methanol or in an acetic acid–water mixture at 65 °C. Dioxygen consumption was monitored by a gas burette system. Colour changes of the initial solutions from orange to blue-green and finally orange-brown were observed in both cases. They are consistent with the variation of the oxidation state of vanadium [V(V)/V(IV)] and the overall reaction can be interpreted in terms of a vanadium-catalysed process assisted by dioxygen. Under dinitrogen the solution remained blue and there was no significant reaction. The results are summarized in Table 1.

Regioselective cleavage of **1a** gave adipic acid or its dimethyl ester (Scheme 1) as the major products in acetic acid or methanol, respectively (runs 1 and 2). As shown in a blank experiment, adipic acid (**2a**) conversion to dimethyl adipate (**2b**) was also catalysed by 'HPA-3'† in methanol (100% yield in 1.5 h).

The *in situ* esterification yield, as determined by comparison of the diester (**2b**) amounts before and after addition of an ethereal solution of diazomethane was about 85–90%. Very low yields (< 1%) of glutaric acid derivatives were obtained. In methanol, the major by-products identified as methyl 6-oxohexanoate (**2c**) and methyl 6,6-dimethoxyhexanoate (**2d**) also arise from the cleavage of the C(O)–CH(OH) bond.

The conversion of the 2-hydroxycyclohexanone dimer to the monomer with accessible hydroxy and carbonyl groups proved to be an important prerequesite for the exclusive scission of this bond. Otherwise, significant amounts of 2-methoxybutanedioate were formed. In fact, the availability of both groups is not necessary for the occurrence of the desired reaction in methanol, as shown in Table 1 (runs 3 and 4). Comparison of the conversion rates (not shown) of 2,2-dimethoxycyclohexanol, a potential intermediate under acidic conditions, and 2-methoxycyclohexanone showed clearly the negative effects of the OH substituent. These results are consistent with a mechanism in which there is substrate pre-coordination to $[VO_2]^+$ species.[2,7]

The use of 'HPA-3' as a catalyst for the aerobic C–C bond cleavage of α-ketols was then applied successfully to a range of representative substrates (Table 2). For all the benzoyl derivatives (**3a–d**), the reactions could be carried out at room temperature with completion of dioxygen uptake within 5 h. Methyl benzoate and/or benzoic acid were formed with 90–100% selectivity. Quantitative yields of other benzoyl derivatives or cyclohexanone are obtained with **3b** or **3d** respectively. In accordance with published results,[2,7] the outcome with 2-hydroxy-2-phenylacetophenone (**3b**, benzoin) was much more sensitive to the nature of the solvent. Significant amounts of 1,2-diphenylethanedione (benzil) were produced in AcOH–H_2O, whereas only carbon–carbon bond cleavage products (benzaldehyde and its dimethyl ketal) and methyl benzoate were formed at room temperature in methanol.

Table 1 Oxidation of 2-hydroxycyclohexanone (**1a**) or its derivatives with dioxygen catalysed by 'HPA-3'[a]

Run	Substrate	Solvent	*t*/h	Conv. (%)[b]	Yield (%)[b]
1	2-Hydroxycyclohexanone	MeOH	10	100	90 (**2a** + **2b**)
2	2-Hydroxycyclohexanone	AcOH–H_2O	3.5	100	80 (**2a**)
3	2,2-Dimethoxycyclohexanol	MeOH	7	100	83 (**2a** + **2b**)
4	2-Methoxycyclohexanone	MeOH	54	67	52 (**2b**)

[a] *Reaction conditions*: substrate (7.7 mmol), 'HPA-3' (0.078 mmol), MeOH (7 ml) or AcOH–H_2O (6.3 : 0.7 ml), dioxygen pressure (0.1 MPa), temperature (65 °C) stirred at 1000 rpm; [b] Conversions (% of substrate consumed) and yields [(mmol of product per mmol substrate) × 100] were determined by GC analysis (OV1701) after the addition of an ethereal solution of diazomethane to the crude mixture using methyl heptanoate as internal standard. Products were identified by GC-MS (RTX5-MS).

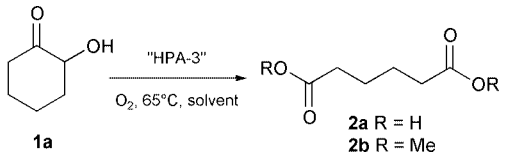

Scheme 1

 DOI: 10.1039/b106969a

Table 2 'HPA-3'-catalysed oxidative cleavage of α-ketols[a]

Run	α-Ketol	Solvent	Conv. (%)[b]	Product(s) [Yield (%)][b]	O_2/Subst. (molar ratio)
5	2-Hydroxyacetophenone[c] (**3a**)	MeOH	100	$PhCO_2Me$ (97)	1.2
6	2-Hydroxyacetophenone[c] (**3a**)	AcOH–H_2O	100	$PhCO_2H$ (100)	1.05
7	2-Hydroxy-2-phenylacetophenone (**3b**)	MeOH	100	$PhCO_2Me$ (110); PhCHO (45); $PhCH(OMe)_2$ (45)	0.77
8	2-Hydroxy-2-phenylacetophenone (**3b**)	AcOH–H_2O	100	$PhCO_2H$ (81); PhCHO (1); PhCOCOPh (47)	0.75
9	2-Hydroxy-2-methylpropiophenone[c] (**3c**)	MeOH	100	$PhCO_2Me$ (97)	0.70
10	2-Hydroxy-2-methylpropiophenone[c] (**3c**)	AcOH–H_2O	100	$PhCO_2H$ (100)	0.50
11	1-Hydroxycyclohexyl phenyl ketone (**3d**)	MeOH	100	$PhCO_2Me$ (100); C_6H_{10}(=O) (100)	0.80
12	1-Hydroxycyclohexyl phenyl ketone (**3d**)	AcOH–H_2O	60	$PhCO_2H$ (54); C_6H_{10}(=O) (60)	0.35

[a] *Reaction conditions*: substrate (7.7 mmol), 'HPA-3' (0.078 mmol), MeOH (7 ml) or AcOH–H_2O (6.3:0.7 ml), dioxygen pressure (0.1 MPa), room temperature. [b] See Table 1. [c] Formaldehyde and acetone or their oxidized derivatives were not determined.

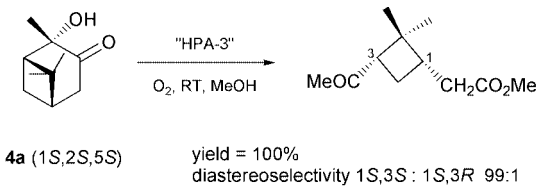

4a (1*S*,2*S*,5*S*) yield = 100%
diastereoselectivity 1*S*,3*S* : 1*S*,3*R* 99:1

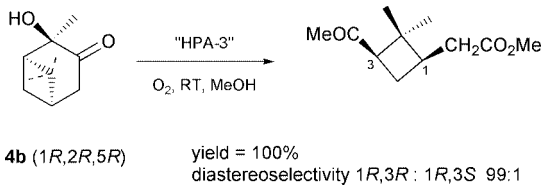

4b (1*R*,2*R*,5*R*) yield = 100%
diastereoselectivity 1*R*,3*R* : 1*R*,3*S* 99:1

Scheme 2

Clean oxidation of **3d** to methyl benzoate or benzoic acid and cyclohexanone was only possible at room temperature; otherwise subsequent cleavage of the cycloalkanone becomes significant.[3] The oxygen consumed–substrate molar ratio was in good agreement with the stoichiometric values (Table 2). The dioxygen uptake for primary α-ketols (**3a**) was roughly twice that for tertiary ones (**3c**,**d**) as expected for pure C–C bond cleavage (runs 6, 10 and 12).

The same experimental procedure was successfully applied to natural compounds. For example, the oxidative cleavage of (1*S*,2*S*,5*S*)-2-hydroxypinan-3-one(**4a**) or its enantiomer (**4b**) led to the diastereoselective formation of methyl esters‡ of the corresponding *cis*-pinonic acids§ with 100% conversion (Scheme 2).

The epimerization of the cyclobutane carbon atom (C3) linked to the acyl group under acidic conditions is well-documented[8] but this competing reaction did not exceed 10% at 65 °C and did not occur at all at room temperature.

Cyclobutane-derived amino-acids and related peptides isolated from natural sources display interesting biological properties, and methyl pinonates are very important chiral cyclobutane synthons. However, stereoselective methodologies based usually on α-pinene oxidation are scant[9] and our approach corresponds to a convenient green alternative.

In conclusion, the present study has proved that the aerobic oxidative cleavage of α-hydroxy ketones (or α-hydroxy ketals) catalysed by 'HPA-3' could replace stoichiometric polluting reagents either for large-scale products or for fine chemicals synthesis. We are currently investigating the mechanism as well as the supported counterpart of these catalysts.

Financial support by the Comité franco-marocain (AI 217/SM/00) is gratefully acknowledged.

Notes and references

† The heteropolyacids 'HPA-3' were prepared according to described procedures.[10] Their elemental analysis gave P, 1.7, Mo, 45.5, V, 7.75% which is consistent with the formula '$H_6[PV_3Mo_9O_{40}]\cdot 11H_2O$'. Solid HPA-*n* and their aqueous solutions are multi-component systems: they contain several polyanions, positional isomers of these, $[VO_2]^+$ and often traces of V(IV).

‡ Methyl esters obtained from the oxidation of (1*S*,2*S*,5*S*) or (1*R*,2*R*,5*R*)-2-hydroxypinan-3-one were characterized by their $[MNH_4]^+$ and $[MH]^+$ signals at 216 and 199 Da, respectively, using GC-MS/CI$^+$ (NH_3). Complete retention of configuration of both asymmetric carbon atoms in the 1*S*,3*S* and 1*R*,3*R* compounds was established by NOE ^{1}H NMR studies. Specific rotations of the diastereoisomeric mixtures isolated from the oxidation of (1*S*,2*S*,5*S*)-2-hydroxypinan-3-one at 65 °C or its enantiomer (1*R*,2*R*,5*R*) at RT were +65.1 deg cm^2 g^{-1}(*c* 2.17, $CHCl_3$) and −81.4 10^{-1} deg cm^2 g^{-1}(*c* 5.03, $CHCl_3$), respectively, in accordance with data for the pure compounds.[11]

§ The IUPAC name for pinonic acid is 3-acetyl-2,2-dimethylcyclobutaneacetic acid.

1 I. V. Kozhevnikov, *Chem. Rev.*, 1998, **98**, 171; M. Misono, *Chem. Commun.*, 2001, 1141.
2 J.-M. Brégeault, B. El Ali, J. Mercier, J. Martin and C. Martin, *C. R. Acad. Sci., Ser. II*, 1988, **307**, 2011; B. El Ali, J.-M. Brégeault, J. Mercier, J. Martin, C. Martin and O. Convert, *J. Chem. Soc., Chem. Commun.*, 1989, 825; J.-M. Brégeault, F. Launay and A. Atlamsani, *C. R. Acad. Sci., Ser. IIc*, 2001, **4**, 11; J.-M. Brégeault, B. El Ali, J. Mercier, J. Martin, C. Martin and O. Mohammedi, in *New Developments in Selective Oxidation*, eds. G. Centi and F. Trifiro, Elsevier Science Publishers, Amsterdam, 1990, p. 205.
3 A. Atlamsani, J.-M. Brégeault and M. Ziyad, *J. Org. Chem.*, 1993, **58**, 5663.
4 M. Golinski, S. Vasudevan, R. Floresca, C. P. Brock and D. S. Watt, *Tetrahedron Lett.*, 1993, **34**, 55; R. Floresca, M. Kurihara, D. S. Watt and A. Demir, *J. Org. Chem.*, 1993, **58**, 2196.
5 M. J. Di Grandi, C. A. Coburn, R. C. A. Isaacs and S. J. Danishefsky, *J. Org. Chem.*, 1993, **58**, 7728; P. W. Clutterbuck and F. Reuter, *J. Chem. Soc.*, 1935, 1467; J. Wrobel, A. Dietrich, B. Gorham and K. Sestanj, *J. Org. Chem.*, 1990, **55**, 2694; S. O. Nwaukwa and P. M. Keehn, *Tetrahedron Lett.*, 1982, **31**, 3135.
6 C. Coin, V. Le Boisselier, I. Favier, M. Postel and E. Dunach, *Eur. J. Org. Chem.*, 2001, 735; M. Kirihara, S. Takizawa and K. Momose, *J. Chem. Soc., Perkin Trans. 1*, 1998, 7.
7 B. El Ali, A. M. El-Ghanam and M. Fettouhi, *J. Mol. Catal. A*, 2001, **165**, 283.
8 M. Petrini, R. Ballini, E. Marcantoni and G. Rosini, *Synth. Commun.*, 1988, **18**, 847.
9 A. G. Moglioni, E. Garcia-Exposito, G. P. Aguado, T. Parella, V. Branchadell, G. Y. Moltrasio and R. M. Ortuno, *J. Org. Chem.*, 2000, **65**, 3934.
10 A. Atlamsani, M. Ziyad and J.-M. Brégeault, *J. Chim. Phys. Phys.-Chim. Biol.*, 1995, **92**, 1344.
11 M. Karpf and C. Djerassi, *J. Am. Chem. Soc.*, 1981, **103**, 302; K. Weinges, S. Schmidbauer and H. Schick, *Chem. Ber.*, 1994, **127**, 1305; O. J. Muscio and C. D. Poulter, *J. Org. Chem.*, 1974, **39**, 3288.

CHEMCOMM Communication
www.rsc.org/chemcomm

Four- and two-electron rules for diatropic and paratropic ring currents in monocyclic π systems

Erich Steiner and Patrick W. Fowler

School of Chemistry, University of Exeter, Stocker Road, Exeter, UK EX4 4QD. E-mail: P.W.Fowler@exeter.ac.uk; E.Steiner@exeter.ac.uk; Fax: +44 1392 263434

Received (in Cambridge, UK) 10th June 2001, Accepted 10th September 2001
First published as an Advance Article on the web 4th October 2001

The π ring current in an even-electron monocycle is dominated by the HOMO–LUMO transition, and hence corresponds to circulation of four electrons in a diatropic (4*n* + 2)-electron, but two in a paratropic (4*n*)-electron cycle.

Ring currents are, according to one widely accepted approach, the defining feature of aromatic systems.[1,2] Calculation of magnetic properties in finite basis sets is bedevilled by the problem of spurious gauge dependence. Distributed-gauge methods offer an alternative to brute-force saturation of the basis, and the particular approach known by the acronym CTOCD-DZ (continuous transformation of origin of current density - diamagnetic zero[3]) has practical and conceptual advantages. In CTOCD-DZ, when calculating the induced current density at a given point, the point itself is taken as the origin of vector potential. Current maps derived with this 'ipsocentric' choice of origin are physically realistic,[4] and can be expressed as sums of the simplest possible orbital contributions.[5] This last property is used here to deduce a simple rule for ring currents in π monocycles.

It will be shown that in Hückel theory: (i) the *diatropic* (*i.e.* diamagnetic) ring current in *aromatic* (4*n* + 2)-electron systems can be attributed to *four* electrons, those in the doubly degenerate HOMO; whereas (ii) the *paratropic* (*i.e.* paramagnetic) ring current in *anti-aromatic* 4*n*-electron systems with bond alternation can be attributed to circulation of the *two* electrons of the non-degenerate HOMO. The proof rests on a specific decomposition[3] of the current density, derived in detail in Ref. 5. Within an ipsocentric formulation, the traditional division of current density into ground-state diamagnetic and excited-state paramagnetic terms is replaced by two excited-state sums, each containing only transitions from occupied to empty orbitals.[5] In an independent-electron model, the first-order change to an occupied orbital ψ_n of an *N*-electron system in an external magnetic field $\boldsymbol{B}$ can be expressed in terms of unoccupied orbitals ψ_p and their energies ε_p as (in atomic units):where $\boldsymbol{l}$ and $\boldsymbol{p}$ are angular and linear momenta, and $\boldsymbol{d}$ is a displacement which is set equal to the position of the electron in the expression for the current density. In this partitioning, the conventional paramagnetic current arises from $\psi_n^{(\mathrm{p})}$, its size depending on accessibility of states *via* rotational transitions, and the diamagnetic current from $\psi_n^{(\mathrm{d})}$, depending on translational transitions.

$$\psi_n^{(1)} = \psi_n^{(\mathrm{p})} + \psi_n^{(\mathrm{d})} = -\frac{1}{2}\sum_{p>N/2}\psi_p \frac{<\psi_p \mid \boldsymbol{l} \mid \psi_n>}{\varepsilon_p - \varepsilon_n} \bullet \boldsymbol{B}$$

$$+\frac{1}{2}\,\boldsymbol{d} \times \sum_{p>N/2}\psi_p \frac{<\psi_p \mid \boldsymbol{p} \mid \psi_n>}{\varepsilon_p - \varepsilon_n} \bullet \boldsymbol{B}$$

For the response of planar conjugated π systems to a perpendicular magnetic field, the relevant operators are for rotation about the field direction, $R_{||}$, and the two translations within the molecular plane, $T_{\perp}$. Orbital contributions to the current density obey a symmetry-based selection rule. An occupied-to-unoccupied transition $\psi_n \rightarrow \psi_p$ gives a *paramagnetic* contribution if the product of symmetries contains a match to $R_{||}$, and a *diamagnetic* ring current contribution if it contains a match to a translation $T_{\perp}$. A transition may be translationally and or rotationally active, or neither.

Using the Hückel approximations for a ring of *N* atoms with equal coulomb parameter α connected by bonds of equal resonance parameter β, the π molecular orbitals and their energies are given by the Frost–Musulin[6] construction, where energies correspond to the vertices of an *N*-gon inscribed point-down in a circle of radius 2β, and the orbitals are sine and cosine combinations associated with an angular momentum quantum number $k = 0, 1, \ldots (N/2)$ (*N* even), $(N-1)/2$ (*N* odd). Closed-shell configurations occur at the aromatic counts of 2, 6, 10 … π-electrons, and, in the same approximation, open shells with two electrons in two degenerate orbitals at anti-aromatic counts 4, 8 … With this characterisation in terms of angular momentum, the ring-current selection rules take on an especially simple form, independent of *N* and details of the point group.

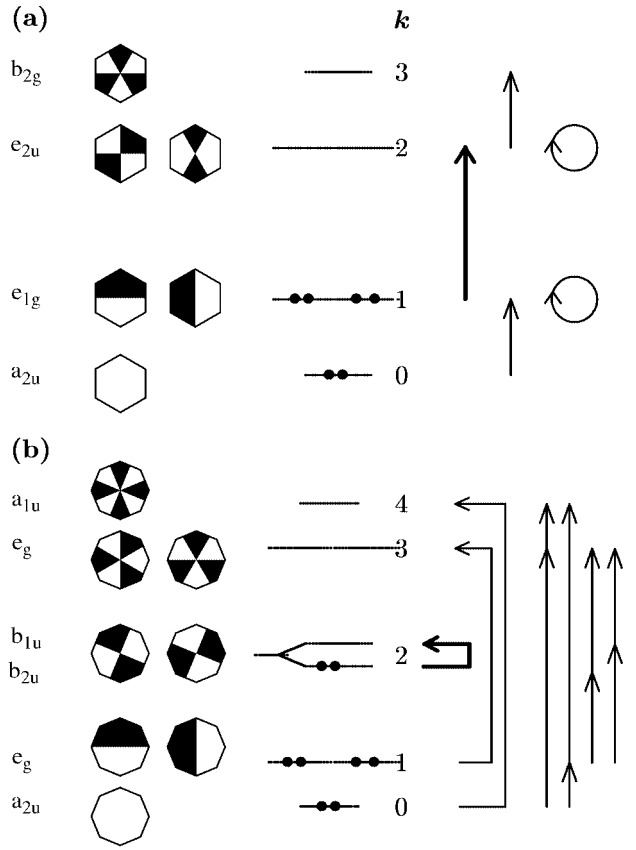

Fig. 1 Orbital energy scheme for (a) benzene (D_{6h}) and (b) planar cyclooctatetraene (D_{4h}), showing symmetries, nodal characteristics, occupancies and *k* values. Symmetry-allowed transitions are indicated by straight (translational) and bent (rotational) arrows, with the dominant HOMO–LUMO transition, responsible for the diatropic and paratropic π ring currents observed in *ab initio* calculations (*cf.* Fig. 2), highlighted.

 DOI: 10.1039/b104847n

To deduce (i), note that, in a closed-shell configuration, either all orbitals with given k are occupied, or all are empty. As $R_{||}$ mixes only orbitals of equal k, it cannot produce occupied-to-virtual transitions, and gives no paramagnetic contribution from any orbital. On the other hand, $T_{\perp}$ operators mix orbitals that differ by ±1 in k, *i.e.* on adjacent rungs of the energy ladder (Fig. 1a). The sole occupied-to-virtual translational transitions in the system are therefore those from HOMO to LUMO. Hence in a $(4n + 2)$-electron monocycle, the ring current is wholly diamagnetic and attributable to the mobility of the HOMO electrons. In all but two trivial cases, the HOMO is doubly degenerate and the system has 4-electron diamagnetism. The exceptions are $C_NH_N^{(N-2)+}$, with 2-electron diamagnetism, and $C_NH_N^{N-}$ anions which have full π systems and hence, in the Hückel model, no available transitions (in practice, their diamagnetism arises from orbitals above the Hückel manifold). In a $(4n + 2)$ system that supports bond alternation, such as $C_{10}H_{10}$ constrained to the plane, the lowering of symmetry to $D_{(2n+1)h}$ allows further mixings, as pairs of levels with mirror-image energies $\alpha \pm \lambda\beta$ become equi-symmetric. The relaxation of symmetry allows new rotational transitions between these pairs and translational transitions between levels differing by 3 in parent k value, but for modest degrees of alternation their contributions remain low because of substantial cancellation in the numerator, and any ring current remains diamagnetic and HOMO–LUMO dominated as in (i).

Statement (ii) is deduced by considering the half-filling of the π system for $N = 4n$. In full D_{Nh} symmetry, there are two non-bonding orbitals and hence an open-shell configuration. The system will distort to lift this degeneracy, as for example by adopting a structure in which alternate bonds have resonance parameters $\beta \pm \delta$. In the reduced $D_{(N/2)h}$ symmetry the HOMO/LUMO pair splits into two non-degenerate components, related by a rotational transition with a small energy denominator and large numerator in the sum over states (since $R_{||}$ transforms HOMO to LUMO (Fig. 1b), thereby producing a strong 2-electron paramagnetic π ring current. The additional transitions introduced by bond alternation are again reduced in importance by poor overlap and large energy gaps. In systems other than neutral half-filled π shells, the geometric distortion that lifts the degeneracy may be different, but it will still split a rotationally connected pair across a small energy gap, and give rise to a dominant 2-electron paramagnetic current contribution. Hence statement (ii) also holds for these other configurations.

The *ab initio* π current density maps† computed for the optimum geometries of the 6-electron systems $C_5H_5^-$, C_6H_6, $C_7H_7^+$, and the planar stationary points on the potential surfaces of $C_{10}H_{10}$ and anti-aromatic C_8H_8 (Fig. 2) all closely match the predictions made here on the basis of Huckel arguments. The isolated C_8H_8 ring is in fact non-planar at equilibrium,[8] but when restricted to the plane or clamped by electronically innocent functional groups[9] it shows exactly the paratropicity described here.[10] Likewise, $C_{10}H_{10}$ has a nonplanar equilibrium geometry but can be forced into planarity.[11] In all cases, the HOMO contribution to the map is almost indistinguishable from the total π current. The present rules, exact within the context of planar equilateral Hückel monocycles, serve in more sophisticated treatments to rationalise the magnitude and sense of computed currents and other magnetic measures of aromaticity, such as the widely used NICS criterion,[2] and give a key to interpretation of a much wider range of systems, where it can also be expected that π ring currents will be dominated by a small number of electrons close to the HOMO–LUMO frontier.[5]

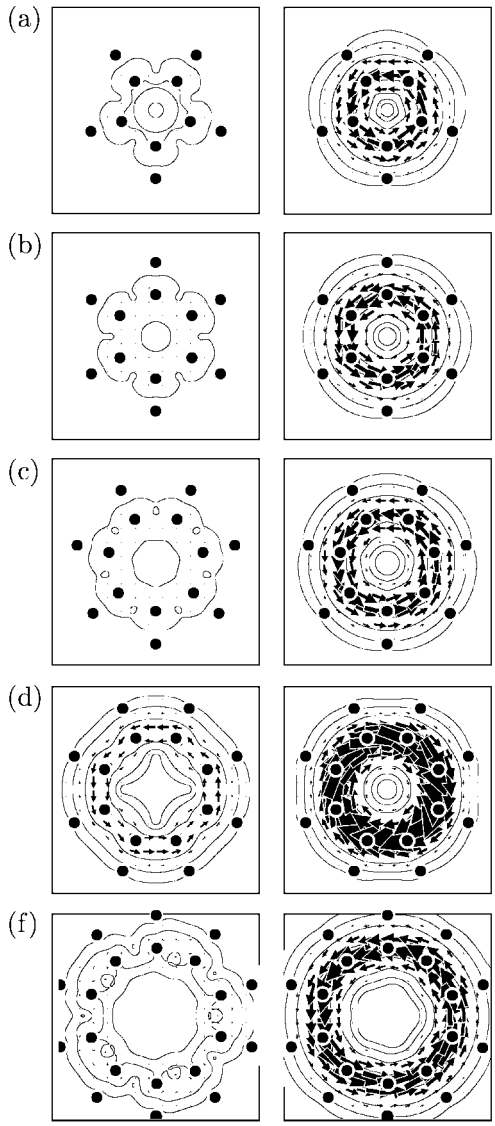

Fig. 2 Computed π ring current maps† for (a) $C_5H_5^-$, (b) C_6H_6, (c) $C_7H_7^+$, (d) planar C_8H_8, (e) planar $C_{10}H_{10}$. Left: contribution of all but the HOMO π electrons. Right: contribution of the HOMO electrons.

Notes and references

† Maps were computed at 6-31G** level using SYSMO[7] as in Ref. 4.

1 P. v. R. Schleyer and H. Jiao, *Pure Appl. Chem.*, 1996, **68**, 209.
2 P. v. R. Schleyer, C. Maerker, A. Dransfeld, H. Jiao and N. J. R. van Eikema Hommes, *J. Am. Chem. Soc.*, 1996, **118**, 6317.
3 T. A. Keith and R. F. W. Bader, *Chem. Phys. Lett.*, 1993, **210**, 223; S. Coriani, P. Lazzeretti, M. Malagoli and R. Zanasi, *Theor. Chim. Acta*, 1994, **89**, 181.
4 E. Steiner, P. W. Fowler and L. W. Jenneskens, *Angew. Chem., Int. Ed.*, 2001, **40**, 362 and references therein.
5 E. Steiner and P. W. Fowler, *J. Phys. Chem.*, 2001, in the press.
6 A. A. Frost and B. J. Musulin, *J. Chem. Phys.*, 1953, **21**, 572.
7 P. Lazzeretti and R. Zanasi, *SYSMO Package*, University of Modena, Italy, 1980. Mapping routines written in Exeter.
8 J. March, *Advanced Organic Chemistry*, John Wiley and Sons, New York, 1986.
9 A. Matsuura and K. Komatsu, *J. Am. Chem. Soc.*, 2001, **123**, 1768.
10 P. W. Fowler, R. W. A. Havenith, L. W. Jenneskens, A. Soncini and E. Steiner, to be published.
11 P. v. R. Schleyer, H. Jiao, H. M. Sulzbach and H. F. Schaefer III, *J. Am. Chem.. Soc.*, 1995, **118**, 2093 and references therein.

CHEMCOMM Communication
www.rsc.org/chemcomm

Catalytic asymmetric Henry reactions—a simple approach to optically active β-nitro α-hydroxy esters†

Christina Christensen, Karsten Juhl and Karl Anker Jørgensen*

Center for Metal Catalysed Reactions, Department of Chemistry, Aarhus University, DK-8000 Aarhus C, Denmark. E-mail: kaj@chem.au.dk

Received (in Cambridge, UK) 4th July 2001, Accepted 19th September 2001
First published as an Advance Article on the web 18th October 2001

The development and potential of a catalytic enantioselective Henry reaction of nitromethane with various α-keto esters catalyzed by chiral bisoxazoline–copper(II) complexes are presented.

The reaction between a carbonyl and a nitro compound, known as the Henry[1] or nitroaldol reaction, constitutes a fundamental carbon–carbon bond forming reaction in organic chemistry which has been applied for the construction of numerous natural products and other useful compounds.[2]

The catalytic asymmetric version of the Henry reaction has been successfully carried out in only a very few cases; Shibasaki *et al*. have in a series of papers shown that rare-earth–lithium–BINOL complexes can be applied as catalysts for the enantioselective reaction of aldehydes with nitroalkanes.[3,4]

This paper presents a new catalytic asymmetric Henry reaction of α-keto esters **1** with nitromethane **2** in the presence of easy-available chiral catalysts [eqn. (1)]. The present reaction is an important new development of the Henry reaction as it demonstrates (*i*) for the first time that ketones react in a catalytic highly enantioselective fashion, (*ii*) the products formed contain a chiral quaternary carbon center, the formation of which is a particularly demanding task in organic synthesis,[5] and (*iii*) highly attractive functionalized optically active β-nitro α-hydroxy esters **3** are formed.

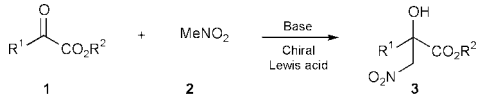

1 2 3

a: R^1 = Me, R^2 = Et
b: R^1 = Et, R^2 = Et
c: R^1 = Et, R^2 = Bn
d: R^1 = $PhCH_2CH_2$, R^2 = Et
e: R^1 = Ph, R^2 = Et
f: R^1 = p-$NO_2C_6H_4$, R^2 = Et

(1)

Different chiral ligands, Lewis acids and bases have been tested as catalyst for the enantioselective Henry reaction of ethyl pyruvate **1a** with nitromethane **2**. The most promising results were found when the chiral bisoxazoline ligands[6] (*S*)-*t*-Bu-BOX **4a**, (*R*)-Ph-BOX **4b** and (4*R*,5*S*)-DiPh-BOX **4c**, were used in combination with copper(II) as the Lewis acid.[7] Table 1 presents some representative results from the screening.

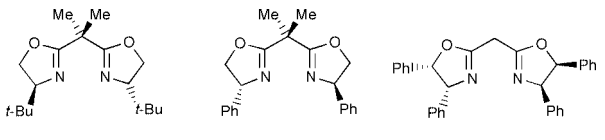

(*S*)-*t*-Bu-BOX **4a** (*R*)-Ph-BOX **4b** (4*R*,5*S*)-DiPh-BOX **4c**

Of the three chiral bisoxazoline–copper(II) catalysts presented for the reaction, the combination of (*S*)-*t*-Bu-BOX **4a** as ligand and $Cu(OTf)_2$ as the Lewis acid gave the most promising results with >95% conversion and 92% ee of the Henry adduct **3a** (entry 1) at rt, compared to >95% conversion and 14% ee for (*R*)-Ph-BOX–$Cu(OTf)_2$ and 11% conversion and 18% ee for (4*R*,5*S*)-DiPh-BOX–$Cu(OTf)_2$ (entries 2, 3). Reduction of the catalyst loading from 20 mol% to 10 mol% does not change the conversion and enantioselectivity of the reaction significantly when using (*S*)-*t*-Bu-BOX–$Cu(OTf)_2$ as the catalyst (entry 4). The conversion and enantioselectivity of the reaction of **1a** with **2** is also dependent on the amount of base relative to the catalyst. A reduction of the amount of Et_3N to 10 mol%, or an increase to 40 mol%, relative to the catalyst (20 mol%) gave a significant reduction in conversion and enantioselectivity for the first combination, and a high conversion and a racemic product **3a** for the latter combination (entries 5, 6). In the presence of NEt_3 and no chiral Lewis acid the reaction proceeds with full conversion (entry 7). The reaction also proceeds well in the presence of (*S*)-*t*-Bu-BOX–$Cu(SbF_6)_2$ as the catalyst: >95% conversion is found and **3a** is obtained with 81% ee (entry 8). Changing the Lewis acid from copper(II) to zinc(II) [(*S*)-*t*-Bu-BOX–$Zn(OTf)_2$] leads to a reaction with only 16% ee of the other enantiomer (entry 9).

Table 1 Some representative results from the screening of reaction conditions for the catalytic enantioselective Henry reaction of ethyl pyruvate **1a** with nitromethane **2** in the presence of Et_3N as the base at room temperature

Entry	Catalyst	Catalyst loading (%)	Base (%)	Conversion (%)[a]	Ee of **3a** (%)[b]
1	(*S*)-*t*-Bu-BOX–$Cu(OTf)_2$	20	20	>95	92
2	(*R*)-Ph-BOX–$Cu(OTf)_2$	20	20	>95	14
3	(4*R*,5*S*)-DiPh-BOX–$Cu(OTf)_2$	20	20	11	18
4	(*S*)-*t*-Bu-BOX–$Cu(OTf)_2$	10	10	84	81
5	(*S*)-*t*-Bu-BOX–$Cu(OTf)_2$	20	10	11	49
6	(*S*)-*t*-Bu-BOX–$Cu(OTf)_2$	20	40	>95	<5
7	—	—	20	>95	—
8	(*S*)-*t*-Bu-BOX–Cu(SbF6)$_2$	20	20	>95	81
9	(*S*)-*t*-Bu-BOX–$Zn(OTf)_2$	20	20	87	−16

[a] Determined by 1H-NMR spectroscopy. [b] Determined by chiral GC using a Chromopack CP-Chiracil (β-PM) column.

The reaction of **1a** with **2** catalyzed by (*S*)-*t*-Bu-BOX–$Cu(OTf)_2$ is base dependent. The results for some representative bases are: Hünigs base 31% conversion, 69% ee; dimethylaniline 14% conversion, 9% ee; *N*-methylmorpholine 65% conversion, 83% ee; Bn_3N 10% conversion, 14% ee, compared to >95% conversion and 92% ee applying Et_3N. It should also be noted that lowering the reaction temperature did not improve the enantioselectivity (at 0 °C: full conversion, 89% ee).

The potential of the reaction is demonstrated for the reaction of the α-keto esters **1a–f** with **2** catalyzed by (*S*)-*t*-Bu–BOX–$Cu(OTf)_2$ as shown in Table 2.‡

Ethyl pyruvate **1a** reacts with nitromethane **2** to give 2-hydroxy-2-methyl-3-nitropropanoic acid ethyl ester **3a** in 95% yield and with 92% ee (Table 2, entry 1). The corresponding ethyl analogue **1b** reacts in a similar way to give the Henry

† Electronic supplementary information (ESI) available: spectroscopic and analytical data. See http://www.rsc.org/suppdata/cc/b1/b105929g/

 DOI: 10.1039/b105929g

Table 2 Catalytic enantioselective addition of nitromethane to various α-keto esters catalyzed by (*S*)-*t*-Bu-BOX–$Cu(OTf)_2$ in the presence of Et_3N as the base

Entry	α-Keto ester	Yield (%)[a]	Ee (%)[b]
1[c]	**1a**	95	92
2[c]	**1b**	46	90
3[d]	**1b**	73	87
4[d]	**1c**	69	87
5[d]	**1d**	47	77
6[c]	**1e**	81	86
7[c]	**1f**	99	93

[a] Isolated yield. [b] Determined by chiral GC or HPLC. [c] Reaction performed at rt. [d] Reaction performed at 50 °C.

adduct **3b** in 46% yield and 90% ee at rt (entry 2). The yield of the Henry adduct is increased to 73% without significant loss in enantioselectivity by heating the reaction mixture to 50 °C (entry 3). In the same manner, the corresponding benzyl ester **1c** gives 69% yield of **3c** with 87% ee (entry 4). The α-keto ester **1d** reacts with **2** giving a moderate yield and enantioselectivty (entry 5) compared to the other reactions presented. The aromatic α-keto esters **1e**,**f** react with **2** in the presence of (*S*)-*t*-Bu-BOX–$Cu(OTf)_2$ as the catalyst to give the optically active Henry adducts in excellent yield and enantioselectivity as 81% and 86% ee of **3e**, and 99% yield and 93% ee of **3f**, respectively, are obtained (entries 6,7).

This new catalytic enantioselective Henry reaction leads to a simple synthetic approach to attractive functionalized optically active β-nitro α-hydroxy esters,[2] while reduction of the nitro functionality gives the corresponding optically active β-amino α-hydroxy esters which are highly attractive compounds in organic chemistry,[8] *e.g.* the side chain in taxol.

In summary, the first catalytic enantioselective addition reaction of α-keto esters with nitromethane has been developed. This approach shows for the first time that ketones undergo catalytic highly enantioselective Henry reactions giving attractive optically active β-nitro α-hydroxy esters having a chiral quaternary carbon center. Further work is in progress to develop, understand and apply this new type of catalytic enantioselective Henry reaction.

We are indebted to The Danish National Research Foundation for financial support.

Notes and references

‡ *Representative experimental procedure*. To a flame dried Schlenk tube $Cu(OTf)_2$ (36.2 mg, 0.100 mmol) and 2,2′-isopropylidenebis[(4*S*)-4-*tert*-butyl-2-oxazoline] (30.9 mg, 0.105 mmol) were added. The mixture was stirred under vacuum for 2 h and filled with N_2. Dry freshly distilled $MeNO_2$ (2 ml) was added and the solution was stirred for 1 h. Ethyl pyruvate **1a** (56 μl, 0.50 mmol) was added followed by the addition of Et_3N (14 μl, 0.1 mmol) and reacted for 16 h under N_2 at rt. The reaction mixture was filtered through a plug of silica with Et_2O. The solvent was removed *in vacuo* and the residue was purified by FC (silica: 10% Et_2O in CH_2Cl_2) to yield 2-hydroxy-2-methyl-3-nitropropanoic acid ethyl ester **3a** as a pale yellow oil (84 mg, 0.475 mmol, 95%) with 92% ee detected by chiral GC using a Chromopack CP-Chiracil (β-PM) column, $\tau_{(minor)}$ = 23.4 min, $\tau_{(major)}$ = 24.1 min, $[\alpha]_D^{23}$ = +10.2° (*c* = 1.19 g per 100 ml in CH_2Cl_2). ^1H NMR (400 MHz, $CDCl_3$) δ 4.83 (d, *J* = 14 Hz, 1H), 4.55 (d, *J* = 14 Hz, 1H), 4.34 (m, 2H), 3.71 (s, 1H), 1.45 (s, 3H), 1.33 (t, *J* = 7.2 Hz, 3H); ^{13}C NMR (100 MHz, $CDCl_3$) δ 173.4, 80.9, 72.3, 62.9, 23.7, 13.8; HRMS $[M + Na]^+$ calcd: $C_6H_{11}NO_5$, 200.0535; found: 200.0282.

1 L. C. Henry, *R. Hebd. Seances Acad. Sci.*, 1895, **120**, 1265.

2 See *e.g.*: D. Seebach, E. W. Lehr and T. Weller, *Chemia*, 1973, **33**, 1; G. Rosini, *Comprehensive Organic Synthesis*, ed. B. M. Trost and C. H. Heathcook, Pergamon Press, Oxford, 1991, Vol. 2, p. 321; M. Shibasaki and H. Gröger in *Comprehensive Asymmetric Catalysis I-III*, ed. E. N. Jacobsen, A. Pfaltz and H. Yamamoto, Springer-Verlag, Berlin–Heidelberg, 1999, Chapter 29.3; F. A. Luzzio, *Tetrahedron*, 2001, **57**, 915.

3 See *e.g.*: H. Sasai, T. Suzuki, S. Arai, T. Arai and M. Shibasaki, *J. Am. Chem. Soc.*, 1992, **114**, 4418; H. Sasai, T. Suzuki, N. Itoh and M. Shibasaki, *Tetrahedron Lett.*, 1993, **34**, 851; H. Sasai, T. Tokunaga, S. Watanabe, T. Suzuki, N. Itoh and M. Shibasaki, *J. Org. Chem.*, 1995, **60**, 7388; K. Iseki, S. Oishi, H. Sasai and M. Shibasaki, *Tetrahedron Lett.*, 1996, **37**, 9081; T. Arai, Y. M. A. Yamada, N. Yamamoto, H. Sasai and M. Shibasaki, *Chem. Eur. J.*, 1996, **2**, 1368.

4 See also: R. Chinchialla, C. Nájera and P. Sánches-Agulló, *Tetrahedron: Asymmetry*, 1994, **5**, 1393; A. P. Davis and K. J. Dempsey, *Tetrahedron: Asymmetry*, 1995, **6**, 2829.

5 For a review about the catalytic formation of molecules with quaternary carbon centers: E. J. Corey and A. Guzman-Perez, *Angew. Chem., Int. Ed.*, 1998, **37**, 388.

6 For recent reviews see: J. S. Johnson and D. A. Evans, *Acc. Chem. Res.*, 2000, **33**, 325; K. A. Jørgensen, M. Johannsen, S. Yao, H. Audrain and J. Thorhauge, *Acc. Chem. Res.*, 1999, **32**, 605; A. K. Ghosh, P. Mathivanan and L. Cappiello, *Tetrahedron: Asymmetry*, 1998, **9**, 1.

7 The chiral bisoxazoline–copper(II) complexes can also catalyze the highly enantioselective addition of nitro compounds to imines: N. Nishiwaki, K. R. Knudsen, K. V. Gothelf and K. A. Jørgensen, *Angew. Chem., Int. Ed.*, 2001, **40**, 2992.

8 C. Cativiela, M. D. Diez-de-Villegas and J. A. Gálvez, *Tetrahedron: Asymmetry*, 1996, **7**, 529 and references therein.

CHEMCOMM Communication
www.rsc.org/chemcomm

Unexpected solute aggregation in water on dilution

Shashadhar Samal and Kurt E. Geckeler*

Laboratory of Applied Macromolecular Chemistry, Department of Materials Science and Engineering, Kwangju Institute of Science and Technology, 1 Oryong-dong, Buk-gu, Kwangju 500-712, South Korea. E-mail: keg@kjist.ac.kr

Received (in Cambridge, UK) 20th June 2001, Accepted 7th September 2001
First published as an Advance Article on the web 15th October 2001

Studies on cluster–cluster aggregation phenomena in aqueous solutions of fullerene–cyclodextrin conjugates, β-cyclodextrin, sodium chloride, sodium guanosine monophosphate, and a DNA oligonucleotide revealed that there are larger aggregates existent in dilute aqueous solutions than in more concentrated solutions.

There has been recent interest in cluster studies in a variety of compounds in solutions including those of functionalized fullerenes in water. C_{60} functionalized with hydrophilic groups and C_{60} inclusion complexes with γ-cyclodextrin in aqueous solution are known to form clusters and aggregates.[1,2] Molecular dynamics simulations[3] followed by experiments[4] proved the existence of submicrometer-sized clusters in electrolyte solutions. Cluster studies on polyelectrolytes,[5] amphiphilic heteropolymers,[6] and other polymers[7] have been reported. While studying the particle size of water-soluble fullerene–cyclodextrin conjugates by using laser light scattering (LLS) and scanning electron microscopic (SEM) measurements, we observed that the cluster size increased steadily with decreasing concentration of the fullerene compound, in contrast to pristine fullerenes in organic solvents.[8] Interestingly, aqueous solutions of unmodified β-cyclodextrin (CD) showed a similar behavior on dilution. Then we measured the cluster size of sodium chloride, guanosine monophosphate disodium salt (GMP), and a DNA oligonucleotide in water at different concentrations. Surprisingly, we found an inverse relationship between the aggregate size and concentration confirmed for all these solutes. This finding could be of general importance with profound implications on the universal understanding of diverse phenomena involving dilution and dilute solutions.

Recently we reported a new class of water-soluble fullerene–cyclodextrins.[9] Aqueous solutions of these fullerene derivatives have characteristic UV-Vis spectra with a broad peak in the visible region starting from ~400 nm, which was attributed to aggregation of fullerenes in water, as reported for other water-soluble fullerene derivatives.[10] While exploring further the aggregation phenomena in aqueous solutions of fullerene–cyclodextrin conjugates by LLS measurements, we observed clusters, as expected. When the particle size of these clusters was measured† in solution by LLS, after each successive dilution a steady increase in size was noticed. The results for one of the fullerene derivatives, the mono-6-aza-6-deoxy-β-cyclodextrin–[60]fullerene (C_{60} covalently bonded to β-cyclodextrin *via* a bridging nitrogen atom, CDAzF) are presented in Fig. 1. The average particle size (Z_{av} values) increased from 0.55 to 3.255 μm with decreasing concentration of the solution from 0.216 to 0.01 mM, respectively. At the highest concentration of 0.216 mM, the polydispersity was 0.086, which increased to 0.425 when the solution was diluted to 0.043 mM. For all other concentrations, the polydispersity was 1.000. The cause of this unexpected growth of the cluster size on dilution was quite intriguing, and we decided to look into it further.

The LLS studies were conducted for CD solutions of concentrations 14.27 to 0.3524 mM, prepared by dissolving appropriate quantities of the CD solid in water. Interestingly, clusters were found for each solution, their size increasing from 0.393 to 3.12 μm with decreasing solute concentration. Two of these solutions of initial concentrations 14.2 and 7.2 mM were diluted successively with water and the particle size at each dilution measured. For both the solutions the average particle size increased, from 0.393 to 0.915 μm and 0.518 to 1.285 μm, respectively. It could also be seen that the concentration *vs.* particle size curves did not merge into one line and the extent of particle size increase was higher for CD solutions of lower starting concentration than for solutions of higher initial concentration, indicating that the solution history is an important factor in the growth dynamics of the aggregates. Thus, in the aggregation process of the cyclodextrin-appended fullerene derivative, in addition to fullerenes, the macrocyclic ring also plays a vital role.

To determine if this is a phenomenon quite specific for these typical water-soluble fullerene derivatives and cyclodextrins, or a more broad-based one, the effect of dilution on the particle size of some other water-soluble compounds such as NaCl, GMP, and a DNA oligonucleotide was studied. The reason for the above choice of molecules emerged from recent experimental reports of clusters in aqueous medium of a variety of compound classes.[4]

The Z_{av} data at different concentrations for NaCl and DNA are given in Fig. 2. The concentrated aqueous solution of 5.5 M NaCl was diluted with water in successive steps to 0.785 M. The aggregate size was seen to rise from 1.491 to 4.95 μm. The dilution of a 0.2 M GMP solution in water showed a similar rise of aggregate size from 0.193 to 3.506 μm. For aqueous solutions of a DNA oligonucleotide (M_n 9.745, M_w 13.205 kg mol^{-1}; polydispersity 1.335) with an initial concentration of 2.5 g dL^{-1} the average particle size increased from 0.196 to 0.512 μm on dilution. The size did not increase significantly until a concentration of about 0.45 g dL^{-1}, beyond which further dilution led to a rapid growth of the aggregates.

Though the clusters were detected in solution, it would be more conclusive to have visual evidence. Therefore we examined the SEM scans (JEOL, JSM-5800) of Au-coated CD films cast from diluted solutions. However, no spherical particles could be identified. This was expected, as drying of the solutions would result in CD molecules settling down to their

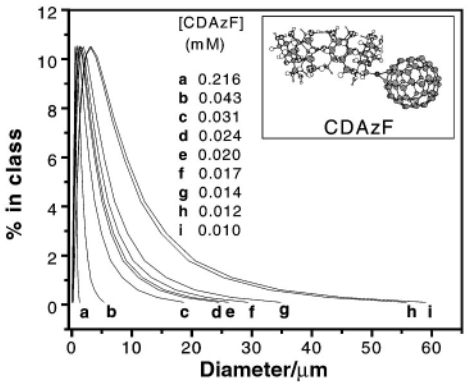

Fig. 1 Dynamic light scattering monomodal distribution plot showing increasing particle size with decreasing mono-6-aza-6-deoxy-β-cyclodextrin–[60]fullerene (CDAzF) concentration.

 DOI: 10.1039/b105399j

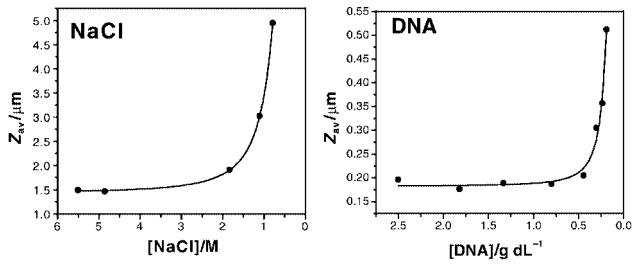

Fig. 2 Increasing Z_{av} values with decreasing concentration for different compound classes.

well identified crystal lattice. We made a comparison of the X-ray powder diffraction patterns of CD, C_{60}, and CDAzF. While both C_{60} and CD had a large number of reflections of strong intensity, the macrofullerene CDAzF was identified as highly amorphous with practically no peaks. Therefore, it was possible that its solutions cast as films might show the clusters. Solutions of the compound CDAzF at the same concentrations as for the LLS studies were cast on clean glass substrates and dried at 60 °C for 12 h under vacuum. The SEM scans clearly showed the clusters and their aggregates (Fig. 3). In the concentrated solution (0.216 mM), the shapes of the particles were irregular. However, on dilution, spherical clusters appeared, which were seen to aggregate in steps resulting in a size increase with decreasing concentration. Similarly, the SEM scans for the DNA film cast from a solution of concentration 1.9 g L^{-1} and dried at room temperature under vacuum clearly showed macroclusters (~0.5–1 μm), consisting of several spherical clusters. Above this concentration, clusters were present, but no cluster–cluster aggregation could be identified. By expecting clusters and their aggregates in the SEM scans, it was implicitly assumed that these aggregates are intrinsically stable in the drying process, *i.e*., that the SEM pictures reflect the 'original' situation. This assumption is not without ground, as very stable clusters have been reported recently,[7b] which, once formed could not be destroyed later by dissolution in water or an aqueous 0.2 M HCl solution at room temperature or by heating under vacuum at high temperature (160 °C).[11]

It appears that there is an equilibrium in the solution between clusters and aggregates of clusters, which is dynamic and dependent on various factors such as concentration, solution history, time, temperature, *etc*. That the steady increase in cluster size was primarily a concentration-related phenomenon, not time-dependent, was ascertained when we measured the cluster size of these compounds in aqueous solutions over three days. The increase in size with time was very small compared to the large and almost instantaneous increase in size on dilution.

Why are clusters formed in solution at all let alone their subsequent aggregation? There are several reports of possible mechanisms of cluster formation. To cite an example, from molecular dynamics simulations it was found that non-neutral ion pairs in a solution of NaCl are stabilized by at least one counter ion, forming large ionic clusters that include the hydration molecules.[3] In spite of several theoretical explanations, the exact nature of the interactions involved in cluster formation is not clearly known.[4] It could be attributed, depending on the nature of the species involved (both solute and solvent), to electrostatic, hydrophilic, or hydrophobic interactions. Aggregation of clusters, leading to formation of macroclusters, could be governed by similar interactions to those responsible for the formation of the clusters. The well-known Stokes–Einstein equation, $D = kT\,(6\pi\eta r_s)^{-1}$, (where k is the Boltzmann constant, D is diffusivity, and r_s, is the radius of particles in a solution of dynamic viscosity η at temperature T) provides the basic relationship that determines the diffusivity of particles. Dilutions leading to decreases in viscosity would apparently increase diffusivity of particles, facilitating the interaction among the clusters leading to cluster–cluster aggregation. On the other hand, this aggregation means an increase in the radius of the particle and consequent decrease in diffusivity. Obviously, the situation is more complex than can be visualized from a simple interpretation of the above equation, and apparently the unusual observation could have a bearing on the dynamics of the process involving clusters and aggregates of clusters. Future experimental and theoretical work would offer suitable explanations for the underlying mechanism.

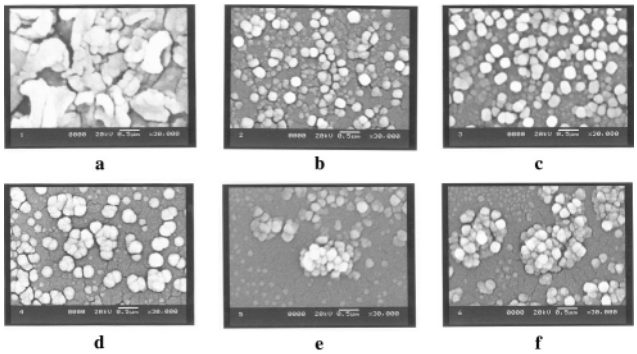

Fig. 3 SEM picture of mono-6-aza-6-deoxy-β-cyclodextrin–[60]fullerene (CDAzF) films cast from aqueous solutions (30000× magnification). [CDAzF] (mM): (a) 0.216, (b) 0.043, (c) 0.031, (d) 0.024, (e) 0.017, (f) 0.013.

The authors express their gratitude to the Korean Federation of Science and Technology and the Ministry of Education for 'brain pool' and 'BK21' projects that provided funding to carry out this work.

Notes and references

† Solutions of the compounds in high purity water (HPLC grade) were filtered using a 0.8 μm syringe filter, and the particle dimensions in solution were measured directly using quasi-elastic light scattering. Measurements (repeated three times) were done on a Malvern instrument (4700C, England), equipped with an Ar^+ laser operating at 700 mW power and 477 nm wavelength, and a computer-controlled correlator, at a 90° accumulation angle. The solutions were thermostatted to 30.0 ± 0.1 °C before each measurement in disposable polystyrene cuvettes. The data were processed using S4700 version PCS v1.26 software, which gives directly the particle size distribution, average particle size, and polydispersity.

1 (*a*) D. M. Guldi, *J. Phys. Chem. A*, 1997, **101**, 3895; (*b*) H. Murakami, M. Shirakusa, T. Sagara and N. Nakashima, *Chem. Lett*., 1999, **8**, 815; (*c*) S. Zhou, C. Burger, B. Chu, M. Sawamura, N. Nagahama, M. Toganoh, U. E. Hackler, H. Isobe and E. Nakamura, *Science*, 2001, **291**, 1944; (*d*) A. S. Boutorine, O. Balland, H. Tokuyama, M. Takasugi, H. Isobe, E. Nakamura and C. Helene, *Proc. Electrochem. Soc*., 1997, **97**, 186.

2 (*a*) T. Anderson, G. Westman, O. Wennerström and M. Sundahl, *J. Chem. Soc., Perkin Trans. 2*, 1994, 1097; (*b*) M. Sundahl, T. Anderson, K. Nilsson, O. Wennerström and G. Westman, *Synth. Met*., 1993, **56**, 3252.

3 (*a*) L. Degreve and F. L. B. da Silva, *J. Chem. Phys*., 1999, **111**, 5150; (*b*) J. L. F. Abascal, F. Bresme and P. Turq, *Mol. Phys*., 1994, **81**, 143.

4 (*a*) Y. Georgalis, A. M. Kierzek and W. Saenger, *J. Phys. Chem. B*, 2000, **104**, 3405; (*b*) L. Li and T. Ogawa, *J. Cryst. Growth*, 2000, **211**, 286.

5 J. Ray and G. S. Manning, *Macromolecules*, 2000, **33**, 2901.

6 E. G. Timoshenko and Y. A. Kuznetsov, *J. Chem. Phys*., 2000, **112**, 8163.

7 (*a*) G. Raos and G. Allegra, *J. Chem. Phys*., 1997, **107**, 6479; (*b*) M. Duval, *Macromolecules*, 2000, **33**, 7862.

8 (*a*) R. S. Ruoff, R. Malhotra and D. L. Huestis, *Nature*, 1993, **361**, 140; (*b*) V. N. Bezmelnitsyn, A. V. Eletsky, M. V. Okun and E. V. Stepanov, *Bull. Russ. Acad. Sci*., 1996, **60**, 1358.

9 (*a*) S. Samal and K. E. Geckeler, *Chem. Commun*., 2000, 1101; (*b*) S. Samal, B.-J. Choi and K. E. Geckeler, *Chem. Commun*., 2000, 1373.

10 M. Brettreich and A. Hirsch, *Tetrahedron Lett*., 1998, **39**, 2731.

11 In spite of this supporting observation, the interpretation of SEM scans should be done with caution, as the aggregates may be destroyed in the drying process.

CHEMCOMM Communication
www.rsc.org/chemcomm

A novel, shape-selective, zeolite-catalyzed synthesis of calix(4)pyrroles†‡

M. Radha Kishan, N. Srinivas, K. V. Raghavan,* S. J. Kulkarni,* J. A. R. P. Sarma and M. Vairamani

Indian Institute of Chemical Technology, Hyderabad-500 007, India. E-mail: kvr@iict.ap.nic.in;sjkulkarni@iict.ap.nic.in

Received (in Cambridge, UK) 28th June 2001, Accepted 6th September 2001
First published as an Advance Article on the web 15th October 2001

Porosity and acidity of molecular sieve Al-MCM-41 (*ca.* 30 Å pore diameter) plays a crucial role in the synthesis of novel calix(4)pyrroles; for the first time, Al-MCM-41 has been used as a solid acid catalyst to produce a number of calix(4)pyrroles with good selectivity and yields where zeolite HY (*ca.* 7.6 Å pore diameter) yields mainly the linear chain dimer and no cyclic products.

Calix(4)pyrroles, which are analogous to calix(4)arenes have gained much attention because of their properties as binders of anionic species, transition metals and neutral substrates.[1–4] Selective synthesis of these calix(4)pyrroles **1**, in high yields by an environmentally clean process is of topical interest, so as to meet the increasing demand of reducing the pollution hazards caused by the usage of homogeneous acid catalysts,[5] which require acid neutralization and tedious work-up procedures. This prompted us to study the macrocyclization reactions for the first time over zeolites,[6] as there are no reports wherein they have been used as catalysts. However, owing to their smaller pore size, they were of limited use in the synthesis of macrocycles. Nevertheless, this objective could be achieved by employing uni-dimensional molecular sieves, Al-MCM-41.[7] Here, we report for the first time the selective synthesis of various novel calix(4)pyrroles over a mesoporous Al-MCM-41 catalyst in an eco-friendly procedure.

An equimolar ratio of pyrrole and ketone was refluxed in dichloromethane over Al-MCM-41§ (Table 1). When cyclohexanone condensed with pyrrole, tetraspirocyclohexyl calix(4)pyrrole **1a**, was obtained with high yield and selectivity. Along with **1a**, the acyclic oligomers, linear dimer, trimer and tetramer (**1b**, **1c** and **1d**) were also observed. The higher reactivity and selectivity of **1a** (*ca.* 14.20 Å)[8] in Al-MCM-41 is attributed to the large pore size (*ca.* 30 Å) and high surface area (980 $m^2\ g^{-1}$). In line with this, a very low yield and selectivity were observed in HY, HZSM-5(30) and SAPO-5 zeolites as they have smaller pore sizes than the product **1a**, *viz.* 7.5, 5.6 and 7.3 Å, respectively (Scheme 1).

In the case of HY zeolite, **1b** is the major product while some amounts of **1c** and **1d** are also observed (Table 1). However, no amount of cyclic **1a** was observed. In the case of HZSM-5(30), again **1b** was the major product along with a minor component of **1a** and negligible amounts of **1c** and **1d**. It is believed that **1a** is formed due to a surface reaction. In fact, this was confirmed by surface poisoning carried out in the form of silylation with tetraethyl orthosilicate (TEOS) following the chemical vapour

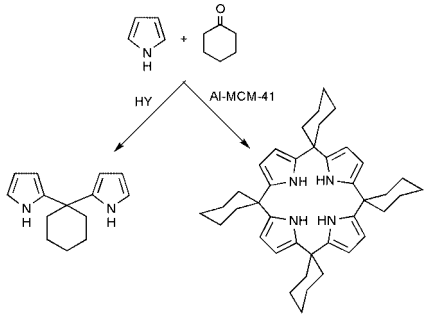

Scheme 1 Shape-selective synthesis of tetraspirocyclohexyl calix(4)pyrrole over MCM-41 and HY catalysts.

† Electronic supplementary information (ESI) available: selected analytical and spectral data for compounds **1**–**10**. Table S1: results of Monte Carlo simulations. Fig. S1: cross-sectional view of the supercell of Al-MCM-41 in which the relative orientations of **1a** and other molecules are seen. See http://www.rsc.org/suppdata/cc/b1/b105690p/

‡ IICT Communication No. 4641.

Table 1 Reaction conditions and percentage of yield of various calix(4)pyrroles over MCM-41 catalysts

Catalyst	Ketone	Time/h	Conversion of pyrrole (%)	Products yield (wt%)		
				Cyclic tetramer	Linear dimer	Others[a]
Al-MCM-41	Cyclohexanone	10	95.0	70.3 (**1a**)	12.3 (**1b**)	12.4
HY	Cyclohexanone	10	87.9	—	62.7 (**1b**)	16.2
HZSM-5(30)	Cyclohexanone	10	69.6	10.7 (**1a**)	53.0 (**1b**)	5.9
HZSM-5(30)[b]	Cyclohexanone	10	82.3	—	61.2 (**1b**)	21.1
SAPO-5	Cyclohexanone	10	16.0	—	11.6 (**1b**)	4.4
Al-MCM-41[c]	Cyclohexanone	10	93.0	64.7	7.5	20.8
Al-MCM-41	Cyclopentanone	20	74.3	62.7 (**2a**)	4.3 (**2b**)	7.3
Al-MCM-41	Cycloheptanone	72	69.8	26.7 (**3a**)	27.4 (**3b**)	15.7
Al-MCM-41	Cyclooctanone	120	78.0	8.3 (**4a**)	46.0 (**4b**)	23.7
Al-MCM-41	2-Methyl cyclohexanone	10	60.2	5.1 (**5a**)	33.8 (**5b**)	21.3
Al-MCM-41	Acetone	10	95.0	70.3 (**7a**)	12.3 (**7b**)	12.4
Al-MCM-41	Cyclohexanone + Acetone	10	92.7	8.0 (**6a**) 21.9 (**1a**) 3.1 (**7a**)	40.6 (**6b**) 12.2 (**7b**)	6.9
Al-MCM-41	Ethyl acetoacetate	72	—	Trace (**8a**)	—	—

Standard reaction conditions include pyrrole : ketone (1 : 1 mole ratio) in dichloromethane solvent (20 ml). [a] Includes linear trimer and tetramer. [b] Catalyst surface was poisoned by chemical vapour deposition with tetraethyl orthosilicate (TEOS). [c] Al-MCM-41 external surface was passivated using Ph_2SiCl_2

 DOI: 10.1039/b105690p

deposition method. However, in order to show that the macrocyclization is actually taking place inside the large pores of Al-MCM-41, the external surface of the mesoporous framework was treated with Ph_2SiCl_2 under non-diffusive conditions.[9] Yields of the cyclized product were comparable to those of the unpassivated Al-MCM-41. It is also interesting to note that SAPO-5, a mild acidic catalyst having a similar pore size as that of HY produced a lower conversion, indicating that the stronger acidic medium facilitates the condensation reaction. Other experiments involving Si/Al catalysts also resulted in low yields as well as selectivity for **1a**.

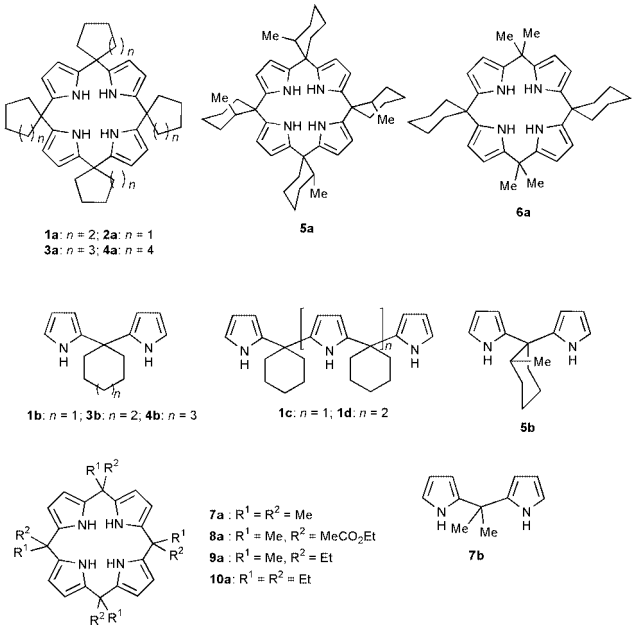

The selective syntheses of calixpyrroles over various molecular sieves were also studied by molecular simulations and the results are exactly comparable. The sorption studies[10] involving HY zeolite indicate very high loading for only **1b** (Table S1) indicating relatively free translation and rotational motion along the channels of HY. In fact, higher oligomers were not loaded during the entire length of the simulation. As expected, cyclic **1a** could not be formed even inside the supercage as its molecular size is larger than the reaction cavity size. For Al-MCM-41, when **1a**, **1b**, **1c** and **1d** are considered as sorbents along with the reactants pyrrole and cyclohexanone, the two reactants constitute a major portion of the total sorbents and decreasing concentrations of **1b**, **1c**, **1d** and **1a** were observed. This is significant given that the average energy of **1a** is much lower than the other oligomers. The stabilization energy of **1a** is consistently lower than all other products and this stabilization energy is equal to that of the single sorbent **1a** simulation run. In the presence of other oligomers and reactants, *i.e.* in the initial stages of the reaction, a maximum amount of **1b** is formed. However, subsequent reactions produce linear trimer and tetramers. These readily condense with another cyclohexanone to form highly stabilized cyclic **1a**.

The synthesis of substituted calix(4)pyrroles was also attempted by condensation of various cyclic ketones with pyrrole over Al-MCM-41 and the results are shown in Table 1. Higher and lower cylic ketones were used in the reaction with pyrrole on Al-MCM-41 in dichloromethane solvent. With cyclopentanone, tetraspirocyclopentyl calix(4)pyrrole **2a** was produced. When the ring size is increased further, the reactivity and selectivity decrease. The increased ring size could have some severe electronic and/or steric effects on the reactivity. However, when cycloheptanone and cyclooctanone were used, initially, dimers **3b** and **4b** were formed even after 10 h. When the reaction was continued for over 3 and 5 days, the respective cyclic tetramers tetraspirocycloheptyl calix(4)pyrrole **3a** and tetraspirocyclooctyl calix(4)pyrrole **4a** were formed and when 2-methyl cyclohexannone was used, tetraspiro(2-methylcyclohexyl) calix(4)pyrrole **5a** was obtained. Incidentally, this is the first report on the formation of a number of macrocyclic compounds such as **3a**, **4a**, **5a** and **7a**. All the cyclic and acyclic oligomers were fully characterized by MS, HR-MS, ^{1}H and ^{13}C NMR spectroscopy.

In the case of acetone, octamethyl calix(4)pyrrole **7a** was produced in higher yields.[11] Increasing the chain length of the ketones on either or both sides, *i.e.* by taking methyl ethyl ketone and pentan-3-one, tetramethyltetraethyl calix(4)pyrrole **9a** and octaethyl calix(4)pyrrole **10a** are observed after 3 and 5 days respectively. This could also be due to the same factors as observed in cylic ketones of higher ring size.

A type of structural mimicry was attempted when pyrrole was refluxed in dichloromethane with a 1 : 1 mixture of cyclohexanone and acetone. A minor component, cyclic tetramethyl dicyclohexyl calix(4)pyrrole **6a**, consisting of two acetone and cyclohexanone units alternately, was formed along with major **1a** and minor **7a** products. Similarly, when a β-keto ester, ethylacetoacetate was used only traces of functionalized calixpyrrole **8a**, which was confirmed by HR-MS, were formed.

The regenerability and reusability studies of the catalyst have shown that constant yields and selectivities can be obtained even after as many as 5–6 cycles. The powder X-ray diffraction patterns are very similar before and after the reaction, indicating the robustness of the catalyst. The present investigations can be extended in terms of varying the pore size and acidity in order to optimize the yield and selectivity of calix($n \geqslant 4$)pyrroles of definite size and shape. Further work along these lines is in progress.

In conclusion, a versatile, novel, shape selective, eco-friendly and simple protocol for the preparation of calix(4)pyrroles and novel calix(4)pyrroles has been achieved using mesoporous molecular sieves as catalysts.

M. R. K. is thankful to CSIR, India, for a Senior Research Fellowship.

Notes and references

§ *General procedure for the condensation reaction*: equimolar (1 : 1) amounts of pyrrole (7.2 mmol) and ketone were dissolved in 20 ml dichloromethane taken in a 100 ml round bottomed flask. To this, 0.5 g of the calcined and dried catalyst was added and the reaction mixture was allowed to reflux for 10 h/days depending on the reaction. After the reaction the catalyst was separated by filtration and washed thoroughly with 100 ml dichloromethane (20 × 5). The solvent was then removed under reduced pressure to give a viscous residue. Products were separated by column chromatography using silica (100-200 mesh size) with *n*-hexane as eluent. Quantification was done using the CAMAG HPTLC system and compared with isolated yields.

1 V. V. Chelintzev and B. V. Toronov, *J. Russ. Phys. Chem. Soc*., 1916, **48**, 105.
2 C. Floriani, *Chem Commun*., 1996, 1257.
3 P. A. Gale, J. L. Sessler and V. Král, *Chem Commun*., 1998, 1.
4 P. A. Gale, J. L. Sessler, V. Lynch and P. I. Sansom, *Tetrahedron Lett*., 1996, **37**, 7881.
5 P. Rothenmund and C. L. Gage, *J. Am. Chem. Soc*., 1955, **77**, 3340.
6 Y. V. Subba Rao, S. J. Kulkarni, M. Subrahmanyam and A. V. Rama Rao, *J. Org. Chem*., 1994, **59**, 3998.
7 C. T. Kresge, M. E. Leonowicz, W. J. Roth, J. C. Vartuli and J. S. Beck, *Nature*, 1992, **359**, 710.
8 The farthest distance between the two diagonally attached atoms.
9 B. F. G. Johnson, S. A. Raynor, D. S. Shephard, T. Mashmeyer, J. M. Thomas, G. Sankar, S. Bromley, R. Oldroyd, L. Gladden and M. D. Mantle, *Chem Commun*., 1999, 1167.
10 Molecular modeling studies were performed using Cerius^2, which is based on Monte-Carlo simulations. Sorption of **1a** and other linear oligomers in Al-MCM-41 and HY zeolite were modelled with Monte Carlo simulation methods. The structure of **1a** was established from single crystal X-ray structure analysis and was verified with the structure already deposited in the Cambridge Structural Database.
11 M. Radha Kishan, S. J. Kulkarni, M. Rama Krishna Prasad, N. Srinivas, G. Kamalakar and K. V. Raghavan, partly presented in 13th International Zeolite Conference (IZC), 8–13 July, 2001, Montpellier, France.

CHEMCOMM Communication
www.rsc.org/chemcomm

Highly effective epoxidation of alkenes with Ti-containing soluble polymers

G. Blanco-Brieva,[a] J. M. Campos-Martín,[a] M. P. de Frutos[b] and J. L. G. Fierro*[a]

[a] *Instituto de Catálisis y Petroleoquímica, CSIC, Campus Cantoblanco, 28049 Madrid, Spain. E-mail: jlgfierro@icp.csic.es; Fax: +34 915854760*
[b] *Centro de Investigación y Desarrollo, Repsol-YPF, Embajadores 183, 28045 Madrid, Spain*

Received (in Cambridge, UK) 19th June 2001, Accepted 13th September 2001
First published as an Advance Article on the web 15th October 2001

Ti-containing polysiloxane epoxidation catalysts have been prepared by controlled hydrolysis of titanium- and alkylsilane precursors. These polysiloxanes exhibit very high yields to epoxides in the epoxidation reaction of primary alkenes with organic hydroperoxides.

Epoxides, particularly propylene oxide, are a class of commodity chemicals of enormous importance in the chemical industry. The oxidation of alkenes to the corresponding epoxide in liquid phase with organic hydroperoxides in the presence of a catalyst is well known. Generally, hydrocarbon-soluble organometallic compounds of transition metals can be employed as the homogeneous catalyst. Examples are vanadium or molybdenum compounds.[1] Other alternatives include the use of heterogeneous catalysts such as a chemical combination of titania–silica,[2] titanium incorporated in a zeolite framework (*i.e.* Tiβ)[3] or into the framework or grafted mesoporous silicas.[4] Although homogeneous titanium-containing epoxidation catalysts are known,[5] the selectivity to the alkene oxide obtained with such catalysts is significantly lower than those obtained with the above heterogeneous catalysts, some improvements having been found with polyorganometallosiloxane synthesized in a neutral solvent such as toluene. However, selectivity and conversion are still lower than with heterogeneous catalysts[6] and, despite more recent attempts with titano–silsesquioxanes,[7] these compounds continue to be tedious, expensive and time-consuming to prepare.

It is by now widely accepted that the active site for epoxidation in titanium-containing materials is of tetrahedral nature. This makes it very important to have a method for preparing the catalysts that will avoid the formation of titanium in octahedral coordination. In this report, we describe a new method for the synthesis of a homogeneous catalyst for the epoxidation of alkenes with a high yield of hydroperoxide to epoxide.

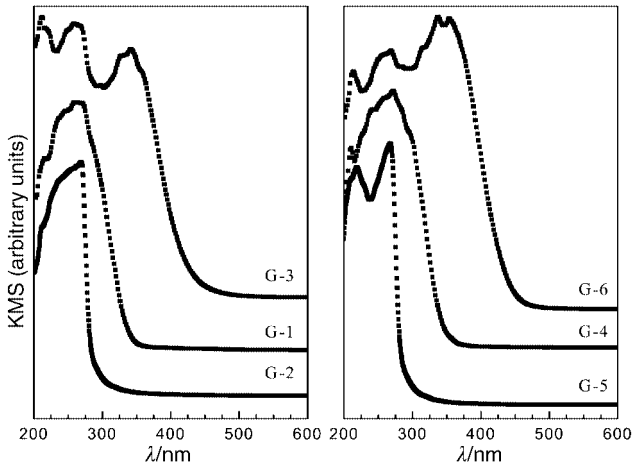

Fig. 1 Diffuse reflectance spectra (Kubelka–Munk–Schuster function) of the catalysts recorded with a Shimadzu UV-2100 spectrometer without pretreatment.

The catalysts were prepared in the following manner: 1.25 mmol of titanium(IV) precursor (titanium isopropoxide or titanium tetrachloride) was added to 100 ml of solvent (toluene or THF) under a nitrogen atmosphere and the solution was stirred for 15 min at rt. Then, 50 mmol of silicon precursor was added. Following this, 6 ml of water was added dropwise for 2 h and a clear solution was obtained, when a halogenated precursor was employed, 80 mmol of sodium carbonate was added to neutralize the HCl byproduct and excess Na_2CO_3 was removed by centrifugation at 6000 rpm for 20 min. The solvent was removed at 363 K under reduced pressure. For comparative purposes a polysiloxane was prepared without the addition of a titanium precursor in toluene (called B). Samples were also prepared in the presence of Hacac, which was added together with a titanium precursor. The Ti-loading of the catalysts was close to 1 wt % determinated by ICP-AES. The IR spectra of these titanopolysiloxanes showed bands characteristic of the aromatic ring as well as that of the Si–O bond. A clear band located at 920 cm^{-1}, associated with Ti–O–Si[8] linkages could also be discerned. A broad band was observed between 3700–3200 cm^{-1} with a shoulder at 3625 cm^{-1}, suggesting the

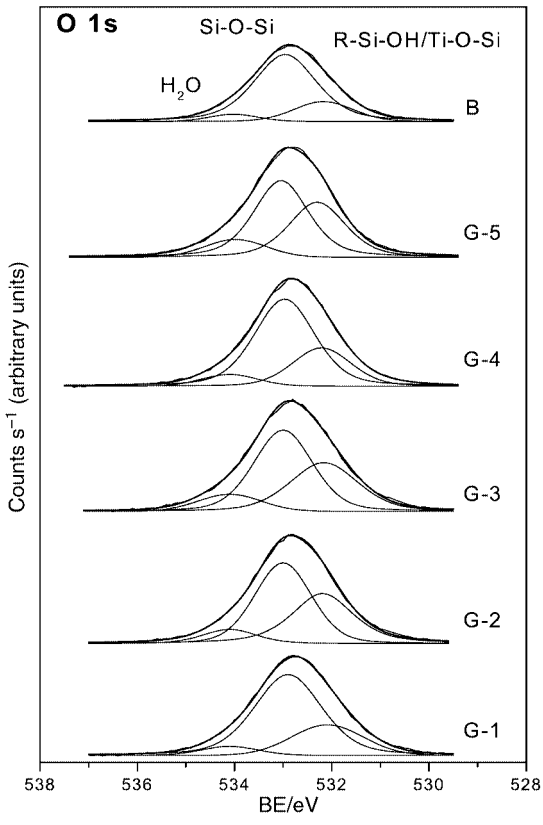

Fig. 2 O 1s core-level spectra of outgassed samples at rt acquired with a VG Escalab 200R spectrometer. The binding energies (BE) were referenced to the C 1s peak at 284.9 eV.

 DOI: 10.1039/b105362k

Table 1 Catalysts prepared, titanium contents, reaction data in the epoxidation of oct-1-ene by ethylbenzene hydroperoxide (EBHP) at 393 K

Catalyst	Titanium precursor	Silicon precursor	Solvent	Ti/wt %	Reaction time/min	% Conversion of EBHP	% Selectivity to epoxide[e]
B	—	PhSiCl[c]	Toluene	—	—	—	—
G-1	$TiCl_4$	PhSiCl[c]	Toluene	0.6	120	87	80
G-2	$TiCl_4$	PhSiCl[c]	THF	0.9	60	100	97
G-3[a]	$TiCl_4$	PhSiCl[c]	Toluene	0.9	90	95	90
G-4	$Ti(iPro)_4$[b]	PhSiMet[d]	Toluene	1.1	90	100	83
G-5	$Ti(iPro)_4$[b]	PhSiMet[d]	THF	0.8	90	100	95
G-6[a]	$Ti(iPro)_4$[b]	PhSiMet[d]	Toluene	1.1	60	100	91

[a] Hacac was added during the synthesis. [b] $Ti(iPro)_4$: titanium isopropoxide. [c] PhSiCl: phenyltrichlorosilane. [d] PhSiMet: phenyltrimethoxysilane. [e] Based on the EBHP consumed.

presence of phenyl-bonded silanol.[9] Catalysts G-3 and G-6 exhibited additional weak bands in the region from 1600 to 1200 cm^{-1} due to the presence of Hacac, which remains strongly adsorbed on the Ti(IV) sites[10] even after the titanopolysiloxane has been formed.

The electronic spectra (Fig. 1) of samples G-1, G-2, G-4 and G-5 showed a band centred around 250 nm, typical of Ti(IV) located in a slightly distorted tetrahedral environment,[11] although the catalysts prepared without the coordinating agent (G-1 and G-4) displayed a weak shift to higher wavelengths. This was attributed to the formation of polymeric titanium species. Despite this, the electronic spectra of samples G-3 and G-6 proved to be different, showing an additional band at about 400 nm characteristic of Ti(IV) in an octahedral environment.[11] The origin of the octahedral coordination lies in the fact that Hacac binds to Ti(IV) sites, as already confirmed by IR spectroscopy.

The photoelectron spectra of the Ti 2p core-level showed a single component for the most intense Ti $2p_{3/2}$ peak at a binding energy of 460.1 eV, corresponding—in accordance with the electronic spectra—to Ti(IV) sites in tetrahedral coordination.[12] No octahedrally coordinated Ti(IV) species (binding energy of Ti $2p_{3/2}$ peak at around 459 eV[11]) were observed in samples G-3 and G-6. A tentative explanation for this is that under the ultrahigh vacuum conditions required to pretreat the samples prior to recording the photoelectron spectra, the Hacac ligands of samples G-3 and G-6 bound to the Ti(IV) site could be lost, thus changing the original coordination $Ti(IV)_{oct} \rightarrow Ti(IV)_{tet}$. However, significant differences were observed in the O 1s line profiles (Fig. 2). This peak could be resolved into three components: the first at 534.1 eV, typical of oxygen in molecular water (H–O–H); a second at 533.0 eV, assigned to oxygen in Si–O–Si bonds, and a third at 532.3 eV, which could be ascribed to oxygen in terminal groups of the R–Si–O–H phenyl-bonded or even Si-O-Ti type.[13] The latter component (532.3 eV) increases with the increase in Ti content (sample B *vs*. sample G-1), and even more so in the catalysts prepared in the presence of THF or Hacac. The intensity of the component with a binding energy of 532.3 eV is higher than expected for the formation of Ti–O–Si bonds exclusively. This effect suggests that titanium incorporation into polysiloxane, with the corresponding Ti–O–Si bond formation, modifies the structure of polysiloxane, more OH groups being developed within the polymer.[9] This is in agreement with the electronic spectra of the titanopolysiloxane samples G-1 and G-5, in which polymeric titanium species (Ti–O–Ti–O–) were observed, with a subsequent decrease in the formation of Ti–O–Si bonds.

In a typical epoxidation run, 45 g of oct-1-ene and 33 g of a solution of 33 wt% of ethylbenzene hydroperoxide (EBHP) in ethylbenzene were heated to the reaction temperature (393 K), after which 0.30 g of catalyst was added, and was immediately completely dissolved. The organic compounds were analyzed on GC-FID equipment. Ethylbenzene hydroperoxide concentrations were measured by standard iodometric titration. All the catalysts afforded high conversions of ethylbenzene hydroperoxide (in most cases above 95%) (Table 1). However, the compounds prepared from halogenated precursors exhibited conversion levels of EBHP that were even higher than with the alkoxide precursors (G-1 *vs*. G-4). The presence of compounds that can coordinate with titanium during the preparation of titanopolysiloxanes elicited an enhancement in the selectivity to the epoxide (G-1 *vs*. G-2 and G-3, and G-4 *vs*. G-5 and G-6, respectively). In the catalysts prepared in the presence of THF or Hacac, titanium remained as isolated units in tetrahedral coordination to oxygen, as already confirmed by the UV-visible and photoelectron spectra, while those prepared in the absence of these compounds (G-1 and G-4) exhibited polymeric titanium species. The behavior of catalysts prepared with THF or Hacac was different. Thus, the values of EBHP conversion and selectivity to epoxide were found to be very high for the catalysts prepared in the presence of ether (G-2 and G-5) and somewhat lower for those prepared in the presence of Hacac (G-3 and G-6), possibly because the Hacac molecule, still present in the coordination sphere of Ti(IV)as confirmed by FTIR and DRS UV-Vis spectra, hinders the adsorption of reactants (hydroperoxide and alkene) on the active site and hence the reaction rate decreases. It is remarkable that the G-2 catalyst exhibited almost quantitative conversion of EBHP to epoxide.

Notes and references

1 H. Mimoun, M. Mignard, P. Brechotand and L. Saussine, *J. Am. Chem. Soc*., 1986, **108**, 3711; U. Masahiro and H. Yasuhiko, Atlantic Richfield Co., US 4593012, 1986.
2 H. P. Wulf and F. Wattimena, Shell Oil Compamy, US 4367342, 1983; R. A. Sheldom, *J. Mol. Catal*., 1980, **7**, 107; M. Tamura, K. Yanmauchi and K. Ichida, Sumitomo Chemical Company, EP 0734764, 1996.
3 M. A. Camblor, M. Constantini, A. Corma, L. Gilbert, P. Esteve, A. Martinez and S. Valencia, *Chem. Commun*., 1996, 1339; R. Hutter, D. C. M. Dutroit, T. Mallat, M. Schneider and A. Baiker, *J. Chem. Soc., Chem. Commun*., 1995, 163.
4 T. Blasco, A. Corma, M. T. Navarro and J. Perez-Pariente, *J. Catal*., 1995, **156**, 65; A. Baker, D. Dutoit and R. Hutter, Hoffman-La Roche AG, WO 9609117, 1996; P. T. Tanev, M. Chibwe and T. J. Pinnavaia, *Nature*, 1994, 321; T. Maschemeyer, F. Rey, G. Sankar and J. M. Thomas, *Nature*, 1995, **378**, 159.
5 P. E. Bost, M. Constantini and G. Lartigau, Rhone-Poulenc S.A., US 3870729, 1975.
6 C. S. Bell and H. P. Wulf, US 38735780, 1975.
7 P. P. Pescarmona, J. C. vander Waal, I. E. Maxwell and T. Maschmeyer, *Angew. Chem., Int. Ed*., 2001, **40(4)**, 740; M. C. Klunduk, T. Maschmeyer, J. M. Thomas and B. F. G. Johnson, *Chem. Eur. J*., 1995, **5(3)**, 1481.
8 A. Haoudi-Mazzah, P. Dhamelincourt, J. Gnado and A. Mazzah, *J. Raman Spectrosc*., 1995, **26**, 1027.
9 J. F. Brown, *J. Am. Chem. Soc*., 1965, **87**, 4317.
10 K. Nakamoto, *Infrared and Raman Spectra of Inorganic and Coordination Compounds*, 5th Edition, John Wiley and Sons Inc., New York, 1997, p. 93, Part B.
11 F. Geobaldo, S. Bordiga, A. Zechina, E. Giamello, G. Leofanti and G. Petrini, *Catal. Lett*., 1992, **16**, 109.
12 T. Blasco, M. A. Camblor, J. L. G. Fierro and J. Perez-Pariente, *Microporous Mater*., 1994, **16**, 109.
13 J. R. Sohn, H. J. Jang, M. Y. Park, E. H. Park and S. E. Park, *J. Mol. Catal*., 1994, **93**, 149.

CHEMCOMM Communication
www.rsc.org/chemcomm

Electrochemical evidence of H· produced by ultrasound

Peter R. Birkin,*[a] John F. Power[a] and Timothy G. Leighton[b]

[a] *Chemistry Department, University of Southampton, Highfield, Southampton, UK SO17 1BJ. E-mail: prb2@soton.ac.uk*
[b] *Institute of Sound and Vibration Research, University of Southampton, Highfield, Southampton, UK SO17 1BJ. E-mail: tgl@isvr.soton.ac.uk*

Received (in Cambridge, UK) 7th August 2001, Accepted 18th September 2001
First published as an Advance Article on the web 15th October 2001

Electrochemical evidence of H· produced by cavitation as the result of ultrasonic irradiation of an aqueous solution is presented.

The production of radical species[1] through the generation of high temperatures and pressure created in the interior of a collapsing cavitation bubble is one of the fundamental pieces of evidence for the phenomena classed as sonochemistry. These high temperature and pressures (estimated† to be around 5000 K and 500 atm)[2,3] are thought to break down the solvent matrix according to reaction (1).

$$H_2O \rightarrow OH\cdot + H\cdot \quad (1)$$

The radical species generated, which have been detected in a number of ways including spin trapping experiments performed by Riesz and coworkers,[1,4] have been suggested as possible pollutant destruction agents owing to their extremely high redox potential (*e.g.* OH· radicals,[5] E° = +2.8 V). However, less evidence is available for the use and detection of H· even though in principle it is generated in equivalent quantities when compared to OH· in the primary solvent degradation step [see reaction (1)]. The chemical nature of these two radical species is quite different.[6–9] As an example, the OH· radical species is known to initiate a number of different reactions within solution[10–12] while in contrast the H· atom can be rapidly consumed directly by molecular oxygen.[13] Indeed less attention has been placed on H· perhaps due to these quenching reactions.

Electrochemical evidence for the production of radical species is limited. Compton and coworkers provided evidence for OH· through a *sono*-EC' reaction involving the electrochemical generation of a radical species (from the electroreduction of fluorescein) which in turn was re-oxidised by OH· produced by ultrasound.[14] However, to the knowledge of the authors, no direct electrochemical evidence for H· appears in the literature. We present here for the first time an electrochemical method for the detection of H· produced by cavitation as the result of ultrasonic irradiation of an aqueous electrolyte solution.

Hart and Heinglein showed that it was possible to detect H· production[15] [measuring $HO_2\cdot$, see reaction (4)] using a system containing Cu^{2+}. In the electrochemical system reported here, a Cu^{2+} solution is also employed. Reaction (2) is thought to be the main process occurring as the H· diffuses into the liquid phase of the mixture employed. The rate constant for the above reaction was determined to be 9.1×10^7 dm^3 mol^{-1} s^{-1}.[16] There are several competing reactions.[3–7] Cu^+ can also be produced by reaction (4). However, the production of $HO_2\cdot$ can also be attributed to H· generation [see reaction (3)]. $HO_2\cdot$ can be generated from both products of reaction (1). However, in the absence of a scavenger for OH·, reaction (6) dominates and the geminate recombination product is preferentially formed.[16] In addition reaction (5) requires the presence of significant H_2O_2 concentrations and if this reaction was very important a non-linear response in Fig. 1 would be expected. Also $HO_2\cdot$ can be consumed by reaction (7). Under these considerations it is expected that the dominant reaction pathway leading to the formation of Cu^+ will involve the generation of H·.

$$Cu^{2+} + H\cdot \rightarrow Cu^+ + H^+ \quad (2)$$

$$H\cdot + O_2 \rightarrow HO_2\cdot \quad (3)$$

$$Cu^{2+} + HO_2\cdot \rightarrow Cu^+ + H^+ + O_2 \quad (4)$$

$$OH\cdot + H_2O_2 \rightarrow HO_2\cdot + H_2O \quad (5)$$

$$OH\cdot + OH\cdot \rightarrow H_2O_2 \quad (6)$$

$$HO_2\cdot + HO_2\cdot \rightarrow H_2O_2 + O_2 \quad (7)$$

In order to stabilise the Cu^+ species a solution containing a high Cl^- concentration was employed. The complex that forms ($CuCl_2^-$) is stable and can be electrochemically detected as shown in reaction (8) ($Cu^{2+}/CuCl_2^-$, $E_{1/2}$ = +231 mV *vs.* SCE as measured under similar conditions).

$$CuCl_2^- \rightarrow Cu^{2+} + 2Cl^- + e^- \quad (8)$$

In order to detect the generated product ($CuCl_2^-$) a pump was used to remove small quantities of liquid from the reactor and then pass this solution through a flow cell where electrochemical detection of the products could be achieved. This method has a number of advantages when compared to employing electrochemical detection of sonochemically generated products directly within the reactor. First, the mass transfer characteristics of the flow cell can be well characterised. Second, employing electrochemistry within an ultrasonic reactor, although producing efficient mass transfer close to the cavitation phenomena, leads to non-steady state mass transfer characteristics (particularly for microelectrodes) or mass transfer characteristics that require careful calibration. These two problems are avoided by employment of a flow cell.

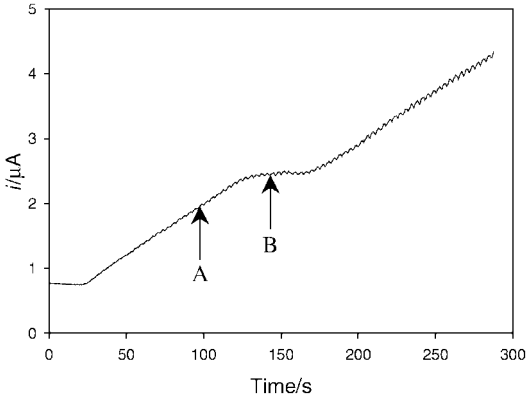

Fig. 1 Plot showing the current as a function of time for the electrochemical detection of Cu^+ produced by H· capture. The solution contained 10 mmol dm^{-3} $CuSO_4$ in 1.5 mol dm^{-3} NaCl. The experiment was performed under aerobic conditions at 25 °C. The electrode (0.071 cm^2) was held at +1 V *vs.* SCE. The solution in the reactor was exposed to 125 kHz ultrasound. The applied drive voltage amplitude was 100 V (corresponding to a measured pressure amplitude of 421 kPa).‡ Ultrasonic irradiation of the liquid was initiated at time t = 0 s, terminated at 'A' and re-started at 'B'.

 DOI: 10.1039/b107617p

A 3 mm diameter glassy carbon electrode was held at +1 V *vs.* SCE§ (a potential sufficient to oxidise any $CuCl_2^-$ produced by the reaction of $H^\cdot$ with Cu^{2+} present within the solution). Fig. 1 shows the current time response for the glassy carbon electrode employed within the flow cell. The solution contained Cu^{2+} in a high [Cl^-] media. Ultrasonic irradiation of the solution was initiated at time $t = 0$. A *ca.* 25 s lag time was observed before any $CuCl_2^-$ was detected at the electrode. This corresponds to the time taken for the solution to pass through the piping to the flow cell. The current at $t = 25$ s is seen to deviate anodically from its initial steady state condition. This is due to the electrochemical oxidation of the $CuCl_2^-$ produced by the radical trap reaction. The gradient of the current time plot at this point is constant indicating a steady production of $CuCl_2^-$ and therefore $H^\cdot$ within the ultrasonic reactor. If the ultrasonic irradiation of the solution was terminated (at time $t = 100$ s) then, after the lag time produced by the piping, the current time trace was observed to plateau out. This indicates that in the absence of ultrasonic irradiation of the solution, no significant background reactions could be observed. If the ultrasonic irradiation of the solution was repeated (time $t = 145$ s) then the current was observed to deviate anodically, indicating that it was possible to produce further quantities of $CuCl_2^-$ and hence $H^\cdot$ within the ultrasonic reactor. The gradients of the two current–time anodic deviations were the same indicating that the rate of Cu^+ production was identical in both cases. It is possible to determine the rate of $CuCl_2^-$ production from the slope of these current time transients.[17] In the example shown in Fig. 1 the rate of $CuCl_2^-$ production was 320 nmol dm^{-3} s^{-1}. This procedure can be repeated under a variety of different conditions. Fig. 2 shows how the rate of $CuCl_2^-$ production can vary as a function of $CuSO_4$ concentration. Below *ca.* 20 mmol dm^{-3} $CuSO_4$ it is apparent that the rate of production of $CuCl_2^-$ is dependent on the concentration of Cu^{2+}. Above 20 mmol dm^{-3} the rate of $CuCl_2^-$ production appears to be independent of Cu^{2+} concentration. This is consistent with other measurements (*e.g.* the Fricke reaction, known to be sensitive to $OH^\cdot$ radical production, showed Fe^{3+} productions rates up to *ca.* 250 nmol dm^{-3} s^{-1}) performed on other electrochemical trapping systems.[17]

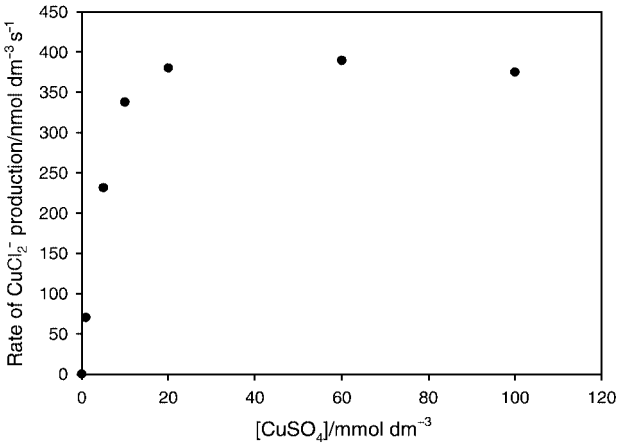

Fig. 2 Plot showing the variation in the rate of $CuCl_2^-$ production as a function of [$CuSO_4$]. The irradiated solution contained 1.5 mol dm^{-3} NaCl. The ionic strength of the solution was maintained at 1.6 mol dm^{-3} using Na_2SO_4. The frequency was fixed at 125 KHz and the drive voltage amplitude was 100 V. The aerobic solution was thermostated at 25 °C.

The results shown here demonstrate that it is possible to detect the sonochemical production of $H^\cdot$ electrochemically using a coupled chemical reaction. The criteria for this detection method are that the products of the trapping reaction are stable over the experimental timescale (as ensured by the presence of high [Cl^-]) and that a product of the trapping reaction is electrochemically active.

The sensitivity of the electrochemical flow system enables very small quantities of sonochemically generated products to be detected. This method enables electrochemically active radical trap generation rates within the nmol dm^{-3} s^{-1} range to be measured. This method can be extended to a number of different products of sonochemical reactions.[17]

Notes and references

† The estimates of the conditions within the interior of a collapsing cavitation bubble are a matter of some debate.[18] The estimation presented by Flint and Suslick relied on the measurement of sonoluminescent emission from silicone oil. The spectra obtained were fitted to a rotation vibration model for a C_2 diatomic molecule.[2] Other authors have assigned differing single value temperatures to the interior of a sonoluminescing bubble.[19,20] However, if the collapse is sufficiently rapid, the pressure and temperature within the bubble will be spatially non-uniform,[21] in which case assignment of a single value temperature is inappropriate.

‡ This pressure was measured with a Bruel & Kjaer 8103 hydrophone placed within the cell. Note that, owing to the modal nature of the sound field the pressure will vary throughout the cell depending on the particular mode excited under the physical conditions within the system.

§ This high potential was employed as it avoided unwanted electrochemical interference presumably from other sonochemical products.

1 K. Makino, M. M. Mossoba and P. Riesz, *J. Phys. Chem.*, 1983, **87**, 1369.
2 E. B. Flint and K. S. Suslick, *Science*, 1991, **253**, 1397.
3 K. S. Suslick and D. A. Hammerton and R. E. Cline, *J. Am. Chem. Soc.*, 1986, **108**, 5641.
4 K. Makino, M. M. Mossoba and P. Riesz, *J. Am. Chem. Soc.*, 1982, **104**, 3537.
5 H. N. McMurray and B. P. Wilson, *J. Phys. Chem. A*, 1999, **103**, 3955.
6 M. Gutierrez, A. Henglein and J. K. Dohrmann, *J. Phys. Chem.*, 1987, **91**, 6687.
7 A. Henglein, *Ultrasonics*, 1987, **25**, 6.
8 K. Makino, M. M. Mossoba and P. Riesz, *Radiat. Res.*, 1983, **96**, 416.
9 M. Anabar and I. Precht, *J. Phys. Chem.*, 1964, **68**, 1460.
10 K. S. Suslick, *Sci. Am.*, 1989, **260**, 62.
11 T. J. Mason and J. P. Lorimer, *Sonochemistry, Theory, Applications and Uses of Ultrasound in Chemistry*, Ellis Horwood, Chichester, 1988.
12 H. Fricke and E. J. Hart, *Radiation Dosimetry*, ed. F. H. Attix and W. C. Roesch., Academic Press, London, 1966, vol. 2, ch. 12.
13 E. J. Hart and A. Henglein, *J. Phys. Chem.*, 1985, **89**, 4342.
14 J. C. Eklund, D. N. Waller, T. O. Rebbitt, F. Marken and R. G. Compton, *J. Chem. Soc., Perkin Trans. 2*, 1995, **2**, 1981.
15 E. J. Hart and A. Henglein, *J. Phys. Chem.*, 1987, **91**, 3654.
16 G. Mark, A. Tauber, L. A. Rudiger, H. P. Schuchmann, D. Schulz, A. Mues and C. von Sonntag, *Ultrasonics Sonochem.*, 1998, **5**, 41.
17 P. R. Birkin, J. F. Power and T. G. Leighton, *Anal. Chem.*, submitted.
18 T. G. Leighton, *The Acoustic Bubble*, Academic Press, London, 1994.
19 A. J. Walton and G. T. Reynolds, *Adv. Phys.*, 1984, **33**, 595.
20 J. Šponer, *Stud. Biophys.*, 1990, **137**, 91.
21 G. J. Ball, B. P. Howell, T. G. Leighton and M. J. Schofield, *Shock Waves*, 2000, **10**, 265.

CHEMCOMM Communication
www.rsc.org/chemcomm

Tuneable electrochemical interactions between polystyrenes with anthracenyl and tetrathiafulvalenyl sidechains

Hugues Augier de Cremiers,[ab] Gilles Clavier,[a] Faysal Ilhan,[a] Graeme Cooke[b] and Vincent M. Rotello*[a]

[a] *University of Massachusetts, Department of Chemistry, Amherst, MA 01002, USA. E-mail: rotello@chem.umass.edu*
[b] *Heriot-Watt University, Department of Chemistry, Riccarton, Edinburgh, Scotland, UK EH14 4AS*

Received (in Columbia, MO, USA) 23rd July 2001, Accepted 5th September 2001
First published as an Advance Article on the web 15th October 2001

Polymer 4 and its monomeric counterpart 3 exhibit electrochemically tuneable interactions with anthracene polymer 2 and a structurally similar monomer 1 as seen by the variation of the oxidation waves of TTF groups and the fluorescence of the anthracene.

The fabrication of nanostructured materials is a promising area for the production of new molecular devices.[1] One of the more appealing approaches for the preparation of assemblies of this size scale has relied upon the use of supramolecular polymer–polymer interactions.[2] The advantages of such assemblies over their molecular brethren stems from the myriad of supramolecular architectures which can be generated through intra- and inter-polymer interactions, which can be fine-tuned by the introduction of suitable functionalities. So far, the polymer–polymer interactions approach has been limited to block copolymers capable of forming nanotubes,[3] templates for nanolithography,[4] mushrooms,[5] or micelles.[6] The development of polymer systems whereby side chain functionality plays a pivotal role is a complementary technique which allows higher aggregates to form *via* interchain interactions. This technique has been used recently for the elaboration of layer by layer surface coatings,[7] polymeric nanoparticles[8] or giant vesicles.[9]

Despite the various examples of the use of polymers for the fabrication of supramolecular assemblies, the introduction of units allowing the reversible formation of new architectures by an external physical stimuli has surprisingly received little attention.[10] Electrochemistry is rapidly emerging as an important tool for supramolecular assembly,[11] and therefore, should provide a versatile and convenient method of reversibly modulating the structure and properties of electro-active macromolecules in solution. Polymers incorporating the tetrathiafulvalene (TTF) moiety are particularly attractive materials for fabricating electrochemically controlled architectures, mainly due to this moieties ability to exist in three stable oxidation states (TTF^0, $TTF^{\cdot+}$ and TTF^{2+})[12] which will allow the formation of π-complexes with electron deficient polymers in its neutral state[13] and electron rich polymers in its electron deficient states.[14]

Here, we describe the tuneable interactions between polystyrene derivatives **2** and **4** bearing anthracene and TTF electroactive groups, respectively, in their side chains, which are capable of reversibly forming polymer aggregates in solution under electrochemical control. Polymer **2** has been shown to exist as a folded structure in chloroform, due to aromatic–aromatic interactions between the side chains.[15] The weak interactions between the electron rich anthracene side chains provide the possibility of forming stronger complexes with electrochemically generated electron-deficient moieties of suitably functionalised polymers, thereby leading to control of inter-polymer interactions in solution. Polymer **4** was targeted as a suitable candidate for the latter, and was synthesised using a similar approach to **2,** by coupling a random 1 : 1 copolymer of styrene and 4-aminomethylstyrene to 4-fluorocarbonyl-TTF.[16] Our attempt to synthesise the fully substituted polymer gave a material which proved insoluble in common organic solvents. When only 25% of the amino sites were functionalised with TTF, the polymer obtained was poorly soluble in dichloromethane (DCM), however, subsequent reaction with an excess of acetic anhydride gave the soluble polymer **4**. Monomeric analogues **1** and **3** were synthesised analogously to **2** and **4** and were used as reference compounds in our study.

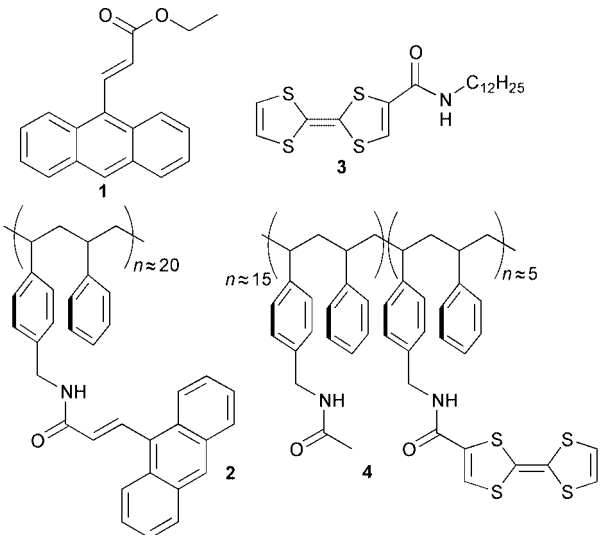

The solution electrochemistry of polymer **4** in DCM displays the two expected oxidation waves for the TTF unit at 487 and 866 mV, corresponding to the formation of the radical cationic and dicationic states, respectively. These peaks are shifted to a lower potential than those of **3** (499 and 981 mV, respectively), presumably due to interactions between the TTF units and the polymer backbone.

The solution electrochemistry of **3** and **4** were then investigated in the presence of the electron rich anthracene derivatives **1** and **2** (Table 1). It can be seen that the oxidation of monomer **3** is barely affected by the presence of the anthracene derivative **1**. This result is expected for the two monomers, where strong interactions are entropically unfavourable. However with polymer **2**, the second oxidation potential of

Table 1 Variation in mV of the oxidation waves of the TTF units of **3** and **4** in the presence of anthracene **1** or **2**[a]

	1	**2**
3	−2 and +1	−2 and +10
4	−10 and +24	−26 and +24

[a] Square waves recorded in dry DCM under argon atmosphere; decamethylferocene was used as reference and $NBu^n_4ClO_4$ as electrolyte (0.1 M). The concentrations of **1**, **2**, **3** and **4** were adjusted to obtain an overall concentration of 10^{-4} M in anthracene and TTF.

 DOI: 10.1039/b106588m

3 is shifted to a higher potential. This can be explained by the fact that the electron rich character of the anthracene side-chains promotes the formation of complexes between the electron deficient radical cation of the TTF and the polymer. Further oxidation is therefore more difficult due to an encapsulation of the radical cation by the polymer.

For polymer **4**, however, the variations in solution electrochemistry are more pronounced upon the addition of **1** or **2**. Surprisingly, the first oxidation is made easier by the presence of the anthracene. On the other hand, the dication formation is less favourable. We determined, by GPC, that the TTF substituted polymer **4** exists in solution as a rather extended structure† allowing easy interactions between its side chains and the monomeric anthracene **1**. It is noteworthy that despite the high electron density of both units, there are interactions between them in the neutral state thus lowering the first oxidation potential of the TTF. It is remarkable that this effect is enhanced when both polymers are mixed. Such favourable interactions between two π-rich units on a polymer is probably due to their similar structure and electronic properties. The interactions between the anthracene and the TTF radical cations make the second oxidation harder to achieve, which is in accordance with the data observed for the monomeric TTF **3** and the polymer **2**. However, the complexes between the polymeric species are stronger, as depicted by the greater shift in the second oxidation waves.

The behaviour of the anthracene derivatives **1** and **2** in the presence of the TTF systems were then studied by fluorescence spectroscopy as it was expected that the interactions between the two moieties would quench the emission of the anthracene. The spectra of molecules **1** and **2** were recorded in the presence of an increasing amount of **3** or **4** and their corresponding radical cations which were electrochemically generated prior to their addition to **1** or **2**. A typical result is presented in Fig. 1 for the polymer **2**.

The fluorescence of **1** did not display any change when either **3** or **4** were added supporting the previous observations that very weak, if any, interactions are taking place. On the other hand, it is apparent from Fig. 1 that the fluorescence of the polymer **2** is quenched with an increasing amount of TTF. Moreover, this process is more efficient with the monomeric TTF **3** than the polymer **4**. This is due to the folded structure of **2** which can accommodate the incorporation of monomeric species within its core but must undergo a large reorganisation to interact efficiently with the polymer **4**. Furthermore, this curve could not be fitted to a simple 1:1 binding mode,

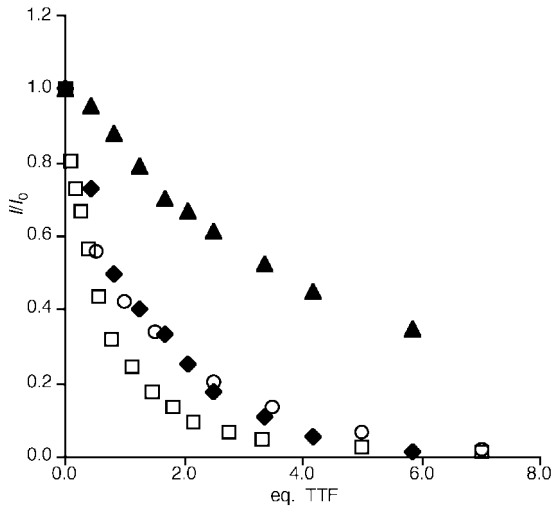

Fig. 1 Variation of the fluorescence of **2** in DCM upon addition of **3** (◆), $\mathbf{3}^{\cdot+}$ (□), **4** (▲) and $\mathbf{4}^{\cdot+}$ (○). [anthracene] = 10^{-4} M.

reflecting the multiple site aspect of polymer **2**. It is remarkable that the lower efficiency of the quenching when both polymers are present does not reflect the larger change in the oxidation waves. It can be inferred that despite the easier access of the monomers to the core of polymer **2** leading to a greater quenching, the formation of multiple interactions between two polymer chains gives an assembly which is thermodynamically more stable and probably give rise to the formation of discrete aggregates in solution. When the radical cation of the TTF moieties of **3** and **4** was generated prior to the addition to the anthracene systems, a steep initial decrease in the fluorescence intensity was observed, which is indicative of the much stronger binding as expected between π-rich anthracene units and π-deficient $TTF^{\cdot+}$ units.

In conclusion, we used two polymers with suitable side-chains as good models for the study of redox-controlled polymer–polymer interactions in solution. We have shown that a 'polymer effect' can be detected where weak interactions are established between the π-rich polymers **2** and **4** allowing a lowering of the first oxidation of the TTF. These interactions are enhanced upon oxidation of the TTF moiety of polymer **4**, thereby evoking strong donor–acceptor interactions between **2** and $\mathbf{4}^{\cdot+}$, respectively. It is anticipated that ordered aggregates are formed *via* redox controlled polymer–polymer interactions and will provide good models for the fabrication of novel devices, and their exploitation as such will be reported in due course.

Notes and references

† Polymer **4** presents a retention time which is consistent with its expected molecular weight obtained for the original copolymer of *p*-chloromethylstyrene and styrene. A folded structure would have given a longer retention time. For an example of the use of GPC for the determination of the size of a polymer in solution see ref. 15.

1 J.-M. Lehn, in *Supramolecular Chemistry*, VCH Press, New York, 1995.
2 S. I. Stupp, *Macromol. Symp.*, 1997, **117**, 1.
3 J. Raez, R. Barjovanu, J. A. Massey, M. A. Winnik and I. Manners, *Angew. Chem., Int. Ed.*, 2000, **39**, 3862.
4 R. D. Peters, X. M. Yang, Q. Wang, J. J. de Pablo and P. F. Nealey, *J. Vac. Sci. Technol. B*, 2000, **18**, 3530.
5 S. I. Stupp, V. LeBonheur, K. Walker, L. S. Li, K. E. Huggins, M. Keser and A. Amstutz, *Science*, 1997, **276**, 384.
6 N. Sommerdijk, S. J. Holder, R. C. Hiorns, R. G. Jones and R. J. M. Nolte, *Macromolecules*, 2000, **33**, 8289; Y. F. Tu, X. H. Wan, D. Zhang, Q. F. Zhou and C. Wu, *J. Am. Chem. Soc.*, 2000, **122**, 10 201.
7 Y. Shimazaki, M. Mitsuishi, S. Ito and M. Yamamoto, *Langmuir*, 1997, **13**, 1385; L. Wang, S. Cui, Z. Wang, X. Zhang, M. Jiang, L. Chi and H. Fuchs, *Langmuir*, 2000, **16**, 10 490.
8 G. Zhang, A. Niu, S. Peng, M. Jiang, Y. Tu, M. Li and C. Wu, *Acc. Chem. Res.*, 2001, **34**, 249.
9 F. Ilhan, T. H. Galow, M. Gray, G. Clavier and V. M. Rotello, *J. Am. Chem. Soc.*, 2000, **122**, 5895.
10 Examples of the introduction of an electroactive species in the polymer have been published but without electrochemical studies. See for example: G. N. Tew, M. U. Pralle and S. I. Stupp, *Angew. Chem., Int. Ed.*, 2000, **39**, 517.
11 A. Kaifer and M. Gómez-Kaifer, *Supramolecular Electrochemistry*, Wiley-VCH, Weinheim, 1999.
12 M. R. Bryce, *Adv. Mater.*, 1999, **11**, 11.
13 M. B. Nielsen, C. Lomholt and J. Becher, *Chem. Soc. Rev.*, 2000, **29**, 153.
14 For an example of the TTF^{2+} interacting with an electron rich macrocycle, see: P. R. Ashton, V. Balzani, J. Becher, A. Credi, M. C. T. Fyfe, G. Mattersteig, S. Menzer, M. B. Nielsen, F. M. Raymo, J. F. Stoddart, M. Venturi and D. J. Williams, *J. Am. Chem. Soc.*, 1999, **121**, 3951.
15 F. Ilhan, M. Gray, K. Blanchette and V. M. Rotello, *Macromolecules*, 1999, **32**, 6159.
16 G. Cooke, V. M. Rotello and A. Radhi, *Tetrahedron Lett.*, 1999, 8611.

CHEMCOMM Communication
www.rsc.org/chemcomm

Novel spermine-based cationic gemini surfactants for gene delivery

Gaël Ronsin,[a] Christele Perrin,[b] Philippe Guédat,[a] Andreas Kremer,[b] Patrick Camilleri*[b] and Anthony J. Kirby[a]

[a] *University Chemical Laboratory, Lensfield Road, Cambridge, UK CB2 1EW*
[b] *SmithKline Beecham Pharmaceuticals, New Frontiers Science Park, Third Avenue, Harlow, Essex, UK CM19 5AW. E-mail: Patrick_Camilleri@sbphrd.com*

Received (in Cambridge, UK) 4th July 2001, Accepted 13th September 2001
First published as an Advance Article on the web 19th October 2001

Two types of spermine-based gemini surfactants have been synthesised; structure–activity studies have shown one type to be far superior in gene transection than the other.

Spermine-based cationic surfactants, such as dioctadecylamidoglycylspermine-4 trifluoroacetic acid (DOGS)[1] and 2,3-dioleoyloxy-*N*-[2-(sperminecarboxamido)ethyl]*N*,*N*-dimethylpropan-1-aminium trifluoroacetate (DOSPA)[2] are commercially available and are widely used for *in vitro* gene transfection studies. The preparation of these surfactants involves multi-step synthetic procedures. In both DOGS and DOSPA the spermine moiety forms the head-group of these surfactants and carries four positive charges. The presence of a multivalent head-group has been reported to favour more efficient gene transfection compared with the monovalent analogues.[2]

As part of a programme[3] aimed at the discovery and development of more efficient tools for gene transfer, we now report the synthesis and biological evaluation of novel spermine-based cationic gemini surfactants. The structure of spermine (**1**, R = R′ = H) allows the synthesis of two isomeric series of cationic gemini surfactants **1** and **2**.

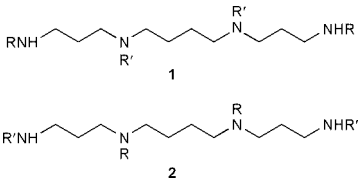

We have synthesised examples of both types of gemini surfactants, varying the length of the hydrocarbon chain and the

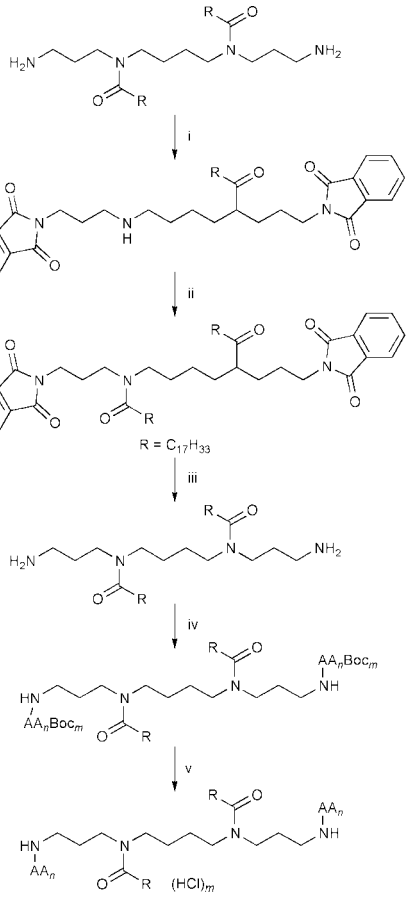

Scheme 1 *Reagents*: i) *N*-ethylcarboxyphthalimide, CH_2Cl_2, rt, 2 h, quant.; ii) oleoyl chloride, pyridine, THF, reflux, 18 h, 35%; iii) hydrazine hydrate, THF–CH_2Cl_2, reflux, 5 h, 88%; iv) SuO-AA-$(AA)_{n-1}Boc_m$, K_2CO_3, THF–H_2O 9 : 1, rt, 20 h, 84–95%; v) conc. HCl, MeOH, rt, 88–93%.

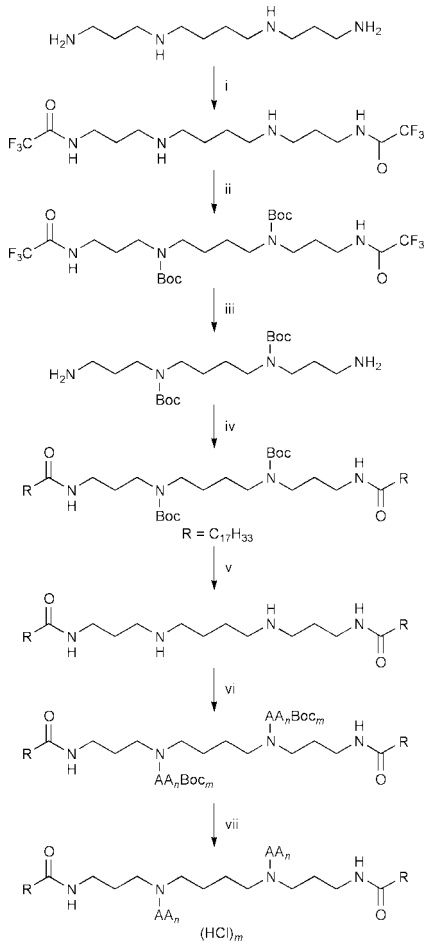

Scheme 2 *Reagents*: i) ethyl trifluoroacetate (4 eq.), H_2O (2 eq.), MeOH, reflux, 98%; ii) Boc_2O, K_2CO_3, THF–H_2O 9 : 1, rt, 20 h, 90%; iii) NH_4OH, MeOH, pH 11, rt, 3 days, 100%; iv) oleoyl succinimidate, Et_3N, THF, TA, 20 h, 60%; v) TFA, CH_2Cl_2, rt, 1 h, 96%; vi) SuO-AA-$(AA)_{n-1}Boc_m$, K_2CO_3, THF–H_2O 9 : 1, rt, 24 h, 67–87%; vii) conc. HCl, MeOH, TA, 1 h, 84–93%.

 DOI: 10.1039/b105936j

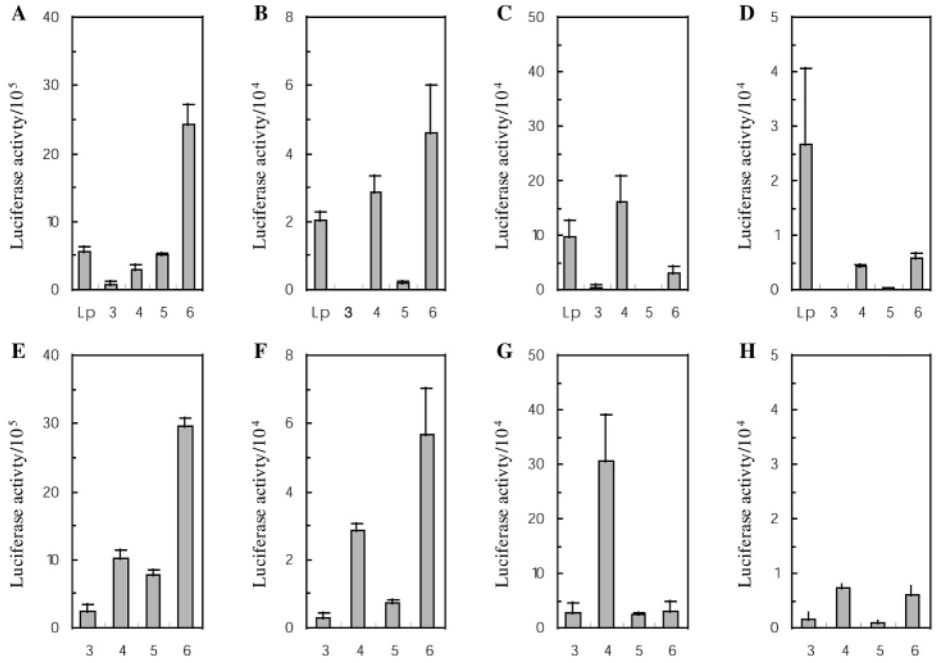

Fig. 1 Structure–activity correlations in different cell lines. Cells were incubated with DNA and gemini surfactants **3–6** at either 4 μM (CHO-DG44, A), or 8 μM (MOPC-315, B; C2C12, C; 1321N1, D). Luciferase activity (in counts per second) was averaged over 4 measurements. As control, Lipofectamine 2000™ (Lp) (Life Technologies) was incubated with DNA (100 ng well^{-1}) and used for transfection. E,F,G and H show the effect of added polylysine on the gene expression efficiency of gemini surfactants in CHO-DG44, MOPC-315, C2C12 and 1321N1 cell lines respectively. Conditions as for A–D, but the luciferase gene was complexed with poly(L-lysine) at a ratio of 1 : 4 (lysine : DNA, w/w), prior to the addition of gemini.

number of basic amino acid residues in the peptide head-group.[4] The general syntheses of **1** and **2** are shown in Schemes 1 and 2. The reagents used in the preparation of these molecules are all commercially available and yields of the various intermediates and final products are generally high. The solubility of these spermine-based detergents in water at neutral pH is better than 1 mg ml^{-1}, making them highly suitable for application to *in vitro* gene delivery.

Mixtures of these dimeric cationic lipids and a luciferase reporter gene were tested for their ability to transfect different types of cells in culture. For the same peptide head-group gemini surfactants of type **2** were found to be considerably better non-viral vectors than type **1**, and the oleoyl ($C_{17}^{\Delta 9}$) chain generally gave the most efficient transfection. Differences in the transfection activity of the two series of isomers are best demonstrated by comparing the isomeric pairs (**3** and **4**), and (**5** and **6**).

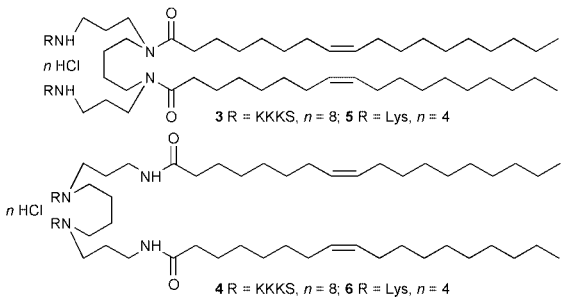

The transfection capabilities of these four gemini surfactants were compared to that of Lipofectamine 2000, a potent commercial cationic lipid formulation recently introduced by Life Technologies. We used four types of mammalian cell, CHO-DG44 (chinese hamster ovary), C2C12 (a mouse muscle cell line), nonadherent MOPC315 (mouse tumour cell line) and 1321N1 (a neuronal cell line). These cell lines were expected to give varying transfection efficiencies under culture conditions. Specific transfection conditions (type and amount of DNA, transfection time, presence and absence of serum) were varied in preliminary experiments for all four different cell lines to optimise transfection efficiency.

As expected, CHO cells were easiest to transfect, whereas the neuronal cells showed the maximum resistance to transfection. Results are shown in Fig. 1 A to D. Although transfection efficacy is assumed to depend on the membrane components of a cell, the lower efficacy of 1321N1 cell transfection could also be partially explained by the shortened transfection time in the absence of serum, compared to other cell lines such as CHO.

The potency of type **1** spermine-based gemini surfactants is much lower than that of corresponding type **2** isomer for all cell lines. Moreover, although surfactant **6** shows the better transfection ability for three of the four cell lines, **4** which contains more positive charges in its head-groups, is the superior gene delivery vector in the case of C2C12 muscle cells. It is also noteworthy that in all four cell lines pre-mixing DNA with either **4** or **6** gave better transfection than the same procedure using Lipofectamine 2000 (used at a concentration recommended by the supplier). These results underline the need to tailor the type of surfactant to the cell type targeted.

It is well known that the addition of polylysine to DNA can enhance the ability of cationic surfactants to deliver genes across cells.[5,6] Fig. 1 E to H show how in some cell lines the transfection activity of multi-valent gemini surfactant **4** increased by a factor of 2 to 4 in the presence of poly(L-lysine), whereas that of **6**, containing only single lysines, was not affected.

These experiments demonstrate the versatility of spermine-based gemini surfactants for the transport of DNA into cells.

This work is a contribution from the European Network on Gemini Surfactants, supported by the TMR Programme of the European Commission.

Notes and references

1 J.-P. Behr, B. Demeneix, J.-P. Loeffler and J. Perez-Mutul, *Proc. Natl. Acad. Sci. USA*, 1989, **86**, 6982.
2 J. G. Lewis, K.-Y. Lin, A. Kothvale, W. M. Flanagan, M. D. Matteucci, B. DePrince, R. A. Mook, R. W. Hendren and R. W. Wagner, *Proc. Natl. Acad. Sci. USA*, 1996, **93**, 3176.
3 This work is a contribution from the European Network on Gemini Surfactants..
4 Patent Application GB 9914045.1.
5 X. Gao and L. Huang, *Biochem.*, 1996, **35**, 1027.
6 C. McGreggor, C. Perrin, M. Monck, P. Camilleri and A. J. Kirby, *J. Am. Chem. Soc.*, in the press.

CHEMCOMM Communication
www.rsc.org/chemcomm

$MoSe_2$ and WSe_2 nanotubes and related structures

Manashi Nath and C. N. R. Rao*

Chemistry and Physics of Materials Unit, Jawaharlal Nehru Centre for Advanced Scientific Research, Jakkur P.O., Bangalore 560 064, India

Solid State and Structural Chemistry Unit, Indian Institute of Science, Bangalore 560 012, India. E-mail: cnrrao@jncasr.ac.in

Received (in Cambridge, UK) 10th August 2001, Accepted 24th September 2001
First published as an Advance Article on the web 5th October 2001

$MoSe_2$ and WSe_2 nanotubes are obtained by the reduction of the corresponding triselenides in hydrogen or by the decomposition of the ammonium selenometallates in a hydrogen atmosphere.

Tenne and coworkers[1,2] have demonstrated that the layered metal disulfides, MoS_2 and WS_2, form fullerene-like nested polyhedra as well as nanotube structures. Nanotubes of these two sulfides have been prepared by treating the oxides, MoO_3 and WO_3, first with a mixture of 5% H_2 + 95% N_2 followed by H_2S around 900 °C.[1–3] It is likely that amorphous trisulfides are formed as intermediates in this process. Accordingly, by heating amorphous MoS_3 or WS_3 or the ammonium thiometallate precursors in hydrogen around 900 °C, we have been able to directly obtain good yields of MoS_2 and WS_2 nanotubes.[4] Fullerene-like structures of the layered Mo and W diselenides have been prepared by the reaction of the oxides with H_2Se and H_2 + N_2 at high temperatures.[2,5] In this communication, we describe our preliminary results on the synthesis of nanotubes and nanorods of $MoSe_2$ and WSe_2 by new routes. Considering that the Mo and W trisulfides are intermediates in the formation of the disulfide nanotubes, we conjectured that the corresponding amorphous triselenides could act as intermediates in the formation of the diselenide nanotubes. We have therefore, examined the hydrogen reduction of amorphous WSe_3 and $MoSe_3$, prepared by the standard procedures.[6] Equally importantly, we have carried out the decomposition of the ammonium selenometallates in a hydrogen atmosphere to obtain the diselenide nanostructures.

Reduction of $MoSe_3$ in a stream of hydrogen (100 sccm) at 850 °C yields nanotubes as evidenced by the low-resolution transmission electron microscope (TEM) images in Fig. 1(a) and (b). Fig. 1(c) shows a TEM image of a nanorod, with a layer separation of 0.64 nm. Hydrogen reduction of WSe_3 at 750 °C yields WSe_2 nanotubes. High-resolution TEM images of some of the nanotube-like structures are shown in Fig. 2(a), (b) and (c), with the lattice fringes corresponding to the expected layer spacing of 0.65 nm. The top image in Fig. 2(c) is that of a WSe_2 nanorod emanating from a precursor particle, while the bottom image in the figure appears to be due to a single-walled nanotube, but the separation between the layers is 0.65 nm. The nanorod shows lattice fringes corresponding to the (002) planes, but the nanoparticle at the tip does not show any lattice planes. Such nanoparticles can act as nucleation centres for the growth of the nanorods or nanotubes. The growth of the nanorod or nanotube starting from the inner core of a particle and proceeding towards the outer edge, is different from that of the carbon nanotubes where the layers grow from the outer edge of the catalyst particle, encapsulating the metal catalyst particle.

The formation of the diselenide nanostructures from the triselenides involves the simple reaction, $MSe_3 + H_2 \rightarrow MSe_2 + H_2Se$ (M = Mo or W). Since the triselenides are formed by the

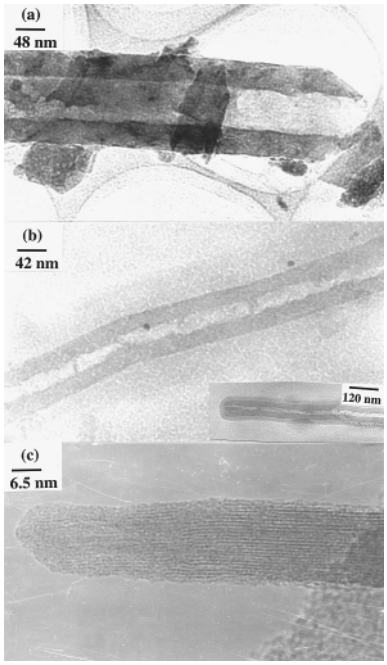

Fig. 1 (a) and (b) TEM images of a $MoSe_2$ nanotubes obtained from the decomposition of $MoSe_3$; (c) high-resolution TEM (HREM) image of a $MoSe_2$ nanorod.

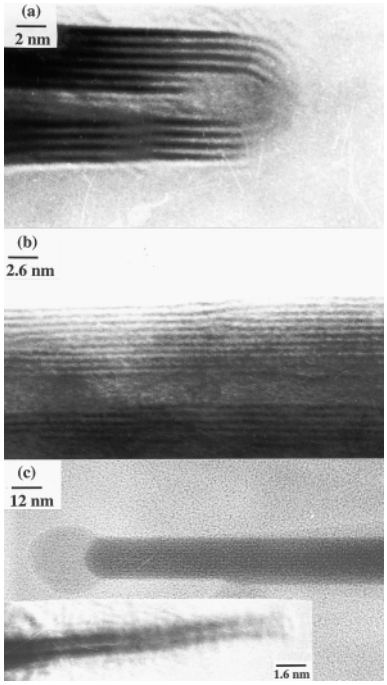

Fig. 2 (a), (b) HREM images of WSe_2 nanotubes obtained by decomposition of amorphous WSe_3 in a flow of H_2; (c) TEM images of a WSe_2 nanorod emanating from the precursor particle (top), and a single-walled WSe_2 nanotube (bottom).

 DOI: 10.1039/b107296j

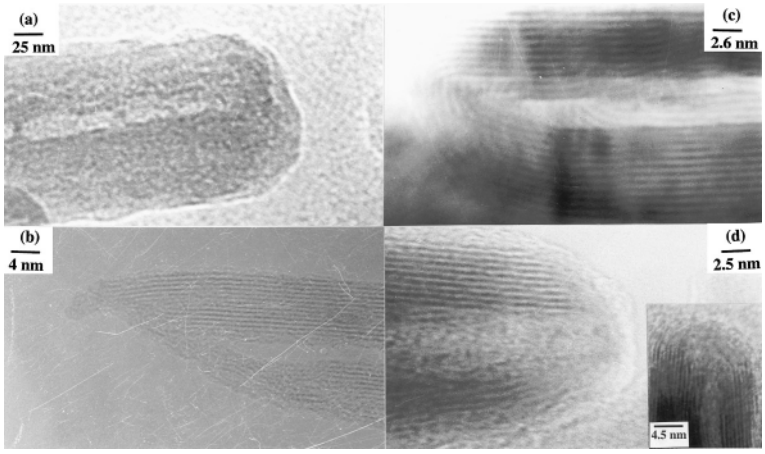

Fig. 3 (a) TEM image of a $MoSe_2$ nanotube obtained by the decomposition of $(NH_4)_2MoSe_4$; (b)–(d), HREM images of $MoSe_2$ nanotubes.

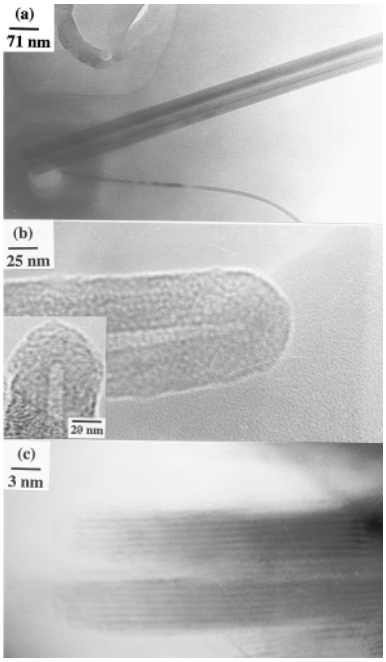

Fig. 4 (a), (b) TEM images of WSe_2 nanotubes obtained by the decomposition of $(NH_4)_2WSe_4$ in a flow of H_2. The nanotube in (a) shows a flat tip. (c) HREM image of a WSe_2 nanotube.

thermal decomposition of ammonium selenometallates, we have directly carried out the reduction of the selenometallates. Fig. 3 shows the TEM images of $MoSe_2$ nanotube structures obtained by heating $(NH_4)_2MoSe_4$ in a flow of H_2 (500 sccm) at 900 °C. The low-resolution image in Fig. 3(a) shows a nanotube closed at one end. The high-resolution images in Fig. 3(b), (c) and (d) show the $MoSe_2$ layers with a spacing of ~0.64 nm corresponding to the (002) planes. Although there is a core in the image in Fig. 3(b), the tube end has an unusual structure. The images in Fig. 3(c) and (d) appear to show closed tips, but the structure of the tip is not clearly evident. Fig. 4(a) and (b) show low-resolution images of WSe_2 nanotubes obtained by the decomposition of $(NH_4)_2WSe_4$ under a flow of H_2 (100 sccm) at 750 °C, the image in Fig. 4(b) showing closed tips. The image in Fig. 4(c) appears to be an open nanotube.

Powder X-ray diffraction (XRD) patterns of the nanotubes and nanorods of $MoSe_2$ and WSe_2 were characteristic of hexagonal structures with $a = 3.28$, $c = 12.82$ Å and $a = 3.29$ and $c = 12.99$ Å, respectively. EDAX analysis of the nanotubes showed the metal : selenium ratio to be close to 1 : 2. Selected area electron diffraction patterns commonly showed Bragg spots corresponding to the (002) and (100) planes, the (103) reflection appearing in only few of them.[7] Diffuse streaking was observed along the rows in some of the patterns.

The present study demonstrates that hydrogen reduction of the triselenides, and more significantly, of the ammonium selenometallates provides a useful route for the synthesis of the $MoSe_2$ and WSe_2 nanotubes. The reaction involved in the latter method is, $(NH_4)_2MSe_4 + H_2 \rightarrow MSe_2 + 2H_2Se + 2NH_3$ (M = Mo, W). In the decomposition of the ammonium selenometallates, the diselenide nanotubes are deposited a small distance away from the location of the starting material indicating that the amorphous triselenide may be acting as a vapor transport agent as well. In conclusion, we have been able to obtain nanotube-like structures of $MoSe_2$ and WSe_2 by the reduction of the amorphous triselenides as well as of the ammonium selenometallates. While we have been able to record a variety of nanotube and nanorod structures, with the former often exhibiting defective structures and variable wall thickness on either side of the core,[3] or loss of structure at the tip, we are presently continuing our studies in an attempt to obtain better images.

Notes and references

1 R. Tenne, L. Margulis, M. Genut and G. Hodes, *Nature*, 1992, **360**, 444; R. Tenne, *Adv. Mater.*, 1995, **7**, 965; Y. Feldman, E. Wasserman, D. J. Srolovitch and R. Tenne, *Science*, 1995, **267**, 222; R. Tenne, M. Homyonfer and Y. Feldman, *Chem. Mater.*, 1998, **10**, 3225.
2 M. Hershfinkel, L. A. Gheber, V. Volterra, J. L. Hutchison, L. Margulis and R. Tenne, *J. Am. Chem. Soc.*, 1994, **116**, 1914; A. Rothschild, J. Sloan and R. Tenne, *J. Am. Chem. Soc.*, 2000, **122**, 5169; A. Rothschild, R. Popovitz-Biro, O. Lourie and R. Tenne, *J. Phys. Chem.*, 2000, **104**, 8976.
3 Y. Q. Zhu, W. K. Hsu, H. Terrones, N. Grobert, B. Chang, M. Terrones, B. Q. Wei, H. W. Kroto, D. R. M. Walton, C. B. Boothroyd, I. Kinloch G. Z. Chen, A. H. Windle and D. J. Fray, *J. Mater. Chem.*, 2000, **10**, 2570.
4 M. Nath, A. Govindaraj and C. N. R. Rao, *Adv. Mater.*, 2001, **13**, 283.
5 T. Srilina, Y. Feldman, M. Homyonfer, J. Sloan, J. L. Hutchison and R. Tenne, *Fullerene Sci. Tech.*, 1998, **6**, 157.
6 S. P. Cramer, K. S. Liang, A. J. Jacobson, C. H. Chang and R. R. Chianelli, *Inorg. Chem.*, 1984, **23**, 1215; A. Wildervanck and F. Jellinek, *Z. Anorg. Allg. Chem.*, 1964, **328**, 309.
7 C. M. Zelenski and P. K. Dorhout, *J. Am. Chem. Soc.*, 1998, **120**, 734.

CHEMCOMM Communication
www.rsc.org/chemcomm

Halogen-free process for the conversion of carbon dioxide to urethanes by homogeneous catalysis

Mahmut Abla, Jun-Chul Choi and Toshiyasu Sakakura*

National Institute of Advanced Industrial Science and Technology (AIST), 1-1-1 Higashi, Tsukuba, Ibaraki 305-8565, Japan. E-mail: t-sakakura@aist.go.jp

Received (in Cambridge, UK) 12th July 2001, Accepted 18th September 2001
First published as an Advance Article on the web 5th October 2001

Carbon dioxide is converted to urethanes (carbamic acid derivatives) through reaction with amine and alcohol catalyzed by tin complexes; the addition of acetals as a dehydrating agent under high CO_2 pressure is the key to achieve high yields.

Polyurethane has many important industrial utilizations and the worldwide production still continues to grow.[1] Current commercial processes for producing polyurethane are based on isocyanate which is synthesized from a primary amine and phosgene [eqn.(1)]. This procedure has the major drawbacks of

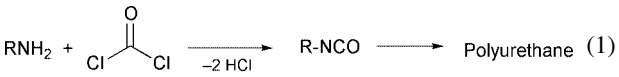

(1)

using highly toxic and corrosive phosgene, and the liberation of hydrogen chloride as a co-product.

From the standpoint of 'green chemistry', significant efforts have been made to find an alternative to the phosgene process. A very attractive substitute for phosgene is carbon dioxide because it is a typical renewable resource.[2,3] In addition, utilization of carbon dioxide is also very fascinating due to its environmentally benign nature (nontoxic, noncorrosive, and nonflammable). In particular, the application of dense carbon dioxide to organic synthesis has recently attracted much interest.[4] Most of the approaches in this context rely on the production of the carbamate anion *via* the reaction of carbon dioxide and amines, followed by the reaction with electrophiles [eqn.(2)].[5–14] However, all these methods require an equimolar

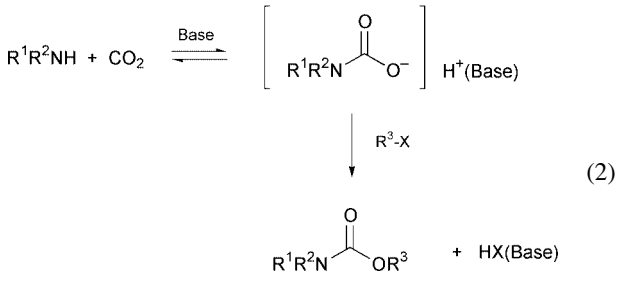

(2)

amount of electrophiles, usually alkyl halides. In this paper, we wish to report urethane synthesis by the reaction of dense carbon dioxide with amines and alcohols [eqn.(3)]. This

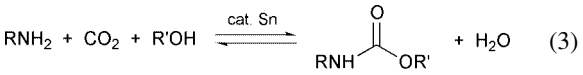

(3)

procedure is not only phosgene-free but also completely halogen-free.

Dialkyl carbonate synthesis from alcohol and CO_2 is catalyzed by metal complexes such as dialkyl(dimethoxy)tin, dialkyl(oxo)tin, and zirconium oxide.[15,16] However, the alcohol conversion is very poor. Similarly, the straightforward reaction of an amine, an alcohol, and carbon dioxide in the presence of dialkyltin compounds produced urethane only in a poor yield although the selectivity was satisfactory (Table 1, run 1).

The low conversion observed in run 1 is presumably attributable to thermodynamic limitations and catalyst deactivation by co-produced water [eqn.(3)]. In order to overcome the low conversion, we have devised a new reaction system utilizing acetals as a chemical dehydrating agent. The idea is schematically represented in Scheme 1; water is trapped by acetal to regenerate alcohol. The conversion of amine was clearly improved by this method without much decrease in the selectivity (Table 1, runs 2 to 4). The larger acetal–amine ratio further promoted the reaction. For example, the reaction of *t*-$BuNH_2$ and EtOH in the presence of two equivalents of 2,2-diethoxypropane led to a high conversion and selectivity, 100 and 84%, respectively (run 5). Since acetals are easily regenerated from acetone, the net reaction can be regarded as an urethane synthesis from CO_2, an amine, and an alcohol. As for the catalyst, dialkoxy(dialkyl)tin and its precursors such as dialkyl(oxo)tin and dialkyl(dichloro)tin exhibited high catalytic activities.[16]†

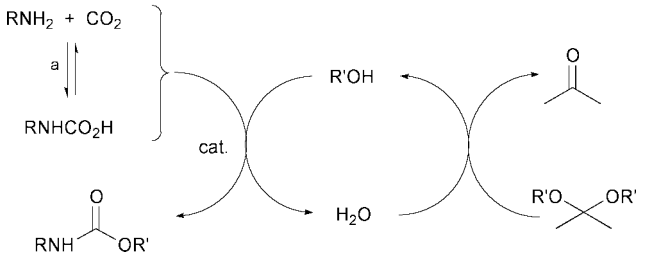

Scheme 1

Table 1 Urethane synthesis from amine, alcohol, and CO_2[a]

Run	Amine	Alcohol	Catalys	Acetal	Conversion (%)	Selectivity[b] (%)
1	*t*-$BuNH_2$	EtOH	Bu_2SnO	None	16	89
2	*t*-$BuNH_2$	EtOH	Bu_2SnO	$Me_2C(OEt)_2$	59	90
3	$CyNH_2$	EtOH	Bu_2SnO	$Me_2C(OEt)_2$	89	64
4	*t*-$BuNH_2$	MeOH	Me_2SnCl_2	$Me_2C(OMe)_2$	74	88
5[c]	*t*-$BuNH_2$	EtOH	Bu_2SnO	$Me_2C(OEt)_2$	100	84
6[d]	*t*-$BuNH_2$	MeOH	Bu_2SnO	None	66	24

[a] *Reaction conditions*: amine (10 mmol), alcohol (100 mmol), acetal (10 mmol), catalyst (0.2 mmol), CO_2 30 MPa, 200 °C, 24 h. [b] Selectivity = (yield of urethane)/conversion × 100. [c] *tert*-Butylamine (5 mmol), ethanol (50 mmol), 2,2-diethoxypropane (10 mmol). [d] *Reaction conditions*: amine (10 mmol), methanol (100 mmol), dimethyl carbonate (10 mmol), catalyst (0.2 mmol), CO_2 30 MPa, 200 °C, 24 h.

 DOI: 10.1039/b106201h

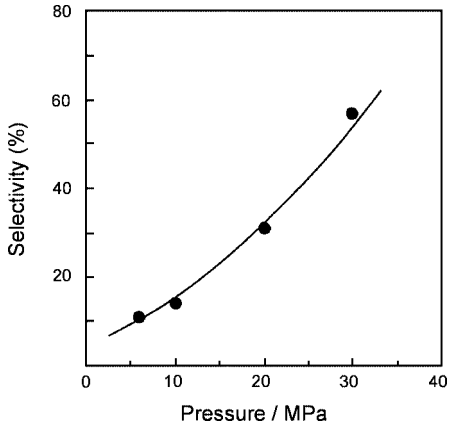

Fig. 1 Pressure effect on the Bu_2SnO-catalyzed urethane synthesis from cyclohexylamine, methanol and 2,2-dimethoxypropane (200 °C, 24 h).

In order to obtain urethane in good yields, dense phase CO_2 under high pressure is necessary as shown in Fig. 1. The major side reactions in Scheme 1 were (i) imine formation from acetone and (ii) alkylation of amines by alcohols. The improvement of the yield under a high pressure is assigned to the depression of side reactions. Thus, high pressure promotes carbamic acid formation (step a, Scheme 1). This will prevent imine formation and amine alkylation resulting in improvement of the urethane selectivity.

A possible mechanism for urethane formation is the reaction of alcohols with isocyanates formed from CO_2 and primary amines [eqn.(4)].[17] The inactivity of secondary amines is

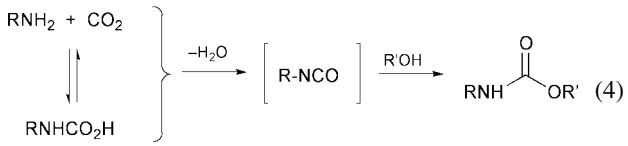

(4)

consistent with this mechanism.[18] In addition, a trace amount of urea was detected in the reaction mixture indicating the participation of isocyanates. On the other hand, the intermediacy of dialkyl carbonate is not very likely because the addition of dialkyl carbonate to the reaction mixture did not improve the urethane yield (Table 1, run 6).

In conclusion, we have succeeded in the catalytic synthesis of urethane directly from carbon dioxide, amines, and alcohols through a halogen-free process. This demonstrates the potential of carbon dioxide as an environmentally benign and easily available phosgene alternative.

This study was supported by Industrial Technology Research Grant Program in 2000 from the New Energy and Industrial Technology Development Organization (NEDO) of Japan.

Notes and references

† All manipulations were carried out under purified argon. In a stainless steel autoclave (20 cm^3 inner volume), carbon dioxide (liquid, 6.5 MPa) was added to a mixture of *tert*-butylamine (10 mmol), a tin complex (0.2 mmol), methanol (100 mmol), and biphenyl (50 mg, internal standard for GC analysis) at room temperature. The initial pressure was adjusted to 30 MPa at 200 °C and the autoclave was heated at that temperature for 24 h. After cooling, product yield was determined by GC and the products were further identified using GC-MS by the comparison of retention times and fragmentation patterns with authentic samples.

1 Polyurethanes had a global demand of 5.1×10^6 tons per year in 1990 with an estimated demand of 8.5×10^6 tons per year in 2000. See, *Synthetic Polymers, Technology, Properties, Applications*, ed. D. Feldman and A. Barbalata, Chapman and Hall, London, 1996, p. 273.

2 P. T. Anastas and J. C. Warner, *Green Chemistry, Theory and Practice,* Oxford University, Oxford, 1998.

3 M. Aresta and E. Quaranta, *CHEMTECH*, 1997, 32.

4 *Chemical Synthesis Using Supercritical Fluids*, ed. P. G. Jessop and W. Leitner, Wiley-VCH, Weinheim, 1999; W. Leitner, *Angew. Chem., Int. Ed. Engl.*, 1995, **34**, 2207; P. G. Jessop, T. Ikariya and R. Noyori, *Science*, 1995, **269**, 1025; P. G. Jessop, T. Ikariya and R. Noyori, *Chem. Rev.*, 1995, **95**, 259; P. G. Jessop, T. Ikariya and R. Noyori, *Chem. Rev.*, 1999, **99**, 475; D. A. Morgensten, R. M. LeLacheur, D. K. Morita, S. L. Borkowsky, S. Feng, G. H. Brown, L. Luan, M. F. Gross, M. J. Burk and W. Tumas, in *Green Chemistry*, ed. P. T. Anastas and T. C. Williamson, ACS Symposium Series 626, American Chemical Society, Washington, DC, 1996, pp. 132–151; J. A. Darr and M. Poliakoff, *Chem. Rev.*, 1999, **99**, 495; W. K. Gray, F. R. Smail, M. G. Hitzler, S. K. Ross and M. Poliakoff, *J. Am. Chem. Soc.*, 1999, **121**, 10711.

5 T. Tsuda, H. Washita, K. Watanabe, M. Miwa and T. Saegusa, *J. Chem. Soc., Chem. Commun.*, 1978, 815; T. Tsuda, K. Watanabe, K. Miyata, H. Yamamoto and T. Saegusa, *Inorg. Chem.*, 1981, **20**, 2728.

6 Y. Yoshida, S. Ishii and T. Yamashita, *Chem. Lett.*, 1984, 1571; Y. Yoshida, S. Ishii, M. Watanabe and T. Yamashita, *Bull. Chem. Soc. Jpn.*, 1989, **62**, 1534.

7 V. G. Parra, F. Sanchez and T. Torres, *Synthesis*, 1985, 282.

8 Y. Hori, Y. Nagano, J. Nakao, T. Fukuhara and H. Taguchi, *Chem. Express*, 1986, **1**, 224.

9 M. Aresta and E. Quaranta, *J. Org. Chem.*, 1988, **53**, 4153; M. Aresta and E. Quaranta, *J. Chem. Soc., Dalton Trans.*, 1992, **48**, 1893; M. Aresta and E. Quaranta, *Tetrahedron*, 1992, **48**, 1515.

10 A. Inesi, V. Mucciante and L. Rossi, *J. Org. Chem.*, 1998, **63**, 1337.

11 A. Belforte and F. Calderazzo, *J. Chem. Soc. Dalton Trans.*, 1989, 1007.

12 W. D. McGhee, B. L. Parnas, D. P. Riley and J. J. Talley, *U.S. Pat.* 5,223,638, June 29, 1993; W. D. McGhee, Y. Pan and D. P. Riley, *J. Chem. Soc., Chem. Commun.*, 1994, 699; W. McGhee, D. Riley, K. Christ, Y. Pan and B. Parnas, *J. Org. Chem.*, 1995, **60**, 2820.

13 M. Yoshida, N. Hara and S. Okuyama, *J. Chem. Soc., Chem. Commun.*, 2000, 151.

14 W. D. McGhee, D. P. Riley, M. E. Christ and K. M. Christ, *Organometallics*, 1993, **12**, 1429.

15 Y. Ikeda, T. Sakahori, K. Tomishige and K. Fujimoto, *Catal. Lett.*, 2000, **66**, 59; J. Kizlink and I. Pastucha, *Collect. Czech. Chem. Commun.*, 1995, **60**, 687; T. Zhao, Y. Han and Y. Sun, *Fuel Process. Technol.*, 2000, **62**, 187.

16 T. Sakakura, J.-C. Choi, Y. Saito, T. Masuda and T. Sako, *J. Org. Chem.*, 1999, **64**, 4506; T. Sakakura, J.-C. Choi, Y. Saito and T. Sako, *Polyhedron*, 2000, **19**, 573; J.-C. Choi, T. Sakakura and T. Sako, *J. Am. Chem. Soc.*, 1999, **121**, 3793; D. Ballivet-Tkatchenko, O. Douteau and S. Stutzmann, *Organometallics*, 2000, **19**, 4563.

17 D. Saylik, M. J. Horvath, P. S. Elmes, W. R. Jackson, C. G. Lovel and K. Moody, *J. Org. Chem.*, 1999, **64**, 3940.

18 Carbamic acids are easily formed from CO_2 and secondary amines. See, F. Fichter and B. Becker, *Ber.*, 1911, **44**, 3481.

CHEMCOMM Communication
www.rsc.org/chemcomm

N-Heterocyclic carbenes can coexist with alkenes and C–H acidic sites

Alois Fürstner,* Helga Krause, Lutz Ackermann and Christian W. Lehmann

Max-Planck-Institut für Kohlenforschung, D-45470 Mülheim/Ruhr, Germany. E-mail: fuerstner@mpi-muelheim.mpg.de; Fax: +49-208-306-2994

Received (in Cambridge, UK) 10th August 2001, Accepted 21st September 2001
First published as an Advance Article on the web 18th October 2001

The isolation of compounds 3 and 7a,b proves that a singlet carbene center can coexist with alkenes or C–H acidic sites in proximity without spontaneous annihilation.

Among the nucleophilic carbenes that can be isolated in pure form,[1] *N*-heterocyclic carbenes (NHC's) of the general structure **1**[2] are rapidly gaining importance as electron-donating ligands

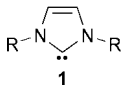

1

for transition metal centers in different oxidation states.[3] Applications of NHC-complexes to catalysis have recently met with considerable success, olefin metathesis[4] and cross coupling chemistry[5] being the most convincing cases.[6] Usually, NHC ligands bearing simple alkyl or aryl substituents R on their N-atoms are employed, although *functionalized* ones may be of even greater preparative appeal. A pertinent example is the ruthenium complex **5** which serves as a 'designer' catalyst for olefin metathesis capable of regenerating itself once the substrate is depleted.[7] The reported synthesis of **5** involves the *in situ* generation of carbene **3** as a *transient* species which is immediately trapped by admixed $(PCy_3)_2Cl_2Ru{=}CHPh$[8] to form product **4**; though easy to carry out, this *in situ* protocol turned out to be rather low yielding (41%). Heating **4** in an inert solvent then effects the intramolecular metathesis of the tethered olefin to form the metallacyclic complex **5**.

To improve the synthesis of this promising catalyst, we were pursuing the *isolation* of compound **3** containing an alkene next to the carbene center. Although cyclopropanation of olefins is a prototype carbene reaction with low activation barrier,[9–11] the preparation of **3** is surprisingly simple. This compound is obtained in essentially quantitative yield as a crystalline solid by treatment of the imidazolium salt **2** with KOt-Bu in THF at 0 °C followed by a standard work-up.[12] The spectral data and the molecular structure in the solid state (Fig. 1) show the *presence of a carbene center in proximity to the intact alkene group*.† Difference maps clearly reveal the location of all hydrogen atoms; the volume element adjacent to the carbene C-atom has no significant electron density. To the best of our knowledge, this is the first example of an isolated carbene that coexists with an olefin in its vicinity.

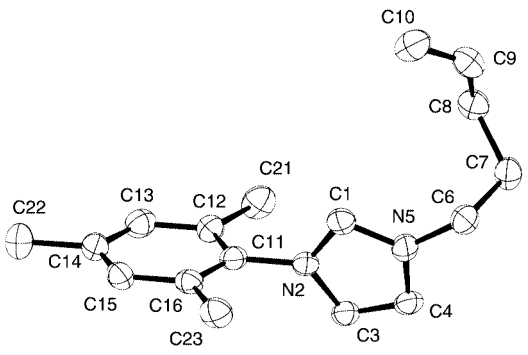

Fig. 1 Molecular structure of **3**.‡ Anisotropic displacement parameters are shown at 50% probability level. There are two independent molecules in the asymmetric unit. The major difference is found in the conformation of the alkyl chain. The torsion angle C6–C7–C8–C9 is 67.6(5)° compared to 177.1(4)° in the second molecule. The difference of the dihedral angles formed between the mesityl and the NHC is 15.8°.

With **3** in hand, it was possible to improve the synthesis of the targeted ruthenium complex **5** (Scheme 1). Thus, reaction of $(PCy_3)_2Cl_2Ru{=}CHPh$ with isolated **3** in toluene affords complex **4** in 86% yield which cyclizes upon heating to form the desired product **5**. The use of toluene instead of *n*-pentane in the latter reaction is beneficial for solubility reasons and constitutes a noteworthy improvement over our original procedure.[7]

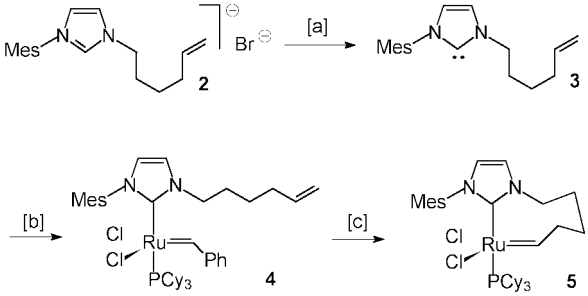

Scheme 1 *Reagents and conditions*: [a] KOt-Bu, THF, 0 °C, 98%; [b] $(PCy_3)_2Cl_2Ru{=}CHPh$, toluene, 0 °C, 86%; [c] *n*-pentane (reflux) or toluene (65 °C), 41–77%; Mes = 2,4,6-trimethylphenyl (= mesityl).

Next, we investigated if other functional groups that are generally believed to be incompatible with free carbenes can similarly be incorporated into NHC's. The insertion of carbenes into acidic C–H bonds is known to be a facile process;[9] therefore the preparation of compounds **7a**,**b** bearing an ester or a nitrile group seemed challenging, in particular since Arduengo[13] has previously reported that closely related dihydroimidazol-2-ylidenes rapidly insert into the acidic C–H bonds of MeCN, $MeSO_2Ph$, $HCCl_3$ or HC≡CH.[14]

Gratifyingly, however, carbenes **7a**,**b** are obtained in excellent yields by deprotonation of the corresponding imidazolium salts **6a**,**b** (Scheme 2),† although they were found to deteriorate within hours even at 0 °C. Reaction of $(PCy_3)_2Cl_2Ru{=}CHPh$[8] with these functionalized carbenes in toluene at ambient temperature provides the novel ruthenium complexes **8** (74%) and **9** (38%).§ The X-ray structure of **8** (Fig. 2) shows the characteristic π–π stacking between the benzylidene ligand and the mesityl group which was previously recognized as a highly

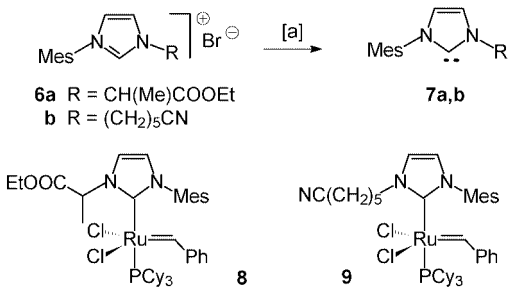

Scheme 2 *Reagents and conditions*: [a] KOt-Bu, THF, −10 °C, 95% (**7a**), 89% (**7b**); Mes = 2,4,6-trimethylphenyl (= mesityl).

 DOI: 10.1039/b107238b

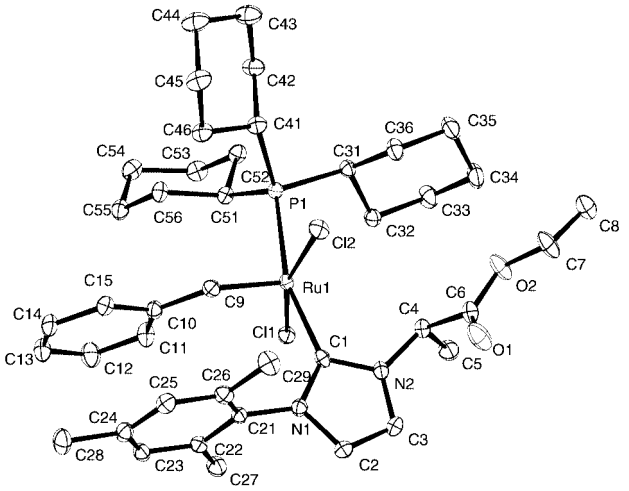

Fig. 2 Molecular structure of complex **8**.‡ Anisotropic displacement parameters are shown at 50% probability level. Selected bond lengths [Å] and angles [°]: Ru1–C9 1.839(2), Ru1–C1 2.066(2), Ru1–Cl2 2.3944(5), Ru1–Cl1 2.4056(5), Ru1–P1 2.4156(6), Cl2–Ru1–Cl1 162.299(19), C1–Ru1–P1 162.02(6).

Table 1 Ring closing metathesis reactions (RCM) using complex **8** as the catalyst; E = COOEt[a]

Substrate	Product	Yield
		91%
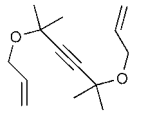	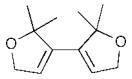	69%
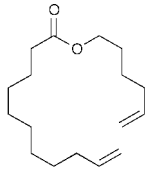	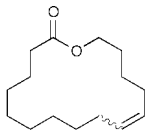	78%[b]

[a] All reactions were performed in toluene at 80 °C using 4–7 mol% of **8**. [b] In CH_2Cl_2 at 40 °C.

conserved structural motif in unsymmetrical NHC-complexes of this type.[7] Moreover, the preliminary data displayed in Table 1 illustrate that complex **8** exhibits promising catalytic activity in prototype metathesis reactions.

We are grateful to the DFG (Leibniz award to A. F.) and the Fonds der Chemischen Industrie for generous financial support.

Notes and references

† *Data for functionalized carbenes*. **3**: ^{1}H NMR (d_8-THF) δ 7.09 (d, 1H, J = 1.5 Hz), 6.90 (s, 2H), 6.83 (d, 1H, J = 1.5 Hz), 5.84 (ddt, 1H, J = 17.0, 10.3, 6.6 Hz), 5.03 (ddt, 1H, J = 17.1, 1.9, 1.6 Hz), 4.94 (ddt, 1H, J = 10.1, 2.1, 1.2 Hz), 4.08 (t, 2H, J = 6.9 Hz), 2.29 (s, 3H), 2.09 (m, 2H), 1.97 (s, 6H), 1.92 (m, 2H); ^{13}C NMR (d_8-THF) δ 217.1, 139.9, 138.9, 137.5, 135.8, 129.5, 121.1, 119.4, 115.2, 50.8, 31.8, 31.6, 21.0, 18.0. **7a**: ^{1}H NMR (d_8-THF) δ 7.25–7.00 (m, 3H), 6.95 (m, 2H), 4.08 (q, 2H, J = 7.1 Hz), 2.30 (s, 3H), 2.30 (br, 3H), 2.01 (s, 6H), 1.19 (t, 3H, J = 7.1 Hz); ^{13}C NMR (d_8-THF) δ 218.2, 138.4, 136.0, 129.5, 128.9, 121.1, 118.3, 59.8, 21.5, 21.1, 17.7, 15.2. **7b**: ^{1}H NMR (d_8-THF) δ 7.11 (d, 1H, J = 1.6 Hz), 6.91 (s, 2H), 6.85 (d, 1H, J = 1.6 Hz), 4.11 (t, 2H, J = 6.9 Hz), 2.35 (t, 2H, J = 6.9 Hz), 2.29 (s, 3H), 1.98 (s, 6H), 1.95–1.80 (m, 2H), 1.75–1.40 (m, 4H).

‡ *Crystal data*. **3**: $C_{17}H_{22}N_2$, M = 254.37 g mol^{-1}, colorless, crystal dimensions 0.26 × 0.22 × 0.11 mm, monoclinic $P2_1/n$ (no. 14), at 100 K a = 9.5288(4), b = 29.1967(15), c = 11.0965(6) Å , β = 94.419(2)°, V = 3078.0(3) Å^3, Z = 8, ρ = 1.098 Mg m^{-3}, μ = 0.065 mm^{-1}, λ = 0.71073 Å, 10536 reflections measured, 3885 unique (R_{int} = 0.148), final R = 0.078, $wR(F^2)$ = 0.209, CCDC 168097. **8**: $C_{42}H_{61}Cl_2N_2O_2PRu$, M = 828.87 g mol^{-1}, red–brown, crystal dimensions 0.18 × 0.12 × 0.02 mm, monoclinic $P2_1/c$ (no. 14), at 100 K a = 17.4060(2), b = 10.2810(1), c = 23.6677(3) Å, β = 96.673(1)°, V = 4206.67(8) Å^3, Z = 4, ρ = 1.309 Mg m^{-3}, μ = 0.573 mm^{-1}, λ = 0.71073 Å, 44732 reflections measured, 15979 unique (R_{int} = 0.075) final R = 0.049, $wR(F^2)$ = 0.113. CCDC 168098. See http://www.rsc.org/suppdata/cc/b1/b107238b/ for crystallographic files in CIF or other electronic format.

§ *Data for ruthenium complexes*. **8**: ^{1}H NMR (CD_2Cl_2) δ 19.16 (s, 1H), 7.82 (br, 2H), 7.53 (m, 1H), 7.42 (m, 1H), 7.12 (t, 2H, J = 7.6 Hz), 6.87 (d, 1H, J = 2.1 Hz), 6.30 (m, 2H), 5.96 (q, 1H, J = 7.4 Hz), 4.40–4.20 (m, 2H), 2.40–2.20 (m, 3H), 2.34 (s, 3H), 2.00–1.50 (m, 15H), 1.99 (d, 3H, J = 7.3 Hz), 1.93 (s, 6H), 1.45–1.00 (m, 15H), 1.33 (t, 3H, J = 7.2 Hz); ^{31}P NMR (CD_2Cl_2) δ 35.6; $C_{42}H_{61}Cl_2N_2O_2PRu$ (915.86) calcd. C, 60.86; H, 7.42; N, 3.38; found C, 60.75; H, 7.38; N, 3.32%; **9**: ^{1}H NMR (C_6D_6) δ 19.75 (s, 1H), 8.17 (br, 2H), 7.60–6.80 (m, 5H), 6.20 (s, 1H), 6.17 (d, 1H, J = 1.8 Hz), 4.54 (t, 2H, J = 7.2 Hz), 3.26 (m, 2H), 2.70–2.50 (m, 3H), 2.30–1.10 (m, 36H), 2.18 (s, 3H), 1.83 (s, 6H); ^{31}P NMR (C_6D_6) δ 34.2; $C_{43}H_{62}Cl_2N_3PRu$ (823.93) calcd. C, 62.68; H, 7.58; N, 5.10; found C, 62.70; H 7.49; N, 4.97%.

1 Review: D. Bourissou, O. Guerret, F. P. Gabbai and G. Bertrand, *Chem. Rev.*, 2000, **100**, 39.
2 A. J. Arduengo, *Acc. Chem. Res.*, 1999, **32**, 913.
3 W. A. Herrmann and C. Köcher, *Angew. Chem., Int. Ed. Engl.*, 1997, **36**, 2162; D. Enders and H. Gielen, *J. Organomet. Chem.*, 2001, **617–618**, 70.
4 Reviews: T. M. Trnka and R. H. Grubbs, *Acc. Chem. Res.*, 2001, **34**, 18; A. Fürstner, *Angew. Chem., Int. Ed.*, 2000, **39**, 3012.
5 C. Zhang, J. Huang, M. L. Trudell and S. P. Nolan, *J. Org. Chem.*, 1999, **64**, 3804; A. Fürstner and A. Leitner, *Synlett*, 2001, 290; S. Lee and J. F. Hartwig, *J. Org. Chem.*, 2001, **66**, 3402; G. A. Grasa and S. P. Nolan, *Org. Lett.*, 2001, **3**, 119; W. A. Herrmann, M. Elison, J. Fischer, C. Köcher and G. R. J. Artus, *Angew. Chem., Int. Ed.*, 1995, **34**, 2371; J. Huang and S. P. Nolan, *J. Am. Chem. Soc.*, 1999, **121**, 9889 and literature cited therein.
6 See also: A. Fürstner and H. Krause, *Adv. Synth. Catal.*, 2001, **343**, 343; H. M. Lee, T. Jiang, E. D. Stevens and S. P. Nolan, *Organometallics*, 2001, **20**, 1255; A. C. Chen, L. Ren, A. Decken and C. M. Crudden, *Organometallics*, 2000, **19**, 3459; J. Louie and R. H. Grubbs, *Chem. Commun.*, 2000, 1479.
7 A. Fürstner, L. Ackermann, B. Gabor, R. Goddard, C. W. Lehmann, R. Mynott, F. Stelzer and O. R. Thiel, *Chem. Eur. J*, 2001, **7**, 3236.
8 P. Schwab, R. H. Grubbs and J. W. Ziller, *J. Am. Chem. Soc.*, 1996, **118**, 100.
9 W. Kirmse, *Carbene Chemistry*, Academic Press, New York, 1971.
10 NHC's rapidly react with electron deficient alkenes, *cf.* D. Enders, K. Breuer, J. Runsink and J. H. Teles, *Liebigs Ann.*, 1996, 2019.
11 For a NHC's with adjacent alkyne groups prepared by a different method see: R. Faust and B. Göbelt, *Chem. Commun.*, 2000, 919.
12 A. J. Arduengo, R. Krafczyk, R. Schmutzler, H. A. Craig, J. R. Goerlich, W. J. Marshall and M. Unverzagt, *Tetrahedron*, 1999, **55**, 14 523.
13 A. J. Arduengo, J. C. Calabrese, F. Davidson, H. V. Rasika Dias, J. R. Goerlich, R. Karfczyk, W. J. Warshall, M. Tamm and R. Schmutzler, *Helv. Chim. Acta*, 1999, **82**, 2348.
14 Note, however, that carbonyl-containing NHC's have previously been invoked as *transient* species in the preparation of metal complexes, *cf.* D. S. McGuinness and K. J. Cavell, *Organometallics*, 2000, **19**, 741; H. Glas, E. Herdtweck, M. Spiegler, A.-K. Pleier and W. R. Thiel, *J. Organomet. Chem.*, 2001, **626**, 100.

CHEMCOMM Communication
www.rsc.org/chemcomm

Direct evidence for the incorporation of univalent indium into high-silica zeolite, H-ZSM-5, by thermal auto-reductive solid-state ion exchange

Magdolna R. Mihályi* and Hermann K. Beyer

Chemical Research Center, Institute of Chemistry, Pusztaszeri út 59-67, Budapest, Hungary 1025. E-mail: rosmag@cric.chemres.hu

Received (in Cambridge, UK) 10th July 2001, Accepted 20th September 2001
First published as an Advance Article on the web 9th October 2001

In mechanical mixtures of H-ZSM-5 and In_2O_3 thermal auto-reductive solid-state ion exchange (AR-SSIE) was found to proceed upon treatment in high vacuum at 840 K resulting in the incorporation of In^+ ions into, and in an increase of the thermal stability of, the zeolitic component.

Recently, zeolites containing cationic indium species have been found to be active and selective catalysts for the reduction of nitric oxides with hydrocarbons in the presence of oxygen.[1] Among the methods for the incorporation of indium cations into zeolites, 'reductive solid-state ion exchange' (R-SSIE) proved to be especially appropriate. This process[2] was found to proceed in mechanical mixtures of crystalline In_2O_3 and H-zeolites in a hydrogen atmosphere at 620–730 K, probably in two steps *via* In_2O, according to

$$In_2O_3 + 2H_2 + 2H^+Z^- \rightarrow 2In^+Z^- + 3H_2O \quad (1)$$

where Z^- represents the fraction of the zeolite framework bearing one negative charge. Also other reductants (*e.g.* ammonia, CO and products formed by a non-oxidative thermal decomposition of templates) induce partial or complete replacement of protons of acidic OH in zeolites.[3,4] It was evidenced that In^+, once incorporated into zeolites by R-SSIE, is oxidized by O_2 to InO^+ which can again be reversibly reduced. Univalent and trivalent indium cations in zeolites can be distinguished from each other by typical IR bands of adsorbed pyridine.[5]

Ogura *et al.*[6] found that in the IR spectra of ground mixtures of In_2O_3 and H-zeolites the intensity of the bands typical of bridging hydroxyls and pyridinium ions decreased upon degassing at 850 K to a higher degree than observed in the case of mere thermal dehydroxylation. They concluded that indium cations were incorporated into the zeolite lattice by conventional solid-state ion exchange (SSIE) according to

$$In_2O_3 + 2H^+Z^- \rightarrow 2InO^+Z^- + H_2O \quad (2)$$

However, these phenomena can be consistently interpreted also in terms of an auto-reductive solid-state ion exchange, according to which In_2O_3 is first converted to In(I) oxide by thermal decomposition and then incorporated as the monovalent cation into the zeolite lattice resulting in the overall reaction:

$$In_2O_3 + 2H^+Z^- \rightarrow 2In^+Z^- + H_2O + O_2 \quad (3)$$

In the present study direct evidence is provided for the incorporation of In^+ cations according to eqn. (3) and the formation of InO^+ cations by subsequent oxidation with oxygen.

The parent H-ZSM-5 was prepared according to procedure B in ref. 7. Na and Al, determined by AAS after digestion with hydrofluoric acid, were found to amount to 0.08 and 0.82 mmol $g_{calc.}^{-1}$, respectively. The amount of acidic bridging hydroxyls (H) was assumed to equal the difference between molar Al and Na content. The parent zeolite (Si/Al = 19.5) and In_2O_3 were intensively ground in amounts corresponding to a molar Al/In ratio of 1.

IR spectra were recorded using the wafer transmission technique. Sample treatments were performed in high vacuum (HV) of about 10^{-3} Pa for 0.5 h between 670 and 840 K. *In situ* oxidation and subsequent reduction of the cationic indium species introduced by auto-reductive SSIE were carried out in oxygen and hydrogen (200 mbar), respectively, for 0.5 h at temperatures indicated in the text. The wafers were contacted *in situ* with pyridine (Py) at 470 K (5.7 mbar) for 0.5 h and then degassed in HV for 0.5 h at temperatures gradually increased between 370 K and 720 K.

Fig. 1 shows the intensity decrease of the band at 3610 cm^{-1}, typical of bridging hydroxyls, upon degassing of H-ZSM-5 with and without In_2O_3 in HV at gradually increasing temperatures. Dehydroxylation of the parent zeolite [Fig. 1, curve (A)] started at about 750 K and approached the 50% level at about 840 K. However, in the presence of In_2O_3 the intensity decrease of the IR band set in at about 720 K, and continued in a more pronounced fashion; by 840 K the degree of dehydroxylation had already reached 70% [Fig. 1, curve (B)]. The additional proton consumption in the presence of In_2O_3 must at least be attributed to the partial replacement of lattice protons by cationic indium species, but actually this process probably proceeds to an even higher degree since incorporation of metal cations into H-zeolites generally results in a greater resistance of remaining bridged hydroxyls to thermal dehydroxylation. Naturally, these results provide no information on whether the replacement of protons proceeds according to eqn. (2) or eqn. (3).

In Fig. 2 the IR spectra of Py adsorbed on H-ZSM-5/In_2O_3 and, for comparison, the parent zeolites are presented. As generally known, the band at 1547 cm^{-1} and the broad absorption zone between 1610 and 1640 cm^{-1} (with maximum absorption around 1635 cm^{-1}) are attributed to the NH stretching and ring vibration mode of pyridinium ions and, hence, are indicative of Brönsted acid sites. The spectra of Py on H-ZSM-5 pretreated, prior to Py adsorption, at only 670 K (spectrum Aa) also exhibited, besides these absorptions, less intense bands at 1446 and 1455 cm^{-1} assigned to the 19b ring vibration of Py interacting with cationic extra-framework aluminium (EF-Al) species and, superimposed on the broad

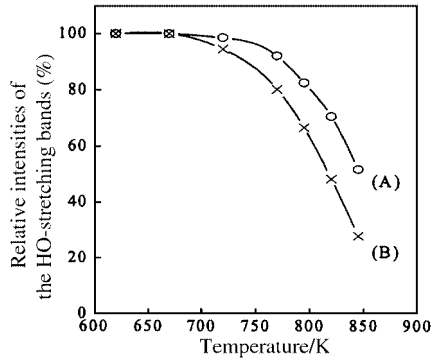

Fig. 1 Relative intensities of the hydroxyl stretching band at 3610 cm^{-1} in spectra of (A) H-ZSM-5 and (B) H-ZSM-5/In_2O_3(H/In = 1) *vs.* degassing temperature.

 DOI: 10.1039/b106081n

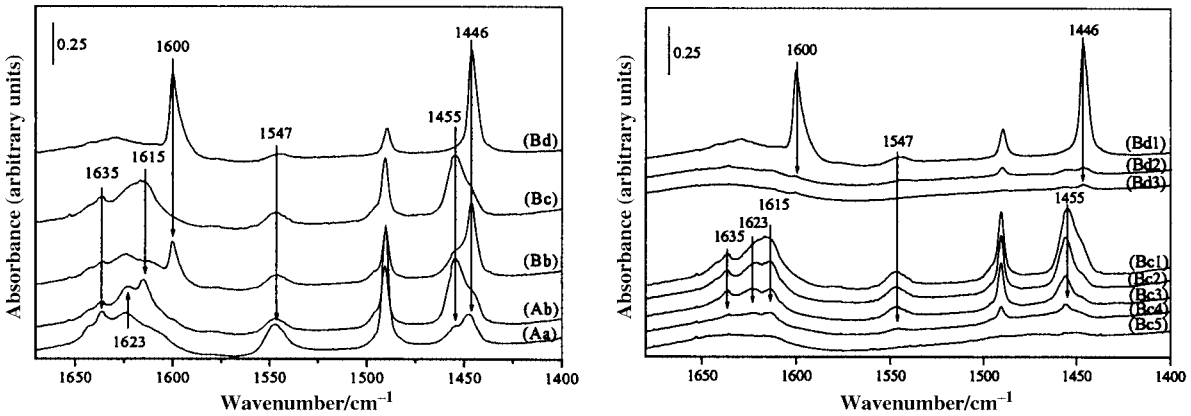

Fig. 2 IR spectra of adsorbed Py retained after degassing at 370 K on (A) H-ZSM-5 and (B) H-ZSM-5/In_2O_3 (H/In = 1) treated prior to Py adsorption in HV (a) at 670 K, (b) at 840 K, (c) at 840 K and subsequently contacted with O_2 at 720 K, and (d) reduced after pretreatment (c) with H_2 at 770 K. Two wafers, (Bc) and (Bd), were submitted to degassing procedures at 370 K (Bc1, Bd1), 470 K (Bc2, Bd2), 570 K (Bc3, Bd3), 670 K (Bc4) and 720 K (Bc5).

pyridinium absorption zone, an additional band at 1625 cm^{-1} attributed to the respective 8a ring vibration mode. According to expectation, the pyridinium bands decreased and the bands typical of Py interacting with EF-Al species increased in intensity upon thermal pretreatment at 840 K (spectrum Ab), *i.e.* at a temperature at which dehydroxylation associated with the release of aluminium from the framework already proceeds. Even a new band appeared at 1615 cm^{-1} which has not been mentioned in earlier reports. It is obviously associated with EF-Al located at a distinct crystallographic site of the ZSM-5 structure. In contrast, the drastic increase in the intensity of the band at 1455 cm^{-1} and the development of a new one at 1615 cm^{-1} upon heat treatment at 840 K was not observed in the spectrum of the H-ZSM-5/In_2O_3 mixture pretreated in the same way, *i.e.* in HV at 840 K [Fig. 2, spectrum (Bb)]. Thus, thermal dehydroxylation seems not to be significantly involved in the process which, nevertheless, results in a considerable reduction of the Brönsted acidity revealed by the intensity decrease of the band at 1547 cm^{-1} and, prior to Py adsorption, of the hydroxyl stretching band at 3610 cm^{-1} (see Fig. 1). In this context it is of great importance that concomitantly with the elimination of acidic hydroxyl groups, rather intense bands develop in the spectrum of adsorbed Py at 1466 and 1600 cm^{-1} (spectrum Bb in Fig. 2) which could earlier[5] be undoubtedly assigned to Py interacting with In^+ located on cation sites of zeolite structures. Thus, the appearance of these bands strongly evidences the incorporation of indium *via* AR-SSIE [eqn. (3)].

Thermal treatment of the H-ZSM-5/In_2O_3 mixture in the presence of O_2 after preceding AR-SSIE, *i.e.* after evacuation at 840 K (spectrum Bb in Fig. 2), resulted in Lewis acid sites of a new type revealed by bands of adsorbed Py at 1455 and around 1615 cm^{-1}, while those typical of In^+ cations disappeared (Fig. 2, spectrum Bc). In an earlier study,[5] these new bands could be assigned to Py interacting with InO^+ ions.

The bands associated with InO^+ appeared at practically the same wavenumbers as those caused by EF-AL (*e.g.* AlO^+). Nonetheless, the distinction of the two different cation species is easily possible by subsequent reduction with H_2 at higher temperature (770 K). According to expectation, such a reductive treatment (and naturally also the preceding oxidation) did not affect the spectra of pure H-ZSM-5, *e.g.* spectra Aa and Ab in Fig. 2 (not illustrated by figures). On the other hand, the same pretreatment procedure resulted in the reappearance of the two bands associated with In^+ cations at the expense of the InO^+ bands in the spectrum of the H-ZSM-5/In_2O_3 mixture (*cf.* spectra Bc and Bd in Fig. 2). Compared to the spectrum monitored after AR-SSIE (Bb in Fig. 2) the bands at 1446 and 1600 cm^{-1} even gained in intensity after the reduction with H_2 pointing to an only partial conversion of the applied In_2O_3 during the preceding heat treatment at 840 K and the completion of the incorporation process by conventional, *i.e.* hydrogen-induced, R-SSIE. After such an oxidation/reduction cycle the zeolitic phase contained only In^+ as lattice cations and even cationic EF-Al species detected in the parent zeolite seem to be displaced by In^+ from their original positions.

Monovalent cations, *e.g.* Na^+, are known to be rather weak Lewis acid sites from which coordinatively bound Py is released at relatively low temperatures. Accordingly, the bands at 1446 and 1600 cm^{-1}, indicative of In^+, practically disappeared upon degassing at temperatures as low as 470 K (*cf.* spectra Bd1–Bd3 in Fig. 2). In contrast, InO^+ proved to be a Lewis site of much higher acid strength since adsorbed Py was fully retained at degassing in HV at 470 K and gradually desorbed only in the temperature range up to 720 K (*cf.* spectra Bc1–Bc5 in Fig. 2).

Interestingly, InO^+-ZSM-5 underwent at least partial auto-reduction when heated in HV at 840 K since after such a treatment the bands typical of Py on In^+ reappeared to some degree at the expense of those attributed to Py on InO^+ (not shown in figures). Knowing this effect the idea may arise that the formation of lattice-stabilized In^+ upon heat treatment of H-ZSM-5/In_2O_3 mixtures could be due to auto-reduction of InO^+ cations previously incorporated into the zeolite structure by conventional SSIE according to eqn. (2). It is evident that the incorporation of indium into ZSM-5 should be unaffected by oxygen if it proceeds according to eqn. (2), but repressed if process (3) is correct. Experimentally it was found that in O_2 (5 mbar), even at 840 K the incorporation of any form of cationic indium ions is completely suppressed. This strongly evidences that auto-reduction of In_2O_3 in the starting mixture is the initial step in the mechanism of the ion-exchange process, and that the reaction route according to eqn. (2) can be excluded.

Notes and references

1 E. Kikuchi, M. Ogura, I. Terasaki and Y. Goto, *J. Catal.*, 1996, **161**, 465.
2 V. Kanazirev and G. L. Price, *Stud. Surf. Sci. Catal.*, 1994, **84C**, 1935.
3 H. K. Beyer, R. M. Mihályi, Ch. Minchev, Y. Neinska and V. Kanazirev, *Microporous Mater.*, 1996, **7**, 333.
4 R. M. Mihályi, G. Pál-Borbély, H. K. Beyer, Ch. Minchev, Y. Neinska and H. G. Karge, *React. Kinet. Catal. Lett.*,, 1997, **60**, 195; Y. Neinska, R. M. Mihályi, V. Mavrodinova, Ch. Minchev and H. K. Beyer, *Phys. Chem. Chem. Phys.*, 1999, **1**, 5761.
5 R. M. Mihályi, H. K. Beyer, Y. Neinska, V. Mavrodinova and Ch. Minchev, *React. Kinet. Catal. Lett.*, 1999, **68**, 355.
6 M. Ogura, N. Aratani and E. Kikuchi, *Stud. Surf. Sci. Catal.*, 1997, **105**, 1593.
7 E. G. Derouane, S. Demmetril, Z. Gabelica and N. Blom, *Appl. Catal.*, 1981, **1**, 201.

CHEMCOMM Communication
www.rsc.org/chemcomm

Room-temperature ionic liquids: a novel versatile lubricant

Chengfeng Ye, Weimin Liu,* Yunxia Chen and Laigui Yu

State Key Laboratory of Solid Lubrication, Lanzhou Institute of Chemical Physics, Chinese Academy of Sciences, Lanzhou 730000, China. E-mail: wmliu@ns.lzb.ac.cn

Received (in Cambridge, UK) 31st July 2001, Accepted 24th September 2001
First published as an Advance Article on the web 10th October 2001

Alkylimidazolium tetrafluoroborates are promising versatile lubricants for the contact of steel/steel, steel/aluminium, steel/copper, steel/SiO_2, Si_3N_4/SiO_2, steel/Si(100), steel/sialon ceramics and Si_3N_4/sialon ceramics; they show excellent friction reduction, antiwear performance and high load-carrying capacity.

Room-temperature ionic liquids were initially developed by electrochemists for use as electrolytes in batteries or for metal electrodeposition. As a non-conventional class of novel solvents, ionic liquids are becoming increasingly important and of particular interest. This is because they have a number of characteristics including negligible volatility, non-flammability, high thermal stability, low melting point, broad liquid range, and controlled miscibility with organic compounds, especially some heterocycle compounds.[1–4] Therefore they have attracted enormous attention as media for green synthesis and been successfully used to realize many important reactions.[5–8]

On the other hand, the above-mentioned properties of ionic liquids make them potent excellent lubricants. The lubricants currently used in industry are restricted in their application. For instance, lubricants for steel/steel contact may be unsuitable for aluminium/ceramics. For example, while alcohol has been successfully used as a lubricant for ceramics and aluminium it behaves poorly for steel. Clearly versatile lubricants would be of great value for the industrial community.

Bearing this in mind and taking into consideration melting point, thermal stability, hygroscopicity and viscosity, we chose 1-methyl-3-hexylimidazolium tetrafluoroborate (denoted L106) and 1-ethyl-3-hexylimidazolium tetrafluoroborate (L206) (see Fig. 1) to evaluate their tribological behavior using an Optimol SRV (SRV is the abridged name for German Schwingung, Reibung, Verschleiss) oscillating friction and wear tester with ball-on-disc configuration.[9]

The SRV test results at a medium load are listed in Table 1. It can be seen that the ionic liquid L106 exhibits excellent tribological performance for steel (SAE-52100), aluminium (Al2024), copper, single crystal SiO_2, single crystal Si(100) and sialon (Si–Al–O–N) ceramics.[10] It exhibits the lowest friction coefficients as compared with the two fluorine-containing lubricants phosphazene (X-1P)[11] and perfluoropolyether (PFPE)[12] which are widely used as lubricants for head/disk interface or space applications. Thus it can be anticipated that ionic liquids might be promising versatile lubricants.

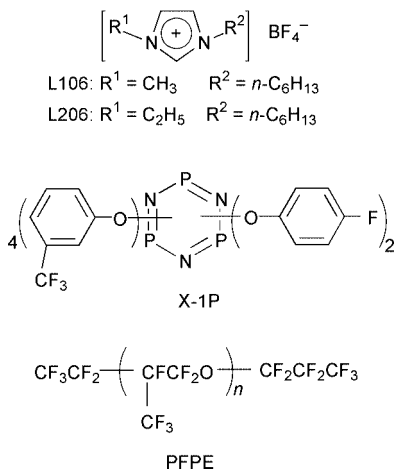

Fig. 1 Molecular structures of the ionic liquids L106 and L206 and traditional lubricants X-1P and PFPE.

Table 1 Friction coefficients for several frictional pairs lubricated with various lubricants (SRV tester, load 50 N, frequency 25 Hz, amplitude 1 mm)

	Friction coefficient		
Frictional pair (ball/disk)	L106	X-1P	PFPE
Steel/steel	0.065	0.098	0.145
Steel/Al	0.040	0.128	—
Steel/Cu	0.025	0.117	0.145
Steel/SiO_2	0.060	0.110	0.132
Si_3N_4/SiO_2	0.083	0.115	0.132
Steel/Si(100)	0.050	0.102	0.145
Steel/sialon	0.065	0.100	0.120
Si_3N_4/sialon	0.065	0.105	0.130

Table 2 shows the SRV test results for the ionic liquid L206, X-1P and PFPE under relatively high loads (≥200 N). The friction coefficient and wear volume loss of a steel disc lubricated by L206 remains at a very low level with increasing load, and the load-carrying capacity of L206 reaches up to 1000 N, much higher than that of X-1P (300 N) or PFPE (400 N).

The ionic liquids L106 and L206 are non-hygroscopic, are air- and water-stable under ambient conditions, and slightly soluble in water; the solubility of L106 in water is *ca.* 0.28 g l^{-1} at 20 °C while L206 has a similar solubility. The solubility of the ionic liquids in water has little effect on the tribological behavior. Moreover, the addition of a small amount of water (≤5 wt%) to the ionic liquids is helpful to improve the antiwear ability for various frictional pairs (steel/steel, steel/aluminium and steel/ceramic) but has little effect on the friction reduction performance.

A question then arises: why do ionic liquids exhibit superior tribological behavior? Noticing the unique dipolar structure, we propose that ionic liquids can be easily adsorbed on the sliding surface of frictional pairs. Subsequently an effective boundary film would form so as to reduce friction and wear. Furthermore, under severe friction conditions, the tetrafluoroborate anion will

Table 2 Tribological properties of ionic liquid L206, X-1P and PFPE for steel/steel contact (SRV tester, load 50 N, frequency 25 Hz, amplitude 1 mm, duration 30 min)

	Friction coefficient			Wear volume/$\times 10^{-4}$ mm^3		
Load/N	L206	X-1P	PFPE	L206	X-1P	PFPE
200	0.060	0.070	0.120	0.05	0.07	0.60
300	0.055	0.065	0.110	0.22	2.21	1.90
400	0.050	—	0.105	0.39	—	5.03
500	0.045	—	—	0.45	—	—
600	0.045	—	—	0.53	—	—

'—' lubrication failure.

 DOI: 10.1039/b106935g

decompose to form anti-scratch components such as fluoride, B_2O_3 and BN. This is confirmed by the B 1s XPS spectra of worn surfaces under different testing conditions (Fig. 2). Only BN is detected in the sliding area of steel/sialon contact lubricated with L106 under 300 N, while both B_2O_3 and BN are detected in the sliding area of Si_3N_4/sialon ceramic contact lubricated with L106 under 80 N.

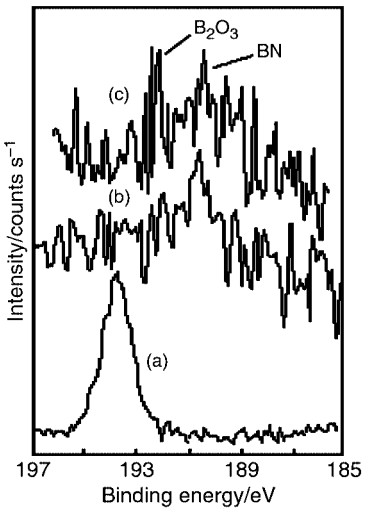

Fig. 2 B 1s spectra of neat L106 on Au (a) and in wear scar of sialon sliding against steel lubricated with L106 under 300 N (b) and of sialon sliding against Si_3N_4 under 80 N (c).

In addition, ionic liquids L106 and L206 have pour points below −55 °C and show no weight loss below 320 °C. Thus, the prominent low temperature fluidity, high temperature stability, low vapor pressure and excellent lubricity makes them an attractive alternative to conventional liquid lubricants.

This work was financially supported by the National Natural Science Foundation of China (Grant No. 59825116) and Chinese Academy of Sciences.

Notes and references

1 T. Welton, *Chem. Rev*., 1999, **99**, 2071.
2 M. J. Earle and K. R. Seddon, *Pure Appl. Chem*., 2000, **72**, 1391.
3 H. Olivier, *J. Mol. Catal. A: Chemical*, 1999, **146**, 285.
4 R. Hagiwara and Y. Ito, *J. Fluorine Chem*., 2000, **105**, 221.
5 J. G. Huddleston, H. D. Willauer, R. P. Swatloski, A E. Visser and R. D. Rogers, *Chem. Commun*., 1998, 1765.
6 T. Fisher, A. Sethi and J. Woolf, *Tetrahedron Lett*., 1999, **40**, 793.
7 M. Earle, P. B. McCormac and K. R. Seddon, *Chem. Commun*., 1998, 2245.
8 V. M. Kobryanskii and S. A. Arnautov, *Chem. Commun*., 1992, 727.
9 W. G. Zhang, W. M. Liu, H. W. Liu, L. G. Yu and Q. J. Xue, *Wear*, 1998, **223**, 143.
10 C. Zhang, W. Y. Sun and D. S. Yan, *J. Eur. Ceram. Soc*., 1999, **19**, 33.
11 B. S. Nader, K. K. Kar, T. D. Morgan, C. E. Pawloski and W. L. Dilling, *Tribol. Trans*., 1992, **35**, 37.
12 W. R. Jones, B. A. Shogrin and M. J. Jansen, *Synth. Lubr*., 2000, 109.

CHEMCOMM Communication
www.rsc.org/chemcomm

$[Ni(R_2pipdt)_2](BF_4)_2$ (R_2pipdt = 1,4-disubstituted-piperazine-3,2-dithione) as useful precursors of mixed–ligand dithiolenes of interest for non-linear optics†‡

Francesco Bigoli,[a] Chin-Ti Chen,[b] Wei-Ching Wu,[b] Paola Deplano,*[c] Maria Laura Mercuri,[c] Maria Angela Pellinghelli,[a] Luca Pilia,[c] Gloria Pintus,[c] Angela Serpe[c] and Emanuele F. Trogu[a]

[a] *Dipartimento di Chimica Generale ed Inorganica, Chimica Analitica, Chimica Fisica, CSSD CNR, Parco Area delle Scienze 17A, I-43100 Parma, Italy*
[b] *Institute of Chemistry, Academia Sinica, Taipei, Taiwan 11529, ROC*
[c] *Dipartimento di Chimica Inorganica ed Analitica, Università di Cagliari, Cittadella di Monserrato, I-09042 Monserrato, Cagliari, Italy. E-mail: deplano@vaxca1.unica.it*

Received (in Cambridge, UK) 9th July 2001, Accepted 27th September 2001
First published as an Advance Article on the web 17th October 2001

A simple method to obtain in high yields mixed-ligand nickel–dithiolene complexes, which show strong negative solvatochromism and negative first molecular hyperpolarizability, and the use of Raman spectroscopy to establish the extent of electronic delocalisation in these complexes, are reported.

Metal–dithiolenes represent a class of compounds of interest in several fields of materials chemistry.[1] Symmetrical bis-dithiolene nickel complexes exhibit an intense electronic transition at low energies assigned to a $\pi \rightarrow \pi^*$ transition between the HOMO and the LUMO, delocalised over both the ligands (R = R′, Scheme 1). This extensive electron-delocalization, while making these complexes useful as near-infrared (NIR) dyes, is irrelevant to intramolecular charge transfer, a crucial factor in generating second order non-linear optical (NLO) properties. It is known[1c] that donor substituents in the parent dithiolene $[Ni(edt)_2]$ (edt = ethylenedithiolate) raise the energy of the HOMO more than that of the LUMO, with a consequent shift of the low-energy band to lower frequencies. However, very strong donor substituents may also force the HOMO to become antibonding and the loss of one or two electrons may be observed, but examples of cations are extremely rare.[1c] On the other hand, electron-withdrawing substituents lower the energy both of the HOMO and the LUMO, and the latter MO may become bonding, leading to the formation of anions, as observed in several cases (mnt,[2a] tdas,[2b] qxd,[2c] dmit,[2d] dsit,[2e] tkr[2f] derivatives, Scheme 2). When R ≠ R′ (unsymmetrical complexes) where R is an electron donating substituent and R′ an electron withdrawing substituent, the resonance form **A** (Scheme 1) may dominate the ground state. In this case the complexes can be described as dithione–dithiolate derivatives with the R′ containing ligand contributing more to the HOMO and R containing one likewise to the LUMO. Thus the electronic transition between the HOMO and the LUMO will have intramolecular CT character, making unsymmetrical complexes potential second-order NLO chromophores.[3]

However $[Ni(R_2C_2S_2)(R'_2C_2S_2)]$ complexes are extremely rare,[4] mainly for the difficulties encountered in the synthetic procedure and in their purification. Among them $[Ni(R_2pipdt)(R'_2C_2S_2)]$ [$R_2C_2S_2$ = 1,4-dialkylpiperazine-3,2-dithione (R_2pipdt); $R'_2C_2S_2$ = maleonitriledithiolate (mnt) and trifluoromethyldithiolate (tfd)] nickel complexes have been prepared by reacting the free R_2pipdt ligand with the neutral complexes $[Ni(mnt)(NH_3)_2]$ and $[Ni(tfd)_2]$, respectively. These complexes show strong negative solvatochromism and negative first molecular hyperpolarizability (β).[5]

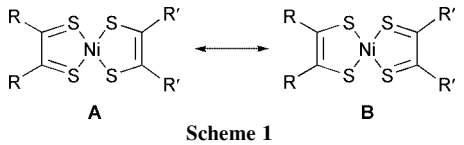

Scheme 1

We report here a simple method to prepare several complexes belonging to this class of potential second-order NLO chromophores, some of them not reported before, by reacting a salt of a nickel–dithiolene dication $[Ni(R_2pipdt)_2](BF_4)_2$ **1** with a salt of a nickel–dithiolene dianion $(Bu_4N)_2[Ni(S_2C_2R'_2)_2]$ **2** as shown in Scheme 2.

$[Ni(Me_2pipdt)_2](BF_4)_2$ (R = Me, **1′**) has been characterized. Structural data[6] show that the most significant bond distances and angles in the $[Ni(Me_2pipdt)_2]^{2+}$ cation fall in the typical range of square-planar nickel–dithiolene complexes (Fig. 1).

This cation has been briefly mentioned in the literature,[1c] but data on its characterisation were missing.

The cyclic voltammogram of **1′** is in agreement with a dithiolene description of this cation, showing four reversible redox steps which are ascribed to mono-electronic processes leading **1′** from the dicationic to the dianionic species.

All the obtained mixed-ligand compounds (**3a**–**f**) shown in Scheme 2 have been characterized by analytical, spectroscopic and electrochemical methods. [Ni(Me$_2$pipdt)(mnt)] (R = Me, **3a′**) has been also structurally characterised[6] (Fig. 2). Complexes **3a′**–**f′** exhibit a low-frequency peak, which shows negative solvatochromism, above 700 nm. Solvatochromic measurements and dipole analysis have been performed on [Ni(Pr$^i_2$pipdt)(dmit)] as described in ref. 5. In Table 1 a comparison of these results with those of [Ni((EH)$_2$-

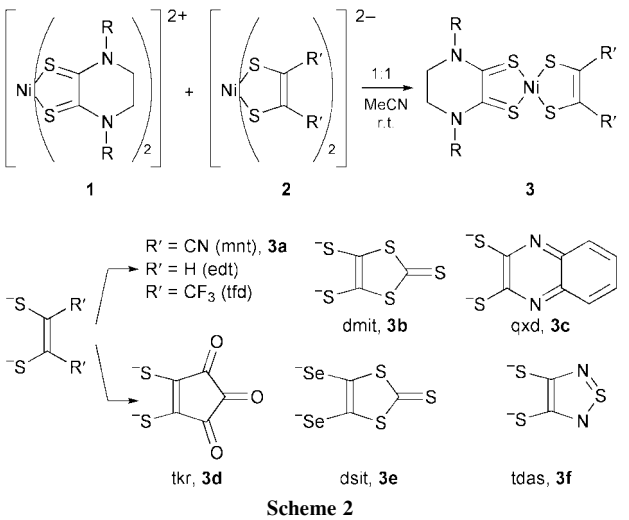

Scheme 2

† Electronic supplementary information (ESI) available: experimental section. See http://www.rsc.org/suppdata/cc/b1/b106064n/
‡ Dedicated to Prof. P. Cassoux, CNRS, Toulouse, for his 60th birthday.

 DOI: 10.1039/b106064n

Table 1

	λ_{max}[a]/nm	10^{-3} ε/ M^{-1} cm^{-1}	μ_{eg}/D	μ_g/D	$\mu_e-\mu_g$/D	d/g ml^{-1}	a/Å	μ_e/D	10^{-30} β_0/esu	Ref.
[Ni(Pr$^i_2$pipdt)(dmit)]	965	10.9	5.9	13	−11	1.51	6.7	2	−130	This work
[Ni((EH)$_2$pipdt)(mnt)]	829	9.8	3.7	16	−10	1.23	7.3	6	−37	5
[Ni(Pr$^i_2$timdt)(mnt)]	883	24.1	6.7	16	~0	1.24	6.8	16	~0	This work

[a] In chloroform; a = Onsager radius (taken as sum of spherical radius of solute and solvent; d = density; μ_{eg} = transition dipole moment; μ_g = ground-state dipole moment; μ_e = excited-state dipole moment. Pr$^i_2$timdt = monoanion of 1,3-diisopropylimidazolidine-2,4,5-trithione;[7] EH = 2-ethylhexyl.

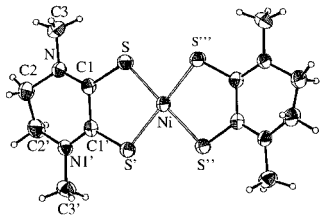

Fig. 1 Molecular structure of the $[Ni(Me_2pipdt)_2]^{2+}$ cation which shows a crystallographic D_2 symmetry. Selected bond distances (Å) and angles(°): Ni–S 2.159(2), S–C(1) 1.688(8), C(1)–C(1′) 1.477(12); S–Ni–S″ 92.08(8), S–Ni–S‴ 87.99(8), S–Ni–S‴ 177.21(8) [′: x, 1/4−y, 1/4−z; ″: ¼−x, y, ¼−z; ‴: ¼−x, ¼−y, z].

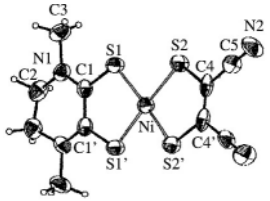

Fig. 2 Molecular structure of **3a′** lying on a two-fold axis. Selected bond distances (Å) and angles (°): Ni–S(1) 2.162(2), Ni–S(2) 2.146(2), S(1)–C(1) 1.700(6), S(2)–C(4) 1.735(6), C(1)–C(1') 1.43(1), C(4)–C(4′) 1.32(1); S(1)–Ni–S(1′) 91.6(1), S(2)–Ni–S(2′) 92.51(8), S(1)–Ni–S(2) 88.21(7), S(1)–Ni–S(2′) 174.3(1) [′ −x, y, ½−z].

Table 2 Cyclic voltammetric data[a]

Complex	E_a/V (1 ← 0)	$E^1_{1/2}$/V (0 ⇌ −1)	$E^2_{1/2}$/V (−1 ⇌ −2)
3a′	+0.900	−0.530	−0.970
3c′	+0.812	−0.595	−1.033
3e′[b]	+0.610	−0.505	−0.966
3f′	+0.820	−0.582	−1.034

[a] Measured at Pt electrodes in MeCN ([b] in DMF), 0.1 M Bu_4NPF_6, scan rate 100 mV s^{-1}, reference electrode: Ag/AgCl.

pipdt)(mnt)][5] and with those obtained on [Ni(Pr$^i_2$timdt)(mnt)] is reported. [Ni(Pr$^i_2$timdt)(mnt)] belongs to a class (**4**) of apparently similar mixed-ligand derivatives, recently prepared by us,[7] where the ligand containing the electron-donating substituent is Pr$^i_2$timdt (formally the monoanion of 1,3-diisopropylimidazolidine, whatever of R_2pipdt. Both [Ni(Pr$^i_2$pipdt)(dmit)] and [Ni((EH)$_2$pipdt)(mnt)] show pronounced negative solvatochromism as indicated by their large negative values of $\mu_e - \mu_g$. The β_0-value found for [Ni(Pr$^i_2$pipdt)(dmit)] is 3× that of [Ni((EH)$_2$pipdt)(mnt)] and it is mainly due to the larger transition dipole moment and longer absorption wavelength. It is reasonable that the direction of the LLCT of these complexes is from the dithiolate-ligand to the dithione-ligand. Instead a β_0-value near to zero is found for [Ni(Pr$^i_2$timdt)(mnt)]. The different behaviour of these apparently similar complexes is related to the extent of the electronic delocalization in class **4** complexes. The low-energy band is thus assigned to a $\pi\rightarrow\pi^*$ transition in class **4** derivatives and to LLCT (dithiolate to dithione) transition in class **3** ones. Accordingly the very similar $E_{1/2}$ values related to the reduction processes of class **3** complexes (Table 2) suggest a prevailing contribution of the Me$_2$pipdt ligand to the LUMO. By contrast, class **4** complexes show corresponding $E_{1/2}$ values at intermediate values between those of the parent symmetrical complexes.[7]

Raman spectra are very diagnostic to distinguish the two classes of complex. The C=C stretch shows a shift to higher frequencies as the negative charge on the complex increases in Ni(mnt)$_2$-complexes.[8a] This peak is found at 1485 for $[Ni(mnt)_2]^{2-}$ and at 1435 cm^{-1} for $[Ni(mnt)_2]^{-}$. [Ni(Me$_2$-pipdt)(mnt)] and [Ni(Pr$^i_2$timdt)(mnt)] exhibit a peak at 1492 and 1425 cm^{-1}, respectively thus suggesting that the mnt ligand bears a −2 formal charge in [Ni(Me$_2$pipdt)(mnt)] which is significantly lowered in [Ni(Pr$^i_2$timdt)(mnt)]. Similarly, comparing the peaks assigned to the C=C stretch of the dmit ligand in [Ni(Pr$^i_2$pipdt)(dmit)] (1445 cm^{-1}) and [Ni(Pr$^i_2$timdt)(dmit)] (1388 cm^{-1}), the position of these bands is near to the frequency of the C=C peaks, respectively, in the dianionic (1435 cm^{-1}) and monoanionic (1390 cm^{-1}) $[Ni(dmit)_2]^{n-}$ complexes.[8b]

The CNR (Materiali Speciali per Tecnologie Avanzate II) is acknowledged for financial support.

Notes and references

1 (*a*) P. Cassoux and L. Valade, *Inorganic Materials*, ed. D. W. Bruce and D. O'Hare, John Wiley & Sons, Chichester, 2nd edn., 1996; (*b*) A. T. Coomber, D. Beljonne, R. H. Friend, J. K. Brédas, A. Charlton, N. Robertson, A. E. Underhill, M. Kurmoo and P. Day, *Nature*, 1996, **380**, 144; (*c*) U. T. Mueller-Westerhoff, B. Vance and D. I. Yoon, *Tetrahedron*, 1991, **47**, 909.

2 (*a*) E. Billig, R. Williams, I. Bernal, J. H. Waters and H. B. Gray, *Inorg. Chem.*, 1964, **3**, 663; (*b*) I. Hawkins and A. E. Underhill, *J. Chem. Soc., Chem. Commun.*, 1990, 1593; (*c*) D. C. Morrison and A. Furst, *J. Chem. Soc.*, 1956, **21**, 470; (*d*) G. Steimecke, H. J. Sieler, R. Kirmse and E. Hoyer, *Phosphorus Sulfur*, 1979, **7**, 49; (*e*) R. M. Olk, A. Rohr, B. Olk and E. Hoyer, *Z. Chem.*, 1988, **28**, 304; (*f*) W. B. Heuer and W. H. Pearson, *J. Chem. Soc., Dalton Trans.*, 1996, 3507.

3 A. Vogler and H. Kunkely, *Angew. Chem., Int. Ed. Engl.*, 1982, **21**, 77.

4 R. Kato, Y. Kashimura, H. Sawa and Y. Okano, *Chem. Lett.*, 1997, 921.

5 C.-T. Chen, S.-Y. Liao, K.-J. Lin and L.-L. Lai, *Adv. Mater.*, 1998, **10**, 334.

6 *Crystal data*: for **1′**: $C_{12}H_{20}B_2F_8N_4NiS_4$, M = 580.89, orthorhombic, *Fddd*, a = 16.646(6), b = 18.189(6), c = 14.887(6) Å, V = 4507(3) Å^3, Z = 8, D_c = 1.712 Mg m^{-3}, μ(Mo-Kα = 1.305 mm^{-1}, T = 293(2) K, 994 reflections measured, 994 unique data. For 326 observed reflections with [$I > 2\sigma(I)$] and 68 parameters the final $R1$ = 0.0750 [$wR2$ = 0.2316 (all data)]. For [Ni(Me$_2$pipdt)(mnt)]: $C_{10}H_{10}N_4NiS_4$, M = 373.17, monoclinic, *C2/c*, a = 15.381(4), b = 13.623(4), c = 7.464(5) Å, β = 106.16(2)°, V = 1502.2(12) Å^3, Z = 4, D_c = 1.650 Mg m^{-3}, μ(Mo-Kα) = 1.837 mm^{-1}, T = 293(2) K. Of a total of 1431 reflections collected, 1330 reflections were independent (R_{int} = 0.021). For 384 observed reflections with [$I > 2\sigma(I)$] and 91 parameters the final $R1$ = 0.0452 [$wR2$ = 0.1215 (all data)]. All data were collected from a Siemens AED diffractometer (Mo-Kα) radiation, λ = 0.71073 Å). The structures were solved by direct methods and refined by full-matrix least squares on F^2. The F(2) atom of the anion in **1′** showed a high thermal parameter. In the final refinement the value of the occupancy factor for the two images of this disordered atom was 0.53 and 0.47, respectively. The unsatisfactory values for **1′** result from the very poor quality of the crystals. CCDC reference numbers 167946 and 167947. See http://www.rsc.org/suppdata/cc/b1/b106064n/ for crystallographic data in CIF or other electronic format.

7 F. Bigoli, P. Cassoux, P. Deplano, M. L. Mercuri, M. A. Pellinghelli, G. Pintus, A. Serpe and E. F. Trogu, *J .Chem. Soc., Dalton Trans*, 2000, 4639 and references therein.

8 (*a*) C. W. Schläpfer and K. Nakamoto, *Inorg. Chem.*, 1975, **14**, 1338; J. L. Wootton and J. I. Zink, *J. Phys. Chem.*, 1995, **99**, 7251; (*b*) K. I. Pokhodnya, C. Faulmann, I. Malfant, R. Andreu-Solano, P. Cassoux, A. Mlayah, D. Smirnov and J. Leotin, *Synth. Met.*, 1999, **103**, 2016.

CHEMCOMM Communication
www.rsc.org/chemcomm

Specific molecular interactions in Pd(II) complexes identify a new approach to the biaxial nematic phase

Laurent Omnès,[a] Bakir A. Timimi,[b] Thomas Gelbrich,[c] Michael B. Hursthouse,[c] Geoffrey R. Luckhurst*[b] and Duncan W. Bruce*[a]

[a] *School of Chemistry, University of Exeter, Stocker Road, Exeter, UK EX4 4QD. E-mail: d.bruce@ex.ac.uk*
[b] *Department of Chemistry and Southampton Liquid Crystal Institute, University of Southampton, Southampton, UK SO17 1BJ*
[c] *Crystallographic Service, Department of Chemistry, University of Southampton, Southampton, UK SO17 1BJ*

Received (in Cambridge, UK) 30th August 2001, Accepted 27th September 2001
First published as an Advance Article on the web 18th October 2001

Liquid-crystalline complexes of Pd(II) allow a new approach to the realisation of the biaxial nematic phase.

In the uniaxial nematic phase (N_u) of liquid crystals, there is no positional order and the unique axes of the molecules are oriented about a director, ***n***. In the *biaxial nematic phase* (N_b) there is, additionally, a correlation of the other molecular axes in a direction perpendicular to ***n*** and so whereas in the N_u phase the physical properties in the plane perpendicular to ***n*** are angle-independent, this is not the case in the N_b phase. Since Freiser's[1] prediction of the existence of an N_b phase, this topic has attracted much interest. Yet despite experimentalists trying to make these predictions come to life, the N_b phase in low-molecular-mass thermotropic liquid crystals remains elusive.

Two main strategies have been developed in the search for the phase. One is based on single-component systems where 'shape biaxiality' is optimised,[2] while the other is suggests that mixtures of two uniaxial nematic phases with non-coincident directors, could lead to the formation of the N_b phase.[3] The latter approach is problematic as such mixtures phase-separate into two uniaxial nematics.

In this communication, we propose a different approach which exploits total *molecular* biaxiality, *i.e.* not simply a shape biaxiality. Thus, we are seeking systems where possibilities for biaxial intermolecular interactions can be built in that lead to the realisation of long-range, orientational correlation in two orthogonal directions.

Fluoro-substitution in thermotropic liquid crystals provides a way of modifying their physical properties.[4,5] Further, the ideas of amphiphilicity and microphase separation are also well-known in liquid crystals,[6] where it is recognised that like parts of a molecule prefer to associate. Indeed, the presence of perfluorocarbon and hydrocarbon chains within the same molecule produces micro-segregation at the molecular level. We wished to use these ideas to design some organopalladium(II) complexes which would, in addition to possessing shape biaxiality, generate localised segregation, so promoting correlations perpendicular to the main nematic director.

The complexes we chose for study are based on the well-known *ortho*-palladated mesogens. We took as our starting point a system described by Espinet and Buey[7] in which dimer **1** is cleaved with the anion of a β-diketonate (Fig. 1). We used trifluoroacetylacetonate (tfac) and obtained the target complex **2** as a 1:1 mixture of isomers as shown by the ^{1}H NMR spectrum.† We were able to obtain single crystals of the dimethoxy derivative (R = R′ = MeO) and found that a single isomer crystallised.‡ However, when the solid-state packing of the molecule was considered, we found that the fluorocarbon parts of the complex remained together (Fig. 2), supporting the approach we were taking.

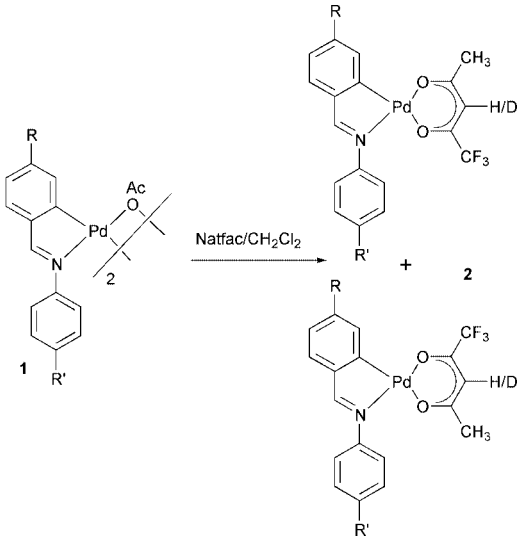

Fig. 1 Synthesis of the target complexes.

While we have made several derivatives of **2**, two are of particular note, namely with R = R′ = $-OC_6H_{13}$ (**2a**) and with R = $-OC_6H_{13}$, R′ = $-C_6H_{13}$ (**2b**). Both showed a monotropic nematic phase [**2a**: Cr • (62.6 • N) • 91.6 • I; **2b**: Cr • (11.7 • N) • 67 • I; temp. in °C]; polarised optical microscopy showed each to have an ill-defined, marbled texture. We then evaluated the thermodynamics of the N–I transition as theory predicts[8] the N_b–I transition to be second order. The enthalpy changes were small [ΔH(**2a**) = 0.20 kJ mol^{-1}; ΔH(**2b**) = 0.17 kJ mol^{-1}] as were the corresponding entropy changes [$\Delta S/R$(**2a**) = 0.075; $\Delta S/R$(**2b**) = 0.072]. It is instructive to compare this behaviour with that of the non-fluorinated analogue of **2a** (*i.e.* prepared using acac) where the N–I transition showed ΔH = 1.0 kJ mol^{-1} and $\Delta S/R$ = 0.30. This significant difference in the $\Delta S/R$ values shows that fluorination causes the transition to become much less strongly first order, providing further evidence supporting our approach.

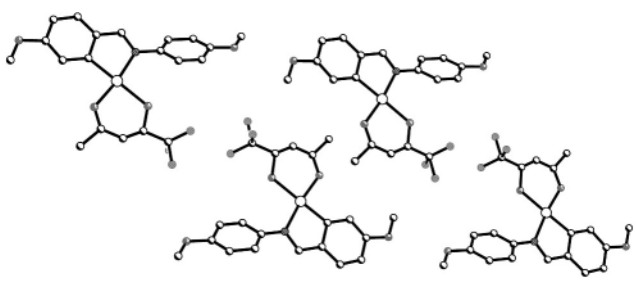

Fig. 2 The packing of **2a** in the solid state.

 DOI: 10.1039/b107775a

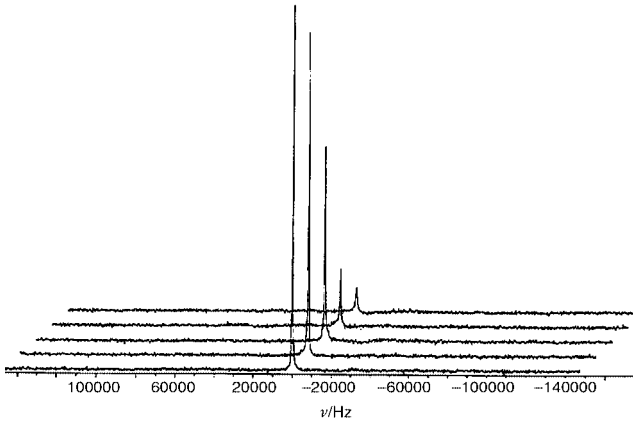

Fig. 3 ^{1}H NMR spectrum of **2a** in the isotropic phase between 365 K (most intense signal) and 335 K (least intense signal).

However, with the biaxial nematic phase, it is characterisation which is at the heart of the question[9] and the one technique which appears to offer unequivocal identification of the N_b phase is ^{2}H NMR spectroscopy.[10] It was, therefore, necessary to introduce deuterium into the complex which we did at the position shown in Fig. 1. Thus, Na^+tfac^- was deuteriated by stirring in CD_3OD–D_2O at room temperature for 4 h before the solvents were removed *in vacuo*. After reaction with **1**, deuteriated **2a** was obtained with 80% deuterium incorporation.

The spectra were measured using a quadrupolar echo sequence, and the sample was brought into the isotropic phase and then cooled slowly; a strong singlet corresponding to the isotropic phase was recorded. However the signal intensity decreased with temperature and 90% of the magnetisation was lost before the nematic phase was reached (Fig. 3). This behaviour normally suggests that the compound is either crystallising or decomposing in the probe, but after the experiment, the sample was checked visually and then by polarised optical microscopy and also by ^{1}H NMR spectroscopy, none of which suggested that either of the two processes had occurred. No definite explanation has yet been given for this experimental observation, although we cannot yet rule out vitrification.

The sample was then further cooled and at the isotropic-to-nematic transition a doublet was observed. The spectra (Fig. 4) showed a small biphasic region and allowed the measurement of the transitional quadrupolar splitting, $\Delta\nu$, even if the signal was rather weak. From the quadrupolar splitting it is possible to calculate S, the order parameter of the long molecular axis and in so doing we made the assumption that the angle between the molecular long axis and the C–D bond was 90°. On calculating values of S, it was found that at the N–I transition, it had a value of 0.105. This compares with typical transition values for a *uniaxial* nematic phase of around 0.35. Note that S is expected to start at zero for a *biaxial* nematic phase if the I → N_b transition is directly at the so-called Landau point. Our results indicate, therefore, a very low order parameter for this nematic phase consistent with the low transitional entropy ($\Delta S/R$), although we cannot say that the phase is biaxial.

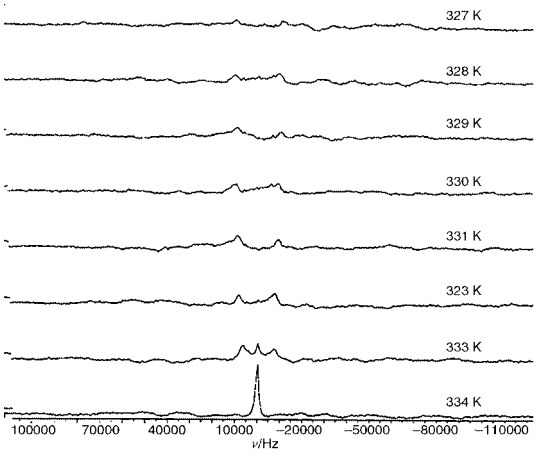

Fig. 4 ^{1}H NMR spectra in the nematic phase.

By comparison, a very similar complex named 'Azpac' (as **2a** but containing an acac ligand and with the imine link replaced by an azoxy function) was studied by ^{2}H NMR spectroscopy some years ago.[11] The deuterons were introduced *via* the aromatic rings of the ligand, here, the order parameter close to the N–I transition was found to be *ca*. 0.4. These results provide further evidence in support of our approach to the generation of biaxial materials.

Further support for this strategy comes from recent results of Monte Carlo simulations by Berardi and Zannoni[12] in which they employed a Gay–Berne potential, modified to enhance side-to-side interactions of Gay–Berne particles. Using this approach, they too were able to stabilise a biaxial nematic phase, although interestingly, when face-to-face interactions were enhanced, a biaxial smectic phase was found. The recent identification[13] of the biaxial SmA phase using such an approach experimentally lends support to their simulations and further lends support to the approach we have identified.

We thank the EU (contract ERBFMRXCT970121), NEDO and the University of Exeter for support (L. O.) and Johnson Matthey for generous loans of precious metal salts.

Notes and references

† All new complexes were satisfactorily characterised by spectroscopic methods and by CHN analysis.

‡ *Crystal data* for **2a**. $C_{20}H_{18}F_3NO_4Pd$, orange block, M_r = 499.75, monoclinic, space group $P2_1/c$, a = 12.8622(12), b = 17.3734(18), c = 8.6466(12) Å, U = 1924.4(4) Å^3, Z = 4, D_c = 1.725 g cm^{-3}, μ = 1.020 mm^{-1}, $F(000)$ = 1000, crystal size 0.07 × 0.05 × 0.05 mm. Data were collected at 150 K, on a Nonius Kappa CCD area detector diffractometer,[14] at the window of a Nonius FR591 rotating anode (λ Mo-Kα = 0.71073 Å). Combined φ and ω scans, frame increment of 2.0°, θ_{max} = 24.00° (index ranges $-14 \leqslant h \leqslant 14$, $-19 \leqslant k \leqslant 18$, $-9 \leqslant l \leqslant 9$). An absorption correction was applied by comparison of multiple and symmetry equivalent reflections, using the program SORTAV[15] (transmission factors = 0.9508/0.9321). A solution was obtained *via* direct methods and refined[16] by full-matrix least squares on F^2, with hydrogens included in idealised positions. 2857 Unique data were produced from 7543 measured reflections (R_{int} = 0.1112). 202 parameters refined to R_1 = 0.1235 and wR_2 = 0.2278 [$I > 2\sigma(I)$] (R_1 = 0.1900 and wR_2 = 0.2482 for all data), with residual electron densities of 1.617 and −0.779 e Å^{-3}. CCDC reference number 170065. See http://www.rsc.org/suppdata/cc/b1/b107775a/ for crystallographic data in CIF or other electronic format.

1 M. J. Freiser, *Phys. Rev. Lett*., 1970, **24**, 1041.
2 K. Praefcke, B. Kohne, B. Gündoğan, D. Singer, D. Demus, S. Diele, G. Pelzl and U. Bakawsky, *Mol. Cryst. Liq. Cryst*., 1991, **198**, 393.
3 A. G. Vanakaras, S. C. McGrother, G. Jackson and D. J. Photinos, *Mol. Cryst. Liq. Cryst*., 1998, **323**, 199.
4 M. Hird and K. J. Toyne, *Mol. Cryst., Liq Cryst*., 1998, **323**, 1.
5 F. Guittard, E. Taffin de Givenchy, S. Geribaldi and A. Cambon, *J. Fluorine Chem*., 1999, **100**, 85.
6 See for example: C. Tschierske, *J. Mater. Chem*., 1998, **8**, 1485.
7 P. Espinet and J. Buey, *J. Organomet. Chem*., 1996, **507**, 137.
8 N. Boccara, R. Mejdani and L. De Seze, *J. Phys*., 1997, **38**, 149.
9 Y. Galerne, *Mol. Cryst., Liq. Cryst*., 1998, **323**, 211.
10 G. R. Luckhurst, *Thin Solid Films*, 2001, **393**, 40.
11 L. Calucci, D. Catalano, M. Ghedini, N. L. Jones, D. Pucci and C. A. Vearcini, *Mol. Cryst. Liq. Cryst*., 1996, **290**, 87.
12 R. Berardi and C. Zannoni, *J. Chem. Phys*., 2000, **113**, 5971.
13 T. Hgemann, J. Kain, S. Diele, G. Pelzl and C. Tschierske, *Angew. Chem., Int. Ed*., 2001, **40**, 887.
14 DENZO: Z. Otwinowski and W. Minor, *Methods in Enzymology, Volume 276, Macromolecular Crystallography*, Part A, ed. C. W. Carter, Jr. and R. M. Sweet, Academic Press, New York, 1997, pp. 307–326, R. Hoaft, COLLECT: Data collection software, Nonius B.V., 1998.
15 R. H. Blessing, *Acta Crystallogr., Sect. A*, 1995, **51**, 33; R. H. Blessing, *J. Appl. Crystallogr*., 1997, **30**, 421.
16 G. M. Sheldrick, SHELXL-97. Program for Refinement of Crystal Structures. University of Göttingen, 1997.

CHEMCOMM Communication
www.rsc.org/chemcomm

Experimental assessment of lanthanide ion donor preference: spectroscopic and theoretical dissection of static charge and dynamic polarisation contributions to axial ligation in a C_4-symmetric chiral europium complex†

James I. Bruce, David Parker* and David J. Tozer

Department of Chemistry, University of Durham, South Road, Durham, UK DH1 3LE. E-mail: david.parker@durham.ac.uk

Received (in Cambridge, UK) 6th July 2001, Accepted 27th September 2001
First published as an Advance Article on the web 17th October 2001

Measurements of the equilibrium constants for ligand exchange (MeCN, 295 K) involving the axial donor in a C_4-symmetric, mono-capped, square antiprismatic cationic Eu complex, supported by calculations based on an electrostatic perturbation model, have been interpreted in terms of a predominant ligand polarisation interaction defined by observation of the hypersensitive $\Delta J = 2$ normalised emission intensity, in association with measurements correlating $\Delta J = 1$ band splitting and ^{1}H NMR dipolar shifts that vindicate Bleaney's theory of magnetic anisotropy.

The correlation of optical and NMR spectral information with the structure of lanthanide complexes in solution has often been frustrated by the extreme sensitivity of the former to apparently minor variations of complex structure.[1,2] Such changes may relate to perturbations in ligand constitution or conformation—thereby defining the local site symmetry and ligand field—or be associated with complex exchange dynamics involving either inter- or intra-molecular processes. The advent of new series of well-defined lanthanide complexes for which intramolecular dynamics and solvent exchange processes are better understood, has afforded an opportunity to clarify this situation.[3] Of particular interest are the series of nine-coordinate lanthanide complexes involving the coordination of C_4-symmetric octadentate macrocyclic ligands, wherein a mono-capped, square antiprismatic coordination environment is adopted. The ninth 'capping' ligand lies along the principal C_4 axis and is susceptible to exchange by other donor ligands.[4] An example is provided by the cationic europium complex (*SSSS*)-[Eu.**1**]$^{3+}$ for

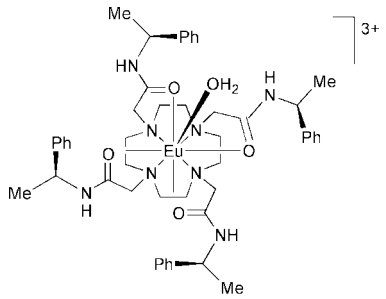

(*SSSS*)-Λ-[Eu.**1**]$^{3+}$

which dynamic NMR, X-ray analysis, CD and CPL spectroscopy have revealed that a dominant species exists in solution, as the Δ-(λλλλ) isomer.[5]† The selection of Eu for study is determined by its favourable spectroscopic characteristics: in emission not only are the $^7F_J \leftarrow {}^5D_0$ spectra the simplest of the paramagnetic lanthanides to interpret, but also the splitting of the two magnetic dipole allowed $\Delta J = 1$ transitions, in C_4 symmetry, is a direct measure of the second-order crystal field parameter, B_2^o.[6] This parameter also determines the dipolar (pseudo-contact) NMR shift in Bleaney's theory of magnetic anisotropy.[7] In axial symmetry, eqn. (1) applies,

$$\delta_{dip} = \frac{-2C_J\beta^2}{(kT)}\left[\frac{3\cos^2\theta - 1}{r^3}B_2^o\right] \quad (1)$$

where $C_J = g^2J(J+1)(2J-1)(2J+3) < J \mid a \mid J' >$. For Eu, analysis of shifted proton NMR resonances that are well-removed from the paramagnetic centre obviates problems associated with any contact shift contribution. Europium emission spectra also provide information on the dipolar polarisability of the ligand donors, by analysis of the hypersensitive $\Delta J = 2$ and $\Delta J = 4$ transitions; the oscillator strength of the $^7F_2 \leftarrow {}^5D_0$ transition is very sensitive to the Eu^{III} coordination environment.[8] However a systematic study of controlled structural variation in a common site symmetry is lacking. With these features in mind, we have measured the equilibrium constant for axial donor exchange with [Eu.**1**]$^{3+}$ in acetonitrile, interpreted changes in the Eu emission and in ^{1}H NMR spectra (CD_3CN, 295 K) and correlated these observations with a simple electrostatic perturbation model.

Addition of eight different oxygen (H_2O, MeOH, $MeNO_2$, DMF, DMSO, pyridine *N*-oxide, HMPA, Ph_3PO) and four nitrogen donors (py, 4-NMe_2py, 4-Mepy, benzylamine) to a solution of [Eu.**1**]$(CF_3SO_3)_3$ in dry acetonitrile (1 mM, 295 K) was monitored by emission spectroscopy. In each case, analysis of the resultant binding isotherms was carried out by a simple least-squares fitting procedure, monitoring changes in the intensity of the $\Delta J = 2$ transition. This allowed an estimate of the free energy change for the ligand exchange process to be determined (Table 1).‡ In addition, ^{1}H NMR spectra were measured at the same concentration of [Eu.**1**]$^{3+}$ (1 mM, 300 MHz, 295 K) adding a sufficient excess of the donor to reach the saturation limit in the corresponding emission spectral analysis. A comparison of ^{1}H NMR hyperfine shifts, in each case, suggested that the complex adopted the same overall structure: the variation with added donor of the shifted ring 'axial', equatorial and diastereotopic NCHH′CO resonances revealed a proportional change (ESI†). That this assumption was valid was corroborated by plotting the chemical shift of the most shifted ring axial proton *vs.* the splitting of the two $\Delta J = 1$ transitions, observed in the corresponding emission spectra. The linearity of this correlation confirms that the observed spectral variations are consistent with an axial donor exchange process in which the site symmetry and overall geometry is conserved. Moreover this correlation vindicates Bleaney's theory[7] demonstrably (Fig. 1).

The ratio of the integrated emission intensities for the $\Delta J = 2/\Delta J = 1$ Eu spectral bands is regarded as a useful parameter that may be used to assess changes in the Eu coordination environment.[1,2,8] The $\Delta J = 1$ transition is magnetic-dipole

† Electronic supplementary information available (ESI) space filling images of [Eu**1**·H_2O], Tables and plots of selected ^{1}H NMR data, emission spectra for [Eu.**1**]$^{3+}$ and examples of least-squares fitting analysis for selected binding isotherms. See http://www.rsc.org/suppdata/cc/b1/b105006k/

 DOI: 10.1039/b105006k

Table 1 Effect of the axial donor on the difference in free energy[ad] for displacement of MeCN compared to the ratio of emission intensities (ΔJ = 2/ΔJ = 1)[b] for Eu emission and the charges on the donor heteroatom in the absence, q, and presence, q^+, of a point charge at 2.5 Å[c]

Axial donor	ΔG^{295}/kJ mol^{-1}	ΔJ = 2/ ΔJ = 1	q	q^+
$MeNO_2$	< 5.5	0.95	0.04	0.16
MeOH	6.6	1.0	0.13	0.20
H_2O	7.8	0.6	0.20	0.26
DMF	11.7	1.9	0.20	0.31
DMSO	14.3	2.8	0.27	0.41
HMPA	18.8	3.2	0.28	0.42
Pyridine[e]	10.7	1.8	0.08	0.23
4-NMe_2py	15.7	3.5	0.11	0.26
4-Mepy	13.0	1.9	0.09	0.24
Pyridine *N*-oxide[f]	17.9	5.2	0.28	0.41
$C_7H_7NH_2$	13.0	1.8	0.19	0.28
MeCN	0	1.1	0.12	0.28

[a] Estimated by iterative least-squares fitting of the variation of emission intensity (λ_{exc} 616 nm) with the concentration of added donor for a solution of [Eu.**1**]$(CF_3SO_3)_3$ in dry MeCN (1 mM, 295 K). [b] Calculated by integrating the emission spectral intensity of [Eu.**1**] (295 K, λ_{exc} = 397 nm). [c] For $MeNO_2$, only unidentate coordination was considered. [d] It should be appreciated that different entropic contributions to the ΔG values shown are expected for each of the donors shown, as well as differential solvation effects. [e] Sterically hindered pyridines, such as 2,5- and 2,6-lutidine did not bind, nor did a representative simple imine, *N*-benzylidenemethylamine. [f] For triphenylphosphine oxide: J ratio = 3.2 and ΔG = 20.1 kJ mol^{-1}.

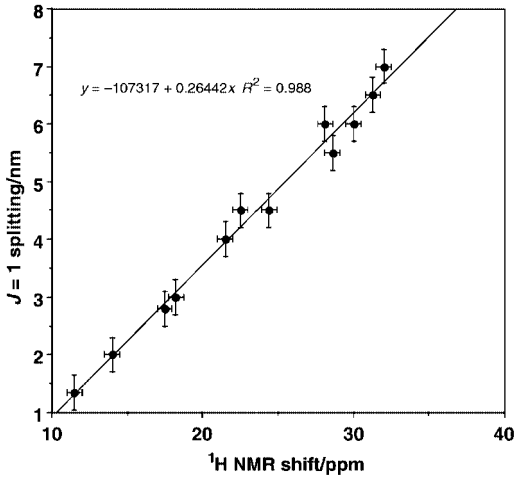

Fig. 1 Correlation of the limiting ^{1}H NMR shift of the most shifted ring axial proton resonance in [Eu**1**]$^{3+}$ (relative to Bu^{t}OH) with the separation of the $A_2 \leftarrow A_1$ and $E \leftarrow A_1$ transitions in the ΔJ = 1 emission bands for eight oxygen and five different nitrogen donors (293 K, MeCN).

allowed and its oscillator strength is generally regarded as being relatively independent of the ligand environment. Values of the ratio are collated in Table 1, and for the oxygen donors in particular, the increases in this ratio correlate quite well with the order of binding affinities (R^2 = 0.91). In the nitrogen donor series, the scope of the analysis was limited by competitive amide de-protonation in strong base, leading to a loss of C_4 symmetry. Nevertheless within the pyridine series, the ΔJ = 2/ΔJ = 1 ratio fell in the order 4-NMe_2py >> 4-Mepy > py consistent with the measured change in binding affinity. In an attempt to rationalise this behaviour, some calculations have been performed using a simple electrostatic model, involving the spatial partitioning of charges on each of the axial donor's atoms. Kohn–Sham density functional theory calculations, using the B97-1[11] exchange-correlation functional and DZP[12] basis set, were performed using the CADPAC[13] program. To reduce the basis set dependence of the calculated charges, each molecule was partitioned into atom centred Voronoi polyhedra,[14] and atomic charges were determined by integrating the charge density within each polyhedron. Calculations were performed at fixed geometries, corresponding to the theoretically optimised structures in the absence of the point charge. These values are given in Table 1 both for the charge on the ligating O or N atom for the isolated molecule in the gas phase (q) and in the presence of an arbitrary (polarising) single point charge (q^+) held 2.5 Å from the ligating donor. The donor atom was oriented towards the putative charge along its stereoelectronically preferred coordination vector. For the oxygen donors, the variation of q^+ followed the sequence of donor affinity (as measured by ΔG for exchange of MeCN) quite closely (R^2 = 0.93), whereas the correlation with q was significantly less good (R^2 = 0.8).

In conclusion, these measurements have allowed a unique assessment of donor atom preference in binding to a typical lanthanide ion. To the extent that the overall binding affinities of the donors examined do *not* correlate with Gutmann's donor number[9] (based on an $SbCl_5$ interaction) nor with Maria and Gal's alternative parameter[10] (based on donation to BF_3), such data could also be considered as the basis for an alternative measure of Lewis basicity, in which there is a dominant contribution from ligand polarisation. Indeed the experimental ΔJ = 2/ΔJ = 1 intensity ratio in complexes of [Eu.**1**]$^{3+}$ with differing axial donors may serve as a useful basis for such an analysis.

We thank EPSRC for support.

Notes and references

‡ Donor exchange was reversible: the position of the equilibrium could be shifted by adding increasing concentrations of more avid donors.

1 (a) Judd–Offelt theory based on a (static) point charge crystal field approximation: B. R. Judd, *Phys. Rev*., 1962, **127**, 750; G. S. Offelt, *J. Chem. Phys*., 1962, **37**, 511; (b) Dynamic ligand polarisation model: S. F. Mason, R. D. Peacock and B. Stewart, *Mol. Phys*., 1975, **30**, 1829; S. F. Mason, *Struct. Bonding (London)*, 1980, **39**, 43; B. Stewart, *Mol. Phys*., 1983, **50**, 161; S. F. Mason and G. E. Tranter, *Chem. Phys. Lett*., 1983, **94**, 29.

2 E. M. Stephens, M. F. Reid and F. S. Richardson, *Inorg. Chem*., 1984, **23**, 4611; M. F. Reid and F. S. Richardson, *J. Chem. Phys*., 1983, **79**, 5735; M. F. Reid and F. S. Richardson, *J. Phys. Chem*., 1984, **88**, 3579; D. R. Foster and F. S. Richardson, *Inorg. Chem*., 1983, **22**, 3996.

3 H. G. Brittain and J. F. Desreux, *Inorg. Chem*., 1984, **23**, 4459; P. Caravan, J. Ellison, T. J. McMurry and R. B. Lauffer, *Chem. Rev*., 1999, **99**, 2293.

4 S. Aime, A. Barge, J. I. Bruce, M. Botta, J. A. K. Howard, J. M. Moloney, D. Parker, A. S. de Sousa and M. Woods, *J. Am. Chem. Soc*., 1999, **121**, 5672; L. DiBari, G. Pintacuda, P. Salvadori, R. S. Dickins and D. Parker, *J. Am. Chem. Soc*., 2000, **122**, 9257. For other examples of the spectroscopic effect of changing donor type (usually more than one donor simultaneously and often with a local symmetry change): J. Lisowski, *Magn. Reson. Chem*., 1999, **37**, 287; J. Lisowski, J. L. Sessler and T. D. Mody, *J. Am. Chem. Soc*., 1995, **117**, 2273.

5 R. S. Dickins, J. A. K. Howard, C. L. Maupin, J. M. Moloney, D. Parker, J. P. Riehl, G. Siligardi and J. A. G. Williams, *Chem. Eur. J*., 1999, **5**, 1095.

6 The separation of the $A_2 \leftarrow A_1$ and $E \leftarrow A_1$ transitions in the Eu ΔJ = 1 manifold for a C_4 symmetric species is determined only by second order crystal-field harmonics. Crystal field parameters of higher order are smallest for Eu amongst the lanthanides: B. R. McGarvey, *J. Magn. Reson*., 1979, **33**, 445; T. A. Babushkina, V. F. Zolin and L. G. Koreneva, *J Magn. Reson*., 1983, **52**, 169.

7 B. Bleaney, *J. Magn. Reson*., 1972, **8**, 91.

8 R. D. Peacock, *Struct. Bonding, (Berlin)*, 1975, **22**, 83; D. E. Henrie, R. L. Fellows and G. R. Choppin, *Coord. Chem. Rev*., 1976, **18**, 199: to a first approximation, the oscillator strength of the $^7F_2 \leftarrow {}^5D_0$ transition is 'considered to be' proportional to the square of the ligand dipolar polarisability, $|\alpha|$.

9 U. Mayer and V. Gutmann, *Struct. Bonding (Berlin)*, 1972, **12**, 113; Y. Marcus, *J. Solution Chem*., 1984, **13**, 599; I. Persson, *Pure Appl. Chem*., 1986, **58**, 1153.

10 P.-C. Maria and J.-F. Gal, *J. Phys. Chem*., 1985, **89**, 1296.

11 F. A. Hamprecht, A. J. Cohen, D. J. Tozer and N. C. Handy, *J. Chem. Phys*., 1998, **109**, 6264.

12 T. H. Dunning, *J. Chem. Phys*., 1970, **53**, 2823.

13 R. D. Amos, I. L. Alberts, J. S. Andrews, S. M. Colwell, N. C. Handy, D. Jayatilaka, P. J. Knowles, R. Kobayashi, G. J. Laming, A. M. Siamndiras, A. J. Stone, M.-D. Su and D. J. Tozer, CADPAC6.5, The Cambridge Analytic Derivatives Package, 1998.

14 A. D. Becke, *J. Chem. Phys*., 1988, **88**, 2547.

CHEMCOMM Communication
www.rsc.org/chemcomm

The nature of the active species in bis(imino)pyridyl cobalt ethylene polymerisation catalysts

Vernon C. Gibson,* Martin J. Humphries, Kilian P. Tellmann, Duncan F. Wass†, Andrew J. P. White and David J. Williams

Department of Chemistry, Imperial College of Science, Technology and Medicine, Exhibition Road, South Kensington, London SW7 2AY, UK

Received (in Cambridge, UK) 20th August 2001, Accepted 14th September 2001
First published as an Advance Article on the web 10th October 2001

Studies on cobalt ethylene polymerisation catalysts bearing bis(imino)pyridine ligands strongly indicate that the activated species is not the anticipated cobalt(II) alkyl cation.

In recent years there has been much interest in late transition metal olefin polymerisation catalysts. Recently, Brookhart and Bennett, and ourselves have independently reported highly active polymerisation[1] and oligomerisation[2] catalysts based on iron and cobalt bearing bis(imino)pyridyl ligands. The activity of the cobalt polymerisation catalyst family, whilst approximately an order of magnitude less than that for their iron relatives, is nevertheless highly respectable for late transition metal olefin polymerisation catalysts. However, the natures of the active sites in both the iron and cobalt systems remain little understood. Here, we report our preliminary findings on the cobalt system.

The activation of the pre-catalyst [$LCoCl_2$] **1** {L = 2,6-[CMe=N(2,6-$C_6H_3Pr^i_2$)]$_2C_5H_3N$} with methylaluminoxane (MAO) produces an initial colour change from yellow–brown to claret, with a subsequent colour change to blue. Addition of ethylene to this solution causes a colour change to aquamarine, concomitant with the onset of polymerisation.[1] An interesting observation is that if the activation with MAO is performed under an argon atmosphere as opposed to dinitrogen, the resulting solution is purple. If this solution is degassed and dinitrogen is then admitted the colour of the solution changes to blue. Degassing returns the original purple colour. Thus the activated species appears to be capable of reversibly binding dinitrogen.

The well-established mode of activation of both early and late transition metal systems [*e.g.* group 4 metallocenes and Ni(α-diimine) catalysts] involves, *via* the action of MAO, the transformation of a metal dihalide fragment L_nMCl_2 into an alkyl cation $[L_nM–R]^+$. If this activation pathway is followed by the cobalt catalyst family, a 15-electron cobalt alkyl cation of the type $[LCoMe]^+$ would be anticipated. Indeed, calculations have been reported based on cationic alkyl species of this type being the active centres.[3] We attempted to synthesise the dimethyl complex [$LCoMe_2$] in order to access a well defined analogue of this hypothesised cobalt(II) alkyl cation. However, the reaction between **1** and methyl Grignard reagents (Scheme 1) affords the reduced species [LCoMe] **2**.

This led us to investigate the reduction of **1** by other means. Clean reduction to the cobalt(I) chloride [LCoCl] **3** is achieved upon reaction of **1** with a suspension of zinc powder in toluene at 50 °C. Both **2** and **3** are claret in colour, and, as with all other cobalt(I) species reported in this study, are highly air- and moisture-sensitive. They are readily oxidised by most chlorinated solvents and other oxidising agents.

The activation of **2** or **3** with MAO affords a blue solution, which also becomes aquamarine on the addition of ethylene to the flask, colour changes that are similar to those observed upon treatment of **1** with MAO. **1–3** all yield identical polyethylene (mol. wt, PDI) when activated with MAO; the same active species thus appears to be present in each case. These observations lead us to conclude that the species produced upon activation of these procatalysts with MAO is a cobalt(I) species rather than cobalt(II).

The addition of ethylene to a sample of the cobalt(I) methyl species **2** in toluene does not lead to the formation of polymer, nor does its NMR spectrum change; **2** is, therefore, not a polymerisation-active species.‡ The addition of Al_2Me_6 does not activate **2** towards ethylene polymerisation, nor does it cause any colour change, thus a stronger Lewis acid (*e.g.* MAO) appears to be required for activation of the catalyst. As a potential model for the activation process, **2** was treated with the Lewis acid $B(C_6F_5)_3$. This afforded a royal blue solution of $[LCo(N_2)][MeB(C_6F_5)_3]$ **4**, thus providing a clue as to the nature of the second colour change in the reaction of **1** with MAO.

Molecular structures of the cobalt(I) species **3**§ and **4**§ have been determined. They are closely related, having approximate C_{2v} symmetry about an axis passing through the pyridyl nitrogen and the cobalt centre (complex **4** is depicted in Fig. 1). In both structures the metal coordination plane extends to include the ligand backbone [from C(11) through C(4) to C(23)], the maximum deviation from planarity being 0.025 Å in **3** and 0.080 Å in **4**. The 2,6-diisopropylphenyl ring systems are in both complexes oriented approximately orthogonally to the coordination plane (by between 82 and 88°). There are no significant differences between the equivalent Co–N bonds to the tridentate ligand in the two structures, or in the C=N double bond lengths. To our knowledge there are no structurally characterised square planar cobalt complexes bearing three nitrogen donors with either a chloride or a dinitrogen ligand in the fourth coordination site reported in the literature. The Co–

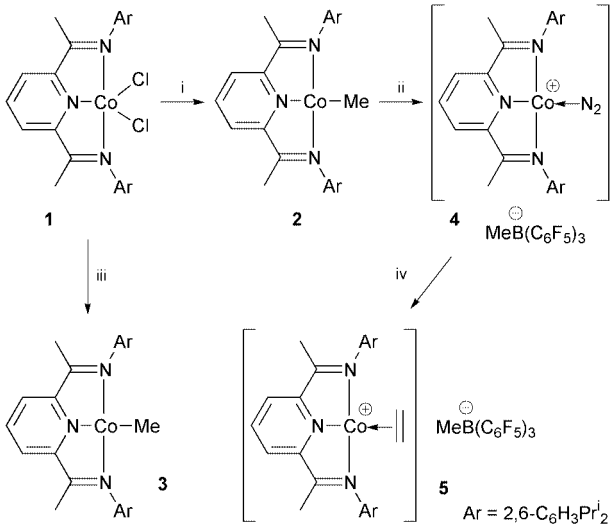

Scheme 1 *Reagents and conditions*: i, 2.5 MeMgBr, Et_2O, −78 °C, 18 h; ii, $B(C_6F_5)_3$, toluene; iii, Zn, toluene, 50 °C, 15 h; iv, C_2H_4, toluene.

† Present address: BP Research Centre, Sunbury on Thames, Middlesex, UK TW16 7LN.

 DOI: 10.1039/b107490c

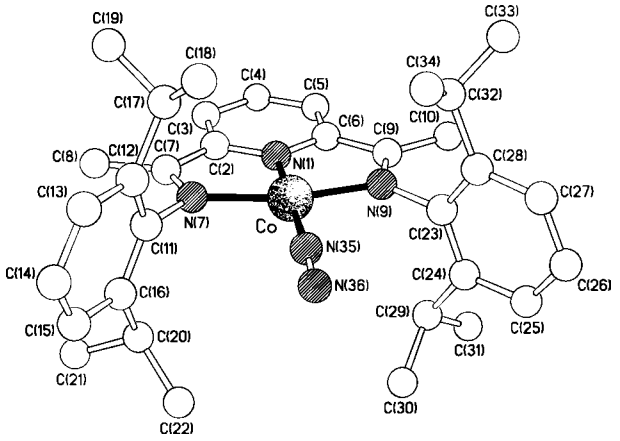

Fig. 1 The molecular structure of **4**. Selected bond lengths (Å) and angles (°) for **4**; Co–N(1) 1.812(3), Co–N(7) 1.915(3), Co–N(9) 1.908(3), Co–N(35) 1.841(3), C(7)–N(7) 1.303(5), C(9)–N(9) 1.303(5), N(35)–N(36) 1.112(6); N(1)–Co–N(7) 81.67(12), N(1)–Co–N(9) 81.68(12), N(1)–Co–N(35) 178.3(2), N(7)–Co–N(9) 163.31(12), N(7)–Co–N(35) 98.23(14), N(9)–Co–N(35) 98.44(14), Co–N(35)–N(36) 175.4(5). For **3**; Co–Cl 2.1807(10), Co–N(1) 1.797(3), Co–N(7) 1.916(3), Co–N(9) 1.912(3), C(7)–N(7) 1.317(5), C(9)–N(9) 1.322(5); Cl–Co–N(1) 179.15(10), Cl–Co–N(7) 98.89(9), Cl–Co–N(9) 98.17(9), N(1)–Co–N(7) 81.35(14), N(1)–Co–N(9) 81.58(14), N(7)–Co–N(9) 162.92(12).

N_2 bond length in **4** is comparable to those observed in tetrahedral cobalt species. In **4** the shortest anion···cation contact is an approximately orthogonal approach of 2.93 Å of one of the pentafluorophenyl fluorine atoms to the pyridyl nitrogen atom. The closest approach of a fluorine atom to the cobalt centre is 3.5 Å.

The addition of ethylene to a toluene solution of **4** causes a colour change to aquamarine, and polymer is formed, although only with low activity (11 g $mmol^{-1}bar^{-1}h^{-1}$). The addition of 10 equiv. of Al_2Me_6 as co-catalyst increases the activity by an order of magnitude (96 g $mmol^{-1}\,bar^{-1}\,h^{-1}$); the resultant polyethylene is identical in molecular weight and molecular weight distribution to that produced by the MAO activated system.

An important question then concerns how the propagating species is formed from **4**. The diamagnetic nature of the cobalt(I) bis(imino)pyridyl system makes it amenable to study by NMR spectroscopy. One useful feature of the ^{1}H NMR spectra is that the chemical shifts of the ligand resonances vary considerably depending on the nature of the substitution at the cobalt centre. The ketimine methyl resonance is particularly sensitive in this respect, with the singlet being observed at δ −1.14 in **2**, δ 0.05 in **3** and δ 1.11 in **4**, a trend which appears to correlate with the electrophilicity of the cobalt centre.

A study of the pre-catalyst **4** by ^{1}H NMR spectroscopy showed that addition of 1 equiv. of ethylene afforded a species identifiable by its ^{1}H NMR spectrum as the ethylene adduct $[LCo(\eta\text{-}C_2H_4)][MeB(C_6F_5)_3]$ **5**. The ketimine signal now occurs at δ 0.73, and a singlet resonance assignable to bound ethylene is present at δ 4.65 (*cf.* δ 5.32 for free ethylene). The ethylene is only weakly bound; if more ethylene is added to the NMR tube then rapid exchange between free and bound ethylene occurs, resulting in an averaged chemical shift for the ethylene hydrogens. The ethylene can be seen to be consumed, with polymer forming on the walls of the NMR tube. At the end of the polymerisation, **5** remains.

There are several conclusions that can be drawn from these observations. Firstly, the species that is initially formed upon activation, and thus the species from which the initation of polymerisation must occur, is a cobalt(I) cation, a species that contains *no* cobalt–C(alkyl) bond. Secondly, the aluminium co-catalyst appears to perform three functions: (i) to reduce the cobalt(II) pre-catalyst to cobalt(I), (ii) to form the cobalt(I) cation by chloride or methide group abstraction (MAO), and (iii) to enhance the stability of the catalyst, and/or the rate of polymerisation. The manner in which polymerisation is initiated from the cobalt(I) cation is currently unclear. One possibility is the reaction of a bound ethylene with a Lewis acid {*cf.* the activation of $[Cp_2Zr(butadiene)]$ by $B(C_6F_5)_3$[4]} to give a zwitterionic cobalt(III) complex. Another possibility is oxidative coupling of two molecules of ethylene to afford a cobaltacyclopentane species, analogous to the commonly postulated active site of the Phillips chromium catalyst system.[5] A third possibility is C–H σ-bond activation of the bound ethylene to afford a cobalt(III) vinyl hydride species, a reaction which has precedence in the chemistry of the group 9 metals.[6] For the first two possibilities it is less clear how **5** would be regenerated during the polymerisation. A common outcome of all of these processes, however, is the oxidation of the cobalt(I) precursor to cobalt(III). Thus, in accord with findings on other cobalt polymerisation systems,[7] and the apparent inactivity of LCo(I)R species, we err in favour of the active species being cobalt(III). Investigations into these possibilities, and other aspects of the chemistry of the cobalt system, will be reported in due course.

BP Chemicals Ltd is thanked for financial support. Dr J. Boyle and Dr G. Audley are thanked for NMR and GPC measurements, respectively.

Notes and references

‡ The longer chain Co(I)–alkyl homologues of **2**, LCoR (where R = Et, Pr^n or Bu^n) have been synthesised and they too are inactive towards ethylene polymerisation.

§ *Crystal data*: for **3**: $C_{33}H_{43}N_3ClCo$, M = 576.1, monoclinic, space group $P2_1/n$ (no. 14), a = 8.819(1), b = 23.121(2), c = 15.744(2) Å, β = 101.08(1)°, V = 3150.7(7) Å^3, Z = 4, D_c = 1.214 g cm^{-3}, μ(Mo-Kα) = 6.54 cm^{-1}, T = 293 K; 4635 independent measured reflections, F^2 refinement, R_1 = 0.046, wR_2 = 0.100, 3253 independent observed reflections [$|F_o| > 4\sigma(|F_o|)$, $2\theta \leqslant 47°$], 343 parameters. For **4**: $[C_{33}H_{43}N_5Co][C_{19}H_3F_{15}B]$, M = 1095.7, triclinic, space group $P\bar{1}$ (no. 2), a = 10.764(1), b = 15.797(1), c = 15.881(1) Å, α = 100.55(1), β = 102.86(1), γ = 98.80(1)°, V = 2534.7(3) Å^3, Z = 2, D_c = 1.436 g cm^{-3}, μ(Cu-Kα) = 35.1 cm^{-1}, T = 183 K; 8102 independent measured reflections, F^2 refinement, R_1 = 0.055, wR_2 = 0.128, 6057 independent observed absorption corrected reflections [$|F_o| > 4\sigma(|F_o|)$, $2\theta \leqslant 126°$], 668 parameters. CCDC reference numbers 169303 and 169304. See http://www.rsc.org/suppdata/cc/b1/b107490c/ for crystallographic data in CIF or other electronic format.

1 (*a*) G. J. P. Britovsek, V. C. Gibson, B. S. Kimberley, G. A. Solan, A. J. P. White and D. J. Williams, *Chem. Commun*., 1998, 849; (*b*) B. L. Small, M. Brookhart and A. M. A Bennett, *J. Am. Chem. Soc*., 1998, **120**, 4049; (*c*) G. J. P. Britovsek, M. Bruce, V. C. Gibson, B. S. Kimberley, P. J. Maddox, S. Mastroianni, S. J. McTavish, C. Redshaw, G. A. Solan, S. Strömberg, A. J. P. White and D. J. Williams, *J. Am. Chem. Soc*., 1999, **121**, 8728.

2 (*a*) B. L. Small and M. Brookhart, *J. Am. Chem. Soc*., 1998, **120**, 7143; (*b*) G. J. P. Britovsek, S. Mastroianni, G. A. Solan, S. P. D. Baugh, C. Redshaw, V. C. Gibson, A. J. P. White, D. J. Williams and M. R. J. Elsegood, *Chem. Eur. J*., 2000, **6**, 2221.

3 P. Margl, L. Q. Deng and T. Ziegler, *Organometallics*, 1999, **18**, 5701.

4 (*a*) B. Temme, G. Erker, J. Karl, H. Luftmann, R. Fröhlich and S. Kotila, *Angew. Chem., Int. Ed. Engl*., 1995, **34**, 1755; (*b*) for a review, see: ; G. Erker, *Acc. Chem. Res*., 2001, **34**, 309.

5 M. P. McDaniel, *Adv. Catal*., 1985, **33**, 47.

6 See, for example: (*a*) P. O. Stoutland and R. G. Bergman, *J. Am. Chem. Soc*., 1985, **107**, 4581; (*b*) S. T. Bely, S. B. Duckett, D. M. Haddleton and R. N. Perutz, *Organometallics*, 1989, **8**, 748; (*c*) C. K. Ghosh, J. K. Hoyano, R. Krentz and W. A. G. Graham, *J. Am. Chem. Soc*., 1989, **111**, 5480; (*d*) R. S. Tanke and R. H. Crabtree, *Inorg. Chem*., 1989, **28**, 3444; (*e*) B. Papenfuhs, N. Mahr and H. Werner, *Organometallics*, 1993, **12**, 4244; (*f*) E. Gutiérrez-Puebla, A. Monge, M. C. Nicasio, P. J. Pérez, M. L. Poveda, L. Rey, C. Ruíz and E. Carmona, *Inorg. Chem*., 1998, **37**, 4538.

7 G. F. Schmidt and M. Brookhart, *J. Am. Chem. Soc*., 1985, **107**, 1443.

CHEMCOMM Communication
www.rsc.org/chemcomm

Catalytic C–F activation of polyfluorinated pyridines by nickel-mediated cross-coupling reactions

Thomas Braun,*[a] Robin N. Perutz*[b] and Marianna I. Sladek[a]

[a] *Fakultät für Chemie, Universität Bielefeld, Postfach 100131, 33501 Bielefeld, Germany. E-mail: thomas.braun@uni-bielefeld.de*
[b] *Department of Chemistry, University of York, York, UK YO10 5DD. E-mail: rnp1@york.ac.uk*

Received (in Cambridge, UK) 24th July 2001, Accepted 20th September 2001
First published as an Advance Article on the web 9th October 2001

The cross-coupling reaction of pentafluoropyridine with tributyl(vinyl)tin affording 2-vinyltetrafluoropyridine by activation of a carbon–fluorine bond is catalysed by [NiF(2-C_5NF_4)(PEt_3)$_2$]; a similar reaction is observed with 2,3,5,6-tetrafluoropyridine.

A variety of methods of activating carbon–fluorine bonds by transition metal centres have been established in the last two decades.[1] However, the formation of new organofluorine compounds *via* C–F activation, followed by functionalisation within the coordination sphere of the metal is still little developed. Nevertheless, catalytic C–F activation has become a reality.[2] Catalytic cycles include the conversion of hexafluorobenzene into pentafluorobenzene and the silylation of pentafluoroacetophenone using rhodium catalysts.[3,4] In the zirconium-initiated oligomerisation of hexafluorobenzene new C–C bonds are formed in addition to the cleavage of C–F bonds.[5] The nickel-mediated cross-coupling of fluorobenzene with ^{i}PrMgCl has also been reported.[6] In this communication we present the first cross-coupling reactions that generate polyfluorinated aromatic compounds by C–F activation. We show that 2,3,5,6-tetrafluoropyridine and pentafluoropyridine can be converted catalytically into the previously unknown 2-vinylfluoropyridine derivatives by cross-coupling reactions. Fluorinated pyridines are of current interest as building blocks in pharmaceuticals, agrochemicals and dyes.[7]

Reaction of $Ni(cod)_2$ with PEt_3 in the presence of pentafluoropyridine yields *trans*-[NiF(2-C_5NF_4)(PEt_3)$_2$] **1**.[8] Treatment of a solution of **1** with $Bu_3SnCH{=}CH_2$ at room temperature results in the slow formation of three products **2**–**4** identified by NMR spectroscopy including ^{1}H–^{1}H and ^{19}F–^{19}F COSY measurements. The ^{31}P NMR spectrum of [Ni{η^2-2-C_5NF_4(CH=CH_2)}(PEt_3)$_2$] **2**, the initial product, exhibits two mutually coupled doublets (J_{PP} = 34 Hz) as found for [Ni{η^2-C_6F_5(CH=CH_2)}(PEt_3)$_2$].† [8] After 1 d of reaction, two further compounds are observed. The ^{19}F and ^{31}P NMR data of these compounds are compatible with their assignment as **3** and **4** (Scheme 1).‡ [8] The ^{19}F NMR spectrum of **3** shows a triplet at δ −367.46 (J_{PF} 47 Hz) characteristic of the metal-bound fluorine.[9] The fluorine ligand is also revealed by a doublet resonance at δ 13.6 (J_{PF} 48 Hz) in the ^{31}P NMR spectrum for the two equivalent phosphorus nuclei. The assignment as a 2-pyridyl nickel derivative is based on the presence of three additional fluorine signals in the ^{19}F NMR spectrum at δ −129.88, −159.78, −163.34. The spectrum shows no signal at *ca.* δ −80, which would be indicative of a fluorine in the *ortho* position to the nitrogen.[8] The ^{31}P NMR data of **4** resemble those for **2**. A ^{1}H–^{31}P COSY NMR spectrum measured at 233 K shows a correlation between the resonance for the olefinic proton at δ −3.58 and the signal in the ^{31}P spectrum at δ 24.4. Treatment of a reaction solution containing **2** as major product with pentafluoropyridine **5** and PEt_3 in the presence of Cs_2CO_3 affords small amounts of free 2-vinyltetrafluoropyridine **6**, which has not been described previously.§ Compound **6** was removed by distillation *in vacuo* and reacted with $Ni(cod)_2$–PEt_3 providing an alternative route to **2**.

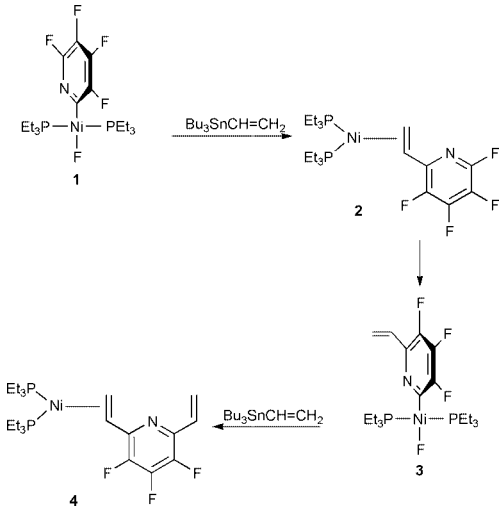

Scheme 1 Reaction of **1** with $Bu_3SnCH{=}CH_2$.

Encouraged by these observations and other stoichiometric coupling reactions which we reported recently,[10] we turned our attention to catalytic cross-coupling methods for the synthesis of **6** (Scheme 2).¶ The coupling of pentafluoropyridine **5** with $Bu_3SnCH{=}CH_2$ in the presence of a nickel catalyst, phosphine and Cs_2CO_3 was investigated. Representative results are summarised in Table 1. The best result is obtained with **1**–PEt_3–Cs_2CO_3 as the catalytic system giving a TON (turnover number) of 4 based on the formation of **6**. All the reactions gave the coupling product **6** together with considerable amounts of 2,3,5,6-tetrafluoropyridine **7**. According to the GC-MS, there were also traces of 4-vinyltetrafluoropyridine, 2-vinyl-3,5,6-trifluoropyridine **8** and 2,6-divinyltrifluoropyridine in the product mixture. We did not observe any significant change in the activity of the catalysts by altering the solvent (NMP, DME, DMF, 1,4-dioxane, benzene) or base (Na_2CO_3, K_3PO_4). The effect of cyclooctadiene or a weakly coordinating alkene such as 3-trifluoromethylstyrene is also negligible. Base may be needed to trap small amounts of HF, formed in side reactions.[12] In a control experiment we discovered that **7** is also formed from PEt_3 and pentafluoropyridine without adding the catalyst and $Bu_3SnCH{=}CH_2$. The concomitant generation of phosphoranes

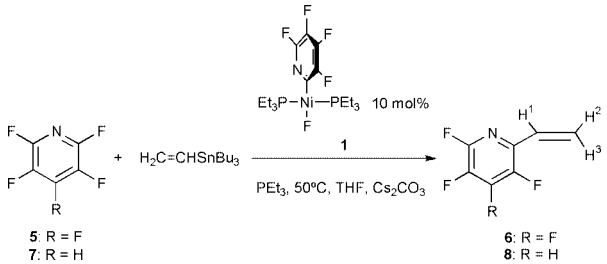

Scheme 2 Catalytic conversion of fluorinated pyridines.

 DOI: 10.1039/b106646c

Table 1 Coupling of fluorinated pyridines with $Bu_3SnCH{=}CH_2$

Entry	Substrate	Catalyst	Phosphine	Yield **6** (%)	TON[a] **6**	Yield **7** (%)
1	**5**	**1**	PEt_3	38	4	20
2	**5**	**1**	PEt_3[b]	22	2	19
3	**5**	**1**	P^tBu_3	40	4	20
4	**5**	[c]	PCy_3	Traces	—	50
5	**5**	$Ni(cod)_2$	PEt_3	18	2	41
6	**5**	$Ni(cod)_2$	PCy_3	—	—	—
7	**5**	$Ni(cod)_2$	P^tBu_3	—	—	—
8	**5**	$Ni(cod)_2$	$Cy_2PCH_2PCy_2$	—	—	4

[a] Determined by NMR with 4-fluorotoluene as external standard, based on **5**. [b] With additive 3-trifluoromethylstyrene. [c] *trans*-[$NiF(2\text{-}C_5NF_4)(PCy_3)_2$].

indicates that formation of **7** might proceed *via* a phosphonium salt.[11]

The formation of traces of 2-vinyl-3,5,6-trifluoropyridine **8** during the reaction suggested that a similar conversion could be obtained by employing **7** as the starting fluoropyridine in place of **5**. In addition the reaction should be cleaner as competing reactions in position 4 might be avoided. Indeed, **7** can be converted selectively into its vinyl derivative **8** in the presence of **1** as catalyst with a TON of 5.¶‖ There is no indication of the formation of trifluoropyridines or of C–H activation, which would lead to 4-vinyltetrafluoropyridine. However, there were also traces of 2,6-divinyl-3,5-difluoropyridine and 2,6-divinyl-trifluoropyridine in the product mixture. The generation of the latter compound can be explained by the use of **1** as catalyst.

The formation of **6** is of special interest since it is very difficult to prepare tetrafluoropyridines substituted in the 2-position.[10,13] We believe that precoordination of pentafluoropyridine at the nickel centre is likely to be a crucial step in the activation of the carbon–fluorine bond, controlling the regioselectivity for attack at the 2-position.[13,14]

In conclusion, we have demonstrated the first catalytic C–C coupling reactions involving C–F activation of a polyfluorinated molecule. While cross-coupling reactions of arylchlorides have been studied extensively, no examples of cross-coupling of polyfluorinated aromatics *via* C–F cleavage had been described.[15] We have shown that the scope of these reactions can be expanded to the activation of a carbon–fluorine bond using a nickel catalyst. The cross-coupling is likely to proceed *via* the formation of **2**–**4** which were observed during stoichiometric reactions. Such a mechanism is fully consistent with the intermediates observed by Espinet *et al*. in their recent study of the mechanism of Stille coupling of C_6F_5OTf.[16]

We would like to acknowledge the EPSRC and the Deutsche Forschungsgemeinschaft (grants BR-2065/1-1 and BR-2065/1-2) for financial support. T. B. also thanks Professor P. Jutzi for his generous support.

Notes and references

† *Selected NMR spectroscopic data for* **2**: ($[^2H_8]$THF): ^1H (500 MHz, 233 K): δ 3.52, 2.11, 1.75 (η^2-H_2C=CH, all br). ^{31}P (202.4 MHz, 300 K): δ 24.9 (d, J_{PP} 34 Hz), 17.1 (d, J_{PP} 34 Hz). ^{19}F (470.4 MHz, 300 K): δ −85.75 (m, 1 F), −145.54 (m, 1 F), −153.79 (m, 1 F), −172.75 (m, 1 F).

‡ *Selected NMR spectroscopic data for* **3** and **4**: **3** ($[^2H_8]$THF, 300 K): ^{31}P (202.4 MHz): δ 13.6 (d, J_{PF} 48 Hz). ^{19}F (470.4 MHz): δ −129.88 (m, 1 F), −159.78 (m, 1 F), −163.34 (m, 1 F), −367.46 (t, J_{PF} 47 Hz, 1 F). **4** ($[^2H_8]$THF): ^1H (500 MHz, 233 K): δ 6.80, 6.23, 5.40 (H_2C=CH, all br), 3.58, 2.30, 1.72 (η^2-H_2C=CH, all br). ^{31}P (202.4 MHz, 300 K) δ 24.4 (d, J_{PP} 37 Hz), 17.4 (d, J_{PP} 34 Hz). ^{19}F (470.4 MHz, 300 K) δ −150.74 (m, 1 F), −153.86 (m, 1 F), −160.12 (d, J_{PF} 17 Hz, 1 F). The signals at δ −153.86 and −150.74 are partially obscured by resonances of **1** and **2**, respectively.

§ *Spectroscopic data for* **6**: ($[^2H_8]$THF, 300K): ^1H (500 MHz): δ 6.90 (ddd, J_{HH} 17, J_{HH} 11, J_{FH} 1 Hz, 1 H, H^1), 6.34 (dm, J_{HH} 16 Hz, 1 H, H^3), 5.69 (dm, J_{HH} 11 Hz, 1 H, H^2). ^{19}F (470.4 MHz): δ −82.32 (m, 1 F), −139.53 (m, 1 F), −148.30 (m, 1 F), −157.80 (m, 1 F). Mass spectrum (EI) *m*/*z* 177 (M^+, 100%).

¶ In a typical catalysis experiment, an NMR tube containing a capillary with $[^2H_8]$THF and 4-fluorotoluene was charged with a solution of **1** in THF (1 mL, 0.03 mmol), pentafluoropyridine (0.31 mmol), $Bu_3SnCH{=}CH_2$ (0.31 mmol), phosphine (0.09 mmol), and Cs_2CO_3 (1 mg). The tube was sealed and put in an oil bath at 50 °C. After 16 h the mixture was cooled to room temperature and analysed by NMR spectroscopy. The solution was then filtered over silica using THF as solvent and analyzed by GC.

‖ *Spectroscopic data for* **8**: ($[^2H_8]$THF, 300K): ^1H (500 MHz): δ 7.88 (m, 1 H, aromatic CH), 6.87 (dd, J_{HH} 17, J_{HH} 11 Hz, 1 H, H^1), 6.29 (d, J_{HH} 17 Hz, 1 H, H^3), 5.57 (d, J_{HH} 11 Hz, 1 H, H^2). ^{19}F (470.4 MHz): δ −91.02 (m, 1 F), −128.12 (m, 1 F), −138.55 (m, 1 F). Mass spectrum (EI) *m*/*z* 159 (M^+, 100%).

1 J. Burdeniuc, B. Jedlicka and R. H. Crabtree, *Chem. Ber./Recl*., 1997, **130**, 145; J. L. Kiplinger, T. G. Richmond and C. E. Osterberg, *Chem. Rev*., 1994, **94**, 373; E. F. Murphy, R. Murugavel and H. W. Roesky, *Chem. Rev*., 1997, **97**, 3425; T. G. Richmond, in *Topics in Organometallic Chemistry*, ed. S. Murai, Springer, New York, 1999, vol. 3, pp. 243–269.
2 T. G. Richmond, *Angew. Chem., Int. Ed*., 2000, **39**, 3241.
3 M. Aizenberg and D. Milstein, *J. Am. Chem. Soc*., 1995, **117**, 8674.
4 Y. Ishii, N. Chatani, S. Yorimitsu and S. Murai, *Chem. Lett*., 1998, 157.
5 B. L. Edelbach, B. M. Kraft and W. D. Jones, *J. Am. Chem. Soc*., 1999, **121**, 10327.
6 Y. Kiso, K. Tamao and M. Kumada, *J. Organomet Chem*., 1973, **50**, C12.
7 *Organofluorine Chemistry: Principles and Commercial Applications*, eds. R. E. Banks, B. E. Smart and J. C. Tatlow, Plenum, New York, 1994.
8 L. Cronin, C. L. Higgitt, R. Karch and R. N. Perutz, *Organometallics*, 1997, **16**, 4920.
9 T. Braun, S. P. Foxon, R. N. Perutz and P. H. Walton, *Angew. Chem., Int. Ed. Engl*., 1999, **38**, 3326.
10 T. Braun, S. Parsons, R. N. Perutz and M. Voith, *Organometallics*, 1999, **18**, 1710; R. Dagani, *Chem. Eng. News*, 2001, **79**, 40.
11 W. Boenigk and G. Hägele, *Chem. Ber*., 1983, **116**, 2418; E. Anders and F. Markus, *Chem. Ber*., 1989, **122**, 113.
12 P. A. McLaughlin and J. K. Verkade, *Organometallics*, 1998, **17**, 5937; M. K. Whittlesey, R. N. Perutz, B. Greener and M. H. Moore, *Chem. Commun*., 1997, 187.
13 S. J. Archibald, T. Braun, J. F. Gaunt, J. E. Hobson and R. N. Perutz, *J. Chem. Soc., Dalton Trans*., 2000, 2013.
14 T. Braun, L. Cronin, C. L. Higgitt, J. E. McGrady, R. N. Perutz and M. Reinhold, *New J. Chem*., 2001, **25**, 19.
15 A. Zapf, A. Ehrentraut and M. Beller, *Angew. Chem., Int. Ed*., 2000, **39**, 4153; and references therein; ; C. Dai and G. C. Fu, *J. Am. Chem. Soc*., 2001, **123**, 2719; and references therein; V. P. W. Böhm, T. Weskamp, C. W. K. Gstöttmayr and W. A. Herrmann, *Angew. Chem., Int. Ed*., 2000, **39**, 1602; E. Shirakawa, K. Yamasaki and T. Hiyama, *Synthesis*, 1998, 1544.
16 A. L. Casado, P. Espinet, A. M. Gallego and J. M. Martinez-Ilarduya, *Chem. Commun*., 2001, 339.

CHEMCOMM
Communication
www.rsc.org/chemcomm

Two different one-dimensional structural motifs in the same coordination polymer: a novel interpenetration of infinite ladders by bundles of infinite chains

Md. Badruz Zaman,† Mark D. Smith and Hans-Conrad zur Loye*

Department of Chemistry and Biochemistry, University of South Carolina, Columbia, SC 29208, USA. E-mail: zurloye@sc.edu

Received (in Cambridge, UK) 12th July 2001, Accepted 11th September 2001
First published as an Advance Article on the web 5th October 2001

A coordination polymer with a novel structural motif consisting of stacks of infinite ladders interpenetrated by bundles of infinite chains is described; geometrical arguments are made for the requirements that can lead to such interpenetration as a function of ligand dimensions.

To date, a large number of one-, two- and three-dimensional infinite frameworks, such as helical, brick wall, ladder, honeycomb, square grid, parquet, diamondoid and more complex 3D connectivities have been generated from tetrahedral, trigonal, and octahedral metal templates in combination with linear and nonlinear bidentate spacers.[1–3] Product topology can often be influenced by selecting the coordination geometry of the metals and the chemical nature of the organic ligands. In particular, the T-joint building block, defined by the coordination of a metal center by three *N*,*N*′-bidentate ligands, has given rise to several isomeric framework types *via* different orientation of the T-joints relative to one another.[4–6]

While different structural isomers can form from T-shaped building blocks, and while it is not unusual to find multiple structural isomers within the same batch of crystals,[4,7] it is quite rare to find two structural motifs within the same crystal structure.[8–11] The use of the long ligand 1,4-bis[(4′-pyridylethynyl)benzene] (**1**)[12] has led to the formation of a highly unusual interpenetrated network in [Cu(**1**)(solv)$(NO_3)_2$] [Cu$(\mathbf{1})_{1.5}(NO_3)_2$]·2solv (solv = solvent; EtOH for **2** and MeOH for **3**) where two dissimilar motifs co-exist in the same structure: stacks of infinite ladders of composition [Cu$(\mathbf{1})_{1.5}(NO_3)_2$] are interpenetrated by infinite chains of composition [Cu(**1**)(solv)$(NO_3)_2$].

A blue solution of $Cu(NO_3)_2{\cdot}3H_2O$ (12.2 mg, 0.05 mmol) in ethanol and/or methanol (3 mL) was carefully layered onto an ethanol and/or methanol (3 mL) solution of 1,4-bis[(4′-pyridylethynyl)benzene] (14.4 mg, 0.05 mmol). Light green precipitates formed immediately. After two weeks, green crystals of **2** and **3** grew at the interface of the two layers and also at the top of the mixture. Single crystals suitable for X-ray analysis were isolated and their structures determined.‡

The one-dimensional ladders are composed of T-shaped building blocks with the copper center in a five-coordinate trigonal bipyramidal environment (Fig. 1a) consisting of three pyridyl nitrogen donors (two axial and one equatorial), one from each of the three ligands, **1**, and two equatorial oxygen donors from two monodentate nitrate ions. The ladders stack in a terraced fashion with an offset of 1/2 the ladder width along the crystallographic *a*-axis and with a close intralayer separation of 6.1 Å.[13] The one-dimensional chains (Fig. 1b) also feature five-coordinate copper, but now in a square pyramidal coordination environment, with the basal plane consisting of two pyridyl nitrogen donors, from two *trans* ligands of **1**, and two oxygen donors from two monodentate nitrate ions. The apical site is occupied by an oxygen donor from a coordinated ethanol (**2**) or methanol (**3**) solvent molecule.

We can consider the ladder to be a 'double-chain', formed *via* the crosslinking of two chains by the ligand, **1**. The square opening is divided into two infinite rectangular channels by the ladders located above and below. These channels in turn are occupied by the single-chains, as shown schematically in Fig. 2, such that the chains fill the square openings in bundles of four. Further supramolecular interactions exist between the two structural motifs in the form of weak O–H···O hydrogen bonds between the coordinated solvent in the chains and the nitrate ions in the ladders (O–O distance = 2.72 Å for **2** and 2.75 Å for **3**). The interpenetration of stacks of ladders by bundles of chains together with the hydrogen bonding between the two distinct one-dimensional structural motifs combine to form the virtual three-dimensional frameworks of **2** and **3**.

It is interesting to note that this structural motif has not previously been observed, a fact that can be accounted for by the geometrical requirement of this double motif. The square openings between the rungs must be large enough to accommodate a bundle of four chains arranged in a 2×2 pattern. With the proviso that both the ladder and the chains that fill the ladder are constructed from the same ligand/metal pair, then the ligand (plus metal bonds) length-to-diameter ratio must fall within a fairly narrow size regime. A simple geometrical argument using space-filling models indicates that a length-to-diameter ratio of 3 : 1 would allow 4 chains to exactly occupy the opening in the ladder. Since in the structures of **2** and **3**, the chains pass through two ladders offset by 1/2, a ratio of 4 : 1 (a loose fit in the ladder

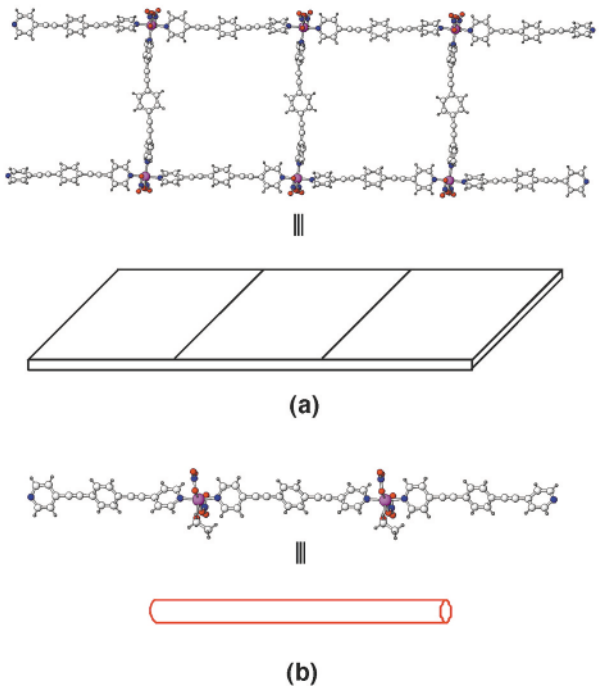

Fig. 1 Perspective view (top) and schematic representation (bottom) of a single (a) ladder motif and (b) chain motif in compounds **2** and **3**.

† On leave from Department of Applied Chemistry and Chemical Technology, University of Dhaka, Dhaka-1000, Bangladesh.

 DOI: 10.1039/b106190a

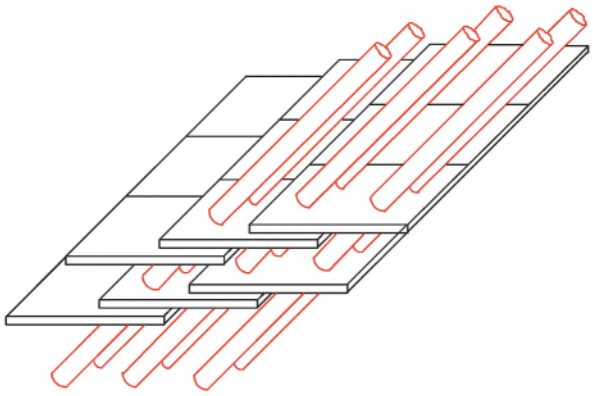

Fig. 2 Schematic view of the terraced stacks of ladders offset by 1/2 relative to each other along the crystallographic *a*-axis. The interpenetration by bundles of chains through the square openings is shown. For clarity only six chains in a square opening of a ladder are presented.

direction and an exact fit in the direction incident to the ladder) is required to allow for the space blocked by the second ladder. The experimentally determined ratio for both **2** and **3** is approximately 4.2 : 1. (The Cu–Cu distance is 20.4 Å while the approximate van der Waals diameter of the ligand (**1**) ranges from 3.40 Å at the most narrow to 6.43 Å at the widest point– yielding a crude 'average' vdW radius of 4.9 Å.)

Interestingly, one might have expected that shorter ligands such as 4,4′-bipyridine, which have been used extensively in the past, would have resulted in the discovery of a 1 × 1 pattern.[8] This would necessarily consist of parallel stacks of ladders without an offset. The fact that this has not been observed suggests that such a structural motif may require some hydrogen bonding between ladders for added stability. Offset systems, as described in this paper, allow for a virtual three-dimensional structure with, apparently, enhanced stability. By extension, longer ligands might form ladders and/or square grids that are interpenetrated by bundles of 9 or 16 chains in 3 × 3 or 4 × 4 patterns, respectively, with ladder offsets of 1/3 and 1/2 (or possibly 1/4). Such structures would require length-to-diameter ratios of at least 6 : 1 and 8 : 1 for 3 × 3 and 4 × 4 patterns, respectively (Fig. 3). Assuming that the 'average' vdW diameter of a typical unencumbered N,N′-bidentate ligand is ~5 Å, the lengths of the requisite ligands (assuming a 2 Å nitrogen–metal distance) would have to be ~26 and ~36 Å, respectively. (The fact that the rings in the ligand result in a 'plank-like' rather than a true 'spherical' shape should be an advantage for this type of offset structure.)

It is likely that the driving force for the formation of this type of interpenetration is the need to fill empty space in the structure. Typically, as suggested by Batten and Robson,[14] longer ligands will lead to more highly interpenetrated structures. The structural motif described in this communication fulfils that suggestion, however, not by using a self-interpenetrated structure, but rather by using two different structures, *i.e.* ladders and chains, that interpenetrate.

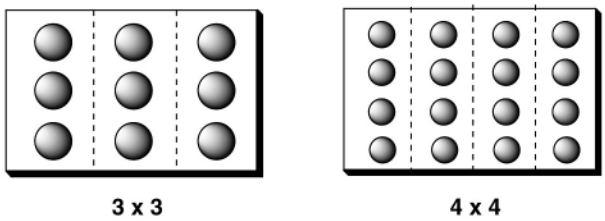

Fig. 3 Schematic representation of 3 × 3 and 4 × 4 bundles interpenetrating a stacked ladder structure. Chains (shaded circles) are running through the stacked ladders where dashed lines indicate the lateral offset of the ladders, 1/3 and 1/4, respectively.

Financial support was provided in part by the National Science Foundation through Grant DMR:9873570 and in part by the South Carolina Commission for Higher Education through Grant CHE:RU00-U25. The Bruker CCD Single Crystal Diffractometer was purchased using funds provided by the NSF Instrumentation for Materials Research Program through Grant DMR:9975623.

Notes and references

‡ *Crystal data* for **2**: $C_{56}H_{48}Cu_2N_9O_{15}$, M = 1214.11, triclinic, space group $P\bar{1}$, a = 12.248(2), b = 13.771(3), c = 18.257(4) Å, α = 108.078(4), β = 97.890(4), γ = 103.139(5)°, V = 2778.1(9) Å^3, Z = 2, T = 293(2) K, μ(Mo-Kα) = 0.842 mm^{-1}, R_1 = 0.052 and wR_2 = 0.094 for 9758 data with $I > 2\sigma(I)$. *Crystal data* for **3**: $C_{53}H_{42}Cu_2N_9O_{15}$, M = 1172.04, triclinic, space group $P\bar{1}$, a = 12.136(1), b = 13.738(2), c = 17.563(3) Å, α = 107.663(3), β = 94.805(4), γ = 104.021(4)°, V = 2667.6(7) Å^3, Z = 2, T = 180(2) K, μ(Mo-Kα) = 0.874 mm^{-1}, R_1 = 0.050 and wR_2 = 0.086 for 7669 data with $I > 2\sigma(I)$. X-Ray intensity data were measured on Bruker SMART APEX CCD-based diffractometer system. Both structures were solved by a combination of direct methods and difference Fourier syntheses, and refined by full-matrix least-squares against F^2, using the SHELXTL software package. All non-hydrogen atoms were refined with anisotropic displacement parameters; hydrogen atoms were placed in idealized positions and refined using a riding model with the exception of the coordinated solvent hydrogens, which were located and refined subject to an O–H distance restraint of 0.9(1) Å and given a U_{eq} value 1.5 times the parent atom. CCDC reference numbers 167941 and 167942. See http://www.rsc.org/suppdata/cc/b1/b106190a/ for crystallographic data in CIF or other electronic format.

Yield for **2**: 18% (crystals only) based on $Cu(NO_3)_2{\cdot}3H_2O$. Elemental analysis (%): calc. C 55.54, H 3.96, N 10.38; found C 53.79, H 3.90, N 10.74. Yield for **3**: 24% (crystals only) based on $Cu(NO_3)_2{\cdot}3H_2O$. Elemental analysis (%): calc. C 54.36, H 3.59, N 10.77; found C 54.14, H 3.61, N 10.52.

1 M. J. Zaworotko, *Chem. Commun.*, 2001, 1.
2 Design of Solids from Molecular Building Blocks: Golden Opportunity for Solid State Chemist, Special issue of *J. Solid State Chem.*, ed. O. M. Yaghi and M. O'Keeffe, 2000, **152**.
3 Y.-B. Dong, M. D. Smith and H.-C. zur Loye, *Angew. Chem. Int. Ed.*, 2000, **39**, 4271.
4 Y.-B. Dong, R. C. Layland, N. G. Pschirer, M. D. Smith, U. H. F. Bunz and H.-C. zur Loye, *Chem. Mater.*, 1999, **11**, 1413.
5 Y.-B. Dong, M. D. Smith, R. C. Layland and H.-C. zur Loye, *Chem. Mater.*, 2000, **12**, 1156.
6 L. Carlucci, G. Ciani and D. M. Proserpio, *J. Chem. Soc., Dalton Trans.*, 1999, 1799.
7 M. B. Zaman, M. D. Smith and H.-C. zur Loye, *Chem. Mater.*, in press.
8 D. Hagrman, R. P. Hammond, R. Haushalter and J. Zubieta, *Chem. Mater.*, 1998, **10**, 2091.
9 C. V. K. Sharma and R. D. Rogers, *Chem. Commun.*, 1999, 83.
10 S. R. Batten, *Curr. Opin. Solid State Mater. Sci.*, 2001, **5**, 107.
11 L. Carlucci, G. Ciani, M. Moret, D. M. Proserpio and S. Rizzato, *Angew. Chem., Int. Ed.*, 2000, **39**, 1506.
12 The N-to-N distance in 1,4-bis[(4′-pyridylethynyl)benzene] (**1**) is 16.5 Å, which is about 9.0 Å longer than 4,4′-bipyridine. The convenient route for the synthesis of **1** is described in J. T. Lin, S.-S. Sun, J. J. Wu, L. Lee, K.-J. Lin and Y. F. Huang, *Inorg. Chem.*, 1995, **34**, 2323.
13 Most of the 4,4′-bipyridine and transition metal square grid architectures have an interlayer separation of 6–8 Å: K. Biradha, K. V. Domasevitch, B. Moulton, C. Seward and M. J. Zaworotko, *Chem. Commun.*, 1999, 1327 and the references therein. The shortest interlayer separation of 4.5 Å is obtained from the longer ligand, 1,4-bis[(4′-pyridyl)biphenyl]; K. Biradha, Y. Hongo and M. Fujita, *Angew. Chem., Int. Ed.*, 2000, **39**, 3843.
14 S. R. Batten and R. Robson, *Angew. Chem., Int. Ed.*, 1998, **37**, 146.

CHEMCOMM
Communication
www.rsc.org/chemcomm

Inorganic–organic interpenetrating frameworks: 4,4′-bipyridine *N*,*N*′-dioxide as a bridging hydrogen-bond acceptor

Alexander J. Blake,* Matthew T. Brett, Neil R. Champness,* Andrei N. Khlobystov, De-Liang Long, Claire Wilson and Martin Schröder*

School of Chemistry, University of Nottingham, University Park, Nottingham, UK NG7 2RD. E-mail: Neil.Champness@nottingham.ac.uk; M.Schroder@nottingham.ac.uk; A.J.Blake@nottingham.ac.uk

Received (in Cambridge, UK) 17th July 2001, Accepted 3rd September 2001
First published as an Advance Article on the web 11th October 2001

4,4′-Bipyridine *N*,*N*′-dioxide (L) acts as a hydrogen-bond acceptor in the compounds {[$M(NO_3)_2(H_2O)_4$]·L_2} (M = Co, Ni) to form doubly-interpenetrated framework materials with sixfold topological connectivity.

Developments in inorganic crystal engineering strategies comprise two major themes, coordination polymer construction[1,2] and the use of hydrogen-bonding between suitable building-blocks.[2,3] The employment of these approaches has led to the development of many unusual materials with extraordinary topological features such as interpenetration.[4] Although these themes can be viewed as quite distinct, they are highly interdependent and should not be considered as distinct approaches to crystal engineering. We have reported recently a range of highly unusual lanthanide coordination polymers using 4,4′-bipyridine *N*,*N*′-dioxide (L) as a bridging ligand,[5,6] and have also demonstrated the versatility of this ligand with d-block metal ions in which four distinct bridging modes, including H-bonding, have been observed in a single framework.[7] L can act as a hydrogen-bond acceptor *via* the N-oxide moiety and thus offers the potential to act as a H-bonding bridge between two H-bond donor building-blocks.[8] In this respect L can be thought of as an antithetic building-block compared to the 4,4′-bipyridinium cation which has been used so elegantly by Orpen and coworkers[9] to bridge halometallates by acting as a H-bond donor (Scheme 1). We now report the use of L to construct three-dimensional H-bonded arrays by linking simple aquo–metal complexes.

Mixing of L with $M(NO_3)_2$ (M = Co, Ni) in aqueous solution affords a single crystalline product following addition of EtOH to the reaction mixture as an antisolvent after *ca.* 5 days. Characterisation of this product confirms the 2 : 1 stoichiometric co-crystallisation of L and the aquated metal ions to afford species of formula {[$M(NO_3)_2(H_2O)_4$]·L_2} (M = Co **1**, Ni **2**). To fully understand the H-bonding role of L and the structural topology of the products single-crystal X-ray structural determinations were carried out for **1** and **2**.† L acts as a H-bond acceptor with eight molecules of L forming O–H···O[N(L)] H-bonds with all eight H-atoms of the four metal-coordinated water molecules (Fig. 1). However, each N-oxide unit acts as a bifurcated acceptor adopting H-bonds to two different water molecules coordinated to independent metal centres (Fig. 2). This results in each [$M(NO_3)_2(H_2O)_4$] unit being bridged by four molecules of L to a further metal-bearing fragment forming a $R^4_4(16)$ H-bonded ring. Thus, each molecule of L bridges a total of four different metal nodes[10] *via* OH···O[N(L)] H-bonds affording a structure of complex topology in which each [$M(NO_3)_2(H_2O)_4$] moiety is linked *via* bridging molecules of L to fourteen further metal-bearing units. This description does not aid structural interpretation and we prefer a view of the structure considering a virtual node positioned centrally between metal centres linked *via* the $R^4_4(16)$ H-bonded ring (Fig. 2). By using this virtual node the structure can be viewed as a network in which (4,4) nets of H_2O-linked L are pillared by [$M(NO_3)_2(H_2O)_4$] units affording a 6-connected net of ReO_3-like topology. In **1** and **2** the large separation between metal centres [13.65 **1**, 13.66 Å **2** (*cis* to bridging L), 15.24 **1**, 15.21 Å **2** (*trans* to L)] allows interpenetration to occur (Fig. 3) thus affording a doubly interpenetrated framework. Six-connected nets of ReO_3 topology based upon coordinate bonds[11] or a

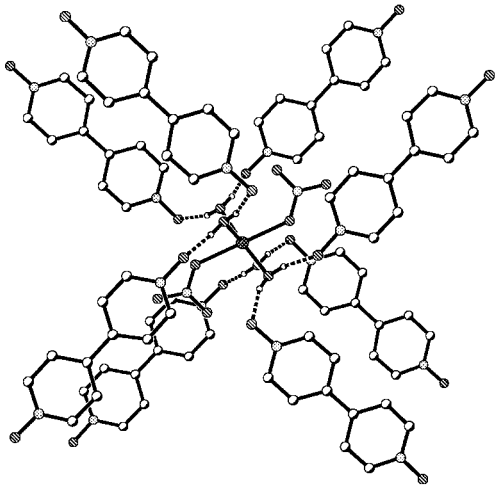

Fig. 1 O–H···O[N(L)] H-bonding observed between each [$M(NO_3)_2(H_2O)_4$] node and eight different molecules of L in **1** and **2**.

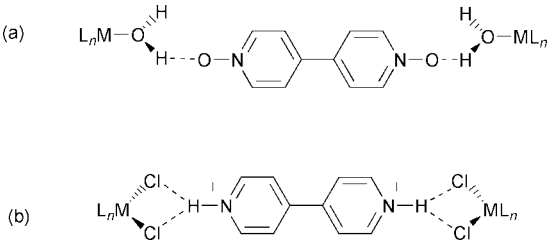

Scheme 1 (a) The O–H···O[N(L)] synthon used by L to construct the H-bonded frameworks **1** and **2** contrasting with (b) the N–H···Cl(M) synthon observed for 4,4′-bipyridinium halometallate systems.[9]

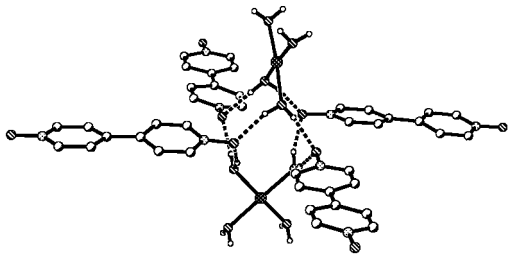

Fig. 2 Bridging between [$M(NO_3)_2(H_2O)_4$] units by four molecules of L, forming a $R^4_4(16)$ H-bonded ring. (L H-atoms and nitrate anions omitted for clarity).

 DOI: 10.1039/b106348k

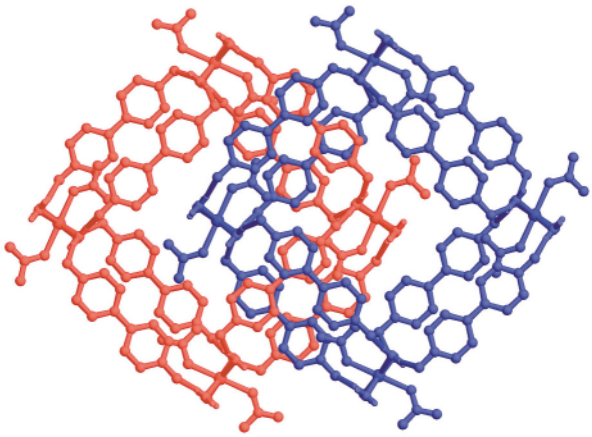

Fig. 3 Double interpenetration of six-connected hydrogen-bonded frameworks observed in **1** and **2**.

combination of H-bonds and coordinate bonds[12] have been observed to exhibit double-interpenetration previously but in only two previous examples has it been based exclusively on H-bonding.[13] The beauty of the current system is its simplicity and the potential for application to a vast range of H-bonded networks due to the large variety of metal–aquo complexes available. **1** and **2** are isotopological and both compounds crystallise in high symmetry (tetragonal) space groups.

The crystallisation conditions are crucial for the successful preparation of the H-bonded frameworks in **1** and **2**. By reacting L with $Co(NO_3)_2{\cdot}6H_2O$ in MeOH, L is sufficiently competitive as a ligand for the metal centre, in the absence of a large excess of water, such that no aquo ligands are coordinated to the metal centre, but only *N*-oxide donors. Structural characterisation by single crystal X-ray diffraction studies† reveals that the product formed exists as a discrete molecular unit, $[Co(L)_6](NO_3)_2$ **3**, in which each metal centre is coordinated by six, independent molecules of L. Each of these ligands coordinates *via* only one of its N-oxide donors leaving the other end of each ligand to engage in π–π interactions with other molecules of L in the solid-state to afford a two-dimensional (3,6) net.[7]

We have shown that L can be used to construct H-bonded frameworks by co-crystallisation with metal–aquo complexes. The large variety of metal–aquo complexes means that the H-bonding synthon reported here has potential for the construction of many new framework families such as that observed in **1** and **2**. We have also demonstrated that by using a coordinating NO_3^- anion we can control the connectivity at the metal-containing H-bonding fragment, thus determining the framework topology. We are currently exploring the variation in anion and metal centre coordination geometries for the construction of new families of H-bonded framework materials.

This work was supported by the EPSRC (UK) and the University of Nottingham.

Notes and references

† *Crystal data*: $\{[Co(NO_3)_2(H_2O)_4]{\cdot}L_2\}$ **1**: $C_{20}H_{24}CoN_6O_{14}$, M = 631.38, tetragonal, space group $I4_1/a$ (no. 88), pink block, a = 19.3309(10), c = 13.4691(7) Å, U = 5033.2(7) Å^3, Z = 8, D_c = 1.666 g cm^{-3}, μ(Mo-Kα) = 0.767 mm^{-1}, T = 150(2) K. 3132 Unique reflections [R_{int} = 0.019] [2374 with $I > 2\sigma(I)$]. Final R = 0.0275, wR_2 (all data) = 0.0896. $\{[Ni(NO_3)_2(H_2O)_4]{\cdot}L_2\}$ **2**: $C_{20}H_{24}NiN_6O_{14}$, M = 631.16, tetragonal, space group $I4_1cd$ (no. 110), pale green block, a = 19.3091(11), c = 13.4271(8) Å, U = 5006.2(8) Å^3, Z = 8, D_c = 1.675 g cm^{-3}, μ(Mo-Kα) = 0.861 mm^{-1}, T = 150(2) K. 2454 Unique reflections [R_{int} = 0.018] [2259 with $I > 2\sigma(I)$]. Final R = 0.0245, wR_2 (all data) = 0.0649. Flack parameter = 0.08(3). $[Co(L)_6](NO_3)_2$ **3**: $C_{60}H_{48}CoN_{14}O_{18}$, M = 1312.05, triclinic, space group $P\bar{1}$ (no. 2), dark red tablet, a = 8.9447(8), b = 11.7160(11), c = 14.0734(13) Å, α = 104.712(3), β = 96.797(2), γ = 98.233(2)°, U = 1393.2(2) Å^3, Z = 1, D_c = 1.564 g cm^{-3}, μ(Mo-Kα) = 0.401 mm^{-1}, T = 298(2) K. 6175 Unique reflections [R_{int} = 0.035] [5351 with $I > 2\sigma(I)$]. Final R = 0.042, wR_2 (all data) = 0.123. CCDC reference numbers 169145–169147. See http://www.rsc.org/suppdata/cc/b1/b106348k/ for crystallographic data in CIF or other electronic format.

1 A. J. Blake, N. R. Champness, P. Hubberstey, W.-S. Li, M. Schröder and M. A. Withersby, *Coord. Chem. Rev.*, 1999, **183**, 117; M. Munakata, L. P. Wu and T. Kuroda-Sowa, *Bull. Chem. Soc. Jpn.*, 1997, **70**, 1727; P. J. Hagrman, D. Hagrman and J. Zubieta, *Angew. Chem., Int. Ed.*, 1999, **38**, 2638; M. Eddaoudi, D. B. Moler, H. Li, B. Chen, T. M. Reineke, M. O'Keeffe and O. M. Yaghi, *Acc. Chem. Res.*, 2001, **34**, 319.

2 B. Moulton and M. J. Zaworotko, *Chem. Rev.*, 2001, **101**, 1629.

3 D. Braga and F. Grepioni, *Acc. Chem. Res.*, 2000, **33**, 601; D. Braga, L. Maini, M. Polito, L. Scaccianoce, G. Cojazzi and F. Grepioni, *Coord. Chem. Rev.*, 2001, **216**, 225.

4 S. R. Batten and R. Robson, *Angew. Chem., Int. Ed.*, 1998, **37**, 1460.

5 D.-L. Long, A. J. Blake, N. R. Champness and M. Schröder, *Chem. Commun.*, 2000, 1369; D.-L. Long, A. J. Blake, N. R. Champness, C. Wilson and M. Schröder, *J. Am. Chem. Soc.*, 2001, **123**, 3401.

6 D.-L. Long, A. J. Blake, N. R. Champness, C. Wilson and M. Schröder, *Angew. Chem., Int. Ed.*, 2001, **40**, 2444.

7 D.-L. Long, A. J. Blake, N. R. Champness and M. Schröder, *Chem. Commun.*, 2000, 2273.

8 R. Thaimattam, D. S. Reddy, F. Xue, T. C. W. Mak, A. Nangia and G. R. Desiraju, *J. Chem. Soc., Perkin Trans. 2*, 1998, 1783.

9 G. R. Lewis and A. G. Orpen, *Chem. Commun.*, 1998, 1873; A. L. Gillon, A. G. Orpen, J. Starbuck, X.-M. Wang, Y. Rodriguez-Martin and C. Ruiz-Perez, *Chem. Commun.*, 1999, 2287; A. L. Gillon, G. R. Lewis, A. G. Orpen, S. Rotter, J. Starbuck, X.-M. Wang, Y. Rodriguez-Martin and C. Ruiz-Perez, *J. Chem. Soc., Dalton Trans.*, 2000, 3897; B. Dolling, A. L. Gillon, A. G. Orpen, J. Starbuck and X.-M. Wang, *Chem. Commun.*, 2001, 567.

10 S. Tanase, M. Andruh, A. Müller, M. Schmidtmann, C. Mathonière and G. Rombaut, *Chem. Commun.*, 2001, 1084.

11 P. C. M. Duncan, D. M. L. Goodgame, S. Menzer and D. J. Williams, *Chem. Commun.*, 1996, 2127; D. M. L. Goodgame, D. A. Grachvogel, I. Hussain, A. J. P. White and D. J. Williams, *Inorg. Chem.*, 1999, **38**, 2057.

12 L. Carlucci, G. Ciani, D. M. Proserpio and A. Sironi, *J. Chem. Soc., Dalton Trans.*, 1997, 1801; C. S. Hong, S.-K. Son, Y. S. Lee, M.-J. Jun and Y. Do, *Inorg. Chem.*, 1999, **38**, 5602; K. Biradha and M. Fujita, *J. Chem. Soc., Dalton Trans*, 2000, 3805.

13 C.-Y. Su, B.-S. Kang, H.-Q. Liu, Q. G. Wang and T. C. W. Mak, *J. Chem. Soc., Dalton Trans.*, 2000, 1857; P. G. Desmartin, A. F. Williams and G. Bernardinelli, *New J. Chem.*, 1995, **19**, 1109.

CHEMCOMM Communication
www.rsc.org/chemcomm

Hydrogen bond directed formation of liquid-crystalline merocyanine dye assemblies

Frank Würthner,*[a] Sheng Yao,[a] Bernd Heise[b] and Carsten Tschierske[c]

[a] *Abteilung Organische Chemie II, Universität Ulm, Albert-Einstein-Allee 11, 89081 Ulm, Germany. E-mail: frank.wuerthner@chemie.uni-ulm.de; Fax: +49 731 5022840*
[b] *Abteilung Experimentelle Physik, Universität Ulm, Albert-Einstein-Allee 11, 89081 Ulm, Germany*
[c] *Institut für Organische Chemie, Martin-Luther-Universität Halle-Wittenberg, Kurt-Mothes-Strasse 2, 06120 Halle/Saale, Germany*

Received (in Cambridge, UK) 19th July 2001, Accepted 29th August 2001
First published as an Advance Article on the web 11th October 2001

Combined interaction of triple hydrogen bonding, dipolar π–π aggregation and micro-segregation in a melamine–barbituric acid dye assembly leads to a columnar mesophase which could be characterized by optical polarising microscopy, differential scanning calorimetry and X-ray diffraction.

The ditopic triple hydrogen bonding motif offered by *N*,*N*′-dialkylmelamines has been applied for the construction of numerous supramolecular architectures.[1–10] Recently we showed that complementary hydrogen bonding to dyes bearing imide functional groups can lead to nano- and mesoscopic assemblies which exhibit luminescence and chiroptical properties.[9,10] In these systems long alkyl chains at the melamine amino groups provide the capability to solubilise even little soluble pigment dyes by means of directional hydrogen bonds which are especially strong in low-polarity solvents. However, upon heating, such weak complexes often disassemble leading to precipitation of insoluble materials. In this communication we introduce the new and easily accessible ditopic melamine **3** bearing a much higher amount of alkyl chains which proved to be well-suited to induce stable thermotropic liquid-crystallinity upon self-assembly with a barbituric acid merocyanine dye.

Melamine **3** is easily available according to Scheme 1 from 2-amino-4,6-dichlorotriazine **1** and tridodecyloxyaniline **2**.†

If a stoichiometric mixture of **3** and merocyanine dye **4** is dissolved in chloroform an amorphous solid is obtained after evaporation (**3·4**). This solid melts at 164 °C. Upon cooling the texture shown in Fig. 1 appears at 151 °C which remains unchanged upon further cooling to room temperature, according to optical polarising microscopy (OPM, Fig. 1).

Further heating–cooling cycles between −30 and 180 °C (DSC, 10 K min^{-1}) showed exclusively the peaks corresponding to the transition between the liquid crystalline and the isotropic phase at 161 °C (ΔH = 4.2 J g^{-1}) upon heating and at 151 °C (ΔH = −4.0 J g^{-1}) upon cooling, confirming the enantiotropic nature of the LC phase and its persistence even at low temperature. XRD studies of the LC phase revealed three Bragg reflections in the small angle region at 2θ = 2.43, 3.61 and 5.02° (CuK_α) corresponding to layer spacings of d = 36.3, 24.5 and 17.6 Å and a diffuse halo in the wide-angle region corresponding to 4–5 Å arising from disordered alkyl chains. The position of the small angle reflections exclude a smectic layer structure. As there are no references to a hexagonal or rectangular 2D lattice we evaluated the pattern under the assumption of an oblique two-dimensional lattice, assigning the observed reflections to (10), (01) and (11) and obtained the lattice parameter a = 38 Å, c = 26 Å and β = 110°.

A hydrogen-bonded circular rosette-type assembly[11] can clearly be ruled out by the small lattice parameters, which are not even sufficient to accommodate the aromatic part (diameter 44 Å) of such an extended architecture. On the other hand, the formation of a columnar mesophase from triple hydrogen-bonded tapes as suggested by Scheme 2 is fully consistent with the X-ray data.

According to Scheme 2 triple hydrogen-bonding, dipolar π–π aggregation and microphase separation ('micro-segregation')[12] of the polar aromatic units and the unpolar alkyl chains are the driving forces for the three-dimensional organisation of **3·4** in the bulk. Thus triple-hydrogen bonding between melamines and barbituric acid dyes affords polymeric tapes similar to related assemblies reported from the Whitesides group in the crystalline state.[1] The dimension of these tapes is in good accordance with the largest lattice parameter of 38 Å obtained by XRD. Typically, owing to the significant polarity contrast between the aromatic and the aliphatic part such tapes are supposed to aggregate giving extended sheets, which would lead to a smectic phase.[13] However, electrostatic and steric considerations have to be taken into account for a reasonable model for **3·4** self-assembly. Firstly, because of the parallel alignment of highly dipolar merocyanine dyes within a hydrogen-bonded tape neighbouring tapes will orient in an antiparallel fashion[14] which also provides more space to accommodate the bulky alkyl chains. Nevertheless, molecular modeling of the dimeric tape assembly shows that infinite growth perpendicular to the tape direction is impossible due to the significant sterical demand of the large number of alkyl chains. The result is a superstructure in which infinite ribbons

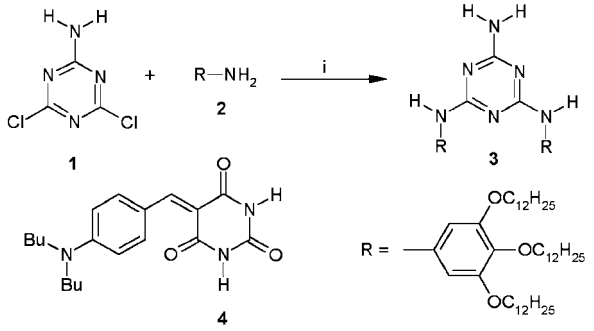

Scheme 1 *Reagents and conditions*: i, $NaHCO_3$, dioxane, reflux, 24 h.

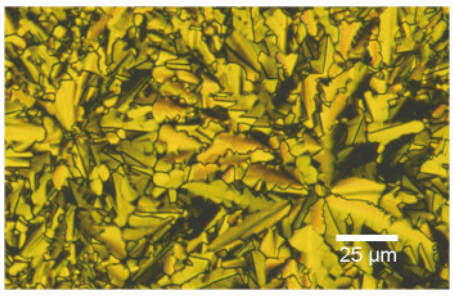

Fig. 1 Optical texture observed between crossed polarisers at 25 °C for the complex **3·4** as obtained upon cooling from the isotropic melt.

 DOI: 10.1039/b106413d

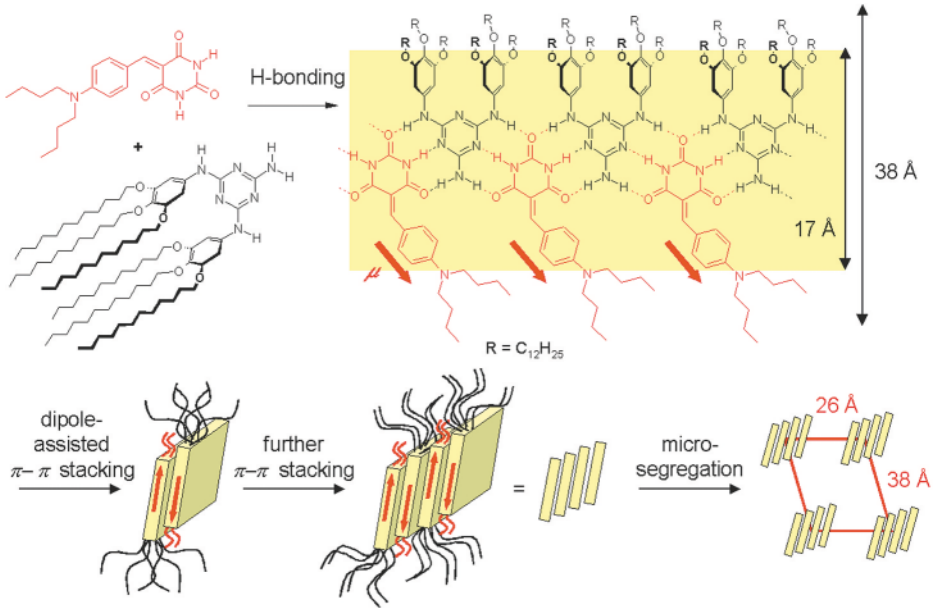

Scheme 2 Formation of a columnar assembly of **3**·**4** based on orthogonal intermolecular interactions involving hydrogen bond-directed growth of tapes (first direction) and dipole-assisted π–π stacking of these tapes to give ribbons (second direction) which finally assemble into a columnar structure by micro-segregation and steric effects. The yellow shaded area represents the π-conjugated part of the assembly.

consisting of 4–6 antiparallel tapes, arranged in a two-dimensional lattice, are separated by the fluid alkyl chains. Within the ribbons the tapes can be tilted as shown in Scheme 2, but also a non-tilted arrangement is possible. All dimensions of the given arrangement are in good agreement with the obtained lattice parameters.

To our knowledge this is the first example of a columnar mesophase formed by hydrogen-bonded rigid tape assemblies. Furthermore, in contrast to all other hydrogen-bonded columnar liquid crystals[15–17] the hydrogen bonds *and* the involved aromatic cores are organised *parallel* to the column long axes.[16] In this respect they represent counterparts to the columnar phases formed by the stacking of disc-like supermolecules in columns, where flat supermolecules are organised *perpendicular* to the column long axis.[17]

In conclusion thermotropic liquid-crystallinity has been achieved for barbituric acid dye–melamine assemblies which enlarges the set of architectures realised by organisation of these complementary building blocks, *i.e.* interfacial monolayers,[3–5] mesoscopic fibers[6] and rosette assemblies.[10] Current work in our group is directed toward further applications of the new amphiphilic melamine **3** for mesophase induction involving other dye molecules.

The authors are grateful to the Deutsche Forschungsgemeinschaft for financial support (grant Wu 317/1).

Notes and references

† Synthesis of 2-amino-4,6-bis[(3,4,5-tridodecyloxyphenyl)amino]-1,3,5-triazine (**3**). Dichlorotriazine **1** (0.165 g, 1.0 mmol) and aniline **2** (1.42 g, 2.2 mmol) were mixed with $NaHCO_3$ (0.193 g, 2.3 mmol) in 20 ml dry dioxane. The mixture was heated at reflux for 24 h and the solvent was evaporated under reduced pressure. To the residue, 50 ml water and 100 ml CH_2Cl_2 were added and the water phase was extracted with another 100 ml CH_2Cl_2. The combined organic phase was washed with 20 ml water and dried. Evaporation of the solvent, column chromatography on silica with toluene–ethyl acetate 1 : 1 and crystallisation from isopropyl alcohol afforded 0.21 g (15%) of pure **3**. Mp 135–136 °C, ^{1}H NMR (400 MHz, $CDCl_3$) δ: 6.93 (br, 2H, NH), 6.66 (s, 4H, Ph-H), 5.02 (br, 2H, NH), 3.83 (t, *J* 6.6, 12H, OCH_2), 1.67 (m, 12H, CH_2), 1.37 (m, 12H, CH_2), 0.91 (m, 96H, CH_2), 0.81 (m, 18H, CH_3). Anal. calc. for $C_{87}H_{158}N_6O_6$ (1384.3): C 75.49, H 11.50, N 6.07; found: C 75.31, H 11.32, N 6.07%.

1 E. E. Simanek, X. Li, I. S. Choi and G. M. Whitesides, *Comprehensive Supramolecular Chemistry, Vol. 9*, ed. J.-M. Lehn, J. L. Atwood, J. E. D. Davies, D. D. MacNicol and F. Vögtle, Pergamon, Oxford, 1996, pp. 595–621.
2 J.-M. Lehn, *Supramolecular Chemistry*, VCH, Weinheim, 1995, pp. 161–179.
3 T. M. Bohanon, S. Denzinger, R. Fink, W. Paulus, H. Ringsdorf and M. Weck, *Angew. Chem., Int. Ed. Engl.*, 1995, **34**, 58.
4 K. Ariga and T. Kunitake, *Acc. Chem. Res.*, 1998, **31**, 371.
5 K. Motesharei and D. C. Myles, *J. Am. Chem. Soc.*, 1998, **120**, 7328.
6 W. Yang, X. Chai, L. Chi, X. Liu, Y. Cao, R. Lu, Y. Jiang, X. Tang, H. Fuchs and T. Li, *Chem. Eur. J.*, 1999, **5**, 1144; Y. W. Cao, X. D. Chai, T. J. Li, J. Smith and D. Li, *Chem. Commun.*, 1999, 1605.
7 R. F. M. Lange, F. H. Beijer, R. P. Sijbesma, R. W. W. Hooft, H. Kooijman, A. L. Spek, J. Kron and E. W. Meijer, *Angew. Chem., Int. Ed.*, 1997, **36**, 969.
8 H.-A. Klok, K. A. Jolliffe, C. L. Schauer, L. J. Prins, J. P. Spatz, M. Möller, P. Timmerman and D. N. Reinhoudt, *J. Am. Chem. Soc.*, 1999, **121**, 7154.
9 F. Würthner, C. Thalacker, A. Sautter, W. Schärtl, W. Ibach and O. Hollricher, *Chem. Eur. J.*, 2000, **6**, 3871.
10 L. J. Prins, C. Thalacker, F. Würthner, P. Timmerman and D. N. Reinhoudt, *Proc. Nat. Acad. Sci. USA*, 2001, **98**, 10 042.
11 The concept of peripheral crowding was applied to explain the preferred formation of circular assemblies between barbituric acids and melamines possessing bulky substituents: C. M. Drain, K. C. Russell and J.-M. Lehn, *Chem. Commun.*, 1996, 337; J. A. Zerkowski, J. C. Seto and G. M. Whitesides, *J. Am. Chem. Soc.*, 1992, **114**, 5473. In a recent paper this view was questioned and evidence for tape-formation even in the presence of bulky substituents was presented: A. G. Bielejewska, C. E. Marjo, L. J. Prins, P. Timmerman, F. de Jong and D. N. Reinhoudt, *J. Am. Chem. Soc.*, 2001, **123**, 7518.
12 C. Tschierske, *J. Mater. Chem.*, 1998, **8**, 1485.
13 Smectic and columnar folic acid derivatives: K. Kanie, T. Yasuda, S. Ujiie and T. Kato, *Chem. Commun.*, 2000, 1899.
14 F. Würthner and S. Yao, *Angew. Chem., Int. Ed.*, 2000, **39**, 1978.
15 Recent reviews: C. M. Paleos and D. Tsiourvas, *Angew. Chem., Int. Ed. Engl.*, 1995, **34**, 1696; T. Kato, *Structure and Bonding, Vol. 96, Molecular Self-Assembly—Organic Versus Inorganic Approach*, ed. M. Fujita, Springer, Berlin, 2000, p. 95.
16 Some aromatic amides form columnar and nematic phases in which the hydrogen bonds are directed along the column axis, whereas the aromatic cores are organised perpendicular to them: J. Malthete, A.-M. Levelut and L. Liebert, *Adv. Mater.*, 1992, **4**, 37; T. Akutagawa, K. Iuchi and Y. Matsunaga, *Liq. Cryst.*, 2000, **27**, 1399.
17 R. Kleppinger, C. P. Lillya and C. Yang, *J. Am. Chem. Soc.*, 1997, **119**, 4097; M. Suarez, J.-M. Lehn, S. C. Zimmerman, A. Skoulios and H. Heinrich, *J. Am. Chem. Soc.*, 1998, **120**, 9526; A. Kraft, A. Reichert and R. Kleppinger, *Chem. Commun.*, 2000, 1015; J. H. K. K. Hirschberg, L. Brunsveld, A. Ramzi, J. A. J. M. Vekemans, R. P. Sijbesma and E. W. Meijer, *Nature*, 2000, **407**, 167; D. Goldmann, R. Dietel, D. Janietz, C. Schmidt and J. H. Wendorff, *Liq. Cryst.*, 1998, **24**, 407.

CHEMCOMM Communication
www.rsc.org/chemcomm

1,3,5-Triarylpent-2-en-1,5-diones for the colorimetric sensing of the mercuric cation

Félix Sancenón, Ramón Martínez-Máñez* and Juan Soto

Departamento de Química, Universidad Politécnica de Valencia, Camino de Vera s/n. 46071, Valencia, Spain. E-mail: rmaez@qim.upv.es

Received (in Cambridge, UK) 13th July 2001, Accepted 14th September 2001
First published as an Advance Article on the web 4th October 2001

The 1,3,5-triarylpent-2-en-1,5-dione group selectively undergoes cyclisation and changes its colour from yellow to magenta upon coordination of Hg^{2+} on a remote site.

The development of sensing systems able to selectively trace the presence of target substrates, is an area of interest, due to its potential application in the development of new methodologies for cation and anion determination.[1] Among straightforward methods for sensing target analytes, those involving colour changes[2] are especially interesting due to their simple use and because they require less expensive equipment than closely related methods involving fluorescence[3] or electrochemical changes.[4] Colorimetric reagents would find direct application in the development of optodes based on absorption changes or disposable dip-stick rapid assays. Despite these attractive features, colorimetric selective reagents for "naked-eye" detection in water are scarce for many cations[5] and anions[6] of importance.

We have recently found that 1,3,5-triarylpent-2-en-1,5-dione derivatives undergo cyclisation to give the 2,4,6-triphenylpyrylium cation upon protonation of the anylinium group or by interaction with certain anions, and we have described a selective ATP colorimetric sensor based on this system.[7] To study the possibility of using similar compounds as chromogenic reagents towards metal ions we have synthesised new 1,3,5-triaryl-2-en-1,5-dione derivatives bearing aza-oxa binding sites and have studied their interaction with metal cations.

Reaction of 2,6-diphenylpyrylium perchlorate with the corresponding aryl aza-oxa derivative (see Scheme 1) gave, after column chromatography on aluminium oxide, the corresponding diketone derivatives L^1 and L^2 in a *ca.* 35% yield.[8] The ^1H NMR spectra of L^1 and L^2 present one characteristic singlet at 4.8 ppm corresponding to the methylene attached directly to one carbonyl and to the double bond. The most characteristic signals in the ^{13}C NMR spectra were two singlets at 190.5 and 196.6 ppm ascribed to the two non-equivalent carbonyl groups. The mass spectra gave molecular ions and fragmentation patterns consistent with the proposed structures. The UV–VIS spectra of L^1 and L^2 show bands in the 200–300 nm range, and a band centred at 380 nm responsible for the yellow colour of the receptors.

The transformation of the penta-1,5-diones to the corresponding pyrylium ions was studied in 1,4-dioxane–water (70 : 30 v/v) mixtures (L^1 and L^2 are not water soluble). A simple method to induce cyclisation is the addition of acid to protonate the amine. Thus, addition of HCl solutions to L^1 or L^2 caused a very significant colour change from yellow to magenta. This change was reflected in the UV–VIS spectrum of the solution that showed a new intense band centred at 550 nm, which was attributed to the highly delocalised pyrylium ring formation.[9] By fitting the plot of the absorption of the band at 550 nm as a function of the pH for compound L^1 (not shown), a logarithm of the stability constant of 4.4 ± 0.2 is obtained for the process $L^1 + H^+ = [HL^1(Cy)]^{2+} + OH^-$. This value is similar to that reported for the protonation of aniline ($\log K = 4.6$), reinforcing the idea that protonation induces diketone-to-pyrylium transformation.

It is known that the cyclisation occurs by electrophilic attack of the C1 carbon to the lone pair of the hydroxylic oxygen of the enol tautomer.[10] The basic idea in this system is that the electrophilic character of the C1 changes, depending on whether the nitrogen atom is protonated or not. Thus, the formation of the pyrylium cation, as described above, is triggered by a protonation event in a remote site (the anilinium group). The nitrogen atom, besides controlling cyclisation upon protonation, is part of a binding site in receptors L^1 and L^2. In this respect, it would also be possible that coordination of metal ions to the nitrogen would also change the electrophilicity of C1. By changing the nature of the binding sites it would be possible to tune the coordination strength between the metal ion and the nitrogen atom. Strong coordination with the amine will induce cyclisation, whereas poor coordination will not. Consequently, we have designed ligand L^1 containing an open-chain binding site and L^2 incorporating a macrocycle, and have studied the effect of metal ion addition on the colour of L^1 and L^2.

The nitrate or perchlorate salts of the cations Li^+, Na^+, K^+, Ba^{2+}, Ca^{2+}, Mg^{2+}, Fe^{3+}, Fe^{2+}, Mn^{2+}, Co^{2+}, Ni^{2+}, Cu^{2+}, Zn^{2+}, Hg^{2+}, Cd^{2+}, Pb^{2+}, Al^{3+}, Cr^{3+} and Sb^{2+} were added to solutions of L^1 or L^2 in dioxane–water (70 : 30 v/v) at pH 6 (pH was buffered with HEPES at a concentration of 0.1 M). Solutions of receptors were prepared in a 10^{-4} M concentration. Very remarkably, the colour change clearly depends on the nature of the binding sites. For instance, Fig. 1(a) shows a photograph

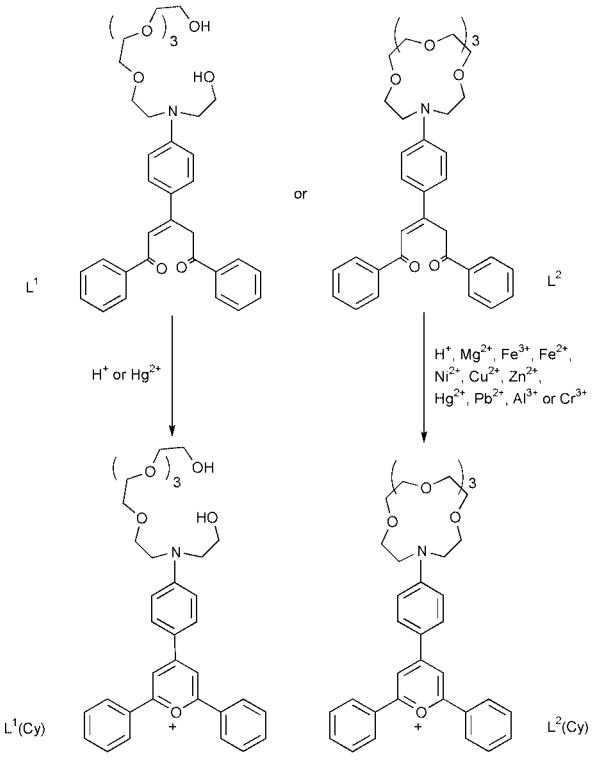

Scheme 1

 DOI: 10.1039/b106941c

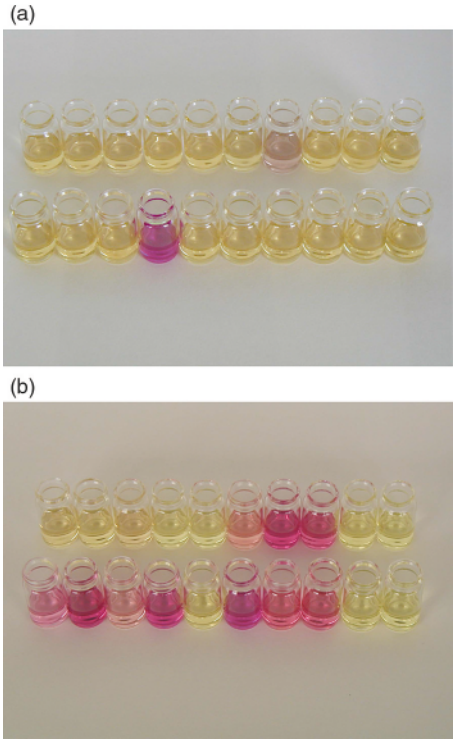

Fig. 1 Colour changes induced on (a) L^1 (1.0×10^{-4} M) and (b) L^2 (1.0×10^{-4} M) at pH 6 (HEPES 0.1 M) in the presence of certain cations in dioxane–water (70:30 v/v) solutions. From left to right and from top to bottom: Li^+, Na^+, K^+, Ba^{2+}, Ca^{2+}, Mg^{2+}, Fe^{3+}, Fe^{2+}, Mn^{2+}, Co^{2+}, Ni^{2+}, Cu^{2+}, Zn^{2+}, Hg^{2+}, Cd^{2+}, Pb^{2+}, Al^{3+}, Cr^{3+}, Sb^{2+} and no cation.

with the colour transformation observed upon addition of stoichiometric amounts of those cations to dioxane–water solutions of L^1. At this pH, a slight change in colour upon addition of Fe^{3+} was found, but the really dramatic effect is observed in the presence of Hg^{2+}. The remaining cations do not induce any significant colour change. This chromogenic behaviour in the presence of Hg^{2+} contrasts with the unspecific colour changes observed, under similar conditions, by using receptor L^2 [see Fig. 1(b)]. In this case, there is at least a partial colour change in the presence of metal cations Mg^{2+}, Fe^{3+}, Fe^{2+}, Ni^{2+}, Cu^{2+}, Zn^{2+}, Hg^{2+}, Pb^{2+}, Al^{3+} and Cr^{3+}.

Ring closure in the presence of metal ions is most likely due to the Lewis acid character of the metals that, when coordinated to the nitrogen atom, might enhance the electrophilic character of the C1 carbon. L^2 probably forms stronger complexes (macrocyclic effect) than L^1, therefore favouring, for many metals, an effective nitrogen–metal interaction. L^1 would form weaker complexes and give poorer nitrogen–metal interactions; therefore, most of the metals do not induce cyclisation. The colour change induced by mercury is not unexpected, bearing in mind the strong complexes (compared with other metal ions) that this cation forms with oxa-aza binding sites. L^1 can be considered as a chromogenic reagent for Hg^{2+} sensing.[11]

In order to appreciate the utility of this system, quantification studies by means of extraction experiments of Hg^{2+} from water using L^1 as extractant in dichloromethane, were carried out. Thus, in a typical experiment, 10 mL of dichloromethane containing L^1 (1×10^{-3} M) were placed in a separatoty funnel with 500 mL of water containing Hg^{2+} and the mixture was shaken for 4 min. When the Hg^{2+} cation goes into the dichloromethane, a colour change in this phase proportional to the mercury concentration in water is observed. Fig. 2 shows the absorbance of dichloromethane phases used to extract Hg^{2+} from aqueous solutions at neutral pH. A good linear range is found with a remarkable detection limit for mercury determination in water of 5×10^{-8} M (10 ppb). From some preliminary fixed interference experiments with competing levels of other cations, we found that only Fe^{3+} competes significantly in the extraction experiments whereas other cations such as Cu^{2+} or Pb^{2+} does not interfere in the mercury cation determination.

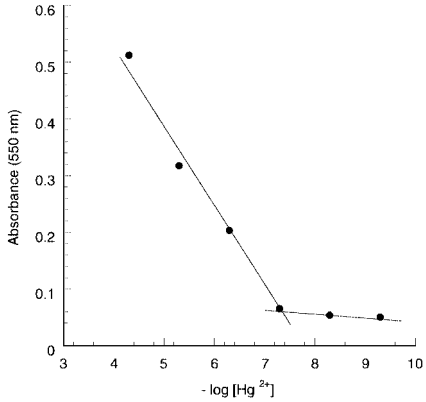

Fig. 2 Extraction experiments. Plot of the absorbance of the dichloromethane phase containing L^1 as a function of the Hg^{2+} concentration in water at neutral pH.

In conclusion, naked-eye sensing of Hg^{2+} has been achieved by using ligands based on 1,3,5-triaryl-2-en-1,5-diones containing a suitable open-chain aza-oxa binding site. Simple extraction experiments allow tracing Hg^{2+} to concentrations that are not far from the maximum contaminant level for mercury in drinking water (2 ppb) set by the United States Environmental Protection Agency (EPA).

We should like to thank the DGICYT (proyecto PB95-1121-C02-02, 1FD97-0508-C03-01 and AMB99-0504-C02-01) for support. F. S. also thanks the Ministerio de Educación y Cultura for a Doctoral Fellowship.

Notes and references

1 A. P. De Silva, H. Q. N. Gunaratne, T. Gunnlaugsson, A. J. M. Huxley, C. P. McCoy, J. T. Rademacher and T. E. Rice, *Chem. Rev.*, 1997, **97**, 1515; P. D. Beer and P. A. Gale, *Angew. Chem., Int. Ed.*, 2001, **40**, 486.

2 M. Takagi and K. Ueno, *Top. Curr. Chem.*, 1984, **121**, 39; H. G. Löhr and F. Vögtle, *Acc. Chem. Res.*, 1985, **18**, 65.

3 For recent works on fluorescent sensing of metals, see: T. Hirano, K. Kikuchi, T. Higuchi and T. Nagano, *Angew. Chem., Int. Ed.*, 2000, **39**, 1052; K. Rurack, M. Kollmannsberger, U. Resch-Genger and J. Daub, *J. Am. Chem. Soc.*, 2000, **122**, 968; G. K. Walkup, S. C. Burdette, S. J. Lippard and R. Y. Tsien, *J. Am. Chem. Soc.*, 2000, **122**, 5644; J. V. Mello and N. S. Finney, *Angew. Chem., Int. Ed.*, 2001, **40**, 1536; Y. Al Shihadeh, A. Benito, J. M. Lloris, R. Martínez-Máñez, T. Pardo, J. Soto and M. D. Marcos, *J. Chem. Soc., Dalton Trans.*, 2000, 1.

4 For recent works on electrochemical sensing of metals, see: J. M. Lloris, R. Martínez-Máñez, J. Soto, T. Pardo, M. E. Padilla-Tosta, A. Benito and M. D. Marcos, *Polyhedron*, 1999, **18**, 3689; J. M. Lloris, R. Martínez-Máñez, M. E. Padilla-Tosta, T. Pardo, J. Soto, P. D. Beer, J. Cadman and D. K. Smith, *J. Chem. Soc., Dalton Trans.*, 1999, 2359.

5 N. J. van der Veen, R. J. M. Egberink, J. F. J. Engbersen, F. J. C. M. van Veggel and D. N. Reinhoudt, *Chem. Commun.*, 1999, 681; N. Su, J. S. Bradshaw, X. X. Zhang, H. Song, P. B. Savage, G. Xue, K. E. Krakowiak and R. M. Izatt, *J. Org. Chem.*, 1999, **64**, 8855; R. Ibrahim, S. Tsuchiya and S. Ogawa, *J. Am. Chem. Soc.*, 2000, **122**, 12174.

6 D. H. Lee, K. H. Lee and J. I. Hong, *Org. Lett.*, 2001, **3**, 5; H. Miyaji and J. L. Sessler, *Angew. Chem., Int. Ed.*, 2000, **41**, 154; H. Miyaji, W. Sato, J. L. Sessler and V. M. Lynch, *Tetrahedron Lett.*, 2000, **41**, 1369; H. Miyaji, W. Sato and J. L. Sessler, *Angew. Chem., Int. Ed.*, 2000, **39**, 1777; C. B. Black, B. Andrioletti, A. C. Try, C. Ruiperez and J. L. Sessler, *J. Am. Chem. Soc.*, 1999, **121**, 10438; P. A. Gale, L. J. Twyman, C. I. Handlin and J. L. Sessler, *Chem. Commun.*, 1999, 1851.

7 F. Sancenón, A. B. Descalzo, R. Martínez-Máñez, M. A. Miranda and J. Soto, *Angew. Chem., Int. Ed.*, 2001, **40**, 2640.

8 K. E. Krakowiak, J. S. Bradshaw and D. J. Zamecka-Krakowiak, *Chem. Rev.*, 1989, **89**, 929; D. Markovitsi, C. Jallabert, H. Strzelecka and M. Veber, *J. Chem. Soc., Faraday Trans.*, 1990, **86**, 2819.

9 F. Pina, M. J. Melo, M. Maestri, P. Passaniti and V. Balzani, *J. Am. Chem. Soc.*, 2000, **122**, 4496.

10 G. Schwarzenbach and K. Lutz, *Helv. Chim. Acta*, 1940, **23**, 1147; E. N. Marvell, G. Caple, T. A. Gosink and G. Zimmer, *J. Am. Chem. Soc.*, 1966, **88**, 619.

11 For new recent colorimetric chemosensors for Hg^{2+} see: O. Brümmer, J. J. La Clair and K. D. Janda, *Org. Lett.*, 1999, **1**, 415; F. Sancenón, R. Martínez-Máñez and J. Soto, *Tetrahedron Lett.*, 2001, **42**, 4321; O. Brümmer, J. J. LaClair and K. D. Janda, *Bioorg. Med. Chem.*, 2001, **9**, 1067.

CHEMCOMM
Communication
www.rsc.org/chemcomm

Synthesis and characterization of [Bu^{t}NSn(μ-NBu^t)$_2$TeNBu^t](μ$_3$-SnTe), a stannanetellurone with four-coordinate tin

Tristram Chivers* and Gabriele Schatte

Department of Chemistry, University of Calgary, Calgary, Alberta, Canada T2N 1N4

Received (in Purdue, IN, USA) 28th July 2001, Accepted 16th September 2001
First published as an Advance Article on the web 18th October 2001

Treatment of [Li$_2$Te(NBu^t)$_3$]$_2$ with Sn(O$_3$SCF$_3$)$_2$ or SnCl$_2$ in diethyl ether generates the stannanetellurone [Bu^{t}NSn(μ-NBu^t)$_2$TeNBu^t](μ$_3$-SnTe) involving four-coordinate tin with *d*(Sn=Te) = 2.589(1) Å; the two Sn and two Te atoms are in different oxidation states (+II/+IV and +IV/−II, respectively).

The chemistry of 'heavy ketones', a class of compound that involves a double bond between heavier group 14 and 16 elements, has undergone remarkable development recently.[1] Two methods have been exploited to stabilize these highly reactive functionalities. For example, kinetic stabilization by the use of bulky substituents on the Group 14 elements has been applied successfully to the synthesis of germanetellurones involving three-coordinate germanium.[2] In an alternative approach stabilization may be achieved by intramolecular heteroatom coordination.[3] Indeed the only known stannanetellurone involves five-coordinate tin;[4a] attempts to generate a porphyrinatotin telluride were unsuccessful.[4b] In addition to the fundamental interest in the bonding and reactions of these multiply bonded species, tin–tellurium compounds are of interest as potential precursors of the low band gap semiconductor SnTe,[5] which has a variety of applications, *e.g.* as IR detectors or in thermoelectric devices.[6] In this communication we describe the synthesis, spectroscopic characterization and X-ray structure of [Bu^{t}NSn(μ-NBu^t)$_2$TeNBu^t](μ$_3$-SnTe) **1**, the first stannanetellurone involving four-coordinate tin.

The reaction of [Li$_2$Te(NBu^t)$_3$]$_2$[7] with Sn(SO$_3$CF$_3$)$_2$ or SnCl$_2$ in diethyl ether produced **1** as orange, moisture-sensitive crystals.† Yields of pure, crystalline material were only 10–20% as a result of the thermal instability of **1** in solution. An X-ray structure analysis of **1** revealed a tricyclic structure containing a Sn=Te functionality with four-coordinate tin (Fig. 1).‡ Complex **1** contains two tin atoms in different oxidation states, +II[Sn(2)] and +IV[Sn(1)] and two tellurium atoms, also in different oxidation states, −II[Te(1)] and +IV[Te(2)]. The formation of **1** involves the redox process shown in eqn. (1) (X=Cl, O$_3$SCF$_3$).

$$[Li_2Te(NBu^t)_3]_2 + 2SnX_2 \rightarrow [Bu^tNSn(\mu\text{-}NBu^t)_2TeNBu^t](\mu_3\text{-}SnTe) + Bu^tN{=}NBu^t + 4LiX \quad (1)$$
1

In effect, 1 equivalent of the [Te(NBu^t)$_3$]$^{2-}$ anion acts as a bridging, tridentate ligand to the two tin centres while the second equivalent serves as the source of tellurium for the terminal telluride and provides a bridging NBu^t group with the elimination of Bu^{t}N=NBu^t (^{1}H NMR). By contrast, no-sulfur-containing products were identified from the reaction of SnCl$_2$ with the congeneric [S(NBu^t)$_3$]$^{2-}$ dianion.[8]

As expected the Sn–Te bond distance of 2.5918(3) Å in **1** is significantly shorter than the value of 2.618(1) Å found for the previously reported five-coordinate tin complex.[4a] The calculated value for the prototypical three-coordinate tin system H$_2$Sn=Te is 2.543 Å.[1a] Typical Sn–Te single bond distances are in the range 2.73–2.79 Å.[4a,9] Thus the bond contraction in **1** is *ca.* 6%. The geometry at the four-coordinate tin atom Sn(1) is highly distorted tetrahedral with bond angles in the range 76.52(7)–127.51(6)° and the Sn(IV)–N bonds are expectedly *ca.* 0.08 Å shorter than the corresponding Sn(II)–N bonds. In addition, the Te–N bond involving the four-coordinate nitrogen atom N(1) is *ca.* 0.08 Å longer than the mean value of the Te–N bonds involving the three-coordinate nitrogen atoms N(3) and N(4). Taken together these data suggest approximately equal contributions from the resonance forms **A** and **B** to the structure of **1**.

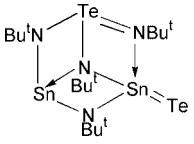

A

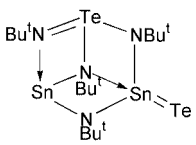

B

An additional structural feature of interest is the existence of weak intermolecular interactions between the Te(−II) and Sn(+II) centres, which gives rise to parallel polymeric strands in the unit cell of **1** (Fig. 2). The Te···Sn distances of 4.5719(3)°, although somewhat longer than the sum of the van der Waals radii (*ca.* 4.2 Å),[10] can be compared with Sn(+II)···Sn(+II) contacts of 4.40–4.42 Å observed for the complex [Sn{NDipp}$_2${Sn(μ-NMe$_2$)}$_2$] (Dipp = 2,6-Pr$^i_2$C$_6$H$_3$).[11]

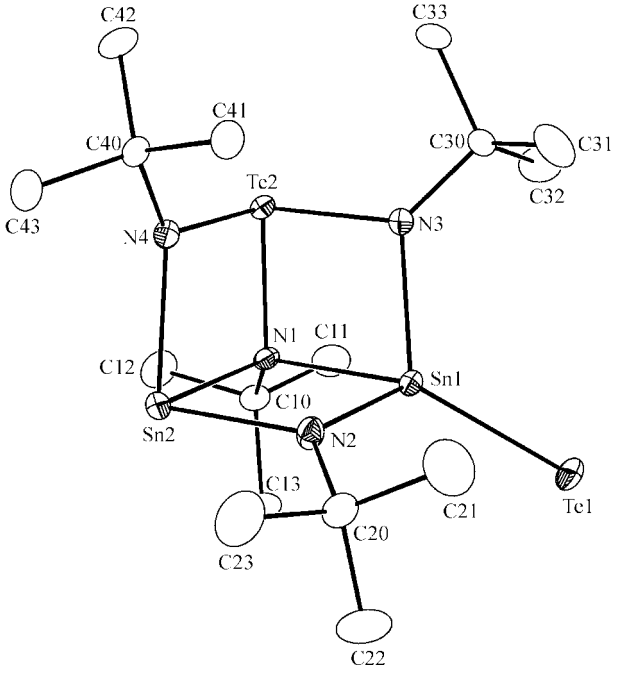

Fig. 1 Molecular structure of [Bu^{t}NSn(μ-NBu^t)$_2$TeNBu^t](μ$_3$-SnTe) **1**. Thermal ellipsoids are drawn at the 30% probability level. Selected bond distances (Å) and angles (°): Sn(1)–N(1) 2.245(2), Sn(1)–N(2) 2.019(2), Sn(1)–N(3) 2.114(2), Sn(2)–N(1) 2.326(2), Sn(2)–N(2) 2.103(2), Sn(2)–N(4) 2.181(2), Sn(1)–Te(1) 2.5918(3), Te(2)–N(1) 2.043(2), Te(2)–N(3) 1.978(3), Te(2)–N(4) 1.951(2); N(4)–Te(2)–N(3) 104.72(9), N(4)–Te(2)–N(1) 83.20(8), N(3)–Te(2)–N(1) 84.40(8), N(2)–Sn(2)–N(4) 96.87(8), N(2)–Sn(2)–N(1) 78.45(8), N(4)–Sn(2)–N(1) 72.02(7), N(2)–Sn(1)–N(1) 82.11(8), N(2)–Sn(1)–N(3) 108.70(9), N(3)–Sn(1)–N(1) 76.52(7), N(1)–Sn(1)–Te(1) 127.39(5), N(2)–Sn(1)–Te(1) 127.51(6), N(3)–Sn(1)–Te(1) 119.20(6).

 DOI: 10.1039/b106867a

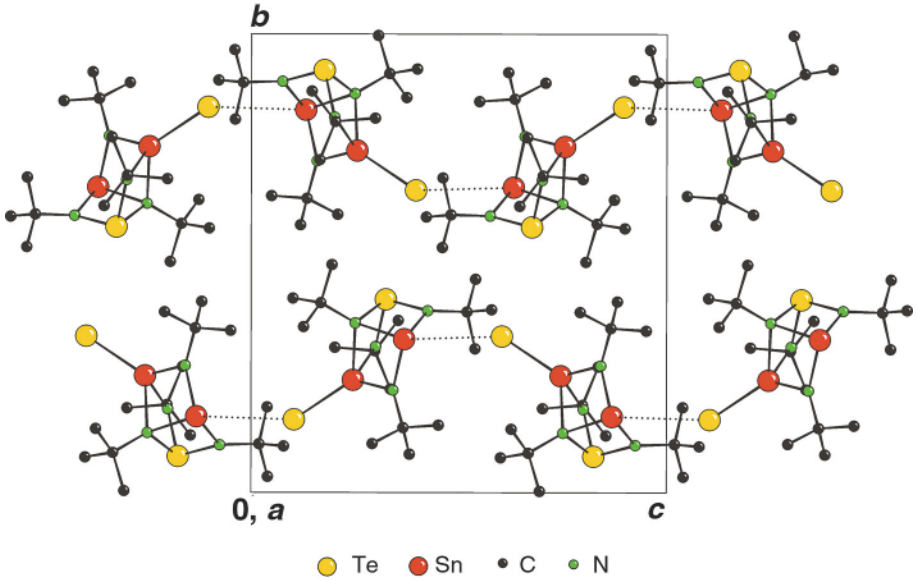

Fig. 2 View of the unit cell of **1** looking down the *a* axis.

The ^{1}H, ^{119}Sn and ^{125}Te NMR spectra in d_8-thf indicate that **1** is fluxional in solution. The ^{1}H NMR spectrum at 23 °C shows two singlets in the ratio 1:3. The broad, more intense, signal is resolved into two resonances with relative intensities 1:2 at −60 °C. In order to observe the expected resonances for inequivalent tin and tellurium environments in **1** it was necessary to record the ^{119}Sn and ^{125}Te NMR spectra at low temperatures. The ^{119}Sn NMR spectrum at −60 °C exhibits two broad resonances at δ −429.7 and +364.6 assigned to the Sn(IV) and Sn(II) centres, respectively. The ^{125}Te NMR spectrum at −60 °C also reveals two resonances at δ +1891.3 and −384.6. The former resonance falls within the range of δ 1500–1900 typical for the tris(*tert*-butylimido)tellurite ligand in metal complexes.[12] The resonance at δ *ca.* −385 is assigned to the terminal telluride ligand. The ^{125}Te NMR chemical shifts for terminal tellurido complexes of p-block elements span a very wide range: δ +1000 to +1140 for three-coordinate germanetellurones,[2] δ −2030 for a five-coordinate stannatellurone[4a] and δ −840 to −495 for R_3PTe (R = alkyl, aryl, dialkylamino).[13] The one-bond ^{119}Sn–^{125}Te NMR coupling could not be resolved in either the ^{119}Sn or ^{125}Te NMR spectra even at −80 °C. These NMR data indicate the occurrence of a fluxional process involving exchange of Te(1) between Sn(IV) and Sn(II) sites. The line-widths of the ^{119}Sn NMR resonances increase from *ca.* 300 to *ca.* 2200 Hz when the concentration of a d_8-thf solution is increased fourfold, consistent with an intermolecular process. A similar exchange process has been reported for R_3PTe (R = alkyl, aryl) in the presence of the corresponding phosphine (R_3P).[13]

A preliminary TGA experiment showed that **1** decomposes with essentially quantitative formation of $Bu^tN{=}NBu^t$ in the temperature range 180–400 °C. Investigations of related *tert*-butylimidotin tellurides as potential single-source presursors of SnTe are in progress.

We thank the NSERC (Canada) for financial support and Dr R. MacDonald (University of Alberta) for help with the X-ray structure determination of **1**.

Notes and references

† *Synthesis* of **1**: a mixture of $\{Li_2[Te(NBu^t)_3]\}_2$[7] (0.300 g, 0.423 mmol) and $Sn(O_3SCF_3)_2$ (0.353 g, 0.846 mmol) was placed in a Schlenk vessel. Addition of diethyl ether (10 mL) to this mixture produced a red solution with small amounts of a black deposit and a white precipitate. After 3 h at 23 °C the solution was filtered and the volume of the filtrate was reduced to *ca.* 3 mL. After 1 d at −19 °C colourless crystals of $Li[O_3SCF_3]{\cdot}OEt_2$ (X-ray structure) (0.181 g) were obtained. After 4 d red plate-like crystals of **1** were formed. A second recrystallization from thf at −19 °C produced X-ray quality crystals after 10 d. Complex **1** is obtained in *ca.* 10% yield from $\{Li_2[Te(NBu^t)_3]\}_2$ and $SnCl_2$ by using a similar procedure. ^{1}H NMR (d_8-thf, −60 °C) δ 1.547 (9 H, Bu^t), 1.464 (9 H, Bu^t), 1.421 (18 H, Bu^t); ^{1}H NMR (d_8-thf, 23 °C) δ 1.490 (9 H, Bu^t), 1.475 (br, 27 H, Bu^t); ^{119}Sn NMR (d_8-thf, −60 °C) δ −429.7(s), +364.6(s); ^{125}Te NMR (d_8-thf, −60 °C) δ −384.6 (s), +1891.3(s).

‡ *Crystal data* for **1**: $C_{16}H_{36}N_4Sn_2Te_2$, M = 777.07, monoclinic, space group $P2_1/n$ (no. 14), a = 10.2669(2), b = 16.4668(3), c = 14.9671(3) Å, β = 94.6721(6)°, V = 2521.97(8) Å^3, T = 173(2) K, space, Z = 4, μ(Mo-Kα) = 4.255 mm^{-1}. Crystal dimensions 0.18 × 0.18 × 0.10 mm. Data were collected on a Nonius Kappa CCD 4-circle Kappa FR540C diffractometer. Structure was solved by direct methods (SHELXS-97) and refined by full-matrix least-squares methods on F^2 with SHELXL97-2. 13494 reflections measured, 7314 unique (R_{int} = 0.0190), 6157 observed [$I \geqslant 2.00\sigma(I)$]. The final R_1 and wR_2 (all data) values were 0.0249 and 0.0528, respectively.

CCDC reference number 171259. See http://www.rsc.org/suppdata/cc/b1/b106867a/ for crystallographic data in CIF or other electronic format.

1 (*a*) R. Okazaki and N. Tokitoh, *Acc. Chem. Res.*, 2000, **33**, 625; (*b*) M. C. Kuchta and G. Parkin, *Coord. Chem. Rev.*, 1998, **176**, 323.
2 N. Tokitoh, T. Matsumoto and R. Okazaki, *J. Am. Chem. Soc.*, 1997, **119**, 2337.
3 M. Kuchta and G. Parkin, *J. Chem. Soc., Chem. Commun.*, 1994, 1351.
4 (*a*) W.-P. Leung, W.-H. Kwok, L. T. C. Law, Z.-Y. Zhou and T. C. W. Mak, *Chem. Commun.*, 1996, 505; (*b*) L. M. Berreau and L. K. Woo, *J. Am. Chem. Soc.*, 1997, **117**, 1314.
5 P. Boudjouk, M. P. Remington, Jr., D. G. Grier, W. Triebold and B. R. Jarabek, *Organometallics*, 1999, **18**, 4534; P. Boudjouk, D. J. Seidler, D. Grier and G. J. McCarthy, *Chem. Mater.*, 1996, **8**, 1189.
6 S. S. Fouad, A. Y. Morsy, H. S. Soliman and G. A. Ganainy, *J. Mater. Sci. Lett.*, 1994, **13**, 82.
7 T. Chivers, X. Gao and M. Parvez, *Angew. Chem., Int. Ed. Engl.*, 1995, **34**, 2549; T. Chivers, X. Gao and M. Parvez, *Inorg. Chem.*, 1996, **35**, 4336.
8 R. Fleischer and D. Stalke, *Organometallics*, 1998, **17**, 832.
9 A. Schäfer, M. Weidenbruch, W. Saak, S. Pohl and H. Marsmann, *Angew. Chem., Int. Ed. Engl.*, 1991, **30**, 834; H. Puff, B. Breuer, W. Schuh, R. Sievers and R. Zimmer, *J. Organomet. Chem.*, 1987, **332**, 279; A. Blecher and M. Dräger, *Angew. Chem., Int. Ed. Engl.*, 1979, **18**, 677.
10 A. Bondi, *J. Phys. Chem.*, 1964, **68**, 441.
11 R. E. Allan, M. A. Beswick, G. R. Coggan, P. R. Raithby, A. E. H. Wheatley and D. S. Wright, *Inorg. Chem.*, 1997, **36**, 5202.
12 T. Chivers, M. Parvez and G. Schatte, *Inorg. Chem.*, 2001, **40**, 540; T. Chivers, M. Parvez, G. Schatte and G. P. A. Yap, *Inorg. Chem.*, 1999, **38**, 1380.
13 C. H. W. Jones and R. D. Sharma, *Organometallics*, 1987, **6**, 1419.

CHEMCOMM
Communication
www.rsc.org/chemcomm

Efficient intramolecular general acid catalysis: a preview from a crystal structure

Andrew D. Bond, Anthony J. Kirby* and Encina Rodriguez

University Chemical Laboratory, Cambridge UK CB2 1EW

Received (in Cambridge, UK) 30th August 2001, Accepted 21st September 2001
First published as an Advance Article on the web 19th October 2001

The crystal stucture of acetal acid 5 reveals changes in geometry representing progress along the reaction coordinate for acetal cleavage.

We are interested in intramolecular general acid catalysis by the COOH group (**1**), and have developed systems where this is

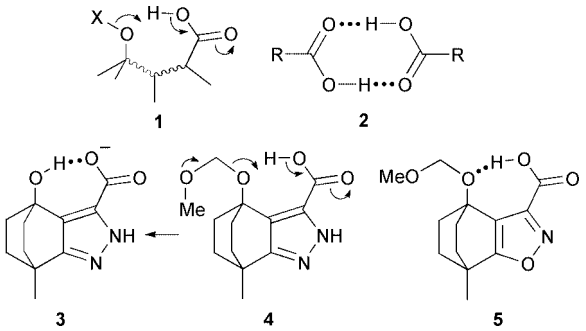

highly efficient.[1,2] We believe that the key to high efficiency is that proton transfer takes place within a strong hydrogen bond, and have varied the geometry to try to optimise this feature. However, we could never observe the geometry of the relevant hydrogen bond in crystal structures because carboxylic acids prefer to crystallise as the dimer **2**, the double intermolecular H-bond reinforcing the intrinsic preference for the *Z*-geometry.[3] We report a first useful exception to this rule, an acetal with an intramolecular hydrogen bond strong enough to reinforce the anomeric effect, and to initiate the structural changes that will lead to acetal cleavage.

We recently obtained the structure of the product anion (**3**) of our most efficient such reaction to date, the hydrolysis of **4**. As expected it shows an almost linear intramolecular hydrogen bond from the OH to the carboxylate as acceptor.[2] We now report the structure (Fig. 1) of the reactive acetal **5**, closely related to **4**.[4] This is the first example of a carboxylic acid that makes an intramolecular hydrogen bond to an aliphatic oxygen acceptor in the solid state. [5] Low-temperature single-crystal X-ray diffraction of **5** allowed the location and free isotropic refinement of the proton in the key hydrogen bond; the isotropic displacement parameter of H(2O) refines to 0.078 Å^2, comparable to values for other hydrogen atoms in the molecule.

Acetal **5** has the same basic geometry as the methoxymethyl acetal **4**, but is expected to be a considerably stronger carboxylic acid because of the electron-deficient nature of the isoxazole ring.[1] The intramolecular hydrogen bond is not precisely linear (O(2)–O(4) = 2.625(3) Å, O(2)–H(2O) = 0.89(5) Å, O(2)–H(2O)···O(4) = 162(4)°), primarily because the proton is displaced significantly out of the mean plane of the O–C–C–C–O system. [6] This may be a remnant of the stereoelectronic preference for aliphatic oxygen to form H-bonds in the tetrahedral direction:[7] it is not obviously the result of crystal packing.

The pattern of C–O bond lengths at the acetal group centre shows that the CH_2–O bond (C(11)–O(4), Fig. 1) to the eventual leaving group, at 1.424(3) Å, is significantly longer than the MeO–CH_2 bond O(5)–C(11), (1.383(4) Å).[8] Evidently the hydrogen bond polarises the acetal group and thus enhances the anomeric effect in the direction $MeO^+{=}CH_2$ $^-$OR. Such 'desymmetrisation' of an acetal by H-bonding has not been observed previously. (Potential effects of hydrogen bonding on the anomeric effect have been discussed by Lemieux[9] in the context of the *exo*-anomeric effect of glycoside OH groups as H-bond donors, but the only published example of which we are aware in which the anomeric effect is reinforced by H-bond donors is the observation by Alder *et al.* of systematic bond length changes in two N–C–N systems.[10])

The good correlation[11] between the length of the CH_2–OX bond in methoxymethyl acetals $MeOCH_2$–OX and the pK_a of HOX, the conjugate acid of the leaving group, allows us (not without significant reservations[8]) to estimate an effective pK_a of 10 for the leaving group oxygen. (The effective pK_a of the leaving group in the transition state for the hydrolysis of **4** is about 4.[2]) The bond angle at the leaving group oxygen (C(11)–O(4)–C(5), 118.6(2)°) is close to trigonal and the acetal torsion angle around the stretched C–O bond is 88.0(3)°. (The other is typically gauche, at 68.0(4)°.) The leaving group oxygen may be thought to be behaving more like a phenol[12] than a tertiary alcohol oxygen, with the third (hydrogen) bond causing the trigonal geometry. In fact the near-trigonal bond angle at oxygen is typical for methoxymethyl acetals of tertiary alcohols (the 6 examples in the Cambridge Structural database have a mean angle of 118.6 ± 0.7°), no doubt for steric reasons.

This system (**5**) displays significant progress along the reaction coordinate of the reaction of interest, and offers the sort of detailed structural information we need for analysis, and as a basis for improving efficiency further—which means optimis-

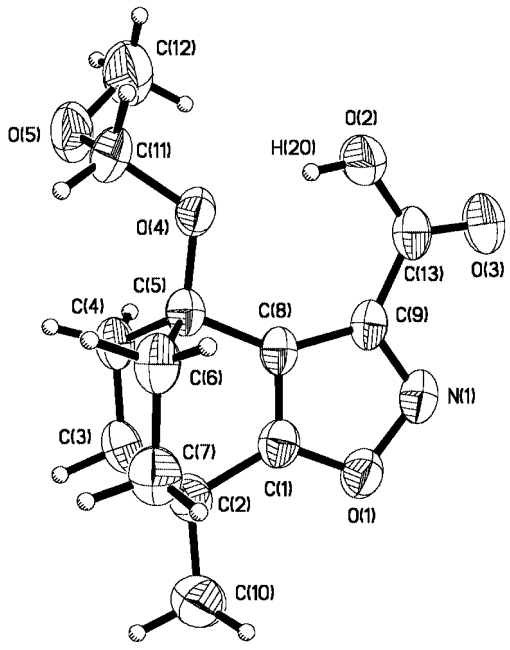

Fig. 1 Molecular conformation of the acetal acid **5** showing displacement ellipsoids at the 30% probability level.[13]

 DOI: 10.1039/b107787b

ing the hydrogen bond in the transition state. The intramolecular hydrogen bond we see in the crystal may not make a major contribution to the ground state in aqueous solution: in water, hydrogen-bonding solvation disrupts all but the strongest intramolecular hydrogen bonds. It is however, clearly the first committed species on the reaction coordinate.

Notes and references

1 A. J. Kirby and A. Parkinson, *J. Chem. Soc., Chem. Commun*., 1994, 707.

2 E. Hartwell, D. R. W. Hodgson and A. J. Kirby, *J. Am. Chem. Soc*., 2000, **122**, 9326.

3 L. Eberson, in *The Chemistry of Carboxylic Acids and Esters*, ed. S. Patai, Wiley, New York, 1969, pp. 211–340.

4 We have not measured rates of hydrolysis of **5**. From our results in the aromatic series we can expect the isoxazole system to be more reactive than weaker carboxylic acids derived from other heterocyclic systems, such as **4**, with similar geometries.

5 We could find no comparable intramolecular hydrogen bond in the Cambridge Structural Database (Version 5.21, April 2001). The closest analogue of **5** is fluorenone-1-carboxylic acid (M. L. Cote, R. A. LaLancette and H. W. Thompson, *Acta Crystallogr., Sect. C*, 1996, **52**, 1585), based on a similar 6,5-fused system geometry, where the acceptor is the ketone oxygen.

6 The deviation from planarity is significant, even considering the relatively large imprecision of the hydrogen atom position derived from the X-ray results. The O–H···O distance is longer (2.713 Å) in the anion **3** (as expected for the more electron-rich system), and almost linear (angle at H 175°), with little deviation from planarity.

7 A. J. Kirby, *The Anomeric Effect and Related Stereoelectronic Effects at Oxygen*, Springer-Verlag, Berlin and Heidelberg, 1983.

8 Mean values of of 1.3975 ± 0.0155 and 1.4077 ± 0.0065 Å for these two bond lengths, for the six acetals $MeOCH_2OR$ derived from tertiary alcohols ROH for which accurate structures are available, suggest there may also be a small steric contribution to the extension of the CH_2–OR bond. (Other things being equal the O derived from the tertiary alcohol ROH should be the better *n*-donor.)

9 J.-P. Praly and R. U. Lemieux, *Can. J. Chem*., 1987, **65**, 213.

10 R. W. Alder, T. M. G. Carniero, R. W. Mowlam, A. G. Orpen, P. A. Petillo, D. J. Vachon, G. R. Weisman and J. M. White, *J. Chem. Soc., Perkin Trans. 2*, 1999, 589.

11 P. G. Jones and A. J. Kirby, *J. Chem. Soc., Chem. Commun*., 1986, 444, give the correlation as $BL = 1.462 - 3.7 \times 10^{-3}\ pK_a$.

12 The geometry of the methoxymethyl group is closely similar to that of methoxymethoxy-3,5-dinitrobenzene (P. G. Jones, G. M. Sheldrick, A. J. Kirby and A. J. Briggs, *Acta Crystallogr., Sect. C*, 1985, 41, 1377).

13 Crystal data for **5**: $C_{13}H_{17}NO_5$, $M = 267.28$, monoclinic, space group $P2_1/n$, $a = 11.5493(8)$, $b = 8.4256(4)$, $c = 13.4272(11)$ Å, $\beta = 98.756(3)$ °, $U = 1291.4(2)$ Å^3, $T = 180(2)$ K, $Z = 4$, $D_c = 1.375$ g cm^{-3}, μ(Mo-Kα) = 0.106 mm^{-1}. Of 6633 reflections measured, 2812 were unique ($R_{int} = 0.0817$) and were used in all calculations. H(2O), associated with the hydroxy group, was located in a difference Fourier map and refined with an isotropic displacement parameter and without restraint. The final $wR2 = 0.2505$ (all data), $R1 = 0.0819$ [$F^2 > 2\sigma(F^2)$] and goodness-of-fit on F^2, $S = 1.087$. CCDC 169817. See http://www.rsc.org/suppdata/cc/b1/b107787b/ for crystallographic files in .cif or other electronic format.

CHEMCOMM Communication
www.rsc.org/chemcomm

Novel polymer-supported 2-(diphenylmethylsilyl)ethoxymethyl chloride (DSEM-Cl) linker†

Kyungjin Kim* and Bingbing Wang

Roche Research Center, Hoffmann-La Roche, Inc., Nutley, NJ 07110, USA.
E-mail: kyungjin.kim@roche.com

Received (in Cambridge, UK) 25th July 2001, Accepted 29th August 2001
First published as an Advance Article on the web 17th October 2001

A synthetic method to prepare a novel polymer-supported 2-(diphenylmethylsilyl)ethoxymethyl chloride (DSEM-Cl) linker and its applications are described.

The selection of an appropriate linker is an important factor when considering synthetic design on solid phase. Several efforts to develop new solid supports and linkers have been reported.[1] In a previous communication, we reported synthetic strategies for the preparation of polymer-supported 2-(trialkylsilyl)ethanol linkers **1** and their functionalized silyl linkers with an application to ketopiperazine synthesis.[2] Herein we wish to report a synthetic method to prepare a novel polymer-supported 2-(diphenylmethylsilyl)ethoxymethyl chloride (DSEM-Cl) linker **2c** and its applications in our continuing efforts to explore new silyl linkers.

2-(Trimethylsilyl)ethoxymethyl chloride (SEM-Cl) has frequently been utilized in solution phase as a protection group for amines, alcohols, phenols and carboxy groups.[3] We considered that it would be worthwhile to develop a supported SEM linker based on the virtues of SEM-Cl. Our initial efforts were directed towards the preparation of polymer-supported 2-(trialkylsilyl)-ethoxymethyl chlorides **2** containing different alkyl substituents and the investigation of their stability in a broad range of chemistries (Scheme 1). After careful examination, we found that a pre-mixture of paraformaldehyde and HCl(g) could be employed as an efficient method for chloromethylation of **1**.[4] Three polymer-supported 2-(trialkylsilyl)ethoxymethyl chlorides **2** were carefully synthesized to avoid protodesilation during chloromethylation in acidic media.[5] Dimethylphenyl-substituted silyl linker **2a** proved labile under acidic conditions, yielding only a low loading (0.13 mmol g^{-1}). The diisopropylphenyl functional group of **2b** was observed to impede the attachment of starting material to the solid support, necessitating harsh reaction conditions. Finally, 2-(diphenylmethylsilyl)ethoxymethyl chloride (DSEM-Cl) **2c** showed good stability and reactivity with optimal loading capacity (0.64–0.74 mmol g^{-1}). The progress of the reaction was monitored by FT-IR spectroscopy with the disappearance of the O–H stretch at 3428 cm^{-1}. In addition, the structure of polymer-supported DSEM-Cl **2c** was confirmed using HR-MAS (high resolution magic angle spinning) ^{1}H-NMR analysis, in which methylene protons of O–CH_2–Cl were observed at 5.60 ppm.[6]

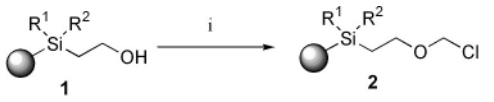

1 **2**

Entry	R^1	R^2	Yield*
2a	CH_3	CH_3	15%
2b	*i*-Propyl	*i*-Propyl	90%
2c	CH_3	C_6H_5	>70%

*The loading yield was determined by Cl analysis

Scheme 1 *Reagents and conditions*: i, HCl(g), paraformaldehyde, DME, 0 °C, 1 h.

We then examined the utility of immobilized DSEM linker **2c** for various functional groups (Table 1). Acid (entries 1 and 2), alcohol (entries 3 and 4), phenol (entry 5), amine (entry 6) and heterocyclic amide (entries 7 and 8) were successfully attached onto **2c** in good yields.[7] The unreacted chloromethyl functionality on resin was capped with methanol to avoid undesired side reactions. Acidic cleavage using a solution of TFA–CH_2Cl_2 proved efficient in providing the corresponding starting material in good yield (entries 1–7). Interestingly, the removal of the DSEM protecting group from the purine-supported linker (entry 8) showed strong stability in acetic acid, however 2-fluoro-6-chloropurine started to be released from the solid support in 50% trifluoroacetic acid–CH_2Cl_2 with 66% purity.[8] To improve purity, microwave irradiation was employed, since we anticipated that using a high temperature for a short time period would avoid other side reactions.[9] The resin suspension in 50% TFA–CH_2Cl_2 was irradiated for 3 min at 100 °C. As expected, 2-fluoro-6-chloropurine **3** was successfully recovered in quantitative yield with 93% purity. This new DSEM linker is expected to make up for the weak points of trityl and tetrahydropyranyl (THP) linkers, which show thermal and acid sensitivity when aromatic heterocycles are loaded onto the linker.

Polymeric DSEM-supported 2-fluoro-6-chloropurine **4** was then utilized to synthesize a number of 2,6-disubstituted purines

Table 1 Loading and cleavage of **2c** on various functional groups

Entry	Starting material	Loading yield (%)	Recovered yield (%)
1	Fmoc-Ala-OH	64[a]	85[d]
2	Fmoc-Phe-OH	61[a]	86[d]
3	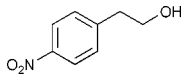	94[a]	70[d]
4	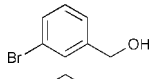	81[b]	93[d]
5	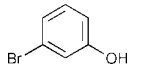	99[b]	93[e]
6	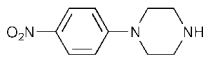	66[a]	99[d]
7	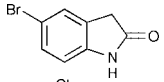	64[a,b]	92[e]
8	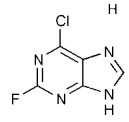	92[a,c]	99[f]

The loading yield was determined by [a] N-, [b] Br-, [c] F-analysis. Acidic cleavage was performed in a solution of [d] 5% TFA–CH_2Cl_2, [e] 50% TFA–CH_2Cl_2, [f] 50% TFA–CH_2Cl_2 with microwave irradiation for 3 min at 100 °C.

† Electronic supplementary information (ESI) available: HR-MAS ^{1}H-NMR spectra of resins **1c** and **2c**; loading and cleavage of **2c** on various functional groups. See http://www.rsc.org/suppdata/cc/b1/b106767b/

 DOI: 10.1039/b106767b

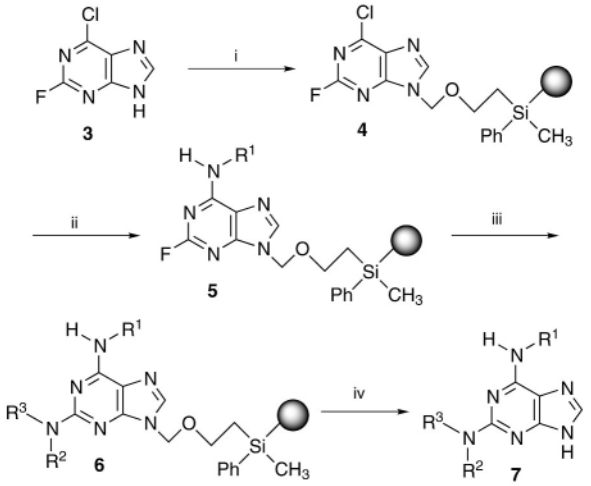

Scheme 2 *Reagents and conditions*: i, **2c**, 2-*tert*-butylimino-2-diethylamino-1,3-dimethylperhydro-1,3,2-diazaphosphorine (BEMP), THF, 0 °C to rt, 3 h, 92%; ii, R^1NH_2, diisopropylethyl amine, 1 : 1 n-butanol–DMSO, 50 °C, rt, overnight; iii, R^2R^3NH, DIPEA, 1-methyl-2-pyrrolidinone, microwave irradiation; iv, 1 : 1 TFA–CH_2Cl_2, microwave irradiation, 3 min, 100 °C.

on solid phase (Scheme 2). Nucleophilic amination of **4** with benzylamine or isobutylamine proceeded successfully under the described conditions to provide **5**. Subsequent amination at C2 has been reported to require longer reaction time and higher temperature due to decreased reactivity at C2. Therefore, we applied microwave-assisted heating to enhance reaction rates. Several variations of solvents and irradiation times were examined in a parallel format *en route* to **6** using a Smith Synthesizer™. Microwave irradiation in 1-methyl-2-pyrrolidinone at 180 °C followed by a sequential microwave-assisted linker cleavage provided a good yield of **7** with high purity (Table 2).

Table 2 2,6-disubstituted purine **7** synthesis on solid phase

R^1	R^2/R^3	Microwave condition[a]	Y[b]/P[c]
Benzylamine	Morpholine	180 °C, 10 min	70/90
	N-Methylpiperazine	180 °C, 20 min	85/94
	4-Fluorophenethylamine	180 °C, 40 min	80/92
	3-Bromoaniline	200 °C, 40 min	n.a.[d]
Isobutylamine	Morpholine	180 °C, 10 min	74/95
	N-Methylpiperazine	180 °C, 20 min	89/89
	4-Fluorophenethylamine	180 °C, 40 min	82/89
	3-Bromoaniline	200 °C, 40 min	n.a.[d]

[a] Nucleophilic amination of **5** proceeded using microwave heating to provide **6** under the described conditions. [b] Isolated yield was determined after acidic cleavage of **6** based on loading capacity of **4** (0.74 mmol g^{-1}). [c] Purity score was determined by LC/MS–ELSD. [d] Starting material recovered.

In conclusion, we have successfully synthesized a new polymer-supported DSEM-Cl linker **2c**. Protection and deprotection of the DSEM linker on various functional groups was successful. Microwave-assisted linker cleavage proved to enhance the cleavage process. In particular, sequential microwave applications, utilized at the amination and linker cleavage steps, greatly accelerated the 2,6-disubstitituted purine synthesis. The DSEM-Cl linker **2c** is a promising new candidate for the protection of hydroxy and nitrogen functional groups in solid phase synthesis. In comparison with other acid-labile linkers, we envision that the new silyl linker will offer several advantages, such as stability in various reaction conditions including basic and moderately acidic media as well as elevated thermal conditions.[10] Our efforts toward the development of applications of support-bound DSEM linkers **2** are ongoing.

We are grateful to all combinatorial and NLCI group members who made this work possible. We wish to thank Dr Harald Schroeder of PRBT at Basel for providing HR-MAS NMR spectra of **1c** and **2c**.

Notes and references

1 For reviews see: (*a*) B. J. Backes and J. A. Ellman, *Curr. Opin. Chem. Biol*., 1997, **1**, 86; (*b*) I. W. James, *Tetrahedron*, 1999, **55**, 4855; (*c*) D. Hudson, *J. Comb. Chem*., 1999, **1**, 333; (*d*) D. Hudson, *J. Comb. Chem*., 1999, **1**, 403.

2 (*a*) B. Wang and K. Kim, *Book of Abstract, 220th ACS National Meeting*, Washington DC, 20–24 August, 2000, ORGN-231; B. Wang, L. Chen and K. Kim, *Tetrahedron Lett*., 2001, **42**, 1463.

3 T. W. Greene and P. G. M. Wuts, *Protective Groups in Organic Synthesis*, John Wiley & Sons, Inc., 1999 and references therein.

4 The preparative method of polymer-supported SEM-Cl was modified based on the precedent in solution phase: (*a*) B. H. Lipshutz and J. J. Pegram, *Tetrahedron Lett*., 1980, **21**, 3343; (*b*) E. J. Corey, J. Gras and P. Ulrich, *Tetrahedron Lett*., 1976, 809.

5 General synthetic procedure for support-bound 2-(trialkylsilyl)ethoxymethyl chlorides **2**: 11.1 g of pararformaldehyde in 150 mL of 1,2-dimethoxyethane, glyme (DME) was treated with dry HCl gas at 0 °C until a clear solution resulted, at which time 4.57 g of silylethanol resin **1** was slowly added to the mixture. The suspension was stirred for 1 h and then filtered. The resin was washed with dry DME, CH_2Cl_2 and diethyl ether and dried *in vacuo* to provide **2**. The prepared silyl linkers **2** are stable in a refrigerator over 6 months.

6 The resins **1c** and **2c** were swollen in $CDCl_3$. All experiments were performed at 297 K on a DRX-400 Bruker 400 MHz spectrometer equiped with a 4 mm HR MAS probe using a 4 kHz spinning rate.

7 More details are available in electronic supplementary information (ESI).

8 Purity was determined by a C18 reverse phase HPLC column, WR-C18 3 μ 120 Å (30 × 3.2 mm) of ES Industries in 10–90% CH_3CN–H_2O containing 0.02% TFA and monitored at 215 nm using a UV detector and by SEDEX 55 evaporative light scattering detector (ELSD). Purity scores reported herein are based on ELSD.

9 Smith Synthesizer™ of Personal Chemistry Inc., in which the reaction time and temperature can be precisely controlled was used for microwave applications.

10 To compare with the approach derived from Wang linker, purine **3** was loaded onto the linker, following the same conditions, to provide the corresponding support-bound **4a** in 76% yield (*loading* 1.12 mmol g^{-1}). Interestingly, both with and without microwave irradiation, only N9-substituted core **4b** derived from the linker was identified in quantitative yield with high purity (> 82%).

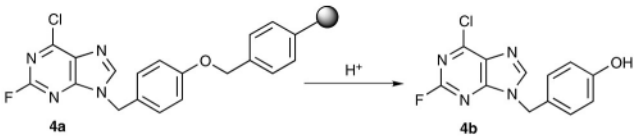

4a **4b**

CHEMCOMM Communication
www.rsc.org/chemcomm

Control of methanol oxidation by ionic behavior in supercritical water

Masaru Watanabe,[a] Kiwamu Sue,[b] Tadafumi Adschiri,[b] Hiroshi Inomata,*[a] Richard Lee Smith, Jr.[a] and Kunio Arai[ab]

[a] *Research Center of Supercritical Fluid Technology, Tohoku University, 07 Aoba, Aramaki, Aoba-ku, Sendai, 980-8579, Japan. E-mail: inomata@scf.che.tohoku.ac.jp; Fax: +81-22-217-7282; Tel: +81-22-217-7282*

[b] *Department of Chemical Engineering, Tohoku University, 07 Aoba, Aramaki, Aoba-ku, Sendai, 980-8579, Japan. Fax: +81-22-217-7246; Tel: +81-22-217-7246*

Received (in Cambridge, UK) 25th April 2001, Accepted 21st September 2001
First published as an Advance Article on the web 17th October 2001

In supercritical water the rate of methanol oxidation was controlled by ionic behavior as follows: the oxidation rate of methanol decreased with increasing proton and hydroxide ion concentration, possibly due to stabilization of the reactant, while that of CO was suppressed by added protons and enhanced by added hydroxide ions.

Supercritical water oxidation (SCWO) has been known to be a promising method for complete decomposition of organic compounds in water without emission of toxic pollutants.[1,2] One of the reasons why SCWO is suitable as an oxidation medium is that organic species and oxygen are completely miscible in water above its critical point (647 K and 22.1 MPa).[3,4] Another reason is that water reacts with O_2 to generate OH radicals at temperatures greater than 773 K,[5] which is highly active as an oxidant. On the other hand, around the critical temperature of water, the rate of complete oxidation of a hydrocarbon is suppressed with increasing water density and the yields of partial oxidation products such as CO and aldehyde increase with increasing water density.[6] This phenomenon cannot be explained solely by a free radical reaction mechanism. Ionic reaction of an organic compound, such as protonation and dehydration of some alcohols, proceeds in supercritical water near its critical point, that is, around 673 K.[7] Thus, the effect of ionic behaviour of an organic compound on oxidation in supercritical water must be taken into consideration. In this study, the effect of water density, acid, and base on methanol oxidation was examined and a possible reaction pathway of methanol oxidation in supercritical water near its critical point was proposed.

Methanol (99.7%), 1 mol L^{-1} of NaOH aqueous solution, and 1 mol L^{-1} of H_2SO_4 solution were purchased from Wako Pure Chemical and used without further purification. Pure water, which was distilled after deionization, had a conductivity 1×10^{-5} S m^{-1}. The batch type reactor (SS316) used in this study has been described previously.[8] Briefly, 1.0–3.1 g water, 0.03 g of methanol, an amount of acid (H_2SO_4) solution or base (NaOH) solution, and a given amount of O_2 (molar ratio: O_2–methanol = 3 : 1) were loaded into a batch type reactor (internal volume: 6 mL). Pressures (P_w) were calculated from the water densities (ρ_w) and steam tables.[9] The reactor was immersed in a fluidized sand bath (673 K) and the reaction was started. After a given time, the reactor was taken out from the sand bath and put into a water bath (room temperature), and then the reaction was stopped. After cooling the reactor, a stop valve on the reactor was connected with a gas sampling system and the gaseous product was collected and analyzed by gas chromatography with a thermal conductivity detector (GC-TCD) (Shimadzu GC-7A and Hitachi GC163). After gas sampling, an amount of water was added into the reactor and the liquid product was recovered and analyzed by gas chromatography with a flame ionization detector (GC-FID) (HP 6890). For all the experiments in this study, the detected products were H_2, CO, and CO_2, in agreement with the results of Anitescu *et al.*[10] The proton concentration ($[H^+]$) and ion product (K_w) of pure water was calculated by the method of Marshall and Franck.[11] The proton concentration with acid and base was calculated from the ion product of water,[11] the equilibrium constant,[12,13] and the activity coefficient.[14]

Corrections were applied for heat-up time and reactor dead space. Heat-up time (*ca.* 1 min) was subtracted from the actual run time. Corrections for dead space were estimated by using separate runs at reaction times of 540 s. The amount of CO and CO_2 obtained at 540 s was used to estimate available reactants at 120 s and 240 s.

Fig. 1 shows results at 673 K and 0.16 g cm^{-3}. In this figure, the calculated results using the model proposed by Anitescu *et al.*[10] are also shown. As shown in Fig. 1, the agreement between the experimental results and the model was good. Table 1 summarizes the experimental conditions and yields. Experiments were run for 120–540 s at a range of water densities without catalysts and also with acid and base catalysts. Methanol yield without catalyst increased with increasing water density and rapidly decreased with time at all the water densities. With acid or base catalyst, the methanol yield was higher than that without catalyst at the same water density. CO yield without catalyst decreased with reaction time but increased in the presence of acid and decreased in the presence of base. CO_2 yield was relatively low in the presence of acid and high in the presence of base. H_2 yield at all the reaction times increased with increasing water density without catalyst, while acidic conditions gave more or less the same yields as neutral conditions. H_2 yield was highest under alkaline conditions.

To consider the effect of water density, acid, and alkali on the methanol oxidation, the rate constants (k_1 and k_2) of eqn. (1) were evaluated by fitting the data in a similar manner to that of Anitescu *et al.*[10]

$$CH_3OH \xrightarrow{k_1} CO \xrightarrow{k_2} CO_2 \qquad (1)$$

Fig. 2 shows the rate constants as a function of proton concentration. While the value of k_1 exhibited a maximum with proton concentration, k_2 decreased linearly with increasing proton concentration. As suggested by Antal *et al.*,[7] alcohols tend to be protonated in supercritical water. If the stability of protonated alcohol for oxidation is higher that of a molecular alcohol, the oxidation rate (k_1) of the protonated alcohol is expected to be lower than that of unprotonated alcohol. An

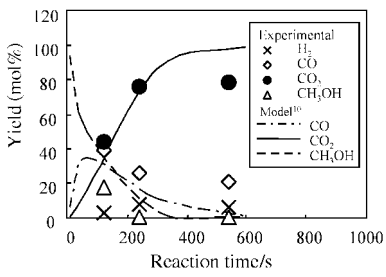

Fig. 1 Experimental results at 673 K and 0.16 g cm^{-3}.

 DOI: 10.1039/b103728p

Table 1 Summary of experimental conditions and data (673 K)

P_w/MPa	ρ_w/g cm^{-3}	log (K_w/mol^2 L^{-2})	Catalyst	log ([H$^+$]/ mol L^{-1})	Reaction time/s	CH_3OH yield (mol%)	CO yield (mol%)	CO_2 yield (mol%)	H_2 yield (mol%)
25	0.16	−21.00	None	−10.50	120	17.7	38.8	43.5	2.5
					240	0	25.3	76.2	7.5
					540	0	21.0	79.3	5.5
30	0.35	−15.85	None	−7.93	120	23.6	49.6	26.8	4.1
					240	0	40.3	63.9	13.3
					540	0	35.2	64.8	9.4
40	0.52	−13.90	None	−6.55	120	43.3	32.1	24.6	15.8
					240	0	21.9	42.5	25.3
					540	0	29.4	70.6	22.6
30	0.35	−15.85	0.08 mol L^{-1} H_2SO_4	−3.94	120	69.4	21.2	9.4	19.3
					240	28.1	49.9	22.0	18.4
					540	0	59.1	41.0	12.3
30	0.35	−15.85	0.1 mol L^{-1} NaOH	−13.21	120	40.7	16.0	43.3	28.0
					240	20.0	6.0	74.1	38.3
					540	0	2.6	97.4	52.4

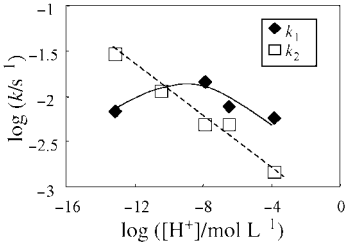

Fig. 2 Dependence of k_1 and k_2 on proton concentration.

alcohol possibly dissociates into the alkoxide ion and a proton in the presence of alkali in supercritical water because alcohols are weak acids.[15] Like the protonated alcohol, an alkoxide ion is expected to be more stable than the molecular alcohol towards oxidation. Thus the k_1 value was also low at the lowest proton concentration (in NaOH solution).

For the oxidation of CO into CO_2 (for k_2), there are two pathways: one is direct oxidation and the other is the water gas shift reaction ($CO + H_2O \rightleftharpoons CO_2 + H_2$). As shown in Fig. 2, the rate of conversion of CO to CO_2 decreased with increasing proton concentration. Analogously to methanol, CO oxidation seemed to be suppressed by increased proton concentration. Some ionic effects on the water gas shift in sub- and supercritical water have been studied. Rice *et al.*[16] and Sato *et al.*[17] examined the effect of water density (pressure) on the rate of the water gas shift reaction. While Sato *et al.*[17] reported that the rate of water gas shift reaction was independent of pressure up to 30 MPa and 673 K, Rice *et al.*[16] reported that the rate of the water gas shift reaction drastically increased with increasing pressure above 30 MPa at 683 K. Ross *et al.*[18] and Elliott *et al.*[19] suggested that the water gas shift reaction must be promoted by alkali (that is, OH^- ion) in sub- and supercritical water. The ion product of water increases drastically above 30 MPa both at 673 and 683 K.[11] Thus the rate of the water gas shift reaction is expected to depend on OH^- concentration. Fig. 3 shows the dependence of H_2 yield on OH^- concentration. The yield of H_2 (540 s) increased with increasing OH^- concentration. If the formation of H_2 were solely due to the water gas shift reaction, then the H_2 yield would be comparable with the CO_2 yield. The high H_2 yield indicates that the rate of the water gas

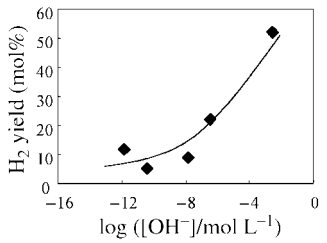

Fig. 3 Dependence of H_2 yield (540 s) on OH^- concentration.

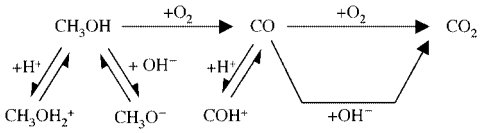

Fig. 4 Proposed mechanism of methanol oxidation in supercritical water.

shift reaction is possibly enhanced by high water density and added alkali.

Based on these results a mechanism for methanol oxidation in supercritical water can be proposed as follows (Fig. 4). Methanol is stabilized to some extent by ionic species that promote its protonation or its dissociation. Then, after methanol is oxidized to CO, the CO is stabilized by the presence of protons. The CO is oxidized to CO_2, however, hydroxide ions promote conversion of CO to CO_2 *via* the water gas shift reaction. This shows that addition of ionic species in supercritical water can have broad application in organic syntheses.

Notes and references

1 H. M. Freeman, *Standard Handbook of Hazardous Waste Treatment and Disposal*, McGraw-Hill, New York, 1989.
2 D. W. Tedder and F. G. Pohland, *ACS Symposium Series 518: Emerging Technologies in Hazardous Waste Management III*, American Chemical Society, Washington DC, 1993.
3 T. M. Seward and E. U. Franck, *Ber. Bunsenges. Phys. Chem.*, 1981, **85**, 2.
4 G. M. Schneider, *Ber. Bunsenges. Phys. Chem.*, 1972, **76**, 325.
5 P. E. Savage, *Chem. Rev.*, 1999, **99**, 603.
6 M. Watanabe, M. Mochiduki, S. Sawamoto, T. Adschiri and K. Arai, *J. Supercrit. Fluids*, 2001, **20**, 257.
7 M. J. Antal, Jr., M. Carlsson, X. Xu and D. G. Anderson, *Ind. Eng. Chem. Res.*, 1998, **37**, 3820.
8 K. Arai, T. Adschiri and M. Watanabe, *Ind. Eng. Chem. Res.*, 2000, **39**, 4967.
9 L. Haar, J. S. Gallagher and G. S. Kell, *NBC/NRC Steam Tables*, Hemisphere, Washington DC, 1984.
10 G. Anitescu, Z. Zhang and L. L. Tavlarides, *Ind. Eng. Chem. Res.*, 1999, **38**, 2231.
11 W. L. Marshall and E. U. Franck, *J. Phys. Chem. Ref. Data*, 1981, **10**, 295.
12 T. Xiang, K. P. Johnston, W. T. Wofford and E. F. Gloyna, *Ind. Eng. Chem. Res.*, 1996, **35**, 4788.
13 P. C. Ho and D. A. Palmer, *J. Solution Chem.*, 1996, **25**, 711.
14 R. T. Pabalan and K. S. Pitzer, *Geochim. Cosmochim. Acta*, 1987, **25**, 2429.
15 R. T. Morrison and R. N. Boyd, *Organic Chemistry*, 6th edn., Prentice-Hall, New York, 1992.
16 S. F. Rice, R. R. Steeper and J. D. Aiken, *J. Phys. Chem. A*, 1998, **102**, 2673.
17 T. Sato, S. Kurosawa, T. Adschiri and K. Arai, *Kagaku Kogaku Ronbunshu*, 1999, **25**, 993 (in Japanese).
18 D. S. Ross, J. E. Blessing, Q. C. Nguyen and G. P. Hum, *Fuel*, 1984, **63**, 1206
19 D. C. Elliott, R. T. Hallen and L. J. Sealock, Jr., *Ind. Eng. Chem. Prod. Res. Dev.*, 1983, **22**, 431.

CHEMCOMM
Communication
www.rsc.org/chemcomm

Reversible trapping of acid and base vapours into an amphoteric crystalline material

Dario Braga,*[a] Gianna Cojazzi,[b] Dario Emiliani,[a] Lucia Maini[a] and Fabrizia Grepioni*[c]

[a] *Dipartimento di Chimica G. Ciamician, University of Bologna, Via Selmi 2, 40126 Bologna, Italy. E-mail: dbraga@ciam.unibo.it*
[b] *Centro CNR per la Fisica delle Macromolecole, c/o Dipartimento di Chimica G. Ciamician, Via Selmi 2, 40126 Bologna, Italy*
[c] *Dipartimento di Chimica, University of Sassari, Via Vienna 2, 07100 Sassari, Italy. E-mail: grepioni@ssmain.uniss.it*

Received (in Cambridge, UK) 2nd August 2001, Accepted 20th September 2001
First published as an Advance Article on the web 18th October 2001

Exposure of the solid zwitterion $[Co^{III}(\eta^5\text{-}C_5H_4CO_2H)(\eta^5\text{-}C_5H_4CO_2)]$ to hydrated vapours of volatile acids (HCl, CF_3CO_2H, HBF_4) or bases (NH_3, NMe_3, NH_2Me) quantitatively produces the corresponding salts; the heterogeneous reactions are fully reversible, as the acid or base molecules can be removed by thermal treatment, regenerating the starting material.

Crystal engineering with inorganic and organometallic building blocks[1–3] allows construction of robust crystal architectures. Robustness is a prerequisite for the preparation of nanoporous materials able to withstand removal of guest molecules.[4] Zeolitic type materials are being extensively studied in the quest for solid state sensors, reservoirs, filters and sieves to be used to detect or trap small molecules.[5–7] An alternative to nanoporosity for controlled uptake and release of small molecules could be afforded by heterogeneous gas–solid reactions.[8] Solid-state reactions, however, often imply profound transformations in the chemical and physical nature of the solid material and rarely are of practical use, unless fully reversible.

Here we report that the low-cost, water soluble and robust organometallic zwitterion $[Co^{III}(\eta^5\text{-}C_5H_4CO_2H)(\eta^5\text{-}C_5H_4CO_2)]$, **1**, undergoes fully reversible heterogeneous reactions with the hydrated vapours of a variety of acids (*e.g.* HCl, CF_3CO_2H, HBF_4) and bases (*e.g.* NH_3, NMe_3, NH_2Me), with formation of the corresponding salts. The acid or base molecules can be removed by mild thermal treatment, regenerating **1**. Since no decomposition is observed after several uptake/release cycles, the organometallic material behaves as a *reversible* amphoteric trap towards both acid and base hydrated vapours *via* the gas–solid reaction. The reaction of solid carboxylic acids with ammonia and amines have been the subject of elegant pioneering studies.[9]

The organometallic zwitterion **1** is easy to handle and is thermally stable up to a temperature of 506 K.[10] The heterogeneous reactions of **1** with hydrated vapours of HCl or NH_3 to give the compounds **2** and **3** are depicted in Fig. 1.

Complete conversion of the neutral crystalline **1** (1–10 mg) into the crystalline salt **2** is attained after 5 min of exposure to vapours† of 36% aqueous HCl. Formation of **2** in the heterogeneous reaction is easily assessed by comparison of the observed X-ray powder diffraction pattern‡ with that calculated on the basis of the single-crystal structure determined previously.[11] The formation of **2** from **1** requires that the O–H···O bonds involving the protonated $–CO_2H$ group and the deprotonated $–CO_2^-$ of neighbouring zwitterion molecules are replaced, upon absorption of HCl, by $^+O–H\cdots Cl^-$ interactions between the $–CO_2H$ groups on the fully protonated organometallic cation $[Co^{III}(\eta^5\text{-}C_5H_4CO_2H)_2]^+$ and the Cl^- anions.

Crystalline **2** can be converted back to **1** by heating the sample for 1 h at 440 K in an oil-bath under low pressure (10^{-2} mbar). A thermogravimetric analysis (TGA) shows that **2** releases one water molecule and one HCl molecule per molecular unit at 394 and 498 K, respectively [see Fig. 2(a)]. The powder diffractogram of the final product corresponds

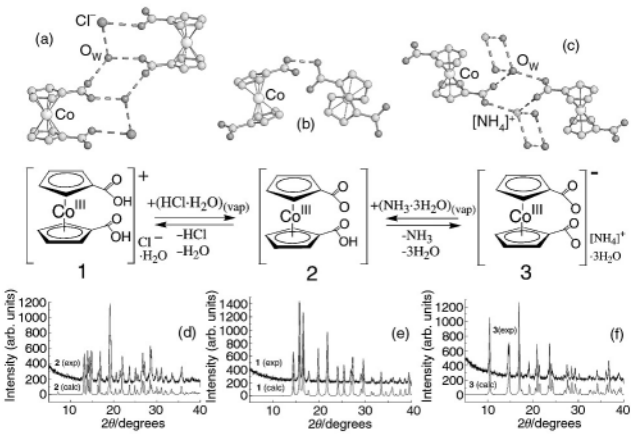

Fig. 1 Schematic representation of the uptake and release of hydrated vapours of HCl and NH_3 by crystalline $[Co^{III}(\eta^5\text{-}C_5H_4CO_2H)(\eta^5\text{-}C_5H_4CO_2)]$ **1**. The different relative arrangement of the organometallic moieties in the solid state is shown for **2** (a), **1** (b) and **3** (c). Hydrogen atoms not shown. Experimental X-ray powder diffraction patterns for **2** (d), **1** (e) and **3** (f), measured after each uptake–release cycle, are compared with the powder patterns calculated on the basis of the single crystal structures.

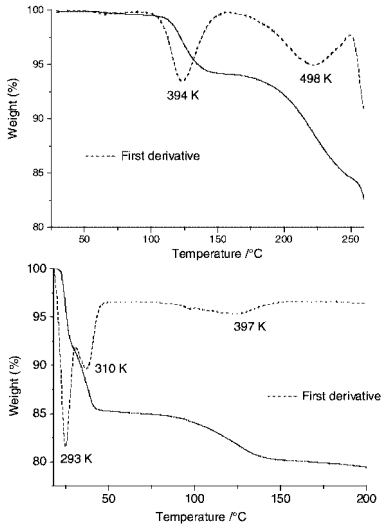

Fig. 2 Thermogravimetric analyses (TGA) corresponding to the **2** → **1** (a) and **3** → **1** (b) solid state processes. The loss in weight at 394 and 498 K in the **2** → **1** process corresponds to one water and one HCl molecules per formula unit, respectively. The loss in weight at 293, 310 and 397 K in the **3** → **1** process corresponds to a total of 3.5 water and one NH_3 molecule per molecular unit.

 DOI: 10.1039/b106984e

Table 1 Reaction of **1** with hydrated acid and base vapours

Acid[a]	Exposure time[b]	ν_{CO}[c]/cm^{-1}	Base[a]	Exposure time[b]	ν_{CO}[c]/cm^{-1}
HCl (37%)	5 min	1733s, 1707s	NH_3 (30%)	5 min	1610s
CF_3CO_2H (99%)	1 h	1723s, 1706s	NH_2Me (30%)	1 h	1610s
HBF_4 (54%)	16 h	1736s, 1708s	NMe_3 (30%)	1 h	1612s

[a] Concentration of the solution given in parenthesis. [b] Uptake time for a complete conversion of 10 mg of **1**, all processes are fully reversible. [c] Diagnostic CO stretching frequencies (KBr) for reaction products; neutral **1** is characterized by a band at 1714s cm^{-1}.

precisely to that of form **1**. Crystalline **1** can be cycled through several absorption and release processes of HCl without decomposition or detectable formation of amorphous material.

Incidentally, since compound **2** is the precursor for the synthesis of **1**,[10] the solid state conversion **2** → **1** represents an alternative an more convenient way to obtain the anhydrous zwitterion **1** directly from solid **2**.

The behaviour of **1** towards NH_3 is remarkably similar: **1** (1–10 mg) quantitatively transforms into the hydrated ammonium salt **3** upon 5 min exposure to vapours† of 30% aqueous ammonia. Single crystals of **3** for X-ray structure determination‡ can be obtained if the reaction of **1** with ammonia is carried out in aqueous solution.

As in the case of **2**, formation of **3** in the heterogeneous reaction is assessed by comparison of the observed and calculated (see caption to Fig. 1) X-ray powder patterns of **3**. The salt is characterized by the presence of charge-assisted $^+$N–H$\cdots$O$^-$ interactions between the ammonium cation and the deprotonated –CO_2^- groups on the organometallic anion.

As in the case of the reaction with HCl, absorption of ammonia is a fully reversible process: upon thermal treatment (1 h at 373 K, ambient pressure) crystalline **3** converts quantitatively into **1**. Repeated thermogravimetric analyses (TGA)§ show that **3** releases between 3 and 3.5 water molecules and 1 molecule of NH_3 per formula unit in the temperature range 293–397 K [see Fig. 2(b)]. The slight excess of water is probably due to humidity absorbed on the surface. All attempts to remove the water in excess (under low pressure) also resulted in a partial loss of the crystallization water. The powder diffractogram of the product after thermal treatment corresponds precisely to that of form **1**.

IR spectroscopy can also be utilized to quickly detect formation of the organometallic cation or anion when **1** is reacted with volatile acids or bases, as spectra in KBr show diagnostic bands for the CO stretching at 1733s and 1707s in **2**, and 1610s cm^{-1} in **3** (see Table 1). In the release process, these bands are replaced by the stretching at 1714s cm^{-1} characteristic of the zwitterionic form **1**.

Heterogeneous acid–base reactions are, obviously, well known. However, system **1** represents, to the best of our knowledge, the first example of an organometallic solid that can withstand both processes, behaving as a fully reversible 'amphoteric trap' towards a variety of hydrated vapours of acids and bases. It is worth pointing out that the process relies on the possibility of 'switching' between O–H$\cdots$O hydrogen bonds in neutral **1** and charge-assisted $^+$O–H$\cdots$X$^-$ or O$^-\cdots$[H–NR_3]$^+$ hydrogen bonds.

The experiments with ammonia or hydrogen chloride have been examined in depth. We are currently exploring the reactivity of solid **1** towards other acid and basic vapours beside those reported above. The dependence on the composition of the vapour phase on the exposure time and on the surface area is also being investigated.

The bottom-up construction of solid-state sensors, filters and sieves for small molecules is an attractive prospective of crystal engineering. While many nanoporous systems irreversibly decompose upon removal of guest molecules because of loss of stability,[12] our gas–solid reaction *exploits* the reversible interconversion between a molecular crystal and different crystalline salts where **1** can convert into either a cation or an anion, depending on the acid–base reaction. The control on solid-state reactions that can be used to trap environmentally dangerous or poisonous molecules is an attractive goal for solid-state chemistry and crystal engineering.

We thank MURST (projects Supramolecular Devices and Solid Supermolecule), the Universities of Bologna (project Innovative Materials) and Sassari for financial support.

Notes and references

† Exposure to HCl or NH_3 hydrated vapours was attained by allowing the vapours of the corresponding aqueous solutions contained in a round-bottom flask to pass into a filter funnel, in which a glass sample holder containing powder **1** was placed: in this way the powder and the solution were not in contact; the reaction took place in a closed system. Elemental analysis for **3** (single crystals): Found: C, 41.13; H, 5.34; N, 4.01. Calc.: C, 41.51; H, 5.23; N, 4.03%.

‡ Powder data were collected on a Philips PW-1100 automated diffractometer with Cu-Kα radiation, graphite monochromator. The program PowderCell 2.2 was used for calculation of X-ray powder patterns [PowderCell programmed by W. Kraus and G. Nolze (BAM Berlin) © subgroups derived by Ulrich Müller (Gh Kassel)]. The solid state structure of $[(C_5H_4CO_2)_2Co][NH_4]\cdot 3H_2O$ **3** was determined at 223 K by single crystal X-ray diffraction on a Nonius CAD4 diffractometer equipped with an Oxford Cryostream device and a graphite-monochromator (Mo-Kα radiation, λ = 0.71073 Å). *Crystal data*: triclinic, space group $P\bar{1}$, Z = 1, a = 6.442(6), b = 7.007(4), c = 9.120(4) Å, α = 68.79(4), β = 89.06(5), γ = 69.72(7)°, V = 357.2(4) Å^3, 1252 independent reflections (1338 measured), R_1 = 0.0381, wR_2 = 0.1050, GOF = 1.111. One of the O_{water} atoms in the asymmetric unit shares its position with the N atom of the $[NH_4]^+$ cation, and the two atoms were refined with an occupancy factor of 0.5. All non-H atoms refined anisotropically. The SHELX-97 package was used for structure solution and refinement based on F^2 (G. M. Sheldrick, SHELX-97, Program for Crystal Structure Determination; University of Göttingen, Göttingen, Germany, 1997).

CCDC reference number 166132. See http://www.rsc.org/suppdata/cc/b1/b106984e/ for crystallographic data in CIF or other electronic format.

§ The TGA experiments were carried out on a Perkin-Elmer TGA-7 instrument in open Al pans under N_2 atmosphere.

1 Proceedings of the Dalton Discussion on Inorganic Crystal Engineering, *J. Chem. Soc. Dalton Trans*., 2000, 3705.
2 D. Braga and F. Grepioni, *Acc. Chem. Res*., 2000, **33**, 601.
3 D. Braga, F. Grepioni and G. R. Desiraju, *Chem. Rev*., 1998, **98**, 1375.
4 V. A. Russell, C. C. Evans, W. Li and M. D. Ward, *Science*, 1997, **276**, 575; K. T. Holman, A. M. Pivovar, J. A. Swift and M. D. Ward, *Acc. Chem. Res*., 2001, **34**, 107.
5 O. M. Yaghi, G. Li and H. Li, *Nature*, 1995, **378**, 703.
6 S.-i. Noro, S. Kitagawa, M. Kondo and K. Seki, *Angew. Chem., Int. Ed*., 2000, **39**, 2082.
7 B. F. Abrahams, B. F. Hoskins, D. M. Michail and R. Robson, *Nature*, 1994, **369**, 727.
8 M. Albrecht, M. Lutz, A. L. Speck and G. van Koten, *Nature*, 2000, **406**, 970; M. Albrecht, R. A. Gossage, M. Lutz, A. L. Speck and G. van Koten, *Chem. Eur. J*., 2000, **6**, 1431.
9 I. C. Paul and D. Y. Curtin, *Acc. Chem. Res*., 1973, **6**, 217; R. S. Miller, D. Y. Curtin and I. C. Paul, *J. Am. Chem. Soc*., 1974, **96**, 6340.
10 D. Braga, G. Cojazzi, L. Maini, M. Polito and F. Grepioni, *Chem. Commun*., 1999, 1949.
11 D. Braga, L. Maini, M. Polito, M. Rossini and F. Grepioni, *Chem. Eur. J*., 2000, **6**, 4227.
12 S. C. Zimmermann, *Science*, 1997, **276**, 543.

CHEMCOMM Communication
www.rsc.org/chemcomm

Abnormal binding in a carbene complex formed from an imidazolium salt and a metal hydride complex

Stephan Gründemann, Anes Kovacevic, Martin Albrecht, Jack W. Faller* and Robert H. Crabtree*

Department of Chemistry, 225 Prospect Street, Yale University, New Haven, CT 06520-8107, USA. E-mail: robert.crabtree@yale.edu

Received (in Purdue, IN, USA) 24th August 2001, Accepted 24th September 2001
First published as an Advance Article on the web 18th October 2001

2-Pyridylmethylimidazolium salts and $IrH_5(PPh_3)_2$ give an $[(N–C)IrH_2(PPh_3)_2]^+$ species with the imidazole ring bound in the 'wrong way': at C-5, not the expected C-2.

N-Heterocyclic carbenes have adopted an increasing role as ligands in homogeneous catalysis and organometallic chemistry.[1–3] Previous examples have always shown C-2 metal binding (**1**)—the same structure as in the free carbenes isolated by Arduengo *et al.*[4] C-4(5) binding as in **2** has not been considered as a likely alternative because the free carbenes always have a C-2 structure (**3**) and the adjacent nitrogens were considered to strongly stabilize both the free carbene in **3** and the M–C bond in **1** (Scheme 1).

In recent work, Sini, Eisenstein and Crabtree[5] reported DFT (B3PW91) calculations on 2- *vs.* 4(5)-binding of **1** and **2** (R = H), where a much less stable C-bound isomer was shown to result from metal binding to the 4(5) position as in **2**. The free 'carbene' at C-4(5) was calculated to lie at +20.0 kcal mol^{-1} above the C-2 carbene. With $PtCl_3^-$ bound {**1** or **2**; ML_n = $[PtCl_3]^-$}, the C-4(5) complex was calculated to lie even higher, +23.3 kcal mol^{-1} above the C-2 complex.

Previous synthetic routes from the precursor imidazolium salt most often include deprotonation to give the free carbene as intermediate;[1–3] since **3** is the stablest form of the carbene,[4,5] this route is likely always to give the C-2 bound complex, **1**. Direct metallation of imidazolium salts has also previously always occurred at the 2-position,[6] including in our own prior work.[6c]

In this communication, we report the facile reaction of the imidazolium precursor salt with a metal hydride to give a 'carbene' of type **2** with the metal attached at the 'wrong' carbon, C-5 not C-2. **2** could also be regarded as a metallated imidazolium salt.

$IrH_5(PPh_3)_2$ **4** is known[7] to react with substituted pyridines (L′) in refluxing C_6H_6 *via* loss of H_2 to give the trihydrides $(L')IrH_3(PPh_3)_2$ (**5**). Since the pyridine-substituted imidazolium salts **6a**,**b** are readily available[8] from the *N*-alkylimidazole and 2-bromomethylpyridine, followed by Br/BF_4 anion exchange, we looked at their reaction with **4**. This occurred readily under similar conditions as before (refluxing THF, 2 h, recrystalization from THF–pentane) but to give the chelating carbene complex, **7** with the metal bound at C-5, not C-2 as expected [eqn. (1)].†

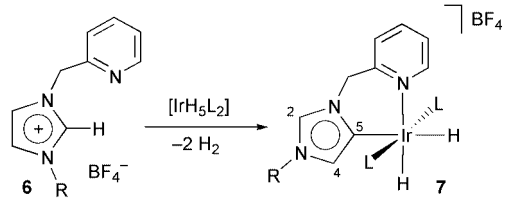

(1)

[**a** R = Pr^i, **b** R = Bu^n; L = PPh_3]

The identity of the product **7a** is suggested by the spectroscopic data (298 K), particularly ^1H NMR spectroscopy in $CDCl_3$ where a low field signal of unit intensity (8.72 ppm) is assigned to the imidazole 2 proton, while a signal at higher field

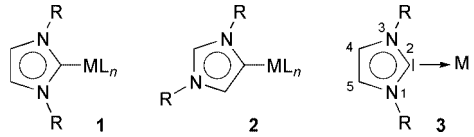

Scheme 1

also of unit intensity (5.17 ppm) is assigned to the 4-proton. The metal bound hydrides show very different shifts reflecting the large differences of the *trans* ligands (−10.83 ppm, tentatively[7] assigned to be *trans* to the metal-bound carbon, and −21.49 ppm, *trans* to pyridine). The $J(HH')$ of 5 Hz is typical[9] for a *cis* MH_2 arrangement, and the $J(PH)$ of 18–20 Hz is typical of a *cis* $M(PR_3)H$ arrangement. The presence of a metal bound carbene follows from the $^{13}C\{^1H\}$ spectra where the C-5 carbon is low field shifted (141.07 ppm compared to *ca.* 122 ppm in the precursor imidazolium salt). Moreover, this resonance appears as a triplet as a result of coupling to ^{31}P [$J(PC)$ 7.1 Hz]. In contrast, the C-2 carbon underwent a high field shift to 129.55 ppm, which does not suggest metallation of this carbon. As expected for equivalent phosphorus nuclei only one singlet (21.4 ppm) is observed in the $^{31}P\{^1H\}$ NMR spectra. The similarity of the NMR data of **7b** with those of **7a** leaves no doubt that they have similar structures and all data are consistent with structure **7**.

The X-ray structure‡ (Fig. 1) defines the situation unambiguously for **7a**. The Ir is attached to the imidazole 5-carbon, equivalent to C(7) in crystallographic numbering, as shown by the locations of the benzylic and Pr^i ring substituents that define the nitrogen positions; Pr^i is not adjacent to the M–C bond so the complex is of non-Arduengo type. The C–C distances in the ring are normal for an imidazolium and the Ir–C(7) bond [2.100(6) Å] is essentially single, so there is little if any Ir–C π-bonding. Other distances and angles are unremarkable.

The crystallographic data show that the molecule is chiral owing to the non-planarity of the pyridine–carbene ligand. The six- and five-membered rings of the chelate ligand are oriented at a dihedral angle of 146°. The NMR spectra, however, are consistent with a molecule with a plane of symmetry as isopropyl methyl protons and the bridge methylene protons of the ligand are equivalent; likewise there is also only a single ^{31}P resonance. This suggests a rapid interconversion on the NMR timescale (at 298 K) that corresponds to racemization *via* a boat–boat six-membered ring flip.

Complex **7** has so far shown no tendency to rearrange to the 2-isomer. Heating a DMSO solution of **7b** to 100 °C for 1 h did not show any change. At 160 °C, however, gradual decomposition of the material was observed without rearrangement of the ligand binding mode. It is still unclear if **7** is a thermodynamic or a kinetic product. The > 20 kcal mol^{-1} energy favoring 2- *vs.* 5-binding [numbering as in eqn. (1)] found[5] for the $[PtCl_3]^-$ derivative seems rather too large to be reversed by change of metal and substituents and **7a**,**b** seem most likely to be kinetic products. If so, abnormal 4(5)-binding may only be a risk for any path not involving deprotonation, such as direct metallation.

 DOI: 10.1039/b107881j

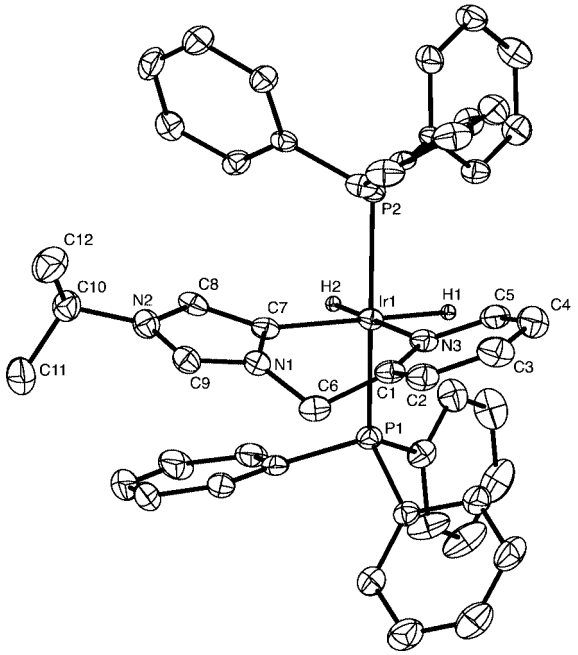

Fig. 1 Molecular structure of the cation of **7a** showing 50% probability thermal ellipsoids. Only the metal-bound hydrogens (calculated positions) are shown. Selected distances (Å) and angles (°): Ir(1)–P(1) 2.287(2), Ir(1)–P(2) 2.301(2), Ir(1)–N(3) 2.193(5), Ir(1)–C(7) 2.100(6), N(1)–C(6) 1.461(7), N(1)–C(7) 1.404(7), N(1)–C(9) 1.335(8), N(2)–C(8) 1.390(8), N(2)–C(9) 1.327(8), N(2)–C(10) 1.459(8); N(3)–Ir(1)–C(7) 89.3(2), P(1)–Ir(1)–P(2) 163.86(6).

We cannot exclude **7a**,**b** being thermodynamic products, however, in which case other carbenes currently considered Arduengo type may in fact be bound at C-4(5). Whatever the origin of the effect, care must clearly be taken in future not to assume 2-substitution always takes place in carbenes derived from imidazolium salts.

We gratefully acknowledge financial support from the Deutsche Akademie der Naturforscher Leopoldina (BMBF-LPD 9901/8-37; S.G.), Swiss National Foundation (M. A.), and the US DOE and NSF (R. H. C., J. W. F.).

Notes and references

† *Typical synthesis*: a mixture of **6b** (BF_4 salt, 54 mg, 0.18 mmol) and $IrH_5(PPh_3)_2$ (129 mg, 0.18 mmol) in THF (8 ml) was refluxed in air for 2.3 h. After 20 min a clear solution is obtained. After the reaction mixture had cooled to room temperature it was layered with 10 ml heptane. Over a period of 12 h, crystals of **7b** formed which were filtered off and dried *in vacuo*. Yield: 124 mg (68%). The complex can be recrystallized from THF/pentane.

Spectroscopic data for **6a**: ^{1}H NMR ($CDCl_3$, 298 K): δ 9.17 (s, 1H, NCHN), 8.55 (d, $^3J_{HH}$ 4.6 Hz, 1H, py-H), 7.77 (dt, $^3J_{HH}$ 7.7, $^4J_{HH}$ 1.7 Hz, 1H, py-H), 7.66 (d, $^3J_{HH}$ 7.9 Hz, 1H, py-H), 7.59 (s, 1H, imid-H), 7.31 (dd, $^3J_{HH}$ 7.6 , $^3J_{HH}$ 5.0 Hz, 1H, py-H), 7.25 (s, 1H, imid-H), 5.51 (s, 4H, CH_2), 4.65 (septet, $^3J_{HH}$ 6.8 Hz, 1H, CH), 1.61 (t, $^3J_{HH}$ 6.8 Hz, 6H, CH_3). ^{13}C{^{1}H} NMR ($CDCl_3$, 298 K): δ 152.38 (C_{py}), 149.90 (C_{py}), 137.85 (C_{py}), 135.08 (NCN), 124.05 (C_{py}), 123.84 (C_{py}), 123.04 (C_{imid}), 119.83 (C_{imid}), 54.17 (CH_2), 53.56 (C_{Pr^i}), 22.68 (C_{Pr^i}).

For **6b**: ^{1}H NMR ($CDCl_3$, 298 K): δ 9.09 (s, 1H, NCHN), 8.51 (d, $^3J_{HH}$ 4.6 Hz, 1H, py-H), 7.73 (dt, $^3J_{HH}$ 7.7, $^4J_{HH}$ 1.8 Hz , 1H, py-H), 7.58 (d, $^3J_{HH}$ 7.8 Hz, 1H, py-H), 7.53 (s, 1H, imid-H), 7.32 (s, 1H, imid-H), 7.27 (dd, $^3J_{HH}$ 7.7, $^3J_{HH}$ 4.8 Hz, 1H, py-H), 5.49 (s, 4H, CH_2), 4.19 (t, $^3J_{HH}$ 7.5 Hz, 2H, Bu-H), 1.89–1.81 (m, 2H, Bu-H), 1.39–1.30 (m, 2H, Bu-H), 0.93 (t, $^3J_{HH}$ 7.5 Hz, 3H, Bu-H). ^{13}C{^{1}H} NMR ($CDCl_3$, 298 K): δ 152.25 (C_{py}), 149.77 (C_{py}), 137.86 (C_{py}), 136.37 (NCN), 124.06 (C_{py}), 123.80 (C_{py}), 122.93 (C_{imid}), 121.75 (C_{imid}), 54.00 (CH_2), 49.93 (C_{Bu}), 31.81 (C_{Bu}), 19.34 (C_{Bu}), 13.30 (C_{Bu}).

For **7a**: ^{1}H NMR ($CDCl_3$, 298 K): δ 8.72 (s, 1H, NCHN), 8.23 (d, 1H, $^3J_{HH}$ 5.5 Hz, py-H), 7.37–7.14 (m, 32H, py-H, Ph-H), 6.07 (t, $^3J_{HH}$ 6.3 Hz, py-H), 5.17 (s, 1H, imid-H), 4.70 (s, 2H, CH_2), 4.25 (septet, 1H, $^3J_{HH}$ 6.5 Hz, CH), 1.19 (d, 6H, $^3J_{HH}$ 6.5 Hz, CH_3), −10.83 (dt, $^2J_{PH}$ 19.6, $^3J_{HH}$ 4.9 Hz, Ir-H), −21.49 (dt, $^2J_{PH}$ 18.6, $^3J_{HH}$ 4.9 Hz, Ir–H). ^{13}C{^{1}H} NMR ($CDCl_3$, 298 K): δ 161.78 (C_{py}), 153.10 (C_{py}), 141.07 (t, J_{PC} 7.1 Hz, $C_{carbene}$), 137.04 (C_{py}), 134.93 (t, J_{PC} = 26.3 Hz, C_{Ph}), 133.55 (t, J_{PC} 6.0 Hz, C_{Ph}), 132.40 (C_{Ph}), 129.55 (NCN), 127.84 (t, J_{PC} 5.8, C_{Ph}), 125.87 (C_{imid}), 124.15 (C_{imid}), 123.56 (C_{py}), 55.03 (CH_2), 50.47 (C_{Pr^i}), 22.94 (C_{Pr^i}). ^{31}P{^{1}H} NMR ($CDCl_3$, 298 K): δ 21.36.

For **7b**: ^{1}H NMR ($CDCl_3$, 298 K): δ 8.71 (s, 1H, NCHN), 8.19 (d, $^3J_{HH}$ 5.1 Hz, 1H, py-H), 7.37–7.15 (m, 32H, py-H, Ph-H), 6.07 (t, $^3J_{HH}$ 5.9 Hz, 1H, py-H), 5.03 (s, 1H, imid-H), 4.72 (s, 2H, CH_2), 3.63 (t, $^3J_{HH}$ 6.9 Hz, 1H, CH_2), 1.47 (m, 2H, CH_2), 1.17 (m, 2H, CH_2), 0.90 (t, $^3J_{HH}$ 7.7 Hz, CH_3), −10.89 (dt, $^2J_{PH}$ 19.6, $^3J_{HH}$ 5.1 Hz, Ir-H), −19.61 (dt, $^2J_{PH}$ 18.4, $^3J_{HH}$ 5.1 Hz, Ir-H). ^{13}C{^{1}H} NMR ($CDCl_3$, 298 K): δ 161.77 (C_{py}), 153.07 (C_{py}), 141.30 (t, J_{PC} 6.9 Hz, $C_{carbene}$), 137.09 (C_{py}), 134.96 (t, J_{PC} = 26.3, C_{Ph}), 133.79 (C_{Ph}), 133.61 (t, J_{PC} 6.0, C_{Ph}), 129.59 (NCN), 127.86 (t, J_{PC} 4.7, C_{Ph}), 126.13 (C_{imid}), 125.90 (C_{py}), 124.18 (C_{py}), 55.08 (CH_2), 47.89 (C_{Bu}), 31.96 (C_{Bu}), 19.36 (C_{Bu}), 13.37 (C_{Bu}). ^{31}P{^{1}H} NMR ($CDCl_3$, 298 K): δ 21.39.

‡ *Crystal data* for **7a**: $C_{48}H_{47}BF_4IrN_3P_2$, M = 1006.89, colorless crystal, primitive monoclinic cell with dimensions: a = 9.4493(2), b = 20.6687(6), c = 22.0865(6) Å, β = 90.160(2)° and V = 4313.6(2) Å^3; Z = 4; μ(Mo–Kα) = 3.223 mm^{-1}; D_c = 1.550 g cm^{-3}. The systematic absences of: $h0l$: $l \neq \pm 2n$ and $0k0$: $k \neq \pm 2n$ uniquely determine the space group to be $P2_1/c$ (no. 14). 38573 reflections measured (KappaCCD diffractometer, T = 183 K). The structure was solved by direct methods and expanded using Fourier techniques. The non-hydrogen atoms were refined anisotropically. Hydrogen atoms were included at calculated positions (including the Ir hydrides), but not refined. The final cycle of full-matrix least-squares refinement on F was based on 4789 observed reflections [$I > 3.00\sigma(I)$] and 532 variable parameters and converged with unweighted and weighted agreement factors of R = 0.033 and R_w = 0.035 (S = 0.905). CCDC reference number 171283. See http://www.rsc.org/suppdata/cc/b1/b107881j/ for crystallographic data in CIF or other electronic format.

1 D. Bourissou, O. Guerret, F. P. Gabbai and G. Bertrand, *Chem. Rev.*, 2000, **100**, 39.
2 W. A. Herrmann, C. P. Reisinger and M. Spiegler, *J. Organomet. Chem.*, 1998, **557**, 93.
3 C. W. Bielawski and R. H. Grubbs, *Angew. Chem., Int. Ed.*, 2000, **39**, 2903; P. B. Hitchcock, M. F. Lappert and P. Terreros, *J. Organomet. Chem.*, 1982, **239**, C26; H. M. Lee, T. Jiang, E. D. Stevens and S. P. Nolan, *Organometallics*, 2001, **20**, 1255.
4 A. J. Arduengo, R. L. Harlow and M. Kline, *J. Am. Chem. Soc.*, 1991, **113**, 361.
5 G. Sini, O. Eisenstein and R. H. Crabtree, *Inorg. Chem.*, submitted.
6 (*a*) H. J. Schönherr and H. W. Wanzlick, *Chem. Ber.*, 1970, **103**, 1037; (*b*) K. M. Lee, C. K. Lee and I. J. B. Lin, *Angew. Chem., Int. Ed.*, 1997, **36**, 1850; (*c*) E. Peris, J. A. Loch, J. Mata and R. H. Crabtree, *Chem. Commun.*, 2001, 201.
7 E. Peris, J. C. Lee, J. R. Rambo, O. Eisenstein and R. H. Crabtree, *J. Am. Chem. Soc.*, 1995, **117**, 3485.
8 A. A. D. Tulloch, A. A. Danopoulos, S. Winston, S. Kleinhenz and G. Eastham, *J. Chem. Soc., Dalton Trans.*, 2000, 4499.
9 S. Gründemann, H.-H. Limbach, G. Buntkowsky, S. Sabo-Etienne and B. Chaudret, *J. Phys. Chem. A*, 1999, **103**, 4752.

CHEMCOMM Communication
www.rsc.org/chemcomm

p-Sulfonatocalix[6]arene is an effective coacervator of poly(allylamine hydrochloride)

Vincent Ball,[a] Mathias Winterhalter,[b] Florent Perret,[c] Guy Esposito[c] and Anthony W. Coleman*[c]

[a] *Institut Charles Sadron, Unité propre 22 CNRS, 6 rue Boussingault, 67083, Strasbourg Cedex, France. E-mail: ball@ics.u-strasbg.fr; Fax: (0033) 3 88 41 40 99; Tel: (0033) 3 88 41 40 12*

[b] *Institut de Pharmacologie et de Biologie Structurale, Unité Mixte de Recherche 5089, 205 route de Narbonne, 31077, Toulouse, France. E-mail: winter@ipbs.fr; Fax: (0033) 5 61 33 58 86; Tel: (0033) 5 61 33 58 22*

[c] *Institut de Biologie et de Chimie des Protéines, Unité propre 412 CNRS, 7 Passage du Vercors, 69367, Lyon, France. E-mail: aw.coleman@ibcp.fr; Fax: (0033) 4 72 72 26 90; Tel: (0033) 4 72 72 26 40*

Received (in Cambridge, UK) 17th July 2001, Accepted 3rd September 2001
First published as an Advance Article on the web 11th October 2001

p-Sulfonatocalix[6]arene is shown to form insoluble complexes with poly(allylamine hydrochloride) when the charge balance between the negative calixarene sulfonate groups matches the positive charge carried by the polyelectrolyte, this makes this glycosylaminoglycan analog an interesting candidate for controlled release systems in the case of proteins encapsulated in mesoscopic complexes with polyelectrolytes.

Calixarenes are one of the major classes of host molecules in supramolecular chemistry, together with cyclodextrins and crown ethers.[1] The interest in these molecules is increasing in view of the possibility of preparing water soluble derivatives.[2] Among these are the *p*-sulfonatocalix[*n*]arenes, denoted $\mathbf{1}_n$, where *n* is the number of linked aromatic rings.[3] These molecules complex organic compounds as well as inorganic ions in water[4] and are possible candidates for heparin mimics,[5] since as with heparin they display a high density of negatively charged sulfonate groups and could hence possess an antithrombotic activity.[5] Moreover the synthetic pathway to these compounds[6] is rather simple when compared to that leading to heparin and they display essentially no immune response.[7] It is well known that arginine and lysine play a key role in the sequences present in heparin recognition sites.[8] Recently, the interactions between $\mathbf{1}_4$, $\mathbf{1}_6$, and $\mathbf{1}_8$ with these single amino acids[9] as well as with their small oligomers[10] have been investigated by means not only of NMR spectroscopy to determine the stoichiometry as well as the localisation of the amino acids within the hydrophobic cavity, but also by means of isothermal microcalorimetry (ITC) to determine the standard enthalpy and entropy variations associated with complex formation. To our knowledge, the interactions between $\mathbf{1}_n$ and large cationic homopolymers in solution have never been investigated. This is of prime importance not only from a fundamental point of view, to study the influence of the correlation between the cationic groups on the complexation process, but also from a more practical point of view for the controlled release in protein–polyelectrolyte complexes.[11,12] It has been shown, that enzymes can be stabilised for long range storage when wrapped in a polyelectrolyte network,[12] but is it possible to remove the polyelectrolyte around the protein without denaturation of the enzyme? For this reason, we give here our first results describing the interactions between $\mathbf{1}_6$ and poly(allylamine hydrochloride), PAH, in a pH 7.4 Tris (10 mM)–NaCl 0.1 M buffer. Under these conditions we assume that the phenolic groups on $\mathbf{1}_6$ are not ionised. Our results were obtained by combining several physicochemical techniques aimed to describe not only the structure of the obtained mesoscopic complexes but also their formation mechanism. In order to understand the influence of the chain length upon the interactions with $\mathbf{1}_6$, two different molecular weight polymers were used, PAHS, M_w = 15 kDa and PAHL, M_w = 70 kDa.†

At a constant PAH concentration of 2.2×10^{-6} M for PAHL and 4.3×10^{-6} M for PAHS, the addition of $\mathbf{1}_6$,[6] leads to a progressive increase of the solution turbidity (Fig.1),‡ and levelling off at a given mixing ratio *r* (defined as the number of provided $\mathbf{1}_6$ to the number of initially present PAH molecules). Simultaneously with the turbidity increase, the average size of the (polydisperse) particles increases as determined by means of dynamic light scattering (DLS): the initial PAHS and PAHL have an hydrodynamic radius around 4 and 8.5 nm respectively,‡ however at r = 37.3 for PAHL, the solution contained particles of hydrodynamic radius around 10 and 99 nm which contribute to about 60% of the scattered intensity (data not shown). For PAHS at r = 12.4, the solution contains particles of the same size and also particles around 370 nm in radius (12% of the scattered intensity). For PAHL and PAHS the plateau of the turbidity isotherms are reached for r = (200 ± 30) and r = (40 ± 10) respectively (Fig. 1).

Taking into account the presence of 6 negative charges from the sulfonate groups on $\mathbf{1}_6$ and the DP of the two PAHs, these *r* values correspond to the electrical neutralisation of the polymer with a full release of the condensed chloride counter ions. This assumption was furthermore checked by means of laser Doppler electrophoresis (LDE),‡ operated under conditions of constant current, 5 mA (Fig. 2): for low *r* values the ζ potential is positive as expected in the presence of an excess of positively charged PAH whereas for high *r* the negative ζ potential reflects mainly the presence of a large excess of $\mathbf{1}_6$. The charge inversion occurs again around r = 200 for PAHL and r = 40 for PAHS (Fig. 2).

At *r* values higher than this threshold, the obtained particles sediment in about 10 to 15 min after their preparation. Hence, these particles could not be characterised by means of DLS. At lower *r* values, no sedimentation is observed even after a few hours despite the particle size increase at least in the dilute polyelectrolyte concentration regime: we are in presence of

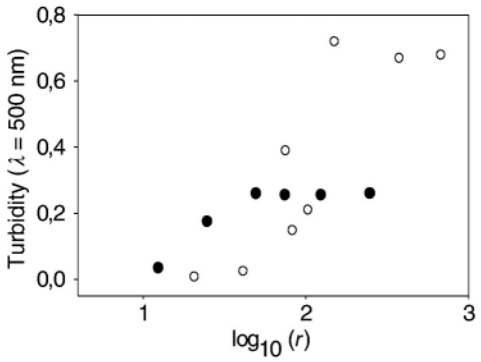

Fig. 1 Evolution of the turbidity (at λ = 500 nm) as a function of *r* for PAHL (○) and PAHS (●) at constant PAH concentration.

 DOI: 10.1039/b106361h

phase separation[13] *when neutral complexes are formed.* The used PAHL and PAHS display an average hydrodynamic radius close to 8 and 4 nm, implying that the increase in size originates from $\mathbf{1_6}$ induced intermolecular bridging. This is not unrealistic on the basis of the preferential double partial cone conformation of $\mathbf{1_6}$.[14] The obtained mesoscopic complexes are irreversible not only under dilution with Tris–NaCl buffer as displayed by a linear decrease of the turbidity with the dilution ratio (data not shown) but also by addition of either PAH or $\mathbf{1_6}$, when the plateau level of the binding isotherm is reached. The irreversibility of this process upon dilution was also checked by centrifugation of the particles (prepared at r = 44.4 for PAHL), removal of the supernatant, replacement by Millipore water and redispersion of the particles. Three centrifugation, supernatant removal, redispersion in water cycles were performed, the particles were then dried for 28 h at 110° and analysed by means of elemental analysis: they contained 33.2 C, 5.7 N, 5.0 H, 6.5 S and 13.47% Cl, whereas the initial PAH had 37.9% Cl and no sulfur content. This implies that sulfonate molecules remain bound to the PAH even after extensive rinsing and that a significant number of Cl^- counter ions have been released. Turbidity experiments performed in the absence of buffer but at 0.1 M NaCl and by varying the pH showed that the turbidity became lower than 0.01 at pH higher than 11.5 with a gradual decrease beginning after pH 9: hence the complexes are dissociated by neutralisation of the primary amine groups of PAH. These observations all point to strong interaction of electrostatic nature taking place between $\mathbf{1_6}$ and PAH. This was checked by means of ^{1}H NMR spectroscopy‡ where it appears that the signals due to $\mathbf{1_6}$ (at δ = 7.37 and 3.86 ppm) practically disappear and the peaks become broader when r is lower than 200 for PAHL and 30 for PAHS (data not shown). Hence only the unbound $\mathbf{1_6}$ molecules are seen (at high enough r) and those bound to PAH are not able to relax after radio frequency excitation. ITC‡ revealed that the dilution heat of PAHL into the Tris–NaCl buffer was slightly endothermic ($\Delta H_{\mathrm{dil,\ PAHL}}$ = 66.2 kJ mol^{-1}). The enthalpy variation associated with the reaction is equal to (−18100 ± 1500) kJ mol^{-1}, meaning that the average enthalpy per $\mathbf{1_6}$ molecule amounts to −90.5 kJ mol^{-1}. This value is 4 times larger than the binding enthalpy for lysine–$\mathbf{1_6}$ complex formation.[10] Each $\mathbf{1_6}$ molecule interacts on average with 6 monomer units (indeed the solution extracted from the calorimeter cell displays strong turbidity, we are hence in the plateau region of Fig. 1), the binding interaction per site amounts hence to about −15 kJ mol^{-1}, which is only about 1.5 times smaller than for lysine–$\mathbf{1_6}$ complexation. To conclude whether this smaller enthalpy variation per interaction site originates from intrinsic differences between the side chain of PAH and lysine or from a contribution due to the constraints imposed by the polymer chain, we will perform the same kind of ITC experiments with poly(L-lysine hydrobromide). Note that the interaction enthalpy is the same when PAHS is employed instead of PAHL. Thus if any chain effect should occur, it must take place for smaller degrees of polymerisation. Hence we have demonstrated the occurrence of strong and irreversible electrostatically driven interactions between PAH and $\mathbf{1_6}$ at pH 7.4, leading to phase separation when the polymer is neutralised by the appropriate number of $\mathbf{1_6}$ molecules. The interactions between $\mathbf{1_6}$ and PAH may be used in order to quantitatively release proteins bound inside protein–PAH complexes[11] as will be shown in a forthcoming study.

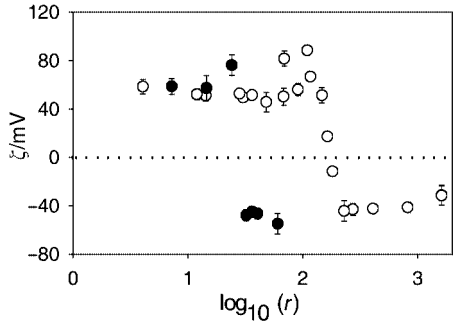

Fig. 2 ζ potential of the PAH–$\mathbf{1_6}$ complexes in Tris–NaCl buffer as a function of r: PAHL (○) and PAHS (●), the dotted line corresponds to ζ = 0. The error bars correspond to the standard deviation of the mean (n = 10).

Notes and references

1 V. Böhmer, *Angew. Chem., Int. Ed. Engl.*, 1995, **34**, 713.
2 A. Arduini, A. Pochini, S. Reverberi and R. Ungaro, *J. Chem. Soc., Chem. Commun.*, 1984, 981.
3 S. Shinkai, S. Mori, T. Tsubaki, T. Sone and O. Manabe, *Tetrahedron Lett.*, 1984, **25**, 5315.
4 C. D. Gutsche, *Monographs in Supramolecular Chemistry, Calixarenes*, The Royal Society of Chemistry, London, 1989.
5 Genelabs Technologies Inc., *US Pat.*, 93-07441, WO 94-03165.
6 S. Shinkai, K. Araki, T. Tsubaki, T. Arimura and O. Manabe, *J. Chem. Soc., Perkin Trans. 1*, 1987, 2297.
7 M. H. B. Grote Gansey, A. S. de Haan, E. S. Bos, W. Verboom and D. N. Reinhoudt, *Bioconjugate Chem.*, 1999, **10**, 613.
8 H. E. Conrad, *Heparin binding proteins*, Academic Press, San Diego, 1997.
9 N. Douteau-Guével, A. W. Coleman, J.-P. Morel and N. Morel-Desrosiers, *J. Chem. Soc., Perkin Trans. 2*, 1999, 629.
10 N. Douteau-Guével, F. Perret, A. W. Coleman, J.-P. Morel and N. Morel-Desrosiers, submitted for publication.
11 V. Ball, M. Winterhalter, P. Schwinte, Ph. Lavalle, J.-C. Voegel and P. Schaaf, submitted for publication..
12 M. M. Andersson and R. Hatti, *J. Biotechnol.*, 1999, **72**, 21.
13 L. Piculell and B. Lindman, *Adv. Colloid Interface Sci.*, 1992, **41**, 149.
14 J. L. Atwood, D. L. Clark, R. K. Juneja, G. W. Orr, K. D. Robinson and R. L. Vincent, *J. Am. Chem. Soc.*, 1992, **114**, 7558.

CHEMCOMM Communication
www.rsc.org/chemcomm

Tetra-*N*-propylammonium perruthenate: a case study in catalyst recovery and re-use involving tetraalkylammonium salts

Steven V. Ley,* Chandrashekar Ramarao and Martin D. Smith

University Chemical Laboratories, Lensfield Road, Cambridge, UK CB2 1EW.
E-mail: svl1000@cam.ac.uk

Received (in Cambridge, UK) 3rd September 2001, Accepted 13th September 2001
First published as an Advance Article on the web 18th October 2001

The use of tetraalkylammonium salts or imidazolium ionic liquids in catalytic oxidations of alcohols with tetra-*N*-propylammonium perruthenate allows recovery and reuse of the oxidant; this concept may find application in the recovery of other homogenous catalysts.

The application of reagents in sub-stoichiometric quantities to perform fundamental transformations is one of the cornerstones upon which modern organic chemistry is constructed. This approach, *via* either heterogeneous or homogeneous catalysis, is environmentally and economically advantageous although there are well-documented problems associated with the removal of homogenous catalysts from reaction mixtures. Methods to circumvent this issue generally rely on covalent attachment of catalytic materials to polymeric backbones;[1] this approach has proven to be effective in certain cases but necessitates modification of the catalyst structure and this can lead to a loss of efficacy.[2] Ionic liquids have been proposed as 'green' solvents for organic synthesis due to the ease with which they can be recycled and reused whilst offering an inert, dipolar media compatible with much of conventional chemistry.[3] These properties have been reflected in their use in a range of reactions including Suzuki cross-couplings,[4] Heck reactions,[5,6] oxidation processes[7,8] and Diels–Alder reactions.[9,10] Recent reports of their utility in the immobilisation of transition metal catalysts[11] prompted us to extend these investigations to encompass reagents for the selective oxidation of alcohols. The use of tetra-*N*-propylammonium perruthenate (TPAP) as a homogenous and versatile reagent for the catalytic oxidation of alcohols has previously been reported;[12] in this communication we disclose a system that permits recycling and reuse of TPAP. A recent report describes attempts to develop a recyclable variant of TPAP through its entrapment in a complex sol–gel matrix; this method severely curtails the activity of the catalyst relative to solution-phase TPAP.[13] Our initial investigations centred on the use of imidazolium ionic liquids to permit immobilisation of the ruthenium catalyst, Table 1. TPAP oxidation (10 mol%) of benzyl alcohol in CH_2Cl_2 in the presence of 1-ethyl-3-methyl-1*H*-imidazolium hexafluorophosphate ([emim][PF_6]) and pre-dried *N*-methylmorpholine *N*-oxide (NMO) as co-oxidant proceeded smoothly; when the reaction was deemed to be complete (*via* TLC), diethyl ether was added to the solution with stirring. The insolubility of solid [emim][PF_6] in ethereal solvents results in sequestration of the catalyst, observed as the

Table 1 Oxidation of alcohols with TPAP in the presence of [emim][PF_6] or Et_4NBr†

Substrate	Run	Method	Reaction time	Conversion[a] (isolated)	Method	Reaction time	Conversion[a] (isolated)
	**1**	**A**‡	20 min	>95 (96)	**B**§	5 min	>95 (95)
	2		30 min	>95 (94)		30 min	>95 (96)
	3		30 min	>95 (95)		30 min	>95 (93)
	4		30 min	>95 (98)		30 min	>95 (97)
	5		40 min	>95 (94)		50 min	>95 (93)
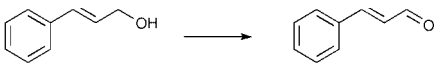	**1**	**A**‡	1 h	>95 (95)	**B**§	30 min	>95 (95)
	2		3 h	>95 (88)		3 h	>95 (95)
	3		9 h	>95 (85)		12 h	>95 (95)
	4		16 h	70		30 h	85
	5		3 days	85		—	—
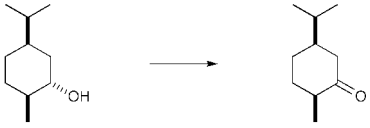	**1**[b]	**A**‡	2.5 h	>95 (89)	**B**§	2 h	>95 (84)
	2		24 h	40		3 h	>95 (87)
	3		—	—		3 days	66
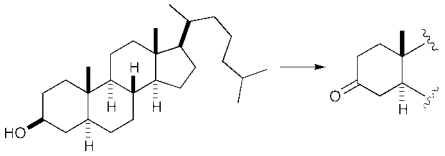	**1**[bc]	**A**‡	15 min	>95 (94)	**B**§	1 h	>95 (96)
	2		3 h	>95 (86)		3 h	>95 (93)
	3		5 h	>95 (96)		24 h	68
	4		24 h	54			
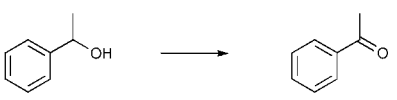	**1**	**B**§	20 min	>95 (96)	**C**¶	6 h	>95 (99)
	2		1 h	>95 (94)		12 h	>95 (97)
	3		7 h	82		16 h	>95 (98)
	4		12 h	56		16 h	75
	5		3 days	33		16 h	52
	6		—	—		2 days	>95 (96)

[a] Determined by 400 MHz ^{1}H NMR spectroscopy.[b] In the presence of 4 Å sieve contained in an Irori MicroKan™ reactor.[c] Performed on a 1 mmol scale.

 DOI: 10.1039/b107966m

precipitation of a black–green suspension. The clear supernatant liquid containing the oxidation products can be recovered by simply decanting and the remaining solid containing the ruthenium catalyst can be reused after drying. It was found that reuse of the catalyst was viable when applied to the oxidation of trivial substrates such as benzyl alcohol; the reaction was repeated five times without significant loss of catalytic activity. Similar results were obtained with cinnamyl alcohol but a significant slowing of the reaction was observed during the fourth recycling. Although these results were encouraging, the high cost of this particular imidazolium species[14] prompted us to search for an alternative and it was reasoned that the use of another weakly coordinating salt such as a tetraalkylammonium halide could be appropriate. Tetraalkylammonium halides have been utilized as molten salts at elevated temperatures (T > 150°C) in non-aqueous Heck reactions[15] and are cheap and readily available.[16] Oxidation of benzyl alcohol with TPAP under standard conditions (10 mol% catalyst, CH_2Cl_2, NMO, RT) in the presence of tetraethylammonium bromide (prepared by pre-drying under vacuum) afforded benzaldehyde in essentially quantitative yield. Recovery and reuse of the catalyst was found to be simple *via* the procedure described previously; the catalyst could be reused five times for simple oxidations such as this without any noticeable loss of activity. Oxidation of cinnamyl alcohol proceeded smoothly in yields comparable to those achieved with the imidazolium salt. After three recycles, however, there was a noticeable loss of activity culminating in only 85% conversion after 30 h reaction time.[17] The reasons for this loss of activity are not clear, although it has been postulated that black insoluble material produced during these oxidations could be colloidal ruthenium.[18] In an attempt to ascertain the scope and limitations of these conditions, the oxidation of a non-activated secondary alcohol was also attempted. The oxidation of menthol was rapid and high yielding for two catalyst repetitions in the presence of Et_4NBr but the reaction slowed significantly afterwards with only 66% conversion being observed after 3 days. This was still superior to the results observed with the use of the imidazolium species. The conversion of dihydrocholesterol to dihydrocholesterone was also successful in the presence of both alkylammonium and imidazolium salts. Similarly good results were obtained with the oxidation of *sec*-phenethyl alcohol; the starting material was rapidly and quantitatively oxidized to acetophenone, and the procedure could be repeated without incident. Encouraged by the outcome of these reactions, it was decided to examine the aerobic co-oxidation of TPAP in an attempt to enable isolation of the products without the need for separation from a co-oxidant. Aerobic co-oxidation of ruthenium(VII) derivatives has been reported in oxygenated toluene at 80°C.[18–20] However, these conditions were found to lead to catalyst decomposition and hence incomplete oxidation. In contrast, performing the reaction under moderate oxygen pressure (30–40 bar) in dichloromethane at room temperature resulted in rapid, clean oxidation of *sec*-phenethyl alcohol. Repetition of this process could also be achieved, and three cycles were performed with consistently good catalyst performance. The reaction was stopped after 16 h to gauge the extent of reaction in both the fourth and fifth recycles and showed that the activity of the catalyst was declining over time. If extended reaction times were employed, however, it was found that complete conversion to the ketone was still attained.

In this paper it has been demonstrated that both Et_4NBr and [emim][PF_6] may be used to enable the recovery and reuse of tetra-*N*-propylammonium perruthenate. The ease with which this procedure can be employed for oxidations with oxygen or *N*-methylmorpholine *N*-oxide as co-oxidant augurs well for its application in clean synthetic procedures.

We would like to thank Syngenta for a postdoctoral fellowship (to CR), Pembroke College, Cambridge for a fellowship (to MDS) and the Novartis Research fellowship (to SVL).

Notes and references

† As with all TPAP oxidations, care should be exercised upon addition of the oxidant to reaction mixtures as heat may be evolved. Mixing of neat ionic liquids and TPAP is not recommended; it has been observed that this reaction can be violent and exothermic.‡ Method A: representative procedure: TPAP (0.25 mmol) was added cautiously to a stirring solution of alcohol (2.5 mmol), *N*-methylmorpholine *N*-oxide (3.75 mmol) and [emim][PF_6] (0.5 g) in CH_2Cl_2 (5 mL). The solution was stirred at RT under an atmosphere of argon until TLC indicated the completion of the reaction. Et_2O (40 mL) or petroleum ether (40 mL) was added and the mixture vigorously stirred for 10 min. The mixture was allowed to stand for 5 min when the clear supernatant liquid was decanted (through a filter paper), concentrated and filtered through a plug of silica gel (10 mm × 10 mm), eluting with Et_2O to afford *the aldehyde or ketone*. The catalyst mixture was dried under vacuum before reuse.

§ Method B: representative procedure: as for method A but with tetra-*N*-ethylammonium bromide in place of [emim][PF_6].

¶ Method C: representative procedure: TPAP (0.25 mmol) was added cautiously to a stirring solution of alcohol (2.5 mmol) and Et_4NBr (0.5 g) in CH_2Cl_2 (5 mL). The solution was stirred at RT under an atmosphere of oxygen (40 Bar) until TLC indicated the completion of the reaction. Et_2O (40 mL) was added and the mixture vigorously stirred for 10 min. The mixture was allowed to stand for 5 min when the clear supernatant liquid was decanted (through a filter paper) and concentrated to afford *the aldehyde or ketone*. The catalyst mixture was dried under vacuum before reuse.

1 S. V. Ley, I. R. Baxendale, R. N. Bream, P. S. Jackson, A. G. Leach, D. A. Longbottom, M. Nesi, J. S. Scott, R. I. Storer and S. J. Taylor, *J. Chem. Soc., Perkin Trans. 1*, 2000, 3815.
2 B. Clapham, T. S. Reger and K. D. Janda, *Tetrahedron*, 2001, **57**, 4637.
3 K. R. Seddon, *J. Chem. Technol. Biotechnol.*, 1997, **68**, 351.
4 C. J. Mathews, P. J. Smith and T. Welton, *Chem. Commun.*, 2000, 1249.
5 A. J. Carmichael, M. J. Earle, J. D. Holbrey, P. B. McCormac and K. R. Seddon, *Org. Lett.*, 1999, **1**, 997.
6 V. Calo, A. Nacci, L. Lopez and N. Mannarini, *Tetrahedron Lett.*, 2000, **41**, 8973.
7 J. Howarth, *Tetrahedron Lett.*, 2000, **41**, 6627.
8 G. S. Owens and M. M. Abu-Omar, *Chem. Commun.*, 2000, 1165.
9 M. J. Earle, P. B. McCormac and K. R. Seddon, *Green Chem.*, 1999, **1**, 23.
10 T. Fischer, A. Sethi, T. Welton and J. Woolf, *Tetrahedron Lett.*, 1999, **40**, 793.
11 C. E. Song and E. J. Roh, *Chem. Commun.*, 2000, 837.
12 S. V. Ley, J. Norman, W. P. Griffith and S. P. Marsden, *Synthesis*, 1994, 639.
13 M. Pagliaro and R. Ciriminna, *Tetrahedron Lett.*, 2001, **42**, 4511.
14 Price for [emim][PF_6]: £88.40 for 5 g (Aldrich, 2001).
15 W. A. Herrmann and V. P. W. Bohm, *J. Organomet. Chem.*, 1999, **572**, 141.
16 Price for Et_4NBr: £38.70 for 1 kg (Aldrich, 2001).
17 Upon mixing TPAP and the imidazolium species in CH_2Cl_2, formation of an uncharacterised insoluble black precipitate was observed. In our hands this material did not catalyze the oxidation of alcohols.
18 I. Marko, A. Gautier, I. Chelle-Regnaut, P. R. Giles, M. Tsukazaki, C. J. Urch and S. M. Brown, *J. Org. Chem.*, 1998, **63**, 7576.
19 R. Lenz and S. V. Ley, *J. Chem. Soc., Perkin Trans. 1*, 1997, 3291.
20 B. Hinzen, R. Lenz and S. V. Ley, *Synthesis*, 1998, 977.

CHEMCOMM Communication
www.rsc.org/chemcomm

Luminescence and photocatalytic properties of a platinum(II)–quaterpyridine complex incorporated in Nafion membrane

Xiao-Hong Li,[a] Li–Zhu Wu,*[a] Li–Ping Zhang,[a] Chen-Ho Tung[a] and Chi-Ming Che[b]

[a] *Technical Institute of Physics and Chemistry, The Chinese Academy of Sciences, Beijing 100101, China. E-mail: g217@ipc.ac.cn*

[b] *Department of Chemistry and the HKU-CAS Joint Laboratory on New Materials, The University of Hong Kong, Pokfulam Road, Hong Kong*

Received (in Cambridge, UK) 26th June 2001, Accepted 19th September 2001
First published as an Advance Article on the web 11th October 2001

The non-emissive platinum(II)–quaterpyridine complex shows strong photoluminescence at room temperature upon incorporation into Nafion membrane; this complex is stabilized toward photochemical decomposition in Nafion even in the presence of oxygen, and can be used as a sensitizer to generate singlet oxygen to oxidize alkenes.

Luminescent square planar d^8 platinum(II)–polypyridine complexes may oligomerize in solution leading to supramolecular architectures whose photophysical properties can be used to elucidate ligand–ligand (π–π) and metal–metal interactions.[1–4] However, in many cases they are weak emitters or even non-emissive in fluid solution at room temperature.[1–5] Thus, many researchers have diverted their attention to exploit new complexes which show strong luminescence at room temperature.[4–6] Here we report an approach to enhance the room-temperature luminescence from Pt(II)–polypyridine complexes. Our approach involves the use of Nafion membrane as the rigid matrix. Upon incorporation into the membrane, the non-emissive platinum(II)–quaterpyridine complex $[Pt(QP)](CF_3SO_3)_2$ (QP = 2,2′:6′,2″:6″,2‴-quaterpyridine) exhibits strong photoluminescence at room temperature. Furthermore, this complex in Nafion is stable and can be used as a photosensitizer to generate singlet oxygen.

Nafion represents a family of polymers which consists of a perfluorinated backbone and short pendant chains terminated by sulfonic groups. When swollen in water, the structure of Nafion is believed to resemble that of an inverse micelle.[7] The water-swollen Nafion can incorporate high concentrations of organic and inorganic compounds, thus raising the possibility of obtaining high local concentrations of substrates. The complex $[Pt(QP)](CF_3SO_3)_2$ was successfully incorporated into water-swollen Nafion (in sodium form, Nafion-Na^+) by immersing the membrane samples in an aqueous suspension of the platinum complex. The concentration of the platinum complex in the membrane was measured by its absorption spectrum, assuming that the absorption spectra obey Beer's law in the concentration range studied. Although this complex has a low solubility in water, its concentration in the water-swollen Nafion-Na^+ can be rather high (*ca.* 2×10^{-5} mol/g Nafion). It is likely that the molecules of this complex are primarily solubilized in the hydrophobic perfluorocarbon backbone region close to the fluorocarbon/water interface.

The absorption spectrum of $[Pt(QP)](CF_3SO_3)_2$ in acetonitrile has been described previously by one of the authors.[8] This complex shows intense absorption bands in the high-energy region ($\lambda < 325$ nm) which are assigned to intraligand ^{1}IL(π, π*) transitions, and moderately intense low-energy bands ranging from 320 to 370 nm which can be assigned to spin-allowed metal-to-ligand charge-transfer transitions (^{1}MLCT) involving a dπ platinum orbital as the donor orbital and π* quaterpyridine orbital as the acceptor orbital. Upon incorporation into Nafion membrane, all of the absorption bands are slightly blue-shifted (*ca.* 2 nm) compared with those in acetonitrile solution. Furthermore, weak absorption bands from 375 to 450 nm were observed at high complex loading level and attributed to the absorption of oligomerized species based on the fact that excitation with light in this wavelength region exclusively leads to excimeric emission (see below).

At room temperature, a degassed acetonitrile solution of $[Pt(QP)](CF_3SO_3)_2$ shows no emission upon excitation at 358 nm due to molecular distortion which results in nonradiative decay. This situation is quite different when the complex is incorporated into Nafion membrane. In water-swollen Nafion membrane and in a nitrogen atmosphere, this complex shows a very weak emission. However, after removal of the absorbed water by evaporation under vacuum, the dry complex–Nafion sample exhibits a strong luminescence in a nitrogen atmosphere. Possibly, the rigid matrix in dry Nafion causes the deactivation process *via* molecular distortion to be blocked. Fig. 1 shows the emission spectra of dry Nafion samples at room temperature. At low complex loading (*ca.* 1×10^{-7} mol/g Nafion) the Nafion sample shows a structured emission with λ_{max} at 476, 513 and 544 nm. and lifetime of *ca.* 3.42 μs. The long emission lifetime suggests that the transition involved is a spin-forbidden process. The vibrational progression is *ca.* 1330 cm^{-1}, which corresponds to the C=C and C=N stretching modes, the dominant high-frequency acceptor modes of LC levels involving polypyridine-type ligands.[5] Thus, this emission is assigned to be associated to the ^{3}IL (π, π*) state of the coordinated quaterpyridine ligand. At high loading a broad emission band centered at 600 nm (τ = 2.58 μs) prevails in addition to the structured ^{3}IL emission (Fig. 1). The broad

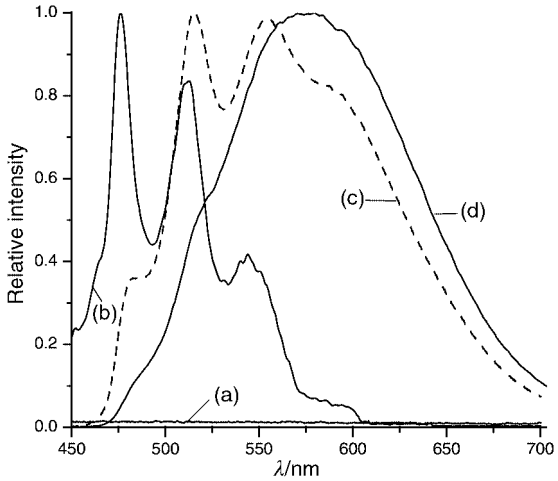

Fig. 1 The normalized emission spectra of $[Pt(QP)](CF_3SO_3)_2$ incorporated in Nafion at different concentrations and excitation wavelength: (a) in acetonitrile, 1×10^{-5} M, λ_{ex} = 358 nm; (b) in Nafion, 1×10^{-7} mol/g Nafion, λ_{ex} = 358 nm; (c) in Nafion, 1.4×10^{-5} mol/g Nafion, λ_{ex} = 358 nm; (d) in Nafion, 1.4×10^{-5} mol/g Nafion, λ_{ex} = 410 nm.

 DOI: 10.1039/b105601h

Table 1 Photooxidation of alkenes sensitized by Nafion-incorporated $[Pt(QP)](CF_3SO_3)_2$ (7.02×10^{-6} mol/g Nafion) in acetonitrile solution.

Substrate	Photoirradiation time/h	Product	Yield (%)[c]
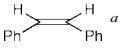 [a]	5	PhCHO	100
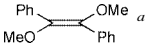 [a]	2	$PhCO_2Me$	100
 [b]	5	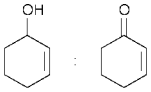	18:82

[a] The concentration is 10^{-2} M. [b] The concentration is 10^{-1} M. [c] Yields were calculated based on the consumption of the substrates.

emission overlaps on the ^{3}IL emission when the complex is excited with light of wavelength < 375 nm. However, the broad emission becomes dominant at an excitation wavelength > 380 nm (Fig. 1). Since this broad emission occurs only at high loading, it is attributed to excimeric species originating from π–π interactions between the partially stacked quaterpyridine ligands in the oligomers. In other words, the broad emission originates from excitation of the oligomerized species, differently from the ^{3}IL emission which originates from excitation of the 'isolated' monomers. The oligomerization of square planar d^8 metal complexes has been well precedented.[1–6]

The rigid matrix of Nafion stabilizes the $[Pt(QP)](CF_3SO_3)_2$ complex towards photochemical decomposition. At room temperature in aerated acetonitrile solution, this complex is photochemically unstable. For example, photoirradiation of the solution within 2 h resulted in a significant decrease in absorption. However, photolysis of the complex in dry Nafion membrane immersed in acetonitrile led to no change in the absorbance of $[Pt(QP)](CF_3SO_3)_2$ over a period of 10 h. The matrix-stabilized complex was used as a photosensitizer to generate singlet oxygen and to oxidize alkenes such as *trans*-stilbene, *trans*-1,2-dimethoxystilbene and cyclohexene. The photosensitized oxidations were carried out in oxygen-saturated solution of the substrate in acetonitrile in which $[Pt(QP)](CF_3SO_3)_2$ incorporated Nafion membranes were suspended. Photoirradiation of the complex yields the photooxidation products as shown in Table 1. All the products were identified by GC–MS. Significantly, the platinum complex–Nafion sample was easily separated from the solution, and could be used for many cycles without loss of activity. We propose that this photooxidation of alkenes proceeds *via* singlet oxygen mechanism. Acetonitrile can moderately swell the complex–incorporated Nafion membrane and thus enables oxygen to diffuse into the membrane from the solvent. Interaction between oxygen and the ^{3}IL excited state of the complex results in energy transfer to generate singlet oxygen, which diffuses back to the solution to oxidize the alkenes. This proposal is supported by EPR spectroscopy. It has been established that 2,2,6,6-tetramethylpiperidine (TMP) reacts with singlet oxygen to give the stable free radical nitroxide, which can be readily detected by EPR spectroscopy.[9] Thus, we dissolved TMP in oxygen-saturated acetonitrile, and immersed the complex-incorporated Nafion membrane in the solution. Fig. 2 shows the EPR spectrum obtained after 400 s irradiation of the solution and clearly evidenced the nitroxide free radical. This obsevation shows that singlet oxygen was generated in the Nafion membrane and diffused into the solution to react with TMP to give the nitroxide radical.

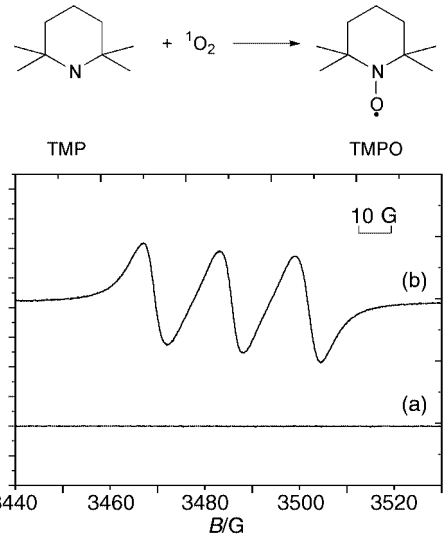

Fig. 2 EPR spectrum of nitroxide radical generated by irradiation of the Nafion-incorporated complex immersed in an oxygen-saturated acetonitrile solution of TMP: (a) in the dark; (b) after the sample was irradiated for 400 s.

Financial support from the Ministry of Science and Technology of China (grant No. G2000078104 and No. G2000077502) and the National Nature Science Foundation of China are gratefully acknowledged. We also acknowledge support from the University of Hong Kong and the Hong Kong Research Grants Council [HKU7298/99P].

Notes and references

1 J. A. Bailey, M. G. Hill, R. E. Marsch, V. M. Miskowski, W. P. Schaefer and H. B. Gray, *Inorg. Chem.*, 1995, **34**, 4591.
2 D. G. Nocera, *Acc. Chem. Res.*, 1995, **28**, 209.
3 S. D. Cummings and R. Eisenberg, *Inorg. Chem.*, 1995, **34**, 2007.
4 M. G. Hill, J. A. Bailey, V. M. Miskowski and H. B. Gray, *Inorg. Chem.*, 1996, **35**, 4585.
5 G. Arena, G. Calogero, S. Campagna, L. Monsù Scolaro, V. Ricevuto and R. Romeo, *Inorg. Chem.*, 1998, **37**, 2763.
6 L. Z. Wu, T. C. Cheung, C. M. Che, K. K. Cheung and M. H. W. Lam, *Chem. Commun.*, 1998, 1127.
7 C. H. Tung and J. Q. Guan, *J. Am. Chem. Soc.*, 1998, **120**, 11874 and references therein..
8 C. W. Chan and C. M. Che, *Inorg. Chem.*, 1992, **31**, 4874.
9 H. R. Li, L. Z. Wu and C. H. Tung, *J. Am. Chem. Soc.*, 2000, **122**, 2446 and references therein..

CHEMCOMM
Communication
www.rsc.org/chemcomm

Super-microporous organic-integrated silica prepared by non-electrostatic surfactant assembly

Mark D. McInall,[a] Jennifer Scott,[a] Louis Mercier*[a] and Patricia J. Kooyman[b]

[a] *Department of Chemistry and Biochemistry, Laurentian University, Sudbury, Ontario, Canada P3E 2C6*

[b] *National Centre for High Resolution Electron Microscopy, Delft University of Technology, Delft, The Netherlands*

Received (in Purdue, IN, USA) 28th June 2001, Accepted 24th September 2001
First published as an Advance Article on the web 11th October 2001

Hybrid organo-silica materials possessing uniform nanoscale porosity in the super-micropore size range (1.0–2.0 nm diameter) have been prepared using neutral alkylamine and non-ionic alkyl(phenyl)polyethylene oxide surfactants as structure-directing agents.

The preparation of functionalized derivatives of surfactant-assembled nanoporous silica (including MCM-41,[1] HMS,[2] MSU-X[3,4] and SBA[5]) has been achieved by the incorporation of various moieties inside the pore channels of these mesostructures.[6] Recently, the reported syntheses of new mesostructures (designated HMM,[7] UOFMN,[8] PMO[9,10] or BSQM[11]) in which organic groups are integrated *within* the framework of mesoporous materials has opened up new prospects for the design of functional materials with uniform framework porosity.[7–13]

Reported methods to prepare organic-integrated mesostructures have thus far tended to produce materials with large mesoscale pore channels (>2.0 nm). It has been suggested that this pore size range may be too large to allow useful size- and shape-based separation/catalytic applications, and that materials possessing uniform-sized pores in the 1.0–2.0 nm size range (the *super-micropore* regime) may be better suited for such tasks.[14] Unfortunately, relatively few materials with uniform pore channels in this size domain have been described.[14]

Super-microporous hybrid organo-silica materials (hereafter designated Laurentian University Organic-Integrated Silica, or LUOIS) were synthesized using alkylamine surfactants[2] and bis(triethoxysilyl)ethane [$(EtO)_3Si–CH_2CH_2–Si(OEt)_3$, BTSE], producing organo-silica analogs of HMS silica. One such material, designated HMS-OIS-C8, was prepared by stirring BTSE (6.6 mmol) in an aqueous solution of octylamine (2.9 mmol in 25 mL water) for 24 h. Another LUOIS, denoted HMS-OIS-C12, was synthesized by stirring BTSE (7.6 mmol) in a solution of dodecylamine (3.4 mmol in 45 mL water and 5 mL ethanol) with trimethylbenzene (TMB, 3.4 mmol) for 24 h. LUOIS materials were also prepared by non-ionic surfactant assembly (*i.e.* N^0I^0),[3,4] producing organo-silica analogs of MSU-X silica. The first of these, hereafter designated MSU-2-OIS(N), was prepared by stirring BTSE (2.7 mmol) in a neutral pH solution of Triton-X100 non-ionic surfactant (0.68 mmol in 25 mL water) until a completely clear solution was obtained (12–24 h), after which NaF (0.22 mmol) was added to catalyze the silicate cross-linking and subsequent precipitation of the final product. Two other materials, MSU-2-OIS(A) and MSU-1-OIS(A), were prepared by stirring BTSE (2.7 mmol) in aqueous solutions of Triton-X100 and Brij-76 non-ionic surfactants (0.68 mmol in 25 mL water), respectively, to which was added HCl (0.2 mol L^{-1}) until the final pH reached 4.0 and 5.0, respectively. After ageing for 4 h, NaF (0.22 mmol) was added to form the solid product. For the purpose of comparison, purely siliceous samples of HMS, MSU-1 and MSU-2 were also prepared by replacing BTSE with a bimolar amount of TEOS in each of the previously outlined synthesis procedures. The LUOIS materials and their pure silica counterparts were washed free of surfactant by Soxhlet extraction over ethanol, and then characterized by powder X-ray diffraction (XRD), solid-state ^{29}Si and ^{13}C NMR spectroscopy, N_2 sorptometry and transmission electron microscopy (TEM).

The XRD patterns of all the LUOIS materials featured single diffraction peaks at low 2θ diffraction angles (in the range 1.8–2.4°), suggestive of mesostructures with uniform wormhole-motif pore channels.[2–4] ^{29}Si MAS NMR spectra of the samples in all cases showed two signals at -63 and -58 ppm which can be assigned to T^3 [*i.e.* $–CH_2–Si(OSi)_3$] and T^2 [$–CH_2–Si(OSi)_2OH$] sites, respectively. This observation, in addition to the absence of any Q^4 [*ca.* -110 ppm, $Si(OSi)_4$] and Q^3 signals [*ca.* -100 ppm, $Si(OSi)_3OH$] in these spectra, attests to the hydrolytic stability of the Si–C bonds under the synthesis conditions used to prepare these materials. TEM images of the LUOIS materials confirmed the wormhole-motif structure (Fig. 1), and showed that their pore channels were quite uniform in size.

The pore diameters of the LUOIS materials were, however, much smaller than those of purely siliceous mesostructures, in the super-micropore size range (10–20 Å, Table 1, Fig. 2). The pore structures and diameters of LUOIS materials distinguish these structures from previously reported hybrid mesostructures,[7–13] which typically possess pore channels with diameters similar to those of electrostatically-assembled mesostructures such as MCM-41 (20–30 Å).[7–13] Extensive TEM investigation of the LUOIS materials verified that the porous domains of the materials were extensive and that they contained very little or no amorphous xerogel phases. The surface areas and framework mesopore volumes of the LUOIS materials (calculated from their N_2 adsorption isotherms) were very high

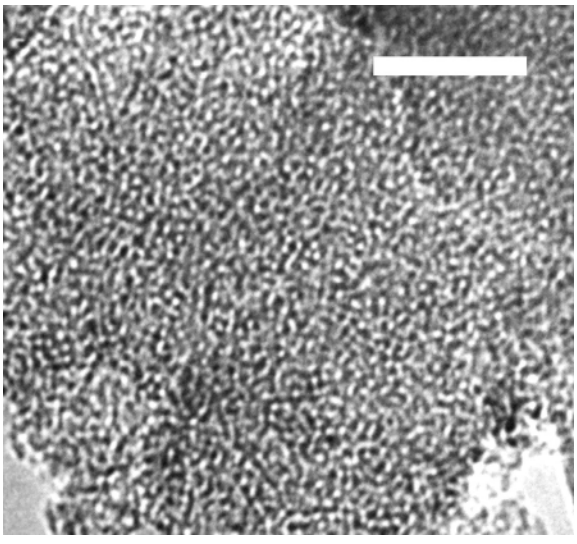

Fig. 1 Representative transmission electron micrographs of a LUOIS hybrid organo-silica mesostructure (HMS-OIS-C12). The white scale bar corresponds to 30 nm.

 DOI: 10.1039/b105718a

Table 1 Physical and surface characteristics of silica mesostructures and their LUOIS analogs

Material	Synthesis pH	*d*-Spacing[a]/Å	BET surface area/m^2 g^{-1}	Pore volume/cm^3 g^{-1}	Pore diameter[b]/Å	Wall thickness[c]/Å
HMS-C8	*ca.* 10	30.9	1345	0.59	22	9
HMS-OIS-C8	*ca.* 10	36.4	926	0.46	(*ca.* 13)	*ca.* 23
HMS-C12	*ca.* 8	42.8	964	0.87	34	9
HMS-OIS-C12	*ca.* 8	43.8	812	0.46	(*ca.* 17)	*ca.* 27
MSU-2(N)	7.0	46.9	1089	0.56	29	18
MSU-2-OIS(N)	7.0	46.9	738	0.33	20	27
MSU-2(A)	4.0	42.0	1227	0.75	30	12
MSU-2-OIS(A)	4.0	39.4	1058	0.47	(*ca.* 10)	*ca.* 29
MSU-1(A)	5.0	51.0	1225	0.77	32	19
MSU-1-OIS(A)	5.0	55.0	818	0.44	16	38

[a] *d*-Spacings = d_{100} (from XRD patterns).[b] Pore sizes were calculated using the Broekhoff–DeBoer pore size distribution model (> 20 Å),[15] or the BJH model (≤20 Å). Pore diameters in parentheses were estimated from TEM micrographs of the samples.[c] Wall thickness = *d*-spacing − pore diameter.

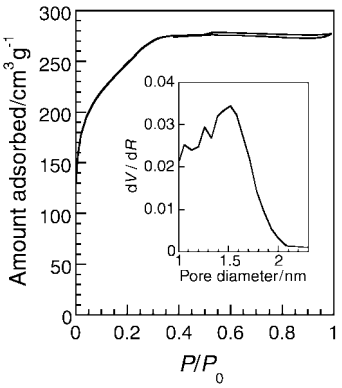

Fig. 2 Nitrogen adsorption–desorption isotherm and pore size distribution (inset) of a LUOIS material (MSU-1-OIS).

(Table 1), as is characteristic of most surfactant-assembled mesostructures.[1–14] The isotherms, however, do not usually exhibit the sharp Type IV inflexion typically observed for pure silica mesostructures. They instead exhibit Type I-like isotherms which are likely due to the microporous dimensions of the pore channels (< 20 Å) (Fig. 2). Despite having comparable framework lattice spacings to those of their pure silica counterparts (Table 1), the smaller pore diameters of the LUOIS materials suggests that these mesostructures have considerably thicker framework walls, lower surface areas and diminished pore volumes than those of pure silica mesostructures (Table 1).

That the LUOIS materials have smaller pore channel diameters than their electrostatically-assembled UOFMN/HMM/PMO counterparts can be related to the different assembly mechanisms involved in the formation of these various materials. The framework-forming precursors of UOFMN, HMM and PMO are expected to be negatively charged (owing to the high assembly pH of their synthesis) and thus strongly bound by electrostatic interaction with the cationic head groups of the alkylammonium surfactant micelles (*i.e.* S^+I^- assembly). This leads to the formation of materials which are structurally similar to pure silica mesostructures (*e.g.* MCM-41) prepared under similar conditions. In contrast, the precursors of the LUOIS materials are likely to be mostly uncharged under the synthesis conditions used, and are thus weakly interacting with the head groups of the surfactants (*viz.* by H-bonding) through S^0I^0 and N^0I^0 assembly interactions.[2,3] Moreover, these BTSE-based precursors are much more hydrophobic than the pure silica precursors involved in the formation of pristine HMS and MSU-X materials. Hence, we postulate that the combined effect of precursor hydrophobicity and the weak interaction between the precursors and micelle head groups results in the penetration of some of these precursors within the hydrophobic core of the surfactant micelles. Thus, materials with significantly reduced pore diameters are produced upon final condensation of these precursors.

The absence of any surfactant signal in the ^{13}C NMR spectra of the LUOIS materials demonstrates the ability of ethanol extraction to remove all of the assembly surfactant from the as-synthesized materials. In contrast, the acid extraction technique used for the electrostatically-assembled UOFMN materials failed to remove the surfactant entirely from the pore channels.[8] The weak surfactant–framework interaction apparent in the LUOIS materials is thus conducive for the preparation of compositionally pure organic-integrated nanoporous silica.

The integration of functional groups within the frameworks of mesostructured oxides can be useful for a wide variety of potential applications (*i.e.*, shape-selective adsorption and catalysis). Non-electrostatic assembly methodologies provide the required flexibility to prepare organic-integrated mesostructures with controlled pore sizes in both the supermicropore and mesopore size regimes, and may allow the successful incorporation of functional groups (such as highly electrophilic moieties) that may be unstable in the harsh, highly basic/acidic conditions typically used in electrostatic organosilica preparations.[7–13]

M. M., J. S. and L. M. would like to thank the Natural Sciences and Engineering Research Council of Canada (NSERC) for financial support. P. J. K. also wishes to acknowledge the support of the NWO (The Netherlands). We also gratefully acknowledge Collin Kowalchuk (University of Western Ontario) for providing the NMR spectra of the samples. Finally, we thank Dr Stephen Bagshaw for helpful discussions.

Notes and references

1 C. T. Kresge, M. E. Leonowicz, W. J. Roth, J. C. Vartuli and J. S. Beck, *Nature*, 1992, **359**, 710.
2 P. T. Tanev and T. J. Pinnavaia, *Science*, 1995, **267**, 865.
3 S. A. Bagshaw, E. Prouzet and T. J. Pinnavaia, *Science*, 1995, **269**, 1242.
4 C. Boissiere, A. van der Lee, A. El Mansouri, A. Larbot and E. Prouzet, *Chem. Commun.*, 1999, 2047.
5 D. Zhao, Q. Huo, J. Feng, B. F. Chmelka and G. D. Stucky, *J. Am. Chem. Soc.*, 1998, **120**, 6024.
6 K. Moller and T. Bein, *Chem. Mater.*, 1998, **10**, 2950.
7 S. Inagaki, S. Guan, Y. Fukushima, T. Ohsuna and O. Terasaki, *J. Am. Chem. Soc.*, 1999, **121**, 9611.
8 B. J. Melde, B. T. Holland, C. F. Blanford and A. Stein, *Chem. Mater.*, 1999, **11**, 3302.
9 T. Asefa, M. J. MacLachlan, N. Coombs and G. A. Ozin, *Nature*, 1999, **402**, 867.
10 C. Yoshina-Ishii, T. Asefa, M. J. MacLachlan, N. Coombs and G. A. Ozin, *Chem. Commun.*, 2000, 2539.
11 Y Lu, H. Fang, N. Doke, D. A. Loy, R. A. Assink, D. A. LaVan and C. J. Brinker, *J. Am. Chem. Soc.*, 2000, **122**, 5258.
12 S. Guan, S. Inagaki, T. Ohsuna and O. Terasaki, *J. Am. Chem. Soc.*, 2000, **122**, 5660.
13 T. Asefa, C. Yoshina-Ishii, M. J. MacLachlan and G. A. Ozin, *J. Mater. Chem.*, 2000, **10**, 1751.
14 S. A. Bagshaw and A. R. Hayman, *Chem. Commun.*, 2000, 533.
15 J. C. P. Broekhoff and J. H. de Boer, *J. Catal.*, 1968, **10**, 377.

CHEMCOMM Communication
www.rsc.org/chemcomm

Regioselective synthesis of substituted 3,4-dihydro-2*H*-thiines from α,β-unsaturated oxathiolanes and styrene derivatives

Sébastien Kerverdo,[a] Michel Loiseau,[a] Louisette Lizzani-Cuvelier[a] and Elisabet Duñach*[b]

[a] *Laboratoire Arômes, Synthèses et Interactions, Université de Nice-Sophia Antipolis, 06108 Nice Cedex 2, France*

[b] *Laboratoire de Chimie Bio-organique, UMR CNRS 6001, Université de Nice-Sophia Antipolis, 06108 Nice Cedex 2, France. E-mail: dunach@unice.fr*

Received (in Cambridge, UK) 30th July 2001, Accepted 24th September 2001
First published as an Advance Article on the web

A one-step $TiCl_4$-mediated regiospecific synthesis of thiine derivatives is effected in good yields by a tandem cyclisation-fragmentation reaction.

In the last few years, thiine derivatives have received considerable attention as building blocks in organic synthesis, in particular for the construction of natural product skeletons.[1] The synthesis of six-membered ring sulfur-containing heterocycles may proceed through hetero Diels–Alder-type (HDA) reactions involving either thioaldehydes or thioketones or their α,β-unsaturated analogs, 1-thiabuta-1,3-dienes.[2–4] However, in contrast to the homologous oxygenated substrates, thioaldehydes and their derivatives (unless conveniently substituted by electron-withdrawing substituents[5–7]) present very low stability and tend to dimerise and polymerise easily.[8] In most cases, these highly reactive thio-compounds are not isolated but generated and trapped *in situ* by the diene or the dienophile.[9]

We present here the use of α,β-unsaturated oxathiolanes as precursors for unsaturated thioketone analogs (thienium cations), as heterodienes in Diels–Alder cycloadditions for the construction of α,β-unsaturated thianes, as shown in Scheme 1. To our knowledge, no report on the utilization of oxathiolanes for hetero Diels–Alder reactions has been reported. The related use of other heterocycles for HDA reaction has been recently described.[10]

The reaction of the oxathiolane **1**[11] in the presence of 1 equiv. of $TiCl_4$ in dichloromethane at −48 °C, followed by the addition of styrene, afforded, after hydrolysis by aqueous KOH and purification, 2,4-diphenyl-3,4-dihydro-2*H*-thiine, **3a**, in 65% isolated yield. The cycloaddition was completely regioselective and gave a mixture of two *cis–trans* stereoisomers in a 1 : 1 ratio. The formation of the thiine derivative **3a** occurred with loss of the C_2H_4O fragment of the starting oxathiolane.

This cycloaddition–fragmentation process was extended to several substituted styrene derivatives, and the results and yields of the corresponding thiine derivatives **3** are presented in Table 1.

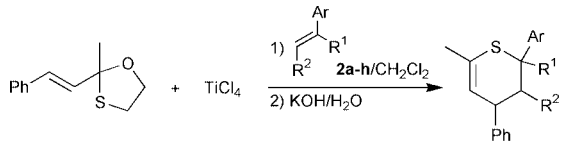

1 **3a-h**

2a, 3a Ar = Ph, R^1 = H, R^2 = H
2b, 3b Ar = Ph, R^1 = H, R^2 = Me
2c, 3c Ar = Ph, R^1 = Me, R^2 = H
2d, 3d Ar = *p*-MePh, R^1 = H, R^2 = H
2e, 3e Ar = *p*-MeOPh, R^1 = H, R^2 = H
2f, 3f Ar = *p*-ClPh, R^1 = H, R^2 = H
2g, 3g Ar = *p*-FPh, R^1 = H, R^2 = H
2h, 3h Ar = Ph, R^1 = Ph, R^2 = H

Scheme 1

A regiospecific reaction occurred in all the examples examined; the aryl group of the styrene derivative always being located at the 2-position of the cyclic sulfide.

A stereoselective cycloaddition was observed with β-methylstyrene **2b** (entry 2), for which the two phenyl groups of **3b** are exclusively *trans* diequatorial. In contrast, α-methylstyrene **2c** (entry 3) afforded **3c** in 76% yield as a 45 : 55 *cis–trans* mixture. *cis–trans* ratios were calculated by ^{1}H-NMR and by GC. The diastereomeric assignments were based on the NOESY ^{1}H-NMR correlations between H-2 and H-4 protons.

Electron-donating (entries 4, 5) as well as electron-deficient substituents (entries 6, 7) on the *para* position of the aryl ring of **2** were compatible with the reaction conditions, and gave the corresponding thiine derivatives **3** with stereoselectivities generally in favor of the *trans* isomer. The *p*-methoxystyrene **2e** led to a poor yield due to its partial polymerisation. The coordination of the methoxy group to Ti(IV) could explain the change in reactivity. Indeed, the formation of **3** did not occur in a coordinating solvent such as Et_2O. It is interesting to note that the presence of a *p*-chloro substituent in **2f** (entry 6) reversed the stereochemical outcome of the reaction.

The reaction of **1** with sterically hindered 1,1-diphenylethylene gave **3h** in 69% isolated yield, after crystallisation in ethanol. Thus, the cyclisation does not seem particularly influenced by the steric hindrance of the substrates. However, no reaction occurred between **1** and oct-1-ene under the reaction conditions.

By the present procedure, 2,4-diaryl substituted dihydrothiapyrans **3** could be prepared for the first time.

The order of addition of the reactants was an important feature of this reaction. When the styrene derivative was added at the beginning of the reaction polymerisation occurred and compound **3** was formed in low yields.

The addition of $TiCl_4$ to **1** led to a poorly stable orange precipitate in dichloromethane at low temperature, which was attributed to the formation of a titanium(IV) alcoholate–thienium cation intermediate of type **A**, presumably involving the cleavage of the C–O bond of the heterocycle (Scheme 2). Upon addition of the styrene derivative, the precipitate slowly disappeared with the plausible formation of an intermediate of type **B**. When the reaction was quenched by aqueous potassium

Table 1 $TiCl_4$-mediated cycloaddition–fragmentation reaction between oxathiolane **1** and substituted styrene derivatives **2**[12]

Entry	Olefin	Time/h	Isolated yield (%) of **3**	Ratio *cis–trans*
1	**2a**	2	65	50 : 50
2	**2b**	10	65	100 : 0
3	**2c**	0.5	76	45 : 55
4	**2d**	1.5	72	20 : 80
5	**2e**	2.5	29	36 : 64
6	**2f**	8	55	57 : 43
7	**2g**	1	43	44 : 56
8	**2h**	5	69	—

 DOI: 10.1039/b106882m

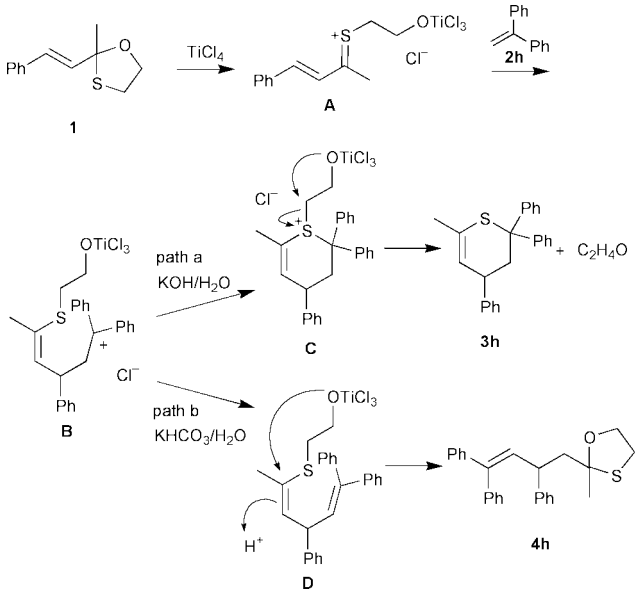

Scheme 2

hydroxide (path a), thiine **3** was formed with fragmentation of the C_2H_4O unit, presumably of ethylene oxide, *via* intermediate **C**. However, upon hydrolysis by aqueous potassium bicarbonate, the 4,5-unsaturated oxathiolane **4h** could be isolated in 25% yield in the case of 1,1-diphenylethylene as the dienophile, *via* path b. To explain the formation of **4h** the intermediate formation of **D** can be proposed.

The *in situ* generation of a thienium salt **A** from stable oxathiolanes in the presence of Lewis acids seems an interesting alternative to 1-thiabuta-1,3-diene equivalents. The formation of a thienium cation intermediate from a dimethyl-substituted six-membered ring oxathiane has also been proposed.[10]

Work is in progress to further extend the cyclisation–fragmentation process to other substrates and to get a better understanding of the mechanism of the reaction.

Notes and references

1 P. Metzner, *Top. Curr. Chem.*, 1999, **204**, 127.
2 L. F. Tieze and G. Kettschau, *Top. Curr. Chem.*, 1997, **189**, 1.
3 T. Saito, M. Kawamura and J. Nishimura, *Tetrahedron Lett.*, 1997, **38**, 3231.
4 T. Saito, K. Takekawa and T. Takahashi, *J. Chem. Soc., Chem Commun.*, 1999, 449.
5 J. Prabhakaran, H. Lhermitte, J. Das, T. K. Sasi-Kumar and D. S. Grierson, *Synlett*, 2000, **5**, 658.
6 I. L. Pinto, D. R. Buckle, H. K. Rami and D. G. Smith, *Tetrahedron Lett.*, 1992, **33**, 7597.
7 A. Marchand, D. Mauger, A. Guingant and J. P. Pradère, *Tetrahedron Asymmetry*, 1995, **6**, 853.
8 K. B. Lipkowitz and B. P. Mundy, *Tetrahedron Lett.*, 1977, **18**, 3417.
9 E. Block and S. H. Zhao, *Tetrahedron Lett.*, 1990, **31**, 5003.
10 K. Nishide, S. Ohsugi and M. Node, *Tetrahedron Lett.*, 2000, **41**, 371.
11 Compound **1** was prepared by a method adapted from the synthesis of G. H. Wilson, M. G. Huang and W. W. Schloman, Jr, *J. Org. Chem.*, 1968, **33**, 2133.
12 Typical procedure for the synthesis of **3**: to a vigorously stirred solution of **1** (1.0 mmol) in dichloromethane (10 ml) at −48 °C under inert atmosphere was added a CH_2Cl_2 solution of titanium tetrachloride (1.0 mmol). After formation of an orange precipitate, the styrene derivative **2** was added dropwise. After the complete disappearance of the precipitate, the solution was quenched with an aqueous solution of potassium hydroxide (1.0 M). The aqueous layer was extracted twice with diethyl ether. The organic layers were dried over $MgSO_4$, and the solvent was removed *in vacuo*. The crude product was purified by silica gel column chromatography with a mixture of hexane–diethyl ether (99 : 1) as the eluent. In the case of **3b** and **3h**, the products were purified by crystallisation in ethanol. The compounds were analysed by ^1H and ^{13}C-NMR, mass spectrometry and HRMS.

CHEMCOMM Communication
www.rsc.org/chemcomm

$[(PPh_3)Ag(CB_{11}H_6Y_6)]$ (Y = H, Br): highly active, selective and recyclable Lewis acids for a hetero-Diels–Alder reaction†

Catherine Hague, Nathan J. Patmore, Christopher G. Frost,* Mary F. Mahon and Andrew S. Weller*

Department of Chemistry, University of Bath, Bath, UK BA2 7AY. E-mail: c.g.frost@bath.ac.uk; a.s.weller@bath.ac.uk

Received (in Cambridge, UK) 25th July 2001, Accepted 1st October 2001
First published as an Advance Article on the web 17th October 2001

The complex $[(PPh_3)Ag(CB_{11}H_6Br_6)]$ 1 is an effective and selective catalyst (0.1 mol% loading) for a hetero-Diels–Alder reaction, which shows a marked dependence on the presence of trace amounts of water, while addition of Ag[Y] [Y = $CB_{11}H_{12}$, $CB_{11}H_6Br_6$, O_3SCF_3] to a phosphine functionalised support gives an efficient and recyclable Lewis acid catalyst for this transformation.

Cationic silver(I)–phosphine complexes have been used as effective promoters for a wide-range of organic transformations including allylation, aldol, ene and glycosylation reactions, asymmetric aldol reactions, Mukaiyama aldol reactions, asymmetric allylations and hetero-Diels–Alder reactions.[1] It is well established that these reactions are accelerated by other Lewis acids (for example; Ti, B, Al and Sn complexes). However, many of these established catalysts are sensitive to air, water and product inhibition and consequently are used in a low substrate/catalyst ratio. The use of silver(I)–phosphine complexes can provide a practical solution to this problem, as many complexes are stable in air and retain activity in the presence of reaction product. Nevertheless, the best examples from the literature routinely employ high catalytic loadings (5–10 mol%) to achieve competitive rates and product yields. We are interested in developing silver(I) Lewis acids partnered with the carborane anion [1-*closo*-$CB_{11}H_{12}]^-$ and derivatives,[2] in the anticipation that the weakly coordinating nature of these anions will reveal enhanced activity for these systems. As the hetero-Diels–Alder reaction is one of the most useful methods for the synthesis of bioactive heterocycles we chose to test the new complexes in this challenging reaction.

We report here the synthesis of two new silver(I)–phosphine complexes containing $[CB_{11}H_{12}]^-$ and $[CB_{11}H_6Br_6]^-$ respectively and their use as efficient catalysts at low loadings for a hetero-Diels–Alder reaction. Additionally, we report that this methodology may be transferred to a solid support with good activity, low leaching and promising recycleability.

Addition of 1 equivalent of PPh_3 to a CH_2Cl_2 solution of $Ag[CB_{11}H_6Br_6]$ or $Ag[CB_{11}H_{12}]$ affords the new complexes $(PPh_3)Ag(CB_{11}H_6Br_6)$ **1** and $(PPh_3)Ag(CB_{11}H_{12})$ **2**, respectively, in good yields after recrystallisation from CH_2Cl_2–hexanes. Both complexes have been fully characterised‡ by multinuclear NMR spectroscopy, microanalysis and X-ray crystallography. In solution the complexes display C_{5v} symmetry in both the ^{11}B and $^1H\{^{11}B\}$ NMR spectra, showing that the $\{AgPPh_3\}^+$ fragment is fluxional over the cage surface, as has been observed previously for other *exo* polyhedrally bound $\{Ag(PPh_3)\}$ fragments.[3] The $^{31}P\{^1H\}$ NMR spectra show a pair of concentric doublets for both **1** and **2**: $J(AgP_{average})$ 715 Hz and $J(AgP_{average})$ 743 Hz, respectively. The solid state structure of complex **1** is shown in Fig. 1.§ In the asymmetric unit, the silver is ligated by one phosphine and the three bromine atoms

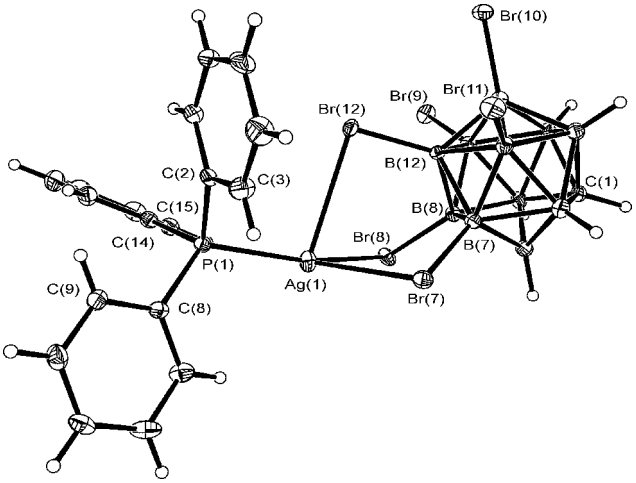

Fig. 1 Solid state structure of complex **1**. Ellipsoids are shown at the 50% probability level. Selected bond lengths (Å) and angles (°): Ag(1)–Br(7) 2.8710(5), Ag(1)–Br(8) 2.6963(5), Ag(1)–Br(12) 3.0953(5), Ag(1)–P(1) 2.4032(10); P(1)–Ag(1)–Br(7) 117.44(3), P(1)–Ag(1)–Br(8) 155.55(3), Br(8)–Ag(1)–Br(7) 87.471(14).

that radiate from the B(7)–B(8)–B(12) triangular face of the cage. Bond lengths and angles are unremarkable, aside from the fact that the silver centre appears to have a vacant site lying roughly opposite to B(12). Examination of the supramolecular structure revealed that this site is filled by a long Ag(1)–Br interaction [Ag(1)–Br(11)′ 3.4901(5) Å], affording a ribbon-like structure in the lattice (ESI†). The asymmetric unit found for **2** is grossly similar to **1**, the $\{AgPPh_3\}$ fragment interacting with the cage through three 3-centre–2-electron Ag–H–B, interactions.

We have investigated the reaction between *N*-benzylidene aniline **I** and Danishefsky's diene **II** (Scheme 1) using as catalysts the silver complexes **1**, **2** and, for comparison, $(PPh_3)Ag(OTf)$ (OTf = O_3SCF_3). In the absence of any catalyst there was only a trace (< 5%) of product after 24 h at room temperature. On the bench (2 h, room temperature, 1 mol% catalyst, CH_2Cl_2) both complexes **1** and **2** afforded essentially quantitative (> 99%) yields of **III** on workup, while $(PPh_3)Ag(OTf)$ gave **III** in 70% yield. However, it was only when catalyst loadings were reduced to 0.1 mol% and the reactions were monitored by NMR spectroscopy that the efficiency of complex **1**, in particular, for this transformation was revealed.

Fig. 2 shows a plot of time *vs*. reaction course for complexes **1**, **2** and $(PPh_3)Ag(OTf)$. $[(PPh_3)Ag(ClO_4)$ was also tested, not

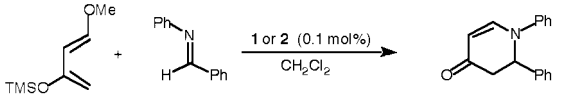

Scheme 1

† Electronic supplementary information (ESI) available: Fig. S1: extended solid state structure apparent in **1**. Figs. S2 and S3: bar charts showing isolated yield of product **III** using supported catalysts **3**–**5** in the absence and presence of water. See http:www/rsc.org/suppdata/cc/b1/b106719b/

 DOI: 10.1039/b106719b

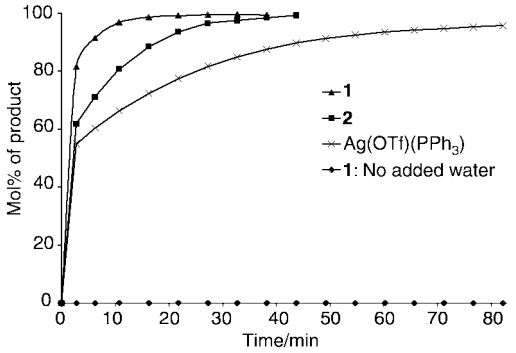

Fig. 2 Relative rates of reaction CD_2Cl_2 solutions, 0.1 mol% **1**, **2** and $(PPh_3)Ag(OTf)$, 50 mol% added H_2O. Also shown: **1** with no added water.

shown here, and showed a very similar time dependent profile to $(PPh_3)Ag(OTf)$.] It is clear that complex **1** gives the fastest rate of catalysis, the reaction being complete in ~15 min, yielding a turnover frequency (TOF) of *ca.* 4000 h^{-1}. Complex **2** is slower than **1**, with complete reaction effected after 50 min, while $(PPh_3)Ag(OTf)$ does not attain 100% conversion, even after 80 min. Although these results reflect the previously enunciated relative weakly coordinating properties of carborane anions,[2] especially the halogenated examples,[4] it is pleasing to see that these ideas can be applied to a synthetically useful transformation, using well defined catalysts.

Importantly, and somewhat surprisingly, we have found that water plays an important role in this reaction. When these NMR experiments are performed in rigorously dry solvent (CD_2Cl_2, vacuum distilled from CaH_2), no catalysis occurs (Fig. 2). Addition of a substoichiometric (1 μl, 50 mol%, unoptimised) amount of H_2O to the sample immediately initiates catalysis. While water-accelerated catalysis is becoming appreciated more widely,[5] we currently can only speculate as to its rôle in this system. These results, however, implicate a polarised, silver-bound water molecule in the catalytic process, with the resulting Lewis-assisted Brønsted-acid similar to that previously reported in lanthanide catalysed aromatic electrophilic substitutions[6] and the catalytic role of coordinated water in certain zeolites.[7] Consonant with this idea, when the reaction was repeated in the presence of the hindered base 2,6-di-*tert*-butyl-4-methylpyridine no product was formed, while a control experiment taking **I** and **II** with just 50 mol% water also resulted in no product formation. On the bench, it is probably adventitious water that is made available to the reaction.

Catalyst **1** is also selective for imines over aldehydes in this reaction. A competition experiment demonstrated preferential activation of imine **I** in the presence of an equimolar amount of benzaldehyde. Thus, after 15 min at room temperature the product arising from reaction with the imine was isolated in 70% yield whilst the aldehyde adduct was produced in only 5% yield.

Polymer supported Lewis acids have been recently attracting significant attention as they represent one method of generating clean, efficient and re-usable catalysts.[8] However, the incorporation of the Lewis acidic sites onto the polymer often requires a multistep synthesis. Given that one of the most popular supports is polymer bound triphenylphosphine,[9] we were interested to see if the high activity and efficiency shown by complexes **1** and **2** could be transferred to this support. Stirring a CH_2Cl_2 solution of Ag[Y][Y = $CB_{11}H_{12}$ **3**, $CB_{11}H_6Br_6$ **4**, OTf **5**] with commercially available resin (Fluka) afforded a material that was an efficient catalyst in all three cases for the hetero-Diels–Alder reaction under investigation.¶ Moreover, all the resins were shown to be re-usable over at least three catalyst runs (>95% isolated yield, *vide infra*). In concert with this, low leaching levels (0.3% Ag, by AAS) where also determined, while the supernatant from freshly prepared and filtered supported catalyst afforded only trace product (<5%) when used in the reaction. These supported catalysts also show a significant dependence on the presence of water. If no water is added then catalyst performance drops off rapidly on the second and third runs, however with 10 mol% water high yields of >95% are afforded over three consecutive cycles (ESI†). At the relatively high catalyst loadings (10 mol%) used in these preliminary experiments the counter ion effects observed in the homogeneous system are not observed.

In conclusion, we have demonstrated that silver(I)–phosphine complexes partnered by carborane anions based on $[CB_{11}H_{12}]$ are effective and active catalysts in a hetero-Diels–Alder transformation, and that water dramatically effects the observed rate of reaction. These catalysts may also be supported on commercially available resin to give active and recyclable Lewis acid catalysts. Full details of the synthesis, solution and solid state structures of **1** and **2** along with comparisons of the catalytic performance when other common anions are partnered with silver(I)–phosphines will be reported in due course.[10]

A. S. W. thanks the Royal Society for a University Research Fellowship. The EPSRC and JERI are thanked for providing funds for the purchase of a diffractometer. The referees are thanked for useful comments.

Notes and references

‡ NMR data (CD_2Cl_2 solutions, 22 °C, 300 MHz). Complex **1**: $^1H\{^{11}B\}$, δ 7.52–7.22 (15H, m, C_6H_5), 2.73 (1H, s br, CH_{cage}), 2.43 (5H, BH). $^{11}B\{^1H\}$, δ −2.09 (1B), −6.59 (5B), −16.88 (5B). $^{31}P\{^1H\}$, δ 16.52 [1P, d d, $J(Ag^{109}P)$ 766, $J(Ag^{107}P)$ 664 Hz]. IR/cm^{-1} (KBr): 2608vs (BH), 2593s (BH). Calc. for $C_{19}H_{21}B_{11}AgPBr_6$: C, 23.1; H, 2.12. Found: C, 22.6; H 2.17%. Complex **2**: $H\{^{11}B\}$, δ 7.52–7.29 (15H, m, C_6H_5), 2.55 (1H, s br, CH_{cage}), 2.25 (1H, s br, BH), 1.85 (10H, 5 + 5 coincidence, BH): $^{11}B\{^1H\}$. δ −10.27 (1B, s br), −11.18 (5 B), −12.02 (5 B). $^{31}P\{^1H\}$, δ 18.70 [1P, dd, $J(Ag^{109}P)$ 795, $J(Ag^{107}P)$ 691 Hz]. IR/cm^{-1} (KBr): 2565vs (BH), 2517s (sh) (BH), 2372m (BH). Calc. for $C_{19}H_{27}B_{11}AgP$: C, 44.5; H, 5.30. Found: C, 44.3; H, 5.19%.

§ *Crystallographic data*: for **1**: $C_{19}H_{21}AgB_{11}Br_6P$, M = 986.57, λ = 0.71073 Å, monoclinic, space group $P2_1/c$, a = 8.8950(10), b = 24.4140(4), c = 14.4170(3) Å, β = 102.0720(10)°, U = 3061.60(9) Å^3, Z = 4, T = 150(2) K, D_c = 2.140 g cm^{-3}, μ = 8.554 mm^{-1}, $F(000)$ = 1848, crystal: 0.10 × 0.10 × 0.05 mm, 7253 unique reflections (R_{int} = 0.0519), R_1 = 0.0358, wR_2 = 0.0783 [$I > 2\sigma(I)$]. For **2**: $C_{19}H_{27}AgB_{11}P$, M = 513.16, λ = 0.71073 Å, triclinic, space group $P\bar{1}$, a = 10.282(2), b = 10.988(2), c = 11.308(2) Å, α = 76.22(3), β = 75.25(3), γ = 75.61(3)°, U = 1175.7(4) Å^3, Z = 2, T = 150(2) K, D_c = 1.450 g cm^{-3}, μ = 0.932 mm^{-1}, $F(000)$ = 516, crystal 0.20 × 0.20 × 0.10 mm, 5374 unique reflections (R_{int} = 0.0387), R_1 = 0.0316, wR_2 = 0.0757 [$I > 2\sigma(I)$].

CCDC reference numbers 171721 and 168828. See http://www.rsc.org/suppdata/cc/b1/b106719b/ for crystallographic data in CIF or other electronic format.

¶ *General procedure*: ~3 mmol g^{-1} polymer-bound PPh_3 (Fluka, 200–300 mesh) with a slight excess of Ag[Y] in CH_2Cl_2 was used to generate the polymer bound catalyst. After washing with CH_2Cl_2 and drying *in vacuo*, catalytic runs were performed using *ca.* 10 mol% catalyst and 10 mol% H_2O in CH_2Cl_2 (5 ml) (1 h, room temp.). The support was recycled by cannula filtration of the supernatent under argon and drying *in vacuo*.

1 *Lewis Acids in Organic Synthesis*, ed. H. Yamamoto, Wiley-VCH, Weinheim, 2000; P. Buonora, J. C. Olsen and T. Oh, *Tetrahedron*, 2001, **57**, 6099.
2 C. A. Reed, *Acc. Chem. Rev.*, 1998, **31**, 133.
3 D. D. Ellis, A. Franken, P. A. Jellis, J. A. Kautz and F. G. A. Stone, *J. Chem. Soc., Dalton Trans.*, 2000, 2509; D. D. Ellis, J. C. Jeffery, P. A. Jellis, J. A. Kautz and F. G. A. Stone, *Inorg. Chem.*, 2001, **40**, 2041.
4 C. A. Reed, K. C. Kim, R. D. Bolskar and L. J. Mueller, *Science*, 2000, **289**, 101.
5 S. Ribe and P. Wipf, *Chem. Commun.*, 2001, 299.
6 A. G. M. Barrett, D. C. Braddock, J. P. Henschke and E. R. Walker, *J. Chem. Soc., Perkin Trans. 1*, 1999, 873.
7 H.-M. Kao, C. P. Grey, K. Pitchumani, P. H. Lakshminarasimhan and V. Ramamurthy, *J. Phys. Chem. A.*, 1998, **102**, 5627.
8 S. V. Ley, A. R. Baxendale, R. N. Bream, P. S. Jackson, A. G. Leach, D. A. Longbottom, M. Nesi, J. S. Scott, R. I. Storer and S. J. Taylor, *J. Chem. Soc., Perkin Trans. 1*, 2000, 3815; S. Itsuno, in *Lewis Acids in Organic Synthesis*, ed. H. Yamamoto, Wiley-VCH, Weinheim, 2000.
9 A. C. Comely, S. E. Gibson and N. J. Hales, *Chem. Commun.*, 2000, 305.
10 C. Hague, N. J. Patmore, J. H. Cotgreave, M. F. Mahon, C. G. Frost and A. S. Weller, manuscript in preparation.

CHEMCOMM Communication
www.rsc.org/chemcomm

Novel small organo-P–S/Se heterocycles

Petr Kilian, Alexandra M. Z. Slawin and J. Derek Woollins*

Department of Chemistry, University of St. Andrews, Fife, UK KY16 9ST.
E-mail: jdw3@st-andrews.ac.uk

Received (in Cambridge, UK) 9th August 2001, Accepted 25th September 2001
First published as an Advance Article on the web 18th October 2001

Oxidative addition of elemental sulfur and selenium to cyclomonocarbatetraphosphines $(PhP)_4CR_2$ (R = H, Me) afforded novel five- and four-membered heterocycles $PhP(E)CH_2PhP(E)E_2$ (E = S, Se) and $PhP(Se)CMe_2$-PhP(Se)Se.

Although the chemistry of cyclophosphines $(R'P)_n$ (R′ = alkyl, aryl; n = 3–6) has been studied extensively, tetraphospholanes $(R'P)_4CR_2$ have received less attention, despite their ease of access from cyclophosphines.[1] Due to the stability of the endocyclic P–C bond they are a valuable source of $PhPCR_2PPh$ moiety as shown herein for oxidative addition reactions with elemental sulfur and selenium (Scheme 1). Four- and five-membered heterocycles described here represent only the third known heterocycle with the atomic sequence PCPSe (and the first X-ray structure determination reported), whilst the heterocyclic sequence PCPSeSe is the first example. The parallels in S chemistry are also scarce; PCPS rings were prepared using low-coordinate phosphorus starting compounds such as diphosphaallene,[2] phosphanylidene[3] and thioxophosphane with phosphonium ylide.[4] The only known heterocyclic compound with the PCPSS atomic sequence, **9**, has been isolated in low yield as a side product in the reaction of sulfur and diphosphaallene with stabilizing bulky supermesityl side groups.[2a] Partially sulfur oxidised derivatives $(PhP)_4CH_2S$ and $(PhP)_4CH_2S_2$ were obtained from the reaction of $(PhP)_4CH_2$ with lower molar amounts of sulfur.[5]

Our aim was to obtain thermodynamically stable products, thus all the reactions were performed in refluxing toluene (under N_2). Treatment of $(PhP)_4CH_2$ with 8 equivalents of sulfur and a catalytic amount of DBU, followed by fractional crystallisation afforded colourless crystals of **1** in a moderate yield (40%, Scheme 1).[6]

Crystallographic analysis of **1** (Fig. 1)[7] reveals the formation of a five–membered PCPSS heterocycle with a *trans*-geometry of exocyclic phenyl and sulfur substituents. The central heterocycle has an envelope shape, with S(2) atom lying 1.1 Å out of the plane defined by the other ring atoms (mean deviation of this plane is 0.04 Å), which is in contrast to the half-chair conformation found in the only known PCPSS heterocycle **9**.[2a]

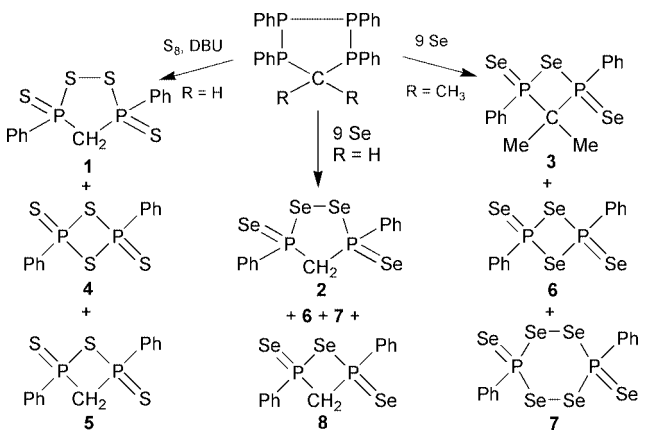

Scheme 1

The internal bond lengths in **1** are comparable to those in **9**. The envelope shape however accounts to significant changes in internal bond angles, the P–C–P angle as well as PSSP dihedral angle are substantially decreased in **1** [P–C–P angle in **1** 114.47(9)°; 119.6(4)° in **9**; PSSP dihedral angle in **1** 49.48(3)°; 54.8(1)° in **9**]. Also the S(3)–P(1)–C(2) and S(4)–P(2)–C(8) angles of 115° are decreased due to lower steric hindrance of phenyl *vs.* supermesityl substituent in **9** (corresponding angles 126°). The shortest intermolecular contacts in **1** are 3.47 Å [S(2)···S(3)], which is less than twice the van der Waals radius for sulfur (3.70 Å).

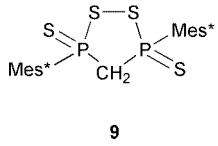

9

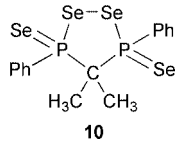

10

The $^{31}P\{^1H\}$ NMR spectrum of **1** (in $CDCl_3$) shows a singlet at δ 80.3. A minor singlet (*ca.* 4% intensity) with a very similar shift of δ 80.9 has been also observed in the spectrum, belonging to a less energetically favourable conformation or *cis*-isomer of **1**. The ^1H NMR spectrum of **1** contains multiplets for the phenyl ring protons and a triplet for the CH_2 group [δ 3.9, ^2J(HP) 9.9 Hz]. These spectral data are in a very good agreement with those reported for **9** [δ_P 87.6, $\delta_H(CH_2)$ 3.96, ^2J(HP) 9.6 Hz].[2a]

Treatment of $(PhP)_4CH_2$ with 9 equivalents of grey selenium in boiling toluene, hot filtration to remove insoluble **6** and unreacted selenium, concentration of the filtrate *in vacuo* and cooling afforded the orange crystalline solid **2** in 94% yield (Scheme 1). The minor impurities, heterocycles **7** and **8**, can be removed by recrystallisation from hot toluene.[8]

Crystallographic analysis[7] reveals **2** to be almost isostructural with **1** (Fig. 1). The central heterocycle has again envelope

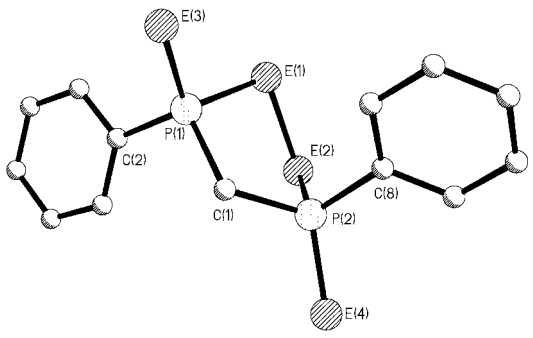

Fig. 1 Molecular structure of **1** (E = S) and **2** (E = Se). H atoms omitted for clarity. Selected bond lengths (Å) and angles (°) for **1** and **2** (values in square brackets): P(1)–C(1) 1.839(2) [1.830(7)], P(2)–C(1) 1.839(2) [1.839(6)], P(1)–E(1) 2.1160(7) [2.249(2)], P(2)–E(2) 2.1095(7) [2.247(2)], E(1)–E(2) 2.0667(7) [2.338(1)], P(1)–C(2) 1.810(2) [1.809(7)], P(2)–C(8) 1.810(2) [1.828(8)], P(1)–E(3) 1.9394(7) [2.100(2)], P(2)–E(4) 1.9419(7) [2.100(2)], P(1)–C(1)–P(2) 114.47(9) [116.7(4)], P(1)–E(1)–E(2) 97.07(3) [93.40(6)], P(2)–E(2)–E(1) 95.73(3) [91.97(6)], E(1)–P(1)–C(1) 102.71(6) [105.2(2)], E(2)–P(2)–C(1) 100.90(6) [102.7(2)], C(2)–P(1)–E(3) 114.86(6) [114.0(2)], C(8)–P(2)–E(4) 114.78(7) [114.0(2)], E(1)–P(1)–E(3) 107.16(3) [106.82(9)], E(2)–P(2)–E(4) 107.77(3) [107.91(9)].

 DOI: 10.1039/b107214e

conformation, with Se(2) lying 1.27 Å out of plane defined by other ring atoms (mean deviation of this plane is 0.04 Å). The PCP angle, P···P distance and PSeSeP torsion angle vary little from the corresponding values in **1**, as expected the ring dimensions are increased due to larger radii of Se atoms (see *e.g.* differences in Se–Se and S–S bond length for **2** and **1**), however Se(3)–P(1)–C(2) and Se(4)–P(2)–C(8) angles (114°) show no significant change when compared with corresponding angles in **1**. The shortest intermolecular contacts in **2** are 3.48 Å [Se(2)···Se(3)].

The $^{31}P\{^{1}H\}$ NMR spectrum of **2** comprises of a singlet (δ_P 43, in $CDCl_3$) with symmetric sets of selenium satellites. The satellite spectrum is generated mainly from two distinct isotopomers with one ^{77}Se atom in exo- or endo-positions of the ring, both having an AXX′ pattern (A = ^{77}Se, X = P). Simulation of the satellite spectra enabled determination of all four P–Se coupling constants[9] as well as a homonuclear P–P coupling [^2J(PP) ±34.1 Hz].

By the treatment of $(PhP)_4CMe_2$ with 9 equivalents of grey selenium in the same manner as **2** (including work-up procedures), orange crystalline **3** has been obtained in 68% yield (Scheme 1).[10] Crystallographic analysis of **3** (Fig. 2)[7] reveals that oxidation of $(PhP)_4CMe_2$ proceeds surprisingly with the formation of a four-membered PCPSe ring. The unit cell contains two independent molecules, in both the central ring is folded (17 and 28° along the Se···C diagonal) with phenyl and exocyclic selenium substituents in *trans* configuration. No X-ray structure determination of a PCPSe ring has been reported up to date, the nearest parallels found are PCPS rings, both thiadiphosphetanes with known X-ray data[2b,4] show *cis* configuration and folded geometry of the central ring (19.2 and 29.4° along C···S diagonal). Internal P–Se bond lengths in **3** [2.274(2)–2.283(2) Å] are slightly increased with respect to **2** [2.247(2) and 2.249(2) Å] however they are comparable with **6** [2.276(2) and 2.284(2) Å].[11] In contrast, the internal P–Se–P angles in **3** (77.7 and 76.0° for each molecule in the unit cell) are substantially decreased when compared with corresponding angle in the planar PSePSe heterocycle **6** (85.5°).[11] The shortest intermolecular contacts in **3** are 3.59 Å [Se(1)···Se(2)].

$^{31}P\{^{1}H\}$ NMR examination of the mixture after the reaction did not show any reasonably intense signals at lower field, assignable to related five-membered heterocycle **10**. The $^{31}P\{^{1}H\}$ NMR spectrum of **3** comprises of a singlet (δ_P 52, in $CDCl_3$) with two symmetric sets of selenium satellites of AXX′ (Se_{exo}) and AX_2 (Se_{endo}) pattern (A = ^{77}Se, X = P). The simulation of the AXX′ satellite subspectrum enabled determination of a homonuclear P–P coupling, whose magnitude is surprisingly low [^2J(PP) < ±2 Hz].[12] The ^1H NMR spectrum of **3** ($CDCl_3$, 25 °C) shows a second-order A_3B_3XX' pattern (A, B = CH_3 protons, X, X′ = P) at δ 1.3, confirming magnetic inequivalence of methyl groups protons as a consequence of the folded geometry of the central heterocycle.

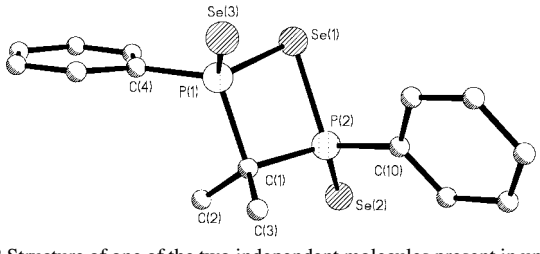

Fig. 2 Structure of one of the two independent molecules present in unit cell of **3**. H atoms omitted for clarity. Selected bond lengths (Å) and angles (°) for the molecule with less folded central heterocycle: P(1)–C(1) 1.915(7), P(2)–C(1) 1.910(6), P(1)–Se(1) 2.279(2), P(2)–Se(1) 2.283(2), P(1)–C(4) 1.825(7), P(2)–C(10) 1.817(7), P(1)–Se(3) 2.096(2), P(2)–Se(2) 2.101(2), P(1)–C(1)–P(2) 96.9(3), P(1)–Se(1)–P(2) 77.73(7), Se(1)–P(1)–C(1) and Se(1)–P(2)–C(1) 91.4(2), C(1)–P(1)–Se(3) 114.4(2), C(1)–P(2)–Se(2) 115.1(2), C(1)–P(1)–C(4) 110.2(3), C(1)P(2)–C(10) 108.9(3), C(4)–P(1)–Se(3) 112.3(2), C(10)–P(2)–Se(2) 113.0(3), Se(1)–P(1)–C(4) 109.0(2), Se(1)–P(2)–C(10) 107.5(3), Se(1)–P(1)–Se(3) 117.70(9), Se(1)–P(2)–Se(2) 118.74(9), C(2)–C(1)–C(3) 113.2(6). For parameters of second molecule in the independent unit see crystallographic data in CIF format.

Studies to employ new soluble P–Se heterocycles in our reagent program for C=O to C=Se transformations are now underway.

We are grateful to the EPSRC for financial support.

Notes and references

1 M. Baudler, J. Vesper, P. Junkes and H. Sandmann, *Angew. Chem. Int. Ed. Engl.*, 1971, **10**, 940; M. Baudler, E. Tolls, E. Clef, B. Kloth and D. Koch, *Z. Anorg. Allg. Chem.*, 1977, **435**, 21; *Synth. React. Inorg. Met. Org. Chem.*, 1977, **7**, 253.

2 (*a*) K. Toyota, Y. Ishikawa, M. Yoshifuji, K. Okada, K. Hosomi and K. Hirotsu, *Chem. Lett.*, 1991, 2213; (*b*) K. Toyota, M. Yoshifuji and K. Hirotsu, *Chem. Lett.*, 1990, 643.

3 N. M. Yousif, *Phosphorus, Sulfur Silicon Relat. Elem.*, 1989, **46**, 169.

4 G. Jochem, A. Schmidpeter, F. Kulzer and S. Dick, *Chem. Ber.*, 1995, **128**, 1015.

5 M. Baudler, J. Vesper, B. Kloth, D. Koch and H. Sandmann, *Z. Anorg. Allg. Chem.*, 1977, **431**, 39.

6 $^{31}P\{^{1}H\}$ NMR examination of the reaction mixture before recrystallisation indicated presence of two side products **4** (s, δ_P 17.3) and **5** (s, δ_P 29.8). Full spectral and structural characterisation of **5** is the subject of our continuating studies. Compound **1** is soluble in dichloromethane and toluene, correct C, H microanalysis were obtained; mp 153–155 °C; MS (EI, sampled neat) 358 (M^+, base peak), 326 (M − S), 294 (M − 2S), 262 (M − 3S); IR (KBr disc) 769 cm^{-1} (vs, $\nu_{P=S}$).

7 *Crystal data*: for **1**: $C_{13}H_{12}P_2S_4$, M = 358.41, space group $P2_1/c$, monoclinic, a = 9.8833(6), b = 8.8370(5), c = 18.375(1) Å, β = 94.948(1)°, U = 1598.9(2) Å^3, T = 293 K, Z = 4, μ(Mo-Kα) = 0.777 mm^{-1}, 6688 reflections measured, 2276 unique (R_{int} = 0.0121) which were used in all calculations. The final R was 0.0228 for $I > 2\sigma(I)$ and $wR(F^2)$ was 0.0649 for all data. For **2**: $C_{13}H_{12}P_2Se_4$, M = 546.01, monoclinic, space group $P2_1/c$, a = 10.016(1), b = 8.9836(5), c = 18.677(5) Å, β = 93.687(1)°, U = 1677.2(5) Å^3, T = 293 K, Z = 4, μ(Mo-Kα) = 8.924 mm^{-1}, 9054 reflections measured, 3481 unique (R_{int} = 0.1376) which were used in all calculations. The final R was 0.0632 for $I > 2\sigma(I)$ and $wR(F^2)$ was 0.1677 for all data. For **3**: $C_{15}H_{16}P_2Se_3$, M = 495.10, orthorhombic, space group $Pna2_1$, a = 17.7582(3), b = 27.4561(2), c = 7.1512(1) Å, U = 3486.72(8) Å^3, T = 293 K, Z = 8, μ(Mo-Kα) = 6.501 mm^{-1}, 14916 reflections measured, 4885 unique (R_{int} = 0.0522) which were used in all calculations. The final R was 0.0347 for $I > 2\sigma(I)$ and $wR(F^2)$ was 0.0876 for all data. CCDC reference numbers 169264–169266. See http://www.rsc.org/suppdata/cc/b1/b107214e/ for crystallographic data in CIF or other electronic format.

8 The identity of by-products **7** and **8** has been established by single crystal X-ray structure analyses and NMR, their details together with their rational syntheses and NMR spectra will be published elsewhere. Compound **2** is only slightly soluble in cold dichloromethane and toluene. It is stable under dry nitrogen atmosphere, on exposition to air it decomposes with deposition of a red selenium. Recrystallised product gave correct C, H microanalysis; mp decomp. above 180 °C; MS (EI, sampled neat) 546 (M^+), 468 (M − Se + 1); IR (KBr disc) 555 cm^{-1} (s, $\nu_{P=Se}$).

9 Further selected NMR data for **2**: $^1J(PSe_{exo})$ ±775 Hz, $^3J(PSe_{exo})$ ±11 Hz, $^1J(PSe_{endo})$ ±342 Hz, $^2J(PSe_{endo})$ ±13 Hz. Magnitudes of ^1J(PSe) coupling constants have been confirmed by measurement of ^{77}Se NMR spectra of **2**; $\delta(^{77}Se)$ −114 (d, Se_{exo}) and 494 ppm (d, Se_{endo}); ^1H NMR: δ 4.4 [t, CH_2, ^2J(HP) 9.2 Hz]; $^{13}C\{^{1}H\}$ NMR: δ 52.2 [t, CH_2, ^1J(CP) 27.3 Hz].

10 Compound **3** is stable under N_2 atmosphere, it is well soluble in dichloromethane and toluene. Correct C, H microanalysis were obtained; mp 211–214 °C; MS (EI, sampled neat) 496 (M^+); IR (KBr disc) 553 cm^{-1} (m, $\nu_{P=Se}$).

11 P. Bhattacharyya, A. M. Z. Slawin and J. D. Woollins, *J. Chem. Soc. Dalton Trans.*, 2001, 300.

12 Further selected NMR data for **3**: $^1J(PSe_{exo})$ ±804 Hz, $^1J(PSe_{endo})$ ±243 Hz, inner lines of AXX′ subspectrum were hidden under intensive central line, prohibiting determination of $^3J(PSe_{exo})$ coupling. Magnitudes of ^1J(PSe) coupling constants have been confirmed by measurement of ^{77}Se NMR spectra of **3**; $\delta(^{77}Se)$ −96 (d, Se_{exo}) and 506 (t, Se_{endo}); ^1H NMR: δ 1.2–1.5 (m, 2 × CH_3); $^{13}C\{^{1}H\}$ NMR: δ 63.2 [t, CP_2, ^1J(CP) 29.3 Hz], 26.8 (s, 2 × CH_3).

CHEMCOMM Communication
www.rsc.org/chemcomm

Catalysis in supercritical CO_2 using dendrimer-encapsulated palladium nanoparticles†

Lee K. Yeung,[a] C. Ted Lee Jr.,[b] Keith P. Johnston,*[b] and Richard M. Crooks*[a]

[a] *Department of Chemistry, Texas A&M University, P.O. Box 30012, College Station, TX 77842-3012, USA. E-mail: crooks@tamu.edu*

[b] *Department of Chemical Engineering, University of Texas, Austin, Austin, TX 78712 USA. E-mail: kpj@che.utexas.edu*

Received (in Columbia, MO, USA) 5th June 2001, Accepted 2nd August 2001
First published as an Advance Article on the web 17th October 2001

Dendrimer-encapsulated nanoparticles are shown to be versatile catalysts for both the hydrogenation of styrene and Heck heterocoupling of iodobenzene and methacrylate in supercritical CO_2 ($scCO_2$).

Here we present the first examples of catalysis in pure liquid or supercritical CO_2 ($scCO_2$) using soluble metal nanoparticles. The catalysts are composites consisting of functionalized poly(propylene imine) (PPI) dendrimers and Pd(0) nanoparticles. The perfluoropolyether-functionalized dendritic host is responsible for solubilizing the 1–2 nm diameter catalytic Pd(0) nanoparticles in $scCO_2$. The versatility of these dendrimer-encapsulated catalysts (DECs)[1] is illustrated by performing two very different chemical reactions. First, in the presence of hydrogen, the catalyst is effective for the hydrogenation of olefins, such as the reduction of styrene to ethylbenzene. Second, iodobenzene can be coupled with methylacrylate, which is a benchmark reaction for the synthetically useful Heck coupling,[2] to yield exclusively methyl 2-phenylacrylate **1** (Scheme 1). The selectivity for **1** is remarkable when compared with standard palladium complexes[2] or colloidal nanoparticles[3–6] used for Heck couplings in organic solvents, which result in only *cis*- and/or *trans*-cinnamate **2** (Scheme 1). When used in hydrocarbon/fluorocarbon solvents the same Pd-based DECs yield only *trans*-formylcinnamate.[7]

The use of liquid or $scCO_2$ as an alternative to hydrocarbon solvents is attractive because CO_2 is both inexpensive and environmentally benign.[8] Additionally, by changing the density, and thus the 'solvent power' of $scCO_2$, the reaction rates, product distribution,[9] and yields can be tuned,[10–12] and therefore there is intense interest in catalysts and chemical processes that are compatible with this 'green solvent'.[13] There are two approaches for the utilization of liquid and $scCO_2$ as a solvent for both hydrogenation[14–19] and Heck[20–22] reactions. One of these involves the use of CO_2-soluble coordination complexes, and the other utilizes Pd metal on a solid substrate such as carbon.

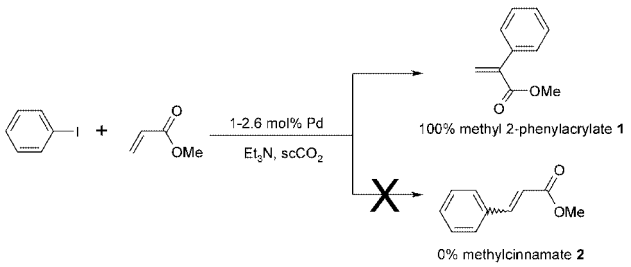

Scheme 1

The DECs used for both the hydrogenation and Heck chemistry described here consisted of Pd(0) nanoparticles sequestered within fifth-generation poly(propylene imine) (PPI) dendrimers having perfluoro-2,5,8,11-tetramethyl-3,6,9,12-tetraoxapentadecanoyl perfluoropolyether chains covalently attached to their periphery.[23] The general method used to prepare these materials has previously been reported and the specific procedures used in this work are provided in the ESI†.[1,7] Importantly, the dark-brown DECs (dry) could be easily solublized in liquid- and $scCO_2$ (dull-orange solution), and there were no obvious signs of aggregation or precipitation. Note that we and others have recently prepared and characterized Ag[24,25] and CdS[26] nanoparticles in $H_2O/scCO_2$ microemulsions as well as in pure CO_2 solvent[27] utilizing perfluorinated surfactants as either the sole emulsifier or as a co-surfactant.

Although synthetically trivial, the hydrogenation of styrene to ethylbenzene is a convenient example for demonstrating the catalytic activity of DECs.[11] With the novel catalyst (1–2.6 mol% Pd), the progress of styrene reduction was followed by capillary gas chromatography (GC) and shown to be complete in under 4 h (Fig. 1). Evidence of catalyst decomposition, such as Pd(0) precipitation, was not apparent at the end of the reaction. The ethylbenzene could be recovered after depressurization of the reaction vessel and was confirmed by NMR spectroscopy to be the only product.

To demonstrate the versatility of $scCO_2$-soluble DECs, the same catalyst was shown to be active for a Heck-type coupling reaction. In the presence of triethylamine (TEA) and the DEC (1–2.6 mol% Pd), methylacrylate (MA) reacted with iodobenzene (PhI) at 75 °C and 5000 psi, forming methyl 2-phenylacrylate **1**. The progress of the reaction was followed by GC using *n*-decane as an internal reference (Fig. 2). The DECs stopped producing **1** after about 24 h when 57% of the iodobenzene was consumed. This corresponds to a turnover number (TON) of *ca.* 22 (TON = mol of substrate/mol of Pd).

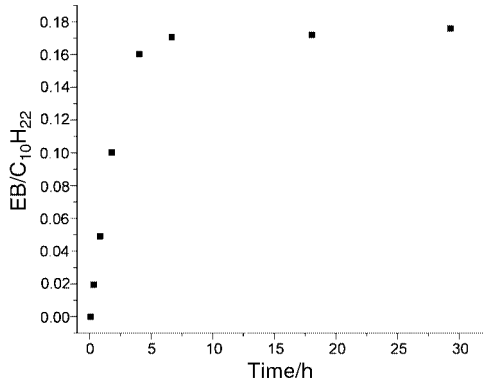

Fig. 1 Gas chromatographic data showing the appearance of ethylbenzene (EB) from the DEC catalyzed reduction of styrene in a supercritical H_2/CO_2 mixture with *n*-decane ($C_{10}H_{22}$) as an internal standard.

† Electronic supplementary information (ESI) available: DEC synthesis and specific reaction conditions used for the hydrogenation and Heck reactions. See http://www.rsc.org/suppdata/cc/b1/b106594g/

 DOI: 10.1039/b106594g

Although this TON does not approach values obtained in other solvent systems,[28] it is comparable to previous reports of Heck catalysis in $scCO_2$ using both soluble complexes and heterogeneous catalysts.[20–22]

Importantly, even after 52 h the $scCO_2$ Heck reaction solution did not show evidence of Pd(0) precipitates or other catalyst decomposition products. The DECs and product were recovered by slowly venting the CO_2 followed by washing the depressurized reaction vessel with 1,1,2-trichlorotrifluoroethane (CFC-113). ^{1}H NMR analysis of the extract revealed a mixture of the *n*-decane internal GC reference, the starting materials (PhI and MA), and methyl 2-phenylacrylate **1**, but no evidence of byproducts or other impurities[29,30]

Prior to drying and loading into the CO_2 reactor, the CFC-113 DEC solution is dark-brown. However, the recovered CFC-113 solution was dull-orange in color, reminiscent of the color of the Pd(II)-containing PPI dendrimers [from which the Pd(0)-containing DECs were prepared].[1] This color change suggests that the Pd is oxidized from Pd(0) to Pd(II) during the course of the Heck reaction. Indeed, upon treatment of the recovered Pd(II)-containing DEC solution with an excess of $NaBH_4$, the solution turned dark-brown, UV-VIS spectroscopy indicated the formation of intradendrimer nanoparticles, and the solution remained precipitate free. We also noted that the Pd-containing DEC can be subjected to the reaction conditions described above, but in the absence of substrate, and then recovered without signs of Pd(0) oxidation. These findings provide a reasonable hypothesis for the cause of reaction termination and the low TON.

It is widely accepted that the last step in the catalytic Heck cycle involves the reductive elimination of the halide from the Pd metal and neutralization of the resulting acid.[31,32] Moreover, the use of excess tertiary amine has led to rate enhancements for a Heck-type coupling reaction resulting from both the neutralization effect of the base and weak ligand–complex stabilization.[33] We propose that at the start of the reaction in $scCO_2$, the inherently more basic[34] and proximal tertiary amines of the dendrimer neutralize the eliminated acid more effectively than the slightly less basic TEA. However, an equilibrium develops in which the interior tertiary amine hydrogen iodide salt disproportionates back to the free amine and acid, resulting in Pd(0) oxidation and halting the catalytic cycle. In fact, past studies have shown that stronger bases lead to increased rates and completion of Heck reactions because dissociation to the free base and acid is not a concern.[32,35]

To summarize, we have described the first example of catalytically active nanoparticles solublized in environmentally benign $scCO_2$. This versatile catalyst is able to reduce styrene exclusively to ethylbenzene and to catalyze the carbon–carbon bond forming Heck reaction. Although the conditions have not been optimized, it is clear that DECs can select for particular products (*e.g.*, methyl 2-phenylacrylate for the Heck reaction). The high selectivity is due in part to the steric environment the dendrimer template imposes on the reaction intermediates, but primarily results from the $scCO_2$ solvent in view of our recent finding that the same DEC in an organic/fluorocarbon solvent system yields exclusively the *trans*-coupled isomer.[7]

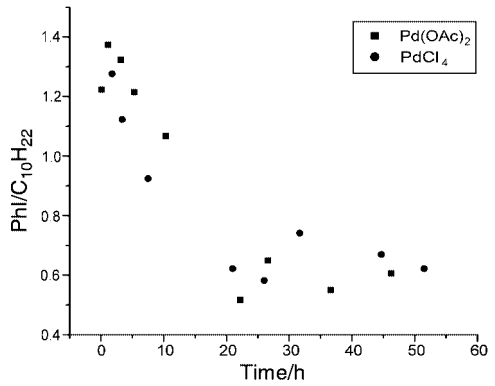

Fig. 2 Gas chromatography data showing the disappearance of the limiting reagent (PhI) for the Heck reaction as a function of time. The two sets of data correspond to independently run reactions using DECs prepared from different molecular sources of palladium, $Pd(OAc)_2$ and K_2PdCl_4.

We gratefully acknowledge support from the Office of Naval Research (R. M. C.) and the STC program of the NSF under Agreement No. CHE-9876674 (K. P. J.). We also acknowledge Prof. Victor Chechik (University of York) whose preliminary work with DECs in $scCO_2$ contributed greatly to our progress in this area.

Notes and references

1 R. M. Crooks, M. Zhao, L. Sun, V. Chechik and L. K. Yeung, *Acc. Chem. Res*., 2001, **34**, 181, and references therein.
2 A. deMeijere and F. E. Meyer, *Angew. Chem., Int. Ed. Engl*., 1994, **33**, 2379.
3 M. Beller, H. Fischer, K. Kuehlein, C. P. Reisinger and W. A. Herrmann, *J. Organomet. Chem*., 1996, **520**, 257.
4 M. T. Reetz and G. Lohmer, *Chem. Commun*., 1996, 1921.
5 M. T. Reetz and E. Westermann, *Angew. Chem., Int. Ed*., 2000, **39**, 165.
6 S. Klingelhöfer, W. Heitz, A. Greiner, S. Oestreich, S. Förster and M. Antonietti, *J. Am. Chem. Soc*., 1997, **119**, 10116.
7 L. K. Yeung and R. M. Crooks, *Nano Lett*., 2001, **1**, 14.
8 M. A. McHugh and V. J. Krukonis, *Supercritical Fluids Extraction: Principles and Practice*, Butterworth-Heinmann, MA, 2nd edn., 1993.
9 W. Leitner, *Top. Curr. Chem*., 1999, **206**, 107.
10 C. A. Eckert and K. Chandler, *J. Supercrit. Fluids*, 1998, **13**, 187.
11 G. B. Jacobson, C. T. Lee Jr, K. P. Johnston and W. Tumas, *J. Am. Chem. Soc*., 1999, **121**, 11902.
12 A. A. Clifford, *Chemical Sythesis in Supercritical Fluids*, ed. W. Leitner and P. G. Jessop, Wiley-VCH, Weinheim, 1999, p. 54.
13 P. G. Jessop, T. Ikariya and R. Noyori, *Chem. Rev*., 1999, **99**, 475.
14 P. G. Jessop, T. Ikariya and R. Noyori, *Nature*, 1994, **368**, 231.
15 S. Kainz, A. Brinkmann, W. Leitner and A. Pfaltz, *J. Am. Chem. Soc*., 1999, **121**, 6421.
16 S. Lange, A. Brinkman, P. Trautner, K. Woelk, J. Bargon and W. Leitner, *Chirality*, 2000, **12**, 450.
17 R. J. Bonilla, B. R. James and P. G. Jessop, *Chem. Commun*., 2000, 941.
18 L. Devetta, A. Giovanzana, P. Canu, A. Bertucco and B. J. Minder, *Catal. Today*, 1999, **48**, 337.
19 M. G. Hitzler and M. Poliakoff, *Chem. Commun*., 1997, 1667.
20 N. Shezad, R. S. Oakes, A. A. Clifford and C. M. Rayner, *Tetrahedron Lett*., 1999, **40**, 2221.
21 D. K. Morita, D. R. Pesiri, S. A. David, W. H. Glaze and W. Tumas, *Chem. Commun*., 1998, 1397.
22 S. Cacchi, G. Fabrizi, F. Gasparrini and C. Villani, *Synlett*., 1999, 345.
23 A. I. Cooper, J. D. Londono, G. Wignall, J. B. McClain, E. T. Amulski, J. S. Lin, A. Dobrynin, M. Rubinstein, A. L. C. Burke, J. M. J. Frechet and J. M. DeSimone, *Nature*, 1997, **389**, 368.
24 M. Ji, X. Chen, C. M. Wai and J. L. Fulton, *J. Am. Chem. Soc*., 1999, **121**, 2631.
25 N. Kometani, Y. T. Toyoda, K. Asami and Y. Yonezawa, *Chem. Lett*., 2000, **6**, 682.
26 J. D. Holmes, P. A. Bhargava, B. A. Korgel and K. P. Johnston, *Langmuir*, 1999, **15**, 6613.
27 P. S. Shah, J. D. Holmes, R. C. Doty, K. P. Johnston and B. A. Korgel, *J. Am. Chem. Soc*., 2000, **122**, 4245.
28 I. P. Beletskaya and A. V. Cheprakov, *Chem. Rev*., 2000, **100**, 3009.
29 M. B. Watson and G. W. Youngson, *J. Chem. Soc., Perkin Trans. 1*, 1972, **12**, 1597.
30 ^{1}H NMR 200 MHz (CFC-113 with acetone-d_6) δ 3.71 (s, 3H), 5.81 (d, 1H, *J* 1.6 Hz), 6.32 (d, 1H, *J* 1.6 Hz), 7.13 (m, 2H), 7.32 (m, 1H), 7.70 (m, 2H).
31 W. Smadja, S. Czernecki, G. Ville and C. Georgoulis, *Organometallics*, 1987, **6**, 166.
32 A. J. Chalk and S. A. Magennis, *J. Org. Chem*., 1976, **41**, 273.
33 R. Benhaddou, S. Czernecki and G. Ville, *Chem. Commun*., 1988, 247.
34 R. C. Van Duijvenbode, M. Borkovec and G. J. M. Koper, *Polymer*, 1998, **39**, 2657.
35 J. B. Melpolder and R. F. Heck, *J. Org. Chem*., 1976, **41**, 265.

Typeset and printed by Black Bear Press Limited, Cambridge, England

CHEMCOMM
Feature Article
www.rsc.org/chemcomm

The stabilisation and reactivity of indium trihydride complexes

Cameron Jones

Department of Chemistry, University of Wales, Cardiff, P.O. Box 912, Park Place, Cardiff, UK CF10 3TB

Received (in Cambridge, UK) 10th August 2001, Accepted 4th September 2001
First published as an Advance Article on the web 3rd October 2001

Indium trihydride complexes were unknown prior to 1998. This article focuses on the development of this field over the last 4 years. Emphasis is placed on strategies employed to stabilise such complexes, their structure, properties and use in inorganic and organic synthesis. Throughout, comparisons are drawn with the chemistries of related lighter group 13 metal trihydride complexes. A number of similarities and differences have been observed in these comparisons which have been rationalised in terms of the properties of the group 13 elements involved.

Introduction

The importance of boron trihydride complexes to organic[1] and inorganic[2] synthesis is unquestionable and thoroughly documented. It was not really until the early seventies that the chemistry of corresponding aluminium trihydride (alane) and gallium trihydride (gallane) complexes received any significant attention[3] and even then this waned towards the end of that decade. In the late 1980s a resurgence of interest in alane and gallane coordination chemistry occurred, probably because of an increased accessibility to routine X-ray crystallography around that time. The resulting systematic study of these compounds allowed an understanding of their properties that was not previously possible. This area has been covered by several reviews which revealed that major differences exist between the coordination chemistry of alane and gallane.[4–6] These differences revolve around the fact that, although of a similar size, aluminium is more electropositive than gallium as a result of a 'd-block' contraction of the electron cloud in the latter (Table 1). Therefore, the AlH_3 unit is more Lewis acidic than the GaH_3 unit and thus it prefers coordination numbers of 5 or 6 as opposed to 4, or in rare instances 5, for GaH_3. Correspondingly, the M–H bonds in gallane complexes are more covalent (less hydridic) than in alane complexes. These properties, and others, have been exploited in recent years to the point where Lewis base adducts of alane and gallane are now widely utilised in a variety of areas which include organic, inorganic[4–6] and materials chemistry. With regards to the latter, the potential volatility and clean decomposition pathways of the complexes have led to them becoming commercially available as precursors to the pure group 13 metal or to 13/15 semiconductor materials (*e.g.* AlN). This area has been recently reviewed.[7]

Table 1 Some properties of the Group 13 elements

	B	Al	Ga	In	Tl
Covalent radius/Å[a]	0.88	1.25	1.25	1.50	1.55
Electronegativity					
Pauling[a]	2.04	1.61	1.81	1.78	2.04
Allred and Rochow[a]	2.01	1.47	1.82	1.49	1.44
Mean bond enthalpies					
M–H/kJ mol^{-1}[b]	373	287	260	225	180
M–C/kJ mol^{-1}[a]	365	274	245	162	125

[a] Ref. 6. [b] Ref. 27.

It seemed logical that if stable InH_3 (indane) complexes could be prepared they may find a range of applications similar to their lighter group 13 congeners. Despite this and until our involvement in the field no such complexes had been reported, probably because of a general belief that they would not be stable species under normal conditions, given the frailty of the In–H bond (Table 1). This is at odds with early reports from Wiberg *et al*. that indane and indeed thallane (TlH_3) can exist at room temperature, albeit in an associated form, $[(MH_3)_n]$.[8] However, based on theoretical studies[9] which predict In_2H_6 to be thermodynamically unstable in the gas and solid states, these claims are thought to be doubtful. It is noteworthy that monomeric indane has been synthesised in a solid argon matrix and a number of its properties investigated.[10] The results of this study generally mirrored those predicted by earlier theoretical work.

Although no well characterised indane complexes had been reported prior to 1998, a handful of compounds containing In–H bonds, **1**–**6**, had been previously crystallographically characterised.[11–16] These are mentioned here for purposes of comparison but also because they show that compounds containing In–H bonds are not necessarily only low temperature stable species. This point is perhaps best illustrated by the intramolecularly base stabilised complex, **4**, which is neutral and contains a terminal In–H bond but still is stable in the solid state until 90 °C.[14] Other compounds containing In–H bonds that have been reported include $MInH_4$, M = Li–Cs;[17] $Li[InH_{4-n}Ph_n]$, n = 1 or 2[18] and $[InCl_2H(THF)]$[19,20] though the degree of characterisation of these compounds is variable. In addition, in the last two years the Downs and Himmel group at Oxford have made major advances into the understanding of indium hydride chemistry by preparing and studying a variety of unusual organo-, chloro-, amido- and phosphido-complexes in solid argon matrices.[21–26]

This review covers our efforts since 1997 to stabilise and explore the reactivity of indium trihydride complexes. We

Cameron Jones was born in Perth, Australia in 1962. He completed both his BSc (1982) and BSc (Hons.) (1984) degrees at the University of Western Australia. From 1985–1987 he worked as a Research Officer at the University Department of Surgery at Royal Perth Hospital. His PhD degree (1989–1992) was gained from Griffith University, Brisbane, under the supervision of Professor Colin L. Raston. He then moved to a postdoctoral research assistantship (1992–1994) at Sussex University under the supervision of Professor John F. Nixon FRS. From 1994–1998 he held a lectureship at The University of Wales, Swansea before moving to a Readership in Inorganic Chemistry at Cardiff University where he remains. His research interests include the chemistry of the heavier group 13 hydrides and the low coordination chemistry of heavier group 15 elements.

DOI: 10.1039/b107285b

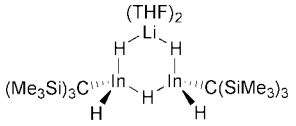

1

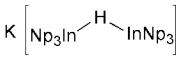

Np = neopentyl

2

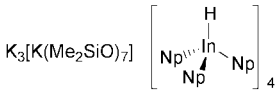

3

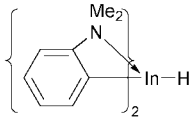

4

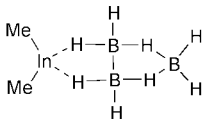

5

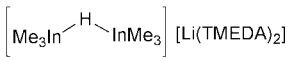

6

originally became interested in this area as we were intrigued by what structural and reactivity differences these complexes would show to their aluminium and gallium counterparts, especially considering the larger covalent radius of indium and its intermediate electronegativity (Table 1). Moreover, the thermal stability of compounds such as **4** gave us encouragement and it seemed that given the right ligand environment some success could be had. This proved to be the case and what we have found is that the coordination chemistry of indane can be similar but also significantly different to that of alane and gallane.

Stabilisation strategies

It is perhaps a misconception that the paucity of indium hydride complexes is wholly due to the weakness of the In–H bond (Table 1). This must be part of the reason but as pointed out by Downs and Pullham, the In–H bond is actually stronger than the In–C bond and indium trialkyls and their complexes are common place and generally thermally stable.[27] These authors suggested that the facile decomposition of the heavier group 13 binary hydrides may be partly kinetic in origin in that M–H–M bridges are easily formed, much more so than M–C–M bridges, and that such intermolecular association could lower the energy barrier to decomposition to $M_{(s)}$ and $H_{2(g)}$.

This argument could also be applied to indane complexes, [L → InH_3], if comparisons are drawn with their alane analogues, [L → AlH_3]. These are well known to associate through hydride bridges[4,5] and it is quite possible that such an associative process could occur prior to ligand (L) loss which in the case of indane complexes would invariably lead to decomposition to indium metal and H_2 gas. It has been calculated that the strengths of the bonds between normal donors (*e.g.* tertiary amines) and the InH_3 unit should be weak (< 100 kJ mol^{-1}) and certainly less than the strength of the In–H bond.[28] This situation would favour ligand loss in the aforementioned associative decomposition mechanism but also in a dissociative mechanism involving ligand loss from monomeric [L → InH_3]. It seems likely that a dissociative pathway is more likely given the relative instability of gallane complexes [L → GaH_3] for which intermolecular hydride bridges are not favoured.

It was thought logical that the formation of room-temperature stable indane complexes would require the use of a ligand with two major characteristics. Firstly, it would have to be a strong Lewis base. This would allow the formation of a relatively strong L–In bond, thus disfavouring ligand loss. This, in turn, would help circumvent the formation of intermolecular hydride bridges as the indium centre would be more electronically satisfied. Secondly, the ligand would need to be sterically bulky. This would help prevent the formation of intermolecular hydride bridges while at the same time protecting the InH_3 unit from attack from oxygen and moisture.

Preparation and properties

Group 15 donor complexes

Our original strategy was to employ ligands that had been successfully used to stabilise the AlH_3 and GaH_3 fragments, *viz.* tertiary amines and phosphines. With regards to tertiary amines, a theoretical study had suggested these would be far superior to phosphines as ligands with respect to their binding energy to the InH_3 unit (*e.g.* [$InH_3(NH_3)$] 91 kJ mol^{-1}, [$InH_3(PH_3)$] 35 kJ mol^{-1}).[28] Two synthetic routes to tertiary amine complexes were employed which involved (i) salt elimination from the reaction of $LiInH_4$ with a trialkylammonium chloride or (ii) ligand displacement from *in-situ* generated [$InH_3(NMe_3)$]. It is noteworthy that in route (i) $LiInH_4$ is generated *in-situ* (from the reaction of $InBr_3$ and LiH) and the by-product, LiBr, is soluble in diethyl ether. These reactions do not appear to work when NaH or KH are used, or if they are carried out in THF.

The only success achieved with tertiary amines was in the preparation of complexes **7**–**9** (Scheme 1), none of which are

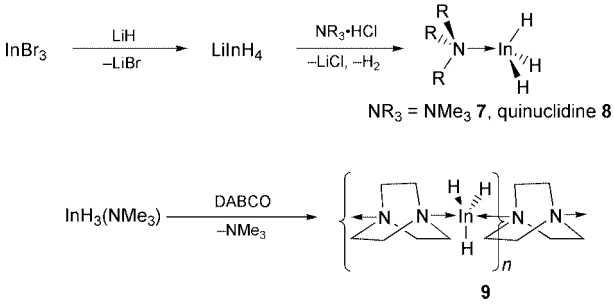

Scheme 1

stable at room temperature. In fact **7** is only stable below −30 °C and in dilute solutions (< 0.1 M) and so could not be properly characterised.[29,30] Compounds **8** and **9** are unstable below *ca.* 0 °C in the solid state, decomposing to In metal, H_2 gas and returning the free tertiary amine.[31] This is perhaps surprising considering the alane analogues of these compounds are very thermally stable and do not decompose until 170 °C (mp 110–112 °C)[32] and > 200 °C respectively.[33] Little data could be obtained on either compound but their IR spectra display very strong, broad In–H stretching absorptions at 1640 cm^{-1} and 1650 cm^{-1} which are at considerably lower frequency than normally seen for tertiary amine–alane complexes (*ca.* 1700–1800 cm^{-1}).[4,5] This is in line with the relative strengths of the M–H bonds. It is noteworthy that very stable ionic aluminium hydride complexes, *e.g.* $[AlH_2(L)]^+[AlH_4]^-$, L = tetramethylcyclam (decomp. 243–246 °C) or pmdeta (decomp. 182 °C),[34] can be formed from the reaction of [$AlH_3(NMe_3)$] with polydentate tertiary amines. Interestingly, a number of similar reactions have been carried out with [$InH_3(NMe_3)$] but all led to decomposition below < −15 °C.[31] It is not known why this occurs but it is clear that indane is different to alane in this respect.

Although tertiary phosphines are much poorer donors than tertiary amines towards alane, both ligand types have a similar donor ability toward gallane. Despite theoretical studies which have predicted that tertiary phosphines would be poorer donors than amines toward indane,[28] the preparation of a series of complexes was attempted (Scheme 2). It was found that both 1:1 and 2:1 complexes could be prepared using a ligand displacement route but reactions of PR_3/HCl with $LiInH_4$ proved fruitless even though a similar route can be used to form gallane complexes.[35]

In general, the phosphine–indane complexes possessed remarkable thermal stability (*cf.* gallane chemistry) that

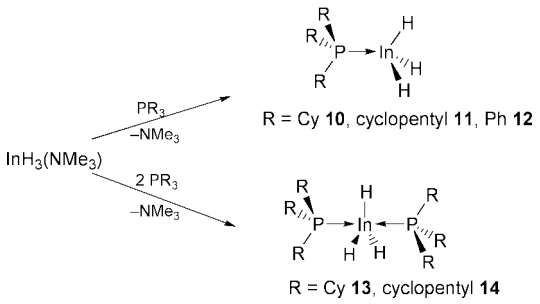

Scheme 2

increased with the σ-donating and steric properties of the phosphine ligand. The 1 : 1 and 2 : 1 PCy_3 adducts were the most stable in the solid state (**10** decomp. 50 °C and **13** decomp. 37 °C) though all complexes decomposed to indium, $H_{2(g)}$ and the free phosphine.[36] Remarkably, crystalline samples of **10** proved to be completely stable to the atmosphere at room temperature over a 24 hour period. The apparently greater stability of phosphine–indane adducts over their amine analogues is probably due to a combination of factors. Firstly, the phosphines that have been employed are much bulkier than the amines used. Secondly, the electronegativity of In, intermediate between that of Al and Ga, and its greater covalent radius might make the InH_3 unit a softer Lewis acid than alane and therefore prefer phosphine coordination, as does gallane. However, unlike gallane, indane appears to take on higher coordination numbers, which is a well documented feature of alane chemistry. Indeed, it appears that indane prefers even higher coordination numbers than alane as the latter cannot form a 2 : 1 adduct with PCy_3 (*cf.* **13**). These trends were further examined with the attempted preparation of an arsine–indane complex, $[InH_3(AsCy_3)]$, however, not surprisingly, no stable adduct could be obtained.[31]

Both **10** and **13** have been crystallographically characterised and in the case of **10** the hydride ligands were located. Although not terribly accurate, the average In–H distance was found to be 1.68 Å which is significantly longer than M–H bonds in alane and gallane adducts (*e.g.* $[AlH_3(PCy_3)]$ 1.53 Å and $[GaH_3(PCy_3)]$ 1.48 Å).[4] Most significantly, the geometry around the indium centre is a flattened tetrahedron (av. P–In–H 101.4°; av. H–In–H 116.2°). Similar flattenings are common for alane and gallane complexes and imply that the MH_3 units are relatively weak Lewis acids. In **13** the phosphine donors take up the axial positions of a trigonal bipyramid and the In–P bond lengths are some 0.34 Å longer than in **10**. This significant difference was put down to a combination of steric and electronic factors.

All the phosphine–indane complexes mentioned here displayed strong In–H stretching absorptions in what is now known to be the normal region for InH_3 complexes (*ca.* 1630–1690 cm^{-1}). Of the data obtained so far there seems to be an inverse correlation between the strength of the donor ligand and the position of this band. In several cases the resonances for the hydride ligands were observed in ^1H NMR spectra of the complexes though these were significantly broadened due to the quadrupolar nature of the indium centre to which they are bonded (^{115}In 95%, I = 9/2; ^{113}In 5%, I = 9/2). Again, a trend is emerging which points to these resonances occurring at *ca.* 1 ppm to lower field than for corresponding Al and Ga complexes, *e.g.* $[MH_3(PCy_3)]$, M = Al δ 4.32 ppm; Ga δ 4.25 ppm; In δ 5.61 ppm. At present there is no explanation for this observation.

Carbene complexes

Although phosphine complexes such as **10** and **13** are stable at room temperature in the solid state they are not in solution which makes an investigation of their further chemistry difficult. We began looking at the use of imidazol-2-ylidenes, or 'Arduengo carbenes' as they are sometimes known, for this purpose. These room temperature stable carbenes were seen as potentially ideal in that they are extremely nucleophilic, easy to prepare, can incorporate bulky N-substituents and are known to behave like classical Lewis bases in combination with main group Lewis acids.[37] These properties have led to their use in the stabilisation of a variety of main group complexes including $[AlH_3(IMes)]$, IMes = $:CN(Mes)C_2H_2N(Mes)$, Mes = mesityl, which melts at 246 °C.[38] This is *ca.* 100–150 °C greater than the decomposition temperatures of normal tertiary amine–alane complexes.[4,5] To predict if these carbenes would have a similar stabilising effect toward the InH_3 fragment DFT studies have been carried out on the model carbene–indane adduct, $[InH_3\{CN(H)C_2H_2N(H)\}]$, and have found the ligand binding energy to be 110.8 kJ mol^{-1} which can be compared to values of 64.5 kJ mol^{-1} and 58.2 kJ mol^{-1} for $[InH_3(NMe_3)]$ and $[InH_3(PMe_3)]$ respectively.[39] Therefore it seemed likely that carbene–indane adducts might well be more stable than either tertiary amine or phosphine adducts.

Our initial approach was to carry out hydride/halide exchange reactions on 1 : 1 and 2 : 1 carbene adducts of indium halides. Several of these adducts, **15** and **16**, were prepared and structurally characterised[40] but when treated with a variety of hydride sources, *e.g.* LiH, $LiInH_4$, $LiAlH_4$ *etc.* no reaction was observed (Scheme 3). More success was had when the same

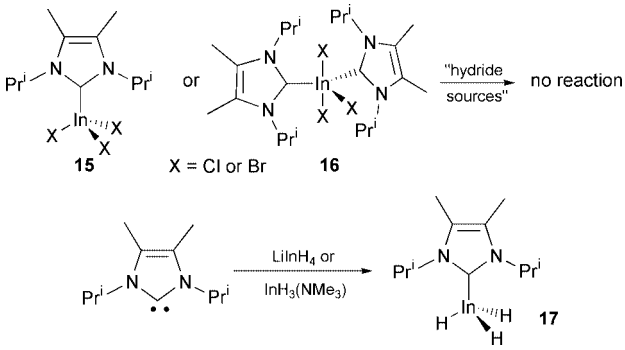

Scheme 3

carbene was treated with $LiInH_4$ or $[InH_3(NMe_3)]$ which afforded the first carbene–indane adduct, **17**.[29,30] The latter reaction was a simple ligand displacement but in the former a thermally unstable by-product, thought to be a complex indium hydride species, was formed. Despite the aforementioned theoretical predictions, complex **17** proved to be disappointingly unstable in that it decomposed above −5 °C in the solid state and −20 °C in solution. However, the decomposition products did not include the free carbene, but a complex mixture of products that contained organoindium species. Therefore it was thought that in this case decomposition proceeded *via* metallation of the carbene isopropyl substituents by the InH_3 unit.

Accordingly the mesityl substituted carbene, IMes **18**, was employed in identical reactions as it was thought that it would be sterically less viable for any formed adduct to decompose *via*. metallation of the N-substituents. This indeed proved to be the case and the reactions depicted in Scheme 4 yielded **19** in up to a 86% yield.[41] Interestingly in the reaction of **18** with $LiInH_4$,

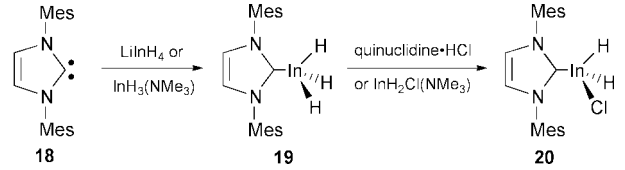

Scheme 4

LiH was the by-product which contrasts with the previously mentioned reaction. Moreover, when $[InH_3(NMe_3)]$ was reacted with two equivalents of either IMes or $:CN(Pr^i)C_2H_2N(Pr^i)$ only the 1:1 adducts were formed. This is perhaps not surprising on steric grounds but contrasts with the formation of the 2:1 indium halide adducts, **16**, and is evidence for the weaker Lewis acidity of the InH_3 unit relative to InX_3, X = Cl or Br.

Complex **19** proved to be remarkably stable in that it remained intact in the solid state up to 115 °C (*cf.* $[AlH_3(IMes)]$ mp 246 °C,[38] $[GaH_3(IMes)]$ 214 °C decomp.[41]) and can be heated as a toluene solution for up to 2.5 hours before decomposition is complete. The decomposition of **19** in solution has been studied and in no case does this occur *via* metallation reactions (*cf.* the facile decomposition of **17**). In fact, this decomposition is solvent dependent. For example, heating toluene solutions of **19** afforded In metal, H_2 gas and returned the free ligand in a similar manner to the decomposition of Lewis base adducts of alane and gallane.[4,5] However, in THF and in the presence of a catalytic amount of indium metal, decomposition occurs *via* hydrogen transfer from the InH_3 unit to the carbene ligand to give indium metal and the dihydroimidazole, $H_2CN(Mes)C_2H_2N(Mes)$. More surprising is the decomposition of **19** in CH_2Cl_2 which gives high yields of $[InCl_3(IMes)]$ as a result of chloride abstraction from the solvent.

The crystal structures of both **17** and **19** have been reported though in both the hydride ligands were not located. Both are monomeric with In–C bond lengths in the normal region for indium alkyls. In each there is a degree of delocalisation over the NCN fragment of the carbene ligands which is manifested by an opening of this angle relative to that in the free carbene. The NMR and IR data for the compounds confirmed the presence of the hydride ligands and the latter revealed the In–H stretching absorptions (**17** 1640 cm^{-1}; **19** 1640 cm^{-1}) to be at the low end of the normal range. This observation is in line with the highly nucleophilic nature of the ligands which should weaken the In–H bonds in the complexes relative to phosphine–indane complexes for example. In addition, the deuteride analogue of **19**, $[InD_3(IMes)]$, has been prepared and its IR spectrum shows a strong In–D stretch at 1180 cm^{-1}, which is shifted by the expected amount from the corresponding In–H stretch. Finally, if one of the hydride ligands of **19** is substituted with a chloride, the resulting complex, **20** (Scheme 4), shows an In–H stretch at a significantly higher frequency (1737 cm^{-1}) which is no doubt a result of the chloride ligand drawing electron density away from the In centre, thus strengthening the two In–H bonds relative to those in **19**.

Recently we have extended this work to investigate the interaction of bidentate carbenes with indane. The rationale here was that alane forms very stable ionic species of the type $[AlH_2(L)]^+[AlH_4]^-$ with polydentate donors[34] and we thought a similar outcome might result with indane. However, the reaction of **21** with either $[InH_3(NMe_3)]$ or $LiInH_4$ only gave the indane rich 2:1 adduct, **22** (Scheme 5) under any stoichiometry of reactants.[31] This is in line with our previous observation that the InH_3 fragment will only form four-coordinate adducts with nucleophilic carbene ligands. By contrast, when the same carbene is reacted with $InBr_3$ in any stoichiometry it forms a five-coordinate chelate complex, **23**, which again implies that InH_3 is a weaker Lewis acid than indium trihalides.

Unfortunately, **22** did not prove to be very thermally stable as it decomposes slowly above 0 °C. However, in its crystal structure the hydride ligands were located for the first time in a carbene–indane complex. As expected, the tetrahedral geometry about the In centres is much less flattened (C–In–H 105.7° av., H–In–H 112.9° av.) than in the phosphine adduct, **10**, which gives evidence for the relative strength of the donors (carbene > phosphine) in these complexes. The In–H distances (1.72 Å av.) are close to those in **10**.

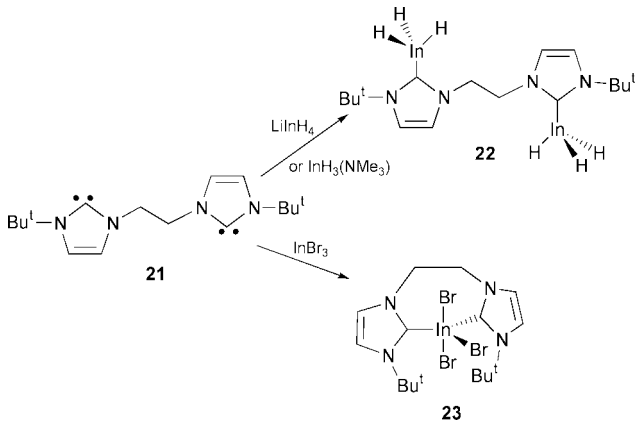

Scheme 5

Reactivity

Use in inorganic synthesis

Now that room temperature stable indane complexes have been developed it is of great interest to investigate their further reactivity and compare it to alane and gallane chemistry. To date only preliminary and largely unconnected steps have been made in this direction which, in the case of inorganic synthesis, are summarised in Scheme 6. There is no doubt that a more complete picture will soon emerge in this respect.

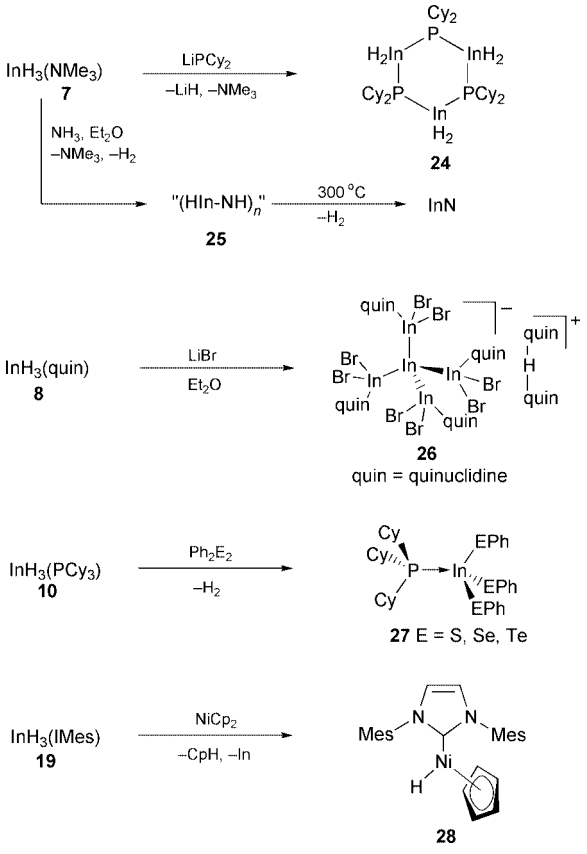

Scheme 6

The *in-situ* generated indane complex, **7**, reacts with $LiPCy_2$ to give the trimeric phosphido–indium hydride complex, **24**.[36a] This proved to be moderately stable in the solid state (decomp. 64 °C) but did not decompose in solution as hoped to give InP and cyclohexane but instead afforded $In_{(s)}$, H_2 and PCy_2H. X-Ray crystallography confirmed its structure and the location of the hydride ligands gave an average In–H bond length of 1.71 Å for the complex. When NH_3 was passed through an ethereal

solution of **7** at −30 °C an amorphous white precipitate immediately deposited which is thought to be some form of imido–indane polymer, **25**. This is stable at room temperature but when heated at 300 °C yields relatively pure nanocrystalline InN as determined by X-ray powder diffractometry.[31] This result mimics similar work with alane and gallane complexes[7] and with development could offer a facile route into other group 13–15 materials, *e.g.* InP from the reaction of **7** with PH_3.

One of the most interesting reactions we have encountered is the controlled decomposition of [InH_3(quinuclidine)] **8** at −30 °C in the presence of LiBr, the by-product in the synthesis of the $LiInH_4$ precursor to **8**. At this temperature over 5 days the solution slowly changes from colourless to deep orange and orange diamagnetic crystals of **26** deposit in 15% yield. These are unstable above 0 °C and probably form from a combination of H_2 elimination and H/Br exchange.[31] The crystal structure shows the anion to consist of a tetrahedron of 4 indium atoms around a central In. Each of the outer indium atoms is coordinated by two bromides and a quinuclidine giving an average In oxidation state of 1.4. The cation consists of two quinuclidine molecules coordinated to a proton in a linear fashion. Interestingly, a neutral gallium relation of this complex, [$Ga_5Cl_7(OEt_2)_5$], has been reported by Schnöeckel and coworkers to have arisen from the controlled decomposition/redistribution of metastable [$Ga^{I}Cl(OEt_2)$].[42] There is no precedent for the formation of **26** in alane or gallane chemistry and it offers the exciting possibility of preparing sub-valent indium hydride compounds *via* the controlled decomposition of indane complexes.

Other reactions that have been investigated include the use of the phosphine–indane complex, **10**, in the formation of a series of monomeric tris(chalcogenolato)indium complexes, **27**, all of which were crystallographically characterised.[36a] Finally, the interaction of the carbene–indane complex, **19**, with transition metal complexes is being systematically examined in the hope that low valent transition metal fragments can be oxidatively inserted into the In–H bond. Although no indium containing products have yet been obtained, a noteworthy result from this study has come from the reaction of **19** with nickelocene.[39] This effected both a hydride and a carbene transfer to the nickel centre with a concomitant loss of cyclopentadiene to form **28**.

Use in organic synthesis

Boron and aluminium hydride complexes are invaluable reducing agents in organic synthesis. Even gallium trihydride complexes have found a niche as chemoselective reductants as a result of the lesser polarity of the Ga–H bond relative to the Al–H bond.[43] It was of considerable interest to us to examine the exploitation of indane complexes as selective reducing agents given the chemical and physical differences they show to their lighter group 13 analogues. This seemed especially timely considering the recent emergence of indium and its complexes as reagents in organic synthesis.[6,44] Indeed, the selective reducing abilities of several indium hydride complexes had been previously confirmed though in these instances the active species were invariably prepared *in-situ*, were not thermally stable and were poorly characterised.[18–20,45] It was apparent that if easily prepared, room temperature stable indane complexes did show selectivity in organic reductions they might be of real use to organic chemists.

Indium has an electronegativity between that of Al and Ga. Therefore it might be expected that the In–H bond has a polarity between that of Al–H and Ga–H bonds. As a result, indane complexes could display a degree of chemoselectivity in the reduction of organic functionalities. This proved to be the case as both **10** and **19** readily reduce ketones but showed no activity towards a variety of ester functionalities that are readily reduced by alane complexes.[46] In addition, the debromination qualities of **10** toward 2,4′-dibromoacetophenone (57% C–Br cleavage) are mid way between those of alane complexes, which quantitatively effect α C–Br cleavage, and gallane complexes which show only minimal activity towards alkyl bromides. It is noteworthy that [$BH_3(NMe_3)$] is completely inactive towards this substrate. In addition, the reduction of styrene oxide by **10** highlights an intermediate regioselectivity of this reductant (reduction product mixture: 56% 1-phenylethanol, 44% 2-phenylethanol) over [$GaH_3(PCy_3)$] which gives 99% of the secondary alcohol and [AlH_3(quinuclidine)] which yields 37% of the primary alcohol as a reduction product.

Indium has a greater covalent radius (1.50 Å) than either aluminium or gallium (1.25 Å) which means that like alane but unlike gallane, indane should form hypervalent complexes as has been demonstrated with the preparation of **13**. It was thought this preference could lead to indane complexes showing diastereoselectivity in the reduction of potentially chelating bifunctional substrates. This has been confirmed with the reductions of benzoin, benzil and benzoin methyl ether by **10**, all of which occur with >99% disastereoselectivity. These results suggest a chelation of the substrate to the indium centre of the complex which allows a directed hydride delivery leading to the observed result.[46]

Efforts have also been made to examine the enantioselectivity of indane reductions using the *in-situ* generated complexes [InH_3{PPh_2((+)-neomenthyl)}] and [InH_3((−)-sparteine)]. Unfortunately, when a range of prochiral ketone substrates were employed no significant enantiomeric excesses were observed.[31] This work is now moving towards the use of chiral carbene–indane complexes for this purpose.

Outlook

In the past 4 years the stabilisation of indane complexes has been achieved and their structure, bonding, properties and reactivity have begun to be explored and understood. This work has showed that indane complexes display many similarities to their alane and gallane counterparts but also significant differences which can often be accounted for by examining the properties of the group 13 elements themselves. Now that reasonably stable indane complexes have been developed their further chemistry should be systematically explored. Areas in which they might be especially useful include their employment as precursors to sub-valent indium hydride complexes (*cf.* **26**) which are currently unknown. In addition, our preliminary work suggests they might find valuable use as materials precursors, as have alane and gallane complexes.

Of course the obvious question for the future is can stable TlH_3 (thallane) or other thallium hydride complexes be formed? It would perhaps be thought that the weakness of the Tl–H bond and the potential for thallane complexes to undergo reductive elimination of hydrogen would argue against this. However, we have recently prepared the first carbene–thallium complexes, *e.g.* [$TlCl_3$(IMes)] (decomp. 208 °C), which are remarkably stable under normal conditions and show little desire to undergo reductive decomposition processes.[47] This again raises the question, would a complex such as [TlH_3(IMes)] be isolable under normal conditions? Only time will tell.

Acknowledgements

Thanks go to my current and former postgraduate students and postdoctoral colleagues who made this work possible through their perseverance and attention to detail. The results reported in this article would not have been possible without them. Their names are cited in the references. Funding for this work was

from the EPSRC who I must thank for their continuing support.

Notes and references

1 (*a*) H. C. Brown, *Hydroboration*, Benjamin Reading, MA, 1962; (*b*) I. Beletskaya and A. Pelter, *Tetrahedron*, 1997, **53**, 4957.
2 T. P. Fehlner, *J. Chem. Soc., Dalton Trans*., 1998, 1525.
3 E. Wiberg and E. Amberger, *Hydrides of the Elements of Main Groups I–IV*, Elsevier, London, 1971.
4 M. G. Gardiner and C. L. Raston, *Coord. Chem. Rev*., 1997, **166**, 1.
5 C. Jones, G. A. Koutsantonis and C. L. Raston, *Polyhedron*, 1993, **12**, 1829.
6 *Chemistry of Aluminium, Gallium, Indium and Thallium*, ed. A. J. Downs, Blackie, Glasgow, 1993.
7 J. A. Jegier and W. L. Gladfelter, *Coord. Chem. Rev*., 2000, **206–207**, 631.
8 (*a*) E. Wiberg and M. Schmidt, *Z. Naturforsch., Teil B*, 1957, **12**, 54; (*b*) E. Wiberg, O. Dillmann, H. Nöth and M. Schmidt, *Z. Naturforsch., Teil B*, 1957, **12**, 56, 59; (*c*) E. Wiberg, O. Dillmann and M. Schmidt, *Z. Naturforsch., Teil B*, 1957, **12**, 60.
9 P. Hunt and P. Schwerdtfeger, *Inorg. Chem*., 1996, **35**, 2085.
10 P. Pullumbi, Y. Bouteiller, L. Manceron and C. Mijoule, *Chem. Phys*., 1994, **185**, 25.
11 A. G. Avent, C. Eaborn, P. B. Hitchcock, J. D. Smith and A. C. Sullivan, *J. Chem. Soc., Chem. Commun*., 1986, 988.
12 O. T. Beachley, S. L. Chao, M. R. Churchill and R. F. See, *Organometallics*, 1992, **11**, 1486.
13 M. R. Churchill, C. H. Lake, S. L. Chao and O. T. Beachley, *J. Chem. Soc., Chem. Commun*., 1993, 1577.
14 C. Kümmel, A. Meller and M. Noltemeyer, *Z. Naturforsch., Teil B*, 1996, **51**, 209.
15 S. Aldridge, A. J. Downs and S. Parsons, *Chem. Commun*., 1996, 2055.
16 D. E. Hibbs, M. B. Hursthouse, C. Jones and N. A. Smithies, *Organometallics*, 1998, **17**, 3108.
17 S. I. Bakum, S. F. Kuznetsova and V. P. Tarasov, *Zh. Neorg. Khim*., 1997, **44**, 346.
18 M. Yamada, K. Tanaka, S. Araki and Y. Butsugan, *Tetrahedron Lett*., 1995, **36**, 3169.
19 T. Miyai, K. Inoue, M. Yasuda, I. Shibata and A. Baba, *Tetrahedron Lett*., 1998, **39**, 1929.
20 K. Inoue, M. Yasuda, I. Shibata and A. Baba, *Tetrahedron Lett*., 2000, **41**, 113.
21 H.-J. Himmel, A. J. Downs, T. M. Greene and L. Andrews, *Organometallics*, 2000, **19**, 1060.
22 H.-J. Himmel, A. J. Downs, J. C. Green and T. M. Greene, *J. Chem. Soc., Dalton Trans*., 2001, 535.
23 H.-J. Himmel, A. J. Downs and T. M. Greene, *Inorg. Chem*., 2001, **40**, 396.
24 H.-J. Himmel, A. J. Downs and T. M. Greene, *J. Am. Chem. Soc*., 2000, **122**, 9793.
25 H.-J. Himmel, A. J. Downs and T. M. Greene, *J. Am. Chem. Soc*., 2000, **122**, 922.
26 H.-J. Himmel, A. J. Downs and T. M. Greene, *Chem. Commun*., 2000, 871.
27 A. J. Downs and C. R. Pullham, *Chem. Soc. Rev*., 1994, 175.
28 M. Chaillet, A. Dargelos and C. J. Marsden, *New J. Chem*., 1994, **18**, 693.
29 D. E. Hibbs, M. B. Hursthouse, C. Jones and N. A. Smithies, *Chem. Commun*., 1998, 869.
30 M. D. Francis, D. E. Hibbs, M. B. Hursthouse, C. Jones and N. A. Smithies, *J. Chem. Soc., Dalton Trans*., 1998, 3249.
31 M. L. Cole, PhD Thesis, Cardiff University, 2001.
32 C. Jones, PhD Thesis, Griffith University, 1992.
33 E. C. Ashby, *J. Am. Chem. Soc*., 1964, **86**, 1883.
34 J. L. Atwood, K. D. Robinson, C. Jones and C. L. Raston, *J. Chem. Soc., Chem. Commun*., 1991, 1697.
35 J. L. Atwood, K. D. Robinson, F. R. Bennett, F. M. Elms, G. A. Koutsantonis, C. L. Raston and D. J. Young, *Inorg. Chem*., 1992, **31**, 2673.
36 (*a*) M. L. Cole, D. E. Hibbs, C. Jones and N. A. Smithies, *J. Chem. Soc., Dalton Trans*., 2000, 545; (*b*) D. E. Hibbs, C. Jones and N. A. Smithies, *Chem. Commun*., 1999, 185.
37 C. J. Carmalt and A. H. Cowley, *Adv. Inorg. Chem*., 2000, **50**, 1.
38 A. J. Arduengo III, H. V. R. Dias, J. C. Calabrese and J. Davidson, *J. Am. Chem. Soc*., 1992, **114**, 9724.
39 C.D. Abernethy, S.T. Howard, and C. Jones, unpublished results.
40 S. J. Black, D. E. Hibbs, M. B. Hursthouse, C. Jones, K. M. A. Malik and N. A. Smithies, *J. Chem. Soc., Dalton Trans*., 1997, 4313.
41 C. D. Abernethy, M. L. Cole and C. Jones, *Organometallics*, 2000, **19**, 4852.
42 D. Loos, H. Schnöeckel and D. Fenske, *Angew. Chem., Int. Ed. Engl*., 1993, **32**, 1059.
43 C. L. Raston, A. F. H. Siu, C. J. Tranter and D. J. Young, *Tetrahedron Lett*., 1994, **35**, 5915.
44 M. R. Pitts, J. R. Harrison and C. J. Moody, *J. Chem. Soc., Perkin Trans. 1*, 2001, 955.
45 M. Yamada, T. Horie, M. Kawai, H. Yamamura and S. Araki, *Tetrahedron*, 1997, **53**, 15 685.
46 C. D. Abernethy, M. L. Cole, A. J. Davies and C. Jones, *Tetrahedron Lett*., 2000, **41**, 7567.
47 M. L. Cole, A. J. Davies and C. Jones, *J. Chem. Soc., Dalton Trans*., 2001, 2451.

CHEMCOMM
Communication
www.rsc.org/chemcomm

Intramolecular electron conduction along DNA strands and their temperature dependency in a DNA-aligned cast film

Hajime Nakayama,[a] Hiroyuki Ohno[b] and Yoshio Okahata[a]

[a] *Department of Biomolecular Engineering, Tokyo Institute of Technology, Nagatsuda, Midori-ku, Yokohama 226-8501, Japan. E-mail: yokahata@bio.titech.ac.jp*
[b] *Department of biotechnology, Tokyo University of Agriculture & Technology, Koganei, Tokyo, 184-8588, Japan*

Received (in Cambridge, UK) 13th August 2001, Accepted 20th September 2001
First published as an Advance Article on the web 22nd October 2001

Electroconductivity along a long DNA strand (*ca.* 10 μm length) in a DNA-aligned cast film of DNA–lipid complex was measured on a comb-type electrode (5 μm distance), and it could be reversibly regulated by temperatures across 70 °C.

DNA is interesting as a conducting molecule along double strands. There have been many approaches to study the electric conductivity along a DNA strand.[1–9] Barton and co-workers reported in pioneer work that photoinduced charge transfer between donors and acceptors immobilized at both ends of DNA strands could be observed in homogeneous aqueous solution.[1] Photoinduced or long range charge transfer along DNA molecules has also been studied in aqueous solution.[2,3] Conductivities of a DNA monolayer on Au electrode have been studied by cyclic voltammogram[4] or atomic force microscopy (AFM)[5] in aqueous solution. Fink and Schonenberger measured directly the electrical conductivity of dry DNA fibers across two electrodes separated by the very short distance of 8 nm.[6] Recently, superconductivities of DNA fibers across a sub-micronic slit on mica plate has been reported.[7] The conductivity values obtained in these studies are roughly in the wide range of 1–10^{-5} S cm^{-1} and are still a matter of controversy. This is due to the widely spread measurement methods or media depending on different sample preparations. We have reported that a large, self-standing DNA film (10 × 10 cm, 20–100 μm thick), in which DNA strands aligned in one direction, could be prepared by casting from organic solution of DNA–cationic lipid complexes.[8] We observed high anisotropic conductivity along the DNA strands in the film.[9] The DNA-aligned film has many advantages as an electric conducting material, being large, flexible, self-standing and thermo-stable.

In this communication, we report molecular level evidence of *electron* conductivity through DNA strands in the DNA-aligned cast film prepared from two different length of DNAs (*ca.* 0.2 and 10 μm per molecule), by measuring direct or alternating currents on a comb-type electrode plate (5 μm distance between two electrodes) at different temperatures.

The DNA-aligned cast film was prepared as follows.[8,9] Two different lengths of DNA were extracted and purified from salmon testes: *ca.* 0.2 μm length, average *M* 3 × 10^5, 500 bps *ca.* 10 μm length, *M* 2 × 10^7, 30 000 bps. An aqueous solution of DNA^{n-} $n Na^+$ and an aqueous solution of 1.1 eq. mol of a cationic amphiphile (**1**) were mixed at rt and the precipitated DNA–lipid polyion complex (1 : 1 ratio of phosphate anion to cationic lipid) was collected and solubilized in chloroform–ethanol (4 : 1 v/v). The solution (40 mg mL^{-1}, 4 wt%) was cast on a Teflon plate and the solvent was evaporated slowly under saturated vapor at rt. The obtained self-standing film (*ca.* 60 μm thick) was transparent, water-insoluble, and physically stable below 150 °C. The DNA film could be stretched mechanically 3–5 times in length at rt. From X-ray diffraction, polarized microscopy, and polarized absorption spectra measurements, DNA strands were aligned with a distance of 41 Å along the stretching direction as shown schematically in Fig. 1.[8] The distance between stacked base pairs of DNAs in the film was 3.4 Å, similar to the native DNAs in aqueous solution. The stretched film was still transparent and physically strong. The orientation of DNA strands in the film disappeared on heating to 150 °C (glass transition temperature, T_g = 135 °C).

The stretched DNA film (5 × 5 mm, 20 ± 5 μm) was put on a comb-type electrode plate, in which the distance between two electrodes is 5 μm. The dc conductivity was measured using an ammeter (R8340A, Advantest, Co., Tokyo) at 20 °C in a dry box. Typical results are shown in Fig. 2. When the stretched DNA film prepared from long DNA strands (10 μm length, 30,000 bps) was put on the comb-type electrodes with the DNA strand axis aligned perpendicularly to the electrodes, large ohmic currents (0–0.7 mA) were observed that increased linearly with increasing applied voltage in the range of −0.5–+0.5 V. The conductivity was calculated from the slope to be 5 × 10^{-3} S cm^{-1}. The currents were constant during measurements and did not decrease for at least 10 min. In contrast, when the same film prepared from the long DNA was placed with DNA strands aligned *parallel* to the two electrodes, electric current was hardly observed even at voltages up to 100 mV (less than 0.001 mA or 10^{-6} S cm^{-1}, data not shown).[9] When the DNA-aligned film prepared from the short DNA molecules (0.2 μm length, 500 bps) was put perpendicularly to the electrodes, very small ohmic currents (0–1 μA, 10^{-6} S cm^{-1}) were observed depending on applied voltage, and the current diminished within 5 s (Fig. 2B). The constant, large, and ohmic currents along the long DNA strands indicate electron conduction along DNA strands aligned in the film, since one 10 μm DNA molecule can be expected to bridge the distance of 5 μm between two electrodes in the film. In contrast, the short 0.2 μm DNA strands could not bridge two electrodes and only very small and immediately-diminished currents were observed due to the rate-limiting diffusion of impurity ions between inter-molecular short DNA strands in the film.

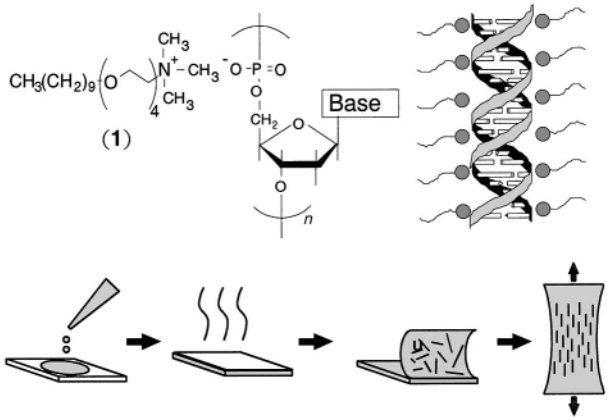

Fig. 1 Schematic illustration of a DNA aligned film prepared from casting organic soluble DNA–lipid (**1**) complex with subsequent uniaxial stretching.

 DOI: 10.1039/b107228e

Fig. 3 shows temperature dependences of Cole–Cole plots of DNA-aligned cast film with the DNA strands placed perpendicularly to the two comb-type electrodes. Alternating currents were measured by using a universal impedance analyzer (Model 53131A, Hewlett Packard, CO. Tokyo) by changing the frequencies from 10 Hz to 10 MHz at 20–100 °C in a dry box. With the film prepared from the long DNA (10 μm molecular length), the apparent resistances at the zero imaginary of impedance were constant at 400 Ω independent of temperature from 25 to 60 °C (Fig. 3A). When the film prepared from the short DNA (0.2 μm length) was employed, in which DNA molecules cannot bridge two electrodes, the resistance was greatly increased to 100–650 kΩ depending on temperature (Fig. 3B). The conductance (σ) obtained from the resistance is plotted against temperature in Fig. 4. The conductance obtained from the long DNA film was 10^{-3} S cm^{-1}, consistent with that obtained by direct current measurements (Fig. 2), and was independent of temperature from 20 to 60 °C. In contrast, the conductance of the short DNA film was very small and increased linearly with increasing temperatures (10^{-7} to 10^{-5} S cm^{-1}). Thus, the temperature-independent conductance of the long DNA film again indicates electron conductance along intramolecular DNA strands. The temperature-dependent conductance of the short DNA film shows the small ionic transportation between short DNA molecules.

When the film prepared from the long DNAs was heated above 60 °C, the conductance decreased drastically to 10^{-6} S cm^{-1}, but reverted to the original value when the temperature was decreased to below 60 °C (curve A in Fig. 4). When the film was heated above 135 °C, the conductivity diminished and did not revert to the original value, since the orientation of the DNA strands in the film disappeared above T_g = 135 °C. This indicates that the anisotropic conductivity along DNA strands can be switched *on* and *off* reversibly depending on whether the temperature is below or above 70 °C. Since the intermolecular orientation of DNA strands in the film does not change below 135 °C, this reversible conductivity change can be explained by reversible changes in intramolecular stacking of base pairs of DNA strands aligned in the film.

In summary, we could directly observe the switchable electron conduction along intramolecular DNA strands by using DNA-aligned cast film on a comb-type electrode. This was possible because of the large area and self-standing, physically strong, and thermotropic liquid crystalline nature of the DNA-aligned cast film.

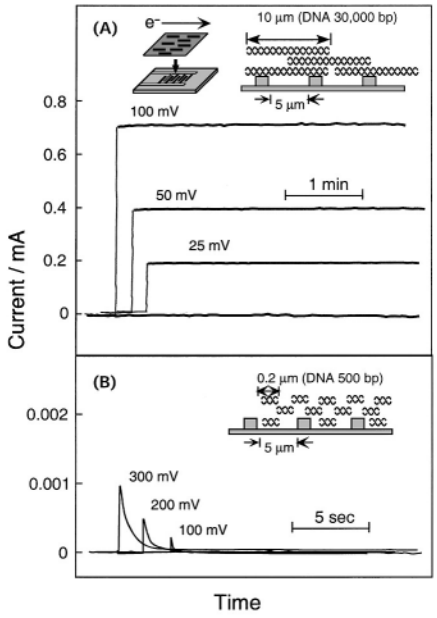

Fig. 2 Direct currents of DNA-aligned films (5 × 5 mm, thickness 20 ± 5 μm) on a comb-type electrode (distance between two electrodes: 5 μm) at 25 °C in a dry box. (A) The film prepared from long DNA strands (10 μm, 30 000 bps) and (B) from short DNA strands (0.2 μm, 500 bps). Both films aligned perpendicularly to the two electrodes.

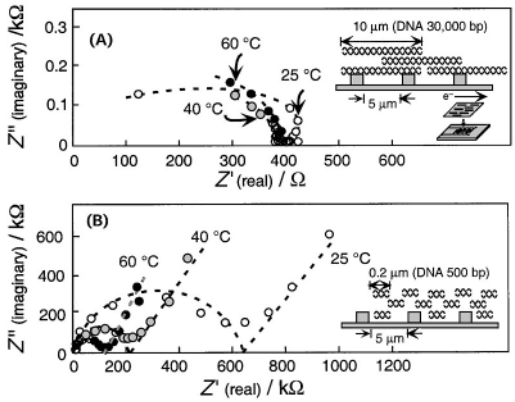

Fig. 3 Cole–Cole plots (10 Hz to 10 MHz frequencies) of alternating currents of the DNA-aligned film placed perpendicularly to the comb-type electrode (5 μm distance). (A) The film prepared from long DNA molecules (10 μm, 30,000 bps) and (B) from short DNA molecules (0.2 μm, 500 bps).

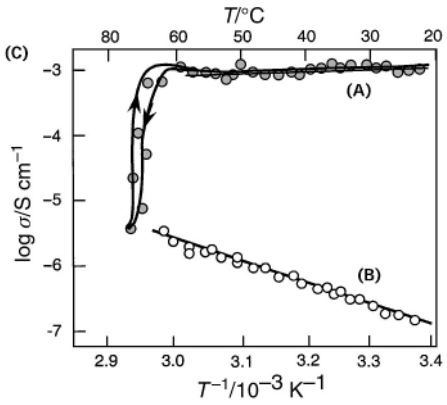

Fig. 4 Temperature dependence of alternating conductivities of **Fig. 3**. (A) The film prepared from long DNA molecules (10 μm, 30 000 bps) and (B) from short DNA molecules (0.2 μm, 500 bps).

Notes and references

1 C. J. Murphy, M. R. Arkin, Y. Jenkins, N. D. Ghatlia, S. H. Bossmass, N. J. Turro and J. K. Barton, *Science*, 1993, **262**, 1025; R. E. Homlin, P. E. Dandliker and J. K. Barton, *Angew. Chem., Engl. Int. Ed.*, 1997, **36**, 2714; S. O. Kelly, N. M. Jackson, M. G. Hill and J. K. Barton, *Angew. Chem., Int. Ed.*, 1999, **38**, 941.

2 F. D. Lewis, R. L. Letsinger and M. R. Wasielewski, *Acc. Chem. Res.*, 2001, **34**, 159.

3 G. B. Shuster, *Acc. Chem. Res.*, 2000, **33**, 253; B. Giese, *Acc. Chem. Res.*, 2000, **33**, 631.

4 G. Hartwith, D. J. Caruana, T. de L. Woodyear, Y. Wu, C. N. Campbell and A. Heller, *J. Am. Chem. Soc.*, 1999, **121**, 10 803.

5 D. J. Wold and C. D. Frisbie, *J. Am. Chem. Soc.*, 2000, **122**, 2970.

6 H.-W. Fink and C. Schonenberger, *Nature*, 1999, **398**, 407.

7 A. Y. Kasumov, M. Kociak, S. Gueron, B. Roeulet, V. T. Volkov, D. V. Klinov and H. Bouchiat, *Science*, 2001, **291**, 280.

8 K. Ijiro and Y. Okahata, *J. Chem. Soc., Chem. Commun.*, 1992, 1339; K. Tanaka and Y. Okahata, *J. Am. Chem. Soc.*, 1996, **118**, 10 679; Y. Okahata, T. Kobayashi and K. Tanaka, *Langmuir*, 1996, **12**, 1326; Y. Okahata and K. Tanaka, *Thin Solid Films*, 1996, **284/285**, 6.

9 Y. Okahata, T. Kobayashi, K. Tanaka and M. Shimomura, *J. Am. Chem. Soc.*, 1998, **120**, 6165; Y. Okahata, T. Kobayashi, H. Nakayama and K. Tanaka, *Supramol. Sci.*, 1998, **5**, 317; Y. Okahata and H. Nakayama, *Proc. Jpn. Acad. Ser. B*, 2000, **76**, 145.

CHEMCOMM Communication
www.rsc.org/chemcomm

Configurational ordering of a cationic dinuclear triple helicate by chiral TRISPHAT anions†

Jérôme Lacour,* Jonathan J. Jodry and David Monchaud

Département de Chimie Organique, Université de Genève, quai Ernest Ansermet 30, CH-1211 Genève 4, Switzerland. E-mail: Jerome.Lacour@chiorg.unige.ch; Fax: (41-22) 328-73-96

Received (in Cambridge, UK) 10th September 2001, Accepted 25th September 2001
First published as an Advance Article on the web 22nd October 2001

Chiral TRISPHAT anions behave as efficient asymmetric hosts controlling with high efficiency the configuration of a cationic dicobalt(II) triple helicate—de up to 82%.

Helicate derivatives made by the self-assembly of polydentate organic ligands and metal ions have received much attention over the last two decades.[1] They are chiral and the helical enantiomers are characterized by their *plus* (*P*) or *minus* (*M*) handedness. To obtain chiral helicates in a predominant *P* or *M* configuration, the most common strategy, apart from resolution, has been to add stereogenic elements to the backbone of the ligands. Intramolecular diastereoselective interactions occur between the enantiopure strands and lead to the preferred formation of one diastereomer.[2] To date, there are several examples of high selectivity in the formation of double and triple helicates, in which enantiopure ligands completely control the configuration. The stereogenic elements are introduced either on the coordinating units, on the bridging elements or on a chiral template linking the strands together.[3]

An alternative strategy to control the configuration of the charged chiral complexes is to consider their asymmetric ion pairing with chiral counter-ions; intermolecular diastereoselective interactions controlling the stereoselectivity (Pfeiffer effect). However this approach, although efficient, has been essentially used with small molecules and simple coordination complexes.[4] Recently, Raymond *et al*. reported the asymmetric induction of chiral pyridinium cations onto an anionic dinuclear Ga(III) triple-stranded helicate, the extent of the diastereoselectivity being determined by chiroptical measurement.[5]‡ Herein, we report that the asymmetric induction of chiral counter-ions onto a triple helicate can be indeed an efficient process, a good level of configurational ordering from TRISPHAT **1** anions onto a cobalt(II) dinuclear triple helicate being observed in solution (diastereomeric excess (de) ≤ 82%, determined by ^{1}H NMR).

Previously, we reported the synthesis and resolution of D_3-symmetric tris(tetrachlorobenzenediolato)phosphate(V) anion **1** or TRISPHAT.[6] Associated with mononuclear ruthenium(II) or iron(II) tris(diimine) complexes, it is an efficient NMR chiral shift, resolving and asymmetric inducing agent.[7] However, in these studies, D_3-symmetric mononuclear complexes were used. It was then debatable whether **1** would behave as a good asymmetric inducer for cationic polynuclear helicates of more complex structure and geometry.

Chiral di- and polynuclear helicates of Fe(II), Ni(II) and Cu(I) racemize more slowly (factor 10^{-6}) than their mononuclear equivalents.[8] Their association with chiral anions has therefore led to their resolution into separated enantiomers rather than an asymmetric induction from the anions.[9] To perform our projected study, we thus derived a known configurationally stable helicate—Elliott's dinuclear iron(II) derivative **2** (Fig. 2, $[Fe_2(\mathbf{L})_3]^{4+}$, **L** = 1,2-bis[4-(4′-methyl-2,2′-bipyridyl)]-ethane)—into a configurationally labile dinuclear cobalt(II) derivative (**3**, $[Co_2(\mathbf{L})_3]^{4+}$).[10]

The synthesis of complexes [**3**][Δ-**1**]$_4$ was achieved in a single step as follows.† Treatment in hot water of $CoSO_4{\cdot}7H_2O$ with 1.5 equiv. of ligand **L** afforded a yellow solution of [**3**][SO_4]$_2$. Extraction of the cationic helicate **3** from the aqueous layer into the organic layer [CH_2Cl_2–acetone (25 : 1)], using 2 equiv. of [cinchonidinium][Δ-**1**], gave the desired complex [**3**][Δ-**1**]$_4$ as the major product, which was further purified by recrystallization.

The efficiency of anions **1** as chiral inducers was then simply demonstrated by ^{1}H NMR. Solutions of [**3**][Δ-**1**]$_4$ (0.50 mM) were prepared in mixtures of $CDCl_3$ and [D_6]-DMSO (100% to 20%) and analyzed. Due to the presence of the chiral TRISPHAT anions, we were able to distinguish between the diastereomeric pairs [*P*-**3**][Δ-**1**]$_4$ and [*M*-**3**][Δ-**1**]$_4$ as the spectra showed partial or complete separation for the signals of the chiral cation.§·¶ The diastereoselectivity of the asymmetric ion pairing between [*P*-**3**][Δ-**1**]$_4$ and [*M*-**3**][Δ-**1**]$_4$ was then directly calculated by the integration of the respective signals (Fig. 3). Upon decreasing solvent polarity (lower % DMSO), one diastereomer became predominant up to 82% de (diastereomeric ratio 10.1 : 1 in 20% [D_6]–DMSO–$CDCl_3$, Table 1). The study could not be performed in lower polar mixtures as compound [**3**][Δ-**1**]$_4$ precipitated in such solvent conditions.

So, with the decrease of the polarity of the solvent combination, a highly asymmetric induction took place in solution.‖ The equilibrium ([*P*-**3**][Δ-**1**]$_4$ ⇄ [*M*-**3**][Δ-**1**]$_4$) was

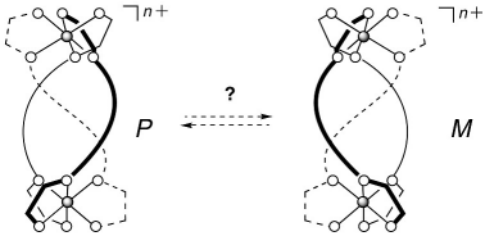

Fig. 1

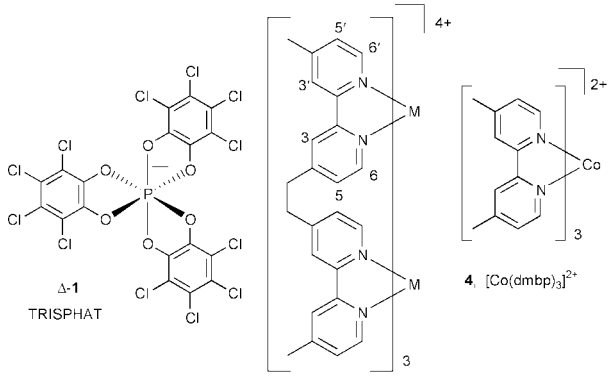

2, $[Fe_2(L)_3]^{4+}$
3, $[Co_2(L)_3]^{4+}$

Fig. 2

† Electronic supplementary information (ESI) available: synthesis and analytical data for compounds [**3**][Δ-**1**]$_4$ and [**4**][Δ-**1**]$_2$. See http://www.rsc.org/suppdata/cc/b1/b108110a/

 DOI: 10.1039/b108110a

consequently shifted towards the preferred diastereomer. The increase in diastereoselectivity as the polarity decreases is interpreted as the result of closer interactions between the ions.[11] Unfortunately, despite our efforts, we did not succeed in obtaining reliable solution CD spectra of complex [**3**][Δ-**1**]$_4$.†† Finally, to evaluate the efficiency of the chiral recognition of dinuclear helicate **3** by TRISPHAT anions, we measured the asymmetric induction of anions **1** onto mononuclear $[Co(dmbp)_3]^{2+}$ equivalent (Fig. 2, **4**, dmbp = 4,4′-dimethyl-[2,2′]bipyridinyl). Association of **4** with TRISPHAT was realized in a similar manner to **3**.† ^{1}H NMR analysis of salt [**4**][Δ-**1**]$_2$ in mixtures of [D$_6$]-DMSO–$CDCl_3$ revealed two sets of signals and, as for helicate **3**, a strong dependence of the diastereoselectivity as a function of the polarity of the solvent medium was observed (Table 1). In rather low-polar solvent conditions (7.5% DMSO–$CDCl_3$), only one of the two diastereomers was observed by ^{1}H-NMR (dr > 96%); its absolute configuration being [Δ-**4**][Δ-**1**]$_2$ as determined by CD analysis (0.1% DMSO–$CHCl_3$, 4.5 × 10^{-6} M).

Although the comparison of the diastereoselectivity of the association of TRISPHAT anions **1** and cations **3** and **4** was limited to a rather small range of solvent polarity, interesting observations could be made. In 20% [D$_6$]-DMSO–$CDCl_3$, a higher selectivity for complex [**3**][Δ-**1**]$_2$ (dr 10.1 : 1) than that for [**4**][Δ-**1**]$_2$ (dr 4.0 : 1) (Table 1) was determined. The stronger electrostatic attraction, due to the higher charge of the helicate, and the synergy resulting from mechanical coupling at both metal centers, all contribute to a higher asymmetric induction.

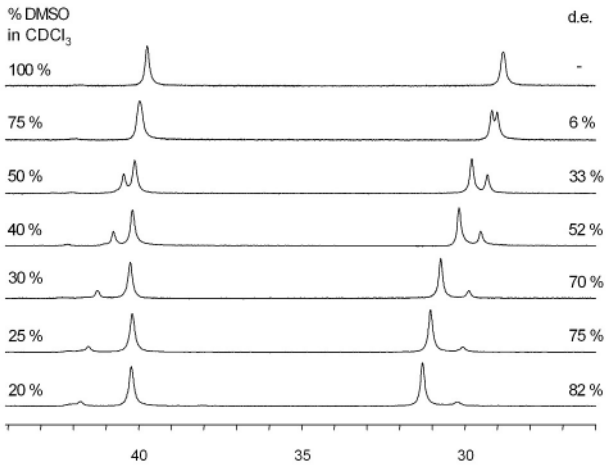

Fig.3 ^{1}H NMR spectra (δ 44–27 ppm) of [**3**][Δ-**1**]$_4$ in mixtures of [D$_6$]DMSO–$CDCl_3$.

Table 1 Asymmetric induction (diastereoselectivity) from TRISPHAT anions **1** onto dinuclear helicate **3** or mononuclear complex **4** as function of the percentage of DMSO in chloroform

	dr		de (%)	
% [D$_6$]DMSO	[**3**][Δ-**1**]$_2$	[**4**][Δ-**1**]$_2$	[**3**][Δ-**1**]$_2$	[**4**][Δ-**1**]$_2$
50	2.0 : 1	[a]	33	[a]
40	3.2 : 1	[a]	52	[a]
30	5.7 : 1	2.0 : 1	70	33
20	10.1 : 1	4.0 : 1	82	60
15	[a]	8.6 : 1	[a]	79
12.5	[a]	13.9 : 1	[a]	87
10	[a]	22.5 : 1	[a]	92
7.5	[a]	> 49 : 1	[a]	> 96
5	[a]	> 49 : 1	[a]	> 96

[a] Not measured.

In conclusion, we have shown that the association with chiral triple helicate **3** and a stoichiometric amount of four chiral counterions **1** is sufficient to lead to an efficient asymmetric induction ^{1}H NMR allowing an unambiguous determination of the diastereoselectivity.

We thank the Swiss National Science Foundation, the Federal Office for Education and Science (COST D11), the 'Société Académique de Genève' for financial support, and more particularly the 'Fondation de Famille Sandoz' for a professorship.

Notes and references

‡ A correlation between solid-state and solution circular dichroism (CD) spectra was used to determine the extent of the diastereoselectivity.

§ In lower polar solvent conditions, contact ion pairs are formed between **1** and **3**, and the resulting short-range diastereomeric interactions lead to a non-equivalence of the enantiomers of the cation.

¶ Due to the broadening of the signals induced by paramagnetic metal centers, only two sets of signals could be analyzed properly (δ ~41 and ~30 ppm).

‖ Low-temperature experiments—which possibly have led to an improved selectivity—could not be performed due to the low solubility of the complex and the use of DMSO as co-solvent.

†† Complex [**3**][Δ-**1**]$_4$ seems to decompose in 20% DMSO–$CHCl_3$ at the 5 × 10^{-6} M concentration required for accurate solution CD measurements. As helicate **3** is formally an 'extended dimer' of mononuclear complex **4**, for which we have observed a high homochiral asymmetric induction in favor of [Δ-**4**][Δ-**1**]$_4$, we believe that [*P*-**3**][Δ-**1**]$_4$ is the preferred diastereomeric ion pair.

1 C. Piguet, G. Bernardinelli and G. Hopfgartner, *Chem. Rev.*, 1997, **97**, 2005; A. F. Williams, *Chimia*, 2000, **54**, 585; M. Albrecht, *Chem. Eur. J.*, 2000, **6**, 3485; A. Williams, *Chem. Eur. J.*, 1997, **3**, 15; D. L. Caulder and K. N. Raymond, *J. Chem. Soc., Dalton Trans.*, 1999, 1185.

2 U. Knof and A. von Zelewsky, *Angew. Chem., Int. Ed.*, 1999, **38**, 302.

3 P. Baret, D. Gaude, G. Gellon and J.-L. Pierre, *New J. Chem.*, 1997, **21**, 1255; C. Provent, S. Hewage, G. Brand, G. Bernardinelli, L. J. Charbonniere and A. F. Williams, *Angew. Chem., Int. Ed.*, 1997, **36**, 1287; E. C. Constable, T. Kulke, G. Baum and D. Fenske, *Inorg. Chem. Commun.*, 1998, **1**, 80; H. Murner, A. von Zelewsky and G. Hopfgartner, *Inorg. Chim. Acta*, 1998, **271**, 36; G. Baum, E. C. Constable, D. Fenske, C. E. Housecroft and T. Kulke, *Chem. Eur. J.*, 1999, **5**, 1862; W. Zarges, J. Hall, J.-M. Lehn and C. Bolm, *Helv. Chem. Acta*, 1991, 1843; R. Annunziata, M. Benaglia, M. Cinquini, F. Cozzi, C. R. Woods and J. S. Siegel, *Eur. J. Org. Chem.*, 2001, 173.

4 P. Pfeiffer and K. Quehl, *Chem. Ber.*, 1931, **64**, 2667; S. Kirschner and N. Ahmad, *J. Am. Chem. Soc.*, 1968, **90**, 1910; S. Kirschner, N. Ahmad, C. Munir and R. J. Pollock, *Pure Appl. Chem.*, 1979, **51**, 913; D. J. Owen, D. VanDerveer and G. B. Schuster, *J. Am. Chem. Soc.*, 1998, **120**, 1705.

5 R. M. Yeh, M. Ziegler, D. W. Johnson, A. J. Terpin and K. N. Raymond, *Inorg. Chem.*, 2001, **40**, 2216.

6 J. Lacour, C. Ginglinger, C. Grivet and G. Bernardinelli, *Angew. Chem., Int. Ed. Engl.*, 1997, **36**, 608.

7 J. Lacour, J. J. Jodry, C. Ginglinger and S. Torche-Haldimann, *Angew. Chem., Int. Ed.*, 1998, **37**, 2379; J. Lacour, C. Goujon-Ginglinger, S. Torche-Haldimann and J. J. Jodry, *Angew. Chem., Int. Ed.*, 2000, **39**, 3695.

8 L. J. Charbonnière, A. F. Williams, U. Frey, A. E. Merbach, P. Kamalaprija and O. Schaad, *J. Am. Chem. Soc.*, 1997, **119**, 2488; L. J. Charbonnière, M.-F. Gilet, K. Bernauer and A. F. Williams, *Chem. Commun.*, 1996, 39.

9 L. J. Charbonniere, G. Bernardinelli, C. Piguet, A. M. Sargeson and A. F. Williams, *J. Chem. Soc., Chem. Commun.*, 1994, 1419; B. Hasenknopf and J.-M. Lehn, *Helv. Chem. Acta*, 1996, **79**, 1643; G. Rapenne, B. T. Patterson, J.-P. Sauvage and F. R. Keene, *Chem. Commun.*, 1999, 1853; J. Lacour, S. Torche-Haldimann, J. J. Jodry, C. Ginglinger and F. Favarger, *Chem. Commun.*, 1998, 1733; J. J. Jodry and J. Lacour, *Chem. Eur. J.*, 2000, **6**, 4297.

10 B. R. Serr, K. A. Andersen, C. M. Elliott and O. P. Anderson, *Inorg. Chem.*, 1988, **27**, 4499.

11 A. Loupy and B. Tchoubar, *Salt Effects in Organic and Organometallic Chemistry*, 1st ed., VCH, Weinheim, 1992.

CHEMCOMM Communication
www.rsc.org/chemcomm

Single-source precursors to ternary silver indium sulfide materials

Theivanayagam C. Deivaraj,[a] Jin-Ho Park,[b] Mohammmad Afzaal,[b] Paul O'Brien*[b] and Jagadese J. Vittal*[a]

[a] *Department of Chemistry, 3 Science Drive 3, National University of Singapore, Singapore. E-mail: chmjjv@nus.edu.sg*
[b] *The Manchester Materials Science Centre and Department of Chemistry, The University of Manchester, Oxford Road, Manchester, UK M13 9PL. E-mail: paul.obrien@man.ac.uk*

Received (in Cambridge, UK) 1st August 2001, Accepted 1st October 2001
First published as an Advance Article on the web 24th October 2001

Compounds of type $[(Ph_3P)_2AgIn(SC\{O\}R)_4]$ (R = Me (1), Ph (2)) are excellent single-source precursors for $AgInS_2$ bulk materials by pyrolysis and $AgIn_5S_8$ films by aerosol assisted chemical vapour deposition (AACVD).

In the past two decades chemists have been interested in synthesizing effective molecular precursors for various metal chalcogenides.[1–4] However, the possibility of single-source precursors for silver indium sulfide materials has been unexplored. Both $AgInS_2$ and $AgIn_5S_8$ are known to be semiconducting.[5–8] $AgInS_2$ finds applications as linear and nonlinear optical materials. The band gap of $AgIn_5S_8$ is 1.80 eV (300 K) and has been identified as making it a suitable candidate for photovoltaic solar cell applications.[9] Thin films of these sulfides have been obtained by spray pyrolysis[10,11] which also deposits Ag_2S.[10] Various metal monothiocarboxylates have been used as single-source precursors for metal sulfides.[12–14] Hence we attempted to synthesize bimetallic thiocarboxylate compounds as single-source molecular precursors to silver indium sulfides. Here we report the synthesis and characterization of compounds of the type $[(Ph_3P)_2AgIn(SCOR)_4]$ [R = Me (**1**), Ph (**2**)] along with the results of AACVD experiments.

The compounds were synthesized by reacting $[(Ph_3P)_2AgCl]_2$ and $InCl_3{\cdot}4H_2O$ with four molar equivalents of $Na^+RC\{O\}S^-$.† The structure of compound **2** (as its chloroform solvate) has been determined unequivocally by X-ray crystallography.‡

A view of **2** is shown in Fig. 1. Compound **2** consists of $(Ph_3P)_2Ag$ and $In(SC\{O\}Ph)_2$ units bridged by two $PhC\{O\}S^-$ ligands through μ-*S* bridging. The Ag(I) centre has distorted tetrahedral geometry with a P_2AgS_2 core while In(III) adopts distorted octahedral coordination geometry with two terminal $PhC\{O\}S^-$ anions chelating to In(III). The $AgInS_2$ ring is essentially planar with the two benzoyl groups attached to the S atoms in *anti* fashion.

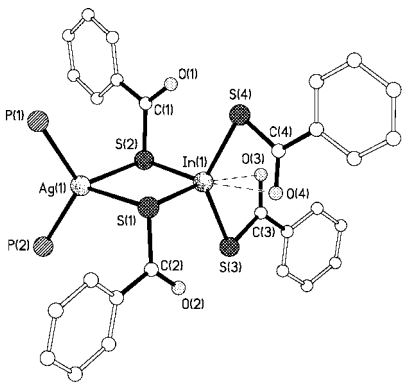

Fig. 1 Molecular structure of compound **2**. All hydrogen atoms and the phenyl rings on the triphenylphosphine ligand have been deleted for clarity. Selected bond distances (Å) and angles (°): Ag(1)–S(1), 2.7032(8); Ag(1)–S(2), 2.7173(8); Ag(1)–P(1), 2.4649(8); Ag(1)–P(2), 2.4573(1); In(1)–S(1), 2.5421(8); In(1)–S(2), 2.5352(2); In(1)–S(3), 2.4594(9); In(1)–S(4), 2.4571(9); In(1)–O(3), 2.672(2); In(1)–O(4), 2.664(3); S(1)–Ag(1)–S(2), 87.20(2), P–Ag(1)–S, 104.47(3)–117.61(3); P(2)–Ag(1)–P(1), 122.44(3); S(2)–In(1)–S(1), 87.20(2); S(3)–In(1)–S(1), 108.76(3); S(4)–In(1)–S(1), 101.05(3); S(3)–In(1)–S(2), 99.53(3); S(4)–In(1)–S(2), 111.23(3); S(4)–In(1)–S(3), 134.75(3); S–In–O, 59.98(6)–170.67(6); In(1)–S(1)–Ag(1), 89.05(2); In(1)–S(2)–Ag(1), 88.88(2).

The residual weights observed for **1** and **2** in thermogravimetric analyses indicate the formation of $AgInS_2$. The decomposition occurs in unresolved multiple steps in the temperature range 132–315 °C for **1** and 175–328 °C for **2**. X-Ray powder diffraction (XRPD) of the final residue obtained from pyrolysis of compounds **1** and **2** indicated the formation of orthorhombic $AgInS_2$, JCPDS: 25-1328 (Fig. 2).§ I-III-VI_2 materials are known to prefer tetragonal structures and hence the formation of the high temperature orthorhombic $AgInS_2$ phase is interesting.[4,15]

However, aerosol assisted chemical vapour deposition (AACVD) of a THF solution of compound **1** yielded $AgIn_5S_8$.¶ Films on glass deposited at 400 and 450 °C from the precursor were found to be transparent and adherent (Scotch tape test) with a dark red colour.

XRPD analysis (step size; 0.04° per 2 s) confirmed that the films were found to be cubic-$AgIn_5S_8$ (JCPDS 25-1329) with a preferred orientation along (311) (Fig. 3). Scanning electron

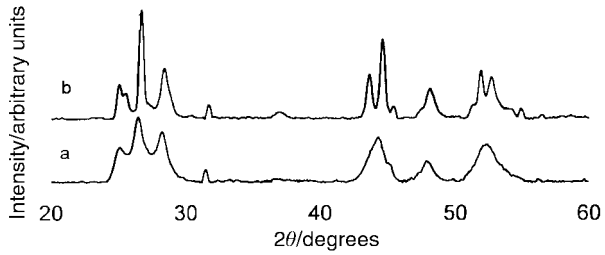

Fig. 2 X-Ray powder diffraction of $AgInS_2$ formed by pyrolysis of compounds (a) **1** and (b) **2**.

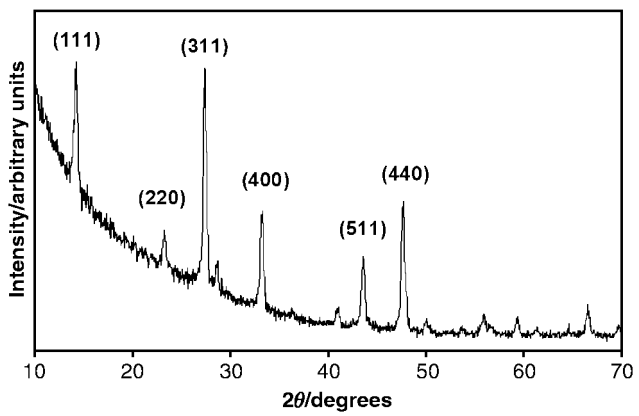

Fig. 3 X-Ray powder diffraction of $AgIn_5S_8$ thin films formed from compound **1**.

 DOI: 10.1039/b106923c

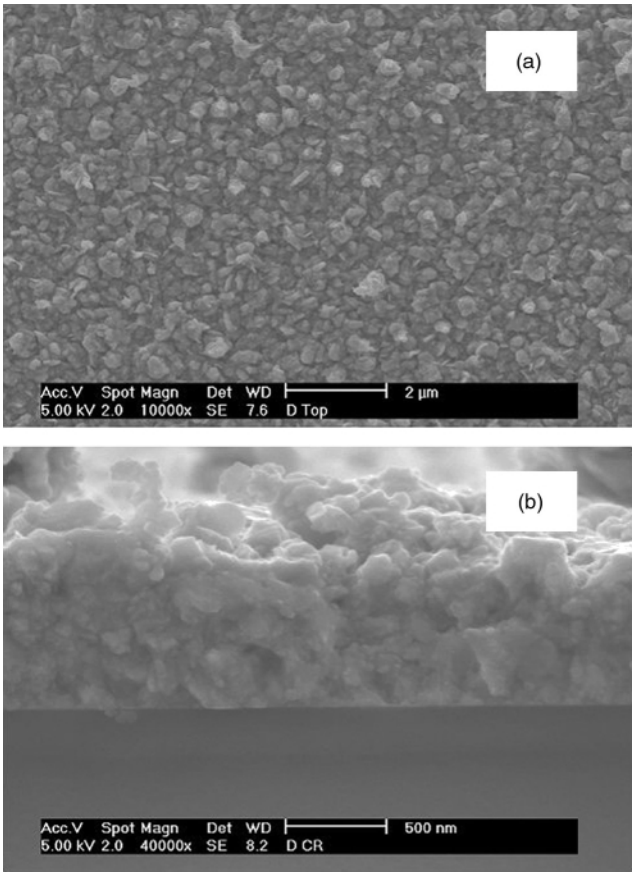

Fig. 4 SEM images of the film on glass grown at 400 °C from compound **1** (a): top view, (b): cross view.

microscopy (SEM) studies showed there is a dramatic change in the morphologies of films grown at 400 and 450 °C. The morphology of films grown at 450 °C consists of thin plate-like particles, perpendicularly laid down onto the substrate with random orientation. However, with decreasing growth temperature from 450 to 400 °C, the morphology was dense and no longer were plate-like particles formed (Fig. 4). Growth rate and average particle size of the films grown at 400 °C were *ca*. 0.3 μm h^{-1} and *ca*. 0.5 μm.

In conclusion, $[(Ph_3P)_2Ag(\mu\text{-}SC\{O\}Me\text{-}S)_2In(SC\{O\}Me)_2]$ (**1**) is shown to be a suitable single-source precursor for the deposition of cubic $AgIn_5S_8$ films on glass substrates by AACVD at 400 and 450 °C. The films grown at 400 °C were dense on a glass substrate. Similar results have also been obtained for **2**.

The significance of the current study is two fold. First of all, we have isolated and characterized bimetallic compounds containing In(III) and Ag(I) for the first time. Secondly, their potential use as single source precursors to silver indium sulfide has been clearly demonstrated. To the best of our knowledge no single-source precursors have been reported for silver indium sulfides previously in the literature. Further studies of novel single-source precursors for the growth of I–III–VI thin films are in hand.

J. J. V. would like to thank the National University of Singapore for a research grant (Grant No. R-143-000-084-112) and P. O. B. thanks EPRSC, UK for support.

Notes and references

† *Synthesis* of **1** and **2**: indium chloride tetrahydrate (0.10 g, 0.34 mmol) dissolved in 12 mL MeOH was added to a CH_2Cl_2 solution (25 mL) of $\{(PPh_3)_2AgCl\}_2$ (0.23 g, 0.17 mmol). To this solution was added NaSC{O}Me prepared *in situ* by mixing 97.5 μL (1.36 mmol) of CH_3\{O\}CSH and 0.031 g (1.36 mmol) of sodium in 15 mL of MeOH. The solvents were removed by a flow of N_2. The product was extracted into 20 mL of CH_2Cl_2, filtered immediately, layered with 40 mL of petroleum ether (bp 35–60 °C) and allowed to stand at 5 °C overnight. The creamy precipitate thus formed was filtered off and washed with petroleum ether (bp 35–60 °C) and Et_2O and dried under vacuum. Yield: 0.37 g (76%). Anal. Calc. for $C_{44}H_{42}O_4S_4P_2AgIn$ (*M* 1047.71): C, 50.44; H, 4.02; S, 12.24. Found: C, 50.52; H, 4.02; S, 12.79%. ^{1}H NMR ($CDCl_3$): δ 2.24 (s, 12H, CH_3), 7.28–7.41 (m, 30H, $(C_6H_5)_3P$). ^{13}C NMR ($CDCl_3$): δ for thioacetato ligand: 34.1 ($CH_3C\{O\}S$), 206.8 ($MeC\{O\}S$); for the PPh_3: 129.4 (C_3, ^3J(P–C) = 9.8 Hz), 130.8 (C_4), 132.1 (C_1, ^1J(P–C) = 25.1 Hz), 134.1 (C_2, ^2J(P–C) = 16.3 Hz). ^{31}P NMR: δ 8.03. Compound **2** was also obtained by a procedure similar to that described for **1** but PhC{O}SH was used instead of MeC{O}SH. Yield: 79%. Anal. Calc. for $C_{64}H_{50}O_4S_4P_2AgIn$ (*M* 1296.0): C, 59.31; H, 3.89; S, 9.90. Found: C, 58.36; H, 3.80; S, 9.66%. ^{13}C NMR ($CDCl_3$): δ for thiobenzoato ligand: 127.8 ($C_{2/6}$ or $C_{3/5}$), 129.2 ($C_{2/6}$ or $C_{3/5}$), 132.8 (C_4), 138.0 (C_1); for the PPh_3: 128.7 (C_3, ^3J(P–C) = 9.8 Hz), 129.9 (C_4), 132.3 (C_1, ^1J(P–C) = 22.9), 133.7 (C_2, ^2J(P–C) = 16.3). ^{31}P NMR: δ 7.28(s).

‡ *Crystal data* for **2**·$CHCl_3$: triclinic, $P\bar{1}$; a = 12.7284(5); b = 14.3145(6); c = 18.7071(7) Å; α = 90.716(1); β = 99.624(1); γ = 110.728(1)°; V = 3133.4(2) Å^3; Z = 2; D_c = 1.500 g cm^{-3}; R_1 = 0.0486; wR_2 = 0.0802. CCDC reference number 169235. See http://www.rsc.org/suppdata/cc/b1/b106923c/ for crystallographic data in CIF or other electronic format.

§ Pyrolysis experiments were performed in a quartz or Pyrex glass reactor using a horizontal tube furnace. The samples were heated to 300 °C under a dynamic vacuum of *ca*. 0.5 Torr.

¶ Thin films of silver indium sulfide were grown on borosilicate glass slides by AACVD. The growth apparatus consisted of a flask containing the solution with a pipette connected to an argon flow which was used as the propellant and carrier gas. The flask was attached, *via* reinforced tubing, to a silica tube containing the glass substrates, which were heated in a tube furnace. $[(Ph_3P)_2Ag(\mu\text{-}SCOMe)_2In(SCOMe)_2]$ (**1**) (~20 mg) was dissolved in tetrahydrofuran (20 mL) at room temperature, and injected into the growth apparatus, with the substrate at 400 or 450 °C. The system was allowed to run for 1 h, with a constant argon flow rate of 140 sccm (carrying the precursor from flask to substrate), at which point the substrates, thin coatings, were collected.

1 M. Bochmann, *Chem. Vap. Deposition*, 1996, **2**, 85.
2 P. O'Brien and R. Nomura, *J. Mater. Chem.*, 1995, **5**, 1761.
3 A. N. Gleizes, *Chem. Vap. Deposition*, 2000, **6**, 155.
4 M. Lazell, P. O'Brien, D. J. Otway and J. H. Park, *J. Chem. Soc., Dalton Trans.*, 2000, 4479.
5 S. C. Abrahams and J. L. Bernstein, *J. Chem. Phys.*, 1973, **59**, 1625.
6 I. Yonenaga, K. Sumino, E. Niwa and K. Masumoto, *J. Cryst. Growth*, 1996, **167**, 616.
7 A. Usujima, S. Takeuchi, S. Endo and T. Irie, *Jpn. J. Appl. Phys., Part 2*, 1981, **20**, 505.
8 Y. Ueno, Y. Hattori, M. Ito, T. Sugiura and H. Minoura, *Sol. Energy Mater. Sol. Cells*, 1992, **26**, 229.
9 N. M. Gasanly, A. Serpengüzel, A. Aydinli, O. Gürlü and I. Yilmaz, *J. Appl. Phys.*, 1999, **85**, 3198.
10 M. Ortega-López, A. Morales-Acevedo and O. Solorza-Feria, *Thin Solid Films*, 2001, **385**, 120.
11 M. Gorska, R. Beaulieu, J. J. Loferski and B. Roessler, *Thin Solid Films*, 1980, **67**, 341.
12 G. Shang, M. J. Hampden-Smith and E. N. Duesler, *Chem. Commun.*, 1996, 1733.
13 M. D. Nyman, M. J. Hampden-Smith and E. N. Duesler, *Inorg. Chem.*, 1997, **36**, 2218.
14 M. D. Nyman, K. Jenkins, M. J. Hampden-Smith, T. T. Kodas, E. N. Duesler, A. L. Rheingold and M. L. Liable-Sands, *Chem. Mater.*, 1998, **10**, 914.
15 C. C. Landry, J. Lockwood and A. R. Barron, *Chem. Mater.*, 1995, **7**, 699.

CHEMCOMM Communication
www.rsc.org/chemcomm

Mesoporous silica-immobilized aluminium chloride as a new catalyst system for the isopropylation of naphthalene

X. S. Zhao,*[a] G. Q. Lu[b] and C. Song[c]

[a] *Department of Chemical and Environmental Engineering, National University of Singapore, Singapore 119260. E-mail: chezxs@nus.edu.sg*
[b] *Centre for Nanomaterials and Department of Chemical Engineering, University of Queensland, St Lucia, Qld 4072, Australia*
[c] *Applied Catalysis in Energy Laboratory, Department of Energy and Geo-Environmental Engineering, Pennsylvania State University, University Park, PA 16802, USA*

Received (in Cambridge, UK) 20th July 2001, Accepted 27th September 2001
First published as an Advance Article on the web 24th October 2001

Mesoporous MCM-41 silica immobilized aluminium chloride shows high catalytic activity and selectivity in the Friedel–Crafts alkylation of naphthalene with isopropanol.

Liquid phase Fridel–Crafts isopropylation of naphthalene over $AlCl_3$ catalysts is widely used in the chemical industry to manufacture 2,6-diisopropylnaphthalene (2,6-DIPN), an important chemical intermediate for making monomers of advanced polymers.[1] While $AlCl_3$ is catalytically efficient and readily available commercially, it has a number of drawbacks: (1) $AlCl_3$ catalyzes the formation of the desired 2,6-DIPN and the undesired 2,7-diisopropylnaphthalene (2,7-DIPN) in a thermodynamic ratio (2,6-:2,7-DIPN = 1:1), requiring a costly separation step to isolate the 2,6 isomer; (2) significant quantities of other isopropylated derivatives such as 2-isopropylnaphthalene (2-IPN) are formed, which must also be separated and removed or recycled; (3) $AlCl_3$ is a stoichiometric reagent that cannot be regenerated and has to be hydrolyzed and disposed of, resulting in a large volume of solid waste. As a result, there has been an interest in finding environmentally friendly alternative catalyst systems.[1–3]

Immobilization of aluminium chloride onto inorganic support materials has been studied previously.[4–8] Of particular interest is the observation that aluminium chlorides immobilized on silica gel and on mesoporous HMS are highly active in the liquid-phase alkylation of aromatic molecules while the selectivity towards the formation of monoalkylates is considerably better than under homogeneous conditions, and the immobilized catalyst systems are recoverable and reusable.[7,8] Therefore, we initiated our investigation on the immobilization of aluminium chloride on mesoporous MCM-41[9] for the liquid-phase alkylation of naphthalene.

The pure-silica MCM-41 support was prepared using cetyltrimethylammonium bromide† as the template according to the method described by Beck *et al.*[9] Two immobilized catalysts designed as $AlCl_x$/MCM-41 and $AlCl_x$/MCM-41(ESM) (ESM refers for external surface modification) respectively were prepared. The preparation of $AlCl_x$/MCM-41 was similar to that reported by Clark *et al.*[8] The procedures of preparing catalyst $AlCl_x$/MCM-41(ESM) are described as follows. The external surface of the MCM-41 support was modified by silylation, using trimethylchlorosilane. It was achieved by modifying the as-synthesized MCM-41 sample before template removal (the template acts as protecting species equivalent to the protecting groups in the organic synthesis). The detailed modification procedures have been described previously.[10] After modification of the external surface, the surfactant template was removed by solvent extraction using 1 M HCl in ethanol at 50 °C under stirring (1 g of MCM-41 in 50 ml of solution), followed by calcination at 450 °C to achieve the maximum density of internal surface silanol groups[11] while maintaining the external surface-attached trimethylsilyl groups without burning off (according to thermogravimetric analysis, the thermal decomposition temperature of the trimethylsilyl species is about 650 °C). Aluminium chloride was grafted onto the internal surface of the MCM-41 support by refluxing benzene (99.99%) containing anhydrous $AlCl_3$ (BDH) and the support ($AlCl_3$:support:benzene = 2 g:5 g:100 ml) at room temperature for 4 h. No reaction occurred on the external surface because the silanol groups on the external surface had already been poisoned during the silylation step. The solid was filtered off, washed with benzene and dried at 110 °C. Other catalysts involved in this study included H/MCM-41 (Si:Al = 15:1) and H/Mordenite (Si:Al = 13:1).

The catalysts were characterized using the techniques of ICP-AES (Spectroflame Model P), XPS (PHI Model 560 XPS/SAM/SIMS I), XRD (PW 1050 diffractometer, Cu Kα radiation), Nitrogen adsorption (NOVA 1200, Quanta Chrome), and solid-state NMR (Bruker MSL 300 spectrometer). The properties of the catalysts are shown in Table 1.

The isopropylation of naphthalene was carried out in a Parr batch reactor equipped with a temperature controller. Naphthalene (0.02 mol), isopropanol (0.04 mol) and fresh catalyst (1.5 g) were loaded in an autoclave containing 200 ml of cyclohexane (solvent). The reaction temperature was 200 °C and the pressure was autogenous. After 4 h, the reactor was cooled to room temperature, and the liquid products were analyzed using a GC-FID with a DB-17 column (30 m × 0.25

Table 1 Physical and chemical properties of catalysts

Sample	Surface area/$m^2\ g^{-1}$	Pore volume/ml g^{-1}	Pore diameter/nm	Atomic ratio[a]		
				$Al:Si_{Bulk}$	$Al:Si_{XPS}$	$Cl:Al_{XPS}$
$AlCl_x$/MCM-41	723	0.67	2.3	0.019	0.023	1.56
$AlCl_x$/MCM-41(ESM)	778	0.70	2.0	0.020	0.021	2.08
Parent MCM-41	1230	1.2	3.0	Nil	Nil	N/A
H/MCM-41	1040	1.1	3.0	0.058	0.064	0
H/Mordenite	444	0.32	0.65 × 0.70[12]	0.076	0.075	0

[a] The atomic ratio of Al:Si was measured using both ICP-AES (denoted $Al:Si_{Bulk}$) and XPS (denoted $Al:Si_{XPS}$) while the atomic ratio of Cl:Al was measured using XPS only.

 DOI: 10.1039/b106499c

Table 2 Catalytic properties of catalysts

Catalyst	Conv.[a] (mol%)	DIPN yield (mol%)	DIPN selectivity (mol%)			Other products[c] (mol%)
			2,6	2,6:2,7	Other[b]	
$AlCl_x$/MCM-41	88.5	65.5	41.0	2.20	40.4	34.3
$AlCl_x$/MCM-41(ESM)	85.2	72.3	60.9	2.82	17.5	27.7
$AlCl_3$	96.4	56.3	36.7	0.986	26.1	43.7
H/MCM-41	60.4	38.4	38.6	1.64	37.9	61.6
H/Mordenite	84.8	44.5	44.3	2.00	33.6	55.4

[a] Conversion of naphthalene. [b] Other DIPN isomers. [c] Other products except DIPNs including MIPN, tri-, and tetra-IPNs, *etc*.

mm). Product identification was carried out using a GC/MS system. Comparisons of the catalytic performance of the catalysts are summarized in Table 2.

Table 1 shows that both the pure-silica and the aluminosilicate MCM-41 materials are of high quality with a pore diameter of 3.0 nm. As expected, immobilization of aluminium chloride on MCM-41 silica resulted in a reduction of surface area, pore volume, and pore diameter. The chemical analysis data further prove the attachment of aluminium chloride on the surface of the MCM-41 silica. The Al contents analyzed using ICP-AES are consistent with that analyzed using XPS.

It can be seen from Table 2 that the highest activity was observed on $AlCl_3$ while the lowest activity was observed on H/MCM-41. The two immobilized catalysts exhibit a reasonable catalytic activity, similar to that of H/Mordenite. Despite a slightly lower activity for catalysts $AlCl_x$/MCM-41 and $AlCl_x$/MCM-41(ESM) compared to $AlCl_3$, there are significant differences in the yield and selectivity of products. With $AlCl_x$/MCM-41 and $AlCl_x$/MCM-41(ESM) as the catalysts, DIPNs were the major products, whereas the other catalysts produced a large amount of other products. Very remarkably, $AlCl_x$/MCM-41(ESM) catalyzed the formation of 72.3% DIPNs with a selectivity of 2,6-DIPN of 60.9% while $AlCl_x$/MCM-41 produced 65.5% DIPNs with a selectivity of 2,6-DIPN of 41.0%. The significant enhancement of selectivity towards 2,6-DIPN after modification of the external surface of the MCM-41 support is explicable only in terms of the differences in the pore-opening size and the nature of the external surfaces of the two catalysts. The selective modification of the external surface of the MCM-41 support resulted in a reduction of the pore-opening size (see Table 1) and the poisoning of the external catalytically active sites. The former probably enabled shape-selectivity while the latter led to the avoidance of the catalytic reaction taking place on the external surface of the $AlCl_x$/MCM-41(ESM) catalyst.

After the 4 h reaction, catalyst $AlCl_x$/MCM-41(ESM)† was filtered off, washed with hot benzene and calcined at 450 °C for 2 h. Subsequent characterization using ^{27}Al NMR and catalytic tests were carried out. The chemical shifts of ^{27}Al before and after the 4 h reaction were found to be about 53.0 and 52.2 ppm, respectively, indicating that the immobilized aluminium chloride species had hardly changed. It was also observed that both the activity and selectivity towards 2,6-DIPN remained unchanged.

Overall, the results discussed above demonstrate that immobilization of aluminium chloride on mesoporous MCM-41 silica can create substantial density of acidic sites, which are catalytically responsible for the liquid-phase isopropylation of naphthalene. Most remarkably, a significant increase in selectivity towards 2,6-DIPN can be achieved through the use of external surface-silylated MCM-41 support. The immobilized catalyst system is recyclable and reusable without observable loss in activity and selectivity, demonstrating its promise as an environmentally friendly alternative catalyst for the isopropylation of naphthalene.

We thank the University of Queensland for partial financial support and the Australian Academy of Science for traveling support (*via* the program Scientific Visit to North America for Young Australian Scientists). X. S. Z. wishes to acknowledge Ms Lim Hwee Ling for her help during manuscript revision.

Notes and references

† The IUPAC name for cetyl is hexadecyl.

1 J. A. Cusumano, *CHEMTECH*, 1992, 482.
2 R. A. Sheldon and R. S. Downing, *Appl. Catal., A*, 1999, **189**, 163.
3 C. Song, *Stud. Surf. Sci. Catal.*, 1998, **113**, 163.
4 R. S. Drago and E. E. Getty, *J. Am. Chem. Soc.*, 1988, **110**, 3311.
5 E. E. Getty and R. S. Drago, *Inorg. Chem.*, 1990, **29**, 1186.
6 S. Sato and G. E. Maciel, *J. Mol. Catal. A: Chem.*, 1995, **101**, 153.
7 J. H. Clark, K. Martin, A. J. Teasdale and S. J. Barlow, *J. Chem. Soc., Chem. Commun.*, 1995, 2037.
8 J. H. Clark, P. M. Price, K. Martin, D. J. Macquarrie and T. W. Bastock, *J. Chem. Res.*, 1997, 430.
9 J. S. Beck, C. Vartuli, W. J. Roth, M. E. Leonowicz, C. T. Kresge, K. D. Schmitt, C. T.-W. Chu, D. H. Olson, E. W. Sheppard, S. B. McCullen, J. B. Higgins and J. L. Schlenker, *J. Am. Chem. Soc.*, 1992, **114**, 10834.
10 X. S. Zhao, G. Q. Lu and X. J. Hu, *Chem. Commun.*, 1999, 1391.
11 X. S. Zhao and G. Q. Lu, *J. Phys. Chem. B*, 1998, **102**, 1556.
12 W. M. Meier, D. H. Olson and Ch. Baerlocher, *Zeolites*, 1996, **12**, 153.

CHEMCOMM Communication
www.rsc.org/chemcomm

Bidentate lactate binding in aqueous solution in a cationic, heptadentate lanthanide complex: an effective chiral derivatising agent

Rachel S. Dickins,* Christine S. Love and Horst Puschmann

Department of Chemistry, University of Durham, South Road, Durham, UK DH1 3LE. E-mail: R.S.Dickins@durham.ac.uk

Received (in Cambridge, UK) 13th July 2001, Accepted 1st October 2001
First published as an Advance Article on the web 16th October 2001

The X-ray crystal structures of cationic, heptadentate lanthanide complexes of holmium and ytterbium bound to lactate are reported and the observed bidentate chelation in the solid state is consistent with near-IR CD (Yb) and solution NMR measurements; the complexes are shown to act as aqueous chiral derivatising agents for α-hydroxy acids.

In vivo detection of lactate is of prime importance in the diagnosis, grading and therapeutic monitoring of diseases such as cancer, stroke and heart disease.[1] Magnetic resonance spectroscopy (MRS) offers a non-invasive means of analysing lactate concentration *in vivo* but suffers from limitations due to insensitivity and the requirement of long acquisition times for a good signal to noise ratio. Furthermore the lactate resonances are often masked by overlapping lipid resonances for example, which has severely limited the role of MRS in the clinic. In order to improve the diagnostic potential of MRS it would be highly advantageous to utilise the enhanced shifting and relaxation properties of paramagnetic shift reagents, designed to bind strongly and selectively to lactate, to effect spectral resolution and also allow rapid acquisition times to be implemented giving increased signal intensity.

Lanthanide complexes of heptadentate ligands *e.g.* **1**, possess two bound water molecules and have been reported to show high affinity for oxy-anions, and in particular lactate.[2]

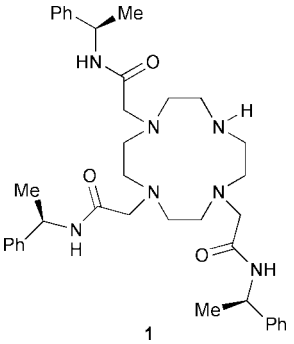

1

They form well-defined, relatively stable complexes in aqueous solution, are amenable to NMR and luminescence studies and are good candidates for assessment as MRS reagents for lactate. With this model in mind we set out to examine the shifting ability of a series of such lanthanide complexes. Herein we report the crystal structures of the first examples of lactate-bound lanthanide complexes and describe preliminary near-IR CD and ^{1}H NMR studies of [Yb.**1**]$^{3+}$($CF_3SO_3^-$)$_3$.†

There are only 13 examples of metal-containing lactate species reported and none involves a rare earth ion.[3] The ytterbium complex of (*RRR*)-**1** in the presence of lactate crystallised in the *P*1 space group in the triclinic system with the unit cell comprising of [Yb.**1**]$^{3+}$, one lactate molecule, two triflate counter ions and three water molecules. The complex adopts a monocapped square antiprismatic geometry (twist angle = 40°) with the tetraazacyclododecane ring in the usual [3333] conformation in which the four nitrogen atoms are roughly coplanar, directed towards the lanthanide ion and occupy four coordination sites (average Ln–N 2.573 Å) (Fig. 1).

The oxygen atoms of the pendent arms lie approximately in the same plane (average Yb–O 2.299 Å) and define three coordination sites. The average values of the macrocyclic N–C–C–N and the pendent arm N–C–C–O torsion angles are +57.6 and −26.4 respectively, showing the complex has crystallised in the Λ(δδδδ) form. The lactate binds in a bidentate manner with the hydroxyl oxygen occupying the axial position above the lanthanide ion (Yb–O 2.461 Å)[4] and one of the carboxylate oxygens binding in the same plane as the O3 face (Yb–O 2.278 Å) completing the nine-coordinate sphere. The lactate bound holmium complex was isostructural with lactate–[Yb.**1**]$^{3+}$ with Ho–O distances of 2.469 and 2.317 Å to the lactate OH and carboxylate oxygens, respectively.

The local coordination environment about the lanthanide centre may be probed by CD. Yb absorbs in the near-IR region and exhibits sensitive CD bands centred around 980 nm due to magnetically allowed $^2F_{7/2} \rightarrow {}^2F_{5/2}$ transitions.[5] The CD spectrum of [Yb.**1**]$^{3+}$ (20 mM, H_2O) exhibited two peaks at 972.5 and 996.0 nm (Fig. 2). On the addition of ten equivalents of sodium lactate (100 mM, H_2O) the peak at 972.5 nm was shifted to longer wavelength, increased in intensity by 80% and was resolved into two peaks at 975.0 and 979.5 nm. The peak at 996.0 nm displayed a 40% increase in intensity and was shifted to a shorter wavelength of 990.5 nm. Changing the nature of the donor atom, on lactate addition, from a neutral water to a charged carboxylate greatly affects the electronic properties of the lanthanide ion resulting in modulation of the crystal field splitting and hence the observed changes in CD.

Analysis of [Yb.**1**]$^{3+}$ by ^{1}H NMR spectroscopy (293 K, D_2O, 200 MHz) revealed eight broadened singlet resonances to high frequency corresponding to the four most shifted axial and

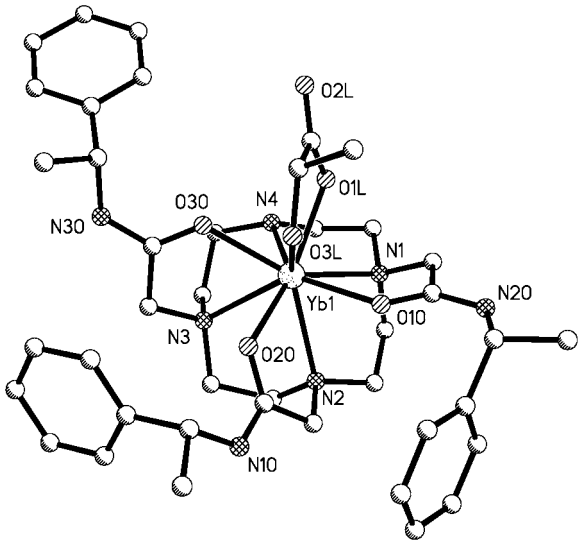

Fig. 1 Structure of [Yb.**1**]$^{3+}$ showing bidentate chelation of (*S*)-lactate.

 DOI: 10.1039/b106262j

equatorial ring protons [Fig. 3(a)]. On the addition of 0.25 equivalents of Na (*S*)-lactate to [Yb.**1**]$^{3+}$ an additional set of axial and equatorial ring resonances appeared which may be attributed to the lactate bound species which is in slow exchange on the NMR timescale with the free form [Fig. 3(b)]. Subsequent incremental additions of lactate resulted in an increase in the bound to free ratio and after addition of 1.0 equivalent only the bound form was observed [Fig. 3(c)]. Two additional singlet resonances were also evident at +58 ppm, integrating to one proton and attributed to the CH of the bound lactate, and at +20 ppm, integrating to three protons and subsequently attributed to the methyl resonance of the bound lactate.[6] The expected Me doublet was not resolved due to the broadening effect of the paramagnetic ion. The induced paramagnetic shift, which for Yb is largely due to dipolar contributions and can be approximated to having a $(3\cos^2 - 1)$ r^{-3} dependence, suggests the lactate CH lies closer to the principal axis of the complex than the Me group. This is consistent with the X-ray data.[7]

Following addition of 2.5 equivalents of racemic lactate to [Yb.**1**]$^{3+}$, a 1:1 mixture of diastereomeric complexes was observed by ^{1}H NMR [Fig. 3(d)], consistent with the very similar formation constants measured for (*R*)- and (*S*)-lactate with [Eu.**1**]$^{3+}$.[2] The CH and Me lactate resonances are clearly resolved for the *R* and *S* diastereoisomers ($\Delta\Delta\delta \sim 10$ ppm) and

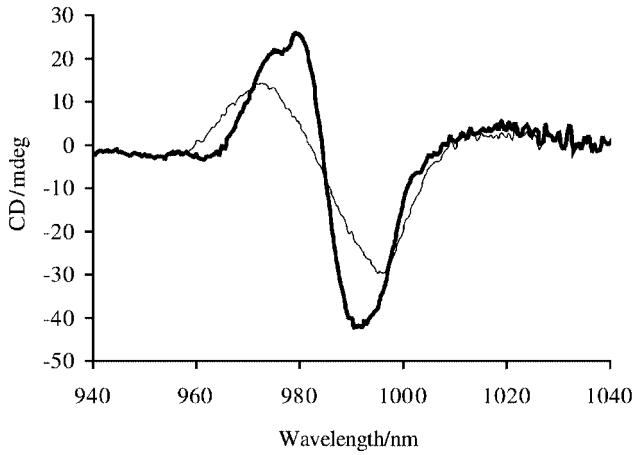

Fig. 2 Circular dichroism spectra of [Yb.**1**]$^{3+}$ (diaqua species) and in the presence of 10 equiv. (*S*)-lactate (bold).

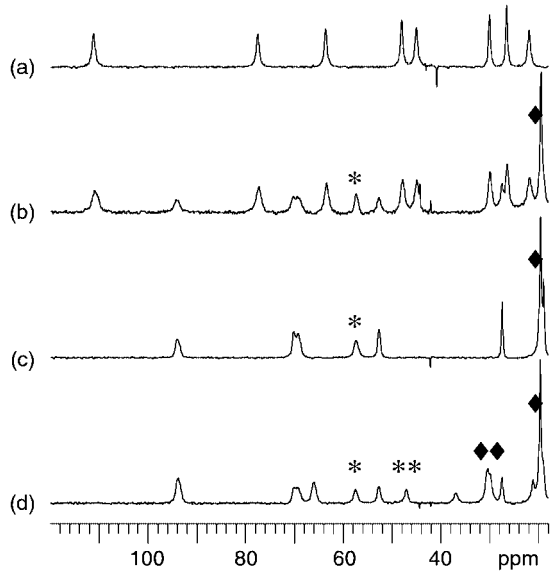

Fig. 3 Partial ^{1}H NMR spectra of (a) [Yb.**1**]$^{3+}$ (diaqua species) showing four axial and four equatorial ring protons; (b) in the presence of 0.25 equiv. (*S*)-lactate [(*) (*S*)-lactate CH, (◆) (*S*)-lactate CH_3]; (c) 1 equiv. of (*S*)-lactate; (d) 2.5 equiv. of racemic lactate [(**) (*R*)-lactate CH, (◆◆) (*R*)-lactate CH_3].

experienced large lanthanide induced shifts; the CH resonating at +48 and +58 ppm (*cf.* +4.1 ppm in the free form) and the Me resonating at +30 and +20 ppm for (*R*)- and (*S*)-lactate, respectively (*cf.* +1.3 ppm in the free form). A lack of enantioselectivity in complex formation was also observed following addition of the sterically more demanding (*R*)- and (*S*)-mandelic acid to [Yb.**1**]$^{3+}$. Similar behaviour is exhibited with related alkyl and aryl α-hydroxy acids. A difference of 16 ppm was observed for the mandelic *ortho*-phenyl ring protons which appeared at +37.0 and +20.5 ppm for the *R* and *S* complexes, respectively.[6] The very large shifts and chemical shift non-equivalence for this unique NMR 'chiral derivatising agent' may be compared to the much smaller $\Delta\Delta\delta$ values reported for shift reagents which are generally around 1 ppm and often < 0.1 ppm. Moreover there are very few examples of water-soluble chiral shift reagents,[8] the majority of studies being performed in organic media and those reported are mainly based around neutral and anionic systems. Sasaki and coworkers, for example, has reported an aqueous cationic chiral lanthanide shift reagent to separate enantiomeric signals based upon bpba[9] which exhibits $\Delta\Delta\delta$ values of < 0.15 ppm.

In summary, the substituents alpha to the α-hydroxy acid in the Ln-bound complex fall within the 'McConnell' cone and so are susceptible to large dipolar shifts. The apparent absence of kinetic resolution in complex formation with racemic α-hydroxy acids substrates augurs well for the development of such complexes as NMR chiral derivatising agents. By reducing the effective charge demand at the Ln centre chiral shift reagents (*i.e.* lower affinity and fast exchange on the NMR timescale) may also be envisaged.

We thank the University of Durham for support, Prof. J. A. K. Howard for use of crystallographic facilities and the Royal Society for a Dorothy Hodgkin Fellowship (RSD).

Notes and references

† *Crystal data* for [Yb.**1**]$^{3+}$: $C_{44}H_{64}F_6N_7O_{15}S_2Yb$; M_r = 1282.18; T = 100(2) K; triclinic, space group $P1$; a = 11.287(2), b = 11.9208(19), c = 12.407(3) Å, a = 64.712(16), β = 77.152(19), γ = 62.720(10)°, V = 1340.8(5) Å^3; D_c = 1.597 Mg m^{-3}; Z = 1; μ(Mo-Ka) = 1.913 mm^{-1}; reflections collected/unique 15088/11065 [R_{int} = 0.0277]; final R indices [$I > 2\sigma(I)$]: R_1 = 0.0321 and wR_2 = 0.0760 [11036]; R indices (all data): R_1 = 0.0325 and wR_2 = 0.0761. For [Ho.**1**]$^{3+}$: $C_{44}H_{64}F_6N_7O_{15}S_2Ho$; M_r = 1274.07; T = 100(2) K; triclinic, space group $P1$; a = 11.280(2), b = 11.950(4), c = 12.423(3) Å, a = 64.82(2), β = 76.837(4), γ = 62.38(2)°, V = 1341.9(6) Å^3; D_c = 1.577 Mg m^{-3}; Z = 1; μ(Mo-Ka) = 1.643 mm^{-1}; reflections collected/unique 14284/10965 [R_{int} = 0.0185]; final R indices [$I > 2\sigma(I)$]: R_1 = 0.0239 and wR_2 = 0.0640 [10951]; R indices (all data): R_1 = 0.0239 and wR_2 = 0.0641. Data collected on a Bruker SMART CCD 1K area detector diffractometer. CCDC reference numbers 172449 and 172450. See http://www.rsc.org/suppdata/cc/b1/b106262j/ for crystallographic data in CIF or other electronic format.

1 M. Stubbs, *Acta Oncologica*, 1999, **38**, 845; D. E. Saunders, *Br. Med. Bull.*, 2000, **56**, 334; J. W. Pritchard, *NMR Biomed.*, 1991, **4**, 99.
2 J. I. Bruce, R. S. Dickins, L. J. Govenlock, T. Gunnlaugsson, S. Lopinski, M. P. Lowe, D. Parker, R. D. Peacock, J. J. B. Perry, S. Aime and M. Botta, *J. Am. Chem. Soc.*, 2000, **122**, 9674.
3 Cambridge Structural Database, October 2000 Release: F. H. Allen and O. Kennard, *Chem. Des. Automation News*, 1993, **8**, 30.
4 In the monoaqua Yb complex of the related tetraamide, the Yb–OH_2 distance was 2.44 Å; A. S. Batsanov, A. Beeby, J. I. Bruce, J. A. K. Howard, A. M. Kenwright and D. Parker, *Chem. Commun.*, 1999, 1011.
5 F. S. Richardson, *Inorg. Chem.*, 1980, **19**, 2806.
6 Confirmed by independent COSY ^{1}H NMR experiments.
7 From the crystal data: for lactate Me: θ = 22.64°, r = 4.87 Å; for lactate CH: θ = 25.62°, r = 3.929 Å, where θ is the mean angle with respect to the principal (z') axis.
8 M. Watanabe, T. Hasegawa, H. Miyake and Y. Kojima, *Chem. Lett.*, 2001, 4; R. Hazama, K. Umakoshi, C. Kabuto, K. Kabuto and Y. Sasaki, *Chem. Commun.*, 1996, 157; R. Hulst, N. Koen de Vries and B. L. Feringa, *J. Org. Chem.*, 1994, **59**, 7453.
9 bpba = *N,N'*-Bis(2-pyridylmethyl)-*N,N'*-1,2-ethanediylbis(alaninate); K. Ogasawara, K. Omata, K. Kabuto, T. Hasegawa, Y. Kojima and Y. Sasaki, *Org. Lett.*, 2000, **2**, 3543.

CHEMCOMM Communication
www.rsc.org/chemcomm

The first zinc-promoted, environmentally friendly, and highly efficient acetoxyallylation of aldehydes in aqueous ammonium chloride

Marco Lombardo,* Rugiada Girotti, Stefano Morganti and Claudio Trombini*

Dipartimento di Chimica 'G.Ciamician', University of Bologna, Bologna, Italy.
E-mail: trombini@ciam.unibo.it; Fax: +39 051 2099456; Tel: +39 051 2099513

Received (in Cambridge, UK) 9th August 2001, Accepted 20th September 2001
First published as an Advance Article on the web 15th October 2001

An exceptionally mild acetoxyallylation of aldehydes in water promoted by zinc is reported, using 3-bromo-1-acetoxyprop-1-ene as starting material; simple diastereoselectivity mainly depends on the nature of the aldehyde.

In any synthetic plan, carbon–carbon bond forming reactions are the most important and valuable transformations. If the construction of a carbon–carbon bond is carried out in water at ambient temperature, we also meet some basic requirements of green chemistry,[1] such as preventing hazardous waste (organic solvents), optimising synthetic efficiency by reducing derivatisation reactions (protection–deprotection *etc*.) and minimising energy consumption. The Henry nitroaldol reaction[2] has been known for a long time as a prototype of these reactions, allowing for example the direct use of unprotected aldoses,[3] but only in the 1980s did the use of water in organic chemistry enjoy an outbreak in terms of studies and applications.[4] A lot of attention has been devoted to the allylation of carbonyl compounds in water,[5] by generating allylic organometallic reagents, particularly tin, zinc, indium and even magnesium[6] species, and reacting them with carbonyl compounds. Two general protocols are available: the *in situ* Barbier procedure where the allylic species is formed in the presence of the carbonyl compound, or the stepwise Grignard procedure where the organometallic compound is preformed and then added to the aldehyde. Again, sugars may be used without derivatisation, as demonstrated by the synthesis of higher sugars,[7] sialic acid derivatives,[8] and *C*-branched sugars in water.[9] To the best of our knowledge, no report is available in the literature on Barbier reactions in water using 3-halo-1-alkoxyprop-1-enes **1**, which could ensure a straightforward access to 3-alkoxy-1-en-4-ols **2**,[10] attractive building blocks for the synthesis of polyoxo compounds [eqn. (1)].

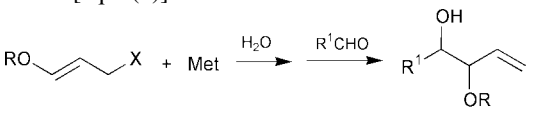

(1)

1 **2**

A possible reason why chemists are discouraged from attempting this reaction could be based on the sensitivity towards acidic conditions of the enol ether functionality in **1**. In fact, both Barbier protocols involving zinc and indium operate in acidic media; zinc requires the NH_4Cl–H_2O system to give the best results, while indium salts formed during the oxidative addition undergo acidic hydrolysis which lowers the pH by up to 3.

Considering that enol esters are supposed to be somewhat more stable than enol ethers under acidic conditions, we envisaged 3-bromo-1-acetoxyprop-1-ene (**3**) as a promising candidate for the acetoxyallylation of aldehydes. Preparation of **3** as a 35:65 *E*/*Z* isomer mixture,† was carried out by the $ZnCl_2$ catalysed 1,4-bromoacetylation of propenal with acetyl bromide [eqn. (2)].[11]

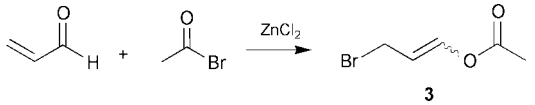

(2)

3

We were delighted by the observation that **3** was compatible with aq. ammonium chloride solutions and that the reaction of **3** with zinc was very rapid and exothermic. On this basis, a simple, fast and environmentally benign Barbier protocol was developed (Scheme 1);‡ preliminary results are collected in Table 1.

As shown in the reaction mechanism, once **4** is formed in water at pH = 5, a few reaction channels are possible: *E*/*Z* metallotropic isomerisation, protonation, Wurtz-like dimerisation, addition to an electrophile, if present. In the presence of an aldehyde, nucleophilic addition to the carbonyl group is faster than protonation or dimerisation. Of course, in the absence of the aldehyde, **4** completely decomposes within 30 min. Data presented in Table 1 deserve a few comments: i) with reference to the general economy criteria, the overall procedure is simple, fast and makes use of inexpensive reagents; ii) the procedure is based on **3**, an easily available starting material obtained in 70% yield in multigram scale, iii) side-products are limited to some Wurtz coupling product (< 10% based on **3**), and iv) the product is a selectively monoprotected diol, namely a 3-acetoxy-1-en-4-ol **5**, a straightforward precursor of the parent 1-en-3,4-diol by simple hydrolysis (quantitative in 2 h using K_2CO_3 in MeOH–H_2O 9:1). All these features make **3** highly competitive with alkoxylated organometallic derivatives **6a–f**,[12] whose forma-

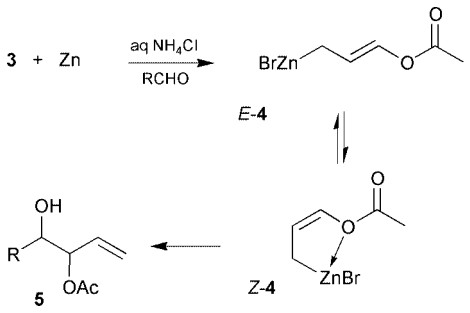

Scheme 1

Table 1 Zinc-mediated acetoxyallylation of aldehydes under Barbier conditions in aq. NH_4Cl

Run	Aldehyde	*T* (°C)[a]	**5** Yield (%)	*syn*:*anti*
				65:35
1	Benzaldehyde	22	90 (75)[b]	(70:30)[b]
2	2-Furaldehyde	2	81	80:20
3	*p*-Tolualdehyde	24	60[c]	60:40
4	*p*-Anisaldehyde	24	72[c]	70:30
5	(*E*)-PhCH=CHCHO	20	81	60:40
6	*n*-C_6H_{13}CHO	22	84	30:70
7	*n*-$C_{11}H_{23}$CHO	20	42	25:75
8	$PhCH_2CH_2CHO$	22	81	30:70
9	$(CH_3)_2CHCH_2CHO$	22	76	30:70
10	*c*-C_6H_{11}CHO	22	83	10:90
11	Benzaldehyde	4	80	70:30

[a] External bath temperature ± 1 °C. [b] Reaction carried out with indium in H_2O; reaction time = 6 h. [c] *Syn*-**5** partially undergoes acetyl transfer (~10%) to 4-acetoxy-1-en-3-ol.

 DOI: 10.1039/b106759a

tion generally requires metalation of protected allyl ethers with alkyllithiums followed by transmetalation.

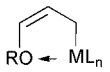

6a : RO = MeO, ML_n = $BIpc_2$
6b : RO = MeO, ML_n = $InCl_2$
6c : RO = MeO, ML_n = $FeCp(CO)_2$
6d : RO = TBSO, ML_n = $SnBu_3$
6e : RO = sugarO, ML_n = $SnBu_3$
6f : RO = sugarO, ML_n = $AlEt_3$

Indium may replace zinc (Table 1, run 1) but the overall process is slower and does not produce a significant improvement both in terms of yield and selectivity. With indium a Grignard protocol in THF seems to represent a more appropriate reaction system and results will be published independently.

Even though the stereochemical outcome of these reactions, in terms of simple diastereoselectivity, is not exceptional, an interesting difference comes out with respect to the use of **6a–f**. In fact, all the **6a–f** species are denoted by a remarkable *syn*-selectivity, independent of the aldehyde used, with *syn–anti* ratios in the 70 : 30–99 : 1 range. Invariably, the stereopreference for the formation of the *syn*-adduct is discussed in terms of a preferred formation of a *Z*-configurated organometallic species **6**, stabilised by internal coordination, which adds to the aldehyde following the classical chair-like Zimmerman-type transition state.

Results reported in Table 1 show that, starting from **3**, the simple diastereopreference depends on the nature of the aldehyde, saturated aldehydes mainly affording *anti* adducts (runs 6–10), and aromatic or α,β-unsaturated aldehydes leading to *syn* adducts (runs 1–5). No attempt was made to detect the actual structure of the intermediate **4**, anyway, in analogy to **6**, we believe that (*Z*)-**4** should enjoy thermodynamic stabilisation by zinc–oxygen coordination and should represent the most abundant isomer in the reaction mixture. On a purely speculative basis, we believe that the most important contribution to the observed diastereoselectivity is given by twist–boat transition states (TSs) **A** and **B** (Fig. 1) rather than by Zimmerman chair-like TSs which could not enjoy the through space stabilising O → Zn interaction present in **A** and **B**. **A** holds the sterically demanding R group in the *anti* position relative to the acetoxy group, so leading to the *anti* adduct, while **B** eclipses the unsaturated substituent with the acetoxy group with a likely stabilisation by π–π stacking interaction.

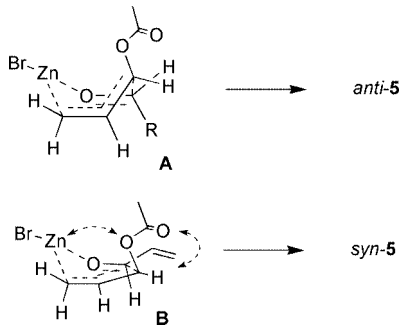

Fig. 1 Proposed transition states for the addition of **4** to aldehydes.

In conclusion, a new promising route to monoacetylated 1-en-3,4-diols based on 3-bromo-1-acetoxyprop-1-ene (**3**) is reported; this protocol joins an excellent efficiency in terms of yield, cost and time, to the use of typical environmentally benign conditions, such as the use of water as a solvent at room temperature.

This work was supported by MURST-Rome (National Project 'Stereoselezione in Sintesi Organica. Metodologie e Applicazioni') and University of Bologna (funds for selected topics).

Notes and references

† Anhydrous $ZnCl_2$ (0.068 g, 0.5 mmol) was added at −20 °C to a solution of freshly distilled propenal (3.32 mL, 50 mmol) and acetyl bromide (3.73 mL, 50 mmol) in anhydrous CH_2Cl_2 (40 mL). The reaction was stirred for 2 h at 0 °C and quenched at 0 °C by addition of aq. $NaHCO_3$. After extraction (CH_2Cl_2), 3-bromo-1-acetoxyprop-1-ene (**3**) was isolated by distillation (bp = 69–71 °C/22 mmHg) as a 35 : 65 mixture of *E*/*Z* isomers in 70% yield. (*Z*)-**3**. ^{1}H NMR (300 MHz, $CDCl_3$) δ 2.22 (s, 3H), 4.09 (dd, J = 0.3, 8.1 Hz, 2H), 5.24 (dt, J = 6.3, 8.1 Hz, 1H), 7.19 (dt, J = 0.3, 6.3 Hz, 1H); ^{13}C NMR (75 MHz, $CDCl_3$) δ 20.5, 23.5, 109.3, 136.9, 166.9. (*E*)-**3.** ^{1}H NMR (300 MHz, $CDCl_3$) δ 2.16 (s, 3H), 3.99 (dd, J = 0.3, 8.1 Hz, 2H), 5.70 (dt, J = 8.1, 12.3 Hz, 1H), 7.19 (dt, J = 0.3, 12.3 Hz, 1H); ^{13}C NMR (75 MHz, $CDCl_3$) δ 20.5, 28.4, 111.1, 139.0, 167.2.

‡ In a typical experimental procedure, an aldehyde (1 mmol) and **3** (1.5 mmol) are added to a sat aq. solution of NH_4Cl (5 ml). Zinc powder (1.5 mmol) is added and completely dissolves within 2 min. The reaction is checked after 15 min and products are extracted with ether after 30 min. The monoacetylated diol **5** is isolated by flash-chromatography in the 75–90% yield range. All new compounds were fully characterised by ^{1}H NMR, ^{13}C NMR and high resolution mass spectrometry; *syn–anti* stereorelationships were assigned after hydrolysis to 1-en-3,4-diols (Ref. 12).

1 P. T. Anastas and J. C. Warner, *Green Chemistry: Theory and Practice*, Oxford University Press, New York, 1998.
2 R. Ballini and G. Bosica, *J. Org. Chem.*, 1997, **62**, 425.
3 H. H. Baer, *Adv. Carbohydrate Chem. Biochem.*, 1969, **24**, 67.
4 A. Lubineau, J. Augé and Y. Queneau, *Synthesis*, 1994, 741; C. H. Li and T. H. Chan, *Tetrahedron*, 1999, **55**, 11149.
5 C. J. Li, *Tetrahedron*, 1996, **52**, 5643.
6 C. J. Li and W. C. Zhang, *J. Am. Chem. Soc.*, 1998, **120**, 9102.
7 E. Kim, D. M. Gordon, W. Schmid and G. M. Whitesides, *J. Org. Chem.*, 1993, **58**, 5500.
8 T. H. Chan and M. B. Isaac, *Pure Appl. Chem.*, 1996, **68**, 919.
9 Y. Canac, E. Levoirier and A. Lubineau, *J. Org. Chem.*, 2001, **66**, 3206.
10 A. R. Katritzky, M. Piffl, H. Lang and E. Anders, *Chem. Rev.*, 1999, **99**, 665.
11 M. Neuenschwander, P. Bigler, K. Christen, R. Iseli, R. Kyburz and H. Mühle, *Helv. Chim. Acta*, 1978, **61**, 2047.
12 **6a**: P. Ganesh and K. M. Nicholas, *J. Org. Chem.*, 1997, **62**, 1737; **6b**; T. Hirashita, T. Kamei, T. Horie, H. Yamamura, M. Kaway and S. Araki, *J. Org. Chem.*, 1999, **64**, 172; **6c**; S. Jiang, G. E. Agoston, T. Chen, M. P. Cabal and E. Turos, *Organometallics*, 1995, **14**, 4697; **6d**; G. E. Keck, D. E. Abbott and M. R. Wiley, *Tetrahedron Lett.*, 1987, **28**, 139; **6e**; W. R. Roush and M. S. VanNieuwenhze, *J. Am. Chem. Soc.*, 1994, **116**, 8536; **6f**; J.-I. Chika and H. Takei, *Tetrahedron Lett.*, 1998, **39**, 605.

CHEMCOMM Communication
www.rsc.org/chemcomm

Layer-by-layer assembly of metal-mediated multiporphyrin arrays

Dong-Jin Qian,* Chikashi Nakamura and Jun Miyake

Tissue Engineering Research Center, National Institute of Advanced Industrial Science and Technology, 1-1-1 Higashi, Tsukuba, Ibaraki 305-8562, Japan. E-mail: dongjin-sen@aist.go.jp

Received (in Cambridge, UK) 24th July 2001, Accepted 1st October 2001
First published as an Advance Article on the web 24th October 2001

Two types of multiporphyrin arrays, mediated by $PdCl_4^{2-}$ complex ions at the air–water interface, were alternately transferred onto solid supports to form three-dimensional organized multilayers by a layer-by-layer method.

The architecture of multiporphyrin arrays has attracted much attention in the developing biomimetic chemistry of photosynthetic reaction centers, as well as in developing potential materials for optical, photoelectrochemical and sensor applications.[1,2] The methodology commonly used for preparing multiporphyrin arrays is *via* linkages including ethyne-type organic groups and transition metal ions between porphyrins and/or metal ions.[3,4] Recently, efforts have been made on the preparation of three-dimensional (3D) organized multiporphyrin arrays. One interesting strategy by Sharma *et al*. was using solvent molecule inclusion in crystals of multiporphyrin arrays to control the interlayer separation of 2D layers.[5] However, examples of 3D multiporphyrin arrays prepared and characterized are much rarer.

In the present communication, a layer-by-layer (LBL) technique, developed from the Langmuir–Blodgett (LB) method, was used to build 3D multilayers of two types of multiporphyrin arrays. The 2D multiporphyrin arrays were prepared by using $PdCl_4^{2-}$ complex ions as linkages between porphyrins at the air–water interface. Compared to synthesis in solution, the present method is more rapid and efficient in forming multiple porphyrins with network structure, and more easily available and controllable in building 3D layered multilayers.

The used porphyrins were 5,10,15,20-tetrakis(4-pyridyl)-21*H*,23*H*-porphine (TPyP) and 5,10,15,20-tetrakis(4-carboxymethyloxyphenyl)-21*H*,23*H*-porphine (TCPP), as shown in Fig. 1. Preparation of 2D multiporphyrin arrays and LBL deposition were performed with the use of a KSV 5000 minitrough at 20 °C. Since the monolayer could not be transferred by the vertically dipping method, we used a horizontal lifting technique.[6]

Fig. 2 shows the π–A isotherms for TPyP and TCPP monolayers on pure water and 0.3 mM K_2PdCl_4 subphase surfaces. By extrapolating the tangent on the isotherms at a fixed point (20 mN m^{-1}) to zero surface pressure ($A_{\pi\rightarrow 0}$), the mean TPyP and TCPP molecular areas were obtained and are summarized in Table 1. Based on single-crystal structures of simple tetraarylporphyrins, the expected mean molecular areas of Langmuir monolayers would be about 0.9 nm^2 if the porphyrin rings lie vertical to the aqueous surface, and about 2.25 nm^2 if the porphyrin rings lie parallel.[7] Here, the mean TPyP and TCPP areas are about 0.55–0.65 nm^2 on pure water surface, smaller than 0.9 nm^2, which may be ascribed to a tilted and overlapped arrangement of the porphyrin rings.[8] On the other hand, the mean TPyP and TCPP areas are about 1.4–1.8 nm^2 on the 0.3 mM K_2PdCl_4 subphase surfaces, a value between 0.9 and 2.25 nm^2, which may be ascribed to the formation of Pd–TPyP and Pd–TCPP multiporphyrin arrays.[9] The Pd–TPyP multiporphyrin array is based on a coordination of Pd to N atoms of pyridyl groups of TPyP, and that of Pd–TCPP on reaction of Pd with $-CO_2H$ groups of TCPP.[10]

Layer-by-layer deposition was performed by alternately transferring monolayers of the Pd–TPyP and Pd–TCPP multiporphyrin arrays onto a hydrophobic glass substrate surface by the horizontal lifting technique.[6,11] Fig. 3 shows the absorption spectra of 1–8 layers of the assembled 3D Pd–TPyP and Pd–TCPP LBL multilayers. Each spectrum consists of a strong Soret band (425–465 nm) together with several Q-bands ranging from 500 to 700 nm. Table 1 summarizes the spectral data. We have reported that the TPyP Soret band in dilute solution appears at 417 nm, and that in its LB film transferred from a pure water surface, it red shifts to 442 nm.[9] Here, the TPyP Soret band in the LBL multilayers of Pd–TPyP multiporphyrin arrays red shifts to 430 nm. That is, there is a smaller red shift for the Pd-mediated multiporphyrin arrays than that for the LB films from a pure water surface. Similar red shift results

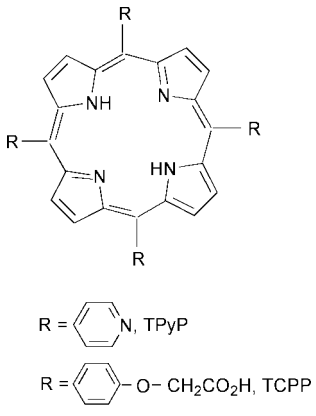

Fig. 1 Molecular structure of porphyrins used in this study.

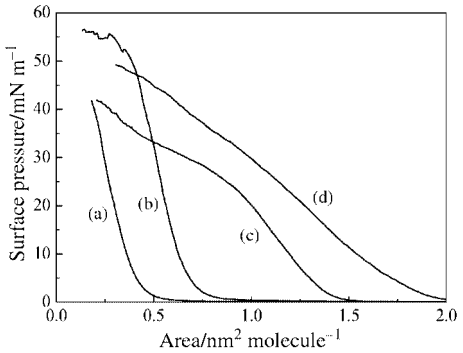

Fig. 2 π–A isotherms for TPyP and TCPP monolayers on pure water and 0.3 mM K_2PdCl_4 subphase surfaces. (a) TCPP, water; (b) TPyP, water; (c) TCPP, K_2PdCl_4; and (d) TPyP, K_2PdCl_4.

Table 1 Mean molecular area (A), absorption characteristics and tilted angle (θ) of the porphyrins

Porphyrin	Subphase	A/nm^2	Soret band/nm	θ/°
TPyP	Water	0.65	442	30
	K_2PdCl_4	1.75	430	42
TCCP	Water	0.45	430	32
	K_2PdCl_4	1.35	426, 462	51

 DOI: 10.1039/b106716h

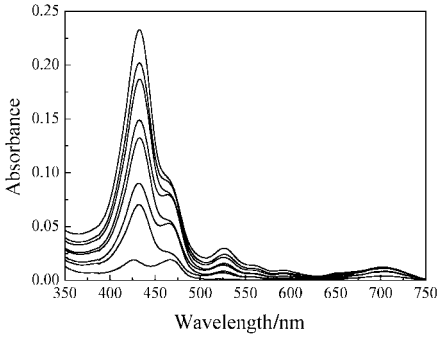

Fig. 3 Absorbance spectra for the LBL multilayers of Pd–TPyP and Pd–TCPP multiporphyrin arrays. From bottom to top: Pd–TCPP and Pd–TPyP layers assembled alternately.

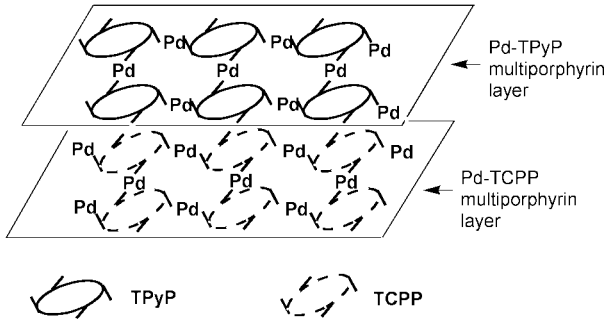

Fig. 4 Schematic model of LBL multilayers of Pd–TPyP and Pd–TCPP multiporphyrin arrays.

are also observed from the absorption spectra of TCPP in solution, LB film and Pd–TCPP LBL multilayers. It is clear that the porphyrins exist in a monomer form in dilute solution and that a peak shift of the Soret band corresponds to the formation of aggregates, which can be explained by exciton theory.[12] This theory points out that the red shift of the Soret band relates to the side-to-side electronic coupling between the respective porphyrins; the stronger the electronic coupling the larger the red shift. Thus, the electronic coupling is weaker in the LBL multilayers of the Pd–TPyP and Pd–TCPP multiporphyrin arrays than that in the TPyP and TCPP LB films from a pure water surface. This weakened electronic coupling is due to the linkage of Py–Pd–Py or CO_2–Pd–CO_2 between two porphyrin rings, which enlarges the porphyrin–porphyrin distance in the Pd-mediated multiporphyrin arrays as indicated in their π–A isotherms.

Close inspection of Fig. 3 reveals that there is a large increase at 430 nm between each even layer due to the deposition of a Pd–TPyP multiporphyrin array, and a large increase at 460 nm between each odd layer due to the deposition of a Pd–TCPP multiporphyrin array. The absorption at 460 nm corresponds to protonated TCPP.[13] If we define the absorption intensity at 430 nm, $A_{sum} = A_i + A_{i+1}$ (number of layers, i = 1, 3, 5 and 7), we observe a linear growth of A_{sum} with increasing number (i + 1) of the deposited layers. Thus, we conclude that 3D multiporphyrin arrays can be constructed by the LBL method. Furthermore, the fact that spectral features of either Pd–TPyP or Pd–TCPP multiporphyrin arrays are retained separately in their LBL multilayers indicates that the electronic coupling among the interlayers of Pd–TPyP and Pd–TCPP multiporphyrin arrays is weak.

The orientation of TPyP and TCPP rings, commonly expressed by the tilted angle, θ, between the mean porphyrin plane and the substrate surface, plays an important part in the description of the organization of the LBL multilayers, and was estimated by measuring polarized UV–VIS spectra of the transferred monolayers at different incidence angles.[14] According to the equation by Yoneyame *et al.*,[14] we calculated that θ_{LBL} was *ca.* 42 and 51° for TPyP and TCPP rings in the LBL multiporphyrin multilayers and 30 and 32° for TPyP and TCPP LB monolayers from a pure water interface, respectively. That is, θ_{LBL} is larger than θ_{LB}, from which, if there were no linkage between porphyrin rings, the mean porphyrin area in LBL multilayers should be smaller than that in LB monolayers from a pure water surface ($\cos\theta_{LBL} < \cos\theta_{LB}$). However, from the π–A isotherms, quite large TPyP or TCPP areas are observed in the LBL multilayers. Thus, we conclude that not the orientation angle but the Py–Pd–Py or CO_2–Pd–CO_2 linkages dominate the arrangement of TPyP or TCPP in the multiporphyrin arrays. On the basis of the monolayer properties, spectral characteristics and orientation angles, we propose a schematic organization of the 3D LBL multilayers of multiporphyrin arrays (two layers) in Fig. 4. Each Pd ion coordinates with two Py or CO_2^- from different porphyrins, leading to the formation of Pd–TPyP or Pd–TCPP multiporphyrin arrays with unlimited numbers of porphyrin macrocycles.[5,10,15] An electrostatic interaction between the layers of Pd–TPyP and Pd–TCPP might dominate the formation of the 3D LBL multilayers of multiporphyrin arrays.[16]

In summary, we have demonstrated a layer-by-layer method to prepare 3D well-defined, organized multiporphyrin arrays with virtually unlimited numbers of porphyrin macrocycles, features that are relevant to the design of light harvesting model systems and to the development of potential materials for optical and photoelectrochemical applications.

This work was supported by Research and Development Project for Environmental Monitoring Technologies under the Agency of Industrial Science and Technology (AIST), Japan. D.-J. Q. acknowledges the Industrial Technology Trainee Fellowship Program sponsored by the New Energy and Industrial Technology Development Organization (NEDO).

Notes and references

1 R. K. Lammi, A. Ambroise, T. Balasubramanian, R. W. Wagner, D. F. Bocian, D. Holten and J. S. Lindsey, *J. Am. Chem. Soc.*, 2000, **122**, 7579.
2 E. K. L. Yeow, K. P. Ghiggino, J. N. H. Reek, M. J. Crossley, A. W. Bosman, A. P. H. J. Schenning and E. W. Meijer, *J. Phys. Chem. B*, 2000, **104**, 2596.
3 V. S. Y. Lin, S. G. DiMagno and M. J. Therien, *Science*, 1994, **264**, 1105.
4 T. Imamura and K. Fukushima, *Coord. Chem. Rev.*, 2000, **198**, 133.
5 C. V. K. Sharma, G. A. Broker, J. G. Huddleston, J. W. Baldwin, R. M. Metzger and R. D. Rogers, *J. Am. Chem. Soc.*, 1999, **121**, 1137.
6 K. Fukuda, H. Nakahara and T. Kato, *J. Colloid Interface Sci.*, 1976, **54**, 430.
7 A. Ruaudel-Teixier, A. Barraud, B. Belbeoch and M. Roulliay, *Thin Solid Films*, 1983, **99**, 33.
8 H. Chou, C. T. Chen, K. F. Storck, P. W. Bohn and K. S. Suslick, *J. Phys. Chem.*, 1994, **98**, 383.
9 D. J. Qian, C. Nakamura and J. Miyake, *Langmuir*, 2000, **16**, 9615.
10 C. M. Drain and J.-M. Lehn, *J. Chem. Soc., Chem. Commun.*, 1994, 2313.
11 The TPyP and TCPP monolayers on a pure water surface can be also deposited as alternate multilayers with different structural features, where each layer was composed of ordered TPyP or TCPP aggregates but without multiporphyrin arrays.
12 M. Kasha, *Radiat. Res.*, 1963, **20**, 55.
13 H. G. Liu, D. J. Qian, X. S. Feng, Q. B. Xue and K. Z. Yang, *Langmuir*, 2000, **16**, 5079.
14 M. Yoneyama, M. Sugi, M. Saito, K. Ikegami, S. Kuroda and S. Iizima, *Jpn. J. Appl. Phys.*, 1986, **25**, 961.
15 C. M. Drain, F. Nifiatis, A. Vasenko and J. D. Batteas, *Angew. Chem. Int. Ed.*, 1998, **37**, 2344.
16 We failed to assemble 3D multilayers of multiporphyrin arrays by using a single porphyrin (either TPyP or TCPP).

CHEMCOMM
Communication
www.rsc.org/chemcomm

A novel system consisting of Rh–DuPHOS and ionic liquid for asymmetric hydrogenations

Silvina Guernik,[a] Adi Wolfson,[b] Moti Herskowitz,[b] Noam Greenspoon[c] and Shimona Geresh*[d]

[a] *Department of Chemistry, Ben-Gurion University of the Negev, Beer-Sheva, Israel*
[b] *Department of Chemical Engineering, Ben-Gurion University of the Negev, Beer-Sheva, Israel*
[c] *Chemada Fine Chemicals Ltd., Israel. E-mail: geresh@bgumail.bgu.ac.i; Fax: 972-8-6479074*
[d] *Institute for Applied Biosciences, Ben-Gurion University of the Negev, Beer-Sheva, Israel*

Received (in Cambridge, UK) 10th August 2001, Accepted 28th September 2001
First published as an Advance Article on the web 24th October 2001

The ionic liquid [bmim][PF_6] was found to provide extra stability to the air-sensitive chiral catalyst Rh–MeDuPHOS in asymmetric hydrogenation of enamides.

One of the most versatile routes for preparing optically active compounds is asymmetric synthesis, particularly by the use of enantioselective catalysts.[1] Various chiral catalysts including biocatalysts (enzymes and/or microorganisms),[2] chiral transition-metal complexes[3,4] and heterogenized chiral catalysts have been used for the conversion of a prochiral substrate into a chiral product. The chiral complex Rh–DuPHOS[5] has been found to be particularly efficient as a homogeneous catalyst in the asymmetric hydrogenation of enamides. However, as good as its performance is, the rather expensive Rh–DuPHOS is very sensitive to oxidation; hence, an inert atmosphere is required for its preparation and handling, and separation of the complex from reagents and products and recovery of the complex are not easy.

Possible solutions to these drawbacks have focused on the engineering of chiral 'heterogenized' catalysts. Heterogenization of chiral complexes by immobilization in various organic and inorganic supports has been successful, but leaching and stability of the complex still remain severe problems.[6] Another approach was the use of two-phase systems, in which the phase of preference of the complex differs from that of the substrate,[7,8] but only limited success has been achieved.[9,10] In most cases, the activity and enantioselectivity of the chiral complexes are lower than those of the identical homogeneous system as a result of mass transfer limitations. The immobilization of chiral metal complexes in molten salts (ionic liquids) has recently been reported for some enantioselective hydrogenations[10,11] and for the epoxidation of alkenes.[12] Room-temperature ionic liquids (RTIL) have gained increasing interest as 'green' solvents in organic syntheses.[13,14] An ionic liquid such as [bmim][PF_6] (Fig. 1), which has poorly coordinating ions and which is highly polar, nonvolatile, stable in air, and immiscible with both water and nonpolar solvents can serve as a good and environmentally friendly medium for asymmetric hydrogenations. First earlier examples that have appeared in the literature are the asymmetric-catalyzed hydrogenation of 2-phenylacrylic acid in a [bmim][BF_4]–iPrOH system[10] and the Rh–DIOP-catalyzed hydrogenation of α-acetamidocinnamic acid in [bmim][SbF_6] as an ionic liquid to produce (*S*)-phenylalanine (64% ee).[11]

Our approach to performing hydrogenation reactions with the unstable air-sensitive Rh–DuPHOS catalyst was based on 'immobilizing' the Rh–MeDuPHOS complex (Fig. 2) in the air-stable molten salt [bmim][PF_6] (Fig. 1). This ionic liquid was not only a good host for the chiral catalyst, but it also protected the complex from attack by atmospheric oxygen and facilitated easy recycling. Hydrogenation of two model enamide compounds to optically active α-amino acid derivatives was performed in the biphasic system [bmim][PF_6]–iPrOH (Scheme 1). The chiral complex was totally soluble in the ionic liquid phase, and the products were easily recovered in the upper iPrOH phase.†

Results of the asymmetric hydrogenations of methyl α-acetamidoacrylate (**1a**) and of methyl α-acetamidocinnamate (**1b**) with Rh–MeDuPHOS in the [bmim]PF_6–iPrOH system are presented in Table 1. In the first run (entry 3), the enantioselectivities obtained for the two substrates in the ionic liquid were high, the values being similar to those obtained in the homogeneous reaction. Note that for the homogeneous reactions, the transfer of the catalyst into the reactor without an inert atmosphere brought about a significant decrease in the enantioselectivity of the hydrogenation of **1a** (57% ee *vs*. 97% ee) and the conversion dropped almost completely. Two cycles of recycling of the catalyst were performed for both substrates (entries 3 and 4), with the recycling procedure being continued with substrate **1b** for three further cycles (entries 5–7), since the activity and enantioselectivity of the immobilized catalyst after the second run were remarkable. Although the activity of the catalyst decreased after the first cycle, it remained almost constant upon successive cycles, without significant loss of enantioselectivity, even though the fifth cycle was performed after the heterogenized catalyst had been exposed to air for 24 h. It thus appears that the combination of the particularly efficient chiral complex (Rh–MeDuPHOS)[6] with the ionic liquid system used in this study [(bmim)PF_6–iPrOH] provides a promising route to facile asymmetric hydrogenations.

In summary, as an extension of our ongoing efforts to heterogenize chiral catalysts, this work focused on the perform-

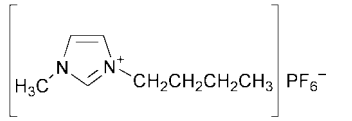

Fig. 1 Butyl-3-methylimidazolium hexafluorophosphate [bmim][PF_6].

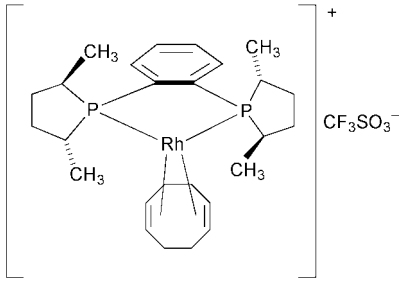

Fig. 2 Rh–(*R*,*R*)-MeDuPHOS complex.

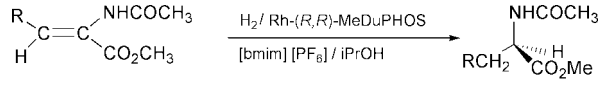

1a. R = H
1b. R = Phenyl

Scheme 1 Asymmetric hydrogenation of enamides catalyzed by Rh–MeDuPHOS complex heterogenized in [bmim][PF_6] ionic liquid.

 DOI: 10.1039/b107292g

Table 1 Asymmetric hydrogenation of enamides with Rh–MeDuPHOS in [bmim][PF_6]–iPrOH

		1a		**1b**	
Entry		Conversion (%)	% ee	Conversion (%)	% ee
1	Homogeneous[a]	100	97 (*R*)	100	99 (*R*)
2	Homogeneous[b]	5	57 (*R*)	—	—
3	Heterogeneous First cycle	100	93 (*R*)	83	96 (*R*)
4	Heterogeneous Second cycle	100	80 (*R*)	64	96 (*R*)
5	Heterogeneous Third cycle			62	95 (*R*)
6	Heterogeneous Fourth cycle			60	94 (*R*)
7	Heterogeneous Fifth cycle[c]			58	94 (*R*)

Reaction conditions for homogeneous catalyst: 25 °C, 2 atm H_2, 7 g iPrOH; reaction time = 5 min. In the heterogeneous system, 5 g of ionic liquid was added; reaction time = 20 min. [a] Preparation of the catalyst and of feeding into the reactor were performed under nitrogen. [b] Catalyst prepared in an inert atmosphere and exposed to air for a few minutes during feeding into the reactor. For cycles 3–7, all manipulations were performed in air. [c] Left to stand in air for 24 h.

ance of the 'immobilized' Rh-DuPHOS complex in an ionic liquid such as [bmim][PF_6] for the asymmetric hydrogenations of enamides. Recycling of the catalyst was possible. Entrapment of the air-sensitive complex in an ionic liquid facilitated its handling without loss of enantioselectivity. At the end of the reaction, the products were easily separated by decantation of the upper iPrOH phase.

We thank the Magneton program for financial support.

Notes and references

† The salt 1-butyl-3-methylimidazolium chloride was prepared under nitrogen according to the method of Huddleston *et al*.[15] with small changes. The [bmim][PF_6] salt was prepared by dropwise addition of HPF_6 (65%) into a precooled aqueous solution of the crude imidazolium salt. After stirring for a few hours, the lower phase was washed with water (×3) until the pH was about 6–7. After separation, the ionic liquid was dissolved in methylene chloride and dried over anhydrous $MgSO_4$. After the methylene chloride was evaporated off, the ionic liquid was characterized by ^{1}H-NMR spectroscopy.

The Rh–MeDuPHOS homogeneous catalyst was prepared as previously described.[5] Homogeneous and biphasic reactions were performed with magnetic stirring in a specially designed 25 ml reactor. In the homogeneous reactions, 10 μmol of the prepared complex were dissolved in 5–7 g of iPrOH. In the biphasic reactions, 5 g of ionic liquid were added to the solution of the complex under nitrogen. The reaction mixture was added to the reactor together with the substrate. The reaction took place at 20–25 °C at a reactor pressure of 2 bars of highly pure hydrogen (99.995%). Re-use of the catalyst was achieved by replacing the iPrOH and insertion of fresh substrate dissolved in iPrOH. Conversion and enantiomeric excess were determined with a Hewlett Packard GC equipped with an Astec Chirasil-Val-L capillary column.

1 A. N. Collins, G. N. Sheldarke and J. Crosby, *Chirality in Industry: The Commercial Manufacture and Application of Optically Active Compounds*, John Wiley, New York, 1995.
2 L. Poppe and L. Novak, *Selective Biocatalysis*, VCH, Weinheim, 1992.
3 R. A. Sheldon, *Chirotechnology*, Marcel Dekker Inc., New York, 1993.
4 R. Noyori, *Asymmetric Catalysis in Organic Synthesis*, John Wiley, New York, 1994.
5 M. J. Burk, J. E. Feaster, W. A. Nugent and R. L. Harlow, *J. Am. Chem. Soc*., 1993, **115**, 10125.
6 K. Fodor, S. G. A. Kolmschot and R. A. Sheldon, *Enantiomer*, 1999, **4**, 497.
7 L. Maat, G. Papadoginakis and R. A. Sheldon, *J. Chem. Soc., Chem. Commun*., 1994, 2659.
8 Y. Chauvin, S. Einloft and H. Olivier, *Ind. Eng. Chem. Res*., 1995, 1149.
9 K. T. Wan and M. E. Davis, *Nature*, 1994, **370**, 449.
10 (*a*) A. L. Monteiro, F. K. Zinn, R. F. De Souza and J. Dupont, *Tetrahedron: Asymmetry*, 1997, 179; (*b*) Y. Chauvin, L. Mussmann and H. Olivier, *Angew. Chem., Int. Ed. Engl*., 1995, 34; (*c*) A. Berger, R. F. De Souza, M. R. Delgado and J. Dupont, *Tetrahedron: Asymmetry*, 2001, **12**, 1825.
11 R. A. Brown, P. Pollet, E. McKoon, C. A. Eckert, C. L. Liotta and P. G. Jessop, *J. Am. Chem. Soc*., 2001, **123**, 1254.
12 C. E. Song and E. J. Roh, *Chem. Commun*., 2000, 837.
13 S. G. Cull, J. D. Holbey, V. Vargas-Mora, K. R. Seddon and G. J. Lye, *Biotech. Bioeng*., 2000, **69**, (2), 227.
14 T. Welton, *Chem. Rev*., 1999, **99**, 2071.
15 J. G. Huddleston, H. D. Willdver, R. P. Swatloski,. A. F. Visser and R. D. Rogers, *Chem. Commun*., 1998, 1765.

CHEMCOMM Communication
www.rsc.org/chemcomm

Rhodium catalysed addition of boronic acids to anhydrides: a new method for the synthesis of ketones

Christopher G. Frost* and Kelly J. Wadsworth

Department of Chemistry, University of Bath, Bath, UK BA2 7AY. E-mail: c.g.frost@bath.ac.uk; Fax: 01225 826231; Tel: 01225 826142

Received (in Cambridge, UK) 22nd August 2001, Accepted 26th September 2001
First published as an Advance Article on the web 24th October 2001

The efficient transmetalation from boron to rhodium is exploited in a new synthesis of aryl and alkenyl ketones.

The rhodium catalysed addition of boronic acids to organic electrophiles has recently emerged as an important tool for organic synthesis.[1] An efficient transmetalation between boron and rhodium permits the addition of organoboronic acids to a range of activated olefins.[2] Significant advances have also been made in the coupling of unactivated olefins in aqueous media.[3] Further to this the addition of aryl boronic acids to aldehydes and imines has been achieved.[4] The mechanism of these transformations is proposed to involve transmetalation between the boronic acid and the rhodium(I) complex to afford an R–Rh(I) species. The nucleophilic R group then adds to the coordinated electrophile yielding either a Rh bound enolate or alkoxide which is subsequently hydrolysed. As part of our research programme developing catalysts for the functionalisation of aromatics, we were interested in the boron–rhodium transmetalation process as a means to promote the equivalent of a Friedel–Crafts acylation reaction of deactivated aryl derivatives. This is a demanding transformation which is not readily achieved by even the most effective Lewis acid catalysts.[5] In this communication we wish to report our development of an efficient rhodium catalysed addition reaction that allows the synthesis of ketones from boronic acids under mild conditions.

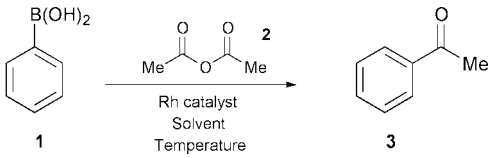

Scheme 1 Rhodium catalysed acylation.

Table 1 Rhodium catalysed addition of **1** to acetic anhydride **2**

Entry	Catalyst	Solvent (Temp./°C)	Yield of 3 (%)
1	—	Dioxane (100)	0
2	[Rh(acac)(ethylene)$_2$]	Dioxane (100)	0
3	[Rh(acac)(ethylene)$_2$]	DME–H_2O (65)	0[a]
4	[Rh(acac)(cod)]	Dioxane (100)	16
5	[Rh(acac)(cod)]	DME–H_2O (65)	18[a]
6	[Rh(acac)(nbd)]	Dioxane (100)	27
7	[Rh(acac)(nbd)]	DME–H_2O (65)	29[a]
8	[Rh(nbd)Cl]$_2$	Dioxane (100)	20
9	[Rh(cod)Cl]$_2$	Dioxane (100)	57
10	[Rh(OAc)$_2$]$_2$	Dioxane (100)	27
11	$RhCl_3·3H_2O$	Dioxane (100)	0
12	[Rh(ethylene)Cl]$_2$	Dioxane (100)	83
13	[Rh(ethylene)Cl]$_2$	DME–H_2O (65)	84[a]
14	[Rh(ethylene)Cl]$_2$	Toluene (100)	17
15	[Rh(ethylene)Cl]$_2$	THF (65)	37
16	[Rh(ethylene)Cl]$_2$	DME (65)	85[b]
17	[Rh(ethylene)Cl]$_2$	DME (20)	76[c]

[a] DME–H_2O (6:1). [b] Yield after 2 hours. [c] Yield after 16 hours.

To demonstrate this concept, initial experiments examined the reaction of phenylboronic acid (1.6 equiv.) **1** with acetic anhydride **2** in the presence of 5 mol% of various rhodium complexes (Scheme 1).[6] As summarised in Table 1, the formation of acetophenone **3** is symptomatic of an effective protocol for ketone synthesis.

The first point to note is that in the absence of catalyst no product formation is observed. It was interesting to learn that the Rh(acac) complexes favoured for addition to activated olefins, were not particularly effective in this case (entries 2–7). Similarly, the use of [Rh(OAc)$_2$]$_2$ and $RhCl_3·3H_2O$ afforded disappointing results (entries 10 and 11). Gratifyingly, the use of [Rh(alkene)Cl]$_2$ complexes showed more promise (entry 9)

Table 2 Rhodium catalysed synthesis of ketones

Entry	Boronic acid	Product	Yield (%)
1	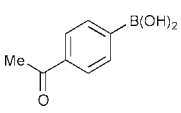	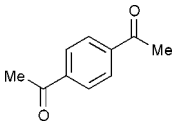	86
2	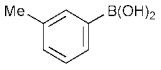	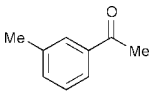	68
3	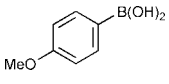	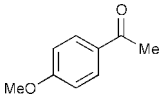	67
4	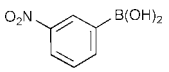	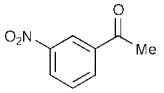	56
5	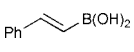	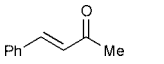	54
6	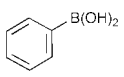	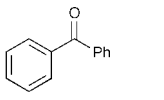	76
7	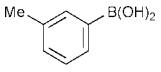	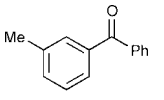	70
8	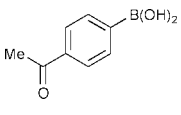	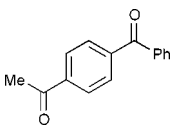	88
9	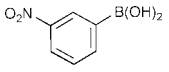	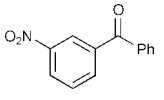	59
10	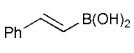	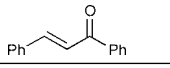	74

 DOI: 10.1039/b107633g

resulting in the formation of **3** in excellent overall yield in the best case (entry 12). The choice of solvent had a clear effect on the efficiency of the reaction (entries 12–16) with the reaction proceeding smoothly in dioxane and 1,2-dimethoxyethane (DME). The insensitivity of this protocol towards air and water (entry 13) is extremely beneficial from a practical perspective. At 65 °C in DME the reaction was complete within two hours, whilst at room temperature the reaction required 24 hours to afford comparable yields (entries 16 and 17). Furthermore, the catalyst loading could be lowered to 1.5 mol% with the product **3** being obtained in an 87% yield after 16 hours. Upon lowering to 0.1 mol% of catalyst, a modest 33% of **3** was isolated after the same period of time.

Under the optimised conditions the reaction was examined with respect to the scope of the boronic acid (Table 2).† An attractive feature of this methodology is the commercial availability of a wide range of boronic acids. An important point to note about the presented reaction is the regiospecific formation of product with the electrophile substituting the boronic acid group. Therefore, whilst electronic effects (inductive and resonance) may influence the rates of the reactions, as a consequence of the nucleophilicity dictating the transmetalation and transfer processes, the composition of product is unaffected by the nature and position of substituent in the starting boronic acid. This offers a significant tactical advantage over Lewis acid catalysed electrophilic substitution processes. Thus, the reaction can be designed to mirror typical electrophilic substitution reactions (Table 2, entry 3). Conversely, the formation of *meta*- or *para*-substituted deactivated aromatics can be achieved in excellent isolated yield (Table 2, entries 1, 2 and 4). The results also confirm the scope of the reaction with the alternative electrophile, benzoic anhydride (Table 2, entries 6–10). Furthermore, the reaction can be extended to alkenylboronic acids with no significant loss in efficiency. At the present time, difficulties have been encountered in extending the methodology to acid chlorides.[7] Further investigations are directed towards accomplishing this and the addition of organoboronic acids to other electrophiles.

In summary, a new rhodium catalysed addition of boronic acids has been developed that allows the synthesis of ketones. This transformation proceeds in good yield for a range of boronic acids. Importantly, this new methodology offers specific advantages over traditional Lewis acid catalysed acylation reactions in that it allows the regiospecific functionalisation of activated, unactivated and deactivated aromatics.

C. G. F. thanks Astra-Zeneca for a generous award from their strategic research fund.

Notes and references

† *General experimental procedure*: to a pressure tube charged with $[Rh(ethylene)Cl]_2$ (0.006 mmol, 1.5 mol%) was added 1,4-dioxane (4 ml), boronic acid (0.56 mmol) and anydride (1 ml of 0.4 M solution). The tube was sealed, placed in a cold oil bath which was then heated to the required temperature and stirred for 16 hours. The mixture was allowed to cool to room temperature then worked up by extracting with ethyl acetate, washing with brine, drying over magnesium sulfate and concentrating *in vacuo*. The crude product was then purified by flash chromatography (ethyl acetate–hexane, 1:8 by volume). All the products have been satisfactorily characterised by ^{1}H NMR, ^{13}C NMR and IR spectroscopy.

1 (*a*) M. Sakai, H. Hayashi and N. Miyaura, *Organometallics*, 1997, **16**, 4229; (*b*) Y. Takaya, M. Osgawara, T. Hayashi, M. Sakai and N. Miyaura, *J. Am. Chem. Soc*., 1998, **120**, 5579; (*c*) S. Sakuma, M. Sakai, R. Itooka and N. Miyaura, *J. Org. Chem*., 2000, **65**, 5951; (*d*) T. Hayashi, T. Senda, Y. Takaya and M. Ogasawara, *J. Am. Chem. Soc*., 2000, **122**, 10716.

2 For an excellent review, see: T. Hayashi, *Synlett*, 2001, 879.

3 M. Lautens, A. Roy, K. Fukuoka, K. Fagnou and B. Martin-Matute, *J. Am. Chem. Soc*., 2001, **123**, 5358.

4 (*a*) M. Sakai, M. Ueda and N. Miyaura, *Angew. Chem., Int. Ed*., 1998, **37**, 3279; (*b*) M. Ueda and N. Miyaura, *J. Org. Chem*., 2000, **65**, 4450; (*c*) A. Fürstner and H. Krause, *Adv. Synth. Catal*., 2001, **343**, 343.

5 (*a*) *Lewis Acids in Organic Synthesis*, ed. H. Yamamoto, Wiley-VCH, Weinheim, 2000; (*b*) C. J. Chapman, C. G. Frost, J. P. Hartley and A. J. Whittle, *Tetrahedron Lett*., 2001, **42**, 773.

6 All rhodium salts were purchased (Aldrich, Strem) and used as received.

7 For corresponding palladium catalysed protocol, see: (*a*) C. S. Cho, K. Itotani and S. Uemura, *J. Organomet. Chem*., 1993, **433**, 253; (*b*) N. A. Bumagin and D. N. Korolev, *Tetrahedron Lett*., 1999, **40**, 3057; (*c*) M. Haddach and J. R. McCarthy, *Tetrahedron Lett*., 1999, **40**, 3109.

CHEMCOMM Communication
www.rsc.org/chemcomm

A convenient imino aldol reaction in ethyl alcohol catalyzed by a cation-exchange resin

Makoto Shimizu,* Susumu Itohara and Emi Hase

Department of Chemistry for Materials, Mie University, Tsu, Mie 514-8507, Japan

Received (in Cambridge, UK) 24th July 2001, Accepted 26th September 2001
First published as an Advance Article on the web 25th October 2001

Imino aldol reaction of ketene silyl acetals with imines proceeds smoothly to give β-amino esters in good yields under the influence of a cation-exchange resin in ethanol, and the work-up of the reaction consists only of a simple filtration followed by concentration of the crude mixture and purification.

Cation-exchange resins have been found to be excellent activators for imino aldol reaction of ketene silyl acetals with imines in dichloromethane or in some cases in isopropyl alcohol.[1] Although a variety of activators for such transformations have been reported,[2] polymer supported catalysts such as ion-exchange resins have not received much attention for promotion of imino aldol reaction until recently.[3] Use of ion-exchange resins offers several advantages in organic synthesis,[4] *e.g.* simplification of reaction procedures, easy separation of products without discharging harmful waste water, repeated use, and so on. In our previous report, a cation-exchange resin, in particular Amberlyst® 15 DRY, having a large surface area (45 m^2 g^{-1}), was found to be one of the most useful resins that promoted aldol type reaction, where the addition reactions proceeded with high chemoselectivity in the presence of two kinds of imines and/or nucleophiles. From an environmental point of view, however, this reaction needs modifications, because it is carried out in dichloromethane as a solvent and an equimolar amount of a cation-exchange resin is needed in most cases. Recent papers describing imino aldol reaction carried out in water or organic solvent–water as a convenient system[5] prompted us to report our approach which reduces harmful wastes such as waste water containing metal ions and organic wastes. We wish to report herein a convenient imino aldol reaction using a cation-exchange resin as a recyclable catalyst in ethanol as a solvent.

First, reaction of the imine **2a** and the ketene silyl acetal **1a** was chosen as a model for comparison of solvents, and the results are shown in Table 1. Among the alcohols examined the use of ethyl alcohol proved to be the most effective, whereas in methyl alcohol the ketene silyl acetal **1a** hydrolized to some extent and in *tert*-butyl alcohol the desired reaction proceeded very slowly.

Table 1 Effects of solvent[a]

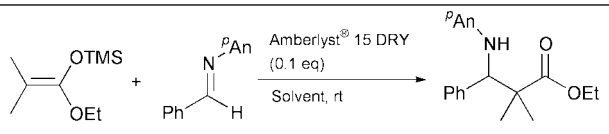

1a **2a** **3aa**

Entry	Solvent	Time/h	Yield (%)[b]
1	EtOH	10.5	99
2	*i*-PrOH	11.0	81
3[c]	*t*-BuOH	11.5	30
4	MeOH	12.5	66

[a] The reaction was carried out according to the typical experimental procedure. [p]An = *p*-anisyl (*p*-methoxyphenyl). [b] Isolated yield. [c] Amberlyst® 15 DRY (0.2 eq.) was used.

Examples of the Amberlyst® 15 DRY catalyzed imino aldol reactions of ketene silyl acetals with imines in ethyl alcohol are shown in Table 2.† In the reactions of ketene silyl acetal **1a** with the imines derived from aromatic amines, the addition reaction proceeded smoothly to afford β-amino esters **3** in moderate to high yields. However, the imine derived from benzyl amine did not give the addition product in good yield (entry 7). A moderate diasteroselectivity was observed in the reaction of the ketene silyl acetal **1b** derived from propionate (entry 8). Ketene silyl thioacetals also worked well to give the corresponding adducts in good yields (entries 9 and 10).

The present reaction conditions were also effective for the addition of ketene silyl acetal **1a** to the imine equivalent **2h** derived from formaldehyde,[6] and the β-amino ester was obtained in 66% yield. As shown in Scheme 1, the *in situ* preparation of a relatively unstable imine could be used for the present addition, and the adduct was formed in good yield.

Furthermore, Amberlyst® 15 DRY was recovered by simple filtration after the reaction, and could be reused at least four times without loss of activity.‡ The results are shown in Table 3.

Regarding the chemoselectivity, the ketene silyl acetal **1a** reacted with the anisyl imine **2a** preferentially even in the presence of benzaldehyde to give β-amino ester **3aa** in 83% yield, and none of the adduct **4** arising from benzaldehyde was detected.[7]

Competition reactions between two kinds of imines were examined next. Amberlyst® 15 DRY selectively promoted the

Table 2 Imino aldol reaction promoted by Amberlyst® 15 DRY in EtOH[a]

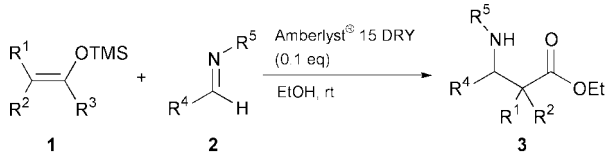

1 **2** **3**

1b: R^1 = H, R^2 = Me, R^3 = OEt
1c: R^1 = H, R^2 = Me, R^3 = SEt
1d: R^1 = R^2 =H, R^3 = SEt

2b: R^4 = (*E*)-PhCH=CH, R^5 = *p*-An
2c: R^4 = PhCO, R^5 = *p*-An
2d: R^4 = 2-Furyl, R^5 = *p*-An
2e: R^4 = 2-Thienyl, R^5 = *p*-An
2f: R^4 = Ph, R^5 = *p*-ClPh
2g: R^4 = Ph, R^5 = Bn

Entry	1	2	Time/h	Yield (%)[b]
1	**1a**	**2a**	10.5	99
2	**1a**	**2b**	24.5	73
3	**1a**	**2c**	18.0	81
4	**1a**	**2d**	23.5	69
5	**1a**	**2e**	9.0	57
6	**1a**	**2f**	4.0	94
7	**1a**	**2g**	24.0	27
8	**1b**	**2a**	16.5	60[c]
9	**1c**	**2a**	9.0	96[d]
10	**1d**	**2a**	20.5	86

[a] The reaction was carried out according to the typical experimental procedure. [b] Isolated yield. [c] *syn*:*anti* = 39:61. [d] *syn*:*anti* = 48:52.

 DOI: 10.1039/b106662e

addition to anisyl imine in the presence of the tosyl **2j** or ethoxycarbonyl imine **2k** with an electron-withdrawing *N*-substituent. One of the reasons for the chemoselectivity may be due to the difference in the ability of the imino nitrogen to be protonated by the catalyst. A better chemoselectivity between the imines **2a** and **2k** was observed in the present case than that in the previous report, showing that the present reaction conditions are much milder than the previous ones.

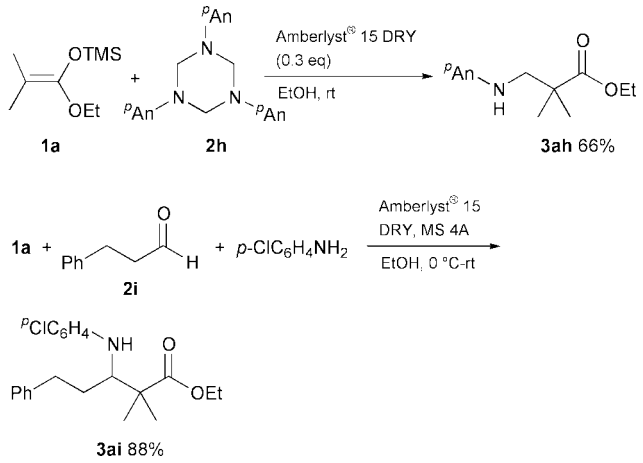

Scheme 1

Table 3 Reuse of Amberlyst® 15 DRY[a]

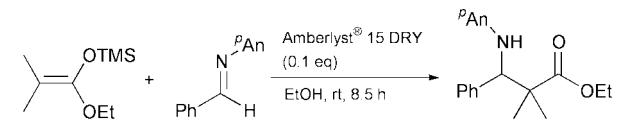

Run	1st	2nd	3rd	4th
3aa (%)[b]	98	93	97	94

[a] The reaction was carried out according to the typical experimental procedure. [b] Isolated yield.

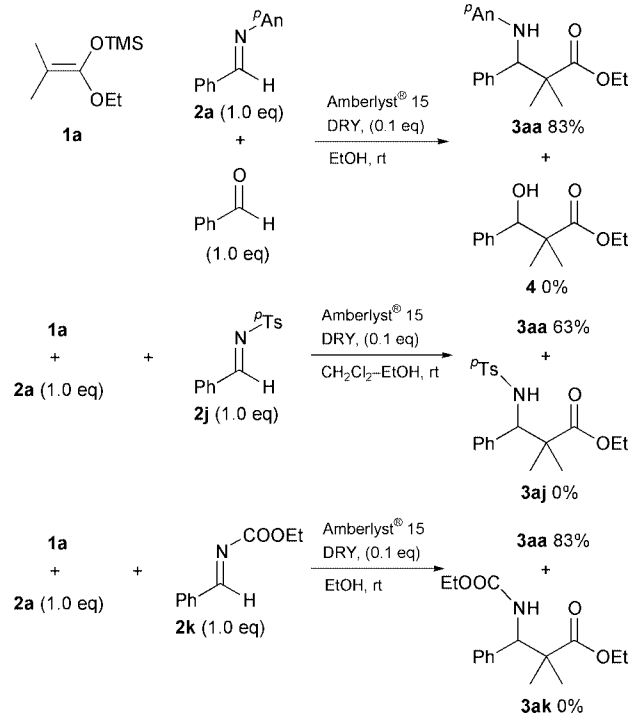

Scheme 2

This work was supported by a Grant-in-Aid for Scientific Research from the Ministry of Education, Science, Sports, and Culture, Japan, and a grant from the Nagase Science and Technology Foundation.

Notes and references

† A typical experimental procedure is as follows: to a suspension of Amberlyst® 15 DRY (4.3 mg, 0.02 mmol of the sulfonic acid portion, washed with EtOH and dried *in vacuo* at 100 °C) and aldimine **2a** (42.3 mg, 0.2 mmol) in EtOH (1.0 ml) was added a solution of ketene silyl acetal **1a** (45.2 mg, 0.24 mmol) in EtOH (1.0 ml) at room temperature under an argon atmosphere. After being stirred at room temperature for 10.5 h, the suspension was filtered through a Celite pad. The filtrate was concentrated *in vacuo* to afford a crude oil. Purification on preparative silica gel TLC (*n*-hexane–AcOEt = 10 : 1, as an eluent) gave the adduct **3aa** (64.7 mg, 99%) as a colorless oil.

‡ The sulfonic acid groups on the recovered resin are involved in the salt formation with amine moieties,[8] and therefore, such salts may be also responsible for the present imino aldol reaction. We are currently investigating such salt formation in more detail.

1 M. Shimizu and S. Itohara, *Synlett*, 2000, 1828.

2 I. Ojima, S. Inaba and K. Yoshida, *Tetrahedron Lett*., 1977, **18**, 3643; R. A. Pilli and D. Russowsky, *Chem. Commun*., 1987, 1053; G. Guanti, E. Narisano and L. Banfi, *Tetrahedron Lett*., 1987, **28**, 4331; T. Mukaiyama, K. Kashiwagi and S. Matsui, *Chem. Lett*., 1989, 1397; T. Mukaiyama, H. Akamatsu and J. S. Han, *Chem. Lett*., 1990, 889; M. Onaka, R. Ohno, N. Yanagiya and Y. Izumi, *Synlett*, 1993, 141; K. Ishihara, M. Miyata, K. Hattori, T. Tada and H. Yamamoto, *J. Am. Chem. Soc*., 1994, **116**, 10 520; S. Kobayashi, M. Araki, H. Ishitani, S. Nagayama and I. Hachiya, *Synlett*, 1995, 233; M. Shimizu, K. Kume and T. Fujisawa, *Chem. Lett*., 1996, 545; R. Hayakawa and M. Shimizu, *Chem. Lett*., 1999, 591.

3 S. Kobayashi, S. Nagayama and T. Busujima, *Tetrahedron Lett*., 1996, **37**, 9221; L. Yu, D. Chen, J. Li and P. G. Wang, *J. Org. Chem*., 1997, **62**, 3575; S. Kobayashi and S. Nagayama, *J. Am. Chem. Soc*., 1998, **120**, 2985; N. Tanaka and Y. Masaki, *Synlett*, 2000, 406.

4 A. Akelah and D. C. Sherrington, *Chem . Rev*., 1981, **81**, 557; S. J. Shuttleworth, S. M. Allin and P. K. Sharma, *Synthesis*, 1997, 1217; B. Baruah, M. P. Dutta, A. Boruah, D. Prajapati and J. S. Sandhu, *Synlett*, 1999, 409; J.-J. Young, L.-J. Jung and K.-M. Cheng, *Tetrahedron Lett*., 2000, **41**, 3415.

5 T.-P. Loh and L.-L. Wei, *Tetrahedron Lett*., 1998, **39**, 323; S. Kobayashi, T. Busujima and S. Nagayama, *Synlett*, 1999, 545; T. Akiyama, J. Takaya and H. Kagoshima, *Synlett*, 1999, 1045; K. Manabe, Y. Mori and S. Kobayashi, *Synlett*, 1999, 1401; T. Akiyama, J. Takaya and H. Kagoshima, *Synlett*, 1999, 1426; K. Manabe and S. Kobayashi, *Org. Lett*., 1999, **1**, 1965; T. Akiyama, J. Takaya and H. Kagoshima, *Tetrahedron Lett*., 2001, **42**, 4025.

6 D. D. Reynolds and B. C. Cossar, *J. Heterocycl. Chem*., 1971, 597.

7 Preferential activation of aldimine in the presence of aldehyde, see: H. Nakamura, H. Iwama and Y. Yamamoto, *J. Am. Chem. Soc*., 1996, **118**, 6641; S. Kobayashi and S. Nagayama, *J. Org. Chem*., 1997, **62**, 232; S. Kobayashi and S. Nagayama, *Synlett*, 1997, 653; S. Kobayashi and S. Nagayama, *J. Am. Chem. Soc*., 1997, **119**, 10 049; T. Akiyama and J. Iwai, *Synlett*, 1998, 273.

8 Y.-S. Liu, C. Zhao, D. E. Bergbreiter and D. Romo, *J. Org. Chem*., 1998, **63**, 3471.

CHEMCOMM
Communication
www.rsc.org/chemcomm

Ferrimagnetic-like ordering in a unique three-dimensional coordination polymer featuring mixed azide/carboxylate-bridged trinuclear manganese(II) clusters as subunits†

Hong-Ji Chen,[ab] Zong-Wan Mao,[a] Song Gao*[c] and Xiao-Ming Chen*[a]

[a] *School of Chemistry & Chemical Engineering, Zhongshan University, Guangzhou 510275, China. E-mail: cescxm@zsu.edu.cn*
[b] *Department of Chemistry, Jinan University, Guangzhou 510632, China*
[c] *State Key Laboratory of Rare Earth Materials Chemistry and Applications, College of Chemistry and Molecular Engineering, Peking University, Beijing 100871, China. E-mail: gaosong@pku.edu.cn*

Received (in Cambridge, UK) 16th July 2001, Accepted 11th September 2001
First published as an Advance Article on the web 25th October 2001

The crystal structure of the coordination polymer $[Mn_3(N_3)_2(nta)_4(H_2O)_2]_n$ (nta = nicotinate) consists of trinuclear subunits bridged by mixed μ-1,1-azide and μ-carboxylate-*O,O* groups, which are linked by μ_3-nta-*N,O,O* ligands into a three-dimensional network exhibiting ferrimagnetic-like ordering.

The family of azide-bridged transition metal complexes has been investigated widely in the past decade due to its magnetic properties and potential applications.[1–3] A number of synthetic strategies utilizing different organic spacers for propagating new motifs have been used to produce a large number of azide-bridged complexes.[1–4] Among them the end-to-end (EE) coordination mode affords antiferromagnetic exchange interactions,[2] the end-on (EO) coordination mode shows ferromagnetic exchange interactions,[3] and some alternating azide-bridged modes give interesting magnetic properties.[1] These complexes include dinuclear,[1a] trinuclear[4] and tetranuclear[3a] species, as well as one-,[1b] two-[1c,2a,3b–d] and three-dimensional[2b] coordination frameworks. So far no azide-bridged trinuclear Mn^{II} complex has been documented; in contrast, carboxylate-bridged trinuclear manganese complexes have been widely investigated as models for a variety of metalloenzymes[5] and often show antiferromagnetic interactions.[6] Meanwhile, very few complexes containing mixed azide and carboxylate bridges have been reported.[7] In this communication, we report the synthesis, crystal structure and magnetic properties of a unique three-dimensional complex $[Mn_3(N_3)_2(nta)_4(H_2O)_2]_n$ (**1**)‡ featuring mixed azide/carboxylate-bridged trinuclear Mn^{II} clusters as subunits.

Single-crystal X-ray diffraction§ shows that **1** consists of a three-dimensional covalent network constructed by linear Mn^{II}_3 subunits (Fig. 1), in which each Mn^{II} atom is coordinated in a distorted octahedral geometry. The central Mn(1) atom, being located at a crystallographic inversion centre, is coordinated by two *trans*-related nitrogen atoms [Mn(1)–N(3) 2.184(2) Å] from two azide groups and four carboxy oxygen atoms [Mn(1)–O(2B) 2.212(2) Å and Mn(1)–O(4) 2.257(2) Å] from nta groups. Each of the two terminal Mn^{II} atoms is coordinated by a μ-1,1-azide nitrogen atom [Mn(2)–N(3A) 2.233(2) Å], two nitrogen atoms [Mn(2)–N(1C) 2.292(3), Mn(2)–N(2D) 2.321(2) Å] from two nta ligands, two oxygen atoms [Mn(2)–O(1) 2.150(2), Mn(2)–O(3) 2.194(2) Å] from two other nta ligands, and an aqua ligand [Mn(2)–O(1W) 2.206(2) Å]. The central Mn^{II} atom is linked to each terminal Mn^{II} atom by a μ-azide and a *syn-syn* μ-carboxylate bridge [Mn···Mn 3.861(1) Å, Mn–N–Mn 118.6(1)°]. The aqua ligand is hydrogen bonded [O(1W)···O(4) 2.772(3), O(1W)···O(1E) 3.003(3) Å] to two oxygen atoms from adjacent nta ligands [O(1W)···O(4B) 2.772(3), O(1W)···O(1E) 3.003(3) Å]. The nta ligands act in two kinds of tridentate-*N,O,O′* modes, either utilizing the pyridyl nitrogen atom and the two carboxy oxygen atoms (*syn-anti*) to bridge Mn^{II} atoms from adjacent trinuclear units to form a two-dimensional sheet (Fig. 1S),† or using both carboxy oxygen atoms (*syn-syn*) to bridge a pair of intracluster metal atoms and the pyridyl nitrogen atom to link a metal atom from an adjacent sheet, which link layers into a three-dimensional network (Fig. 2). The shortest intercluster Mn···Mn distance is 6.771(1) Å.

The EPR spectrum of powdered **1** at room temperature shows a broad isotropic signal at $g = 2.018$. The variable-temperature magnetic susceptibility of **1** from 5 to 300 K was measured at 5 kOe, as shown in Fig. 3(a). The magnetic susceptibility above 18 K obeys the Curie–Weiss law with a Weiss constant, $\theta = -19.26$ K, and a Curie constant, $C = 14.49$ cm^3 mol^{-1} K. The C value is slightly higher than the value (13.1 cm^3 mol^{-1} K) of three non-interacting Mn^{II} ions with $g = 2.0$. The $\chi_m T$ decreases continuously with decreasing temperature and reaches a minimum of 6.64 cm^3 mol^{-1} K near 12 K. Upon a further decrease of temperature, however, the $\chi_m T$ rises quickly. This is a characteristic ferrimagnetic-like behavior. Usually the EO azide bridge should promote ferromagnetic interaction for an angle between 100 and 105°.[1a] In **1**, however, the Mn–N–Mn angle of the EO azide bridge is 118.63(9)°, which is much larger than the above-mentioned range of bond angles, giving an antiferromagnetic interaction within the trinuclear unit. In addition, the *anti-anti* carboxylate bridges also promote an antiferromagnetic interaction.[5] Therefore, the ferrimagnetic-like behavior ought to arise from competitions between intra-

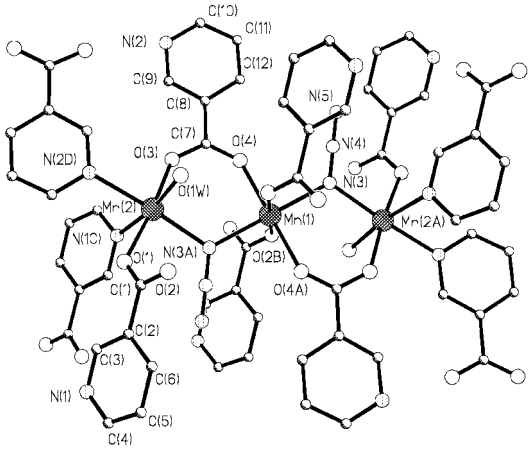

Fig. 1 Perspective view of the trinuclear unit in **1** projected approximately along the *a*-axis.

† Electronic supplementary information (ESI) available: the theoretical expressions of the intra-/inter-molecular magnetic interactions, two-dimensional view of **1**, temperature dependence of ac magnetic susceptibility and field dependence of magnetization at 1.97 K. See http://www.rsc.org/suppdata/cc/b1/b106314f/

 DOI: 10.1039/b106314f

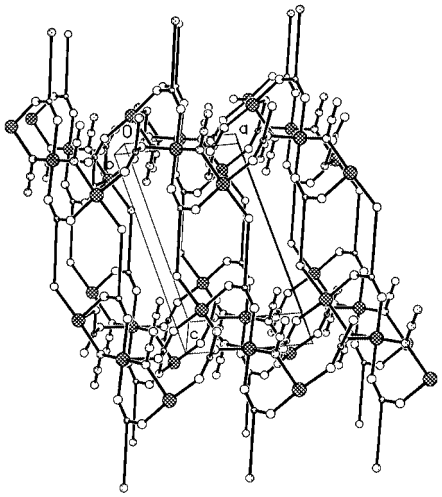

Fig. 2 Perspective view of the three-dimensional framework of **1** viewed along the *b*-axis. The aromatic rings are simplified by sticks for clarity.

cluster antiferromagnetic and inter-cluster ferromagnetic interactions.

To evaluate the intra- and inter-cluster super-exchange coupling constants in **1**, a trinuclear Mn^{II} model[8] including a mean field approximation term was used, with the J and J' referring to the intra- and inter-cluster coupling constants, respectively.† The experimental data fitted well [Fig. 3(a)], and led to the following parameters: $J/k = -2.20$ K, $J'/k = 0.326$ K, $g = 2.01$ and $R = 7.16 \times 10^{-4}$ ($R = \Sigma[(\chi_m)_{obs} - (\chi_m)_{calc}]^2/\Sigma[(\chi_m)_{obs}]^2$). The negative value of J and the small positive value of J' imply that there is an antiferromagnetic exchange interaction within the trimers and a ferromagnetic exchange interaction among the trimers through nta bridges, respectively.

The temperature dependence of the magnetization measured in a low field of 100 Oe showed an abrupt increase in M at *ca.* 3.7 K, indicating a long-range magnetic ordering occurring [Fig. 3(b)]. The temperature dependence of *ac* magnetic susceptibilities verifies the magnetic phase transition at almost the same temperature 3.7 K (T_c), defined as the point where non-zero out of phase χ appears distinctly. The field dependence of the magnetization (0–70 kOe) measured at 1.97 K shows a rapid increase of the magnetization, expected for a magnet, reaching 4.98 $N\beta$ per Mn_3 at 25 kOe, very close to the expected value of 5 $N\beta$ for an anti-parallel alignment of three Mn^{II} magnetic moments in a linear Mn_3 cluster with $S_T = 5/2$. The magnetization increases further above 25 kOe as the spins begin to deviate from antiferromagnetic coupling and align with the applied field. No detected hysterestic loop was observed, typical of a soft magnet.

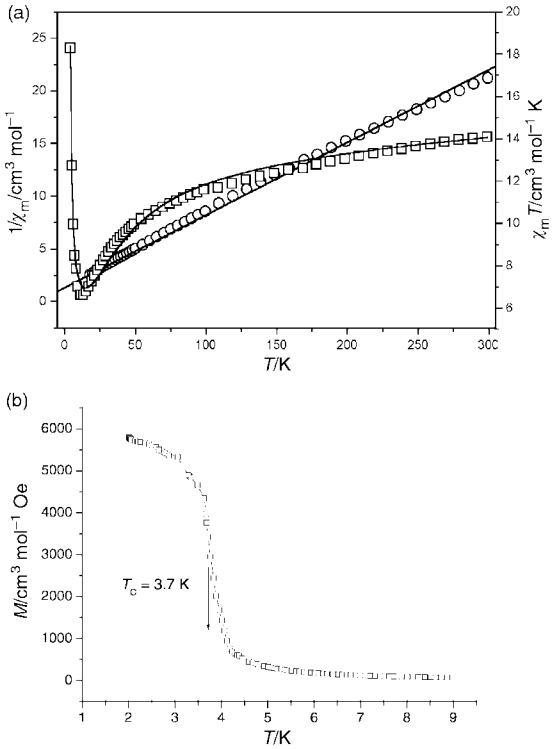

Fig. 3 Temperature dependence of the magnetic susceptibility of **1** (a) measured at 5 kOe and of magnetization (b) of **1** measured at 100 Oe.

In summary, weak ferrimagnetic interactions among the antiferromagnetically correlated Mn_3 clusters lead to a long-range ferromagnetic-like ordering: this is essentially due to increasing structural dimensions when going from an isolated cluster to a supercluster.[8]

The authors gratefully acknowledge the NSFC (No. 29971033), State Key Project for Fundamental Research (G1998061305), the Ministry of Education of China for support of this work and the Chemistry Department of CUHK for donation of the diffractometer.

Notes and references

‡ An aqueous solution (5 cm^3) of $Mn(NO_3)_2$ (3.0 mmol) was added to an ethanol solution (8 cm^3) of ntaH (4.0 mmol). After mixing for 5 min, an aqueous solution (2 cm^3) of NaN_3 (2.0 mmol) was slowly added. The resulting mixture (pH ~ 7) was stirred for 10 min at room temperature and then allowed to evaporate in air. Pale yellow crystals of **1** were obtained in a week (58% yield). Calc. for $C_{24}H_{20}Mn_3N_{10}O_{10}$ (**1**): C, 37.28, H, 2.61, N, 18.11; found: C, 37.30, H, 2.63, N, 18.09%. IR data (cm^{-1}): 3442m, 3327m, 3069w, 2069vs, 1613vs, 1563vs, 1393vs, 1286w, 1196w, 1158w, 1096w, 1044w, 841w, 760m, 697m, 637w, 557w, 439w. **CAUTION.** *Metal azide complexes are potentially explosive. Only a small amount of material should be prepared and should be handled with caution.*

§ *Crystal data* for **1**: $M_r = 773.32$, triclinic, space group $P\bar{1}$; $a = 6.771(2)$, $b = 10.158(6)$, $c = 11.635(4)$ Å; $\alpha = 73.210(3)$, $\beta = 74.570(4)$, $\gamma = 87.800(2)°$; $V = 737.9(5)$ Å^3 and $Z = 1$, $D_c = 1.740$ g cm^{-3}, μ(Mo-Kα) = 1.338 mm^{-1}. The data collections were carried out on a Siemens R3m diffractometer using graphite-monochromated Mo-Kα ($\lambda = 0.71073$ Å) radiation at 293(2) K. The structure solutions and full-matrix least-squares refinements based on F^2 were performed with the SHELX-97 program package,[9] giving a final $R1$ value of 0.0408 for 214 parameters and 3041 unique reflections with $I \geq 2\sigma(I)$ and $wR2$ of 0.1162 for all 3553 reflections. CCDC reference number 170949. See http://www.rsc.org/suppdata/cc/b1/b106314f/ for crystallographic data in CIF or other electronic format.

1 (*a*) J. Ribas, M. Monfort, B. K. Ghosh and X. Solans, *Angew. Chem., Int. Ed. Engl.*, 1994, **33**, 2087; (*b*) Z. Shen, J.-L. Zuo, Z. Yu, Y. Zhang, J.-F. Bai, C.-M. Che, H.-K. Fun, J. J. Vittal and X.-Z. You, *J. Chem. Soc., Dalton Trans.*, 1999, 3393; (*c*) Z. Shen, J.-L. Zuo, S. Gao, Y. Song, C.-M. Che, H.-K. Fun and X.-Z. You, *Angew. Chem., Int. Ed.*, 2000, **39**, 3633.

2 (*a*) A. Escuer, R. Vicente, M. A. S. Goher and F. A. Mautner, *Inorg. Chem.*, 1996, **35**, 6386; (*b*) F. A. Mautner, R. Cortes, L. Lezama and T. Rojo, *Angew. Chem., Int. Ed. Engl.*, 1996, **35**, 78.

3 (*a*) J. Ribas, M. Monfort, R. Costa and X. Solans, *Inorg. Chem.*, 1993, **32**, 695; (*b*) J. L. Manson, A. M. Arif and J. S. Miller, *Chem. Commun.*, 1999, 1479; (*c*) X. Hao, Y. Wei and S.-W. Zhang, *Chem. Commun.*, 2000, 2271; (*d*) G. D. Munno, M. Julve, G. Viau, F. Lloret, J. Faus and D. Viterbo, *Angew. Chem., Int. Ed. Engl.*, 1996, **35**, 1807; (*e*) R. Cortés, K. Urtiaga, L. Lezama, J. L. Pizarro, M. I. Arriortua and T. Rojo, *Inorg. Chem.*, 1997, **36**, 5016.

4 M. H. W. Lam, Y. Y. Tang, K. M. Fung, X. Z. You and W. T. Wong, *Chem. Commun.*, 1997, 957; J. C. Liu, D. G. Fu, J. Z. Zhuang, X. Z. Duan and X. Z. You, *J. Chem. Soc., Dalton Trans.*, 1999, 2337.

5 K.-F. Hsu and S.-L. Wang, *Inorg. Chem.*, 2000, **39**, 1773; R. L. Rardin, P. Poganiuch, A. Bino, D. P. Goldberg, W. B. Tolman, S.-C. Liu and S. J. Lippard, *J. Am. Chem. Soc.*, 1992, **114**, 5240.

6 V. L. Pecoraro, *Manganese Redox Enzymes*, VCH Publishers Inc., New York, 1992.

7 L. K. Thompson, S. S. Tandon, F. Lloret, J. Cano and M. Julve, *Inorg. Chem.*, 1997, **36**, 3301; M.-Y. Chow, Z.-Y. Zhou and T. C. W. Mak, *Inorg. Chem.*, 1992, **31**, 4900.

8 O. Kahn, *Molecular Magnetism*, VCH Publishers Inc., New York, 1993, p. 211; S. Menage, S. E. Vitols, P. Bergerat, E. Codjovi, O. Kahn, J.-J. Girerd, M. Guillot, X. Solans and T. Calvet, *Inorg. Chem.*, 1991, **30**, 2666.

9 G. M. Sheldrick SHELX-97, Program for X-ray crystal structure determination and refinement, Göttingen University, Germany, 1997.

CHEMCOMM
Communication
www.rsc.org/chemcomm

Stereospecific oxidation by Compound I of Cytochrome P450 does not proceed in a concerted synchronous manner

Sam P. de Visser, François Ogliaro and Sason Shaik*

Department of Organic Chemistry and the Lise Meitner-Minerva Center for Computational Quantum Chemistry, The Hebrew University of Jerusalem, 91904 Jerusalem, Israel.
E-mail: sason@yfaat.ch.huji.ac.il; Fax: +972-2-6584680; Tel: +972-2-6585909

Received (in Cambridge, UK) 26th June 2001, Accepted 1st October 2001
First published as an Advance Article on the web 25th October 2001

Calculations show that the transition structure for the synchronous oxygen transfer by Compound I is a second order saddle point. The process is unlikely.

Cytochrome P450 specializes in vital oxygen transfer reactions such as alkane hydroxylation and alkene epoxidation.[1,2] One of the attractive features of the enzyme is its overwhelmingly stereospecific reactions. However, the stereospecifity is occasionally incomplete resulting in some loss of stereochemical integrity of the alkene or alkane.[1] These findings led to the formulation of mechanistic schemes that involve competing concerted and stepwise monooxygenations mediated by the primary active species of the enzyme, so called Compound I (Cpd I),[1,2] and/or by secondary oxidants, *e.g.* the iron-hydroperoxo species.[3] The concerted reactions are generally described in terms of *a synchronous oxygen insertion* (Scheme 1, bottom), while the formation of an intermediate carbon radical remains a controversial issue since the estimated lifetime of the putative species is too short.[1,4] Using alkene epoxidation as an archetypal mechanism, this paper addresses the feasibility of synchronous mono-oxygenations[3] by Cpd I *vis-à-vis* the alternative mechanistic hypothesis that invokes the existence of radical species in the reaction process.

Cpd I is a high valent iron-oxo species that possesses three unpaired electrons, coupled to closely lying quartet and doublet spin states. The adjacency of the states renders Cpd I prone to two state reactivity (TSR). Indeed, our recent study of ethene epoxidation (Scheme 1),[5] revealed TSR in which the two spin states are close throughout the reaction path. The bond activation was found to occur along an *asynchronous trajectory of oxygen insertion*. On the quartet spin surface this trajectory leads to a stable intermediate radical complex, in two different oxidation states of iron; Fe^{IV} and Fe^{III} (^{4}**2-IV** and ^{4}**2-III**). Ring closure of these radical complexes to produce the epoxide complex (^{4}**3**) proceeds with substantial barriers. These barriers, especially for ^{4}**2-III**, endow the intermediates with a finite lifetime, sufficient to undergo loss of stereochemistry of the olefin and other side reactions.[5] The doublet state reaction proceeds along the same asynchronous trajectory, but exhibits tiny barriers (if at all existent) for the ring closure step. As such, it is essentially an '*effectively concerted*' process, leading to stereospecific epoxidation. The question now is whether there exists a competitive concerted synchronous mechanism that can also account for the observed stereospecifity? *An answer to this question can decide between the two alternative mechanistic hypotheses* and is expected to shed light on mechanistic puzzles generated by use of radical clocks and mutant enzymes.[1–4]

To answer this question we performed density functional calculations.[6] We used both restricted and unrestricted B3LYP hybrid density functional methods. The Los Alamos effective core potential (ECP) was employed and coupled with the double-ζ LACVP basis set for iron and an all-electron 6-31G basis set for C, H, O and N.[7] We also investigated the availability of concerted oxygen insertion in CH_4 hydroxylation,[8] as well as in C_2H_4 epoxidation by dioxygen.

The transition state for the concerted ethene epoxidation (^{4}**TS3**) is depicted in Fig. 1. It was further ascertained that the transition state ^{4}**TS3** is indeed connected to the ground states of the reactants (^{4}**1** + CH_2=CH_2) and product ^{4}**3**. Alongside we show the corresponding transition states for the asynchronous process (^{4,2}**TS1**). Underneath the drawings we indicate the corresponding barriers. The barrier for the synchronous reaction is 7.2 kcal mol^{-1} higher than the one for the asynchronous process. Inclusion of zero point energy correction leads to a difference of 4.1 kcal mol^{-1}, in favor of the asynchronous reaction. The free energy barrier at 298 K is 3.6 kcal mol^{-1} in

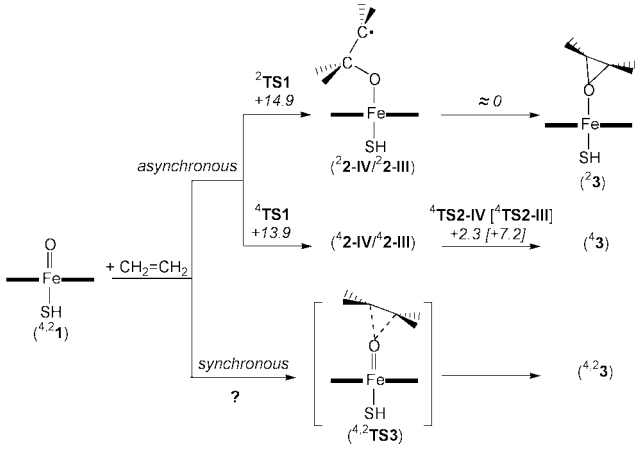

Scheme 1 Asynchronous and synchronous reaction paths. The barriers of the transition states are written above the arrows in kcal mol^{-1}.

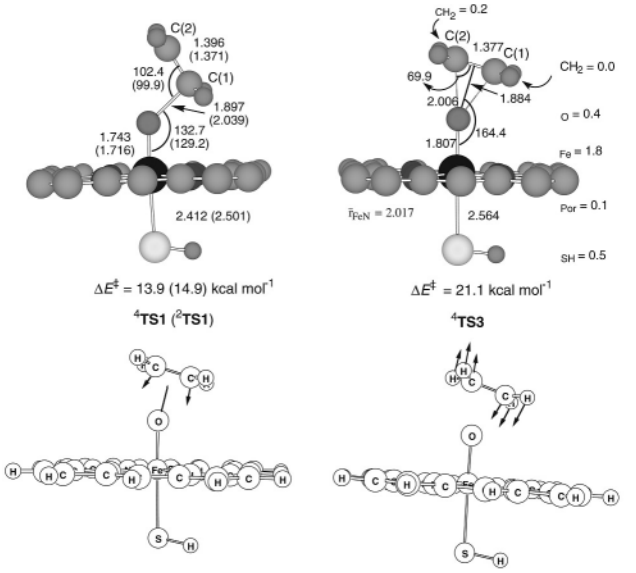

Fig. 1 Optimized geometries (Å and degrees) of ^{4,2}**TS1** and ^{4}**TS3** and imaginary modes of ^{4}**TS3** (bottom). Group spin densities (ρ) of ^{4}**TS3** are noted near the structure.

 DOI: 10.1039/b105571m

favor of the asynchronous processes. Thus, ^{4}**TS3** may become accessible only at high temperatures (T > 600 K), certainly unavailable in the enzymatic reaction. All attempts to locate ^{2}**TS3** failed, and upon removal of the synchronous constraints the structure collapsed into ^{2}**TS1**.

A frequency analysis on ^{4}**TS3** revealed two imaginary modes (see Fig. 1) with magnitude i607 cm^{-1} and i44 cm^{-1}. The first mode is the motion that connects ^{4}**TS3** to the epoxide product by a synchronous formation of two C–O bonds. The second one is a cartwheel rotation of C_2H_4. This vector drives the system towards the asynchronous ^{4}**TS1** transition state, and subsequently to the radical intermediate (^{4}**2–IV**/^{4}**2-III**, in Scheme 1) in which only one C-O bond is formed. The instability of ^{4}**TS3** toward conversion to ^{4}**TS1** is apparent in fact from the electronic structure. As shown in Fig. 1, even though the two C–O bonds are identical (2.006 Å), nevertheless the radical character on C(2) is larger than on C(1), in accord with the fate of ^{4}**TS3** to collapse to the radical intermediate on C(2) (by C(1)–O bond formation).

The epoxidation of C_2H_4 by dioxygen reveals clearly the problem with the synchronous concerted mechanism. Two synchronous pathways were explored in C_{2v} symmetry; an in-plane attack and a side-on attack, along with the asynchronous path (see definitions given in Scheme 2 for Cpd I + C_2H_4). The resulting two transition states for the synchronous paths were found to be geometrically similar to the one found for Cpd I + C_2H_4 (^{4}**TS3**). More so, both exhibit the same types of imaginary frequencies. Here too, the barrier for the asynchronous stepwise mechanism is lower, by 11.3 and 10.7 kcal mol^{-1}, respectively, than the barriers for the concerted attacks. In fact, this is a general finding among analogous mono-oxygenation processes. Thus, in water formation by the reactions of O_2 with H_2, and of FeO^+ with H_2, the concerted oxygen insertion transition states are second-order saddle points; one of their imaginary modes leads to the stepwise asynchronous transition state.[9] Notably, in both reactions, the barrier for the asynchronous path is lower than the corresponding barrier for the synchronous process by 15 and 2 kcal mol^{-1}.[9] Finally, we explored the concerted hydroxylation of CH_4 by Cpd I. Here too, structures leading to synchronous oxygen insertion into the C–H bond were extremely high. They invariably collapsed onto the asynchronous transition state for the hydrogen abstraction, reported before,[8] and were found to be analogous to Groves' rebound mechanism in its TSR formulation.

The existence of a second imaginary frequency in the concerted transition states of such processes is rooted in electronic structure. This instability derives from the fact that the addition of O to C_2H_4 (or H_2) is a forbidden process.[10] Sevin and Fontecave used molecular orbital arguments to show that this 'forbiddeness' remains effective in the C_{2v} reaction paths of Cpd I with C_2H_4.[11] Additional insight is provided by valence bond (VB) arguments in Scheme 2. The Fe=O bond of Cpd I possesses the same bonding as the dioxygen molecule, with two unpaired electrons in π* type orbitals made from d_{xz}–p_x and d_{yz}–p_y overlaps.[8] In each of the two major resonance structures, the oxygen carries one electron in p_x and two in p_y or *vice versa*. In addition, there is a lone pair along the FeO axis (z-axis). When the alkene approaches the oxygen to make two bonds synchronously as in **a**, the transition state will encounter a repulsive 4-electron interaction. In the side-on approach as in **b** the concerted transition state encounters with either one of the two resonance structures of FeO a repulsive 4-electron interaction and an unfavorable 3-electron interaction. The latter shown in **b** involves a 3-electron/3-center structure in a cyclic orbital array, which is an unstable situation (recall the D_{3h} form of H_3 is on top of a conical intersection and of high energy compared with the linear structure). Faced with these two evils, the transition state assumes the open structure **c** which resembles a radical attack on the π-CC bond and is the **TS1**structure.[5] *There is then, a fundamental reason why the concerted oxygen insertion processes are less favorable than the stepwise mechanisms.*

Since the synchronous pathway is unavailable, the stereospecifity of P450 oxidations[1–4] must originate in the *effectively concerted but asynchronous mechanism* of the doublet state (Scheme 1). Occasional loss of stereochemistry and side products originate, in turn, in the asynchronous and stepwise quartet state process. The interplay of the low-spin and high-spin components of the TSR provide also a lucid rationale[5,8] for the ultrashort lifetime observed in radical probe experiments in these mechanisms.[1–4] Furthermore, the observed *cis* selectivity[1] can also be accounted for by an asynchronous side-on transition state, obtained from ^{2,4}**TS1** by a 90° rotation around C–O.

In conclusion, therefore, the computational results make a choice between mechanistic alternatives and provide support for the asynchronous nature of olefin epoxidation and the C–H hydroxylation by the primary oxidant of P450 and generally by Cpd I iron-oxo species.[5,8]

The research was supported by the Israel Science Foundation (ISF) and the Ministry of Science, Culture and Sport. F. O. thanks the European Union for a Marie Curie Fellowship.

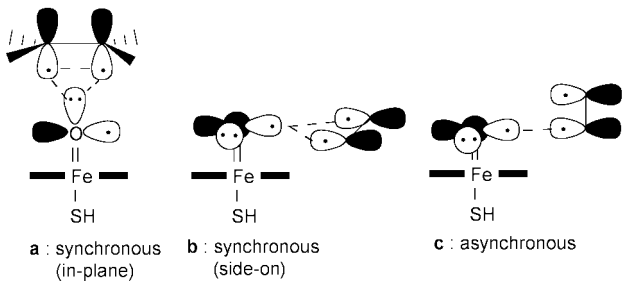

Scheme 2

Notes and references

1 J. T. Groves, Y.-Z. Han, in *Cytochrome P450: Structure, Mechanism and Biochemistry*, ed. P. R. Ortiz de Montellano, Plenum Press, New York, 2nd edn., 1995, p. 3.
2 *The Porphyrin Handbook*, ed. K. M. Kadish, K. M. Smith and R. Guilard, Academic Press, San Diego, 2000, vol. 4; chapters. 26–28, 30 and 31.
3 A. D. N. Vaz, D. F. McGinnity and M. J. Coon, *Proc. Natl. Acad. Sci. USA*, 1998, **95**, 3555.
4 M. Sono, M. P. Roach, E. D. Coulter and J. H. Dawson, *Chem. Rev.*, 1996, **96**, 2841.
5 S. P. de Visser, F. Ogliaro, N. Harris and S. Shaik, *J. Am. Chem. Soc.*, 2001, **123**, 3037.
6 *Jaguar 4.1*, Schrödinger, Inc., Portland, Oregon, 1998.
7 J. P. Hay and W. R. Wadt, *J. Chem. Phys.*, 1985, **82**, 99.
8 F. Ogliaro, N. Harris, S. Cohen, M. Filatov, S. P. de Visser and S. Shaik, *J. Am. Chem. Soc.*, 2000, **122**, 8977.
9 (*a*) M. Filatov, W. Reckien. S. D. Peyerimhoff and S. Shaik, *J. Phys. Chem. A*, 2000, **104**, 12014; (*b*) M. Filatov and S. Shaik, *J. Phys. Chem. A*, 1998, **102**, 2835.
10 R. B. Woodward and R. Hoffmann, *The Conservation of Orbital Symmetry*, Academic Press, New York, 1970.
11 A. Sevin and M. Fontecave, *J. Am. Chem. Soc.*, 1986, **108**, 326.

CHEMCOMM Communication
www.rsc.org/chemcomm

Regioselective cyclization of α,ω-alkynoic acids catalysed by TpRu complexes: synthesis of endocyclic enol lactones [Tp = hydrotris(pyrazolyl)borate]†

Manuel Jiménez-Tenorio,[a] M. Carmen Puerta,[a] Pedro Valerga,*[a] F. Javier Moreno-Dorado,[b] Francisco M. Guerra[b] and Guillermo M. Massanet[b]

[a] *Departamento de Ciencia de Materiales e Ingeniería Metalúrgica y Química Inorgánica, Facultad de Ciencias, Universidad de Cádiz, Apartado 40, 11510 Puerto Real, Cádiz, Spain. E-mail: pedro.valerga@uca.es; Fax: 34 956 016288; Tel: 34 956 016340*

[b] *Departamento de Química Orgánica, Facultad de Ciencias, Universidad de Cádiz, Apartado 40, 11510 Puerto Real, Cádiz, Spain. Fax: 34 956 016288; Tel: 34 956 016374*

Received (in Cambridge, UK) 24th July 2001, Accepted 27th September 2001
First published as an Advance Article on the web 25th October 2001

The σ-enynyl complex [TpRu{C(Ph)=C(Ph)C≡CPh}(P-Me^{i}Pr$_2$)] efficiently catalyses the regioselective cyclization of α,ω-alkynoic acids to yield endocyclic enol lactones having ring size up to 12 atoms.

Enol lactones are present in a number of biologically active natural products. Whereas some compounds contain the exocyclic enol lactone substructure,[1] other natural products contain an endocyclic enol lactone ring, *e.g.* eresmofarfugin A,[2] and all products containing the isocoumarin ring system.[3,4] Endocyclic enol lactones are useful intermediates in the synthesis of more complex natural products such as the alkaloid (−)-aspidospermidine.[5] The cyclization of α,ω-acetylenic acid precursor represents one effective synthetic approach to enol lactone systems.[6] Silver salts and mercuric salts have been used as catalysts, but their utility suffers from limited scope, drastic conditions and poor selectivity.[7] Transition metal complexes have shown to catalyse efficiently the cyclization of α,ω-alkynoic acids to give enol lactones of 5- and 6-member rings, with variable degree of regio- and stereoselectivity depending upon the catalyst used and the particular alkynoic acid [eqn. (1)].[8–11]

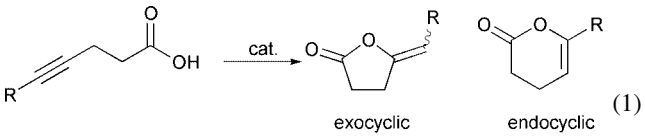

(1)

In the case of terminal alkynoic acids (R = H), the metal-catalysed cyclization reaction yields exclusively exocyclic enol lactones. This can be interpreted in terms of the regioselective Markovnikov addition of the carboxylic acid to the terminal alkyne.[12] Alternatively the *anti*-Markovnikov addition would produce the corresponding endocyclic enol lactone. However, *anti*-Markovnikov addition products have never been observed to any significant extent, hence the use of this synthetic route for the general preparation of enol lactones seems to be very limited. We have recently reported the σ-enynyl complexes [TpRu{PhC=C(R)C≡CPh}(PMe^{i}Pr$_2$}] [R = Ph, H; Tp = hydrotris(pyrazolyl)borate(1−)] and their ability to catalyse the dimerisation and even cross-coupling of alkynes.[13] We have now found that [TpRu{PhC=C(Ph)C≡CPh)(PMe^{i}Pr$_2$}] (**1**) catalyses the regioselective cyclization of HOOCCH$_2$(CH$_2$)$_n$C≡CH (*n* = 1, 2, 3, 7) to the corresponding endocyclic enol lactones. Results are shown in Table 1 (entries 1–4).‡ The cyclization takes place smoothly in refluxing toluene in 6 h, and 2% catalyst load. Analytical samples of the lactones were isolated by solvent removal followed by preparative HPLC. In the case of larger lactone rings, the catalyst load and reaction time were increased to 10% and 24 h respectively, diluting the substrate concentration to *ca.* 0.05 M in order to prevent the formation of linear oligomers. As shown in Table 1, endocyclic enol lactones were the only product generated when catalyst **1** was used. So far, our catalyst has proven to be able to cyclize ring systems of up to 12 atoms. This constitutes an efficient method for the synthesis of macrocyclic enol lactones, with the potential ability for accessing even larger cyclic systems. In these cases, the cyclization is not stereoselective, and mixtures of the endocyclic *Z*- and *E*-enol lactones are obtained (entry 4).§ The complex [TpRuH(PPh$_3$)$_2$] (**2**)[14] can also cyclize alkynoic acids to enol lactones (Table 1, entries 5–8). However, with pentynoic acid the only exception, the cyclization is not regioselective, and mixtures of endocyclic (*anti*-Markovnikov) and exocyclic (Markovnikov) enol lactones are obtained. Detailed studies carried out on rhodium and iridium complexes, supported by X-ray crystal structure determinations of some iridium model catalytic intermediates,[11] have led to a mechanistic proposal for the catalytic cyclization of alkynoic acids leading to exocyclic enol lactones.[10,11] Based upon these observations, we can propose in our case a similar catalytic cycle to account for the formation of exocyclic enol lactones (Scheme 1, pathway A). Compound **2** dissociates one PPh$_3$ molecule followed by insertion of the alkynoic acid into the Ru–H bond. The resulting alkenyl complex releases alkenoic acid (10-undecenoic acid has been isolated from runs

Table 1 Catalysed cyclization of alkynoic acids to enol lactones

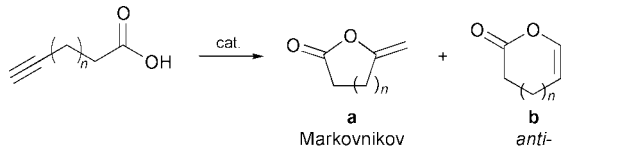

Entry	Catalyst	*n*	Product ratio a:b	Total yield (%)
1	**1**	1	0:100	97
2	**1**	2	0:100	95
3	**1**	3	0:100	45[a]
4	**1**	7	0:100[b]	84
5	**2**	1	0:100	98
6	**2**	2	47:53	95
7	**2**	3	32:68	50[a]
8	**2**	7	13:87[c]	79

[a] The remaining yield corresponds to 7-oxoheptanoic acid. [b] As a mixture of *Z*/*E* isomers in the ratio 51:49. [c] As a mixture of *Z*/*E* isomers in the ratio 41:59.

† Electronic supplementary information available: selected spectral data for enol lactone derivatives. See http://www.rsc.suppdata/cc/b1/b106647c/

 DOI: 10.1039/b106647c

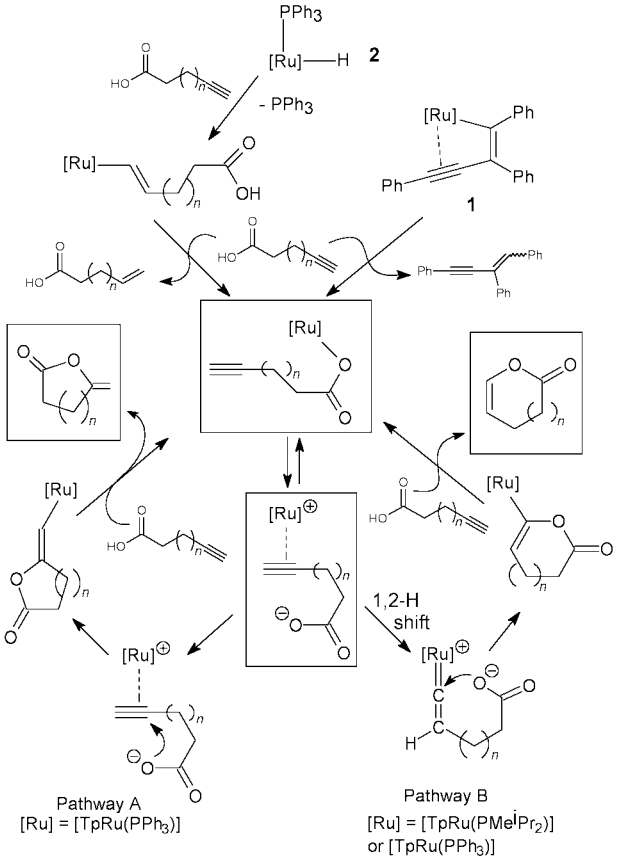

Scheme 1 Proposed mechanism for the cyclization of alkynoic acids to exocyclic enol lactones (pathway A) or endocyclic enol lactones (pathway B) catalysed by the complexes **1** and **2**.

involving undecynoic acid) upon reaction with another alkynoic acid molecule, furnishing a coordinatively unsaturated carboxylate complex which seems to be the actual catalytic species. An alternative pathway must be figured out in order to explain the regioselective formation of endocyclic enol lactones. Dixneuf and co-workers have developed ruthenium-based catalysts which can give either Markovnikov or *anti*-Markovnikov addition of acids or other organic substrates to terminal alkynes in a regioselective fashion.[12] The *anti*-Markovnikov addition takes place when the terminal carbon atom of the alkyne becomes electrophilic, this being feasible if a ruthenium–vinylidene intermediate species is generated at some stage during the catalytic process.[12] Therefore, we assume that in our case, a fast alkyne to vinylidene rearrangement takes place, most likely *via* a concerted 1,2-hydrogen shift (Scheme 1, pathway B).[15] In this fashion, the terminal carbon of the alkyne becomes electrophilic, and hence the carboxylate group attacks at this position. Ring closure yields an endocyclic alkenyl complex. As in pathway A, reaction with another alkynoic acid molecule releases the enol lactone and regenerates the coordinatively unsaturated carboxylate complex. It appears that the fast isomerization to vinylidene prior to carboxylate attack is the key step in the regioselective formation of endocyclic enol lactones. In the case of catalyst **1**, the presence of highly basic phosphine PMe^iPr_2 prompts the fast alkyne to vinylidene tautomerisation. In fact, we have already observed that facile alkyne to vinylidene rearrangement takes place at the $\{[TpRuCl(PMe^iPr_2)]\}$ moiety furnishing neutral vinylidene complexes $[TpRu{=}C{=}CHR(Cl)(PMe^iPr_2)]$ (R = Ph, Bu^t, $SiMe_3$).[13] For catalysts **2**, the alkyne to vinylidene rearrangement possibly occurs at a slower rate, similar to that of the attack of the carboxylate on the π-alkyne, so both pathways A and B of Scheme 1 might operate simultaneously. Further investigations are currently in progress in order to expand the applicability of these catalytic reactions, and in order to find additional information in support of our proposal for the reaction sequence in the catalytic cycle.

We thank the M.E.C./M.C.Y.T. of Spain (DGICYT, Projects PB97-1357, PB97-1360) for financial support, and Johnson Matthey plc for generous loans of ruthenium trichloride.

Notes and references

‡ *General procedure*. A round bottom flask fitted with a condenser was loaded with 0.02 equiv. of the catalyst and dry toluene (5 mL), and the mixture was heated at 100 °C under argon. Then, 1 equiv. of alkynoic acid dissolved in dry toluene (2 mL) was added. The reaction mixture was refluxed for 6 h and then allowed to cool to rt. Cyclohexane (5 mL) was added and the solvent removed using reduced pressure. In the case of octynoic and undecynoic acids, the catalyst load and reaction time were increased to 10% and 24 h respectively, diluting the substrate concentration to *ca*. 0.05 M in order to prevent the formation of linear oligomers. The ratio of the different products present in the crude was established by integration of the signals in the ^{1}H NMR spectrum. Pure samples of the lactones were obtained by preparative HPLC.

§ There is evidence for the formation of *Z*- and *E*-stereoisomers also in case of the 8-membered lactone ring, but the *E*-stereoisomer is strained, and tends to open up during the purification process yielding 7-oxoheptanoic acid (Table 1, entry 3).

1 C. P. Mason, K. R. Edwards, R. E. Carlson, J. Pignatello, F. K. Gleason and J. M. Wood, *Science*, 1982, **215**, 400.
2 T. Motoo, Y. Shiotani, M. Tanaka, K. Nakashima and M. Sono, *Tetrahedron Lett*., 2000, **41**, 1797.
3 D. Mal, M. Bandyopadhyay, S. K. Ghorai and K. Datta, *Tetrahedron Lett*., 2000, **41**, 3677; L. Wang and W. Shen, *Tetrahedron Lett*., 1998, **39**, 7625.
4 S. P. Waters and M. Kozlowski, *Tetrahedron Lett*., 2001, **42**, 3567.
5 A. G. Schultz and L. Pettus, *J. Org. Chem*., 1997, **62**, 6855.
6 G. A. Krafft and J. A. Katzenellebogen, *J. Am. Chem. Soc*., 1981, **103**, 5459.
7 With silver: U. Dalla and P. Pale, *New J. Chem*., 1999, **23**, 803; Y. Ogawa, M. Maruno and T. Wakamatsu, *Synlett*, 1995, 871; with mercury: A. Jellal, J. Grimaldi and M. Santelli, *Tetrahedron Lett*., 1984, **25**, 3179; M. Yamamoto, *J. Chem. Soc., Perkin Trans. 1*, 1981, 582.
8 T. Wakabayashi, Y. Ishii, K. Ishikawa and M. Hidai, *Angew. Chem., Int. Ed. Engl*., 1986, **35**, 2123; M. Cavicchioli, D. Bouyssi and G. Balme, *Tetrahedron Lett*., 1996, **37**, 1429.
9 S. Elgafi, L. D. Field and B. A. Messerle, *J. Organomet. Chem*., 2000, **607**, 97 and references therein.
10 D. M. T. Chan, T. B. Marder, D. Milstein and N. J. Taylor, *J. Am. Chem. Soc*., 1987, **109**, 6385 and references therein.
11 T. B. Marder, D. M. T. Chan, W. C. Fultz, J. C. Calabrese and D. Milstein, *J. Chem. Soc., Chem. Commun*., 1987, 1885.
12 C. Bruneau and P. H. Dixneuf, *Chem. Commun*., 1997, 507.
13 M. A. Jiménez Tenorio, M. Jiménez Tenorio, M. C. Puerta and P. Valerga, *Organometallics*, 2000, **19**, 1333.
14 M. A. Jiménez Tenorio, M. Jiménez Tenorio, M. C. Puerta and P. Valerga, *Inorg. Chim. Acta*, 1997, **259**, 77.
15 I. de los Ríos, M. Jiménez Tenorio, M. C. Puerta and P. Valerga, *J. Am. Chem. Soc*., 1997, **119**, 652 and references therein.

CHEMCOMM
Communication
www.rsc.org/chemcomm

The tetramethylpiperidinyl-1-oxide anion (TMPO$^-$) as a ligand in lanthanide chemistry: synthesis of the per(TMPO$^-$) complex $[(ONC_5H_6Me_4)_2Sm(\mu\text{-}ONC_5H_6Me_4)]_2$

William J. Evans,* Jeremy M. Perotti, Robert J. Doedens and Joseph W. Ziller

Department of Chemistry, University of California, Irvine, CA 92697-2025, USA. E-mail: wevans@uci.edu

Received (in Purdue, IN USA) 28th July 2001, Accepted 14th September 2001
First published as an Advance Article on the web 25th October 2001

$(C_5Me_5)_3Sm$ reacts with the free radical 2,2,6,6-tetramethylpiperidinyl-1-oxy (TMPO) to form $(C_5Me_5)_2$ and the per nitroxide $[(\eta^1\text{-}ONC_5H_6Me_4)_2Sm(\mu\text{-}\eta^1:\eta^2\text{-}ONC_5H_6Me_4)]_2$

Recent studies of the chemistry of $(C_5Me_5)_3M$ complexes[1] have shown that these sterically crowded molecules can function as reducing agents, even though the metal is not redox active. This sterically induced reduction[2] is likely to occur *via* a half reaction like that shown in equation (1). For example, $(C_5Me_5)_3Sm$ reduces C_8H_8 according to equation (2).[3]

$$(C_5Me_5)_3M \rightarrow e^- + 1/2\ (C_5Me_5)_2 + [(C_5Me_5)_2M]^+ \quad (1)$$

$$2(C_5Me_5)_3Sm + C_8H_8 \rightarrow (C_5Me_5)Sm(C_8H_8) + (C_5Me_5)_2 + (C_5Me_5)_3Sm \quad (2)$$

To probe the mechanism of the Sm(III) reduction reaction and to explore the possibility that radical intermediates are involved, the reaction of $(C_5Me_5)_3Sm$ with the commonly-used free radical trapping agent 2,2,6,6-tetramethylpiperidinyl-1-oxy (TMPO)[4–10] was studied. We report here the unexpected result that TMPO can replace all of the C_5Me_5 groups in $(C_5Me_5)_3Sm$ to form an unusual per(TMPO$^-$) metal complex.

Reaction of $ONC_5H_6Me_4$ with $(C_5Me_5)_3Sm$ in toluene gave crystals of a yellow complex, **1**.† Examination of the mother-liquor by ^{1}H NMR spectroscopy revealed the formation of the reduction byproduct expected from equations (1) and (2), namely, $(C_5Me_5)_2$, but no signals were observed which could be attributed to products such as $(C_5Me_5)_2Sm(ONC_5H_6Me_4)$ or $(C_5Me_5)ONC_5H_6Me_4$. Instead, X-ray crystallography† revealed that $ONC_5H_6Me_4$ had been reduced with formation of a bimetallic homoleptic samarium complex, $[(\eta^1\text{-}ONC_5H_6Me_4)_2Sm(\mu\text{-}\eta^1:\eta^2\text{-}ONC_5H_6Me_4)]_2$ **1**, Fig. 1, in which TMPO$^-$ anions were the sole ligands, equation (3). Although several metal complexes of TMPO and TMPO$^-$ have been reported in the literature,[5–11] to our knowledge this is the first example

$$2(C_5Me_5)_3Sm + 6\ ONC_5H_6Me_4 \rightarrow Sm_2(ONC_5H_6Me_4)_6 + 3(C_5Me_5)_2 \quad (3)$$

of a per(TMPO$^-$) metal complex and the first example in which TMPO is a ligand for the large electropositive lanthanide elements. The only homoleptic TMPO system we could find in the literature is the boron system, $B(ONC_5H_6Me_4)_3$.[9]

Complex **1**, which has a center of inversion, has four terminal TMPO$^-$ ligands bound only through oxygen. Two bridging TMPO$^-$ units connect the two samarium centers *via* bridging oxygen atoms and each also coordinates to one samarium with its nitrogen atom. This gives each samarium a formal coordination number of 5. Both of these coordination modes are precedented in $ONC_5H_6Me_4$ metal chemistry.[5–10] The overall structure of **1** is reminiscent of bimetallic alkoxide-bridged lanthanide and yttrium structures such as $[(Ph_3CO)_2Ln(\mu\text{-}OCPh_3)]_2$, and $[(Ph_3SiO)_2Ln(\mu\text{-}OSiPh_3)]_2$.[11] This comparison indicates that the TMPO$^-$ anion is comparable in steric bulk to large alkoxide ligands. The 2.110(5) and 2.124(5) Å terminal Sm–O ($ONC_5H_6Me_4$) bond lengths are shorter than the 2.295(4) and 2.354(4) Å bridging Sm–O distances as expected. The 2.537(6) Å Sm–N bond length is significantly longer than the Sm–O bonds in **1** as expected for a Sm ← NR_3 donor bond. The Sm–N bond is shorter than typical bonds of this type in samarium metallocenes,[12] which is consistent with the fact that the formal coordination number of samarium in $Sm_2(ONC_5H_6Me_4)_6$ is much less than in the metallocenes. The difference in length between the Sm–N bond and the bridging Sm–O distances is similar to that observed in several high valent transition metal complexes in which TMPO$^-$ is bound side-on.[7,8,10] The three N–O bond lengths in **1** (1.434(7), 1.433(8), and 1.427(8) Å) are similar and are nearly 0.15 Å longer than the corresponding 1.283(9) Å bond length in the structure of the isolated free radical,[4] which is consistent with the formation of TMPO$^-$ anions.[7,8]

The isolation of **1** shows that $ONC_5H_6Me_4$ readily replaces C_5Me_5 in organolanthanide complexes and the reduced nitroxyl can function as the sole ligand in lanthanide compounds.

We thank the National Science Foundation for funding.

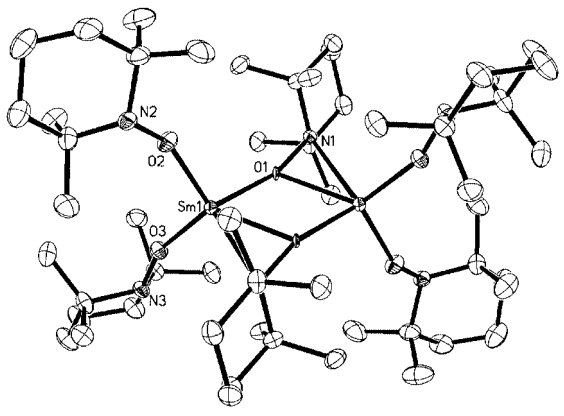

Fig. 1 Thermal ellipsoid plot for $[(\eta^1\text{-}ONC_5H_6Me_4)_2Sm(\mu\text{-}\eta^1\text{:}\eta^2\text{-}ONC_5H_6Me_4)]_2$, **1**, with ellipsoids drawn at the 50% probability level (all hydrogen atoms have been omitted for clarity).

Notes and references

† *Synthesis* of **1**: under a N_2 atmosphere, an H-shaped reaction vessel was charged in one side-arm with $(C_5Me_5)_3Sm$ (42 mg, 0.075 mmol), dissolved in 12 mL of toluene and with neat $ONC_5H_6Me_4$ (71 mg, 0.45 mmol) in the other. The H-tube was evacuated to the vapor pressure of the solvent and the $ONC_5H_6Me_4$ containing side-arm was placed in an 80 °C bath. $(C_5Me_5)_3Sm$ reacted with the $ONC_5H_6Me_4$ vapor over several days to form yellow crystals (32 mg, 68% yield) and $(C_5Me_5)_2$ (21 mg, 99%). Anal. Calcd. for $C_{27}H_{54}N_3O_3Sm$: Sm, 24.29. Found: Sm, 25.10%. IR (thin film from toluene, cm^{-1}): 2964m, 2930w, 2876w, 1544s, 1455m, 1413s, 1297w, 1262s, 1089s br, 1019s br, 803s, 741w, 699s.

Crystallographic data for **1**: $C_{27}H_{54}N_3O_3Sm$, M = 619.08, triclinic, a = 10.3838(11), b = 11.9579(13), c = 12.8023(14) Å, α = 85.934(2), β = 83.450(2), γ = 66.8500(10)°, V = 1451.5(3) Å^3, T = 163(2) K, space group $P\bar{1}$, Z = 2, μ(Mo-Kα) = 2.053 mm^{-1}, 15 802 reflections measured on a

 DOI: 10.1039/b106869p

Siemens CCD diffractometer, 6872 unique (R_{int} = 0.0366) which were used in all calculations. The final $R1$ was 0.0591 ($I > 2.0\sigma(I)$) and $wR2$ (all data) was 0.1655. The SMART program package was used to determine the unit-cell parameters and for data collection (30 s per frame counting time for a sphere of diffraction data). The raw frame data were processed using SAINT and SADABS to yield the reflection data file. Subsequent calculations were carried out using the SHELXTL program. The structure was solved by direct methods and refined on F^2 by full-matrix least-squares techniques. CCDC reference numbers 170799 and 170800. See http://www.rsc.org/suppdata/cc/b1/b106869p/ for crystallographic data in CIF or other electronic format.

1 W. J. Evans, G. W. Nyce and J. W. Ziller, *Angew. Chem., Int. Ed.*, 2000, **39**, 240.
2 W. J. Evans, *Coord. Chem. Rev.*, 2000, **206–207**, 263.
3 W. J. Evans, K. J. Forrestal and J. W. Ziller, *J. Am. Chem. Soc.*, 1998, **120**, 9273.
4 P. A. Capiomont and J. Lajzerowicz-Bonneteau, *Acta Crystallogr., Sect. B*, 1974, **30**, 2160.
5 G. C. Forbes, A. R. Kennedy, R. E. Mulvey and P. J. A. Rodger, *Chem. Commun.*, 2001, 1400.
6 L. B. Volodarsky, V. A. Reznikov and V. I. Ovcharenko, *Synthetic Chemistry of Stable Nitroxides*, CRC Press, Boca Raton, FL, 1994.
7 M. H. Dickman and R. J. Doedens, *Inorg. Chem.*, 1982, **21**, 682 and references therein.
8 P. Jaitner, W. Huber, G. Huttner and O. Scheidesteger, *J. Organomet. Chem.*, 1983, **259**, C1.
9 M. Armbrecht, W. Maringgele, A. Meller, N. Noltemeyer and G. M. Sheldrick, *Z. Naturforsch., Teil B*, 1985, **40**, 1113.
10 P. Jaitner, W. Huber, A. Gieren and H. Betz, *J. Organomet. Chem.*, 1986, **311**, 379.
11 W. J. Evans, R. E. Golden and J. W. Ziller, *Inorg. Chem.*, 1991, **30**, 4963.
12 H. Schumann, E. C. E. Rosenthal, J. Demtschuk and G. A. Molander, *Organometallics*, 1998, **17**, 5324 and references therein.

CHEMCOMM Communication
www.rsc.org/chemcomm

Novel photohydration of non-conjugated aryl/olefin bichromophores within cyclodextrin cavities

Otman Benali, M. Consuelo Jiménez, Miguel A. Miranda* and Rosa Tormos

Departamento de Química-Instituto de Tecnología Química UPV-CSIC, Universidad Politécnica de Valencia, Apdo 22012, 46071 Valencia, Spain. E-mail: mmiranda@qim.upv.es; Fax: 34 963879349; Tel: 33 963877340

Received (in Cambridge, UK) 27th July 2001, Accepted 8th October 2001
First published as an Advance Article on the web 25th October 2001

Cyclodextrin media are used to achieve photochemical water addition to isolated, acyclic double bonds *via* intramolecular interaction with excited arenes.

Cyclodextrins (CD) are known to form inclusion complexes with a variety of organic guests, whose chemical reactivity may become significantly modified due to interaction with the CD hosts. In particular, the photochemical properties of a number of substrates are sensitive to the CD microenvironment. In this context, the modified polarity inside the cavities and the imposed steric constraints are among the main factors governing the photoreactivity of CD inclusion complexes.[1,2]

Most of the photochemical processes performed within the CD microvessels involve formation of radicals or radical pairs. These include the Norrish type I or type II photoreactions[1,3,4] and the photo-Fries and photo-Claisen rearrangements.[1,5,6] Inside CD, some of these processes appear to occur with remarkable chemo- and/or regio-selectivity. The potential of CD as chiral reaction media, to bring about enantioselective photoreactions (albeit with modest ee) has also been explored.[7,8]

Photochemical processes involving generation of polar intermediates inside CD (for instance, carbocations, radical cations or zwitterions) are much less common. This is not surprising, as the interior of CD cavities is markedly hydrophobic. Actually, when these charged intermediates are formed in the CD microenvironment, their escape to the bulk of the aqueous solution occurs in the nanosecond timescale.[9]

With this background, the purpose of the present work was to investigate the photochemical behaviour of the CD complexes of a series of arene/olefin bichromophoric compounds; their structures are shown in Chart 1.

In organic solution, compounds **1a** and **1c** are known to photocyclise to 5-membered ring products,[10–13] while **1b** undergoes di-π-methane photorearrangement[14] and compound **1d** is essentially unreactive.[15]

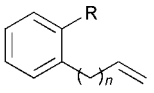

1a-d

a: R = OH, *n* = 1
b: R = OCH_3, *n* = 1
c: R = NH_2, *n* = 1
d: R = OH, *n* = 2

Chart 1

By contrast, it will be shown that the photoreactivity of the β-CD inclusion complexes of the allyl derivatives in aqueous media is dramatically modified. Under these conditions, a novel hydration of the acyclic olefin moiety is by far the predominating photoprocess.

Compound **1a** was purchased from Merck, while **1b–d** were prepared by known procedures.[13,16,17] Irradiation of **1a–d** was carried out using the quartz-filtered light of a medium pressure mercury lamp for 1 h. Parallel experiments were performed in homogeneous solution (hexane or acetonitrile, 5 mM) and in β-cyclodextrin–water (*ca.* 1.5 mM **1a–d** and 7 mM CD). The results are shown in Table 1 and Chart 2.

Photolysis of **1a** in hexane afforded dihydrobenzofuran **2a** (Table 1, entry 1).[18] In acetonitrile (Table 1, entry 2), a 4:1 mixture of **2a** and the cyclopropane **3a** was obtained. Photoproduct **2a** is known to arise *via* intramolecular proton transfer,[10,12] while **3a** is the di-π-methane photorrearrangement product.[19] Formation of **3a** in acetonitrile is consistent with the previously reported enhancement of the rearrangement in polar solvents.[20] Irradiation of **1a** in β-CD–water resulted in a much higher conversion, together with a dramatic change in the product distribution (Table 1, entry 3). In this case, cyclisation to **2a** was totally suppressed, to the benefit of alcohols **4a** and **5a**, the hydration products of **3a** and **1a**, respectively. Lower amounts of **3a** were also obtained. The same trend was observed with α and γ-CD (Table 1, entries 4 and 5), although photohydration was less efficient than with β-CD. Control experiments were run leaving **1a**–CD in the dark and irradiating emulsions of **1a** in water for 1 h. Under these conditions, **1a** remained unreacted.

Table 1 Photochemistry of compounds **1a–c**

				Product yield (%)[b]					
Entry	Substrate	Conditions[a]	Conversion (%)	**2**	**3**	**4**	**5**	**6**	**7**
1	**1a**	A	22	100	—	—	—	—	—
2	**1a**	B	34	80	20	—	—	—	—
3	**1a**	C	95	—	11	20	69	—	—
4	**1a**	D	85	13	28	16	43	—	—
5	**1a**	E	56	24	37	4	35	—	—
6	**1b**	A	55	—	100	—	—	—	—
7	**1b**	B	42	—	100	—	—	—	—
8	**1b**	C	58	—	27	36	37	—	—
9	**1c**	A	54	53	—	—	—	47	—
10	**1c**	B	57	81	—	—	—	19	—
11	**1c**	C	94	33	—	—	55	4	8

[a] A: Hexane, B: acetonitrile, C: β-CD–water, D: α-CD–water, E: γ-CD–water. [b] The photoproducts were identified by comparison of the GC retention times and MS spectra with those of authentic samples and quantitated by GC, using adequate standards.

 DOI: 10.1039/b106847b

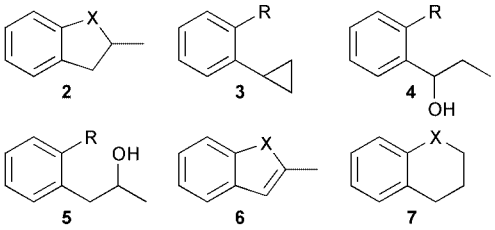

Chart 2

Photohydration of the allylic double bond is a remarkable result. Monosubstituted, non-conjugated acyclic olefins are unable to absorb light of $\lambda > 200$ nm, employed under the usual irradiation conditions. Neither direct nor sensitized irradiation of acyclic or large ring cyclic alkenes results in addition of protic solvents;[21] the only reported process is *E*/*Z* isomerization, which is a hidden non-observable process in the case of monosubstituted olefins such as **1a–d**. Only tri- or tetraalkyl substituted olefins (through their Rydberg excited states), medium-ring cycloalkenes and conjugated aryl olefins undergo addition of nucleophilic solvents *via* photoprotonation.[21–23]

Obviously, although the reacting moiety involved in photohydration is the isolated double bond, the phenolic substructure is the only light-absorbing chromophore. On the other hand, the phenolic singlet (*ca*. 103 kcal mol^{-1}) lies well below the lowest olefin singlet.[24] Thus, excitation of the allyl group by simple singlet–singlet energy transfer is thermodynamically disfavoured.

A possible pathway leading to **5a** could involve excited state proton transfer from the phenolic hydroxy group to the allylic double bond. The resulting zwitterion might undergo either cyclisation to **2a** or nucleophilic attack of water to the cationic center. This is reasonable and would be closely related to the behaviour of **1a** in homogeneous solution. However, if this were the only operating mechanism, methylation of the OH group should result in the suppression of photoproduct **5a**. In order to check this possibility, the photochemistry of **1b** was studied under the same conditions. Irradiation of **1b** in hexane and acetonitrile (Table 1, entries 6 and 7 respectively) gave rise to cyclopropane **3b** as the only product. By contrast, in cyclodextrin media (Table 1, entry 8) the alcohols **4b** (36%) and **5b** (37%) were obtained. These results indicate that in homogeneous solution the di-π-methane photorrearangement is the only occurring process, while inside β-CD it has to compete with photohydration. To make sure that **4b** is formed by secondary photohydration of **3b**, this compound was irradiated in the presence of β-CD. As a matter of fact, alcohol **4b** was the only product under these conditions.

A comparison between the results given in entries 3 and 8 (Table 1) clearly shows that excited state proton transfer is not the only operating mechanism. As photohydration also occurs in the case of the methylated derivative **1b** there must be other pathway(s) leading to **5**. In this context, photohydration might involve an intramolecular charge transfer exciplex. Although such a species was not detected when recording the fluorescence spectra of **1b**, intramolecular exciplex emission has been observed in closely related systems.[25] Moreover, it is generally assumed that non-detectable intramolecular exciplexes are involved in a variety of arene/alkene photoreactions.[26]

As allyl anilines undergo intramolecular electron transfer (rather than proton transfer) in their excited states,[13] **1c** was selected as a probe to check whether this type of process also contributes to photohydration. As expected,[13] direct photolysis of **1c** in hexane (Table 1, entry 9) afforded indoline **2c**, together with its secondary oxidation product **6c**. In acetonitrile (Table 1, entry 10), the same two products were obtained, although in a different ratio. However, when photolysis of **1c** was carried out in β-CD–water **5c** was the major product. Lower amounts of **2c**, **6c** and the tetrahydroquinoline **7c** were also obtained (Table 1, entry 11). These results indicate that intramolecular excited state electron transfer also contributes to photohydration, although to a lesser extent than proton transfer.

Finally, to gain some insight into the influence of the interchromophoric distance on the efficiency of photohydration, the photochemistry of **1d** was investigated in organic solution as well as in aqueous medium, in the presence of β-CD. Under these conditions, **1d** was found to be photostable.[27] This shows that increasing the distance between the phenol and the allyl moieties prevents the intramolecular excited state interaction required for photohydration.

In summary, a novel photohydration of non-conjugated aryl/olefin bichromophores has been observed in constrained media. Intramolecular excited state interaction (most likely exciplex formation) is responsible for activation of the otherwise unreactive olefin. The occurrence of photohydration inside the hydrophobic CD pockets might indicate that the olefin moiety is directed towards the bulk of the solution, remaining accessible to water. Current studies are aimed at disclosing this point, at extending the reaction to other systems and to investigate a possible stereoselectivity of CD-mediated photohydration.

We thank support from the Spanish DGES (PB97-0339).

Notes and references

1 P. Bortolus and S. Monti, *Adv. Photochem*., 1996, **21**, 1.
2 V. Ramamurthy, *Photochemistry in Organized and Constrained Media V*, ed. V. Ramamurthy, VCH Publishers, Cambridge, UK, 1991.
3 S. Sing, G. Usha, C. H. Tung, N. J. Turro and V. Ramamurthy, *J. Org. Chem*., 1986, **51**, 941.
4 B. N. Rao, N. J. Turro and V. Ramamurthy, *J. Org. Chem*., 1986, **51**, 460.
5 A. V. Veglia and R. H. De Rossi, *J. Org. Chem*., 1993, **58**, 4941.
6 A. M. Sánchez, A. V. Veglia and R. H. De Rossi, *Can. J. Chem*., 1997, **75**, 1151.
7 K. Vizvardi, K. Desmet, I. Luyten, P. Sandra, G. Hoornaert and E. Van der Eycken, *Org. Lett*., 2001, **3**, 1173.
8 Y. Inoue, T. Wada, N. Sugahara, K. Yamamoto, K. Kimura, L.-H. Tong, X.-M. Gao, Z.-J. Hou and Y. Liu, *J. Org. Chem*., 2000, **65**, 8041.
9 R. S. Murphy and C. Bohne, *Photochem. Photobiol*., 2000, **71**, 35.
10 G. Fráter and H. Schmid, *Helv. Chim. Acta*, 1967, **50**, 255.
11 W. M. Horspool and P. L. Pauson, *J. Chem. Soc, Chem. Commun*., 1967, 195.
12 A. Shani and R. Mechoulam, *Tetrahedron*, 1971, **27**, 601.
13 U. Koch-Pomeranz, H. Schmid and H.-J. Hansen, *Helv. Chim. Acta*, 1977, **60**, 768.
14 N. Miyamoto, M. Kawanisi and H. Nozaki, *Tetrahedron Lett*., 1971, 2565.
15 M. T. Bosch-Montalvá, L. R. Domingo, M. C. Jiménez, M. A. Miranda and R. Tormos, *J. Chem. Soc., Perkin Trans. 2*, 1998, 2175.
16 Compound **1b** was prepared by treating **1a** with methyl iodide.
17 P. Yates and T. S. Macas, *Can. J. Chem*., 1988, **66**, 1
18 Other minor products (yields less than 5%) have been previously identified upon irradiation of **1a** for longer irradiation times. See M. A. Miranda and R. Tormos, *J. Org. Chem*., 1993, **58**, 3304.
19 T. Kitamura, T. Imagawa and M. Kawanisi, *Tetrahedron*, 1978, **34**, 3451.
20 M. C. Jiménez, M. A. Miranda and R. Tormos, *Chem. Commun*., 2000, 2341.
21 P. J. Kropp, Photoreactions of alkenes in protic media, in, *CRC Handbook of Organic Photochemistry and Photobiology*, eds. W. M. Horspool and P.-S. Song, CRC Press, Boca Raton, 1995, p. 105.
22 M. Fischer and P. Wan, *J. Am. Chem. Soc*., 1999, **121**, 4555.
23 M. Fischer and P. Wan, *J. Am. Chem. Soc*., 1998, **120**, 2680.
24 S. L. Murov, I. Carmichael and G. L. Hug, *Handbook of Photochemistry*, 2nd Edition, Marcel Dekker, Inc, New York, 1993.
25 F. Galindo, M. C. Jiménez, M. A. Miranda and R. Tormos, *Chem. Commun*., 2000, 1747.
26 A. Gilbert and J. Baggot, *Essentials of Molecular Photochemistry*, Blackwell Scientific Publications, Oxford, 1991.
27 However, longer irradiation times lead to small amounts of six- and seven-membered ring photoproducts (see ref. 15).

CHEMCOMM Communication
www.rsc.org/chemcomm

β-Peptides as catalysts: poly-β-leucine as a catalyst for the Juliá–Colonna asymmetric epoxidation of enones

Paul E. Coffey,[a] Karl-Heinz Drauz,[b] Stanley M. Roberts,*[a] John Skidmore[a] and John A. Smith[c]

[a] *Department of Chemistry, University of Liverpool, Liverpool, UK L69 7ZD. E-mail: smrsm@liv.ac.uk*
[b] *Degussa-Hüls AG, Rodenbacher Chaussee 4, D-63457 Hanau-Wolfgang, Germany*
[c] *School of Biological Sciences, University of Liverpool, Liverpool, UK L69 7ZB*

Received (in Cambridge, UK) 17th July 2001, Accepted 26th September 2001
First published as an Advance Article on the web 25th October 2001

Poly-β-leucines have been evaluated as catalysts for the Juliá–Colonna asymmetric epoxidation of enones; the β³-isomer was found to be an effective catalyst for the epoxidation of chalcone (70% ee) and some analogues.

Peptides, generated from α-amino acids, can adopt a number of stable conformations such as the α-helix and β-sheet. In combination these secondary structural units allow a protein to adopt a defined tertiary structure, which can lead to catalytic behaviour. Recent work by Seebach,[1] Gellman[2] and others,[3] as well as earlier studies,[4] has shown that peptides generated from β-amino acids (so called β-peptides) show similar secondary structural characteristics to their natural counterparts. This suggests that, in principle, the β-analogues of proteins may exhibit related catalytic behaviour. It is notable that short β-peptides show promise as therapeutic agents as they can exhibit similar biological profiles to α-peptides with increased stability to peptidases, leading to improved bioavailability.[5] Careful tuning of β-amino acid structure has allowed a wide range of structural units to be reliably prepared using the β-peptide backbone.

Work initiated by Juliá and Colonna[6a] has shown that polyamino acids, typically containing 30 or more identical residues of α-leucine or α-alanine, are capable of catalysing the Weitz–Scheffer epoxidation of enones with remarkable levels of asymmetric control.[6] More recently, modifications have been made to the original reaction conditions[6b] and as a result the method is now applicable to a wide range of *trans*-enones.[6c] As part of an ongoing program investigating and developing this transformation, β-analogues of the Juliá–Colonna poly-α-leucine catalysts have been prepared, in order to evaluate their potential as asymmetric catalysts.

The addition of a methylene unit to an α-amino acid generates two possible structurally-isomeric β-amino acids. Seebach has termed these β² and β³ depending on which carbon bears the side chain.[1] In order to prepare the two isomeric β-leucine polymers, the monomer amino acids β²-(**1**) and β³-leucine (**2**) were required in enantiomerically enriched form (Fig. 1).

Following the method of Seebach, β²-leucine **1** was prepared by amidomethylation of **3** with *N*-(chloromethyl)benzamide using the Evans auxiliary to control the formation of the stereocentre (Scheme 1).†[7] The β³ isomers are generally synthesised using an Arndt–Eistert homologation of the corresponding α-amino acids.[8] Thus, we were able to prepare protected β³-leucines **6a** and **6b** from the corresponding α-amino acids **5a** and **5b**. Compound **6a** was then deprotected to afford **2** {$[\alpha]_D^{22}$ +35 (*c* 1.0, H_2O) lit.[9] +34.7 (*c* 1.0, H_2O}} (Scheme 1).

Poly-α-amino acids are typically prepared from the corresponding monomers by activation as the *N*-carboxyanhydride, followed by polymerisation using a nucleophilic initiator.[10] This approach is less effective in the case of β-amino acids[10] and even employing recent synthetic improvements[11] a pure sample of the β³-leucine *N*-carboxyanhydride could not be prepared.

We have shown that a 20-mer of poly-L-α-leucine, prepared using solid phase synthesis, exhibits similar catalytic activity to material generated by polymerisation of L-leucine NCA.[12] Moreover, Seebach has shown that solid phase techniques can be used to prepare β-peptides.[8] Thus, solid phase automated peptide synthesis was carried out using the two isomeric Fmoc protected β-leucines† to afford two 20-mer peptides β²-Leu_{19}-α-Leu-R **7** and β³-Leu_{19}-α-Leu-R **8**.‡[13]

The polymers **7** and **8** were tested under two sets of reaction conditions; first, a triphasic protocol, consisting of aqueous NaOH and H_2O_2 and a solution of the substrate in toluene,[6a] and

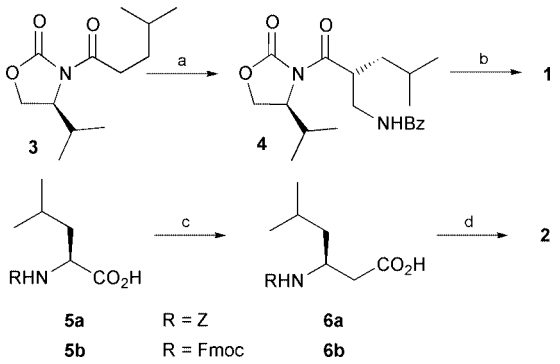

Scheme 1 Synthesis of isomeric β-leucines. *Reagents and conditions*: (a) $TiCl_4$, TEA, $ClCH_2NHBz$, DCM, –10 °C, 53%; (b) i. H_2O_2, LiOH, THF, H_2O, 0 °C, 82%; ii. aq. HCl, AcOH, 110 °C, 86%; (c) i. isobutylchloroformate, TEA, THF, Et_2O, 0 °C; ii. CH_2N_2, Et_2O; iii. Na_2CO_3, $Na_2S_2O_3$, AgO_2CCF_3, dioxane, H_2O, 53% over three steps where R = Fmoc; (d) HBr, AcOH, 110 °C, 90% where R = Z.

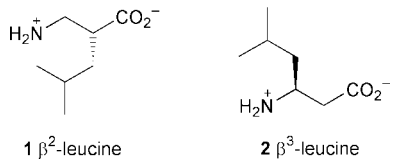

Fig. 1 Isomeric β-leucine monomers.

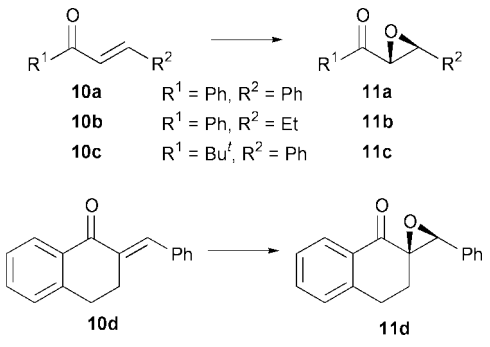

Scheme 2 Epoxidations.

 DOI: 10.1039/b106368p

Table 1 Epoxidation of enones using poly-β-amino acid catalysts

Entry	Substrate	Catalyst	Activation	Conditions	Major product	Time/h	Conversion (%)[a]	Ee (%)[b]
1	**10a**	α-Leu-R	None	Biphasic[c]	**11a**	1.5	66	89
2	**10a**	β^2-Leu_{19}-α-Leu-R **7**	None	Biphasic[c]	**11a**	4	21	3
3	**10a**	β^3-Leu_{19}-α-Leu-R **8**	None	Biphasic[c]	**11a**	1.5	20	23
4	**10a**	β^3-Leu_{19}-α-Leu-R **8**	None	Triphasic[d]	**11a**	4	15	25
5	**10a**	β^3-Leu_{19}-α-Leu-R **8**	Aq. NaOH–PhMe[e]	Triphasic[d]	**11a**	24	92	70
6	**10a**	β^3-Leu_{20}-R **9**	DBU–PhMe[f]	Biphasic[c]	**11a**	24	96	39
7	**10a**	β^3-Leu_{20}-R **9**	Aq. NaOH–PhMe[e]	Biphasic[c]	**11a**	24	77	20
8	**10b**	β^3-Leu_{20}-R **9**	DBU–PhMe[f]	Triphasic[d]	**11b**	24	98	15
9	**10b**	$\beta^3$$Leu_{20}$-R **9**	DBU–PhMe[f]	Biphasic[c]	**11b**	24	98	28
10	**10c**	β^3-Leu_{20}-R **9**	DBU–PhMe[f]	Biphasic[c]	**11c**	24	10	85
11	**10d**	β^3-Leu_{20}-R **9**	DBU–PhMe[f]	Triphasic[d]	**11d**	24	25	22
12	**10d**	β^3-Leu_{20}-R **9**	DBU–PhMe[f]	Biphasic[c]	**11d**	24	35	9

[a] Determined by HPLC. [b] Determined by chiral HPLC, major enantiomer **11**. [c] Substrate (0.24 mmol), urea–H_2O_2 (28 mg), DBU (56 μl), catalyst (100 mg) in THF (1 ml). [d] Substrate (0.24 mmol), catalyst (100 mg), 30% aq. H_2O_2 (0.7 ml), 4 M aq. NaOH (0.5 ml) and PhMe (1 ml). [e] Catalyst (100 mg) stirred with 4 M aq. NaOH (0.5 ml) and toluene (1 ml) for 70 hours, then filtered and dried. [f] Catalyst (100 mg) stirred with DBU (56 μl) in THF (1 ml) for 16 hours then reagents for reaction added directly.

secondly, biphasic conditions, employing urea–H_2O_2 and DBU in THF.[6b] Like their α-analogues, the poly-β-leucines proved to be insoluble in both organic and aqueous solvents.§

In the first instance, the poly-β-amino acids were tested as catalysts for the epoxidation of chalcone (**10a**) (Scheme 2). Under the biphasic conditions, with catalysis by α-Leu_{20}-R, the (2*R*,3*S*)-epoxide **11a** was obtained (66% conversion, 89% ee) after 1.5 hours (Table 1, entry 1). Catalysis using β^2-Leu_{19}-α-Leu-R **7** afforded essentially racemic epoxide under the same conditions; moreover, the rate of reaction was considerably diminished (entry 2). On the other hand, the β^3-Leu_{19}-α-Leu-R catalyst **8** gave a significant ee of (2*R*,3*S*)-**11a** under both biphasic (23% ee) and triphasic (25% ee) reaction conditions, albeit still with a decreased rate (entries 3 and 4 respectively).

Previous studies have shown that the activity of poly-α-amino acid catalysts can be improved by various washing procedures.[14] Two such activations were investigated with the catalyst **8** and a third 20-mer: β^3-Leu_{20}-R **9**. In the first procedure the catalyst was stirred for 70 hours in a mixture of 4 M aq. NaOH and toluene, before filtering, washing and drying;[14] in the second it was stirred with DBU in toluene for 16 hours before adding the reagents for epoxidation directly. Both activation procedures significantly increased the enantioselectivity of the catalysed epoxidation reaction. For example, NaOH–PhMe-activated **8** catalysed the epoxidation of **10a** with 92% conversion and 70% ee under the triphasic conditions (entry 5).¶

The catalyst **9** was tested against a range of other substrates **10b–d**. Using DBU–PhMe-activated **9** the ees for the epoxidation of the β-ethyl enone **10b** were somewhat lower than for chalcone (entries 6, 8 and 9); under the biphasic conditions the ethyl epoxide **11b** had an ee of 28% (entry 9). On the other hand, under similar conditions the *tert*-butyl ketone **10c** was epoxidised in a high ee (entry 10), however the reaction rate was significantly retarded, with only 10% conversion to the epoxide **11c** being obtained after 24 hours. The final substrate investigated was 2-benzylidene-3,4-dihydronaphthalen-1(2*H*)-one (**10d**). In this case the triphasic reaction conditions gave an ee of 22%; however the reaction was again slow (entry 11).

In conclusion, peptides generated from β-amino acids exhibit catalytic behaviour analogous to that shown by poly-α-amino acids. Specifically, poly-β^3-leucine catalyses the epoxidation of (*E*)-α,β-enones with significant enantioselectivity. Although this methodology is not competitive with the poly-α-amino acid analogues it is possible that variation of the β-amino acid monomer may lead to altered catalytic behaviour. Results of such studies and approaches to preparing poly-β-amino acids *via* polymerisation reactions will be reported in due course.

Notes and references

† Fmoc β^2-leucine was prepared from **1** using FmocCl under standard conditions {$[\alpha]_D^{22}$ = +12 (*c* 1.0, $CHCl_3$) lit.[8] +10.8 (*c* 0.6, $CHCl_3$)}.

‡ The oligoleucines were linked *via* a hydroxymethylphenoxyacetic acid linker to PEG and thence to polystyrene resin (loading 0.18 mmol g^{-1}). These oligomers are represented as Leu_n-R where R = linker–PEG–resin.

§ The poly-β-amino acids remained attached to the support; the solubility of the non-immobilised material was not investigated.

¶ Ees using activated β^2-Leu_{19}-α-Leu-R **7** remained below 10%.

1 D. Seebach and J. L. Matthews, *Chem. Commun*., 1997, 2015 and references therein.

2 S. H. Gellman, *Acc. Chem. Res*., 1998, **31**, 173 and references therein.

3 M. García-Alveraz, A. Martínez de Ilarduya, S. León, C. Alemán and S. Muñoz-Guerra, *J. Phys. Chem. A*, 1997, **101**, 4215; B. W. Gung, D. Zou, A. M. Stalcup and C. E. Cottrell, *J. Org. Chem*., 1999, **64**, 2176.

4 See for example: J. Kovacs, R. Ballina, R. L. Rodia, D. Balasubramamnian and J. Applequist, *J. Am. Chem. Soc*., 1965, **87**, 119; J. D. Glickson and J. Applequist, *J. Am. Chem. Soc*., 1971, **93**, 3276; F. Chen, G. Lepore and M. Goodman, *Macromolecules*, 1974, **7**, 779; M. Narita, M. Doi, K. Kudo and Y. Terauchi, *Bull. Chem. Soc. Jpn*., 1986, **59**, 3553.

5 M. Werder, H. Hauser, S. Abele and D. Seebach, *Helv. Chim. Acta*, 1999, **82**, 1774.

6 (*a*) S. Juliá, J. Masana and J. C. Vega, *Angew. Chem., Int. Ed. Engl*., 1980, **19**, 929; (*b*) B. M. Adger, J. V. Barkley, S. Bergeron, M. W. Cappi, B. E. Flowerdew, M. P. Jackson, R. McCague, T. C. Nugent and S. M. Roberts, *J. Chem. Soc., Perkin Trans. 1*, 1997, 3501; (*c*) M. J. Porter, S. M. Roberts and J. Skidmore, *Bioorg. Med. Chem*., 1999, **7**, 2145.

7 D. Seebach, S. Abele, K. Gademann, G. Guichard, T. Hintermann, B. Jaun, J. L. Matthews and J. V. Schreiber, *Helv. Chim. Acta*, 1998, **81**, 932.

8 For a recent example see: G. Guichard, S. Abele and D. Seebach, *Helv. Chim. Acta*, 1998, **81**, 187.

9 T. Yamada, S. Kuwata and H. Watanabe, *Tetrahedron Lett*., 1978, **19**, 1813.

10 H. R. Kricheldorf, *α-Aminoacid-N-Carboxy-Anhydrides and Related Heterocycles: Syntheses, Properties, Peptide Synthesis, Polymerisation*, Springer-Verlag, Berlin, 1987.

11 J. Cheng, J. W. Ziller and T. J. Deming, *Org. Lett*., 2000, **2**, 1943.

12 M. W. Cappi, W.-P. Chen, R. W. Flood, Y.-W. Liao, S. M. Roberts, J. Skidmore, J. A. Smith and N. M. Williamson, *Chem. Commun*., 1998, 1159.

13 It was judged that the single α-leucine residue at the *C*-terminus would play no role in the reaction, see: P. A. Bentley, M. W. Cappi, R. W. Flood, S. M. Roberts and J. A. Smith, *Tetrahedron Lett*., 1998, **39**, 9297.

14 See for example: J. V. Allen, K. H. Drauz, R. W. Flood, S. M. Roberts and J. Skidmore, *Tetrahedron Lett*., 1999, **40**, 5417.

CHEMCOMM Communication
www.rsc.org/chemcomm

Reduction of tris(benzene-1,2-dithiolate)molybdenum(VI) by hydroxide ions in dry tetrahydrofuran solution

Antonio Cervilla,*[a] Francisco Pérez-Pla[b] and Elisa Llopis[a]

[a] *Departamento de Química Inorgànica, ICMUV, PO Box 2085, Polígono La Coma, Paterna, Valencia, Spain. E-mail: Antonio Cervilla@.uv.es; Fax: 34963983633*
[b] *Departamento de Química-Física, Universidad de Valencia, Dr. Moliner 50, 46100-Burjasot, Valencia, Spain*

Received (in Cambridge, UK) 10th July 2001, Accepted 4th October 2001
First published as an Advance Article on the web 25th October 2001

Tris(benzene-1,2-dithiolate)molybdenum(VI) reacts rapidly and quantitatively with tetrabutylammonium hydroxide to yield the corresponding Mo(V) and Mo(IV) complexes and hydrogen peroxide; the reaction has been executed in dry tetrahydrofuran where the reaction rate shows a fair dependence on complex and OH^- concentrations.

Tris(dithiolene) complexes of transition metals have been the subject of considerable attention since they were first reported.[1] While early interest focused primarily on the facile one-electron redox reactions which these complexes undergo, more recently the scope has expanded to areas ranging from bioinorganic chemistry to materials science.[2]

Surprisingly little is known about the interaction of this class of compounds with hydroxide ions. Kawashima *et al.*[3] first reported the reduction of neutral $M(tdt)_3$ complexes (M = Re, Mo, and W; tdt = toluene-3,4-dithiolate) dissolved in acetone or THF by aqueous NaOH, but little more than the formation of the corresponding one-electron reduced complex was described. Confirmation of the occurrence of this reaction was subsequently provided by Sellmann *et al.*[4] who reacted $Mo(bdt)_3$ (bdt = benzene-1,2-dithiolate) with NaOH in methanol. The reaction yields the $[Mo(bdt)_3]^-$ or $[Mo(bdt)_3]^{2-}$ complex, depending upon the ratio in which NaOH and $Mo(bdt)_3$ are mixed, and it was thought to proceed by oxidation of methanol to methanal, although this hypothesis has not been tested.

We were surprised to find that addition of n-Bu_4NOH to a THF solution of neutral $Mo(bdt)_3$ caused its conversion to the monoanionic $[Mo(bdt)_3]^-$ complex and then to the dianionic $[Mo(bdt)_3]^{2-}$ complex. All these complexes have been thoroughly characterised elsewhere in solid[5] and in solution.[4] Because the whole reaction was complete in less than 20 s in excess of base, both reduction processes have been studied by stopped-flow spectrophotometry. A general treatment of spectrophotometric data has been used to investigate the kinetics of the reaction. The solution absorption spectra of authenticated Mo(VI), Mo(V), and Mo(IV) complexes were fitted to a Gaussian function basis set within the 400–800 nm region.[6] The calculated optical densities $\varepsilon_i(\lambda)$ were used to analyse the $Mo(bdt)_3$–n-Bu_4NOH system spectrum at each time and to deduce the variation of molybdenum complex concentrations with time.† In all cases the sums of the Mo complex concentrations were equal to the initial $Mo(bdt)_3$ concentration and the resulting c_i *vs.* time curves were subject to further kinetic analysis by using a non-linear least-squares method.[7]

The monitoring of an equimolecular $Mo(bdt)_3$–n-Bu_4NOH reaction system is presented in Fig. 1a. On the basis of comparisons with authentic samples of $Mo(bdt)_3$ and $[Mo(bdt)_3]^-$, it was concluded that the latter complex is the only molybdenum product formed. This was further supported by HPLC which enabled the separation of $Mo(bdt)_3$ from $[Mo(bdt)_3]^-$ in a reaction mixture where no other peaks were detected. Finally, GC–FID did not show peaks other than that from the THF, indicating that this solvent is not involved in the redox process.

All evidence indicates that no absorbing intermediates are formed in appreciable quantities. First, as can be seen in Fig. 1, repetitive UV–Vis scans show tight isosbestic behaviour. Secondly, and more significantly, the kinetics treatment

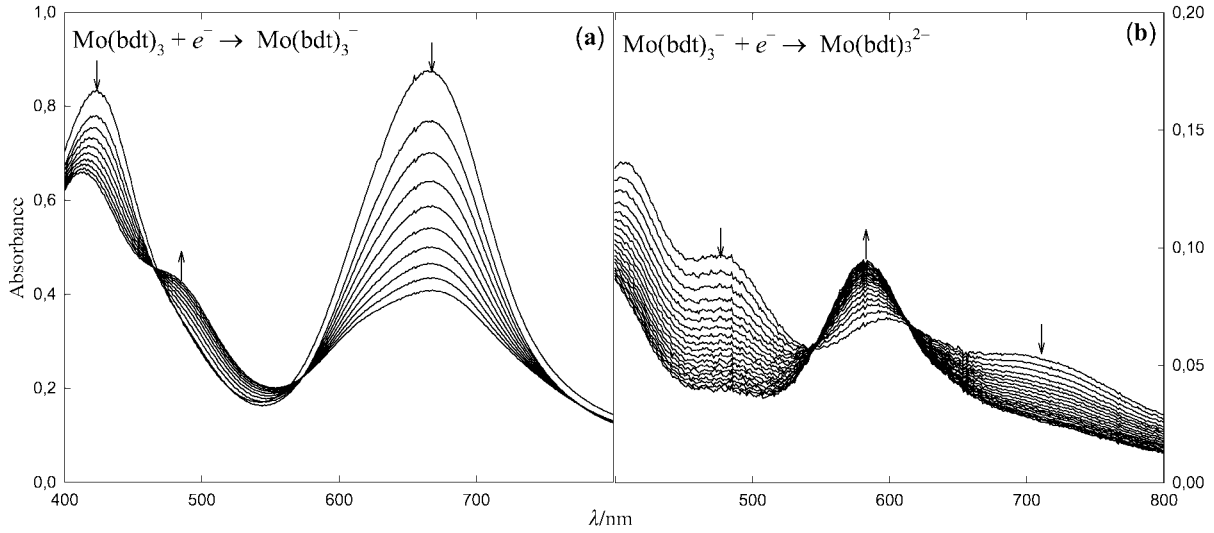

Fig. 1 Repetitive diode-array UV-scans from reaction mixtures in dry THF containing: (a) $Mo(bdt)_3$ 3.38×10^{-5} mol dm^{-3} and n-Bu_4NOH 3.38×10^{-5} mol dm^{-3} (spectra taken every 0.2 s, shown every 1 s, T = 300.2 K). (b) $Mo(bdt)_3^-$ 1.16×10^{-5} mol dm^{-3}, n-Bu_4NOH 3.28×10^{-4} mol dm^{-3} (spectra taken every 0.5 s, shown every 10 s, T = 301.2 K).

 DOI: 10.1039/b106123m

described here is capable of reproducing any of these experimental spectra satisfactorily by using only the component Gaussian functions of the $Mo(bdt)_3$ and $Mo(bdt)_3^-$ spectra.

The kinetics of the Mo(VI)–Mo(V) transformation were investigated with Bu_4NOH–$Mo(bdt)_3$ mole ratios of 0.4–1.3. At higher ratios, a further reduction of the formed Mo(V) complex with excess *n*-Bu_4NOH led to the Mo(IV) complex. Because of this limitation on the ratio of reactants, the kinetics data were treated in complete form, fitting the Mo(VI) and Mo(V) concentration *vs.* time curves to the integrated form of the $d[Mo^{VI}]/dt = -k[Mo^{VI}]^p[OH^-]^q$ equation by using non-linear regression methods. An excellent fit was obtained over a wide range of conditions for $p = 2$, $q = 1$, and $k = (5.0 \pm 0.2) \times 10^8$ s^{-1} mol^{-2} dm^6 at 27 °C. Reaction orders were also corroborated by applying the initial rate method.

The second-order dependence on $[Mo(bdt)_3]$ suggests a two-electron reduction of hydroxide ions to hydroperoxide ions that were actually identified in separate experiments [reaction (1)].

$$2\ Mo(bdt)_3 + 3\ OH^- \longrightarrow 2\ Mo(bdt)_3^- + HO_2^- + H_2O \quad (1)$$

The experiments were performed in biphasic systems by dissolving $Mo(bdt)_3$ in the organic phase and extracting the produced H_2O_2 as HO_2^- in the aqueous basic phase. Thus, when a 2.0×10^{-3} M solution of $Mo(bdt)_3$ in THF–toluene mixture (70:30) was added to a 0.1 M aqueous solution of NaOH over a period of 4 h, H_2O_2 could be detected and spectrophotometrically analysed by reacting an aliquot of the aqueous phase with a solution of $TiOSO_4$ in 25% H_2SO_4–H_2O. The transmittance at 405 nm due to the yellow peroxotitanyl cation indicated the presence of H_2O_2 in yields of 80–90% based on the initial $Mo(bdt)_3$ concentration, while no formation of H_2O_2 was detected in the absence of $Mo(bdt)_3$.

The second-order dependence on $[Mo(bdt)_3]$ is consistent with a mechanism having a bimolecular Mo complex interaction as the rate-limiting step. Taking into account that the current spectrophotometric results do not show that OH^- binds to Mo through the oxygen, we suggest as a reasonable pathway the association of one hydroxide ion with two neutral $Mo(bdt)_3$ molecules by hydrogen bonding to the co-ordinated sulfur atoms of the ligands.‡[1,2] The μ-hydroxo $Mo(bdt)_3\cdots HO^-\cdots Mo(bdt)_3$ species thus formed may pass through a highly concerted transition state in which the interaction with another OH^- ion would lead to a polar group-transfer reaction,[8] dominated by HO···OH bond making and metal reduction, to yield the $[Mo(bdt)_3]^-$ radical ($<g> = 2.006$; $<A>$ ($^{95,97}Mo$) $= 26.6 \times 10^{-4}$ cm^{-1}) and H_2O_2‡[3] which in basic solution forms the HO_2^- ion. An Eyring plot of the rate constant k determined at a series of temperatures gives an excellent straight line from which $\Delta H^{\neq} = 37.9 \pm 0.8$ kJ mol^{-1} and $\Delta S^{\neq} = -39 \pm 3$ J K^{-1} mol^{-1} are deduced. The $\Delta S^{\neq}$ value is consistent with the proposed associative transition-state.

As estimated from standard reduction potential data, the overall reaction (1) must be exergonic at least in acetonitrile solution. In fact, the redox potential for the reduction of HO_2^- to OH^- ions has been reported to be −0.11 V *vs.* ENH, [1 M $(Bu_4N)OH$, pH 30.4],[8] whereas the measured redox potential for the $Mo(bdt)_3$–$Mo(bdt)_3^-$ pair was found to be +0.610 V by cyclic voltammetry.[5] Thus, reaction (1) lies indeed far to the right.

However, the $[Mo(bdt)3]^{1-/2-}$ reduction potential is considerably more negative (−0.040 V) than that of the $[Mo(bdt)_3]^{0/1-}$ couple, and thus the former reduction must have a smaller driving force and a relatively slower reactivity. This was confirmed by monitoring the reaction of (Bu_4N)-$[(Mo(bdt)_3]$ with Bu_4NOH, which also proceeds cleanly with well-defined isosbestic points upon addition of excess base (Fig. 1b). By using the procedure indicated above, these spectra were simulated and the concentration of each complex evaluated as a function of time. The disappearance rate of $[Mo(bdt)_3]^-$ parallels the appearance rate of $[Mo(bdt)_3]^{2-}$ for all runs, but it should be noted that both rates become negligible a few seconds after the reaction starts (*ca.* 15 s), and also that a complete conversion does not take place even when an excess of *ca.* 20 equivalents of base are initially present. These observations can be plausibly explained when the equilibrium shown in reaction (2) is assumed.

$$2\ Mo(bdt)_3^- + 3\ OH^- \rightleftharpoons 2\ Mo(bdt)_3^{2-} + HO_2^- + H_2O \quad (2)$$

Support for the occurrence of this equilibrium comes from the fact that final complex concentrations are dependent on the initial Bu_4NOH concentration ($K = (1.2 \pm 0.3) \times 10^3$ mol^{-1} dm^3 at 298 K). A first analysis of the kinetic data seems to indicate a reversible process in which the rate of $[Mo(bdt)_3]^-$ reduction is first-order in both $[Mo(bdt)_3]^-$ and $[Mo(bdt)_3]^{2-}$ concentrations, being the rate constants dependent on the concentration of base.

In summary, on the basis of this and other works,[3,4] it should no longer be considered unusual to react a higher valent molybdenum tris(dithiolene) compound with hydroxide ions to produce a lower valent molybdenum tris(dithiolene) compound. Moreover, such electron-transfer processes have also been observed to occur with tungsten, *e.g.* $W(bdt)_3$, and this will be the basis of a later publication. Further investigations of the reactivity of $Mo(bdt)_3$ and related compounds in solvents other than THF may clarify whether the observed reactivity is relevant to that of molybdenum cofactor (Moco).[2]

Notes and references

† The molybdenum complex concentrations were calculated by minimising the following least-squares equation with respect to the concentration of the Mo(VI–IV) complexes:

$$\phi(c_1, c_2, \ldots, c_n; \lambda) = \sum_{k=1} (A(\lambda_k) - l \sum_{i=1} \varepsilon_i(\lambda_k) c_i)^2$$

where $A(\lambda)$ is the reaction mixture absorbance at wavelength λ, l is the optical pathway, and $\varepsilon_i(\lambda)$ and c_i, $i \in \{1\ldots3\}$, are the optical densities and concentrations of $Mo(bdt)_3$, $Mo(bdt)_3^-$, and $Mo(bdt)_3^{2-}$ species. The calculations were performed using the C++ Linux programs GssKin and GssFit. Free copies of the program are supplied under request.

‡ (1) $Mo(bdt)_3 + OH^- \underset{k_{-1}}{\overset{k_1}{\rightleftharpoons}} Mo(bdt)_3\cdots OH^-$ (fast)

(2) $Mo(bdt)_3\cdots OH^- + Mo(bdt)_3 \underset{k_{-2}}{\overset{k_2}{\rightleftharpoons}} Mo(bdt)_3\cdots OH^-\cdots Mo(bdt)_3$ (fast)

(3) $Mo(bdt)_3\cdots OH^-\cdots Mo(bdt)_3 + OH^- \xrightarrow{k_3} 2Mo(bdt)_3^- + H_2O_2$ (rls)

1 R. P. Burns and C. A. McAuliffe, *Adv. Inorg. Chem. Radiochem.*, 1979, **22**, 303; J. A. McCleverty, *Progr. Inorg. Chem.*, 1968, **10**, 49.
2 C. Collison, C. D. Garner and J. A. Joule, *Chem. Soc. Rev.*, 1996, **25**, 25; P. Falaras, C. Mitsopoulou, D. Argyropoulos, E. Lyris, N. Psaroudakis, E. Vrachnou and D. Katakis, *Inorg. Chem.*, 1995, **34**, 4536 and references therein.
3 M. Kawashima, M. Koyama and T. Fujinaga, *J. Inorg Nucl. Chem.*, 1976, **38**, 801.
4 D. Sellmann and L. Zapf, *Z. Naturforsch. B*, 1985, **40B**, 380.
5 A. Cervilla, E. Llopis, D. Marco and F. Pérez-Pla, *Inorg. Chem.*, in press.
6 P. Gans, *Data Fitting in the Chemical Sciences*, John Wiley & Sons, Chichester, 1992, chap. 8.
7 F. F. Pérez Pla, J. F. Bea Redón and R. Valero, *Chemometrics and Intelligent Laboratory Systems*, 2000, **53**, 1.
8 J. A. McCleverty, *Encyclopedia of Inorganic Chemistry*, ed. R. B. King, John Wiley & Sons, New York, 1994, p. 2304.

CHEMCOMM Communication
www.rsc.org/chemcomm

Direct oxidation of sulfur-containing fuels in a solid oxide fuel cell

Hyuk Kim, John M. Vohs and Raymond J. Gorte*

Department of Chemical Engineering, University of Pennsylvania, Philadelphia, PA 19104, USA. E-mail: gorte@seas.upenn.edu

Received (in Purdue, IN, USA) 27th June 2001, Accepted 27th September 2001
First published as an Advance Article on the web 25th October 2001

Solid-oxide fuel cells with Cu–ceria anodes are shown to provide stable power generation through the direct oxidation of hydrocarbon fuels having sulfur levels similar to that in gasoline and can be regenerated by steam after being poisoned with higher sulfur levels.

The economical development of fuel cells for the near future depends on the use of hydrocarbon fuels, usually through the reforming of those fuels to hydrogen. However, most hydrocarbon fuels available today contain significant levels of sulfur. For example, approximately 10 ppm of sulfur-containing compounds are added to natural gas as an odorant. In the case of gasoline, regulations in most of the US allow 300 ppm of sulfur.[1] Even with new regulations to avoid poisoning the automotive catalytic converter, gasoline will still contain at least 20 ppm for the foreseeable future.[1] For military applications, logistical fuels can be as high as 10 000 ppm S. This sulfur represents a serious complication for fuel-cell developers, since sulfur levels must be in the ppb range for a reasonable lifetime in proton-exchange membrane (PEM) fuel cells and <1 ppm for many solid-oxide fuel cells (SOFC).[2] Indeed, for SOFC operation at 1023 K and lower, it is reported that the H_2S concentration must be below 0.05 ppm.[3] Depending on the fuel, removal of sulfur can require a complex hydrodesulfurization reactor and always requires a trap that must be periodically serviced.[2]

Direct, electrochemical oxidation of hydrocarbons, without first reforming them to H_2, is theoretically possible in an SOFC because O^{2-} is the species that diffuses through the electrolyte. An SOFC generates electricity through the reduction of O_2 to O^{2-} anions at the cathode, transfer of the anions through an electrolyte that is an electronic insulator (usually yttria-stabilized zirconia, YSZ), and finally the oxidation of the O^{2-} anions by the fuel at the anode. The anode in conventional designs is a ceramic–metallic (cermet) composite of Ni and yttria-stabilized zirconia (YSZ) which is an electronic conductor due to Ni and ionic conductor due to YSZ. However, Ni catalyzes formation of graphite from hydrocarbons; and, except for a narrow range of operating temperatures and only for methane,[4] carbon formation with Ni-based anodes is unavoidable unless steam or oxygen is fed along with the hydrocarbon.

By substituting Ni with Cu, we were able to show that carbon formation is essentially eliminated for hydrocarbon fuels,[5,6] including fuels that are liquids at room temperature such as *n*-decane, toluene and synthetic diesel.[6] While Cu provides the high electronic conductivity necessary for good anode performance, Cu–YSZ anodes are not active for the oxidation of hydrocarbons.[7] To provide activity for hydrocarbon oxidation, we have found it necessary to add ceria to the anode.[5–7] Ceria appears to help catalyze the oxidation reactions.

The fuel cells used in this study were prepared by tape-casting methods according to procedures described elsewhere.[7] Briefly, a YSZ wafer was prepared having a dense layer, 60 μm thick, supported by a porous layer, 400 μm thick. A 50:50 mixture of YSZ and LSM ($La_{0.8}Sr_{0.2}MnO_3$, Praxair Surface Technologies) powders was pasted onto the dense side of the wafer to form the cathode. Cu and ceria were then added to the porous side of the YSZ wafer, in separate steps, using wet impregnation of aqueous nitrate solutions to a final concentration of 10 wt% ceria and 20 wt% Cu, followed by heating in air at 750 K to form the oxides. Au was used to form the electrical contacts at the anode so as to avoid questions about catalytic activity. Finally, the cell with an active surface area of 0.25 cm^2 was sealed onto a 1.2 cm alumina tube using a zirconia-based adhesive.

As described in a previous paper, room-temperature liquids were introduced into the anode compartment using a syringe pump, and the liquids were vaporized in the oven used to maintain the temperature of the cell at 973 K.[6] The effect of fuel concentration and hydrocarbon type on the curves of potential *vs.* current are shown elsewhere.[6] In order to simulate a realistic, sulfur-containing fuel, this study used pure *n*-decane to which thiophene was added to achieve the desired level of sulfur. The sulfur contents are reported as the weight fraction of S in ppm. Because of the low surface area of the anode, it was not possible for us to reduce the flow rates to the point where fuel conversion was high. In the experiments reported here, the liquid flow rate was maintained at 1.0 ml h^{-1}, implying that the conversion to CO_2 and H_2O was never higher than 3%. Analysis by gas chromatography of the effluent from the cell showed that CO_2 was formed in an amount equal to the O^{2-} flux through the electrolyte.[5,6]

To control the composition of the fuel in the anode compartment and to maintain flow, dry N_2 was introduced into the anode compartment with the liquids. The fuel concentration was either 50 mol% *n*-decane in N_2 or 5 mol% *n*-decane. These correspond to the *n*-decane concentrations that would be obtained at 10 and 50% conversion if pure *n*-decane were fed to the anode and only CO_2 and H_2O were formed by reaction.

The effect of sulfur on the Cu is shown in Fig. 1. Here, the resistance between the two Au wires, pasted on opposite sides of the Cu cermet, 0.5 cm apart, was measured as a function of time. Initially, the resistance was high because the Cu was in the form of an oxide. As the temperature of the cermet was ramped in flowing H_2, the resistance dropped to metallic levels. At 16 h, while holding the sample at 973 K, the fuel was switched to 50 mol% *n*-decane (5000 ppm S), while the resistance was measured for an additional 24 h. The results demonstrate that

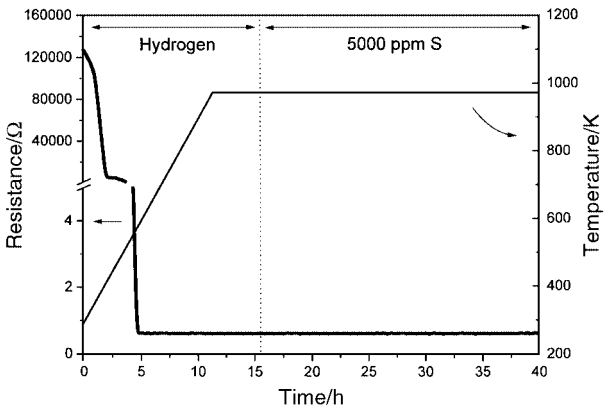

Fig. 1 The resistance measured across 0.5 cm of the Cu–ceria–YSZ cermet as a function of time. The feed to the anode was pure H_2 for the first 16 h and was then switched to 50 mol% *n*-decane containing 5000 ppm S.

 DOI: 10.1039/b105713h

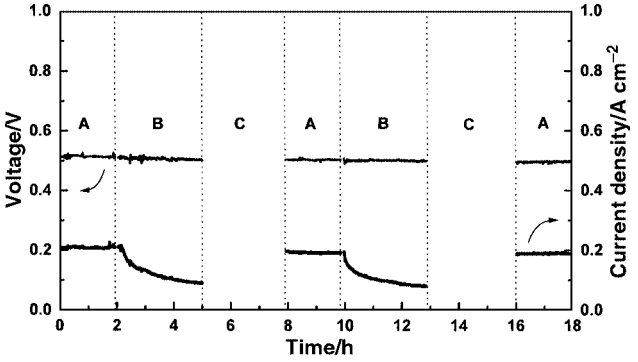

Fig. 2 Single cell performance as a function of time at 973 K, holding the cell potential at 0.5 V. The feed to the anode was: (A) 50 mol% *n*-decane in N_2; (B) 50 mol% *n*-decane, having 5000 ppm S; (C) 50 mol% H_2O in N_2.

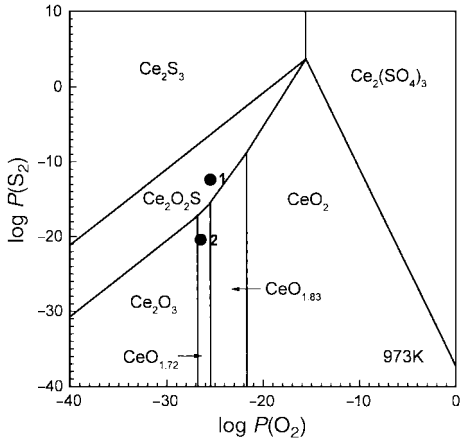

Fig. 3 The Ce–O–S phase diagram at 973 K. Points 1 and 2 correspond to the experimental conditions described in the text.

the presence of sulfur at these levels gave rise to no measurable changes in the resistance, implying that the Cu was not strongly affected. This result is not surprising, given that equilibrium calculations demonstrate that Cu_2S formation is not favorable under these conditions. While surface sulfides are reported to be more stable than bulk Cu_2S,[8] their presence would probably have no effect on anode performance, since the role of Cu appears to be only that of providing electronic conductivity.[7] It is also noteworthy that Cu has been added to the anodes of molten-carbonate fuel cells to improve the sulfur tolerance.[9]

As discussed elsewhere, ceria is an important component in the anode, probably because of its catalytic properties for hydrocarbon oxidation, and is essential for achieving good power densities for hydrocarbon fuels.[7] Fig. 2 shows the performance of the cell upon switching from 50 mol% *n*-decane (0 ppm S) to 50 mol% *n*-decane (5000 ppm S), while holding the cell potential at 0.5 V. The current density began to drop dramatically upon the introduction of sulfur and could not be restored by simply switching back to the sulfur-free fuel. However, the cell could be completely restored to its original performance level by introducing steam (50 mol% in N_2) at 973 K. As shown in Fig. 2, the cell could be poisoned and restored, repeatedly, using this procedure.

The phase diagram for ceria, calculated from the data of Dwivedi and Kay and shown in Fig. 3,[10] shows the likely cause for the sulfur poisoning. To calculate the equilibrium O_2 pressure at the anode, we used the equation for the complete oxidation of *n*-decane to CO_2 and H_2O and the conversion calculated from the current density, 1.5%. The equilibrium S_2 pressure was determined from the reaction $C_4H_4S + 2H_2 = \frac{1}{2}S + C_4H_4$, using literature values for C_4H_4S.[11] We further assumed that $P(H_2)$ and $P(C_4H_8)$ were present at the same

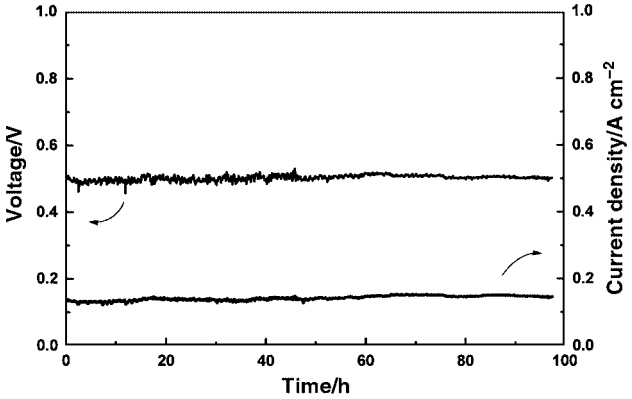

Fig. 4 Single cell performance as a function of time at 973 K, holding the cell potential at 0.5 V. The feed to the anode was 5 mol% *n*-decane containing 100 ppm S.

concentrations as *n*-decane. With these assumptions, $P(O_2)$ and $P(S_2)$ would be $10^{-25.5}$ and $10^{-12.6}$ atm, respectively, and cerium should exist as Ce_2O_2S, point 1 in Fig. 3. Heating Ce_2O_2S in steam should remove sulfur and restore CeO_2.

An obvious implication of the phase diagram is that a more modest level of sulfur should not affect the ceria in the anode. This is demonstrated in Fig. 4, which shows the cell performance in 5 mol% *n*-decane (100 ppm S). The calculated $P(O_2)$ and $P(S_2)$ for this experiment ($10^{-26.6}$ and $10^{-20.3}$ atm) are shown in point 2 of Fig. 3. Holding the cell potential at 0.5 V, Fig. 4 shows that the current density was slightly lower because of the lower fuel concentration,[6] but remained constant for 100 h in this fuel mixture. Even though the total exposure of the ceria to sulfur over this period was significant, sulfur at this concentration seems to have no effect on anode performance.

The results are extremely encouraging in that they demonstrate that fuels with moderate levels of sulfur can be used in SOFCs having anodes made from Cu and ceria. For applications with natural gas and low-sulfur gasoline, it will probably not be necessary to desulfurize or trap the sulfur before introducing it to the anode. Even for high-sulfur, logistical fuels, it may be necessary to remove only some of the sulfur. Furthermore, we have shown that a cell which has been poisoned by sulfur-containing fuels can be restored by passing steam over the anode. The implications of this for distributed-power and portable-power applications, where complex and bulky fuel-processing equipment is difficult to incorporate, are enormous.

We are grateful to the Office of Naval Research for funding.

Notes and references

1 S. Thompson and J. B. McCarthy, *Sulfur in Gasoline*, 1999, http://www.cnie.org/nle/eng-51.html 1.
2 J. H. Hirschenhofer, D. B. Stauffer, R. R. Engleman and M. G. Klett, *Fuel Cell Handbook*, US Department of Commerce, Springfield, VA, 4th edn., 1998, pp. 7-2 to 7-43.
3 Y. Matsuzaki and I. Yasuda, in *SOFC VII, Proc. 7th Int. Symp.*, Electrochemical Society, Penninton, NJ, 2001, vol. 2001-16, p. 769.
4 E. Perry Murray, T. Tsai and S. A. Barnett, *Nature*, 1999, **400**, 649.
5 S. Park, J. M. Vohs and R. J. Gorte, *Nature*, 2000, **404**, 265.
6 H. Kim, S. Park, J. M. Vohs and R. J. Gorte, *J. Electrochem. Soc.*, 2001, **148**, A693.
7 R. J. Gorte, S. Park, J. M. Vohs and C. Wang, *Adv. Mater.*, 2000, **12**, 1465.
8 C. H. Bartholomew, P. K. Agrawal and J. R. Katzer, *Adv. Catal.*, 1982, **31**, 135.
9 L. G. Marianowski, G. L. Anderson and E. H. Camara, *US Pat.*, 5 071 718, 1991.
10 D. K. Dwivedi and D. A. R. Kay, *Metall. Trans. B*, 1984, **15**, 523.
11 G. Waddington, J. W. Knowlton, D. W. Scott, G. D. Oliver, S. S. Todd, W. N. Hubbard, J. C. Smith and H. M. Huffman, *J. Am. Chem. Soc.*, 1949, **71**, 797.

CHEMCOMM Communication
www.rsc.org/chemcomm

Manganese as a template: a new synthesis of corrole

Martin Bröring* and Christian Hell

Institut für Anorganische Chemie, Universität Würzburg, Am Hubland D-97074. Würzburg, Germany. E-mail: Martin.Broering@mail.uni-wuerzburg.de

Received (in Cambridge, UK) 14th August 2001, Accepted 2nd October 2001
First published as an Advance Article on the web 22nd October 2001

The reaction of 2,2′-bisdipyrrins 1, 2, and 3 with manganese(II) acetate tetrahydrate and molecular dioxygen yields the manganese(III)corroles 4, 5 and 6, which are readily demetalated to the respective free-base corroles.

The chemistry of corrole, the one-carbon short analogue of porphyrin, is currently one of the most flourishing fields in the porphyrin area.[1] Ever since the unexpected observation by Vogel *et al.* in 1994, that this trisanionic ligand stabilises unusually high oxidation states of transition metal centers like Fe(IV), Cu(III), and Co(IV),[2] the interest in this particular macrocycle has continuously increased. The synthetic pathways leading to corroles, however, are still rather small in number, albeit a large body of work has been conducted in recent years towards general approaches to differently substituted corroles, mainly by the groups of Paolesse[3] and Gross.[4] Very recently, the first applications of corroles as ligands in catalytically active transition metal complexes have appeared in the literature,[5] and the first multi-macrocyclic architectures using corroles as building blocks have also been achieved.[6] Today, the major methods used for the preparation of corroles are the oxidative cyclization of α,ω-didesoxybiladienes-*a*,*c* as described by Murakami,[7] and the strategy of Gross *et al.*, who developed the non-catalysed condensation of pyrrole and aromatic aldehydes as a one step procedure.[4] In the course of studies towards a synthetic entry into the corrole and corrin field, Johnson *et al.* attempted to cyclize 2,2′-bisdipyrrin complexes of Pd(II) as early as 1960, but received a palladium(II)-10-oxacorrole instead.[8] Here we report, that by simply changing the metal ion to manganese the desired formation of corroles from 2,2′-bisdipyrrins[9] can in fact be observed.

As 3,3′,4,4′,8,8′,9,9′-octaethyl-10,10′-dimethyl-2,2′-bisdipyrrin **1** is treated with manganese(II) acetate tetrahydrate under aerobic conditions in boiling DMF, varying amounts of **4** build up over the course of several hours. Purging the hot reaction mixture with dioxygen accelerates the reaction significantly, so that within five minutes the cyclization is complete. After chromatography and recrystallization from diethyl ether–*n*-hexane, **4** is obtained as violet crystals in 23% yield (Scheme 1). The material obtained this way is identical in every respect with the manganese(III)octaethylcorrole reported earlier.[10] When applying the very same conditions to other α,ω-dimethyl-2,2′-bisdipyrrins,[9] substituted manganese(III)corroles can be prepared. For example, *meso*-diphenyl- and *meso*-di-*p*-tolyl-2,2′-bisdipyrrins **2** and **3** are cyclized to the manganese(III)-5,15-diarylcorroles **5** and **6** in 18 and 19% yield, respectively.[11,12]

As we experienced at an initial stage of the project, the manganese(III)corroles appear remarkably prone to oxidation by chlorinated solvents (Scheme 2). Thus, simply performing the chromatographic work-up of **4** on silica with a dichloromethane–methanol mixture as the eluent directly gave the known chloro-manganese(IV) complex **7**[1b] as the only product, albeit in diminished yield (17%). This observation provides yet another example for the ease of stabilisation of high oxidation states through the trisanionic corrole ligand.

Free base corroles are readily released from the manganese complexes by simple acid induced demetallation. For example, treatment of **4** with HBr in acetic acid yields the well-known octaethylcorrole **8** quantitatively within 10 min (Scheme 3).[7] This clean demetalation protocol makes the newly found manganese induced cyclization a useful synthetic tool towards

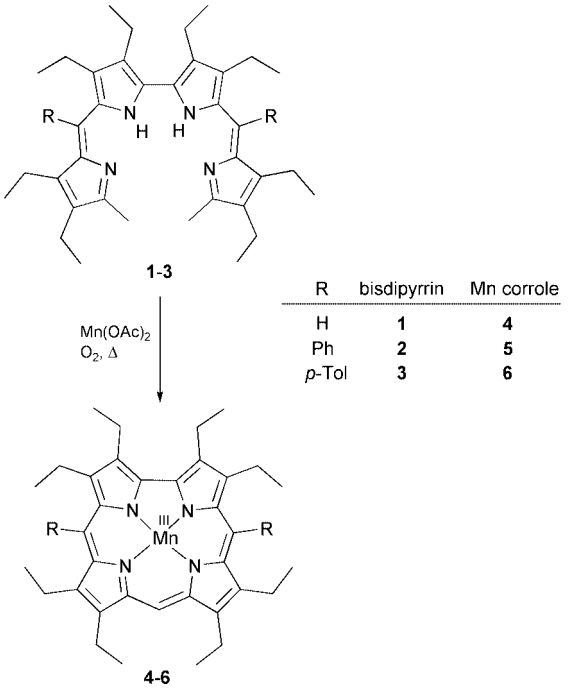

R	bisdipyrrin	Mn corrole
H	1	4
Ph	2	5
p-Tol	3	6

Scheme 1

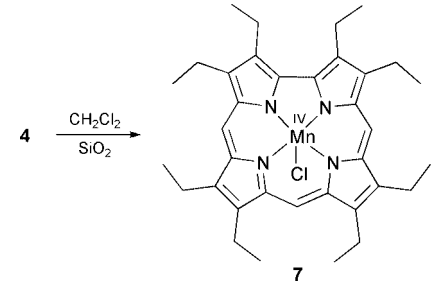

Scheme 2

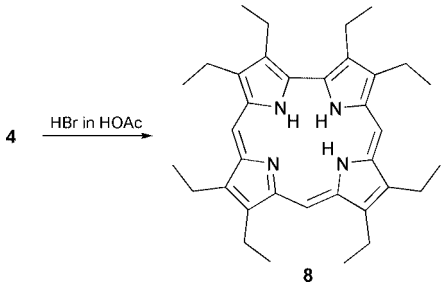

Scheme 3

 DOI: 10.1039/b107362c

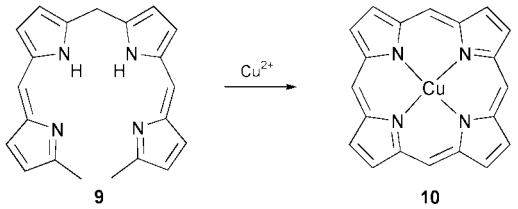

Scheme 4

substituted corrole ligands, some which are hardly or not at all accessible by any other of the corrole forming reactions known today.

Although the mechanistic details of the Mn(II)–O_2 induced cyclization of 2,2′-bisdipyrrins are still in question, the formation of **4**–**6** points to an analogous oxidative transformation in the porphyrin field, namely the reaction of *a*,*c*-biladienes **9** with several metal salts or oxidants to yield porphyrins **10** (Scheme 4). This valuable transformation, initially found by Johnson *et al*.,[13] has been thoroughly investigated and mechanistically explained by Smith.[14] It appears highly probable, that a related sequence of steps occurs also in the case of 2,2′-bisdipyrrin cyclization. As a major difference to the macrocyclization of *a*,*c*-biladienes we believe, that in our case a templating action of the metal ion—prior to or after partial oxidation—is crucial to the reaction. Most probably, the 2,2′-bisdipyrrin unit will not stabilise the tense, helical conformation necessary for ring closure on its own, but rather retain the ability of an almost free rotation around the central pyrrole–pyrrole axis. Additionally, it is quite questionable, whether the terminal methyl groups of a 2,2′-bisdipyrrin in a closed, quasi-macrocyclic conformation would have sufficient overlap without being forced by a central metal ion.

Further studies towards an understanding of the C_1 extrusion, the use of other metal ions and/or co-oxidants, and the application of the new macrocyclization in the synthesis of tailor-made and functionalized corroles and metallocorroles are currently in progress.

This work was funded by the Deutsche Forschungsgemeinschaft (Emmy-Noether-Programm) and the Fonds der Chemischen Industrie. We thank Professor Helmut Werner for his generous support.

Notes and references

1 (*a*) R. Paolesse, in *The Porphyrin Handbook*, ed. K. M. Kadish, K. M. Smith and R. Guilard, Academic, San Diego, CA, 2000, vol. 2, ch. 11, p. 201–232 ; (*b*) C. Erben, S. Will and K. M. Kadish, in *The Porphyrin Handbook*, ed. K. M. Kadish, K. M. Smith and R. Guilard, Academic, San Diego, CA, 2000, vol. 2, ch. 12, p. 233–300.

2 E. Vogel, S. Will, A. Schulze-Tilling, L. Neumann, J. Lex, E. Bill, A. X. Trautwein and K. Wieghardt, *Angew. Chem., Int. Ed. Engl*., 1994, **33**, 731; S. Will, J. Lex, E. Vogel, V. A. Adamian, E. Van Caemelbecke and K. M. Kadish, *Inorg. Chem*., 1996, **35**, 5577; S. Will, J. Lex, E. Vogel, H. Schmickler, J.-P. Gisselbrecht, C. Haubtmann, M. Bernard and M. Gross, *Angew. Chem., Int. Ed. Engl*., 1997, **36**, 357.

3 R. Paolesse, S. Licoccia, M. Fanciullo, E. Morgante and T. Boschi, *Inorg. Chim. Acta*, 1993, **203**, 107; R. Paolesse, S. Licoccia, G. Bandoli, A. Dolmella and T. Boschi, *Inorg. Chem*., 1994, **33**, 1171; V. A. Adamian, F. D'Souza, S. Licoccia, M. L. Di Vona, E. Tassoni, R. Paolesse, T. Boschi and K. M. Smith, *Inorg. Chem*., 1995, **34**, 532; R. Paolesse, L. Jaquinod, D. J. Nurco, S. Mini, F. Gagone, T. Boschi and K. M. Smith, *Chem. Commun*., 1999, 1307.

4 Z. Gross, N. Galili and I. Saltsman, *Angew. Chem., Int. Ed*., 1999, **38**, 1427; Z. Gross, N. Galili, L. Simkhovich, I. Saltsman, M. Botoshansky, D. Blaser, R. Boese and I. Goldberg, *Org. Lett*., 1999, **1**, 599; for related work, see also:; D. T. Gryko, *Chem. Commun*., 2000, 2243; R. Paolesse, S. Nardis, F. Sagone and R. G. Khoury, *J. Org. Chem*., 2000, **66**, 550; D. T. Gryko and K. Jadach, *J. Org. Chem*., 2001, **66**, 4267; C. V. Asokan, S. Smeets and W. Dehaen, *Tetrahedron Lett*., 2001, **42**, 4483.

5 Z. Gross, L. Simkhovich and N. Galili, *Chem. Commun*., 1999, 599; Z. Gross, G. Golubkov and L. Simkhovich, *Angew. Chem., Int. Ed*., 2000, **39**, 4045; G. Golubkov, J. Bendix, H. B. Gray, A. Mahammed, I. Goldberg, A. J. DiBilio and Z. Gross, *Angew. Chem., Int. Ed*., 2001, **40**, 2132.

6 R. Paolesse, R. K. Pandey, T. P. Forsyth, L. Jaquinod, K. R. Gerzevske, D. J. Nurco, M. O. Senge, S. Licoccia, T. Boschi and K. M. Smith, *J. Am. Chem. Soc*., 1996, **118**, 3869; F. Jérome, C. P. Gros, C. Tardieux, J.-M. Barbe and R. Guilard, *Chem. Commun*., 1998, 2007; R. Paolesse, A. Macagnano, D. Monti, P. Tagliatesa and T. Boschi, *J. Porph. Phthal*., 1998, **2**, 501; F. Jérome, C. P. Gros, C. Tardieux, J.-M. Barbe and R. Guilard, *New J. Chem*., 1998, 1327; R. Paolesse, F. Sagone, A. Macagnano, T. Boschi, L. Prodi, L. Mantalti, N. Zaccheroni, F. Boletta and K. M. Smith, *J. Porph. Phthal*., 1999, **3**, 364.

7 Y. Murakami, Y. Matsuda, K. Sakata, S. Yamada, Y. Tanaka and Y. Aoyama, *Bull. Chem. Soc. Jpn*., 1981, **54**, 163.

8 A. W. Johnson and R. Price, *J. Chem. Soc*., 1960, 1649; A. W. Johnson and I. T. Kay, *Proc. Chem. Soc*., 1961, 168.

9 M. Bröring, *Synthesis*, 2000, 1291; M. Bröring, D. Griebel, C. Hell and A. Pfister, *J. Porph. Phthal*., 2001, **5**, 708.

10 K. M. Kadish, V. A. Adamian, E. Van Caemelbecke, E. Gueletii, S. Will, C. Erben and E. Vogel, *J. Am. Chem. Soc*., 1998, **120**, 11986.

11 *Spectroscopic data* for **5**: mp. 252 °C (decomp.); MS (FAB): *m*/*z* 726.4, M^+; calc. for $C_{47}H_{51}N_4Mn$: C 77.66, H 7.07, N 7.71; found: C 77.21, H 7.25, N 7.53%.

12 *Spectroscopic data* for **6**: mp. 294 °C (decomp.); MS (FAB): *m*/*z* 754.5, M^+; calc. for $C_{49}H_{55}N_4Mn$: C 77.96, H 7.34, N 7.42; found: C 77.97, H 7.52, N 7.44%.

13 A. W. Johnson and I. T. Kay, *J. Chem. Soc. C*, 1961, 2418.

14 K. M. Smith, in *The Porphyrin Handbook*, ed. K. M. Kadish, K. M. Smith and R. Guilard, Academic, San Diego, CA, 2000, vol. 1, ch. 3, p. 119–148.

CHEMCOMM Communication
www.rsc.org/chemcomm

Synthesis and electrochemical properties of novel dimeric fullerenes incorporated in a 2,3-diazabicyclo[2.2.2]oct-2-ene framework

Yasujiro Murata, Mitsuharu Suzuki and Koichi Komatsu*

Institute for Chemical Research, Kyoto University, Uji, Kyoto 611-0011, Japan.
E-mail: komatsu@scl.kyoto-u.ac.jp; Fax: +81-774-38-3178; Tel: +81-774-38-3172

Received (in Cambridge, UK) 6th September 2001, Accepted 9th October 2001
First published as an Advance Article on the web 25th October 2001

Novel dimeric fullerenes incorporated in a 2,3-diazabicyclo[2.2.2]oct-2-ene framework, with and without direct inter-fullerene-cage bonds, were synthesized and fully characterized spectroscopically; the electronic communication between the two fullerene cages was clarified by differential pulse voltammetry.

Dimeric fullerene compounds are attracting current interest not only from the structural curiosity but also concerning their electrochemical properties, as the partial structure of fullerene polymers.[1] In some of such compounds having direct C–C bond(s) between the fullerene cages has been reported the occurrence of electronic communication between the fullerene units upon electroreduction.[2,3] We recently reported electronic communication in a dimeric compound without the direct C–C bond between the fullerene cages.[4] Herein we report the synthesis and properties of new dimeric fullerenes incorporated in a 2,3-diazabicyclo[2.2.2]oct-2-ene framework, with and without the covalent bonds directly between the two cages.

The synthesis of dimeric compound **2** was conducted by the solid-state reaction of fullerene C_{60} with 0.5 equiv. of di(2-pyridyl)-1,2,4,5-tetrazine (Scheme 1). The key intermediate **1**[4a,5] was found to be formed quantitatively under the high-speed vibration milling (HSVM) conditions[4,6] for 30 min. The [4 + 2] cycloaddition of resultant **1** with C_{60} was achieved by heating the solid mixture of **1** and C_{60} at 150 °C for 2 h. After flash chromatography over SiO_2, the dimeric compound **2**† without inter-cage bonds was obtained in 27% yield along with 40% of recovered C_{60}. This dimeric compound **2** was obtained only by the solid-state reaction, in which the highest concentration of the reactants without any solvation can cause the closest contact of the reacting species. The reaction in solution has been reported to result in only hydrogenation of **1**.[5,7]

The structure of **2** was determined based on the following spectral data.† The MALDI-TOF MS spectrum showed a molecular ion peak at *m*/*z* 1649 with the isotopic distribution pattern identical to the calculated one for $C_{132}H_8N_4$ as shown in Fig. 1. The ^{1}H NMR exhibited only one type of 2-pyridyl group. The ^{13}C NMR showed 33 signals (one signal overlapped) in the sp^2 carbon region and 2 signals in the sp^3 carbon region. These data support the structure of **2** having C_{2v} symmetry with two C_{60} cages rigidly fixed in close proximity by incorporation in a 2,3-diazabicyclo[2.2.2]oct-2-ene framework. Although it was expected that extrusion of a nitrogen molecule from **2** and the addition of another molecule of C_{60} would give a C_{60} trimeric compound, like triptycene having fullerene instead of benzene, **2** was found to be stable in the solid state at temperatures as high as 250 °C. Such nitrogen extrusion was observed only under the MALDI-TOF MS conditions as shown in Fig. 1.

When a solution of **2** in *o*-dichlorobenzene (ODCB) was irradiated with room light for 3 h, a novel C_{60} dimer **3**‡ with direct inter-cage bonds was formed quantitatively by the intramolecular [2 + 2] cycloaddition[8] (Scheme 1). This reaction was monitored by UV-vis spectra which displayed decreasing absorption at 329 nm and increasing absorption at 441 nm with isosbestic points at 312, 353, and 535 nm as shown in Fig. 2. The ^{1}H NMR spectrum of **3** showed two types of 2-pyridyl groups and the ^{13}C NMR spectrum exhibited 61 signals (five signal overlapped) in the sp^2 carbon region and 6 signals in the sp^3 carbon region. These data support the structure of **3** having

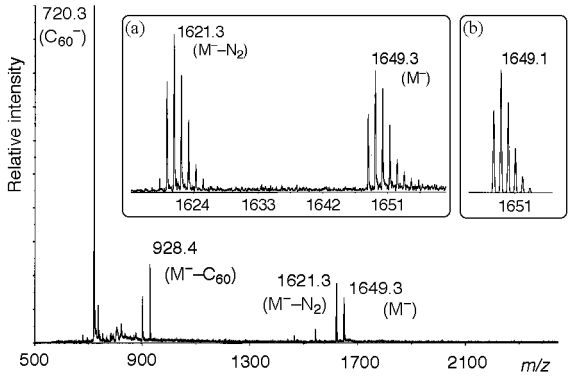

Fig. 1 MALDI-TOF MS spectrum of **2** in a dithranol matrix (negative-ion reflector mode); inset (a) molecular-ion region, (b) a theoretical isotropic pattern for $C_{132}H_8N_4$.

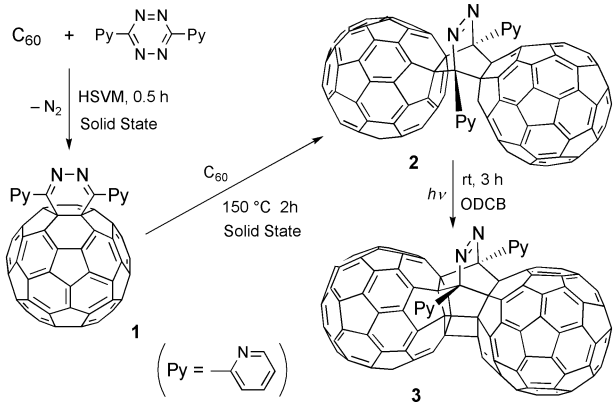

Scheme 1

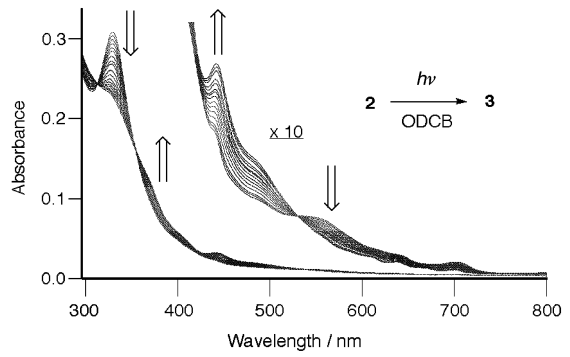

Fig. 2 Time-dependent UV-vis spectral changes observed upon irradiation of **2** (in ODCB, 3.06×10^{-5} M) with room light for 3 h.

 DOI: 10.1039/b107922k

C_s symmetry with two C_{60} cages directly connected by sharing a newly formed cyclobutane ring. It was found that dimeric compound **3** does not revert to **2** either under the thermal (in ODCB, 100 °C, 2 h) or photochemical (visible light) conditions. This observation was supported by theoretical calculations which show that the relative energy of **3** is lower than that of **2** by 4.24 kcal mol^{-1} at the B3LYP/3-21G level of theory.[9]

The redox properties of these dimeric compounds were studied by differential pulse voltammetry in ODCB in order to investigate the possible electronic communication between the two fullerene cages closely located to each other.[2–4] As shown in Fig. 3, **2** displayed three sets of reduction peaks, each of which consisted of two closely located reduction peaks (−1.09, −1.15, −1.52, −1.58, −2.11, and −2.19 V *vs*. Fc/Fc$^+$), indicating that the reduction takes place stepwise on each fullerene cage due to the small but clear electronic communication between two cages. However, **3** showed two sets of two reduction peaks (−1.11, −1.20,−1.56, and −1.63 V) and then two isolated reduction peaks at −2.03 and −2.32 V. The difference in voltage between the fifth and sixth reduction peaks for **3** is quite large, suggesting that the electronic interaction is large after the fifth reduction because of the effects of Coulombic repulsion between the negatively charged fullerene cages. Although the reason for the close distance between the third and fourth reduction peaks compared with that between the first and second peaks is not clear, the overall reduction profile of **3** is quite similar to that of C_{121} reported by Dragoe.[3]

In summary, novel fullerene dimers **2** and **3** were synthesized using a solid-state reaction as a key technique. The intramolecular [2 + 2] reaction in **2** forming a cyclobutane ring readily took place photochemically to give **3**. The newly formed cyclobutane ring was found to be thermally and electrochemically stable, which is in sharp contrast to the ready cleavage of the [2 + 2] bonds upon heating[6c,8] or reduction[4b,6c] in dimer C_{120} and in compounds with a related structure.

This work was supported by a Grant-in-Aid for COE Research on Elements Science (No. 12CE2005) from the Ministry of Education, Culture, Sports, Science and Technology of Japan.

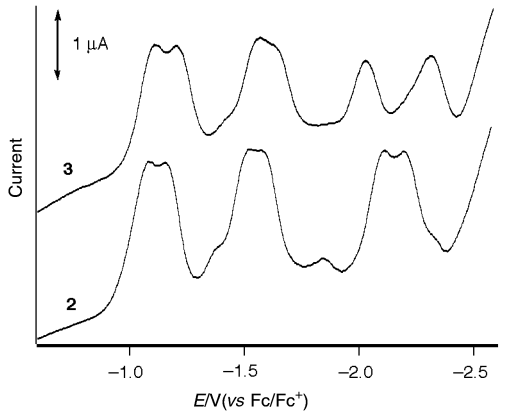

Fig. 3 Differential pulse voltammograms of **2** and **3** in ODCB solution (2×10^{-4} M) containing 0.1 M Bu_4NBF_4; scan rate, 0.02 V s^{-1}.

Notes and references

† *Spectroscopic data for* **2**: UV-vis (ODCB) λ_{max} (log ε) 329 nm (5.01), 438sh (3.79), 551sh (3.38), 702 (2.72); ^{1}H NMR (300 MHz, CS_2–acetone-d_6 (7 : 1)) δ 9.77 (d, 1H), 8.56 (d, 1H), 8.09 (m, 1H), 7.35 (m, 1H); ^{13}C NMR (75 MHz, ODCB-d_4) δ 151.44, 148.34, 146.17, 145.45, 143.29, 142.87, 142.21, 141.92, 141.78, 141.45, 141.39, 141.07, 140.78, 140.72, 140.68, 140.36, 140.11, 139.66, 138.46, 138.20, 138.02, 137.96, 137.60, 137.30, 136.83, 136.31, 135.60, 135.15, 134.16, 132.37, 132.25, 130.27, 119.11, 69.81, 67.22; MS (MALDI-TOF, negative, dithranol) *m*/*z* 1649.

‡ *Spectroscopic data for* **3**: UV-vis (ODCB) λ_{max} (log ε) 326sh nm (4.89), 441 (4.43), 483sh (3.69), 638sh (2.75), 668 (2.48), 701 (2.37); ^{1}H NMR (300 MHz, CS_2–acetone-d_6 (7 : 1)) δ 9.51 (m, 1H), 9.45 (m, 1H), 8.63 (m, 1H), 8.35 (m, 1H), 8.11 (m, 1H), 7.87 (m, 1H), 7.43 (m, 1H), 7.12 (m, 1H); ^{13}C NMR (150 MHz, ODCB-d_4) δ 157.23, 151.07, 150.79, 150.60, 149.17, 148.77, 148.46, 148.38, 148.08, 147.71, 147.20, 147.15, 146.72, 146.69, 146.65, 146.54, 146.36, 145.97, 145.93, 145.35, 145.30, 145.21, 145.20, 145.11, 145.01, 144.93, 144.71, 144.64, 144.60, 145.55, 144.34, 144.30, 144.02, 143.97, 143.62, 143.52, 143.48, 143.15, 142.90, 142.85, 142.82, 142.72, 142.59, 142.51, 142.44, 142.42, 142.09, 141.78, 140.15, 140.14, 140.07, 139.49, 139.23, 138.19, 136.79, 136.54, 136.44, 134.86, 134.76, 123.58, 122.71, 83.25, 80.95, 80.25, 71.74, 71.54, 66.44; MS (MALDI-TOF, negative, dithranol) *m*/*z* 1649.

1 J. L. Segura and N. Martín, *Chem. Soc. Rev*., 2000, **29**, 13.
2 (*a*) A. L. Balch, D. A. Costa, W. R. Fawcett and K. Winkler, *J. Phys. Chem*., 1996, **100**, 4823; (*b*) J. C. Hummelen, B. Knight, J. Pavlovich, R. González and F. Wudl, *Science*, 1995, **269**, 1554; (*c*) N. Dragoe, H. Shimotani, M. Hayashi, K. Saigo, A. Bettencourt-Dias, A. L. Balch, Y. Miyake, Y. Achiba and K. Kitazawa, *J. Org. Chem*., 2000, **65**, 3269.
3 N. Dragoe, H. Shimotani, J. Wang, M. Iwaya, A. Bettencourt-Dias, A. L. Balch and K. Kitazawa, *J. Am. Chem. Soc*., 2001, **123**, 1294.
4 (*a*) K. Komatsu, Y. Murata and N. Kato, *Fullerenes 2000, Volume 9, Functionalized Fullerenes*, ed. N. Matrin, M. Maggini and D. M. Guldi, Electrochemical Society, Pennington, N.J., 2000, pp. 20–27; (*b*) Y. Murata, N. Kato and K. Komatsu, *J. Org. Chem*., 2001, **66**, in press.
5 The reaction in solution was reported: G. P. Miller and M. C. Tetreau, *Org. Lett*., 2000, **2**, 3091.
6 For the reactions under the high-speed vibration milling conditions, see: (*a*) G.-W. Wang, Y. Murata, K. Komatsu and T. S. M. Wan, *Chem. Commun*., 1996, 2059; (*b*) G.-W. Wang, K. Komatsu, Y. Murata and M. Shiro, *Nature*, 1997, **387**, 583; (*c*) K. Komatsu, G.-W. Wang, Y. Murata, T. Tanaka, K. Fujiwara, K. Yamamoto and M. Saunders, *J. Org. Chem*., 1998, **63**, 9358; (*d*) K. Komatsu, Y. Murata, G.-W. Wang, T. Tanaka, N. Kato and K. Fujiwara, *Fullerene Sci. Technol*., 1999, **7**, 609; (*e*) Y. Murata, N. Kato, K. Fujiwara and K. Komatsu, *J. Org. Chem*., 1999, **64**, 3483; (*f*) K. Komatsu, K. Fujiwara, Y. Murata and T. Braun, *J. Chem. Soc., Perkin Trans. 1*, 1999, 2963; (*g*) K. Komatsu, K. Fujiwara and Y. Murata, *Chem. Commun*., 2000, 1583; (*h*) K. Komatsu, K. Fujiwara and Y. Murata, *Chem. Lett*., 2000, 1016.
7 The transformation of **1** has been studied in this laboratory and will be reported elsewhere. For the preliminary results, see ref. 4a.
8 J. Knol and J. C. Hummelen, *J. Am. Chem. Soc*., 2000, **122**, 3226.
9 M. J. Frisch, G. W. Trucks, H. B. Schlegel, G. E. Scuseria, M. A. Robb, J. R. Cheeseman, V. G. Zakrzewski, J. A. Montgomery, Jr., R. E. Stratmann, J. C. Burant, S. Dapprich, J. M. Millam, A. D. Daniels, K. N. Kudin, M. C. Strain, O. Farkas, J. Tomasi, V. Barone, M. Cossi, R. Cammi, B. Mennucci, C. Pomelli, C. Adamo, S. Clifford, J. Ochterski, G. A. Petersson, P. Y. Ayala, Q. Cui, K. Morokuma, D. K. Malick, A. D. Rabuck, K. Raghavachari, J. B. Foresman, J. Cioslowski, J. V. Ortiz, A. G. Baboul, B. B. Stefanov, G. Liu, A. Liashenko, P. Piskorz, I. Komaromi, R. Gomperts, R. L. Martin, D. J. Fox, T. Keith, M. A. Al-Laham, C. Y. Peng, A. Nanayakkara, C. Gonzalez, M. Challacombe, P. M. W. Gill, B. Johnson, W. Chen, M. W. Wong, J. L. Andres, C. Gonzalez, M. Head-Gordon, E. S. Replogle and J. A. Pople, *Gaussian 98, Revision A.7*, Gaussian, Inc., Pittsburgh PA, 1998.

CHEMCOMM Communication
www.rsc.org/chemcomm

Chelating alkoxy-N-heterocyclic carbene complexes of silver and copper†

Polly L. Arnold,* Andrew C. Scarisbrick, Alexander J. Blake and Claire Wilson

School of Chemistry, The University of Nottingham, University Park, Nottingham, UK NG7 2RD. E-mail: Polly.Arnold@nott.ac.uk

Received (in Cambridge, UK) 31st August 2001, Accepted 27th September 2001
First published as an Advance Article on the web 22nd October 2001

Incorporation of an alkoxide functional group into an N-heterocyclic carbene (NHC) ligand allows the synthesis of the first anionic NHC chelating ligands, which react to give the first neutral, molecular silver(I) alkoxide carbene complex, and a copper(I) derivative containing the first non-macrocyclic, square planar Cu(I) centres.

The surge in recent research focused on stable N,N′-dialkylated heterocyclic carbenes (NHC) has been fuelled in part by results that show that these strong σ-donor ligands can significantly increase the reactivity of many homogeneous catalysts.[1] The straightforward synthesis of the imidazolium precursors has pushed these phosphine replacements to the forefront of catalyst design.

To date, almost all NHC ligand tuning has involved N-functionalisation with chiral hydrocarbyl groups, or other pendant neutral donor ligands (a second NHC or pyridyl, phosphine, carbonyl or ether groups).[2] These derivatives have been used almost entirely to enhance the catalytic properties of the platinum group metals. Surprisingly, only monodentate NHC 'solvated' adducts of more electropositive metals have been characterised.

We have targeted the first NHC-based chelate ligand that incorporates a hard, anionic functional group, in this case an alkoxide. Despite the calculated strength of the Cu(I)–carbene bond (319 kJ mol^{-1}) and the involvement of the copper carbene fragment in a number of important catalytic processes,[3] remarkably few copper carbene complexes have been reported, and their synthesis is not always trivial.[4] We report herein a one-pot synthesis of the imidazolium precursor to a mixed alkoxide/carbene ligand, and the observation that the combination of the anionic binding site with the NHC provides easy access to stable silver and copper carbene complexes.

Simplicity and atom efficiency is achieved by using functionalised epichlorohydrin as the source of the anionic alkoxide binding site. The combination of an imidazolium and alcohol group has been achieved in two previous instances, but neither targeted a metal–alkoxide product.[5] The zwitterionic diimidazolium salt **1** (the proligand) is accessible as a hygroscopic cream-coloured powder from the one-pot reaction of two equivalents of *N-tert*-butylimidazole with 2-chloromethyl-2-phenyloxirane at 100 °C for 24 h, followed by washing with dry THF, eqn. (1).‡ Recrystallisation from CH_2Cl_2–THF

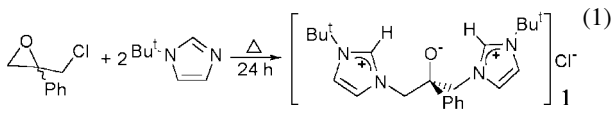

(1)

produces colourless crystals of **1**·HCl·3H_2O, the structure of which, as determined by X-ray crystallography, is shown in Fig. 1.§

Ionic silver NHC adducts, already recognised as valuable transmetallation reagents in NHC chemistry, may be directly

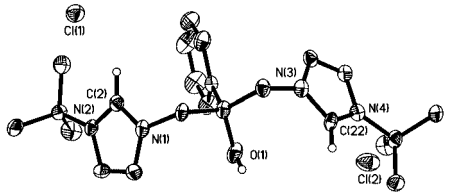

Fig. 1 Ellipsoid plot of the molecular structure of [**1**H]$^+$Cl$^-$, solvent H_2O and peripheral hydrogens omitted for clarity, 30% probability. Selected distances (Å) and angles (°); O1–C10 1.433(8), N–C(2, 22) range 1.301(7) to 1.338(7), N–C(2, 22)–N 109.4(5), 109.1(5).

accessed by treating the imidazolium precursor salt with a basic silver salt such as silver oxide.[6] The diimidazolium **1** is readily deprotonated upon treatment with Ag_2O to afford the neutral silver(I) alkoxide carbene **2** within 4 h at room temperature in dichloromethane, if activated 4 Å molecular sieves are added, Scheme 1.‡ Complex **2** is modestly light and air sensitive ($t_{1/2}$ ~ 12 h for a powdered sample on the bench).

The halide-free, neutral, silver alkoxy-carbene **2** Ag–NHC complex should be an ideal vehicle for the transfer of the alkoxide-functionalised carbene to other metals using the driving force of silver halide precipitation. Noting the failure of copper halides and simple derivatives to react with other ionic Ag–NHC reagents,[4] we looked to copper halides as a suitable test for the transmetallation reactions of **2**.

Accordingly, treatment of a concentrated dichloromethane solution of **2** with one equivalent of copper iodide furnishes a red solution from which, after filtration to remove silver iodide, dark red crystals of the neutral copper alkoxide-carbene **3** may be isolated in 85% yield, see Scheme 1.§ Upon deprotonation, as expected, the chemical shift of the carbenoid C shifts to higher frequency by about 40 ppm, to the characteristic $C_{carbene}$ values of 179 (**2**) and 181 ppm (**3**). It is broadened in **2**, presumably due to coupling to the silver nuclei and non-rigidity in the complex (the ^{1}H NMR spectrum of **2** also shows broadening of the shifts at 300 K).

A single crystal X-ray structure determination of the copper complex **3** shows the dinuclear solid-state structure, Fig. 2, and confirms that the copper centre is co-ordinated by both the alkoxide and two carbene centres.

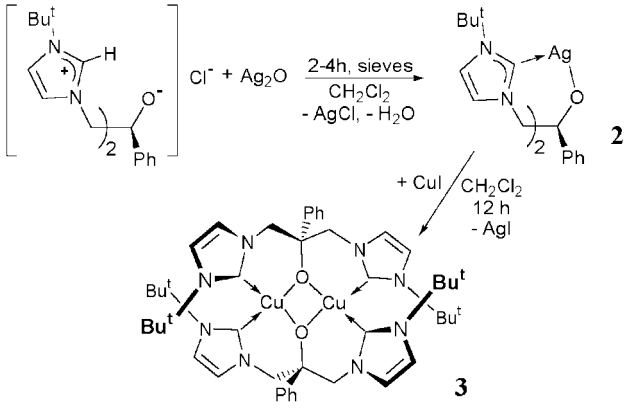

Scheme 1 Synthesis of the copper carbene complex **3**.

† Electronic supplementary information (ESI) available: spectroscopic data for **1**–**3**, cyclic voltammetry. See http://www.rsc.org/suppdata/cc/b1/b107855k/

 DOI: 10.1039/b107855k

The most notable feature in the structure is that the Cu(I) centres exhibit nearly square planar geometry, the angle between the CuO_2 and CuC_2 planes is 14.0(2)°. We can find only two four-co-ordinate Cu(I) complexes in the literature which achieve this degree of planarity. Each is found as one metal of an M_2O_2 core in the centre of a dinucleating compartmental macrocycle; the analogous plane–plane angle in each is 11.9°.[7]

The average Cu–$C_{carbene}$ distance of 1.963(4) Å is at the upper end of the C(sp^3)–Cu(I) bond distance range, confirming the absence of π-character in the bond.[8] In comparison to the imidazolium geometries, each carbene ring displays a lengthened $C_{carbene}$–N bond and narrowed N–$C_{carbene}$–N angle, concomitant with the increase in p character of the N–C bond after deprotonation.[9]

Since the Cu(I)–alkoxide bond is not regarded as particularly stable, it is interesting that this tridentate ligand, which combines hard alkoxide and soft NHC functionalities, is so effective in stabilising the Cu(I) centres, and in such an unexpected geometry. The near planarity of each Cu(I) centre suggests the oxidation to Cu(II) might be accessible. The cyclic voltammogram of a CH_2Cl_2 solution shows two irreversible oxidations at +0.435 and +0.850 V *vs*. Fc^+/Fc, whilst that in acetonitrile shows a quasireversible first oxidation at +0.717 V, and a second irreversible oxidation at 1.06 V *vs*. Fc/Fc^+. The proximity of the *tert*-butyl groups appears not to allow absolute square planarity of a smaller Cu(II) ion, but how the peculiar electronic structure of the carbenes influences the frontier MOs of the complex **3** clearly needs to be addressed.

Importantly, deprotonation of the imidazolium protons in **1** with Ag_2O is completely selective and does not require forcing conditions. The use of silver carbenes instead of free NHCs is becoming increasingly widespread, both as a method to avoid unselective deprotonations of N-functionalised NHCs, and due to the tolerance to air and moisture of both precursors and the silver salts.[10] The synthesis of **2** is driven by precipitation of silver chloride which is readily removed. Thus this neutral silver alkoxycarbene contrasts with previously reported silver–carbene salts (which tend to retain silver halide, forming $[NHCAg]^+[AgHal_2]^-$ ion pairs) and should provide access to a range of alkoxide-supported NHC metal complexes.[10]

To conclude, we have described a one-pot reaction to combine two imidazolium heterocyclic cations with an alkoxide anion. Deprotonated, this forms the first chelating ligand to bind to a metal through an anionic alkoxide bond as well as through the N-heterocyclic carbene group. Structural studies have shown an unusual near-planar conformation for the copper(I) derivative—unprecedented in non-macrocyclic complexes.

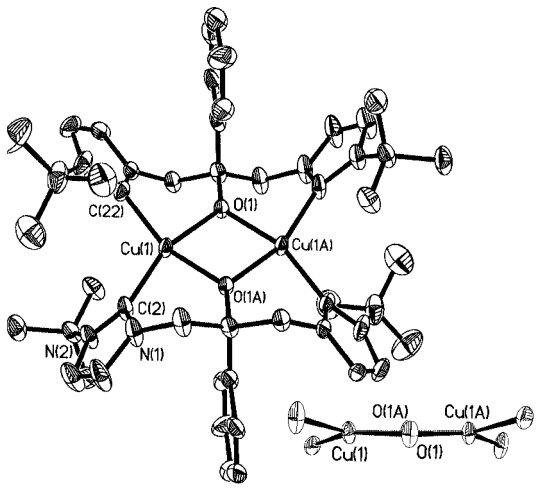

Fig. 2 Ellipsoid plot of the molecular structure of **3**, and side view of the Cu_2 core, 30% probability. Selected distances (Å) and angles (°); Cu–Cu 3.1122(9), Cu–O 1.941(2), 1.959(2), Cu–C(2, 22) 1.960(4), 1.966(4), N–C(2, 22) range 1.349(5) to 1.364(5), Cu–O–Cu 105.88(11), O–Cu–O 74.12(11), O(1A)–Cu–C(2) 87.88(14), O(1)–Cu–C(22) 89.40(15), C(2)–Cu–C(22) 110.27(18), N–C(2, 22)–N 105.0(3), 106.2(4).

We thank the EPSRC National Crystallography Service and Dr E. S. Davies for advice on the cyclic voltammetry experiments.

Notes and references

‡ *Selected data for* **1**: hygroscopic cream-coloured powder, yield 70%, 1.86 g, mp 121–124 °C. δ_H (300 MHz, $CDCl_3$): 9.83 (s, 1H, NCHN), 7.59 (s, 2H, C*H*CH), 7.07 (s, 2H, CHC*H*), 7.55 (m, 5H, Ph), 5.38 (d, 2H, NCH_2), 5.22 (d, 2H, NCH*H*), 1.62 (s, 18H, $C(CH_3)_3$). δ_C (75.5 MHz, $CDCl_3$) 136.8 ($C_{2,22}$H imz). IR (fluorocarbon mull) ν/cm^{-1} 1548(m), 1466(w), 1375(m). MS (ES): *m*/*z* 417 ($[M - Cl]^+$, 59%), 381 ($[M - Cl]^+$, 67%), 325 ($[M - Cl - Bu^t + H]^+$, 25%), 257 ($[M - Cl - Bu^tC_3H_2N_2]^+$, 100%). Anal. Calc. for $C_{23}H_{34}N_4OCl_2{\cdot}2H_2O$: C, 56.44; H, 7.82. Found: C, 56.67; H, 7.59%. *Selected data for* **2**: white powder, yield 61%, 0.255 g. δ_H (300 MHz, $CDCl_3$): 7.45 (d, 2H), 7.31 (t, 1H), 7.26 (d, 2H, Ph), 7.30 (s, 2H), 6.93 (s, 2H, NCH), 4.77 (dd, 4H, NCH_2), 1.56 (s, 18H, $C(CH_3)_3$). δ_C (75.5 MHz, $CDCl_3$) 180.5 (br, $C_{carbene}$). IR (fc mull) ν/cm^{-1} 1568(w), 1446(m), 1410(m), 1370(m). MS (ES): *m*/*z* 487 ($[M]^+$, 2%), 269 ($[M - Bu^t_2(CH)_2Ph]^+$, 100%), 257 ($[Bu^timCH_2PhCOH]^+$, 97%). Anal. Calc. for $C_{23}H_{31}N_4OAg{\cdot}1.7CH_2Cl_2$: C, 46.96; H, 5.49. Found: C, 47.35; H, 5.31%.

Selected data for **3**: dark red crystals, yield 85%, 97 mg. δ_H (300 MHz, CD_2Cl_2): 7.27, 6.91 (br m, 9H, Ph, im), 4.80 (br m, 4H, CH_2), 1.55 (s, 18H, Bu^t). δ_C (75.5 MHz, CD_2Cl_2) 177 (br, $C_{carbene}$). IR (fc mull) ν/cm^{-1} 1562(w), 1446(m), 1384(m). MS (ES): *m*/*z* 443 ($[M]^+$, 98%), 397 ($[M - C_3H_2N_2Bu^t + Ph]^+$, 100%), 257 ($[M - CuC_3H_2N_2Bu^t]^+$, 39%). Anal. Calc. for $C_{23}H_{31}N_4OCu{\cdot}CH_2Cl_2$: C, 54.60; H, 6.30. Found: C, 54.91; H, 6.37%.

§ *Crystal data for* **1**·HCl: $C_{23}H_{34}N_4OCl_2{\cdot}3H_2O$, M = 507.49, monoclinic, space group *Cc* (no. 9), a = 20.5270(6), b = 11.3091(4), c = 13.0364(4) Å, β = 110.933(2)°, U = 2826.6(2) Å^3, T = 150(2) K, Z = 4, D_c = 1.193 g cm^{-3}, μ(Mo-Kα) = 0.262 mm^{-1}, 10342 unique reflections (R_{int} 0.043) used in all calculations. Final R_1 [4294 $F > 4\sigma(F)$] = 0.0747 and *wR* (all F^2) was 0.216. *Crystal data for* **3**: $C_{46}H_{62}N_8O_2Cu_2$, M = 886.12, monoclinic, space group *C*2/*c* (no. 15), a = 21.330(2), b = 12.2341(13), c = 25.177(3) Å, β = 112.38(2)°, U = 6075(2) Å^3, T = 150(2) K, Z = 4, D_c = 0.969 g cm^{-3}, μ(Mo-Kα) = 0.734 mm^{-1}, 5347 unique reflections (R_{int} 0.036) used in all calculations. Final R_1 [3738 $F > 4\sigma(F)$] = 0.0594 and *wR* (all F^2) was 0.156. CCDC reference numbers 169965 and 169966. See http://www.rsc.org/suppdata/cc/b1/b107855k/ for crystallographic data in CIF or other electronic format.

1 σ-bonding: J. C. Green, R. G. Scurr, P. L. Arnold and F. G. N. Cloke, *Chem. Commun*., 1997, 1963; recent reviews: W. A. Herrmann and C. Kocher, *Angew. Chem., Int. Ed. Engl*., 1997, **36**, 2163; L. T. Li and S. M. Ma, *Chin. J. Org. Chem*., 2001, **21**, 75.

2 S. Lee and J. F. Hartwig, *J. Org. Chem*., 2001, **66**, 3402; W. A. Herrmann, C. P. Reisinger and M. Spiegler, *J. Organomet. Chem*., 1998, **557**, 93; R. E. Douthwaite, M. L. H. Green, P. J. Silcock and P. T. Gomes, *Organometallics*, 2001, **20**, 2611; A. A. D. Tulloch, A. A. Danopoulos, G. J. Tizzard, S. J. Coles, M. B. Hursthouse, R. S. Hay-Motherwell and W. B. Motherwell, *Chem. Commun*., 2001, 1270; A. M. Magill, D. S. McGuinness, K. J. Cavell, G. J. P. Britovsek, V. C. Gibson, A. J. P. White, D. J. Williams, A. H. White and B. W. Skelton, *J. Organomet. Chem*., 2001, **617**, 546; H. F. Lang, J. J. Vittal and P. H. Leung, *J. Chem. Soc., Dalton Trans*., 1998, 2109.

3 C. Boehme and G. Frenking, *Organometallics*, 1998, **17**, 5801; M. P. Doyle and D. C. Forbes, *Chem. Rev*., 1998, **98**, 911; M. Buhl, F. Terstegen, F. Loffler, B. Meynhardt, S. Kierse, M. Muller, C. Nathe and U. Luning, *Eur. J. Org. Chem*., 2001, 2151; B. F. Straub and P. Hofmann, *Angew. Chem., Int. Ed*., 2001, **40**, 1288.

4 A. J. Arduengo, H. V. R. Dias, J. C. Calabrese and F. Davidson, *Organometallics*, 1993, **12**, 3405; A. A. D. Tulloch, A. A. Danopoulos, S. Kleinhenz, M. E. Light, M. B. Hursthouse and G. Eastham, *Organometallics*, 2001, **20**, 2027.

5 J. Schwarz, V. P. W. Bohm, M. G. Gardiner, M. Grosche, W. A. Herrmann, W. Hieringer and G. Raudaschl-Sieber, *Chem. Eur. J*., 2000, **6**, 1773; H. Glas, E. Herdtweck, M. Spiegler, A. K. Pleier and W. R. Thiel, *J. Organomet. Chem*., 2001, **626**, 100.

6 H. M. J. Wang and I. J. B. Lin, *Organometallics*, 1998, **17**, 972.

7 R. R. Gagne, L. M. Henling and T. J. Kistenmacher, *Inorg. Chem*., 1980, **19**, 1226; M. Shinoura, S. Kita, M. Ohba, H. Okawa, H. Furutachi and M. Suzuki, *Inorg. Chem*., 2000, **39**, 4520.

8 A Cu–C_{sp^3} single bond distance (1.90–1.96 Å) is expected if the carbene binds through a pure σ-lone pair. The three structurally characterised Cu–NHC complexes have shorter Cu–$C_{carbene}$ distances.

9 A. J. Arduengo, *Acc. Chem. Res*., 1999, **32**, 913.

10 A. A. D. Tulloch, A. A. Danopoulos, S. Winston, S. Kleinhenz and G. Eastham, *J. Chem. Soc., Dalton Trans*., 2000, 4499; D. J. Nielsen, K. J. Cavell, B. W. Skelton and A. H. White, *Organometallics*, 2001, **20**, 995.

CHEMCOMM Communication
www.rsc.org/chemcomm

Intercalation and controlled release of pharmaceutically active compounds from a layered double hydroxide†

Aamir I. Khan, Lixu Lei, Alexander J. Norquist and Dermot O'Hare*

Inorganic Chemistry Laboratory, South Parks Road, Oxford, UK OX1 3QR. E-mail: dermot.ohare@chem.ox.ac.uk

Received (in Cambridge, UK) 20th July 2001, Accepted 10th October 2001
First published as an Advance Article on the web 19th October 2001

A series of pharmaceutically active compounds including diclofenac, gemfibrozil, ibuprofen, naproxen, 2-propylpentanoic acid, 4-biphenylacetic acid and tolfenamic acid can be reversibly intercalated into a layered double hydroxide, initial studies suggest that these materials may have application as the basis of a novel tuneable drug delivery system.

In order for drug therapy to be most effective the desired pharmacological response must be obtained at the target without harmful interactions at other sites.[1] This requires the correct amount of drug to be absorbed into the body and transported to the target with control of the drug rate input in order to produce the correct dosage. Ideally the delivery of the drug to other tissues should be minimised or prevented, however this is rarely achieved owing to the complex nature of these processes.[2] Modern controlled release systems are usually polymer based with mechanisms of release regulated by diffusion, bioerosion, degradation and swelling or the production of osmotic pressure. Exposing the polymer–drug mixture to the gastrointestinal fluid results in the diffusion of the drug from the tablet or capsule and the polymers are excreted. Certain polymer–drug complexes undergo bio-erosion or degradation when they pass through the gastrointestinal tract. Swelling or the generation of osmotic pressure occurs with other polymer–drug formulations upon contact with gastrointestinal fluid resulting in the release or expulsion of the drug.[3]

Controlled release systems have many advantages but also have disadvantages. The main advantage is the decreased fluctuation in drug concentration resulting in reduced toxicity. In addition, the reduction in the number of doses may lead to lower patient care time and also to the use of a smaller amount of drug. However, disadvantages include the increased amount of time required to achieve therapeutic blood concentrations, dose dumping and usually an increase in the cost.[3] Not all drugs are suitable for controlled release systems—those not suitable are drugs with very short or very long half lives, poor absorption through the gastrointestinal tract and low solubility.[4] Controlled release systems are most useful for drugs that are taken on an extended basis such as drugs used to treat cardiovascular disorders and arthritis. Layered double hydroxides (LDHs) represented by the general formula $[M^{II}_{(1-x)}M^{III}_{x}(OH)_2]$-$[A^{n-}_{x/n}]\cdot zH_2O$ or $[M^{I}M^{III}_2(OH)_6][A^{n-}_{1/n}]\cdot zH_2O$, where M^{I}, M^{II} and M^{III} are mono-, di- and tri-valent metal cations, respectively, are now well established as excellent anion-exchange materials and their extensive intercalation chemistry has widespread applications in areas such as heterogeneous catalysis,[5,6] optical materials,[7,8] biomimetic catalysis,[9,10] separation science[11,12] and as DNA reservoirs.[13,14]

Here we report the reversible intercalation of a number of active cardiovascular and anti-inflammatory agents into a layered double hydroxide and the results of an initial study into the use of these drug–inorganic hybrid materials as a novel tuneable drug delivery system.

As a number of well known cardiovascular, anti-inflammatory and analgesic agents are either carboxylic acids or carboxylic derivatives we were interested in investigating whether these compounds could be ion-exchange intercalated in a layered double hydroxide. $[LiAl_2(OH)_6]Cl\cdot H_2O$ reacts with 2 equivalents of either the sodium salts of diclofenac, gemfibrozil, ibuprofen, naproxen, 2-propylpentanoic acid, 4-biphenylacetic acid or tolfenamic acid (Table 1) in H_2O at 60 °C for 1–2 h to give a LDH–drug intercalation compound. The solid products are isolated by filtration and then washed with an excess of deionised water and then acetone. In each case full anion exchange of the interlayer Cl^- anions and intercalation of these pharmaceutically active compounds has taken place. In each case the products are first stage intercalation compounds and they have all been fully characterised using X-ray powder diffraction (XRD), elemental microanalysis, IR spectroscopy and thermogravimetric analysis. The observed interlayer spacings for the drug–LDH intercalates are shown in Table 1, the values are consistent with the formation of bilayer arrangement for all the drug molecules with the positively charged $[LiAl_2(OH)_6]^+$ layers of the host lattice. In all cases the intercalated anions can be quantitatively recovered from the host lattice by treatment of the intercalates with either an aqueous solution of M_2CO_3 (M = Na or Li) or addition of dilute HCl. In the case of treatment with an alkali metal carbonate, the alkali metal salt of the organic guest ions goes into solution and

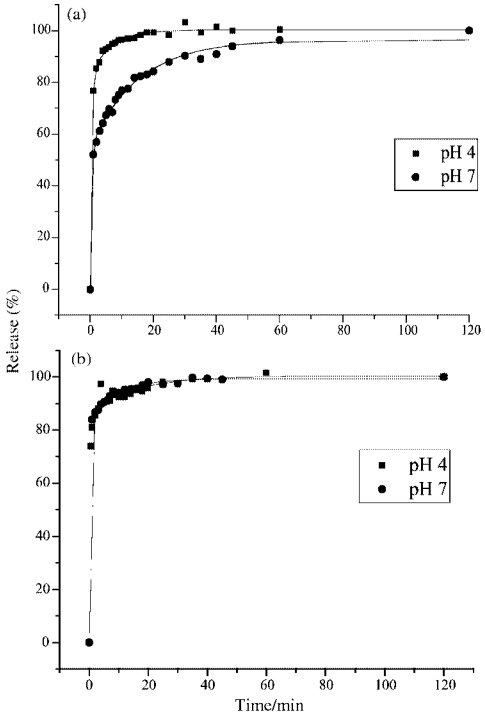

Fig. 1 Release profiles for (a) diclofenac at pH 4 and pH 7 and (b) gemfibrozil at pH 4 and pH 7.

† Electronic supplementary information (ESI) available: Fig. S1: X-ray diffraction patterns of (a) $[LiAl_2(OH)_6]Cl\cdot H_2O$ and (b) LDH/Ibuprofen intercalate. See http://www.rsc.org/suppdata/cc/b1/b106465g/

 DOI: 10.1039/b106465g

Table 1 Summary of the guest molecule used and the analytical and structural data of the LDH–drug intercalation compounds

Guest	Molecular structure of guest[a]	Interlayer spacing/Å[b]	Elemental analysis: found (calc.)[c]
4-Biphenylacetic acid ($C_{14}H_{12}O_2$)	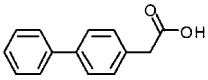	20.4	C, 30.77 (30.77); H, 5.16 (5.20); $x = 0.58$, $y = 2$
Diclofenac ($C_{14}H_{10}Cl_2NaNO_2$)	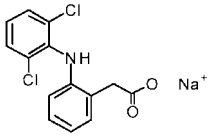	22.3	C, 30.91 (30.92); H, 4.12 (3.91); N, 2.60 (2.58); $x = 0.72$, $y = 1$
Gemfibrozil ($C_{15}H_{22}O_3$)	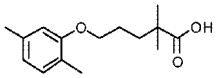	23.2	C, 35.35 (35.36); H, 6.56 (6.65); $x = 0.69$, $y = 1$
Ibuprofen ($C_{13}H_{18}O_2$)	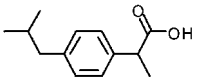	22.7	C, 31.92 (31.98); H, 6.15 (5.99); $x = 0.75$, $y = 3$
Naproxen ($C_{14}H_{14}O_3$)	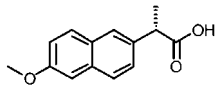	21.5	C, 27.91 (28.08); H, 4.98 (4.99); $x = 0.48$, $y = 1$
2-Propylpentanoic acid ($C_8H_{16}O_2$)		18.7	C, 14.78 (14.82); H, 5.77 (6.04); $x = 0.35$, $y = 1$
Tolfenamic acid ($C_{14}H_{12}ClNO_2$)	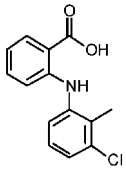	21.9	C, 23.24 (23.18); H, 5.25 (5.29); N, 1.90 (1.93); $x = 0.46$, $y = 3$

[a] Neutral guest molecules were converted to the sodium salt prior to intercalation. [b] Based on hexagonal cell: $\alpha = \beta = 90$, $\gamma = 120°$, $a = b = 5.1$ Å and $c = 2 \times d_{(002)}$ [c] Based on the general formula $Li_xAl_2(OH)_6[drug]_x \cdot yH_2O$

the solid phase is quantitatively converted to $[LiAl_2(OH)_6](CO_3)_{0.5}\cdot H_2O$ as indicated by the XRD data which shows a series of 00*l* reflections corresponding to an interlayer spacing of 7.51 Å. Addition of dilute aqueous HCl solution to the LDH–drug complex results in dissolution of the inorganic host and precipitation of the neutral form of the guest acid.

Given that these ions could be recovered intact from the LDH host we were interested to see if this could form the basis of a drug reservoir and controlled release system. Therefore, we performed a series of experiments in order to quantitatively monitor the kinetics of release of the guest ions under conditions which would resemble physiological conditions. Deintercalation of the drugs from the LDH was performed by the addition of the drug–LDH complex to 250 ml of phosphate buffer solution at 37 °C of pH 7 or pH 4. A mass of 0.025 g of the LDH–drug complex was used for 4-biphenylacetic acid, diclofenac and tolfenamic acid and a larger amount of 0.1 g for naproxen and gemfibrozil. Aliquots were removed from the reaction mixture at regular intervals and solution UV–Vis absorption spectroscopy was used to quantify the concentration of the de-intercalated ions in the aqueous phase. Fig. 1 shows release profile plots for the deintercalation of diclofenac and of gemfibrozil on addition of phosphate buffer at pH 4 and pH 7. At pH 4 the measured release of diclofenac and gemfibrozil is very fast with almost full deintercalation observed in less than 10 min. Surprisingly, the release curve for gemfibrozil at pH 7 is almost identical to the profile recorded at pH 4. At pH 7 the release of diclofenac is much slower and only after 28 min is 90% of the drug released into solution. Table 2 is a summary of the release profiles for all the different guest ions that we have intercalated in $[LiAl_2(OH)_6]Cl\cdot H_2O$.

In summary, the results show that the intercalation of pharmaceutically active compounds that form stable anions is a feasible approach for the storage then subsequent controlled release of bioactive agents. We anticipate that there will be tremendous scope for fine tuning the intercalation and de-intercalation kinetics in these materials by employing different LDHs with differing charge densities and basicities.

Table 2 Release profile data

	Release times/min[a]			
	pH 4		pH 7	
Guest molecules	t_{50}[b]	t_{90}[b]	t_{50}[b]	t_{90}[b]
Diclofenac (λ_{max} = 279 nm)	1	4	1	28
Naproxen (λ_{max} = 317, 330 nm)	1	9	1	17
Gemfibrozil (λ_{max} = 275 nm)	1	5	1	5
Tolfenamic acid (λ_{max} = 290 nm)	1	21	1	23
4-Biphenylacetic acid (λ_{max} = 290 nm)	1	2	1	35

[a] Release (%) = $(I_t/I_{max}) \times 100$, at λ_{max}. [b] t_{50} and t_{90} are the times for 50 and 90% release, respectively.

Notes and references

1 C. R. Gardner, *Biomaterials*, 1985, **6**, 153.
2 L. F. Prescott, *Novel Drug Delivery*, 1989, 1.
3 V. V. Ranade, *J. Clin. Pharm.*, 1991, **31**, 2.
4 J. E. Shaw, *Annu. Rep. Med. Chem.*, 1980, **15**, 302.
5 V. R. L. Constantino and T. J. Pinnavaia, *Catal. Lett.*, 1994, **23**, 361.
6 A. Corma, V. Fornes, F. Rey, A. Cervilla, E. Llopis and A. Ribera, *J. Catal.*, 1995, **152**, 237.
7 M. Ogawa and K. Kuroda, *Chem. Rev.*, 1995, **95**, 399.
8 H. Tagaya, S. Sato, T. Kuwahara, J. Kadokawa, K. Masa and K. Chiba, *J. Mater. Chem.*, 1994, **4**, 1907.
9 B. Sels, D. De Vos, M. Buntinx, F. Pierard, A. Kirsch-De Mesmaeker and P. Jacobs, *Nature*, 1999, **400**, 855.
10 L. Ukrainczyk, M. Chibwe, T. J. Pinnavaia and S. A. Boyd, *Environ. Sci. Technol.*, 1995, **29**, 439.
11 A. M. Fogg, V. M. Green, H. G. Harvey and D. O'Hare, *Adv. Mater.*, 1999, **11**, 1466.
12 A. M. Fogg, J. S. Dunn, S. G. Shyu, D. R. Cary and D. O'Hare, *Chem. Mater.*, 1998, **10**, 351.
13 J. H. Choy, S. Y. Kwak, Y. J. Jeong and J. S. Park, *Angew. Chem., Int. Ed.*, 2000, **39**, 4042.
14 J. H. Choy, J. S. Park, S. Y. Kwak, Y. J. Jeong and Y. S. Han, *Mol. Cryst. Liq. Cryst. Sci. Technol., Sect. A*, 2000, **341**, 425.

CHEMCOMM Communication
www.rsc.org/chemcomm

Unusual electronic absorption changes in the 800–2200 nm region by intramolecular dimer radical cations from photoirradiated *meso*-2,4-bis[4-(4′-nitrostyryl)pyridinium]pentane ditetraphenylborates during storage in the dark

Sang Hyun Park[a] and Toshihiko Nagamura*[b]

[a] *Department of Electronic Materials Science, The Graduate School of Electronic Science and Technology, Shizuoka University, 3-5-1 Johoku, Hamamatsu 432-8011, Japan*
[b] *Molecular Photonics Laboratory, Research Institute of Electronics, Shizuoka University, 3-5-1 Johoku, Hamamatsu 432-8011, Japan*

Received (in Cambridge, UK) 23rd August 2001, Accepted 8th October 2001
First published as an Advance Article on the web 26th October 2001

Electronic absorption spectra were remarkably changed in the broad near-infrared region for photoirradiated *meso*-2,4-bis[4-(4′-nitrostyryl)pyridinium]pentane ditetraphenylborates during storage in the dark, which was attributed to conformational changes of the intramolecular dimer radical cations between sandwich and partially overlapped types.

We have been studying absorption spectra changes in the visible and near-infrared (NIR) regions due to photoinduced electron transfer.[1–12] We reported, for the first time, a charge resonance (CR) band as a broad absorption with a peak in the NIR region upon steady photolysis of 4-substituted styrylpyridinium tetraphenylborate (TPB^-) in organic solutions at rt as a result of electronic interaction between a photogenerated styrylpyridinyl radical and a parent styrylpyridinium cation.[4] The CR band characterized by its absorption spectrum in the NIR region had been known for dimer radical cations only between the neutral aromatic compound and its oxidized form as a transient species or a stable one at near 77 K, until we reported the CR band between a substituted styrylpyridinium cation and its photoreduced form.

The peak wavelength of the CR band corresponding to twice the stabilization energy of dimer radical cations is affected by many factors such as the extent of overlapping of two chromophores, the conformation, or the electronic distribution. Intramolecular dimer radical cations are especially interesting since it is possible to control the CR band by the structure of the connecting unit. The intramolecular dimer radical cation is one of the promising candidates for materials with large refractive index and/or absorption changes in the 1300–1600 nm region together with fast responses, which are greatly needed for near future all-optical data processing.

Recently we reported the formation of intramolecular dimer radical cations in 1,3-bis[4-(4′-nitrostyryl)pyridinium]propane ditetraphenylborates (SPPr).[7] Two types of intramolecular CR bands, sandwich and partially overlapped, were observed in SPPr upon steady photolysis. Two chromophores connected by a trimethylene bridge in SPPr showed much more efficient intramolecular CR interactions compared with those having shorter or longer alkyl bridges, *e.g.*, ethane, butane and hexadecane.[7,9] A shift of the peak wavelength was observed from 1742 to 1505 nm in 3 h after steady photolysis of SPPr, although the absorbance at each wavelength was very weak.[7] Yamamoto *et al.* studied the intramolecular CR band for several chromophores linked with a tri-methylene chain in organic solutions at rt by ns laser photolysis.[13–17] They observed sandwich and partially-overlapped dimer radical cations for carbazole, pyrene, naphthalene, anthracene and phenanthrene as transient species with lifetimes of a few ms. Peak wavelengths of the intramolecular CR band observed in these measurements are between 1050 and about 2000 nm depending on chromophores and the type of overlapping.[13–17] No shift of the CR band was, however, observed after flash photolysis to indicate any change in conformation or overlapping of the two chromophores.

We now report unusual absorption changes in 800–2200 nm due to the intramolecular CR band of styrylpyridinyl radicals, formed by steady photolysis of newly synthesized *meso*-2,4-bis[4-(4′-nitrostyryl)pyridinium]pentane ditetraphenylborates (*m*-SPPe), during storage in the dark in solutions at rt, clearly indicating a change in conformation and overlapping of the two chromophores in dimer radical cations.

Synthesis of tetraphenylborate (TPB^-) salts of *m*-SPPe will be published elsewhere. The purity was confirmed by 300 MHz NMR and HPLC. Absorption spectra were recorded on a Hitachi U-3500 spectrophotometer upon irradiation *in vacuo* by a Hamamatsu 150 W Hg-Xe lamp through a band pass filter (λ_{ex} = 405 nm) at rt. All absorption spectra reported were the difference between those after and before irradiation. Fig. 1 shows absorption spectra just after irradiation of *m*-SPPe in acetonitrile (ACN) at room temperature. The visible absorption band was assigned to styrylpyridinyl radical formation[3–8] by photoinduced electron transfer from TPB^- which is known to be decomposed after oxidation.[4,10,11] Two bands at 920 and 1734 nm in the NIR region were attributed to a sandwich form and a partially overlapped one of intramolecular dimer radical cations, respectively, in comparison with those observed in SPPr[7] and from the fact that both of them disappeared upon introduction of air. Two chromophores in the sandwich form I and II as shown in Fig. 2 can interact with each other to give the CR band at 920 nm. An example of the partially overlapped form is shown in Fig. 2 III, which will give the CR band at 1734

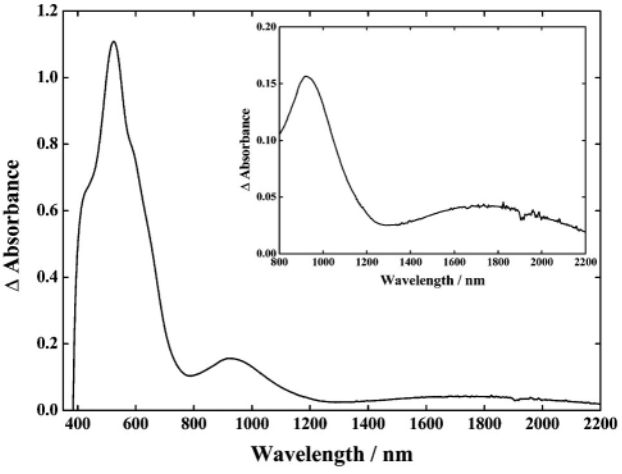

Fig. 1 Difference absorption spectra in 400–2200 nm region after irradiating *m*-SPPe in ACN solution (0.25 mM) through a band pass filter (405 nm) for 4 min. The inset shows the enlarged spectra in the 800–2200 nm region.

 DOI: 10.1039/b107504g

nm with a lower stabilization energy (34.4 kJ mol^{-1}) than the sandwich form (64.8 kJ mol^{-1}). The overlap of π-orbitals of both chromophores at the trimethylene bridge is maximized, and known as Hirayama's rule.[18] The CR bands of *m*-SPPe are stronger by a factor of 1.3 at 920 nm and of 2.1 at 1734 nm as compared with those of SPPr studied under the same conditions.[7] These results clearly indicate that two additional methyl groups in *m*-SPPe contributed to the conformational confinement of both sandwich-type and partially overlapped intramolecular dimer radical cations formed just after irradiation.

Very interestingly, the absorption spectra of *m*-SPPe irradiated for 4 min changed dramatically during storage in the dark at rt as shown in Fig. 3. The strong band at 920 nm decayed monotonically and a very broad band with a peak at 1559 nm and a shoulder at 1300 nm appeared concomitantly. The less stabilized partially overlapped dimer radical cation with a peak at 1734 nm, which is most probably caused by the excess energy in photoreaction products, also seemed to shift to 1559 nm at the initial stage of storage in the dark. The absorbance of the new band increased gradually until 20 h at the expense mostly of the band at 920 nm with an isosbestic point at 1060 nm for spectra **b–d**. Then it decayed very slowly in the dark due to radical reactions, surviving even after 100 h as shown in Fig. 3 (**e**). The maximum absorbance of the newly observed CR band at 1559 nm was about 4.5 times larger than that at 1734 nm and exceeded even the initial absorbance of the sandwich form at 920 nm. This broad band with a peak at 1559 nm can be assigned to thermodynamically stabilized partially overlapped dimer radical cations which were formed from both the non-thermalized partially overlapped one and from the sandwich-type formed just after photoinduced electron transfer. Such change from the sandwich-type to the partially overlapped is most probably due to electronic repulsion. These changes in the NIR region during storage in the dark showed strong temperature dependences. No changes were observed below 15 °C, most probably because of a high energy barrier. Similar spectral changes were observed in SPPr, but absorbance of the new band at 1505 nm was smaller, about 80%, than the band at 1742 nm and was less than a half of the sandwich form.[7] The lifetime of the new band in SPPr was much shorter.[7] These results confirmed again the remarkable effect of two methyl groups at the 2- and 4-positions of *m*-SPPe on the conformational confinement of two chromophores forming dimer radical cations.

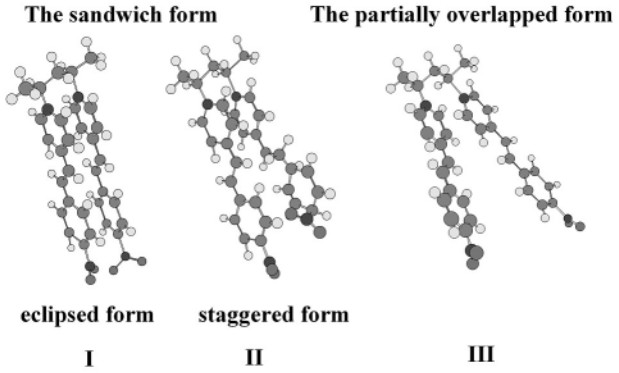

Fig. 2 Proposed models of the sandwich (I and II) and partially overlapped (III) forms of imtramolecular dimer radical cations in *m*-SPPe.

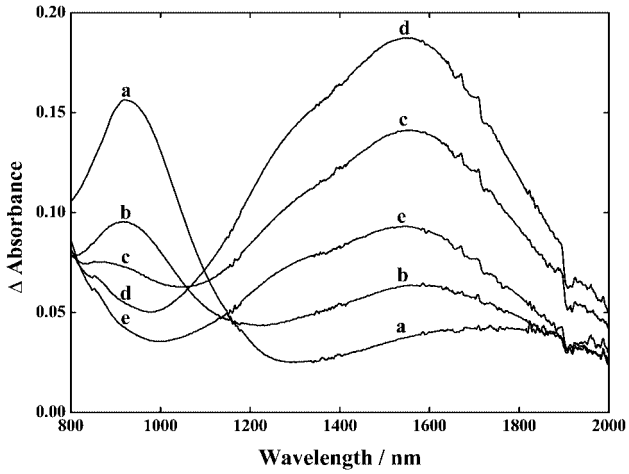

Fig. 3 Difference absorption spectra changes in 800–2000 nm region of *m*-SPPe irradiated for 4 min. (**a**) Just after irradiation, (**b–e**) after storing in the dark for (**b**) 2 h, (**c**) 6 h, (**d**) 20 h, and (**e**) 100 h.

Unusual spectral changes in the NIR region were reproducible in successive cycles of photoexcitation at least several times, because each photoreaction was limited to only a small conversion of less than 10%. The change of a counter ion from TPB$^-$ to bromide, which shows reversible transient electron transfer, will give a totally reversible system upon pulsed laser excitation.

In conclusion, we have achieved unusual absorption changes in the broad NIR region, which finally gave an absorption with a peak at 1559 nm, by newly synthesized *m*-SPPe during storage in the dark at rt. Two methyl groups at the 2- and 4-positions of *m*-SPPe greatly contributed to the conformational confinement of two chromophores in the intramolecular dimer radical cation between a photogenerated styrylpyridinyl radical and a parent styrylpyridinium cation. The absorbance and stability of the CR band were remarkably increased as compared with the 1,3-propane derivative. Such strong absorption change in the NIR region can be used to control the complex refractive index in the molecular photonic device proposed by us[19–23] at the wavelength compatible with the present light communication.

This work was partly supported by the Grant-in-Aid for Scientific Research on Priority Areas 'Molecular Synchronization for Design of New Materials System' (No. 11167242, 13022230) from the Ministry of Education, Science, Sports and Culture, Japan.

Notes and references

1 T. Nagamura and K. Sakai, *J. Chem. Soc., Chem. Commun.*, 1986, 810.
2 T. Nagamura, *Pure Appl. Chem.*, 1996, **68**[7], 1449.
3 H. Inoue, H. Sakaguchi and T. Nagamura, *Appl. Phys. Lett.*, 1998, **73**, 10.
4 T. Nagamura, A. Tanaka, H. Kawai and H. Sakaguchi, *J. Chem. Soc., Chem. Commun.*, 1993, 599.
5 T. Nagamura, T. Ichihara and H. Kawai, *J. Phys. Chem.*, 1996, **100**, 9370.
6 H. Kawai and T. Nagamura, *J. Chem. Soc., Faraday Trans.*, 1998, **94**, 167.
7 T. Nagamura, S. Kashihara and H. Kawai, *Chem. Phys. Lett.*, 1998, **294**, 167.
8 H. Kawai and T. Nagamura, *Mol. Cryst. Liq. Cryst.*, 2000, **344**, 209.
9 S. H. Park, H. Kawai and T. Nagamura, *J. Photopolym. Sci. Technol.*, 2000, **13(2)**, 197.
10 W. S. Xia, H. Kawai and T. Nagamura, *J. Photochem. Photobiol. A.*, 2000, **136**, 35.
11 S. H. Park and T. Nagamura, *J. Photopolym. Sci. Technol.*, 2001, **14**(2), 227.
12 S. H. Park and T. Nagamura, *Mol. Cryst. Liq. Cryst.*, in press.
13 M. Yamamoto, Y. Tsujii and A. Tsuchida, *Chem. Phys. Lett.*, 1989, **154**, 559.
14 A. Tsuchida, T. Ikawa, M. Yamamoto, A. Ishida and S. Takamuku, *J. Phys. Chem.*, 1995, **99**, 14 793, and references cited therein.
15 A. Tsuchida, Y. Tsujii, S. Ito, M. Yamamoto and Y. Wada, *J. Phys. Chem.*, 1989, **93**, 1244.
16 Y. Tsujii, A. Tsuchida, S. Ito and M. Yamamoto, *Macromolecules*, 1991, **24**, 4061.
17 A. Tsuchida, H. Takamura, M. Yamamoto, B. Lee, T. Ikeda and S. Tazuke, *Bull. Chem. Soc. Jpn.*, 1992, **65**, 909.
18 F. Hirayama, *J. Chem. Phys.*, 1965, **42**, 3163.
19 T. Nagamura and T. Hamada, *Appl. Phys. Lett.*, 1996, **69**, 1191.
20 K. Sasaki and T. Nagamura, *Appl. Phys. Lett.*, 1997, **71**, 434.
21 K. Sasaki and T. Nagamura, *J. Appl. Phys.*, 1998, **83**, 2894.
22 T. Nagamura and K. Sasaki, *Mol. Cryst. Liq. Cryst.*, 2000, **344**, 199.
23 T. Nagamura, T. Adachi, I. Yoshida, H. Inoue, H. Heckmann and M. Hanack, *Mol. Cryst. Liq. Cryst.*, in press.

CHEMCOMM
Communication
www.rsc.org/chemcomm

$Cu_4\{CH_3C(OH)(PO_3)_2\}_2(C_4H_4N_2)(H_2O)_4$: a novel, three-dimensional copper diphosphonate with metamagnetism†

Ping Yin,[a] Li-Min Zheng,*[a] Song Gao[b] and Xin-Quan Xin[a]

[a] *State Key Laboratory of Coordination Chemistry, Coordination Chemistry Institute, Nanjing University, Nanjing 210093, P. R. China. E-mail: lmzheng@netra.nju.edu.cn*

[b] *State Key Laboratory of Rare Earth Materials and Applications, College of Chemistry and Molecular Engineering, Peking University, Beijing 100871, P. R. China*

Received (in Cambridge, UK) 26th July 2001, Accepted 4th October 2001
First published as an Advance Article on the web 26th October 2001

A novel, three-dimensional copper diphosphonate $Cu_4\{CH_3C(OH)(PO_3)_2\}_2(C_4H_4N_2)(H_2O)_4$ (1) incorporating an organic pyrazine ligand has been hydrothermally synthesized, which exhibits antiferromagnetic ordering below 4.2 K and metamagnetic behavior.

Continuous attention has been paid to the porous materials based on metal phosphonates owing to their potential applications in exchange, sorption and catalysis, *etc*.[1] Several approaches, including the direct reaction between metal ions and suitable mono- or di-phosphonic acids[2–6] and the reaction through template influences,[7,8] have been employed to explore novel phosphonate compounds with porous or open framework structures. The approach using a second ligand, either inorganic or organic, however, has not been well documented. Only a few zirconium phosphonates have been prepared by introducing small anions of phosphate (PO_4^{3-}) or phosphite (HPO_3^{2-}) into the inorganic layers and thus creating large pore sizes.[9,10] A vanadium copper phosphonate containing a terminal organic ligand (2,2′-bipyridine) has also been reported recently.[11] Based on 1-hydroxyethylidenediphosphonate [$CH_3C(OH)(PO_3)_2^{4-}$, $hedp^{4-}$] and a pyrazine (pz) bridging ligand, herein we describe the synthesis and crystal structure of a novel copper phosphonate compound $Cu_4\{CH_3C(OH)(PO_3)_2\}_2(C_4H_4N_2)(H_2O)_4$ (**1**) with an open framework structure. The magnetic properties of this compound have been investigated.

The hydrothermal reaction of $Cu(NO_3)_2$, 50% $hedpH_4$, pyrazine, NaOH and H_2O in a molar ratio of 1:1.3:1:4:444 (pH ≈ 3) at 140 °C for 48 h afforded blue, needle-like crystals of **1** as a single phase. Thermal analysis showed a one-step weight loss (9.3%) below 230 °C, corresponding to the removal of four water molecules (calc. 8.9%). Single crystal structural determinations‡ reveals a three-dimensional open framework structure composed of $\{Cu_4(hedp)_2(H_2O)_2\}_n$ layers connected by pyrazine bridges (Fig. 1). The copper(II) phosphonate layer consists of $\{Cu_3(hedp)_2(H_2O)_2\}$ double chains linked by $\{CuO_4\}$ units (Fig. 2). Within the double chain, two types of Cu atoms are found. The Cu(1) atom, sitting on an inversion center, is chelated by two equivalent $hedp^{4-}$ groups using two of its six phosphonate oxygens [O(1) and O(4)]. Each $hedp^{4-}$ group behaves as a bis(chelating) ligand to bridge Cu(1) and Cu(2) atoms, forming $\{Cu_3(hedp)_2\}$ trimer units. The neighboring trimers are fused together by the coordination of the phosphonate oxygen O(3) to the equivalent Cu(2) atom, hence forming an infinite chain along the [100] direction with a ladder-like motif. The chain is reminiscent of that observed in $(NH_4)_2Cu_3(hedp)_2(H_2O)_4$.[12] These chains are connected through $\{Cu(3)O_4\}$ units by sharing the remaining phosphonate oxygen [O(6)] of hedp. The remaining two sites of $\{Cu(3)O_4\}$ are filled with two water molecules. The Cu(3) atom sits on an inversion center. Consequently, a two-dimensional network structure of copper phosphonate is constructed with zigzag fluctuation in the *ab* plane (Fig. 2). The layers are linked by pyrazine bridging ligands, leading to a three-dimensional open framework structure (Fig. 1). All the Cu–O and Cu–N bond lengths are normal, although the Cu(2)–O(1w) distance is longer than usual [Cu(2)–O(1w) 2.368 Å].

The temperature dependent molar magnetic susceptibilities of **1** are shown in Fig. 3. The observed $\chi_M T$ value per Cu_4 unit at 280 K is 1.8 cm^3 K mol^{-1}, slightly higher than the value of

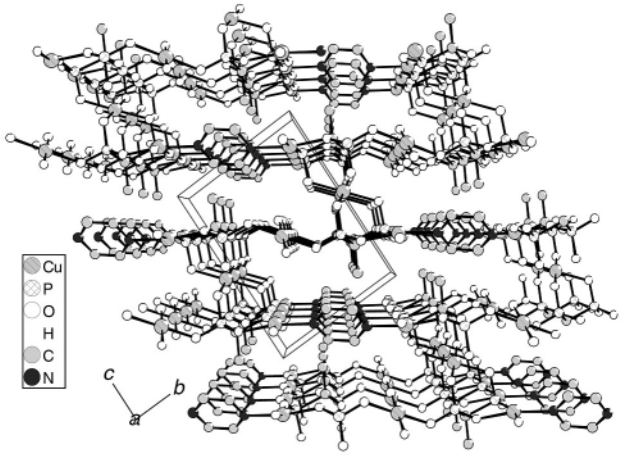

Fig. 1 Structure **1** viewed along the *a*-axis.

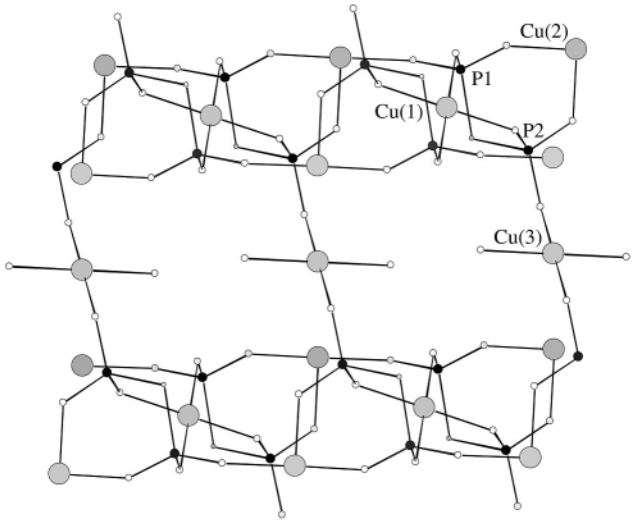

Fig. 2 One layer of copper phosphonate in structure **1**. For clarity, the atoms are shown with arbitrary radii and the C2, O7 and all H atoms are omitted.

† Electronic supplementary information (ESI) available: views of structure **1**, temperature dependence of ac magnetic susceptibility and field dependence of magnetization of **1**. See http://www.rsc.org/suppdata/cc/b1/b106780j/

 DOI: 10.1039/b106780j

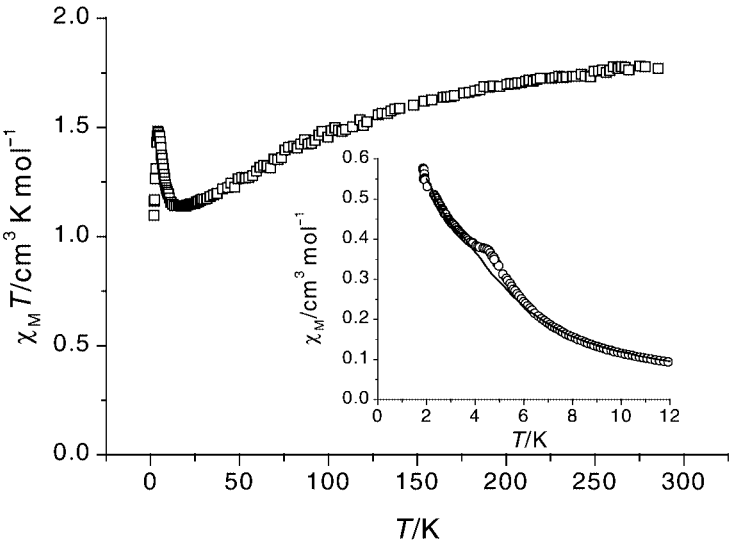

Fig. 3 Temperature dependence of the magnetic susceptibility of **1** [$\chi_M T$ at 10 kOe (□); χ_M at 10 kOe (—); χ_M at 500 Oe (○)].

1.5 expected for four spin-only Cu(II) ions with S = 1/2, g = 2.0, and correspond to g = 2.2. Upon cooling down, the $\chi_M T$ decreases regularly and reaches a minimum of 1.14 cm^3 K mol^{-1} at 17.7 K. This is characteristic of a dominant ferrimagnetic behavior. Below 17.7 K, a sharp maximum of 1.48 cm^3 K mol^{-1} is found at 4.2 K followed by a drop to 1.1 cm^3 K mol^{-1} at 2 K, suggesting a magnetic phase transition. As shown in the inset of Fig. 3, there appears a shoulder peak around 4.5 K in the χ_M *vs*. T curve measured at low field (500 Oe) while without any anomaly at high field (10 kOe, line), which indicates the antiferromagnetic (AF) ordering at low field. The AF transition is further evidenced by the in phase of zero-field ac magnetic susceptibility $\chi_M'(T)$, which has a peak at *ca*. 4.2 K under H_{ac} = 5 Oe and frequencies of 111, 199, 355, 633 and 1111 Hz. No detected out-of-phase signal and frequency dependence were observed, excluding any ferromagnetic phase and glassy behavior.

Low-dimensional ferrimagnetism is generally related to uncompensated sublattices giving a net magnetic moment in the ground state. Although more common in bimetallic systems, ferrimagnetic behavior has also been observed in homometallic chain systems containing discrete species with an odd number of interacting metal ions or complicated alternating sequences of ferro-/antiferro-magnetic interactions.[13,14] With regard to structure **1**, the Cu···Cu distance over the pyrazine bridge (6.8 Å) is much longer than that over the O–P–O bridges (*ca*. 4.7 Å). The magnetic behavior of **1** is mainly attributed to the phosphonate layer which is composed of $\{Cu_3(hedp)_2(H_2O)_2\}$ double chains linked by $\{Cu(3)O_4\}$ units. The saturation magnetization of **1** at 1.93 K is 2.3 $N\beta$ per Cu_4 unit, far from the value of 4.4 $N\beta$ anticipated for four independent S = 1/2 spins with g = 2.2, but close to the value of 2.2 $N\beta$ based on the assumption that the exchange within the $\{Cu_3(hedp)_2(H_2O)_2\}$ double chain is antiferromagnetic and the exchange between the chain and the Cu(3) atom is ferromagnetic (Fig. 2). At very low temperature, the inter-layer antiferromagnetic couplings through the pyrazine bridge and/or the space must be considered. It is this interaction that yields a weak, three-dimensional AF ordering state below 4.2 K. By carefully looking at the M *vs*. H curve in the low field range, a metamagnetic behavior was observed with a critical field of *ca*. 2–3 kOe at 1.93 K. Compound **1** switches from an AF ground state to a ferrimagnetic-like state when a field is larger than the critical field.

The authors thank the National Natural Science Foundation of China (No. 29901003, 29823001) and State Key Project for Fundamental Research (G1998061305) for financial support, and Mr Yong-Jiang Liu for crystal data collection.

Notes and references

‡ *Crystal data*: $C_8H_{20}Cu_4N_2O_{18}P_4$, M = 810.3, triclinic, space group $P\bar{1}$, a = 6.248(2), b = 8.035(3), c = 11.014(4) Å, α = 86.035(6), β = 87.889(6), γ = 82.809(5)°, V = 547.1(3) Å^3, Z = 1, D_c = 2.459 g cm^{-3}, μ(Mo-Kα) = 42.2 cm^{-1}, λ = 0.71073 Å. A crystal of dimensions 0.20 × 0.04 × 0.04 mm was selected for indexing and intensity data collection at 298 K. Total number of measured and observed independent reflections [$I_o > 2\sigma(I)$] are 2823, 1909 (R_{int} = 0.0679). Least-squares refinements were based on F^2 and converged at R_1 = 0.0468, wR_2 = 0.1211.

CCDC reference number 169230. See http://www.rsc.org/suppdata/cc/b1/b106780j/ for crystallographic data in CIF or other electronic format.

1 G. Cao, H. Hong and T. E. Mallouk, *Acc. Chem. Res.*, 1992, **25**, 420; G. Alberti, *Comprehensive Supramolecular Chemistry*, ed. J. M. Lehn, Pergamon, Elsevier Science, Ltd., Oxford, 1996, vol. 7; A. Clearfield, *Progress in Inorganic Chemistry*, ed. K. D. Karlin, John Wiley & Sons, Inc., New York, 1998, vol. 47, pp. 371–510.
2 J. Le Bideau, C. Payen, P. Palvadeau and B. Bujoli, *Inorg. Chem.*, 1994, **33**, 4885.
3 S. Drumel, P. Janvier, D. Deniaud and B. Bujoli, *J. Chem. Soc., Chem. Commun.*, 1995, 1051.
4 J. Akimoto, Y. Kiyozumi and F. Mizukami, *Angew. Chem., Int. Ed. Engl.*, 1995, **34**, 1199.
5 D. L. Lohse and S. C. Sevov, *Angew. Chem., Int. Ed. Engl.*, 1997, **36**, 1619.
6 M. Riou-Cavellec, M. Sanselme and G. Férey, *J. Mater. Chem.*, 2000, **10**, 745.
7 V. Soghomonian, Q. Chen, R. C. Haushalter and J. Zubieta, *Angew. Chem., Int. Ed. Engl.*, 1995, **34**, 223.
8 L.-M. Zheng, H.-H. Song and X.-Q. Xin, *Comments Inorg. Chem.*, 2000, **22**, 129.
9 G. Alberti, U. Costantino, F. Marmottini, R. Vivani and P. Zappelli, *Angew. Chem., Int. Ed. Engl.*, 1993, **32**, 1357.
10 A. Clearfield, D. M. Poojary, B. Zhang, B. Zhao and A. Derecskei-Kovacs, *Chem. Mater.*, 2000, **12**, 2745.
11 R. C. Finn and J. Zubieta, *J. Chem. Soc., Dalton Trans.*, 2000, 1821.
12 L.-M. Zheng, H.-H. Song, C.-Y. Duan and X.-Q. Xin, *Inorg. Chem.*, 1999, **38**, 5061.
13 M. Drillon, E. Coronado, M. Belaiche and R. L. Carlin, *J. Appl. Phys.*, 1988, **63**, 3551.
14 M. A. M. Abu-Youssef, A. Escuer, M. A. S. Goher, F. A. Mautner, G. J. Reiß and R. Vicente, *Angew. Chem., Int. Ed.*, 2000, **39**, 1624.

CHEMCOMM Communication
www.rsc.org/chemcomm

Conjugate addition of arylsilanes to unsaturated carbonyl compounds catalyzed by rhodium in air and water

Tai-Sheng Huang and Chao-Jun Li*

Department of Chemistry, Tulane University, New Orleans, Louisiana, 70118. E-mail: cjli@tulane.edu

Received (in Cambridge, UK) 10th July 2001, Accepted 19th September 2001
First published as an Advance Article on the web 22nd October 2001

$ArSiCl_3$ and Ar_2SiCl_2, believed to be unstable in aqueous media, reacted efficiently with α,β-unsaturated ketones and esters in air and water (in the presence of sodium fluoride and a rhodium catalyst), giving good to excellent yields of the desired conjugate addition products.

Currently, there is a wide interest in searching for alternative media and processes for chemical and organic synthesis. As a result of the natural abundance of water as well as the inherent advantages of using water as a solvent, interest has been growing in studying organic reactions in water.[1] Recently, in our ongoing 'green' chemistry research program, namely, the use of environmentally friendly reagents, solvents, and processes for organic reactions, we have been interested in developing transition-metal catalyzed carbon–carbon bond formations under the quasi-natural conditions of air and water.[2] Such reactions have the advantages of simplifying protection–deprotection steps, easy recycling of the catalyst solution, and convenient conducting of the reaction. A general requirement for performing such reactions is that the reagent is air- and water-stable, readily available, and less toxic (nontoxic if possible).

Conjugate addition of organometallic reagents to α,β-unsaturated carbonyl compounds is an important means for C–C bond formation in organic synthesis.[3] This reaction was once limited to organocopper chemistry but now is possible with other organometallic compounds through the use of transition metal catalysts.[4] Recently we found that, in the presence of a rhodium catalyst, α,β-unsaturated esters and ketones reacted with arylbismuth, aryltin (and vinyltin), and aryllead reagents in aqueous media to give the corresponding conjugate addition products in an air atmosphere.[5] The method has been used in synthesizing natural and unnatural α-amino acids.[6] However, organotin, organolead, and organobismuth reagents are rather toxic in spite of the fact that they are very efficient in the quasi-natural conditions of water and air. Therefore we felt it was highly desirable to search for the less toxic reagents instead of tin, lead, or bismuth.

Silicon has drawn the attention of chemists for many years due to its low cost, large abundance, and nontoxic properties. The application of silicon and organic silicon compounds for synthetic purposes has been growing in scope due to their relatively high stability and the ability to tailor chemo-, regio-, and stereoselectivities by combining these reagents with appropriate catalysts. Widely recognized reactions attributed to the use of silicon include organosilane based reduction chemistry,[7] cross-coupling reactions,[8] allylsilanes chemistry,[9] as protecting groups,[10] and the chemistry of silyl enolates.[11] Recently, transition-metal catalyzed conjugate additions involving allylsilanes were studied under an inert gas atmosphere and anhydrous conditions.[12] However, conjugate addition with arylsilicon compounds has not been reported due to their lower reactivity, especially in the presence of air and water. Herein we wish to report a highly efficient conjugate addition reaction with arylsilanes in air and water in the presence of sodium fluoride and catalyzed by rhodium catalysts (eqn. 1).

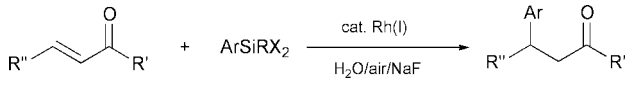

(1)

Initially, phenyltrimethylsilane was chosen to react with 2-cyclohexen-1-one in the presence of a catalytic amount of $(COD)_2RhBF_4$ in water because of its high stability in aqueous media. However no reaction was observed, even after refluxing for several days in the presence of sodium fluoride. Knowing that arylsilyl halides undergo transmetalation with palladium complexes with the aid of fluoride ions *via* five-coordinate silicates in the cross-coupling reaction with aryl- or alkenylhalides,[13] we selected phenyltrichlorosilane as a phenylating reagent despite the fact that phenyltrichlorosilane was thought to be unstable in water. Subsequently, it was discovered that, when cyclohex-2-en-1-one was stirred with phenyltrichlorosilane and a catalytic amount of $(COD)_2RhBF_4$ in the presence of an excess amount of NaF at refluxing conditions overnight in water, a smooth reaction occurred to give the conjugate addition product in 54% isolated yield. Unlike the triphenylbismuth reaction, virtually no biphenyl product was observed with the silicon reagent. No reaction was observed without the catalyst or fluoride. At room temperature the reaction also ceased to proceed completely. Interestingly, the use of different fluoride salts also affected the reaction progress. Fluoride salts such as lithium fluoride, sodium fluoride and potassium fluoride were tested, and sodium fluoride appeared to be the most effective for this reaction. Among the rhodium catalysts screened, $(COD)_2RhBF_4$ and $(COD)_2RhCl$ were effective while others such as $[(CO)_2RhCl]_2$, $(PPh_3)_3RhCl$, and $(C_2H_4)_2Rh(acac)$ were not. It is noteworthy that the yield of this reaction was dramatically improved to almost 100% when (4 equivalents) Ph_2SiCl_2 was used instead of $PhSiCl_3$ (Table 1). The use of 1 equivalent of the silicon reagent decreased the yield somewhat (67%). It is noteworthy that essentially identical results were obtained with either Ph_2SiCl_2 or $Ph_2Si(OH)_2$ as the phenylating reagent, which implies that hydrolysis of the silyl chloride does

Table 1 Effects of reagents and catalyst on conjugated addition of cyclohex-2-en-1-one

$ArMR_n$	Conditions	Yield (%)
$PhSiCl_3$	H_2O/reflux/$(COD)_2RhBF_4$/NaF	54
Ph_2SiCl_2	H_2O/reflux/$(COD)_2RhBF_4$/NaF	97
$PhMeSiCl_2$	H_2O/reflux/$(COD)_2RhBF_4$/NaF	95
$PhSiMe_3$	H_2O/reflux/$(COD)_2RhBF_4$/NaF	0
Ph_2GeCl_2	H_2O/reflux/$(COD)_2RhBF_4$/NaF	0
$PhGeCl_3$	H_2O/reflux/$(COD)_2RhBF_4$/NaF	0
$PhSiCl_3$	H_2O/reflux/$(COD)_2RhBF_4$/KF	48
$PhSiCl_3$	H_2O/reflux/$(COD)_2RhBF_4$/LiF	Trace
$PhSiCl_3$	H_2O/reflux/$(COD)_2RhBF_4$/NaOH	< 10
$PhSiCl_3$	H_2O/reflux/$(COD)_2RhBF_4$	0
Ph_2SiCl_2	H_2O/rt/$(COD)_2RhBF_4$/NaF	Trace
Ph_2SiCl_2	H_2O/reflux/$[(CO)_2RhCl]_2$/NaF	0
Ph_2SiCl_2	H_2O/reflux/$(CH_2{=}CH_2)_2$ Rhacac/NaF	0
Ph_2SiCl_2	H_2O/reflux/$(PPh_3)_3RhCl$/NaF	0
Ph_2SiCl_2	H_2O/reflux/NaF	0

 DOI: 10.1039/b106768k

Table 2 Conjugated addition with arylsilanes in air and water[a]

Entry	Carbonyl derivative	Silane	Product	Yield (%)
1		Ph_2SiCl_2	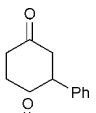	97
2		Ph_2SiCl_2	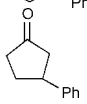	81
3		Ph_2SiCl_2	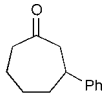	95
4	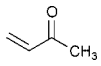	Ph_2SiCl_2	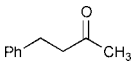	34
5	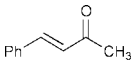	Ph_2SiCl_2	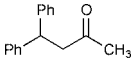	87
6	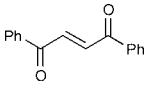	Ph_2SiCl_2	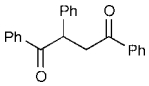	96
7	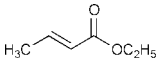	Ph_2SiCl_2	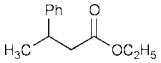	71
8	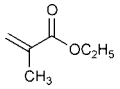	Ph_2SiCl_2	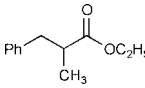	61
9	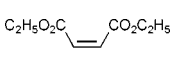	Ph_2SiCl_2	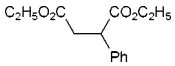	85
10	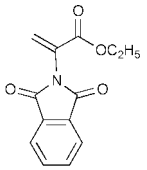	Ph_2SiCl_2	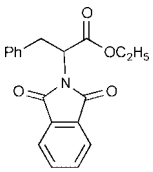	94
11		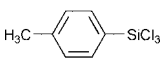	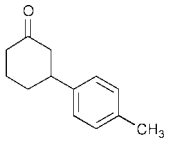	47
12	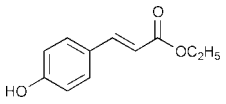	Ph_2SiCl_2	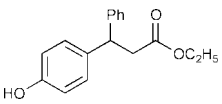	61

[a] All reactions were carried out at refluxing conditions with isolated yields after column chromatography on silica gel.

not affect the reaction. Under the same reaction conditions, no reaction was observed with analogous germanium compounds. With the optimal reaction conditions in hand, several α,β-unsaturated carbonyl compounds were examined with Ph_2SiCl_2 (or $TolSiCl_3$ for entry 11) under these conditions (Table 2). Both ketones (linear and cyclic) and esters were effective as the electron-withdrawing functional groups. Compounds bearing a hydroxy group reacted as expected without the need of protection.

The following procedure is representative. A mixture of cyclohex-2-en-1-one (0.25 mmol), diphenyldichlorosilane (253 mg, 1.0 mmol), NaF (210 mg, 5.0 mmol) and $(COD)_2RhBF_4$ (5.6 mg, 0.013 mmol) in 5 mL of water was stirred at 100 °C for 12 h under an air atmosphere. The reaction mixture was extracted with ethyl acetate. After the combined solvent was dried and concentrated *in vacuo*, the residue was purified by silica gel chromatography eluting with hexanes–ethyl acetate (5 : 1) to give 42.2 mg (97%) of the desired product.

In conclusion, a highly effective conjugate addition of diphenyldichlorosilane to α,β-unsaturated ketones and esters was achieved by using a rhodium catalyst in the presence of sodium fluoride in air and water. The scope (such as asymmetric synthesis), mechanism, and synthetic applications of this reaction are currently under investigation.

We are grateful to the NSF (CAREER) and the NSF-EPA Joint Program for a Sustainable Environment for partial support of this research.

Notes and references

1 C. J. Li and T. H. Chan, *Organic Reactions in Aqueous Media*, John Wiley & Sons, New York, 1997A. Lubineau, J. Auge and Y. Queneau, *Synthesis*, 1994, 741; *Organic Synthesis in Water*, ed. P. A. Grieco and P. A. Blackie Academic & Professional, Glasgow, 1998.

2 C. J. Li, *Chem. Rev.*, 1993, **93**, 2023; C. J. Li and T. H. Chan, *Tetrahedron*, 1999, **55**, 11149; C. J. Li, *Tetrahedron*, 1996, **52**, 5643.

3 P. Perlmutter, *Conjugate Addition Reactions in Organic Synthesis*, Pergamon, Oxford, UK, 1992J. A. Kozlowski, in *Comprehensive Organic Synthesis*, ed. D. M. Trost and I. Fleming, Pergamon, Oxford, UK, 1992, **4**, p. 169.

4 C. Petrier, J. C. de Souza Barbosa, C. Dupuy and J. L. Luche, *J. Org. Chem.*, 1985, **50**, 5761; J. J. Eshelby, P. J. Crowley and P. J. Parsons, *Synlett*, 1993, 279; J. Schwartz, D. B. Carr, R. T. Hansen and F. M. Dayrit, *J. Org. Chem.*, 1980, **45**, 3053; J. Westermann and K. Nickisch, *Angew. Chem., Int. Ed. Engl.*, 1993, **32**, 1368; S. Flemming, J. Kabbara, K. Nickisch, H. Neh and J. Westermann, *Synthesis*, 1995, 317.

5 S. Venkatraman and C. J. Li, *Tetrahedron Lett.*, 2001, **42**, 781; S. Venkatraman, Y. Meng and C. J. Li, *Tetrahedron Lett.*, 2001, **42**, 4459; T. Huang, Y. Meng, S. Venkatraman, D. Wang and C. J. Li, *J. Am. Chem. Soc.*, 2001, **123**, 7451.

6 T. S. Huang and C. J. Li, *Org. Lett.*, 2001, **3**, 2037.

7 D. N. Kursanov, Z. N. Parnes and N. M. Loim, *Synthesis*, 1974, 633; J. L. Fry, S. B. Silverman and M. Orfanopoulos, *Org. Synth. Collect.*, 1990, **7**, 393.

8 H. Matsuhashi, M. Kuroboshi, Y. Hatanaka and T. Hiyama, *Tetrahedron Lett.*, 1994, **35**, 6507; Y. Hatanaka and T. J. Hiyama, *J. Am. Chem. Soc.*, 1990, **112**, 7793; H. Urata and T. Fuchikami, *Tetrahedron Lett.*, 1991, **32**, 91.

9 H. Sakurai, *Pure Appl. Chem.*, 1982, **54**, 1; G. A. Molander and K. O. Cameron, *J. Org. Chem.*, 1993, 5931; *Comprehensive Organic Synthesis*, ed. B. M. Trost and I. Fleming, Pergamon, Oxford, 1991, Vol. 2, Part 2.2, p. 563C. E. Masse and J. S. Panek, *Chem. Rev.*, 1995, **95**, 1293.

10 L. Blanco, P. Amice and J. M. Conia, *Synthesis*, 1976, 196; H. R. Kricheldorf and A. Fehrle, *Synthesis*, 1974, 422; M. Lalonde and T. H. Chan, *Synthesis*, 1985, 817.

11 T. Mukaiyama, *Pure Appl. Chem.*, 1983, **55**, 1749; K. Koga, *Pure Appl. Chem.*, 1994, **66**, 1487.

12 H. Nakamura, H. Iwama and Y. Yamamoto, *J. Am. Chem. Soc.*, 1996, **118**, 6641 and refs therein.

13 J. Yoshida, K. Tamao, M. Takahashi and M. Kumada, *Tetrahedron Lett.*, 1978, 2161; Y. Hatanaka, K. Goda, Y. Okahara and T. Hiyama, *Tetrahedron*, 1994, **50**, 8301.

CHEMCOMM Communication
www.rsc.org/chemcomm

First chiral selenium ylides used for asymmetric conversion of aldehydes into epoxides

Hiroya Takada,[a] Patrick Metzner*[a] and Christian Philouze[b]

[a] *Laboratoire de Chimie Moléculaire et Thio-organique (UMR CNRS 6507), ISMRA-Université, 6, boulevard du Maréchal Juin, 14050 Caen, France. E-mail: metzner@ismra.fr; Fax: +33 231 452 877*
[b] *LEDSS (UMR CNRS 5616), Université Joseph Fourier, BP 53, 38041 Grenoble 9, France*

Received (in Cambridge, UK) 9th July 2001, Accepted 8th October 2001
First published as an Advance Article on the web 26th October 2001

Enantioenriched selenonium ylides have been generated by addition of benzyl bromide to C_2 symmetric (2*R*,5*R*)-2,5-dimethylselenolane in the presence of NaOH, and subsequently reacted with a variety of aldehydes to give oxiranes with excellent enantiomeric excesses (a catalytic version has been achieved); also, an aliphatic cyclic hypervalent dibromoselenurane structure has been demonstrated by X-ray analysis.

The reaction of selenium ylides with carbonyl compounds provides epoxides.[1,2] Since the initial report by Krief and his group[3] in 1974, it has rarely been exploited[4,5] and, to our knowledge, no asymmetric version is available. We wished to introduce a chiral selenide for the conversion of aldehydes into oxiranes with absolute stereocontrol. This raises several challenges. Few enantioenriched selenides have been synthesized so far.[6] An interesting question is the stereochemical course: will it differ, due to the possible [2 + 2]cycloaddition for the key step, leading to 4-membered ring intermediates with a hypervalent selenium atom (oxaselenetanes),[7] or will it be similar to that of the sulfur analogue,[8] with classical betaines as intermediates?[9,10]

We anticipated favourable kinetics of the epoxidation sequence as compared to the sulfur series. For the first step, a high nucleophilicity of selenides towards benzyl halides has been reported.[11] Deprotonation of the selenonium salt will probably be facilitated,[12] as a result of the higher polarizability of selenium. For the third step, addition of the ylide to the carbonyl group, we found no accurate data in the literature, but a fair reactivity was hoped for in relation to polarizability, bond lengths and dissociation energies.

Our study has been based on our results[13,14] with C_2 symmetric sulfur ylides, prepared from (+)-(2*R*,5*R*)-2,5-dimethylthiolane and possible comparisons. Therefore we embarked on the synthesis of the selenium analogue and its use for the epoxidation reaction.

Enantiopure selenolane **1** has been prepared in two easy steps from commercially available (2*S*,5*S*)-hexanediol.† Activation of both hydroxy groups into mesylates and subsequent double nucleophilic substitution with lithium selenide[15,16] (generated *in situ* from selenium and $LiBEt_3H$) provided the crude selenolane quantitatively. Isolation of **1** proved problematic in relation to volatility and azeotrope formation with solvents. We converted **1** by addition of bromine into a stable crystalline 'dibromide'[17,18] **2** (Scheme 1). A selenurane structure was suggested by the single NMR signal observed for the two methyl groups. We were able to grow single crystals (mp: 93.5–94.5 °C) and the X-ray analysis demonstrated the Se^{IV} hypervalent[19] arrangement (Fig. 1). A trigonal bipyramid[20] was observed with the two electron withdrawing groups (bromine atoms) in apical positions, a reduced C–Se–C angle[21,22] of 89.9° and the lone pair in equatorial position. To our knowledge, this is the first structural determination of an aliphatic cyclic dibromoselenurane.

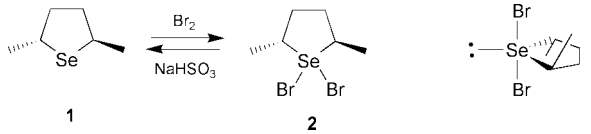

1 2

Scheme 1

Selenolane **1** was regenerated by reaction with aqueous sodium hydrogensulfite in 70% overall yield.

The expoxidation reaction was carried out in a very simple, one pot procedure. Selenolane **1**, benzyl bromide, an aldehyde, and sodium hydroxide were reacted at ambient temperature in a 9 : 1 mixture of Bu^tOH and water as solvent (Scheme 2).‡ With a stoichiometric amount of selenide (Table 1), the reaction time is shorter than for the corresponding sulfide: after 2 h, a 51% yield of stilbene oxide was isolated. After 24 h, oxiranes were obtained in 71–97% yields (Table 1, entries 2–4). Excellent enantiomeric excesses were attained: 92–93%.

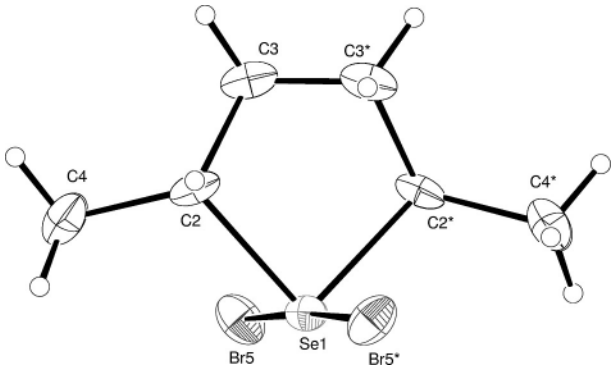

Fig. 1 X-Ray crystal structure of selenurane **2**.§ Selected interatomic distances (Å), bond angles (°) and torsion angles (°): Br–Se(1) 2.570(1), Se(1)–C(2) 2.013(7), C(2)–C(3) 1.53(1); Br–Se(1)–Br 176.4, Br–Se(1)–C(2) 93.4, Br–Se(1)–C(2) 89.2, C(2)–Se(1)–C(2) 89.9(4), Se(1)–C(2)–C(3) 103.0(5), C(2)–C(3)–C(3) 109.3(6).

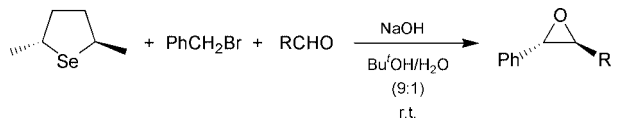

Scheme 2

Table 1 Asymmetric synthesis of epoxides from aldehydes[a]

Entry	Aldehyde	Conditions	Yield (%)	dr *trans* (%)	ee (*S*,*S*) (%)
1	Benzaldehyde	2 h	51	1 : 1.4	92
2	Benzaldehyde	24 h	71	1 : 2	92
3	4-Tolualdehyde	24 h	86	1 : 1.4	93
4	2-Naphthaldehyde	24 h	97	1 : 1	92

[a] All reactions were performed with selenolane **1** (0.20 mmol), benzyl bromide (0.40 mmol), aldehyde (0.20 mmol) and NaOH (0.40 mmol).

 DOI: 10.1039/b106063p

Table 2 Catalytic asymmetric benzylidenation of various aldehydes[a]

Entry	Aldehyde	Yield (%)	dr *trans* (%)	ee[b] (*S*,*S*) (%)
1	Benzaldehyde	91	1 : 1	91
2	4-Tolualdehyde	97	1 : 1	92
3	2-Naphthaldehyde	97	1 : 1	92
4	4-Chlorobenzaldehyde	97	1 : 1	76
5	4-Trifluoromethylbenzaldehyde	76	1 : 1	83
6	(*E*)-Cinnamaldehyde	66	1 : 1	94
7	2-Furaldehyde	67	1 : 1	93
8		65[c]	1 : 1	92
9	2-Thiophenecarboxaldehyde	72	1 : 1	94
10		86[c]	1 : 1	94

[a] All reactions were performed with selenolane **1** (0.020 mmol, 20 mol% to aldehyde), benzyl bromide (0.40 mmol), aldehyde (0.20 mmol) and NaOH (0.40 mmol) at rt for 7 days. [b] Enantiomeric excesses were determined by chiral HPLC using a Daicel AD column. [c] Reaction time: 4 h.

These results led us to achieve a catalytic procedure.[23–25] Using 0.2 equivalent of selenolane **1** and eight aldehydes, at ambient temperature for a maximum of 7 days, good to excellent yields of oxiranes (65–97%) were obtained (Table 2). For the more reactive heteroaromatic aldehydes (entries 8, 10) the reaction time could be optimized to 4 h. Enantiomeric excesses were 91–94% (entries 1–3, 6–10), except for aldehydes bearing electron-withdrawing groups (entries 4, 5).

As compared to the sulfur analogues,[13,14] this series leads to enhanced reactivity and higher asymmetric induction, with the same absolute configuration.

Another feature is the diastereoselectivity,[26] which has almost not been addressed so far in the selenium series.[1,2] Under stoichiometric conditions, the *trans* oxirane was the major isomer but to a much lesser extent than with sulfides (for the example of benzaldehyde: excess of 18–34% instead of 86%). The catalytic series provides an equal abundance of *trans* and *cis* oxiranes, for most cases. This trend towards the *cis* isomer is reminiscent of the reaction of unstabilized sulfur ylides with aliphatic aldehydes, and of the Wittig reaction of unstabilized phosphoranes with aldehydes. The higher reactivity observed here with selenonium ylides leads us to propose early transition states, and possible hypervalent oxaselenetane intermediates.[7,27]

In conclusion this first report of chiral selenium ylides demonstrates that they can provide efficient asymmetric induction for the synthesis of epoxides. They exhibit marked differences with sulfur ylides. The catalytic version is competitive with previous methods in the sulfur series.[23–25,28–30]

We thank CNRS and PunchOrga ('Réseau inter-régional du Pôle Universitaire Normand de Chimie Organique') for support.

Notes and references

† *Experimental data for* **1**: pale yellow oil; δ_H (250 MHz, $CDCl_3$) 1.45 (6H, d, *J* 6.6 Hz, 2 Me), 1.57–1.63 (2H, m), 2.25–2.30 (2H, m), 3.77–3.85 (2H, m, 2 CH); δ_C (62.9 MHz, CDCl3) 21.3, 38.2, 39.3; ν_{max} (NaCl)/cm^{-1} 2966, 2950, 2920, 1090, 1046, 1030, 1000, 990, 802; $[\alpha]_D^{22}$ +166 (*c* 1.31 in $CHCl_3$); HRMS (EI) *m*/*z* calcd. 164.0104, found 164.0131. **2**: yellow needles; mp 93.5–94.5 °C; δ_H (250 MHz, $CDCl_3$) 1.83 (6H, d, *J* 6.9 Hz, 2 Me), 2.29–2.36 (m, 2H), 2.67–2.76 (m, 2H), 4.85–4.93 (m, 2H); δ_H (250 MHz, C_6D_6) 1.49 (6H, d, *J* = 6.6 Hz, 2 Me), 1.65–1.71 (m, 2H), 1.96–2.04 (m, 2H), 4.40–4.47 (m, 2H); δ_C (62.9 MHz, $CDCl_3$) 20.1, 39.4, 78.7; δ_C (62.9 MHz, C_6D_6) 18.7, 39.8, 79.1; ν_{max} (KBr)/cm^{-1} 2920, 1440, 1370, 1090, 1046, 1030, 1000, 990, 802; $[\alpha]_D^{22}$ +64.4 (*c* 0.41 in CHCl3); HRMS (EI) *m*/*z* calcd. ($M^+ - Br$) 242.9287, found 242.9241.

‡ *Representative experimental procedure*: to a solution of selenolane **1** (0.020 mmol) in a 9 : 1 mixture of Bu^{t}OH and water (0.80 mL) were added benzyl bromide (48 μL, 0.40 mmol), benzaldehyde (20 μL, 0.20 mmol) and powdered NaOH (16 mg, 0.40 mmol). The reaction mixture was stirred at room temperature for 24 h then water was added. The aqueous phase was extracted with CH_2Cl_2. The combined organic layers were dried over $MgSO_4$ and then concentrated to dryness. Purification by silica gel column chromatography (eluent diethyl ether–ethyl acetate) gave the expected oxirane. The ee was determined by HPLC analysis on a Daicel Chiralpak AD column (9 : 1 n-hexane–propan-2-ol).

§ *Crystal data for* **2**: $C_3H_6BrSe_{0.5}$. *M* = 161.46, tetragonal, space group $P4_32_12$, at 293.2 K, *a* = 9.009(3), *b* = 9.009(3), *c* = 12.21(1) Å, *V* = 991.0(7) Å 3 , *Z* = 8, *F*(000) = 608.00, μ(MoKα) = 0.7107 cm^{-1}, D_{calc} = 2.164 g cm^{-3}, final *R* values R_1 = 0.0452 (all data), wR_2 = 0.0358. CCDC 167809. See http://www.rsc.org/suppdata/cc/b1/b106063p/ for electronic files in .cif or other electronic format.

1 A. Krief, in *The Chemistry of Organic Selenium and Tellurium Compounds*, ed. S. Patai, New York, 1987, vol. 2, p. 675.
2 A. Krief, W. Dumont, D. Van Ende, S. Halazy, D. Labar, J.-L. Laboureur and T. Q. Lê, *Heterocycles*, 1989, **28**, 1203.
3 W. Dumont, P. Bayet and A. Krief, *Angew. Chem., Int. Ed. Engl.*, 1974, **13**, 274.
4 K. Takaki, M. Yasumura and K. Negoro, *Angew. Chem., Int. Ed. Engl.*, 1981, **20**, 671.
5 C. Paulmier, *Selenium Reagents and Intermediates in Organic Synthesis*, Pergamon Press, Oxford, 1986.
6 T. Wirth, *Tetrahedron*, 1999, **55**, 1.
7 T. Kawashima and R. Okazaki, *Synlett*, 1996, 600.
8 A.-H. Li, L.-X. Dai and V. K. Aggarwal, *Chem. Rev.*, 1997, **97**, 2341.
9 F. Volatron and O. Eisenstein, *J. Am. Chem. Soc.*, 1987, **109**, 1.
10 M. K. Lindvall and A. M. P. Koskinen, *J. Org. Chem.*, 1999, **64**, 4596.
11 E. Maccarone and G. Perrini, *J. Chem. Soc., Perkin Trans. 2*, 1983, 1605.
12 W. von E. Doering and A. K. Hoffmann, *J. Am. Chem. Soc.*, 1955, **77**, 521.
13 K. Julienne, P. Metzner, V. Henryon and A. Greiner, *J. Org. Chem.*, 1998, **63**, 4532.
14 K. Julienne, P. Metzner and V. Henryon, *J. Chem. Soc., Perkin Trans. 1*, 1999, 731.
15 J. A. Gladysz, J. L. Hornby and J. E. Garbe, *J. Org. Chem.*, 1978, **43**, 1204.
16 E. Honda, T. Iwamura, S.-i. Watanabe, T. Kataoka, O. Muraoka and G. Tanabe, *J. Chem. Soc., Perkin Trans. 1*, 2001, 529.
17 L. J. Benjamin, C. H. Schiesser and K. Sutej, *Tetrahedron*, 1993, **49**, 2557.
18 G. T. Morgan and F. H. Burstall, *J. Chem. Soc.*, 1929, 1096.
19 N. Furukawa and S. Sato, in *Chemistry of Hypervalent Compounds*, ed. K.-y. Akiba, New York, 1999, p. 241.
20 E. L. Muetterties and R. A. Schunn, *Quart. Rev.*, 1966, **20**, 245.
21 J. D. McCullough and R. E. Marsh, *Acta Crystallogr.*, 1950, **3**, 41.
22 J. D. McCullough and G. Hamburger, *J. Am. Chem. Soc.*, 1941, **63**, 803.
23 V. K. Aggarwal, *Synlett*, 1998, 329.
24 V. K. Aggarwal, in *Comprehensive Asymmetric Catalysis*, ed. E. Jacobsen, A. Pfaltz and H. Yamamoto, Berlin, 1999, vol. 2, p. 679.
25 J. Zanardi, C. Leriverend, D. Aubert, K. Julienne and P. Metzner, *J. Org. Chem.*, 2001, **66**, 5620.
26 V. K. Aggarwal, S. Calamai and G. J. Ford, *J. Chem. Soc., Perkin Trans. 1*, 1997, 593.
27 F. Ohno, T. Kawashima and R. Okazaki, *Chem. Commun.*, 1997, 1671.
28 V. K. Aggarwal, E. Alonso, G. Hynd, K. M. Lydon, M. J. Palmer, M. Porcelloni and J. R. Studley, *Angew. Chem., Int. Ed.*, 2001, **40**, 1430.
29 R. Hayakawa and M. Shimizu, *Synlett*, 1999, 1328.
30 T. Saito, D. Akiba, M. Sakairi and S. Kanazawa, *Tetrahedron Lett.*, 2001, **42**, 57.

CHEMCOMM Communication
www.rsc.org/chemcomm

The radical-chain addition of aldehydes to alkenes by the use of *N*-hydroxyphthalimide (NHPI) as a polarity-reversal catalyst

Shinya Tsujimoto, Takahiro Iwahama, Satoshi Sakaguchi and Yasutaka Ishii*

Department of Applied Chemistry, Faculty of Engineering & High Technology Research Center, Kansai University, Suita, Osaka 564-8680, Japan. E-mail: ishii@ipcku.kansai-u.ac.jp

Received (in Corvallis, OR, USA) 20th August 2001, Accepted 3rd October 2001
First published as an Advance Article on the web 29th October 2001

Hydroacylation of simple alkenes with aldehydes *via* a radical process was successfully achieved by the use of *N*-hydroxyphthalimide (NHPI) as a polarity-reversal catalyst. Thus, 5-tridecanone was obtained by the reaction of oct-1-ene with pentanal in the presence of small amounts of NHPI and dibenzoyl peroxide (BPO).

Intermolecular radical-chain addition of aldehydes to alkenes is the simplest methodology for the synthesis of long-chain unsymmetrical ketones, but employment of this method is usually difficult for the synthesis of simple aliphatic ketones.[1–3] The hydroacylation between alkenes and aldehydes *via* a radical process involves the following reaction sequences: (i) hydrogen abstraction from an aldehyde by a radical initiator to form an acyl radical (**A**), (ii) addition of the acyl radical to alkene leading to a β-oxocarbon radical (**B**), and (iii) abstraction of the aldehydic hydrogen atom from another aldehyde by **B,** generating ketone and acyl radical **A** (Scheme 1).

In this radical-chain reaction, if the R′ is an alkyl or an electron-donating group (EDG), step (iii) becomes a sluggish process, since the abstraction of the aldehydic hydrogen atom by nucleophilic radical **B** (Nu·) proceeds with difficulty. In contrast, if the R′ is an electron-withdrawing group (EWG), this step proceeds smoothly because of the ease of aldehydic hydrogen abstraction by an electrophilic radical **B** (El·).[2] Acyl radicals, which are nucleophilic in nature, are known to add more easily to electron-deficient alkenes than normal alkenes.[3] As a result, the hydroacylation of simple alkenes with aldehydes *via* a radical process proceeds with difficulty. Recently, the hydroacylation of alkenes, particularly electron-rich alkenes, with aldehydes has been reported to be achieved by the use of methyl thioglycolate ($HSCH_2CO_2Me$) which acts as a polarity-reversal catalyst. For instance, the addition of butanal to isopropenyl acetate using di-*tert*-butyl hyponitrite (TBHN) as an initiator and methyl thioglycolate as the polarity-reversal catalyst at 60 °C produces 1-acetoxyhexan-3-one in good yield.[4,5]

In a previous paper, we reported that NHPI under dioxygen serves as an efficient carbon radical generation catalyst from alkanes. In this reaction, we found that the hydrogen atom attached to the hydroxyimide moiety of NHPI is easily abstracted by a radical species to generate phthalimide *N*-oxyl (PINO) which abstracts the hydrogen atom from alkanes to give alkyl radicals.[6] Therefore, if the adduct radical **B** in Scheme 1 can abstract the hydrogen atom from NHPI, NHPI is expected to serve as a polarity-reversal catalyst in analogy with methyl thioglycolate. The hydrogen atom of the hydroxylimide moiety adjacent to two carbonyl groups may be easily abstracted by a nucleophilic radical rather than an electrophilic one, and the resulting PINO would behave as an electrophilic radical that can efficiently abstract the aldehydic hydrogen atom. In this paper, we wish to report the radical-chain hydroacylation of simple alkenes with aldehydes assisted by NHPI [eqn. (1)].

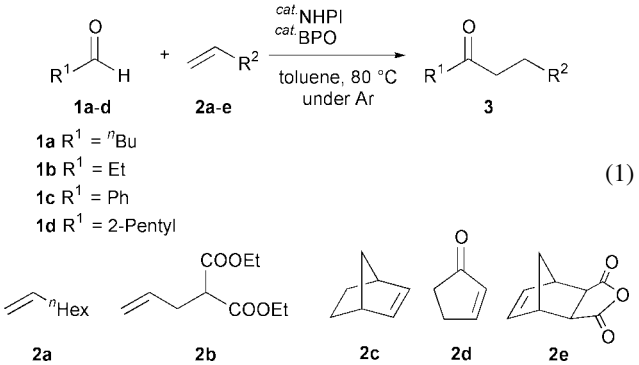

(1)

A solution in dry toluene (0.5 mL) containing pentanal (**1a**) (6 mmol), oct-1-ene (**2a**) (2 mmol), NHPI (0.2 mmol) and dibenzoyl peroxide (BPO) (0.1 mmol) was stirred at 80 °C under argon. After 12 h, additional BPO (0.1 mmol) in toluene (0.5 mL) was added to the reaction system and the mixture was allowed to react at that temperature for 12 h.† The reaction gave tridecan-5-one (**3aa**) in 78% yield at 77% conversion (Table 1, Run 1). In the absence of NHPI, the reaction gave **3aa** in lower conversion and yield (Run 2). This indicates that the NHPI enhances the chain transfer reaction of step (iii) shown in Scheme 1.

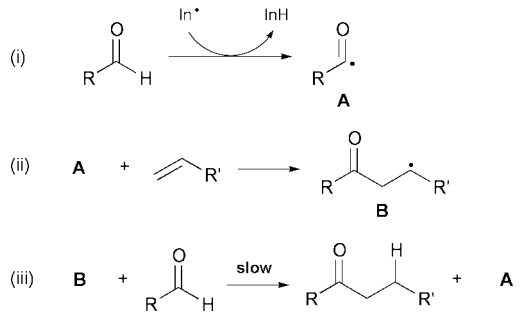

Scheme 1

Table 1 Reaction of pentanal (**1a**) with oct-1-ene (**2a**) using various catalysts in toluene at 80 °C in the presence of BPO[a]

Run	Catalyst	Conv. (%)	Yield (%)[b]
1	NHPI	77	78
2	—	63	48
3	3F-NHPI[c]	79	80
4	4Cl-NHPI[d]	72	78
5	NHSI[e]	78	65
6[f]	NHPI	67	75
7[g]	NHPI	72	88
8[g]	—	53	58

[a] Reaction was run as described text. [b] Based on **1a** reacted. [c] 3F-NHPI = 3-fluoro-*N*-hydroxyphthalimide. [d] 4Cl-NHPI = 4-chloro-*N*-hydroxyphthalimide. [e] NHSI = *N*-hydroxysuccinimide. [f] BPO (0.2 mmol) was added at once at the start of the reaction. [g] BPO (0.2 mmol) was added over 18 h using a syringe pump.

 DOI: 10.1039/b107548a

Table 2 Hydroacylation of alkenes with aldehydes catalyzed by NHPI[a]

Run	Aldehyde	Alkene	Conv. (%)	Product	Yield (%)
1	**1a**	**2b**	91	**3ab**	67
2[b]	**1a**	**2b**	91	**3ab**	80
3	**1a**	**2c**	90	**3ac**	73
4	**1a**	**2d**	>99	**3ad**	53
5	**1a**	**2e**	>99	**3ae**	92
6	**1b**	**2a**	58	**3ba**	73
7	**1c**	**2a**	30	**3ca**	90
8[c]	**1c**	**2a**	33	**3ca**	83

[a] See Table 1a. [b] Chlorobenzene was used as a solvent. [c] Reaction condition was 90 °C.

Several NHPI derivatives and *N*-hydroxysuccinimide (NHSI) were examined as catalysts (Runs 3 to 5). Among them, 3-fluoro-*N*-hydroxyphthalimide (3F-NHPI) gave the best result (Run 3). When the radical initiator BPO (0.2 mmol) was added in one portion, **3aa** was formed in slightly lower yield (Run 6). It was found that the gradual addition of BPO (0.2 mmol) in toluene (0.5 mL) using a syringe-pump over a period of 18 h afforded **3ab** in higher yield (88%) in 72% conversion (Run 7).

On the basis of these results, the reactions of various aldehydes with alkenes were run under the same conditions as Run 1 in Table 1 (Table 2). Diethyl allylmalonate (**2b**) and norbornene (**2c**) were reacted with **1a** giving the corresponding adducts, **3ab** and **3ac**, respectively, in good yields (Runs 1–3). α,β-Unsaturated ketone, **2d**, afforded the 1,4-adduct **3ad** in slightly lower yield.‡ 5-Norbornene-2,3-dicarboxylic anhydride (**2e**) resulted in adduct **3ae** in high selectivity (Run 5).§ The reaction of benzaldehyde (**1c**) with **2a** produced 1-phenyloctan-2-one (**3ca**) in high selectivity, although the conversion was not high (30%) (Run 7). Treatment of 2-methylpentanal (**1d**) with **2a** catalyzed by NHPI gave the corresponding coupling product **3da** (8%) and 4-methyldodecane (**4**) (42%) [eqn. (2)]. It is reported that the isoamylacyl radical was easily decarbonylated to an isoamyl radical and CO.[7] Therefore, **4** would be produced by the addition of an isoamyl radical, which is generated by decarbonylation of **1c**, to **2a**.

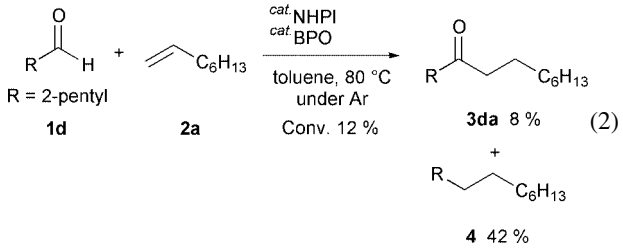

A possible reaction path for the NHPI-catalyzed hydroacylation of alkenes with aldehydes is shown in Scheme 2. The reaction may be initiated by the hydrogen atom abstraction from aldehyde by the radical initiator (In·), giving an acyl radical **C** which then adds to an alkene to afford a β-oxocarbon radical **D**. The resulting radical **D** having a nucleophilic character abstracts the hydrogen atom from NHPI leading to ketone and PINO. The abstraction of the hydrogen atom from aldehyde by the PINO forms the acyl radical **C** and NHPI. An alternative formation of PINO from NHPI and radical initiator (In·) may also be possible.

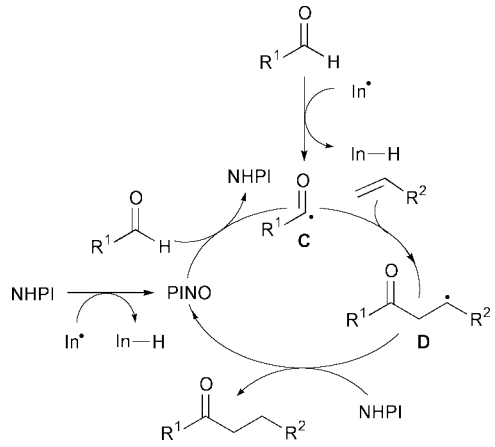

Scheme 2

In conclusion, we have developed a facile catalytic method for hydroacylation of alkenes using NHPI which acts as a polarity-reversal catalyst. Further extension of this method is now underway.

This work was partly supported by a Grant-in-Aid for Scientific Research (S) (No. 13853008) from Japan Society for the Promotion of Science (JSPS).

Notes and references

† *A typical procedure for reaction of pentanal* ***1a*** *with oct-1-ene* ***2a***. To a solution in dry toluene (0.5 mL) containing pentanal (**1a**) (6 mmol) were added oct-1-ene (**2a**) (2 mmol), NHPI (0.2 mmol) and dibenzoyl peroxide (BPO) (0.1 mmol) and the reaction mixture was stirred at 80 °C under argon. After 6 h, additional BPO (0.1 mmol) in toluene (0.5 mL) was added to the reaction system and allowed to react under stirring at that temperature for 12 h. The reaction was quenched with wet diethyl ether, and products were isolated by column chromatography on silica gel (*n*-hexane–AcOEt = 7 : 1) affording tridecan-5-one (**3aa**) (238 mg, 60% yield) as a colorless liquid.

‡ *Spectral data* for **3ad**. ^{1}H NMR δ 3.34–3.22 (m, 1H), 2.69–1.93 (m, 8H), 1.64–1.53 (m, 2H), 1.39–1.26 (m, 2H), 0.91 (t, J = 7.3 Hz, 3H); ^{13}C NMR δ 216.6, 210.7, 47.4, 41.1, 39.9, 37.3, 25.8, 25.4, 22.1, 13.6.

§ *Spectral data* for **3ae**. ^{1}H NMR δ 4.09–3.41 (m, 2H), 2.99–2.87 (m, 2H), 2.62–2.39 (m, 4H), 2.07–2.02 (m, 1H), 1.74–1.48 (m, 4H), 1.36–1.23 (m, 2H), 0.90 (t, J = 7.3 Hz, 3H); ^{13}C NMR δ 209.1, 171.6, 171.4, 49.3, 49.1, 48.1, 42.6, 41.0, 39.8, 39.6, 27.6, 25.6, 22.1, 13.6.

1 M. S. Kharasch, W. H. Urry and B. M. Kuderna, *J. Org. Chem.*, 1949, **14**, 248.
2 M. Tracy and Jr. Patrick, *J. Org. Chem.*, 1952, **17**, 1009; P. Gottschalk and D. C. Neckers, *J. Org. Chem.*, 1985, **50**, 3498.
3 H.-S. Dang and B. P. Roberts, *J. Chem. Soc., Chem. Commun.*, 1996, 2201; H.-S. Dang and B. P. Roberts, *J. Chem. Soc., Perkin Trans. 1*, 1998, 67.
4 V. Paul, B. P. Roberts and C. R. Willis, *J. Chem. Soc., Perkin Trans. 2*, 1989, 1953; R. P. Allen, B. P. Roberts and C. R. Willis, *Chem. Commun.*, 1989, 1387; B. P. Roberts, *Chem. Soc. Rev.*, 1999, **28**, 25.
5 Another approach to understand controlling factors of the reactivity for the radical hydrogen abstraction has been made by A. A. Zavitsas; A. A. Zavitsas, *J. Chem. Soc., Perkin Trans. 2*, 1998, 499.
6 Y. Yoshino, Y. Hayashi, T. Iwahama, S. Sakaguchi and Y. Ishii, *J. Org. Chem.*, 1997, **62**, 6810; S. Sakaguchi, T. Takase, T. Iwahama and Y. Ishii, *Chem. Commun.*, 1998, 2037, and references therein.
7 C. Chatgilialogu, D. Crich, M. Komatsu and I. Ryu, *Chem. Rev.*, 1999, **99**, 1991.

CHEMCOMM
Communication
www.rsc.org/chemcomm

The first bismuth phosphonate cluster. X-Ray single crystal structure of $[(Bu^tPO_3)_{10}(Bu^tPO_3H)_2Bi_{14}O_{10}\cdot 3C_6H_6\cdot 4H_2O]$†

Michael Mehring* and Markus Schürmann

Universität Dortmund, Lehrstuhl für Anorganische Chemie II D-44221. Dortmund, Germany. E-mail: mmeh@platon.chemie.uni-dortmund.de

Received (in Cambridge, UK) 9th August 2001, Accepted 8th October 2001
First published as an Advance Article on the web 26th October 2001

The reaction of triphenylbismuth and *tert*-butylphosphonic acid gives the bismuth phosphonate phase $(Bu^tPO_3H)_3Bi$ and the first bismuth phosphonate cluster $[(Bu^tPO_3)_{10}(Bu^tPO_3H)_2Bi_{14}O_{10}\cdot 3C_6H_6\cdot 4H_2O]$.

In the past three decades phosphate and phosphonate ligands have been widely used to prepare polynuclear oxo anions such as vanadates and molybdates.[1] A fascinating example of this class of compounds is the cluster $[V_{18}O_{25}(H_2O)_2(PhPO_3)_{20}Cl_4]^{4-}$.[2] In addition to the soluble metallaoxo anions, poorly soluble oxo–vanadium phosphonates such as $[VO(PhPO_3)\cdot H_2O]_n$ have also been reported.[3] The latter phosphonate forms a layered structure with well-defined internal void spaces and coordination sites which are accessible for organic molecules such as alcohols. Similarly, zirconium phosphates and phosphonates are composed of two-dimensional layered structures and show properties which make them useful as ion exchangers, sorbents, sensors, proton conductors, non-linear optical materials, photochemically active materials, catalysts, and hosts for the intercalation of a broad spectrum of guests.[4] Several other metal phosphonates which exhibit two- and three-dimensional structures in the solid state have been reported, including recent examples of Al, Zn, Cu, and Ga, among others.[4,5] The only bismuth phosphonate characterised by a single crystal X-ray structure analysis is $Bi(O_3PC_2H_4CO_2)\cdot H_2O$ which has a two-dimensional layered structure.[6] The chemistry of uncharged organophosphonate clusters which are soluble in common organic solvents and serve as molecular models for phosphate and phosphonate based materials is more recent.[7,8]

Herein we report our results on the reaction of $BiPh_3$ with $Bu^tPO_3H_2$ which was undertaken initially in order to obtain soluble organobismuth phosphonate compounds *via* the elimination of benzene. A 1 : 1 mixture of $BiPh_3$ and $Bu^tPO_3H_2$ was heated at 50 °C for three days in THF to give a suspension. The solid material was filtered off and the solvent removed *in vacuo*. The residue was dissolved in $CHCl_3$/benzene and by slow evaporation of the solvent colourless single crystals of $[(Bu^tPO_3)_{10}(Bu^tPO_3H)_2Bi_{14}O_{10}\cdot 3C_6H_6\cdot 4H_2O]$‡ (**1**) were obtained in low yield. The major product was identified as $(Bu^tPO_3H)_3Bi$ (**2**) which can be prepared almost quantitatively by choosing the appropriate stoichiometry. EDX analysis of analytically pure **2** shows a phosphorus-to-bismuth ratio of approximately 3 : 1 and in the ^{31}P MAS NMR only one signal at δ 36.0 is observed. The IR spectrum of **2** shows a broad absorption (3100 cm^{-1}) in the ν(P–OH) region. In the PO_3 vibration domain three strong absorption bands at 1066, 1017 and 934 cm^{-1} are observed. The absorption band at 1192 cm^{-1} is indicative for a P=O group. The TGA shows a weight loss of 4.7% in the temperature range 230–320 °C as a result of a condensation reaction of the Bu^tPO_3H moieties (weight loss calc. for 1.5 H_2O 4.6%). In the range 400–470 °C cleavage of the C–P bonds occurs (weight loss 27.9%; calc. for three Bu^t groups 27.6%). Additional weight loss in the temperature range 320–400 °C (1.8%) and 480–550 °C (2.7%) was observed giving a ceramic yield at 550 °C of 62.9% which is lower than the calculated ceramic yield for $Bi(PO_3)_3$ of 71.9%. The X-ray powder diffraction data show broad diffraction peaks which are indicative for the bismuth phosphonate phase **2** to be amorphous.

The single crystal X-ray structure analysis of **1**§ revealed the formation of a bismuth phosphonate oxo cluster containing 14 bismuth atoms and 12 *tert*-butylphosphonate groups (Fig. 1). In the crystal structure of **1** (space group *Immm* with $Z = 2$) the cluster, the water and the benzene molecules show *mmm* symmetry.

Two of the phosphonate groups are not fully deprotonated and give two Bu^tPO_3H units which form strong hydrogen bonds to adjacent Bu^tPO_3 groups with O(2')–O(2'E) and O(2'A)–O(2'D) distances of 2.327 Å. The molecular formulation $[(Bu^tPO_3)_{10}(Bu^tPO_3H)_2Bi_{14}O_{10}\cdot 3C_6H_6\cdot 4H_2O]$ (**1**) was confirmed by elemental analysis. The 10 μ_3-oxygen atoms are most likely the result of partial hydrolysis of $BiPh_3$ caused by residual water present in $Bu^tPO_3H_2$. The difficulty to obtain water-free $Bu^tPO_3H_2$ was previously noticed in context with the synthesis of *tert*-butylphosphonate clusters of titanium.[8,9] Cluster **1** shows D_{2h} symmetry which results in the observation of only two crystallographically independent phosphonate groups, four independent bismuth atoms, Bi(1)–Bi(4), and three independent μ_3-oxygen atoms, O(3)–O(5). The μ_3-oxygens O(3)–O(5) are incorporated inside the cluster and show Bi–O distances in the range 2.093(16)–2.237(9) Å. The oxygen O(3) is trigonal planar coordinated which is indicated by the sum of the O–Bi–O angles Σ 360.0°, whereas the μ_3-oxygens O(4) and O(5) show sums of the O–Bi–O angles of Σ 342.7 and 339.2°, respectively. The coordination geometry both at Bi(2) and Bi(4) is best described as a square pyramid with four phosphorus-bonded oxygen

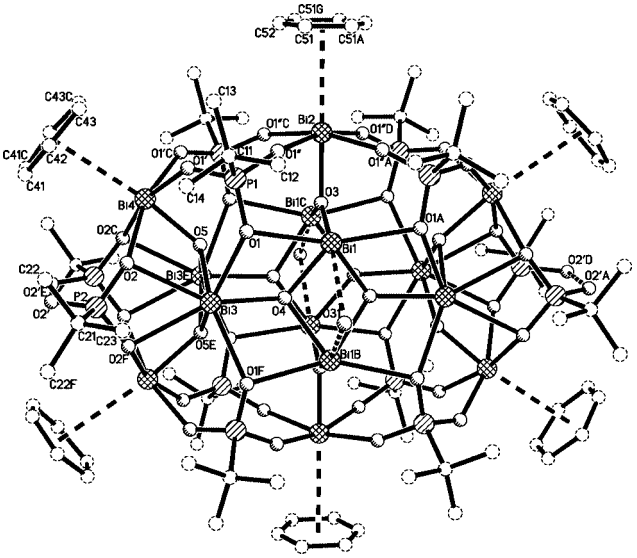

Fig. 1 General view of **1** showing the molecular structure and the atom numbering scheme (symmetry transformations used to generate equivalent atoms: a = *x*, *y*, −*z* + 1; b = −*x*, *y*, −*z* + 1; c = *x*, −*y*, *z*; d = *x*, −*y*, −*z* + 1; e = −*x*, −*y*, *z*; f = −*x*, *y*, *z*; g = 1 − *x*, −*y*, *z*).

† Electronic supplementary information (ESI) available: Fig. S1: XRD pattern for **2**. See http://www.rsc.org/suppdata/cc/b1/b107220j/

 DOI: 10.1039/b107220j

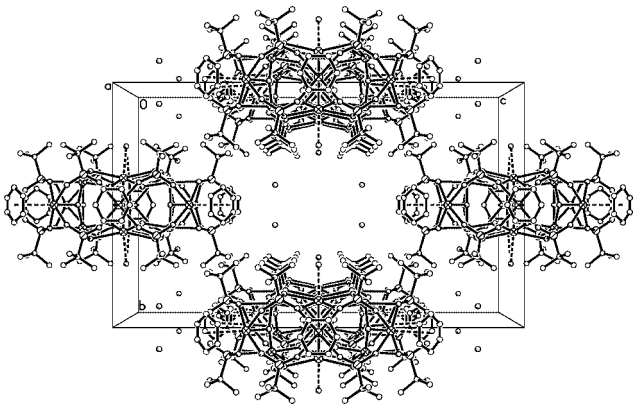

Fig. 2 Packing diagram of **1**. The view along the *a*-axis highlights the channels which are partially filled with water molecules. A one-dimensional copolymer of the bismuth-containing cluster and benzene extends along the *a*-axis.

atoms occupying the corners of the base. The corresponding bond distances Bi(2)–O(P) and Bi(4)–O(P) are in the range 2.212(11)–2.439(11) Å. The apex of each of the pyramids is occupied by an oxygen atom with Bi(2)–O(3) and Bi(4)–O(5) bond distances of 2.093(16) and 2.119(12) Å, respectively. In addition, both Bi(2) and Bi(4) are each coordinated to a benzene molecule with Bi–C distances in the range 3.428–3.459 and 3.376–3.564 Å, respectively, which is comparable with the bismuth–benzene coordination in $BiCl_3 \cdot C_6H_6$ with Bi–C distances in the range 3.219–3.621 Å.[10] The benzene molecules coordinated to Bi(2) link adjacent clusters to give a linear polymeric arrangement with a Bi–benzene$_{centroid}$ distance of 3.194 Å. A similar polymeric structure with collinear bismuth atoms and arene centers was recently reported for $[Bi_2(O_2CCF_3)_4](C_6Me_6)$.[11] The benzene molecules coordinated to Bi(4), Bi(4A), Bi(4B) and Bi(4C) and having an occupancy of 0.5 occupy a void built up by four chains of the bismuth clusters. The coordination geometry at Bi(1) is best described as that of a strongly distorted square pyramid with four phosphorus-bonded oxygen atoms occupying the corners of the base (Bi–O(P) 2.237(9)–2.577(10) Å). The O(1)–Bi(1)–O(1A) angle of 147.8(5)° deviates strongly from the ideal value of 90° indicating a stereochemically active lone pair. The apex of the pyramid is occupied by a μ_3-oxygen with a Bi(1)–O(3) distance of 2.228(6) Å. In addition, a water molecule is weakly coordinated to Bi(1) with a Bi(1)–O(31) distance of 3.066 Å. The coordination environment of Bi(3) consists of four phosphonate-oxygens and three μ_3-oxygens. The Bi–O(P) distances are in the range 2.555(10)–2.664(10) Å and the Bi–O distances amount to 2.208(13)–2.231(7) Å. In the crystal lattice huge voids extend along the *a*-axis at (0,0,0) and (0,1/2,1/2) which are partially filled with water molecules (Fig. 2). The IR spectrum of **1** shows a broad absorption band in the region 3000–3500 cm^{-1} which is indicative for OH vibrations in agreement with the single crystal X-ray structure analysis. Only two strong and relatively broad absorption bands are observed at 1059 and 970 cm^{-1}, which are assigned with caution to ν(P–O–Bi) vibrations. A ν(P=O) absorption band is observed at 1190 cm^{-1}.

In conclusion, the single crystal X-ray structure analysis of the first bismuth phosphonate cluster **1** is reported which, to the best of our knowledge, is the largest bismuth containing cluster reported so far and a rare example of a linear π-coordination copolymer of a main group metal cluster and an arene molecule. We have shown that novel hybrid organic–inorganic bismuth compounds are easily accessible under mild reaction conditions starting from a commercially available organobismuth compound and phosphonic acids.

We are grateful to Professor Dr K. Jurkschat (Universität Dortmund, Lehrstuhl für Anorganische Chemie II) for his generous support.

Notes and references

‡ *Synthesis* of $[(Bu^tPO)_3)_{10}(Bu^tPO_3H)_2Bi_{14}O_{10} \cdot 3C_6H_6 \cdot 4H_2O$ (**1**) and $(Bu^tPO_3H)_3Bi$ (**2**): to a solution of $BiPh_3$ (900 mg, 2.04 mmol) in 20 mL of THF was added $Bu^tPO_3H_2$ (282 mg, 2.04 mmol). The reaction mixture was stirred at 50 °C for three days to give a cloudy solution. The precipitate was isolated by filtration and dried *in vacuo* to give 280 mg (66%) of **2** as a colourless solid. The solvent was removed to give a slightly yellow oil which was dissolved in a $CHCl_3$/benzene mixture. Slow evaporation of the solvent afforded colourless crystals of analytically pure **1** (20 mg). A second crop of crystals (25 mg) contained small amounts of the starting material $BiPh_3$ as impurity. **1**: Decomp. > 200 °C. IR (KBr) ν/cm^{-1}: 3400br, 2950m, 2903w, 2867w, 1643w, 1479m, 1403w, 1362w, 1190m, 1059s, 970s, 831w, 656m, 498s, 331w. Anal. Found: C, 15.9; H, 2.7. Calc. C, 15.8; H, 2.7%. **2**: Decomp. > 150 °C. IR (KBr) ν/cm^{-1}: 3100br, 2970m, 2906w, 2870w, 1479m, 1395w, 1365w, 1192m, 1066s, 1017s, 934s, 830w, 729w, 694w, 657m, 507m, 331w. ^{31}P MAS NMR (161.98 MHz): δ 36.0. Anal. Found: C, 23.3; H, 4.7. Calc. C, 23.2; H, 4.9%.

§ *Crystal data for* **1**: $C_{66}H_{136}Bi_{14}O_{50}P_{12}$, M = 5027.11, crystal size 0.05 × 0.03 × 0.03 mm^3, orthorhombic, space group *Immm*, Z = 2, a = 15.628(1), b = 17.977(2), c = 30.189(3), V = 8481.4(13) $Å^3$, D_c = 1.968 g cm^{-3}, $F(000)$ = 4548, μ(Mo-Kα) = 0.7107 mm^{-1}, T = 171(1) K, $3.31 \leqslant 2\theta \leqslant 25.35$, Completeness to 2θ: 99.2%, max./min. residual electron density: 1.516/−1.244 e $Å^{-3}$. Data were collected on a Nonius Kappa CCD diffractometer. Of a total of 18370 reflections collected, 4236 reflections were independent (R_{int} = 0.098). The structure was solved by direct methods (SHELXS97)[12] and successive difference Fourier syntheses. Refinement applied full-matrix least-squares methods SHELX97.[13] Final $R1$ = 0.054 (for 4236 reflections $I > 2\sigma(I)$) and $wR2$ = 0.130 (all data). The H atoms were placed in geometrically calculated positions using a riding model with U_{iso} constrained at 1.2 for non-methyl groups and 1.5 for methyl groups times U_{eq} of the carrier C atom. Disordered solvent molecules of benzene and water were found with occupancies of 0.25 (O(21)) and of 0.5 (C(41), C(42), C(43)), whereas all solvent molecules, except O(31), were refined isotropically. CCDC 162527. See http://www.rsc.org/suppdata/cc/b1/b107220j/ for crystallographic data in CIF or other electronic format.

1 M. I. Khan and J. Zubieta, *Prog. Inorg. Chem.*, 1995, **43**, 1.
2 J. Salta, Q. Chen, Y.-D. Chang and J. Zubieta, *Angew. Chem.*, 1994, **106**, 781; J. Salta, Q. Chen, Y.-D. Chang and J. Zubieta, *Angew. Chem., Int. Ed.*, 1994, **33**, 757.
3 G. Huan, J. Jacobson, J. W. Johnson and E. W. Corcoran Jr., *Chem. Mater.*, 1990, **2**, 91.
4 (*a*) G. Alberti, M. Casciola, U. Costantino and R. Vivani, *Adv. Mater.*, 1996, **8**, 291; (*b*) A. Clearfield, *Prog. Inorg. Chem.*, 1998, **47**, 371.
5 For selected recent examples, see: (*a*) A. Cabeza, M. A. G. Aranda, S. Bruque, D. M. Poojary, A. Clearfield and J. Sanz, *Inorg. Chem.*, 1998, **37**, 4168; (*b*) F. Fredoueil, M. Evain, M. Bujoli-Doeuff and B. Bujoli, *Eur. J. Inorg. Chem.*, 1999, 1077; (*c*) J. Zhu, X. Bu, P. Feng and G. D. Stucky, *J. Am. Chem. Soc.*, 2000, **122**, 11563; (*d*) M. Bujoli-Doeuff, M. Evain, F. Fayon, B. Alonso, D. Massiot and B. Bujoli, *Eur. J. Inorg. Chem.*, 2000, 2497; (*e*) C. V. K. Sharma and A. Clearfield, *J. Am. Chem. Soc.*, 2000, **122**, 1558.
6 P. Janvier, S. Drumel, Y. Piffard and B. Bujoli, *C. R. Acad. Sci, Paris*, 1995, 29.
7 Selected examples: (*a*) M. G. Walawalkar, H. W. Roesky and R. Murugavel, *Acc. Chem. Res.*, 1999, **32**, 117; (*b*) V. Chandrasekhar and S. Kingsley, *Angew. Chem.*, 2000, **112**, 2410; V. Chandrasekhar and S. Kingsley, *Angew. Chem., Int. Ed.*, 2000, **39**, 2320; (*c*) M. R. Mason, *J. Cluster Sci.*, 1998, **9**, 1.
8 (*a*) G. Guerrero, M. Mehring, P. H. Mutin, F. Dahan and A. Vioux, *J. Chem. Soc., Dalton Trans.*, 1999, 1537; (*b*) M. Mehring, G. Guerrero, F. Dahan, P. H. Mutin and A. Vioux, *Inorg. Chem.*, 2000, **39**, 3325.
9 M. G. Walawalkar, S. Horchler, S. Dietrich, D. Chakraborty, H. W. Roesky, M. Schäfer, H. G. Schmidt, G. M. Sheldrick and R. Murugavel, *Organometallics*, 1998, **17**, 2865.
10 W. Frank, J. Schneider and S. Müller-Becker, *J. Chem. Soc., Chem. Commun.*, 1993, 799.
11 W. Frank, V. Reiland and G. J. Reiß, *Angew. Chem.*, 1998, **110**, 3154; W. Frank, V. Reiland and G. J. Reiß, *Angew. Chem., Int. Ed.*, 1998, **37**, 2984.
12 G. M. Sheldrick, *Acta Crystallogr., Sect, A*, 1990, **46**, 467.
13 G. M. Sheldrick, University of Göttingen, 1997.

CHEMCOMM
Communication
www.rsc.org/chemcomm

Two alternative products from the intercalation of alkali metals into cation-defective Ruddlesden–Popper oxysulfides

Sophie G. Denis and Simon J. Clarke*

Inorganic Chemistry Laboratory, Department of Chemistry, University of Oxford, South Parks Road, Oxford, UK OX1 3QR. E-mail: simon.clarke@chem.ox.ac.uk

Received (in Cambridge, UK) 23rd August 2001, Accepted 9th October 2001
First published as an Advance Article on the web 26th October 2001

Sodium may be topotactically inserted into the perovskite layers (under thermodynamic control) or the rock-salt layers (under kinetic control) of the cation-deficient $n = 2$ Ruddlesden–Popper oxysulfides $Ln_2Ti_2O_5S_2$ with concomitant reduction of Ti^{IV}.

Intercalation is important in the modification of materials properties. Reductive topotactic insertion of alkali metals into transition metal oxides[1] and sulfides[2] is central to battery technology.[3] Layered sulfides and oxyhalides,[2,4] and layered oxides such as Ruddlesden–Popper (R–P) phases consisting of perovskite slabs separated by rock-salt layers, accept non-redox intercalants to increase the separation of the slabs[5] or exfoliate them.[6] Some R–P phases, such as $Sr_3Ru_2O_7$,[7] undergo topotactic *oxidative* intercalation of fluorine into the rock-salt layers.

Oxysulfides contain anions with different sizes and chemical requirements which order crystallographically, often resulting in layered structures. Two groups[8,9] have reported the cation-defective $n = 2$ R–P oxysulfides $Ln_2Ti_2O_5S_2$ (Ln = Pr–Er, Y). These contain vacant sites 12-coordinated by oxygen in perovskite slabs, which are separated by LnS rock-salt layers (**1**). Here we show that lithium and sodium intercalate into the vacant sites in the perovskite slabs with reduction of Ti^{IV}. While reductive intercalation of alkali metals into partially filled rock-salt layers of R–P oxides is known,[10] we show here that reductive intercalation of sodium into *new sites* in filled rock-salt layers is also possible in the oxysulfides. The synthetic conditions determine the destination of the Na intercalants: thermodynamic control favours insertion into the perovskite slab, whereas kinetic control favours insertion into the rock-salt layers.

All manipulations were carried out in an argon-filled dry box or under nitrogen using Schlenk techniques. The brown oxysulfides were prepared† on the 5 g scale for Ln = Nd, Y by reacting stoichiometric amounts of Ln_2O_3, TiO_2 and TiS_2 in evacuated silica tubes at 1100 °C. Lithium intercalation was carried out by reacting the powders with excess *n*-BuLi (2.5 M in hexane) or lithium naphthalide (0.05 M in THF) at between 20 and 50 °C for 0.5–11 days. Sodium intercalation was carried out either by exposing the oxysulfide to excess sodium vapour at 600 °C in a sealed nickel container for 4–10 days, or by reacting the powder with excess sodium naphthalide (0.05 M in THF) at 50 °C for 3–7 days. The products were black or blue-black powders and were analysed chemically† and using powder X-ray diffraction (PXRD) and powder neutron diffraction (PND).‡ Magnetic susceptibility measurements§ were carried out on the products of intercalation into diamagnetic $Y_2Ti_2O_5S_2$, **1** (Fig. 1).

The PXRD patterns of the Na intercalates and the products of Li intercalation at 50 °C were indexed on the tetragonal unit cell of the starting material in space group *I*4/*mmm* suggesting that intercalation is topotactic. The products of lower temperature Li intercalation were less Li-rich and were orthorhombic (*Immm*); lattice parameters and compositions are given in Table 1. In the products of reaction with *n*-BuLi or Na vapour, the *a* parameter increases by 2–3 % whereas the *c* parameter decreases by 1–2 %, consistent with reduction of Ti^{IV} and insertion into the perovskite slabs (**2**). The products of Na intercalation using Na naphthalide (**3**) are dramatically different: the *a*-axis decreases by 1% and the *c*-axis increases by 25% (6 Å). The only topotactic change which can give rise to this involves insertion into the rock-salt layers.[7] The products of Li intercalation using Li naphthalide or *n*-BuLi were indistinguishable from one another. This suggests that Na is too large to intercalate into the perovskite blocks under mild conditions to give the thermodynamic product; the product of Na naphthalide intercalation may be converted into a product indistinguishable from the product of Na vapour intercalation by annealing for 6 days at 600 °C in an evacuated silica tube. The Li intercalates are the most air sensitive, and the brown colour of the starting material was apparent after a few seconds' exposure to air. Decomposition of the Na naphthalide intercalate was apparent after a few minutes, and the product had a PXRD pattern characteristic of $Ln_2Ti_2O_5S_2$, but enhanced 00*l* reflection intensities with the sample mounted in flat plate geometry showed that deintercalation exfoliates the crystallites. The products of Na vapour intercalation are air stable for many days.

Rietveld refinements against PND data of the structures of the $Na_xY_2Ti_2O_5S_2$ phases **2** and **3** are shown in Fig. 2. The structures‡ are compared in Fig. 1 with that of the parent $Y_2Ti_2O_5S_2$, **1**. Insertion into the perovskite slabs to produce **2** was predicted[9] based on the reactivity of Ti^{IV} and other early transition metal oxides. Reductive intercalation into completely new sites to produce **3** is, to our knowledge, unprecedented, and is surprising as it involves a change in the Y^{3+} ion coordination from 9 [4 × S at 2.8048(2) Å, 1 × S at 2.9395(6) Å and 4 × O at 2.4277(2) Å] to 8 [4 × S at 2.9404(7) Å and 4 × O at 2.3008(5) Å] with cleavage of the longest Y–S bond. The Ti coordination also changes substantially: in **1**, Ti can be considered 6-coordinate [4 × O at 1.9427(1) Å, 1 × O at 1.7941(4) Å and 1 × S at 2.8741(6) Å]. The long axial Ti–S bond is broken completely on intercalation of sodium into the rock-salt layers, increasing to 3.312(1) Å, and in **3** Ti is unambiguously in square pyramidal coordination by O [4 × O at 1.9814(6) Å and 1 × O at 1.809(1) Å]. On intercalation of Na into the perovskite slabs (**2**), the Ti–O bonds lengthen [4 × O at

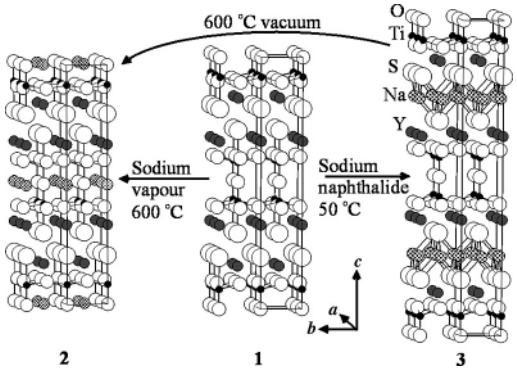

Fig. 1 Structures of $Y_2Ti_2O_5S_2$, **1**, and its sodium intercalates.

 DOI: 10.1039/b107659k

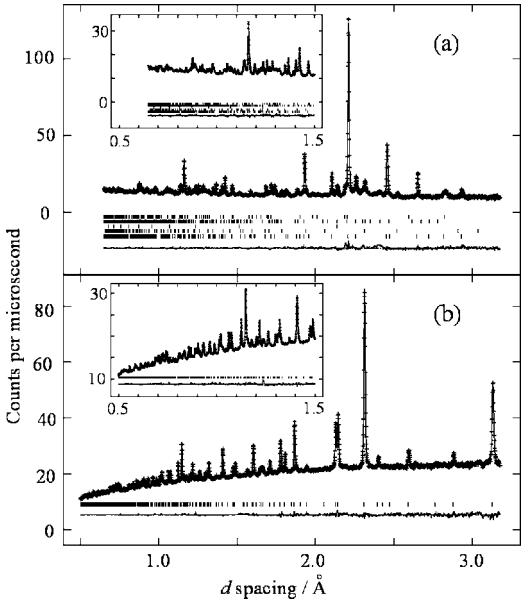

Fig. 2 Rietveld refinements against powder neutron diffraction data (2θ = 145°) for: (a) **2** (Na vapour): χ^2 = 1.62, wR_p = 0.018, $R(F^2)$ = 0.055; tick marks are for $NaY_2Ti_2O_5S_2$ (bottom-most), and impurities $Y_2Ti_2O_7$, vanadium sample holder, and poorly crystalline $YTiO_3$ and $NaYS_2$ (topmost); (b) **3** (Na naphthalide): χ^2 = 1.31, wR_p = 0.007, $R(F^2)$ = 0.086.

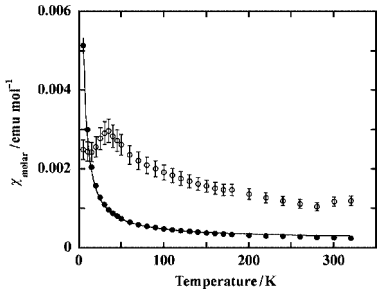

Fig. 3 Magnetic susceptibility of **2** (Na vapour intercalation) (○) and **3** (Na naphthalide intercalation) (●). The fit is to $\chi = \chi_0 + C/T$ with χ_0 = 2.2(1) × 10^{-4} emu mol^{-1} and a Curie constant corresponding to 5% of Ti ions behaving as S = ½ moments. The anomaly in the susceptibility of **2** is an artefact of the correction§ for the $YTiO_3$ impurity.

1.9699(4) Å, 1 × O at 1.883(2) Å] and the Ti–S bond shortens to 2.732(3) Å. In **2** Na is surrounded by four O atoms at 2.7282(1) Å in the *ab* plane; the eight more distant O atoms in the TiO_2 sheets were best modelled as a split site such that on average four would be located 2.772(1) Å from Na. In the Na naphthalide intercalate, **3**, Na is tetrahedrally coordinated by four S atoms at 2.796(1) Å. Refinement of the Na occupancy for **2** indicated a composition of $Na_{1.04(1)}Y_2Ti_2O_5S_2$ with the vacant site in the perovskite slab fully occupied. The composition of **3** refined to $Na_{1.02(1)}Y_2Ti_2O_5S_2$ with the tetrahedral site 50% occupied by Na so that short Na–Na contacts of 2.64 Å across shared tetrahedral edges are avoided. Compound **3** is poorer in Na than suggested by chemical analysis (Table 1). This discrepancy is under investigation: while no additional crystalline phases were observed in diffraction studies of **3**, the sloping background in Fig. 2(b) shows that an H-containing species remains after washing with THF. Rietveld refinement showed that the site in the perovskite blocks was 4(1)% occupied in **3**.

Compounds **2** and **3** both have Ti in a formal oxidation state of +3.5. The main contribution to both magnetic susceptibilities§ (Fig. 3) is a temperature-independent term comparable in magnitude to that of reduced metallic titanates that lie close to the metal–insulator boundary, such as $LaTiO_3$.[11]

Compound **3** bears some similarity to the oxysulfides prepared by Zhu and *et al.*[12] in which transition metal-containing perovskite slabs are separated by Cu_2S_2 layers. We are currently investigating further the synthesis, properties and ion-exchange chemistry of the intercalates described here.

Table 1 Lattice parameters and compositions from chemical analysis† for tetragonal (*I*4/*mmm*) or orthorhombic (*Immm*) intercalates

Compound	x	a/Å	b/Å	c/Å
$Nd_2Ti_2O_5S_2$	—	3.84906(1)		23.0005(1)
$Li_xNd_2Ti_2O_5S_2$[a]	0.72(3)	3.98956(8)	3.89125(8)	22.5217(6)
$Li_xNd_2Ti_2O_5S_2$[a]	0.94(3)	3.98855(9)	3.93880(8)	22.4003(6)
$Li_xNd_2Ti_2O_5S_2$[a]	1.38(4)	3.98263(2)		22.3066(2)
$Na_xNd_2Ti_2O_5S_2$[b]	0.92(4)	3.93112(2)		22.7024(2)
$Na_xNd_2Ti_2O_5S_2$[c]	1.46(5)	3.81337(2)		28.8881(3)
$Y_2Ti_2O_5S_2$ **1**	—	3.76956(1)		22.80557(9)
$Na_xY_2Ti_2O_5S_2$ **2**[b]	1.00(5)	3.85823(8)		22.5926(6)
$Na_xY_2Ti_2O_5S_2$ **3**[c]	1.43(5)	3.73088(5)		28.8193(5)

Synthetic methods: [a] *n*-BuLi in hexane.[b] Na vapour.[c] Na naphthalide in THF.

We thank the UK EPSRC (grant GR/N18758) for funding and access to ISIS. S. J. C. thanks the Royal Society and the Nuffield Foundation for further financial support.

Notes and references

† Y_2O_3 (Aldrich 99.99%), Nd_2O_3 (ALFA 99.99%), TiO_2 (Aldrich 99.9+%); TiS_2 was prepared by reacting Ti (ALFA 99.99%) with S (ALFA 99.9995%) at 600 °C for 3–4 days in evacuated silica tubes. Analysis for lithium and sodium (Table 1) was carried out using a Thermo Elemental Atomscan 16 ICP analyser. The alkali metal ions were leached out by boiling the materials in 20% nitric acid solution.

‡ PXRD data were collected using a Siemens D5000 diffractometer operating with CuKα radiation in Debye–Scherrer geometry and the sample sealed in a glass capillary. PND data were collected using the Polaris diffractometer at ISIS, UK; 0.25–2 g samples were sealed in vanadium containers. Rietveld refinement was carried out against neutron data collected at 35, 90 and 145° 2θ ($0.5 < d < 8$ Å) using GSAS: A. Larson and R. B. von Dreele, *The General Structure Analysis System*, Los Alamos National Laboratory, Los Alamos, NM, 1985. *Crystal data*: for $Y_2Ti_2O_5S_2$ **1**: T = 25 °C, tetragonal, space group *I*4/*mmm* (no. 139), a = 3.76956(1) Å, c = 22.80557(9) Å, Z = 2; Y (0 0 0.333589(9)), Ti (0 0 0.07867(2)), O1 (0 0.5 0.099313(8)), O2 (0 0 0), S (0 0 0.20469(2)). For $NaY_2Ti_2O_5S_2$ **2** (Na vapour): T = 25 °C, tetragonal, space group *I*4/*mmm* (no. 139), a = 3.85823(8) Å, c = 22.5926(6) Å, Z = 2; Y (0 0 0.33258(4)), Ti (0 0 0.08335(8)), O1 (0 0.4371(3) 0.40264(5)) (50% occupied split site), O2 (0 0 0), S (0 0 0.20429(8)), Na (0 0 0.5). For $NaY_2Ti_2O_5S_2$ **3** (Na naphthalide): T = 25 °C, tetragonal, space group *I*4/*mmm* (no. 139), a = 3.73088(5) Å, c = 28.8193(5) Å, Z = 2; Y (0 0 0.36732(2)), Ti (0 0 0.06278(5)), O1 (0 0.5 0.08596(3)), O2 (0 0 0), S (0 0 0.17774(5)), Na (0 0.5 0.25) (occupancy 0.509(5)).

§ Magnetic susceptibility data were measured using a Quantum Design MPMS2 SQUID magnetometer. The susceptibility of **2** was determined from the differences in moments measured at 4.5 and 5.0 T due to the presence of 4 mol% of ferromagnetic $YTiO_3$[13] impurity. Compound **3** contained a small Ni impurity and was measured at 2.0 and 3.0 T.

1 A. M. Chippindale, P. G. Dickens and A. V. Powell, *Prog. Solid State Chem.*, 1994, **21**, 133.
2 B. W. Eichhorn, in *Progress in Inorganic Chemistry*, ed. K. D. Karlin, Wiley, New York, 1994, vol. 42.
3 P. G. Bruce, *Chem. Commun.*, 1997, 1817.
4 P. Palvadeau, L. Coic, J. Rouxel and J. Portier, *Mater. Res. Bull.*, 1978, **13**, 221; K. Song and S. M. Kauzlarich, *Chem. Mater.*, 1994, **6**, 386.
5 R. A. Mohan Ram and A. Clearfield, *J. Solid State Chem.*, 1994, **112**, 288.
6 R. E. Schaak and T. E. Mallouk, *Chem. Mater.*, 2000, **12**, 3429.
7 R. K. Li and C. Greaves, *Phys. Rev. B*, 2000, **62**, 3811.
8 M. Goga, R. Seshadri, V. Ksenofontov, P. Gütlich and W. Tremel, *Chem. Commun.*, 1999, 979.
9 C. Boyer, C. Deudon and A. Meerschaut, *C. R. Acad. Sci. Paris, Ser. II*, 1999, **2**, 93.
10 A. R Armstrong and P. A. Anderson, *Inorg. Chem.*, 1994, **33**, 4366; K. Toda, M. Takahashi, T. Teranishi, Z.-G. Ye, M. Sato and Y. Hinatsu, *J. Mater. Chem.*, 1999, **9**, 799.
11 D. A. Crandles, T. Timusk and J. E. Greedan, *Phys. Rev. B*, 1991, **44**, 13 250.
12 W. J. Zhu, P. H. Hor, A. J. Jacobson, G. Crisci, T. A. Albright, S.-H. Wang and T. Vogt, *J. Am. Chem. Soc.*, 1997, **119**, 12 398.
13 J. E. Greedan, *J. Less-Common Met.*, 1985, **111**, 335.

CHEMCOMM Communication
www.rsc.org/chemcomm

New basic mesoporous silica catalyst obtained by ammonia grafting

Yoshitaka Inaki,[a] Yoshiyasu Kajita,[a] Hisao Yoshida,*[a] Kenji Ito[b] and Tadashi Hattori[a]

[a] *Department of Applied Chemistry, Graduate School of Engineering, Nagoya University, Nagoya 464-8603, Japan. E-mail: yoshidah@apchem.nagoya-u.ac.jp*
[b] *Department of Molecular Design and Engineering, Graduate School of Engineering, Nagoya University, Nagoya 464-8603, Japan*

Received (in Cambridge, UK) 6th August 2001, Accepted 10th October 2001
First published as an Advance Article on the web 29th October 2001

NH_3-treated mesoporous silica (FSM-16) contains $SiNH_2$ sites which exhibit basic catalytic activity for Knoevenagel condensation; $SiNH_2$ and SiOH pair sites formed at lower NH_3-treatment temperatures exhibit higher turnover frequencies (TFs) in comparison with $SiNH_2$ single sites.

The development of solid base catalysts is now becoming active[1–5] to replace liquid bases for the production of fine chemicals in industrial processes, since solid bases are easy to recycle and are environment friendly.[6]

Mesoporous silica materials such as FSM-16[7] and MCM-41[8] developed in the last decade have high surface area (*ca.* 1000 m^2 g^{-1}) and regular nanometer size pores (2–10 nm), and thus provide suitable fields for functional guest components and large reaction spaces. It was reported that amino functionalised MCM-41 obtained by silylation catalysed the Knoevenagel condensation,[1] a typical base catalysed reaction.[1–6] However, this method requires complicated manipulation, and produces a waste solution. In order to obtain basic catalysts, simple routes have been reported *e.g.*, thermal treatments at above 1023 K for amorphous aluminophosphates[2] or zeolites[3] in a flow of NH_3, leading to the formation of $–NH_2$ and/or –NH– sites. We report here a new simple method to obtain basic mesoporous silica catalysts through NH_3 adsorption on evacuated silica surfaces. The present method can lead to pair sites of $SiNH_2$ and SiOH, which exhibit higher TFs in comparison with $SiNH_2$ single sites.

Siliceous mesoporous silica (Si/Al > 5000), FSM-16, was prepared in the same manner as in previous reports,[9] and the structure was confirmed by its XRD pattern and N_2 adsorption isotherm; the BET surface area was 850 m^2 g^{-1}.

FSM-16 was treated in O_2 (100 Torr, 1 Torr = 133 Pa) at a given temperature for 1 h and evacuated for 1 h at the same temperature (pre-evacuation). Then NH_3-treatment was carried out; evacuated FSM-16 was exposed to 30 Torr gaseous NH_3 for 30 min at 473 or 923 K in a closed system, and evacuated for 30 min at the same temperature. The sample after NH_3-treatment is denoted as FSMN. FSMN samples showed almost the same clear XRD pattern as that of FSM-16.

For the measurement of FTIR spectra, sample powders were pressed (30 kg cm^{-2}) into self-supported disks of 5–10 mg cm^{-2}. Temperature programmed desorption (TPD) was carried out for FSMN at a rate of 5 K min^{-1} in a flow of He (60 ml min^{-1}).

The Knoevenagel condensation [eqn. (1)] was carried out as follows. The powder catalyst was added to a toluene (2.5 ml)

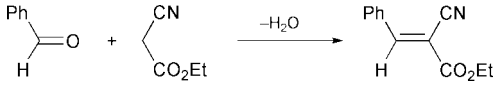

(1)

solution of benzaldehyde (0.7 mmol) and ethyl cyanoacetate (0.5 mmol), then the reaction mixture was stirred at 323 K. Products were analyzed by gas chromatography (GC) employing dodecane as an internal standard.

Table 1 shows the results of the Knoevenagel condensation. The reaction occurred on all FSMN samples (entries 1–6), while reaction did not occur over unmodified FSM-16 (entry 7). ^1H NMR and GC did not detect any by-products, confirming the progress of the selective reaction. Moreover, basic species did not elute during the reaction, since the filtrate after the reaction over the active catalyst did not exhibit any activity (entry 8). These results indicate that NH_3 molecules are stabilised on FSM-16 to function as base catalytic sites.

The catalytic activity of FSMN increased with increasing the pre-evacuation temperature for FSM-16 prior to NH_3-treatment at 473 K (entries 1–3). Increase of the pre-evacuation temperature from 923 K (entry 4) to 1073 K (entry 5) prior to NH_3-treatment at 923 K also enhanced the activity. These results suggest that the sites on which NH_3 molecules are stabilised would be generated by evacuation at higher temperature. NH_3-treatment temperature also influenced the catalytic activity. Increase of the treatment temperature from 473 K

Table 1 Results of the Knoevenagel condensation[a]

Entry	Sample		Pre-evacuation temperature/K	NH_3-treatment temperature/K	Reaction		$SiNH_2$[b]/μmol g^{-1}	TF/h^{-1}
	Name	Weight/g			Time/h	Yield (%)		
1	FSMN-1	0.1	673	473	0.5	4.0	1.06	283[e]
2	FSMN-2	0.1	873	473	0.5	12	15.3	78.6
3	FSMN-3	0.1	1073	473	0.5	16	21.2	75.5
4	FSMN-4	0.1	923	923	0.5	30	124	24.1
5	FSMN-5	0.1	1073	923	0.5	35	140	25.0
6	FSMN-5[c]	0.05	1073	923	0.5	19	140	27.1
7	FSM-16	0.1	1073	—	18	0.0	0.0	0.0
8	filtrate[d]	—	—	—	72	0.0	—	0.0

[a] The reaction mixture (2.5 ml toluene as solvent, 0.7 mmol benzaldehyde, 0.5 mmol ethyl cyanoacetate and 100 mg powdered catalyst as standard) was stirred at 323 K. [b] Values were estimated by using the absorption coefficient of the $SiNH_2$ band at 1553 cm^{-1}. The coefficient was calculated in terms of molar amount of desorbed NH_3 in NH_3-TPD above 923 K per decreased amount of the integrated intensity of the $SiNH_2$ band for FSM-16N-5 above 923 K. [c] This sample was the same as that in entry 5 but the sample weight used for the reaction was halved (50 mg). [d] The filtrate was isolated from the mixture after the reaction for 30 h over FSM-16N-5. [e] Very high TF would be due to the underestimation of the $SiNH_2$ band.

 DOI: 10.1039/b107131a

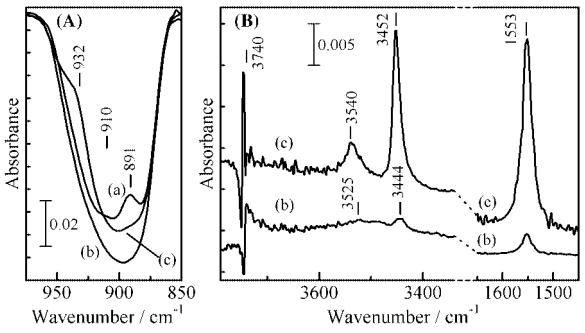

Fig. 1 (A) FTIR spectra of FSM-16 after evacuation at 1073 K (a), followed by NH_3-treatment at 473 K (b) and 923 K (c). (B) Difference spectra (b) and (c) obtained by subtraction of the spectrum (Aa) from (Ab) and (Ac), respectively. The intensity was normalised by the sample weight.

(entries 1–3) to 923 K (entries 4 and 5) enhanced the activity significantly. When a half amount of the sample of FSMN-5 (entry 5) was used, about half activity was observed (entry 6).

Fig. 1 shows the FTIR spectra of FSM-16. Evacuation at high temperature such as 1073 K gave rise to the absorption band at 891 cm^{-1} with a small band at 910 cm^{-1} (Fig. 1Aa). These bands were assigned to the strained siloxane bridge formed by dehydroxylation of the isolated hydroxy groups [eqn. (2)].[10]

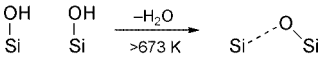

(2)

Intensities of the strained siloxane bands increased with increasing the evacuation temperature above 673 K. After NH_3-treatment at 473 K, the strained siloxane bands at 891 and 910 cm^{-1} completely disappeared (Fig. 1Ab), and new absorption bands were generated at 1553 and 3444 cm^{-1} with a very weak band at 3525 cm^{-1} (Fig. 1Bb). These new bands could be assigned to bending, symmetric stretching and asymmetric stretching vibrations of $SiNH_2$, formed by dissociative chemisorption of NH_3 on the strained siloxane bridges [eqn. (3)].[10]

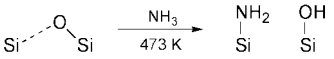

(3)

At the same time, the intensity of the SiOH band at 3740 cm^{-1} increased (Fig. 1Bb) upon NH_3-treatment, indicating that the reaction of eqn. (3) occurred during NH_3-treatment at 473 K. We confirmed that the reaction of eqn. (3) occurs even at r.t. as reported previously.[10] In the present study, NH_3-treatment was performed at 473 K to exclude physisorption of NH_3. No N–H bands other than the $SiNH_2$ bands were observed.

Higher temperature NH_3-treatment at 923 K resulted in generation of three intense bands at 3540, 3452 and 1553 cm^{-1} (Fig. 1Bc). These could be also assigned to $SiNH_2$ bands.[10] Also the Si–N stretching of $SiNH_2$ was observed at 932 cm^{-1} (Fig. 1Ac). Morrow *et al*. proposed that reaction can occur to form $SiNH_2$ [eqn. (4)] at high temperatures such as 923 K.[10] In the present case, much stronger $SiNH_2$ bands were formed (Fig. 1Bc) than at 473 K (Fig. 1Bb). However, the SiOH band intensity did not increase so much (Fig. 1Bc), and the strained siloxane band at 891 cm^{-1} decreased only partially (Fig. 1Ac). These results suggest that the reaction of eqn. (4) should mainly occur at 923 K rather than that of eqn. (3).

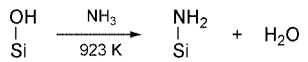

(4)

The amounts of $SiNH_2$ sites were estimated by using NH_3-TPD (see footnote *b* in Table 1) and are listed in Table 1. The yield in the Knoevenagel condensation increased with increasing the amount of $SiNH_2$ sites (Table 1), suggesting that $SiNH_2$ sites are the basic active sites catalysing this reaction.

Fig. 2 shows a plot of the product yield in the Knoevenagel condensation *vs*. the amount of $SiNH_2$. It is noteworthy that the

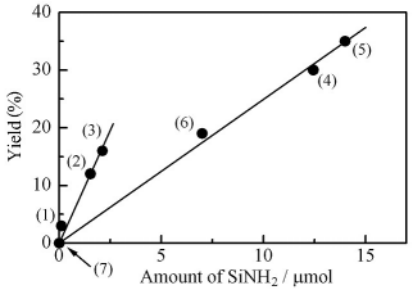

Fig. 2 Product yield for Knoevenagel condensation *vs*. the amount of $SiNH_2$ sites. The numbers in the plots correspond to the entry number in Table 1.

plot gives two straight lines (Fig. 2) the slopes of which are dependent upon the NH_3-treatment temperature. A steep slope was obtained by NH_3-treatment at 473 K (entries 1–3), while the less steep slope was obtained at 923 K (entries 4–6). The activity per amount of $SiNH_2$ (TF) was three times higher for the former than for the latter as shown in Table 1.

As mentioned above, pair sites of $SiNH_2$ and SiOH were formed at 473 K (Fig. 1Bb), while $SiNH_2$ sites with only few SiOH were formed at 923 K (Fig. 1Bc). Angeletti *et al*. proposed that the Knoevenagel condensation over propylamine catalyst bound on a silica surface was promoted by participation of residual surface silanols.[4] Therefore, in the present study, higher TFs for FSMN treated at 473 K (entries 1–3) would be attributed to the presence of SiOH with neighbouring $SiNH_2$ basic sites.

It can be concluded that NH_3-grafted mesoporous silica, FSMN, exhibits base catalytic activity for Knoevenagel condensation. The active basic site is $SiNH_2$ and higher pre-evacuation temperature and higher NH_3-treatment temperature are effective to form larger amounts of $SiNH_2$. Higher TFs were obtained for the FSMN on which pair sites of $SiNH_2$ and SiOH were formed by low temperature NH_3-treatment [eqn. (3)] in comparison with that for $SiNH_2$ single sites formed by high temperature NH_3-treatment [eqn. (4)].

Notes and references

1 D. Brunel, *Microporous Mesoporous Mater*., 1999, **27**, 329; B. M. Choudary, M. L. Kantam, P. Sreekanth, T. Bandopadhyay, F. Figueras and A. Tuel, *J. Mol. Catal. A*, 1999, **142**, 361.

2 M. J. Climent, A. Corma, V. Fornés, A. Frau, R. Guil-López, S. Iborra and J. Primo, *J. Catal*., 1996, **163**, 392; S. Delsarte, A. Auroux and P. Grange, *Phys. Chem. Chem. Phys*., 2000, **2**, 2821.

3 S. Ernst, M. Hartmann, S. Sauerbeck and T. Bongers, *Appl. Catal. A*, 2000, **200**, 117.

4 E. Angeletti, C. Canepa, G. Martinetti and P. Ventullo, *J. Chem. Soc., Perkin Trans. 1*, 1989, 105.

5 A. Corma, V. Fornés, R. M. Martín-Aranda, H. García and J. Primo, *Appl. Catal*., 1990, **59**, 237; K. R. Kloetstra, M. van Laren and H. van Bekkum, *J. Chem. Soc., Faraday Trans*., 1997, **93**, 1211; D. J. Macquarrie and D. B. Jackson, *Chem. Commun*., 1997, 1781; U. Rymsa, M. Hunger, H. Knözinger and J. Weitkamp, *Stud. Surf. Sci. Catal*., 1999, **125**, 197; S. Sebti, R. Nazih, R. Tahir, L. Salhi and A. Saber, *Appl. Catal. A*, 2000, **197**, L187.

6 H. Hattori, *Chem. Rev*., 1995, **95**, 537; K. Tanabe and W. F. Hölderich, *Appl. Catal., A*, 1999, **181**, 399.

7 S. Inagaki, Y. Fukushima and K. Kuroda, *J. Chem. Soc., Chem. Commun*., 1993, 680.

8 J. S. Beck, J. C. Vartuli, W. J. Roth, M. E. Leonowicz, C. T. Kresge, K. D. Schmitt, C. T.-W. Chu, D. H. Olson, E. W. Sheppard, S. B. McCullen, J. B. Higgins and J. L. Schlenker, *J. Am. Chem. Soc*., 1992, **114**, 10834.

9 Y. Inaki, H. Yoshida, K. Kimura, S. Inagaki, Y. Fukushima and T. Hattori, *Phys. Chem. Chem. Phys*., 2000, **2**, 5293; Y. Inaki, H. Yoshida and T. Hattori, *J. Phys. Chem. B*, 2000, **104**, 10304.

10 B. A. Morrow, I. A. Cody and L. S. M. Lee, *J. Phys Chem*., 1976, **80**, 2761.

CHEMCOMM Communication
www.rsc.org/chemcomm

Ruthenium-catalysed asymmetric hydrosilylation of ketoximes using chiral oxazolinylferrocenylphosphines

Izuru Takei,[a] Yoshiaki Nishibayashi,[b] Youichi Ishii,[c] Yasushi Mizobe,[a] Sakae Uemura*[b] and Masanobu Hidai*[d]

[a] *Institute of Industrial Science, The University of Tokyo, Komaba, Meguro-ku, Tokyo 153-8505, Japan*
[b] *Department of Energy and Hydrocarbon Chemistry, Graduate School of Engineering, Kyoto University, Yoshida, Sakyo-ku, Kyoto 606-8501, Japan*
[c] *Department of Chemistry and Biotechnology, Graduate School of Engineering, The University of Tokyo, Hongo, Bunkyo-ku, Tokyo 113-8656, Japan*
[d] *Department of Materials Science and Technology, Faculty of Industrial Science and Technology, Science University of Tokyo, Noda, Chiba 258-8510, Japan*

Received (in Cambridge, UK) 19th July 2001, Accepted 10th October 2001
First published as an Advance Article on the web 22nd October 2001

Chiral ruthenium(II) complexes, $RuCl_2(PPh_3)$(oxazolinylferrocenylphosphine), have been found to be effective catalysts for asymmetric hydrosilylation of ketoximes to give the corresponding primary amines in good yields with high enantioselectivities (up to 89% ee) after acid hydrolysis.

Optically active *primary* amines are one of the most useful synthetic intermediates of natural compounds and pharmaceutical drugs.[1] However, the *direct* enantioselective synthesis of optically active *primary* amines with high enantioselectivities is limited only to the hydroboration of ketoxime ethers[2] and the kinetic resolution of *racemic primary* amines.[3] A catalytic hydrogenation of ketoximes producing directly the chiral *primary* amines has been reported by several groups, but no sufficient results have been achieved until now.[4] This is in sharp contrast to the enantioselective hydrogenation and transfer hydrogenation of imines catalysed by transition metal complexes with chiral ligands to afford the corresponding *secondary* amines with high enantioselectivities.[5,6] As an alternative *direct* enantioselective synthesis of chiral *primary* amines, Brunner and co-workers developed the rhodium-catalysed asymmetric hydrosilylation of ketoximes using DIOP (2,3-*O*-isopropylidene-2,3-dihydroxy-1,4-bis(diphenylphosphino)butane) as a chiral ligand, but enantioselectivities of the produced *primary* amines were moderate (up to 36% ee).[7] On the other hand, we have recently disclosed that the ruthenium(II)- and iridium(I)-catalysed asymmetric hydrosilylation of imines by using oxazolinylferrocenylphosphines[8] (**1**) as chiral ligands gave the corresponding *secondary* amines with high enantioselectivities after acid hydrolysis (up to 89% ee).[9] As an extension of our studies, we have now investigated the ruthenium(II)-catalysed asymmetric hydrosilylation of ketoximes by using **1** as chiral ligands and have found that the corresponding chiral *primary* amines were produced successfully. Preliminary results are described here.

Treatment of 1-tetralone oxime[10] (**3a**) with 3 equiv. of diphenylsilane in THF in the presence of [$RuCl_2(PPh_3)$·**1a**] (**2a**) (1 mol%) at rt for 24 h afforded 1,2,3,4-tetrahydro-1-naphthylamine (**4a**) in 46% GLC yield with 74% ee (*R*) after acid hydrolysis (Scheme 1; Table 1, run 1).[11] The ee value of **4a** was determined by GLC analysis of the corresponding trifluoroacetamide. The relatively low yield of **4a** to the high conversion of **3a** is considered to be due to the formation of unidentified side products together with 1-tetralone, which was probably formed after the hydrolysis of some intermediates. The addition of AgOTf (1 mol%; OTf = OSO_2CF_3) to the reaction system slightly increased the yield of **4a** (Table 1, run 2). The use of **2b**, bearing *i*-Pr substituted oxazoline, in place of **2a** caused a decrease of the catalytic activity (Table 1, run 3). The ruthenium complex having an oxazolinylphenylphosphine[12] (**1c**) without planar chirality showed a quite low enantioselectivity (Table 1, run 4), compared with that having an oxazolinylferrocenylphosphine (**1a** and **1b**). Reaction in the presence of 2 mol% of **2a** and AgOTf in DME (1,2-dimethoxyethane) gave the best enantioselectivity (up to 83% ee) (Table 1, runs 5 and 6). It is noteworthy that none of the oxazolinylphosphines (**1a**, **1b**, and **1c**) worked effectively as chiral ligands for the rhodium- and iridium-catalysed asymmetric hydrosilylation of ketoximes. For example, the ee values of **4a** obtained by using rhodium and iridium catalysts having **1a** were only 8% (*S*) and 5% (*R*), respectively. Furthermore, no reaction occurred when the ruthenium complex with DIOP was employed under the same reaction conditions, in contrast to Brunner's results[7] described above (Rh-catalysed: up to 36% ee).

Asymmetric hydrosilylation of other ketoximes with diphenylsilane was investigated in the presence of **2** and AgOTf.[13] Typical results are summarised in Table 2. Reactions of 1-indanone oxime (**3b**) and 1-benzosuberon oxime (**3c**) proceeded smoothly, but only moderate enantioselectivities were obtained (Table 2, runs 3–5). In the case of acetophenone

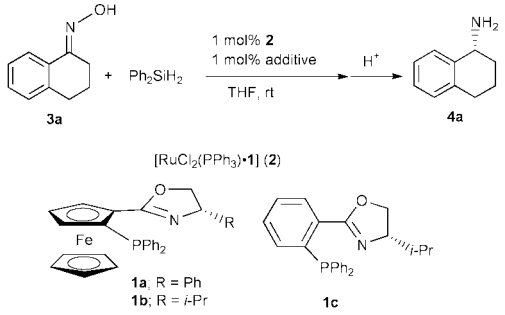

Scheme 1 Asymmetric hydrosilylation of ketoximes.

Table 1 Ruthenium-catalysed asymmetric hydrosilylation of 1-tetralone oxime (**3a**)[a]

Run	Catalyst/ mol%	Additive/ mol%	Reaction time/h	Conv. of **3a** (%)	Yield of **4a** (%)[b]	ee of **4a** (%)[c]
1	**2a** (1)	—	24	>95	46	74 (*R*)
2	**2a** (1)	AgOTf(1)	18	>95	50	78 (*R*)
3	**2b** (1)	AgOTf(1)	80	>95	45	74 (*R*)
4	**2c** (1)	AgOTf(1)	40	77	44	23 (*R*)
5	**2a** (2)	AgOTf(2)	15	>95	71	79 (*R*)
6[d]	**2a** (2)	AgOTf(2)	24	>95	65	83 (*R*)

[a] All reactions were carried out in the presence of a catalyst and an additive using ketoxime **3a** (1.0 mmol) and Ph_2SiH_2 (3.0 mmol) in THF (5 ml) at rt.[b] GLC yield.[c] Determined by GLC analysis of the corresponding trifluoroacetamide.[d] DME was used in place of THF.

 DOI: 10.1039/b106435p

Table 2 Ruthenium-catalysed asymmetric hydrosilylation of ketoximes (**3**)[a]

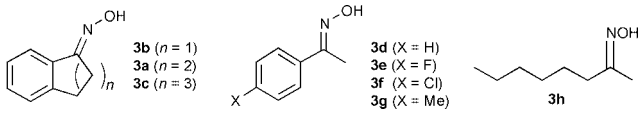

Run	Ketoxime	Catalyst	Solvent	Reaction time/h	Conv. of **3** (%)	Yield of **4** (%)[b]	ee of **4** (%)[c]
1	**3a**	**2a**	THF	20	>95	50	79 (*R*)
2	**3a**	**2a**	DME	25	>95	62	83 (*R*)
3	**3b**	**2a**	DME	40	>95	26	18 (*R*)
4	**3b**	**2b**	DME	40	>95	10	35 (*R*)
5	**3c**	**2a**	THF	90	>95	45	60 (*R*)
6	**3d**	**2a**	THF	20	>95	5	58 (*R*)
7	**3d**	**2b**	THF	40	>95	21	89 (*R*)
8	**3e**	**2b**	THF	25	>95	22	61 (*R*)
9	**3f**	**2b**	THF	25	70	26	74 (*R*)
10	**3g**	**2b**	DME	40	>95	15	69 (*R*)
11	**3h**	**2a**	THF	90	>95	6	12 (*R*)

[a] All reactions were carried out in the presence of catalyst (0.010 mmol) and AgOTf (0.010 mmol) using ketoxime **3** (0.50 mmol) and Ph_2SiH_2 (2.0 mmol) in solvent (5 ml) at rt.[b] GLC yield.[c] Determined by GLC analysis of the corresponding trifluoroacetamide.

oxime (**3d**),[14] the best enantioselectivity of 89% ee was achieved (Table 2, run 7). Introduction of a *p*-halogeno or *p*-methyl substituent to the aromatic ring of acetophenone oxime slightly decreased the enantioselectivity (Table 2, runs 8–10). When **2b** was used in place of **2a** as catalyst, a slightly better enantioselectivity was obtained in several cases (Table 2, runs 7–10). Dialkyl ketoxime (**3h**) was also converted into the corresponding dialkyl amine, but unfortunately in low yield with low enantioselectivity (Table 2, run 11).

In summary, we have developed the highly enantioselective ruthenium(II)-catalysed hydrosilylation of ketoximes to give the corresponding *primary* amines with high enantioselectivities (up to 89% ee) after hydrolysis. This may provide a versatile method for the straightforward synthesis of chiral *primary* amines because of the ready accessibility of ketoximes by reaction of ketones with hydroxylamine. Further work is currently in progress aiming at the elucidation of the reaction mechanism and broadening the scope of this asymmetric hydrosilylation.

This work was supported by Grant-in-Aid for Scientific Research (Nos. 09102004 and 12750747) from the Ministry of Education, Culture, Sports, Science and Technology, Japan.

Notes and references

1 For recent reviews, (*a*) E. Juaristi, J. Escalante, J. L. Le-Romo and A. Reyes, *Tetrahedron: Asymmetry*, 1998, **9**, 715; (*b*) E. Juaristi, J. L. Le-Romo, A. Reyes and J. Escalante, *Tetrahedron: Asymmetry*, 1999, **10**, 2441.

2 (*a*) S. Itsuno, M. Nakano, K. Miyazaki, H. Masuda, K. Ito, A. Hirao and S. Nakahama, *J. Chem. Soc., Perkin Trans. 1*, 1985, 2039; (*b*) S. Itsuno, Y. Sakurai, K. Ito, A. Hirao and S. Nakahara, *Bull. Chem. Soc. Jpn.*, 1987, **60**, 395; (*c*) Y. Sakito, Y. Yoneyoshi and G. Suzukamo, *Tetrahedron Lett.*, 1988, **29**, 223.

3 (*a*) M. T. Reetz and C. Dreisbach, *Chimia*, 1994, **48**, 570 and references cited therein; (*b*) S. Takayama, S. T. Lee, S.-C. Hung and C.-H. Wong, *Chem. Commun.*, 1999, 127; (*c*) S. Arai, S. Bellemin-Laponnaz and G. C. Fu, *Angew. Chem., Int. Ed.*, 2001, **40**, 234.

4 (*a*) P. Krasik and H. Alper, *Tetrahedron: Asymmetry*, 1992, **3**, 1283; (*b*) A. C. Chan, C.-C. Chen, C.-W. Lin, Y.-C. Lin, M.-C. Cheng and S.-M. Peng, *J. Chem. Soc., Chem. Commun.*, 1995, 1767.

5 (*a*) S. Kobayashi and H. Ishihara, *Chem. Rev.*, 1999, **99**, 1069; (*b*) T. Ohkuma, M. Kitamura and R. Noyori, in *Catalytic Asymmetric Synthesis*, ed. I. Ojima, Wiley-VCH, New York, 2000, ch. 1.

6 (*a*) K. Tani, J.-I. Onouchi, T. Yamagata and Y. Kataoka, *Chem. Lett.*, 1995, 955; (*b*) S. Kainz, A. Brinkmann, W. Leitner and A. Pfaltz, *J. Am. Chem. Soc.*, 1999, **121**, 6421; (*c*) K. Abdur-Rashid, A. J. Lough and R. H. Morris, *Organometallics*, 2001, **20**, 1047; (*d*) N. Uematsu, A. Fujii, S. Hashimoto, T. Ikariya and R. Noyori, *J. Am. Chem. Soc.*, 1996, **118**, 4916; (*e*) X. Verdaguer, U. E. W. Lange, M. T. Reding and S. L. Buchwald, *J. Am. Chem. Soc.*, 1996, **118**, 6784; (*f*) X. Verdaguer, U. E. W. Lange and S. L. Buchwald, *Angew. Chem., Int. Ed.*, 1998, **37**, 1103.

7 (*a*) H. Brunner and R. Becker, *Angew. Chem., Int. Ed.*, 1984, **23**, 222; (*b*) H. Brunner, R. Becker and S. Gauder, *Organometallics*, 1986, **5**, 739.

8 (*a*) Y. Nishibayashi and S. Uemura, *Synlett*, 1995, 79; (*b*) Y. Nishibayashi, K. Segawa, Y. Arikawa, K. Ohe, M. Hidai and S. Uemura, *J. Organomet. Chem.*, 1997, **545–546**, 381 and references cited therein.

9 (*a*) Y. Nishibayashi, I. Takei, S. Uemura and M. Hidai, *Organometallics*, 1998, **17**, 3420; (*b*) I. Takei, Y. Nishibayashi, Y. Arikawa, S. Uemura and M. Hidai, *Organometallics*, 1999, **18**, 2271.

10 In the present study, the prochiral ketoximes were used as formed from the corresponding ketones and hydroxylamine liberated from hydroxylammonium chloride.[7] A single isomer of each ketoxime was tentatively assigned as (*E*)-form from the following arguments: G. L. Karabatsos and N. Hsi, *Tetrahedron*, 1967, **23**, 1079; K. Maruoka, T. Miyazaki, M. Ando, Y. Matsumura, S. Sakane, K. Hattori and H. Yamamoto, *J. Am. Chem. Soc.*, 1983, **105**, 2831; D. L. Boger and W. L. Corbett, *J. Org. Chem.*, 1992, **57**, 4777; K. D. Sugi, T. Nagata, T. Yamada and T. Mukaiyama, *Chem. Lett.*, 1997, 493.

11 When the reaction of **3a** (2.50 mmol) with diphenylsilane (10.0 mmol) was carried out under the same reaction conditions, **4a** was isolated in 67% yield (70% GLC yield) with 80% ee.

12 G. Helmchen and A. Pfaltz, *Acc. Chem. Res.*, 2000, **33**, 336 and references cited therein.

13 A typical procedure for ruthenium-catalysed asymmetric hydrosilylation of ketoximes is as follows. In a 20 ml flask were placed catalyst **2a** (10.3 mg, 0.010 mmol; 2.0 mol%) and AgOTf (2.6 mg, 0.010 mmol; 2.0 mol%) under N_2. Anhydrous DME (5 ml) was added, and then the mixture was magnetically stirred at rt for 1 h. After the addition of 1-tetralone oxime (**3a**) (80 mg, 0.50 mmol), diphenylsilane (2.0 mmol) was slowly added at rt and the mixture was stirred at rt for an appropriate time. The mixture was then quenched with MeOH (1.0 ml), stirred at rt for 30 min, and subsequently hydrolysed by the addition of 1 N HCl aq. The mixture was extracted with water (50 ml), and 3 N NaOH aq. (20 ml) was added to the aqueous solution to obtain a free amine. This solution was extracted with diethyl ether (50 ml × 3) and the extract was dried over anhydrous $MgSO_4$. For GLC analysis of the yield of **4a**, *n*-tetradecane was added as an internal standard. The optical purity was determined by GLC analysis of the corresponding trifluoroacetamide on a cyclodextrin phase (Chiraldex GT-A, 30 m). The absolute configuration of **4a** was determined by an optical rotation..

14 Acetophenone oxime (**3d**) was assigned as the (*E*)-isomer by ^{1}H NMR; F. G. Bordwell and G.-Z. Ji, *J. Org. Chem.*, 1992, **57**, 3019.

CHEMCOMM
Communication
www.rsc.org/chemcomm

Multi-component coupling reactions: synthesis of a guanidine containing analog of the hexahydropyrrolo[3,2-*c*]quinoline alkaloid martinelline

Robert A. Batey* and David A. Powell

Department of Chemistry, University of Toronto, 80 St George Street, Toronto, Ontario, Canada M5S 3H6. E-mail: rbatey@chem.utoronto.ca

Received (in Cambridge, UK) 15th August 2001, Accepted 19th September 2001
First published as an Advance Article on the web 23rd October 2001

A multi-component coupling reaction is used to synthesize a highly functionalized guanidine containing pyrroloquinoline analog of martinelline that displays bradykinin B2 receptor antagonist activity.

The martinelline alkaloids **1**[1] (Fig. 1) have attracted a considerable amount of interest from the synthetic community,[2–4] much of which stems from the unique biological activity and unprecedented (in nature) hexahydropyrrolo[3,2-*c*]quinoline core of these natural products. Martinelline was the first naturally occurring, non-peptidic bradykinin receptor antagonist to be identified and antagonists of the bradykinin B2 receptor have been implicated as potential therapeutics for pain, rhinitis, shock and asthma.[5] Hence martinelline and derivatives thereof offer significant potential as novel pharmaceutical agents. Despite considerable work towards the synthesis of the tricyclic core,[2] only recently has a 29 step total synthesis of (−)-martinellic acid **1b** been achieved.[3] Furthermore, there are no reported structure–activity relationship studies on synthetic analogs of **1a** and **1b**.

We recently reported a one pot protocol towards the hexahydropyrrolo[3,2-*c*]quinoline core of martinelline utilizing a lanthanide triflate[6,7] catalyzed formal hetero Diels–Alder reaction (Povarov reaction)[8] between an aniline, aldehyde and a protected endocyclic enamine component (*N*-CBz 2-pyrroline).[4] In all cases an approximate 1:1 mixture of *endo*:*exo* diastereomers[9] was observed using $Dy(OTf)_3$ in MeCN. Moreover, conversion of the deprotected pyrrolidine nitrogen to a trisubstitued guanidine proved to be problematic. An alternative strategy to introduce the *N*-1 guanidine from an appropriately functionalized 2-pyrroline was thus required. We now report the first use of a synthetic equivalent to a 2-pyrroline, which employs an *N*-thiocarbamoyl group to improve the *exo*-selectivity of the hetero Diels–Alder reaction and provides a means to introduce the challenging *N*-1 trisubstituted guanidine functionality. A simplified analogue of **1a** which displays similar biological activity to the natural product is synthesized using this strategy.

One approach to improve the diastereoselectivity of the key 3-component Povarov reaction is to modify the *N*-substituent on the 2-pyrroline component. This approach initially appears to be problematic, as the synthesis and isolation of the requisite *N*-substituted-2-pyrrolines by dehydration of the corresponding hemiaminals requires harsh conditions (acid catalysis with reflux) and often proceeds in low yields. We considered that cyclic hemiaminals could however serve as *in situ* equivalents of *N*-substituted-2-pyrrolines under the mildy Lewis acidic conditions employed for the 3-component coupling reaction. Since thioureas are useful guanidine precursors, a *N*-thiocarbamoyl group was considered an ideal choice for this purpose. Synthesis of the pyrrolidine carbothioic acids (Scheme 1) was accomplished through reaction of the sodium anion of 2-pyrrolidinone with benzylisothiocyanate. The resulting lactam was reduced with 1.5 equiv. of DIBAL-H in CH_2Cl_2 at −78 °C to furnish the lactamol **2**. Lactamol **2** was found to be unstable when stored for extended periods of time and was converted to the methyl ether **3**, which could be stored for up to 8 months at room temperature without significant decomposition.

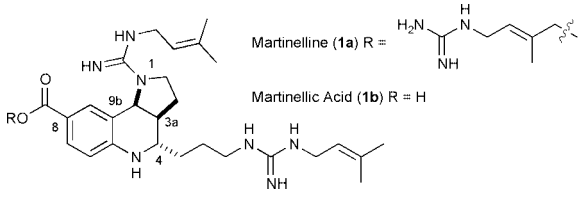

Fig. 1 Martinelline alkaloids (IUPAC numbering).

As desired, both **2** and **3** serve as endocyclic enamine equivalents in the lanthanide triflate catalyzed Povarov reaction. Lewis acid promoted loss of water from **2** or MeOH from **3** generates *in situ N*-substituted-2-pyrroline which reacts with the 2-azadiene, generated *in situ* from the aldehyde and aniline components, affording pyrroloquinoline **4** as a 7:3 mixture of *exo*:*endo* diastereomers (Table 1). This is the first example, to our knowledge, of the use of N-protected hemiaminals as dienophile precursors in hetero Diels–Alder reactions of this type and offers a significant improvement in both the range of protected endocyclic enamines and facility with which they can be employed as dienophiles.[10] This observation is of potential importance for combinatorial applications of such 3-component coupling reactions.

We envisioned the conversion of thiourea **4** to the trisubstituted guanidine through a modified Rathke procedure. Accordingly, 3-component coupling product *exo*-**4b** was ethy-

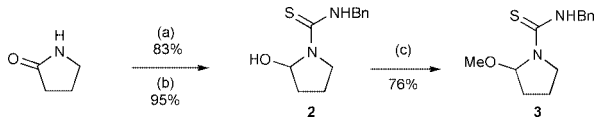

Scheme 1 *Reagents and conditions*: (a) i) NaH, THF, 0 °C, 20 min., ii) BnNCS, −78 °C to 25 °C 16 h; (b) DIBAL-H, −78 °C, 2 h; (c) $HC(OMe)_3$, PPTS (cat.), MeOH, rt, 4 h.

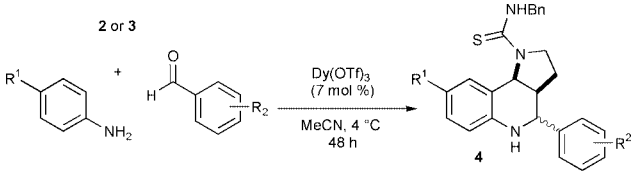

4	R^1	R^2	Yield (%)[a]	dr[b] (*exo*:*endo*)
a	H	3,4-Cl	74	76:24
b	MeOOC	3,4-Cl	80	70:30
c	MeOOC	H	81	70:30
d	Teoc[c]	3,4-Cl	64	72:28

[a] Yield based on **2**, within ± 5% of the yields based on **3**. [b] dr determined by ^1H NMR of the crude reaction mixture. [c] Teoc = $(CH_3)_3SiCH_2CH_2OOC$–.

 DOI: 10.1039/b107431h

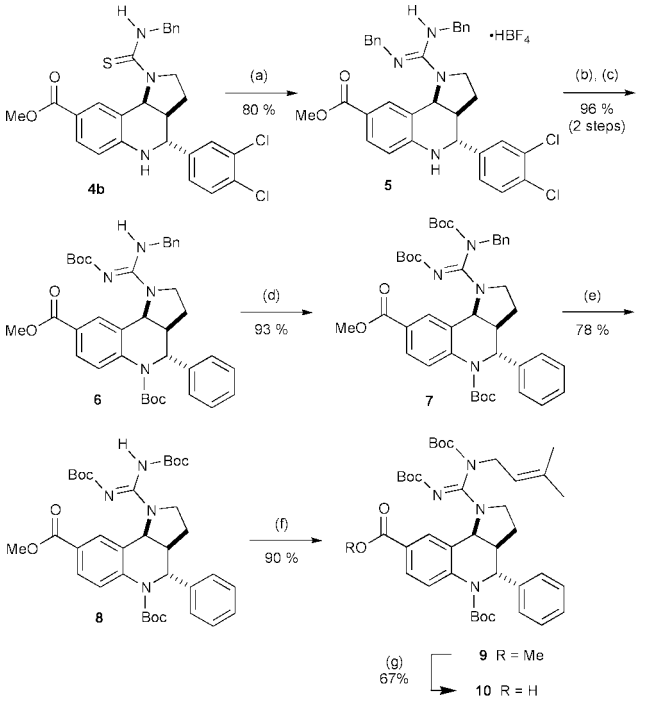

Scheme 2 *Reagents and conditions*: (a) i) $Et_3O^+BF_4^-$ (1.0 equiv.), CH_2Cl_2, rt, 1 h; ii) $BnNH_2$, MeCN, 75 °C, 20 h; (b) Boc_2O, DMAP, Cs_2CO_3, CH_2Cl_2, rt, 24 h; (c) $Pd(OH)_2$ (10 mol%), H_2, Et_3N, MeOH, rt, 5 h; (d) Boc_2O, DMAP (5 mol%), CH_2Cl_2, 4 h; (e) $Pd(OH)_2$ (50 mol%), H_2, Et_3N, MeOH, rt, 24 h; (f) 4-bromo-2-methylbutene, K_2CO_3, MeCN, 50 °C, 4 h; (g) *t*-BuOK, H_2O, THF, 70 °C, 5 h.

lated with 1.0 equiv. of triethyloxonium tetrafluoroborate[11] and the crude mixture refluxed with benzylamine in MeCN for 20 h to afford guanidinium salt **5** in 80% yield (Scheme 2). Debenzylation of the guanidine was accomplished through a modification of a procedure first outlined by Isobe.[12] First the guanidine and aniline nitrogens were acylated with Boc_2O under basic conditions. The benzyl groups were then removed sequentially with hydrogenation over Pearlman's catalyst. Treatment with catalytic $Pd(OH)_2$ and Et_3N in MeOH gave the monodebenzylated guanidine **6** in quantitative yield. Perhaps not surprisingly, the aryl chloride was also reduced under these conditions. Acylation of the guanidine at the more nucleophilic nitrogen gave **7**, which on hydrogenation gave the fully protected guanidine compound **8**. The isoprenyl side chain was installed through nucleophilic displacement of bromide from 4-bromo-2-methylbutene under basic conditions. Finally, the methyl ester **9** was hydrolyzed with *t*-BuOK–H_2O in THF[13] to afford carboxylic acid **10** in 67% yield.

The side chain **11** was installed through Mitsunobu coupling with acid **10** to give ester **12** which was deprotected with TFA–CH_2Cl_2 to yield the highly functionalized model compound **13** as its TFA salt (Scheme 3).[14] The binding affinities of (±)-**13** against human bradykinin B1 and human and rat B2 receptors were determined with IC_{50} values of >10 μm, 1.7 μm and 2.4 μm respectively. Similar selectivity for the B2 over the B1 receptors is shown for (±)-**13** and martinelline.[1] The B2 binding affinity of (±)-**13** is between that of martinelline and martinellic acid, suggesting that the guanidine containing C-8 ester side chain is of greater importance for B2 receptor antagonist activity than the C-4 aliphatic guanidine side chain.

In conclusion, these model studies have demonstrated the convergent synthesis of a highly functionalized derivative of martinelline containing 2 of the 3 guanidine side chains and a phenyl group in place of the C-4 aliphatic guanidine side chain. In addition, the first biological studies reported on a synthetic analog of martinelline are presented. Further application of this methodology towards the synthesis of martinelline, martinellic acid and analogs thereof will be reported in due course.

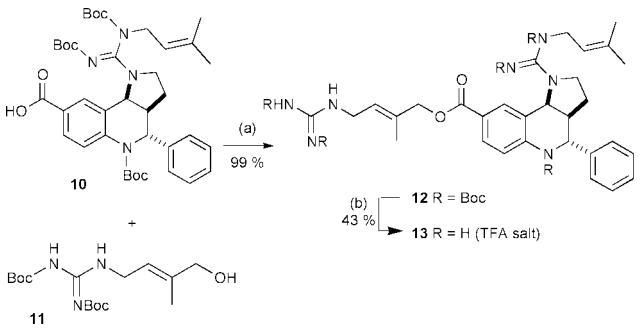

Scheme 3 *Reagents and conditions*: (a) **11** (1.2 equiv.), PPh_3, DEAD, THF, rt, 2 h; (b) TFA, CH_2Cl_2, rt, 24 h.

We thank Paul D. Simoncic for preliminary studies and the synthesis of **11** and Joanne Butterworth at AstraZeneca for ligand binding studies on **13**. We also thank Dr A. B. Young for mass spectrometric analyses and Dr T. Burrow for NMR analysis of **13**. AstraZeneca, the Natural Science and Engineering Research Council (NSERC) of Canada and the Ontario Research and Development Challenge Fund supported this work. D.A.P. thanks AstraZeneca and NSERC for an Industrial Postgraduate Scholarship.

Notes and references

1 K. M. Witherup, R. W. Ransom, A. C. Graham, A. M. Bernard, M. J. Salvatore, W. C. Lumma, P. S. Anderson, S. M. Pitzenberger and S. L. Varga, *J. Am. Chem. Soc*., 1995, **117**, 6682.

2 (*a*) M. K. Gurjar, S. Pal and A. V. R. Rao, *Heterocycles*, 1997, **45**, 231; (*b*) T. C. T. Ho and K. Jones, *Tetrahedron*, 1997, **53**, 8287; (*c*) M. Hadden and P. J. Stevenson, *Tetrahedron Lett*., 1999, **40**, 1215; (*d*) C. J. Lovely and H. Mahmud, *Tetrahedron Lett*., 1999, **40**, 2079; (*e*) B. B. Snider, Y. Ahn and B. M. Foxman, *Tetrahedron Lett*., 1999, **40**, 3339; (*f*) S. K. Kang, S. S. Park, S. S. Kim, J.-K. Choi and E. K. Yum, *Tetrahedron Lett*., 1999, **40**, 4379; (*g*) K. E. Frank and J. Aubé, *J. Org. Chem*., 2000, **65**, 655; (*h*) M. Nyerges, I. Fejes and L. Töke, *Tetrahedron Lett*., 2000, **41**, 7951; (*i*) C. Escolano and K. Jones, *Tetrahedron Lett*., 2000, **41**, 8951; (*j*) J. A. Nieman and M. D. Ennis, *Org. Lett*., 2000, **2**, 1395; (*k*) B. B. Snider and S. M. O'Hare, *Tetrahedron Lett*., 2001, **42**, 2455; (*l*) H. Mahmud, C. J. Lovely and H. V. R. Dias, *Tetrahedron*, 2001, **57**, 4095; (*m*) M. Hadden, M. Nieuwenhuyzen, D. Potts, P. J. Stevenson and N. Thompson, *Tetrahedron*, 2001, **57**, 5615; (*n*) M. Hadden, M. Nieuwenhuyzen, D. Osborne, P. J. Stevenson and N. Thompson, *Tetrahedron Lett*., 2001, **42**, 6417.

3 D. Ma, C. Xia, J. Jiang and J. Zhang, *Org. Lett*., 2001, **3**, 2189.

4 R. A. Batey, P. D. Simoncic, D. Lin, R. P. Smyj and A. J. Lough, *Chem. Commun*., 1999, 651.

5 Y. Öztürk, *Curr. Pharm. Design*, 2001, **7**, 135.

6 T. Imamoto, *Lanthanides in Organic Synthesis*, Academic Press, London, 1994.

7 S. Kobayashi, H. Ishitani and S. Nagayama, *Synthesis*, 1995, 1195.

8 L. S. Povarov, *Russ. Chem. Rev*., 1967, **36**, 656.

9 The *endo* and *exo* diastereomers are defined based on the Diels–Alder reaction, where H-4 and H-3a have a *cis* and *trans* relationship respectively.

10 In addition, we have found other lactamols, including the CBz protected 2-pyrrolidinol, also serve as enamine equivalents in $Ln(OTf)_3$ catalyzed hetero Diels–Alder reaction of *N*-aryl imines.

11 Methylation of **4b** and heating with benzylamine in MeCN for 20 h gave only the demethylated starting material **4b**, presumably through a demethylative S_N2 attack of benzylamine on the methyl thiouronium salt.

12 (*a*) T. Nishikawa, M. Asai, N. Ohyabu, N. Yamamoto and M. Isobe, *Angew. Chem., Int. Ed. Engl*., 1999, **38**, 3081; (*b*) T. Nishikawa, N. Ohyabu, N. Yamamoto and M. Isobe, *Tetrahedron*, 1999, **55**, 4325.

13 P. G. Gassman and W. N. Schenk, *J. Org. Chem*., 1977, **42**, 918.

14 The ^1H NMR of **13** shows a 1.5 Hz coupling constant between protons H-4 and H-3a, which is similar to the coupling observed in martinelline (<2 Hz, ref. 1). We have also found that analogs of the *endo* series also display coupling constants of <2 Hz between H-4 and H-3a.

CHEMCOMM Communication
www.rsc.org/chemcomm

Hydrogen abstraction from ionic liquids by benzophenone triplet excited states†

Mark J. Muldoon,[a] Andrew J. McLean,*[b] Charles M. Gordon*[a] and Ian R. Dunkin[a]

[a] *Department of Pure and Applied Chemistry, University of Strathclyde, 295 Cathedral Street, Glasgow Scotland, UK G1 1XL. E-mail: c.m.gordon@strath.ac.uk*
[b] *Department of Chemistry and Chemical Engineering, University of Paisley, Paisley Campus, Paisley, Scotland, UK, PA1 2BE. E-mail: mcle-ch0@paisley.ac.uk*

Received (in Cambridge, UK) 30th August 2001, Accepted 2nd October 2001
First published as an Advance Article on the web 31st October 2001

The activation energy for hydrogen abstraction from imidazolium-based ionic liquids is significantly higher than that observed in conventional solvents.

The photochemistry of benzophenone (Bp) has been widely investigated over the past 50 years. Its ability in its excited state to act as an energy transfer donor, electron acceptor or hydrogen atom abstracting agent has been exploited in numerous studies.[1] As part of a continuing study of the influence of ionic liquids[2] on photochemical processes,[3] we now report our initial results on hydrogen abstraction from these solvents by triplet excited state benzophenone (^{3}Bp*). Although ionic liquids are finding increasing use in a wide range of applications, there have been only a few reports on the behaviour of excited state species or reactive intermediates in these media.[3,4] Furthermore, only a handful of photochemical systems have been studied in ionic liquids to date, often with results that are quite different from those observed in conventional solvents.[5]

The ionic liquids used in this study were based on the cations 1-butyl-3-methylimidazolium ([bmim]$^+$), 1-methyl-3-octylimidazolium ([omim]$^+$) and 1-butyl-2,3-dimethylimidazolium ([bmmim]$^+$), combined with the anions $[PF_6]^-$ and $[Tf_2N]^-$ (Tf = CF_3SO_2), chosen to give a moderate degree of structural variation. All are immiscible with water, facilitating their preparation in a 'spectroscopically pure' form.‡ Hydrogen abstraction was studied in five different ionic liquids and three conventional solvents using laser flash photolysis methods.§ Laser excitation (λ_{ex} = 355 nm) of N_2-saturated 5 mM solutions of Bp gave rise to a broad feature with a maximum at λ = *ca.* 525 nm, entirely typical of ^{3}Bp*.[6] This species decayed *via* first order kinetics over several microseconds forming a second, long-lived species that exhibited a slight solvent dependence in its absorption maximum (λ_{max} = 530–550 nm), suggesting formation of the hydrogen abstraction product benzophenone ketyl radical (KR). An example of the spectra obtained is given in the ESI†. The short–lived component formed initially was quenched by naphthalene at a diffusion controlled rate,[7] forming triplet excited state naphthalene (λ_{max} = 425 nm). The decay rate of both components was strongly dependent on oxygen concentration. We are therefore very confident of the assignment of both species (see Scheme 1). The hydrogen abstraction product, benzophenone ketyl radical (KR) is known to exhibit a λ_{max} value around 540 nm (±10 nm), depending on the solvent.[8] The lifetime of KR was orders of magnitude longer than that of ^{3}Bp*.

It is clear that the values of the first order decay rate constant of ^{3}Bp*, k_{obs}, determined in ionic liquids are an order of magnitude *lower* than those observed in the conventional solvents (see Table 1) despite the clear availability of abstractable alkyl hydrogen atoms on the cation substituents. In cyclohexane, toluene and butan-1-ol, we found that the relative amplitudes of absorbances from KR relative to those of ^{3}Bp* were independent of temperature, indicating that ^{3}Bp* decays entirely *via* the hydrogen abstraction process in these solvents. However, the amplitude of the KR signals increased relative to those of ^{3}Bp* with increasing temperature in the ionic liquids. This indicates that not all ^{3}Bp* species decayed *via* a single process in these media. There are two possible mecanisms responsible for this temperature dependence of KR quantum yield: competing decay pathways of the ^{3}Bp* or geminate recombination of the KR and solvent radicals competing with cage escape. The latter seems unlikely despite the high viscosities of the ILs because there is no correlation between the yield of KR and solvent viscosity, η. Consequently it seems more likely that the former mechanism is responsible for the yield effects.

As Scheme 1 shows, ^{3}Bp* can decay *via* two competing processes: H-atom abstraction from the solvent (rate constant k_H) to form KR, and intersystem crossing (ISC, rate constant k_T) giving the ground state. The observed first order rate constant is the sum of these two rate constants (*i.e.*, $k_{obs} = k_H + k_T$). Based on the assumption that the absorbance measured directly after the laser pulse arises entirely from ^{3}Bp*, while the absorbance after several μs arises from KR only, it is possible to calculate the values of k_H and k_T from the intensities of the transient absorption bands for ^{3}Bp* and KR. Values of k_H were then calculated using eqn. (1) where ΔA_H and ΔA_T are the absorbance signals at 530 nm due to KR and ^{3}Bp*, respectively, and $\varepsilon_T/\varepsilon_H$ is the ratio of the molar absorptivities of ^{3}Bp*:KR at 530 nm. The value of $\varepsilon_T/\varepsilon_H$ was taken as 2.4 in all cases.[9]

$$k_H = k_{obs}(\Delta A_H/\Delta A_T)(\varepsilon_T/\varepsilon_H) \quad (1)$$

The values of k_{obs} (and thus k_H) were recorded over the temperature range 3–70 °C in each solvent, and the Arrhenius parameters for H-abstraction were determined. The results are summarised in Table 1.¶

The k_T values listed for the ionic liquids are comparable to that observed in benzene (*ca.* 1.7 × 10^5 s^{-1} at 298 K), an electrophilic solvent in which no hydrogen abstraction occurs. The cationic components of the ILs are also of course electrophilic, suggesting that similar solvation effects are responsible for controlling ^{3}Bp* deactivation in both solvent types. The Arrhenius data for hydrogen abstraction clearly show that the low k_{obs} values in ionic liquids arise from the lower values of k_H in these solvents compared with conventional solvents. It is also clear that there is a significant difference in E_a values between the ionic liquids and those in conventional

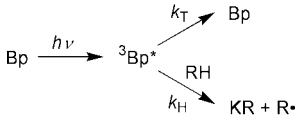

Scheme 1

† Electronic supplementary information (ESI) available: transient spectra of ^{3}Bp* and KR in [omim][Tf_2N]. Purification of starting materials for ionic liquids. Arrhenius plots obtained for H-abstraction by ^{3}Bp* ionic liquids. UV–VIS spectra of Bp in ionic liquids. See http://www.rsc.org/suppdata/cc/b1/b107730a/

 DOI: 10.1039/b107730a

Table 1 Arrhenius data obtained for the abstraction of hydrogen from ^{3}Bp* in a range of solvents

Solvent	η^a/cP	$k_{obs}{}^{bc}$/s^{-1}	Φ^b	$k_T{}^b$/s^{-1}	$k_H{}^b$/s^{-1}	ln A_H	E_a/kJ mol^{-1}
[bmim][PF_6]	330	3.6×10^5	0.57	1.6×10^5	2.0×10^5	22.5 (± 1.1)	25.4 (± 2.5)
[omim][PF_6]	940	4.8×10^5	0.72	1.4×10^5	3.4×10^5	21.7 (± 0.9)	22.2 (± 2.2)
[bmim][Tf_2N]	61	3.2×10^5	0.46	1.8×10^5	1.4×10^5	20.7 (± 1.1)	21.9 (± 2.2)
[bmmim][Tf_2N]	113	7.3×10^5	0.23	5.6×10^5	1.7×10^5	23.1 (± 1.1)	27.3 (± 2.7)
[omim][Tf_2N]	118	1.3×10^6	0.76	5.7×10^5	7.3×10^5	22.3 (± 0.9)	21.6 (± 2.2)
Toluene	0.59	3.1×10^6	1.0	—	2.7×10^6	20.7 (± 0.8)	14.5 (± 2.0)
Cyclohexane	1.02[17]	4.9×10^6	1.0	—	4.9×10^6	21.0 (± 0.7)	13.7 (± 1.7)
Butan-1-ol	2.95	1.1×10^7	1.0	—	1.1×10^7	21.6 (± 0.8)	13.3 (± 2.0)

[a] At 20 °C except where noted. [b] At 23.5 °C. [c] Errors within 5%.

solvents (*ca.* 25 and 15 kJ mol^{-1} respectively). Despite the uncertainty in $\varepsilon_T/\varepsilon_H$, our results indicate that the uniformly low k_H values in ionic liquids arise as a consequence of uniquely high E_a values in these solvents rather than systematic variation in A_H values. The similarities in A_H values suggest that the transition state geometries for H-abstraction are similar in all the solvents in this study.‖ The results show that the activation parameters for H abstraction in the ionic liquids are essentially independent of the anionic component and the availability of the hydrogen atom at the 2-position on the imidazolium ring. Also, the values of k_H are larger for the [omim]$^+$ salts than those with [bmim]$^+$ or [bmmim]$^+$ cations. We therefore conclude that it is more likely that an alkyl chain H atom is being abstracted in the ionic liquids, but cannot currently discriminate its precise location. It should be noted that abstraction of a benzylic H atom would result in the formation of a resonance stabilised radical cation.

Several factors are known to influence the rate constant for H abstraction by aromatic ketone excited states. Firstly, the nπ* or $\pi\pi$* character of the ketone excited state can be influenced by solvent polarity. UV–VIS spectra suggest that no unique interactions are observed in ionic liquids compared with the conventional solvents (see ESI†). Furthermore, there is no evidence that the differences in E_a can be attributed to differences in bond strength of the C–H bonds involved in the abstraction process as has been noted previously.[10] IR and ^{1}H NMR spectra suggest that alkyl CH bonds in the 1,3-dialkylimidazolium salts display essentially the same properties as alkanes, with the exception of the CH_2 group bonded directly to the ring. Finally, there is no evidence for the influence of a charge transfer interaction in the excited state, as the spectra of ^{3}Bp* and KR are essentially identical to those in conventional solvents.

Thus, there is no spectroscopic evidence for uniquely strong interactions between the ILs and Bp or ^{3}Bp*. The similarity in pre-exponential factors for H-abstraction in all solvents suggests that the transition state structure is solvent independent. It is possible that electrostatic interactions between the solvent ions must be broken or disrupted in order to arrive at the common transition state geometry. Small movements of either ion could then result in significant energy costs resulting in the raising of the transition state energy and thereby E_a.

Finally, these results show that the effect of an ionic liquid on a relatively well understood chemical reaction involving low polarity reactants and transition states may be very significant and yet have a subtle origin. We have observed that significant lowering of rate constants for hydrogen abstraction from the solvent can occur despite the absence of any direct solvation effects on reactants. These results also show, however, that ionic liquids cannot be regarded as entirely 'innocent' solvents in the presence of reactive species.

We would like to thank the EPSRC (Grant No. GR/M56852) for financial support and the award of a studentship (M. J. M.), the Royal Society of Edinburgh for the award of a BP Research Fellowship (C. M. G.), and 3M (Minneapolis, MN) for a gift of Li(Tf_2N).

Notes and references

‡ The liquids were prepared following standard literature procedures (see ESI† for details of purification of starting materials).[11]

§ The laser flash photolysis set-up is described elsewhere.[12] All ILs were dried by heating at *ca.* 70 °C under vacuum for several hours prior to preparation of the solutions. Bp (Aldrich) was purified by sublimation. All solutions were thoroughly degassed with nitrogen prior to data collection.

¶ It should be noted that variation from the value of 2.4 estimated for the relative molar absorptivity values does not affect the calculated value of $E_a{}^H$, but only the value of A_H. Arrhenius plots for the ionic liquids may be found in the ESI†.

‖ We cannot directly compare solvent *A* values because of our assumptions regarding the ε ratio and also our lack of current knowledge as to which H atoms are being abstacted from RTILs. Before such comparisons can be made for different solvents, it is necessary to carry out a statistical correction for the relative number of identical, abstractable hydrogen atoms present in each solvent. In this case we cannot 'normalise' the *A* values for the RTILs as we can the conventional solvents. However, were alkyl substituent H atoms being abstracted slightly *higher* values of *A* in RTILs would be calculated than those of the conventional solvents. Were benzylic hydrogen atom abstraction to be dominant, similar values of *A* would be obtained in all solvents. Further research is currently under way in order to clarify this point.

1 See, for example: H. Shizuka and M. Yamaji, *Bull. Chem. Soc. Jpn*, 2000, **73**, 267 and references therein.
2 See: P. Wasserscheid and W. Keim, *Angew. Chem., Int. Ed.*, 2000, **39**, 3772 and references therein.
3 C. M. Gordon and A. J. McLean, *Chem. Commun.*, 2000, 1395.
4 A. Marcinek, J. Zielonka, J. Gebicki, C. M. Gordon and I. R. Dunkin, *J. Phys. Chem. A*, 2001, **105**, 9305; D. Behar, C. Gonzalez and P. Neta, *J. Phys. Chem. A*, 2001, **105**, 7607.
5 H. L. Chum, D. Koran and R. A. Osteryoung, *J. Am. Chem. Soc.*, 1978, **100**, 310; G. Hondrogiannis, C. W. Lee, R. M. Pagni and G. Mamantov, *J. Am. Chem. Soc.*, 1993, **115**, 9828; C. Lee, T. Winston, A. Unni, R. M. Pagni and G. Mamantov, *J. Am. Chem. Soc.*, 1996, **118**, 4919.
6 R. V. Bensasson and J.-C. Gramain, *J. Chem. Soc., Faraday Trans. 1*, 1980, **76**, 1801.
7 A. J. McLean, M. J. Muldoon, C. M. Gordon and I. R. Dunkin, manuscript in preparation.
8 E. J. Land, *Proc. R. Soc. London, Sect. A*, 1968, **305**, 457.
9 The value of 2.4 for the ratio of absorption coefficients was estimated from averages for values of ε_{530} for ^{3}Bp* and KR in conventional solvents.
10 C. M. Previtali and J. C. Scaiano, *J. Chem. Soc., Perkin Trans. 2*, 1972, 1672; L. Giering, M. Berger and C. Steel, *J. Am. Chem. Soc.*, 1974, **96**, 953.
11 J. G. Huddleston, H. D. Willauer, R. P. Swatloski, A. E. Visser and R. D. Rodgers, *Chem. Commun.*, 1998, 1765; P. Bonhôte, A. Das, N. Papageorgiou, K. Kalanasundram and M. Grätzel, *Inorg. Chem.*, 1996, **35**, 1168.
12 A. C. Benniston, P. R. Mackie, L. J. Farrugia, G. Smith, S. J. Teat and A. J. McLean, *New J. Chem.*, 2001, 458.

CHEMCOMM Communication
www.rsc.org/chemcomm

A by-product using TIPS protection—a warning

David J. Barden and Ian Fleming*

Department of Chemistry, Lensfield Road, Cambridge, UK CB2 1EW. E-mail: if10000@cam.ac.uk; Fax: +44 (0)1223 336362; Tel: +44 (0)1223 336372

Received (in Cambridge, UK) 16th August 2001, Accepted 9th October 2001
First published as an Advance Article on the web 31st October 2001

The TIPS derivatives of alcohols are contaminated with more or less of the diisopropyl(*n*-propyl)silyl derivative, which can be a major product when a bad batch of reagent is used, a large excess of reagent is used, and/or the reaction is not taken to completion.

We reported elsewhere a half-expected problem that we met when using the triisopropylsilyl (TIPS) protecting group—the alcohol **1** gave the ortho esters **2** and **3** on attempted silylation.[1] We had expected that acyl migration might be a problem, but we had not expected that it would be the most hindered of the possible alcohol components in equilibrium with each other that would be selected, although there had been two precedents in the silylation of the tetrahedral intermediate produced by intramolecular attack of a secondary alcohol on the carbonyl group of a cyclic imide.[2] The problem was easily overcome in our case by using the pivalate (±)-**4** instead of the acetate, when we obtained cleanly the derivative (±)-**5** with the pivalate on the primary alcohol and the TIPS on the secondary. We now report an entirely different and more general problem when using the TIPS protecting group.

The reactions in Scheme 1 were carried out with racemic material. More recently we have repeated the sequence[3] with enantiomerically enriched material. All the intermediates in the synthetic sequence up to and including the alcohol (+)-**4** were identical (^{1}H-NMR, ^{13}C-NMR, IR, TLC) to the samples prepared earlier, except of course for their optical rotation. We were dismayed, however, when its TIPS derivative gave ^{1}H-NMR and ^{13}C-NMR spectra that were slightly different from those we had measured before. Careful inspection of the ^{1}H-NMR spectrum revealed, downfield of the diagnostic signal from the C-3 proton, a similar signal from a minor component corresponding exactly to the compound (±)-**5** observed in the racemic series. This meant that there was a new product **6** in addition to a little of the right compound (Scheme 2), and that the anomalous spectra were not caused by some unlikely association phenomenon that might have made the enantiomerically enriched materials give different NMR spectra from their racemic counterparts. Furthermore, the next two intermediates in our synthetic sequence also had spectra with the same features—a major product and a slightly different minor product matching the corresponding intermediates in the racemic series.

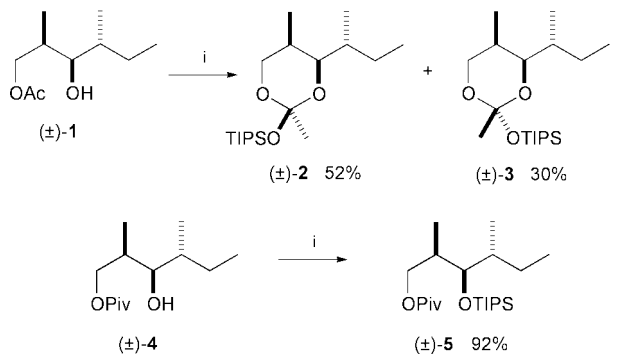

Scheme 1 *Reagents and conditions*: i, Pr$^i_3$SiOTf, 2,6-lutidine, CH_2Cl_2, rt, 30 min.

The presence of a new product might have meant that our enantiomerically enriched material was a diastereoisomer of the alcohol (+)-**4**, with the difference showing up only after TIPS protection; it might have meant that the TIPS and pivalate had exchanged places in this work, even though we knew they had not in the earlier work; finally, it might have meant that there was something wrong with the TIPS reagent. We have now found that it is the last of these explanations—we were the victims of an unfortunate batch of contaminated TIPS triflate.[4] When we repeated the TIPS protection with a different batch of TIPS triflate, the product (+)-**5** now had NMR spectra that were identical to those in the racemic series, and the merest trace of the byproduct was all that we could detect. Order was restored.

We might have left the problem there, but we have noticed that *all* batches of TIPS triflate that we have been able to test have the same problem, usually to a lower extent, making it less noticeable. It is, however, unlikely that we will be the last people to meet this problem, and so we have investigated its nature.

We used 2,4-dimethylpentan-3-ol **7** as a test compound—a secondary alcohol with a similar degree of steric hindrance to that of the alcohol **1**. It too gave two products with the contaminated batch of TIPS triflate, but essentially only one **8** with a good batch of TIPS triflate.[5] The two products could easily be detected in their ^{1}H-NMR spectra by the carbinol proton on C-3, the triplet from the TIPS derivative was at δ3.47 and that from the byproduct at δ3.33. GC-MS showed that the two compounds were isomers. The next clue about what might be wrong came when we found that we could easily control the proportions of the two products by varying the molar proportions of the alcohol **7** and the TIPS triflate reagent. If the contaminated triflate was used in ever larger excess, the amount of byproduct **9** went up proportionately (Scheme 3). We estimate, using the proportion 4:96 of **8**:**9** from the run with the

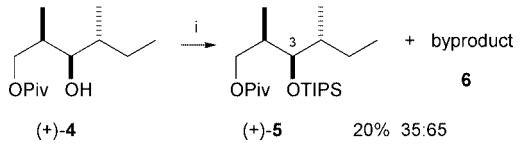

Scheme 2 *Reagents and conditions*: i, 1.25 equiv 'Pr$^i_3$SiOTf', 2,6-lutidine, CH_2Cl_2, rt, 6 h.

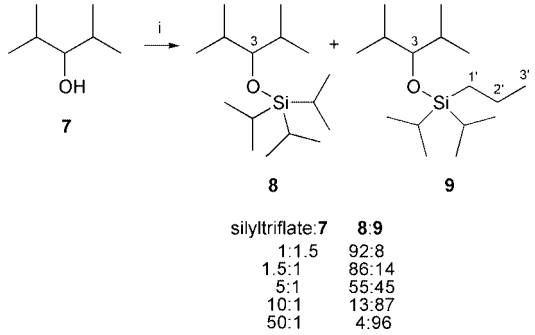

Scheme 3 *Reagents and conditions*: i, Pr$^i_3$SiOTf + Pr$^i_2$Pr^{n}SiOTf (92:8), 2,6-lutidine, CH_2Cl_2, rt, 30 min.

 DOI: 10.1039/b107415f

largest excess of triflate reagent, that the contaminant was reacting nearly 300 times faster than the TIPS triflate.[6] Evidently it was a less hindered silylating agent, and it seemed plausible that it would prove to have a *n*-propyl group in place of one or more of the isopropyl groups.

We confirmed this supposition from the ^{1}H-NMR and ^{13}C-NMR spectra of the silyl ether **9** prepared using the highest ratio of TIPS triflate to alcohol **7**.[7] The ^{13}C-NMR spectrum using the attached proton test showed two methylene signals at δ 15.3 and 17.3 and one methyl signal at δ19.0 from C-1′, C-2′ and C-3′, in addition to the methines and methyls of the isopropyl groups and the carbinol carbon. The ^{1}H-NMR spectrum showed a clear but imperfectly resolved 3-proton triplet at δ0.98 from the 3′ protons of the n-propyl group. In addition there was a 2-proton multiplet at δ 1.42 from the 2′ protons, and a 2-proton multiplet at δ 0.66 from the 1′ protons, neither of which was first-order. An HMQC spectrum showed that the signals assigned to the protons and the carbons of the *n*-propyl group were correlated. None of these signals was present in the spectrum of the pure TIPS derivative **8**. The integrals in the ^{1}H-NMR spectrum showed that there was one *n*-propyl group and not two, a conclusion that was supported by the ^{13}C-NMR spectrum, which showed *two* signals for the methyl groups in the isopropyl groups on silicon, which can only be diastereotopic if there are two isopropyl groups.

When we used an excess (1.5 : 1) of the alcohol **7**, instead of an excess of triflate, the ratio of **8** : **9** was 92 : 8, indicating that our batch of TIPS triflate had been contaminated with about 8% of diisopropyl(*n*-propyl)silyl triflate. A similar experiment with the better reagent indicated that it contained 4% of the impurity, but when this reagent was used in tenfold excess, the ratio of **8** : **9** was a noticeable 42 : 58. It is obviously unwise ever to use an excess of the TIPS reagent. Our original problem with the alcohol (+)-**4** arose, not because we had used a notably large excess of silyl triflate, but because we had failed to allow the reaction to go to completion, another pitfall. We also tested a primary alcohol, 2-methylbutanol, and found that it too gave both silyl ethers. With a tenfold excess of the bad batch, the ratio of TIPS ether to diisopropyl(*n*-propyl)silyl ether was 70 : 30, significantly better than the corresponding ratio 13 : 87 found for the secondary alcohol **7**, as might be expected for a less hindered and therefore less selective nucleophile.

We have been unable to find out how the reagent is made, having been informed only that the method is 'proprietary'. Corey made TIPS triflate by treating triisopropylsilane with triflic acid.[8] The triisopropylsilane had in turn been made by Cunico and Bedell from trichlorosilane and isopropylmagnesium chloride.[9] It seems likely that the alkyl halide used to make the Grignard reagent (or whatever is used commercially) might not always be purely isopropyl. It is also conceivable that the isopropyl Grignard might slowly rearrange to give some *n*-propyl Grignard, and that old batches of Grignard reagent might not reflect the alkyl halide composition that went into them. Furthermore, there is a multiplying factor that makes 1% of the *n*-propyl contaminant in the Grignard reagent lead statistically to 3% of the *n*-propyl impurity in TIPS triflate. It might well be worse than that if there is any selective reactivity in favour of the primary Grignard reagent.

In conclusion, *you are likely to find a byproduct whenever you use TIPS protection*. The problem is worst when (a) an inferior batch of reagent is used, (b) a large excess of reagent is used, (c) the reaction is not taken to completion (d) the alcohol is relatively hindered, and presumably, although we have not tested this, (e) the alcohol is added to the triflate instead of the triflate being added to the alcohol. In our experience, the diisopropyl(*n*-propyl)silyl derivatives have the carbinol proton between 0.05 and 0.14 ppm upfield of the signal from the corresponding signal in the TIPS derivative, and there is always a characteristic multiplet, which is not a first-order triplet, close to δ0.66 from the $SiCH_2$ protons.

Notes and references

1 I. Fleming and A. K. Mandal, *J. Indian Chem. Soc.*, 2000, **77**, 593.

2 W. J. Vloon, J. C. van den Bos, N. P. Willard, G.-J. Koomen and U. K. Pandit, *Recl. Trav. Chim. Pays-Bas*, 1989, **108**, 393; P. A. Grieco, K. J. Henry, J. J. Nunes and J. E. Matt, Jr., *J. Chem. Soc., Chem. Commun.*, 1992, 368.

3 A. K. Mandal, *PhD Thesis*, Cambridge, 1999; to be published when the synthesis of ebelactone-a is complete.

4 Aldrich, batch number 16816TU C1.

5 Following Corey and his co-workers:[8] 2,6-lutidine (0.42 cm^3, 3.6 mmol) and neat silyl triflate (0.15 cm^3, 0.54 mmol) were added successively to the alcohol **7** (0.05 cm^3, 0.36 mmol) in dry DCM (1 cm^3) at 0 °C under nitrogen. After stirring for 30 min at rt, water (2 cm^3) was added, the layers separated and the aqueous layer extracted with DCM (2 × 2 cm^3). The combined organic layers were dried (Na_2SO_4), evaporated under reduced pressure and the residue chromatographed [SiO_2, Et_2O–light petroleum (bp 40–60 °C), 1 : 10] to give the triisopropylsilyl ether **8** quantitatively; R_f(light petroleum) 0.64; ν_{max}(film)/cm^{-1} 1054 (Si–O); δ_H(400 MHz, $CDCl_3$) 3.47 (1 H, t, *J* 4.1, CHOSi), 1.82 (2 H, septet d, *J* 7.0 and 4.1, C*H*CHOSi), 1.15–1.05 (21 H, m, Pr$^i_3$Si), 0.94 (6 H, d, *J* 7.0, *Me*$_A$Me$_B$CHCH) and 0.92 (6 H, d, *J* 7.0, Me$_A$*Me*$_B$CHCH); δ_C(100 MHz, $CDCl_3$) (+ = C or CH_2, − = CH or CH_3) 82.1− (CHOSi), 32.0− (*C*HCHOSi), 20.0− (*Me*$_A$Me$_B$CHCH), 18.5− (Me$_A$*Me*$_B$CHCH), 18.4− (*Me*$_2$CHSi) and 13.5− (SiCH); *m*/*z* (EI) 272 (3%, M$^+$), 229 (100, M − Pr), 187 (33, MH − 2Pr) and 115 (33, M − $SiPr_3$)(Found: M$^+$, 272.2525. $C_{16}H_{36}OSi$ requires *M*, 272.2535). The triisopropylsilyl ether of 2-methylbutanol was prepared similarly; R_f(light petroleum) 0.59; ν_{max}(film)/cm^{-1} 1167 (Si–O); δ_H(400 MHz, $CDCl_3$) 3.55 (1 H, dd, *J* 9.5 and 5.7, C*H*$_A$H$_B$O), 3.48 (1 H, dd, *J* 9.5 and 6.2, CH$_A$*H*$_B$O), 1.6–1.4 (1 H, m, C*H*MeEt), 1.15–1.00 (23 H, m, Pr$^i_3$Si and CHC*H*$_2$Me), 0.90 (3 H, t, *J* 7.3, CHCH$_2$*Me*) and 0.90 (3 H, d, *J* 6.6, CH*Me*Et); δ_C(100 MHz, $CDCl_3$) 68.4+, 37.7−, 25.8+, 18.0−, 16.3−, 12.0− and 11.4− (Found: M$^+$, 244.2229. $C_{14}H_{32}OSi$ requires *M*, 244.2222).

6 The other ratios in Scheme 3 indicate that essentially all the diisopropyl(n-propyl)silyl triflate present has been consumed.

7 Data for the silyl ether **9** prepared on half the scale, using the large excess of the bad batch of triflate and 9 mmol of lutidine, and chromatographed again by preparative TLC to remove the large quantity of siloxane byproducts: R_f(light petroleum) 0.64; ν_{max}($CDCl_3$)/cm^{-1} 1053 (Si–O); δ_H(400 MHz, $CDCl_3$) 3.33 (1 H, t, *J* 4.5, CHOSi), 1.77 (2 H, septet d, *J* 6.9 and 4.5, C*H*CHOSi), 1.42 [2 H, m (not first-order), C*H*$_2$Me], 1.10–0.98 (14 H, m, Pr$^i_2$Si), 0.98 (3 H, t, *J* 7.2, CH$_2$*Me*), 0.91 (6 H, d, *J* 6.9, *Me*$_A$Me$_B$CHCH), 0.88 (6 H, d, *J* 6.9, Me$_A$*Me*$_B$CHCH) and 0.66 [2 H, m (not first-order), $SiCH_2$]; δ_C(100 MHz, $CDCl_3$) 82.3− (CHOSi), 31.8− (*C*HCHOSi), 20.1− (*Me*$_A$Me$_B$CHCH), 19.0− (CH$_2$*Me*), 18.3− (Me$_A$*Me*$_B$CHCH), 18.11− (*Me*$_A$Me$_B$CHSi), 18.07− (Me$_A$*Me*$_B$CHSi), 17.3+ (*C*H$_2$Me), 15.3+ ($SiCH_2$) and 13.5− (SiCH); *m*/*z* (EI) 272 (1%, M$^+$), 229 (100, M − Pr), 187 (72, MH − 2Pr) and 115 (46, M − $SiPr_3$) (Found: M$^+$, 272.2538. $C_{16}H_{36}OSi$ requires *M*, 272.2535).

8 E. J. Corey, H. Cho, C. Rücker and D. H. Hua, *Tetrahedron Lett.*, 1981, **22**, 3455.

9 R. F. Cunico and L. Bedell, *J. Org. Chem.*, 1980, **45**, 4797.

CHEMCOMM Communication
www.rsc.org/chemcomm

Electronic origin of the structural versatility in linear trichromium complexes of dipyridylamide

Noureddine Benbellat, Marie-Madeleine Rohmer* and Marc Bénard*

Laboratoire de Chimie Quantique, UMR 7551, CNRS and Université Louis Pasteur, 4 rue Blaise Pascal, F-67000 Strasbourg, France. E-mail: benard@quantix.u-strasbg.fr; rohmer@quantix.u-strasbg.fr

Received (in Cambridge, UK) 10th July 2001, Accepted 2nd October 2001
First published as an Advance Article on the web 31st October 2001

Spin unrestricted DFT calculations on $Cr_3(dpa)_4Cl_2$ (dpa = dipyridylamide) suggest that the linear $(Cr_3)^{6+}$ metal framework could adopt either a symmetric conformation, or a strongly nonsymmetric one, depending on the nature of the spin coupling between the localized metal electrons.

In a series of recent articles, Cotton, Murillo and co-workers have shown that the linear trimetallic framework of complexes belonging to the $M_3(dipyridylamide)_4L_2$ family (Fig. 1) exhibits an unprecedented structural variability when the metal is Co^{II},[1,2] or Cr^{II}.[3] The case of cobalt complexes, and more especially $Co_3(dpa)_4Cl_2$, has been most extensively documented. It was proved that the same compound can exist with either a symmetrical (*s*) Co3 chain, or an unsymmetrical (*u*) one, solely depending on the crystal form in which it is found.[1] The structural behavior of the chromium complexes $Cr_3(dpa)_4L_2$ and $Cr_3(dpa)_4LL'$ presents strong analogies, and some differences. Complexes with identical axial ligands, including $Cr_3(dpa)_4Cl_2$ (**1**), show a clear preference for the *s* conformation, even though two types of moderately unsymmetrical arrangements (Δd_{Cr-Cr} = 0.064 Å and 0.118 Å at −60 °C) reminiscent of the *u* conformation of $(Co_3)^{6+}$ complexes, were observed in one of the reported crystal structures.[3] However, the two $Cr_3(dpa)_4LL'$ compounds with different ligands in axial position (L = Cl; L′ = BF_4^-, PF_6^-) exhibit extremely unsymmetrical arrangements, with Cr–Cr distances of the order of 2.00 Å and 2.62 Å, respectively. Magnetic measurements confirm that the ground state should be a quintet (*S* = 2), whether the complex is completely symmetrical or extremely unsymmetrical.[3]

$M_3(dpa)_4L_2$ molecules synthesized with other metals (M = Ni, Cu, Ru, Rh) have been structurally characterized in the symmetrical form only.[3] The structural documentation presently available on this family of complexes therefore raises the hypothesis of a common electronic origin to the structural versatility observed for the linear frameworks of $(Co_3)^{6+}$ and $(Cr_3)^{6+}$. Spin unrestricted DFT calculations have therefore been carried out on $Cr_3(dpa)_4Cl_2$ using the ADF program with the BP86 functional and Slater basis sets of triple-ζ plus polarization quality for the valence shells.[4] The obtained results have been compared with those of similar calculations previously reported on the cobalt complexes.[5]

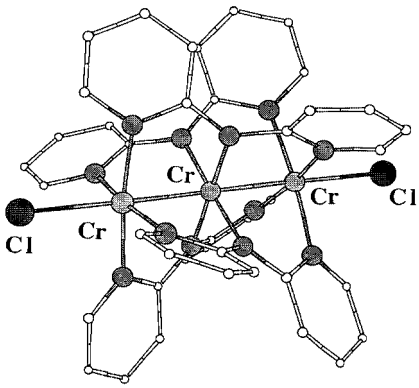

Fig. 1 Schematic representation of $Cr_3(dpa)_4Cl_2$ in the symmetric conformation (D_4 point group).

As for the homologous complex of cobalt, the ground state conformation of an isolated molecule of $Cr_3(dpa)_4Cl_2$ was found to be symmetric (D_4 point group), with optimized structural parameters (Cr–Cr = 2.350 Å; Cr–Cl = 2.560 Å; Cr_{term}–N = 2.094 Å; $Cr_{central}$–N = 2.010 Å) very close to the distances observed in the *s* conformations. A schematic representation of the metal orbitals obtained in the *s* form of the $(Co_3)^{6+}$ and $(Cr_3)^{6+}$ complexes, with their relative ordering, their occupancies and the spin orientation of the d electrons, is displayed in Fig. 2.[6] In both systems, a covalent σ linkage is delocalized over the whole metallic framework by means of a *three-electron three-center bond* involving an all-bonding, doubly occupied σ orbital (σb), and a singly occupied nonbonding orbital (σnb) (Fig. 2). This type of bonding is reminiscent of the π system of the allyl radical and generally yields a delicate balance between symmetry and distortion for the nuclear framework.[5b,7] The overlap between the 3d π and δ orbitals at a distance of 2.350 Å is not sufficient to induce a clear separation between the bonding, nonbonding and antibonding MOs of these types. The six π and the three δ levels[8] are therefore clustered between the σb and the σnb levels. In the cobalt complex, these nine levels are all equally occupied with two electrons, which implies a localization of these 18 d electrons on the metal atoms. In the chromium complex, the nine non-σ d electrons are also equally distributed among the π and δ orbitals, but the occupancy is now one electron per MO

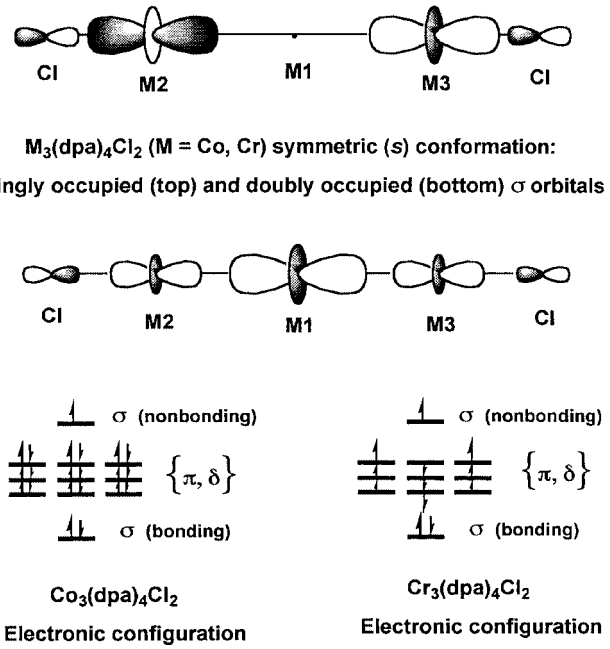

Fig. 2 $M_3(dpa)_4Cl_2$ (M = Co, Cr); symmetric form: sequence of the metal orbitals and their occupancies.[6] Scheme of the doubly occupied, σ-bonding MO and of the singly occupied, σ-nonbonding MO.

 DOI: 10.1039/b106100n

Table 1 Spin-coupling scheme, atomic spin populations and relative energies (kcal mol^{-1}) for various electronic configurations calculated for the symmetric ground state ($\Delta d_{Cr-Cr} = 0$); for a slightly distorted form ($\Delta d_{Cr-Cr} = 0.106$ Å) and for the highly distorted structure (optimized geometry; $\Delta d_{Cr-Cr} = 0.679$ Å)

Structure	*S* value	Spin coupling Atomic spin populations	Relative energies	Electronic configuration
Symmetric $\Delta d_{Cr-Cr} = 0$	2	↑↑↑—↓↓↓—↑↑↑ 3.52 −3.00 3.52	0.0	Type *a*
Nonsymmetric $\Delta d_{Cr-Cr} = 0.106$	2	↑↑↑—↓↓↓—↑↑↑ 3.60 −3.00 3.44	+0.97	Type *a*
Nonsymmetric $\Delta d_{Cr-Cr} = 0.679$	2	↑↑↑↓↓↑↑ 3.79 −2.27 2.50	+4.25	Type *a*
Nonsymmetric $\Delta d_{Cr-Cr} = 0.679$	2	↑↑↑↑↓↓ 3.84 2.17 −2.09	+10.12	Type *b*
Symmetric $\Delta d_{Cr-Cr} = 0$	5	↑↑↑—↑↑↑—↑↑↑ 3.50 2.93 3.50	+30.8	Type *c*

The total molecular spin *S* is defined as $0.5[n(\alpha)-n(\beta)]$, where $n(\alpha)$ and $n(\beta)$ represent the number of electrons with α and β spin, respectively.

(Fig. 2). These nine localized electrons—and the unpaired σ electron—are spin-coupled. The most favorable coupling is antiferromagnetic, with 3.5 electrons with α spin on each terminal chromium atom and three electrons with β spin localized on the central chromium (Table 1, coupling type *a*). The resulting molecular spin state is a quintet ($S = 2$) in agreement with the magnetic measurements. The energetic stabilization due to the antiferromagnetic coupling was estimated by computing the energy associated with the electronic configuration of maximum spin ($S = 5$) assuming the same symmetric structure as optimized for the quintet ground state. The high spin state is destabilized by 30.8 kcal mol^{-1} (Table 1, coupling type *c*).

As for the cobalt complex,[5] the ground state potential energy curve has been calculated with respect to an imposed distortion of the metallic framework by constraining the metal–metal distances to keep fixed, nonsymmetric values, while optimizing all other geometric parameters. The molecule in the distorted conformation belongs to the C_4 point group, and the calculations have been carried out with the C_2 constraints. The obtained curve is very shallow: the destabilization is less than 1 kcal mol^{-1} when Δd_{Cr-Cr} is equal to 0.106 Å and reaches 4.25 kcal mol^{-1} only when the extreme framework distortion observed in $Cr_3(dpa)_4LL'$ complexes is imposed to $Cr_3(dpa)_4Cl_2$. In the latter case, the spin populations assigned to the atoms involved in the 'supershort' Cr–Cr linkage (2.27β and 2.50α for $Cr_{central}$ and for Cr_{term}, respectively) evolve toward values typical of a quadruple bond between two chromium atoms, calculated in the broken symmetry formalism (Table 1). The potential energy curve calculated for $Cr_3(dpa)_4Cl_2$ is practically the same as that calculated in the same conditions for the equivalent complex of cobalt.[5] This should be traced to the identity in both complexes of the driving force to covalent bonding, namely the three-electron three-center linkage. It should therefore be assumed that the strength of the antiferromagnetic interaction, superimposed to the σ bond in the chromium system, is not significantly modified by a distortion of the metal framework.

A different spin arrangement of the unpaired electrons was also found when the observed structure of $Cr_3(dpa)_4Cl(BF_4)$ was taken as an initial guess for the geometry of $Cr_3(dpa)_4Cl_2$ (Table 1, coupling type *b*). The molecular electronic state remains a quintet and the calculated spin density distribution appears quite consistent with the electronic structure proposed by Clérac, Cotton and co-workers for the strongly distorted systems: a metal–metal quadruple bond flanked with an isolated chromium atom accommodating four unpaired spins.[3] At variance with the antiferromagnetic—type *a*—coupling, however, this arrangement of spins is basically nonsymmetric and should favor a distorted structure. In fact, a geometry optimization of $Cr_3(dpa)_4Cl_2$ assuming this electronic configuration resulted in a conformation very close to that reported for $Cr_3(dpa)_4Cl(BF_4)$.[3] The calculated geometrical parameters are as follows: Cr1–Cr2 = 2.671 Å; Cr1–Cr3 = 1.992 Å; Cr2–Cl = 2.526 Å; Cr3–Cl = 2.574 Å; Cr2–N = 2.111 Å; Cr3–N = 2.097 Å; Cr1–N = 2.006 Å. From the energetic viewpoint, the type *b* coupling corresponds to a low-lying excited state for $Cr_3(dpa)_4Cl_2$: at its optimal distorted geometry, this electronic configuration is destabilized by 10.1 kcal mol^{-1} with respect to the symmetric ground state. It is still higher by 5.9 kcal mol^{-1} than the symmetric coupling at the distorted geometry (Table 1), which means that the potential energy surface (PES) of the quintet *ground state* only displays a single minimum, corresponding to the symmetric conformation.

Calculations on $Cr_3(dpa)_4Cl(BF_4)$ are in progress to confirm that the change in axial coordination modifies the energy ordering of the two electronic configurations. It is not excluded in this case that both configurations appear as separate minima on the ground state PES. The structural behavior of the complex would therefore be relevant to the much debated issue of *bond-stretch isomerism*.[9]

Calculations have been carried out in part at the Centre Universitaire et Régional de Ressources Informatiques (CURRI, Université Louis Pasteur, Strasbourg, France) and in part at the IDRIS computer center (CNRS, Orsay, France). We are pleased to thank Professor F. A. Cotton and C. A. Murillo for stimulating discussions and for communicating their most recent results and structures.

Notes and references

1 (*a*) F. A. Cotton, C. A. Murillo and X. Wang, *J. Chem. Soc., Dalton Trans*., 1999, 3327; (*b*) R. Clérac, F. A. Cotton, L. M. Daniels, K. R. Dunbar, K. Kirschbaum, C. A. Murillo, A. A. Pinkerton, A. J. Schultz and X. Wang, *J. Am. Chem. Soc*., 2000, **122**, 6226; (*c*) R. Clérac, F. A. Cotton, S. P. Jeffery, C. A. Murillo and X. Wang, *Inorg. Chem*., 2001, **40**, 1265.

2 R. Clérac, F. A. Cotton, L. M. Daniels, K. R. Dunbar, C. A. Murillo and X. Wang, *J. Chem. Soc., Dalton Trans*., 2001, 386.

3 R. Clérac, F. A. Cotton, L. M. Daniels, K. R. Dunbar, C. A. Murillo and I. Pascual, *Inorg. Chem*., 2000, **39**, 748 and references therein.

4 *ADF User's Guide, Release 1999*, Chemistry Department, Vrije Universiteit, Amsterdam, The Netherlands, 1999.

5 (*a*) M.-M. Rohmer and M. Bénard, *J. Am. Chem. Soc*., 1998, **120**, 9373; (*b*) M.-M. Rohmer, A. Strich, M. Bénard and J.-P. Malrieu, *J. Am. Chem. Soc*., 2001, **123**, 9126. More information on the computational details can be found in these articles.

6 The orbital diagram of Fig. 2 has been slightly simplified with respect to the spin-unrestricted results by assigning the same energy to the occupied α and β spin orbitals.

7 S. Shaik, A. Shurki, D. Danovich and P. C. Hiberty, *Chem. Rev*., 2001, **101**, 1501.

8 The three remaining δ levels are involved as acceptor orbitals in the donation interactions originating in the dpa ligands.

9 (*a*) G. Parkin, *Acc. Chem. Res*., 1992, **25**, 455; (*b*) G. Parkin, *Chem. Rev*., 1993, **93**, 887; (*c*) M.-M. Rohmer and M. Bénard, *Chem. Soc. Rev*., in press.

CHEMCOMM
Communication
www.rsc.org/chemcomm

Direct electrochemistry of pentachlorophenol hydroxylase

Weihong Xie,* John P. Jones, Luet-Lok Wong and H. Allen O. Hill*

Central Chemistry Laboratory, University of Oxford, South Parks Road, Oxford UK OX1 3QH.
E-mail: allen.hill@chem.ox.ac.uk; zxn@pentium.whiov.ac.cn

Received (in Cambridge, UK) 30th August 2001, Accepted 9th October 2001
First published as an Advance Article on the web 31st October 2001

The direct electrochemistry of the flavin-containing monooxygenase, pentachlorophenol hydroxylase (PCPH), at an edge plane graphite electrode was observed and a catalytic response, linear with concentration, was found with the substrate pentachlorophenol (PCP).

Pentachlorophenol hydroxylase (PCPH) isolated from *Sphingomonas chlorophenolica* strain ATCC 53874 is a flavin containing monooxygenase.[1–5] The monomeric enzyme possesses one FAD prosthetic group, and converts pentachlorophenol (PCP) to 2,3,5,6-tetrachlorohydroquinone (TeCH). The enzymatic reaction requires two equivalents of NADPH and one molecule of dioxygen to hydroxylate one molecule of PCP [eqn. (1)].

$$2NADPH + H^+ + O_2 + PCP \rightarrow 2NADP^+ + H_2O + Cl^- + TeCH \quad (1)$$

Herein we describe the direct electrochemistry of PCPH. We hope that the exploitation of PCPH using electrochemical techniques can be used in sensing PCP or converting the pollutant to a less, or non-toxic, substance.

Cyclic voltammetry was performed in a two-compartment electrochemical cell with a working volume of 0.5 ml. The working compartment accommodated the platinum gauze counter electrode in addition to the edge plane pyrolytic graphite working electrode (diameter = 5 mm). A saturated calomel electrode (SCE) was used as a reference in a sidearm, which connected to the working compartment *via* a Luggin capillary. An Autolab PG STAT10 potentiostat (Eco Chemie B.V.) was used to record and control the potential of the working electrode.

The cyclic voltammogram of PCPH in Tris buffer is shown in Fig. 1(a). A redox couple with E_{pc} at −536 mV and E_{pa} at −487 mV ($E_{1/2}$ = −512 mV) is observed. The peak current increases linearly with the square root of the scan rate indicating a diffusion controlled process. A diffusion coefficient of 5.4×10^{-7} cm^2 s^{-1} for PCPH was estimated, which is similar to values observed for other proteins (1.1×10^{-7} cm^2 s^{-1} for *p*-cresolmethylhydroxylase,[6] and 4.5×10^{-7} cm^2 s^{-1} for spinach [2Fe–2S] ferredoxin[7]). The k^0 calculated for the electron transfer between PCPH and the EPG electrode was 7.2×10^{-4} cm s^{-1} which is in the rate constant region for a quasi-reversible process ($10^{-1} > k^0 > 10^{-5}$ cm s^{-1}).[8] In order to be sure that the electrochemical response observed from the enzyme solution was not due to the dissociated coenzyme, the electrochemistry of free FAD was also examined under identical experimental conditions. The cyclic voltammogram [Fig. 1(b)] of free FAD shows two redox couples at −501 and −639 mV. The peak current of the first couple is proportional to the square root of the scan rate only up to 20 mV s^{-1}. A diffusion coefficient estimated from the linear part was 7.1×10^{-6} cm^2 s^{-1}, near the literature values of 4.5×10^{-6} cm^2 s^{-1} [9] and 3.8×10^{-6} cm^2 s^{-1}.[10,11] This value is an order of magnitude larger than that calculated for PCPH. The heterogeneous rate constant k^0 is *ca.* 8.3×10^{-3} cm s^{-1}, which broadly agrees with the literature values of 1.6×10^{-3} cm s^{-1} [11] and 2.0×10^{-3} cm s^{-1}.[12] The peak current of the second couple has a linear relationship with the potential scan rate, indicating that it is likely an adsorption process. The different electrochemical behaviour between PCPH and free FAD therefore suggests that the direct electrochemistry of PCPH observed at the bare EPG electrode was not due to the dissociated coenzyme, FAD.

Electrochemistry of PCPH in the presence of substrate PCP was performed with the enzyme immobilised on the electrode surface. The EPG electrode was protected by a dialysis membrane (MW cut-off 3500 Da) which was fixed on the electrode by an 'O' ring. Modification the electrode was performed by depositing 4 mL (2 mL each time) of the concentrated PCPH (>80 mM) on to the top of the electrode. The enzyme layer was allowed to slightly dry at room temperature, then covered by the membrane. The electrode was then dipped into a solution containing PCP. Cyclic voltammograms were recorded in the presence of the substrate at a scan rate of 10 mV s^{-1}. As shown in Fig. 2, a catalytic response is

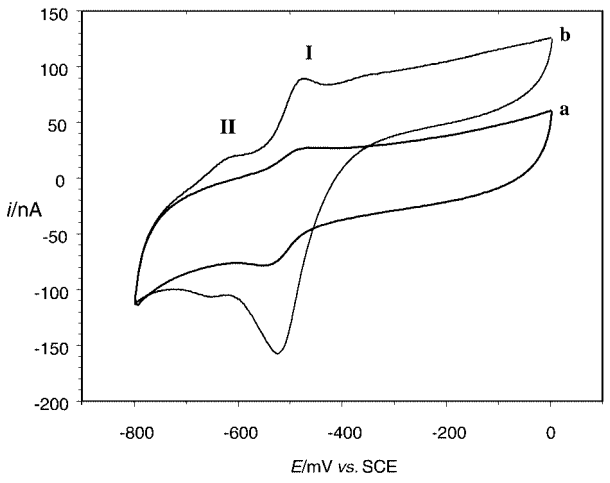

Fig. 1 Cyclic voltammograms recorded at a bare EPG electrode with a scan rate of 20 mV s^{-1} in 50 mM Tris buffer, pH 8.0: (a) 10 μM PCPH, (b) 10 μM FAD.

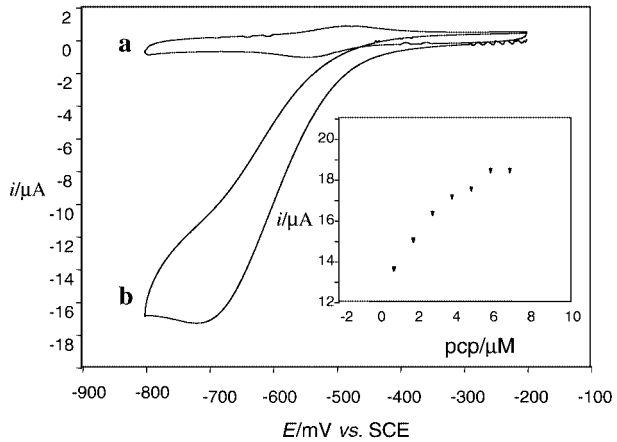

Fig. 2 Cyclic voltammograms of PCPH (4 μl of 200 μM PCP immobilized at an EPG electrode with dialysis membrane (MW cut-off 3500 Da) recorded at a scan rate of 10 mV s^{-1}: (a) in absence of PCP, (b) in the presence of 5 μM PCP; the PCP concentration dependence curve is shown in the inset.

 DOI: 10.1039/b107740f

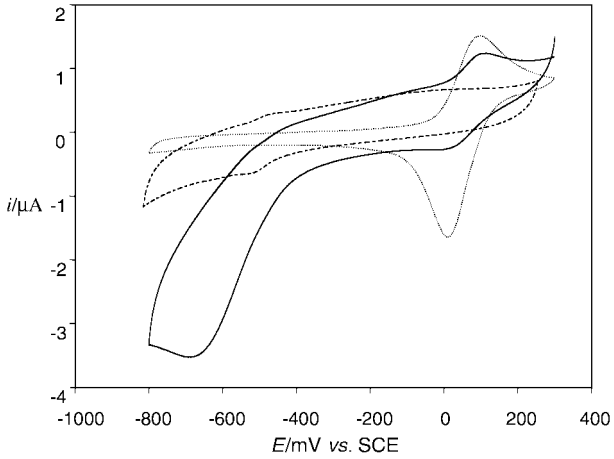

Fig. 3 Cyclic voltammograms recorded at an EPG electrode in 50 mM Tris buffer, pH 7.0, at a scan rate of 20 mV s^{-1}: (1) CV (–·–) was recorded in 45 μM PCPH solution prior to electrolysis, (2) CV (—) was recorded in solution (1) after the electrolysis had been carried out for 120 min, (3) CV (·····) was recorded in 0.1 mM of TeCH solution.

observed and the catalytic current increases with the increase of the concentration of PCP. Cyclic voltammetry carried out at a FAD modified electrode, which was constructed in the same manner as used in the enzyme experiment, showed that the reduction current decreased when PCP was added into the solution. This suggested that free FAD alone could not take part in a catalytic reaction with PCP. The addition of PCP into a deoxygenated enzyme solution did not stimulate a catalytic reaction, while in the present of dioxygen, the addition of PCP aroused a catalytic response, thereby demonstrating the mono-oxygenase function of PCPH.

The electrochemical conversion of PCPH was performed using a 5 mm diameter EPG electrode in a 50 mM Tris buffer solution containing 45 μM PCPH and 80 μM PCP. Prior to electrolysis, the enzyme solution was deoxygenated using Ar. During the reduction, the flow of Ar was stopped, enabling dioxygen to diffuse gradually into the electrochemical cell. The potential of the working electrode was fixed at −800 mV *vs.* SCE for 2 h and the cyclic voltammogram was recorded every 30 min. The measured cyclic voltammogram showed a new redox couple with a mid-point potential of 60 mV after the electrolysis. The peak current of this couple increased slightly when the electrolysis time was prolonged. In order to identify this response, cyclic voltammetry of a 0.1 mM TeCH solution (in 50 mM Tris buffer at pH 7.0) was recorded at the EPG electrode with a scan rate of 20 mV s^{-1}. The response of TeCH is identical to that obtained in the electrolysis experiment (Fig. 3) suggesting that the oxidised product of the reaction is formed. The observation of hydroxylation product at the electrode shows the possibility of designing a bioreactor, which could make use of this electroenzymological process to drive the conversion of PCP.

The author thanks the K. C. Wong Foundation for a Scholarship.

Notes and references

1 S. Fetzner and F. Lingens, *Microbiol. Rev.*, 1994, **58**, 641.
2 L. Y. Xun and C. S. Orser, *J. Bacteriol.*, 1991, **173**, 4447.
3 L. Y. Xun, E. Topp and C. S. Orser, *J. Bacteriol.*, 1992, **174**, 5745.
4 L. Y. Xun, E. Topp and C. S. Orser, *J. Bacteriol.*, 1992, **174**, 2898.
5 C. S. Orser, C. C. Lange, L. Xun and T. C. Zahrt, *J. Bacteriol.*, 1993, **175**, 411.
6 L. H. Guo, H. A. O. Hill, G. A. Lawrance, G. S. Sanghera and D. J. Hopper, *J. Electroanal. Chem.*, 1989, **266**, 379.
7 F. A. Armstrong, H. A. O. Hill and N. J. Walton, *Quart. Rev. Biophys.*, 1986, **18**, 261.
8 J. Heinze, *Angew. Chem., Int. Ed. Engl.*,1984, **23**, 831.
9 R. D. Braun, *J. Electrochem. Soc.*, 1977, **124**, 1342.
10 B. Janik and P. J. Elving, *Chem. Rev.*, 1968, **68**, 295.
11 M. Verhagen and W. R. Hagen, *J. Electroanal. Chem.*, 1992, **334**, 339.
12 C. B. Moore, D.Phil. Thesis, University of Oxford, Oxford, 1996.

CHEMCOMM
Communication
www.rsc.org/chemcomm

Preparation, structure and catalytic properties of a binuclear Pd(0) complex with bridging silylene ligands

Alois Fürstner,* Helga Krause and Christian W. Lehmann

Max-Planck-Institut für Kohlenforschung, D-45470 Mülheim/Ruhr, Germany.
E-mail: fuerstner@mpi-muelheim.mpg.de; Fax: +49-208-306-2994

Received (in Cambridge, UK) 10th September 2001, Accepted 9th October 2001
First published as an Advance Article on the web 31st October 2001

In contrast to the N-heterocyclic carbene (NHC) 1, the homologous N-heterocyclic silylene (NHS) 4 acts as a bridging ligand to Pd(0), giving rise to the dinuclear complex 5 which is catalytically active in Suzuki reactions.

Applications of transition metal complexes bearing N-heterocyclic carbene (NHC) ligands to catalysis have recently met with considerable success,[1,2] with olefin metathesis[3] and cross coupling chemistry being the most pertinent examples.[4,5] Thereby the strong σ-donor properties of the NHC account for the observed gain in activity and stability, while the fact that many catalysts can be conveniently prepared *in situ* from readily accessible precursors renders the procedures particularly user-friendly. Some of the resulting complexes, however, have also been isolated and structurally characterized. Thus, it has been shown that the sterically hindered NHC **1** readily displaces PAr_3 from Pd(0), leading to the formation of the homoleptic, mononuclear 14-electron complex **2** which is catalytically competent for Suzuki cross-coupling reactions (Scheme 1).[6]

As part of our project aiming at the design of novel metal catalysts and their applications to advanced organic synthesis,[7] we became interested in the properties of the homologeous N-heterocyclic silylenes (NHS)[8] as ancillary ligands. Although they promise to exhibit a similarly favorable profile, the catalytic performance of transition metal–NHS complexes is as yet largely unexplored. Outlined below is an exploratory study into palladium chemistry which resulted in the discovery that NHS **4** leads to an entirely different structural motif than its NHC-analogue **1**, without compromising the catalytic activity of the resulting Pd(0) template.

For the preparation of the required NHS, the procedure described by West *et al*. has been modified.[9] Rather than refluxing the dichlorosilane **3** in THF with a large excess of potassium chunks for extended periods of time, its treatment with C_8K[10,11] in THF at ambient temperature turned out highly beneficial (Scheme 2).† Not only does this method lead to the formation of **4** in high yield, but also gives much better reproducible results and requires neither large excess of the reducing agent nor the monitoring of the reaction progress by NMR as recommended in the original publication.[9]

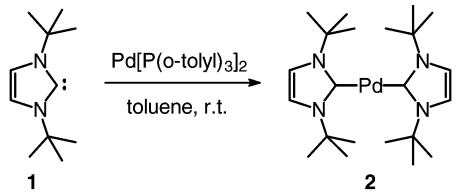

1 2

Scheme 1 Preparation of a homoleptic Pd(0)–NHC complex.[6a]

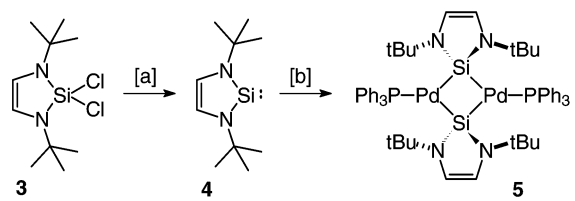

3 4 5

Scheme 2 *Reagents and conditions*: [a] C_8K (2.2 equiv.), THF, rt, 18 h, 67%; [b] $Pd(PPh_3)_4$, rt, 1 h, 50%.

Having secured good access to multigram amounts of **4**, this ligand was reacted with $Pd(PPh_3)_4$ in THF at ambient temperature. ^{31}P NMR spectroscopy revealed the rapid release of PPh_3 accompanied by the virtually quantitative formation of a single new product which was isolated as dark red, air-sensitive crystals in 50% yield (Scheme 2).‡ Its structure in solution can be deduced from the spectroscopic and analytical data. Particularly diagnostic is the ^{29}Si NMR signal which appears as a triplet at δ = 109.5 ppm ($J_{P,Si}$ = 21.5 Hz) indicating a highly symmetrical structure containing *two* PPh_3 ligands at degenerate positions. MS indicates the presence of a dimeric species which was unambiguously identified by X-ray crystallography. Fig. 1 depicts the molecular structure of **5** in the solid state, showing that the silylene moieties act as bridging ligands between two 14-electron Pd(0) centers.§

The dimer is situated upon a crystallographic inversion center. The distance between the Pd atoms (2.65005(17) Å) is shorter than that of Pd(0) in the bulk metal (2.7511 Å), but slightly longer than the distances observed in structurally related, bridged dinuclear Pd(I)-complexes with a linear R_3P–Pd–Pd–PR_3 entity.[12] The co-ordination of the Pd atoms is planar, the sum of the Pd bond angles is 359.8°. The 1,3-diaza-2-silacyclopentene is also essentially planar (with a mean deviation of 0.005 Å) and is oriented perpendicular to the Pd1, Si1, Pd1*, Si1* plane (interplanar angle 94.1°). Its geometry reflects the silylene character of this ligand, with the N–Si–N

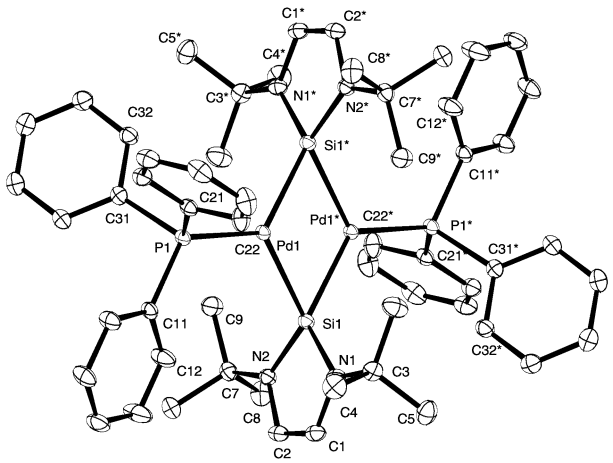

Fig 1 Molecular structure of **5**. Anisotropic displacement parameters are shown at 50% probability level, hydrogen atoms have been omitted for clarity. Selected bond lengths [Å] and angles [°]: Pd1–P1 2.2706(3), Pd1–Si1 2.4154(4), Pd1–Si1* 2.3996(3), Pd1–Pd1* 2.65005(17), Si1–N1 1.7582(11), Si1–N2 1.7630(12), N1–C1 1.3930(17), N2–C2 1.3938(16), C1–C2 1.344(2), Pd1*–Si1–Pd1 66.784(10), Si1*–Pd1-Si1 113.217(10), N1–Si1–N2 88.80(5), C1–N1–Si1 111.97(9), C2–N2–Si1 111.87(9), C2–C1–N1 113.75(12), C1–C2–N2 113.60(12), symmetry transformation used to generate equivalent atoms: * $-x+1, -y, -z$

 DOI: 10.1039/b108132b

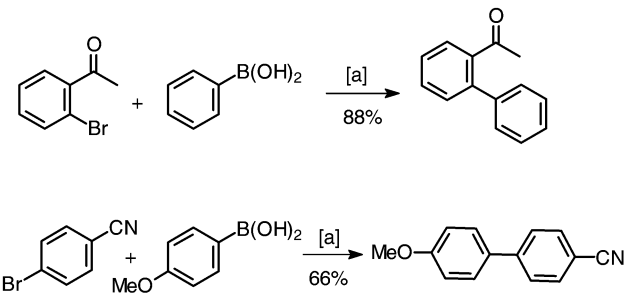

Scheme 3 *Reagents and conditions*: [a] complex **5** (5 mol%), DME, K_2CO_3, 80 °C.

angle being even more acute than in dicarbonyl-bis(1,3-diaza-2-silacyclopentene)nickel[13] and the Si–N distances being also slightly longer.

Although the propensity of silylenes to act as bridging ligands in a variety of stable binuclear complexes is well established,[14] we are not aware of any precedence involving Pd(0). Moreover, the synthesis of **5** favorably compares with that of most other silylene bridged metal(0) complexes¶ which are usually prepared by less convenient indirect routes. Finally, complex **5** seems to be the first case of a NHS–metal complex used as catalyst in organic synthesis. Specifically, it was found to effect Suzuki reactions[15] of aryl boronic acids with bromoarenes in high yield. Two representative examples are depicted in Scheme 3.

Generous financial support by the Deutsche Forschungsgemeinschaft (Leibniz award program) and the Fonds der Chemischen Industrie is gratefully acknowledged. We thank Professor K. Pörschke for a valuable discussion.

Notes and references

† *Preparation* of **4**: To a stirred solution of dichloride **3** (6.04 g, 22.6 mmol) in THF (100 mL) under Ar is added C_8K (6.7 g, 49.7 mmol)[10] in several portions. The resulting suspension is stirred at ambient temperature for 18 h during which its color changes from bronze to black. The insoluble residues are filtered off under Ar and are repeatedly rinsed with THF, the combined filtrates are evaporated and the crude product is purified by sublimation *in vacuo* (bath temperature 60–75 °C, 10^{-1} torr) thus affording silylene **4** as a colorless solid (2.97 g, 67%). Its spectroscopic and analytical data are in full agreement with those reported in the literature.[9]

‡ *Preparation of complex* **5**: To a solution of silylene **4** (345 mg, 1.75 mmol) in THF (40 mL) under Ar is added a solution of $Pd(PPh_3)_4$ (1.69 g, 1.46 mmol) in THF (60 mL) over a period of 30 min and stirring is continued for another 30 min after the addition is complete. The resulting dark red solution is evaporated, the residue is suspensed in hexane (15 mL), the precipitate is filtered off under Ar and is carefully rinsed with hexane in several portions. Drying *in vacuo* affords complex **5** as a dark-red solid (824 mg, 50%). ^{1}H NMR (THF-d_8): δ = 7.21–7.44 (m, 30H), 6.86 (s, 4H), 1.25 (s, 36H); ^{13}C NMR (THF-d_8): δ = 139.8, 139.7, 139.5, 135.2, 135.1, 134.8, 134.7, 129.2, 129.0, 128.8, 128.7, 128.6, 128.4, 121.3, 54.6, 33.8; ^{31}P NMR (THF-d_8): δ = 31.4; ^{29}Si NMR (THF-d_8): 109.5 (t, J = 21.5 Hz); MS (EI): *m*/*z* (rel. intensity) 1130 (0.5, [M$^+$]), 350 (10), 263 (20), 262 (100), 261 (14), 184 (13), 183 (58), 154 (14), 121 (14), 108 (23), 84(4), 77(3), 57(7), 51(4).

§ *Crystal data* for **5**: $C_{56}H_{70}N_4P_2Pd_2Si_2$, M = 1130.12 g mol^{-1}, red–brown, crystal dimensions 0.17 × 0.13 × 0.09 mm, triclinic $P\bar{1}$ (no. 2), at 100 K a = 10.2277(2), b = 10.8525(2), c = 13.8201(2) Å, α = 66.897(1), β = 73.515(1), γ = 89.888(1)°, V = 1342.51(4) Å^3, Z = 1, ρ = 1.398 Mgm^{-3}, μ = 0.814 mm^{-1}, λ = 0.71073 Å. ω-Scans covering reciprocal space up to θ_{max} 33.18° with 93.7% completeness, total of 13730 reflections (9616 unique) with R_{int} = 0.034. Structure solution SHELXS-97, full matrix least-squares based on F^2 using SHELXL-97, final R = 0.026, wR = 0.071, $\triangle\rho_{max}$ 0.7 eÅ^{-3}. CCDC 168806. For crystallographic files in .cif or other electronic format see http://www.rsc.org/suppdata/cc/b1/b108132b/

¶ In this context it is noteworthy that treatment of $Ni(CO)_4$, $Ni(COD)_2$ or $Pt(PPh_3)_4$ with **4** or its benzoanellated analogues is reported to give monomeric rather than bridged dinuclear complexes, *cf.* ref. 8, 13, 16.

1 A. J. Arduengo, *Acc. Chem. Res*., 1999, **32**, 913.
2 (*a*) W. A. Herrmann and C. Köcher, *Angew. Chem., Int. Ed. Engl*., 1997, **36**, 2162; (*b*) D. Enders and H. Gielen, *J. Organomet. Chem*., 2001, **617–618**, 70.
3 (*a*) T. M. Trnka and R. H. Grubbs, *Acc. Chem. Res*., 2001, **34**, 18; (*b*) A. Fürstner, *Angew. Chem., Int. Ed*., 2000, **39**, 3012.
4 (*a*) C. Zhang, J. Huang, M. L. Trudell and S. P. Nolan, *J. Org. Chem*., 1999, **64**, 3804; (*b*) A. Fürstner and A. Leitner, *Synlett*, 2001, 290; (*c*) S. Lee and J. F. Hartwig, *J. Org. Chem*., 2001, **66**, 3402; (*d*) G. A. Grasa and S. P. Nolan, *Org. Lett*., 2001, **3**, 119; (*e*) W. A. Herrmann, M. Elison, J. Fischer, C. Köcher and G. R. J. Artus, *Angew. Chem., Int. Ed*., 1995, **34**, 2371; (*f*) J. Huang and S. P. Nolan, *J. Am. Chem. Soc*., 1999, **121**, 9889 and literature cited therein.
5 For further applications see: (*a*) A. Fürstner and H. Krause, *Adv. Synth. Catal*., 2001, **343**, 343; (*b*) H. M. Lee, T. Jiang, E. D. Stevens and S. P. Nolan, *Organometallics*, 2001, **20**, 1255; (*c*) A. C. Chen, L. Ren, A. Decken and C. M. Crudden, *Organometallics*, 2000, **19**, 3459; (*d*) J. Louie and R. H. Grubbs, *Chem. Commun*., 2000, 1479.
6 (*a*) V. P. W. Böhm, C. W. K. Gstöttmayr, T. Weskamp and W. A. Herrmann, *J. Organomet. Chem*., 2000, **595**, 186; (*b*) L. R. Titcomb, S. Caddick, F. G. Cloke, D. J. Wilson and D. McKerrer, *Chem. Commun*., 2001, 1388.
7 (*a*) A. Fürstner, L. Ackermann, B. Gabor, R. Goddard, C. W. Lehmann, R. Mynott, F. Stelzer and O. R. Thiel, *Chem. Eur. J*., 2001, **7**, 3236; (*b*) L. Ackermann, A. Fürstner, T. Weskamp, F. J. Kohl and W. A. Herrmann, *Tetrahedron Lett*., 1999, **40**, 4787; (*c*) A. Fürstner, O. R. Thiel, L. Ackermann, H.-J. Schanz and S. P. Nolan, *J. Org. Chem*., 2000, **65**, 2204; (*d*) A. Fürstner, O. R. Thiel, N. Kindler and B. Bartkovska, *J. Org. Chem*., 2000, **65**, 7990; (*e*) A. Fürstner, M. Liebl, C. W. Lehmann, M. Picquet, R. Kunz, C. Bruneau and P. H. Dixneuf, *Chem. Eur. J*., 2000, **6**, 1847; (*f*) A. Fürstner, H. Krause, L. Ackermann and C. W. Lehmann, *Chem. Commun*., 2001, 2240
8 For pertinent reviews see: (*a*) B. Gehrhus and M. F. Lappert, *J. Organomet. Chem*., 2001, **617–618**, 209; (*b*) M. Haaf, T. A. Schmedake and R. West, *Acc. Chem. Res*., 2000, **33**, 704.
9 (*a*) M. Denk, R. Lennon, R. Hayashi, R. West, A. V. Belyakov, H. P. Verne, A. Haaland, M. Wagner and N. Metzler, *J. Am. Chem. Soc*., 1994, **116**, 2691; (*b*) M. Haaf, A. Schmiedl, T. A. Schmedake, D. R. Powell, A. J. Millevolte, M. Denk and R. West, *J. Am. Chem. Soc*., 1998, **120**, 12714.
10 (*a*) A. Fürstner and H. Weidmann, *J. Organomet. Chem*., 1988, **354**, 15; (*b*) A. Fürstner, *Angew. Chem., Int. Ed. Engl*., 1993, **32**, 164; (*c*) M. Kira, S. Ishida, T. Iwamoto and C. Kabuto, *J. Am. Chem. Soc*., 1999, **121**, 9722.
11 In his review (ref. 8a), Lappert also mentions the advantages of C_8K in the preparation of other NHS derivatives as unpublished results.
12 (*a*) R. Vilar, D. M. P. Mingos and C. J. Cardin, *J. Chem. Soc., Dalton Trans*., 1996, 4313; (*b*) M. Sommovigo, M. Pasquali, P. Leoni and U. Englert, *Inorg. Chem*., 1994, **33**, 2686; (*c*) P. Leoni, M. Sommovigo, M. Pasquali, P. Sabatino and D. Braga, *J. Organomet. Chem*., 1992, **423**, 263; For a detailed discussion see: (*d*) J. Krause, R. Goddard, R. Mynott and K.-R. Pörschke, *Organometallics*, 2001, **20**, 1992; (*e*) See also: H. Werner, *Adv. Organomet. Chem*., 1981, **19**, 155.
13 M. Denk, R. K. Hayashi and R. West, *J. Chem. Soc., Chem. Commun*., 1994, 33.
14 Reviews: (*a*) T. D. Tilley, *Comments Inorg. Chem*., 1990, **10**, 37; (*b*) W. Petz, *Chem. Rev*., 1986, **86**, 1019; (*c*) C. Zybill, *Top. Curr. Chem*., 1990, **160**, 1; (*d*) P. D. Lickiss, *Chem. Soc. Rev*., 1993, **21**, 271; (*e*) J. Y. Corey and J. Braddock-Wilking, *Chem. Rev*., 1999, **99**, 175.
15 A. Suzuki, *J. Organomet. Chem*., 1999, **576**, 147.
16 (*a*) B. Gehrhus, P. B. Hichcock, M. F. Lappert and H. Maciejewski, *Organometallics*, 1998, **17**, 5599; (*b*) T. A. Schmedake, M. Haaf, B. J. Paradise, D. Powell and R. West, *Organometallics*, 2000, **19**, 3263.

CHEMCOMM Communication
www.rsc.org/chemcomm

Hydrogen-bonded capsules in polar, protic solvents

Alexander Shivanyuk and Julius Rebek, Jr.*

The Skaggs Institute for Chemical Biology and the Department of Chemistry, The Scripps Research Institute, MB-26, 10550 North Torrey Pines Rd., La Jolla, CA 92037, USA. E-mail: jrebek@scripps.edu

Received (in Columbia, MO, USA) 12th July 2001, Accepted 8th August 2001
First published as an Advance Article on the web 19th October 2001

A kinetically stable, dimeric capsule is formed by tetrahydroxyresorcinarene in methanol; it encapsulates tropylium and tetramethylammonium cations.

Molecular capsules held together by hydrogen bonds are stable in organic solvents that do not compete well for donors and acceptors.[1] Ordinarily, the addition of small amounts of highly polar solvents disrupts these capsular hosts and releases their guests. A few monomeric cavitands are able to form inclusion complexes in methanol and in water,[2] and a number of well-defined molecular capsules involving metal co-ordination are stable in alcohols and water.[3] But the presence – even requirement – of water in the assemblies of resorcinarene **1a**[4] is anomalous. Water is an integral part of its hexameric capsules in the solid state, and in wet organic solvents large, polar guests can be encapsulated. [5] Enough additional space is available to co-encapsulate sizable, neutral molecules (Fig. 1). A similar hexameric structure is reported for **1b**[6] in the solid state. Its additional hydroxy groups offer greater possibilities for self-assembly in competitive media and we describe here the behavior of the closely related **1c** in protic solvent mixtures. We have found that **1c** forms dimeric capsules in solution and in the solid state.

Compound **1c** is insoluble in water or dry acetonitrile, but readily dissolves in **wet** acetonitrile (10–20% water), in methanol, or in mixtures of acetonitrile and methanol. Colorless crystals were grown from aqueous acetonitrile. These were unstable without the mother liquor but were, nonetheless, suitable for single crystal X-ray analysis.†

The molecule adopts a slightly distorted cone conformation, stabilized by intramolecular hydrogen bonds. Two molecules of **1c** form a centrosymmetric dimer linked through no less than 16 hydrogen-bonded water molecules (Fig. 2). The overall structure resembles the dimeric capsular assembly known for resorcinarene **1e**,[7] and encapsulates four acetonitrile molecules. Two of them are positioned to engage in CH–π interactions with the aromatic rings; the remaining two are nearly parallel to the plane of bridging carbon atoms and are disordered over two positions. The dipoles of the two ordered acetonitrile molecules are antiparallel and their intermolecular distances are consistent with dipole–dipole interactions. The distances between nitrogen atoms of acetonitrile molecules and selected oxygens of **1c** indicate host–guest hydrogen bonding.

Solution studies were undertaken in methanol and aqueous acetonitrile. The ^{1}H NMR spectrum of **1c** in methanol-d_4 measured at 295 K contains one singlet for the C–H protons of the aromatic rings and one triplet for the methine protons of the bridges. These features are characteristic of the C_{4v}-symmetric cone conformation. The addition of tropylium tetrafluoroborate **2a**$^+$BF$_4^-$ to the solution of **1c** in methanol-d_4 resulted in an intense red color, suggesting a charge-transfer interaction of the tropylium ion with the electron-rich pyrrogallol rings.[8] The UV spectrum showed a charge-transfer absorption maximum at λ = 407 nm. The NMR spectrum gives rise to a broad singlet for the tropylium ion, and its chemical shift depends on the ratio between the host and guest. The complexation equilibrium is fast on the NMR timescale at 295 K but becomes slow at 233 K. At host : guest ratios larger than 2 the ^{1}H NMR spectrum contains two signals for the protons of the bridges in the complexed and free **1c** [Fig. 3(a)]. The ratio between these signals depends on the amount of tropylium cation so that only the complex is detected at [**1c**]/[**2a**$^+$BF$_4^-$] = 2 [Fig. 3(b)]. A singlet at 5.2 ppm corresponds to the protons of the tropylium ion, shifted 4.3 ppm upfield by the shielding of the pyrogallol rings. Integration revealed that two molecules of **1c** complex one **2a**$^+$.[9] The slow exchange of the guest and the large upfield shifts of its resonances are typical for capsular assemblies.[10] Further addition of **2a**$^+$BF$_4^-$ results in a new set of signals for the protons of **1c** which grows at the expense of the set of the 2 : 1 complex [Fig. 3(c)]. After 4 equivalents of the salt were added, no dimeric complex remained. Remarkably, no signals

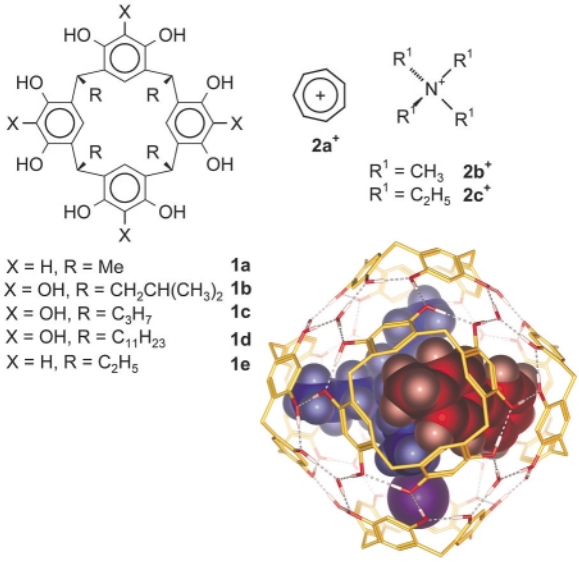

Fig. 1 Line drawings of the resorcinarenes and their guests. The specific complex shown has tetrabutylammonium bromide and *p*-phenyltoluene inside.

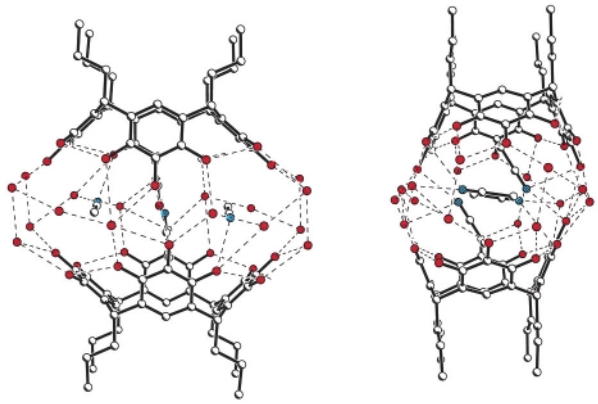

Fig. 2 X-Ray structure of **1c**·3MeCN·5H$_2$O. Symmetry-related water molecules are shown. Hydrogen atoms are omitted for clarity, heteroatoms are darkened and hydrogen bonds are indicated with dashed lines. Only one position of the encapsulated, disordered acetonitriles is indicated, while acetonitriles outside the cavity are not shown.

 DOI: 10.1039/b106793c

for the free tropylium cation were detected at host : guest ratios smaller than 2. Instead, the broad resonance emerged, whose chemical shift depended on the concentration of the tropylium salt [Fig. 3(c)]. This suggests that the new set of signals corresponds to an open, perhaps 1 : 1, complex between the tropylium cation and **1c**, which is in fast exchange with its components. The ESI mass spectrum showed peaks at *m/z* 722, 812 and 1533, corresponding to **1c**, **1c**·**2a** and 2**1c**·**2a**. The same behavior was observed in wet acetonitrile-d_3 (10% of D_2O) although the low temperature NMR studies were somewhat hampered by ice crystallization. The high stability of the dimer and its complicated behavior in the presence of excess **2a**$^+BF_4^-$ prevented the reliable determination of its stability constant.

The ^{1}H NMR spectrum of the more lipophilic resorcinarene **1d** in $CDCl_3$ shows sharp signals and contains one singlet for the aromatic rings and one triplet for the methine protons of the bridges. The addition of solid **2a**$^+BF_4^-$ does not lead to the formation of a lipophilic charge-transfer complex. Neither the color of the solution nor the ^{1}H NMR spectrum of **1d** changes. This is in sharp contrast to the behavior of resorcinarene tetrabenzoates, where encapsulation and charge-transfer take place.[9] However, the addition of methanol-d_4 (20%) results, again, in an intense red color of the solution which is a visual indication of a charge-transfer host–guest interaction. The NMR dilution experiments at 233 K revealed the same characteristics seen for **1c** in pure methanol-d_4. These results strongly suggest that a 2 : 1 complex forms between **1c**, **1d** and **2a**$^+BF_4^-$; in methanol-d_4, in wet acetonitrile-d_3 or in mixtures of $CDCl_3$ and methanol-d_4, the complex has a capsular structure – the methanol or water molecules act as linkers between two resorcinarene molecules in solution, as they do in the solid state (Fig 2).

Finally, the addition of the tetramethylammonium cation **2b**$^+$ gives a kinetically stable (*i.e.* slow exchange on the NMR timescale) 1 : 2 complex with **1c** at 233 K. The NMR signals of the guest's methyl groups are shifted upfield by 3.8 ppm, typical for an encapsulation complex. The octols **1a**, **1e** fail to show a kinetically stable complex with tropylium and tetramethylammonium cations under these conditions. [11] Apparently, the π-basicity and the expanded hydrogen bonding patterns available to the pyrogallol contribute to its more facile capsule formation.

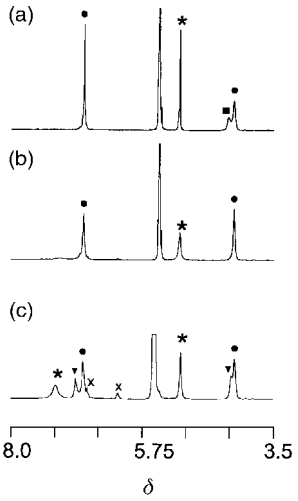

Fig. 3 ^{1}H NMR spectra at 233 K (methanol-d_4, 600 MHz, $[\mathbf{1c}]_{total}$ = 10 mM): (a) 3 **1c** + $C_7H_7^+BF_4^-$; (b) 2 **1c** + $C_7H_7^+BF_4^-$; (c) **1c** + $C_7H_7^+BF_4^-$; (*) tropylium cation; (■) free **1c**; (●) **1c** in a 2 : 1 complex; (▼) **1c** in an open complex; (×) products of methanolysis of the tropylium cation (established by control experiments with $C_7H_7^+BF_4^-$ in methanol-d_4).

In conclusion, the readily available tetrahydroxyresorcinarenes provide easy access to new molecular capsules, stable in protic solutions.[12] The repertoire of encapsulation complexes assembled from these molecules will be reported in the sequel.

We are grateful for support from the Skaggs Foundation and the National Institute of Health. A. S. is a Skaggs Postdoctoal Fellow.

Notes and references

† *X-Ray analysis*: data were recorded with Bruker Smart diffractometer equipped with a CCD-detector, using graphite monochromatized MoKα radiation [λ(MoKα) = 0.71073 Å] at 173 K. The crystal was covered by inert FOMBLIN® oil and mounted in the nylon loop. The structure was solved by direct methods [SHELXS-97 (G. M. Sheldrick, *Acta Crystallogr., Sect. A*, 1990, **46**, 467)] and refinement, based on F^2, was made by full-matrix, least squares techniques [SHELXL-97 (G. M. Sheldrick, SHELXL-97, A program for crystal structure refinement, University of Göttingen, Germany, 1997)].

Crystal data for **1a**: 3MeCN·5H_2O: M = 925.96, crystal size 0.4 × 0.3 × 0.3 mm, triclinic, space group $P\bar{1}$, a = 11.455(1), b = 11.627(1), c = 18.662(2) Å, α = 102.785(2), β = 90.042(2), γ = 102.881(2)°, V = 2360.0(4) Å^3, T = 173(2) K, Z = 2, D_c = 1.303 g cm^{-3}, $2\theta_{max}$ = 56.12°, μ = 0.1 mm^{-1}, $F(000)$ = 984, 639 parameters, $R1$ = 0.0620, $wR2$ = 0.1786 [for 7603 reflections $I > 2\sigma(I)$], $R1$ = 0.0909, $wR2$ = 0.2055 (for 11 082 unique reflections), S = 1.057 , $\Delta\rho$(min./max.)/e Å^{-3} = −0.62/0.56.

CCDC reference number 170259. See http://www.rsc.org/suppdata/cc/b1/b106793c/ for crystallographic data in CIF or other electronic format.

1 For a review on reversible molecular encapsulation see: M. M. Conn and J. Rebek, Jr., *Chem. Rev.*, 1997, **97**, 1647; J. Rebek, Jr., *Chem. Commun.*, 2000, 637; L. R. MacGillivray and J. L. Atwood, *Angew. Chem., Int. Ed.*, 1999, **38**, 1018.

2 T. Haino, D. M. Rudkevich, A. Shivanyuk, K. Rissanen and J. Rebek, Jr., *Chem. Eur. J.*, 2000, **6**, 3797.

3 M. Fujita, K. Umemoto, M. Yoshizawa, N. Fujita, T. Kusukawa and K. Biradha, *Chem. Commun.*, 2001, 509; D. Caulder, R. E. Powers, T. Parac and K. Raymond, *Angew. Chem., Int. Ed.*, 1998, **37**, 1840.

4 L. R. MacGillivray and J. L. Atwood, *Nature*, 1997, **389**, 469.

5 A. Shivanyuk and J. Rebek, Jr., *Proc. Natl. Acad. Sci.*, 2001, **98**, 7662.

6 T. Gerkensmeier, W. Iwanek, C. Agena, R. Frölich, S. Kotila, C. Näther and J. Mattay, *Eur. J. Org. Chem.*, 1999, 2257.

7 K. Murayama and K. Aoki, *Chem. Commun.*, 1998, 607; A. Shivanyuk, K. Rissanen and E. Kolehmainen, *Chem. Commun.*, 2000, 1107; K. N. Rose, L. J. Barbour, G. W. Orr and J. L. Atwood, *Chem. Commun.*, 1998, 407.

8 See, for example: M. Lämsä, J. Pursiainen, K. Rissanen and J. Huuskonen, *Acta Chem. Scand.*, 1998, **52**, 563.

9 A. Shivanyuk, E. F. Paulus and V. Böhmer, *Angew. Chem., Int. Ed.*, 1999, **38**, 2906.

10 In the course of dilution experiments only one signal was observed in the ^{19}F NMR spectrum suggesting that the BF_4^- anion is not encapsulated. See, for example: F. Fochi, P. Jacopozzi, E. Wegelius, K. Rissanen, P. Cozzini, E. Marastoni, E. Fisicaro, P. Manini, R. Fokkens and E. Dalcanale, *J. Am. Chem. Soc.*, 2001, **123**, 7539.

11 The larger tetraethylammonium cation **2c**$^+$ does not form kinetically stable complexes with **1a**, **1c** or **1e** in methanol-d_4.

12 For a timely review, see: L. J. Prins, D. N. Reinhoudt and P. Timmerman, *Angew. Chem., Int. Ed.*, 2001, **40**, 2382.

CHEMCOMM Communication
www.rsc.org/chemcomm

Hydrogen-bonded molecular capsules are stable in polar media

Jerry L. Atwood,* Leonard J. Barbour and Agoston Jerga

Department of Chemistry, University of Missouri-Columbia, Columbia, MO 65211, USA. E-mail: atwoodj@missouri.edu

Received (in Cambridge, UK) 13th July 2001, Accepted 13th August 2001
First published as an Advance Article on the web 19th October 2001

Robust, very large hydrogen-bonded capsules which are even stable in 50 : 50 water–acetone mixtures have been characterized both in solution and in the solid state.

For the spherical enclosure of space by means of hydrogen-bonded organic frameworks, two general approaches have emerged: covalent synthesis[1] and synthesis *via* self-assembly.[2] From our viewpoint, self-assembly has provided an attractive means for constructing large, highly organized chemical entities.[3–5] However, self-assembled capsules based on hydrogen bonding have not previously afforded robust structures, particularly in highly polar solvents. Here, we reveal spherical molecular capsules with outstanding stability in such media.

The synthesis of pyrogallol[4]arenes from the acid-catalyzed condensation of pyrogallol and aldehydes has recently been reported.[6,7] Mattay and co-workers noted that these entities typically crystallize as wave-like 2D polymeric structures held together by hydrogen bonds.[7] Of great interest was the revelation that *C*-isobutylpyrogallol[4]arene, **1a**, formed a spherical hexamer, **2a**, on one occasion. However, all attempts to form the hexamer a second time apparently failed.[7] This was attributed to an inherent instability of hexamer **2a** compared with [(*C*-methylresorcin[4]arene)$_6$(H$_2$O)$_8$], **3**, a very large synthetic molecular capsule.[3] This instability in solvents such as nitrobenzene or acetonitrile was especially noteworthy in view of the comment that hexamer **2** is stabilized by 72 hydrogen bonds.[7] A detailed inspection of **2a** shows that the hexamer, comprised of six molecular building blocks, is held together by 48 intermolecular hydrogen bonds, or by eight hydrogen bonds per molecule. For comparison, **3**, comprised of 14 entities (six resorcin[4]arenes and eight water molecules) is held together by 36 intermolecular hydrogen bonds, or 2.6 hydrogen bonds per molecule. The Rebek tennis balls, softballs, and related capsules are comprised of two identical molecules held together by eight hydrogen bonds, or four hydrogen bonds per molecule.[8] Thus, it seems to us that **2** should in fact be highly stable in solvents such as acetonitrile or nitrobenzene. We anticipate that conditions might be found such that hexamer **2** can enjoy a useful existence even in highly polar media. Surprisingly, even these high expectations for the stability of **2** have been exceeded.

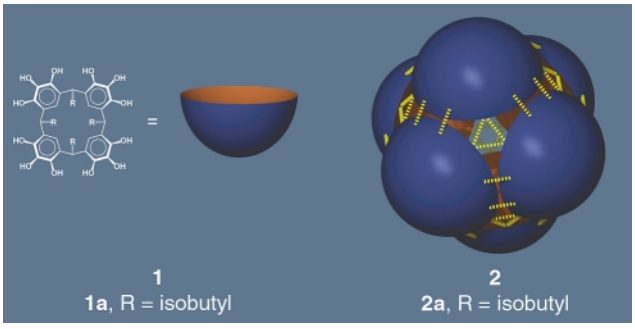

The acid-catalyzed condensation of pyrogallol and isovaleraldehyde proceeded smoothly in 95% ethanol, as reported,[7] and, after stirring for 24 h, a precipitate consisting of *ca*. 25% yield of pure **1** was obtained. No evidence of any hexamer **2** was found in this material. Indeed, it is our view that the initial precipitate is comprised exclusively of the wave-like hydrogen-bonded polymer reported by Mattay.[7] It is possible to convert this material to hexamer **2** by dissolving the initial precipitate in Et$_2$O, acetone or methanol, with a few drops of nitrobenzene or *o*-dichlorobenzene added, followed by crystallization upon slow evaporation. The hexamer may also be obtained by thermal treatment of either the initial precipitate or the initial filtrate. The latter contains *ca*. 1–5% hexamer as determined by NMR analysis. The product in the initial filtrate may be converted to hexamer by extraction with Et$_2$O, followed by evaporation to dryness with subsequent dissolution in methanol. The methanol solution is then heated in a sealed tube to 120–150 °C for at least 12 hours. Methanol may be removed under vacuum to yield a red–brown solid. Colorless hexameric spherical capsules have been obtained utilizing the crystallization procedure described for the initial precipitate.

Conclusive proof for the existence of the hexamer in solution was obtained from an NMR spectroscopic investigation. A representative experiment afforded the ^{1}H NMR spectrum of the hexamer (thermally treated with methanol as described above) in deuterochloroform, which is shown in Fig. 1. For the purpose of this discussion, the most important features in the spectrum are the two methanol peaks labeled **b** and **c**, where **b** is the methyl proton resonance for methanol trapped within the hexameric sphere, and **c** is the methyl proton resonance for methanol in the bulk solvent. The identity of these peaks was proved by a spiking experiment in which additional methanol added to the NMR tube had the effect of increasing the intensity of peak **c**. Similar results were obtained in d^6-acetone, d^6-DMSO and d^8-toluene. It should also be noted that NMR spectra for hexamer **2** synthesized in ethanol or isopropanol also showed two sets of resonances for each inequivalent proton in the ethanol or isopropanol molecules. Indeed, in a pressurized NMR sample tube we observed no change in the intensities of peaks **b** and **c** at 150 °C. These results clearly demonstrate that

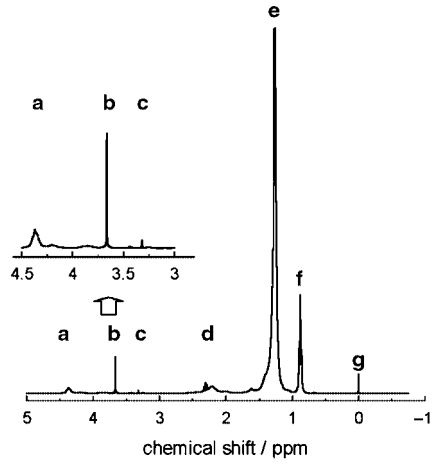

Fig. 1 ^{1}H NMR spectrum of *C*-tridecylpyrogallol[4]arene at room temperature in CDCl$_3$ with TMS. The region of the spectrum displaying the methanol resonances is enlarged in the inset. Peak assignments: **a**, diaryl C–H; **b**, CH$_3$ of guest methanol; **c**, CH$_3$ of methanol in the bulk solvent; **d**, CH$_2$ adjacent to CH in bridging group; **e**, remaining CH$_2$ groups; **f**, terminal CH$_3$ on R; **g**, TMS internal standard.

 DOI: 10.1039/b106250f

(1) methanol molecules within the hexameric sphere do not exchange with methanol in the bulk solvent, or with bulk solvent itself, and (2) the hexameric sphere is stable with methanol as a guest up to at least 150 °C in d^6-acetone.

Using the techniques described above, stable hexameric spheres have been obtained for R = *n*-propyl up to *n*-tridecyl, whereas for R = methyl or ethyl there is no evidence for the existence of hexameric spheres. The solubility of *C*-alkylpyrogallol[4]arenes is low in apolar solvents when the *C*-alkyl group is a short chain (*i.e.* C_3, C_4). Similarly, low solubility occurs in polar solvents when the *C*-alkyl chain is long (*i.e.* C_{10}, C_{13}). It is therefore possible, with the appropriate choice of R-group, to have stable hexameric spheres in polar or apolar solvents. Remarkably, these hexameric spheres are also stable in mixtures of acetone and water to the limit of their solubility. For example, the hexameric sphere for R = *n*-pentyl is stable in a 50% v/v mixture of d^6-acetone and D_2O (precipitation without decomposition occurs with a higher percentage of water). These results show the extraordinary stability of these hydrogen-bonded hexameric spheres in highly polar media. We refer here to the stability of the capsule both with regard to the structural integrity imparted by the hydrogen bonding arrangement, as well as to the failure of the entrapped methanol to exchange with the bulk solvent.

Thus far we have obtained and crystallographically characterized hexameric molecular capsules for R = *n*-propyl, *n*-butyl, isobutyl and *n*-pentyl. In the structure of the *C*-isobutylpyrogallol[4]arene capsule, **2a**,† the capsule completely encloses the space, Fig. 2. The interior volume[9] of the capsule is 1510 Å^3 and can be regarded as the total space available to the guest molecules. Indeed, the X-ray crystal structures reveal nothing more than smears of electron density within the cavity.

The hexameric structure **2** is the only type of capsule that we have observed in the solid state. Furthermore, the NMR experiments reveal that a capsule exists in solution and integration of the methyl proton signal **b** and the diaryl C–H signal **a** are consistent with the enclosure of *ca.* 18 methanol molecules. The free volume of 1510 Å^3, calculated from the solid-state structure, provides enough space for *ca.* 23 methanol molecules. This is based on a van der Waals volume of 36 Å^3 for a single molecule of methanol, and 55% guest-occupancy was recently put forward by Rebek and Mecozzi.[10] This clearly demonstrates that the capsule in solution encloses a comparable amount of space as the solid-state hexameric capsule. Therefore, the only reasonable interpretation is that the solid-state structure **2** is maintained in solution. The only other type of non-porous structure with precedent in this area of chemistry is a dimer.[5,11] While the dimer [*C*-alkylpyrogallol[4]arene]$_2$ has not been observed in the solid state, we modeled and calculated the volume that such a dimer would enclose, should it exist (*ca.* 140 Å^3). This is enough space to enclose two methanol molecules to give a 1 : 1 host : guest ratio, as opposed to the 1 : 4 ratio expected for the hexamer. The 1 : 3 ratio observed in the NMR experiments rules out any structure which provides less available space, such as the dimer. While 23 molecules provide 23/6 or a 1 : 4 host : guest ratio, the observed 18 methanol molecules (1 : 3 host : guest ratio) is quite reasonable, since other unaccounted guests may also be present (*e.g.* non-hexameric **1**, unreacted starting material, colored reaction by-products, other solvents, all in low concentration).

In summary, very large spherical capsules with outstanding stability in highly polar media have been synthesized and characterized reproducibly.

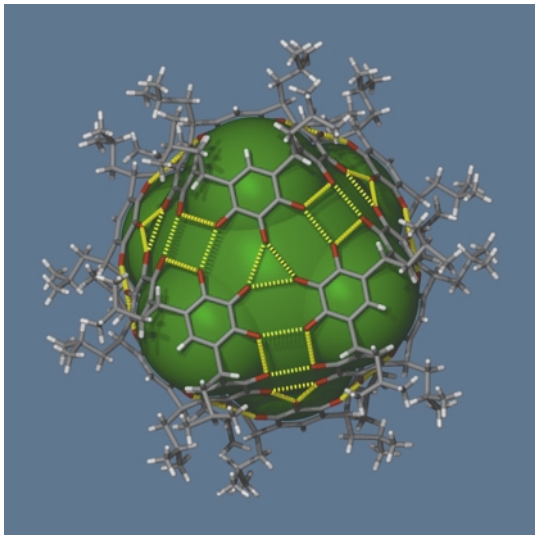

Fig. 2 Stick-bond representation of hexameric capsule with the enclosed space represented in green. Hydrogen bonds are shown as broken yellow cylinders. Orientation is the same as that shown in **2**.

Notes and references

† *Crystal data* for *C*-isobutylpyrogallol[4]arene: M = 905.06, rhombohedral, space group $R\bar{3}$ (the space group for the hexameric capsule reported by Mattay[7] was $P\bar{1}$), $a = b$ = 34.84(2), c = 24.04(3) Å, V = 25268(4) Å^3, Z = 18, μ (Mo-Kα) = 0.066 mm^{-1}. A colorless crystal of dimensions 0.35 × 0.30 × 0.20 mm was used. Intensity data were collected at 173 K on a Bruker SMART CDD diffractometer. Owing to extensive disorder of the contents of the supramolecular cavity as well as the nitrobenzene molecules embedded in the propyl chains, the structure is very poorly resolved. Final refinement converged with R_1 = 0.1482 for 6890 unique reflections [$I > 2\sigma(I)$, $2\theta_{max}$ = 46°]. CCDC reference number 167522. See http://www.rsc.org/suppdata/cc/b1/b106250f/ for crystallographic data in CIF or other electronic format.

1 D. J. Cram, H. J. Choi, J. A. Bryant and C. B. Knobler, *J. Am. Chem. Soc.*, 1992, **114**, 7748; D. A. Makeiff, D. J. Pope and J. C. Sherman, *J. Am. Chem. Soc.*, 2000, **122**, 1337; A. Collet, *Tetrahedron*, 1987, **43**, 5725.

2 M. M. Conn and J. Rebek, *Chem. Rev.*, 1997, **97**, 1647; J. Rebek, *Acc. Chem. Res.*, 1999, **32**, 278; J. Rebek, *Chem. Commun.*, 2000, 637.

3 L. R. MacGillivray and J. L. Atwood, *Nature*, 1997, **389**, 469.

4 L. R. MacGillivray and J. L. Atwood, *Angew. Chem., Int. Ed.*, 1999, **38**, 1019; G. W. Orr, L. J. Barbour and J. L. Atwood, *Science*, 1999, **285**, 1049; M. J. Hardie and C. L. Raston, *J. Chem Soc., Dalton Trans.*, 2000, 2483.

5 K. N. Rose, L. J. Barbour, G. W. Orr and J. L. Atwood, *Chem. Commun.*, 1998, 407; K. Murayama and K. Aoki, *Chem. Commun.*, 1998, 607.

6 Y. Tanaka, M. Miyachi and Y. Kobuke, *Angew. Chem., Int. Ed.*, 1999, **38**, 504.

7 T. Gerkensmeier, W. Iwanek, C. Agena, R. Frohlich, S. Kotila, C. Nather and J. Mattay, *Eur. J. Org. Chem.*, 1999, 2257.

8 R. S. Meissner, J. Rebek and J. Mendoza, *Science*, 1995, **270**, 1485; J. Kang and J. Rebek, *Nature*, 1997, **385**, 50; R. Meissner, X. Garcias, S. Mecozzi and J. Rebek, *J. Am. Chem. Soc.*, 1997, **119**, 77; T. Heinz, D. M. Rubkevich and J. Rebek, *Nature*, 1998, **394**, 764; T. Martin, U. Obst and J. Rebek, *Science*, 1998, **281**, 1842.

9 L. J. Barbour, CAVITY, unpublished computer program.

10 S. Mecozzi and J. Rebek, *Chem. Eur. J.*, 1998, **4**, 1016.

11 J. M. Rivera, T. Martin and J. Rebek, *J. Am. Chem. Soc.*, 2001, **123**, 5213.

CHEMCOMM Communication
www.rsc.org/chemcomm

Hydrothermal synthesis of the first organically templated open-framework uranium phosphate

Janet A. Danis,[ab] Wolfgang H. Runde,[a] Brian Scott,[a] James Fettinger[b] and Bryan Eichhorn[b]

[a] *Environmental and Chemistry Divisions, Los Alamos National Laboratory, Los Alamos, New Mexico 87545, USA. E-mail: jandanis@lanl.gov*
[b] *Department of Chemistry and Biochemistry, University of Maryland, College Park, Maryland 20742, USA. E-mail: b._eichhorn@umail.umd.edu*

Received (in Purdue, IN, USA) 30th July 2001, Accepted 28th September 2001
First published as an Advance Article on the web 31st October 2001

$[(C_2H_5)_2NH_2]_2[(UO_2)_5(PO_4)_4]$ was prepared from U_3O_8, $HONEt_2$ and phosphoric acid under hydrothermal conditions (180 °C, 5 days) and represents the first three-dimensional open-framework uranium phosphate prepared to date.

Microporous phosphates are an important class of materials that are well studied for their use in catalysis and their ability to selectively sorb guest molecules.[1,2] Interest in the preparation of open-framework and porous transition metal phosphates, in particular, has heightened in recent years.[1,3–8] These materials can provide many of the same benefits as traditional zeolites such as accessible internal micropores, size and shape selectivity, rigid frameworks and chemical/thermal stability, and in addition, incorporate potentially catalytically active sites. Uranium phosphates are of interest in areas such as ion exchange[9,10] and protonic conduction.[11,12] Uranium-containing materials, such as uranium oxides, are also known to be effective catalysts.[13,14] The synthesis of 3-D open-framework uranium phosphates is a desirable goal in this regard but there are currently no examples of such materials. Uranyl (UO_2^{2+}) phosphates tend to form 2-D layered structures in both mineral phases and synthetic compounds.

The pentagonal bipyramidal (PBP) geometry common to the uranyl complexes could be combined with the tetrahedral phosphate ion to form a new class of PBP-tetrahedral framework structures. Recent studies have yielded new uranium-(IV) and -(VI) compounds of variable dimensions containing phosphate,[15] molybdate[16] and fluoride;[17–21] including the first two organically templated layered uranyl phosphate compounds.[15] These two-dimensional structures form with charge-balancing organic cations interacting through hydrogen bonds between the layers. Clearfield and co-workers have been investigating the formation of uranium-containing molecular solids incorporating phenylphosphonates and phenylphosphinates to produce linear, layered and tunnel-type frameworks.[22,23] The three-dimensional inorganic uranium frameworks prepared to date are limited to uranium(IV) fluorides.[17–21]

As part of a systematic search for novel uranium phosphate phases, we have employed hydrothermal methods to prepare an organically templated three-dimensional open-framework uranium phosphate. We report here the synthesis and structural characterization of the first example in this class: $[(C_2H_5)_2NH_2]_2[(UO_2)_5(PO_4)_4]$ (**1**). In a concurrent study, O'Hare and coworkers have prepared the first organically templated 3-D uranium phosphite.[24]

The title compound was prepared† from U_3O_8, $HONEt_2$ and phosphoric acid under hydrothermal conditions (180 °C, 5 days, autogenous pressure). The reaction produced a large amount of brown powder and a small amount of tiny, translucent gold-colored crystals of **1**. X-Ray powder diffraction showed the brown powder to be a mixture of U_3O_8 and other unidentified components. The largest of the plate-like crystals measured 0.02 × 0.04 × 0.08 mm^3. The compound is air-stable and has been characterized by single crystal X-ray diffraction.‡ The small size of the crystals and the low crystalline yield of the reaction have hindered further characterization.

$[(C_2H_5)_2NH_2]_2[(UO_2)_5(PO_4)_4]$ is monoclinic, space group *I*2/*m*, and contains a 3-D network of U(VI) distorted octahedra, U(VI) PBPs and phosphate tetrahedra. These vertices form an open-framework structure (Fig. 1) in which the channels are filled with $Et_2NH_2^+$ cations. The structure contains parallel chains of edge-shared PBPs (containing U(1)) that are linked into $UO_2PO_4^-$ sheets in the *xz* plane by virtue of bridging phosphates (Fig. 1). The PBP is defined by two axial uranyl oxygen atoms (U(1)–O = 1.76(1), 1.74(1) Å) and five

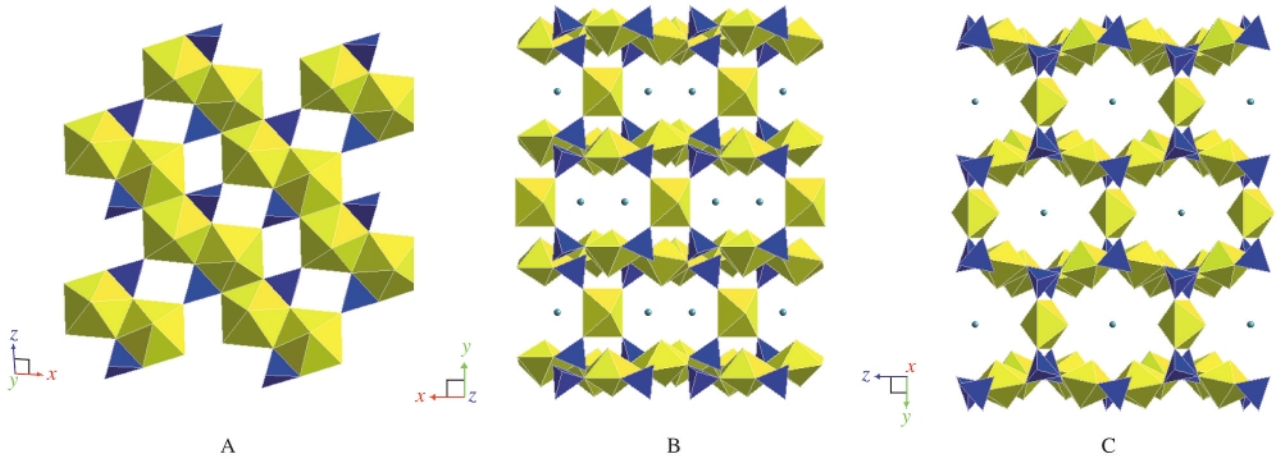

Fig. 1 The 3-D structure of $[(C_2H_5)_2NH_2]_2[(UO_2)_5(PO_4)_4]$ as viewed down (A) the crystallographic *b* axis, (B) the crystallographic *c* axis, and (C) the crystallographic *a* axis. Only nitrogen atoms of $[(C_2H_5)_2NH_2]^+$ are shown for clarity. The yellow polyhedra represent the uranyl distorted octahedra and PBPs. The blue tetrahedra represent phosphate groups and the light blue balls the nitrogen atoms.

 DOI: 10.1039/b106916k

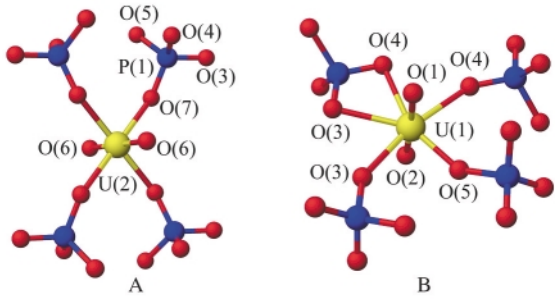

Fig. 2 Ball-and-stick drawings of (A) the distorted octahedron, U(2), and (B) the pentagonal bipyramid, U(1). Selected bond distances (Å): U(1)–O(1) 1.756(14), U(1)–O(2) 1.736(13), U(1)–O(3) 2.348(10), U(1)–O(3′) 2.513(10), U(1)–O(4) 2.382(11), U(1)–O(4′) 2.484(12), U(1)–O(5) 2.225(12), U(2)–O(6) 1.72(2), U(2)–O(7) 2.266(13).

equatorial phosphate oxygens that form the pentagonal plane (Fig. 2B). These five uranium–oxygen bonds are formed by sharing corners with three phosphate tetrahedra and an edge with a fourth tetrahedron. Each PO_4 tetrahedron shares corners with four uranyls and an edge with a fifth.

The $UO_2PO_4^-$ sheets stack along the *y*-axis and are linked into a rigid 3-D structure by the bridging U(2) distorted octahedra (Fig. 1B). The distorted octahedra (Fig. 2A) are defined by two axial uranyl oxygens and four phosphate oxygens from two adjacent $UO_2PO_4^-$ layers. The U(2)–O uranyl distance of 1.72(2) Å is typical of distorted U(VI) octahedra of this type. The U(2) distorted octahedra create a pillaring effect with intersecting tunnels that run along the crystallographic *a* and *c* axes. The 3-D $[(UO_2)_5(PO_4)_4]^{2-}$ uranyl phosphate framework is charge balanced through inclusion of two $Et_2NH_2^+$ cations per formula unit that reside in the tunnels (see Fig. 1B and 1C).

The $UO_2PO_4^-$ sheets of **1** are similar to those of the mineral β-uranophane, $Ca(UO_2)_2(SiO_3OH)_2{\cdot}5H_2O$.[25] In this layered structure, chains of uranyl PBPs are linked into sheets by SiO_3OH^{3-} tetrahedra. The silicate oxygens that are not involved in bonding within the sheet are all protonated and on one side of the sheet whereas the corresponding phosphate oxygens of **1** alternate, pointing above and below the sheet, and are not protonated. The layers of β-uranophane are intercalated with Ca^{2+} ions in contrast to the rigid 3-D framework structure of **1**. The layers of **1** are reminiscent of those in the 2-D uranyl phosphates prepared by O'Hare and co-workers[15] and α-uranophane.[26] The presence and mode of connectivity of the inter-layer uranyl octahedra in **1** also appear in phosphuranylite, $KCa(H_3O)_3(UO_2)_7(PO_4)_4O_4{\cdot}8H_2O$.[27] However, the sheet portion of this mineral contains hexagonal bipyramids and PBPs and is very different from that in **1**.

The formation of the $Et_2NH_2^+$ cations from Et_2NOH presumably occurs through a redox process involving U_3O_8. The use of Et_2NH instead of Et_2NOH in the synthesis of **1** under identical conditions results in smaller crystallites that are not suitable for single-crystal studies by conventional methods.

This work was supported by the LDRD program at Los Alamos National Laboratory.

Notes and references

† Hydrothermal reactions were carried out in Teflon lined 23 mL stainless steel, commercially purchased Parr brand pressure autoclaves. Water was purified in a Millipore MilliQ Ultra-pure water system. U_3O_8, phosphoric acid (85%), diethylhydroxyamine and deionized water were combined in the mol ratio of 1.0:8.0:4.0:496 and reacted under autogenous pressure at 180 °C for 5 days, then ramp cooled at the rate of 5 °C h^{-1}. Single crystals were manually isolated for analysis.

‡ *Crystal data* for $[(C_2H_5)_2NH_2]_2[(UO_2)_5(PO_4)_4]$: $C_8H_{24}N_2O_{26}P_4U_5$, M = 3748.58, monoclinic, *I*2/*m*, a = 9.4442(17), b = 15.449(3), c = 9.5719(17) Å, β = 93.268(3)°, V = 1394.3(4) Å^3, Z = 2, D_c = 4.464 g cm^{-1}, λ = 0.71073 Å, T = 193 K, $5 < 2\theta < 50°$, R (R_w) = 0.0619 (0.1133) for refinement on F^2 using all 1243 unique reflections. The structure was solved and refined using the SHELXTL software package.[28] All atoms were refined anisotropically except for the N and C atoms of the $Et_2NH_2^+$ cation, which were refined isotropically. Hydrogen atoms were placed in idealized positions. There was large thermal motion but no apparent disorder associated with the Et groups.

CCDC reference number 171758. See http://www.rsc.org/suppdata/cc/b1/b106916k/ for crystallographic data in CIF or other electronic format.

1 A. K. Cheetham, G. Férey and T. Loiseau, *Angew. Chem., Int. Ed.*, 1999, **38**, 3268.
2 S. T. Wilson, B. M. Lok, C. A. Messina, T. R. Cannan and E. M. Flanigen, *J. Am. Chem. Soc.*, 1982, **104**, 1146.
3 R. C. Haushalter and L. A. Mundi, *Chem. Mater.*, 1992, **4**, 31.
4 Y. Ma, W. Tong, H. Zhou and S. L. Suib, *Microporous Mesoporous Mater.*, 2000, **37**, 243.
5 J. R. D. Debord, W. M. Reiff, C. J. Warren, R. C. Haushalter and J. Zubieta, *Chem. Mater.*, 1997, **9**, 1994.
6 R. C. Haushalter, V. Soghomonian, J. Zubieta, C. J. O'Connor and Q. Chen, *Science*, 1993, **259**, 1596.
7 D. M. Whang, N. H. Hur and K. Kim, *Inorg. Chem.*, 1995, **34**, 3363.
8 C. N. R. Rao, S. Natarajan and S. Neeroj, *J. Am. Chem. Soc.*, 2000, **122**, 2810.
9 M. M. Olken, R. N. Biagioni and A. B. Ellis, *Inorg. Chem.*, 1983, **22**, 2128.
10 M. Pham-Thi and P. Colomban, *J. Less-Common Met.*, 1985, **108**, 189.
11 B. Morosin, *Acta Crystallogr., Sect. B*, 1978, **34**, 3732.
12 B. Morosin, *Phys. Lett. A*, 1978, **65**, 53.
13 G. J. Hutchins, C. S. Heneghan, I. D. Hudson and S. H. Taylor, *Nature*, 1996, **384**, 341.
14 S. H. Taylor and S. R. O'Leary, *Appl. Catal. B*, 2000, **25**, 137.
15 R. J. Francis, M. J. Drewitt, P. S. Halasyamani, C. Ranganathachar, D. O'Hare, W. Clegg and S. J. Teat, *Chem. Commun.*, 1998, 279.
16 P. S. Halasyamani, R. J. Francis, S. M. Walker and D. O'Hare, *Inorg. Chem.*, 1999, **38**, 271.
17 S. Allen, S. Barlow, P. S. Halasyamani, J. F. W. Mosselmans, D. O'Hare, S. M. Walker and R. I. Walton, *Inorg. Chem.*, 2000, **39**, 3791.
18 R. J. Francis, P. S. Halasyamani and D. O'Hare, *Angew. Chem., Int. Ed.*, 1998, **37**, 2214.
19 (*a*) R. J. Francis, P. S. Halasyamani and D. O'Hare, *Chem. Mater.*, 1998, **10**, 3131; (*b*) P. M. Almond, C. E. Talley, A. C. Bean, S. M. Peper and T. E. Albrecht-Schmidt, *J. Solid State Chem.*, 2000, **154**, 635.
20 (*a*) R. J. Francis, P. S. Halasyamani, J. S. Bee and D. O'Hare, *J. Am. Chem. Soc.*, 1999, **121**, 1609; (*b*) P. M. Almond, L. Deakin, A. Mar and T. E. Albrecht-Schmidt, *J. Solid State Chem.*, 2001, **158**, 87.
21 S. M. Walker, P. S. Halasyamani, S. Allen and D. O'Hare, *J. Am. Chem. Soc.*, 1999, **121**, 10513.
22 D. Grohol, M. A. Subramanian, D. M. Poojary and A. Clearfield, *Inorg. Chem.*, 1996, **35**, 5264.
23 (*a*) D. Grohol, F. Gingl and A. Clearfield, *Inorg. Chem.*, 1999, **38**, 751; (*b*) D. M. Poojary, A. Cabeza, M. A. G. Aranda, S. Bruque and A. Clearfield, *Inorg. Chem.*, 1996, **35**, 1468.
24 M. Doran, S. M. Walker and D. O'Hare, *Chem. Commun.*, 2001, 1988.
25 K. Viswanathan and O. Harnett, *Am. Miner.*, 1986, **71**, 1489.
26 D. Ginderow, *Acta Crystallogr., Sect. C*, 1988, **44**, 421.
27 F. Demartin, V. Diella, S. Donzelli, C. M. Gramaccioli and T. Pilati, *Acta Crystallogr., Sect. B*, 1991, **47**, 439.
28 G. M. Sheldrick, SHELXTL, Program for crystal structure solution and refinement, University of Göttingen, Germany, 1997.

CHEMCOMM Communication
www.rsc.org/chemcomm

Hydroxylated nanoballs: synthesis, crystal structure, solubility and crystallization on surfaces

Heba Abourahma,[a] Anthony W. Coleman,[b] Brian Moulton,[a] Beth Rather,[a] Patrick Shahgaldian[b] and Michael J. Zaworotko*[a]

[a] *Department of Chemistry, University of South Florida, 4202 E Fowler Ave (SCA 400), Tampa, FL, 33620, USA. E-mail: xtal@usf.edu*
[b] *Institut de Biologie et Chimie des Proteines, CNRS UMR5086, 7 Passage du Vercors, Lyon, F69367, France. E-mail: aw.coleman@ibcp.fr*

Received (in Columbia, MO, USA) 5th June 2001, Accepted 26th August 2001
First published as an Advance Article on the web 31st October 2001

The reaction of equimolar amounts of $Cu(NO_3)_2$ and bdc-5-OH (bdc-5-OH = benzene-1,3-dicarboxylate-5-hydroxy) affords hydroxylated nanoballs with high solubility and an ability to form microcrystals on surfaces.

The design and generation of nanoscale polyhedral structures *via* self-assembly represents an approach to synthesis that offers new horizons in the context of synthetic chemistry and its possible impact upon nanotechnology.[1–9] In this context, we have recently reported a design strategy for the one-step synthesis of nanoscale molecules[10] and frameworks[11,12] that are based upon self-assembly of structure building units (SBUs),[13] $M_2(O_2CR)_4$ molecular squares, at their vertices. The discrete structures, which we have termed 'nanoballs', are molecular versions of faceted polyhedra,[14] namely *small rhombihexahedra*, and are depicted schematically in Fig. 1. The key to obtaining 'nanoballs' cleanly and in high yield is that the square SBUs are linked at a 120° angle using the angular bifunctional ligand benzene-1,3-dicarboxylate, bdc. They are distinguished by their nanoscale size, their facile synthesis and the potential for functionalisation at multiple sites: the inner or outer metal centres, the interior cavity, or the bridging ligand. In this contribution we report the first example of a small rhombihexahedron that is functionalised at the bridging ligand, bdc-5-OH serving as the ligand.

The small rhombihexahedron $[(DMSO)(MeOH)Cu_2(bdc\text{-}5\text{-}OH)_2]_{12}$, **1**, formed spontaneously upon the addition of 2,6-dimethylpyridine (2 equivalents) to a methanolic solution of $Cu(NO_3)_2$ (1 equivalent) and H_2bdc-5-OH (1 equivalent). Addition of diethyl ether precipitated a crude product, recrystallization of which from DMSO afforded single crystals of **1** suitable for X-ray crystallography.† The crystal structure of **1** is illustrated in Fig. 2. **1** has DMSO ligands axially bonded to the metal ions that lie at the exterior surface of the nanoball, and MeOH ligands axially bonded to the metal ions that lie at the interior surface of the ball. It has a molecular volume, including solvent sphere, > 17 nm^3 and a molecular weight of 7.43 kDa. The internal cavity has a volume of *ca.* 1 nm^3. Crystals of **1** appear to be stable indefinitely if in contact with the mother-liquor but are highly deliquescent if removed from mother-liquor.

The presence of 24 hydroxy groups on the surface of the nanoball predictably alters the chemical and physical properties when compared to the unsubstituted analogues. For example, **1** is readily soluble in a variety of organic solvents, including methanol, ethanol, *iso*-propyl alcohol, DMF and hot acetonitrile. This has allowed us to grow microcrystals of **1** on mica or glass, *via* evaporation of methanol solutions of **1**.

Atomic force microscopy (AFM) has become one of the most widely used tools for the study of crystal growth and behaviour on surfaces,[15–20] examples include size control of nano-crystals on Langmuir–Blodgett films,[15] protein crystal growth,[16] molecular and nanotribology,[17] statistical analysis of 2-D crystal sizes,[18] dopant effects on crystal growth[19] and annealing effects on crystallisation.[20] AFM studies‡ revealed that the microcrystals of **1** are of quite uniform dimensions and that they are stable even after mild heating.

The images obtained on a mica surface, without thermal treatment, show increasing density of microcrystals with increasing concentration. The micocrystals have an average height of 140 nm with a variation of 30 nm; the roughness (RMS) is 56 nm. The average size is 1.3 μm with a variation of 0.4 μm. In the case of the films prepared on glass, observation on samples not thermally treated gave poor image quality even in the non-contact mode due to the presence of residual solvent forming a strongly bound contamination film. This contamination layer can be removed by heating to 37 or 75 °C during 24 h. The corresponding images are shown in Fig. 3(a) and (b), respectively; the roughness (RMS) is 236 nm and 261 nm. Image analysis shows an average size of 1.4 μm for the sample annealed at 37 °C and again 1.4 μm for that annealed at 75 °C, the variance is 0.4 μm. It is interesting that there is no apparent difference in the crystal sizes either on different substrates or under different thermal treatment. The average heights are 500 and 600 nm, respectively. For the sample treated at 37 °C the height values are randomly distributed about this average. However, for the sample treated at 75 °C there is a clear statistical distribution of heights at 300, 600 and 900 nm. Whilst it is apparent that annealing at higher temperature leads to a higher density of crystals, it is of interest that there is apparently non-crystalline material present between the microcrystals in Fig. 3(a). This situation is analogous to that observed for thermally treated thin films of *tert*-butylcalix[4]arene.[21] It would appear that annealing at the higher temperature gives rise

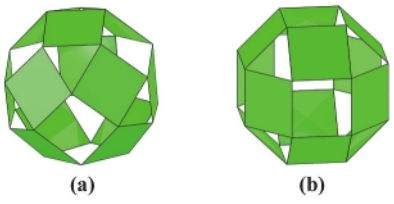

Fig. 1 Schematic representations of the small rhombihexahedra that exist for $[(MeOH)_2Cu_2(bdc)_2]_{12}$, **a**, and $[(Py)(MeOH)Cu_2(bdc)_2]_{12}$, **b**. The two polyhedra differ in the connectivity of the SBUs.

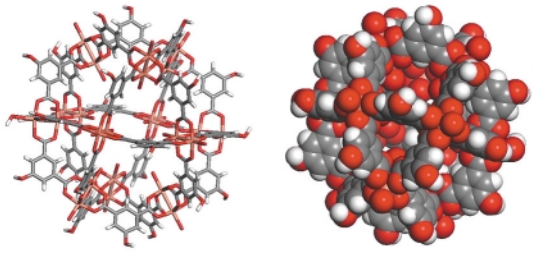

Fig. 2 Crystal structure of $[(DMSO)(MeOH)Cu_2(bdc\text{-}5\text{-}OH)_2]_{12}$ **1**. The connectivity of the SBUs in **1** is the same as in **b**.

 DOI: 10.1039/b106592k

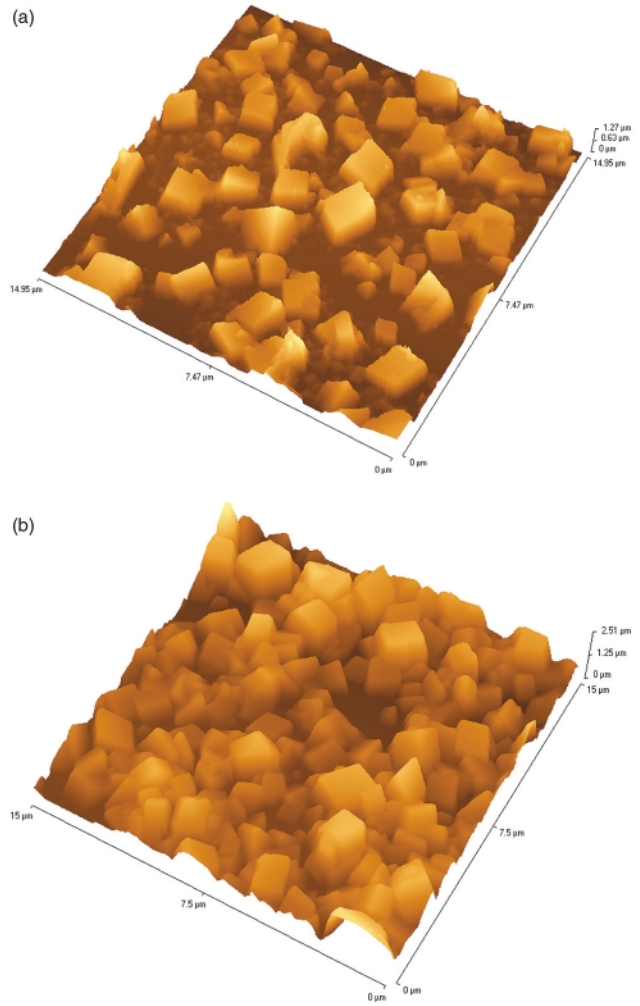

Fig. 3 (a) Non-contact mode AFM image of microcrystals of **1** on glass after annealing at 37 °C for 24 h. (b) Non-contact mode AFM image of microcrystals of **1** on glass after annealing at 75 °C for 24 h.

to a complete crystallisation of the film and that there is a definite self-organisation producing structures for which the heights are multiples of 300 nm. The existence of nanoscale channels in the crystal structure of **1** is a consequence of the inability of spheres to close-pack efficiently and the inherent open structure that must occur for a faceted polyhedron. We are therefore evaluating **1** for possible use in sensors.

We gratefully acknowledge the financial support of UCBL1 (M. Z.), NSF (DMR 0101641, M. Z.) and CNRS and FRM (A. W. C.).

Notes and references

† *Crystallographic data*: intensity data for **1** were collected at 200 K on a Bruker SMART-APEX diffractometer using Mo-Kα radiation (λ = 0.7107 Å). The data were corrected for Lorentz and polarization effects and for absorption using the SADABS program. The structure was solved using direct methods and refined by full-matrix least-squares on $|F|^2$. All non-hydrogen atoms were refined anisotropically and hydrogen atoms were placed in geometrically calculated positions and refined with temperature factors 1.2 times those of their bonded atoms. The calculated density is very low and a reflection of the large amounts of space in the unit cell that are occupied by disordered solvent molecules.

Crystal data for **1**: tetragonal, space group *I*4/*mmm*, $a = b = 31.111(4)$, $c = 35.999(6)$ Å, $V = 34844(8)$ Å^3, $Z = 2$, $D_c = 0.708$ g cm^{-3}, $\mu = 0.778$ mm^{-1}, $F(000) = 7366$, $2\theta_{max} = 42.08°$ ($-30 \leqslant h \leqslant 31$, $-31 \leqslant k \leqslant 31$, $-36 \leqslant l \leqslant 21$). Final residuals (for 296 parameters) were $R1 = 0.1531$ for 5170 reflections with $I > 2\sigma(I)$, and $R1 = 0.2128$, $wR2 = 0.4702$, GOF = 1.679 for all 49928 data. Residual electron density was 1.051 and -0.592 e Å^{-3}.

CCDC reference number 169279. See http://www.rsc.org/suppdata/cc/b1/b106592k/ for crystallographic data in CIF or other electronic format.

‡ *Atomic force microscopy data*: films of **1** were prepared by deposition of 20 µL of a solution of **1** in methanol, at varying concentrations, onto either freshly cleaved mica or freshly cleaned glass slides. Images of deposited films of **1** on mica or glass were collected using a Thermomicroscopes Explorer AFM. Scan sizes from 80 to 5 µm were collected in amplitude detection in the non-contact mode. Cantilevers were HRF with a resonance frequency of 270 kHz, scan rates were 1 Hz. Image resolution was 500 × 500. Images are unfiltered.

1 G. W. Orr, L. J. Barbour and J. L. Atwood, *Science*, 1999, **285**, 1049.
2 L. R. MacGillivary and J. L. Atwood, *Nature*, 1997, **389**, 469.
3 B. Olenyuk, M. D. Levin, J. A. Whitford, J. E. Shield and P. J. Stang, *J. Am. Chem. Soc.*, 1999, **121**, 10434.
4 B. Olenyuk, J. A. Whitford, A. Fechtenkotter and P. J. Stang, *Nature*, 1999, **398**, 796.
5 P. J. Stang, B. Olenyuk, D. C. Muddiman and R. D. Smith, *Organometallics*, 1997, **16**, 3094.
6 N. Takeda, K. Umemoto, K. Yamaguchi and M. Fujita, *Nature*, 1999, **398**, 794.
7 M. Fujita, D. Ogura, M. Miyazawa, H. Oka, K. Yamaguchi and K. Ogura, *Nature*, 1995, **378**, 469.
8 K. Umemoto, K. Yamaguchi and M. Fujita, *J. Am. Chem. Soc.*, 2000, **122**, 7150.
9 M. Eddaoudi, J. Kim, J. B. Wachter, H. K. Chae, M. O'Keeffe and O. M. Yaghi, *J. Am. Chem. Soc.*, 2001, **123**, 4368.
10 B. Moulton, J. Lu, A. Mondal and M. J. Zaworotko, *Chem. Commun.*, 2001, 683.
11 S. A. Bourne, J. Lu, A. Mondal, B. Moulton and M. J. Zaworotko, *Angew. Chem., Int. Ed.*, 2001, **40**, 2111.
12 J. Lu, A. Mondal, B. Moulton and M. J. Zaworotko, *Angew. Chem., Int. Ed.*, 2001, **40**, 2113.
13 O. M. Yaghi, H. L. Li, C. Davis, D. Richardson and T. L. Groy, *Acc. Chem. Res.*, 1998, **31**, 747.
14 A. Holden, *Shapes, Space and Symmetry*, Columbia University Press, New York, 1971.
15 G. Hemakanthi, A. Dhathathreyan, B. U. Nair, T. Ramasami, D. Möbius and T. Schaffer, *Colloid. Surf. A*, 2001, **181**, 115.
16 M. Wiechmann, O. Enders, C. Zeilinger and H.-A. Kolb, *Ultramicroscopy*, 2001, **86**, 159.
17 B. Bhushan, *P. I. Mech. Eng. J.-J. Eng.*, 2001, **215**, 1.
18 B. Li, I. Avrutsky, Y. Zhao and G. Mao, *Colloid. Surf. A*, 2000, **174**, 113.
19 M. Moret, *Mater. Chem. Phys.*, 2000, **66**, 177.
20 B. Heck, T. Hugel, M. Iijima and G. Strobl, *Polymer*, 2000, **41**, 8839.
21 P. Goreloff, R. Lamartine and A. W. Coleman, *Cryst. Eng.*, 1999, **1**, 191.

CHEMCOMM Communication
www.rsc.org/chemcomm

M_2 δ-to-oxalate π* conjugation in oxalate-bridged complexes containing M–M quadruple bonds†‡

Bruce E. Bursten,* Malcolm H. Chisholm,* Christopher M. Hadad,* Jun Li and Paul J. Wilson

Department of Chemistry, The Ohio State University, Newman and Wolfrom Laboratory, 100 W. 18th Avenue, Columbus, OH 43210-1185, USA. E-mail: chisholm@chemistry.ohio-state.edu

Received (in Cambridge, UK) 1st May 2001, Accepted 27th September 2001
First published as an Advance Article on the web 18th October 2001

The electronic structures of oxalate-bridged, quadruply-bonded dimolybdenum and ditungsten compounds have been investigated by a variety of computational methods employing density function theory (gradient corrected and time-dependent) which reveal the consequences of strong mixing of M_2 δ and oxalate π orbitals within extended chains and cyclic structures.

Recently, Cotton and others have reported the solid-state and molecular structures of a wide variety of dinuclear complexes linked by dicarboxylate groups, including dimers, cyclotrimers and cyclotetramers.[1–10] Lehn and coworkers have also reported alkynyl-linked tetranuclear complexes incorporating Ru_2 units.[11] In our earlier work, we have prepared several linked dimolybdenum and ditungsten complexes supported by pivalate ligands and noted the strong electronic communication between the metal centres that arises for oxalate-bridged complexes of the type $(Bu^tCO_2)_3M_2(\mu\text{-}O_2CCO_2)M_2(O_2CBu^t)_3$, where M = Mo and W.[12] We have now investigated the electronic communication in these complexes. These investigations have involved electronic structure calculations employing density functional theory (DFT) using both the Gaussian 98 and the ADF 2000 packages, and use has been made of the rapidly emerging time-dependent density functional theory (TDDFT) method to predict excitation energies for both the cyclic and linear forms. We report here the highlights of these findings.

When two quadruply-bonded M–M groups are linked by a bridging oxalate ligand, the primary interactions between the metals and dicarboxylate unit (aside from the formation of the M–O σ bonds) involve the filled δ orbitals and two of the oxalate π orbitals. There is a filled–filled interaction between the M_2 δ orbitals and one of the filled oxalate π orbitals, shown in **A**, and a donation from the M_2 δ orbital to one of the empty π* orbitals of oxalate, shown in **B**.

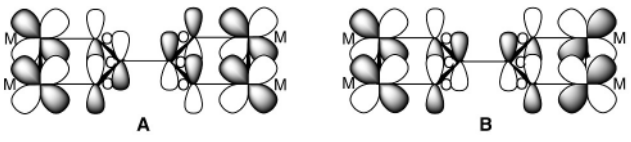

A **B**

The calculated molecular structures of the compound $(HCO_2)_3Mo_2(\mu\text{-}O_2CCO_2)Mo_2(O_2CH)_3$, which we have thus far used to model the previously reported hexa-pivalate complexes, are shown in Fig. 1.

For this work, molecular and electronic structure determinations were performed under either rigid D_2, D_{2h} or D_{4h} symmetry using both the Gaussian 98 and ADF 2000.01 programs, which gave comparable results.[13] It is notable that the oxalate ligand is essentially planar even though the symmetry of the molecule was relaxed to allow twisting about the oxalate C–C bond; and furthermore, the oxalate ligand has a relatively short C–C distance (1.50 Å) compared with 1.57 Å as seen in $K_2C_2O_4\cdot H_2O$.[14,15] Based on the oxalate-based LUMO being C–C π bonding, the planar D_{2h} structure is favoured by the back-bonding that results from the orbital interaction shown in **B**. The geometrical parameters shown in Fig. 1 for the central $Mo_2(\mu\text{-}O_2CCO_2)Mo_2$ core compare well with those recently reported by Cotton and Murillo for formamidinate-supported, oxalate-bridged complexes of Mo_2 and Rh_2.[1,2] The calculations also predict that the 'twisted' D_{2d} structure is not much higher in energy than the D_{2h} form, with an energy difference calculated to be 3.0 (Gaussian 98) and 3.7 (ADF 2000) kcal mol^{-1}. Slightly larger (6–8 kcal mol^{-1}) D_{2h}–D_{2d} energy differences are found in preliminary calculations for the analogous tungsten systems. The small conformational differences seem to correlate well with the observed thermochromism of the low-energy electronic transitions of the oxalate-bridged molecules. The energy of the transition from the b_{2g} HOMO to the b_{3u} oxalate π* orbital will be particularly sensitive to small changes in the C–C torsional angle that can be induced upon cooling. (These symmetry labels refer to D_{2h} symmetry. Under D_2 symmetry, b_{2g} transforms as b_2, and similarly, b_{3u} transforms as b_3.) The calculated energy of that vertical transition for $(HCO_2)_3Mo_2(\mu\text{-}O_2CCO_2)Mo_2(O_2CH)_3$ using TDDFT[13] is 2.76 eV (449 nm) and 2.41 eV (515 nm) as determined by Gaussian 98 and ADF 2000, respectively, which compares reasonably well to the λ_{max} observed for the pivalate complex $(Bu^tCO_2)_3Mo_2(\mu\text{-}O_2CCO_2)\text{-}Mo_2(O_2CBu^t)_3$, namely 2.70 eV (460 nm) at room temperature.[12]

In reactions employing $M_2(O_2CBu^t)_4$ (M = Mo or W) with one equivalent of free oxalic acid, replacement of two pivalate ligands per dinuclear unit occurs leading to higher oligomers, which have yet to be structurally characterized. If substitution proceeds to give *trans* products, a series of compounds can be anticipated which may be conveniently represented as $[M_2]_n(OXA)_{n-1}$, whereas if substitution proceeds in a *cis* manner, as recently seen in the substitution reactions of $Rh_2(O_2CMe)_4$ with a dicarboxylic acid,[4] then molecular squares $[M_2]_4(OXA)_4$ could result. Indeed, Cotton and Murillo, who have employed formamidinate ligands, have shown that squares, cyclotetramers, as well as cyclotrimers can be formed.[2,5–9] There, the *cis*-disposition of the ligands around the

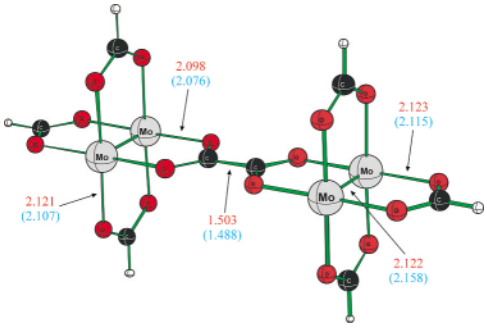

Fig. 1 View of the D_{2h} $[Mo_2]_2(OXA)$ system with selected geometrical data (Å). The Gaussian results are in red and the ADF data are in blue.

† Electronic supplementary information (ESI) available: Table of irreducible representations for $[M_2]_n(OXA)_{n-1}$ for all values of n. Fig. S1: plots of the frontier molecular orbitals of the D_{2h} linear $[Mo_2]_4(OXA)_3$ system and the D_{4h} square $[Mo_2]_4(OXA)_4$ system. See http://www.rsc.org/suppdata/cc/b1/b103898m/

‡ Dedicated to Professor Ernest R. Davidson on the occasion of his 65th birthday.

 DOI: 10.1039/b103898m

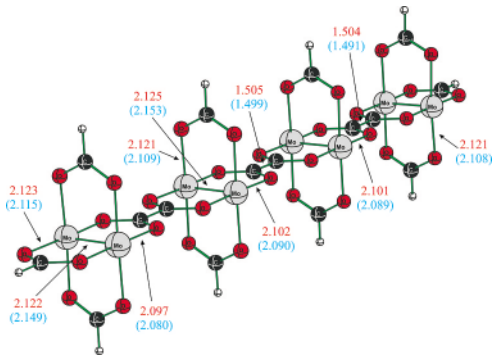

Fig. 2 View of the D_{2h} linear $[Mo_2]_4(OXA)_3$ system with selected geometrical data (Å). The Gaussian results are in red and the ADF data are in blue.

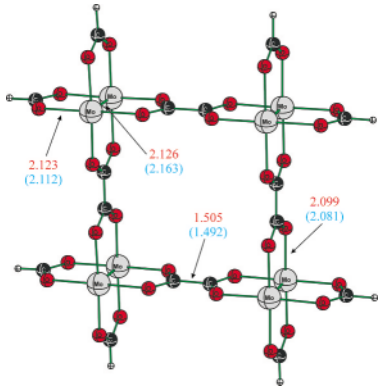

Fig. 3 View of the D_{4h} square $[Mo_2]_4(OXA)_4$ system with selected geometrical data (Å). The Gaussian results are in red and the ADF data are in blue.

M_2 core may be anticipated based on the *trans*-influence order N > O. Irrespective of the substitution pattern, the important electronic and structural features of the resulting compounds arise from extensions of the key orbital interactions shown in **A** and **B**. For D_{2h} planar $[M_2]_n(OXA)_{n-1}$ systems, if n is even the M_2 δ orbitals transform as $n/2$ b_{2g} and $n/2$ b_{3u}, and by contrast, when n is odd they transform as $(n + 1)/2$ b_{2g} and $(n - 1)/2$ b_{3u}. The filled and empty oxalate π orbitals also transform as b_{2g} and b_{3u}, which allows for the formation of a filled δ band and a vacant oxalate π* band. Irreducible representations spanned by the δ and oxalate orbitals are given in Table 1 (ESI†) for all values of n. On the other hand, for a D_{4h} square $[M_2]_4(OXA)_4$ system, the M_2 δ orbitals transform as a_{1g}, b_{2g} and e_u, and the filled and empty oxalate π orbitals transform as a_{2g} b_{2g} e_g and a_{1g} b_{1g} e_u, respectively.

In order to investigate the growth of the band structure in the linear compounds, we examined the electronic structure of the model compound $[Mo_2]_4(OXA)_3$ supported by formate ligands, and also, for comparison, that of the formate-supported cyclic tetramer, $[Mo_2]_4(OXA)_4$. The calculated optimised geometries of the model systems are illustrated in Figs. 2 and 3, respectively, and a comparative description is given in the frontier molecular orbital energy level diagram, Fig. 4.

For both D_{2h} $[Mo_2]_4(OXA)_3$ and D_{4h} $[Mo_2]_4(OXA)_4$, the HOMO is a b_{2g} δ-based orbital, which is raised in energy by interaction with the filled b_{2g} oxalate π orbital. The LUMO for $[Mo_2]_4(OXA)_3$ has b_{3u} symmetry, and that for $[Mo_2]_4(OXA)_4$ has b_{1g} symmetry, and in each case is an oxalate-localised π* orbital which is *totally* uninvolved with the metal atoms. Throughout, the M_2 δ*, π and σ orbitals are largely unperturbed by the oxalate ligands. Plots of the key frontier molecular orbitals for the linear $[Mo_2]_4(OXA)_3$ and the square $[Mo_2]_4(OXA)_4$ system are given as ESI in Fig. S1.†

The lowest energy electronic bands of $M_2(O_2CR)_4$ 'monomers' are due to metal-localised δ → δ* transitions. The presence of the oxalate ligands in $[M_2]_n(OXA)_{n-1}$ chains and $[M_2]_4(OXA)_4$ squares provides a significant electronic perturbation and hence the electronic transitions in these systems will be dominated by M_2 δ → oxalate π* MLCT transitions. In the linear chains, there is a low-energy allowed $b_{2g} \rightarrow b_{3u}$ or $b_{3u} \rightarrow b_{2g}$ transition for all values of n. By contrast, the highly symmetric square $[M_2]_4(OXA)_4$ system has a smaller number of allowed, low-energy transitions. The lowest energy MLCT transition ($b_{2g} \rightarrow b_{1g}$) is rigorously forbidden, but the next lowest transitions are expected to be intense MLCT transitions. The bonding in the formamidinate square $[(HNCHNH)_2M_2(\mu\text{-}O_2CCO_2)]_4$ is qualitatively very similar, underlining the importance of the oxalate ligands in determining the ultimate electronic structure of these systems.

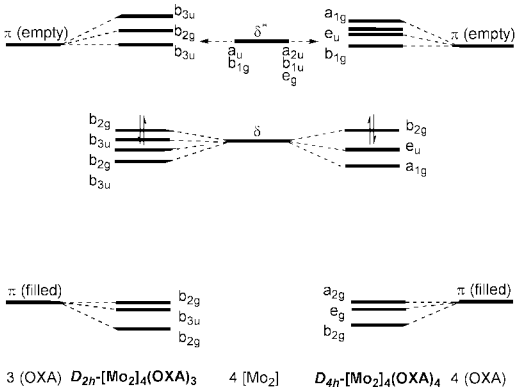

Fig. 4 Qualitative schematic frontier molecular orbital energy level splitting diagram for the D_{2h} linear $[Mo_2]_4(OXA)_3$ system (left), and the D_{4h} square $[Mo_2]_4(OXA)_4$ system (right).

From the above example of perpendicularly linked M–M quadruple bonds, the qualitative features of conjugation involving M_2 δ orbitals and vacant ligand π* orbitals can be anticipated. By contrast, for an axially aligned linear arrangement ~(M_2–bridge–M_2)~, such as found in Lehn's acetylene linked diruthenium chains,[11] the primary conjugation involves the metal π or π* orbitals except when the bridge spans the M_2 unit as in 2,7-dioxynaphthyridine or 1,8-anthracenyldicarboxylate. Thus, investigations of these complexes should also prove most fascinating.

We thank the National Science Foundation for financial support and the Ohio Supercomputing Center for computational resources.

Notes and references

1 F. A. Cotton, C. Lin and C. A. Murillo, *J. Chem. Soc., Dalton Trans.*, 1998, 3151.
2 F. A. Cotton, L. M. Daniels, C. Lin and C. A. Murillo, *J. Am. Chem. Soc.*, 1999, **121**, 4538.
3 S. L. Schiavo, G. Pocsfalvi, S. Serroni, P. Cardiano and P. Piraino, *Eur. J. Inorg. Chem.*, 2000, 1371.
4 J. F. Bickley, R. P. Bonar-Law, C. Femoni, E. J. MacLean, A. Steiner and S. J. Teat, *J. Chem. Soc., Dalton Trans.*, 2000, 4025.
5 F. A. Cotton, C. Lin and C. A. Murillo, *Inorg. Chem.*, 2001, **40**, 472.
6 F. A. Cotton, J. P. Donahue, C. Lin and C. A. Murillo, *Inorg. Chem.*, 2001, **40**, 1234.
7 J. K. Bera, P. Angaridis, F. A. Cotton, M. A. Petrukhina, P. E. Fanwick and R. A. Walton, *J. Am. Chem. Soc.*, 2001, **123**, 1515.
8 F. A. Cotton, C. Lin and C. A. Murillo, *Inorg. Chem.*, 2001, **40**, 478.
9 F. A. Cotton, L. M. Daniels, C. Lin, C. A. Murillo and S.-Y. Yu, *J. Chem. Soc., Dalton Trans.*, 2001, 502.
10 R. P. Bonar-Law, T. D. McGrath, J. F. Bickley, C. Femoni and A. Steiner, *Inorg. Chem. Commun.*, 2001, **4**, 16.
11 K.-T. Wong, J.-M. Lehn, S.-M. Peng and G.-H. Lee, *Chem. Commun.*, 2000, 2259.
12 R. H. Cayton, M. H. Chisholm, J. C. Huffman and E. B. Lobkovsky, *J. Am. Chem. Soc.*, 1991, **113**, 8709.
13 See the accompanying ESI† for full details of the calculational methods employed in this work.
14 D. J. Hodgson and J. A. Ibers, *Acta Crystallogr., Sect. B*, 1969, **25**, 469.
15 G. Jovanovski, J. O. Thomas and I. Olovsson, *Acta Crystallogr., Sect. B: Struct. Sci.*, 1987, **43**, 85.

CHEMCOMM Communication
www.rsc.org/chemcomm

A new structural motif for rigid C_2-symmetrical propeller-shaped 1,2-diamines employing double aromatic π-stacking†

James McNulty,*[a] Rouwei Mo,[a] Alfredo Capretta[a] and Christopher S. Frampton[b]

[a] *Institute of Molecular Catalysis, Department of Chemistry, Brock University, St. Catharines, Ontario L2S 3A1, Canada. E-mail: jmcnulty@chemiris.labs.brocku.ca*
[b] *Roche Products Ltd., 40 Broadwater Rd., Welwyn Garden City, Herts, UK AL7 3AY*

Received (in Corvallis, OR, USA) 23rd July 2001, Accepted 12th September 2001
First published as an Advance Article on the web 23rd October 2001

Utilization of double aromatic π-stacking interactions on a 2,3-diaminobutane framework provides a new motif for structurally rigid C_2-symmetrical propeller-shaped chiral 1,2-diamines.

Catalytic asymmetric carbon–carbon bond forming reactions have emerged as one of the most active areas of research in organic synthesis.[1] In this field, standard reactions such as the addition of diethylzinc to benzaldehyde are investigated as benchmarks upon which to evaluate the relative efficiency of different ligands. Chiral, C_2-symmetrical 1,2-diamines are valuable scaffolds both as auxiliaries and ligands in catalytic asymmetric reactions.[1,2] In particular, sulfonamide derivatives of the ligands 1,2-diaminocyclohexane **1** and 1,2-diamino-1,2-diphenylethane **2** (Fig. 1) have been utilized extensively over the last few years in a large variety of catalytic asymmetric processes.[1]

Kobayashi *et al*. have demonstrated that derivatives of **1** are highly efficient (maximum 99% yield and 99% ee) in promoting the addition of diethylzinc to benzaldehyde.[3] However, applications to other systems involving functionalized aldehydes and/or functionalized organozincs are generally not as efficient. For example, Marshall reported an elegant approach to annonaceous acetogenins employing the addition of a functionalized organozinc reagent to an aliphatic aldehyde, using the Kobayashi catalyst, in 90% ee[4] This result appears to be quite general for functionalized variants of the reaction[5] highlighting the need for the design of new types of chiral ligand incorporating new defined structural motifs.

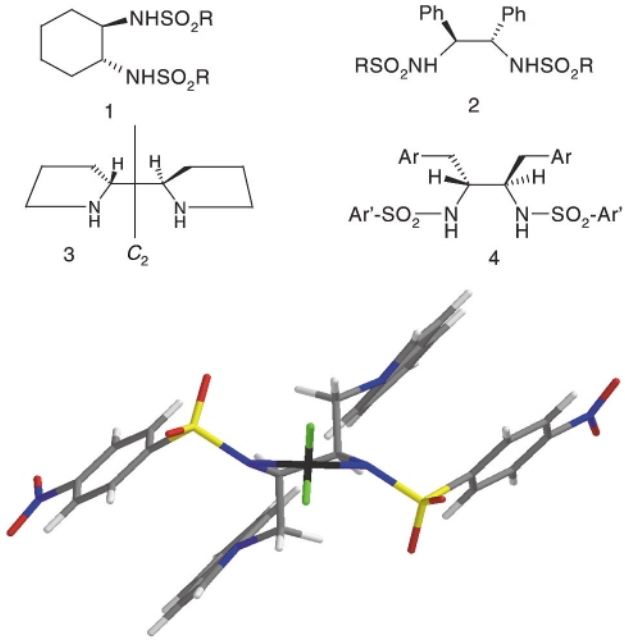

Fig. 1 Design of propeller shaped catalyst **5** as the minimized $ZnCl_2$ complex of ligand **4**.

† Electronic supplementary data (ESI) available: colour figure showing π-stacking in compound **12**. See http://www.rsc.org/suppdata/cc/b1/b106641b/

A central theme of our research is the investigation of novel scaffolds for chiral ligand design.[6] This led us to the concept of developing a new class of chiral ligand having a C_2-symmetrical 1,2-diamine core encompassed within a 2-bladed propeller-shaped architecture exemplified by the 2,2′-bipyrrolidine **3**. Such a structure has analogy with axially chiral 1,4-bidentate ligands (*e.g.* BINAP, BINOL) but is connected *via* sp^3 hybridized atoms and has the stereogenic centre in closer proximity to a coordinated metal. Propeller[7] and helical[8] shaped motifs have found application as ligands in the area of asymmetric catalysis.[1] Current difficulties with the incorporation of a propeller motif into ligand design centre on devising a molecular assembly which will retain a rigid propeller shaped conformation.

We considered that two important factors in the design of such a ligand would be the chemical nature and the control of conformational mobility of the 'blades' of the ligand. One possible molecular assembly which emerged from modelling studies‡ consisted of the incorporation of two different aromatic rings on each 'blade' of the propeller, conformationally restrained by utilization of double intramolecular π-stacking secondary orbital interactions (**4**, Fig. 1). These studies indicated that an arylsulfonamide moiety (Ar′) on each nitrogen would be correctly positioned for donor–acceptor interactions with a second aryl residue (Ar) on the diamine core provided that a methylene spacer was positioned between. Under these constraints, the two Ar residues of **4** could be envisioned to form a π-stack with each arylsulfonamide having an approximate interplanar separation of about 3.5 Å. Complexes of such a ligand **5** would result in the desired conformationally rigid propeller structural motif.[9,10] We chose the electron-rich heterocycle indole as the Ar-substituent at the 1,4-positions in this model study. It was considered advantageous to install the bis-*N*-sulfonamide late in the synthesis allowing for steric or electronic manipulation of the Ar′ π-acceptor and for the introduction of diversity within the ligand set. We now report the synthesis and characterization of ligand **12** from tartaric acid (Scheme 1), confirming the rigid double π-stack both in solution and in the solid state, as well as preliminary application of **12** and analogs **13** and **14** as promoters for the addition of diethylzinc to benzaldehyde. Tartaric acid **6** was converted to the bis-mesylate **7** following literature protocols.[11] Interestingly, substitution using the lithium salt of indole proceeded in refluxing THF to provide only the monosubstituted product while the use of THF–HMPA 4 : 1 gave the desired bis-*N*-alkylated product **8** in high yield. The acetonide was cleaved and the resulting 2,3-diol converted to the bis-mesylate derivative **9**. Conversion to the 2,3-bis-azide was achieved following the protocol of Mosset *et al*.,[11b] reduction of which, using Adam's catalyst, provided the key diamine **11**. Standard

 DOI: 10.1039/b106641b

sulfonylation of the diamine using 4-nitrobenzenesulfonyl chloride gave ligand **12**.

The UV spectra of ligand **12** in CH_3CN exhibited both a bathochromic as well as a significant hyperchromic shift in comparison to indole and 4-nitrobenzenesulfonyl chromophores attributable to a charge-transfer interaction in solution.[12] Further evidence for the π-stacking in solution was provided by the ^{1}H-NMR spectrum. For example, the average chemical shift of the indole C-2 proton of **8**–**11** was δ 6.55 ppm in sharp contrast to that of **12** (δ 6.23 ppm). This shielding is ascribed to the neighbouring ring current anisotropy exerted by the nitrosulfonamide on the stacked indole.[13]

Crystals of **12** suitable for X-ray diffraction were grown from MeOH,§ the molecular structure is shown in Fig. 2. The unit cell consists of two molecules of **12** each of which are doubly intramolecularly π-stacked with an interplanar separation of approximately 3.5Å. The two molecules of **12** are bonded through a rarely observed intermolecular hydrogen bond between the oxygen lone pairs of a nitro substituent and a sulfonamide NH on the other ligand.

Other sulfonamide derivatives such as **13** (4-FC_6H_4-) and **14** (4-MeC_6H_4-) were also readily obtainable from diamine **11**. The addition of diethylzinc to benzaldehyde was investigated in toluene under conditions similar to Kobayashi using these ligands.[3] The adduct (*S*)-1-phenylpropan-1-ol was obtained in ee's of 99% (**12**), 71% (**13**) and 31% (**14**) respectively. Consumption of benzaldehyde was generally complete, however in all cases 5–15% of benzyl alcohol was also produced through competitive β-hydride reduction which may be attributed to steric crowding in the catalysts derived from **12**–**14**.

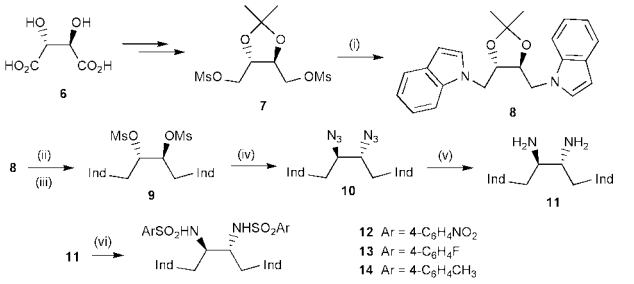

Scheme 1 Synthesis of ligands **12**–**14**. *Reagents and conditions*: (i) indole, LiHMDS, THF–HMPA 4 : 1, −78 °C, 2 h then to 22 °C, 6 h, 81% (ii) MeOH–THF 2 : 1, 0.1 N HCl, 68 °C, 1 h, 86%. (iii) MsCl, Et_3N, CH_2Cl_2, 0 °C, 5 h, 90%. (iv) NaN_3, DMSO, 80 °C, 24 h, 89%. (v) MeOH–H_2O 3 : 2, PtO_2, 1 atm H_2, 22 °C, 8 h, >99%. (vi) $ArSO_2Cl$, Et_3N, CH_2Cl_2, 0 °C, 6 h, 62%. Note: Ind = 1′-indolyl.

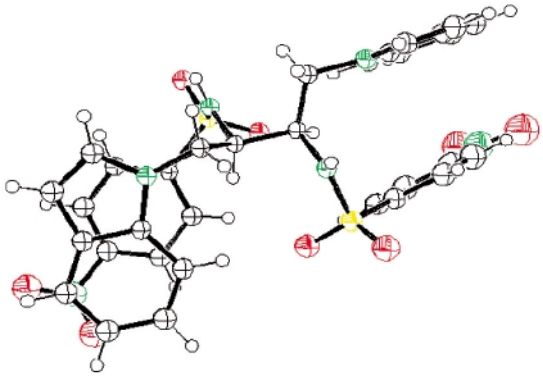

Fig. 2 ORTEP diagram of one molecule of **12** verifying the double intramolecular π-stacking.

In conclusion, we have experimentally confirmed the structure of the double π-stacked chiral 1,2-diamine ligand **12** as a model system for obtaining the C_2-symmetrical propeller motif as well as the preparation of propeller shaped catalysts. An inspiring agreement between the molecular modelling studies‡ and eventual structure of ligand **12** was observed. Preliminary investigations have demonstrated the viability of this structural motif in asymmetric catalysis. Further modifications to the ligand structure based on models **3** and **4** incorporating various donor–acceptor partners as well as applications to functionalized variants of the reaction are in progress.

Financial support of this work by the Natural Sciences and Engineering Research Council of Canada, Research Corporation (Cottrell Scholar Science Award to J. McN) and the Canada Foundation for Innovation is gratefully acknowledged.

Notes and references

‡ Semi-empirical modelling studies were carried out at the restricted Hartree-Fock level using the PM3 Hamiltonian in the Spartan Program (Spartan, v4.0, Wavefunction, Irvine CA, 1995).

§ *Crystal structure determination of* **12**. Cell dimensions and intensities were measured at 123(1) K on a Bruker AXS SMART CCD diffractometer with graphite-monochromated Mo-Kα radiation (λ = 0.71073 Å). $C_{32}H_{28}N_6O_8S_2$. M_r = 688.7, μ = 0.237 mm^{-1}, ρ_c = 1.485 mg m^{-3}, monoclinic, $P2_1$, Z = 4, a = 7.4557(12), b = 26.437 (10), c = 15.693(6) Å, β= 95.10(4)° U = 3080.8(17) Å^3. 34222 reflections measured, θ_{max} = 28.28°, 98.2% complete), 14627 reflections unique (Rint = 0.0322). Final agreement factors for 865 parameters and 1 restraint gave R_1 = 0.0429, wR^2 = 0.1036 and S = 1.008 based on 12813 reflections with $I \geq 2\sigma(I)$. Final difference map +0.316 and –0.315 e Å^{-3}. Absolute structure parameter = −0.04(4) (H. D. Flack, *Acta Cryst*., 1983, **A39**, 876). Programs used Bruker AXS SMART and SAINT control and integration software, SHELXTL Structure solution and refinement (G. M. Sheldrick, University of Göttingen, Germany). CCDC 172111.

1 (*a*) I. Ojima, *Catalytic Asymmetric Synthesis*, Wiley-VCH Inc., New York , 2nd edn., 2000; (*b*) H. Tye, *J. Chem. Soc., Perkin Trans. 1*, 2000, 275 and prior reviews in this series.
2 (*a*) A. Alexakis, I. Aujard, T. Kanger and P. Mangeney, *Org. Synth*., 1998, **76**, 23; (*b*) J. F. Larrow and E. N. Jacobsen, *Org. Synth*., 1997, **75**, 1.
3 H. Takahashi, T. Kawakita, M. Ohno, M. Yoshioka and S. Kobayashi, *Tetrahedron*, 1992, **48**, 5691.
4 J. A. Marshall and H. Jiang, *J. Org. Chem*., 1998, **63**, 7066.
5 For examples using functionalized reagents see: (*a*) C. Lutz and P. Knochel, *J. Org. Chem*., 1997, **62**, 7895; (*b*) S. Nowotny, S. Vettel and P. Knochel, *Tetrahedron Lett*., 1994, **35**, 4539.
6 (*a*) J. McNulty, M. J. Millar, G. Bernardinelli and C. W. Jefford, *J. Org. Chem*., 1999, **64**, 5312; (*b*) A. Robertson, C. Bradaric, C. S. Frampton, J. McNulty and A. Capretta, *Tetrahedron Lett*., 2001, **42**, 2609.
7 (*a*) M. T. Powell, A. M. Porte and K. Burgess, *Chem. Commun*., 1998, 2161; (*b*) C. Moberg, *Angew. Chem., Int. Ed*., 1998, **37**, 249.
8 S. D. Dreher, T. J. Latz, K. C Lam and A. L. Rheingold, *J. Org. Chem*., 2000, **65**, 815.
9 For general discussions on the nature of π–π interactions, see (*a*) C. A. Hunter and J. K. M. Sanders, *J. Am. Chem. Soc*., 1990, **112**, 5525; (*b*) C. A. Hunter, *Angew. Chem., Int. Ed*., 1993, **32**, 1584.
10 For a general review on the use of π-stacking effects in asymmetric synthesis, see G. B. Jones and B. J. Chapman, *Synthesis*, 1995, 475.
11 (*a*) E. A. Mash, K. A. Nelson, S. Van Deusen and S. B. Hemperley, *Org. Synth*., 1989, **68**, 92; (*b*) A. Scheurer, P. Mosset and R. W. Saalfrank, *Tetrahedron: Asymmetry*, 1997, **8**, 1243.
12 N. Kaneta, F. Mitamura, M. Uemura, Y. Murata and K. Komatsu, *Tetrahedron Lett*., 1996, **37**, 5385.
13 The upfield shift of heterobase protons in oligonucleotides is a well known phenomenon and is a result of the stacking of aromatic bases. For examples, see: (*a*) C. H. Lee, F. S. Ezra, N. S. Kondo, R. H. Sarma and S. S. Danyluk, *Biochemistry*, 1976, **15**, 3627; (*b*) R. A. Bell, J. R. Everett, D. W. Hughes, J. M. Coddington, D. Alkema, P. A. Hader and T. Neilson, *J. Biomol. Struct. Dynamics*, 1985, **2**, 693; (*c*) R. A. Bell, J. R. Everett, D. W. Hughes, J. M. Coddington, D. Alkema, P. A. Hader and T. Neilson, *J. Biomol. Struct. Dynamics*, 1985, **2**, 693.

CHEMCOMM
Communication
www.rsc.org/chemcomm

Survival and extinction of delocalised ring currents in clamped benzenes

Patrick W. Fowler,*[a] Remco W. A. Havenith,[a] Leonardus W. Jenneskens,*[b] Alessandro Soncini[a] and Erich Steiner[a]

[a] *School of Chemistry, University of Exeter, Stocker Road, Exeter, UK EX4 4QD. E-mail: P.W.Fowler@exeter.ac.uk; Fax: +44 1392 263434*

[b] *Debye Institute, Department of Physical Organic Chemistry, Utrecht University, Padualaan 8, 3584 CH Utrecht, The Netherlands. E-mail: jennesk@chem.uu.nl; Fax: +31 30 2534533*

Received (in Cambridge, UK) 24th July 2001, Accepted 9th October 2001
First published as an Advance Article on the web 31st October 2001

Direct visualisation of induced current density in clamped benzenes 1–4 distinguishes between saturated clamping groups, for which the central benzene ring retains a conventional diamagnetic ring current, and strongly interacting, unsaturated clamps, for which the central ring supports only the localised circulations expected of a 1,3,5-cyclohexatriene with fully fixed double bonds.

Synthetic chemists have been tantalised for many years by the target of a molecular realisation of 1,3,5-cyclohexatriene (CHT). A popular strategy for conversion of benzene to CHT has been to attempt to tilt the energy balance in favour of the localised form by imposition of geometric constraints.[1] Annelation with rigid clamping groups has produced rings having various degrees of bond alternation, ΔR. If bond equalisation is the signature of aromaticity, then structures such as tris(bicyclo-[2.1.1]hexano)benzene (**1**) and tris(benzocyclobutadieno)benzene (**2**), with ΔR(**1**) = 0.089 Å and ΔR(**2**) = 0.154 Å (X-ray[1]), are *de facto* non-aromatic forms of benzene and hence realisations of CHT.[1] If, on the other hand, magnetic criteria for aromaticity[2] are used, the conclusion is different. From IGLO calculations, it is known that the benzene ring can tolerate a wide range of geometric distortion (*e.g.* $\Delta R \leq 0.165$ Å[2a]) whilst maintaining exaltation of diamagnetisability. We will show here by direct visualisation of the current density maps that **1** retains the ring current of benzene, whereas **2** has the localised magnetic character expected of a CHT ring with fixed double bonds. It will be seen that the same dichotomy in magnetic response is exhibited by simpler model systems[3] tris(cyclobuteno)benzene (**3**, de-localised) and tris(cyclobutadieno)benzene (**4**, localised), and we will give a systematic explanation in terms of an orbital model[4] for sizes and signs of ring currents.

A distributed-origin, coupled Hartree–Fock method such as CTOCD-DZ (continuous transformation of origin of current density, diamagnetic zero[5]) is particularly suited to visualisation and interpretation of ring currents.[6] As the current density at any point is calculated with that point as the origin of vector potential, this *ipsocentric* formulation gives numerically well converged results[5] and lends itself to physically based analysis.[4]

Optimised geometries (RHF/6-31G**) show bond alternations of ΔR(**1**) = 0.096 Å, ΔR(**2**) = 0.152 Å, ΔR(**3**) = 0.015 Å and ΔR(**4**) = 0.182 Å. The SYSMO program[7] was used to calculate current densities (Fig. 1) as in ref 6. In all plots, diamagnetic circulation is shown anti-clockwise.

The computed map (Fig. 1a) for the π current density in **1** exhibits a strong central diamagnetic current in the benzene ring. Despite significant bond alternation imposed by clamping, the D_{3h} benzene moiety of **1** retains the classical π ring current. In contrast, the central ring of **2**, also of D_{3h} symmetry, has only localised π currents (Fig. 1b). Thus, attachment of the unsaturated benzocyclobutadieno clamps to the benzene ring has completely destroyed its delocalised character, and hence on magnetic criteria, removed its aromaticity. Compound **2** does have delocalised currents (π diamagnetic in outer benzene rings, σ paramagnetic[6a] in square rings) but no central ring current.

As Figs. 1c and d show, retention and destruction of a central π ring current can be reproduced in simpler model systems, **3** and **4**. To explain the opposite effects of saturated and unsaturated clamping groups, it is useful to consider orbital contributions to the current density maps. In an ipsocentric formulation, the total current density is partitioned into paramagnetic and diamagnetic orbital contributions, that depend on accessibility of excited states *via* rotational and translational transitions,[4] respectively. In the Hückel picture of the benzene ring, the *sole* active transition is that from HOMO (e_{1g}) to LUMO (e_{2u}), which is translationally allowed and produces four-electron diamagnetism.[4b] In a full, *ab initio* treatment this transition remains overwhelmingly dominant in the diamagnetic π ring current.[4a]

Fig. 2 illustrates the π orbital systems of the molecules **3** and **4**, and reveals the essential difference between the two. Clamping of the benzene ring with saturated groups as in **1** and **3**, imposes a purely geometric constraint, producing bond alternation and lowering the molecular symmetry. The HOMO–LUMO transition is then formally both translationally and rotationally allowed, but as the changes to the orbitals are first-order in ΔR, the transition moments are hardly changed, so that the pattern of currents remains essentially that of free benzene.

On the other hand, an *un*saturated clamping group introduces an extra set of π orbitals around the Fermi level. In **4** the interaction between central and perimeter π systems leads to a manifold of 5 orbitals in which significant but cancelling current density in the central ring arises from a mixture of translational and rotational $\pi \rightarrow \pi^*$ transitions. The $2e''$ HOMO pair gives a strong paramagnetic circulation in the central ring, the $2a_2''$ HOMO-1 gives con-rotating paramagnetic circulations in all three four-membered rings, and the $1e''$ HOMO-2 gives a diamagnetic circulation outside the central ring. The result is the island pattern of circulation on formal double bonds seen in the π map (Fig. 1d), dominated by 10 of the 12 π electrons.

A similar interaction diagram can be constructed for the benzene-annelated derivative **2**. The $2e''$ set corresponding to the HOMO of benzene contributes a diamagnetic current that is quenched by the paramagnetic contribution from $3e''$. A further 8 π electrons in the highest lying occupied orbitals ($4e''$, $3a_2''$, $1a_1''$) account for the discrete diamagnetic circulation on the outer benzene rings.

Orbital analyses also account for the different nucleus-independent chemical shifts[2b] in **1** (−8.0 ppm (0.0 Å)[8] and **2** (−1.1 ppm (1.0 Å)).[9] The strongly diatropic value for **1** and the equivocally diatropic value for the central ring of **2** arise from integrations over distinctly different patterns of total current.

Two general comments can be made. The first concerns bond alternation, used as an indication of benzenoid character of a

 DOI: 10.1039/b106651j

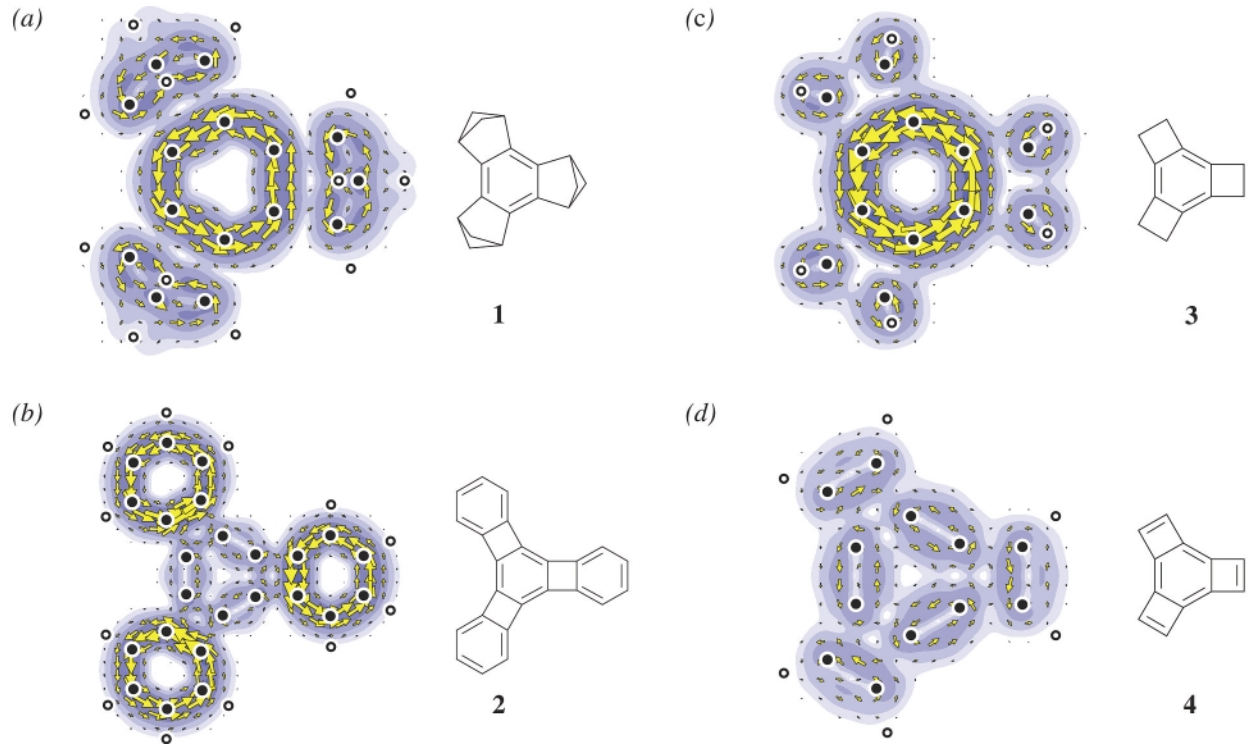

Fig. 1 Maps of π current density in (*a*) tris(bicyclo[2.1.1]hexeno)benzene (**1**), (*b*) tris(benzocyclobutadieno)benzene (**2**), (*c*) tris(cyclobuteno)benzene (**3**) and (*d*) tris(cyclobutadieno)benzene (**4**). Nuclear positions are projected into the plotting plane, $1a_0$ above molecular plane.

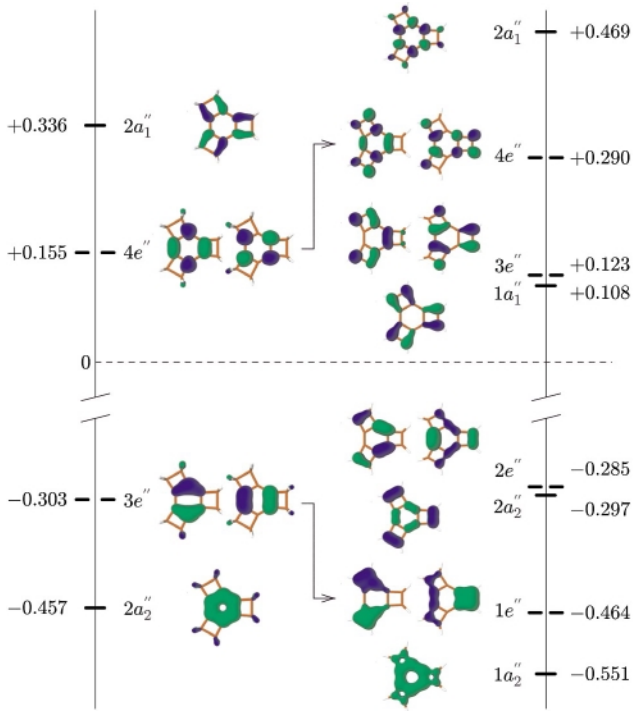

Fig. 2 Highest occupied and lowest unoccupied π molecular orbitals of **3** and **4**, with energies (au) and symmetries. In D_{3h}, translational (diamagnetic) π-π* transitions are $a_1'' \rightarrow e''$, $a_2'' \rightarrow e''$, $e'' \rightarrow (a_1'', a_2'', e'')$ and rotational (paramagnetic) transitions $a_1'' \rightarrow a_2''$, $a_2'' \rightarrow a_1''$, $e'' \rightarrow e''$.

clamped ring. It is clear from the orbital picture that the electronic effect of the clamping groups rather than their rôle as geometrical constraints determines whether the central current will be quenched. Strong bond alternation may be a symptom of either a rigid saturated clamp without significant effect on ring current, or of a strongly interacting unsaturated clamp which, by pushing HOMO and LUMO apart, quenches the current. The (benzo)cyclobutadieno clamp belongs to this latter class, whereas, for example, a set of 3,4-dimethylenecyclobuteno clamps,[3a] with localised π bonds *exo* to the four-membered rings, would be expected not to affect the central benzene current. Calculated maps (not shown here) confirm this expectation.

The second comment is that the orbital picture gives a unified account of both diatropic and paratropic central rings. For example, annelation[8] of cyclooctatetraene (COT) either retains or quenches the central paratropic current,[10] accordingly as the clamps do or do not push apart the closely separated HOMO–LUMO pair of the COT subunit.

Notes and references

1 (*a*) N. L. Frank, K. K. Baldridge and J. S. Siegel, *J. Am. Chem. Soc.*, 1995, **117**, 2102; H.-B. Bürgi, K. K. Baldridge, K. Hardcastle, N. L. Frank, P. Gantzel, J. S. Siegel and J. Ziller, *Angew. Chem., Int. Ed. Engl.*, 1995, **34**, 1454; (*b*) R. Diercks and K. P. C. Vollhardt, *J. Am. Chem. Soc.*, 1986, **108**, 3150; D. Holmes, S. Kumaraswamy, A. J. Matzger and K. P. C. Vollhardt, *Chem. Eur. J.*, 1999, **5**, 3399.

2 (*a*) U. Fleischer, W. Kutzelnigg, P. Lazzeretti and V. Mühlenkamp, *J. Am. Chem. Soc.*, 1994, **116**, 5298; (*b*) P. von R. Schleyer, C. Maerker, A. Dransfeld, H. Jiao and N. J. R. van Eikema Hommes, *J. Am. Chem. Soc.*, 1996, **118**, 6317.

3 (*a*) R. Faust, E. D. Glendening, A. Streitwieser and K. P. C. Vollhardt, *J. Am. Chem. Soc.*, 1992, **114**, 8263; (*b*) A. Stanger, *J. Am. Chem. Soc.*, 1998, **120**, 12034; (*c*) R. Boese, D. Bläser, W. E. Billups, M. M. Haley, A. H. Maulitz, D. L. Mohler and K. P. C. Vollhardt, *Angew. Chem., Int. Ed. Engl.*, 1994, **33**, 313.

4 (*a*) E. Steiner and P. W. Fowler, *J. Phys. Chem. A.*, 2001, **105**, 9553; (*b*) E. Steiner and P. W. Fowler, *Chem. Commun.*, 2001, 2220.

5 (*a*) T. A. Keith and R. F. W. Bader, *Chem. Phys. Lett.*, 1993, **210**, 223; (*b*) S. Coriani, P. Lazzeretti, M. Malagoli and R. Zanasi, *Theoret. Chim. Acta*, 1994, **89**, 181.

6 (*a*) E. Steiner and P. W. Fowler, *Int. J. Quant. Chem.*, 1996, **60**, 609; (*b*) P. W. Fowler, E. Steiner, B. Cadioli and R. Zanasi, *J. Phys. Chem. A*, 1998, **102**, 7297; (*c*) E. Steiner, P. W. Fowler and L. W. Jenneskens, *Angew. Chem., Int. Ed. Engl.*, 2001, **40**, 362.

7 P. Lazzeretti and R. Zanasi, SYSMO package (University of Modena), 1980. Additional routines written in Exeter.

8 A. Matsuura and K. Komatsu, *J. Am. Chem. Soc.*, 2001, **123**, 1768.

9 J. M. Schulman, R. L. Disch, H. Jiao and P. von R. Schleyer, *J. Phys. Chem. A*, 1998, **102**, 8051.

10 P. W. Fowler, R. W. A. Havenith, L. W. Jenneskens, A. Soncini and E. Steiner, to be published.

CHEMCOMM
Communication
www.rsc.org/chemcomm

Successive intramolecular transiminations in an iron(II) complex with chiral tridentate ligands

Tulio Enrique Chavez-Gil,† Mizuomi Yasaka, Tomoko Senokuchi, Masamitsu Sumimoto, Hiromasa Kurosaki and Masafumi Goto*

Faculty of Pharmaceutical Sciences, Kumamoto University, Oe-honmachi 5-1, Kumamoto 862-0973, Japan. E-mail: gotomphi@gpo.kumamoto-u.ac.jp

Received (in Cambridge, UK) 23rd August 2001, Accepted 9th October 2001
First published as an Advance Article on the web 24th October 2001

Two molecules of *S*-2-pyridylmethylidene-1-(2-pyridyl)-ethylamine coordinated to an iron(II) undergo successive transiminations yielding bis[1-(2-pyridyl)ethylidene-2-pyridylmethylamine]iron(II) in acetonitrile.

Biochemical transformations such as transamination and racemization of α-amino acid are mediated by pyridoxal (vitamin B_6).[1] Pyridoxal converts one amino compound to an aldimine by providing aldehyde followed by transimination of the aldimine to a ketimine, a precursor of a keto acid. Metal ions assist these reactions, though the details of their participation *in vivo* is a matter of controversy.[1] 2-Pyridinecarbaldehyde has been reported to promote the transimination by forming an imine bond with aliphatic α-amino acids in the presence of Zn^{II} and Cu^{II}.[2]

Imines, on the other hand, are useful functional groups for the construction of metal chelates because imines are easily derived from carbonyl groups (aldehyde or ketone) and primary amines.[3] Although much attention has been paid to the mechanism for the formation of imine bonds in the presence of metal ions,[3,4] less is known about the conversion of imines thus formed.[5] A translocation of the imine bond in a macrocyclic tetraimine coordinated to Fe^{II} has been described but the nature of the reaction remains ambiguous.[6]

Here, we describe the occurrence and kinetics of a smooth transimination on a low-spin iron(II) with *S*-2-pyridylmethylidene-1-(2-pyridyl)ethylamine, *S*-PMPE. The bis(*S*-PMPE)Fe^{II} perchlorate was isolated as a diastereomeric mixture.‡ The UV–Vis spectrum of CD_3CN solution is almost identical to {Fe[1-(2-pyridyl)ethylidene-2-pyridylmethylamine]$_2$}$^{2+}$, [Fe(PEPM)$_2$]$^{2+}$, but a significant negative Cotton effect at 550 nm and positive-to-negative exciton band around 330 nm were observed in CD spectroscopy. The Cotton effects are in agreement with the Λ-[Fe(phen)$_3$]$^{2+}$ or Λ-[Fe(bpy)$_3$]$^{2+}$.[7] (The assignment of the absolute configuration is based on the chirality of two 1,2-diimine chromophores of the tridentate ligands.) From the ^{1}H NMR spectrum the ratio of the amount of the two diastereomers is 1.0 to 0.8. Based on these, the major and minor compounds are tentatively assigned to the Λ-*mer*- and Δ-*mer*- isomers respectively.

Changes on the ^{1}H NMR spectrum of [Fe(*S*-PMPE)$_2$]$^{2+}$ in CD_3CN at 45 °C are shown in Fig. 1. At first, the spectra (Fig. 1(a)) are composed of two sets of signals because [Fe(*S*-PMPE)$_2$]$^{2+}$ is a mixture of two diastereomers, each of which has C_2 symmetry. In the early reaction stage, the magnitudes of two doublet methyls at δ = 2.42 (peak 1) and 2.57 (peak 4) and two azomethine signals at δ = 10.32 (peak 11) and 10.39 (peak 14) decreased, while those of the two new doublet methyls at δ = 2.44 (peak 2) and 2.48 (peak 3) and azomethine signals at δ = 10.33 (peak 12) and 10.34 (peak 13) increased along with new singlet methyls at δ = 3.40 (peak 6) and 3.43 (peak 7) and AB pattern signals at *ca*. 6.43–6.30 ppm. In the successive stage, the magnitudes of the new signals diminished after reaching maxima and new signals followed, in which only one methyl signal at δ = 3.37 (peak 5) emerged and an AB pattern centered at δ = 6.37 (peak 8) appeared. The final spectrum coincided with that of [Fe(PEPM)$_2$](ClO$_4$)$_2$.[8] These changes are accounted for by consecutive reactions shown in Fig. 2. There are two tridentate ligands, *S*-PMPE, co-ordinated to Fe^{II}. The transimination on one of the ligands of Λ-[Fe(*S*-PMPE)$_2$]$^{2+}$ (**1**) and Δ-[Fe(*S*-PMPE)$_2$]$^{2+}$ (**2**) yields intermediates, Δ-[Fe(*S*-PMPE)(PEPM)]$^{2+}$ (**3**) and Λ-[Fe(*S*-PMPE)(PEPM)]$^{2+}$ (**4**) respectively. In the successive transimination, the remaining *S*-PMPE is converted to PEPM thus forming Λ- and

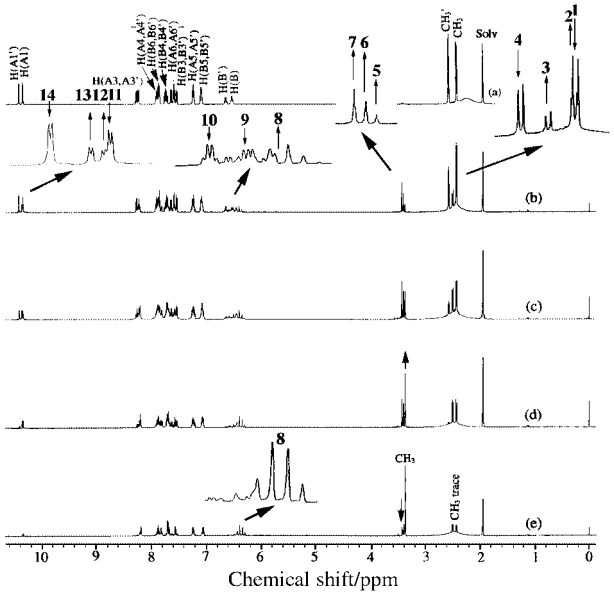

Fig. 1 ^{1}H NMR change of [Fe(*S*-PMPE)$_2$](ClO$_4$)$_2$ in CD_3CN.

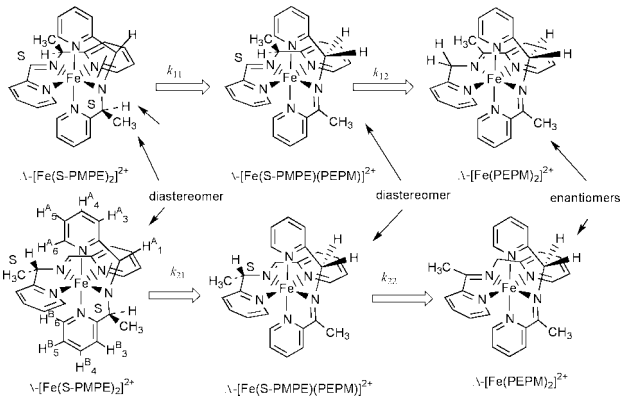

Fig. 2 Pathway of transimination of Λ- and Δ-[Fe(*S*-PMPE)$_2$]$^{2+}$ as detected by NMR and CD spectra in CD_3CN and proton labels.

† A JSPS Foreign Researcher Postdoctoral Fellow from Nov 1997 to Nov 1999. Present Address, University of Puerto Rico, Mayaguez Campus, Department of Chemistry, P.O.Box 9019, Mayaguez, PR 00681.

 DOI: 10.1039/b107502k

Δ-[Fe(PEPM)$_2$]$^{2+}$ (**5** and **6**) which are enantiomers to each other and indistinguishable by NMR spectroscopy.

The CD spectrum of the final stage showed Cotton effects which are very similar to those of [Fe(*S*-PMPE)$_2$]$^{2+}$. This finding supports that the optical activity stems from the configurational effect of two 1,2-diimine chromophores co-ordinated to Fe^{II} because the asymmetric centres in the ligands were lost in the final product and that this reaction proceeds without disruption of the Fe–N bonds.

This conversion was slow in CD_3CN, and the presence of water accelerated the reaction. The reaction was investigated with varying solvents, *i.e.* 90% CD_3CN–H_2O, 90% CD_3CN–D_2O. In the presence of D_2O, however, the intensity of the AB signals (peak 8) due to –CH_2 diminished. These findings support that the product [Fe(PEPM)$_2$]$^{2+}$, undergoes a facile H–D exchange at the methylene hydrogen in the presence of D_2O.

The reaction was accelerated by the presence of organic base. The time course of the reaction was followed by ^{1}H NMR measurements with CD_3CN solution of 2,6-dimethylpyridine and an example is shown in Fig. 3, the curves are drawn based on the first-order consecutive reactions using rate constants derived from a non-linear least-squares method. Increase in the concentration of 2,6-dimethylpyridine resulted in the increase of the rate constant as shown in the inset of Fig. 3. The abscissa, $k_{0,\,obs}$, for each reaction can be ascribed to a small amount of water in the solvent. From the slope of the lines in the inset, second order rate constants are derived: k_{11} = 41.7 ± 0.1; k_{12} = 24.1 ± 0.1; k_{12} = 10.7 ± 0.1; k_{22} = 10.1± 0.1 M^{-1} min^{-1} at 45 °C.

The driving force of this transimination will be the difference in the enthalpy between N(py)=C–CH=N–CH(CH_3)–CH(py) and N(py)=C–CH_2–N=C(CH_3)–C=N(py) co-ordinated to Fe(II). This reaction could occur *via* H$^+$ dissociation by a base yielding a 1,3-diiminate intermediate, N(py)=C–CH=N(Fe^{II})$^-$=C(CH_3)–CH(py), followed by reprotonation from the conjugated acid of the base to the 1,3-diiminate because the rate of each step is proportional to the base. It is noteworthy that the doublet methyls did not show any indication of singlet formation in 10% D_2O–CD_3CN solution due to an H–D exchange at the –CH(CH_3)– site. This will be the consequence of the unidirectional nature of this reaction, *i.e.* reprotonation to the deprotonated species occurs exclusively at the ethylidene site.

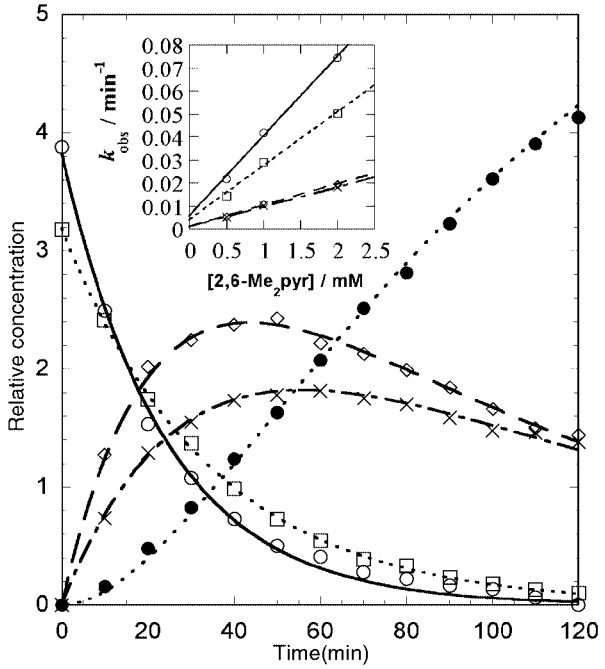

Fig. 3 Time course of transimination of Λ- and Δ-[Fe(*S*-PMPE)$_2$]$^{2+}$ in 1.0 mM 2,6-dimethylpyridine CD_3CN solution at 45 °C: ○, 1; □, 2; ◇, 3; ×, 4; ●, 5 + 6. Inset shows the dependency of first-order rate constants on the concentration of 2,6-dimethylpyridine: ○, k_{11}; □, k_{21} ◇, k_{12}; ×, k_{22}.

These observations led us to measure the rate of H–D exchange in {Fe[pyridylmethylidene-1-(2-pyridyl)methylamine]$_2$}$^{2+}$. This compound has been known for several decades but there seems no report on the H–D exchange on the ligand.[9] In a 10% D_2O–CD_3CN solvent, the H–D exchange occurred at the methylene and azomethine in the presence of 5 mM 2,6-dimethylpyridine at 45 °C. The H–D exchange at the methylene followed successive first-order consecutive reactions (exchange of one of the methylene hydrogens in the initial stage followed by exchange of the remaining hydrogen) with the rate constants of 0.04 min^{-1} and 0.025 min^{-1}. The decay of the azomethine signal occurred more slowly and did not follow simple first-order rate law. The decay was described by two-phase first-order reactions as rate = $A_1\exp(-k_1t)$ + $A_2\exp(-k_2t)$, with k_1 = 0.014 min^{-1} and k_2 = 0.0015 min^{-1}. These results are in accordance with the reaction paths where the H$^+$ is removed from the methylene (or deuterated methylene) solely and reprotonation occurs to a 1,3-diiminate intermediate.

Notes and references

‡ *Experimental procedure*: *S*-2-(1-ethyl)pyridine was synthesized as described in the literature.[10] Λ- and Δ-[Fe(*S*-PMPE)$_2$](ClO_4)$_2$. An acetonitrile solution of Fe(ClO_4)$_2$·6H_2O (0.5 g, 1.4 mmol) in 50 cm^3 was mixed with 3 cm^3 of acetonitrile containing 0.29 g (2.7 mmol) of pyridine-2-aldehyde under argon. After 10 minutes, 0.33 g (2.7 mmol) of *S*-2-(1-ethyl)pyridine in 5 cm^3 of acetonitrile was added dropwise. The mixture was warmed at 60 °C for 10 minutes followed by cooling; addition of 15 cm^3 of diethyl ether yielded violet microcrystals. Yield 0.89g (96.7%). Anal. Calc. for $C_{26}H_{26}N_6FeCl_2O_8$: C, 46.1; H, 3.8; N, 12.4. Found: C, 46.7; H, 3.8; N, 12.1%. FAB-mass *m/z*: $C_{13}H_{13}N_3FeClO_4^+$ requires 366.5; found: 366.5. The signals of the ^{1}H NMR spectrum were assigned as indicated in Fig. 1a on the basis of ^{1}H–^{1}H COSY, ^{1}H–^{13}C HMQC, and ^{1}H–^{13}C HMBC spectra. For the 2,6-dimethylpyridine accelerated reactions, the iron complex was weighed into 2 mm φ NMR tubes and air was eliminated by argon flow through a serum cap. The CD_3CN solution of 2,6-dimethylpyridine was added with a syringe through the serum cap. The sample was mounted to an NMR probe and the measurement was started immediately at 45 °C. The isolated peaks were chosen to measure the peak areas; peak 4 as **1**, peak 14 as **2**, peaks 6, 7, 5 as intermediates and the final product. The relative concentration of each species was calculated based on the area.

1 (*a*) E. C. Constable, *Metals and Ligand Reactivity*, VCH, Weinheim, 1996, p. 116–119; (*b*) A. E. Martell, *Acc. Chem. Res*., 1989, **22**, 115–124; (*c*) Y. Nagata, R. Yoda and U. Matsushima, *Chem. Pharm. Bull*., 1998, **46**, 1849; (*d*) R. F. Zabinski and M. D. Toney, *J. Am. Chem. Soc*., 2001, **123**, 193.

2 L. Casella and M. Gullotti, *Inorg. Chem*., 1983, **22**, 2259.

3 (*a*) T. E. Chavez-Gil, D. L. A. de Faria and H. E. Toma, *Vib. Spectr*., 1998, **16**, 89; (*b*) J. deO. Cabral, M. F. Cabral, M. G. B. Drew, F. S. Escho, O. Haas and S. M. Nelson, *J. Chem. Soc., Chem. Commun*., 1982, 1068.

4 D. S. C. Black, in *Comprehensive Coordination Chemistry*, **Vol. 1**, ed. G. Wilkinson, R. D. Gillard and J. A. McCleverty, Pergamon, Oxford, 1984, pp. 415.

5 M. Goto, Y. Ishikawa, T. Ishihara, C. Nakatake, T. Higuchi, H. Kurosaki and V. L. Goedken, *J. Chem. Soc., Dalton Trans*., 1998, 1213.

6 J. C. Dabrowiak, F. V. Lovecchio, V. L. Goedken and D. H. Busch, *J. Am. Chem. Soc*., 1972, **94**, 5503.

7 S. F. Mason and B. J. Norman, *J. Chem. Soc. (A)*, 1969, 1442.

8 The final ^{1}H NMR coincided with the authentic sample which was prepared from Fe(ClO_4)$_2$·6H_2O, 2-aminomethylpyridine, and 2-acetylpyridine.

9 (*a*) F. Lions and K. V. Martin, *J. Am. Chem. Soc*., 1957, **79**, 2733; (*b*) P. Krumholz, *Inorg. Chem*., 1965, **4**, 757; (*c*) S. M. Nelson and J. Rodgers, *J. Chem. Soc., (A)*, 1968, 272; (*d*) E. Baggio-Saitovitch and M. A. de Paoli, *Inorg. Chim. Acta*, 1978, **27**, 15.

10 J. W. Canary, C. S. Allen, J. M. Castagnetto and Y. Wang, *J. Am. Chem. Soc*., 1995, **117**, 8484.

CHEMCOMM
Communication
www.rsc.org/chemcomm

Selective binding and reversible release of riboflavin by polymer-bound zinc(II) azamacrocycles†

Burkhard König,* Hans-Christoph Gallmeier and Roland Reichenbach-Klinke

Institut für Organische Chemie, Universität Regensburg, Regensburg, Germany. E-mail: Burkhard.Koenig@chemie.uni-regensburg.de; Fax: (+49)941-943-1717; Tel: (+49)941-943-4576

Received (in Cambridge, UK) 23rd August 2001, Accepted 9th October 2001
First published as an Advance Article on the web 31st October 2001

The reversible formation of a coordinative bond between a polymer-bound Lewis-acidic metal complex and a flavin imide moiety allows complete extraction of riboflavin from aqueous solution at physiological pH and its quantitative release at pH 5.

Vitamin B2 (riboflavin) is an important biological redox cofactor and essential for human and animal health. Riboflavin is produced biotechnologically and used in vitamin enriched food and food supplements. This calls for methods that allow the quantitative and selective isolation of riboflavin from aqueous solutions. We report here the synthesis and the properties of a functionalized polymer which reversibly and selectively binds flavins at physiological pH in aqueous solution.[1]

From the work of Kimura[2,3] and others[4] the ability of Lewis-acidic zinc(II)–cyclen complexes to reversibly coordinate imide moieties with high binding strengths is well documented. The binding motif has been used in artificial receptors for barbiturates,[5] thymine[6] and flavins.[4] To immobilize zinc(II)–cyclen as a binding site on a polymer surface we have reacted the protected cyclen derivative **1**[7] with Fractogel® EMD epoxy, a tentagel phase which is derivatized with epoxy groups.[8] Remaining epoxide groups on the polymer were deactivated with excess glycine, the BOC protecting groups of the azamacrocycle were removed by standard methods with trifluoroacetic acid (TFA) and treatment with aqueous zinc(II) perchlorate solution gave the target material, as a stable, white powder (Scheme 1). A loading of 15 mmol of zinc(II) complex per gram of the polymeric material was determined by elemental analysis.‡

Due to the large number of binding sites, high affinity of the polymer to imide-containing molecules was expected even in water. A simple experiment revealed the predicted properties. Buffered aqueous solution of riboflavin (c = 4.9 × 10^{-5} mol L^{-1}) was passed through a column which was filled with the polymer material. For comparison an identical second column was filled with Fractogel® EMD epoxy, which was derivatized with glycine only. As easily observed by the naked eye the flavin was fully retained on the material with zinc(II)–cyclen binding sites (see supporting information† Fig. 3b, left column), while no retention is observed on the reference polymer (Fig. 3b, right column). The flavin is retained on the polymer upon washing with aqueous buffer pH 7.4, but is quantitatively released with aqueous buffer at pH 5.4 (Fig. 3c, left column). Fig. 1 shows the UV spectra of the solutions before and after passage through the column.

Apoproteins of riboflavin-binding proteins, *e.g.* the riboflavin-binding protein of egg white, have been used to determine the amount of riboflavin in mixtures with other compounds.[9] Such proteins show up to nanomolar affinities for the analyte and distinguish between flavin derivatives.[10]

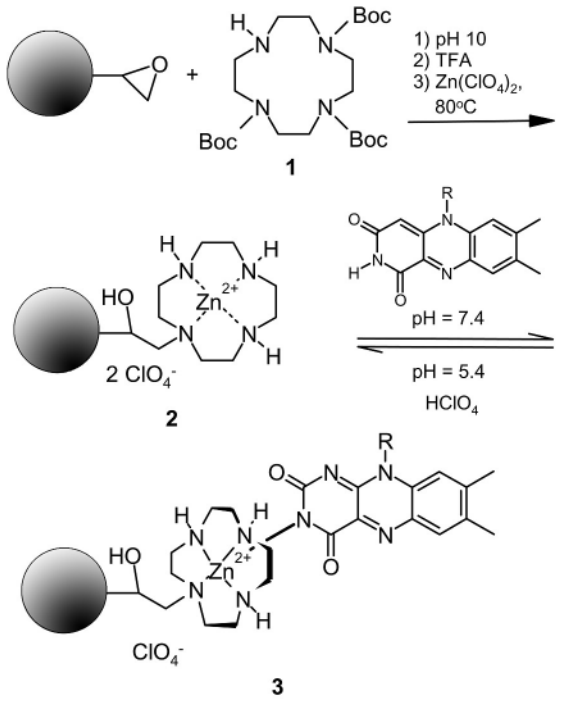

Scheme 1 Synthesis of a zinc(II)–cyclen loaded polymer **2** and binding equilibrium with riboflavin (R = ribityl) or its tetraacetate [R = $CH_2CH(OAc)CH(OAc)CH(OAc)CH_2OAc$].

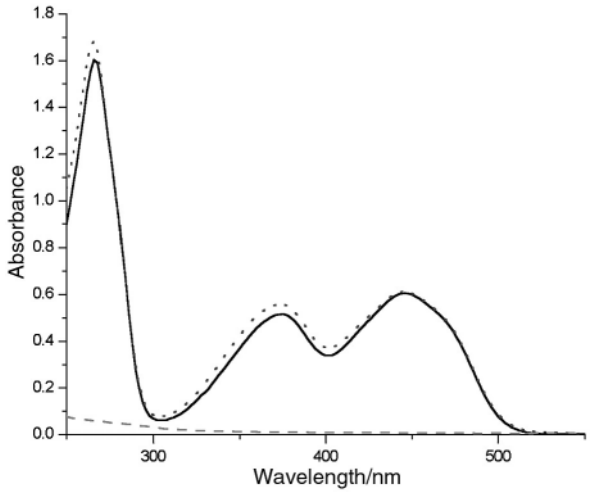

Fig. 1 Absorption spectra of a buffered aqueous solution (pH = 7.4; Tris–HCl) of riboflavin (c = 4,9 × 10^{-5} mol L^{-1}) before passage through the column filled with **2** (——); absorption spectra of the eluate after passage through the column (– – –); absorption spectra of the buffered aqueous solution (pH 4.4; acetate buffer) used to wash the column (· · ·). Solutions to load and to wash the column have the same volume.

† Electronic supplementary information (ESI) available: selective binding and reversible release of riboflavin, Figs. 3 and 4. See http://www.rsc.org/suppdata/cc/b1/b107605a/

 DOI: 10.1039/b107605a

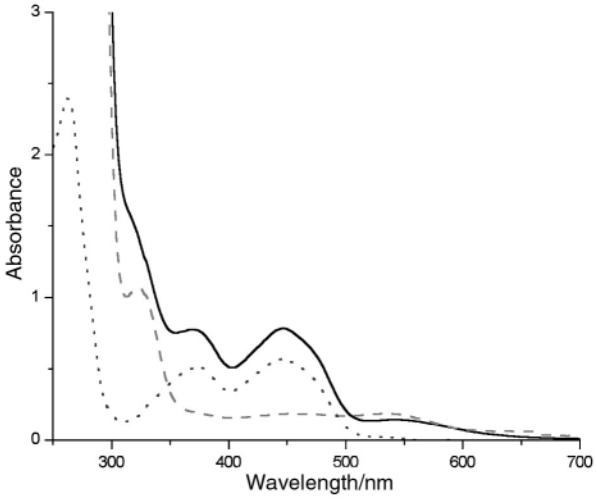

Fig. 2 UV spectra of vitamin drink: (——) before passage through a column filled with **2**; (– – –) filtrate after passage; (· · ·) eluted with aqueous buffer pH 4.4.

Polymer **2** shows an apparent binding constant to riboflavin in the millimolar range at pH 7.4 and its selectivity is restricted to imide recognition.§ However, for many practical purposes this might be sufficient to replace an apoprotein. To demonstrate the ability of **2** to remove riboflavin selectively and quantitatively from a mixture of compounds, the polymer was treated with a solution of a commercial vitamin dietary supplement.[11] The tablets, which have to be dissolved in water to prepare a vitamin drink, contain vitamins B1, B2, B6, B12, C, E, folic acid, biotin, pantothenic acid and nicotinamide in amounts corresponding to the recommended daily amount (RDA) for adults. Additional ingredients are citric acid, sodium bicarbonate, fructose, colour from beetroot, starch, sodium cyclamate and sodium saccharine. The composition of ingredients of this product is typical for similar dietary supplements of this kind. Passage through the column filled with **2** removes riboflavin, as indicated by the disappearance of the typical absorptions in the UV spectra of the filtrate (Fig. 2). Elution of the column with aqueous buffer at pH 4.4 gave a solution of pure riboflavin in the concentration exactly corresponding to the total amount of riboflavin the mixture (tablet) had contained.[12] As verification, 0.21 mg of riboflavin were added to the filtrate which had passed the column and the resulting solution was passed through a second column filled with **2**. The retained riboflavin was eluted with aqueous buffer pH 4.4. From the absorption an overall isolated amount of 0.20 mg was determined, showing within the experimental error a quantitative reisolation.

The functionalized polymer **2** introduced in this paper facilitates the isolation of riboflavin from natural sources[13] and its analytical determination in mixtures.[9] Moreover, it is another example of selective binding of a biological important compound under physiological conditions using artificial receptors within the concept of polyvalence binding sites.

Notes and references

‡ *Preparation of zinc(II)–cyclen loaded Fractogel® EMD epoxy polymer.* Fractogel® EMD epoxy (4.0 g) and **1** (600 mg, 1.27 mmol) were suspended in 80 mL of water buffered to pH 10 with carbonate, and mechanically stirred for 4 d at 40 °C. The polymer was collected by filtration, suspended in 40 mL of aqueous Tris–HCl buffer (pH 8) which contains 0.2 mol L^{-1} glycine and stirred for 2 h at 40 °C. The material was collected by filtration, treated with 20 mL of trifluoroacetic acid for 10 min at rt, filtered and washed with aqueous NaOH (2 M, 50 mL) and water (100 mL) to yield 4.01 g cyclen-loaded polymer. Elemental analysis (C: 53.32, H: 8.02, N: 0.80%) corresponds to 0.14 mmol cyclen for 1 g of material.

A suspension of $Zn(ClO_4)\cdot 6H_2O$ (1.34 g, 3.6 mmol) and the prepared polymer (2.02 g) in 10 mL of water was heated to 80 °C for 3 h, the polymer was collected by filtration and was washed with water and methanol to yield after drying 1.9 g of zinc(II)–cyclen-loaded polymer. Elemental analysis (C: 51.45, H: 7.6, N: 0.85%) corresponds to a polymer loading of 0.15 mmol zinc–cyclen complex for 1 g of polymeric material.

§ The binding constant was determined from the UV absorption of a buffered aqueous solution of riboflavin ($c = 10^{-5}$ mol L^{-1}) after incubating it with a specific amount of **2** for 30 min at room temperature. $K_{app} = 1.2 \times 10^{-3}$ mol L^{-1} (average of several measurements).

1 The use of reversible coordinative bonds for the binding of substrates to polymeric support has very recently been reported by Ley *et al*. in the context of organic synthesis. S. V. Ley, A. Massi, F. Rodriguez, D. C. Horwell, R. A. Lewthaite, M. C. Pritchard and A. M. Reid, *Angew. Chem*., 2001, **113**, 1088; *Angew. Chem., Int. Ed*., 2001, **40**, 1053.

2 M. Shionoya, E. Kimura and M. Shiro, *J. Am. Chem. Soc*., 1993, **115**, 6730.

3 E. Kimura and T. Koike, *Chem. Commun*., 1998, 1495.

4 B. König, M. Pelka, H. Zieg, T. Ritter, H. Bouas-Laurent, R. Bonneau and J.-P. Desvergne, *J. Am. Chem. Soc*., 1999, **121**, 1681.

5 T. Koike, M. Takashige, E. Kimura, H. Fujioka and M. Shiro, *Chem. Eur. J*., 1996, **2**, 617.

6 E. Kimura, M. Murata, N. Katsube, T. Koike and E. Kikuta, *J. Am. Chem. Soc*., 1999, **121**, 5426 and cited references.

7 S. Brandes, C. Gros, F. Denat, P. Pullumbi and R. Guilard, *Bull. Soc. Chim. Fr*., 1996, **133**, 65.

8 Fractogel®EMD is an activated tentagel phase produced by Merck KG, Darmstadt, and designed for the immobilization of proteins.

9 For a fluorometric apoprotein titration of urinary riboflavin, see: J. A. Tillotson and M. M. Bashor, *Anal. Biochem*., 1980, **107**, 214.

10 J. Becvar and G. Palmer, *J. Biol. Chem*., 1982, **257**, 5607.

11 Multivitamin tablets, orange taste, Krüger GmbH, Germany. See supporting information for a detailed list of ingredients. The aqueous solution of the vitamin drink was adjusted to pH 8 by addition of NaOH before separation on **2**.

12 In several experiments the determined amount of riboflavin varied less than 5% from the analysis of the supplier.

13 For an aqueous isolation and purification process for riboflavin, see: J. Grimmer, H. C. Horn (BASF AG), DE 3421714, 985.

CHEMCOMM
Communication
www.rsc.org/chemcomm

Inclusion adducts of 4,4-bis(4′-biphenylyl)cyclohexa-2,5-dienone: a clay mimic organic host

V. S. Senthil Kumar and Ashwini Nangia*

School of Chemistry, University of Hyderabad, Hyderabad 500 046, India. E-mail: ansc@uohyd.ernet.in

Received (in Columbia, USA) 1st July 2001, Accepted 11th October 2001
First published as an Advance Article on the web 24th October 2001

In the lamellar architecture of the title crystal structure mediated by C–H···O hydrogen bonds, 1,2-dimethoxyethane and *n*-hexane are included in the hydrophobic galleries; isostructurality of these clathrates is a unique case of guest mimicry.

Host–guest inclusion compounds provide opportunities for the design of novel open architectures for diverse applications such as chemical separation, reactions and catalysis in a microcavity, and for electrooptic, nonlinear and magnetic materials.[1] Crystal engineering of 2D and 3D robust metal–organic and soft molecular open frameworks offer the promise of tailoring specific structures, functions and properties through functionalised organic molecules.[2] For example, 4-tritylbenzoic acid crystallises *via* a carboxylic acid dimer (O–H···O hydrogen bond) with wheel–axle topology, 4-halophenoxy triazines self-assemble through triangulo halogen synthons (Cl···Cl, Br···Br interaction) as hexagonal channel hosts, and ligands such as 1,3,5-benzenetricarboxylic acid, 4-aminopyridine and 4,4′-bipyridine continue to be exploited in coordination polymer networks.[3] We report herein the construction of a lamellar, C–H···O hydrogen bonded host lattice which includes guest species in the interlayer region, thereby expanding the family of newly emerging neutral, organic clay mimics.[4]

Molecule **1**† [5] (Scheme 1) was designed as a tecton[6] with hydrogen bonding donor–acceptor groups in the quinone ring and biphenyl spacers oriented in the third dimension. It was expected that tecton **1** will self-assemble in a layer motif *via* C–H···O hydrogen bonded tape **2** and the biphenyl groups will constitute the pillars in the resulting 3D open framework. While implementing this molecule → crystal synthetic strategy for a potential host, we are aware that interpenetration[7] competes with guest inclusion during crystallisation and that the latter phenomenon (the goal of this study) occurs in only *ca.* 15% cases.[8] Recrystallisation of **1** from various solvents afforded diffraction quality crystals from 1,2-dimethoxyethane (DME). The X-ray structure of **1**·DME (2:1 stoichiometry, *C*2/*c* space group)‡ contains a C–H···O hydrogen bond chain along [001] (H···O 2.66 Å, C–H···O 160.6°; C–H distance neutron-normalised to 1.083 Å). The second C–H···O bond of the tape is long (3.05 Å, 175.6°) but at the accepted distance limit advocated by Desiraju and Steiner.[9] What is significant from a crystal engineering objective is that the target synthon **2** has been obtained (Fig. 1). The biphenyl groups do not engage in the usual herringbone T-motif or π–π stacking interactions,[10] possibilities that would have resulted in a self-inclusion crystal through interdigitation. Instead, inversion-related biphenyl groups form parallelepiped channels of 8 × 5 Å down the *c*-axis which are occupied by ordered DME guest species (Fig. 2). Host–host and host–guest (Ph)C–H···O hydrogen bonds (2.71, 137.2; 2.57 Å, 159.5) further stabilise the ordered supramolecular structure of **1**·DME. The advantage of building host networks with weak interactions was highlighted in a recent paper on 14 inclusion compounds of tetrakis(4-nitrophenyl)-methane.[11] Open architectures assembled with C–H···O hydrogen bonds have a degree of both stability and flexibility, a combination that results in adaptability and versatility towards guest inclusion.

Continuing further, **1** was recrystallised from *n*-hexane, a solvent isosteric with DME but devoid of hydrogen bonding groups. The crystal structure of **1**·*n*-hexane (2:1) is iso-

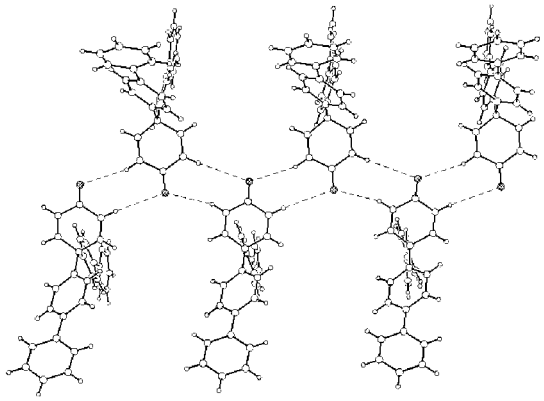

Fig. 1 Crystal structure of **1**·DME (2:1) in the *bc*-plane to show the tape synthon **2**. Guest molecules are not shown for clarity. Notice that the biphenyl groups project in the third dimension.

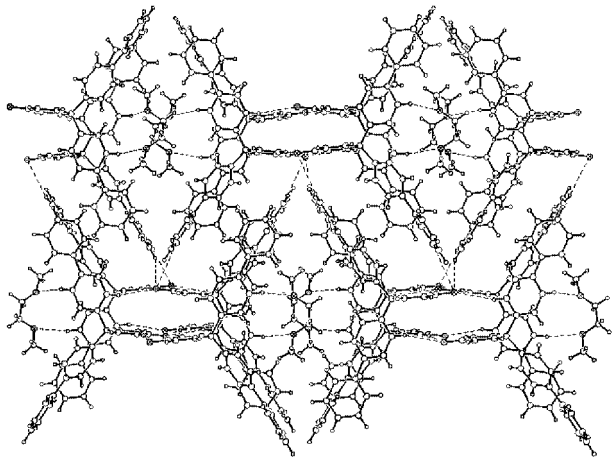

Fig. 2 Crystal structure of **1**·DME (2:1) down the *c*-axis. The network of host–host and host–guest C–H···O hydrogen bonds stabilise the ordered superstructure.

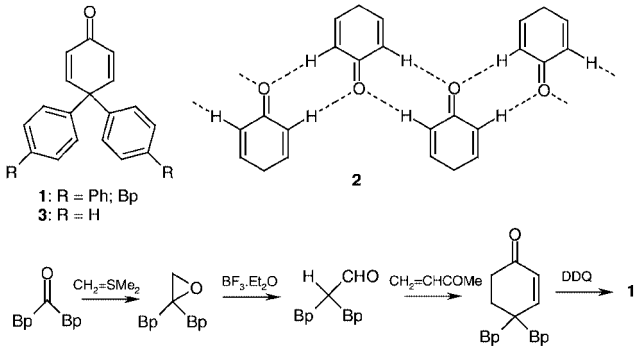

Scheme 1

 DOI: 10.1039/b106598j

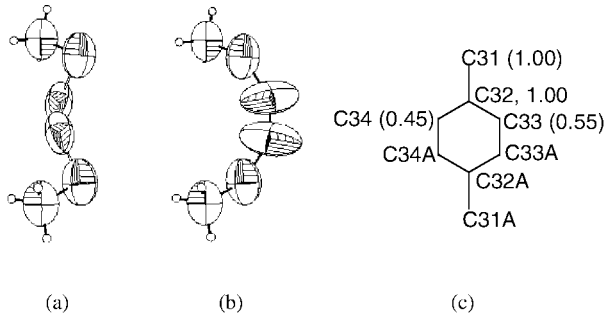

Fig. 3 Displacement ellipsoids at 50% probability of *n*-hexane in **1**·*n*-hexane (2:1). (a) Conformation with 45% occupancy of C34, (b) conformation with 55% occupancy of C33, (c) superposition of both conformers to show the mimicry with 1,4-dimethylcyclohexane (sof of atoms).

morphous‡ with identical arrangement of host atoms in the crystal. The metrics of quinone tape C–H···O bonds are 2.67, 161.9 and 2.99 Å, 175.1°; the (Ph)C–H···O is 2.71 Å, 137.2°. In the channel, *n*-hexane is disordered over two orientations with 55% and 45% occupancy (Fig. 3). The slightly elongated displacement ellipsoid of the C33 atom in a low temperature crystal structure implies that there are other minor conformations that contribute to guest disorder, but it is difficult to assign their exact position because of very low electron density. Using our refinement model, the structure converges (*R* factor 0.0675) with site occupancy factor (sof) of 0.55 and 0.45 for C33 and C34 guest atoms. Notably, neither of the conformations of *n*-hexane trapped in the microcavity correspond to the one in the crystal structure of pure solvent.[12] Superposition of the two conformers (Fig. 3c) suggests that host **1** may be able to separate a mixture of *cis*- and *trans*-1,4-dimethylcyclohexane.§ The guest is present in folded conformations because dimensions of the host cavity (8 × 5 Å) force it to adopt a compact shape.[13] The end-to-end C···C distance in the folded conformations of *n*-hexane is 5.5 Å (5.3 Å in DME) while it is 6.4 Å in the extended zigzag conformation.[12] Energy of the three conformations of *n*-hexane (RHF-631G*)¶ is −235.2718 au (55% population), −235.2933 au (45% population) and −235.3678 au (zigzag). A survey of the Cambridge Structural Database[14] (version 5.21, April 2001 update) shows that this is the first example of structural mimicry between DME and *n*-hexane in a host channel. The host cavity of **1**, which also includes 1,4-dibromobutane,‖ is highly selective towards these guest species. Co-solvents such as EtOAc, Et_2O, $CHCl_3$, CH_2Cl_2 are not included, even when present in large excess.

Finally, we note that while polymorphs of phenyl benzoquinone **3** were found to have divergent, even abstruse, crystal packing in $P\bar{1}$ (Z = 8) and $P2_1$ (Z = 2) space groups,[15] pseudopolymorphs of biphenyl analogue **1** are isostructural. Therefore replacement of geminal phenyl group with biphenyl steers crystal packing towards a recurring (robust) supramolecular synthon[16] and yields a novel, organic host material with clay-like properties. Metric engineering[2] of the lamellar–pillar molecular framework of **1** is a current goal in our studies.

We thank Professor W. T. Robinson and Dr R. Kadirvelraj (University of Canterbury, New Zealand) for X-ray data collection on a Bruker SMART diffractometer. Financial assistance from the DST in the form of a research project (SP/S1/G29/98) and for supporting the Enraf-Nonius X-ray diffractometer facility is acknowledged. VSSK thanks the CSIR for fellowship.

Notes and references

† **1** was synthesised from 4,4′-diphenylbenzophenone using standard reagents and reaction conditions. FT-IR: 1668, 763 cm^{-1}. ^1H NMR: δ 6.45 (d, J 10 Hz, 2 H), 7.20–7.50 (m, 12 H), 7.50–7.70 (m, 8 H). For synthesis of **3**, see ref. 5.

‡ *Crystal data*: (**1**)·$(CH_3OCH_2CH_2OCH_3)_{0.5}$: $(C_{30}H_{22}O)$·$(C_4H_{10}O_2)_{0.5}$, *C*2/*c*, a = 25.464(5), b = 19.751(4), c = 9.770(2) Å, β = 97.72(3)°, Z = 8, V = 4868.9(17) $Å^3$, 5886 unique reflections ($3 < 2\theta < 57°$), final R = 0.0522 for 1352 observed reflections [$I > 2\sigma(I)$] for 308 parameters. Data collected on Enraf-Nonius MACH-3 diffractometer at 293(2) K using Mo-Kα X-rays (λ 0.71073 Å) in the ω scan mode. CCDC 172238. (**1**)·(*n*-hexane)$_{0.5}$: $(C_{30}H_{22}O)$·$(C_6H_{14})_{0.5}$, *C*2/*c*, a = 25.052(5), b = 20.185(4), c = 9.722(2) Å, β = 98.27(3)°, Z = 8, V = 4865.4(17) $Å^3$, 4736 unique reflections ($5 < 2\theta < 53°$), final R = 0.0675 for 2282 observed reflections [$I > 2\sigma(I)$] for 317 parameters. Data collected on a Bruker SMART diffractometer at 168(2) K using MoKα X-rays (λ 0.71073 Å) in the ω-2θ scan mode. For both structures, H-atoms were fixed and structure solution and refinement were done with SHELX-97. CCDC 172239. See http://www.rsc.org/suppdata/cc/b1/b106598j/ for crystallographic files in .cif or other electronic format.

§ Aldrich Chemical Co. USA, mixture of isomers $71.20 per 25g, pure *cis* $227.70 per 25g.

¶ PC Spartan Pro 1.0, Wave function Inc. USA.

‖ (**1**)·$(Br(CH_2)_4Br)_{0.5}$: *C*2/*c*, a = 25.21, b = 20.21, c = 9.84 Å, β = 97.8°, T = 293 K, R = 0.12. The heavy guest disorder in interlayer regions gives a high diffraction R value typical of clays.[4] The presence of 1,4-dibromobutane in crystals was confirmed by NMR (δ 2.0, 3.4).

1 L. R. MacGillivray and J. L. Atwood, *Angew. Chem., Int. Ed.*, 1999, **38**, 1018; P. J. Langley and J. Hulliger, *Chem. Soc. Rev.*, 1999, **28**, 279; Y. Aoyama, *Top. Curr. Chem.*, 1998, **198**, 131.
2 M. J. Zaworotko, *Chem. Commun.*, 2001, 1; K. T. Holman, A. M. Pivovar, J. M. Swift and M. D. Ward, *Acc. Chem. Res.*, 2001, **34**, 107; M. Eddaoudi, D. B. Moler, H. Li, B. Chen, T. M. Reineke, M. O'Keefe and O. M. Yaghi, *Acc. Chem. Res.*, 2001, **34**, 319; A. Nangia, *Curr. Opin. Solid State Mater. Sci.*, 2001, **5**, 115.
3 R. K. R. Jetti, F. Xue, T. C. W. Mak and A. Nangia, *J. Chem. Soc., Perkin Trans. 2*, 2000, 1223; R. K. R. Jetti, A. Nangia, F. Xue and T. C. W. Mak, *Chem. Commun.*, 2001, 919; K. Biradha and M. Fujita, *Chem. Commun.*, 2001, 15; T. J. Prior and M. J. Rosseinsky, *Chem. Commun.*, 2001, 495.
4 E. B. Brouwer, K. A. Udachin, G. D. Enright, J. A. Ripmeester, K. J. Ooms and P. A. Halchuk, *Chem. Commun.*, 2001, 565.
5 H. E. Zimmerman, K. G. Hancock and G. C. Licke, *J. Am. Chem. Soc.*, 1968, **90**, 4892.
6 P. Brunet, M. Simard and J. D. Wuest, *J. Am. Chem. Soc.*, 1997, **119**, 2737.
7 S. R. Batten and R. Robson, *Angew. Chem., Int. Ed.*, 1998, **37**, 1460.
8 A. Nangia and G. R. Desiraju, *Chem. Commun.*, 1999, 605.
9 G. R. Desiraju and T. Steiner, *The Weak Hydrogen Bond in Structural Chemistry and Biology*, OUP, Oxford, 1999.
10 C. A. Hunter, *Chem. Soc. Rev.*, 1994, **23**, 101.
11 R. Thaimattam, F. Xue, J. A. R. P. Sarma, T. C. W. Mak and G. R. Desiraju, *J. Am. Chem. Soc.*, 2001, **123**, 4432.
12 R. Boese, H.-C. Weiss and D. Bläser, *Angew. Chem., Int. Ed.*, 1999, **38**, 988.
13 L. R. MacGillivray, H. A. Spinney, J. L. Reid and J. A. Ripmeester, *Chem. Commun.*, 2000, 517.
14 F. H. Allen and O. Kennard, *Chem. Des. Autom. News*, 1993, **8**, 31.
15 A. Anthony, G. R. Desiraju, R. K. R. Jetti, S. S. Kuduva, N. N. L. Madhavi, A. Nangia, R. Thaimattam and V. R. Thalladi, *Cryst. Eng.*, 1998, **1**, 1.
16 A. Nangia and G. R. Desiraju, *Top. Curr. Chem.*, 1998, **198**, 57.

CHEMCOMM Communication
www.rsc.org/chemcomm

A novel intramolecular through-space interaction between F and CN: a strategy for the conformational control of an acyclic system†

Kiyoharu Nishide,*[a] Yuri Hagimoto,[a] Hiroaki Hasegawa,[a] Motoo Shiro‡[b] and Manabu Node*[a]

[a] *Department of Pharmaceutical Manufacturing Chemistry, Kyoto Pharmaceutical University, Misasagi, Yamashina, Kyoto 607-8414, Japan. E-mail: node@mb.kyoto-phu.ac.jp; Fax: +81-75-595-4775; Tel: +81-75-595-4639*

[b] *Rigaku Corporation, 3-9-12 Matsubara, Akishima, Tokyo 196-0003, Japan*

Received (in Cambridge, UK) 8th August 2001, Accepted 11th October 2001
First published as an Advance Article on the web 2nd November 2001

X-Ray crystallographic analyses of fluorocyanides *anti*-1 and 2 revealed a novel *intramolecular through-space interaction between F and CN* in an acyclic system, which was applied to a stereoselective protonation of acyclic fluorocyanides 2 having flexible conformation.

The discovery of interactions between functional groups, such as hydrogen-bonding, π–π stacking, and CH–π interactions, is a pivotal area of investigation in organic and bioorganic chemistry. In organic synthesis, these interactions have controlled the stereochemistry in Diels–Alder and ene reactions.[1] Based on theoretical studies of the 'Bürgi–Dunitz trajectory' in nucleophilic additions to carbonyl groups,[2] Dunitz *et al*., discovered in 1978 the interaction between the ethereal oxygen and the carbonyl group in 8-methoxy-1-naphthyl methyl ketones.[3a] The newly coined 'nucleophilic–electrophilic interaction' was also found between the nitrogen and the carbonyl carbon and between the oxygen and the cyanide carbon.[3] Recently, intramolecular nonbonded interactions between oxygen and sulfur or selenium in heterocycles have also been observed.[4] Because of their unique characteristics of metabolic inhibition and high lipophilicity, organofluorine compounds are widely used in pharmaco- and agrochemistry. However despite their extensive use, the interaction of fluoride with organofunctional groups has remained virtually unexplored,[5] whereas interactions between fluoride and metals[6] and hydrogen-bonding interactions with fluoride[7] are often observed. We report herein the discovery of *a novel through-space interaction between F and CN*, which serves as a conformational regulation of a flexible acyclic carbon chain.

A molecule having two functional groups with large dipole moments in an acyclic system usually adopts a stable conformer in which the dipole moments oppose each other. However, we have observed the unusual phenomenon in which two functional groups in an acyclic system align to give the maximum dipole moment. Namely, during studies on ferroelectronic crystals,[8] a large spontaneous polarization was observed in liquid crystals doped with optically active 3-fluorocyanide derivatives. It is possible that in this case the two functional groups with large dipole moments aligned in the same direction to make a large spontaneous polarization; therefore, we postulated the existence of a novel through-space interaction between F and CN, as depicted in Fig. 1. In order to prove this hypothesis, we carried out X-ray crystallographic analyses of the crystalline fluorocyanides **1** and **2**.

The crystallographic analysis[9] (see ESI†) of optically active *anti*-**1**, which was prepared from 4-methoxyphenylacetonitrile and (*R*)-epoxyoctane,[10] is shown in Fig. 2. The distance between F and C(1) was found to be 2.890 Å, which is 0.28 Å shorter than the sum (3.17 Å) of their van der Waals radii. The angle between these atoms when projected in the C2–C4 plane was 8.6°. These two functional groups formed an envelope-shaped *pseudo* five-membered ring which includes the three carbons C2–C4. The F moiety of the *pseudo* five-membered ring was distorted toward the CN group. Among the angles concerned with the *pseudo* ring, θ_1 and θ_2 were shorter than a right angle, and θ_4 was found to be less than 180°, unlike the usual cyanide having the linear sp configuration. These data suggest that the lone pair of the fluorine (n_F) is being donated to the π* orbital on the cyanide carbon (π^*_{CN}).

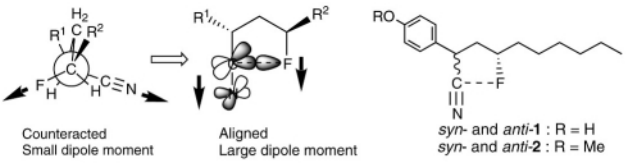

Fig. 1 Novel through-space $n_F \rightarrow \pi^*_{CN}$ interaction to freeze the conformation in an acyclic system.

Unlike the *anti*-**1**, the crystallographic analysis[11] (see ESI†) of the other diastereomer *syn*-**1** has revealed that the angle between these atoms when projected in the C1–C3 plane is −118.6°. Instead of a through-space interaction, an intermolecular hydrogen-bonding between phenolic hydrogen and cyano nitrogen was observed in the packing structure. This suggests that the observed through-space interaction between F and CN is weaker than the hydrogen-bonding interaction. Since the phenol moiety of the *syn*- and *anti*-**1** had drastically affected their conformation through the hydrogen-bonding interaction, we next decided to investigate the conformation of their methyl ethers *syn*- and *anti*-**2**.

The crystallographic analysis[12] (see ESI†) of *anti*-**2** has shown that the distance between F and C(9) is 2.872 Å, which is 0.30 Å shorter than the sum of their van der Waals radii. The conformation of *anti*-**2** was found to be almost the same as that of *anti*-**1**; therefore, the novel through-space interaction was

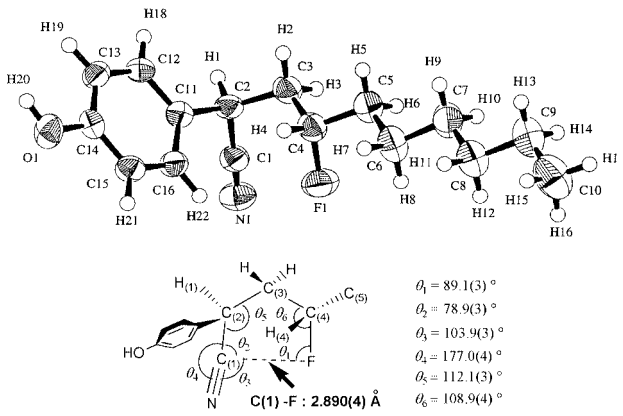

Fig. 2 Crystal structure of *anti*-**1**.

† Electronic supplementary information (ESI) available: experimental procedure for the syntheses of *syn*- and *anti*-**1** and **2**, spectroscopic data for all compounds, a procedure for the stereoselective protonation of **2**, full crystallographic data of *syn*- and *anti*-**1** and *anti*-**2**. See http://www.rsc.org/suppdata/cc/b1/b107213g/

 DOI: 10.1039/b107213g

proved to be independent of the intermolecular hydrogen-bonding of the phenol moiety. However, conformational data on *syn*-**2** in solid state could not be obtained because it is an oil.

Since the through-space interaction between F and CN had been established in the crystal, we turned our attention to the existence of this new interaction in solution. The ^{1}H-NMR signals of the methylene protons (ABXX′ type) in *syn*-**1** were observed at 1.98 and 2.34 ppm in $CDCl_3$, whereas those of *anti*-**1** were at 1.94–2.13 (2H). These chemical shift values and the coupling patterns in *syn*- and *anti*-**1** were very similar to those of the corresponding *cis*-γ-lactone (1.99 and 2.72) and the *trans*-γ-lactone (2.35 and 2.46), respectively.[8a,b] This observation suggests that the through-space interaction also occurs *via* a *pseudo* five-membered ring in both the *syn* and *anti*-fluorocyanides **1** in solution. To demonstrate the conformational control of an acyclic system utilizing this interaction, we investigated the stereoselective protonation of the α-anion of the cyanide derived from an equimolar mixture of *syn*- and *anti*-**2**. Our working hypothesis is that the diastereoselective protonation of the naked anion intermediate[13] with a bulky proton source would give *syn*-**2** preferentially by 1,3-asymmetric induction, based on a chiral carbon bearing a fluorine atom, if the through-space interaction between F and CN existed in the naked anionic molecule in solution. Our results are summarized in Table 1. Bulky phenols as proton sources gave products with higher diastereoselectivity than benzoic acid derivatives. 2,5-Dichlorobenzoic acid gave a product with lower selectivity than did benzoic acid, probably due to its higher acidity. The major diastereomer obtained was *syn*-**2**, with a very significant diastereoselectivity (5.3 : 1). We interpret this result as follows: the 1,3-asymmetric induction would arise from the *pseudo* five-membered ring intermediate formed by the through-space interaction between a lone pair of F and an sp-carbon of the naked α-anion of the cyanide, as in the control experiment under the same reaction conditions using an equimolar mixture of the corresponding *cis*- and *trans*-γ-lactones to give predominantly the *cis*-γ-lactone (94% yield, *cis* : *trans* = 10.6 : 1). From the above experiments, this through-space interaction, even in a solution containing the carbanion, is able to affect the conformational regulation of an acyclic carbon chain, but the ring formed by the interaction is not completely fixed as in the γ-lactone. However, this novel conformational regulation in an acyclic compound is valuable because of (1) the diastereoselective reaction of the α-anion of the 3-fluorocyanide and (2) the stereochemical prediction of the product, both of which are usually difficult in acyclic systems.

In conclusion, we have observed for the first time *a novel intramolecular through-space interaction between F and CN* by X-ray crystallographic analyses of the 1,3-fluorocyanides *anti*-**1** and **2**. Although this through-space interaction is weaker than the hydrogen-bonding interaction, acyclic compounds having flexible conformations were conformationally controlled by this interaction to form the distorted *pseudo* five-membered ring. However, it is particularly noteworthy that the existence of this novel interaction can not be predicted by the semiemperical PM3 calculation of *anti*-**1**, and by *ab initio* MP2 6-31G* and density functional df 6-31G* calculations of the simplified model compound of *anti*-**1**.[14] We also demonstrated the utility of the through-space interaction by a stereoselective protonation of an anion in solution. Further studies on through-space interactions between the functional groups are underway in our laboratory.

Table 1 Stereoselective protonation of the naked α-anion of cyanide[a]

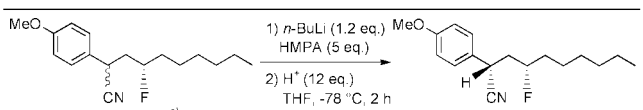

2[a)]

Run	H^+	*syn* : *anti*[b]	Yield (%)[c]
1	Benzoic acid	3.5 : 1	100
2	2,5-Dichlorobenzoic acid	1.9 : 1	90
3	2,6-Diphenylphenol	4.4 : 1	87
4	2,6-Di-*tert*-butyl-*p*-cresol	5.3 : 1	91

[a] *syn* : *anti* = 1.2 : 1. [b] Determined by ^{1}H-NMR of the crude products. [c] Isolated yield.

We are grateful for a Grant-in-Aid (No. 11672126 to K. N.) from the Ministry of Education, Science, Sports and Culture of Japan, in partial financial support of this research. We are also grateful to Professor Tamejiro Hiyama, Kyoto University, for helpful discussions at Sagami Chemical Research Center. We also thank the Japan Energy Corporation, Toda, Saitama, Japan, for its kind gift of (*R*)-epoxyoctane.

Notes and references

‡ Responsible for an X-ray crystallographic analysis of a fine needle of *syn*-**1** on a Rigaku RAXIS-IV imaging plate area detector.

1 (*a*) R. Tripathy, P. J. Carroll and E. R. Thornton, *J. Am. Chem. Soc*., 1990, **112**, 6743; (*b*) D. A. Evans, K. T. Chapman and J. Bisaha, *J. Am. Chem. Soc*., 1988, **110**, 1238; (*c*) J. K. Whitesell, R. M. Lawrence and H.-H. Chen, *J. Org. Chem*., 1986, **51**, 4779.

2 (*a*) H. B. Bürgi, J. D. Dunitz and E. Shefter, *J. Am. Chem. Soc*., 1973, **95**, 5065; (*b*) H. B. Bürgi, J. M. Lehn and G. Wipff, *J. Am. Chem. Soc*., 1974, **96**, 1956; (*c*) H. B. Bürgi, J. D. Dunitz, J. M. Lehn and G. Wipff, *Tetrahedron*, 1974, **30**, 1563.

3 (*a*) W. B. Schweizer, G. Procter, M. Kaftory and J. D. Dunitz, *Helv. Chim. Acta*, 1978, **61**, 2783; (*b*) G. Procter, D. Britton and J. D. Dunitz, *Helv. Chim. Acta*, 1981, **64**, 471.

4 (*a*) F. T. Burling and B. M. Goldstein, *J. Am. Chem. Soc*., 1992, **114**, 2313; (*b*) D. H. R. Barton, M. B. Hall, Z. Lin, S. I. Parekh and J. Reibenspies, *J. Am. Chem. Soc*., 1993, **115**, 5056; (*c*) Y. Nagao, T. Hirata, S. Goto, S. Sano, A. Kakehi, K. Iizuka and M. Shiro, *J. Am. Chem. Soc*., 1998, **120**, 3104 also see references cited therein.

5 A. Wilk, A. Grajkowski, L. R. Phillips and S. L. Beaucage, *J. Am. Chem. Soc*., 2000, **122**, 2149.

6 (CF–Li) (*a*) C.-P. Qian, T. Nakai, D. A. Dixon and B. E. Smart, *J. Am. Chem. Soc*., 1990, **112**, 4602; (*b*) U. Pieper, S. Walter, U. Klingebiel and D. Stalke, *Angew. Chem., Int. Ed. Engl*., 1990, **29**, 209; (Se–F) (*c*) M. Iwaoka, H. Komatsu and S. Tomoda, *Chem. Lett*., 1998, 969; Conformational fixation by Li–F: (*d*) T. Yamazaki, M. Ando, T. Kitazume, T. Kubota and M. Omura, *Org. Lett*., 1999, **1**, 905.

7 For example: (F–HC) (*a*) W. B. Farnham, D. C. Roe, D. A. Dixon, J. C. Calabrese and R. L. Harlow, *J. Am. Chem. Soc*., 1990, **112**, 7707; (F–HN) (*b*) J. P. Snyder, N. S. Chandrakumar, H. Sato and D. C. Lankin, *J. Am. Chem. Soc*., 2000, **122**, 544.

8 (*a*) T. Kusumoto, A. Nakayama, K. Sato, K. Nishide, T. Hiyama, S. Takehara, T. Shoji, M. Osawa, T. Kuriyama, K. Nakamura and T. Fujisawa, *J. Chem. Soc., Chem. Commun*., 1991, 311; (*b*) S. Takehara, T. Kuriyama, K. Nakamura, T. Shoji, T. Fujisawa, M. Osawa, T. Hiyama, T. Kusumoto, A. Nakayama and K. Nishide, *Japan Kokai Tokkyo Koho*, 1990, H02-286673.

9 *Crystal data of anti*-**1**: $C_{16}H_{22}FNO$, M = 263.35, monoclinic, a = 7.855(2), b = 5.462(2), c = 17.607(1) Å, β = 100.90(1)°, V = 741.7(3) Å^3, T = 23 °C, space group $P2_1$ (#4), Z = 2, R = 0.055, Rw = 0.084. CCDC 169361.

10 The syntheses of *syn*- and *anti*-**1** and **2** from *p*-methoxyphenylacetonitrile and (*R*)-epoxyoctane (91% ee) are described in ESI.†

11 *Crystal data of syn*-**1**: $C_{16}H_{22}FNO$, M = 263.35, orthorhombic, a = 7.509(1), b = 35.774(4), c = 5.596(1) Å, V = 1503.3(4) Å^3, T = −130 °C, space group $P2_12_12_1$ (#19), Z = 4, R = 0.043, Rw = 0.057. CCDC 169362.

12 *Crystal data of anti*-**2**: $C_{17}H_{24}FNO$, M = 277.38, monoclinic, a = 7.696(4), b = 5.627(3), c = 18.628(2) Å, β = 95.02(2)°, V = 803.6(6) Å^3, T = 23 °C, space group $P2_1$ (#4), Z = 2, R = 0.081, Rw = 0.192. CCDC 169360. See http://www.rsc.org/suppdata/cc/b1/b107213g/ for crystallographic data in .cif or other electronic format.

13 The usual lithium anion is considered to have the known intra- and/or intermolecular Li–F coordination.[6]

14 All three theoretical calculations showed that the most stable conformer had the angle (*ca*. 120°) between CN and F when projected in the C1–C3 plane. The relative energy differences between the conformers having the through-space interaction and the most stable conformers were 2.72 kcal mol^{-1} (PM3), 1.34 kcal mol^{-1} (MP2 6-31G*), and 2.12 kcal mol^{-1} (df 6-31G*).

CHEMCOMM
Communication
www.rsc.org/chemcomm

A model complex of a possible intermediate in the mechanism of action of peptide deformylase: first example of an (N_2S)zinc(II)–formate complex†

SeChin Chang,[a] Roger D. Sommer,[b] Arnold L. Rheingold[b] and David P. Goldberg*[a]

[a] *Department of Chemistry, The Johns Hopkins University, 3400 N. Charles Street, Baltimore, MD 21218, USA. E-mail: dpg@jhu.edu*

[b] *Department of Chemistry and Biochemistry, University of Delaware, Newark, DE 19716, USA*

Received (in Cambridge, UK) 30th July 2001, Accepted 27th September 2001
First published as an Advance Article on the web 2nd November 2001

The synthesis and crystallographic characterization of a new (N_2S)zinc–alkyl complex and (N_2S)zinc–formate complex is described; the bonding mode of the formate complex has implications for the mechanism of action of the enzyme peptide deformylase.

The zinc ion is the active metal in a considerable number of metalloenzymes, and the details of its catalytic function are of great interest to a continually expanding audience.[1,2] In many of these enzymes (*e.g.* carbonic anhydrase, thermolysin, carboxypeptidase A), a tetrahedral zinc(II) center is bound by an N_xO_y ligand set and a fourth catalytically active H_2O/OH^- ligand.[2] Much less commonly found, however, is the presence of a cysteinate sulfur ligand as part of a mixed N,S environment. One example of this uncommon coordination environment comes from the bacterial enzyme peptide deformylase (PDF), which has a [(His_2Cys)$M^{II}(OH_2)$] active site.[3] Intriguingly, PDF is the first example of a metallopeptidase that utilizes an iron(II) ion *in vivo*,[4] although its structural and functional characteristics indicate that it rightfully belongs in the mononuclear zinc(II) enzyme family.[5] Even more interestingly, the Zn(II) form of the enzyme is remarkably less active ($k_{cat}/K_m \sim 10^2$ smaller for the same substrate) than the Fe(II) form.[6]

Through a synthetic analogue approach, we intend to address the underlying principles that may be responsible for the unusual selection of iron(II) by PDF and the low reactivity found for Zn(II)–PDF. Also of interest is the role that the unusual thiolate donor plays. The effect of a thiolate donor on the structure and reactivity of model compounds capable of hydrolysis[7] is essentially unknown because of a dearth of well-defined N_xS_y-M(II)X (X ≠ N,S) complexes.[8] Herein is described the synthesis and structural characterization of a new reactive N_2S(alkythiolate)zinc(II)–alkyl complex [(PATH)-Zn(CH_3)] **1** (PATH = 2-methyl-1-[methyl-(2-pyridin-2-yl-ethyl)amino]propane-2-thiolate)[8] which serves as a useful synthon for the preparation of the carboxylate complexes [(PATH)Zn(O_2CH)] **2** and [(PATH)Zn(O_2CCH_3)] **3**. Complex **2** represents the best model to date of a PDF–formate species, which may be an important intermediate in the mechanism of deformylation.[3] Also, to our knowledge **2** is the first crystallographically characterized four-coordinate zinc(II)–formate complex. Intriguingly, the bonding mode of the formate ligand in **2** provides a plausible rationale for the strikingly low reactivity of the Zn(II) form of PDF.‡

As shown in Scheme 1, the synthesis of the zinc alkyl complex **1** proceeds smoothly by the addition of $Zn(CH_3)_2$ to PATH-H (thiol form) in toluene. Recrystallization of **1** from toluene at −20 °C resulted in X-ray quality crystals,§ and the molecular structure is shown in Fig. 1. Compound **1** is a discrete zinc–alkyl species with the zinc bound in a distorted tetrahedral geometry. The PATH–Zn(II) bond distances and angles in **1** are similar to those previously observed in [(PATH)ZnBr] and [(PATH)Zn(NCS)].[8] A search of the Cambridge Crystallographic Database shows that **1** is the first reported structure of an (N_2S)zinc–alkyl complex.[9] The Zn–C bond length of 1.987(2) Å for **1** is not much different from that observed for the four-coordinate (N_3)Zn–CH_3 compounds [N_3 = substituted tris(pyrazolyl)borate, Tp^R], *e.g.* *d*(Zn–C) = 1.971(4) Å in [($Tp^{t\text{-}Bu}$)Zn(CH_3)][10] and 1.981(8) Å in [($Tp^{Me,Me}$)Zn(CH_3)],[10] or the NS_2 complex [($pzBm^{Me}$)Zn(CH_3)], [$pzBm^{Me}$ = bis(mercaptoimidazolyl)(pyrazolyl)hydroborato] with *d*(Zn–C) = 1.988(4) Å.[11] Thus the Zn–C distance appears to be insensitive to the other ligands in the coordination sphere.

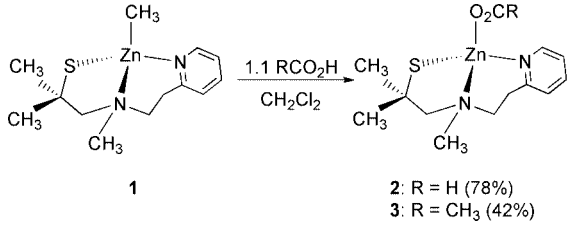

1 **2**: R = H (78%) **3**: R = CH_3 (42%)

Scheme 1

One might expect the thiolate donor of PATH to make the zinc(II) ion more electron-rich as compared to an N_3 donor ligand. Although this effect is not reflected in a comparison of Zn–C bond lengths, an examination of the ^{1}H NMR data is

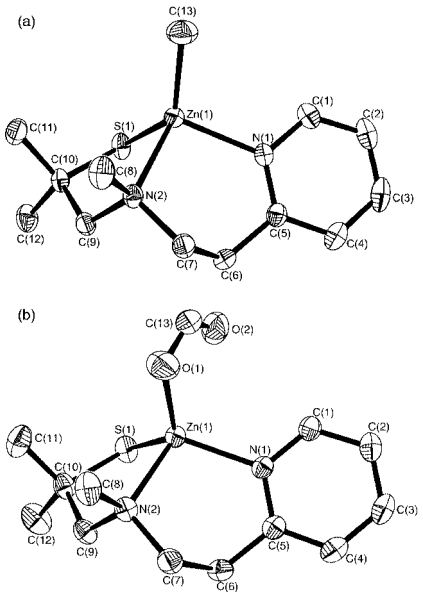

Fig. 1 (a) Thermal ellipsoid plot of [(PATH)Zn(CH_3)] showing 50% probability level. Hydrogen atoms have been omitted for clarity. (b) Thermal ellipsoid plot of [(PATH)Zn(O_2CH)] showing 50% probability level. Hydrogen atoms have been omitted for clarity.

† Electronic supplementary information (ESI) available: synthesis and characterisation of compounds **1**–**3**. See http://www.rsc.org/suppdata/cc/b1/b106865m/

 DOI: 10.1039/b106865m

enlightening. The ^{1}H NMR spectrum of **1** reveals an upfield shift of δ −0.19 in C_6D_6 (δ −0.82 in $CDCl_3$) for the Zn–CH_3 group, as compared to [(Tp^{Me,Me})Zn(CH_3)] [δ +0.28 (C_6D_6)], or [(Tp$^{t\text{-}Bu}$)Zn(CH_3)] [δ +0.54 (C_6D_6)].[10] These data are in line with **1** having a more electron-rich zinc(II) ion than the analogous N_3 complexes. In addition, the Zn–CH_3 peak of **1** is significantly further upfield in comparison to the only other (N_2S)zinc(II) alkyl complex, [(L3S)Zn(CH_3)] [δ −0.55 ($CDCl_3$)],[9] or even the (NS_2) complex [(pzBm^{Me})Zn(CH_3)] [δ −0.63 ($CDCl_3$)].[11]

Addition of 1 equivalent of either formic or acetic acid to **1** in CH_2Cl_2 gives the formate complex **2** and the acetate complex **3**, respectively, *via* protonolysis of the terminal methyl ligand. The ^{1}H NMR spectrum of **2** in $CDCl_3$ reveals a downfield singlet at δ 8.44 for the formate ligand, and that of **3** shows an O_2CCH_3 resonance at δ 2.02. Peaks due to the PATH ligand in **2** and **3** retain the diastereotopic pattern seen for **1** as well as for other [(PATH)ZnX] (X = Br, NCS) complexes,[8] indicative of a monomeric complex with a pseudo-tetrahedral zinc center. Recrystallization of **2** from CH_2Cl_2–hexanes led to the X-ray structure shown in Fig. 1, which reveals the expected monomeric zinc structure.§ Although a crystal structure of **3** has yet to be obtained, the NMR data suggest it has the same monomeric structure as **2**. It is clear that the PATH ligand has a remarkable ability to favor the formation of biologically relevant, monomeric zinc model complexes without the steric encumbrance or constrained tripodal platform of other 'tetrahedral enforcer' ligands.[1]

The most interesting feature of the structure of **2** is revealed in an examination of the bonding mode of the formate ligand, which can be classified as bidentate (or more strictly anisobidentate), as opposed to monodentate, based on the differences in the Zn–O distances (Δd = 0.605 Å) and the M–O–C(13) angles ($\Delta\theta$ = 27.8°).[12] In contrast, the related N_2S complex [(L3S)Zn(O_2CCH_3)], which has recently been prepared,[9] contains an O_2CCH_3 ligand which is bonded in a monodentate fashion (Δd = 0.947 Å, $\Delta\theta$ = 44.2°). The N_2S ligand in [(L3S)Zn(O_2CCH_3)] provides more steric encumberance near the zinc ion than does the PATH ligand, and therefore steric constraints may be the cause of the monodentate bonding in [(L3S)Zn(O_2CCH_3)].[13,14]

The enzyme carbonic anhydrase (CA) contains a $(His)_3$-Zn(II)(OH_2) site, and the reactivity of metal-substituted derivatives follows the order: Zn > Co >> Cu ~ Cd ~ Hg.[15] Data from biochemical[16] and model compound studies[15] indicate that the low reactivity of the latter metals correlates with a bidentate bonding mode of the product molecule (HCO_3^- anion). Bidentate bonding likely makes the displacement of HCO_3^- by H_2O in the final step of the mechanism of action of CA more difficult when compared to a monodentate-bound species. It was suggested that the presence of the thiolate ligand in [(L3S)Zn(O_2CCH_3)] favors monodentate coordination, and hence a cysteinate-containing CA may be inherently more reactive.[9] The bidentate structure of **2** clearly conflicts with these findings.

Importantly, the bidentate motif of **2** correlates nicely with the low reactivity of Zn(II)-PDF. Based on the electron-rich nature of the zinc ion in **1** as indicated by the ^{1}H NMR data, one might expect that **2** would exhibit a monodentate bonding mode. However, the structure of **2** suggests that the inherent (*i.e.* purely electronic) preference of an N_2S(alkylthiolate)–zinc(II) center is to coordinate a carboxylate ligand *via* a more *bidentate* mode. In analogy with CA, it may be more difficult for an incoming water molecule to displace a bidentate-bound formate ligand in Zn(II)–PDF, resulting in the inhibition of the mechanism of action of the enzyme. In fact, the existence of a PDF–formate complex was implicated in the mechanism of PDF and experimental evidence for it has been described.[3]

In conclusion, we have prepared the new (N_2S)zinc alkyl compound **1** as a useful synthetic precursor to other N_2S–Zn(II) complexes. A good model of an enzyme-formate complex has been prepared, and the X-ray structure reveals a rather unexpected anisobidentate bonding mode for the formate ligand. These results imply that this bonding mode may be operative in Zn(II)–PDF, providing a possible explanation for its low reactivity. Further model studies to address this point, including the synthesis of an analogous (N_2S)iron(II)–formate complex, are warranted.

Financial support from the NIH (Grant GM 62309) is gratefully acknowledged.

Notes and references

‡ Spectroscopic and analytical data for the new compounds are consistent with the proposed structures.

§ *Crystal data* for [(PATH)Zn(CH_3)] **1** (colorless prisms, 0.30 × 0.20 × 0.20 mm): $C_{13}H_{22}N_2SZn$, M = 303.76, monoclinic, space group = $P2_1/n$, a = 7.9486(7), b = 15.0809(15), c = 12.1088(12) Å, β = 90.958(2)°, V = 1451.3(2) Å^3, Z = 4, T = 173(2) K, μ = 1.818 m^{-1}, 6945 reflections collected, 3276 independent reflections (R_{int} = 0.0243), final R indices [$I > 2\sigma(I)$], $R1$ = 0.0320, 0.0390 (all data), $wR2$ = 0.0697, 0.0722 (all data), GOF (on F^2) = 1.127.

For [(PATH)Zn(O_2CH)] **2** (colorless plate, 0.40 × 0.20 × 0.20 mm): $C_{13}H_{20}N_2O_2SZn$, M = 333.74, monoclinic, space group = $P2_1/n$, a = 8.3772(4), b = 15.7976(8), c = 11.6276(6) Å, β = 93.0170(10)°, V = 1536.66(13) Å^3, Z = 4, T = 173(2) K, μ = 1.733 m^{-1}, 7382 reflections collected, 3449 independent reflections (R_{int} = 0.0239), final R indices [$I > 2\sigma(I)$], $R1$ = 0.0284, 0.0365 (all data), $wR2$ = 0.0800, 0.0906 (all data), GOF (on F^2) = 0.650. CCDC reference numbers 169231 and 169232. See http://www.rsc.org/suppdata/cc/b1/b106865m/ for crystallographic data in CIF or other electronic format.

1 G. Parkin, *Chem. Commun*., 2000, 1971.
2 W. N. Lipscomb and N. Sträter, *Chem. Rev*., 1996, **96**, 2375.
3 A. Becker, I. Schlichting, W. Kabsch, D. Groche, S. Schultz and A. F. V. Wagner, *Nat. Struct. Biol*., 1998, **5**, 1053.
4 P. T. R. Rajagopalan, X. C. Yu and D. Pei, *J. Am. Chem. Soc*., 1997, **119**, 12 418.
5 T. Meinnel, C. Lazennec and S. Blanquet, *J. Mol. Biol*., 1995, **254**, 175.
6 P. T. R. Rajagopalan, S. Grimme and D. Pei, *Biochemistry*, 2000, **39**, 779.
7 H. Kurosaki, T. Tawada, S. Kawasoe, Y. Ohashi and M. Goto, *Bioorg. Med. Chem. Lett*., 2000, **10**, 1333.
8 S. Chang, V. V. Karambelkar, R. C. diTargiani and D. P. Goldberg, *Inorg. Chem*., 2001, **40**, 194.
9 The synthesis of [(L3S)Zn(CH_3)] [L3SH = bis(3,5-dimethylpyrazolyl)(1-methyl-1-sulfanylethyl)methane] was recently described, although a crystal structure was not obtained: B. S. Hammes and C. J. Carrano, *J. Chem. Soc., Dalton Trans*., 2000, 3304.
10 A. Looney, R. Han, I. B. Gorrell, M. Cornebise, K. Yoon, G. Parkin and A. L. Rheingold, *Organometallics*, 1995, **14**, 274.
11 C. Kimblin, B. M. Bridgewater, T. Hascall and G. Parkin, *J. Chem. Soc., Dalton Trans*., 2000, 1267.
12 Bidentate: Δd < 0.3 Å, $\Delta\theta$ < 14°; anisobidentate: 0.3 < Δd < 0.6 Å, 14 < $\Delta\theta$ < 28°; monodentate: Δd > 0.6 Å, $\Delta\theta$ > 28°. G. J. Kleywegt, W. G. R. Wiesmeijer, G. J. Van Driel, W. L. Driessen, J. Reedijk and J. H. Noordik, *J. Chem. Soc., Dalton Trans*., 1985, 2177.
13 A comparison of the pK_a values for formic acid (3.75) and acetic acid (4.76) implies that an acetate ligand is more likely to coordinate in a bidentate mode than a formate ligand, and thus the nature of the acids in **2** and [(L3S)Zn(O_2CCH_3)] does not account for their difference in bonding modes. An example of a Cu(II) system in which the bonding mode of carboxylic acids correlates with pK_a can be found in: D. J. Darensbourg, M. W. Holtcamp, E. M. Longridge, B. Khandelwal, K. K. Klausmeyer and J. H. Reibenspies, *J. Am. Chem. Soc*., 1995, **117**, 318.
14 The bonding mode of the formate ligand in the complex ([Tp$^{t\text{-}Bu}$)-Zn(O_2CH)] was assigned as monodentate, although an X-ray structure was not obtained; see ref 10.
15 C. Kimblin, V. J. Murphy, T. Hascall, B. M. Bridgewater, J. B. Bonanno and G. Parkin, *Inorg. Chem*., 2000, **39**, 967 and references therein.
16 For the crystal structure of a Co(II)–CA–bicarbonate complex and a discussion of this point, see: K. Håkansson and A. Wehnert, *J. Mol. Biol*., 1992, **228**, 1212.

Typeset and printed by Black Bear Press Limited, Cambridge, England

CHEMCOMM
Feature Article
www.rsc.org/chemcomm

Catalytic reactions in ionic liquids

Roger Sheldon

Laboratory of Organic Chemistry and Catalysis, Delft University of Technology, Julianalaan 136, Delft BL-2628, The Netherlands. E-mail: secretariat-ock@tnw.tudelft.nl

Received (in Cambridge, UK) 10th August 2001, Accepted 11th September 2001
First published as an Advance Article on the web 18th October 2001

The chemical industry is under considerable pressure to replace many of the volatile organic compounds (VOCs) that are currently used as solvents in organic synthesis. The toxic and/or hazardous properties of many solvents, notably chlorinated hydrocarbons, combined with serious environmental issues, such as atmospheric emissions and contamination of aqueous effluents is making their use prohibitive. This is an important driving force in the quest for novel reaction media. Curzons and coworkers,[1] for example, recently noted that rigorous management of solvent use is likely to result in the greatest improvement towards greener processes for the manufacture of pharmaceutical intermediates. The current emphasis on novel reaction media is also motivated by the need for efficient methods for recycling homogeneous catalysts. The key to waste minimisation in chemicals manufacture is the widespread substitution of classical 'stoichiometric' syntheses by atom efficient, catalytic alternatives.[2] In the context of homogeneous catalysis, efficient recycling of the catalyst is a *conditio sine qua non* for economically and environmentally attractive processes. Motivated by one or both of the above issues much attention has been devoted to homogeneous catalysis in aqueous biphasic[3,4] and fluorous biphasic[5] systems as well as in supercritical carbon dioxide.[6] Similarly, the use of ionic liquids as novel reaction media may offer a convenient solution to both the solvent emission and the catalyst recycling problem.[7,8]

Historical development

What are ionic liquids? Quite simply, they are liquids that are composed entirely of ions. Molten sodium chloride, for example, is an ionic liquid but a solution of sodium chloride in water is an ionic solution. The term molten salts, which was previously used to describe such materials, evokes an image of high-temperature, viscous and highly corrosive media. The term ionic liquid, in contrast, implies a material that is fluid at (or close to) ambient temperature, is colourless, has a low viscosity and is easily handled, *i.e.* a material with attractive properties for a solvent. Room temperature ionic liquids are generally salts of organic cations, *e.g.* tetraalkylammonium, tetraalkylphosphonium, *N*-alkylpyridinium, 1,3-dialkylimidazolium and trialkylsulfonium cations (Fig. 1).

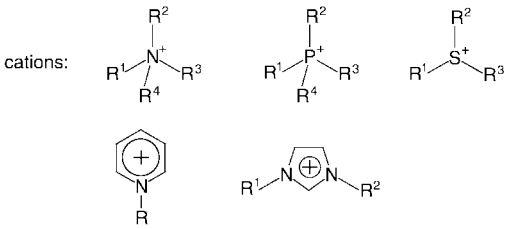

Fig. 1 Structures of ionic liquids.

In order to be liquid at room temperature, the cation should preferably be unsymmetrical, *e.g.* R^1 and R^2 should be different alkyl groups in the dialkylimidazolium cation. The melting point is also influenced by the nature of the anion (see Table 1).

Table 1 Melting points of some dialkylimidazolium salts

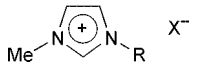

R	X	mp/°C
Me	Cl	125
Et	Cl	87
n-Bu	Cl	65
Et	NO_3	38
Et	$AlCl_4$	7
Et	BF_4	6
Et	CF_3SO_3	−9
Et	$(CF_3SO_3)_2N$	−3
Et	CF_3CO_2	−14
n-Bu	CF_3SO_3	16

Room temperature ionic liquids are not new. Ethylammonium nitrate, which is liquid at room temperature (but usually contains 200–600 ppm water) was first described in 1914.[9] In the late 1940s, *N*-alkylpyridinium chloroaluminates were studied as electrolytes for electroplating aluminium. These systems were reanimated by the groups of Hussey,[10] Osteryoung[11] and Wilkes[12] in the late 1970s. The first examples of ionic liquids based on dialkylimidazolium cations were reported in the early 1980s by Wilkes and coworkers.[12] They contained

Roger Sheldon was born in Nottingham (UK) in 1942. After receiving a PhD in Organic Chemistry from Leicester University (1967) he spent two years as a postdoc with Professor Jay Kochi in the USA. From 1969–1980 he was with Shell Research in Amsterdam and from 1980–1990 he was R&D Director of DSM Andeno. In 1991 he moved to his preent position as Professor of Organic Chemistry and Catalysis at the Delft University of Technology. His research interests are focused on the application of catalytic methodologies—homogeneous, heterogeneous and enzymatic—in organic synthesis, particularly in relation to fine chemicals production. He has widely promoted the concepts of E factors and atom efficiency for assessing the environmental impact of chemical processes. He is the author of ca. 300 scientific publications, numerous patents and three books on the subject of catalysis and chirotechnology. He is the Editor-in-Chief of Journal of Molecular Catalysis B: Enzymatic and Chairman of the Editorial Board of Green Chemistry. Among other distinctions he was recently awarded a Doctor Honoris Causa from the Russian Academy of Sciences.

DOI: 10.1039/b107270f

chloroaluminate anions ($AlCl_4^-$ or $Al_2Cl_7^-$) and proved to be useful catalysts/solvents for Friedel–Crafts acylations.[13] However, a serious obstacle for widespread use of these ionic liquids is the high reactivity of the chloroaluminate anion towards water.

The first example of the new ionic liquids, that currently are receiving so much attention as novel media for homogeneous catalysis, ethylmethylimidazolium tetrafluoroborate (emimBF_4)† was reported by Wilkes *et al.* in 1992.[14] The synthesis of the corresponding hexafluorophosphate followed shortly thereafter.[15] In contrast to the chloroaluminate salts the fluoroborates and hexafluorophosphates are stable towards hydrolysis. Subsequently, 1,3-dialkylimidazolium salts containing a wide variety of anions, *e.g.* $CF_3SO_3^-$, $[CF_3SO_2]_2N^-$, $CF_3CO_2^-$, $CH_3CO_2^-$, $PhSO_3^-$ and many more have been prepared.[16]

Ionic liquids can be prepared by direct quaternisation of the appropriate amine or phosphine. Different anions can subsequently be introduced by anion exchange. It is beyond the scope of this review to discuss in detail the synthesis of ionic liquids and the reader is referred to excellent reviews for many details.[17–20] It is important to note, however, that ionic liquids, owing to their non-volatile nature, cannot be purified by distillation. Consequently, they should be produced in high purity. For example, if synthesis involves exchange of chloride ions it is important that no chloride ions remain in the product as they may seriously impede catalysis by strongly coordinating to low valent transition metal complexes.

The hydrophilicity/lipophilicity of an ionic liquid can be modified by a suitable choice of anion, *e.g.* bmimBF_4 is completely miscible with water while the PF_6 salt is largely immiscible with water. The lipophilicity of dialkylimidazolium salts, or other ionic liquids, can also be increased by increasing the chain length of the alkyl groups.[21]

Ionic liquids containing 'fluorous ponytails' have even been described.[22] When these are added to conventional ionic liquids they facilitate emulsification with perfluorocarbons. This provides the possibility of performing (catalytic) reactions in ionic liquids/perfluorocarbon biphasic systems.

Catalysis in ionic liquids: general considerations

Room temperature ionic liquids exhibit many properties which make them potentially attractive media for homogeneous catalysis:

- They have essentially no vapour pressure, *i.e.* they do not evaporate and are easy to contain.
- They generally have reasonable thermal stability. While tetraalkylammonium salts have limited thermal stability, owing to decomposition *via* the Hoffmann elimination, emimBF_4 is reportedly stable up to 300 °C and emim-$(CF_3SO_2)_2N$ up to 400 °C.[16a] In other words many ionic liquids have liquid ranges of more than 300 °C, compared to the 100 °C liquid range of water.
- They are able to dissolve a wide range of organic, inorganic and organometallic compounds.
- The solubility of gases, *e.g.* H_2, CO and O_2, is generally good which makes them attractive solvents for catalytic hydrogenations, carbonylations, hydroformylations, and aerobic oxidations.
- They are immiscible with some organic solvents, *e.g.* alkanes, and, hence, can be used in two-phase systems. Similarly, lipophilic ionic liquids can be used in aqueous biphasic systems.
- Polarity and hydrophilicity/lipophilicity can be readily adjusted by a suitable choice of cation/anion (see earlier) and ionic liquids have been referred to as 'designer solvents'.[7]
- They are often composed of weakly coordinating anions, *e.g.* BF_4^- and PF_6^- and, hence, have the potential to be highly polar yet non-coordinating solvents. They can be expected, therefore, to have a strong rate-enhancing effect on reactions involving cationic intermediates.
- Ionic liquids containing chloroaluminate ions are strong Lewis, Franklin and Brønsted acids. Protons present in emim$AlCl_4$ have been shown to be superacidic with Hammett acidities up to −18.[23] Such highly acidic ionic liquids are, nonetheless, easily handled and offer potential as non-volatile replacements for hazardous acids such as HF in several acid-catalysed reactions.

Faced with these numerous potential benefits one may wonder if ionic liquids have any problems associated with their use. Atmospheric emissions may not be an issue but, when used on an industrial scale, small amounts of ionic liquids will inevitably find their way into the environment *via* the proverbial 'mechanical losses'. So, what is known about their potential environmental impact? A cursory examination of the literature reveals a dearth of information regarding the biodegradability and toxicity of ionic liquids. A prerequisite for industrial use is, therefore, the generation of appropriate data to enable the assessment of the potential environmental impact of ionic liquids.

Another question which arises in any discussion of ionic liquids as reaction media pertains to the isolation of soluble reaction products. Volatile products can be separated by distillation. Non-volatile products, on the other hand, can be separated by solvent extraction. Although this seems paradoxical—using an ionic liquid to avoid atmospheric emissions and subsequently using a volatile organic solvent to extract the product—it could have environmental benefits. For example, substituting an environmentally unacceptable solvent by an ionic liquid as the reaction medium, followed by extraction with a more benign organic solvent would constitute an environmental benefit. In this context it is worth noting the use of supercritical carbon dioxide to extract products from ionic liquids, which is currently the focus of attention.[24] Quite remarkably, $scCO_2$ is highly soluble (up to 60 mol%) in bmimPF_6 while the latter is insoluble in $scCO_2$. Naphthalene, for example, was recovered quantitatively from bmimPF_6 by $scCO_2$ extraction, without any contamination of the extract by the ionic liquid.

One can envisage various scenarios for catalysis in and/or by ionic liquids:

- Monophasic systems in which the catalyst and substrate are dissolved in the ionic liquid.
- Monophasic systems in which the ionic liquid acts as both the solvent and the catalyst, *e.g.* dialkylimidazolium chloroaluminates as Friedel–Crafts catalysts (see later).
- Biphasic systems in which the catalyst resides in the ionic liquid and the substrate/product in the second phase or *vice versa*.
- Mono- or biphasic systems in which the anion of the ionic liquid acts as a ligand for the homogeneous catalyst, *e.g.* a sulfonated phosphine ligand (see later).
- Triphasic systems comprising, for example, an ionic liquid, water and an organic phase in which the catalyst resides in the ionic liquid, the substrate and product in the organic phase and salts formed in the reaction are extracted into the aqueous phase, *e.g.* in Heck reactions (see later).

The first example of homogeneous transition metal catalysis in an ionic liquid is the platinum catalysed hydroformylation of ethene in tetraethylammonium trichlorostannate, described by Parshall in 1972.[25] This ionic liquid (referred to as a molten salt back in those days) has a melting point of 78 °C. These results were largely ignored for two decades. The potential of ionic liquids as novel media for homogeneous catalysis became more widely appreciated largely due to the pioneering studies and extensive promotion of the groups of Seddon[17] and Chauvin and Olivier-Bourbigou[18] and, more recently, the groups of Welton[19]

and Keim and Wasserscheid.[20] In the last five years their use as novel media for, *inter alia*, catalytic hydrogenations, hydroformylations, isomerisations, olefin dimerisations, oligomerisations and polymerisations and Heck couplings, has been rapidly expanding. The salient features of these studies will be reviewed in the ensuing discussion, with emphasis on their potential as clean synthetic methodologies.

Hydrogenation

The first example of catalytic hydrogenation in an ionic liquid was reported by Chauvin *et al*. in 1995.[26] A solution of the cationic [Rh nbd(Ph_3P)$_2$]PF_6 complex [nbd = norbornadiene (bicyclo[2.2.1]hepta-2,5-diene)] in bmimPF_6 or bmimSbF_6 was shown to be an effective catalyst for the biphasic hydrogenation of pent-1-ene. Reaction rates were up to five times higher than in acetone as solvent which was attributed to the formation of an unsolvated cationic rhodium(III) dihydride complex with two free coordination sites in the nonsolvating ionic liquid. In contrast, poor results were obtained with bmimBF_4 which was ascribed to the presence of trace amounts of strongly coordinating chloride ions in their sample of this ionic liquid. The catalyst solution in the ionic liquid could be reused with rhodium losses below the detection limit of 0.02%.

Similarly, advantage was taken of the biphasic system to perform the selective hydrogenation of cyclohexadiene. The solubility of cyclohexadiene in bmimSbF_6 is about five times that of cyclohexene and, hence, the latter was obtained in 98% selectivity at 96% conversion.

Dupont and coworkers[27] performed the biphasic hydrogenation of cyclohexene with Rh(cod)$_2BF_4$ (cod = cycloocta-1,5-diene) in ionic liquids. They observed roughly equal rates (turnover frequencies of *ca*. 50 h^{-1}) in bmimBF_4 and bmimPF_6 (presumably their bmimBF_4 was chloride-free).

The same group showed that $RuCl_2(Ph_3P)_3$ in bmimBF_4 is an effective catalyst for the biphasic hydrogenation of olefins, with turnover frequencies up to 540 h^{-1}.[28] Similarly, (bmim)$_3$-Co$(CN)_5$ dissolved in bmimBF_4 catalysed the hydrogenation of butadiene to but-1-ene, in 100% selectivity at complete conversion.[28]

More recently, the ruthenium-catalysed hydrogenation of sorbic acid to *cis*-hex-3-enoic acid (Reaction 1) was achieved in a biphasic bmimPF_6–methyl *tert*-butyl ether system.[29]

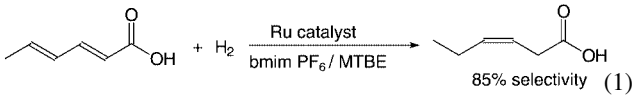

85% selectivity (1)

The ruthenium cluster, $[H_4Ru(\eta^6\text{-}C_6H_6)_4]$ $[BF_4]_2$ in bmimBF_4 was shown to be an effective catalyst for the hydrogenation of arenes, to the corresponding cycloalkanes, at 90 °C and 60 bar.[30] The cycloalkane product formed a separate phase which was decanted and the ionic liquid phase, containing the catalyst, could be repeatedly recycled.

Enantioselective hydrogenation in ionic liquids is of particular interest as it could provide a means for facile recycling of metal complexes of expensive chiral ligands. In their original study Chauvin *et al*.[26] reported that [Rh(cod)(−)-(diop)]PF_6 catalysed the enantioselective hydrogenation of α-acetamidocinnamic acid to (*S*)-phenylalanine, in 64% ee, in a biphasic bmimSbF_6–isopropyl alcohol (Reaction 2). The observed

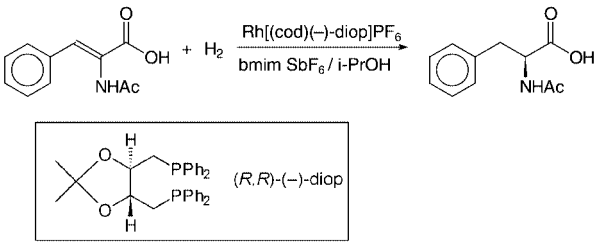

(2)

enantioselectivity is what one would expect with diop which is not a particularly good ligand for this reaction. The product, contained in the isopropyl alcohol, could be separated quantitatively and the recovered ionic liquid, containing the catalyst, reused.

Similarly, Dupont and coworkers[31] extended their studies of ruthenium-catalysed hydrogenations in ionic liquids to enantioselective reactions. The chiral [$RuCl_2$(*S*)-BINAP]$_2NEt_3$ complex was shown to catalyse the asymmetric hydrogenation of 2-phenylacrylic acid and 2-(6-methoxy-2-naphthyl)acrylic acid in bmimBF_4–isopropyl alcohol. The latter afforded the anti-inflammatory drug, (*S*)-naproxen, in 80% ee (Reaction 3). The

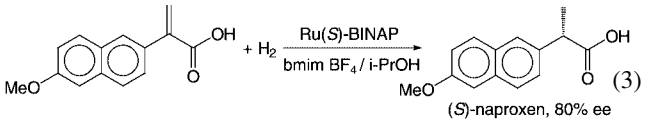

(*S*)-naproxen, 80% ee (3)

product could be quantitatively separated and the recovered ionic liquid catalyst solution recycled several times without any significant change in activity or selectivity.

An interesting recent development is the use of a biphasic ionic liquid–supercritical CO_2 for catalytic hydrogenation[32,33] and other processes (see later). Tumas and coworkers[32] showed that the catalytic hydrogenation of olefins could be conducted in a biphasic bmimPF_6–scCO_2 system. The ionic liquid phase containing the catalyst was separated by decantation and reused in up to four consecutive batches.

Jessop and coworkers[33] extended this concept to the asymmetric hydrogenation of tiglic acid (Reaction 4) and the precursor of the antiinflammatory drug ibuprofen (Reaction 5) using Ru$(OAc)_2$(tolBINAP) as the catalyst.

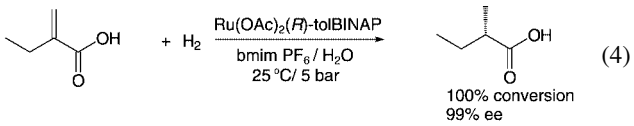

100% conversion
99% ee (4)

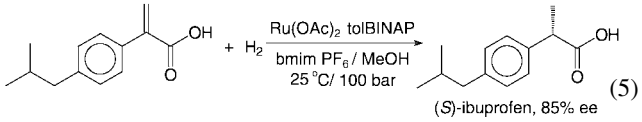

(*S*)-ibuprofen, 85% ee (5)

They found that Reaction 4 was more selective in a bmimPF_6–water biphasic mixture while Reaction 5 gave poor enantioselectivities in the wet ionic liquid. In this case the best result (85% ee) was obtained using methanol as cosolvent at 100 bar H_2 pressure. In both cases the product was separated by scCO_2 extraction when the reaction was complete. The different solvent effects observed with the two substrates was assumed to be due to the solubility of H_2 in the reaction mixture. The hydrogen concentration dependence of asymmetric catalytic hydrogenation with ruthenium BINAP complexes is known to be dependent on the substrate.[34] Class I substrates such as the ibuprofen precursor give higher enantioselectivities at high H_2 concentration while class II substrates, exemplified by tiglic acid, give higher enantioselectivities at low H_2 concentrations.

Hydroformylation

Hydroformylation of propene in an aqueous biphasic system, using a water-soluble rhodium complex of the sodium salt of trisulfonated triphenylphosphine (tppts) forms the basis of the Ruhr Chemie Rhone Poulenc process for the manufacture of butanal.[35] Unfortunately this process is limited to C_2 to C_5 olefins owing to the very low solubility of higher olefins in water. Hence, one can envisage that the use of an appropriate ionic liquid could provide the basis for biphasic hydroformylation of higher olefins.

As noted earlier, Parshall showed, in 1972, that platinum-catalysed hydroformylations could be performed in tetraethylammonium trichlorostannate melts.[25] More recently, Waffenschmidt and Wasserscheid[36] studied the platinum-catalysed hydroformylation of oct-1-ene in bmimSnCl$_3$ (Reaction 6)

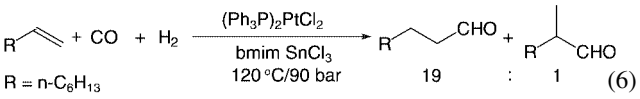

(6)

which is liquid at room temperature. Despite the limited solubility of oct-1-ene in the ionic liquid, high activities (TOF = 126 h^{-1}) were observed together with a remarkably high regioselectivity (n/iso = 19). The product was recovered by phase separation and no leaching of platinum was observed.

The ruthenium- and cobalt-catalysed hydroformylation of internal and terminal olefins in molten tetra-*n*-butylphosphonium bromide was reported by Knifton in 1987.[37] More recently, the rhodium-catalysed hydroformylation of hex-1-ene was conducted in molten phosphonium tosylates, *e.g.* Bu$_3$PEt$^+$TsO$^-$ and Ph$_3$PEt$^+$TsO$^-$ having melting points of 81–83 °C and 94–95 °C, respectively, at 120 °C and 40 bar.[38] Advantage was taken of the higher melting points of these 'ionic liquids' to decant the product from the solid catalyst medium at room temperature.

Chauvin and coworkers[26] investigated the rhodium-catalysed biphasic hydroformylation of pen-1-tene in bmimPF$_6$. High activities (TOF = 333 h^{-1} compared with 297 h^{-1} in toluene) were observed with the neutral Rh(CO)$_2$(acac)–Ph$_3$P as the catalyst precursor but some leaching of the catalyst into the organic phase occurred. This could be avoided by using Rh(CO)$_2$acac with tppts or tppms (monosulfonated triphenylphosphine) as the catalyst precursor, albeit at the expense of rate (TOF = 59 h^{-1} with tppms). Higher activities (TOF = 810 h^{-1}) and high regioselectivity (n/iso = 16) were observed in the biphasic hydroformylation of oct-1-ene in bmimPF$_6$ using cationic cobaltocenium diphosphine ligands but some catalyst leaching (< 0.5%) was observed.[39]

Better results were obtained with cationic guanidine-modified diphosphine ligands containing a xanthene backbone.[40] Xanthene-based diphosphine ligands with large bite angles (P–metal–P ~ 110°) are known to give high selectivities (≥98%) towards the linear aldehyde.[41] Biphasic hydroformylation of oct-1-ene, using rhodium complexes of these ligands in bmimPF$_6$ (Reaction 7), afforded high regioselectivities (*ca.* 20)

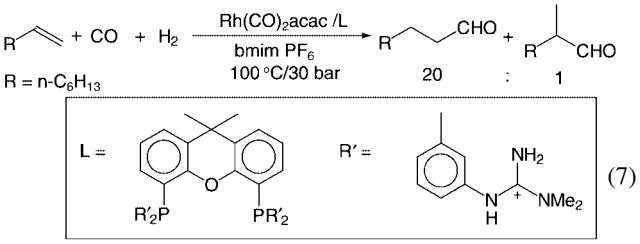

(7)

and the catalyst could be recycled ten times (resulting in an overall turnover number of 3500) without detectable (< 0.07%) leaching of Rh to the organic phase.

The group of Olivier-Bourbigou[42] has recently explored the use of a wide range of ionic liquids, based on imidazolium and pyrrolidinium cations and weakly coordinating anions, for the biphasic hydroformylation of hex-1-ene catalysed by rhodium complexes of modified phosphine and phosphite ligands. The latter are, in contrast, unstable in aqueous biphasic media. The rate and regioselectivity could be optimized by choosing a suitable combination of cation, anion and phosphine or phosphite ligand. Rhodium leaching was minimised by modification of the ligands with cationic (guanidinium or pyridinium) or anionic (sulfonate) groups.

Another interesting recent development is the rhodium-catalysd biphasic hydroformylation of oct-1-ene in bmimPF$_6$–scCO$_2$ in a continuous flow process.[43] Because of the low solubility of Rh–tppms and Rh–tppts complexes in the ionic liquid, [pmim]$^+$Ph$_2$PC$_6$H$_4$SO$_3^-$ (pmim = 1-propyl-3-methylimidazolium) was synthesised and used together with Rh$_2$(OAc)$_4$ as the catalyst precursor. Aldehydes were produced at a constant rate for 72 h albeit with moderate regioselectivity (n/iso = 3.8). Analysis of recovered products revealed that < 1 ppm Rh is leached into the organic phase.

The monophasic hydroformylation of methylpent-3-enoate in bmimPF$_6$ has been reported.[44] The linear aldehyde product (Reaction 8) is a precursor of adipic acid in an alternative

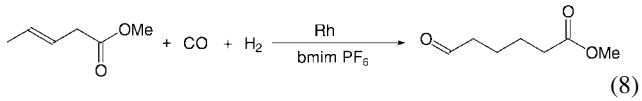

(8)

butadiene-based route. The product was removed by distillation (0.2 mbar/110 °C) and the ionic liquid recycled ten times without significant loss in activity.

Alkoxycarbonylation

Much less attention has been focused on carbonylation reactions in ionic liquids. The biphasic palladium-catalysed alkoxycarbonylation of styrene (Reaction 9) in bmimBF$_4$–cyclohexane has been reported.[45] Very high regioselectivities (≥99.5% iso) were obtained, using PdCl$_2$(PhCN)$_2$ in combination with (+)-neomenthyldiphenylphosphine and toluene-*p*-sulfonic acid, under mild conditions (70 °C and 10 bar).

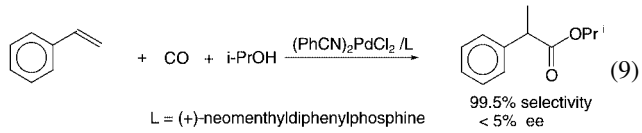

(9)

More recently, the palladium-catalysed alkoxycarbonylation and amidocarbonylation of aryl bromides and iodides in bmimBF$_4$ and bmimPF$_6$ has been described.[46] Enhanced reactivities were observed compared to conventional media and the ionic liquid–catalyst could be recycled.

Olefin dimerisation and oligomerisation

The nickel-catalysed dimerisation of lower olefins in ionic liquids containing chloroaluminate anions is probably the most investigated reaction in ionic liquids.[18,26,47–49] As early as 1990 the group of Chauvin at the Institut Francais du Petrole (IFP) reported the nickel-catalysed dimerisation of propene in bmimAlCl$_4$.[47] The catalyst precursor consisted of L$_2$NiCl$_2$ (L = Ph$_3$P or pyridine) in combination with EtAlCl$_2$ (bmimCl–AlCl$_3$–EtAlCl$_2$ = 1 : 1.2 : 0.25). The active catalyst is a cationic nickel(II) complex, [LNiCH$_2$CH$_3$]$^+$AlCl$_4^-$, formed by reaction of L$_2$NiCl$_2$ with EtAlCl$_2$. Since ionic liquids promote the dissociation of ionic metal complexes it was envisaged that they would have a beneficial effect on this reaction.[18]

This proved to be the case: at 5 °C and atmospheric pressure productivities (> 250 kg dimers per g Ni) much higher than those observed in organic solvents were achieved.[18,47,48] The mixture of dimers obtained, containing 2,3-dimethylbutene as the major component (83%), has commercial importance as the precursor of octane boosters for reformulated gasoline. It has been produced since the mid-seventies by the IFP 'Dimersol' process (25 units worldwide with a production of 3.4 × 10^6 tons per annum) in a single-phase solvent-free medium.

The methodology was subsequently extended to the dimerisation of butenes. The isooctene product constitutes the feedstock for the manufacture of isononanols (plasticizers) by

hydroformylation. A productivity of > 100 kg dimers per g Ni was obtained at 10 °C.

Conducting these dimerisations as biphasic reactions in ionic liquids affords several benefits:[18] a better selectivity to dimers (owing to their low solubility in the ionic liquid), a better use of the catalyst components and, hence, reduced disposal costs, substantially reduced reactor size, no corrosion and broader scope (to less reactive, higher olefins).

The nickel-catalysed biphasic dimerisation of olefins in ionic liquids is being offered for licensing by IFP under the acronym 'Difasol process' and is likely to be the first large scale application of biphasic catalysis in ionic liquids.

Wasserscheid and Keim[20,50] have developed alternative, alkylaluminium-free nickel catalysts for the linear dimerisation of but-1-ene. A turnover frequency of 1240 h^{-1} and a dimer selectivity of 98% (64% linearity) was observed at 25 °C. More recently, the same group reported[51] the use of cationic nickel complexes for the biphasic oligomerisation of ethene to higher α-olefins in bmimPF_6 (Reaction 10). The products separated as

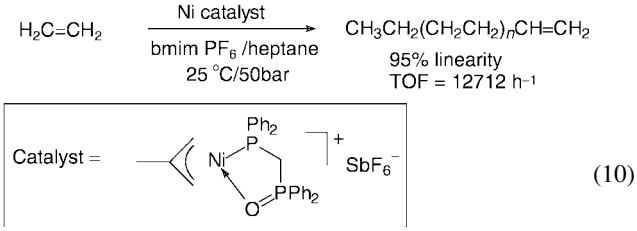

(10)

a clear and colourless layer and the catalyst-containing ionic liquid could be recycled with leaching below the detection limit (0.1%).

The palladium-catalysed dimerisation of butadiene to octa-1,3,6-triene and octa-1,3,7-triene is industrially important as the products have a wide range of applications, *e.g.* as comonomers and in the synthesis of plasticizers, adhesives and fragrances. Since these octatrienes rapidly polymerise in the presence of air, separation of the product from the homogeneous catalyst, *e.g.* by distillation, presents a serious problem. This would seem, therefore, to be an attractive target for biphasic catalysis in an ionic liquid.

Dupont and coworkers[52] have reported that $PdCl_2$–Ph_3P (1:4) catalyses the biphasic dimerisation of butadiene (Reaction 11)

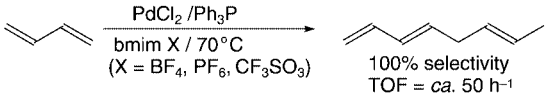

(11)

in bmimX (X = BF_4, PF_6 or CF_3SO_3) at 70 °C, affording octa-1,3,6-triene in 100% selectivity.

The same group reported[53] that when the reaction is performed with $(bmim)_2PdCl_4$ in bmimBF_4–H_2O (roughly 1 : 1 v/v) selective telomerisation resulted to afford octa-2,7-dien-1-ol (Reaction 12). As is also observed in other mono- and

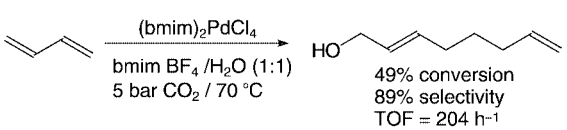

(12)

biphasic telomerisations of butadiene, the presence of carbon dioxide was essential for high activity. Using 5 bar CO_2 a turnover frequency of 204 h^{-1} and a selectivity of 89% (11% octa-1,3,6-triene) at 49% conversion was observed at 70 °C. Interestingly, the reaction is monophasic under the reaction conditions but cooling the mixture to 5 °C produces two phases and the ionic liquid phase can be separated and recycled. This methodology is a potentially attractive alternative to the aqueous biphasic telomerisation of butadiene developed by Kuraray.[3,4]

Heck reactions

The Heck and related C–C coupling reactions are of major importance in organic synthesis and are finding wide application in the manufacture of fine chemicals.[54] The first example of a Heck coupling in an ionic liquid was reported by Kaufmann *et al.* in 1996.[55] Butyl *trans*-cinnamate was produced in high yield by reaction of bromobenzene with butyl acrylate in molten tetraalkylammonium and tetraalkylphosphonium bromide salts (Reaction 13). No formation of palladium metal was observed

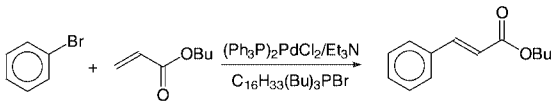

(13)

and the product was isolated by distillation from the ionic liquid.

Herrmann and Böhm[56] subsequently showed that molten Bu_4NBr (mp 103 °C) is a particularly suitable reaction medium for Heck reactions, affording superior results compared with commonly used organic solvents such as DMF. For example, in the reaction of bromobenzene with styrene, using diiodobis(1,3-dimethylimidazolin-2-ylidine)palladium(II) as the catalyst, the yield of stilbene was increased from 20% in DMF to 99% in Bu_4NBr under otherwise identical conditions. The product was separated by distillation and the catalyst containing ionic liquid recycled up to 13 times without significant loss of activity.

Seddon and coworkers[57] performed Heck couplings in bmimPF_6 or *n*-hexylpyridinium PF_6 using $PdCl_2$ or $Pd(OAc)_2$–Ar_3P as the catalyst and Et_3N or $NaHCO_3$ as the base.

For example, $Pd(OAc)_2$–Ph_3P-catalysed coupling of 4-bromoanisole with ethyl acrylate (Reaction 14) in bmimPF_6 at 140 °C, afforded ethyl 4-methoxycinnamate in 98% yield.

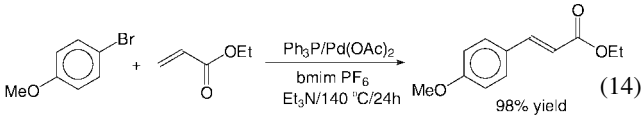

(14)

The high solubility of the catalyst in the ionic liquid allows for product isolation by extraction into a hydrocarbon, *e.g.* hexane or toluene. Furthermore, if water is added a triphasic system is obtained in which the salt formed in the reaction, Et_3NHBr, is extracted into the aqueous phase.

It was also noted that palladium complexes of imidazolylidene carbenes, formed by reaction of the base with the imidazolium cation, may be implicated in these reactions.[57]

This was later confirmed by Xiao and coworkers[58] who observed a significantly enhanced rate of the Heck coupling in bmimBr compared to the same reaction in bmimBF_4. This difference could be explained by the formation of the corresponding palladium–carbene complexes (which were isolated and characterised) in the former but not in the latter. The isolated carbene complexes were shown to be active catalysts when redissolved in bmimBr. Presumably, the formation of the carbene in bmimBr can be attributed to the stronger basicity of bromide compared to tetrafluoroborate.

The Heck arylation of electron-rich enol ethers generally leads to a mixture of regio isomers owing to competition between cationic and neutral pathways, leading to α- and β-arylation, respectively (Reaction 15). The ionic pathway is favoured with aryl triflates but these are less available and much more expensive than the corresponding chlorides and bromides. The ionic pathway would also be expected to be favoured by conducting the reaction in an ionic liquid and this proved to be the case. Thus, Xiao and coworkers[59] achieved > 99% selectivity to the α-arylation product in the Heck coupling of 1-bromonaphthalene to butyl vinyl ether in bmimBF_4 (Reaction 15). In contrast, the same reaction in toluene, acetonitrile, DMF or DMSO afforded mixtures of the α- and β-regio isomers. A range of 4-substituted bromobenzenes were similarly shown to give α-/β-regioselectivities of > 99%.

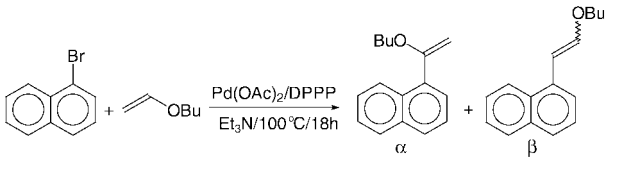

Solvent	Conv. (%)	α/β
bmim BF_4	50	> 99/1
toluene	23	46/54
acetonitrile	36	69/31
DMF	100	60/40
DMSO	100	75/25

(15)

Similarly, palladium-catalysed Stille[60a] and Negishi[60b] couplings and nickel-catalysed coupling of aryl halides[61] in $bmimBF_4$ and $bmimPF_6$, respectively, have also been described.

Palladium-catalysed allylic substitution

Palladium-catalysed allylic substitution by carbon nucleophiles constitutes another synthetically useful method for the generation of C–C bonds. These reactions have also been performed in ionic liquids, both in a mono- and biphasic system, using $Pd(OAc)_2$–Ph_3P (with K_2CO_3 as base) in $bmimBF_4$ (Reaction 16)[62] and $PdCl_2$–tppts in bmimCl–methylcyclohexane (Reaction 17),[63] respectively. In the latter case distinct advantages

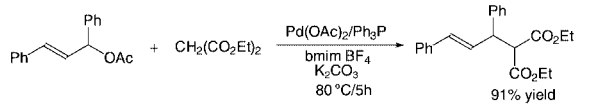

(16)

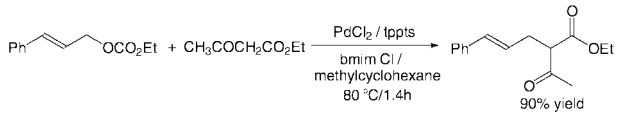

(17)

compared to the corresponding aqueous biphasic system were noted: an order of magnitude higher activity and improved selectivity owing to suppression of the competing reaction with water as a nucleophile and a much decreased phosphonium salt formation (by reaction of tppts with the Pd–allyl complex).

Reaction (16) has also been performed using chiral ferrocenylphosphine complexes of palladium, in $bmimPF_6$.[64] The product was obtained in moderate enantioselectivity (62–74% ee), which was higher than that observed in conventional solvents.

Catalytic oxidations

Considering the commercial importance of catalytic oxidations, and the fact that ionic liquids are expected to be relatively inert towards autoxidation with O_2, surprisingly little attention has been devoted to performing such reactions in ionic liquids. The $Ni(acac)_2$-catalysed aerobic oxidation of aromatic aldehydes, to the corresponding carboxylic acids, in $bmimPF_6$ has been described.[65] However, rather high (3 mol%) catalyst loadings were used and this can hardly be considered a challenging oxidation.

The methyltrioxorhenium (MTO)-catalysed epoxidation of olefins with the urea–H_2O_2 adduct (UHP) in $emimBF_4$ has been reported.[66] Both the UHP and the MTO are soluble in $emimBF_4$ and the medium remains homogeneous throughout the reaction. It should be noted, however, that the substrates were generally highly reactive olefins and when the more challenging dec-1-ene was used, a long reaction time (72 h) was needed for moderate conversion (46%) using 2 equivalents of oxidant. When 30% aq. H_2O_2 was used as the oxidant this led to ring opening of sensitive epoxides.

Asymmetric Jacobsen-Katsuki epoxidation, with NaOCl catalysed by a chiral Mn Schiff's base complex has been conducted in $bmimPF_6$.[67] However, dichloromethane was required as a cosolvent, as the ionic liquid solidifies at the reaction temperature (0 °C), which nullifies one of the primary incentives for using an ionic liquid. The ionic liquid, containing the catalyst, could be recovered and recycled 4 times albeit with a significant loss in yield.

A more recent, and very exciting development, is the electroassisted biomimetic activation of molecular oxygen by a chiral Mn Schiff's base complex in $bmimPF_6$ described by Gaillon and Bedioui.[68] Evidence was provided for the formation of the highly reactive oxomanganese(v) intermediate that could transfer its oxygen to an olefin. This would appear to offer potential for clean, electrocatalytic oxidations with molecular oxygen in ionic liquid media.

Lewis and Brønsted acid catalysis in ionic liquids

Ionic liquids containing chloroaluminate ($AlCl_4^-$, $Al_2Cl_7^-$) anions are strong Lewis acids and if protons are present they are superacidic (see earlier). Coupled with the fact that they are relatively easy to handle this makes these materials attractive non-volatile alternatives for standard Lewis acid catalysts, such as $AlCl_3$, and hazardous Brønsted acids such as HF. The ionic liquid can function as both a catalyst and a solvent for acid catalysed processes. Since Lewis and Brønsted acid-mediated processes generally involve cationic intermediates, *e.g.* carbenium and acylium ions, one would also expect to see substantial rate enhancements in ionic liquids. Indeed, some of the first reactions to be studied in ionic liquids were Friedel–Crafts alkylations and acylations. Wilkes and coworkers[69] showed that ionic liquids derived from the reaction of emimCl with $AlCl_3$ exhibit a wide range of Lewis acidity depending on the molar ratio of reactants. A 1:1 mixture affords the tetrachloroaluminate, $emimAlCl_4$, which is referred to as being neutral and is not active as a Friedel–Crafts catalyst. In contrast, the 2:1 adduct, $emimAl_2Cl_7$ is strongly acidic and was shown to be very active in Friedel–Crafts alkylations and acylations.[69] For example, a mixture of benzene, acetyl chloride and $emimAl_2Cl_7$ in the molar ratio 1.1:1.0:0.5 (*i.e.* less than a stoichiometric amount of the ionic liquid) afforded complete conversion to acetophenone in less than 5 minutes at room temperature. Spectral evidence suggested the formation of the free acylium cation, CH_3CO^+, in the ionic liquid medium.

The Friedel–Crafts alkylation of benzene with long chain α-olefins is used industrially for the manufacture of more than two million tons of linear alkylbenzenes worldwide. The products are the precursors of the corresponding alkylbenzene sulfonates which are widely used as surfactants. Traditionally the reaction is performed using liquid HF or $AlCl_3$ as the catalyst. The production of linear alkylbenzenes using chloroaluminate ionic liquids has been described.[17a] The potential to retrofit existing installations with the ionic liquid catalyst offers enormous benefits with regard to reduced catalyst consumption, ease of product separation and elimination of caustic quenching associated with catalyst leaching. Chloroaluminate ionic liquids modified with HCl were recently shown[70] to give higher rates and more favourable product distributions in Friedel–Crafts alkylations, which was attributed to the superacidities of these media. In this context it is also worth mentioning the work of Hölderich *et al.*[71] who showed that ionic liquids immobilised on inorganic supports (SiO_2, Al_2O_3, TiO_2, ZrO_2) are effective catalysts for Friedel–Crafts alkylation of aromatics. Activities

were higher than those observed with a conventional zeolite catalyst and no leaching of the ionic liquid from the surface was observed. Reactions were performed in batch, continuous liquid-phase and continuous gas-phase operation. For example, alkylation of benzene with dodecene afforded the mono-alkylated product in 98% selectivity at 99% conversion at 80 °C.

Seddon and coworkers[72] studied the Friedel–Crafts acylation of toluene, chlorobenzene and anisole with acetyl chloride in emimAl_2Cl_7 and obtained excellent regioselectivities to the *para* isomer (Reaction 18). Similarly, the fragrance chemical, traseolide, was obtained in 99% yield as a single isomer (Reaction 19). It should be noted, however, that the question of

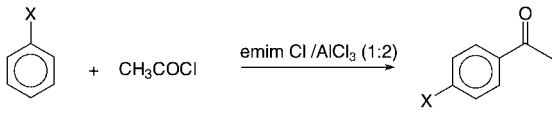

R	Temp/°C	Time/h	Yield(%)
MeO	−10	0.25	99
Me	20	1	98
Cl	20	24	97

(18)

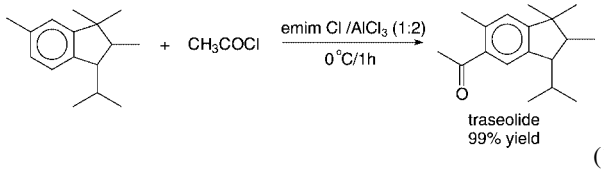

(19)

product recovery from the reaction medium still needs to be addressed in these systems. As in conventional $AlCl_3$-promoted acylations the ketone product forms a strong complex with the chloroaluminate ionic liquid.

Lanthanide triflates, in particular $Sc(OTf)_3$, have been widely studied as water-tolerant Lewis acids in a variety of transformations, including Friedel–Crafts alkylations and acylations.[73] Song and coworkers[74] have recently shown that $Sc(OTf)_3$ catalyses the Friedel–Crafts alkylation of aromatics with olefins in hydrophobic ionic liquids, *e.g.* bmimPF_6 and bmimSbF_6. In contrast, no reaction was observed in common organic solvents, water or hydrophilic ionic liquids such as bmimBF_4 or bmimOTf. For example, reaction of benzene with cyclohexene (Reaction 20) afforded cyclohexylbenzene in 92% yield at

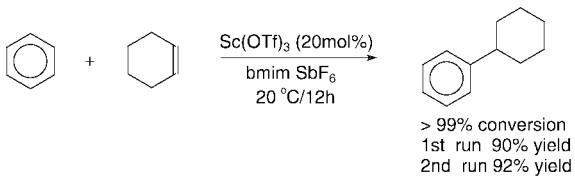

(20)

> 99% cyclohexene conversion in bmimSbF_6 at 20 °C for 12 h. The product formed a separate layer and, after phase separation, the ionic liquid phase, containing the catalyst, was recycled to afford 92% yield of cyclohexylbenzene at > 99% conversion. Although high catalyst loadings (20 mol%) were used the ease of separation and recycling of the catalyst offers potential environmental and economic benefits.

The same group has recently reported[75] that $Sc(OTf)_3$ catalyses Diels–Alder reactions in bmimX (X = BF_4, SbF_6 or OTf), in this case at much lower catalyst loadings (0.2 m%). In contrast to the Friedel–Crafts alkylation (see above) the product did not form a separate phase and was recovered by extraction with ether. It was shown, however, that the ionic liquid containing the catalyst could be recycled eleven times without loss of activity (Reaction 21). Furthermore, improved *endo*/*exo* selectivities were observed with cyclic dienes.

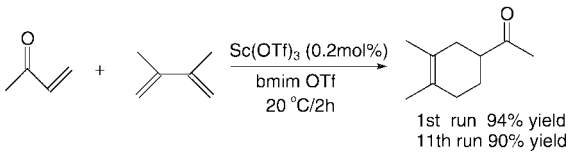

(21)

Another reaction catalysed by Lewis acids is the cycloaddition of carbon dioxide to epoxides, affording cyclic carbonates. It was recently reported that this reaction is catalysed by bmimBF_4.[76] When propene oxide was allowed to react with CO_2 (2.5 MPa) at 110 °C for 6 h in the presence of bmimBF_4 (2.5 mol%), propene carbonate was obtained in 100% yield (Reaction 22).

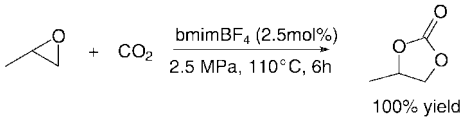

(22)

The propene carbonate was distilled from the reaction mixture and the ionic liquid catalyst recycled four times with only a minor loss in activity.

Protons in acidic ionic liquids have acidities greater than those of H_2SO_4 or liquid HF.[8,17,18] They are, for example, able to protonate benzene to the cyclohexadienyl cation. The acidic ionic liquid, bmimAl_2Cl_7, catalyses the alkylation of ethene with isobutane[18] whereas neither HF nor H_2SO_4 is effective for this reaction. The major product is 2,3-dimethylbutane (75–86%) which has a higher octane number than the products of alkylation of higher olefins. The product forms a separate upper phase and the ionic liquid is readily recycled.

Olefin oligomerisation and polymerisation is also promoted by these strongly acidic ionic liquids, *e.g.* high molecular weight polyisobutene is readily obtained from isobutene.[17] The catalytic activity and degree of polymerisation is determined by the chain length of the alkyl group in the 1-alkyl-3-methylimidazolium or *N*-alkylpyridinium cation which provides a convenient mechanism for controlling the product distribution. Polyisobutene is a commercially important lubricant and the ionic liquid process has several advantages compared with the conventional process which employs a supported or dissolved $AlCl_3$ catalyst. The polymer forms a separate phase and is readily separated and reused which obviates the need for an aqueous wash and, hence, reduces waste and costs. Moreover, the process can be easily retrofitted into existing production facilities.

The electrophilic nitration of aromatics, using a variety of nitrating agents, has also been investigated in ionic liquid solvents.[77] It was noted that nitration in ionic liquids constitutes a useful alternative to classical methods owing to easier product isolation and recovery of the ionic liquid and avoidance of problems associated with the neutralisation of large quantitities of acid.

Many synthetically important rearrangement reactions are catalysed by Brønsted or Lewis acids and, hence, may benefit from using acidic ionic liquids as solvents and/or catalysts. For example, the Beckmann rearrangement of ketoximes in ionic liquids, in the presence of catalytic amounts (20 mol%) of phosphorus compounds (*e.g.* P_2O_5) was recently reported.[78]

The ionic liquid tributylhexylammonium bis(trifluoromethylsulfonyl) amide was shown[79] to be a useful solvent for the acid-catalysed cyclotrimerisation of veratryl alcohol. The methodology obviates the need for large quantities of organic solvent and strongly dehydrating acids and provides the cyclotriveratrylene (CTV) in high yield and purity. CTV is of interest as a supramolecular host compound that complexes a variety of guest molecules.

Biocatalysis in ionic liquids

Attention has recently been focused on the use of enzymes in ionic liquids. It was already noted in 1984[80] that the enzyme alkaline phosphatase is relatively stable in a 4:1 (v/v) mixture of triethylammonium nitrate and water. More recently, Lye and coworkers[81] reported a two-phase biotransformation in which $bmimPF_6$ acts as a reservoir for the substrate while the biocatalyst—whole cells of *Rhodococcus* R312—is present in the aqueous phase. Shortly thereafter two reports of enzymatic conversions in an ionic liquid medium appeared.[82,83]

Erbeldinger *et al.*[82] reported the thermolysin-catalysed synthesis of *Z*-aspartame (Reaction 23) in $bmimPF_6$ containing

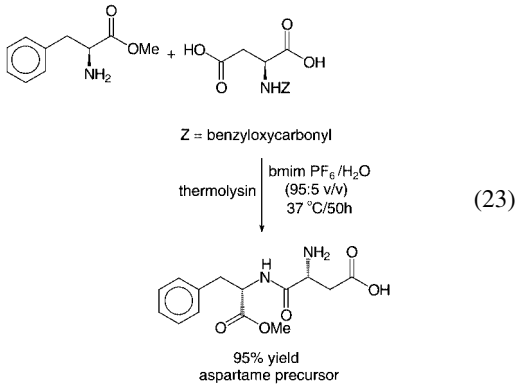

(23)

5% (v/v) water. The enzyme displayed excellent stability when suspended in the ionic liquid and the activity was equal to that observed in ethyl acetate–water. A small amount of the enzyme (< 3.2 mg mL^{-1}) which dissolved in the ionic liquid was completely inactive.

We showed[83] that *Candida antarctica* lipase is able to catalyse a variety of transformations—transesterification, ammoniolysis and perhydrolysis—in $bmimBF_4$ or $bmimPF_6$ in the absence of water. Reactions were performed with the free (NOVO SP525) or immobilized enzyme (Novozyme 435). Reaction rates were comparable with or better than those observed in conventional organic media. For example, the reaction of octanoic acid with ammonia, in $bmimBF_4$ at 40 °C, gave complete conversion to octanamide in 4 days compared to 17 days for the same conversion using ammonium carbamate in methyl isobutyl ketone.[84]

The epoxidation of cyclohexene by peroxyoctanoic acid, generated *in situ* by Novozyme 435-catalysed reaction of octanoic acid with 60% aqueous H_2O_2, proceeded smoothly in $bmimBF_4$ (Reaction 24).

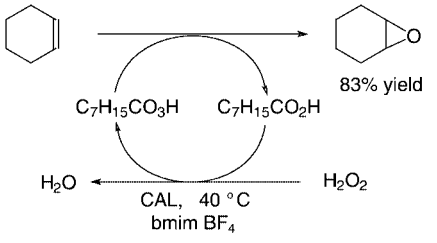

(24)

Subsequently, other groups have reported on lipase-catalysed enantioselective transesterification of chiral alcohols (Reaction 25) in ionic liquids.[85–87] Kragl and coworkers[85] investigated the

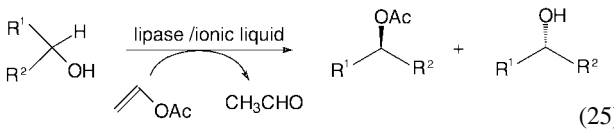

(25)

kinetic resolution of 1-phenylethanol with nine different lipases in ten different ionic liquids. Good activities and, in many cases, improved enantioselectivities were observed compared with the same reaction in MTBE (methyl *tert*-butyl ether). Rates and/or enantioselectivities were dependent on the anion as was also observed by Itoh and coworkers.[86] It was also shown that the product could be extracted with ether and the ionic liquid ($bmimPF_6$), containing the suspended enzyme, could be recycled.[86] Similarly, Kim and coworkers[87] observed markedly enhanced enantioselectivities in *Candida antarctica* and *Pseudomonas cepacia* lipase-catalysed transesterifications of chiral alcohols in $bmimBF_4$ and $bmimPF_6$.

Based on these initial studies the use of enzymes in ionic liquids would appear to open up a new field of nonaqueous enzymology. Ionic liquids could have added benefits for performing biotransformations with highly polar substrates, *e.g.* carbohydrates and amino acids, which are sparingly soluble in common organic solvents. We are currently investigating the scope with regard to type of enzyme, transformation and the effect of the structure of the ionic liquid.

Concluding remarks

Catalysis in ionic liquids is an exciting and burgeoning area of research (many of the references in this review are from 2000 and 2001) which holds considerable potential for industrial application. The use of ionic liquids as reaction media for catalytic transformations or, in some cases, as the catalyst itself can have a profound effect on activities and selectivities. Furthermore, precision tuning of reactions can be achieved by a suitable combination of cation and anion, *i.e.* they are truly 'designer solvents'. In the majority of cases studied the ionic liquid, containing the catalyst could be readily recycled. They provide a medium for performing clean reactions with minimum waste generation. As was remarked by Seddon[8] they could, quite literally, revolutionise the methodology of synthetic organic chemistry.

Notes and references

† We have adopted the abbreviations used by many (but not all) authors for dialkylimidazolium cations, *viz.*, emim for ethylmethylimidazolium, bmim for butylmethylimidazolium, *etc.*

1 A. D. Curzons, D. J. C. Constable, D. N. Mortimer and V. L. Cunningham, *Green Chem.*, 2001, **3**, 1.
2 For leading references see: R. A. Sheldon, *Pure Appl. Chem.*, 2000, **72**, 1233; R. A. Sheldon, *Chem. Ind. (London)*, 1997, 12.
3 *Aqueous Phase Organometallic Catalysis*, eds. B. Cornils and W. A. Herrmann, Wiley-VCH, Weinheim, 1998.
4 G. Papadogianakis and R. A. Sheldon, *Specialist Periodical Reports Catalysis*, Vol. 13, Senior Reporter J. J. Spivey, Royal Society of Chemistry, Cambridge, 1997, pp. 114–193.
5 I. T. Horvath and J. Rabai, *Science*, 1994, **266**, 72.
6 *Chemical Synthesis using Supercritical Carbon Fluids*, ed. P. G. Jessop and W. Leitner, VCH/Wiley, Weinheim, 1999; W. Leitner, *Top. Curr. Chem.*, 1999, **206**, 107.
7 M. Freemantle, C&EN, March 30, 1998, p. 32; May 15, 2000, p. 37; January 1, 2001, p. 21; H. Carmichael, *Chem. Brit.*, January 2000, p. 36.
8 K. Seddon, *Molten Salt Forum*, 1998, **5–6**, 53.
9 P. Walden, *Bull. Acad. Imper. Sci. (St. Petersburg)*, 1914, p. 1800; cited in S. Sugden and H. Wilkins, *J. Chem. Soc.*, 1929, p. 1291.
10 C. L. Hussey, *Adv. Molten Salt Chem.*, 1983, **5**, 185.
11 H. L. Chum, V. R. Kock, L. L. Miller and R. A. Osteryoung, *J. Am. Chem. Soc.*, 1975, **97**, 3264; J. Robinson and R. A. Osteryoung, *J. Am. Chem. Soc.*, 1979, **101**, 323.
12 J. S. Wilkes, J. A. Levinsky, R. A. Wilson and C. A. Hussey, *Inorg. Chem.*, 1982, **21**, 1263.
13 J. A. Boon, J. A. Levinsky, J. L. Pflug and J. S. Wilkes, *J. Org. Chem.*, 1986, **51**, 480.
14 J. S. Wilkes and M. J. Zaworotko, *J. Chem. Soc., Chem. Commun.*, 1992, 965.
15 J. Fuller, R. T. Carlin, H. C. De Lang and D. Haworth, *J. Chem. Soc., Chem. Commun.*, 1994, 299.
16 (*a*) P. Bonhôte, A. P. Dias, N. Papageorgiou, K. Kalyanasundaram and M. Grätzeb, *Inorg. Chem.*, 1996, **35**, 1168; (*b*) V. R. Koch, C. Nanjundiah, G. B. Appetecchi and B. Scrosati, *J. Electrochem. Soc.*, 1995, **142**, 116; (*c*) D. R. Macfarlane, J. Golding, S. Forsyth and G. B. Deacon, *Chem. Commun.*, 2001, 1430.

17 J. D. Holbrey and K. R. Seddon, *Clean Prod. Process.*, 1999, **1**, 223; K. R. Seddon, *J. Chem. Technol. Biotechnol.*, 1997, **68**, 351.
18 Y. Chauvin and H. Olivier-Bourbigou, *CHEMTECH*, September 1995, p. 26.
19 T. Welton, *Chem. Rev.*, 1999, **99**, 2071.
20 P. Wasserscheid and W. Keim, *Angew. Chem., Int. Ed.*, 2000, **39**, 3772.
21 J. G. Huddleston, A. E. Visser, W. M. Reichert, H. D. Willauer, G. A. Broker and R. D. Rogers, *Green Chem.*, 2001, **3**, 156; see also S. V. Dzyuba and R. A. Bartsch, *Chem. Commun.*, 2001, 1466.
22 T. L. Merrigan, E. D. Bates, S. C. Dorman and J. H. Davis, *Chem. Commun.*, 2000, 2051.
23 G. P. Smith, A. S. Dworkin, R. M. Pagni and S. P. Zingg, *J. Am. Chem. Soc.*, 1989, **111**, 525.
24 L. A. Blanchard, D. Hancu, E. J. Beckman and J. F. Brennecke, *Nature*, 1999, **399**, 28; L. A. Blanchard and J. F. Brennecke, *Ind. Eng. Chem. Res.*, 2001, **40**, 287.
25 G. W. Parshall, *J. Am. Chem. Soc.*, 1972, **94**, 8716.
26 Y. Chauvin, L. Mussman and H. Olivier, *Angew. Chem., Int. Ed. Engl.*, 1995, **34**, 2698.
27 P. A. Z. Suarez, J. E. L. Dullins, S. Einloft, R. F. de Souza and J. Dupont, *Polyhedron*, 1996, **15**, 1217.
28 P. A. Z. Suarez, J. E. L. Dullins, S. Einloft, R. F. de Souza and J. Dupont, *Inorg. Chim. Acta*, 1997, **255**, 207.
29 S. Steines, B. Drießen-Hölscher and P. Wasserscheid, *J. Prakt. Chem.*, 2000, **342**, 348.
30 P. J. Dyson, D. J. Ellis, D. G. Parker and T. Welton, *Chem. Commun.*, 1999, 25.
31 A. L. Monteiro, F. K. Zinn, R. F. de Souza and J. Dupont, *Tetrahedron: Asymmetry*, 1997, **8**, 177.
32 F. Liu, M. B. Abrams, R. T. Baker and W. Tumas, *Chem. Commun.*, 2001, 433.
33 R. A. Brown, P. Pollet, E. McKoon, C. A. Eckert, C. L. Liotta and P. G. Jessop, *J. Am. Chem. Soc.*, 2001, **123**, 1254.
34 R. Noyori, *Asymmetric Catalysis in Organic Synthesis*, Wiley, New York, 1994.
35 E. G. Kuntz, *CHEMTECH*, 1987, 570.
36 H. Waffenschmidt and P. Wasserscheid, *J. Mol. Catal. A: Chemical*, 2000, **164**, 61.
37 J. F. Knifton, *J. Mol. Catal.*, 1987, **43**, 65.
38 N. Karodia, S. Guise, C. Newlands and J. A. Anderson, *Chem. Commun.*, 1998, 2341.
39 C. Brasse, U. Englert, A. Salzer, H. Waffenschmidt and P. Wasserscheid, *Organometallics*, 2000, **19**, 3818.
40 P. Wasserscheid, H. Waffenschmidt, P. Machnitzki, K. W. Kottsieper and O. Steltzer, *Chem. Commun.*, 2001, 451.
41 P. W. N. M. van Leeuwen, P. C. J. Kamer, J. N. H. Reek and P. Dierkes, *Chem. Rev.*, 2000, 100.
42 F. Favre, H. Olivier-Bourbigou, D. Commereuc and L. Saussine, *Chem. Commun.*, 2001, 1360.
43 M. F. Sellin, P. B. Webb and D. J. Cole-Hamilton, *Chem. Commun.*, 2001, 781.
44 W. Keim, D. Vogt, H. Waffenschmidt and P. Wasserscheid, *J. Catal.*, 1999, **186**, 481.
45 D. Zim, R. F. de Souza, J. Dupont and A. L. Monteiro, *Tetrahedron Lett.*, 1998, **39**, 7071.
46 E. Mizushima, T. Hayashi and M. Tanaka, *Green Chem.*, 2001, **3**, 76.
47 Y. Chauvin, B. Gilbert and I. Guibard, *J. Chem. Soc., Chem. Commun.*, 1990, 1715.
48 Y. Chauvin, S. Einloft and H. Olivier, *Ind. Eng. Chem. Res.*, 1995, **34**, 1149.
49 Y. Chauvin, H. Olivier, C. N. Wyrvalski, L. C. Simon and R. F. de Souza, *J. Catal.*, 1997, **165**, 275; see also L. C. Simon, J. Dupont and R. F. de Souza, *J. Mol. Catal.*, 1998, **175**, 215.
50 B. Ellis, W. Keim and P. Wasserscheid, *Chem. Commun.*, 1999, 337.
51 P. Wasserscheid, C. M. Gordon, C. Hilgers, M. J. Muldoon and I. R. Dunkin, *Chem. Commun.*, 2001, 1186.
52 S. M. Silva, P. A. Z. Suarez, R. F. de Souza and J. Dupont, *Polymer Bull.*, 1998, **40**, 401.
53 J. E. L. Dullins, P. A. Z. Suarez, S. Einloft, R. F. de Souza, J. Dupont, J. Fischer and A. De Cian, *Organometallics*, 1998, **17**, 815.
54 For a recent review see: I. P. Beletskaya and A. V. Cheprakov, *Chem. Rev.*, 2000, **100**, 3009.
55 D. E. Kaufmann, M. Nouroozian and H. Henze, *Synlett*, 1996, 1091.
56 W. A. Herrmann and V. P. W. Böhm, *J. Organometal. Chem.*, 1999, **572**, 141; V. P. W. Böhm and W. A. Herrmann, *Chem. Eur. J.*, 2000, **6**, 1017.
57 A. J. Carmichael, M. J. Earle, J. D. Holbrey, P. B. McCormac and K. R. Seddon, *Org. Lett.*, 1999, **1**, 997.
58 L. Xu, W. Chen and J. Xiao, *Organometallics*, 2000, **19**, 1123.
59 L. Xu, W. Chen, J. Ross and J. Xiao, *Org. Lett.*, 2001, **3**, 295.
60 (*a*) S. T. Handy and X. Zhang, *Org. Lett.*, 2001, **3**, 233; (*b*) L. Sirieix, M. Ossberger, P. Betzmeier and P. Knochel, *Synlett*, 2000, 1613.
61 J. Howarth, P. James and J. Dai, *Tetrahedron Lett.*, 2000, **41**, 10 319.
62 W. Chen, L. Xu, C. Chatterton and J. Xiao, *Chem. Commun.*, 1999, 1247; L. Ross, W. Chen, L. Xu and L. Mao, *Organometallics*, 2001, **20**, 138.
63 C. de Bellefon, E. Pollet and P. Grenouillet, *J. Mol. Catal. A: Chemical*, 1999, **145**, 121.
64 S. Toma, B. Gotov, I. Kmentova and E. Solcaniova, *Green Chem.*, 2000, **2**, 151.
65 J. Howarth, *Tetrahedron Lett.*, 2000, **41**, 6627.
66 G. S. Owens and M. M. Abu-Omar, *Chem. Commun.*, 2000, 1165.
67 C. E. Song and E. J. Roh, *Chem. Commun.*, 2000, 837.
68 L. Gaillon and F. Bedioui, *Chem. Commun.*, 2001, 1458.
69 J. A. Boon, J. A. Levisky, J. L. Pflug and J. S. Wilkes, *J. Org. Chem.*, 1986, **51**, 480.
70 K. Qiao and Y. Deng, *J. Mol. Catal. A: Chemical*, 2001, **171**, 81.
71 C. DeCastro, E. Sauvage, M. H. Valkenberg and W. F. Hölderich, *J. Catal.*, 2000, **196**, 86.
72 C. J. Adams, M. J. Earle, G. Roberts and K. R. Seddon, *Chem. Commun.*, 1998, 2097.
73 For reviews see: S. Kobayashi, *Synlett*, 1994, 689; S. Kobayashi, *Eur. J. Org. Chem.*, 1999, 15.
74 C. E. Song, W. H. Shim, E. J. Roh and J. H. Choi, *Chem. Commun.*, 2000, 1695.
75 C. E. Song, W. H. Shim, E. J. Roh, S. Lee and J. H. Choi, *Chem. Commun.*, 2001, 1122.
76 J. Peng and Y. Deng, *New J. Chem.*, 2001, **25**, 639.
77 K. K. Laali and V. J. Gettwert, *J. Org. Chem.*, 2001, **66**, 35.
78 J. Peng and Y. Deng, *Tetrahedron Lett.*, 2001, **42**, 403.
79 J. L. Scott, D. R. MacFarlane, C. L. Raston and C. M. Teoh, *Green Chem.*, 2000, **2**, 123.
80 D. K. Magnusson, J. W. Bodley and D. F. Adams, *J. Sol. Chem.*, 1984, **13**, 583.
81 S. G. Cull, J. D. Holbrey, V. Vargas-Mora, K. R. Seddon and G. J. Lye, *Biotechnol. Bioeng.*, 2000, **69**, 227; for a related study see: A. G. Fadeev and M. M. Meagher, *Chem. Commun.*, 2001, 295.
82 M. Erbeldinger, A. J. Mesiano and A. J. Russell, *Biotechnol. Progr.*, 2000, **16**, 1131.
83 R. Madeira Lau, F. van Rantwijk, K. R. Seddon and R. A. Sheldon, *Org. Lett.*, 2000, **2**, 4189.
84 M. J. J. Litjens, A. J. J. Straathof, J. A. Jongejan and J. J. Heijnen, *Chem. Commun.*, 1999, 1255.
85 S. H. Schofer, N. Kaftzik, P. Wasserscheid and U. Kragl, *Chem. Commun.*, 2001, 425.
86 T. Itoh, E. Akasaki, K. Kudo and S. Shirakami, *Chem. Lett.*, 2001, 262.
87 K. W. Kim, B. Song, M. Y. Choi and M. J. Kim, *Org. Lett.*, 2001, **3**, 1507.

CHEMCOMM
Communication
www.rsc.org/chemcomm

A surprisingly mild and versatile method for palladium-catalyzed Suzuki cross-couplings of aryl chlorides in the presence of a tri*aryl*phosphine†

Shih-Yuan Liu, Michael J. Choi and Gregory C. Fu*

Department of Chemistry, Massachusetts Institute of Technology, Cambridge, Massachusetts 02139 USA. E-mail: gcf@mit.edu

Received (in Corvallis, OR, USA) 30th August 2001, Accepted 21st September 2001
First published as an Advance Article on the web 8th November 2001

In the presence of new air-stable triarylphosphine 2, palladium-catalyzed Suzuki reactions of a wide array of aryl chlorides can be accomplished in uniformly good yield, including couplings of very sterically demanding and electronically deactivated substrates; activated aryl chlorides can be coupled at room temperature. In terms of scope and mildness, Pd–2 compares well with other catalyst systems that have been described for Suzuki reactions of aryl chlorides, thereby establishing that triarylphosphines should be regarded as fertile ground for future ligand-design efforts for palladium-catalyzed couplings of aryl chlorides.

The palladium-catalyzed cross-coupling of organic halides/triflates with organoboron reagents [Suzuki reaction; *e.g.*, eqn. (1)] is a powerful and widely used method for carbon–carbon

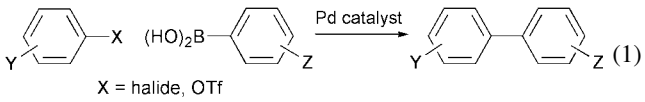

(1)

bond formation.[1] Until recently, aryl chlorides, an attractive class of substrates due to their low cost and ready availability,[2] were generally not suitable coupling partners in palladium-catalyzed Suzuki reactions.[3] However, during the past few years this deficiency has been remedied through the use of ligands such as electron-rich, sterically hindered phosphines[4] and carbenes.[5,6]

The low reactivity of aryl chlorides in palladium-catalyzed coupling reactions is often ascribed to their reluctance to oxidatively add to palladium, and the unusual effectiveness of strongly electron-donating ligands in achieving Suzuki cross-couplings of aryl chlorides is consistent with this hypothesis. Thus, at the time that we initiated our studies, there were no examples of Suzuki reactions of unactivated aryl chlorides by palladium catalysts that bear tri*aryl*phosphines,[7,8] which are generally significantly less electron-rich than tri*alkyl*phosphines.

In this communication, we describe our discovery that a wide array of palladium-catalyzed Suzuki reactions of aryl chlorides can be achieved through the use of a new ferrocene-derived triarylphosphine (**2**). In the presence of this air-stable, sterically demanding ligand, we can effect the Suzuki cross-coupling of activated aryl chlorides at rt, and we can accomplish reactions of unactivated aryl chlorides, including sterically hindered and electron-rich substrates, at 70 °C.

Phosphine **1**, previously reported by Price and Simpkins,[9] serves as a moderately efficient ligand for the palladium-catalyzed coupling of *p*-chlorotoluene with *o*-tolylboronic acid (37% yield by GC after 24 h at 70 °C; Table 1, entry 1). An increase in the steric demand of the bottom ring of the ligand (Cp → Cp*; **2**) leads to a substantial increase in reactivity (entry 2 *vs.* entry 1).[10] The TMS group is an important contributor to

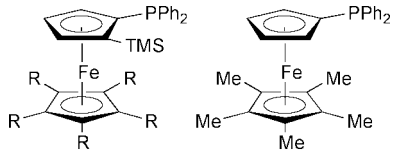

the unusual reactivity of **2**, as demonstrated by the slow coupling that we observe when we employ the corresponding non-silylated ligand (**3**; entry 3). Entry 4 establishes that PPh_3 is not useful under these conditions.

New triarylphosphine **2**, which is air- and moisture-stable both in the solid state and in solution, serves as a remarkably versatile ligand for Suzuki cross-couplings of aryl chlorides. As shown in Table 2, a variety of chlorides, including hindered (entries 2–5) and electronically deactivated (entry 6) ones, react with a range of boronic acids in very good yield. The sterically demanding coupling that is illustrated in entry 5, which furnishes a tri-*ortho*-substituted biaryl in 93% yield, is especially worthy of note.[11,12]

We have determined that, in the presence of triarylphosphine **2**, Suzuki cross-couplings of activated aryl chlorides can be accomplished at rt. To date, only a few other ligands have achieved this objective.[13] For room-temperature couplings, use of $Pd(OAc)_2$ as the palladium source and an ~1:1 ratio of Pd:ligand provide the highest reactivity among the conditions that we have examined. With these conditions, we can effect Suzuki cross-couplings of a range of activated aryl chlorides, including heteroaryl (entry 2) and *ortho*-substituted (entry 3) substrates, with arylboronic acids in excellent yield (Table 3).

In summary, we have prepared a new, air-stable triarylphosphine (**2**), and we have established that it serves as an

Table 1 Suzuki reaction of an unactivated aryl chloride: triarylphosphines as ligands

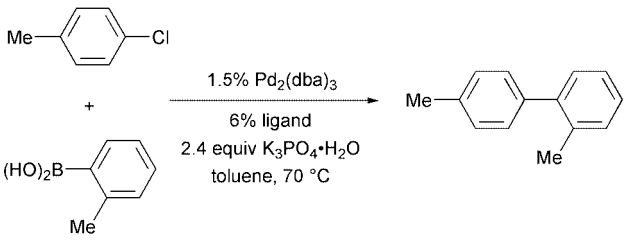

Entry	Ligand	% Yield by GC after 24 h[a]
1	**1**	37
2	**2**	87
3	**3**	8
4	PPh_3	< 2

[a] Average of two runs.

† Electronic supplementary information (ESI) available: experimental procedures and compound characterization data. See http://www.rsc.org/suppdata/cc/b1/b107888g/

 DOI: 10.1039/b107888g

Table 2 Scope of the Suzuki reaction of unactivated aryl chlorides catalyzed by Pd–triarylphosphine **2**

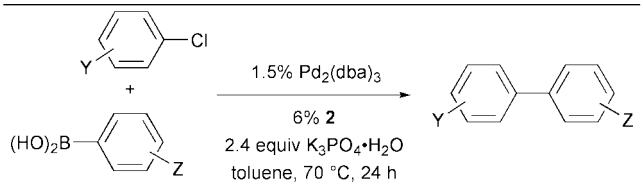

Entry	Aryl chloride	Arylboronic acid	Isolated yield[a]
1	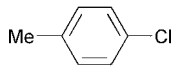	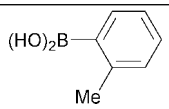	90%
2	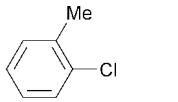	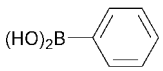	86%
3	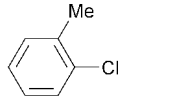	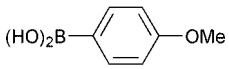	82%
4	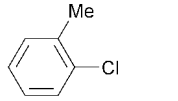	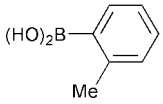	95%
5	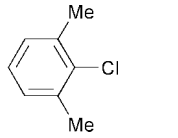	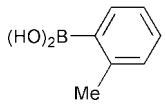	93%
6	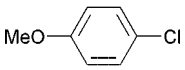	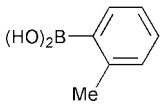	88%

[a] Average of two runs.

Table 3 Suzuki reaction of activated aryl chlorides at room temperature

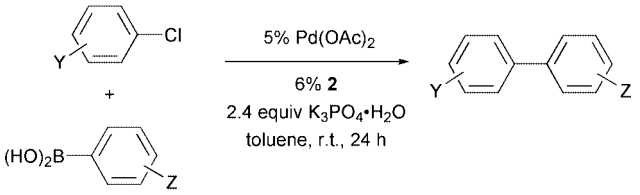

Entry	Aryl chloride	Arylboronic acid	Isolated yield[a]
1	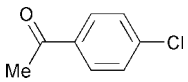	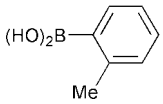	89%
2	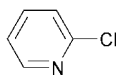	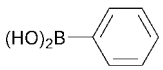	93%
3	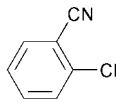	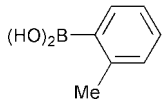	95%

[a] Average of two runs.

effective ligand in palladium-catalyzed Suzuki couplings of aryl chlorides. In the presence of Pd–**2**, a diverse array of substrates, including hindered, heteroaryl, and electronically deactivated chlorides, react in uniformly good yield. The ability of this system to achieve cross-couplings of activated aryl chlorides at rt is particularly noteworthy. Because **2** is a tri*aryl*phosphine, the high reactivity of Pd–**2** (in terms of scope and mildness, comparable to sterically demanding trialkylphosphines and greater than carbene ligands) is unexpected. In view of the ease with which the structure of **2** can be modified, we anticipate that further enhancements in reactivity will be possible, as well as the design of effective ligands for asymmetric catalysis.

Support has been provided by Bristol-Myers Squibb, Merck, the National Institutes of Health (National Institute of General Medical Sciences, R01-GM62871), Novartis, and Pfizer. We thank Frontier Scientific for donating arylboronic acids.

Notes and references

1 For reviews, see: N. Miyaura and A. Suzuki, *Chem. Rev.*, 1995, **95**, 2457; A. Suzuki, *J. Organomet. Chem.*, 1999, **576**, 147; N. Miyaura, in *Advances in Metal-Organic Chemistry*, ed. L. S. Liebeskind, JAI, London, 1998, Vol. 6, pp. 187–243; A. Suzuki, in *Metal-Catalyzed Cross-Coupling Reactions*, ed. F. Diederich, P. J. Stang, Wiley-VCH, New York, 1998, Chapter 2.

2 For a general discussion, see: V. V. Grushin and H. Alper, *Chem. Rev.*, 1994, **94**, 1047; R. Stürmer, *Angew. Chem., Int. Ed.*, 1999, **38**, 3307.

3 For an overview, see: A. F. Littke, C. Dai and G. C. Fu, *J. Am. Chem. Soc.*, 2000, **122**, 4020.

4 For early work, see: (*a*) D. W. Old, J. P. Wolfe and S. L. Buchwald, *J. Am. Chem. Soc.*, 1998, **120**, 9722; J. P. Wolfe, R. A. Singer, B. H. Yang and S. L. Buchwald, *J. Am. Chem. Soc.*, 1999, **121**, 9550; (*b*) A. F. Littke and G. C. Fu, *Angew. Chem., Int. Ed.*, 1998, **37**, 3387, ref. 3; (*c*) X. Bei, H. W. Turner, W. H. Weinberg, A. S. Guram and J. L. Petersen, *J. Org. Chem.*, 1999, **64**, 6797.

5 For early work, see: W. A. Herrmann, C.-P. Reisinger and M. Spiegler, *J. Organomet. Chem.*, 1998, **557**, 93; T. Weskamp, V. P. W. Bohm and W. A. Herrmann, *J. Organomet. Chem.*, 1999, **585**, 348; C. Zhang, J. Huang, M. L. Trudell and S. P. Nolan, *J. Org. Chem.*, 1999, **64**, 3804.

6 For other early work, see: F. Firooznia, C. Gude, K. Chan and Y. Satoh, *Tetrahedron Lett.*, 1998, **39**, 3985. See also: G. Y. Li, *Angew. Chem., Int. Ed.*, 2001, **40**, 1513.

7 For a single example of a Suzuki coupling of an *activated* aryl chloride by a Pd–triarylphosphine catalyst, see: P. Kocovsky, S. Vyskocil, I. Cisarova, J. Sejbal, I. Tislerova, M. Smrcina, G. C. Lloyd-Jones, S. C. Stephen, C. P. Butts, M. Murray and V. Langer, *J. Am. Chem. Soc.*, 1999, **121**, 7714.

8 As our investigation was nearing completion, Richards described one Suzuki coupling of an unactivated aryl chloride (*p*-chlorotoluene) and one reaction of an activated aryl chloride (*p*-chloronitrobenzene) that proceed in good yield by GC at 60 °C, using a Pd–tris(2-methylferrocenyl)phosphine catalyst: T. E. Pickett and C. J. Richards, *Tetrahedron Lett.*, 2001, **42**, 3767. This catalyst furnishes modest yields in couplings of deactivated and *ortho*-substituted aryl chlorides (< 50% by GC).

9 D. Price and N. S. Simpkins, *Tetrahedron Lett.*, 1995, **36**, 6135.

10 For a related observation of a change in reactivity upon conversion of a remote Cp group to a C_5Ph_5 group, see: Q. Shelby, N. Kataoka, G. Mann and J. Hartwig, *J. Am. Chem. Soc.*, 2000, **122**, 10 718.

11 Suzuki cross-couplings that efficiently generate tri-*ortho*-substituted biaryls are very uncommon, especially with aryl chlorides as substrates. For a discussion, see ref. 3.

12 This catalyst system is also very active for Suzuki reactions of aryl bromides. For example, in the presence of 0.25% Pd_2dba_3–0.5% **2**, the cross-coupling of 2-bromo-*m*-xylene with *o*-tolylboronic acid proceeds in 99% isolated yield after 24 h at rt. To the best of our knowledge, only P(*t*-Bu)$_3$ has been shown to effect a room-temperature Suzuki reaction of an unactivated aryl bromide to generate a tri-*ortho*-substituted biaryl (ref. 3).

13 Only Buchwald's aryldialkylphosphines are effective for room-temperature couplings of unactivated aryl chlorides: ref. 4*a*. See also: ref. 4*b* (six examples); D. Zim, A. L. Monteiro and J. Dupont, *Tetrahedron Lett.*, 2000, **41**, 819 (two examples); P. Kocovsky, S. Vyskocil, I. Cisarova, J. Sejbal, I. Tislerova, M. Smrcina, G. C. Lloyd-Jones, S. C. Stephen, C. P. Butts, M. Murray and V. Langer, *J. Am. Chem. Soc.*, 1999, **121**, 7714 (one example).

CHEMCOMM Communication
www.rsc.org/chemcomm

Linear dichroism for the detection of single base pair mutations†

David J. Halsall,[a] Alison Rodger*[b] and Timothy R. Dafforn[c]

[a] *Department of Clinical Biochemistry, Addenbrooke's Hospital, Hills Rd, Cambridge, UK CB2 2XY*
[b] *Department of Chemistry, University of Warwick, Coventry, UK CV4 7AL. E-mail: a.rodger@warwick.ac.uk; Fax: (+44) 24 76524112*
[c] *Department of Haematology, Cambridge Institute of Medical Research, Wellcome Trust/MRC Building, Hills Rd, Cambridge, UK CB2 2XY*

Received (in Cambridge, UK) 30th August 2001, Accepted 8th October 2001
First published as an Advance Article on the web 8th November 2001

Flow linear dichroism is shown to be able to detect single base mismatches in a polymerase chain reaction (PCR) amplimers from exon 10 of the human β-glucocerebrosidase gene (associated with Gaucher disease) over a kilobase long with no post PCR manipulation.

The need to detect sequence variations in human genes has increased with the continuing identification of disease-causing mutations and the use of DNA polymorphisms, especially single nucleotide polymorphisms (SNPs), to assist genetic mapping strategies.[1] Despite improvements in technologies available for detecting and identifying SNPs, all suffer from either expense (reagents and time) or low sensitivity/accuracy.[2–6] We aimed to identify an inherent optical signal from DNA that is sensitive to distortions in DNA structure, and to demonstrate that this signal can be used to detect point mutations in PCR products. Existing absorbance (on thermal denaturation) and circular dichroism methods are of value for oligonucleotides,[7,8] but not for polynucleotides (100's of bases). Here we present data describing the use of flow linear dichroism[8,9] (LD) to detect structural distortions caused by mismatching of base pairs in DNA helices.

An LD signal is produced by measuring the difference in absorbance of light linearly polarised parallel and perpendicular to an orientation direction. LD signals are positive for transitions whose polarization is along the direction of orientation and negative for those perpendicular to it. In this case, the dichroic signal is generated by aligning DNA fragments in solution by induced laminar flow. The signal from the π–π* transitions of the DNA bases is expected to be negative as the bases lie more perpendicular than parallel to the DNA helix axis which is also the orientation axis. However, an additional factor that must be considered when analysing the data below is that all absorbance spectroscopic measurements involve measuring what light the sample causes not to reach the photomultiplier tube. These are a combination of true absorbance and apparent absorbance—scattering. In most cases the true absorbance dominates the scattering effects as is the case for calf thymus DNA linear dichroism. However, with the PCR products that form the subject of this paper, the total LD signal is three orders of magnitude smaller than with the calf thymus DNA so the scattering effect dominates. With flow LD the scattering effect is always positive.[10]

In this study we have used two mutations within the human gene β-glucocerebrosidase that are associated with Gaucher disease. These mutations were found in 32/92 and 15/92 alleles respectively from UK patients diagnosed with Gaucher disease.[11] This large, clinically relevant, gene spans 7 kilo bases of genomic DNA and is comprised of 11 exons. At least 138 different types of mutation have been found to be associated with Gaucher disease, and the UK population is particularly heterogeneous for these. DNA-based diagnosis and family screening for this disease is currently limited by available methodology.

Genomic DNA was prepared from peripheral leucocytes of patients previously confirmed to be a compound heterozygote (h1/h2) for the L444P and R463C point mutations (A to C and G to T, see Fig. S1 ESI for full details) in the β-glucocerebrosidase gene (Entrez AF023268), from patients heterozygous for each mutation (h1/wt and h2/wt), and a control without either mutation (wt/wt), using conventional methods.[12] A 1353 bp amplimer encompassing these mutations was generated by PCR. Mutations were confirmed using restriction digestion and cycle sequencing (ABI big dye cycle sequencing reagents and an ABI 310 capillary zone sequencer) using the previously published primers and methods.[11]

Heteroduplexes were generated by re-heating each PCR reaction to 95 °C for 5 min, incubating at 72 °C for 20 min and allowing to cool to 25 °C over 3 h. As the patients were heterozygous for these mutations heteroduplices of each mutant (h1/wt and h2/wt) with the normal sequence were produced from the single heterozygous patients and a heteroduplex containing two mismatches (h1/h2) from the compound heterozygous patient.

The LD spectra of the samples were measured using a JASCO J-715 spectropolarimeter. The sample was aligned within the light beam using a custom made stirred cell.[13] The stirred cell consists of a cylindrical cross section stainless steel sleeve with opposing quartz apertures embedded in the cylinder walls. A cylinder of quartz is mounted centrally (with a 0.5 mm annular gap) with respect to its circular face on a rotating spindle within the sleeve. The speed of rotation of the spindle and hence the quartz cylinder is controlled electronically to allow the sample solution to be maintained with the highest possible degree of alignment without inducing turbulent flow. LD measurements were made directly in PCR buffer. The signals derived from the PCR amplimers are corrected for concentration, as determined by PICO green binding (Molecular Probes, Oregon), and are directly comparable (50 μg mL^{-1}); the calf thymus DNA (Sigma) was at a concentration of 300 μM (determined using the extinction coefficient at 258 nm of 6600 cm^{-1} mol^{-1} dm^3).

LD spectra of wt/wt, h1/wt, h2/wt and h1/h2 are shown in Fig. 1a. All 4 samples showed a negative maximum of similar magnitude at 260 nm that is characteristic of the signal from the lowest energy π–π* transitions of the DNA bases when the bases are oriented approximately perpendicular[14] to the DNA helix axis. The spectra of the short PCR amplimers also show *positive* maxima at 230 nm that is of a greater magnitude relative to the 260 nm band and of a different sign from the LD signal of the much larger DNA fragments obtained from calf thymus (Fig. 1b). The amplitudes of the 230 nm peak observed from the PCR derived amplimers show a trend related to the number of mismatched base pairs in each sample, h1/h2 having the lowest amplitude. Upon addition of 50% glycerol to the DNAs to increase the sample viscosity, the flow orientation increases the true absorbance LD signal by an order of

† Electronic supplementary information (ESI) available: Figures S1–S4. See http://www.rsc.org/suppdata/cc/b1/b107830p/

 DOI: 10.1039/b107830p

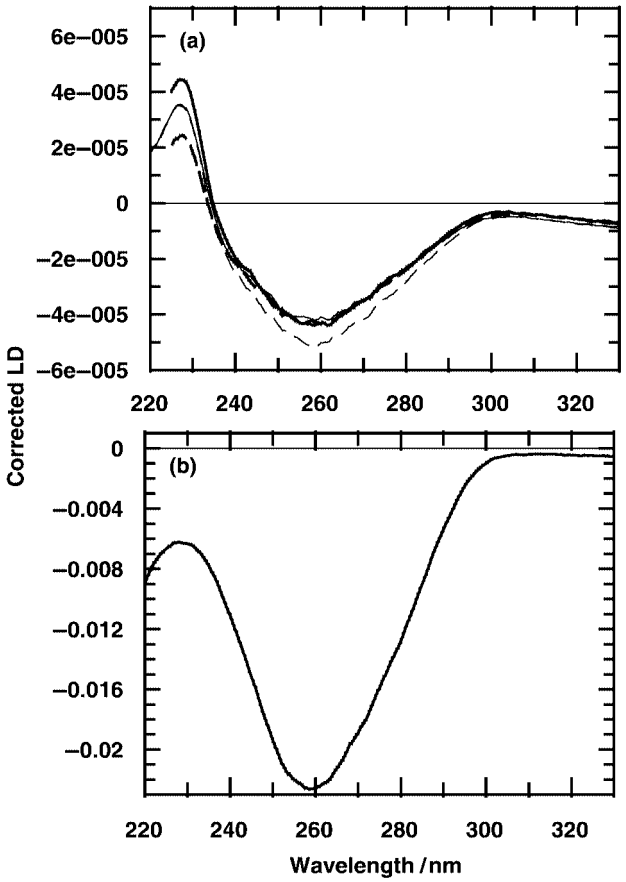

Fig. 1 (a) Flow LD spectra of wt/wt (*thick solid line*), h1/wt (*thin solid line*), h2/wt (*thin dashed line*), and h1/h2 (*thick dashed line*) at 50 μg mL^{-1} in Bio-extract PCR buffer at 1750 rpm. The maximum at 230 nm changes in intensity with respect to the number of mis-matches present. (b) Flow LD spectra of Calf thymus DNA. Corrected LD denotes the signal is corrected for concentration differences. The units for the LD are the absorbance readings directly from the instrument. Pathlength is 1 mm.

magnitude making LD absorbance signal dominant over the scattering signal (see Fig. S2 ESI). Residual primers have no LD signal and the starting genomic DNA sequence has an incredibly small (2–3 orders of magnitude smaller than the PCR products) signal (data not shown). The effect of flow rate is given in Figs. S3 and S4 of the ESI.

The effect of single base pair mismatches on the conformation of linear sections of DNA is most likely due to induced local flexibility around the mismatched region. Existing techniques for detecting single mutations such as Differential Gradient Gel Electophoresis[3] and denaturing HPLC[4] rely on the fact that the local disruption in structure is propagated through the DNA molecule and effects hydrodynamic behaviour. The limitation of these techniques is that as the length of the DNA molecule increases the difference in behaviour of the mismatched and complementary DNA is reduced. By way of contrast our data show that linear dichroism relies on changes in hydrodynamic properties having an effect on the spectroscopy of the DNA itself. We have demonstrated that, although the 260 nm minimum is essentially unaffected by base pair mismatches, the amplitude of the maximum at 230 nm is sensitive to such changes and these can be detected in a DNA amplimer of greater than a kilobase in length. This exceeds the length at which previous techniques have been shown to be effective.

As 230 nm corresponds to an absorbance minimum for DNA and we see a positive maximum in the LD signal, these observations imply that light scattering is dominating the 230 nm signal whereas at 260 nm the intrinsic LD signal dominates the scattering. The intensity of the 230 nm signals is therefore dominated by the volume of the DNA. wt/wt is largest and h1/h2 the smallest. If the 230 nm signals are normalised by dividing by the 260 nm signal we have:

$$LD_{230\ nm}: \text{wt/wt} > \text{h1/wt} > \text{h2/wt} > \text{h1/h2}$$

The h1 mutation involves replacing an A:T base pair with C:T which could retain two hydrogen bonds if the helix were pulled in. The h2 mutation can retain at most one hydrogen bond and needs to accommodate an extra N–H bond within the base-pairing region. These differences presumably result in h1/wt being stiffer than h2/wt (so having a larger intrinsic LD) and less bent (so having a larger scattering term).

Increasing the viscosity of the sample also has the effect of increasing alignment of the DNA molecules, so increasing the intrinsic LD signal. The heteroduplex and homoduplex DNA appear equivalent in glycerol, the increased viscosity overriding the differences in flexibility seen in less viscous solutions and the larger LD signal swamps the scattering effects.

These data provide evidence for the exciting prospect that LD spectroscopy may be a powerful tool for use as a pre-screen to detect base pair mis-matches, and even distinguishing different mismatches, in comparatively long pieces of DNA. The major advantage of this technique is that it exploits an inherent optical property in combination with the hydrodynamic properties of the DNA helix. This allows the information derived from LD spectra to be less dependent on the length of the DNA (and may even be enhanced for longer DNAs in contrast to other techniques) and hence allows the possibility that the technique will be applicable to whole gene searches. These experiments were deliberately designed to use PCR products directly demonstrating that no post-amplification modification is necessary. For these particular mutations no other technique can distinguish between these disease-causing mutations so efficiently. How widely applicable this technique is to other mutations awaits the results of further studies.

Notes and references

1 P. Y. Kwok and Z. J. Gu, *Mol. Med. Today*, 1999, **5**, 538.
2 M. Orita, H. Iwahana, H. Kanazawa, K. Hayashi and T. Sekiya, *Proc. Natl. Acad. Sci. U.S.A.*, 1989, **86**, 2766.
3 R. M. Myers, T. Maniatis and L. S. Lerman, *Methods Enzymol.*, 1987, **155**, 501.
4 W. Liu, D. I. Smith, K. J. Rechtzigel, S. N. Thibodeau and C. D. James, *Nucleic Acids Res.*, 1998, **26**, 396.
5 A. Lambrinakos, K. E. Humphrey, J. J. Babon, T. P. Ellis and R. G. H. Cotton, *Nucleic Acids Res.*, 1999, **27**, 1866.
6 T. P. Ellis, K. E. Humphrey, M. J. Smith and R. G. H. Cotton, *Hum. Mutat.*, 1998, **11**, 345.
7 R. Lyng, A. Rodger and B. Nordén, *Biopolymers*, 1992, **32**, 1201.
8 B. Nordén, M. Kubista and T. Kurucsev, *Q. Rev. Biophys.*, 1992, **25**, 51.
9 A. Rodger and B. Nordén, *Circular dichroism and linear dichroism*, Oxford University Press, Oxford, 1997.
10 M. Ardhammar, N. Mikati and B. Nordén, *J. Am. Chem. Soc.*, 1998, **120**, 9957.
11 C. E. Hatton, A. Cooper, C. Whitehouse and J. E. Wraith, *Arch. Dis. Child.*, 1997, **77**, 17.
12 S. A. Miller, D. D. Dykes and H. F. Polesky, *Nucleic Acids Res.*, 1988, **16**, 1215.
13 A. Rodger, *Methods Enzymol.*, 1993, **226**, 232.
14 P. J. Chou and W. C. Johnson, *J. Am. Chem. Soc.*, 1993, **115**, 1205.

CHEMCOMM Communication
www.rsc.org/chemcomm

Visible light-induced photoepoxidation of propene by molecular oxygen over chromia–silica catalysts

Chizu Murata, Hisao Yoshida* and Tadashi Hattori

Department of Applied Chemistry, Graduate School of Engineering, Nagoya University, Nagoya 464-8603, Japan. E-mail: yoshidah@apchem.nagoya-u.ac.jp

Received (in Cambridge, UK) 5th September 2001, Accepted 9th October 2001
First published as an Advance Article on the web 8th November 2001

Highly dispersed chromate species on silica catalyse the selective epoxidation of propene to propene oxide (PO) by molecular oxygen under visible light irradiation with the same quantum yield as that under UV light irradiation.

Currently propene epoxidation is performed by two liquid phase processes: the chlorohydrin process and the hydroperoxide process.[1] These processes have some problems of by-products, wastes, *etc*. The direct gas phase epoxidation of propene by molecular oxygen, which is the most simple process without these problems, is desirable. Recently some workers reported new approaches for propene epoxidation using O_2 and H_2.[2] However, it is evident that using only O_2 is more advantageous, and many researchers have attempted epoxidation of propene using only O_2.[3]

On the other hand, 'photoepoxidation' of propene using only O_2 over TiO_2,[4] Ba-Y type zeolite,[5] Nb_2O_5/SiO_2,[6] MgO/SiO_2 and SiO_2[7] has been reported. However, these activities were low and it was not clear whether the reaction proceeded catalytically. We have found that isolated tetrahedral Ti species on titania–silica catalytically promoted the selective photoepoxidation of propene by molecular oxygen.[8] However, the isolated tetrahedral Ti species absorb only UV light ($\lambda < 250$ nm), and the reaction proceeded only under UV irradiation. Artificial UV light sources tend to be expensive, and the UV light component in sunlight reaching the surface of the earth is relatively small. Thus, it is significant to develop a visible light-driven photocatalyst for epoxidation of propene. It is known that Cr species have LMCT absorption in the visible light region, and recently NO decomposition and propane oxidation over Cr-containing mesoporous silica molecular sieves (Cr-HMS) under visible light irradiation have been reported.[9,10] In our previous screening study of silica-supported metal oxide catalysts for propene photoepoxidation, CrO_x/SiO_2 (1.5 mol% as Cr) showed high propene conversion, but low selectivity for PO.[11]

In the present study, we prepared chromia–silica catalysts containing a very small amount (0.1 mol%) of Cr by the sol–gel method or impregnation method, and examined the propene photoepoxidation activity and the dependence of the activity on the wavelength of photoirradiation.

CrO_x–SiO_2 binary oxide was prepared by hydrolysis of a mixed solution of $Si(OC_2H_5)_4$ and $Cr(NO_3)_3{\cdot}9H_2O$ dissolved in ethylene glycol followed by calcination at 773 K in flowing air for 5 h.[12] CrO_x/SiO_2 supported oxides were prepared by impregnation method with amorphous silica and $Cr(NO_3)_3{\cdot}9H_2O$ aqueous solution, followed by calcination in the same way.[11] CrO_x–SiO_2 and CrO_x/SiO_2 are denoted as Cr–Si(x) and Cr/Si(x) respectively, where x is mol% of Cr; $n_{Cr}/(n_{Cr} + n_{Si}) \times 100$. Prior to each reaction test and spectroscopic measurement, the sample was treated with 100 Torr oxygen at 773 K for 1 h, followed by evacuation at 673 K for 1 h. The photoepoxidation of propene was performed with a conventional closed system (123 cm^3) and 200 W Xe lamp in the same manner as previously reported.[8]The wavelength of photoirradiation light was limited by using TOSHIBA UV-cut glass filters: UV-31 and Y-43, which allow the transmission of light with $\lambda > 310$ nm and 430 nm, respectively. The distribution of the intensity of light from the Xe lamp was measured using a Hamamatsu Photonic Multi-Channel Analyzer C7473 with a CCD sensor. Diffuse reflectance UV-vis spectra of the pretreated samples were measured *in vacuo* on a JASCO V-570 spectrophotometer at room temperature.

Fig. 1 shows diffuse reflectance UV-vis spectra of Cr/Si(0.1), Cr–Si(0.1) and Cr/Si(1.5). All samples showed three absorption bands centred around 245, 330 and 460 nm, which were assigned to the LMCT (from O^{2-} to Cr^{6+} charge transfer) transitions of chromate species.[9] Cr/Si(1.5) and Cr–Si(0.1) showed an additional absorption band in the 580–800 nm region assigned to the d–d transition of octahedral Cr^{3+} in Cr_2O_3 clusters.[9] Weckhuysen *et al*. reported that monochromate and dichromate species existed over Cr/SiO_2 0.2 wt% (0.23 mol%), and, with increasing Cr loading, additional polychromate (trichromate, tetrachromate, *etc*.) species and Cr_2O_3 clusters were formed.[13] Since Cr/Si(0.1) contained 0.09 wt% of Cr and exhibited a spectrum without an absorption band at 580–800 nm, Cr/Si(0.1) would have dispersed chromate species (monochromate and/or dichromate) most abundantly. The additional very weak absorption band at 580–800 nm in the spectrum of Cr–Si(0.1) indicates that a very small amount of polychromate species and Cr_2O_3 clusters would also be formed on Cr–Si(0.1). Over Cr/Si(1.5), larger amounts of polychromate species and Cr_2O_3 clusters would exist, illustrated by the stronger band at 580–800 nm in the spectrum.

Table 1 shows the results of photooxidation of propene over chromia–silica catalysts. The major products were propene oxide (PO), ethanal, CO and CO_2. Small amounts of propanal, acetone, acrolein, 2-propanol, ethene and butene were also observed. Cr/Si(1.5) showed very high selectivity for CO_x and low selectivity for PO (run 1) as previously reported.[11] Cr/Si(0.1) and Cr–Si(0.1) showed much higher selectivity for PO than Cr/Si(1.5) when they were compared at similar conversion (runs 2 and 3). This indicates that chromia–silica catalysts containing a very small amount (0.1 mol%) of Cr were efficient for the photoepoxidation of propene. Cr–Si(0.1) showed slightly lower selectivity for PO and higher selectivity for ethanal than Cr/Si(0.1). These results on the photoreaction and the UV-vis spectra indicate that dispersed chromate species on SiO_2 should be effective in the photoepoxidation of propene, while polychromate species and Cr_2O_3 clusters should promote

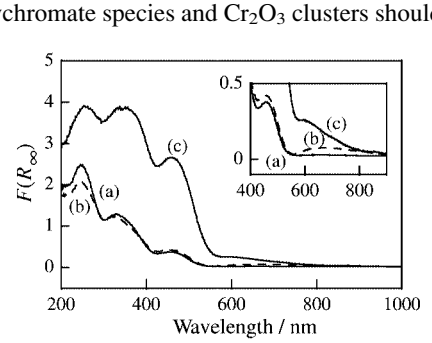

Fig. 1 Diffuse reflectance UV-vis spectra of chromia–silica catalysts. (a) Cr/Si(0.1), (b) Cr–Si(0.1) (broken line) and (c) Cr/Si(1.5). The samples were evacuated at 673 K.

 DOI: 10.1039/b108063f

Table 1 Results of the photooxidation of propene over the chromia–silica catalyst[a]

Run	Catalyst	SA[b]/ $m^2\ g^{-1}$	Filter	Time[c]/h	Conv.[d] (C%)	PO yield (C%)	Selectivity[f] (C%)[e] PO	Propanal	Acetone	Acrolein	Ethanal	HC	CO_x
1	Cr/Si(1.5)[g]	573	no	1	16.9	0.6	3.7	1.7	1.9	4.8	15.2	8.9	61.5
2	Cr/Si(0.1)	537	no	2	16.7	7.3	44.0	2.7	5.8	4.3	17.9	3.7	19.6
3	Cr–Si(0.1)	382	no	2	17.8	5.7	32.0	4.6	5.3	4.8	22.2	5.2	19.5
4	Cr–Si(0.1)	382	UV-31	2	12.5	4.2	33.9	9.2	3.5	5.0	30.7	2.4	14.8
5	Cr–Si(0.1)	382	Y-43	2	7.7	2.5	31.8	9.2	3.0	5.8	30.8	3.3	15.7

[a] Catalyst 0.2 g, propene 100 μmol, O_2 200 μmol, reaction time 2 h. [b] BET surface area. [c] Reaction time. [d] Conversion. [e] Based on introduced propene. [f] PO, propene oxide; HC, ethene + butenes; CO_x, CO + CO_2. A very small amount of 2-propanol was also observed, but is not shown here. [g] From ref. 11.

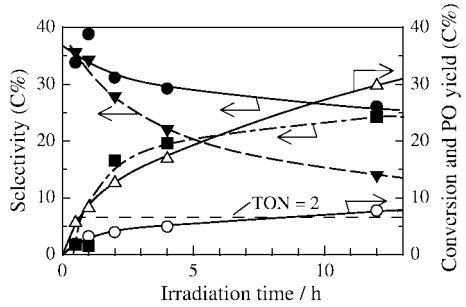

Fig. 2 Time course of photooxidation of propene over Cr–Si(0.1). Conversion (△), PO yield (○), and selectivity to propene oxide (●), ethanal (▼) and CO + CO_2 (■).

the oxidation of propene to by-products such as ethanal and CO_x. In addition, the turnover number, TON = (the amount of produced PO) / (the amount of Cr on sample), exceeded 2 after 12 h irradiation over Cr–Si(0.1) (Fig. 2), which indicated that this reaction proceeded catalytically.

The effective wavelength for photoepoxidation of propene over the Cr–Si(0.1) catalyst was examined using UV cut-off filters (Table 1, runs 4 and 5). Even under visible light ($\lambda > 430$ nm) irradiation (run 5), the conversion and PO yield almost reached half of the run without the filter (run 3). This means that visible light is sufficient to promote photoepoxidation of propene over chromia–silica catalysts. By using the UV cut-off filters, selectivity for PO was not significantly changed, but ethanal selectivity increased and CO_x selectivity decreased. As shown in Fig. 2, in the range of conversion 7–18% (1–4 h) ethanal selectivity decreased and CO_x selectivity increased with increasing conversion, but selectivity to PO was not so affected by the conversion. The differences in ethanal and CO_x selectivity among runs 3–5 can be attributed to the difference in conversion, not in the wavelength of light. In other words, the product distribution would not be affected by the wavelength of light, which suggests that the chromate species excited by UV or visible light catalyse the photoepoxidation of propene *via* the same mechanism, regardless of the absorbed wavelength. The relative amount of photons absorbed by Cr–Si(0.1) was estimated from summing the products of absorption intensity of

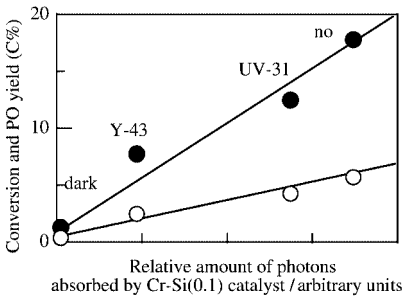

Fig. 3 The plot of conversion (●) and PO yield (○) in photooxidation of propene over Cr–Si(0.1) against the relative amount of photons absorbed by Cr–Si(0.1).

Cr–Si(0.1) and light intensity irradiated from the Xe lamp through UV cut-off filters at each wavelength. With increasing the relative amount of photons absorbed by Cr–Si(0.1), the conversion and PO yield increased linearly (Fig. 3). This result means that chromate species excited by UV or visible light would be equally efficient in the photoepoxidation of propene; that is, the quantum yield of photoepoxidation under visible light would be equal to that under UV light. Thus, exclusion of UV light changed neither the selectivity nor the quantum yield of propene photoepoxidation over chromate species. Therefore, it is suggested that chromate species excited by UV or visible light identically catalyse the photoepoxidation of propene, although the energy of photons was different at each wavelength. This should mean that the energy of visible light is sufficient to promote photoepoxidation of propene, that is, to activate oxygen and/or propene on the catalyst.

In conclusion, highly dispersed chromate species on SiO_2 were found to catalyse propene epoxidation by molecular oxygen under photoirradiation, and even under visible light irradiation. Chromate species excited by visible light would promote propene epoxidation identically to those excited by UV light.

This work was partly supported by a Grant-in-Aid for Encouragement of Young Scientists from the Ministry of Education, Culture, Sports, Science and Technology (MEXT), Japan.

Notes and references

1 G. Centi, F. Cavani and F. Trifirò, in *Selective Oxidation by Heterogeneous Catalysis*, Kluwer Academic/Plenum Publishers, New York, 2001, p. 101.
2 Y. Wang and K. Otuka, *J. Catal.*, 1995, **157**, 450; T. Hayashi, K. Tanaka and M. Haruta, *J. Catal.*, 1998, **178**, 566.
3 G. Lu and X. Zuo, *Catal. Lett.*, 1999, **58**, 67; T. A. Nijhuis, S. Musch, M. Makkee and J. A. Moulijn, *Appl. Catal. A*, 2000, **196**, 217; K. Murata and Y. Kiyozumi, *Chem. Commun.*, 2001, 1356.
4 P. Pichat, J. Herrmann, J. Disdier and M. Mozzanega, *J. Phys. Chem.*, 1979, **83**, 3122.
5 F. Blatter, H. Sun and H. Frei, *Catal. Lett.*, 1995, **35**, 1; F. Blatter, H. Sun, S. Vasenkov and H. Frei, *Catal. Today*, 1998, **41**, 297; Y. Xiang, S. C. Larsen and V. H. Grassian, *J. Am. Chem. Soc.*, 1999, **121**, 5063.
6 T. Tanaka, H. Nojima, H. Yoshida, H. Nakagawa, T. Funabiki and S. Yoshida, *Catal Today*, 1993, **16**, 297.
7 H. Yoshida, T. Tanaka, M. Yamamoto, T. Funabiki and S. Yoshida, *Chem. Commun.*, 1996, 2125; H. Yoshida, T. Tanaka, M. Yamamoto, T. Yoshida, T. Funabiki and S. Yoshida, *J. Catal.*, 1997, **171**, 351.
8 H. Yoshida, C. Murata and T. Hattori, *Chem. Commun.*, 1999, 1551.
9 B. M. Weckhuysen, A. A. Verberckmoes, A. L. Buttiens and R. A. Schoonheydt, *J. Phys. Chem.*, 1994, **98**, 579; B. M. Weckhuysen, I. E. Wachs and R. A. Schoonheydt, *Chem. Rev.*, 1996, **96**, 3327.
10 H. Yamashita, K. Yoshizawa, M. Ariyuki, S. Higashimoto, M. Che and M. Anpo, *Chem. Commun.*, 2001, 435.
11 H. Yoshida, C. Murata and T. Hattori, *J. Catal.*, 2000, **194**, 364.
12 A. Ueno, H. Suzuki and Y. Kotera, *J. Chem. Soc., Faraday Trans. 1*, 1983, **79**, 127.
13 B. M. Weckhuysen, R. A. Schoonheydt, J-M Jehng, I. E. Wachs, S. J. Cho, R. Ryoo, S. Kijlstra and E. Poels, *J. Chem. Soc., Faraday Trans.*, 1995, **91**, 3245.

CHEMCOMM
Communication
www.rsc.org/chemcomm

Reactivity in polynuclear transition metal chemistry as a means to obtain high-spin molecules: substitution of μ_4-OH^- by η^1,μ_4-N_3^- increases nine times the ground-state *S* value of a nonanuclear nickel(II) cage

Giannis S. Papaefstathiou,[a] Albert Escuer,*[b] Ramon Vicente,[b] Merce Font-Bardia,[c] Xavier Solans[c] and Spyros P. Perlepes*[a]

[a] *Department of Chemistry, University of Patras, 26504 Patras, Greece. E-mail: perlepes@patreas.upatras.gr*
[b] *Departament de Qhimica Inorganica, Universitat de Barcelona, Diagonal 647,08028 Barcelona, Spain. E-mail: aescuer@kripto.qui.ub.es*
[c] *Departament de Crystallografia i Mineralogia, Universitat de Barcelona, Marti Franqués s/n, 08028 Barcelona, Spain*

Received (in Cambridge, UK) 19th July 2001, Accepted 9th October 2001
First published as an Advance Article on the web 8th November 2001

The reaction of di-2-pyridyl ketone, $(2\text{-py})_2CO$, with $Ni(O_2CMe)_2{\cdot}4H_2O$ yields the cage $[Ni_9(OH)_2(O_2CMe)_8\{(2\text{-py})_2CO_2\}_4]$, which reacts further with N_3^- ions to give the structurally similar cluster $[Ni_9(N_3)_2(O_2CMe)_8\{(2\text{-py})_2CO_2\}_4]$ containing extremely rare η^1,μ_4-N_3^- groups; magnetic studies reveal that the spin ground state of the latter is nine times the ground state of the former.

The study of molecules with unusually large numbers of unpaired electrons has taken on added impetus in the last five years,[1–3] since it has been realised that a fairly large ground-state *S* value is one of the necessary requirements for molecules to be able to function as magnetizable magnets (single-molecule magnets, SMMs) below a critical temperature.[4] In most polynuclear clusters, magnetic exchange interactions are mainly propagated by bridging OH^-, O^{2-}, RO^- or RCO_2^- ligands, or a combination of two or more of these groups.[4] These ligands often cause antiferromagnetic interactions and, thus, it is necessary to arrange the metal ions and the bridging groups in an appropriate manner so that they can give a high-spin ground state for the system.[4] No systematic attempts have been made to replace the above mentioned bridging ligands in a known cluster with other groups that are more prone to ferromagnetic coupling, for example end-on N_3^-, and, in general, the reactivity chemistry of polynuclear 3d-metal complexes is practically unexplored. We herein describe a novel OH^--bridged, nonanuclear nickel(II) cluster with an $S = 1$ ground state and its reaction with azide ions, which leads to substitution of the μ_4-OH^- ligands and yields a structurally similar cluster with an $S = 9$ ground state.

Reaction of di-2-pyridyl ketone, $(2\text{-py})_2CO$, with 2 equivalents of $Ni(O_2CMe)_2{\cdot}4H_2O$ in DMF under reflux resulted in a green solution from which $[Ni_9(OH)_2(O_2CMe)_8\{(2\text{-py})_2CO_2\}_4]{\cdot}19H_2O$ **1**† precipitated within 4 days in *ca.* 60% yield. The double deprotonation of the *gem*-diol form of di-2-pyridyl ketone (formed *in situ* in the *presence* of the metal ions) is a consequence of the high $MeCO_2^-$ to $(2\text{-py})_2C(OH)_2$ ratio (4 : 1) used in the reaction. The $RCO_2^-/(2\text{-py})_2CO_2^{2-}$ ligand 'blend' has resulted in a variety of high-nuclearity species in cobalt(II)[5] and copper(II)[6] chemistry.

Complex **1**‡ (Fig. 1) has a fourfold axis passing through Ni(1). The nine Ni^{II} atoms adopt the topology of two square pyramids sharing a common apex at Ni(1) and are held together by four $\eta^1:\eta^3:\eta^3:\eta^1:\mu_5$ (**A**) $(2\text{-py})_2CO_2^{2-}$ ligands. Each Ni···Ni edge of the bases of the pyramids is further bridged by one *syn, syn* $\eta^1:\eta^1:\mu_2$ acetate. The four acetate ligands create a concave cavity in each pyramid's base, into which a very rare μ_4-OH^- is effectively trapped capping the square base. A

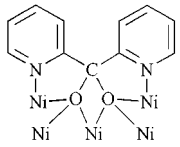

A

salient feature of the structure is the coordination number eight (square antiprismatic geometry) around Ni(1).

The dc $\chi_M T$ product of **1** shows a continuous decrease from the room temperature value of 11.47 cm^3 K mol^{-1} down to 0.40 cm^3 K mol^{-1} at 2 K (Fig. 2), indicating a dominant antiferromagnetic superexchange pattern. A first approach to quantify the magnetic exchange interactions in **1** has been performed by means of the full-matrix diagonalisation program CLUMAG,[7] applying the Hamiltonian (1):

$$H = -J_1(S_1S_2 + S_1S_3 + S_1S_4 + S_1S_5 + S_1S_6 + S_1S_7 + S_1S_8 + S_1S_9) - J_2(S_2S_3 + S_3S_4 + S_4S_5 + S_5S_2 + S_6S_7 + S_7S_8 + S_8S_9 + S_9S_6) - J_3(S_2S_4 + S_3S_5 + S_6S_8 + S_7S_9) \quad (1)$$

in which S_1 corresponds to the central metal site [Ni(1)], and S_2, S_3, S_4, S_5 and S_6, S_7, S_8, S_9 correspond to the Ni^{II} atoms placed at the two square bases [Ni(2), Ni(2b), Ni(2c), Ni(2d) and Ni(3), Ni(3b), Ni(3c), Ni(3d), respectively]. In this scheme (**B**), J_1

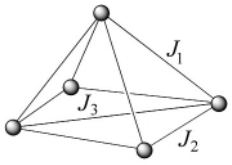

B

relates the central with the peripheral spins, whereas J_2 and J_3 relate the neighboring and the opposite spins, respectively, in each base. To reduce the deviation of the data due to the zero field splitting effect, the fit was performed in the 300–12 K temperature range. The best fit parameters obtained are $J_1 = 6.0$ cm^{-1}, $J_2 = 18.0$ cm^{-1} and $J_3 = -57.0$ cm^{-1} for a *g* value of 2.30. The strong antiferromagnetic interaction J_3 is consistent with the large Ni–O–Ni angles of *ca.* 140°, whereas the weak to moderate ferromagnetic interactions J_1 and J_2 were expected for the observed Ni–O–Ni angles that are slightly larger than 90°.[8] The ground state of **1**, obtained from the low temperature data and magnetization measurements ($M/N\beta$ value of 1.05 under an external field of 5 T at 2 K) is $S = 1$.

We have wondered whether the end-on azido ligand, a well known ferromagnetic coupler, would be incorporated into the

 DOI: 10.1039/b106472j

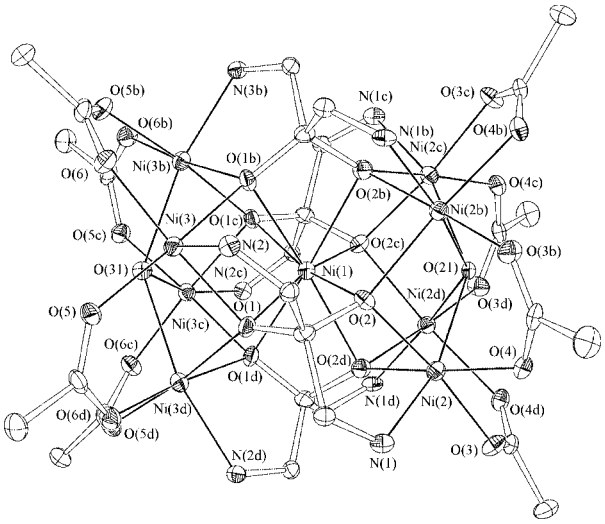

Fig. 1 ORTEP representation of complex **1** at the 20% probability level. Letters b, c and d refer to equivalent positions. b: *x*, $-y + 1/2$, *z*. c: $-x + 1/2$, $-y + 1/2$, *z*. d: $-x + 1/2$, *y*, *z*.

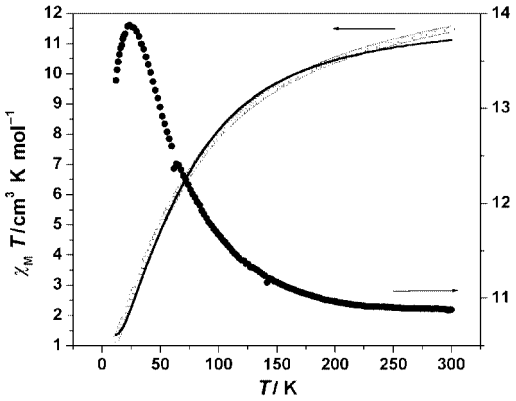

Fig. 2 Plots of $\chi_M T$ *vs.* *T* for complexes **1** (left *y* axis, open circles) and **2** (right *y* axis, solid circles). The solid line is a fit of the data to the appropriate theoretical expression; see text for fitting parameters.

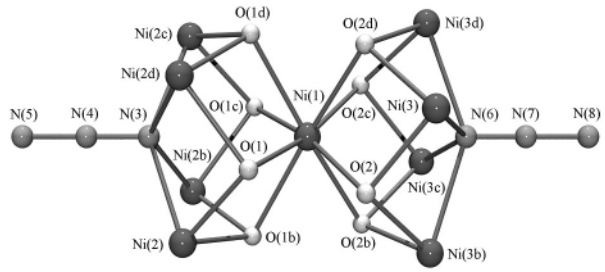

Fig. 3 The molecular structure of complex **2**. For clarity, only the Ni^{II} atoms, nitrogen atoms of the azido ligands and triply bridging oxygen atoms of $(2\text{-py})_2CO_2^{2-}$ are shown. Symmetry transformations used to generate equivalent atoms: b: *x*, $-y + 1/2$, *z*. c: $-x + 1/2$, $-y + 1/2$, *z*. d: $-x + 1/2$, *y*, *z*.

Ni_9 cage skeleton replacing the hydroxo ligands, which cause the strong antiferromagnetic interaction J_3 (see **B**). This has, indeed, turned out to be the case. Reaction of **1** with 2–3 equivalents of NaN_3 in DMF–MeOH (2 : 1 v/v) gave green crystals of $[Ni_9(N_3)_2(O_2CMe)_8\{(2\text{-py})_2CO_2\}_4]\cdot 4DMF\cdot 4.5H_2O$ **2**† in 80% yield.

Complex **2**‡ (Fig. 3), which also has a fourfold axis passing through Ni(1), bears striking structural similarity to **1**, the main difference being the replacement of the μ_4-OH^- ligands of the latter by the η^1,μ_4-N_3^- ligands in the former. Such η^1,μ_4 azido ligands had been totally unknown and were first observed in the recently reported[9] nonanuclear cage $[Co_9(N_3)_2(O_2CMe)_8\{(2\text{-py})_2CO_2\}_4]$ **3**.

Complexes **1** and **2** join a handful of structurally characterized discrete, non-organometallic nonanuclear Ni^{II} complexes with O,N-ligation.[10–13]

The dc $\chi_M T$ product of **2** increases from the room temperature value of 10.87 cm^3 K mol^{-1} to a maximum of 13.88 cm^3 K mol^{-1} at 24 K, and then decreases continuously down to 2 K (Fig. 2). This behaviour is compatible with a moderate ferromagnetic coupling; the low-temperature decrease of the magnetic moment is associated with the anisotropy of the Ni^{II} ions. Magnetization data collected for **2** show a rapid increase of $M/N\beta$ upon increasing the external field, reaching a value of 9.59 at 5 T. Thus, the magnetic data for **2** should be associated with ferromagnetic coupling mediated by the η^1,μ_4-N_3^- ligand (giving a total *S* value of nine times the local spin), assuming ferromagnetic coupling between the central and the peripheral Ni^{II} ions (as in **1**); this assumption is reasonable because the structural parameters of complexes **1** and **2** do not differ much. The low temperature fall in $\chi_M T$ might be very exciting and the study of the relaxation behaviour of **2** is in progress.

In conclusion, the structures of both **1** and **2** feature very rare characteristics, such as the coordination number 8 for the central Ni^{II} ion, the μ_5 coordination mode of $(py)_2CO_2^{2-}$, and the η^1,μ_4 coordination mode of both the hydroxo and azido ligands. However, the most remarkable result of this work is the fact that rational reactivity chemistry of a polynuclear complex results in a new cluster of the same nuclearity, which retains the structural identity of and has much more attractive magnetic properties than the starting material. The described N_3^- for OH^- substitution has the potential for general application in the area of high-spin molecules.

This work was supported by CICYT (Grant BP96/0163) and the Research Committee of the University of Patras (C. Caratheodory Programme, No 1941).

Notes and references

† The air-dried complexes analysed satisfactorily (C, H, N).

‡ *Crystal data*: for **1**: $C_{60}H_{96}N_8O_{45}Ni_9$, M = 2177.67, tetragonal, space group *P*4/*ncc* (no. 130), $a = b$ = 17.785(8), c = 27.313(3) Å, U = 8639(6) Å^3, T = 293 K, Z = 4, μ(Mo-Kα) = 2.013 mm^{-1}, 37752 reflections measured, 7038 unique (R_{int} = 0.082). The final $wR2(F^2)$ was 0.1703 for 4166 reflections with $I > 2\sigma(I)$.

For **2**: $C_{72}H_{93}N_{18}O_{32.5}Ni_9$, M = 2258.75, tetragonal, space group *P*4/*n* (no. 85), $a = b$ = 17.841(8), c = 14.008(3) Å, U = 4459(3) Å^3, T = 293 K, Z = 2, μ(Mo-Kα) = 1.947 mm^{-1}, 24451 reflections measured, 5241 unique (R_{int} = 0.038). The final $wR2(F^2)$ was 0.1052 for 3417 reflections with $I > 2\sigma(I)$.

CCDC reference numbers 169286 and 169287. See http://www.rsc.org/suppdata/cc/b1/b106472j/ for crystallographic data in CIF or other electronic format.

1 G. L. Abbati, A. Cornia, A. C. Fabretti, A. Caneschi and D. Gatteschi, *Inorg. Chem.*, 1998, **37**, 1430.
2 G. Aromi, M. J. Knapp, J.-P. Claude, J. C. Huffman, D. N. Hendrickson and G. Christou, *J. Am. Chem. Soc.*, 1999, **121**, 5489.
3 R. E. P. Winpenny, *Comments Inorg. Chem.*, 1999, **20**, 233.
4 G. Christou, D. Gatteschi, D. N. Hendrickson and R. Sessoli, *MRS Bull.*, 2000, **25**, 1.
5 A. Tsohos, S. Dionyssopoulou, C. P. Raptopoulou, A. Terzis, E. G. Bakalbassis and S. P. Perlepes, *Angew. Chem., Int. Ed.*, 1999, **38**, 983.
6 V. Tangoulis, C. P. Raptopoulou, S. Paschalidou, E. G. Bakalbassis, S. P. Perlepes and A. Terzis, *Angew. Chem., Int. Ed. Engl.*, 1997, **36**, 1083.
7 D. Gatteschi and L. Pardi, *Gazz. Chim. Ital.*, 1993, **123**, 231.
8 J. M. Clemente-Juan, B. Chansou, B. Donnadieu and J.-P. Tuchagues, *Inorg. Chem.*, 2000, **39**, 5515.
9 G. S. Papaefstathiou, S. P. Perlepes, A. Escuer, R. Vicente, M. Font-Bardia and X. Solans, *Angew. Chem., Int. Ed.*, 2001, **40**, 884.
10 V. Tangoulis, E. Diamantopoulou, E. G. Bakalbassis, C. P. Raptopoulou, A. Terzis and S. P. Perlepes, *Mol. Cryst. Liq. Cryst.*, 1999, **335**, 463.
11 A. Pajunen, I. Mutikainen, H. Saarinen and M. Orama, *Z. Kristallogr.*, 1999, **214**, 217.
12 D. M. J. Doble, C. H. Benison, A. J. Blake, D. Fenske, M. S. Jackson, R. D. Kay, W.-S. Li and M. Schroder, *Angew. Chem., Int. Ed. Engl.*, 1999, **38**, 1915.
13 E. K. Brechin, S. G. Harris, S. Parsons and R. E. P. Winpenny, *Angew. Chem., Int. Ed. Engl.*, 1997, **36**, 1967.

CHEMCOMM Communication
www.rsc.org/chemcomm

Stoichiometric water splitting into H_2 and O_2 using a mixture of two different photocatalysts and an IO_3^-/I^- shuttle redox mediator under visible light irradiation

Kazuhiro Sayama,[a] Kazuaki Mukasa,[b] Ryu Abe,[a] Yoshimoto Abe[b] and Hironori Arakawa*[a]

[a] *Photoreaction Control Research Center (PCRC), National Institute of Advanced Industrial Science and Technology (AIST), Central 5, 1-1-1 Higashi, Tsukuba, Ibaraki 305-8565, Japan. E-mail: h.arakawa@aist.go.jp*

[b] *Faculty of Science and Technology, Science University of Tokyo, Yamazaki 2641, Noda, Chiba 278-8514, Japan*

Received (in Cambridge, UK) 23rd August 2001, Accepted 8th October 2001
First published as an Advance Article on the web 29th October 2001

The stoichiometric splitting of water into H_2 and O_2 (H_2/O_2 = 2) under visible light irradiation (λ > 420 nm) took place for the first time using a mixture of Pt-WO_3 and Pt-$SrTiO_3$ (Cr–Ta-doped) photocatalysts and an IO_3^-/I^- shuttle redox mediator.

The construction of an efficient artificial photosynthesis system for solar energy conversion and storage is one of the fascinating goals to solve the global energy problem. The splitting of water into H_2 and O_2 stoichiometrically (H_2/O_2 = 2) is the most fundamental and important reaction in artificial photosynthesis. So far, many semiconductor photocatalysts such as Pt-TiO_2 have been reported for water splitting under UV light irradiation.[1,2] However, development of a photocatalyst system working under visible light irradiation (λ > 400 nm) is indispensable from the viewpoint of efficient solar energy utilization. Unfortunately, such a reliable and reproducible photocatalyst system has not been established yet.

Recently, we reported a unique synergy effect of two different TiO_2 photocatalysts suspended in NaI aqueous solution for the water splitting reaction under UV light in a one-pot cell.[3] In this system, H_2 was formed on Pt-TiO_2(anatase) accompanied by the oxidation of I^- to IO_3^-, and O_2 was formed on TiO_2(rutile) accompanied by the reduction of IO_3^- to I^-, therefore, I^- and IO_3^- ions acted as electron carrier shuttles between two photoexcitation systems, as shown in the following equations:

$$6H^+ + 6e^- \rightarrow 3H_2 \text{ (conduction band of Pt-}TiO_2\text{(anatase))} \quad (1)$$

$$I^- + 6OH^- + 6h^+ \rightarrow IO_3^- + 3H_2O \text{ (valence band of Pt-}TiO_2\text{(anatase))} \quad (2)$$

$$IO_3^- + 3H_2O + 6e^- \rightarrow I^- + 6OH^- \text{ (conduction band of } TiO_2\text{(rutile))} \quad (3)$$

$$6OH^- + 6h^+ \rightarrow {}^3/_2O_2 + 3H_2O \text{ (valence band of } TiO_2\text{(rutile))} \quad (4)$$

Here, we report the first stoichiometric decomposition of water into H_2 and O_2 under only visible light (λ > 420 nm) using a mixture of two different photocatalysts, Pt-WO_3 and Pt-$SrTiO_3$(Cr–Ta-doped) in NaI aqueous solution.

Commercial WO_3 powder (99.999% purity), supplied from Kojundo Chemical Co., was used as one of the photocatalysts. $SrTiO_3$ powder doped with Cr and Ta ions was prepared by the calcination of a mixture of Cr_2O_3 (Cr: 1 mol% of Ti), Ta_2O_5 (Ta: 1 mol% of Ti), $SrCO_3$ and TiO_2 at 1100 °C in air.[4] Pt-loaded catalyst was prepared by the photodeposition of H_2PtCl_6 on the catalysts in aqueous solution. The photocatalytic reaction was performed in a one-pot Pyrex glass cell connected to a closed gas-circulating system. A suspension of catalyst powder (0.2 g) in NaI (100 mmol l^{-1}) or $NaIO_3$ (4 mmol l^{-1}) aqueous solution (250 ml) in the cell was degassed completely. The visible light irradiation was performed using a Xe lamp (300 W, CERMAX-LX-300) through a 420 nm cutoff filter (HOYA Glass Co.). The evolution of H_2 and O_2 was detected by on-line gas chromatography (TCD, molecular sieve 5A, argon carrier). The I^-, IO_3^- and I_3^- ions were analyzed by ion-chromatography and UV-vis spectroscopy.

There are some reports on unique mixed-oxide semiconductor photocatalysts that could produce H_2 under visible light irradiation using methanol as a sacrificial reagent,[4–6] suggesting a negative conduction band potential compared to the H^+ reduction potential to H_2. First, we investigated these mixed-oxide semiconductors such as $SrTiO_3$(Cr–Ta-doped),[4] $In_2Zn_9O_{12}$,[5] $InNbO_4$,[6] *etc.* for H_2 formation using I^- ion as a reversible electron donor. Pt-loaded $SrTiO_3$(Cr–Ta-doped) showed catalytic activity, with H_2 evolution from NaI aqueous solution. The initial rate of H_2 evolution was 0.8 μmol h^{-1}, but the evolution rate decreased gradually and stopped after 20 h from the start of irradiation, as shown in Fig. 1(a). No H_2 evolution was observed without NaI. In the case of Pt-TiO_2(anatase), the IO_3^- ion was mainly produced by the oxidation of I^-.[3] The IO_3^- ion was also observed in solution after the photoreaction on Pt-$SrTiO_3$(Cr–Ta-doped). O_2 evolution was not detected. This catalyst had a broad absorption band in the visible light region and the absorption edge extended to more than 700 nm. H_2 evolution was observed under visible light even through a 500 nm cutoff filter. The catalyst itself was stable after a long reaction time, and the activity of the used catalyst was recovered by replacing the reaction solution with a new NaI aqueous solution. The H_2 formation was significantly suppressed (< 0.1 μmol h^{-1}) when a small amount of $NaIO_3$ (0.1 mmol l^{-1}) was added to the initial NaI reaction solution (100 mmol l^{-1}). Therefore, it is speculated that the decrease in

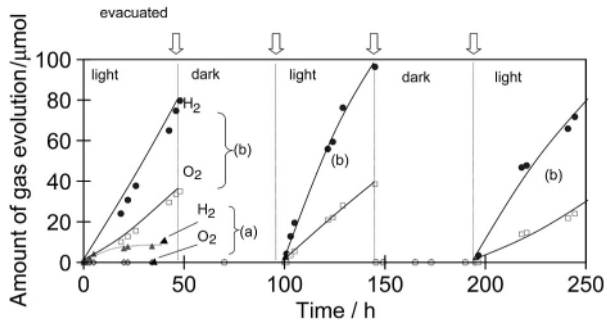

Fig. 1 Reaction time course of the photocatalytic splitting of water into H_2 and O_2 under visible light (λ > 420 nm, 3.1 W, window area: 16 cm^2). (a) 0.2 g of Pt(0.3 wt%)-$SrTiO_3$ doped with Cr and Ta (both 1 mol% of Ti) was suspended in the NaI aqueous reaction solution (100 mmol l^{-1}, 250 ml, pH = 7.0). (b) Both 0.2 g of Pt(0.3 wt%)-$SrTiO_3$ doped with Cr and Ta (both 1 mol% of Ti) and 0.2 g of Pt(1 wt%)-WO_3 were suspended in the NaI aqueous reaction solution (100 mmol l^{-1}, 250 ml, pH = 7.0). The magnetic stirring was continued during the light irradiation and in the dark.

 DOI: 10.1039/b107673f

H_2 evolution rate was caused by the accumulation of IO_3^-. By analogy with the mixed system of Pt-TiO_2(anatase) and TiO_2(rutile) described in reference 3, we added TiO_2(rutile) powder as an O_2 evolution photocatalyst into the Pt-$SrTiO_3$(Cr–Ta-doped) suspension in NaI aqueous solution. TiO_2(rutile) had the ability to reduce IO_3^- to I^-, resulting in O_2 evolution. After TiO_2(rutile) addition it was found that both H_2 and O_2 gases were evolved (H_2: 3.1 μmol h^{-1}, O_2: 1.5 μmol h^{-1}) under UV irradiation for a long time.

Next, in order to utilize visible light for photocatalytic O_2 evolution, we investigated various kinds of narrow bandgap semiconductor photocatalysts (WO_3, In_2O_3, Bi_2O_3, Fe_2O_3, $BiVO_4$, $CuWO_4$, $NiWO_4$, $SrWO_4$ *etc*.) instead of TiO_2(rutile), using the IO_3^- ion as an electron acceptor. It was found that the Pt-loaded WO_3 catalyst showed the best activity for O_2 evolution under visible light irradiation in $NaIO_3$ aqueous solution. No H_2 gas evolution was observed. The initial O_2 evolution rate was very high (84 μmol h^{-1}), and the rate decreased gradually with decreasing levels of the IO_3^- ion and with increasing I^- ions. More than 96% of the IO_3^- ions were reduced to I^-, accompanied by O_2 evolution, after a reaction time of 70 h. The O_2 evolution continued until most of the IO_3^- ions were consumed even if an excess of I^- was present in the solution during the reaction. Therefore, it is considered that the undesirable backward reaction, oxidation of I^- to IO_3^- by holes in the valence band, was very slow on this catalyst under these reaction conditions compared to the oxidation of water to O_2. The band gap of the WO_3 was *ca*. 2.7 eV, and the catalyst absorbed visible light up to 460 nm. O_2 gas was evolved under visible light even through a 440 nm cutoff filter but was negligible through a 460 nm cutoff filter, suggesting that the dependence of the activity on the wavelength of the incident light was in accord with the absorption spectrum.

Finally, we added the Pt-WO_3 photocatalyst into the Pt-$SrTiO_3$(Cr–Ta-doped) suspension in NaI aqueous solution. It was found that both H_2 and O_2 gases evolved under visible light, as shown in Fig. 1(b). The stoichiometric ratio of evolved H_2 and O_2 (2 : 1) was constant from the start of irradiation to more than 250 h. For the mixed catalysts, the H_2 evolution rate over Pt-$SrTiO_3$(Cr–Ta-doped) (1.8 μmol h^{-1}) was higher than that over Pt-$SrTiO_3$(Cr–Ta-doped) alone (0.8 μmol h^{-1}), suggesting that the added Pt-WO_3 effectively eliminated the IO_3^- ion from the solution by reduction to I^-. Both H_2 and O_2 gases were evolved using a 440 nm cutoff filter, but only H_2 evolution was observed using a 460 nm cutoff filter because the Pt-WO_3 catalyst could not work at $\lambda > 460$ nm. The concentration of introduced I^- ion (100 mmol l^{-1}) did not change, and formation of the IO_3^- ion was negligible during the reaction. For the first time, stoichiometric water splitting has taken place over oxide semiconductor photocatalysts under visible light irradiation, and the presence of three components, Pt-$SrTiO_3$(Cr–Ta-doped), Pt-WO_3 and NaI, was essential. The rates of H_2 and O_2 evolution under monochromatic light through a bandpass filter (420.7 nm, 57 mW) were 0.21 and 0.11 μmol h^{-1}, respectively. Therefore, the quantum efficiency was estimated to be *ca*. 0.1% at 420.7 nm.

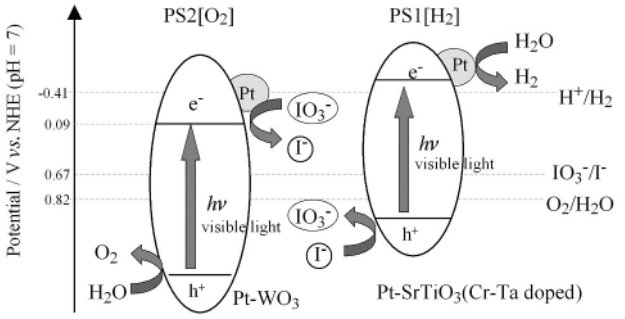

Fig. 2 Speculated reaction mechanism for the water splitting using a mixture of Pt-$SrTiO_3$, Pt-WO_3 and NaI aqueous solution.

Fig. 2 shows the speculated reaction mechanism. By analogy with the Pt-TiO_2–NaI system described in reference 3, it is considered that the IO_3^-/I^- redox pair may act as an electron carrier between two photocatalysts because it has an appropriate redox potential (0.67 V (*vs*. NHE, pH = 7)). The conduction band potential of WO_3 is +0.09 V (*vs*. NHE, pH = 7),[7] and the redox potential of H^+/H_2 is −0.41 V (*vs*. NHE, pH = 7). Therefore, the electron in the conduction band of WO_3 has the ability to reduce IO_3^- to I^-, but it cannot reduce H^+ to H_2. Though the I_3^-/I^- redox pair also seemed to be suitable as an electron carrier from its redox potential, it did not contribute to this reaction because any gas evolution on Pt-WO_3 or on Pt-$SrTiO_3$(Cr–Ta-doped) did not take place in I_3^- aqueous solution. The details of the band structure of Pt-$SrTiO_3$(Cr–Ta-doped) and the reaction mechanism are under investigation by means of photoelectrochemical measurement.

Notes and references

1 K. Yamaguchi and S. Sato, *J. Chem. Soc., Faraday Trans. 1*, 1985, **81**, 1237.
2 K. Sayama and H. Arakawa, *J. Chem. Soc., Chem. Commun*., 1992, 150.
3 R. Abe, K. Sayama, K. Domen and H. Arakawa, *Chem. Phys. Lett*., 2001, **344**, 339.
4 T. Ishii, S. Nakagawa, H. Kato and A. Kudo, *Abstract of the Japan Chemical Society Spring Meeting*, 2000, **78**, 32.
5 A. Kudo and I. Mikami, *Chem. Lett*., 1998, 1027.
6 Z. Zou, J. Ye and H. Arakawa, *Chem. Phys. Lett*., 2000, **332**, 271.
7 H. P. Maruska and A. K. Ghosh, *Sol. Energy*, 1978, **20**, 443.

CHEMCOMM Communication
www.rsc.org/chemcomm

A low cost route to hexagonal mesostructured carbon molecular sieves

Seong-Su Kim and Thomas J. Pinnavaia*

Department of Chemistry and Center for Fundamental Materials Research, Michigan State University, East Lansing, MI 48824, USA. E-mail: pinnavai@cem.msu.edu

Received (in Columbia, MO, USA) 30th July 2001, Accepted 2nd October 2001
First published as an Advance Article on the web 29th October 2001

A mesoporous carbon molecular sieve with a hexagonal framework structure (denoted C-MSU-H) has been prepared using a MSU-H silica template that can be assembled from a low cost soluble silicate precursor at near-neutral pH conditions.

Porous carbons with high surface areas, large pore volumes, and chemical inertness are useful in many materials application areas, including water and air purification, adsorption, catalysis, and energy storage.[1,2] It has been recently demonstrated that a new class of carbon molecular sieves can be prepared through the use of mesostructured silica[3] as a host to template the carbon structure. The subsequent removal of the silica host by dissolution methods allowed the carbon replica to be recovered intact. A number of carbons with hexagonal,[4] cubic,[5] wormhole[6] and foam-like[7] framework mesostructures have now been reported. Zeolites also have been used to form microstructured carbon replicas.[8] Among these templated carbons, the CMK-3 materials[4] templated in the mesopores of hexagonal SBA-15 silicas[9] are especially attractive for catalytic and adsorption applications, in part, because they possess very large mesopores, thick framework walls and an interconnected channel structure. Although SBA-15 can be assembled using readily available and biodegradable tri-block copolymers of propylene oxide and ethylene oxide as the structure director, the structure is formed under strongly acidic conditions from cost intensive silicon alkoxides as the silica precursor. Since the silica mesostructure is destroyed in the preparation of a templated carbon, it is desirable to develop more efficient synthetic routes to the mesostructured silica templates.

In an effort to replace the silicon alkoxides with low-cost sodium silicate for the synthesis of SBA-15, we recently achieved the high-yield synthesis of highly ordered mesoporous silica molecular sieves (denoted MSU-H) with large framework mesopores (7.6–11.9 nm) under near neutral pH conditions using sodium silicate as the silica precursor.[10] MSU-H mesostructures are isostructural with SBA-15, although the fundamental particle size of MSU-H (300–500 nm) is somewhat small in comparison to SBA-15 (>1.0 μm). Also, we have shown that the framework pore size, intraparticle textural porosity, and interconnected channel size of MSU-H silicas can be tailored by a favorable choice of the initial synthesis temperature and post-synthesis hydrothermal treatment methods.[11]

In the present work we demonstrate the preparation of a mesostructured carbon molecular sieve (denoted C-MSU-H) using MSU-H silica as the nanoscale template. For comparison purposes, we compare the textural properties of the C-MSU-H carbon with those of CMK-3 templated by SBA-15.

MSU-H and SBA-15 silicas were synthesized as reported previously.[9,10] MSU-H was prepared at 60 °C from Pluronic P123 surfactant and sodium silicate (27% SiO_2, 14% NaOH) using a reaction stoichiometry of 1 SiO_2:0.016 P123:0.8 CH_3COOH:0.76 NaOH:230 H_2O and a reaction time of 20 h. SBA-15 was assembled under acidic conditions and a reaction stoichiometry of 1.00 TEOS:0.017 P123:6.0 HCl:195 H_2O. The mixture was allowed to react at 35 °C for 20 h, then at 100 °C for 24 h. The surfactants were removed from the as-made MSU-H and SBA-15 mesostructures by calcination at 600 °C for 4 h and 500 °C for 6 h, respectively. Carbon replication of the MSU-H mesostructure was performed at 900 °C using sucrose in the presence of sulfuric acid as the carbon source, as described by Ryoo and coworkers.[4,5b] The carbon/silica composites were washed twice with 5 wt% hydrofluoric acid at room temperature to remove the silica templates. Elemental analysis of C-MSU-H and CMK-3 gave C/H molar ratio of 7.9 and 6.8, respectively.

Fig. 1 illustrates the powder X-ray diffraction patterns of calcined MSU-H and SBA-15 silicas and the corresponding C-MSU-H and CMK-3 carbon replicas. The calcined MSU-H and SBA-15 silicas exhibited resolved *hkl* reflections consistent with two-dimensional hexagonal symmetry and unit cell dimensions of 122 and 116 Å, respectively. The C-MSU-H and CMK-3 carbons also exhibited hexagonal structural order and unit cell dimensions of 109 and 100 Å, respectively. Interestingly, the structural shrinkage experienced in the replication of a mesostructured silica into a mesostructured carbon is somewhat smaller for the MSU-H system ($\sim$10% shrinkage) than for the SBA-15 system ($\sim$13% shrinkage).

Fig. 2 illustrates the N_2 adsorption–desorption isotherms and BJH pore size distribution plots (insert) determined from the adsorption branch of the N_2 isotherms for the calcined silicas and carbon replicas. The values of the BET surface area, total pore volume, pore diameter, and wall thickness are listed in Table 1. The adsorption–desorption isotherm for the C-MSU-H carbon is similar to that of CMK-3 carbon. The pore volume is 1.26 $cm^3\ g^{-1}$ and the BET surface area is 1228 $m^2\ g^{-1}$ for the C-MSU-H carbon. The values are a little higher than a pore volume of 1.10 $cm^3\ g^{-1}$ and a BET surface area of 1190 $m^2\ g^{-1}$ for CMK-3 using SBA-15. The pore size distribution obtained for the C-MSU-H carbon from N_2 adsorption is compared with that for CMK-3. The result indicates that the C-MSU-H is mesoporous with a quite narrow pore size distribution centered at 39 Å, while the distribution for CMK-3 is centered at 35 Å.

Thermogravimetric weight changes were recorded to determine the thermal stability and phase purity of the mesostructured carbons in air. As can be seen in Fig. 3, the C-MSU-H and CMK-3 carbons exhibited nearly identical weight change

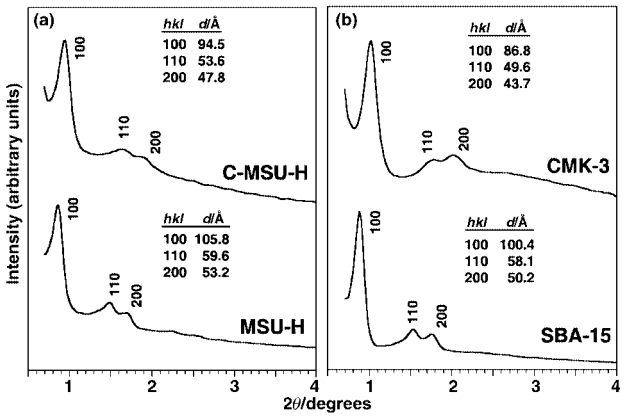

Fig. 1 XRD patterns of (a) MSU-H silica and the C-MSU-H carbon replica and (b) SBA-15 silica and the CMK-3 carbon replica.

 DOI: 10.1039/b107896h

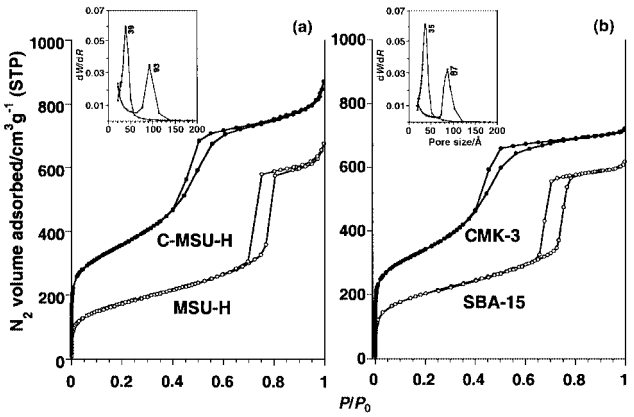

Fig. 2 N_2 adsorption–desorption isotherms for (a) MSU-H silica and C-MSU-H carbon replica and (b) SBA-15 silica and CMK-3 carbon replica. The insert provides the BJH pore size distribution calculated from the adsorption branch of the N_2 isotherm.

Table 1 Structural properties of MSU-H and SBA-15 silica templates and the corresponding mesostructured C-MSU-H and CMK-3 carbon replicas

Sample	*d* Spacing/ nm	Pore size[a]/ nm	Wall thickness[b]/ nm	S_{BET}/m^2 g^{-1}	Total pore volume/ cm^3 g^{-1}
MSU-H	10.6	9.3	2.9	625	0.97
SAB-15	10.0	8.7	2.8	718	0.93
C-MSU-H	9.5	3.9	7.1	1228	1.26
CMK-3	8.7	3.5	6.5	1190	1.10

[a] Calculated from the adsorption branch of the N_2 isotherm. [b] Determined from the difference between the unit cell parameter ($a_0 = 2d_{100}/\sqrt{3}$) and the framework pore size.

profiles. A significant loss in weight loss corresponding to the oxidation of the carbon occurred in a narrow temperature range between 550 and 650 °C. Thus, the oxidation temperatures for these carbons are significantly higher than the reported burning temperature of C_{60} (425 °C), but lower than those of multiwalled carbon nanotubes (700 °C) and highly graphitized carbon fibers (up to 800 °C).[12]

In summary, a new route to templated carbon molecular sieves (C-MSU-H) has been developed using MSU-H silica as the template without compromising the textural properties of the carbon replica. Thus, C-MSU-H carbons should be considerably more cost-efficient to prepare on an industrial scale in comparison to CMK-3 carbons, because the silica template is easily assembled from readily available sodium silicate.

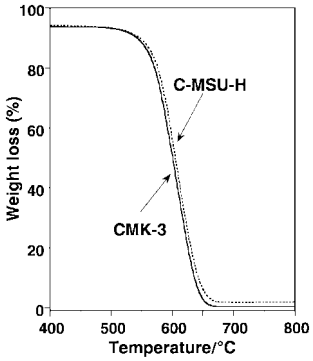

Fig. 3 Thermogravimetric curves for the calcination of C-MSU-H and CMK-3 carbons in air. The heating rate was 5.0 °C min^{-1}.

The support of this research by NIEHS grant ESO 4911C is gratefully acknowledged. Support of the National Science Foundation in the form of equipment purchased under NSF-CRG grant CHE-9903706 also is gratefully acknowledged.

Notes and references

1 C. R. Bansal, J.-B. Donnet and F. Stoeckli, *Active Carbon*, Marcel Dekker, New York, 1998.
2 H. C. Foley, *J. Microporous Mater.*, 1995, **4**, 407.
3 C. T. Kresge, M. E. Leonowicz, W. T. Roth, J. C. Vartuli and J. S. Beck, *Nature*, 1992, **359**, 710.
4 S. Jun, S. H. Joo, R. Ryoo, M. Kruk, M. Jaroniec, Z. Liu and T. Ohsuma and O. Terasaki, *J. Am. Chem. Soc.*, 2000, **122**, 10712.
5 (*a*) J. Lee, S. Yoon, T. Hyeon, S. M. Oh and K. B. Kim, *Chem. Commun.*, 1999, 2177; (*b*) R. Ryoo, S. H. Joo and S. Jun, *J. Phys. Chem., B*, 1999, **103**, 7743; (*c*) S. B. Yoon, J. Y. Kim and J.-S. Yu, *Chem. Commun.*, 2001, 559.
6 J. Lee, S. Yoon, S. M. Oh, C.-H. Shin and T. Hyeon, *Adv. Mater.*, 2000, **12**, 359.
7 J. Lee, K. Sohn and T. Hyeon, *J. Am. Chem. Soc.*, 2001, **123**, 5146.
8 (*a*) T. Kyotani, T. Nagai, S. Inoue and A. Tomita, *Chem. Mater.*, 1997, **9**, 609; (*b*) S. A. Johnson, E. S. Brigham, P. J. Ollivier and T. E. Mallouk, *Chem. Mater.*, 1997, **9**, 2448; (*c*) Z. Ma, T. Kyotani and A. Tomita, *Chem. Commun.*, 2000, 2365.
9 D. Zhao, Q. Huo, J. Feng, B. F. Chmelka and G. D. Stucky, *J. Am. Chem. Soc.*, 1998, **120**, 6024.
10 S.-S. Kim, T. R. Pauly and T. J. Pinnavaia, *Chem. Commun.*, 2000, 1661.
11 S.-S. Kim, A. Karkamkar, T. J. Pinnavaia, M. Kruk and M. Jaroniec, *J. Phys. Chem., B*, 2001, **105**, 7663.
12 (*a*) L. S. K. Pang, J. D. Saxby and S. P. Chatfield, *J. Phys. Chem.*, 1993, **97**, 6941; (*b*) P. M. Ajayan, T. W. Ebbesen, T. Ichihashi, S. Iijima, K. Tanigaki and H. Hiura, *Nature*, 1993, **362**, 522; (*c*) M. S. Dresselhaus, G. Dresselhaus, K. Sugihara, I. L. Spain and H. A. Goldberg, *Graphite Fibers and Filaments*, Springer, New York, 1988.

CHEMCOMM Communication
www.rsc.org/chemcomm

Tuning the recovery of an Rh-containing catalyst with silica-based (poly) amine ion exchangers

Jurjen Kramer, Ana Ríos García, Willem L. Driessen* and Jan Reedijk

Leiden Institute of Chemistry, Leiden University, P.O. Box 9502 2300 RA. Leiden, The Netherlands. E-mail: driessen@chem.leidenuniv.nl

Received (in Cambridge, UK) 19th September 2001, Accepted 12th October 2001
First published as an Advance Article on the web 29th October 2001

Highly efficient Rh-recovery from different adsorption media has been effected with silica-based (chelating) ion exchangers containing (poly) amine functionalities; recoveries have been found to correlate well with the stability of the metal-to-ligand complexes.

Rh-containing homogeneous catalysts play an important role in the improvement of many important industrial processes, such as hydroformylation and hydrogenation reactions.[1] As these catalysts are widely used and since Rh is a very scarce element, the efficient separation of the used metal-containing catalyst from product streams is of paramount importance. However, the complete recovery of the often very low concentration of catalyst is a difficult task. A highly efficient technique for the recovery of low concentrations of metal ions is ion exchange, due to the ease of separation of the adsorbed metal ions from the product stream. Earlier findings indicated that silica is a very suitable backbone, due to its high chemical and thermodynamical stability and fast recovery kinetics.[2]

One of the difficulties is to find optimal binding. This means, the ligands′ binding capacity should be sufficiently strong. On the other hand, if the coordination is too strong, the desorption becomes very difficult, as previous studies on the recovery of two Rh-containing model catalyst with ion exchangers that possessed ligands with both N and S donor atoms already pointed out.[3]

Amine ligands are known to coordinate well to platinum group metals and a number of studies have focussed on their application, mainly as anionic extractants for hydrometallurgical purposes.[4,5] The efficient recovery of Rh almost always proved to be the bottleneck, though. The Rh extraction is complicated due to its chemical behaviour in chloride media, and desorption of the loaded ion exchangers is often incomplete or only possible under very harsh elution conditions.[6,7]

This communication describes our first investigations on the tuning of the recovery of $RhCl_3$, which is both used as a catalyst precursor and as a real catalyst,[8–11] with silica-based ion exchangers containing (poly) amine functionalities.

The ion exchangers used for this investigation contain a monoamine (**1**), ethylenediamine (**2**), diethylenetriamine (**3**)[12] and propylenediamine (**4**) functionalities (Table 1).†

In order to gain insight into the stability of the binding of the different ligands with the Rh metal-ions, distribution coefficients have been measured at different pH values (Fig. 1).[3] Clearly, the log *D* values of ion exchangers **1** and **4** are much lower than of **2** and **3**. The stability of Rh-complexes with the latter two ion exchangers proved to be some 3–10 times higher over the entire tested pH range (Fig. 1).

An explanation for the observed behaviour lies in the ability of **2** and **3** to form highly stable chelate rings with Rh, whereas **1** can only coordinate in a monodentate fashion. Another striking feature is the observed log *D* difference between **2** and **4**. The experiment clearly demonstrates, that the complex formation of ligands that contain five-membered chelate rings with Rh metal-ions is favoured over those forming six-membered rings. This is in agreement with previous findings on metal ion selectivity, that already indicated the preference of relatively large metal ions to coordinate with chelating ligands *via* five-membered rings whereas relatively small transition metals prefer larger, six-membered rings.[13]

At low pH (< 2), the amines are protonated[14] and binding will probably proceed *via* an ion association way, with positively charged amine ligands binding in an ionic fashion to a negatively charged Rh complex of the type $[RhCl_{6-n}(H_2O)_n]^{(3-n)-}$ (with *n* generally 0–2).[6] The somewhat lower log *D* values at pH 1–2, are caused by the presence of Cl^- ions from the HCl/NaCl buffers which compete with the metal ions for binding to the ion exchangers. At higher pH, HOAc/NaOAc buffers have been used, and these coordinate less strongly to the Rh metal-ions. Still, the acetate ions, present in increasing amounts with increasing pH, also compete when the ligand to metal complexes are weaker (Fig. 1, **1** and **4**).

For the recovery of Rh, ion exchangers **1**–**4** were added to a fresh solution of $RhCl_3{\cdot}3H_2O$‡ in water, 1 M HCl or EtOH (absolute), to study the effect of the adsorption medium on the stripping possibility. The desorption was done in 2 M HNO_3, as it proved to be the most effective stripping agent. The results are depicted in Fig. 2. Since the ligand concentrations vary significantly between the different ion exchangers (see Table 1) it is more correct to not only look at the uptake capacity (*C*, mmol g^{-1}) but to compare the ligand occupation (*L*, %) as well. This value is defined in the following way: *L* (%) = [uptake capacity (*C*) for M^{n+} (mmol g^{-1})]/[ligand concentration (mmol/g silica)].

The maximum ligand capacities have been found to increase with increasing ligand concentration. A maximum of over 0.5 mmol g^{-1} ion exchanger could be extracted (> 50 mg Rh/g ion exchanger). The extraction percentage is clearly very dependent on the adsorption medium; the Rh adsorption in water and ethanol proved to be much more efficient (about 40–70%) than

Table 1 Ion exchanger characteristics

Ion exchanger	Grafted group	Ligand conc./ mmol g^{-1}[a]
1	$-(CH_2)_3NH_2$	1.14
2	$-(CH_2)_3NHCH_2CH_2NH_2$	1.02
3	$-(CH_2)_3NH(CH_2CH_2NH)_2H$	0.63
4	$-(CH_2)_3NH_2CH_2CH_2CH_2NH_2$	0.68

[a] Based on the N content.

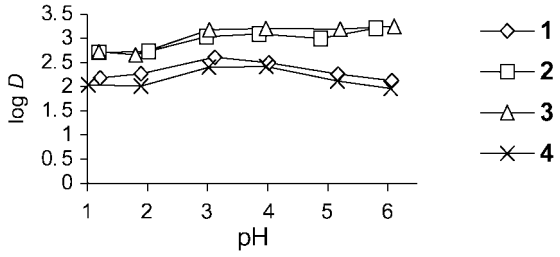

Fig. 1 The distribution coefficients for Rh^{3+} uptake using ion exchangers **1**–**4**. *D* = (mmol M^{n+}/g of dry ion exchanger)/(mmol M^{n+}/ml of solution). The ligand to metal ratio is 5 : 1.

 DOI: 10.1039/b108457g

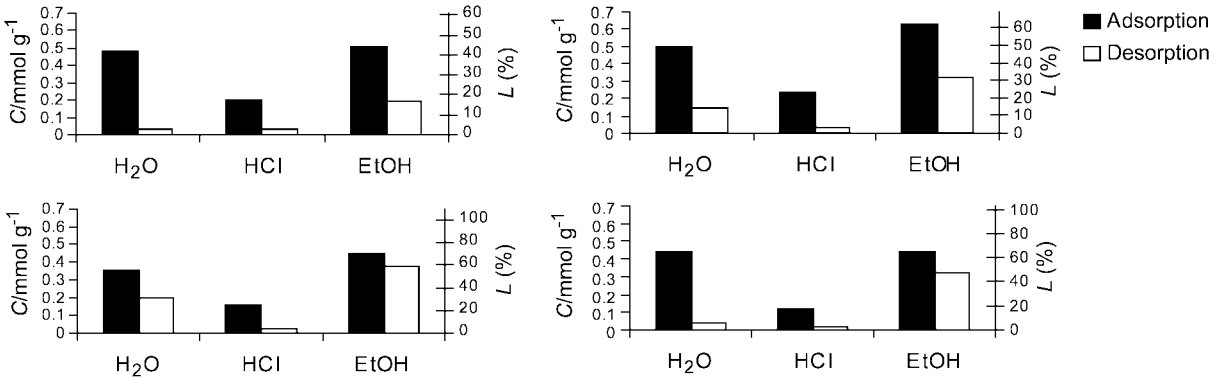

Fig. 2 Recovery experiments of Rh^{3+}-loaded ion exchangers **1** (top left), **2** (top right), **3** (bottom left) and **4** (bottom right).§ Black bars indicate the loaded ion exchangers after adsorption of Rh^{3+} in H_2O, 1 M HCl or absolute EtOH for 48 h. White bars indicate the amount of Rh^{3+} left on the ion exchanger after desorption in 2 M HNO_3 for 48 h. *Reagents and conditions*: adsorption: $RhCl_3{\cdot}3H_2O$ (an amount, corresponding to a ligand to metal ratio of 1 : 1) in 50 ml of solvent (H_2O, 1 M HCl or absolute EtOH), 200 mg ion exchanger, agitation for 2 days. Desorption: 100 mg loaded ion exchanger, 50 ml 2 M HNO_3, agitation for 2 days.

in 1 M HCl (maximum 25%). The difference can be explained by a different extraction mechanism under the adsorption conditions, as discussed above. The large amounts of chloride ions strongly compete with the metal ions for the positively charged binding sites. The possible coordination of more than one ligand to a single Rh metal-ion might be an explanation for the inability of any of the ion exchangers to attain a 100% ligand occupancy.

The desorption possibility (Fig. 2, right bars), after Rh adsorption in water, increased in the following way: **3** ≪ **2** ≪ **4** = **1**

The stripping percentages range from 45% when the diethylenetriamine ion exchanger **3** is used to >90% for the monoamine ion exchanger **1**. Evidently, the formation of five-membered chelate rings has a strongly negative effect on the desorption. This effect already becomes clear with ethylenediamine but is more strongly displayed when multiple chelate rings are formed. Apparently, the six-membered chelate rings, that ion exchanger **4** forms with the metal ions, are stable enough for good adsorption (64%), but not too stable, to prevent easy desorption.

These desorption differences are absent when the adsorption was performed in 1 M HCl, demonstrating the absence of binding in a chelate fashion under these conditions. Although the adsorptions were much lower, a good desorption was obtained with all the ion exchangers (>80%).

The desorption, after adsorption in ethanol, proved to be very difficult for all the ion exchangers used. This has most probably to do with partial reduction of the Rh metal ions in this solvent, as reported by Hernan *et al.*[15] and Kriek *et al.*[16]

In conclusion, it is shown that very efficient recovery of Rh^{3+} has been achieved with amine-containing ion exchangers that form complexes with log *D* values lying roughly between 2.0 and 2.5. Both the ligand capacity and the elution percentage of the metal ion have proven to be very dependent on the adsorption conditions.

The work is currently being extended to the possible application in a continuous system. This implies that important factors such as adsorption and desorption kinetics, successive recovery and the use of other Rh-containing catalysts will be investigated.

Financial support comes from the IOP (Innovation Oriented Research Programme, The Netherlands) Environmental Technology/Heavy Metals cluster Separation, project number IZW97411. Dr W. Buijs (DSM-Research) is acknowledged for stimulating discussions. Mr J. J. M. van Brussel is thanked for his technical assistance.

Notes and references

† A mixture of 3-chloropropyltrimethoxysilane (83 mmol) and 1,3-diaminopropane (250 mmol) was heated under argon at 150 °C for 6 h. After cooling, the white solid phase was filtered off and the liquid phase was purified by vacuum distillation (bp 112–114 °C/1 mm Hg). Yield 5.18 g (22%).^{1}H NMR (300 MHz, $CDCl_3$): δ 0.61 (t, 2H, $SiCH_2$) 1.00 (br s, 2H, NH_2), 1.21 (t, 9H, OCH_2CH_3), 1.55–1.65 (m, 4H, $SiCH_2CH_2$, $NHCH_2CH_2CH_2NH_2$), 2.59–2.64 (2 × t, 4H, CH_2NHCH_2), 2.74 (t, 2H, CH_2NH_2), 3.80 (q, 6H, OCH_2CH_3). Subsequent immobilisation was performed similarly to ion exchangers **1**–**3**.[12]

‡ As $RhCl_3$ shows extensive aquation (the formation of kinetically rather inert aquochloro complexes) with time, freshly prepared $RhCl_3$-solutions (<10 min old) were always used. Furthermore, hardly any variation in the pH has been observed.

§ The determinations of the uptake capacities and desorption, are based upon the metal content on the ion exchangers, established by concentrated acid digestion as previously described.[3]

1 B. Cornils and W. A. Herrmann, *Applied Homogeneous Catalysis with Organometallic Compounds*, ed. B. Cornils and W. A. Herrmann, VCH Publishers, NY, 1996, vol. 29.
2 H. J. Hoorn, P. deJoode, D. J. Dijkstra, W. L. Driessen, H. Kooijman, N. Veldman, A. L. Spek and J. Reedijk, *J. Mater. Chem.*, 1997, **7**, 1747.
3 J. Kramer, A. Scholten, W. L. Driessen and J. Reedijk, *Inorg. Chim. Acta*, 2001, **315**, 183.
4 G. P. Demopoulos, *Hydrometallurgy*, 1989, **82**, 165.
5 I. A. Kovalev, L. V. Bogacheva, G. I. Tsysin, A. A. Formanovsky and Y. A. Zolotov, *Talanta*, 2000, **52**, 39.
6 E. Benguerel, G. P. Demopoulos and G. B. Harris, *Hydrometallurgy*, 1996, **40**, 135.
7 M. S. Alam, K. Inoue and K. Yoshizuka, *Hydrometallurgy*, 1998, **49**, 213.
8 H. J. Borg, L. C. A. Vandenoetelaar and J. W. Niemantsverdriet, *Catal. Lett.*, 1993, **17**, 81.
9 J. Blum, *Russ. Chem. Bull.*, 1993, **42**, 1619.
10 M. Lin and A. Sen, *Nature*, 1994, **368**, 613.
11 M. M. Mdleleni, R. G. Rinker and P. C. Ford, *Inorg. Chim. Acta*, 1998, **270**, 345.
12 J. Kramer, W. L. Driessen, K. R. Koch and J. Reedijk, *Hydrometallurgy*, to be submitted.
13 P. Comba, *Coord. Chem. Rev.*, 1999, **185–186**, 81.
14 B. K. Tait and D. P. Shillington, *S. Afr. J. Chem.*, 1992, **45**, 17.
15 P. Hernan, C. del Pino and E. Ruiz-Hitzky, *Chem. Mater.*, 1992, **4**, 49.
16 R. J. Kriek, W. J. Engelbrecht and J. J. Cruywagen, *J. S. Afr. Inst. Min. Metall.*, 1995, 75.

CHEMCOMM
Communication
www.rsc.org/chemcomm

Silicon-29 diffusion-ordered NMR spectroscopy (DOSY) as a tool for studying aqueous silicates

Robin K. Harris,*[a] Katherine A. Kinnear,[b] Gareth A. Morris,*[b] Marc J. Stchedroff,*[b] Abdolraouf Samadi-Maybodi[c] and Naser Azizi[ac]

[a] *Department of Chemistry, University of Durham, South Road, Durham, UK DH1 3LE. E-mail: r.k.harris@durham.ac.uk*
[b] *Department of Chemistry, University of Manchester, Oxford Road, Manchester, UK M13 9PL. E-mail: g.a.morris@man.ac.uk*
[c] *Department of Chemistry, Faculty of Basic Sciences, University of Mazandaran, P.O. Box 311, Babolsar, Iran*

Received (in Cambridge, UK) 13th September 2001, Accepted 12th October 2001
First published as an Advance Article on the web 30th October 2001

The first use of silicon-29 diffusion-ordered NMR spectroscopy (DOSY) is reported, in a study of the speciation of aqueous silicates.

Aqueous silicate solutions are extensively used in industry, with applications in the preparation of detergents, adhesives and coatings. The diversity of silicate chemistry familiar from the solid phase extends also to solution, with alkaline solutions of silica forming a wide range of species from the silicate monomer through small oligomers up to colloids.[1] Silicon-29 NMR is a useful tool in the study of such species,[2–6] although the modest (negative) magnetogyric ratio, low natural abundance (4.7%) and long spin–lattice relaxation times of this spin-1/2 nucleus pose some experimental obstacles. At natural abundance of ^{29}Si, there are difficulties also in attempting to link together different signals for the same species. The dependence of the rate of self-diffusion on molecular size, shape and solvation makes high-resolution diffusion-ordered NMR spectroscopy (DOSY),[7–9] in which pulsed field gradient spin–echo experiments are used to construct a two-dimensional plot of signal strength as a function of chemical shift and of diffusion coefficient, a natural candidate as a method of studying silicate speciation.

Experiments were carried out at room temperature (21 °C) and 99.34 MHz using a 5 mm broadband probe (Nalorac Corporation) equipped with a 0.6 T m^{-1} actively shielded gradient coil in a 500 MHz Varian Unity spectrometer. To enable field-frequency locking, solutions were made up in H_2O–D_2O mixtures; samples were stored in plastic vials to avoid contamination with ions leached from glassware. Spectra were measured using the bipolar pulse pair stimulated echo (BPPSTE) pulse sequence,[9] with a 90° pulse duration of 20 μs.

Fig. 1 shows the DOSY spectrum of a sample of 0.5 mol kg^{-1} ^{29}Si enriched silicate in 1 mol kg^{-1} aqueous (90% H_2O/10% D_2O) tetramethylammonium hydroxide (TMAOH), prepared by dissolving enriched silica ($^{29}SiO_2$, 99.35%, Cambridge Isotope Laboratories, Inc.) in TMAOH (Aldrich) at 70 °C overnight. Two-parameter exponential fitting of peak height as a function of gradient strength squared was used to extract a diffusion coefficient D for each detected peak. The DOSY spectrum was then constructed by taking the NMR lineshape from the lowest gradient spectrum in the NMR (horizontal) dimension for each peak and giving it a Gaussian shape, with a width determined by the estimated standard error in D, centred on the fitted diffusion coefficient D in the diffusion (vertical) dimension.

The result is clear resolution of the four principal species found in this system, the monomeric silicate unit **1** (the Q^0 species, where the superscript indicates the number of siloxane bridges to a given silicon centre), the cyclic trimer **3** (Q^2), the prismatic hexamer **7** (Q^3) and the cubic octamer **8** (Q^3). As

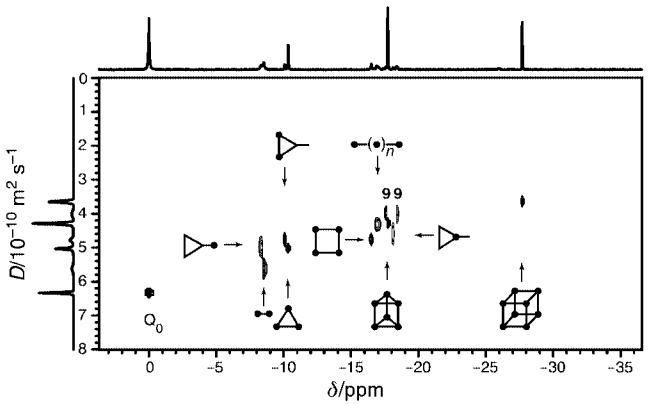

Fig. 1 99.34 MHz ^{29}Si DOSY spectrum of 0.5 mol kg^{-1} ^{29}Si-enriched silicate in 1 mol kg^{-1} aqueous tetramethylammonium hydroxide, measured as described in the text, with (top) the normal ^{29}Si spectrum and (side) the integral projection onto the diffusion axis. 10 BPPSTE spectra of 320 transients each were measured in a total time of 7 h, using gradient pulses of duration 1.5 ms and amplitude from 0.1 to 0.6 T m^{-1}, and a diffusion time Δ of 0.5 s. Chemical shifts are referenced to the Q^0 signal at 0 ppm.

expected, the diffusion coefficients decrease as the number of silicate units in the species increases, with the cubic octamer having the slowest diffusion of these species. Magnetic equivalence causes each of the species to display a single line, making their signals the most prominent in the spectrum. The dimer **2** and cyclic tetramer **6** are also seen, at lower concentration, as are signals from several species displaying multiplet structure due to scalar (Si,Si) coupling. Here the ability of the DOSY technique to identify signals from the same species is apparent, all three signals from species **5** appearing, as expected, at similar positions in the diffusion domain. Similarly, the two signals marked '9' in Fig. 1 appear at the same diffusion coefficient, and at the chemical shifts tentatively assigned in ref. 5 to the pentacyclic heptamer **9** (though the Q^2 signal cannot be identified). One limitation of the technique is illustrated by the remaining peak, from the inner silicate units of linear oligomers **4**, where a number of signals from different species coincide in the NMR dimension and hence show an averaged diffusion coefficient (the terminal silicate signals of the linear oligomers are obscured by the terminal silicate signal of **5**).

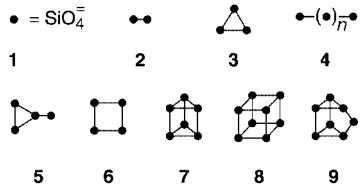

 DOI: 10.1039/b108325m

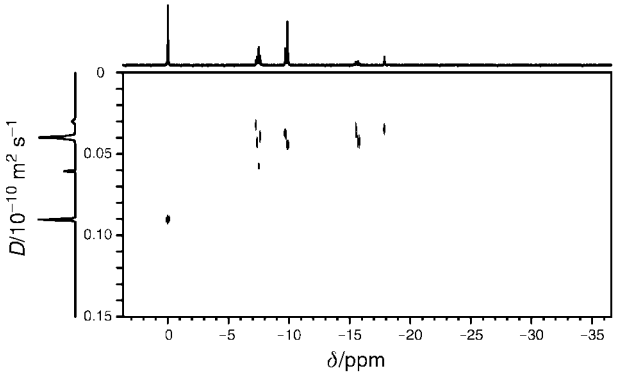

Fig. 2 99.34 MHz ^{29}Si DOSY spectrum of 13 mol kg^{-1} natural abundance silicate in 13 mol kg^{-1} aqueous NaOH. 10 BPPSTE spectra of 480 transients each were measured in a total time of 10 h, using gradient pulses of duration 5.8 ms and amplitude from 0.1 to 0.6 T m^{-1}, and a diffusion time Δ of 1.3 s.

Fig. 2 shows the DOSY spectrum at natural abundance of a sample containing 13 mol kg^{-1} silicate (34% SiO_2 by weight) and 13 mol kg^{-1} NaOH (Aldrich) in HDO, again prepared by dissolution of silica (produced by hydrolysis of silicon tetrachloride (99.8% purity; Janssen Chemical Co.) using doubly distilled water) in alkaline solution at 70 °C overnight. Here, once again, well-resolved signals are seen, but without multiplet structure, and at diffusion coefficients almost two orders of magnitude lower. The spectrum is dominated by low coordination species (Q^0, Q^1 and Q^2), and signal intensities are broadly consistent with the known silica content, suggesting that most if not all of the silicate species are NMR visible. The chemical shifts and DOSY correlations are consistent with a mixture of species **1**, **2**, **3**, **4** and **5**; such assignments could be tested by homonuclear correlation on an enriched sample. The sharp lines suggest short rotational correlation times, whereas such slow diffusion is normally associated with large (colloidal) particles. In practice Stokes' law, which represents the solution as a continuous medium and from which size estimates are generally derived *via* the Stokes–Einstein relation, is not applicable to such concentrated solutions of strongly interacting particles, in which obstruction effects outweigh viscous drag. The unrealistic radii which this relation produces for species in concentrated sodium silicate solutions have been noted previously.[6]

^{29}Si DOSY is potentially a highly effective tool for studying speciation in silicate solutions, where sensitivity permits, allowing the separation of signals of different species and the estimation of their relative sizes. The principal limitations of the technique are the difficulty of extracting useful diffusion data for strongly overlapping NMR signals, the limited receptivity of the ^{29}Si nucleus, and the complications (line broadening, diffusional averaging) caused by chemical exchange. As comparison between Figs. 1 and 2 shows, a wide range of different sizes of aggregate is accessible to study.

G. A. M. thanks the EPSRC for grant GR/M16863 and N. A. is grateful to the Iranian Ministry of Education for a Scholarship. We thank Dr A. M. Kenwright for helpful discussions.

Notes and references

1 *Soluble Silicates*, ed. J. S. Falcone, ACS Symp. Ser. 194, Washington D.C., 1982.
2 G. Engelhardt, D. Zeigan, H. Jancke, D. Hoebbel and W. Wieker, *Z. Anorg. Allg. Chem.*, 1975, **418**, 17.
3 R. K. Harris and R. H. Newman, *J. Chem. Soc., Faraday Trans. 2*, 1977, **73**, 1204.
4 R. K. Harris and C. T. G. Knight, *J. Chem. Soc., Faraday Trans. 2*, 1983, **79**, 1525.
5 R. K. Harris and C. T. G. Knight, *J. Chem. Soc., Faraday Trans. 2*, 1983, **79**, 1539.
6 E. K. F. Bahlmann, R. K. Harris, K. Metcalfe, J. W. Rockliffe and E. G. Smith, *J. Chem. Soc., Faraday Trans.*, 1997, **93**, 93.
7 C. S. Johnson Jr., *Prog. Nucl. Magn. Reson. Spectrosc.*, 1999, **34**, 203.
8 H. Barjat, G. A. Morris, S. Smart, A. G. Swanson and S. C. R. Williams, *J. Magn. Reson., Ser. B*, 1995, **108**, 170.
9 M. D. Pelta, H. Barjat, G. A. Morris, A. L. Davis and S. J. Hammond, *Magn. Reson. Chem.*, 1998, **36**, 706.

CHEMCOMM
Communication
www.rsc.org/chemcomm

Reversible encapsulation of multiple, neutral guests in hexameric resorcinarene hosts

Alexander Shivanyuk and Julius Rebek, Jr*

The Skaggs Institute for Chemical Biology and The Department of Chemistry, The Scripps Research Institute, MB-26, 10550 North Torrey Pines Rd., La Jolla, CA 92037 USA. E-mail: jrebek@scripps.edu

Received (in Columbia, MO, USA) 6th August 2001, Accepted 2nd October 2001
First published as an Advance Article on the web 8th November 2001

A variety of aromatic guest molecules are co-encapsulated with Bu_4SbBr in an assembly of six resorcinarene subunits.

Resorcinarenes are known to form huge, hexameric hydrogen bonded capsules in the crystalline state.[1] The hexamer of **1a** reported by MacGillivray and Atwood[1a] resembles a cube with six resorcinarenes as its sides and eight water molecules at its 'corners' (Fig. 1). Through NMR studies in water-saturated $CDCl_3$, we recently showed that six molecules of **1b** assemble to encapsulate appropriately sized tetraalkylammonium or phosphonium salts.[2] Here we report that covalent antimony(v) bromides **2**[3] also induce capsule formation and leave enough room inside to reversibly co-encapsulate various aromatic guests.

The ^{1}H NMR spectrum of resorcinarene **1b** in *water-saturated* $CDCl_3$ is shown in Fig. 2A. The expected sets of signals for the protons of resorcinol rings, methine bridges, hydroxy groups and water (at 3.0 ppm) are present.[4] Addition of Bu_4SbBr results in the formation of a complex having high kinetic stability (Fig. 2B): separate signals for bound and free guest are present and the exchange rates are slow on the NMR timescale (600 MHz, 313 K). The large upfield shifts of the guest signals are the earmarks of encapsulation. Integration of the appropriate signals at different host–guest ratios clearly shows that one molecule of **2a** is complexed by six(!) molecules of **1b**. The broadened resonance of water is found at 3.0 ppm and indicates that it, too, is an integral component of the assembly.[5] A similar complex is formed between **1b** and the tetraphenyl derivative **2b**, but the less polar Bu_4Si and Bu_4Ge are not encapsulated within **1b**.

Reversible encapsulation in the liquid state occurs optimally when ~55% of the space in the host is occupied by guests.[6] One molecule of Bu_4SbBr (V = 314 Å^3) or Ph_4SbBr (V = 340 Å^3) leaves enough space in the cavity of **6**$\cdot$$8H_2O$ (V = 1375 Å^3) for occupancy by appropriate smaller guest molecules. This co-encapsulation was confirmed by NMR spectroscopy.

The addition of benzene to the complex resulted in splitting of the signals for the methylene protons of encapsulated Bu_4SbBr and the appearance of a broadened singlet at 5.9 ppm (Fig. 3A). The 1D-GOESY experiment established that the latter peak corresponds to the protons of encapsulated benzene molecules (Fig. 3B). The relatively small upfield shift of −1.2 ppm suggests that, on average, the benzene molecule(s) are situated at some distance from the magnetically anisotropic regions of the hexameric capsule.[7] At higher concentrations of benzene the protons of encapsulated Bu_4SbBr emerge as three sets of signals (Fig. 3C).[8] The set **c** appears at the expense of the set **b** and the original set **a**. Analogous behavior was observed on the addition of toluene and *p*-xylene. No encapsulation of benzene, toluene or *p*-xylene could be detected in absence of Bu_4SbBr; the principal guest determines the properties of the inner space of the capsule.

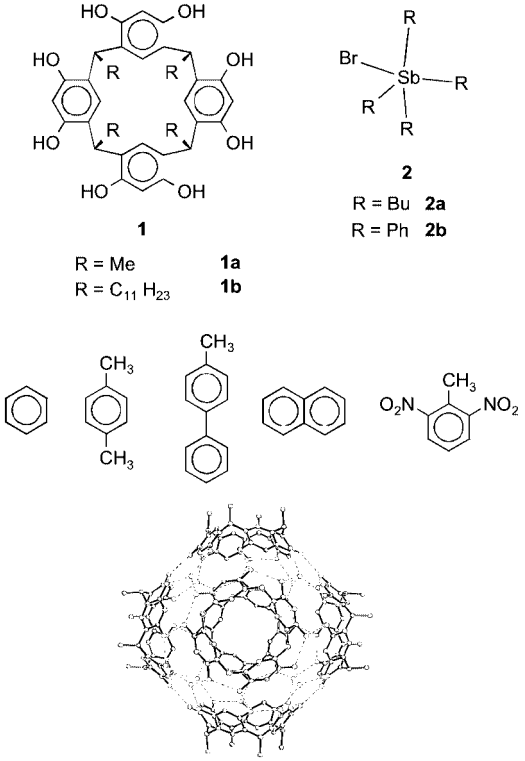

Fig. 1 Resorcinarenes, their guests and the crystal structure of the hexameric capsule **6**$\cdot$$8\ H_2O$.[1a]

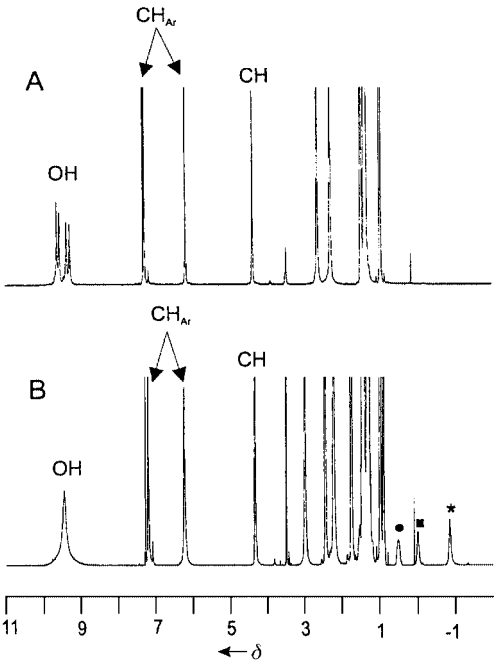

Fig. 2 The ^{1}H-NMR spectra in $CDCl_3$ saturated with H_2O (600 MHz, 313 K): A) **1b**; B) **1b** + Bu_4SbBr. The signals of encapsulated Bu_4SbBr are marked with an asterisk (methyl groups) and solid square and circle (methylene groups).

 DOI: 10.1039/b109464p

Addition of 4-phenyltoluene to the complex 6**1b**·Bu_4SbBr gives rise to an additional set of signals for the methylene groups of encapsulated Bu_4SbBr (Fig. 3D). Further addition of 4-phenyltoluene increases the new set of signals at the expense of the original set (Fig. 3E). Through 1D-GOESY-experiments it was shown that the singlet at −0.75 ppm corresponds to the methyl protons of encapsulated 4-phenyltoluene $\Delta\delta = -3.05$ ppm.

To probe the dimensions and the character of the remaining space in the Bu_4SbBr complex, a range of guests were added. Amongst those also encapsulated were ethylbenzene, *p*-xylene, propylbenzene, amylbenzene, nitrobenzene, 4-nitrotoluene, 2,6-dinitrotoluene, naphthalene, biphenyl, anthracene and azulene. Those not encapsulated include heptylbenzene, 1,4-dimethyl-2,6-dinitrobenzene, hexamethylbenzene, trans-stilbene, azobenzene, *p*-terphenyl. The longest guest co-encapsulated with Bu_4SbBr appears to be 4-phenyltoluene, since the slightly longer 4,4′-dimethylbiphenyl was not encapsulated under the same conditions. Hexafluorobenzene, cyclohexane and pentane were also not encapsulated suggesting that not only the size and shape of the aromatic guest but also its polarity and polarizability determines its co-inclusion with Bu_4SbBr.

Hexameric capsule encapsulating tetraphenylantimony bromide **2b** is also able to include benzene, toluene, *p*-xylene, however no encapsulation of *p*-phenyltoluene occurred. This difference in binding properties of 6 : 1 complexes of **2b** and **2a** is caused most probably by a larger volume of **2b** which does not leave enough space for the co-encapsulation of *p*-phenyltoluene.

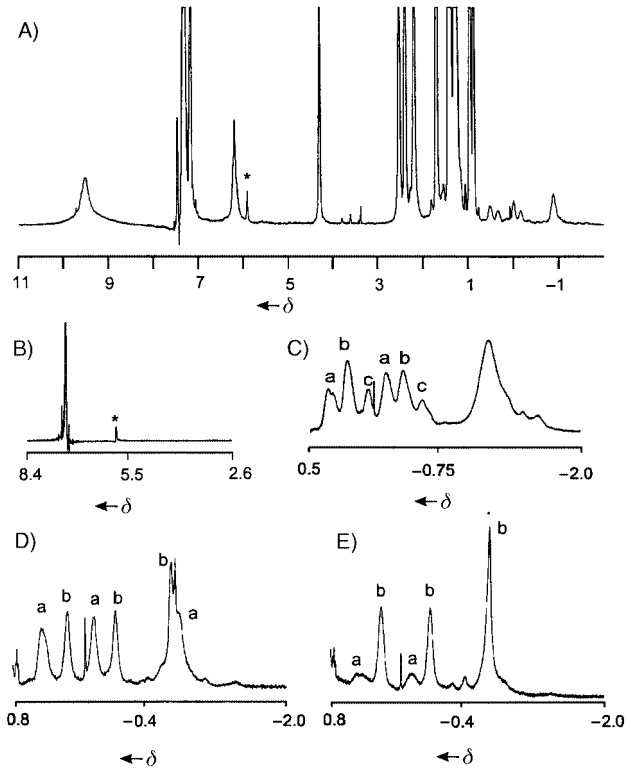

Fig. 3 (A) The ^{1}H-NMR spectrum of **1b** + Bu_4SbBr + 60 equiv. benzene; (B) 1D-GOESY spectrum with saturation of the benzene signal; the signal of encapsulated benzene is indicated by an asterisk. (C) Up-field window of the spectrum in the presence of 20% of benzene-d_6. (D) **1b** + Bu_4SbBr + 13 equiv. 4-phenyltoluene; (E) **1b** + Bu_4SbBr + 42 equiv. 4-phenyltoluene. The signal of the methyl protons of the encapsulated guest is marked by an asterisk.

The resorcinarenes hold a special place among modules for molecular recognition: their chemical modifications provided the first cavitands,[9] then carcerands[10] and hydrogen bonded capsules.[11] More than a decade ago Aoyama and co-workers[12] described the formation of *stoichiometric* (1 : 1) complexes of **1b** (Fig. 1) with dicarboxylic acids, sugars and even steroids in $CDCl_3$ solution. We now see that the resorcinarene **1b** is capable of hexameric assembly and encapsulates sizable molecules, independent of their hydrogen bonding abilities but dependent on the presence of water. The principal guest **2** fine tunes the binding properties of the hexameric cavity, and is essential for further encapsulation of smaller, aromatic guests.

We are grateful to the Skaggs Research Foundation and The National Institutes of Health for financial support. A. S. is a Skaggs Postdoctoral Fellow.

Notes and references

1 (*a*) L. R. MacGillivray and J. L. Atwood, *Nature*, 1997, **389**, 469; (*b*) T. Gerkensmeier, W. Iwanek, C. Agena, R. Frolich, S. Kotila, C. Nather and J. Mattay, *Eur. J. Org. Chem.*, 1999, 2257.

2 A. Shivanyuk and J. Rebek Jr., *Proc. Natl. Acad. Sci. USA*, 2001, **98**, 7762.

3 O. Knop, B. R. Vincent and T. S. Cameron, *Can. J. Chem.*, 1989, **67**, 63; G. Ferguson, C. Glidewell, L. Douglas and S. Matcalfe, *J. Chem. Soc., Perkin. Trans.*, 1988, 731.

4 Y. Tanaka and Y. Aoyama, *Bull. Chem. Soc. Jpn.*, 1990, **63**, 3343.

5 Carefully dried resorcinarene 1b is *insoluble* in $CDCl_3$ dried over molecular sieves, but heating the mixture gives a gel that dissolves immediately after addition of water. In $CDCl_3$ with a little water, resorcinarene **1b** shows a very broad and featureless spectrum characteristic of ill-defined hydrogen bonded aggregates. The addition of guests **2** to this solution results in very broad signals for the complexed species; these sharpen when water is added.

6 A. S. Mecozzi and J. Rebek Jr., *Chem. Eur. J.*, 1998, **4**, 1016.

7 This shift is about one half of that seen with carcerands and hemicarcerands (J. Ayub and J. C. Sherman, *Chem. Rev.*, 1999, **99**, 931) dimeric self-assembling capsules of cavitands (R. G. Chapman, G. Olovsson, J. Trotter and J. C. Sherman, *J. Am. Chem. Soc.*, 1998, **120**, 6252) or calix[4]arene tetraurea derivatives (B. C. Hamman, K. D. Shimizu and J. Rebek Jr., *Angew. Chem., Int. Ed. Engl.*, 1996, **35**, 1326; O. Mogck, E. F. Paulus, V. Böhmer, I. Thondorf and W. Vogt, *Chem. Commun.*, 1996, 2533; L. Frish, S. E. Matthews, V. Böhmer and Y. Cohen, *J. Chem. Soc., Perkin Trans. 2*, 1999, 669).

8 The addition of benzene-d_6 resulted in the same changes, although the signal of encapsulated benzene was absent.

9 J. R. Moran, S. Karbach and D. J. Cram, *J. Am. Chem. Soc.*, 1982, **104**, 5826.

10 J. C. Sherman, C. C. Knobler and D. J. Cram, *J. Am. Chem. Soc.*, 1991, **113**, 2194; D. J. Cram and J. M. Cram, *Container Molecules and their Guests*, Royal Society of Chemistry, Cambridge, 1994.

11 M. M. Conn and J. Rebek Jr., *Chem. Rev.*, 1997, **97**, 1647; J. C. Sherman, *Tetrahedron*, 1995, **51**, 3395; T. Heinz, D. M. Rudkevich and J. Rebek Jr., *Nature*, 1998, **394**, 764; A. Shivanyuk, E. F. Paulus and V. Böhmer, *Angew. Chem.*, 1999, **111**, 3091; *Angew. Chem., Int. Ed.*, 1999, **38**, 2906.

12 Y. Aoyama, Y. Tanaka, H. Toi and H. Ogoshi, *J. Am. Chem. Soc.*, 1988, **110**, 634; Y. Aoyama, Y. Tanaka and S. J. Sugahara, *J. Am. Chem. Soc.*, 1989, **111**, 5397.

CHEMCOMM Communication
www.rsc.org/chemcomm

Nearly pure blue photoluminescent poly{2,7-[9-{3,5-bis[3,5-bis(benzyloxy)benzyloxy]benzyl}-9-(3,6-dioxaoctyl)]fluorene} in film†

Hong-Zhi Tang,[a] Michiya Fujiki,*[ab] Zhong-Biao Zhang,[ab] Keiichi Torimitsu[b] and Masao Motonaga[a]

[a] *CREST-JST, 3-1 Wakamiya, Morinosato, Atsugi, Kanagawa 243–0198, Japan*
[b] *NTT Basic Research Laboratories, NTT Corporation, 3-1 Wakamiya, Morinosato, Atsugi, Kanagawa 243-0198, Japan. E-mail: fujiki@will.brl.ntt.co.jp*

Received (in Cambridge, UK) 6th September 2001, Accepted 11th October 2001
First published as an Advance Article on the web 30th October 2001

The first unsymmetrically substituted polyfluorene bearing a bulky poly(benzyl ether) dendron and less bulky 3,6-dioxaoctyl groups in the 9-position was designed and synthesized, which gives almost a pure bluish photoluminescence with negligible weak greenish excimer emission around 520 nm even in a thermally annealed thin solid film.

Recently, π-conjugated polyfluorene (PF) has been attracting intensive interest due to its bluish photo/electro-luminescence properties with high quantum yield.[1] However, greenish excimer emission and significant fluorescence quenching generally occur for this blue light emitter in a solid film.[2] Among the methods to avoid the detrimental π-aggregation behavior,[3] much effort has been made to introduce bulky dendrons like poly(benzyl ether) (Fréchet-type) or polyphenylene into the conjugated polymer backbone, *i.e*., end-capping of poly[2,7-(9,9-di-*n*-hexyl)fluorene][4] and symmetrically 9,9-bis-substituting PFs.[5] The resulting PFs have been found to significantly suppress the excimer emission even in their thermally annealed solid films. In addition to these symmetrically 9,9-bis-substituted PFs, the unsymmetrically substituted PF having two different side groups in the 9-position has also attracted much attention.[6] As an example, a PF bearing two different methyl and 4-cyanobutyl groups in the 9-position was designed and synthesized towards water-soluble conjugated polymer.[6b] Based on the assumption that a regio-random PF bearing two different substituents in the 9-position may significantly suppress the π-aggregation in a solid film to decrease the greenish excimer emission and the combination of bulky dendrons with less bulky groups will increase the luminophore density, thereby producing a strong luminescence, we have designed and synthesized a new unsymmetrically substituted PF **4** (Scheme 1) bearing semiflexible bulky poly(benzyl ether) dendrons and linear 3,6-dioxaoctyl groups in the 9-position. We now report that **4** emits almost a pure blue color photoluminescence even in a thermally annealed thin solid film, while the greenish excimer emission was drastically suppressed even compared to the corresponding 9,9-bis-dendron-substituted **5**.

The synthetic procedures are outlined in Scheme 1. The resulting 2,7-dibromo-9-lithiofluorene from 2,7-dibromofluorene (**1**) (Aldrich) and 2-fold lithium diisopropylamide (LDA) (Aldrich) was reacted with an equivalent amount of 1-bromo-3,6-dioxaoctane (Lancaster) at −60 to 25 °C in THF, yielding 2,7-dibromo-9-(3,6-dioxaoctyl)fluorene (**2**).[7] Using the phase transfer catalyst, triethylbenzyl ammonium chloride (Kanto), the monomer **3** was synthesized from **2** and 3,5-bis[3,5-bis(benzyloxy)benzyloxy]benzyl bromide (**R-Br**) (TCI). The conversion was almost quantitative, which was evidenced by the complete disappearance of the triplet signal of 9-H at 4.10 ppm in the ^{1}H NMR spectrum. Polymerization was carried out using the zero-valent nickel reagent, bis(1,5-cyclooctadiene)-nickel(0) ($Ni(COD)_2$) (Kanto), and the end-termination was accomplished using 2-bromofluorene (Acros).[8] For a comparison of the photophysical properties with **4**, the two corresponding symmetrically 9,9-bis-substituted **5** and **6** were also synthesized using previouly reported method.[8] The structures of all the synthesized monomers and PFs were confirmed by NMR and elemental analysis.†

PF **4** as well as **5** is highly soluble in common organic solvents, *e.g*., THF, toluene and chloroform, but **6** has limited solubility in THF and toluene although it is readily soluble in chloroform. The molecular weights of **4**, **5** and **6** (soluble part in THF) estimated by gel permeation chromatography (GPC) *versus* the polystyrene standards in THF at 30 °C are M_w = 26,300 (M_w/M_n, 2.0), M_w = 32,700 (M_w/M_n, 1.7), and M_w = 381,300 (M_w/M_n, 2.6), respectively. Differential scanning calorimetry (DSC) (heating at 10 °C min^{-1} at the second run) revealed that **4** and **5** have softening points at around 58 °C and 62 °C, respectively, evidenced by the endothermic peaks, while **6** exhibits a melting point of 182 °C.

As shown in Fig. 1, the UV-vis spectrum of **4** in THF solution exhibits two absorption bands at 386.0 nm (ε = 3.1 × 10^4 (fluorene-repeating-unit)$^{-1}$ dm^3 cm^{-1}) and 284.0 nm (ε = 1.1 × 10^4 (fluorene-repeating-unit)$^{-1}$ dm^3 cm $^{-1}$), probably ascribed to the π–π* transition of the conjugated polymer backbone and the phenylene in the side dendrons, respectively. The $\lambda_{max,abs}$ of **4** exhibits only a slight red shift of 2 nm compared to that of **5** ($\lambda_{max,abs}$, 384.0 nm), implying that the number of bulky dendron side chains does not affect the torsion angle in the conjugated polymer backbone, but shows a large blue shift of 8.5 nm compared to that of **6** ($\lambda_{max,abs}$, 394.5 nm), probably due to the larger steric hindrance impacted by the bulky dendrons than the two less bulky 3,6-dioxaoctyl groups. The photoluminescence (PL) spectrum of **4** in THF solution exhibits the two characteristic sharp peaks at 415.0 and 437.0 nm and a low energy shoulder near 470.0 nm, almost identical to those of the corresponding **5** ($\lambda_{max,emi}$, 414.0 nm, excited at 384.0 nm) and **6** ($\lambda_{max,emi}$, 417.0 nm, excited at 394.5 nm). The quantum yield of **4** in THF is estimated to be 58%, comparable to 54% of **5** and 53% of **6**.†

Fig. 2 compares the UV-vis and PL spectra of **4**–**6** in the thermally annealed thin solid films. The UV-vis spectrum of **4** in the film exhibits no absorption band broadening except for the $\lambda_{max,abs}$ showing a minute red shift of 2.5 nm in comparison to that in THF solution. This is similar to **5** in the film and THF solution. On the other hand, **6** in the solid film gave a UV-vis spectrum with a significantly broadened absorption band and a new absorption peak around 399 nm compared to that in THF solution, indicating that a specific intensive aggregation formed. The PL spectrum of **4** in the film shows two characteristic $\lambda_{max,emi}$s at 423.0 and 447.5 nm and a tail in the range 500 to 700 nm. On the other hand, **5** gave a PL spectrum with a featureless long wavelength emission (excimer emission)

† Electronic supplementary information (ESI) available: characterization data for **2**, **3**, and **4**, and measurement details of the quantum yield in THF solution. See http://www.rsc.org/suppdata/cc/b1/b108097k/

 DOI: 10.1039/b108097k

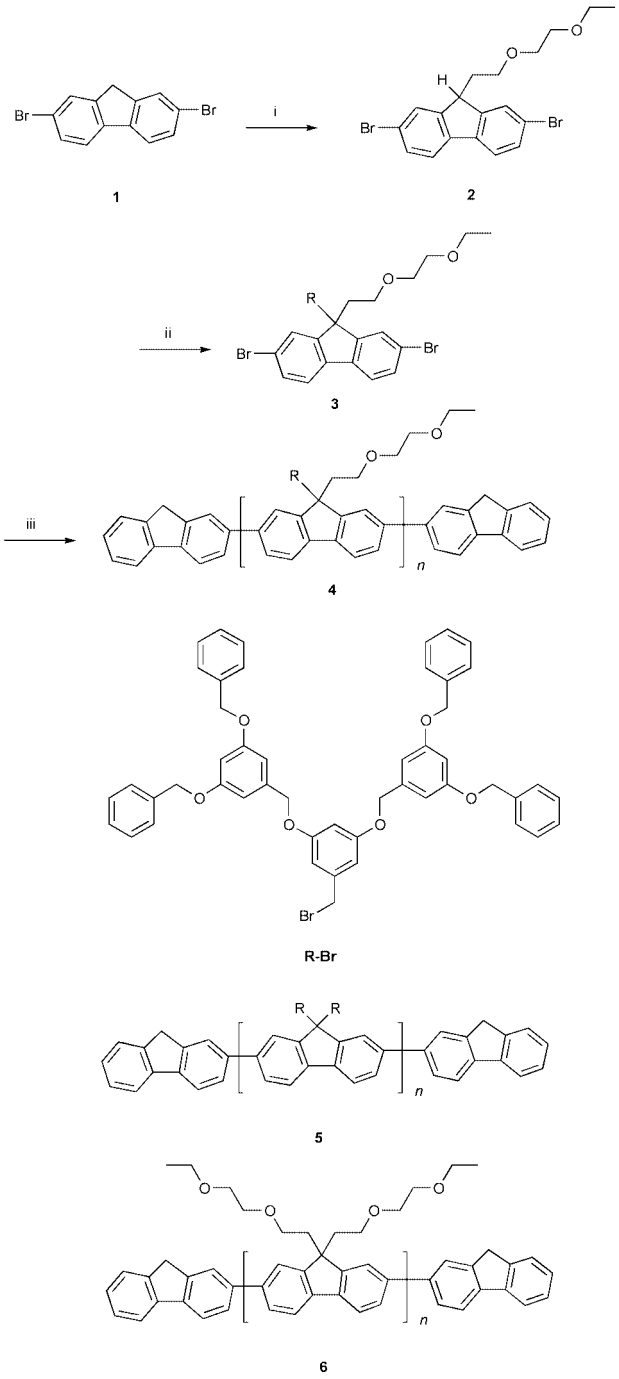

Scheme 1 *Reagents and conditions*: i, 2-equimolar LDA, THF, 1-bromo-3,6-dioxaoctane, −60 to 25 °C, 3 h, 60%; ii, **R-Br**, 50% aq. NaOH, DMSO, triethylbenzyl ammonium chloride, 25 °C, overnight, ~100%; iii, $Ni(COD)_2$–1,1′-bipyridyl (1 : 1, mol/mol), COD, DMF–toluene (1 : 4, v/v), 80 °C, 4 d; 2-bromofluorene in toluene, 4 h, 80%.

band around 520 nm, which is much weaker than that for **6**, indicating that the steric impact of the dendritic substituents significantly suppresses the intermolecular π-stacking of the polymer backbone. The weak excimer emission for **5** could be due to the liquid crystalline property already reported for the poly(phenylenevinylene)s having poly(benzyl ether) dendron side chains.[9] The almost negligible weak excimer emission for **4** in the film might result from an amorphous structure caused by the regio-random backbone structure, which is possibly related to the lower softening point than that of **5**. Thus, the replacement of one dendron with a less bulky substituent in the 9-position enables almost pure blue photoluminescence.

In conclusion, the first well-defined unsymmetrical-substituted **4** bearing bulky poly(benzyl ether) dendron and less bulky 3,6-dioxaoctyl substituents in the 9-position gave almost a pure bluish photoluminescence with negligible weak greenish excimer emission around 520 nm even in the thermally annealed thin solid film, showing the great potential for the construction of large-area blue light emitters.

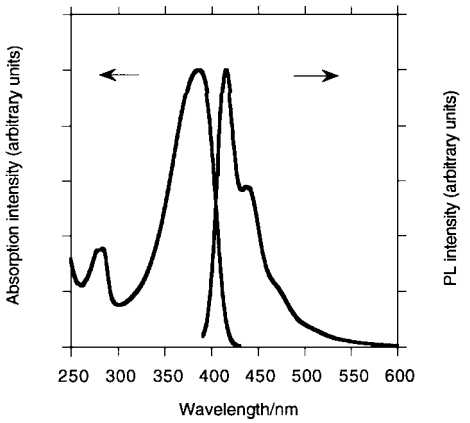

Fig. 1 UV-vis absorption (3.0×10^{-5} mol L^{-1} of the fluorene-repeating-unit) and PL (1.4×10^{-6} mol L^{-1} of the fluorene-repeating-unit) spectra of **4** (excited at 386.0 nm) in THF solution at 25 °C.

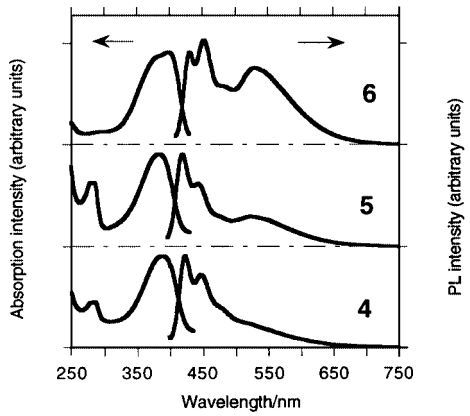

Fig. 2 Normalized UV-vis absorption and PL spectra of **4** (excited at 388.5 nm), **5** (excited at 384.5 nm) and **6** (excited at 399.0 nm) in thin solid films prepared by the spin-coating method from chloroform solution ($\sim 10^{-2}$ mol L^{-1} of the fluorene-repeating-unit) on a quartz substrate upon annealing at 200 °C for 3 h *in vacuo* followed by slow cooling to 25 °C.

We gratefully thank Dr Hideaki Takayanagi for his continuing support. CREST-JST is acknowledged for funding at NTT.

Notes and references

1 (*a*) M. Fukuda, K. Sawada and K. Yoshino, *Jpn. J. Appl. Phys.*, 1989, **28**, L1433Q.-B. Pei and Y. Yang, *J. Am. Chem. Soc.*, 1996, **118**, 7416; (*c*) J. Teetsov and M. A. Fox, *J. Mater. Chem.*, 1999, **9**, 2117.

2 (*a*) J. Huber, K. Müllen, J. Salbeck, H. Schenk, U. Scherf, T. Stehlin and R. Stern, *Acta Polym.*, 1994, **45**, 244; (*b*) M. Grell, D. D. C. Bradley, G. Ungar, J. Hill and K. S. Whitehead, *Macromolecules*, 1999, **32**, 5810.

3 G. Klärner, M. H. Davey, W.-D. Chen, J. C. Scott and R. D. Miller, *Adv. Mater.*, 1998, **10**, 993.

4 G. Klaerner, R. D. Miller and C. J. Hawker, *Polym. Prepr. (Am. Chem. Soc., Polym. Sci. Div.)*, 1998, **39**(2), 1006.

5 (*a*) D. Marsitzky, R. Vestberg, C. J. Hawker and K. R. Carter, *Polym. Prepr. (Am. Chem. Soc., Polym. Sci. Div.)*, 2000, **41**(2), 1344; (*b*) S. Setayesh, A. C. Grimsdale, T. Weil, V. Enkelmann, K. Müllen, F. Meghdadi, E. J. W. List and G. Leising, *J. Am. Chem. Soc.*, 2001, **123**, 946; (*c*) A. C. Grimsdale, A. Herrmann, S. Setayesh, T. Weil and K. Müllen, *Polym. Mater. Sci. Eng.*, 2001, **84**, 6.

6 (*a*) D. M. Johansson, M. Theander, T. Granlund, O. Inganäs and M. R. Andersson, *Macromolecules*, 2001, **34**, 1981; (*b*) B. Liu, Z.-K. Chen, W.-L. Yu, Y.-H. Lai and W. Huang, *Thin Solid Films*, 2000, **363**, 332.

7 (*a*) M. Ranger and M. Leclerc, *Chem. Commun.*, 1997, 1597; (*b*) M. Ranger, D. Rondeau and M. Leclerc, *Macromolecules*, 1997, **30**, 7686; (*c*) M. Ranger and M. Leclerc, *Macromolecules*, 1999, **32**, 3306.

8 H.-Z. Tang, M. Fujiki, M. Motonaga and K. Torimitsu, *Polym. Prepr. (Am. Chem. Soc., Polym. Sci. Div.)*, 2001, **42**(1), 440.

9 Z.-N. Bao, K. R. Amundson and A. J. Lovinger, *Macromolecules*, 1998, **31**, 8647.

CHEMCOMM Communication
www.rsc.org/chemcomm

New fluorocarbon iodides†

Richard D. Chambers,* Julian A. Cooper, Elodie Copin and Graham Sandford*

University of Durham, Department of Chemistry, South Road, Durham, UK DH1 3LE.
E-mail: R.D.Chambers@durham.ac.uk; Graham.Sandford@durham.ac.uk

Received (in Cambridge, UK) 21st August 2001, Accepted 16th October 2001
First published as an Advance Article on the web 8th November 2001

A general, efficient approach for the synthesis of fluorocarbon iodides and di-iodides bearing hydrocarbon groups is described and the synthetic utility of these new systems is demonstrated in reactions with thiols.

Perfluorocarbon iodides (R_FI) have been important for many years as 'building blocks' for the synthesis of various organic compounds containing fluorine.[1–3] For example, they are crucial components in the synthesis of highly efficient surfactants on the industrial scale.[4] Here, we report an approach to the synthesis of fluorocarbon iodides that bear hydrocarbon end-groups and demonstrate the potential of these systems for further synthesis of fluorinated derivatives.

We are exploring the use of the carbon–hydrogen bond as a functional group in efficient free radical chain reactions with fluorinated alkenes,[5] *e.g.* formation of **1** and **2** from cyclohexane,‡ and have begun to explore the chemistry of the resultant fluorinated adducts. It has been demonstrated that stereospecific elimination of hydrogen fluoride[5] from **1** and **2** leads to unsaturated derivatives **3** and **4** respectively. We now find that alkene derivatives **3** and **4** react with a stoichiometric mixture of iodine pentafluoride and iodine, that corresponds to iodine monofluoride, giving fluorinated iodide **5** and di-iodide **6** respectively in efficient processes (Scheme 1).

The mechanism of iodine monofluoride addition is of interest because the process is regiospecific, to the limits of detection by ^{19}F NMR. In principle, we could envisage two possible mechanisms for addition of I–F to **3** (Scheme 2). Route B involves first addition of iodine to the double bond, but the next step would then require selective replacement of iodine at the R–CFI site by fluorine and we see no convincing reason for this to occur. Furthermore, we have been unable to add iodine to **3** to give a di-iodide. In contrast, we find that other additions to **3** involving bromine, iodine monochloride and iodine monobromide are efficient processes and moreover, additions involving ICl and IBr are regiospecific. It is surprising that these electrophilic additions proceed so readily with electron deficient double bonds but the regioselectivity is entirely consistent with an electrophilic process. The developing carbocationic site in intermediate **7a** is stabilised by cyclohexyl and by fluorine, whereas **7b** would be strongly destabilised by the attached trifluoromethyl group and so, consequently, we favour Route A.

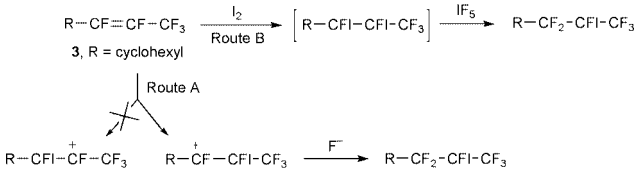

Scheme 2

Novel iodides **5** and **6** react with thiols and di-thiols, most likely *via* an $S_{RN}1$ mechanism,[6] giving thioethers **8a–d**[7] and di-thioethers **9**, mostly in high yields (Scheme 3) and oxidation of the thioether products to the corresponding sulphones was possible using chromium trioxide in acetic acid.

These preliminary results demonstrate that these unusual fluorocarbon iodide 'building blocks' could be used for approaches to a variety of new systems containing fluorinated groups.

We thank EPSRC and the University of Durham (Studentship to E. C.) and the Royal Society (University Research Fellowship to G. S.).

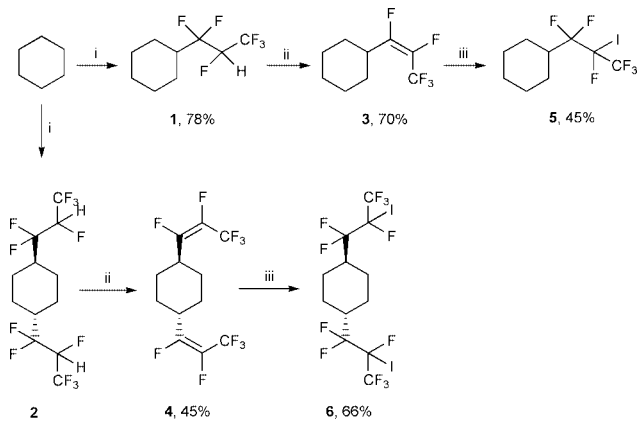

Scheme 1 *Reagents and conditions*: i, CF_2=CF–CF_3, (*t*-BuO)$_2$, 140 °C; ii, t-BuOK, 0 °C; iii, I_2, IF_5, 0 °C.

† Electronic supplementary information (ESI) available: characterisation of new fluorocarbon iodides **5–9**. See http://www.rsc.org/suppdata/cc/b1/b107565a/

Notes and references

‡ Reaction of cyclohexane with two equiv. of hexafluoropropene yields a mixture of 1,3- and 1,4- dihexafluoropropylcyclohexane adducts. However, the *trans*-1,4-diadduct **2** crystallises from the diadduct mixture and can, therefore be readily separated and purified by filtration (see ref. 5).

1 L. E. Deev, T. I. Nazarenko, K. I. Pashkevich and V. G. Ponomarev, *Russ. Chem. Rev.*, 1992, **61**, 40.
2 N. O. Brace, *J. Fluorine Chem.*, 1999, **93**, 1.
3 N. O. Brace, *J. Fluorine Chem.*, 2001, **108**, 147.
4 N. S. Rao and B. E. Baker, in *Organofluorine Chemistry. Principles and Commercial Applications*, ed. R. E. Banks, B. E. Smart and J. C. Tatlow, Plenum, New York, 1994, p. 321.
5 R. D. Chambers, R. W. Fuss, R. C. H. Spink, M. P. Greenhall, A. M. Kenwright, A. S. Batsanov and J. A. K. Howard, *J. Chem. Soc., Perkin Trans. 1*, 2000, 1623.
6 A. E. Feiring, *J. Fluorine Chem.*, 1984, **24**, 191.
7 All compounds were characterised by elemental analysis, NMR and mass spectrometry. For example, **8d**; a yellow oil; bp 292 °C; (Found: C, 48.7; H, 6.3. $C_{26}H_{38}F_{12}S_2$ requires C, 48.6; H, 5.9%); ν_{max}/cm^{-1} 2857 and 2932 (C–H); δ_H 1.0 –2.0 (32H, m, CH_2), 2.20 (2H, m, $CHCF_2$), 2.8 (4H, m, CH_2S); δ_C 24.7 (t, $^3J_{CF}$ 4.2, *C*H_2CH), 25.4 (s, CH_2), 25.5 (s, CH_2), 25.5 (t, $^3J_{CF}$ 4.2, CH_2CH), 25.7 (s, CH_2), 28.5 (s, C-4), 28.8 (s, C-3), 28.9 (s, C-2), 39.0 (s, CH_2S), 42.4 (t, $^2J_{CF}$ 21.7, $CHCF_2$), 101.4 (dm, $^1J_{CF}$ 242.7, CF), 120.6 (ddd, $^1J_{CF}$ 262.1, $^1J_{CF}$ 253.7, $^2J_{CF}$ 24, CF_2), 122.3 (qd, $^1J_{CF}$ 287.6, $^2J_{CF}$ 35.2, CF_3); δ_F −72.8 (3F, m, CF_3), −112.0 and −112.7 (2F, AB, J_{AB} 267.6, CF_2), −158.4 (m, CFS); *m*/*z* (EI$^+$) 642 (M$^+$, 1%), 409 (40), 227 (65), 143 (100).

 DOI: 10.1039/b107565a

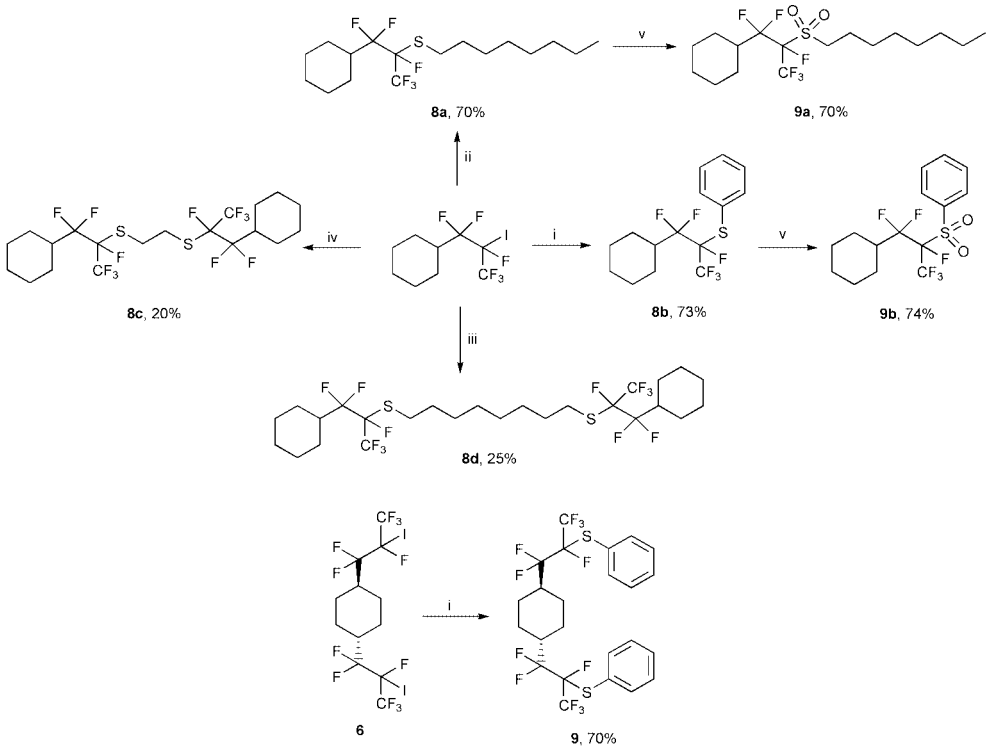

Scheme 3 *Reagents and conditions*: i, PhSNa, DMF, rt; ii, $C_8H_{17}SNa$, DMF, rt; iii, NaS–C_8H_{16}–SNa, DMF, rt; iv, NaS–C_2H_4–SNa, DMF, rt; v, CrO_3, CH_3COOH, reflux, 3 h.

CHEMCOMM Communication
www.rsc.org/chemcomm

Synthesis of a highly thermally stable octupolar polyimide for nonlinear optics†

Thomas Le Bouder,[a] Olivier Maury,[a] Hubert Le Bozec,*[a] Isabelle Ledoux[b] and Joseph Zyss[b]

[a] *Laboratoire de Chimie de Coordination et Catalyse, UMR 6509 CNRS-Université Rennes 1, Institut de Chimie, Campus de Beaulieu 35042. Rennes Cedex, France. E-mail: lebozec@univ-rennes1.fr*
[b] *Laboratoire de Physique Quantique Moléculaire, ENS Cachan, 61 avenue du président Wilson 94235. Cachan, France*

Received (in Cambridge, UK) 6th September 2001, Accepted 10th October 2001
First published as an Advance Article on the web 30th October 2001

A new polyimide with covalently incorporated 4,4′-bis-(dialkylaminostyryl)-2,2′-bipyridine chromophores is described which allows the synthesis of the corresponding NLO octupolar metallo-polymer.

Polymers featuring nonlinear optical (NLO) chromophores are of particular interest due to potential applications in electro-optic devices.[1] A current approach for the design of NLO materials is the covalent attachment of NLO-phores to a polymer backbone, and increasing numbers of side-chain, main-chain and cross-linked polymers have been recently designed.[2] Among them, aromatic polyimides appear to be very promising materials due to their high thermal stabilities and high glass transition temperatures.[3]

Beyond the dipolar approach, recognition in the early nineties of the enlarged potential for nonlinear optics of octupolar chromophores has opened a new field of research.[4] Metal bipyridyl complexes offer many possibilities for the design of non-centrosymmetric octupolar molecules.[5] For instance, large nonlinearities have been demonstrated for octahedral metal complexes[6] and tetrahedral copper(I) complexes[7] possessing 4,4′-bis(dialkylaminostyryl)-2,2′-bipyridines. Despite their interesting properties, so far only the third-order optical nonlinear properties of one polymer containing a substituted 1,3,5-triazine octupole has been reported.[8] We now describe the synthesis, characterisation and preliminary solution NLO activity of the first polyimide functionalised by an octupolar ruthenium trisbipyridyl complex.

To achieve the synthesis of the desired polymer, the preparation of the proper monomer was required. Our approach began with the synthesis of dihydroxy-substituted 4,4′-bis-(dialkylaminostyryl)-2,2′-bipyridine **1a** (x = 1).[9] In order to get more soluble polymers, **1b** (x = 2) was prepared in 74% yield by the same route, *i.e.* from 4,4′-dimethyl-2,2′-bipyridine and *p*-(*N*-butyl-*N*-tetrahydropyranyloxybutyl)aminobenzaldehyde **b** (Scheme 1).[10] NLO polyimides are generally prepared *via* the condensation of a diamino functionalised chromophore with dianhydrides. Therefore, the bis-diamino substituted 4,4′-bis(dialkylaminostyryl)-2,2′-bipyridines **2a** and **2b** were readily prepared (81 and 74% yield, respectively) from **1a** and **1b** using the Mitsunobu reaction and followed by the cleavage of the phthalimido protecting groups with hydrazine. The diamine derivatives were then reacted with hexafluoroisopropylidene diphthalic anhydride (6FDA) in NMP at 25 °C, followed by chemical imidization with Ac_2O–pyridine,[11] to yield the expected polyimides **3a** and **3b**. It is worth noting that the presence of butyl end groups and C_4 linkers in **3b** leads to enhanced solubility in organic solvents (NMP, THF and dichloromethane), as compared to the poor solubility of **3a** in the same solvents. The structure of **3a** and **3b** was confirmed by IR, UV-visible and NMR (^{1}H, ^{19}F) spectroscopies.† In the IR spectra, the polyimides display characteristic absorptions at *ca.* 1780, 1720 and 740 cm^{-1}, attributed to the imide rings, and all the resonance peaks in the ^{1}H NMR spectra can be assigned to the protons of the bipyridine moieties and polymer backbone. Their UV-visible spectra are characterised by a broad intramolecular charge-transfer absorption band at *ca.* 400 nm, comparable to that of the monomer precursors (Table 1). Gel permeation chromatography gave relatively low molecular weights [M_w (**3a**, 9300; **3b**, 19300 Da); M_n (**3a**, 6600; **3b**, 14100 Da)] indicating an average of *ca.* 7 and 14 bipyridine units in **3a** and **3b**, respectively. These polyimides possess excellent thermal stability, with 5% weight losses (Td_5 determined by TGA) occurring above 370 °C. Thermal analysis by DSC also shows that the glass transition temperature (T_g) of **3b** is significantly lower ($\triangle T_g$ = 45 °C) than that of **3a**, in agreement with the more flexible structure of **3b** (Table 1). The metallo-polyimide **4b** was obtained in 92% yield by refluxing **3b** and $(DBAS\text{-}bpy)_2RuCl_2$ (DBAS-bpy = 4′4′-bis(dibutylamino-styryl)-2,2′-bipyridine) in DMF, followed by an exchange of the

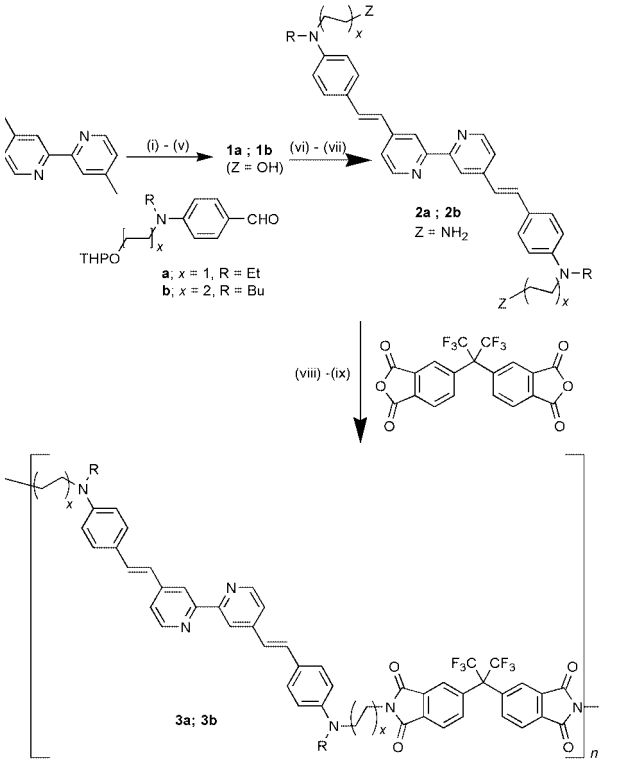

Scheme 1 *Reagents and conditions* (for the synthesis of **1b**–**3b**): i, LDA (2 eq.), THF, −78 °C, 1 h; ii, **b** (2 eq.), THF, −78 °C → rt, 12 h; iii, H_2O, rt, 1 h; iv, PPTS (0.1 eq.), toluene, reflux, 6 h; HCl 6 N (0.5 eq.), EtOH–H_2O, 80 °C, 15 h; vi, PPh_3 (2 eq.), DEAD (2 eq.), THF, rt, 15 h; vii, H_2NNH_2 (10 eq.), THF, reflux, 15 h; viii, 6FDA (1 eq.), NMP, 0 °C → rt, 48 h; ix, pyridine (16 eq.), $(CH_3CO)_2O$ (36 eq.), 60 °C, 15 h.

† Electronic supplementary information (ESI) available: detailed synthetic procedures and complete spectroscopic characterisations of compounds **1**–**4**. See: http://www.rsc.org/suppdata/cc/b1/b108099g/

 DOI: 10.1039/b108099g

Table 1 Optical and thermal properties

Compound	λ_{max} (nm)/ε (L mol^{-1} cm^{-1})[a]	Td_5 (°C)[b]	Tg (°C)[c]
1a	387 (56000)	338	—
1b	398 (54000)	356	—
2a	384 (43000)		—
2b	400 (38000)		—
3a	388	374	210
3b	401	398	165
4b	445–513	358	—[d]

[a] Measured in dichloromethane.[b] Decomposition temperature at 5% weight loss determined by TGA.[c] Determined by DSC.[d] Not observed.

chloride counterions with tris(tetrachlorobenzenediolato)phosphate (TRISPHAT) anions and precipitation in Et_2O (Scheme 2). The use of this anion was found to greatly enhance the solubility of the resulting polymer in solvents such as THF and dichloromethane.[12] The complete coordination of all bipyridine units was confirmed by ^{1}H NMR, which showed an upfield shift of the H_6 protons by *ca*. 1 ppm upon complexation.[12] The UV-visible spectrum is similar to that of the Ru(DBAS-bpy)$_3^{2+}$ monomer with two maxima at 445 and 513 nm due to the overlapping metal to ligand (MLCT) and intra-ligand (ILCT) charge-transfer transitions. This new polymer also displays high thermal stability (Td_5 = 358 °C).

The molecular hyperpolarisability β of the metallo-polyimide **4b** was measured by means of the harmonic light scattering technique (HLS).[13] To circumvent the problems associated with reabsorption of the second harmonic and enhancement of β by two-photon absorption fluorescence, the experiment was performed at a fundamental wavelength of 1.91 μm in dichloromethane.[14] The β value of **4b** is 1300 × 10^{-30} esu, which is approximately 4 times larger than that of the parent octupolar

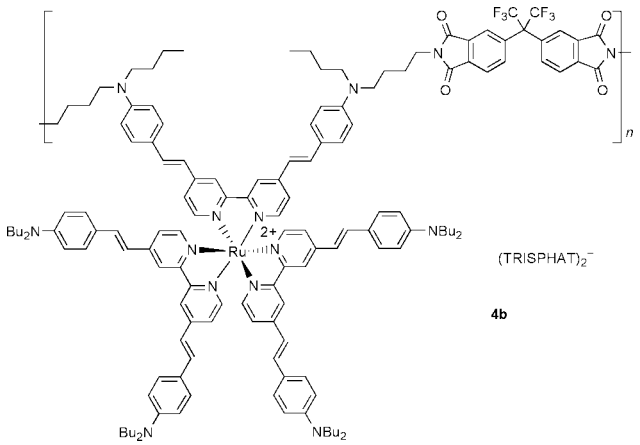

Scheme 2

monomer Ru(DBAS-bpy)$_3^{2+}$ [β(monomer) = 320 × 10^{-30} esu].[15] According to the HLS principle, the number N of individual monomers in **4b** can be inferred from the following relationship $<\beta^2(\text{polymer})> = N <\beta^2(\text{monomer})>$. Thus, a number of *ca*. 16 ruthenium trisbipyridine monomers can be deduced, and it worth noting that this value fits almost perfectly with the average number of 14 obtained from the GPC analysis of **3b**.

In conclusion, we have reported an efficient synthesis of a highly thermally stable octupolar NLO polyimide which exhibits large solution second-order nonlinearity. The designed approach described here also opens the way for the preparation of new push–pull polyimides featuring dipolar chromophores upon complexation of the bipyridyl-polymer ligands to metal complexes.[16] We are continuing to explore the second- and third-order NLO bulk susceptibilities on thin films.

The authors thank the CNET (France-Telecom) and the Conseil Régional de Bretagne for financial support.

Notes and references

1 D. M. Burland, *Chem. Rev., (special issue)*, 1994, **94**, 1; Y. Q. Shi, C. Zhang, H. Zang, J. H. Bechtel, L. R. Dalton, B. H. Robinson and W. H. Steier, *Science*, 2000, **288**, 119.
2 T. J. Marks and M. A. Ratner, *Angew. Chem., Int. Ed.*, 1995, **34**, 155.
3 H. Saadeh, D. Yu, L. M. Wang and L. P. Yu, *J. Chem. Mater*., 1999, **9**, 1865; Z. Liang, L. R. Dalton, S. M. Garner, S. Kalluri, A. Chen and W. H. Steier, *Chem. Mater*., 1995, **7**, 941; D. Yu, A. Gharavi and L. Yu, *J. Am. Chem. Soc*., 1995, **117**, 11680.
4 J. Zyss and I. Ledoux, *Chem. Rev*., 1994, **94**, 77.
5 H. Le Bozec and T. Renouard, *Eur. J. Inorg. Chem*., 2000, 229.
6 C. Dhenaut, I. Ledoux, I. D. W. Samuel, J. Zyss, M. Bourgault and H. Le Bozec, *Nature*, 1995, **374**, 339; F. W. Vance and J. T. Hupp, *J. Am. Chem. Soc*., 1999, **121**, 4047.
7 T. Renouard, H. Le Bozec, I. Ledoux and J. Zyss, *Chem. Commun*., 1999, 871.
8 F. Chérioux, H. Maillotte, P. Audebert and J. Zyss, *Chem. Commun*., 1999, 2083.
9 T. Le Bouder, P. Massiot and H. Le Bozec, *Tetrahedron Lett*., 1998, **39**, 6869.
10 T. Le Bouder, Thesis, University of Rennes, 2000.
11 P. J. A. Kenis, O. F. J. Noordman, N. F. van Hulst, J. F. J. Engbersen, D. N. Reinhoudt, B. H. M. Hams and C. P. J. M. van der Vorst, *Chem. Mater*., 1997, **9**, 596.
12 O. Maury, J. Lacour and H. Le Bozec, *Eur. J. Inorg. Chem*., 2001, 201 and references therein.
13 R. W. Terhune, P. D. Maker and C. M. Savage, *Phys. Rev. Lett*., 1965, **14**, 681; K. Clays and A. Persoons, *Phys. Rev. Lett*., 1991, **66**, 2980.
14 I. D. Morrison, R. G. Denning, W. M. Laidlaw and M. A. Stammers, *Rev. Sci. Instrum*., 1996, **67**, 1445.
15 H. Le Bozec, T. Le Bouder, O. Maury, A. Bondon, I. Ledoux, S. Deveau and J. Zyss, *Adv. Mater*., in press.
16 A. Hilton, T. Renouard, O. Maury, H. Le Bozec, I. Ledoux and J. Zyss, *Chem. Commun*., 1999, 2521; M. Bourgault, K. Baum, H. Le Bozec, G. Pucetti, I. Ledoux and J. Zyss, *New J. Chem*., 1998, 517.

CHEMCOMM
Communication
www.rsc.org/chemcomm

Ferrocene-modified bis(spiropyridopyran)s as synthetic signaling receptors for guanine–guanine dinucleoside derivatives

Masayoshi Takase[a] and Masahiko Inouye*[b]

[a] *Department of Chemistry, Graduate School of Science, Kyoto University, Kyoto 606-8502, Japan*
[b] *Faculty of Pharmaceutical Sciences, Toyama Medical and Pharmaceutical University, Toyama 930-0194, Japan. E-mail: inouye@ms.toyama-mpu.ac.jp*

Received (in Cambridge, UK) 13th August 2001, Accepted 16th October 2001
First published as an Advance Article on the web 30th October 2001

A ferrocene-linked bis(spiropyridopyran) was designed and synthesized, that recognized guanine–guanine dinucleoside derivatives *via* complementary hydrogen bonds in CH_2Cl_2, resulting in the isomerization of the colorless spiropyridopyran as self-indicating receptors.

The recognition and selective binding of nucleobases play essential roles in entire living systems. For example, complementary hydrogen bonds arise in a very specific fashion between purine and pyrimidine bases of the two strands of double-helical DNA in order to store genetic information.[1] Thus, the synthetic models that recognize specific nucleobases and that read-out the recognition event are attracting much attention from the viewpoint of their uses in biological sciences.[2] In this connection, we have reported spiropyridopyrans **1**,[3] isomerization of which to the colored merocyanines **1′** was induced by recognition of guanosine derivatives.[4] To extend this approach to more challenging projects, we focused on the recognition of oligonucleotides. Here we describe the molecular recognition ability and its recognition-induced coloration of a ferrocene-modified bis(spiropyridopyran) **2** for guanine–guanine dinucleosides (Scheme 1).

The choice of ferrocene as a linker was based on the inter-ring spacing of the two Cp rings (0.33 nm),[5] which is near to the spacing between the stacked base pairs.[6] Another advantageous point of the ferrocene skeleton is its restricted conformational flexibility. This may result in the decrease of the entropy loss of **2** upon complexation with dinucleotides.[7] To evaluate the recognition abilities of **2** for dinucleotides in less-polar solvents, lipophilic dinucleoside derivatives were chosen (Fig. 1b). The bulky silyl groups at the 5′ and 3′ ends and the di-*n*-hexylsilylene internucleoside linkage make the dinucleoside soluble in such solvents and prevent their deoxyribofuranoside residues from interacting with the hydrogen-bonding motif of **2**. The decision for utilizing the silylene linkage was based on the similarity of covalent bond radius of tetrahedral silicon (0.117 nm) to that of tetrahedral phosphorus (0.110 nm).[8]

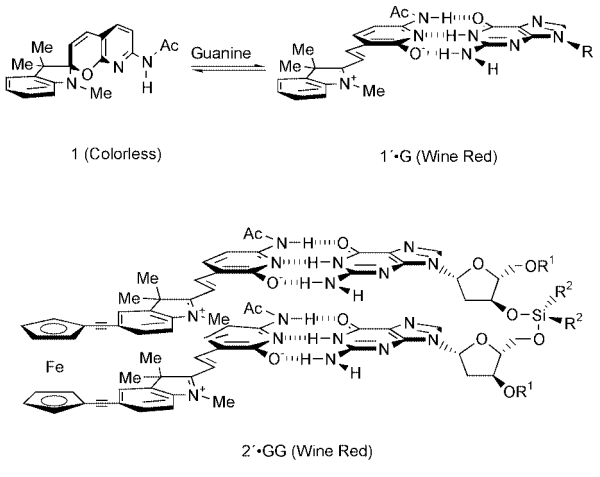

Scheme 1

The 3*H*-indole derivative bearing ethynyl groups at the 5 position was prepared from 4-bromophenylhydrazine by using the Fischer-indole synthesis followed by Sonogashira reaction.[9] Further Sonogashira reaction of the indole with 1,1′-diiodoferrocene[10] gave ferrocene-linked bis(3*H*-indole),[7c] which was methylated at the nitrogen and condensed with 6-acetamido-2-pyridone-3-carbaldehyde[4a] to yield desired bis(spiropyridopyran) **2** (Scheme 2).† The lipophilic dinucleoside derivatives were prepared according to a literature procedure.[8]

The ferrocene-linked bis(spiropyridopyran) **2** showed wine-red color in CH_2Cl_2, indicating that it exists at least partly as the open merocyanine form. This was demonstrated by the ^{1}H NMR spectrum of **2**, in which 10% or less of **2** is present as **2′** on the basis of the integration of the spectrum.‡ Futhermore, the UV-vis spectrum of **2** revealed an absorption maximum around 580 nm ($\varepsilon = 6.9 \times 10^3$) that is unambiguously attributed to the merocyanine chromophore (Fig. 1a; a line of 'none').[4a] In CH_2Cl_2, addition of the guanine–guanine dinucleoside derivative **GG** (10 equiv.) to **2** produced changes in the absorption spectra, and strong absorption bands appeared ($\lambda_{max} = 575$ nm, $\varepsilon = 3.8 \times 10^4$). The change was clearly seen visually, as the wine-red color of **2** dramatically darkened. Unfortunately, the ^{1}H NMR spectrum of the mixture of **2** and **GG** in $CDCl_3$ gave no useful information for the increment of the merocyanine

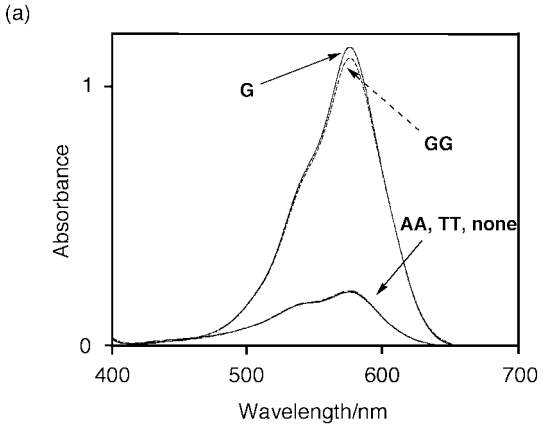

Fig. 1 (a) Electronic absorption spectra of **2** (3.0×10^{-2} mM) in the presence of the lipophilic nucleoside derivatives (3.0×10^{-1} mM) in CH_2Cl_2 at 25 °C. (b) The structures of the dinucleoside derivatives. The guanine–guanine dinucleoside (**GG**) was used as a mixture with 3′–3′ and 5′–5′ homo-coupling dimers. The guanine mononucleoside (**G**) is 3′,5′-bis-*O*-(*tert*-butyldimethylsilyl)deoxyguanosine.

 DOI: 10.1039/b107306k

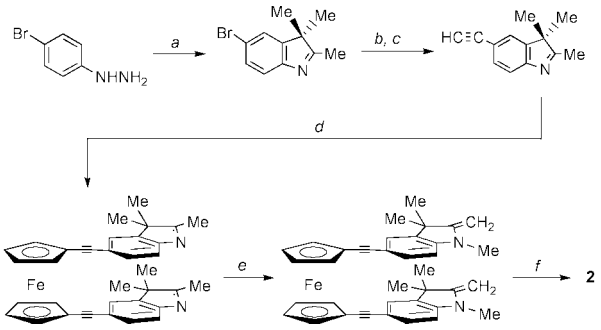

Scheme 2 *Reagents*: (*a*) butan-2-one, AcOH; (*b*) 2-methylbut-3-yn-2-ol, $(Ph_3P)_2PdCl_2$, CuI, Et_2NH; (*c*) NaOH, toluene; (*d*) 1,1′-diiodoferrocene,[10] $(Ph_3P)_2PdCl_2$, $Cu(OAc)_2$, *i*-Pr_2NH; (*e*) MeI, MeCN, then NaOH, H_2O; (*f*) 6-acetamido-2-pyridone-3-carbaldehyde,[4a] EtOH.

form **2′** because of much overlap of the peaks between **2′** and **GG**. The guanine mononucleoside **G** resulted in similar changes to the absorption spectrum, while other mononucleoside (**A**, **T**, **C**) and dinucleoside (**AA** and **TT**) derivatives had absolutely no influence on it (Fig. 1a). These findings indicated that the complementary triple hydrogen bond between the acetamidopyridone anion part of **2′** and guanine bases is critical for selective coloration.

The binding constants were estimated by UV titration at 25 °C using an iterative least-squares curve-fitting with weighting of data points according to the error analysis of Deranleau.[11] The absorbances of the merocyanine forms (575 nm) were monitored as a function of the concentration of guanosine derivatives assuming that all the complexed-spiropyrans exist as merocyanine forms. The association constant between **1′** and **G** displayed 2.4×10^4 M^{-1} ($-\Delta G_{298} = 25.0$ kJ mol^{-1}), while that of **2′** and **GG** was 4.2×10^5 M^{-1} ($-\Delta G_{298} = 32.0$ kJ mol^{-1}). The increment of the binding energy was lower than that predicted by the doubled recognition sites; this may partly result from the electrostatic repulsion between the two zwitterionic merocyanines.

In summary, a ferrocene-modified bis(spiropyridopyran) was developed as a synthetic signaling receptor for guanine–guanine dinucleoside derivatives. The high selectivity for the coloration of the receptor is governed by the hydrogen-bonding complementarity between them. In the future, design and synthesis of the receptors that bind native nucleotides will be expected to show significant practical value.

Notes and references

† **2**: ^{1}H NMR (400 MHz, $CDCl_3$, TMS): δ 1.18 (s, 6 H, $C(CH_3)_2$), 1.33 (s, 6 H, $C(CH_3)_2$), 2.12 (s, 6 H, $COCH_3$), 2.77 (s, 6 H, NCH_3), 4.31 (s, 4 H, Cp-CH), 4.53 (s, 4 H, Cp-CH), 5.67 (d, J = 10.0 Hz, 2 H, pyrane-CH), 6.45 (d, J = 8.0 Hz, 2 H, benzene-CH), 6.83 (d, J = 10.0 Hz, 2 H, pyrane-CH), 7.18 (s, 2 H, benzene-CH), 7.30 (d, J = 8.0 Hz, 2 H, benzene-CH), 7.41 (d, J = 8.0 Hz, 2 H, pyridine-CH), 7.71 (br s, 2 H, NH), 7.72 (d, J = 8.0 Hz, 2 H, pyridine-CH).

‡ **2′** (diagnostic peaks in ^{1}H NMR): 1.73 (s, $C(CH_3)_2$), 2.31 (s, $COCH_3$), 3.62 (s, N^+CH_3). Assignments of the peaks of **2** and **2′** were based on those for **1** and **1′**.[4a]

1 General reviews: (*a*) J. D. Watson, N. H. Hopkins, J. W. Roberts, J. A. Steitz and A. M. Weiner, *Molecular Biology of the Gene, 4th ed*., Benjamin, Menlo Park, 1987; (*b*) B. Alberts, D. Bray, J. Lewis, M. Raff and J. D. Watson, *Molecular Biology of the Cell 3rd ed*., Garland, New York, 1994; (*c*) B. Lewin, *Genes V*, Oxford University, Oxford, 1994.

2 A comprehensive review: *Comprehensive Supramolecular Chemistry*, ed. J. L. Atwood, J. E. D. Davies, D. D. MacNicol and F. Vögtle, Elsevier, Oxford, 1996, vol. 2.

3 General reviews of spiropyrans: (*a*) R. C. Bertelson, in *Photochromism*, ed. G. H. Brown, Wiley-Interscience, New York, 1971, p. 45; (*b*) R. J. Guglielmetti, in *Photochromism, Molecules and Systems*, ed. H. Dürr and H. Bouas-Laurent, Elsevier, Amsterdam, 1990, p. 314; (*c*) R. C. Bertelson, in *Organic Photochromic and Thermochromic Compounds*, ed. J. C. Crano and R. J. Guglielmetti, Plenum, New York, 1999, vol. 1, p. 11.

4 (*a*) M. Inouye, K. Kim and T. Kitao, *J. Am. Chem. Soc*., 1992, **114**, 778; (*b*) M. Inouye, *Coord. Chem. Rev*., 1996, **148**, 265; (*c*) M. Inouye, in *Organic Photochromic and Thermochromic Compounds*, ed. J. C. Crano and R. J. Guglielmetti, Plenum, New York, 1999, vol. 2, p. 393.

5 General reviews of ferrocene: (*a*) A. J. Deeming, in *Comprehensive Organometallic Chemistry*, ed. G. Wilkinson and F. G. A. Stone, Pergamon, Oxford, 1982, vol. 4, p. 475; (*b*) *Ferrocenes*, ed. A. Togni and T. Hayashi, VCH, New York, 1995.

6 A comprehensive review: W. Saenger, *Principles of Nucleic Acid Structure*, Springer-Verlag, New York, 1984.

7 (*a*) M. Inouye, Y. Hyodo and H. Nakazumi, *J. Org. Chem*., 1999, **64**, 2704; (*b*) M. Inouye, M. S. Itoh and H. Nakazumi, *J. Org. Chem*., 1999, **64**, 9393; (*c*) M. Takase and M. Inouye, *Mol. Cryst. Liq. Cryst*., 2000, **344**, 313; (*d*) M. Inouye and M. Takase, *Angew. Chem., Int. Ed*., 2001, **40**, 1746.

8 K. K. Ogilvie and J. F. Cormiew, *Tetrahedron Lett*., 1985, **26**, 4159.

9 Reviews: (*a*) K. Sonogashira, in *Comprehensive Organic Synthesis*, ed. B. M. Trost, I. Fleming, C. H. Heathcock, G. Pattenden, S. V. Ley, S. L. Schreiber, R. Noyori, M. F. Semmelhack, L. A. Paquette and E. Winterfeldt, Pergamon, Oxford, 1991, vol. 3, p. 521; (*b*) K. Sonogashira, in *Metal-Catalyzed Cross-Coupling Reactions*, ed. F. Diederich and P. J. Stang, Wiley-VCH, Weinheim, 1998, p. 203.

10 D. Guillaneux and H. B. Kagan, *J. Org. Chem*., 1995, **60**, 2502.

11 D. A. Deranleau, *J. Am. Chem. Soc*., 1969, **91**, 4044.

CHEMCOMM
Communication
www.rsc.org/chemcomm

More than just a catalyst: a novel role for benzylamine in the sol–gel transcription of organogels†

Arianna Friggeri,[a] Oliver Gronwald,[a] Kjeld J. C. van Bommel,[a] Seiji Shinkai*[a] and David N. Reinhoudt*[b]

[a] *Chemotransfiguration Project, Japan Science and Technology Corporation, Aikawa, Kurume, Fukuoka 839-0861, Japan*
[b] *Chemotransfiguration Project, MESA+ Research Institute, University of Twente, 7500 AE Enschede, The Netherlands*

Received (in Cambridge, UK) 7th September 2001, Accepted 16th October 2001
First published as an Advance Article on the web 8th November 2001

Gelator–catalyst interactions allow the transcription of the organogel structure of methyl-4,6-*O*-(*p*-nitrobenzylidene)-α-D-glucopyranoside (1) into its silica analogue, even in the absence of positive charges or H-bonding sites on the gelator molecule which, until now, were considered indispensable.

Inorganic materials can be shaped into a variety of structures using organic, supramolecular assemblies as templates.[1] Vesicles,[2] organic crystals[3] and phospholipid fibers[4] are just some of the organic templates that have successfully been employed to create interesting silica constructs. In addition, we have found that superstructures formed by organogelators act as excellent templates because of their stable, 'solid-like' aggregation behavior. The growth of helical silica is one of the most striking examples of what can be achieved by using organogel fibers as the template for sol–gel polycondensation of tetraethylorthosilicate (TEOS).[5] It has, however, been shown that the presence of some attractive force between the superstructures and TEOS is indispensable for efficent sol–gel transcription. Therefore, up till now, transcription into silica *via* TEOS polycondensation has been limited to superstructures of molecules that possess a cationic charge in the form of a quaternary ammonium moiety[6] or a metal cation,[5,7] and molecules that possess a H-bonding site in the form of primary amines or combinations of primary and secondary amines.[2,8] The design of new gelators for organogel transcription into silica has, therefore, been strongly limited to molecules containing either positive charges or amino groups.[8] In this paper we show the first example of an organogel that can be successfully transcribed into silica although it does not possess either a positive charge or a H-bonding amino group. We have found that the catalyst for silica formation, *i.e.* benzylamine, can interact with the molecular aggregates of **1**[9] in

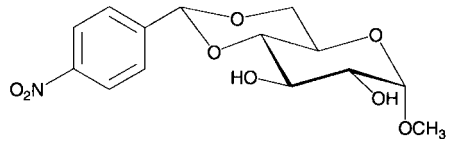

1

the gel fibers, thus providing the driving force necessary for the transcription process. Clear evidence for the gelator–catalyst interaction has been obtained from transmission electron microscopy (TEM), circular dichroism (CD), ^{1}H NMR and FT-IR spectroscopy measurements.

In water, gelator **1** forms a clear gel consisting of a three-dimensional network of curved fibers[9] (Fig. 1a). An aqueous solution containing **1** (0.5 wt%) and benzylamine (ba) in a 1 : 1 ratio also yields a clear gel. However, this particular gel consists of a network of much straighter fibers (Fig. 1b) than those observed for the gel of **1** without benzylamine. The structure of the organogel of **1** is, therefore, altered, to some degree, by the interaction with benzylamine. To transcribe this organic superstructure into silica, polycondensation of TEOS was carried out using an aqueous solution of **1** + ba.[10] After calcination of the sample,[11] TEM images (Fig. 1c and d) showed tubular structures of similar diameter (50–100 nm) and appearance to those observed in the gel samples of **1** + ba, indicating that the transcription was successful. In a sample containing only **1** and TEOS, *i.e.* no catalyst, no silica formation was observed even after several weeks. Apparently, benzylamine can interact with the molecules of **1** in the gel fibers, most likely *via* hydrophobic and/or π–π stacking interactions, making transcription of the organogel possible.

To elucidate the gelation process of **1** with benzylamine, experiments were carried out replacing benzylamine with different catalysts: hydrazine and 3,5-dimethoxybenzylamine. Although an aqueous solution of **1** (0.5 wt%) and hydrazine (in a 1 : 1 ratio) did form a gel, the transcription experiment carried out by adding TEOS to this system yielded only granular silica particles. This result indicates that there is no particular interaction between **1** and hydrazine which can lead to the transcription of the organogel. This observation is in accordance with the assumption that hydrophobic and/or π–π stacking interactions between benzylamine and **1** play a key role in the

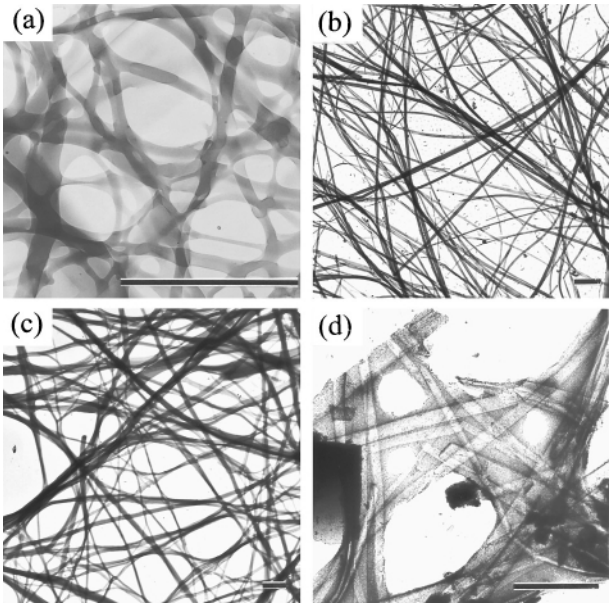

Fig. 1 TEM images of (a) the gel of **1** (scale bar = 0.75 μm), (b) the gel of **1** + ba, (c) the xerogel of **1** + ba + TEOS and (d) the xerogel after calcination (scale bars = 1.50 μm).

† Electronic supplementary information (ESI) available: CD, FT-IR and temperature dependent ^{1}H NMR spectra. See http://www.rsc.org/suppdata/cc/b1/b108148a/

 DOI: 10.1039/b108148a

transcription process. The structure of 3,5-dimethoxybenzylamine is similar to that of benzylamine, however, its bulky methoxy substituents should disturb the stacking of **1** and, therefore, prevent organogel formation. Indeed, an aqueous solution of **1** (0.5 wt%) and 3,5-dimethoxybenzylamine (in a 1 : 1 ratio) did not form a gel upon cooling, but a precipitate and, thus, could not be transcribed. These results strongly indicate that benzylamine interacts with **1** *via* aromatic π–π stacking, without considerable disruption of the gel structure. Such interactions bring a number of amino moieties (from the benzylamine) onto the gel fiber surface thereby providing the stimulus for organogel transcription.

CD spectra of a gel of **1** and of a gel of **1** + ba show slight differences which can be attributed to interactions of the catalyst with **1**. The decrease in spectral intensity for the gel of **1** + ba implies that the chiral superstructure originating from the H-bonding interactions among the sugar moieties of **1** is partially destroyed by bound benzylamine molecules. Furthermore, the appearance of a shoulder (215 nm) on the peak at 212 nm suggests the presence of benzylamine in proximity of, or perhaps even intercalated in the gel fibers.

Additional evidence for the interaction of benzylamine with the gel fibers of **1** was obtained from FT-IR measurements (KBr pellet) of the xerogel of **1** and the xerogel of **1** + ba. The spectrum of the xerogel of **1** shows only a rather broad peak (3750–3100 cm^{-1}) corresponding to H-bonded OH and NH moieties. However, more signals can be distinguished in the spectrum of **1** + ba, *i.e.* shoulders at 3482 cm^{-1} and 3254 cm^{-1}, in comparison with the spectrum of the xerogel of **1** alone. These signals most likely arise from the partial disruption of the H-bonding network of the OH groups in the gel fibers by the interaction of the amino moieties of the catalyst with the gelator molecules within or between the fibers.

To obtain a more detailed picture of the gel of **1** + ba in water, temperature-dependent ^1H NMR spectroscopy was performed. The peaks of the gelator and of the benzylamine appear broadened in the spectrum of the gel at 298 K. This line-broadening effect for the gelator molecules is typical of organogel samples due to the restricted molecular motion in the gel state with respect to the solution state.[12] Moreover, broadening of the benzylamine peak can be attributed to a decreased mobility of some of the benzylamine molecules, deriving from their intercalation in the gel fibers of **1**.[13] However, the integrals for the peaks of the benzylamine and the gelator protons show a 1 : 1 ratio of both components only in the solution state (343 K), while in the gel state (298 K) the amount of benzylamine appears to be approximately 3 times larger than the amount of **1**. This shows that in the gel, the benzylamine molecules are, on average, more mobile than the molecules of **1** and, therefore, only some are incorporated in the gel fibers, while most are probably situated between the fibers. To determine the actual amount of benzylamine trapped in the gel fibers of **1**, xerogels of **1** + ba were prepared by freeze drying the aqueous samples for 8, 14, 18, 24 and 36 h. The samples were then dissolved in CD_2Cl_2 and the ratio of benzylamine to gelator was determined by measuring the integrals of the corresponding aromatic proton peaks in the NMR spectra. The amount of benzylamine in the samples decreased with freeze drying time, to reach a steady value of 10–20% after approximately 14 h (Fig. 2). No further decrease was observed even after freeze drying for 36 h. As a reference, a sample containing only benzylamine and water, but no gelator, was subjected to the same treatment and after 24 h no benzylamine could be detected by NMR spectroscopy. Therefore, the amount of benzylamine intercalated/trapped in the gel fibers of **1** seems to be approximately 10–20% of the total number of gelator molecules. These results are in agreement with the temperature-dependence NMR experiments, which showed only a partial broadening of the signals of the benzylamine protons in the gel state, as well as an increase in the integral ratio of benzylamine to gelator.

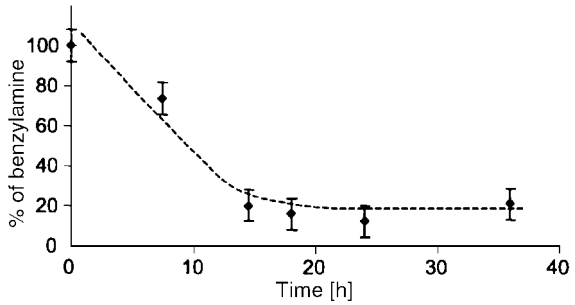

Fig. 2 Percentage of benzylamine in samples of **1** + ba as a function of freeze drying time (---- line to guide the eye).

In conclusion, we have shown that the organogel of a compound which does not contain a positive charge or an amino group can still be transcribed into a silica structure, as long as the catalyst for the polycondensation process can interact with the gelator molecules. Preliminary results using other gelators that do not contain positive charges or amino groups either,[14] indicate that this phenomenon is of a general nature. As a consequence, the transcription of a much broader range of organic superstructures, such as proteins, neutral vesicular aggregates or polysaccharides, *via* the polycondensation of TEOS can now be taken into consideration. Being able to transcribe such entities will undoubtedly lead to a greater variety of inorganic materials with interesting new shapes and properties.

Notes and references

1 For a recent review, see: L. A. Estroff and A. D. Hamilton, *Chem. Mater.*, 2001, **13**, 3227; E. Krämer, S. Förster, C. Göltner and M. Antonietti, *Langmuir*, 1998, **14**, 2027; Y. Zhou, K. Shimizu, J. N. Cha, G. D. Stucky and D. E. Morse, *Angew. Chem., Int. Ed.*, 1999, **38**, 779.

2 S. S. Kim, W. Zhang and T. J. Pinnavaia, *Science*, 1998, **282**, 1302.

3 F. Miyaji, S. A. Davis, J. P. H. Charmant and S. Mann, *Chem. Mater.*, 1999, **11**, 3021.

4 S. L. Burkett and S. Mann, *Chem. Commun.*, 1996, 321.

5 J. H. Jung, Y. Ono and S. Shinkai, *Angew. Chem., Int. Ed.*, 2000, **39**, 1862; J. H. Jung, Y. Ono and S. Shinkai, *Chem. Eur. J.*, 2000, **6**, 4552.

6 Y. Ono, K. Nakashima, M. Sano, Y. Kanekiyo, K. Inoue, J. Hojo and S. Shinkai, *Chem. Commun.*, 1998, 1477.

7 J. H. Jung, Y. Ono, K. Sakurai, M. Sano and S. Shinkai, *J. Am. Chem. Soc.*, 2000, **122**, 8648; J. H. Jung, Y. Ono and S. Shinkai, *Langmuir*, 2000, **16**, 1643.

8 J. H. Jung and S. Shinkai, *J. Chem. Soc., Perkin Trans. 2*, 2000, 2393; J. H. Jung, M. Amaike and S. Shinkai, *Chem. Commun.*, 2000, 2343.

9 O. Gronwald and S. Shinkai, *J. Chem. Soc., Perkin Trans. 2*, 2001, 1933.

10 A sample containing **1** (0.5 wt%, 300 μL H_2O) and benzylamine in a 1 : 1 molar ratio was heated in a sealed tube until a transparent solution was obtained. Upon cooling to rt a clear gel formed. 15 μL of TEOS were added to this gel, the sample was re-heated until transparent, and placed at rt under static conditions for 4 d.

11 The gelator was removed by calcination at 200 °C for 2 h, 500 °C for 2 h under nitrogen, followed by 500 °C for 4 h under aerobic conditions.

12 K. Yoza, N. Amanokura, Y. Ono, T. Akao, H. Shinmori, M. Takeuchi, S. Shinkai and D. N. Reinhoudt, *Chem. Eur. J.*, 1999, **5**, 2722.

13 Analogous to the incorporation of 4-nitrophenol in sodium bis(2-ethylhexyl) sulfosuccinate as reported by M. Tata, V. T. John, Y. Y. Waguespack and G. L. McPherson, *J. Phys. Chem.*, 1994, **98**, 3809.

14 Unpublished results by the same authors.

CHEMCOMM
Communication
www.rsc.org/chemcomm

A cascade of reactions involving anchimeric assistance leads to a highly 'crowded' hexa(alkylcarboxy)benzene†

Gunther Hennrich, Vincent M. Lynch and Eric V. Anslyn*

Department of Chemistry and Biochemistry, The University of Texas at Austin, Austin, TX 78712-1167, USA. E-mail: anslyn@ccwf.cc.utexas.edu; Fax: +1-512-471-7791

Received (in Columbia, USA) 26th June 2001, Accepted 15th October 2001
First published as an Advance Article on the web 8th November 2001

The substitution of hexabromomethylbenzene with 1-adamantyl carboxylate quantitatively leads to the corresponding hexacyl derivative *via* anchimeric assistance by the alkylcarboxy substituents.

Currently, considerable effort is being devoted to the synthesis of hexasubstituted benzene derivatives with a 1,3,5-, 2,4,6-substitution pattern, leading to characteristically preorganized systems.[1] Based on this type of scaffold, we recently presented various receptor molecules for the recognition of small, biologically relevant anions.[2] Such preorganized systems are also useful in the synthesis of macrocycles. By virtue of the alignment of functional groups of a reactant, the closure to the desired ring is facilitated.[3]

Lately, we have been exploring the substitution of the halogen atoms of hexabromomethyl benzene (**1**)[4] in order to create molecules with alternating groups on the phenyl ring. By reacting **1** with equimolar amounts of a bulky, weak nucleophile, we expected to obtain in a first step the respective, monosubstituted pentabromomethyl benzene and/or statistical mixtures of other substitution products.

To our surprise, the reaction of 1-adamantylcarboxylic acid (1-adca) with **1** in a 1 : 1 stoichiometry using caesium carbonate as the base, gave the hexa(alkylcarboxy)benzene **2** in a quantitative yield (Scheme 1), along with the recovery of **1**.[5] There are several effects to explain this result. The use of potassium carbonate instead of caesium carbonate as the base did not significantly affect the yield of the product. Accordingly, we can exclude a caesium induced effect, by which the caesium cation templates a benzene intermediate and brings a carboxylate reactant in proximity to the reaction center.[6] Further, there is no obvious inductive effect that can be invoked as a reason for this results. Therefore, we sought a different explanation.

Hexasubstituted benzenes have been studied extensively, with particular attention having been paid to their distinct conformations, *i.e.* the orientation of the substituents around the benzene core.[7] It was found by X-ray and NMR investigations that the alternation of substituents at the phenyl ring is thermodynamically favoured in persubstituted benzenes, with significant energetic barriers for the rotation of a substituent around the respective *C*(aryl)–*C*(methylene) bond.[8]

As determined for **2** by X-ray crystallography, the molecule lies on a crystallographic inversion center at ½, ½, ½ (Fig. 1).‡ Three molecules of benzene solvate co-crystallize along with **2**. Each molecule of benzene is also situated around a different crystallographic inversion center located at the center of the aromatic ring in the **ab** plane. As can be seen in the figure, the six bulky substituents alternate above and below the plane of the central benzene ring.

The stoichiometry used in the reaction, the mass balance of the products, as well as the identity of the product itself dictates kinetic control of the substitution reaction. The most apparent explanation is anchimeric assistance. Anchimeric assistance by acetoxy groups is a known and well-investigated phenomenon in substitution reactions, involving cyclic dioxonium intermediates,[9] but has so far been disregarded in the syntheses of hexasubstituted benzene derivatives.[10]

Although most commonly 5- or 6-membered rings are invoked in anchimeric assistance reactions, the formation of 7-membered heterocyclic intermediates has been reported.[11]

In our case, we propose that the introduction of a first adamantylcarboxy substituent leads to the monosubstituted adduct, which due to the alternation of the groups around the benzene ring is perfectly poised for an S_N2 displacement of a neigbouring bromide. This forms a 1,3-cycloheptadienium ring, which should be relatively free of ring strain due to the ring size and the *cis*-orientation at the benzene double bond and that of the carboxy group.[12] The attack of each additional carboxy nucleophile is thereby accelerated. Each neighbour group effect is 'handed over' from one carboxy group to the next one (Scheme 2).

However, Siegel has found S_N2 mechanisms are operative in similar systems,[13] and also at this stage we cannot rule out the formation of other intermediates, such as a cyclic bromonium cation.

As a control experiment, trisbromomethyl benzene **3**,[14] which does not allow the formation of the proposed 7-membered ring was subjected to the same reaction as **1**. After 3 h the reaction was still incomplete, *i.e.* starting material was still present, and the main product was identified as the mono-

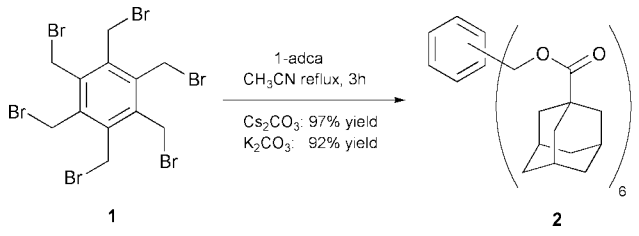

Scheme 1

† Electronic supplementary data (ESI) available: general methods, materials and X-ray data. See http://www.rsc.org/suppdata/cc/b1/b105569k/

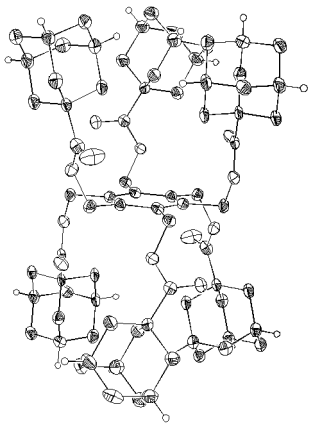

Fig. 1 Displacement ellipsoid (scaled to the 30% probability level) representation of **2**. Most hydrogen atoms have been removed for clarity. The oxygen atoms are shown without shaded segments.

 DOI: 10.1039/b105569k

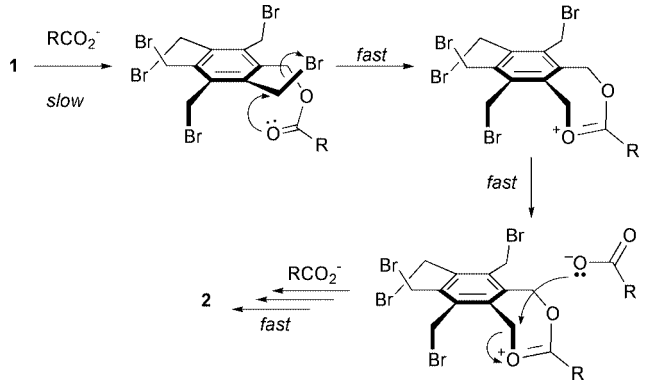

Scheme 2 Formation of a 7-membered 1,3-dioxazolenium ring intermediate during the reaction of **1** yielding **2**.

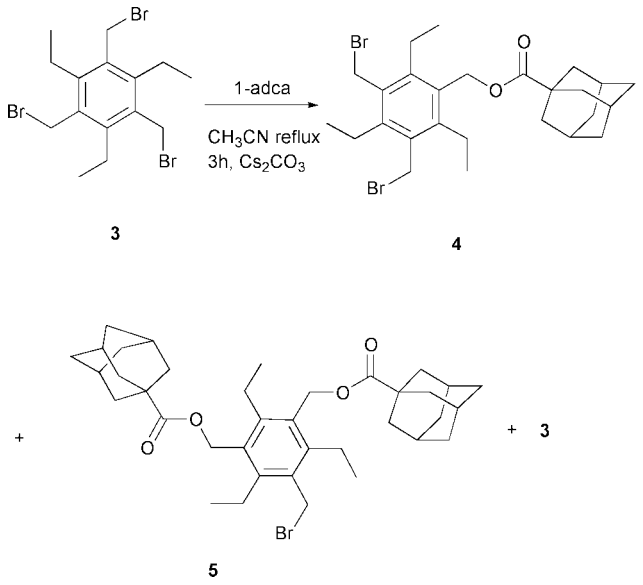

Scheme 3

adamantylcarboxy-derivative with traces of bis-substituted product being present in the reaction mixture (Scheme 3). After a further 5 h of heating, a complex mixture of the expected products was found.

The results reported herein support the necessity of adjacent bromomethyl functions to be present in the starting material, and therefore substantiate a mechanism involving the formation of cyclic intermediates, controlled by anchimeric assistance. Also, the clean and quantitative reaction of **1** giving **2** as the only detectable product points to a mechanism that involves an initial, rate determining step, and the subsequent fast conversion of the remaining bromomethyl groups as with energetically less demanding reactions.

We gratefully acknowledge the financial support by from the Beckman and Welch Foundation.

Notes and references

‡ *Crystallographic summary for* **2**. Very long, colourless lathes were grown by slow cooling from benzene, triclinic, *P*-1 (No. 2), $Z = 1$ in a cell of dimensions: $a = 10.5161(5)$, $b = 11.3542(7)$, $c = 18.823(2)$ Å, $\alpha = 82.191(4)$, $\beta = 79.886(3)$, $\gamma = 63.025(2)°$, $V = 1967.8(3)$ Å^3, $\rho_{calc} = 1.24$ g cm^{-3}, $F(000) = 792$. A total of 11370 reflections were measured, 7389 unique ($R_{int} = 0.078$), Nonus Kappa CCD using graphite monochromatized Mo-Kα radiation ($\lambda = 0.71073$ Å) at −120 °C. The structure was refined on F^2 to an $R_w = 0.233$, with a conventional $R = 0.109$ (3523 reflections with $F_0 > 4[\sigma(F_0)]$), and a goodness of fit = 1.101 for 488 refined parameters. CCDC 166842. See http://www.rsc.org/suppdata/cc/b1/b105569k/ for crystallographic data in .cif or other electronic format.

1 T. Szabo, B. M. O'Leary and J. Rebek, Jr., *Angew. Chem., Int. Ed.*, 1998, **37**, 3410; J. Chin, C. Walsdorff, B. Stranix, J. Oh, H. J. Chung, S.-M. Park and K. Kim, *Angew. Chem., Int. Ed.*, 1999, **38**, 2756; S.-G. Kim and K. H. Ahn, *Chem. Eur. J.*, 2000, **6**, 3399; K. S. Oh, C.-W. Lee, H. S. Choi, S. J. Lee and K. S. Kim, *Org. Lett.*, 2000, **2**, 2679.

2 J. J. Lavigne and E. V. Anslyn, *Angew. Chem., Int. Ed.*, 1999, **38**, 3666; K. Niikura, A. Metzger and E. V. Anslyn, *J. Am. Chem. Soc.*, 1998, **120**, 8533; L. A. Cabell, M. D. Best, J. J. Lavigne, S. E. Schneider, D. M. Perreault, M.-K. Monahan and E. V. Anslyn, *J. Chem. Soc., Perkin Trans. 2*, 2001, 315.

3 A. P. Bisson, V. M. Lynch, M.-K. C. Monahan and E. V. Anslyn, *Angew. Chem., Int. Ed.*, 1997, **36**, 2340; R. D. Ionescu and T. Frejd, *Chem. Commun.*, 2001, 1088; S. Y. Jon, M. Kim, S.-H. Park, W. S. Jeon, J. Heo and K. Kim, *Angew. Chem., Int. Ed.*, 2001, **40**, 2116.

4 J. Zavada, M. Pankova, P. Holy and M. Tichi, *Synthesis*, 1994, 1132.

5 For a general preparation method, spectroscopic data for 2, 3, 4, 5, and for other products obtained by using different carboxylic acids see supplementary material.†

6 A. Ostrowicki, E. Koepp and F. Vögtle, *Top. Curr. Chem.*, 1991, **161**, 38; M. Crescenzi, C. Gallo and L. Mandolini, *J. Phys. Org. Chem.*, 1990, **3**, 428.

7 D. D. MacNicol, A. D. V. Hardy and D. R. Wilson, *Nature*, 1977, **266**, 611; A. D. V. Hardy, D. D. MacNicol and D. R. Wilson, *J. Chem. Soc., Perkin Trans. 2*, 1979, 1011.

8 F. Vögtle and E. Weber, *Angew. Chem., Int. Ed. Engl.*, 1974, **13**, 814; K. V. Kilway and J. S. Siegel, *J. Am. Chem. Soc.*, 1992, **114**, 255; H.-W. Marx, F. Moulines, T. Wagner and D. Astruc, *Angew. Chem., Int. Ed. Engl.*, 1996, **35**, 1701.

9 H. Perst, *Oxonium Ions in Organic Chemistry*, VCH, Weinheim, 1971; M. I. Page, *Chem. Soc. Rev.*, 1973, **2**, 295.

10 U. Rosenthal and W. Schulz, *J. Prakt. Chem.*, 1986, **328**, 335; E. Weber, W. M. Müller and F. Vögtle, *Tetrahedron Lett.*, 1979, **25**, 2335.

11 S. H. Wilen, L. Delguzzo and R. Saferstein, *Tetrahedron*, 1987, **43**, 5094.

12 S. W. Benson, F. R. Cruickshaw, D. M. Golden, G. R. Haugen, H. E. O'Neil, A. S. Rodgers, R. Shaw and R. Walsh, *Chem. Rev.*, 1969, **69**, 279.

13 K. V. Kilway and J. S. Siegel, *Tetrahedron*, 2001, **57**, 3651.

14 A. W. van der Made and R. H. van der Made, *J. Org. Chem.*, 1993, **58**, 1262; A. Metzger, V. M. Lynch and E. V. Anslyn, *Angew. Chem., Int. Ed.*, 1997, **36**, 862.

CHEMCOMM Communication
www.rsc.org/chemcomm

A new one-pot three-component condensation reaction for the synthesis of 5-deaza-5,8-dihydropterins

Mark C. Bagley* and Nivedita Singh

Department of Chemistry, Cardiff University, PO Box 912, Cardiff, UK CF10 3TB. E-mail: bagleymc@cf.ac.uk; Fax: 29 2087 4030; Tel: 29 2087 4029

Received (in Cambridge, UK) 17th September 2001, Accepted 18th October 2001
First published as an Advance Article on the web 13th November 2001

The one-pot cyclocondensation of 2,6-diaminopyrimidin-4-one, an aromatic or aliphatic aldehyde and a β-ketoester in acetic acid, or dimethyl sulfoxide in the presence of zinc(II) bromide, under thermal conditions provided dihydropyrido[2,3-*d*]pyrimidin-4(3*H*)-ones in good yield and with total regiocontrol.

Since the isolation and characterisation of wing pigments of European butterflies at the end of the nineteenth century, the pterins have distinguished themselves as heterocycles of profound chemical and biological significance.[1] The discovery that the pyrazino[2,3-*d*]pyrimidine core of the pterin pigments was shared by the vitamin folic acid[2] caused a dramatic increase

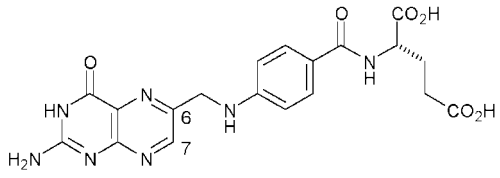

folic acid (*N*-pteroyl-L-glutamic acid)

in interest in this heterocycle in an effort to understand its role in the prevention of disease.[3] Structurally-related folate antagonists[4] have been shown to possess a diverse range of biological properties and they elicit highly species-specific responses as antitumour,[5] antibacterial,[6] anti-inflammatory,[7] and antifungal agents.[8]

Uracil derivatives have been reported in the literature to be versatile building blocks for the synthesis of a wide range of heterocyclic motifs,[9] including pyrazolopyridines,[10] pyrimido- and pyridopyrimidines[11] and pyrazolopyrimidines.[12] Kajino has reported the synthesis of dihydropyrido[2,3-*d*]pyrimidines using 6-aminouracils, but as a one-pot three-component cyclocondensation reaction this procedure suffered from very poor yields and limited substrate tolerance.[13] Since our own studies on this topic, Quiroga revealed the successful three-component cyclocondensation of a 6-aminouracil derivative, benzoylacetonitrile and aldehyde, but this process was only reported for aromatic aldehydes and required microwave irradiation as thermal conditions gave only a poor yield of the pyridopyrimidine product.[14]

As part of our interest in the synthesis of simple nitrogen-containing heterocycles[15] we established a new approach towards the 5-deaza-7-folate heterocycle **1**,[16] based upon a

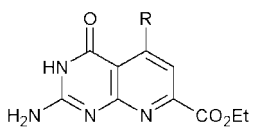

1

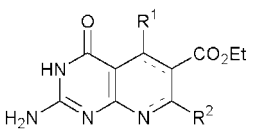

2

modification of the Bohlmann–Rahtz pyridine synthesis,[17] for the rapid assembly of a targeted library of folate antagonists from uracil derivatives. This communication describes a complementary approach towards the 5-deaza-6-folate motif **2** using a new three-component condensation reaction of an aldehyde, β-ketoester and 2,6-diaminopyrimidin-4-one **3**. This novel process prepares the target heterocycle with total regiocontrol, is successful for both aromatic and aliphatic aldehydes, utilises simple experimental conditions and incorporates a number of points of diversity for application in the synthesis of antifolate combinatorial libraries.

A mixture of 2,6-diaminopyrimidin-4-one **3**, benzaldehyde **4a** and ethyl acetoacetate **5** or ethyl benzoylacetate **6** was heated to 110 °C in dimethyl sulfoxide (DMSO) in the presence of zinc(II) bromide. After 72 hours, water was added and the precipitated solid was filtered to give dihydropyrido[2,3-*d*]pyrimidine **9** or **10** in 65 or 53% yield, respectively, as the only isolated reaction product.

In an effort to optimise this process, a range of different temperatures, solvents and acid catalysts were investigated. The choice of solvent for this reaction was limited by the solubility of diaminopyrimidinone **3** but reactions conducted in ethanol or DMSO at room temperature in the absence of a Lewis acid failed completely and gave only unreacted starting material **3**. Other Lewis acids, such as ytterbium(III) trifluoromethanesulfonate or scandium(III) trifluoromethanesulfonate were found generally not to be as efficient in this reaction. However, when a mixture of pyrimidinone **3**, benzaldehyde **4a** and ethyl acetoacetate **5** was stirred in acetic acid at 110 °C 5-deaza-5,8-dihydropterin **9**† was generated in 86% yield (Scheme 1).

Evidence on the mechanistic course of this reaction was obtained by the isolation of intermediate **7**, from a three-component reaction conducted in acetic acid at room temperature, that when stirred with ethyl acetoacetate **5** in acetic acid at 110 °C gave the same product **9**, albeit in only 43% yield. These findings indicated that initial addition to aldehyde **4a** was followed by acetoacetate **8** cyclodehydration in what appeared to be a totally regioselective process. The product **9** or **10**, obtained as a single regioisomer, was identified by ^{1}H and ^{13}C NMR spectroscopic techniques, the former of which clearly

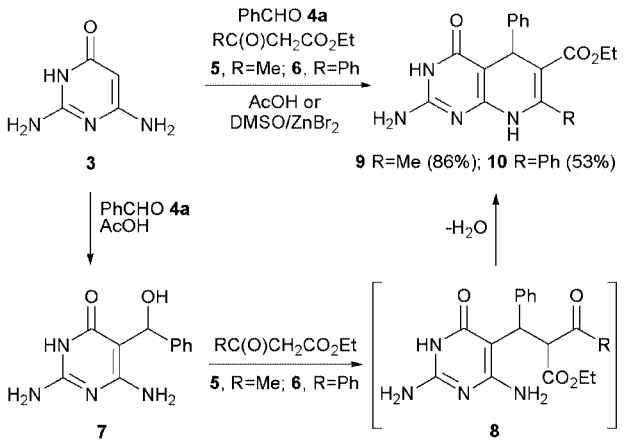

Scheme 1 The three-component cyclocondensation reaction.

 DOI: 10.1039/b108373b

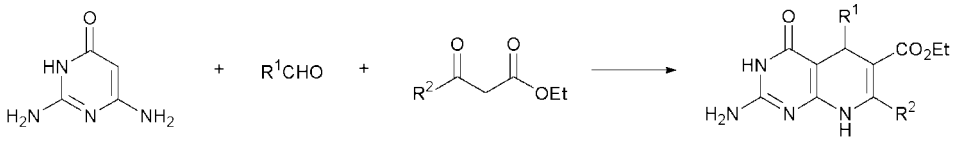

3 **4** **5**, R=Me; **6**, R=Ph **9-20**

Scheme 2 Three-component cyclocondensation of 2,6-diaminopyrimidin-4-one **3**, aldehyde **4** and β-ketoester **5** or **6**.

Table 1 Examining the scope of the three-component cyclocondensation reaction

Entry	R^1	R^2	Solvent	Lewis acid	Temperature/°C	Product	Yield[a](%)
1	Ph	Me	DMSO	$Yb(OTf)_3$	110	**9**	74
2	Ph	Ph	DMSO	$ZnBr_2$	110	**10**	53
3	4-$MeOC_6H_4$	Me	AcOH	None	110	**11**	77
4	4-$MeOC_6H_4$	Me	DMSO	$ZnBr_2$	110	**11**	68
5	4-ClC_6H_4	Me	DMSO	$ZnBr_2$	110	**12**	85
6	4-ClC_6H_4	Me	DMSO	$ZnBr_2$	110	**12**	63
7	2-$NO_2C_6H_4$	Me	AcOH	None	RT	**13**	41[b]
8	2-$NO_2C_6H_4$	Me	DMSO	None	110	**13**	66
9	2-$NO_2C_6H_4$	Me	DMSO	$ZnBr_2$	110	**13**	64
10	3,4-$(MeO)_2C_6H_3$	Me	DMSO	$ZnBr_2$	110	**14**	45
11	3,5-$Me_2C_6H_3$	Me	DMSO	$ZnBr_2$	110	**15**	66
12	3,5-$Me_2C_6H_3$	Me	AcOH	None	110	**15**	73[b]
13	cyclopropyl	Me	DMSO	None	110	**16**	78
14	Et	Me	DMSO	None	110	**17**	80
15	$PhCH_2$	Me	DMSO	None	110	**18**	65
16	Me	Me	DMSO	None	110	**19**	60
17	$MeCH_2CH_2$	Me	DMSO	None[c]	RT	**20**	40
18	$MeCH_2CH_2$	Me	DMSO	None	110	**20**	94

[a] Yield of pure isolated product. [b] Some impurities were evident. [c] The use of a Lewis acid did not improve the yield of reactions conducted at RT.

indicated the presence of the NH (position 8) and deshielded methine (position 5) protons.

In order to examine the scope of this new three-component cyclocondensation reaction, 2,6-diaminopyrimidin-4-one **3**, a range of aromatic and aliphatic aldehydes **4** and ethyl acetoacetate **5** or ethyl benzoylacetate **6** was stirred at room temperature or heated to 110 °C in DMSO with zinc(II) bromide or in acetic acid for 72 hours to give dihydropyrido[2,3-*d*]pyrimidine **9**–**20**, usually in good to excellent yield (Scheme 2, Table 1). Although aromatic aldehydes gave slightly disappointing results in DMSO, it was found that conducting these reactions in acetic acid or in the presence of zinc(II) bromide usually improved the reaction and gave yields routinely in excess of 70%. Aliphatic aldehydes proved the most predictable, generating the product in reasonable yield as a single regioisomer after 72 hours at 110 °C in DMSO.

This new one-pot three-component cyclocondensation reaction generated 5-deaza-5,8-dihydropterins, bearing a range of different functional groups, under thermal and, where necessary, Lewis acid catalysed conditions. Efforts are now underway to apply this new procedure, that is simple, appropriate for combinatorial methodology and avoids the use of microwave irradiation, to the synthesis of deazapterin libraries and other targeted libraries of inhibitors of folate-dependent enzymes.

Notes and references

† *General experimental procedure for the 3-component cyclo-condensation reaction*. A mixture of 1,3-diaminopyrimidin-4-one **3** (0.20 g, 1.6 mmol), benzaldehyde **4a** (0.15 g, 1.5 mmol) and ethyl acetoacetate **5** (0.18 g, 1.5 mmol) in glacial acetic acid (5 mL) was stirred at 110 °C for 72 h. The mixture was allowed to cool, water (15 mL) was added and the solution was left to stand for 5 h. The precipitate that formed was filtered to give pure *5-deaza-5,8-dihydropterin* **9** (0.41 g, 86%) as a pale yellow solid.

1 F. G. Hopkins, *Nature*, 1889, **40**, 335; *Nature*, 1891, **45**, 197; *Nature*, 1892, **45**, 581.
2 H. K. Mitchell, E. E. Snell and R. J. Williams, *J. Am. Chem. Soc*., 1941, **63**, 2284.
3 J. M. Scott, D. G. Weir and P. Kirke, *Folate and Neural Tube defects. Folate in Health and Disease*, ed. L. B. Bailey, Marcel Dekker, New York, 1994, ch. 12, p. 329–360.
4 E. C. Taylor, D. C. Palmer, T. J. George, S. R. Fletcher, C. P. Tseng, P. J. Harrington and G. P. Beardsley, *J. Org. Chem*., 1983, **48**, 4852; J. I. DeGraw, P. H. Christie, W. T. Colwell and F. M. Sirotnak, *J. Med. Chem*.,1992, **35**, 320; J. I. Borrell, J. Teixidó, J. L. Matallana, B. Martínez-Teipel, C. Colominas, M. Costa, M. Balcells, E. Schuler and M. J. Castillo, *J. Med. Chem*., 2001, **44**, 2366.
5 E. M. Grivsky, S. Lee, C. W. Sigel, D. S. Duch and C. A. Nichol, *J. Med. Chem*., 1980, **23**, 327.
6 J. Matsumoto and S. Minami, *J. Med. Chem*., 1975, **18**, 74; N. Suzuki, *Chem. Pharm. Bull*., 1980, **28**, 761; V. Oakes and H. N. Rydon, *J. Chem. Soc*., 1956, 4433; J. I. DeGraw, R. L. Kisliuk, Y. Gaumont and C. M. Baugh, *J. Med. Chem*., 1974, **17**, 470; A. V. Zakharov, M. Yu. Gavrilov, G. N. Novoselova, M. I. Vakhrin and M. E. Konshin, *Khim.-Farm. Zh*., 1996, **30**, 39.
7 A. B. Deyanov, R. K. Niyazov, F. Y. Nazmetdinov, B. Y. Syropyatov, V. E. Kolla and M. E. Konshin, *Khim.-Farm. Zh*., 1991, **25**, 26.
8 R. E. Heckler and G. P. Jourdan, *Eur. Pat*., 1991, **414**, 386; *Chem. Abstr*., 1991, **115**, 71630.
9 E. Lunt and C. C. Newton, in *Comprehensive Heterocyclic Chemistry*, ed. A. R. Katritzky, C. W. Rees, A. J. Boulton and A. McKillop, Pergamon Press, Oxford, 1984, vol. 3, p. 199, 232, 260–261; J. D. Brown, in *Comprehensive Heterocyclic Chemistry*, ed. A. R. Katritzky, C. W. Rees, A. J. Boulton and A. McKillop, Pergamon Press, Oxford, 1984, vol. 3, 57; T. K. Bradshaw and D. W. Hutchinson, *Chem. Soc. Rev*., 1977, **6**, 43.
10 J. Quiroga, S. Cruz, B. Insuasty and R. Abonía, *Heterocyclic Commun*., 2000, **6**, 275; J. Quiroga, S. Cruz, B. Insuasty, R. Abonía, M. Nogueras, A. Sánchez, J. Cobo and J. N. Low, *J. Heterocyclic Chem*., 2001, **38**, 53.
11 A. J. Thakur, P. Saikia, D. Prajapati and J. S. Sandhu, *Synlett*, 2001, 1299.
12 P. Bhuyan, R. C. Boruah and J. S. Sandhu, *J. Org. Chem*., 1990, **55**, 568.
13 M. Kajino and K. Meguro, *Heterocycles*, 1990, **31**, 2153.
14 J. Quiroga, C. Cisneros, B. Insuasty, R. Abonía, M. Nogueras and A. Sánchez, *Tetrahedron Lett*., 2001, **42**, 5625.
15 M. C. Bagley, J. W. Dale and J. Bower, *Synlett*, 2001, 1149.
16 M. C. Bagley, D. D. Hughes, R. Lloyd and V. E. C. Powers, *Tetrahedron Lett*., 2001, **42**, 6585.
17 F. Bohlmann and D. Rahtz, *Chem. Ber*., 1957, **90**, 2265.

CHEMCOMM Communication
www.rsc.org/chemcomm

Catalytic asymmetric synthesis of cyclopentenones from propargyl malonates and allylic acetate by successive action of homogeneous palladium(II) and cobalt on charcoal catalysts in a one-pot reaction†

Seung Uk Son,[a] Kang Hyun Park,[a] Hwimin Seo,[a] Young Keun Chung*[a] and Sueg-Geun Lee[b]

[a] *School of Chemistry and Center for Molecular Catalysis, Seoul National University, Seoul 151-747, Korea. E-mail: ykchung@plaza.snu.ac.kr; Fax: (+82)2-889-0310; Tel: +82-2-880-6662*
[b] *Korea Research Institute of Chemical Technology, PO Box 107, Yusong, Taejeon 305-600, Korea*

Received (in Cambridge, UK) 30th July 2001, Accepted 17th October 2001
First published as an Advance Article on the web 5th November 2001

The tandem action of a homogeneous chiral Pd(II) catalyst and a heterogeneous Co/C catalyst leads to a two-step one-pot highly enantioselective Pauson–Khand-type reaction.

Much success has been achieved in the field of transition-metal-mediated (or catalyzed) synthesis of cyclopentenones from readily available substrates;[1] however, catalytic asymmetric synthesis is still surprisingly underdeveloped. The use of a chiral titanocene complex (EBTHI)Ti(CO)$_2$ (EBTHI = ethylene-1,2-bis(η^5-4,5,6,7-tetrahydroinden-1-yl)[2] and Co,[3] Rh,[4] and Ir[5] complexes with chiral diphosphines have been recently reported. Demand for the development of a catalytic and enantioselective Pauson–Khand type reaction remains high.

Recently, the tandem use of two kinds of homogeneous catalyst in a one-pot multistep transformation of substrates to products has been reported.[6] The report by Jeong's group has attracted our attention. They used a combination of Pd and Rh catalysts in the preparation of bicyclopentenones from propargyl malonates. The use of Pd-catalyzed asymmetric allylic alkylation[7] to generate enantioselective enynes appears to be quite promising. However, the use of *in situ* generated enantiomerically enriched enynes as substrates in the Pauson–Khand reaction has not been reported even though increasing efforts are being devoted to the development of practical enantioselective versions of the Pauson–Khand reaction.[8]

In this connection, we decided to use the Pd(II)-catalyzed asymmetric allylic alkylation in the synthesis of enantiomerically pure enynes. We report herein that the tandem action of homogeneous chiral Pd(II) catalyst and heterogeneous catalyst Co/C[9] leads to a 'two-step one-pot' highly enantioselective Pauson–Khand-type reaction. The efficiency of this two-step one-pot reaction was studied for **3(Me)** as shown in Scheme 1. Thus, we screened several chiral ligands (Chart 1) to find the best chiral ligand (Table 1).[10] The same reaction was conducted in the presence of dppe to obtain racemic products. All the chiral ligands were effective for Pd-catalyzed asymmetric allylic alkylation. The ee values of **4(Me)** ranged from 83 to 95% at room temperature. As expected, the best ligand was phosphinooxazoline ligand **b**. The best ee value of 96% was obtained when the reaction was conducted at 0 °C in the presence of **b** (entry 3 in Table 1). The absolute configuration of **3(Me)** was easily established by comparison of the observed [α] values with those of the known reactions. The absolute configuration (3*R*,4*S*,5*R*) of the bicyclic enone **4(Me)** was determined by an NMR study. When the reaction in Scheme 1 was carried out stepwise to determine whether the ee value was changed during the carbonylative cyclization, the ee value of the final product was the same as that of the first step and no other diastereomer was found in the second step. Thus, the ee value of the first asymmetric allylic alkylation reaction was maintained during the second cycloaddition reaction. This suggests that the first step is a stereoselective reaction and the second a stereospecific one. The enantioselectivity of this tandem cycloaddition was absolutely dependent on the Pd-catalyzed asymmetric allylic alkylation. This could be a good advantage of this combination of catalysts because the palladium-catalyzed allylic alkylation is one of the most thoroughly and intensively studied catalytic transformations. High yields were observed for all reactions. The yield of the second step was always quantitative. Thus, the turnover number was completely dependent upon the Pd-catalyzed allylic alkylation. For convenience, we used 2.5 mol% of Pd(II) catalyst for studying the reactions.

The success of this tandem catalytic reaction is primarily due to the use of Co/C. In the Pd(II)-catalyzed allylic alkylation reaction, acetic acid was generated. The acid would interact with cobalt species in the solution. When $Co_2(CO)_8$ (20 mol%) instead of Co/C was used as a catalyst, only 2% of the product

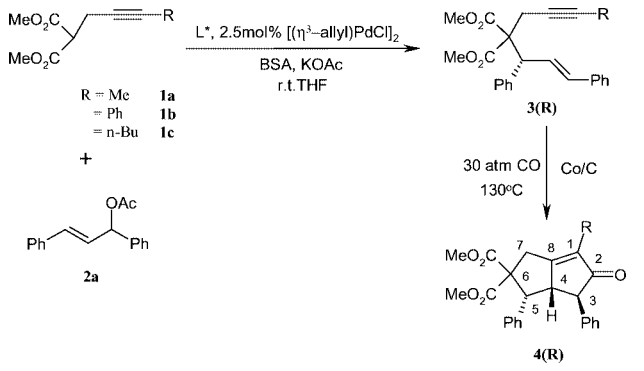

Scheme 1

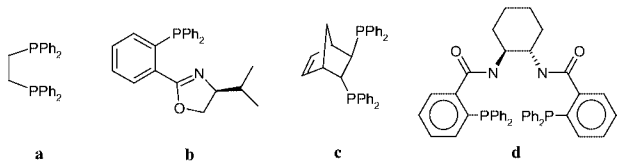

Chart 1

Table 1 Asymmetric one-pot synthesis of bicyclopentenone[a]

Entry	Chiral ligand	Time/h[b]	Yield (%)[c]	Ee (%)[d]
1	**a**	10	74	—
2	**b**	4	81	95
3[e]	**b**	18	95	96
4[f]	**b**	4	2	—
5	**c**	12	81	83

[a] **1a** and **2a** used as substrates. Conditions for the 2nd step: 130 °C, 18 h, 30 atm. CO.[b] Reaction time of the first step at rt.[c] Isolated yield.[d] Diacel OD column was used.[e] Reaction temperature of the first step is 0 °C.[f] 20 mol% $Co_2(CO)_8$ was used instead of Co/C.

† Electronic supplementary information (ESI) available: experimental details. See http://www.rsc.org/suppdata/cc/b1/b106836a/

 DOI: 10.1039/b106836a

Table 2 Asymmetric one-pot synthesis of various cyclopentenones[a]

	Substrates	Product	L*	Base	Time/ h[b]	Yield (%)[c]	Ee (%)[d]
1	**1a 2a**	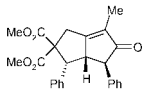 **4(Me)**	**b**	BSA	4	81	95
2	**1b 2a**	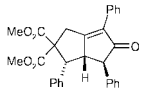 **4(Ph)**	**b**	BSA	6	95	84
3	**1c 2a**	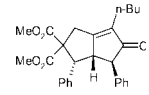 **4(Bu)**	**b**	BSA	4	84	93
4	**1a 2b**	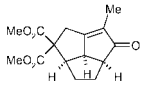 **6(1)**	**a**	BSA	10	95	—
			d	BSA	24	85	33
			d	Cs_2CO_3[e]	12	92	94
5	**1a 2c**	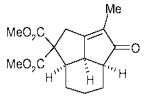 **6(2)**	**a**	BSA	10	95	—
			d	BSA	24	90	36
			d	Cs_2CO_3[e]	12	90	72
6	**1a 2d**	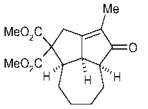 **6(3)**	**a**	BSA	10	89	—
			d	BSA	24	93	4
			d	Cs_2CO_3[e]	12	97	31

[a] Reaction conditions: 6.0 mol% L* , 2.5 mol% $[(\eta^3\text{allyl})PdCl]_2$, 0.2 g Co/C, and THF. Condtions for the 2nd step: 130 °C, 18 h, and 30 atm CO.[b] Reaction time of the first step at rt.[c] Isolated yield.[d] Diacel OD column was used.[e] CH_2Cl_2 as a solvent.

was isolated (entry 4 in Table 1). However, the Co/C was found to be insensitive to acid or base. Generally, for good enantioinduction, low temperatures are required. However, our reaction conditions in the second step seem to be quite harsh, nevertheless no racemization occurred under these reaction conditions. We also examined the catalytic asymmetric carbonylative cyclization of **3(R)** (R = Ph, *n*-Bu) (entries 2 and 3 in Table 2). Under our reaction conditions, **4(R)** were obtained in high yields (84–95%) with high ee values (84–95%). The usefulness of this combination catalyst is highlighted by the

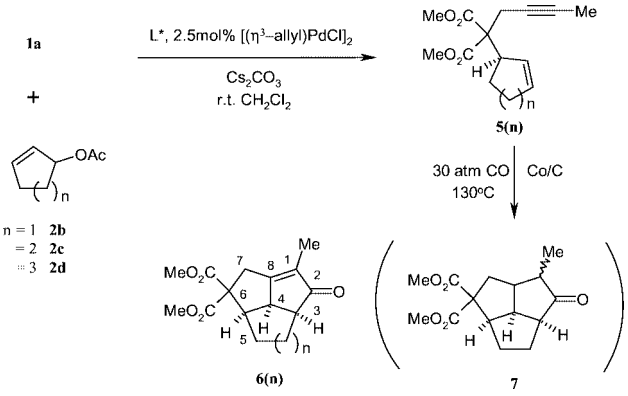

Scheme 2

synthesis of various tricyclic enones **6(*n*)** (*n* = 1–3) (Scheme 2 and entries 4–6 in Table 2).

The intramolecular Pauson–Khand reaction of cyclic enynes having cyclopentenes or cyclohexenes with pendant alkynes has been well studied.[11] Chiral ligand **d** developed by Trost[12] was selected since it is one of the best ligands in the Pd(II)-catalyzed asymmetric reaction of 2-cyclopentenyl, -hexenyl, or -hepenyl acetate with the anion of dimethyl malonate.[13] The reaction was quite sensitive to the base and the solvent used. The best results were obtained when Cs_2CO_3 and dichloromethane were used as a base and a solvent, respectively.[13] Interestingly, substrates **5(2)** and **5(3)** were known not to be cyclized with (EBTHI)-$Ti(CO)_2$.[1] However, fairly high yields (89–97%) were obtained in our case. In the cyclization of **5(1)**, the reduced **7** was obtained as a byproduct provided the generated acetic acid was not removed. In contrast to the high yields, the ee values (31–94%) were quite sensitive to the ring size. As the ring size increases, the ee values decrease. A fairly high ee value of 94% was obtained for **6(1)**. The absolute configuration (3*R*,4*R*,5*S*) of the tricyclic enone **6(*n*)** was determined by comparison with the known reactions.[13] The fused tricyclic systems such as **6(1)** and **6(2)** had been used in the synthesis of natural products.[14]

In summary, we have demonstrated that the tandem action of a homogeneous chiral Pd(II) catalyst and a heterogeneous Co/C catalyst leads to a two-step one-pot highly enantioselective Pauson–Khand-type reaction. The enantiomeric purity of the product depends upon the optical purity of the *in situ* generated enyne. Further synthetic applications of the tandem action of two different catalysts in other reactions are now in progress.

This work supported by the Korea Science and Engineering Foundation (KOSEF) (1999-1-122-001-5), and the KOSEF through the Center for Molecular Catalysis. SUS, KHP, and HS acknowledge receipt of the BK21 fellowship.

Notes and references

1 For recent reviews, see: N. Jeong, in *Transition Metals in Organic Synthesis*, ed. M. Beller and C. Bolm, Wiley-VCH, Weinheim, 1998, vol. 1, p. 560; Y. K. Chung, *Coord. Chem. Rev*., 1999, **188**, 297; K. M. Brummond and J. L. Kent, *Tetrahedron*, 2000, **56**, 3263.
2 F. A. Hicks and S. L. Buchwald, *J. Am. Chem. Soc*., 1996, **118**, 11688.
3 K. Hirori, T. Watanabe, R. Kawagishi and I. Abe, *Tetrahedron Lett*., 2000, **41**, 891.
4 N. Jeong, B. K. Sung and Y. K. Choi, *J. Am. Chem. Soc*., 2000, **122**, 6771.
5 T. Shibata and K. Takagi, *J. Am. Chem. Soc*., 2000, **122**, 9852.
6 R. W. Barnhart and G. C. Bazan, *J. Am. Chem. Soc*., 1998, **120**, 1082; Z. J. A. Komon, X. Bu and G. C. Bazan, *J. Am. Chem. Soc*., 2000, **122**, 1830; N. Jeong, S. D. Seo and J. Y. Shin, *J. Am. Chem. Soc*., 2000, **122**, 10220; P. A. Evans and J. E. Robinson, *J. Am. Chem. Soc*., 2001, **123**, 4609.
7 B. M. Trost and D. L. van Vranken, *Chem. Rev*., 1996, **96**, 395.
8 X. Verdaguer, J. Vázquez, G. Fuster, V. Bernardes-Génisson, A. E. Greene, A. Moyano, M. A. Pericàsa and A. Riera, *J. Org. Chem*., 1998, **63**, 7037; J. Castro, A. Moyano, M. A. Pericàsa, A. Riera, A. Alvarez-Larena and J. F. Piniella, *J. Am. Chem. Soc*., 2000, **122**, 7944.
9 S. U. Son, S.-I. Lee and Y. K. Chung, *Angew. Chem., Int. Ed*., 2000, **39**, 4158.
10 P. Von Matt and A. Pfaltz, *Angew. Chem., Int. Ed. Engl*., 1993, **32**, 566; J. Sprinz and G. Helmchen, *Tetrahedron Lett*., 1993, **34**, 1769; G. J. Dawson, C. G. Frost, J. M. J. Williams and S. J. Coote, *Tetrahedron Lett*., 1993, **34**, 3149.
11 C. Almansa, A. Moyano and F. Serratosa, *Tetrahedron*, 1988, **44**, 2657; J. Macro-Contelles and J. Ruiz, *Tetrahedron Lett*., 1998, **39**, 6393; J. Cassayre and S. Z. Zard, *J. Organomet. Chem*., 2001, **624**, 316.
12 B. M. Trost, D. L. van Vranken and C. Bingel, *J. Am. Chem. Soc*., 1992, **114**, 9327.
13 B. M. Trost and R. C. Bunt, *J. Am. Chem. Soc*., 1994, **116**, 4089; B. M. Trost and R. C. Bunt, *Angew. Chem., Int. Ed. Engl*., 1996, **35**, 99.
14 S. Takano, K. Inomata and K. Ogasawara, *Chem. Lett*., 1992, 443; L. A. Paquette and S. Borrelly, *J. Org. Chem*., 1995, **60**, 6912; J. Cassayre and S. Z. Zard, *J. Am. Chem. Soc*., 1999, **121**, 6072.

CHEMCOMM Communication
www.rsc.org/chemcomm

Multilayer structure of an unsymmetrical monolayer lipid membrane with a 'head-to-tail' interface

Mitsutoshi Masuda* and Toshimi Shimizu

Nanoarchitectonics Research Center (NARC), National Institute of Advanced Industrial Science and Technology (AIST), CREST, Japan Science and Technology Corporation (JST), Tsukuba Central 5, 1-1-1 Higashi, Tsukuba, Ibaraki 305-8565, Japan

Received (in Cambridge, UK) 23rd July 2001, Accepted 9th October 2001
First published as an Advance Article on the web 2nd November 2001

A synthetic unsymmetrical 1-galactosamide bolaamphiphile self-assembles in methanol to form a multilayer structure comprising unsymmetrical monolayer lipid membranes linked *via* a sugar–carboxylic acid H-bonding interface.

Bolaamphiphiles having a hydrophilic group at each end are able to form monolayer lipid membrane (MLM) structures.[1,2] When the bolaamphiphiles are unsymmetrical with two headgroups of different sizes, the resulting MLMs are classified into two categories, 'unsymmetrical' and 'symmetrical', depending on a parallel or antiparallel molecular packing within the layer as shown in Fig. 1. In multilayer structures (such as in the crystalline state), a further two kinds of membrane stacking motifs can be defined depending on the interface between the two surfaces termed 'head-to-head' or 'head-to-tail' (with the larger of the two hydrophilic groups termed the 'head'). Since the dipole moment and spatial void arising from the bulky headgroup are best compensated by an antiparallel packing motif, most synthetic bolaamphiphiles exhibit this kind of packing in the solid phase[3] or (excepting a few examples)[4] form MLMs with random molecular orientation in the disperse phase.[1,5] Even in those cases where unsymmetrical MLMs are formed,[6] each membrane stacks with the head-to-head interface to give the multilayer structures for the same reason. Some attempts have been made to combat this tendency to form unsymmetrical MLMs by the introduction of the multiple H-bonding functional groups into both ends of an unsymmetrical bolaamphiphile.[7]

Recently, we have found that the bolaamphiphilic 1-glucosamide **2** or 1-galactosamide **3** self-assembled to form MLM-based structures in the crystal lattice *via* the formation of multiple sugar and amide H-bond networks,[8,9] with the stereochemistry of the sugar headgroups strongly affecting the intra- and interlayer H-bonding scheme. Our results suggested that similar unsymmetrical sugar-based bolaamphiphiles might be able to self-assemble to form an unsymmetrical MLM with a head-to-tail interface, forming multiple H-bonds between hetero surfaces. In this communication we report the crystal structure obtained from the synthetic unsymmetrical bolaamphiphile **1** having a 1-galactosamide headgroup at one end and a carboxylic acid group at the other (Scheme 1). This bolaamphiphile self-assembled in methanol to form an unsymmetrical MLM-based structure with the formation of intralayer H-bonds between the sugar headgroups and between amide groups. In addition, these MLMs stacked together with a head-to-tail interface directed *via* the formation of interlayer H-bonds between the 1-galactosamide hydroxy and carboxylic acid groups. To the best of our knowledge, only three crystal structures have so far been reported for unsymmetrical bolaamphiphiles with spacers longer than a decamethylene chain[3,6] and only one[6] forms an unsymmetrical MLMs-based structure with a head-to-head interface.

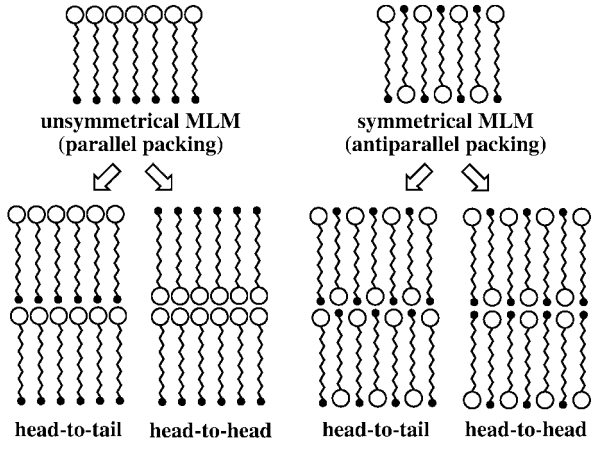

Fig. 1 Monolayer lipid membrane (MLM) formation from unsymmetrical bolaamphiphiles and resultant multilayer structures formed by the stacking of the MLMs.

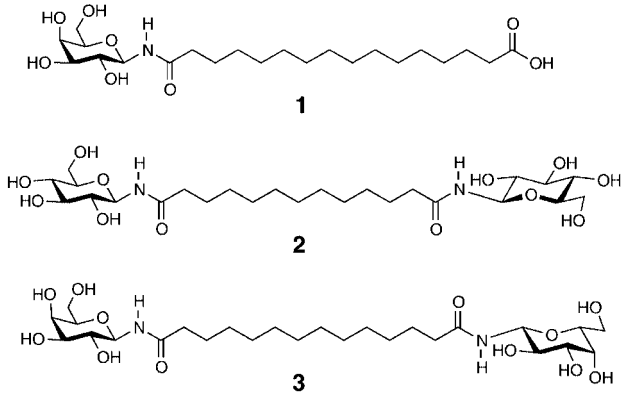

Scheme 1

Single crystals of the unsymmetrical bolaamphiphile **1** suitable for X-ray measurements† were obtained on cooling of a hot methanolic solution (6.1 g ml^{-1} at 40 °C) and the crystal structure is shown in Fig. 2. The bolaamphiphile **1** packed in the parallel arrangement to form the unsymmetrical MLM-based structure in the crystal, with the 1-galactosamide headgroups adopting the same $^4C_1$ chair conformation as reported previously for the symmetrical analogue **3**.[9] The alkylene chain adopts an all-*trans* zigzag conformation which has an inclination of 52° with respect to the normal to the layer plane, again in a similar fashion to that previously reported for the 1-glucosamide **2** and 1-galactosamide **3** bolaamphiphiles.[8,9] The two hydrophilic surfaces of the each unsymmetrical MLM arising from this parallel orientation, one comprising sugar and the other carboxylic acid groups, come into contact and form a complementary H-bonded interface along the *ac* plane.

Among the eleven H-bonds per molecule in crystals, intralayer H-bonds between the sugars and amides stabilize the parallel molecular arrangement within the unsymmetrical MLM structure, whilst interlayer H-bonds between the sugar hydroxy and the carboxylic acid groups stabilize the head-to-tail

 DOI: 10.1039/b106581p

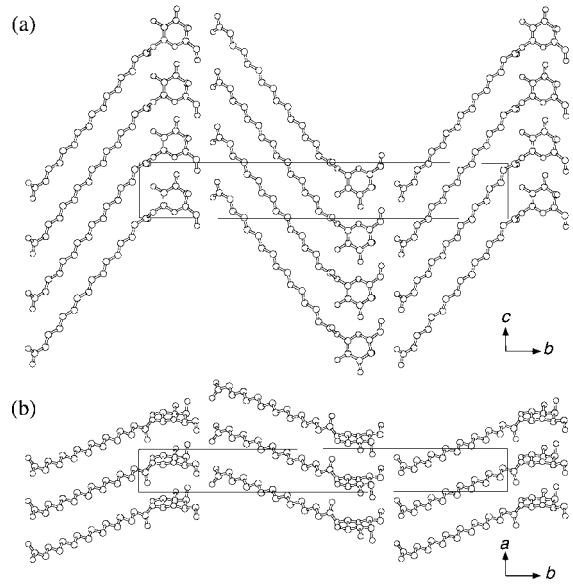

Fig. 2 Molecular packing of **1**, viewed along (a) the *a* axis and (b) the *c* axis. Hydrogen atoms have been omitted for clarity.

membrane interface as shown in Fig. 3. The intralayer H-bonding scheme of **1** exhibited '*N*'-type H-bonds (O-4···H–(O-6)···O-3···O-5) and amide H-bonds (O-2–H···O-7···H–N-1) similar to those characteristic of the pyranose headgroup with 1-amide group found in **2**.[8] The carboxylic and sugar hydroxy groups form interlayer H-bond arrays of O-8···H-O-4 and O-9-H···O-6 resulting in a finite H-bonded chain (O-8···H–O-4···H–O-6···H–O-9) which stabilizes the stacking of unsymmetrical MLMs at the head-to-tail interface. In general, carboxylic acids tend to form cyclic dimers with bifurcated H-bonds[2] and there have been so far very few examples of sugar–carboxylic acid H-bonds except for a carbohydrate-binding protein.[10] Since the axial O-4 hydroxy group seems to be buried under the hydrophilic surface, it forms H-bonds with the less bulky carboxylic acid to form a head-to-tail interface rather than the hydroxy groups of the 1-galactosamide which would give a head-to-head interface. This can be supported by the existence of clathrated water around the O-4 axial group for the head-to-head interface of the symmetrical 1-galactosamide **3**.[9] In contrast, no clathrated water can be found in the solid state structure of the 1-glucosamide **2**.[8] These results indicate that the predominant driving forces for the unsymmetrical MLM structure are the side-by-side aggregation of the 1-galactosamide headgroups *via* H-bond formation between the hydroxy groups and amides and a hydrophobic interaction between tetradecane spacers. The resultant unsymmetrical MLMs stack with a head-to-tail interface, forming H-bonding arrays between residual hydroxy groups of the 1-galactosamide and carboxylic acid groups.

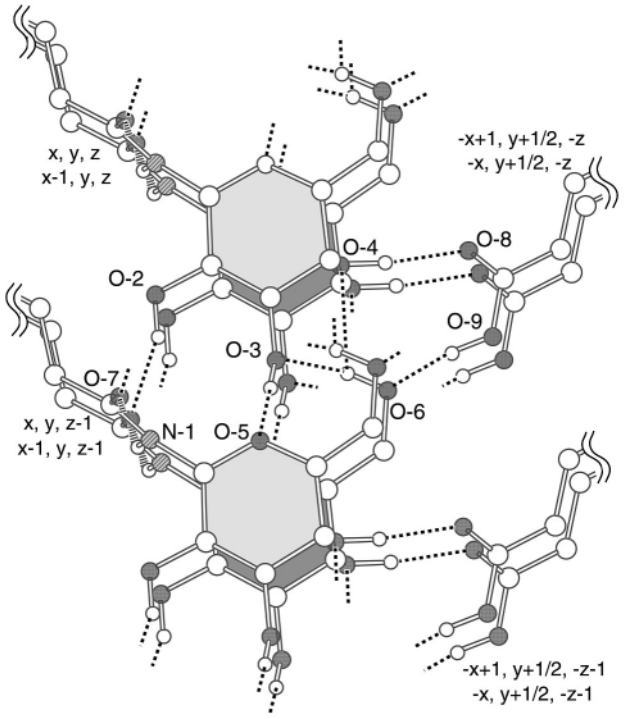

Fig. 3 Three-dimensional H-bond networks formed between β-D-galactosamide and carboxylic acid of **1**, viewed along the *a* direction.

Notes and references

† *Crystal data for* **1**: $C_{22}H_{44}N_1O_8$, M = 450.59, monoclinic $P2_1$, a = 4.90(1) Å, b = 40.139(1) Å, c = 6.289(1) Å, β = 106.48(1)°, V = 1187.3(3) Å^3, Z = 2, D_c = 1.260 g cm^{-3}, μ = 7.79 cm^{-1}, 2038 reflections (θ_{max} = 119.9°) were collected using a Rigaku AFC7R automatic four-circle diffractomater (Cu-Kα radiation, λ = 1.54178 Å, graphite monochoromator) at measured T = 302 K. 1936 unique (R_{int} = 0.014) which were used in all calculations. Refinement using the SHELXS 97 on all data converged at R = 0.031, R_w = 0.047, GOF = 1.27. The covalent O–H and N–H bond lengths were normalized to 0.97 and 1.03 Å respectively. The H-bonds between O–H···O and N–H···O are estimated by the distance between hydrogen and acceptor shorter than 2.33 Å [(O)–H···O] and 2.32 Å [(N)–H···O].[11] The absolute configuration of the molecules is uniquely determined by the known chirality of the D-galactopyranose rings. CCDC 166281. See http://www.rsc.org/suppdata/cc/b1/b106581p/ for crystallographic files in .cif or other electronic format.

1 J.-H. Fuhrhop and D. Fritsch, *Acc. Chem. Res.*, 1986, **19**, 130.
2 (*a*) J.-H. Fuhrhop and J. Köing, *Membranes and Molecular Assemblies: The Synkinetic Approach*, The Royal Society of Chemistry, Cambridge, UK, 1994; (*b*) G. H. Escamilla and G. R. Newkome, *Angew. Chem., Int. Ed. Engl.*, 1994, **33**, 1937.
3 (*a*) P. T. Aigouy, P. Costeseque, R. Sempere and T. Senac, *Acta Cryst.*, 1995, **B51**, 55; (*b*) M. Szafran, Z. Dega-Szafran, A. Katrusiak, G. Buczak, T. Glowiak, J. Sitkowski and L. Stefaniak, *J. Org. Chem.*, 1998, **63**, 2898.
4 (*a*) J.-H. Fuhrhop, H.-H. David, J. Mathieu, U. Liman, H.-J. Winter and E. Boekema, *J. Am. Chem. Soc.*, 1986, **108**, 1785; (*b*) J.-H. Fuhrhop, H. Hungerbühler and U. Siggel, *Langmuir*, 1990, **6**, 1295; (*c*) K. Liang and Y. Hui, *J. Am. Chem. Soc.*, 1992, **114**, 6588.
5 (*a*) J. Song, Q. Cheng, S. Kopta and R. C. Stevens, *J. Am. Chem. Soc.*, 2001, **123**, 3205; (*b*) J. Guilbot, T. Benvegnu, N. Legros and D. Plusquellec, *Langmuir*, 2001, **17**, 613; (*c*) D. A. Jaeger, G. Li, W. Subotkowski and K. T. Carron, *Langmuir*, 1997, **13**, 5563; (*d*) C. Prata, N. Mora, A. Polidori, J.-M. Lacombe and B. Pucci, *Carbohydr. Res.*, 1999, **321**, 15.
6 G. A. Sim, *Acta Cryst.*, 1955, **8**, 833.
7 J.-H. Fuhrhop, D. Spiroski and C. Boettcher, *J. Am. Chem. Soc.*, 1993, **115**, 1600.
8 M. Masuda and T. Shimizu, *Carbohydr. Res.*, 1997, **302**, 139.
9 M. Masuda and T. Shimizu, *Carbohydr. Res.*, 2000, **326**, 56.
10 F. A. Quiocho, *Pure Appl. Chem.*, 1989, **61**, 1293.
11 G. A. Jeffrey and W. Saenger, *Hydrogen Bonding in Biological Structure*, Springer, Berlin, 1991.

CHEMCOMM
Communication
www.rsc.org/chemcomm

Uniform thin films of poly-3,4-ethylenedioxythiophene (PEDOT) prepared by *in-situ* deposition

Dirk Hohnholz,[a] Alan G. MacDiarmid,[a] David M. Sarno[b] and Wayne E. Jones, Jr.*[b]

[a] *Department of Chemistry, University of Pennsylvania, PA 19104, USA*
[b] *Department of Chemistry, State University of New York at Binghamton, Binghamton, NY 13902, USA*

Received (in Columbia, USA) 6th August 2001, Accepted 11th October 2001
First published as an Advance Article on the web 2nd November 2001

***In-situ* deposited thin films of the conducting polymer poly-3,4-ethylenedioxythiophene (PEDOT) have been prepared on hydrophilic and hydrophobic substrates and characterized by UV–Vis spectroscopy, atomic force microscopy and resistivity measurements.**

Conducting polymers have been widely discussed for their potential applications in molecular electronics. The recent development of the highly conductive, stable, and transparent polythiophene derivative poly-3,4-ethylenedioxythiophene (PEDOT) by Jonas *et al.*[1] and its commercialization by Bayer Corp. ('Baytron M, C, P', Bayer Corp.) has resulted in multiple patents, suggesting a new era of electronics based on this class of organic compounds and their derivatives.[2] Even though thin films of various conducting polymers have been extensively studied, the reliable deposition of such films on different surfaces is a continuing challenge due to the poor solubility of many of these polymers in common solvents.[3]

Recently, high quality thin films of conducting polymers have been prepared on substrates by *in-situ* deposition of the polymer from a polymerizing solution of the monomer and an oxidant.[4,5] *In-situ* deposited films of polyaniline and polypyrrole have been shown to be applicable for electronic devices, *e.g.* liquid crystal displays[5] and capacitors.[6] Given the limited solubility of PEDOT, the *in-situ* deposition method would seem to provide an effective means of preparing high quality thin films of this new material. The enhanced transparency of PEDOT to visible wavelengths could lead to new transparent electronic and photonic devices.

Here we report the first example of PEDOT thin films *in-situ* deposited from an acetonitrile solution of the ethylenedioxythiophene (EDOT) monomer and iron(III) chloride oxidant. The PEDOT films, deposited on hydrophilic and hydrophobic substrates, are characterized by UV–Vis–NIR spectroscopy, surface resistivity and atomic force microscopy (AFM).[7]

Commercially available glass microscope slides were rinsed with deionized water and then dipped into a mixture of 100 ml concentrated sulfuric acid and 50 ml 30% hydrogen peroxide ('piranha solution') for 2 h. The fresh hydrophilic surfaces were thoroughly rinsed with deionized water, dried and stored under vacuum. Hydrophobic glass surfaces were obtained by immersing piranha solution-cleaned substrates in a 0.1 wt% solution of dodecyltrichlorosilane in hexane for 5 s, drying and storing under vacuum. Hydrophilic slides were then coated with a composition of 1 ml ethylene glycol and 6 ml 1.3 wt% water dispersion of poly-3,4-ethylenedioxythiophene–polystyrenesulfonic acid (PEDOT–PSS, 'Baytron P', Bayer Corp.) by a single roller application wetted by the PEDOT–PSS. The slides were then dried in a stream of hot air for 2 min to obtain PEDOT–PSS pre-coated substrates. Pieces of a polyethyleneterephtalate (PET) transparency film (Nashua xf-20, Nashua Corp., NH) were cut to the same size as the glass slides and used as substrates without further treatment.

Separate solutions of 0.1 M EDOT ('Baytron M', Bayer Corp.) and 0.2 M iron(III) chloride·$6H_2O$, were prepared in acetonitrile and stirred for at least 20 min until completely clear. In most solvents, EDOT does not polymerize or does so very slowly (*e.g.* water or tetrahydrofuran). Acetonitrile was found to be the only highly polar solvent allowing fast reaction.[8] Each of the four substrates (hydrophilic glass, hydrophobic glass, PEDOT–PSS pre-coated glass, and PET) was suspended in a beaker with 125 ml of the stirred EDOT solution. At room temperature, 125 ml of the $FeCl_3$ solution was added with gentle stirring. The clear solution darkened rapidly (< 20 s) as the oxidative polymerization began, Scheme 1. After 2, 5, 10, 15 and 20 min, one substrate of each type was removed from the polymerizing solution and immersed in de-ionized water for 30 min to stop polymerization and remove residual reactants and un-bound oligomers. These PEDOT covered substrates were dried under air at room temperature for 30 min.

The characteristic electronic transitions for PEDOT on the four different substrates after a 15 min *in-situ* deposition are shown in Fig. 1. Regardless of the substrate, all UV-Vis-NIR absorption spectra exhibit the same general shape with relatively sharp absorptions in the UV at 300–450 nm and an intense, broad absorption at longer wavelengths. The higher energy transitions can be assigned to n–π* transitions in the polymer backbone. The band starting at 700 nm has been described as the free carrier tail.[10] In general, the absorbance of the film increases as a function of the deposition time, indicating continuous growth of the film. This has also been observed for polypyrrole and polyaniline films where maximum absorbances were observed at deposition times of 10–20 min.[5]

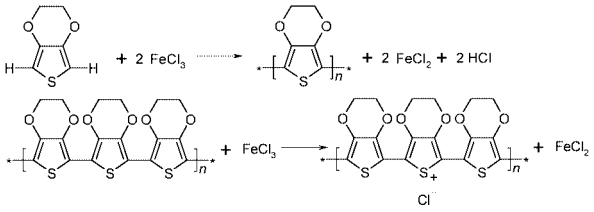

Scheme 1 Oxidative polymerization of EDOT to PEDOT with subsequent doping of the PEDOT polymer.

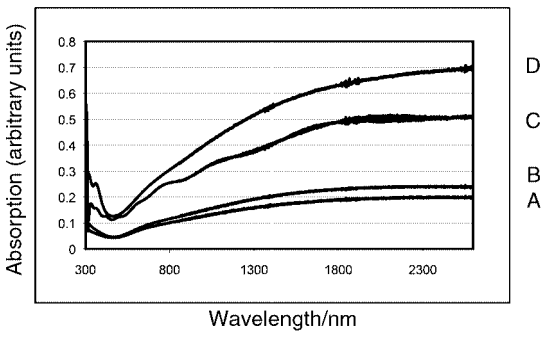

Fig. 1 UV–Vis–NIR absorption spectra of *in-situ* deposited films of PEDOT after 15 min on (A) hydrophilic glass, (B) hydrophobic glass, (C) PET[9] and D) PEDOT–PSS pre-coated glass. Substrates prior to *in-situ* deposition were used as a reference for each spectrum.

 DOI: 10.1039/b107130k

Table 1 Surface resistivity in kΩ cm^{-2} of *in-situ* deposited PEDOT films as a function of substrate type and deposition time

	Deposition time [minutes]				
	2	5	10	15	20
Hydrophilic glass	—[a]	—[a]	4.95 ± 3.6	18.0 ± 4.5[b]	1.8 ± 1.0[b]
Hydrophobic glass	—[a]	—[a]	—[a]	90.0 ± 4.5[b]	4.5 ± 1.35
PET	—[a]	9000 ± 2250	8.1 ± 1.35	1.35 ± 0.18	0.945 ± 0.135
Pre-coated glass	18.0 ± 9.0[c]	1.8 ± 0.45	0.765 ± 0.135	0.585 ± 0.225	0.405 ± 0.045

[a] Measurement out of range (> 13,000 kΩ cm^{-2}).[b] Resistivity measured on extended spots (islands); the majority of the slide showed no measurable resistivity.[c] Initial value of the PEDOT–PSS coating.

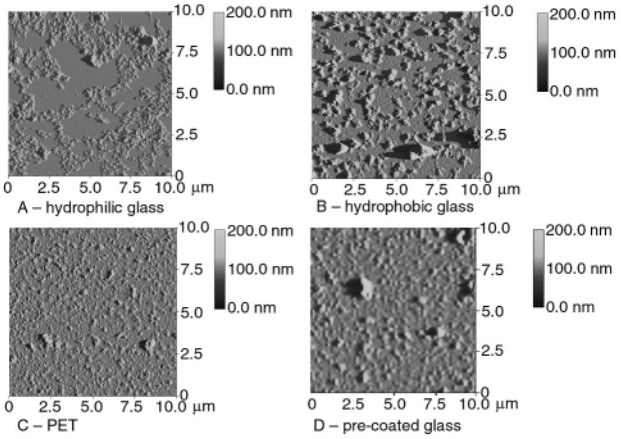

Fig. 2 Amplitude images of the surface morphology of PEDOT films on (A) hydrophilic, (B) hydrophobic, (C) PET, and (D) pre-coated glass substrates after 15 min *in-situ* deposition.

Although there is no significant shift in the spectra as a function of the substrate, there is a large difference in intensity. PEDOT on hydrophilic glass (A) shows the weakest absorption, suggesting the thinnest films, relative to the other three substrates. This result is consistent with the highly polar surface of the glass, which would be expected to interact weakly with the PEDOT polymer during deposition. In fact, following 20 min deposition cycles, the polymer was found to 'flake off' the surface. The three hydrophobic surfaces should facilitate deposition of a thicker, more uniform film, consistent with the absorption spectra (Fig. 1).

Shown in Table 1 are the resistivity values for each film–substrate combination obtained with a Pt 'four-in-line' probe with a constant current source and digital voltmeter.[11] In some cases insufficient surface coverage by PEDOT prevented resistivity determination. The lowest resistivity values were obtained for the PEDOT films *in-situ* deposited on PEDOT–PSS glass slides. A steady decrease of resistivity with increasing deposition time was observed on both PET and PEDOT–PSS pre-coated substrates, indicating continuous and stable film growth. This result is consistent with the stronger UV–Vis absorption for films grown on the pre-coated substrate.

Atomic Force Microscopy (AFM) in 'tapping mode' was used to analyze the surface morphology and film thickness of the *in-situ* deposited PEDOT thin films. Fig. 2 shows the different substrates after a 15 min *in-situ* deposition.

Deposition on hydrophilic glass (A) leads to islands of PEDOT, with only ~50% coverage of the glass surface. The average film thickness, determined by scoring the film with a razor to expose the underlying substrate, was found to be 50 ± 22 nm. In contrast, PEDOT on hydrophobic glass (B) exhibits larger grains, with film thickness of 118 nm ± 36 nm. The particulate nature of these *in-situ* deposited films contrasts with the successful 4-probe measurements on these two samples. While it is possible that a very thin (< 25 nm) surface layer of PEDOT exists, it is more likely that connectivity occurs through adjacent grains on the surface.

The deposition of PEDOT on PET (C) and PEDOT–PSS pre-coated glass (D) leads to uniform films of similar quality, as can be seen in Fig. 2. The thickness of the films deposited on pre-coated glass (D) was 228 ± 32 nm, whereas the thickness of the film on PET (C) could not be measured due to the softness of the plastic substrate. By comparison to the UV–Vis absorption spectra, both films are expected to be nearly the same thickness. PEDOT films on PET and on pre-coated glass showed moderate adhesion with respect to a 'Scotch-tape' test. Surface roughness of both films, calculated as the average variation in height across each sample, was ~60 nm.

In conclusion, we have successfully prepared thin, conducting films of PEDOT by the *in-situ* deposition method, bypassing common application problems associated with low polymer solubility. By varying the substrate on which the deposition occurs, we have identified the importance of surface hydrophobicity in obtaining uniform, highly conducting thin films. A simple and inexpensive method has been developed to reproducibly deposit highly conducting films of PEDOT with uniform thickness on organic substrates such as PET. Further it was observed that pre-coating insulating glass substrates with PEDOT–PSS resulted in highly conducting and uniform, ~230 nm thick films after only 15 min of deposition.

This work was financed jointly by the Office of Naval Research, the Army Resarch Office under the Multidisciplinary University Research Institute (MURI) program, and the National Institute of Health (Grant No. 1RI5ES10106-0).

Notes and references

1 Bayer AG, *Eur. Pat. No.* 339340, 1988 F. Jonas, G. Heywang, W. Schmidtberg, J. Heinze and M. Dietrich, *US Pat. No.* 5035926, 1991.
2 L. Groenendaal, F. Jonas, D. Freitag, H. Pielartzik and J. R. Reynolds, *Adv. Mater.*, 2000, **12**, 481.
3 D. Fichou, *Handbook of Oligo- and Polythiophenes*, Wiley VCH, Weinheim, 1999J. Roncali, *Chem. Rev.*, 1997, **97**, 173.
4 L. A. A. Petterson, F. Carlsson, O. Inganäs and H. Arwin, *Thin Solid Films*, 1998, **313–314**, 356.
5 Z. Huang, P.-C. Wang and A. G. MacDiarmid, *Langmuir*, 1997, **13**, 6480; Z. Huang, P.-C. Wang, J. Feng and A. G. MacDiarmid, *Synth. Met.*, 1997, **85**, 1375.
6 G. Heywang and F. Jonas, *Adv. Mater.*, 1992, **4**, 116.
7 UV–Vis–NIR spectra were recorded using a Perkin–Elmer Model Lambda 9 spectrometer. Surface resistivity was measured with a Keithly M 617 constant current source and HP digital voltmeter. AFM images were obtained with a Digital Instruments, Inc. Nanoscope III.
8 P. M. Lessner, T.-Y. Su, R. S. Hahn and V. Rajasekaran, *US Pat. No.* 6136372, 2000.
9 The slight 'waviness' of spectrum C was found to be inherent to samples using PET transparency film as substrate.
10 Y. Xia, A. G. MacDiarmid and A. J. Epstein, *Macromolecules*, 1994, **27**, 7212; H. J. Ahonen, J. Lukkari and J. Kankare, *Macromolecules*, 2000, **33**, 6787.
11 A. L. Cabrera, W. Garrido-Molina, E. Morales-Leal, J. Espinosa-Gangas, I. K. Schuller and D. Lederman, *Langmuir*, 1998, **14**, 3249.

CHEMCOMM Communication
www.rsc.org/chemcomm

A novel way to prepare ultra-thin polymer films through surface radical chain-transfer reaction

Feng Zhou,[a] Weimin Liu,*[a] Miao Chen[a] and D. C. Sun[b]

[a] *Lanzhou Institute of Chemical Physics, Chinese Academy of Science, Lanzhou, China 730000. E-mail: wmliu@ns.lzb.ac.cn; Fax: +86-931-8277088*
[b] *State University of New York at Binghamton, Binghamton, N. Y, USA 13902-6000*

Received (in Cambridge, UK) 30th August 2001, Accepted 16th October 2001
First published as an Advance Article on the web 2nd November 2001

Radical chain transfer to bonded thiol groups and surface re-initiated polymerization resulted in ultra-thin polymer films.

In-situ grafting polymer films through surface initiated polymerization (SIP) from inorganic substrates are gaining increasing interest in recent years.[1] The key step is to introduce initiating points on substrates surfaces, which can be carried out through the assembly of self-assembly-initiators or the *in-situ* modification of end group functionalized surfaces by using self-assembling techniques.[2] Therefore, most polymerization techniques including conventional free radical polymerization,[3] 'living' radical polymerization based on 'iniferter',[4] 'TEMPO'[5] and 'ATRP',[6] ionic polymerization,[7] ROMP,[8] *etc*. have been realized on surfaces. However, most of these SIPs require the synthesis of self-assembly-initiator molecules with complex structures. Thus, the formation of initiating points on surfaces often involves many reaction steps. Radical chain-transfer reaction is widely used in molecular weight control, synthesis of end group functionalized polymers and macromonomers, *etc*.[9] and has once been used for the modification of solid substrates *via* the so-called radical transfer addition of olefin derivatives.[10] Here we report that it may also serve as the intermediate reaction for surface induced polymerization to fabricate covalently attached polymer films with the emphasis on planar substrates.

Surface bonded thiol groups were used as the radical chain transfer agents because of their relative high chain transfer constant. A widely used silane coupling reagent, mercaptopropyltrimethoxylsilane (MPS), was used to prepare thiol-terminated silica or silicon wafer (denoted as HS–silica and HS–silicon) according to the corresponding published procedures[11] using toluene as the solvent. The grafting amount of MPS on silica surface (S_{BET}, 250 $m^2\ g^{-1}$) was about 0.9 mmol g^{-1} from elemental analysis. HS–silicon had a water contact angle of 70°, which indicated a complete coverage of thiol-terminated monolayer. *In-situ* polymerization was carried out in a 20 ml mixture of methyl methacrylate (MMA), azodiisobutylnitrile (AIBN) as the initiator and toluene at 60 °C for a certain time in the presence of HS–silica or HS–silicon. The molar ratio of MMA : AIBN (100 : 1) and the volume ratio of MMA : toluene (1 : 2) were kept constant. The thiol terminated silica or silicon wafers and the polymer film modified silica/silicon (denoted as polymer-silica or polymer-silicon) were extracted with CH_2Cl_2 to ensure the removal of all unbonded species. The basic strategy of this novel process is depicted in Scheme 1.

The obvious Raman shift at 2577 cm^{-1} for HS–silica was attributed to the stretching vibration of S–H (Fig. 1a). After polymerization, its intensity decreased dramatically but still could be detected, indicating that radical chain transfer to (a part of, but not all) thiol groups occurred. The other absorbance bands characteristic of PMMA proved that MMA was grafted onto silica surface. The normalized transmittance FTIR of HS–silicon, PMMA–silicon and spin-cast PMMA film as a control for the selected region between 3200 and 1500cm^{-1} also indicated that a layer of PMMA was formed on silicon wafer (Fig. 1b).

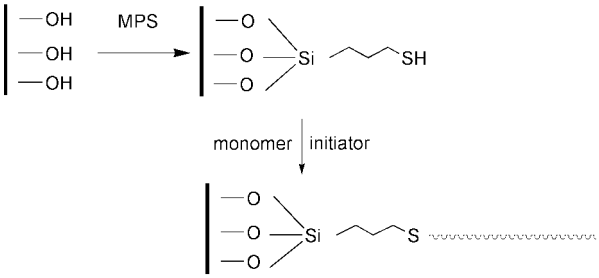

Scheme 1 Reaction procedures of *in-situ* grafting polymer film through radical chain transfer reaction.

The role of silica-carried thiol groups as the potential chain-transfer agents was verified by measuring the molecular weight of the free polymers formed simultaneously in the bulk solution. As is shown in Fig. 2, increasing the amount of HS–silica

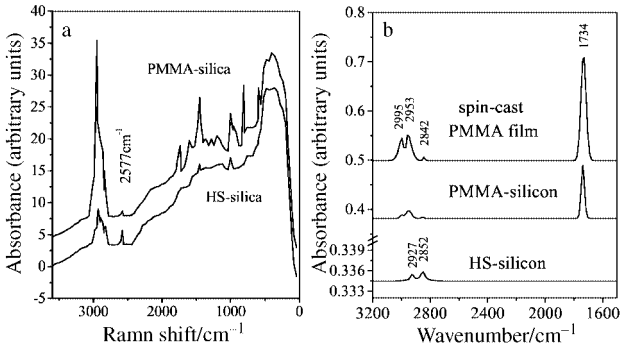

Fig. 1 (a) Raman spectra of HS–silica, PMMA–silica and (b) normalized transmittance FTIR of HS–silicon, PMMA–silicon as well as spin-cast PMMA film.

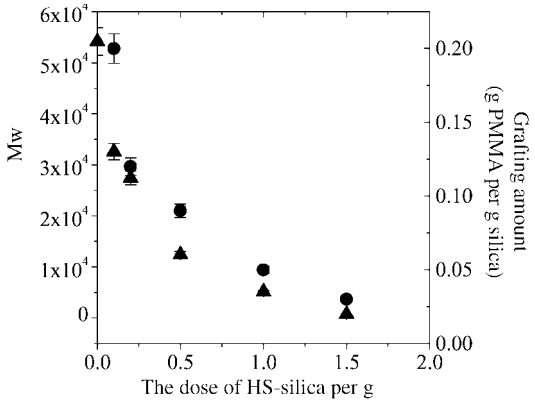

Fig. 2 Weight average molecular weight (▲) of free PMMA and the grafting amount (●) of PMMA *versus* the dose of HS–silica.

 DOI: 10.1039/b107831n

reduced the weight-average molecular weight of the free polymer. The results confirmed that silica-carried thiol groups played a similar role as the other thiol compounds, of being effective chain-transfer agents in polymerization. The grafting amount[12] of polymer also decreased with increasing the dose of HS–silica, closely resembling the variation of the molecular weight of the free polymer.

Our hypothesized reaction procedures were also confirmed by XPS. After polymerization of MMA for 24 h on silicon wafers, no peaks characteristic of Si_{2p} and S_{2p} were detected. This indicated that the substrate was completely covered by a polymer layer of at least 5 nm. (In fact, the film thickness was about 27 nm.) But this is not the case with the silica surface. The evaluation[13] of the film thickness from the attenuation of Si_{2p} of PMMA–silica (even the sample having the maximum grafting amount in Fig. 2) showed a very thin polymer film of less than 2 nm. We attributed the ineffectiveness of the method on silica surfaces, against that on silicon wafers, to the different rate of termination. Propagating chains on silica surfaces were easily formed and simultaneously terminated by the chain transfer reaction because of the relatively high contents of thiol groups in polymerization systems and also the mobility of silica-carried thiol groups. But on planar substrates, the possibility of radical chain transfer could be reduced because of the two-dimension restriction of thiol groups and also the absence of effective chain transfer agents in bulk solution, which made the propagating chains on planar substrates less likely to be terminated.

Grafting polymerization on silicon wafers was found to occur during the first two hours, resulting in more than 90% of the thickness obtained with 24 h of polymerization time. The contact mode AFM topography of a 27 nm thick PMMA film revealed a homogeneous and smooth polymer film with an rms roughness of 0.207 nm.

The advantage of this method was its capability to realize polymerization of a wide range of monomers in both non-aqueous and aqueous solutions. Table 1 lists several examples of the obtained polymer films and the corresponding contact angles and film thicknesses. We aimed to fabricate surfaces with different lypohydrophilic characters by co-polymerization of monomer pairs using different molar ratios. Fig. 3 shows that the method was effective. By simply varying the composition of the monomer pairs, the wetting behavior of the resulting copolymer films could be changed in a highly controlled fashion. Therefore, radical chain transfer reaction and surface re-initiated polymerization provides a means to control the physical properties of polymer films.

In conclusion, we have demonstrated for the first time that (1) radical chain transfer to thiol-terminated self-assembled monolayer and (2) surface re-initiated radical polymerization on both silica surface and silicon wafers truly occurred and ultra-thin polymer films with nanometer dimensions resulted. The method is a new addition to SIP, applicable to the polymerization of a wide range of monomers (especially functionalized monomers) and workable in situations where other SIPs are inconvenient to use. The method has potential applications in tailoring the chromatographic properties of solid supports, enhancing the biocompatibility of substrate surfaces, lubricating microelectromechanical systems (MEMS), the chemical modification of electrodes, *etc*.

Table 1 The static contact angles of water and thicknesses of the obtained polymer films

Film	Solvent	Contact angle	Thickness (Å)
PMMA	Toluene	70	274
PSt	Toluene	90	225
PTDMA	Toluene	94	62
PBuA	Toluene	96	134
PAN	THF	40	1356
PAA	THF	27	135
	Water	16	295
PAn	Water	46	125
	DMF	47	145

Time: 24 h; Temperature: 60 °C. For the polymerization in water $(NH_4)_2S_2O_8$ was used as the initiator. PMMA: poly(methyl methacrylate); PSt: polystyrene; PTDMA; poly(tetradecanyl methacrylate); PAN: polyacrylonitrile; PAA: poly(acrylic acid); PBuA: poly(butyl acrylate); PAN: polyacrylanitrile; THF: tetrahydrofuran; DMF: *N*,*N*′-dimethylformamide.

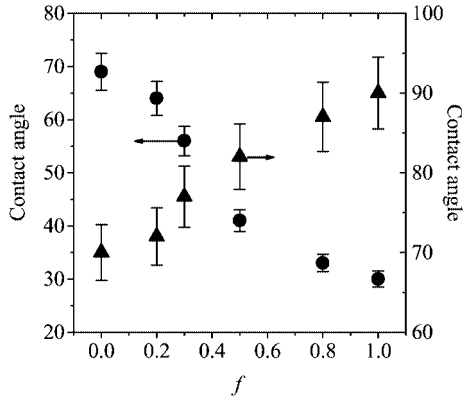

Fig. 3 The contact angle of copolymer film as a function of the molar percentage (*f*) of AA in AA–MMA pair (●) and of St in St–MMA pair (▲).

The research was supported by Natural Science Foundation of China (Grants No. 59825116).

Notes and references

1 B. Zhao and W. J. Brittain, *Prog. Polymer Sci*., 2000, **25**, 677.
2 F. Schreiber, *Prog. Surface Sci*., 2000, **65**, 151.
3 O. Pruker and J. Ruhe, *Macromolecules*, 1998, **31**, 592.
4 B. de Boer, M. P. Simon and E. W. Werts van der Vegte, *Macromolecules*, 2000, **33**, 349.
5 M. Husseman, M. Morrison, D. Benoit, J. Prommer, C. M. Mate, W. D. Hinsberg, J. L. Kedrick and C. J. Hawker, *J. Am. Chem. Soc*., 2000, **122**, 1844.
6 P. Zhou, G. Q. Chen, C. Z. Li, F. S. Du, Z. C. Li and F. M. Li, *Chem. Commun*., 2000, 797; A. Marsh, A. Khan, M. Garcia and D. M. Haddleton, *Chem. Commun*., 2000, 2083.
7 B. Zhao and W. J. Brittain, *J. Am. Chem. Soc*., 1999, **121**, 3557; R. Jordan, A. Ulman, J. F. Kang, M. H. Rafailovich and J. Sokolov, *J Am. Chem. Soc*., 1999, **121**, 1016.
8 M. Weck, J. J. Jackiw, R. R. Rossi, R. S. Weiss and R. H. Grubbs, *J. Am. Chem. Soc*., 1999, **121**, 4088.
9 Y. Ysukahara, Y. Nakanishi, Y. Yamashita, Y. Ohtani, H. Nakashima, Y. F. Luo, T. Ando and S. Tsuge, *Macromolecules*, 1991, **24**, 2493; A. J. Yamazaki, M. Song, F. M. Winnik and J. L. Brash, *Macromolecules*, 1998, **31**, 109.
10 C. E. Song, J. S. Lim, S. C. Kim, K. J. Lee and D. Y. Chi, *Chem. Commun*., 2000, 2415.
11 C. Rosini, C. Bertucci, D. Pini, P. Altemura and P. Salvadori, *Tetrahedron Lett*., 1985, **26**, 3361; N. Balachander and C. N. Sukenik, *Langmuir*, 1990, **6**, 1621.
12 The grafting amount was obtained from thermogravimetric analysis. The selected temperature range was from room temperature to 600 °C up to which the alkyl chains were nearly all decomposed. (See G. J. Kluth, M. M. Sung, and R. Maboudian, *Langmuir,* 1997, **13**, 3775.) The contribution of MPS was subtracted from the total weight loss of PMMA–silica.
13 J. D. Andrade, *Surface and Interfacial Aspects of Biomedical Polymers, Surface Chemistry and Physics*; Plenum Press, New York, 1985, Vol. 1, p. 176.

CHEMCOMM Communication
www.rsc.org/chemcomm

Dissociative cycloelimination, a new selenium based pericyclic reaction

Lars Henriksen* and Søren Jakobsen

Department of Chemistry, University of Copenhagen, Universitetsparken 5, DK-2100 Copenhagen, Denmark. E-mail: larsh@kiku.dk

Received (in Cambridge, UK) 24th August 2001, Accepted 19th October 2001
First published as an Advance Article on the web 13th November 2001

The stereospecific oxidation of hydrazine into *cis*-diimide and the catalytic disproportionation of hydrogen peroxide effected by selenoxides are suggested to involve a dissociative cycloelimination from an intermediary selenurane.

One consequence of the high polarizability of the selenium nucleus is the occurrence under mild conditions of pericyclic reactions involving selenium. Three reactions of this type, *i.e.* the [2,3]-sigmatropic shift,[1] the ene-reaction[2] and the cycloelimination,[3] were described shortly after the recognition of the concept of pericyclic reactions. More recently[4] we have found evidence for a dissociative analogue of the ene-reaction (Scheme 1) in the *ortho*-specific substitution in phenols effected by neutral benzeneselenenic acid (while more reactive phenylselenenium ion equivalents attacks a variety of donor-activated aromats with high *para*-selectivity).[5] In consequence, a dissociative analogue of the cycloelimination reaction might also be feasible. The selenuranes formed from a selenoxide and a nucleophile having a labile hydrogen atom in a vicinal position, *e.g.* hydrogen peroxide, hydrazines and hydroxylamines, are the most obvious substrates for this type of reaction (Scheme 2). In fact, all three types of compound react with selenoxides at ambient temperature. The present paper discusses the evidence for a dissociative cycloelimination step in the reactions of phenyl methyl selenoxide (**1a**) and phenyl anisyl selenoxide (**1b**)[6] with hydrazine and hydrogen peroxide as substrates.

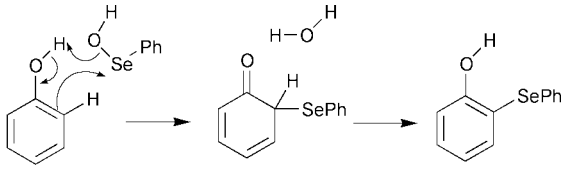

Scheme 1

The reaction of hydrazine with a variety of oxidants has been shown to proceed *via* diimide (**2**) which exists in *cis* and *trans* isomeric forms with a high barrier for interconversion. Only the thermodynamically less stable *cis*-**2** can transfer a pair of hydrogen atoms to a double bond through a pericyclic transition state. Therefore exhaustive alkene hydrogenation with **2** normally requires a large excess of hydrazine and oxidant. (See ref. 7 for a review of diimide chemistry.) Only one previous example of the specific generation of *cis*-**2** has appeared.[8]

Since the dissociative cycloelimination path (Scheme 2, Y = Z = NH) predicts a stereospecific formation of *cis*-**2**, the hydrazine oxidation furnishes a test of our hypothesis. We found that the reaction of **1a** with hydrazine in methanol (Scheme 3) produced 1 mol of N_2 per 2 moles of selenoxide (path **a**) while the same reaction in the presence of an excess of alkene (prop-2-en-1-ol) gave 1 mol of N_2 per mol of selenoxide

Scheme 2

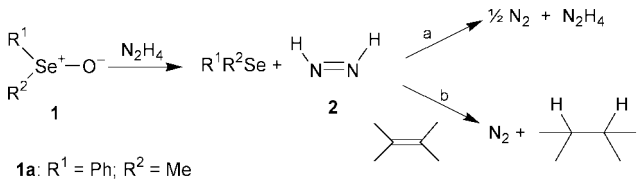

1a: R^1 = Ph; R^2 = Me
1b: R_1 = Ph; R_2 = 4-MeOC$_6$H$_4$

Scheme 3

(path **b**). The observed quantitative transfer of hydrogen to the alkene shows that *cis*-**2** is produced specifically. The rate of evolution of nitrogen does not follow a simple reaction order but is approximately constant during the first 60% of the reaction indicating the presence of an intermediate, presumably **2**, at a steady-state concentration. Plots of the reaction fraction against time for cases **a** and **b** are almost superimposable, showing that the bimolecular disporportionation of **2** into hydrazine and dinitrogen is fast even at a very low concentration.

The preparative use of *cis*-**2** generated by the hydrazine–selenoxide reaction is illustrated by the examples shown in Scheme 4. The reaction of **1a** (2.3 mmol) and hydrazine hydrate (5 mmol) with azobenzene (**3**) (2.1 mmol) in ethanol (3 ml) at 300 K gave complete decolourisation in 14 min. 1,2-Diphenylhydrazine (**4**) (93%) was isolated from the reaction mixture. This result confirms the specific formation of *cis*-**2**. It further demonstrates that a nucleophilic addition to the selenoxide precedes the elimination step. While **4** is very readily oxidized and is, in fact, slowly converted into **3** by selenoxides it is not sufficiently nucleophilic to compete with hydrazine in the initial addition step. The conversion of 3-(2-furyl)propenoic acid (**5**) into 3-(2-furyl)propanoic acid (**6**) with **1** and **5** in the molar ratio 1 : 1 is included as a model for the reduction of a less reactive hydrogen acceptor. In this case the reduction yields increase with an increasing reaction period (Table 1) in accord with a disproportionation (second order in **2**) competing with the hydrogen transfer to the alkene (first order in **2**). The rate of diimide generation qualitatively displays the same dependence

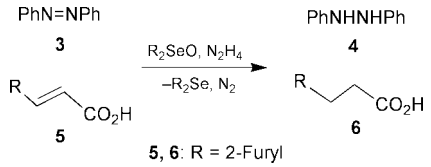

5, **6**: R = 2-Furyl

Scheme 4

Table 1 Yield *versus* reaction period in the conversion of **5** into **6**

Selenoxide	Conditions	Reaction time/h	Reduction/ %[a]
1b	**5**, MeOH	0.8	38
1a	**5**, Na-salt, 67% aq. MeOH	2.0	63
1b	**5**, Na-salt, MeOH	2.5	71
1b	**5**, Na-salt, 67% aq. MeOH	48	92 (77)[b]

[a] Calculated from the molar ratio, N_2/**1**. [b] Isolated, pure compound.

 DOI: 10.1039/b107688b

upon the identity of **1** and the solvent composition as found in the hydrogen peroxide reaction (see later). It may thus be regulated by varying the identity of the selenoxide and/or changing the composition of the medium to suit the hydrogenation of alkenes with varying reactivities.

Since the kinetics of the hydrazine oxidation are not simple we turned to the reaction of **1** with hydrogen peroxide in order to obtain additional information on the medium dependence of the addition–cycloelimination sequence. It has been reported[9] that hydrogen peroxide is disproportionated into water and dioxygen with selenoxides as catalysts. We suggest that the catalytic cycle involves a reversible addition of hydrogen peroxide to **1** with formation of selenurane (**7**), a cycloelimination giving dioxygen and selenide (**8**) and a reoxidation step (Scheme 5). This sequence is supported by the observation[10] that *tert*-butyl hydroperoxide lacking the vicinal hydrogen atom necessary for the elimination does not give a similar reaction and by our observation that **8** is present in the reaction mixtures at steady-state concentrations depending on the identity of the medium. The rate of oxygen evolution is first order in hydrogen peroxide with an apparent rate constant proportional to the concentration of the selenoxide. Some representative second order rate constants are given in Table 2. This type of kinetics can be reconciled with either of three situations: (i) rate determining addition to give **7** (k_1); (ii) rate determining elimination to give **8** (k_2) preceded by the formation of **7** in a rapid equilibrium, (iii) rate determining reoxidation to **1** (k_3). The three steps appear to have comparable rates and depending upon the medium either one may be rate determining. The concentration of **8** is very low in neutral or acidic methanol showing that k_3 cannot be rate determining. Addition of triethylamine gives an unchanged initial rate which subsequently falls off to about one third. At the latter stage ^{77}Se NMR shows **8** and **1** in the approximate ratio 2:1 thus indicating a slow reoxidation. The reaction of **1b** in methanol is acid catalysed while that of **1a** is not. This indicates a rate determining addition step for **1b**, at least in the absence of acid, in accord with the report that the racemization of optically active **1b**, assumed to occur by reversible selenurane formation, requires acid catalysis[6] while **1a** is racemized by water alone.[11,12]

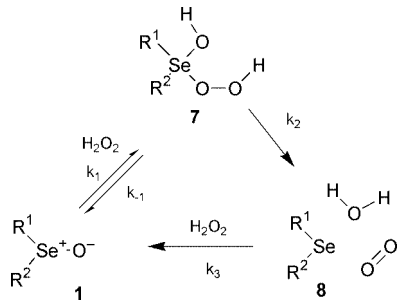

Scheme 5

Table 2 Second order rate constants[a] (10^2 k/s^{-1} M^{-1} = 10^2 k_{obs} [**1**]$^{-1}$) for the selenoxide catalyzed decomposition of hydrogen peroxide at 300 K

Selenoxide	**1a**		**1b**	
Conditions	Neutral	4M AcOH	Neutral	4M AcOH
Solvent:				
94% MeOH	3.7	3.7	0.60	5.2
80% MeOH	1.5	1.7	0.43	1.5
60% MeOH	0.5	0.5	0.18	0.55
96% THF	2.0	5.8	0.36	0.95
90% THF	2.0	4.2		0.50
84% THF	2.0	3.2		

[a] Reproducibility ± 20%.

In THF the reactions of both **1a** and **1b** are acid catalysed. This is hardly surprising. The formation of **7** is not an elementary process but also involves a proton transfer step which requires a proton donating component in the medium. Two observations suggest that the elimination step may be rate determining at high reaction rates. The reactions of **1a** in neutral and **1a** and **1b** in acidic methanol are more strongly inhibited by water than the reactions of **1b** in neutral methanol and **1a** in THF. Moreover, the order of reactivities **1a**:**1b** is reversed in acidic 94% methanol.

While the three-stage mechanism of hydrogen peroxide decomposition seems established it cannot in the absence of stereochemical information be finally shown that the elimination step is pericyclic. However, the observation that triethylamine does not increase the initial rate in the reaction of **1a** is a strong argument against an acyclic, base or solvent assisted reaction. The dissociative cycloelimination step calls for the oxygen molecule to be produced in the singlet state. We were unable to detect oxygen consumption by singlet oxygen acceptors such as furanes. However, this cannot be taken as an argument against the pericyclic reaction. The oxygen molecule is generated in a solvent cage together with a molecule of **8** which, in analogy with diethyl sulfide[13] is expected to be a powerful quenching agent for singlet oxygen.

In conclusion, a dissociative cycloelimination reaction is indicated by the stereospecific oxidation of hydrazine with **1** to give *cis*-**2**. The same mechanism is compatible with the features of the selenoxide (or selenide) catalysed disproportionation of hydrogen peroxide in which case the disproportionation releases no reactive intermediates into the reaction medium, a feature of possible interest in selenium biochemistry.

Notes and references

1 K. B. Sharpless and R. F. Lauer, *J. Am. Chem. Soc.*, 1973, **94**, 7154.
2 K. B. Sharpless and R. F. Lauer, *J. Am. Chem. Soc.*, 1974, **95**, 2697.
3 D. Neville Jones, D. Mundy and R. D. Whitehouse, *J. Chem. Soc., Chem. Commun.*, 1972, 86.
4 L. Henriksen, *Tetrahedron Lett.*, 1994, **35**, 7057.
5 L. Henriksen and N. Stuhr-Hansen, *Phosphorus, Sulfur*, 1998, **136–138**, 175.
6 N. Stuhr-Hansen, H. O. Sørensen, L. Henriksen and S. Larsen, *Acta Chem. Scand.*, 1997, **51**, 1186.
7 D. J. Pasto and R. T. Taylor, *Org. React.*, 1991, **40**, 91.
8 K. Kondo, S. Murai and N. Sonoda, *Tetrahedron Lett.*, 1977, **42**, 3727.
9 H. J. Reich, S. Wollowitz, J. E. Trend, F. Chow and D. F. Wendelborn, *J. Org. Chem.*, 1978, **43**, 1697.
10 T. Hori and K. B. Sharpless, *J. Org. Chem.*, 1978, **43**, 1689.
11 F. Davis, J. Billmers and O. Stringer, *Tetrahedron Lett.*, 1983, **24**, 3191.
12 F. Davis, O. Stringer and J. McCauley, Jr, *Tetrahedron*, 1985, **41**, 4747.
13 R. W. Denny and A. Nickon, *Org. React.*, 1973, **20**, 133.

CHEMCOMM Communication
www.rsc.org/chemcomm

Regiocontrolled deprotonative-zincation of bromopyridines using aminozincates

Tatsushi Imahori, Masanobu Uchiyama, Takao Sakamoto and Yoshinori Kondo*

Graduate School of Pharmaceutical Sciences, Tohoku University, Aobayama, Aoba-ku, Sendai 980-8578, Japan. E-mail: ykondo@mail.pharm.tohoku.ac.jp

Received (in Cambridge, UK) 11th September 2001, Accepted 19th October 2001
First published as an Advance Article on the web 13th November 2001

Regiochemistry in the deprotonation of bromopyridines was found to be greatly influenced by the choice of metal amide base, and DA-zincate and TMP-zincate turned out to be excellent complementary practical agents for regioselective metalation of bromopyridines.

Deprotonative metalation has been widely used as a facile method for regioselective functionalization of various aromatic compounds.[1] Regioselective metalation has also been important in pyridine chemistry and pyridine derivatives have been employed as attractive functional molecules for supramolecular chemistry.[2] Much work has been done on selective lithiation using lithium diisopropylamide (LDA) and other bases,[3] including investigations by Effenberger and co-workers who reported that the lithiation of 2-bromopyridine proceeds mainly at the 3-position together with partial lithiation at the 4-position using LDA in THF at −78 °C. These lithiospecies were trapped by trimethylsilyl chloride using an *in situ* method (Scheme 1).[4]

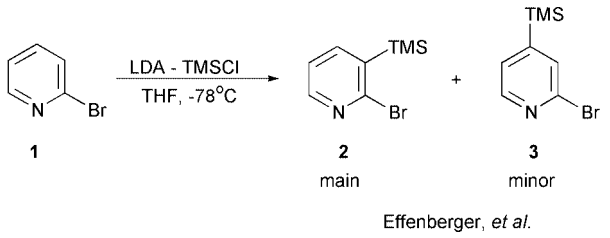

Scheme 1

In order to investigate regiochemistry in the deprotonative metalation of pyridine, we screened metalating agents and solvents in the lithiation of 2-bromopyridine. To our surprise, when we carried out the reaction of 2-bromopyridine (**1**) with LTMP and TMSCl using an *in situ* method at −78 °C in Et_2O, the 6-TMS derivative (**4**) was obtained exclusively in 65% yield (Scheme 2). Related to this unique regioselectivity, Fort and co-workers recently reported a unique selective lithiation at the 6-position of 2-chloropyridine or 2-methoxypyridine using a n-BuLi and lithium dimethylaminoethoxide mixed reagent in hexane;[5] however their method is considered to be difficult to apply to the lithiation of 2-bromopyridine due to the likely competition with the bromine–lithium exchange reaction. To the best of our knowledge, the reaction described above is the first example of the regioselective deprotonative-lithiation of 2-bromopyridine at the 6-position. This complete reversal of the regioselectivity by changing only the amide base and solvent (LDA in THF *vs.* LTMP in Et_2O) is noteworthy.

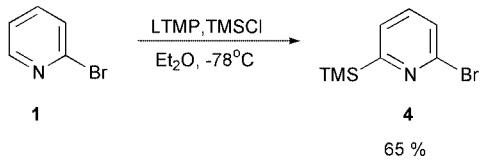

Scheme 2

In some cases, pyridinyllithiums with a bromo substituent are known to be unstable due to the formation of pyridyne,[4b,6] lithium migration[7] and so on. In order to overcome these side reactions, the *in situ* method is effective by the existence of an electrophile in the metalation process, but the range of electrophiles has been limited. We therefore focused our interest on the use of organozincate chemistry in the metalation of bromopyridines, seeking a wider scope of direct functionalization. We recently disclosed that TMP-zincate is a highly chemoselective base for aromatic metalation in the presence of electrophilic substituents such as alkoxycarbonyl or cyano groups and that it has also been found to be effective for α-metalation of N-heteroaromatics[8] in connection with our recent studies on selective aromatic metalation.[9]

Intrigued by the above result on regioselective lithiation, we turned our interest to the selective zincation of bromopyridines using TMP-zincate (lithium di-*tert*-butyltetramethylpiperidinozincate) and DA-zincate (lithium di-*tert*-butyldiisopropylaminozincate). The reaction of 2-bromopyridine (**1**) with TMP-zincate in Et_2O proceeded at room temperature and treatment with I_2 gave 2-bromo-6-iodopyridine (**6**) in 86% yield together with a trace amount of 2-bromo-3-iodopyridine (**8**). In contrast, when DA-zincate was employed as a metalating agent and the reaction was carried out at −20 °C, the metalation proceeded at the 3-position preferentially and 2-bromo-3-iodopyridine (**8**) was obtained in 72% avoiding the formation of 2,3-pyridyne (Scheme 3). The intermediary bromopyridinylzincates **5** and **7** are relatively stable under those reaction conditions, and thus the selective conversion without side reactions to the corresponding bromoiodides was achieved.

The zincation of 3-bromopyridine was also examined and it was found that TMP-zincate and DA-zincate show completely different regioselectivity (Scheme 4). Namely, the reaction of 3-bromopyridine (**9**) with TMP-zincate in THF at room temperature proceeded at the 2-position exclusively and treatment with I_2 gave 3-bromo-2-iodopyridine (**11**) in 68% yield, whereas the zincation of **9** with DA-zincate occurred predominantly at the 4-position and treatment with I_2 gave 3-bromo- 4-iodopyridine (**13**) in 66% yield together with a trace amount of **11**. It is noteworthy that these results suggest that the pyridinylzincates **10** and **12** cause no formation of pyridyne[4b,6] throughout the reactions, even at room temperature.

Limited examples of the preparation of these bromoiodopyridines using conventional methods are known but they sometimes require tricky steps or multi steps and particularly no report on the preparation of 2-bromo-6-iodopyridine from 2-bromopyridine has appeared so far.[10] The present regioselective zincation is considered to provide a new effective direct methodology.

In summary, regiocontrolled deprotonative metalation of pyridine was achieved with excellent regioselectivity by choosing one of the tunable aminozincates, and highly regioselective transformation of bromopyridines was accomplished. Further studies are underway for understanding the origin of the regioselectivity by the change of amide bases[11] and

 DOI: 10.1039/b108252n

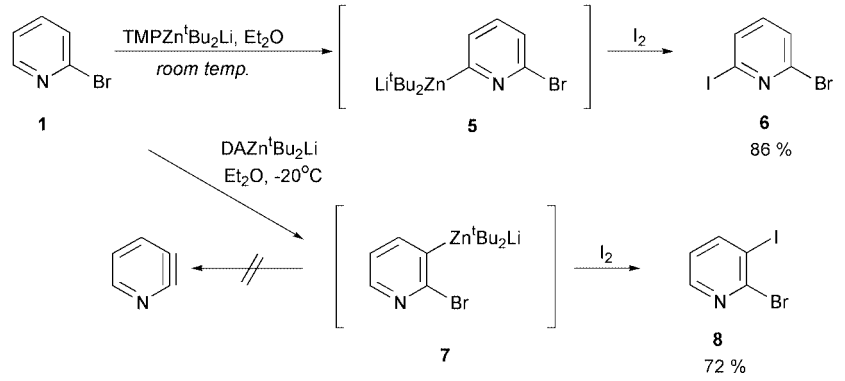

Scheme 3

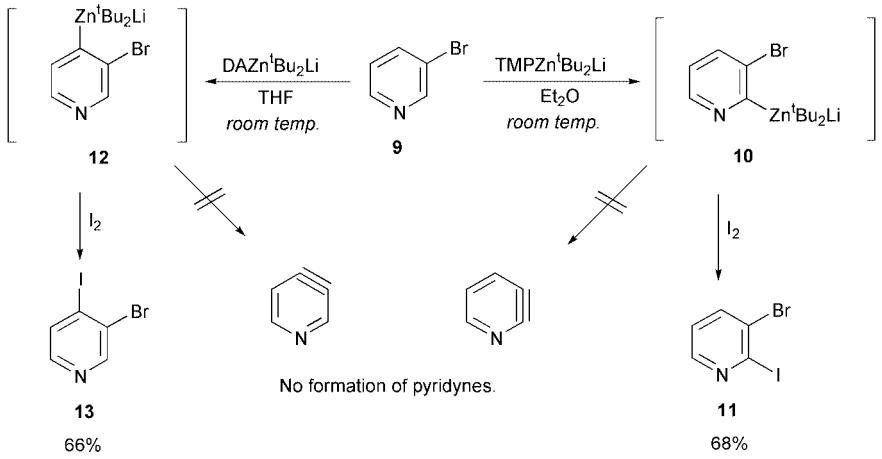

Scheme 4

also for applying the methodology for the preparation of unique functional molecules using new carbon–carbon bond forming reactions.

This work was partly supported by the Grant-in-Aid for Scientific Research (No. 12672047 and No. 12557198) from the Ministry of Education, Culture, Sports, Science and Technology, Japan and by the Tokuyama Science Foundation.

Notes and references

1 (*a*) H. Gilman and R. L. Bebb, *J. Am. Chem. Soc.*, 1939, **61**, 109; (*b*) G. Wittig and G. Fuhrman, *Chem. Ber.*, 1940, **73**, 1197; (*c*) B. J. Wakefield, *The Chemistry of Organolithium Compounds*, Pergamon, Oxford, 1974; (*d*) B. J. Wakefield, *Organolithium Method*, Academic Press, London, 1988; (*e*) V. Snieckus, M. Gray and M. Tinkl, in *Comprehensive Organometallic Chemistry II*, ed. F. G. Abel, F. G. A. Stone, G. Wilkinson and A. McKillop, Pergamon Press, Oxford, 1995, Vol. 1, p. 1; (*f*) V. Snieckus, *Chem. Rev.*, 1990, **90**, 879; (*g*) H. W. Gschwend and H. R. Rodrigues, *Heteroatom Facilitated Lithiations. Org. React. (N.Y.)*, 1979, **26**, 1.

2 J.-M. Lehn, *Supramolecular Chemistry*, VCH, Weinheim, 1995.

3 (*a*) D. L. Comins and S. O'Conner, *Adv. Heterocycl. Chem.*, 1988, **44**, 199; (*b*) G. Queguiner, F. Marsais, V. Snieckus and J. Epsztajn, *Adv. Heterocycl. Chem.*, 1991, **52**, 187; (*c*) G. Rewcastle and A. R. Katritzky, *Adv. Heterocycl. Chem.*, 1993, **56**, 155; F. Mongin and G. Queguiner, *Tetrahedron*, 2001, **57**, 4059.

4 (*a*) F. Effenberger and W. Daub, *Chem. Ber.*, 1991, **124**, 2119; (*b*) G. W. Gribble and M. G. Saulnier, *Tetrahedron Lett.*, 1980, **21**, 4137; For *in situ* trapping with TMSCl see: T. D. Krizan and J. C. Martin, *J. Am. Chem. Soc.*, 1983, **105**, 6155; S. Caron and J. M. Hawkins, *J. Org. Chem.*, 1998, **63**, 2054.

5 (*a*) S. Choppin, P. Gros and Y. Fort, *Org. Lett.*, 2000, **2**, 803; (*b*) P. Gros and Y. Fort, *J. Chem. Soc., Perkin Trans. 1*, 1998, 3515; (*c*) P. Gros, Y. Fort and P. Caubere, *J. Chem. Soc., Perkin Trans. 1*, 1997, 3071.

6 (*a*) H. Hart, *Supplement C2, The Chemistry of Triple Bonded Functional Groups*, Wiley, Chichester, 1994, p. 1113; (*b*) M. G. Reinecke, *Tetrahedron*, 1982, **38**, 427.

7 M. Mallet, G. Branger, F. Marsais and G. Queguiner, *J. Organomet. Chem.*, 1990, **382**, 319.

8 Y. Kondo, M. Shilai, M. Uchiyama and T. Sakamoto, *J. Am. Chem. Soc.*, 1999, **121**, 3539.

9 (*a*) Y. Kondo, N. Takazawa, C. Yamazaki and T. Sakamoto, *J. Org. Chem.*, 1994, **59**, 4717; (*b*) Y. Kondo, M. Fujinami, M. Uchiyama and T. Sakamoto, *J. Chem. Soc., Perkin Trans. 1*, 1997, 799; (*c*) M. Uchiyama, M. Koike, M. Kameda, Y. Kondo and T. Sakamoto, *J. Am. Chem. Soc.*, 1996, **118**, 8733; (*d*) M. Uchiyama, M. Kameda, O. Mishima, N. Yokoyama, M. Koike, Y. Kondo and T. Sakamoto, *J. Am. Chem. Soc.*, 1998, **120**, 4934; (*e*) Y. Kondo, T. Komine, M. Fujinami, M. Uchiyama and T. Sakamoto, *J. Comb. Chem.*, 1999, **1**, 123; (*f*) Y. Kondo, M. Asai, T. Miura and M. Uchiyama, *Org. Lett.*, 2001, **3**, 13.

10 For a recent excellent preparation of 2-bromo-6-iodopyridine using halogen–magnesium exchange of 2,6-dibromopyridine, see: F. Trecourt, G. Breton, V. Bonnet, F. Mongin, F. Marsais and G. Queguiner, *Tetrahedron*, 2000, **56**, 1349.

11 Relating to the regioselectivity of deprotonative-zincation of bromopyridines, it was also found that the concentration of the aminozincate is critical for obtaining high selectivity. Further studies on this interesting effect are in progress.

CHEMCOMM Communication
www.rsc.org/chemcomm

Ion-carrier controlled precipitation of calcium phosphate in giant ABA triblock copolymer vesicles

Marc Sauer,[a] Thomas Haefele,[a] Alexandra Graff,[a] Corinne Nardin[a] and Wolfgang Meier*[ab]

[a] *Department of Physical Chemistry, University of Basel, Klingelbergstrasse 80 CH-4056. Basel, Switzerland. E-mail: wolfgang.meier@unibas.ch*
[b] *School of Engineering and Science, International University of Bremen, Campus Ring 1 28759. Bremen, Germany*

Received (in Cambridge, UK) 30th August 2001, Accepted 22nd October 2001
First published as an Advance Article on the web 7th November 2001

An ionophore assisted metal-ion transport across block copolymer membranes has been used to control the local Ca^{2+} concentration during precipitation of calcium phosphate in giant block copolymer vesicles.

The controlled formation of inorganic minerals within organic or polymeric matrices is successfully used by nature to design biological composite materials such as bone or teeth.[1] Many of the mineralized tissues formed by organisms have superior mechanical properties. Therefore it has been tempting for a long time to mimic their design principles during fabrication of synthetic (so-called 'biomimetic') materials. Although the detailed mechanisms of biomineralization are still not clarified various models have been suggested that increase our understanding of these biological processes.[2] A key step in the control of mineralization employed by almost all organisms is an initial allotment of space. This is usually achieved by cellular membranes, predeposited macromolecular matrix frameworks or vesicles. Subsequently minerals are precipitated under controlled conditions within the individual compartments. Vesicular structures are one of the most investigated *in vitro* templates in biomimetic mineralization. Furthermore they also play a crucial role in biological processes such as epiphyseal cartilage or embryonic bone growth.[1] Phospholipid vesicles have been successfully used to mineralize and precipitate inorganic solids, such as *e.g.* calcium phosphate[3] or iron oxide[4] within their interior.

Ion transport across the membranes of lipid vesicles can be controlled by lipophilic ion carriers. This allows control of the local ion concentration inside the vesicles during mineralization.[5] Similar to biological systems, also during biomimetic mineralization, specific interactions between the matrix forming material and the crystal planes of the growing nuclei are of crucial importance[6] for the structure and morphology of the newly formed minerals. The high diversity of block copolymer chemistry (*i.e.*, the ease to modify their chemical constitution or attach certain functionalities) makes the self assembled superstructures of amphiphilic block copolymers ideally suited as templates for biomimetic mineralization.[7] Recently we could show that even membrane proteins can be functionally reconstituted in block copolymer membranes.[8] Similar to nature, such membrane proteins could potentially be used to tune, for example, the interactions between the matrix and minerals or to control the local ion concentration during precipitation in block copolymer vesicles. The latter could be achieved by incorporating ion carriers or specific ion channels or pumps into the membrane. As a preliminary example of this, we report here on ion carrier-assisted precipitation of calcium phosphate in giant poly(2-methyloxazoline)–poly(dimethylsiloxane)–poly(2-methyloxazoline) (PMOXA–PDMS–PMOXA)[9] triblock copolymer vesicles. In this work, phosphate anions are encapsulated within the vesicles during their formation. Since the Ca^{2+} ions from the external solution are not able to permeate the triblock copolymer membranes, precipitation of calcium phosphate in the vesicle interior requires a transport system (see Fig. 1 for a schematic representation). As representative model systems we used three different ionophores that should enable selective or unselective calcium transport from the bulk medium into the intravesicular space. Lasalocid A (X537A, from Fluka)[10] and *N*,*N*-dicyclohexyl-*N*′,*N*′-dioctadecyl-3-oxapentane-1,5-diamide (ETH5234, from Buchs)[11] transport cations *via* a carrier mechanism, where the former shows no specific selectivity and the latter is highly selective for calcium ions. Alamethicin (U22324, from Sigma)[12] is a channel forming peptide that transports cations and anions unselectively.

To facilitate observation of the precipitated calcium phophate we used giant unilamellar PMOXA–PDMS–PMOXA triblock copolymer vesicles prepared by electro-formation. Here, usually a thin film of polymer is phoresed from conductive glasses or adjactent platinum electrodes by an alternating current into the aqueous solution.[13] To obtain giant vesicles in higher yields we used a slightly modified set-up based on a two-electrode cell that had originally been designed for EPR studies.[14] The cell consists of a helically wound (0.5 mm diameter) gold wire electrode and a 0.5 mm diameter straight platinum wire supported by two Teflon holders. 2 ml (concentration: 10 g L^{-1} polymer) of a chloroformic PMOXA–PDMS–PMOXA solution was sprayed onto the gold electrode and the polymer formed a thin film which was dried by blowing a stream of nitrogen over the wire for about 1 min. Afterwards the electrodes were immersed in 2.2 ml phosphate buffer (50 mM K_3PO_4, 10 mM Hepes, 10 mM KCl; pH adjusted to 7.4 with KOH). Giant vesicles were prepared by applying an ac voltage of 5 V at a frequency of 10 Hz for 2 h followed by 30 min at 5 V and 5 Hz. Phase contrast microscopy investigations indicated that the resulting dispersion contained giant vesicles with diameters between 1 and 2 μm in a very high density. Subsequently non-encapsulated phosphate ions can be removed by dialysis against buffer solution (10 mM Hepes, 110 mM KCl, pH = 7.4). After addition of 2 ml of a calcium chloride solution (50 mM $CaCl_2$, 10 mM Hepes, 35 mM KCl; pH adjusted to 7.4 with KOH) the sample was divided into four aliquots of 1 ml. The first aliquot was mixed with 18 μl of a U22324 solution (1.28 mM in ethanol), the second with 18 μl of an X537A solution (0.44 mM in ethanol) and the third with 18 μl of an ETH5234 solution (0.41 mM in ethanol). As a control experiment we added 18 μl

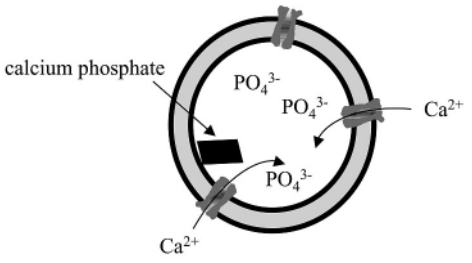

Fig. 1 Schematic representation of ion-carrier controlled precipitation of calcium phosphate in block copolymer vesicles.

 DOI: 10.1039/b107833j

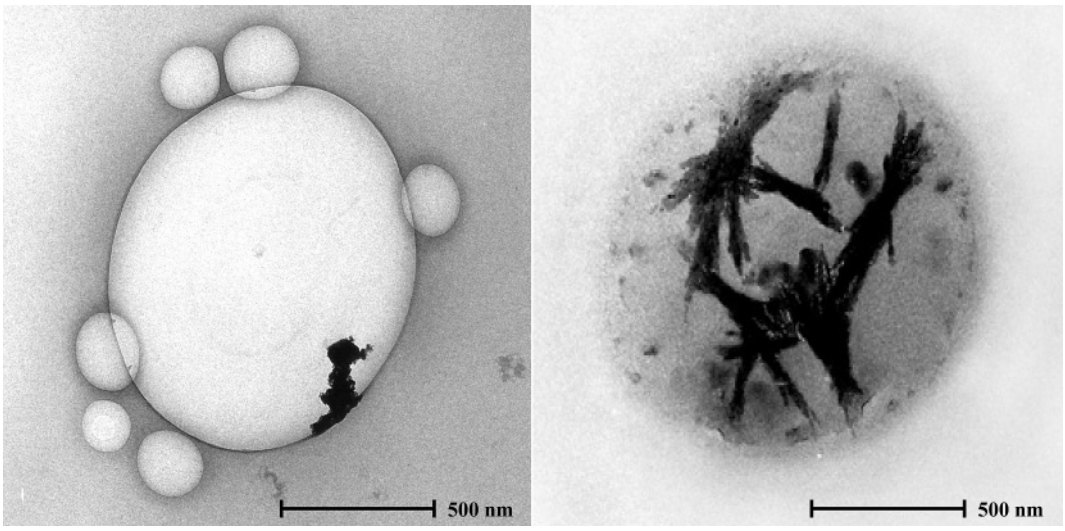

Fig. 2 Transmission electron micrograph of phosphate loaded PMOXA–PDMS–PMOXA triblock copolymer giant vesicles after 1 (left) and 24 h (right) of incubation with $CaCl_2$-solution in the presence of the ion carrier ionophore U22324.

of pure ethanol to the fourth aliquot. All samples were incubated at 4 °C and investigated after 1 and 24 h by transmission electron microscopy. To avoid rupturing of the vesicles the samples were kept in a hydrated state during the preparation procedure. In the control experiment without ionophore no precipitation of calcium phosphate occurred. This is in contrast to observations with any of the three used ionophores in which formation of crystals could be observed within the vesicular structures. This clearly shows that the ionophores play a crucial role for the transport of Ca^{2+} ions across the polymer membranes. Fig. 2 shows a representative transmission electron micrograph of phosphate containing triblock copolymer vesicles after 1 and 24 h of incubation with $CaCl_2$-solution in the presence of U22324. As can directly be seen already after only 1 h calcium phosphate crystals start to grow at the inner surface of the polymer membrane. After 24 h a considerable fraction of the vesicle interior is filled with needle-like calcium phosphate crystals. Longer incubation times did not lead any detectable further growth of the crystals. Obviously after 24 h the encapsulated phosphate ions have already been consumed. This is also reflected by the fact that the volume of the minerals was always in reasonable agreement with the starting concentration of phosphate in the vesicle. Moreover, the inorganic crystals are clearly confined to the inner cavity of the vesicles thus indicating that crystal growth is limited by the shells of the block copolymer vesicles.

In conclusion, we have successfully applied ionophores to control ion concentration within ABA triblock copolymer vesicles during mineralization of calcium phosphate. Although the ionophores are still rather simple ′vehicles′ to transport ions across polymer membranes we believe that the concept of combining artificial block copolymer membranes with natural membrane proteins holds great potential for biomimetic mineralization.

The possibility to incorporate additional design criteria to the block copolymers is straightforward, *e.g.*, functional groups that lead to special surface characteristics of the resulting vesicles which could be used to control the morphology of the resulting minerals. In this context it is also interesting to note that nature provides many more specific, unspecific and ligand gated channels or pumps (that can additionally be genetically modified!) which can be reconstituted in block copolymer superstructures thus providing a unique tool to control the permeation of ions across polymer membranes. Moreover, the resulting combination of the enormous mechanical stability of block copolymer aggregates with the specifity and efficiency of naturally occurring membrane proteins could even be a helpful tool to get a closer insight into the principles of biomineralization.

Financial support from the Swiss National Science foundation is gratefully acknowledged.

Notes and references

1 H. A. Lowenstam and S. Weiner, *On Biomineralization*, Oxford University Press, Oxford, 1989.
2 F. Z. Cui, Y. Zhang and Q. Cai, *Mater. Res. Soc. Symp. Proc.*, 2000, **599**, 317.
3 E. D. Eanes, A. W. Hailer and J. L. Costa, *Calcif. Tissue Int.*, 1984, **36**, 421.
4 S. Mann, J. P. Hannington and R. J. P. Williams, *Nature*, 1986, **324**, 565.
5 B. R. Heywood and E. D. Eanes, *Calcif. Tissue Int.*, 1987, **41**, 192.
6 L. Addadi and S. Weiner, *Angew. Chem., Int. Ed. Engl.*, 1992, **31**, 153.
7 H. Coelfen and M. Antonietti, *Langmuir*, 1998, **14**, 582.
8 W. Meier, C. Nardin and M. Winterhalter, *Angew. Chem.*, 2000, **112**, 4747.
9 For detailed polymer synthesis and characterization, see: C. Nardin, T. Hirt, J. Leukel and W. Meier, *Langmuir*, 2000, **16**, 1035.
10 T. R. Hinds and F. F. Vincenzi, *Cell Calcium*, 1985, **6**, 265.
11 Y. Qin, Y. Mi and E. Bakker, *Anal. Chim. Acta*, 2000, **421**, 201.
12 M. K. Matthew, R. Nageraj and P. Balaram, *J. Membr. Biol.*, 1982, **65**, 13.
13 P. L. Luisi and P. Walde, *Giant Vesicles*, Wiley, Chichester, 2000.
14 H. Ohya-Nishiguchi, *Bull. Chem. Soc. Jpn.*, 1979, **52**(7), 2064.

CHEMCOMM Communication
www.rsc.org/chemcomm

Decreased methane formation from the hydrogenation of carbon monoxide using zeolite/cobalt–manganese oxide composite catalysts

Meleri Johns,[a] Philip Landon,[a] Tony Alderson[b] and Graham J. Hutchings*[a]

[a] *Department of Chemistry, Cardiff University, Cardiff, UK CF10 3TB. E-mail: hutch@cardiff.ac.uk*
[b] *Advantica Technologies Ltd., Ashby Road, Loughborough, Leics., UK LE11 3GR*

Received (in Cambridge, UK) 14th September 2001, Accepted 17th October 2001
First published as an Advance Article on the web 13th November 2001

A composite catalyst comprising a physical mixture of a zeolite and a cobalt/manganese oxide Fischer–Tropsch catalyst decreases the formation of methane in the hydrogenation of carbon monoxide without significantly affecting conversion.

The Fischer–Tropsch synthesis, in which carbon monoxide is hydrogenated to linear C_{2+} hydrocarbons, continues to attract considerable research attention.[1,2] Part of this revival in interest has been due to the commercialisation of the Shell Middle Distillate Synthesis in Malaysia in 1993,[3] as well as the recent interest in the use of air blown methane partial oxidation technology which eliminates the requirement for pure oxygen in the overall process.[4] However, the main interest concerns the utilisation of remote natural gas reserves using the Fischer–Tropsch synthesis as a liquefaction process. In this process, methane is partially oxidised to CO + H_2 which is then converted to liquid hydrocarbons.[1,2] It is essential that the yield of methane, which can be a significant by-product in the Fischer–Tropsch synthesis, is minimised. Previously, catalysts that favour carbon–carbon bond formation have been preferred for minimisation of methane, but the products produced are typically waxes which require further processing.[1–3] Use of chain limiting Fischer–Tropsch catalysts,[1,5,6] *e.g.* Fe/MnO or Co/MnO, can produce liquid hydrocarbons with decreased methane formation and, in particular, the Co/MnO catalyst gives propene as the major product. Previously, many studies[7–10] have attempted to modify the product distribution of Fischer–Tropsch catalysts by supporting them on zeolites, but this approach did not lead to a marked decrease in methane yields, and most emphasis has concerned the synthesis of C_{6+} products. In these earlier studies, the catalysts were typically prepared by impregnation of the zeolite and the use of a composite of the zeolite with a chain limiting Fischer–Tropsch catalyst as a simple physical mixture has been largely neglected. We have now addressed this type of catalyst and, surprisingly, we have observed that methane formation is significantly decreased with the composite catalyst Co/MnO:H-ZSM-5. Furthermore, we show the active sites present in the composite catalyst can be formed reversibly, indicating that new catalyst sites are formed at the interface between the zeolite and Co/MnO particles.

Carbon monoxide hydrogenation (CO:H_2 = 1:1 mol ratio) was investigated using a Co/MnO catalyst (Co:Mn = 1:1, prepared by coprecipitation[5]) physically mixed with boron nitride (Co/MnO:BN = 1:1 by wt) using a standard laboratory microreactor operating at atmospheric pressure. Under these reaction conditions (Table 1, experiment 1) the formation of methane as a by-product is the preferred reaction. No reaction was observed for CO hydrogenation over boron nitride or H-ZSM-5 in the absence of Co/MnO. The catalyst performance was found to be stable for ≥100 h time-on-stream. In a subsequent experiment (Table 1, experiment 2), a physical mixture of pellets (600–1000 μm) of Co/MnO and zeolite H-ZSM-5 (Si:Al ratio = 80) was tested under identical reaction conditions and it is apparent that the selectivity of methane is decreased by a factor of 2, without any significant effect on conversion being observed. Use of the sodium-exchanged form of zeolite (Table 1, experiment 3) also decreased the selectivity to methane but, in this case, the conversion of carbon monoxide was significantly decreased. Use of zeolite H-ZSM-5 with a higher concentration of acid sites (Si:Al = 30) also showed decreased methane formation (Table 1, experiment 4). Interestingly, a physical mixture of Co/MnO with silicalite (the aluminium-free form of ZSM-5) did not give any marked reduction in the formation of methane (Table 1, experiment 5). This indicates that the acidity of the zeolite is an important factor with respect to the reduction in methane formation. Similar effects of decreased methane formation were observed when the Co/MnO catalyst was mixed as a physical mixture with zeolite β and, to a lesser extent, with zeolite Y (Table 1, experiments 6 and 7). This indicates the effect can be observed with several zeolites.

In a subsequent set of experiments, we demonstrate that the active sites responsible for the decreased methane formation can be produced reversibly. In this experiment, a physical mixture of pellets of the Co/MnO catalyst (600–1000 μm) with zeolite H-ZSM-5 powder (Si/Al = 80) were reacted for *ca.* 100 h and the product selectivities by carbon number are given in Fig. 1. Following reaction, the catalyst was cooled in dry N_2 and the

Table 1 CO hydrogenation over Co/MnO : zeolite composite catalysts[a]

Expt. no.	Catalyst[b]	CO conversion (%)	Product selectivity (wt%)												
			CH_4	C_2H_4	C_2H_6	C_3H_6	C_3H_8	C_4H_8	C_4H_{10}	C_5H_{10}	C_5H_{12}	C_{6+}	Ethanal	Propanal	Butanal
1	Co/MnO:BN	14.8	38.7	2.5	3.7	12.8	2.8	13.6	1.0	6.5	9.3	9.0	tr[c]	tr	0
2	Co/MnO:H-ZSM-5(80)	15.6	19.2	5.6	3.1	6.5	6.6	20.4	8.2	10.8	15.3	3.8	0	0.5	0
3	Co/MnO:Na-ZSM-5(80)	1.0	24.9	8.9	tr	9.8	13.3	2.2	27.9	12.2	tr	tr	0.4	1.7	1.0
4	Co/MnO:H-ZSM-5(30)	8.1	18.2	8.1	3.1	9.3	7.9	15.8	13.4	7.0	13.1	4.8	0.	0.1	0
5	Co/MnO:silicalite	9.4	34.6	3.5	4.3	13.3	3.4	5.7	12.1	1.8	12.6	8.7	0	0.1	0
6	Co/MnO:zeolite Y	13.4	32.6	2.2	4.1	12.6	3.7	2.4	12.7	0.7	17.9	10.6	0	0.2	0.4
7	Co/MnO:zeolite β	3.4	22.3	3.3	1.7	2.6	1.6	39.4	2.4	24.8	1.8	0.1	0	tr	tr

[a] *Reaction conditions*: 206 °C, CO:H_2 = 1:1 mol ratio, GHSV = 200 h^{-1}, P = 101 kPa. Data recorded at *ca.* 100 h time-on-stream. [b] All catalysts physical mixtures (1:1 by wt) of pellets of the individual components (600–1000 μm), zeolites obtained commercially from PQ Corporation, zeolite Y (Si/Al ratio = 4.3), zeolite β (Si/Al ratio = 2.5). [c] tr = trace.

 DOI: 10.1039/b108353h

Table 2 CO hydrogenation over Co/MnO:H-ZSM-5 composite catalysts[a]

Expt. no.	Catalyst	Time on line/h	CO conversion (%)	Product selectivity (wt%)												
				CH_4	C_2H_4	C_2H_6	C_3H_6	C_3H_8	C_4H_8	C_4H_{10}	C_5H_{10}	C_5H_{12}	C_{6+}	Ethanal	Propanal	Butanal
1	Co/MnO : BN	178	8.6	13.9	11.9	3.5	21.8	8.8	10.6	5.4	6.9	4.7	7.9	1.1	1.6	3.9
2	Co/MnO : BN	396	12.4	12.2	8.8	3.2	22.6	9.1	11.8	6.1	9.3	5.8	10.7	0.9	2.4	1.2
3	Co/MnO : BN	461	11.4	11.2	8.8	3.3	23.1	9.0	12.2	6.5	10.7	6.3	7.9	0.8	2.2	1.4
4	Co/MnO : H-ZSM-5(80)	178	16.0	8.8	13.6	3.2	24.9	10.8	9.4	7.5	5.4	6.4	6.2	1.0	0.8	2.1
5	Co/MnO : H-ZSM-5(80)	410	11.0	9.7	9.2	4.1	24.2	9.6	11.6	9.1	7.5	4.9	6.6	1.0	0.8	2.1

[a] *Reaction conditions*: 206 °C, CO : H_2 = 1 : 1 mol ratio, GHSV = 4400 h^{-1}, P = 2.2 MPa.

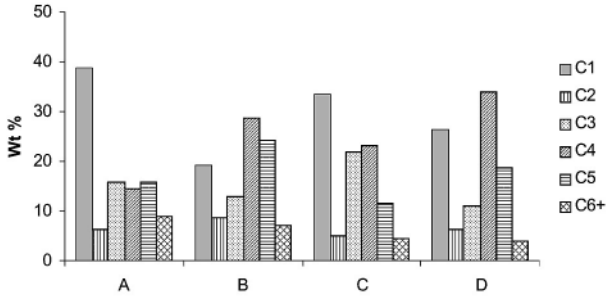

Fig. 1 Selectivity for C_1–C_{6+} hydrocarbons for the hydrogenation of CO. (a) Co/MnO : BN (1 : 1 by wt) physical mixture, (b) Co/MnO:H-ZSM-5 (Si/Al = 80, 1 : 1 by wt) physical mixture, (c) Co/MnO recovered by sieving following experiment (b) mixed with fresh boron nitride as physical mixture (1 : 1 by wt), (d) Co/MnO recovered by sieving following experiment (c) mixed with fresh H-ZSM-5 (Si/Al = 80) as physical mixture (1 : 1 by wt). Reaction conditions: 206 °C, CO = H_2 = 1 : 1 mol ratio, GHSV = 200 h^{-1}, 101 kPa.

Co/MnO catalyst was separated by sieving from the H-ZSM-5 and the catalyst was tested again for CO hydrogenation following mixing with boron nitride powder (1 : 1 physical mixture) and it is clear that, in the absence of the zeolite, the methane selectivity is significantly enhanced and is similar to that observed for the fresh Co/MnO:BN catalyst mixture (Fig. 1). It is, of course, possible that not all the H-ZSM-5 has been removed by the sieving procedure and this may account for the small differences observed. After reaction for a further 100 h, the Co/MnO catalyst was cooled in dry N_2 and was again separated by sieving and it was then mixed with fresh zeolite H-ZSM-5 (Si/Al = 80) in a simple physical mixture (Co/MnO:H-ZSM-5 = 1 : 1 by wt). The results (Fig. 1) clearly show that the methane selectivity is significantly decreased and the higher hydrocarbons, particularly C_3, are enhanced.

The effect was also observed when the catalysts were tested at a higher pressure using the same contact time (Table 2). At the higher pressure, methane formation is much lower when the Co/MnO catalyst is tested alone (Table 2, experiment 1). This is because carbon–carbon bond formation is favoured as the reaction pressure is increased.[1,2] However, the methane selectivity is still decreased when zeolite H-ZSM-5 (Si/Al = 80) is physically mixed with the Co/MnO catalyst. Although the effect is much less marked, it was observed over extended catalyst testing for periods of up to 1000 h.

It is interesting to consider the origin of this effect. We consider that the physical interaction of the Co/MnO and the zeolite particles creates new active sites at the interface. These sites comprise a combination of a strong acid together with a CO hydrogenation catalyst. The origin of the effect may be similar to the reduction in methane formation that is observed when ethene is added to CO hydrogenation when Co/MnO is used as catalyst[11] and may involve the activation of the C–H bonds of hydrocarbon, including methane, by polarisation at the interface between the zeolite and the Co/MnO.

We thank Dr S. Jones for useful discussions and Advantica Technologies Ltd. and the EPSRC for financial support.

Notes and references

1 J. P. Hindermann, G. J. Hutchings and A. Kiennemann, *Catal. Rev.-Sci. Eng*., 1993, **35**, 1.
2 M. E. Dry, *Appl. Catal. A*, 1996, **138**, 319.
3 I. Wender, *Fuels Prod. Technol*., 1996, 238.
4 M. A. Agee, *Stud. Surf. Sci. Catal*., 1998, **119**, 931.
5 R. G. Copperthwaite, G. J. Hutchings, M. van der Reit and J. Woodhouse, *Ind. Eng. Chem. Res*., 1987, **26**, 869.
6 G. J. Hutchings, M. van der Riet and R. Hunter, *J. Chem. Soc., Faraday Trans. 1*, 1989, **85**, 2875.
7 P. D. Caesar, J. A. Brennan, W. E. Garwood and J. Ciric, *J. Catal*., 1979, **56**, 274.
8 R. L. Varma, N. N. Bakhshi and J. F. Matthews, *Ind. Eng. Chem. Res*., 1990, **29**, 1753.
9 G. Calleja, A. De Lucas and R. Van Gricken, *Appl. Catal*., 1991, **68**, 11.
10 S. Bessell, *Stud. Surf. Sci. Catal*., 1994, **81**, 461.
11 M. van der Riet, R. G. Copperthwaite and G. J. Hutchings, *J. Chem. Soc., Faraday Trans. 1*, 1987, **83**, 2963.

CHEMCOMM Communication
www.rsc.org/chemcomm

Synthesis of cyclopentadienones catalyzed by methylidynetricobalt nonacarbonyl

Takumichi Sugihara,* Akihito Wakabayashi, Hiroko Takao, Hiroshi Imagawa and Mugio Nishizawa

Faculty of Pharmaceutical Sciences, Tokushima Bunri University, Yamashiro-cho, Tokushima 770-8514, Japan. E-mail: taku@ph.bunri-u.ac.jp; Fax: +81-88-655-3051; Tel: +81-88-622-9611

Received (in Cambridge, UK) 4th September 2001, Accepted 23rd October 2001
First published as an Advance Article on the web 7th November 2001

Easily prepared and air-stable methylidynetricobalt nonacarbonyl could be used as a catalyst for the intramolecular [2+2+1]-cocyclization of diynes and carbon monoxide producing cyclopentadienones.

Cyclopentadienones are anticipated versatile building blocks in synthetic organic chemistry due to the formal ease in introduction of a variety of functionalities at all positions on the ring.[1,2] Since the compounds have *anti*-aromatic nature, availability would seem to be troublesome. The assistance of transition metal complexes in the [2+2+1]-cocyclization of alkynes and carbon monoxide appears as a promising method to prepare cyclopentadienones.[3] In most cases, however, a stoichiometric amount of complex is required, since the newly formed cyclopentadienone tends to remain coordinated onto the metal.[4,5] Unexpectedly we were led to discover that the cocyclization of alkynes and carbon monoxide can be catalysed by certain polynuclear cobalt carbonyl complexes.

At first, we chose **1** as a substrate and investigated the cyclization catalyzed by polynuclear cobalt carbonyl complexes under various conditions. The results are shown in Table 1.

Since some alkylidynetricobalt nonacarbonyls[6] **4** were known to catalyze the Pauson-Khand reaction without any additive,[7,8] we first chose these clusters as catalysts for the cyclization. When the structurally simplest methylidynetricobalt nonacarbonyl (**4a**) was used, the desired **2**[9] was produced in 24% yield along with **3** even under an argon atmosphere (Entry 1). More than half of the carbon monoxide in the cluster was incorporated into the products. Whereas the catalytic activity was not increased dramatically under 1 atm pressure of carbon monoxide (Entry 2), the reaction under 20 atm of carbon monoxide proceeded in a good yield (Entry 3). It should be mentioned that **4a** was also recovered in 70% yield by silica gel column chromatography (Entry 3). Since the reaction of **1** in the presence of 0.01 equiv. of **4a** produced **2** in 32% yield, a certain amount of **4a** was required to complete the reaction and **4a** was recyclable under these conditions. Among the solvents investigated (such as THF, DME, CH_2Cl_2, MeCN, DMF, and EtOH) toluene seemed to be the best for this reaction in terms of the yield of **2** and the recovery of **4a**. When the reaction was carried out at 120 °C for 48 h, only **3** was obtained and **4a** was not recovered at all (Entry 4). The prolonged reaction time at higher temperature brought about the decomposition of the cluster, which might have promoted isomerization of one of the alkenes to produce **3**. A variety of clusters was also investigated. Whereas the thermally stable clusters, such as **4b–e**, did not catalyze the cyclization (Entries 5–8), ones having hydrogen and bromine brought about fruitful results (Entries 3 and 9). While it is known that treatment of **4f** in refluxing toluene gave **4g**, **4g** itself also catalyzed the cyclization but the yield was lower than the case of **4f** (Entry 10). Finally, dicobalt octacarbonyl **5** and tetracobalt dodecacarbonyl **6** also catalyzed the cyclization (Entries 11 and 12), although the catalytic activity was less than **4a**. The difference of reactivity between **4a**, **5**, and **6** was also observed in the cyclization of **7** (Scheme 1). When **4a** was used as a catalyst, the desired **8** was produced in 48% yield along with the recovery of **7**, whereas the reaction with **5** or **6** was not fruitful. Since the cluster is more stable against auto-oxidation than the binary cobalt carbonyl complexes such as **5** and **6**, placing one carbon unit in the core brings stability and reactivity. Methylidynetricobalt nonacarbonyl showed the best catalytic activity in the cyclization.

Table 1 Cyclization of **1** catalyzed by cobalt complexes[a]

Entry	Catalyst	Atmosphere (atm)	Temp. (°C)	Time (h)	Yield (%) **2**	**3**	**1**
1	**4a**[b]	Ar(1)	reflux	10	24	5	51
2	**4a**[b]	CO(1)	reflux	10	32	4	45
3	**4a**[c]	CO(20)	95	10	96	—	—
4	**4a**	CO(20)	120	48	—	89	—
5	**4b**	CO(20)	95	10	—	—	99
6	**4c**	CO(20)	95	10	—	—	100
7	**4d**	CO(20)	95	10	—	—	98
8	**4e**	CO(20)	95	10	—	—	98
9	**4f**	CO(20)	95	10	80	2	11
10	**4g**	CO(20)	95	10	53	4	42
11	**5**	CO(20)	95	10	73	5	15
12	**6**	CO(20)	95	10	55	8	36

[a] A 0.125 M solution of **1** and 0.015 equiv. of the catalyst was stirred. [b] A 0.05 equiv. of the catalyst was used. [c] **4a** was recovered in 70% yield.

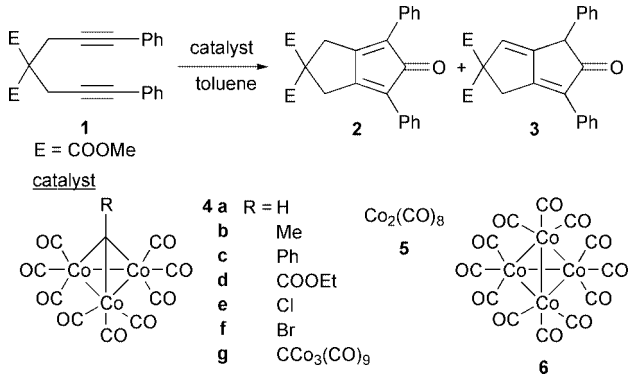

The conditions for the catalytic synthesis of cyclopentadienones were fixed and were applied for various substrates. The intermolecular cyclization of diphenylacetylene, 1-phenyl-2-triethylsilylacetylene, bis(trimethylsilyl)acetylene, and bis-

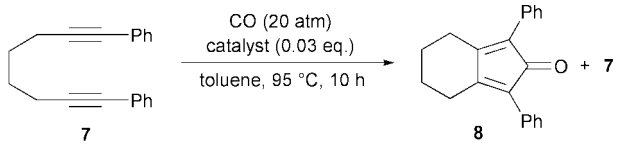

$Co_3(CO)_9(\mu^3\text{-}CH)$	**4a**	48%	45%
$Co_2(CO)_8$	**5**	3%	96%
$Co_4(CO)_{12}$	**6**	3%	95%

Scheme 1

 DOI: 10.1039/b107985a

Table 2 The cyclization of diynes catalyzed by methylidynetricobalt nonacarbonyl[a]

Entry	S.M.	**4a** (mol%)	Product	Yield (%)	Recovery of S. M. (%)
1	**9**	1.5	**10**	70	15
2	**9**	3.0	**10**	92	—
3	**11**	1.5	**12**	92	—
4	**13**	1.5	**14**	90	—
5	**15**	1.5	**16**	62	29
6	**17**	1.5	**18**	85	8
7	**19**	1.5	**20**	45	34
8	**21**	1.5	**22**	88	—
9	**23**	3.0	**24**	72	—
10	**25**	3.0	**26**	70	—
11	**27**	3.0	**28**	83	—
12	**29**	3.0	**30**	84	—
13	**31**	3.0	**32**	35	60

[a] All reactions were carried out in a 0.125 M solution of toluene at 95 °C under 20 atm of carbon monoxide in the presence of **4a**.

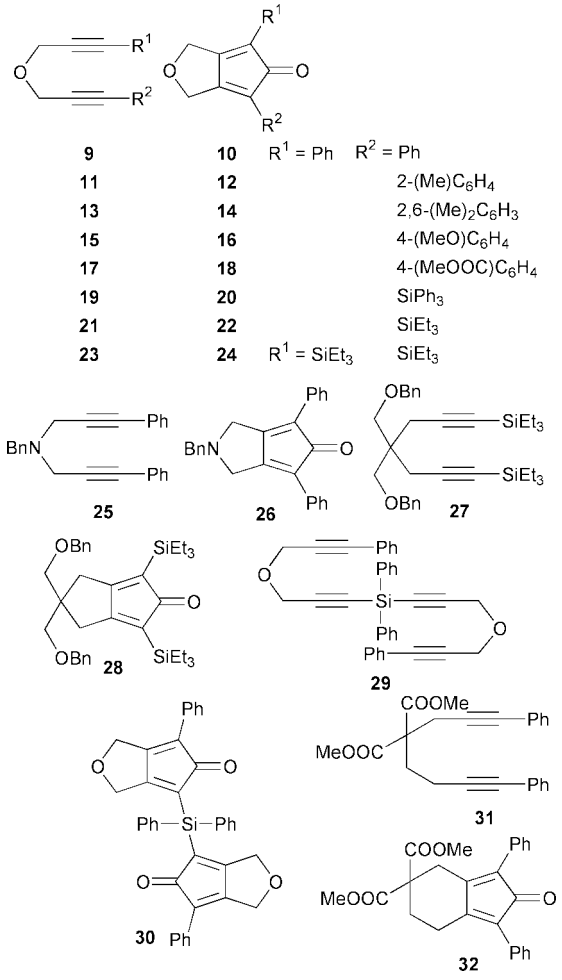

(triphenylsily)acetylene did not produce the cyclopentadienones and recovered the starting alkynes and **4a**. When oct-4-yne was treated under the same conditions, hexa(*n*-propyl)benzene was produced in 99% yield.[10] The cyclization could proceed only when the diynes with three or four atoms' tether had an aromatic or silyl group on both termini of the alkynes (Table 2). In all cases shown in Table 2, the desired cyclopentadienones[9] were produced in good yields.

In conclusion, we have developed a method for catalytic synthesis of cyclopentadienones by methylidynetricobalt nonacarbonyl. The cluster combines the advantages of being both easy to handle and catalytically active.

This work is supported in part by grants from the Asahi Glass Foundation and the Ministry of Education, Science, Sports, and Culture, Japan. TS gratefully thanks Professor Masahiko Yamaguchi at the Graduate School of Pharmaceutical Sciences, Tohoku University, Japan for his helpful discussion.

Notes and references

1 For reviews, see: M. A. Ogliaruso, M. G. Romanelli and E. I. Becker, *Chem. Rev*., 1965, **65**, 261.

2 (*a*) L. S. Liebeskind and A. Bombrum, *J. Am. Chem. Soc*., 1991, **113**, 8736; (*b*) D. Mackay, D. Papadopoulos and N. J. Taylor, *J. Chem. Soc., Chem. Commun*., 1992, 325; (*c*) H.-J. Knölker, E. Baum and J. Heber, *Tetrahedron Lett*., 1995, **36**, 7647; (*d*) T. Jikyo, M. Eto and K. Harano, *Bull. Chem. Soc. Jpn*., 1997, **45**, 1961; (*e*) J. D. Rainier and J. E. Imbriglio, *Org. Lett*., 1999, **1**, 2037.

3 [Fe] (*a*) E. Weiss and W. Hübel, *J. Inorg. Nucl. Chem*., 1959, **11**, 42; (*b*) E. Weiss, R. Merényi and W. Hübel, *Chem. Ber*., 1962, **95**, 1170; (*c*) W. Hübel and R. Merényi, *Chem. Ber*., 1963, **96**, 930; (*d*) A. J. Pearson and R. A. Dubbert, *J. Chem. Soc., Chem. Commun*., 1991, 202; (*e*) A. J. Pearson, R. J. Shively and R. A. Dubbert, *Organometallics*, 1992, **11**, 4096; (*f*) A. J. Pearson and R. J. Shively, *Organometallics*, 1994, **13**, 578; (*g*) A. J. Pearson and A. Perosa, *Organometallics*, 1995, **14**, 5178; (*h*) A. J. Pearson and X. Yao, *Synlett*, 1997, 1281; (*i*) H.-J. Knölker, J. Heber and C. H. Mahler, *Synlett*, 1992, 1002; (*j*) H.-J. Knölker and J. Heber, *Synlett*, 1993, 924; (*k*) H.-J. Knölker, *J. Prakt. Chem*., 1994, **336**, 277; [Co]; (*l*) H. Yamazaki and N. Hagihara, *J. Organomet. Chem*., 1967, **7**, 21; (*m*) H. Yamazaki and N. Hagihara, *J. Organomet. Chem*., 1970, **21**, 431; (*n*) E. R. F. Gesing, J. P. Tane and K. P. C. Vollhardt, *Angew. Chem., Int. Ed. Engl*., 1980, **19**, 1023; (*o*) T. Shibata, T. Ohta and K. Soai, *Tetrahedron Lett*., 1998, **39**, 5785; (*p*) T. Shibata, K. Yamashita, K. Takagi, T. Ohta and K. Soai, *Tetrahedron*, 2000, **56**, 9259; [Ni]; (*q*) K. Tamao, K. Kobayashi and Y. Ito, *J. Org. Chem*., 1989, **54**, 3517; (*r*) K. Tamao, K. Kobayashi and Y. Ito, *Synlett*, 1992, 539.

4 Cyclization was shown to proceed in a catalytic manner when the resulting cyclopentadienones were transformed into stable molecules to reduce their coordinating ability. See: (*a*) S. H. Hong, J. W. Kim, D. S. Choi, Y. K. Chung and S.-G. Lee, *Chem. Commun*., 1999, 2099; (*b*) S. U. Son, S.-J. Paik, S. I. Lee and Y. K. Chung, *J. Chem. Soc., Perkin Trans. 1*, 2000, 141; (*c*) S. U. Son, D. S. Choi and Y. K. Chung, *Org. Lett*., 2000, **2**, 2097; (*d*) S. U. Son and Y. K. Chung, *J. Org. Chem*., 2000, **65**, 6142.

5 Recently, Shibata *et al*. reported the synthesis of cyclopentadienones catalyzed by iridium complexes. See, T. Shibata, K. Yamashita, H. Ishida and K. Takagi, *Org. Lett*., 2001, **3**, 1217.

6 For reviews, see: (*a*) B. R. Penfold and B. H. Robinson, *Acc. Chem. Res*., 1973, **6**, 73; (*b*) D. Seyferth, *Adv. Organomet. Chem*., 1976, **14**, 97; (*c*) R. D. W. Kemmitt and D. R. Russell, in *Comprehensive Organometallic Chemistry, Vol. 5* (Eds. G. Wilkinson, F. G. A. Stone and E. W. Abel), Pergamon Press, Oxford, 1982, p. 1.

7 T. Sugihara and M. Yamaguchi, *J. Am. Chem. Soc*., 1998, **120**, 10782.

8 T. Sugihara, M. Yamaguchi and M. Nishizawa, *Chem. Eur. J*., 2001, **7**, 1589.

9 The cyclopentadienones shown here were quite stable stored in dichloromethane, benzene, and toluene solution. In the concentrated state, Diels–Alder-type dimerization proceeded.

10 The [2+2+2]-cyclotrimerization of alkynes catalyzed by alkylidynetricobalt nonacarbonyl was reported, although the catalytic activity was low and the reaction conditions were vigorous. See, R. S. Dickson and G. R. Tailby, *Aust. J. Chem*., 1970, **23**, 229.

CHEMCOMM
Communication
www.rsc.org/chemcomm

EPR and NMR spectroscopic studies of $[MoL_2(MeC{\equiv}CMe)Cp]^z$ (L = P-donor ligand, z = 0 and 1): fluxionality in a metal–alkyne redox pair

Christopher J. Adams,[a] Neil G. Connelly[a] and Philip H. Rieger[b]

[a] *School of Chemistry, University of Bristol, Bristol, UK BS8 1TS. E-mail: Neil.Connelly@bristol.ac.uk*
[b] *Department of Chemistry, Brown University, Rhode Island, RI 02912, USA*

Received (in Cambridge, UK) 20th September 2001, Accepted 19th October 2001
First published as an Advance Article on the web 13th November 2001

Variable temperature NMR and EPR spectroscopic studies provide rates and activation parameters for alkyne rotation and oscillation, respectively, in the fluxional redox pair $[Mo\{P(OMe)_3\}_2(MeC{\equiv}CMe)Cp][BF_4]$ (diamagnetic) and $[Mo\{P(OMe)_3\}_2(MeC{\equiv}CMe)Cp]$ (paramagnetic).

Although 'piano-stool' alkyne complexes of molybdenum[1–4] were first formulated as 16-electron species, with the alkyne acting as a two-electron donor, it was soon recognised that this ligand could act as a four-electron donor, thus bringing the formal electron count to 18.[5] The crystal structures of $[Mo\{P(OMe)_3\}_2(\eta^2\text{-}HC{\equiv}CBu^t)Cp]^+$ [6] and $[Mo\{(MeO)_2PO\text{-}BF_2OP(OMe)_2\}(\eta^2\text{-}PhC{\equiv}CPh)Cp]^+$ [7] show the alkyne aligned parallel to one of the metal–phosphorus bonds, as in isoelectronic tungsten and vanadium species.[8,9]

If maintained in solution this geometry would lead to different environments for R′ and R″ in an alkyne R′C≡CR″ and, therefore, separate signals in the ^{1}H NMR spectrum even when R′ = R″. At room temperature, however, only one signal is often observed due to a propeller-like rotation [Fig. 1(a)] of the alkyne ligand rendering R′ and R″ equivalent. In some cases this rotation process is frozen out at low temperature, and an activation energy, $\Delta G^{\ddagger}$, can be estimated from the coalescence temperature of the appropriate signals in the ^{1}H NMR spectrum, *e.g. ca.* 60 and 47 kJ mol^{-1} for $[Mo(dppe)(\eta^2\text{-}MeC{\equiv}C\text{-}Me)Cp][PF_6]$[1] and $[Mo(dmpe)(\eta^2\text{-}MeC{\equiv}CMe)Cp][BF_4]$,[4] respectively.

We have recently described the effects of electron-transfer on the structures of metal–alkyne complexes *via* single crystal X-ray diffraction studies of the redox pairs $[Cr(CO)_2(\eta\text{-}PhC{\equiv}CPh)(\eta\text{-}C_6Me_6)]^z$, $[Mo(CO)_2(\eta\text{-}PhC{\equiv}CPh)Tp']^z$ [10] and $[WX(CO)(MeC{\equiv}CMe)Tp']^z$ (X = Cl and Br; z = 0 or 1).[11] This communication reports the *solution* behaviour of the redox pair $[Mo\{P(OMe)_3\}_2(\eta^2\text{-}MeC{\equiv}CMe)Cp][BF_4]$, $\mathbf{1}^+[BF_4]^-$, and $[Mo\{P(OMe)_3\}_2(\eta^2\text{-}MeC{\equiv}CMe)Cp]$, **1** (and related complexes) where NMR and EPR spectroscopic studies allow the fluxional behaviour of the diamagnetic and paramagnetic species respectively to be quantified and compared.

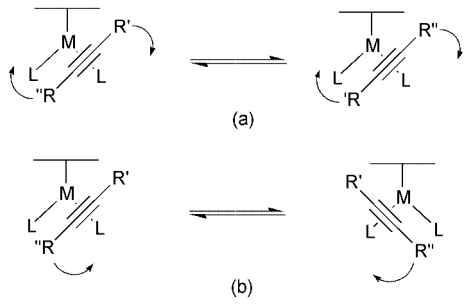

Fig. 1 (a) Propeller-like rotation, and (b) oscillation, of the coordinated alkyne of $[ML_2(R'C{\equiv}CR'')Cp]$ (L = PR_3). The horizontal line denotes the Cp ligand.

Variable temperature ^{1}H NMR spectroscopic studies of $\mathbf{1}^+[BF_4]^-$ in CD_3OD show that the room temperature singlet (δ 3.03) attributable to the alkyne methyl groups becomes two signals (δ 2.93, 3.11) below about 200 K. Line shape analysis[12] of spectra recorded at 2 K intervals between 208 and 188 K gives $\Delta H^{\ddagger}$ = 40.9(2) kJ mol^{-1} and $\Delta S^{\ddagger}$ = 9(1) J mol^{-1} K^{-1}, and (at 298 K) a rate constant, k, of 1.2 × 10^6 s^{-1} for the propeller-like rotation. Similar values in CD_2Cl_2 show that there is relatively little solvent effect on this intramolecular process (Table 1).

These results do not, however, show that the alkyne is stationary at 188 K as the ^{1}H NMR spectrum still shows the two $P(OMe)_3$ ligands to be equivalent; a stationary alkyne aligned with one of the M–P bonds, as in the crystal structures noted above[6,7] would create different environments for the two phosphite ligands, as well as for R′ and R″. Thus, a second fluxional process, namely an oscillation of the alkyne [Fig. 1(b)] which renders the two phosphite ligands magnetically equivalent while R′ and R″ remain inequivalent, still operates at this temperature.

Cyclic voltammetry shows that $\mathbf{1}^+[BF_4]^-$ undergoes reversible reduction at −1.25 V *vs.* SCE at a platinum electrode in dichloromethane. Accordingly, complex **1** was generated by adding solid $[Co(\eta\text{-}C_5Me_5)_2]$ ($E^{o\prime}$ = −1.48 V)[13] to a frozen solution of $\mathbf{1}^+[BF_4]^-$ in a 2:1 mixture of thf–CH_2Cl_2 and allowing the mixture to thaw slowly. Surprisingly, the EPR spectra of the resulting solution of **1** are similar to the NMR spectra of $\mathbf{1}^+[BF_4]^-$ in that they too reveal a temperature-dependent fluxional process. (The observation of fluxional behaviour for paramagnetic organometallic complexes on the EPR timescale is very unusual.[14,15])

At 280 K the EPR spectrum of **1** [Fig. 2(a)] shows a triplet ($<A^{31}P>$ = 11.25 G), resulting from coupling of the unpaired electron to two equivalent phosphorus nuclei and arising from either alkyne oscillation or rotation. As the temperature is lowered to 160 K the triplet gradually becomes a doublet due to

Table 1 Activation parameters for, and rates of, fluxional processes for metal–alkyne complexes

Complex	$\Delta H^{\ddagger}$/kJ mol^{-1}	$\Delta S^{\ddagger}$/mol^{-1} K^{-1}	k/s^{-1}[a]
$[Mo\{P(OMe)_3\}_2(\eta^2\text{-}MeC{\equiv}CMe)Cp]^+$, $\mathbf{1}^{+b}$	40.9(2)	9(1)	1.2 × 10^6
$[Mo\{P(OMe)_3\}_2(\eta^2\text{-}MeC{\equiv}CMe)Cp]^+$, $\mathbf{1}^{+c}$	39.5(4)	−2(2)	6.0 × 10^5
$[Mo\{P(OMe)_3\}_2(\eta^2\text{-}MeC{\equiv}CMe)Cp]$ **1**	13.2(3)	−14(2)	1.0 × 10^9
$[Mo\{P(OMe)_3\}_2(\eta^2\text{-}PhC{\equiv}CPh)Cp]$	21.6(4)	−4(2)	1.3 × 10^9
$[Mo\{P(OMe)_3\}_2(\eta^2\text{-}DC{\equiv}CBu^t)Cp]$	24.7(7)	−5(3)	3.2 × 10^8

[a] At 298 K. [b] In CD_3OD. [c] In CD_2Cl_2

 DOI: 10.1039/b108561c

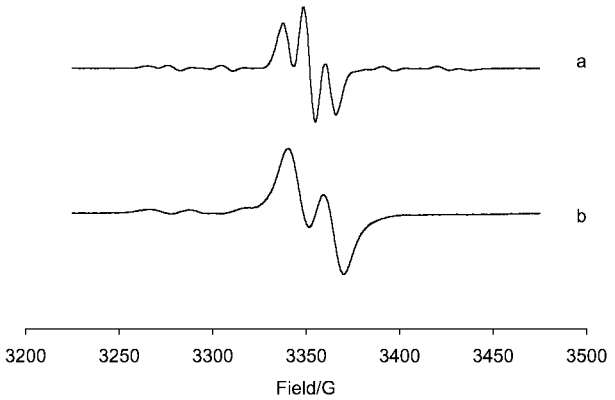

Fig. 2 The EPR spectra of **1** at (a) 280 K and (b) 160 K.

coupling to only one phosphorus nucleus ($<A^{31P}>$ = 18.8 G) [Fig. 2(b)], now implying a stationary alkyne ligand. Line shape analysis[14] of spectra recorded at 10 K intervals from 240 to 160 K gives values for the fluxional process of $\Delta H^{\ddagger}$ = 13.2(3) kJ mol^{-1} and $\Delta S^{\ddagger}$ = −14(2) J mol^{-1} K^{-1}, and a rate constant k (at 298 K) of 1.0 × 10^{9} s^{-1}. {Similar results were obtained for [Mo{P(OMe)$_3$}$_2$(η^2-PhC≡CPh)Cp] and [Mo{P(OMe)$_3$}$_2$(η^2-DC≡CBu^t)Cp] (in toluene) (Table 1)}.

Given that EHMO calculations, based on the crystal structure of [Mo{P(OMe)$_3$}$_2$(η^2-HC≡CBu^t)Cp]$^+$, show that the barrier to alkyne oscillation is significantly lower than the barrier to rotation we conclude that the fluxional process observed for **1** involves alkyne oscillation. It is therefore apparent that the fluxional behaviour involving the metal–alkyne units of **1**$^+$ and **1** involve different processes, *i.e.* alkyne rotation in the monocation and a much faster oscillation process in the neutral species.

The EHMO calculations also indicate that although the SOMO of **1** is based largely on the metal, there is a significant amount of unpaired electron density on the alkyne. In agreement, coupling to the alkyne H atom ($<A^{1H}>$ = 4.2 G between 210 and 310 K) as well as to the phosphorus atoms ($<A^{31P}>$ *ca.* 18.4 G at lower temperatures, for the single P coupling) is observed in the EPR spectrum of [Mo{P(OMe)$_3$}$_2$(η^2-HC≡CBu^t)Cp]. Thus, *C*-based radical-like behaviour is anticipated for **1** and related paramagnetic alkyne complexes.

We thank the EPSRC for a Postdoctoral Research Associateship (to C. J. A.).

Notes and references

1 J. A. Segal, M. L. H. Green, J.-C. Daran and K. Prout, *J. Chem Soc., Chem. Commun*., 1976, 766.
2 M. L. H. Green, J. Knight and J. A. Segal, *J. Chem. Soc., Dalton Trans*., 1977, 2189.
3 M. Bottrill and M. Green, *J. Chem. Soc., Dalton Trans*., 1977, 2365.
4 S. R. Allen, P. K. Baker, S. G. Barnes, M. Green, L. Trollope, L. Manojlovic-Muir and K. W. Muir, *J. Chem. Soc., Dalton Trans*., 1981, 873.
5 J. L. Templeton and B. C. Ward, *J. Am. Chem. Soc*., 1980, **102**, 3288; J. L. Templeton, *Adv. Organomet. Chem*., 1989, **29**, 1.
6 S. R. Allen, R. G. Beevor, M. Green, A. G. Orpen, K. E. Paddick and I. D. Williams, *J. Chem. Soc., Dalton Trans*., 1987, 591.
7 G. Brauers, F. J. Feher, M. Green, J. K. Hogg and A. G. Orpen, *J. Chem. Soc., Dalton Trans*., 1996, 3387.
8 F. R. Kreissl, W. J. Sieber, P. Hofmann, J. Riede and M. Wolfgruber, *Organometallics*, 1985, **4**, 788.
9 B. Hessen, A. Meetsma, F. van Bolhuis, J. H. Teuben, G. Helgesson and S. Jagner, *Organometallics*, 1990, **9**, 1925.
10 I. M. Bartlett, N. G. Connelly, A. G. Orpen, M. J. Quayle and J. C. Rankin, *Chem. Commun*., 1996, 2583.
11 I. M. Bartlett, S. Carlton, N. G. Connelly, D. J. Harding, O. D. Hayward, A. G. Orpen, C. D. Ray and P. H. Rieger, *Chem. Commun*., 1999, 2403.
12 J. A. Pople, W. G. Schneider and H. J. Bernstein, *High-resolution Nuclear Magnetic Resonance*, McGraw-Hill, New York, 1959, pp. 218–224.
13 N. G. Connelly and W. E. Geiger, *Chem. Rev*., 1996, **96**, 877.
14 N. W. Duffy, R. R. Nelson, M. G. Richmond, A. L. Rieger, P. H. Rieger, B. H. Robinson, D. R. Tyler, J. C. Wang and K. Wang, *Inorg. Chem*., 1998, **37**, 4849.
15 S. D. Ittel, P. J. Krusic and P. Meakin, *J. Am. Chem. Soc*., 1978, **100**, 3264.

CHEMCOMM Communication
www.rsc.org/chemcomm

Epoxidation of allylic alcohols in aqueous solutions of non surfactant amphiphilic sugars

Cécile Denis,[a] Khalid Misbahi,[a] Abdelali Kerbal,[b] Vincent Ferrières[a] and Daniel Plusquellec*[a]

[a] *Ecole Nationale Supérieure de Chimie de Rennes, Synthèses et Activations de Biomolécules, CNRS UMR 6052, Institut de Chimie de Rennes, Avenue du Général Leclerc F-35700. Rennes, France. E-mail: daniel.plusquellec@ensc-rennes.fr; Fax: (+33 0) 2 99 87 13 98; Tel: (+33 0) 2 99 87 13 01*
[b] *Laboratoire de Chimie Organique, Faculté des Sciences, Dhar Elmehrez, Fès, Morocco*

Received (in Cambridge, UK) 14th September 2001, Accepted 15th October 2001
First published as an Advance Article on the web 15th November 2001

A variety of cyclic and acyclic allylic alcohols undergo efficient chemo-, regio- and/or stereoselective epoxidations in neutral aqueous solutions of amphiphilic carbohydrates (sucrose, L-arabinose, methyl or ethyl β-D-fructopyranoside) by using dilute hydrogen peroxide in the presence of molybdic or tungstic salts.

Epoxides are versatile building blocks for organic synthesis, because the epoxide group can be readily opened to produce vicinal functionalities. Chemo-, regio-, diastereo- and enantioselective processes have therefore been developed over the last decades for the synthesis of oxiranes.[1] Traditionally, the conversion of an alkene into an epoxide is performed by using peroxycarboxylic acids or *tert*-butyl hydroperoxide in conjunction with transition metal catalysts in organic solvents.[1] Nevertheless the need for reducing the amounts of toxic waste from chemical processes requires the use of environmentally friendly solvents and reagents. In this context, intensive efforts have been developed in the field of organic synthesis in water.[2,3] In this communication, we report a novel and very simple route for epoxidation of allylic alcohols by aqueous hydrogen peroxide[4] in the presence of molybdic or tungstic salts[5] in neutral aqueous solutions of non surfactant amphiphilic carbohydrates.

Reactions were carried out in water solutions of selected carbohydrates, *e.g.* sucrose **1**, α-L-arabinopyranose **2** and methyl or ethyl β-D-fructopyranoside **3a**,**b** (Fig. 1). Recent reinvestigation of sucrose conformation in water reveals the existence of an interresidue water-bridge.[6] This conformation resembles that found in the crystal[7] and in polar aprotic solvents.[8] Applying the Oxford Molecular MAD program[9] to that conformation of sucrose revealed the outside section of the fructose moiety to be hydrophobic in type.[10]

The composition of an equilibrated mixture of L-arabinose **2** in water greatly favours pyranoses (60% α, 35% β) over furanoses (3% α, 2% β) at 25 °C.[11] In the most abundant α-pyranose form, L-arabinose **2α** is characterised by an arrangement of hydroxy, methine and methylene groups which divides the molecule into hydrophobic and hydrophilic surfaces. This expectation is clearly corroborated by computation of the hydrophilicity potential. Moreover, we have synthesised methyl and ethyl β-D-fructopyranosides **3a** and **3b**, respectively, according to a procedure recently developed in our laboratory.[12]

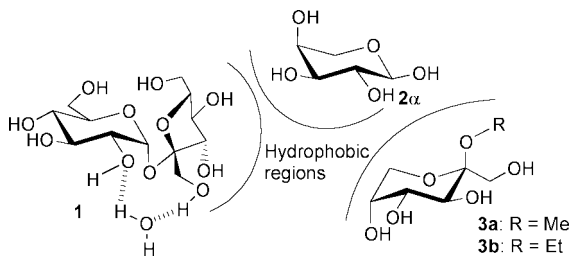

Fig. 1 Structure and hydrophobic areas of amphiphilic carbohydrates **1**–**3**.

Carbohydrates **1**–**3a**,**b** display therefore facial amphiphilicity and apolar organic compounds are expected to interact in aqueous media with the hydrophobic regions of these sugars in order to minimise unfavourable interactions with water. Aqueous solutions of amphiphilic carbohydrates are therefore expected i) to enhance the solubility of allylic alcohols and ii) to localise and to orientate the organic substrates.

Epoxidations of allylic alcohols (Fig. 2, 1 mmol) were performed with 30% hydrogen peroxide (10 mmol) in the presence of molybdic acid or sodium tungstate (0.1 mmol) in aqueous buffered solutions (20 mL, pH7, phosphate buffer)

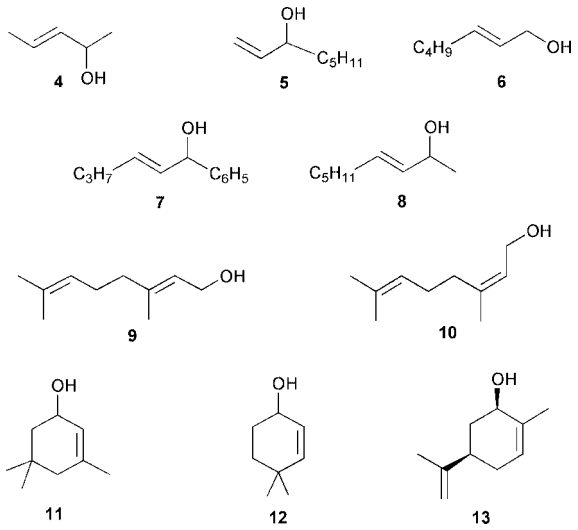

Fig. 2 Selected allylic alcohols **4**–**13**.

containing 20 mmol (molar solutions) of sugar additives. Indeed epoxidations were therefore carried out in dilute ~2% aqueous hydrogen peroxide. The reactions were stirred for 12–72 h (Table 1) at +2 °C and the products were then easily extracted with diethyl ether and their purity was determined by capillary GLC analysis. To compare our system with previously described aqueous solutions of surfactants,[13] some epoxidations were carried out under the same conditions without any amphiphilic carbohydrate.

Results of the epoxidation of a number of acyclic and cyclic allylic alcohols are reported in Table 1. Simple allylic alcohols **4**–**8** (entries 1–6) afforded the corresponding epoxides in high conversion yields when reactions were performed in the presence of carbohydrates **1** or **2**. It is noteworthy that no enone formation was observed[14] (see for example entry 2) and that conversion of the less reactive terminal olefin **5**[1] was dramatically enhanced in the presence of sucrose additive (entries 2, 3). Moreover, under the present conditions, no triol, resulting from oxirane opening, could be detected.

In order to extend our investigation on the regioselectivity of the reaction, geraniol **9** and nerol **10** were chosen as typical polyolefinic substrates that are sparingly soluble in pure water

 DOI: 10.1039/b108352j

Table 1 Epoxidation of allylic alcohols with H_2O_2–metal catalyst in aqueous neutral solutions of glycosidic additives at + 2 °C

Entry	Alcohol	Additive	Metal catalyst	Reaction time (h)	Conversion (%)	Epoxide : ketone ratio	Isolated yield (%)
1	**4**	**1**	Mo^{+6}	24	100	>99 : 1	75
2	**5**	**1**	Mo^{+6}	72	78	>99 : 1[a]	72
3	**5**	—	Mo^{+6}	72	30	>99 : 1	28
4	**6**	**1**	W^{+6}	24	100	95 : 5	83
5	**7**	**1**	Mo^{+6}	72	92	>99 : 1	83
6	**8**	**2**	Mo^{+6}	72	97	>99 : 1	88
7	**9**	**1**	Mo^{+6}	48	94	>99 : 1	92
8	**10**	**1**	Mo^{+6}	48	98	>99 : 1	92
9	**11**	**2**	Mo^{+6}	24	97	90 : 10	80
10	**11**	**3a**	W^{+6}	48	100	97 : 3	86
11	**11**	**3b**	W^{+6}	48	100	97 : 3	85
12[b]	**11**	**3b**	W^{+6}	48	100	98 : 2	84
13	**12**	**1**	W^{+6}	72	100	83 : 17	80
14	**13**	**2**	Mo^{+6}	24	70	87 : 13	66
15	**13**	—	Mo^{+6}	48	72	60 : 40	68
16	**13**	**3a**	Mo^{+6}	24	70	85 : 15	67

[a] Oxirane oxidation in CH_2Cl_2 gave 51 : 49.[14b] [b] Recycled aqueous solution from entry 11.

but highly soluble in 1 M sucrose solutions. A site-selective epoxidation occurred at the least electron-rich allylic double bond and pure 2,3-epoxy-geraniol and -nerol were isolated in high yields (entries 7, 8). Unfortunately, epoxidation of geraniol **9** in the presence of sucrose gave 2,3-epoxygeraniol with modest enantioselectivity (ee = 10% determined by polarimetry). Our results obtained in neutral media therefore compare favourably with previous work performed with peracids in strongly alkaline media[13] or with transition metal catalysed epoxidations in organic solvents.[15,16]

Oxidations of six-membered cyclic substrates (Table 1, entries 9–15) indicated that enone formation competed with epoxidation. The ratio of oxirane to ketone showed a pronounced dependence on both substrates and reaction conditions as exemplified by entries 14 and 15. The best chemoselectivities were attained by using tungsten(VI) catalyst in the presence of sugar additives. Moreover, it is important to mention that solutions containing fructosides and catalyst could be recycled for further experiments without loss of conversion yield, chemoselectivity and stereoselectivity (entry 12).

The results presented here suggest OH-assisted epoxidation of allylic alcohols, presumably related to the formation of an intermediate in which the olefinic alcohol is most likely coordinated to the metal *via* the hydroxy group. Such an intermediate was previously suggested for tungsten catalysed epoxidations in protic media.[16,17] The next step was therefore to ascertain whether sugar–substrate and/or intermediate interactions were strong enough to promote stereodiscrimination in the epoxidation reaction. Some significant results for the epoxidation of representative cyclic and acyclic allylic alcohols are listed in Table 2. The data indicate that acyclic alcohols **4–8** gave mixtures of *erythro*/*threo* epoxides. Nevertheless, epoxidation in glycosidic aqueous media generates stereoselectively *erythro* enriched epoxy alcohols. This outcome is the same as for metal catalysed systems in organic solvents but is opposite to that obtained using peroxyacids in organic media.[16]

Table 2 Diastereoselective epoxidations of allylic alcohols in aqueous neutral solutions of carbohydrates **1–3**

Entry	Substrate	Additive	Metal catalyst	dr[a] *erythro* : *threo* (*cis* : *trans*)	mCPBA or analogues (lit.)
1	**4**	**1**	Mo^{+6}	68 : 32	30 : 70[13]
2	**5**	**1**	Mo^{+6}	68 : 32	38 : 62[14]
3	**8**	**1**	Mo^{+6}	62 : 38	36 : 64[14]
4	**11**	**2**	Mo^{+6}	(99 : 1)	(95 : 5)[18]
	11	**3a** or **3b**	W^{+6}	(>99 : 1)	(95 : 5)[18]
5	**12**	**1**	W^{+6}	(95 : 5)	
6	**12**	**3a** or **3b**	W^{+6}	(>99 : 1)	
7	**13**	**2**	Mo^{+6}	(94 : 6)	(90 : 10)
8	**13**	—	Mo^{+6}	(89 : 11)	

[a] dr: diastereoisomeric ratio were determined by GLC. *erythro*/*threo* refers to acyclic substrates whereas *cis*/*trans* to cyclic products.

In the case of cyclohex-2-enols **11–13** the epoxidation was highly stereoselective when compared with the results obtained by a peracid epoxidation (Table 2). In particular, allylic alcohols **11–12** gave exclusively the product where epoxide and OH functions are *cis* to each other when the reactions were performed in aqueous solutions of D-fructose derivatives **3a** or **3b** in the presence of Mo^{+6} or W^{+6} catalyst. Once again, comparison of *cis* : *trans* ratio underlines the role played by arabinose as additive (entries 7 and 8).

The predictable sense of the addition to cyclic olefins can be rationalised by means of a model where hydrophobic interactions are probably involved between the most hydrophobic face of the cyclic alcohol and that of sugar additive. These interactions may account for the enhanced stereoselective hydroxy directed epoxidation of cyclic allylic alcohols observed herein.

In conclusion, it was shown that dilute hydrogen peroxide together with molybdenum(VI) or tungsten(VI) salts is an efficient system for the chemo-, regio- and stereoselective epoxidation of allylic alcohols in aqueous solutions of carbohydrates characterised by a facial amphiphilicity.

Notes and references

1 For a review, see for instance: A. S. Rao, in *Comprehensive Organic Synthesis*, ed. B. M. Trost and I. Fleming, Pergamon, Oxford, 1991, Vol. 7, pp. 357–387.
2 C. J. Li, *Chem. Rev.*, 1993, **93**, 2023; A. Lubineau, J. Augé, H. Bienaymé and Y. Queneau, *Synthesis*, 1994, 741; A. Lubineau, *Chem. Ind.*, 1996, 123.
3 C. Denis, B. Laignel, D. Plusquellec, J. Y. Le Marouille and A. Botrel, *Tetrahedron Lett.*, 1996, **37**, 53.
4 G. Strukul, in *Catalytic Oxidation with Hydrogen Peroxide as Oxidant*, Kluwer Academic Publishers, 1992 R. A. Sheldon, in *Applied Homogeneous Catalysis with Organometallic Compounds*, ed. B. Cornils and W. A. Hermans, VCH Weinheim, 1996J. Brinksma, R. Hage, J. Kerschner and B. L. Feringa, *Chem. Commun.*, 2000, 537.
5 K. Sato, M. Aoki, M. Ogawa, T. Hasimoto and R. Noyori, *J. Org. Chem.*, 1996, **61**, 8310.
6 S. Immel and F. W. Lichtenthaler, *Liebigs Ann.*, 1995, 1925; S. B Engelsen, C. Hervé du Penhoat and S. Pérez, *J. Phys. Chem.*, 1995, **99**, 13334.
7 J. C. Hanson, L. C. Sieker and L. H. Jensen, *Acta Crystallogr., Sect. B*, 1973, **29**, 797; G. M. Brown and H. A. Levy, *Acta Crystallogr., Sect. B*, 1973, **29**, 790.
8 J. C. Christofides and D. B. Davies, *Chem. Commun.*, 1985, 1553.
9 MAD V23, Oxford Molecular Ltd, Magdalen Centre, Oxford Science Park, Oxford OX4 4GA, England.
10 F. W. Lichtenthaler and S. Immel, *Int. Sugar J.*, 1995, **97**, 12.
11 S. A. Galena, M. J. Blandamer and J. B. F. N. Engberts, *J. Org. Chem.*, 1992, **57**, 1995.
12 V. Ferrières, T. Benvegnu, M. Lefeuvre, D. Plusquellec, G. Mackenzie, M. J. Watson, J. A Haley, J. W. Goodby, R. Pindak and M. K. Durbin, *J. Chem. Soc., Perkin Trans. 2*, 1999, 951.
13 F. Fringuelli, R. Germani, F. Pizzo, F. Santinelli and G. Sanelli, *J. Org. Chem.*, 1992, **57**, 1198; M. Nakaruma, N. Tsutsui and T. Takeda, *Tetrahedron Lett.*, 1984, **25**, 3231.
14 B. E. Rossiter, T. R. Verhoeven and K. B. Sharpless, *Tetrahedron Lett.*, 1979, 4733; W. Adam, F. Prechtl, M. J. Richter and A. K. Smerz, *Tetrahedron Lett.*, 1993, **34**, 8427.
15 K. B. Sharpless and R. C. Michaelson, *J. Am. Chem. Soc.*, 1973, **95**, 6136.
16 K. B. Sharpless and T. R. Verhoeven, *Aldrichimica Acta*, 1979, **12**, 63.
17 D. Prat and R. Lett, *Tetrahedron Lett.*, 1986, **27**, 707; D. Prat, B. Delpech and R. Lett, *Tetrahedron Lett.*, 1986, **27**, 711.
18 P. Chantemps and J. L. Pierre, *Tetrahedron*, 1976, **32**, 549.

CHEMCOMM
Communication
www.rsc.org/chemcomm

Exploiting modularity in template-controlled synthesis: a new linear template to direct reactivity within discrete hydrogen-bonded molecular assemblies in the solid state

Giannis S. Papaefstathiou, Alex J. Kipp and Leonard R. MacGillivray*

Department of Chemistry, University of Iowa, Iowa City, Iowa 52242-1294, USA. E-mail: len-macgillivray@uiowa.edu

Received (in Columbia, MO, USA) 14th May 2001, Accepted 30th September 2001
First published as an Advance Article on the web 7th November 2001

Co-crystallization of 1,8-naphthalenedicarboxylic acid (1,8-nap) with *trans*-1,2-bis(*n*-pyridyl)ethylene (*n,n′*-bpe) (*n* = 2 or 4) yields a discrete four-component molecular assembly, 2(*n,n′*-bpe)·2(1,8-nap) 1, that is held together by four O–H···N hydrogen bonds where the dicarboxylic acid, serving as a linear template, directs alignment of olefins in the solid state for [2 + 2] photoreaction.

Molecules that function as linear templates[1,2] are emerging as tools for applying principles of molecular recognition,[3] supramolecular chemistry,[4] and self-assembly[5] for the control of covalent-bond-making processes that lead to the design of molecules,[6] oligomers,[7] and polymers[8] in solution[6a,d,7] and the solid state.[6b,c,8] In addition to facilitating stereo- and regiocontrolled positioning of reactive sites with atomic-level precision, linear templates are promising tools for gaining control of reactivity that approaches the nanometer-scale level, and beyond (*i.e.* > 10 Å),[9] owing to an ability of such molecules to enforce predetermined topologies upon reactants, circumventing problems of molecular entanglement[10] that can lead to poor selectivities and product yields. Indeed, to extend linear templates beyond the reach of current synthetic methodologies,[1] it will be necessary to exploit the inherent modularity of such a template approach[9] by devising templates, reactants, and reactions that may be readily interchanged. Moreover, by establishing such synthetic flexibilities, ready access to molecules and materials not accessible using traditional approaches to synthesis may be realized.[6–8]

We are utilizing linear templates to control reactivity in molecular solids.[6b] In particular, we have revealed the ability of resorcinol, and derivatives, to function as linear templates in the solid-state by organizing, by way of hydrogen bonds, olefins attached to symmetrically substituted bipyridines in position for [2+2] photoreaction.[11] By enforcing reaction to occur within a discrete molecular assembly,[5] this approach eliminates many vexatious problems of intermolecular forces that have made such topochemical designs unreliable,[11] providing a reliable means to make covalent bonds in solids. Such an ability to deliberately control chemical reactivity offers a prospect of eliminating waste organic solvent in molecular synthesis (*i.e.* green chemistry)[12] and gaining access to molecules less obtainable, or completely inaccessible, in solution.

We are currently identifying molecules that function as linear templates. Owing to the modularity of the approach, we reasoned that it should be possible to engineer molecules that possess structures largely preorganized,[13] in a similar way to resorcinol, to align olefins within discrete assemblies, giving rise to template libraries.[8] Here, we reveal the ability of 1,8-naphthalenedicarboxylic acid (1,8-nap), in 2(4,4′-bpe)·2(1,8-nap) **1a** and 2(2,2′-bpe)·2(1,8-nap) **1b** (where 4,4′-bpe = *trans*-1,2-bis(4-pyridyl)ethylene, 2,2′-bpe = *trans*-1,2-bis(2-pyridyl)ethylene), to function, in a similar way to resorcinol, as a linear hydrogen bond donor template. Following work of Feldman and Campbell,[14] we anticipated that co-crystallization of 1,8-nap with either 4,4′-bpe or 2,2′-bpe would yield a four-component molecular assembly held together by four O–H···N hydrogen bonds (Scheme 1) where 1,8-nap, owing to the proximity of the carboxylic acid groups along the naphthalene scaffold,[14] would juxtapose two bipyridines in the solid for [2 + 2] photoreaction. To our knowledge, 1,8-nap represents the second example of a molecule that functions as a linear template by controlling reactivity within a discrete hydrogen-bonded molecular assembly in the solid-state.[6b]† In addition to increasing the synthetic flexibility of this approach, such observations provide structure criteria for controlling reactivity that approaches the nanometer-scale level,[6–8] which is of growing interest.

Addition of 1,8-nap (0.017 g) to methanol (2 mL) in the presence of either 4,4′-bpe (0.015 g) or 2,2′-bpe (0.015 g) yielded, upon slow cooling, colorless crystals of **1a** and **1b**, respectively, suitable for X-ray analysis. The formulations of **1a** and **1b** were confirmed by ^{1}H NMR spectroscopy and single-crystal X-ray diffraction.‡

ORTEP perspectives of **1a** and **1b** are shown in Fig. 1. The components of **1a** and **1b** have assembled, in a similar way to 2(4,4′-bpe)·2(resorcinol) and 2(2,2′-bpe)·2(resorcinol),[6b] to form discrete molecular assemblies, of dimensions ~5.5 × 6.4 × 26.3 and 5.5 × 11.1 × 19.3 Å, respectively, held together by four O–H···N hydrogen bonds. In addition to a primary O–H···N interaction, each carboxylic acid group, each of which is twisted out of the plane of the naphthalene unit, participates in a C–H···O hydrogen bond with each pyridyl ring.[15,16] In this arrangement, two molecules of 4,4′-bpe and 2,2′-bpe lie stacked adjacent to 1,8-nap where the olefins of each complex are separated by 3.73 and 3.91 Å, respectively. These separations

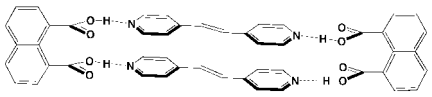

2(4,4'-bpe)·2(1,8-nap)

Scheme 1

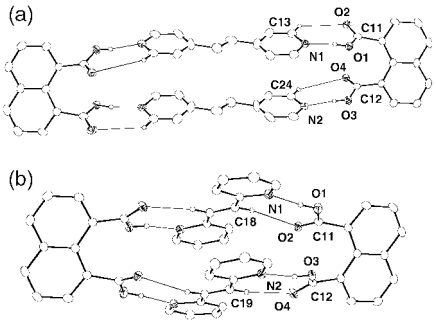

Fig. 1 ORTEP perspectives of molecular assemblies: (a) **1a** and (b) **1b**. Selected interatomic distances (Å) for **1a**: O(1)···N(1) 2.598(4), O(3)···N(2) 2.612(4), C(13)···O(2) 3.497(5), C(24)···O(4) 3.562(4); for **1b**: O(1)···N(1) 2.658(2), O(3)···N(2) 2.601(2), C(18)···O(2) 3.396(2), C(19)···O(4) 3.287(2). Twist angles of carboxylic acid groups (°): **1a**, 51.2 (C11), 50.9 (C12); **1b**, 53.0 (C11), 52.2 (C12).

 DOI: 10.1039/b106584j

are within the distance criterion of Schmidt for [2 + 2] photoreaction.[11] Notably, in the case of **1a**, the olefins are disordered across two sites (occupancies: 70 : 30) while the olefins of **1b** are ordered and parallel. Olefins of nearest-neighbor molecular assemblies of **1a** and **1b** are offset and separated by 4.81 and 4.09 Å, respectively. Indeed, UV irradiation of powdered crystalline samples of **1a** and **1b**, each for a period of 7 h (Rayonet reactor, 300 nm Hg lamp), produces, stereospecifically (100% yield), *rctt*-tetrakis(4-pyridyl)cyclobutane (4,4′-tpcb) and *rctt*-tetrakis(2-pyridyl)cyclobutane (2,2′-tpcb), respectively, as determined by ^{1}H NMR spectroscopy.

To confirm the structure of each product, a portion of each photolyzed solid (0.0010 g) was dissolved in methanol (5 mL) and single crystals of (4,4′-tpcb)·2(1,8-nap) **2a** and (2,2′-tpcb)·2(1,8-nap) **2b** were grown, after a period of approximately three days, by way of slow solvent evaporation. The formulations of **2a** and **2b** were confirmed by ^{1}H NMR spectroscopy and single-crystal X-ray diffraction.‡

ORTEP perspectives of **2a** and **2b** are shown in Fig. 2. As in the case of **1a** and **1b**, the components of **2a** and **2b** assemble by way of O–H···N and C–H···O hydrogen bonds, the carboxylic acid groups being twisted out of the plane of the naphthalene unit. For **2a**, one carboxylic acid group participates in an O–H···O hydrogen bond, in the form of a carboxylic acid dimer, with a neighboring diacid. As a consequence of these forces, the components of **2a**, in contrast to **1a**, assemble to form a one-dimensional hydrogen-bonded polymer along the crystallographic *a*-axis. This contrasts (4,4′-tpcb)·2(resorcinol)[6b] where the template, owing to the flexibility of the hydroxy groups, forms a discrete assembly with 4,4′-tpcb. We attribute the formation of the polymer **2a** to the rigidity of the diacid which, presumably, is less able to participate, in a similar way to (4,4′-tpcb)·2(resorcinol), in two O–H···N interactions with two *cis*-pyridyl groups of the product. In the case of **2b**, the components assemble, in a similar way to **1b**, to form a discrete molecular assembly held together by four O–H···N and four C–H···O hydrogen bonds where the O–H···N forces involve, in contrast to **1b**, two *trans*-pyridyl groups of the photoproduct.§

In this report, we have identified the ability of 1,8-nap to function as a linear template in the solid state, controlling reactivity within a discrete molecular assembly held together by hydrogen bonds. With these observations realized, we are currently utilizing the molecule as a template for conducting solid-state synthesis by design.[6b] With a library of linear templates now emerging,[8] it may be possible to utilize this approach for the designed synthesis of molecules of increasing complexity (*e.g.* nanosystems).[7] In the case of the solid state, our observations suggest an ability to organize molecules with precision and flexibility that rivals the liquid phase, providing routine access to molecular species less available in solution.[9]

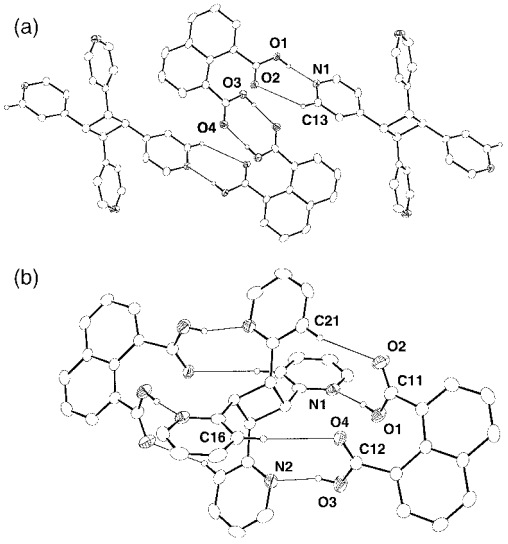

Fig. 2 ORTEP perspectives of the photoproducts: (a) **2a** and (b) **2b**. Selected interatomic distances (Å) for **2a**: O(1)···N(1) 2.607(3), O(3)···O(4) 2.619(3), C(13)···O(2) 3.474(4); for **2b**: O(1)···N(1) 2.651(2), O(3)···N(2) 2.667(2), C(21)···O(2) 3.196(3), C(16)···O(4) 3.722(3). Twist angles of carboxylic acid groups (°): **2a**, 48.5 (C11), 50.2 (C12); **2b**, 41.0 (C11), 48.8 (C12).

We are grateful for financial support from the University of Iowa. We thank Dr Michael J. Zaworotko (University of South Florida) for collection of the X-ray data for **2a**.

Notes and references

† A conceptually similar approach has been described that has involved infinite assemblies (see ref. 6*c*).

‡ *Crystal data*: for **1a**: monoclinic, space group $P2_1/c$, a = 7.599(2), b = 29.271(6), c = 9.106(2) Å, β = 106.611(4)°, U = 1941.0(8) Å^3, D_c = 1.36 g cm^{-3}, Mo-Kα radiation (λ = 0.71070 Å) for Z = 4. Least-squares refinement based on 1412 reflections with $I_{net} > 2.0\sigma(I_{net})$ (out of 2539 unique reflections) led to a final value of R = 0.053. For **1b**: monoclinic, space group $P2_1/c$, a = 7.303(1), b = 23.187(3), c = 11.425(1) Å, β = 98.070(3)°, U = 1915.4(4) Å^3, D_c = 1.38 g cm^{-3}, Mo-Kα radiation (λ = 0.71070 Å) for Z = 4. Least-squares refinement based on 2325 reflections with $I_{net} > 2.0\sigma(I_{net})$ (out of 2500 unique reflections) led to a final value of R = 0.031. For **2a**: triclinic, space group $P\bar{1}$, a = 8.377(2), b = 11.294(2), c = 11.685(2) Å, α = 99.45(3), β = 105.12(3), γ = 109.73(3)°, U = 965.1(3) Å^3, D_c = 1.37 g cm^{-3}, Mo-Kα radiation (λ = 0.71070 Å) for Z = 1. Least-squares refinement based on 2182 reflections with $I_{net} > 2.0\sigma(I_{net})$ (out of 2509 unique reflections) led to a final value of R = 0.049. For **2b**: monoclinic, $P2_1/n$, a = 10.059(2), b = 15.456(3), c = 12.414(3) Å, β = 97.39(3)°, U = 1914.0(7) Å^3, D_c = 1.38 g cm^{-3}, Mo-Kα radiation (λ = 0.71070 Å) for Z = 2. Least-squares refinement based on 2405 reflections with $I_{net} > 2.0\sigma(I_{net})$ (out of 2493 unique reflections) led to a final value of R = 0.043. CCDC reference numbers 172617–172620. See http://www.rsc.org/suppdata/cc/b1/b106584j/ for crystallographic data in CIF or other electronic format.

§ The photoproduct of **2b** adopts a conformation where the nitrogen atoms of *cis*-pyridyl groups point in opposite directions which, in addition to the rigidity of 1,8-nap, may account for the discrete assembly.

1 T. R. Kelly, C. Zhao and G. J. Bridger, *J. Am. Chem. Soc.*, 1989, **111**, 3744.
2 S. Anderson and H. L. Anderson, in *Templated Organic Synthesis*, ed. F. Diederich and P. J. Stang, Wiley-VCH, New York, 2000, pp. 1–38.
3 J. Rebek Jr., *Angew. Chem., Int. Ed. Engl.*, 1990, **29**, 245.
4 J.-M. Lehn, *Supramolecular Chemistry*, Wiley-VCH, Weinheim, 1995.
5 M. C. T. Fyfe and J. F. Stoddart, *Acc. Chem. Res.*, 1997, **30**, 393.
6 (*a*) D. M. Bassani, X. Sallenvae, V. Darcos and J.-P. Desvergne, *Chem. Commun.*, 2001, 1446; (*b*) L. R. MacGillivray, J. L. Reid and J. A. Ripmeester, *J. Am. Chem. Soc.*, 2000, **122**, 7817; (*c*) S. Ohba, H. Hosomi and Y. Ito, *J. Am. Chem. Soc.*, 2001, **123**, 6441; (*d*) D. M. Bassani, V. Darcos, S. Mahony and J.-P. Desvergne, *J. Am. Chem. Soc.*, 2000, **122**, 8795.
7 (*a*) E. A. Archer, N. T. Goldberg, V. Lynch and M. J. Krische, *J. Am. Chem. Soc.*, 2000, **122**, 5006; (*b*) E. A. Archer, A. E. Sochia and M. J. Krische, *Chem. Eur. J.*, 2001, **7**, 2059.
8 (*a*) J. Xiao, M. Yang, J. W. Lauher and F. W. Fowler, *Angew. Chem., Int. Ed.*, 2000, **39**, 2132; (*b*) J. J. Kane, J. John, R.-F. Liao, J. W. Lauher and F. W. Fowler, *J. Am. Chem. Soc.*, 1995, **117**, 12003.
9 K. E. Drexler, *Proc. Natl. Acad. Sci. USA*, 1981, **78**, 5275.
10 C.-T. Chen, P. Gantzel, J. S. Siegel, K. K. Baldridge, R. B. English and D. M. Ho, *Angew. Chem., Int. Ed. Engl.*, 1995, **34**, 2657.
11 G. M. J. Schmidt, *Pure Appl. Chem.*, 1971, **27**, 647.
12 P. T. Anastas and J. C. Warner, in *Green Chemistry: Theory and Practice*, Oxford University Press, New York, 1998.
13 D. J. Cram, *Science*, 1988, **240**, 760.
14 K. S. Feldman and R. F. Campbell, *J. Org. Chem.*, 1995, **60**, 1924.
15 C. V. K. Sharma and M. J. Zaworotko, *Chem. Commun.*, 1996, 2655.
16 L. R. MacGillivray, M. M. Siebke and J. L. Reid, *Org. Lett.*, 2001, **3**, 1257.

CHEMCOMM
Communication
www.rsc.org/chemcomm

Synthesis and DNA-binding properties of dinuclear platinum(II)–amine complexes of 1,7-dicarba-*closo*-dodecaborane(12)†

Susan L. Woodhouse and Louis M. Rendina*

Department of Chemistry, The University of Adelaide, Adelaide 5005, Australia. E-mail: lou.rendina@adelaide.edu.au

Received (in Cambridge, UK) 6th September 2001, Accepted 19th October 2001
First published as an Advance Article on the web 7th November 2001

The first examples of platinum(II)–amine complexes containing a dicarba-*closo*-dodecaborane(12) (carborane) moiety are described; preliminary *in vitro* DNA-binding experiments indicate that the complexes are capable of targetting plasmid DNA.

Boron Neutron Capture Therapy (BNCT) is a bimodal cancer treatment that is currently undergoing clinical trials in several countries, including the US, Japan, Sweden, The Netherlands and Finland.[1] The therapy makes use of thermal neutrons of low kinetic energy (<0.025 eV) and ^{10}B-containing drugs, and it exploits the unusual capacity of the ^{10}B nucleus (natural abundance = 19.8%) to undergo neutron capture (NC) reactions as a consequence of its extremely large effective nuclear cross-section (3837 barns). The immense amount of kinetic energy (*ca*. 2.4 MeV) that accompanies the primary fission products ($^{7}Li^{3+}$ and $^{4}He^{2+}$) is dissipated in a very small volume, and the potential application of the NC reaction to the selective destruction of cancer cells is the subject of intensive research. Previous studies have demonstrated that if ^{10}B-compounds are localized near the nucleus of a cell, then cellular damage is maximized.[2] To date, a number of organic compounds tethered to boron-rich moieties such as dicarba-*closo*-dodecaboranes(12) (carboranes), *e.g*. alkylating agents,[3] bibenzimidazole groove binders,[4] acridine dyes,[5] and polyamines,[5a,6] are known to target DNA, but their success in BNCT has yet to be demonstrated.[1a] To our knowledge, the use of boron-containing metal complexes as potential DNA-targetting agents in BNCT is without any precedent. Herein we describe the synthesis and DNA-binding properties of novel, dinuclear platinum(II)–amine complexes of 1,7-carborane that are related to the DNA cross-linking agents reported by Farrell and co-workers.[7]

The synthetic methodology employed in the preparation of the bridging 1,7-bis(3-aminopropyl)-1,7-carborane ligand and its platinum(II) derivatives **6** and **7** is presented in Scheme 1. The protocol for the ligand synthesis was based upon that reported by Sjöberg and coworkers for the preparation of 1,12-bis(3-aminopropyl)-1,12-carborane.[8] The reaction of ^{n}BuLi with 1,7-carborane in THF solution at −78 °C, followed by the addition of oxetane and subsequent hydrolysis with $HCl_{(aq)}$, afforded the dipropanol **1** in 62% yield. Bromination of **1** using CBr_4 and PPh_3 in CH_2Cl_2 solution at 0 °C gave the dibromo compound **2** (86%), which was readily converted to the diiodo species **3** (92%) by means of a metathesis reaction employing NaI in acetone solution. Alkylation of di-*tert*-butyliminodicarboxylate, $HN(BOC)_2$, with **3** was carried out under basic phase-transfer conditions and afforded the di-substituted, BOC-protected amine **4** (75%). Treatment of **4** with 3 M HCl in ethyl acetate solution gave the amine **5**·2HCl as a white crystalline solid in 69% yield. Addition of $K_2CO_{3(aq)}$ to **5**·2HCl afforded the free amine **5** as a slightly unstable, white solid (76%). All compounds were fully characterised by ^{1}H, ^{13}C{^{1}H} and ^{11}B{^{1}H} NMR spectroscopy and microanalysis.

† Electronic supplementary information (ESI) available: experimental section. See http://www.rsc.org/suppdata/cc/b1/b108081d/

Treatment of **5** with two equivalents of the labile precursor complex *trans*-$[PtCl(dmf)(NH_3)_2]OTf$ led to the formation of **6** as an off-white solid.‡ Alternatively, use of the mixed-halogeno species *cis*-$[PtCl_2I(NH_3)]^-$, formed *in situ* from the reaction of $[PtCl_3(NH_3)]^-$ and KI in aqueous solution,[9] afforded the chloro–iodo analogue of **7**.‡ Subsequent treatment of this

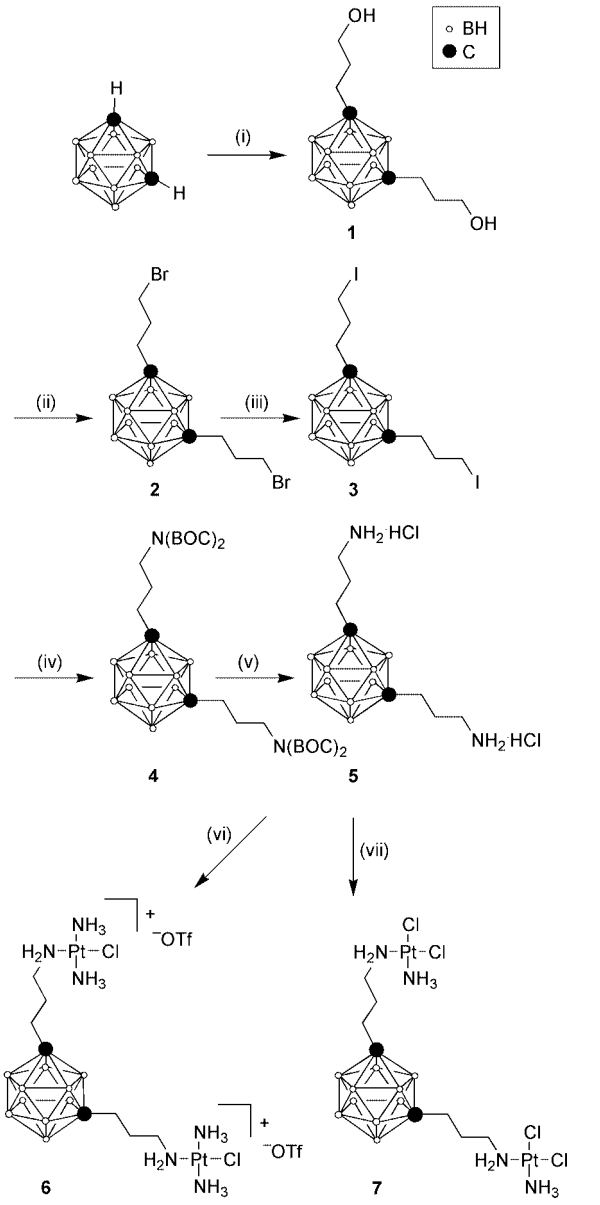

Scheme 1 *Reagents*: (i) ^{n}BuLi, oxetane, H_3O^+; (ii) CBr_4, PPh_3; (iii) NaI; (iv) $HN(BOC)_2$, NaOH, Bu_4NHSO_4; (v) 3 M HCl in EtOAc; (vi) $K_2CO_{3(aq)}$, *trans*-$[PtCl(dmf)(NH_3)_2]OTf$; (vii) $K_2CO_{3(aq)}$, *cis*-$[PtCl_2I(NH_3)]^-$, $AgNO_3$, $HCl_{(aq)}$.

 DOI: 10.1039/b108081d

complex with $AgNO_3$ in DMF solution, followed by the addition of $HCl_{(aq)}$ to the resulting tetra(nitrato) species gave the target complex **7** as a bright-yellow solid. The new complexes were fully characterised by ^{1}H, $^{13}C\{^{1}H\}$ and $^{11}B\{^{1}H\}$ NMR spectroscopy and microanalysis. Furthermore, **6** and **7** exhibited singlet $^{195}Pt\{^{1}H\}$ NMR resonances that lie in the range observed for complexes with a PtN_2Cl_2 and PtN_3Cl coordination sphere, respectively.[10]§

In order to assess the DNA-binding characteristics of **6** and **7**, preliminary plasmid DNA-binding experiments were conducted using a well-established *Eco* RI restriction endonuclease assay that monitored platinum binding at (or near) its unique restriction site in linearized pBR322 DNA.[11] For comparative purposes, we also investigated the DNA-binding characteristics of the archetypal, cross-linking agent *cis*-$[PtCl_2(NH_3)_2]$. These experiments confirm that **6** (Fig. 1) and **7** are capable of targetting plasmid DNA. The concentration of platinum complex required to achieve 20% inhibition of DNA cleavage by the enzyme is 3, 14 and 49 μM for **6**, *cis*-$[PtCl_2(NH_3)_2]$, and **7**, respectively. The inhibition of *Eco* RI activity by **6** at a concentration that is considerably less than *cis*-$[PtCl_2(NH_3)_2]$ and **7** is most likely the result of its rapid kinetics of DNA-binding. Similar effects have been reported previously with dinuclear platinum(II) complexes bridged by α,ω-diaminoalkane ligands.[12] At platinum concentrations greater than *ca*. 3.3 μM for **6**, considerable streaking of the DNA is observed (Fig. 1). This effect is also consistent with the rapid and effective (covalent¶) binding by the dicationic complex to the polyanionic DNA molecule, resulting in extensive charge neutralization. Further work to elucidate the nature of the Pt–DNA adduct(s) formed by **6** and **7**, including their quantification, is in progress.

In conclusion, **6** and **7** are the first examples of platinum(II)–amine complexes containing a carborane moiety, and they represent a new class of boron-containing DNA-binding agents for potential application in BNCT. The NC properties and biological studies involving selected platinum complexes will be reported in due course.

We thank Mr D. Sykiotis (The University of Adelaide) for assistance with the DNA-binding studies, Dr N. E. Dixon (Australian National University) for advice regarding the DNA-binding experiments, Prof. N. P. Farrell (Virginia Commonwealth University, US) for advice regarding the synthesis of **7** and DNA-binding studies, Prof. S. Sjöberg (Uppsala University, Sweden) for advice regarding the ligand synthesis, and Prof. B. J. Allen (Cancer Care Centre, Sydney, Australia) for many useful discussions. We are grateful to Johnson Matthey for the generous loan of $K_2[PtCl_4]$. We also thank the Australian Research Council and the Anti-Cancer Foundation of South Australia for financial support.

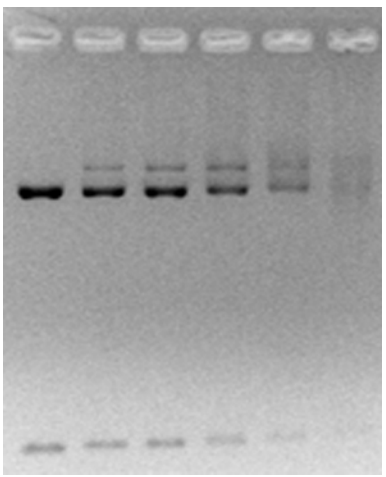

Fig. 1 Gel electrophoresis experiment. Lanes correspond to linear pBR322 DNA samples that were incubated with increasing concentrations of **6** (0, 1.2, 1.6, 2.3, 3.3 and 4.0 μM) for 2 h at 37 ± 0.1 °C, followed by spin dialysis and treatment with *Eco* RI restriction endonuclease.

Notes and references

‡ Note that the use of the isomeric 1,2-carborane derivative in the complexation reactions with platinum(II) precursors resulted in extensive decomposition accompanied by the formation of platinum metal. We are now in the process of investigating the various factors that may contribute to the reduction process, and the results of this study will be reported in due course.

§ $^{195}Pt\{^{1}H\}$ NMR data (d_7-DMF): δ −2410 and −2156 for **6** and **7**, respectively.

¶ Note that electrostatic interactions alone are unlikely to account for the strong binding of **6** to DNA. These would be reversed with the high NaCl concentrations used in the quenching of the Pt–DNA reactions, and under the conditions of the gel electrophoresis experiment.

1 For recent reviews, see: (*a*) A. H. Soloway, W. Tjarks, B. A. Barnum, F.-G. Rong, R. F. Barth, I. M. Codogni and J. G. Wilson, *Chem. Rev.*, 1998, **98**, 1515; (*b*) M. F. Hawthorne, *Mol. Med. Today*, 1998, 174; (*c*) G. W. Kabalka, *Expert Opin. Ther. Pat.*, 1998, **8**, 545; (*d*) J. A. Coderre and G. M. Morris, *Radiat. Res.*, 1999, **151**, 1; (*e*) R. F. Barth, A. H. Soloway, J. H. Goodman, R. A. Gahbauer, N. Gupta, T. E. Blue, W. L. Yang and W. Tjarks, *Neurosurgery*, 1999, **44**, 433.

2 (*a*) T. Hartman and J. Carlsson, *Radiother. Oncol.*, 1994, **31**, 61; (*b*) D. Gabel, S. Foster and R. G. Fairchild, *Radiat. Res.*, 1987, **111**, 14; (*c*) T. Kobayashi and K. Kanda, *Radiat. Res.*, 1982, **91**, 77.

3 (*a*) Y. Yamamoto and N. Sadayori, *Bioorg. Med. Chem. Lett.*, 1996, **6**, 9; (*b*) Y. Yamamoto, N. Asao, M. Megura, N. Tsukada, H. Nemoto, N. Sadayori, J. G. Wilson and H. Nakamuru, *J. Chem. Soc., Chem. Commun.*, 1993, 1201; (*c*) Y. Yamamoto and H. Nakamura, *J. Med. Chem.*, 1993, **36**, 2232; (*d*) F. Haslinger and A. H. Soloway, *J. Med. Chem.*, 1966, **9**, 792; (*e*) A. H. Soloway and D. N. Butler, *J. Med. Chem.*, 1966, **9**, 411.

4 (*a*) S. A. Bateman, D. P. Kelly, R. F. Martin and J. M. White, *Aust. J. Chem.*, 1999, **52**, 291; (*b*) D. P. Kelly, S. A. Bateman, R. F. Martin, M. E. Reum, M. Rose and A. R. D. Whittaker, *Aust. J. Chem.*, 1994, **47**, 247; (*c*) M. Argentini, D. F. Dos Santos, R. Weinreich and H.-J. Hansen, in *Advances in Neutron Capture Therapy*, ed. B. Larsson, J. Crawford and R. Weinreich, Elsevier, Amsterdam, The Netherlands, 1997, vol. II, Chemistry and Biology, p. 82.

5 (*a*) H. Ghaneolhosseini, W. Tjarks and S. Sjöberg, *Tetrahedron*, 1998, **54**, 3877; (*b*) M. A. Davis and A. H. Soloway, *J. Med. Chem.*, 1967, **10**, 730.

6 (*a*) J. Cai, A. H. Soloway, R. F. Barth, D. M. Adams, J. R. Hariharan, I. M. Wyzlic and K. Radcliffe, *J. Med. Chem.*, 1997, **40**, 3887; (*b*) J. Cai and A. H. Soloway, *Tetrahedron Lett.*, 1996, **37**, 9283; (*c*) J. R. Hariharan, I. M. Wyzlic and A. H. Soloway, *Polyhedron*, 1995, **14**, 823.

7 N. Farrell, *Comments Inorg. Chem.*, 1995, **16**, 373.

8 H. Ghaneolhosseini, W. Tjarks and S. Sjöberg, *Tetrahedron*, 1997, **53**, 17519.

9 A. J. Kraker, J. D. Hoeschele, W. L. Elliott, H. D. H. Showalter, A. D. Sercel and N. Farrell, *J. Med. Chem.*, 1992, **35**, 4526.

10 (*a*) N. Farrell and Y. Qu, *Inorg. Chem.*, 1989, **28**, 3416; (*b*) Y. Qu and N. Farrell, *Inorg. Chem.*, 1992, **31**, 930.

11 (*a*) K. A. Skov, H. Adomat, D. C. Konway and N. P. Farrell, *Chem. Biol. Interact.*, 1987, **62**, 117; (*b*) N. P. Farrell, S. G. de Almeida and K. A. Skov, *J. Am. Chem. Soc.*, 1988, **110**, 5018; (*c*) J. A. Broomhead, L. M. Rendina and L. K. Webster, *J. Inorg. Biochem.*, 1993, **49**, 221.

12 (*a*) N. Farrell, Y. Qu, L. Feng and B. Van Houten, *Biochemistry*, 1990, **29**, 9522; (*b*) N. Farrell, T. G. Appleton, Y. Qu, J. D. Roberts, A. P. Soares Fontes, K. A. Skov, P. Wu and Y. Zou, *Biochemistry*, 1995, **34**, 15480.

CHEMCOMM Communication
www.rsc.org/chemcomm

How van der Waals bonds orient molecules in zeolites

Ewout Kemner,* Ignatz M. de Schepper and Gordon J. Kearley

Interfaculty Reactor Institute, Mekelweg 15 2629 JB, Delft, The Netherlands.
E-mail: kemner@iri.tudelft.nl

Received (in Cambridge, UK) 26th June 2001, Accepted 3rd October 2001
First published as an Advance Article on the web 9th November 2001

We show that weak bonds are responsible for the way a molecule is held in a zeolite, and for its reactivity.

How is a guest molecule held in a zeolite cage? What is the bonding? How does this affect the reactivity of the guest? To answer these questions in a coherent manner we must examine the topology of electron density between the host and the guest, and then reconsider what we mean by 'bonding'. Using the approach pioneered by Bader,[1] we reveal only weak H-bonds and even weaker van der Waals bonds between the host and the guest. Yet the reactivity of the guest (ferrocene in the present case) is dramatically increased when it is in the zeolite.[2,3] The popular concept is that the increased reactivity of the guest arises from changes in its electronic structure is incorrect in the present case, and it is the orientation in which the guest ferrocene molecule is held that renders it vulnerable to attack. Analyses of this type in which we separate the electronic and steric effects may have a general impact on the study of catalytic systems. In the current study the guest molecule is ferrocene, $Fe(C_5H_5)_2$, (an iron atom 'sandwiched' by two identical parallel cyclopentadienyl C_5H_5 rings) held within the host lattice of NaY zeolite, $Na_x(AlO_2)_x(SiO_2)_{192-x}$. The original interest in this system stems from its use as a preparative route by which iron may be included in the zeolite. The ferrocene molecules occupy 'supercages' (shown in Fig. 1) in the zeolite which have a diameter of about 12 Å, and each of these contains four sodium ions on its walls (see Fig. 1). We have recently determined the position of the ferrocene molecule in the supercage of NaY zeolite to be 0.87 Å above a line joining two sodium ions, using powder X-ray and neutron diffraction[4] (see Fig. 1). The question immediately arises as to why the ferrocene molecule does not lie on the line joining two sodium ions since then it would optimize the Coulombic interaction between the π-systems of the aromatic rings and the sodium ions. Such a position would also lead to considerably shorter hydrogen bonds between the cyclopentadienyl hydrogen atoms and the oxygen atoms of the zeolite. Where is the energy-gain in leaving the ferrocene molecule almost 1 Å above the Na^+–Na^+ vector, and how can we quantify this? One possibility would be to map out the potential-energy hypersurface of the ferrocene along its normal-mode vectors. A subsequent examination of this map for all atom pairs would reveal the origin of the observed ferrocene position. A far more convenient approach is a direct examination of the electron density for evidence of bonds between the ferrocene molecule and the zeolite cage. An analysis of the electron density should be able to account for the observed location of the ferrocene molecule, and more important, the increased reactivity with respect to the pure compound.

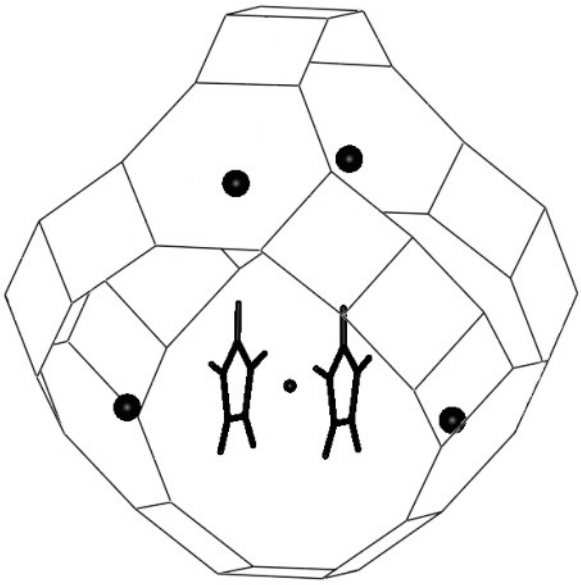

Fig. 1 Location and orientation of a ferrocene molecule (bold) inside a NaY zeolite supercage. The four spheres show the positions of the sodium ions on the walls of the zeolite supercage.

The first step in the analysis is to ensure that the atomic positions derived from crystallography do indeed correspond to the energy minimum, and that there is consistency between observation and calculation. We achieve this by modelling a realistic fraction of the zeolite containing the ferrocene (Fig. 2). Various constraints are possible which would allow relaxation in the immediate environment around the ferrocene molecule. For convenience we chose the outer H-atoms (which had been introduced artificially) as a rigid container for the model. The energy of the system is then minimised with respect to the ferrocene position using *ab initio* density functional theory (Dmol[3] within the suite Cerius[2]).[5] We use the local density approximation, Perdew Wang functionals, the DND basis set,[5] and an atomic cutoff radius of 5.5 Å. After optimization of the geometry we find that there is no significant difference in the atomic positions from diffraction experiments and DFT calculations.

The DFT calculations also provide the total electron density $\rho(\boldsymbol{r})$ map for the model, which we use to perform a topological analysis, and hence obtain a straightforward definition of bonds between atoms. We start by locating the critical points in the electron density, that is, where the gradient of the electron density $\nabla\rho(\boldsymbol{r})$ vanishes. In addition to the maxima associated with atom positions, there are also saddle points where the curvature is positive in one direction and negative in the two

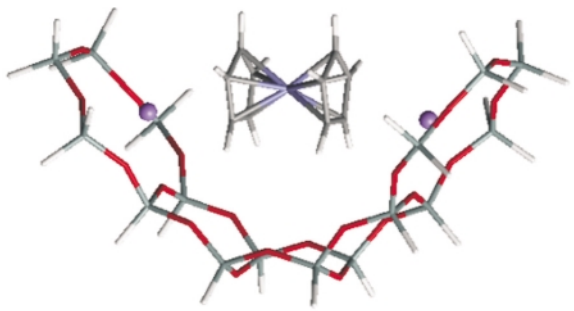

Fig. 2 Illustration of the zeolite fragment consisting of oxygen (red) and silicon (grey) atoms and the ferrocene molecule as used for DFT calculations. Sodium ions are represented by purple spheres. The oxygen atoms adjacent to the zeolite framework have been replaced by hydrogen atoms (white).

 DOI: 10.1039/b105611p

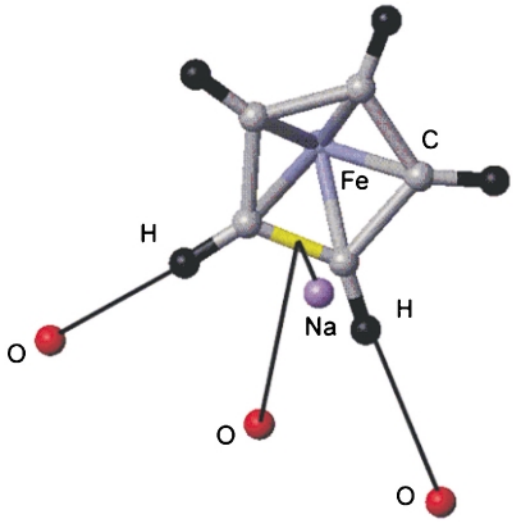

Fig. 3 Interaction paths between a ferrocene-C_5H_5 ring and atoms in the zeolite framework. We find two paths from a hydrogen atom (black) of the ring to an oxygen atom (red) of the framework. There are also two paths from a sodium ion (purple) and an oxygen atom to the centre of a carbon-carbon bond in the ring (yellow).

others. Saddle points are located somewhere in between the nuclei and are usually termed 'bond critical points'. The next step is to identify 'gradient paths', *i.e.* curves such that the gradient vector $\nabla\rho(\boldsymbol{r})$ is tangent to it in every point. These paths are roughly analogous to ridges in a mountainous landscape. Some of these originate at a bond critical point and lead to atoms (peaks, in our analogy), and these correspond to bonds. We perform this topological analysis on the electron density with the program FAST,[6] the results for the bond critical points and paths for the model being shown in Fig. 3.

All of the bonds that one normally would expect in the zeolite framework and in the ferrocene molecule, are found as expected, but what is of interest here are the bonds that we find between the ferrocene and the zeolite framework. These go *via* the cyclopentadienyl rings. There are four connecting each cyclopentadienyl ring of the ferrocene molecule and the zeolite framework (see Fig. 3). Two of these are between a hydrogen atom of the ring and an oxygen atom of the framework, and these correspond to weak hydrogen bonds. The other two paths are somewhat unusual, and to our knowledge, unique. Essentially, these join both a sodium ion and an oxygen atom of the zeolite to the same point, that point being the center of a bond between two carbon atoms. These bonds lie in a mirror plane of the system, and if this symmetry is broken the van der Waals bonds go to one of the carbon atoms, and the real situation at room temperature corresponds to fluxionality of bonding to the alternative carbon atoms. These bonds are not artefacts of the basis set in that although the details of the density maps vary with the level of calculation, even the most basic calculations still show the van der Waals bonds.

It seems clear that the unexpected position of the ferrocene molecule arises from an interaction of the carbon atoms of the ferrocene with the sodium ions and the oxygen atoms of the zeolite. It should be emphasised that many gradient paths in the electron density eventually flatten out, and hence disappear, but in the present case they actually continue as bond-paths. This makes it possible to express these arguments in more chemical terms. The energy associated with the formation of these new bonds more than compensates for the weakening of the hydrogen bond and the weaker interaction of the aromatic π-system with the sodium ion. The length of these bonds and the charge density in the bond critical points are collected in Table 1, and these allow a quantitative comparison of the different types of bond. For example, the electron density at the critical point of the strong covalent bond between two carbon atoms in benzene amounts to 0.33 e/a_0^3, and of the bond between oxygen and hydrogen in a water molecule 0.39 e/a_0^3.[1] An ionic bond has a rather lower value, for example 0.036 e/a_0^3 in case of NaCl,[1] whilst hydrogen bonds normally have a values for the electron density between 0.001–0.035 e/a_0^3.[7] In the present case the hydrogen bond between the ferrocene hydrogen and the zeolite oxygen is also within this range, 0.0081 e/a_0^3, and further, the C···O distance is comparable with that found in C–H···O hydrogen bonds.[7] Similar values for the electron density at bond critical points are found in van der Waals molecules, for example 0.0077 e/a_0^3 between Ar and HF and 0.0099 e/a_0^3 between Ne and HF. These are comparable with the values we find for the interaction between the sodium and oxygen and the center of the C–C bond of 0.0057 e/a_0^3. However, we find distances that are >3 Å, which is somewhat longer than the corresponding distances in Ne/HF (2.11 Å) and Ar/HF (2.56 Å).

Table 1 Pathlength and electron density ρ at the bond critical points for the interaction lines between a cyclopentadienyl ring and the zeolite framework

	Pathlength/Å	ρ (e/a_0^3) at bond critical point
H–O	2.63	0.0081
Ring–O	3.49	0.0057
Ring–Na	3.15	0.0057

Bonds between π-bondings and positive ions have been observed before,[8] and a Bader analysis has been reported for hydrogen bonds with a π-bond.[9] However, to our knowledge the binding between the π-cloud of an aromatic ring and an ion always involves the centre of the ring. In the present case the iron atom may well distort the π-cloud in such a way that two edge-bonds plus the involvement of an extra oxygen atom is energetically more favourable. We stress that these novel bonds should not be thought of as the primary interaction between the ferrocene and the zeolite. They are secondary to the main Coulomb and hydrogen bond interactions, which play the primary role in holding the ferrocene molecule in its place. It follows that rather long weak bonds are responsible for the displacement of the ferrocene molecule from the expected position. All bonds between the ferrocene and the zeolite are weak and the bonding within the ferrocene itself is virtually unchanged from that of the isolated molecule. Inspection of Fig. 1 reveals a large 'free volume' on the side of the ferrocene molecule furthest from the cage fragment as shown in Fig. 2, which is an attractive site for any potential reactants. It is even conceivable that without the van der Waals bonds, the ferrocene would be held deeper in the zeolite cage where it would be less accessible to attack, and in this way very weak bonds could play a crucial role in catalysis.

Notes and references

1 R. F. W. Bader, *Atoms in Molecules. A Quantum Theory*, Clarendon Press, Oxford, 1990.
2 G. A. Ozin and J. Godber, *J. Phys. Chem.*, 1989, **93**, 878.
3 A. R. Overweg *et al.*, *J. Phys. Chem. B*, 1999, **103**, 4298.
4 E. Kemner *et al.*, submitted.
5 B. Delley, *J. Chem. Phys.*, 1995, **92**, 508.
6 http://www.nas.nasa.gov/Software/FAST/
7 U. Koch and P. L. A. Popelier, *J. Phys. Chem.*, 1995, **99**, 9747.
8 J. C. Ma and D. A. Dougherty, *Chem. Rev.*, 1997, **97**, 1303.
9 I. Rozas, I. Alkorta and J. Elguero, *J. Phys. Chem. A*, 1997, **101**, 945.

CHEMCOMM Communication
www.rsc.org/chemcomm

Silver(I) carboxylates: versatile inorganic analogs of carboxylic acids for supramolecular network formation†

Lee Brammer,*‡ Michael D. Burgard, Colin S. Rodger, John K. Swearingen and Nigam P. Rath

Department of Chemistry and Biochemistry, University of Missouri–St. Louis, 8001 Natural Bridge Road, St. Louis, MO 63121-4499, USA

Received (in Cambridge, UK) 18th September 2001, Accepted 16th October 2001
First published as an Advance Article on the web 15th November 2001

Dimeric motifs formed by silver(I) carboxylates, illustrated here by the unit $Ag_2(CF_3CO_2)_2$, resemble the well known dimerization of carboxylic acids, *i.e.* '$H_2(RCO_2)_2$', but exhibit greater flexibility, while permitting further elaboration into neutral coordination networks through linkage of the silver centres *via* ditopic ligands.

The molecular level design of new materials, synthetic receptors and biomimetic systems has proceeded apace in the past decade under the banner of the multidisciplinary fields of supramolecular chemistry[1] and crystal engineering.[2] Fundamental to such an approach is the need for interactions between molecular building blocks that are sufficiently reliable to permit some degree of predictability and control over the formation of supramolecular assemblies and networks.[3] To convey this idea Desiraju has introduced the term supramolecular synthon,[4] often applied to structural units comprising weaker, and thus inherently *flexible*, non-covalent linkages. The carboxylic acid dimer, the archetypal synthon, illustrated as **I** in its symmetric

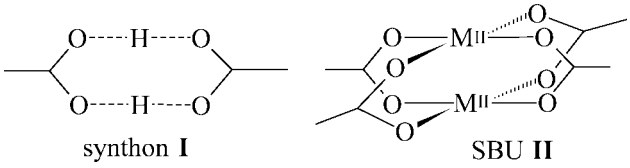

form, is a mainstay of organic crystal engineering[2a] and is beginning to see some applications in organometallic systems.[2b,5] A related concept conveyed by Yaghi is that of the secondary building unit (SBU),[6] as exemplified by the square 4-connected unit **II**. SBU **II** is known for a variety of divalent transition metals, M^{II}, and has been applied to the synthesis of *rigid* metal–organic frameworks.[6]

In this report, we highlight a middle ground in the form of a versatile inorganic analog of synthon **I** in which the hydrogen-bonded protons that link the two carboxylate groups are replaced by Ag^+ ions, an idealised symmetric example of which is shown as **III**. However, in contrast to protons, the

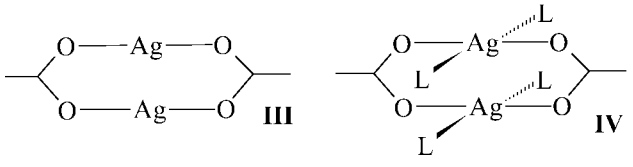

coordination sphere of the Ag^+ ions is not satisfied by the two oxygen atoms, and additional bridging by the oxygen atoms typically leads to polymeric or oligomeric structures for simple silver(I) carboxylates.[7] Thus, we surmised that the silver carboxylate dimers might serve as a useful new building block through occupation of these additional coordination sites at each silver center by neutral polytopic ligands (**IV**). Here we illustrate the case where L is a ditopic ligand capable of forming a linear linkage between two metal centers. This leads to a new SBU (**V**) with approximately square connectivity about the central $Ag_2(RCO_2)_2$ unit, self-assembly of which generates a 2D-network (**VI**).

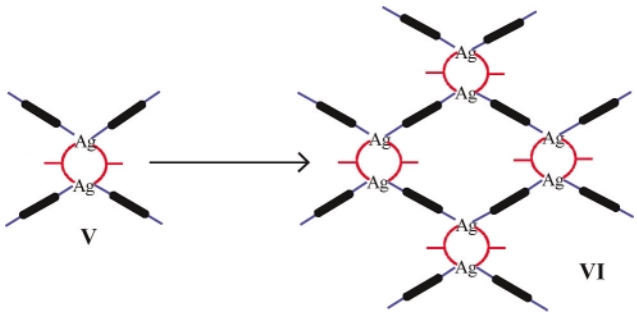

The three examples presented herein, $Ag(O_2CCF_3)L$ [L = 1,4-diazabicyclooctane (DABCO) **1**, tetramethylpyrazine (TMP) **2**, pyrazine (pyraz) **3**] (ESI†),[8] are archetypes for this approach using a small carboxylate anion. In each compound, pairs of silver centers are linked *via* carboxylate bridges. Each silver ion is further coordinated by two neutral ditopic ligands that provide linkages to two further silver centers resulting in assembly of the SBUs into a 2D grid of tiled rhomboids with an Ag_2 dimer at each node [Fig. 1(a)–(c)]. The structures of **1** and **2** adopt a staggered arrangement of layers [Fig. 1(d) and (e)] in which the anions occupy the interlayer space with each CF_3 group oriented toward the center of a rhomboid in an adjacent layer. The pairs of silver ions in **1** and **2** are bridged by a slipped version of the idealised synthon **III**, employing only one oxygen atom from each carboxylate anion. The structure of **3** differs in that the layers are now aligned to give a channel structure. This alignment appears to be permitted due to the stacking of the planar pyrazine ligands (face-to-face separation 4.34 Å). The versatility of the silver carboxylate bridge is further illustrated in **3** by its adaptation from the discrete linkage seen in **1** and **2** to an infinite linkage that lies mid-way between the ring [$R^2_2(8)$] and chain [C(4)] arrangements[9] well known for the (organic) carboxylic acid analog. This permits cross-linking of the 2D network [Fig. 1(c)] into a 3D network [Fig. 1(f)]. In contrast to **1** and **2**, the anions in **3** are oriented parallel to the layers.

Importantly, it is apparent that the integrity of the silver(I) carboxylate dimer, and thus its structure-directing role, can be maintained within a variety of related bridging carboxylate coordination modes.[10] This offers the prospect of both control and reliability of the overall structural arrangement while maintaining some flexibility. These traits are often cited as being advantages offered by hydrogen bonds rather than by coordination bonds in supramolecular chemistry.[11] It should also be emphasized that the approach described here differs from the predominant approach to coordination networks, especially those involving silver(I) ions.[12] Rather than using

† Electronic supplementary information (ESI) available: synthesis, characterization and crystal data for **1**–**3**; displacement ellipsoid plots; figures showing carboxylate coordination modes. See http://www.rsc.org/suppdata/cc/b1/b108448h/

‡ Current address: Department of Chemistry, University of Sheffield, Sheffield, UK S3 7HF. E-mail: lee.brammer@sheffield.ac.uk

 DOI: 10.1039/b108448h

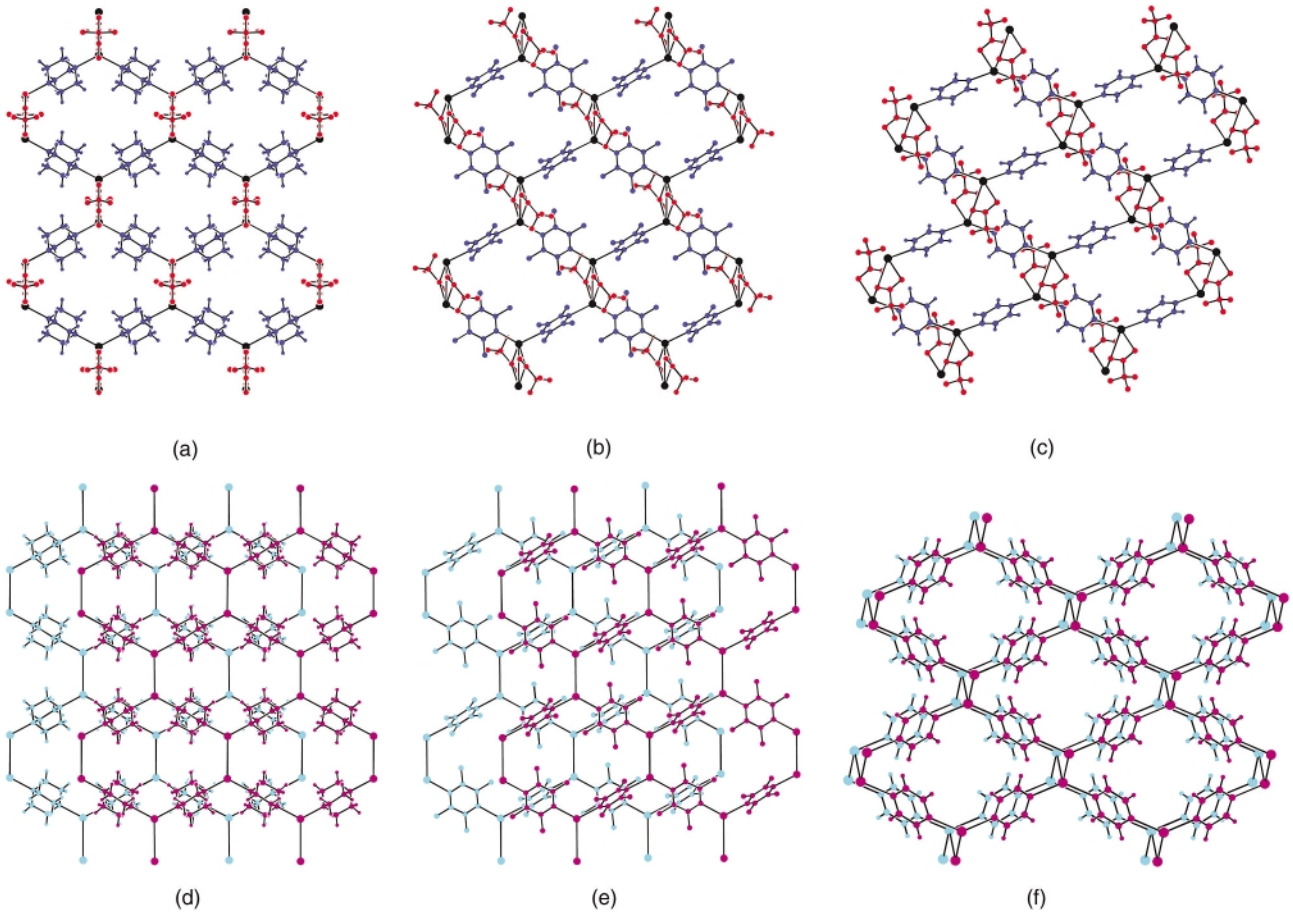

Fig. 1 View of a single layer: (a) **1**, (b) **2**, (c) **3** (Ag: black, anions: red, ligands: blue). Stacking of two adjacent layers (anions omitted): (d) **1**, (e) **2**, (f) **3**. Methyl hydrogen atoms not shown for **2**. Dimensions: Ag–Ag (bridged), vertical (Ag···Ag) and horizontal (Ag_2···Ag_2) dimensions of rhomboids, and interlayer separation, respectively. **1**: 3.75, 10.63, 12.58, 6.20 Å; **2**: 3.82, 10.83, 13.02, 6.47 Å; **3**: 4.00, 8.95, 13.22, 7.01 Å.

weakly coordinating anions to avoid disruption of a cationic network formed from Ag^+ centers and neutral polytopic ligand connectors, as is the common practice, here we have deliberately used the anions as an integral part of the final *neutral* network.[13] Therein, this approach provides a new avenue to the construction of neutral frameworks that complements the recent approaches of the groups of Yaghi[6] and Cotton[14] in linking pairs of *divalent* transition metal ions *via* polycarboxylate units to yield a variety of networks, polygons and polyhedra. Thus, this approach utilizes what might be considered a 'soft' or adaptable SBU (**V**) that appears to offer reliable 2D network formation coupled with flexibility of the silver(I) carboxylate linkage, permitting accommodation of the specific packing demands of the network for a given ditopic ligand, L.

We are currently exploring a variety of extensions of this approach including changing the length of the linkages, the use of polytopic connectors, and the provision of additional network links through use of polycarboxylate anions, with a view to developing adaptable cavity and channel-containing network solids.

Support for this work from the NSF (CHE-9988184) is gratefully acknowledged.

Notes and references

1 *Comprehensive Supramolecular Chemistry*, series ed. J.-M. Lehn; volume ed. J. L. Atwood, J. E. D. Davies, D. D. MacNicol and F. Vögtle, Pergamon, Oxford, 1996.

2 (*a*) G. R. Desiraju, *Crystal Engineering: The Design of Organic Solids*, Elsevier, New York, 1989; (*b*) D. Braga, F. Grepioni and G. R. Desiraju, *Chem. Rev*., 1998, **98**, 1375.

3 F. H. Allen, W. D. S. Motherwell, P. R. Raithby, G. P. Shields and R. Taylor, *New J. Chem*., 1999, **23**, 25.

4 Hereafter contracted to *synthon*. See: G. R. Desiraju, *Angew. Chem., Int. Ed. Engl*., 1995, **34**, 2311.

5 L. Brammer, J. C. Mareque Rivas, R. Atencio, S. Fang and F. C. Pigge, *J. Chem. Soc., Dalton Trans*., 2000, 3855; D. Braga, L. Maini and F. Grepioni, *Angew. Chem., Int. Ed*., 1998, **37**, 2240.

6 M. Eddaoudi, D. B. Moler, H. Li, B. Chen, T. M. Reineke, M. O'Keeffe and O. M. Yaghi, *Acc. Chem. Res*., 2001, **34**, 319; M. Eddaoudi, J. Kim, J. B. Wachter, H. K. Chae, M. O'Keeffe and O. M. Yaghi, *J. Am. Chem. Soc*., 2001, **123**, 4368.

7 *e.g*. R. S. Griffin, J. D. Ellett Jr., J. G. Bullitt and J. S. Waugh, *J. Chem. Phys*., 1972, **57**, 2147.

8 CCDC reference numbers 171148–171150. See http://www.rsc.org/suppdata/cc/b1/b108448h/ for crystallographic data in CIF or other electronic format.

9 For graph set notation see: J. Bernstein, R. E. Davis, L. Shimoni and N.-L. Chang, *Angew. Chem., Int. Ed. Engl*., 1995, **34**, 1555.

10 This is confirmed by examination of simple silver(I) carboxylates in the Cambridge Structural Database. For further discussion of silver carboxylate coordinate modes, also see (*a*) X.-M. Chen and T. C. W. Mak, *J. Chem. Soc., Dalton Trans*., 1991, 1219; (*b*) D. S. Sagatys, G. Smith, R. C. Bott, D. E. Lynch and C. H. L. Kennard, *Polyhedron*, 1993, **12**, 709.

11 C. B. Aakeröy, *Acta Crystallogr., Sect. B*, 1997, **53**, 569.

12 A. J. Blake, N. R. Champness, P. Hubberstey, W.-S. Li, M. A. Withersby and M. Schröder, *Coord. Chem. Rev*., 1999, **183**, 117; L. Carlucci, G. Ciani, D. M. Proserpio and A. Sironi, *J. Am. Chem. Soc*., 1995, **117**, 4562; L. Carlucci, G. Ciani, P. Macchi, D. M. Proserpio and S. Rizzato, *Chem. Eur. J*., 1999, **5**, 237; K. A. Hirsch, S. R. Wilson and J. Moore, *J. Am. Chem. Soc*., 1997, **119**, 10401.

13 Robson has used the trigonal $C(CN_3)^-$ anion as a structurally active component of the coordination networks comprising silver(I) and neutral ligands: S. R. Batten, B. F. Hoskins and R. Robson, *New J. Chem*., 1998, **22**, 173.

14 F. A. Cotton, L. M. Daniels, C. Lin and C. A. Murillo, *J. Am. Chem. Soc*., 1999, **121**, 4538; F. A. Cotton, C. Lin and C. A. Murillo, *Chem. Commun*., 2001, 11; F. A. Cotton, C. Lin and C. A. Murillo, *J. Chem. Soc., Dalton Trans*., 2001, 499.

CHEMCOMM Communication
www.rsc.org/chemcomm

Synthesis of *p*-benzylcalix[4]arene and its sulfonated water soluble derivative

Mohamed Makha[a] and Colin L. Raston*[b]

[a] *School of Chemistry, Monash University, Clayton, Victoria 3800, Australia*
[b] *School of Chemistry, University of Leeds, Leeds, UK LS2 9JT.*
E-mail: c.l.raston@chemistry.leeds.ac.uk; Fax: +44 0113 2336401; Tel: +44 0113 233655

Received (in Columbia, USA) 13th July 2001, Accepted 1st October 2001
First published as an Advance Article on the web 7th November 2001

p-Benzylcalix[4]arene is formed in good yield by a direct "one pot" reaction involving *p*-benzylphenol and formaldehyde, selectively converted to the corresponding chlorosulfonyl and sulfonate analogues.

There is a growing interest in cyclooligomeric compounds called calix[*n*]arenes.[1] These bowl shaped (usually $n = 4, 5$) or more flexible ($n \geqslant 6$) macrocycles can form a diverse range of molecular assemblies. The synthesis of calixarenes has been widely investigated by Gutsche *et al.* and others, leading to well-established procedures for their preparation in reasonable yields.[2,8] However, these focus mainly on *p*-^{t}Bu- calix[*n*]arenes derived from base or acid catalysed condensation of *p*-^{t}Bu-phenol and formaldehyde, leading to the major calixarenes (n = 4, 5, 6, and 8) and other higher calixarenes.[2,3] In contrast, the direct syntheses of calixarenes derived from other *p*-alkylphenols are not extensively investigated and are generally formed in low yields;[6] this is an impediment to developing their chemistry. Base catalysed condensation of *p*-benzylphenol and formaldehyde, for example, leads to a mixture of *p*-benzylcalix-[5,6,8]arenes in 33%, 16% and 12% yields respectively,[5–7] as well as *p*-benzylcalix[7 and 10]arenes,[4,9,10] with no evidence for the formation of the *p*-benzylcalix[4]arene. Herein we report the synthesis of *p*-benzylcalix[4]arene as the first 'major' calixarene of the *p*-benzylcalix[*n*]arene family now available in good yield. The calix[4]arene is new and its availability offers scope for further elaboration such as *O*-alkylation, aromatic substitution of the benzyl groups, and as a receptor molecule, both aspects being established herein with the synthesis of the water soluble sulfonated *p*-benzylcalix[4]arene and the formation of a discrete 1 : 1 complex of the calixarene with C_{60} (Scheme 1).

The rigid cone structure of the phenolic-containing array with the flexibility of the benzyl moieties, offers scope for complexation of a range of substrates, of varying shape and electronic characteristics.

The base induced condensation reaction of *p*-benzylphenol and formaldehyde, proceeds smoothly and quickly relative to the similar condensation of its *p*-^{t}Bu-phenol analogue.[2] Oligomerization of *p*-benzylphenol formed at 120 °C using aqueous formaldehyde as the reaction medium with a catalytic amount of sodium hydroxide, affording a clear beige glass, consisting exclusively of *p*-benzylcalix[8]arene as the sole calixarene formed (TLC, NMR), with the consumption of all the starting phenol. Other products presumably are linear oligomers, noting that corresponding oligomers are formed in the condensation of *p*-^{t}Bu-phenol. Upon addition of diphenyl ether to this material and increasing the temperature quickly to 260 °C over half-an-hour and holding the temperature at reflux for 3 hours affords *p*-benzylcalix[4]arene, **1** in 60% isolated yield.†

It is noteworthy that the outcome of the reaction changes dramatically when either the ramping period or the reflux temperature is altered. For instance when the ramping is over one hour instead of half-an-hour and the reflux temperature is 220 °C instead of 260 °C and even over an extended period of reflux (10 h) the conversion to *p*-benzylcalix[4]arene accounts for only 16% of the starting material.

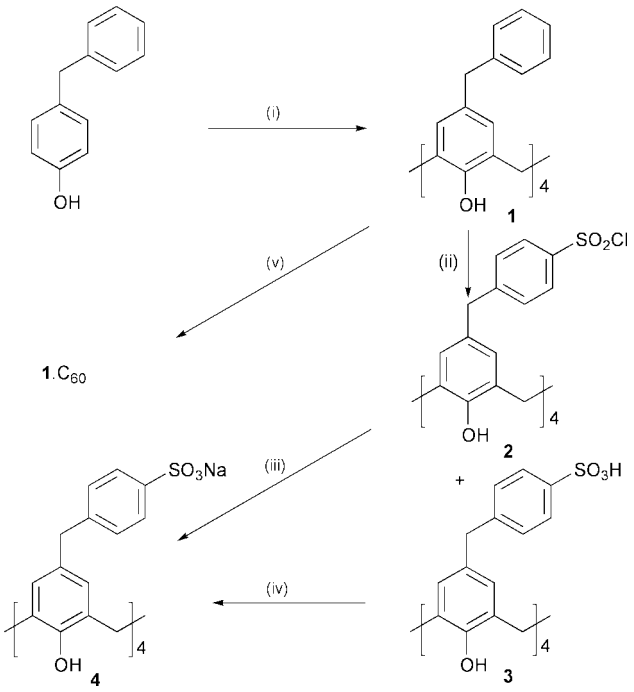

Scheme 1 Reagents and conditions: (i) Ph_2O, NaOH, H_2CO, 260 °C, 3 h; (ii) Anh. DCM, $ClSO_3H$, rt, 5 h, Argon; (iii) Py–H_2O, $NaHCO_3$, 100 °C; (iv) NaOH; (v) C_{60}, Tol.

The organic free solvent condensation to give the *p*-benzylcalix[8]arene also depends on the reaction conditions, notably, the molar ratio of the base to *p*-benzylphenol and the amount of formaldehyde used. Interestingly, this reaction always gives *p*-benzylcalix[8]arene in varying amounts which is easily separated, precipitating from the reaction mixture upon addition of acetonitrile. The mother liquor contains a mixture of *p*-benzylcalix[4,5,6,7]arenes which can be recycled and, if desired, separated (Table 1).

The ready availability of compound **1** allowed the preparation of the water soluble sulfonated derivative. This adds a novel lipophilic and highly charged calixarene to the expanding

Table 1 Product distribution of solvent free base induced condensation of *p*-benzylphenol (10 g) and formaldehyde (15 ml) using different molar ratios of base to *p*-benzylphenol at 110 °C

Molar ratio	*p*-Benzylcalix[*n*]arene distributions
0.045 NaOH	$n = 8$, 30%[a]
0.045 KOH	$n = 8$, 30%[a]
0.26 NaOH	$n = 8 > 6 > 4 > 7$
0.26 KOH	$n = 8 > 7 > 4$
0.34 NaOH	$n = 8 > 5 > 4$
0.34 KOH	$n = 6 > 5 > 8$

[a] Isolated yield, no other calixarenes present.

 DOI: 10.1039/b106161p

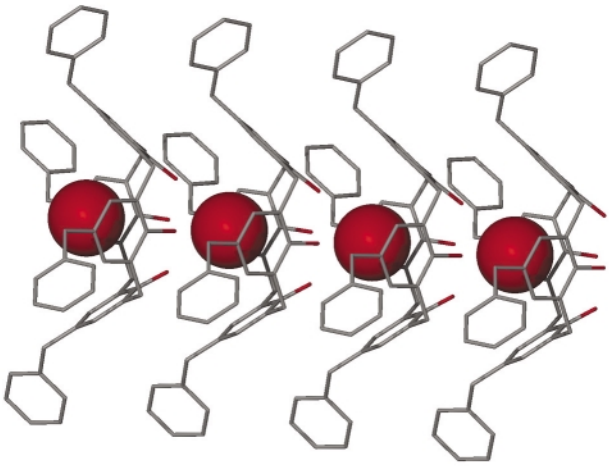

Fig. 1 Molecular structure of *p*-benzylcalix[4]arene showing the inclusion of water (space filling) within a self inclusion leading to a columnar array (hydrogen atoms have been removed for clarity).

chemistry of the water soluble calixarenes. The sulfonated *p*-benzylcalix[4]arene was prepared using the chlorosulfonation approach, isolated either in 60% yield as the sulfonic acid **3**, which slowly absorbs moisture as a deliquescent solid or as the sodium salt **4**. The chlorosulfonyl analogue, **2** can be intercepted and isolated in 30% yield (this yield can be improved under dry forcing reaction condition).†

The structure of *p*-benzylcalix[4]arene (Fig. 1) was established using diffraction data,‡ and shown to be an inclusion complex with water sandwiched between calixarenes in a columnar array, Fig. 1. The water resides deep in the cavity of the cone conformation, hydrogen bonded to the lower rim hydroxy groups. This is different to the water inclusion complex of sulfonated calix[4]arene with water in the cavity whereby the O–H groups are H-bonded (H$\cdots\pi$) to adjacent aromatic rings.[11,12] Another structural feature is the columnar π-stacking of the 1 : 1 supermolecules.

The C_{60} inclusion complex of **1** was prepared by slow evaporation of an equimolar toluene solution of both components. While crystals suitable for X-ray-diffraction studies were available, solution of the structure has proved elusive. Nevertheless, the structure is likely to be similar to those reported by Atwood *et al.*[13,14] where the fullerenes form columnar arrays. Indeed the cell dimensions are remarkably similar for the 1 : 1 complex of C_{60} with *C*-ethylphenylcalix[4]resorcinarene (tetragonal, $a = b = 18.9296(7)$, $c = 27.2702(13)$ Å,[13] and tetragonal, $a = b = 19.2183(3)$, $c = 27.7911(6)$ Å for **1**.C_{60}). Moreover, the similarity of the two cells supports the assignment of the 1 : 1 ratio of the two components.

In conclusion, we have demonstrated the accessibility of *p*-benzylcalix[4]arene in good yield and its water soluble sulfonated derivatives, opening the challenge to expand and diversify the chemistry. Moreover, the results give insight into the advantage of organic solvent free oligomerisation reactions.[15,16]

We are grateful to the Australian Research Council for support of this work.

Notes and references

† *Synthesis* of compound **1**. *p*-Benzylcalix[4]arene was prepared by an adapted method described in ref. 2. A mixture of *p*-benzylphenol (20.1 g, 0.109 mol), 13 ml of formaldehyde solution and (0.19 g, 0.0049 mol) of 10 M sodium hydroxide was stirred and heated at 120 °C for *ca.* 2 h forming a gummy beige material. 165 ml of warm diphenyl ether was added and the contents were heated first for 2 h at 120 °C, before ramping the temperature to 260 °C over half-an-hour. Refluxing at 260 °C was maintained for 3 h forming a dark amber solution, and the mixture then allowed to cool to rt. Diphenyl ether was evaporated and the viscous material obtained was washed and dried *in vacuo* affording an amber oil which crystallized slowly on standing, and upon addition of acetone (150 ml), *p*-benzylcalix[4]arene, **1** was obtained as a micro-crystalline white powder. Yield 60%, mp 204.5–205.6 °C, MS (ESI$^+$): *m/z* 807.34 [M.Na$^+$], 844.44 [M(H_2O).K$^+$], $C_{56}H_{48}O_4$ (784.34). ^{1}H NMR ($CDCl_3$, 300 MHz) δ 3.39 (d, 4H, Ar-CH_2-Ar), 3.76 (s, 8H, Ar-CH_2-Ph), 4.18 (d, 4H, Ar-CH_2-Ar), 6.78 (s, 8H; Ar-H), 7.11–7.30 (m, 20H, Ph), 10.13 (s, 4H, OH), ^{13}C NMR: ($CDCl_3$, 300 MHz) δ 32.1 (Ar-CH_2-Ar), 41.3 (ArCH_2-Ph), 126.2 (Ar), 128.4 (Ar), 128.6 (Ar), 129.0 (Ar) 129.5 (Ar), 134.7 (Ar), 141.3 (Ar), 147.2 (Ar-OH). *Synthesis* of compounds **2** and **3**. To a solution of *p*-benzylcalix[4]arene (0.4 g, 0.51 mmol) dissolved in 20 ml of dry dichloromethane, 1 ml of chlorosulfonic acid was added dropwise. The biphasic mixture was stirred at rt for *ca.* 5 h with formation of a viscous amber coloured material. The reaction mixture was poured over ice, and the organic phase was separated, treated successively with 1 M sodium bicarbonate ($\times$ 2), brine solution ($\times$ 2), water and dried ($MgSO_4$) affording the tetrachlorosulfonyl of *p*-benzylcalix[4]arene, **2**. Yield 56%, decomp. 180–195 °C, MS (ESI$^+$): *m/z* 1201.9 [M.Na$^+$], 1218.1 [M.K$^+$], $C_{56}H_{44}O_{12}S_4Cl_4$ (1179.01). ^{1}H NMR ($CDCl_3$, 300 MHz) δ 3.45 (d, 4H, Ar-CH_2-Ar, J_{AB} 13.2 Hz), 3.87 (s, 8H, Ar-CH_2-Ph), 4.24 (d, 4H, Ar-CH_2-Ar), 6.79 (s, 8H, Ar-H), 7.36 (AA′XX′, 8H, Ph-H), 7.94 (AA′XX′, 8H, Ph-H), 10.15 (s, 4H; OH), ^{13}C NMR ($CDCl_3$, 300 MHz) δ 32.1 (Ar-CH_2-Ar), 41.3 (ArCH_2-Ph), 127.4 (Ar), 128.7 (Ar), 129.8 (Ar), 130.1 (Ar) 132.7 (Ar), 142.4 (Ar), 147.9 (Ar), 149.7 (Ar-OH). The aqueous phase was filtered and treated with activated charcoal ($\times$ 2) leaving a clear light amber solution. Water was evaporated affording a deliquescent light gray solid, which crystallized from acetone to afford the sulfonic acid of *p*-benzylcalix[4]arene, **3**. Yield 80% decomp. 166–170 °C, MS (ESI$^+$): *m/z* 1105.2 [M.H$^+$], 1127.2 [M.Na$^+$], $C_{56}H_{48}S_4O_{16}$ (1104.2). ^{1}H NMR (d_6-DMSO, 300 MHz) δ 3.68 (s, 8H; Ar-CH_2-Ph), 4.08 (br s, 8H, Ar-CH_2-Ar), 6.25 (br s, COH/SOH, shifts downfield with increasing [H_2SO_4]), 6.88 (s, 8H, Ar-H), 7.15 (AA′XX′, 8H, Ph-H), 7.53 (AA′XX′, 8H, Ph-H), ^{13}C NMR (d_6-DMSO, 300 MHz) δ 49.2 (Ar-CH_2-Ar), 49.5 (ArCH_2-Ph), 126.2 (Ar), 128.7 (Ar), 129.1 (Ar), 129.7 (Ar) 134.2 (Ar), 143.2 (Ar), 145.3 (Ar), 148.2 (Ar-OH). Compound **4** was prepared by titration of compound **3** with 1 M sodium hydroxide to neutral pH. Treatment with methanol afforded sodium sulfonates of *p*-benzylcalix[4]arene, **4**, decomp. 200–210 °C. ^{1}H NMR (CD_3OD, 300 MHz) δ 3.65–3.95 (m, 8H, Ar-CH_2-Ar), 3.81 (s, 8H, Ar-CH_2-Ph), 4.82 (s, 4H, COH), 6.90 (s, 8H, Ar-H), 7.22 (AA′XX′, 8H, Ph-H), 7.73 (AA′XX′, 8H, Ph-H).

‡ *Crystal data*. Crystals of **1** for X-ray structural determination were grown from a moist acetone–propan-2-ol solution of *p*-benzylcalix[4]arene affording [*p*-benzylcalix[4]arene]·[H_2O]$_{0.5}$: $C_{56}H_{48}O_{4.5}$, space group *P*4/*n*, $a = b = 19.0703(3)$, $c = 5.6631(11)$ Å, $V = 2059.4(6)$ Å^3, $T = 173(2)$ K, $\rho_{calc.} = 1.279$ g cm^{-3}, $\mu = 0.080$ cm^{-1} (no correction), $Z = 2$, Mo-K$_\alpha$ radiation, $2\theta_{max} = 50°$ (1484 observed, $I > 2\sigma(I)$, 139 parameters, no restraints, $R_1 = 0.0455$, $wR_2 = 0.1245$ (all data), Data were collected at 173(1) K on an Enraf-Nonius Kappa CCD diffractometer. The structure was solved by direct methods (SHELXS-97) and refined with a full matrix least-squares refinement on F^2 (SHELXL-97), hydrogens included at calculated positions, $S = 1.079$. CCDC 172616. See http://www.rsc.org/suppdata/cc/b1/b106161p/ for crystallographic data in .cif or other electronic format.

1 C. D. Gutsche, *Calixarenes Revisited*, Royal Society of Chemistry, Cambridge, 1998; V. Bohmer, *Angew. Chem., Int. Ed. Engl.*, 1995, **34**, 713.
2 C. D. Gutsche and M. Iqbal, *Org. Synth.*, 1990, **68**, 234.
3 D. R. Stewart and C. D. Gutsche, *J. Am. Chem. Soc.*, 1999, **121**, 4136.
4 J. L. Atwood, M. J. Hardie, C. L. Raston and C. A. Sandoval, *Org. Lett.*, 1999, **1**, 1523.
5 J. L. Atwood, L. J. Barbour, C. L. Raston and C. A. Sandoval, *Chem. Eur. J.*, 1999, **5**, 990.
6 B. Souley, Z. Asfari and J. Vicens, *Polish. J. Chem.*, 1992, **66**, 959.
7 P. J. Nichols, C. L. Raston, C. A. Sandoval and D. J. Young, *Chem. Commun.*, 1997, 1839.
8 D. R. Stewart and C. D. Gutsche, *OPPI BRIEFS*, 1993, **25**, 137.
9 (*a*) Z. Asfari and J. Vicens, *Makromol Chem. Rapid Commun.*, 1989, **10**, 181; (*b*) Y. Nakamoto and S. Ishida, *Makromol Chem. Rapid Commun.*, 1982, **3**, 705.
10 I. E. Lubitov, E. A. Shokova and V. V. Kovalev, *Synlett*, 1993, 647.
11 J. L. Atwood, F. Hamada, K. D. Robinson, G. W Orr and R. L. Vincent, *Nature (London)*, 1991, **349**, 683.
12 A. Drljaca, M. J. Hardie and C. L. Raston, *J. Chem. Soc., Dalton Trans.*, 1999, 3639.
13 K. N. Rose, L. J. Barbour, G. W. Orr and J. L. Atwood, *Chem. Commun.*, 1998, 407.
14 L. J. Barbour, G. W. Orr and J. L. Atwood, *J. Chem. Soc., Chem. Commun.*, 1997, 1439.
15 G. Rothenberg, A. P. Downie, C. L. Raston and J. L. Scott, *J. Am. Chem. Soc.*, 2001, **123**, 8701.
16 B. A. Roberts, G. W. V. Cave, C. L. Raston and J. L. Scott, *Green Chem.*, in press.

CHEMCOMM Communication
www.rsc.org/chemcomm

An extended chain structure formed by covalently linking polyoxovanadate cages with tetrahedral six rings

Xiqu Wang, Lumei Liu, Ge Zhang and Allan J. Jacobson*

Department of Chemistry and Materials Research Science and Engineering Center, University of Houston, Houston, TX 77204-5641, USA. E-mail: ajjacob@uh.edu

Received (in Cambridge, UK) 13th September 2001, Accepted 24th October 2001
First published as an Advance Article on the web 15th November 2001

The compound $Cs_{10.5}[(V_{16}O_{40})(Si_{4.5}V_{1.5}O_{10})]\cdot 3.5H_2O$ is the first example of an extended structure in which a polyoxometallate anion is linked by an extended tetrahedral unit.

A promising approach to the synthesis of new microporous compounds is to connect nanoscale 'cores' with extended linking groups *via* covalent bonds. Yaghi and coworkers have used this concept in the synthesis of a number of microporous phases in which metal–oxo cores have been connected with multifunctional organic linking groups. The compound $(benzenedicaboxylate)_3Zn_4O$ is a recent example.[1] We have explored a similar approach using preformed vanadium borophosphate anions linked by metal cations into three-dimensional structures.[2] Others have synthesized compounds where polyoxovanadate ions are linked in a similar way.[3–5] A combination of both approaches in which polyoxoanion clusters are *covalently* linked to form stable microporous structures would be of special interest since polyoxovanadates are known to adopt a wide variety of structures with shapes ranging from cages to bowls, baskets, and belts.[6–8] A great diversity of framework topologies is therefore possible. Precedents for this strategy are found in the known compounds based on $Mo_4O_4^{4+}$ and $V_5O_9^{2+}$ 'cores' linked by single phosphate anions[9,10] and in the related structures of the minerals pharmacosiderite[11] and phosphovanadylite.[12] Here, we report the first example (to our knowledge) of an extended structure in which a polyoxovanadate ion is linked covalently by an extended tetrahedral linking unit. We note that chains of oxobridged cluster units have been previously reported.[13,14] The compound $Cs_{10.5}[(V_{16}O_{40})(Si_{4.5}V_{1.5}O_{10})]\cdot 3.5H_2O$ **1** contains a linear chain of $V_{16}O_{40}^{16-}$ anion shells linked by $(Si_{4.5}V_{1.5}O_{10})^{5.5+}$ six-rings and represents a first step towards the synthesis of three-dimensional expanded structures based on polyoxoanions.

In a typical synthesis of compound **1**, a mixture was prepared by mixing 0.14 g fumed silica, 0.26 g $VOSO_4\cdot 3H_2O$ and 1 ml H_2O. The mixture was then sealed together with 0.5 ml CsOH 50 wt% aqueous solution in a flexible Teflon bag in air. The bag was subsequently sealed in a steel reaction vessel filled with water to about 60% volume, and heated at 240 °C for 3 days. After cooling to room temperature over 3 h, the products were filtered off, washed with water, and dried in air. Dark-brown plate-like crystals of **1** were recovered as a minor phase together with blue crystals of $Cs_2(VSi_4O_{11})\cdot 3H_2O$ (VSH-2),[15] and were characterized with electron microprobe analysis, IR spectra† and single crystal X-ray diffraction.‡

In the crystal structure of **1**, two eight-membered rings of VO_5 tetragonal pyramids that share basal edges are fused together perpendicularly to form a cage. Two opposite windows of the cage are each capped by an additional VO_5 pyramid forming a spherical shell of composition $[V_{16}O_{40}]$ (Fig. 1).

The shell can be considered as a derivative of the α-Keggin cluster shell $[V_{12}O_{36}]$. The six square windows of the α-Keggin shell can be capped by V=O groups to form a $[V_{18}O_{42}]$ shell.[16] Substitution of two VO_5 pyramids of the $[V_{18}O_{42}]$ shell by Si_2O_7 dimers leads to the $[V_{16}Si_4O_{46}]$ unit of **1**. The spherical

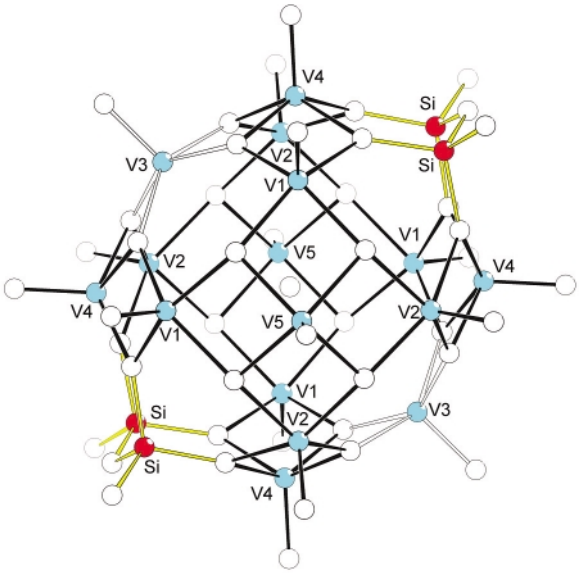

Fig. 1 The spherical shell $[V_{16}Si_4O_{46}]$ in **1**. Empty circles are oxygen atoms. The two eight-rings of square pyramids (vertical and horizontal) are plotted with black solid bonds.

shell $[V_{16}Si_4O_{46}]$ in **1** has the symmetry 2/*m* and has a water molecule located at the shell center. The shortest distances from the water oxygen to the shell oxygen and vanadium atoms are 3.52 and 3.57 Å, respectively. Neighboring $[V_{16}Si_4O_{46}]$ shells are linked together by $(V_{1.5}Si_{0.5})O_4$ tetrahedra to form infinite chains running along [001]. The $(V_{1.5}Si_{0.5})O_4$ tetrahedra share corners with the SiO_4 tetrahedra of the shells to form a six-membered ring that has the symmetry 2/*m* (Fig. 2). Alternatively the chain may be described as made up of $[V_{16}O_{40}]$ cluster anions that are linked by single six-rings of composition $[Si_{4.5}V_{1.5}O_{10}]$. Efforts to solve the V,Si cation disorder in the $(V_{1.5}Si_{0.5})O_4$ tetrahedra by refinements in lower symmetry space groups were unsuccessful. Caesium cations and water molecules occupy the space between the chains.

The SiO_4 tetrahedron in **1** has regular Si–O bond lengths 1.604–1.630 Å and O–Si–O angles 105.8–112.3°. The $(V_{1.5}Si_{0.5})O_4$ tetrahedron has an average V–O bond length of 1.69 Å and a bond valence sum (bvs) of 5.45 v.u. calculated using bond valence parameters for V^{5+}–O bonds.[17] The high bvs value is a result of the partial substitution of Si^{4+} for V^{5+}. The chemical composition was confirmed by electron microprobe analysis and is consistent with the occupancies refined

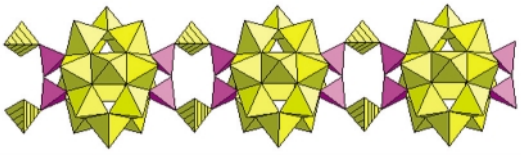

Fig. 2 The one-dimensional chain in **1**; $(V_{1.5}Si_{0.5})O_4$ tetrahedra are hatched.

 DOI: 10.1039/b108303a

from the X-ray data. The VO_5 pyramids have apical V=O bond lengths 1.602–1.633 Å and basal V–O bond lengths 1.908–2.017 Å. Bond valence sums calculated for the V atoms of the pyramids are in the range 4.03–4.20 v.u., in agreement with their V^{4+} characters.

The $[V_{16}Si_4O_{46}]$ unit of **1** has four silicate tetrahedral corners available for further covalent bonding, and therefore, can readily be linked into a chain. In contrast, in the related Keggin cluster derivatives $[As^{III}_{2n}V^{IV}_{18-n}O_{42}]^{4-}$, n = 3, 4 where n VO_5 pyramids of a $[V_{18}O_{42}]$ shell are replaced by As_2O_5 trigonal pyramid dimers, the clusters cannot link because of the presence of the electron lone pairs on As(III).[18,19] The tetrahedral configuration of the four As_2O_5 groups in $[As^{III}_8V^{IV}_{18}O_{42}]^{4-}$, however, points to possibilities for similar substitution by Si_2O_7 groups to form, for example, clusters of composition $[Si_8V_{14}O_{50}]$. Such clusters could favor formation of three-dimensional framework structures in which each cluster functions as a super-tetrahedron.

In summary, we have synthesized hydrothermally a novel one-dimensional silicovanadate that demonstrates the possibility of decorating cage-like polyvanadate clusters with silicate tetrahedra and linking them covalently into extended structures. This example suggests a synthetic route to novel microporous materials by using polymetalate nanoclusters as building units.

We thank the National Science Foundation (DMR9805881), the R. A. Welch Foundation for financial support. This work made use of MRSEC/TCSUH Shared Experimental Facilities supported by the National Science Foundation under Award Number DMR-9632667 and the Texas Center for Superconductivity at the University of Houston.

Notes and references

† Electron mocroprobe analysis was carried out with a JEOL 8600 electron microprobe operating at 15 keV with a 10 μm beam diameter and a beam current of 30 nA. Observed atomic ratios (based on V = 17.5): Cs : Si : V = 10.20 : 4.52 : 17.5. Infrared data (cm^{-1}): 629(w), 702(s), 945(s), 980(vs), 1020(s), 1633(m), 3462(m).

‡ *Crystal data* for **1**: M = 3276.4, orthorhomic, space group *Pnnm*, a = 19.351(2), b = 12.803(1), c = 13.189(1) Å. Dark-brown plate, crystal size 0.11 × 0.07 × 0.02 mm. Mo-Kα radiation (λ = 0.71073 Å), μ = 8.32 mm^{-1}, $2\theta_{max}$ = 57°, $R(F)$ = 0.055/0.143 for 1911/3964 observed ($I > 2\sigma(I)$)/all unique reflections and 269 variables.

Intensities were measured on a SMART platform diffractometer equipped with a 1K CCD area detector using graphite-monochromatized Mo-Kα radiation at 20 °C. Absorption correction was made using the program SADABS. The structure was solved with direct methods and refined using SHELXTL.[20–22]

CCDC reference number 171147.

See http://www.rsc.org/suppdata/cc/b1/b108303a/ for crystallographic data in CIF or other electronic format.

1 H. Li, M. Eddaoudi, M. O'Keeffe and O. M. Yaghi, *Nature*, 1999, **402**, 276.
2 J. Do, R. P. Bontchev and A. J. Jacobson, *Inorg. Chem.*, 2000, **39**, 4305.
3 M. I. Khan, E. Yohannes and D. Powell, *Chem. Commun.*, 1999, 23.
4 M. I. Khan, E. Yohannes and R. J. Doedens, *Angew. Chem., Int., Ed.*, 1999, **38**, 1292.
5 M. I. Khan, *J. Solid State Chem.*, 2000, **152**, 105.
6 M. T. Pope and A. Müller, *Angew. Chem., Int. Ed. Engl.*, 1991, **30**, 34.
7 A. Müller, F. Peters, M. T. Pope and D. Gatteschi, *Chem. Rev.*, 1998, **98**, 239.
8 W. G. Klemperer, T. A. Marquart and O. M. Yaghi, *Angew. Chem., Int. Ed. Engl.*, 1992, **31**, 49.
9 R. C. Haushalter, K. G. Strohmaier and F. W. Lai, *Science*, 1989, **246**, 1289.
10 M. Khan, L. M. Meyer, M. Linda, R. C. Haushalter, A. L. Schweitzer, J. Zubieta and J. L. Dye, *Chem. Mater.*, 1996, **8**, 43.
11 E. A. Behrens, D. M. Poojary and A. Clearfield, *Chem. Mater.*, 1996, **8**, 1236.
12 M. D. Medrano, H. T. Evans Jr., H.-R. Wenk and D. Z. Piper, *Am. Mineral.*, 1998, **83**, 889.
13 A. Müller, M. Koop, P. Schiffels and H. Bögge, *Chem. Commun.*, 1997, 1715.
14 B. Yan, Y. Xu, X. Bu, N. Goh, L. Chia and G. Stucky, *J. Chem. Soc., Dalton Trans.*, 2001, 2009.
15 X. Wang, L. Liu and A. J. Jacobson, *Angew. Chem., Int., Ed.*, 2001, **40**, 2174.
16 A. Müller, M. Penk, R. Rohlfing, E. Krickemeyer and J. Döring, *Angew. Chem., Int. Ed. Engl.*, 1990, **29**, 926.
17 N. E. Brese and M. O'Keeffe, *Acta Crystallogr., Sect. B*, 1991, **47**, 192.
18 G. Huan, M. A. Greaney and A. J. Jacobson, *Chem. Commun.*, 1991, 260.
19 A. Müller and J. Döring, *Z. Anorg. Allg. Chem.*, 1991, **595**, 251.
20 SAINT, Program for Data Extraction and Reduction, Siemens Analytical X-ray Instruments Inc., Madison, WI, 1996.
21 G. M. Sheldrick, SADABS, Program for Siemens Area Detector Absorption Corrections, University of Göttingen, Germany, 1997.
22 G. M. Sheldrick, SHELXTL, Program for Refinement of Crystal Structures, Siemens Analytical X-ray Instruments Inc., Madison, WI, 1994.

CHEMCOMM Communication
www.rsc.org/chemcomm

Protein–calixarene interactions: complexation of Bovine Serum Albumin by sulfonatocalix[*n*]arenes

Leila Memmi,[a] Adina Lazar,[a] Arnaud Brioude,[b] Vincent Ball[c] and Anthony W. Coleman*[a]

[a] *Institut de Biologie et Chimie des Protéines, CNRS-UCBL1, UMR 5086, 7 passage du Vercors, Lyon cedex 07, F69367, France. E-mail: aw.coleman@ibcp.fr*
[b] *Dept. Physique de Materiaux, CNRS6UCBL1, UMR 5586, 43 bvd 11 Nov. 1918, Villeurbanne, F69622, France*
[c] *Institut Charles Sadron, Unité propre 22 CNRS, 6 rue Boussingault, 67083 Strasbourg Cedex, France. E-mail: ball@ics.u-strasbg.fr*

Received (in Columbia, MO, USA) 14th August 2001, Accepted 2nd October 2001
First published as an Advance Article on the web 15th November 2001

The complexation of Bovine Serum Albumin with sulfonatocalix[*n*]arenes has been demonstrated by means of electrospray mass spectrometry, dynamic light scattering and atomic force microscopy; with sulfonatocalix[4]arene one strong and two weaker binding sites are detected; the effects on the structure of thin films formed by surface deposition of BSA show that the sulfonatocalix[*n*]arenes act to reticulate the films and produce essentially planar systems.

During the last few years there has been a rising interest in the application of *p*-sulfonatocalix[*n*]arenes as bioactive molecules, reports on the action of these molecules include chloride ion-channel blocking,[1] anti-thrombotic[2] and anti-viral effects,[3] the lack of cell cytotoxicity[4] and the inhibition of enzymatic activity of lysyl-oxidase.[5] These effects have been measured *in vitro* or on the pure proteins themselves. However in order to cross over to *in vivo* activity one interesting experiment remains; do these molecules interact with the most common of the physiological proteins, the Serum Albumins? The Serum Albumins are a class of globular circulating proteins with a molecular mass of 67 kDa and molecular size of $4 \times 4 \times 14$ nm.[6] A major role of these proteins is their adhesion at surfaces forming anchors for subsequent formation of protein films. In addition it has been demonstrated that the Serum Albumins possess a wide number of different binding sites for cations and anions. In the case of anion binding three strong binding sites for fatty acids are located at Arg117, Lys351 and Lys475,[7] three weaker anion binding sites have also been identified, these may include the salicylate binding sites, Lys199 and Arg 222.[8] We have previously studied the formation of films at surfaces by the Serum Albumins and have demonstrated that molecular recognition of cations plays a determinant role in the structuring of such films.[9] In this communication we report on the complexation of Bovine Serum Albumin by the sulfonatocalix[*n*]-arenes.

Fig. 1 shows the mass spectrum† of BSA in the presence of sulfonatocalix[4]arene **1** at a molar ratio of 1:4. The observed molecular mass of BSA at 66.5 kDa is in agreement with literature.[6] Additional peaks showing specific complexation[10] and corresponding to the 1:1 (67.2 kDa), 1:2 (68.1 kDa) complexes and a very weak peak due to a 1:3 (68.8 kDa) complex are observed, the intensity of the 1:1 being the greatest. For **2** (not shown) with BSA only a weak signal for the 1:1 complex is observed and for **3** no complexation is observed by ES–MS. The steric hindrance for **2** and **3** reduces their access to the anion binding sites and inhibits complexation, in contrast to **1** for which one strong binding site is sterically available.

Surface plasmon resonance studies show that the complexation of BSA with **2** has no effect on the adhesion properties of the protein (data not shown).‡

Sulfonatocalixarenes **1**, **2** and **3** in aqueous solution cause precipitation of BSA at 2.36 mM concentration with molar rations above 1:6, 1:4 and 1:3 respectively, in the presence of a Tris buffer at 10 mM, pH 7.4 and 150 mM NaCl such precipitation is not observed. Indeed dialysis§ showed complexation of 36 molecules of **2** (5.0 mL at 9.1×10^{-4} mol L^{-1}) to BSA (1.0 mL at 2.9×10^{-5} mol^{-1}, and hence **2**/BSA = 157). This higher number of molecules of **2** bound to BSA in comparison with the distribution found by ES–MS shows either the occurrence of additional non-specific complexation which cannot be detected by mass spectrometry or an effect due to the variation in ionic strength. Microcalorimetry§ titration of BSA with **2** shows an exothermic interaction with a standard enthalpy of interaction equal to (-8600 ± 200) kJ mol^{-1} at 304 K in the presence of 10 mM Tris and NaCl 150 mM at pH 7.4 indicating an average enthalpy of -239 kJ mol^{-1} per bound **2**. The measurement of the titration curve of BSA by **2** is in progress.

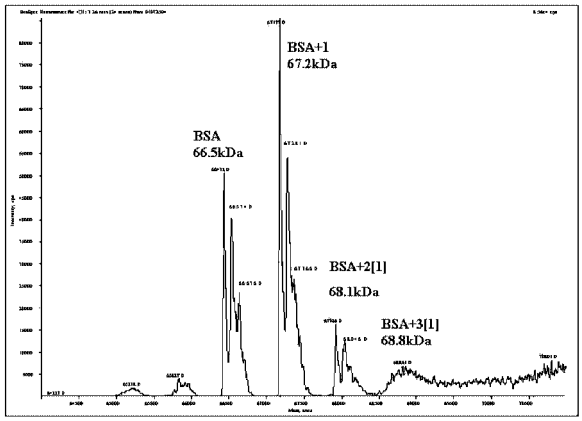

Fig. 1 ES–MS spectrum of the BSA–**1** complexes at a molar ratio of 1:4.

The results of studies using photon correlation spectroscopy¶ are given in Fig. 2(a) and (b).

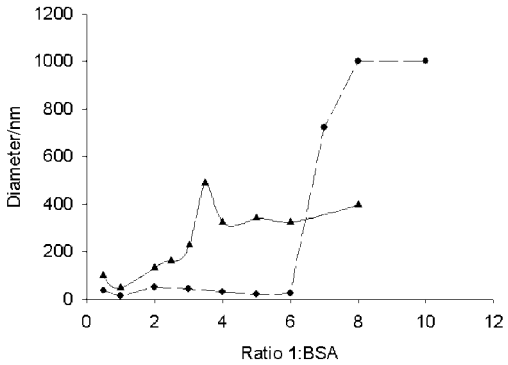

Fig. 2 PCS titration curves for BSA:**1**, (a) in buffer (●) and (b) in the absence of buffer (▲).

 DOI: 10.1039/b109190p

It appears clearly that the average size reaches a maximum at a **2**/BSA ratio of about 3 in the presence of water and that the Tris–NaCl buffer delays the occurrence of strong aggregation. However, at high **2**/BSA ratios in the presence of tris–NaCl, a large increase in size is also observed in possible correlation with the high number of bound **2** and the high observed exothermicity observed under these conditions. Hence the Cl^- counter ions delay the complexation. In pure water a specific binding of three calixarenes per BSA is hence detected both by ESMS and PCS, however higher **2**/BSA ratios also induce non-specific binding and finally protein precipitation. This suggested that mixtures of **2** and BSA dissolved in water should be contacted with mica surfaces after drying of the solutions. The effect of **2** on the structure of films prepared by deposition of a 1 : 1 solution on mica were studied by non-contact mode AFM.‖ The images for BSA alone and in the presence of **2** are shown in Fig. 3(a) and (b), respectively. For BSA alone a highly irregular cracked surface with large linear structures is observed with an rms roughness of 1236 nm. In the presence of **2** a planar unfractured film with rms roughness of 2.8 mn is observed.

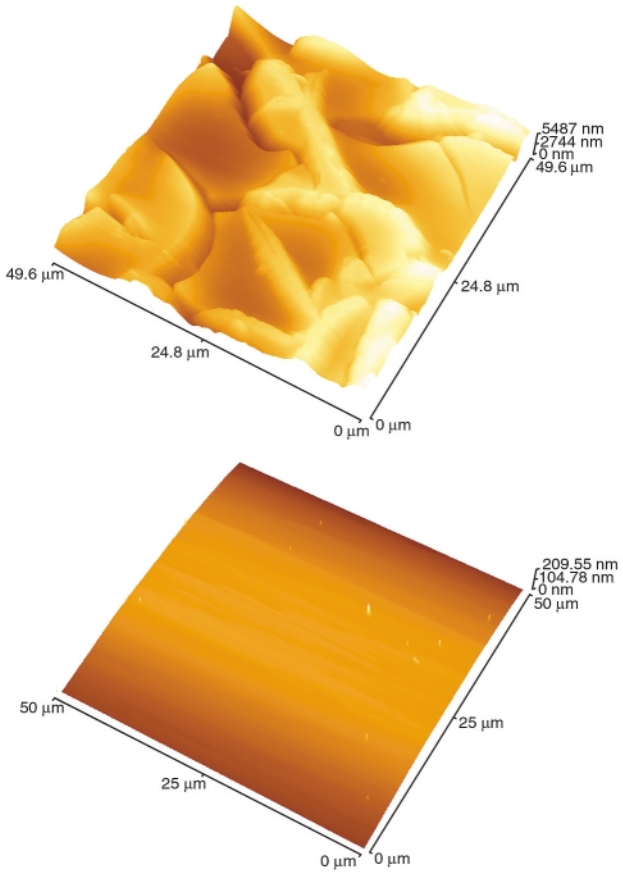

Fig. 3 (a) AFM image of a film of BSA at 50 µm scan range and (b) AFM image of a BSA–sulfonatocalix[4]arene film at 50 µm scan range.

Optical measurements have shown that the films are typically 4–6 µm in thickness.

From the above it has been shown that BSA complexes with sulfonatocalix[*n*]arenes; this involving multiple binding for sulfonatocalix[4]arene, complexation of which leads to aggregation of the protein and in the case of film formation to stabilisation of the film. We plan also to study the structure of films like those shown in Fig. 3 by means of small angle X-ray scattering. Indeed, it cannot be totally excluded that the sulfonatocalix[*n*]arenes induce some crystallisation of the proteins since high concentrations of sodium sulfate are used to crystallise a number of proteins with acidic isoelectric points, such as albumins.[11]

We thank the Fondation pour la Recherche Medicale for support for the AFM.

Notes and references

† Electrospray mass spectrometry was carried out on a Sciex API 165 spectrometer, the solvent was H_2O–MeOH–HCO_2H (50 : 50 : 0.1), with a BSA concentration of 10 pmol μl^{-1}. The spectra were deconvoluted to obtain the molecular masses.

‡ Surface plasmon resonance was carried on a Texas Instruments SPREETA 256 channel system at 20 °C using a flow cell.

§ Non-contact mode imaging was performed using a Themomicroscopes Explorer system; using a 11 µ linearised scanner, Si cantilevers with resonant frequencies of 159 kHz were used, the scan rate was 1.2 Hz.

¶ Photon correlation spectroscopy was carried out on a Malvern 4700C spectrometer equipped with a Siemens 40mW laser at 633 nm, values were measured at 90 °C in 10 mm cells using a thermostated bath at 25 °C.

‖ Equilibrium dialysis experiments were performed at 298 K with Spectra R Cellulose Ester membranes (cut off: 10000 Da) for a duration of 45 h. Unbound **2** was quantified by UV spectroscopy at λ = 300 nm.

The microcalorimetry experiments (Microcal Omega MC-2, Microcal) were performed in presence of a huge excess of **2** (3.3 mM) in the cell so allowing the assumption that all the added protein is bound to **2**. The small dilution heat of BSA (-20 kJ mol^{-1}) is taken into account in the quoted reaction enthalpy.

1 A. K. Singh, R. K. Juneja, J. L. Atwood and R. J. Bridges, *Biophys. J.*, 1993, **64**, 17; J. L. Atwood, R. J. Bridges, R. K. Juneja and A. K. Singh, *US Pat.*, 5 489 612, 1996.
2 K. M. Hwang, Y. M. Qi, S. Y. Liu, T. C. Lee, W. Choy and J. Chen, *US Pat.*, 5 409 959. 1995.
3 K. M. Hwang, Y. M. Qi, S. Y. Liu, T. C. Lee, W. Choy and J. Chen, *US Pat.*, 5 196 452, 1991.
4 F. Perret, P. Shahgaldian, M. Mazorana and A. W. Coleman, *Abstracts, IISC-10*, Fukuoka, Japan, July 2000.
5 D. J. S. Hulmes, E. Aubert-Foucher and A. W. Coleman, *Fr. Pat.*, FR 98.10074, 1998.
6 T. Peters, Jr., *All about Albumin*, Academic Press, San Diego, CA, 1996.
7 G. V. Richieri, A. Anel and A. M. Kleinfeld, *Biochemistry*, 1993, **32**, 7574.
8 G. Sudlow, D. J. Birkett and D. N. Wade, *Mol. Pharmacol.*, 1976, **12**, 1052.
9 C. C. Annarelli, L. Reyes, J. Fornazero, J. Bert, R. Cohen and A. W. Coleman, *Cryst. Eng*, 2000, **3**, 173.
10 J. A. Loo, *Mass Spectrom. Rev.*, 1997, **16**, 1.
11 M. G. Cacace, E. M. Landau and J. J. Ramsden, *Q. Rev. Biophys.*, 1997, **30**, 241.

CHEMCOMM Communication
www.rsc.org/chemcomm

Formation of a novel porphyrin–gold nanoparticle network film induced by IR light irradiation

Mami Yamada, Akiyoshi Kuzume, Masato Kurihara, Kenya Kubo and Hiroshi Nishihara*

Department of Chemistry, School of Science, The University of Tokyo, Tokyo 113-0033, Japan. E-mail: nisihara@chem.s.u-tokyo.ac.jp

Received (in Cambridge, UK) 24th July 2001, Accepted 30th October 2001
First published as an Advance Article on the web 15th November 2001

IR light irradiation of a mixed toluene solution of ammonium salt-stabilized gold nanoparticles with 3.8 ± 0.8 nm core diameter and a porphyrin thioacetate derivative affords a thin photoactive film of the cluster–porphyrin network.

Many attempts to construct 2D/3D structures of nanometer-scale metal particles[1] have been made in order to attain more advanced properties brought about by collective interaction among the assembled metal particles for use in electronic and photochemical devices.[2] Current research is moving into a new stage of functionalization by introducing redox and photoactive species into metal nanoparticle arrays so that the specific properties of metal nanoparticles associated with the electronic state of surrounding functional molecules are changeable upon an applied potential[3] or light.[4] From this viewpoint, we previously reported on an electrochemical procedure effective in fabricating redox-active gold[1e,5] and palladium[6] nanoparticle films.

In this report, we present a new approach by which a photofunctional nanoparticle film is constructed. The system consists of a combination of an octylammonium bromide-covered gold nanoparticle (**1**) and a new porphyrin derivative, mesotetra(5-thioacetylpentyl)porphyrin, with four alkyl chains terminated with a thioacetate group (**2**) (Scheme 1). It is expected that heat activation can produce aggregation of **1** bridged by **2** based on the fact that the adsorption force of the ammonium salt on the gold nanoparticle surface is weaker than that of thiolate. Heating a toluene solution of the mixture caused substantial coagulation, and resulted in precipitation at the bottom of the vessel. In this study, we successfully introduced an extra perturbation of 'light irradiation' in addition to heating, in order to control the cohesion process of the nanoparticles to form a film on a specific part of the substrate. The film formation process, along with the morphological and photochemical properties of the constructed film, is reported.

A toluene solution of **1** was prepared by use of the single-phase method employed in our previous report.[6] In brief, $AuCl_3$ (29 mg, 0.097 mmol) dissolved in a micelle solution of tetraoctylammonium bromide (0.53 g, 0.97 mmol) in degassed toluene (90 cm^3) was reduced by 1.0 mol dm^{-3} lithium triethylborohydride (0.73 mmol) in THF (0.73 cm^3), and stirred for 2 h. The mixture was diluted with 150 cm^3 toluene and then dried with a requisite amount of Na_2SO_4 to give a dark red solution of **1**, which was used without isolation, in order to avoid irreversible aggregation, for further experiments. The core diameter of the particles determined by transmission electron micrograph (TEM) images was 3.8 ± 0.8 nm. The core size was sensitive to the total concentration used in the synthetic procedure; *e.g.* it was diminished to 2.9 ± 0.8 nm in a ten times more dilute solution with the same mol ratio of the starting materials. The solution was stable for a few weeks in the absence of air, water and light. The porphyrin derivative **2**[7] equipped with four adsorptive units around a rigid planar porphyrin moiety to generate a chemically tight combination with **1**, was synthesized by a nucleophilic substitution reaction between potassium thioacetate and mesotetra(5-chloropentyl)porphyrin[8] in a yield of 87%.

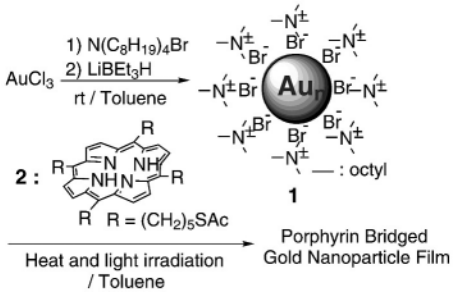

Scheme 1

Fig. 1A displays time-resolved UV–VIS spectra of a mixed solution of **1** (15 cm^3) and **2** in toluene (38 μmol dm^{-3}/5 cm^3) with incident light of D_2 + W lamps for 2 h with simultaneous heating at 50 °C.[9] The formation of a purple thin film on the inner wall of the UV quartz cell was observed, and corresponded to a gradual increase of the absorption in the range of 500–900 nm (Fig. 1A). A film is formed in a circle where the irradiated light strikes indicating that the irradiation process is essential for formation of this film. The thus prepared film exhibits a red-shifted surface plasmon band of assembled **1** at 576 nm, and a sharp Soret band due to the porphyrin moiety of **2** at 420 nm (ε_{max} = 2.4 × 10^5 dm^3 mol^{-1} cm^{-1}), confirming that the film is essentially composed of porphyrin-bridged gold nanoparticles (Fig. 1A inset). Assuming that the molar absorp-

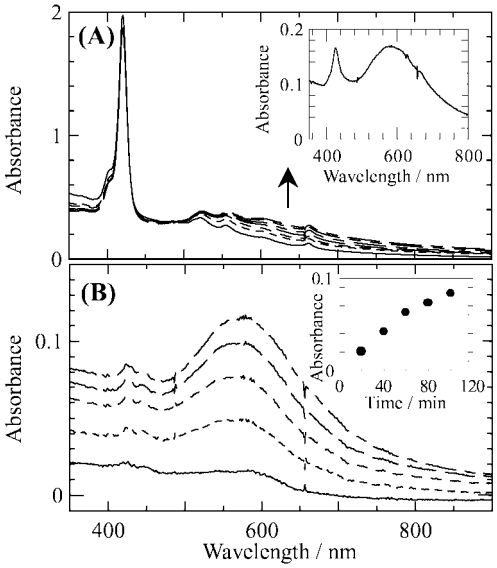

Fig. 1 (A) UV–VIS spectral changes of a mixture of **1** and **2** with incident light at every 20 min intervals for 2 h with simultaneous heating at 50 °C (from bottom to top). (Inset) The UV–VIS spectrum of the prepared film after the measurement. (B) UV–VIS spectrum of the porphyrin-bridged gold nanoparticle film on the wall of the UV cell prepared using an a Xe lamp (from bottom to top for 20, 40, 60, 80 and 100 min) with simultaneous heating at 50 °C in a mixture of **1** and **2**. (Inset) Correlation between the absorption intensity at 420 nm of the film and the irradiation time.

 DOI: 10.1039/b106682j

tion coefficient of the synthesized gold nanoparticles, ε_{max}, is *ca.* 1.2×10^7 dm^3 mol^{-1} cm^{-1},[10] the molar ratio of **1** to **2** in the film is calculated to be 1 : 19. The coverage of **1** is 1.6×10^{-11} mol cm^{-2}, corresponding to 4 layers having a total thickness of 25 nm based on an inter-particle spacing of 6.2 nm, as estimated from scanning tunneling microscopy (STM) (*vide infra*).

Fig. 1B shows the UV–VIS spectra of the films stuck on the inside of the cell prepared using an Xe lamp with different irradiation times.[11] The spectra present two bands, derived from **1** and **2**, respectively, similar to those shown in Fig. 1A, and the intensity of the absorption bands grows almost linearly with increase in irradiation time (Fig. 1B inset). The molar ratio of **1** to **2** is 1 : 7.5, indicating that the film contains fewer porphyrin moieties than that prepared using the D_2 + W lamps, as noted above, and in addition the film formation process depends on the light source.

Additional experiments were carried out for a detailed elucidation of the mechanism of film formation, and the following results were obtained: (i) the film cannot be constructed without a binding ligand of **2**, and insoluble black precipitates were collected at the bottom of the cell; (ii) there is no dependence of film formation on the wavelength of irradiated light between 360 and 840 nm; and (iii) light blocked by an infrared cut filter cannot produce a film. These results indicate that the main factor involved in film formation is 'the thermal energy of molecular vibration' in the quartz of the UV cell provided by IR light irradiation, which generates a specifically heated area of the inner wall. Consequently, the isolated and/or partially gathered nanoparticles are stuck on the irradiated spot, connected by a thioacetate group of porphyrin ligands, and the nanoparticle networks grow gradually in a three-dimensional direction.

The top of Fig. 2 shows an STM image of the porphyrin-bridged gold nanoparticle film prepared by photoirradiation with an Xe lamp for 1 h. It can be seen that many spherical particles are closely packed to cover the HOPG surface over an area *ca.* 100 nm^2. The average inter-particle distance shown in Fig. 2 (bottom) is 6.2 nm, which is reasonable compared with the expected value (6.0 nm) when **1** is bridged with **2** (the core diameter of the nanoparticle is 3.8 nm and the porphyrin linker length is 2.2 nm). This finding proves that the gold nanoparticles exist individually in the film without decomposition or flocculation by light irradiation.

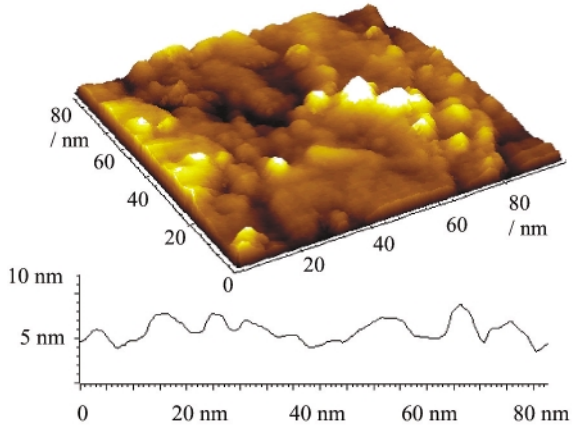

Fig. 2 STM image of a multilayer porphyrin-bridged gold nanoparticle film on HOPG (top), and a cross-sectional profile of the film (bottom). The image was taken at a current of 0.3 nA and a bias of 0.5 V with a Pt/Ir tip.

Film formation also occurs for larger gold nanoparticles with a 5.6 nm core diameter prepared by the method of Fink *et al.*[12] This demonstrates that this technique is possibly useful for film formation in a designated area. We also examined the photochemical properties of the film using an interdigitated array microelectrode,[13] which shows that the photocurrent response is switchable by light irradiation, and involves a reliable increase of conductivity in 30%. It can be deduced that the excited electrons of the porphyrin units induce faster electron transfer through the film.

In conclusion, we have synthesized a new porphyrin thioacetate derivative that can connect to ammonium salt-covered gold nanoparticles. The porphyrin-bridged gold nanoparticle films were formed on the substrate in a mixed toluene solution of the porphyrin and nanoparticles, and formation was induced by IR light irradiation.

This work was supported by Grants-in-Aid for Scientific Research (Nos. 11309003 and 12874085) from the Ministry of Culture, Education, Science, Sports, and Technology, Japan, and the Tokyo Ohka Foundation.

Notes and references

1 (*a*) S. Peschel and G. Schimid, *Angew. Chem., Int. Ed. Engl.*, 1995, **34**, 1442; (*b*) C. J. Kiely, J. Fink, M. Brust, D. Bethell and D. J. Shiffrin, *Nature*, 1998, **396**, 444; (*c*) M. Kahav, A. N. Shipway and I. Willner, *J. Chem. Soc., Perkin. Trans. 2*, 1999, 1925; (*d*) F. P. Zamborini, J. F. Hicks and R. W. Murray, *J. Am. Chem. Soc.*, 2000, **122**, 4514; (*e*) M. Yamada, T. Tadera, K. Kubo and H. Nishihara, *Langmuir*, 2001, **17**, 2363.

2 (*a*) D. L. Feldheim, K. C. Grabar, M. J. Natan and T. E. Mallouk, *J. Am. Chem. Soc.*, 1996, **118**, 7640; (*b*) J. T. Heroves, N. Ulman and S. G. Boxer, *Science*, 1997, **275**, 651.

3 D. I. Gittins, D. Bethell, D. J. Schiffrin and R. J. Nichols, *Nature*, 2000, **408**, 6808.

4 M. Lahav, T. Gabriel, A. N. Shipway and I. Willner, *J. Am. Chem. Soc.*, 1999, **121**, 258.

5 (*a*) T. Horikoshi, M. Itoh, M. Kurihara, K. Kubo and H. Nishihara, *J. Electroanal. Chem.*, 1999, **473**, 113; (*b*) M. Yamada, K. Kubo and H. Nishihara, *Chem. Lett.*, 1999, 1335.

6 M. Yamada, I. Quiros, J. Mizutani, K. Kubo and H. Nishihara, *Phys. Chem. Chem. Phys.*, 2001, **3**, 3377.

7 *Characterization data* for **2**: ^{1}H NMR ($CDCl_3$): δ −2.69 (s, 2H), 1.82 (m, 16H), 2.32 (m, 12H), 2.51 (m, 8H), 2.93 (t, *J* 4.1 Hz, 8H), 4.93 (t, *J* 7.3 Hz, 8H), 9.45 (s, 8H). UV–VIS (toluene): λ_{max} 420, 521, 555, 602, 662 nm; FAB-MS: *m*/*z* 887.31 ($C_{48}H_{62}O_4N_4S_4$ requires 887.31). Anal. Calc. for $C_{48}H_{62}O_4N_4S_4$: C, 64.97; H, 7.04; N, 6.31; S, 14.46. Found: C, 64.73; H, 7.05; N, 6.30; S, 14.36%.

8 M. Onoka, T. Shinoda, Y. Izumi and E. Nolen, *Chem. Lett.*, 1993, 117.

9 The UV–VIS absorption spectra were recorded with an Agilent 8453 UV-Visible Spectroscopy System that used two light sources (a deuterium and tungsten lamp) and a diode-array detector.

10 M. J. Hostetler, J. E. Wingate, C.-J. Zhong, J. E. Harris, R. W. Vachet, M. R. Clark, J. D. Londono, S. J. Green, J. J. Stokes, G. D. Wignall, G. L. Glish, M. D. Porter, N. D. Evans and R. W. Murray, *Langmui*, 1998, **14**, 17.

11 A sample solution in a UV quartz cell heated at 50 °C was irradiated with an intensity reduced light using an USHIO 500 W xenon short arc lamp 500D-O.

12 J. Fink, C. J. Kiely, D. Bethell and D. J. Schiffrin, *Chem. Mater.*, 1998, **10**, 922.

13 H. Nishihara, F. Dalton and R. W. Murray, *Anal. Chem*, 1991, **63**, 2955.

CHEMCOMM Communication
www.rsc.org/chemcomm

Si-BEZA – catalytic pyridinium triflate: a mild and powerful agent for the silylation of alcohols

Tomonori Misaki, Minoru Kurihara and Yoo Tanabe*

School of Science, Kwansei Gakuin University, 1-1-155 Uegahara, Nishinomiya, Hyogo 662-8501, Japan

Received (in Cambridge, UK) 16th August 2001, Accepted 9th October 2001
First published as an Advance Article on the web 5th November 2001

A highly efficient method of silylation using a novel agent, *Si*-BEZA (silylbenzamide), together with a pyridinium triflate catalyst was developed, wherein a variety of silyl groups can be introduced into sterically crowded alcohols under mild conditions.

The silylation of alcohols is indispensable for organic syntheses as the most reliable protective method.[1–3] Despite the well-established method, there still remains a strong need for improved efficiency. In view of the restrictions involved during elaborate syntheses of complex compounds, the development of mild and efficient silylation methods has become increasingly important for: (1) smooth silylation against sterically crowded and functionalized alcohols under mild conditions, (2) introduction of bulky silyl groups into unreactive alcohols, and (3) mild alternatives to some bulky-sized silyl triflates, one of the most powerful agents, because the preparation of silyl triflates sometimes requires tedious procedures.

Thus, we were prompted to explore a more efficient system. Consistent with the interest in the mild and effective silylations,[4,5] we wish to introduce here a novel, efficient, and powerful silylation agent, *Si*-BEZA [**1**, *O*-(trisubstituted silyl)benzamide] together with catalytic $PyH^{+}\cdot OTf^{-}$ (**2**, pyridinium triflate). The present method is of general interest, because it covers several types of silylations [TMS, TES, TBMDS, TIPS (triisopropylsilyl), and TBDPS (*tert*-butyldiphenylsilyl)] against sterically crowded, functionalized, aliphatic, allylic, and phenolic hydroxy groups under mild conditions.

Preparation and handling of both *Si*-BEZA (**1a–e**) and $PyH^{+}\cdot OTf^{-}$ (**2**) are quite easy (Table 1).† Compared with the

Table 1 Preparation of *Si*-BEZA[a]

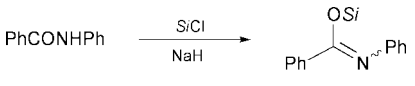

Si-BEZA (**1**)

Si-BEZA (**1**)	Yield (%)	Purification
TMS- (**1a**)	54	Distillation[b]
TES- (**1b**)	48	Distillation[b]
TBDMS- (**1c**)	83	Recrystallization[c]
TIPS- (**1d**)	74	Chromatography[d]
TBDPS- (**1e**)	74	Chromatography[d]

[a] In MeCN at 20 to 25 °C for 10 h. Molar ratio; benzamide:*Si*Cl:NaH = 1.0:1.0:1.0.[b] By Kügelrohr.[c] From hexane.[d] Use of neutral alumina.

Table 2 Silylation of alcohols using *Si*-BEZA with $PyH^{+}\cdot OTf^{-}$ catalyst[a]

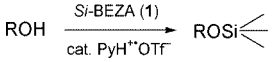

Alcohol	*Si*-BEZA (**1**)	cat. $PyH^{+}\cdot OTf^{-}$ (equiv.)	Solv.	Temp./°C	Time/min	Yield[b] (%)
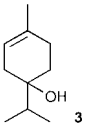	**1a** (TMS)	0.05	THF	25	5	95
	1b (TES)	0.1	THF	25	10	99
	1c (TBDMS)	0.2	THF	50	150	96
3						
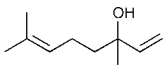	**1c**	0.2	THF	25	30	99
	1d (TIPS)	0.2	THF	50	840	97
4						
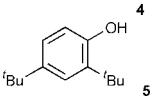	**1a**	0.05	BTF[c]	25	5	99
	1b	0.1	BTF[c]	25	10	99
	1c	0.2	BTF[c]	50	60	99
5	**1c**	0.2	THF	50	60	10 ~ 20
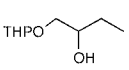	**1e** (TBDPS)	0.1	THF	25	30	98
6						
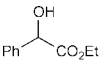	**1e**	0.1	THF	25	30	99
7						
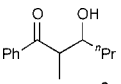	**1e**	0.1	THF	25	60	90
8						
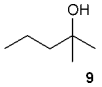	**1e**	0.2	THF	50	1200	23
	1e	0.4	THF	Reflux	2400	83[d]
9						

[a] Molar ratio; alcohol:**1** = 1.0:1.5.[b] Isolated.[c] Benzotrifluoride.[d] 5.0 equiv. of **1e** was used.

 DOI: 10.1039/b107447b

corresponding silyl triflates (especially, TBDMS, TIPS, and TBDPS), **1c–e** are considerably moisture-insensitive. Without catalyst **2**, the reaction did not proceed. Namely, *Si*-BEZA (**1**), itself, is adequately stable and **2** acts as a useful trigger. An analogous pyridinium salt, PPTS did not promote the silylation. Diphenylammonium triflate[6] is also a good catalyst, we chose **2** due to its convenience. Careful NMR experiments of **1c** revealed that the structure was not an *N*-TBDMS amide but a *O*-TBDMS imidate. The high silylation potential originated from the strong driving force of the reactive *O*-silyl imidate transformed into thermodynamically stable benzamide with the release of the silyl moiety. Table 2 lists the results of the silylation of sterically crowded (silylation-resistant) and/or functionalized alcohols.‡ Indeed, silylation-resistant terpinen-4-ol (**3**), linalool (**4**), and 2,4-di-*tert*-butylphenol (**5**) were successfully silylated in excellent yield under mild conditions. In the case of **5**, BTF solvent was more suitable than THF. Several functionalized alcohols, *i.e.*, allylic **4**, tetrahydropyranyl **6**, ester **7** and aldol **8** tolerated the present conditions. To our knowledge, this is the first example of the bulky TBDPS group being practically introduced into a tertiary alcohol **9**.[7]

The present method has another practical merit of easy work-up procedure. After the reaction was completed, solid benzanilide was easily filtered from the mixture containing the desired silyl ester and/or separated by standard column chromatography. Two parallel experiments for silylations using TIPS-BEZA (**1d**) with linalool (**4**) and *o*-cresol (**10**) demonstrate that the ability of **1d** is considered to rival or surpass the most powerful method using *Si*OTfs–2,6-lutidine[8] under standard conditions (Figs. 1 and 2). Small amounts of polymerization

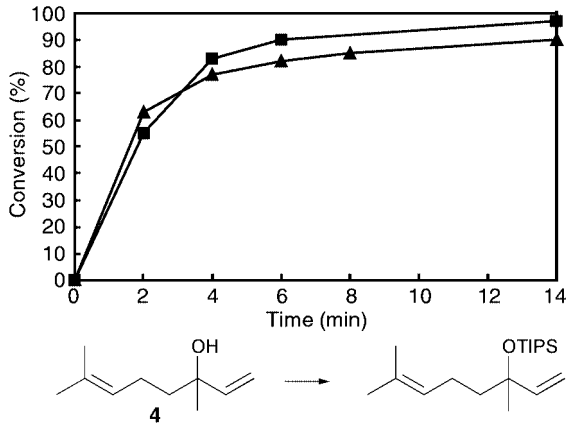

Fig. 1 Comparable experiments of triisopropylsilylation of linalool (**4**) conversion (GC%) ■: TIPS-BEZA (**1d**; 1.5 equiv.)–PyH$^+$·OTf$^-$ (**2**; 0.2 equiv.)–THF, 50 °C. ▲: TIPSOTf (1.5 equiv.)–2,6-lutidine (2.5 equiv.)–DMF, 50 °C.

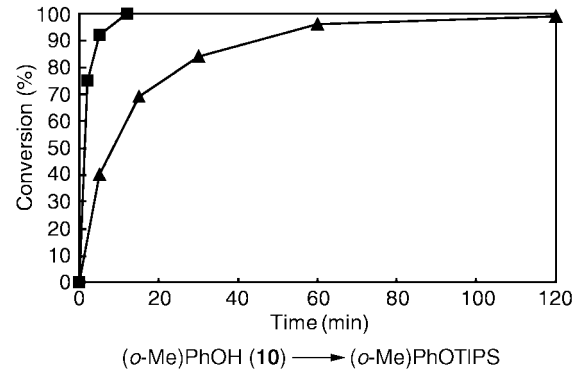

Fig. 2 Comparable experiments of triisopropylsilylation of *o*-cresol (**10**) conversion (GC%) ■: TIPS-BEZA (**1d**; 1.5 equiv.)–PyH$^+$·OTf$^-$ (**2**; 0.2 equiv.)–BTF, 25 °C. ▲: TIPSOTf (1.5 equiv.)–2,6-lutidine (2.5 equiv.)–CH_2Cl_2, 25 °C

was found to occur, when linalool (**4**) was subjected to silylation using TIPSOTf–2,6-lutidine (Fig. 1).

In conclusion, this original reagent, *Si*-BEZA (**1**), with catalytic PyH$^+$·OTf$^-$ (**2**) is structurally simple, yet, exhibits powerful and highly efficient silylations.

This research was partially supported by a Grant-in-Aid for Scientific Research on Priority Areas (A) 'Exploitation of Multi-Element Cyclic Molecules' and on Basic Areas (C) from the Ministry of Education, Culture, Sports, Science and Technology, Japan.

Notes and references

† Benzanilide was added to a stirred suspension of NaH (1.0 equiv.) in MeCN (*ca.* 0.5 M) at 0–5 °C and stirred at rt for 1 h. To the mixture was added silyl chloride (1.0 equiv.) at 0–5 °C, followed by stirring at room temp. for 2–10 h. After evaporation of MeCN, the residue was extracted with hexane, and NaCl and the small amount of benzanilide remaining were removed. Hexane was evaporated to give crude *Si*-BEZA (**1a–e**), which was purified by distillation (TMS, TES), recrystallization from hexane (TBDMS), or neutral alumina column chromatography with hexane–ether (*ca.* 20 : 1) (TIPS, TBDPS). TfOH was added to a stirred solution of pyridine (1.0 equiv.) in toluene at 0–5 °C and stirred at rt for 15 min. Toluene was evaporated to give the crude solid, which was washed with ether to give pure PyH·OTf$^-$. TMS-BEZA (**1a**); yellow oil; 190 °C (oven temp.) at 0.2 mmHg; ^{1}H NMR (300 MHz, $CDCl_3$) δ −0.26–0.69 (9H, br s), 6.62–8.16 (10H, m); ^{13}C NMR (75 MHz, $CDCl_3$) δ 0.22, 120.21—123.89 (br), 126.98—131.48 (br), 148.01. TES-BEZA (**1b**); yellow oil; 200 °C (oven temp.) at 0.2 mmHg; ^{1}H NMR (300 MHz, $CDCl_3$) δ 0.07–1.41 (15H, m), 6.50–8.12 (10H, m); ^{13}C NMR (75 MHz, $CDCl_3$) δ 5.01, 6.56, 120.17–131.78 (br), 148.00. TBDMS-BEZA (**1c**); Colorless crystals; mp 73–74 °C; ^{1}H NMR (300 MHz, −40 °C, $CDCl_3$) δ −0.29 (3.7H, s), 0.39 (2.3H, s), 0.79 (5.6H, s), 0.99 (3.4H, s), 6.68–7.99 (10H, m); (20 °C, $CDCl_3$) δ −0.52–1.57 (15H, m), 6.53–8.36 (10H, m); (140 °C, d^7-DMF) 0.16 (6H, s), 0.94 (9H, s), 6.78–6.86 (2H, m), 6.91–6.99 (1H, m), 7.15–7.24 (2H, m), 7.27–7.40 (3H, m), 7.54–7.65 (2H, m). ^{13}C NMR (100 MHz; −40 °C, $CDCl_3$) δ −4.89, −4.23, 17.87, 18.19, 25.36, 25.73, 120.88, 122.14, 122.51, 123.34, 127.62, 128.00, 128.26, 128.33, 128.89, 129.56, 129.77, 130.74, 131.51, 135.16, 146.95, 148.29, 154.28, 156.40; (20 °C, $CDCl_3$) δ −4.28, 18.26, 25.79, 120.18–123.72 (br), 126.61–130.79 (br), 147.87 (not *amide* but *imidate*). ^{29}Si NMR (80 MHz; −40 °C, TMS) δ 23.10, 23.25. ^{15}N-enriched TBDMS-BEZA (**1c**) was prepared from ^{15}N-aniline (>99% purity). ^{15}N NMR of this sample (40 MHz; −40 °C, CH_3NO_2) δ −123.43, −123.29. TIPS-BEZA (**1d**); pale yellow oil; ^{1}H NMR (300 MHz, $CDCl_3$) δ 0.84–1.61 (21H, m), 6.63–7.62 (10H, m); ^{13}C NMR (75 MHz, $CDCl_3$) δ 12.43, 18.16, 120.73–122.81 (br), 127.80, 128.90, 129.46, 129.81, 148.47. TBDPS-BEZA (**1e**); pale yellow viscous oil; ^{1}H NMR (300 MHz, $CDCl_3$) δ 0.83–1.46 (9H, m), 6.24–7.90 (20H, m); ^{13}C NMR (75 MHz, $CDCl_3$) δ 19.59, 27.30, 120.78, 122.49, 127.39, 127.86, 128.70, 129.40, 129.51, 130.01, 133.08, 135.17, 135.54, 147.60, 154.76.

‡ A typical procedure. TBDMS-BEZA (**1c**; 476 mg, 1.5 mmol) was added to a stirred solution of terpinen-4-ol (**3**; 154 mg, 1.0 mmol) and PyH·OTf$^-$ (46 mg, 0.2 mmol) in THF (2.0 cm^3) at 20–25 °C. After stirring at 50 °C for 2.5 h, the mixture was quenched with water and extracted twice with ether. The combined organic phase was washed with water, brine, dried (Na_2SO_4) and concentrated. The obtained crude oil was purified by SiO_2-column chromatography (hexane) to give 1-(*tert*-butyldimethylsiloxy)-1-isopropyl-4-methyl-3-cyclohexene (257 mg, 96%). Colorless oil. ^{1}H NMR (300 MHz, $CDCl_3$) δ 0.03 (3H, s), 0.06 (3H, s), 0.87 (9H, s), 0.88 (3H, d, *J* 6.7 Hz), 0.89 (3H, d, *J* 6.7 Hz), 1.61–2.30 (10H, m), 5.20–5.25 (1H, m). ^{13}C NMR (75 MHz, $CDCl_3$) δ −2.33, −2.04, 17.06, 17.15, 18.65, 23.07, 26.00, 28.78, 32.23, 33.79, 35.92, 75.72, 119.40, 133.49.

1 T. W. Green and P. G. M. Wuts, *Protective Groups in Organic Synthesis*, 3rd. edn., Wiley, New York, 1999, pp. 113–148.
2 P. Kocienski, *Protecting Groups*, Thieme, Stuttgart, 1994, p. 28.
3 B. A. D'Sa and J. G. Verkade, *J. Am. Chem. Soc.*, 1996, **118**, 12832.
4 Y. Tanabe, M. Murakami, K. Kitaichi and Y. Yoshida, *Tetrahedron Lett.*, 1994, **35**, 8409; Y. Tanabe, H. Okumura, A. Maeda and M. Murakami, *Tetrahedron Lett.*, 1994, **35**, 8413.
5 D. A. Johnson and L. M. Taubner, *Tetrahedron Lett.*, 1996, **37**, 605.
6 K. Wakasugi, T. Misaki, K. Yamada and Y. Tanabe, *Tetrahedron Lett.*, 2000, **41**, 5249; J. Otera, *Angew. Chem., Int. Ed.*, 2001, **40**, 2044.
7 Fluka Fine Chemical Co. Ltd., *Chemika, Silylating Agents*, 1995.
8 E. J. Corey, H. Cho, C. Rücker and D. H. Hua, *Tetrahedron Lett.*, 1981, **22**, 3455.

CHEMCOMM Communication
www.rsc.org/chemcomm

The first example of a diazaarsolyl anion: structure and coordination polymerisation of the aromatic metallacycle benzo[1,3,2]diazaarsolyl lithium·2THF

Michael A. Paver,* Jonathan S. Joy and Michael B. Hursthouse

Department of Chemistry, University of Southampton, Highfield, Southampton, UK SO17 1BJ. E-mail: M.A.Paver@soton.ac.uk

Received (in Cambridge, UK) 25th September 2001, Accepted 23rd October 2001
First published as an Advance Article on the web 15th November 2001

The first example of an aromatic diazaarsolyl anion 1 has been synthesised and structurally characterised; the X-ray crystal structure of 1 exhibits planar metallacyclic fragments which link together to generate a coordination polymer *via* bridging lithium cations.

Over the past few years the chemistry of metal–imido species and anionic ligand systems based on p block element imido frameworks have received much attention.[1,2] As part of our recent research into the reactivities of distibine-dimethylamido derivatives we reported the synthesis and structural characterisation of 1,3-[(RNLi)Sb]$_2$(μ-NR)(CH$_2$)$_3$·RNHLi, a chiral bimetallic imido-/amido-bridged cage structure of interlocking six-membered rings, incorporating the co-complexation of primary lithium amide.[3] In relation to this work we have also investigated the chemistry of (Me$_2$N)$_2$AsCH$_2$As(NMe$_2$)$_2$. In contrast to the iminophosphanes, compounds containing an As–N double bond are very rare.[4–7] The first stable compound containing an As^{III}N double bond to be structurally characterised was reported by Lappert, Hitchcock and coworkers, namely As(=NAr)(NHAr) where Ar = C$_6$H$_2$^{t}Bu$_3$-2,4,6. In this case the As–N p_π–p_π bond is stabilised by both steric bulk and electronic factors.[5] Subsequently, Roesky and coworkers reported bis[2,4,6-tris(trifluoromethyl)phenyl]iminoarsane which is only kinetically stabilised by bulky groups,[6] as is the very recently reported (2,4,6-^{t}Bu$_3$C$_6$H$_2$)N=As–N(SiMe$_3$)$_2$.[7]

Here we report the unexpected outcome of the reaction between (Me$_2$N)$_2$AsCH$_2$As(NMe$_2$)$_2$ and 1,2-H$_2$N(C$_6$H$_4$)NHLi (1 : 4 equiv.) which instead of generating the expected diarsine-based polyimido anion, yields the aromatic metallacycle, benzo[1,3,2]diazaarsolyllithium·2THF, [C$_6$H$_4$N$_2$As·Li(THF)$_2$]$_\infty$ **1** (Scheme 1).†

Clearly the reaction involves cleavage of the bridging methylene group, the by-product presumably being an, as yet unidentified, methyl arsine species. Attempts to prepare **1** by an alternative route, namely the reaction of As(NMe$_2$)$_3$ with 1,2-H$_2$N(C$_6$H$_4$)NHLi (1 : 1 equiv.), have failed indicating that the methylene bridged diarsine plays an important role with a differing pattern of reactivity to its mononuclear counterpart. Previous studies indicate that the reactivity of As(NMe$_2$)$_3$ towards primary lithium amides differs markedly from that of Sb(NMe$_2$)$_3$, requiring acid catalysis from an excess of primary amine in order to react, *e.g.*, in the synthesis of {As(N^{t}Bu)$_3$}$_2$Li$_6$.[8] However, all attempts to prepare **1** utilising various stoichiometries of lithium amide and free amine have also failed.‡

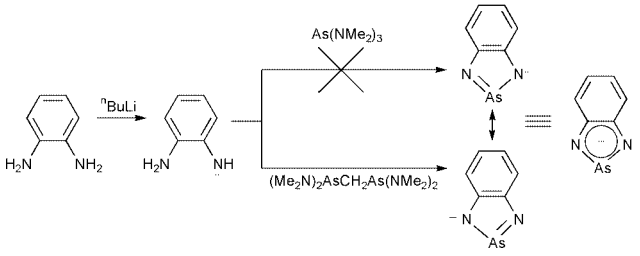

Scheme 1

The X-ray structure of **1** reveals planar anionic C$_6$H$_4$N$_2$As metallacycles that are linked together *via* bridging Li(THF)$_2^+$ units to form a two-dimensional coordination polymer (see Fig. 1). This is the first example of an aromatic diazaarsolyl anion to be structurally characterised. The neutral phosphorus analogue of **1**, 1*H*-benzo[1,3,2]diazaphosphole, has been reported, but readily oligomerises to a tetrameric form requiring Lewis acid stabilisation or thermolysis to retain the monomeric unit.[9] As a result of a direct synthesis of the (more synthetically useful) anion, we believe that the aromatic nature of **1**, leads to its inherent stability with respect to oligomerisation without the need for any steric protection.

Unlike As(=NAr)(NHAr) (Ar = C$_6$H$_2$^{t}Bu$_3$-2,4,6)[5] and (2,4,6-^{t}Bu$_3$C$_6$H$_2$)N=As–N(SiMe$_3$)$_2$[7] [As=N 1.714(7), 1.708(3); As–N 1.745(7), 1.822(2) Å, respectively] where there are clear distinctions between the arsenic–nitrogen single and double bonds (even though some conjugation is evident), in **1** the As–N bonds are virtually identical [As(1)–N(1) 1.786(3), As(1)–N(2) 1.789(3) Å]. Thus there is complete delocalisation within the N$_2$As unit, with the bond order being intermediate between single (calculated at 1.87 Å[10]) and double bond character {av. 1.71(1) Å for the previous two compounds, *cf.* 1.73 Å[11] in [(Me$_3$SiO)$_2$AsN]$_3$}. The sum of the angles about N(1) and N(2) (av. 359.7(5)°) are also consistent with the planar nature of the metallacycle, indicating a sp^2 hybridisation. Within this ring the C–N distances (av. 1.36 Å) are also consistent with comparable literature aromatic systems.[12] The angle about As [93.87(12)°] indicating predominant use of p-orbitals in bonding, is in line with those found in arsole derivatives, *e.g.*, 86.96° in η^5-(Me$_4$C$_4$As)Li·TMEDA.[13]

The coordination polymerisation of **1**, caused by N–Li–N bridging of Li(THF)$_2^+$ units with neighbouring metallacyclic anions is comparable to that seen in the anionic phosphorus cyclen complex, [(C$_8$H$_{16}$P)(Li·THF)]$_\infty$.[14] The Li–N distances

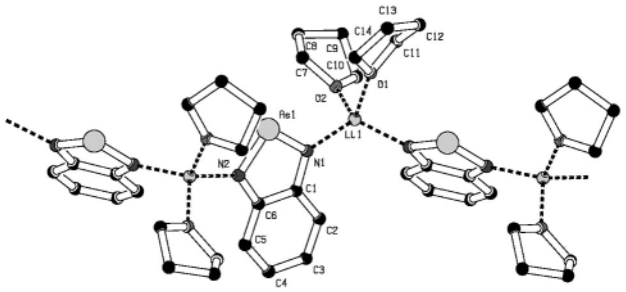

Fig. 1 Selected bond lengths (Å) and angles (°) for compound **1**. Hydrogen atoms have been omitted for clarity: As(1)–N(1) 1.786(3), As(1)–N(2) 1.789(3), C(1)–N(1) 1.364(4), C(6)–N(2) 1.363(4), Li(1)–N(1) 2.003(6), Li(1)–N(2) 2.043(6), Li(1)–O(1) 1.992(6), Li(1)–O(2) 1.974(5); N(1)–As(1)-N(2) 93.87(12), N(1)–C(1)-C(6) 115.6(3), N(2)–C(6)–C(1) 115.6(3), C(1)–N(1)–As(1) 107.4(2), C(6)–N(2)–As(1) 107.4(2), O(2)–Li(1)–O(1) 97.1(2), O(2)–Li(1)–N(1) 108.3(2), O(1)–Li(1)-N(1) 112.8(3), O(2)–Li(1)–N(2) 112.3(3), N(1)–Li(1)–N(2) 121.3(3).

 DOI: 10.1039/b108593j

[range 2.003(6)–2.043(6) Å] are within the expected values.[15] The preparation of **1** *via* such a pathway to directly generate a stable anion may allow the syntheses of heavier metal homologues, which would otherwise be unstable with respect to oligomerisation in the protonated form. Additionally, the ligand chemistry of **1** is currently being investigated with a range of metal centres.

We thank the EPSRC for a project studentship (J. S. J) and the National X-ray Crystallographic Service (M. B. H and Dr S. Coles).

Notes and references

† *Crystal data* for $C_{28}H_{40}As_2Li_2N_4O_4$ **1**: M_r = 660.36, orthorhombic space group $Pna2_1$, a = 11.830(2), b = 8.6933(17), c = 14.914(3) Å, U = 1533.8(5) Å^3, Z = 2, μ = 2.217 mm^{-1}, crystal size 0.18 × 0.16 × 0.10 mm, T = 150(2) K; refinement of 3225 unique reflections ($2\theta \leqslant 27.48°$, R_{int} = 0.0454) against 182 parameters gave R_1 = 0.0328 and wR_2 = 0.0699 [$I > 2\sigma(I)$] (R_1 = 0.0454 and wR_2 = 0.0747 for all data).

Data were collected on a Nonius KappaCCD area detector diffractometer, at the window of a Nonius FR591 rotating anode [λ (Mo-Kα) = 0.71073 Å]. Corrections were applied to account for absorption effects by means of comparing multiple and equivalent reflections. Solutions were obtained *via* direct methods and refined by full-matrix least-squares on F_o^2, with hydrogens included in idealised positions and refined using the Riding model.

CCDC reference number 173021.

See http://www.rsc.org/suppdata/cc/b1/b108593j/ for crystallographic data in CIF or other electronic format.

‡ *Synthesis* of **1**: all manipulations were undertaken under an inert nitrogen atmosphere. 1,2-Diaminobenzene (0.43 g, 4 mmol) was dissolved in dry toluene and ^{n}BuLi (4 mmol) added to give a white precipitate which was stirred, with gentle warming, for *ca*. 30 min. Subsequently $(Me_2N)_2$-$AsCH_2As(NMe_2)_2$ (0.34 g, 1 mmol) was added and the mixture stirred at 100 °C for 2 h to yield a pale green precipitate. The toluene was removed *in vacuo* and the mixture dissolved in 30 cm^3 of THF to yield a blue solution. Reduction to *ca*. 15 ml and storage at 5 °C overnight yielded a crop of colourless plates of **1** in 30% yield (relative to 1,2-diaminobenzene, 1st batch). ^{1}H NMR (300 MHz; DMSO-d_6; 25 °C) δ 7.51–6.85 (m, 4H, ArH), 3.61 (m, 8H, –CH_2CH_2O–), 1.75 (m., 8H, –CH_2CH_2O–); ^{13}C NMR (75 MHz; DMSO–d_6; 25 °C) δ 114.6–135.1 (Ar), 67.1 (–CH_2CH_2O–), 25.2 (–CH_2CH_2O–). Satisfactory analyses (C, H, N) were obtained for all samples of **1**.

1 M. A. Beswick and D. S. Wright, *Coord. Chem. Rev*., 1998, **176**, 373.
2 M. A. Paver, C. A. Russell and D. S. Wright, *Angew. Chem., Int. Ed. Engl*., 1995, **34**, 1545.
3 S. J. Coles, M. B. Hursthouse, J. S. Joy and M. A. Paver, *J. Chem. Soc., Dalton Trans*., 2000, 3239.
4 H. G. Ang and F. K. Lee, *Polyhedron*, 1989, **8**, 1461; S. K. Vasisht, M. Sood, P. K. Verma, T. Kaur and K. Usha, *Phosphorus, Sulfur, Silicon*, 1990, **47**, 349; S. K. Vasisht, T. P. Kaur, K. Usha, J. Kaushal and K. Bandhu, *Phosphorus, Sulfur, Silicon*, 1995, **107**, 189.
5 P. B. Hitchcock, M. F. Lappert, A. K. Rai and H. D. Williams, *Chem. Commun*., 1986, 1633.
6 J.-T. Ahlemann, A. Künzel, H. W. Roesky, M. Noletmeyer, L. Markovskii and H.-G. Schmidt, *Inorg. Chem*., 1996, **35**, 6644.
7 C. Kruppa, M. Nieger, B. Ross and I. Väth, *Eur. J. Inorg. Chem*., 2000, 165.
8 M. A. Beswick, S. J. Kidd, M. A. Paver, P. R. Raithby, A. Steiner and D. S. Wright, *Inorg. Chem. Commun*., 1999, **2**, 612.
9 C. Malavaud, T. M'Pondo, L. Lopez, J. Barrans and J.-P. Legros, *Can. J. Chem*., 1984, **62**, 43.
10 V. Schomaker and D. P. Stevenson, *J. Am. Chem. Soc*., 1941, **63**, 37; L. K. Krannich, U. Thewalt, W. J. Cook, S. R. Jain and H. H. Sisler, *Inorg. Chem*., 1973, **12**, 2304.
11 M. Baier, P. Bissinger and H. Schmidbaur, *Chem. Ber*., 1993, **126**, 351.
12 C. Lambert, F. Hampel and P. v. R. Schleyer, *J. Organomet. Chem*., 1993, **455**, 29; L. D. Brown, J. A. lbers and A. R. Siedle, *Inorg. Chem*., 1978, **17**, 3026.
13 S. C. Sendlinger, B. S. Haggerty, A. L. Rheingold and K. H. Theopold, *Chem. Ber*., 1991, **124**, 2453.
14 M. Lattman, M. M. Olmstead, P. P. Power, D. W. H. Rankin and H. E. Robertson, *Inorg. Chem*., 1988, **27**, 3012.
15 K. Gregory, P. v. R. Schleyer and R. Snaith, *Adv. Inorg. Chem*., 1991, **37**, 47.

CHEMCOMM Communication
www.rsc.org/chemcomm

Bis[hydrotris(pyrazol-1-yl)borato]titanium(II): a stable Tp_2M complex of singular reactivity†

Ajay Kayal, Joshi Kuncheria and Sonny C. Lee*

Department of Chemistry, Princeton University, Princeton, New Jersey 08544, USA. E-mail: sclee@princeton.edu

Received (in Purdue, IN, USA) 10th September 2001, Accepted 22nd October 2001
First published as an Advance Article on the web 15th November 2001

Tp_2Ti [Tp = hydrotris(pyrazol-1-yl)borate] is a stable hard donor complex of divalent titanium that shows controlled reaction chemistry with simple chalcogen oxidants.

The homoleptic bis-complexes of hydrotris(pyrazol-1-yl)borate ($[Tp_2M]^{0,+}$) are founding compounds in the expansive metal chemistry of polypyrazolylborate ligands.[1] The first of these simple, symmetric species date back to Trofimenko's disclosure of the ligand class,[2] and neutral Tp_2M complexes of divalent metal ions (or equivalently substituted pyrazole homologues) are now known for almost all of the 3d (V to Zn) and three 4, 5d elements (Ru, Cd, Hg), as well as for a number of alkaline earths (Be–Ba), rare earths (Sm, Eu, Yb) and metalloids (Sn, Pb).[1,3] We report here the extension of this chemical series to the uncommon, reactive divalent oxidation state of titanium.†

The reaction of $TiCl_2(TMEDA)_2$[4] with 2 equivalents of potassium hydrotris(pyrazol-1-yl)borate (KTp) in benzene immediately affords a deep red solution from which Tp_2Ti (**1**) can be isolated as a dark red, analytically pure, microcrystalline solid in excellent (>90%) yield (Scheme 1). A crystal structure analysis‡ reveals the expected bis(κ^3-Tp) structure, with approximate molecular D_{3d} symmetry and octahedral microsymmetry about the Ti(II) center; the average Ti–N bond distances§ are comparable to values previously observed for Ti(II)–N(aromatic) contacts.[5–7] Compound **1** is paramagnetic and, as a polycrystalline solid, obeys the Curie–Weiss law (30–300 K) for an $S = 1$ state ($\mu_{eff} = 2.62\ \mu_B$). Under rigorously anaerobic, aprotic conditions, the complex is soluble, stable, and well-defined in a variety of solvents. The ^{1}H NMR spectrum of **1** consists of four paramagnetically shifted signals (C_6D_6: δ −43.1 (6H), 1.2 (6H), 13.1 (2H), 16.1 (6H)), as expected for a D_{3d} symmetric structure, that can be fully assigned to corresponding hydrogens through ^{1}H{^{11}B} NOE difference spectroscopy. The intense purple–red color of the complex arises from broad charge-transfer bands in the near UV and visible regions of its electronic absorption spectrum (CH_2Cl_2: λ_{max} = 256, 390 (sh), 513, 590 (sh) nm, with ε_M = 7400, 1650, 3170, 1610 dm^3 mol^{-1} cm^{-1} respectively). Complex **1** exhibits two reversible electrochemical oxidations at −1.28 and +1.20 V *vs.* SCE (MeCN, 0.1 M (n-Bu_4N)ClO_4). Oxidation with $AgPF_6$ in CH_2Cl_2 allows chemical access to the trivalent state as crystalline, transparent yellow $[Tp_2Ti](PF_6)$ (**2**) (Scheme 1). The cyclic voltammogram of the oxidized complex

† Electronic supplementary information (ESI) available: synthetic details for compounds **1**–**5**. See http://www.rsc.org/suppdata/cc/b1/b108115b/

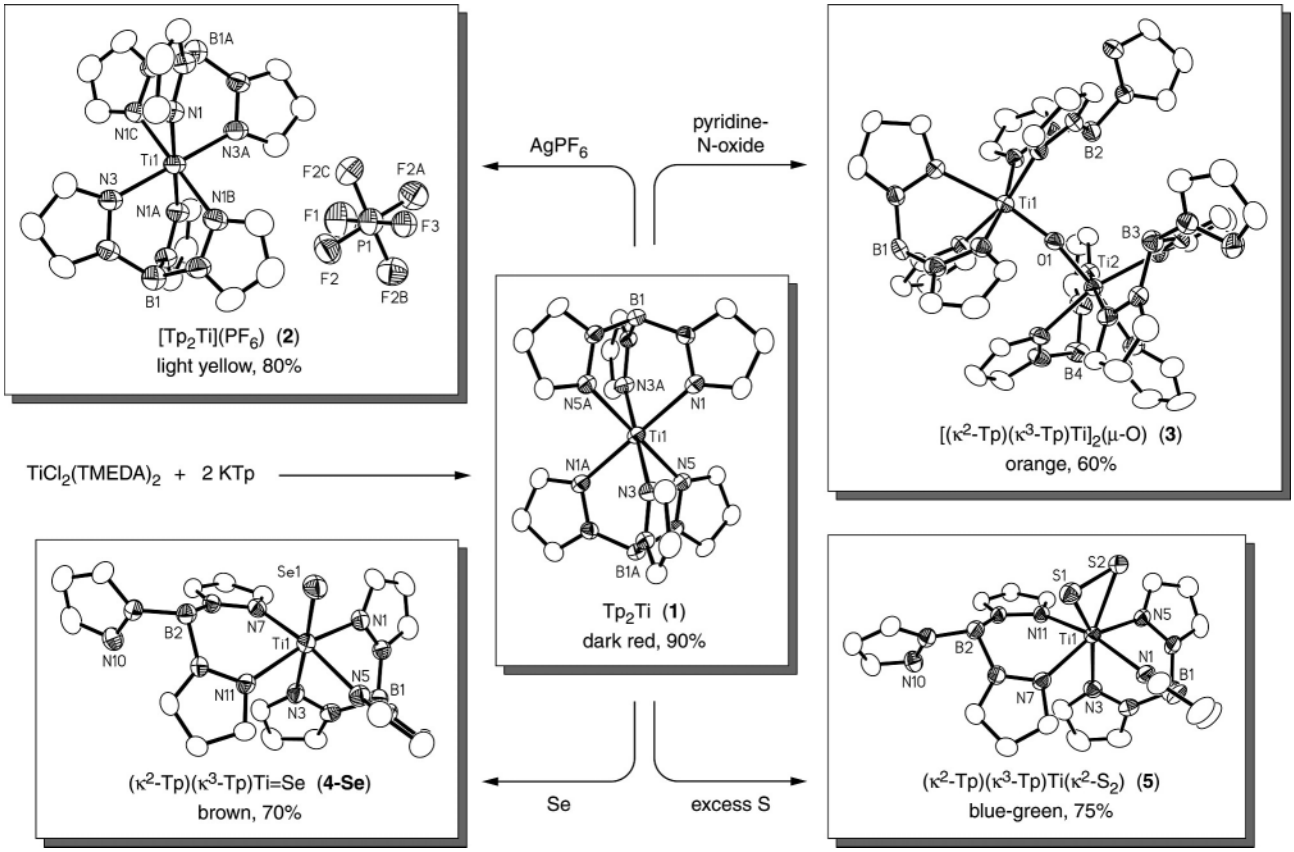

Scheme 1

 DOI: 10.1039/b108115b

shows one reversible reduction and one reversible oxidation at potentials matching those of the two oxidative couples measured for **1**; this allows definite assignment of the lower potential as the Ti(II)/Ti(III) couple. We are aware of only one other report of a reversible Ti(II)/Ti(III) couple, measured for $Ti(OAr)_2(bipy)_2$ (Ar = 2,6-diisopropylphenyl) in THF at −0.86 V *vs.* SCE.[7,8] Although a precise comparison is not possible due to the use of different electrochemical solvents, the aryloxide complex appears to have a moderately higher oxidation potential,[8] perhaps as a result of π-acidity in its bipyridyl ligands.

Stable, isolable complexes of divalent titanium typically require the presence of π-acceptors and/or soft donor ligands to support the reduced metal ion;[9] Ti(II) centers ligated solely by hard donors (as in **1**) are rare[4–7] and often undergo progressive, spontaneous decomposition in solution.[4] We ascribe the exceptional stability of complex **1**, which remains unchanged in toluene solution even after prolonged heating (90 °C, 1 week, dinitrogen atmosphere), to the effectiveness of the bis(κ^3-Tp) ligation in maintaining a coordinatively saturated metal center. This intrinsic stability of the bis-chelate structure might be expected to preclude further chemistry, and indeed, we know of no documented reactivity in transition metal Tp_2M complexes other than electron transfer.[10] Studies with simple chalcogen reagents, however, establish the Tp_2Ti environment as an effective platform for metal-centered chemistry.†

Exposure of **1** in benzene solution to atmospheric dioxygen results in an immediate color change and eventual separation of oxo-bridged Ti(III) dimer $[(\kappa^2\text{-Tp})(\kappa^3\text{-Tp})Ti]_2(\mu\text{-O})$ (**3**) as light orange crystals (Scheme 1). The same product can be obtained by treatment of **1** with 0.5 equivalents of pyridine *N*-oxide in benzene; excess pyridine *N*-oxide (to 6 equivalents) has no effect on the reaction outcome. Analogous oxidations with elemental sulfur and selenium are marked by more varied, stoichiometry-dependent behavior. Complex **1** reacts with 0.5 equivalents of yellow sulfur or gray selenium to form as yet unidentified but homologous paramagnetic species.[11] At 1 equivalent of sulfur, a rapid (minutes) reaction yields the terminal sulfido Ti(IV) monomer (κ^2-Tp)(κ^3-Tp)Ti=S (**4-S**) along with limited amounts of the disulfido Ti(IV) complex (κ^2-Tp)(κ^3-Tp)Ti(κ^2-S_2) (**5**); although the two products co-crystallize inseparably, crystal structure and NMR analyses allow unambiguous identification of the individual components. The use of excess sulfur (12 equivalents) also generates a mixture of **4-S** and **5** at first, but in this case the terminal sulfide ligand slowly (hours) transforms to disulfide, allowing isolation of pure **5** (Scheme 1). Finally, reactions of **1** with 1–20 equivalents of selenium lead exclusively to the selenium homologue of **4-S**, (κ^2-Tp)(κ^3-Tp)Ti=Se (**4-Se**) (Scheme 1). The reaction chemistry of complex **1** is well-behaved, with spectroscopically clean conversions and high isolated yields (60–80%) of pure crystalline products.

In solution, the terminal chalcogenido complexes **4-S** and **4-Se** present nearly identical $^1H\{^{11}B\}$ NMR spectra with 2 B–H and 12 sharp, well-resolved pyrazole-H resonances in a 2:2:1:1 pyrazole ratio; this signal pattern is consistent with the C_s symmetric structures found in the solid state (*vide infra*). The spectra also display weak, broad features (< 5% of the total signal intensity) that have been linked through variable-temperature EXSY experiments to intermediates in dynamic processes which exchange all pyrazole positions of the parent structure. The room-temperature NMR spectra of the other reaction products are also characteristic, but less interpretable due to line broadening from paramagnetism (Ti(III) dimer **3**) and pronounced fluxionality (disulfido complex **5**).

Despite differences in their solution NMR spectra, the solid-state structures of the chalcogen reaction products all share the same distinctive (κ^2-Tp)(κ^3-Tp)TiL architecture, where bidentate binding of one Tp chelate allows incorporation of the entering ligand within an octahedral coordination sphere. (For comparative purposes, the κ^2-S_2 fragment of seven-coordinate **5** is regarded as one ligand of a six-coordinate metal center.) The unbound pyrazole arm and the chalcogen ligand are *trans*-oriented in the (κ^2-Tp)Ti metallocycle, indicating that the change in Tp binding mode is not a simple substitution of one donor for another, but reflects a more substantive rearrangement of the coordination sphere. The *trans*-influences of bridging oxo and terminal selenido ligands give rise to long Ti–N(*trans*) bonds in complexes **3** and **4-Se**; increased Ti–N distances are also evident for the three meridional pyrazole donors coplanar with the κ^2-disulfido ligand of complex **5**, due presumably to non-orthogonal, '*trans*-like' orbital interactions as well as steric effects that exist when five ligands occupy the same coordination plane. The structural metrics of these complexes are otherwise typical for their respective donor sets.‡§

In conclusion, the venerable Tp_2M structure type offers new, extensible chemistry as a stabilizing yet reactive coordination environment for divalent titanium.

We thank Drs A. K. Verma and I. Pelczer for experimental assistance and helpful discussions, and the Arnold and Mabel Beckman Foundation (Beckman Young Investigator Award) and the NSF (CAREER CHE-9984645) for their generous support.

Notes and references

‡ *Crystal data*: CCDC reference numbers 172870–172874. See http://www.rsc.org/suppdata/cc/b1/b108115b/ for crystallograpic data in CIF or other electronic format.

§ Selected structural metrics (Å or °, averaged for equivalent sites). **1**: Ti–N 2.216(2). **2**: Ti–N 2.114(3). **3**: Ti–N(*cis*) 2.171(3), Ti–N(*trans*) 2.257(3), Ti–O 1.811(3); Ti1–O–Ti2 167.4(1). **4-Se**: Ti–N(*cis*) 2.146(4), Ti–N(*trans*) 2.278(4), Ti=Se 2.255(1). **5**: Ti–N(axial) 2.143(3), Ti–N(meridional) 2.230(3), Ti–S 2.32(2), S–S 2.011(1).

1 S. Trofimenko, *Scorpionates—The Coordination Chemistry of Polypyrazolylborate Ligands*, Imperial College Press, London, 1999; P. T. Edelmann, *Angew. Chem., Int. Ed.*, 2001, **40**, 1656.
2 S. Trofimenko, *J. Am. Chem. Soc.*, 1966, **88**, 1842.
3 T. J. Brunker, T. Hascall, A. R. Cowley, L. H. Rees and D. O'Hare, *Inorg. Chem.*, 2001, **40**, 3170.
4 J. J. H. Edema, R. Duchateau, S. Gambarotta, R. Hynes and E. Gabe, *Inorg. Chem.*, 1991, **30**, 154.
5 M. A. Araya, F. A. Cotton, J. H. Matonic and C. A. Murillo, *Inorg. Chem.*, 1995, **34**, 5424.
6 L. K. Woo, J. A. Hays, V. G. Young Jr., C. L. Day, C. Caron, F. D'Souza and K. M. Kadish, *Inorg. Chem.*, 1993, **32**, 4186.
7 L. D. Durfee, P. E. Fanwick, I. P. Rothwell, K. Folting and J. C. Huffman, *J. Am. Chem. Soc.*, 1987, **109**, 4720.
8 The Ti(II)/Ti(III) redox potential of $Ti(OAr)_2(bipy)_2$ was measured at −0.95 V *vs.* Ag/AgCl using 0.1 M (n-Bu_4N)PF_6 in THF, and referenced against the ferrocene/ferrocinium couple at +0.47 V;[7] this can be adjusted to −0.86 V *vs.* SCE, since Fc/Fc^+ = +0.56 V *vs.* SCE under the same conditions. The solvent effect can be approximated by comparing the Fc/Fc^+ couple in MeCN (+0.40 V *vs.* SCE) and THF (+0.56 V *vs.* SCE) to give an estimated Ti(II)/Ti(III) potential of *ca.* −1.0 V *vs.* SCE in MeCN. We ignore here the trivial differences in potential that arise from the use of different supporting electrolyte anions. For reference potentials, see: N. G. Connelly and W. E. Geiger, *Chem. Rev.*, 1996, **96**, 877.
9 Some examples of Ti(II) complexes with soft ligands: F. G. N. Cloke, J. R. Hanks, P. B. Hitchcock and J. F. Nixon, *Chem. Commun.*, 1999, 1731; P. B. Hitchcock, F. M. Kerton and G. A. Lawless, *J. Am. Chem. Soc.*, 1998, **120**, 10264; J. R. Hagadorn and J. Arnold, *Organometallics*, 1998, **17**, 1355; R. Duchateau, S. Gambarotta, N. Beydoun and C. Bensimon, *J. Am. Chem. Soc.*, 1991, **113**, 8986; J. A. Jenson, S. R. Wilson, A. J. Schultz and G. S. Girolami, *J. Am. Chem. Soc.*, 1987, **109**, 8094; L. B. Kool, M. D. Rausch, H. G. Alt, M. Herberhold, U. Thewalt and B. Wolf, *Angew. Chem., Int. Ed. Engl.*, 1985, **24**, 394.
10 Chemical reactivity does occur in divalent lanthanoid congeners, where large metal ion radii allow facile expansion of coordination spheres: A. C. Hillier, S. Y. Liu, A. Sella and M. R. J. Elsegood, *J. Alloys Compd.*, 2000, **303–304**, 83; J. Takats, *J. Alloys Compd.*, 1997, **249**, 52.
11 The sulfur and selenium reaction products show near identical paramagnetically shifted ^1H NMR signatures different from that of oxo-dimer **3**.

CHEMCOMM Communication
www.rsc.org/chemcomm

Hydrophobic ionic liquids incorporating *N*-alkylisoquinolinium cations and their utilization in liquid–liquid separations

Ann E. Visser, John D. Holbrey and Robin D. Rogers*

Department of Chemistry and Center for Green Manufacturing, The University of Alabama, Tuscaloosa, AL 35487, USA. E-mail: rdrogers@bama.ua.edu; Fax: +1 (205) 348 0823; Tel: +1 (205) 348 4323

Received (in Columbia, USA) 4th September 2001, Accepted 8th October 2001
First published as an Advance Article on the web 6th November 2001

The first examples of Room Temperature Ionic Liquids (RTIL) containing fused polycyclic *N*-alkylisoquinolinium cations ([C$_n$isoq]$^+$) in combination with the bis(perfluoroethylsulfonyl)imide anion ([BETI]$^-$) have been synthesized, characterized, and utilized in liquid–liquid partitioning from water; these salts have unexpectedly low melting points and give high distribution ratios for aromatic solutes, especially chlorobenzenes, between the RTIL and water.

The growth in recent attention given to Room Temperature Ionic Liquids (RTIL) stems from the unique properties inherent to this new class of solvents and their potential to replace volatile organic solvents. RTIL may exhibit miniscule vapor pressure, high thermal stability, unique miscibilities,[1] and a wide temperature range for the liquid phase. In addition, the composite RTIL cations and anions significantly affect the IL miscibility with other solvents (*e.g.*, water), and also the solubility of these solvents in the IL.[2] For aqueous–organic separations, relatively hydrophobic RTIL can be considered as replacements for traditional VOCs while maintaining the basis for biphasic separation.[3–8] Solute partitioning studies indicate that organic solutes have an affinity for the RTIL phase, correlating with their octan-1-ol–water log *P* values,[2,5] or hydrophobicity.

The range of hydrophobic RTIL has, until recently, been limited and largely focused on systems containing imidazolium and pyridinium cations,[9] imidazolium cations have exceptional advantages for electrochemical applications.[10] The number of available RTIL systems has increased due to the incorporation of a large range of different weakly coordinating anions.[11,12] Using perfluorinated anions has led to ionic liquids with attractive properties (hydrophobicity and low viscosity) for applications beyond electrochemistry.[13] Clearly, however, new classes of RTIL are needed, both to further our understanding of RTIL in general and also to find the appropriate combination of physical properties and performance geared towards industrial application.

In this work, a homologous series of *N*-alkylisoquinolinium salts containing linear alkyl substituents from butyl to octadecyl were prepared with the bis(perfluoroethylsulfonyl)imide ([BETI]$^-$) anion. It was hoped that the extended aromatic system present in these RTIL would lead to specific interactions with other aromatic species that could improve specific separations, *e.g.* in the removal of aromatics from hydrocarbon feedstocks.[1]

The salts were prepared by metathesis from the corresponding chloride salts and were isolated as colorless liquids that separated from aqueous solution. The physical properties for the [C$_n$isoq][BETI] RTIL are summarized in Table 1. The thermal properties are of particular interest. TGA results show the onset of thermal decomposition begins around 400 °C from where they decompose in the liquid state with a single continuous weight loss with little variation with increasing alkyl chain length. The salts displayed DSC cooling and heating profiles typical for ionic liquids[14] showing a glass transition on cooling and an exothermic transition on heating (corresponding to crystallization) followed by a sharp melting transition of the crystalline phase. The variation in glass transitions and melting point with chain length and anion are shown graphically in Fig. 1. Glass transition temperatures generally increase progressively with increasing alkyl-chain length (*n*) owing, perhaps, to the additional energy required to reorient larger cations in the glassy state.

Table 1 Characterization of the [C$_n$isoq][BETI] RTIL[a]

n	Water content (wt%)	Mole fraction water	Melting point (T_g/°C)	Glass transition (T_g/°C)	Density/ g cm^{-3}
4	1.77	0.36	−62.0	−85.2	1.23
6	1.62	0.35	−77.3	−84.0	1.20
8	1.49	0.35	−68.1	−79.4	1.17
10	0.69	0.20	−59.3	−77.8	1.09
12	0.66	0.20	−51.0	−75.4	1.08
14	0.61	0.20	−49.7	−66.7	1.07
16	0.47	0.16	−48.6	−61.8	1.05
18	0.41	0.15	−47.2	−59.3	1.05

[a] Data measured for RTIL equilibrated against water.

For the series [C$_n$isoq][BETI], melting points are affected by the alkyl chain length and decrease from n = 4 to 6. This observation may be associated with a possible destabilization of the crystalline state. With further lengthening of the alkyl chain, the melting point increases monotonically, associated with the increasing stability of the crystal state through alkyl–alkyl interactions.

The observed decrease in melting points with increasing alkyl chain length to a minimum for the C$_6$-derivatives and then increasing melting point for longer alkyl chain derivatives has been observed as a general feature of organic salts containing an alkyl-chain substituent.[15] The reasons behind this trend are not well understood but it is believed to be a combination of competing factors which influences the stability of the crystal lattice and therefore the melting point; destabilization of cation packing on increasing chain length, and increased chain–chain packing stabilization through microphase separation.

All the [C$_n$isoq][BETI] RTIL prepared were relatively hydrophobic and separated from water upon metathesis from the Li[BETI] salt as colorless liquids containing around 1%

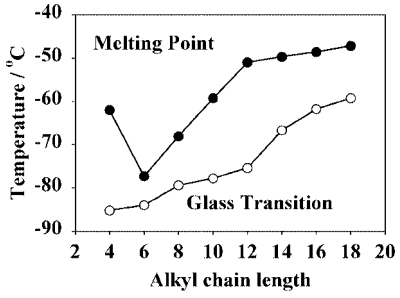

Fig. 1 Glass transition temperatures (○) and melting points (●), for [C$_n$isoq][BETI] RTIL determined on cooling and heating cycles respectively, by differential scanning calorimetry.

 DOI: 10.1039/b109340c

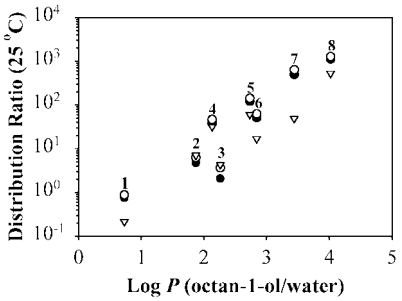

Fig. 2 Distribution ratios for ^{14}C-labeled organic solutes (1, phthalic acid; 2, benzoic acid; 3, salicylic acid; 4, benzene; 5, toluene; 6, chlorobenzene; 7, dichlorobenzene; 8, trichlorobenzene) in [C_8isoq][BETI]–water (●), [C_{14}-isoq][BETI]–water (○), or [C_4mim][PF_6]–water (∇) as a function of the solutes' octan-1-ol–water log *P* value.

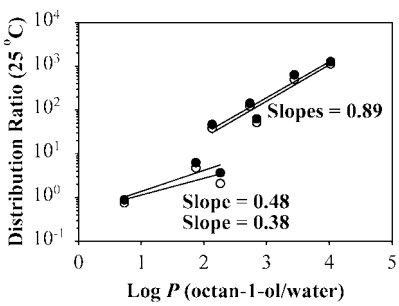

Fig. 3 Linear regression of the distribution ratios from Fig. 2 for the sets of acid (lower points 1–3) and aromatic (upper points 4–8) solutes partitioned between [C_8isoq][BETI]–water (●) or [C_{14}isoq][BETI]–water (○).

(wt.) of water. The water content of the RTILs corresponds to approximately 0.35–0.15 mole fraction. With increasing chain length, the salts become less dense and increasingly hydrophobic (see Table 1) as the contribution from the alkyl-chain to the liquid structure increases.

The octyl- and tetradecyl-substituted RTIL were used in liquid–liquid separation for a series of aromatic solutes and the results are compared to [C_4mim][PF_6]–water systems in Fig. 2. As the solute hydrophobicity increases (as noted by the octan-1-ol–water partition coefficient, log *P*), the general trend is for an increase in the distribution ratios for the organic solutes. Using log *P* provides at best only a general parameter for comparing solute partitioning behavior in these systems since, the environment in an ionic liquid is clearly different from that in octan-1-ol. Certain solutes, (*e.g.*, benzoic and salicylic acids) may interact *via* hydrogen bonding and partition as complex species, hence the break in the trend for those solutes.

The data in Table 1 indicate that the [C_{14}isoq][BETI] RTIL is the most hydrophobic and, in fact, the data in Fig. 2 show a slight increase in the distribution ratios for most hydrophobic solutes in liquid–liquid systems with that RTIL. It is of particular interest to note that the distribution ratios for substituted aromatics with the isoquinolinium systems are higher than with [C_4mim][PF_6] as the extracting phase.[2] With [C_{14}isoq][BETI], the distribution ratio for 1,2,4-trichlorobenzene is 1280 compared to 524 with [C_4mim][PF_6].[2] For the series of solutes (*e.g.*, carboxylic acids or substituted aromatics) examined here, the slope of the carboxylic acid partitioning data (0.44) is approximately half that of the aromatic hydrocarbons and halogenated aromatic solutes (0.89), as shown in Fig. 3. It is not yet clear whether the enhanced distribution ratios, particularly for aromatic species, are due to the hydrophobicity in the isoquinolinium RTIL or to increased aromatic interactions.

This series of new, hydrophobic ionic liquids based on the *N*-alkylisoquinolinium† cation and the [BETI]$^-$ anion has been characterized and the thermal properties of the salts have been described. All the salts are hydrophobic and are liquids at room temperature, prompting the investigation of their use as a component for aqueous-IL two-phase separation systems. The availability of ionic liquids containing a conjugated aromatic core in particular, offers significant potential opportunities for the separation of aromatic compounds from aqueous or hydrocarbon sources.

This research has been supported by the U. S. Environmental Protection Agency's STAR program through grant number R-82825701-0. Additional support was provided from the PG Research Foundation.

Notes and references

† Chloride salts were prepared by *N*-alkylation of isoquinoline with the respective alkyl chloride. The *N*-alkylisoquinolinium salts were prepared by metathesis in aqueous solution from the respective chloride salts with Li[BETI] (3 M). Distribution ratios are measured as the radioactivity in the lower(RTIL) phase divided by the radioactivity in the upper (aqueous) phase, the standard radiochemical assay utilized is described elsewhere.[2] Water content, melting point, thermal decomposition, and density measurements were perfomed as described in the literature.[2]

1 M. S. Selvan, M. D. McKinley, R. H. Dubois and J. L. Atwood, *J. Chem. Eng. Data*, 2000, **45**, 841.
2 J. G. Huddleston, A. E. Visser, W. M. Reichert, H. D. Willauer, G. A. Broker and R. D. Rogers, *Green Chem.*, 2001, **3**, 156.
3 A. E. Visser, R. P. Swatloski, S. T. Griffin, D. H. Hartman and R. D. Rogers, *Sep. Sci. Technol.*, 2001, **36**, 785.
4 S. Dai, Y. H. Ju and C. E. Barnes, *J. Chem. Soc., Dalton Trans.*, 1999, 1201.
5 J. G. Huddleston, H. D. Willauer, R. P. Swatloski, A. E. Visser and R. D. Rogers, *Chem. Commun.*, 1998, 1765.
6 A. E. Visser, R. P. Swatloski and R. D. Rogers, *Green Chem.*, 2000, **2**, 1.
7 A. E. Visser, R. P. Swatloski, W. M. Reichert, S. T. Griffin and R. D. Rogers, *Ind. Eng. Chem. Res.*, 2000, **39**, 3596.
8 A. E. Visser, R. P. Swatloski, W. M. Reichert, R. D. Rogers, R. Mayton, S. Sheff, A. Wierzbicki and J. H. Davis, Jr., *Chem. Commun.*, 2001, 135.
9 S. N. V. K. Aki, J. F. Brennecke and A. Samanta, *Chem. Commun.*, 2001, 413.
10 J. S. Wilkes and C. L. Hussey, *Selection of Cations for Ambient Temperature Chloroaluminate Molten Salts Using MNDO Molecular Orbital Calculations*, Report FJSRL-TR-82-0002, 1982, USAF Academy, CO.
11 J. S. Wilkes and M. J. Zaworotko, *Chem. Commun.*, 1992, 965.
12 A. S. Larsen, J. D. Holbrey, F. S. Tham and C. A. Reed, *J. Am. Chem. Soc.*, 2000, **122**, 7264.
13 P. Bonhôte, A.-P. Dias, N. Papageorgiou, K. Kalyanasundaram and M. Grätzel, *Inorg. Chem.*, 1996, **35**, 1168.
14 J. Sun, M. Forsyth and D. R. McFarlane, *J. Phys. Chem. D*, 1998, **102**, 8858.
15 J. D. Holbrey and K. R. Seddon, *J. Chem. Soc., Dalton Trans.*, 1999, 2133.

CHEMCOMM Communication
www.rsc.org/chemcomm

Synthesis of a new hollandite-type manganese oxide with framework and interstitial Cr(III)

Stanton Ching,*[a] Peter F. Driscoll,[a] Katarzyna S. Kieltyka,[a] Michael R. Marvel[a] and Steven L. Suib[b]

[a] *Department of Chemistry, Connecticut College, New London, CT 06320, USA. E-mail: sschi@concoll.edu*
[b] *Department of Chemistry, University of Connecticut, Storrs, CT 06269, USA*

Received (in Purdue, IN, USA) 30th August 2001, Accepted 23rd October 2001
First published as an Advance Article on the web 15th November 2001

Hollandite with Cr(III) in both tunnel and framework sites has been prepared hydrothermally from layered manganese oxide precursors.

Hollandite-type manganese oxides are one-dimensional tunneled materials that consist of 2 × 2 arrangements of edge-shared MnO_6 octahedra with cations occupying the interstitial voids. They have been widely studied for potential applications in catalysis, cation sorption, chemical sensing, and rechargeable battery technology.[1,2] By far, the most common and easily prepared member of this class is cryptomelane, a specific hollandite with K^+ in the tunnels. The prevalence of cryptomelane can be attributed to the widespread use of potassium salts in manganese oxide syntheses and stabilization from an excellent fit of K^+ in the 2 × 2 tunnels.[3] Hollandite-type manganese oxides have been prepared with other alkali and alkaline earth cations in the tunnels,[4,5] but similar routes have not been developed for hollandites with interstitial transition metal cations. Here we report the hydrothermal synthesis of the transition-metal-containing Cr-hollandite from a layered manganese oxide precursor. The formation of the 2 × 2 hollandite material is unusual because previous studies have found this route to yield the related 3 × 3 tunneled manganese oxide, todorokite.[6–8]

The overall synthetic scheme for Cr-hollandite is shown in Fig. 1. A 1.69 g (10.0 mmol) sample of $MnSO_4{\cdot}H_2O$ was dissolved in 20 mL of water in a plastic bottle and treated with 30 mL of aqueous 6 M NaOH to produce tan-colored $Mn(OH)_2$. A solid mixture of 1.89 g (7.0 mmol) $K_2S_2O_8$ and 0.38 g (1.4 mmol) pulverized $CrCl_3{\cdot}6H_2O$ was then added very slowly with stirring over a 45 min period. The resulting grey–black slurry of Cr-doped Na-birnessite was aged for two days before being isolated by filtration and washed three times with water. The Na-birnessite was then immediately slurried with 100 mL of 0.25 M $Cr(NO_3)_3$ and stirred overnight to yield Cr-buserite, which was isolated in a very slow filtration step. Hydrothermal

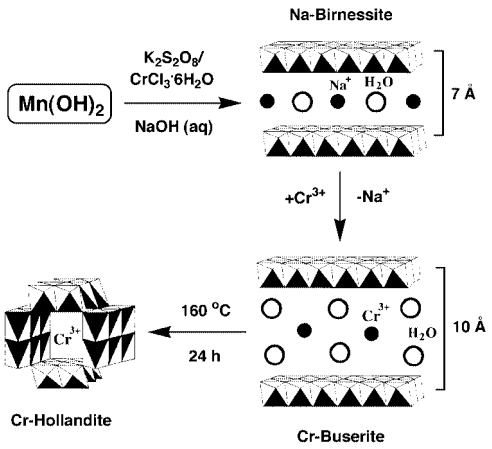

Fig. 1 Synthetic scheme for Cr-hollandite.

treatment of Cr-buserite at 160 °C for 24 h ultimately led to the transformation into Cr-hollandite, of which *ca.* 0.8 g (*ca.* 70% based on Mn) could be isolated.

The structures of Na-birnessite and Cr-buserite were confirmed by powder X-ray diffraction data collected on a Scintag PDS 2000 diffractometer using Cu-Kα radiation. The diffraction pattern for Na-birnessite displayed characteristic peaks at 7.14 and 3.57 Å, which correspond to the interlayer spacing. In the pattern of Cr-buserite, peaks were observed at 9.63, 4.81 and 3.21 Å due to interlayer expansion from a second layer of water molecules being established in the gallery region. Scanning electron microscopy images reveal plate-like morphologies for both Na-birnessite and Cr-buserite, which are typical of these layered materials.

The Cr^{3+} ion was introduced in the synthesis of Na-birnessite as an isomorphous dopant in the manganese oxide framework. Similar modifications with other transition metal cations have been applied to birnessite and buserite materials to promote the formation of 3 × 3 tunneled todorokite materials.[6–8] Elemental analysis of the Cr-doped Na-birnessite revealed a Cr/Mn ratio of 0.13, which compared favorably to the 0.14 ratio used in the reactants and was taken to indicate that most of the Cr^{3+} became incorporated in the manganese oxide structure. After ion exchange, a Cr/Mn ratio of 0.32 was determined for Cr-buserite. No soluble Mn was detected from the reaction, which suggested that the ion exchange process occurred topotactically without contributions from redox reactions involving the manganese oxide framework.[3,9] From the Cr : Mn ratios in Cr-doped Na-birnessite and Cr-buserite, it was determined that 44% of the total Cr^{3+} was doped into the manganese oxide framework while 56% was contained between the layers.

Hydrothermal treatment of Cr-buserite resulted in the collapse of the layered framework and formation of tunneled Cr-hollandite. The hollandite-type manganese oxide structure was confirmed by X-ray diffraction, Fig. 2. The peaks were indexed to a tetragonal structure, which is analogous to the observed patterns for cryptomelane (K-hollandite).[4] Scanning electron microscopy revealed needle-like formations of Cr-hollandite with thickness in the range 100–400 nm. By comparison, cryptomelane also has a fibrous morphology, but with thinner particles that are much less than 100 nm.[10,11] A thermogravimetric profile showed essentially no weight loss (< 0.5%) up to 300 °C, indicating a lack of interstitial water. A weight loss of 7% from 400 to 620 °C was assigned to the formation of M_2O_3 while a further weight loss of 4% from 620 to 800 °C was due to the appearance of Mn_3O_4.

The chemical formula of $Cr_{0.30}MnO_{2.41}$ was determined for Cr-hollandite using data from elemental analysis (14.4% Cr, 50.3% Mn) and the thermogravimetric results which showed the absence of water. There was no detectable Na in the material. The 0.30 Cr/Mn ratio indicated some loss of interstitial chromium during the hydrothermal treatment of Cr-buserite (Cr/Mn = 0.32). This was verified by an observed light yellow color in the Cr-holladite filtrate and detection of soluble Cr by atomic absorption spectroscopy. There was no detectable Mn in

 DOI: 10.1039/b107887a

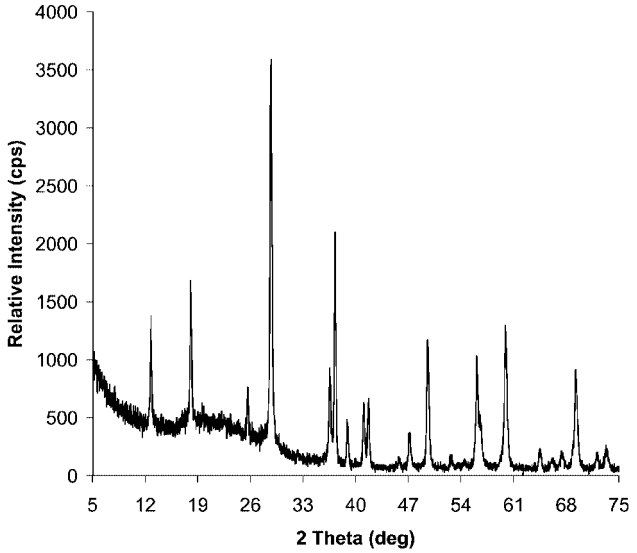

Fig. 2 Powder X-ray diffraction pattern for Cr-hollandite. The *d*-spacings in Å and indices (*hkl*) are provided: 6.95 (110), 4.92 (200), 3.48 (220), 3.12 (310), 2.46 (400), 2.42 (211), 2.32 (330), 2.20 (420), 2.17 (301), 1.93 (510), 1.84 (411), 1.64 (600), 1.63 (431), 1.54 (521), 1.44 (002), 1.36 (640).

the filtrate, indicating that Cr^{3+} was expelled from the interstitial region rather than from the manganese oxide framework. Thus, the Cr-hollandite formula can be expressed as $Cr_{0.16}(Cr_{0.14}Mn)O_{2.41}$ to show the distribution of chromium between tunnel and framework sites. Difficulties in sample preparation prevented a standard analysis of the average Mn oxidation state, but a value of 3.9 could be obtained indirectly from the chemical formula determined for Cr-hollandite. Cryptomelane samples have similar oxidation states. Considering the presence of Cr(III) in the $Cr_{0.14}Mn$ composition of the tunneled framework, the average oxidation state on each metal center in the framework is 3.8.

The synthesis of Cr-doped Na-birnessite is the key step in the overall preparative scheme for Cr-hollandite. The degree of crystallinity in Na-birnessite, as determined by X-ray diffraction peak intensities, correlates well with the crystallinities of buserite and hollandite obtained in subsequent steps. Slow addition of the $K_2S_2O_8/CrCl_3{\cdot}6H_2O$ oxidant/dopant mixture is critical to achieving high quality Na-birnessite, as rapid addition produced amorphous manganese oxide. In related birnessite syntheses, rapid addition of $K_2S_2O_8$ and divalent cation dopants (Mg^{2+}, Co^{2+}, Ni^{2+}, Cu^{2+}) resulted in the formation of feitknechtite, a layered MnOOH material.[8] A number of other oxidants have been used to prepare Na-birnessite and these can presumably be substituted for $K_2S_2O_8$ in this synthesis.[1] $CrCl_3{\cdot}6H_2O$ was chosen as the other solid reagent with $K_2S_2O_8$ because it was less hygroscopic than other water-soluble Cr(III) salts. The effect of aging on Cr-doped Na-birnessite was interesting, since aging has been typically used to promote greater crystallinity in birnessites.[12,13] However, in this case the most crystalline birnessites were obtained when aging was carried out between zero and three days, with the optimum time being about two days. Prolonged aging yielded birnessite with poorly crystallinity or amorphous manganese oxide.

Successful syntheses of Cr-hollandite were dependent on having Cr^{3+} both as an isomorphous framework dopant and a gallery cation in the birnessite and buserite precursors. Na-birnessite with Cr^{3+} as a framework dopant could be ion exchanged with divalent cations such as Mg^{2+}, Co^{2+}, Ni^{2+} and Cu^{2+}. However, the resulting buserites were converted to feitknechtite (layered MnOOH) upon hydrothermal treatment, as determined by the appearance of a prominent X-ray diffraction peak at 4.70 Å.[8,12,13] Similar results were obtained when divalent cations were doped in the manganese oxide framework and Cr^{3+} was exchanged into the interlayer gallery. Interestingly, there was no evidence of the 3 × 3 tunneled todorokite phase from the hydrothermal reaction, even though

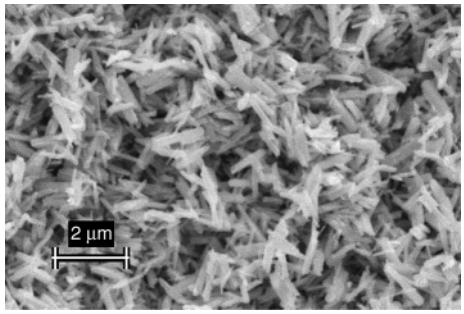

Fig. 3 Scanning electron microscope image of Cr-hollandite.

this phase is favored when the divalent cations occupy both framework and interlayer sites in buserite.[8] Attempts were also made to prepare Cr-hollandite in the absence of framework dopants. In these cases, some conversion of undoped Cr-buserite to Cr-hollandite was observed, but the process was slow and incomplete.

In addition to presenting the first example of a Cr-containing hollandite, the hydrothermal synthesis also provides a route to 2 × 2 tunneled manganese oxides that contain a high level of framework dopant. The cryptomelane framework has been doped with a variety of foreign cations, but the amounts are typically low (0.01–0.5% substitution of total manganese) using redox precipitation methods.[11] Significant improvement of up to 16% has been reported for Fe^{3+} in cryptomelane through calcination of Fe-doped K-birnessite.[14] The framework doping of Cr^{3+} in Cr-hollandite represents a 12% substitution of total manganese.

Overall, the hydrothermal synthesis of Cr-hollandite from Cr-buserite is very unusual, especially given all the precedents that show buserite acting as a precursor to todorokite. Hydrothermal routes to todorokite are known with a variety of tunnel cations, including alkali metals (Li^+, Na^+),[15] alkaline earth metals (Mg^{2+}, Ca^{2+}, Sr^{2+}, Ba^{2+}),[15] transition metals (Mn^{2+}, Co^{2+}, Ni^{2+}, Cu^{2+}, Zn^{2+}),[6–8,15] and even lanthanides (Eu^{3+}, Tb^{3+}).[15] It is not yet clear why Cr^{3+} is able to direct this reaction toward the hollandite structure, but such information would undoubtedly be valuable in designing syntheses of tunneled manganese oxides.

This research was supported by the Research Corporation and the donors of the Petroleum Research Fund, administered by the American Chemical Society. The Keck Foundation is also acknowledged for providing summer stipends for P. F. D., K. S. K, and M. R. M.

Notes and references

1 Q. Feng, H. Kanoh and K. Ooi, *J. Mater. Chem.*, 1999, **9**, 319.
2 S. L. Brock, N. Duan, Z. R. Tian, O. Giraldo, H. Zhou and S. L. Suib, *Chem. Mater.*, 1998, **10**, 2619.
3 Q. Feng, H. Kanoh, Y. Miyai and K. Ooi, *Chem. Mater.*, 1995, **7**, 148.
4 R. Giovanoli and B. Balmer, *Chimia*, 1981, **35**, 53.
5 R. Giovanoli and M. Faller, *Chimia*, 1989, **43**, 54.
6 D. C. Golden, C. C. Chen and J. B. Dixon, *Clays Clay Miner.*, 1987, **35**, 271.
7 Y. F. Shen, S. L. Suib and C. L. O'Young, *J. Am. Chem. Soc.*, 1994, **116**, 11020.
8 S. Ching, K. S. Krukowska and S. L. Suib, *Inorg. Chim. Acta* , 1999, **294**, 123.
9 Q. Feng, H. Kanoh, Y. Miyai and K. Ooi, *Chem. Mater.*, 1995, **7**, 1722.
10 C. C. Chen, D. C. Golden and J. B. Dixon, *Clays Clay Miner.*, 1986, **34**, 565.
11 R. N. DeGuzman, Y. F. Shen, E. J. Neth, S. L. Suib, C. L. O'Young, S. Levine and J. M. Newsam, *Chem. Mater.*, 1994, **6**, 815.
12 J. Luo, A. Huang, S. H. Park, S. L. Suib and C. L. O'Young, *Chem. Mater.*, 1998, **10**, 15261.
13 J. Luo, Q. Zhang and S. L. Suib, *Inorg. Chem.*, 2000, **39**, 741.
14 J. Cai, J. Liu, W. S. Willis and S. L. Suib, *Chem. Mater.*, 2001, **13**, 2413.
15 J. Luo, Q. Zhang, A. Huang, O. Giraldo and S. L. Suib, *Inorg. Chem.*, 1999, **38**, 6106.

CHEMCOMM
Communication
www.rsc.org/chemcomm

Inducing structural polarity using fluorinated organics: X-ray crystal structures of *p*-XC_6F_4CN (X = Cl, Br, I)†

Andrew D. Bond,[a] Joanna Griffiths,[a] Jeremy M. Rawson*[a] and Jürg Hulliger[b]

[a] *Department of Chemistry, University of Cambridge, Lensfield Road, Cambridge, UK CB2 1EW. E-mail: jmr31@cus.cam.ac.uk*

[b] *Department of Chemistry and Biochemistry, The University of Berne, Freiestrasse 3, Berne CH 3012, Switzerland*

Received (in Cambridge, UK) 23rd August 2001, Accepted 16th October 2001
First published as an Advance Article on the web 6th November 2001

Non-centrosymmetric structures are promoted through the use of perfluoroaromatics containing structure-directing CN···X (X = Br, I) supramolecular synthons.

There has been considerable interest over a number of years in the design of organic molecules for non-linear optic (NLO) applications, particularly frequency doubling through second harmonic generation (SHG).[1] For materials to exhibit SHG a (macroscopically) non-centrosymmetric crystal is required.[1] Considerable efforts in crystal engineering have led to the design of well defined polar molecular chains[2] but the antiparallel alignment of these supramolecular dipoles tends to generate centrosymmetric structures.[3] An approach to favour the co-parallel alignment of molecular chains is inclusion into channel-like hosts such as PHTP.[4] In this case molecules in separate channels are essentially non-interacting and crystal polarity evolves through a stochastic process (Markov theory).[3,4] A natural development of this concept is the design of molecular chains bearing lateral substituents which minimise interactions between chains, favouring co-parallel or non-centrosymmetric structures.[3] Here we report the structures of *p*-XC_6F_4CN (X = Cl, Br, I) in which the CN···X interaction is utilised as a structure-directing synthon[5] and the fluorinated substituents reduce inter-chain interactions.

The nitrile *p*-BrC_6F_4CN is commercially available (Lancaster). The related nitriles, *p*-ClC_6F_4CN and *p*-IC_6F_4CN were prepared according to literature methods.[6] C_6F_5CN is a liquid at room temperature and its low-temperature crystal structure has been reported recently.[7] The other halo-derivatives are solids and were crystallised by slow sublimation (1 atm, 45–28 °C).

The CN···X interaction (X = Br, I) is a well characterised supramolecular synthon[5] but is less structure-directing for the less polarisable more electronegative halogens (F, Cl). The structures of *p*-BrC_6F_4CN and *p*-IC_6F_4CN are isomorphous (space group $Pna2_1$) and exhibited some tendency for racemic twinning. Amongst the samples, single crystals of both compounds were found which did not exhibit twinning (on the basis of their Flack parameter). Both *p*-BrC_6F_4CN and *p*-IC_6F_4CN contain a single molecule in the asymmetric unit of unexceptional geometry.‡ The solid state structures of both derivatives exhibit characteristic chain motifs, with molecules linked *via* CN···X interactions [$d_{N\cdots X}$ = 3.157(7) and 3.128(7) Å for Br and I analogues]. Within error (3 esd's), these are close to the sum of the van der Waals radii (3.14–3.44 Å in the case of *p*-BrC_6F_4CN and 3.36–3.73 Å for the iodo derivative). The chain-like motif for *p*-BrC_6F_4CN is illustrated in Fig. 1. There appear to be no significant directional intermolecular interactions between molecules in different chains, with N···F, F···F and C···F contacts all greater than the sum of the van der Waals radii. The shortest of the intermolecular Br···F contacts [at 3.413(5) Å] and the corresponding I···F contacts [at 3.521(5) Å] falls beyond or at the longer end of the range expected for an X···F non-bonded contact (2.84–3.22 Å for Br···F and 3.06–3.51Å for I···F).

The chains run co-parallel across the unit cell diagonal and lie approximately in the *bc* plane, with Br···N–C angles of 164.8°. A second set of co-parallel chains run across the unit cell diagonal, approximately bisecting the *b* and *c* cell edges (Fig. 2). These two planes form acute angles of 75.9° and 73.4° for *p*-

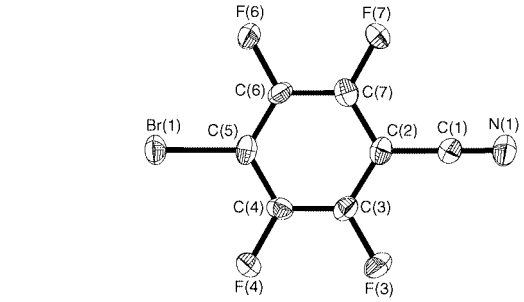

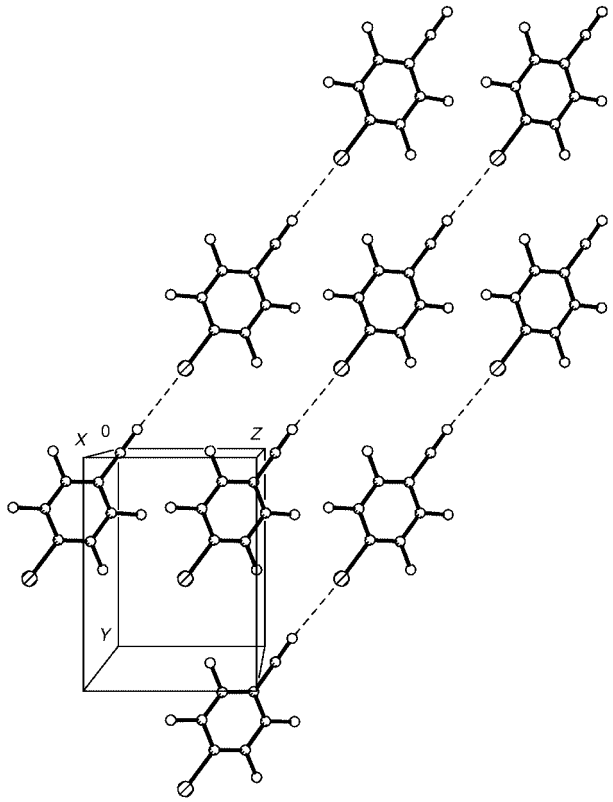

Fig. 1 Crystal structure of *p*-BrC_6F_4CN viewed in the *bc* plane. Top: the asymmetric unit with atom labelling.

† Electronic supplementary data (ESI) available: the crystal structure of *p*-BrC_6F_4CN in .pdb format. See http://www.rsc.org/suppdata/cc/b1/b107665p/

 DOI: 10.1039/b107665p

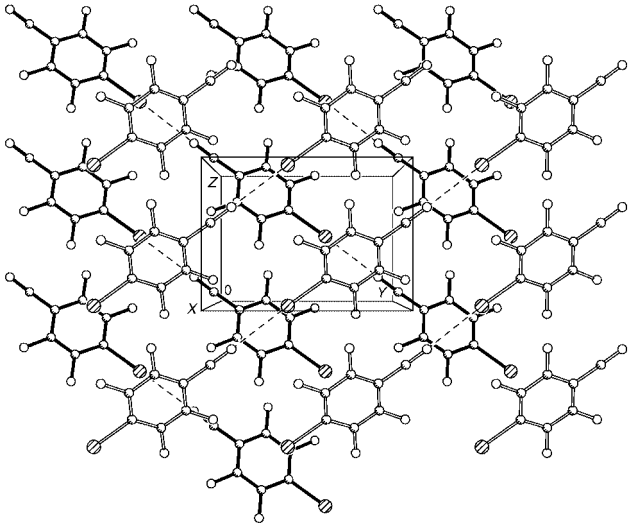

Fig. 2 View of *p*-IC_6F_4CN viewed in the *bc* plane, illustrating the non-colinear alignment of molecular chains.

BrC_6F_4CN and *p*-IC_6F_4CN respectively, generating a macroscopically polar structure. This is in marked contrast to the hydrogenated analogue, *p*-IC_6H_4CN which crystallises in the centrosymmetric space group *I*2/*a* [*p*-BrC_6H_4CN crystallises in the non-centrosymmetric space group *Am*, but exhibits some structural disorder].[5]

In contrast to the bromo and iodo derivatives, the fluoro[7] and chloro analogues adopt rather different structures, consistent with the less structure-directing nature of the CN···X interaction for the lighter halogens. In both these cases the cyanide prefers close contacts with the π system of the aromatic ring rather than the polarisable electron density of the heavier halogens (Fig. 3). The CN···centroid contacts in *p*-FC_6F_4CN and *p*-ClC_6F_4CN are 3.071 and 3.110 Å respectively.

For the current series of derivatives, *p*-XC_6F_4CN (X = F, Cl, Br, I), the structures of the heavier halogens are dictated by CN···X interactions similar to those reported elsewhere,[5] whereas for the lighter halogens a tendency for CN···π type interactions are observed. The structure-directing CN···X interactions generate polar chains in both bromo and iodo derivatives. The inclusion of the perfluorinated aromatic substituent leads to minimal inter-chain interactions (as exemplified by all major interchain interactions greater than or equal to the sum of the van der Waals radii). The CN···X interaction (X = Br, I) faciliates a co-parallel alignment of chains forming polar molecular sheets. In the current systems, the sheets do not align co-parallel but are oriented at approximately 75° with respect to each other but, nevertheless, render the structures non-centrosymmetric and macroscopically polar.

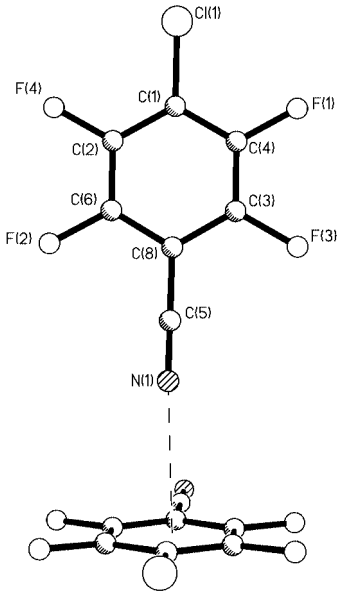

Fig. 3 Crystal structure of *p*-ClC_6F_4CN, illustrating the CN···π interaction.

Confirmation of acentric packing in *p*-BrC_6F_4CN was obtained from an SHG test using a Continuum SLI-10 nanosecond pulsed Nd:YAG laser (1064 nm). The qualitative measurement of frequency doubling utilised single crystals, crushed between two glass slides at a peak power of 30 MW cm^{-2}. Previous studies have indicated that there is no clear trend in the molecular second order susceptibility, β, on perfluorination of the aromatic ring.[8] Further experiments are underway to characterise fully the NLO activity of these materials.

The present studies indicate that perfluorinated aromatics containing structure-directing CN···X synthons can be utilised to generate macroscopically polar structures which we have shown to be SHG active. The current series of molecules are not particularly rod-like in nature and perfect co-parallel alignment of molecular chains is not observed. We are currently persuing perfluorobiphenyl derivatives and related systems in which the co-parallel alignment of molecular chains should be preferred.

We thank the EPSRC for financial support (A. D. B., J. G.).

Notes and references

‡ *Crystal data* for ClC_6F_4CN: C_7ClF_4N, M = 209.53, orthorhombic, space group $Pca2_1$, a = 11.7854(9), b = 6.2300(4), c = 10.0333(4) Å, U = 736.68(8) Å^3, T = 180(2) K, Z = 4, D_c = 1.889 g cm^{-3}, μ(Mo-Kα) = 0.534 mm^{-1}. Of 3607 reflections measured, 1464 were unique (R_{int} = 0.0444) and were used in all calculations. The final *wR*2 = 0.0980 (all data), *R*1 [$F^2 > 2\sigma(F^2)$] = 0.0349. Absolute structure (Flack) parameter = 0.04(9). CCDC 170505. *Crystal data* for BrC_6F_4CN: C_7BrF_4N, M = 253.99, orthorhombic, space group $Pna2_1$, a = 14.6736(12), b = 8.2804(5), c = 6.1368(5)Å, U = 745.64(10)Å^3, T = 180(2) K, Z = 4, D_c = 2.263 g cm^{-3}, μ(Mo-Kα) = 5.529 mm^{-1}. Of 4047 reflections measured, 1647 were unique (R_{int} = 0.0679) and were used in all calculations. The final *wR*2 = 0.1002 (all data), *R*1 [$F^2 > 2\sigma(F^2)$] = 0.0447. Absolute structure (Flack) parameter = 0.05(2). CCDC 170504. *Crystal data* for IC_6F_4CN: C_7IF_4N, M = 300.98, orthorhombic, space group $Pna2_1$, a = 15.252(2), b = 8.5160(6), c = 6.1817(7) Å, U = 802.92(15)Å^3, T = 180(2) K, Z = 4, D_c = 2.490 g cm^{-3}, μ(Mo-Kα) = 4.003 mm^{-1}. Of 4924 reflections measured, 1699 were unique (R_{int} = 0.0499) and were used in all calculations. The final *wR*2 = 0.1051 (all data), *R*1 [$F^2 > 2\sigma(F^2)$] = 0.0417. Absolute structure (Flack) parameter = 0.05(5). CCDC 170503. See http://www.rsc.org/suppdata/cc/b1/b107665p/ for crystallographic files in .cif or other electronic format.

1 C. Bosshard, K. Sutter, P. Pretre, J. Hulliger, M. Florsheimer, P. Kaatz and P. Gunter, *Organic Nonlinear Optical Materials*, Gordon and Breach, Basel, 1995.
2 S. R. Marder, B. Kippelen, A. K.-Y. Jen and N. Peyhambarian, *Nature*, 1997, **388**, 845.
3 J. Hulliger, P. J. Langley and S. W. Roth, *Cryst. Eng.*, 1999, **1**, 177; J. Hulliger, O. König and R. Hoss, *Adv. Mater.*, 1995, **7**, 719.
4 V. Ramamurthy and D. F. Eaton, *Chem. Mater.*, 1994, **6**, 1128; J. Hulliger, S. W. Roth, A. Quintel and H. Bebie, *J. Solid State Chem.*, 2000, **152**, 49.
5 G. R. Desiraju and R. L. Harlow, *J. Am. Chem. Soc.*, 1989, **111**, 6757.
6 J. M. Birchall, R. N. Haszledine and M. E. Jones, *J. Chem. Soc. (C)*, 1971, 1343.
7 A. D. Bond, J. E. Davies, J. Griffiths and J. M. Rawson, *Acta Crystallogr.*, 2001, **E57**, 231..
8 C. C. Henderson, P. A. Cahill, T. C. Kowalczyk and K. D. Singer, *Chem. Mater.*, 1993, **5**, 1059.

CHEMCOMM Communication
www.rsc.org/chemcomm

Electrochemistry of chalcogen compounds: prediction of antioxidant activity

Gregory I. Giles,[a] Karen M. Tasker,[a] Russell J. K. Johnson,[a] Claus Jacob,*[a] Chris Peers[b] and Kim N. Green[b]

[a] *School of Chemistry, University of Exeter, Stocker Road, Exeter, UK EX4 4QD. E-mail: C.Jacob@ex.ac.uk; Fax: +44 (0)1392 263434; Tel: +44 (0)1392 263462*
[b] *Institute for Cardiovascular Research, University of Leeds, Leeds, UK LS2 9JT*

Received (in Cambridge, UK) 4th September 2001, Accepted 19th October 2001
First published as an Advance Article on the web 15th November 2001

Synthesis and characterisation of organochalcogens has demonstrated a high correlation between their electrochemical oxidation potential on the glassy carbon electrode, their activity in bioassays and an unprecedented antioxidant activity in neuronal cell culture (EC_{50} ~ 20 nM) making electrochemical methodology a valuable tool in drug design for Alzheimer's and related diseases.

Oxidative stress is a biochemical condition present in several human disorders, including Alzheimer's disease.[1] It is the manifestation of an imbalance in an organism's biochemical redox-processes that results in the production of high concentrations of reactive oxygen (ROS), nitrogen and sulfur species. Various antioxidant strategies are used to treat oxidative stress related disorders, *e.g.* by supplementation with artificial 'one shot' antioxidants (vitamin C, penicillamine) that react *stoichiometrically* with stressors to form non-toxic species.[2] Recent studies have indicated that catalytic antioxidants that mimic the action of the selenium enzyme glutathione peroxidase (GPx) are considerably more effective. GPx catalyses the reaction of toxic peroxides with glutathione (GSH) to form oxidised glutathione (GSSG) and water. Most synthetic GPx mimics incorporate a Se or Te atom within an organic framework and their catalytic redox cycle consists of the initial oxidation of a chalcogen atom, in the process reducing peroxide to water, followed by regeneration of the catalyst *via* reduction with two equivalents of thiols.[3–5]

Only a few attempts have so far been made to link the electrochemical redox potentials of these agents with antioxidant activity, among them cyclic voltammetry (CV) to characterise tellurides and selenides in organic solvents and polarography of diselenides on mercury electrodes.[6,7] A fast, widely applicable and reliable method to *predict* biochemical and biological activity is, however, still lacking and a requirement for an accurate prediction is that antioxidants are compared under conditions closely resembling a biological environment. The results presented in this communication show that oxidation potentials can be obtained in aqueous media on the glassy carbon graphite electrode (GE) for both mono- and di-chalcogens and that there is a good correlation between these potentials and biochemical activity in oxidation assays. This data can be used to predict antioxidant activity in cell culture experiments indicative of Alzheimer's disease.

The redox-behaviour of a number of structurally related mono- and di-chalcogens has been investigated (Table 1). Compounds **1** and **2** were purchased from Aldrich and **3**–**6** and **10** were synthesised according to established procedures.[8] **7** and **9** were synthesised by the reduction of **6** with sodium borohydride followed by the addition of either a stoichiometric amount of 1,3-dibromopropane (**7**) or an excess of the reagent (**9**). Compound **8** was synthesised by stirring **10** in excess acetic anhydride over 20 h. Cyclic voltammograms of organochalcogens (50 μM) were recorded in 50 mM potassium phosphate buffer (pH 7.4) containing 30% methanol (due to the limited solubility of the organochalcogens in aqueous media) using a standard Ag/AgCl reference electrode, a Pt counter electrode and a GE (BAS) that was thoroughly cleaned and polished (Al_2O_3) after each scan.

Most chalcogen compounds studied displayed only one irreversible oxidation peak between 0 and +1200 mV *vs.* Ag/AgCl (Table 1) with the exception of **10**, which also exhibited a reduction peak at +270 mV and a second oxidation peak at +820 mV. The value for the first oxidation potential (*E*pa) ranged from +300 to +1400 mV with a clearly observable trend, the tellurides having the lowest potential averaging around +400 mV, increasing to approximately +900 mV for the selenides and +1200 mV for the sulfides. Interestingly, both mono- and di-chalcogens displayed an oxidation peak, allowing comparison of the two species. In aqueous solution anodic oxidation of these chalcogens is an irreversible process that involves the formation of the intermediate radical species rapidly followed by reaction with water to form the chalcogen- or dichalcogen oxide.[4,9] The formation of such species (*e.g.* disulfide *S*-oxides, selenoxides) is frequently observed in biochemical studies[3] and has been implicated in catalytic antioxidation (*e.g.* oxidative activation of ditellurides, selenylsulfides).[4] On the assumption that the ease of radical formation correlates with the ease of oxidation of the

Table 1 Correlation between *E*pa and the biochemical activity of compounds **1**–**10**. Cyclic voltammograms were recorded at a scan rate of 200 mV s^{-1}. MT (0.5 μM) was incubated with *t*-BuOOH (500 μM) and catalyst (200 nM, 100 nM for **7** to allow for the presence of two tellurium catalytic sites) in the presence of PAR (100 μM) in 20 mM HEPES-Na^+, pH 7.5 at 25 °C (N_2 purged). The reaction was continuously monitored for 60 min at 500 nm (Cary50/Varian). Initial rates (*r*) were calculated between 0 and 10 min

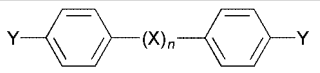

Comp.	X	*n*	Y	*E*pa/mV	*r* × 10^{-10} M s^{-1}
1	S	1	H	+1366	1.0
2	S	2	OCH_3	+1176	1.3
3	Se	1	OCH_3	+753	0.1
4	Se	2	OCH_3	+1000	3.8
5	Te	1	OCH_3	+368	4.3
6	Te	2	OCH_3	+578	9.3
7	Te	1	[a]	+527	11.6
8	Te	1	$O(O)CCH_3$	+448	5.5
9	Te	1	[a]	+694	6.7
10	Te	1	OH	+299	14.1

Exp. error 10%. [a] Structures for **7** and **9** given below.

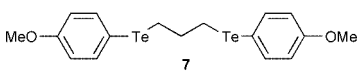

7

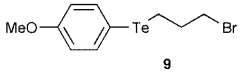

9

 DOI: 10.1039/b107972g

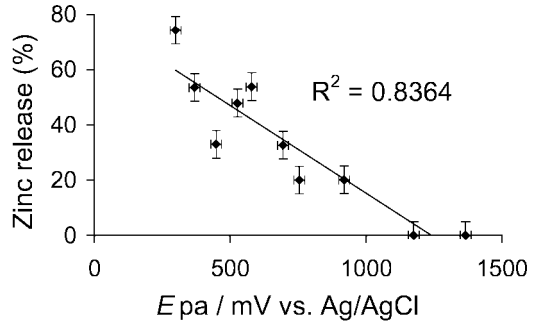

Fig. 1 Correlation between *E*pa and % zinc transfer from MT (experimental details given in legend of Table 1). A value for the maximum zinc release was obtained by incubation with 10 μM ebselen. The value for zinc release after 60 min was expressed as a percentage of the maximum zinc release and plotted as a function of the catalyst's (separately determined) oxidation potential. Experiments were repeated (N = 3) and error bars (SD) applied for zinc release as well as *E*pa.

chalcogen *in vivo* *E*pa has the potential to be used as a predictor of biological activity.

Organochalcogens were evaluated for GPx-like activity *via* their ability to catalyse the reaction of *tert*-butyl hydrogen peroxide (*t*-BuOOH) with the thiol protein metallothionein (MT) (this redox assay is increasingly used since it provides excellent reproducibility).[10,11] Zinc release from MT occurs upon oxidation of the thiol ligands and is detected spectrophotometrically in the presence of the chromophoric dye 4-(2-pyridylazo)resorcinol (PAR). Agents catalysing this process can be evaluated according to both the initial rate and the total extent of zinc release. Maximum zinc release from 0.5 μM MT was calculated by incubation with 10 μM ebselen (2-phenyl-1,2-benzisoselenazol-3[2*H*]-one) and the amount of zinc release for different antioxidants compared to this theoretical maximum.[11] Table 1 and Fig. 1 indicate that *E*pa correlated well with the activity in the bioassay, with the lowest potentials associated with the highest activity. A similar correlation was observed in a standard GPx assay monitoring thiophenol oxidation by hydrogen peroxide in methanol (data not shown).[12] Among the agents tested, **10** had the lowest *E*pa and also one of the highest activities. It was therefore tested in PC12 cell culture indicative of Alzheimer's disease and compared with other antioxidants.

PC12 cells were cultured as previously described.[13,14] 24 h prior to study aliquots were exposed to 100 nM amyloid beta peptide (residues 1–40) ($A\beta P_{(1-40)}$) and varying concentrations of antioxidants. $A\beta P_{(1-40)}$ causes dramatic and selective enhancement of Ca^{2+} channel activity in these cells *via* a mechanism which involves increased production of ROS.[13,14] Ca^{2+} channel currents were recorded using the whole-cell patch clamp technique, with 20 mM Ba^{2+} as charge carrier. Currents were evoked by applying 200 ms ramps (−100 mV to +100mV, 0.2 Hz) from −80 mV holding potential, measured at the peak of the current–voltage relationship (+20 mV) and corrected for cell size to yield current densities (p*A*/p*F*, means ± sem).[14] Cell viability was determined using a standard 3-(4,5-dimethylthiazol-2-yl)-2,5-diphenyltetrazolium bromide (MTT) assay and at this dose of $A\beta P_{(1-40)}$ does not result in cell kill. The antioxidants tested reversed the current augmentation induced by $A\beta P_{(1-40)}$ without any detectable loss of cell viability (Fig. 2). The naturally occurring antioxidant melatonin exhibited the least potency (EC_{50} ~30 μM), whereas the commonly used selenium based anti-inflammatory agent ebselen (*E*pa determined as +1044 mV) showed increased potency (EC_{50} ~1 μM). In line with a variation in *E*pa of approximately 700 mV, compound **10** by far exceeded the activity of ebselen and, astonishingly, was active in nanomolar concentrations (EC_{50} ~20 nM). The diselenide **4** was also found to be highly active in cell culture, albeit considerably less active than **10**, in line with its higher oxidation potential (+ 1000 mV) and lower bioassay activity (EC_{50} ~160 nM). In accordance with a high oxidation potential (*E*pa = +1155 mV) the commonly studied Se-compound selenocystamine proved rather inactive (EC_{50} ~10 μM).

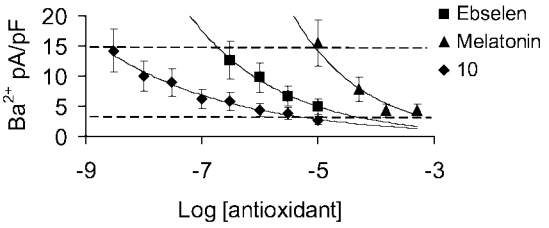

Fig. 2 Effect of antioxidant concentration on current augmentation of PC12 cells with $A\beta P_{(1-40)}$. The plot shows the preventive effect of different concentrations of antioxidants. The lower dashed line indicates current density in control cells, whilst the upper dashed line represents currents observed following 24 h incubation with 100 nM $A\beta P_{(1-40)}$.

These experiments have demonstrated that antioxidants selected on the basis of electrochemical redox-behaviour and their activity in bioassays are also likely to be highly active in cell cultures. Compound **10** exhibited the lowest *E*pa and the most promising antioxidant activity in the *in vitro* bioassays. It also showed a remarkable activity when compared to ebselen and melatonin in cell culture while showing little cell toxicity, demonstrating that this compound is among the best antioxidants available to date in cultured cells mimicking Alzheimer's disease. It is expected that this combination of chalcogen-electrochemistry with organoselenide and organotelluride catalysts will provide a new methodology for innovative antioxidant research in Alzheimer's disease.

This work was financially supported by the EPSRC (GR/N22007), the MRC, an Alzheimer's Society Innovation Grant, the Wellcome Trust, the Royal Society and the University of Exeter.

Notes and references

1 L. M. Sayre, *Curr. Opin. Chem. Biol.*, 1999, **4**, 220.
2 M. Miki, *Methods Enzymol.*, 1994, **234**, 542.
3 G. Mugesh and H. B. Singh, *Chem. Soc. Rev.*, 2000, **29**, 347; G. I. Giles, K. M. Tasker and C. Jacob, *Free Radic. Biol. Med.*, 2001, **31**, 1279.
4 L. Engman, *J. Am. Chem. Soc.*, 1992, **114**, 9737.
5 K. M. Vessman, M. Ekstrom, M. Berglund and C.-M. Andersson, *J. Org. Chem.*, 1995, **60**, 4461.
6 L. Engman, J. Persson, C. M. Andersson and M. Berglund, *J. Chem. Soc., Perkin Trans. 2*, 1992, 1309; I. A. Cotgreave, P. Moldeus, L. Engman and A. Hallberg, *Biochem. Pharmacol.*, 1991, **42**, 1481; L. Engman, D. Stern, H. Frisel, K. Vessman, M. Berglund, E. Bengt and C.-M. Andersson, *Bioorg. Med. Chem.*, 1995, **3**, 1255; C.-M. Andersson, A. Hallberg, M. Linden, R. Brattsand, P. Moldeus and I. Cotgreave, *Free Radical Biol. Med.*, 1994, **16**, 17.
7 J. Ludvík and B. Nygård, *J. Electroanal. Chem.*, 1997, **423**, 1.
8 H. Suzuki and T. Nakamura, *Synthesis*, 1992, **6**, 549; L. Engman and J. Persson, *J. Organomet. Chem.*, 1990, **388**, 71; L. Engman and J. Persson, *Synth. Commun.*, 1993, **23**, 445.
9 B. Svensmark and O. Hammerich, in *Organic Electrochemistry*, eds. H. Lund and M. M. Baizer, Marcel Dekker, Inc., New York, 3rd edn., 1991, p. 659.
10 C. Jacob, W. Maret and B. L. Vallee, *Proc. Natl. Acad. Sci. U.S.A.*, 1999, **96**, 1910.
11 C. Jacob, G. E. Arteel, T. Kanda, L. Engman and H. Sies, *Chem. Res. Toxicol.*, 2000, **13**, 3; C. Jacob, W. Maret and B. L. Vallee, *Biochem. Biophys. Res. Commun.*, 1998, **248**, 569.
12 M. Iwaoka and S. Tomoda, *J. Am. Chem. Soc.*, 1994, **116**, 2557.
13 S. C. Taylor, T. F. C. Batten and C. Peers, *J. Biol. Chem.*, 1999, **274**, 31217.
14 K. N. Green and C. Peers, *J. Neurochem.*, 2001, **77**, 953.

CHEMCOMM Communication
www.rsc.org/chemcomm

Electro-oxidation of methanol on platinum–organic metal complex mixed catalysts in acidic media†

Tatsuhiro Okada,*[a] Yoshifumi Suzuki,[b] Takuji Hirose,[c] Takako Toda[d] and Takeo Ozawa[b]

[a] *National Institute of Advanced Industrial Science and Technology, Higashi 1-1-1, Central 5, Tsukuba, Ibaraki 305-8565, Japan. E-mail: okada.t@aist.go.jp*
[b] *Department of Electrical Engineering, Chiba Institute of Technology, Tsudanuma, Narashino, Chiba 275-0016, Japan*
[c] *Department of Applied Chemistry, Faculty of Engineering, Saitama University, 255 Shimo-Ohkubo, Urawa, Saitama 338-8570, Japan*
[d] *Japan Science and Technology Corporation, Honmachi 4-1-8, Kawaguchi, Saitama 332-0012, Japan*

Received (in Cambridge, UK) 6th August 2001, Accepted 25th October 2001
First published as an Advance Article on the web 15th November 2001

Novel mixed catalysts systems have been developed using a platinum tetraammine complex with a cobalt or nickel quinolyldiamine complex supported on graphite powder and heat treated at 600 °C in argon atmosphere, for the methanol oxidation reaction in direct methanol fuel cells.

The methanol oxidation reaction (MOR) is of great technological interest because of its potential application to direct methanol fuel cells (DMFCs).[1] DMFCs have an advantage over polymer electrolyte fuel cells utilizing hydrogen gas generated through a methanol reformer, because the system can be made much simpler. However, in order to accomplish the DMFC reaction, the methanol fuel should undergo the six-electron oxidation process on the electrode catalyst given by eqn. (1).

$$CH_3OH + H_2O \rightarrow CO_2 + 6H^+ + 6e^- \quad (1)$$

This is extremely difficult to control, and therefore leads to a high overpotential. Moreover, the reaction is strongly hindered by adsorbed CO, which occurs on the catalyst surface when Pt based catalysts are used.[2,3] Electrode catalysts free from CO poisoning are thus desired in order to realize high conversion efficiency in the DMFC.

Several types of MOR electrocatalysts have been proposed including platinum based alloy catalysts[4,5] or platinum finely dispersed on oxides such as TiO_2, MoO_2, WO_3, *etc*.[6] New base catalysts have also been proposed, *e.g*. mixtures of nickel–tungsten alloy and WC prepared from nickel tungstate.[7] The best catalyst known so far is Pt–Ru alloy (50/50), the function of Ru being as sites of oxygen containing species, and capable of CO elimination by oxidation.[8–11] However, a low natural abundance of Ru is a drawback of this catalyst for practical uses.

Here, the possibility of constituting a new class of catalysts is pursued using new components that may possess novel functions. We select organic metal complexes as candidates, because these could provide the possibility to generate new functions such as CO removal by selective oxidation or strong coordination, compared to metal alloy catalysts *etc*., by manipulating molecular structures.

An aqueous mixture of 8-hydroxyquinoline (2.90 g, 0.02 mol), *o*-phenylenediamine (1.08 g, 0.01 mol) and sodium disulfate (3.08 g, 0.02 mol) was refluxed for a week at 110 °C. Recrystalization from methanol gave *N*-8-quinolyl-*o*-phenylenediamine (mqph) as an amber colored crystals (ESI†). Equimolar amounts of mqph and cobalt acetate tetrahydrate were added at room temperature in ethanol under nitrogen atmosphere in a glass flask, and the resulting solution was concentrated and refrigerated to obtain cobalt *N*-8-quinolyl-*o*-phenylenediamine diacetate [Co(mqph)] as a claret or reddish purple powder.

Mixed catalysts were prepared from the platinum precursor, platinum tetraammine chloride $Pt(NH_3)_4Cl_2{\cdot}xH_2O$, and the cobalt complex Co(mqph) in various mixing ratios. Mixing ratios used were $Pt(NH_3)_4Cl_2{\cdot}xH_2O$/Co(mqph) = 100/0, 80/20, 60/40, 50/50, 40/60, 20/80 and 0/100 (on a weight basis). 10 mg of the mixed catalyst and 40 mg of graphite powder (1–2 μm, Aldrich) were mixed in 0.5 cm^3 of ethanol in a mortar, dried in air at 80 °C for 60 min and then heat-treated in Ar atmosphere at 600 °C for 2 h in a furnace. 5 mg of the powder thus obtained (denoted Pt–Co(mqph)/C] was mixed with 100 mg of 5% Nafion solution (Aldrich) together with 0.1 cm^3 of ethanol, to obtain an ink of the mixture. 0.01 cm^3 of this mixture was transferred to the disk electrode [6 mm diameter, basal plane of high-density pyrolytic graphite (BHPG)]. The overall loading of the mixed catalyst was 1.8×10^{-4} g cm^{-2}, for the apparent electrode area of BHPG.

Electrochemical measurements were conducted in a glass cell consisting of a three-electrode system in 1 mol dm^{-3} CH_3OH–0.05 mol dm^{-3} H_2SO_4 at 25 °C, in deaerated conditions under N_2. The working electrode was the catalyst supported BHPG disk, the counter electrode was a platinum plate and a saturated calomel electrode (SCE) was used as the reference electrode. The electrode was pretreated by cyclic potential scanning between −300 and 1200 mV *vs*. SCE (+316 mV on the RHE scale) at 100 mV s^{-1}. Potentials were scanned in the anodic direction at a scan rate of 1 mV s^{-1} for the polarization measurement in the potential range −200 to 1000 mV.

Fig. 1 shows the polarization curves of MOR for mixed catalysts Pt–Co(mqph)/C of various mixing ratios. The total catalyst amount corresponds to 12% Pt/C in the case of 100/0 mixing ratio. The polarization curves were reproducible to within 10%. Compared with Pt/C or Co(mqph)/C alone, 40/60 → 60/40 mixtures revealed extraordinarily high MOR current density indicating cooperative phenomena between two components.

On the other hand, using the organic complex $Co(NH_3)_6Cl_3$ in place of Co(mqph) as a precursor material led to no MOR activity. In this system, the activity did not exceed that of pure Pt. The initial structure of the complex thus clearly affects the catalytic function after the heat treatment.

XRD showed evidence of inter-metallic compounds between Pt and Co for the mixed system of Pt and $Co(NH_3)_6Cl_3$ after heat treatment, but not for the mixed system of Pt and Co(mqph). According to X-ray photoelectron spectroscopy (XPS), Co 2p and N 1s peaks for Pt–Co(mqph)/C mixed catalysts were identified as Co coordinated by N ligands. As anticipated from the temperature of heat treatment of the catalyst, only a small extent of demetallation of the Co complex was observed after the heat treatment, but major peaks indicated coordinated states between Co and N. The particle size of the

† Electronic supplementary information (ESI) available: reaction scheme for the preparation of mqph and spectroscopic data. See http://www.rsc.org/suppdata/cc/b1/b10/b107132g/

 DOI: 10.1039/b107132g

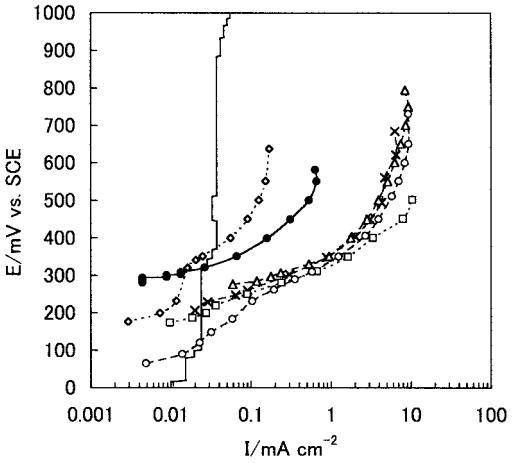

Fig. 1 Polarization curves of methanol oxidation on mixed catalysts Pt–Co(mqph)/C with various mixing ratios. Solution: 1 mol dm^{-3} CH_3OH–0.05 mol dm^{-3} H_2SO_4 at 25 °C, under deaerated conditions (N_2). $Pt(NH_3)_4Cl_2{\cdot}xH_2O$/Co(mqph) ratios: (●) 100/0, (×) 80/20, (△) 60/40, (□). 50/50, (○): 40/60, (◇) 20/80, (——) 0/100.

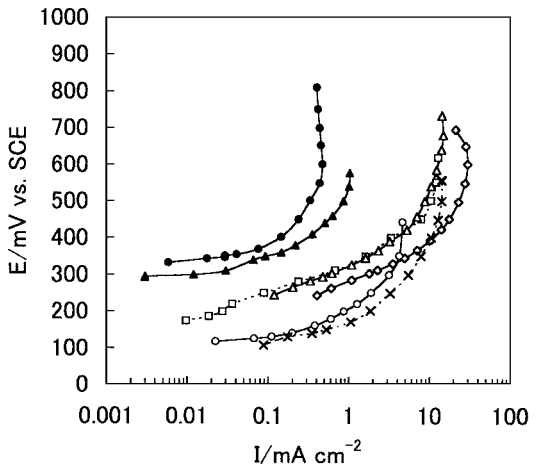

Fig. 2 Comparison of performances of methanol oxidation electrocatalysts: (□) 50/50 Pt–Co(mqph)/C, (◇) 50/50 Pt–Ni(mqph)/C, (△) 50/50 Pt–Fe(mqph)/C, (▲) 50/50 Pt–$Co(NH_3)_6Cl_3$/C, (●) 10% Pt/C (Aldrich), (○) 10% Pt–Ru/C (Shinshu Univ.), (×) 20% Pt–Ru/C (E-TEK).

mixed catalysts tended to be smaller than for pure Pt/C after the heat treatment, but did not solely account for the difference in observed MOR activity. The role of the graphite supporting material may be important for the stability of complexes at high temperature.

In Fig. 2, MOR performances are compared for several types of mixed catalysts of platinum and M(mqph) (M = Fe^{3+}, Co^{2+} and Ni^{2+}) complexes. Results for 10% Pt/C (Aldrich), 10% Pt–Ru/C (Shinshu University) and 20% Pt–Ru/C (E-TEK) are also included. The amount of mixed catalyst corresponds to 10% on C. Among the three central metals of the M(mqph) complex prepared as precursors, Ni showed the best MOR activity. The MOR activity of Pt-Ni(mqph)/C of 50/50 ratio is very promising far exceeding the performance of Pt–Ru in terms of current density.

To our knowledge, there have been no reports concerning methanol oxidation utilizing organic metal complexes in acidic media. Only methanol oxidation on a nickel porphyrin complex has been reported in basic media for methanol sensors, with polymerized nickel porphyrin functioning as 3-D Ni(II)/Ni(III) redox centers.[12] It is discovered for the first time that mixed catalysts of platinum and organic metal complexes exhibit very high catalytic ability for MOR, which could have very high potential considering the wide variety and applicability of such organic complexes. The function and mechanism of the organic complex in promoting the reaction is not clear at this stage, but some concerted process is likely. Further study on the detailed mechanism, the longevity of the catalysts and search for other combinations of platinum (or other metals) and organic complex mixed catalysts is now under progress.

We thank Professor Yoshio Takasu of Shinshu University for supplying Pt–Ru/C catalysts.

Notes and references

1 S. Wasmus and A. Küver, *J. Electroanal. Chem.*, 1999, **461**, 14.
2 H. A. Gasteiger, N. Markovic, P. N. Ross, Jr. and E. J. Cairns, *J. Phys. Chem.*, 1993, **97**, 12 020.
3 T. Frelink, W. Visscher, A. P. Cox and J. A. R. van Veen, *Electrochim. Acta*, 1995, **40**, 1537.
4 M. M. P. Janssen and J. Moolhuysen, *Electrochim. Acta*, 1976, **21**, 861.
5 M. M. P. Janssen and J. Moolhuysen, *Electrochim. Acta*, 1976, **21**, 869.
6 P. K. Shen and A. C. C. Tseung, *J. Electrochem. Soc.*, 1994, **141**, 3082.
7 G. T. Burnstein, C. J. Barnett, A. R. J. Kucernak and K. R. Williams, *Electrochem. Soc. Lett.*, 1996, **143**, L139.
8 M. Watanabe and S. Motoo, *J. Electroanal. Chem.*, 1975, **60**, 267.
9 A. Aramata, M. Matsuda and T. Kodera, *J. Electrochem. Soc.*, 1989, **136**, 3288.
10 P. S. Kauranen, E. Skou and J. Munk, *J. Electroanal. Chem.*, 1996, **404**, 1.
11 D. Chu and S. Gilman, *J. Electrochem. Soc.*, 1996, **143**, 1685.
12 A. Ciszewski and G. Milczarek, *J. Electroanal. Chem.*, 1997, **426**, 125.

CHEMCOMM Communication
www.rsc.org/chemcomm

Deep desulfurization of diesel fuel by extraction with ionic liquids

A. Bösmann, L. Datsevich, A. Jess,* A. Lauter, C. Schmitz and P. Wasserscheid

Institut für Technische und Makromolekulare Chemie, RWTH Aachen, Sammelbau Chemie, Worringer Weg 1, D-52074 Aachen, Germany, E-mail: jess@itmc.rwth-aachen.de

Received (in Cambridge, UK) 17th September 2001, Accepted 24th October 2001
First published as an Advance Article on the web 15th November 2001

A new approach for the deep desulfurization of diesel fuels by extraction with ionic liquids is described.

In recent years deep desulfurization of diesel fuel has attracted much attention due to the gradual reduction of the statutory sulfur content in most western countries. In 2005 the max. S-content will be limited down to 10–50 ppm compared to today's value of 500 ppm S. These efforts aim to limit SO_2 emission from diesel engines and to protect equipment from corrosion. Moreover, lower sulfur content of diesel fuels would allow the use of other catalysts for the reduction of NO_x emissions.

In industry, desulfurization of diesel is actually carried out by hydrotreating. Generally, this allows the elimination of aliphatic and alicyclic sulfur compounds.[1] However, dibenzothiophene (DBT) and especially 4,6-alkyl-substituted DBTs are difficult to convert into H_2S due to the sterically hindered adsorption of these compounds on the catalyst surface.[2–4] The expenses (hydrogen pressure, reactor size) to meet future legal specifications with classical hydrotreating processes are therefore high. Thus, alternative ways for the production of low or even ultra-low sulfur contents in diesel oil are attractive.

In the present paper, the use of ionic liquids (ILs) for the selective extraction of sulfur compounds from diesel fuel is described for the first time. ILs are low melting (< 100 °C) salts which represent a new class of non-molecular, ionic solvents.[5,6] Up to now, ILs have been mainly studied with respect to biphasic homogeneous catalysed processes. The range of known and available ILs has been expanded so that many different candidates are accessible today.[7,8]

In a first set of experiments, the desulfurization of a model diesel oil obtained by dissolving 500 ppm DBT in *n*-dodecane was investigated. Based on the initial idea to extract the sulfur compound by chemical interaction, the extraction with Lewis- and Brønsted-acidic ILs was studied. As Lewis-acidic ILs, acidic mixtures of 1-*n*-butyl-3-methylimidazolium ([BMIM]) chloride and 1-ethyl-3-methylimidazolium ([EMIM]) chloride[8] with $AlCl_3$ (molar ratio [cation]Cl/$AlCl_3$ = 0.35/0.65) were investigated. A 1 : 1 (mol/mol) mixture of two trialkylammonium methanesulfonate salts was tested as Brønsted-acidic ILs. All ILs formed a biphasic system with the model oil at room temperature. Application of the methanesulfonate melt had the additional advantage of having an easy analytical control of IL leaching into the (for this specific experiment S-free) oil, although this was never observed.

For the extraction experiments, the IL was added to an excess of model oil in a mass ratio of 1/5. The obtained biphasic mixture was then stirred at room temperature. Samples were taken every 5 min. However, it was found that the extraction process proceeded quickly. Consequently, the final sulfur concentration was reached after 5 min and longer stirring did not result in lower sulfur contents. All sulfur contents presented were determined with an Antek Pyroreactor 771, which was equipped with an Antek UV-sulfur-detector 714. Repeated measurements indicated an average error of this method of ± 5 ppm.

The results of a single extraction step with selected Lewis- and Brønsted-acidic ILs are presented in Table 1. All ILs under investigaton showed good properties to extract DBT out of the model oil. The comparison of the extraction experiments with the two different chloroaluminate melts suggests a certain influence of the ionic liquid's cation (compare entries a and b in Table 1). The relatively good extraction properties of the Brønsted-acidic methanesulfonate mixture indicates both good extraction power for DBT and no (or at least not measurable) leaching of the ionic liquid into the model oil. The solubility of hydrocarbons in ILs compared to S-compounds is very low.

Table 1 Desulfurization of model diesel fuel (500 ppm sulfur in *n*-dodecane) by extraction with Lewis- and Brønsted-acidic ionic liquids[a]

Entry	Ionic liquid	Sulfur content/ ppm
a	[BMIM]Cl/$AlCl_3$ = 0.35/0.65[b]	275
b	[EMIM]Cl/$AlCl_3$ = 0.35/0.65	335
c	[HN(C_6H_{11})Et_2][CH_3SO_3]/[$HNBu_3$][CH_3SO_3] = 1/1	310

[a] *General conditions*: room temperature, mass ratio model oil/IL = 5/1, extraction time: 15 min, initial sulfur content 500 ppm. [b] Mol/mol.

In order to understand in more detail the observed DBT extraction, the extraction with the neutral methanesulfonate mixture [N(C_6H_{11})Et_2Me][CH_3SO_3]/[NBu_3Me][CH_3SO_3] = 1/1 (C_6H_{11} = cyclohexyl) under otherwise identical conditions was investigated. The latter was obtained in a simple manner by mixing equimolar amounts of N(C_6H_{11})Et_2 and NBu_3 with a stoichiometric amount of methanesulfonic acid methylester. Surprisingly, the sulfur content of the model oil was found to be as low as 300 ppm after a single extraction step. This demonstrates—at least for the methanesulfonate melts under investigation—that the ionic liquid's extraction power for DBT is not uniquely based on chemical interactions involving the acid proton.

Encouraged by these results, different cation/anion combinations of neutral ILs in the extraction of DBT were tested. Selected results of an anion variation with ILs of the general type [BMIM][anion] are given in Table 2.

The data indicate that the desulfurization is hardly affected by the chemical nature of the anion. Only the IL with the somewhat bigger octylsulfate ion showed significantly better extraction properties. From these results it can be concluded that the size of the ions is rather important for the extraction effect. This

Table 2 Comparison of different anions in the desulfurization process of a model diesel oil (500 ppm sulfur in *n*-dodecane) by extraction with neutral ionic liquids of the general type [BMIM][anion][a]

Entry	Anion	Sulfur content/ppm
a	$[PF_6]^-$	440
b	$[CF_3SO_3]^-$	430
c	$[BF_4]^-$	420
d	Cl^-	410
e	$[MeSO_4]^-$	410
f	$[MeSO_3]^-$	410
g	$[OcSO_4]^-$	350

[a] *General conditions*: 60 °C (except entry d: 80 °C), mass ratio model oil/IL = 5/1, reaction time 15 min, initial sulfur content: 500 ppm.

 DOI: 10.1039/b108411a

Table 3 Comparison of different cations in the extraction of DBT from *n*-dodecane with different tetrafluoroborate ionic liquids[a]

Cation	Sulfur content/ppm
[EMIM]	450
[BMIM]	420
[OMIM]	380

[a] *General conditions*: 50 °C, mass ratio model oil/IL = 5/1, reaction time 15 min, initial sulfur concentration 500 ppm; [OMIM] = 1-methyl-3-*n*-octylimidazolium.

Table 4 Multistage desulfurization of predesulfurized (real) diesel oil[a]

Stage	[BMIM]Cl/$AlCl_3$	$[HN(C_6H_{11})Et_2]$-$[CH_3SO_3]$/$[HNBu_3]$-$[CH_3SO_3]$ = 1/1	[BMIM]-[octylsulfate]
1	375	375	375
2	220	330	320
3	160	300	280
4	130	270	260
5	75	240	235

[a] 60 °C, mass ratio diesel oil/IL = 5/1, reaction time: 15 min.

assumption was further supported by extraction experiments with different tetrafluoroborate salts (Table 3).

In this context, it is important to note that the comparison of different ILs in Tables 2 and 3 is based on equal mass ratio model oil/IL. A comparison on the base of equal molar levels would show an even more pronounced effect of the cation's/anion's size on the extraction power of the ILs. A possible explanation for this behaviour may be that the physical solubility of DBT in the IL is dependent on steric factors in the IL.

In order to check the feasibility of our concept for a deep desulfurization process, we tried to reach very low sulfur levels by application of a multistage extraction process (mixer–settler-system). For these experiments the best IL candidate [BMIM]Cl/$AlCl_3$: 0.35/0.65 was chosen as extraction medium. The desulfurized model oil from the first extraction step was again treated with fresh ionic liquid. This process was repeated up to four times. The results with different mass ratios model oil/IL are presented in Fig. 1.

As expected, Fig. 1 shows that a lower mass ratio of model oil to ionic liquid results in lower sulfur contents. However, sulfur contents below 50 ppm can be reached for all mass ratios if the number of extraction steps is high enough. The almost linear relationship of log(S-content) *vs*. the number of extraction steps indicates that the extraction can be formally described by a partition coefficient according to Nernst's law. This is confirmed by re-extraction experiments (mixture of IL with extracted S-compound and S-free *n*-dodecane): The same distribution of sulfur (ratio of concentration in IL to concentration in *n*-dodecane) is obtained, which was tested by the re-extraction of DBT from the loaded ionic liquid $[HN(C_6H_{11})Et_2][CH_3SO_3]/[HNBu_3][CH_3SO_3]$ = 1/1 with in this case S-free *n*-dodecane. In this context NMR measurements of the used ILs confirm also that the extracted DBT remains unreacted. Thus regeneration of the ILs should be generally achievable, although more systematic experiments are needed.

In a technical extraction process, the IL, which has been loaded with organic sulfur components in the extraction column (or mixer–settler-system), would be continuously regenerated in a second column, and then pumped back into the extraction unit. Thus the potential to regenerate the IL is an important aspect. Interesting re-extraction media are probably light alkanes (C_2–C_5) or supercritical CO_2, as these solvents can be easily recovered and separated from the higher boiling sulfur compounds by evaporation. The organic sulfur would than be converted into elemental sulfur by the common Claus-process.

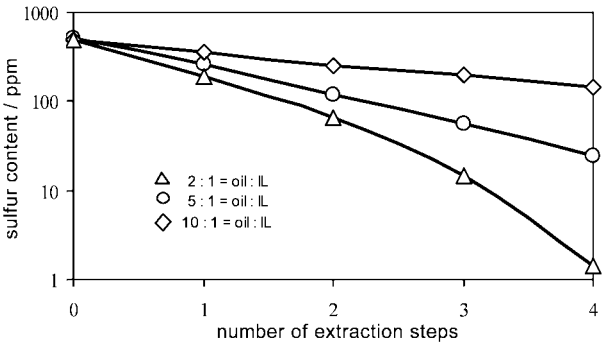

Fig. 1 Multistage desulfurization of model diesel oil (500 ppm sulfur in *n*dodecane) by the IL [BMIM]Cl/$AlCl_3$ (0.35/0.65; different mass ratios oil/IL) at room temperature.

Subsequently, the new desulfurization concept was tested by additional experiments with a 'real' predesulfurised diesel oil (without additives, sulfur content: 375 ppm). As expected, the extraction of real diesel oil is much more complicated due to its complex chemical composition including many different sulfur compounds and other impurities like organic nitrogen and oxygen compounds.

Nevertheless, the results of experiments with predesulfurized diesel are also promising. As shown in Table 4, the Lewis-acidic ionic liquid [BMIM]Cl/$AlCl_3$: 0.35/0.65 showed much higher efficiency in the sulfur extraction from real diesel in comparison to the methanesulfonate and octylsulfate melts.

This indicates that Lewis acid–base interactions enhance the extraction power of the IL here. Nevertheless, the extraction power of the neutral methanesulfonate and octylsulfate melts is still remarkable. However, more extraction steps are necessary in case of 'real' diesel oil to reach future technical sulfur content specifications (< 50 ppm). The use of $AlCl_3$-free ILs is particularly promising as the use of $AlCl_3$ in desulfurization is probably unlikely to be accepted by refiners.

In conclusion, the presented results show a new approach for the deep desulfurization of diesel oil, especially with regard to those sulfur compounds that are very difficult to remove by common hydrodesulfurization techniques. Traces of such sulfur compounds could easily be removed. The new method is based on the extraction of the sulfur compounds with ILs. The application of very mild process conditions (low pressure and temperature) is an additional advantage of this new approach in comparison to traditional HDS.

Generally the extraction of polarizeable compounds by ionic liquids may be a possibility to isolate valued products which reside in complex mixtures of a multitude of different organic substances as is likely to occur in aromas and scents.

Present work is directed towards a deeper understanding of the extraction properties of ILs, and to identify inexpensive, unchlorinated IL systems with enhanced extraction power.

The authors acknowledge Miro refinery/Karlsruhe, Germany for the donation of the predesulfurized diesel oil.

Notes and references

1 S. Zaczepinski, Exxon Diesel Oil Deep Desulfurization (DODD), in *Handbook of Petroleum Refining Processes*, ed. R. A. Meyers, McGraw-Hill, New York, 1996, ch. 8.7.
2 C. Kwak, J. J. Lee, J. S. Bae, K. Choi and S. H. Moon, *Appl. Catal. A*, 2000, **200**, 233.
3 R. Shafi and G. J. Hutchings, *Catal. Today*, 2000, **59**, 423.
4 X. Ma, K. Sakanishi and I. Mochida, *Ind. Eng. Chem. Res.*, 1994, **33**, 218.
5 P. Wasserscheid and W. Keim, *Angew. Chem., Int. Ed.*, 2000, **39**, 3772.
6 T. Welton, *Chem. Rev.*, 1999, **99**, 2071.
7 J. D. Holbrey and K. R. Seddon, *Clean Products Processes*, 1999, **1**, 223.
8 Many ionic liquids are commercially available nowadays. For example, [BMIM]Cl and [EMIM]Cl can be purchased from Solvent Innovation GmbH, Cologne, Germany (www.solvent-innovation.de).

CHEMCOMM Communication
www.rsc.org/chemcomm

Design of silica-coated microcapsules for bioencapsulation

Thibaud Coradin, Emilie Mercey, Laurent Lisnard and Jacques Livage*

Laboratoire de Chimie de la Matière Condensée, CNRS-UMR 7574, 4 place Jussieu, F-75252 Paris cedex 05, France. E-mail: livage@ccr.jussieu.fr

Received (in Cambridge, UK) 13th September 2001, Accepted 24th October 2001
First published as an Advance Article on the web 15th November 2001

Alginate-based microcapsules are coated with silica, providing enhanced mechanical resistance, protein diffusion and allowing enzyme immobilization.

The design of microcapsules for cell encapsulation is a major challenge for tissue transplantation.[1] The most popular device is based on alginic acid, a copolymer of guluronic and mannuronic acids, that can be prepared as gel beads in the presence of divalent metals such as Ca^{2+}.[2] Additional coating with poly(L-lysine) and liquefaction of the inner-core alginate by complexing Ca^{2+} (*i.e.* with citrate) leads to the formation of hollow capsules with a semi-permeable membrane.[3] The strengthening of this membrane is made possible by using other polycationic systems[4] or adding a second alginate layer.[5]

The possibility to coat alginate/poly-lysine capsules with silica was studied in order to improve their mechanical properties. This strategy was based on our recent work showing that poly-lysine is able to favor the condensation of silica.[6]

The principle of preparation of the microcapsules is illustrated in Scheme 1. Ca^{2+}/alginate beads, *ca.* 4 mm in diameter, were prepared by the dropwise addition of an aqueous solution of alginic acid (1.5 wt%) to a solution of $CaCl_2$ (0.1 M). Beads were then placed into a solution of poly-lysine, alginate or silica (0.1 w/v%) with a Tris·HCl buffer (0.05 M, pH = 7.2) and citrate (0.05 M).

Alginate/poly-lysine coated with alginate (APA), with sodium silicate (APS) and colloidal silica (APC) were prepared.† The sodium silicate concentration was limited to 30 mM to avoid solution gelation during the coating process. APC beads could be prepared with a concentration up to 60 mM from Ludox sols (Aldrich). The contact time between the poly-lysine/alginate beads and silica solutions was optimized at 2 h in order to obtain a complete and homogeneous coating.

The presence of silica was ascertained by IR spectroscopy showing the appearance of a band at 1100 cm^{-1}, corresponding to the stretching vibration mode of $[SiO_4]$ tetrahedra, and confirmed by energy dispersive X-ray analysis.

Scanning electron micrographs of dried APA, APS ([Si] = 30 mM) and APC ([Si] = 60 mM) are shown in Fig. 1. Sodium silicate condensation leads to a smooth coating whereas silica particles lead to a more granular surface. Fig. 1 also shows the homogeneous 10 μm thick membrane of APS.

The mechanical strength of the hollow capsules was investigated by stirring 100 beads at 300 rpm in 50 mL Tris·HCl buffer and counting fractured capsules at selected intervals of time. As shown in Fig. 2, sodium silicate coating enhances membrane resistance when compared to alginate whereas colloidal silica does not appear to be suitable for long-term use. This is consistent with SEM studies and suggests that sodium silicate is highly condensed at the poly-lysine interface whereas the colloid coating consists of silica particles adsorbed on the polyamine chain with only weak interparticle bonding.

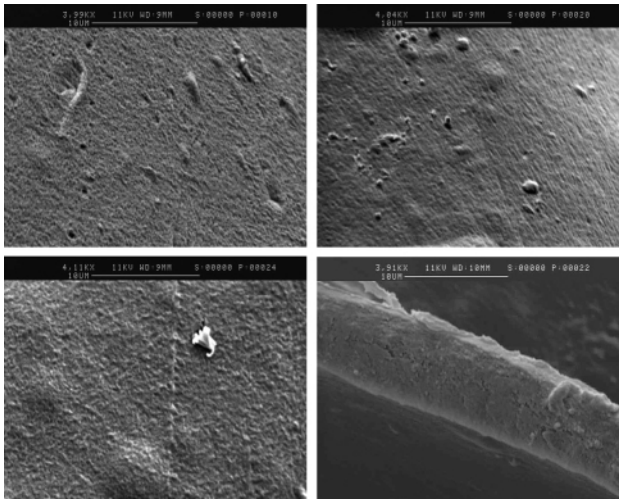

Fig. 1 Scanning electron micrographs of (top left) APA, (top right) APS, (bottom left) APC surfaces and (bottom right) APS membrane (bar = 10 μm).

The existence of a molecular weight cut-off for diffusion through the membrane is a key feature for cell transplantation since small substrates or products should be able to diffuse through the membrane, whereas larger molecules such as antibodies should not be able to interact with the immobilized species.[1] The diffusion of myoglobin (≈20 kDa) in the beads was followed by the intensity decrease of its absorption band at λ = 409 nm. Fig. 2 shows that protein diffusion is easier in silica coated beads. In contrast, following the same procedure, no diffusion of a larger protein, Bovine Serum Albumin (≈70 kDa) could be observed after 2 h.‡ Differences in diffusion properties arise from the porosity of the external coating. Silica gels obtained from sodium silicate or Ludox have been shown to be in the mesoporous range (50–100 Å).[7] Layer-by-layer coating by polyelectrolytes of opposite charge can lead to dense membranes if the charge density of both polymers is optimized.[8] This is the case at pH 7 where carboxylate groups from

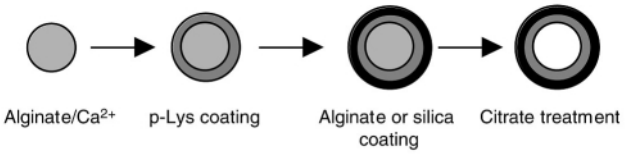

Scheme 1 Schematic representation of the step-by-step formation of hollow beads.

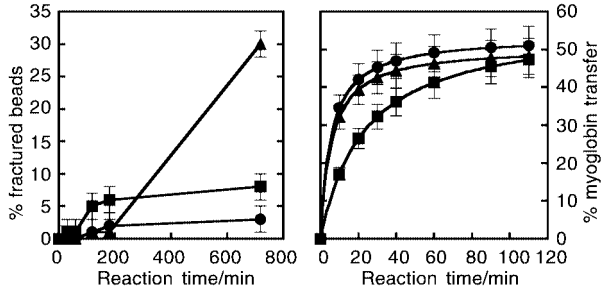

Fig. 2 Comparison of (left) mechanical resistance and (right) myoglobin diffusion for APA (■), APS (●) and APC (▲) empty beads.

 DOI: 10.1039/b108324b

alginic acid ($pK_a \approx 5$) and amino groups from the poly-lysine side chains ($pK_a \approx 9$) are mostly ionised.

The final issue to be raised is the biocompatibility of these materials. Sol–gel silica has already been demonstrated to be suitable for cell encapsulation.[9] We have recently reported that encapsulation of *E. coli* bacteria within sol–gel matrices obtained from sodium silicate and Ludox precursors led to a limited lysis of the cell membrane.[10] This effect was assigned to the confinement of the cell within the silica network rather than to the reaction conditions which were very similar to those used in this work (pH ≈ 7, ionic strength < 0.2 M, room temp., low silica content). As a first step, we have studied the encapsulation of β-galactosidase in APS beads. The catalytic activity of this enzyme can be measured *via* the hydrolysis of 4-nitrophenyl-β-D-galactopyranoside that yields the formation of *p*-nitrophenol, a yellow compound that can be easily titrated by UV–VIS spectroscopy.[10] Moreover, the enzyme should be too large (≈ 135 kDa) to be leached out of the beads. The enzyme was introduced in the initial alginate solution before the formation of Ca^{2+}/alginate beads. The enzymatic activity§ of β-galactosidase in filled and empty APS beads was found to be 1.2 ± 0.2 U mg^{-1} and 1.0 ± 0.2 U mg^{-1}, respectively. A comparison with the activity of a solution of β-galactosidase in Tris·HCl buffer (1.8 ± 0.2 U mg^{-1}) shows that enzymes are not severely denaturated during the entrapment process. After rinsing the beads, they could be re-used, leading to similar enzymatic activities, therefore demonstrating that no leaching occurs during the activity measurements. Therefore, it suggests that partial leaching of β-galactosidase took place during the gelation of alginate droplets in aqueous $CaCl_2$. Moreover, it was observed that adding β-galactosidase leads to weakening of the membrane. Beads could be partially damaged during the citrate treatment, a fact that could account for the difference between filled and empty capsules.

Such an association of mineral and bioorganic components, mimicking Nature's strategy to design composite materials,[11] appears therefore very promising. Further work will now focus on size reduction of capsules and cytocompatibility investigations.

Notes and references

† 10 mL of a 1.5 wt% alginic acid solution (Fluka) was added dropwise through a 0.9 mm needle to 100 mL of a 0.1 M solution of $CaCl_2$. After 1 h stirring, *ca*. 600 beads were recovered and washed with 0.05 M Tris·HCl (pH = 7.2) buffer. They were then placed in contact for 30 min with a 0.01 w/v% poly-lysine (≈ 30 kDa) solution prepared in 0.85 wt% NaCl. After recovering and washing, beads were added for 6 min to a 0.03 wt% solution of alginic acid (APA) or 2 h in a dilute solution of sodium silicate (Riedel-de Haen) (APS) or Ludox sols (Aldrich) (APC). The dissolution of the inner-core alginate was performed by complexing Ca^{2+} ions with citrate (0.05 M). After washing, beads were kept in Tris·HCl buffer.

‡ It was checked that similar experiments using fractured beads led to a very small decrease in the protein content of the solution. This therefore indicates that the observed decrease is due to the diffusion of the proteins inside the beads and not to adsorption on their surface.

§ Enzymatic activity is given in U per mg of enzyme in the starting alginate solution. 1 U corresponds to the hydrolysis of 1 μmol of 4-nitrophenyl-β-D-galactopyranoside per minute.

1 *Immobilised Living Cell Systems. Modelling and Experimental Methods*, ed. R. G. Willaert, G. V. Baron and L. De Backer, Wiley, Chichester, 1996; H. Uludag, P. De Vos and P. A. Tresco, *Adv. Drug Deliv. Rev.*, 2000, **42**, 29.

2 A. Haug, B. Larsen and O. Smidsrod, *Acta Chem. Scand.*, 1972, **26**, 79.

3 F. Lim and A. M. Sun, *Science*, 1980, **210**, 909.

4 Y. J. Wang, *Mater. Sci. Eng., C*, 2000, **13**, 59.

5 M. F. A. Goosen, G. M. O'Shea, H. M. Gharapetian, S. Chou and A. M. Sun, *Biotechnol. Bioeng.*, 1985, **27**, 146.

6 T. Coradin and J. Livage, *Colloids Surf., B*, 2001, **21**, 329.

7 R. K. Iler, *The Chemistry of Silica: Solubility, Polymerization, Colloid and Surfaces Properties, and Biochemistry*, Wiley, New York, 1979.

8 H. Möhwald, *Colloids Surf., A*, 2000, **171**, 25; A. Bartkowiak and D. Hunkeler, *Chem. Mater.*, 1999, **11**, 2486.

9 J. Livage, *C. R. Acad. Sci. Paris Ser. IIb*, 1996, **322**, 217; E. J. A. Pope, K. Braun and C. M. Peterson, *J. Sol-Gel Sci. Technol.*, 1997, **8**, 635; K. S. Finnie, J. R. Bartlett and J. L. Woolfrey, *J. Mater. Chem.*, 2000, **10**, 1999; G. Carturan, R. Dal Monte and M. Muraca, *Mater. Res. Soc. Symp. Proc.*, 2000, **628**, CC10.1.1.

10 A. Coiffier, T. Coradin, C. Roux, O. Bouvet and J. Livage, *J. Mater. Chem.*, 2001, **11**, 2039.

11 *Biomineralization, Chemical and Biochemical Perspectives*, ed. S. Mann, J. Webb and R. J. P. Williams, VCH, Weinheim, 1989.

CHEMCOMM Communication
www.rsc.org/chemcomm

Diastereo- and enantioselective synthesis of α,β-disubstituted γ-nitro methyl sulfonates†

Dieter Enders,*[a] Otto Mathias Berner,[a] Nicola Vignola[a] and Jan Willem Bats[b]

[a] *Institut für Organische Chemie der RWTH Aachen, Professor-Pirlet-Strasse 1, D-52074 Aachen, Germany. E-mail: enders@rwth-aachen.de; Fax: +49-241-8092 127*

[b] *Institut für Organische Chemie der Universität Frankfurt, Marie-Curie-Strasse 11, D-60439 Frankfurt am Main, Germany*

Received (in Cambridge, UK) 24th September 2001, Accepted 22nd October 2001
First published as an Advance Article on the web 15th November 2001

A novel asymmetric synthesis of highly enantioenriched homotaurine precursors has been developed *via* diastereoselective Michael addition of lithiated enantiopure sulfonates to nitroalkenes by using 1,2:5,6-di-*O*-isopropylidene-α-D-allofuranose as chiral auxiliary.

Recently, we have reported a highly efficient asymmetric synthesis of α-substituted methyl sulfonates by α-alkylation of lithiated enantiopure sulfonates using 1,2:5,6-di-*O*-isopropylidene-α-D-allofuranose as easily available chiral auxiliary.[1] We have now extended this new methodology to asymmetric Michael additions using nitroalkenes as acceptors leading to α,β-disubstituted γ-nitro methyl sulfonates.

Homotaurine (3-aminopropanesulfonic acid) is the sulfonic acid equivalent of γ-aminobutyric acid (GABA), which is of great importance in the regulation of neurological disorders.[2] Consequently, homotaurine possesses many pharmacological effects, increasing for example the synthesis of dopamine in the brain.[3] Furthermore, the γ-aminosulfonic acids can provide interesting applications in the area of peptide mimetics. We envisioned to gain access to γ-aminosulfonic acid precursors *via* an asymmetric Michael reaction to nitroalkenes. In recent years, a great variety of asymmetric Michael additions have been developed,[4] including nitroalkenes as excellent acceptors, which are easily obtained *via* the Henry reaction[5] and subsequent dehydration. In addition to being very reactive, the nitro group can be converted into a broad range of functionalities such as the amino group.[6] Although several reports of enantioselective Michael additions to nitroalkenes do exist,[7] no asymmetric 1,4-additions of metalated sulfonates bearing a chiral auxiliary have been reported so far.

As is depicted in Scheme 1, the enantiopure sulfonates **1**[1] were metalated with *n*-butyllithium in tetrahydrofuran and allowed to react with nitroalkenes[8,9] at −(90–95) °C to obtain the highest diastereoselectivity. In addition, any side reactions are minimized by using low temperatures, mainly the attack of *n*-butyllithium on the sulfonate moiety. For this reason, exactly one equivalent of base must be utilized. After the reaction is quenched, the aqueous phase must be extracted several times with dichloromethane (TLC control) to ensure high yield, as some of the Michael adducts have a solubility in water. The Michael adducts **2** were obtained in very good to excellent yields (84–99%) and high diastereoselectivities of 80–88% (Table 1). Only three of the possible four diastereoisomers could be detected. In the case of **2a**, for example, a ratio of 88.5:7.5:4 was obtained. Further increase in diastereoselectivity could be achieved either *via* preparative HPLC or recrystallization (ds = 84–≥ 99%). In the case of compound **2d**, preparative HPLC purification resulted in a mixture of the two major diastereomers. If the two diastereomers would remain as such rather than enantiomers *after* the cleavage of the auxiliary, then a possible separation at a later stage would still provide enantiomerically pure products (*vide infra*).

† Dedicated to Professor Helmut Zahn on the occasion of his 85th birthday.

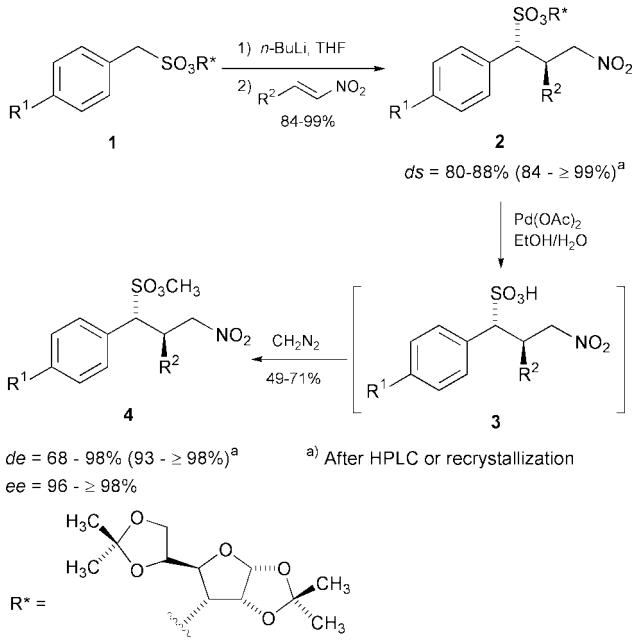

Scheme 1

Originally, the removal of the chiral auxiliary to form the corresponding sulfonic acids **3** was achieved by refluxing the Michael adducts in an EtOH–H_2O solution containing 20 mol% $Pd(OAc)_2$ for 12 h. In contrast to the alkylation products,[1] care must be taken when the reaction is performed. The liberated sulfonic acid can cause a Meyer reaction[10] to occur, which converts the primary nitro group into a carboxylic acid. The yields could be significantly increased if additional H_2O was added to the reaction. This reduces the side reactions allowing an increase of reaction time which results in higher yields (Table 2). In analogy, it has been reported that additional H_2O slows the related Nef-reaction.[11] Also elementary Pd^0 can be used to achieve cleavage of the auxiliary indicating that

Table 1 Asymmetric Michael addition of sulfonates **1** to nitroalkenes to afford the 1,4-adducts **2**

Product **2**	R^1	R^2	Yield (%)	ds (%)[a]	$[\alpha]_D$ (*c*, $CHCl_3$)[b]
a	H	Et	88	88 (≥99)[c]	+86.2 (0.98)
b	H	*n*-Pr	90	86 (≥99)[c]	+81.2 (0.82)
c	H	*i*-Pr	84	86 (≥99)[d,e]	+101.0 (1.15)
d	H	$Ph(CH_2)_2$	99	80 (84)[f]	+75.0 (1.10)
e	*t*-Bu	Et	91	87 (≥98)[d]	+80.7 (0.94)

[a] In brackets after HPLC. [b] All optical rotations were measured in Uvasol grade $CHCl_3$ at rt. [c] Determined by HPLC using a chiral stationary phase (Daicel AD, *n*-heptane/isopropyl alcohol 95:5). [d] Determined by ^{13}C NMR. [e] After recrystallization. [f] Estimated by ^1H NMR and ^{13}C NMR.

 DOI: 10.1039/b108567k

elementary palladium may be required for the reaction. To obtain the final product in a more accessible form, the sulfonic acids **3** were converted with diazomethane to the corresponding methyl sulfonates **4**. The methyl groups can be considered as suitable 'protecting groups' due to their ability to be easily cleaved under mild conditions. The title methyl sulfonates **4** were obtained in moderate to good yields and as virtually pure stereoisomers (Table 2).

Table 2 Removal of the chiral auxiliary to form the title methyl sulfonates

Product **4**	R^1	R^2	Yield (%)[a]	ds (%)[b]	ee (%)[c]	$[\alpha]_D$ (*c*, $CHCl_3$)[d]
a	H	Et	53 (71)	≥98	≥98	+33.1 (0.72)
b	H	*n*-Pr	56 (70)	≥98	≥98	+25.3 (1.15)
c	H	*i*-Pr	49	≥98	≥98	+49.6 (0.73)
d	H	$Ph(CH_2)_2$	58	68 (93)[e]	≥98	+24.4 (0.62)
e	*t*-Bu	Et	51 (63)	≥98	≥96	+27.6 (0.81)

[a] Yields in paranthesis are obtained by using an EtOH–H_2O-solution as solvent. [b] Measured by ^1H NMR and ^{13}C NMR. [c] Based on de values of the Michael adducts. [d] All optical rotations were measured in Uvasol grade $CHCl_3$ at rt. [e] After recrystallization.

NOE-studies of the products revealed that the protons at the α and β positions are *anti* to each other. The absolute configuration of the newly formed stereogenic centers was established unambiguously as *R*,*R* by X-ray crystallography.‡ The stereochemistry of the major diastereomer of other Michael adducts is expected to be also *R*,*R* and is based on the assumption of an uniform mechanism operating in the addition to nitroalkenes. Further evidence is obtained for this assumption by the fact that the related electrophilic substitution under α-alkylation[1] shows the same relative topicity.

To confirm that the cleavage of the auxiliary occurs in the presence of a nitro group without epimerization of the α-position of the sulfonyl group, compound **2d**, which consists of only the two major diastereomers in a ratio of 84:16, was chosen as a case study. If the reaction is truly epimerization free, then the ratio should be identical after the cleavage reaction. After treatment with $Pd(OAc)_2$ and diazomethane the ratio remained the same. Indeed, the result is in accordance with the reported racemization-free cleavage of the auxiliary in the case of the alkylated products.[1] This also proves that the two major diastereomers of the Michael addition are in an *anti* and *syn* relation to each other. The diastereomeric ratio could be easily increased to 97:3 *via* recrystallization from an ether–pentane mixture.

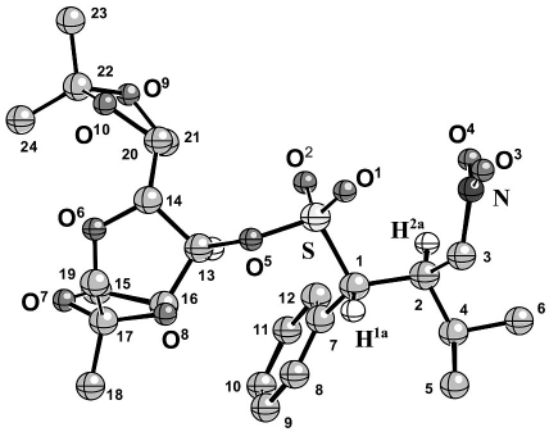

Fig. 1 X-Ray crystal structure of **2c**.‡

In conclusion, the described asymmetric Michael addition provides an efficient route to optically active α,β-disubstituted γ-nitro methyl sulfonates in good overall yields as well as excellent diastereomeric and enantiomeric excesses. The title compounds are valuable bifunctional building blocks and constitute highly enantioenriched precursors of pharmacologically interesting homotaurine derivatives.

This work was supported by the Deutsche Forschungsgemeinschaft (SFB 380) and the Fonds der Chemischen Industrie. We thank Degussa AG, BASF AG, Bayer AG and Aventis for the donation of chemicals. The NOE-measurements by Dr J. Runsink are gratefully acknowledged.

Notes and references

‡ *Crystal data* for **2c**: single crystals were obtained by recrystallization from a diethyl ether–petrol ether mixture (6:4). The substance ($C_{24}H_{35}NO_{10}S$ M_r = 529.59) crystallized in the orthorhombic space group $P2_12_12_1$, a = 9.7493(9), b = 15.7940(15), c = 17.251(2) Å, V = 2656.4(5) Å^3, Z = 4, ρ_{calcd} = 1.324 g cm^{-3}, $F(000)$ = 1128, T = 143(2) K. Data collection: A single crystal (colorless transparent block with dimensions 0.32 × 0.40 × 0.60 mm) was measured on a SIEMENS SMART diffractometer at a temperature of about −130 °C. Repeatedly measured reflections remained stable. An empirical absorption correction was made using the program SADABS. The correction factor ranged from 0.973 to 1.000. Equivalent reflections were averaged. Friedel opposites were not averaged. $R(I)$internal = 0.040. The structure was determined by direct methods using the program SHELXS. The H atoms were placed at calculated positions and were treated as riding atoms. The segment containing atoms O9, C22, C23 and C24 was found to be disordered over two possible conformations. Atoms in this group were refined with a split atom model. The occupancy factor of atoms O9, C22, C23 and C24 refined to 0.644(4). The occupancy factor of atoms O9′, C22′, C23′ and C24′ was 0.356(4). The structure was refined on F^2 values using the program SHELXL97. The final difference density was between −0.34 and +0.54 e Å^{-3}. The absolute configuration of the structure was confirmed by the value of the Flack x-parameter (x = 0.04(5)). CCDC 167504. See http://www.rsc.org/suppdata/cc/b1/b108567k/ for crystallographic files in .cif or other electronic format.

1 D. Enders, N. Vignola, O. M. Berner and J. W. Bats, *Angew. Chem.*, 2001, in press.
2 P. Krogsgaard-Larsen in *Comprehensive Medicinal Chemistry, Vol. 3*, ed. P. G. Sammes and J. B. Taylor, Pergamon, Oxford, 1990, 493.
3 A. Kalir and H. H. Kalir, in *The Chemistry of Functional Groups. The Chemistry of Sulfonic acids, esters and their Derivatives*, ed. S. Patai and Z. Rappoport, John Wiley & Sons, New York, 1991, 767.
4 For general reviews on asymmetric Michael additions see: (*a*) B. E. Rossiter and N. M. Swingle, *Chem. Rev.*, 1992, **92**, 771; (*b*) B. L. Feringa and J. F. G. A. Jansen, in *Stereoselective Synthesis (Houben-Weyl)*, ed. G. Helmchen, R. W. Hoffmann, J. Mulzer and E. Schaumann, 4th edn., Vol. E21b, Thieme, Stuttgart, 1995, 2104; (*c*) J. Leonard, E. Diez-Barra and S. Merino, *Eur. J. Org. Chem.*, 1998, 2051.
5 For a recent review see: F. A. Luzzio, *Tetrahedron*, 2001, **57**, 915.
6 (*a*) D. Seebach, E. W. Colvin, F. Lehr and T. Weller, *Chimia*, 1979, **33**, 1; (*b*) N. Ono, *The Nitro Group in Organic Synthesis*, Wiley-VCH, New York, 2001.
7 For some recent examples see: (*a*) H. Schäfer and D. Seebach, *Tetrahedron*, 1995, **51**, 2305; (*b*) D. Enders and T. Otten, *Synlett*, 1999, 747 and literature cited therein; (*c*) D. Enders, P. Teschner and G. Raabe, *Synlett*, 2000, 637; (*d*) D. Enders, L. Tedeschi and J. W. Bats, *Angew. Chem.*, 2000, **112**, 4774; *Angew. Chem., Int. Ed.*, 2000, **39**, 4605.
8 D. Lucent, S. Sabelle, O. Kostelitz, T. Le Gall and C. Mioskowski, *Eur. J. Org. Chem.*, 1999, 2583.
9 Aromatic nitroalkenes can also be used as Michael acceptors but at the present time the asymmetric inductions are still unsatisfactory.
10 V. Meyer and C. Wurster, *Ber.*, 1873, **6**, 1168.
11 S. F. Sun and T. J. Holland, *Tetrahedron*, 1971, **27**, 323.

CHEMCOMM
Communication
www.rsc.org/chemcomm

FRET probes to monitor phospholipase A_2 activity

Oliver Wichmann and Carsten Schultz*

Max-Planck-Institut für molekulare Physiologie, Otto-Hahn-Str. 11, 44227 Dortmund, Germany. E-mail: carsten.schultz@embl-heidelberg.de; Fax: 49 6221 387518; Tel: 49 6221 387210

Received (in Cambridge, UK) 23rd August 2001, Accepted 21st September 2001
First published as an Advance Article on the web 7th November 2001

Phosphatidylethanolamine and -choline derivatives equipped with fluorescent donor–acceptor pairs of dyes connected to the tips of the fatty acids were synthesised and shown to be suitable substrates for phospholipase A_2.

Phospholipase A_2 is a central enzyme in intracellular signal transduction and digestion and a major constituent of various venoms.[1] The Ca^{2+}-dependent cytosolic phospholipases A_2 ($cPLA_2$) regulate the biosynthesis of eicosanoides by specifically cleaving off arachidonic acid from the *sn*-2 position.[2] Because of the involvement of both cytosolic and secretory isoenzymes in diseases like inflammation and allergies,[3] the monitoring of PLA_2 enzyme activity is crucial for the development of PLA_2 inhibitors as drug candidates. We aim towards the preparation of probes that allow real-time monitoring, that are concentration-independent due to ratio measurements of two emission wavelengths, and which exhibit significant specificity in favour of PLA_2 over other phospholipases. We therefore looked for a pair of matching fluorophores that would allow fluorescence resonance energy transfer (FRET) with an excitation wavelength close to common laser bands, a large difference in emission wavelengths and a good match of the donor emission and the acceptor excitation spectra. We chose the pair consisting of 7-nitrobenz-2-oxa-1,3-diazole amine (NBD-amine) and Nile red, because NBD can be excited with the 458 or 488 nm argon-ion laser lines and the membrane stain Nile red emits above 600 nm in lipophilic environment and is more lipophilic than other red dyes like rhodamine. The fatty acid of the *sn*-1 position was altered to an ether to avoid PLA_1 substrate properties. The fatty acid chain length was held above C_{10} for favorable substrate properties when treated with secretory PLA_2.[4] Previously published probes relied on interdye quenching or excimer formation. A choline compound had two identical BODIPY® dyes attached as esters and served to monitor $cPLA_2$ activity during zebra fish development.[5] A similar probe relied on the excimer formation of two pyrene dyes. After separation of the dyes due to enzymatic ester hydrolysis, the pyrenes emit at much shorter wavelengths.[6] However, the short excitation wavelength required is often not favourable in microscope applications.

In order to synthesize phospholipid derivatives equipped with two matching dyes we started from the commercially available 2,3-isopropylidene-*sn*-glycerol **1** which was treated with sodium hydride in DMF and subsequently alkylated with 1,12-dibromododecane. After acidic hydrolysis of the acetonide the Nile red 2-*O*- or 3-*O*-hydroxy derivative[7] was coupled to the alkyl chain, respectively, to give the diol **2** in an overall yield of 58%. Regioselective *tert*-butyldimethylsilyl (TBDMS) protection of the primary hydroxy group of **2** was achieved in moderate yield. 11-NBD-aminoundecanoic acid was linked with the help of triisopropylphenylsulfonyl nitrotriazole (TPSNT)† and three equiv. of methylimidazole in dichloromethane to give the fully protected glycerol derivative **3** in excellent yield (86%).[8] For this reaction the method appears to be clearly superior to esterifications with carbodiimides like DCC or DIC (35–75% yield). Deprotection of the *sn*-3 position was achieved best with 10% aq. HCl in a dichloromethane–ethanol mixture at rt (78% yield plus 12% recovery of **3**).[9] Under these conditions acyl migration could be limited to a minimum (Scheme 1). Several attempts to introduce ethanolamino phosphate or choline phosphate headgroups *via* phosphorous(v) reagents failed probably due to the sensititvity of the dyes under the reaction conditions. We then employed several ethanolamine-containing phosphorous(III) reagents which required intermediate protection of the latter negatively charged phosphate oxygen and the amino group. An approach with an

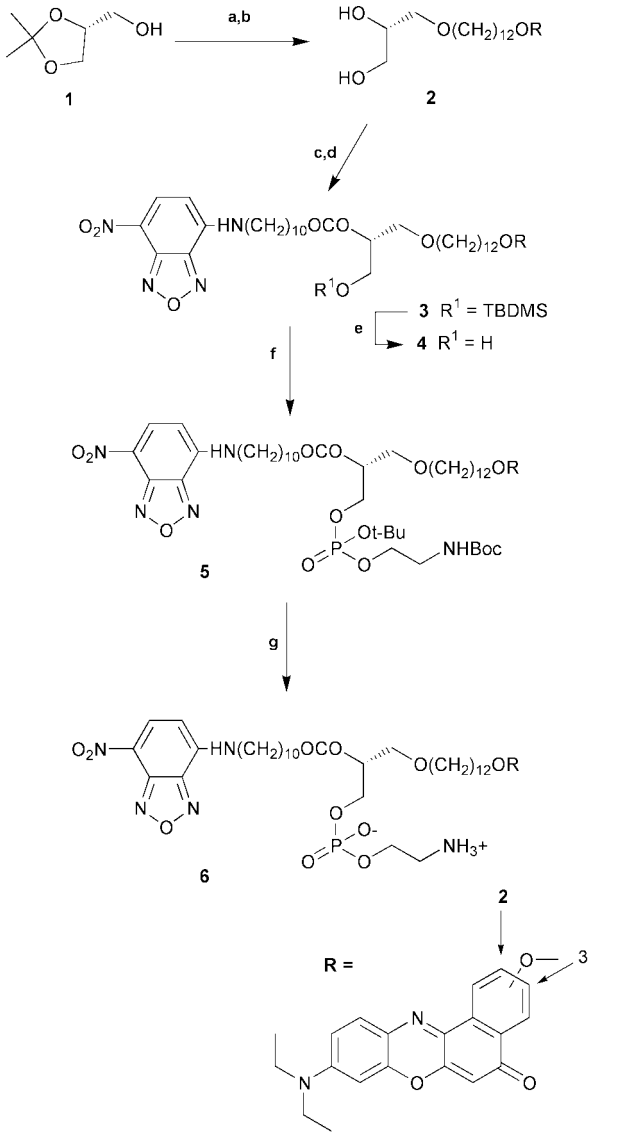

Scheme 1 *Reagents and conditions (rt unless otherwise stated):* (a) *(i)* NaH, DMF, then 1,12-dibromododecane, 1 d, *(ii)* TFA, MeOH, 72% from **1**; (b), 2-hydroxy Nile red, DMF, K_2CO_3, 65 °C, 3 h, 81%; (c) TBDMS-Cl, imidazole, DMF, 12 h, 66%; (d) 11-NBD-aminoundecanoic acid, 1.5 eq. TPSNT, 3 eq. methylimidazole, CH_2Cl_2, 7 h, 86%; (e) 10% aq. HCl, CH_2Cl_2–EtOH 1 : 1 (v/v), 3 h, 78%; (f) *(i)* **7**, tetrazole, DMF, 12 h; *(ii)* *tert*-BuOOH, 0.5 h; (g) 5% TFA, CH_2Cl_2, 0.5 h, 55% from **4**. The synthesis of the 2-*O*-linked derivative **6a** is shown.

 DOI: 10.1039/b107670c

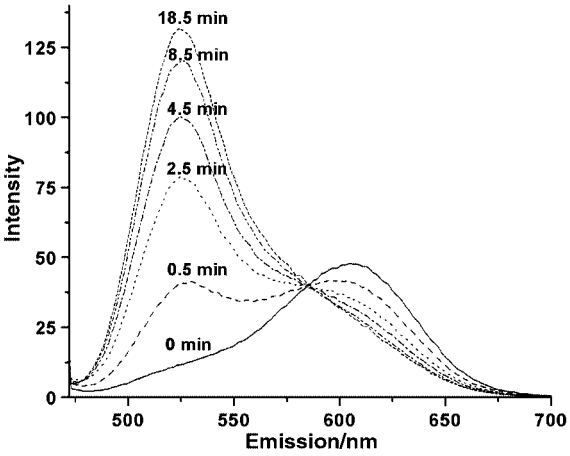

Fig. 1 Rapid change in the emission spectra of probe **6a** after the addition of honey bee PLA_2.

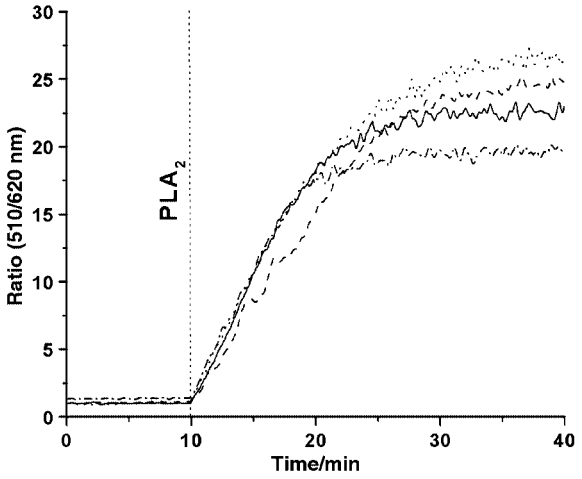

Fig. 2 Emission ratio change 510/620 nm over time, depicted for the four probes **6a** (solid line) and **6b** (dot dash line), as well as **9a** (dotted line) and **9b** (dashed line). (n = 3 for each trace).

allyl group on the phosphate and Fmoc protection of the amino group failed, because under deprotecting conditions (piperidine, followed by palladium(0)), the ethylamino group was presumably lost. More successful was the use of a novel reagent: *tert*-butyl *tert*-butyloxycarbonylaminoethyl *N*,*N*-diisopropyl phosphoramidite (**7**) which was prepared for the first time from the commercially available *tert*-butyl *N*,*N*,*N*′,*N*′-diisopropyl phosphordiamidite and Boc-protected ethanolamine in the presence of ½ equiv. diisopropyl ammonium tetrazolide.[10] The phosphitylation with **7** and subsequent oxidation with *t*-BuOOH was successful, but due to some instability of the protected phospholipid **5** on silica we decided to remove the protecting groups without further purification. A sample of **5** was purified for analysis. The final phosphatidyl ethanolamines **6a** and **6b** were generated after treatment with TFA in dichloromethane and purification on silica (DCM–MeOH–H_2O, 80:20:1.5, v/v/v). In order to introduce the choline phosphate head group, we prepared *tert*-butyl trimethylammomiumethyl *N*,*N*-diisopropyl phosphoramidite as its tosylate (**8**). Phosphitylation and oxidation proceeded as described above and the *tert*-butyl protecting group was removed instantly to give the phosphatidylcholine (**9a**) and (**9b**), respectively. Purification on silica (DCM–MeOH–H_2O, 65:35:3, v/v/v) was successful to give homogenous **9** in 40% yield.

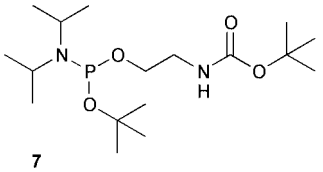

7

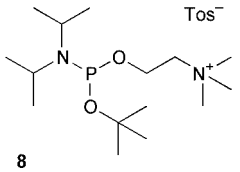

8

The ethanolamine and choline derivatives **6** and **9**, each with the 2- (**a**) and 3-*O*-linkage (**b**) of the Nile red dye, respectively, were dispersed with the help of micelles from Triton X-100 in the presence of calcium chloride (100 mM) and the mixture was buffered with Tris–HCl to pH 7.5 at 37 °C. Addition of one unit of PLA_2 from honey bee venom led to a rapid increase in NBD fluorescence at 520 nm and a decrease of the Nile red fluorescence at 600 or 610 nm (Fig. 1, 2-*O*-linked **6a** shown), respectively. After about 20 min no further change was monitored, indicating that the hydrolysis was complete. Consequently, TLC analysis showed NBD fluorescence only for the NBD-labelled undecanoic acid. The overall change in the emission ratio 520/620 nm was 20- to 30-fold (Fig. 2), depending on the dye linkage (2-*O*-linkage gave slightly better separated emission maxima and hence larger ratio changes).

Equimolar concentrations (1 μM) of the competitive PLA_2 inhibitor MJ33 (ref. 11) reduced the hydrolysis rate by about 40% (data not shown) indicating that inhibitor and fluorescent probe bound to the enzyme with similar kinetics.

In conclusion, the PLA_2 probes presented here fulfil all criteria of a true FRET probe for real-time monitoring. Future experiments in vesicles and living cells and particularly the use of a membrane-permeable derivative to non-disruptively load the dye into cells will allow interesting experiments for drug searches, including high throughput screening in living cells.

We thank the Deutsche Forschungsgemeinschaft (Schu 943/3-1) and the Fonds der Chemischen Industrie for financial support.

Notes and references

† Mesitylene sulfonyl nitrotriazole (MSNT) was used for attaching amino acids or dicarboxylic acids to Wang resin.[8] The bulky triisopropylphenylsulfonyl nitrotriazole (TPSNT) was usually preferred for condensation reactions on phosphates.[12]

1 E. A. Dennis, *J. Biol. Chem.*, 1994, **269**, 13057; E. A. Dennis, *Trends Biochem. Sci.*, 1997, **22**, 1.
2 C. C. Leslie, *J. Biol. Chem.*, 1997, **272**, 16709.
3 S. Yedgar, D. Lichtenberg and E. Schnitzer, *Biochim. Biophys. Acta*, 2000, **1488**, 182.
4 L. Yu and E. A. Dennis, *J. Am. Chem. Soc.*, 1992, **114**, 8757.
5 S. A. Farber, E. S. Olson, J. D. Clark and M. E. Halpern, *J. Biol. Chem.*, 1999, **274**, 19338.
6 M. S. Fernández and J. A. Juárez, *Biochim. Biophys. Acta*, 1994, **1192**, 132; W. R. Burack, Q. Yuan and R. L. Biltonen, *Biochemistry*, 1993, **32**, 583.
7 For the synthesis of Nile red dyes see: N. N. Alekseev, V. S. Bezborodov, A. Y. Gorolenko, L. S. Novikov and N. P. Shcors, *J. Org. Chem. USSR*, 1986, **21**, 2047; M. S. Briggs, I. Bruce, J. N. Miller, C. J. Moody, A. C. Simmonds and E. Swann, *J. Chem. Soc., Perkin Trans. 1*, 1997, 1051.
8 B. Blankemeyer-Menge, M. Nimtz and R. Frank, *Tetrahedron Lett.*, 1990, **31**, 1701.
9 L. W. Leung, C. Vichèze and R. Bittman, *Tetrahedron Lett.*, 1998, **39**, 2921.
10 W. Bannwarth and A. Trzeciak, *Helv. Chim. Acta*, 1989, **70**, 175.
11 M. K. Jian, W. Tao, J. Rogers, C. Arenson, H. Eibl and B.-Z. Yu, *Biochemistry*, 1991, **30**, 10256.
12 M. J. Gait and S. G. Popov, *Tetrahedron Lett.*, 1980, **21**, 2841; J. A. J. den Hartog, R. A. Wijnands, J. H. van Boom and R. Crea, *J. Org. Chem.*, 1981, **46**, 2242.

CHEMCOMM Communication
www.rsc.org/chemcomm

Polymer supported chromium porphyrin as catalyst for polycarbonate formation in supercritical carbon dioxide

Louise M. Stamp,[a] Stephan A. Mang,[a] Andrew B. Holmes,*[a] Kevin A. Knights,[b] Yolanda R. de Miguel*[b] and Ian F. McConvey[c]

[a] *Melville Laboratory for Polymer Synthesis, New Museums Site, Pembroke Street, Cambridge, UK CB2 3RA. E-mail: abh1@cus.cam.ac.uk; Fax: + 44 1223 334866; Tel: +44 1223 334370*
[b] *Department of Chemistry, King's College London, Strand, London, UK WC2R 2LS. E-mail: yolanda.demiguel@kcl.ac.uk; Fax: + 44 2078 481180; Tel: +44 2078 482810*
[c] *AstraZeneca, Process Research and Development, Macclesfield, Cheshire, UK SK10 2NA*

Received (in Cambridge, UK) 15th August 2001, Accepted 25th October 2001
First published as an Advance Article on the web 15th November 2001

A new polymer-supported chromium porphyrin has been prepared and fully characterised; its catalytic activity and recyclability were investigated for the ring-opening copolymerisation of 1,2-cyclohexene oxide (CHO) and carbon dioxide (CO_2).

The synthesis of polycarbonates by copolymerisation of carbon dioxide and epoxides, was first reported in 1969 by Inoue *et al.*[1] More recently, Darensbourg *et al.*[2] synthesised these polymers using supercritical carbon dioxide ($scCO_2$) as both a solvent and a reactant, thereby eliminating the need for toxic volatile organic solvents in this process. Beckman and colleagues[3,4] have also prepared polycarbonates, including products that were found to be soluble in $scCO_2$. The physical properties of compressed carbon dioxide make it an attractive alternative solvent and reagent for application in polymer synthesis owing to its high diffusivity, low viscosity and readily attainable supercritical region (T_c of 31 °C, P_c of 73 atm).[5] The plasticisation effects of CO_2 on polymeric materials also make it an interesting choice as a solvent for polymer supported reactions.[6] The use of supported catalysts in supercritical CO_2 is an emerging field.[7,8]

In recent years, many supported catalysts have been developed for use in organic synthesis[9] and for polymer-assisted solution-phase parallel synthesis.[10] Furthermore, in the drive towards the development of more environmentally friendly or Green Chemistry,[11] supported transition metal catalysts offer many advantages over their homogeneous counterparts. Herein we report the synthesis of an Argogel® supported chromium porphyrin **2b** and the study of its catalytic activity in the copolymerisation of 1,2-cyclohexene oxide (CHO) **1** and CO_2 (Scheme 1) and compare our results with previously investigated systems.[12]

The attachment of the porphyrin onto Argogel chloride beads, *via* an ether linkage, was achieved in 75% yield, following three treatments of the beads with a phenol-functionalised porphyrin **2a**.[13] (using potassium carbonate as base and catalytic potassium iodide in DMF, at 80 °C for 3 days). The metallation using chromium(II) chloride (in DMF, at 45 °C for 3 days) proceeded in 67–78% yield to give the new polymer-bound chromium porphyrin catalyst **2b**.

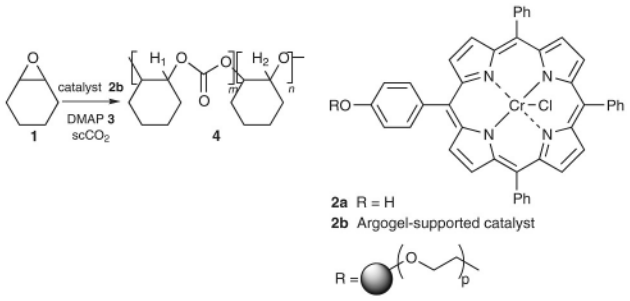

Scheme 1 Copolymerisation of CHO **1** and $scCO_2$ using the supported chromium porphyrin catalyst **2b** and DMAP **3**.

Before testing this catalyst, control experiments were carried out (in the absence of catalyst), using Argogel chloride beads, to probe for any unexpected activity of the blank resin. The beads were therefore exposed to reaction conditions in $scCO_2$ (90 °C, 200 bar, 72 h) analogous to those to be used for the polymerisations. These control experiments were carried out with and without stirring using 100 mg of the polymer support. The beads were analysed by Scanning Electron Microscopy (SEM), which showed that they remained intact except when stirring was applied. A breakdown of the spherical morphology of the particles was observed due to stirring. Further control experiments determined that the presence of both the supported catalyst **2b** and 4-dimethylaminopyridine (DMAP **3**) was essential for polymerisation (Table 1, entries 1–3).

After these control experiments were completed, the ring opening copolymerisation of 1,2-cyclohexene oxide (CHO) **1** and CO_2 to form the copolymer poly(cyclohexene carbonate-*co*-cyclohexene ether) **4** was investigated using catalyst **2b** under various reaction conditions (Table 1).

The number average molecular weight (M_n) (determined by conventional polystyrene-calibrated gel permeation chromatography (GPC) in chloroform) and the yield of the polymer varied greatly according to the conditions applied. It appeared that the polymerisation was near to completion after 24 hours as indicated by both the M_n and the yield (even though an improvement to 78% was observed after 120 h; Table 1, Entry 8). In addition, it was observed that increasing the temperature and the pressure of the CO_2 led to greater molecular weights and higher yields. This is probably due to the fact that, although a constant volume of CHO **1** and a constant amount of the catalysts **2b** and **3** were used in all cases, the effective mole fraction of CHO **1** decreased, since more moles of CO_2 were present in reactions at elevated pressures.

Variation of the reaction conditions appeared to have little effect on the percentage of CO_2 incorporated into the polymer backbone (determined by the ratio of H_1 to H_2 using ^{1}H NMR spectroscopy) which always remained $m > 90$ % (Scheme 1, **4**). Very low polydispersities (determined by GPC) were observed, ranging between 1.2 and 1.7. However, there was no obvious trend observed relating to the increase of the temperature, pressure and the reaction time. Average molecular weights and yields varied according to the batch of beads used for polymerisation (Table 1, entries 11 and 16). This can be attributed to the variable loading of the porphyrin attachment onto the polymer support as well as the variation of the amount of chromium introduced during metallation, which was determined by microanalysis.

Experiments were also carried out in order to investigate the recyclability of the solid supported chromium porphyrin catalyst **2b** (Table 2, entries 1–6). After a reaction,† the polymer

 DOI: 10.1039/b107400h

Table 1 Preliminary studies of the copolymerisation of cyclohexene oxide **1** and $scCO_2$[a]

Entry	Time/h	Temp/°C	*P*/bar	*m* (%)	M_n[b]/g mol^{-1}	(M_w/M_n)	Yield (%)	Comments
1	24	90	170			[c]		**2b**, no Cr
2	24	90	170			[c]		Without **2b**
3	24	90	170			[c]		Without **3**
4	8	90	170	96	4400	1.3	38	[d]
5	24	90	170	97	7100	1.7	62	[d]
6	48	90	170	99	5300	1.7	60	[d]
7	72	90	170	97	5800	1.3	69	[d]
8	120	90	170	96	6500	1.7	78	[d]
9	24	60	170	96	4000	1.5	26	[d]
10	24	70	170	96	4700	1.4	37	[d]
11	24	90	170	97	7100	1.7	62	[d]
12	24	100	170	93	3300	1.3	72	[d]
13	24	90	35	91	2200	1.2	5	[e]
14	24	90	85	95	2800	1.2	13	[e]
15	24	90	140	93	3300	1.2	17	[e]
16	24	90	170	92	2700	1.3	21	[e]
17	24	90	210	94	3400	1.2	32	[e]

[a] Conditions: χ(CHO) (volume fraction of monomer) = 25 %w/v, N_{cat} (amount of catalyst) = 100 mg (average loading = 0.14 mmol g^{-1}). [b] Relative to polystyrene (PS) standards. [c] Recovered monomer. [d] Chromium porphyrin beads (batch 1, loading 0.14 mmol g^{-1}). [e] Chromium porphyrin beads (batch 2, loading 0.06 mmol g^{-1}).

4 was solubilised in acetone allowing the beads to be filtered, washed and dried for re-use.

Polymerisations were also carried out using an Irori Kan™ reactor[14] to encapsulate the porphyrin beads (Table 2, entries 7–10). This not only allowed the use of a stirrer bar, thereby preventing damage to the beads, but also facilitated their recovery.

Table 2 shows that the chromium porphyrin beads **2b** can successfully be recycled, although a decrease in molecular weight and yield is observed. This may be due to leaching of the metal from the porphyrin or decomposition of the beads leading to loss of porphyrin. Mild colouration of the polycarbonate also suggested minor leaching of the chromium metal. However, the solid supported catalyst appeared to prevent the polymer products becoming intensely green as was observed when the soluble chromium perfluorinated porphyrin was used.[12] The use of an Irori Kan™ reactor[14] to encapsulate the beads appeared to result in higher molecular weights and yields of the polycarbonate. This is likely to be due to thorough mixing of the reagent in the vessel.

In summary, we have presented a new supported chromium porphyrin **2b** as a catalyst in the ring opening copolymerisation of 1,2-cyclohexene oxide **1** and CO_2. The results are comparable to those reported for a CO_2-soluble tetra(pentafluorophenyl)chromium porphyrin catalyst. However, as well as being recyclable, the supported catalyst showed efficiencies of up to 5.5 kg of polymer/1 g of chromium, thus demonstrating this new system to be superior to those previously reported.[12]

Table 2 Recyclability experiments of the polymer-supported catalyst **2b** for the copolymerisation of CHO **1** and CO_2[a]

Entry	Cycle	*m* (%)	M_n[b]/g mol^{-1}	(M_w/M_n)	Yield (%)
1	1	95	3600	1.3	56
2	2	94	3000	1.4	40
3	3	93	2300	1.1	25
4	1	94	4000	1.4	55
5	2	94	3500	1.2	50
6	3	89	1500	1.3	6
7	1	95	5000	1.2	64
8	2	95	3700	1.1	64
9	3	93	2000	1.1	47
10	4	88	1400	1.1	7

[a] Conditions: P = 170 bar, Temp = 90 °C, χ(CHO) (volume fraction of monomer) = 25 %w/v, N_{cat} (amount of catalyst) = 100 mg (batch 3, loading = 0.18 mmol g^{-1}). [b] Relative to PS standards.

We thank AstraZeneca (L. Stamp), DERA (S. Mang), King's College London (K. Knights), the Royal Society (Dorothy Hodgkin Fellowship to Y. de Miguel), EPSRC (Swansea Mass Spectrometry Service) and the Commission of the EU (Brite-Euram BRRT-CT98-5089 'RUCADI') for generous funding. We are also grateful to Professor J. K. M. Sanders, Dr A. I. Cooper and Dr M. Eamon Colclough for their interest in this work.

Notes and references

† In a typical experiment a 10 cm^3 stainless steel reactor was charged with CHO **1** (2.4 g), DMAP **3** (5 mg) and supported catalyst **2b** (100 mg). The reactor was filled to capacity with liquid CO_2 and heated to the desired temperature. Then the reaction mixture was pressurised with further CO_2. After the allotted time the reaction was allowed to cool and then vented into acetone (50 cm^3). The remaining contents of the reactor were added to this solution and the beads were collected by filtration. The polymer solution was concentrated to 10 cm^3 and precipitated into hexane, filtered and dried to constant weight. The polymeric products were characterised by ^{1}H NMR spectroscopy and GPC.

1 S. Inoue, T. Tsuruta and H. J. Koinuma, *J. Polym. Sci., Polym. Lett.*, 1969, **7**, 287.
2 D. J. Darensbourg, N. W. Stafford and T. J. Katsurao, *J. Mol. Catal., A*, 1995, **104**, L1.
3 M. Super, E. Berluche, C. Costello and E. Beckman, *Macromolecules*, 1997, **30**, 368.
4 T. Sarbu, T. Styranec and E. J. Beckman, *Nature*, 2000, **405**, 165.
5 J. L. Kendall, *Chem. Rev.*, 1999, **99**, 543.
6 A. I. Cooper, *J. Mater. Chem.*, 2000, **10**, 207.
7 A. Baiker, *Chem. Rev.*, 1999, **99**, 453.
8 N. J. Meehan, A. J. Sandee, J. N. H. Reek, P. C. J. Kamer, P. W. N. M. van Leeuwen and M. Poliakoff, *Chem. Commun.*, 2000, 1497.
9 Y. R. de Miguel, *J. Chem. Soc., Perkin Trans. 1*, 2000, **24**, 4213, and references therein.
10 L. A. Thompson, *Curr. Opin. Chem. Biol.*, 2000, **4**, 324.
11 J. H. Clark, *Pure Appl. Chem.*, 2001, **73**, 103.
12 S. Mang, A. I. Cooper, M. E. Colclough, N. Chauhan and A. B. Holmes, *Macromolecules*, 2000, **33**, 303.
13 H. Uno, K. Takata and Y. Mizutani, *Reactive Polym.*, 1991, **15**, 121.
14 K. C. Nicolau, J. A. Pfefferkorn, H. J. Mitchell, A. J. Roecker, S. Barluenga, G.-Q. Cao, R. L. Affleck and J. E. Lillig, *J. Am. Chem. Soc.*, 2000, **122**, 9954.

CHEMCOMM Communication
www.rsc.org/chemcomm

Intramolecular addition of acyl radicals to α-substituted vinylogous carbonates: demonstrating the effect of ring size on acyclic stereocontrol†

P. Andrew Evans,*[a]‡ Sushil Raina[b] and Khalid Ahsan[a]

[a] *Department of Chemistry, Indiana University, Bloomington, IN 47405, USA. E-mail: paevans@indiana.edu; Fax: +1(812) 855-8300*
[b] *Department of Chemistry and Biochemistry, University of Delaware, Newark, DE 19716, USA*

Received (in Corvallis, USA) 14th July 2001, Accepted 18th September 2001
First published as an Advance Article on the web 9th November 2001

The level of stereocontrol obtained in the reduction of the free radical derived from the intramolecular addition of an acyl radical to an α-branched vinylogous carbonate is dependent upon the ring-size of the cyclic ether.

The stereoselective construction of cyclic ethers remains an important area of interest due to the ubiquity of this structural motif in biologically significant natural and unnatural molecules.[1] In the course of our studies focused on the intramolecular addition of acyl radicals[2] to vinylogous carbonates[3,4] and sulfonates,[5] we anticipated that we could expand the synthetic utility of the former through the examination of α-branched derivatives, which should provide access to an additional stereogenic center.[6,7] The ability to control the relative and absolute configuration of acyclic stereogenic centers in free radical addition reactions represents an important method in asymmetric synthesis.[8] Herein, we report that the level of stereocontrol in the intramolecular addition of acyl radicals, derived from the selenoesters **1a–c** (n = 0–2), to α-substituted vinylogous carbonates, is directly dependent upon the ring size of the resulting cyclic ether **2/3a–c** (eqn. 1).

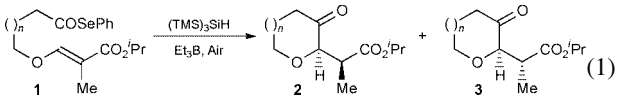

(1)

Table 1 outlines the results for the preliminary study. Treatment of **1a–c** with tris(trimethylsilyl)silane[9] and triethylborane in the presence of air, furnished the cyclic ethers **2/3a–c** in excellent yield. Interestingly, the tetrahydrofuran-3-one **2a/3a** and tetrahydrooxepin-3-one **2c/3c** were furnished with only modest diastereocontrol irrespective of reaction temperature (Entries 1/2 and 5/6). This trend in selectivity was somewhat surprising given the precedent for this type of free radical reduction in tetrahydrofuran derivatives.[5–7] Conversely, the tetrahydropyran-3-ones **2b/3b** were afforded with excellent diastereoselectivity, favoring the *syn*-isomer **2b** (Entry 3). Furthermore, the diastereoselectivity could be further improved by lowering the reaction temperature (−20 °C), which is in sharp contrast to the tetrahydrofuran-3-one **2a/3a** and tetrahydrooxepin-3-one **2c/3c** derivatives (Entry 4 *vs* 2/6).§ The origin of the stereoselectivity may be rationalized using the static model for allylic strain,[7] in which the ketone is responsible for promoting *re*-face reduction of the radical (Fig. 1). The difference in selectivity between the various ring sizes may be attributed to conformation, which presumably alters the relative orientation of the carbonyl relative to the incipient radical. This observation is likely to provide a useful guide in understanding the factors that influence stereocontrol in acyclic radical reductions involving the intramolecular addition of acyl radicals.

Table 1 Intramolecular additions of acyl radical to α-substituted vinylogous carbonates†

Entry	Acyl selenide **1**[a]	n =	Temp./°C	Conc./M	Ratio of **2** : **3**[b]	Yield (%)[c]
1	**a**	0	22	0.02	3 : 1	84
2	″	″	−20	″	4 : 1	76
3	**b**	1	22	0.01	21 : 1	80
4	″	″	−20	″	46 : 1	82
5	**c**	2	22	0.005	7 : 1	81
6	″	″	−20	″	8 : 1	37

[a] All reactions carried out in hexane on a 0.5 mmol reaction scale. [b] Ratios of diastereoisomers determined by capilliary GLC. [c] Isolated yields.

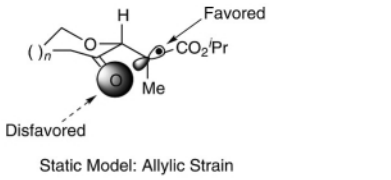

Fig. 1

The ability to undertake the stereoselective synthesis of tetrahydropyran-3-ones in this manner prompted the extension of this study as outlined in Scheme 2. The benzylidene acetal **8** was expected to promote the formation of *cis*-2,6-disubstituted tetrahydropyran-3-one **9a** in accord with previous studies and thus determine whether the more conformationally rigid system would deviate from the excellent stereoselectivity obtained in the simple acyclic radical reduction in eqn. 1.

The acyl selenide **8** required for this study was prepared from the secondary alcohol **4** derived from deoxy-D-ribose (Scheme 1).[10] Ozonolysis of the α,β-unsaturated ester **4** followed by *in situ* reductive work-up furnished the diol, which was selectively

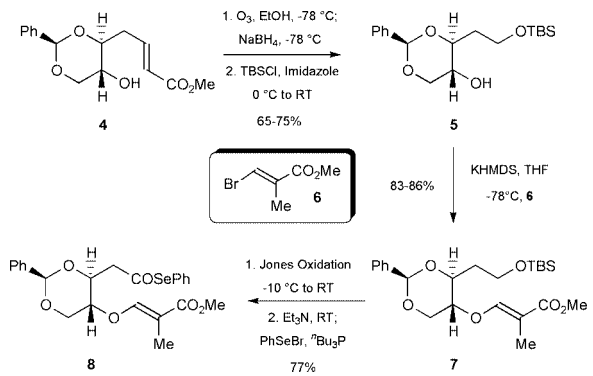

Scheme 1

† Electronic supplementary information (ESI) available: spectral data (IR, ^{1}H and ^{13}C NMR) and high resolution MS for **1/2a-c**, **7–10**. See http://www/rsc.org/suppdata/cc/b1/b106766b/

‡ Current Address: Indiana University.

 DOI: 10.1039/b106766b

protected as the primary *tert*-butyldimethylsilyl ether **5** in 65–75% overall yield from **4**. Treatment of **5** with potassium hexamethyldisilazide followed by the β-bromomethacrylate **6**, furnished the vinylogous carbonate **7** in 83–86% yield. Oxidation of the primary *tert*-butyldimethylsilyl ether **7** with Jones reagent afforded the carboxylic acid,[11] which was then converted to the acyl selenide **8**, using the Crich protocol in 77% yield from **7**.[12] The chemoselectivity of the oxidation is pertinent given that the benzylidene acetal and vinylogous carbonate are susceptible to acid-catalyzed hydrolysis.

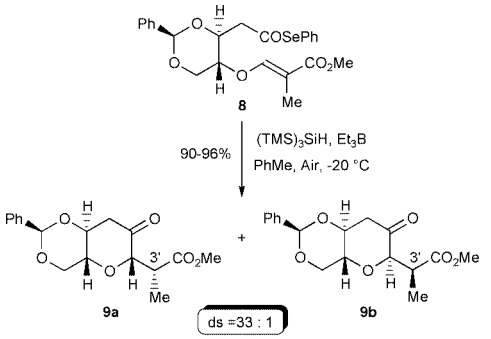

Scheme 2

The acyl selenide **8** was then subjected to the optimized cyclization conditions, as outlined in Scheme 2. Treatment of the acyl selenide **8** in an analogous manner to **1b**, at −20 °C, furnished the cyclic ethers **9a**/**b** in 90–96% yield, with 33 : 1 diastereoselectivity (by HPLC) at C-3′ favoring **9a**. The stereochemical outcome is consistent with the model outlined in Fig. 1.

The relative configuration of the radical cyclization–reduction was proven unequivocally through X-ray crystallography of the tricyclic lactone **10** (Fig. 2).¶ Reduction of the cyclic ketone **9a** with K-Selectride at −78 °C resulted in an *in situ* lactonization, to afford **10** in 90% yield with ⩾19 : 1 diastereoselectivity for the *cis*-lactone (eqn. 2).

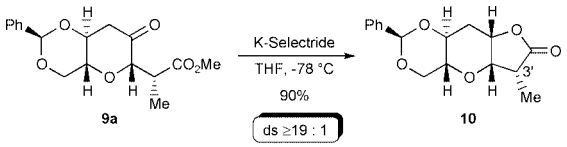

(2)

In conclusion, we have demonstrated that the level of stereocontrol in the reduction of the insipient radical derived from the *intra*molecular addition of an acyl radical to a α-substituted vinylogous carbonate is dependent on the relative ring-size of the cyclic ether. The ability to achieve excellent acyclic stereocontrol in 6-*exo* acyl radical addition reactions is likely to have considerable synthetic utility, particularly for the construction of *C*-glycosides.

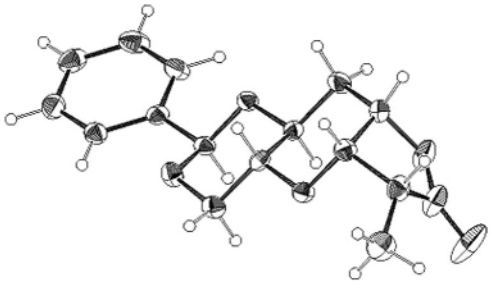

Fig. 2 Thermal ellipsoid plot of **10** (50% probability thermal ellipsoids).‖

We sincerely thank the National Institutes of Health (GM58877) for generous financial support. We also thank Zeneca Pharmaceuticals for *an Excellence in Chemistry Award*, Eli Lilly for a *Young Faculty Grantee Award*, GlaxoWellcome for a *Chemistry Scholar Award* and Novartis Pharmaceuticals for an *Academic Achievement Award*. The Camille and Henry Dreyfus Foundation is also thanked for a *Camille Dreyfus Teacher-Scholar Award* (PAE).

Notes and references

§ The relative configuration of the major diastereoisomer **2a–c** was confirmed by NMR after conversion to the corresponding *cis*-lactone in an analogous manner to that described in eqn. 2.

¶ Correspondence regarding the X-ray crystallography should be addressed to: Arnold L. Rheingold, Department of Chemistry and Biochemistry, University of Delaware, Newark, DE 19716, USA.

‖ *Crystal structure data for* **10**, ($C_{16}H_{18}O_5$): monoclinic, $P2_1$, a = 8.4891(2), β = 17.5380(3), c = 14.1931(2) Å, b = 93.9331(7), V = 2108.09(6), Z = 6, Z' = 3, T = 198(2) K, D_{calc} = 1.372 g cm^{-1}, colorless plate, *GOF* = 0.904, *R(F)* = 0.058 for 6032 observed independent reflections (2.9° ⩽ 2θ ⩽ 56.9°). CCDC 172435. See http://www.rsc.org/suppdata/cc/b1/b10676b/ for crystallographic data in .cif or other electronic format.

1 For reviews on cyclic ether syntheses, see: (*a*) C. J. Moody and M. Davies, in *Studies in Natural Product Chemistry*, ed. Atta-ur-Rahman, Elsevier, Amsterdam, 1992, **vol. 10**, pp. 201–239; (*b*) J.-C. Harmange and B. Figadère, *Tetrahedron: Asymmetry*, 1993, **4**, 1711; (*c*) E. Alvarez, M.-L. Candenas, R. Perez, J. L. Ravelo and J. D. Martin, *Chem. Rev.*, 1995, **95**, 1953; (*d*) J. O. Hoberg, *Tetrahedron*, 1998, **54**, 12631 and pertinent refereces cited therein.

2 For recent reviews on acyl radicals, see: (*a*) I. Ryu, N. Sonoda and D. P. Curran, *Chem. Rev.*, 1996, **96**, 177; (*b*) C. Chatgilialoglu, D. Crich, M. Komatsu and I. Ryu, *Chem. Rev.*, 1999, **99**, 1991 and pertinent references cited therein.

3 (*a*) P. A. Evans and J. D. Roseman, *Tetrahedron Lett.*, 1995, **36**, 31; (*b*) P. A. Evans and J. D. Roseman, *J. Org. Chem.*, 1996, **61**, 2252; (*c*) P. A. Evans, J. D. Roseman and L. T. Garber, *J. Org. Chem.*, 1996, **61**, 4880. ; For an example of an acyl radical cyclization in the total synthesis of (−)-kumausallene, see: P. A. Evans, V. S. Murthy, J. D. Roseman and A. L. Rheingold, *Angew. Chem., Int. Ed.*, 1999, **38**, 3175 and pertinent references within these articles.

4 For related examples of radical additions to β-alkoxyacrylates, see: (*a*) alkyl radicals: E. Lee, S.-K. Yoo, H. Choo and H. Y. Song, *Tetrahedron Lett.*, 1998, **39**, 317; (*b*) Lewis acid catalyzed addition of alkyl radicals: Y. Yuasa, W. Sato and S. Shibuya, *Synth. Commun.*, 1997, **27**, 573; (*c*) photosensitized electron-transfer addition of aldehydes: G. Pandey, S. Hajra, M. K. Ghorai and R. Kumar, *J. Org. Chem.*, 1997, **62**, 5966; (*d*) SmI_2 reduction of aldehydes: N. Hori, H. Matsukura, G. Matsuo and T. Nakata, *Tetrahedron Lett.*, 1999, **40**, 2811; (*e*) alkyl radicals from selenoacetals: M. Sasaki, T. Noguchi and K. Tachibana, *Tetrahedron Lett.*, 1999, **40**, 1337.

5 (*a*) P. A. Evans and J. D. Roseman, *Tetrahedron Lett.*, 1997, **38**, 5249; (*b*) P. A. Evans and T. Manangan, *Tetrahedron Lett.*, 1997, **38**, 8165; (*c*) P. A. Evans and T. Manangan, *J. Org. Chem.*, 2000, **65**, 4523.

6 For a closely related rationale for the reduction of β-alkoxy-α-halomethacrylates, see: Y. Guindon, J.-F. Lavallée, L. Boisvert, C. Chabot, D. Delorme, C. Yoakim, D. Hall, R. Lemieux and B. Simoneau, *Tetrahedron Lett.*, 1991, **32**, 27; for semiempirical calculations on this type of radical reduction reaction, see: K. Durkin, D. Liotta, J. Rancourt, J.-F. Lavallée, L. Boisvert and Y. Guindon, *J. Am. Chem. Soc.*, 1992, **114**, 4912.

7 For a related example of an alkyl radical addition to a β-alkoxymethacrylate, see: E. Lee and S. J. Choi, *Org. Lett.*, 1999, **1**, 1127.

8 D. P. Curran, N. D. Porter and B. Giese, in *Stereochemistry of Radical Reactions: Concepts, Guidelines and Synthetic Applications*, VCH Publishers, New York, 1995, pp. 147–177.

9 (*a*) C. Chatgilialoglu, *Acc. Chem. Res.*, 1992, **25**, 188; (*b*) C. Chatgilialoglu, C. Ferreri and T. Gimisis, in *The Chemistry of Organic Silicon Compounds*, ed. S. Rappoport and Y. Apeloig, Wiley, London, 1998, **vol. 2**, chapter 25, pp. 1539.

10 K. C. Nicolaou, C. A. Veale, C.-K. Hwang, J. Hutchinson, C. V. C. Prasad and W. W. Ogilvie, *Angew. Chem., Int. Ed. Engl.*, 1991, **30**, 299.

11 P. A. Evans, J. D. Roseman and L. T. Garber, *Synth. Commun.*, 1996, **26**, 4685.

12 The acyl selenides were prepared from carboxylic acids, see D. Batty and D. Crich, *Synthesis*, 1990, 273.

CHEMCOMM Communication
www.rsc.org/chemcomm

The promotion of hydrolysis of acetylsalicylic acid in AOT/near-critical propane microemulsion

Zameer Shervani* and Yutaka Ikushima

Supercritical Fluid Research Center, National Institute of Advanced Industrial Science and Technology, 4-2-1 Nigatake, Miyagino-ku, Sendai 983-8551, Japan. E-mail: z.shervani@aist.go.jp

Received (in Cambridge, UK) 24th August 2001, Accepted 22nd October 2001
First published as an Advance Article on the web 8th November 2001

A significant acceleration of the hydrolysis of acetylsalicylic acid was accomplished by the introduction of an AOT/near-critical propane microemulsion at lower W_0 values; the rate constant at W_0 = 1 was found to be 54 times that in aqueous buffer medium in the presence of imidazole catalyst.

In recent years, high pressure microemulsions prepared in near-critical and supercritical hydrocarbons or carbon dioxide have been applied to various fields such as organic synthetic reactions[1,2] and synthesis of nanometer-sized metal and metal oxide particles[3,4] from industrial and scientific points of view. It is well known that the advantages of near-critical (NC) and supercritical fluids (SCFs) as the dispersed phase for microemulsion preparation are their higher diffusivities and lower viscosities compared to conventional solvents.[5] In addition, their physical properties such as density,[6,7] viscosity,[8] diffusivity and dielectric constant[9] can be varied widely by simply changing the temperature and pressure of the system. In this communication we demonstrate for the first time that the introduction of a sodium bis(2-ethylhexyl) sulfosuccinate (AOT) microemulsion into near-critical propane leads to a significant acceleration of hydrolysis even at low W_0 compared with aqueous buffer solution in the presence of catalyst.† *In situ* UV-vis was employed for the determination of the rate constant of the reaction as a function of the water content of the microemulsion at a fixed temperature and pressure of 310 K and 25 MPa, respectively. The appearance of a band at 298.6 nm has been assigned to the expected hydrolysis product salicylic acid and the absorbance of this band was followed as a function of time for kinetics measurement, with spectra being recorded at different reaction times, for the determination of the degree of conversion.

Fig. 1 shows the pseudo first-order rate constant (k) of hydrolysis of acetylsalicylic acid carried out in various reaction media. A dramatic enhancement in the rate constant is observed in an AOT/NC propane microemulsion containing imidazole compared to a micoemulsion without imidazole or an aqueous buffer media. The reaction in the microemulsion containing imidazole at W_0 = 1 is 54 times faster than in aqueous buffer. The rate constant in aqueous buffer remains unchanged on addition of imidazole catalyst, whereas in the microemulsion system it greatly increased in the presence of catalyst. In a separate experiment monitoring percentage conversion *vs.* reaction time, it was noticed that the conversion of acetylsalicylic acid into salicylic acid in the microemulsion at W_0 = 1 reached 100% after 33 min while in aqueous buffer it took 61 h for 100% conversion in the presence of imidazole catalyst. The W_0 dependence of the rate constant shows that the reaction is significantly accelerated (Fig. 2) by decreasing the W_0 value in the microemulsion system, especially in the region below W_0 = 4, which is contrary to the W_0 dependence on the reaction rate for enzyme catalyzed hydrolysis or esterifications.[10,11] In the AOT/propane microemulsion medium in the presence of imidazole, a considerably higher reaction rate was observed at low water content (W_0 = 1) since the small water soluble imidazole and acetylsalicylic acid molecules can be solubilized inside the smaller cores of microemulsion droplets consisting of a small amount of water W_0 = 1. As the water content is increased in the microemulsion, the concentration of imidazole and acetylsalicylic acid is decreased and therefore the rate of reaction decreases. The higher values of the rate constant observed in the microemulsion compared to that in aqueous solution is attributed to the compartmentalization of water soluble imidazole and acetylsalicylic acid in the aqueous core of the microemulsion droplets as a result of which the local concentration of reactants is increased compared to that in neat aqueous medium. The enhancement of the reaction rate due to compartmentalization of imidazole catalyst and substrate acetylsalicylic acid was confirmed after conducting the concentration dependent hydrolysis reaction in AOT/propane microemulsion and aqueous buffer media. In both media, the rate constant increased with increasing the concentration of imidazole and acetylsalicylic acid (Fig. 3). This shows that the compartmentalization of solutes in the core of microemulsion droplets is responsible for the higher reaction rate and decreased reaction time. The mechanism of the hydrolysis reaction using

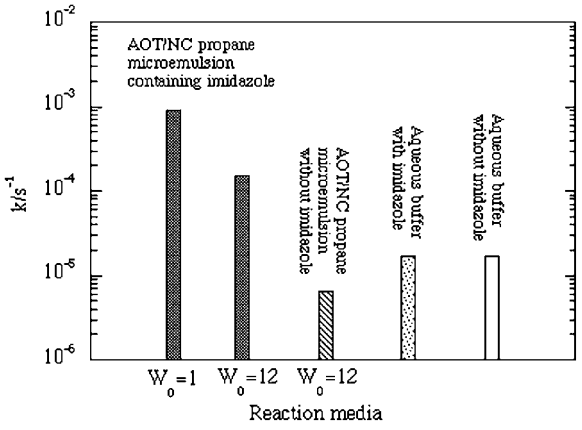

Fig. 1 Pseudo first-order rate constant (k/s^{-1}) of hydrolysis of acetylsalicylic acid in aqueous buffer and in AOT/propane microemulsion (25 MPa) at 310 K.

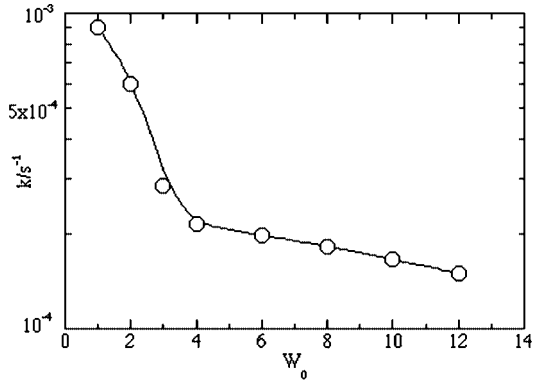

Fig. 2 W_0 dependence of the rate constsnt of hydrolysis of acetylsalicylic acid in AOT/NC propane microemulsion at 25 MPa and 310 K.

 DOI: 10.1039/b103695p

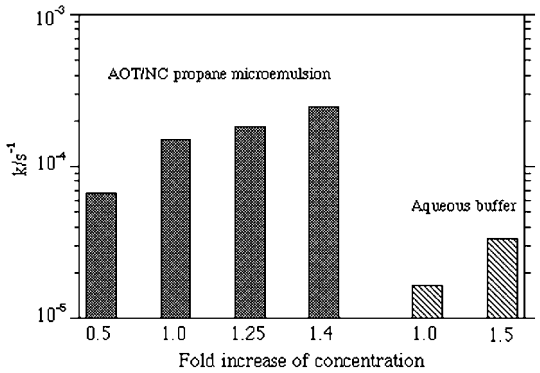

Fig. 3 Rate constant (k/s^{-1}) *vs*. fold increase in the concentration of acetylsalicylic acid and imidazole in AOT/NC propane microemulsion (W_0 = 12, P = 39.2 MPa) and in aqueous buffer at 310 K.

imidazole catalyst has been proposed to be a general acid–base catalysis reaction involving the transferral of a proton in the transition state.

Fig. 4 compares the rate constants of the hydrolysis of acetylsalicylic acid in AOT/NC propane and AOT/hexane microemulsions. The rate constant in the propane system is higher than in hexane. This can be be attributed to the decrease in the microviscosity of the water/AOT interface in the NC propane system similar to the reduced microviscosity observed in a perfluoropolyether ammonium carboxylate (PFPE-$CO_2^-NH_4^+$)/carbon dioxide microemulsion.[12]

In conclusion, high pressure microemulsion systems can be used as reaction media for hydrolysis reactions leading to the enhancement of catalytic activity as compared to aqueous buffers and normal microemulsion systems. The water content of the microemulsion has a strong influence on the hydrolysis of acetylsalicylic acid in presence of imidazole catalyst. The reaction is faster in low water containing microemulsions than in microemulsions of larger water content. The promotion of the hydrolysis in the microemulsion has been proved to be due to the compartmentalization of the water soluble catalyst and substrate in the cores of microemulsion droplets which also explains the dependence of the rate constant on the water content of the system. Increasing the amount of water in the microemulsion dilutes the reactants so lowering the rate constant and slowing the reaction.

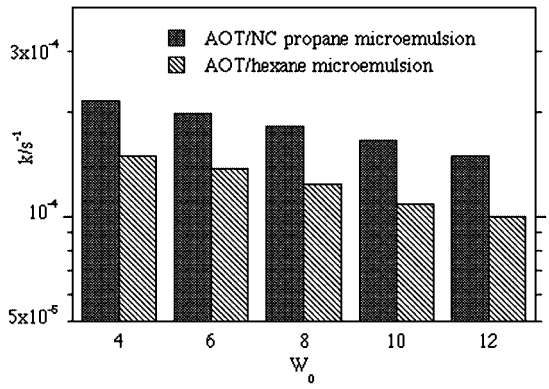

Fig. 4 A comparison of pseudo-first order rate constant (k/s^{-1}) of hydrolysis of acetylsalicylic acid in the presence of imidazole in AOT/hexane and AOT/propane (25 MPa) systems at 310 K.

Notes and references

† *Experimental procedure*: a high pressure UV cell of 2.2 ml volume fitted with a pair of sapphire windows was used as the reactor. After adding AOT, acetylsalicylic acid, imidazole and water the high pressure cell was closed and propane at 25 MPa was pressurized inside the cell. The concentrations of AOT, acetylsalicylic acid and imidazole was estimated as 0.1, 2.5×10^{-4} and 2.5×10^{-2} M, respectively. The temperature of the reaction was controlled within ±0.2 °C with a temperature controller attached to the cell. The reaction mixture was stirred continuously during the measurement by a Teflon-coated bar driven by an outside magnet. A schematic diagram of the high pressure cell used as the reactor has been given elsewhere.[13] The increase in the absorbance was recorded *vs*. the reaction time with a Jasco V-570 spectrometer. The percentage conversion was determined by the intensity of 298.6 nm band. W_0 represents the water content of the microemulsion and is the molar ratio of water to AOT. 100 mM phosphate buffer was used to adjust the water content of the microemulsion and also as the aqueous reaction medium. The reactions in aqueous buffer and in AOT/hexane microemulsions were carried at 310 K and at ambient pressure.

1 Y. Ikushima, Z. Shervani, N. Saito and M. Arai, *J. Colloid Interface Sci*., 1997, **191**, 177.
2 J. D. Holmes, D. C. Steytler, G. D. Rees and B. H. Robinson, *Langmuir*, 1998, **14**, 6371.
3 M. Ji, X. Chen, C. M. Wai and J. L. Fulton, *J. Am. Chem. Soc*., 1999, **121**, 2631.
4 C. B. Roberts and J. P. Cason, *J. Phys. Chem. B*, 2000, **104**, 1217.
5 E. Klesper, *Angew. Chem., Int. Ed. Engl*., 1978, **17**, 738.
6 S. Peter and G. Brunner, *Angew. Chem., Int. Ed. Engl*., 1978, **17**, 746.
7 E. Stahl, W. Schilz, E. Schutz and E. Willing, *Angew. Chem., Int. Ed. Engl*., 1978, **17**, 731.
8 J. Eastoe, B. H. Robinson, A. J. W. G. Visser and D. C. Steytler, *J. Chem. Soc., Faraday Trans*., 1991, **87**, 1899.
9 G. M. Schneider, *Angew. Chem., Int. Ed. Engl*., 1978, **17**, 716.
10 P. J. Cunnah, M. R. Aires-Barros and J. M. S. Cabral, *Biocatal. Biotransform*., 1996, **14**, 125.
11 C. Oldfield, *Biotechnol. Genetic Eng. Rev*., 1994, **12**, 255.
12 R. G. Zielinski, S. R. Kline, E. W. Kaler and N. Rosov, *Langmuir*, 1997, **13**, 3934.
13 Z. Shervani and Y. Ikushima, *J. Supercrit. Fluids*, 1998, **13**, 375.

CHEMCOMM Communication
www.rsc.org/chemcomm

Bimetallic-induced tail-to-tail dimerization and C–H activation of methyl acrylate†‡

Pierre Braunstein,*[a] Michael J. Chetcuti*[a] and Richard Welter[b]

[a] *Laboratoire de Chimie de Coordination, UMR CNRS 7513, Université Louis Pasteur, 4 rue Blaise Pascal F-67070. Strasbourg Cédex, France. E-mail: braunst@chimie.u-strasbg.fr; chetcuti@chimie.u-strasbg.fr*

[b] *Groupe Composés métalliques et densités électroniques, UMR CNRS 7513, Université Louis Pasteur, 4 rue Blaise Pascal F-67070. Strasbourg Cédex, France*

Received (in Cambridge, UK) 30th August 2001, Accepted 19th October 2001
First published as an Advance Article on the web 7th November 2001

An organometallic complex resulting from tail-to-tail dimerization and C–H activation of methyl acrylate (MA), $[Mo(CO)_2Cp\{\eta^3\text{-}(MeO_2C)CH{=}CH{=}CHCH_2(CO_2Me)]$ 2, has been fully characterized from the reaction of the heterobimetallic complex $[Cp^*Ni{=}Mo(\mu\text{-}CO)(CO)_2Cp]$ with MA and an exclusively η^3-allyl bonding mode of the coupled ligand was established for the first time by X-ray diffraction; formation of 2 is accompanied by that of the μ_3-alkylidyne-capped cluster $[NiMo_2(\mu_3\text{-}CCH_2CO_2Me)(CO)_4Cp^*Cp_2]$ 3 which results from a double C–H activation of the CH_2 group of MA; none of these reactions occur with the corresponding homodinuclear complexes.

Methyl acrylate (CH_2=CHC(O)OMe = MA) plays an increasingly important role in the copolymerization of olefins[1] and its catalytic tail-to-tail dimerization represents an attractive alternative route to adipic acid from C_3 feedstocks. Its activation by metal complexes is therefore of significant current interest.

Reaction of the paramagnetic heterobimetallic complex $[Cp^*Ni{=}Mo(\mu\text{-}CO)(CO)_2Cp]$ **1** (Cp = η-C_5H_5, Cp* = η-C_5Me_5)[2] with an excess of MA (THF, reflux) afforded the new compounds **2** (20% yield) and **3** (18% yield based on Ni) (Scheme 1).†

The structure of **2** (Fig. 1)§ revealed that the organic ligand MeOC(O)CH=CH=CHCH$_2$C(O)OMe (*i*) has formed by C–C coupling and C–H bond activation of two methyl acrylate moieties leading to their tail-to-tail dimerization and (*ii*) that it is only η^3-allylically *exo*-bound to a $CpMo(CO)_2$ fragment. The methoxycarbonyl group bonded to the sp^2-hybridized carbon is essentially coplanar with the allylic carbon atoms while the other is perpendicular. One H is lost from one molecule of MA and a formal 1,2-hydrogen migration takes place in the other. The H atom is likely eliminated with a Cp* ligand to form isolated Cp*H.

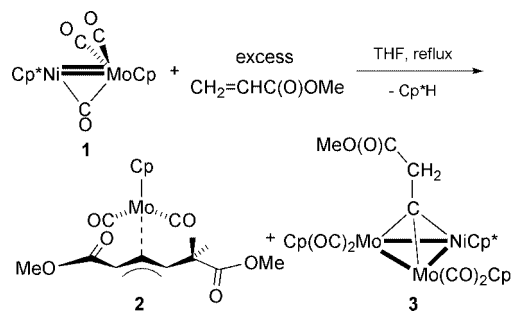

Scheme 1

The other complex isolated (Scheme 1)† is the μ_3-alkylidyne capped mixed-metal cluster $[NiMo_2(\mu_3\text{-}CCH_2CO_2Me)(CO)_4Cp^*Cp_2]$ **3** (Fig. 2).§ In this 48e cluster, each Mo atom is bonded to a Cp ligand and to two CO ligands, and the Ni to its Cp* ligand. The cluster has no (C_1) symmetry. The Ni–Mo bonds (2.63 Å, av.) and the Mo–Mo bond (2.9343(4) Å) are in the range for normal single bonds between these metals. As in **2**, the C(O)OMe group in **3** is not involved in any bonding interaction with any metal. The asymmetry observed in the solid-state for **3** is maintained in solution, as is reflected in the NMR spectra.†

The organic ligand in **3** is derived from MA by activation of both CH_2 protons: again 1,2-migration of one H and loss of the other have occurred, generating the triply-bridging $\equiv CCH_2C(O)OMe$ fragment. There appears to be no precedent in the literature for such activation of MA to afford structures like those of **2** and **3**.

MA dimerization has been observed with complexes of Ni,[3] Pd,[4] Rh,[5] Ru[6–8] and Sm,[9] but few organometallic intermediates have been isolated. An Rh(III) complex which contains a dimerized MA ligand was characterized but both an allylic interaction and chelation *via* a carbonyl function were noted; the latter was thought to be responsible for its inactivity towards excess MA.[5c] Carbon–carbon bond formation at polynuclear metal centers has been much investigated but fewer studies have targeted alkenes as compared to alkynes[10] and we are not aware of any complexes similar to **2** that were isolated from such reactions. The potential of multicenter activation of organic substrates is further illustrated by the recent thermal cleavage (in contrast to our case of C–C coupling) of the C=C double

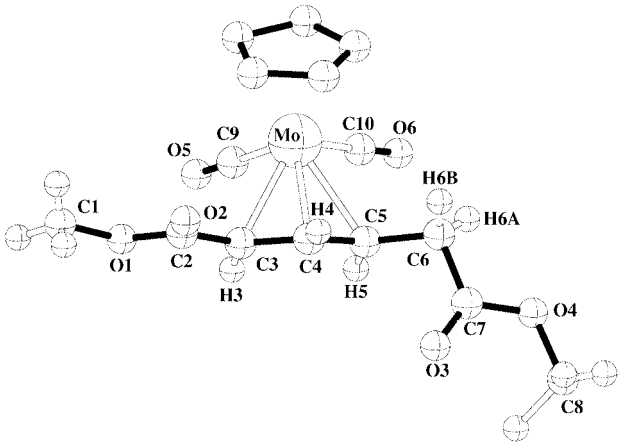

Fig. 1 Crystalmaker® plot of the structure of the allylic complex $[Mo(CO)_2(\eta^3\text{-}MeOC(O)CH{=}CH{=}CHCH_2C(O)OMe)Cp]$ **2** (covalent radii for all atoms except for H). Cp hydrogen atoms are not shown; selected bond lengths (Å) and angles (°): Mo–C(3) 2.328(2), Mo–C(4) 2.238(2), Mo–C(5) 2.379(2), C(3)–C(4) 1.419(3), C(4)–C(5) 1.406(3), C(5)–C(6) 1.510(3); C(3)–C(4)–C(5) 118.6(2), C(9)–Mo–C(10) 78.75(9).

† Electronic supplementary information (ESI) available: preparation and selected data for **2** and **3**. See http://www.rsc.org/suppdata/cc/b1/b107827p/

‡ Dedicated to Prof. C. Moïse (Dijon) on the occasion of his 60th birthday, with warmest wishes.

 DOI: 10.1039/b107827p

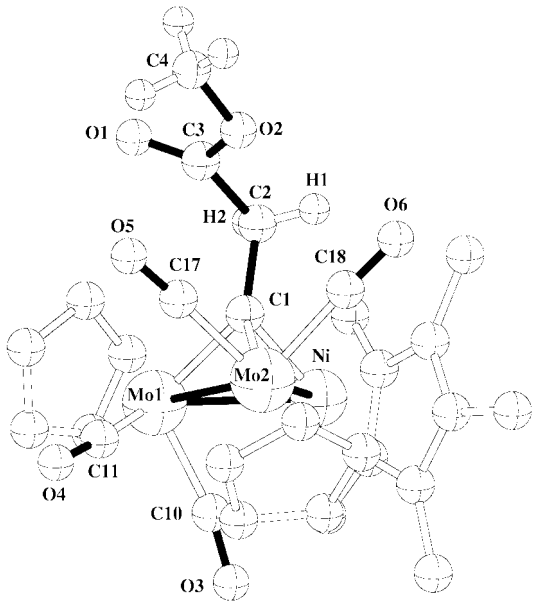

Fig. 2 Crystalmaker® plot of the structure of the alkylidyne cluster $[NiMo_2(\mu_3\text{-}CCH_2CO_2Me)(CO)_4Cp^*Cp_2]$ **3** (covalent radii for all atoms except for H). Only the alkylidyne ligand hydrogen atoms are shown; selected bond lengths (Å) and angles (°): Ni–Mo(1) 2.6282(5), Ni–Mo(2) 2.6309(5), Mo(1)–Mo(2) 2.9343(4), Ni–C(1) 1.891(3), Mo(1)–C(1) 2.090(4), Mo(2)–C(1) 2.131(3); Mo(1)–Mo(2)–Ni 56.04(1), Mo(1)–Ni–Mo(2) 67.83(2), Ni–Mo(1)–Mo(2) 56.13(1), Ni–C(1)–C(2) 119.6(2), Mo(1)–C(1)–C(2) 131.4(3), Mo(2)–C(1)–C(2) 134.6(3), C(10)–Mo–C(11) 87.6(2), C(17)–Mo–C(18) 87.5(2).

bond of methyl acrylate mediated by a triruthenium pentahydride cluster which afforded a μ_3-alkyne, μ_3-methylidyne cluster.[11]

To address the need for a heterometallic species, we examined the reactivity of MA separately with each of the closely related metal–metal bonded homodinuclear complexes $[Cp^*Ni(\mu\text{-}CO)]_2$ and $[CpMo(CO)_3]_2$ and with the triply bonded, unsaturated complex $[Cp(OC)_2Mo{\equiv}Mo(CO)_2Cp]$ under similar reaction conditions. In all cases the metal complexes and ligand were recovered essentially unchanged. Since the reaction of Scheme 1 occurs under thermal conditions, we do not believe that the paramagnetic nature of **1** is responsible for its reactivity. Furthermore, the multiple metal–metal bond character of **1** alone is not sufficient, as shown by the lack of reaction of the Mo≡Mo complex. The coordinatively saturated complex $[Cp^*(OC)Ni\text{–}Mo(CO)_3Cp]$ was not investigated as it decarbonylates under these thermal reaction conditions to generate **1**.

Although the detailed reaction mechanism leading to the C–H activations of MA and C–C bond formation observed here remains unknown, the reactions observed here could occur at the heterometallic core or, alternatively, fragmentation of the Ni–Mo multiple bond could generate reactive species not readily acccessible from the Ni_2 or Mo_2 complexes. Nevertheless, pure **1** is thermally stable in refluxing THF. This study represents a clear example of a heterobimetallic complex showing enhanced reactivity as compared to that of its homodinuclear congeners.[12]

This work was supported by the CNRS and the Ministère de la Recherche (also *via* an associate research position to M. J. C.) and we are also grateful to the COST D-17 programme of the European Commission (DG-XII).

Notes and references

§ *Crystal data* for **2**: $C_{15}H_{11}MoO_6$, M = 383.18, monoclinic, space group $P2_1/c$, a = 11.0224(2), b = 18.5428(4), c = 7.93560(10) Å, β = 106.7923(10)°, V = 1552.77(5) Å^3, Z = 4, D_c = 1.639 g cm^{-3}, μ = 0.869 mm^{-1}, $F(000)$ = 764, λ(Mo-Kα) = 0.71073 Å, T = 293(2) K. Yellow prism, dimensions 0.15 × 0.12 × 0.10 mm. A total of 11066 reflections were collected with $2.90 < \theta < 34.98°$. R = 0.0389, R_w = 0.0951, GOF = 1.051, maximum residual electron density 0.839 e Å^{-3}. Out of the 6803 unique reflections, 5384 had intensities $I > 2\sigma(I)$.

For **3**: $C_{28}H_{30}Mo_2NiO_6$, M = 713.11, monoclinic, space group $P2_1/c$, a = 10.3564(3), b = 16.6644(4), c = 15.3764(5) Å, β = 90.4249(11)°, V = 2653.64(5) Å^3, Z = 4, D_c = 1.785 g cm^{-3}, μ = 1.674 mm^{-1}, $F(000)$ = 1432, λ(Mo-Kα) = 0.71073 Å, T = 180(2) K. Black prism, dimensions 0.1 × 0.1 × 0.1 mm. A total of 16458 reflections were collected with $2.78 < \theta < 30.06°$. R = 0.0466, R_w = 0.0922, GOF = 0.823, maximum residual electron density 0.535 e Å^{-3}. Out of the 7737 unique reflections, 5611 had $I > 2\sigma(I)$.

CCDC reference numbers 162868 and 162869.

See http://www.rsc.org/suppdata/cc/b1/b107827p/ for crystallographic data in CIF or other electronic format.

1 (*a*) G. J. P. Britovsek, V. C. Gibson and D. F. Wass, *Angew. Chem., Int. Ed.*, 1999, **38**, 428; (*b*) S. D. Ittel, L. K. Johnson and M. Brookhart, *Chem. Rev.*, 2000, **100**, 1169; (*c*) A. Michalak and T. Ziegler, *Organometallics*, 2001, **20**, 1521.

2 M. J. Chetcuti, B. E. Grant, P. E. Fanwick, M. J. Geselbracht and A. M. Stacy, *Organometallics*, 1990, **9**, 1343.

3 G. Wilke, *Angew. Chem., Int. Ed. Engl.*, 1988, **27**, 185.

4 (*a*) G. Oehme and H. Pracejus, *J. Organomet. Chem.*, 1987, **320**, C56; (*b*) I. Guibert, D. Neibecker and I. Tkatchenko, *J. Chem. Soc., Chem. Commun.*, 1989, 1850.

5 (*a*) M. Brookhart and S. Sabo-Etienne, *J. Am. Chem. Soc.*, 1991, **113**, 2777; (*b*) M. Brookhart and E. Hauptman, *J. Am. Chem. Soc.*, 1992, **114**, 4437; (*c*) E. Hauptman, S. Sabo-Etienne, P. S. White, M. Brookhart, J. M. Garner, P. J. Fagan and J. C. Calabrese, *J. Am. Chem. Soc.*, 1994, **116**, 8038; (*d*) T. Kaneko, T. Kanke, S. Kiyooka and K. Isobe, *Chem. Lett.*, 1997, 23.

6 (*a*) R. J. McKinney and M. C. Colton, *Organometallics*, 1986, **5**, 1080; (*b*) B. Patzke and R. Sustmann, *J. Organomet. Chem.*, 1994, **480**, 65; (*c*) C. Strehblow, T. Schupp and R. Sustmann, *J. Organomet. Chem.*, 1998, **561**, 181; (*d*) G. L. Tembe, P. A. Ganeshpure and S. Satish, *React. Kinet. Catal. Lett.*, 1998, **63**, 151.

7 C. Y. Ren, W. C. Cheng, W. C. Chan, C. H. Yeung and C. P. Lau, *J. Mol. Catal.*, 1990, **59**, L1.

8 C. S. Yi and N. Liu, *J. Organomet. Chem.*, 1998, **553**, 157.

9 H. Yasuda, H. Yamamoto, K. Yokota, S. Miyake and A. Nakamura, *J. Am. Chem. Soc.*, 1992, **114**, 4908.

10 (*a*) M. J. Chetcuti, P. E. Fanwick, S. R. McDonald and N. P. Rath, *Organometallics*, 1991, **10**, 1551; (*b*) G. C. Bruce, S. A. R. Knox and A. J. Phillips, *J. Chem. Soc., Chem. Commun.*, 1990, 716; (*c*) S. A. R. Knox, *J. Cluster Sci.*, 1992, **3**, 385.

11 T. Takemori, A. Inagaki and H. Suzuki, *J. Am. Chem. Soc.*, 2001, **123**, 1762.

12 (*a*) P. Braunstein and J. Rosé, *Catalysis and Related Reactions with Compounds containing Heteronuclear Metal–Metal Bonds*, in *Comprehensive Organometallic Chemistry II*, ed. E. W. Abel, F. G. A. Stone and G. Wilkinson, Pergamon, Oxford, 1995, vol. 10, p. 351; ; (*b*) M. J. Chetcuti, *Heterodinuclear Compounds, in Comprehensive Organometallic Chemistry II*, ed. E. W. Abel, F. G. A. Stone and G. Wilkinson, Pergamon, Oxford, 1995, **vol. 10**, p. 23; (*c*) T. Nakajima, I. Shimizu, K. Kobayashi, H. Koshino and Y. Wakatsuki, *Inorg. Chem.*, 1997, **36**, 6440; (*d*) P. Braunstein and J. Rosé, *Heterometallic Clusters in Catalysis*, in *Metal Clusters in Chemistry*, ed. P. Braunstein, L. A. Oro and P. R. Raithby, Wiley–VCH, Weinheim, 1999, vol. 2, p. 616; (*e*) N. Wheatley and P. Kalck, *Chem. Rev.*, 1999, **99**, 3379; (*f*) L. H. Gade, *Angew. Chem., Int. Ed.*, 2000, **39**, 2659; (*g*) J. R. Torkelson, O. Oke, J. Muritu, R. McDonald and M. Cowie, *Organometallics*, 2000, **19**, 854; (*h*) P. Braunstein, M. Knorr, G. Reinhard, U. Schubert and T. Stährfeldt, *Chem. Eur. J.*, 2000, **6**, 4265; (*i*) P. Braunstein, J. Durand, M. Knorr and C. Strohmann, *Chem. Commun.*, 2001, 211.

CHEMCOMM Communication
www.rsc.org/chemcomm

Efficient heterogeneous catalytic intramolecular Tishchenko reaction of *o*-phthalaldehyde to phthalide with alkaline earth oxides

Tsunetake Seki and Hideshi Hattori*

Center for Advanced Research of Energy Technology, Hokkaido University, Kita-13, Nishi-8, Kita-ku, Sapporo 060-8628, Japan. E-mail: hattori@carbon.caret.hokudai.ac.jp

Received (in Cambridge, UK) 10th October 2001, Accepted 30th October 2001
First published as an Advance Article on the web

The heterogeneous catalytic systems realized by alkaline earth oxides are successfully applicable to the highly efficient intramolecular Tishchenko lactonization of *o*-phthalaldehyde to phthalide.

The heterogeneous catalytic Tishchenko reaction using solid bases involves the dimerizarion of aldehydes yielding the corresponding esters initiated by the interactions of polarized carbonyl groups of aldehydes with surface acidic and basic sites of solid bases. The adaptability of solid base catalysts to the Tishchenko reaction has been demonstrated in several investigations.[1] Most of previous development of efficient catalysis for Tishchenko reaction, however, has been confined to homogeneous catalytic systems. Recent articles dealing with homogeneous catalyses have reported considerable improvements in activities for the dimerization of aldehydes in comparison with traditional aluminium alkoxides catalysts.[2,3] Solid base catalysts, unlike these homogeneous catalysts, can be easily separated from the reaction mixture after carrying out the reaction, and are inexpensive and environmentally benign. These excellent properties emphasize the importance of the replacement of homogeneous catalyses with heterogeneous ones both in the laboratory and in industrial processes utilizing Tishchenko esterification.

Although several studies have been conducted on the *intermolecular* Tishchenko reaction over solid base catalysts as mentioned above, there have been no reports of the *intramolecular* Tishchenko reaction which results in cyclization.[2,4] In addition, to our knowledge, in the field of heterogeneous basic catalysis, there has been only one report dealing with intramolecular cyclization (dehydration of monoethanolamine to ethylenimine).[5] Here we report the intramolecular Tishchenko reaction of *o*-phthalaldehyde to phthalide using alkaline earth oxides as powerful and highly selective heterogeneous catalysts. The general reaction equation is shown in Scheme 1.

Experimental procedures are as follows: MgO, CaO, SrO and BaO were prepared from $Mg(OH)_2$, $Ca(OH)_2$, $SrCO_3$ and $BaCO_3$, respectively, by thermal decomposition at elevated temperatures *in vacuo*. The pretreatment temperatures and surface areas of the catalysts examined are listed in Table 1. To a Schlenk tube containing the alkaline earth oxide pretreated (10 or 50 mg) was added a benzene (1 mL) solution of *o*-phthalaldehyde (1 mmol) under N_2 at room temperature. Then the reaction mixture was warmed to 313 K and stirred for a prescribed reaction time. The resulting solution, after alkaline earth oxide was separated, was analyzed by GC equipped with a DB-1 column (total length: 60 m; diameter: 0.25 mm) to determine the yield (%) of phthalide. The product was identified by ^{1}H NMR and GC–MS analysis.

The catalytic activities of alkaline earth oxides for the intramolecular Tishchenko reaction of *o*-phthalaldehyde to phthalide are given in Table 1. To compare the activities of alkaline earth oxides, *o*-phthalaldehyde was treated with 10 mg of each alkaline earth oxide at 313 K for 60 min (entries 1, 3, 5 and 7). Barium oxide did not furnish the corresponding lactone at all (entry 7). Magnesium oxide and SrO showed almost equal moderate activities (entries 1 and 5). In contrast, however, CaO exhibited an excellent activity (entry 3). It should be emphasized that MgO, CaO and SrO yielded phthalide selectively (intermolecular Tishchenko dimerization products were not observed by GC–MS analysis). In an attempt to attain a synthetically satisfactory level of yield, the amount of MgO, CaO, and SrO was increased without changing the reaction temperature. Thus, when the reaction was carried out at 313 K with 50 mg of CaO, the reaction proceeded instantaneously, and phthalide was obtained quantitatively in a short time of 15 min (entry 4). Under the same conditions, MgO and SrO also furnished pthalide in excellent yields of 91 and 86%, respectively (entries 2 and 6).

In summary we have shown that efficient heterogeneous catalytic lactonization of dialdehydes can be realized by using alkaline earth oxides through the intramolecular Tishchenko reaction of *o*-phthalaldehyde to phthalide.

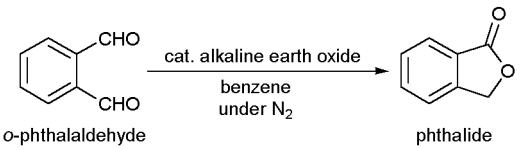

Scheme 1 Heterogeneous catalytic intramolecular Tishchenko reaction of *o*-phthalaldehyde to phthalide with alkaline earth oxides.

Table 1 Activities of alkaline earth oxides for the intramolecular Tishchenko reaction of *o*-phthalaldehyde to phthalide[a]

Entry	Catalyst	Catalyst weight/mg	Pretreatment temperature/K	Surface area[b]/m^2 g^{-1}	Reaction time/min	Reaction temp./K	Yield[c] (%)
1	MgO	10	873	267	60	313	15
2	MgO	50	873	267	15	313	91
3	CaO	10	873	48	60	313	59
4	CaO	50	873	48	15	313	Quantitative
5	SrO	10	1273	12	60	313	15
6	SrO	50	1273	12	15	313	86
7	BaO	10	1273	2	60	313	0

[a] Reactant: 1 mmol of *o*-phthalaldehyde; solvent, 1 mL of benzene. All reactions were carried out under N_2. [b] Surface areas were determined by the BET method. [c] Yield was determined by the GC analysis of the resulting solution and was calculated by the equation: yield (%) = {(mol% of phthaide)/[(mol% of *o*-phthalaldehyde) + (mol% of phthalide)]} × 100.

 DOI: 10.1039/b109249a

This work is supported by a Grant-in aid for Scientific Research of Ministry of Education, Science, Sports, and Culture, Japan.

Notes and references

1 (*a*) K. Tanabe and K. Saito, *J. Catal*., 1974, **35**, 247; (*b*) H. Tsuji, F. Yagi, H. Hattori and H. Kita, *J. Catal*., 1994, **148**, 759; (*c*) H. Handa, T. Baba, H. Sugisawa and Y. Ono, *J. Mol. Catal*., 1998, **134**, 171; (*d*) H. Kabashima, H. Tsuji, S. Nakata, Y. Tanaka and H. Hattori, *Appl. Catal*., 2000, **194–195**, 227; (*e*) T. Seki, K. Akutsu and H. Hattori, *Chem. Commun*., 2001, **11**, 1000.

2 (*a*) S. Onozawa, T. Sakakura, M. Tanaka and M. Shiro, *Tetrahedron*, 1996, **52**, 4291; (*b*) T. Ooi, T. Miura, K. Takaya and K. Maruoka, *Tetrahedron Lett*., 1999, **40**, 7695; (*c*) M. R. Bürgstein, H. Berberich and P. W. Roesky, *Chem. Eur. J*., 2001, **7**, 3078.

3 For the use of traditional aluminium alkoxides as catalysts, see: (*a*) W. Tischtschenko, *Chem. Zentralbl*., 1906, **77**, **I**, 1309; (*b*) W. C. Child and H. Adkins, *J. Am. Chem. Soc*., 1925, **47**, 798; (*c*) F. J. Villani and F. F. Nord, *J. Am. Chem. Soc*., 1947, **69**, 2605; (*d*) L. Lin and A. R. Day, *J. Am. Chem. Soc*., 1952, **74**, 5133; (*e*) T. Saegusa and T. Ueshima, *J. Org. Chem*., 1968, **33**, 3310.

4 S. H. Bergens, D. P. Fairlie and B. Bosnich, *Organometallics*, 1990, **9**, 566.

5 M. Ueshima, H. Yano and H. Hattori, *Sekiyu Gakkaishi* (*J. Jpn. Petroleum Inst*.), 1992, **35**, 362.

CHEMCOMM Communication
www.rsc.org/chemcomm

Thermal stability of an SiO_2-coated Rh catalyst and catalytic activity in NO reduction by CO

Masanori Ikeda,* Teruoki Tago, Masahiro Kishida and Katsuhiko Wakabayashi

Department of Materials Process Engineering, Graduate School of Engineering, Kyushu University, 6-10-1 Hakozaki, Higashi-ku, Fukuoka 812-8581, Japan. E-mail: mikeda@chem-eng.kyushu-u.ac.jp

Received (in Cambridge, UK) 1st August 2001, Accepted 25th August 2001
First published as an Advance Article on the web

An SiO_2-coated Rh catalyst with SiO_2 thickness of 13 nm has much higher stability against sintering of Rh and SiO_2 than sol–gel and impregnation Rh/SiO_2 catalysts; it exhibits the highest activity in the NO–CO reaction among these catalysts after thermal treatment.

The efficiency and life-time of a supported metal catalyst is influenced by the thermal stability of the metal particles. At high temperatures, sintering of metal particles causes deactivation of the catalyst. Sintering is a serious problem especially for automotive catalysts because they are exposed to exhaust gases at high temperatures. There is no method that completely inhibits sintering. However, it is considered that physical prevention of the migration of metal particles can effectively restrain sintering. For instance, sol–gel catalysts are known to have high resistance to the sintering of metal particles.[1–3] Such catalysts have metal particles that are incorporated into the framework of the support or partially embedded in the support.[1,2] Such a structure restrains the migration of metal particles, leading to inhibition of sintering.

We developed a preparation method for supported metal catalysts using a water-in-oil microemulsion (ME method) and reported that Rh particles of an Rh/SiO_2 catalyst prepared by this method were partially embedded into SiO_2 supports.[4] Furthermore, we successfully synthesized Rh nanoparticles wholly coated by a nanometer-scale SiO_2 layer using a specific microemulsion system.[5] It is expected that such a structure results in high resistance to sintering since the migration of the Rh particles is prevented by the SiO_2 layer. In the present study, we compared the sintering behaviors of SiO_2-coated Rh particles (SC) with catalysts prepared by the microemulsion (ME) method, sol–gel (SG) method and the impregnation (IMP) method. In addition, the catalytic activities of the particles in NO reduction by CO were also compared with those of the other catalysts before and after thermal treatment. It has been reported that similar silica-coated metal particles have been synthesized,[6–8] but the present report is the first to describe SC particles used as a catalyst.

The starting materials for Rh and SiO_2 were $RhCl_3{\cdot}3H_2O$ and tetraethyl orthosilicate (TEOS), respectively for all the catalysts. The SC and ME catalysts were prepared using the same procedure as reported previously.[4,5] A microemulsion system of polyoxyethylene (n = 15) cetyl ether (226 g, 0.5 M)/cyclohexane and polyoxyethylene (n = 5)–*p*-nonylphenyl ether (22 g, 0.5 M)/hexan-1-ol were used for the preparation of the SC and ME catalysts, respectively. The molar ratios of surfactant to water (for hydrolysis of TEOS) were 3 and 6 for the SC and ME catalysts, respectively.

The SG catalyst was prepared using the following procedure. A mixture of TEOS (37 g) and ethanol (20 ml) were stirred at 70 °C for 10 min. A solution of $NH_3{\cdot}H_2O$ (1 ml) and distilled water (20 ml) were added to the mixture and stirred at 70 °C for 30 min. An aqueous $RhCl_3$ solution (0.38 M, 2.6 ml) was added to the mixture and stirred at 70 °C for 1 h to obtain a gel containing the Rh precursor. The gel was then dried at 70 °C for 12 h. The IMP catalyst was prepared by the usual procedure. The SiO_2 support was prepared using the ME method employing a microemulsion system of polyoxyethylene (n = 15) cetyl ether/cyclohexane.

In all methods, the dried samples were calcined under an air flow at 500 °C for 2 h and reduced at 450 °C for 1 h. The Rh loading was 1 wt% for the ME SG and IMP catalysts and 10 wt% for the SC catalyst. For the NO–CO reaction, the SC catalyst was mixed with silica (the same silica as the support of the IMP catalyst) to 1 wt% Rh content.

To investigate the thermal stability of Rh particles against sintering, air calcination of all the catalysts was conducted at 900 °C for 12 h under air flow. The mean Rh particle size of the Rh/SiO_2 catalysts was determined by powder X-ray diffraction (XRD) using a Rigaku RINT 2500 instrument. BET surface areas were measured by nitrogen adsorption at −196 °C using a Shimadzu Tristar 3000 instrument at 55 °C. The amount of CO uptake by the Rh particles was measured by CO chemisorption. Transmission electron microscopy (TEM) images of the catalysts were taken with a JOEL JEM 2000FX.

Catalytic activity was measured using a quartz tubular reactor. The reactant gas mixture was composed of 10 000 ppm NO, 10 000 ppm CO and He as a balance, while the gas-flow rate was 100 ml min^{-1} (SV = 30000 ml $g\text{-}cat^{-1}$ h^{-1}). The effluent gas was directly routed to a gas chromatograph (Shimadzu GC-8A) for on-line analysis.

Table 1 shows the Rh particle sizes determined by XRD before and after thermal treatment. Both the Rh particle size after the thermal treatment and the difference in the Rh particle size before and after the thermal treatment, $\triangle D$, could be ranked in the following order according to size: SC < ME < SG < IMP. Fig. 1 shows TEM photographs of these catalysts after thermal treatment. The sequence of mean Rh particle sizes determined by TEM photographs was the same as that determined by XRD. In the IMP catalyst [Fig. 1(a)], several Rh particles of size >20 nm were observed. In the SG catalyst, most Rh particles remained small (*ca.* 5 nm) after thermal treatment, which indicates that the SG catalyst has a higher resistance to sintering than does the IMP catalyst, although some Rh particles were as large as those of the IMP catalyst. In the ME catalyst [Fig. 1(c)], most of Rh particles remained small (*ca.* 4 nm) after thermal treatment while a few Rh particles of size *ca.* 15 nm were observed. Therefore, the ME catalyst has a higher resistance to the sintering than does the SG catalyst. In

Table 1 Rh particle sizes and BET surface areas of catalysts prepared *via* different routes

	Rh particle size/nm			BET surface area/m^2 g^{-1}	
Cat.	Before[a]	After[b]	ΔD[c]/nm	Before[a]	After[b]
SC	3.4	5.7	2.3	246	170
ME	3.8	6.8	3.0	24	18
SG	6.8	10.1	3.3	231	34
IMP	6.6	11.0	4.4	73	51

[a] Value before thermal treatment. [b] Value after thermal treatment at 900 °C for 12 h. [c] The difference in Rh particle sizes before and after thermal treatment.

 DOI: 10.1039/b106797d

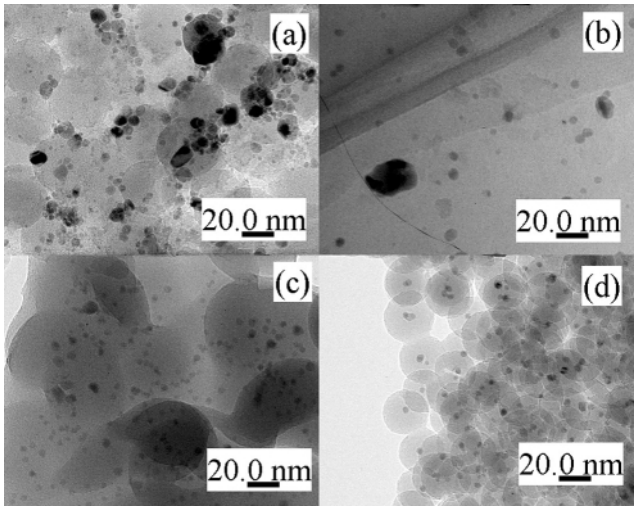

Fig. 1 TEM photographs of the Rh/SiO_2 catalysts after thermal treatment at 900 °C for 12 h: (a) IMP, (b) SG, (c) ME, (d) SC.

the SC catalyst [Fig. 1(d)], however, all the Rh particles were covered by the SiO_2 layer and remained small even after the thermal treatment. It is concluded that migration of Rh particles of the SC catalyst was restrained by the SiO_2 layer, resulting in the highest resistance to sintering.

Fig. 2 shows the temperatures for 50% NO conversion in NO reduction by CO, T_{50}, before and after thermal treatment. The sequence of relative activity before thermal treatment was IMP < SC < ME < SG. It was noted that the SC catalyst showed an activity as high as that of the IMP catalyst although the Rh particles of the SC catalyst were fully covered by the SiO_2 layer. This result indicates that the reactant gases were accessible to the Rh particles. The amount of CO uptake of the SC catalyst (13.9 μmol g^{-1}) was of the same order as found for the IMP catalyst (16.5 μmo g^{-1}).

The IMP catalyst was considerably deactivated by the thermal treatment as can be seen from Fig. 2. The main reason for the deactivation is due to the sintering of the Rh particles as shown in Table 1. T_{50} of the ME and SG catalysts also considerably increased despite their high resistance to sintering. In contrast to these catalysts, T_{50} of the SC catalyst having the highest resistance to sintering increased only slightly and was the lowest after the thermal treatment. Accordingly, the SC

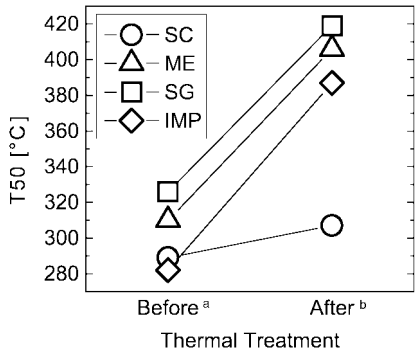

Fig. 2 T_{50} values in the NO–CO reaction over the Rh/SiO_2 catalysts. [a] Values before thermal treatment; [b] Value after thermal treatment at 900 °C for 12 h.

catalyst had the highest activity of these catalysts after the thermal treatment. As to the difference in activity between the three types of catalysts, this is difficult to explain in terms of Rh particle size since the difference is attributable to changes in several physical and physico-chemical factors. One of the most important factors may be metal–support interactions. It was reported that sol–gel catalysts with metal particles embedded in silica supports showed stronger metal–support interaction than impregnation catalysts,[9] leading to the existence of $M^{\delta+}$ species in the catalyst. In another report, it was shown that the presence of $Rh^{\delta+}$ in the catalyst improved catalytic activity in the NO–CO reaction.[10] Rh–SiO_2 interactions might differ between the catalysts causing the differences in catalytic activity.

In addition, we considered that the thermal stability of the SiO_2 support might affect the catalytic activity since the reactant gases are accessed on the Rh surface through the SiO_2 pores. The BET surface areas of these catalysts are given in Table 1. For the SG catalyst, the area was drastically decreased upon thermal treatment while for the ME catalyst the initial low surface area was further lowered upon thermal treatment. On the other hand, the area of the SC catalyst after thermal treatment was still substantial. The CO uptake of these catalysts were 3.1, 0.2 and 0.2 μmol g^{-1} for the SC, ME and SG catalysts, respectively. These results suggest that the SiO_2 pores of the ME and SG catalysts are decreased upon thermal treatment while the pores are less affected in the SC catalyst. It is clear that the SC catalyst has a high SiO_2 thermal stability. The reason for this is not clear, but such high thermal stability may be derived from the thin SiO_2 layer. The thickness of SiO_2 layer of the SC catalyst used in the reactions is *ca.* 13 nm [Fig. 1(d)]. The BET surface area of this SC catalyst decreased upon thermal treatment from 246 to 170 m^2 g^{-1} (Table 1). On another SC catalyst with an SiO_2 thickness of 22 nm, however, the BET surface area drastically decreased upon thermal treatment from 91 to 3 m^2 g^{-1}. The difference suggests that the thinner SiO_2 layer shows a higher resistance to blockage of silica pores upon thermal treatment. Such high thermal stability of SiO_2 in the SC catalyst as well as high resistance to sintering of Rh particles led to high activity after thermal treatment.

In conclusion, the SiO_2-coated Rh catalyst with SiO_2 thickness of 13 nm showed a much higher stability against sintering of Rh and SiO_2 than sol–gel and impregnation Rh/SiO_2 catalysts. As a result, this catalyst had the highest activity in NO reduction by CO after thermal treatment at 900 °C for 12 h.

Notes and references

1 M. Azomoza, T. Lopez, R. Gomez and R. D. Gonzalez, *Catal. Today*, 1992, **15**, 547.
2 P. Bosch, T. Lopez, V.-H. Lara and R. Gomez, *J. Mol. Catal.*, 1993, **80**, 299.
3 I. H. Cho, S. B. Park, S. J. Cho and R. Ryoo, *J. Catal.*, 1998, **173**, 295.
4 M. Kishida, T. Hanaoka, H. Hagata and K. Wakabayashi, *Catal. Today*, 1998, **45**, 203.
5 M. Kishida, T. Tago, T. Hatsuta and K. Wakabayashi, *Chem. Lett.*, 2000, **9**, 1108.
6 L. M. Liz-Marzán, M. Giersig and P. Mulvaney, *Langmuir*, 1996, **12**, 4329.
7 M. Giersing, T. Ung, L. M. Liz-Marzán and P. Mulvaney, *Adv. Mater.*, 1997, **9**, 570.
8 T. Li, J. Moon, A. A. Morrone, J. J. Mecholsky, D. R. Talham and J. H. Adair, *Langmuir*, 1999, **15**, 4328.
9 T. Lopez, M. Villa and R. Gomez, *J. Phys. Chem.*, 1991, **95**, 1690.
10 W. C. Hecker and A. T. Bell, *J. Catal.*, 1983, **84**, 200.

CHEMCOMM
Communication
www.rsc.org/chemcomm

A new, highly fluorescent terpyridine which responds to zinc ions with a large red-shift in emission†

Wendy Goodall and J. A. Gareth Williams*

Department of Chemistry, University of Durham, South Road, Durham, UK DH1 3LE. E-mail: j.a.g.williams@durham.ac.uk

Received (in Cambridge, UK) 17th September 2001, Accepted 24th October 2001
First published as an Advance Article on the web

A sequence of three metal-catalysed aryl coupling reactions leads to the new ligand 4′-(4-*N*,*N*-diphenylaminophenyl)-2,2′:6′,2″-terpyridine, the intense ICT emission of which undergoes a large red-shift upon binding of zinc ions, providing a unique response over other common metal ions.

Sensitive and selective fluorescent probes for metal ions are important in clinical analyses, including the study of the physiological roles of metal ions.[1] With a large number of cellular functions having been identified for zinc over the past decade, probes of cellular Zn^{2+} concentration are of increasing interest.[2] The luminescence of some transition metal complexes of terpyridines is well established including applications to chemical sensing (*e.g.* for pH, halide and metal ions[3,4]). On the other hand, terpyridine ligands themselves have generally not been considered for use as fluorescent sensors, possibly owing to an expected lack of selectivity (given the diverse range of metal ions they are able to bind) and perhaps also to the fact that few terpyridines are strongly emissive at wavelengths other than in the UV, with short-wavelength excitation being required. We report here on the use of palladium-catalysed cross-couplings of aryl boronates with 4′-bromoterpyridine, to construct novel, 4′-substituted terpyridines in high yield.[5] In particular, this methodology has been used to prepare the compound 4′-(4-*N*,*N*-diphenylaminophenyl)-2,2′:6′,2″-terpyridine, a highly fluorescent new ligand whose emission is affected very distinctively upon binding of zinc ions.

4-Bromo-*N*,*N*-diphenylaniline was prepared by a copper(I)-catalysed Ullmann coupling of diphenylamine with 4-bromoiodobenzene in the presence of 1,10-phenanthroline (Scheme 1, ESI†). Under these conditions, substitution occurs specifically at the iodine atom. Conversion to the neopentyl boronate was accomplished by a palladium-catalysed reaction with bis(neopentyl glycolato)diboron. Finally, a Suzuki-type coupling of the boronate with 4′-bromoterpyridine, (readily accessible in multigram quantities†), led to the desired compound in 66% yield. The use of cross-coupling reactions in this way offers an attractive, divergent route to new 4′-aryl-substituted terpyridines and, indeed, the *N*,*N*-dimethyl analogue (designated L^2) was prepared similarly from 4′-triflate-terpyridine upon reaction with commercially available 4-(dimethylamino)benzeneboronic acid.

The lowest energy absorbance maxima of the two compounds in solution (Table 1) display a very small red-shift with increasing solvent polarity. In contrast, the fluorescence maxima undergo very large shifts to longer wavelengths. Such behaviour is strongly indicative of intramolecular charge transfer (ICT) character in the emissive excited states of these compounds. The fluorescence of L^2 and its non-methylated ($-NH_2$) analogue has been interpreted in this way in a contemporary report, where a semi-empirical MO calculation revealed that the amino substituent raises the energy level of the pendent phenyl to such an extent that the lowest energy excited state corresponds to an ICT (π_{Ph}–π^*_{tpy}) transition, as opposed to the locally excited states (π_{tpy}–π^*_{tpy}) of other 4′-aryl-substituted terpyridines.[6] The present results indicate that the diphenylamino substituent has a similar effect, with comparable emission wavelength maxima in each solvent. However, whereas the emission intensity of L^2 is greatly reduced in polar solvents such as ethanol, L^1 is strongly fluorescent in all solvents investigated. This difference is strikingly clear upon comparing the fluorescence quantum yields in ethanol: 0.009 and 0.25, respectively. Given that the fluorescence lifetimes of the two compounds in this solvent are the same within experimental error (Table 1), the much smaller quantum yield of L^2 is most likely due to a reduction in the efficiency of formation of the emissive ICT state in L^2, following excitation to the initially populated excited state, rather than enhanced non-radiative deactivation. It is well-established that ICT emission from dialkylamino-substituted aromatics of the 'push–pull' type (for example, the classic compound dimethylaminobenzonitrile), requires a dynamic relaxation of the initially populated state through twisting of the dialkylamino group, coupled with electron transfer from the amino nitrogen to the remote π* orbital of the acceptor moiety. In alcohol solutions which can hydrogen bond to the N atom of the donor, it has been shown that the twisting process may be partially inhibited owing to the requirement for simultaneous breakage of such a hydrogen bond.[7] Given the basicity of dimethylaniline compared to non-basic triphenylamine (pK_a values of the conjugate acids are 5.15 and *ca.* −5 respectively), such hydrogen bonding is to be expected in L^2 but may be absent (or only very weak) in

Table 1 Photophysical properties of ligands L^1 and L^2 in solvents of varying polarity

	Cyclohexane	THF	DCM	EtOH
L^1				
λ_{max}[a]/nm (absorbance)	356	360	361	362
λ_{max}[b]/nm (emission)	392 (414 sh)	453	472	513
τ_f[c]/ns	1.2	3.4	4.0	2.5
ϕ_f[d]	0.36	0.51	0.58	0.25
L^2				
λ_{max}[a]/nm (absorbance)	337	346	348	348
λ_{max}[b]/nm (emission)	369 (385 sh)	469	470	531
τ_f[c]/ns	1.7	5.2	5.2	2.6
ϕ_f[d]	0.31[e]	0.22	0.27	0.009

[a] Absorbance of longest wavelength absorption band. [b] Upon excitation into the lowest energy absorption band. [c] Fluorescence lifetimes were measured in the frequency domain using an Instruments S.A. Flurolog τ-3 instrument; estimated uncertainty ± 0.2 ns. [d] Fluorescence quantum yields were measured using an Instruments S.A. Fluoromax, with an excitation wavelength of 350 nm and excitation and emission band-passes set to 2.5 nm in each case; quinine sulfate was used as the standard (ϕ = 0.546 in 1 M H_2SO_4[11]); estimated uncertainty ±20%. [e] Measured using an excitation wavelength of 340 nm: a steeply decreasing absorbance profile at 350 nm in cyclohexane prohibits the reliable use of this wavelength.

† Electronic supplementary information (ESI) available: details of synthetic details and characterisation and plots of: (i) the decrease in fluorescence as a function of pH for the two ligands L^1 and L^2, and (ii) the increase in the intensity of fluorescence of L^1 at 620 nm as a function of added zinc, including the method used for determination of K_{ass}. See http://www.rsc.org/suppdata/cc/b1/b108408a/

 DOI: 10.1039/b108408a

L^1, such that formation of the ICT state may be inhibited in the former but not in the latter.

Acidification of an ethanolic solution of L^1 led to a change from colourless to yellow, with a substantial hypochromic shift in the longest wavelength absorption band to 430 nm (Fig. 1). The fluorescence emission band underwent a comparable red-shift (from 513 to 642 nm, Fig. 2), but the integrated emission intensity was enormously decreased, by a factor of >200 when excited at the isosbestic point (387 nm). The red-shift in emission may be attributed to the stabilisation of the charge-transfer state which is expected to occur upon protonation of the terpyridine, as the electron acceptor properties of the latter are enhanced. Monitoring of the emission intensity at 513 nm in the presence of increasing concentrations of trifluoroacetic acid led to a pH profile with a single inflection point at 3.3, probably associated with diprotonation of the terpyridine. Ligand L^2 behaved similarly, but with a smaller change in intensity and with a subtle displacement of the profile to higher pH.†

Addition of zinc(II) ions (as zinc triflate) to a solution of L^1 in ethanol–water (9/1) led to an effect on the absorbance and emission maxima comparable to that of acid, namely a large shift to longer wavelengths (Figs. 1 and 2). In this case, however, the fluorescence intensity was not reduced to the same extent. Terpyridines are well-known to possess quite high affinity for Zn^{2+}, although the 2:1 complexes they form are kinetically more labile than those of transition metal ions with partially-filled d sub-shells such as iron(II). That the binding of zinc to L^1 leads to red-shifts similar to those induced by protonation is not surprising, since the positive charge on the metal ion will similarly promote the ICT process from pendent amine to terpyridine. On the other hand, the markedly higher emission intensity of the zinc complex is intriguing (Fig. 2). It is likely that this is due to the greater rigidity of the zinc complex, compared to the diprotonated terpyridine, which will serve to reduce the efficacy with which C–C stretching vibrations are able to act as energy accepting modes for deactivation of the excited state.[8] Although fluorophores with ICT excited states have been considered previously for pH and metal ion sensing,[9] the system described here is very unusual in that the proton or metal ion binds to the moiety which acts as the acceptor (rather than the donor) in the charge transfer process.

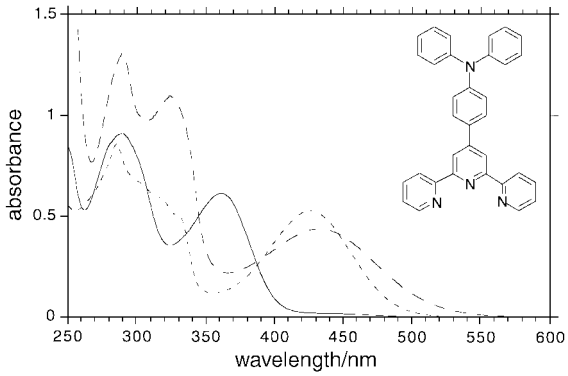

Fig. 1 UV–VIS absorbance spectra of L^1 (——); L^1 after addition of trifluoroacetic acid to pH 0.7 (— —); after addition of Zn^{2+} (5 equivalents of zinc triflate) (- - -). [L^1] = 6.7 μM in ethanol.

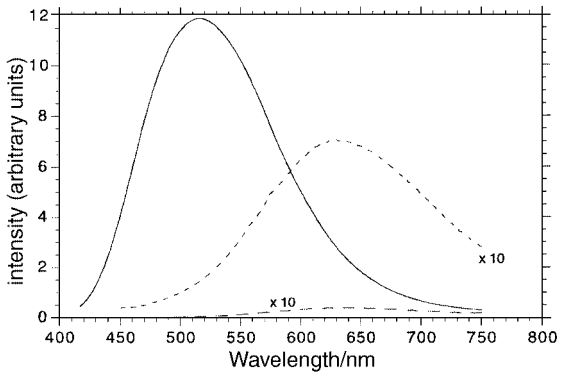

Fig. 2 Fluorescence emission spectra of L^1 (——), L^1 in the presence of H^+ (— —) (×10), and L^1 in the presence of Zn^{2+} (- - -) (×10) at the concentrations in ethanol given in the caption to Fig. 1. Samples were excited at the isosbestic point (387 nm) with excitation and emission band-passes set to 2.5 nm. Spectra shown are corrected for the wavelength dependence of the photomultipler tube.

The fluorescence responds sensitively to zinc ions; preliminary estimates indicate an apparent 2:1 (ligand:Zn^{2+}) association constant of $(4.3 \pm 0.6) \times 10^9$ dm^6 mol^{-2}.† However, although the emission profile changes dramatically (Fig. 2), excitation at the isosbestic point actually leads to a net decrease in the intensity at the new maximum (630 nm), owing to the higher emissivity of the ligand and the broadness of its fluorescence band. On the other hand, the changes in the absorption spectra which accompany formation of the zinc complex are synergistic, such that excitation at 415 nm (close to the absorbance maximum of the zinc complex) allows a 5-fold increase in the emission intensity at 630 nm to be achieved. The *ratio* of the emission intensity at 630 nm to that at 513 nm increases by a factor of 12 under these conditions; such ratiometric fluorimetry, where the ratio of signals at two emission or excitation wavelengths is monitored, is highly desirable in practical sensors, in order to cancel out variations in intensity arising from background changes in the analytical environment.[1]

The response to zinc is unique among the metal ions investigated (with the single exception of Cd^{2+}).‡ The addition of calcium and magnesium ions (competing ions when zinc sensors are used in physiological studies[2]) gave no change in the fluorescence of L^1, probably owing to the low affinity of these metal ions for terpyridines. On the other hand, paramagnetic transition metal ions such as Fe^{2+}, Ni^{2+} and Cu^{2+}, led to quenching of the fluorescence of both bands, as did the heavy metal ion Pb^{2+}. Thus, ligand L^1 offers a set of responses which render it encouraging for study as a potential sensory system for zinc, although a water-soluble analogue would be required in order to allow use in physiological studies.

We thank the University of Durham, EPSRC and the Royal Society for support.

Notes and references

‡ The effect of other metal ions was tested at concentrations equal to that required to bring about the maximum response for zinc(II). Cd^{2+} induced similar changes to that of Zn^{2+}, binding significantly more strongly.

1 See, for example, *Principles of Fluorescence Spectroscopy*, ed. J. R. Lakowicz, Kluwer Academic/Plenum, New York, 2nd edn., 1999.
2 S. C. Burdette and S. J. Lippard, *Coord. Chem. Rev.*, 2000, **216–217**, 333.
3 F. Barigelletti, L. Flamigni, M. Guardigli, J.-P. Sauvage, J.-P. Collin and A. Sour, *Chem. Commun.*, 1996, 1329; F. Barigelletti, L. Flamigni, G. Calogero, L. Hammarström, J.-P. Sauvage and J.-P. Collin, *Chem. Commun.*, 1996, 2334.
4 M. Licini and J. A. G. Williams, *Chem. Commun.*, 1999, 1943; W. Goodall and J. A. G. Williams, *J. Chem. Soc., Dalton Trans.*, 2000, 2893.
5 Previously we reported on Suzuki couplings of pre-coordinated terpyridines: C. J. Aspley and J. A. G. Williams, *New J. Chem.*, 2001, 1136.
6 T. Mutai, J.-D. Cheon, S. Arita and K. Araki, *J. Chem. Soc., Perkin Trans. 2*, 2001, 1045.
7 A. M. Brun, A. Harriman, Y. Tsuboi, T. Okada and N. Mataga, *J. Chem. Soc., Faraday Trans.*, 1995, **91**, 4047.
8 An increase in the emission intensity of a donor–acceptor β-diketone ligand, upon binding of Mg^{2+}, has similarly been accounted for in terms of structural restriction reducing the contribution of skeletal C–C stretching vibrations in deactivating the excited state: Y. Sato, M. Morimoto, H. Segawa and T. Shimidzu, *J. Phys. Chem.*, 1995, **99**, 35.
9 For example, crowns appended with acceptor chromophores; J. F. Letard, R. Lapouyade and W. Rettig, *Pure Appl. Chem.*, 1993, **65**, 1705.
10 S. R. Meech and D. Phillips, *J. Photochem.*, 1983, **23**, 193.

CHEMCOMM Communication
www.rsc.org/chemcomm

The bond cover approach to chemical topology†

Steven H. Bertz

Complexity Study Center, Mendham, NJ 07945 USA. E-mail: sbertz@ispcorp.com

Received (in Corvallis, OR, USA) 13th August 2001, Accepted 8th October 2001
First published as an Advance Article on the web

Bond covers based on substructures can be used to guide retrosynthetic analysis and give greater insight into the principle of convergence.

Topology is of growing interest in chemistry.[1] It has been proposed that molecular topology might have a significant effect on chemical synthesis;[2,3] thus, Corey and Cheng posited, 'The existence of alternative paths through a molecular skeleton as a consequence of the presence of cyclic subunits gives rise to a topological complexity which is proportional to the degree of internal connectivity.'[4] The concept of topological complexity has been generalized to include all the structural features that contribute to skeletal complexity, *e.g.* multiple bonds and branching in addition to rings.[5] Herein we address the problem of finding a measure of topological complexity by introducing an approach to chemical topology based on mathematical entities known as edge covers.[6–8] For chemical applications we call them bond covers.

A *substructure* of a molecule is a structure that has all its atoms and bonds in the molecule. For our applications the substructures are *connected*, meaning all pairs of atoms are the termini of at least one path. (The methane subgraph is trivially connected to itself by a path of length 0.[6]) We follow the precedent of Gordon and Kennedy,[9] who named substructures after the molecules they become when any incomplete valences are satisfied by hydrogen. For example, butane has four methane substructures, three ethane, two propane and one butane. (It follows from the above definition that a molecule is a substructure of itself.) We also adopt the common practice of representing molecules and substructures as hydrogen-suppressed structural formulas,[5] in which hydrogen atoms and the bonds to them are omitted.

We define a *bond cover* of a molecule as a set of substructures such that every bond in the molecule is in at least one of the substructures. In a *minimal bond cover* (or simply *minimal cover*) each substructure is essential, *i.e.* the removal of any substructure results in a set that no longer contains all the bonds in the molecule. A special case of minimal cover is a *partition*, in which each bond in the molecule is in exactly one of the substructures, so that no two substructures have a bond in common. The total number of covers K_T, minimal covers K_T^{min} and partitions P_T follow the order, $K_T > K_T^{min} > P_T$, except for ethane ($K_T = K_T^{min} = P_T = 1$) and propane ($K_T = 5$, $K_T^{min} = P_T = 2$). The corresponding numbers of kinds of covers are K_S, K_S^{min} and P_S, respectively.

These definitions are illustrated for cyclopropane **1** with the aid of Fig. 1. The minimal bond covers are 1{3 ethane}, 3{propane + ethane}, 3{2 propane} and 1{cyclopropane}, where the coefficient of a pair of braces gives the number of covers of that kind. (Henceforth, a 1 will not be shown explicitly.) Bond covers are the same kind when they contain the same substructures in equal numbers; they do not have to be isomorphic.[5–8] In this example $K_S^{min} = 4$ and $K_T^{min} = 8$. They are all partitions except 3{2 propane}, which have overlapping bonds; consequently, $P_S = 3$ and $P_T = 5$. An example of a bond cover of **1** that is not minimal is {cyclopropane + ethane}, since the ethane substructure can be removed and {cyclopropane} is also a cover. As far as all possible covers are concerned, $K_S = 28$ and $K_T = 109$ (*cf.* ESI†).

The values of K_T, K_T^{min} and P_T increase monotonically with the numbers of atoms, bonds, rings and branches, *e.g.* K_T^{min} (P_T) = 1 (1) for ethane, 2 (2) for propane, 5 (4) for butane, 13 (8) for pentane and 34 (16) for hexane, members of the homologous series of *n*-alkanes; 8 (5) for cyclopropane **1**, 30 (12) for cyclobutane **2**, 97 (27) for cyclopentane and 285 (58) for cyclohexane, members of a homologous series (cycloalkanes) which have an additional bond and ring compared to the corresponding *n*-alkanes; and 8 (5) for 2-methylpropane, 49 (15) for 2,2-dimethylpropane and 522 (52) for $K_{1,5}$ (the graph in which one point is joined to five other points, *i.e.* the hypothetical '2,2,2-trimethylpropane'), members of a homologous series (stars) where branching is greater than in the corresponding *n*-alkanes (except for methane, ethane and propane, which are *n*-alkanes and stars). Also, it can be shown that these indices increase with the introduction of multiple bonds; therefore, they are general indices of topological complexity. As a more sophisticated example, the [2]catenane of **1** has $K_T^{min} = 8 \times 8 = 64$ and $P_T = 5 \times 5 = 25$, compared to $K_T^{min} = 8 + 8 = 16$ and $P_T = 5 + 5 = 10$ for two isolated molecules of **1**. Minimal covers grow in number much less rapidly than covers, and partitions are particularly easy to enumerate.

Indices based on bond covers can be used to infer that topology has a significant role in synthesis, *e.g.* in the case of strategic bond disconnections. *Strategic bonds* are those that give a significant simplification when disconnected in the retrosynthetic (antithetic) direction.[4,10,11] When chosen on the basis of experience, they are *heuristic strategic bonds*, and when identified by using mathematical methods like the ones discussed here, they are *topological strategic bonds*. The question is, to what extent are they the same? According to Corey *et al.*,[10] 'the most desirable bond disconnections in the antithetic manipulation of structure are those in which the following structural features are minimized: (i) appendages, (ii) appendages carrying chiral centers, (iii) rings of medium or large size, and (iv) bridged rings.'

For any complexity index C, a change in complexity ΔC is calculated as the sum of index values for the products minus the sum for the starting materials, ΔC(reaction) = ΣC(products) − ΣC(starting materials). A negative value indicates overall simplification in a reaction or disconnection. Construction reactions are characterized by significant increases in complexity,[12] and their retrosynthetic transforms and disconnections by significant decreases. Several transforms can have the same

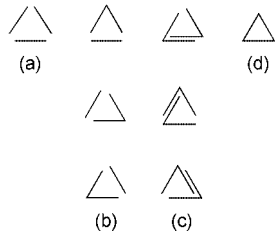

Fig. 1 Minimal bond covers of cyclopropane **1**: (a) {3 ethane}, (b) {propane + ethane}, (c) {2 propane}, and (d) {cyclopropane}.

† Electronic supplementary information (ESI) available: all possible covers for cyclopropane and 2-methylpropane. See http://www.rsc.org/suppdata/cc/b1/b107339g/.

 DOI: 10.1039/b107339g

disconnection, and the advantage of the latter is functional groups do not have to be included explicitly, unless they contain bonds that are made or broken. Thus, disconnections most clearly reveal topological changes. (We follow Corey *et al.*,[4,10] and differentiate 'transform' and 'disconnection'; some authors use them synonymously.)

Cyclobutane **2** (P_T = 12, K_T^{min} = 30) and methylcyclopropane **3** (P_T = 13, K_T^{min} = 39) are the results of the two possible 1-bond disconnections of bicyclobutane **4** (P_T = 43, K_T^{min}(**4**)). (*Cf.* Fig. 2.) For **4** ⇒ **2**, which breaks the fusion bond, ΔP_T(fusion) = ΔP_T(**4** ⇒ **2**) = P_T(**2**) − P_T(**4**) = −31, and for **4** ⇒ **3**, which breaks one of the four equivalent 'exendo'[4] bonds, ΔP_T(exendo) = ΔP_T(**4** ⇒ **3**) = P_T(**3**) − P_T(**4**) = −30. (Whereas $\Delta\Delta P_T$ = ΔP_T(**4** ⇒ **2**) − ΔP_T(**4** ⇒ **3**) = –1 is small, $\Delta\Delta K_T^{min}$ = [30 – K_T^{min}(**4**)] − [39 − K_T^{min}(**4**)] = −9 is substantial.) We conclude that the fusion bond is the topological strategic bond, as it gives the larger simplification. It was eliminated as the heuristic strategic bond in the general case, owing to the difficulty of forming the synthetic precursors when they are medium or large rings (*vide supra* iii, *cf.* rule 2A).[10]

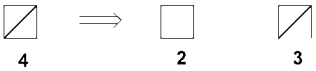

Fig. 2 The 1-bond retrosynthetic disconnections of bicyclobutane **4** to cyclobutane **2** and methylcyclopropane **3**.

The changes in the indices for the 1-bond and 2-bond disconnections of **3** are summarized in Table 1 (*cf.* Fig. 3). Since all the disconnections proceed from the same molecule, they are named according to the result, *e.g.* (a) stands for **3** ⇒ butane. Of the 1-bond disconnections (a)–(c), the one (a) that breaks the bond adjacent to the methyl substituent to afford butane gives the greatest simplification (ΔP_T = −9, ΔK_T^{min} = −34). Disconnection (b) to 2-methylpropane does not minimize appendages (*vide supra* i), and it gives less simplification (ΔP_T = −8, ΔK_T^{min} = −31).‡ The 2-bond disconnections (d) and (e) cannot be ranked by minimal covers, since the resulting systems have the same number of them (ΔP_T = −11, ΔK_T^{min} = −37); nevertheless, (d) and (e) are more efficient than the 1-bond disconnection (c) into two pieces (ΔP_T = −8, ΔK_T^{min} = −31).‡ The tie between (d) and (e) can be broken by considering the total number of covers K_T for the disconnected products. For propane they are {2 ethane}, {propane}, 2{propane + ethane} and {propane + 2 ethane}, and K_T = 5. For ethane K_T = 1, and for methane K_T = 0.§ Both disconnections have the same starting material **3**; thus, for (d) ΔK_T = 5 − K_T(**3**) and for (e) ΔK_T = 2 – K_T(**3**). Since K_T(**3**) > K_T^{min}(**3**) = 39, the latter is the negative number with the larger absolute value, indicating greater simplification ($\Delta\Delta K_T$ = −3). Therefore, the disconnection that results in two pieces of equal complexity is the most efficient. This is the topological basis for the heuristic of convergence.[11,12] Overall, the order of simplification is (e) > (d) > (a) > (b) > (c).¶

Table 1 Index values for the molecules of Fig. 3[a]

System	P_T	K_T^{min}	K_T
3 (methylcyclopropane)	13	39	K_T(**3**)
Butane (a)	4 (−9)	5 (−34)	46 (46 − K_T(**3**))
2-Methylpropane (b)	5 (−8)	8 (−31)	109 (109 − K_T(**3**))
1 + methane[b] (c)	5 (−8)	8 (−31)	109 (109 − K_T(**3**))
Propane + methane[b] (d)	2 (−11)	2 (−37)	5 (5 − K_T(**3**))
2 Ethane (e)	2 (−11)	2 (−37)	2 (2 − K_T(**3**))

[a] The values in parentheses are the changes in the indices for the disconnections (a)–(e) of **3** into the other systems. [b] For methane every index is 0.§

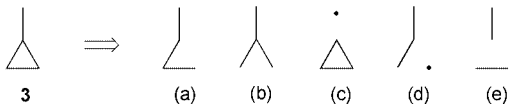

Fig. 3 The 1-bond (a)–(c) and 2-bond (d)–(e) retrosynthetic disconnections of methylcyclopropane **3**: (a) butane, (b) 2-methylpropane, (c) cyclopropane + methane, (d) propane + methane, and (e) 2 ethane.

For large molecules it is very difficult to determine all possible covers or even all possible minimal covers. Fortunately, there are subsets of all possible substructures that can be used to construct novel covers. For example, Bone and Villar[13] limited substructures to maximal ones (*cf.* induced subgraphs[6]), *i.e.* two atoms are bonded in a substructure whenever they are bonded in the structure. Another approach is to use substructures that are cliques or bicliques.[8] In a clique each atom is bonded to every other atom. In a biclique the atoms can be labeled with an asterisk or left unlabeled (*cf.* alternant hydrocarbons[5]) in such a way that each labeled atom is bonded to every unlabeled atom, and *vice versa*.

Bertz and Sommer proposed the number of kinds of subgraphs (substructures) of the molecular graph (structure) as a measure of diversity,[2] and Bone and Villar used the number of kinds of maximal substructures.[13] The number of kinds of covers or partitions might also be useful in this regard.

The author thanks C. Zamfirescu (CUNY) for assistance with checking the calculations, T. Sommer (Brandeis) for helpful discussions and W. F. Wright for valuable literature searches.

Notes and references

‡ When methane is ignored, disconnections (b) and (c) cannot be distinguished, since **1** and 2-methylpropane have the same number of bonds and the same symmetry (Supplementary Information). If methane is assigned K_T = 1,§ then (b) is more efficient.

§ Following Harary,[6] we generally do not include the trivial graph K_1 (methane) as a subgraph (substructure) in covers, hence K_T = 0 for methane. Some mathematicians include it,[7] in which case K_T = 1.

¶ Disconnection (d) represents two isomorphic disconnections, *i.e.* they have the same initial and final states. They can be differentiated by labeling the bonds that are broken in **3**. In the first, the bond joining the methyl and cyclopropyl groups is broken, along with the distal cyclopropane bond. In the second, the distal cyclopropane bond and one of the bonds adjacent to it are broken. The latter corresponds to the reaction of methylene and propene. (Disconnection (d) is drawn to suggest this reaction.) The former corresponds to the (theoretical) reaction of methane with allene, *e.g. via* cyclopropylidene.[14]

1 *Molecular Catenanes, Rotaxanes and Knots: A Journey through the World of Molecular Topology*, ed. J.-P. Sauvage and C. Dietrich-Buchecker, Wiley-VCH, Weinheim, 1999 (title systems); M. V. Diudea and G. Katona, *Advances in Dendritic Macromolecules*, 1999, **4**, 135 (title systems); N. C. Seeman, *Angew. Chem., Int. Ed.*, 1998, **37**, 3220 (DNA); A. P. Klyagina, *Russ. J. Coord. Chem. (Transl. of Koord. Khim.)*, 1995, **21**, 586 (molecular orbitals).

2 S. H. Bertz, *J. Am. Chem. Soc.*, 1981, **103**, 3599; S. H. Bertz, *Chem. Commun.*, 1981, 818; S. H. Bertz and T. J. Sommer, *Chem. Commun.*, 1997, 2409.

3 S. H. Bertz, *Chemical Applications of Topology and Graph Theory*, ed. R. B. King, Elsevier, Amsterdam, 1983, pp. 206–221; S. H. Bertz and T. J. Sommer, *Organic Synthesis: Theory and Applications, vol. 2*, ed. T. Hudlicky, JAI Press, Greenwich, CT, 1993, pp. 67–92.

4 E. J. Corey and X.-M. Cheng, *The Logic of Chemical Synthesis*, Wiley, New York, 1989, p. 37.

5 N. Trinajstić, *Chemical Graph Theory, 2nd ed.*, CRC Press, Boca Raton, FL, 1992; *Chemical Applications of Graph Theory*, ed. A. T. Balaban, Academic Press, London, 1976.

6 F. Harary, *Graph Theory*, Addison-Wesley, Reading, MA, 1969.

7 T. A. McKee and F. R. McMorris, *Intersection Graph Theory*, SIAM, Philadelphia, 1999.

8 S. H. Bertz and C. M. Zamfirescu, *Commun. Math. Comput. Chem. (MATCH)*, 2000, **42**, 39.

9 M. Gordon and J. W. Kennedy, *J. Chem. Soc., Faraday Trans. 2*, 1973, **69**, 484.

10 E. J. Corey, W. J. Howe, H. W. Orf, D. A. Pensak and G. Petersson, *J. Am. Chem. Soc.*, 1975, **97**, 6116.

11 S. Warren, *Organic Synthesis: The Disconnection Approach*, Wiley, Chichester, 1982.

12 J. B. Hendrickson, *J. Am. Chem. Soc.*, 1977, **99**, 5439; S. H. Bertz, *J. Am. Chem. Soc.*, 1982, **104**, 5801.

13 R. G. A. Bone and H. O. Villar, *J. Comput. Chem.*, 1997, **18**, 86.

14 William C. Shakespeare and R. P. Johnson, *J. Org. Chem.*, 1991, **56**, 6377.

CHEMCOMM Communication
www.rsc.org/chemcomm

Preparation of a novel core–shell nanostructured gold colloid–silk fibroin bioconjugate by the protein *in situ* redox technique at room temperature†

Yong Zhou,[a] Wenxing Chen,[b] Hideaki Itoh,[a] Kensuke Naka*[a] Qingqing Ni,[b] Hideki Yamane[b] and Yoshiki Chujo*[a]

[a] *Department of Polymer Chemistry, Graduate School of Engineering, Kyoto University, Yoshida, Sakyo-ku, Kyoto, 606-8501, Japan. E-mail: ken@chujo.synchem.kyoto-u.ac.jp*
[b] *Division of Advanced Fibro-Science, Kyoto Institute of Technology, Mastugasaki, Sakyo-ku, Kyoto 606-8585, Japan*

Received (in Cambridge, UK) 4th September 2001, Accepted 24th October 2001
First published as an Advance Article on the web

A novel core–shell gold colloid–silk fibroin (SF) bioconjugate was prepared by the protein *in situ* redox technique at room temperature, in which the tyrosine (Tyr) residue of the SF, having strong electron donating properties, *in situ* reduced Au(III) ions to Au colloids showing a stable and highly monodispersed nature.

Recently, the immobilization of proteins and enzymes on nanocolloidal substrates has received much attention in biotechnology, biochemistry and medicine. The general route to protein–metal colloid conjugates involves a simple solution-mixing process of proteins with metal colloidal sols formed prior to the mixing.[4] The thiol or amine functional groups in the protein bind with the metal nanoparticle surface, leading to the formation of the bioconjugate. However, due to the inhomogeneous dispersion between the protein and the metal colloid, the resulting conjugates always show large aggregated structures either in solution or in dried state, which is not a promising indication for the application of such bioconjugates. To the best of our knowledge, until now, no definite core–shell nanostructured metal colloid–protein bioconjugates have, as yet, been reported.

Here, we report, for the first time, the preparation of a novel core–shell nanostructured gold colloid–silk fibroin (SF) bioconjugate by the protein *in situ* redox technique at room temperature. The tyrosine residue (Tyr) component in the SF, having strong electron donating properties, *in situ* reduced Au(III) ions to Au colloids displaying a stable and highly monodispersed nature. The SF is secreted from the silk gland of the silkworm *Bombyx mori*. The SF possesses many special properties that are desirable for food, cosmetics, medical and biological materials, which attracts the wide interest of scientists in many disciplines including biology, polymer materials, iatrology, the chemical industry *etc*., and has led to a recent upsurge in researching SF.[5] With the incorporation of colloidal gold nanoparticles, the present SF will be expected to exhibit new bioactivity and applications in biotechnology.

In a typical preparation of the core–shell nanostructured gold colloid–SF bioconjugate by the protein *in situ* redox technique, 5 ml of an SF aqueous solution (10 mg ml^{-1}) (ESI†) was added dropwise to 5 ml of an aqueous solution of $HAuCl_4$ (2 mmol l^{-1}). The pH of the mixture solution was adjusted to 9–10 with KOH to prevent cross-linked aggregation of the SF [the isoelectric point (pI) of the SF is *ca*. 4.58–5.00].[5] The solution was stirred for 6 h at room temperature and the reaction mixture changed gradually from yellow to purple with stirring, indicating the formation of the gold colloid *via* oxidation of the SF. The resulting aqueous solution of the Au colloid–SF bioconjugate was stable with no precipitation being observed for more than three months at room temperature under air. A similar SF aqueous solution in the absence of $AuCl_4^-$ was allowed to stand at room temperature under air and flocculent precipitates appeared in the solution after a week. This result indicates that the presence of a large number of *in situ* produced Au colloids rendered high stability of the protein against aggregation.

Fig. 1 shows a typical transmission electron microscopy (TEM) image of the core–shell nanostructured Au colloid–SF bioconjugate produced by the present protein *in situ* redox technique at room temperature. It is evident that the gold nanoparticles are evenly coated with the SF to form core–shell nanostructrured bioconjugates. The spherical core–shell Au–SF nanostructures of 45 nm average size were essentially monodispersed. No large aggregation structure of the protein was observed in the present Au colloid–SF bioconjugate. The nanostructured bioconjugate particles were in contact with each other, a consequence of the solvent evaporation process required for TEM analysis, and not due to performed aggregation in solution. The gold nanoparticle cores of 15 nm average size with a narrow size distribution are well separated from each other *via* the coating of the SF. The thickness of the SF was *ca*.

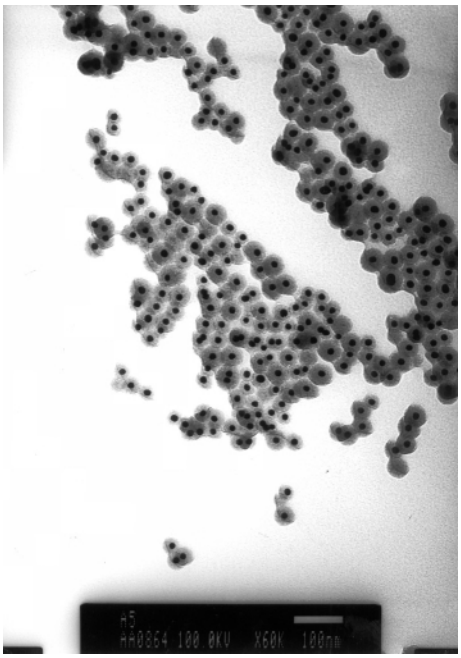

Fig. 1 Typical transmission electron microscopy (TEM) image of the core–shell nanostructured Au colloid–SF bioconjugate produced by the present protein *in situ* redox technique at room temperature.

† Electronic supplementary information (ESI) available: contents of various amino acid residues in the SFP, UV–VIS absorption spectra, and preparation of the SF solution. See http://www.rsc.org/suppdata/cc/b1/b108013j/

 DOI: 10.1039/b108013j

15 nm. The oxidized SF stabilized the gold nanoparticles and prevented the close approach of the particles *via* both steric and electrostatic stabilization mechanisms.[6] Mulvaney and coworkers have also reported similar interesting core–shell nanostructures of silica-coated gold particles.[7]

It has been reported that three conformations occur for silk fibroin: random coil, α-helix form (silk fibroin I) and β-sheet form (silk fibrion II).[5] The α-helix form is a crankshaft pleated structure while the β-sheet form is an antiparallel pleated sheet structure. Previous atomic force microscopy (AFM) measurements revealed that a single SF molecule is rod shaped with length 60 nm, width 15 nm and height 0.3 nm with long smaller chains extending from the ends.[8] The rod shape can be ascribed to the α-helix form of the SF. The SF molecule with a random-coil conformation has a hydrodynamic radius of *ca.* 20 nm.[9] Many factors can induce the transformation of the SF conformation. Bhat *et al.*[10*a*] and Tsukada *et al.*[10*b*] investigated the conformation transition induced by solvents and other treatments *via* infrared (IR) spectroscopy and X-ray diffractometry. Yu and Li studied the conformation change of a single silk fiber in different parts of silkgland under stress and provided a relevant model.[11] They found that under stretching, the α-helix form can be completely destroyed and partially turned into a random coil conformation. In the present reaction system, the TEM image demonstrates that the SF employed displayed a rod shape, which may be associated with the α-helix fibroin conformation. During the formation of the core–shell Au–SF nanostructured bioconjugate, the oxidation of the SF may promote the transformation of the SF conformation from the α-helix form to the random-coil form. The random-coil form is expected to facilitate the attachment of the SF molecular chain onto the gold nanoparticle to form the core–shell nanostructure. Based on the thickness of the SF of *ca.* 15 nm, it is deduced that one shell may be constructed by one SF molecular chain; this requires clarification by AFM measurements.

The SF is composed of 18 types of amino acid residues, which arrange in a specific sequence in the SF molecular chain.[5] The total content of glycine (Gly, 44.60 mol%), alanine (Ala, 29.40 mol%), serine (Ser, 12.10 mol%) and tyrosine (Tyr, 5.17 mol%) comprised more than 90 mol% of the whole composition of the SF (ESI†).[12] In the preparation of the present core–shell nanostructured Au colloid–SF bioconjugate at room temperature, according to the molecular structures and contents of various amino residues in the SF, the most probable amino acid residue which contributed to the reduction of $AuCl_4^-$ is believed to be the Tyr residue. It is well known that the cresol component of the Tyr residue is very easily oxidized into the quinone in air, displaying strong electron donating properties. In addition, in the present solution of pH 9–10, the cresol components may be transformed partially to phenoxide anions, increasing the electron density in the π–π* transition of the Tyr residues, favorable for electron transfer from Tyr to Au(III). Although the Ser residue contains a methanol group, widely used as a reducing agent for the preparation of metal nanoparticles, this reduction process proceeds only at elevated temperatures. To confirm our assumption, two model compounds, *p*-cresol and methanol, were added to two similar $AuCl_4^-$ solutions in the absence of the SF. The results show that the *p*-cresol can reduce $AuCl_4^-$ ions into gold nanoparticles very quickly within 30 s at room temperature while methanol did not. As a result, it can be concluded that the Tyr residue in the SF molecular chain was responsible for the reduction of the $AuCl_4^-$ in the preparation of the present core–shell nanostructured Au colloid–SF bioconjugate.

For further corroboration of the role of the Tyr residue in reduction of Au(III), UV–VIS absorption spectra (ESI†) were measured. The UV–VIS absorption spectra of an aqueous solution of pure SF displayed a strong absorption band at *ca.* 276 nm, assigned mainly to the π–π* transition of the Tyr residue in the SF molecular chain.[13] This band strongly red shifted to 288 nm with the reduction of the $AuCl_4^-$ and formation of the core–shell nanostructured Au colloid–SF bioconjugate. Further results demonstrate that the partial conversion of the cresol components of the Tyr to phenoxide anions at pH 9–10 did not induce the red shift. Therefore, the most probable reason for the red shift would be electron transfer from the residue to the Au(III) ions. A similar red shift, from 258 to 269 nm, was also observed in the UV–VIS absorption spectra of *p*-cresol (as a model compound) before and after the reduction of Au(III) ions. The strong absorption band at 521 nm in the core–shell nanostructred Au colloid–SF bioconjugate can be assigned to the surface plasmon resonance of the produced gold colloid. The absorption band maximum of the present Au colloid in the bioconjugate is well consistent with results for Au sols of 3–20 nm in size.[14] It has been demonstrated that adsorbate-induced aggregation of metal colloids leads to increased absorption at longer wavelengths and broadening of the primary absorption band, and often to the appearance of a secondary absorption peak that is red-shifted relative to the primary absorption band.[15] In the present study, no absorption at longer wavelength was observed, and the absorption band was symmetrical. The absorption spectrum of the Au colloid–SF bioconjugate did not change in shape, absorption maximum or intensity even after three months, indicative of the high stability of the gold nanoparticle in the bioconjugate.

In summary, a novel core–shell nanostructured gold colloid–silk fibroin (SF) bioconjugate has been prepared by the protein *in situ* redox technique at room temperature. The tyrosine (Tyr) residue in the SF *in situ* reduced $AuCl_4^-$ to Au colloids showing a stable and highly monodispersed nature. Simultaneously, the oxidized SF molecular chain attached to the surface of the Au nanoparticle forms the core–shell nanostructured bioconjugate. The present protein *in situ* redox technique may be extended to prepare other core–shell nanostructured metal colloid–SF bioconjugates.

We thank Professor T. Fukuda and Dr M. Tsujii (Kyoto University) for the TEM measurements.

Notes and references

1 F. Caruso and H. Mohwald, *J. Am. Chem. Soc.*, 1999, **121**, 6039.
2 M. Horisberger, in *Preparation of Biological Specimens for Scanning Electron Microscopy*, ed. J. A. Murphy and G. M. Roomans, Scanning Electron Microscopy, Inc., Chicago, IL, 1984, pp. 315.
3 *Colloidal Gold: Principles, Methods, and Applications*, ed. M. A. Hayat, Academic Press, New York, 1989 (in three volumes).
4 A. Gole, C. Dash, V. Ramakrishnan, S. R. Sainkar, A. B. Mandale, M. Rao and M. Sastry, *Langmuir*, 2001, **17**, 1674.
5 R. M. Robson, in *Handbook of Fiber Chemistry*, ed. M. Lewin and E. M. Pearce, Marcel Dekker, New York, 2nd edn., 1998.
6 A. Dalmia, C. L. Lineken and R. F. Savinell, *J. Colloid Interface Sci.*, 1998, **205**, 535.
7 T. Ung, L. M. Liz-Marzán and P. Mulvaney, *J. Phys. Chem. B*, 2001, **105**, 3441; L. M. Liz-Marzán, M. Giersig and P. Mulvaney, *Chem. Commun.*, 1996, 731; L. M. Liz-Marzán, M. Giersig and P. Mulvaney, *Langmuir*, 1996, **12**, 4329.
8 S. I. Inoue, J. Magoshi, T. Tanaka, Y. Magoshi and M. Becker, *J. Polym. Sci., Part B: Polym. Phys.*, 2000, **38**, 1436.
9 K. S. Hossain, N. Nemoto and J. Magoshi, *Langmuir*, 1999, **15**, 4114.
10 (*a*) N. V. Bhat and S. M. Ahirrao, *J. Polym. Sci., Polym. Chem. Ed.*, 1983, **21**, 1273; (*b*) M. Tsukada, Y. Gotoh, M. Nagura, N. Minoura, N. Kasai and G. Freddi, *J. Polym. Sci., Part B: Polym. Phys.*, 1994, **32**, 961.
11 T. Y. Yu and G. X. Li, *Acta Polym. Sinica*, 1993, **4**, 415.
12 F. Lucas, *Nature*, 1966, **210**, 952.
13 C. M. Stoscheck, *Methods Enzymol*, 1990, **182**, 50.
14 J. A. Creighton and D. G. Eadon, *J. Chem. Soc., Faraday Trans.*, 1991, **87**, 3881.
15 J. A. Creighton, C. G. Blatchford and M. G. Albrecht, *J. Chem. Soc., Faraday Trans.*, 1979, **75**, 790.

Typeset and printed by Black Bear Press Limited, Cambridge, England

CHEMCOMM
Feature Article
www.rsc.org/chemcomm

Ligand-controlled self-assembly of polynuclear lanthanide–oxo/hydroxo complexes: from synthetic serendipity to rational supramolecular design

Zhiping Zheng

Department of Chemistry, The University of Arizona, Tucson, Arizona 85721, USA. E-mail: zhiping@u.arizona.edu

Received (in Cambridge, UK) 3rd September 2001, Accepted 4th October 2001
First published as an Advance Article on the web 23rd November 2001

Lanthanide ions and complexes occupy a special position in developing synthetic nucleases capable of catalyzing the hydrolytic cleavage of RNA or DNA. Stimulated by a number of serendipitous lanthanide complexes that feature the common active-site structure of dinuclear metallo-phosphodiesterases, rational design and synthesis of polynuclear lanthanide–hydroxo species *via* ligand-controlled hydrolysis of the lanthanide ions were attempted. The efforts yielded a series of highly sophisticated yet structurally well-defined lanthanide–hydroxo complexes. These materials are potentially applicable to the study of biomimetic catalysis of phosphate diester cleavage. Research highlights are described in this Feature Article.

Introduction

Polynuclear metal complexes exhibit a fascinating variety of unusual symmetries and structural patterns.[1] The biological relevance of some of these compounds and their potentially important applications as advanced materials add to their interest and significance.[2,3] Ligand-controlled hydrolysis is a time-honored approach to these unique chemical entities.[4] In this method, auxiliary ligands occupy part of the metal coordination sphere, thereby reducing the number of sites available for water coordination and preventing extensive hydrolysis from occurring. As a result, finite-size polynuclear complexes rather than intractable metal hydroxides and/or oxides can be crystallized and structurally characterized. Several classes of ligands have been utilized in this capacity, among which carboxylates, polyketonates, polyamines, polyols, pyridonate and alkoxides are prominent.[5–10] Spectacular examples in transition metal chemistry, such as molecular cages and wheels, have been reported.[11,12] These novel complexes exhibit rather interesting magnetic properties owing to the presence of a large number of unpaired electrons.[3–12]

Despite the impressive progress in the preparation of polynuclear complexes of the d-block elements, the number of large, polynuclear lanthanide complexes is still rather limited.[13,14] Lanthanide elements, bearing special electronic and spectroscopic properties mainly associated with their 4f electronic configurations, represent a unique series of metals in the Periodic Table. The position of mononuclear lanthanide complexes in a number of important areas has been firmly established,[15] but polynuclear lanthanide complexes are expected to find such niche applications as precursors in sol–gel technology,[16] new radiographic agents,[17] and metalloenzyme mimics.[18] Great prospects notwithstanding, the high expectations have been compromised by our current limited synthetic ability; the formation of polynuclear lanthanide complexes cannot yet be controlled and is frequently characterized by random self-organization.[13,14,19]

The story begins

Our efforts to create structurally well-defined polynuclear lanthanide complexes were stimulated by the potential to develop synthetic nucleases that are capable of hydrolyzing RNA or DNA through the cleavage of the phosphate diester bonds.[20] X-Ray analysis of many phosphodiesterases indicates that these important metalloenzymes possess two or three divalent metal ions, such as Zn^{II}, in the active site.[20] It is generally agreed that the catalysis occurs *via* substrate activation by the electropositive metal ions, followed by nucleophilic attack by the activated hydroxo ligands (Fig. 1). Numerous

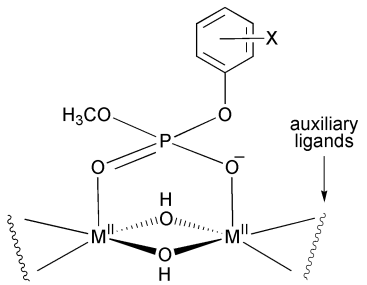

Fig. 1 A possible activation mechanism of a phosphate diester substrate by the dinuclear active site of a metallo-phosphodiesterase.

synthetic models have appeared in the literature in mimicking the dinuclear structural motif, most of which utilize transition metal ions, most notably Zn^{II}, Cu^{II} and Co^{III}, to activate the substrate.[21] Trivalent lanthanide ions (Ln^{III}) are expected to be more effective in this capacity due to their strong Lewis acidity and the kinetic lability of their complexes. Elegant studies in this vein have been carried out by Chin, Schneider, Martell and others.[18] However, the ease of lanthanide ion hydrolysis and the propensity for lanthanide–hydroxo species to form polynuclear aggregates in solution render unambiguous identification of the catalytically active species extremely difficult, if at all possible. There exist, nevertheless, a number of structurally characterized dinuclear[22] and tetranuclear[23] lanthanide–hydroxo complexes

Zhiping Zheng received his B.S. (1987) and M.S. (1990) in Chemistry from Peking University, Beijing, China. He obtained his Ph.D. from UCLA (1995) with Professor M. Frederick Hawthorne. After conducting postdoctoral research with Professor Richard H. Holm at Harvard University, he joined the faculty of The University of Arizona in 1997. His current research is focused on supramolecular inorganic chemistry and its materials applications, which involves the elaboration of polynuclear lanthanide complexes, transition metal clusters, dendrimers, and nanocrystallites.

DOI: 10.1039/b107971a

whose core components (Fig. 2) feature the desired diamond-shaped dinuclear lanthanide–hydroxo motif. However, these species were either synthetic serendipity or accidents, and general synthetic guidelines are lacking, and not surprisingly, there were no studies of their catalytic potentials.

Toward the ultimate goal of achieving non-enzymatic hydrolysis of phosphate diesters using *structurally well-defined* lanthanide catalysts, we have recently embarked on a design and synthesis tour of lanthanide–hydroxo complexes whose core structure resembles that of the active site of phosphodiesterases. We were particularly interested in the tetranuclear species whose constituent lanthanide ions and triply bridging hydroxo groups occupy the alternate vertices of a distorted cube. Structurally, it may be viewed as the dimeric form of the dinuclear species. More importantly, a complex featuring this core may be catalytically more potent on per molecule basis due to the extra Lewis acidic metal ions. The three seemingly unrelated literature precedents[23] further stimulated our interest. That distinctly different routes yielded the common structural motif led to our suspicion that the cubane-like core may actually be a standard feature of this type of chemistry, analogous to its extensively studied d-block counterparts.[24]

The presence of the hydroxo ligands suggests that these tetranuclear clusters may be synthesized *via* hydrolytic reactions of the lanthanide ions. However, hydrolysis of the lanthanide ions is commonly perceived as rather limited and unpredictable with intractable precipitates of lanthanide hydroxides and/or oxohydroxides as the end products.[25] Probably due to this very concern of extensive and uncontrollable hydrolysis, aqueous lanthanide coordination with organic ligands have been carried out almost exclusively under acidic conditions, typically below pH 5.[26] However, in light of the increasing number of unexpected and structurally characterized polynuclear lanthanide–oxo/hydroxo species,[13,14*a*,19,22,23] we deemed a systematic investigation of the hydrolytic reactions of these unique metal ions to be not only worthwhile, but also important.

Providing further inspiration for this endeavor is the great success of creating polynuclear transition metal complexes using the hydrolytic approach.[4] In such an approach, certain types of supporting ligands are necessary to control the hydrolysis in order to avoid the possible formation of intractable products. It is the subtle balance between the hydrolysis of a transition metal ion and its coordination with a chelating ligand that affords the novel high-nuclearity complexes. *We submit that an analogous ligand-controlled hydrolytic approach should be applicable to the lanthanide ions, provided that suitable supporting ligands are identified.* Our efforts have been concentrated on utilizing α-amino acids as auxiliary ligands to control the hydrolysis.[27] This exploratory synthesis has produced a number of spectacular and unprecedented polynuclear lanthanide–hydroxo complexes which may find important applications in biotechnology and chemotherapy. Research highlights are summarized in this Feature Article.

The story of α-amino acids – self-assembly of complexes featuring the $[Ln_4(\mu_3\text{-}OH)_4]$ core

The specific choice of α-amino acids as hydrolysis-limiting auxiliary ligands is mainly based on their biological relevance. It is reasonable to hypothesize that the metal coordination environment of the native enzyme can be better modeled by using such biological building blocks. In addition, lanthanide coordination with α-amino acids has been extensively investigated.[28] These studies have been conducted almost exclusively under low-pH (below 5) conditions. Typically, only the carboxylate group coordinates the lanthanide ion, as shown by more than 50 crystal structures of such complexes.[28*a*] The great variety of α-amino acids due to the presence of different side-group(s), some of which being potentially lanthanide-coordinating, is especially beneficial for systematic studies of lanthanide complexation with this unique class of ligands.

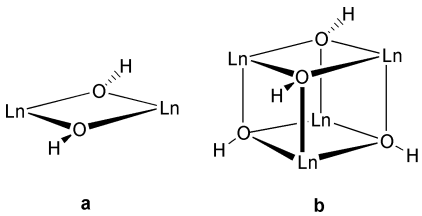

Fig. 2 Core components of crystallographically characterized dinuclear (a) and tetranuclear (b) lanthanide–hydroxo species.

The validity of this ligand-controlled hydrolytic approach was tested in a series of proof-of-concept syntheses, using a variety of α-amino acids, including glycine, alanine, valine, phenylalanine, tyrosine, proline, glutamic acid and aspartic acid as the supporting ligands.[29–34] The zwitterionic structures of these amino acids are shown in Fig. 3.

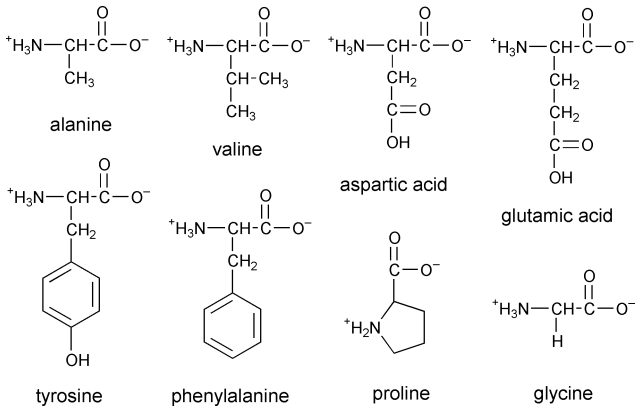

Fig. 3 Zwitterionic structures of the α-amino acids discussed in this article.

In a representative synthesis, a lanthanide chloride or perchlorate is mixed with an α-amino acid in aqueous solution. The mixture is subjected to hydrolysis with dilute NaOH. The end point of the reaction is indicated by the formation of an incipient but permanent precipitate, presumably of lanthanide hydroxide and/or oxohydroxide. Although the addition of base is seemingly arbitrary, lanthanide–amino acid (other than tyrosine) complexes composed of a cubane-like $[Ln_4(\mu_3\text{-}OH)_4]^{8+}$ core have invariably been obtained as crystalline solids upon slow concentration of the supernatant at room temperature. The ORTEP drawing of the cationic complex[35] formed by $Yb(ClO_4)_3$ and phenylalanine (Phe), representative of all the single-cubane complexes, is depicted in Fig. 4.†

The cluster core is 'camouflaged' by six phenylalanine ligands through bridging carboxylate groups, and the metal coordination sphere is completed by aqua ligands. The amino groups remain protonated, presumably affecting lanthanide complexation *via* electrostatic and steric effects. Because the amino groups do not participate in direct coordination with the lanthanide ion, the interaction of an α-amino acid with a lanthanide ion is structurally reminiscent of that of a carboxylic acid.[36] However, with carboxylic acids as supporting ligands, lanthanide acetates are typically obtained. These well-studied lanthanide materials exist in polymeric forms in the solid state, often featuring carboxylate-bridged dinuclear lanthanide units as the fundamental building blocks.[36] It is thus of interest to note that finite-size cluster-type polynuclear lanthanide–hydroxo complexes are generally isolated with the use of N-containing supporting ligands,[37] including α-amino acids. It is reasonable to assume that the higher water-solubility of lanthanide complexes with such ligands is due to possible hydrogen bonding interactions involving the N atom(s). In the case of α-amino acids, the zwitterionic character of these unique ligands

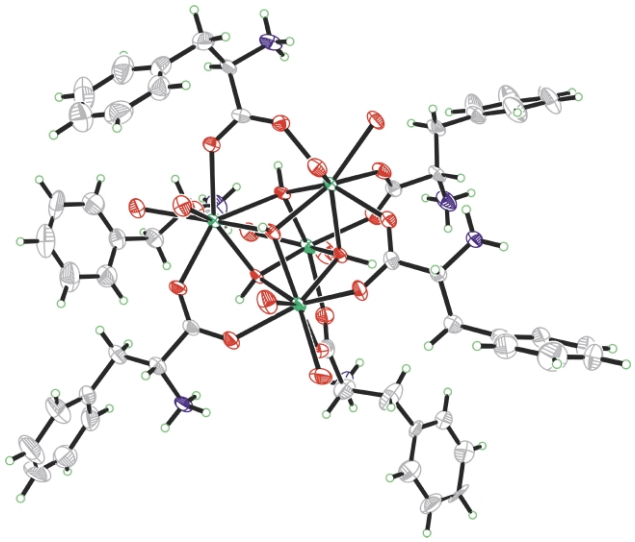

Fig. 4 An ORTEP representation of the cationic complex $[Yb_4(\mu_3\text{-}OH)_4(Phe)_6(H_2O)_7]^{8+}$. The cubane-like tetranuclear Yb^{III}-hydroxo core is apparent.†

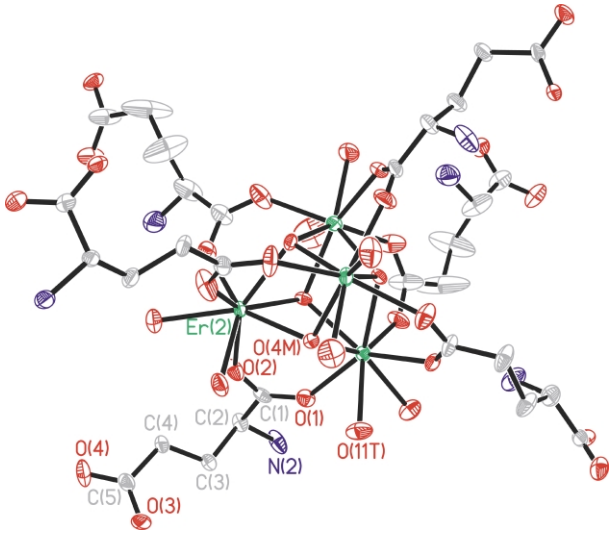

Fig. 5 An ORTEP drawing of the elementary building unit of $[Er_4(\mu_3\text{-}OH)_4(Glu)_3(H_2O)_8]^{5+}$. Three symmetry-related glutamic acid "arms" are included to complete the coordination of the cuboid $[Er_4(\mu_3\text{-}OH)_4]^{8+}$core.

is expected to further contribute to the better water solubility of their complexes. As a result, a lanthanide complex with such ligands remains soluble in solution instead of precipitating out as less soluble coordination polymers. Addition of base to such a solution is expected to deprotonate the aqua ligands. Condensation of the lanthanide–hydroxo species thus generated eventually leads to the formation of the cluster-type lanthanide–hydroxo complexes.

The story of the networking glutamic acid

Having established that the cuboid $[Ln_4(\mu_3\text{–}OH)_4]^{8+}$ cluster is a common structural motif in lanthanide complexes, we entertained the idea of using this motif as a secondary building unit[38] for the creation of supramolecular assemblies with porosity. The practice of constructing such open framework structures is stimulated by the hope that these porous materials will display a range of molecular sieve, ion exchange and catalytic properties that are comparable to (or perhaps more extensive than) those observed in zeolites. As compared with the large amount of work concerning the construction of coordination networks of d-block metal ions with polydentate ligands, crystal engineering involving lanthanide ions remains relatively unexplored at the present time,[39] and the use of lanthanide clusters as building blocks is unknown. Nevertheless, by employing appropriate supporting ligands, it may be possible to assemble the $[Ln_4(\mu_3\text{-}OH)_4]^{8+}$ cluster units into zeolite-like polymeric forms, whereby the high coordination requirement and Lewis acidity of the lanthanide ions may be of important use for both laboratory research and industrial processes.

In this effort, an α-amino acid with more than one carboxylate group is necessary in order to support the hydrolytic formation of the $[Ln_4(\mu_3\text{-}OH)_4]^{8+}$ cluster and to bridge individual cluster units. A three-dimensional (3-D) network may be anticipated from such extended interactions between the carboxylate ligands and the lanthanide–hydroxo cluster core. As expected, by treating a mixture of $Er(ClO_4)_3$ and L-glutamic acid with aqueous NaOH to the point of incipient precipitation, a 3-D porous network comprised of discrete $[Er_4(\mu_3\text{-}OH)_4]^{8+}$ units and cluster-linking glutamate ligands, $[Er_4(\mu_3\text{-}OH)_4(Glu)_3(H_2O)_8][ClO_4]_5$ (Glu = glutamate), was obtained.[30] The structure of the complex was determined by single-crystal X-ray diffraction, and the elementary constituent of the open framework is depicted in Fig. 5. The cubane-like $[Er_4(\mu_3\text{-}OH)_4]^{8+}$ building block is apparent, resembling its previously reported analogues. The six carboxylate groups ligating a particular cube are of two different types, one being α and the other (of the side chain) being γ to the amino moiety; each glutamate ligand contributes one carboxylate group for the coordination of one $[Er_4(\mu_3\text{-}OH)_4]^{8+}$ cluster while using the remaining one to coordinate an adjacent lanthanide cluster cube. The 3-D open framework exhibits nearly parallelogram-shaped pore apertures with approximate dimensions of 4.4 × 9.1 Å for channels in the *c* direction (Fig. 6). Although the network structure is the result

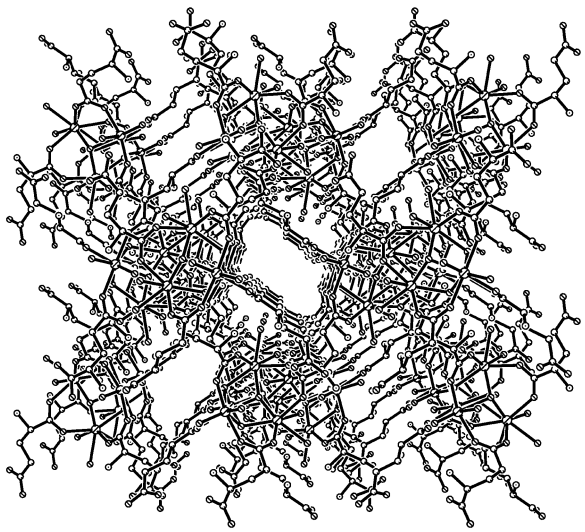

Fig. 6 3-D porous framework structure of $[Er_4(\mu_3\text{-}OH)_4(Glu)_3(H_2O)_8]^{5+}$, shown along the *c* axis. The channel dimensions are approximately 4.4 × 9.1 Å.

of self-assembly, the $[Er_4(\mu_3\text{-}OH)_4]^{8+}$ core may be *formally* considered as a *prefabricated* and *transferable* building block for the assembly of the extended structure. An analogous extended channel structure has also been obtained by the hydrolytic reaction of $Dy(ClO_4)_3$ using L-aspartic acid as supporting ligand,[34] which further supports our synthetic design in using the cubane-like units as building blocks for the extended solid state materials.

The unique story of tyrosine – anion-templated self-assembly of multi-cubane complexes

Using lanthanide perchlorates, analogous hydrolytic reactions with tyrosine as the supporting ligand were carried out in an effort to evaluate the possible effect(s) of the side-group of an α-amino acid has on the metal coordination.[29,32] To our great surprise, complexes featuring a single lanthanide–hydroxo

cluster core were not obtained. Instead, the reactions produced a series of pentadecanuclear lanthanide–hydroxo complexes.

As a representative of these pentadecanuclear complexes, the sophisticated structure of an Eu^{III} complex is described in detail below. As shown in Fig. 7, the complex, containing 15 Eu^{III} ions

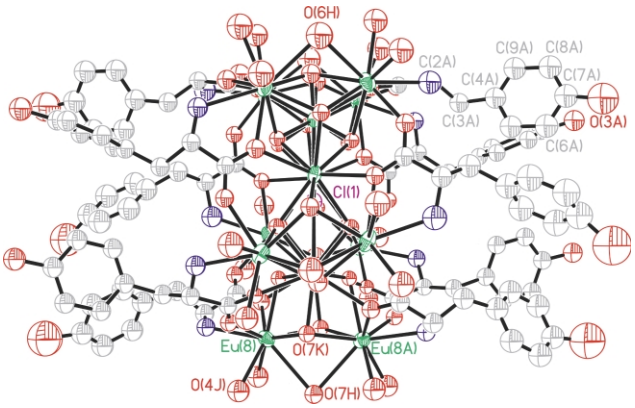

Fig. 7 A perspective view of the pentadecanuclear Eu^{III}–hydroxo complex with tyrosinato ligands. The cationic complex is formulated as $[Eu_{15}(\mu_3\text{-}OH)_{20}(\mu_5\text{-}Cl)(\mu_3\text{-}Tyr)_{10}(OH)_2(\mu\text{-}H_2O)_5(H_2O)_{18}]^{12+}$ (Tyr = tyrosinato ligand). Color legend: chlorine (purple).

and 10 tyrosinato ligands in addition to the hydroxo and aqua ligands associated with the hydrolysis, crystallizes as discrete barrel-shaped molecular units with space between these barrels filled with solvent water. The core component of the complex, formulated as $[Eu_{15}(\mu_3\text{-}OH)_{20}(\mu_5\text{-}Cl)]^{24+}$, consists of five vertex-sharing $[Eu_4(\mu_3\text{-}OH)_4]^{8+}$ cubane units centered on a μ_5-Cl^- 'axle' (Fig. 8). The metal ions are assembled into a layered

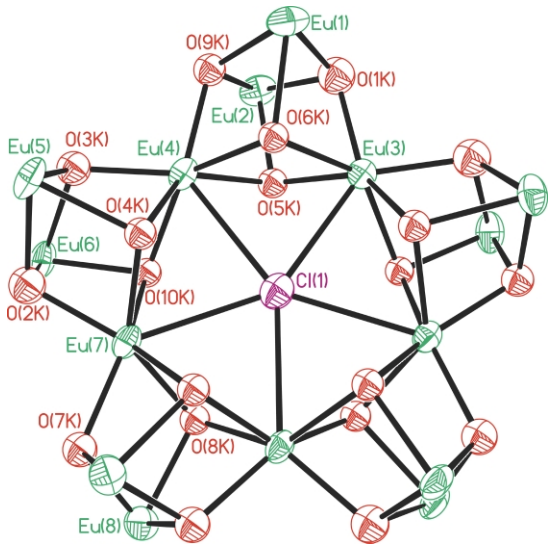

Fig. 8 An ORTEP drawing of the wheel-like core structure showing five vertex-sharing cuboid $[Eu_4(\mu_3\text{-}OH)_4]^{8+}$ units centered on a μ_5-Cl^- ion.

arrangement; each of the three parallel layers contains five Eu^{III} ions that occupy the vertices of a nearly perfect pentagon. The average Eu–Eu separation within the two outer layers is 6.331 Å, while that in the middle layer is 3.896 Å. The average Eu–Cl distance of 3.314 Å is significantly longer than the sum of the van der Waals radii of Cl^- (1.81 Å)[40] and Eu^{III} (0.95 Å),[40b] reflecting the primarily ionic interactions between the halide and the lanthanide ions. The coordination sphere of the Eu^{III} ion is completed by hydroxo and aqua ligands. Thus, each of the 10 Eu^{III} ions in the outer layers has a coordination number (CN) of nine, and the coordination polyhedra can be best described as monocapped square antiprismatic, while the inner-layer Eu^{III} centers also have a CN of nine, forming irregular square antiprisms monocapped by the central chloride ion.

The tyrosinato ligands can be divided into two equivalent groups, each of which extends their 4-hydroxybenzyl side-chains in the direction perpendicular to the crystallographically imposed C_2 axis. The side-chains do not participate in the coordination. The coordination mode of the tyrosinato ligand with Eu^{III} is significant: each acts as a tridentate ligand by utilizing both its amino and carboxylate groups. The ligand can be described as a $\mu_3:\eta^1:\eta^2:\eta^1$ anion (Fig. 9), not only linking

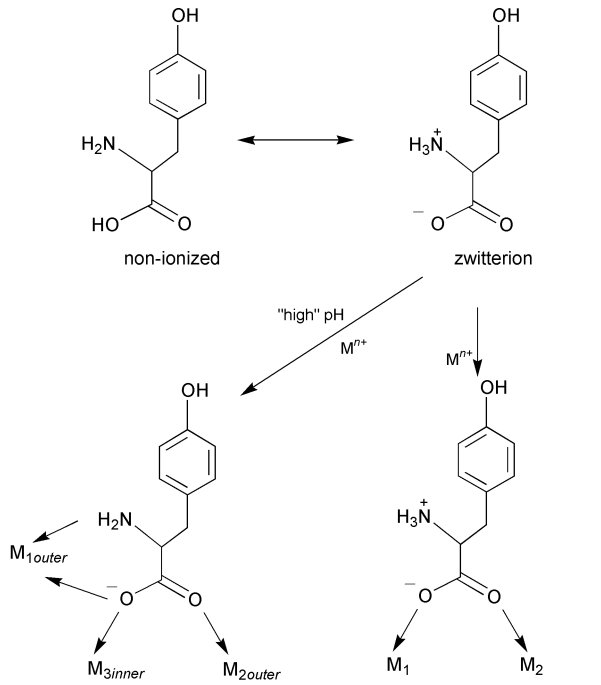

Fig. 9 Comparison of the lanthanide-coordination modes of tyrosine-based ligands under different pH conditions.

two neighboring Eu^{III} within the same (outer) layer, but also coordinating a third Eu^{III} ion in the middle layer through one of the carboxylate oxygen atoms. Such a mode has not been observed prior to our work.

The formation of the pentadecanuclear complex was unexpected, as only complexes containing discrete cubane unit(s) were obtained with other supporting α-amino acids,[30,33–35] including the closely related phenylalanine.[35] It is not yet understood why tyrosine is so unique in this capacity, but work is in progress to elucidate the possible causes. The incorporation of a μ_5-Cl^- ion was even more surprising because no Cl^- was utilized in the original synthesis which involved only $Ln(ClO_4)_3$, tyrosine and NaOH. A possible source of the mystifying Cl^- was an impurity present in the perchloric acid used for the digestion of lanthanide oxides. Template effects exerted by Cl^-, presumably in minute amount in the original synthesis, were thus suspected, and subsequently corroborated by the improved synthesis, in both product yield and purity, with the presence of added Cl^-. Thus, *the formation of the pentadecanuclear complex may be best understood as chloride-templated self-assembly of the lanthanide ions with the assistance of tyrosinato ligands.*

Stimulated by these findings, the potential roles of other anionic species in promoting the assembly of similar or distinct complexes were explored.[32] It has since been found that the composition of the resulting complex is profoundly affected by the anionic species present in the reaction mixture, but is independent of the lanthanide ions. For example, analogous pentadecanuclear complexes featuring a μ_5-Br^- were obtained when Br^- was involved. Except for the substitution of Br^- (van der Waals radius, 1.96 Å)[40] for Cl^-, the cationic complexes are isostructural to their Cl^--containing cognates. The Br^- simultaneously coordinates the five inner-layer Ln^{III} ions in a perfectly planar and previously unknown fashion (Fig. 10). The Ln–Br distances are also significantly longer than the corresponding sum of the van der Waals radii.

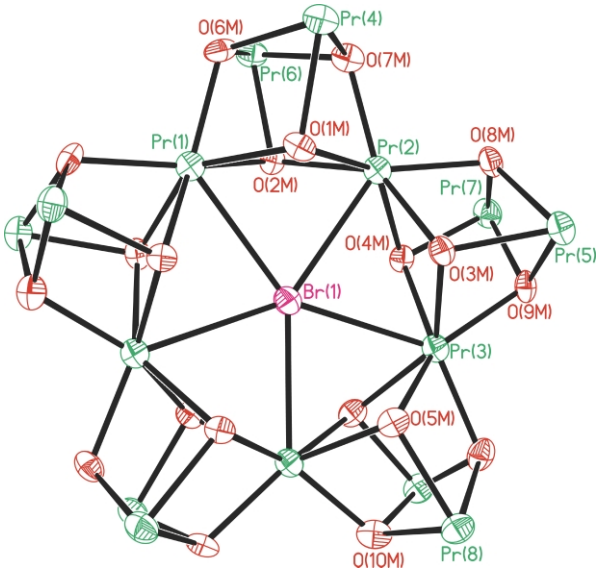

Fig. 10 An ORTEP drawing of the wheel-like core structure of the pentadecanuclear Pr^{III}–hydroxo complex showing five vertex-sharing $[Pr_4(\mu_3\text{-}OH)_4]^{8+}$ units centered on a μ_5-Br^- ion. Color legend: bromine (purple).

When I^- was employed, however, dodecanuclear complexes were isolated; the surprising product featured a cyclic core composed of four vertex-sharing $[Ln_4(\mu_3\text{-}OH)_4]^{8+}$ cubanes and two I^- guests (Fig. 11). In contrast to the single Cl^- or Br^- that

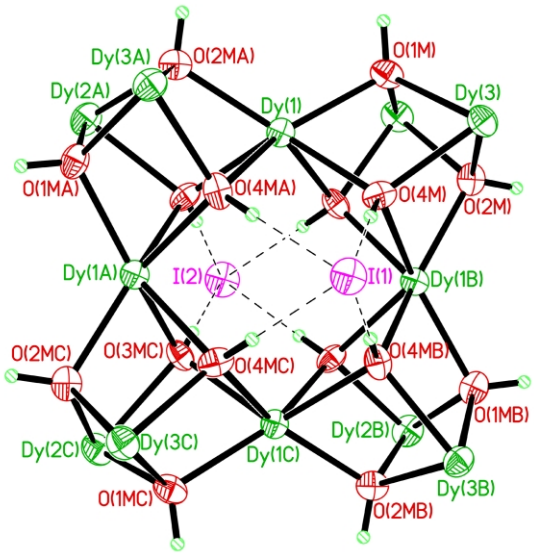

Fig. 11 An ORTEP representation of the core component of the dodecanuclear Dy^{III}–hydroxo complex showing four vertex-sharing $[Dy_4(\mu_3\text{-}OH)_4]^{8+}$ units in a square-shaped arrangement. Two I^- ions are found in the complex, one on each side of the square and interacting with the μ_3-OH groups in a μ_4-I^- fashion. Color legend: iodine (purple).

was situated in the center of the five-cubane wheel, the I^- ions were located on both sides of wheel plane formed by the lanthanide ions. The distances between the iodide ion and the hydrogen atoms of the μ_3-OH groups are almost the same as the corresponding sum of the van der Waals radii, indicating a very compact core structure and likely a hitherto unknown supramolecular motif. Eight tyrosinato ligands cap the wheel structure, four on each side (Fig. 12). The coordination mode of the tyrosinato ligands is identical to that in the Cl^- and Br^--containing complexes. Although the formation of a smaller cubane-wheel is counterintuitive, this observation may be understood in terms of the energetically insurmountable constraints between adjacent cubane units if a larger wheel were formed.

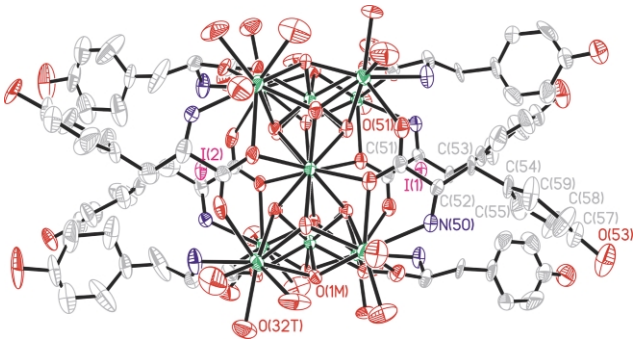

Fig. 12 A perspective view of the cationic dodecanuclear Dy^{III}–hydroxo complex, $[Dy_{12}(\mu_3\text{-}OH)_{16}(I)_2(\mu_3\text{-}Tyr)_8(H_2O)_{20}]^{10+}$.

The identity of the multi-cubane complex is clearly dependent on the nature of the halide ion utilized. However, the templating roles of these spherical anions in establishing the wheel-like complexes remain to be confirmed because the key criterion of a legitimate template is the influence of both of its size and shape on the product distribution.[41] Specifically, can one expect a different product with the presence of a non-spherical anion? Further, what outcome may one anticipate when two different types of anions coexist in the reaction mixture? To answer these questions, a reaction with the trigonal planar NO_3^- (1.79 Å),[40] which is of similar size to Cl^-, was executed.[32,42] The analogous hydrolytic reaction using $Er(NO_3)_3$ and tyrosine produced a known and structurally characterized, tyrosine-free cationic complex $[Er_6(\mu_6\text{-}O)(\mu_3\text{-}OH)_8(NO_3)_6(H_2O)_{12}]^{2+}$ (Fig. 13) which was obtained pre-

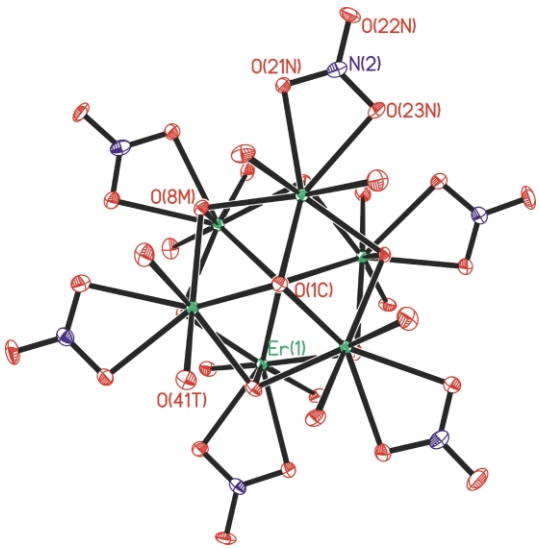

Fig. 13 An ORTEP representation of the cationic complex $[Er_6(\mu_6\text{-}O)(\mu_3\text{-}OH)_8(NO_3)_6(H_2O)_{12}]^{2+}$.

viously by the thermal decomposition of hydrated $Er(NO_3)_3$ followed by hydrolysis of the decomposition products.[43] The core component of this compound is a face-capped octahedral $[Er_6(\mu_6\text{-}O)(\mu_3\text{-}OH)_8]^{8+}$ unit with an interstitial μ_6-oxo group. Its assembly is presumably templated by the μ_6-oxo group whose origin is unclear, but is probably from hydroxide or water. These results clearly indicate the general importance of spherical anionic species in governing the formation of polynuclear lanthanide complexes.[13,14a]

The most convincing evidence supporting the halide template effects was provided by the tyrosine-limited hydrolytic reaction of $Gd(NO_3)_3$ in the presence of competitive Cl^-: Structural determination by X-ray crystallography established that the pentadecanuclear Cl^--containing complex was the sole product with non-coordinating NO_3^- as counter ions. This finding, coupled with the inability to produce a multi-cubane complex in the absence of a halide ion suggests that the halide ion must be

a stabilizing factor along the reaction coordinate to the 'wheel'-structured complexes, and hence, a kinetic template.[41]

It has long been recognized in the chemistry of lanthanide alkoxides that the presence of a 'central spherical negative charge density' accounts for the driving force for product formation.[13] However, the exact roles played by these anionic species have not yet been investigated. We have discovered several lines of evidence that point convergently to the superior ability of halide ions in templating the formation of unprecedented lanthanide–hydroxo complexes. Our work thus provides a stimulating demonstration of the under-appreciated templating roles of anions in self-assembly processes,[44] and should aid in future work in assembling novel lanthanide complexes by utilizing templating anions of different *size* and *geometry*.

Controlled or not? Direct hydrolysis of lanthanide nitrates and perchlorates

The isolation of polynuclear complexes containing the cubane-like $[Ln_4(\mu_3\text{-}OH)_4]^{8+}$ unit firmly establishes the critical importance of the organic ligands in controlling the hydrolysis of the lanthanide ions. However, the isolation of the tyrosine-free complex, $[Er_6(\mu_6\text{-}O)(\mu_3\text{-}OH)_8(NO_3)_6(H_2O)_{12}](NO_3)_2$, from a hydrolytic reaction involving $Er(NO_3)_3$, tyrosine and NaOH was unexpected and intriguing. Admittedly, this and related hexanuclear complexes[43,45] are structurally drastically different from the cubane-like tetranuclear species. But are tyrosine or any organic ligands really necessary in controlling the hydrolysis of the lanthanide ions? Is the equivalent polyoxometalate chemistry[46] of the lanthanide ions a reasonable conceptual stretch? If so, how extensive is this chemistry?

The answers to these interesting questions were provided by the isolation of the same hexanuclear complex from the direct hydrolysis of $Er(NO_3)_3$ [eqn. (1)]:[42]

$$Er(NO_3)_3 + NaOH(aq) \rightarrow [Er_6(\mu_6\text{-}O)(\mu_3\text{-}OH)_8(NO_3)_6(H_2O)_{12}](NO_3)_2 \quad (1)$$

Insolubility of this and analogous nitrate-containing complexes[43] in organic solvents and the strong coordination of nitrato ligands to the lanthanide ions preclude the potential use of these clusters in further research. Our efforts have therefore concentrated on the direct hydrolysis of lanthanide perchlorates. Although these starting materials are potentially explosive, they have been utilized extensively in lanthanide research because of their water solubility and the weakly coordinating nature of ClO_4^-. The latter is essential for the preparation of novel oxo–hydroxo lanthanide precursors for future work.

Indeed, the direct hydrolysis of $Nd(ClO_4)_3$ and $Gd(ClO_4)_3$ afforded two new molecular oxo–hydroxo clusters.[42] Shown in Fig. 14 is the structure of the cationic cluster complex obtained from the reaction of $Nd(ClO_4)_3$ with aqueous NaOH. Established by X-ray diffraction, the cationic cluster core, formulated as $[Nd_6(\mu_6\text{-}O)(\mu_3\text{-}OH)_8(H_2O)_{24}]^{8+}$, is comprised of an octahedron of Nd^{III} centered on a μ_6-oxo ligand. Each of the triangular metal faces is capped by a μ_3-OH ligand. The metal coordination sphere is completed with four aqua ligands. Thus, each Nd^{III} is coordinated to nine oxygen atoms: one interstitial oxo unit, four face-capping hydroxo groups, and four terminal aqua ligands. Overall, the complex is structurally similar to the Lindquist-type hexametalates of transition elements with the distinction of having eight face-capping hydroxo groups instead of 12 edge-bridging oxo ligands. To the best of our knowledge, this is the first molecular lanthanide cluster with *only coexisting* oxo, hydroxo and aqua ligands. Such hydrous species are the simplest and most fundamental forms of $[Ln_6(\mu_6\text{-}O)(\mu_3\text{-}OH)_8]^{8+}$ core-containing clusters and may be useful precursors for various substituted clusters in future work, including the construction of open framework structures using the octahedral clusters as building blocks. In fact, the octahedral core appears to be another common structural motif in lanthanide oxo-

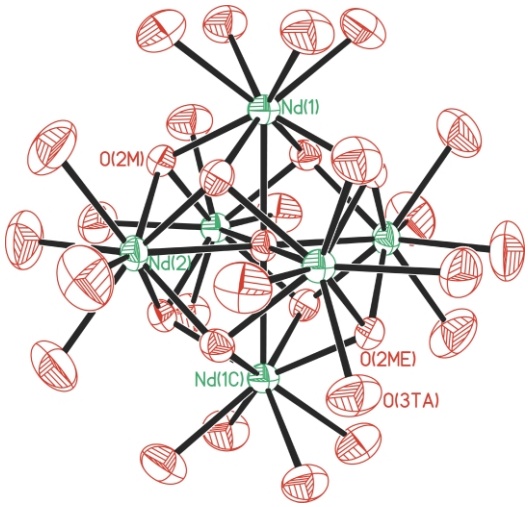

Fig. 14 An ORTEP drawing of $[Nd_6(\mu_6\text{-}O)(\mu_3\text{-}OH)_8(H_2O)_{24}]^{8+}$, a cationic complex featuring a face-capped hexanuclear cluster core and containing only water-based ligands.

hydroxides, as demonstrated by our group[42] and others.[43,45] Its presence has also been recognized in a polymeric cyanide-bridged lanthanide-transition metal complex reported by Shore and coworkers.[47]

In stark contrast to the extensive chemistry of the closely related lanthanide oxo–alkoxides,[16a,48] the closely related chemistry of lanthanide oxo–hydroxides has essentially been unexplored. Thus, our demonstration of the direct hydrolysis of the lanthanide ions leading to hexanuclear lanthanide oxo–hydroxo complexes is significant. The structural integrity, the highly ordered arrangement of paramagnetic centers and the anticipated substitutional lability of the cluster terminal aqua ligands portend their applications as structural and functional building blocks for a variety of lanthanide-containing materials.

New tricks for an old dog – unusual lanthanide–EDTA coordination under high-pH conditions

Prompted by the close relationship between polyaminopolycarboxylic acids (PAPCs) and α-amino acids, we set out to re-evaluate, under much higher pH conditions however, the classical coordination chemistry of the lanthanide ions with PAPCs. If the solution pH condition can have such significant influence on the outcome of the well-established lanthanide–amino acid coordination chemistry, one should not be surprised if some new but admittedly hard-to-predict results are to be obtained with this venerable class of ligands[49] under similarly altered pH conditions.[50] In this section, we illustrate how the otherwise well-established chemistry can be profoundly affected by simply increasing the pH of the reaction mixture.

Our initial foray has been focused on ethylenediamine-*N,N,N′,N′*-tetraacetic acid (H_4EDTA), one of the most studied PAPCs. Lanthanide–EDTA complexes, represented by the general chemical formula $M[Ln(EDTA)(H_2O)_m]\cdot nH_2O$ (M = an alkali metal ion), have invariable 1 : 1 (EDTA : Ln) composition.[51] Structural analyses always reveal a hexadentate EDTA ligand with two coordinating nitrogen atoms and four oxygens of the unidentate carboxylate groups (**A**, Fig. 15). The O(aqua)–Ln–O(aqua) bond angles range from 70.0 to 83.3°, which are very close to the corresponding O(μ_3–OH)–Ln–O(μ_3–OH) angles (ranging from 68.1 to 76.8°) in the $[Ln_4(\mu_3\text{–}OH)_4]^{8+}$ unit. An intriguing question then arises: *Can a cubane-like tetranuclear lanthanide–hydroxo cluster be assembled from a mononuclear trisaqua lanthanide complex with EDTA?*

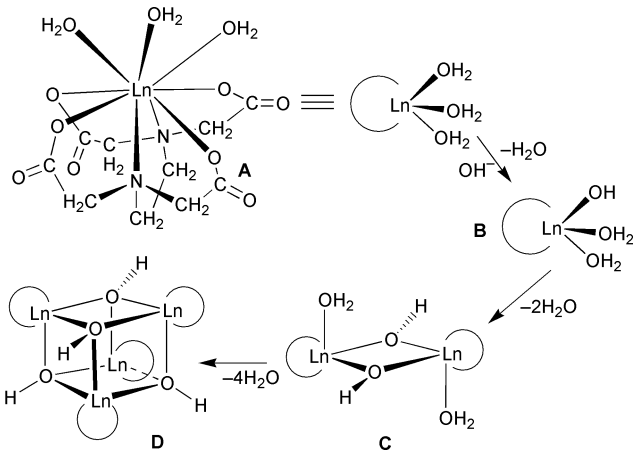

Fig. 15 A proposed mechanism for the self-assembly of a tetranuclear lanthanide–hydroxo complex with EDTA from its corresponding mononuclear aqua complex.

It seemed plausible that if the pH of a lanthanide-EDTA reaction mixture is raised, the aqua ligand(s) of the initially formed nine-coordinate complex would be deprotonated, giving rise to a hydroxo complex of lanthanide with EDTA (**B**, Fig. 15). Bimolecular reactions of species **B** leads to the formation of the μ_2-OH bridged, diamond-shaped intermediate (**C**, Fig. 15), for which a number of literature precedents exist.[22] Subsequent condensation of two of such dinuclear units would afford a tetranuclear lanthanide cluster, bearing the familiar cuboid $[Ln_4(\mu_3\text{–}OH)_4]^{8+}$ unit whose metal centers are capped by EDTA ligands (**D**, Fig. 15).

This hypothesis was validated: The La^{III}–EDTA complex, formulated as $Na_{10}[La_4(\mu_3\text{–}OH)_4(EDTA)_4](ClO_4)_2$, was obtained by mixing $La(ClO_4)_3$ and $Na_2H_2EDTA{\cdot}2H_2O$ in an aqueous solution and subsequently adjusting the pH of the reaction mixture to about 13 with dilute aqueous NaOH.[31] The molecular structure of the anionic cluster was established by X-ray diffraction and is shown in Fig. 16, wherein the presence of

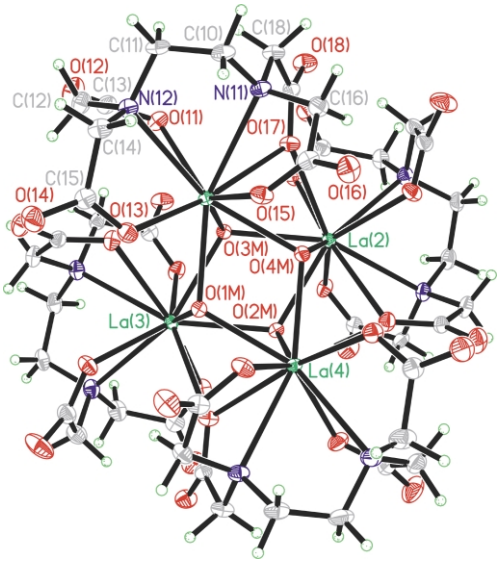

Fig. 16 An ORTEP representation of the anionic complex $[La_4(\mu_3\text{-}OH)_4(EDTA)_4]^{8-}$ featuring the familiar cubane-like $[La_4(\mu_3\text{-}OH)_4]^{8+}$ core.

a cubane-like $[La_4(\mu_3\text{–}OH)_4]^{8+}$ core is quite clear. Each metal vertex is capped by an EDTA ligand whose coordination mode is unusual: the EDTA ligand is hexadentate (a, Fig. 17), but with one of its four coordinating oxygen atoms bridging a second La^{III} ion. The two non-bridged La^{III} pairs (La1–La4 and La2–La3) correspond to a metal–metal separation of 4.278 Å, which is significantly longer than the other four (3.975 Å). Each La^{III} ion has a CN = 10, and its coordination polyhedron may be best described as a bicapped square antiprism. Although the

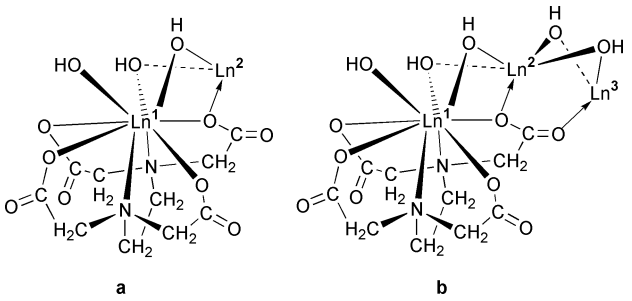

Fig. 17 The well-known hexadentate mode of an EDTA ligand to Ln^1 with the unprecedented bridging modes to additional lanthanide ions (Ln^2 and Ln^3).

complex is not exactly the one originally targeted, its formation can be readily rationalized based on the proposed condensation mechanism. An isostructural tetranuclear hydroxo complex of Pr^{III} with EDTA has been obtained;[52] the Pr^{III} ion in this complex is also 10-coordinate.

Since one EDTA ligand contributes six coordinating atoms, only two aqua ligands would be possible for a lanthanide ion that prefers a coordination number of eight. A complex featuring the diamond-shaped lanthanide–hydroxo core would be the expected product, and the reaction would terminate at the stage of **C** upon increasing the pH of the reaction mixture. Indeed, a dinuclear Er^{III}–hydroxo complex was isolated from a reaction mixture of $Na[Er(EDTA)(H_2O)_2]$ (formed at pH 6) with KOH at pH 13–14.[52] The structure of the complex, formulated as $K_4[(EDTA)Er(\mu\text{-}OH)_2Er(EDTA)]$, has been determined by X-ray diffraction, and that of the anionic core component is depicted in Fig. 18.

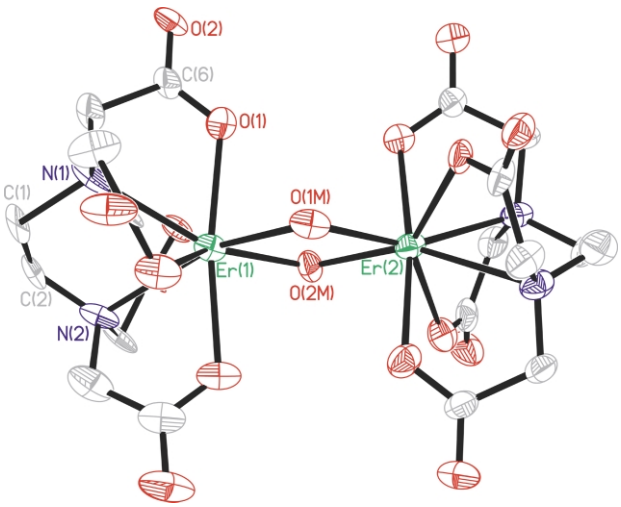

Fig. 18 An ORTEP representation of the diamond-shaped dinuclear Er^{III}–hydroxo complex with EDTA, $[(EDTA)Er(\mu\text{-}OH)_2Er(EDTA)]^{4-}$.

The observation of ten-coordinate La^{III} and Pr^{III} in both of the tetranuclear complexes merits further discussion. While the high coordination number is not so unusual for La^{III}, ten-coordinate Pr^{III} is rather rare. It appears that the previously unknown bridging interaction by one of the EDTA carboxylato oxygens is a prerequisite for the formation of the cubane-like structure. What can one anticipate when a lanthanide ion preferring a CN = 9 is utilized in an analogous reaction? On the one hand, since a CN = 10 is very unlikely, it is a reasonable assessment that the tetranuclear complex will not form. On the other hand, since such a lanthanide ion may not be satisfied with a CN = 8, one may expect a coordination environment different from that of the dinuclear Er^{III} complex (Fig. 18). Once again, our efforts to seek answer to this question yielded pleasantly surprising results. A dodecanuclear complex composed of four vertex-sharing $[Nd_4(\mu_3\text{–}OH)_4]^{8+}$ cubanes and eight EDTA

ligands was isolated from an aqueous mixture of EDTA and $Nd(ClO_4)_3$ at pH 14.[27,31]

The crystal structure of the anionic cluster complex, formulated as $\{[Na(H_2O)_2]_4[Nd_{12}(\mu_3\text{–}OH)_{16}(EDTA)_8]\}^{8-}$, is shown in Fig. 19. Its skeletal structure is identical to those of the

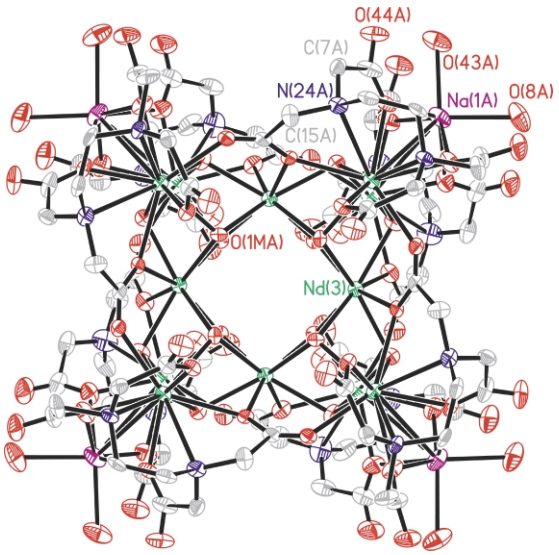

Fig. 19 An ORTEP representation of the dodecanuclear Nd^{III}–hydroxo complex featuring four vertex-sharing $[Nd_4(\mu_3\text{-}OH)_4]^{8+}$ units in a square-shaped arrangement. The anionic complex is formulated as $\{[Na(H_2O)_2]_4[Nd_{12}(\mu_3\text{–}OH)_{16}(EDTA)_8]\}^{8-}$. Color legend: sodium (purple).

diiodide complexes obtained from the tyrosine-supported hydrolytic reaction of $Ln(ClO_4)_3$ (Ln = Dy^{III}, Er^{III}) with templating I^-.[32] The EDTA ligands occupy the vertices of a perfect tetragon, each capping one of the eight non-shared Nd^{III}. One may alternatively view the structure as a sandwich made with a four-cubane 'patty' and two slices of EDTA 'bread'. The coordination mode of EDTA ligands in this complex is significant: each EDTA molecule acts as a *heptadentate* ligand (b, Fig. 17) as opposed to the well-known hexadentate one. One of the carboxylate groups together with the nitrogen atom to which it is bound can be described as $\mu_3:\eta^1:\eta^2:\eta^1$, a coordination mode first observed in the aforementioned lanthanide-tyrosine complexes,[29,32] but unprecedented for EDTA. Hydroxo ligands complete the Nd^{III} coordination sphere. Thus, each inner-layer Nd^{III} ion has a CN of 8, forming an irregular square antiprism, while each outer layer Nd^{III} ion has a CN of 10, and its coordination polyhedron may be best described as a bicapped square antiprism. Both eight- and ten-coordinate Nd^{III} are uncommon; the metal ion is predominantly nine-coordinate with tricapped trigonal prism being the most frequently observed structure. Even more intriguing are the unprecedented co-existence of these rare coordination numbers and the accompanying absence of the commonly observed nine-coordination.

The square opening, clearly shown in Fig. 19, could potentially permit entry by a guest molecule or ion. The strong preference of Nd^{III} for nine-coordinate geometry coupled with the high affinity of a lanthanide ion for F^- suggests that a fluoride-containing complex with the anionic guest species sitting in the square-shaped opening is possible.[53]

What the story tells us

The research described here was initially stimulated by the observation of several aesthetically pleasing polynuclear lanthanide–hydroxo complexes that were characterized as synthetic serendipity or accidents. The ultimate goal of making high-nuclearity lanthanide complexes aimed at potential applications in biomedical science and advanced technologies drove us to study the lanthanide coordination with biologically relevant ligands under near physiological and even high pH conditions. A variety of novel lanthanide–hydroxo complexes have been isolated and structurally characterized. The results clearly illustrate that otherwise well-established chemistry can be profoundly affected by simply altering the reaction pH.

The following are the principal results and conclusions from the research described above.

1. Ligand-controlled hydrolysis of the lanthanide ions is a new avenue in lanthanide coordination chemistry. It is a valid and highly efficient approach to the assembly of finite-size polynuclear lanthanide–hydroxo complexes.
2. α-Amino acids are a novel class of supporting ligands for controlling the hydrolysis of the lanthanide ions. Under near physiological pH conditions, lanthanide complexation with amino acids may be achieved *via* only the carboxylate group or simultaneous coordination by both the carboxylate and amino moieties.
3. Lanthanide–amino acid complexes generated under near neutral conditions typically exist as discrete polynuclear lanthanide–hydroxo clusters, whereas their low-pH counterparts are in mononuclear, dinuclear or noncluster polynuclear forms. It is the high-pH conditions that promote the formation of the large molecular clusters. These complexes may be viewed as the precursors to stepwise, controllable sol–gel materials syntheses.
4. The cuboid $[Ln_4(\mu_3\text{-}OH)_4]^{8+}$ cluster, complementing its *d*-block counterparts, is a common structural motif in lanthanide coordination compounds. Extended supramolecular structures can be assembled by using the $[Ln_4(\mu_3\text{-}OH)_4]^{8+}$ cluster cores as building blocks.
5. Octahedral $[Ln_6(\mu_6\text{-}O)(\mu_3\text{-}OH)_8]^{8+}$ core-containing clusters with an interstitial μ_6-O ligand can be assembled *via* direct hydrolysis of lanthanide nitrates and perchlorates in the absence of any organic supporting ligands.
6. Spherical anionic species are important in templating the formation of wheel-like lanthanide cluster complexes.
7. pH conditions exert a strong and general influence on the outcome of lanthanide coordination chemistry, as demonstrated by the isolation of unprecedented EDTA–lanthanide complexes from otherwise well-established chemistry.

The story continues with an open end

The results detailed above suggest extensive and promising coordination chemistry of the lanthanide ions under physiological or higher pH conditions. Many important questions, both fundamental and practical, remain to be answered. For example, why is tyrosine so unique in that it uses both amino and carboxylate groups for simultaneous lanthanide coordination? Why are pentadecanuclear or dodecanuclear complexes composed of corner-sharing cuboid $[Ln_4(\mu_3\text{-}OH)_4]^{8+}$ cluster units formed with tyrosine ligands while monocluster complexes are generated with carboxylate-only coordination when other amino acids are utilized? Although the steric effect due to the side group of the amino acid may play an important role, answers to these questions are not yet available. Further, how extensively applicable to other metals and ligands is the hydrolytic approach to polynuclear complexes? What properties may be expected of these novel lanthanide-containing materials? From the work discussed herein, it is clear that 'high'-pH lanthanide coordination chemistry represents a rich field of research that can be exploited to create novel lanthanide-containing materials with desirable properties. There are ample opportunities for investigation and high expectation for a broad range of applications of these novel polynuclear lanthanide complexes, including the well-characterized structural platform for potential development of lanthanide-based synthetic phosphodiesterases.

Acknowledgements

I wish to thank my collaborators, students and postdoctoral associates whose names appear in the references and whose contributions made the described work possible and enjoyable. Financial support from Research Corporation, The American Chemical Society, China Bridge International–North America, Chinese National Natural Science Foundation and The University of Arizona is gratefully acknowledged. The CCD based X-ray diffractometers were purchased through an NSF grant (CHE-96103474, Arizona) and an NIH grant (1S10RR11937-01, Harvard).

Notes and references

† Note: unless indicated otherwise, color legends are as follows: carbon (gray), lanthanide (green), nitrogen (cyan), oxygen (red). Thermal ellipsoids are represented in 50% probability.

1 R. W. Saalfrank, B. Demleitner, S. Kareth, N. Low and S. Trummer, *Mol. Cryst. Liq. Cryst. Sci. Technol., Sect. A*, 2001, **356**, 71; A. Müller and P. Kögerler, *Coord. Chem. Rev.*, 1999, **182**, 3; D. L. Caulder and K. N. Raymond, *J. Chem. Soc., Dalton Trans.*, 1999, 1185; R. E. P. Winpenny, *Chem. Soc. Rev.*, 1998, **27**, 447.
2 S. J. Lippard, *Angew. Chem., Int. Ed. Engl.*, 1988, **27**, 344.
3 D. Gatteschi, R. Sessoli and A. Cornia, *Chem. Commun.*, 2000, 725; A. Müller, F. Peters, M. T. Pope and D. Gatteschi, *Chem. Rev.*, 1998, **98**, 239; D. Gatteschi, A. Caneschi, L. Pardi and R. Sessoli, *Science*, 1994, **265**, 1054.
4 G. L. Abbati, A. Cornia, A. C. Fabretti, A. Caneschi, D. Gatteschi, *Inorg. Chem.*, 1998, **37**, 3759 and references therein.
5 G. Christou in *Magnetism: A Supramolecular Function*, ed. O. Kahn, NATO ASI Series 484, Kluwer Academic, Dordrecht, 1996, pp. 383–409.
6 A. Caneschi, A. Cornia, A. C. Fabretti and D. Gatteschi, *Angew. Chem., Int. Ed.*, 1999, **38**, 1295.
7 R. Bhula and D. C. Weatherburn, *Angew. Chem., Int. Ed. Engl.*, 1991, **30**, 688.
8 M. Cavalluzzo, Q. Chen and J. Zubieta, *J. Chem. Soc., Chem. Commun.*, 1993, 131.
9 D. P. Goldberg, A. Caneschi, C. D. Delfs, R. Sessoli and S. J. Lippard, *J. Am. Chem. Soc.*, 1995, **117**, 5789.
10 S. Parsons and R. E. P. Winpenny, *Acc. Chem. Res.*, 1997, **30**, 89.
11 K. L. Taft, A. Caneschi, L. E. Pence, C. D. Delfs, G. C. Papaefthymiou and S. J. Lippard, *J. Am. Chem. Soc.*, 1993, **115**, 11753; R. E. P. Winpenny, *Comments Inorg. Chem.*, 1999, **20**, 233.
12 S. P. Watton, P. Fuhrmann, L. E. Pence, A. Caneschi, A. Cornia, G. L. Abbati and S. J. Lippard, *Angew. Chem., Int. Ed.*, 1997, **36**, 2774; A. L. Dearden, S. Parsons and R. E. P. Winpenny, *Angew. Chem., Int. Ed.*, 2001, **40**, 151.
13 R. Anwander, *Angew. Chem., Int. Ed.*, 1998, **37**, 599 and references therein.
14 (*a*) C. G. Pernin and J. A. Ibers, *J. Cluster Sci.*, 1999, **10**, 71; (*b*) D. Freedman, J. H. Melman, T. J. Emge and J. G. Brennan, *Inorg. Chem.*, 1998, **37**, 4162.
15 N. Sabbatini, M. Guardigli and J.-M. Lehn, *Coord. Chem. Rev.*, 1993, **123**, 201; C. Benelli, A. Caneschi, D. Gatteschi and L. Pardi, in *Magnetic Molecular Materials*, ed. D. Gatteschi, O. Kahn, J. S. Miller and F. Palacio, NATO ASI Series 198, Kluwer Academic, Dordrecht, 1991, pp 233–244; J.-C. G. Bunzli and G. R. Choppin, *Lanthanide Probes in Life, Chemical and Earth Science*, Elsevier, Amsterdam, 1989; D. Parker and J. A. G. Williams, *J. Chem. Soc., Dalton Trans.*, 1996, 3613.
16 (*a*) L. G. Hubert-Pfalzgraf, *New J. Chem.*, 1995, **19**, 727; (*b*) P. Chanaud, A. Julbe, P. Vaija, M. Persin and L. Cot, *J. Mater. Sci.*, 1994, **29**, 4244.
17 S. Yu and A. Watson, *Chem. Rev.*, 1999, **99**, 2353.
18 N. H. Williams, B. Takasaki, M. Wall and J. Chin, *Acc. Chem. Res.*, 1999, **32**, 485; K. G. Ragunathan and H.-J. Schneider, *Angew. Chem., Int. Ed. Engl.*, 1996, **35**, 1219; P. E. Jurek, A. M. Jurek and A. E. Martell, *Inorg. Chem.*, 2000, **39**, 1016; S. J. Oh, K. H. Song, D. Whang, K. Kim, T. H. Yoon, H. Moon and J. W. Park, *Inorg. Chem.*, 1996, **35**, 3780; M. J. Komiyama, *Biochemistry*, 1995, **118**, 665; K. Bracken, R. A. Moss and K. G. Ragunathan, *J. Am. Chem. Soc.*, 1997, **119**, 9323.
19 M. R. Bürgstein and P. W. Roesky, *Angew. Chem., Int. Ed.*, 2000, **39**, 549; R. Anwander, F. C. Munck, T. Piermeier, W. Scherer, O. Runte and W. A. Herrmann, *Inorg. Chem.*, 1997, **36**, 3545.
20 N. Straeter, W. N. Lipscomb, T. Klabunde and B. Krebs, *Angew. Chem., Int. Ed. Engl.*, 1996, **35**, 2025.
21 P. Molenveld, J. F. J. Engbersen and D. N. Reinhoudt, *Chem. Soc. Rev.*, 2000, **29**, 75.
22 E. Baraniak, R. St. L. Bruce, H. C. Freeman, N. J. Hair and J. James, *Inorg. Chem.*, 1976, **15**, 2226; M. D. Grillone, F. Benetollo and G. Bombieri, *Polyhedron*, 1991, **10**, 2171; R. Wang, J. Zhao, T. Jin, G. Xu, Z. Zhou and X. Zhou, *Polyhedron*, 1998, **17**, 43.
23 T. Dubé, S. Gambarotta and G. Yap, *Organometallics*, 1998, **17**, 3967; X. M. Chen, Y. L. Wu, Y. X. Tong, Z. Sun and D. N. Hendrickson, *Polyhedron*, 1997, **16**, 4265; J. C. Plakatouras, I. Baxter, M. B. Hursthouse, K. M. Abdul Malik, J. McAleese and S. R. Drake, *J. Chem. Soc., Chem. Commun.*, 1994, 2455.
24 R. H. Holm, *Adv. Inorg. Chem.*, 1992, **38**, 1; J. E. McGrady, *J. Chem. Soc., Dalton Trans.*, 1999, 1393.
25 S. A. Cotton, *Lanthanides and Actinides*, Macmillan, London, 1991.
26 S. P. Sinha, *Complexes of the Rare Earths*, Pergamon, New York, 1966.
27 R. Wang and Z. Zheng, *Comments Inorg. Chem.*, 2000, **22**, 1.
28 (*a*) R. Wang, F. Gao and T. Jin, *Chem. Bull.*, 1996, **10**, 14 and references therein; (*b*) J. Reuben, in *Handbook on Physics and Chemistry of Rare Earths*, ed. K. A. Gschneidner, Jr. and L. Eyring, North-Holland, Amsterdam, 1979, vol. 4, pp. 515–552.
29 R. Wang, T. Jin, Z. Zheng and R. J. Staples, *Angew. Chem., Int. Ed.*, 1999, **38**, 1813.
30 R. Wang, H. Liu, M. D. Carducci, T. Jin, C. Zheng and Z. Zheng, *Inorg. Chem.*, 2001, **40**, 2743.
31 R. Wang, T. Jin and Z. Zheng, *Acta Chim. Sinica*, 2000, **58**, 1481.
32 R. Wang, H. D. Selby, H. Liu, Z. Zheng, M. D. Carducci, T. Jin, J. W. Anthis and R. J. Staples, *Inorg. Chem.*, submitted.
33 B. Ma, D. Zhang, S. Gao, T. Jin and C. Yan, *New J. Chem.*, 2000, **24**, 251.
34 B. Ma, D. Zhang, S. Gao, T. Jin, C. Yan and G. X. Xu, *Angew. Chem., Int. Ed.*, 2000, **39**, 3644.
35 H. Liu, R. Wang, M. D. Carducci and Z. Zheng, unpublished results.
36 A. Ouchi, Y. Suzuki, Y. Ohki and Y. Koizumi, *Coord. Chem. Rev.*, 1988, **92**, 29.
37 X. Chen, S. M. J. Aubin, Y. Wu, Y. Yang, T. C. W. Mak and D. N. Hendrickson, *J. Am. Chem. Soc.*, 1995, **117**, 9600; X. Chen, Y. Wu, Y. Tong and X. Huang, *J. Chem. Soc., Dalton Trans.*, 1996, 2443; Q. Liu, S. Gao, J. Li, Q. Zhou, K. Yu, B. Ma, S. Zhang, X. Zhang and T. Jin, *Inorg. Chem.*, 2000, **39**, 2488.
38 M. Eddaoudi, D. Moler, H. Li, T. M. Reineke, M. O'Keeffe and O. M. Yaghi, *Acc. Chem. Res.*, 2001, **34**, 319.
39 For selected representative work, see: T. M. Reineke, M. Eddaoudi, M. Fehr, D. Kelley and O. M. Yaghi, *J. Am. Chem. Soc.*, 1999, **121**, 1651; D. L. Long, A. L. Blake, N. R. Champness, C. Wilson and M. Schröder, *Angew. Chem., Int. Ed.*, 2001, **40**, 2444; C. V. Krishnamohan Sharma and R. D. Rogers, *Chem. Commun.*, 1999, 83; L. Pan, X. Y. Huang, J. Li, Y. G. Wu and N. W. Zheng, *Angew. Chem., Int. Ed.*, 2000, **39**, 527; L. Pan, E. B. Woodlock, X. T. Wang and C. Zheng, *Inorg. Chem.*, 2000, **39**, 4174; S. S. Y. Chui, A. Siu, X. Feng, Z. Y. Zhang, T. C. W. Mak and I. D. Williams, *Inorg. Chem. Commun.*, 2001, **4**, 467; L. Ma, O. R. Evans, B. M. Foxman and W. B. Lin, *Inorg. Chem.*, 1999, **38**, 5837.
40 (*a*) R. D. Shannon, *Acta Crystallogr., Sect. A*, 1976, **32**, 751; (*b*) Y. Marcus, *J. Chem. Soc., Faraday Trans.*, 1991, **87**, 2995.
41 A. Anderson, H. L. Anderson and J. K. M. Sanders, *Acc. Chem. Res.*, 1993, **26**, 469; D. H. Busch and N. A. Stephenson, *Coord. Chem. Rev.*, 1990, **100**, 119.
42 R. Wang, M. D. Carducci and Z. Zheng, *Inorg. Chem.*, 2000, **39**, 1836.
43 Z. Žák, P. Unfried and G. Giester, *J. Alloys Compds.*, 1994, **205**, 235; G. Giester, P. Unfried and Z. Žák, *J. Alloys and Compds.*, 1997, **257**, 175.
44 *Supramolecular Chemistry of Anions*, ed. A. Bianchi, K. Bowman-James and E. García-España, Wiley-VCH, New York, 1997; P. D. Beer and P. A. Gale, *Angew. Chem., Int. Ed.*, 2001, **40**, 486.
45 D. Zhang, B. Ma, T. Jin, S. Gao, C. Yan and T. C. W. Mak, *New J. Chem.*, 2000, **24**, 61.
46 Thematic issue on polyoxometalates, *Chem. Rev.*, 1998, **98**, No. 1.
47 J. Liu, E. A. Meyers and S. G. Shore, *Inorg. Chem.*, 1998, **37**, 5410.
48 W. J. Evans and M. S. Sollberger, *J. Am. Chem. Soc.*, 1986, **108**, 6095; K. G. Caulton and L. G. Hubert-Pfalzgraf, *Chem. Rev.*, 1990, **90**, 969.
49 G. R. Choppin and P. J. Wong, in *Coordination Chemistry: A Century of Progress*, ed. G. B. Kauffman, ACS Symposium Series 565, Washington, DC, 1994, pp 346–360.
50 C. Djordjevic and N. Vuletic, *Inorg. Chem.*, 1980, **19**, 3049.
51 N. Sakagami, Y. Yamada, T. Konno and K. Okamoto, *Inorg. Chim. Acta*, 1999, **288**, 7 and references therein.
52 H. D. Selby, R. Wang, B. K. Roland, M. D. Carducci and Z. Zheng, unpublished results.
53 L. Niinistö, in *Systematics and the Properties of the Lanthanides*, ed. S. P. Sinha, NATO ASI Series C No. 109, Reidel, Dordrecht, 1982, pp. 125–152.

CHEMCOMM Communication
www.rsc.org/chemcomm

Template route toward a novel nanostructured superionic conductor film; AgI nanorod/γ-Al_2O_3

Woo Lee,[a] Han-Ill Yoo[b] and Jin-Kyu Lee*[a]

[a] *School of Chemistry and Molecular Engineering, Seoul National University, Seoul 151-747, Korea. E-mail: jinklee@snu.ac.kr*
[b] *Solid State Ionics Research Laboratory, School of Materials Science and Engineering, Seoul National University, Seoul 151-742, Korea*

Received (in Cambridge, UK) 11th September 2001, Accepted 29th October 2001
First published as an Advance Article on the web 8th November 2001

A hierarchically structured composite ion conductor film (AgI nanorod/γ-Al_2O_3) was chemically prepared using nanoporous anodic aluminium oxide (AAO) as a template, where ion conducting AgI nanorods (av. diameter = 75 nm) are periodically aligned within a hexagonally organized insulating Al_2O_3 matrix.

Composite solid electrolytes, where ion conducting solids (such as AgI, AgCl, AgBr, LiI, CuCl, *etc.*) are heterogeneously mixed with an insulating solid dispersant (such as γ-Al_2O_3, SiO_2, MgO, *etc.*), have attracted much research attention due to their markedly enhanced conductivity with respect to pristine ion conducting solids themselves.[1–3] Among many composite ion conductor systems, AgI/γ-Al_2O_3 composite solid electrolytes have been extensively studied and impedance measurements revealed a maximum conductivity enhancement by a factor of 10^3–10^4, even at room temperature, compared with pristine β-AgI.[3] It is generally accepted that interface interactions between the ionic conductor (AgI) and insulator (γ-Al_2O_3) play a key role in governing the transport behaviour.[2] Although it has been suggested quite recently that such an enhanced conductivity is a consequence of the formation of an interfacial conducting phase (*e.g.*, 7H polytype of AgI with stacking fault arrangement), the microscopic mechanism or the origin of the enhancement in ionic conductivity is, as yet, not clear.[4] The interfacial interaction between particles could be maximized by reducing the size of particles down to 140 nm, since the surface of fine particles with high specific surface area are not only structurally unsaturated but also chemically labile and so can be easily converted to metastable phases. Previously, the fabrication of such composite ion conductors have been simply achieved by mechanically mixing and grinding the constituent materials (*i.e.* AgI and γ-Al_2O_3) and then hydrostatically pressing the resulting solid mixture, which does not, however, ensure homogeneous mixing of the components.[4,5]

Herein we report the synthesis and characterization of a hierarchically structured composite ion conductor film (AgI nanorod/Al_2O_3), where ion conducting AgI nanorods are homogeneously and periodically aligned within an insulating Al_2O_3 matrix with hexagonally organized configuration. A novel composite conductor was realized using porous anodic aluminium oxide (AAO) as a template, the structure of which is characterized by a closely packed regular array of hexagonal columnar cells with uniform nanoholes each of which contains a long cylindrical nanochannel.[6] The synthetic procedure for the preparation of the AgI nanorod/AAO composite is schematically presented in Fig. 1.

The nanoporous anodic aluminium oxide (AAO) template was prepared by a two-step anodization technique as described previously.[7] A field emission scanning electron microscopic (FE-SEM; Hitachi S-4300) image of the as-prepared AAO indicated that the template contained a well-organized hexagonal array of cylindrical pores with an average pore diameter of 75 nm and a pore density of 1×10^{10} cm^{-2} (Fig. 2(a)). According to XRD (Philips PW3710) pattern of the as-prepared AAO, the nanoporous AAO turned out to be X-ray amorphous, showing a broad spectral feature over the 2θ range 15–35°. However, the corresponding FT-IR (Bomem DA 8) spectrum showed a characteristic Al–O vibration of γ-Al_2O_3 with a shoulder at *ca.* 1180 cm^{-1} and strong absorption bands at 600–900 cm^{-1}.[8]

The Ag nanorod/AAO composites were fabricated *via* the electrodeposition of silver within the pores of the alumina template. A through-hole AAO membrane was used in the preparation of the Ag nanorod array. Initially, a layer (*ca.* 120 nm thick) of Ag was thermally evaporated onto one side of membrane to make the surface electrically conductive. This

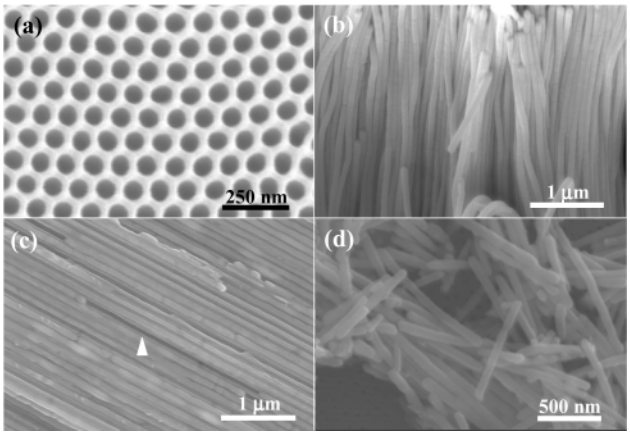

Fig. 2 FE-SEM images of (a) AAO template, (b) Ag nanorods after removing the AAO template, (c) cross-sectional image of AgI nanorod/AAO, and (d) AgI nanorods after removing the AAO template.

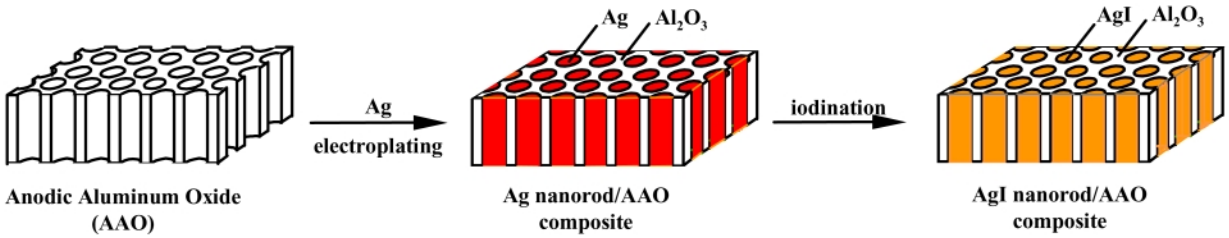

Fig. 1 Scheme for the fabrication of the AgI nanorod/AAO composite.

 DOI: 10.1039/b108230m

conducting layer functions as the working electrode in the electrodeposition of silver. After this, Ag was electroplated using a commercial plating solution (Technic silver 1025A and B) at room temperature. Electrodeposition of silver on the nanoporous AAO membrane produced large arrays of silver nanowires with a uniform diameter and a very large aspect ratio. As evidenced by FE-SEM investigation, the average diameter of the resulting metal nanowires is highly consistent with the average pore diameter (75 nm) of the alumina template used in the electrodeposition (Fig. 2(b)).

Fabrication of the silver iodide nanorod array was readily achieved by utilizing the solid–gas reaction between metallic silver nanorods and gaseous iodine. This reaction is known as iodization or iodination of silver;[9] a typical metal oxidation process where iodine serves as an oxidant. The net reaction can be expressed by eqn. (1):

$$2\ \mathrm{Ag(s)} + \mathrm{I_2(g)} \rightarrow 2\ \mathrm{AgI(s)} \qquad (1)$$

Typically, iodination was carried out by heating a vacuum sealed Pyrex tube containing 2 g of elemental iodine and a piece (0.5×1 cm^2) of Ag nanorod/AAO composite film in a constant temperature furnace (150 °C) for 24 h. After completion of the reaction, the resulting AgI nanorod/AAO composite was isolated after subliming the excess iodine, thoroughly washing with acetone and water to remove the residual elemental iodine, and finally drying under vacuum.

A representative cross-sectional FE-SEM image of the AgI nanorod/AAO is shown in Fig. 2(c). Some of the nanochannels (white triangle marks in Fig. 2(c)) of AAO were not filled with AgI nanorods probably due to the mechanical force applied to the film in order to obtain the cross-sectional image of the AgI nanorod/AAO composite film. An FE-SEM image of AgI nanorods freed from alumina by dissolving the oxide matrix with 0.5 M NaOH solution is shown in Fig. 2(d). Unlike the image of Ag nanorods in Fig. 2(b), the direction of the rod axis of individual AgI nanorods is rather arbitrary and the length of each nanorod is relatively short. Such morphological evolution can be attributed to the brittle nature of ionic AgI nanorods compared to metallic Ag nanorods and to the external stress exerted during the processes of eliminating the alumina matrix and drying the resulting AgI nanorods. Each of AgI nanorods in the nanochannels of the AAO matrix, however, is expected to have a high aspect ratio aligning its rod axis perfectly orthogonally with respect to the surface of AAO.

The phase of the synthesized nanorods was checked by TEM and X-ray diffraction (XRD). A selected area electron diffraction (SAED) pattern of the present AgI nanorods indicated that the sample is polycrystalline showing diffuse ring patterns. According to the estimated lattice spacings from the diffraction rings, the sample is mainly composed of a hexagonal wurtzite type β-AgI and this assignment was confirmed by XRD. Typical XRD spectra of Ag nanorod/AAO and AgI nanorod/AAO composites are presented in Fig. 3, together with the spectrum of commercial AgI for comparison. Broad spectral features in the 2θ range 15–35° were observed for the Ag nanorod/AAO and AgI nanorod/AAO composite samples, which originated from amorphous alumina (Al_2O_3). The XRD spectrum of the Ag nanowire/AAO composite showed well defined (111), (200) and (220) lines at 2θ = 38.8, 44.1 and 64.7°, respectively, revealing pure metallic silver (JCPDS code # 03-0931). On the other hand, it is evident from the present XRD patterns that the iodination reaction on the Ag nanorod/AAO composite gives rise to significant changes in the diffraction patterns. According to our XRD analysis, the observed diffraction peaks in the AgI nanorod/AAO composite could be indexed to the β-AgI structure with lattice parameters a = 4.6 Å and c = 7.5 Å (JCPDS code # 09-0374), consistent with the analytical result of the SAED pattern.

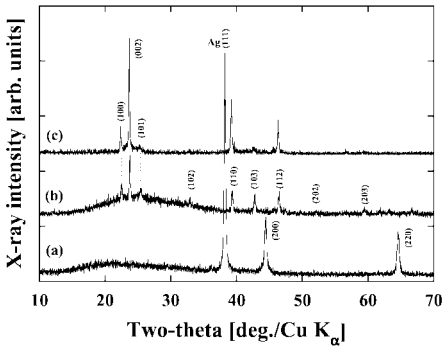

Fig. 3 Cu-Kα powder X-ray diffraction (XRD) pattern of (a) Ag nanorod/AAO, (b) AgI nanorod/AAO composite film, and (c) commercially available AgI.

Our preliminary results on ionic conductivity measurements revealed that the present AgI nanorod/AAO composite showed a three orders of magnitude enhanced ionic conductivity ($\sigma_{(28\ ^\circ\mathrm{C})} = (1.67 \pm 0.03) \times 10^{-3}\ \Omega^{-1}\ \mathrm{cm}^{-1}$) compared with pristine β-AgI, which is comparable with the previously reported maximum values in physically prepared AgI/Al_2O_3 composite ion conductors.[3]

It has been pointed out that the interfacial effect together with size and texture are responsible for conductivity enhancement in composite ion conductors. Unlike the inhomogeneous structure of physically prepared conventional composite ion conductors, the present sample has a novel geometric structure, where ion conducting nanorods with high aspect ratio are periodically embedded in the nanochannels of porous anodic aluminium oxide (AAO). Moreover, the interfaces formed by the AgI nanorods and the walls of cylindrical nanochannels of AAO are expected to act as well defined, isolated, and discrete conduction channels, leading to a markedly enhanced ionic conductivity. Therefore, the present AgI nanorods/AAO composite film might provide a good model system for elucidating the origin of the conductivity enhancement as well as the mechanism governing the transport behaviour in composite conductors.

We are quite certain that our underlying concept to develop novel nanostructured composite ion conductors can be readily extended to other solid electrolyte systems such as LiI and CuCl. We are at present investigating the transport properties of the present composite conductor with variation of the physical dimensions of the AgI nanorods, such as rod diameter and length.

This work was supported by the grant from the Interdisciplanary Research Program (Grant No. 1999-2-121-004-5) of the KOSEF. W. Lee is grateful for the award of a BK21 fellowship.

Notes and references

1 C. C. Liang, *J. Electrochem. Soc.*, 1973, **120**, 1289.
2 T. Jow and J. B. Wagner, *J. Electrochem. Soc.*, 1979, **126**, 1963.
3 K. Shahi and J. B. Wagner, *J. Electrochem. Soc.*, 1981, **128**, 6.
4 J.-S. Lee, S. Adams and J. Maier, *Solid State Ionics*, 2000, **136–137**, 1261.
5 N. F. Uvarov, P. Vanek, M. Savinov, V. Zelezny, V. Studnicka and J. Petzelt, *Solid State Ionics*, 2000, **127**, 253.
6 F. Li, L. Zhang and R. M. Metzger, *Chem. Mater.*, 1998, **10**, 2470.
7 H. Masuda and M. Satoh, *Jpn. J. Appl. Phys.*, 1996, **35**, L126.
8 J. A. Cadsden, *Infrared spectra of minerals and related inorganic compound*, Butterworths, London, 1975, p. 43.
9 P. S. Kumar, P. B. Dayal and C. S. Sunandana, *Thin Solid Films*, 1999, **357**, 111.

CHEMCOMM Communication
www.rsc.org/chemcomm

1,4-Benzenedicarboxylate derivatives as links in the design of paddle-wheel units and metal–organic frameworks

Matthew E. Braun, Cory D. Steffek, Jaheon Kim, Paul G. Rasmussen and Omar M. Yaghi*

Department of Chemistry, University of Michigan, Ann Arbor, MI 48109-1055, USA.
E-mail: oyaghi@umich.edu

Received (in Columbia, MO, USA) 5th September 2001, Accepted 6th November 2001
First published as an Advance Article on the web 30th November 2001

The square grid structure of MOF-2, constructed from paddle-wheel units of Zn(II) and 1,4-benzenedicarboxylate (BDC) links, persists for 2-amino-1,4-benzenedicarboxylate (ABDC) links but not for the sterically demanding 2,3,5,6-tetramethyl-1,4-benzenedicarboxylate (TBDC); the dihedral angle between planes of the benzene and carboxylate groups play a determining role in the formation of the paddle-wheel motif.

Extensive progress has been achieved in the synthesis of metal–organic frameworks (MOFs).[1–6] In particular MOFs of carboxylates have been designed to have permanent porosity in the absence of guests.[7–10] The first such material was constructed from paddle-wheel secondary building units (SBUs) and ditopic benzene links.[7a] Namely, Zn(BDC)·(DMF)(H_2O) (termed MOF-2) in which the benzene ring of BDC (1,4-benzenedicarboxylate) (Fig. 1a) is essentially in the same plane as the carboxylates (dihedral angle, Θ = 5.5°), a feature that allows the formation of a porous 4^4 square network with one dimensional channels of 7.8 Å cross-section (Fig. 1a–c). Our interest in design of MOFs led us to consider whether other derivatives of BDC can form this structural motif. In particular we focused on 2-amino-1,4-benzenedicarboxylate (ABDC) and 2,3,5,6-tetramethyl-1,4-benzenedicarboxylate (TBDC), since the substituents on benzene were expected to result in rotation of the carboxylates out of the plane containing the benzene ring to give larger Θ. In this report, we show that the size of substituents, and Θ are critical parameters in the formation of paddle-wheel units and ultimately their reticulated MOFs.

The ABDC and TBDC compounds were prepared using identical procedures: slow diffusion of a mixture containing chlorobenzene–trimethylamine (700:1 v/v) into an *N*,*N*′-dimethylformamide (DMF)–chlorobezene (5/5 mL) solvent mixture containing $Zn(NO_3)_2·6H_2O$ (55 mg, 0.185 mmol) and H_2ABDC (1 equiv.) or H_2TBDC (1 equiv.) at room temperature results after 4–7 days in the formation of Zn(ABDC)(DMF)·$(C_6H_5Cl)_{0.25}$ (MOF-46) or $Zn_2(TBDC)_2(H_2O)_{1.5}(DMF)_{0.5}$·(DMF)($H_2O$), (MOF-47). These compounds were formulated and characterized by elemental microanalysis† and single crystal X-ray diffraction.‡

To fully appreciate the structures of MOF-46 and -47, it is important to consider first the structure of MOF-2 in which the paddle-wheel M–O–C core cluster is considered a square SBU (Fig. 1b) that is polymerized into square grids by benzene ditopic links (Fig. 1c). We sought to learn whether the paddle-wheel and thus the square grid can be produced from other BDC derivatives. Our approach required relating the dihedral angle, Θ of the benzene ring of the ligand to the distance, *d* between the

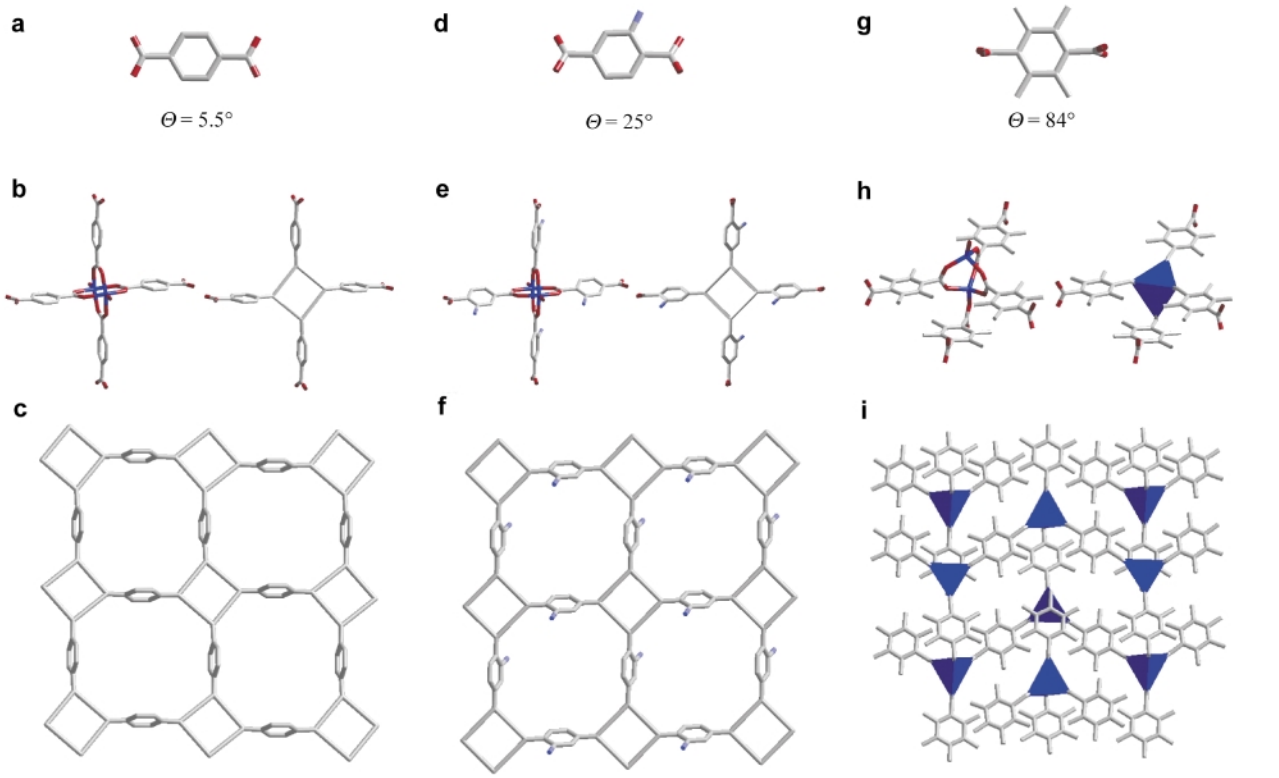

Fig. 1 The assembly of Zn(II) with BDC derivatives having a dihedral angle Θ to produce MOF-2 (a–c), MOF-46 (d–f) and MOF-47 (g–i). Zn(II) (blue) is connected to carboxylate O (red) with carboxylate C (gray) forming square (MOF-46) and tetrahedral (MOF-47) SBUs, which are linked by functionalized benzene units (N, light blue in d–f). All hydrogen atoms have been omitted for clarity.

 DOI: 10.1039/b108031h

substituent groups (g_1 and g_2) of contiguous BDC units of the same paddle-wheel. This is illustrated below and d is derived accordingly.

The general equation for d can be obtained by using $d = \{(x_1 - x_2)^2 + (y_1 - y_2)^2 + (z_1 - z_2)^2\}^{1/2}$ with the limiting condition, $\{l(1 + \tan 15°)\}/2 \geqslant R$. In case when g_1 and g_2 are the same functional groups and $(180° - \Theta_1) = \Theta_2$, this equation is simplified to $d = [2(l - (r+\sigma)/2 - \{3^{1/2}(r+\sigma)/2\}\sin\Theta_1)^2 + 3(r + \sigma)^2\cos^2\Theta_1]^{1/2}$.

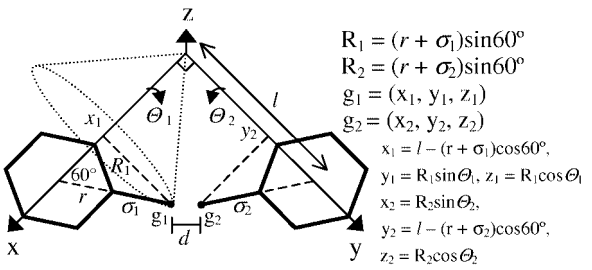

Here l = the distance between the center of the SBU and the center of the benzene ring, R = the radius of the trajectory of the circle generated by rotating the substituent group along the x- or y-axis by the dihedral angle, Θ. Thus to obtain a square grid structures as in MOF-2, functionalization of BDC should use groups that do not allow d to have value less than the summation of the van der Waals radii of g_1 and g_2.

For ABDC, $\Theta_1 = 25°$, $\Theta_2 = (180 - 25)°$, $l = 5.495$ Å, $r = 1.342$ Å and $\sigma = 1.40$ Å result in $d = 6.17$ Å which is enough to accommodate the $-NH_2$ groups. Then in principle, a paddle-wheel and an MOF-2 type structure can form. Reactions that are known to yield the paddle-wheel were utilized to make MOF-46. Indeed, the single crystal structure of the amino-benzene allows the formation of the expected motif (Fig. 1d–f), where the square layers are stacked along the c-axis, and DMF axial ligands fill the space in between adjacent layers. Due to the larger size of DMF relative to water (present in MOF-2 as an axial ligand), the $(CH_3)_2N$– groups pertrude into the channels of MOF-46. In this way, the pores have periodic arrays of $(CH_3)_2N$– and $–NH_2$ functionalities decorating the internal walls.

On the other hand, for TBDC, $\Theta_1 = 84°$, $\Theta_2 = (180 - 84)°$, $l = 5.309$ Å, $r = 1.398$ Å and $\sigma = 1.50$ Å result in $d = 2.00$ Å which is smaller than twice the van der Waals radii of the $–CH_3$ groups, 4.0 Å. Therefore it is not possible to produce an analogous framework. This is essentially a consequence of having methyl groups on both *ortho*-C atoms which inhibit the formation of the paddle-wheel structure at such a large dihedral angle. In fact, the van der Waals distance across the pores is 8.076–6.771 Å in MOF-2; well below that needed (9.329 Å) for TBDC units to replace BDC in that structure. Instead, MOF-47 is constructed from tetrahedral SBUs (Fig. 1g–i), a geometry known to be best in spacing apart sterically demanding groups.

Three carboxylate groups from three TBDC units are bound in a dimonodentate fashion to two Zn centers. One zinc center is also bound to a terminal water molecule, while the other is linked by an additional carboxylate in a monodentate fashion. Following the SBU structure analysis scheme, the carboxylate C atoms in the M–O–C cluster of MOF-47 forms a tetrahedral SBU. A closely related SBU is known in molecular complexes and other MOFs.[11,12] However, in this case, where it is expected that a tetrahedral SBU leads to the formation of a tetrahedral 4-connected 3-D network such as diamond, we find that the structure forms a double layer motif. Two TBDC units are bound entirely through dimonodentate coordination to Zn centers, and the remaining two units are each bound to Zn in both dimonodentate and monodentate fashion. One water and one DMF molecule per formula unit fill the space between the layers.

Thermogravimetric analysis on MOF-46 and -47 show that the DMF ligands in MOF-46, and the guests in MOF-47 can be removed upon heating to >50 °C: a weight loss of 41% was observed for MOF-46 in the range 50–310 °C corresponding to the loss of one DMF and 0.25 C_6H_5Cl (Calc.: 41%), and a sharper weight loss of 21% was measured for MOF-47 in the range 50–90 °C, which is attributed to the loss of 1.5 DMF and one water (Calc.: 21%). Both frameworks completely decompose above 350 °C.

This study demonstrates that the pores in MOFs can be functionalized with potentially reactive groups ($–NH_2$) without changing the SBU or the underlying framework topology (MOF-46). It is clear from the structure of MOF-47 that TBDC is too bulky to have the paddle-wheel arrangement or the square grid structure observed in MOF-2.

Notes and references

† Elemental microanalyses: MOF-46: Anal. Calc. for $Zn(C_8H_5O_4N)(DMF)(ClC_6H_5)_{0.25}$: C, 39.2; H, 4.15; N, 8.71. Found: C, 39.36, H, 4.24, N, 8.83. MOF-47: Anal. Calc. for $Zn_2(C_{12}H_{12}O_4)_2(H_2O)_{1.5}(DMF)_{0.5}(DMF)(H_2O)$: C, 47.10; H, 5.44; N, 2.89. Found: C, 47.49; H, 5.11, N, 2.54%.

‡ *Crystallographic data*: MOF-46: monoclinic, $C2/m$, $a = 11.2043(9)$, $b = 15.0516(12)$, $c = 8.0275(7)$ Å, $\beta = 111.706(1)°$, $U = 1257.79(18)$ Å^3, $Z = 4$, $R_{int} = 0.0278$, $D_c = 1.762$ g cm^{-3}, μ(Mo-Kα) = 1.977 mm^{-1}, $R1$ ($I > 2\sigma(I)$) = 0.0433, $wR2$ (all data) = 0.1227.

MOF-47: monoclinic, $P2_1/c$, $a = 11.3033(7)$, $b = 16.0291(10)$, $c = 17.5346(11)$ Å, $\beta = 92.546(1)°$, $U = 3173.8(3)$ Å^3, $Z = 4$, $R_{int} = 0.0719$, $D_c = 1.519$ g cm^{-3}, μ(Mo-Kα) = 1.574 mm^{-1}, $R1$ ($I > 2\sigma(I)$) = 0.0554, $wR2$ (all data) = 0.1544.

CCDC reference numbers 172613 and 172614.

See htttp://www.rsc.org/suppdata/cc/b1/b108031h/ for crystallographic data in CIF or other electronic format.

1 (*a*) S. Batten and R. Robson, *Angew. Chem., Int. Ed.*, 1998, **37**, 1460; (*b*) J. Hagrman, D. Hagrman and J. Zubieta, *Angew. Chem., Int. Ed.*, 1999, **38**, 2638; (*c*) S. Kitagawa and M. Kondo, *Bull. Chem. Soc. Jpn.*, 1998, **71**, 1739; (*d*) M. Eddaoudi, D. Moler, H. Li, B. Chen, T. Reineke, M. O'Keeffe and O. M. Yaghi, *Acc. Chem. Res.*, 2001, **34**, 319; (*e*) B. Moulton and M. Zaworotko, *Chem. Rev.*, 2001, **101**, 1629.

2 L. R. MacGillivray, R. H. Groeneman and J. L. Atwood, *J. Am. Chem. Soc.*, 1998, **120**, 2676

3 O. Evans and W. Lin, *Inorg. Chem.*, 2000, **39**, 2189.

4 L. Carlucci, G. Ciani, D. M. Proserpio and S. Rizzato, *Chem. Comm.*, 2001, 1198.

5 Z. Xu, Y. Kiang, S. Lee, E. Lobkovsky and N. Emmott, *J. Am. Chem. Soc.*, 2000, **122**, 8376.

6 (*a*) T. Y. Niu, X. Q. Wang and A. J. Jacobson, *Angew. Chem., Int. Ed.*, 1999, **38**, 1934; (*b*) J. A. Lu, W. T. A. Harrison and A. J. Jacobson, *Chem. Commun.*, 1996, 399; (*c*) C. Livage, C. Egger and G. Férey, *Chem. Mater.*, 2001, **13**, 410.

7 (*a*) H. Li, M. Eddaoudi, T. L. Groy and O. M. Yaghi, *J. Am. Chem. Soc.*, 1998, **120**, 8571; (*b*) H. Li, M. Eddaoudi, M. O'Keeffe and O. M. Yaghi, *Nature*, 1999, **402**, 276; (*c*) M. Eddaoudi, H. Li and O. M. Yaghi, *J. Am. Chem. Soc.*, 2000, **122**, 1391.

8 K. Seki, *Chem. Commun.*, 2001, 1496.

9 S. S. Y. Chui, S. M. F. Lo, J. P. H. Charmant, A. G. Orpen and I. D Williams, *Science*, 1999, **283**, 1148.

10 M. Kondo, M. Shimamura, S. Noro, S. Minakoshi, A. Asami, K. Seki and S. Kitagawa, *Chem. Mater.*, 2000, **12**, 1288.

11 (*a*) O. M. Yaghi, C. E. Davis, G. Li and H. Li, *J. Am. Chem. Soc.*, 1997, **119**, 2861; (*b*) J. Kim, B. Chen, T. M. Reineke, H. Li, M. Eddaoudi, D. B. Moler, M. O'Keeffe and O. M. Yaghi, *J. Am. Chem. Soc.*, 2001, **123**, 8239.

12 (*a*) W. Clegg, D. R. Harbron, C. D. Homan, P. A. Hunt, I. R. Little and B. P. Straughan, *Inorg. Chim. Acta.*, 1991, **186**, 51; (*b*) W. Clegg, I. R. Little and B. P. Straughan, *J. Chem. Soc., Chem. Commun.*, 1985, 73; (*c*) W. Clegg, I. R. Little and B. P. Straughan, *J. Chem. Soc., Dalton Trans.*, 1986, 1283.

CHEMCOMM
Communication
www.rsc.org/chemcomm

Metal–organic frameworks constructed from pentagonal antiprismatic and cuboctahedral secondary building units

David T. Vodak, Matthew E. Braun, Jaheon Kim, Mohamed Eddaoudi and Omar M. Yaghi*

Materials Design and Discovery Group, Department of Chemistry, University of Michigan, Ann Arbor, MI 48109-1055, USA. E-mail: oyaghi@umich.edu

Received (in Columbia, IN, USA) 24th September 2001, Accepted 6th November 2001
First published as an Advance Article on the web 30th November 2001

Two crystalline metal–organic frameworks formulated as $Zn_6(NDC)_5(OH)_2(DMF)_2{\cdot}4DMF$, MOF-48, and $Zn_7(m\text{-}BDC)_6(OH)_4(H_2O)_2{\cdot}6DMF{\cdot}4H_2O$, MOF-49, (NDC = 1,4-naphthalenedicarboxylate; *m*-BDC = 1,3-benzenedicarboxylate) have been synthesized and fully characterized by single crystal X-ray diffraction studies, which reveal that the frameworks are constructed from pentagonal antiprismatic (MOF-48) and cuboctahedral (MOF-49) secondary building units respectively, however, both are reticulated into 3-D structures having the B network of CaB_6.

In the chemistry of metal–organic frameworks (MOFs), especially where metal ions have been joined by polytopic carboxylate links, M–O–C clusters generally result in which the carboxylate C atoms define the shape of what is referred to as a secondary building unit (SBU).[1–4] Such entities have been recognized and used as tools for simplifying complex structures,[5] and in cases where reaction conditions can be directed to give specific SBU geometries; they have the potential to allow for the assembly of MOFs by design.[6–8] Furthermore, the size of SBU constructs is directly related to achieving optimal porosity and rigidity of MOFs including the design of periodic arrays of open metal sites within their voids.[6–10] With the long-term goal of understanding the factors affecting the composition, topology, shape and size of SBUs, we have begun to explore synthetic routes that may lead to new SBUs. Here we report two 3-D metal carboxylate frameworks prepared by linking Zn(II) with 1,4-naphthalenedicarboxylate (NDC), and *m*-benzenedicarboxylate (*m*-BDC) to give MOF-48 and MOF-49, respectively. We find that these MOFs are constructed from pentagonal antiprismatic and cuboctahedral SBUs; however, both form 6-connected CaB_6 type networks rather than 10- and 12-connected networks that one might expect to find based on the geometry of their respective SBUs. We show that pairwise connections between SBUs in MOF-48 and 49 provide the means for these frameworks to adopt networks of lower connectivity.

Vapour diffusion from a mixture of H_2O_2 (0.40 mL, 40% in water) and chlorobenzene–triethylamine (20 mL/1 mL) into a clear solution of *N*,*N*′-dimethylformamide (DMF)/chlorobenzene (5 mL/5 mL) containing $Zn(NO_3)_2{\cdot}6H_2O$ (0.029 g, 0.097 mmol) and NDC acid (0.015 g, 0.069 mmol) gives, after 7 d, cube-like crystals of MOF-48 in 33% yield (based on NDC acid). MOF-49 was prepared by dissolving $ZnCl_2$ (0.060 g, 0.44 mmol) and *m*-BDC acid (0.040 g, 0.261 mmol), in that order, in DMF (5 mL). This solution was subjected to dropwise addition of a mixture of 0.6 M aqueous methylamine–acetonitrile (2 mL/5 mL). The resulting clear solution was left undisturbed for three days at room temperature to give hexagonal shape crystals in 27% yield (based on *m*-BDC acid). MOF-48 and 49 were formulated and characterized by elemental microanalysis† and X-ray single crystal diffraction studies.‡

MOF-48, $Zn_6(NDC)_5(OH)_2(DMF)_2{\cdot}4DMF$, is constructed from hexameric units composed of four tetrahedral and two octahedral Zn(II) centres, where a total of ten NDC links doubly bridge the zinc atoms in a dimonodentate fashion (Fig. 1a). Each cluster has an inversion centre, which relates two zinc trimer units in which the zinc centres are further joined by a triply bridging μ_3–OH group. One terminal DMF ligand is bound to each of the octahedral zinc centres. The assignment of μ_3-OH was based on the near tetrahedral angles around the central O (110.8(6), 114.0(4), 114.0(4)°), which are in the range of those found in molecular complexes.[11]

It is useful to connect the points-of-extension (the carboxylate C atoms) in the hexameric units, a process that leads to SBUs having pentagonal antiprismatic geometry (Fig. 1b). Each SBU is connected to six other SBUs to give a 3-D framework having 6.2 Å diameter[12] 1-D channels where four DMF guests per formula unit reside (Fig. 1c). It is important to note that in addition to two single NDC connections along [001] between SBUs, there are eight pairwise connections (Fig. 1c). Here each pair of NDC links connecting two SBUs can be considered topologically as a single ditopic link, in essence a doubly reinforced link. Since each SBU acts as a six connector, the structure of MOF-48 has the topology of a decorated B network of CaB_6.[13]

The crystal structure of MOF-49, $Zn_7(m\text{-}BDC)_6(OH)_4(H_2O)_2{\cdot}6DMF{\cdot}4H_2O$, is constructed from a unit composed of four tetrahedral and three octahedral Zn(II) centres in which two identical units, each composed of two tetrahedra and one octahedron, are joined together by an octahedron (Fig. 2a). Within each such unit, the carboxylates of four *m*-BDC links bridge the zinc centres in a dimonodentate fashion, and an additional two links bind as monodentate to the tetrahedral zinc

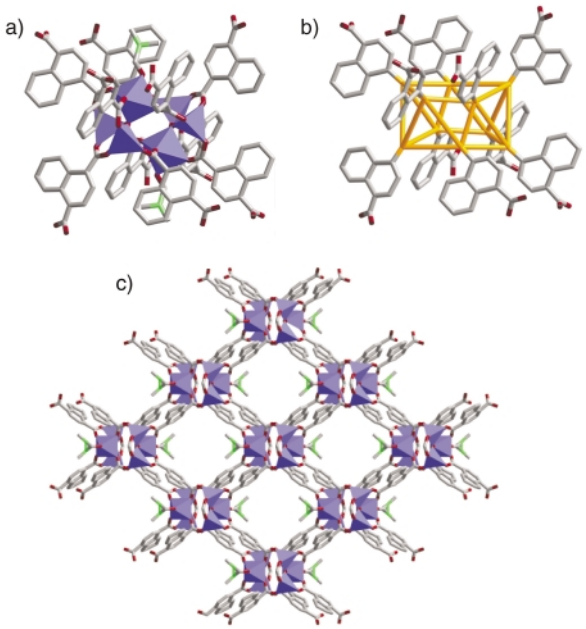

Fig. 1 MOF-48: (a) $Zn_6(NDC)_5(OH)_2(DMF)_2$ unit showing the coordination around four tetrahedral and two octahedral zinc atoms. (b) A pentagonal antiprism SBU is shown in orange. (c) Extended structure shown along [001], DMF guests and all hydrogen atoms have been omitted for clarity. (colour scheme: C, grey; O, red; Zn, blue in polyhedral form).

 DOI: 10.1039/b108684g

centres. Each unit also contains two μ_3-OH groups (their identity was confirmed as in MOF-48) and only one terminal water ligand bound to each octahedral centre.

In the crystal structure of MOF-49, a total of twelve carboxylates per formula unit in which carboxylate C atoms are found to lie on the vertices of a large, distorted cuboctahedral SBU (Fig. 2b). Here each SBU is bridged to six others *exclusively* through pairwise connections resulting in an extended framework having a topology similar to MOF-48, in that it is also related to the B network of CaB_6. MOF-49 contains a 3-D porous system with 3.5–5.5 Å diameter voids, where six DMF and four water molecules per formula unit reside as guests.

It is instructive to note that although the SBUs observed in MOF-48 and -49 have overall geometries generally associated with higher coordination (10 and 12), their large size combined with the short link do not allow for high coordination of the SBU in the solid state, as that would be sterically disfavoured. Instead the SBUs are reticulated into frameworks having six-coordination around each SBU; this made possible by the pairwise binding of links. Another factor that may be operating here was revealed upon close examination of distances between benzene rings of pair members: distances in the ranges 3.246–3.634 Å (MOF-48) and 3.315–3.725 Å (MOF-49) were found—values that indicate strong π–π intermolecular forces, and point to the possibility of their relevance in achieving lower coordination SBUs. It will be necessary to use *branched* links in order to attain SBUs with higher coordination as recently demonstrated for seven coordinated SBUs in MODF-1.[14]

Calculations of the space occupied by guests in MOF-48 and -49 indicate that it represents 50% of the crystal volume. The mobility of guests within their frameworks was assessed by thermal gravimetric studies: Here, 8.711 mg (MOF-48) and 17.23 mg (MOF-49) were heated over a range of 30–400 and 30–650 °C, respectively. For MOF-48, 25.8% weight loss was observed in the range 50–380 °C, which is equivalent to the loss of six DMF molecules per formula unit (calc.: 22.6%) representing four DMF guests and two DMF ligands. While for MOF-49, 16.95% weight loss was observed in the range 30–140 °C, which is equivalent to the loss of 3.5 DMF guests and four water guests per formula unit (calc.: 17.34%) representing the 3.5 DMF guest molecules and four water guest molecules found in the air-dried samples subjected to elemental microanalysis.† Experimentation is currently underway to examine whether the evacuated forms of MOF-48 and -49 can maintain their porosity in the absence of guests.

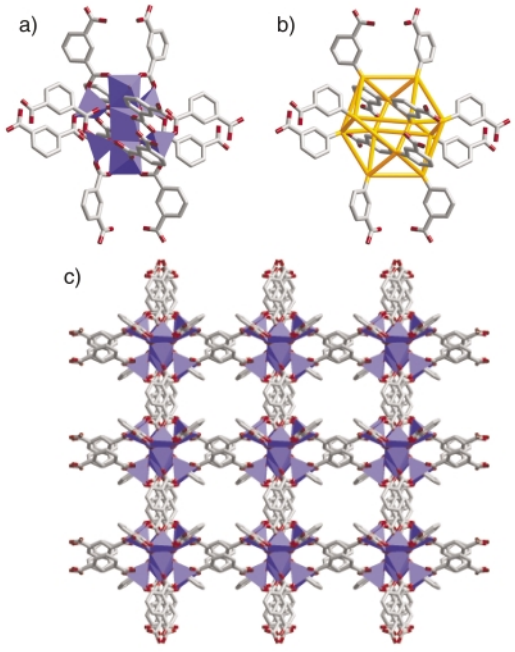

Fig. 2 MOF-49: (a) $Zn_7(m\text{-}BDC)_6(OH)_4(H_2O)_2$ unit showing the coordination around four tetrahedral and three octahedral zinc atoms. (b) A cuboctahedron SBU is shown in orange. (c) Extended structure along [001], DMF and water guests and all hydrogen atoms have been omitted for clarity (same colour scheme and drawing conditions as in Fig. 1).

This study has prompted us to focus on examining the role of intermolecular forces and the geometry of the link on the symmetry, size and coordination number of SBUs, aspects central to design of MOFs.

We acknowledge support of this work by the National Science Foundation.

Notes and references

† Elemental microanalysis: MOF-48. Calc. for $Zn_6(C_{12}H_6O_4)_5(OH)_2\cdot(DMF)_2\cdot 4DMF$: C, 48.40; H, 3.85; N, 4.34. Found: C, 48.52; H, 3.74; N, 4.46%. MOF-49. Calc. for $Zn_7(m\text{-}BDC)_6(OH)_4(H_2O)_2\cdot 3.5DMF\cdot 4H_2O$: C, 32.40; H, 3.70; N, 2.62. Found: C, 32.65; H, 3.72; N, 2.63%.

‡ *Crystallographic data*: MOF-48: $Zn_6(C_{12}H_6O_4)_5(OH)_2(DMF)_2\cdot 4DMF$, M = 1935.65, monoclinic, space group $C2/m$, a = 19.5043(16), b = 16.4817(14), c = 14.6396(12) Å, β = 95.902(2)°, U = 4681.2(7) Å^3, Z = 2, μ(Mo-Kα) = 1.586 mm^{-1}, D_c = 1.373 g cm^{-3}, T = 173(2) K $R1$ ($I > 2\sigma(I)$) = 0.0939 and $wR2$ (all data) = 0.2546.

MOF-49: $Zn_7(m\text{-}BDC)_6(OH)_4(H_2O)_2\cdot 6DMF\cdot 4H_2O$, M = 2013.43, monoclinic, space group $P2/c$, a = 13.509(2) Å, b = 11.9838(19, c = 27.039(4) Å, β = 93.459(3)°, U = 4369.4(12) Å^3, Z = 2, μ(Mo-Kα) = 1.977 mm^{-1}, D_c = 1.530 g cm^{-3}, T = 153(2) K, $R1$ ($I > 2\sigma(I)$) = 0.0983, $wR2$ (all data) = 0.2720.

CCDC reference numbers 171766 and 171767.

See http://www.rsc.org/suppdata/cc/b1/b108684g/ for crystallographic data in CIF or other electronic format.

1 M. Eddaoudi, D. B. Moler, H. Li, B. Chen, T. M. Reineke, M. O'Keeffe and O. M. Yaghi, *Acc. Chem. Res.*, 2001, **34**, 319.
2 S. A. Bourne, J. J. Lu, A. Mondal, B. Moulton and M. J. Zaworotko, *Angew. Chem., Int. Ed.*, 2001, **40**, 2111.
3 P. Ayyappan, O. R. Evans and W. B. Lin, *Inorg. Chem.*, 2001, **40**, 4627.
4 J. S. Seo, D. Whang, H. Lee, S. I. Jun, J. Oh, Y. J. Jeon and K. Kim, *Nature*, 2000, **404**, 982.
5 J. Kim, B. Chen, T. M. Reineke, H. Li, M. Eddaoudi, D. B. Moler, M. O'Keeffe and O. M. Yaghi, *J. Am. Chem. Soc.*, 2001, **123**, 8239.
6 H. Li, M. Eddaoudi, M. O'Keeffe and O. M. Yaghi, *Nature*, 1999, **402**, 276.
7 B. Chen, M. Eddaoudi, S. T. Hyde, M. O'Keeffe and O. M. Yaghi, *Science*, 2001, **291**, 1021.
8 B. Chen, M. Eddaoudi, T. M. Reineke, J. W. Kampf, M. O'Keeffe and O. M. Yaghi, *J. Am. Chem. Soc.*, 2000, **122**, 11559.
9 T. M. Reineke, M. Eddaoudi, M. Fehr, D. Kelley and O. M. Yaghi, *J. Am. Chem. Soc.*, 1999, **121**, 1651.
10 T. M. Reineke, M. Eddaoudi, D. Moler, M. O'Keeffe and O. M. Yaghi, *J. Am. Chem. Soc.*, 2000, **122**, 4843.
11 (*a*) J. Tao, M. L. Tong, J. X. Shi, X. M. Chen and S. W. Ng, *Chem. Commun.*, 2000, 2043; (*b*) W. Clegg, D. R. Harbron, C. D. Homan, P. A. Hunt, I. R. Little and B. P. Straughan, *Inorg. Chim. Acta.*, 1991, **186**, 51; (*c*) J. Hermann and A. Erxleben, *Inorg. Chim. Acta.*, 2000, **304**, 125.
12 Van der Waals radii of C (1.70 Å) and O (1.40 Å) were employed in determination of distance parameters. A. Bondi, *J. Phys. Chem.*, 1964, **68**, 441.
13 M. O'Keeffe, M. Eddaoudi, H. Li, T. M. Reineke and O. M. Yaghi, *J. Solid State Chem.*, 2000, **152**, 3.
14 H. K. Chae, M. Eddaoudi, J. Kim, S. I. Hauck, J. F. Hartwig, M. O'Keeffe and O. M. Yaghi, *J. Am. Chem. Soc.*, 2001, **123**, 11483.

CHEMCOMM Communication
www.rsc.org/chemcomm

Thin dense Pd membranes supported on α-Al_2O_3 hollow fibers

X. L. Pan,*[a] G. X. Xiong,[a] S. S. Sheng,[a] N. Stroh[b] and H. Brunner[b]

[a] *State Key Laboratory of Catalysis, Dalian Institute of Chemical Physics, Chinese Academy of Sciences, Dalian, 116023, P.R.China. E-mail: panxiulian@163.net*

[b] *Fraunhofer Institute for Interfacial Engineering and Biotechnology, Nobelstrasse 12, Stuttgart D-70569, Germany*

Received (in Cambridge, UK) 17th September 2001, Accepted 26th October 2001
First published as an Advance Article on the web 9th November 2001

Macroporous α-Al_2O_3 hollow fibers are used as supports for thin dense Pd membranes; these membranes show a high and stable H_2 flux in permeance studies.

The increasing demand for H_2 as an energy carrier or chemical in the petroleum industry has promoted research interest in H_2 production, purification and utilization all over the world.[1] As an advanced technology with a compact apparatus and high efficiency, metallic Pd-based membranes have occasionally been applied to separate and purify H_2 for electronic, metallurgic and fine chemical applications.[2] However, the commercialization of Pd-based technology on a large scale does not appear to be likely in the near future, although this technology has been shown to have great potential[3–5] in last four decades. The high cost of membranes, still too low permeability and long-term stability and low separation area/volume ratios are some of most important obstacles[6,7] to wide acceptance in industry.

Hollow fibers (HFs) are known for their much higher separation area/volume ratios, in comparison to other geometries such as plates, discs, tubes and multichannels.[8] The objective of this work was to deposit ultrathin dense Pd membranes on macroporous α-Al_2O_3 HFs since thin membranes can reduce the cost and improve H_2 permeability.

α-Al_2O_3 HFs are produced by a spinning-extrusion technique.[9] Typical HFs have an outer diameter of 700–800 μm, an inner diameter of 500–600 μm and an average pore size of 0.2 μm. Boehmite sol was modified with palladium complexes.[10] A modified sol prepared in this manner was coated on HF surfaces by a dip-coating process, based on capillary forces of the support pores,[11] while applying a vacuum on the inner side of the HFs. The particle size of the sol was 60–100 nm, which was smaller than the size of support pores. Therefore with the aid of the vacuum on the inner side of the HFs, there was some penetration of sol particles into the pores, which improved the adhesion between the top layer and the support. After calcination at 750 °C in static air, the average pore size of Pd/γ-Al_2O_3 was determined by the N_2 adsorption–desorption technique to be around 5.7 nm. SEM micrographs of these porous Pd/γ-Al_2O_3 membranes showed a very smooth surface. No defects or pinholes were observed in the scanned area. Both the narrow pore size distribution and smooth surface of the substrate make it possible to deposit ultrathin Pd membranes without defects.[12] After reduction in flowing H_2 at 200 °C, substrates with palladium species uniformly distributed in γ-Al_2O_3 were used for electroless plating.

The electroless plating process was developed by Rhoda,[13] which is based on an autocatalytic reaction between $[Pd(EDTA)]^{2-}$ and hydrazine. The palladium seeds introduced during modification of the boehmite sol act as catalysts for the chemical reaction and as nuclei for deposition and growth of Pd membranes. Fig. 1 shows SEM micrographs of a thin dense Pd membrane supported on a porous Pd/γ-Al_2O_3/α-Al_2O_3 HF. The surface of the porous substrate was fully covered by a continuous Pd membrane, which grew by nucleation at and growth of the small palladium crystals. No defects or pinholes were observed on the surface. The Pd membrane was around 0.6 μm thick after 1 h deposition, as can be seen from Fig. 1(b).

Gas permeation through dense Pd/ceramic HFs were measured at 335–400 °C with the permeate side set at atmospheric pressure. These membranes are composed of a 2–3 μm thick Pd membrane and a porous substrate, comprising of a mesoporous Pd/γ-Al_2O_3 layer (3–4 μm thick) supported on α-Al_2O_3. Each layer contributes some resistance to gas transport, which is defined as the reciprocal of H_2 permeance. The substrate has an H_2 permeance of 170–200 $m^3\ m^{-2}\ h^{-1}\ bar^{-1}$ while that of the dense Pd membrane is 8.8 $m^3\ m^{-2}\ h^{-1}\ bar^{-1}$ at 400 °C. Therefore the resistance of the substrates can be neglected, since it represents only 5% of the total resistance. H_2 transport through the composite membranes can thus be essentially discussed in terms of the Pd membrane itself.

H_2 transport through a Pd membrane follows a solution–diffusion mechanism, which involves several steps: (1) reversible dissociative adsorption of H_2 on the membrane surface; (2) diffusion of atomic hydrogen in the bulk metal under the driving force of concentration gradients; (3) recombination of hydrogen atoms to molecules on the opposite surface and desorption into the gas phase. The H_2 flux can be described by the integration of Fick's law [eqn. (1)]:

$$J = (D/l)(P_h^n - P_l^n) \quad (1)$$

where D is the diffusion coefficient, l is the membrane thickness, P_h and P_l are the pressures on each side of membrane

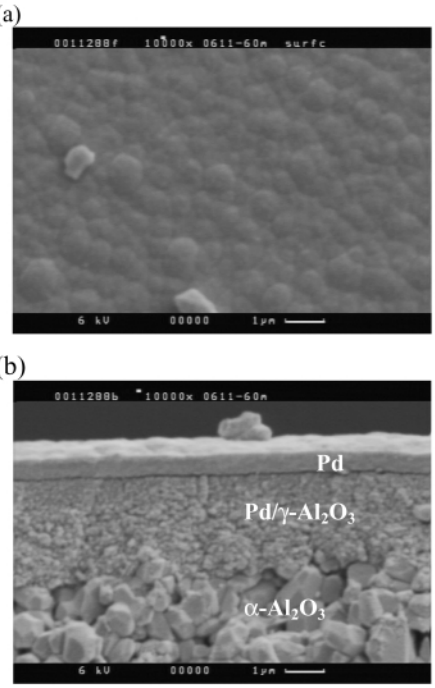

Fig. 1 SEM micrographs of a dense Pd membrane on a ceramic hollow fiber: (a) surface view; (b) cross-sectional view.

 DOI: 10.1039/b108395c

and n is the pressure exponent, which reflects the mechanism of H_2 transport. In thick membranes, the surface process of H_2 adsorption and desorption is very fast compared to the bulk diffusion and H_2 transport is often controlled by the bulk diffusion. In this case, $n = 0.5$, so that H_2 permeance is proportional to the square root of H_2 pressures on either side of the membrane.[3] With a decrease of membrane thickness, the resistance of the bulk diffusion reduces, so that the resistance of the surface process becomes increasingly significant. When both the surface process and bulk diffusion control H_2 transport, $0.5 < n < 1$. With a further decrease of membrane thickness, the surface process dominates, and n tends to unity.

As seen in Fig. 2(a), the H_2 permeance shows a linear relationship with the pressure difference across the membranes in the temperature range 335–400 °C, indicating that $n = 1$. This implies that the reaction of hydrogen with the Pd surface is the rate-determining step rather than bulk diffusion.[14] The thin Pd membrane (2–3 μm) reduces the resistance of bulk diffusion of hydrogen in the metal, so that the surface process becomes the rate-determining step. Moreover, Fig. 2(a) shows that the H_2 permeance increases with temperature: from 6.5 $m^3\ m^{-2}\ h^{-1}\ bar^{-1}$ at 335 °C to 8.8 $m^3\ m^{-2}\ h^{-1}\ bar^{-1}$ at 400 °C. These membranes have a fairly high permance compared to thick membranes previously investigated.[15,16] Fig. 2(b) shows the Arrhenius relation of H_2 permeance as a function of the temperature in the range 335–400 °C. The activation energy for H_2 transport was calculated to be 15.8 kJ mol^{-1}, similar to a recently reported value.[17]

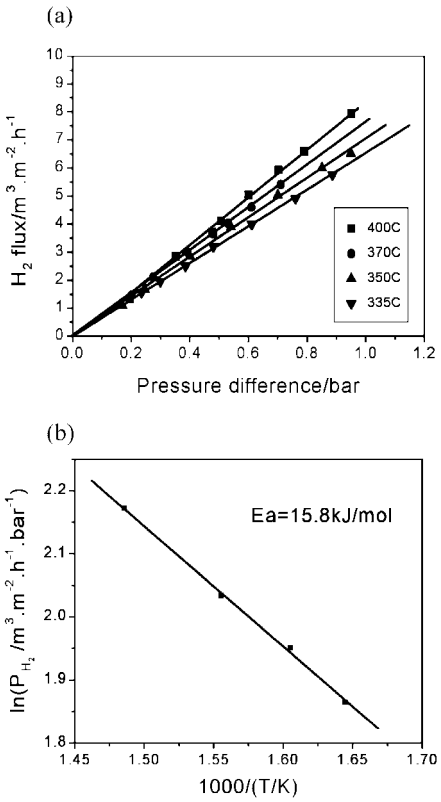

Fig. 2 H_2 transport through ultrathin Pd/ceramic hollow fiber membranes: (a) influence of the temperature and pressure difference; (b) Arrhenius relation between the H_2 permeance and temperature in the range 335–400 °C.

For applications in industry, membranes should have a good long-term stability, which was tested here for H_2 permeation at 430 °C for 660 h. Before applying high temperatures, no He flux was detected at a pressure difference of 1.2 bar at room temperature. This implies that these membranes are fairly gas-tight. At 430 °C, N_2 permeance was detected as 0.019 $m^3\ m^{-2}\ h^{-1}\ bar^{-1}$. This might be attributed to some leakage through the sealing at high temperatures or formation of defects during heating. There is probably some stress in the ultrathin Pd layer after the electroless deposition which may be released during heating, which might cause small defects. Either possible defects or possible leakage through the sealing will lead to transport of inert gases. After 660 h H_2 permeation, there was only a slight decrease in H_2 permeance, which remained > 11 $m^3\ m^{-2}\ h^{-1}\ bar^{-1}$. The ideal separation factor $\alpha(H_2/N_2)$ (defined as the ratio of permeances of pure H_2 to pure N_2) was > 1000. Such membranes are applicable in catalytic reactions to enhance conversions and/or selectivities.[18]

In conclusion, ultrathin dense Pd membranes have been successfully deposited on hollow fiber substrates. The resulting composite membranes not only provide high separation area/volume ratios, but also reduce the cost and improve the permeability with a high separation factor. These membranes show a good durability in H_2 permeation, which is important for industrial applications in H_2 separation and membrane catalysis.

We gratefully acknowledge Mr N. Specognia for SEM measurements and Dr A. Goldbach for many discussions and constructive suggestions in this work.

Notes and references

1 F. Barbir and T. Gomez, *Int. J. Hydrogen Energy*, 1996, **21**, 891.
2 R. R. Bhave, *Inorganic Membranes Synthesis, Characteristics and Applications*, Van Nostrand Reinhold, New York, 1991.
3 J. Shu, B. P. A. Grandjean, A. van Neste and S. Kaliaguine, *Can. J. Chem. Eng.*, 1991, **69**, 1036.
4 V. M. Gryaznov, *Platinum Met. Rev.*, 1986, **30**, 68.
5 G. Saracco, H. W. J. P. Neomagus, G. F. Versteeg and W. P. M. van Swaaij, *Chem. Eng. Sci.*, 1999, **54**, 1997.
6 J. Zaman and A. Chakma, *J. Membrane Sci.*, 1994, **92**, 1.
7 J. N. Armor, *J. Membrane Sci.*, 1998, **147**, 217.
8 L. Cot, *Proc. 5th Int. Conf. Inorg. Membranes*, Tokyo, Japan, 1998.
9 A. Goldbach, T. Mauer and N. Stroh, *Keram. Z.*, 2001, **53**, 16.
10 H.-B. Zhao, X. G. Xiong, J. H. Gu, S. S. Sheng, H. Bauser, N. Stroh and K. Pflanz, *Catal.Today*, 1995, **25**, 237.
11 A. F. M. Leenaars and A. J. Burggraaf, *J. Colloid Interface Sci.*, 1985, **105**, 27.
12 S. Uemiya, *Sep. Purif. Methods*, 1999, **28**, 51.
13 R. N. Rhoda, *Trans. Inst. Met. Finish.*, 1958–1959, **36**, 82.
14 R. C. Hurlbert and J. O. Konecny, *J. Chem. Phys.*, 1961, **34**, 655.
15 A. G. Knapton, *Plat. Met. Rev.*, 1977, **21**, 44.
16 A. J. de Rosset, *Ind. Eng. Chem.*, 1990, **52**, 525.
17 A. Li, W. Liang and R. Hughes, *Catal. Today*, 2000, **56**, 45.
18 W. S. Yang and G. Xiong, *Curr. Opin. Solid State Mater. Sci.*, 1999, **4**, 103.

CHEMCOMM
Communication
www.rsc.org/chemcomm

The crystal structure and physical properties of β-(BDA-TTP)$_2$FeCl$_4$ [BDA-TTP = 2,5-bis(1,3-dithian-2-ylidene)-1,3,4,6-tetrathiapentalene]

Jun-ichi Yamada,*[a] Takashi Toita,[a] Hiroki Akutsu,[a] Shin'ichi Nakatsuji,[a] Hiroyuki Nishikawa,[b] Isao Ikemoto[b] and Koichi Kikuchi*[b]

[a] *Department of Material Science, Faculty of Science, Himeji Institute of Technology, 3-2-1 Kouto, Kamigori-cho, Ako-gun, Hyogo 678-1297, Japan. E-mail: yamada@sci.himeji-tech.ac.jp*
[b] *Department of Chemistry, Graduate School of Science, Tokyo Metropolitan University, Hachioji, Tokyo 192-0397, Japan*

Received (in Cambridge, UK) 14th June 2001, Accepted 29th October 2001
First published as an Advance Article on the web 9th November 2001

The title charge-transfer (CT) salt exhibits metallic conducting behavior with a metal-to-insulator (MI) transition at 113 K, and its magnetic properties reveal that it is an antiferromagnet below the Néel temperature, T_N = 8.5 K.

Recent studies on the development of molecular magnetic conductors by combining organic π-electron donors and inorganic magnetic anions have resulted in a new class of CT salts with multifunctional properties such as antiferro- and ferro-magnetic organic metallic behavior,[1,2] and antiferromagnetic organic metals exhibiting superconductivity.[3] However, these CT salts, in which magnetic order and metallic conductivity coexist, are derived from tetrachalcogenafulvalene (TCF) donors. Meanwhile, the successful formation of metallic or superconducting CT materials consisting of non-TCF donors and magnetic anions remains as a challenging subject in this research area.[4] The Fe-containing BDA-TTP salts in this regard would be promising candidates, because we have already found that BDA-TTP, a sulfur-based π-donor containing no TTF functionalities, produces superconducting salts with relatively large anions, such as SbF_6^-, AsF_6^-, and PF_6^-.[5] In this paper we report on the preparation and crystal structure of β-(BDA-TTP)$_2$FeCl$_4$ and also on its electrical conducting and magnetic properties.

Electrocrystallization of BDA-TTP (0.08 mmol) with Et_4N-$FeCl_4$ (0.43 mmol) in 5% EtOH–PhCl (60 mL) by the controlled-current method[6] gave two types of crystals; preliminary X-ray analyses revealed that the black plate crystals had a β-type structure [designated as β-(BDA-TTP)$_2$FeCl$_4$] while the more pale black plate-like crystals are solvated with composition (BDA-TTP)$_3$FeCl$_4$·PhCl.†

Fig. 1(a) shows the crystal structure of β-(BDA-TTP)$_2$FeCl$_4$, which consists of one $FeCl_4^-$ anion and two crystallographically independent BDA-TTP molecules. In this salt, the BDA-TTP molecules and the $FeCl_4^-$ anions are arranged in alternating layers along the *b* axis, so that the Fe···Fe distance between the most adjacent anions along the *b* axis [19.535(6) Å] is significantly longer than those along the *a* and *c* axes [6.227(3) and 7.731(4) Å]. Two independent BDA-TTP molecules have similar molecular structures, in both of which the two outer dithiane rings adopt nonequivalent chair conformations: their respective dihedral angles around the intramolecular sulfur-to-sulfur axis in one BDA-TTP molecule are 38.6 and 13.0°, and the corresponding angles in the other are 39.1 and 13.0° (Fig. 2). Thus one dithiane ring of each independent BDA-TTP molecule is much flatter than that of each BDA-TTP molecule in the superconducting BDA-TTP salts.[5] The BDA-TTP molecules form slipped stacks along the

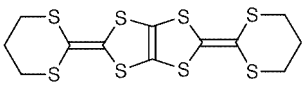

BDA-TTP

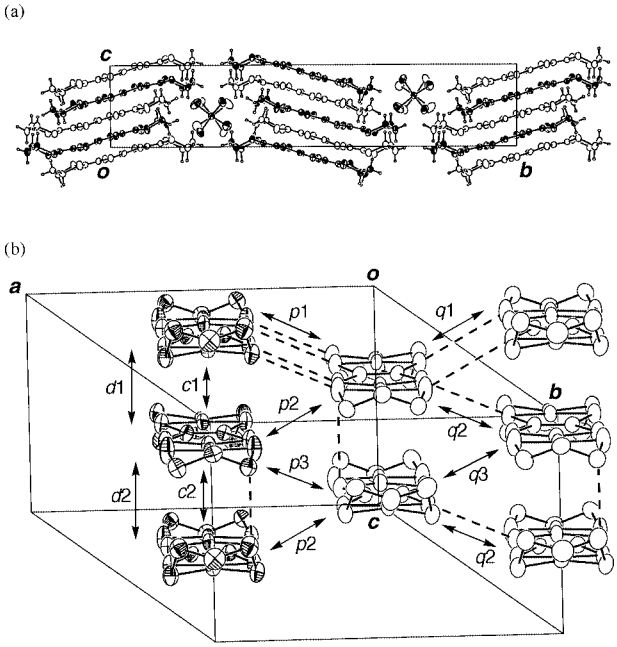

Fig. 1 (a) Crystal structure of β-(BDA-TTP)$_2$FeCl$_4$ viewed down the *a* axis; open circles indicate the back molecules. (b) Donor arrangement of β-(BDA-TTP)$_2$FeCl$_4$. Hydrogen atoms are omitted for clarity. The interplanar distances of the BDA-TTP column are 3.56 (*d*1) and 3.89 (*d*2) Å. Intermolecular S···S contacts (< 3.70 Å) are drawn by broken lines. The values of intermolecular overlap integrals ($\times 10^{-3}$) *c*1, *c*2, *p*1, *p*2, *p*3, *q*1, *q*2 and *q*3 are 14.4, 13.5, 1.88, −7.34, 3.44, 6.99, −5.62 and 5.49, respectively.

c axis with some dimerization (average interplanar distances of 3.56 and 3.89 Å), so as to avoid the steric hindrance of the less flat dithiane ring. There is only one S···S contact shorter than the sum of van der Waals radii (3.70 Å) within the stack, while several short intermolecular S···S contacts exist between stacks (Fig. 1(b)). These S···S contacts, however, do not always reflect the magnitude of the intermolecular overlap integrals, calculated on the donor layer in the *ac* plane by the extended Hückel method.[7] It is noteworthy that the largest overlap integral (14.4 $\times 10^{-3}$) is almost equal to those found in the superconducting

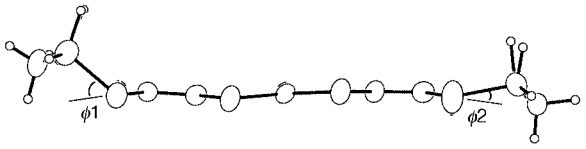

Fig. 2 Molecular structure of one BDA-TTP unit in β-(BDA-TTP)$_2$FeCl$_4$. The dihedral angles ϕ1 and ϕ2 are 38.6 and 13.0°, whereas the corresponding angles in the other BDA-TTP are 39.1 and 13.0°.

 DOI: 10.1039/b105264k

BDA-TTP salts,[5] suggesting that the BDA-TTP molecules in this salt are also packed loosely.

The four-probe resistivity of β-(BDA-TTP)$_2$FeCl$_4$ as a function of temperature indicated that this salt, with a room-temperature conductivity (σ_{rt}) of 9.4 S cm^{-1}, is metallic from room temperature down to 113 K, at which temperature it undergoes a sharp MI transition (Fig. 3). Although the reason of this MI transition is not clear, the charge separation between two independent donors in the column may be considered as a cause. Fig. 4 shows the temperature dependence of the magnetic susceptibility of this salt measured by using a SQUID magnetometer at 1000 Oe from 300 to 2 K. The susceptibility can be well fitted to the Curie–Weiss law over the whole temperature range 40–300 K, and the values of the Curie and Weiss constants are 4.48 emu K mol^{-1} and −15.1 K, respectively. The fitted Curie constant is close to the value of 4.38 emu K mol^{-1} calculated for a high-spin Fe^{3+} ion (S = 5/2, g = 2.0), so that the Fe in the anion certainly dominates the measured magnetization. Below 40 K, the susceptibility increased to a maximum near 8.5 K, after which it decreased rapidly. As shown in the inset of Fig. 4, the susceptibilities, which were measured under magnetic fields (1000 Oe) applied along the directions approximately parallel to the *a*, *b* and *c* axes, were anisotropic below near 8.5 K, indicating antiferromagnetic ordering with T_N of near 8.5 K. Below T_N, the easy spin axis seems to lie close to the intrastacking *c*-direction of the donor molecules. So, considering that the shortest Fe···Fe distance along the *c* axis is longer than 6 Å, the donor molecules could mediate the observed antiferromagnetic order between the Fe^{3+} ions.[8]

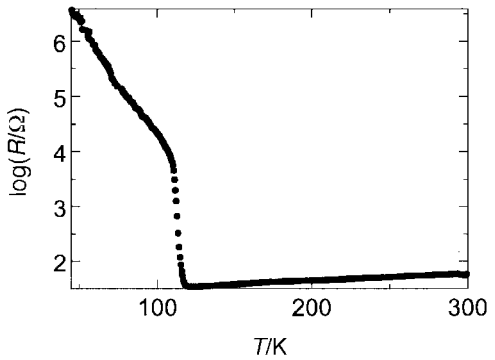

Fig. 3 Temperature dependence of the resistance of β-(BDA-TTP)$_2$FeCl$_4$.

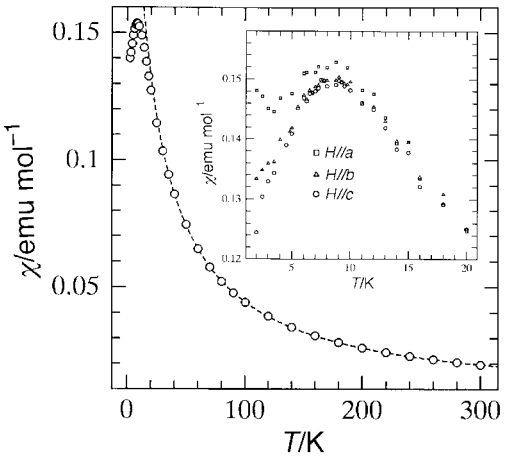

Fig. 4 Temperature dependence of the susceptibility of β-(BDA-TTP)$_2$FeCl$_4$. The dashed line is a Curie–Weiss fit (see text). The inset shows magnetic anisotropies in magnetic fields approximately parallel to the *a*, *b* and *c* axes (*H*//*a*, *H*//*b*, and *H*//*c*).

On the other hand, the solvated (BDA-TTP)$_3$FeCl$_4$·PhCl salt is a semiconductor with a thermal activation energy of 0.11 eV (σ_{rt} = 2.0 × 10^{-2} S cm^{-1}) and exhibited Curie–Weiss behavior from 300 to 2 K. The fitted Curie constant is 4.42 emu K mol^{-1} and the Weiss constant is –0.35 K, suggesting very weak antiferromagnetic interaction between the Fe moments. The structural characteristics of this salt will be report elsewhere.

In conclusion, following the discovery of superconducting BDA-TTP salts, we found a new BDA-TTP salt that displays metallic conductivity as well as antiferromagnetism. To search for a new system capable of enhancing further the interaction between conduction π-electrons of donors and localized d-spins of anions, the preparation of CT salts composed of BDA-TTP or related π-donors and other magnetic anions is currently underway.

Notes and references

† *Crystal data* for (BDA-TTP)$_2$FeCl$_4$: $C_{24}H_{24}S_{16}FeCl_4$, M = 1023.04, monoclinic, space group $P2_1/a$, a = 12.452(7), b = 38.72(1), c = 7.731(4) Å, β = 91.17(4)°, U = 3727(3) Å^3, Z = 4, D_c = 1.823 g cm^{-3}, μ(Mo-Kα) = 1.611 mm^{-1}, T = 295 K, R = 0.0407 and R_w = 0.112 for 4289 observed reflections with $I > 3\sigma(I)$ from 8692 unique reflections ($2.10 < \theta < 27.76°$). Max./min. residual electron density 0.118/−0.265 e Å^{-3}. *Crystal data* for (BDA-TTP)$_3$FeCl$_4$·PhCl: $C_{42}H_{41}S_{24}FeCl_5$, M = 1548.29, monoclinic, space group $P2_1$, a = 9.7717(15), b = 35.639(6), c = 8.8584(14) Å, β = 92.085(3)°, U = 3083.0(8) Å^3, Z = 2, D_c = 1.668 g cm^{-3}, μ(Mo-Kα) = 1.308 mm^{-1}, T = 293 K, R = 0.0484 for 3828 reflections [$I > 2\sigma(I)$] and R_w = 0.1005 for 6441 unique reflections ($2.81 < \theta < 28.33°$). Max./min. residual electron density 0.073/−0.329 e Å^{-3}. The data were collected on a Rigaku AFC7R diffractometer for (BDA-TTP)$_2$FeCl$_4$ and on a Bruker SMART-APEX three-circle diffractometer, equipped with a CCD area detector for (BDA-TTP)$_3$FeCl$_4$·PhCl. The structures were solved by direct methods and refined by full-matrix least-squares analysis. The structure of (BDA-TTP)$_3$FeCl$_4$·PhCl was refined as a racemic twin with the twin parameters refining to 0.69(5). All diagrams and calculations were performed using SHELXTL software. CCDC reference numbers 166357 and 166358. See http://www.rsc.org/suppdata/cc/b1/b105264k/ for crystallographic data in CIF or other electronic format.

1 T. Enoki, T. Umeyama, A. Miyazaki, H. Nishikawa, I. Ikemoto and K. Kikuchi, *Phys. Rev. Lett.*, 1998, **81**, 3719.

2 E. Coronado, J. R. Galán-Mascarós, C. J. Gómez-Garciá and V. Laukhin, *Nature*, 2000, **408**, 447; J. Nishijo, E. Ogura, J. Yamaura, A. Miyazaki, T. Enoki, T. Tanaka, Y. Kuwatani and M. Iyoda, *Solid State Commun.*, 2000, **116**, 661.

3 T. Otsuka, A. Kobayashi, Y. Miyamoto, J. Kiuchi, N. Wada, E. Ojima, H. Fujiwara and H. Kobayashi, *Chem. Lett.*, 2000, 732; H. Fujiwara, E. Fujiwara, Y. Nakazawa, B. Z. Narymbetov, K. Kato, H. Kobayashi, A. Kobayashi, M. Tokumoto and P. Cassoux, *J. Am. Chem. Soc.*, 2001, **123**, 306.

4 For an attempt to settle this subject see:M. Iwamatsu, T. Kominami, K. Ueda, T. Sugimoto, T. Adachi, H. Fujita, H. Yoshino, Y. Mizuno, K. Murata and M. Shiro, *Inorg. Chem.*, 2000, **39**, 3810.

5 J. Yamada, M. Watanabe, H. Akustu, S. Nakatsuji, H. Nishikawa, I. Ikemoto and K. Kikuchi, *J. Am. Chem. Soc.*, 2001, **123**, 4174.

6 H. Anzai, J. M. Delrieu, S. Taksaki, S. Nakatsuji and J. Yamada, *J. Cryst. Growth*, 1995, **154**, 145; H. Nishikawa, T. Sato, T. Kodama, I. Ikemoto, K. Kikuchi, H. Anzai and J. Yamada, *J. Mater. Chem.*, 1999, **9**, 693.

7 T. Mori, *Bull. Chem. Soc. Jpn.*, 1998, **71**, 2509.

8 H. Tanaka, T. Adachi, E. Ojima, H. Fujiwara, K. Kato, H. Kobayashi, A. Kobayashi and P. Cassoux, *J. Am. Chem. Soc.*, 1999, **121**, 11243.

CHEMCOMM
Communication
www.rsc.org/chemcomm

Self-assembly of a chloro-bridged helical coordination polymer achieved from a ferrocenyl-containing double-helicate

Fang Chen-jie,[a] Duan Chun-ying,*[a] Guo Dong,[a] He Cheng,[b] Meng Qing-jin,*[a] Wang Zhe-ming[b] and Yan Chun-hua[b]

[a] *Coordination Chemistry Institute, The State Key Laboratory of Coordination Chemistry, Nanjing University, Nanjing, 210093, P.R. China. E-mail: duancy@nju.edu.cn*
[b] *The State Key Laboratory of Rare Earth Materials Chemistry and Applications of Peking University, College of Chemistry and Molecular Engineering, Peking University, Beijing, 100871, P.R. China*

Received (in Cambridge, UK) 10th September 2001, Accepted 26th October 2001
First published as an Advance Article on the web 8th November 2001

A new chloro-bridged single-helical chain has been constructed from a ferrocenyl-containing tetranuclear double-helical architecture *via* self-assembly

Helical complexes have elegantly illustrated how the specific formation of architecturally complex assemblies are directed by the interplay between relatively simple parameters such as the stereoelectronic preference of the metal and the disposition of the binding sites of the helicands (helicating ligands).[1] While the basic features of the design necessary to assemble a double helix are now fairly well established,[2] the design and control of assembly of the helical unit into a multi-helical array represents a considerable synthetic challenge.[3,4] Sophisticated supramolecular targets will require the ability to assemble small molecular units which may be further aggregated in a controlled fashion. To achieve this, a five-coordinated copper(II) ion is chosen to build the unsaturated double helicate, which contains binding sites on its interior. It is suggested that the five-coordinate geometry of the copper(II) ion may prevent the formation of a triple helicate and that the metal centers incorporated into the helicate framework will not use all of their coordination sites in the construction process. We reasoned that these unused coordinated sites might then be bound by additional mono- or bi-dentate coordinated ligands such as bridging groups or anions. Here we report what we believe to be a unique helical structure motif in inorganic supramolecular architectures through self-assembly, where single-helical 1D chains are constructed from double-helicates *via* chloro-bridging.

The chosen ligand designed here is an easy-to-prepare ferrocenyl-containing imine-based bis-bidentate system. The introduction[5] of a ferrocenediyl unit as a spacer to separate the two metal binding sites is chosen not only because such a spacer is suitable to assemble double-helices, but also because molecules containing metallocene units can retain a particular metal ion at its coordination site whilst undergoing a concurrent redox change.

An ethanol solution of $CuCl_2{\cdot}2H_2O$ was added to a mixture of diacetylferrocene and 2-hydrazinopyridine in absolute methanol followed by addition of NH_4BF_4; after 24 h, dark-red crystals of **1** were obtained.† In the electronspray mass spectrum of **1**, a peak at *m/z* 1066.5, corresponding to the $[Cu_2(L - H)_2Cl]^+$ cation, in which one of the hydrogen atoms attached to the imine nitrogen atom in each ligand is lost, indicates the formation of a 2:2 (ligand:metal) coordination stoichiometry. An X-ray crystallographic study‡ has unequivocally confirmed the existence of a tetranuclear cationic unsaturated double helicate.

Fig. 1 shows one of the two enantionmers of the double helicate. Each ligand wraps around the two copper(II) cations with a copper–copper separation of 8.4 Å and the two iron centers are separated by a distance of 6.4 Å. The four metal centers are co-planar and form a slightly distorted rhombus with sides of 5.2 and 5.3 Å. Each copper center is coordinated to two pyridyl imine units, one from each ligand, to form the unsaturated double helicate while the fifth coordination site is occupied by a chloride ion. The value of the topological parameter[6] τ of *ca.* 0.6 indicates an intermediate structure between square pyramidal and trigonal bipyramidal for copper but more towards the trigonal bipyramidal limit. The EPR spectrum of the complex also indicates a trigonal bipyramidal stereochemistry.[7] The pyridines are twisted by *ca.* 39° from the Cp rings to which they are attached with dihedral angles between the two pyridine rings in each ligand being *ca.* 38° on average. It is interesting that the helicate is also stabilized by intramolecular π–π stacking interactions between the pyridine rings of one ligand and the Cp rings of the other. The dihedral angles of the stacked pairs lie in the range 17.4–33.5° with center-to-center separations of the stacked pairs in the range 3.47–3.81 Å.

The most distinctive structural feature of the complex in the solid state is that each enantiomer of the double helicate links to its symmetry-related equivalents to form an infinite monochiral helical polymer (Fig. 2) *via* single chloro-bridges. The bridging chloride coordinates to two copper centers with a Cu–Cl–Cu angle of 124.6(1)° and Cu···Cu separation of *ca.* 4.29 Å. It is particularly striking that the helices in one chain are all of a single enantiomer. Each chain exhibits a crystallographic 2_1 single helix with a pitch twice that of the crystal cell *b* axis. The chains lie parallel to each other and align themselves along

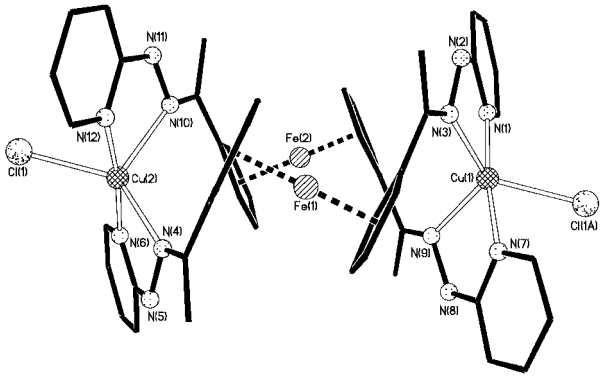

Fig. 1 Molecular structure of the double helicate with hydrogen atoms omitted for clarity. Selected bond lengths (Å) and angles (°): Cu(1)–N(1) 1.921(8), Cu(1)–N(7) 1.959(9), Cu(1)–N(3) 2.079(8), Cu(1)–N(9) 2.130(8), Cu(1)–Cl(1A) 2.443(3), Cu(2)–N(6) 1.936(9), Cu(2)–N(12) 1.940(8), Cu(2)–N(4) 2.099(8), Cu(2)–N(10) 2.196(9), Cu(2)–Cl(1) 2.404(3); N(1)–Cu(1)–N(7) 173.0(3), N(1)–Cu(1)–N(3) 79.8(4), N(7)–Cu(1)–N(3) 105.1(4), N(1)–Cu(1)–N(9) 102.6(3), N(7)–Cu(1)–N(9) 79.6(4), N(3)–Cu(1)–N(9) 118.3(3), N(1)–Cu(1)–Cl(1A) 89.9(3), N(7)–Cu(1)–Cl(1A) 83.2(2), N(3)–Cu(1)–Cl(1A) 136.8(2), N(9)–Cu(1)–Cl(1A) 104.8(2), N(6)–Cu(2)–N(12) 173.3(4), N(6)–Cu(2)–N(4) 79.1(4), N(12)–Cu(2)–N(4) 101.9(3), N(6)–Cu(2)–N(10) 106.5(4), N(12)–Cu(2)–N(10) 78.9(4), N(4)–Cu(2)–N(10) 118.3(3), N(6)–Cu(2)–Cl(1) 89.7(3), N(12)–Cu(2)–Cl(1) 85.1(2), N(4)–Cu(2)–Cl(1) 138.6(2). (Symmetry code A: $-x$, $-0.5 + y$, $0.5 - z$).

 DOI: 10.1039/b108206j

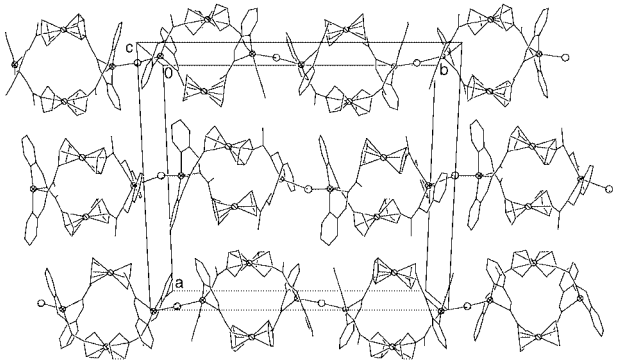

Fig. 2 Molecular packing along the *b*–*c* plane showing the one-dimensional mono-helical chains; solvent molecules, hydrogen atoms and anions are omitted for clarity.

the (0,1,0) direction. It is interesting that the pyridine ring containing nitrogen atom N(1) is almost parallel to the related pyridine ring containing nitrogen atom N(6A) (symmetry code A: $-x$, $-0.5 + y$, $0.5 - z$) of an adjacent double-helicate in an adjacent chain (dihedral angle between the two planes is *ca.* 6.4°) with a close intermolecular separation between the stacked pair of *ca.* 3.5 Å. Although these stacking interactions are weak compared to the metal–nitrogen and metal–chlorine coordination bonds,[8] such interactions may well be important in the molecular assembly of double helicates and mono-helical chains.

Bridged biferrocenes have been proven to be good candidates for mixed-valence compounds. Differential pulse voltammetry of **1** (Fig. 3) shows two peaks with half-wave potentials ($E_{1/2}$) at 0.75 and 0.58 V, respectively, corresponding to the two single-electron oxidations of the ferrocene moieties. The ΔE value of *ca.* 0.17 V indicates strong interactions between two ferrocene moieties. A similar separation ΔE has also been found for the two single electron reductions (Cu^{II}/Cu^{I}) with two peaks at 0.29 and 0.14 V, respectively.

The assembly of helical units into a multi-helical array is interesting in terms of controlled aggregation of helices. The generation of a helical motif derived from an inexpensive and readily prepared ferrocene containing ligand enables extension of self-assembly through the use of helicates as building blocks by judicious design and control. The development of new ligand systems containing functional ferrocene groups and the application to aggregation of small supramolecular units into large multi-helical arrays are in progress.

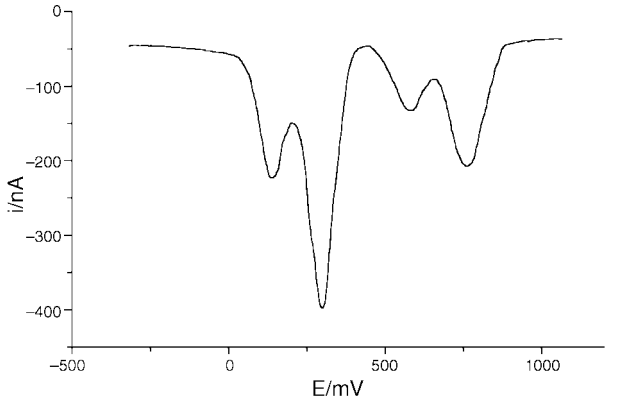

Fig. 3 Differential pulse voltammetry for the complex (1.0×10^{-3} M) in DMF containing *n*-Bu_4NClO_4 (0.1 M) (ferrocene as external standard, *vs.* AgCl/Ag).

This work is supported by the National Natural Science Foundation of China.

Notes and references

† *Preparation* of $[Cu_2L_2Cl][BF_4]_3{\cdot}H_2O$ **1**: an ethanol solution (10 ml) of $CuCl_2{\cdot}2H_2O$ (0.17 g, 1 mmol) was added to a mixture of diacetylferrocene (0.13 g, 0.5 mmol) and 2-hydrazinopyridine (0.11 g, 1 mmol) in 15 mL absolute methanol after refluxing for 2 h. After further refluxing for 1 h, NH_4BF_4 was added and reflux continued for a further 1 h. The reactant solution was allowed to stand overnight, after which dark-red crystals suitable for structural studies were obtained and dried under vacuum. Calc. for $C_{48}H_{50}B_3ClCu_2F_{12}Fe_2N_{12}O$: C, 42.8; H, 3.8; N, 12.5. Found: C, 42.6; H, 4.3; N, 12.5%.

‡ *Crystal data*: $C_{48}H_{50}B_3ClCu_2F_{12}Fe_2N_{12}O$, monoclinic, space group $P2_1/c$, a = 23.443(5), b = 24.577(5), c = 21.329(4) Å, β = 115.80(4), U = 11064(4) Å^3, Z = 8, D_c = 1.616 Mg m^{-3}, $F(000)$ = 5440, μ = 1.410 mm^{-1}. 14212 independent reflections measured, 7597 observed [$F > 4\sigma(F)$]. Final refinement converged at $R1$ = 0.0704, $wR2$ = 0.1420, respectively. Intensities were collected on an Enraf-Nonius CCD system[9] with graphite-monochromated Mo-Kα radiation (λ = 0.71073 Å). Data were reduced using HKL Denzo and maXus programs and a semi-empirical absorption correction from ψ-scans was applied. The structure was solved by direct methods and refined on F^2 by full-matrix least-squares methods using SHELXTL version 5.0.[10] Anisotropic thermal parameters were refined for non-hydrogen atoms. BF_4^- anions and lattice water molecules were refined assuming disordered contributions. CCDC reference number 164148. See http://www.rsc.org/suppdata/cc/b1/b108206j/ for crystallographic data in CIF or other electronic format.

1 J.-M. Lehn, *Supramolecular Chemistry—Concept and Perspectives*, VCH, Weinheim, 1995; E. C. Constable, *Polynuclear Transition Metal Helicates in Comprehensive Supramolecular Chemistry*, ed. J. P. Sauvage, Elservier, Oxford, 1996, vol. 9, pp 213–252.
2 C. Piguet, G. Bernardinelli and G. Hopfgartner, *Chem. Rev.*, 1997, **97**, 2005.
3 L. J. Childs, N. W. Alcock and M. J. Hannon, *Angew. Chem., Int. Ed.*, 2001, **40**, 1079; J. D. Ranford, J. J. Vittal, D. Wu and X. Yang, *Angew. Chem., Int. Ed.*, 1999, **38**, 3498; M. A. Withersby, A. J. Blake, N. R. Champness, P. Hubberstey, W. Liand and M. Schroder, *Angew. Chem., Int. Ed.*, 1997, **36**, 2327; E. C. Constable, M. Neuburger, L. A. Whall and M. Zehnder, *New J. Chem.*, 1998, **22**, 2190.
4 K. Bowyer, K. A. Porter A. D. Rae, A. C. Willis and S. B. Wild, *Chem. Commun.*, 1998, 1153; O. Mamula, A. V. Zelewsky, T. Bark and G. Bernardinelli, *Angew. Chem., Int. Ed.*, 1999, **38**, 2945; T. Ezuhara, K. Endo and Y. Aoyama, *J. Am. Chem. Soc.*, 1999, **121**, 3279.
5 (*a*) C. J. Fang, C. Y. Duan, C. He and Q. J Meng, *Chem. Commun.*, 2000, 1187; (*b*) C. J. Fang, C. Y. Duan, H. Mo, C. He, Q. J Meng, Y. J. Liu, Y. H. Mei and Z. M. Wang, *Organometallics*, 2001, **20**, 2525; (*c*) M. Buda, J.-C. Moutet, E. Saint-Aman, A. De Cian, J. Fisher and R. Ziessel, *Inorg. Chem.*, 1998, **37**, 4146.
6 A. W. Addison, T. N. Rao, J. Reedijk, J. V. Rijn and G. C. Verschoor, *J. Chem. Soc., Dalton, Trans.*, 1984, 1349.
7 The EPR spectrum of the complex in frozen DMF shows an intense $g_\perp$ signal with resolution of the four copper hyperfine lines, $g_\perp$ = 2.2379, and a very intense $g_\parallel$ signal with $g_\parallel$ = 2.0004.
8 Z. H. Liu, C. Y. Duan, J. Hu and X. Z. You, *Inorg. Chem.*, 1999, **38**, 1719; G. R. Desiraju, *Angew. Chem., Int. Ed. Engl.*, 1995, **34**, 2311.
9 "Collect" data collection software, Delft, Nonius B. V., The Netherlands, 1998.
10 Siemens, SHELXTL, Version 5.0, Siemens Industrial Automation, Inc. Analytical Instrumentation, Madison, WI, 1995.

CHEMCOMM Communication
www.rsc.org/chemcomm

The tetrameric macrocycle $[\{P(\mu\text{-}N^tBu)\}_2NH]_4$

Alan Bashall,[a] Emma L. Doyle,[b] Catherine Tubb,[b] Sara J. Kidd,[b] Mary McPartlin,[a] Anthony D. Woods[b] and Dominic S. Wright*[b]

[a] *School of Chemistry, University of North London, London, UK N7 8DB*
[b] *Chemistry Department, University of Cambridge, Lensfield Road, Cambridge, UK CB2 1EW. E-mail: dsw1000@cus.cam.ac.uk.*

Received (in Cambridge, UK) 28th August 2001, Accepted 25th October 2001
First published as an Advance Article on the web 22nd November 2001

The 1:1 reaction of the symmetrical dimers $[ClP(\mu\text{-}N^tBu)]_2$ 1 and $[H_2NP(\mu\text{-}N^tBu)]_2$ 2 in thf–Et_3N gives the tetrameric macrocycle $[\{P(\mu\text{-}N^tBu)\}_2NH]_4$ 3 (67%); consisting of four $P_2(\mu\text{-}N^tBu)_2$ rings linked by *endo* N–H groups.

Although the study of macrocyclic organic ligands, such as crown ethers, calixarenes and cyclophanes,[1] is an ever-growing field of research, in comparison there are very few counterparts based on frameworks other than those of carbon. A major problem in such inorganic systems is establishing general and selective synthetic strategies to cyclic inorganic frameworks that avoid polymerisation or other undesired modes of aggregation. Mercuracarborands[2] and cyclic s-block amides[3] are two recently explored classes of inorganic ligands that behave as Lewis acids in their coordination of various anions. Particularly rare, however, are inorganic macrocycles which have the ability to act as Lewis bases; for example certain cyclophospha(v)zenes, such as $[P(NMe_2)_2N]_6$,[4] and Si/N macrocyles of the type $[(R_2Si)NH]_4$.[5] In earlier work we characterised the neutral Group 15 macrocycle $[\{Sb(\mu\text{-}NR)\}_2(\mu\text{-}NR)]_6$ (R = 2-$MeOC_6H_4$), composed of six $[Sb(\mu\text{-}NR)]_2$ rings linked into a cyclic structure by μ-NR groups.[6] Owing to the more robust nature of P–N bonds compared to other Group 15 element–nitrogen bonds, we have more recently begun to extend studies in this area to related cyclophospha(III)zanes,[7,8] with the aim of producing more generally useful and (possibly) air-stable ligand arrangements. We report here the selective, high yielding synthesis of a neutral cyclophospha(III)zane macrocycle $[\{P(\mu\text{-}N^tBu)\}_2NH]_4$ **3**, *via* the reaction of $[ClP(\mu\text{-}N^tBu)]_2$ **1** with $[NH_2P(\mu\text{-}N^tBu)]_2$ **2** (Scheme 1).

The dimer $[ClP(\mu\text{-}N^tBu)]_2$ **1** is readily prepared by the 1:3 stoichiometric reaction of PCl_3 with $^tBuNH_2$ in thf (67%).† This method is different from that reported in the literature, involving the reaction of $^tBuNH_2$, PCl_3 and Et_3N (3:2:3 equivalents, respectively).[8] However, very little of the monochloride $[^tBuNHP(\mu\text{-}N^tBu)PCl]$[7,8] is isolated after distillation of **1** from the reaction, despite the use of excess of $^tBuNH_2$. The slow addition of **1** to a saturated solution of NH_3 in thf–Et_3N at −78 °C produces $[NH_2P(\mu\text{-}N^tBu)]_2$ **2**.† Very few impurities are present in the ^1H and ^{31}P NMR spectra of the crude product (obtained in 48% yield), which can be used without further purification. The 1:1 stoichiometric reaction of **1** with **2** in thf–Et_3N was followed by variable-temperature ^1H and ^{31}P NMR spectroscopy. This study showed that the conversion to the macrocyle $[\{P(\mu\text{-}N^tBu)\}_2NH]_4$ **3** is *ca.* 100% efficient (with only minor traces of other products being generated). The selectivity of this reaction and the almost quantitative formation of **3** can be attributed to the known preference for the phosphazane dimers $[XP(\mu\text{-}NR)]_2$ to adopt the *cis* isomer in solution and in the solid state,[8,9] *i.e.* pre-organisation of the precursors. Indeed, the *cis* isomer of **1** has previously been shown to be preferred[10] and, although the structure of **2** is not known at this stage, the relatively low ^{31}P chemical shift observed (δ 100.2) is strongly indicative of a *cis* conformation (normally in the range δ 96–108; *cf.* δ 166–185 for *trans* isomers).[11] Subsequent scaling up of the reaction allows **3** to be obtained in 67% (crude) yield (the overall conversion of PCl_3 and $^tBuNH_2$ to **3** being *ca.* 30%).† Again, ^1H and ^{31}P NMR studies reveal that the crude product is extremely pure (estimated 95–100%, over several reactions). The ^{31}P NMR spectrum of **3** shows that a single species exists in solution, with a singlet resonance being observed at δ 129.5 over a wide temperature range. This chemical shift compares to δ 117.2 for the related dimer $[\{P(\mu\text{-}N^tBu)\}_2N^tBu]_2$.[12] Compound **3** is relatively air-stable, air-exposure for greater than *ca.* 6 h leading only to slight decomposition, with the appearance of minor new resonances in both the ^{31}P and ^1H NMR spectra.

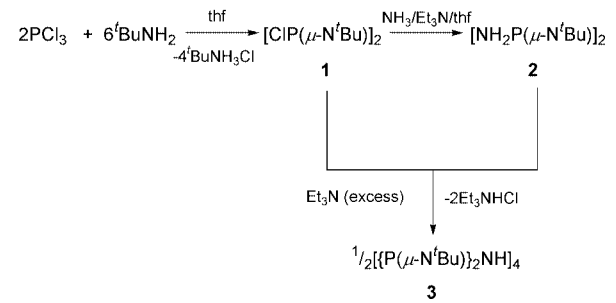

Scheme 1

The low-temperature X-ray structure of **3** shows that its macrocyclic backbone arises from cyclic tetramerisation of four $[\{P(\mu\text{-}N^tBu)\}_2NH]$ units [Fig. 1(a)].‡ Although these units are crystallographically independent, the pattern of bond lengths and angles in **3** is very regular. As a result, the twelve atoms of the $(P\cdots P\text{–}N)_4$ fragment defining the macrocycle deviate by only *ca.* 0.07 Å from their mean plane, and the transannular N···N separation between opposite pairs of N centres differ by only *ca.* 0.067 Å (mean 5.221 Å). The planes of the four $[P(\mu\text{-}N^tBu)]_2$ rings are aligned almost exactly perpendicular to the macrocyclic plane (the associated dihedral angles with respect to the macrocyclic plane being in the range 87.0–93.2°), giving the ligand periphery of **3** an overall torus-shape. The only noticeable distortion in the structure of **3** arises from the steric crowding of the ^{t}Bu groups above and below the macrocycle. As a consequence, two of the four ^{t}Bu groups on either side [attached to N(1) and N(5), and N(4) and N(8)] are forced out of the planes of their P_2N_2 rings. However, this distortion has only a marginal effect on the P–N bonding within the P_2N_2 ring units; resulting in small variations in the associated P–(μ-N) bond lengths (by *ca.* 0.03 Å) and P–N–P angles (by *ca.* 2°).

The closest relatives to **3** are cyclophosphazanes of the type $[\{P(\mu\text{-}NR)\}_2NR]_2$, consisting of two $P_2(\mu\text{-}NR)_2$ rings linked into a cyclic arrangement by bridging NR groups.[12,13] The formation of a tetrameric macrocyle for **3** (as opposed to a cyclic dimer, $[\{P(\mu\text{-}N^tBu)\}_2NH]_2$) primarily results from the presence of sterically undemanding NH groups linking the $[P(\mu\text{-}N^tBu)]_2$ units; this allows the *cis* conformation of the constituent units to be retained in **3**, without producing steric congestion at the centre of the macrocylic cavity. It is interesting in this regard that the increased steric effects associated with the NR groups linking the $[Sb(\mu\text{-}NR)]_2$ units in $[\{Sb(\mu\text{-}NR)\}_2(\mu\text{-}NR)]_6$[6] (R = 2-$MeOC_6H_4$, Ph) results in the adoption of a *trans* conformation

 DOI: 10.1039/b107650g

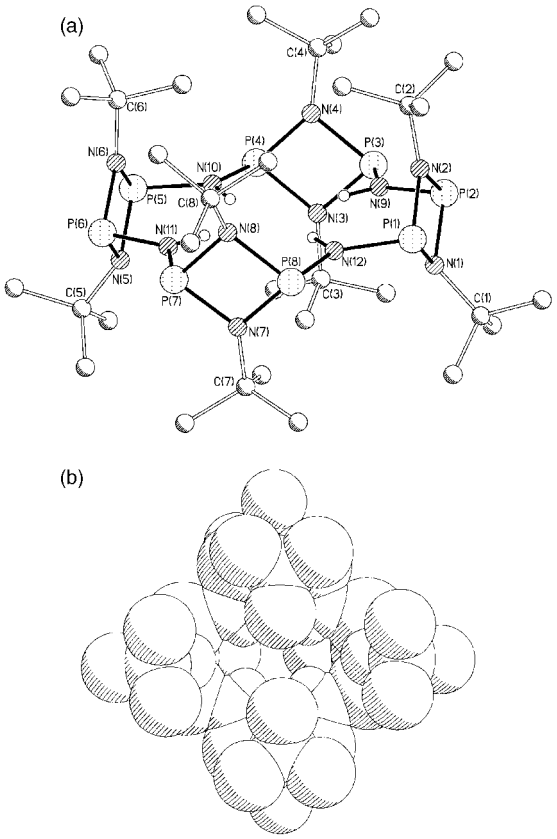

Fig. 1 (a) Structure of $[\{P(\mu\text{-}N^tBu)\}_2NH]_4$ **1** (side view). Key bond lengths (Å) and angles (°); P–N(9–12) mean 1.703 [range 1.697(2)–1.709(2)], ring P–N mean 1.725 [range 1.710(2)–1.740(2)], N(9)···N(11) 5.255(4), N(10)···N(12) 5.188(4), P–N(9,10,11,12)–P mean 127.8, endocyclic N–P(1–8)–N mean 81.4, exocyclic N–P(1–8)–N mean 103.5, P–{μ–N(1–8)}–P mean [range 97.6(1)–99.6(1)]; (b) Space-filling diagram (top view).

for these constituents. This *trans* conformation provides the most probable reason for the greater size of the macrocyles obtained in these cases, since the formation of a smaller ring composed of *trans* constituents would be more strained.

The presence of four N–H protons within the macrocyclic structure of **3** is reminiscent of a tetraazacyclotetradecane (*i.e.* based on $[CH_2CH_2NH]_4$),[14] while the molecules possess a ligand periphery that is analogous (spatially) to calixarenes.[1] Although the macrocyclic cavity of **3** is apparently sterically crowded [Fig. 1(b)], the rearrangement of the ligand framework to accommodate metal centres (upon deprotonation) may well be anticipated. This is suggested by the observed flexibility of the μ-N^{t}Bu groups within **3**. Studies of the coordination behaviour of **3** and of related P/N ligands are underway.

We gratefully acknowledge the EPSRC for financial support.

Notes and references

† *Syntheses*: **1**: to a solution of freshly distilled PCl_3 (16.6 ml, 0.190 mol) in thf (300 ml) at −78 °C was added dropwise ^{t}BuNH$_2$ (60 ml, 0.571 mmol) (the addition taking *ca.* 1 h). The mixture was stirred for a further 4 h at this temperature, then allowed to stir at room temperature for 12 h. The solvent was removed under vacuum and the colourless, crystalline mass formed was carefully distilled through a 10 cm Vigreaux column under vacuum (since the product rapidly solidifies, the condenser should not be cooled). The major fraction (86 °C, 2.0 mmHg) was collected (the minor 96 °C fraction is $[^tBuNHP(\mu\text{-}N^tBu)]_2$). Yield 17.6 g (67%, based on P supplied). ^{1}H NMR (d_6-benzene, +25 °C, 400.16 MHz), δ 1.25 (s, ^{t}BuN). ^{31}P NMR (d_6-benzene, +25 °C, 161.98 MHz), δ 207.6 (s).

2: A concentrated solution of NH_3 in thf–Et_3N was produced by condensing NH_3 gas into a mixture of thf (450 ml) and Et_3N (40 ml) at 25 °C for *ca.* 40 min. To this solution (at −78 °C) was added a solution of **1** (10.0 g, 36.4 mmol) in thf (250 ml) at −78 °C. After stirring at this temperature (3 h), the mixture was allowed to warm to room temperature and stirring was continued (12 h). The solvent was removed under vacuum and to the dried solid was added *n*-pentane (400 ml). The insoluble ammonium salts were removed by filtration and the filtrate reduced under vacuum to *ca.* 120 ml, whereupon precipitation of **2** occurred. This first batch was filtered off and dried under vacuum. A second batch was obtained by further reduction of the solvent to *ca.* 50 ml. Total yield 4.15 g (48%). Mp 110–115 °C. IR (Nujol, NaCl), ν/cm^{-1} 3402 (doublet, m), 3291 (doublet, m) (N–H str.). ^{1}H NMR (d_6-benzene, +25 °C, 400.16 MHz), δ 2.41 (d, $^2J_{^{31}P-H}$ 7.9 Hz, 2H, NH_2), 1.46 (s, 9H, ^{t}BuN). ^{31}P NMR (d_6-benzene, +25 °C, 161.98 MHz), δ 100.2 (s). ^{13}C NMR (100.1 MHz, d_8-toluene, rel. 80% H_3PO_4–D_2O), δ 51.33 (t, $^1J_{C-^{31}P}$ 13.3 Hz, C_α of ^{t}Bu), 31.17 (t, $^2J_{C-^{31}P}$ 6.8 Hz, Me of ^{t}Bu). Found C 40.1, H 9.2, P 25.5, Cl 0.2; Calc. C 40.8, H 9.3, P 26.3, Cl 0.0% (satisfactory N analysis could not be obtained, despite repeated attempts). The crude reaction product is of high purity and can be used in further reactions without purification.

3: A solution of **1** (0.50 g, 2.12 mmol) in thf (20 ml) was added dropwise to a solution of **2** (0.58 g, 2.12 mmol) in thf (100 ml) and Et_3N (1 ml) at −78 °C. The mixture was stirred for 3 h at this temperature and allowed to warm to room temperature before being stirred further (12 h). The solvent was removed under vacuum and the solid extracted with *n*-pentane (100 ml) and filtered. The filtrate was reduced to dryness under vacuum to give **3** as a white powder (0.62 g, 67%). Crystals of **3** were obtained from *n*-pentane–thf at 25 °C. The following data refer to the crude material. Partial melting *ca.* 130 °C, decomp. *ca.* 170 °C. IR (Nujol, NaCl), ν/cm^{-1} 3582 (sharp, w) (N–H str.). ^{1}H NMR (d_6-benzene, +25 °C, 400.16 MHz), δ 4.86 (s, 1H, N–H), 1.54 (s, 18H, ^{t}BuN). ^{31}P NMR (d_6-benzene, +25 °C, 161.98 MHz), δ 129.5 (s) (minor impurities may be seen at *ca.* δ 120, 75 and 0). Electrospray MS (+ve ion), *m/z* = 877.4 (tetramerH$^+$) (dominant), 658.4 (trimerH$^+$) (minor) (no dimerH$^+$). Satisfactory C, H and P analysis were obtained. ^{1}H and ^{31}P NMR spectroscopy indicate that the crude product obtained from the reaction without further purification is *ca.* 95–100% pure.

‡ *Crystal data* for **3**: $C_{32}H_{76}N_{12}P_8$, M = 876.81, orthorhombic, space group $P2_12_12_1$, Z = 4, a = 13.3936(2), b = 17.1372(4), c = 21.7137(5) Å, V = 4983.92(18) Å^3, μ(Mo–Kα) = 0.315 mm^{-1}, T = 180(2) K. Data were collected on a Nonius Kappa CCD diffractometer. Of a total of 25299 reflections collected, 8699 were independent (R_{int} = 0.040). The structure was solved by direct methods and refined by full-matrix least squares on F^2.[15] Final $R1$ = 0.036 [$I > 2\sigma(I)$] and wR 2 = 0.079 (all data).

CCDC reference number 172095.

See http://www.rsc.org/suppdata/cc/b1/b107650g/ for crystallographic data in CIF or other electronic format.

1 *Comprehensive Supramolecular Chemistry*, ed. J. M. Lehn, vol. 1, ch. 2 (crown ethers); vol. 2, ch. 4 (calixarenes); vol. 2, ch. 5 (cyclophanes), Pergamon, Oxford, 1995.

2 M. F. Hawthorne and Z. Zheng, *Acc. Chem. Res.*, 1997, **30**, 267.

3 R. E. Mulvey, *Chem. Commun.*, 2001, 1049.

4 W. C. Marsh, N. L. Paddock, C. J. Stewart and J. Trotter, *Chem. Commun.*, 1970, 1190; J. P. O'Brien, R. W. Allen and H. R. Allcock, *Inorg. Chem.*, 1979, **18**, 1130.

5 E. Egert, H. Hasse, U. Klingebiel, C. Lensen, D. Schmit and G. M. Sheldrick, *J. Organomet. Chem.*, 1986, **315**, 19; T. Kottke, U. Klingebiel, M. Noltemeyer, U. Pieper and S. Walter, *Chem. Ber.*, 1991, **124**, 1941; G. S. Smith and L. E. Alexander, *Acta Crystallogr.*, 1963, **16**, 1015; H.-J. Rakebraudt, U. Klingebiel, M. Noltemeyer, U. Wenzel and D. Mootz, *J. Organomet. Chem.*, 1996, **524**, 237; V. G. Shklover, Yu. T. Struchkov, B. A. Astapov and K. A. Andianov, *Zh. Strukt. Khim.*, 1979, **20**, 102; transannular N···N separations in uncoordinated (symmetrical) species are *ca.* 3.57–4.25 Å.

6 M. A. Beswick, M. K. Davies, M. A. Paver, P. R. Raithby, A. Steiner and D. S. Wright, *Angew. Chem., Int. Ed. Engl.*, 1996, **35**, 1508; R. Bryant, S. C. James, J. C. Jeffery, N. C. Norman, G. A. Orpen and U. Weckermann, *J. Chem. Soc., Dalton Trans.*, 2000, 4007.

7 A. Bashall, M. A. Beswick, B. R. Elvidge, S. J. Kidd, M. McPartlin and D. S. Wright, *Chem. Commun.*, 2000, 1439.

8 L. Stahl, *Coord. Chem. Rev.*, 2000, **210**, 203, and references therein.

9 I. Silaghi-Dumitrescu and I. Haiduc, *Phosphorus, Sulfur Silicon*, 1994, **91**, 21.

10 K. W. Muir and J. F. Nixon, *Chem. Commun.*, 1971, 1405.

11 A. Tarassoli, M. L. Thomson, R. C. Haltiwanger, T. G. Hill and A. D. Norman, *Inorg. Chem.*, 1988, **27**, 3382, and references therein.

12 J. K. Brask, T. Chivers, M. L. Krahn and M. Parvez, *Inorg. Chem.*, 1999, **38**, 290.

13 O. J. Scherer, K. Andres, C. Kruger, Y.-H. Tsay and G. Wolmerhauser, *Angew. Chem., Int. Ed. Engl.*, 1980, **19**, 571.

14 See for example: J. H. Reibenspier, *Acta Crystallogr., Sect. C*, 1992, **48**, 1717; T. Sakuri, K. Kobayashi, K. Tsuboyama and S. Tsuboyama, *Acta Crystallogr., Sect. B*, 1978, **34**, 1144; transannular N···N separations in uncoordinated species of the type $[CR_2CR_2NH]_4$ are *ca.* 4.07–4.29 Å (Cambridge crystallographic data base).

15 SHELXTL PC version 5.03, Siemens Analytical Instruments, Madison, WI, 1994.

CHEMCOMM Communication
www.rsc.org/chemcomm

Stacking of a benzenehexacarboxylic acid core in the crystal structure of benzenehexacarboxylic acid α-aminomethyl isobutyrate amide (MA-Aib$_6$)–sodium nitrate complex†

Subramania Ranganathan,*[ab] K. M. Muraleedharan,[a] C. H. Chandrashekhar Rao,[a] M. Vairamani,[c] Isabella L. Karle[d] and Richard D. Gilardi[d]

[a] *Discovery Laboratory, Indian Institute of Chemical Technology, Hyderabad 500 007, India*
[b] *Jawaharlal Nehru Center for Advanced Scientific Research, Bangalore 560 007, India*
[c] *Mass Spectrometry Laboratory, Indian Institute of Chemical Technology, Hyderabad 500 007, India*
[d] *Laboratory for the Structure of Matter, Naval Research Laboratory, Washington, DC 20375-5341, USA*

Received (in Columbia, MO, USA) 20th August 2001, Accepted 4th October 2001
First published as an Advance Article on the web 22nd November 2001

MA-Aib$_6$ forms discrete stacks with sandwiched water, sodium and nitrate ions, presenting a novel profile, where nine out of the 12 binding sites, of the six amides present, are involved in bonding with water, sodium and nitrate ions, with no inter-amide hydrogen bonding. This is the first example of the stacking of a benzenehexacarboxylic acid core.

The design and synthesis of conformationally constrained organic scaffoldings/templates that can potentiate controlled growth to protein secondary structure motifs, is of current interest.[1] Such structural mimics are important for the design of simple, low molecular weight pharmaceutical agents.[2] The present communication reports the synthesis of benzenehexacarboxylic acid α-aminomethyl isobutyrate amide (MA-Aib$_6$, $C_6[CONHC(CH_3)_2COOMe]_6$ (**1**) and the determination of its structure by X-ray crystallography. The choice of α-aminomethyl isobutyrate as the first spacer was logical because of the known ability of the Aib residue to control the growth of secondary structures.[3]

The tertiary carbon center present in Aib resisted the introduction of all the six units in a single step. The best conditions afforded only MA-Aib$_5$ mono imide (**2**), which, on *in situ* treatment with further Aib gave **1**. Thus, the reaction of hexamellitoyl chloride[4] with Aib-OMe under carefully defined conditions followed by chromatography on silica gel column and elution with ethylacetate–hexane afforded nearly pure MA-Aib$_6$ in 41% yield.[5] Re-chromatography under the same conditions afforded fine needles, mp 256–258 °C, that separated from the eluent (Fig. 1).

The crystal structure[6] of MA-Aib$_6$ (**1**) (Fig. 2) shows its assembly to layered stacks along a two-fold screw axis where molecules of MA-Aib$_6$ on the one hand and water and sodium nitrate on the other, form alternate layers (Fig. 2). The ester groups, projected vertically, do not participate in the assembly. The twelve α-methyl groups from each molecule form a neat ring around the stack. The pattern of the stack is repeated every 14.3 Å. Each stack is quite independent of the others and there are no hydrogen bonds between stacks or any interdigitation.

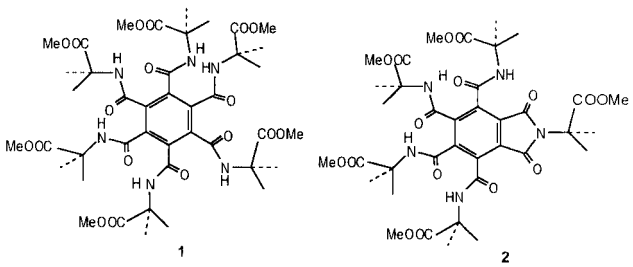

Fig. 1 Structure of **1** and **2**.

† Respectfully dedicated to Darshan Ranganathan, who passed away on June 4, 2001, her sixtieth brithday.

In the stack, shown with a central MA-Aib$_6$ flanked by two neighbors as presented in Fig. 2, the aromatic rings are tilted slightly along the two-fold screw axis by 2.9°. The sodium ion is penta-coordinated to two proximate carbonyls of the upper layer (Na···O30, 2.472 Å; Na···O40, 2.488 Å) and a single carbonyl from the middle layer (Na···O0, 2.255 Å), as well as to both water molecules (Na···W3, 2.463 Å, Na···W4, 2.415 Å). The short Na···O0 distance of 2.255 Å is found in penta-coordinated Na^+ complexes[7] but not for tetra- or hexa-complexes. The water molecules are, in addition, bonded to carbonyls from the middle layer (W3···O10, 2.872 Å; W4···O50, 2.813 Å), the NH of the upper layer (W3···N21, 3.011 Å; W4···N51, 2.996 Å) and the nitrate ion (W3···O1S, 3.102 Å; W4···O2s, 2.824 Å). In turn, the nitrate ion is an acceptor for the NH of the middle layer (N31···O1s, 2.984 Å) and NH in the upper layer (N1···O2S, 2.805 Å). Thus, of the twelve binding sites available in the hexa-amide **1**, five carbonyl groups and four NH units are used in a unique manner; while N11 and N41 do not participate in any manner. The absence of any inter amide hydrogen bonding and the strong involvement of the nitrate counter ion in the assembly are particularly noteworthy.

A schematic profile of the stacking is presented in Fig. 3.

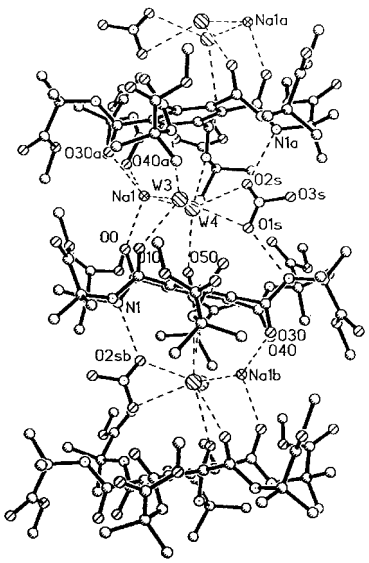

Fig. 2 The crystal structure of **1**. A Na^+ ion, NO_3^- ion and two water molecules (W_3 and W_4) are also indicated. The columnar stacking of molecules **1** alternating with Na^+ and NO_3^- ions and two water molecules. The dashed lines indicate the five ligands to Na^+ and hydrogen bonds between water molecules, the NO_3^- ion and **1**.

 DOI: 10.1039/b109465n

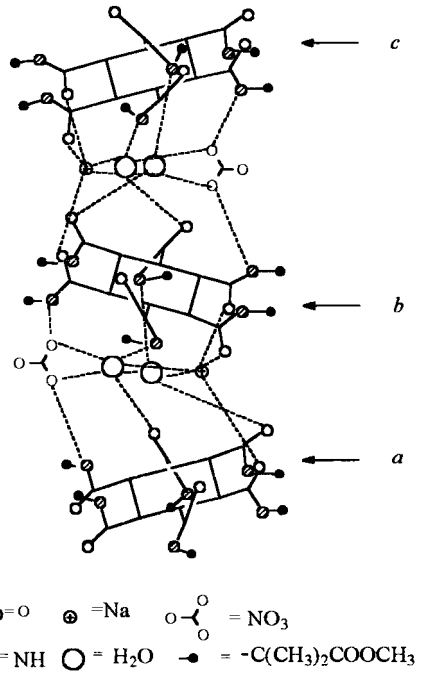

Fig. 3 Schematic drawing of the layered structure in a stack.

Using a sample of the crystal, the presence of sodium nitrate was confirmed by using positive and negative ion mass spectrometry. By negative ion mass spectrometry, the source of sodium nitrate was traced to the silica gel used for chromatography.[8] Chromatographically pure MA-Aib$_6$, freed of nitrate[9] when allowed to stand in ethyl acetate with dissolved sodium nitrate, deposited needles identical to that used for crystallographic studies.[10]

Futher experiments have shown that in the complexation of **1**, the nature of the metal ion is important. Thus, under identical conditions lithium nitrate formed the complex whereas potassium nitrate did not.[11] However it is very likely that in the assembly of **1** the nitrate ion, being large and with dispersed charge, plays a controlling role to the extent that the expected hydrogen bonding involving the amide bonds is not seen.

To the best of our knowledge, this is the first report of achieving the stacking of a benzenehexacarboxylic acid core. Crystallographic data currently available relating to mellitic acid, its esters and metal salts are unexceptional.[12]

Financial support was provided by the National Institutes of Health Grant GM-30902, the Office of Naval Research and the Department of Science and Technology, New Delhi.

Notes and references

1 J. P. Schneider and J. W. Kelly, *Chem. Rev.*, 1995, **95**, 2169; G. Tuchscherer, L. Scheibler, P. Dumy and M. Mutter, *Biopolymers (Peptide Sci.)*, 1998, **47**, 63.

2 R. Hirschmann, *Angew. Chem., Int. Ed. Engl.*, 1991, **30**, 1278; R. Hirschmann, P. A. Sprengeler, T. Kawasaki, J. W. Leahy, W. C. Shakespeare and A. B. Smith, III, *J. Am. Chem. Soc.*, 1992, **114**, 9699; R. Hirschmann, P. A. Sprengeler, T. Kawasaki, J. W. Leahy, W. C. Shakespeare and A. B. Smith, III, *Tetrahedron*, 1993, **49**, 3665; R. Hirschmann, K. C. Nicolaou, S. Pietreanico, E. M. Leahy, J. Salvino, B. Arison, M. A. Cichy, P. G. Spoors, W. C. Shakespeare, P. A. Sprengeler, P. Hamley, A. B. Smith, III, T. Reisine, K. Raynor, L. Maechlecr, C. Donaldson, W. Vale, R. M. Freidinger, M. A. Cascieri and C. D. Strader, *J. Am. Chem. Soc.*, 1993, **115**, 12 550; N. Beeley, *Tib. Tech.*, 1994, **12**, 213; W. M. Kazmierski, *Tib. Tech.*, 1994, **12**, 216; M. Goodman and S. Ro, in *Burgers's Medicinal Chemistry and Drug Discovery*, ed. M. E. Wollf, Wiley, New York, 1995, vol. 1, pp. 803; G. Muller, *Angew. Chem., Int. Ed. Engl.*, 1996, **35**, 2767; R. Haubner, D. Finsinger and H. Kessler, *Angew. Chem., Int. Ed. Engl.*, 1997, **36**, 1374.

3 E. Benedetti, *Biopolymers (Peptide Sci.)*, 1996, **40**, 3; I. L. Karle, *Biopolymers (Peptide Sci.)*, 1996, **40**, 157; I. L. Karle, *Acc. Chem. Res.*, 1999, **32**, 693

4 Mellitic acid [1.62 g, 4.73 mmol] was digested with PCl_5 [9.8 g, 47 mmol] at 150 °C for 24 h, excess reagent and $POCl_3$ distilled off, the residue triturated with dry benzene [5 × 10 ml] and dried to give 1.8 g [84%] of hexamellitoyl chloride mp 245–247 °C, whose structure was confirmed by methanolysis to mellitic acid hexamethyl ester and comparison with an authentic sample.

5 A solution of hexamellitoyl chloride [0.48 g, 1.1 mmol] in dry CH_2Cl_2 (20 mL) and triethylamine (1 mL, 6.7 mmol) were simultaneously added, in drops, over a period of 0.5 h to an ice cooled and stirred solution of α-amino isobutyric acid methyl ester, generated *in situ* by addition of triethylamine (1 mL, 6.7 mmol) to an ice cooled and stirred solution of α-amino isobutyric acid methyl ester hydrochloride (1.48 g, 9.67 mmol) in dry CH_2Cl_2 (65 mL). The reaction mixture was left sitrred at room temperature for two days. After this period another batch of α-amino isobutyric acid methyl ester, precisely generated as described above from the hydrochloride (1.48 g, 9.67 mmol) in dry CH_2Cl_2, was introduced, the mixture left stirred for 2 d at rt, washed successively with saturated $NaHCO_3$ (2 × 15 mL), 2 N H_2SO_4 (2 × 15 mL), water (2 × 15 mL), dried ($MgSO_4$) and the residue chromatographed on silica gel. Elution with hexane–EtOAc = 8:2 afforded 0.420 g (41%) of nearly pure MA-Aib$_6$ (**1**), mp 247–250 °C; δ_H (200 MHz, DMSO-d$_6$) 1.68 (s, 36H), 3.71 (s, 18H), 7.00 (br, 6H); FAB-MS (*m/z*) (%) 959 (M + Na$^+$) (60), 820 (M + H$^+$ − Aib) (44), 703 (M + H$^+$ − 2Aib) (100), 586 (M + H$^+$ − 3Aib) (8). Further elution gave 0.100 g (11%) of **2**, mp 203–205 °C. When the second batch was not added, work up afforded exclusively 33% of **2**, mp 203–205 °C; δ_H (200 MHz, $CDCl_3$) 1.66, 1.77, 1.88 (s, s, s, 30H), 3.68, 3.73, 3.78 (s, s, s, 15H), 7.13 (br, 4H); FAB-MS (*m/z*) (%) 842 (M + Na$^+$) (77), 703 (M + H − Aib) (100%), 586 (M + H$^+$ − 2Aib) (24).

6 *Crystal data* for **1**: $C_{42}H_{60}N_6O_{18}\cdot 2H_2O\cdot NaNO_3$, space group *Pna*2$_1$, a = 14.286(1) Å, b = 14.614(1) Å, c = 24.800(5) Å, V = 5177.9 Å^3, D_c = 1.352 g cm^{-3}, Cu-Kα radiation, λ = 1.54178 Å. Least squares refinement on F^2, R_1 = 0.0512 for 4480 data [$|F| > 4.0\sigma(F)$] and wR_2 = 0.1388 for all data. Data collection at 293 °C. CCDC 173157. See http://www.rsc.org/suppdata/cc/b1/b109465n/ for crystallographic files in .cif or other electronic format.

7 I. L. Karle, *Biochemistry*, 1974, **13**, 2155.

8 Silica gel (2.0 g), used for chromatography, was triturated with ethyl acetate (5 mL), filtered and the clear filtrate evaporated. Negative ion Ms of the residue clearly showed presence of nitrate and the positive ion Ms that of sodium ion.

9 Chromatographically pure MA-Aib$_6$ (0.005 g, mp 247–250 °C) was triturated with distilled water (3 × 2 mL), centrifuged and dried *in vacuo* to afford sample, mp 238–239 °C which was shown to be totally free of sodium nitrate by Ms.

10 Sodium nitrate (0.005 g) in water (2 mL) was shaken with ethyl acetate (2 mL), the layers separated and the organic layer filtered through cotton to give a clear solution in which salt freed MA-Aib$_6$ from the above experiment was dissolved and left aside. Fine needles, mp 256–258 °C, identical to that used for crystallographic studies were slowly deposited. These were demonstrated to contain sodium nitrate by positive and negative ion mass spectrometry.

11 The conditions used were similar to that described above. Unlike sodium nitrate, crystals were not deposited with lithium nitrate and potassium nitrate, on standing. Solvents were evaporated, the residue washed with water to remove uncomplexed salts, centrifuged, dried and the resulting fine powders, when analyzed by both positive and negative ion mass spectra, clearly showed complexation with lithium nitrate and the absence of this with potassium nitrate. In view of the exclusive preference of the amide groups for hydrogen bonding with nitrate ions seen with **1**, the lithium nitrate complex is likely to have a structure similar to that with sodium nitrate.

12 K. A. Bezja and D. Grdenic, *Nature*, 1960, **185**, 756; S. F. Darlow, *Nature*, 1960, **186**, 542; S. F. Darlow, *Acta Crystallogr.*, 1961, **14**, 159; V. A. Uchtman and R. Jandacek, *J. Inorg. Chem.*, 1980, **19**, 350; H. A. Endres and A. Knieszner, *Acta. Crystallogr., Sect. C.*, 1984, **40**, 770; C. Robl and W. F. Kuhs, *J. Solid State Chem.*, 1991, **92**, 101; C. Robl and S. Hentschel, *Z. Naturforsch. Teil B*, 1991, **46**, 1188; C. Robl and S. Hentschel, *Z. Naturforsch. Teil B*, 1992, **47**, 1561; L. P. Wu, M. Munakata, M. Yamamoto, T. K. Sowa and M. Maekawa, *J. Coord. Chem.*, 1996, **37**, 361; L. P. Wu, M. Munakata, M. Yamamoto, T. K. Sowa, M. Maekawa and Y. Suenaga, *Inorg. Chem. Acta*, 1996, **249**, 183; J. A. Harnisch, L. M. Thomas, I. A. Cuzei and R. J. Angelici, *Inorg. Chim. Acta*, 1999, **286**, 207.

CHEMCOMM
Communication
www.rsc.org/chemcomm

A periodic mesoporous organosilica containing electron acceptor viologen units

Mercedes Álvaro, Belén Ferrer, Vicente Fornés and Hermenegildo García*

Instituto de Tecnología Química CSIC-UPV and Departamento de Química UPV, Avda de los Naranjos s/n, 46022 Valencia, Spain. E-mail: hgarcia@qim.upv.es

Received (in Cambridge, UK) 3rd October 2001, Accepted 30th October 2001
First published as an Advance Article on the web 22nd November 2001

A periodic structured organosilica solid of the MCM-41 type containing 4,4′-bipyridinium presumably inserted on the walls that is stable after surfactant removal has been prepared; the ability of bipyridinium units to act as electron acceptor termini has been demonstrated by observation of the radical cation in the photochemical and thermal activation of the as-synthesized material.

Since the first report describing the preparation of periodic mesoporous silica of the MCM-41 type[1] there has been considerable amount of work aimed at exploiting the possibilities of these materials to host organic guests. The target was to produce hybrid solids with functional properties derived from the response of the organic guest confined in a regular compartmentalised space provided by the MCM-41 silicate. In this regard, recent reports have described the preparation of periodic mesoporous organosilica (PMO) in which the organic component occupies framework positions in the walls rather than in the empty voids of the hexagonal channels.[2–5] This paves the way for the preparation of a new type of innovative organic–inorganic hybrid materials for which a vast potential can be foreseen. In the present communication we describe a new PMO incorporating 4,4′-bipyridinium units that implemented the solid with unique electron acceptor ability as well as photo- and thermo-chromic responses characteristic of viologen derivatives.[6]

Viologens are the most widely used electron acceptor units in a variety of charge transfer complexes and electron transfer processes. The corresponding radical cations are very well documented and have as the most characteristic properties a relatively high stability and an intense blue–green colour.[7]

The preparation of the solid of the MCM-41 type incorporating 4,4′-bipyridinium units (BP∝PMO) was accomplished following basically the same procedure described in the literature for similar solids having methylene groups covalently linked to the walls.[5]

Our strategy to attempt the covalent binding of viologen to the silica walls consisted in the attachment of trimethoxysilylpropyl groups to the nitrogen atoms of 4,4′-bipyridine by nucleophilic substitution as indicated in Scheme 1.† Subsequently, the silyilated viologen precursor (BP) was used in combination with TEOS in the synthesis of the BP∝PMO, using cetyltrimethylammonium bromide (CTABr) as the structure directing agent. The molar proportions of the precursor gels used in a preferred preparation are: 1.00 Si: 114 H_2O: 8.0 NH_3 (20 wt%): 0.12 CTABr. TEOS as the silica source and BP were used in the following mol ratios: 0.85:0.15, 0.95:0.5 and 0.99:0.01. The formation of the solid was carried out at 80 °C in a closed 25 ml polyethylene container.

Thermogravimetric analysis coupled with differential scanning calorimetry conducted in air shows three distinctive peaks. The first between 150 and 250 °C corresponding to a loss of 30% in weight was attributed to the decomposition of the CTABr surfactant based on the reports on analogous PMO materials.[8] A second exothermic jump between 250 and 450 °C (11.5% weight, for the BP∝PMO with the maximum BP content) probably corresponds to the concurrent loss of residual surfactant and viologen. The final peak in the thermogravimetry (4% weight) is most probably due to desorption of water generated by condensation of silanol groups.

The presence of viologen in BP∝PMO is clearly revealed in the IR spectrum of the solid (Fig. 1). The strongest band characteristic of BP appears at 1650 cm^{-1}. Its intensity remains unaltered upon outgassing at 200 °C under 10^{-2} Pa for 1 h, conditions under which a large part of the template has been desorbed [see Fig. 1(b)]. Other characteristic bands of weak to medium intensity also appear in the aromatic region of the IR spectrum corresponding to BP.[9]

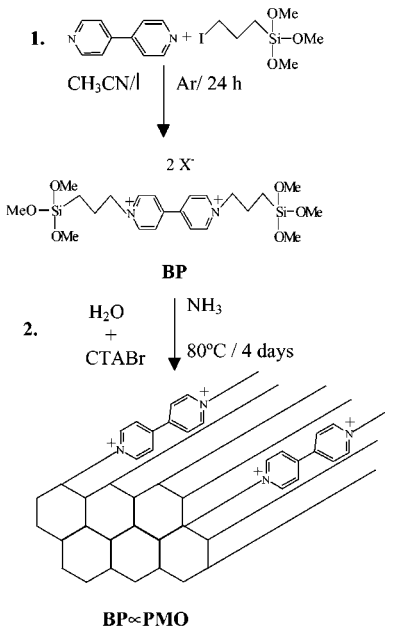

Scheme 1

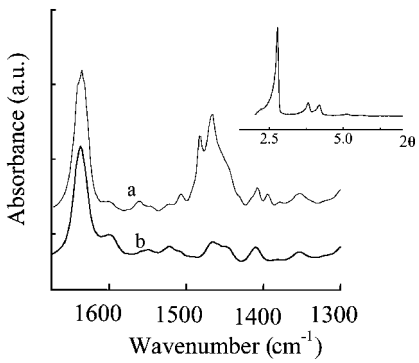

Fig. 1 FT-IR spectra of as-synthesised BP∝PMO (TEOS:BP 0.85:0.15) recorded at r.t. (a) and after outgassing at 200 °C for 1 h at 10^{-2} Pa (b). The decrease in the intensity of the 1470 cm^{-1} band corresponds to the desorption of the structure directing agent. The inset shows the powder X-ray diffraction spectrum of as-synthesized BP∝PMO.

 DOI: 10.1039/b108964c

The periodic structure of the as-synthesized BP∝PMO was assessed by powder X-ray diffraction wherein a sharp peak appearing at $2\theta = 3°$ characteristic of the d_{100} reflection is clearly observed[8] (inset of Fig. 1). Removal of the structure directing agent was accomplished by solid–liquid extraction using dilute acid in ethanol. The resulting solid exhibits the same characteristic X-ray diffraction peak as the as-synthesised powder and a BET surface area of 930 m^2 g^1 having a mononodal pore distribution around 3.8 nm and a total pore volume of 0.88 ml g^{-1}. These values are within the expected range for a typical MCM-41 solid. The fact that BP is not removed in the extraction treatment that removes CTA^+ and the ordering evidenced by X-ray diffractogram indicates that BP is strongly bound to the solid walls.

Of note in the observation in the UV–VIS spectrum of as-synthesised BP∝PMO, together with a sharp peak at 280 nm due to the pyridinium rings, was the presence of a featureless, broad band $\lambda_{max} = 400$ nm. This weak, broad band is characteristic of the formation of a charge transfer (CT) complex between the bipyridinium units and accompanyging halide as electron acceptor and donor components, respectively. This type of CT complex between viologen and halides has been reported in the literature[7] and evidences the ability of this new BP∝PMO material to promote the formation of CTC complexes.[10]

The novel opportunities of our BP∝PMO can be exemplified considering the efficiency of the generation of the $BP^{\cdot+}$ radical cation. Thus 308 nm laser excitation of powdered BP∝PMO in a sealed cell gives rise to the formation of the corresponding radical cation as assessed by diffuse reflectance UV–VIS spectroscopy (Fig. 2). The intensity of the band grows gradually upon irradiation until a maximum is reached. An estimation of the maximum percentage of radical ion generation can be obtained by comparing the intensity of the reflectance corresponding to the residual neutral viologen precursor at 280 nm with that of 600 nm characteristic of the radical ion, both corrected by the relative extinction coefficient of the bands. From this data it can be concluded that the transformation of the neutral BP into $BP^{\cdot+}$ radical cation is in practice complete $[(I_{280}/\varepsilon_{280})/(I_{600}/\varepsilon_{600})] < 0.1$. Concerning the nature of the electron donor site, we can conclusively rule out I^- as the electron donor, since none of the corresponding oxidised I_2 and $I_2^{\cdot-}$ species were observed in the optical spectrum.[11] In this context, the fact that a silicate framework can provide an electron to the excited state of viologens is not without precedent.[12] Importantly, not only has such high efficiency of $BP^{\cdot+}$ generation in aluminosilicates not been reported previously, but also the $BP^{\cdot+}$ does not significantly decay even one month after generation.

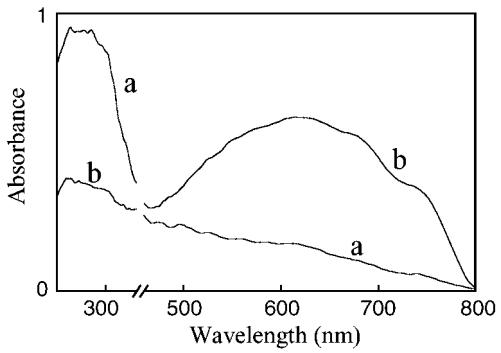

Fig. 2 Diffuse reflectance UV–VIS spectra of as-synthesized BP∝PMO (TEOS : BP 0.85 : 0.15) in a sealed cell before (a) and after 10 min (b) 308 nm laser irradiation. The sharp band at 290 nm is characteristic of BP while the broad band in the region 500–800 nm is due to the corresponding radical cation. Note that the increase of the latter upon irradiation is accompanied by a decrease of the 290 nm band.

The other unprecedented observation, that can give an idea of the potential of our BP∝PMO material, derived from its ability to stabilize $BP^{\cdot+}$, is thermal generation of the viologen radical cation. As far as we are aware, the only related precedent claiming the thermal generation of a viologen radical cation included in a porous aluminosilicate was published by Yoon as a note in his review on CT complexes in zeolites, which appeared in 1993.[7] No later confirmation of this interesting observation has been ever reported. In our case, just the simple outgassing of the BP∝PMO at room temperature develops a slight blue tint visually indicating the spontaneous generation of some $BP^{\cdot+}$. Upon heating at increasing temperatures (25–150 °C) under an Ar stream the intensity of the color increases and the diffuse reflectance UV–VIS spectrum provides evidence for the formation of the radical ion together with an enhancement of the CT complex. Upon cooling at room temperature apparently the radical cation decays but an enhanced concentration of CT complexes remains. This cycling can be repeated without noticeable loss in the ability to generate $BP^{\cdot+}$ radical cations.

In summary, our contribution derives from the seminal reports on PMO[2–5] that we have shown it can be applicable to covalently insert viologen in MCM-41 walls. While we describe the synthesis of the BP∝PMO and some properties of the as-synthesised material concerning its ability to stabilise radical cations, it is obvious that a range of further possibilities will be available after removal of the surfactant, emptying the channels of BP∝PMO. Preliminary experiments have shown that the template can be extracted from the solid without removing BP^{++}, as expected according to its covalent bonding. The empty voids of this BP∝PMO material could then be used to assemble different types of CT complexes having viologen imprinted in the walls as the acceptor unit.

Financial support by the Spanish CICYT (H. G., M. A. T. 2000, 1768-002-01) is gratefully acknowledged. B. F. thanks the Spanish Ministry of Education for a scholarship.

Notes and references

† BP was fully characterized by analytical and spectroscopic data: combustion analysis: theoretical (%) for $C_{22}H_{38}I_2N_2O_6Si_2$: C, 35.9; N, 3.8; H, 5.2; experimental: C, 35.1; N, 3.8; H, 5.2; IR: 1450, 1500, 1550 and 1650 cm^{-1}; ^1H NMR (CD_3OD): δ 9.17 (4H, d), 8.59 (4H, d), 4.63 (4H, t), 3.47 (18H, s), 2.07 (4H, m) and 0.63 (4H, m); ^{13}C NMR (CD_3OD): δ_C 151.4, 147.1, 128.4, 65.1, 51.2, 26.4 and 6.8.

1 J. S. Beck, J. C. Vartuli, W. J. Roth, M. E. Leonowicz, T. C. Kresge, K. D. Schmitt, C. T.-W. Chu, D. H. Olson, E. W. Sheppard, S. B. McCullen, J. B. Higgins and J. L. Schlenker, *J. Am. Chem. Soc.*, 1992, **114**, 10834–10843.
2 M. J. MacLachlan, T. Asefa and G. A. Ozin, *Chem. Eur. J.*, 2000, **6**, 2507–2511.
3 S. Inagaki, S. Guan, Y. Fukushima, T. Oshuna and O. Terasaki, *J. Am. Chem. Soc.*, 1999, **121**, 9611–9614.
4 B. J. Melde, B. T. Holland, C. F. Blandford and A. Stein, *Chem. Mater.*, 1999, **11**, 3302–3308.
5 C. Yoshina-Ishii, T. Asefa, N. Coombs, M. J. MacLachlan and G. A. Ozin, *Chem. Commun.*, 1999, 2539–2540.
6 J. A. Monk, *The Viologens: Physicochemical Properties, Synthesis and Applications of the Salts of 4,4′-Bipyridine*, Wiley, New York, 1998.
7 K. B. Yoon, *Chem. Rev.*, 1993, **93**, 321–339.
8 T. Asefa, M. J. MacLachlan, N. Coombs and G. A. Ozin, *Nature*, 1999, **402**, 867–871.
9 A. Corma, *Chem. Rev.*, 1995, **95**, 559–614.
10 K. B. Yoon, T. J. Huh and J. K. Kochi, *J. Phys. Chem.*, 1995, **99**, 7042–7053.
11 O. Horvath, J. H. Fendler and K. L. Stevenson, *Inorg. Chem.*, 1993, **32**, 227–230.
12 M. Alvaro, H. García, S. García, F. Marquez and J. C. Scaiano, *J. Phys. Chem.*, 1997, **101**, 3043–3051.

CHEMCOMM Communication
www.rsc.org/chemcomm

Cooperative directing effect of OH anions and polymerized DABCO cations in the formation of the $Ge_{16}O_{32}(OH)^{-}(C_6H_{12}N_2H)^{+}(C_6H_{12}N_2)\cdot 1.125H_2O$ zeotype

Manuela E. Medina, Marta Iglesias, M. Angeles Monge* and Enrique Gutiérrez-Puebla*

Instituto de Ciencia de Materiales de Madrid, CSIC Cantoblanco. E-28049 Madrid, Spain. E-mail: amonge@icmm.csic.es; egutierrez@icmm.csic.es

Received (in Cambridge, UK) 24th July 2001, Accepted 30th October 2001
First published as an Advance Article on the web 22nd November 2001

$Ge_{16}O_{32}(OH)^{-}(C_6H_{12}N_2H)^{+}(C_6H_{12}N_2)\cdot 1.125H_2O$ results from a simultaneous cation and anion templating effect during the zeotype formation; the structure shows a linear arrangement of the organic species along the channels as well as the existence of Ge_4O_8 tetramers with confined OH^- anions in the middle of large germanium cages.

The possibility of designing new open frameworks increases greatly for germanium zeotypes. The co-existence of different coordination polyhedra around the Ge atom (tetrahedron, octahedron and trigonal bipyramid) implies different charged frameworks.[1–8] The hydroxy group is involved in the formation of some new germanium zeotypes but not much attention has been paid to its role. In the previously reported ICMM3[7] the OH^- group was confined inside a six germanium cage, and the templating effect of this group was suggested.

The use of $(DABCO)^{+}(C_6H_{13}N_2)$ and DABCO derivatives as structure-directing agents (SDA) for zeolite synthesis has resulted in many high-silica products. The occurrence of a polymerization process has also been shown in solutions of DABCO at temperatures $\geqslant$ *ca.* 170 °C in the presence of an 'initiator', for instance ammonium salts.[9] In the synthesis of the beta zeolite a similar process has been suggested.[10] High-germanium compounds, zeotypes such as ASU-9,[2] or ICMM4[11] have been obtained by using DABCO as an SDA. In these compounds DABCO molecules or *dabconium* cations are isolated without any evidence of polymerization processes. Following our studies on this subject, we focus our attention on the effect of both OH^- and *dabconium* ions in zeolite formation, as well as on the acid–base bifunctional character that these templates confer to the zeotype.

ICMM5 was synthesized hydrothermally, and variations in the procedure were explored especially to avoid the presence of ASU-9[2] and ICMM4[11] the synthesis of which also involves DABCO (Table 1). Finally, by tuning the amount of water as a reactant and optimizing the reaction conditions ICMM5 was obtained as the sole product of the reaction. The purity of the resulting solid product was confirmed by PXRD.

TGA–DTA in N_2 atmosphere (50 ml min^{-1}) shows that the compound is stable up to 250 °C. A progressive weight loss of 12.5%, was then observed between 250 and 600 °C accompanied by an endothermic effect corresponding to the loss of both DABCO molecules, the OH group and water molecules, to give crystalline GeO_2 at 600 °C. PXRD and IR spectra show that the structure is maintained after heating to 400 °C for 1 h in air and collapses into amorphous GeO_2, after prolonged heating.

Table 1 Variation in gel composition and obtained products; Temp. = 150 °C and time = 5 days; EG = ethylene glycol

GeO_2	DABCO	H_2O	$PrNH_2$	EG	pH	Products
1	2.8	112	—	14	8.5	ASU-9[2]
1	2.8	112	—	—	9.5	ASU-9 + ICMM4
1	2.8	112	1.3	—	11	ICMM4[11]
1	2.8	2.9	25	—	12	ICMM5
1	2.8	0.14	25	—	12.6	GeO_2
1	2.8	—	25	—	—	GeO_2

Upon determining the crystal structure,† the composition was found to be $Ge_{16}O_{32}(OH)^{-}(C_6H_{12}N_2H)^{+}(C_6H_{12}N_2)\cdot 1.125H_2O$ [ICMM5]. In ICMM5 there are nine unique Ge sites, all exhibiting tetrahedral coordination [Ge–O 1.715(9)–1.784(8) Å; O–Ge–O 99.2(4)–119.9(4)° Ge–O–Ge 123.4(4)–147.0(6)°]. Connections among tetrahedra give rise to cages formed by 24 Ge atoms. The cages are made up of three different kind of rings (eight 6R, eight 5R and three R4). Linkages among cages along the *a* and *b* directions produce cubane 4–4 units which are displaced relative to each other in the *c* direction as required by the $I4_1/amd$ spatial group symmetry. The zeolite framework can be thought to consist of a combination of 5–3 + 4–4 SBUs that gives rise to a 3-D system of 12R intersecting tunnels (Fig. 1).

Inside each cage, one O atom is situated on a twofold axis, and corresponds to a confined OH^- anion (H atom located by difference Fourier synthesis. The O weakly interacts with the four Ge atoms of the central 4R of the cage at distances of 2.32(1) and 2.52(1) Å ($r_{Ge} + r_O$ = 1.9 Å).

This framework, that has been also described[10] for $(Me_3N)_6[Ge_{32}O_{64}]\cdot 4.5H_2O$ (FOS-5), is very similar to that of beta zeolite, both showing tetragonal symmetry, with 5–3 and single 4R SBUs and a 3-D system of 12R channels. Nevertheless, there are some important differences: (1) besides the 5–3 and 4R, ICMM5 bears double 4–4 cubane units. (2) Due probably to the templating effect of the OH^- anion,[7] cages of 24 Ge atoms, which do not exist in beta zeolite, are formed. (3) In ICMM5 the 12R channels are circular and equally sized in the three directions, while in beta zeolite, they are smaller in the [001] than in the [100] direction.

It is important to note the role of the OH^- anion on these new germanium cages. During the zeotype formation, some GeO_5

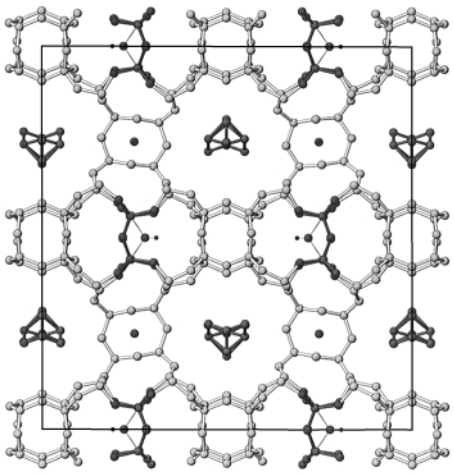

Fig. 1 View of the structure of $Ge_{16}O_{32}(OH)^{-}(C_6H_{12}N_2H)^{+}(C_6H_{12}N_2)\cdot 1.125H_2O$ [ICMM5] along the [010] direction, where the Ge_4O_8 tetramers and confined OH^- anions in the middle of the cages as well as the rows of DABCO molecules and dabconium cations, are in black. Thin lines do not indicate an actual bond but the shorter OH^-–Ge distances.

 DOI: 10.1039/b106671b

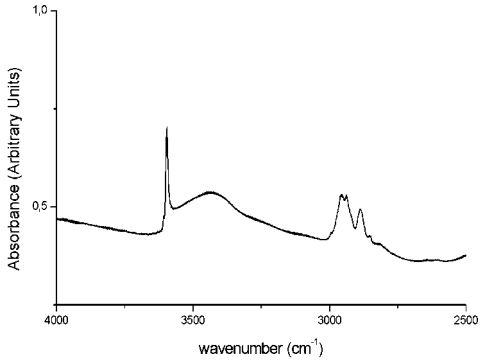

Fig. 2 Infrared spectrum of ICMM5.

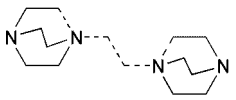

Scheme 1

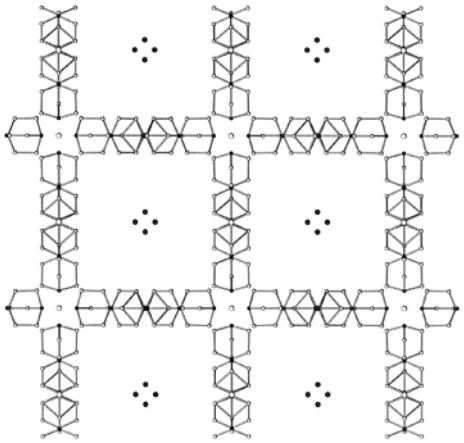

Fig. 3 View of the templates along [001] showing the disposition of the DABCO molecules and dabconium cations along the channels. Black and grey circles are the OH^- anions and water molecules respectively.

pentacoordinate species are formed, in which the fifth coordination position is occupied by an OH^- anion. In some cases this OH^- is only bonded to one Ge atom, usually giving laminar structures as in ICMM4 where the OH^- clearly forms part of a charged framework. Frequently hydroxy groups interact with more than one Ge, creating around it clusters of GeO_4 tetrahedra that give rise to new cages. When the zeotype is built up these OH^- anions remain confined inside the cages. Depending on the distances between the oxygen atom and the surrounding Ge atoms the tetrahedra become distorted to a greater or lesser degree, distortion ranging from the nearly regular tetrahedra as in the current ICMM5, to what can be considered trigonal bypiramids when including the fifth Ge–O interaction.[7,11] It seems quite probable that the presence of these hydroxy groups stabilizes the formation of new cages in gemanium zeotypes, but the point is to know to what extent they are either mere templates or anions belonging to the framework and thus, giving charged structures. Anyway, their existence implies the presence of cations, in this case, protonated molecules of DABCO.

Probably due to the difficulty of obtaining this compound free of ASU-9, in FOS-5, no total characterization of the material is reported. It could be that in that compound, the oxygen atoms inside the cages belong to OH^- anions instead of water molecules. ICMM5 was finally obtained as the sole product of the reaction. The presence of both OH^- anions and dabconium cations are clearly observed in the IR spectrum. Besides the characteristic C–N, C–C and C–H bands, it exhibits a very sharp peak at 3580 cm^{-1} and a band at ~2700 assigned to the stretching vibrations of the OH groups and to the characteristic N–H vibrations of an amine in its protonated form, respectively (Fig. 2); $\delta(NH^+)$ at ~1530 cm^{-1} is also observed.

We propose that in the reaction mixture for preparing ICMM5 the DABCO molecule might behave as in the beta zeolite synthesis.[10]

In fact in the single crystal structure solution of ICMM5 we have found, apart from the thermal some positional disorder around these molecule (Scheme 1). This model of disorder assumes the coexistence of both dabconium cations and polyethylene piperazine and does not allow a determination of the number of polymerized monomers in the crystal.

Although propylamine is probably involved in the polymerization process, perhaps as the 'initiator', its role is not fully clear. The arrangement of the DABCO molecules (Fig. 3) is in accord with a certain degree of polymerization and indicates clearly the directing effect of these molecules in the formation of the 3-D system of straight large rings.

The acid–base bifunctional character of ICMM5 has been tested in reactions catalyzed by basic sites (Michael addition) and acid sites (isomerization of epoxides). ICMM5 catalyzes the Michael addition of acrolein or methyl vinyl ketone and nitroethane at 313 K, in toluene yielding, after 20 h reaction, 62–54% Michael adduct. The rearrangement of styrene oxide over ICMM5, in acetone at 313 K was successful, giving 50% of phenylacetaldehyde after 20 h. XRPD spectra of the material after the catalytic tests, show in both cases that the structure remains unchanged.

If abstraction of the nearest environment of the OH^- (black part in Fig. 1), and of the deformation that it provokes in the framework is made, the result is a more symmetric zeolite with double the amount of equivalent 12R channels along the [100] and [010] directions. The *a* and *b* cell parameters would be one half of their value, as occurs in beta zeolite. In the actual ICMM5, rows of dabconium cations run along one half of these channels and the other half is occupied by the $Ge_4O_8(OH)^-$ tetramers giving rise to the 24 Ge cages. The result can be considered a 2×2 superstructure derived from the beta zeolite.

In view of this, we conclude that in the initial steps of the zeotype constitution, the hydroxy group induces $Ge_4O_8(OH)^-$ tetramer formation, which could take part in an anion templating effect, similar to that of the organic cations (dabconium cations in ICMM5) in the structural building formation.

This work was supported by the Spanish CICYT MAT1999-0892. M. E. M. thanks the MCYT for her grant.

Notes and references

† *Crystal data* for ICMM5: $(H_2O)_{1.125}(OH)^-[C_6H_{13}N_2]^+[C_6H_{12}N_2]$-$Ge_{16}O_{32}$, tetragonal, space group $I4_1/amd$ a = 25.973(2), c = 27.088(2) Å, V = 18274(2) Å^3, Z = 22, M_w = 1936.1, D_c = 1.938 Mg cm^{-3}, μ(Mo-Kα) = 7.18 mm^{-1}. Crystal dimensions: 0.10 × 0.10 × 0.02 mm. CCDC reference number 168740. See http://www.rsc.org/suppdata/cc/b106671b/ for crystallographic data in CIF or other electronic format.

1 C. Cascales, E. Gutiérrez-Puebla, M. A. Monge and C. Ruiz-Valero, *Angew. Chem.*, 1998, **110**, 135; C. Cascales, E. Gutiérrez-Puebla, M. A. Monge and C. Ruiz-Valero, *Angew. Chem., Int. Ed.*, 1998, **37**, 129.
2 H. Li and O. Yaghi, *J. Am. Chem. Soc.*, 1998, **120**, 10 569.
3 X. Bu, P. Feng, T. E. Gier, D. Zhao and G. D. Stucky, *J. Am. Chem. Soc.*, 1998, **120**, 13 389.
4 H. Li, M. Eddaoudi and O. Yaghi, *Angew. Chem., Int. Ed.*, 1999, **38**, 653.
5 C. Cascales, E. Gutiérrez-Puebla, M. Iglesias, M. A. Monge and C. Ruiz-Valero, *Angew. Chem.*, 1999, **111**, 2592; C. Cascales, E. Gutiérrez-Puebla, M. Iglesias, M. A. Monge and C. Ruiz-Valero, *Angew. Chem., Int. Ed.*, 1999, **38**, 2436.
6 X. Bu, P. Feng and G. D. Stucky, *Chem. Mater.*, 2000, **12**, 1811.
7 C. Cascales, E. Gutiérrez-Puebla, M. Iglesias, M. A. Monge, C. Ruiz-Valero and Natalia Snejko, *Chem. Commun.*, 2000, 2145.
8 T. Conradsson, M. S. Dadachov and X. Zou, *Micropourous Mesoporous Mater.*, 2000, **41**, 183.
9 E. F. Rasvodovskii, A. V. Nekrasou, L. M. Pushchaeva, L. S. Morozova and M. A. Markevich, *J. Macromol. Sci. A. Chem.*, 1974, **8**, 241.
10 P. Caullet, J. Hazm, J. L. Guth, J. F. Joly, J. Lynch and F. Raatz, *Zeolites*, 1992, **12**, 240.
11 C. Cascales, B. Gomez-Lor, E. Gutiérrez-Puebla, M. Iglesias, M. A. Monge, C. Ruiz-Valero and N. Snejko, *Chem. Mater.*, 2001, in press.

CHEMCOMM Communication
www.rsc.org/chemcomm

Diastereoselective synthesis of 5 *R* and 5 *S* TT pyrimidine h[5](6-4) pyrimidone photoproducts; structural analogues of the mutagenic UV-induced TT (6-4) photolesion

Sandra Karina Angulo Matus,[ab] Leticia Quintero,*[b] Jean-Louis Fourrey[a] and Pascale Clivio*[a]

[a] *Institut de Chimie des Substances Naturelles, CNRS, 1 Avenue de la Terrasse, 91190 Gif sur Yvette, France. E-mail: pascale.clivio@icsn.cnrs-gif.fr*

[b] *Centro de Investigacíon de la Facultad de Ciencias Quimicas, Universidad Autónoma de Puebla, 72570 Puebla, Mexico*

Received (in Cambridge, UK) 28th August 2001, Accepted 26th October 2001
First published as an Advance Article on the web 22nd November 2001

Two pyrimidine (6-4) pyrimidone photoproduct derivatives, highly valuable to probe the substituent influence during polymerase replicative bypass, were prepared; one (1a) by diastereoselective Raney nickel reductive desulfurization of the s[5](6-4) adduct of TpT (3) and the other (1b) by alkaline treatment of 1a.

Pyrimidine (6-4) pyrimidone photoproducts are one of the major mutagenic UV-induced DNA damage produced at adjacent pyrimidine sites.[1] These photoproducts are formed by a [2 + 2] cycloaddition between the 5,6-double bond of the 5′-pyrimidine and the carbonyl (thymine) or imine (cytosine) of the 3′-pyrimidine yielding an unstable four membered heterocycle (oxetane or azetidine) that spontaneously rearranges to transfer the heteroatom onto the C5 position of the 5′-pyrimidine base (Scheme 1). Among the four possible bipyrimidine sites, 5′-thymine-containing-sequences (TC and TT) are the most reactive.[2] Comparison of the mutagenic properties of (6-4) adducts produced at these sites, when embedded in a same sequence context, allowed some insights into structure–mutagenicity relationships.[3,4] It appeared that the 5′-pyrimidine base retained its coding properties (95% A insertion) whereas incorporation of G opposite the 3′-pyrimidone was favoured (89% for the TT (6-4) adduct, and 71% for the TC (6-4)). However, the 18% variation could not be attributed to any substituent since photoproduct structures differed at more than one position (X_2 at C5 of the saturated thymine and R_2 at C5 of the pyrimidone) (Scheme 1). Thus, neither the influence of the 5′-pyrimidine C5 substituent, and *a fortiori* nor its stereochemistry, on nucleotide insertion during trans-lesion synthesis (TLS) could be established from these experiments.

Analogues of the (6-4) photoproducts, differently substituted at the C5 position of the saturated thymine base portion, when incorporated into oligonucleotides, would be highly valuable to study in detail structure–mutagenicity relationships. In a first approach, we considered that analogues of the (6-4) TpT adduct bearing an hydrogen atom instead of the hydroxy group at the dihydropyrimidine 5-position (**1a** or **1b**) would be very useful to study the impact of this latter group during TLS. We envisaged that such analogues could be obtained by reductive desulfurization of the known s[5](6-4) adduct of TpT (**3**).[5]

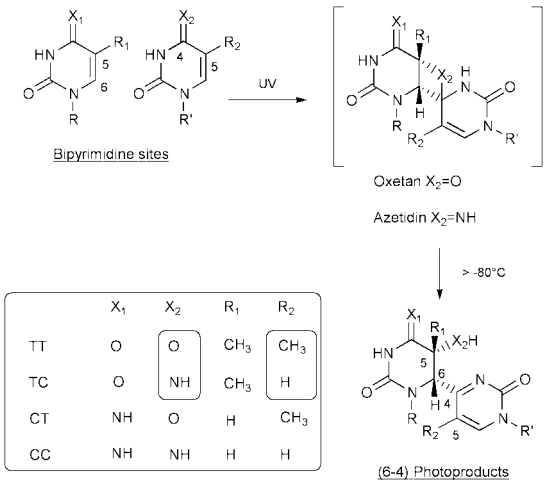

	X_1	X_2	R_1	R_2
TT	O	O	CH_3	CH_3
TC	O	NH	CH_3	H
CT	NH	O	H	CH_3
CC	NH	NH	H	H

Scheme 1

Raney nickel is a reagent of choice to reduce sulfur compounds.[6] Thus, treatment of a methanolic solution of the thietane **4**,[5] in equilibrium with its opened form **3**, with Raney nickel led rapidly to the formation of a major product (**1a**) together with a minor compound (**1b**) (Scheme 2) in a *ca.* 9 : 1 ratio as judged by ^{1}H NMR and HPLC analysis.[7] ^{1}H NMR signals of **1a** were strictly superimposable to those of the product that we previously obtained upon 254 nm irradiation of the s[5]Dewar photoproduct **2**.[8] The tentatively assigned *R* stereochemistry at C5 of **1a** was herein confirmed from a set of NMR data. The configuration of Tp C6 is retained since H6 gives an NOE with Tp H3′. It is known that dihydropyrimidines adopt half chair conformations, N1–C2–N3–C4 atoms in the plane and the C5 and the C6 atoms on each side of the plane (Fig. 1).[9] The 7 Hz coupling constant between H6 and H5, a value typical of an ax/eq coupling, could accommodate only with a C5 *R* configuration. NOEs between the two methyl groups and between Tp H6 and pT CH_3 showed the conformation of the 5′-thymine ring to be in an half chair with C5 atom above and C6 atom below the N1-C4 mean plane (Fig. 1, B). It is worth mentioning that this conformation is the same as the one recently observed by X-ray crystallography of the (6-4) adduct of TpT[10] and obtained by molecular modelling.[11] The ^{13}C NMR spectrum of **1a**, compared to the one of the natural (6-4) photoproduct of TpT,[12] ascertained the proposed structure and its stereochemistry at C5. All the ^{13}C NMR chemical shifts matched those of the (6-4) TpT adduct except C5, C6 and the methyl of the Tp part. In particular, carbon C5 (40 ppm) experienced a shielding of 34 ppm in agreement with removal of the α-effect produced by C5 hydroxy substitution in 5,6-dihydropyrimidine derivatives.[13] The methyl (δ 10.5 ppm) was also shielded compared to the corresponding one of the TpT (6-4) adduct (δ 26.4 ppm). This difference cannot be attributed solely to the removal of a β-effect due to OH substitution which is around 9 ppm (comparison between 5-hydroxy-5,6-dihydropyrimidine and 5,6-dihydropyrimidine) but is due to a *gauche* relationship with the bulky pyrimidone C6 substituent, confirming a *cis* relationship between the Tp methyl and the pyrimidone.[13] Carbon C6 (δ 53.3 ppm) experienced a 5.8 ppm shielding when compared to the corresponding one in the (6-4) adduct of TpT, a β-effect magnitude in agreement with that observed between 5-hydroxy-5,6-dihydrothymidine and 5,6-dihydrothymidine.[13] Interestingly, upon storage in D_2O, the H-5 atom of **1a** experienced an isotopic exchange that occurred with retention of configuration.

 DOI: 10.1039/b107773m

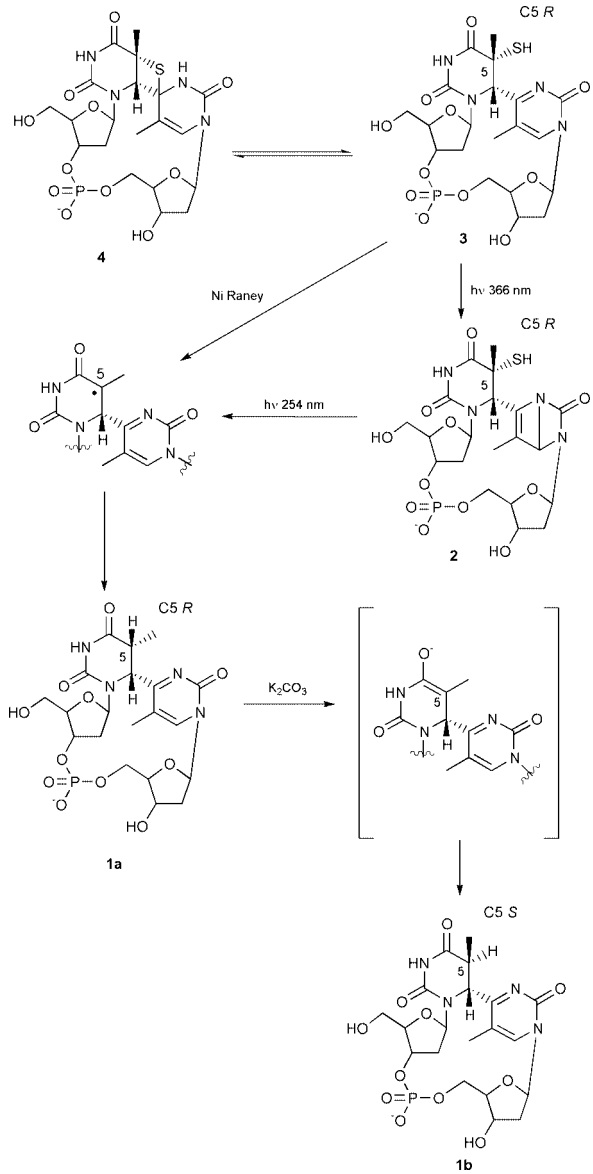

Scheme 2

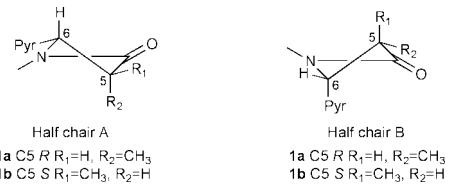

Fig. 1

Compound **1b** also belongs to the pyrimidone type as attested by its UV chromophore (absorption at 322 nm). Its ^{1}H NMR spectrum displayed two methyl signals at 2.23 and 1.51 ppm, one of which being a doublet, evidencing that this compound was either a conformer or a diastereoisomer of **1a**. Its saturated H6 proton (5.02 ppm) appeared as a singlet indicating an eq/eq relationship between H6 and H5, fitting the half chair B with methyl in β position and ruling out **1a** in the half chair A conformation. Finally, deshielding of the ^{13}C NMR methyl signal (17.7 ppm) compared to the corresponding one of **1a** confirmed the *trans* substitution and hence that **1b** is the C5 diastereoisomer of **1a**.

The reductive desulfurization step proceeded not only in high yield (73%) but also with an excellent diastereoselectivity. Attempts to fully explain the observed diastereoselectivity are, at this stage, premature since the stereochemical course of desulfurization, in cyclic systems, using Raney nickel is not fully understood[14] and would require additional experiments which are beyond the scope of this work. Moreover, our case is particularly complex for the reduction occurs at a potentially isomerizable center. However we propose, to interpret the observed diastereoselectivity, that the major C5 *R* diastereoisomer **1a** could result from a stereoselective hydrogen atom transfer on the less hindered face of the C5 radical (Scheme 2).

Raney nickel desulfurization of **3** yielded **1a** in good yield, we then attempted to define conditions affording **1b** on a preparative scale. Since it is known that 5,6-dihydrothymine derivatives isomerize at C5 under alkaline conditions,[15] we thought that **1a** could be converted into **1b** at high pH. Treatment of the water solution of the **1a**–**1b** 9 : 1 mixture with K_2CO_3 (0.15 M) at rt indeed led to the full conversion of **1a** into **1b**. C5 epimerization of **1a** is likely to proceed through an enol intermediate (Scheme 2). Our results seem to indicate that at neutral pH, this enol preferentially equilibrates with its kinetic form **1a** (protonation on the less hindered side of the dihydropyrimidine) whereas at basic pH, the thermodynamic species (**1b**) is highly favoured. This hypothesis could explain the 10% formation of **1b** since the desulfurization reaction was achieved using crude Raney nickel reagent.

In conclusion, we have developed a straightforward method to prepare either the C5 *R* or *S* h^5(6-4) photoproduct of TpT sites at the dinucleotide level. This result is extremely important since **1b**, when incorporated into oligonucleotides, could directly probe the impact of the C5 hydroxy group of the (6-4) dithymine lesion on its mutagenic properties. Oligonucleotides containing **1a**[16] would be also very important to examine the stereochemical effect of the methyl group on mutagenesis. We are confident that these (6-4) analogues will find a number of other applications in the biophysical and biological fields of (6-4) photolesions.

We thank CONACYT (Mexico) for a doctoral fellowship to S. K. A. M.

Notes and references

1 E. C. Friedberg, G. C. Walker and W. Siede, in *DNA Repair and Mutagenesis*, ASM Press, Washington, D. C., 1995, p. 24.
2 T. Douki and J. Cadet, *Biochemistry*, 2001, **40**, 2495.
3 J. E. LeClerc, A. Borden and C. W. Lawrence, *Proc. Natl. Acad. Sci. USA*, 1991, **88**, 9685.
4 M. J. Horsfall and C. W. Lawrence, *J. Biol. Chem.*, 1994, **235**, 465.
5 P. Clivio, J.-L. Fourrey, J. Gasche and A. Favre, *J. Am. Chem. Soc.*, 1991, **113**, 5481.
6 G. R. Pettit and E. E. van Tamelen, in *Organic Reactions*, ed. A. C. Cope, J. Wiley & Sons, Inc., New York, 1962, Vol. 12, p. 356; H. Hauptmann and W. F. Walter, *Chem. Rev.*, 1962, **62**, 347.
7 HPLC conditions: 4 × 250 mm, 5μ, Kromasile C18 column, 0 to 10% acetonitrile in 0.05 M ammonium acetate in 15 min, rt of **1a**: 17.1 min; rt of **1b**: 16.6 min.
8 P. Clivio and J.-L. Fourrey, *Chem. Commun.*, 1996, 2203.
9 J. Cadet, L. Voituriez, F. E. Hruska, L.-S. Kan, F. A. A. M. De Leeuw and C. Altona, *Can. J. Chem.*, 1985, **63**, 2861 and references cited.
10 H. Yokoyama, R. Mizutani, Y. Satow, Y. Komatsu, E. Ohtsuka and O. Nikaido, *J. Mol. Biol.*, 2000, **299**, 711.
11 J.-S. Taylor, D. S. Garrett and M. J. Wang, *Biopolymers*, 1988, **27**, 1571.
12 R. E. Rycyna and J. L. Alderfer, *Nucleic Acids Res.*, 1985, **13**, 5949.
13 M. Berger, J. Cadet and J. Ulrich, *Can. J. Chem.*, 1985, **62**, 6.
14 W. A. Bonner and R. A. Grimm, in *The Chemistry of Organic Sulfur Compounds*, ed. N. Kharasch and C. Y. Meyers, Pergamon Press, New York, 1966, Vol. 2, p. 35.
15 V. Skaric and J. Matulic-Adamic, *Helv. Chim. Acta*, 1983, **66**, 687.
16 For the incorporation of **1a** into oligonucleotides the synthesis should be accomplished using non-alkaline protocols.

CHEMCOMM Communication
www.rsc.org/chemcomm

Mesoporous VO_x–SbO_x/SBA-15 synthesized by a two-stage grafting method and its characterization

Kake Zhu,[a] Zhuona Ma,[a] Yan Zou,[a] Wuzong Zhou,[b] Tong Chen[c] and Heyong He*[a]

[a] *Department of Chemistry, Fudan University, 220 Handan Road, Shanghai 200433, P. R. China. E-mail: heyonghe@fudan.edu.cn*
[b] *Department of Chemistry, School of Chemistry, University of St. Andrews, St. Andrews, UK KY16 9ST*
[c] *Department of Chemistry, Xiamen University, Xiamen 361005, P. R. China*

Received (in Cambridge, UK) 17th August 2001, Accepted 1st November 2001
First published as an Advance Article on the web 22nd November 2001

Bi-metallic VO_x–SbO_x/SBA-15, which may be used as a site-isolated model catalyst, is successfully prepared by a two-stage grafting method using a vanadium matallocene and $SbCl_5$ as precursors.

SBA-15[1,2] is a purely siliceous mesoporous molecular sieve with high thermal and hydrothermal stabilities and is a potential support in catalysis. Grafting methods are widely used to prepare catalysts on supporting materials. The catalysts prepared in this way are often highly active and selective. In mesoporous molecular sieves the active metal species are dispersed evenly on the inner walls of the pores and appear to be less likely to form large clusters at reaction temperatures as they are usually bonded with the surface silanols. Although single metals are relatively easy to graft on the support, there are only a few reports on grafting bimetallic clusters as they are difficult to prepare.[3–6] V–Sb mixed oxide catalysts have been extensively studied for their activities of propane ammoxidation to acrylonitrile. However, the surface areas of these materials are still no more than 21 $m^2\ g^{-1}$.[7] Mixed-oxide catalysts have been rationalized in terms of the site isolation theory, *i.e.* the isolation of active V moieties in the structure is a key factor for obtaining a catalyst with high selectivity.[8] Here we present a two-stage grafting method to prepare V–Sb bimetallic oxide on the support of mesoporous SBA-15 with isolated V and Sb active centers. Our aim is to obtain a new type of catalyst to further study its catalytical activities and reaction mechanisms in comparison with conventional mixed-oxide catalysts.

The synthesis of SBA-15 was carried out using the literature method.[1–2] Prior to grafting, SBA-15 was calcined to remove the surfactant, resulting in *ca.* 15% Si atoms remaining as silanols as detected by ^{29}Si MAS NMR spectroscopy. The amount of the two precursors, bis(cyclopentadienyl)vanadium dichloride and $SbCl_5$ was calculated according to the molar ratio of SiOH:V:Sb = 5:1:1, *i.e.* utilizing all silanols (Scheme 1). The grafting process was conducted in a similar method as used by Maschmeyer *et. al.*[9] and Kang *et al.*[10] for grafting Ti and V, respectively, on other mesoporous silicates. SBA-15 was dehydrated at 423 K for 2 h under vacuum and then added to chloroform containing 10 wt% bis(cyclopentadienyl)vanadium dichloride under dry nitrogen. The sample was kept in chloroform solution for 2 h under stirring to enable the V species to diffuse into the SBA-15 pores. Triethylamine was then added to activate the grafting reaction. After 3 h, a 10 wt% $SbCl_5$ chloroform solution was added to the now brown mixture and allowed to react for 3 h. The grafted sample was washed with chloroform and filtered off, and then washed with water to hydrolyse and to remove HCl. The sample was finally dried and calcined in air at 773 K for 3 h, to form VO_x–SbO_x/SBA-15 (Scheme 1). SbO_x/SBA-15 and VO_x/SBA-15 were prepared in a similar manner.

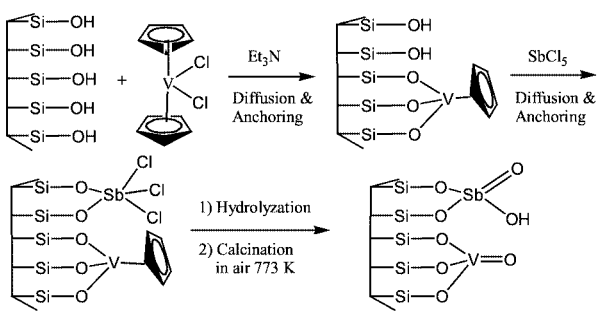

Scheme 1

XRD patterns of all grafted SBA-15 samples (Fig. 1) show well-resolved patterns with a prominent peak at *ca.* 1.0° and two weak peaks at *ca.* 1.6 and 1.7°, confirming that the SBA-15 structure was maintained.

The N_2 adsorption isotherms of all materials (Fig. 2) give typical type IV adsorption isotherms with a H1 hysteresible

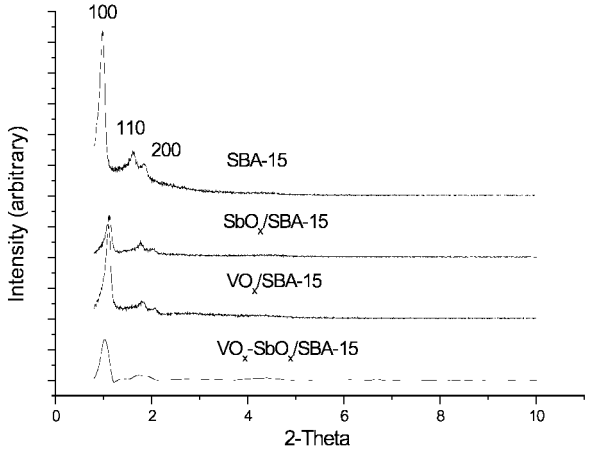

Fig. 1 X-Ray powder diffraction patterns for SBA-15, SbO_x/SBA-15, VO_x/SBA-15 and VO_x–SbO_x/SBA-15.

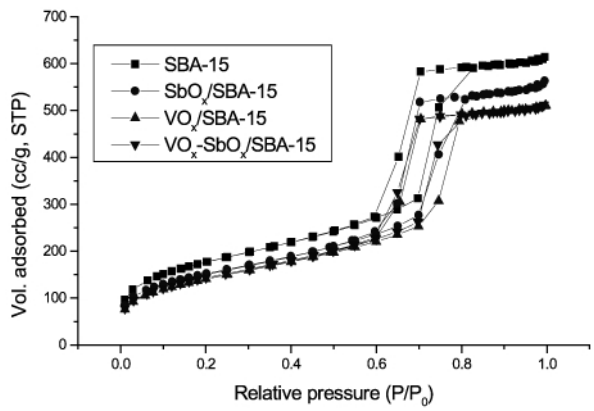

Fig. 2 N_2 adsorption isotherms for SBA-15, SbO_x/SBA-15, VO_x/SBA-15 and VO_x–SbO_x/SBA-15.

 DOI: 10.1039/b107487n

Table 1 Pore structural parameters of SBA-15, SbO_x/SBA-15, VO_x/SBA-15 and VO_x–SbO_x/SBA-15 calculated from the desorption branch of the nitrogen adsorption isotherms and the molar compositions by ICP

Sample	A_{BET}/ $m^2\ g^{-1}$	A_{BJH}/ $m^2\ g^{-1}$	V_{BJH}/ $cm^3\ g^{-1}$	D_{BJH}/ Å	Si/metal
SBA-15	706	716	1.10	61.3	
SbO_x/SBA-15	512	578	0.81	56.0	15.3
VO_x/SBA-15	548	600	0.89	59.4	21.9
VO_x–SbO_x/SBA-15	520	584	0.81	55.6	53.6(V) 44.1(Sb)

loop. The BET surface area of SBA-15 was 706 $m^2\ g^{-1}$, and decreased to 512, 548 and 520 $m^2\ g^{-1}$ for the samples SbO_x/SBA-15, VO_x/SBA-15 and VO_x–SbO_x/SBA-15, respectively (Table 1). This decreasing trend is also shown by the mesopore surface areas (A_{BJH}). Such a trend can be explained by two factors: the addition of the metals increases the density of the samples and decreases the pore size, as shown by the decreasing trend of V_{BJH} and D_{BJH}. The BJH pore size distribution is narrow, indicating that the pore structure remains regular and unchanged after the grafting process. The elemental content of each sample was determined by ICP (Table 1). The values of Si/metal indicate that in all three grafted samples not all of the precursor molecules reacted with the available silanols.

Fig. 3 shows the UV Raman spectra of the four samples. The bands at *ca*. 490 cm^{-1} are assigned to three Si siloxane rings.[11] For both VO_x–SbO_x/SBA-15 and VO_x/SBA-15 the bands at *ca*. 1035 cm^{-1} arise from the (support–Si–O–)$_3$V=O species[11] illustrated in the final product (Scheme 1). Bands at 930 cm^{-1} assignable to dinuclear vanadium complexes[12] were not observed, since the cyclopentadienyl ring prevents vanadium from bonding with other metal centers. The XPS binding energies of Sb $3d_{3/2}$ for SbO_x/SBA-15 and VO_x–SbO_x/SBA-15 are 540.0 and 540.5 eV, respectively. The former is the same as that reported previously by Benvenutti *et al.*,[13] for the Sb structure is shown in the final product (Scheme 1). The latter is slightly higher which may be caused by the weak interaction between the V and Sb species.

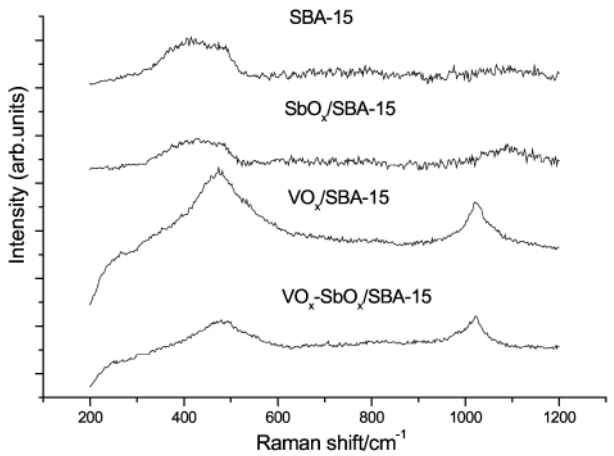

Fig. 3 UV Raman spectra for SBA-15, SbO_x/SBA-15, VO_x/SBA-15, and VO_x–SbO_x/SBA-15.

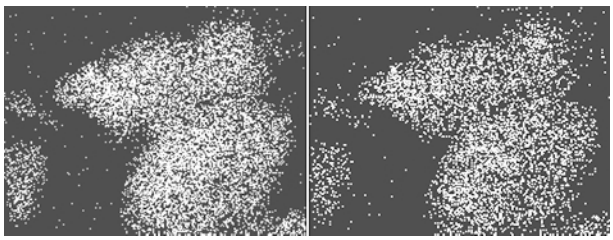

Fig. 4 Elemental mapping images of VO_x–SbO_x/SBA-15; left: Sb, right V.

VO_x–SbO_x/SBA-15 was also studied by elemental mapping. Fig. 4 shows that the grafted metals are evenly spread in the support. In the preparation of VO_x–SbO_x/SBA-15 the amount of two precursors was calculated to react with all silanols. However, the ICP analysis shows that V and Sb had not reacted completely. Therefore, all these results indicate that the metal species do not associate together during the calcination process at 773 K and confirm our expectation of isolated metal centers in the grafted samples (Scheme 1).

In conclusion, bimetallic VO_x–SbO_x/SBA-15 has been successfully prepared by a two-stage grafting method using the vanadium matallocene and $SbCl_5$ as precursors. SbO_x/SBA-15 and VO_x/SBA-15 were also synthesised and characterized for comparison. The structure of SBA-15 is retained after the grafting and calcination processes. The material may be used as a site-isolated model catalyst, *e.g.* for the ammoxidation of propane.

We acknowledge the Li Ka Shing Foundation for the Cheung Kong Scholars Programme, National Natural Sciences Foundation Committee of China for the National Science Fund for Distinguished Young Scholars (grant No. 20005310) and financial support from the Ministry of Education of China.

Notes and references

1 D. Zhao, J. Feng, Q. Huo, N. Melosh, G. H. Fredrickson, B. F. Chmelka and G. D. Stucky, *Science*, 1998, **279**, 548.
2 D. Zhao, Q. Huo, J. Feng, B. F. Chmelka and G. D. Stucky, *J. Am. Chem. Soc.*, 1998, **120**, 6024.
3 M. Ichikawa, in *Dynamic Aspects in Heterogeneous Catalysis*, ed. K. Tamaru, Plenum, New York, 1994, p. 149.
4 A. Fukuoka, T. Kimura, N. Kosugi, H. Kuroda, Y. Minai, Y. Sasaki, T. Tominaga and M. Ichikawa, *J. Catal.*, 1990, **126**, 434.
5 W. H. H. Sachtler and M. Ichikawa, *J. Phys. Chem.*, 1986, **90**, 475.
6 R. D. Oldroyd, G. Sankar, J. M. Thomas and D. Ozkaya, *J. Phys. Chem. B*, 1998, **102**, 1849.
7 G. Centi, P. Mazzoli and S. Perathoner, *Appl. Catal. A: Gen.*, 1997, **165**, 273.
8 J. Nilsson, A. R. Landa-Canovas, S. Hansen and A. Andersson, *J. Catal.*, 1999, **186**, 442.
9 T. Maschmeyer, F. Rey, G. Sanker and J. M. Thomas, *Nature*, 1995, **378**, 159.
10 K. K. Kang and W. S. Ahn, *J. Mol. Catal. A: Chem.*, 2000, **159**, 403.
11 K. J. Chao, C. V. Wu, H. Chang, L. J. Lee and S.-F. Hu, *J. Phys. Chem.*, 1997, **101**, 6341.
12 G. Xiong, C. Li, H. Y. Li, Q. Xin and Z. C. Feng, *Chem. Commun.*, 2000, 677.
13 E. V. Benvenutti, Y. Gushikem and C. U. Davanzo, *J. Chem. Soc., Faraday Trans.*, 1992, **88**, 3193.

CHEMCOMM Communication
www.rsc.org/chemcomm

Metallo-phosphorylation of olefins: reaction of diethyl chlorophosphate with zirconocene–ethylene complex†

Chanjuan Xi,* Mingming Ma and Xiaodong Li

Key Laboratory for Bioorganic Phosphorus Chemistry of Ministry of Education, Department of Chemistry, Tsinghua University, Beijing 100084, China. E-mail: cjxi@tsinghua.edu.cn; Fax: +86-10-62566383; Tel: +86-10-62782695

Received (in Cambridge, UK) 29th August 2001, Accepted 23rd October 2001
First published as an Advance Article on the web 9th November 2001

Zirconocene–ethylene complex Cp_2Zr ($CH_2=CH_2$) reacted with chlorophosphate to form zircono-ethylphosphonate, which could be converted into various functionalized ethylphosphonates.

Introduction of a heteroatom to multiple carbon–carbon bonds is attractive from the synthetic viewpoint.[1] In this regard, a particularly attractive and interesting subject is the simultaneous introduction of a metal and another heteroatom to multiple carbon–carbon bonds, since it is a more versatile and elegant synthetic elaboration. While the related carbometallation of multiple carbon–carbon bonds has been extensively studied,[2] only a few reactions for the preparation of such a complex, which contains a metal and a heteroatom to a carbon–carbon bond, have been studied. In this paper, we would like to report a novel reaction of zirconocene–ethylene complex $Cp_2Zr(CH_2=CH_2)$ with chlorophosphate to form zircono-ethylphosphonate **(1)** (Scheme 1), which can be converted into various functionalized ethylphosphonates.

A typical experiment was carried out as follows. To a solution of zirconocene–ethylene complex $Cp_2Zr(CH_2=CH_2)$,[3] generated by the reaction of Cp_2ZrCl_2 with 2 equiv. of EtMgBr in THF, was added one equiv. of diethyl chlorophosphate. The reaction mixture was kept at room temperature for 24 hours, and then it was quenched with 2M HCl. Purification of crude product was carried out by column chromatography on silica gel (ethyl acetate–petroleum ether = 2:1). Ethylphosphonate **(2a)** was obtained in 87% yield.

The product ethylphosphonate did not come from the reaction of EtMgBr with chlorophosphate: hydrolysis was replaced by iodination of the reaction mixture and 2-iodoethylphosphonate **(2b)** was obtained in 85% yield, which suggested that the intermediate of the reaction of zirconocene–ethylene complex with chlorophosphate contains a Zr–C bond before hydrolysis.

Zircono-ethylphosphonate could be converted into functionalized ethylphosphonate by coupling with various electrophiles such as I_2, NBS, acyl chloride and allyl bromide. The various reactions are summarized in Table 1. The reaction of zircono-ethylphosphonate with I_2 or NBS gave 2-iodoethylphosphonate or 2-bromoethylphosphonate **(2c)** in 85% and 73% yields, respectively. Moreover, treatment of zircono-ethylphosphonate with allyl bromide obtained **(2d)** in 77% yield, in which the new carbon–carbon bond was formed. It is noteworthy that without CuCl the reaction of zircono-ethylphosphonate with acyl chloride did not proceed. The zircono-ethylphosphonate requires initial reaction with CuCl to give the alkylcopper reagent,[4] which then undergoes smooth reaction with acyl chloride to give **(2e)**. This is due to the different reactivity of the carbon attached to zirconium in the zircono-ethylphosphonate.

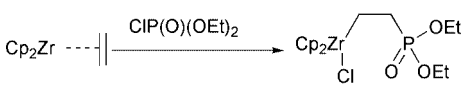

(1)

Scheme 1

The reaction of zirconocene–ethylene complex Cp_2Zr ($CH_2=CH_2$) with various unsaturated compounds such as alkynes,[5] alkenes,[3] ketone, and nitriles,[6] in which the reactions afforded five-membered zirconacycles was investigated. To elucidate the intermediate of this reaction, the reaction of $Cp_2Zr(CH_2=CH_2)$ with chlorophosphate was followed by ^{31}P NMR spectroscopy. Immediately following the addition of chlorophosphate at −78 °C, the reaction mixture was analysed by ^{31}P NMR. The ^{31}P NMR spectrum showed only one peak at 3.2 ppm, which was confirmed to be due to the phosphorus of the chlorophosphate. Then, the reaction mixture was stirred for 10 minutes from −78 °C to room temperature. Three peaks appeared in the ^{31}P NMR spectrum. One appeared at 3.2 ppm and another at −3.8 ppm. The latter signal is consistent with phosphorus of coordination number five.[7] The third signal was at 33.7 ppm and was assigned to the phosphorus of zircono-ethylphosphonate **(1)**. Following continuous stirring of the reaction mixture for 30 minutes at room temperature, the peak at 3.2 ppm completely disappeared and the peak at 33.7 ppm increased. Finally, the peak at −3.8 ppm disappeared after the reaction mixture was stirred for 24 hours at room temperature.

Based on the above results, a proposed reaction mechanism is shown in Scheme 2. The reaction of Cp_2ZrCl_2 with 2 equiv. of EtMgBr gives Cp_2ZrEt_2, which smoothly decomposes at 0 °C to give resonance hybrids Cp_2Zr-ethylene and zirconacyclopropane **(3)**.[3] The Zr–C bond of zirconacyclopropane **(3)** reacts with chlorophosphate to form five-membered zirconacycle **(4)**. Then, elimination of chloride from zirconacycle **(4)** takes place to form zircono-ethylphosphonate.

Table 1 Reaction of a mixture of Cp_2ZrEt_2 and chlorophosphate with electrophiles

Entry	Electrophile	*T*/°C	Time/h	Product	Yield (%)[a]
1	HCl	rt	1	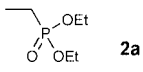 **2a**	87 (63)
2	I_2	rt	3	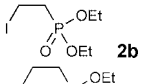 **2b**	85 (60)
3	NBS	rt	3	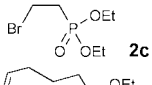 **2c**	73 (49)
4		rt	6	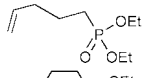 **2d**	77 (56)
5[b]	MeCOCl	50	6	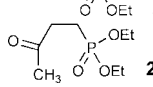 **2e**	64 (45)

[a] GC yields. Isolated yields are given in parentheses; [b] CuCl (1 equiv.) was added.

† Electronic supplementary data available: experimental procedure and NMR data. See http://www.rsc.org/suppdata/cc/b1/b107755d/

 DOI: 10.1039/b107755d

To further explore this reaction, other olefins were used. During the course of our study, we found that styrene also reacted with chlorophosphate in the presence of zirconocene species. When Cp_2ZrBu_2 (Negishi reagent) was treated with 2 equiv. of styrene and chlorophosphate successively, 2-phenylethylphosphonate was observed in 43% yield. In this case, the reaction proceeded *via* the β, β′ carbon–carbon bond cleavage of the zirconacyclopentane.[8]

Further investigations are still in progress in this area.

We are grateful to the National Natural Sciences Foundation of China (20172032) and Tsinghua University for financial support.

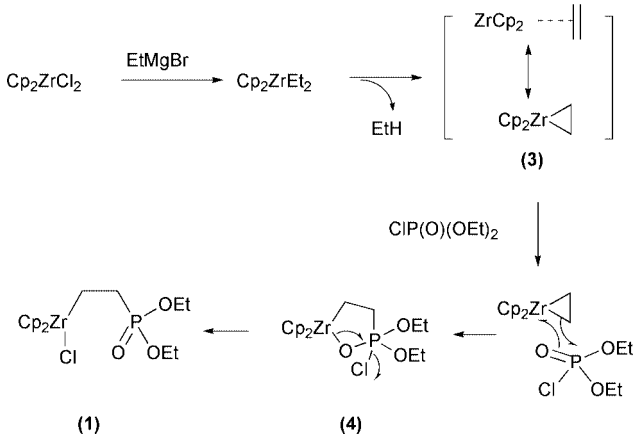

Scheme 2

Notes and references

1 (*a*) J. P. Collman, L. S. Hegedus, J. R. Norton and R. G. Finke, *Principles and Applications of Organotransition Metal Chemistry*, University Science Books, Hill Valley, 1987; (*b*) T. Hiyama and T. Kusumoto, in *Comprehensive Organic Synthesis*, eds. B. M. Trost and I. Fleming, Pergamon Press, Oxford, 1991, Vol. 8. Chapter 3.12; (*c*) Y. Ura, R. Hara and T. Takahashi, *Chem. Lett.*, 1998, 195; (*d*) L.-B. Han and M. Tanaka, *Chem.Commun.*, 1999, 395; (*e*) L.-B. Han and M. Tanaka, *Chem. Lett.*, 1999, 863.

2 (*a*) E. Negishi, *Pure Appl. Chem.*, 1981, **53**, 2333; (*b*) J. Normant and A. Alexakis, *Synthesis*, 1981, 841; (*c*) T. Takahashi, C. Xi, Y. Ura and K. Nakajima, *J. Am. Chem. Soc.*, 2000, **122**, 3228; (*d*) U. M. Dzhemilev and O. S. Vostrikova, *J. Organomet. Chem.*, 1985, **285**, 43.

3 (*a*) T. Takahashi, T. Seki, Y. Nitto and M. Saburi, *37th Symposium on Organometallic Chemistry*, Osaka, Japan, 1990, 172; (*b*) T. Takahashi, T. Seki, Y. Nitto, M. Saburi, C. J. Rousset and E. Negishi, *J. Am. Chem. Soc.*, 1991, **113**, 6266; (*c*) T. Takahashi, N. Suzuki, M. Kageyama, Y. Nitto, M. Saburi and E. Negishi, *Chem. Lett.*, 1991, 1579.

4 (*a*) T. Takahashi, M. Kotora, K. Kasai and N. Suzuki, *Organometallics*, 1994, **13**, 4183; (*b*) K. Kasai, M. Kotora, N. Suzuki and T. Takahashi, *J. Chem. Soc., Chem. Commun.*, 1995, 109.

5 T. Takahashi, M. Kageyama, V. Denisov, R. Hara and E. Negishi, *Tetrahedron Lett.*, 1993, **34**, 687.

6 T. Takahashi, Z. Xi, C. J. Rousset and N. Suzuki, *Chem. Lett.*, 1993, 1001.

7 (*a*) J. G. Verkade and L. D. Quin, *Phosphorus-31 NMR Spectroscopy in Stereochemical Analysis*, VCH Publishers, Inc., 1987, Vol. 8; (*b*) D. G. Gorenstein, *Phoshorus-31 NMR*, Academic Press, Inc., 1984.

8 (*a*) T. Takahashi, M. Tamura, M. Saburi, Y. Uchida and E. Negishi, *J. Chem. Soc., Chem. Commun.*, 1989, 852; (*b*) E. Negishi, D. R. Swanson and T. Takahashi, *J. Chem. Soc., Chem. Commun.*, 1990, 1254; (*c*) N. Suzuki, C. J. Rousset, K. Aoyagi, M. Kotora and T. Takahashi, *J. Organomet. Chem.*, 1994, **473**, 117.

CHEMCOMM Communication
www.rsc.org/chemcomm

Fluorescent photoinduced electron transfer (PET) sensing of anions using charge neutral chemosensors†

Thorfinnur Gunnlaugsson,*[a] Anthony P. Davis[ab] and Mark Glynn[a]

[a] *Department of Chemistry, Trinity College Dublin, Dublin 2, Ireland. E-mail: gunnlaut@tcd.ie*
[b] *School of Chemistry, University of Bristol, Cantock's Close, Bristol, UK BS8 1TS*

Received (in Cambridge, UK) 23rd August 2001, Accepted 23rd October 2001
First published as an Advance Article on the web 9th November 2001

We demonstrate for the first time that the charge neutral anthracene based fluorescent sensors 1a–c, having an aromatic or aliphatic thiourea moiety as an anion receptor, show *ideal* PET sensor behaviour where the anthracene fluorescence emission is selectively quenched upon titration with AcO^-, $H_2PO_4^-$ and F^- but not by Cl^- and Br^- in DMSO.

There is great interest in the design and synthesis of luminescent based chemosensors for on-line and real time detection of physiologically important ions and molecules,[1] and for environmental monitoring of harmful pollutants.[2] While numerous fluorescent and metal based delayed luminescent sensors for cations and organic molecules have emerged from the fields of supramolecular and coordination chemistry,[3] sensors for selective detection of anions are still relatively rare, despite the fact that several elegant examples of anion receptors have been reported over the years.[4] These, however, often involve the synthesis of complex and challenging organic hosts from scaffolds such as cholic acid,[5] calixarenes and peptides.[6] Luminescent anion sensing has recently been achieved[4] through the use of anion receptors composed, for example, from metal based Lewis acid centres,[7] calix[4]pyrroles,[8] thiouronium[9] and protonated quinoxaline,[10] amine[11] or polyamine moieties,[12] but the use of simple and easily synthesised electroneutral anion receptors for such sensing has been less investigated.[13] Intrigued by this fact, we set out to develop the charge neutral chemosensors **1a–c**, employing the criteria of PET sensing using the *fluorophore–spacer–receptor* model developed by de Silva for the detection of cations.[14] A few research groups have attempted to develop PET anion sensors.[11–13,15] But, to the best of our knowledge no such systems, employing neutral anion receptors, have yet been reported that show *ideal* PET behaviour, *i.e.* (*i*) only the quantum yield (intensity) and lifetime of the fluorescence emission should be modulated upon ion recognition due to (*ii*) changes in the free energy of electron transfer (ΔG_{PET}) between the excited state of the fluorophore and the receptor upon ion recognition, and (*iii*) no changes should be observed in the absorption spectra of the fluorophore.[14]

The three PET chemosensors **1a–c**, were easily made in good yield from readily available starting materials, Scheme 1. The 9-aminomethyl anthracene **2**, synthesised by reducing 9-cyanoanthracene using B_2H_6 in THF, was reacted in dry CH_2Cl_2 at room temperature, under an inert atmosphere with an equimolar amount of 4-(trifluoromethyl)phenyl-, phenyl- and methyl isothiocyanate respectively, **3a–c**, yielding **1a–c** as off-white solids that were purified by crystallisation from CH_2Cl_2. For comparable UV-Vis binding studies, the thiourea receptor **4** was prepared in an analogous way from ethylamine. All products were analysed by conventional methods.† The three different isothiocyanates **3a–c**, were chosen with the aim of being able to modulate or tune the acidity of the thiourea receptor moiety, which would lead to different *receptor–analyte* complex stability and hence different binding constants. Of the three chemosensors, **1a** was expected to show the strongest binding due to this effect, and **1c** the least. We initially investigated the binding of **1a** using $(C_4H_9)_4N(O_2CCH_3)$, since AcO^- is known to form strong directional hydrogen bonding with thiourea, as well as having a functional group of great biological relevance.[16] The ^1H NMR of **1a** in DMSO-d_6, showed two sharp signals at 9.62 ppm and 8.36 ppm for the thiourea hydrogens. These were substantially shifted downfield upon addition of $0.1 \rightarrow 2$ equivalents of $(C_4H_9)_4N(O_2CCH_3)$ ($\Delta\delta$ = 1.92 and 1.66 ppm respectively after 1 eq.) signifying the formation of a 1 : 1 binding through hydrogen bonding with a log β = 3.2.†

The fluorescence emission spectra of **1a** when titrated with AcO^- in DMSO displayed typical PET behaviour. In the absence of AcO^- the fluorescence emission spectra consisted of three sharp bands at 443, 419 and 397 nm, with a shoulder at 473 nm, when excited at 370 nm with Φ_F = 0.1037.‡ Upon addition of the AcO^- ($0 \rightarrow 32$ mM), the intensity of these bands gradually decreased with no other spectral changes being observed (*i.e.* no spectral shifts or formation of new emission bands), Fig. 1a. Using PET nomenclature, the emission can be said to being *ca.* 70% (at 443 nm) '*switched off*', with Φ_F = 0.0070. Concurrently, the absorption spectra of **1a**, consisting of bands at 390, 370, 352 and 336 nm, was hardly affected by the addition of AcO^-.† This confirms the insulating role of the methylene spacer, which minimises any ground state interactions between the fluorophore and the anion receptor. Similar emission and absorption effects were observed for **1b** and **1c**. When the fluorescence titrations of **1a–c** were carried out in CH_3CN, CH_3CO_2Et or THF, the emission was also quenched upon addition of AcO^- but the degree of quenching was somewhat smaller. In EtOH, which is a highly competitive hydrogen bonding solvent, no binding was observed between **1a** and AcO^-. Furthermore, *no* exciplex emission was observed in any of these solvents; in contrast, Teramae *et al.* have recently shown that a pyrene analogue of **1c**, is a ratiometric anion

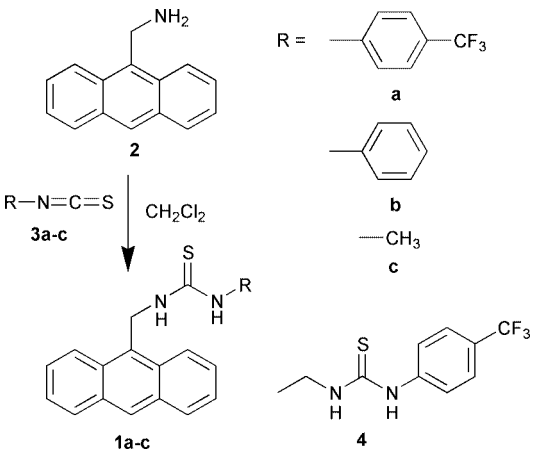

Scheme 1 The synthesis of **1a–c**. **4** was made in a similar way.

† Electronic supplementary data (ESI) available: ^1H, ^{13}C NMR for **1a–c** and UV-Vis and NMR titration results for **1a** are available as electronic supplementary information (ESI). See http://www.rsc.org/suppdata/cc/b1/b107608f/

 DOI: 10.1039/b107608f

indicator based on the control of intramolecular exciplex emission.[13]

To investigate the selectivity and the sensitivity of the sensor towards biologically important anions, we carried out a series of titrations using $N(C_4H_9)_4^+$ salts of F^-, Cl^-, Br^- and $H_2PO_4^-$ in DMSO. In the case of $H_2PO_4^-$ and F^- the fluorescence emission was quenched by *ca.* 50 (Φ_F = 0.0156) and 90% Φ_F = 0.0011) respectively (at 443 nm), but only minor quenching (<7%) was observed when titrated with Cl^- (Φ_F = 0.108) or Br^- (Φ_F = 0.088), ruling out a quenching by heavy atom effect. We propose that the quenching is likely to be due to the modulations of ΔG_{PET} upon anion sensing. This can be regarded as an enhancement in the rate of electron transfer from the HOMO of the thiourea–anion complex to the anthracene excited state, upon anion recognition *i.e*, the reduction potential of the thiourea is increased causing PET to become competitively more viable, which causes the fluorescence emission to be quenched or *'switched off'*.§ Plotting the fluorescence intensity changes (at 443 nm) as a function of log [anion] further supports this view. Fig. 1b, shows several features commonly seen for PET cation sensors *e.g.* the profiles for AcO^-, $H_2PO_4^-$ and F^- are all sigmoidal, the quenching occurs over two log concentration units, which is consistent with 1 : 1 binding and simple equilibrium. From these changes the binding constant log β for **1a** was measured to be 3.35 (±0.05) for F^-, 2.55 (±0.05) for AcO^- and 2.05 (±0.05) for $H_2PO_4^-$.‡ Similar binding constants were found for **4a** by measuring the changes in its absorption spectra at 286 nm. Importantly, **1a** shows good anion selectivity with AcO^- being recognised over $H_2PO_4^-$, but both represent families of biological important anions. The fact that **1a** shows higher affinity and more efficient quenching for F^- than AcO^- is not surprising, since its high charge density and small size enables it to form strong hydrogen bonding with the thiourea receptor. Measurements using **1b** and **1c** and the same anions showed similar results. For **1b**, the same selectivity trend was observed as for **1a**, with smaller binding constants due to the reduced acidity of the thiourea protons. For **1c** the order of selectivity and the sensitivity was somewhat different with $H_2PO_4^-$ (log β = 2.05 (±0.05)) being selectively detected over AcO^- (log β = 1.75 (±0.05)). These results show that the anion sensor's affinity can be controlled by simple design.[16]

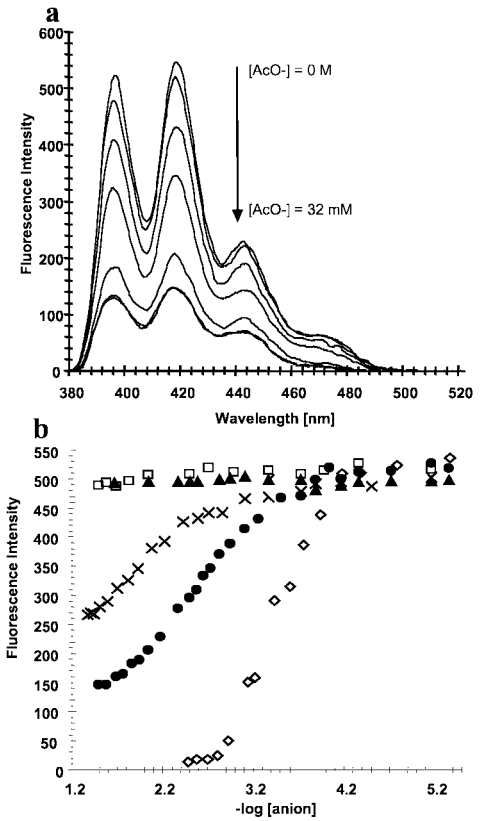

Fig. 1 (a) The changes in the fluorescence spectra of **1a** in DMSO upon addition of acetate. From top: [AcO^-] = 0, 92 μM, 550 μM, 1.8 mM, 8.9 mM, 26 mM, 32 mM. (b) Titration profile for **1a** showing the changes in the fluorescence emission as a function of added anion: ◇ = F^-, ● = AcO^-, × = $H_2PO_4^-$, □ = Cl^-, ▲ = Br^-, when measured at 443 nm. All titrations were repeated two to three times to ensure reproducibility.

In conclusion, the simple fluorescent PET anion chemosensors **1a–c** show *ideal* PET sensing behaviour upon ion recognition, *e.g.* only the fluorescence emission is *'switched off'* in the presence of AcO^-, $H_2PO_4^-$ and F^-. **1a–c** are a very important contribution to the fast growing field of supramolecular anion recognition and sensing.

We thank Enterprise Ireland, Kinerton Ltd, and TCD for financial support, Dr Hazel M. Moncrieff for helpful discussion and Dr John E. O'Brien for NMR.

Notes and references

‡ **1a–c** Φ_F were measured by comparison with anthracene (Φ_F = 0.27 in EtOH); D. F. Eaton, *Pure Appl. Chem.*, 1988, **60**, 1107. log β was determined from the equation:
$\log [(I_{max} - I_F)/(I_F - I_{min})] = \log [anion] - \log \beta$.
§ CV measurements on **4** showed two irreversible oxidative waves. Accurate ΔG_{ET} could not be determined from these measurements. We investigated the PET dependence of **1a** by comparing the Φ_F of **1a** with that of 9-methylanthracene (9MA), which lacks the anion receptor. In the absence of AcO^- the Φ_F of 9MA was found to be 0.284 in DMSO. This suggests that PET is active in **1a** prior to the anion recognition, but becomes even more efficient after anion recognition. In contrast, the addition of 40 mM of AcO^- to 9MA did not affect the Φ_F.

1 *Chemical Sensors and Biosensors for Medical and Biological Applications*, U. S. Spichiger-Keller, Wiley-VCH, 1998 Weinheim; Germany.
2 C. F. Mason, *Biology of Freshwater Pollution*, 2nd. edn., Longman, New York, 1991.
3 A. P. de Silva, D. B. Fox, A. J. M. Huxley and T. S. Moody, *Coord. Chem. Rev.*, 2000, **205**, 41; T. Gunnlaugsson, D. A. Mac Dónaill and D. Parker, *Chem. Commun.*, 2000, 93.
4 P. A. Gale, *Coord. Chem. Rev.*, 2001, **213**, 79; P. A. Gale, *Coord. Chem. Rev.*, 2000, **199**, 181; P. D. Beer and P. A. Gale, *Angew. Chem. Int. Ed.*, 2001, **40**, 486; F. P. Schmidtchen and M. Berger, *Chem. Rev.*, 1997, **97**, 1609; P. D. Beer, *Chem. Commun.*, 1996, 689.
5 A. P. Davis and L. J. Lawless, *Chem. Commun.*, 1999, 9; A. P. Davis, J. J. Perry and R. P Williams, *J. Am. Chem. Soc.*, 1997, **119**, 1793.
6 J. L. Atwood, K. T. Holman and J. W. Steed, *Chem. Commun.*, 1996, 1401; A. Metzger and E. V. Anslyn, *Angew. Chem. Int. Ed.*, 1998, **37**, 649.
7 L. Fabbrizzi, M. Licchelli, G. Rabaioli and A. Taglietti, *Coord. Chem. Rev.*, 2000, **205**, 85; P. D. Beer, V. Timoshenko, M. Maestri, P. Passaniti and V. Balzani, *Chem. Commun.*, 1999, 1755; R. S. Dickens, T. Gunnlaugsson, D. Parker and R. D. Peacock, *Chem. Commun.*, 1998, 1643.
8 P. Anzenbacher Jr., K. Jursíková and J. L. Sessler, *J. Am. Chem. Soc.*, 2000, **122**, 9350; H. Miyaji, P. Anzenbacher Jr., J. L. Sessler, E. R. Bleasdale and P. A. Gale, *Chem. Commun.*, 1999, 1723.
9 Y. Kubo, M. Tsukahara, S. Ishihara and S. Tokita, *Chem. Commun.*, 2000, 653.
10 P. E. Kruger, P. R. Mackie and M. Nieuwenhuysen, *J. Chem. Soc., Perkin Trans. 2*, 2001, 1079; C. B. Blake, B. Andrioletti, A. C. Try, C. Ruiperez and J. L. Sessler, *J. Am. Chem. Soc.*, 1999, **121**, 10438.
11 H. Xie, S. Yi, X. Yang and S. Wu, *New J. Chem.*, 1999, **23**, 1105.
12 D. H. Vance and A. W. Czarnick, *J. Am. Chem. Soc.*, 1994, **116**, 9397; M. E. Huston, E. U. Akkaya and A. W. Czarnick, *J. Am. Chem. Soc.*, 1989, **111**, 8735.
13 S. Nishizawa, H. Kaneda, T. Uchida and N. Teramae, *J. Chem. Soc., Perkin Trans. 2*, 1998, 2325.
14 A. P. de Silva, H. Q. N. Gunaratne, T. Gunnlaugsson, A. J. M. Huxley, C. P. McCoy, J. T. Rademacher and T. E. Rice, *Chem. Rev.*, 1997, **97**, 1515.
15 C. R. Cooper, N. Spencer and T. D. James, *Chem. Commun.*, 1998, 1365.
16 P. Bühlmann, S. Nishizawa, K. P. Xiao and Y. Umezawa, *Tetrahedron*, 1997, **53**, 1647.

CHEMCOMM
Communication
www.rsc.org/chemcomm

Intermolecular hydroacylation of acrylate esters: a new route to 1,4-dicarbonyls†

Michael C. Willis* and Selma Sapmaz

Department of Chemistry, University of Bath, Bath, UK BA2 7AY. E-mail: m.c.willis@bath.ac.uk; Fax: (+44) (0)1225 826231; Tel: (+44) (0)1225 826568

Received (in Cambridge, UK) 31st August 2001, Accepted 15th October 2001
First published as an Advance Article on the web 22nd November 2001

1,4-Dicarbonyl compounds can be prepared using a Rh(I) mediated hydroacylation reaction between (2-aminopicolyl)imines and acrylate esters followed by acid hydrolysis.

The transition metal catalysed hydroacylation reaction in which an aldehyde and an alkene are combined to generate a ketone is a relatively unexplored process. The main limitation of this reaction is the instability of the proposed acyl-metal intermediates and the resulting competitive decarbonylation pathway.[1] Intramolecular variants of the process utilising pent-4-en-1-als as substrates, leading to cyclopentanones as products, have been extensively studied,[2] however reports leading to larger ring sizes[3] or intermolecular examples are scarce.[4] Recently the Jun group have reported the use of a reaction system employing Wilkinson's complex and 2-aminopicoline as catalysts that allows intermolecular hydroacylation to proceed.[5] The success of the Jun system is attributed to the intermediacy of a picolylimine capable of forming a chelate stabilised acylrhodium species.[6] The majority of hydroacylation reactions reported to date utilise unfunctionalised alkenes as substrates thus generating simple ketones as products. We speculated that the use of alkenes substituted directly with either an ester or ketone group would provide direct access to the synthetically challenging 1,4-dicarbonyl array (Scheme 1). These 1,4-difunctionalised motifs are synthetically useful intermediates for the preparation of substituted furans,[7] butyrolactones[8] and succinate derivatives.[9] Such 1,4-dicarbonyl systems are not straightforward to prepare and the approach presented here can be considered as the equivalent of an acyl-anion addition to an enoate.[10] The related hydroformylation reaction has been reported although in these cases, by definition, only a single carbon unit corresponding to the CO molecule is introduced.[11] Using variously substituted and functionalised aldehydes in the corresponding hydroacylation reaction would allow the addition of functionalised carbon chains.[12] In this communication we report our progress towards this goal.

To assess the feasibility of the process we elected to study the reactions of imine **1** as an aldehyde equivalent and thus limit decarbonylation. The reaction of **1** with methyl acrylate under a variety of reaction conditions is summarised in Table 1. Reactions were conducted in a sealed tube using Wilkinson's complex as the catalyst. Upon completion the reaction mixtures were treated directly with 1.0 M HCl to liberate the required 1,4-dicarbonyl adducts. Optimal conditions involved heating a THF solution of the substrates at 135 °C for 6 hours with 10 mol% catalyst (entry 1). Under these conditions the desired product was isolated in 73% yield as a single regioisomer. Lowering the catalyst loading or reaction temperature or decreasing the reaction time resulted in less efficient processes (entries 2–4). The reaction also proceeds if toluene is employed as solvent although a more complex reaction mixture is produced resulting in lower yields (entry 5). Chlorobenzene was also evaluated but resulted in only low conversion to product. The use of 1,4-dioxane allowed a reasonable yield of the desired product to be isolated however solubilty problems were encountered that were not observed with THF.

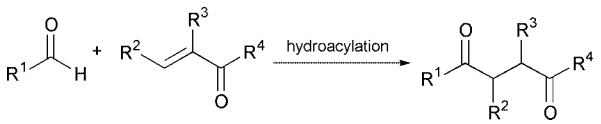

Scheme 1

† Electronic supplementary information (ESI) available: experimental details. See http://www.rsc.org/suppdata/cc/b1/b107852f/

In order to probe the generality of the process a range of substituted enoates were evaluated in the reaction with imine **1** (Table 2). Variation in the ester group is tolerated well, with Me and ^{t}Bu esters both delivering the expected adducts in good yields (entries 1 and 2).[13] Entry 3 demonstrates the tolerance towards amides with *N,N*-dimethylacrylamide generating the corresponding product in 74% yield. The introduction of substituents to the β-position of the alkene significantly reduces the reaction efficiency with methyl crotonate and cinnamate delivering the desired adducts in 24% and 10% yield respectively (entries 4 and 5). Substitution at the α-position has a similar effect on the reaction efficiency with methyl methacrylate yielding 16% of the requisite product (entry 6). A β-substituent could be successfully introduced if it was sufficiently activating, thus the use of *N*-methyl maleimide as the alkene component generated the desired hydroacylation product in 81% yield (entry 7).

The generality with respect to the imine component was next explored; we were particularly interested in assessing the influence of electron withdrawing and donating substituents on the aryl ring. A selection of 2-amino-3-methylpyridylimines bearing a range of substituents were readily prepared and evaluated in the reaction with methyl acrylate (Table 3). Electron withdrawing groups such as -NO_2 and -CN had a beneficial effect on the rate of the reaction with good yields of the desired products being obtained in only 20 and 80 min respectively (entries 2 and 3). Electron donating substituents

Table 1 Reaction of imine **1** with methyl acrylate[a]

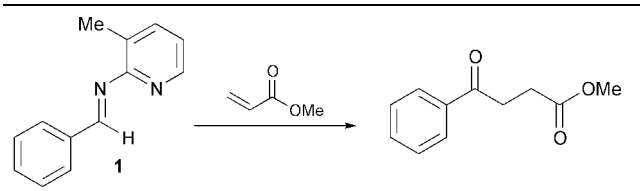

Entry	Temp./°C	Solvent	Time/h	Yield (%)
1	135	THF	6	73
2[b]	135	THF	6	47
3	70	THF	7	48
4	135	THF	4	59
5	135	PhMe	6	56

[a] *Conditions*: imine **1** (1.0 eq.), methyl acrylate (2.0 eq), sealed tube, $RhCl(PPh_3)_3$ (10 mol%) followed by HCl (1.0 M). [b] $RhCl(PPh_3)_3$ (5 mol%).

 DOI: 10.1039/b107852f

had a smaller influence on the rate of reaction; a -OMe substituent had minimal effect compared to the parent phenyl system with an 83% yield being achieved after 6 h (entry 4). *para*-Methyl and -bromo groups are also well tolerated delivering the corresponding 1,4-dicarbonyls in 98% and 85% yield respectively (entries 5 and 6). Exchange of a phenyl for the more electron rich naphthyl derived imine again showed little difference with the naphthyl derived adduct being obtained in 86% yield after 6 h reaction (entry 7).

The reason for the rate accelerations observed with the nitro- and cyano-substituted imines is unclear although destabilisation of the chelated intermediate is a possibility. Given these rate accelerations we were interested to see if these more reactive imines would allow α- and β-substituted acrylate esters to be employed as substrates. Unfortunately, although a rate acceleration was observed little difference in yield was obtained, with the nitro-substituted imine delivering products from reaction with methyl crotonate and methyl methacrylate in only 22% and 14% yield respectively.

The use of diimine **2**, prepared in good yield from benzene-1,4-dicarboxaldehyde, offers a potential starting point for two directional synthesis[14] and allowed a double hydroacylation to be attempted. Pleasingly, the required tetracarbonyl product **3** was isolated in 76% yield after 6 hours reaction.[15]

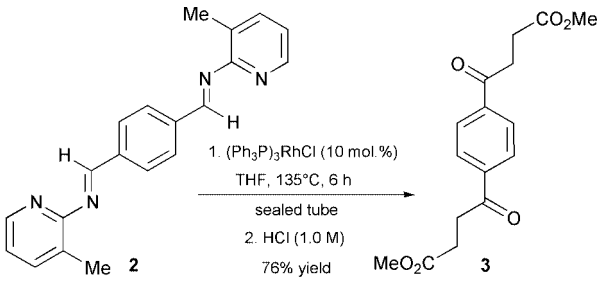

In conclusion, we have demonstrated the general viability of the intermolecular hydroacylation of acrylate esters as a new regioselective route to 1,4-dicarbonyl systems. The imine component of the reaction can tolerate a range of substituents including electron donating and electron withdrawing groups. The enoate component can contain a variety of ester groups as well as amide functionalities with little effect on yield, however, introduction of simple α- or -substituents reduces the efficiency of the reactions. Efforts to expand the substrate tolerance, to identify more efficient catalyst systems and to develop a process that can utilise aldehydes directly are underway in our laboratory and will be reported in due course.

The EPSRC are thanked for financial support of this project. We also thank the EPSRC Mass Spectrometry service at the University of Wales, Swansea, for analyses and Johnson Matthey PLC for the loan of rhodium salts.

Table 2 Reaction between **1** and various alkenes using $RhCl(PPh_3)_3$[a]

Entry	Alkene	Product	Time/h	Yield (%)
		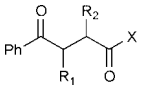		
1	X = OMe	$R_1 = R_2 = H$	6	73
2	X = O^{t}Bu	$R_1 = R_2 = H$	6	71
3	X = NMe_2	$R_1 = R_2 = H$	6	74
4	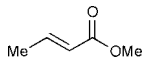	R_1 = Me, R_2 = H X = OMe	18	24
5	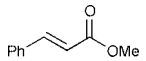	R_1 = Ph, R_2 = H X = OMe	12	10
6	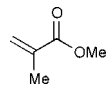	R_1 = H, R_2 = Me X = OMe	12	16
7[b]	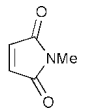	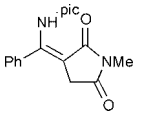	6	81

[a] *Conditions*: imine **1** (1.0 eq.), alkene (2.0 eq), THF, 135 °C, sealed tube, $RhCl(PPh_3)_3$ (10 mol%) followed by HCl (1.0 M). [b] Product isolated as enamine. pic = 3-picolin-2-yl.

Table 3 Variation in imine substituent[a]

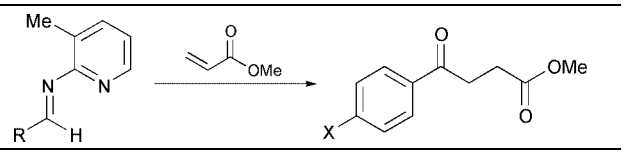

Entry	R	Time/h	Yield (%)
	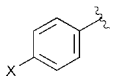		
1	X = H	6 h	73
2	X = NO_2	20 min	80
3	X = CN	80 min	80
4	X = OMe	6 h	83
5	X = Me	6 h	98
6	X = Br	6 h	85
7	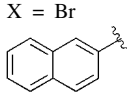	6 h	86

[a] *Conditions*: imine (1.0 eq.), methyl acrylate (2.0 eq), THF, 135 °C, sealed tube, $RhCl(PPh_3)_3$ (10 mol%) followed by HCl (1.0 M).

Notes and references

1 J. M. O'Connor and M. Junning, *J. Org. Chem.*, 1992, **57**, 5075.
2 For leading refs, see: (*a*) R. W. Barnhart, D. A. McMorran and B. Bosnich, *Inorg. Chim. Acta*, 1997, **263**, 1; (*b*) B. Bosnich, *Acc. Chem. Res.*, 1998, **31**, 667; (*c*) M. Fujio, M. Tanaka, X.-M. Wu, K. Funakoshi, K. Sakai and H. Suemune, *Chem. Lett.*, 1998, 881.
3 For examples, see: A. D. Aloise, M. E. Layton and M. D. Shair, *J. Am. Chem. Soc.*, 2000, **122**, 12610; K. P. Gable and G. A. Benz, *Tetrahedron Lett.*, 1991, **32**, 3473.
4 For leading refs, see: H. Lee and C.-H. Jun, *Bull. Korean Chem. Soc.*, 1995, **16**, 66; C. P. Lenges, P. S. White and M. Brookhart, *J. Am. Chem. Soc.*, 1998, **120**, 6965; T. Kondo, M. Akazome, Y. Tsuji and Y. Watanabe, *J. Org. Chem.*, 1990, **55**, 1286; T. Kondo, N. Hiraishi, Y. Morisaki, K. Wada, Y. Watanabe and T.-A. Mitsudo, *Organometallics*, 1998, **17**, 2131.
5 C.-H. Jun, D.-Y. Lee, H. Lee and J.-B. Hong, *Angew. Chem., Int. Ed.*, 2000, **39**, 3070.
6 J. W. Suggs, *J. Am. Chem. Soc.*, 1979, **101**, 489.
7 W. Friedrichsen, 'Furans and their benzo derivatives: synthesis', in *Compr. Heterocycl. Chem. II*, ed. C. W. Bird, Elsevier, Oxford, 1996.
8 E.-I. Negishi and M. Kotora, *Tetrahedron*, 1997, **53**, 6707.
9 R. E. Babine and S. L. Bender, *Chem. Rev.*, 1997, **97**, 1359.
10 D. Seebach, *Angew. Chem.*, 1979, **91**, 259; *Umpoled Synthons. A Survey of Sources and Uses in Synthesis*, ed. T. A. Hase, Wiley, New York, 1987.
11 For examples, see: G. Fremy, E. Monflier, J.-F. Carpentier, Y. Castanet and A. Mortreux, *Angew. Chem., Int. Ed. Engl.*, 1995, **34**, 1474; C. W. Lee and H. Alper, *J. Org. Chem.*, 1995, **60**, 499; Y. Hu, W. Chen, A. M. B. Osuna, J. Xiao, A. M. Stuart and E. G. Hope, *Chem. Commun.*, 2001, 725.
12 For an example of an intramolecular hydroacylation of an acrylate ester see ref. 2(*a*).
13 All new compounds have been characterised, see ESI for details.†
14 For a review, see: S. R. Magnuson, *Tetrahedron*, 1995, **51**, 2167.
15 The preparation of **3** serves as a general procedure: a solution of imine **2** (282 mg, 1.79 mmol) in THF (1 mL) was added to a solution of $RhCl(PPh_3)_3$ (167 mg, 10 mol %) in THF (1 mL) at room temperature and stirred for 1 h. Methyl acrylate (480 μL, 5.37 mmol) in THF (2 mL) was added and the reaction vessel flushed with argon. The reaction tube was sealed and then heated at 135 °C for 6 h. The reaction was cooled to room temperature, diluted with EtOAc (20 mL), poured into aqueous HCl (1 M, 20 mL) and extracted with EtOAc (3 × 20 mL). The organic portions were washed with brine (20 mL), dried ($MgSO_4$) and evaporated *in vacuo*. The residue was purified by flash chromatography (SiO_2, 25% EtOAc–petrol) to give **3** (212 mg, 76%) as pale yellow plates.

CHEMCOMM Communication
www.rsc.org/chemcomm

Facile enantioselective synthesis of a key homoallylic alcohol building block for polyketide synthesis: TiF_4–BINOL catalyzed allylsilylation with allyl trimethylsilane

Jeffrey W. Bode,[a] Donald R. Gauthier Jr.[a] and Erick M. Carreira*[a]

Laboratorium für Organische Chemie, ETH-Zentrum, Universitätstrasse 16, CH-8092 Zürich, Switzerland. E-mail: carreira@org.chem.ethz.ch

Received (in Cambridge, UK) 5th September 2001, Accepted 1st November 2001
First published as an Advance Article on the web 22nd November 2001

The titanium fluoride–BINOL catalyzed asymmetric allylsilylation of α,α-disubstituted aldehydes provides facile access to highly functionalized, chiral building blocks, which following simple recrystallization affords a key versatile starting material for polyketide synthesis in 96% ee.

Polyketides constitute a large class of naturally occurring structures with diverse, biological activities of importance to human medicine. As a consequence of the common biosynthetic pathways through which these structures are assembled there are often a number of recurring structural patterns in the form of 1,3-dicarbonyls, 1,3-hydroxy carbonyls, and 1,3-diols derived from acetate, propionate, or isobutyrate. Access to fragments that function as building blocks for the synthesis of these structures has resulted in many useful asymmetric synthetic enantioselective and diastereoselective methods.[1] The majority of these address the construction of acetate and propionate derived subunits, while many fewer are available for the preparation of isobutyrate derived subunits. We have recently reported the enantioselective TiF_4–BINOL catalyzed allylsilylation of aldehydes employing allyltrimethylsilane to afford adducts in useful selectivities and yields.[2] In our initial communication, the catalytic, enantioselective allylsilation of $^iPr_3Si$-protected 2,2-dimethyl-3-hydroxypropanal furnished the adduct in 93% yield, albeit in only 84% ee. The importance of such building blocks led us to initiate a program of study aimed at developing methods that would provide for their ready access. Herein we report investigations of this process furnishing fragments possesing the isobutyrate structural motif found in polyketide-derived natural products (eqn. 1). Importantly,

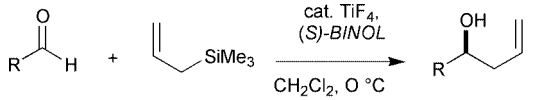

(1)

1 **2** **3**

the approach described herein furnishes optically active, crystalline adducts from commercially available reagents, and as such should find use in the ongoing studies towards the development of efficient routes and strategies to polyketide-derived natural products, such as aplasmomycin[3] byrostatins[4] epothilones,[5] mycalamides,[6] and boromycin.[7]

Among the critical advantages offered by the allylation reaction we have developed are: (1) the commercial availability of the ligand ((*R*)- or (*S*)- BINOL), metal (TiF_4), and allyltrimethylsilane; (2) the single step, *in situ*, preparation of the active catalyst from BINOL, TiF_4; (3) the low toxicity of allylsilane as compared to the alternative and often utilized allylstannane reagents; and (4) the volumetric efficiency of the process. In our preliminary laboratory screening of substrate scope for this transformation it was noted that the method was particularly effective for the enantioselective allylation of hindered, aliphatic non-enolizable aldehydes, affording adducts consistently in useful levels of enantiopurity.

The specific use of protected 2,2-dimethyl-3-hydroxypropionaldehyde in the allylation reaction provides access to the recurring structural isobutyrate motif found in polyketide-derived natural products. In an effort to identify the appropriate protecting group strategy that would provide crystalline material in high optical purity, we prepared a number of aldehyde substrates possessing a variety of protecting groups. Preparation of the necessary aldehydes was readily achieved by monoprotection of the 2,2-dimethypropane-1,3-diol, an inexpensive commodity chemical, followed by oxidation with either catalytic TEMPO[8] or catalytic TPAP.[9]

The allylation reaction of these substrates afforded adducts in 55–97% yield and 84–91% ee as shown in eqn. (2) and Table 1.[10,11] It is interesting to note that *O*-silyl, *O*-benzyl, and ester protecting groups all proved to be stable to and compatible with the allylation reaction. Also noteworthy is the ability to utilize both acetate (entry 6) and nitro (entry 5) moieties without complication by potentially competing reactions. Of the various adducts isolated, the 2-naphthoate protected adduct **5g** was isolated as a white crystalline solid in 91% ee and in 97% yield, following desilylation of the adduct. Importantly, after simple recrystallization, product was isolated enriched to 96% ee, as determined by chiral HPLC analysis. Additionally, the same reaction could be carried out with 5 mol% of the titanium catalyst on an 80 mmol scale, with the product isolated in 92% ee and in 72% yield.

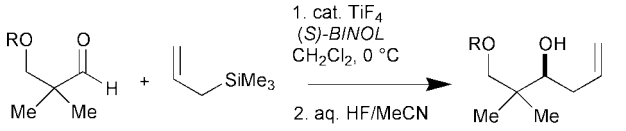

(2)

4a-g **2** **5a-g**

In an effort to demonstrate the versatility of these adducts, we have carried out a number of facile, high yielding transformations. Hydrolysis of the naphthoate esters with potassium carbonate in methanol led to diol **6**, which following protection

Table 1 TiF_4–BINOL catalyzed allyl silylation of **5a–g**

Entry	Substrate	Product	% ee	Yield
1	R = $^iPr_3Si$ **4a**	**5a**	84%[a]	93%
2	R = $^tBuMe_2Si$ **4b**	**5b**	86%[a]	48%
3	R = $PhCH_2$ **4c**	**5c**	89%[b]	55%
4	R = PhCO **4d**	**5d**	88%[a]	85%
5	R = *p*-$NO_2C_6H_4CH_2$ **4e**	**5e**	88%[c]	69%
6	R = MeCO **4f**	**5f**	90%[c]	85%
7	R = 2-Naphthoyl **4g**	**5g**	91%[c] (96%)[d]	97%

[a] Determined by GC analysis of the Mosher ester. [b] Determined by ^1H NMR analysis of the Mosher ester. [c] Determined by chiral HPLC analysis (Chiradex OD). [d] Following recrystallization.

 DOI: 10.1039/b107995f

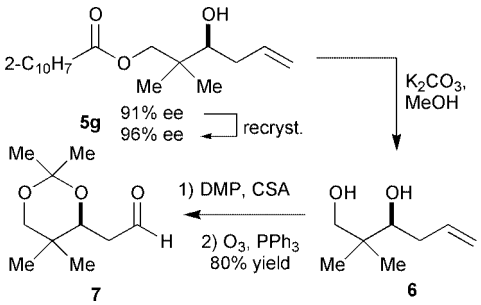

Scheme 1 Elaboration of adduct **6g** to diol **7**.

as the corresponding acetonide and ozonolytic cleavage of the olefin afforded chiral aldehyde **7** in 80% overall yield (Scheme 1). Alternatively, ozonolysis could be performed directly on the allyl adduct and the resulting aldehyde protected *in situ* as dioxolane **8** in 80% yield. Following saponification and selective oxidation of the primary hydroxy moiety, aldehyde **9** was obtained in 80% yield (Scheme 2).

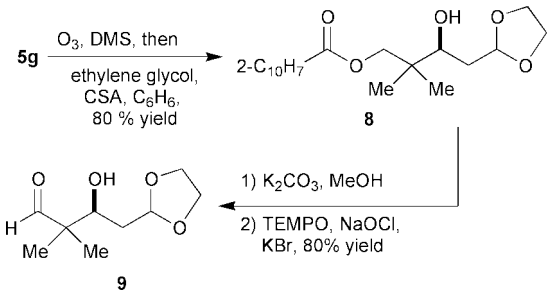

Scheme 2 Elaboration of adduct **6g** to aldehyde **10**.

In summary, the TiF_4–BINOL catalyzed allylsilylation of protected aldehydes provides facile access to highly functionalized building blocks in high enantiopurity. These results demonstrate the possibility of employing this reaction for the preparation of significant quantities of chiral starting materials and attests to the tolerance of this catalyst towards a number of potentially reactive functionalities. Importantly, the synthesis study described herein furnishes optically active, crystalline adducts from commercially available reagents, and as such should find applications in the development of increasingly efficient strategies to polyketide-derived natural products.

Support has been provided by generous funds from the ETH, the Kontaktgruppe für Forschungsfragen (KGF), Hoffmann-La Roche, and Merck. J. W. B. is grateful to the National Science Foundation (USA) for a predoctoral fellowship.

Notes and references

1 (*a*) *Catalytic Asymmetric Synthesis*, ed. I. Ojima, VCH, New York, 1993; (*b*) R. Noyori, *Asymmetric Catalysis in Organic Synthesis*, Wiley, New York, 1994.
2 D. R. Gauthier and E. M. Carreira, *Angew. Chem., Int. Ed. Engl.*, 1996, **35**, 2363–2365.
3 F. Matsuda, N. Tomiyoshi, M. Yanagiya and T. Matsumoto, *Tetrahedron Lett.*, 1986, **27**, 6345–6347.
4 M. Kageyama, T. Tamura, M. H. Nantz, J. C. Roberts and P. Somfai, *J. Am. Chem. Soc.*, 1990, **112**, 7407–7409.
5 G. H. Höfle, N. Bedorf, H. Steinmetz, D. Schonburg, K. Gerth and H. Reichenbach, *Angew. Chem., Int. Ed. Engl.*, 1996, **35**, 1567–1569.
6 N. B. Perry, J. W. Blunt, M. H. G. Munro and L. K. Pannell, *J. Am. Chem. Soc.*, 1988, **110**, 4850–4851.
7 H. Maehr, L. Leach, L. Yarmchuk and L. M. Mitrouic, *J. Antibiot.*, 1979, **32**, 361–367.
8 P. L. Anelli, C. Biffi, F. Montanari and S. Quici, *J. Org. Chem.*, 1987, **52**, 2559–2562.
9 W. P. Griffith, S. V. Ley, G. P. Whitcombe and A. D. White, *J. Chem. Soc., Chem. Commun.*, 1987, 1625–1627.
10 Experimental procedure for naphthalene-2-carboxylic acid (3*S*)-hydroxy-2,2-dimethylhex-5-enyl ester. To a suspension of TiF_4 (0.25 g, 2.0 mmol, 5.0 mol%) in 10 ml CH_3CN was added (*S*)-BINOL (1.15 g, 4.00 mmol, 10.0 mol%) and the mixture stirred 15 min before the solvent was removed under reduced pressure. After 10 min at 1.0 torr, the residue was dissolved in 10 ml CH_2Cl_2 and cooled to 0 °C. To this solution was added allyltrimethylsilane (12.7 ml, 80.0 mmol, 2.00 equiv.) and stirred 1 h to give a dark precipitate to which aldehyde **4g** (10.3 g, 40.0 mmol, 1.00 equiv.) was added neat in two portion to give a dark red-orange solution. This solution was allowed to stir 5 days at 0 °C at which time analysis by ^{1}H NMR showed the reaction to be complete. The reaction mixture was diluted with 2:1 pentane:ether (500 ml), filtered over silica gel and eluted with 2:1 pentane:Et_2O (500 ml). Following rotary evaporation, the resulting residue was treated with 5:95:1.5 HF:MeCN:H_2O (80 ml) for 0.5 h, dissolved in Et_2O (200 ml), washed with 2 M NaOH (2 × 50 ml), brine (100 ml), dried over Na_2SO_4, and concentrated to give a yellow oil (11.65 g, 98% yield). Purification by crystallization from hexanes provided **5g** (8.30 g, 72% yield) as a white solid in 92% ee. (Determined by chiral HPLC analysis Chiradex OD), 98:2 hexanes–iPrOH. $[\alpha]_D^{25}$ (*c* 0.950, $CHCl_3$) = +11.9; mp 46.5 °C; 1H NMR (300 MHz, $CDCl_3$) d 8.61 (s, 1H), 8.06 (dd, *J* = 8.7, 1.6, 1 H), 7.97 (d, *J* = 7.78, 1 H), 7.92 (d, *J* = 8.7, 1 H), 7.60–7.53 (m, 2 H), 5.97-5.83 (m, 1 H), 5.19 (d, *J* = 8.6, 1 H), 5.14 (s, 1 H), 4.48 (d, *J* = 10.9, 1 H), 4.13 (d, *J* = 10.9, 1 H), 3.59 (td, *J* = 8.4, 3.4, 1 H), 2.45–2.39 (m, 1 H), 2.20 (d, *J* = 3.4, 1 H), 2.17–2.12 (m, 1 H), 1.10 (s, 3H), 1.07 (s, 3H); ^{13}C NMR (75 MHz, $CDCl_3$): 167.0, 136.1, 135.6, 132.5, 131.1, 129.4, 128.3, 128.2, 127.8, 127.5, 126.7, 125.2, 118.0, 74.1, 71.2, 38.7, 36.2, 21.8, 19.4; IR (KBr) 3493, 3068, 2971, 2892, 1683, 1475, 1373, 1274, 1230, 1198, 905, 776; EI-MS: 298.1 $(M)^+$; Anal. Calcd. for ($C_{19}H_{22}O_3$) C, 76.48; H, 7.43%; found, C, 76.64; H, 7.26%.
11 At the current level of development the process works optimally with non-enolizable aldehydes. Enolizable aldehydes furnish adducts, albeit in reduced yields and selectivities.

CHEMCOMM
Communication
www.rsc.org/chemcomm

A new 'hybrid' molecular square composed of alternating multiply-bonded dinuclear and mononuclear corners

Jitendra K. Bera,[a] Bradley W. Smucker,[a] Richard A. Walton[b] and Kim R. Dunbar*[a]

[a] *Department of Chemistry, Texas A&M University, P.O. Box 30012, College Station, TX 77842-3012 USA. E-mail: dunbar@mail.chem.tamu.edu*

[b] *Department of Chemistry, Purdue University, 1393 Brown Building, West Lafayette, IN47907-1393, USA*

Received (in Columbia, MO, USA) 26th June 2001, Accepted 6th September 2001
First published as an Advance Article on the web 22nd November 2001

The incorporation of both dinuclear (M_2) and mononuclear (M′) units into molecular squares has been achieved by reacting a triply bonded Re_2(II,II) complex that possesses two *cis* isonicotinate donor ligands with Pt(II) molecules that contain substitutionally labile *cis* triflate groups.

The use of dicarboxylate bridging ligands to link quadruply bonded dimetal complexes into open-chain oligomers and polymers was first reported by Chisholm and coworkers over ten years ago.[1] Recently, several other research groups have demonstrated that cyclic architectures with M_2^{n+} units located at the vertices are also accessible from this chemistry.[2] The use of dimetal units in addition to square-planar[3] and octahedral[4] mononuclear building blocks in the design of metallocyclophanes, such as triangles and squares, opens up new prospects for research in this area including the possibility of incorporating mixed-nuclearity precursors into the same molecule. Herein we report the structure of a 'hybrid' molecular square from geometrically designed Re_2(II,II) and Pt(II) starting materials, the first such molecule of its kind to be reported.

In considering the goal of connecting M_2 and M′ units, one approach that occurred to us is to use a ligand such as isonicotinate that can bind to three metal atoms as depicted in Scheme 1. We reasoned that if a suitable dimetal complex with two *cis* isonicotinate ligands could be prepared, then the dangling pyridine groups would be available for further coordination to a square-planar metal center. In this vein, the new compound *cis*-$Re_2Cl_2(\mu\text{-dppm})_2(\mu\text{-}O_2CC_5H_4N)_2$ (**1**) was synthesized from *cis*-$Re_2Cl_2(\mu\text{-dppm})_2(\mu\text{-}O_2CCH_3)_2$[5] [dppm = bis(diphenylphosphino)methane] and isonicotinic acid in ethanol and characterized by NMR spectroscopy, electrochemistry† and X-ray crystallography.‡ As shown in Fig. 1, the *cis* conformation of the parent acetate complex is retained in complex **1**, the result of which is the presence of two orthogonal, uncoordinated pyridine groups of the isonicotinate ligands.

Compound **1** was reacted in a 1:1 ratio with the mononuclear complexes *cis*-$Pt[P(C_2H_5)_3]_2(O_3SCF_3)_2$[6] and $Pt(dbbpy)(O_3SCF_3)_2$[7] (dbbpy = 4,4′-di-*tert*-butyl-2,2′-bipyridine), both of which contain *cis*, labile triflate ligands, to yield complexes **2**§ and **3**,¶ respectively. The ^1H NMR spectra of these products established that the $Re_2Cl_2(\mu\text{-dppm})_2(\mu\text{-}O_2CC_5H_4N)_2$ and PtL_2 units (where L_2 is $[P(C_2H_5)_3]_2$ or dbbpy) are present in a 1:1 ratio. Crystals of $[cis\text{-}Re_2(O_3SCF_3)_2(\mu\text{-dppm})_2(\mu\text{-}O_2CC_5H_4N)_2Pt(dbbpy)]_2[O_3SCF_3]_4$ (**3**),‡ obtained as a CH_2Cl_2–H_2O solvate, revealed that the structure of the cation is a molecular square consisting of alternating $[(dppm)_2Re^{II}_2]$ and $[(dbbpy)Pt^{II}]$ units at the vertices and isonicotinate ligands along the edges (Fig. 2). This is the first example of a 'hybrid' molecular square involving multiply bonded dimetal units in combination with mononuclear units.

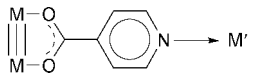

Scheme 1

The molecule, which resides on a crystallographic inversion center, is considerably distorted from ideality as clearly illustrated by various metrical parameters within the molecule. For example, the Pt1–Pt1′ diagonal is 11.97 Å whereas the diagonal defined by the midpoints of the two Re_2 units is 13.26 Å. The vertex angles subtended by the Re_2 units are less than the ideal value of 90° [O(1)–Re(2)–O(4) 80.9(7), O(2)–Re(1)–O(3) 79.8(7)°], a situation that leads to a bending of the isonicotinate ligands to accommodate ring closure.

Cyclic voltammetric studies in 0.1 M $^nBu_4NPF_6$–CH_2Cl_2 solutions of the new molecular squares revealed that both compounds exhibit two reversible one-electron oxidations; these are located at $E_{1/2}$ = +0.67 and +0.80 V for **2** (Fig. 3) and at $E_{1/2}$ = +0.54 and +0.67 V for **3**. The parent compound **1** exhibits a single one-electron oxidation at $E_{1/2}$ = +0.45 V (ΔE_p = 60 mV) under the same conditions. The fact that the molecular squares exhibit two closely spaced oxidation processes ($\Delta E_{1/2}$ = 130 mV for both **2** and **3**) is an indication of weak electronic coupling (comproportionation constant[8] K_c = 158) of the Re^{II}_2 units through the Pt^{II} centers.

The results of this study demonstrate the feasibility of preparing novel types of cyclic molecules based on the self-assembly of multiply bonded dimetal units with mononuclear building blocks. Further prospects for incorporating electron-rich metal–metal bonded complexes into cyclic architectures that contain a second type of reactive metal site are attractive ones that are being actively pursued in our laboratories.

K. R. D. gratefully acknowledges the National Science Foundation (PI grant, NSF CHE-99O6583; CCD diffract-

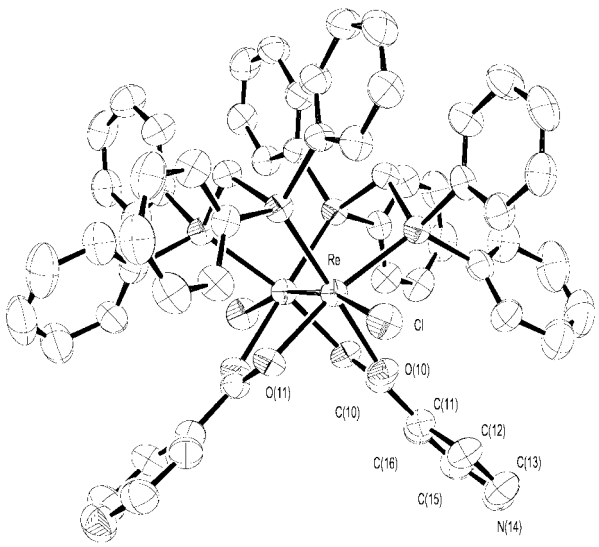

Fig. 1 ORTEP representation of the structure of **1** with important atoms labeled. The thermal ellipsoids are drawn at the 50% level. Some important bond distances (Å) and angles (°): Re–Re′ 2.3271(4), Re–O(11) 2.145(4), Re–O(10) 2.173(4), Re–P(1) 2.3958(16), Re–P(2) 2.4001(16), Re–Cl 2.5170(16), O(10)–Re–O(11) 82.43(17).

 DOI: 10.1039/b106600p

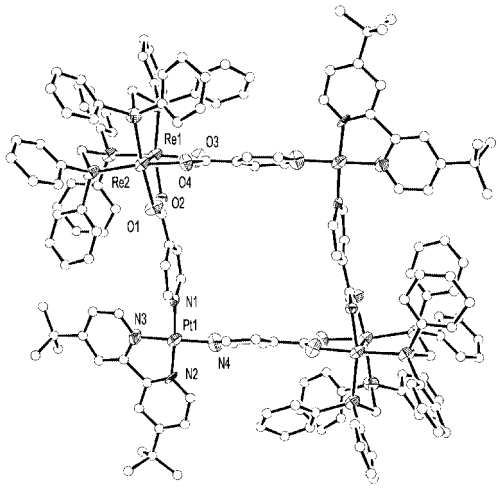

Fig. 2 Thermal ellipsoid plot of the cationic unit of **3** with important atoms labeled. The thermal ellipsoids are drawn at the 50% level except for the carbon atoms which are represented as circles of arbitrary radius. The C, O, F and S atoms of the triflate anions were removed for the sake of clarity. Selected bond distances (Å) and bond angles (°): Re(1)–Re(2) 2.2839(15), Pt(1)–N(2) 1.96(2), Pt(1)–N(1) 1.99(2), Pt(1)–N(4) 2.00(2), Pt(1)–N(3) 2.01(2), Re(1)–O(2) 2.086(17), Re(1)–O(3) 2.099(17), Re(2)–O(1) 2.109(17), Re(2)–O(4) 2.122(16), N(1)–Pt(1)–N(4) 89.0(9), O(2)–Re(1)–O(3) 80.9(7), O(1)–Re(2)–O(4) 79.8(7).

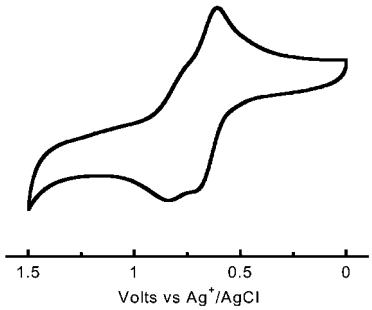

Fig. 3 Cyclic voltammogram of **2** recorded at a scan rate of 100 mV s^{-1} in 0.1 M $^nBu_4NPF_6$–CH_2Cl_2 solution on a CHI Electrochemical Workstation with a Pt disk working electrode, Pt-wire auxiliary electrode and a Ag/AgCl reference electrode.

ometer, CHE-9807975) as well as the Welch Foundation (A-1449) for support of this project. R. A. W. thanks the John A. Leighty Endowment Fund for support of this work.

Notes and references

† *Synthesis* of *cis*-$Re_2Cl_2(\mu\text{-dppm})_2(\mu\text{-}O_2CC_5H_4N)_2$ **1**: a mixture of *cis*-$Re_2Cl_2(\mu\text{-dppm})_2(\mu\text{-}O_2CCH_3)_2$ (0.103 g, 0.08 mmol) and isonicotinic acid (0.037 g, 0.30 mmol) was refluxed in ethanol for two days. The red crystals obtained were filtered off and washed with ethanol (3 × 5 mL) and diethyl ether (3 × 5 mL). Yield: 108 mg (87%). Anal. Calc. for $C_{66}H_{64}Cl_2N_2O_6P_4Re_2$ (**1**•$2C_2H_5OH$): C, 51.16; H, 4.17; N, 1.81. Found: C, 50.84; H, 4.10; N, 1.50%. ^{1}H NMR (in CD_2Cl_2): δ 5.05 and 6.51 (m, 4H, –CH_2– of dppm); 6.9–7.2, 7.46, 7.63 (m, 40H, Ph of dppm); 7.82 and 8.74 (m, 8H, isonicotinate), 1.25 (t, 6H, –CH_3, EtOH), 3.70 (q, 4H, –CH_2–, EtOH). ^{31}P{^{1}H} NMR (CD_2Cl_2): δ −9.36.

‡ *Crystal data*: for **1**•$2C_2H_5OH$: $C_{66}H_{64}Cl_2N_2O_6P_4Re_2$, M = 1548.46, monoclinic, space group $C2/c$ (no. 15), a = 28.2880(16), b = 10.1028(3), c = 23.7579(13) Å, β = 114.1577(18)°, V = 6195.1(10) Å^3, Z = 4, T = 295 ± 1 K, D_c = 1.660 g cm^{-3}, μ = 4.198 mm^{-1}, 22927 reflections (7023 unique, R_{int} = 0.063) with 2θ = 55.0°, 372 variables, R = 0.050 [6642 data, $I > 2\sigma(I)$], $wR(F_o^2)$ = 0.120, GoF = 1.008. Routine experimental details on data collection, solution and refinement procedures are reported elsewhere.[9]

For **3**•$2.37(CH_2Cl_2)$•$1.18(H_2O)$: $C_{170.36}H_{156.72}Cl_{4.74}F_{24}N_8O_{33.18}P_8Pt_2Re_4S_8$, M = 5110.00, monoclinic, space group $P2_1/c$ (no. 14), a = 20.218(4), b = 28.529(6), c = 20.218(4) Å, β = 98.78(3)°, V = 11525(4) Å^3, Z = 2, T = 110 ± 2 K, D_c = 1.473 g cm^{-3}, μ = 3.562 mm^{-1}, 70586 reflections (19136 unique R_{int} = 0.2771) with 2θ = 55.0°, 1138 variables, R = 0.094 [5748 data, $I > 2\sigma(I)$], $wR(F_o^2)$ = 0.2230, GoF = 0.870. The data were collected on a Siemens SMART CCD diffractometer with graphite monochromated Mo-Kα (λ = 0.71073 Å) radiation. The data were corrected for Lorentz and polarization effects. The frames were integrated with the Siemens SAINT software package,[10] and the data were corrected for absorption using the SADABS program.[11] The structure was solved by direct methods and refined using the program in the Bruker SHELXTL v5.1 software package.[12] Hydrogen atoms were placed in calculated positions and constrained with isotropic thermal parameters. The minimal electron density in the cavity of the square was assigned as a partially occupied H_2O. The partially occupied dichloromethane and water molecules sites and one carbon atom of a phenyl group were refined isotropically.

CCDC reference numbers 166127 and 166128. See http://www.rsc.org/suppdata/cc/b1/b106600p/ for crystallographic data in CIF or other electronic format.

§ *Synthesis* of [*cis*-$Re_2Cl_2(\mu\text{-dppm})_2(\mu\text{-}O_2CC_5H_4N)_2\{Pt(P(C_2H_5)_3\}_2]_2$-$[O_3SCF_3]_4$ **2**: a mixture of **1** (0.095 g, 0.07 mmol) and $Pt\{P(C_2H_5)_3\}_2(O_3SCF_3)_2$ (0.052 g, 0.07 mmol) was stirred in CH_2Cl_2 for 8–10 h. The red solution was concentrated and treated with diethyl ether to yield a solid that was collected by filtration, washed with fresh diethyl ether (3 × 5 mL) and recrystallized from CH_2Cl_2–diethyl ether: Yield: 140 mg (92%). Anal. Calc. for $C_{152}H_{164}Cl_4F_{12}N_4O_{20}P_{12}Pt_2Re_4S_4$: C, 41.76; H, 3.78; N; 1.28. Found: C, 42.18; H, 3.81; N, 1.89%. ^{1}H NMR (CD_2Cl_2): δ 5.05 and 6.43 (m, 4H, –CH_2– of dppm); 6.8–7.2, 7.41, 7.59 (m, 40H, Ph of dppm); 7.91 and 8.76 (m, 8H, isonicotinate), 1.20 (m, 18H, –CH_3 of PEt_3) and 2.18 (m, 12H, –CH_2– of PEt_3). ^{31}P{^{1}H} NMR (CD_2Cl_2): δ −10.07, +18.12.

¶ *Synthesis* of [*cis*-$Re_2(O_3SCF_3)_2(\mu\text{-dppm})_2(\mu\text{-}O_2CC_5H_4N)_2Pt(dbbpy)]_2[O_3SCF_3]_4$ **3**: a procedure similar to that described for **2** was employed using 0.095 g (0.07 mmol) of **1** and 0.052 g (0.07 mmol) of $Pt(dbbpy)(O_3SCF_3)_2$. Single crystals were grown by slow diffusion of Et_2O into a solution of **3** in CH_2Cl_2. Yield of isolated crystals is 42%. ^{1}H NMR ($CDCl_3$): δ 5.05 and 6.50 (m, 4H, –CH_2– of dppm); 6.8–7.2, 7.42, 7.60 (m, 40H, Ph of dppm); 8.01 and 8.80 (m, 8H, isonicotinate), 8.19, 8.28, 9.42 (m, 6H, aromatic, dbbpy), 1.45 (m, 18H, CH_3 of dbbpy) ^{31}P{^{1}H} NMR ($CDCl_3$): δ −9.88.

1 R. H. Cayton, M. H. Chisholm, J. C. Huffman and E. B. Lobkovsky, *J. Am. Chem. Soc.*, 1991, **113**, 8709; for recent works on dicarboxylate bridged M_2^{n+} complexes, see: F. A. Cotton, C. Lin and C. A. Murillo, *J. Chem. Soc., Dalton Trans.*, 1998, 3151; F. A. Cotton, L. M. Daniels, C. Lin and C. A. Murillo, *Chem. Commun.*, 1999, 841; F. A. Cotton, C. Lin and C. A. Murillo, *Inorg. Chem.*, 2001, **40**, 472; F. A. Cotton, J. P. Donahue, C. Lin and C. A. Murillo, *Inorg. Chem.*, 2001, **40**, 1234; F. A. Cotton, C. Lin and C. A. Murillo, *Chem. Commun.*, 2001, 11.

2 F. A. Cotton, L. M. Daniels, C. Lin and C. A. Murillo, *J. Am. Chem. Soc.*, 1999, **121**, 4538; R. P. Bonar-Law, T. D. McGrath, N. Singh, J. F. Bickley and A. Steiner, *Chem. Commun.*, 1999, 2457; J. F. Bickley, R. P. Bonar-Law, C. Femoni, E. J. MacLean, A. Steiner and S. J. Teat, *J. Chem. Soc., Dalton Trans.*, 2000, 4025; J. K. Bera, P. Angaridis, F. A. Cotton, M. A. Petrukhina, P. E. Fanwick and R. A. Walton, *J. Am. Chem. Soc.*, 2001, **123**, 1515; F. A. Cotton, C. Lin and C. A. Murillo, *Inorg. Chem.*, 2001, **40**, 478; F. A. Cotton, L. M. Daniels, C. Lin, C. A. Murillo and S. Y. Yu, *J. Chem. Soc., Dalton Trans.*, 2001, 502; F. A. Cotton, C. Lin and C. A. Murillo, *Inorg. Chem.*, 2001, **40**, 575.

3 M. Fujita, *Chem. Soc. Rev.*, 1998, **27**, 417; S. Leininger, B. Olenyuk and P. J. Stang, *Chem. Rev.*, 2000, **100**, 853; P. J. Stang and B. Olenyuk, *Acc. Chem. Res.*, 1997, **30**, 502. See also references therein.

4 R. V. Slone, J. T. Hupp, C. L. Stern and T. E. Albrecht-Schmitt, *Inorg. Chem.*, 1996, **35**, 4096; S. Bélanger, J. T. Hupp, C. L. Stern, R. V. Slone, D. F. Watson and T. G. Carrell, *J. Am. Chem. Soc.*, 1999, **121**, 557; C. S. Campos-Fernandez, R. Clérac and K. R. Dunbar, *Angew. Chem., Int. Ed.*, 1999, **38**, 3477 and reference therein; X. H. Bu, H. Morishita, K. Tanaka, K. Biradha, S. Furusho and M. Shionoya, *Chem. Commun.*, 2000, 971; J. R. Galán-Mascarós and K. R. Dunbar, *Chem. Commun.*, 2001, 217.

5 A. R. Cutler, D. R. Derringer, P. E. Fanwick and R. A. Walton, *J. Am. Chem. Soc.*, 1988, **110**, 5024.

6 P. J. Stang, K. Chen and A. M. Arif, *J. Am. Chem. Soc.*, 1995, **117**, 8793.

7 G. S. Hill, L. M. Rendina and R. J. Puddephatt, *J. Chem. Soc., Dalton Trans.*, 1996, 1809.

8 D. E. Richardson and H. Taube, *Inorg. Chem.*, 1981, **20**, 1278.

9 J. K. Bera, S. S. Lau, P. E. Fanwick and R. A. Walton, *J. Chem. Soc., Dalton Trans.*, 2000, 4277.

10 SAINT, Program for area detector absorption correction, Siemens Analytical X-Ray Instruments Inc., Madison, WI, USA, 1994–1996.

11 G. M. Sheldrick, SADABS, Program for Siemens area detector absorption correction, University of Göttingen, Germany, 1996.

12 G. M. Sheldrick, SHELXTL, An integrated system for solving, refining and displaying crystal structures from diffraction data (Revision 5.1), University of Göttingen, Germany, 1985.

CHEMCOMM
Communication
www.rsc.org/chemcomm

Synthesis of dinucleoside pyridylphosphonates involving palladium(0)-catalysed phosphorus–carbon bond formation as a key step

Tommy Johansson[a] and Jacek Stawinski*[ab]

[a] *Department of Organic Chemistry, Arrhenius Laboratory, Stockholm University, S-106 91 Stockholm, Sweden. E-mail: js@organ.su.se*
[b] *Institute of Bioorganic Chemistry, Polish Academy of Sciences, Noskowskiego 12/14, 61-704 Poznan, Poland*

Received (in Cambridge, UK) 28th September 2001, Accepted 30th October 2001
First published as an Advance Article on the web 23rd November 2001

Dinucleoside 3-pyridylphosphonates, as well as their 2- and 4-pyridyl positional isomers, have been synthesised using a palladium(0)-catalysed cross coupling strategy.

A pyridine ring is found in many natural products, *e.g.* in pyridine alkaloids, vitamins (niacin, pyridoxal), nicotinamide adenine dinucleotide phosphate (NADP), and constitutes a functionality often present in drugs (*e.g.* isoniazid—antitubercular activity; sulfapyridine—antibacterial and antiviral properties; pyrilamine—antihistaminic drug).[1]

These prompted us to develop a synthetic method for incorporation of a pyridine moiety in the form of pyridylphosphonate functionality (Chart 1) into natural product derivatives. Since the position of the phosphonyl group on the pyridine ring may be important for biological activity, all three isomeric compounds of type **1**, **2**, and **3** should be accessible for chemical and biological studies.

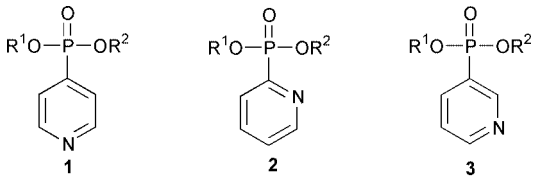

Chart 1

Recently, we have developed efficient and general protocols for the preparation of dinucleoside 2-pyridyl-[2] and 4-pyridylphosphonates[3] but, unfortunately, 3-pyridylphosphonates of type **3** cannot be prepared by these methods.

Introduction of a phosphonyl group into the 3-position of a pyridine ring is rather difficult and the few methods available for this purpose are usually low yielding.[4] Encouraged by the promising results of Hirao *et al.*[5] in the synthesis of diethyl 3-pyridylphosphonate **3**, we have embarked on a more detailed investigation of chemistry and stereochemistry of this palladium(0)-catalysed reaction, as a viable way for preparing dinucleoside pyridylphosphonates **6**–**8**.

We set out to prepare dinucleoside 3-pyridylphosphonates **6**, for which there was no synthetic method available. This required considerable experimentation to develop the best conditions of solvents and reagents, as well as the nature and quantity of the catalyst. Eventually, the use of equimolar amounts of dinucleoside H-phosphonate **4** and 3-bromopyridine **5a** in the presence of 0.2 equiv. of $Pd(PPh_3)_4$, and 1.2 equiv. of triethylamine (TEA) under reflux in THF, was found to serve most needs.† Using these conditions, a cross coupling of dinucleoside H-phosphonate **4** with 3-bromopyridine **5a** (Scheme 2) in the presence of a base (TEA) catalysed by the added $Pd(PPh_3)_4$ proceeded quantitatively (^{31}P NMR) and afforded the desired 3-pyridylphosphonate derivatives **6** in *ca.* 85% yield.

A palladium(0) catalytic cycle[6] expected for this type of reaction and supported by ^{31}P NMR experiments, is depicted in Scheme 1. It seemed that the most energy demanding step in this cycle was the ligand substitution, *i.e.* the formation of a *trans*-adduct **B** *via* nucleophilic attack of a phosphorus nucleophile on the initial intermediate, *trans*-adduct **A**. Since the only intermediate observed by ^{31}P NMR spectroscopy during the course of the reaction was that of *trans*-adduct **A** [δ_P = 24.2 ppm], the two consecutive steps in which **B** collapsed to the pyridylphosphonate products (see Scheme 1), both had to be fast.‡

To investigate the stereochemical outcome of this palladium(0)-catalysed cross coupling, separate diastereomers of dinucleoside H-phosphonate **4** were subjected to the reaction with 3-bromopyridine **5a** (Scheme 2). We found that the P–C bond formation was completely stereospecific as the R_P diastereomer **4a**, (δ_P = 6.9 ppm) afforded exclusively the diastereomer **6a**, (δ_P = 16.3 ppm), while the S_P diastereomer **4b** (δ_P = 8.6 ppm) produced the other diastereomer of 3-pyridylphosphonate **6b** (δ_P = 17.2 ppm).

To find out if the formation of the P–C bond in this reaction occurred with retention or with inversion of configuration at the phosphorus center in **4**, we decided to synthesise separate diastereomers of dinucleoside 2-pyridylphosphonates **7** and 4-pyridylphosphonates **8** using palladium(0) chemistry and compare them with the same compounds obtained in another way.[2,3]

Dinucleoside 4-pyridylphosphonates **8** were prepared using the protocol developed for 3-pyridylphosphonate **6**, by reacting separate diastereomers of dinucleoside H-phosphonate **4** with

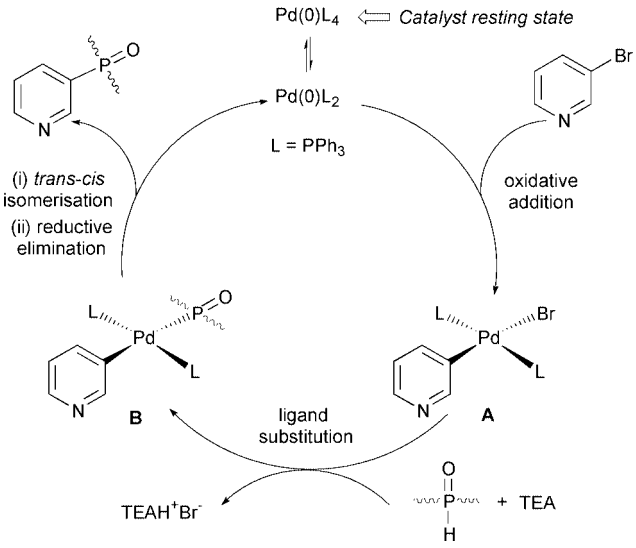

Scheme 1

 DOI: 10.1039/b108857m

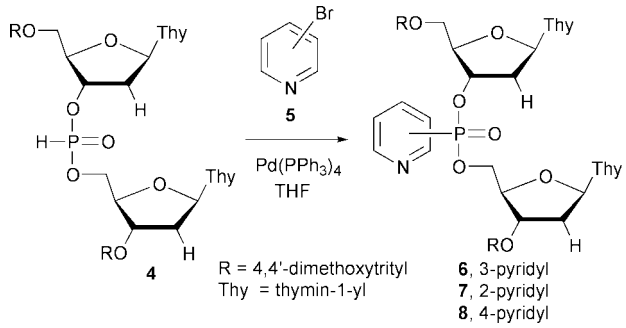

4a, (R_P) ("fast") (δ_P = 6.9 ppm)
4b, (S_P) ("slow") (δ_P = 8.6 ppm)
5a, 3-bromopyridine
5b, 2-bromopyridine
5c, 4-bromopyridine

6a, (R_P) ("fast") (δ_P = 16.3 ppm)
6b, (S_P) ("slow") (δ_P = 17.2 ppm)
7a, (R_P) ("fast") (δ_P = 10.6 ppm)
7b, (S_P) ("slow") (δ_P = 11.0 ppm)
8a, (R_P) ("fast") (δ_P = 15.0 ppm)
8b, (S_P) ("slow") (δ_P = 16.0 ppm)

Scheme 2

4-bromopyridine **5c** in the presence of $Pd(PPh_3)_4$. The reactions were stereospecific and afforded products **8**§ with the same stereochemistry as those formed in the reaction of H-phosphonates **4** with the pyridine–trityl chloride–DBU reagent system.[3] Since the latter provided products **8** most likely with retention of configuration at the phosphorus center,[3] we could tentatively conclude that the palladium(0)-catalysed cross coupling of H-phosphonate **4** with 4-bromopyridine **5c**, and probably also that with 3-bromopyridine **5a**, occurred with the same stereochemistry, *i.e.* with retention of configuration of the phosphorus center of **4**.

Attempted preparation of dinucleoside 2-pyridylphosphonate **7** by a palladium(0)-catalysed coupling of H-phosphonate **4** with 2-bromopyridine **5b**, turned out to be a more difficult task as the protocol developed for the 3-pyridyl isomer **6** afforded the desired product in less than 30% (^{31}P NMR analysis).

Inspired by the recent findings of Hartwig *et al.*[7] that chelating, sterically hindered phosphines are superior (in terms of yields and kinetics) ligands in palladium(0)-catalysed *N*-arylation of amines, we replaced in our catalytic system triphenylphosphine by 1,1′-bis(diphenylphosphino)ferrocene (DPPF). With this modification, the efficiency of 2-pyridylphosphonates **7** formation increased to *ca* 80% (^{31}P NMR analysis) and **7a** and **7b** were isolated in >50% yield.¶‖ By comparing the stereochemistry of 2-pyridylphosphonates **7** formed in this and in a DBU-catalysed reaction,[2] we conclude that both of them provided products with the same stereochemistry at the phosphorus centre. Thus, palladium(0)-catalysed formation of the P–C bond in this instance also most likely occurred with retention of configuration as was found for 3- and 4-pyridylphosphonates **6** and **8**.

It is worth noting that using DPPF in the synthesis of 3-pyridylphosphonates **6** shortened the reaction time from 4 to 2 h.†† Unfortunately, due to separation problems, yields of the isolated products **6** were lower (*ca.* 55%) than those where triphenylphosphine acted as a ligand.

In conclusion, we have developed a new method for the preparation of dinucleoside pyridylphosphonates **6**–**8** based on a palladium(0)-catalysed cross coupling of the corresponding H-phosphonate diesters **4** and halopyridines **5**. The reaction is stereospecific, occurring most likely with retention of configuration and can be considered as a general entry to isomeric pyridylphosphonate derivatives.

We are indebted to Professor P. J. Garegg for his interest in this work. Financial support from the Swedish Natural Science Research Council and the Swedish Foundation for Strategic Research is gratefully acknowledged

Notes and references

† *Typical protocol for the preparation of dinucleoside 3-pyridylphosphonates* **6**. Dry, degassed (argon) THF was used throughout and the reactions were carried out under an atmosphere of argon. A separate diastereomer **4a** or **4b**, (0.529 mmol), $Pd(PPh_3)_4$ (0.20 equiv.), triethylamine (1.2 equiv.) and 3-bromopyridine (1.0–1.2 equiv.) in freshly distilled and degassed THF (10 mL) was refluxed for 4–5 h. After concentration and partition of the reaction mixture between sat. aq. $NaHCO_3$ and CH_2Cl_2, the product was purified by silica gel column chromatography using a stepwise gradient of methanol (0.5–5%) in CH_2Cl_2 containing 0.1% TEA. White solids, purity >98% (^{1}H NMR). **6a** (85% from **4a**, probably R_P diastereomer). HRMS [M + H]$^+$, found 1212.4376. $C_{67}H_{67}N_5O_{15}P$ requires 1212.4371. **6b** (80% from **4b**, probably S_P diastereomer). HRMS [M + H]$^+$, found 1212.4373. $C_{67}H_{67}N_5O_{15}P$ requires 1212.4371. Some diagnostic spectral data (in $CDCl_3$) [compound, δP; δH(H-2 py); δH1′; δC(C-3 py) (J_{CP})]: **6a**, 16.3 ppm; 8.42–8.75 ppm (with pyr-H6, 2H); 6.38 (1H) & 6.26 (1H) ppm; 123.68 ppm (190 Hz). **6b**, 17.2 ppm; 8.86 ppm (1H); 6.39 (1H) & 6.20 (1H) ppm; 123.61 ppm (189 Hz).

‡ The same course of the reaction was observed when H-phosphonate **4** was allowed to react with a separately prepared intermediate **A**[8] in THF under reflux in the presence of TEA.

§ Compounds **8a** (from **4a**, 66% yield) and **8b** (from **4b**, 69% yield) were identical to those obtained in another way.[3] White solids, purity >98% (^{1}H NMR).

¶ The reaction was carried out as described above for 3-pyridylphosphonates **6**, with the exception that $Pd(PPh_3)_4$ was replaced by 0.2 equiv. of $Pd(OAc)_2$ and 0.4 equiv. of DPPF. Compounds **7a** (from **4a**, 54% yield) and **7b** (from **4b**, 51% yield) were identical to those obtained in another way.[2]

‖ The stereochemical course of the reaction was the same as that with $Pd(PPh_3)_4$. In contradistinction to DPPF, conformationally more flexible 1,3-bis(diphenylphosphino)propane (DPPP) was found to be unreactive, which may indicate the importance of rigidity of the ligand in this reaction.

†† With chelating ligands such as DPPF, oxidative addition (Scheme 1) results in the formation of *cis*- rather than *trans*-adducts (of type **A**). This may change geometry and electron distribution in the adduct and facilitate substitution of bromide by a phosphorus nucleophile, which was assumed to be the rate-determining step for the catalytic cycle.

1 *The Merck Index*, Merck & Co, Inc., Rahway, NJ, 1989.
2 T. Johansson, A. Kers and J. Stawinski, *Tetrahedron Lett.*, 2001, **42**, 2217.
3 A. Kers and J. Stawinski, *Tetrahedron Lett.*, 1999, **40**, 4263.
4 R. D. Bennett, A. Burger and W. A. Volk, *J. Org. Chem.*, 1958, **23**, 940.
5 T. Hirao, T. Masunaga, Y. Ohshiro and T. Agawa, *Synthesis*, 1981, 56.
6 C. Amatore and A. Jutand, *Acc. Chem. Res.*, 2000, **33**, 314.
7 M. S. Driver and J. F. Hartwig, *J. Am. Chem. Soc.*, 1996, **118**, 7217.
8 P. Fitton and E. A. Rick, *J. Organomet. Chem.*, 1971, **28**, 287.

CHEMCOMM Communication
www.rsc.org/chemcomm

Novel and catalytic oxidation of internal epoxides to α-diketones

Sylvain Antoniotti[a] and Elisabet Duñach*[b]

[a] *Laboratoire Arômes, Synthèses et Interactions, Université de Nice-Sophia Antipolis, Parc Valrose, 06108 Nice cedex 2, France*

[b] *Laboratoire de Chimie Bio-Organique, UMR CNRS 6001,Université de Nice-Sophia Antipolis, Parc Valrose, 06108 Nice cedex 2, France. E-mail: dunach@unice.fr*

Received (in Cambridge, UK) 10th July 2001, Accepted 15th October 2001
First published as an Advance Article on the web 23rd November 2001

A catalytic system based on Bi(0)–Cu(OTf)$_2$ is efficient for the selective one-pot oxidation of 1,2-disubstituted epoxides to α-diketones under molecular oxygen and DMSO.

The ring opening of epoxides,[1] including stereo-, regio- and enantioselective aspects, has been widely reported for the functionalization of organic compounds. However, the oxidative ring opening of oxiranes has been poorly explored, the oxirane ring being difficult to oxidize selectively. Within epoxide oxidations, the formation of α-hydroxy ketones in the presence of dimethyl sulfoxide and an activating agent has been reported to occur in moderate yields.[2] The oxidative cleavage of the C–C bond of oxiranes can lead to aldehydes or to carboxylic acids, by a Ce(IV)-mediated reaction[3] or by a Bi(III)-catalysed process,[4] respectively. To our knowledge, no report in the literature deals with the direct and catalytic transformation of epoxides to α-diketones.[5]

We recently reported the use of Bi(0) under oxidative conditions for the synthesis of carboxylic acids from α-hydroxy acids or terminal aryl epoxides involving the oxidative cleavage of the terminal C–C bond.[6] However, the reaction conditions were not well adapted to disubstituted epoxides.

We describe here a novel and simple methodology based on the use of catalytic amounts of Bi(0) and Cu(OTf)$_2$ (or TfOH), able to oxidize internal epoxides to α-diketones in one step, under relatively mild conditions, using molecular oxygen–DMSO according to Scheme 1.

This reaction involves Bi(III)/Bi(0) as the catalytic system; the possibility of using commercially available Bi(0) powder is interesting, due to its availability, its low cost and its low toxicity.[7]

The results of the oxidation of several 1,2-disubstituted epoxides are presented in Table 1. The reactions are carried out in DMSO at 100 °C and under an oxygen pressure of 1 atm in the presence of 5–10 mol% of Bi(0) powder and 2.5–20 mol% of Cu(Otf)$_2$ or TfOH as the additives. Interestingly, the black Bi(0) powder is dissolved in the organic medium containing the epoxide, affording a light yellow homogeneous solution, provided that the reaction is run under oxygen.

Cyclic, as well as linear 1,2-disubstituted epoxides led to the corresponding 1,2-diketones in good yields. For five and six-membered ring epoxides (entries 1–3, 6), the use of Cu(OTf)$_2$ (2.5–8 mol%) as the additive afforded the best results as compared to the use of other Lewis acids, such as $BiCl_3$, Li(NTf$_2$) or TfOH. Thus, epoxide **1a** afforded 74% isolated yield of cyclohexane-1,2-dione **1b**, whereas the same epoxide led to partial polymerisation in the presence of TfOH or Li(NTf$_2$) as the additives. On the other hand, for larger cycles (n = 12, **5a**) or linear epoxides such as **4a**, with less ring strain, the use of TfOH instead of Cu(OTf)$_2$ resulted in the best yields (entries 4, 5). The main by-products in the oxidation of **4a** and **5a** were the corresponding ketones (5–10% to 29% re-

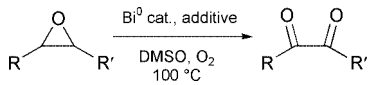

Scheme 1

Table 1 Bi-catalysed oxidation of epoxides under O_2 (1 atm) in DMSO at 100 °C

Entry	Epoxide	Bi(0) (equiv.)	Additive (equiv.)	Time (h)	Product	Yield
1	 **1a**	0.08	Cu(OTf)$_2$ (0.025)	2	 **1b**	74%
2	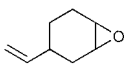 **2a**	0.05	Cu(OTf)$_2$ (0.08)	1.3	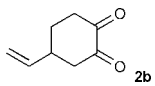 **2b**	77%
3	 **3a**	0.08	Cu(OTf)$_2$ (0.06)	2.3	 **3b**	48%
4	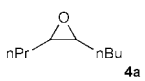 **4a**	0.10	TfOH (0.2)	2.3	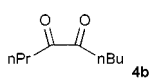 **4b**	83%
5	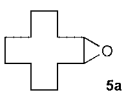 **5a**	0.06	TfOH (0.09)	7.0	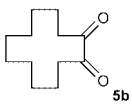 **5b**	70%
6	 **6a**	0.06	Cu(OTf)$_2$ (0.07)	2	 **6b**	52%

 DOI: 10.1039/b106110k

spectively), issued from the epoxide isomerisation in acidic medium.[8] No other by-products were detected.

The oxidation of unsaturated epoxides **2a** and **3a** indicated that olefin functions were not modified by the catalytic system.

The α-diketones in five or six-membered rings were mainly found in their enol form according to ^{1}H-NMR analysis (in $CDCl_3$ at 20 °C). Particularly in the case of entry 3, only the 1,2-dihydroxybenzene form was observed. However, diketones **4b** and **5b** were present with low enolisation (respectively 36 and 30%) under the same analytical conditions.

When a terminal epoxide such as 1-octene oxide was treated under the Bi(0)–$Cu(OTf)_2$ oxidation conditions (as for entry 1), the expected α-keto aldehyde underwent further C–C cleavage leading to a mixture of heptanal and heptanoic acid in 80% overall yield. This result was consistent with our previous observations on the reactivity of terminal epoxides.[6]

The presence of Bi(0) was essential for the preparation of the α-diketone. In the absence of bismuth, **1a** did not lead to **1b** but afforded 2-hydroxycyclohexanone in 55% yield. On the other hand, no diketone was obtained in the absence of O_2 (reactions under N_2) or in the absence of DMSO (reactions in DMF). This result indicates that DMSO would act as the oxygen transfer agent to the epoxide. Accordingly, dimethyl sulfide is evolved in the oxidation process. It was also shown that without any additive, the epoxide was unreactive.

In order to check if Bi(III) species were involved in the catalytic cycle, the reaction of **1a** was carried out in the presence of Bi(III)-mandelate,[9] replacing Bi(0) (conditions of entry 1). The reaction also afforded **1b**, but in low yield (10%). This result was taken to indicate that the reaction could proceed through a Bi(0)/Bi(III) redox couple, in agreement with recent results.[6] We observed that the Bi(0) oxidative dissolution (presumably to Bi(III)) needed molecular oxygen as well as the presence of the epoxide and the additive. Under nitrogen, the black Bi(0) precipitate persisted, and the epoxide oxidation to the α-diketone did not take place.

For the reaction mechanism, still under investigation, we propose the initial oxidative oxirane ring opening to an α-hydroxy ketone intermediate catalysed by the system $Cu(OTf)_2$ [or TfOH]–DMSO. The presence of a strong acid (Lewis or protic one) to activate the oxirane ring seems an important feature of this process. The presence of weakly coordinating triflate species could also have an important role in the reaction. DMSO, in association to the acid, effects the oxidative ring opening.

In a second step, in the presence of Bi(III), presumably issued from Bi(0) oxidative dissolution, a redox reaction affords the α-diketone by oxidation of the ketol. The reduced bismuth species are reoxidized to Bi(III) under molecular oxygen. The use of oxygen at the pressure of 1 atm as the oxidant in this step is an interesting aspect of the process. Recently, another Bi(III)–O_2 system has proven its efficiency in the deprotection of *S,S*-acetals.[10]

In conclusion, a new synthetic transformation is described, involving the oxidative ring opening of epoxides to α-diketones, in a combined Bi(0)–$Cu(OTf)_2$ catalytic system under O_2–DMSO. The process uses commercially available reagents in a one-pot reaction under relatively mild conditions.

S. A. thanks the French Ministry of Research for a doctoral fellowship.

Notes and references

General procedure for epoxide oxidation. A mixture of bismuth(0) (0.5 mmol) and the additive (0.5 mmol) in DMSO (15 ml) is heated at 100 °C under O_2 (1 atm). The epoxide (5mmol) in DMSO (5 ml) is then introduced through a serum cap and the mixture is stirred at this temperature until complete consumption of the epoxide (monitored by GC). The reaction mixture is hydrolysed with brine (50 ml) and extracted with diethyl ether (3 × 50 ml). The combined organic layers are dried over $MgSO_4$ and evaporated. The product is purified by column chromatography over silica gel with dichloromethane as the eluent. The products are identified by ^{1}H and ^{13}C NMR and mass spectroscopy, and compared with authentic commercial samples or literature data.

1 (*a*) S. Rampalli, S. S. Chaudhari and K. G. Akamanchi, *Synthesis*, 2000, **1**, 78; (*b*) V. Kesevan, D. Bonnet-Delpon and J. P. Bégué, *Tetrahedron Lett.*, 2000, **41**, 2895; (*c*) S. E. Denmark, P. A. Barsanti, K.-T. Wong and R. A. Stavenger, *J. Org. Chem.*, 1998, **63**, 2428; (*d*) S. Matsunaga, J. Das, J. Roels, E. M. Vogl, N. Yamamoto, T. Iida, K. Yamaguchi and M. Shibasaki, *J. Am. Chem. Soc.*, 2000, **122**, 2252.

2 T. M. Santusso and D. Swern, *J. Org. Chem.*, 1975, **40**, 2764.

3 S. C. Roy and S. Adhikari, *Indian J. Chem.*, 1992, **31B**, 459.

4 T. Zevaco, E . Duñach and M. Postel, *Tetrahedron Lett.*, 1993, **34**, 2601.

5 For catalytic oxidation of other substrates to α-diketones, see for example: (*a*) F. A. Kham, B. Prabhudas, J. Dash and N. Sahu, *J. Am. Chem. Soc.*, 2000, **122**, 9558; (*b*) C. M. Amon, M. G. Banwell and G. L. Gravatt, *J. Org. Chem.*, 1987, **52**, 4851.

6 C. Coin, V. Le Boisselier, I. Favier, M. Postel and E. Duñach, *Eur. J. Org. Chem.*, 2001, 735.

7 N. Irwing-Sax and R. J. Bewis, in *Dangerous properties of industrial materials*, Van Nostrand Reinhold, New York, 1989, 283.

8 (*a*) B. C. Ranu and U. Jana, *J. Org. Chem.*, 1998, **63**, 8212; (*b*) A. M. Anderson, J. M. Blazek, P. Garg, B. J. Payne and R. S. Mohan, *Tetrahedron Lett.*, 2000, **41**, 1527.

9 T. Zevaco and M. Postel, *Synth. React. Inorg. Met.-Org. Chem.*, 1992, **22**, (2&3), 289.

10 N. Komatsu, A. Taniguchi, M. Uda and H. Suzuki, *Chem. Commun.*, 1996, 1847.

CHEMCOMM Communication
www.rsc.org/chemcomm

Periodic large mesoporous organosilicas from lyotropic liquid crystal polymer templates†

Haoguo Zhu, Deborah J. Jones, Jerzy Zajac, Jacques Rozière* and Roger Dutartre

Laboratoire des Agrégats Moléculaires et Matériaux Inorganiques, UMR CNRS 5072, Université Montpellier II, Place Eugène Bataillon, 34095, Montpellier cedex 5, France.
E-mail: debtoja@crit.univ-montp2.fr

Received (in Cambridge, UK) 31st July 2001, Accepted 9th October 2001
First published as an Advance Article on the web 13th November 2001

Periodic large mesopore organosilicas have been obtained for the first time using bridged silsesquioxane $(RO)_3SiCH_2CH_2Si(OR)_3$ precursors and triblock copolymers as structure-directing species in acid media.

Recently, beneficial properties of ordered mesoporous materials and hybrid organic–inorganic frameworks have been combined in an interesting class of materials possessing organic fragments fused 'within' the mesoporous framework, denoted periodic mesoporous organosilicas (PMO) through the surfactant-templated condensation of bifunctional organosiloxane presursors $(R'O)_3SiRSi(OR')_3$.[1–5] The development of PMOs offers an opportunity for fine-tuning porous structure, surface and framework characteristics by the judicious choice of the organic groups incorporated, and the synthesis conditions employed, and their properties may open new opportunities in catalysis, separations and advanced materials design. To date, the pore diameters of all reported PMOs are in the range of 2–4 nm,[1–4] however PMOs with larger pores are desirable for a variety of possible applications such as hosts for chemical reactions, uses in separations, immobilisation or encapsulation involving large molecules *etc*. Usually, ordered mesoporous silica phases with large pores are synthesised by using triblock copolymers as templates in strong acid (2 M HCl).[6] The charge density on organosilicate species formed by hydrolysis and oligomerisation of organosiloxanes under strong acid conditions is lower than that on the silicate species formed from tetraethoxysilane (TEOS),[1] and at low surfactant concentrations, no inorganic–organic interaction-induced long-range ordering of block polymers into templates occurs to help organise inorganic polymerising species. Thus the organosiloxane precursors are hydrolysed, and polymerised disordered structures and scattered pore-size distributions are obtained in such experimental conditions. An alternative route towards ordered mesoporous ceramic nanostructures is the utilisation of reformed lyotropic liquid crystal phases as structure-directing media.[7–11] For direct liquid crystal templating, surfactant concentrations are high enough to form long-range ordered assemblies even in the absence of silica–surfactant interactions. Thus, it is not necessary to create strong interactions between surfactant arrays and inorganic species because such interactions may disrupt the already existing long-range ordering of surfactant arrays.[9] Non-ionic block copolymers are very suitable for use in preparing ordered PMO materials by direct liquid crystal templating.[7,9] Feng *et al.* have reported large mesopore silicas using non-ionic Pluronic surfactants as templates in the triblock copolymer–alcohol–water ternary system.[9] In this communication, we report the synthesis of PMO systems with large tunable mesopores and a narrow pore size distribution using pre-existing polymeric liquid crystal phases as templates in the binary triblock copolymer–water system.

In a typical synthesis, colloidal ethanesilica was prepared by mixing an aqueous dilute HCl solution (pH 2) with bis(triethoxysilyl)ethane (BTE). Pluronic P123 ($M_{av} = 5800$), $EO_{20}PO_{70}EO_{20}$ was then added to the mixture, and the ethanol from the hydrolysis of BTE was removed under vacuum. The mass ratio was H_2O/HCl (1.0):P123 (0.8):BTE (3.2). As expected, the use of lyotropic polymer templates for the synthesis of nanocomposites has the advantage that macroscopic, optically transparent monoliths are obtainable, and crack-free monoliths can be obtained in considerable size. They are stable in air and due to their low-k dielectric and transparent properties, may have possible use in optical, electronic or other advanced applications.[5,12] The mesoporous ethanesilica materials were investigated by powder X-ray diffraction (PXRD), as shown in Fig. 1. After hydrothermal treatment and extraction of surfactant,[9] the long-range ordering of the sample is improved. The presence of (100), (110) and (200) peaks in the diffraction patterns is characteristic of well-ordered, 2-D hexagonal mesoporous monolithic materials. The ^{29}Si MAS NMR spectrum (see ESI†) of the hybrid mesoporous materials shows a broad ^{29}Si resonance at −56.5 ppm and a shoulder at −64.2 ppm, corresponding to trifunctional (−56.5 ppm, $RSiO_2(OH)$; −64.2 ppm, $RSiO_3$) silicon.[1–5] There was no evidence of tetrafunctional Q silicons between −90 and −120 ppm, and the absence of SiO_4 species such as $Si(OH)(OSi)_3$ and $Si(OSi)_4$ confirms that no cleavage of the carbon–silicon bond of the BTE starting organosilane compound has occurred during hydrolysis and polymerisation. The presence of T^2 Si atoms was indicative of incomplete condensation of the organosilane precursor, unreacted silanol groups still being present. On the other hand, a high concentration of silanol may be desirable for post-synthesis functionalisation of the mesoporous wall structure.[9] FT-IR spectroscopy† also supported this result, showing the appearance of absorption bands assigned to C–Si streching modes (ν(C–Si), 1273 cm^{-1}), while the broad absorption band at 1000–1200 cm^{-1} (ν(Si–O–Si)) indicates the formation of

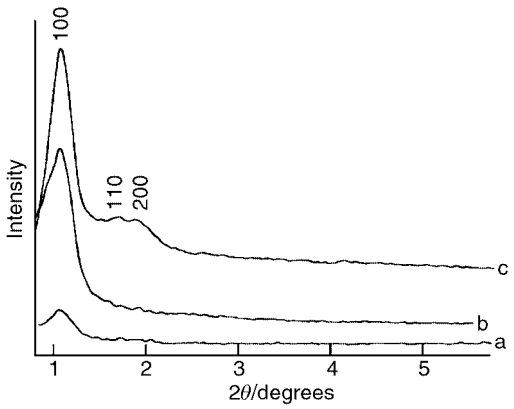

Fig. 1 Powder X-ray diffraction patterns of as-synthesised and surfactant-extracted hexagonal mesophases prepared from a P123/water system (51 wt%). (a) As-synthesised organosilica–surfactant mesophase before hydrothermal treatment; (b) as (a), hydrothermally treated at 100 °C for 24 h; (c) as (b), hydrothermally treated at 100 °C for 24 h, and then solvent extracted.

† Electronic supplementary information (ESI) available: TEM image, MAS NMR and FT-IR spectra, and BJH pore size distribution for PMO materials. See http://www.rsc.org/suppdata/cc/b1/b106938c/

 DOI: 10.1039/b106938c

siloxane bonds. Residual silanol groups are evidenced by the ν(Si–OH) streching vibration at 900 cm^{-1}.[13] It is important to note that all silicon atoms are covalently connected to carbon atoms. Powder X-ray diffraction and TEM images of the materials showed that the structural integrity and order of the material is well maintained. In acid media, a slow and moderate condensation of organosilica units probably facilitates the ordering of the organic fragments due to a rigidity of the siloxane network that is lower when it consists of T^2 substructures than when it contains fully condensed T^3 substructures. In silica–block copolymer systems, hydrothermal treatment can lead to an enhancement of mesoscopic ordering and a reduction in shrinkage after removing surfactants. In the present case, after hydrothermal treatment at 100 °C for 24 h and solvent extraction, the materials showed an intensity enhanced diffraction pattern. TEM investigation of PMOs confirmed that they were well organised and have a 2-D *P6mm* hexagonal structure (Fig. 2). In the hexagonal range of the surfactant/water binary system,[14] an increase in surfactant concentration leads to an expansion in the mesopore size. With a ratio of PO/EO > 1, the increase in the hydrophobic volume exceeds the increase in hydrophilic volume, and the pore size can be tuned in the range of 5.8–7.7 nm through changing the concentration of the block copolymers. The N_2 adsorption isotherms at 77 K of the materials show a typical type IV isotherm with a clear H1-type hysteresis loop at high relative pressures and a vertical capillary condensation step at about P/P_0 = 0.75 (Fig. 3), suggesting that the materials have very regular mesoporous channels despite their large pore size. Quantitative analysis shows that the Brunauer–Emmett–Teller (BET) surface area is 957 m^2 g^{-1}, the total pore volume 1.37 cm^3 g^{-1}, and the most probable pore diameter 7.7 nm (BJH model). In conjunction with the unit cell dimension of 9.3 nm estimated from PXRD and TEM, this provides a wall thickness of *ca.* 1.6 nm. The wall thickness is in agreement with results on related systems.[2,15]

Thermogravimetric analysis of surfactant–organosilica mesophases shows a weight loss at 35–80 °C corresponding to the removal of physically adsorbed water and a weight loss at 150–250 °C corresponding to the elimination of surfactant. TGA data for solvent-extracted PMOs show a major weight loss at 200–300 °C corresponding to the decomposition and release of ethane fragments from the hybrid framework. This suggests that the thermal decomposition of surfactants may have a detrimental effect on organic groups in the PMO framework.[15]

In conclusion, a novel large pore size highly ordered PMO material has been synthesised for the first time, and is being investigated for the possible applications in immobilisation and encapsulation of large molecules.

H. Z. thanks the French government for a post-doctoral award.

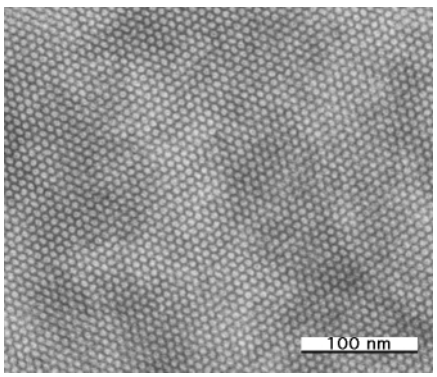

Fig. 2 Transmission electron micrograph of mesoporous organosilica after surfactant extraction.

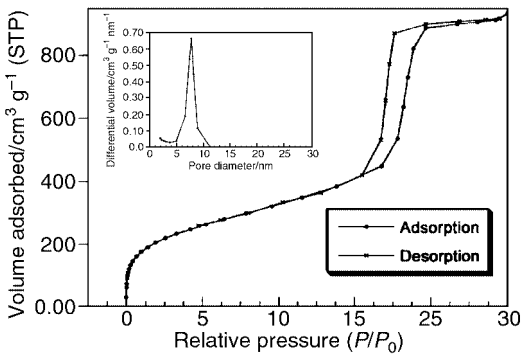

Fig. 3 Nitrogen adsorption–desorption isotherms at 77 K and (inset) BJH pore-size distribution plot for the mesoporous organosilica.

Notes and references

1 S. Inagaki, S. Guan, Y. Fukushima, T. Ohsuna and O. Terasaki, *J. Am. Chem. Soc.*, 2000, **122**, 823.

2 B. J. Melde, B. T. Hollande, C. F. Blanford and A. Stein, *Chem. Mater.*, 1999, **11**, 3302.

3 (*a*) T. Asefa, M. J. MacLachlan, N. Coombs and G. A. Ozin, *Nature*, 1999, **402**, 867; (*b*) M. J. MacLachlan, T. Asefa and G. A. Ozin, *Chem. Eur. J.*, 2000, **6**, 2507; (*c*) T. Asefa, M. J. MacLachlan, H. Gondley, N. Coombs and G. A. Ozin, *Angew. Chem., Int. Ed.*, 2000, **39**, 1808.

4 A. Sayari, S. Hamoudi, Y. Yang, J. L. Moudrakovski and J. R. Ripmeester, *Chem. Mater.*, 2000, **12**, 3857.

5 Y. Lu, H. Fan, N. Doke, D. A. Loy, R. A. Assink, D. A. LaVan and C. J. Brinker, *J. Am. Chem. Soc.*, 2000, **122**, 5258.

6 D. Zhao, Q. Huo, J. Feng, B. F. Chmelka and G. D. Stucky, *J. Am. Chem. Soc.*, 1998, **120**, 6024.

7 (*a*) G. S. Attard, J. C. Glyde and C. G. Göltner, *Nature*, 1995, **378**, 366; (*b*) C. G. Göltner, S. Henke, M. C. Weissenberger and M. Antonietti, *Angew. Chem., Int. Ed.*, 1998, **37**, 613.

8 P. V. Braun, P. Osenar and S. I. Stupp, *Nature*, 1996, **380**, 325.

9 (*a*) P. Feng, X. Bu, G. D. Stucky and D. J. Pine, *J. Am. Chem. Soc.*, 2000, **122**, 994; (*b*) P. Feng, X. Bu and D. J. Pine, *Langmuir*, 2000, **16**, 5304.

10 (*a*) N. A. Melosh, P. Davidson and B. F. Chmelka, *J. Am. Chem. Soc.*, 2000, **122**, 823; (*b*) N. A. Melosh, P. Lipic, F. S. Bates, F. Wudl, G. D. Stucky, G. H. Fredrickson and B. F. Chmelka, *Macromolecules*, 1999, **32**, 4332.

11 (*a*) P. Yang, D. Zhao, D. I. Margolese, B. F. Chmelka and G. D. Stucky, *Nature*, 1998, **396**, 152; (*b*) J. Rozière, M. Jacquin, M. Brandhorst, R. Dutartre, D. J. Jones and J. Zajac, *J. Mater. Chem.*, 2001, **11**, 3262.

12 B. Lebeau, C. E. Fowler, S. R. Hall and S. Mann, *J. Mater. Chem.*, 1999, **9**, 2279.

13 A. C. Franville, D. Zambon, R. Mahiou and Y. Troin, *Chem. Mater.*, 2000, **12**, 428.

14 B. Chu and Z. Zhou, in *Nonionic Surfactant: Polyoxyalkylene Block Copolymer*, ed. V. M. Nace, Surface Science Series Vol. 60, Marcel Dekker, New York, 1996.

15 M. Kruk, M. Jaroniec, S. Guan and S. Inagaki, *J. Phys. Chem. B*, 2001, **105**, 681.

CHEMCOMM Communication
www.rsc.org/chemcomm

Synthesis and characterization of [4$_6$]paracyclophanedodecayne derivative

Masakazu Ohkita,* Kohta Ando and Takashi Tsuji*

Division of Chemistry, Graduate School of Science, Hokkaido University, Sapporo 060-0810, Japan. E-mail: ohkita@sci.hokudai.ac.jp and tsuji@sci.hokudai.ac.jp

Received (in Cambridge, UK) 11th September 2001, Accepted 29th October 2001
First published as an Advance Article on the web 13th November 2001

[4$_6$]paracyclophanedodecayne derivative 1 having a novel belt-shaped fully conjugated π-system was photochemically generated from the corresponding hexakis(Dewar benzene) precursor 7 as a highly strained but isolable compound.

Recently much attention has been focused on the design and construction of novel carbon-rich materials with unusual structural, electronic and optical properties.[1] Despite the fascinating structural features, however, π-conjugated carbon-rich macrocycles with a cylindrical structure still remain as a synthetic challenge, although several attempts to prepare related belt-shaped molecules such as cyclacenes,[2] cyclic paraphenylenes[3] and [8.8]paracyclophaneoctayne[4] have been reported. Remarkable examples are cyclic paraphenylacetylenes prepared by Kawase and Oda.[5] The generation of cyclo[*n*]carbons[6] and related polyyne-bridged cyclophanes[7] under mass spectroscopic conditions have also been proposed. In this communication we report the synthesis and characterization of the first [4$_6$]paracyclophanedodecayne derivative **1b**, in which six *p*-phenylene and butadiyne units are alternately connected to form a highly unsaturated cylindrical π-conjugated system. A key feature in the present approach is exploitation of a Dewar benzene as an angular *p*-phenylene synthon.[8] Thus, macrocycle **1b** was photochemically generated from the corresponding hexakis(Dewar benzene) compound **7** as a highly strained but isolable compound.

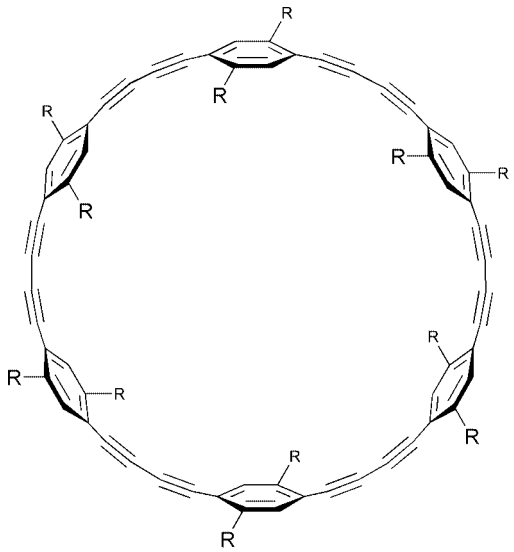

1a R = H
1b R = $CH_2OSiMe_2(t\text{-Bu})$

Synthesis of the precursor **7**, which also represents a rare example of oligo(Dewar benzene)s,[8,9] was achieved by using Dewar benzene building block **2**[8] as outlined in Scheme 1. Successive Pd-catalyzed couplings of **2** with TMS–acetylene and TIPS–acetylene gave unsymmetrical monomer unit **3**,

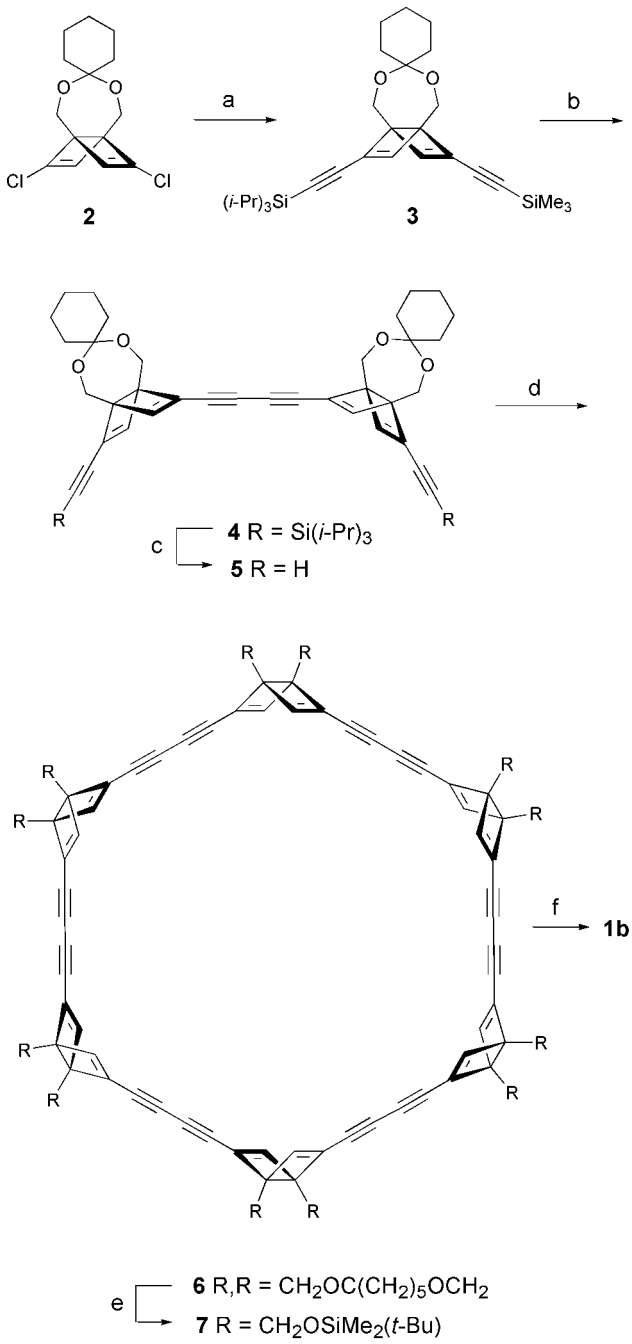

Scheme 1 *Reagents and conditions*: (a) (i) Me_3SiCCH, $Pd(PPh_3)_4$, CuI, Et_3N, rt; (ii) $(i\text{-Pr})_3SiCCH$, $Pd(PPh_3)_4$, CuI, Et_3N, rt, 54% (two steps); (b) $Cu(OAc)_2$, CuCl, Py, rt, 85%; (c) Bu4NF, THF, 0 °C; (d) $Cu(OAc)_2$, CuCl, Py, 60 °C, syringe-pump, 15% (two steps); (e) (i) 1 N HCl, THF, rt, (ii) $CF_3SO_3SiMe_2(t\text{-Bu})$, Et3N, rt, 69% (two steps); (f) *hν*, benzene, 12 °C, 100%. Although compounds **4**–**7** are inseparable mixtures of diastereomers, only those with the highest symmetry are illustrated for clarity.

 DOI: 10.1039/b108253c

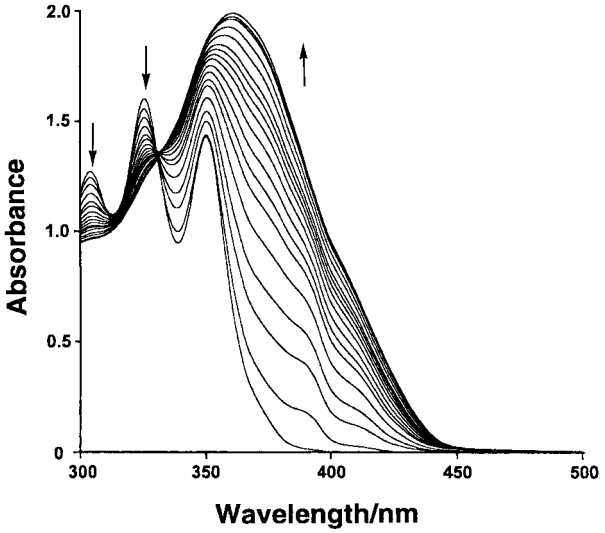

Fig. 1 UV-vis spectral changes observed upon irradiation of **7** in benzene through Pyrex at 30 s intervals.

which was converted to dimer unit **4** by an *in situ* selective deprotection–oxidative coupling sequence.[10] After the removal of the TIPS groups, **5** was subjected to the modified Eglinton coupling[10] under pseudo-high-dilution conditions to afford cyclic hexamer **6** in 15% yield as a mixture of diastereomers after purification by preparative GPC. In this macrocylization, a larger cyclic oligomer, to be assigned as octamer, was also formed as a minor product (5–8% yield). Acid hydrolysis of **6** followed by silylation of the resulting polyol afforded hexakis(Dewar benzene) derivative **7**.

Aromatization of **7** was found to proceed smoothly and cleanly under photochemical conditions to afford **1b**.† Thus, ^{1}H NMR monitoring of the photolysis showed that irradiation of **7** in $CDCl_3$ with a high-pressure mercury lamp through Pyrex at ambient temperature led to the formation of a single product in a nearly quantitative yield. The marked down-field shift observed for the resonance signals due to the olefinic protons (δ 6.80–6.83) and the CH_2OTBS methylene protons (δ 4.00) to δ 7.58 and δ 4.80, respectively, are consistent with the aromatization of the Dewar benzene units. The UV-vis spectral changes recorded during the photolysis of **7** in benzene are shown in Fig. 1; the isosbestic point observed is also indicative of the clean conversion of **7** into **1b**.‡ Macrocycle **1b** was isolated as a rather air-sensitive pale yellow solid which decomposed gradually within several days upon standing in solution or in the solid state under air at room temperature. Although attempts to determine the molecular mass of **1b** by mass spectroscopy with routine ionization methods (EI, FD, FAB) failed, it was successfully determined by ESI-MS as a complex with Na^+. Compound **1b** exhibits simple ^{1}H and ^{13}C NMR spectra in $CDCl_3$ at 25 °C, four singlets in the former and nine lines in the latter, suggesting fast rotation of the *p*-phenylene units on the NMR time scale at this temperature.§ Since to date we have been unable to obtain single crystals of **1b** suitable for X-ray diffraction study, we carried out semiempirical PM3 calculations for model compound **1a** to gain structural information about **1b**. As shown in Fig. 2, the optimized structure of **1a** adopts a cylindrical conformation possessing a well-defined cavity of about 15 Å diameter. The strained nature of **1a** is mainly reflected in the deviation of the acetylene moieties from linearity and the calculated C≡C–C(sp^2) and C≡C–C(sp) bond angles are 170.8° and 171.2°, respectively.

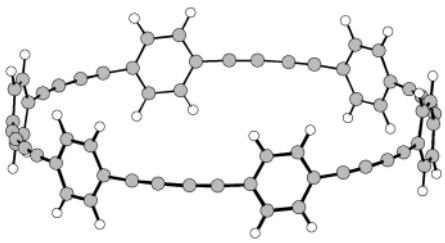

Fig. 2 PM3 optimized structure of **1a**.

In conclusion, we have successfully synthesized and characterized [4$_6$]paracyclophanedodecayne derivative **1b**, possessing the most unsaturated cylindrical π-conjugated system ever isolated. The present results clearly demonstrate the high synthetic potential of our Dewar benzene building block approach for the construction of strained phenylene macrocycles that are difficult to prepare from planar benzene derivatives.

This work was supported by Grants-in-Aid for Scientific Research (No. 09640620 and 12640508) from the Ministry of Education, Science, Sports and Culture of Japan.

Notes and references

† *Spectroscopic data* for **1b**; ν_{max} (KBr)/cm^{-1} 2928, 2852 and 1096; δ_H (300 MHz, $CDCl_3$) 0.12 (36 H, s), 0.94 (54 H, s), 4.80 (24 H, s) and 7.58 (12 H, s); δ_C (75 MHz, $CDCl_3$) −5.28, 18.42, 25.96, 62.79, 81.97, 86.34, 120.30, 130.15 and 142.72; *m*/*z* (ESI) 2499.1 (M + Na^+, 100%); λ_{max} (benzene)/nm 360 (log ε_{em} 5.02); λ_{em} (excitation at 360 nm, benzene)/nm 442 and 468 sh.

‡ It is not clear at present whether the aromatization of the Dewar units in **7** proceeds as a one-photon process or in a stepwise fashion.

§ The limited solubility of **1b** hampered its NMR measurement at lower temperature.

1 R. Faust, *Angew. Chem., Int. Ed.*, 1998, **37**, 2825; U. H. F. Bunz, Y. Rubin and Y. Tobe, *Chem. Soc. Rev.*, 1999, **28**, 107; U. H. F. Bunz, *Chem. Rev.*, 2000, **100**, 1605; *Topics in Current Chemistry*, ed. A. de Meijere, Springer-Verlag, Heidelberg, 2000, vol. 35.

2 F. H. Kohnke, J. P. Mathias and J. F. Stoddart, *Top. Curr. Chem.*, 1993, **165**, 1; R. M. Cory and C. L. McPhail, *Tetrahedron Lett.*, 1996, **37**, 1987 and references cited therein.

3 R. Friederich, M. Nieger and F. Vögtle, *Chem. Ber.*, 1993, **126**, 1723.

4 M. M. Haley and B. L. Langsdorf, *Chem. Commun.*, 1997, 1121.

5 T. Kawase, H. R. Darabi and M. Oda, *Angew. Chem., Int. Ed. Engl.*, 1996, **35**, 2664.

6 Y. Rubin, C. B. Knobler and F. Diederich, *J. Am. Chem. Soc.*, 1990, **112**, 1607; Y. Rubin, C. B. Knobler and F. Diederich, *J. Am. Chem. Soc.*, 1990, **112**, 4966; Y. Rubin, M. Kahr, C. B. Knobler and F. Diederich, *J. Am. Chem. Soc.*, 1991, **113**, 495; Y. Tobe, T. Fujii, H. Matsumoto, K. Naemura, Y. Achiba and T. Wakabayashi, *J. Am. Chem. Soc.*, 1996, **118**, 2758; Y. Tobe, H. Matsumoto, K. Naemura, Y. Achiba and T. Wakabayashi, *Angew. Chem., Int. Ed Engl.*, 1996, **35**, 1800.

7 Y. Rubin, T. C. Parker, S. I. Khan, C. L. Holliman and S. W. McElvany, *J. Am. Chem. Soc.*, 1996, **118**, 5308; Y. Rubin, T. C. Parker, S. J. Pastor, S. Jalisatgi, C. Boulle and C. L. Wilkins, *Angew. Chem., Int. Ed.*, 1998, **37**, 1226; Y. Tobe, N. Nakagawa, K. Naemura, T. Wakabayashi, T. Shida and Y. Achiba, *J. Am. Chem. Soc.*, 1998, **120**, 4544.

8 M. Ohkita, K. Ando, K. Yamamoto, T. Suzuki and T. Tsuji, *Chem. Commun.*, 2000, 83; M. Ohkita, K. Ando, T. Suzuki and T. Tsuji, *J. Org. Chem.*, 2000, **65**, 4385.

9 T. Tsuji, M. Ohkita and S. Nishida, *J. Am. Chem. Soc.*, 1993, **115**, 5284; T. Tsuji, M. Ohkita, T. Konno and S. Nishida, *J. Am. Chem. Soc.*, 1997, **119**, 8425; H. Kawai, T. Suzuki, M. Ohkita and T. Tsuji, *Angew. Chem., Int. Ed.*, 1998, **37**, 817; H. Kawai, T. Suzuki, M. Ohkita and T. Tsuji, *Chem. Eur. J.*, 2000, **6**, 4177.

10 D. O'Krongly, S. R. Denmade, M. Y. Chiang and R. Breslow, *J. Am. Chem. Soc.*, 1985, **107**, 5544; A. de Meijere, S. Kozhushkov, T. Haumann, R. Boese, C. Puls, M. J. Cooney and L. T. Scott, *Chem. Eur. J.*, 1995, **1**, 124.

CHEMCOMM
Communication
www.rsc.org/chemcomm

Highly enantioselective synthesis *via* dynamic kinetic resolution under transfer hydrogenation using Ru(η⁶-arene)-*N*-perfluorosulfonyl-1,2-diamine catalysts: a first insight into the relationship of the ligand's pK_a and the catalyst activity

Barbara Mohar,[a] Alain Valleix,[b] Jean-Roger Desmurs,[c] Marc Felemez,[d] Alain Wagner*[d] and Charles Mioskowski*[bd]

[a] *National Institute of Chemistry, Hajdrihova 19 SI-1001. Ljubljana, Slovenia*
[b] *CEA-Service des Molécules Marquées F-91191. Gif sur Yvette, France*
[c] *Rhodia Chimie, 85 Avenue Freres Perret F-69192. Saint Fons, France*
[d] *UMR 7514 du CNRS, Faculté de Pharmacie, 74 Route du Rhin F-67401. Strasbourg, France. E-mail: alwag@aspirine.u-strasbg.fr; mioskowski@bioorga.u-strasbg.fr; Fax: +33 3 90 24 43 06; Tel: +33 3 90 24 42 95*

Received (in Cambridge, UK) 30th August 2001, Accepted 22nd October 2001
First published as an Advance Article on the web 13th November 2001

β-(3,4-Dimethoxyphenyl)serine methyl ester was obtained in high diastereomeric and enantiomeric excesses under transfer hydrogenation using chiral Ru(η⁶-arene)-*N*-perfluorosulfonyl-1,2-diamine catalysts.

Catalytic transfer hydrogenation using propan-2-ol or formic acid as hydrogen source has become one of the most significant tools for asymmetric reduction of ketones.[1,2] This method is a powerful alternative to asymmetric hydrogenation using molecular hydrogen with chiral Ru(II)-bisphosphane catalysts[3] due to its practical simplicity and the possibility of using easily accessible and less sensitive ligands. Applications include the asymmetric reduction of aromatic[4] or α,β-acetylenic ketones[5] and, more recently, transfer hydrogenation of benzils into chiral hydrobenzoins *via* a dynamic kinetic resolution.[6] Most of these articles deal with Noyori's chiral catalyst Ru(II)-TsDPEN[7] (TsDPEN = *N*-tosyl-1,2-diphenylethylenediamine). However, although very efficient, this catalyst suffers from long reaction time and general low activity.

In an attempt to improve the performance of this catalytic system, we thought to modify the diamine ligand by introducing electron-withdrawing fluorosulfonyl groups, despite some discouraging results reported on the use of triflate substituted ligand **4d**.[4]

In order to evaluate the performance of our catalysts we investigated the transfer hydrogenation of the racemic *threo*-β-hydroxy-α-amino acids **1**[8] for the synthesis of the *threo*-**2** isomer[9] *via* a dynamic kinetic resolution (Scheme 1).

Several ligands (*S,S*)-**4a–e** and (*S,S*)-**5a–e** were prepared starting from homochiral 1,2-diphenylethylenediamine and *trans*-1,2-diaminocyclohexane, respectively. The β-keto-α-amino ester **1** was subjected to transfer hydrogenation in the presence of the reference Ru(II)-TsDPEN catalyst[4] in a 5:2 formic acid–triethylamine azeotrope yielding *threo*-**2** in 94% ee and with high 95:5 *threo/erythro* ratio. Curiously, the catalyst prepared *in situ* by heating TsDPEN ligand **4a** and $[RuCl_2(p\text{-cymene})]_2$ in propan-2-ol in the presence of triethylamine,[4b] led to only 20% conversion compared with 80% for the catalyst prepared without a base (Table 1, entry 1). Changing the arylsulfonyl group in the diamine ligand from toluene-*p*-sulfonyl to a more electron-withdrawing *p*-trifluoromethylben-

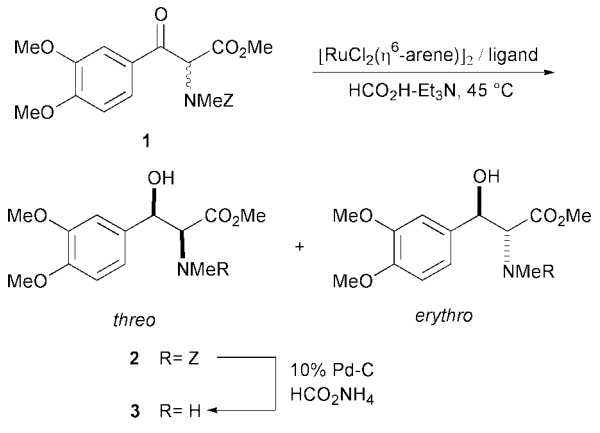

Scheme 1

Table 1 Stereoselective transfer hydrogenation of β-keto-α-methylamino acid ester **1** by chiral Ru(η⁶-arene)-*N*-perfluorosulfonyl-1,2-diamine catalysts

Ligands

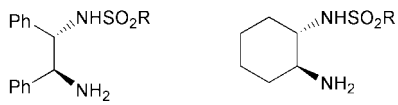

(*S,S*)-**4a-e** (*S,S*)-**5a-e**

a: R= *p*-CH_3-C_6H_4-
b: R= *p*-CF_3-C_6H_4-
c: R= C_6F_5
d: R= CF_3
e: R= $CF_2CF_2CF_2CF_3$

	Ru-catalyst			Product **2**		
Entry	Ligand	η⁶-arene	Time (h)	Conv.[a] (%)	*threo/ erythro*[b]	Ee[c] (%)
1	**4a**	*p*-Cymene	72	80	95/5	94
2	**4b**	*p*-Cymene	72	100	95/5	90
3	**4c**	*p*-Cymene	72	90	95/5	94
4	**4c**	Benzene	72	95	78/22	50
5	**4d**	*p*-Cymene	35	100	95/5	98
6	**4e**	*p*-Cymene	27	100	95/5	>99
7	**5a**	*p*-Cymene	95	50	95/5	88
8	**5b**	*p*-Cymene	95	65	95/5	88
9	**5d**	*p*-Cymene	72	95	95/5	97
10	**5d**	benzene	72	100	88/12	86
11	**5e**	*p*-Cymene	40	100	95/5	>99
12	**5e**	Benzene	40	100	84/16	90
13	**5e**	*p*-Cymene	40	100	95/5	99[d]

[a] Reactions were carried out at 45 °C with S/C (substrate/catalyst) = 40.[b] Conversion and *threo/erythro* ratio were determined by ^{1}H NMR spectroscopy.[c] Enantiomeric purity of *threo*-**2** was determined by HPLC (Daicel Chiralpack AD) of the Z-deprotected compound **3**.[d] S/C = 100.

 DOI: 10.1039/b107822b

zenesulfonyl resulted in a remarkable improvement of activity leading to 100% conversion, but with 90% ee (entry 2).

The catalyst prepared from the pentafluorobenzenesulfonamide ligand **4c** and [$RuCl_2$(*p*-cymene)] gave 94% ee of *threo*-**2** (entry 3), but it was less reactive than the catalyst prepared from **4b**. Changing the η^6-arene ligand from *p*-cymene to benzene slightly increased the catalyst activity, while stereoselectivity dropped significantly (entries 3, 4). Using the triflate substituted ligand **4d** in combination with η^6-*p*-cymene, led to total conversion of **1** in 35 h yielding *threo*-**2** in 98% ee (entry 5). The nonaflate-substituted ligand **4e**, despite its higher steric bulkiness with respect to **4d**, gave practically enantiomerically pure *threo*-**2** in only 27 h (entry 6).

The cyclohexyldiamine ligand series **5a–e** led to similar stereoselectivities compared with the diphenylethylenediamine ligands **4a–e**, but necessitated longer reaction times (entries 7–11). The most active catalyst was prepared with the nonaflate substituted ligand **5e** and η^6-*p*-cymene leading to 100% conversion in 40 h with >99% ee (entry 11).

These results show that the stereoselectivity and the catalyst activity are very much influenced by the sulfonamide group and by the η^6-arene of the catalyst. Moreover, the η^6-arene has a profound influence on the diastereoselectivity (*e.g.* entries 3, 4). In an attempt to rationalize our results we determined pK_a values of the diamine ligands[10] (Table 2).

We found that the sulfonyl function does not only affect the acidity of the sulfonamide NH group, but also affects the basicity of NH_2. As expected, the sulfonamide groups display large pK_a variations from 7.4 to 4.5 for ligands **4a–e** and from 8.4 to 3.0 for ligands **5a–e**. The pK_a values of NH_2 range from 11.1 to 8.3 and from 9.4 to 5.7 for **4a–e** and **5a–e**, respectively. Correlation of these pK_a's and the catalysis results revealed that the activity of the catalyst is improved by a decrease of the pK_a of the sulfonamide group and by a decrease of the basicity of the NH_2. For example, the most active catalyst in the cyclohexanediamine series (100% conversion in 40 h with >99% ee) was prepared from the mono nonaflate ligand **5e** which showed the lowest pK_{a1} = 3.0 and pK_{a2} = 5.7 values. The poorest catalyst in this series (50% conversion in 95 h with 88% ee) was prepared from the ligand **5a** showing the highest pK_{a1} = 8.4 and pK_{a2} = 9.4 values. The catalyst prepared from ligands showing intermediate pK_a values (*e.g.* 5.6 and 6.5 for **5d**) proved to have an intermediate reactivity (95% conversion in 72 h with 97% ee). The same correlation is observed in the diphenylethylendiamine series.

Table 2 pK_a values of ligands **4,5-a,b,d,e**[a]

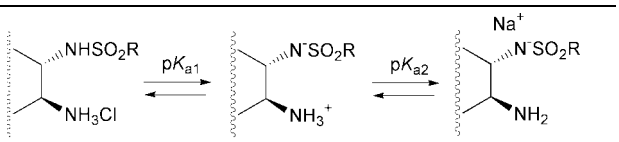

Ligand		**a**	**b**	**d**	**e**
4	pK_{a1}	7.4	—[b]	4.5	4.5
pK_{a2}	11.1	—	8.3	8.5	
5	pK_{a1}	8.4	8.3	5.6	3.0
pK_{a2}	9.4	9.3	6.5	5.7	

[a] pK_a values were determined potentiometrically. [b] The ligand was not soluble under titration conditions.

Although these preliminary results have to be extended to other families of ligands and catalytic systems, pK_a measurements might become a useful tool for ligand design and mechanistic investigations.

In summary, in this work we show that introducing a better electron-withdrawing group on the Noyori's TsDPEN ligand strongly improves the catalyst activity and stereoselectivity in transfer hydrogenation of a β-keto-α-amino acid **1** *via* dynamic kinetic resolution. In particular, the catalyst prepared from the nonaflate ligand **4e** proved to be much more active than the TsDPEN ligand and gave >99% ee. Moreover, the activity and enantioselectivity were found to be influenced by the ligand's pK_a values.

Notes and references

1 For reviews, see:G. Zassinovich, G. Mestroni and S. Gladiali, *Chem. Rev.*, 1992, **92**, 1051; M. Willis and H. Tye, *J. Chem. Soc. Perkin Trans. 1*, 1999, 1109; M. J. Palmer and M. Wills, *Tetrahedron: Asymmetry*, 1999, **10**, 2045.

2 L. Schwink, T. Ireland, K. Püntener and P. Knochel, *Tetrahedron: Asymmetry*, 1998, **9**, 1143; Y. Jiang, Q. Jiang and X. Zhang, *J. Am. Chem. Soc.*, 1998, **120**, 3817; C. Frost and P. Mendonça, *Tetrahedron: Asymmetry*, 1999, **10**, 1813; K. Murata and T. Ikariya, *J. Org. Chem.*, 1999, **64**, 2186; A. Aitali, S. Allaoud, A. Karim, C. Meliet and A. Mortreux, *Tetrahedron: Asymmetry*, 2000, **11**, 1367; C. G. Frost and P. Medonça, *Tetrahedron: Asymmetry*, 2000, **11**, 1845; D. Maillard, C. Nguefack, G. Pozzi, S. Quici, B. Valadé and D. Sinou, *Tetrahedron: Asymmetry*, 2000, **11**, 2881; R. Noyori and T. Ohkuma, *Angew. Chem., Int. Ed.*, 2001, **40**, 40.

3 T. Naota, H. Takaya and S.-J. Murahashi, *Chem. Rev.*, 1998, **98**, 2599.

4 S. Hashiguchi, A. Fujii, J. Takehara, T. Ikariya and R. Noyori, *J. Am. Chem. Soc.*, 1995, **117**, 7562; A. Fujii, S. Hashiguchi, N. Uematsu, T. Ikariya and R. Noyori, *J. Am. Chem. Soc.*, 1996, **118**, 2521; R. Noyori and S. Hashiguchi, *Acc. Chem. Res.*, 1997, **30**, 97; K. Everaere, J.-F. Carpentier, A. Mortreux and M. Bulliard, *Tetrahedron: Asymmetry*, 1998, **9**, 2971.

5 K. Matsumura, S. Hashiguchi, T. Ikariya and R. Noyori, *J. Am. Chem. Soc.*, 1997, **119**, 8738.

6 K. Murata, K. Okano, M. Miyagi, H. Iwane, R. Noyori and T. Ikariya, *Org. Lett.*, 1999, **1**, 1119.

7 The catalyst precursor, the catalyst, and its reactive species have been identified and their structures were confirmed by X-ray crystal analysis. See: K.-J. Haack, S. Hashiguchi, A. Fujii, T. Ikariya and R. Noyori, *Angew. Chem. Int. Ed. Engl.*, 1997, **36**, 285.

8 L-*threo*-β-(3,4-Dihydroxyphenyl)-*N*-methyl serine and its methyl ester were found to be antiparkinsonian and antidepressive agents. See: EP 218,440; EP 112,606. For hypoglycemic action, see:Y. Hioki, A. Nakajima, T. Fukuroda, H. Ohasi and M. Yano, *Jpn. J. Pharmacol.*, 1995, **69**, 251. ; For other activities, see: M. A. Blaskovich, G. Evindar, N. G. W. Rose, S. Wilkinson, Y. Luo and G. A. Lajoie, *J. Org. Chem.*, 1998, **63**, 3631 and references cited therein.

9 Catalytic hydrogenation of the related methyl 2-(benzyloxycarbonylamino)-3-(3,4-methylenedioxyphenyl)-3-oxopropanoate was conducted with [$RuBr_2$(*R*)-BINAP] under 100 atm of hydrogen to give a 99:1 diastereomeric ratio and 92% ee of the corresponding *threo* compound. See: R. Noyori, T. Ikeda, T. Ohkuma, M. Widhalm, M. Kitamura, H. Takaya, S. Akutagawa, N. Sayo, T. Saito, T. Taketomi and H. Kumobayashi, *J. Am. Chem. Soc.*, 1989, **111**, 9134.

10 Two pK_a's were determined: pK_{a1} corresponds to deprotonation of the sulfonamide group, since it is similar to pK_a's of trifluoromethanesulfonamides (*ca.* 5.8); pK_{a2} is comparable with the pK_{a2} value of 1,2-diamine salt (*ca.* 9.9).

CHEMCOMM Communication
www.rsc.org/chemcomm

One-step syntheses of very large cage-type molecules from aromatic sub-units†

Howard M. Colquhoun,*[a] Fabio Arico[a] and David J. Williams*[b]

[a] *Department of Chemistry, University of Reading, Whiteknights, Reading, UK RG6 6AD. E-mail: h.m.colquhoun@rdg.ac.uk*
[b] *Department of Chemistry, Imperial College, South Kensington, London, UK SW7 2AY. E-mail: djw@ic.ac.uk*

Received (in Cambridge, UK) 7th September 2001, Accepted 23rd October 2001
First published as an Advance Article on the web 13th November 2001

Polycondensation of a trifunctional, ketone-activated fluoroarene with bis- or tris-phenoxides under *pseudo*-high dilution conditions affords a series of very large macropolycyclic aromatic ether ketones; isolation and characterisation of these materials by NMR, MALDI-TOF MS and, for one example (after reduction of the carbonyl groups to methylene linkages) by X-ray crystallography, confirms that polycondensations which would normally lead to highly branched or cross-linked polymers can also give rise to large, closed-network molecules.

The synthetic and structural relationships between linear aromatic polymers and their macrocyclic homologues have been intensively investigated over the past decade,[1] work focusing mainly on the potential of macrocyclic ring-opening polymerisation for reactive fabrication of linear polymers. The reverse reaction—ring closing depolymerisation—has however also been explored for application in the recovery and recycling of high-value condensation polymers.[2] Macrocyclic aromatic oligo-amides are, in addition, of considerable value for the generation of novel supramolecular architectures including catenanes,[3] rotaxanes,[4] and knots.[5] We now describe some preliminary experiments which demonstrate that the ring–chain relationship can be extended to a third dimension. Thus, polycondensations involving trifunctional monomers, which would normally afford highly branched or even fully cross-linked polymers, are here shown also to give, under *pseudo*-high dilution conditions, a series of very large aromatic cage-type molecules.[6]

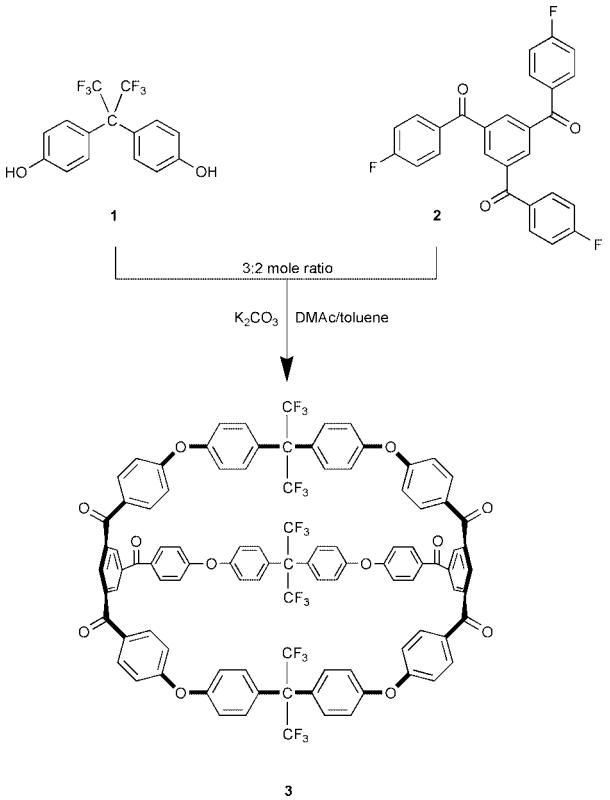

Scheme 1

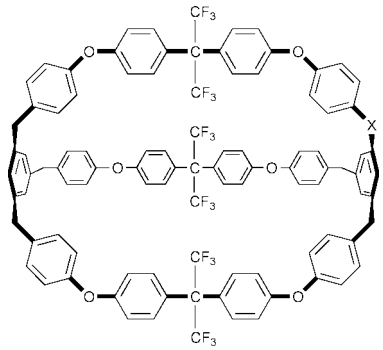

Reaction of 4,4′-hexafluoroisopropylidenediphenol (**1**) with 1,3,5-tris(4-fluorobenzoyl)benzene (**2**) was carried out by slow addition of a solution of the two monomers (3 : 2 mole ratio) in dimethylacetamide (DMAc) to potassium carbonate in refluxing DMAc–toluene, with continuous azeotropic removal of water (Scheme 1). A complex mixture of oligomeric and polymeric materials was obtained but the macrobicyclic cage-compound **3** (mp 450 °C) could be isolated straightforwardly from this mixture, albeit in low yield (~5%) , by column chromatography.

Spectroscopic analyses of **3** by MALDI-TOF MS and by ^{1}H and ^{13}C NMR were entirely consistent with the structure shown in Scheme 1, but efforts to obtain single crystals suitable for X-ray analysis were unsuccessful. However, reduction of the carbonyl groups in **3** to methylene linkages using triethylsilane and trifluoroacetic acid (Scheme 1)[7] afforded the fully-reduced cage-compound **4** (42% yield), together with a compound (**5**) in 21% yield in which one ketone group remains unreduced.† Compounds **4** and **5** were readily separated by column chromatography, and **4** eventually yielded crystals suitable for X-ray analysis.‡ Its structure is shown in Fig. 1, from which it is evident that the composition and topology proposed for this compound (and thus by inference for **3**) are correct.

The molecule adopts a semi-collapsed and flattened conformation with no obvious intramolecular interactions other than a weak π-stacking arrangement between a pair of aromatic ether-containing ring systems in the two adjacent arms of the

† Electronic supplementary data (ESI) available: analytical and spectroscopic data for compounds **3**–**5** and **8**. See http://www.rsc.org/suppdata/cc/b1/b108124c/

 DOI: 10.1039/b108124c

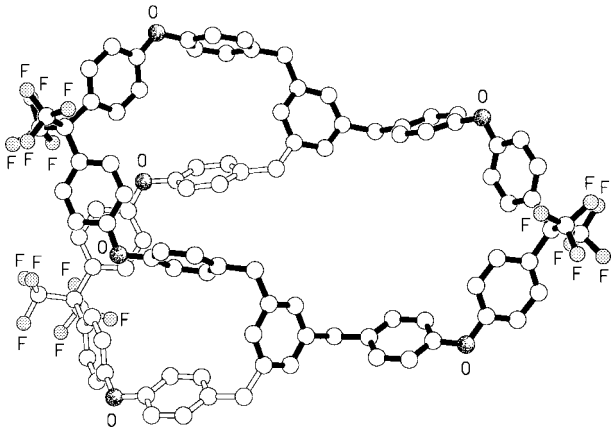

Fig. 1 Molecular structure of the reduced cage-compound **4** (hydrogen atoms are omitted for clarity).

macrocycle. The hexafluoroisopropylidene-linked aromatic residues here display a consistently skewed conformation, but the diarylene-ether units have geometries that range from symmetrically-skewed to near-orthogonal.

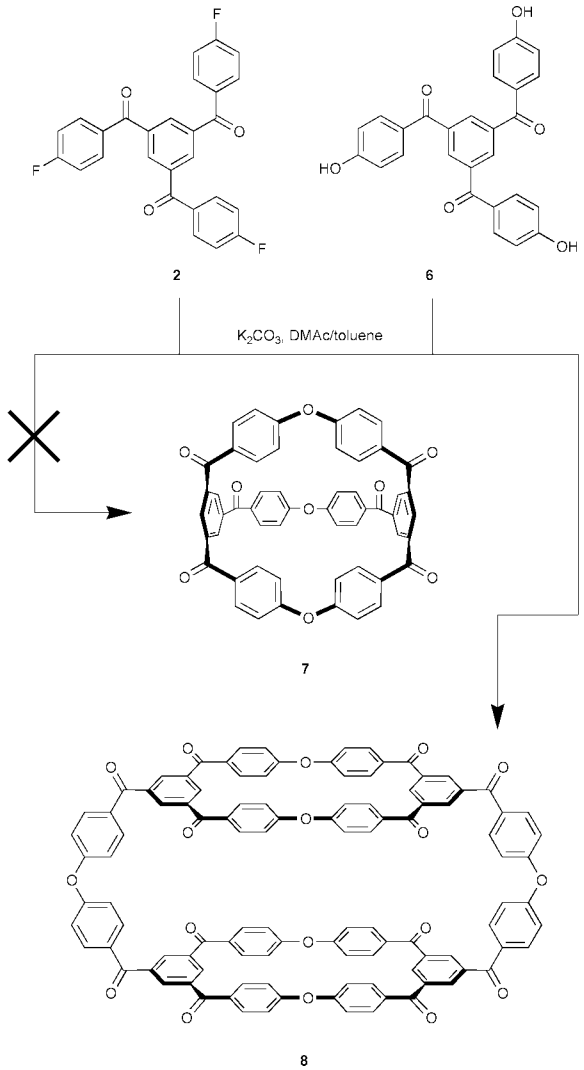

Scheme 2

An analogous polycondensation between the trifluoro-compound **2** and tris-phenol **6** (derived from **2** by hydrolysis with potassium hydroxide in DMSO) afforded not the expected cage-compound **7**—a direct analogue of **3**—but its macrotricyclic dimer **8** (Scheme 2). This compound was isolated in pure form by column chromatography (4% yield) and characterised in detail.† It shows a sharp, clearly-defined melting point by DSC at the astonishingly high temperature of 556 °C, reflecting both extreme rigidity of the molecular structure and a quite remarkable thermal stability. The MALDI-TOF spectrum of the original product mixture showed a strong $[M + Na]^+$ peak for compound **8**, but gave no evidence for the monomeric cage **7**. The MALDI-TOF analysis did however indicate the presence of higher polycyclic oligomers of **7**, including the macro-polycyclic trimer and tetramer. Evidence to date, mainly from the ^1H NMR spectra of partially-resolved chromatographic fractions, suggests that the higher-order polycyclic oligomers of **7** comprise increasing numbers of the structural repeat (a six-ring macrocycle with a two-ring linking umit) found in oligomer **8**.

This approach to large, closed-network molecules is clearly not restricted to the aromatic polyetherketone systems described here, but should be generally applicable to *any* type of branching polycondensation, including esterification, amidation and imidation. Such possibilities are currently under investigation, as are the potential applications of these molecules in supramolecular assembly and in cage-opening polymerisation.

We thank Professor F. H. Kohnke of the University of Messina for stimulating discussions.

Notes and references

‡ *Crystal data* for **4**: $C_{99}H_{66}F_{18}O_6.0.75\ CH_2Cl_2$, M_r = 1757.21, triclinic, $P\bar{1}$, a = 14.291(3), b = 17.673(4), c = 20.181(3) Å, α = 97.04(2), β = 109.61(1), γ = 112.31(2)°. V = 4255(1) Å^3, T = 293 K, Z = 2, D_c 1.371 g cm^{-3}, μ(Cu-Kα) = 1.371 mm^{-1}, F(000) = 1803. Independent measured reflections 11444. R_1 = 0.077, wR_2 = 0.166 for 5472 independent observed reflections [$2\theta \leq 115°$, $I > 2\sigma(I)$]. CCDC 171849. See http://www.rsc.org/suppdata/cc/b1/b108124c/ for crystallographic files in .cif format.

1 D. J. Brunelle, in *New Methods of Polymer Synthesis*, ed. J. R. Ebdon and G. C. Eastmond, Blackie, London, 1995, p. 197; Y. F. Wang and A. S. Hay, *Macromolecules*, 1997, **30**, 182; M. Chen, I. Guzei, A. L. Rheingold and H. W. Gibson, *Macromolecules*, 1997, **30**, 2516; H. O. Krabbenhof, D. J. Brunelle and E. Pearce, *J. Appl. Polym. Sci.*, 1997, **66**, 2251; H. M. Colquhoun, C. C. Dudman, M. Thomas, C. A. O′Mahoney and D. J. Williams, *J. Chem. Soc., Chem. Commun.*, 1990, 336; H. Jiang, T. Chen, Y. Qi and J. Xu, *Polym. J.*, 1998, **30**, 300; T. Takekoshi and J. M. Terry, *J. Polym. Sci., Polym. Chem. Ed.*, 1997, **35**, 759.

2 A. Ben-Haida, I. Baxter, H. M. Colquhoun, P. Hodge, F. H. Kohnke and D. J. Williams, *Chem. Commun.*, 1997, 1533; A. Ben-Haida, I. Baxter, H. M. Colquhoun, P. Hodge, F. H. Kohnke and D. J. Williams, *Chem. Commun.*, 1998, 2213; P. Hodge, Z. Yang, A. Ben-Haida and C. S. McGrail, *J. Mater. Chem.*, 2000, **10**, 1533.

3 A. G. Johnston, D. A. Leigh, L. Nezhat, J. P. Smart and M. D. Deegan, *Angew. Chem., Int. Ed. Engl.*, 1995, **34**, 1212.

4 C. Heim, A. Affield, M. Neiger and F. Vögtle, *Helv. Chim. Acta*, 1999, **82**, 746.

5 O. Safarowsky, M. Nieger, R. Frölich and F. Vögtle, *Angew. Chem., Int. Ed.*, 2000, **39**, 1616.

6 A number of smaller, semi-aromatic cage-type molecules (4–8 aromatic rings) have previously been obtained by branching polycondensations involving benzylic halides. See: N. Kon, H. Takemura, K. Otsuka, K. Tanoue, S. Nakashima, M. Yasutake, K. Tani, J. Kimoto, T. Shinmyozu and T. Inazu, *J. Org. Chem.*, 2000, **65**, 3708; F. Vögtle, S. Ibach, M. Nieger, C. Chartroux, T. Kruger, H. Stephan and K. Gloe, *Chem. Commun.*, 1997, 1809; G. Hohner and F. Vögtle, *Chem. Ber.*, 1977, **110**, 3052.

7 C. T. West, S. J. Donnelly, D. A. Kooistra and M. P. Doyle, *J. Org. Chem.*, 1973, **38**, 2675.

CHEMCOMM Communication
www.rsc.org/chemcomm

Ruthenium-catalysed oxidative cyclisation of 2-aminobenzyl alcohol with ketones: modified Friedlaender quinoline synthesis

Chan Sik Cho,*[a] Bok Tae Kim,[b] Tae-Jeong Kim[b] and Sang Chul Shim*[b]

[a] *Research Institute of Industrial Technology, Kyungpook National University, Taegu 702-701, Korea*
[b] *Department of Industrial Chemistry, College of Engineering, Kyungpook National University, Taegu 702-701, Korea. E-mail: scshim@kyungpook.ac.kr*

Received (in Cambridge, UK) 10th October 2001, Accepted 26th October 2001
First published as an Advance Article on the web 13th November 2001

2-Aminobenzyl alcohol is oxidatively cyclised with an array of ketones in dioxane at 80 °C in the presence of a catalytic amount of a ruthenium catalyst and KOH to afford the corresponding quinolines in high yields.

Many synthetic routes are well documented for the formation of quinolines since the quinoline nucleus plays an important role as an intermediate for the design of many pharmacologically active compounds.[1,2] Besides conventional named methods such as Skraup, Döbner-von Miller, Conrad-Limpach, Friedlaender and Pfitzinger syntheses,[1] homogeneous transition metal-catalysed synthetic methods have been attempted because of the wide availability of substrate.[3] We have also reported on the formation of quinolines *via* a ruthenium-catalysed alkyl group transfer from alkylamines to the nitrogen atom of anilines (amine exchange reaction).[4] During the course of our ongoing studies on ruthenium catalysis,[5,6] in connection with this report, we recently found an unusual type of ruthenium-catalysed transfer hydrogenation of ketones by alcohols under the molar ratio of alcohol : ketone = 3 (Scheme 1).[7] It was suggested that the reaction proceeds *via* a sequence involving oxidation of alcohol to aldehyde and cross aldol reaction of aldehyde with ketone to form an α,β-unsaturated ketone which is subsequently hydrogenated to the product by a dihydridoruthenium (RuH_2) generated by the initial oxidation of the starting alcohol. Prompted by these findings and intrigued by the diverse reactivities of ruthenium catalysts, we have directed our attention to the application of this methodology to the synthesis of N-heterocycles. Herein we report a modified Friedlaender quinoline synthesis *via* a ruthenium-catalysed oxidative cyclisation of 2-aminobenzyl alcohol with ketones.[8]

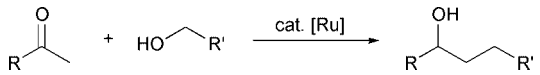

Scheme 1

Table 1 Ruthenium-catalysed oxidative cyclisation of **1** with **2** under various ruthenium catalysts[a]

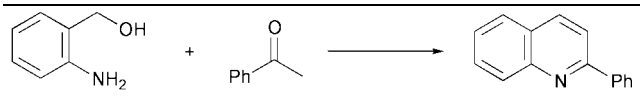

1 **2** **3**

Run	Ruthenium catalysts	*T*/°C	GLC yield (%)[b]
1	$RuCl_2(PPh_3)_3$	25	40
2	$RuCl_2(PPh_3)_3$	50	63
3	$RuCl_2(PPh_3)_3$	80	94
4[c]	$RuCl_2(PPh_3)_3$	80	73
5	$RuCl_3{\cdot}nH_2O$–$3PPh_3$	80	85
6	$RuCl_3{\cdot}nH_2O$–1.5 dppm	80	50
7	$RuH_2(PPh_3)_4$	80	91
8	$Ru_3(CO)_{12}$	80	34
9	$Cp^*RuCl_2(CO)$[d]	80	29
10	$Cp^*RuCl(CO)(PPh_3)$[d]	80	65
11	$RuCl_2(=CHPh)(PCy_3)_2$	80	99

[a] Reaction conditions: **1** (1 mmol), **2** (2 mmol), ruthenium catalyst (1 mol% based on **1**), KOH (1 mmol), for 1 h, under argon. [b] Based on **1**. [c] [**2**] : [**1**] = 1. [d] Cp* = η^5-C_5Me_5

The results of several attempted oxidative cyclisations of 2-aminobenzyl alcohol (**1**) with acetophenone (**2**) are listed in Table 1. Typically, **1** was subjected to react with **2** in the

Table 2 Ruthenium-catalysed synthesis of quinolines from **1** and ketones[a]

Ketones	Quinolines	Yield (%)[b]
	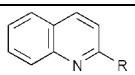	
R = Ph	R = Ph	97
R = 2-MeC_6H_4	R = 2-MeC_6H_4	94
R = 3-MeC_6H_4	R = 3-MeC_6H_4	96
R = 4-MeC_6H_4	R = 4-MeC_6H_4	96
R = 4-$MeOC_6H_4$	R = 4-$MeOC_6H_4$	94
R = 4-FC_6H_4	R = 4-FC_6H_4	97
R = 3-$CF_3C_6H_4$	R = 3-$CF_3C_6H_4$	98
R = 4-$NO_2C_6H_4$	R = 4-$NO_2C_6H_4$	40
R = 2-HOC_6H_4	R = 2-HOC_6H_4	50[c]
R = 4-CNC_6H_4	R = 4-CNC_6H_4	70
R = 2-naphthyl	R = 2-naphthyl	99
R = 2-furanyl	R = 2-furanyl	94
R = 2-thiophenyl	R = 2-thiophenyl	78
R = 2-pyridyl	R = 2-pyridyl	89
R = Me	R = Me	76[d]
R = pentyl	R = pentyl	69[e]
R = phenethyl	R = phenethyl	79[f]
R = *i*-Pr	R = *i*-Pr	72
	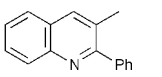	86
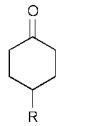	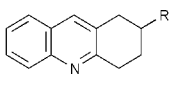	
R = H	R = H	66
R = Ph	R = Ph	97
	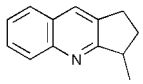	74
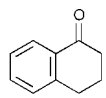	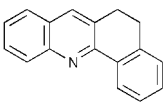	90
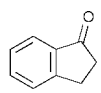	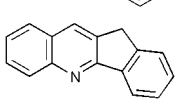	86

[a] Reaction conditions: **1** (1 mmol), ketone (2 mmol), $RuCl_2(=CHPh)(PCy_3)_2$ (0.01 mmol), KOH (1 mmol), 80 °C, for 1 h, under argon. [b] Isolated yield based on **1**. [c] For 15 h. [d] [Acetone] : **1** = 5. [e] 3-Butyl-2-methylquinoline was also formed in 30% yield. [f] 3-Benzyl-2-methylquinoline was also formed in 20% yield.

 DOI: 10.1039/b109245f

presence of a catalytic amount of a ruthenium catalyst (1 mol% based on **1**) and KOH to afford 2-phenylquinoline (**3**). The reaction was monitored until **1** had disappeared on TLC, which occurred within 1 h. The product yield increased with increase in reaction temperature up to 80 °C (runs 1–3). Tuning the molar ratio of **2** to **1** was critical for the effective formation of **3**. Upon using equimolar amounts of **1** and **2**, the yield of **3** was lower than that when the molar ratio of 2 was used (run 4). This could be due to partial consumption of **2** leading to 1-phenylethanol by transfer hydrogenation of **2** by **1**. Of various ruthenium catalysts employed, $RuCl_2(=CHPh)(PCy_3)_2$ is the choice of preference for the effective formation of **3** (runs 5–11). In all cases, **3** was formed in moderate to high yields with concomitant formation of 1-phenylethanol by transfer hydrogenation of **2** by **1** ranging from 5–12%.† [9]

Given suitable reaction conditions, a series of ketones were screened in order to scrutinise the reaction scope, and several representative results are summarised in Table 2. Alkyl aryl ketones were readily cyclised with **1** irrespective of the examined functional groups on the aromatic ring to afford the corresponding 2-arylquinolines in excellent to good yields. The quinoline yield was not greatly affected by the position of the substituent on the aromatic ring of ketones, whereas the electronic nature of that had some relevance to the product yield. Lower reaction rate and yield were observed with acetophenones having nitro, hydroxy and cyano functional groups on the aromatic ring. With alkyl heteroaryl ketones, the corresponding quinolines were also formed in high yields. In the reaction of dialkylketones, the corresponding quinolines were obtained as a regioisomeric mixture, favoring cyclisation at less-hindered position over α-methylene.[6,7,10] An array of alkyl aryl, cyclic and benzo-fused cyclic ketones having only the methylene reaction site also afforded the corresponding products ranging from 66–97%.

As to the reaction pathway, this seems to proceed *via* an initial oxidative addition of ruthenium to O–H bond of **1** followed by β-hydrogen elimination to give 2-aminobenzaldehyde. The precedents of such an oxidative addition have been well documented in several transfer hydrogenation reactions.[9]

In summary, we have demonstrated that 2-aminobenzyl alcohol can be oxidatively cyclised with an array of ketones in the presence of a ruthenium catalyst to give quinolines in high yields. The present reaction is a novel transition metal-catalysed Friedlaender quinoline synthesis.

The present work was supported by the Basic Research Program of the Korea Science and Engineering Foundation (R01-2000-00044). C.S.C. gratefully acknowledges a MOE-KRF Research Professor Program (2001-050-D00015).

Notes and references

† *General experimental procedure*: a mixture of 2-aminobenzyl alcohol (1 mmol), ketone (2 mmol), $RuCl_2(=CHPh)(PCy_3)_2$ (0.01 mmol) and KOH (1 mmol) in dioxane (3 ml) was placed in a 5 ml screw-capped vial. The system was flushed with argon and allowed to react at 80 °C for 1 h. The reaction mixture was filtered through a short silica gel column (ethyl acetate), washed with brine and dried over Na_2SO_4. Removal of the solvent left a crude mixture, which was separated by column chromatography (silica gel, ethyl acetate–hexane mixture) to give quinolines.

1 J. Jones, *Comprehensive Heterocyclic Chemistry*, ed. A. R. Katritzky and C. W. Rees, Pergamon, New York, 1984, vol. 2, pp. 395–510.
2 H. Amii, Y. Kishikawa and K. Uneyama, *Org. Lett.*, 2001, **3**, 1109.
3 For the formation of quinolines catalysed by transition metals such as Pd, Rh, Ru and Fe, see: ref. 4d.
4 (*a*) C. S. Cho, B. H. Oh and S. C. Shim, *Tetrahedron Lett.*, 1999, **40**, 1499; (*b*) C. S. Cho, B. H. Oh and S. C. Shim, *J. Heterocycl. Chem.*, 1999, **36**, 1175; (*c*) C. S. Cho, J. S. Kim, B. H. Oh, T.-J. Kim and S. C. Shim, *Tetrahedron*, 2000, **56**, 7747; (*d*) C. S. Cho, B. H. Oh, J. S. Kim, T.-J. Kim and S. C. Shim, *Chem. Commun.*, 2000, 1885.
5 C. S. Cho, H. K. Lim, S. C. Shim, T. J. Kim and S. C. Shim, *Chem. Commun.*, 1998, 995; C. S. Cho, J. H. Kim and S. C. Shim, *Tetrahedron Lett.*, 2000, **41**, 1811; C. S. Cho, J. H. Kim, T.-J. Kim and S. C. Shim, *Tetrahedron*, 2001, **57**, 3321; C. S. Cho, T. K. Kim, S. W. Yoon, T.-J. Kim and S. C. Shim, *Bull. Korean Chem. Soc.*, 2001, **22**, 545.
6 C. S. Cho, B. T. Kim, M. J. Lee, T.-J. Kim and S. C. Shim, *Angew. Chem., Int. Ed.*, 2001, **40**, 958.
7 C. S. Cho, B. T. Kim, T.-J. Kim and S. C. Shim, *J. Org. Chem.*, in press.
8 P. Friedlaender, *Chem. Ber.*, 1882, **15**, 2572;; For a review, see: C.-C. Cheng and S.-J. Yan, *Org. Reactions*, 1982, **28**, 37.
9 For recent reviews, see: R. Noyori and S. Hashiguchi, *Acc. Chem. Res.*, 1997, **30**, 97; T. Naota, H. Takaya and S.-I. Murahashi, *Chem. Rev.*, 1998, **98**, 2599; M. Palmer and M. Wills, *Tetrahedron: Asymmetry*, 1999, **10**, 2045.
10 Exclusive regioselective Friedlaender quinoline synthesis using β-keto phosphonates has recently been reported: Y. Hsiao, N. R. Rivera, N. Yasuda, D. L. Hughes and P. J. Reider, *Org. Lett.*, 2001, **3**, 1101.

CHEMCOMM Communication
www.rsc.org/chemcomm

A novel synthesis of substituted bicyclo[2.2.2]octenones and 3,3-sigmatropic shift: a general and stereoselective entry into functionalized *cis*-decalins

Vishwakarma Singh* and Sridhar Iyer

Department of Chemistry, Indian Institute of Technology Bombay, Mumbai 400 076, India

Received (in Cambridge, UK) 8th October 2001, Accepted 26th October 2001
First published as an Advance Article on the web 14th November 2001

Synthesis of bicyclo[2.2.2]octenones 4a–d, 9 and their Cope rearrangement to substituted *cis*-decalins 3a–d, 12, is described.

Recently, several diterpene alkaloids such as **1**, **2** were isolated from marine sponges of the genus *Agelas*.[1–3] Some members of this family exhibit interesting biological activities such as cytotoxicity, antimicrobial activity and inhibition of Na, K-ATPase.[2a,c,4] Interestingly, these alkaloids contain a *cis*-decalin framework similar to *cis*-cleoradanes.[5] In view of the isolation of these interesting diterpenes and cleoradanes[5] which have a *cis*-decalin skeleton containing contiguous stereocentres, there has been a growing interest in the development of new stereoselective methods for the synthesis of substituted *cis*-decalins.[6–10]

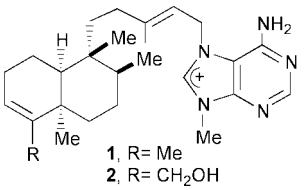

1, R= Me
2, R= CH_2OH

We thought to develop a general and flexible route to *cis*-decalins of type **3** having stereochemically defined substituents, olefinic linkages and a carbonyl group. It was considered that *cis*-decalins such as **3** could be directly obtained *via* a Cope rearrangement of an appropriately designed bicyclo[2.2.2]octenone system of type **4** with an *endo* vinyl moiety and other substituents, in a highly stereocontrolled fashion (Scheme 1). It may be worth mentioning that, while there are no routes to advanced bicyclo[2.2.2]octenones of type **4**, synthesis of even simpler bicyclic precursors involves cycloaddition of ketene equivalents with dienes followed by addition of a vinyl group.[9b,c]

In this communication, we wish to report a new method for the synthesis of bicyclo[2.2.2]octenones of type **4** that directly introduces a vinyl group on to the bicyclic frame and also permits introduction of methyl and other alkyl substituents, and their Cope rearrangement leading to a general, flexible and stereoselective route to highly substituted *cis*-decalins.

Conceptually, the desired bicyclooctenones of type **4** should be available *via* inverse electron demand cycloaddition of cyclohexa-2,4-dienones of type **5** with acyclic 1,3-dienes. Though, there are some methods for preparation of 6,6-disubstituted cyclohexadienones of type **5** *viz*., the alkylation[11a] of

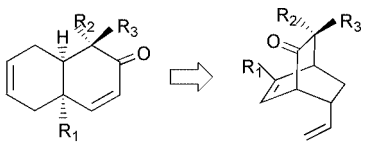

3 **4**

Scheme 1

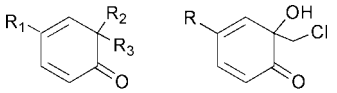

5 **6**

o-substituted phenols and rearrangement of epoxyfulvene,[11b] these methods are not easily adaptable. We therefore, developed an indirect route to the bicyclic systems of type **4** by *in-situ* generation of cyclohexa-2,4-dienone **6** and butadiene, their cycloaddition, and manipulation of the resulting adduct.

Thus, the addition of sulfolene **8** to a solution of the readily available[12] dimer **7a** in *o*-dichlorobenzene at 140 °C followed by chromatography of the reaction mixture gave the adduct **9a** as a major product. The structure of the adduct was deduced from its spectroscopic and analytical data.† While, the *endo*-stereochemistry of the adduct **9a** was proved through its Cope rearrangement (*vide infra*), orientation of the chloromethyl and hydroxy group was suggested on the basis of general tendency of cyclohexa-2,4-dienones during their cycloaddition and comparison with analogous compounds.[13] Although yield of the above cycloaddition is moderate, the generation of molecular complexity in a single step is noteworthy.

Manipulation of the functional groups of **9a** enabled the stereoselective introduction of alkyl substituents at the carbon bearing hydroxy and chloromethyl groups. Thus, the adduct **9a** was easily converted into epoxyketone **10a** in a quantitative fashion. Treatment of **10a** with zinc in dry dioxane containing ammonium chloride gave the compound **11a** as a result of deoxygenation of the oxirane ring.[14]

Alkylation of **11a** with allyl bromide in the presence of NaH–THF gave a mixture of *syn–anti* (85 : 15) isomers from which the *syn* isomer **4a** was isolated in major amounts. Such type of stereoselectivity in alkylation has been also observed by Stork and Paquette.[15] Alkylation of **11a** with propargyl bromide also gave the propargyl analogue **4c** in a selective fashion, which was converted into the dione **4d** by hydration of the acetylene moiety (Scheme 2). Similarly, more substituted bicyclic precursor **4b** with a methyl group at C-8, and an allyl and a methyl group at C6 was synthesized from the dimer **7b** (Scheme 2). Thus, the present methodology provides a novel and stereoselective route to bicyclic frameworks with an *endo* vinyl moiety, stereochemically defined substituents and a carbonyl group.

Next 3,3-sigmatropic rearrangement of **9a**, and **4a–d** was examined. Thus, a solution of **9a** in *o*-dichlorobenzene was heated at ~ 170 °C which smoothly furnished the bicyclic enone **12** in quantitative yield. Similarly, other bicyclic compounds **4a–d** also underwent 3,3-sigmatropic shifts to give the highly substituted *cis*-decalins **3a–d** (Scheme 3). The structures of all the products were clearly revealed from their spectral data.†

In summary, we have described a new and efficient synthesis of bicyclooctenones of type **4a–d**, **9** with vinyl, methyl and other alkyl substituents and their Cope rearrangement leading to a stereoselective route to substituted *cis*-decalins (**3a–3d**, **12**). This strategy is flexible and adaptable since it permits incorporation of a methyl group at the ring junctions in the

 DOI: 10.1039/b109116f

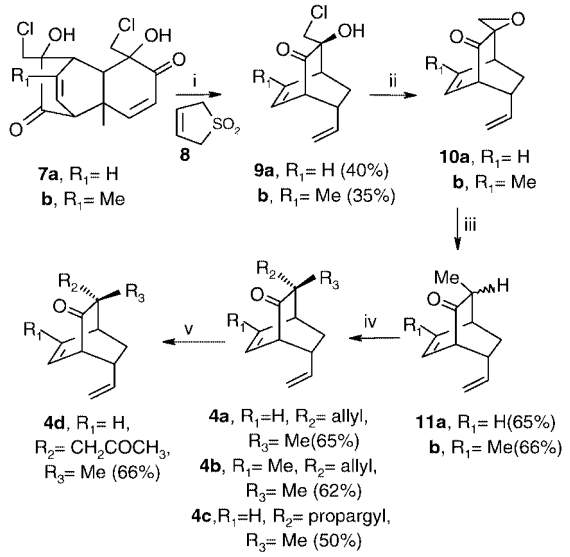

Scheme 2 *Reagents/conditions*: i, 140 °C, *o*-dichlorobenzene; ii, KOH, CTAB (cetyltrimethylammonium bromide), $CHCl_3$–H_2O, quantitative; iii, Zn, NH_4Cl, dry dioxane, △; iv, NaH, THF, △, allyl bromide (for **4a**,**b**), propargyl bromide (for **4c**); v, MeOH, HgO, 4%H_2SO_4.

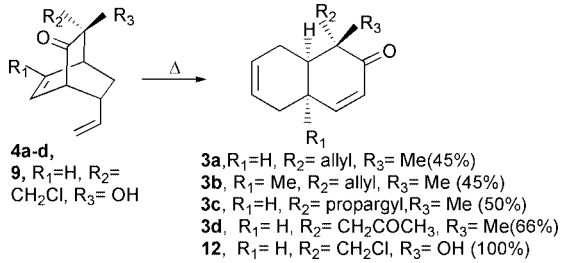

Scheme 3

decalin framework by appropriate selection of the starting precursors of type **7**.

We are grateful to Department of Science and Technology, New Delhi for financial support. We also thank RSIC, IIT Bombay for spectral data.

Notes and references

† All the compounds were thoroughly characterized with the help of spectral and analytical data. Selected data for **4b**: ν_{max}/cm^{-1} 1719,1657; δ_H(300 MHz, $CDCl_3$) 5.90–5.69 (m, 3H), 5.12–4.80 (m, 4H), 2.97(dd, *J* 7 & 3, 1H), 2.54–2.44 (m, 2H), 2.24 (d of part of an AB system, J_{AB} 14 & *J* 8, 1H), 2.07 (d of part of an AB system, J_{AB} 14 & *J* 8, 1H), 1.90 (d, *J* 1.5, 3H), 1.82–1.69 (m, 2H), 1.02 (s, 3H); δ_C(75 MHz, $CDCl_3$) 216.45, 147.12, 140.55, 134.03, 120.54, 118.17, 115.11, 54.32, 47.31, 46.46, 43.16, 42.05, 26.60, 21.33, 19.46; *m*/*z* 216(M^+). **4d**: ν_{max}/ cm^{-1} 1715; δ_H(300 MHz, $CDCl_3$) 6.50 (superimposed dd, *J* 7.2, 1H, γ H of β, γ-enone group), 6.04 (superimposed dd, *J* 7.2, 1H, β H of β, γ-enone moiety), 5.58–5.46 (m, 1H, olefinic proton), 4.98 (d, *J* 16.5, 1H, olefinic proton), 4.92 (d, *J* 10.8, 1H, olefinic proton), 3.28 (m, 1H), 3.08 (d, *J* 6.6, 1H), 2.65 (part of an AB system merged with a multiplet, J_{AB} 16.5, total 2H, methylene and methine H), 2.38 (part of an AB system, J_{AB} 16.5, 1H, methylene), 2.25–2.22 (m, 1H), 2.06 (s, 3H, $COCH_3$), 1.25–1.20 (m merged on to a singlet, total 4H, CH_3 and methine); δ_C(75 MHz, $CDCl_3$+CCl_4) 213.50 (CO), 206.23 (CO), 140.73, 138.93, 125.13, 114.49 (olefinic carbons), 54.50, 50.29, 45.30, 40.02, 38.38, 31.89, 28.33, 20.94; *m*/*z* 218 (M^+). **3b**: ν_{max}/cm^{-1} 1670; δ_H(400 MHz, $CDCl_3$) 6.73 (d, *J* 10, 1H, β H of α, β-enone group), 5.89 (d, *J* 10, 1H, α H of α, β-enone moiety), 5.80–5.74 (m, 1H, olefinic proton), 5.70–5.63 (m, 1H, olefinic proton), 5.60–5.48 (m, 1H, olefinic proton), 5.20–5.00 (m, 2H, olefinic proton), 2.80 (dd, *J* 13 &5.5 Hz, 1H), 2.30–2.20 (m, 1H), 2.20–2.02 (overlapped m, 4H), 1.99–1.90 (m, 1H), 1.15 (s, 3H, CH_3), 1.01 (s, 3H, CH_3); δ_C(100 MHz, $CDCl_3$) 203.90, 159.16, 135.09, 126.03, 125.78, 123.25, 117.54, 48.88, 41.83, 38.71, 34.89, 34.27, 28.82, 22.20, 20.71; *m*/*z* 216 (M^+). **3d**: mp. 71–72 °C. ν_{max}/cm^{-1} 1713, 1675; δ_H(300 MHz, $CDCl_3$) 6.65 (m of d, *J* 10.2, 1H, β H of α, β-enone group), 5.95 (dd, *J* 10.2 and ~2.5, 1H, α H of α, β-enone moiety), 5.80–5.72 (m, 1H, olefinic proton), 5.68–5.60 (m, 1H, olefinic proton), 3.02 (br m, 1H), 2.74 (part of an AB system, J_{AB} 15, 1H, methylene), 2.62–2.40 (m merged with a part of an AB system, J_{AB} 15, total 3H), 2.22–2.04 (s merged with a m, total 5H), 1.78–1.60 (m merged with the signal due to H_2O present in $CDCl_3$, 1H), 1.2 (s, 3H, CH_3); δ_C(75 MHz, $CDCl_3$) 206.82, 202.41 (CO), 153.82, 128.60, 126.78, 125.10 (olefinic carbons), 48.92, 47.68, 37.96, 32.37,31.99, 30.97, 23.73, 18.72. Mass (*m*/*z*): 218 (M^+).

1 J. D. Faulkner, *Nat. Prod. Rep.*, 2000, **17**, 7.
2 (*a*) X. Fu, F. J. Schmitz, R. S. Tanner and M. Kelly-Borges, *J. Nat. Prod.*, 1998, **61**, 548; (*b*) T. Iwagawa, M. Kaneko, H. Okamura, M. Nakatani and R. W. M. van Soest, *J. Nat. Prod.*, 1998, **61**, 1310; (*c*) H. Wu, H. Nakamura, J. Kobayashi, M. Kobayashi, Y. Ohizumi and Y. Hirata, *Bull. Chem. Soc., Jpn.*, 1986, **59**, 2495.
3 N. Shoji, A. Umeyama, M. Teranaka and S. Arihara, *J. Nat. Prod.*, 1996, **59**, 448.
4 K. Ishida, M. Ishibashi, H. Shigemori, T. Sasaki and J. Kobayashi, *Chem. Pharm. Bull.*, 1992, **40**, 766.
5 A. T. Merritt and S. V. Ley, *Nat. Prod. Rep.*, 1992, **9**, 243.
6 (*a*) W. C. Liu and C. C. Liao, *Synlett*, 1998, 912; (*b*) P.-Yi. Hsiu and C. C. Liao, *J. Chem. Soc., Chem. Commun.*, 1997, 1085.
7 (*a*) E. Piers, M. L. Breau, Y. Han, G. L. Plourde and W. L. Yeh, *J. Chem. Soc., Perkin Trans. 1*, 1995, 963; (*b*) O. Z. Pereira and T. H. Chan, *J. Org. Chem.*, 1994, **59**, 6710; (*c*) H.-J. Liu and Y. Han, *Tetrahedron Lett.*, 1993, **34**, 423.
8 (*a*) Y. Sato, S. Watanabe and M. Shibasaki, *Tetrahedron Lett.*, 1992, **33**, 2589; (*b*) H. Bouchard and J. Y. Lallemand, *Tetrahedron Lett.*, 1990, **31**, 5151.
9 (*a*) W. P. Jackson and S. V. Ley, *J. Chem. Soc., Perkin Trans. 1*, 1981, 1516; (*b*) D. A. Evans and A. M. Golob, *J. Am. Chem. Soc.*, 1975, **97**, 4765; (*c*) D. A. Evans, W. L. Scott and L. K. Truesdale, *Tetrahedron Lett.*, 1972, 121.
10 J. Bonjoch, J. Cuesta, S. Diaz and A. Gonzalez, *Tetrahedron Lett.*, 2000, 5669.
11 (*a*) A. G. Schultz, J. P. Dittami, S. O. Myong and C. K. Sha, *J. Am. Chem. Soc.*, 1983, **105**, 3273; (*b*) K. Alder, H. F. Flock and A. Lessenich, *Chem. Ber.*, 1957, **90**, 1709.
12 (*a*) V. Singh and A. V. Bedekar, *Synth. Commun.*, 1989, **19**, 107; (*b*) E. Adler and K. Holmberg, *Acta Chem. Scand.*, 1974, **28b**, 465.
13 M. R. Caira, A. V. Bedekar and V. Singh, *J. Chem. Cryst.*, 1995, **25**, 583.
14 For a brief discussion on the mechanism of keto-epoxide reduction,V. Singh, *Acc. Chem. Res.*, 1999, **32**, 324.
15 (*a*) G. Stork and N. H. Baine, *Tetrahedron Lett.*, 1985, 5927; (*b*) L. A. Paquette, C. S. Ra and T. W. Silvestri, *Tetrahedron*, 1989, **45**, 3099.

CHEMCOMM Communication
www.rsc.org/chemcomm

Metal-mediated formation of liquid crystals: synthesis, structural and thermal analysis of palladium(II) complexes of crown thioether derivatives†

Heiko Richtzenhain,[a] Alexander J. Blake,[a] Duncan W. Bruce,*[b] Ian A. Fallis,[c] Wan-Sheung Li[a] and Martin Schröder*[a]

[a] *School of Chemistry, The University of Nottingham, University Park, Nottingham, UK NG7 2RD. E-mail: m.schroder@nottingham.ac.uk*
[b] *School of Chemistry, The University of Exeter, Stocker Road, Exeter, UK EX4 4QD*
[c] *Department of Chemistry, University of Wales, Cardiff, PO Box 912, Cardiff, UK CF10 3TB*

Received (in Cambridge, UK) 2nd August 2001, Accepted 17th October 2001
First published as an Advance Article on the web 23rd November 2001

Oligo(benzoate) derivatives of *cis*- and *trans*-$(RO)_2$[14]aneS$_4$, *trans*-$(RO)_2$[16]aneS$_4$, and their corresponding Pd(II) complexes reveal metal-induced mesomorphic behaviour which can be rationalised by conformational locking of the ligand on complexation.

The formation of mesogenic materials from functionalised macrocyclic ligands is the subject of considerable current interest.[1–8] Examples have been reported using N-functionalised aza crowns which afford columnar mesophases,[2–6] although these systems tend to use the aza crown as a central building core for attachment of peripheral groups and the amide nitrogen atoms are generally poor donors to metal ions. Metal ion binding can, however, be facilitated by reduction of the amide linkers of the ligand to tertiary amines. In this way, for example, Lattermann and coworkers have reported[7] the formation of columnar rectangular phases for the octahedral complexes $[M(CO)_3(R_3[9]aneN_3)]$ (R = alkoxybenzyl; M = Cr, Mo, W), while the symmetric functionalisation of polyaza macrocycles to give a range of columnar mesophases has also been reported by the groups of Latterman, Ringsdorf and Goodby.[8]

We were interested in developing functionalised thioether S-donor crowns as potential mesogenic materials. Unlike the N-donor systems, these have to be functionalised on the C-backbone, and although this is not always synthetically straightforward, it affords the polythioether donor core intact and available for metal complexation. A direct comparison can, therefore, also be made between the mesogenic mesomorphic properties of metal-free and metal-complexed materials. Furthermore, the ability of thioether macrocycles to coordinate to a wide variety of metal ions has been demonstrated,[9] and functionalisation of the periphery of the ligand does not appear to alter significantly the complexation properties of the resultant thioether crown.[10] Very little work has been reported on the synthesis of mesomorphic thioether crowns,[1,11,12] and we report herein the synthesis and thermal behaviour of a range of ligands and Pd(II) complexes of oligo(benzoate) ester derivatives.

Compounds **1**–**9** (Scheme 1) were prepared from the corresponding pure *cis* and *trans* dialcohols[13] *via* esterification with the appropriate carboxylic acid, acid chloride or acid anhydride. The reaction of equimolar amounts of $[Pd(MeCN)_4](BF_4)_2$ and each of **1**–**9** in MeCN–CH_2Cl_2 gave yellow solids which afforded yellow crystals upon crystallisation from MeCN–Et_2O. The purity of both the macrocyclic ligand and the corresponding Pd(II) complex was confirmed by ^{1}H and ^{13}C NMR spectroscopy, mass spectrometry (EI, FAB, ES) and by elemental analysis after consecutive recrystallisations. The thermal behaviour of the ligands and their Pd(II) complexes was studied by polarised optical microscopy. None of the ligands showed any mesomorphism, all simply melting directly to the isotropic phase. However, on complexation to Pd(II), the thermal behaviour changed markedly. Thus, while all the complexes of the *cis*-ligands and the two complexes of the *trans*-functionalised ligand with methoxy chains (**1** and **7**) were non-mesomorphic, the remaining complexes were indeed found to be mesomorphic (Table 1), showing monotropic nematic or SmC phases. These phases can be observed clearly by polarised optical microscopy, although decomposition does occur when samples are kept at elevated temperatures for prolonged periods.

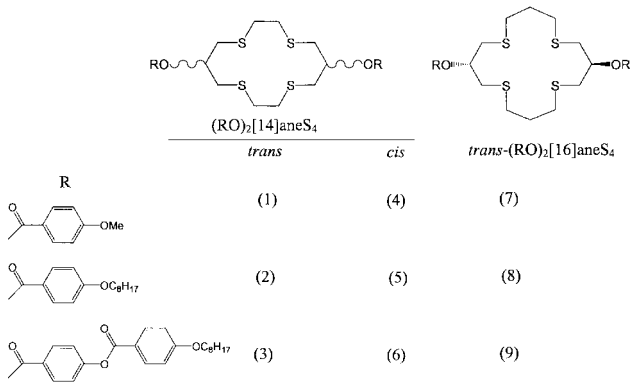

Scheme 1

On complexation to Pd(II), the macrocyclic ring becomes conformationally locked and acts as a rigid spacer which couples the terminal mesogenic groups together. Thus, for $[Pd(\mathbf{3})](BF_4)_2$ all four terminal phenyl groups are now part of the same anisotropic unit connected *via* the central complexed crown. The overall anisotropy is now sufficiently high to allow mesomorphism, and a monotropic nematic phase is observed, whereas the metal free ligand simply melts. Furthermore, $[Pd(\mathbf{2})](BF_4)_2$ is also mesomorphic giving a monotropic smectic SmC phase confirming that only two phenyl ester functions are required for mesomorphism. Interestingly, $[Pd(\mathbf{3})](BF_4)_2$ and

Table 1 Summary of polarising microscopic data for polyphenylester derivatives of *trans*- and *cis*-$(HO)_2$[14]aneS$_4$ and *trans*-$(HO)_2$[16]aneS$_4$

1	Cryst · 169 · I	$[Pd(\mathbf{1})](BF_4)_2$	Cryst · 273(decomp)
2	Cryst · 117 · I	$[Pd(\mathbf{2})](BF_4)_2$	Cryst · 222 · I · (164) · (S_c)
3	Cryst · 192 · I	$[Pd(\mathbf{3})](BF_4)_2$	Cryst · 280 · I · (242) · (N)
4	Cryst · 162 · I	$[Pd(\mathbf{4})](BF_4)_2$	Cryst · 242(decomp)
4	Cryst · 108 · I	$[Pd(\mathbf{4})](BF_4)_2$	Cryst · 242(decomp)
6	Cryst · 192 · I	$[Pd(\mathbf{6})](BF_4)_2$	Cryst · 244 · I(decomp)
7	Cryst · 144 · I	$[Pd(\mathbf{7})](BF_4)_2$	Cryst · 269(decomp)
8	Cryst · 101 · I	$[Pd(\mathbf{8})](BF_4)_2$	Cryst · 244 · I · (144) · (S_c)
9	Cryst · 171 · I	$[Pd(\mathbf{9})](BF_4)_2$	Cryst · 260 · I · (238) · (N)

† Electronic supplementary information (ESI) available: Figs. 1–3 with full captions, Fig. 4: view of the packing of $[Pd(\mathbf{7})][BF_4]_2$. Fig. 5: schematic of undulating layers in $[Pd(\mathbf{7})][BF_4]_2$. See http://www.rsc.org/suppdata/cc/b1/b107027b/

 DOI: 10.1039/b107027b

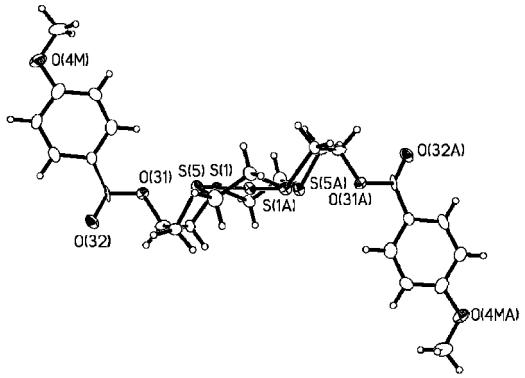

Fig. 1 View of the structure of $[Pd(\mathbf{1})]^{2+}$ with numbering scheme adopted.

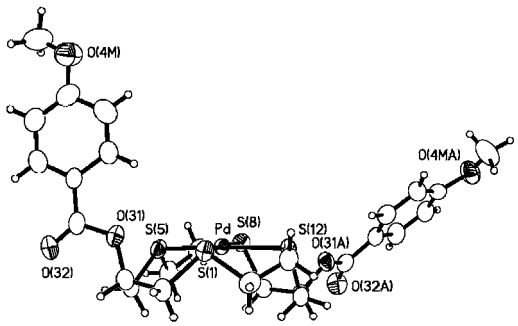

Fig. 2 View of the structure of $[Pd(\mathbf{4})]^{2+}$ with numbering scheme adopted.

$[Pd(\mathbf{9})](BF_4)_2$ are very rare examples of ionic species showing a thermotropic nematic phase.[14]

Further support for the above arguments comes from crystal structure determinations on model anisate derivatives $[Pd(\mathbf{1})](BF_4)_2$, $[Pd(\mathbf{4})](BF_4)_2$ and $[Pd(\mathbf{7})](BF_4)_2$.‡ The structure of $[Pd(\mathbf{1})](BF_4)_2$ shows an S-shaped conformation for the complexed *trans*-ligand (Fig. 1). A zigzag arrangement of cations in the packing diagram is observed as a consequence of the *trans* configuration of the functionalised macrocycle which adopts a [3434] conformation. The Pd(II) cation occupies a crystallographic inversion centre and therefore lies precisely in the S_4 mean plane. No aromatic π–π stacking is observed, although such interactions have been observed for the free ligand **1** where the macrocycle also adopts a [3434] configuration.[1] In contrast, the structure determination of *cis*-$[Pd(\mathbf{4})](BF_4)_2$ reveals a U-shaped cation with the phenyl groups pointing away from the macrocycle which adopts a [3434] conformation (Fig. 2) as for $[Pd(\mathbf{1})]^{2+}$. The Pd(II) ion exhibits a square planar geometry and is displaced out of the S_4 mean plane by 0.0365 Å. The dihedral angle between the mean plane of the phenyl rings and the S_4 mean plane is 82.6(2)° (C1P–C6P) and 41.5(2)° (C1P′–C6P′), with a dihedral angle between the two phenyl rings of 77.5(2)°. This results in the observed twisted U-shaped conformation for the complexed ligand. As in $[Pd(\mathbf{1})]^{2+}$, there are no aromatic π–π interactions between the phenyl groups in $[Pd(\mathbf{4})](BF_4)_2$ (Fig. 4, ESI†), although this is observed for the metal-free ligand which adopts a [223223] conformation.[1]

There is clearly, therefore, a direct conformational and configurational difference between the *cis* and *trans* isomers, which is reflected in mesophase formation. It is of course dangerous to attempt to correlate directly solid-state effects and potential structural features in the mesophase itself, particularly since monotropic behaviour is observed in each case. However, it is tempting to suggest that *trans*-isomers are more favorably disposed towards the formation of nematic mesophases. This is supported further by the results of a structure determination of $[Pd(\mathbf{7})](BF_4)_2$ which shows (Fig. 3) a similar S-shaped configuration to that of *trans*-$[Pd(\mathbf{1})](BF_4)_2$. The central Pd(II) cation occupies a crystallographic inversion centre and therefore lies precisely in the S_4 plane The central Pd(II) cation lies

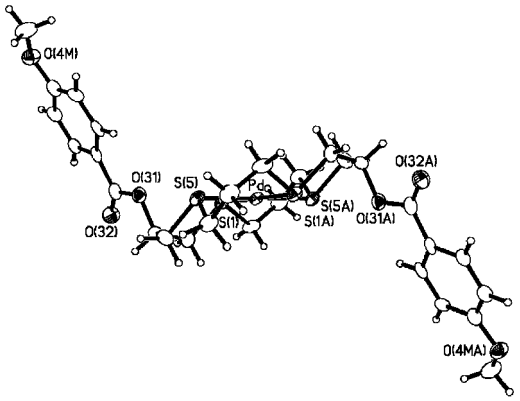

Fig. 3 View of the structure of $[Pd(\mathbf{7})]^{2+}$ with numbering scheme adopted.

in the mean S_4 plane of the macrocycle which adopts a [5353] conformation. Interestingly, however, the packing diagram of $[Pd(\mathbf{7})](BF_4)_2$ shows undulating layers of cations *via* π–π interactions of 3.326 Å with an offset angle of some 64.1° (Fig. 5, ESI†). This confirms that there are clear structural differences between 14- and 16-membered ring systems.

In conclusion, we have demonstrated the ability of a metal ion to induce mesomorphism in non-mesomorphic ligands, defining a sensing function for the ligands. Further, while both *cis* and *trans* isomers of related highly anisotropic macrocycles have been shown previously to be mesomorphic,[1] the conformational locking of the macrocycle resulting from complexation now discriminates between the isomers leading to mesomorphic complexes of *trans*-ligands, and non-mesomorphic complexes of *cis*-ligands.

This work was supported by the EPSRC and by the University of Nottingham.

Notes and references

‡ CCDC reference numbers 145062–145064. See http://www.rsc.org/suppdata/cc/b1/b107027b/ for crystallographic data in CIF or other electronic format.

1 A. J. Blake, D. W. Bruce, I. A. Fallis, S. Parsons and M. Schröder, *J. Chem. Soc., Chem. Commun.*, 1994, 2471; A. J. Blake, D. W. Bruce, I. A. Fallis, S. Parsons, H. Richtzenhain, S. A. Ross and M. Schröder, *Phil. Trans. R. Soc. London A*, 1996, **354**, 395; A. D. Pidwell, S. R. Collinson, S. J. Coles, M. B. Hursthouse, M. Schröder and D. W. Bruce, *Chem. Commun.*, 2000, 955.

2 J. Malthête, A.-M. Levelut and J.-M. Lehn, *J. Chem. Soc., Chem. Commun,*, 1985, 1794; J. Malthête, A.-M. Levelut and J.-M. Lehn, *J. Chem. Soc., Chem. Commun.*, 1992, 1434.

3 C. Mertesdorf and H. Ringsdorf, *Liq. Cryst.*, 1989, **5**, 1757.

4 C. Mertesdorf and H. Ringsdorf, *Liq. Cryst.*, 1991, **3**, 337.

5 G. Lattermann, *Mol. Cryst. Liq. Cryst.*, 1990, **182**, 299.

6 G. Lattermann, S. Schmidt and B. Gallot, *J. Chem. Soc., Chem. Commun.*, 1992, 1091.

7 S. Schmidt, G. Lattermann, R. Kleppinger and J. H. Wendorff, *Liq. Cryst.*, 1994, **16**, 693; S. Schmidt, G. Lattermann, R. Kleppinger and J. H. Wendorff, *Adv. Mater.*, 1992, **4**, 30.

8 U. Stebani, G. Latterman, M. Wittenberg, R. Festag and J. H. Wendorff, *Adv. Mater.*, 1994, **6**, 572; H. Fisher, S. S. Ghosh, P. A. Heiney, N. C. Maliszewskyj, T. Plesnivy, H. Ringsdorf and M. Seitz, *Angew. Chem., Int. Ed. Engl.*, 1995, **34**, 795; R. P. Tuffin, K. J. Toyne and J. W. Goodby, *J. Mater. Chem.*, 1995, **5**, 2093; R. P. Tuffin, K. J. Toyne and J. W. Goodby, *J. Mater. Chem.*, 1996, **6**, 1271.

9 A. J. Blake and M. Schröder, *Adv. Inorg. Chem.*, 1990, **35**, 1; A. J. Blake, R. O. Gould, M. A. Halcrow and M. Schröder, *Acta Crystallogr. Sect B*, 1993, **49**, 1652 and references therein.

10 R. J. Smith, G. D. Adams, A. P. Richardson, H.-J. Kuppers and P. J. Blower, *J. Chem. Soc., Chem. Commun.*, 1991, 475; R. J. Smith, S. N. Salek, M. J. Went, P. J. Blower and N. J. Barnard, *J. Chem. Soc., Dalton Trans.*, 1994, 3165.

11 F. Neve and M. Ghedini, *J. Mater. Chem.*, 1994, **6**, 70.

12 F. Neve and M. Ghedini, *Inorg. Chim. Acta*, 1994, **217**, 1.

13 V. B. Prett, G. H. Leggett, T. H. Cooper, P. R. Reed, D. Sumeteang, L. A. Ochrymowycz and D. B. Rorabacher, *Inorg. Chem.*, 1988, **27**, 2164.

14 F. Neve, *Adv. Mater.*, 1996, **8**, 277; B. Donnio and D. W. Bruce, *Struct. Bonding (Berlin)*, 1999, **95**, 193.

CHEMCOMM Communication
www.rsc.org/chemcomm

A new cofacial binucleating macropolycycle: segregated *versus* encapsulated complexation†

Lorenzo Tei,[a] Alexander J. Blake,[a] Francesco A. Devillanova,[b] Alessandra Garau,[b] Vito Lippolis,*[b] Claire Wilson[a] and Martin Schröder*[a]

[a] *School of Chemistry, The University of Nottingham, University Park, Nottingham, UK NG7 2RD. E-mail: m.schroder@nottingham.ac.uk*

[b] *Dipartimento di Chimica Inorganica ed Analitica, University of Cagliari, Complesso Universitario di Monserrato, S.S. 554 Bivio per Sestu 09042. Monserrato (Ca), Italy*

Received (in Cambridge, UK) 20th September 2001, Accepted 29th October 2001
First published as an Advance Article on the web 14th November 2001

A new cofacial binucleating macropolycycle combining, for the first time, the distinctive coordination properties of [9]aneN$_3$ (1,4,7-triazacyclononane) with those of phenol-based compartmental macrocycles is reported together with binuclear Cd^{II} and Y^{III} complexes, which show segregated and encapsulated complexation, respectively.

The design and synthesis of phenol-based binucleating compartmental macrocycles and the preparation of their homo- and hetero-dinuclear complexes incorporating bridging phenolate donors have important applications in several fields of chemical research.[1] In particular, binuclear complexes with transition metal ions in close proximity can show fascinating magnetic properties[2] and can serve as synthetic analogues of bimetallic biosites.[3] Furthermore, homo- and hetero-dinuclear lanthanide complexes with phenol-based compartmental macrocycles have proved to be useful models in studying the nature and applications of such compounds in lasers,[4] phosphors,[5] tunable photonic devices,[6] and in molecular recognition processes which govern Ln^{III} cation pairing events.[7] Variation of the building blocks[1,8] has afforded compartmental ligands incorporating lateral chains such as 2,2′-bipyridyl,[9] triethylenetetraamine[10] or 1,8-diamino-3,6-dioxaoctane.[11] Interestingly, there are no reports of pre-formed macrocycles being introduced as part of the lateral chains bridging the two phenolic units to give binucleating compartmental or cofacial macropolycycles.

We report herein the synthesis of H_2L and its coordination to Cd^{II} and Y^{III}. H_2L represents a new cofacial binucleating macropolycycle in which, for the first time, the particular coordination properties of [9]aneN$_3$ are combined with those of phenol-based compartmental macrocycles. Thus, direct [2 + 2] Schiff-base condensation of one mol equivalent of 1,4-bis(2-aminoethyl)-1,4,7-triazacyclononane, **3**, with one mol equivalent of 2,6-diformyl-4-methylphenol in MeOH gives, after partial removal of the solvent and addition of light petroleum, the cofacial macropolycycle H_2L in 78% yield as confirmed by ^{1}H, ^{13}C NMR spectroscopy, FAB mass spectrometry and analytical data† (Scheme 1). **3** was synthesised in overall 88% yield by reaction of 1-(*p*-tolylsulfonyl)-1,4,7-triazacyclononane **1** with two equivalents of *N*-tosylaziridine and subsequent detosylation of **2** with concentrated sulfuric acid. The ligand **3** has been reported previously,[12] but only as a by-product of the synthesis of the tris-pendant arm-species 1,4,7-tris(2-aminoethyl)-1,4,7-triazacyclononane. Our synthesis of **3** represents a selective and efficient methodology to the synthesis of asymmetric amine-functionalised [9]aneN$_3$ derivatives.

H_2L is characterised by two large adjacent chambers each with potential N_5O_2 donacity capable of accommodating metal ions with large ionic radii. We sought to determine whether H_2L behaves as a compartmental macrocycle encapsulating and bringing together two metal ions in close proximity, or as a segregated system leaving the metal ions separated within two independent N_5O-donating sites.

Reaction of H_2L with two mol equivalents of both $Cd(NO_3)_2{\cdot}4H_2O$ and Me_4NOH in MeOH–$CHCl_3$ (2 : 1 v/v) under reflux gives yellow plate crystals on partial removal of solvent and diffusion of Et_2O vapour into the remaining solution. The single crystal X-ray structure of $[Cd_2(L)](NO_3)_2{\cdot}$2MeOH confirms‡ the formation of a binuclear complex lying on a two-fold rotation axis with each six coordinate Cd^{II} ion bound to an N_5O donor set within a distorted octahedral environment (Fig. 1). Each Cd^{II} is coordinated to three N-donors of the triaza ring [Cd–N 2.342(3)–2.511(3) Å], to two imine nitrogen atoms [Cd–N(13) 2.293(3) and Cd–N(43) 2.313(3) Å] and to one phenolate oxygen [Cd–O(17) 2.283(2) Å]. The two N_5O-donating chambers of the macropolycycle act, therefore, as isolated donor sets and the phenolate oxygens do not bridge the metal ions. However, the phenolate O-donors are involved in a strong hydrogen-bond with a methanol molecule [H(1M)···O(17) 1.70 Å, O(1M)–H(1M)···O(17) 172°] which is also hydrogen-bonded to the secondary N–H of the triazacyclononane ring [H(7)···O(1M) 2.34 Å, N(7)–H(7)···O(1M) 139°] to form a six-membered ring including the Cd^{II} ion. Significantly, the two aromatic rings of the macropolycycle are stacked with a perpendicular distance of 3.342(4) Å between the mean planes of the rings and a distance of 3.428(4) Å between the centres of the rings (Fig. 1). This face-to-face π–π interaction and additional hydrogen-bonding force the donor atoms of the anionic ligand L^{2-} to assume a peculiar disposition with the phenolate oxygens twisted in opposite directions [twist angle 81.1(3)°] and each pointing towards an individual metal ion. As a result, the phenolate O-donors cannot bridge the Cd^{II}

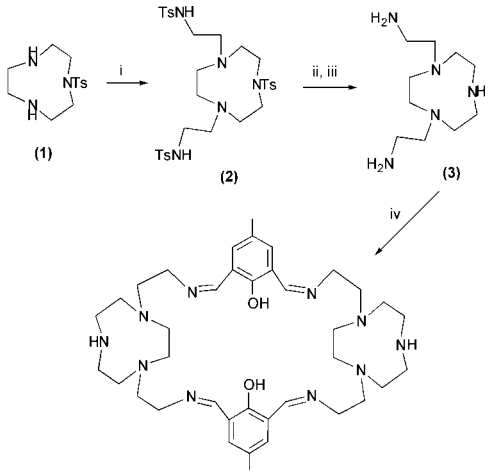

Scheme 1 *Reagents and conditions*: i, TsN(CH$_2$)$_2$, CH$_3$CN, reflux 3 h, 96% yield, ii, conc. H_2SO_4, 110 °C, 72 h; iii, Amberlite IRA-416, 93% overall yield from **2**; iv, 4-methyl-2,6-diformylphenol, MeOH, reflux 2 h, 78% yield.

† Electronic supplementary information (ESI) available: spectroscopic and crystallographic data. See http://www.rsc.org/suppdata/cc/b1/b108549m/

 DOI: 10.1039/b108549m

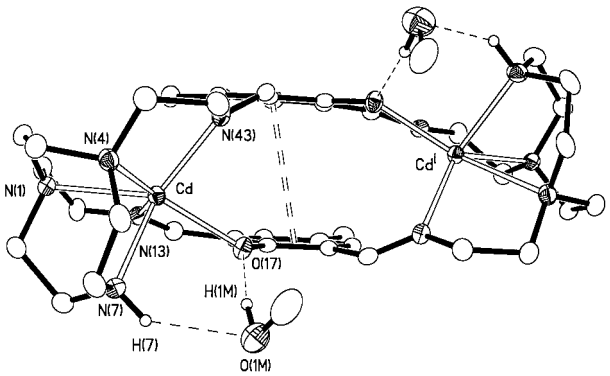

Fig. 1 Structure of $[Cd_2(L)](NO_3)_2{\cdot}2MeOH$ with numbering scheme adopted. Nitrate anions and hydrogen atoms on carbon atoms have been omitted for clarity. Hydrogen bonds and the face to face π–π interaction are drawn as single and double dashed lines, respectively. Displacement ellipsoids are drawn at 50% probability. Symmetry operation: i = $-x + 1$, y, $-z + 1/2$.

centres, which are, therefore, segregated each within its own N_5O-donor chamber [Cd···Cd distance 7.017(1) Å].

Reaction of H_2L with $Y(NO_3)_3{\cdot}6H_2O$ in a 1:2 molar ratio under the same conditions as above afforded yellow crystals. The single crystal X-ray structure of $[Y_2(L)(OH)][Y(NO_3)_4(MeOH)_2](NO_3)_2{\cdot}2MeOH$ shows‡ the complex cation lying across a two-fold rotation axis with $[Y(NO_3)_4(MeOH)_2]^-$ and two nitrate counter-anions (Fig. 2). The two Y^{III} centres in the cation lie within the two N_5O donating chambers of L^{2-} and are bridged not only by the phenolate oxygen atoms but also by a hydroxy group. To our knowledge the cation $[Y_2(L)(OH)]^{3+}$ represents one of the few structurally characterised homobinuclear lanthanide complexes with phenol-based compartmental macrocycles.[9,10] Each Y^{III} ion in $[Y_2(L)(OH)]^{3+}$ is eight coordinate and bound to three N-donors from the triazacyclononone framework [Y(1)–N 2.436(9)–2.655(7) Å], two azomethine nitrogen atoms [Y(1)–N(13) 2.418(8) and Y(1)–N(24) 2.472(8) Å], two phenolate oxygens [Y(1)–O(21) 2.391(6) and Y(1)–O(21^{i}) 2.322(6) Å] and a hydroxy O-donor [Y(1)–O(1) 2.277(7) Å]. This coordination mode is similar to that observed for the binuclear Lu^{III} and Dy^{III} complexes with the iminophenolate cryptate obtained by the template Schiff-base condensation of tris(2-aminoethyl)amine and 4-methyl-2,6-diformylphenol, where three phenolate oxygens bridge a pair of adjacent lanthanide ions [Lu···Lu 3.447(1) Å, Dy···Dy 3.4840(4) Å].[13] In the case of the binuclear Pr^{III}, Gd^{III} and La^{III} complexes of phenol-based compartmental macrocycles with 1,8-diamino-3,6-dioxaoctane[11] and 2,2′-bipyridine[9] as lateral chains, the two metal centres are bridged only by the two phenolate oxygen atoms, with nitrate and acetate anions completing the coordination sphere. The Pr···Pr, Gd···Gd and La···La distances are 4.05, 3.97 and 4.135(12) Å, respectively, whereas in $[Y_2(L)(OH)]^{3+}$ the Y···Y distance is significantly shorter at

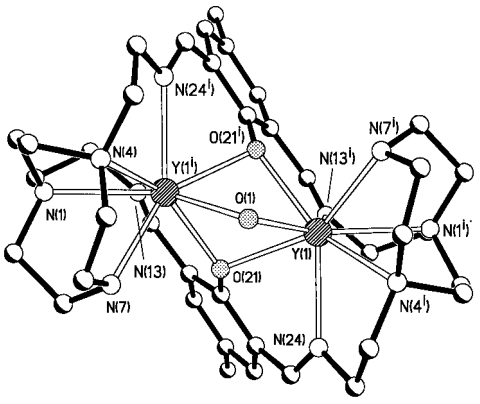

Fig. 2 Structure of $[Y_2(L)(OH)]^{3+}$ with numbering scheme adopted. Hydrogen atoms have been omitted for clarity. Symmetry operation: i = $-x + 1$, y, $-z + 3/2$.

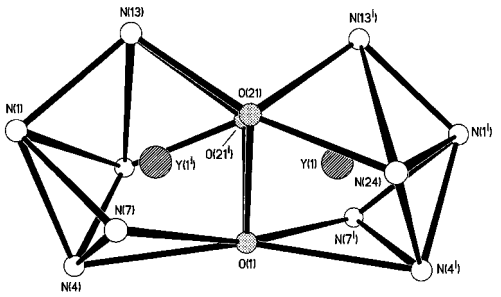

Fig. 3 View of the coordination polyhedra in $[Y_2(L)(OH)]^{3+}$.

3.4295(19) Å, which is considerably shorter than distances reported for binuclear lanthanide complexes.[13] The three bridging oxygen atoms in $[Y_2(L)(OH)]^{3+}$ form an almost equilateral triangle [O(21)···O(21^{i}) 2.747(13) Å and O(21)···O(1) 2.721(12) Å, O(1)–O(21)–O(21^{i}) 59.7(2)° and O(21)–O(1)–O(21^{i}) 60.6(4)°], and the two Y^{III} ions lie 1.716(5) Å out of this O_3 plane. Therefore, the coordination polyhedron at each metal ion can best be described as monocapped distorted dodecahedral (Fig. 3).

The work described herein represents the first example of a phenol-based compartmental system incorporating [9]aneN_3 to afford a large cofacial macropolycycle capable of forming binuclear complexes in which the two metal centres can be segregated or encapsulated. Furthermore, since H_2L can be synthesised directly without using templating metal ions, heterodinuclear complexes may be targeted, and this is currently under investigation.

We thank the EPSRC and University of Nottingham for support.

Notes and references

‡ CCDC reference numbers 171456 and 171457. See http://www.rsc.org/suppdata/cc/b1/b108549m/ for crystallographic data in cif or other electronic format.

1 P. Zanello, S. Tamburini, P. A. Vigato and G. A. Mazzocchin, *Coord. Chem. Rev.*, 1987, **77**, 165; A. J. Atkins, D. Black, A. J. Blake, A. Martin-Becerra, S. Parsons, L. Ruiz-Ramirez and M. Schröder, *Chem. Commun.*, 1996, 457; H. Okawa, H. Furutachi and D. E. Fenton, *Coord. Chem. Rev.*, 1998, **174**, 51.
2 O. Kahn, *Struct. Bonding (Berlin)*, 1987, **68**, 89.
3 D. E. Fenton and H. Okawa, *Perspect. Bioinorg. Chem.*, 1993, **2**, 81.
4 L. F. Johnson and H. J. Guggeinheim, *Appl. Phys. Lett.*, 1971, **19**, 44; S. A. Pollack and D. B. Chang, *J. Appl. Phys.*, 1988, **64**, 2885.
5 H. S. Kiliaan, F. P. Vanherwijnen and G. Blasse, *J. Solid State Chem.*, 1988, **74**, 39.
6 J. P. Desvergne, F. Fages, H. Bouaslaurent and P. Marsau, *Pure Appl. Chem.*, 1992, **64**, 1231.
7 K. D. Matthews, R. A. Fairman, A. Johnson, K. V. N. Spence, I. A. Kahwa, G. L. McPherson and H. Robotham, *J. Chem. Soc., Dalton Trans.*, 1993, 1719.
8 H. Adams, D. E. Fenton, S. R. Haque, S. L. Heath, M. Ohba, H. Okawa and S. E. Spey, *J. Chem. Soc., Dalton Trans.*, 2000, 1849; U. Casellato, S. Tamburini, P. Tomasin, P. A. Vigato, S. Aime, A. Barge and M. Botta, *Chem. Commun.*, 2000, 145; M. Yonemura, H. Okawa, M. Ohba, D. E. Fenton and L. K. Thompson, *Chem. Commun.*, 2000, 817; H. Furutachi, S. Fujinami, M. Suzuki and H. Okawa, *J. Chem. Soc., Dalton Trans.*, 1999, 2197; S. Kita, H. Furutachi and H. Okawa, *Inorg. Chem.*, 1999, **38**, 4038.
9 Z. Wang, J. Reibenspies and A. E. Martell, *Inorg. Chem.*, 1997, **36**, 629.
10 I. A. Kahwa, J. Selbin, T. C. Y. Hsieh and R. A. Laine, *Inorg. Chim. Acta*, 1986, **118**, 179; I. A. Kahwa, F. R. Fronczek and J. Selbin, *Inorg. Chim. Acta*, 1987, **126**, 227.
11 I. A. Kahwa, S. Folkes, D. J. Williams, S. V. Ley, C. A. Omahoney and G. L. McPherson, *J. Chem. Soc., Chem. Commun.*, 1989, 1531; P. Guerriero, P. A. Vigato, J. C. G. Bunzli and E. Moret, *J. Chem. Soc., Dalton Trans.*, 1990, 647; K. D. Matthews, I. A. Kahwa and D. J. Williams, *Inorg. Chem.*, 1994, **33**, 1382.
12 L. R. Gahan, G. A. Lawrence and A. M. Sargeson, *Aust. J. Chem.*, 1982, **35**, 1119.
13 C. Platas, F. Avecilla, A. de Blas, and T. Rodriguez-Blas, C. F. G. C. Geraldes, E. Toth, A. E. Merbach and J.-C. Bunzli, *J. Chem. Soc., Dalton Trans.*, 2000, 611 and references therein.

CHEMCOMM Communication
www.rsc.org/chemcomm

Kinetic resolution of secondary alcohols *via* chiral Pd(II)-complex-catalysed enantioselective benzoylation using CO and organobismuth(V) compound

Yoshihiro Miyake, Tomochika Iwata, Kang-Go Chung, Yoshiaki Nishibayashi and Sakae Uemura*

Department of Energy and Hydrocarbon Chemistry, Graduate School of Engineering, Kyoto University, Sakyo-ku, Kyoto 606-8501, Japan. E-mail: uemura@scl.kyoto-u.ac.jp

Received (in Cambridge, UK) 5th September 2001, Accepted 30th October 2001
First published as an Advance Article on the web 23rd November 2001

A novel method for kinetic resolution of racemic secondary alcohols *via* their enantioselective benzoylation (up to 48% ee) has been explored using CO, $Ph_3Bi(OAc)_2$, a catalytic amount of chiral Pd(II)-complex and AgOAc.

Kinetic resolution of secondary alcohols through enantioselective acylation is one of the most valuable methods for obtaining optically active alcohols and their derivatives in organic synthesis. In this field, enzymatic methods have widely been used to synthesise several natural products and bio-active compounds.[1] However, structural variations of substrates are limited because of high substrate specificity in enzymatic reactions. Recently, non-enzymatic methods using effective chiral catalysts for asymmetric acylation of alcohols have also been studied intensively.[2]

The carbonylative acylation of alcohols using carbon monoxide (CO) is an alternative tool for the preparation of esters and the various methods catalysed by transition metals have been reported.[3] However, the application of carbonylative acylation to kinetic resolution of racemic alcohols has not yet been reported so far, to the best of our knowledge.[4] We have previously reported transition metal-catalysed carbonylative benzoylation of methanol with phenyl-heteroatom compounds under an atmospheric pressure of carbon monoxide.[5] These findings led us to apply this catalytic system to asymmetric reactions. We have now investigated Pd(II)-complex-catalysed kinetic resolution of secondary alcohols[6] with phenyl-heteroatom compounds using optically active oxazolynylferrocenyl phosphine **L** as a chiral ligand [eqn. (1)].[7] Preliminary results are reported here.

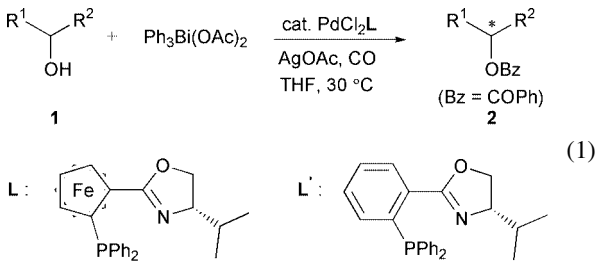

(1)

At first, we examined phenyl-heteroatom compounds such as $PhB(OH)_2$ and $PhSnMe_3$ which have been used as phenylating reagents in some asymmetric reactions by other groups.[8] However, these compounds were not effective for the enantioselective carbonylative acylation. Eventually it was disclosed that organobismuth(V) compound $Ph_3Bi(OAc)_2$ was quite useful for this purpose. Thus, the reaction of secondary alcohols **1** with $Ph_3Bi(OAc)_2$ in the presence of $PdCl_2$**L** catalyst under CO atmosphere proceeded smoothly to give the enantio-enriched benzoyl esters **2** [eqn. (1)].† Typical results are shown in Table 1. Treatment of 1-phenylethanol (**1a**) with $Ph_3Bi(OAc)_2$ (0.6 equiv.) in tetrahydrofuran (THF) under CO (5 atm) in the presence of AgOAc and a catalytic amount of $PdCl_2$**L** afforded 1-phenylethyl benzoate (**2a**) in 34% yield with 19% ee. The unreacted alcohol **1a** was recovered in 52% yield with low enantioselectivity (8% ee). Other solvents such as CH_2Cl_2, Et_2O and CH_3CN and reoxidants such as $CuCl_2$

Table 1 Palladium-catalysed kinetic resolution of *sec*-alcohols[a]

	2		**1**	
sec-Alcohol (**1**)	Yield (%)[b]	Ee (%)[c]	Yield (%)[b]	Ee (%)[c]
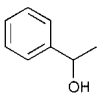	34	19[d]	52	8[e]
(**1a**) 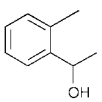	29	25	43	13
(**1b**) 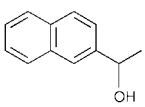	30	18	70	11
(**1c**) 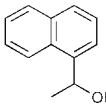	20	19	67	13
(**1d**) 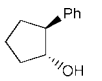	37	28	36	11
(**1e**)[f] 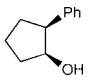	29	38	32	18
(**1f**)[g] 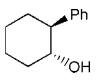	32	39[h]	46	23[i]
(**1g**)[f] 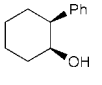	21	48	45	5
(**1h**)[g]				

[a] Reaction conditions: **1** (0.50 mmol), $Ph_3Bi(OAc)_2$ (0.30 mmol), $PdCl_2$**L** (0.050 mmol), AgOAc (1.5 mmol), THF (25 mL) at 30 °C under CO atmosphere (5 atm) for 48 h. [b] Isolated yield. [c] Determined by HPLC or GLC analysis using suitable chiral columns. [d] Absolute configuration is *R*. [e] Absolute configuration is *S*. [f] THF (10 mL) was used. [g] THF (5 mL) was used. [h] Absolute configuration is 1*R*, 2*S*. [i] Absolute configuration is 1*S*, 2*R*.

 DOI: 10.1039/b107904b

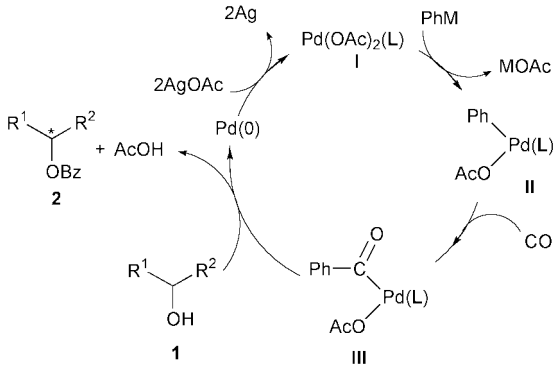

Scheme 1

$Cu(OAc)_2$ and ammonium cerium(IV) nitrate were not effective. The reaction of **1a** using the bidentate phosphine ligands such as (*R*)-(+)-2,2′-bis(diphenylphosphino)-1,1′-binaphthyl (BINAP) hardly proceeded and only a trace amount of **2a** was obtained. When other benzylic alcohols **1b–d** were used as substrates, the corresponding esters (**2b–d**) were obtained with similar enantioselectivities (19–25% ee). The reaction of cyclic alcohols such as **1e–h** proceeded slower than that of benzylic alcohols and it was necessary to carry out in a slightly higher concentration of **1** to obtain moderate enantioselectivies. In this reaction system, planar chirality of **L** might have some effect on enantioselectivity, and actually the reaction of **1g** using **L′**[9] in place of **L** gave **2g** in 38% yield with 16% ee. The best enantioselectivity was achieved when **1h** was treated with $Ph_3Bi(OAc)_2$ under similar conditions (up to 48% ee of **2h** in 21% yield; s = 3.2[10]).

A plausible reaction pathway is shown in Scheme 1. The reaction of the Pd(II) complex (**I**) with $Ph_3Bi(OAc)_2$ (PhM) affords the phenylpalladium species (**II**) *via* transmetallation followed by migratory insertion of CO to give the benzoylpalladium species (**III**). The attack of **1** to **III** results in the formation of the enantio-enriched **2** together with the Pd(0) species. The Pd(0) species is reoxidized to **I** by AgOAc.

In summary, we have demonstrated the Pd(II)-catalysed kinetic resolution of racemic secondary alcohols using CO and organobismuth(V) compound. Although the enantioselectivity is not yet satisfactory, our catalytic system may provide a novel methodology for kinetic resolution of racemic alcohols. Moreover, only a few example are known to use organobismuth compounds in asymmetric reaction[11] and so the reaction presented here might also be interesting from the viewpoint of organobismuth chemistry. Further work is now in progress aiming to construct a more effective chiral environment for enantioselective carbonylative acylation.

Notes and references

† *General procedure for enantioselective benzoylation of secondary alcohols*: To a solution of $PdCl_2$**L** (32.9 mg) and AgOAc (250.4 mg) in THF were added secondary alcohol **1** (0.50 mmol) and $Ph_3Bi(OAc)_2$ (167.5 mg, 1.50 mmol), and then the mixture was transferred into a 50 mL stainless-steel autoclave. Carbon monoxide (5 atm) was charged and the solution was stirred at 30 °C for 48 h. The resulting mixture was filtered through Florisil and Celite and the filtrate was concentrated under reduced pressure. Purification of the residue by column chromatography gave the benzoyl ester **2** and the unreacted **1**. Enantiomeric excess was determined by GLC or HPLC analysis using suitable chiral columns.

1 For reviews of enantioselective acylation of alcohols by enzymes, see: K. Drauz and H. Waldmann, *Enzyme Catalysis in Organic Synthesis: A Comprehensive Handbook*, VCH, New York, 1995; H. G. Davies, R. H. Green, D. R. Kelly and S. M. Roberts, *Biotransformations in Preparative Organic Chemistry*, Academic Press Ltd., London, 1989.

2 For representative examples of non-enzymatic catalytic enantioselective acylation, see: E. Vedejs, O. Daugulis and S. T. Diver, *J. Org. Chem.*, 1996, **61**, 430; E. Vedejs and J. A. MacKay, *Org. Lett.*, 2001, **3**, 535; J. C. Buble, H. A. Latham and G. C. Fu, *J. Am. Chem. Soc.*, 1997, **119**, 1492; S. Bellemin-Laponnaz, J. Tweddell, J. C. Ruble, F. M. Breitling and G. C. Fu, *Chem. Commun.*, 2000, 1009; T. Oriyma, Y. Hori, K. Imai and R. Sasaki, *Tetrahedron Lett.*, 1996, **37**, 8543; T. Sano, H. Miyata and T. Oriyama, *Enantiomer*, 2000, **5**, 119; T. Kawabata, M. Nagato, K. Takasu and K. Fuji, *J. Am. Chem. Soc.*, 1997, **119**, 3169; S. J. Miller, G. T. Copeland, N. Papaioannou, T. E. Horstmann and E. M. Ruel, *J. Am. Chem. Soc.*, 1998, **120**, 1629; F. Iwasaki, T. Maki, W. Nakamura, O. Onomura and Y. Matsumura, *Org. Lett.*, 1999, **1**, 969; A. C. Spivey, T. Fekner and S. E. Spey, *J. Org. Chem.*, 2000, **65**, 3154 and references cited therein.

3 H. M. L. Colquhoun, D. J. Thompson and M. V. Twigg, *Carbonylation: Direct Synthesis of Carbonyl Compounds*, Plenum Press, New York, 1991.

4 Some examples of enantioselective intramolecular lactonization using CO and Pd(II)-catalyst have been reported, see: T. Suzuki, Y. Uozumi and M. Shibasaki, *J. Chem. Soc., Chem. Commun.*, 1991, 1593.

5 C. S. Cho, T. Ohe and S. Uemura, *J. Organomet. Chem.*, 1995, **496**, 221; C. S. Cho, K. Tanabe, O. Itoh and S. Uemura, *J. Org. Chem.*, 1995, **60**, 274; C. S. Cho, Y. Yoshimori and S. Uemura, *Bull. Chem. Soc. Jpn.*, 1995, **68**, 950.

6 Quite recently, two examples of Pd(II)-catalysed oxidative kinetic resolution of secondary alcohols have been reported, see: D. R. Jensen, J. B. Pugsley and M. S. Sigman, *J. Am. Chem. Soc.*, 2001, **123**, 7475; E. M. Ferreira and B. M. Stoltz, *J. Am. Chem. Soc.*, 2001, **123**, 7725.

7 For our representative examples, see: Y. Nishibayashi and S. Uemura, *Synlett*, 1995, 79; Y. Nishibayashi, K. Segawa, K. Ohe and S. Uemura, *Organometallics*, 1995, **14**, 5486; I. Takei, Y. Nishibayashi, Y. Arikawa, S. Uemura and M. Hidai, *Organometallics*, 1999, **18**, 2271; Y. Nishibayashi, I. Takei, S. Uemura and M. Hidai, *Organometallics*, 1999, **18**, 2291; K.-G. Chung, Y. Miyake and S. Uemura, *J. Chem. Soc., Perkin Trans. 1*, 2000, 15; K.-G. Chung, Y. Miyake and S. Uemura, *J. Chem. Soc., Perkin Trans. 1*, 2000, 2725 and references cited therein.

8 Y. Takaya, M. Ogasawara, T. Hayashi, M. Sakai and N. Miyaura, *J. Am. Chem. Soc.*, 1998, **120**, 5579; M. Sakai, M. Ueda and N. Miyaura, *Angew. Chem., Int. Ed.*, 1998, **37**, 3279; T. Hayashi, T. Senda, Y. Takaya and M. Ogasawara, *J. Am. Chem. Soc.*, 1999, **121**, 11591; T. Hayashi and M. Ishigedani, *J. Am. Chem. Soc.*, 2000, **122**, 976; T. Hayashi, T. Senda and M. Ogasawara, *J. Am. Chem. Soc.*, 2000, **122**, 10716.

9 G. Helmchen and A. Pfaltz, *Acc. Chem. Res.*, 2000, **33**, 336.

10 Selectivity factor (s) was calculated from the yield and the ee value of the benzoyl ester **2**, see: H. B. Kagan and J. C. Fiaud, *Top. Stereochem.*, 1988, **18**, 249.

11 H. Brunner, U. Obermann and P. Wimmer, *Organometallics*, 1989, **8**, 821.

CHEMCOMM
Communication
www.rsc.org/chemcomm

Pyrazine dioxide bridged two-dimensional antiferromagnets $[M(NCS)_2(pzdo)_2]$ (M = Mn, Co; pzdo = pyrazine dioxide)†

Hao-Ling Sun,[a] Bao-Qing Ma,[a] Song Gao*[a] and Gang Su[b]

[a] *State Key Laboratory of Rare Earth Materials Chemistry and Applications & PKU-HKU Joint Laboratory on Rare Earth Materials and Bioinorganic Chemistry, College of Chemistry and Molecular Engineering, Peking University, Beijing 100871, China. E-mail: gaosong@pku.edu.cn*

[b] *Department of Physics, The Graduate School of the Chinese Academy of Sciences, P.O. Box 3908, Beijing 100039, China*

Received (in Cambridge, UK) 14th August 2001, Accepted 17th October 2001
First published as an Advance Article on the web 23rd November 2001

Two 2D coordination polymers $[M(NCS)_2(pzdo)_2]$ (M = Mn, Co; pzdo = pyrazine dioxide) bridged by pzdo ligand are synthesized, which are found to exhibit antiferromagnetic ordering below 8.4 and 11.2 K, respectively.

The construction of molecule-based magnets through a coordination polymer approach is a particular area of contemporary materials research. Judicious choice of bridges is a crucial factor to generate fascinating structures and unusual magnetic properties. Cyano, azido, oxalato and recently emerging dicyanamide ligands have been demonstrated to transmit magnetic interactions efficiently as bridges, and among their coordination polymers, numerous long-range ordering magnetic molecular materials were obtained.[1] Although pyrazine (pyz) and 4,4′-bipyridine have been widely used to build multi-dimensional network, fewer complexes with magnetic ordering have been afforded. In a recent communication the 3D $Mn(N_3)_2(pzdo)$,[2] in which pzdo supports the azide layer in the third direction, has been reported to display a spin-flop state and a higher antiferromagnetic ordering temperature (T_N = 62 K), which is remarkably higher than that for the well separated 2D quadratic azide sheet $[Mn(minc)_2(N_3)_2]_n$[3] (minc = methyl isonicotinate) and is comparable with that of the azide-bridged exclusively 3D compound $[N(CH_3)_4][Mn(N_3)_3]$.[4] By contrast, in a 2D analogous $Mn(N_3)_2(pyz)$ constructed *via* μ-1,1-N_3 and μ-pyz ligands, a lower magnetic ordering temperature (T_N = 2 K) was observed.[5] This signifies that pzdo might have better capability of tuning magnetic coupling than pyz. In order to elucidate the role of the pzdo ligand in mediating magnetic interplay, the 2D coordination polymers $[M(NCS)_2(pzdo)_2]$ (M = Mn **1**, Co **2**) were prepared‡ and their magnetic properties investigated.

X-Ray diffraction analysis§ revealed that **1** and **2** are isomorphous and consist of a 2D quadratic network (Fig. 1). Each metal ion is located at an inversion center and coordinated with four O atoms from bridging pzdo ligands and two terminal NCS^- groups, forming a compressed octahedral environment in which two N atoms lie in axial positions. The NCS^- group is almost linear with an N–C–S angle of 178.8° and bound to metal ion in a bent fashion with C–N–M angles of 161.1–162.1°. The bridging pzdo ligands adopt a *trans* mode similar to 4,4′-bipyridine dioxide in ref. 6(*a*), and extends the structure into a layer with M···M separations being within the range 8.257–8.604 and 8.107–8.461 Å for **1** and **2**, respectively. The 2D grid is similar to that found in $M(NCS)_2(pyz)_2$ (M = Mn, Co, Fe, Ni),[7] in which the pyz connects the metal ions to give a square lattice (intra-sheet M···M distance is *ca.* 7.3 Å).

As demonstrated previously, a striking feature of O,O-bifunctional ligands is their strong capability of forming hydrogen bonds compared with the corresponding N,N-ligands.[6] In both **1** and **2**, the O atom of pzdo not only coordinates with the metal ion, but forms weak hydrogen bonds with hydrogens of pzdo molecules from an adjacent layer [O2···H2a 2.564 Å, C2a–H2a···O2 159.3°; O1···H4b 2.355 Å, C4b–H4b···O1 144.21°: $a = -x+1, -y, -z, b = -x, -y, -z$]. Whereas in the corresponding pyz complexes[7] this feature is pronouncedly absent, its presence here links the 2D sheets into a 3D network with the nearest interlayer M···M separation being 6.940 and 6.892 Å for **1** and **2**, respectively.

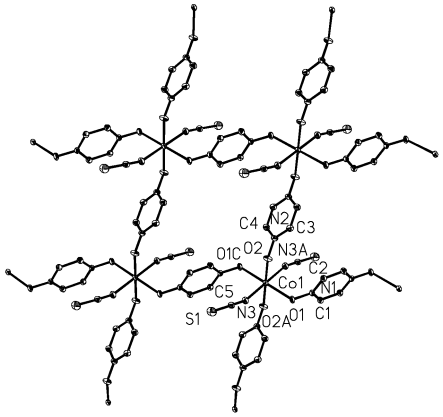

Fig. 1 Two-dimensional grid for **2**. Selected bond distances (Å) and angles (°): Mn(1)–N(3) 2.114(4), Mn(1)–O(1) 2.208(3), Mn(1)–O(2) 2.226(3). For **2**: Co(1)–N(3) 2.045(2), Co(1)–O(1) 2.1116(15), Co(1)–O(2) 2.1315(16).

The variable-temperature magnetic susceptibility χ_M for a collection of small crystals of **1** and **2** was measured in the temperature range 1.8–300 K (Fig. 2). At room temperature, the $\chi_M T$ values of **1** and **2** are 4.34 and 2.73 $cm^3\ mol^{-1}$ K, well consistent with the values of 4.38 and *ca.* 3.0 $cm^3\ mol^{-1}$ K expected for an uncoupled Mn^{2+} ion, and an octahedral high-spin Co^{2+} ion,[8] respectively. The value of χ_M increases as the temperature is lowered, reaching a maximum at *ca.* 12.9 and

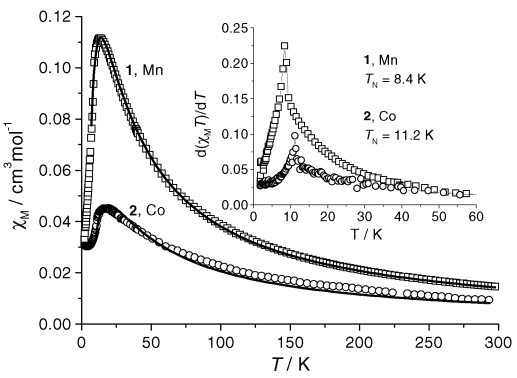

Fig. 2 Temperature dependence of magnetic susceptibility for **1** (□), and **2** (○). Solid lines correspond to calculated curves based on the Lines' model. Inset: $d(\chi_M T)/dT$ *vs.* *T* for **1** and **2**.

† Electronic supplementary information (ESI) available: Fig. S1: two types of coordination mode for pzdo. Fig. S2: perspective view of compound **2** along the [010] direction. See http://www.rsc.org/suppdata/cc/b1/b107334f/

 DOI: 10.1039/b107334f

17.2 K, for **1** and **2**, respectively, indicative of antiferromagnetic interactions between metal ions. The Neel temperatures, T_N, of **1** and **2** were determined from the sharp peak of $d(\chi_M T)/dT$ at 8.4 and 11.2 K, respectively, shown in the inset of Fig. 2.[9] The higher T_N of **2** may be related to the single-ion anisotropy of Co(II) ion. The best fitting of the magnetic data above 7 and 10 K using the Lines' model[10] for a quadratic layer gave the following results: for **1** (Mn), $J = -1.063(3)$ cm^{-1}, $g = 2.033(2)$ with $R = 1.9 \times 10^{-4}$; for **2** (Co), $J = -3.34(3)$ cm^{-1}, $g = 2.35(1)$ with $R = 2.8 \times 10^{-3}$ {$R = \Sigma[(\chi_M)_{obs} - (\chi_M)_{calcd}]^2/\Sigma(\chi_M)_{obs}^2$}. Although $M(NCS)_2(pyz)_2$ (M = Mn, Co) have 2D grids similar to **1** and **2**, no maximum was observed in their χ_M–T plots.[7b]

The field dependence of the magnetization for **1** at different temperatures below T_N (8.4 K) shows a pronounced sigmodial shape, especially at lower temperature (Fig. 3). The behavior is due to a spin-flop transition as observed in ref. 2. The magnetization below T_N increases very slowly with increasing field due to antiferromagnetic ordering, and then increases quickly for a transition from an antiferromagnet to a spin-flop state at a transition field around 30–35 kOe, which is also determined by the maximum of the ac susceptibilty χ' (inset of Fig. 3). The magnetization is only 1.6 $N\beta$ at 70 kOe, far from the saturation value of 5 $N\beta$ for the Mn^{2+} ion, suggesting an antiferromagnetic ordering again. In contrast to **1**, the field dependence of the magnetization for **2** at different temperatures below and around T_N (11.2 K) all show a linear slow increase, as shown in Fig. 4, and no spin flop state was observed. The magnetization under 70 kOe at 1.8 K is only 0.52 $N\beta$, also far from the saturation value of *ca.* 2.5 $N\beta$ expected for a Co^{2+} with $S_{eff} = 1/2$, and $g = 5.0$,[8b] this being further evidence supporting the antiferromagnetic ordering of **2**.

It was well documented that the ordering temperature of a 3D antiferromagnet is slightly lower than $T(\chi_{max})$.[11] Although the hydrogen bonding between layers in **1** and **2** could have a crucial contribution to the magnetic ordering, the antiferromagnets possess obviously 2D characteristics, as the ratio of $T_N/T(\chi_{max})$, 0.646 and 0.649 for **1** and **2**, respectively, is quite low. In summary, compared with corresponding 2D pyz-bridged paramagnetic complexes, the title 2D quadratic networks constructed by pzdo exhibit antiferromagnetic ordering.

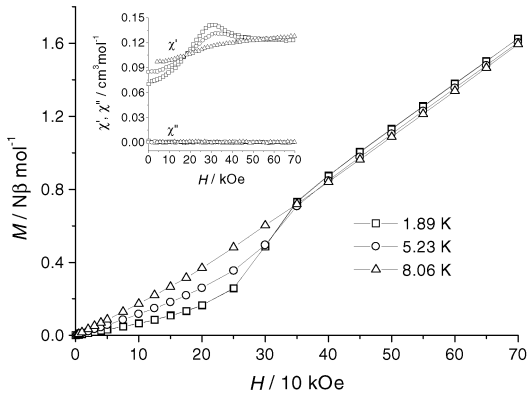

Fig. 3 Field dependence of magnetization and ac magnetic susceptibility at different temperatures for **1**.

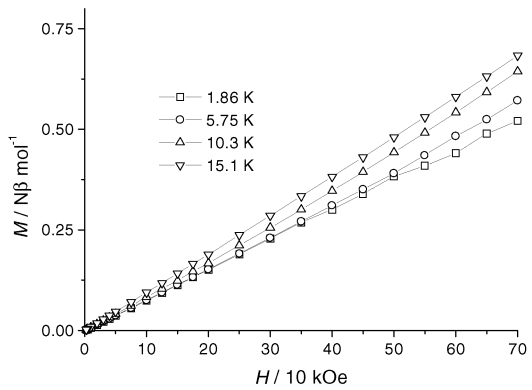

Fig. 4 Field dependence of magnetization at different temperatures for **2**.

This work was partly supported by the State Key Project of Fundamental Research (G1998061305), the National Science Fund for Distinguished Young Scholars.

Notes and references

‡ *Syntheses*: $Mn(NCS)_2(pzdo)_2$ **1**: this was carried out by mixing an aqueous solution of $MnCl_2 \cdot 4H_2O$ (0.5 mmol, 12.5 ml) with a aqueous solution of NaNCS (2.5 mmol, 12.5 ml). After stirring for 1 h at *ca*. 80 °C an aqueous solution of pzdo (0.50 mmol, 10 ml) was added. The resulting solution was allowed to stand at room temperature after stirring for 0.5 h. After two weeks, a prismatic, purple, X-ray quality single crystal was obtained (yield 60%) (Calc.: C, 30.08; H, 2.02, N, 21.05. Found: C, 30.12; H, 2.16; N, 20.09%).

$Co(NCS)_2(pzdo)_2$ **2**: this was obtained by mixing an aqueous solution of $Co(NCS)_2$ (0.25 mmol, 2.85 ml), with an aqueous solution of pzdo (0.50 mmol, 10 ml). The resulting solution was allowed to stand at room temperature after stirring for 0.5 h. After several days red prismatic crystals appeared (yield, 70%) (Calc.: C, 30.39; H, 2.04; N, 21.26. Found: C, 30.47; H, 2.117; N, 20.45%).

§ *Crystal data*: compound **1**: $C_{10}H_8MnN_6O_4S_2$, $M = 395.28$, triclinic, space group $P\bar{1}$, $a = 6.9405(2)$, $b = 7.1938(3)$, $c = 8.2566(4)$ Å, $\alpha = 82.237(3)$, $\beta = 66.892(3)$, $\gamma = 74.971(3)°$, $U = 365.94(3)$ Å^3, $Z = 1$, $D_c = 1.794$ Mg m^{-3}, μ(Mo-Kα) = 1.216 mm^{-1}, $F(000) = 199$, GoF = 1.219. A total of 6971 reflections were collected and 1662 are unique ($R_{int} = 0.0353$). $R1$ and $wR2$ are 0.0443 and 0.1209, respectively, for 107 parameters and 1518 reflections [$I > 2\sigma(I)$].

Compound **2**: $C_{10}H_8CoN_6O_4S_2$, $M = 399.27$, triclinic, space group $P\bar{1}$, $a = 6.8922(14)$, $b = 7.1528(14)$, $c = 8.1074(16)$ Å, $\alpha = 82.49(3)$ $\beta = 67.26(3)°$, $\gamma = 74.06(3)°$, $U = 354.31(12)$ Å^3, $Z = 1$, $D_c = 1.871$, $\mu = 1.536$ mm^{-1}, $F(000) = 201$, GoF = 0.999. A total of 7110 reflections were collected and 1664 are unique ($R_{int} = 0.040$). $R1$ and $wR2$ are 0.0306 and 0.0722, respectively, for 107 parameters and 1406 reflections [$I > 2\sigma(I)$].

The data were collected on a Nonius Kappa CCD with Mo-Kα radiation ($\lambda = 0.71073$ Å) at 293 K. The structures were solved by direct methods and refined by a full matrix least squares technique based on F^2 using the SHELXL 97 program.

CCDC reference numbers 169675 and 16976.

See http://www.rsc.org/suppdata/cc/b1/b107334f/ for crystallographic data in CIF or other electronic format.

1 For examples: (*a*) O. Kahn, *Molecular Magnetism*, VCH, New York, 1993; (*b*) *Magnetic Molecular Materials*, ed. D. Gatteschi, O. Kahn, J. S. Miller and F. Palacio, Kluwer, Dordrecht, Netherlands, 1991. (*c*) *Molecular Magnetism: From Molecular Assemblies to the Devices*, ed. E. Coronado, P. Delhaes, D. Gatteschi and J. S. Miller, NATO ASI Series, E321, Kluwer Academic, Dordrecht, 1996; (*d*) *Molecule-Based Magnetic Materials*, ed. M. M.Turnbull, T. Sugimoto and L. K. Thompson, American Chemical Society, Washington, DC, 1996; (*e*) *Magnetism: A Supramolecular Function*, ed. O. Kahn, NATO ASI Series, C484, Kluwer Academic, Dordrecht, 1996; (*f*) *Metal-Organic and Organic Molecular Magnets*, ed. P. Day and A. E. Underhill, in *Philos. Trans. R. Soc. London A*, 1999, **357**, 2849.

2 B. Q. Ma, H. L. Sun, S. Gao and G. Su, *Chem. Mater.*, 2001, **13**, 1946.

3 (*a*) A. Escuer, R. Vicente, M. A. S. Goher and F. A. Mautner, *J. Chem. Soc., Dalton Trans.*, 1997, 4431; (*b*) A. Escuer, R. Vicente, M. A. S. Goher and F. A. Mautner, *Inorg. Chem.*, 1995, **34**, 5707.

4 F. A. Mautner, R. Cortes, L. Lezama and T. Rojo, *Angew. Chem., Int. Ed. Engl.*, 1996, **35**, 78.

5 J. L. Manson, A. M. Arif and J. S. Miller, *Chem. Commun.*, 1999, 1479.

6 (*a*) B. Q. Ma, S. Gao, H. L. Sun and G. X. Xu, *J. Chem. Soc., Dalton Trans.*, 2001, 130; (*b*) B. Q. Ma, S. Gao, H. L. Sun and G. X. Xu, *Cryst. Eng. Comm.*, 2001, 35.

7 (*a*) J. A. Real, G. D. Munno, M. C. Munoz and M. Julve, *Inorg. Chem.*, 1991, **30**, 2701; (*b*) F. Lloret, M. Julve, J. Cano and G. D. Munno, *Mol. Cryst. Liq. Cryst.*, 1999, **334**, 569; (*c*) J. Lu, T. Paliwala, S. C. Lim, C. Yu, T. Niu and A. J. Jacobson, *Inorg. Chem.*, 1997, **36**, 923.

8 (*a*) A. T. Casey and S. Mitrs, in *Theory and Application of Molecular Paramagnetism*, ed. E. A. Boudreaux and L. N. Mulay, J. Willey and Sons, New York, 1976, p. 135; (*b*) W. K. Robinson and S. A. Friedberg, *Phys. Rev.*, 1960, **117**, 402.

9 (*a*) M. E. Fisher, *Proc. R. Soc. London A*, 1960, **254**, 66; (*b*) M. E. Fisher, *Philos. Mag.*, 1962, **7**, 1731.

10 M. E. Lines, *J. Phys. Chem. Solids*, 1970, **31**, 101.

11 G. C. DeFotis, E. D. Remy and C. W. Scherrer, *Phys. Rev. B*, 1990, **41**, 9047.

CHEMCOMM
Communication
www.rsc.org/chemcomm

Synthesis of heterogeneous palladium catalyst assemblies by molecular imprinting

Andrew N. Cammidge,*[a] Nicholas J. Baines[a] and Richard K. Bellingham[b]

[a] *Wolfson Materials and Catalysis Centre, School of Chemical Sciences, University of East Anglia, Norwich, UK NR4 7TJ. E-mail: a.cammidge@uea.ac.uk*
[b] *GlaxoSmithKline Pharmaceuticals, Old Powder Mills, Nr. Leigh, Tonbridge, Kent, UK. E-mail: Richard.K.Bellingham@gsk.com*

Received (in Cambridge, UK) 19th September 2001, Accepted 1st November 2001
First published as an Advance Article on the web 23rd November 2001

Molecular imprinting can be used to prepare heterogeneous catalysts which mimic their homogeneous counterparts.

Synthetic organic chemistry is now so far advanced that reagent combinations are available to perform a huge spectrum of transformations. Transition metal catalysis features heavily in this arsenal.[1] Homogeneous reactions are often preferred for laboratory scale preparations and the majority of mechanistic elucidations and optimisation studies have been carried out in solution phase. Frequently, however, problems are encountered when taking an optimised laboratory procedure and scaling it up. To take advantage of precedent knowledge, there is a tendency to carry out reactions in homogeneous solution enabling reaction products, yields, rates and safety to be easily predicted. This approach is extremely successful in terms of the synthetic transformation. However, the use of expensive and toxic (*e.g.* palladium) homogeneous catalysts suffers from prohibitive drawbacks. The most important of these, on an industrial scale, is contamination of the final product by trace quantities of the metal. An obvious alternative is the use of heterogeneous catalysis where a polymeric ligand is employed.[2,3] Such catalysts have clear advantages over their homogeneous counterparts. The catalyst is easily separated from the reaction medium, and leaching into the medium (and hence product) is often reduced. Current polymeric ligand/catalyst assemblies are, however, often unsuitable because it is impossible to translate optimised reaction conditions from homogeneous to heterogeneous systems. In homogeneous systems the catalyst/ligand stoichiometry and geometry are uniform across each 'active site' (for a particular intermediate or transition state). Current commercial systems present ligands in non-uniform spatial disposition. This random geometry influences the reaction profile of each active site leading to catalyst inefficiency and unpredictability. The alternative approach has been to attach multidentate ligands to solid supports. These systems, however, have rigid coordination geometry and transfer of the reactions from homogeneous conditions to the solid phase is often not straightforward.

The accepted catalytic cycle for a palladium catalysed cross-coupling reaction is shown in Fig. 1.[4] It is clear that homogeneous reaction protocols have inbuilt flexibility. Ligand stoichiometry and geometry are dynamic throughout the catalytic cycle. A number of features should be noted; (i) Pd(0) complexes favour tetrahedral geometry whereas Pd(II) complexes favour square-planar geometry. (ii) Oxidative addition to Pd(0) complexes bound to four phosphine ligands is slow. (iii) Reductive elimination to yield product takes place from the *cis* complex. It is surprising, perhaps, that these combined factors have not been examined before in the design of efficient polymeric ligand assemblies.

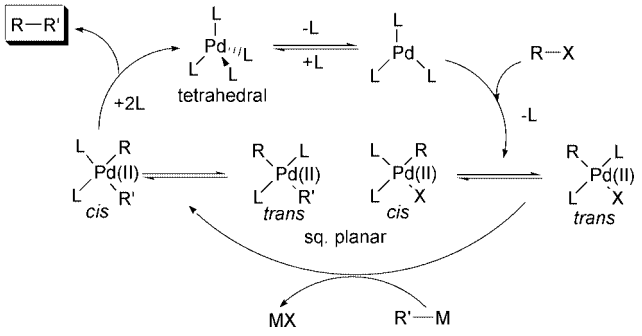

Fig. 1 Catalytic cycles for a cross-coupling reaction.

We reasoned that an ideal solid catalyst could be realised by preassembly of the ligand around the metal followed by polymerisation (molecular imprinting[5,6]). In this way the preferred ligand geometry can be tailored depending on the reaction to be catalysed (the rate limiting step can be accelerated). We chose to investigate palladium-catalysed cross- coupling reactions and aimed to assemble (two) phosphine ligands in a '*cis* square-planar' geometry in order to accelerate reductive elimination (often the rate limiting step) and minimise competing pathways leading to sideproducts.

The catalysts were prepared as outlined in Schemes 1–3. We selected a simple, polymerisable phosphine ligand (**1**) for investigation because we expected its synthesis to be relatively straightforward and it is closely related to triphenylphosphine (which is perhaps the most widely used ligand in coupling reactions and whose complexation chemistry is well-documented). Synthesis of **1**[7] was achieved by reaction of the Grignard reagent from 4-chlorostyrene with chlorodiphenylphosphine. This reaction was complicated by polymerisation of starting material and product due to the exothermic nature of both the Grignard reagent formation and its addition to the chlorophosphine. In practice, formation of the Grignard reagent stops below *ca.* 30 °C, and polymerisation becomes a problem above 40 °C. Nevertheless, under carefully controlled conditions a yield of around 60% could be achieved.

2:1 Complexes of the polymerisable phosphine ligand to palladium(II) were synthesised following modifications to the procedures reported for the simple triphenylphosphine complexes.[8] These latter procedures, which use high temperatures, had to be modified to prevent premature polymerisation of the ligand/complex. Consequently, **1** was stirred in warm (40 °C) ethanol. K_2PdCl_4 (in minimum water) was added and the mixture stirred for 3 h. The precipitate which formed was filtered off and purified by careful recrystallisation to give the pure bis-(**1**)–palladium dichloride which was fully characterised. Our strategy relied on the incorporation of the bis-(**1**)–palladium complex into the polymer matrix in its *cis*-form. The dichloride was therefore converted to its catecholate salt **2** by treatment with catechol/KOH in a mixed solvent system. The pure product precipitated from the mixture and was stored in the dark (Scheme 1).

The final polymers were designed to be rigid (preventing relaxation of the imprinted site) so a high proportion of crosslinker was employed in the polymer synthesis. Initial experiments employed methylmethacrylate as monomer (*ca.*

 DOI: 10.1039/b108464j

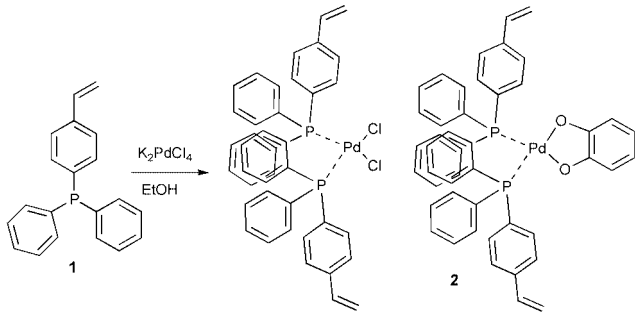

Scheme 1

25%), ethylene glycol dimethacrylate as crosslinker (*ca.* 25%) and butanol as porogenic solvent (50%). To this mixture was added palladium complex **2** (initially 0.5% Pd by weight) and the mixture polymerised (AIBN initiation) at ~ 60 °C for 6 h. Polymerisation proceeded smoothly but it was evident that **2** was not homogeneously distributed throughout the polymer (some precipitation and sedimentation of the complex occurred). Use of trichloroethane as solvent enabled a homogeneous solution to be obtained at the polymerisation temperature. However, polymerisation led to a homogeneous 'gel' (rather than a macroporous network polymer). These transparent polymers were not investigated further because we envisaged a macroporous structure being crucial to achieve efficient delivery and removal of reactants/products to and from the catalytic site.

A second series of polymers was prepared employing styrene (25%), divinyl benzene (25%) and butanol (50%). Addition of 0.5% **2** followed by polymerisation led to a macroporous polymer in which the complex was clearly distributed throughout. However, there was still some evidence of poor solubility (precipitation) of the complex when higher Pd loadings were attempted. Switching to cyclohexanol as porogen enabled polymers to be prepared in which the palladium loading could be increased (we chose 5% as maximum). The initial polymer blocks were crushed and washed (to remove porogen and any unbound species) to produce the catalysts as yellow/green powders (Scheme 2).

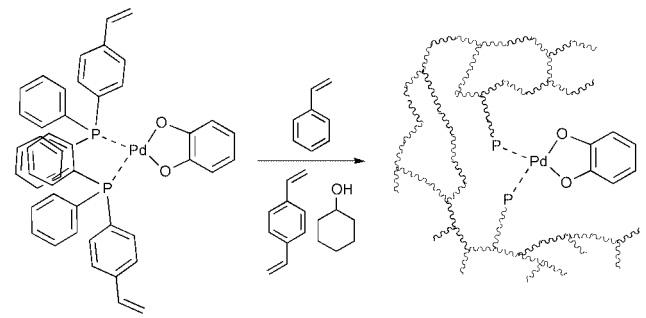

Scheme 2

The Suzuki reaction[4] between *p*-bromoanisole and phenyl boronic acid was chosen as a model reaction (Scheme 3). The standard reaction conditions were as follows: a mixture of *p*-bromoanisole, phenyl boronic acid (1.2 equivalents), palladium catalyst (3 mol% Pd) and sodium carbonate were stirred in refluxing DME–water (4 : 1) for 3 h. The mixture was allowed to cool and filtered to re-isolate the catalyst. The product was isolated either by precipitation (addition of water) or by extraction (dichloromethane) and column chromatography.

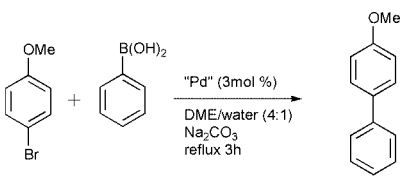

Scheme 3

Under these conditions the catalyst prepared from commercial ligand† led to yields of 46–56%. Re-use of the catalyst led to a slight reduction in the isolated yield (56 → 45%). The catalysts prepared by molecularly imprinting **2** led to consistently higher yields (76–81%). Furthermore, the reaction yield was essentially unaffected by repeated use (catalyst was re-used five times in one series of experiments, giving 80% yield in the fifth experiment) and catalyst loading (0.5 and 5% gave very similar high yields). It is particularly noteworthy that control homogeneous experiments (using $PdCl_2$ and PPh_3) gave yields comparable with the commercial ligand (*i.e.* ~55%, much lower than with the molecularly imprinted polymer). The crude reaction mixture (after filtration) was analysed and found to contain only 1 ppm Pd (0.1 ppm on reuse).

A similar improved performance was observed with 4-nitrobromobenzene and the results were even more impressive with 2-bromoanisole which gave 47% yield (not optimised) with the imprinted catalyst but less than 10% when the commercial ligand was employed under identical conditions. Stille[9] reactions using the same bromides with tributylphenyltin gave only trace quantities of coupled product with the catalyst prepared from commercial ligand. Under identical conditions, both the molecularly imprinted catalyst **2** and homogeneous catalyst gave similarly high yields (65–95%).

In conclusion, we have demonstrated that catalysts prepared by molecular imprinting are clearly far superior to those prepared from traditional polymeric ligands. Their performance is comparable, and often superior, to related homogeneous catalysts. Although it is quite early to draw conclusions it seems likely that the semi-rigid ligand geometry is responsible for the improved performance. Complex **2** is incorporated into the polymer matrix in its square-planar geometry [Pd(II)]. The catalytically active Pd^0 species is therefore slightly strained (tetrahedral). It seems reasonable to suggest that the rate of oxidative addition (the slow step in some cases[10]) is thereby accelerated (having only two phospines per site also serves to increase this rate). Similarly, enforced *cis*-geometry is likely to increase the rate of reductive elimination and minimise side-reactions. The molecularly imprinted catalyst efficiently retains the metal and catalyst efficiency is retained after continual use. This combination of properties makes this new generation of heterogeneous catalysts extremely attractive.

Notes and references

† Commercial polymer bound triphenylphosphine (Aldrich) was treated with K_2PdCl_4 and washed exhaustively to give an orange–yellow solid (12.5% Pd by weight).

1 *Comprehensive Organometallic Chemistry II*, ed. E. W. Abel, F. G. A. Stone and G. Wilkinson, Pergamon Press, New York, 1995.
2 B. Clapham, T. S. Reger and K. D. Janda, *Tetrahedron*, 2001, **57**, 4637.
3 R. Farina, *Can. J. Chem.*, 2000, **78**, 957.
4 N. Miyaura and A. Suzuki, *Chem. Rev.*, 1995, **95**, 2457.
5 For recent overviews, see: (*a*) K. Severin, *Curr. Opin. Chem. Biol.*, 2000, **4**, 710; (*b*) M. J. Whitcombe, C. Alexander and E. N. Vulfson, *Synlett*, 2000, 911.
6 N. M. Brunkan and M. R. Gagne, *J. Am. Chem. Soc.*, 2000, **122**, 6217.
7 (*a*) C. A. Fyfe, H. C. Clark, J. A. Davies, P. J. Hayes and R. E. Wasylishen, *J. Am. Chem. Soc.*, 1983, **105**, 6577; (*b*) R. Rabinowitz and R. Marcus, *J. Org. Chem.*, 1961, **36**, 4157.
8 (*a*) J. C. Bailar Jr. and H. Itatani, *Inorg. Chem.*, 1618, **4**, 1965; (*b*) O. Gandolfi and J. Blum, *Inorg. Chim. Acta*, 1983, **80**, 103.
9 V. Farina, V. Krishnamurthy and W. J. Scott, *Org. React (N.Y.)*, 1997, **50**, 1.
10 D. Milstein and J. K. Stille, *J. Am. Chem. Soc.*, 0000, **101**, 4992.

CHEMCOMM
Communication
www.rsc.org/chemcomm

A solution-phase route to a tetraethynylated (cyclobutadiene)cyclopentadienylcobalt complex with a *para*-(1,3,2,4)-substitution pattern†

Matthew Laskoski, Jason G. M. Morton, Mark D. Smith and Uwe H. F. Bunz*

Department of Chemistry and Biochemistry, The University of South Carolina, Columbia, South Carolina 29208, USA, E-mail: Bunz@mail.chem.sc.edu

Received (in Cambridge, UK) 1st October 2001, Accepted 22nd October 2001
First published as an Advance Article on the web 23rd November 2001

The synthesis of a tetraethynylated, CpCo-stabilized cyclobutadiene complex *via* a metalation/carbonylation/alkynylation route is reported; this synthetic sequence allows, for the first time, the solution phase synthesis of a tetraethynylcyclobutadiene(cyclopentadienyl)cobalt derivative, and sorts the four alkyne substituents into two *para*-related groups.

We have a long-standing commitment in carbon rich organometallics,[1] concentrating our efforts on synthesis, reactions, and properties of multiply alkynylated cyclobutadiene complexes as building blocks for nano-scale carbon-rich[2] objects. Tetraethynylcyclobutadiene(cyclopentadienyl)cobalt complexes[3–7] are valuable due to their robustness, ease of handling and their potential to form super-polycyclic[3,8] organometallic materials. However, the synthesis of these complexes is tedious, requiring a gas-phase flash vacuum pyrolysis step that bottlenecks the amount of tetraethynyl available.[3] These species invariably display a *ortho,ortho*-substituent pattern of their four substituents, a witness to their genesis by a Bergman-type rearrangement. To expand the chemistry of tetraethynylcyclobutadiene(cyclopentadienyl)cobalt complexes, a solution-phase synthesis with control of their regiochemistry would be advantageous.[9]

Reaction of the ethynylated dioxane **1** with $CpCo(CO)_2$ followed by desilylation furnishes a mixture of the two isomeric acetals **2a** and **2b** in a 3.5 : 1 ratio in a combined yield of 95% (Scheme 1).[9] BuLi cleanly metalates **2b** at the cyclobutadiene ring and leaves the Cp-ring intact. We attribute the facile

† Electronic supplementary information (ESI) available: experimental, including details of preparation and spectroscopic characterization of all new compounds. See http://www.rsc.org/suppdata/cc/b1/b109848a/

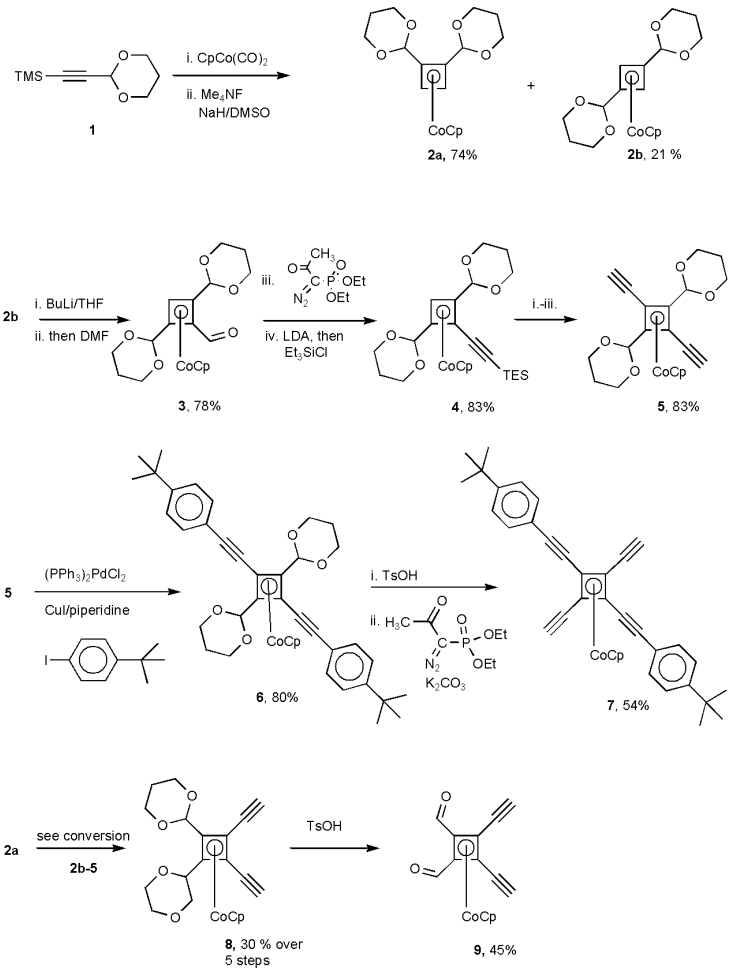

Scheme 1

 DOI: 10.1039/b109848a

metalation of the four-ring to the enhanced s-character of the C–H-bonds *and* the *ortho*-metalating power of the two acetal groups, that drive this deprotonation reaction selectively.[10]

Workup of the formed anion with DMF provided the complex **3** in 78% yield after chromatography. Ohira's reagent[11] converts the aldehyde group of **3** into an alkyne that is further protected by lithiation and reaction with triethylchlorosilane to give **4**. Repetition of the metalation/carbonylation/alkynylation process with **4** as substrate furnishes the *para*-diyne **5**, in which the protecting group is lost during the K_2CO_3-promoted Ohira reaction. Pd-catalyzed arylation transforms **5** into **6** (80% yield). In the last steps of the reaction sequence, the acetal groups are cleaved off **6**, and a double Ohira reaction converts the intermediate dialdehyde into the title compound **7** in 54% yield.

As a proof of this concept we explored the chemistry of the major isomer **2a** and have transformed it in an analogous reaction sequence into complex **9**, in which two free alkyne groups and two free aldehyde functionalities reside on the cyclobutadiene complex. This material is surprisingly stable and can be manipulated in air at ambient temperature. The dialdehyde **9** is an attractive building block for further elaboration of linear, cyclic and star-shaped organometallic cyclobutadiene architectures.

The tetrayne **7** is stable and can be handled under ambient laboratory conditions without decomposition. Due to the unusual tetragonal symmetry of the ligand we performed a single crystal X-ray structure determination. Suitable needle-shaped specimen were grown from dichloromethane.‡ Fig. 1 shows the ORTEP of **7**; bond lengths and bond angles are in excellent agreement with literature reported values for alkynylated cyclobutadiene complexes.[1,3,4] The four-membered ring is square with angles in the range of 89–91°, and, typical for cyclobutadiene complexes, the alkyne groups are bent away on average by 10° from the side of the cyclopentadienylcobalt fragment. This feature is observed in other tetraalkynylated cyclobutadiene complexes and is attributed to electronic effects.[4]

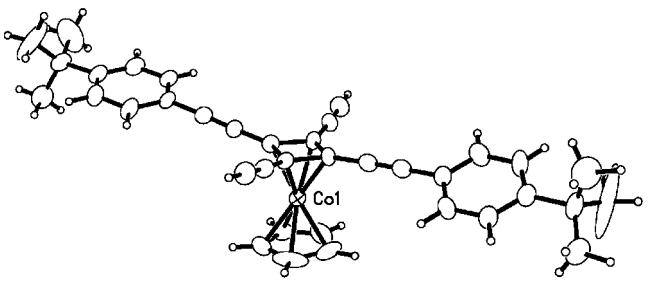

Fig. 1 ORTEP of the tetraethynylated cyclobutadiene complex **7**. Bond lengths and bond angles are in excellent agreement with literature reported values for multiply alkynylated cyclobutadiene complexes.

In conclusion, we have developed a solution-phase route to tetraethynylated, CpCo-stabilized cyclobutadiene complexes. We have executed a stepwise solution-phase synthesis for the hitherto unknown *para*-substituted complex **7**, and could show with the transformation of **2a** into **9** that it will work similarly in the case of the corresponding *ortho*-substituted substrate **2a**. With this methodology, almost complete control over the regiochemistry of the substitution of cyclopentadienylcobalt-stabilized cyclobutadiene complexes is achieved. In future we will report upon the use of these building blocks for novel organometallic oligomers, polymers, cycles and polycycles.

U. H. F. B. and M. L. thank the National Science Foundation (CAREER CHE 9981765, 2000–2003). U. H. F. B. is a Camille Dreyfus Teacher–Scholar (2000–2004).

Notes and references

‡ CCDC reference number 171473. See http://www.rsc.org/suppdata/cc/b1/b109848a/ for crystallographic data in CIF or other electronic format.

1 U. H. F. Bunz, Y. Rubin and Y. Tobe, *Chem. Soc. Rev.*, 1999, **28**, 107; U. H. F. Bunz, *Top. Curr. Chem.*, 1999, **201**, 131; U. H. F. Bunz, *Synlett*, 1997, 1117.

2 For reviews, see: F. Diederich and L. Gobbi, *Top. Curr. Chem.*, 1999, **201**, 44; F. Diederich and Y. Rubin, *Angew. Chem., Int. Ed. Engl.*, 1992, **31**, 1101; F. Diederich, *Nature*, 1994, **369**, 199.

3 M. Altmann, G. Roidl, V. Enkelmann and U. H. F. Bunz, *Angew. Chem., Int. Ed. Engl.*, 1997, **36**, 1107; U. H. F. Bunz, G. Roidl, M. Altmann, V. Enkelmann and K. D. Shimizu, *J. Am. Chem. Soc.*, 1999, **121**, 10 719; U. H. F. Bunz and V. Enkelmann, *Organometallics*, 1994, **13**, 3823.

4 M. Laskoski, G. Roidl, M. D. Smith and U. H. F. Bunz, *Angew. Chem., Int. Ed.*, 2001, **40**, 1460.

5 M. M. Haley, J. J. Pak and S. C. Brand, *Top. Curr. Chem.*, 1999, **201**, 82.

6 R. Diercks, J. C. Armstrong, R. Boese and K. P. C. Vollhardt, *Angew. Chem., Int. Ed. Engl.*, 1986, **25**, 268.

7 J. D. Tovar, N. Jux, T. Jarrosson, S. I. Kahn and Y. Rubin, *J. Org. Chem.*, 1997, **62**, 3432; N. Jux, K. Holczer and Y. Rubin, *Angew. Chem., Int. Ed. Engl.*, 1996, **35**, 1985; Y. Tobe, K. Kubota and K. Naemura, *J. Org. Chem.*, 1997, **62**, 3430.

8 Z. Wu, S. Lee and J. S. Moore, *J. Am. Chem. Soc.*, 1992, **114**, 8730; M. M. Haley, S. C. Brand and J. J. Pak, *Angew. Chem., Int. Ed. Engl.*, 1997, **36**, 835.

9 J. R. Fritch and K. P. C. Vollhardt, *Organometallics*, 1982, **1**, 590.

10 U. Bunz, *Organometallics*, 1993, **12**, 3594.

11 S. Ohira, *Synth. Lett.*, 1989, **19**, 561; D. F. Taber and Y. Wang, *J. Am. Chem. Soc.*, 1997, **119**, 22; S. Müller, B. Liepold, G. J. Roth and H. J. Bestmann, *Synlett*, 1996, 521; the reagent was originally introduced by Seferth *et al.*: D. Seyferth, R. S. Marmor and P. Hilbert, *J. Org. Chem.*, 1971, **36**, 1379; D. G. Brown, E. J. Velthuisen, J. R. Commerford, R. G. Brisbois and T. R. Hoye, *J. Org. Chem.*, 1996, **61**, 2540.

CHEMCOMM Communication
www.rsc.org/chemcomm

Incorporation of conjugated polydiacetylene systems into organic–inorganic quantum-well structures

Yuko Takeoka,*[ab] Keisuke Asai,[bc] Masahiro Rikukawa[ab] and Kohei Sanui[ab]

[a] *Department of Chemistry, Sophia University, 7-1 Kioi-cho, Chiyoda-ku, Tokyo 102-8554, Japan. E-mail: y-tabuch@sophia.ac.jp*
[b] *CREST, Japan Science and Technology Corporation, 4-1-8 Hon-cho, Kawaguchi, Saitama, 332-0012, Japan*
[c] *Department of Quantum Engineering and Systems Science, The University of Tokyo, 7-3-1 Hongo, Bunkyo-ku, Tokyo 113-8656, Japan*

Received (in Cambridge, UK) 24th September 2001, Accepted 1st November 2001
First published as an Advance Article on the web 23rd November 2001

A new type of organic–inorganic semiconductor heterostructure has been successfully fabricated by incorporating a polydiacetylene backbone into layered perovskite compounds by solid-state polymerization.

Much attention has been paid recently to the synthesis and characterization of organic–inorganic layered perovskites because of their exceptional properties and the tunability of their structure.[1–3] Layered perovskites with the general formula $(RNH_3)_2PbBr_4$ (R; C_nH_{2n+1}) naturally form a quantum-well structure consisting of a lead bromide semiconductor sheet sandwiched between organic insulator layers as shown in Fig. 1(a). The layered structure is self-organized through the neutralization of $[PbBr_6]^{4-}$ with organic ammonium in an orientation determined by the hydrogen bonds, and by a van der Waals interaction between adjacent organic ammoniums. Because the insulating organic layers have a wide band gap, excitons are confined in the inorganic $[PbBr_6]^{4-}$ layer; these provide strong photoluminescence with high optical nonlinearity, characteristics with potential applications in optical devices.[4–8] Organic–inorganic perovskites have a wide variety of possible combinations of inorganic and organic parts. Organic materials with specific functionality are combined on a molecular scale with an inorganic matrix with other target properties, creating an organic–inorganic composite with either a combination of the useful properties or one in which new phenomena arise from the interaction between the organic and inorganic components.[9] In this study, we tried to incorporate polydiacetylene systems into the organic–inorganic perovskites. The incorporation of diacetylenic species into the layered perovskites provides the potential for solid-state polymerization through the activation of the materials by an external energy source, as shown in Fig. 1(b). In a one-dimensional conjugated polymer, a Frenkel exciton is produced by optical excitation, whereas Wannier–Mott excitons can be formed under the same conditions in 2D inorganic perovskite quantum wells. The fabrication of such organic-inorganic heterostructures has been long anticipated, ever since Agranovich *et al.* reported the possibility of the existence of a new excitonic state, denoted a hybrid exciton.[10] It is thought that the hybrid exciton can be formed at the interface in organic–inorganic semiconductor heterostructures by the resonant mixing of Frenkel and Wannier exciton states, providing the features of both excitons, and exhibiting a strong nonlinear phenomenon at resonance. However, although hybrid excitons have been investigated theoretically, there are, as yet, no reports on the actual creation of hybrid excitons because of the difficulty in sample preparation. Herein, we report the novel preparation method of organic–inorganic semiconductor heterostructures by topochemical polymerization of polydiacetylenes into layered perovskites.

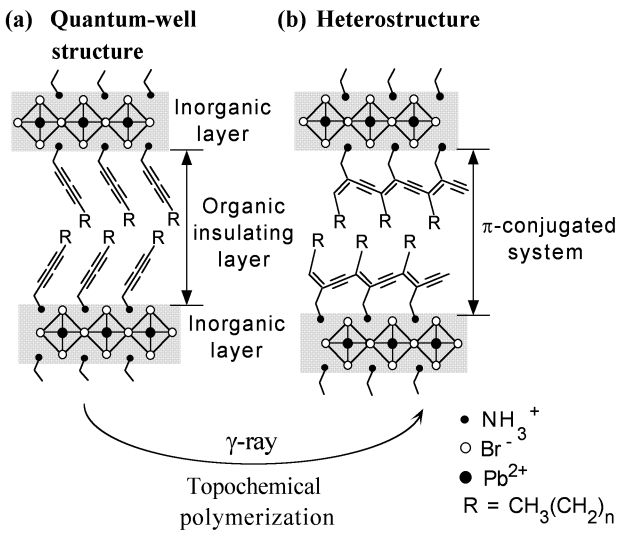

Fig. 1 Model of solid state polymerization performed in layered perovskites $(CH_3(CH_2)_nC{\equiv}CC{\equiv}C(CH_2)NH_3)_2PbBr_4$, DAPbBr(*n*–1), catalyzed by γ-irradiation.

Organic–inorganic perovskites $(CH_3(CH_2)_nC{\equiv}CC{\equiv}C(CH_2)_mNH_3)_2PbBr_4$ [abbreviated DAPbBr(*n*–*m*)], which contain aminodiacetylene organic moieties, were employed as monomer samples. As carefully designed reactant crystal structures are required for topochemical polymerization, we examined the incorporation of various diacetylenic amines into the layered perovskite structure. The diacetylenic amines were synthesized according to the method of Tsibouklis *et al.*[11] DAPbBr(*n*–*m*) were successfully obtained as both powders and thin films by reacting the corresponding alkylammonium bromides $CH_3(CH_2)_nC{\equiv}CC{\equiv}C(CH_2)_mNH_3Br$ with a stoichiometric amount of $PbBr_2$ in *N*,*N*-dimethylformamide (DMF). Powder samples were obtained as precipitates by pouring the reaction solutions into acetone. Films were spin-coated onto SiO_2 from DMF solutions. Solid-state polymerization was carried out using a ^{60}Co γ-source (dose rate 22.3 kGy h^{-1}) at room temperature. Specimens were placed in a glass tube, which was evacuated to 10^{-5} Torr in order to avoid oxidation during γ-irradiation. Polymerizability was monitored by UV–VIS spectra and X-ray diffraction. The DAPbBr(*n*–*m*) films exhibited a clear characteristic X-ray diffraction pattern indicative of a layered perovskite structure consisting of inorganic semiconductor layers of lead bromide and organic insulating layers of diacetylenic ammonium $CH_3(CH_2)_nC{\equiv}CC{\equiv}C(CH_2)_mNH_3^+$. In order to investigate the ability of the diacetylenic ammonium in the perovskites to polymerize, the spin-coated films were irradiated with γ-rays. The polymerization behavior of diacetylenes in DAPbBr(*n*–*m*) was found to be dependent on the alkyl chain length and the position of the diacetylenic unit in the hydrocarbon chains. The results of the

 DOI: 10.1039/b108536k

solid state polymerization of $CH_3(CH_2)_nC{\equiv}CC{\equiv}C(CH_2)_mNH_3^+$ are given in Table 1 together with the *d*-spacing of layered perovskites, as determined by powder X-ray diffraction, for the spin-coated films of both monomer and polymer forms.

In the $m = 1$ compounds, aminodiacetylenes with longer alkyl groups (carbon number $n \geqslant 13$) undergo polymerization under γ-irradiation. Colorless and transparent spin-coated films of DAPbBr(13–1) in monomer form turned red after γ-irradiation. The optical absorption spectra of DAPbBr(13–1) spin-coated film at 19 Mrad irradiation are shown in Fig. 2. The monomer sample exhibited a sharp exciton peak at 378 nm, attributed to the two-dimensional quantum-well structure based on PbBr. After γ-irradiation, a broad peak due to π–π* transitions of polydiacetylene also appeared at around 550 nm, along with the persistent initial exciton peak of perovskite. This implies that a π-conjugated system was successfully incorporated into the quantum-well layered perovskite structure. Exarhos *et al*. and other researchers have reported a method of estimating conjugation length by correlating the observed solid state absorption peak of the π–π* transition.[12,13] By fitting the absorption data obtained for DAPbBr(13–1) to their model, we estimate the conjugation length of polydiacetylene introduced into the perovskite structures to be 22 monomer units. Fig. 3 shows the X-ray diffraction patterns of DAPbBr(13–1) in the monomer and polymerized form. Each spin-coated film produces a series of (00l) diffraction patterns, evidence that the layered structure of alkylammonium cations and lead bromide layers remains intact after topochemical polymerization. The powder X-ray diffraction patterns of the polymerized DAPbBr(13–1) exhibit peaks at 2.60° with $d = 33.4$ Å; however, no peak attributable to the monomer structure was observed. The *d*-spacing increment of 2.7 Å observed after polymerization occurs as a result of conformation changes such as changes in the tilt angle of alkyl groups and the extent of their interdigitation. The polymerizability of DAPbBr(*n*–1) with a shorter alkyl chain was dramatically lower than that with the long alkyl chain (Table 1). DAPbBr(2–1) produced a weak absorbance at shorter wavelengths in addition to an initial exciton peak from the quantum well after γ-irradiation, due to the formation of oligomers rather than a polymer backbone. In the case of DAPbBr(1–1) with short alkylammonium groups, the layered structure was not maintained during the polymeric reaction because of the weak interaction between alkyl chains. The development of polymerization behavior that is dependent on the length of alkyl chains connected to the diacetylene unit is controlled by the presence or absence of favorable orientation for the polymerization via 1,4-addition. Layered structures of DAPbBr(13–1) and DAPbBr(15–1) are well-arranged for polymerization because of the strong self-organization properties of long alkyl chains. In other words, longer alkyl chains favor a molecular arrangement appropriate for topochemical polymerization.

Table 1 Polymerizability of layered perovskites containing aminodiacetylenes DAPbBr(*n*–*m*) catalyzed by γ-irradiation

		After γ-irradiation	
n–*m*	Monomer *d*-Spacing/Å	*d*-Spacing/Å	Polymerizability (conjugation length)
1–1	17.3	Collapse	—
2–1	18.4	16.7	—
13–1	30.7	33.4	○(22 units)
15–1	37.7	38.1	○(27 units)
11–3	31.1	Same as monomer	—

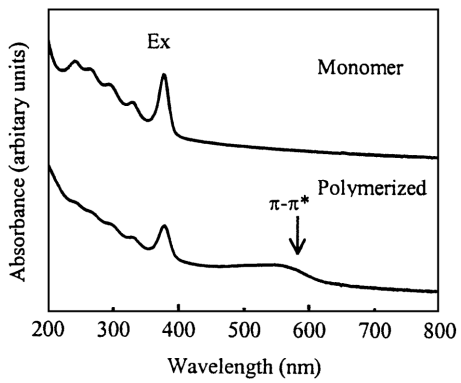

Fig. 2 UV–VIS spectra of spin-coated layered perovskite DAPbBr(13–1) films of monomer and polymerized form (after 19 Mrad γ-irradiation).

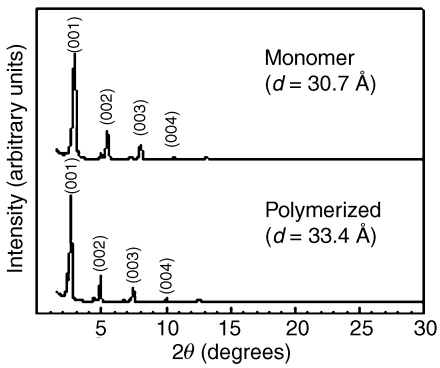

Fig. 3 X-Ray diffraction patterns of DAPbBr(13–1) spin-coated films of monomer and polymerized form.

We compared the polymerizability between DAPbBr(13–1) and DAPbBr(11–3), which have the same total alkyl chain length (*i.e.* $n + m = 14$). Polymerizability is dependent on the spacer length between the butadiyne unit and ammonium groups. DAPbBr(11–3) exhibited no change in the lamellar structure or spectrum after γ-irradiation, indicating that polymerization does not proceed in DAPbBr(11–3). As there are no prominent differences in molecular arrangement between DAPbBr(11–3) and DAPbBr(13–1), the difference in polymerizability is thought to be derived from the packing and flexibility of the diacetylenic ammoniums. Molecules in DAPbBr(13–1) have more freedom to pack in a favorable manner for the reaction, allowing a higher degree of reorganization during the polymerization process.

In summary, we have described a novel method of preparing organic–inorganic semiconductor structures based on layered perovskites. We have successfully incorporated π-conjugated systems using the architecture of diacetylenic ammoniums. We have recently extended this achievement to the production of a hybrid exciton feature, the report on which shall be presented in the near future.

Notes and references

1 D. Mitzi, C. Feild, W. Harrlson and A. Guloy, *Nature*, 1994, **369**, 467.
2 J. Calabrese, N. L. Jones, R. L. Harlow, D. Thorn and Y. Wang, *J. Am. Chem. Soc.*, 1991, **113**, 2328.
3 G. C. Papavassiliou, I. B. Koutselas, A. Terzis and M. H. Whango, *Solid State Commun.*, 1994, **91**, 695.
4 T. Ishihara, J. Takahashi and T. Goto, *Solid State Commun.*, 1989, **69**, 933.
5 C.-Q. Xu, T. Kondo, H. Sakakura, K. Kumata, Y. Takahashi and R. Ito, *Solid State Commun.*, 1991, **79**, 245.
6 M. Era, S. Morimoto, T. Tsutsui and S. Saito, *Appl. Phys. Lett.*, 1994, **65**, 676.
7 Y. Takeoka (nee Y. Tabuchi), K. Asai, M. Rikukawa, K. Sanui and K. Ishigure, *J. Phys. Chem. Solids*, 2000, **61**, 837.
8 Y. Takeoka (nee Y. Tabuchi), K. Asai, M. Rikukawa, K. Sanui and K. Ishigure, *Nonlinear Opt.*, 2000, **25**, 449.
9 P. Day and R. D. Ledsham, *Mol. Cryst. Liq. Cryst.*, 1982, **86**, 163.
10 V. Agranovich, R. Atanasov and F. Bassani, *Solid State Commun.*, 1984, **92**, 295.
11 J. Tsibouklis, C. Pearson, Y. P. Song, J. Yarwood, M. Petty and J. Feast, *J. Mater. Chem.*, 1993, **3**, 97.
12 G. Exarhos, W. Rien Jr. and R. Baughman, *J. Am. Chem. Soc.*, 1976, **98**, 481.
13 H. Kuhn, *J. Chem. Phys.*, 1949, **17**, 1198.

CHEMCOMM Communication
www.rsc.org/chemcomm

Discovery of new solid phase sulfur oxidation catalysts using library screening†

Stuart D. Green,[a] Chiara Monti,[b] Richard F. W. Jackson,*[ab] Michael S. Anson[c] and Simon J. F. Macdonald[c]

[a] *Department of Chemistry, Bedson Building, The University of Newcastle, Newcastle upon Tyne, UK NE1 7RU*
[b] *Department of Chemistry, Dainton Building, University of Sheffield, Brook Hill, Sheffield, UK S3 7HF. E-mail: r.f.w.jackson@shef.ac.uk*
[c] *GlaxoSmithKline, Gunnels Wood Road, Stevenage, Hertfordshire, UK SG1 2NY*

Received (in Cambridge, UK) 19th September 2001, Accepted 31st October 2001
First published as an Advance Article on the web 23rd November 2001

The discovery of a new solid-supported ligand 5 for the catalytic asymmetric oxidation of aryl alkyl sulfides in up to 72% ee using Ti(O^{i}Pr)$_4$ and aqueous H_2O_2 is reported.

The asymmetric synthesis of alkyl aryl sulfoxides has been the subject of much investigation, following the initial reports by Kagan[1] and Modena[2] on the use of a modified Sharpless reagent for the oxidation of alkyl aryl sulfides using alkyl hydroperoxides. More recent work has focussed on the use of H_2O_2 as the oxidant, with the first successful catalytic system discovered by Bolm using the combination of the amino alcohol-derived Schiff base **1** with vanadium.[3,4] An oxidation catalyst that

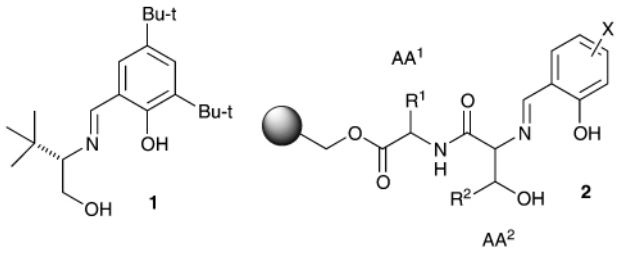

combines high catalytic efficiency and high enantiomeric excess remains an important goal.[5] The recent development of combinatorial methods for the discovery of new asymmetric catalysts offers a potential solution.[6] The great success that has been achieved by Hoveyda and Snapper in various asymmetric C–C bond forming processes by parallel synthesis of peptide–Schiff base libraries[7] suggested that an optimisation of the Bolm system using these techniques might be possible.

The apparent requirement for a hydroxy group in the ligand (presumably to coordinate to vanadium) suggested structure **2** as an appropriate generic ligand, which would be amenable to solid phase synthesis by standard coupling techniques. We planned on exploring five variables in this modular catalyst design, namely the solid support, amino acid 1, hydroxy amino acid 2, the salicylaldehyde and the choice of metal, with vanadium as the obvious starting point. Our initial library fixed the solid support as Wang, screened a series of L-amino acids (Gly, Ala, Val, Leu, Ile, Phe) as amino acid 1, serine and threonine as amino acid 2, and a series of salicylaldehyde derivatives [3,5-dibromosalicylaldehyde, 2-hydroxynaphthaldehyde, 3,5-di-*tert*-butylsalicylaldehyde (DtBS), 3,5-dichlorosalicylaldehyde, 5-nitrosalicylaldehyde and 3,5-dinitrosalicylaldehyde]. All the ligands were prepared in parallel using standard techniques. The library of 72 ligands was tested in the vanadium-catalysed oxidation of methyl phenyl sulfide **3a** using hydrogen peroxide. We employed two different reaction protocols; in the first, 1 equiv. of VO(acac)$_2$ was simply added to a suspension of the ligand in CH_2Cl_2, followed by addition of H_2O_2 and methyl phenyl sulfide **3a** (Scheme 1); in the second, the ligand was preincubated with a solution of VO(acac)$_2$, and the resin was then filtered and added to the reaction mixture.‡ The latter protocol gave results that were as good as, or better than, the first protocol, so the latter protocol was used in all subsequent experiments.

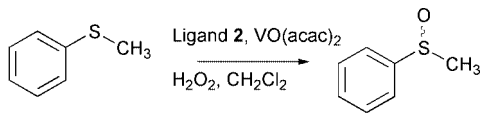

3a **4a**

Scheme 1 Asymmetric oxidation of methyl phenyl sulfide.

The results from this initial screening indicated that all the ligands were good catalysts for the oxidation, with conversions to the sulfoxide **4** ranging from 56 to 93%, but with the best ee a modest 11% (Wang-Phe-Ser-DtBS). The corresponding threonine derivative (Wang-Phe-Thr-DtBS) gave racemic sulfoxide **4**. As a final check, we also prepared the *allo*-threonine derivative (Wang-Phe-Thr*-DtBS),§ which gave excellent conversion to the sulfoxide, with an improved ee of 17%. Since these results were a substantial improvement on either threonine or serine, we felt that we had identified the optimum amino acid AA^2. We now attempted to optimise this ligand by use of the positional scanning method of Hoveyda and Snapper.[7] A library of 18 salicylaldehyde derivatives was screened, and the results unfortunately confirmed that we had already identified the best component. Finally, we prepared another library (Wang-AA^1-Thr*-DtBS) in which 19 different D- and L-amino acids were used as AA^1, including those with and without functionality. This resulted in the discovery that the use of D-Phe gave a much improved ee of 23%, at a conversion of 89%. Thus, the optimised structure for the asymmetric oxidation of methyl phenyl sulfide **3a** had the structure Wang-D-Phe-Thr*-DtBS **5**. Although this ligand had the advantage that it could be rapidly assembled, and easily removed from the reaction mixture allowing straightforward product isolation, the ee was simply far too low to be useful.

At this stage, we felt it appropriate to explore whether metal ions other than vanadium might be more effective. We therefore screened a series of metals for their ability to catalyse the oxidation of methyl phenyl sulfide by aqueous hydrogen peroxide in the absence of added ligand, and unsurprisingly Mo(VI), W(VI), V(IV) and Ti(IV) all proved effective (with Ti(IV) interestingly being the least effective). When the ligand that had been optimised for the vanadium-catalysed oxidation was tested with these metals, it immediately became clear that the combination of Wang-D-Phe-Thr*-DtBS and Ti(Oi-Pr)$_4$ was a much more effective asymmetric catalyst, giving a reproducible ee of between 62 and 64% (*R*-isomer in excess), with high

† Electronic supplementary information (ESI) available: HPLC conditions. See http://www.rsc.org/suppdata/cc/b1/b108487a/

 DOI: 10.1039/b108487a

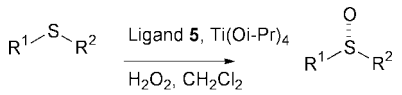

3 4

Scheme 2 Asymmetric oxidation of alkyl aryl sulfides.

Table 1 Asymmetric oxidation of alkyl aryl sulfides

Sulfide	R^1	R^2	Sulfoxide	Conversion[a]	ee (%)[a]
3a	Ph	CH_3	**4a**	100%	64
3b	Ph	Et	**4b**	96%	64
3c	Ph	Pr	**4c**	90%	57
3d	4-$CH_3OC_6H_4$	CH_3	**4d**	85%	63
3e	4-ClC_6H_4	CH_3	**4e**	90%	58
3f	4-BrC_6H_4	CH_3	**4f**	70%	53
3g	4-$O_2NC_6H_4$	CH_3	**4g**	61%	64
3h	4-NCC_6H_4	CH_3	**4h**	90%	45
3i	2-Naphthyl	CH_3	**4i**	87%	72

[a] Conversions and ee values were measured using chiral phase HPLC. HPLC conditions are provided in the supplementary material.

conversion. Clearly the low rate of the background reaction is important. Schiff-base titanium complexes are effective for sulfur oxidation,[8–10] and very recently it has been reported that Ti(salen) complexes can be very effective in the same process using hydrogen peroxide as the oxidant.[11]

Since the behaviour of solid-supported ligands and their solution phase counterparts can differ, we converted the optimum ligand into the corresponding methyl ester **6** by treatment with NEt_3 in DMF–MeOH. Use of this solution phase ligand gave an identical 64% ee in the oxidation of methyl phenyl sulfide **3a** to the solid phase analogue (which is therefore a superior catalyst from a practical point of view).

Rather than screening all our previous libraries in the titanium-catalysed oxidation reaction, we tested the corresponding serine, threonine and *O-tert*-butyl threonine derivatives, Wang-D-Phe-Ser-DtBS (27% ee), Wang-D-Phe-Thr-DtBS (23% ee) and Wang-D-Phe-Thr(t-Bu)-DtBS (0% ee) in the titanium-catalysed oxidation of methyl phenyl sulfide **3a**. These results confirm both the importance of the free hydroxyl group and the influence of the stereogenic centre at C-3 of the *allo*-threonine residue.

In order to establish how strongly the titanium was complexed to the solid phase ligand, we incubated a solution of $Ti(Oi\text{-}Pr)_4$ in CH_2Cl_2 with the ligand **5**. The resin was then washed 5 times, and the titanium concentration in each of the washings was measured by ICP-AES. While some residual titanium was detectable in the first washing, in all the four subsequent washings the titanium concentration was below the background level (< 1 ppm). This suggested that leaching of titanium from the resin was minimal, and that as a consequence the catalyst combination of ligand **5** and Ti might be reusable.

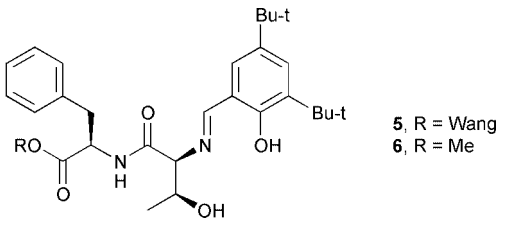

Provided the resin was not allowed to dry out, the catalyst could be reused without erosion of conversion or ee (first run, 62% ee, second run, 64% ee), although the ee did degrade with subsequent runs with the same sample of catalyst.

The ee of our catalyst system was comparable with the original results reported by Bolm, so we decided to investigate its scope in the oxidation of a variety of other alkyl aryl sulfides (Scheme 2), and our results are reported in Table 1. The ee values are remarkably consistent, and indicate the utility of the catalyst. Some overoxidation to the sulfone was observed in the case of **3d** (13%) and **3g** (22%), but in all other cases the amount of sulfone was less than 5%.

We thank EPSRC for the award of a research grant (GR/M13633), GlaxoSmithKline and the EPSRC for an Industrial CASE studentship (S. D. G.), and the Commission of the European Union (IHP Network HPRN-CT-2000-00014) for support of a studentship (C. M.).

Notes and references

‡ *General procedure for solid phase asymmetric oxidation of sulfides*. The solid phase ligand (0.015 mmol) was weighed into an Altech tube. Anhydrous CH_2Cl_2 (2.0 ml) was added, followed by the metal salt (0.05 mmol). After 20 min, the resin was filtered, and anhydrous CH_2Cl_2 (2.0 ml) was added to wash the resin. After one min the resin was filtered. A dry reaction tube with a magnetic stirrer was purged and filled with nitrogen three times. Then the resin was added in the reaction tube, followed by distilled CH_2Cl_2 (2.0 ml), the sulfide (1 mmol), and 30% H_2O_2 in water (1.1 mmol) and the mixture was stirred for 5–16 h, depending on the substrate. A sample (1–2 μl) was then removed, and diluted with 10% IPA–heptane, for analysis by HPLC.† To isolate the products, the reaction was worked up by quenching with 10% Na_2SO_3 solution (5 ml). The reaction mixture was extracted with Et_2O (2×10 ml), and the extracts were combined and dried ($MgSO_4$); the solvent was removed under reduced pressure. The crude product was purified by silica flash chromatography (Et_2O–MeOH 95 : 5) to leave the product as a white solid.

§ We found that use of Wang-Tle- Thr*-DtBS also gave an improved ee of 18%, but since resin loading of *tert*-leucine is less straightforward, we used commercially available Fmoc-L-phenylalanine resin for the subsequent libraries.

1 P. Pitchen, E. Dunach, M. N. Deshmukh and H. B. Kagan, *J. Am. Chem. Soc.*, 1984, **106**, 8188.
2 F. Di Furia, G. Modena and R. Seraglia, *Synthesis*, 1984, 325.
3 C. Bolm and F. Bienewald, *Angew. Chem., Int. Ed. Engl.*, 1995, **34**, 2640.
4 For applications and modifications of this process, see: C. Bolm, G. Schlingloff and F. Bienewald, *J. Mol. Catal. A: Chem.*, 1997, **117**, 347; C. Bolm and F. Bienewald, *Synlett*, 1998, 1327; D. A. Cogan, G. C. Liu, K. J. Kim, B. J. Backes and J. A. Ellman, *J. Am. Chem. Soc.*, 1998, **120**, 8011; A. H. Vetter and A. Berkessel, *Tetrahedron Lett.*, 1998, **39**, 1741; J. Skarzewski, E. Ostrycharz and R. Siedlecka, *Tetrahedron: Asymmetry*, 1999, **10**, 3457; N. N. Karpyshev, O. D. Yakovleva, E. P. Talsi, K. P. Bryliakov, O. V. Tolstikova and A. G. Tolstikov, *J. Mol. Catal. A: Chem.*, 2000, **157**, 91.
5 H. B. Kagan, 'Asymmetric Oxidation of Sulfides', in *Catalytic Asymmetric Synthesis*, ed. I. Ojima, Wiley, VCH, New York, 2000, p. 327.
6 S. Dahmen and S. Bräse, *Synthesis*, 2001, 1431.
7 B. M. Cole, K. D. Shimizu, C. A. Krueger, J. P. A. Harrity, M. L. Snapper and A. H. Hoveyda, *Angew. Chem., Int. Ed. Engl.*, 1996, **35**, 1668; K. D. Shimizu, B. M. Cole, C. A. Krueger, K. W. Kuntz, M. L. Snapper and A. H. Hoveyda, *Angew. Chem., Int. Ed. Engl.*, 1997, **36**, 1703; K. D. Shimizu, M. L. Snapper and A. H. Hoveyda, *Chem., Eur. J.*, 1998, **4**, 1885; J. R. Porter, W. G. Wirschun, K. W. Kuntz, M. L. Snapper and A. H. Hoveyda, *J. Am. Chem. Soc.*, 2000, **122**, 2657; S. J. Degrado, H. Mizutani and A. H. Hoveyda, *J. Am. Chem. Soc.*, 2001, **123**, 755; J. R. Porter, J. F. Traverse, A. H. Hoveyda and M. L. Snapper, *J. Am. Chem. Soc.*, 2001, **123**, 984; C. A. Luchaco-Cullis, H. Mizutani, K. E. Murphy and A. H. Hoveyda, *Angew. Chem., Int. Ed.*, 2001, **40**, 1456.
8 A. Colombo, G. Marturano and A. Pasini, *Gazz. Chim. Ital.*, 1986, **116**, 35.
9 S. Colonna, A. Manfedi, M. Spadoni, L. Casella and M. Gullotti, *J. Chem. Soc., Perkin Trans. 1*, 1987, 71.
10 K. Nakajima, C. Sasaki, M. Kojima, T. Aoyama, S. Ohba, Y. Saito and J. Fujita, *Chem. Lett.*, 1987, 2189.
11 B. Saito and T. Katsuki, *Tetrahedron Lett.*, 2001, **42**, 3873.

CHEMCOMM Communication
www.rsc.org/chemcomm

Octaalkynyltetra[6,7]quinoxalinoporphyrazines: a new class of photosensitisers with potential for photodynamic therapy

Frieder Mitzel,[a] Simon FitzGerald,[b] Andrew Beeby[b] and Rüdiger Faust*[a]

[a] *Department of Chemistry, University College London, 20 Gordon Street, London, UK WC1H OAJ. E-mail: r.faust@ucl.ac.uk*
[b] *Department of Chemistry, University of Durham, South Road, Durham, UK DH1 3LE*

Received (in Cambridge, UK) 24th October 2001, Accepted 30th October 2001
First published as an Advance Article on the web 23rd November 2001

Acetylene-substituted tetra[6,7]quinoxalinoporphyrazines, obtained in two steps from dialkynyl-1,2-diones and 1,2-diamino-4,5-dicyanobenzene, show intense absorptions in the near infrared and have photooxidising properties that make them promising candidates as agents active in photodynamic therapy.

Photodynamic therapy (PDT) is an increasingly valuable method for the treatment of a variety of conditions, among them various forms of cancer, age-related macular degeneration, and, most recently, atherosclerosis.[1–4] At the core of PDT lies the generation of reactive oxygen species by energy transfer from a photosensitiser embedded in the malignant tissue which is irradiated with external light of appropriate wavelength. The reactive oxygen species in turn cause significant cellular damage and thereby ultimately lead to the eradication of the pathogenic tissue. Sensitisers suitable for biomedical applications of this type must meet the minimum requirements of accessibility by light in a biological matrix and of efficient induction of photooxidation. These requirements lead to the definition of a therapeutic window of *ca.* 650–800 nm in the absorption of practical PDT agents. Current applications largely exploit the photosensitising action of functionalised porphyrins such as a mixture of haematoporphyrin derivatives HpD, which is marketed under the tradename Photofrin®.[5] Despite the success of this drug in PDT, efforts are continuing to devise photosensitisers with an improved photochemical profile with respect to that of Photofrin®,[6] whose role in PDT is somewhat limited, among other things, by its low-intensity absorption around 630 nm.

We wish to present here octaalkynyltetra[6,7]quinoxalinoporphyrazines **1a–c** as a new class of photosensitisers which, by virtue of their concise and flexible synthesis and their (photo)chemical properties, are promising candidates as effective PDT agents. As such, **1a–c** represent viable alternatives to some of the phthalo- and naphthalocyanines that are currently being investigated as second generation sensitisers for PDT[6,7] and are a significant advancement over the corresponding octaalkynylphthalocyanines[8,9] and tetrapyrazinoporphyrazines previously reported.[10]

The syntheses of the quinoxalinoporphyrazines **1** are summarised in Scheme 1 and follow a route similar to the one outlined for the related octaalkynyltetrapyrazinoporphyrazines.[10] Key step in the preparation of the new acetylenic chromophores is the condensation of the dialkynyl-1,2-diones **4a–c**[11] with 1,2-diamino-4,5-dicyanobenzene **3** followed by a base-induced cyclotetramerisation of the intermediate quinoxalines to the porphyrazine framework. The alkyl-substituted derivative was prepared for comparison.† The new chromophores are deep blue (**1a**, **1d**) or green (**1b**, **1c**) solids that show good solubility in common organic solvents (CH_2Cl_2, THF).

The electron absorption spectra of compounds **1a–d** in THF are dominated by two transitions, namely the higher-energy *B*-band and the lower-energy *Q*-band, that in case of **1a–c** stretches into the near infrared (Fig. 1). The influence of peripheral substituents on the appearance of the UV–Vis–NIR

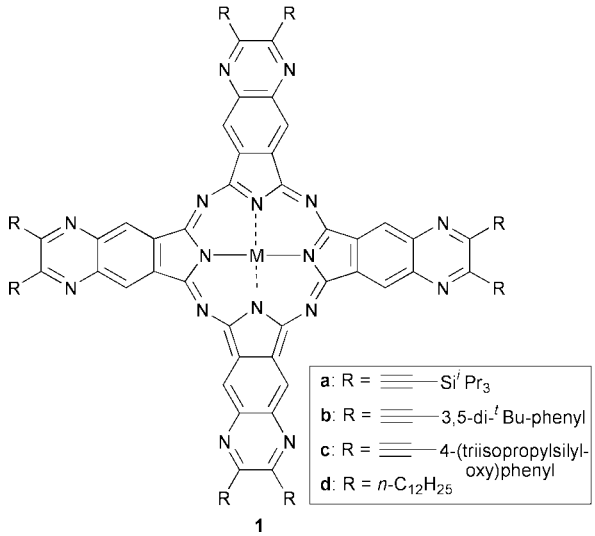

1

spectra of the tetra[6,7]quinoxalinoporphyrazines is quite remarkable. Whereas non-acetylenic **1d** shows a *B*-band at 364 nm (ε = 132 000 M^{-1} cm^{-1}) and a *Q*-band at 735 nm (ε = 431 000 M^{-1} cm^{-1}), the corresponding maxima of acetylenic compound **1a** (M = Mg, *B*-band: 388 nm, ε = 288 000 M^{-1} cm^{-1}; *Q*-band at 770 nm, ε = 512 000 M^{-1} cm^{-1}) are significantly batho- and hyperchromically shifted. This indicates that the π-system of the main chromophore of **1a** extends beyond the periphery of the polyazamacrocycle and includes the acetylene substituents. However, an extension of the π-system of **1a** by the appendage of terminal aryl groups to the acetylene units as, for example, in **1b** (*B*-band: 394 nm, ε = 306 000 M^{-1} cm^{-1}; *Q*-band: 770 nm, ε = 517 000 M^{-1} cm^{-1}, THF) does not result in a further bathochromic shift of the *Q*-band. In comparison to octaalkynyltetrapyrazinoporphyrazines[10] and −phthalocyanines,[8,9] whose *Q*-band absorption

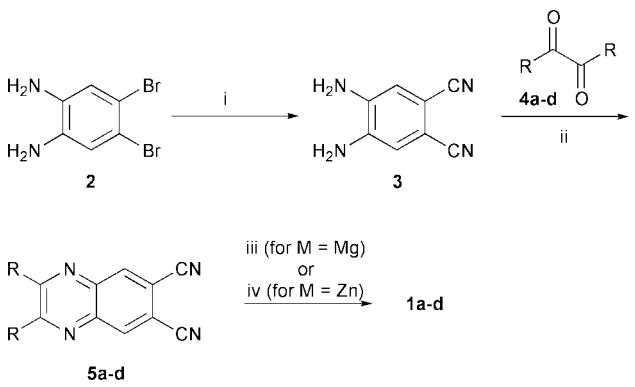

2 **3** **5a-d**

Scheme 1 *Reagents and conditions*: i, CuCN, DMF, 140 °C, 15 h, 25%; ii, AcOH, rt., 20 min, 66–80%; iii, $Mg(OBu)_2$, BuOH, reflux, 1 h, 22–41%; iv, LiOPent, PentOH, reflux, 1 h, then $Zn(OAc)_2$, PentOH, reflux, 3 h, 44%.

 DOI: 10.1039/b109742n

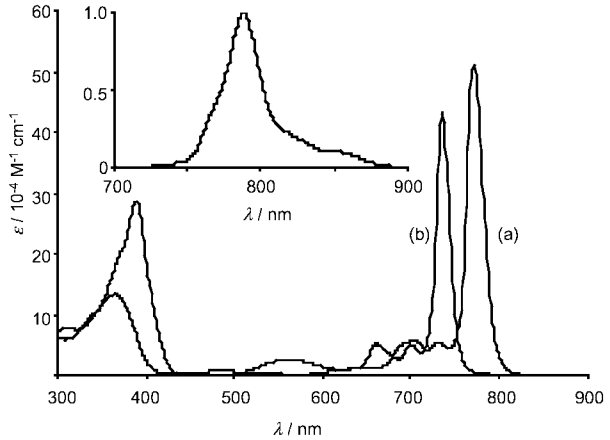

Fig. 1 Electronic absorption spectra of **1a** (a) and **1d** (b) in THF at 298 K. The inset shows the fluorescence spectrum of **1a** in THF at 298K upon irradiation at 388 nm.

maxima centre around 670 nm and 720 nm, respectively, the significantly red-shifted absorption of **1a–c** will allow the use of more deeply penetrating light for the excitation of **1a–c** in biological tissue. In addition, the high molar extinction coefficients associated with their NIR absorptions suggest a more detailed exploration of their suitability for PDT applications. Furthermore, the photostability of the compounds is satisfactory. Their aerated solutions in hexanol show very little degradation upon irradiation with light at a fluence rate of 50 mW cm^{-2} for several hours (*e.g.* 92% of the initial absorption of **1a** (M = Zn) at longest wavelength maximum still present after 4h irradiation). In light of the fluorescence at 790 nm that the alkynyl-substituted compounds **1a–c** exhibit upon irradiation at either their respective *B*- or *Q*-bands (Fig. 1), usage of this class of compounds as fluorescent probes in biological tissue or diagnostic tools in PDT can also be envisioned.

A qualitative evaluation of the photooxidising ability of **1a** (M = Zn) was performed using the singlet oxygen quencher 1,3-diphenylisobenzofuran (DPBF).[12] Hence, an aerated solution of **1a** (M = Zn) and DPBF (120-fold molar excess) in hexan-1-ol was exposed to filtered light (cut-off < 550 nm) of a slide projector lamp while monitoring the 413 nm absorption of DPBF (Fig. 2). No or little photooxidation of DPBF is observed in the absence of either light, **1a** (M = Zn) or oxygen (traces a–c, Fig. 2). However, significant photodegradation of DPBF occured in the presence of **1a** (M = Zn) and oxygen

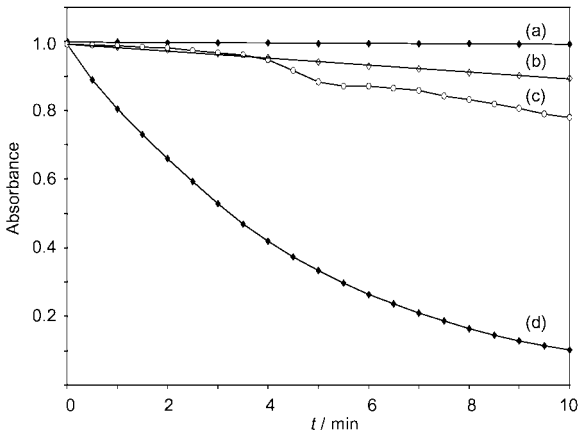

Fig. 2 Photooxidation of 1,3-diphenylisobenzofuran (DPBF) with **1a** (M = Zn) in hexanol at 298 K; c_o(DPBF) = 4.5×10^{-5} mol l^{-1}, c_o (**1a**) = 4.0×10^{-7} mol l^{-1}, light source: slide projector lamp (24 V, 250 W), cut-off filter <550 nm. The absorption at 413 nm was monitored in an aerated solution of **1a** (M = Zn) and DPBF upon irradiation (trace d); trace a, in the absence of light; trace b, in the absence of **1a** (M = Zn); trace c, in the absence of oxygen.

Table 1 Fluorescence lifetimes τ_f, fluorescence quantum yields Φ_f and singlet oxygen quantum yields Φ_Δ for selected tetra[6,7]quinoxalinoporphyrazines[a]

Compound	τ_f/ns	Φ_f[b]	Φ_Δ[c]
1a (M = Mg)	4.3 ± 0.1	0.46	0.19
1a (M = Zn)	2.4 ± 0.1	0.25	0.56
1d (M = Mg)	5.3 ± 0.1	0.59	0.15

[a] All measurements were performed in aerated THF at 298 K. [b] Absolute values (±10%) relative to cresyl violet in MeOH (Φ_f = 0.54) and disulfonated aluminium phthalocyanine in H_2O (Φ_f = 0.40) standards. [c] Obtained by time-resolved phosphorescence measurements using excitation at λ_{ex} = 355 nm. Values are relative to perinaphthenone (Φ_Δ = 0.97) and have an error of ±10%.

(trace d, Fig. 2), clearly demonstrating the photooxidising ability of the zinc quinoxalinoporphyrazine. The corresponding magnesium derivative **1a** (M = Mg) shows a markedly reduced photosensitising effect.

As shown in Table 1, these qualitative findings are further substantiated by the photophysical data obtained for compounds **1a** (M = Mg, Zn) and **1d** (M = Mg). Whereas the magnesium porphyrazinato complexes are strong fluorophores with only limited singlet oxygen producing capacity, the corresponding zinc complex **1a** (M = Zn) is a very efficient singlet oxygen sensitiser with a singlet oxygen quantum yield of Φ_Δ = 0.56. In fact, this value is comparable with that determined for photofrin (Φ_Δ = 0.57 in benzene)[1] and significantly exceeds that determined for silicon naphthalocyanine (Φ_Δ = 0.35 in benzene),[1] an analogue of **1** that has been investigated in the context of PDT applications.

The short and flexible synthesis of alkynyl-substituted quinoxalinoporphyrazines coupled with their high intensity absorption and their emission in the near infrared make them interesting candidates for future PDT applications. While the lipophilicity of the prototypical compounds presented here will require an administration *via*, for example, liposomal formulations, further adaptations of the chromophores to the requirements set by biological environments can be easily achieved by exploiting, for example, the chemistry of the protected phenol functionality in **1c**. Work along these lines is currently under way.

We wish to acknowledge University College London for the provision of a Provost Studentship to F. M. and the EPSRC for a studentship to S. F. We thank Dr A. J. MacRobert for helpful discussions.

Notes and references

† All new compounds are fully characterised by spectroscopic and analytical data. Detailed procedures for their syntheses will be reported elsewhere.

1 R. Bonnett, *Chem. Soc. Rev.*, 1995, **24**, 19–33.
2 T. J. Dougherty, C. J. Gomer, B. W. Henderson, G. Jori, D. Kessel, M. Korbelik, J. Moan and Q. Peng, *J. Natl. Cancer Inst.*, 1998, **90**, 889–905.
3 L. Milgrom and A. J. MacRobert, *Chem. Br.*, May 1998, 45–50.
4 R. Bonnett, *Rev. Contemp. Pharmacother.*, 1999, **10**, 1–17.
5 I. J. MacDonald and T. J. Dougherty, *J. Porphyrins Phthalocyanines*, 2001, **5**, 105–129.
6 H. Ali and J. E. van Lier, *Chem. Rev.*, 1999, **99**, 2379–2450.
7 M. Peeva, M. Shopova, N. Stoichkova, N. Michailov, D. Wöhrle and S. Müller, *J. Porphyrins Phthalocyanines*, 1999, **3**, 380–387.
8 D. S. Terekhov, K. J. M. Nolan, C. R. McArthur and C. C. Leznoff, *J. Org. Chem.*, 1996, **61**, 3034–3040.
9 R. Faust and F. Mitzel, *J. Chem. Soc., Perkin Trans. 1*, 2000, 3746–3751.
10 R. Faust and C. Weber, *J. Org. Chem.*, 1999, **64**, 2571–2573.
11 R. Faust, C. Weber, V. Fiandanese, G. Marchese and A. Punzi, *Tetrahedron*, 1997, **53**, 14655–14670.
12 P. B. Merkel and D. R. Kearns, *J. Am. Chem. Soc.*, 1975, **97**, 462–463.

CHEMCOMM Communication
www.rsc.org/chemcomm

New nucleoside based solid supports. Synthesis of 5′,3′-derivatized thymidine analogues†

M. de Champdoré,[a] L. De Napoli,[a] G. Di Fabio,[a] A. Messere,[b] D. Montesarchio[a] and G. Piccialli*[c]

[a] *Dipartimento di Chimica Organica e Biochimica, Università degli Studi di Napoli 'Federico II', via Cynthia 4, 80126 Napoli, Italy*
[b] *Dipartimento di Scienze Ambientali, Seconda Università di Napoli, via Vivaldi 43, 81100 Caserta, Italy*
[c] *Facoltà di Scienze, Università del Molise, via Mazzini 8, 86170 Isernia, Italy. E-mail: picciall@unina.it; Fax: 39-081-674393; Tel: 39-081-674127/6/5*

Received (in Cambridge, UK) 8th August 2001, Accepted 19th October 2001
First published as an Advance Article on the web 26th November 2001

Two new thymidine based polymeric supports, in which the nucleosides have been anchored through the thymine moiety to a β-hydroxy thioether functionalized resin *via* a Mitsunobu reaction, have been prepared. A simple and efficient solid-phase synthesis of 5′,3′-bis-derivatized thymidine analogues has so been developed, following methodologies well established in peptide and oligonucleotide chemistry and is here proposed for the preparation of a variety of different nucleoside conjugate products.

Combinatorial chemistry allows the study of the properties of many classes of compounds much faster than a classical serial analysis. The combinatorial approach to the simultaneous polymer-supported synthesis of chemical compounds has allowed the rapid screening of a plethora of different substrates, speeding up lead identification and optimisation, and resulting in fundamental developments in biomedicinal chemistry.[1] Combinatorial syntheses are often carried out as sequential, high fidelity condensation and addition reactions on solid-phase linked scaffolds which are typically polyfunctional molecules.[2] In this frame nucleosides can be regarded as very useful scaffolds to be incorporated into polymeric supports for combinatorial libraries[3] since they contain functional groups which can be differently manipulated and stereogenic centres useful for a defined spatial presentation of the various substituents. In addition, the biomedical potential of nucleoside derivatives is well known. Therefore nucleosides are particularly attractive as platforms for the design of primary screening libraries. Aiming at the synthesis of new functionalized solid supports for combinatorial libraries of chimeric biomolecules incorporating nucleoside moieties (*e.g.* nucleoside analogues, conjugates or other hybrids), we turned our attention to *ad hoc* modified polymeric supports linking suitably protected nucleoside derivatives in which the ribosidic functions are susceptible of further modifications. In order to attach to polymeric supports nucleosides through the base, we have investigated the possibility of immobilizing thymidine derivatives in the solid phase by reacting the imino function of the thymine moiety. For this purpose, the Mitsunobu reaction[4] of aliphatic alcohols with amidic or imidic species may be particularly useful for an efficient *N*-alkylation of pyrimidine nucleoside derivatives; this approach has been also successfully exploited by us in order to glycosylate the N-3 position of uridine derivatives.[5] Starting from our previous experiments, we first tested the solid phase Mitsunobu condensation between sugar protected thymidine **3** and a commercially available hydroxy Tentagel® resin (0.24 meq g^{-1}, **1**, Scheme 1), a polymeric support largely employed in peptide and oligonucleotide synthesis. Such reaction gave satisfactory incorporation yields of the thymidine residue (80% yields by DMT test) but did not result in a practically feasible route, since no mild reaction conditions were found for the final detachment of the intact nucleoside from the solid phase.

Therefore we have devised an alternative synthetic scheme involving the Mitsunobu reaction of β-hydroxyethylthioether Tentagel resin **2**‡ with thymidine derivatives **3** and **4** (Scheme 1) to yield nucleoside derivatized supports **5** and **6**, respectively. Such supports have been designed to allow a simple and efficient release of the nucleosidic material *via* a β-elimination reaction by mild alkaline treatment on the alkylthioethyl function in **5** or **6**, once oxidized to sulfone. We report herein a general synthetic strategy to obtain a variety of thymidine-containing hybrid molecules by exploiting supports **5** and **6** which can form phosphoester or glycosidic linkages using the OH functions, and amide or phosphoramidate bonds exploiting the N_3 group, previously reduced to amine.

Thymidine derivatives **3** and **4** were loaded onto resin **2** in the presence of PPh_3 and DEAD in THF–DCM to produce supports **5** and **6**. The DMT test showed in both cases a typical loading of 0.17 meq g^{-1} (90% yield). To transiently mask the 3′-hydroxy moiety in support **5** (Scheme 1), the *tert*-butyldimethylsilyl (TBDMS) group was employed in view of its well established orthogonality to DMT and its stability under both acidic and mild basic conditions as well as during the steps involved in the glycosidic[6] and phosphotriester[7] linkage formation. The best results in the removal of TBDMS were obtained under treatment with $Et_3N{\cdot}3HF$ (overnight, rt) as verified by coupling the 3′-OH with 2′-deoxycytidine phosphoramidite building block by standard automated phosphoramidite protocol[7] (Scheme 2). The coupling yield was almost quantitative (98%) as checked by DMT cation quantitation on **7** and in no case loss of nucleosidic material was observed. Then the thioether function of the support was oxidized with a mClPBA solution[8] (0.5 M in DCM, 1 h, rt) and, after detritylation of the 5′-OH groups, complete detachment from the support was achieved by treatment with conc. aq. ammonia solution (18 h, 60 °C) giving the desired 3′–3′ phosphodiester linked dinucleotide **8**. The crude detached material was purified by reverse phase HPLC and the identity of isolated **8** was ascertained by ^1H, ^{31}P NMR and MS data.

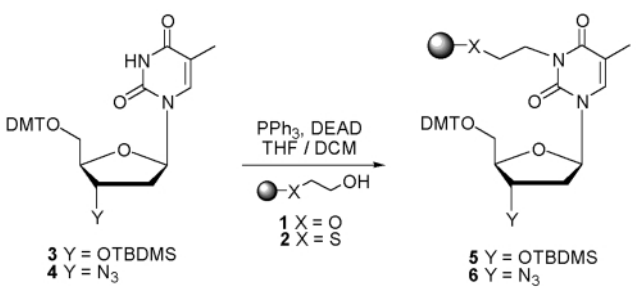

Scheme 1 Solid support functionalization by the Mitsunobu approach.

† Electronic supplementary information (ESI) available: experimental details. See http://www.rsc.org/suppdata/cc/b1/b107200p/

 DOI: 10.1039/b107200p

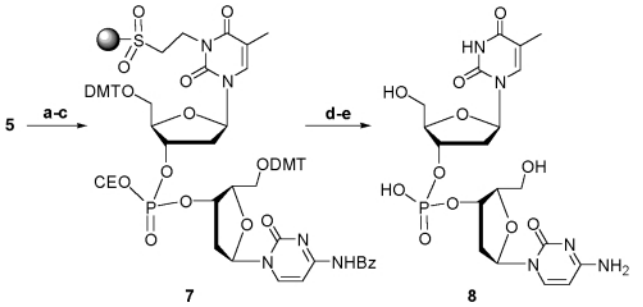

Scheme 2 **a**: $Et_3N{\cdot}3HF$, THF, overnight, rt; **b**: coupling with dC phosphoramidite building block; 0.1 M tetrazole; I_2–THF–H_2O; **c**: 0.5 M mClPBA in DCM, 1 h, rt; **d**: 1% DCA in DCM; **e**: NH_4OH, 18 h, 60 °C.

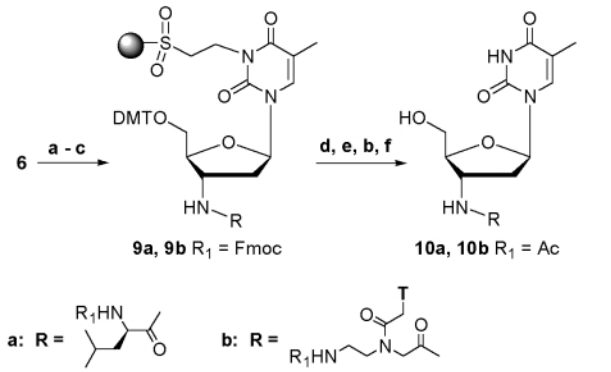

Scheme 3 **a**: FmocNH–amino acid or Fmoc-T(PNA)-OH, DIC, HOBt, nBu$_3$P; **b**: Ac_2O–Py (1 : 1, v/v); **c**: 0.5 M mClPBA in DCM, 1 h, rt; **d**: 1% DCA in DCM; **e**: 20% piperidine in DMF; **f**: NH_4OH, 18 h, 60 °C.

To test the efficiency of support **6** in the synthesis of 3′-amino derivatized thymidine analogues, we first prepared two different thymidine hybrids, **10a** and **10b** (Scheme 3), incorporating at the generated 3′-amino group an aminoacid or a PNA residue, respectively. To this purpose, the 3′-azido function in **6** was reduced to amine and directly coupled in a one pot reaction[9] with Fmoc-Leu-OH (83% yield) or Fmoc-T(PNA)-OH (84% yield) in the presence of DIC–HOBt and PBu_3 in DMF, leading to supports **9a** and **9b**, respectively. After capping with Ac_2O and Fmoc removal on a weighed sample of the supports, the coupling yield was measured by the Kaiser test.[10] Acetylation of the amino functions was followed by thioether oxidation, DMT and Fmoc removal and detachment from supports **9a** and **9b**, which gave **10a** and **10b**, respectively, whose structures have been confirmed by ^{1}H NMR and MS data.

In order to test the compatibility of the synthesized supports with both peptide and oligonucleotide solid phase synthetic strategies, support **9a** was then employed in the synthesis of **11** (Scheme 4), a hybrid dinucleotide having a classical 3′–5′ phosphodiester linkage, by reaction with 2′-deoxyadenosine phosphoramidite building block. Once both DMT and Fmoc protecting groups had been removed by standard methods, acetylation of the support, followed by the above described procedures for the detachment and deprotection, produced **12** (81% yield). On another batch of functionalized support **11**, after amino function deprotection, coupling with Fmoc-Phe-OH was carried out in the presence of DCCI–HOBt in DMF–DCM following a standard Fmoc protocol. DMT and Fmoc removal, followed by acetylation and detachment from the solid support, produced hybrid **13** (73% yield). After HPLC purification, **12** and **13** were characterized by ^{1}H, ^{31}P NMR and MS data.

In conclusion we have reported the synthesis of two new thymidine based solid supports (**5** and **6**) in which the nucleosides are anchored to the solid support through the base, so that both the 5′ and 3′ functions are available for further manipulation. A convenient β-hydroxyethyl-thioether **2** was

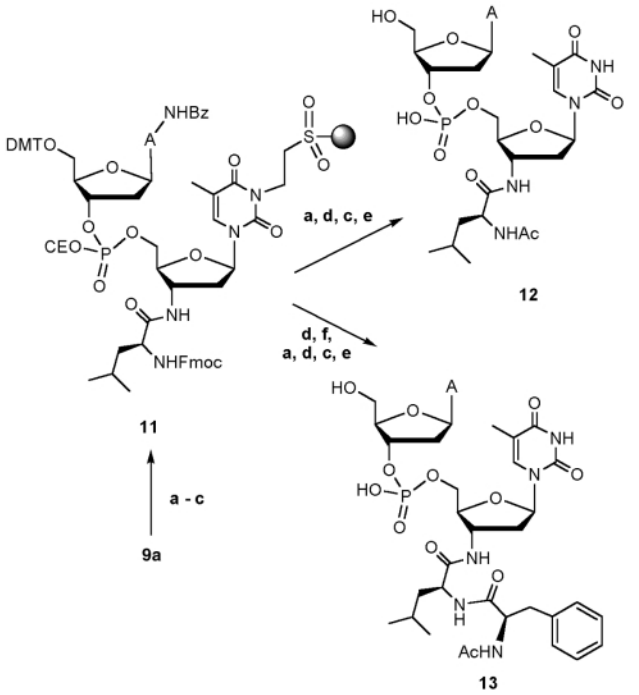

Scheme 4 **a**: 1% DCA in DCM; **b**: coupling with dA phosphoramidite building block; 0.1 M tetrazole; I_2–THF–H_2O; **c**: Ac_2O–Py (1 : 1, v/v); **d**: 20% piperidine in DMF; **e**: NH_4OH, 18 h, 60 °C; **f**: Fmoc-Phe-OH, DCCI, HOBt, 6 h, rt.

synthesized and inserted in the solid phase allowing a high yield incorporation of the protected thymidine building blocks by Mitsunobu reaction and, after the desired derivatization at the 3′ and/or 5′ functions, the total release of the nucleosidic material by a classical ammonia treatment. Starting from these supports we have devised a versatile synthetic strategy to obtain a variety of thymidine hybrids following well established peptide and oligonucleotide chemistry. In principle this methodology can be easily exploited to link any other amido or imino-functionalized heterocycle to a solid support.

Further studies are currently in progress to extend the Mitsunobu reaction to anchor other nucleosides on polymeric supports.

We acknowledge MURST, CNR and Regione Campania for grants in support of this investigation and C.I.M.C.F., Università degli Studi di Napoli 'Federico II', for the NMR facilities.

Notes and references

‡ A CPG support with a linker similar to **2** is commercially available from Glen Research with 0.06 meq g^{-1} loading in which the thioether function is already oxidized to sulfone.

1 M. A. Gallop, R. W. Barret, W. J. Dower, S. P. A. Foder and E. M. Gordon, *J. Med. Chem.*, 1994, **37**, 1233.
2 For example, C. Kallus, T. Opatz, T. Wunberg, W. Schmidt, S. Henke and H. Kunz, *Tetrahedron Lett.*, 1999, **40**, 7783.
3 W. Zhou, A. Roland, Y. Jin and R. P. Iyer, *Tetrahedron Lett.*, 2000, **41**, 441.
4 O. Mitsunobu, *Synthesis*, 1981, 1.
5 L. De Napoli, G. Di Fabio, A. Messere, D. Montesarchio, G. Piccialli and M. Varra, *J. Chem. Soc., Perkin Trans. 1*, 1999, 3489.
6 K. Toshima and K. Tatsuta, *Chem. Rev.*, 1993, **93**, 1503.
7 *Oligonucleotides and Analogues: A Practical Approach*, ed. F. Eckstein, IRL Press, Oxford, UK, 1991.
8 M. Yamada, T. Miyajima and H. Horikawa, *Tetrahedron Lett.*, 1998, **39**, 289.
9 J. P. Malkinson, R. A. Falconer and I. Toth, *J. Org. Chem.*, 2000, **65**, 5249.
10 E. Kaiser, R. L. Colescott, C. D. Bossinger and P. I. Cook, *Anal. Biochem.*, 1970, **34**, 595.

CHEMCOMM
Communication
www.rsc.org/chemcomm

Silicon-bridged bis(cyclohexadienyl) iron complexes: the first structurally characterised [1⁴]ferrocenophane†

Tony Hascall, Mark J. Drewitt and Dermot O'Hare*

Inorganic Chemistry Laboratory, University of Oxford, South Parks Road, Oxford, UK OX1 3QR. E-mail: dermot.ohare@chem.ox.ac.uk

Received (in Cambridge, UK) 4th September 2001, Accepted 9th October 2001
First published as an Advance Article on the web 26th November 2001

Reaction of the Me_2Si bridged bis(6,6-dimethylcyclohexadienyl) dianion with $FeCl_2$·1.5THF gives mono-, di- and tetrametallic complexes; $\{[Me_2Si(DMCh)_2]Fe\}_4$ is the first crystallographically characterised [1⁴]metallocenophane.

[1^n]Metallocenophanes, molecules consisting of n metallocene units joined by single atom bridges,[1] are of interest for several reasons. For example, it is now well established that strained, ring-tilted, [1¹]ferrocenophanes (*ansa*-bridged ferrocenes) undergo thermal, anionic and metal-catalysed ring-opening polymerisation (ROP),[2,3] yielding well-defined, high molecular weight, soluble metal-containing polymers. Oligomeric [1^n]ferrocenophanes are also of considerable interest due to, for example, their novel structural properties and the possibility of metal–metal interactions.[1,4] To date, polymerisation reactions have been limited to metallocenophanes containing cyclopentadienyl rings. We are interested in developing new ligand systems that could offer more flexibility and diverse substitution patterns in order to extend this chemistry.

As part of this research, we have studied metal complexes of the 6,6-dimethylcyclohexadienyl anion (DMCh),[5] which are related to 'open metallocenes'[6] as the ligand can bind to the metal centre though an η⁵-pentadienyl moiety. The dimethylcyclohexadienyl ferrocene analogue, $(DMCh)_2Fe$, has been reported;[5] however, metallocenophanes with bridged cyclohexadienyl ligands are unknown, although recently titanium complexes of the 'constrained geometry' ligand Me_2Si(Bu^{t}N)DMCh have been reported.[7]

A silicon-bridged bis-dimethylcyclohexadienyl ligand was synthesized according to Scheme 1. Thus, addition of 2 equiv. of the potassium salt $K^+(DMCh)^-$ [5,8] to Me_2SiCl_2 gave dimethylbis(dimethylcyclohexadienyl)silane, the NMR spectrum of which (ESI†) is consistent with a C_{2v} symmetric 1,4-diene, indicating reaction has taken place exclusively at the 3-position of the cyclohexadienyl rings. The ligand could be deprotonated with 2 equiv. Bu^{t}Li to yield $Me_2Si(DMChLi)_2$. Reaction of this dianion with $FeCl_2$·1.5THF in THF gives a complex mixture, presumably containing products due to reduction by the DMCh anion[5] as well as insoluble polymeric material. Three products, however, could be isolated: the [1]ferrocenophane analogue, $[Me_2Si(DMCh)_2]Fe$ **1** as well as dimeric and tetrameric species.

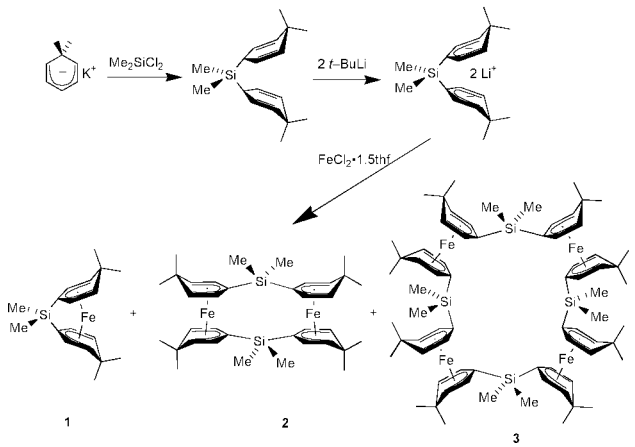

Scheme 1

The three products could be separated by virtue of their differing solubilities, and have been characterised by X-ray crystallography‡ in addition to NMR, and microanalysis (ESI†). The monomer **1** is highly soluble in pentane. Its structure (Fig. 1) reveals it to be analogous to a ring-tilted *ansa*-bridged ferrocene. As an indication of the strain in **1**, the value of α, the angle between the average planes defined by the pentadienyl carbons, is 14.5°. For comparison, an angle of 20.8° was observed between the Cp rings in the analogous $[Me_2Si(C_5H_4)_2]Fe$.[9] Thus, on this basis, the replacement of Cp rings with DMCh would appear to have reduced the strain somewhat. Conversely however, the average value of β, the angle between each plane and the bridging atom–bridgehead bond, is slightly greater for $[Me_2Si(DMCh)_2]Fe$ (40.0°) than $[Me_2Si(C_5H_4)_2]Fe$ (37.0°). This deviation from planarity of the sp² bridgehead atom of **1** is also reflected in its ^{13}C NMR resonance, which is found at δ 47.4, an upfield shift relative to unbridged compounds. For comparison, the corresponding value for $(DMCh)_2Fe$ is δ 77.9.[5] It should also be noted that, in general, bis-pentadienyl iron complexes prefer to adopt a *gauche* eclipsed conformation, in which the pentadienyl units are rotated relative to each other by a conformation angle χ of *ca.* 60°.[6] While the structure of $(DMCh)_2Fe$ has not been reported, the related 6-*tert*-butylcyclohexadienylferrocene analogue exhibits such a conformation.[10] In contrast, the silicon bridge of $[Me_2Si(DMCh)_2]Fe$ constrains the DMCh rings to be *syn*-eclipsed ($\chi \approx 0$), thus representing a potential additional source of strain in this molecule.

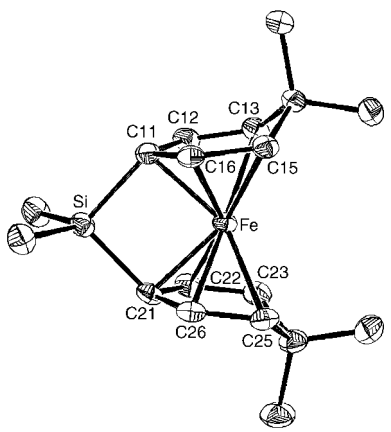

Fig. 1 Molecular structure of $[Me_2Si(DMCh)_2]Fe$ **1**. Selected bond lengths (Å): Fe–C11 2.038(2), Fe–C12 2.052(2), Fe–C13 2.166(2), Fe–C15 2.131(2), Fe–C16 2.038(2), Fe–C21 2.037(2), Fe–C22 2.042(2), Fe–C23 2.149(2), Fe–C25 2.152(2), Fe–C26 2.045(2), Si–C11 1.902(2), Si–C21 1.897(2).

† Electronic supplementary information (ESI) available: experimental details and NMR spectroscopic data. See http://www.rsc.org/suppdata/cc/b1/b107874g/

 DOI: 10.1039/b107874g

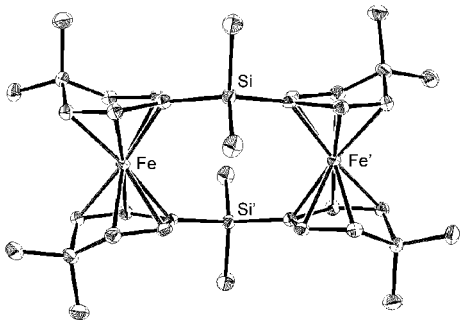

Fig. 2 Molecular structure of $\{[Me_2Si(DMCh)_2]Fe\}_2$ **2**. Labelling scheme for pentadienyl carbons is analogous to that in Fig. 1. Primed atoms are generated by symmetry. Selected bond lengths (Å): Fe–C11 2.094(2), Fe–C12 2.051(2), Fe–C13 2.117(2), Fe–C15 2.133(2), Fe–C16 2.056(2), Fe–C21 2.108(2), Fe–C22 2.056(2), Fe–C23 2.115(2), Fe–C25 2.125(2), Fe–C26 2.057(2), Si–C11 1.876(2), Si–C21′ 1.876(2).

In addition to the monomer **1**, air stable dimeric and tetrameric species are also obtained in low but reproducible yields. The oligomers are much less soluble in hydrocarbon solvents, and can be separated by fractional crystallisation from CH_2Cl_2. The structure of the dimer $\{[Me_2Si(DMCh)_2]Fe\}_2$ **2** (Fig. 2),‡ reveals a molecule on an inversion centre, in which the two halves of the dimer are crystallographically equivalent. The formation of **2** allows significant relief of the strain observed in the *ansa*-bridged species **1**, as demonstrated by an angle α of 5.4°, and an average value of β of 6.5°. The silicon bridged cyclopentadienyl [1²]ferrocenophane, $\{[Me_2Si(C_5H_4)_2]Fe\}_2$, which was reported simultaneously by three groups,[11–13] has a similar ring tilt [α = 4.9(3)°].[12] In both cases, the ring tilt is opposite to that of the monomeric species; the greatest inter-ring separation is observed at the silicon-bridged end of the ring. Furthermore, $\{[Me_2Si(DMCh)_2]Fe\}_2$ is able to adopt the preferred *gauche* eclipsed conformation with an angle χ of 50.7°. Such a conformation is presumably also favoured to reduce steric interactions between the Me_2Si groups; indeed a similar conformation is observed in the structure of $\{[Me_2Si(C_5H_4)_2]Fe\}_2$. The Fe···Fe separation in $\{[Me_2Si(DMCh)_2]Fe\}_2$ is 5.496(1) Å, which is greater than in the cyclopentadienyl analogue (*ca.* 5.17 Å).[11,12]

The third product that can be isolated is the silicon-bridged cyclic tetramer $\{[Me_2Si(DMCh)_2]Fe\}_4$ **3** which is unprecedented in cyclopentadienyl chemistry. The CH_2-bridged parent [1⁴]ferrocenophane has been reported,[14,15] and we have reported the synthesis of a partially methylated analogue,[16] but, to our knowledge, there are no examples of structurally characterized [1⁴]metallocenophanes.§ The structure of $\{[Me_2Si(DMCh)_2]Fe\}_4$ is shown in Fig. 3.‡ It crystallises in the tetragonal space group *P*4/*n* and lies on a crystallographic 4-fold axis. Thus, as with the dimer, the asymmetric unit of $\{[Me_2Si(DMCh)_2]Fe\}_4$ is a single $(DMCh)_2Fe$ unit. The four iron atoms are by necessity coplanar, and the overall shape of the molecule resembles a square. The angle between the planes (α) for each unit is 8.75°, perhaps indicating slightly more strain than in the dimer, while the average β is 5.1°. The Fe···Fe distance between neighbouring iron centres is 6.320(1) Å, a greater separation than in the dimer, while the The Fe···Fe separation across the ring is 8.938(1) Å. Interestingly, while the ^{1}H NMR spectrum of the [1⁴]ferrocenophane $\{[CH_2(C_5H_4)_2]Fe\}_4$ shows only one peak due to the Cp protons,[14,15] the pentadienyl protons of $\{[Me_2Si(DMCh)_2]Fe\}_4$ **3** are observed as eight separate resonances, varying considerably in chemical shift from δ 1.24 to δ 5.35 (C_6D_6). Presumably the upfield-shifted resonances correspond to the protons which are located toward the interior of the cavity, in analogy to the NMR spectra of cyclophanes. The fact that all of the ring protons in $\{[Me_2Si(DMCh)_2]Fe\}_4$ are chemically inequivalent at room temperature suggests the molecule is conformationally rigid, which could perhaps explain why replacement of Cp with DMCh groups has facilitated crystallisation of a [1⁴]metallocenophane analogue.

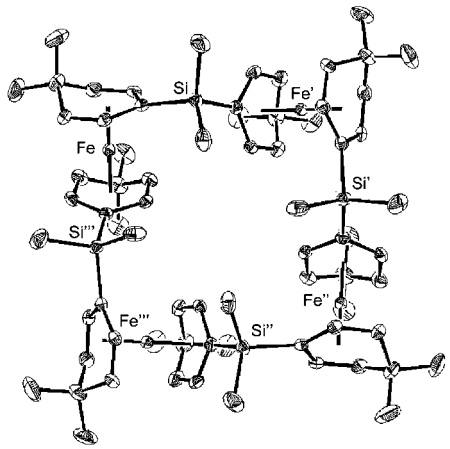

Fig. 3 Molecular structure of $\{[Me_2Si(DMCh)_2]Fe\}_4$ **3**. Labelling scheme for pentadienyl carbons is analogous to that in Fig. 1. Primed atoms are generated by symmetry. Selected bond lengths (Å): Fe–C11 2.090(2), Fe–C12 2.057(2), Fe–C13 2.132(2), Fe–C15 2.131(2), Fe–C16 2.051(2), Fe–C21 2.092(2), Fe–C22 2.057(2), Fe–C23 2.139(2), Fe–C25 2.121(2), Fe–C26 2.056(2), Si–C11 1.870(2), Si–C21′ 1.873(2).

We thank Dr Steve Barlow for many helpful discussions, and the EPSRC for financial support and the award of a studentship (M. J. D).

Notes and references

‡ *Crystal data*: for $[Me_2Si(DMCh)_2]Fe$ **1**: $C_{18}H_{26}SiFe$, monoclinic, space group $P2_1/c$, a = 12.5115(3), b = 8.2107(2), c = 16.9607(4) Å, β = 103.003(1)°, V = 1697.7(1) Å³, 150 K, Z = 4, D_c = 1.277 g cm^{-3}, μ(Mo-Kα) = 0.948 mm^{-1}, 6818 total (3853 independent) reflections, R = 0.0302 and R_w = 0.0795 for 3422 reflections with $I > 4\sigma(I)$.

For $[Me_2Si(DMCh)_2]Fe_2$ **2**: $C_{36}H_{52}Si_2Fe_2$, monoclinic, space group $P2_1/n$, a = 9.597(1), b = 15.977(1), c = 11.106(1) Å, β = 105.185(1)° V = 1643.4(2) Å³, 150 K, Z = 2, D_c = 1.319 g cm^{-3}, μ(Mo-Kα) = 0.979 mm^{-1}, 6425 total (3749 independent) reflections, R = 0.0355 and R_w = 0.0858 for 3359 reflections with $I > 4\sigma(I)$.

For $[Me_2Si(DMCh)_2]Fe_4$: $C_{72}H_{104}Si_4Fe_4$, tetragonal, space group $P4/n$, a = 19.243(1), c = 9.649(1) Å, V = 3573.0(5) Å³, 150 K, Z = 2, D_c = 1.213 g cm^{-3}, μ(Mo-Kα) = 0.901 mm^{-1}, 4072 total, independent reflections, R = 0.0355 and R_w = 0.0787 for 2998 reflections with $I > 4\sigma(I)$.

CCDC reference number 170500–170502.

See http://www.rsc.org/suppdata/cc/b1/b107874g/ for crystallographic data in CIF or other electronic format.

§ The existence of a crystal structure of a mixed iron–cobalt [1⁴]metallocenophane has been mentioned in a review, but apparently has not been published; see ref. 1.

1 U. T. Mueller-Westerhoff, *Angew. Chem., Int. Ed. Engl.*, 1986, **25**, 702.
2 I. Manners, *Chem. Commun.*, 1999, 857.
3 P. Nguyen, P. Gomez-Elipe and I. Manners, *Chem. Rev.*, 1999, **99**, 1515.
4 S. Barlow and D. O'Hare, *Chem. Rev.*, 1997, **97**, 637.
5 P. T. Di Mauro and P. T. Wolczanski, *Organometallics*, 1987, **6**, 1947.
6 R. D. Ernst, *Comments Inorg. Chem.*, 1999, **21**, 285; R. D. Ernst, *Chem. Rev.*, 1988, **88**, 1255; R. D. Ernst, *Acc. Chem. Res.*, 1985, **18**, 56; R. D. Ernst, *Struct. Bonding (Berlin)*, 1984, **57**, 1.
7 S. G. Feng, J. Klosin, W. J. Kruper, M. H. McAdon, D. R. Neithamer, P. N. Nickias, J. T. Patton, D. R. Wilson, K. A. Abboud and C. L. Stern, *Organometallics*, 1999, **18**, 1159.
8 P. T. Di Mauro and P. T. Wolczanski, *Polyhedron*, 1995, **14**, 149.
9 W. Finckh, B. Z. Tang, D. A. Foucher, D. B. Zamble, R. Ziembinski, A. Lough and I. Manners, *Organometallics*, 1993, **12**, 823.
10 K. C. Sturge and M. J. Zaworotko, *J. Chem. Soc., Chem. Commun.*, 1990, 1244.
11 J. W. Park, Y. S. Seo, S. S. Cho, D. M. Whang, K. M. Kim and T. Y. Chang, *J. Organomet. Chem.*, 1995, **489**, 23.
12 D. L. Zechel, D. A. Foucher, J. K. Pudelski, G. P. A. Yap, A. L. Rheingold and I. Manners, *J. Chem. Soc., Dalton Trans.*, 1995, 1893.
13 M. Herberhold and T. Bartl, *Z. Naturforsch., Teil B*, 1995, **50**, 1692.
14 U. T. Mueller-Westerhoff and G. F. Swiegers, *Chem. Lett.*, 1994, 67.
15 T. J. Katz, N. Acton and G. Martin, *J. Am. Chem. Soc.*, 1969, **91**, 2804.
16 S. Barlow and D. O'Hare, *Organometallics*, 1996, **15**, 3885.

CHEMCOMM Communication
www.rsc.org/chemcomm

Seven membered rings *via* intramolecular Pauson–Khand reactions†

Leticia Pérez-Serrano, Luis Casarrubios, Gema Domínguez and Javier Pérez-Castells*

Departamento de Química Orgánica y Farmacéutica, Facultad de Ciencias Experimentales y de la Salud, Universidad San Pablo-CEU, Urb. Montepríncipe, Boadilla del Monte 28668-. Madrid, Spain. E-mail: jpercas@ceu.es; Fax: 34913510475; Tel: 34913724788

Received (in Cambridge, UK) 10th September 2001, Accepted 29th October 2001
First published as an Advance Article on the web 14th November 2001

Seven membered rings are obtained with good yields by intramolecular Pauson–Khand reactions of some aromatic compounds.

The intramolecular Pauson–Khand reaction is becoming an important tool for the synthesis of natural products.[1] Shortcomings such as low conversions, limited scope and lack of efficient catalytic versions are currently being circumvented by the use of new promotion methods and catalytic conditions. Efforts in this field are directed to achieve efficient catalytic versions of this reaction,[2] and to widen the reaction scope.[3] In the intermolecular version of this reaction, only five and six membered rings annulated to the cyclopentenone ring can be obtained with good conversions. Only very recent examples show the formation, although in very low yields, of some medium sized rings.[4,5] In our ongoing program devoted to extend the use of the intramolecular Pauson–Khand reaction to aromatic substrates, we have introduced benzenes[6] and indoles[7]as part of the enyne skeleton. With these substrates we have obtained polycyclic aromatic systems where the Pauson–Khand reaction formed a five or six membered ring annulated to the cyclopentenone ring. However, many aromatic natural products bear seven membered rings in their structures, examples being the indole alkaloids shown in Fig. 1.

The difficulty in achieving medium sized rings *via* Pauson–Khand reactions seems to be related to the low population of the reactive conformation. The planarity of the aromatic rings may have a decisive influence on the reactivity of enynes connected through them. Furthermore, the new way of promotion of the Pauson–Khand reaction introduced by us, based on the addition of molecular sieves to the reaction medium, is probably based on the adsorption of the substrate favouring the preorganisation of the alkene and alkyne moieties for cyclization.[8] We believed then that it was worth trying to form seven membered rings in these systems and in this paper we show the first results of these attempts.

A group of enynoindoles were obtained starting from methyl 2-indolocarboxylate. The synthesis of these substrates was carried out following our previous work with similar compounds.[7] These compounds were submitted to Pauson–Khand reactions under three different conditions: cooperative trimethylamine *N*-oxide (TMANO)–molecular sieves promotion at room temperature (A), molecular sieves in refluxing toluene (B), and thermal promotion in refluxing toluene (C). The results are summarised in Table 1.

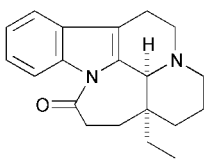

Homoeburnamonine

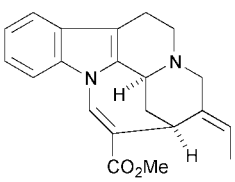

Apogeissoschizine

† Electronic supplementary data (ESI) available: spectroscopic and analytical characterization of compounds **5–8** and **10**. See http://www.rsc.org/suppdata/cc/b1/b108134a/

The results show the first case described of the formation of a seven membered ring *via* intramolecular Pauson–Khand reaction with good yield. That is the conversion of **2** into **6**.[9] Compound **2** appears to have several structural features that favour the cyclization process. Not only the planarity of the indole nucleus, but also the nitrogen and the buttressing effect of the OTBS group, are probably responsible for this result.[10] Compounds **1** and **3**, with groups different from the OTBS present in **2**, do react although with moderate conversions, whereas compound **4** reacts slightly better. Comparing the three reaction conditions used, the positive effect of the molecular sieves is clear and conditions B (cooperative thermal–molecular sieves promotion) are best.

In all the examples in Table 1 only one stereoisomer was obtained. The stereochemistries of compounds **5–7** were determined by NOE experiments.[11]

In view of this results we prepared a series of aromatic enynes structurally related to compound **2**. The compounds, depicted in Fig. 2, were reacted under conditions A and B. Only compound **9**, the one most closely related to compound **2** , reacted with a good yield (80%) to give **10**, as an only diastereoisomer.

Compounds **11–13** decomposed after few hours of reaction. The cobalt–hexacarbonyl complex was not detected in the reaction of compound **14**, probably due to the basic nitrogen in the imidazole. Compound **15** gave small amounts (*ca.* 10%) of

Table 1 Pauson–Khand reaction of enynoindoles. Formation of seven membered rings

Substrate[b]	Product	Yields (%)[a] A	B	C
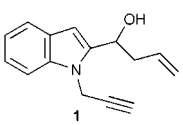 1	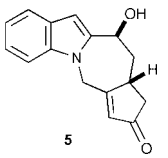 5	20	10	—
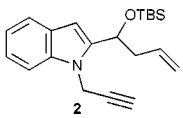 2	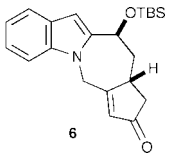 6	65	75	40
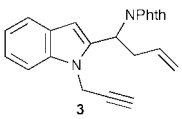 3	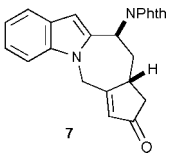 7	10	30	—
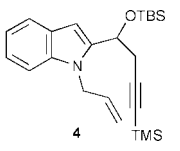 4	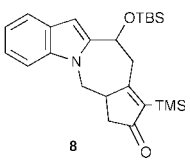 8	15	40	10

[a] In pure product after purification by column chromatography with correct spectroscopic data (^{1}H, ^{13}C NMR, IR).[b] Phth = Phthalimido

 DOI: 10.1039/b108134a

a mixture of isomers that may correspond to the expected seven membered ring diastereomeric compounds, or to related bridged compounds similar to those recently described by Lovely.[12] Finally in compound **16** a competitive Nicholas-type reaction took place allowing the recovery of the corresponding phenol.

In summary, herein we describe the first examples of the obtention of seven membered rings *via* intramolecular Pauson–Khand reactions with good yields and total diastereoselectivity. We are actually trying to understand the structural requirements of the substrates that favour this cyclization. A number of aromatic substrates have been tested and reactions observed in a few of them. We are currently trying to increase the scope of this synthesis so that interesting applications to the synthesis of natural products can be devised.

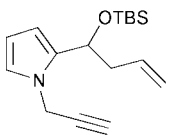

9

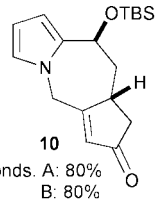

10

Conds. A: 80%
B: 80%

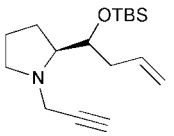

11

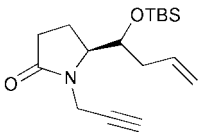

12

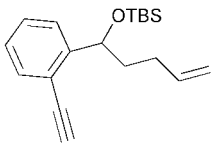

13

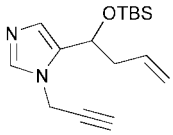

14

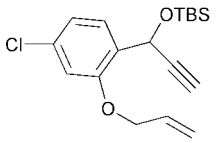

15

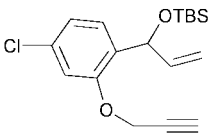

16

The authors are grateful to the DGES (MEC Spain, PB98-0053) and the Universidad San Pablo-CEU (2/99) for financial support. A predoctoral fellowship from the Universidad San Pablo-CEU is gratefully acknowledged by L. P.-S.

Notes and references

1 For recent reviews see: T. Sugihara, M. Yamaguchi and M. Nishizawa, *Chem.-Eur. J.*, 2001, **7**, 1589; K. M. Brummond and J. L. Kent, *Tetrahedron*, 2000, **56**, 3263; O. Geis and H.-G. Schmalz, *Angew. Chem., Int. Ed.*, 1998, **37**, 911; S. T. Ingate and J. Marco-Contelles, *Org. Proc. Prep. Int.*, 1998, 123.

2 Some recent examples of catalytic Pauson–Khand reaction with cobalt complexes: M. E. Kraft, L. V. R. Bonaga and C. Hirosawa, *J. Org.Chem.*, 2001, **66**, 3004; A. C. Comely, S. E. Gibson, A. Stevenazzi and N. J. Hales, *Tetrahedron Lett.*, 2001, **42**, 1183; T. Rajesh and M. Periasamy, *Tetrahedron Lett.*, 1999, **40**, 817.

3 J. Wang, M. L. Falck-Pedersen, C. Romming and K. Undheim, *Synth. Commun.*, 2001, **31**, 1141; S. G. Van Ornum, M. M. Bruendl, H. Cao, M. Reddy, D. S. Grubisha, D. W. Bennet and J. M. Cook, *J. Org. Chem.*, 2000, **65**, 1957.

4 M. E. Kraft, Z. Fu and L. V. R. Bonaga, *Tetrahedron Lett.*, 2001, **42**, 1427; M. Ahmar, C. Locatelli, D. Colombier and B. Cazes, *Tetrahedron Lett.*, 1997, **38**, 5281.

5 Another attempt to obtain seven membered rings: C. Mukai, H. Sonobe, J. S. Kim and M. Hanoaka, *J. Org. Chem.*, 2000, **65**, 6654.

6 L. Pérez-Serrano, J. Blanco-Urgoiti, L. Casarrubios, G. Domínguez and J. Pérez-Castells, *J. Org. Chem.*, 2000, **65**, 3513.

7 L. Pérez-Serrano, P. González-Pérez, L. Casarrubios, G. Domínguez and J. Pérez-Castells, *Synlett*, 2000, 1303.

8 L. Pérez-Serrano, L. Casarrubios, G. Domínguez and J. Pérez-Castells, *Org. Lett.*, 1999, **1**, 1187.

9 Spectroscopic data for compound **6** follow: ^{1}H NMR ($CDCl_3$) δ −0.13 (s, 3H), 0.15 (s, 3H), 0.90 (s, 9H), 1.56 (dd, 1H, J_1 = 13.2, Hz, J_2 = 12.6 Hz), 2.08 (dd, 1H, J_1 = 19.2 Hz, J_2 = 2.2 Hz), 2.55–2.63 (m, 1H), 2.77 (dd, 1H, J_1 = 19.2 Hz, J_2 = 6.6 Hz), 3.62–3.71 (m, 1H), 4.98 (d, 1H, J = 13.5 Hz), 5.21 (d, 1H, J = 6.0 Hz); 5.27 (d, 1H, J = 13.5 Hz), 6.10 (s, 1H), 6.36 (s, 1H), 7.10 (t, 1H, J = 7.7 Hz), 7.25 (t, 1H, J = 8.2 Hz), 7.38 (d, 1H, J = 8.2 Hz), 7.57 (d, 1H, J = 7.7 Hz); ^{13}C NMR δ($CDCl_3$) 207.8, 174.6, 141.2, 136.6, 131.9, 127.1, 121.9, 120.9, 119.5, 108.5, 101.0, 66.9, 44.2, 42.8, 41.4, 38.4, 25.7, 18.0, −5.1, −5.4; IR (neat) ν 2920, 1710, 1460 cm^{-1}.

10 This effect may act as the well known *gem* effect. See:M. E. Jung, *Synlett*, 1999, 843.

11 We have described similar diastereoselectivity in related indole compounds. See ref 7. We have not determined the relative stereochemistry of compound **8**.

12 C. J. Lovely, H. Seshadri, B. R. Wayland and A. W. Cordes, *Org. Lett.*, 2001, **3**, 2607.

CHEMCOMM Communication
www.rsc.org/chemcomm

Expansion of structural and functional diversities of DNA using new 5-substituted deoxyuridine derivatives by PCR with superthermophilic KOD Dash DNA polymerase†

Hiroaki Sawai,* Akiko N. Ozaki, Fumie Satoh, Tutomu Ohbayashi, Mohammad M. Masud and Hiroaki Ozaki

Department of Applied Chemistry, Gunma University, Kiryu, Gunma 376-8515, Japan. E-mail: sawai@chem.gunma-u.ac.jp

Received (in Cambridge, UK) 30th August 2001, Accepted 26th October 2001
First published as an Advance Article on the web 14th November 2001

KOD Dash DNA polymerase can accept triphosphates of new deoxyuridine derivatives bearing a C5-substituent group *via* an α-methylene linker as a substrate in the polymerase chain reaction (PCR) yielding the corresponding functionalized DNA effectively, while other conventional DNA polymerases cannot tolerate the modification of the substrate.

Modified oligonucleotides with a thymidine analogue bearing a functional group at the C5 position are important tools for biological and biochemical studies.[1–5] If modified DNA can be prepared by PCR from the substrate analogue using DNA polymerase, the resulting modified DNA could be used as a DNA probe by attachment of a reporter group, and as a DNA catalyst or as a DNA aptamer by *in vitro* selection. However, examples of functionalized DNA prepared from modified deoxynucleotides are limited, because DNA polymerases accept a limited range of molecular structures as substrate. Some DNA polymerases can use 5′-triphosphates of modified 2′-deoxyuridines with a C5-side chain carrying a propenyl or propynyl group.[6-13] Reduction of the double or triple bond of the C5 propenyl or alkynyl substituted 2′-deoxyuridines completely inhibits their function as a substrate.[12] These results indicate that an sp or sp^2 hybridized carbon at the α-position of the C5-substituted 2′-deoxyuridine is required as a substrate for DNA polymerases.[6–13] The differences in reactivity of C5-substituted 2′-deoxyuridine triphosphates as substrates may be due to the steric effect of a large side-group, or to the ionic effect of a substituting group. The substrate activity may also depend on the kind of DNA polymerase.

Previously, we reported the synthesis of thymidine analogues bearing an sp^3-hybridized carbon at the C5 α-position with an amino-linker arm, and their introduction into oligodeoxyribonucleotides using a DNA synthesizer.[14,15] Very recently, we found that triphosphates of the thymidine analogues could be accepted by KOD Dash DNA polymerase as a substrate in the primer-extension reaction. The enzyme is a hyperthermophilic DNA polymerase, originally isolated from the extremely thermophilic archaeum, *Pyrococcus kodakaraensis*.[16] Here we present studies of modified DNA synthesis by PCR from the thymidine analogues and their substrate efficiency during PCR using KOD Dash and some other thermostable DNA polymerases. The C5-substituted 2′-deoxyuridine derivatives bearing several functional groups were prepared easily from 5-methoxycarbonylmethyl-2′-deoxyuridine.[14] Hexamethylenediamine, ethylenediamine, tris(2-aminoethyl)amine or histamine was introduced at the C5 position by an ester–amide exchange reaction with 5-methoxycarbonylmethyl-2′-deoxyuridine, and the terminal amino group was blocked by a trifluoroacetyl group.[15] The 5′-triphosphates of the analogues were synthesized by a one-pot method described by Ludwig.[17] The terminal amino-protecting group, CF_3CO, was removed by treatment with concentrated aqueous ammonia quantitatively at low temperature. The resulting terminal amino group was further modified by reaction with a functional molecule such as a biotin-succinimide ester. The nucleotides were confirmed by ESI-Mass spectrum, ^1H and ^{31}P NMR spectra. The amino group is largely in the protonated state at neutral pH, and could contribute to interaction of the anionic-charged backbone of nucleic acids and may function as a general acid catalyst in the DNA catalyst. Hydrolysis of the 5′-triphosphate of 5-methoxycarbonylmethyl-2′-deoxyuridine with sodium hydroxide gave the 5′-triphosphate of 5-carboxylmethyl-2′-deoxyuridine. The carboxylic acid has a negative charge under neutral conditions and could enhance the interaction with a cationic-charged molecule.

We examined the incorporation of the modified thymidine triphosphates in place of TTP during the PCR using four thermostable DNA polymerases, KOD Dash, Taq, Tth, and Vent DNA polymerases. pUC18 plasmid DNA, and DNA **A**, 5′-GGAAACAGCTATGACCATGATTAC-3′ and DNA **B**, 5′-CGACGTTGTAAAACGACGGCCAGT-3′ were used as a template and primers, respectively, for the PCR assay. The PCR with the natural substrate demonstrated formation of the 108 base pair DNA product when using any DNA polymerase, as expected (Fig. 1). The formation of full-length plasmid DNA (2686 bp) was also observed under high enzyme concentration or prolonged reaction time, under which the polymerization could go over the primer yielding the full-length one. Vent DNA polymerase yielded only a small amount of the DNA product because it hydrolyzed the DNA with its strong exonuclease activity. The modified substrates, **1** and **2**, worked as a substrate in the PCR forming the 108mer DNA when using KOD DNA polymerase, although a large quantity of the enzyme was

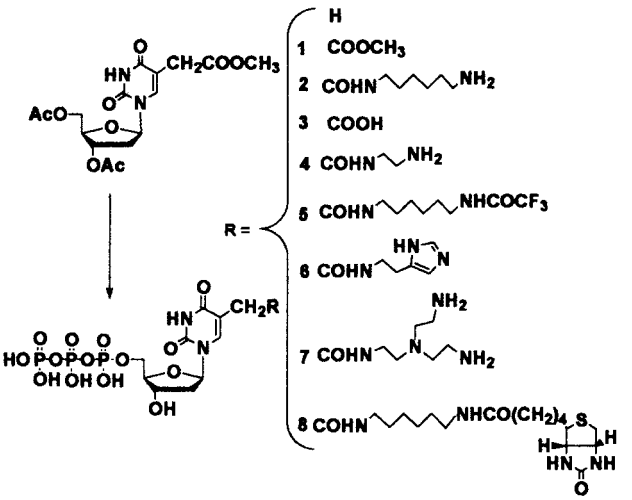

† Electronic supplementary information (ESI) available: sequencing of the PCR products (108mer DNA) from substrates **1** and **2**. See http://www.rsc.org/suppdata/cc/b1/b107838k/

 DOI: 10.1039/b107838k

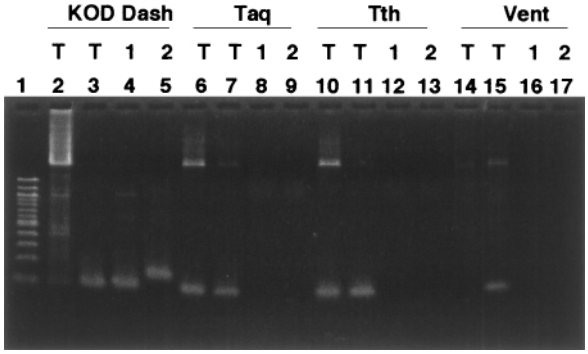

Fig. 1 PCR assays of TTP and its analogs with several DNA polymerases. The mixture (20 μl) for PCR contained 0.5 ng DNA template (pUC18 2686bp), 0.2 μM of each primer, natural dNTPs or modified dNTP mix (0.2 mM of each nucleotide) and 0.5 or 0.05 unit of DNA polymerase in the buffer supplied by the maker for the DNA polymerase reaction. PCR assays were carried out at 94 °C for 1 min, 30 cycles of 94 °C for 30 s–52 °C for 30 sec–74 °C for 1 min, and 74 °C for 5 min for KOD Dash and Vent DNA polymerases; 94 °C for 1 min, 30 cycles of 94 °C for 30 s–52 °C for 30 s–74 °C for 2 min, and 74 °C for 5 min for Taq and Tth DNA polymerases. The reaction mixture was quenched by addition of formamide-dye solution and PCR products were analyzed by 2% agarose gel electrophoresis and visualized by staining with ethidium bromide. 0.5 unit of DNA polymerase was used for the PCR assays except for lanes3, 7, 11 and 15 where 0.05 unit of DNA polymerase was used. Lane 1: Marker DNA (100–1200 bp); lane 2–5: KOD dash DNA polymerase; lane 6–9: Taq DNA polymerase: lane 10–13, Tth DNA polymerase; lane14–17, Vent DNA polymerase. Lanes 2, 3, 6, 7, 10, 11, 14 and 15: TTP + dATP + dCTP + dGTP; lanes 4, 8, 12 and 16: **1** + dATP + dCTP + dGTP; lanes 5, 9, 13 and 17: **2** + dATP + dCTP + dGTP.

required for synthesis of the modified DNA compared with the unmodified one. However, the other widely-used DNA polymerases could not accept these modified substrates and no 108mer modified DNA was obtained. Successful PCR with this template and primers requires the incorporation of 49 modified substrates with a single stretch of four successive thymidine residues. PCR products were obtained on a large scale from the modified substrates, **1** and **2**, and sequenced using a Thermo sequenase radiolabelled terminator-sequencing kit in the usual manner. We confirmed that the sequence of the modified DNAs was the same as that of the template DNA and no mutation took place during the PCR.

Further studies with the modified substrates, **3**–**8**, were carried out using the KOD Dash DNA polymerase to assess the structural feature that can be accepted as a substrate in the PCR. Fig. 2 shows the results of PCR with the modified substrate along with the control reactions with the natural substrate in the presence or absence of the template. The PCR product DNA 108mer was obtained from the modified substrate with a neutral methoxy group (**1**), a terminal protected amine (**5**), or a cationic terminal amine (**2** and **4**). The compound **2** bears a long linker while the compound **4** has a short linker. DNA 108mer with a negative-charged carboxylate at the C5 position of the thymidine residue was also formed from the substrate **3**, although less efficiently under the same condition. However, KOD Dash DNA polymerase could not allow the incorporation of the modified substrate with histamine (**6**) or multi-charged tris(aminoethyl)amine (**7**), probably because of a bulky group with a short linker. The thymidine derivative with biotin at the C5 position *via* a long linker (**8**) was accepted by the enzyme forming the corresponding 108mer DNA. The modified DNA products showed mobility shift on electrophoresis depending on the mass increase and the charge associated with the modified bases.

In conclusion, we found that several new thymidine analogues bearing an sp^3 hybridized carbon at the α-position of the C5-sidearm were good substrates for KOD Dash DNA polymerase yielding the corresponding PCR products. The

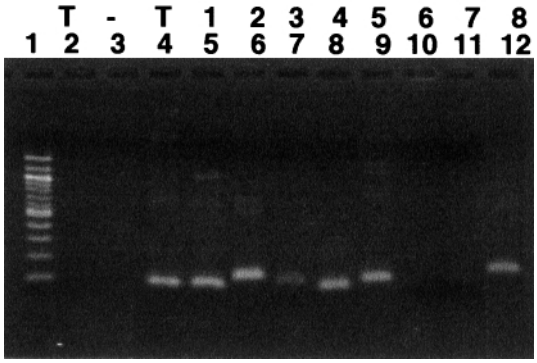

Fig. 2 PCR assays of several TTP analogs using KOD Dash DNA polymerase. PCR assays were carried out in the same way as those in Fig. 1 at 94 °C for 1 min, 30 cycles of 94 °C for 30 s–52 °C for 30 s–74 °C for 1 min, and 74 °C for 5 min for the modified TTP; 94 °C for 1 min, 30 cycles of 94 °C for 30 s–52 °C for 5 s–74 °C for 5 s, and 74 °C for 5 min for the natural TTP. Lane 1: Marker DNA (100–1200 bp); lane 2: negative control without template: TTP + dNTP; lane 3: negative control without TTP: dNTP; lane 4: positive control: TTP + dNTP ; lane 5: **1** + dNTP lane 6: **2** + dNTP: lane 7: **3**+dNTP; lane 8: **4** + dNTP ; lane 9: **5** + NTP; lane 10: **6** + dNTP; lane 11: **7** + dNTP; lane 12: **8** + dNTP (dNTP: dATP + dCTP + dGTP).

thymidine analogues bear various functional groups with a positively charged terminal amino group, negatively charged carboxy group, or neutral ester and amide groups. In contrast to KOD Dash DNA polymerases, conventional DNA polymerases used in this study gave no PCR product from the thymidine analogues. The finding that KOD Dash DNA polymerase tolerates the modification of the substrates could expand the variety of nucleotide analogues that may be used for the synthesis of modified DNA libraries, which will be useful for *in vitro* selection of the functionalized DNA.

Notes and references

1 J. L. Ruth, in *Oligonucleotides and Analogues*, ed. F. Eckstein, IRL Press, Oxford, 1991, pp. 255–282.
2 S. Verma and F. Eckstein, *Ann. Rev. Biochem.*, 1998, **67**, 99.
3 G. B. Dreyer and P. B. Dervan, *Proc. Nat. Acad. Sci. U.S.A.*, 1985, **82**, 968.
4 D. J. Hurley and Y. Tot, *J. Am. Chem. Soc.*, 1998, **120**, 2194.
5 U. Asseline, E. Bonfils, D. Dupret and N. T. Thuong, *Bioconjugate Chem.*, 1996, **7**, 369.
6 R. P. Langer, A. A. Waldrop and D. C. Ward, *Proc. Nat. Acad. Sci. U.S.A.*, 1981, **78**, 6633.
7 J. A. Latham, R. Johnson and J. J. Toole, *Nucleic Acids Res.*, 1994, **22**, 2817.
8 K. Sakthivel and C. F. Barbas III, *Angew. Chem., Int. Ed.*, 1998, **37**, 2872.
9 T. R. Battersby, D. N. Ang, P. Burgstaller, S. C. Jurczyk, M. T. Bowser, D. D. Buchanan, R. T. Kennedy and S. A. Benner, *J. Am. Chem. Soc.*, 1999, **121**, 9781.
10 T. S. Godovikova, D. M. Kolpashchikov, T. N. Orlova, V. A. Richter, T. M. Ivanova, S. L. Grochovsky, T. V. Nasedkina, L. S. Victorova and A. I. Poletaev, *Bioconjugate Chem.*, 1999, **10**, 529.
11 D. M. Perrin, T. Garestier and C. Helene, *Nucleoside Nucletides*, 1999, **18**, 377.
12 S. E. Lee, A. Sidrov, T. Gourlain, N. Mignet, S. J. Thorpe, J. A. Brazier, M. J. Dickman, D. P. Hornby, J. A. Grasby and D. M. Williams, *Nucleic Acids Res.*, 2001, **29**, 1565.
13 T. Gourlain, A. Sidrov, N. Mignet, S. J. Thorpe, S. E. Lee, J. A. Grasby and D. M. Williams, *Nucleic Acids Res.*, 2001, **29**, 1898.
14 H. Sawai, A. Nakamura, S. Sekiguchi, K. Yumoto, M. Endoh and H. Ozaki, *J. Chem. Soc., Chem. Commun.*, 1994, 1997.
15 H. Ozaki, A. Nakamura, M. Arai, M. Endoh and H. Sawai, *Bull. Chem. Soc. Jpn.*, 1995, **68**, 1981.
16 M. Takagi, M. Nishioka, H. Kakihara, M. Kita, H. Inoue, B. Kawakami, M. Oka and T. Imanaka, *Appl. Environmental Microbiol.*, 1997, **63**, 4504; (The enzyme is commercially available from Toyobo Inc.).
17 J. Ludwig, *Acta Biochem. Biophys. Acad. Sci. Hung.*, 1981, **16**, 131.

CHEMCOMM Communication
www.rsc.org/chemcomm

Unprecedented catalytic enantioselective trapping of arene oxides with dialkylzinc reagents†

Fabio Bertozzi,[a] Paolo Crotti,[a] Federica Del Moro,[a] Ben L. Feringa,*[b] Franco Macchia[a] and Mauro Pineschi*[a]

[a] *Dipartimento di Chimica Bioorganica e Biofarmacia, Università di Pisa, Via Bonanno 33, 56126, Pisa, Italy. E-mail: pineschi@farm.unipi.it; Fax: +3905043321*
[b] *Department of Organic and Molecular Inorganic Chemistry, Stratingh Institute, University of Groningen, Nijenborgh 4, NL9747, AG Groningen, The Netherlands*

Received (in Cambridge, UK) 24th September 2001, Accepted 30th October 2001
First published as an Advance Article on the web 15th November 2001

The first catalytic enantioselective trapping of symmetrical and racemic arene oxides with organometallic reagents is reported.

Arene oxide has been subjected to several studies since the demonstration that this class of compounds is formed from aromatic hydrocarbons by the microsomial enzyme fraction from mammalian liver.[1] Much interest, therefore, has been generated concerning the solution chemistry of arene oxide. The nucleophiles utilized in these studies were in most cases heteronucleophiles such as water, alcohols, thiols and amines.[2] There are only few reports dealing with ring-opening reactions of arene oxide carried out with organometallic reagents.[2a,3] Moreover, none of these procedures employing organometallic reagents are catalytic or enantioselective.

We have recently reported a new kinetic resolution of cyclic vinyl oxiranes,[4] a desymmetrization of symmetrical methylidene cycloalkene oxides[5] and a new catalytic regiodivergent kinetic resolution (RKR)[6] based on dialkylzinc reagents and chiral copper complexes of phosporamidite ligands.[7] In the RKR, a single chiral catalyst induces the formation of a distinct regioisomer from each substrate enantiomer with a high ee. The procedure was useful to gain insight into the reaction mechanism of this particular kind of copper-catalyzed allylic alkylation, pointing to reductive elimination as the regio- and stereodetermining step of the addition reaction.

We herein report an unprecedented catalytic and enantioselective desymmetrization of symmetrical arene oxides **1a,b** with hard alkylmetal, and a new, highly enantioselective RKR starting from the racemic arene oxide **8** (Schemes 1, 2 and 3).

Benzene oxide (**1a**) and indan-8,9-oxide (**1b**) were examined as symmetrical arene-oxide substrates (Schemes 1 and 2). Benzene oxide is known to exist in equilibrium with its tautomeric valence structure, the oxepin **1a′**. This compound exists mainly as oxepin at room temperature, even if the oxide component 1a determines the reactions of the system with most agents.[3]

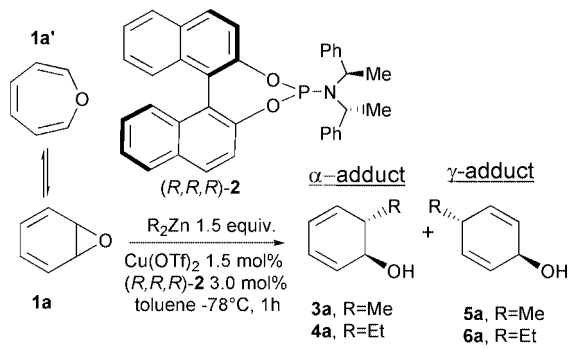

Scheme 1

† Electronic supplementary information (ESI) available: experimental details. See http://www.rsc.org/suppdata/cc/b1/b108541g/

Table 1 Enantioselective trapping-ring-opening of benzene oxide **1a** with R_2Zn[a]

Entry	Substrate	R	Ratio α:γ	Yield (%)[b]	ee (%)[c]
1	**1a**	Me	69:31	85	93
2	**1a**	Et	38:62	88	64

[a] *Conditions*: all reactions were run in accordance with the typical procedure (see ref. 8).[b] Yields are determined on the basis of weight, ^{1}H NMR and GC analysis of the crude reaction mixture.[c] Determined by GC on CSP.

Epoxide **1a** was allowed to react at −78 °C (1 h, 95% conversion) with Me_2Zn (1.5 equiv.) in the presence of a catalytic amount of $Cu(OTf)_2$ (0.015 equiv.) and the chiral ligand (*R,R,R*)-**2** (0.030 equiv.) to give a crude reaction mixture consisting of the not previously synthesized regioisomeric dienols (1*S*,6*S*)-**3a** (α-adduct) and **5a** (γ-adduct) (entry 1, Table 1).[8] The reaction with Et_2Zn gave a slightly different result, with a predominance of the achiral γ-adduct **6a** (entry 2, Table 1).[9] The substituted enantioenriched dihydroaromatic α-adducts (1*S*,6*S*)-**3a** (93% ee) and (1*S*,6*S*)-**4a** (64% ee) were obtained with a complete *anti* stereoselectivity.[10]

Indan 8,9-oxide (**1b**), containing a tetrasubstituted epoxide is known to exist only in the oxide form. The copper-phosphoramidite catalyzed addition of R_2Zn at −78 °C to **1b** (3 h, 95% conversion) gave a *ca*. 80:20 mixture of the corresponding α- and γ-adducts **3b**:**5b** (R = Me) and **4b**:**6b** (R = Et) (Scheme 2).[11]

It is remarkable that the α-adducts **3b** (≥95% ee) and **4b** exclusively derive from an *anti*-stereoselective 1,6-addition pathway (and therefore more appropriately called ε-adducts, Scheme 2). This unexpected regiochemical behavior could be of interest to gain further insight into the interconversion between the regioisomeric (σ-allyl)copper(III) complexes of type **7A–C** that are formed during the oxidative step.[12] Considering the conjugate nature of the starting epoxide, this interconversion between the regioisomeric (σ-allyl)copper(III) complexes of type **7A–C** probably occurs by means of an intermediate delocalized (π-allyl)copper(III) species of type **7D**.[13] In this biased framework the attack at the tertiary carbon terminus atom of **7D** to give **7B** is not favourable for steric reasons, while the attack at the secondary terminus of **7D** to give the (σ-allyl)copper(III) complex **7C** could be highly favoured. The subsequent rate limiting reductive elimination step on **7C** affords the ε-adducts **3b,4b** (1,6-addition products), as observed.

Naphthalene 1,2-oxide (**8**) seems to exist only in the oxide form and it is very prone to spontaneous epoxide ring-opening and aromatization. Despite its extreme chemical reactivity, the addition of Et_2Zn (1.5 equiv.) to racemic **8** in the presence of $Cu(OTf)_2$ (0.015 equiv.) and chiral ligand (*R,R,R*)-**2** (0.030

 DOI: 10.1039/b108541g

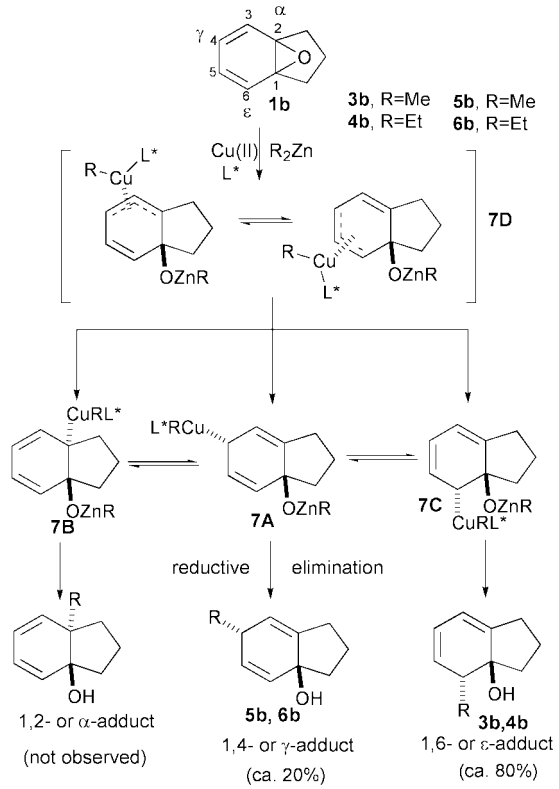

Scheme 2

equiv.) proceeded very cleanly to afford a 66:34 mixture of regioisomeric dihydronaphthols **9** (γ-adduct) and **10** (α-adduct), the latter with a remarkable enantioselectivity (>98% ee) (Scheme 3).[11,14] On the other hand, the addition of Et_2Zn to racemic **8** catalyzed by a copper complex with the racemic ligand (*S,S,S*)(*R,R,R*)-**2** afforded with almost complete (>96%) regioselectivity the racemic γ-adduct **9**. A complete examination of these results clearly indicates that also arene oxide *rac*-**8** exhibits a complementary enantiomer-dependent regioselectivity typical of a RKR process, in which the α-adduct **10** is obtained from the less reactive enantiomer (1*S*,2*R*)-**8** of the racemic substrate, while the γ-adduct derives from the more reactive (1*R*,2*S*)-**8**.[6,14]

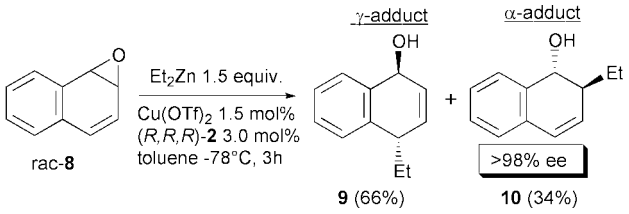

Scheme 3

In summary, the present work describes an unprecedented catalytic and enantioselective trapping of symmetrical and racemic arene oxides. This method offers a new route to enantioenriched dihydroaromatic alcohols, not easily accessible by means of other synthetic methods. An examination of the regiochemical outcome indicated that a 1,6-addition mode may be operative in a biased system such as indan 8,9-oxide for this particular kind of allylic alkylation.

We gratefully acknowledge funding by the MURST (Rome), the University of Pisa, and Merck (2000 ADP Chemistry Award to P. C.).

Notes and references

1 (*a*) D. M Jerina, J. W. Daly, B. Witkop, P. Zaltzman-Niremberg and S. Udenfriend, *J. Am. Chem. Soc.*, 1968, **90**, 6525; (*b*) D. M. Jerina and J. W. Daly, *Science*, 1974, **185**, 573; (*c*) T. C. Bruice and P. Y. Bruice, *Acc. Chem. Res.*, 1976, **9**, 378; (*d*) D. R. Boyd and D. M. Jerina, in *Small Ring Heterocycles, Part 3, Chemistry of Heterocyclic Compounds*, vol. 42, ed. A. Hassner, Wiley, New York, 1985, p. 197.

2 (*a*) A. M. Jeffrey, H. J. C. Yeh, D. M. Jerina, R. M. DeMarinis, C. H. Foster, D. E. Piccolo and G. A. Berchtold, *J. Am. Chem. Soc.*, 1974, **96**, 6929; (*b*) G. H. Posner and D. Z. Rogers, *J. Am. Chem. Soc.*, 1977, **99**, 8214; (*c*) M. J. McManus and G. A. Berchtold, *J. Am. Chem. Soc.*, 1985, **107**, 2977; (*d*) For recent enzymatic transformations, see: D. R. Boyd, J. T. G. Hamilton, N. D. Sharma, J. S. Harrison, W. C. McRoberts and D. B. Harper, *Chem. Commun.*, 2000, 1481; (*e*) S. K. Balani, I. N. Brannigan, D. R. Boyd, N. D. Sharma, F. Hempenstall and A. Smith, *J. Chem. Soc., Perkin Trans. 1*, 2001, 1091; (*f*) T. Hudlicky, D. Gonzales and D. T. Gibson, *Aldrichimica Acta*, 1999, **32**, 34, and references therein.

3 E. Vogel and H. Günther, *Angew. Chem., Int. Ed.*, 1967, **6**, 385.

4 (*a*) F. Bertozzi, P. Crotti, B. L. Feringa, F. Macchia and M. Pineschi, *Synthesis*, 2001, 483; (*b*) F. Badalassi, P. Crotti, F. Macchia, M. Pineschi, A. Arnold and B. L. Feringa, *Tetrahedron Lett.*, 1998, **39**, 7795.

5 F. Bertozzi, P. Crotti, F. Macchia, M. Pineschi, A. Arnold and B. L. Feringa, *Org.Lett.*, 2000, **2**, 933.

6 F. Bertozzi, P. Crotti, F. Macchia, M. Pineschi and B. L. Feringa, *Angew. Chem., Int. Ed. Engl.*, 2001, **40**, 930 and references therein..

7 For an overview of phosphoramidite in catalytic asymmetric conjugate addition, see: B. L. Feringa, *Acc. Chem. Res.*, 2000, **33**, 346.

8 *Typical procedure*: a solution of $Cu(OTf)_2$ (5.8 mg, 0.015 mmol) and **2** (16.2 mg, 0.03 mmol) in anhydrous toluene (2 ml) was stirred at room temperature for 40 min. The colorless solution was cooled to −78 °C and subsequently additioned with a solution of arene oxide (1.0 mmol) in toluene (0.5 ml) and 1.5 mmol of R_2Zn (solution in toluene). The reaction was followed by GC analysis and quenched with saturated aqueous NH_4Cl (see the Supporting Information for further details).

9 The conjugate γ-adducts **5a** and **6a** were obtained only in a mixture with regioisomeric α-adducts **3a** and **4a**. In our hands, it was not possible to isolate in a pure state the achiral γ-adducts **5a** and **6a**, or some simple derivatives of theirs, probably due to a rapid aromatization process.

10 The *anti*-stereochemistry of **3a** was demonstrated by comparison with the product obtained by the addition of MeLi to benzene oxide **1a**, a reaction that is known to proceed with *syn*-stereoselectivity[2a].

11 It is worthy of mention that all the corresponding "blank reactions", performed on epoxides **1a,b** and **8** in the same reaction conditions but in the absence of the chiral ligand (*R,R,R*)-**2**, afforded the corresponding rearranged phenols as the main product (phenol from **1a**, 4-indanol from **1b**, and 1-naphthol from **8**).

12 For very recent experimental evidence supporting the intervention of Cu(III) intermediates, see: A. S. E. Karlström and J.-E. Bäckwall, *Chem. Eur. J.,* 2001, **7**, 1981 and references therein. Even if not indicated in Scheme 2 for the sake of simplicity, the copper(III) complexes **7A–D** are probably cationic species with OTf^- as a possible counterion.

13 The interconversion between the regioisomeric (σ-allyl)copper(III) complexes of type **7A–C** could be reasonably explained also by the intervention of suprafacial 1,3-shifts.

14 All the attempted analyses of the enantiopurity of alcohol **9** both by HPLC- and GC-CSPs gave extensive decomposition of the compound. The absolute configuration of compound (1*R*,2*S*)-**10** was demonstrated by a single crystal X-ray analysis after derivatization of the enantiomer (1*S*,2*R*)-**10** with a chiral auxiliary derived from 4,5-dichlorophthalic acid and (1*S*,2*R*,4*R*)-(−)-2,10-camphorsultam. Details of the procedure will be reported separately in a forthcoming paper.

CHEMCOMM Communication
www.rsc.org/chemcomm

Separation of Pd complexes from a homogeneous solution using zeolite membranes

D. Turlan,[a] E. P. Urriolabeitia,[b] R. Navarro,[b] C. Royo,[a] M. Menéndez[a] and J. Santamaría*[a]

[a] *Department of Chemical Engineering, University of Zaragoza, 50.009 Zaragoza, Spain. E-mail: iqcatal@posta.unizar.es*
[b] *Department of Inorganic Chemistry, ICMA, University of Zaragoza, 50.009 Zaragoza, Spain*

Received (in Cambridge, UK) 4th October 2001, Accepted 6th November 2001
First published as an Advance Article on the web 26th November 2001

A silicalite membrane has been used to separate a homogeneous catalyst from its mixture with solvent and product of the Heck reaction.

Square-planar complexes of Pd(II) play a central role in many catalyzed C–C bond coupling reactions.[1] Research on the Heck arylation of olefins catalyzed by Pd(II) complexes has developed intensely in recent years[2] mainly due to the use of C,P-[3] and C,N-orthometallated Pd(II) derivatives,[4] which provide very high turnover rates. The main problem remains the recovery of the catalyst, which is required for economic reasons (high cost of noble-metal catalysts), and for obvious process and environmental considerations. One of the ideas put forward to facilitate the separation of solvent and reaction products from the catalysts is catalyst heterogenization, which involves some form of attachment of the catalyst to a solid support. However, although some interesting results have been reported,[2,5] heterogenization is difficult to achieve, and it is often detrimental to catalytic performance.

As an alternative, the use of membranes capable of retaining the homogeneous catalyst has been proposed. Giffels *et al.*[6] used solvent-resistant polymeric membranes to retain homogeneous catalysts (oxazaborolidines). However, in order to have the catalyst rejected by the membrane, molecule enlargement by derivatisation was necessary. De Smet *et al.*,[7] used the same membranes under optimum conditions and were able to retain Ru–BINAP and Rh–EtDUPHOS catalysts without the need for derivatisation. However, optimum membrane use was strongly limited in terms of temperature (below 40 °C), which restricts the range of possible applications, considering not only reaction temperature, but also membrane regeneration treatments. Clearly, it would be highly desirable to retain homogeneous catalysts with a membrane that is both solvent and temperature resistant.

In this work, we have used zeolite membranes to separate homogeneous catalysts from liquid solutions. Zeolites are hydrated aluminosilicates with a framework structure. A variety of zeolites have been synthesized as membranes, with pore sizes in the 0.3 to 0.8 nm range.[8] Silicalite was chosen as the zeolite material for this work, in view of its pores of 0.55 nm, well below the size of usual homogeneous catalysts, but still able to permeate many of the usual solvents and products.

The membranes were grown on the inner side of 11 mm internal diameter porous stainless steel tubular supports. The synthesis procedure was as described in a previous work[9] except for the fact that Ludox AS400 was used as the Si source and the molar proportions in the synthesis gel were 280 H_2O:10 SiO_2:0.22 NaOH:0.5 TPABr, where TPABr represents the template (tetrapropylammonium bromide). After synthesis the template was removed by heating the membrane at 460 °C for 8 h using a 1 °C min^{-1} heating rate. The membranes were characterized by measuring N_2 and SF_6 permeances, as the N_2/SF_6 ideal selectivity (ratio of permeances) is customarily used as an indication of membrane quality. X-Ray diffraction (Rigaku/Max System) revealed that silicalite was the only crystalline material formed on the membrane. Scanning electron microscopy analysis (JEOL JSM 6400) and Si concentration profiling by electron-probe microanalysis (EPMA), indicated that the thickness of the zeolite layer was between 10 and 20 μm, depending on the preparation procedure and the number of synthesis. Table 1 gives the characteristics of the two membranes used in this work. Membrane 1 is a lower quality membrane, as ascertained from its much higher permeance (in spite of a higher zeolite loading), and from the notably lower value of the ideal N_2/SF_6 selectivity. Thus, a considerable number of inter-crystalline defects can be expected on membrane 1. On the other hand, the ideal N_2/SF_6 selectivity of membrane 2 was 26, which for MFI membranes on stainless steel supports, indicates a low concentration of inter-crystalline defects.

Table 1 Some characteristics of the membranes used in this work

Membrane	Zeolite weight gain after synthesis (mg/g of membrane)	N_2 permeance/ mol min^{-1} m^{-2} bar^{-1}	N_2/SF_6 ideal selectivity
1	19	1.37×10^{-6}	10.1
2	11	1.53×10^{-7}	26.2

To carry out separation experiments, the liquid mixture containing the catalyst was loaded at the inner side of the tubular support, *i.e.* in contact with the zeolite layer. The feed pressure was then increased to a value between 2 and 2.3 bar, while keeping the outer side at atmospheric pressure. The system temperature was maintained at −2 °C, to minimize evaporation of the permeated liquid during the experiment (which typically lasted 24–36 h). The initial liquid mixture, the liquid remaining on the feed side of the membrane after permeation (retentate) and the liquid collected at the permeate side were analyzed by V-UV spectrophotometry. The detection limit for the Pd complex with this procedure corresponded to a concentration of 10^{-7} M.

In this work, reaction experiments have not been carried out. Instead, the zeolite membrane was used to separate Pd complexes in mixtures representing possible post-Heck reaction scenarios (Pd complex plus solvent, plus a possible reaction product). From the huge variety of possible Pd catalysts and solvents,[2] we have chosen as an example the Heck reaction of 4-bromobenzonitrile with methyl acrylate [eqn. (1)]:

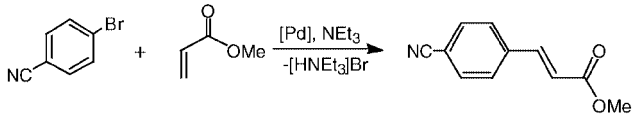

(1)

Typical conditions are reported in the literature (*e.g.* 0.02% mol catalyst/mol sustrate, dimethylacetamide (DMA) as a solvent, and >99% yield after 1 h at 135 °C).[3d] Our choice of $[Pd(\mu\text{-}Cl)(PPh_3)_2]_2(BF_4)_2$ as a catalyst was based on the well known ability of bis-phosphine derivatives of Pd^{II} to catalyse this

 DOI: 10.1039/b109030p

Table 2 Results of permeation experiments with membrane 2. Concentration of catalyst $\{[Pd(\mu\text{-}Cl)(PPh_3)_2]_2(BF_4)_2\}$ and product (4-cyanomethylcinnamate) in the feed to the membrane separator and on the retentate and permeate liquids after permeation. The solvent was dichloromethane in both experiments

	Feed		Retentate		Permeate	
Experiment	Catalyst conc./M	Product conc./M	Catalyst conc./M	Product conc./M	Catalyst conc./M	Product conc./M
1	3.2×10^{-5}	—	9.5×10^{-5}	—	$< 10^{-7}$	—
2	1.1×10^{-5}	5.9×10^{-3}	7.9×10^{-5}	7.9×10^{-3}	$< 10^{-7}$	3.6×10^{-3}

reaction and on the minimum molecular diameter (calculated using CONQUEST™ software across three different perpendicular planes from its X-ray data in the Cambridge Crystallographic Data Centre)[10] which was 1.22 nm, *i.e.* considerably larger than the zeolite pores. On the other hand, the molecular dimensions of the resulting product (4-cyanomethylcinnamate), calculated between the *meta* H atoms are approximately 0.42 nm, and therefore this molecule is able to transit the zeolite pore network. Similarly, the solvents used (DMA and dichloromethane) have kinetic diameters smaller than the zeolite pores.

The first mixture used (Pd complex, DMA, product) corresponds to usual post-reaction conditions: a solid $[HNEt_3]Br$ phase, and a liquid containing a typical solvent (DMA) and the catalyst (and almost nothing else, given the high yields achieved). The second mixture used (Pd complex, dichloromethane, product) contained dichloromethane instead of DMA. While dichlorometane could also be used as a solvent,[2] it is more frequently employed in the post-reaction workup: after vacuum evaporation of the solvent (*e.g.* DMA), water and dichloromethane are used as extractants to obtain, respectively, an aqueous phase with $[HNEt_3]Br$ and an organic phase containing the product and Pd complex in dichloromethane. This organic phase was the second feed mixture used in this work.

Separation experiments using the first mixture as feed were unsuccessful. Permeation rates were extremely low, and the concentration of Pd complex in the permeate was similar to that in the feed solution. This suggests that the DMA solvent was strongly adsorbed in the zeolite pores, blocking them for the permeation of catalyst and product; that permeation took place mainly through non-selective intercrystalline voids. By contrast, good separation was obtained in experiments where dichloromethane was used as a solvent. Binary solvent/catalyst mixtures were readily separated, even at catalyst concentrations much higher than those usually employed for reaction (experiment 1, Table 2). Although the concentration of $[Pd(\mu\text{-}Cl)(PPh_3)_2]_2(BF_4)_2$ increased three-fold as a consequence of solvent permeation through the membrane, complete catalyst retention was observed, within the limits of detection of the V-UV analyser. A separate experiment was performed using ternary mixtures, with concentrations of catalyst and product at typical end-of-reaction levels. The initial pale-yellow feed solution was separated into a strongly coloured retentate and a transparent permeate. The V-UV analysis (experiment 2, Table 2) confirmed the complete retention of the Pd complex, the concentration of which increased seven-fold in the retentate. The retention of Pd occurred simultaneously with the permeation of both solvent and product. Again, the product concentration in the retentate was higher than in the permeate due to the faster solvent permeation. In spite of the small pressure drop across the membrane (*ca.* 1 bar) high permeation fluxes were obtained (average values of 1.6 kg m^{-2} h^{-1}). Finally, as expected, the results of the separation experiment with the defective membrane 1 (not shown) were unsuccessful, demonstrating that this membrane was unable to retain the catalyst.

In conclusion, given suitable conditions, zeolite membranes can separate homogeneous catalysts from their mixtures with solvents and products. A membrane quality above a certain threshold is required, and also suitable membrane characteristics (pore size, absence of undesired adsorption). We believe that this concept can be applied to a variety of systems, both as a post-reaction separation step and also in a continuous reaction-separation scenario.

Financial support from DGICYT, Spain, (Projects PPQ2000-1337 and PB98-1595-C02-01) is gratefully acknowledged. R. N. and E. P. U. wish to thank Professor J. Forniés for invaluable logistic support.

Notes and references

1 (*a*) J. Tsuji, *Palladium Reagents and Catalysts, Innovations in Organic Synthesis*, John Wiley and Sons, Chichester, UK, 1996; (*b*) J. L. Malleron, J. C. Fiaud and J. Y. Legros, *Handbook of Palladium-Catalyzed Organic Reactions*, Academic Press, San Diego, CA, USA, 1997; (*c*) M. Beller and C. Bolm, *Transition Metals for Organic Synthesis, Building Blocks and Fine Chemicals*, Wiley-VCH, Weinheim, Germany, 1998; (*d*) J. Hagen, *Industrial Catalysis, A Practical Approach*, Wiley-VCH, Weinheim, Germany, 1999.

2 I. P. Beletskaya and A. V. Cheprakov, *Chem. Rev.*, 2000, **100**, 3009.

3 (*a*) W. A. Herrmann, C. Brossmer, K. Öfele, C. P. Reisinger, T. Priermeier, M. Beller and H. Fischer, *Angew. Chem., Int. Ed. Engl.*, 1995, **34**, 1844; (*b*) M. Beller, H. Fischer, W. A. Herrmann, K. Öfele and C. Brossmer, *Angew. Chem., Int. Ed. Engl.*, 1995, **34**, 1848; (*c*) W. A. Herrmann, C. Brossmer, C. P. Reisinger, T. Riermeier, K. Öfele and M. Beller, *Chem. Eur. J.*, 1997, **3**, 1357; (*d*) W. A. Herrmann, V. P. W. Böhm and C. P. Reisinger, *J. Organomet. Chem.*, 1999, **576**, 23.

4 (*a*) M. Ohff, A. Ohff and D. Milstein, *Chem. Commun.*, 1999, 357; (*b*) H. Weissman and D. Milstein, *Chem. Commun.*, 1999, 1901; (*c*) X. Gai, R. Grigg, M. I. Ramzan, V. Sridharan, S. Collard and J. E. Muir, *Chem. Commun.*, 2000, 2053; (*d*) M. Nowotny, U. Hanefeld, H. VanKoningsveld and T. Maschmeyer, *Chem. Commun.*, 2000, 1877; (*e*) A. A. D. Tulloch, A. A. Danopoulos, R. P. Tooze, S. M. Cafferkey, S. Kleinhenz and M. B. Hursthouse, *Chem. Commun.*, 2000, 1247.

5 (*a*) D. J. Bayston, J. L. Fraser, M. R. Ashton, A. D. Baxter, M. E. C. Polywka and E. M. Moses, *J. Org. Chem.*, 1998, **63**, 3137; (*b*) I. F. J. Vankelecom and P. A. Jacobs, in *Inmobilisation of chiral catalysts*, ed. D. De Vos, I. F. J. Vankelecom and P. A. Jacobs VCH, Weinheim, 2000.

6 G. Giffels, J. Beliczey, M. Felder and U. Kragl, *Tetrahedron: Asymmetry*, 1998, **9**, 691.

7 K. De Smet, S. Aerts, E. Ceulemans, I. F. J. Vankelekom and P. A. Jacobs, *Chem. Commun.*, 2001, 597.

8 (*a*) J. Coronas and J. Santamaría, *Sep. Purif. Methods*, 1999, **28**, 127; (*b*) J. Caro, M. Noack, P. Kolsch and R. Schafer, *Microporous Mesoporous Mater.*, 2000, **38**, 3.

9 E. Piera, J. Coronas, M. Menéndez and J. Santamaría, *Chem. Commun.*, 1999, 1309.

10 F. H. Allen and O. Kennard, *Chem. Des. Autom. News*, 1993, **8**, 31.

CHEMCOMM Communication
www.rsc.org/chemcomm

An approach to the synthesis of organically templated open-framework metal sulfates by the amine–sulfate route

Amitava Choudhury, Jayaraman Krishnamoorthy and C. N. R. Rao*

[a] *Chemistry and Physics of Materials Unit, Jawaharlal Nehru Centre for Advanced Scientific Research, Jakkur P.O., Bangalore 560 064, India and Solid State and Structural Chemistry Unit, Indian Institute of Science, Bangalore 560 012, India. E-mail: cnrrao@jncasr.ac.in*

Received (in Cambridge, UK) 30th August 2001, Accepted 30th October 2001
First published as an Advance Article on the web 26th November 2001

The first organically templated cadmium sulfates, $[C_4N_2H_{12}][CdCl_2SO_4]\cdot H_2O$ and $[C_4N_2H_{12}]_4[Cd_3Cl_{10}(SO_4)_2(H_2O)]\cdot 3H_2O$, consisting of infinite linear chains and a quasi-2D layer formed by strip-like units respectively, have been synthesized and characterized.

Amongst the variety of open-framework inorganic materials, the metal phosphates constitute one of the largest families.[1] In these materials, the phosphate tetrahedra share corners with the metal–oxygen polyhedra to build networks. Besides the phosphates, open framework 3D metal arsenates,[2] phosphites[3] and germanates[4] have been reported in the literature. Recently, an organically templated zinc selenite with a layered structure has also been reported.[5] One would expect the sulfate tetrahedra to be able to play a role similar to the phosphate tetrahedra, but no open-framework sulfates are known hitherto. We were, therefore, interested in exploring whether open-framework metal sulfates can be synthesized by employing an appropriate strategy. Since the reactions carried out under standard hydrothermal conditions in the presence of amines were not effective, we attempted to synthesize sulfate-based networks by reacting organoammonium sulfates with metal ions. In adopting this approach, we were guided by the significant success achieved in the synthesis of open-framework metal phosphates[6,7] and oxalates[8] by the reaction of metal ions with organoammonium phosphates and oxalates, respectively. In this communication, we report the first success we have had in synthesising two cadmium sulfates, with chain and layer structures, by the reaction of piperazinium sulfate with cadmium chloride. The results suggest that it may indeed be possible to obtain sulfate-based open-framework structures by this route.

Piperazine sulfate, $[H_2N(CH_2)_4NH_2]SO_4\cdot H_2O$ (PIPS), prepared by the reaction of the amine with H_2SO_4,† was characterized by IR spectroscopy and single crystal X-ray diffraction. The structure of PIPS can be described as a 3-D supramolecular network formed by strong N–H···O, O–H···O and C–H···O hydrogen bonds between the diprotonated piperazine, SO_4^{2-} anion and water molecules. Compounds $[C_4N_2H_{12}][CdCl_2SO_4]\cdot H_2O$ **I** and $[C_4N_2H_{12}]_4[Cd_3Cl_{10}(SO_4)_2(H_2O)]\cdot 3H_2O$ **II**, synthesized by the reaction of PIPS with Cd^{2+} ions in butan-2-ol–water under hydrothermal conditions,† were characterized by single-crystal X-ray diffraction,‡ powder X-ray diffraction (PXRD), thermogravimetric analysis (TGA), IR spectroscopy and CHN analysis.

The asymmetric unit of **I** contains 15 non-hydrogen atoms with one crystallographically distinct Cd and S atom each in the asymmetric unit. The Cd atom is six-coordinated by four Cl and two O neighbors, the structure being built up of isolated infinite chains of $[CdCl_2SO_4]^{2-}{}_n$ running along the *b*-axis. In the $[CdCl_2SO_4]^{2-}$chain, $CdCl_4O_2$ octahedra share edges in *trans*-fashion *via* their Cl atoms, and the SO_4 tetrahedra are grafted on to the chain in a symmetrical bridge. The two Cd–μ-Cl–Cd linkages between the adjacent Cd atoms lead to infinite linear chains of *trans*-edge-sharing $CdCl_4O_2$ octahedra. The *trans* orientation of the bridging Cl atom creates a zigzag {–Cd–μ-Cl–Cd–μ-Cl–Cd–} backbone to the linear chain of $CdCl_2O_4$ octahedra. The pairwise canting of the Cd–O bonds gives rise to a helical arrangement responsible for the chirality of the structure. Two of the sulfate oxygens bond to two adjacent Cd sites of the edge-shared $CdCl_4O_2$ in the common symmetrical bridging mode as shown in Fig. 1(a), thus forming a synthetic analogue of the linarite chain.[11] The 1-D chains along the *b*-axis are arranged parallel to one another in the *bc*-plane to form a layer-like arrangement. Such layers are stacked one over the other along the *a*-axis, with the diprotonated amine molecules and the water molecules located in the inter-layer space. The amine and water molecules interact strongly with the inorganic framework through N–H···O and O–H···O hydrogen bonding to stabilize the 3-D structure shown in Fig. 1(b).

The asymmetric unit of **II** contains 33 non-hydrogen atoms with four amine fragments, each corresponding to half-units of piperazine and three water molecules as extra-framework moieties. Two of the four amine fragments and one water molecule are disordered. The structure can be visualized as two parallel chains made up of $CdCl_3O_3$, $CdCl_3O_2$ and SO_4 units, running along the [010] direction. These chains are connected by $CdCl_6$ octahedra, giving rise to an anionic quasi 2-D layer. The structure contains three crystallographically distinct cadmium atoms and one sulfur atom. Cd(1) exists as $CdCl_3O_3$, Cd(2) is penta-coordinated as $CdCl_3O_2$ and Cd(3) is hexa-coordinated as $CdCl_6$. Cd(1) forms two Cd–O–S, and two Cd–Cl bonds besides one Cd–Cl–Cd bond with the neighboring S(1) and Cd(3) atoms. Hexa-coordination is satisfied by bonding to a H_2O molecule. Cd(2) forms a similar connectivity with the

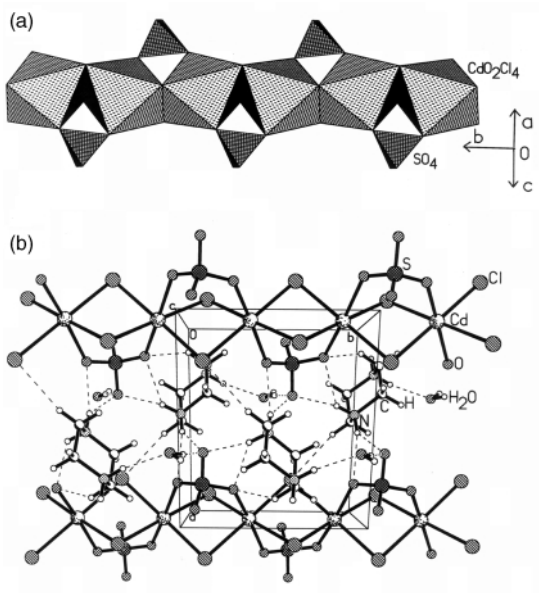

Fig. 1 (a) The inorganic part of **I**, $[CdCl_2SO_4]^{2-}{}_n$ showing the linarite-type chain along the *b*-axis. (b) Illustration of the chain arrangement and the amine molecules along the *c*-axis in **I**. Dotted lines represent hydrogen bonding.

 DOI: 10.1039/b107820h

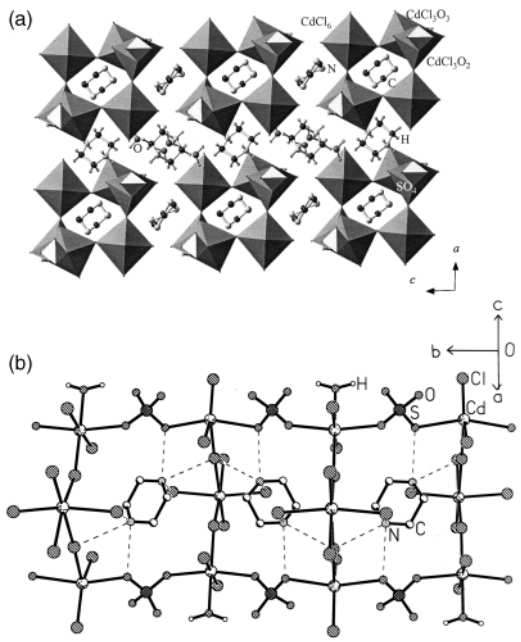

Fig. 2 (a) The quasi 2-D layer of $[C_4N_2H_{12}]_4[Cd_3Cl_{10}(SO_4)_2(H_2O)]\cdot 3H_2O$, **II** with the amine molecules sitting in the middle of the eight-membered aperture. (b) The arrangement of strips in **II** viewed along the *b*-axis.

neighbouring Cd(3) and S(1) but has a distorted trigonal bipyramidal coordination due to absence of a water molecule. Cd(3) on the other hand forms two Cd–Cl–Cd bonds with the two c*is* Cl atoms neighbouring Cd(1) and Cd(2) in addition to four Cd–Cl terminal bonds. The connectivity between $Cd(1)Cl_3O_2(H_2O)$ and $Cd(2)Cl_3O_2$ polyhedra is brought about by the SO_4 tetrahedron *via* corner sharing to form a chain along the *b*-axis. Two such chains are linked by $Cd(3)Cl_6$ octahedron *via* corner sharing between $Cd(1)Cl_3O_2(H_2O)$ and $Cd(2)Cl_3O_2$ polyhedra to form a strip-like quasi 2-D layer. Since the two Cl atoms of the bridging $Cd(3)Cl_6$ octahedra connecting the two chains are in *cis* orientation, the $Cd(3)Cl_6$ octahedra project themselves above and below the plane of the two chains alternately. Such a linkage creates eight-membered apertures within the *strip* in which heavily disordered piperazine moieties reside as shown in Fig. 2(a). These *strips* are held together by N–H···O and C–H···O hydrogen bonds in the *bc*-plane to form a layer-like arrangement. Protonated piperazine and water molecules present between the layers stabilise the 3-D structure [Fig. 2(b)].

To our knowledge the linarite-type chain **I** and the *strip*-like quasi-2D layer **II**, are the first members of the organically templated open-framework metal sulfate family. While there are a few piperazinium templated inorganic hosts, there is only one report of piperazine templated sulfate, comprising a dimer of VO_6 octahedra and SO_4 tetrahedra but this compound does not possess an extended structure.[11] Infinite chains of $[M(T\phi_4)\phi_2]$ stoichiometry in the linarite group minerals[12] are rather rare and generally occur in layered structures such as in iron phosphates[13] and gallium phosphates[14] and in the minerals tsumcorite and bermanite. Such a chain, not known in the metal phosphates, could act as the building block to form higher dimensional structures. It has been shown recently[15,16] that 1-D zinc phosphate ladders and 1-D tancoite type gallium phosphate chains undergo facile transformations to form 3-D open-framework structures. The strip structure of the compound formed in **II**, forming a quasi 2-D layer is unusual and has been found in a open-framework cobalt phosphate.[7]

Notes and references

† *Synthesis*: $[H_2N(CH_2)_4NH_2]SO_4\cdot H_2O$ (PIPS), was prepared by mixing a 1 M aqueous solution of piperazine with 1 M H_2SO_4. (CCDC reference number 170834).

In order to synthesize **I**, 0.1835 g of $CdCl_2\cdot H_2O$ was dissolved in a butan-2-ol-H_2O mixture (2.5 ml/0.49 ml) under constant stirring. To this solution was added 0.5031 g of PIPS and the stirring continued for several hours to obtain a homogeneous mixture. The final mixture with a molar ratio of 1 $CdCl_2\cdot H_2O$: 2.73 PIPS : 30 butan-2-ol : 30 H_2O was transferred into a 7-ml PTFE-lined acid digestion bomb and heated at 423 K for 48 h. **II** was synthesized at a slightly higher temperature (453 K) starting with a reaction mixture of the composition 1 $CdCl_2\cdot H_2O$: 2.75 PIPS : 28.32 butan-2-ol): 36 H_2O. The products contained colorless rod-shaped crystals, suitable for single crystal X-ray diffraction. TGA revealed that both **I** and **II** lose the water molecules in the range 100–150 °C range, with a sharp weight loss around 300° C due to the loss of amine molecules and HCl (calc. 41.25%, obs. 47.58% for **I**; calc. 48.64%, obs. 42.52% for **II**). The dense cadmium sulfate in the case of **I** and chlorosulfate for **II** decompose to CdO at 600 °C. CHN analysis confirmed the amount of organic amine present in both the compounds (Found: C, 12.93; H, 3.79; N, 7.54. Calc.: C, 12.46; H, 3.66; N, 7.26% for **I**. Found: C, 14.72; H, 4.36; N, 8.62%. Calc.: C, 14.68; H, 4.31; N, 8.56% for **II**).

‡ *Crystal data:* $[C_4N_2H_{12}][CdCl_2SO_4]\cdot H_2O$ **I**: M_r = 385.54, monoclinic, space group $P2_1$ (no. 4), a = 9.3500(4), b = 7.4689(3), c = 9.4289(4) Å, β = 116.134(10)°, V = 591.14(4) Å^3, Z = 4, μ = 2.478 mm^{-1}, D_c = 2.166 g cm^{-3}. A total of 2509 reflections were collected in the θ range 2.41–23.24 and merged to give 1582 unique data (R_{int} = 0.021) of which 1539 with $I > 2\sigma(I)$ were considered to be observed. Final R = 0.022, R_w = 0.054 and S = 1.06 were obtained for 144 parameters.

$[C_4N_2H_{12}]_4[Cd_3Cl_{10}(SO_4)_2(H_2O)]\cdot 3H_2O$, **II**: M_r = 1308.54, monoclinic, space group $P2_1/m$ (no.11), a = 12.578(2), b = 13.093(4), c = 13.006(3) Å, β = 94.58(2)°, V = 2135.0(9) Å^3, Z = 4, μ = 2.261 mm^{-1}, D_c = 1.995 g cm^{-3}. A total of 8916 reflections were collected in the θ range 1.57–23.28 and merged to give 3216 unique data (R_{int} = 0.052) of which 2467 with $I > 2\sigma(I)$ were considered to be observed. Final R = 0.058, R_w = 0.095 and S = 1.05 were obtained for 246 parameters.

The structures were solved by direct methods using SHELXS-86[9] and full-matrix-least-squares structure refinement against $|F^2|$ was carried out using SHELXTL-PLUS[10] package of programs. Two amine molecules and one water molecule in **II** being disordered were refined isotropically. CCDC reference numbers 171678 and 171679. See http://www.rsc.org/suppdata/cc/b1/b107820h/ for crystallographic data in CIF or other electronic format.

1 A. K. Cheetham, G. Férey and T. Loiseau, *Angew. Chem., Int. Ed.*, 1999, **38**, 3268.
2 S. Ekambaram and S. Sevov, *Inorg. Chem.*, 2000, **39**, 2405.
3 S. Fernandez, J. L. Mesa, J. L. Pizarro, L. Lezama, M. I. Arriortua, R. Olazcuaga and T. Rojo, *Chem. Mater.*, 2000, **12**, 2092; J. A. Rodgers and W. T. A. Harrison, *Chem. Commun.*, 2000, 2385.
4 B. A. Reisner, A. Tripathi and J. B. Parise, *J. Mater. Chem.*, 2001, **11**, 887; X. Bu, P. Feng, T. E. Gier, D. Zhao and G. D. Stucky, *J. Am. Chem. Soc.*, 1998, **120**, 13389.
5 W. T. A. Harrison, M. L. F. Phillips, J. Stanchfield and T. M. Nenoff, *Angew. Chem., Int. Ed.*, 2000, **39**, 3808.
6 S. Neeraj, S. Natarajan and C. N. R. Rao, *Angew. Chem., Int. Ed.*, 1999, **38**, 3480; C. N. R. Rao, S. Natarajan and S. Neeraj, *J. Solid State Chem.*, 2000, **153**, 302.
7 C. N. R. Rao, S. Neeraj and S. Natarajan, *J. Am. Chem. Soc.*, 2000, **122**, 2810.
8 R. Vaidhyanathan, S. Natarajan and C. N. R. Rao, *J. Chem. Soc., Dalton Trans.*, 2001, 699.
9 G. M. Sheldrick, *SHELXS-86 Program for crystal structure determination*, University of Götingen, 1986; G. M. Sheldrick, *Acta Crystallogr., Sect. A*, 1990, **35**, 467.
10 G. M. Sheldrick, *SHELXTL-PLUS Program for Crystal Structure Solution and Refinement*, University of Götingen, Götingen, Germany, 1993.
11 M. I. Khan, S. Cevik and R. J. Doedens, *Inorg. Chim. Acta.*, 1999, **292**, 112.
12 Von H. G. Bachmann and J. Zemann, *Acta. Crystallogr.*, 1961, **14**, 747; F. C. Hawthorne, *Z. Kristallogr.*, 1990, **192**, 1; F. C. Hawthorne, *Acta. Cristallogr., Sect. B*, 1994, **50**, 481.
13 M. Cavellec, D. Riou, J. M. Greneche and G. Férey, *Inorg. Chem.*, 1997, **36**, 2187; Z. A. D. Lethbridge, P. Lighfoot, R. E. Morris, D. S. Wragg, P. A. Wright, Åke Kvick and G. Vaughnan, *J. Solid State Chem.*, 1999, **142**, 455.
14 R. H. Jones, J. M. Thomas, H. Qisheng, M. B. Hursthouse and J. Chen, *J. Chem. Soc., Chem. Commun.*, 1991, 1520.
15 C. N. R. Rao, S. Natarajan, A. Choudhury, S. Neeraj and A. A. Ayi, *Acc. Chem. Res.*, 2001, **34**, 80.
16 R. I. Walton, F. Millange, D. O'Hare, C. Paulet, T. Loiseau and G. Férey, *Chem. Mater.*, 2000, **12**, 1977; R. I. Walton, F. Millange, A. Le bail, T. Loiseau, C. Serre, D. O'Hare and G. Férey, *Chem. Commun.*, 2000, 203.

CHEMCOMM
Communication
www.rsc.org/chemcomm

A preparative strategy for supramolecular inclusion compounds by combination of dimer formation of isonicotinic acid and coordination bonding

Ryo Sekiya and Shin-ichi Nishikiori*

Department of Basic Science, Graduate School of Arts and Sciences, The University of Tokyo, 3-8-1 Komaba, Meguro, Tokyo 153-8902, Japan. E-mail: cnskor@mail.ecc.u-tokyo.ac.jp

Received (in Cambridge, UK) 19th September 2001, Accepted 6th November 2001
First published as an Advance Article on the web 16th November 2001

A new inclusion compound host $[Ni(SCN)_2(isoH)_2]$, whose cavity is suitable to include large aromatic guests, has been synthesized by a method of combining the dimer formation of isonicotinic acid by double hydrogen bonds with a 1D Ni thiocyanato complex.

Hydrogen bonding has been widely used in the preparation of supramolecular compounds because of its flexibility and availability.[1] However, there are two drawbacks which need to be considered: its weak bonding force and difficulty in predicting the bonding scheme which is easily affected by the surroundings. These are serious problems in designing hosts for a target guest. A method of solving these problems is to use multiple hydrogen bonds. As such a candidate, a dimer structure of two carboxylic acids connected by two hydrogen bonds might be promising and the key compound reported in this paper is isonicotinic acid (isoH, 4-pyridinecarboxylic acid). In recent studies for building multi-dimensional polymeric metal complexes, nicotinic acid and its derivatives have been sometimes used as building blocks because of their versatile coordination behavior and ability to form hydrogen bonds.[2,3] In the case of isoH, as shown in Fig. 1, double hydrogen bonds connect two isoH molecules to make a long flat building block with two coordination sites. If these building blocks can be arrayed at appropriate intervals then large spaces can be formed between the blocks. To make such a structure, we considered a combination of the isoH dimer and a 1D complex of $[M(SCN)_2]$.[4] In the 1D complex, all equatorial sites of a divalent octahedral metal ion (M) are occupied by SCN^- ambidentate ligands which link adjacent M ions to make an infinite 1D double chain structure, and the axial sites of M are available for bonding isoH dimers. An assembly of the isoH dimers and the 1D complexes generates a 2D network host complex with rectangular grids as shown in Fig. 2. Considering the dimensions of the grid, which has a large height (*ca.* 16.5 Å) and a narrow width (*ca.* 5.5 Å), the host is expected to be suitable for including large aromatic molecules. The narrow width of the grid also has an additional significance since its narrowness prevents formation of an interpenetrating structure for the 2D network complex. It is well known that the formation of an interpenetrating structure of networks with large grids fills up space that could have been available for a guest so that the networks can no longer function as a host.[5]

In our preparative experiments using Ni, Cu and Cd as divalent metal ions,[3,6] a series of targeted inclusion compounds $[Ni(SCN)_2(isoH)_2]\cdot 1/2G$ was obtained, where G is a guest such as anthracene, naphthalene, pyrene, perylene, biphenyl, styrene, anthraquinone, azobenzene, *etc*.† As an example, the crystal structure of an anthracene inclusion compound $[Ni(SCN)_2(isoH)_2]\cdot 1/2C_{14}H_{10}$ (**1**), whose space group is $P\bar{1}$, is shown in Fig. 3.‡ The host of **1** has the same structural framework shown in Fig. 2. There are two types of Ni ions, Ni(1) and Ni(2), which lie on independent inversion centers of the crystal. Both Ni ions have an octahedral coordination structure coordinated by four SCN^- ligands at the equatorial sites and two isoH molecules at the axial sites. Each SCN^- ligand makes a bridge between Ni(1) and Ni(2). A bent bridge structure of the SCN^- ligand forms the doubly bridged chain structure of a 1D $[Ni(SCN)_2]$ complex running along the *b* axis of the crystal (Fig. 3(a)). The 1D $[Ni(SCN)_2]$ complexes are linked by isoH dimer blocks which are formed by double hydrogen bonds as shown in Fig. 2. This linkage is formed between Ni(1) and Ni(2) in independent 1D $[Ni(SCN)_2]$ complexes and runs along the [0 1 2] direction of the crystal. As a result, a 2D network complex extending over the *bc* plane is built up. Fig. 3(a) shows the structure of the 2D network. The distance between two Ni ions in the linkage is 16.239(2) Å, and the span between adjacent Ni ions in the 1D $[Ni(SCN)_2]$ complex is 5.506(1) Å. The whole crystal structure is a layered structure of the 2D network complexes stacked along the *a* axis as shown in Fig. 3(b). This layered structure leads to channel-like cavities parallel to the *a* axis delineated by the rectangular grids of the 2D networks. Anthracene molecules, the centers of which lie at different independent inversion centers of the crystal, are arrayed in the channel-like cavities, in which each anthracene molecule is sandwiched between isoH dimer blocks.

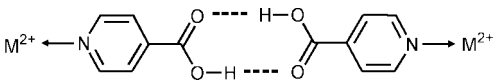

Fig. 1 An isonicotinic acid dimer as a building block.

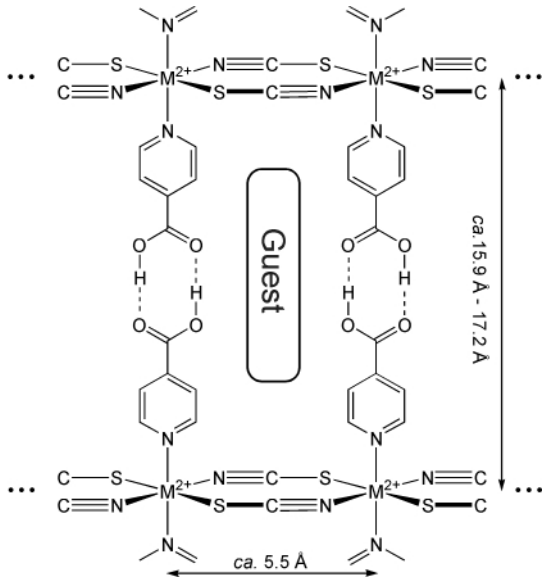

Fig. 2 A 2D network host complex formed by combination of the isonicotinic acid dimers and 1D $[M(SCN)_2]$ complexes.

Our preparative strategy is considered to be applicable to other isoH derivatives. To confirm this, we prepared a pyrene inclusion compound $[Ni(SCN)_2(acrylH)_2]\cdot 1/2C_{16}H_{10}$ (**2**) using 3-(4-pyridinyl)-2-propenoic acid (acrylH) instead of isoH.

 DOI: 10.1039/b108458e

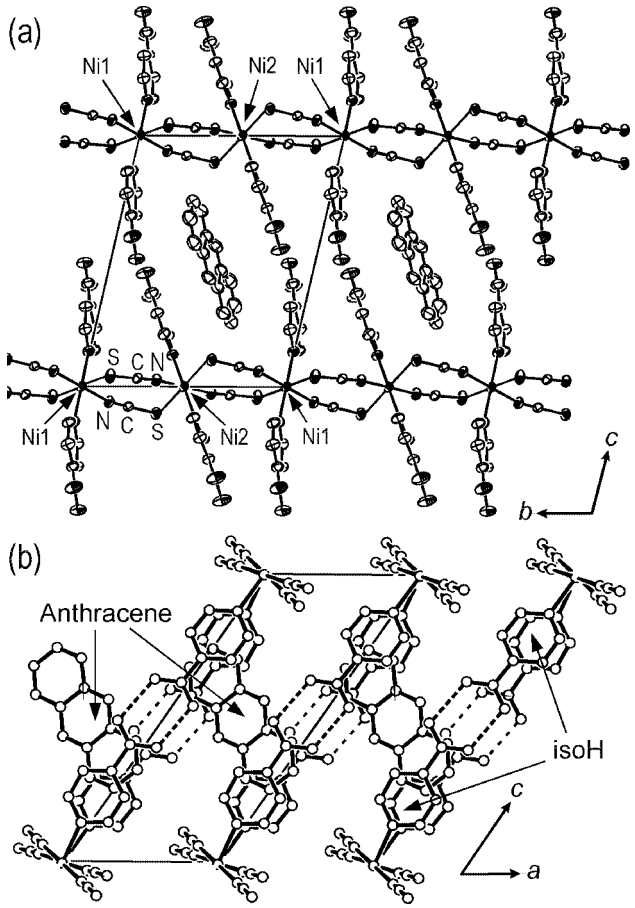

Fig. 3 Crystal structure of $[Ni(SCN)_2(isoH)_2]\cdot 1/2C_{14}H_{10}$ **1**. (a) A view along the *a* axis showing the structure of a 2D network complex extending over the *bc* plane. 1D $[Ni(SCN)_2]$ complexes and –Ni(1)–(isoH dimer)–Ni(2)– linkages run along the *b* axis and the [0 1 2] direction, respectively. (b) A view along the *b* axis. The 2D network complexes are stacked along the *a* axis. The lengths of the double hydrogen bonds indicated by dashed lines are 2.569(4) and 2.639(4) Å.

Fig. 4 shows the crystal structure of **2**.‡ The host structures of **2** and **1** are closely structurally related. The distance between two Ni ions linked by the acrylH dimer is 20.928(1) Å, so that the host of **2** has a potential for including larger aromatics.

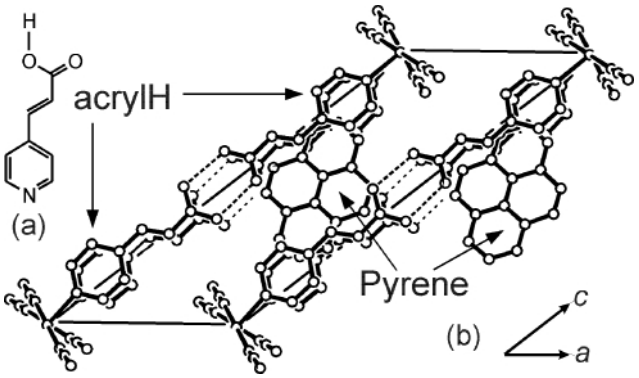

Fig. 4 (a) 3-(4-Pyridinyl)-2-propenoic acid (acrylH). (b) Crystal structure of $[Ni(SCN)_2(acrylH)_2]\cdot 1/2C_{16}H_{10}$ **2** viewed along the *b* axis. The lengths of the double hydrogen bonds indicated by dashed lines are 2.610(4) and 2.636(4) Å.

In conclusion, by means of dimer formation of isoH molecules, a long flat building block that acts as a bidentate ligand has been generated. By assembly of this building block and a 1D $[Ni(SCN)_2]$ complex, a new type of host has been prepared. This preparative strategy is applicable to other isoH derivatives. As an example, a host with an acrylH dimer building block has been prepared. Moreover, another type of structural development, where a molecule with two carboxylic acids is inserted into the isoH dimer building block, is possible. This type of host will be reported elsewhere.

Support of this work by a Grant-in-Aid for Scientific Research(A) Project No. 12354008 from Japan Society for the Promotion of Science is gratefully acknowledged.

Notes and references

† *Preparation*: to 100 mL of acetonitrile suspended with $NiCl_2\cdot 6H_2O$ (1.50 g, 6.3 mmol), KSCN (1.52 g, 15.6 mmol) was added with vigorous stirring. After refluxing the solution for 1 h, precipitated KCl was filtered off and then isoH (1.30 g) and a guest were added to the solution. Crystals of the inclusion compounds were obtained after slow evaporation of the solvent over a period of a few weeks at room temperature.

‡ *Crystal data* for $[Ni(SCN)_2(isoH)_2]\cdot 1/2C_{14}H_{10}$ **1**: $C_{21}H_{15}N_4NiO_4S_2$, M = 510.2, triclinic, space group $P\bar{1}$ (no.2), a = 7.2337(7), b = 11.013(1), c = 16.727(2) Å, α = 104.590(3), β = 54.736(5), γ = 97.602(8)°, U = 1052.7(2) Å^3, T = 293 K, Z = 2, μ(Mo-Kα) = 1.16 mm^{-1}, 9235 reflections measured, 4652 unique (R_{int} = 0.030) which were used in all calculations. The final $wR(F^2)$ = 0.1408 (all data). In the other guest inclusion compounds described in the text, isostructural hosts were confirmed by X-ray diffraction the structures of which will be reported elsewhere. For $[Ni(SCN)_2(acrylH)_2]\cdot 1/2C_{16}H_{10}$ **2**: $C_{26}H_{19}N_4NiO_4S_2$, M = 574.28, triclinic, space group $P\bar{1}$ (no.2), a = 8.9991(8), b = 11.0440(6), c = 21.322(1) Å, α = 101.551(2), β = 37.779(2), γ = 99.392(1)°, U = 1271.9(2) Å^3, T = 293 K, Z = 2, μ(Mo-Kα) = 0.968 mm^{-1}, 12148 reflections measured, 5772 unique (R_{int} = 0.032) which were used in all calculations. The final $wR(F^2)$ = 0.113 (all data). CCDC reference numbers 171788 and 171789. See http://www.rsc.org/suppdata/cc/b1/b108458e/ for crystallographic data in CIF or other electronic format.

1 (*a*) P. Dauber and A. T. Hagler, *Acc. Chem. Res.*, 1980, **13**, 105; (*b*) G. R. Desiraju, *Acc. Chem. Res.*, 1991, **24**, 290; (*c*) C. B. Aakeröy and K. R. Seddon, *Chem. Soc. Rev.*, 1993, 397; (*d*) D. Braga, F. Grepioni, P. Sabatino and G. R. Desiraju, *Organometallics*, 1994, **13**, 3532; (*e*) C. B. Aakeröy and M. Nieuwenhuyzen, *J. Am. Chem. Soc.*, 1994, **116**, 10983; (*f*) J. C. MacDonald and G. M. Whitesides, *Chem. Rev.*, 1994, **94**, 2383; (*g*) G. R. Desiraju, *Angew. Chem., Int. Ed.*, 1995, **34**, 2311; (*h*) G. R. Desiraju, *Acc. Chem. Res.*, 1996, **29**, 441; (*i*) R. K. R. Jetti, F. Xue, T. C. W. Mark and A. Nangia, *J. Chem. Soc., Perkin Trans. 2*, 2000, 1223; (*j*) B. Moulton and M. J. Zaworotko, *Chem. Rev.*, 2001, **101**, 1629.

2 (*a*) M. A. S. Goher and T. C. W. Mak, *Inorg. Chim. Acta*, 1985, **101**, L27; (*b*) L. R. MacGillivray, R. H. Groeneman and J. L. Atwood, *J. Am. Chem. Soc.*, 1998, **120**, 2676; (*c*) C. B. Aakeröy, A. M. Beatty and D. S. Leinen, *Angew. Chem., Int. Ed.*, 1999, **38**, 1815; (*d*) O. R. Evans and W. Lin, *Inorg. Chem.*, 2000, **39**, 2189.

3 G. Yang, H.-G. Zhu, B.-H. Liang and X.-M. Chen, *J. Chem. Soc., Dalton Trans.*, 2001, 580.

4 (*a*) M. Taniguchi, M. Shimoi and A. Ouchi, *Bull. Chem. Soc. Jpn.*, 1986, **59**, 2299; (*b*) A. Ouchi and M. Taniguchi, *Bull. Chem. Soc. Jpn.*, 1988, **61**, 3347; (*c*) H.-J. Chen. G. Yang and X.-M. Chen, *Acta Crystallogr., Sect. C*, 1999, **55**, 2012; (*d*) N. Mondal, M. K. Saha, S. Mitra and V. Gramlich, *J. Chem. Soc., Dalton Trans.*, 2000, 3218; (*e*) M. Kabešová, M. Dunaj-Jurco and J. Soldanova, *Inorg. Chim. Acta.*, 1987, **130**, 105; (*f*) C. A. White, G. P. A. Yap, N. P. Raju, J. E. Greedan and R. J. Crutchley, *Inorg. Chem.*, 1999, **38**, 2548; (*g*) T. K. Maji, I. R. Laskar, G. Mostafa, A. J. Welch, P. S. Mukherjee and N. R. Chaudhuri, *Polyhedron*, 2001, **20**, 651; (*h*) C.-X. Ren, H.-L. Zhu, G. Yang and X.-M. Chen, *J. Chem. Soc., Dalton Trans.*, 2001, 85.

5 (*a*) R. Robson, in *Comprehensive Supramolecular Chemistry*, ed. J. L. Atwood, J. E. D. Davies, D. D. MacNicol, F. Vögtle, F. Toda and R. Bishop, Pergamon, Oxford, 1996, vol. 6, ch. 22, pp. 733–755; (*b*) S. R. Batten and R. Robson, *Angew. Chem., Int. Ed.*, 1998, **37**, 1460 and references therein.

6 L. Tchertanov and C. Pasard, *Acta Crystallogr., Sect. B*, 1997, **53**, 904.

CHEMCOMM Communication
www.rsc.org/chemcomm

Unique formation of two different W/Ag/S clusters from the same components *via* a low heating temperature solid state reaction and a solution reaction and their third-order NLO properties in solution†

Hong Yu,[a] Qing-Feng Xu,[a] Zhen-Rong Sun,[b] Shun-Jin Ji,[a] Jin-Xiang Chen,[a] Quan Liu,[a] Jian-Ping Lang*[a] and Kazuyuki Tatsumi[c]

[a] *Suzhou University, Department of Chemistry and Chemical Engineering, 1 Shizi Street Suzhou 215006. Jiangsu, P. R. China. E-mail: jplang@suda.edu.cn*
[b] *Key Laboratory for Optical & Magnetic Resonance Spectroscopy, Department of Physics, East China Normal University, Shanghai 200062, P. R. China*
[c] *Research Center for Materials Science and Department of Chemistry, Graduate School of Science, Nagoya University, Furo-Cho, Chikusa-ku Nagoya 464-8602, Japan*

Received (in Cambridge, UK) 9th August 2001, Accepted 5th November 2001
First published as an Advance Article on the web 16th November 2001

Reaction of $(NH_4)_2[WS_4]$, $[Ag(MeCN)_4](PF_6)$ and dppm (molar ratio = 1:2:4) in the solid state at 110 °C followed by extraction with CH_2Cl_2 yielded a hexanuclear neutral cluster $[(WS_4)_2Ag_4(dppm)_3]$ 1, while the same materials when mixed directly in CH_2Cl_2 produced a tetranuclear cluster salt $[WS_4Ag_3(dppm)_4](PF_6)$ 2; both compounds showed modest third-order optical nonlinearities.

Over the last three decades, the chemistry of group 6 and 11 mixed-metal sulfide clusters has been attractive due to their potential applications in industrial catalytic systems, biochemical systems, and new materials.[1–9] Many of these clusters are usually synthesized from common solution reactions. However, some others could be prepared by a method denoted 'low heating temperature solid state reaction'.[9a] In this method, $(NH_4)_2[MS_4]$ (M = Mo, W) is allowed to react with copper(I) or sliver(I) salts and other organic ligands at low temperatures (~100 °C). The resulting solid state products are extracted using certain solvents (*e.g.* CH_2Cl_2) to isolate Mo(W)/Cu(Ag)/S clusters. However, this procedure always invoked a question whether the final products are really generated from the solid state reactions. The problem may be tackled by running reactions with the same components both in the solid state and in solution. So far, only a few reactions have been explored to yield positive results.[9b] Herein we report another example of the distinct formation of two W/Ag/S clusters, $[(WS_4)_2Ag_4(dppm)_3]$ (**1**) and $[WS_4Ag_3(dppm)_4](PF_6)$ (**2**), which were isolated from reactions of $(NH_4)_2[WS_4]$ with $[Ag(MeCN)_4](PF_6)$ and dppm in the solid state and in CH_2Cl_2, respectively, along with their crystal structures and third-order NLO properties in solution.

The solid state reaction of $(NH_4)_2[WS_4]$, $[Ag(MeCN)_4](PF_6)$ and dppm in the molar ratio of 1:2:4 was carried out in an open Pyrex tube at 110 °C. During these reactions, an argon stream was introduced in to the tube to remove the NH_3, H_2S and MeCN gases evolved. The reaction mixture gradually became partly molten and its brown yellow color deepened in 1 d. After it was cooled to room temperature, the sintered solid was extracted with CH_2Cl_2 and filtered. Layering Et_2O onto the filtrate led to the formation of the hexanuclear brown yellow cluster **1** in 22% yield.‡ As shown in Fig. 1, the structure of **1** consists of two WS_4Ag_2 cluster fragments and three dppm ligands.§ One dppm links Ag(1) and Ag(2) within a WS_4Ag_2 fragment while the other two interconnect Ag atoms between two WS_4Ag_2 fragments. Such a cluster framework is unprecedented in thiometallates. In the structures of the two WS_4Ag_2 fragments, each WS_4 unit acts as a tridentate ligand, coordinate two Ag atoms while one W=S unit remains intact. The average W–μ_2-S bond length is 0.06 Å longer than the W=S bond, but is 0.07 Å shorter than the W–μ_3-S bond. The two planar WS_2Ag rhombs in each cluster fragment are folded with a dihedral angle of 74–76°. The WS_4Ag_2 core structure is rare. There are only two examples with Cu found in $[WS_4Cu_2(dppm)_3]$[9b] and $[ReS_4(CuNCS)_2]^-$.[10] The Ag atoms of the two WS_4Ag_2 fragments show different coordination geometries. In the fragment containing W(1), each Ag adopts a distorted tetrahedral coordination geometry with two P (dppm), a μ_2-S and a μ_3-S atom. However, the two Ag atoms in the fragment containing W(2) are coordinated by a P (dppm), a μ_2-S and a μ_3-S atom to form an approximately trigonal planar geometry. Because of the different coordination geometries of the Ag atoms, the W(1)–Ag(1) and W(1)–Ag(2) distances in one fragment are slightly longer than those of the W(2)–Ag(3) and W(2)–Ag(4) bonds in the other fragment. The mean W–Ag length (3.0406 Å) of **1** is longer than that observed in $[(WS_4)_2Ag_4(PPh_3)_4]$.[11] The average Ag–S and Ag–P lengths in the fragment containing W(1) are 0.13 and 0.08 Å longer than those of the corresponding bonds in the fragment containing W(2).

On the other hand, upon stirring a mixture of $(NH_4)_2[WS_4]$, $[Ag(MeCN)_4](PF_6)$ and dppm (molar ratio = 1:2:4) in CH_2Cl_2

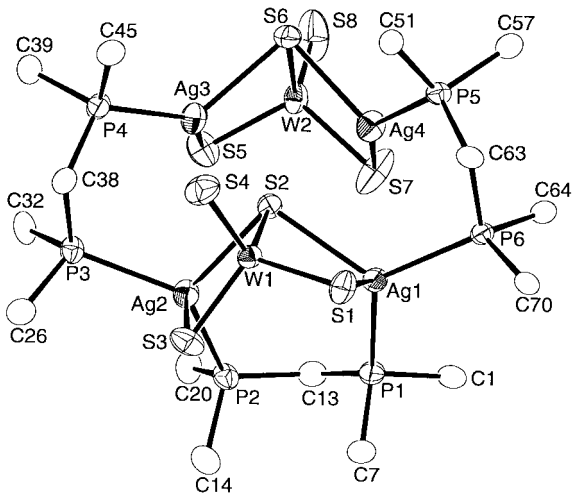

Fig. 1 Molecular structure of the neutral cluster **1**, with labelling scheme and 50% thermal ellipsoids. All phenyl groups are represented by their pivotal C atoms for clarity. Selected bond lengths (Å): W(1)–Ag(1) 3.1500(6), W(1)–Ag(2) 3.1179(5), W(2)–Ag(3) 2.9422(6), W(2)–Ag(4) 2.9523(5), W–S_t(av.) 2.136, W–μ_2-S(av.) 2.197, W–μ_3-S(av.) 2.264, Ag–S(av.) 2.595, Ag–S(av.) 2.438.

† Electronic supplementary information (ESI) available: experimental: general comments, synthesis of complexes, third-order NLO measurements, time response spectra. See http://www.rsc.org/suppdata/cc/b1/b107251j/

 DOI: 10.1039/b107251j

at room temperature for 1 d, there still remained some unreacted $(NH_4)_2[WS_4]$, which was filtered off. Concentration of the filtrate followed by layering with Et_2O on to the solution gave rise to a tetranuclear yellow complex **2** in 52% yield.‡ An X-ray analysis§ revealed that three Ag atoms of the $[WS_4Ag_3(dppm)_4]^+$ cation of **2** are bound to a tetrahedral WS_4 unit at three S–S edges (Fig. 2). The resulting WAg_3 skeleton is approximately T-shaped with an Ag(2)–W–Ag(3) angle of 159.90(2)°. Although such a WS_4Ag_3 core structure has not been observed previously, it is similar to those of analogous Cu clusters such as $[WS_4Cu_3(dppm)_2Br_2]$[9b] and $[WS_4(CuNCS)_3]^{2-}$.[12] In the structure of $[WS_4Ag_3(dppm)_4]^+$, the two of the four S atoms are doubly bridging, and the other two are triply bridging. Two of the four dppm ligands are bidentate while the other two are monodentate. The η^1-coordination of dppm is not especially rare, and is found in some dppm-containing complexes.[9b,13] The average W–Ag (3.0873 Å), Ag–S (2.625 Å) and Ag–P (2.281 Å) bond distances are close to those of the corresponding bonds of **1**.

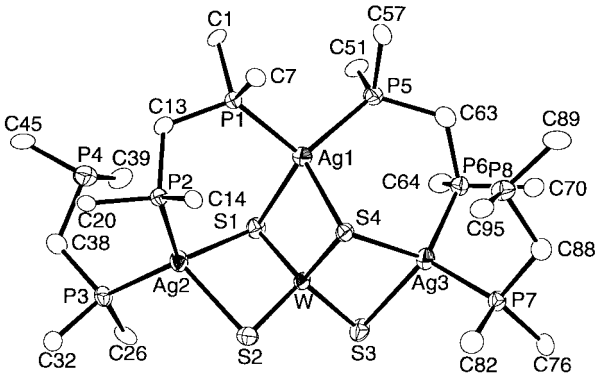

Fig. 2 Structure and labelling of the cluster cation of **2**. Thermal ellipsoids are drawn at the 50% probability level. All phenyl groups are represented by their pivotal C atoms for clarity. Selected bond lengths (Å) and angles (°): W–Ag(av.) 3.0873, W–μ_2-S(av.) 2.188, W–μ_3-S(av.) 2.233, Ag–S(av.) 2.625, Ag–S(av.) 2.281; Ag(2)–W–Ag(3) 159.90(2).

A preliminary study on the third-order NLO properties of **1** and **2** was carried out by a three-dimensional degenerate four-wave mixing (3D DFWM) technique, using a pulsed laser beam (λ = 532 nm) from a frequncy-doubled picosecond pulse mode-locked Nd:YAG laser. The third-order NLO susceptibility $\chi^{(3)}$ was obtained by comparing the measured signals for solutions of **1** and **2** with that for CS_2 as a reference, under the same experimental conditions. The $\chi^{(3)}$ values for **1** (1.0×10^{-3} M) in $CHCl_3$ and **2** (1.0×10^{-3} M) in MeCN, are 2.259×10^{-14} and 5.611×10^{-15} esu, respectively. Although these low concentration solution $\chi^{(3)}$ values are not larger than that reported for $[MoOS_3(CuNCS)_3]^{2-}$,[14] it is expected that higher $\chi^{(3)}$ values could be attained if the clusters could be deposited as thin films *via* CVD techniques. Research into this aspect is currently under way.

This work is supported by the Key Laboratory of Organic Chemistry of Jiangsu Province at Suzhou University.

Notes and references

‡ Satisfactory characterisation data have been obtained for compounds **1** and **2**.

§ *Crystal data*: for **1**·CH_2Cl_2: $C_{76}H_{68}Ag_4Cl_2P_6S_8W_2$, M = 2293.77, triclinic, space group $P\bar{1}$, a = 11.7123(8), b = 14.328(2), c = 25.193(2) Å, α = 90.615(3), β = 90.8288(9), γ = 105.6047(6)°, U = 4070.9(6) Å^3, T = 193 K, Z = 2, μ(Mo-Kα) = 4.19 mm^{-1}, 18404 reflections measured, 18386 unique which were used in all calculations. The final R values are R = 0.041, R_w = 0.056 ($I > 1.0\sigma(I)$). For **2**·$2C_6H_6$·Et_2O: $C_{116}H_{110}Ag_3F_6OP_9S_4W$, M = 2548.59, triclinic, space group $P\bar{1}$, a = 12.699(1), b = 21.258(2), c = 21.340(2) Å, α = 82.731(4), β = 76.2750(6), γ = 86.250(1)°, U = 5547.8(8) Å^3, T = 193 K, Z = 2, μ(Mo-Kα) = 1.82 mm^{-1}, 24943 reflections measured, 24049 unique which were used in all calculations was observed. The final R values are R = 0.060, R_w = 0.071 ($I > 1.0\sigma(I)$). The structures were solved by direct methods (**1**) and heavy-atom Patterson methods (**2**), and expanded using Fourier techniques. All non-hydrogen atoms (except those of CH_2Cl_2 in **1**, and those of F atoms, C_6H_6 and Et_2O molecules in **2**) were refined anisotropically. All hydrogen atoms except those on Et_2O were placed on calculated positions (C–H = 0.97 Å) and refined isotropically. In the case of **2**, the relatively high thermal parameters of the F atoms of the PF_6^- anion indicated signs of disorder. However attempts to refine this disorder failed to improve the R values. CCDC reference numbers 169233 and 169234. See http://www.rsc.org/suppdata/cc/b1/b107251j/ for crystallographic data in CIF or other electronic format.

1 A. Müller, E. Diemann, R. Jostes and H. Bögge, *Angew. Chem., Int. Ed. Engl.*, 1981, **20**, 934.
2 *Molybdenum Enzymes, Cofactors and Model Systems*, ed. E. I. Stiefel, D. Coucouvanis and W. E. Newton, ACS Symposium Series 535, American Chemical Society, Washington DC, 1993.
3 Y. Jeannin, F. Sécheresse, S. Bernes and F. Robert, *Inorg. Chim. Acta*, 1992, **198–200**, 49.
4 C. D. Scattergood, P. G. Bonney, J. M. Slater, C. D. Garner and W. Clegg, *J. Chem. Soc., Chem. Commun.*, 1987, 1749.
5 R. Hernandez-Molina and A. G. Sykes, *J. Chem. Soc., Dalton Trans.*, 1999, 3137.
6 M. D. Curtis, *Appl. Organomet. Chem.*, 1992, **6**, 429.
7 X.-T. Wu, P.-C. Chen, S.-W. Du, N.-Y. Zhu and J.-X. Lu, *J. Cluster Sci.*, 1994, **5**, 265.
8 S. Shi, W. Ji, S. H. Tang, J. –P. Lang and X. –Q. Xin, *J. Am. Chem. Soc.*, 1994, **116**, 3615.
9 (*a*) J.-P. Lang and X.-Q. Xin, *J. Solid State Chem.*, 1994, **108**, 118; (*b*) J.-P. Lang and K. Tatsumi, *Inorg. Chem.*, 1998, **37**, 6308.
10 A. Müller, E. Krickemeyer, A. Hildebrand, H. Bögge, K. Schneider and M. Lemke, *J. Chem. Soc., Chem. Commun.*, 1991, 1685.
11 A. Müller, H. Bögge and E. Koniger-Ahlborn, *J. Chem. Soc., Chem. Commun.*, 1978, 739.
12 J. M. Manoli, C. Potvin, F. Sécheresse and S. Marzark, *Inorg. Chim. Acta*, 1988, **150**, 257.
13 J. C. Fettinger, S. P. Mattamana, R. Poli and R. D. Rogers, *Organometallics*, 1996, **15**, 4211.
14 S. Shi, W. Ji, W. Xie, T.-C. Chong, H.-C. Zeng, J.-P. Lang and X.-Q. Xin, *Mater. Chem. Phys.*, 1995, **39**, 298.

CHEMCOMM Communication
www.rsc.org/chemcomm

Sonochemical synthesis of titania whiskers and nanotubes

Yingchun Zhu,[a] Hongliang Li,[a] Yuri Koltypin,[a] Yaron Rosenfeld Hacohen[b] and Aharon Gedanken*[a]

[a] *Department of Chemistry, Bar-Ilan University, Ramat-Gan 52900, Israel. E-mail: gedanken@mail.biu.ac.il*
[b] *Department of Materials and Interfaces, Weizmann Institute of Science, Rehovot 76100, Israel*

Received (in Cambridge, UK) 3rd October 2001, Accepted 30th October 2001
First published as an Advance Article on the web 30th November 2001

A process has been developed for the formation of titania whiskers and nanotubes with the assistance of sonication; titanate whiskers are obtained as a slender sheet with a length of about 1 μm and a width of 60 nm; arrays of titania whiskers with a diameter of 5 nm are prepared from the titanate whiskers; titania nanotubes with a diameter of about 5 nm, and a length of 200–300 nm are also synthesized.

Nanostructured materials have received much attention because of their novel properties which differ from those of bulk materials. Recently, there has been great interest in controlling the shapes of materials and in finding novel properties. One-dimensional (1D) materials are an important category of nanostructured materials and have been widely researched yielding various special structures such as nanotubes, nanorods, nanowires and nanobelts *etc*.[1–5] The materials in nanotube form include carbon, NbS_2, TaS_2, NB, MoS_2, SiO_2, Al_2O_3, MoO_3, WO_3, ZrO_2 and TiO_2. Many other materials can be prepared in the form of rods or wires such as MgO, Fe_2O_3, CaO, MgO, ZnO, GaN and CdSe, of which titania is one of the most extensively researched materials.

Titania, as a semiconductor, shows high photocatalytic activity and is widely used as a catalyst and carrier of catalysts.[6] In addition, titania finds applications in the fields of sensors, new types of solar cells, electrochromic devices, and antifogging and self-cleaning devices.[7–9] The performance of titania in its various applications depends on its crystalline phase state, dimensions and morphology.[10] Many attempts have been made to control the structure of titania. The methods to prepare 1D-structured titania include mainly template synthesis,[11,12] supramolecular assembles,[13] hydrothermal synthesis[14] and inductive synthesis.[15]

In the current paper, both titania whiskers and nanotubes have been synthesized by sonicating titania particles in NaOH aqueous solution followed by washing with deionized water and dilute HNO_3 aqueous solution. This process is more convenient than template methods in which special templates are required which then have to be removed. In addition, the products obtained using template and supramolecular assembly methods have thick walls (40–150 nm) and large diameters (150–600 nm), while the nanotubes obtained in our process have a diameter of 5 nm and a wall thickness of *ca.* 1.3 nm. As is well known, small dimensions are very important for nanostructured materials. Hydrothermal methods can prepare nanotubes with thin walls and small diameters, but take a long time to do so. The current process can prepare titanate whiskers that are an important precursor for other titanates[16] and titania whiskers are obtained from the titanate. Particularly, this process can shape the products as whiskers or nanotubes, or a mixture of whiskers and nanotubes by controlling the operation process. The samples are characterized by X-ray diffraction (XRD) using Co-Kα radiation, transmission electron microscopy (TEM), high-resolution transmission electron microscopy (HRTEM), and energy-dispersive X-ray spectra (EDS).

The precursors for the preparation of titania whiskers and nonotubes are titania particles with an average diameter of about 20 nm, which are prepared by the hydrolysis of titanium butoxide and heat-treatment at 650 °C for 1 h. The X-ray diffraction analysis in Fig. 1(a) shows that the raw titania powder is a mixture of 17% anatase and 83% rutile, estimated according to the formula $X_A = [1 + 1.26\ (I_R/I_A)]^{-1}$.[17]

In a typical synthesis, 150 mg titania powder with diameter 20 nm and 30 mL of 10 M NaOH aqueous solution were placed in a Teflon vessel. The mixture was sonicated by the direct immersion of a 560 W titanium horn for 80 min to prepare titania whiskers. The temperature during sonolysis was about 80 °C. The precipitate was washed with 0.1 M HNO_3 aqueous solution and deionized water. To prepare titania tubes, the mixture was sonicated at 280 W for 60 min. The sonicated solution in the teflon vessel was then placed in an oil-bath and maintained at 110 °C for 4 h. The precipitate was separated by centrifugation and washed with a 0.1 M HNO_3 aqueous solution and deionized water. The product was further dried under vacuum for 12 h.

Fig. 2(a) shows TEM images of the as-prepared whiskers, which are obtained by washing the sonication product with 0.1 M HNO_3 aqueous solution for 2 h and deionized water for 6 h. The as-prepared product has a slender sheet structure with a length of about 1 μm and a width of 60 nm. HRTEM analysis shows that the product has a layered crystal structure. The stoichiometry of the product is estimated to be $H_3Ti_3O_{7.5}$ according to elemental analysis. The IR spectrum shows a stretching vibration of O–H around 3400 cm^{-1} and a bending vibration of H–O–H around 1630 cm^{-1}, which imply the presence of water. The total weight loss from TGA agrees well with the estimated stoichiometry but the weight loss steps are not very well resolved. XRD analysis [Fig. 1(c)] shows broad reflections at 7.64, 5.43, 3.50, 3.02, 2.56, 2.23 and 1.86 Å. The diffraction pattern is close to that of $H_2Ti_3O_7$.[16] The product may be assigned as $H_2Ti_3O_7{\cdot}0.5H_2O$ according to the foregoing results. When the product is further washed with water for 8 h, arrays of whiskers with a diameter of 5 nm are obtained as

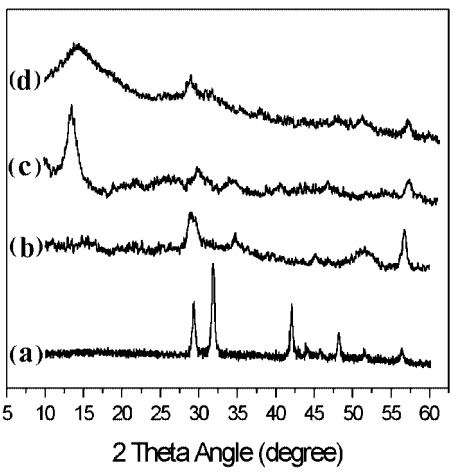

Fig. 1 XRD patterns of as-prepared samples: (a) titania particles, (b) titania whiskers, (c) $H_2Ti_8O_{17}$ whiskers, (d) nanotubes.

 DOI: 10.1039/b108968b

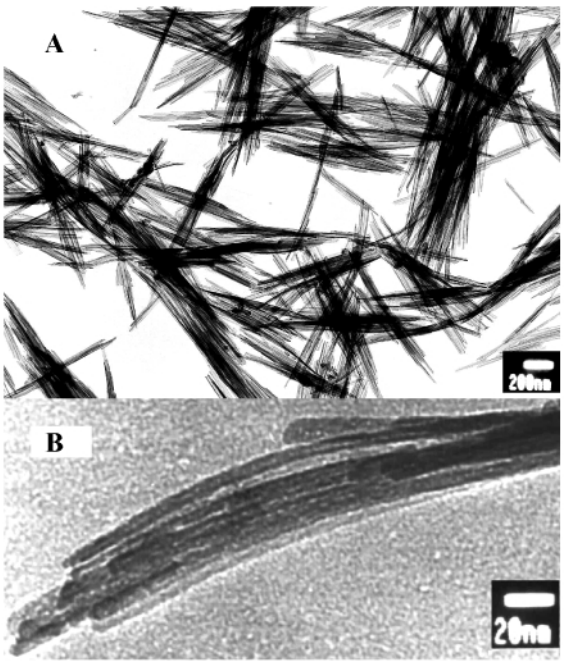

Fig. 2 TEM images of (a) titanate and (b) TiO_2 whiskers.

shown in Fig. 2(b). XRD analysis [Fig. 1(b)] shows that the product is TiO_2 (B) as discovered by Marchand *et al.*[18]

The powders shown in Fig. 3(a) are prepared by sonicating the mixture for 60 min, heat-treating it at 110 °C for 4 h and then washing the product with 0.1 M HNO_3 aqueous solution for 2 h and deionized water for 14 h. The products contain open-ended tubular structures with a diameter of about 5 nm and a length between 200 and 300 nm. XRD analyses show that the phase of the nanotubes is intermediate between $H_2Ti_3O_7{\cdot}0.5H_2O$ and TiO_2 (B). The energy-dispersive X-ray spectra (EDS) indicate that the sample consists of Ti and O in a ratio of 1 : 2 and that Na is absent from the sample.

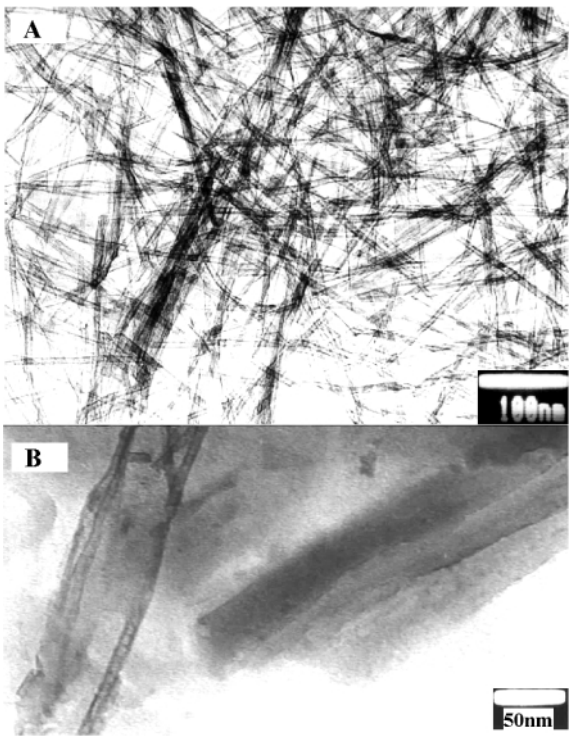

Fig. 3 TEM images of (a) titania nanotubes, (b) powders obtained by heat-treating sonicated products for 4 h at 110 °C followed by washing with water for 5 min.

The processes of formation of titania whiskers and tubes are proposed as follows. When the raw material of titania particles reacts with the NaOH aqueous solution under sonication, some of the Ti–O–Ti bonds are broken and layered titanates are formed, in which titanium–oxygen octahedra form layered lattices and the interlayered regions are occupied by alkali metal ions.[19] When the titanates react with 0.1 M HNO_3 aqueous solution and deionized water, ion exchange and dehydration reactions take place, leading to the formation of the compound $H_2Ti_3O_7{\cdot}0.5H_2O$ as shown in Fig. 1(c).[16] When the products are further dehydrated, titania is formed as proved in Fig. 1(b).[18] The role of sonication is not only to accelerate the reaction between the raw material and the NaOH aqueous solution but also leads to the oriented growth of titanate due to the extreme conditions.[20] It is found that no titanate whiskers can be obtained without sonication.

When the raw material of titania particles is sonicated with the NaOH aqueous solution under conditions of low power, thin small titanate sheets are formed. When the products are heated at 110 °C for 4 h, the small titanate sheets increase in size. The titanate sheets are exfoliated into nanosheets and the nanosheets roll into nanotubes when they are washed with water. The layered structure of the titanate sheets and nanotubes formed at the edge of the sheet are shown in Fig. 3(b). It is assumed that residual electrostatic repulsion due to Ti–O–Na bonds may lead to connection between the ends of the sheets and thus to the formation of a tube structure.[14] The process takes a shorter reaction time and produces longer nanotubes compared to the hydrothermal method for which 20 h are required to prepare titania nanotubes.

Preliminary results show that an effective process has been developed for the preparation of titania whiskers and nanotubes with the assistance of sonication. Further study is being performed to clarify the effect of different experimental parameters on the formation of titania whiskers and nanotubes.

Y. Z. thanks the Fred and Barbara Kort Sino–Israel Postdoctoral Fellowship Foundation for financial support and the China Scholarship Council for its support. A. G. thanks the German Ministry of Science for the support of this work through the Deutsche–Israeli DIP program.

Notes and references

1 S. Iijima and T. Ichihashi, *Nature*, 1993, **363**, 603.
2 P. M. Ajayan, O. Stephan, P. Redlich and C. Colliex, *Nature*, 1995, **375**, 564.
3 O. A. Nerushev, M. Sveningsson, L. K. L. Falk and F. Rohmund, *J. Mater. Chem.*, 2001, **11**, 1122.
4 L. Dloczik, R. Engelhardt, K. Ernst, S. Fiechter, I. Sieber and R. Konenkamp, *Appl. Phys. Lett.*, 2001, **78**, 3687.
5 Z. W Pan, Z. R. Dai and Z. L. Wang, *Science*, 2001, **291**, 1947.
6 A Fujishima and K. Honda, *Nature*, 1972, **37**, 238.
7 M. Gratzel, *Nature*, 1991, **353**, 737.
8 G. Hodes, I. D. J. Howell and L. M. Peter, *J. Electrochem. Soc.*, 1993, **139**, 3136.
9 R. Wang, K. Hashimoto and A. Fujishima, *Nature*, 1997, **388**, 431.
10 A. Narayanasamy, V. A. Maroni and R. W. Siegel, *J. Mater. Res.*, 1989, **4**, 1246.
11 P. Hoyer, *Langmuir*, 1996, **12**, 1411.
12 B. B. Lakshmi, P. K. Dorhout and C. R. Martin, *Chem. Mater.*, 1997, **9**, 857.
13 S. Kobayashi, K. Hanabusa, N. Hamasaki, M. Kimura, H. Shirai and S. Shinkai, *Chem. Mater.*, 2000, **12**, 1523.
14 T. Kasuga, M. Hiramatsu, A. Hoson, T. Sekino and K. Niihara, *Adv. Mater.*, 1999, **11**, 1307.
15 Y. C. Zhu and C. X. Ding, *Nanostruct. Mater.*, 1999, **11**, 427.
16 H. Izawa, S. Kikkawa and M. Koizumi, *J. Phys. Chem.*, 1982, **86**, 5023.
17 R. A. Spurr and H. Myers, *Anal. Chem.*, 1957, **29**, 760.
18 R. Marchand, L. Brohan and M. Tournoux, *Mater. Res. Bull.*, 1980, **15**, 1129.
19 S. Andersson and A. D. Wadsley, *Acta Crystallogr.*, 1961, **14**, 1245.
20 K. S. Suslick, S. B. Choe, A. A. Cichowlas and M. W. Grinstaff, *Nature*, 1991, **353**, 414.

CHEMCOMM Communication
www.rsc.org/chemcomm

A flexible access to highly functionalised boronates

Heraclio Lopez-Ruiz and Samir Z. Zard*

Laboratoire de Synthèse Organique associé au CNRS, Ecole Polytechnique, 91128 Palaiseau, France. E-mail: zard@poly.polytechnique.fr; Fax: +33 (0)1 6933 3851; Tel: +33 (0)1 6933 4872

Received (in Cambridge, UK) 23rd October 2001, Accepted 6th November 2001
First published as an Advance Article on the web 30th November 2001

The radical addition of various xanthates to allyl or vinyl boronates occurs smoothly in the presence of a small amount of lauroyl peroxide as initiator to give good yields of usefully functionalised boronates.

The emergence of the poweful palladium induced coupling of boronates with halides, the Suzuki–Miyaura reaction, has caused a renewed interest in the chemistry of boronic acid derivatives.[1] Access to boronates has so far relied heavily on ionic and organometallic processes, with radical reactions playing only a very minor part.[2] The Kharasch addition of halides to vinyl boronates was reported by Matteson some years ago and has been used occasionally since.[3] In one, more recent work, simple radicals generated using stannane chemistry or through the Barton decarboxylation were found to add to vinyl boronates.[4] Ring-closures of radicals α-to the boron atom have also been described.[5] Recent theoretical studies seem to indicate that boronates have a much lower stabilising influence on an adjacent radical, in comparison to boron groups with less donating substituents.[6] In the present communication, we describe a flexible approach to functionalised boronates by application of the xanthate transfer radical addition[7] to both allyl and vinyl boronates.

The radical addition sequence is summarised in Scheme 1 for the case of allyl boronate **2**. Thus, radical **R**·, generated from xanthate **1** by the action of the initiator, undergoes addition to the least hindered end of the terminal olefin to give a new radical **3**, which then engages in a reversible addition–fragmentation process leading to adduct **4** with the concomitant regeneration of radical **R**· to propagate the chain. Addition to the unactivated olefinic bond is possible because **R**· is *not* competitively consumed by reaction with xanthate **1** (this reaction is both reversible and degenerate) and its effective lifetime in the medium is therefore significantly increased. Fragmentation of intermediate adduct radical **3** to give olefin **5** and high energy boryl radical **6** did not seem likely in the light of a recent ESR study of radicals adjacent to boronates.[6]

Indeed, when a small amount of lauroyl peroxide was added portion-wise to a refluxing, concentrated solution of xanthate **1a** (1 M) and a 1.5 to 2-fold excess of allyl boronate **2** in 1,2-dichloroethane, a smooth reaction occured to produce adduct **4a** in high yield (Table 1).† The same transformation could be accomplished with a number of other xanthates containing various functional groups, including ketones, esters, nitriles, and even heterocyclic rings, as shown by the varied examples compiled in the Table 1. The yields have not been optimised but nevertheless are generally quite good.

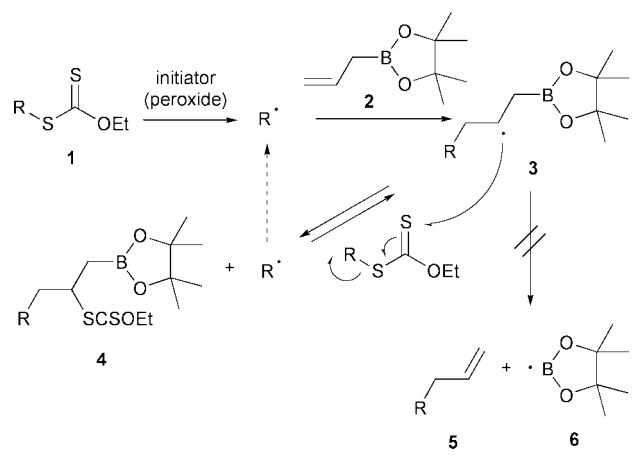

Scheme 1

The xanthate group in the adduct can be efficiently reduced off either by treatment with a stoichiometric amount of lauroyl peroxide in isopropanol,[8] as illustrated by the conversion of **4e** into **7e**, or by using the more traditional tributyltin hydride as in the reduction of **4a** into **7a** (Scheme 2). The former, tin-free procedure is more convenient for large scale work or for producing samples destined for biological testing. The presence of the xanthate group can alternatively be exploited to create another carbon–carbon bond, for example through a ring closure onto an aromatic ring.[9] For instance, addition over a period of one hour of a stoichiometric quantity of lauroyl peroxide to a refluxing solution of adducts **4a** or **4b** in chlorobenzene resulted in the formation of tetralones **8a** and **8b** in 35 and 42% yield respectively.

Finally, by performing the first radical addition on a vinyl boronate such as **9**, the relative position of the various functions present in the initial xanthate with respect to the boronate group can be easily and conveniently modified. The synthesis of compounds **10a** and **10b** (Scheme 3) provides two examples where the xanthate and the boronate groups are now in a geminal disposition.

Table 1 Synthesis of boronates **4**

Xanthate **1**	Boronate **4**	Yield (%)
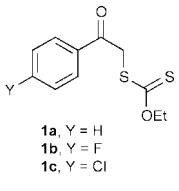 **1a**, Y = H **1b**, Y = F **1c**, Y = Cl	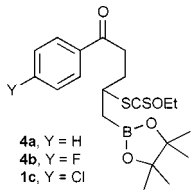 **4a**, Y = H **4b**, Y = F **1c**, Y = Cl	**4a** (94) **4b** (78) **4c** (78)
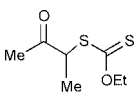 **1d**	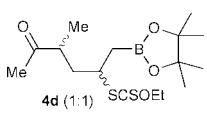 **4d** (1:1)	(63)
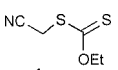 **1e**	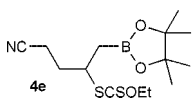 **4e**	(85)
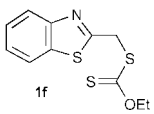 **1f**	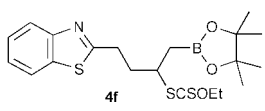 **4f**	(68)
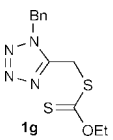 **1g**	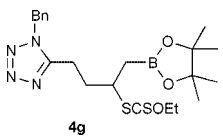 **4g**	(70)

 DOI: 10.1039/b109637k

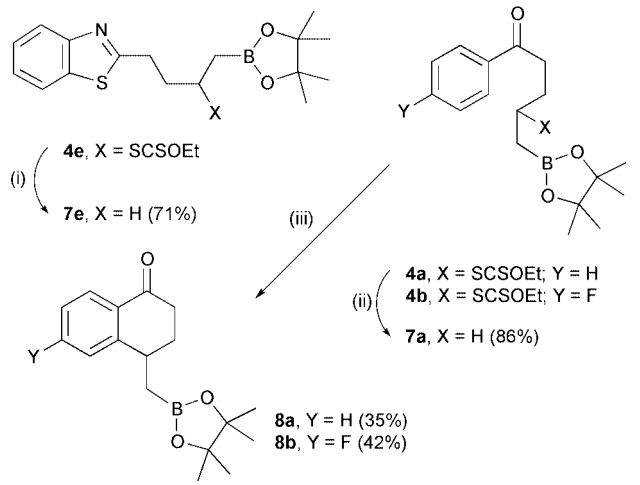

Scheme 2 *Reagents*: (i) lauroyl peroxide (100–110 mol%) propan-2-ol, reflux; (ii) Bu_3SnH, toluene, reflux; (iii) lauroyl peroxide (100–110 mol%), chlorobenzene, reflux.

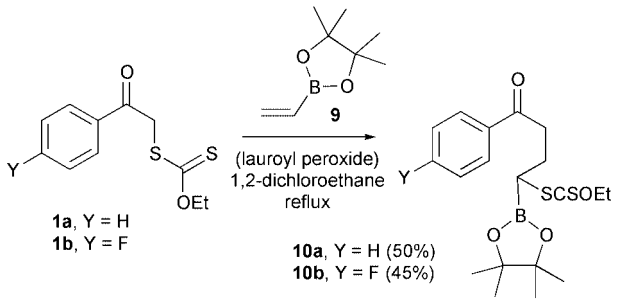

Scheme 3

The present approach to boronates is simple, yet efficient and flexible. A broad variety of densely functionalised, otherwise inaccessible boronates can be rapidly prepared using cheap and readily available starting materials and reagents.

Notes and references

† *General procedure for the radical addition to allyl and vinyl boronates* **2** *and* **9**. A solution of xanthate **1** (1 mmol) and ally or vinyl boronate **2** or **9** (1.5 mmol) in 1,2-dichloroethane (*ca.* 1 mL) was heated to reflux for 15 min. Lauroyl peroxide (10 mmol%) was then added every 1 h until almost complete consumption of the xanthate. The solvent was removed under reduced pressure and the residue purified by chromatography on silica to give the corresponding adduct **4** or **10**.

Representative spectral and analytical data. (**4a**): ^{1}H NMR (300 MHz, $CDCl_3$): 7.95 (d, J = 6.6 Hz, 2H, H arom), 7.52 (m, 1H, H arom), 7.45 (m, 2H, H arom), 4.62 (m, 2H, OCH_2CH_3), 4.03 (m, 1H, CHS), 3.13 (m, 2H, CH_2CH_2), 2.27–2.10 (m, 2H, CH_2CH_2), 1.39 (t, J = 7.2 Hz, 3H, OCH_2CH_3), 1.37 (d, J = 8.1 Hz, 2H, CH_2B), 1.24 (12H, $4CH_3$). ^{13}C NMR (75 MHz, $CDCl_3$): 214.3, 199.4, 136.9, 133.1, 128.6, 128.2, 83.7, 69.7, 47.5, 36.2, 30.7, 24.9, 13.8. IR (cm^{-1}) ν: 1686 (C=O). Anal. Calc. for $C_{20}H_{29}BO_4S_2$: C, 58.82; H, 7.16. Found: C, 58.85, H, 7.16%.

(**4e**): ^{1}H NMR (300 MHz, $CDCl_3$): 4.67 (q, J = 7.2 Hz, 2H, OCH_2CH_3), 3.99 (m, 1H, CHS), 2.18 (t, J = 7.6 Hz, 2H, $NCCH_2$), 2.12 (m, 2H, $NCCH_2CH_2$), 1.43 (t, J = 7.2 Hz, 3H, OCH_2CH_3), 1.32 (d, J = 7.5 Hz, 2H, CH_2B), 1.25 (bs, 12H, $4CH_3$). ^{13}C NMR (75 MHz, $CDCl_3$): 188.0, 119.4, 83.9, 70.1, 46.4, 32.2, 24.8, 15.1, 13.8. IR (cm^{-1}) ν: 2247. Anal. Calc. for $C_{14}H_{24}BNO_3S_2$: C, 51.07; H, 7.35. Found: C, 51.33, H, 7.47%.

(**10b**): ^{1}H NMR (300 MHz, $CDCl_3$): 7.95-8.10 (m, 2H, H arom), 7.1–7.25 (m, 2H, H arom), 4.55–4.70 (3H, OCH_2CH_3, CHS), 3.18, (t, J = 6.0 Hz, 2H, CH_2CH_2), 2.15–2.37 (m, 2H, CH_2CH_2), 1.4 (t, J = 7.5 Hz, 3H, OCH_2CH_3), 1.28 (bs, 12H, $4CH_3$). ^{13}C NMR (75 MHz, $CDCl_3$): 199.5, 179.3, 136.9, 133.1, 128.6, 128.1, 84.4, 70.13, 37.3, 29.6, 24.9, 14.18. IR (cm^{-1}) ν: 1684, 1598, 1226, 1050. Anal. Calc. for $C_{19}H_{26}BFO_4S_2$: C, 55.34; H, 6.36. Found: C, 55.83, H, 6.07.

(**7e**) A solution of xanthate adduct **4e** (0.23 mmol) in propan-2-ol (1 mL) was heated to reflux for 15 min. Lauroyl peroxide (10 mol%) was then added every 1 h until almost complete consumption of the xanthate (100–110 mol%). The solvent was removed under reduced pressure and the product isolated by chromatography over silica gel with heptane–ethyl acetate (9 : 1). ^{1}H NMR (300 MHz, $CDCl_3$): 7.97 (d, J = 7.2 Hz, 1H, H arom), 7.82 (d, J = 8.1 Hz, 1H, H arom), 7.47 (m, 1H, H arom), 7.33 (m, 1H, H arom), 3.12 (t, J = 7.5 Hz, 2H, CH_2), 1.80 (m, 2H, CH_2), 1.63 (m, 2H, BCH_2), 1.26 (s, 12H, CH_3) 0.90 (m, 2H, CH_2). ^{13}C NMR (75 MHz, $CDCl_3$): 179.0,172.7, 153.0, 125.8, 124.6, 122.4, 121.4, 83.0, 34.1, 31.9, 29.6, 24.8. Anal. Calc. for $C_{17}H_{24}BNO_2S$: C, 64.36; H, 7.63. Found: C, 64.35, H, 8.21%.

1 (*a*) N. Miyaura and A. Suzuki, *Chem. Rev.*, 1995, **95**, 2457; (*b*) A. Suzuki, *J. Organomet. Chem.*, 1999, **576**, 147.

2 (*a*) D. S. Matteson, *Stereodirected Synthesis with Organoboranes*, Springer, Berlin, 1995; (*b*) D. S. Matteson, *J. Organomet. Chem.*, 1999, **581**, 51; M. Nakamura, K. Hara, T. Hatakeyama and E. Nakamura, *Org. Lett.*, 2001, **3**, 3137 and references there cited.

3 (*a*) D. S. Matteson, *J. Am. Chem. Soc.*, 1959, **81**, 5004; D. S. Matteson, *J. Am. Chem. Soc.*, 1960, **82**, 4228; (*b*) D. S. Matteson and J. D. Liedtke, *J. Org. Chem.*, 1963, **28**, 1924; (*c*) M. Vaultier, A. El Louzi, S. Lafquih-Titouani and M. Soufiaoui, *Synlett*, 1991, 267; N. Guennouni, C. Rasset-Deloge, B. Carboni and M. Vaultier, *Synlett*, 1992, 581; (*d*) F. Lhermite and B. Carboni, *Synlett*, 1996, 377.

4 N. Guennouni, F. Lhermite, S. Cochard and B. Carboni, *Tetrahedron*, 1995, **51**, 6999.

5 (*a*) R. A. Batey, B. Pedram, K. Yong and G. Baquer, *Tetrahedron Lett.*, 1996, **37**, 6847; (*b*) R. A. Batey and D. V. Smil, *Angew. Chem., Int. Ed.*, 1999, **38**, 1798.

6 J. C. Walton, A. J. McCarroll, Q. Chen, B. Carboni and R. Nziengui, *J. Am. Chem. Soc.*, 2000, **122**, 5455 and references there cited.

7 (*a*) S. Z. Zard, *Angew. Chem., Int. Ed. Eng.*, 1997, **36**, 672; (*b*) B. Quiclet-Sire and S. Z. Zard, *Phosphorus, Sulfur Silicon*, 1999, **153–154**, 137.

8 A. Liard, B. Quiclet-Sire and S. Z. Zard, *Tetrahedron Lett.*, 1996, **37**, 5877.

9 A. Liard, B. Quiclet-Sire, R. N. Saicic and S. Z. Zard, *Tetrahedron Lett.*, 1997, **38**, 1759.

CHEMCOMM Communication
www.rsc.org/chemcomm

Carbamate synthesis by solid-base catalyzed reaction of disubstituted ureas and carbonates

Sunil P. Gupte, Anand B. Shivarkar and Raghunath V. Chaudhari*

Homogeneous Catalysis Division, National Chemical Laboratory, Pune-411008, India.
E-mail: rvc@ems.ncl.res.in

Received (in Cambridge, UK) 5th September 2001, Accepted 31st October 2001
First published as an Advance Article on the web 3rd December 2001

A simple and efficient methodology to prepare carbamates has been demonstrated for the first time from symmetrical ureas and organic carbonates in the presence of solid base catalysts.

Carbamates are compounds of growing interest because of their applications in the agrochemicals industry as herbicides, fungicides and pesticides, in the pharmaceuticals industry as drug intermediates and in the polymer industry, in the synthesis of polyurethane. The commercial production of urethane is almost exclusively based on phosgene technology, however, due to worldwide awareness of pollution hazards of phosgene and pollution prevention laws adopted by Governmental agencies it is most essential to substitute it by environmentally benign routes. Efforts have continuously been made for the replacement of the phosgene route with routes such as reductive carbonylation of nitro aromatics and oxidative carbonylation of amines which have shown some promise. However, the former route will suffer from a lack of economical viability in the near future[1] while the latter suffers from hazards in handling of carbon monoxide and oxygen under high pressures. Carbamate synthesis has also been accomplished by several-pot reaction methods such as Hofmann rearrangement from amides,[2] by reaction of chloroformates and amines catalyzed by zinc,[3] and from alcohols to unsubstituted carbamates by treatment with trichloroacetyl isocyanate, followed by hydrolysis on Al_2O_3.[4] Recently, the use of carbon dioxide to replace phosgene has been attracting attention of research workers mainly due to its non-hazardous nature and safety in handling under pressure. Usually powerful organic bases[5] (*e.g.* *N*-cyclohexyl-*N*′,*N*′,*N*″,*N*″-tetramethylguanidine *etc*.) or additives such as crown ethers[6] are required to stabilize carbamate anion generated during amine and CO_2 reaction. This difficulty was partly overcome by using tetraethylammonium hydrogen carbonates (TEAHC),[7] and a combination of potassium carbonate and onium salts[8] as catalysts for the synthesis of carbamates from alkyl halides and amines. However, these methods at present are not attractive for bulk production of carbamates as they utilize only stoichiometric quantities of reagents and generate salts as by-products, which are not easy to dispose.

Recently, two industrially very important methods have been reported for the synthesis of carbamates *viz*., alcoholysis of ureas[9] and carboxylation of amines.[10] We were interested in developing methods for the synthesis of carbamates utilizing solid catalysts, as they are industrially important due to their potential in replacing conventional acid/base catalysts. The use of solid acid/base catalysts for synthesizing organic intermediates and fine chemicals is gaining increasing awareness and is a field of intense research activity.[11] While, working on reactions of alcoholysis of urea (i) and carboxylation of amines (ii) to carbamic acid esters (Scheme 1), we realized that, reactions (i) and (ii) both show poor atom economy and in each case alcohol or amine is produced as a byproduct reducing the functional group efficiency of the reagent. One way of improving the atom economy in reactions (i) and (ii) is to eliminate the use of alcohols and amines. Therefore, we were interested in effecting the conversion of disubstituted ureas and carbonates to carbamates utilizing the total functionality of both the urea and the carbonate. In this communication, we report for the first time, a new methodology for the synthesis of carbamates from substituted ureas and organic carbonates using a highly efficient and simple catalyst system [Scheme 1, eqn. (iii)].† This novel protocol has 100% atom economy while using an environmentally benign reactant source.

Surprisingly, the reaction between aromatic ureas and carbonates has not been studied[12] previously. A non-catalytic reaction between *N*,*N*′-diphenylurea and diphenyl carbonate gave only traces of *N*-phenyl phenyl carbamate after 24 h at 150 °C (see Table 1, entry 1). During the course of our investigations for screening of catalysts it was observed that basic catalysts such as triphenyl phosphine, sodium phenolate *etc*. were more effective than classical acid catalysts such as Lewis acids ($FeCl_3$, $AlCl_3$ *etc*.) and solid acid catalysts such as acidic Al_2O_3 (entry 4). However, heterogeneous basic catalysts *e.g*. Mg–Al hydrotalcite, Li–MgO, $PbZrO_3$, the Na form of zeolite ZSM-5 and amorphous catalyst grade silica gel were found to give excellent results amongst the catalysts examined, which are summarized in Table 1. Most of the catalyst screening and recycling of catalyst studies were carried out aiming for industrially important phenyl *N*-phenyl carbamate (PPC) as the product and for this purpose *N*,*N*′-diphenyl urea (DPU) and diphenyl carbonate (DPC) were chosen as model substrates (entries 2–9). From the catalysts screened, amorphous silica gel was found to be the most suitable catalyst because of its commercial availability, low cost and ease in recycling. Therefore, further studies were carried out using silica gel catalyst. The generalized applicability of the method is also verified and is evident from the range of carbamates synthesized from different ureas and carbonates (Table 1). Aromatic substituted ureas were also found to react smoothly with DPC giving the corresponding carbamates in excellent to high yields (entries 10–14). However, reaction between DPU and dimethyl carbonate (DMC) gave only a poor yield of *N*-phenyl methyl carbamate (entry 15). Interestingly, industrially important *N*-methyl methyl carbamate is produced in excellent yield from dimethyl urea and DMC (entry 16), while dimethyl urea and dibutyl carbonate require highly basic potassium supported silica gel catalyst for excellent yields of carbamate (entry 17). In general it was observed from screening of the substrates that, excellent yields of carbamates are obtained, when an aromatic urea was reacted with an aromatic carbonate and likewise for aliphatic derivatives. Catalyst screening experiments indicated that the basicity of the catalysts plays a vital role in their

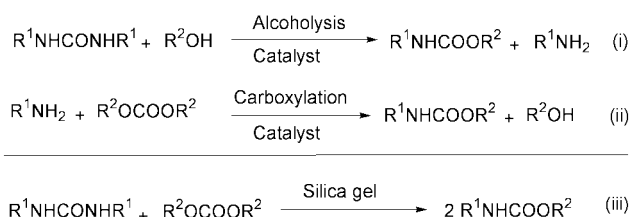

Scheme 1 Carbamate synthesis from urea and carbonate.

 DOI: 10.1039/b107947f

Table 1 Solid base catalysed carbamate synthesis from ureas and carbonates[a]

Entry	R^1 (urea)	R^2 (carbonate)	Catalyst	Time/h	Yield[b] (%)
1	C_6H_5	C_6H_5	None	24	Trace
2	C_6H_5	C_6H_5	Silica gel[c]	3	81
				8	96
3	C_6H_5	C_6H_5	Silica gel[d]	3	23
4	C_6H_5	C_6H_5	Al_2O_3 (acidic)[e]	3	0
5	C_6H_5	C_6H_5	5% Pb on silica gel[c]	3	18
6	C_6H_5	C_6H_5	$PbZrO_3$[f]	3	92
7	C_6H_5	C_6H_5	Mg–Al hydrotalcite[g,h]	3	95
8	C_6H_5	C_6H_5	Na-ZSM-5 (Si/Al = 130)[h]	4	79
9	C_6H_5	C_6H_5	Li–MgO[i]	3	90
10	4-$CH_3C_6H_4$	C_6H_5	Silica gel[c]	8	89
11	2-ClC_6H_4	C_6H_5	Silica gel[c]	8	73
12	3-ClC_6H_4	C_6H_5	Silica gel[c]	8	79
13	4-ClC_6H_4	C_6H_5	Silica gel[c]	8	89
14	4-$NO_2C_6H_4$	C_6H_5	Silica gel[c]	8	91
15	C_6H_5	CH_3[j]	Silica gel[c]	8	18
16	CH_3	CH_3[j]	Silica gel[c]	8	81
17	CH_3	C_4H_9	5%K-Silica gel[c,k]	8	80

[a] *Reaction conditions*: urea: 3.16 mmol; carbonate: 15.4 mmol; catalyst: 200 mg; solvent: carbonate; temperature: 150 °C; agitation: 1000 rpm. [b] Isolated. [c] Silica gel from W.R.Grace, USA. [d] Silica gel from Davisil, Aldrich. [e] Activated, Brockmann-1, Aldrich. [f] 0.9 mmol. [g] Mg/Al ratio: 3 : 1. [h] Synthesized in our laboratory using a standard procedure. [i] Prepared by wet impregnation of lithium acetate on magnesium acetate followed by calcination in air at 750 °C (Li/Mg = 0.1). [j] A 50 cm^3 autoclave was used with 30 bar nitrogen pressure and 15 cm^3 of dimethyl carbonate. [k] Wet impregnation of K_2CO_3 on silica gel followed by calcinations in air at 500 °C.

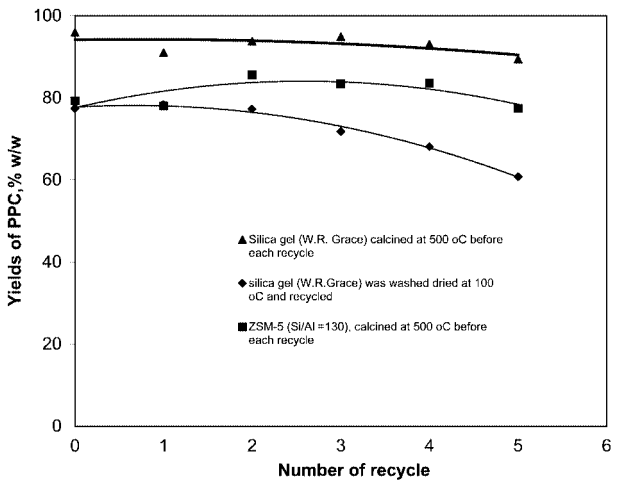

Fig. 1 Catalyst recycle runs.

activity. Also, from the earlier literature, it is known that basic catalysts are highly efficient for reactions involving carbonates (*e.g.* carbomethoxylation, *trans*-esterification and methylation).[13] The solid-base catalysts tested were all found to give excellent yields of carbamates, however, we believe that for exceptional activity, dual acid/base sites on the solid support are necessary. For catalysts having only basic sites (*e.g.* PPh_3, K_2CO_3, NaOH) only moderate yields of carbamates could be realised.[14] The activity of silica gel catalyst can be attributed to the interactions of organic urea and carbonate with silanol groups on the silica gel surface.[15] The variation in activity of silica gel catalysts procured from two different sources *viz.* W.R.Grace & Co., and Davisil (entries 2 and 3 of Table 1) is thought to be due to the difference in distribution of silanol groups in these two silica gels. Na-ZSM-5 catalysts with Si/Al ratio of 130 essentially behaved like SiO_2 since at these high ratios of Si/Al, Al atoms no longer contribute to a major extent to the framework structure of the zeolite. The activity in these zeolites is likely to be due to basic sites created by oxygen atoms while Al contributes to the Lewis acid sites.[16] Common urea and *N*-methyl urea were also examined for carbamate synthesis from DPC, however, the carbamates formed were unstable and at the end of the reaction ill characterized white solids could only be isolated.

The reusability of catalysts was tested for silica gel and Na-ZSM-5 catalyst and the results are shown in Fig. 1. The results show excellent reusability of both the catalysts for up to five recycles. Calcination for silica gel considerably improves the catalyst activity over simply drying and recycling of the catalyst.

In summary the protocol presented here is environmentally benign, simple and involves inexpensive reagents and can be effectively applied to large-scale synthesis of carbamates in high yield.

Notes and references

† *Experimental procedure:* A symmetrical urea (3.16 mmol), aromatic dicarbonate (155.6 mmol) and W.R.Grace silica gel catalyst (200 mg) were added to a well flushed and dried reaction vessel (50 cm^3) equipped with a stirrer and reflux condenser. The contents were heated under stirring up to 150 °C and kept for 8 h while an inert atmosphere was maintained. After cooling to room temperature, the solid mass was dissolved in acetone, filtered to separate the catalyst and the carbamate isolated in pure form by column chromatography (silica gel, ethyl acetate–chloroform 0.2 : 9.8). All the products were fully characterized by elemental analysis, ^1H NMR, ^{13}C NMR, IR, GC–IR and comparison with authentic samples whenever possible. Recycling of catalyst was carried out by filtration of catalyst from the crude reaction mixture in acetone followed by drying of catalyst and calcination 500 °C for 3 h.

1 F. Paul, *Coord. Chem. Rev.*, 2000, **203**, 310.
2 Y. Matsumura, T. Maki and Y. Satoh, *Tetrahedron Lett.*, 1997, **38**, 8879.
3 J. Yadav, G. Reddy, M. Reddy and H. Meshram, *Tetrahedron Lett.*, 1998, **39**, 3259.
4 P. Kocovsky, *Tetrahedron Lett.*, 1986, **27**, 5521.
5 W. D. McGhee, Y. Pan and D. P. Riley, *J. Chem. Soc., Chem. Commun.*, 1994, 699.
6 M. Aresta and E. Quaranta, *Tetrahedron*, 1992, **48**, 1515.
7 A. Inesi, V. Mucciante and L. Rossi, *J. Org. Chem.*, 1998, **63**, 1337.
8 M. Yoshida, N. Hara and S. Okuyama, *J. Chem. Soc., Chem. Commun.*, 2000, 151.
9 K. Kongen, C. Arihito, S. Kashun and R. Akyasu, *Jpn. Kokai Tokkyo Koho*, JP 08198815 A2 6th Aug, 1996.
10 A. E. Gurgiolo, *US Pat.*, 4 268 683, 1981; Z. H. Fu and Y. Ono, *J. Mol. Catal.*, 1994, **91**, 399; I. Vauthey, F. Valot, C. Gozzi and M. Lemaire, *Tetrahedron Lett.*, 2000, **41**, 6347.
11 K. Tanabe and W. F. Holderich, *Appl.Catal. A*, 1999, **181**, 399.
12 P. Molina and A. Tarraga, *Comprehensive Organic Functional Group Transformations*, Pergamon Press, Oxford, 1997, vol. 5, p. 981.
13 Y. Ono, *App.Catal. A*, 1997, **155**, 133.
14 These catalysts gave a PPC yield of 25–30% under the experimental conditions employed in this work.
15 T. Suzuki, H. Tomon and M. Okazaki, *Chem. Lett.*, 1994, 2151.
16 D. Barthomeuf, *J. Phys. Chem*, 1984, **88**, 42; M. Selva, P. Undo and A. Perosa, *J. Org. Chem.*, 2001, **66**, 677.

CHEMCOMM Communication
www.rsc.org/chemcomm

Sequential entrapment of PNA and DNA in lipid bilayers stacks

Vidya Ramakrishnan,[a] Maya Sable,[a] Moneesha D'Costa,[b] Krishna N. Ganesh*[b] and Murali Sastry*[a]

[a] *Materials Chemistry Division, National Chemical Laboratory, Pune-411 008, India. E-mail: sastry@ems.ncl.res.in; Fax: +91 20 5893952; Tel: +91 20 5893044*
[b] *Organic Chemistry (Synthesis) Division, National Chemical Laboratory, Pune-411 008, India. E-mail: kng@ems.ncl.res.in; Fax: +91 20 5893153; Tel: +91 20 5893153*

Received (in Cambridge, UK) 4th September 2001, Accepted 1st November 2001
First published as an Advance Article on the web 19th November 2001

Sequential immobilization of single stranded DNA and complementary PNA molecules in thermally evaporated fatty amine films is demonstrated and evidence for their *in-situ* hybridization is presented.

In a pioneering report, Nielsen and co-workers demonstrated that the entire sugar-phosphate backbone in DNA could be replaced by an *N*-(2-aminoethyl)glycine based polyamide structure and that the DNA bases could be attached to the peptide backbone yielding a class of molecules known as peptide nucleic acids (PNA).[1] Since the discovery of this DNA mimic and subsequent demonstration that PNA molecules obey the Watson–Crick base pairing rules[2] and that they bind with higher affinity to complementary oligonucleotides, PNA has emerged as one of the most suitable candidates for DNA diagnostic[3] and therapeutic applications.[4,5] In this communication, we show for the first time that PNA may be immobilized in thermally evaporated lipid films by simple immersion of the lipid film in the PNA solution and furthermore, that this may be extended to a sequential PNA–DNA immobilization strategy for DNA detection.

Oligonucleotides corresponding to the sequence AGTGATCTAC (**1**) and AGTGATCCAC (**2**) were synthesized as described elsewhere.[6] The PNA oligomer H-GTAGATCACT-$NH(CH_2)_2$-COOH was synthesized manually.[7] **1** is complementary to the PNA sequence while **2** is a single mismatch sequence to the PNA sequence. Pre-formed DNA–PNA solutions were obtained by mixing equimolar quantities of **1** and PNA solution under standard hybridization conditions. 250 Å thick octadecylamine (ODA, Aldrich) films were thermally evaporated onto gold-coated 6 MHz AT-cut quartz crystals, and quartz substrates for quartz crystal microgravimetry (QCM) and UV-melting measurements respectively.[8] The thickness of the films was cross-checked using ellipsometry.

UV-melting experiments on the ODA–DNA/PNA conjugate films were carried out as a test of hybridization. Unlike in the case of hybridization of complementary DNA strands where fluorescent intercalators such as ethidium bromide are routinely used,[6] reports on the use of intercalators for the detection of PNA–DNA hybrids are relatively scarce.[9] Fig. 1A shows plots of the UV-melting data recorded from ODA films in which preformed PNA–DNA duplexes were entrapped (triangles); an ODA film with sequential immobilization of **1** and PNA (squares); an ODA film with **2** and PNA intercalated sequentially (circles) and an ODA film first immersed in PNA followed by **1** (diamonds).[10] The specificity of base-pairing in the DNA–PNA complexes within the ODA matrix is reflected in the lowering of T_m in the case of single base pair mismatch DNA (**2**) with PNA which is much lower (49 °C) than the T_m of complementary DNA (**1**) with PNA (59 °C). Introduction of a single base pair mismatch in the DNA sequence leads to destabilization of the DNA–PNA complex with a lowering of the melting transition temperature. An interesting result of the investigation is the fact that the melting transition of DNA (**1**)–PNA hybrids in the lipid matrix (66 °C, squares) is much higher than the T_m of the ODA film in which preformed DNA–PNA duplexes were incorporated (59 °C, triangles). Another important observation is that the order of immobilization of PNA and DNA in the ODA matrix is not of much consequence (T_m of PNA–DNA hybrids formed by first entrapping PNA and then DNA = 68 °C, diamonds) in the extent of hybridization. The increased stability of the PNA–DNA hybrids formed in the ODA bilayers *vis-à-vis* the duplexes formed in solution and then entrapped within the lipid may be due to the following reason. During sequential immobilisation of DNA followed by PNA (or *vice-versa*), electrostatic attachment of DNA to the ODA monolayer would leave free and exposed the bases on the DNA molecules. Fig. 1B shows a schematic of the expected molecular structure of the ODA–DNA monolayer within the bilayer assemblies after entrapment of PNA. This mode of organization would then enable facile hydrogen bonding of the complementary PNA molecules with the immobilized DNA (Fig. 1B), a process not so easily done in solution. It is also possible that entrapment of pre-formed PNA–DNA complexes would lead to some orientational disorder within the ODA matrix and therefore reduced binding with the lipid. This would be reflected in terms of a lowering of the melting transition temperature as observed in this study. The UV-melting measurements clearly demonstrate that PNA–DNA immobilization and hybridization occurs within the confines of ODA bilayer stacks and furthermore, that it is sensitive to single base mismatches in the DNA sequence.

Fig. 2 presents quartz crystal microgravimetry (QCM) data of the diffusion of the DNA and PNA molecules into the fatty amine films during immersion of the ODA-coated QCM crystals in 1 μM aqueous solutions of **1** followed by PNA (triangles); **2** followed by PNA (squares) and preformed PNA–DNA complexes (circles).[11] In all cases, it is observed that there is extremely rapid diffusion of the DNA and PNA molecules into the lipid matrix. While the diffusion of DNA molecules (both **1** and **2**) into the ODA film is not surprising and may be explained in terms of attractive electrostatic interaction between

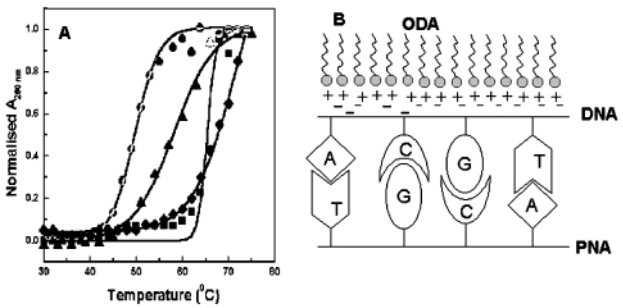

Fig. 1 A) UV melting data for 250 Å thick ODA films on quartz after immersion in 1 μm solutions of **2** followed by PNA (circles); preformed PNA–DNA complexes (triangles); **1** followed by PNA (squares) and PNA followed by **1** (diamonds). The solid lines are sigmoidal fits to the data. B) Schematic showing possible microscopic structure of DNA–ODA composite monolayer binding with complementary PNA.

 DOI: 10.1039/b107727a

the negatively charged DNA phosphate groups and protonated amine groups in the lipid matrix,[12] the significant intake of the extremely weakly charged PNA is clearly due to other interactions. The large PNA uptake is all the more interesting since the presence of DNA molecules **1** and **2** in the ODA matrix should effectively block binding sites with the ODA molecules. It is tempting to attribute the PNA diffusion into the ODA matrix to interactions arising from hybridization of the PNA molecules with the already immobilized DNA. However, a comparison of the QCM curves from the sequential immersion of the ODA films in **1** and **2** followed by immersion in PNA solution (triangles and squares respectively, Fig. 2) reveals that the mass uptake due to PNA alone (the mass increase in the second part of the QCM mass uptake curves) is similar in both cases. This clearly shows that hybridization alone cannot account for the diffusion of PNA into the DNA–ODA films and entropic factors/other interactions drive the diffusion of PNA into the lipid matrix. Indeed, immersion of the ODA films first into PNA solution followed by DNA (data not shown) resulted in significant PNA entrapment further attesting to the above fact. Even though QCM may be used to determine the presence of DNA and PNA molecules in the ODA matrix, it is clearly insufficient in determining whether hybridization had occurred between the entrapped PNA and DNA molecules. Equilibration of the number density of preformed PNA–DNA complexes in the ODA matrix (circles) occurs on time-scales similar to that observed for the single-stranded DNA molecules **1** and **2** as well as PNA. The lower mass uptake in this case (preformed PNA–DNA complexes) may be due to duplex structure preventing complete neutralization of the negative charge on the DNA by the positively charged ODA matrix. Further experiments are required to clarify this point. From the QCM measurements presented in Fig. 2, optimum times of immersion of the ODA films in the different DNA and PNA solutions were determined and used in the preparation of ODA–DNA/PNA composite films for UV melting measurements (Fig. 1A).

To conclude, it has been demonstrated that DNA and PNA molecules may be entrapped in thermally evaporated fatty amine films thus leading to a potentially exciting and novel protocol for the entrapment of oligonucleotides and their analogues. This strategy has been shown to lead to the hybridization of complementary PNA–DNA sequences in the lipid matrix in a sequential immobilization experiment. The specificity of hybridization within the lipid matrix is good and may be easily detected by UV-melting measurements. The possibility of depositing patterned lipid films and entrapping different PNA sequences in the different elements makes this approach promising for gene sequencing by hybridization techniques. A highlight of this approach is that it is both PNA and DNA friendly — no (fairly complicated) thiolation of these molecules needs be done, as is required in other gold film-based immobilization strategies.[3b]

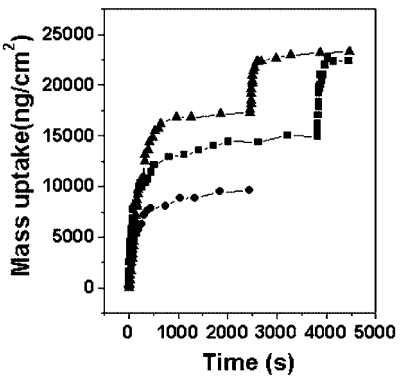

Fig. 2 QCM mass uptake data recorded during immersion of 250 Å thick ODA films in 1 μm solutions of preformed PNA–DNA complexes (circles); sequential immersion in **2** followed by PNA (squares) and **1** followed by PNA (triangles).

V. R. thanks the Council of Scientific and Industrial Research (CSIR), Government of India for financial support.

Notes and references

1 (*a*) P. E. Nielsen, M. Egholm, R. H. Berg and O. Buchardt, *Science*, 1991, **254**, 1497; (*b*) M. Egholm, O. Buchardt, P. E. Nielsen and R. H. Berg, *J. Am. Chem. Soc.*, 1992, **114**, 1895.

2 M. Egholm, O. Buchardt, L. Christensen, C. Behrens, S. M. Freier, D. A. Driver, R. H. Berg, S. K. Kim, B. Norden and P. E. Nielsen, *Nature*, 1993, **365**, 566.

3 (*a*) P. E. Nielsen, *Curr. Opin. Biol.*, 2001, **12**, 16; (*b*) J. Wang, P. E. Nielsen, M. Jiang, X. Cai, J. R. Fernandes, D. H. Grant, M. Ozsoz, A. Beglieter and M. Mowat, *Anal. Chem.*, 1997, **69**, 5200.

4 (*a*) B. Hyrup and P. E. Nielsen, *Bioorg. Med. Chem.*, 1996, **4**, 5; (*b*) K. N. Ganesh and P. E. Nielsen, *Curr. Org. Chem.*, 2000, **4**, 931.

5 (*a*) S. E. Hamilton, C. G. Simmons, I. S. Kathiriya and D. R. Corey, *Chemistry and Biology*, 1996, **6**, 343; (*b*) C. Nastruzzi, R. Cortesi, E. Esposito, R. Gambari, M. Borgatti, N. Bianchi, G. Feriotto and C. Mischiati, *J. Controlled Release*, 2000, **68**, 237.

6 M. Sastry, V. Ramakrishnan, M. Pattarkine, A. Gole and K. N. Ganesh, *Langmuir.*, 2000, **16**, 9142.

7 Merrifield resin derivatized with β-alanine (0.013 meq g^{-1}) employing the standard Boc-protection strategy was used in the synthesis. Cleavage from the solid support using the TFA–TFMSA cleavage procedure yielded the PNA oligomer with a free carboxylic acid at its 'C' terminus. The oligomer was purified by RP-FPLC and its purity rechecked by RP-HPLC and confirmed by MALDI-TOF mass spectroscopy.

8 The films were deposited in an Edwards E306A vacuum coating unit operated at a pressure of better than 1×10^{-7} Torr. The thickness of the deposited films was monitored *in-situ* using an Edwards quartz crystal microbalance (*QCM*).

9 J. Wang, E. Palecek, P. E. Nielsen, G. Rivas, X. Cai, H. Shirashi, N. Dontha, D. Luo and P. A. M. Farias, *J. Am. Chem. Soc.*, 1996, **118**, 7667.

10 The UV melting experiments were carried out on Perkin Elmer Lambda 15 UV/VIS spectrophotometer fitted with a Julabo water circulator with programmed heating accessory. The quartz substrates bearing the films were cut so as to fit into the cuvette normally used for liquid samples. The DNA–ODA films were heated at a rate of 0.5 °C per minute and the thermal denaturation of the duplex was followed by monitoring changes in the absorbance at 260 nm as a function of temperature. A 250 Å thick ODA film on quartz was taken as the reference.

11 This was achieved by *ex-situ* measurement of the QCM resonance frequency after thorough washing and drying of the crystals using an Edwards FTM5 frequency counter. This frequency counter had a resolution and stability of 1 Hz. The frequency change (Δf) was converted to mass loading (Δm) using the relationship $\Delta m = 12.1\ \Delta f$ (ng cm^{-2}).

12 M. Sastry, V. Ramakrishnan, M. Pattarkine and K. N. Ganesh, *J. Phys. Chem. B*, 2001, **105**, 4409.

CHEMCOMM
Communication
www.rsc.org/chemcomm

Immobilisation of ruthenium cluster catalysts *via* novel derivatisations of ArgoGel resins†

Catherine M. G. Judkins,[a] Kevin A. Knights,[b] Brian F. G. Johnson,*[a] Yolanda R. de Miguel,*[b] Robert Raja[a] and John Meurig Thomas[c]

[a] *Chemistry Department, University of Cambridge, Lensfield Road, Cambridge, UK CB2 1EW. E-mail: bfgj1@cam.ac.uk*
[b] *Chemistry Department, King's College London, Strand, London, UK WC2R 2LS. E-mail: yolanda.demiguel@kcl.ac.uk*
[c] *Royal Institution of Great Britain, Davy Faraday Research Laboratory, 21 Albemarle Street, London, UK W1X 4BS*

Received (in Cambridge, UK) 17th July 2001, Accepted 29th October 2001
First published as an Advance Article on the web 19th November 2001

The ruthenium cluster moiety $[Ru_6C(CO)_{17}]$ has been attached to ArgoGel polymer beads using supported phosphine ligands and crown ether interactions with ammonium salt functionalities; these show promising results as hydrogenation catalysts for clean chemical conversions.

The immobilisation of catalysts on solid supports represents a major step in the development of cleaner chemical conversions.[1,2] Active materials thus prepared are considerably easier to handle, retrieve and recycle than their homogeneous counterparts. In addition, they may also exhibit improved activities and selectivities over those found for their homogeneous analogues.[3] An approach used frequently in the development of novel heterogeneous catalysts is the chemical linking of the active moiety to the available functional groups of polymer beads. The choice of support plays an important role in the 'tunability' of such heterogenised catalysts to a particular process. For example, some catalytic processes have been performed using rigid polymer backbones[4a] which barely swell in solvents whereas others require more flexibility in the support.[4b] Amphiphilic polystyrene based resins containing polyethylene glycol (PEG) grafts show great potential as supports for metal cluster based catalytic systems. The PEG component provides the vital flexibility needed to minimise steric congestion of the metals as well as the ability to swell in a variety of solvents, thus enabling maximum access to catalytic sites. Metal clusters and their nanoparticle equivalents are known to possess good catalytic properties in a variety of hydrogenation processes and, in general, their activity is well documented and moderately well understood.[5] In this communication we report the functionalisation of ArgoGel (AG) resins by three different methods and subsequent treatment with the $[Ru_6C(CO)_{17}]$ moiety. Initial studies into their catalytic potential are also described.

Previous research has shown that the cluster $[Ru_6C(CO)_{17}]$ can be coordinated to benzo-18-crown-6 and the well-known host properties of the crown can be used to connect the cluster moiety $[Ru_6C(CO)_{14}(\eta^6\text{-}C_{16}H_{24}O_6)]$ **1** to an ammonium functionalised chain.[6] This strategy has enabled the site-directed deposition of clusters onto mesoporous silica (MCM-41) containing ammonium bearing tethers.[7] Building on these observations, we treated the ArgoGel amine resin with acid to generate terminal ammonium groups to act as sites onto which **1** could be attached.

Protonation of ArgoGel amine was achieved by treating the beads with an excess of HCl (12 M in water) or $HBF_4{\cdot}OEt_2$ to yield the ammonium bearing beads **2** and **3** (see Scheme 1) respectively in quantitative yield as shown by single bead FTIR, gel-phase ^{1}H HR-MAS NMR and microanalysis (see ESI‡).

† Electronic supplementary information (ESI) available: footnotes to the text. See http://www.rsc.org/suppdata/cc/b1/b106336g/

The colourless beads **2** and **3** were treated with **1** (1.5 equivalents) to give the dark red beads **4** and **5**. The IR spectra of the single bead materials showed sharp resonances at 2079, 1978 and 1833 cm^{-1} (for **4**) and 2044, 2009 and 1805 cm^{-1} (for **5**), indicating the presence of carbonyl groups of the attached ruthenium cluster. The presence of ruthenium was confirmed by X-EDS and ICP-AES analysis. This showed the mass percentage of ruthenium on the beads to be 2.96% (0.049 mmol g^{-1}) for **4** and 1.72% (0.028 mmol g^{-1}) for **5**, which corresponds to a 14% site coverage of **1** on resin **4** and an 8% site coverage of **1** on resin **5**.

A preliminary test of the performance of resin **4** in the catalytic hydrogenation of cyclohexene to cyclohexane resulted in exceptionally high turnovers (TOF = 6520 h^{-1}) and high selectivities for cyclohexane (>99%). The catalytic potential of this material was further investigated in the transfer hydrogenation of ketones (cyclohexanone and benzophenone). It is noteworthy to mention here that these reactions were carried out without the aid of conventionally used external reducing agents or hydrogen sources such as propan-2–ol or formic acid.[8] Remarkably high turnovers were also observed for the hydrogenation of cyclohexanone and benzophenone (3846 and 3191 h^{-1} respectively) and exceedingly high selectivities (>99%) for cyclohexanol and diphenylmethanol respectively (see ESI for reaction conditions§). This indicates good site isolation and accessibility of the ruthenium complexes in the porous organic matrix. The re-use of resin **4** in the above-mentioned hydrogenations did not result in appreciable loss in catalytic activity or selectivity. Further, to rule out the possibility of leaching, in a typical experiment using benzophenone as the substrate, the solid catalyst was filtered off from the reaction mixture after 8 h while hot (373 K) and the reaction was continued with the resulting filtrate for a further 12 h. The kinetics revealed no change in conversion or product selectivity and the resulting filtrate (at the end of the reaction, 20 h) was independently

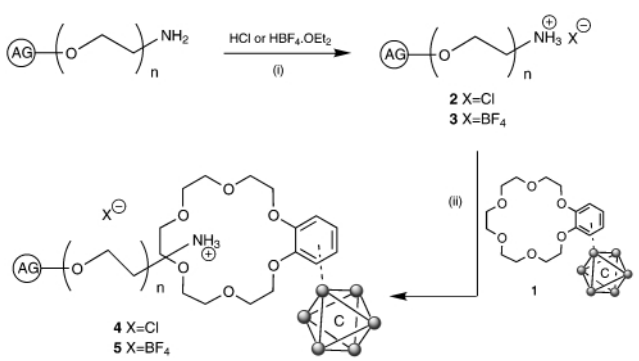

Scheme 1 Preparation of **4** and **5**: *Reagents and conditions*: i, THF, overnight; ii, CH_2Cl_2, room temp., 48 h, N_2.

 DOI: 10.1039/b106336g

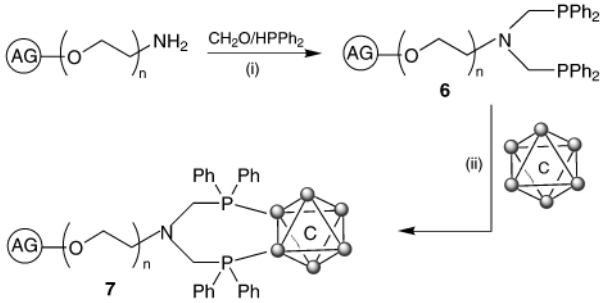

Scheme 2 Preparation of **6** and **7**: *Reagents and conditions*: i, MeOH, PhMe, 65 °C (3 h), room temp. (15 h), Ar; ii, CH_2Cl_2, room temp., 5 days, Ar.

analysed by ICP-AAS for the presence of free ruthenium. Only trace amounts (< 3 ppb) were detected. Moreover, a comparison of the SEM images of the beads before and after catalysis showed no change in the spherical morphology.

The next stage in our bead functionalisation strategy was to increase the loading and strength of binding of the ruthenium cluster to the bead. Conversion of each of the available NH_2 sites on the ArgoGel amine resin to two phosphine groups can effectively double the number of coordination sites available for metal binding and thereby should increase the loading and catalytic activity. In the case of $[Ru_6C(CO)_{17}]$ the stronger bidentate coordination is expected.[9] Diphenylphosphine was treated with paraformaldehyde according to a literature procedure[10] and the phosphido-Mannich intermediate thus formed was added to ArgoGel amine to give the supported phosphine ligand **6** (Scheme 2). The peaks in the ^{31}P NMR spectrum at δ −26 and −27 indicated formation of the supported phosphine ligand. The appearance of two signals was believed to correspond to the bidentate phosphine **6** and some monodentate –$NHCH_2PPh_2$ sites (see ESI¶). Gel-phase ^{1}H HR-MAS NMR spectroscopy showed the presence of phenyl protons at δ 7.48 and 7.82 and a doublet at δ 3.53 (J = 11.5 Hz) which confirmed the presence of the NCH_2PPh_2 species. Microanalysis showed the amounts of N and P to be 0.76 and 2.10%, respectively. This corresponds to 0.54 mmol/g N and 0.68 mmol/g P; a N:P ratio of 1:1.3 showing that not all N–H sites were completely converted. This is in good agreement with the ^{31}P NMR results.

An excess of $[Ru_6C(CO)_{17}]$ was added to a swirled suspension of **6**, resulting in the formation of the dark red beads **7**. NMR, IR and X-EDS all gave evidence that the desired product had formed (see ESI‖). The ^{31}P NMR spectrum showed no peaks at δ −26 and −27 , indicating that all available phosphine sites had coordinated. The new peaks at δ 16 and 24 ppm assigned to different coordination modes of the cluster to the phosphine ligand. ICP-AES analysis showed the beads to be 7.43% by mass ruthenium (0.12 mmol g^{-1}), which corresponds to a site coverage of cluster (assuming bidentate coordination) of 41%.

Since the phosphine bearing beads improved the amount of deposition of ruthenium cluster, an alternative route starting from ArgoGel chloride beads was proposed. In the synthetic procedure, $KPPh_2$ was freshly prepared[11] (from KH and $HPPh_2$) and was added to a suspension of ArgoGel chloride to give the phosphine derivatised beads **8** (Scheme 3). The ^{31}P NMR spectrum showed a peak at δ −21 , indicating the presence of the uncoordinated phosphine functionality (see ESI††). The gel-phase ^{1}H HR-MAS NMR spectra clearly showed the phosphorus bound phenyl groups at δ 7.47 and 7.75 and peaks for the –$OCH_2CH_2PPh_2$ and –CH_2PPh_2 protons at δ 3.64 and 2.48, respectively. Microanalysis showed the mass percentage of phosphorus to be 1.25 (0.40 mmol g^{-1}).

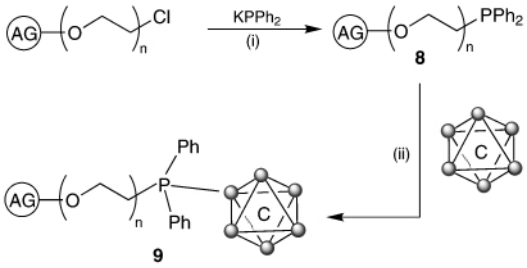

Scheme 3 Preparation of **8** and **9**: *Reagents and conditions*: i, THF, room temp., 30 h, N_2; ii, CH_2Cl_2, room temp, 5 days, N_2.

Treatment of **8** with an excess of $[Ru_6C(CO)_{17}]$ yielded the desired dark red product **9** which was characterised by IR, NMR, microanalysis and X-EDS. ICP-AES showed a larger mass percent of ruthenium on the bead (14.8%, 0.24 mmol g^{-1}) compared with the ArgoGel amine systems, which corresponds to a site coverage of 82%. This was reinforced by X-EDS analysis and the results from microanalysis imply that only one phosphine coordinates per cluster (see ESI‡‡). The ^{31}P NMR spectrum showed no peak at δ −21, indicating that all free phosphine sites had coordinated, giving rise to the new signal at δ 15. The IR spectrum showed the ruthenium carbonyl peaks at the lower wavenumbers of 1965 and 1789 cm^{-1}.

In summary, we have shown the successful derivatisation of two types of commercially available polymer resins which can be used as substrates in heterogeneous catalysis and have demonstrated how the method of functionalisation affects the loading of cluster. Resin **4** exhibits remarkably high activities and selectivities for the hydrogenation of olefins and for the transfer hydrogenation of ketones, without the need for external reducing agents. Further work is in progress to evaluate the catalytic potential of **5**, **7** and **9** as hydrogenation catalysts for a number of diverse organic chemical transformations.

We wish to thank for financial support the EPSRC and ICI (C. M. G. J.), King's College London (K. A. K.) and the Royal Society for a Dorothy Hodgkin Fellowship (Y. D. M). We gratefully acknowledge the assistance of Dr T. Brain (SEM, X-EDS), Jon Cobb and Duncan Howe (NMR), and Dr D.S. Wright and Richard A. Layfield.

Notes and references

1 S. V. Ley, I. R. Baxendale, R. N. Bream, P. S. Jackson, A. G. Leach, D. A. Longbottom, M. Nesi, J. S. Scott, R. I. Storer and S. J. Taylor, *J. Chem. Soc., Perkin Trans. 1*, 2000, **23**, 3815.
2 Y. R. de Miguel, *J. Chem. Soc., Perkin Trans. 1*, 2000, 4213.
3 D. R. Patel and R. N. Ram, *Indian J. Chem. Technol.*, 2000, **7**, 280.
4 (*a*) T. Y. Zhang and M. J. Allen, *Tetrahedron Lett.*, 1999, **40**, 5813; (*b*) P. Hodge, *Chem. Soc. Rev.*, 1997, **26**, 417.
5 R. J. Puddephatt, in *Metal Clusters in Chemistry*, ed. P. Braunstein, L.A. Oro and P.R. Raithby, Wiley-VCH, Weinheim, 1999, vol. 2, ch. 2, p. 605.
6 B. F. G. Johnson, C. M. G. Judkins, J. M. Matters, D. S. Shephard and S. Parsons, *Chem. Commun.*, 2000, 1549.
7 D. S. Shephard, W. Zhou, T. Maschmeyer, J. M. Matters, C. L. Roper, S. Parsons, B. F. G. Johnson and M. J. Duer, *Angew. Chem., Int. Ed.*, 1998, **37**, 2719.
8 K. Polborn and K. Severin, *Chem. Eur. J.*, 2000, **6**, 4604.
9 T. Adatia, G. Conole, S. R. Drake, B. F. G. Johnson, M. Kessler, J. Lewis and M. McPartin, *J. Chem. Soc., Dalton Trans.*, 1997, 669.
10 M. T. Reetz, G. Lohmer and R. Schwickardi, *Angew. Chem., Int. Ed., Engl.*, 1997, **36**, 1526.
11 R. G. Nuzzo, S. L. Haynie, M. E. Wilson and G. M. Whitesides, *J. Org. Chem.*, 1981, **46**, 2861.

CHEMCOMM
Communication
www.rsc.org/chemcomm

Regiospecific high yield reductive coupling of diynes to give a luminescent rhodium complex†

Jonathan P. Rourke,*[a] Andrei S. Batsanov,[b] Judith A. K. Howard[b] and Todd B. Marder*[b]

[a] *Department of Chemistry, University of Warwick, Coventry, UK CV4 7AL. E-mail: j.rourke@warwick.ac.uk*

[b] *Department of Chemistry, University of Durham, South Road, Durham, UK DH1 3LE. E-mail: todd.marder@durham.ac.uk*

Received (in Cambridge, UK) 25th September 2001, Accepted 6th November 2001
First published as an Advance Article on the web 30th November 2001

Reaction of 2 equivalents of 1,4-bis(*p*-tolylethynyl)buta-1,3-diyne with [$(PMe_3)_4Rh(–C{\equiv}CSiMe_3)$] gives the unusual, highly luminescent *mer,cis*-[tris(trimethylphosphine)trimethylsilylethynyl-2,5-bis(*p*-tolylethynyl)-3,4-bis(*p*-tolyl)rhodacyclopenta-2,4-diene] 5 in quantitative yield which has been fully characterised by ^1H and $^{31}P\{^1H\}$ NMR, IR, UV–VIS and luminescence spectroscopies, elemental analysis and single crystal X-ray diffraction.

Rigid rod conjugated systems, such as 1,4-bis(phenylethynyl)benzenes,[1–12] 9,10-bis(phenylethynyl)anthracenes[13,14] and 2,5-bis(phenylethynyl)thiophenes,[2] display interesting structural, electronic, non-linear optical and luminescent properties. The same can be expected from structurally similar 2,5-bis(phenylethynyl)metallacyclopentadienyl derivatives **2A** (Scheme 1), which can be prepared by a reductive coupling of

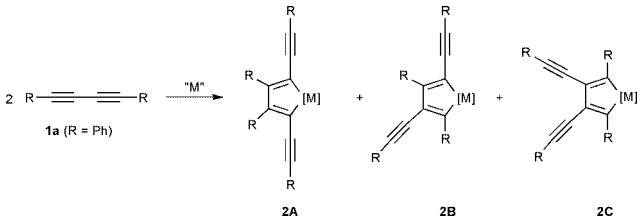

Scheme 1

two diarylbuta-1,3-diyne molecules **1** on a transition metal centre.[15–22] However, in the few reported syntheses of such compounds, various products are formed, including two other isomers of **2** (**B** and **C**), and the yields of the desired isomer **2A** are small: 1.5–4% in the reaction of diphenylbuta-1,3-diyne **1a** with $[Ru_3(CO)_{10}(NCMe)_2]$ in the presence of Me_3NO {[M] = $Ru(NMe_3)(CO)_3$} and 2% in the reaction of **1a** with $[CpCo(PPh_3)_2]$ at 60 °C {[M] = $CoCp(PPh_3)$}, although the reaction of the latter with hexa-2,4-diyne yields 32% of **2A**. The only other analogous monometallic compounds of which we are aware[23] are those containing titanium and zirconium for which isomer **2A** is not observed.[21,22] In the course of our work on rhodium alkynyl complexes,[24–29] we developed a high-yield one-pot synthesis of a luminescent complex **5** *via* the reaction sequence in Scheme 2.

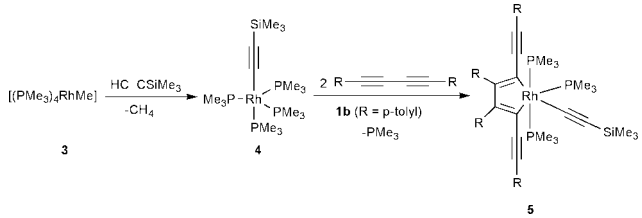

Scheme 2

† Electronic supplementary information (ESI) available: absorption, emission and luminescence spectra for **5**. See http://www.rsc.org/suppdata/cc/b1/b108625a/

Reaction of $[(PMe_3)_4RhMe]$ **3**[30] (20 mg, 4.74×10^{-5} mol) with $HC{\equiv}CSiMe_3$ (6.7 µl, 4.74×10^{-5} mol) in THF (1 ml), gave the alkynyl complex **4** in quantitative yield with loss of methane.[25,26,29] To this, a solution of two equivalents (21.8 mg) of 1,4-bis(*p*-tolyl)buta-1,3-diyne **1b** in THF (2 ml) was added. The reaction was monitored *in situ* by $^{31}P\{^1H\}$ NMR spectroscopy, which showed a partial conversion into a new $(PMe_3)_3Rh^{III}$ complex **5**. After stirring for 2 min, all solvent was removed *in vacuo* and the residue was redissolved in THF (3 ml), thus facilitating the reaction by removing the liberated, volatile PMe_3. This cycle was repeated five times, until the NMR spectra showed the conversion to be complete. Bright yellow product **5** was isolated in 95% yield (40 mg) after recrystallisation from THF–hexane.‡

An X-ray diffraction study of **5**§ revealed a distorted octahedral coordination of the Rh atom (Fig. 1) with a meridonal disposition of the three phosphine ligands. The rhodacyclopentadiene ring is nearly planar: the Rh atom deviates by 0.13 Å from the C(15)C(16)C(17)C(18) plane.

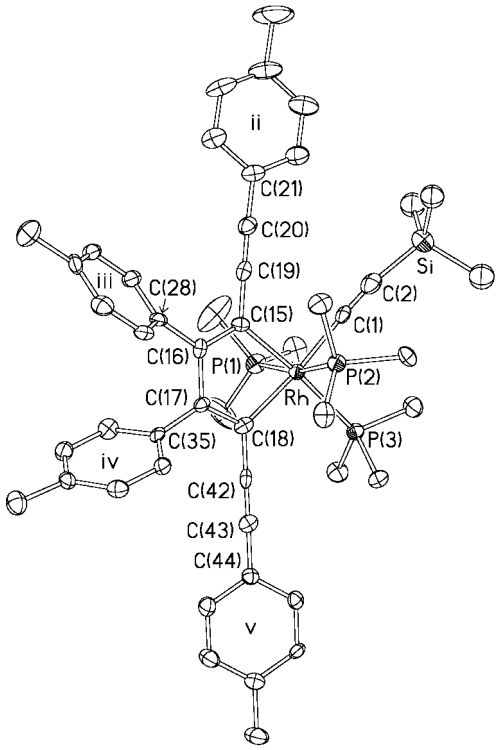

Fig. 1 Molecular structure of **5** showing 50% thermal ellipsoids. The rotational disorder of $P(1)Me_3$ and $SiMe_3$ groups is not shown (H atoms are omitted). Selected bond lengths (Å) and angles (°): Rh–P(1) 2.322(2), Rh–P(2) 2.325(1), Rh–P(3) 2.372(1), Rh–C(1) 2.068(6), Rh–C(15) 2.087(5), Rh–C(18) 2.110(5), C(2)–Si 1.848(7), C(20)–C(21) 1.426(7), C(43)–C(44) 1.432(7); P(1)–Rh-P(2) 168.39(5), C(1)–Rh–C(18) 173.5(2), C(15)–Rh–P(3) 173.9(2), C(1)–Rh–P(2) 85.3(1), P(1)–Rh–P(3) 96.67(5), C(15)–Rh–C(18) 78.8(2).

 DOI: 10.1039/b108625a

Benzene rings *iii* and *iv,* immediately attached to the metallacycle, are inclined to the latter plane by 50 and 66° (due to steric overcrowding), while rings *ii* and *v* are inclined by only 10 and 22°, permitting π-electron conjugation along the 'rod'. Thus, in the metallacycle, the formally double bonds C(15)=C(16) [1.382(6) Å] and C(17)=C(18) [1.389(6) Å] are longer than in cyclopentadiene[31] (1.344 Å) and its derivatives[32] (average 1.341 Å). The C(16)–C(17) bond [1.465(6) Å] is relatively short compared with non-conjugated, *i.e.* non-planar, butadiene moieties[32] (1.478 Å). The C(15)–C(19) and C(18)–C(42) bonds [av. 1.415(7) Å] are short for a C(sp)–C(sp^2) bond[32] (1.431 Å). The alkyne bonds C(19)≡C(20) and C(42)≡C(43) [av. 1.214(7) Å] are longer than the standard value[32] (1.181 Å) as well as the non-conjugated C(1)≡C(2) bond [1.167(7) Å]. Although each of these differences is on the margin of statistical significance, they are all consistent with the model of conjugation. The alkynyl ligand lies close to the rhodacyclopentadiene plane, *trans* to the Rh–C(18) bond, which is longer [2.110(5) Å] than the Rh–C(15) bond [2.087(5) Å] due to the *trans*-influence. The $SiMe_3$ group and the P(1)Me_3 ligand are rotationally disordered, each between two orientations in 1 : 1 and 3 : 1 ratios, respectively.

The $^{31}P\{^1H\}$ NMR spectrum† of **5** displays a doublet of doublets and a doublet of triplets consistent with a meridonal $(PMe_3)_3Rh^{III}$ coordination, where the unique phosphine is *trans* to a Rh–C σ-bond ($^1J_{RhP}$ 82 Hz). The ^1H NMR spectrum indicated four non-equivalents *p*-tolyl groups, three meridonal PMe_3 ligands and a $SiMe_3$ group. Thus, the solution NMR data is entirely consistent with the solid-state structure.

The bright yellow compound **5** displays several intense absorptions in the UV–VIS spectrum with peaks at 480 (ε 36 000), 452 (ε = 43 000), 434 (ε = 31 000), 333 (ε = 36 000) and 312 nm (ε = 55 000 $dm^3\ mol^{-1}\ cm^{-1}$). We noted that NMR samples of **5** in benzene or THF emitted green light when exposed to ordinary fluorescent room lighting. An examination of the luminescence spectra revealed that excitation at 452 nm gave rise to emission bands at 500 and 532 nm (green), whereas excitation at 333 nm showed these two bands as well as stronger emissions at 366 and 384 nm. The absorption spectrum and the emission spectrum resulting from 452 nm excitation are remarkably similar in wavelength and extinction coefficients to those observed previously for 9,10-bis(4-MeSC_6H_4C≡C)anthracene.[13] This is an exciting finding in light of the considerable current interest in luminescent organometallics,[2,33,34] which may have applications as the emissive material in OLEDs. Further photophysical studies on this and related compounds are underway in order to elucidate the nature of the states giving rise to the absorption and emission in **5**.

We have prepared a rare example of a 2,5-bis(arylethynyl)metallacyclopentadiene *via* the regiospecific reductive coupling of two butadiynes at a rhodium centre. The highly luminescent compound is formed in quantitative yield in minutes at room temperature. Solid samples of **5** appear relatively stable to the atmosphere, making this an attractive system for further study and possible applications. The compound offers exciting opportunities for functionalisation at the metal bound alkynyl ligand, the phosphines, and the starting diyne **1**, as well as the possibility of changing the metal centre from Rh to Co or Ir, all of which should allow tuning of the luminescent properties of the system.

J. A. K. H. thanks EPSRC for a Senior Research Fellowship. We thank Mr Simon FitzGerald and Dr Andrew Beeby for assistance with the luminescence specta, Mrs J. Dostal for the elemental analysis, Dr Dmitri S. Yufit for assistance with the structural analysis and Dr Paul J. Low for many helpful discussions and a preprint of ref. 23.

Notes and references

‡ *NMR data*: δ_P (80.96 MHz, C_6D_6) −8.81 (2P, dd, $^1J_{RhP}$ 99, $^2J_{PP}$ 30 Hz), −23.22 (1P, dt, $^1J_{RhP}$ 82, $^2J_{PP}$ 30 Hz). δ_H (200.1 MHz, C_6D_6): 7.74 [2H, (AB)′, Ar], 7.43 [2H, (AB)′, Ar], 7.34 [2H, (AB)′, Ar], 7.23 [2H, (AB)′, Ar], 7.06 [2H, (AB)′, Ar], 7.03 [2H, (AB)′, Ar], 6.99 [2H, (AB)′, Ar], 6.92 [2H, (AB)′, Ar], 2.08 (6H, s, Me), 2.03 (3H, s, Me), 2.01 (3H, s, Me), 1.77 (9H, d, *J* 8 Hz, PMe_3 *trans* to C), 1.38 (18H, vt, *J* 3 Hz, PMe_3 *trans* to PMe_3), 0.42 (9H, s, TMS). Calc. for $C_{50}H_{64}P_3RhSi$: C, 68.65; H, 7.14. Found: C, 67.56; H, 7.26%. IR (solid-state): ν(C≡C) 2160, 2128, 2021 cm^{-1}.

§ *Crystal data* for $C_{50}H_{64}P_3RhSi$ **5**: yellow prismatic crystal (0.46 × 0.09 × 0.07 mm) grown by diffusion of hexane into a THF solution, M = 888.92, orthorhombic, space group *Pbca* (no 61), a = 10.500(2), b = 19.180(1), c = 47.927(6) Å, V = 9652(2) $Å^3$, Z = 8, μ = 0.51 mm^{-1}, T = 120 K, SMART 1K CCD area detector, Mo-$K\alpha$ radiation, 41968 reflections (7981 independent, R_{int} = 0.095), SHELXTL software (Bruker AXS, Madison, WI, 1997), least squares refinement against F^2 of all data, final R = 0.067 [5801 reflections with $F^2 > 2\sigma(F^2)$], $wR(F^2)$ = 0.112. CCDC reference number 171634. See http://www.rsc.org/suppdata/cc/b1/b108625a/ for crystallographic data in CIF or other electronic format.

1 P. Nguyen, Z. Yuan, L. Agocs, G. Lesley and T. B. Marder, *Inorg. Chim. Acta*, 1994, **220**, 289.
2 M. S. Khan, A. K. Kakkar, N. J. Long, J. Lewis, P. Raithby, P. Nguyen, T. B. Marder, F. Whittmann and R. H. Friend, *J. Mater. Chem.*, 1994, **4**, 1227.
3 P. Nguyen, G. Lesley, T. B. Marder, I. Ledoux and J. Zyss, *Chem. Mater.*, 1997, **9**, 406.
4 C. Dai, P. Nguyen, T. B. Marder, A. J. Scott, W. Clegg and C. Viney, *Chem. Commun.*, 1999, 2493.
5 U. H. F. Bunz, *Chem. Rev.*, 2000, **100**, 1605.
6 Z. L. Donhauser, B. A. Mantooth, K. F. Kelly, L. A. Bumm, J. D. Monnell, J. J. Stapleton, D. W. Price, A. M. Rawlett, D. L. Allara, J. M. Tour and P. S. Weiss, *Science*, 2001, **292**, 2303.
7 S. M. Dirk, D. W. Price, S. Chanteau, D. V. Kosynkin and J. M. Tour, *Tetrahedron*, 2001, **57**, 5109.
8 J. Kim and T. M. Swager, *Nature*, 2001, **411**, 1030.
9 C. Schmitz, P. Posch, M. Thelakkat, H. W. Schmidt, A. Montak, K. Feldman, P. Smith and C. Weder, *Adv. Funct. Mater.*, 2001, **11**, 41.
10 S. Lahiri, J. L. Thompson and J. S. Moore, *J. Am. Chem. Soc.*, 2000, **122**, 11315.
11 M. Levitus, K. Schmieder, H. Ricks, K. D. Shimizu, U. H. F. Bunz and M. A. Grace-Garibay, *J. Am. Chem. Soc.*, 2001, **123**, 4259.
12 H. Li, D. R. Powell, T. K. Firman and R. West, *Macromolecules*, 1998, **31**, 1093.
13 P. Nguyen, S. Todd, D. v. d. Biggelaar, N. J. Taylor, T. B. Marder, F. Wittmann and R. H. Friend, *Synlett.*, 1994, 299.
14 T. Kawai, T. Saski and M. Irie, *Chem. Commun.*, 2001, 711.
15 T. Shimura, A. Ohkubo, K. Aramaki, H. Uekusa, T. Fujita, S. Ohba and H. Nishihara, *Inorg. Chim. Acta*, 1995, **230**, 215.
16 T. Fujita, H. Uekusa, A. Ohkubo, T. Shimura, K. Aramaki, H. Nisihara and S. Ohba, *Acta Crystallogr., Sect. C*, 1995, **51**, 2265.
17 M. I. Bruce, N. N. Zaitseva, B. W. Skelton and A. H. White, *Inorg. Chim. Acta*, 1996, **250**, 129.
18 M. I. Bruce, B. W. Skelton, A. H. White and N. N. Zaitseva, *J. Organomet. Chem.*, 1998, **558**, 197.
19 S. P. Tunik, E. V. Grachova, U. R. Denisov, G. L. Starova, A. B. Nikol'skii, F. M. Dolgushin, A. I. Yanovsky and Y. T. Struchkov, *J. Organomet. Chem.*, 1997, **536**, 339.
20 A. A. Koridze, U. I. Zdanovich, N. V. Andrievskaga, Y. Siromakhova, P. V. Petrovski, M. G. Ezernitskaya, F. M. Dolgushin, A. I. Yanovsky and Y. T. Struchkov, *Russ. Chem. Bull.*, 1996, **45**, 1200.
21 U. Rosenthal, P.-M. Pellny, F. G. Kirchbauer and V. V. Burlakov, *Acc. Chem. Res.*, 2000, **33**, 119.
22 D. P. Hsu, W. M. Davis and S. L. Buchwald, *J. Am. Chem. Soc.*, 1993, **115**, 10394.
23 P. J. Low and M. I. Bruce, *Adv. Organomet. Chem.*, 2001, **48**, 71.
24 T. B. Marder, D. Zargarian, J. C. Calabrese, T. Herskovitz and D. Milstein, *Chem. Commun.*, 1987, 1484.
25 D. Zargarian, P. Chow, N. J. Taylor and T. B. Marder, *J. Chem. Soc., Chem. Commun.*, 1989, 540.
26 P. Chow, D. Zargarian, N. J. Taylor and T. B. Marder, *J. Chem. Soc., Chem. Commun.*, 1989, 1545.
27 H. B. Fyfe, M. Mlekuz, D. Zargarian, N. J. Taylor and T. B. Marder, *J. Chem. Soc., Chem. Commun.*, 1991, 188.
28 J. P. Rourke, D. W. Bruce and T. B. Marder, *J. Chem. Soc., Dalton Trans.*, 1995, 317.
29 J. P. Rourke, G. Stringer, P. Chow, R. J. Deeth, D. S. Yufit, J. A. K. Howard and T. B. Marder, *Organometallics*, 2001, in press.
30 D. L. Thorn, *Organometallics*, 1985, **4**, 192.
31 T. Haumann, J. Benet-Buchholz and R. Boese, *J. Mol. Struct.*, 1996, **374**, 299.
32 F. H. Allen, O. Kennard, D. G. Watson, L. Brammer, A. G. Orpen and R. Taylor, *J. Chem. Soc., Perkin Trans. 2*, 1987, S1.
33 V. W.-W. Yam, *Chem. Commun.*, 2001, 789.
34 S. Lamansky, P. J. Djurovish, D. Murphy, F. Abdel-Razzaq, H. E. Lee, C. Adachi, P. E. Burrows, S. R. Forrest and M. E. Thompson, *J. Am. Chem. Soc.*, 2001, **123**, 4304.

CHEMCOMM
Communication
www.rsc.org/chemcomm

A pH-responsive hydroquinone-functionalised glassy carbon electrode

Xinhao Yang,[a] Simon B. Hall,*[a] Anthony K. Burrell[ab] and David L. Officer[a]

[a] *Nanomaterial Research Centre, Institute of Fundamental Sciences, Massey University, Private Bag 11 222, Palmerston North, New Zealand. E-mail: s.b.hall@massey.ac.nz; Fax: 64 6 350 5682; Tel: 64 6 350 5917*

[b] *Actinide, Catalysis and Separations Chemistry, C-SIC, Mail Stop J514, Los Alamos National Laboratory, Los Alamos, NM 87545, USA. E-mail: Burrell@lanl.gov; Fax: 1 505-667-9905; Tel: 1 505 665 9342*

Received (in Cambridge, UK) 6th September 2001, Accepted 31st October 2001
First published as an Advance Article on the web 30th November 2001

A pH-responsive electrode may be formed by covalent modification of glassy carbon by reduction of a diazonium salt hydroquinone precursor, followed by chemical demethylation.

Early methods for chemically modifying carbon surfaces involved vigorous oxidation processes[1–3] leading to the formation of superficial oxygenated functional groups.[4] These functionalities were then reacted further to effect attachment of the target molecule. The exact nature and number of oxygenated functional groups formed by this method was difficult to control, and corrosion of the carbon surface was often observed.[5] An alternative reductive strategy for electrochemically modifying carbon surfaces has been developed by Pinson *et al.*[6,7] This method makes it possible to graft a wide variety of functionalised aryl groups onto carbon surfaces, which allows the attachment of a broad spectrum of substances and shows great promise for a variety of applications.[8,9]

Here, we report the first synthesis of *trans*-2′,5′-dimethoxylstilbene-4-diazonium tetrafluoroborate **3** (Scheme 1), followed by the electrochemical reduction of **3** on the glassy carbon surface to form a monolayer. Chemical demethylation forms a hydroquinone-substituted stilbene-grafted glassy carbon (GC) electrode that is pH-responsive (Scheme 2).

The synthetic route to **3** is shown in Scheme 1. The compounds **1** and **2** were prepared as described previously.[10,11] The diazonium salt **3** was prepared using standard chemistry.†

Fig. 1 shows voltammograms recorded at a GC electrode for a 0.1 M solution of Bu_4NBF_4 in acetonitrile (curve a) and for the first cycle in the presence of 5 mM **3** (Curve b). A broad (500 mV at half height) and irreversible reduction peak located at 500 mV *vs*. Ag/AgCl is observed in a similar manner to those reported previously for other diazonium compounds.[7–9] This corresponds to the one electron reduction of the diazonium functionality. When further cyclic voltammograms are recorded this peak diminishes markedly. Grafting was performed over 20 min on a freshly polished GC electrode at a potential of −0.7 V *vs.* Ag/AgCl to form a complete layer on the GC surface. The broad reduction wave in Fig. 1 is not observed in cyclic voltammograms recorded directly after this potentiostatic grafting process.

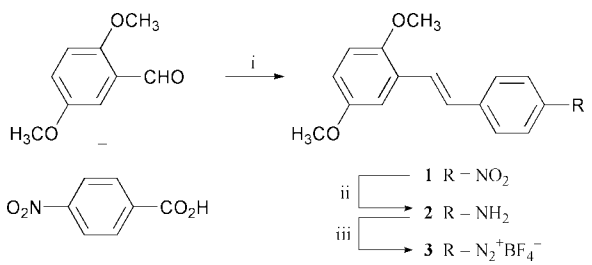

Scheme 1 *Reagents and conditions*: i, piperidine, reflux; ii, $FeSO_4$; iii, HBF_4, $NaNO_2$.

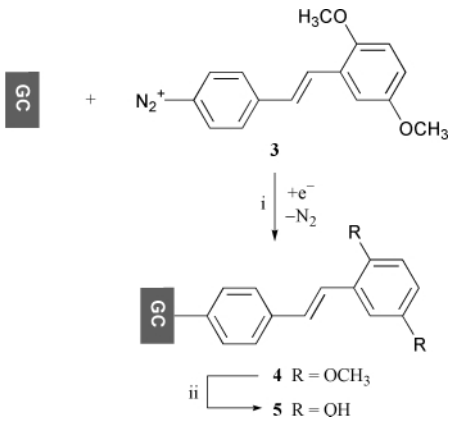

Scheme 2 *Reagents and conditions*: i, CH_3CN, −0.7 V *vs.* Ag/AgCl; ii, CH_2Cl_2, BBr_3, then H_2O.

Fig. 2 shows a series of cyclic voltammograms in an aqueous buffer over a range of sweep rates for a grafted GC electrode after demethylation to give the hydroquinone **5**. The anodic and cathodic peak potentials (−26 mV and −156 mV *vs.* Ag/AgCl respectively) are independent of sweep rate. It is noted that redox activity is not observed for the GC-grafted dimethoxy derivative **4**. Furthermore, the anodic and cathodic peak currents are directly proportional to sweep rate, and integration of the peak areas (after background subtraction) yields a constant charge density of 3.1 + 0.1 C m^{-2} (3.0 to 3.3 C m^{-2} for three replicate electrodes). These observations are consistent with a fixed quantity of **5** adhered to the electrode surface and

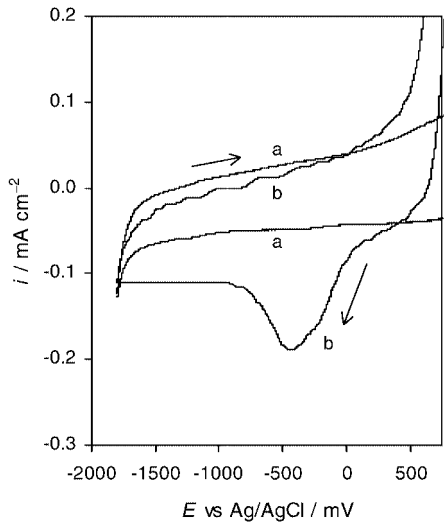

Fig. 1 Cyclic voltammograms in absence (curve a) and presence (curve b) of 5 mM **3** on a freshly polished glassy carbon electrode in a 0.1 M solution of Bu_4NBF_4 in acetonitrile. v = 200 mV s^{-1}.

 DOI: 10.1039/b107921b

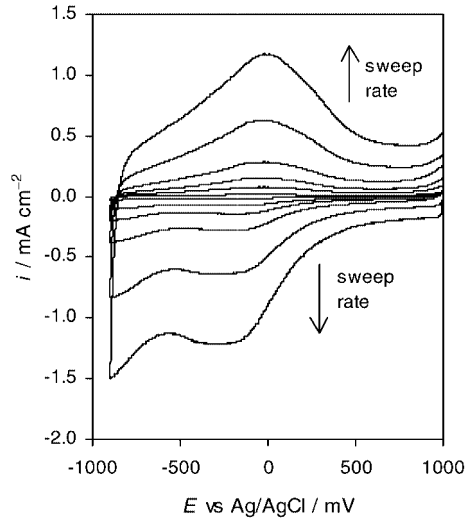

Fig. 2 Cyclic voltammograms for a glassy carbon electrode grafted with **5** in 0.1 M Bu_4NBF_4 in acetonitrile for a series of potential sweep rates: 10, 50, 100, 200, 500 and 1000 mV s^{-1}.

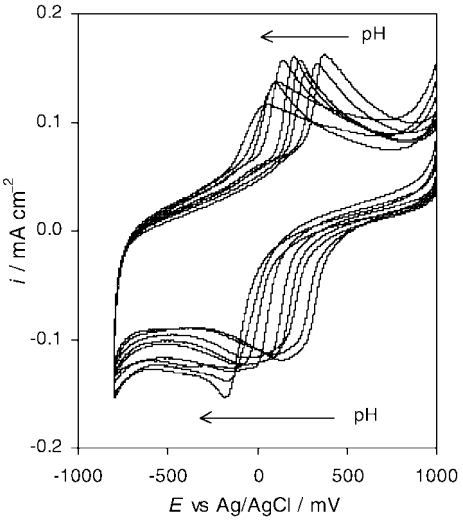

Fig. 3 Cyclic voltammograms for a glassy carbon electrode grafted with **5** in a range of 0.1 M phosphate buffers with pH: 2.65, 4.40, 4.41, 5.25, 6.00, 7.21, 8.16, 9.35 and 10.11. 0.1 M v = 200 mV s^{-1}.

indicate a coverage of 1.6×10^{-9} mol cm^{-2} for the grafted hydroquinone based on a 2 electron redox process. This is consistent with the coverage found by Pinson *et al.* for the formation of a close pack layer of grafted 4-nitrophenyl groups on glassy carbon ($\Gamma = 1.4 \times 10^{-9}$ mol cm^{-2}).[6]

The effects of solution hydrodynamics on a grafted hydroquinone GC rotating disc electrode were examined. Here, the charge associated with the anodic and cathodic peaks does not vary with electrode rotation rate. This is consistent with the redox process being attributable to a firmly tethered surface species rather than a solution species.

Fig. 3 shows cyclic voltammograms for the grafted electrode in a range of aqueous 0.1 M phosphate buffers. Again, the charge associated with the anodic and cathodic peaks does not vary with alteration of solution conditions. There is a progressive cathodic shift in the anodic and cathodic peaks with increase in pH (48.8 and 51.8 mV $decade^{-1}$ respectively). These shifts do not agree well with the expected 58.15 mV $decade^{-1}$ at 20 °C and show poor linearity. However, the open circuit potential of the grafted electrode in these buffers shows good agreement with a slope of 56.18 mV $decade^{-1}$ and good linearity ($r^2 = 0.997$). In comparison, freshly polished bare GC electrodes show only small slopes of *ca.* 10 mV $decade^{-1}$. Consequently, we attribute the pH-sensing utility to the grafted hydroquinone.

In conclusion, we have directly tethered a novel pH-sensing hydroquinone moiety to glassy carbon. The hydroquinone entity is formed after the diazonium grafting reaction from a dimethoxystilbene residue so that the hydroquinone does not impede the coupling process. A Nernstian response for the grafted hydroquinone is found indicating that direct attachment does not alter the hydroquinone couple. Future exploitation of this effect by grafting **3** on other carbon materials such as graphite and carbon could lead to the development of a pH-sensor.

The authors wish to acknowledge the Massey University Research Fund (1998) for financial support of Xinhao Yang.

Notes and references

† *Selected data* for **3**: IR: (KBr): $\nu_{N\equiv N}$ 2212 cm^{-1}, $\nu_{C=C}$ 1622 cm^{-1}. ^1H NMR (DMSO-d_6, TMS) δ: 8.62 (d, 2H, ArH), 7.13 (d, 2H, ArH), 7.93–7.53 (app q, AB system, 2H, HC=CH), 7.31 (d, 1H, Ar′H), 7.05–7.00 (m, 2H, Ar′H), 3.85 (s, 3H, OCH_3) and 3.78 (s, 3H, OCH_3). Analysis calculated for $C_{16}H_{15}N_2O_2BF_4$: C 54.24, H 4.24, N 7.91; found: C 54.29, H 4.31, N 7.82.

1 J. B. Donnet and P. Ehrburger, *Carbon*, 1977, **15**, 143.
2 A. D. Jannakoudakis, P. D. Jannakoudakis, E. Theodoridou and J. O. Besenhard, *J. Appl. Chem.*, 1990, **20**, 619.
3 M. L. Bowers and B. A. Yenser, *Anal. Chim. Acta*, 1991, **243**, 43.
4 R. W. Murray, *Electroanal. Chem.*, 1984, **13**, 191.
5 E. Fitzer, K. H. Geigl, W. Heitner and R. Weiss, *Carbon*, 1987, **18**, 389; W. P. Hoffman, W. C. Curley, T. W. Owens and H. T. Phan, *J. Mater. Sci.*, 1991, **26**, 4545.
6 H. Delamar, R. Hitmi, J. Pinson and J.-M. Saveant, *J. Am. Chem. Soc.*, 1992, **114**, 5883.
7 P. Allongue, B. Desbat, O. Fagebaume, M. Delamar, R. Hitmi, J. Pinson and J.-M. Saveat, *J. Am. Chem. Soc.*, 1997, **119**, 201; M. Delamar, G. Desarmot, O. Fagebaume, R. Hitmi, J. Pinson and J.-M. Saveant, *Carbon,*, 1997, **35**, 801.
8 A. J. Downard and A. D. Roddick, *Electroanalysis*, 1995, **7**, 376; A. J. Downard and A. D. Roddick, *Electroanalysis*, 1997, **9**, 693.
9 C. Bourdillon, M. Delamar, C. Demaille, R. Hitmi, J. Moiroux and J. Pinson, *J. Electroanal. Chem.*, 1992, **336**, 113.
10 H. Ulrich and A. A. R. Sayigh, *J. Org. Chem.*, 1966, **31**, 4146.
11 W. J. Farrissey Jr., F. P. Recchia and A. A. R. Sayigh, *J. Org. Chem.*, 1969, **34**, 2785.

CHEMCOMM
Communication
www.rsc.org/chemcomm

New cyclodextrin dimer and trimer: formation of biphenyl excimer and their molecular recognition

Ken Sasaki, Masahiko Nagasaka and Yasuhisa Kuroda*

Department of Polymer Science, Kyoto Institute of Technology, Matsugasaki, Sakyo-ku, Kyoto 606-8585, Japan. E-mail: ykuroda@ipc.kit.ac.jp

Received (in Cambridge, UK) 5th September 2001, Accepted 1st November 2001
First published as an Advance Article on the web 16th November 2001

New cyclodextrin oligomers bridged with biphenyl moieties are synthesized, among which only the doubly bridged dimer shows excimer formation behaviour in an aqueous solution.

Oligomeric cyclodextrins are one of the most attractive host molecules to provide expanded binding sites showing characteristic specificity. Among possible cyclodextrin oligomers, the dimers have been most extensively investigated.[1] Another interesting aspects of these cyclodextrin oligomers may be potential activities to control the recognition specificity by using conformational change of the relatively large recognition space of the host. The variety of linker moieties connecting the cyclodextrin recognition sites make it possible to create unique specificity and functions compared with rather monotonous recognition abilities of original cyclodextrins. Here we report new types of dimeric and trimeric cyclodextrins bridged with biphenyl moieties which are soluble both in water and various types of organic solvents. The dimer shows unique conformational change which is accompanied by excimer formation between two biphenyl moieties.

The cyclodextrin used in this work is per-*O*-methyl-6A,6D-diamino-β-cyclodextrin (**1**) which is known to be soluble not only in aqueous solution but also in various types of organic solvents.[2] The new doubly bridged cyclodextrin oligomers, **2** and **3**, were obtained from the reaction of **1** with 4,4′-biphenyldicarbonyl chloride in THF in 30% and 9% yields respectively (Scheme 1). The single bridged dimer **4** is also prepared by a similar reaction to the reference compound. One of the great advantages of permethylated cyclodextrin in these syntheses is that the preliminary purification of these products may be performed on a normal silica-gel column which is able to manage relatively large-scale reaction products. The 1H NMR and mass spectra of these compounds show satisfactory agreement with the expected structures.† The electronic spectra of these oligomeric cyclodextrins show quite a normal absorption of the biphenyl moiety at 282 nm in water, of which molar absorption coefficients are roughly proportional to the number of chromophors in the molecule, *i.e.* log ε of **2**, **3** and **4** are 4.70, 4.88 and 4.49 respectively (Fig. 1a). In contrast, an interesting

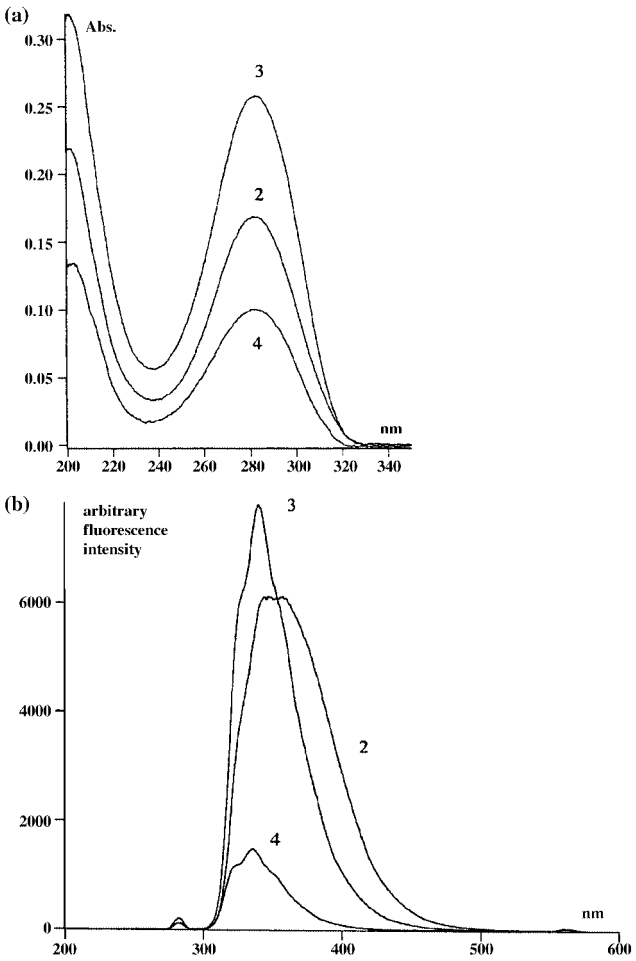

Fig. 1 a) Electronic spectra of cyclodextrin oligomers **2**, **3** and **4** in H_2O. b) Fluorescence spectra of cyclodextrin oligomers **2**, **3** and **4** in H_2O (λ_{ex} = 282nm). [**2**] = [**3**] = [**4**] = 3.4×10^{-6} M.

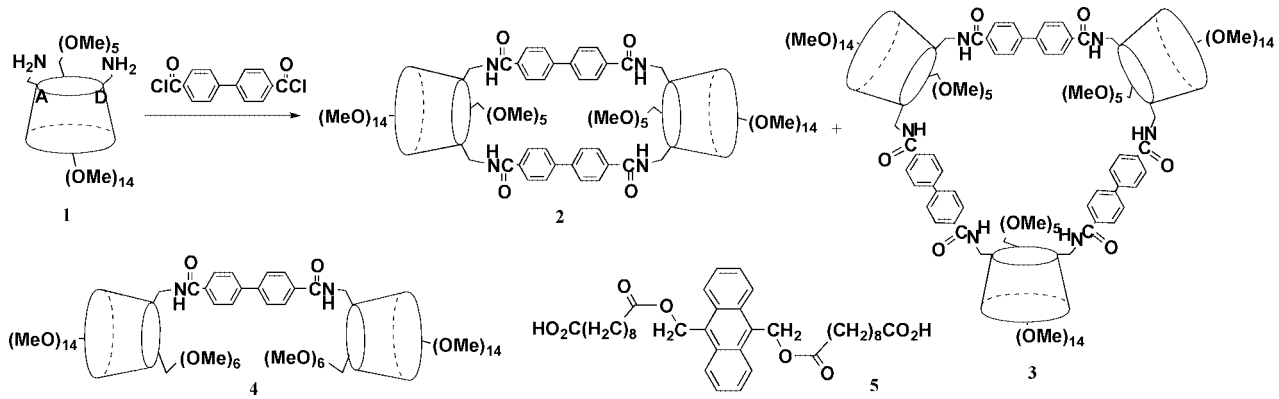

Scheme 1 Cyclodextrin oligomers and substrate.

 DOI: 10.1039/b107987e

difference is observed in the fluorescence spectra of these compounds. As shown in Fig. 1b, the shapes of the fluorescence spectra of **3** and **4** are essentially identical but that of **2** is quite different from others. The red shifted and broadening spectrum of **2** is similar to that of the recently reported biphenyl excimer adsorbed on clay.[3] Since **3** and **4** show no such behaviour, only the closed structure of **2** may assist to associate two biphenyl groups in the parallel mode to generate the excimer emission. It is interesting to understand whether such modified emission of **2** comes from a rigid conformation similar to that of biphenyl molecules strongly adsorbed on clay or from rather simple equilibrium between flexible conformations of **2**. In order to clarify the origin of the driving force of the excimer formation, the fluorescence spectra in different solvents were compared. Interestingly, the fluorescence of **2** in MeOH and $CHCl_3$ becomes the same as that of the monomeric biphenyl group. The observation is quite different from that reported for the 1,3-bis(biphenyl)propane system, where the excimer formation is controlled by the solvent microviscosities.[4] The results indicate that the present cyclodextrin dimer **2** has at least two conformers, the stacked form and the separate form, and the major driving force to control the equilibrium between these two forms is expected to be hydrophobic character (see Scheme 2). This conformational change is also confirmed by measurement of the variable temperature fluorescence spectra in the aqueous solution. The spectra show successive changes from an excimer fluorescence to a monomeric one during temperature change between 273 K and 348 K. The intensities of the spectra at 348 K are *ca*. 1/10 of that at 273 K and the processes are completely reversible. The preliminary analyses of these temperature dependent spectral changes assuming the two-state equilibrium give -8 ± 2 kcal mol^{-1} and -26 ± 5 e.u. for ΔH and ΔS for the present conformational change. The observed entropy change shows rather negative values, which is in contrast to the positive one sometimes observed for the typical hydrophobic processes.[4] The result indicates that the contacting surface of the biphenyl groups may not be wide enough to get large entropy gain during the association process. The thermodynamic parameters also show that *ca.* 50% of **2** in aqueous solution takes the stacked form at room temperature.‡

Finally the molecular recognition of the present new cyclodextrin oligomers is investigated by using the anthracence derivative **5** having two hydrophobic alkyl chains. The association constants for **2**, **3** and **4** determined by spectroscopic titration were 5200 ± 500, 27000 ± 2000 and 8600 ± 500 M^{-1}, respectively. Although the electronic spectra of an anthracene unit at 350–400 nm show slight red shifts with clear isosbestic

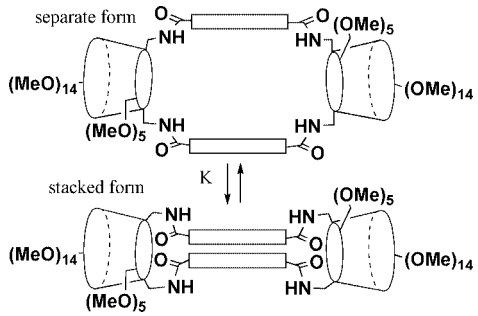

Scheme 2

points on addition of these oligomeric cyclodextrins, simple permethylcyclodextrin results in practically no appreciable spectral change of the present anthracene absorption. In spite of the fact that **5** is not necessarily optimised as the best substrate for the present new host molecules, the observed recognition shows interesting behaviour. The largest binding of **3** may suggest that the effects of the statistical enhancement of binding are due to three cyclodextrin units in the molecule and entropic advantage due to two-points fixation of the cyclodextrins at A,D-positions. In contrast, the similar or rather smaller association constants of **2** compared with non-cyclic dimer host **4** may indicates that the entropic advantage is largely cancelled by the extra energy for opening the stacked form of **2** during the association processes.§

Thus the present results show the unique properties of the present new cyclodextrin oligomers and interesting possibilities for controlling the conformations of these cyclodextrin oligomers. Further investigations of the detailed thermodynamic properties of these systems are now under way in our laboratory.

Notes and references

† The products are mixtures of the possible isomers which have different combinations of the positions bridged with the biphenyl moieties (bp), *i.e.* (A-bp-D)$_2$ and (A-bp-A)(D-bp-D) for **2** and (A-bp-D)$_3$ and (A-bp-A)(D-bp-D)(A-bp-D) for **3**. In the present stage the isomers are not separated even by using HPLC. Spectroscopic data of the mixtures, **2**: ^{1}H NMR (500 MHz. $CDCl_3$) δ 7.89–7.51 (16H, m, biphenyl), 5.32–4.98 (14H, m, C1-H), 4.60–2.75 (199H, m, other cyclodextrin H), HRMS(FAB) *m/z* calcd for $C_{150}H_{232}O_{70}N_4$ 3209.4717, found 3209.4680 (Δ = −1.2ppm), **3**: ^{1}H NMR (500 MHz. CDCl3) δ 7.95–7.63 (24H, m, biphenyl), 5.35–5.02 (21H, m, C1-H), 4.50–2.90 (300H, m, other cyclodextrin H), HRMS(FAB) *m/z* calcd for $C_{225}H_{348}O_{105}N_6$ 4816.2142, found 4816.2158 (Δ = +0.3ppm).

‡ The fluorescence of **2** in H_2O at room temperature may contain the excimer fluorescence and the monomeric one which originates from not only the separate form but also the stacked one in a hydrophobic environment.[6]

§ The fluorescence of the anthracene moiety in **5** increases in intensity by 30–50% on addition of the present hosts, indicating some energy transfer from the biphenyl moieties to the guest molecule.

1 For the first example of cyclodextrin dimer, see: I. Tabushi, Y. Kuroda and K. Shimokawa, *J. Am. Chem. Soc.*, 1979, **101**, 1614; For recent examples, see the following articles and references cited therein, R. Breslow, S. Halfon and B. Zhang, *Tetrahedron*, 1995, **51**, 377; Y. Okabe, H. Yamamura, K. Obe, K. Ohta, M. Kawai and K. Fujita, *J. Chem. Soc., Chem. Commun.*, 1995, 581; F. Veneam, A. E. Rowan and R. J. M. Nolte, *J. Am. Chem. Soc.*, 1996, **118**, 257; C. A. Haskard, B. L. May, T. Kurucsev, S. F. Lincoln and C. J. Easton, *J. Chem. Soc., Faraday Trans.*, 1997, **93**, 279; H. Yamamura, S. Yamada, K. Kohno, N. Okuda, S. Araki, K. Kobayashi, R. Katakai, K. Kano and M. Kawai, *J. Chem. Soc., Perkin Trans. 1*, 1999, 2943; S.-H. Chiu, S. C. Myles, R. L. Garrell and J. F. Stoddart, *J. Org. Chem.*, 2000, **65**, 2792.

2 Y. Kuroda, O. Kobayashi, Y. Suzuki and H. Ogoshi, *Tetrahedron Lett.*, 1989, **51**, 7225; For reduction of the diazidecyclodextrin precursor, see: A. T. Moore and H. N. Rydon, *Org. Synth.*, 1973, 586.

3 A. P. P. Cione, J. C. Scaiano, M. G. Neumann and F. Gessner, *J. Photochem. Photobiol A*, 1998, **118**, 205.

4 J. Emert, C. Behrens and M. Goldenberg, *J. Am. Chem. Soc.*, 1979, **101**, 771.

5 G. Nemethy and H. A. Scheraga, *J. Chem. Phys.*, 1962, **36**, 3401; G. Nemethy, *Angew. Chem., Int. Ed. Engl.*, 1967, **6**, 195.

6 A. Ueno, K. Takahashi and T. Osa, *J. Chem. Soc., Chem. Commun.*, 1980, 921.

CHEMCOMM Communication
www.rsc.org/chemcomm

Zn nanobelts: a new quasi one-dimensional metal nanostructure

Yewu Wang,* Lide Zhang, Guowen Meng, Changhao Liang, Guozhong Wang and Shuhui Sun

Institute of Solid State Physics, Chinese Academy of Sciences, Hefei 230031, P. R. China. E-mail: ywwangcn@china.com

Received (in Cambridge, UK) 11th September 2001, Accepted 6th November 2001
First published as an Advance Article on the web 19th November 2001

A large quantity of metal Zn nanobelts have been synthesized by a simple approach, which involves thermal decomposition of ZnS powder, followed by Zn deposition.

Low dimensional systems represent one of the most important frontiers in advanced materials research.[1–3] Quasi one-dimensional (1D) nanostructured materials, such as nanowires and / or nanotubes, have been successfully synthesized and have received much attention due to their peculiar optical, electrical, thermoelectric properties and potential applications in nanodevices.[4–7] Recently, semiconducting oxide nanobelts, a new group of 1D nanomaterials with a rectangular cross section, have been synthesized, and their morphology is distinctly different from those of nanowires and nanotubes.[8] The nanobelts could be an ideal system for fully understanding dimensionally confined transport phenomena in functional oxides. Through confinement of metals to quasi one-dimension, a variety of changes in their characteristics are induced.[9] Therefore, to fully study the fundamental physical and chemical properties of quasi-1D metal systems, the synthesis of metal nanostructures including nanowires, nanotubes and nanobelts are very important. Up to now, considerable effort has been focused on the synthesis of metal nanowires and nanotubes.[9–14] However, there have been no reports about metal nanobelt synthesis. In this communication, we describe the fabrication of a new quasi-1D metal nanostructure: Zn nanobelts. Successful synthesis of Zn nanobelts will open up the possibility of fully studying physical and chemical properties of quasi-1D metal nanomaterial systems.

A silicon wafer (5 × 10 mm) was used as a substrate for the growth of Zn nanobelts. The substrate was cleaned by a standard treatment in piranha solution (30% H_2O_2–20% H_2SO_4) and rinsed with de-ionized water. Yumoto *et al.* have used pure Zn metal bars as raw materials to fabricate Zn crystals.[15] This method, however, can not produce quasi-one-dimensional Zn crystals such as ribbons or whiskers owing to the fast production of Zn vapor. The produced rate of Zn vapor formed from pure ZnS powder decomposition by thermal evaporation is much slower than the rate of Zn vapor from Zn powder.[16] In order to control the produced rate of Zn vapor, pure ZnS and C powders were used as raw materials in our experiment to synthesize Zn nanobelts. The ZnS was mixed with graphite powder (mass ratio about 1 : 1) and placed in the middle of an alumina boat, and the cleaned Si substrate was placed next to the mixed starting raw powder along the downstream side of flowing argon. The alumina boat, covered with a quartz plate to maintain a higher vapor pressure, was placed in the center of a quartz tube that was inserted in a horizontal tube furnace. Prior to heating, the system was flushed with high purity Ar for 1 h to eliminate O_2, and pumped down to 5×10^{-5} Torr. Then, under a constant flow of high purity Ar gas (100 sccm), the furnace was rapidly heated to 1000 °C (about 5 min) and held at this temperature for 120 min, and subsequently cooled to room temperature. It was observed that white sponge-like products appeared on the surface of the Si substrate.

The synthesized products were characterized using scanning electron microscopy [(SEM) JEOL JSM-6300], X-ray diffraction diffractmetry [(XRD) MXP18AHF], high-magnification TEM [(HRTEM) JEOL-2010] and energy-dispersed X-ray spectrometry (EDS). For HRTEM observation, the products were ultrasonically dispersed in ethanol and a drop of this solution was then placed on a Cu grid coated with a holey carbon film.

SEM observation (Fig. 1a) revealed that the product consisted of a large quantity of wirelike nanostructures. XRD measurement (Fig. 1b) shows that the product is hexagonal structured Zn with lattice constants of a = 0.2655 nm and c = 0.4928 nm, consistent with the standard values for bulk Zn.[17] It should be noted that no diffraction peaks from ZnO or other impurities have been found in our samples. The morphology, structure and composition of the synthesized products have been characterized in detail using SEM, HRTEM, selected area electron diffraction (SAED) and EDS. A low-magnification SEM image (Fig. 2a) of the synthesized products shows that the wirelike nanostructures have typical lengths in the range of several to several tens of micrometers. A representative high-magnification SEM image (Fig. 2b) of a Zn wirelike nanostructure reveals that its geometrical shape is beltlike, distinct from previously reported nanowires and nanotubes, and its thickness is about 20 nm. It can be seen (Fig. 3a and b) that each nanobelt has a uniform width along its entire length, and the typical widths of the nanobelts are in the range 40–200 nm. No nanoparticles were observed at the ends of the nanobelts. The SAED pattern and HRTEM image (Fig. 3c) reveal that the Zn nanobelts are structurally uniform and single crystalline. The SAED pattern (Fig. 3c, inset) recorded perpendicular to the nanobelt long axis could be indexed for the [010] zone axis of

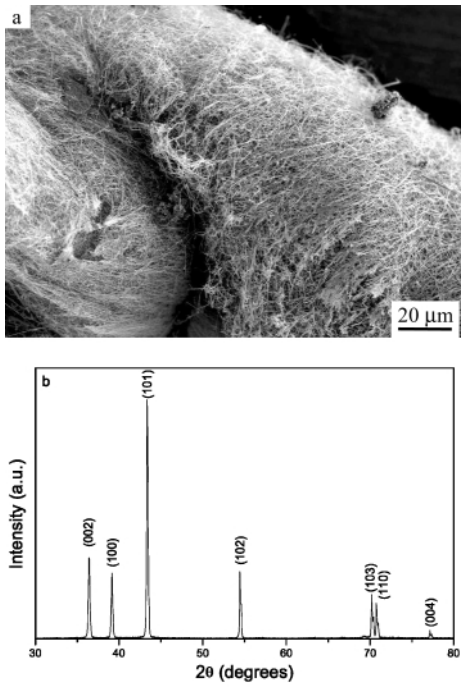

Fig. 1 (a) A typical SEM image of bulk of Zn nanobelts. A large amount of the nanobelts are distributed homogeneously on the Si substrate. (b) XRD pattern taken on the bulk of the Zn nanobelts. The numbers above the peaks correspond to the (*hkl*) values of the hexagonal structure.

 DOI: 10.1039/b108158f

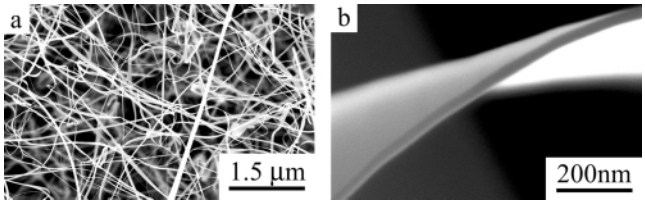

Fig. 2 SEM images of the Zn nanobelts showing their geometrical shapes and thickness. (a) a low-magnification SEM image of the synthesized Zn nanobelts. (b) a high-magnification SEM image of a Zn nanobelt, revealing the shape characteristics of the belt.

single crystalline Zn and suggests that the nanobelt growth occurs along the <100> direction. In addition, Fig. 3c also shows a lattice-resolved HRTEM image of a Zn nanobelt with a width of *ca.* 100 nm; this image clearly reveals the (001) and (101) atomic planes with separations of 0.4894and 0.2099 nm, respectively. We have also used EDS to address the composition of the nanobelts. EDS analysis (Fig. 4) demonstrates that the nanobelts contain only Zn, and no any other element is found. The Cu peaks are generated by the copper grid.

The question arises as to how the Zn nanobelts are formed. There exist several models to explain the growth for crystalline whiskers including dislocation and vapor–liquid–solid (VLS) mechanisms.[18–21] In the present case, however, none of the above mechanisms seem suitable to account for the growth of the Zn nanobelts. This is because first, no evidence of dislocations was found in our analysis, and second, there were no nanoparticles observed on any ends of the Zn nanobelts. In addition, the only source material used in our experiment is pure ZnS and graphite powder. Therefore, it is likely that the Zn nanobelts follow a growth mechanism similar to the vapor–solid

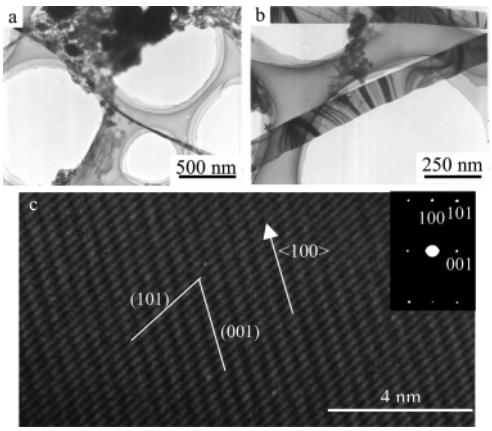

Fig. 3 TEM and HRTEM images of the Zn nanobelts: (a and b) images of several straight and twisted Zn nanobelts. (c) HRTEM image of a Zn nanobelt which shows that the nanobelts are single crystalline and free from dislocation and defects. (Inset) The corresponding electron diffraction pattern recorded with the electron beam perpendicular to the long axis of a belt, showing the growth direction to be <100>.

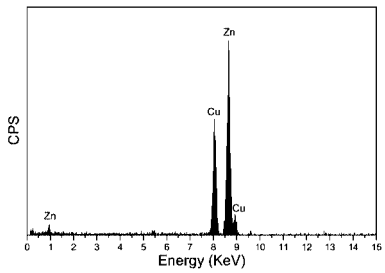

Fig. 4 EDX spectra recorded at the position of the white dot in Fig. 3b.

(VS) mechanism[8–22] First, the unidirectional motion of the Zn atom cloud driven by the carrying gas is a key factor in the preferational 1D growth of the Zn nanobelts. Secondly, the relatively high-saturated vapor pressure of Zn guarantees the concentration of this element necessary for the further growth of the Zn nanobelts. The Zn vapor is generated by the reaction of eqn. (1) at high temperature (1000 °C):

$$\mathrm{ZnS\ (s)} \rightarrow \mathrm{Zn\ (g)} + \mathrm{S\ (g)} \quad (1)$$

$$\mathrm{C\ (s)} + 2\mathrm{S\ (g)} \rightarrow \mathrm{CS_2\ (g)} \quad (2)$$

The Zn vapor is transported to, and deposited on, the surface of Si substrate in the relatively low temperature zone to form nanobelts due to the epitaxial growth of crystals. Meanwhile, the CS_2 vapor [eqn. (2)] is carried away from the furnace by the flowing Ar.

In conclusion, vapor transport has been employed to synthesize single crystalline Zn nanobelts with well-defined morphology distinct from those of metal nanowires and nanotubes. The synthesis of those single crystalline metal nanobelts may open up new possibilities for experimental and theoretical understanding of dimensionally confined transport phenomena of quasi-1D metal nanomaterials.

Notes and references

1 (*a*) A. P. Alivisatos, *Science*, 1996, **271**, 937–937; (*b*) L. Lu, M. L. Sui and K. Lu, *Science*, 2000, **287**, 1463–1466.
2 (*a*) C. Dekker, *Phys. Today*, 1999, **52**, 22–28; (*b*) Y. Cui and C. M. Lieber, *Science*, 2001, **291**, 851–853.
3 (*a*) J. Hu, T. W. Odom and C. M. Lieber, *Acc. Chem. Res.*, 1999, **32**, 435–445; (*b*) X. F. Duan, Y. Huang, Y. Cui, J. F. Wang and C. M. Lieber, *Nature*, 2001, **409**, 66–69.
4 (*a*) X. F. Duan and C. M. Lieber, *Adv. Mater.*, 2000, **12**, 298–302; (*b*) P. M. Ajayan, *Chem. Rev.*, 1999, **99**, 1787–1799.
5 M. S. Gudiksen and C. M. Lieber, *J. Am. Chem. Soc.*, 2000, **122**, 8801–8802.
6 C. C. Chen and C. C. Yeh, *Adv. Mater.*, 2000, **12**, 778–741.
7 Y. Y. Wu and P. D. Yang, *Chem. Mater.*, 2000, **12**, 605–607.
8 Z. W. Pan, Z. R. Dai and Z. L. Wang, *Science*, 2001, **291**, 1947–1949.
9 (*a*) N. H. Huang, A. Choudrey and P. D. Yay, *Chem. Commun.*, 2000, 1063–1064; (*b*) M. Nishizawa, V. P. Menon and C. R. Martin, *Science*, 1995, **268**, 700–702; (*c*) T. M. Whitney, J. S. Jing, P. C. Searson and C. L. Chien, *Science*, 1993, **261**, 1316–1319; (*d*) E. Braun, Y. Eichen, U. Sivan and G. Ben-Yoseph, *Nature*, 1998, **391**, 775–778.
10 Z. B. Zhang, D. Gekhtman, M. S. Dresselhaus and J. Y. Ying, *Chem. Mater.*, 1999, **11**, 1959–1665.
11 W. K. Hsu, J. Li, H. Terrones, M. Terrones, N. Grobert, Y. Q. Zhu, S. Trasobares, J. P. Hare, C. J. Pickett, H. W. Kroto and D. R. W. Watton, *Chem. Phys. Lett.*, 1999, **301**, 159–166.
12 B. Nikoobakht, Z. L. Wang and M. A. El-sayed, *J. Phys. Chem. B*, 2000, **104**, 8635–8640.
13 C. J. Brumlik, V. P. Meron and C. R. Martin, *J. Mater. Res.*, 1994, **9**, 1174–1183.
14 C. J. Brumlik and C. R. Martin, *J. Am. Chem. Soc.*, 1991, **113**, 3174–3175.
15 H. Yumoto and R. R. Hasiguti, *J. Cryst. Growth*, 1986, **75**, 289–294.
16 R. K. Willardson and H. L. Goering, *Compound Semiconductors*, Reinold, New York, 1962.
17 Powder Diffraction File, Inorganic Vol. No PD1S-SiRB, 4-831 file, Published by the Joint Committee on Powder Diffraction Stardards USA, Swarthmere, PA.
18 A. M. Morales and C. M. Lieber, *Science*, 1998, **279**, 208–211.
19 J. D. Holines, K. P. Johnston, R. C. Doty and B. A. Korgel, *Science*, 2000, **25**, 1471–1473.
20 H. Y. Peng, Z. W. Pan, L. Xu, X. H. Fan, N. Wang, C. S. Lee and S. T. Lee, *Adv. Mater.*, 2001, **13**, 317–320.
21 H. Z. Zhang, Y. C. Kong, Y. Z. Wang, X. Du, Z. G. Bai, T. T. Wang, D. P. Yu, Y. Ping, Q. L. Hang and S. Q. Feng, *Solid State Commun.*, 1999, **109**, 677–682.
22 M. Satoh, N. Tanaka, Y. Veda, S. Ohshio and H. Saitoh, *Jpn. J. Appl. Phys.*, 1999, **38**, L586–589.

CHEMCOMM Communication
www.rsc.org/chemcomm

Light-harvesting metal dendrimers appended with additional organic chromophores: a tetranuclear heterometallic first-generation dendrimer exhibiting unusual absorption features†

Nathan D. McClenaghan, Frédérique Loiseau, Fausto Puntoriero, Scolastica Serroni and Sebastiano Campagna*

Dipartimento di Chimica Inorganica, Chimica Analitica e Chimica Fisica, Università di Messina, Via Sperone 31, Messina, I-98166 Italy. E-mail: photochem@chem.unime.it

Received (in Cambridge, UK) 9th October 2001, Accepted 31st October 2001
First published as an Advance Article on the web 30th November 2001

A new tetranuclear heterometallic complex carrying six pyrenyl chromophores at the periphery has been prepared: this species is an example of a new class of light-harvesting metal dendrimer, in which multinuclear metal dendrimers are surrounded by additional purely organic chromophores.

Dendrimers based on Ru(II) and Os(II) polypyridine complexes have recently attracted a great deal of interest because they can play the role of light-harvesting antenna systems in artificial solar energy conversion schemes.[1–4] Most of the light-harvesting metal-based dendrimers reported so far essentially belong to two general categories: (i) species in which the metal-based chromophores are present in all the positions of the dendrimeric array[1,5] and (ii) species in which a single metal-based chromophore is located at the core of the dendrimer, surrounded by purely organic wedges bearing chromophores at the periphery (Fig. 1).[2,5] In the latter case (ii), the light energy absorbed by the peripheral organic chromophores is transferred to the central metal-based chromophore by energy transfer processes which can be mediated either (a) by the organic dendritic framework by superexchange pathways or (b) by direct coulombic interactions allowed *via* dendritic folding. In the former case (i), both center-to-periphery or periphery-to-center energy transfer processes have been reported, the efficiency of which depends on the energy gradient within the dendritic metal branches. In both cases, strict requirements must be fulfilled for efficient energy transfer, for example the correct energy gradient within the multimetal array [for (i)-type dendrimers] or suitable distance and nature of the dendritic framework [for (ii)-type dendrimers].

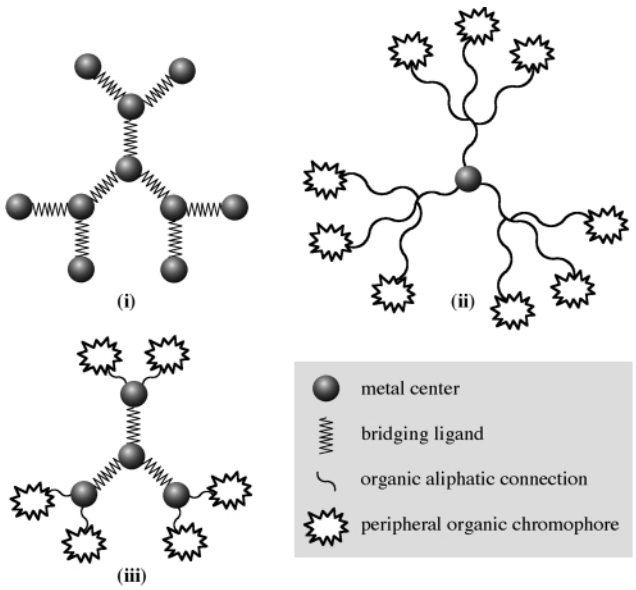

Fig. 1 Representation of metal-based light-harvesting dendrimers.

Here we report the synthesis and the absorption spectra and luminescence properties of a new tetranuclear mixed-metal dendrimeric complex **1** bearing six pyrenyl chromophores at the periphery (Fig. 2). Compound **1** belongs to the first-generation of a large class of luminescent and redox-active metal dendrimers based on the 2,3-dpp bridging ligand [2,3-dpp = 2,3-bis(2′-pyridyl)pyrazine],[1,5,6] and can also be regarded as a new type of light-harvesting dendrimer [(iii) in Fig. 1], coupling some properties of the two types of dendrimers (i) and (ii) discussed above. The four metal-based subunits constitute a (i)-type dendrimer, and the six appended pyrenyl chromophores resemble the peripheral subunits of (ii)-type dendrimers. This new approach allows us to obtain a dendrimer containing three 'layers' of chromophores (from the outer layer to the inner one: six pyrenyl units, three Ru-based chromophores and one Os-based one) in fewer synthetic steps.[6]

The synthesis of **1** is an application of the 'complexes as ligands/complexes as metals' synthetic approach.[7] The procedure is identical to that used for the synthesis of $[Os\{(\mu\text{-}2,3\text{-}dpp)Ru(bpy)_2\}_3]^{8+}$ **2** (bpy = 2,2′-bipyridine).[8] Apparently, the presence of the pyrenyl subunits does not affect the reactivity of the complex-metal species, giving similar yields under analogous reaction conditions.

The absorption spectrum of **1** is shown in Fig. 3, where the spectrum of **2** is also reported for comparison purposes. As expected, at longer wavelengths than 550 nm the spectra of **1** and **2** are almost coincident, with the absorption feature at about 550 nm receiving contributions from spin-allowed metal-to-ligand charge-transfer (MLCT) transitions (namely, Ru→μ-2,3-dpp and Os→μ-2,3-dpp CT) and the long tail which extends towards the IR region assigned to spin-forbidden MLCT transitions involving the Os(II) chromophore.[1,8] In **1**, the intense

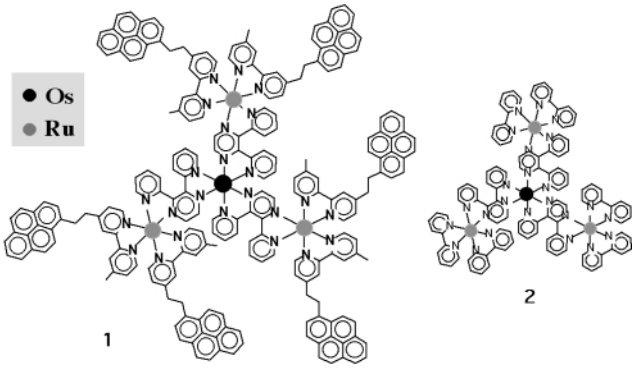

Fig. 2 Structural formula of **1** and of the tetranuclear compound **2**, used as a reference. For simplicity, the charges of the complexes are omitted.

† Electronic supplementary information (ESI) available: synthesis of 4-methyl-4′-[2-(1-pyrenyl)ethyl]-2,2′-bipyridine and synthetic scheme for **1**. See http://www.rsc.org/suppdata/cc/b1/b109068b

 DOI: 10.1039/b109068b

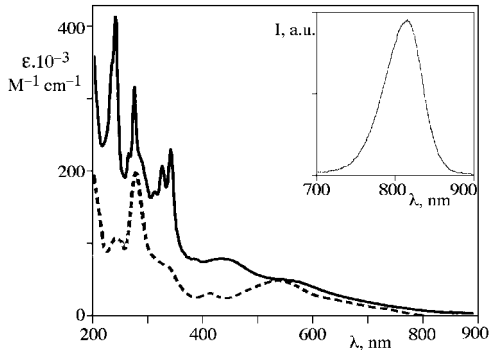

Fig. 3 Absorption spectra in acetonitrile of **1** (——) and **2** (- - - -). In the inset, the luminescence spectrum of **1** is shown.

and structured absorption peaks in the 310–350 nm region and at 239 nm can be mainly assigned to pyrene-centered transitions, 1La and 1Bb, respectively.[9,10] The broad absorption band around 320 nm which is present in **2**, assigned to 2,3-dpp centered (π–π^*) transitions[1,8] is obscured in **1** by the more intense pyrene-centered ^{1}La bands. Finally, the band peaking at 279 nm in **1** receives contributions from both the peripheral pyrenyl chromophores and the four metal subunits of the tetranuclear structure, containing the bpy-centered π–π^* absorption feature, already present in **2**.[6,8]

From the above discussion it appears that **1** significantly absorbs more than **2** in the UV region, confirming our expectations. However, Fig. 3 also shows that **1** absorbs significantly more than **2** in the region 400–550 nm. Indeed the absorption spectrum of **1** exhibits an intense broad band in that region (molar absorption of the band maximum, 8×104 M^{-1} cm^{-1}), which includes the Ru→bpy charge-transfer (CT) band peaking at 420 nm in **2**, but that clearly receives additional contributions from other transitions. To rationalize this behavior it should be considered that the pyrene subunits of **1** are good electron donor groups, in that they can be oxidized at about +1.2 V *vs*. SCE,[11] whereas the polypyridine ligand bpy and expecially the bridged 2,3-dpp are very good electron acceptors (reversible reduction process for 2,3-dpp is around −0.60 V *vs.* SCE).[6,8] The ethylene chains connecting bpy and pyrenyl subunits are flexible enough to allow direct interactions between the pyrenyl subunits with bpy and 2,3-dpp (for 2,3-dpp, CPK models suggest that conformations in which this latter ligand and pyrene can lie in almost parallel planes separated by < 360 pm are possible[12]). Therefore, intramolecular pyrene-to-bpy and/or pyrene-to-μ-2,3-dpp CT transitions (with the latter at lower energy) are possible. The intensity of such transitions can be relatively high: for example, CT transitions in [3,3]paracyclophane–quinhydrones lead to a molar absorbance of between 10^3 and 10^4 M^{-1} cm^{-1} depending on solvent polarity.[13] Significant charge transfer transitions from pyrenyl subunits to polypyridine ligands coordinated to Pt(II) have been recently reported, although in this latter case the pyrene and the polypyridine ligands were directly connected.[14] Similar transitions were also found in the adducts of dibenzyl ether dendrimers with fullerenes.[15] Since the number of such CT transitions in **1** can be high, the relatively intense broad band in the 400–550 nm region is tentatively assigned to these type of transitions (together with contributions from Ru→bpy CT transitions). This somewhat unexpected result is very interesting: the light-harvesting properties of **1** compared to **2** are improved by the presence of the additional peripheral chromophores much more than initially foreseen, due to the coming into play of visible absorption bands which arise from new intercomponent (supramolecular) CT transitions.

The luminescence properties of **1** (deoxygenated acetonitrile at room temperature: λ_{max} = 860 nm; τ = 16 ns; $\Phi = 5 \times 10^{-4}$. The uncorrected luminescence spectrum is shown in the inset of Fig. 3) are practically identical to those of **2** (λ_{max} = 860 nm; τ = 18 ns; $\Phi = 5 \times 10^{-4}$).[8] Therefore, the emission of **1** is assigned to the same excited state responsible for emission of **2**, that is the triplet Os→μ-2,3-dpp CT level.[8] The constancy of the luminescence lifetime and quantum yield on passing from **2** to **1** indicates that the pyrenyl subunits do not affect the luminescence properties of the Os core. Interestingly, the excitation spectrum closely matches the absorption spectrum, demonstrating that the light energy absorbed by the Ru-based chromophores and the peripheral pyrene subunits is quantitatively channelled to the Os core, which plays the role of the energy trap. Taken together, the absorption properties and the energy transfer processes occurring in **1** and the comparison of these data with those of the parent complex **2**, it appears that the presence of suitable peripheral organic chromophores can lead to metal dendrimers which would be better artificial antenna systems compared to the species reported so far.

In conclusion, we have prepared a new type of light-harvesting metal dendrimer, **1**, which couples the structural properties of former studied metal dendrimers. The new compound **1** exhibits better properties compared to the species previously reported, as far as the antenna properties are concerned, owing to the absorption of the additional organic chromophores and also to new absorption features originating from the interaction of the pyrene peripheral subunits with the tetranuclear metal-based core. Work is in progress to study in further detail the photophysical processes and to prepare larger and more complex systems of this type.

We thank MIUR (Project: Fotosintesi artificiale. Processi elementari in sistemi antenna e per separazione di carica), the CNR and the European Community (TMR on Network on nanometer size metal complexes) for financial support. F. L. also thanks the Marie Curie fellowships program.

Notes and references

1 V. Balzani, S. Campagna, G. Denti, A. Juris, S. Serroni and M. Venturi, *Acc. Chem. Res.*, 1998, **31**, 26 and references therein.
2 F. Vögtle, M. Pleovets, M. Nieger, G. C. Azzellini, A. Credi, L. De Cola, V. Marchis, M. Venturi and V. Balzani, *J. Am. Chem. Soc.*, 1999, **121**, 6290.
3 E. C. Constable, *Chem. Commun.*, 1997, 1073.
4 F. Barigelletti and L. Flamigni, *Chem. Soc. Rev.*, 2000, **29**, 1.
5 (*a*) A. Juris, in *Electron Transfer in Chemistry*, ed. V. Balzani, Wiley-VCH, Weinheim, 2001, vol. 3, p. 655, and references therein; (*b*) V. Balzani, P. Ceroni, A. Juris, M. Venturi, S. Campagna, F. Puntoriero and S. Serroni, *Coord. Chem. Rev.*, 2001, **219–221**, 545.
6 M. Sommovigo, G. Denti, S. Serroni, S. Campagna, C. Mingazzini, C. Mariotti and A. Juris, *Inorg. Chem.*, 2001, **40**, 3318.
7 S. Serroni, S. Campagna, F. Puntoriero, C. Di Pietro, F. Loiseau and N. D. McClenaghan, *Chem. Soc. Rev.*, in press.
8 S. Campagna, G. Denti, L. Sabatino, S. Serroni, M. Ciano and V. Balzani, *J. Chem. Soc., Chem. Commun.*, 1989, 1500.
9 M. Klessinger and J. Michl, *Excited States and Photochemistry of Organic Molecules*, VCH, Weinheim, 1995.
10 (*a*) W. E. Ford and M. A. J. Rodgers, *J. Phys. Chem.*, 1992, **96**, 2917; (*b*) G. J. Wilson, A. Launikonis, W. H. F. Sasse and A. W.-H. Mau, *J. Phys. Chem. A*, 1997, **101**, 4860; (*c*) J. A. Simon, S. L. Curry, R. H. Schmehl, T. R. Schatz, P. Piotrowiak, X. Lin and R. P. Thummel, *J. Am. Chem. Soc.*, 1997, **119**, 11012; (*d*) M. Hissler, A. Harriman, A. Khatyr and R. Ziessel, *Chem. Eur. J.*, 1999, **5**, 3366; (*e*) D. S. Tyson, K. B. Henbest, J. Bialecki and F. N. Castellano, *J. Phys. Chem. A*, 2001, **105**, 8154.
11 F. Puntoriero, unpublished results.
12 The 2,3-dpp ligand cannot be planar when it plays the role of a bridging ligand, because of steric constrains. As a first approximation we considered the plane of the pyrazine ring as the molecular plane.
13 H. A. Staab, C. P. Herz, C. Krieger and M. Rentea, *Chem. Ber.*, 1983, **116**, 3813.
14 J. F. Michalec, S. A. Bejune, D. G. Cuttell, G. C. Summerton, J. A. Gertenbach, J. S. Field, R. J. Haines and D. R. McMillin, *Inorg. Chem.*, 2001, **40**, 2193.
15 J.-F. Eckert, D. Byrne, J.-F. Nicoud, L. Oswald, J.-F. Nierengarten, M. Numata, A. Ikeda, S. Shinkai and N. Armaroli, *New J. Chem.*, 2000, **24**, 749.

CHEMCOMM
Communication
www.rsc.org/chemcomm

New insight into the dynamic behaviour of manganese ketene complexes: evidence for the scrambling of a carbene moiety over carbonyl ligands†

Yannick Ortin, Yannick Coppel, Noël Lugan,* René Mathieu and Michael J. McGlinchey‡

Laboratoire de Chimie de Coordination du CNRS, 205 route de Narbonne, 31077 Toulouse Cedex 4, France. E-mail: lugan@lcc-toulouse.fr

Received (in Cambridge, UK) 16th October 2001, Accepted 7th November 2001
First published as an Advance Article on the web 30th November 2001

The carbonyl of the ketene ligand in manganese complexes of the type $RCp(CO)_2Mn[\eta^2\text{-}R'(Ph)C{=}C{=}O]$ exchanges rapidly (NMR time-scale) with the CO ligands though a process that involves scrambling of a carbene moiety over the three carbonyl environments.

The formation of a ketene upon CO-insertion into a metal–carbene bond is considered as the key step in several useful synthetic reactions, such as Dötz's benzannulation reaction or the Hegedus β-lactam synthesis.[1] Though the formation of ketene complexes by coupling of CO and carbene ligands on a single metal centre is now well documented,[2,3] it is only recently that the reverse reaction—splitting of a ketene into carbene and CO ligands—has been explicitly observed.[3]

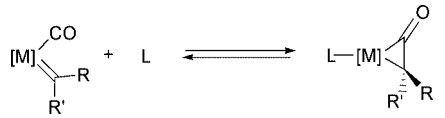

Our current studies on the reactivity of manganese alkynyl–carbene complexes[4] led us to investigate the structures of Mn *ketene* complexes. The present communication provides new insights into the dynamics of the latter species in solution.

The alkynylcarbene complex $RCp(CO)_2Mn{=}C(Ph)C{\equiv}CPh$ (**1**) was reacted with $Co_2(CO)_8$ and, after chromatographic workup, two new species were isolated (Scheme 1). The major product emerged as the cluster $RCpMnCo_2(CO)_6[\mu_3\text{-}\eta^4\text{-}CC(Ph){=}C(Ph)C(O)]$ (**3**), whose structure† exactly parallels that the known $CrCo_2(CO)_9[\mu_3\text{-}\eta^4\text{-}CC(Ph){=}C(OEt)C(O)]$, resulting from thermolysis of the parent group 6 alkynylcarbene complex $(CO)_5Cr[\mu_3\text{-}\eta^3\text{-}{=}C(OEt)C{\equiv}CPh]Co_2(CO)_6$.[5] This strongly suggests that **3** forms *via* the intermediacy of $RCp(CO)_2Mn[\mu_3\text{-}\eta^3\text{-}{=}C(Ph)C{\equiv}CPh]Co_2(CO)_6$ [**2**].

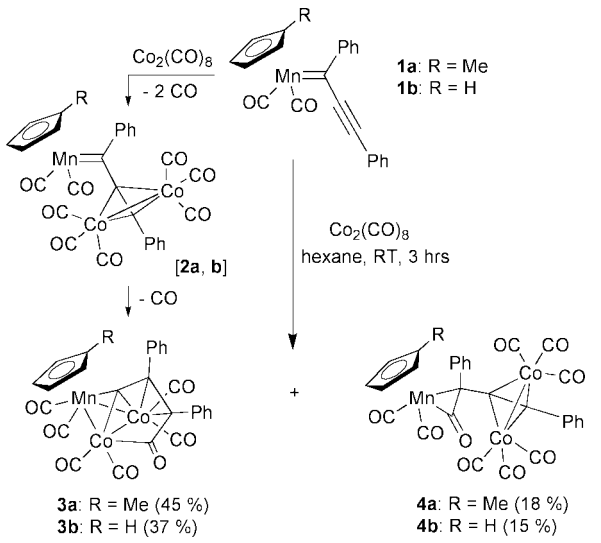

Scheme 1

The structure of the minor product, **4**, was established by X-ray diffraction for R = Me (Fig. 1),§ which revealed it to be a Mn–ketene complex whereby the ketene ligand bears a phenyl substituent and also a phenylalkynyl fragment bonded to a $Co_2(CO)_6$ unit. Without presupposing a mechanism for its formation, which is still to be established,¶ **4** derives from **1** by coordination of the alkyne moiety to a $Co_2(CO)_6$ unit and insertion of a carbonyl into the Mn=C linkage. The ketene adopts the so-called horizontal coordination mode,[6] as expected on electronic grounds.[7] This is evidenced by a value of 68.6° (ideal 90°) for the torsion angle {Cp-centroid}–{Mn}–{middle of C3–C10 vector}–{O3}. Metrical features around the Mn in **4a** are similar to those found in other $RCp(CO)_2Mn$(ketene) complexes.[2c,8]

Unexpectedly, the room temp. ^{13}C NMR spectrum of **4** recorded at 100 MHz showed only one signal in the region where carbonyls—in the broad sense of the term—are usually observed. This signal, observed at δ *ca.* 200, was characteristic only for the CO ligands attached to cobalt, and prompted us to investigate further the structure of **4** in solution. This was conveniently conducted on a ^{13}C-enriched sample of **4b** (R = H), synthesised from $Cp(^{13}CO)_2Mn{=}^{13}C(Ph)C{\equiv}CPh$ and $Co_2(CO)_8$. At 183 K, two additional sets of CO resonances become clearly observable (Fig. 2). The first set, centred at δ 228, is made up of two pairs of signals, C1′ and C2′, and C1″ and C2″, in a 58 : 42 ratio. The second set of signals, centred at δ 249 consists of two singlets, C3′ and C3″, also in a ratio of ~58 : 42. As the temperature is raised, coalescence of C3′ and C3″, C1′ and C2″, and C2′ and C1″ is observed. The C1′ and C2′, and C3′ signals can be attributed to the CO ligands, and to the carbonyl of the ketene ligand, respectively, within one diastereomer of **4b**. The double-primed signals are assigned to the corresponding carbon atoms of the other diastereomer. The fluxional process that permutes C3′ with C3″, C1′ with C2″, and

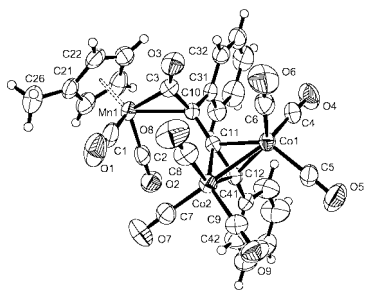

Fig. 1 A perspective view of the complex $MeCp(CO)_2Mn[\mu_3\text{-}\eta^4\text{-}O{=}C{=}C(Ph)C{\equiv}CPh]Co_2(CO)_6$ (**4a**).

† Electronic supplementary information (ESI) available: details of syntheses and spectral characterisation of the new complexes. See http://www.rsc.org/suppdata/cc/b1/b109218a

‡ On sabbatical leave from: Department of Chemistry, McMaster University, Hamilton, Ont., Canada L8S 4M1.

 DOI: 10.1039/b109218a

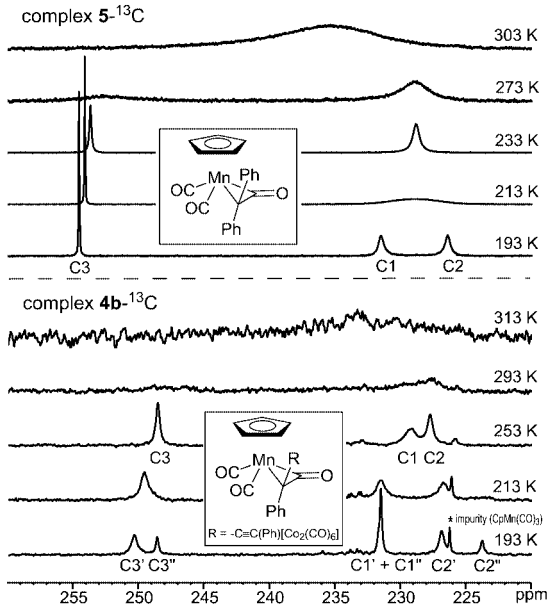

Fig. 2 Selected sections of the ^{13}C NMR spectra (CD_2Cl_2, 100 MHz) of ^{13}C-enriched samples of complexes **4b**-^{13}C (bottom) and **5**-^{13}C (top).

C2′ with C1″ can thus be interpreted in terms of a rapid rotation (NMR time-scale) of the ketene around an axis joining the Mn to the middle of C3–C10 bond. The coalescence behaviour of the C3′/C3″ resonances (and also of the Cp rings within the two diastereomers) led to an energy activation barrier of approximately 10 kcal mol^{-1} for this rotation process. At this stage, it is worth noting that the relative intensity of the C3 signal *vs.* the C1/C2 resonances clearly indicates that ^{13}C has been incorporated into the carbonyl function of the ketene. Above 253 K, the C1, C2 and C3 signals rapidly collapse to give an extremely broad signal located at δ *ca.* 236 ppm at 308 K,‖ suggesting a second type of dynamic exchange now involving the CO ligands attached to Mn *and* the carbonyl of the ketene ligand. This was clearly authenticated by spin saturation transfer experiments between the C1/C2 site and the C3 site.

Suspecting that the above process was more general, we reinvestigated the structure of a ^{13}C-enriched sample of $Cp(^{13}CO)_2Mn(O{=}^{13}C{=}CPh_2)$ (**5**-^{13}C)[8a,9] in solution. Clearly, the variable-temperature ^{13}C NMR spectra show initial coalescence of the CO ligands (C1 and C2) attributable to the rapid ketene rotation, and subsequent coalescence of the CO ligands and the ketene carbonyl (C3) (Fig. 2). The barriers were evaluated as 8.3 kcal mol^{-1} for the ketene rotation, and 12.2 kcal mol^{-1} for the second process. In addition, the J_{CC} value between C3 and the adjacent atom, C10, was found in **5** to be 52 ± 2 Hz at 203 K and 15 ± 2 Hz at 303 K; these data clearly establish the strictly intramolecular nature of the overall exchange process.

Many years ago, Redhouse and Herrmann[8a] did detect a dynamic phenomenon within complex **5** but, with the low-field NMR instrumentation then available, they were unable to observe a limiting low-temperature spectrum. Nor could they detect the ketene carbonyl at δ 254.5 which, unbeknownst to them, was also participating in a fluxional process.

The observation of a dynamic exchange process between the CO ligands and the carbonyl of the ketene in complexes **4** and **5** can be interpreted in terms of rapid transfer (NMR time-scale) of the carbene fragment CPh(R′), where R′ = C≡CPh[$Co_2(CO)_6$] (**4**) or Ph (**5**), over the carbonyl ligands. Scheme 2 intends to illustrate, in a sequential manner, how combinations of ketene rotations and carbene transfers would indeed allow *all three* carbonyls to exchange. Interestingly, we note that for **4b**, when the temperature is raised, the C1 and C2 sites broaden at different rates (see for example Fig. 2, 253 K spectrum). This is likely a consequence of a slight difference in the rate of carbene transfer within each of the diastereomers of **4b** (***1*** ⇆ ***2*** *vs.* ***2*** ⇆ ***3*** in Scheme 2, for instance).

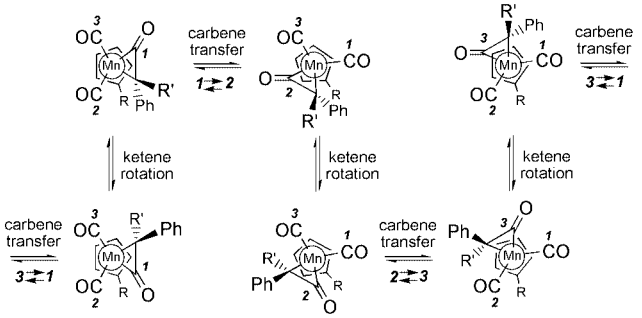

Scheme 2

The carbene transfer could proceed *via* (reversible) cleavage of the ketene into carbene and CO ligands on the Mn centre, as in Grotjahn's Ir system.[3] However, the intramolecular character of the current process would imply the formation of a 20-electron transient species. Alternatively, we suggest that the carbene migration could occur *via* the intermediacy of a 16-electron metallocyclobutan-1,3-dione.

In conclusion, the present observations bring further support to the view of manganese carbonyl ketene complexes as highly fluxional molecules. They are engaged in two independent dynamic processes, which result in the scrambling of the carbene moiety over the three carbonyl ligands.

Notes and references

§ *Crystal data* for **4a**: $C_{30}H_{17}Co_2MnO_9$, M = 694.24, triclinic, space group $P\bar{1}$ a = 9.464(2), b = 10.214(1), c = 14.691(2) Å, α = 81.41(1)°, β = 90.00(1)°, γ = 82.70(1)°, U = 1392.6(8) Å^3, T = 298 K, Z = 2, μ(Mo-Kα) = 1.68 mm^{-1}, 4596 reflections measured, 3863 unique (R_{int} = 0.019). The final $wR(F^2)$ was 0.0565 (all data). CCDC reference numbers 172720 and 172721. See http://www.rsc.org/suppdata/cc/b1/b109218a/ for crystallographic data in CIF or other electronic format.

¶ Complex **4** can be regarded as the result of the insertion of CO into the Mn=C bond of [**2**]. Yet, when **1a** was reacted with $Co_2(CO)_8$ under CO (4 bars, no significant change in the yield of **4a** was observed. Alternatively, carbene transfer from [**2**] to traces of $MeCpMn(CO)_3$ could also have resulted in the formation of **4a**. Such a mechanism has been demonstrated in a specific case,[8b] but does not apply here since treatment of **1a** by $Co_2(CO)_8$ in the presence of $Cp(CO)_3Mn$ produced exclusively **4a**, with no trace of **4b**. At present, we incline to the view that CO insertion proceeds intramolecularly following the initial replacement of a carbonyl ligand in $Co_2(CO)_8$ by the alkynyl unit in **1**. Thus, formation of [**2**] (and then **3**) may in fact compete with that of **4**.

‖ Attempts to record data at higher temperature (in toluene-d_8) became problematic because of partial decomposition during acquisition.

1 F. Z. Dörwald, *Metal Carbenes in Organic Synthesis*, Wiley-VCH, Weinheim, New York, Chichester, Brisbane, Singapore, Toronto, 1999.

2 (*a*) W. A. Herrmann and J. Plank, *Angew. Chem., Int. Ed. Engl.*, 1978, **17**, 525; (*b*) H. Fischer, *Angew. Chem., Int. Ed. Engl.*, 1983, **22**, 874; (*c*) T. W. Bodnar and A. R. Cutler, *J. Am. Chem. Soc.*, 1983, **105**, 5926; (*d*) W. A. Herrmann, J. Plank, G. W. Kreichbaum, M. L. Ziegler, H. Pfisterer, J. L. Atwood and R. D. Rogers, *J. Organomet. Chem.*, 1984, **264**, 327; (*e*) T. Mitsudo, H. Watanabe, T. Sasaki, Y. Takegami and Y. Watanabe, *Organometallics*, 1989, **8**, 368; (*f*) S. E. Gibson, M. F. Ward, M. Kipps, P. D. Stanley and P. A. Worthington, *Chem. Commun.*, 1996, 263.

3 D. B. Grotjahn, G. A. Bikzhanova, L. S. B. Collins, T. Concolino, K.-C. Lam and A. L. Rheingold, *J. Am. Chem. Soc.*, 2000, **122**, 5222.

4 Y. Ortin, Y. Coppel, N. Lugan, R. Mathieu and M. J. McGlinchey, *Chem. Commun.*, 2001, 1690.

5 I. Moldes, J. Ros, M. Rosario Torres, A. Perales and R. Mathieu, *J. Organomet. Chem.*, 1994, **464**, 219.

6 K. G. Caulton, *Coord. Chem. Rev.*, 1981, **38**, 1.

7 B. E. R. Schilling, R. Hoffmann and D. L. Lichtenberger, *J. Am. Chem. Soc.*, 1979, **101**, 585.

8 (*a*) A. D. Redhouse and W. A. Herrmann, *Angew. Chem., Int. Ed. Engl.*, 1976, **15**, 615; (*b*) W. A. Herrmann, J. Plank, M. L. Ziegler and K. Weidenhammer, *J. Am. Chem. Soc.*, 1979, **101**, 3133.

9 W. A. Herrmann, *Angew. Chem., Int. Ed. Engl.*, 1974, **13**, 335.

CHEMCOMM Communication
www.rsc.org/chemcomm

(Bromocarbonyl)sulfenyl bromide, BrC(O)SBr: a novel carbonyl sulfenyl compound formed by the photochemical reaction between Br_2 and OCS isolated together in an Ar matrix

Rosana M. Romano,*[a]† Carlos O. Della Védova[ab]† and Anthony J. Downs[c]

[a] *CEQUINOR (CONICET-UNLP), Departamento de Química, Facultad de Ciencias Exactas, Universidad Nacional de La Plata, 47 esquina 115, 1900, La Plata, Argentina. E-mail: romano@quimica.unlp.edu.ar*

[b] *Laboratorio de Servicios a la Industria y al Sistema Cientifico (UNLP-CIC-CONICET), Departamento de Química, Facultad de Ciencias Exactas, Universidad Nacional de La Plata, 47 esquina 115, 1900, La Plata, Argentina*

[c] *Inorganic Chemistry Laboratory, University of Oxford, South Parks Road, Oxford, UK OX1 3QR*

Received (in Purdue, IN, USA) 10th September 2001, Accepted 29th October 2001
First published as an Advance Article on the web 20th November 2001

The novel (bromocarbonyl)sulfenyl bromide, BrC(O)SBr, is formed by the photochemical reaction between Br_2 and OCS isolated together in an Ar matrix at 15 K.

In the interpretation of the IR spectra of argon matrices containing *syn*-(chlorocarbonyl)sulfenyl bromide, ClC(O)SBr,[1] we proposed several pathways to explain the rich photochemistry of this compound. The photodecomposition of the compound follows apparently two distinct reaction channels, one leading to CO and BrSCl, and the other to OCS and BrCl. One of the ensuing pathways we proposed involves the addition of the interhalogen product BrCl to the OCS molecule either to regenerate ClC(O)SBr or to form the constitutional isomer BrC(O)SCl. To test this proposed mechanism, the following general matrix reaction is currently under investigation [eqn. (1)].

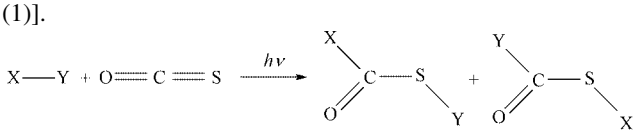

with X, Y = halogen, H (1)

In the case of X = Y = Br, the hypothetical product, BrC(O)SBr, is hitherto unknown. Attempts to prepare it by chemical reactions in different conditions, including low temperatures and from different precursors, failed. This route appears then as a useful way of preparing novel species, and especially those that are short-lived under normal conditions.

In the experiments described here, we have explored the photochemically induced matrix reaction between Br_2 and OCS. Different proportions of gaseous Br_2 and OCS were mixed with an excess of Ar by standard manometric techniques. The gas mixtures were deposited on a cooled CsI window using the pulsed deposition technique,[2,3] and irradiated with broad-band UV-visible light. The reaction was followed by analysis of the FTIR spectrum of the matrix. The experimental arrangements are described elsewhere.[1]

Before irradiation of the matrix, only signals corresponding to the OCS molecule are present in the IR spectrum. These are entirely consistent with results reported previously.[4] Photolysis of the matrix using broad-band UV-visible radiation ($200 \leq \lambda \leq 800$ nm) was observed to produce a decay of the bands associated with the OCS, accompanied by the simultaneous appearance and growth of new absorptions near 2138, 1800, 758, 555, 528, 433, and 418 cm^{-1}. The band near 2138 cm^{-1} is readily identifiable with the formation of free CO,[5] in accordance with the photochemical behavior found previously for OCS under UV light [eqn. (2)]:[4]

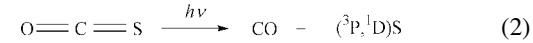

(2)

It was suggested in the study of the matrix photochemistry of ClC(O)SBr that the S atoms in the excited ^1D state react with BrCl to form BrSCl. So, too, in the present study, we note the formation of the SBr_2 molecule, identifiable by its IR band near 418 cm^{-1},[6] and formed presumably *via* eqn. (3):

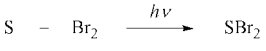

(3)

We can then assign the other four bands that appeared after broad-band UV-visible irradiation of the matrix to the hitherto unknown compound (bromocarbonyl)sulfenyl bromide, BrC(O)SBr, formed in accordance with the general reaction (1), or more specifically in this case with eqn. (4):

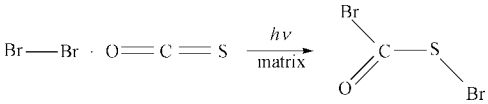

(4)

Thus, the strong absorption near 1800 cm^{-1} is most plausibly identified with a ν(C=O) fundamental of such a compound, and the weaker absorption near 434 cm^{-1} shows a closely spaced doublet pattern highly suggestive of a ν(S–Br) fundamental.[1]

The identity of the new molecule has been confirmed (i) by comparison with the results of density functional theory (DFT) calculations, (ii) by the isotopic shifts due to the naturally occurring atomic pair $^{79}Br/^{81}Br$, and (iii) by reference to the properties of related molecules.[1]

The theoretical calculations were performed using the GAUSSIAN 98 program package[7] under the LINDA parallel execution environment. First, the relative stabilities of the two possible conformational isomers of the BrC(O)SBr molecule, *syn* and *anti*, were investigated. The structures of these two planar forms were fully optimized using different theoretical methods (MP2 and B3LYP) with the 6-31+G* basis set. Both models predict the *syn* form to be more stable than the *anti* one, in agreement with all the available experimental and theoretical evidence regarding the conformational properties of the carbonyl sulfenyl compounds.[1,8–11]

The IR spectra for both conformers of BrC(O)SBr were simulated by the different methods. By comparison of the experimental spectrum with those predicted for the two conformers, we are left in no doubt that the matrix reaction produces not the *anti* but only the *syn* form. Table 1 lists the

† Member of the Carrera del Investigador Científico del Consejo Nacional de Investigaciones Científicas y Técnicas, Argentina.

 DOI: 10.1039/b108218c

Table 1 Experimental IR wavenumbers and intensities for the *syn*-BrC(O)SBr molecule isolated in an Ar matrix and theoretical results obtained with the B3LYP/6-31+G* approximation

Experimental		B3LYP/6-31+G*		
IR	Intensity	IR	Intensity	Assignment
1801.0, 1799.4	0.163 (100%)	1860.8	310 (100%)	ν(C=O)
758.2	0.151 (93%)	763.5	294 (95%)	ν_{as}(Br–C–S)
555.4	0.010 (5%)	550.5	14 (5%)	ν_{s}(Br–C–S)
528.3	0.002 (1%)	548.8	2 (1%)	δ(C=O) oop
433.8, 432.7	0.025 (13%)	428.7, 427.6	40 (13%)	ν(S–^{79,81}Br)
		336.8		δ(S–C=O)
		170.8		δ(S–C–Br)
		113.0		δ(C–S–Br)
		95.0		τ

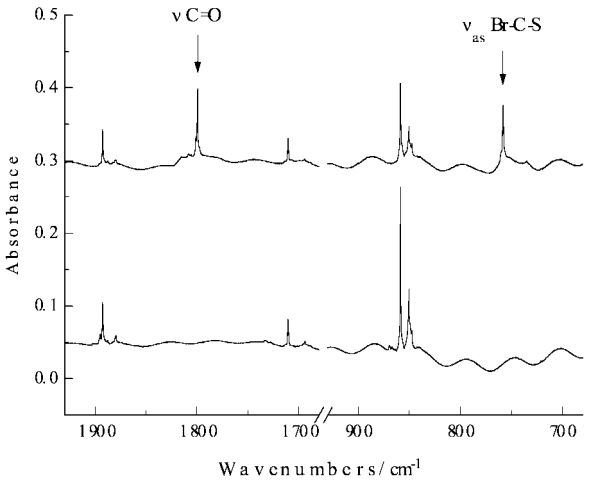

Fig. 1 FTIR spectra of an Ar matrix formed by co-deposition of a gaseous mixture of Br_2, OCS and Ar (10:5:1000) before (bottom) and after (top) photolysis with broad-band UV-visible light ($200 \leq \lambda \leq 800$) for 6 h. The arrows mark bands due to BrC(O)SBr.

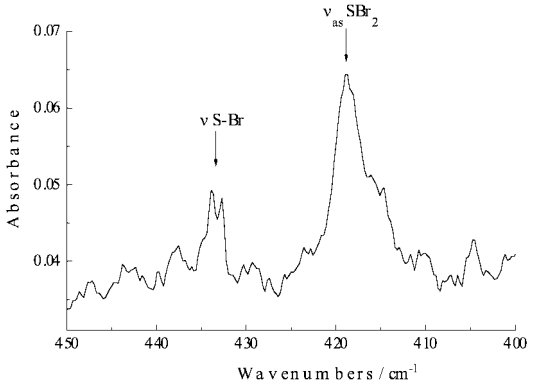

Fig. 2 FTIR spectrum of an Ar matrix formed by co-deposition of a gaseous mixture of Br_2, OCS and Ar (10:5:1000) after photolysis with broad-band UV-visible light ($200 \leq \lambda \leq 800$) for 6 h.

experimental wavenumbers and intensities of the product formed after 6 h of broad-band UV-visible irradiation of the Ar-matrix formed by co-deposition of a gaseous mixture of Br_2, OCS and Ar (10:5:1000), together with the calculated values obtained with the density functional theory method B3LYP/6-31+G*. The assignment of the vibrational modes is also included in the Table.

The excellent agreement between the experimental and simulated spectra thus enables us to confirm the identity of the product. Fig. 1 shows the FTIR spectra of the matrix before and after photolysis in the region where the most intense bands of BrC(O)SBr appeared. The experimental isotopic shift of 1.1 cm^{-1} for the ν(S–Br) band (Fig. 2) is also matched exactly by the predicted one.

Hence the present work confirms that dihalogen molecules react with OCS under matrix conditions [eqn. (1)] as first proposed to account for the matrix photochemistry of ClC(O)SBr, and introduces a novel route to carbonyl sulfenyl compounds.

The authors acknowledge with thanks a British Council-Fundación Antorchas award for British–Argentinian cooperation. C. O. D. V. and R. M. R. thank Consejo Nacional de Investigaciones Científicas y Técnicas (CONICET) (PIP 4695), Agencia Nacional de Promoción Científica y Tecnológica (PICT 122), Comisión de Investigaciones Científicas de la Provincia de Buenos Aires (CIC), and Facultad de Ciencias Exactas, Universidad Nacional de La Plata, for financial support. R. M. R. also is grateful for a Fundación Antorchas grant. In addition, A. J. D. is indebted to the EPSRC for support, including the purchase of equipment.

Notes and references

1 R. M. Romano, C. O. Della Védova, A. J. Downs and T. M. Greene, *J. Am. Chem. Soc.*, 2001, **123**, 5794.
2 M. J. Almond and A. J. Downs, *Adv. Spectrosc.*, 1989, **17**, 1; I. R. Dunkin, *Matrix-Isolation Techniques: A Practical Approach*, Oxford University Press, New York, 1998.
3 R. N. Perutz and J. J. Turner, *J. Chem. Soc., Faraday Trans. 2*, 1973, **69**, 452.
4 M. Hawkins and A. J. Downs, *J. Phys. Chem.*, 1984, **88**, 1527; M. Hawkins and A. J. Downs, *J. Phys. Chem.*, 1984, **88**, 3042; M. Hawkins, J. Almond and A. J. Downs, *J. Phys. Chem.*, 1985, **89**, 3326.
5 H. Dubost, *Chem. Phys.*, 1976, **12**, 139.
6 M. Feuerhahn and G. Vahl, *Inorg. Nucl. Chem. Lett.*, 1980, **16**, 5.
7 M. J. Frisch, G. W. Trucks, H. B. Schlegel, G. E. Scuseria, M. A. Robb, J. R. Cheeseman, V. G. Zakrzewski, J. A. Montgomery Jr., R. E. Stratmann, J. C. Burant, S. Dapprich, J. M. Millam, A. D. Daniels, K. N. Kudin, M. C. Strain, O. Farkas, J. Tomasi, V. Barone, M. Cossi, R. Cammi, B. Mennucci, C. Pomelli, C. Adamo, S. Clifford, J. Ochterski, G. A. Petersson, P. Y. Ayala, Q. Cui, K. Morokuma, D. K. Malick, A. D. Rabuck, K. Raghavachari, J. B. Foresman, J. Cioslowski, J. V. Ortiz, A. G. Baboul, B. B. Stefanov, G. Liu, A. Liashenko, P. Piskorz, I. Komaromi, R. Gomperts, R. L. Martin, D. J. Fox, T. Keith, M. A. Al-Laham, C. Y. Peng, A. Nanayakkara, C. Gonzalez, M. Challacombe, P. M. W. Gill, B. Johnson, W. Chen, M. W. Wong, J. L. Andres, C. Gonzalez, M. Head-Gordon, E. S. Replogle and J. A. Pople, Gaussian 98, Revision A.7, Gaussian Inc., Pittsburgh, PA, 1998.
8 H.-G. Mack, H. Oberhammer and C. O. Della Védova, *J. Phys. Chem.*, 1991, **95**, 4238.
9 C. O. Della Védova, E. H. Cutin, A. H. Jubert, E. L. Varetti and P. J. Aymonino, *Can. J. Spectrosc.*, 1984, **29**, 130.
10 C. O. Della Védova, *J. Raman Spectrosc.*, 1989, **30**, 729.
11 C. O. Della Védova and H.-G. Mack, *Inorg. Chem.*, 1993, **32**, 9.

CHEMCOMM Communication
www.rsc.org/chemcomm

Distinct thermodynamic behaviour of a mesomorphic gold nanoparticle covered with a liquid-crystalline compound

Naoki Kanayama, Osamu Tsutsumi, Akihiko Kanazawa and Tomiki Ikeda*

Chemical Resources Laboratory, Tokyo Institute of Technology, 4259 Nagatsuta, Midori-ku, Yokohama, 226-8503, Japan. E-mail: tikeda@res.titech.ac.jp

Received (in Cambridge, UK) 16th October 2001, Accepted 9th November 2001
First published as an Advance Article on the web 30th November 2001

Gold nanoparticles covered with a liquid-crystalline compound were successfully prepared, exhibiting characteristic double-melting behaviour.

Liquid crystals are attractive materials, since they show unique properties, such as long-range order, cooperative effects and an anisotropic nature in optical and electronic properties, based on a self-organizing nature in a certain temperature range with fluidity.[1] Furthermore, their phase structures and molecular orientations can be controlled easily and quickly by means of various external stimuli.

These dynamic properties of liquid crystals enable us to apply liquid crystals not only to liquid crystal displays but also to various applications. For example, liquid-crystalline materials containing photocromic moieties are employed in photonic applications,[2] such as optical switching and optical storage based on photochemical phase transitions of liquid crystals.[3] Furthermore, by using the self-organizing nature of liquid crystals, highly ordered structures that are difficult to prepare by other methods are constructed. For example, tetraalkylonium salts $[(C_nH_{2n+1})_2(CH_3)_2HetCl]$ (n = 10, 14, 18; Het = N, P)[4] and their metal complex salts[5] $[(C_{18}H_{37})_2(CH_3)_2N]_2[MCl_4]$ (M = Co, Ni, Cu, Zn, Cd) that exhibit thermotropic liquid-crystalline behaviour, were confirmed to form a layered self-assembly built up from alternating layers of various ions and alkyl segments in a smectic phase.

Recently, metal nanoclusters have attracted a great deal of interest since they show unusual properties compared to the bulk metals.[6] Especially, alkanethiolate-protected metal clusters (MPCs)[7] are promising materials, since they can be handled in a similar manner as general organic compounds due to their high stability to light and air, and solubility in conventional organic solvents. Until now, various types of MPCs have been reported and their potential as functional materials have been studied.[8] On the other hand, since the properties of metal nanocluster aggregates is affected by their morphology, various attempts to control their morphology have been performed by means of physical[9] and chemical[10] processes. Now, a control method with reversible and simple processes is desired.

By providing metal nanoclusters with liquid-crystalline properties, we could introduce the self-assembling ability and the reversible control of morphology of their aggregates by external stimuli, as well as the control of their properties by a simple and solvent-free method. The reversible control of the properties of metal nanocluster aggregates will cultivate their potential as functional nanomaterials. In this communication, as a first step, we report the preparation of gold nanoparticles covered with a liquid-crystalline compound *via* a strong gold–sulfur chemical bond, and its characteristic thermodynamic behaviour. The thiol derivative, 10-[(*trans*-(4-pentylcyclohexyl)phenoxy)] decane-1-thiol (5CP10SH, Fig. 1) was synthesized from *p-trans*-(pentylcyclohexyl)phenol (Kanto Chemical Co., Inc. Tokyo, Japan).† 5CP10SH exhibited monotropic liquid-crystalline behaviour showing a nematic phase (43–34 °C) and a smectic phase (34–21 °C) on cooling. Gold nanoparticles covered with 5CP10SH (5CP10MPC) were prepared in toluene by a two-phase reaction analogous to that reported by Brust *et al*.[7] Tetra-*n*-octylammonium bromide was used as a phase transfer reagent, and tetrachloroaurate(III) ion was reduced to Au(0) with sodium borohydride in the presence of 5CP10SH in toluene (feed mole ratio, $AuCl_4^-$: 5CP10SH = 1 : 1). 5CP10MPC was washed with ethanol and acetone several times and dried *in vacuo*. 5CP10MPC was obtained as a black powder, and could be redispersed readily in nonpolar solvents such as chloroform, benzene and hexane. The reduction of tetrachloroaurate(III) ion to Au(0) was confirmed by the appearance of a surface plasmon absorption band at around 510 nm in a UV–VIS absorption spectrum measured in chloroform.

The purity of the gold nanoparticles were confirmed by ^{1}H NMR and thin-layer chromatography (TLC: silica gel plate, mobile phase: chloroform). Fig. 2 shows the ^{1}H NMR spectra of 5CP10SH (a) and 5CP10MPC (b) in $CDCl_3$.

In Fig. 1(b), a proton signal around 2.6 ppm, which can be assigned to α-protons (CH_2SH), disappeared and the broadening of all proton signals was observed. The disappearance of α-protons indicates the formation of a gold–sulfur bonds, and the broadening of the proton signals demonstrates that all 5CP10SH molecules are covalently linked to the gold surface,[11] *i.e.* there are no parent 5CP10SH molecules remaining in 5CP10MPC; TLC supported this result.

The mean diameter of 5CP10MPC was determined to be *ca.* 3 nm by TEM (JOEL JEM-2010F) measurement. Elemental analysis of 5CP10MPC gave C: 29.6%, H: 4.3%, S: 2.9%, Au: 66.3%. The content of gold was estimated from that of the ash. From the elemental analysis result, the composition ratio of 5CP10MPC was estimated as Au : 5CP10S– = 3.4 : 1. To evaluate the mean composition of the gold nanoparticle, we assumed a model with a 3.0 nm diameter for the gold

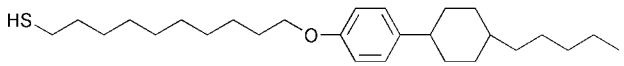

Fig. 1 Chemical structure of 5CP10SH.

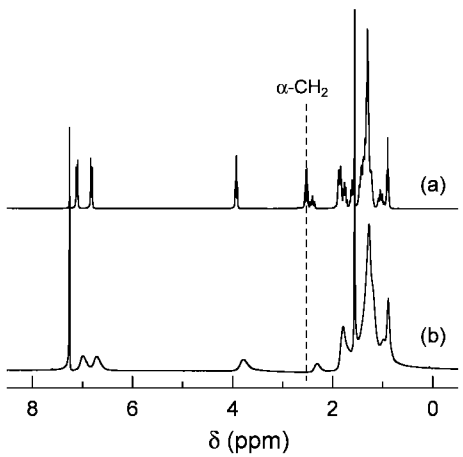

Fig. 2 ^{1}H NMR spectrum of (a) 5CP10SH and (b) 5CP10MPC in $CDCl_3$.

 DOI: 10.1039/b108909a

nanosphere. Taking the gold core as a sphere with density ρ_{Au} (58.01 atoms nm^{-3})[12] covered with an outermost layer of hexagonally close-packed gold atoms (13.89 atoms nm^{-2})[12] with a radius of $R_{CORE} - R_{Au}$ (R_{Au} = 0.145 nm), the model predicts that the core contains about 920 Au atoms, of which 320 atoms lie on the surface. Furthermore, from the result of the elemental analysis, there are 270 of 5CP10S– moieties at the surface of the 3.0 nm gold sphere ($Au_{920}(5CP10S–)_{270}$). From this result, 5CP10S– moieties are very closely packed and form a highly ordered monolayer at the surface of 5CP10MPC.

Next, we examined the thermodynamic behaviour of 5CP10MPC by differential scanning calorimetry (DSC; Seiko I&E SSC-5200 and DSC220C). Fig. 3 shows DSC thermograms of bulk 5CP10SH (a) and 5CP10MPC (b). 5CP10MPC exhibited double phase transition behaviour on heating (74 and 114 °C) and cooling (77 and 110 °C) and showed a mesoscopic phase. The thermodynamic behaviour of 5CP10MPC was quite different from that of bulk 5CP10SH. The phase transition temperatures of 5CP10MPC were high and the mesomorphic phase temperature regions were wide compared with those of 5CP10SH. Since this phase transition behaviour occurred reversibly, we judged these exo- and endo-thermic responses as not due to thermal decomposition of 5CP10MPC (for example, cleavage of the S–Au bond), but to a phase transition of the 5CP10S– moieties at the gold nanoparticle surface. As a reference, we performed DSC measurement of a bare gold nanoparticle.‡ The bare gold nanoparticle exhibited no exo- or endo-thermic response within this temperature region. Badia *et al*. reported thermodynamic behaviour of gold nanoparticles covered with various length alkanethiols (C_{12}, C_{14}, C_{16}, C_{18}, C_{20}).[13] All gold nanoparticles exhibited single phase transition behaviour assigned as an order to disorder phase transition of the alkanethiolate monolayer at the gold nanoparticle surfaces. Furthermore, the 5CP10MPC showed fluidity at the mesophase and optically isotropic state as evidenced by polarizing microscopy.

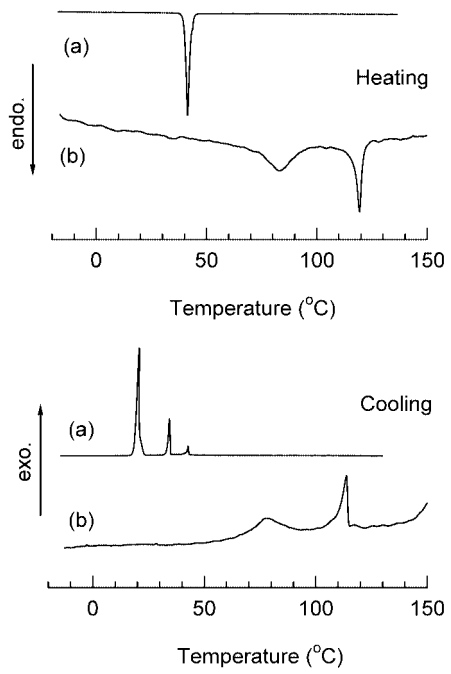

Fig. 3 DSC thermograms of (a) 5CP10SH and (b) 5CP10MPC (scan rate: 5 °C min^{-1}).

The mesomorphic behaviour of the gold nanoparticle indicates the appearance of interaction (cooperative motion) between mesogens at the surface of different gold nanoparticles. By using the mesomorphic behaviour of gold nanoparticles, it might be possible to induce morphological change (interparticle separate, lattice structure *etc*.) of their aggregates. Further detailed studies on the phase transition mechanism of mesogens at the surface of gold nanoparticles and morphological changes of the gold nanoparticle aggregates are in progress.

We thank Professor T. Shiono, Professor H. Kitano and Dr A. Shishido for their useful suggestions and discussions.

Notes and references

† Yield: 61%; elemental analysis calcd for $C_{27}H_{46}OS$, C, 77.4; H, 11.1; S, 7.66. Found: C, 77.8; H, 11.4; S, 7.68%; ^1H NMR (200 MHz in $CDCl_3$) δ 0.9–1.5 (m, 29H, $–CH_2–$, –CH–, $–CH_3$, –SH), 1.7–2.0 (m, 8H, $–CH_2–$), 2.4 (m, 1H, –CH–), 2.6 (q, 2H, $–CH_2SH$), 3.9 (t, 2H, $–OCH_2–$), 6.8 (d, 2H, phenyl), 7.1 (d, 2H, phenyl); FT-IR (KBr pellet method) 3032 (ν(C–H)$_{arom}$), 2952 ($\nu(CH_3)$, 2920 ($\nu_{as}(CH_2)$), 2850 ($\nu_s(CH_2)$), 2555 (ν(S–H), 1610, 1513, 1495 (ν(C=C)), 1465 ($\delta_{as}(CH_2)$), 1246 (ν_{as}(C–O–C)), 1040 cm^{-1} (ν_s(C–O–C)).

‡ Bare gold nanoparticles were prepared by the same method as for 5CP10MPC without 5CP10SH. The bare gold nanoparticles were washed with water, ethanol and acetone several times, and dried *in vacuo*.

1 D. Demus, J. Goodby, G. W. Gray, H.-W. Spiess and V. Vill, *Handbook of Liquid Crystals*, Wiley-VCH, Weinheim, Germany, 1998, vol. 1.

2 B. L. Feringa, *Molecular Switches*, Willey-VCH, Weinhein, Germany, 2001; A. Shishido, O. Tsutsumi, A. Kanazawa, T. Shiono, T. Ikeda and N. Tamai, *J. Am. Chem. Soc.*, 1997, **119**, 7791; T. Yamamoto, A. Ohashi, S. Yoneyama, M. Hasegawa, O. Tsutsumi, A. Kanazawa, T. Shiono and T. Ikeda, *J. Phys. Chem., B*, 2001, **105**, 2308.

3 T. Ikeda and O. Tsutsumi, *Science*, 1995, **268**, 1873.

4 A. Kanazawa, O. Tsutsumi, T. Ikeda and Y. Nagase, *J. Am. Chem. Soc.*, 1997, **119**, 7670; A. Kanazawa, T. Ikeda and J. Abe, *Angew. Chem., Int. Ed.*, 2000, **39**, 612; A. Kanazawa and T. Ikeda, *Coord. Chem. Rev.*, 2000, **198**, 117; A. Kanazawa, T. Ikeda and J. Abe, *J. Am. Chem. Soc.*, 2001, **123**, 1748.

5 A. Kanazawa, T. Ikeda and Y. Nagase, *Chem. Mater.*, 2000, **12**, 3776.

6 J. H. Fendler, *Nanoparticles and Nanostructure Films*, Wiley-VCH, Weinheim, Germany, 1998; G. Schimid, *Clusters and Colloids*, Wiley-VCH, Weinheim, Germany, 1994.

7 M. Brust, M. Walker, D. Bethell, D. J. Schiffin and R. Whyman, *J. Chem. Soc., Chem. Commun.*, 1994, 801.

8 For example: A. C. Templeton, W. P. Wuelfing and R. W. Murray, *Acc. Chem. Res.*, 2000, **33**, 27; W. P. Wuelfing, S. J. Green, J. J. Pietron, D. E. Cliffel and R. W. Murray, *J. Am. Chem. Soc.*, 2000, **122**, 11 465; J. Alvarez, J. Liu, E. Román and A. E. Kaifer, *Chem. Commun.*, 2000, 1151; A. Labande and D. Astruc, *Chem. Commun.*, 2000, 1007; L. Pasquato, F. Rancan, P. Scrimin, F. Mancin and C. Frigeri, *Chem. Commun.*, 2000, 2253; T. Yonezawa, S. Onoue and N. Kimizuka, *Langmuir*, 2001, **17**, 2291.

9 M. Giersig and P. Mulvaney, *J. Phys. Chem.*, 1993, **97**, 6334; J. H. Fendler, *Chem. Mater.*, 1996, **8**, 1616; C. P. Collier, R. J. Saykally, J. J. Shiang, S. E. Hendrichs and J. R. Heath, *Science*, 1997, **277**, 1978.

10 J. J. Storhoff and C. A. Mirkin, *Chem. Rev.*, 1999, **99**, 1849; S. Mann, W. Shenton, M. Li, S. Connolly and D. Fitzmaurice, *Adv. Mater.*, 2000, **12**, 147; A. K. Boal, F. Ilhan, J. E. DeRouchey, T. Thurn-Albrecht, T. P. Russell and V. M. Rotello, *Nature*, 2000, **404**, 746.

11 A. C. Templeton, D. E. Cliffel and R. W. Murray, *J. Am. Chem. Soc.*, 1999, **121**, 7081.

12 R. H. Terrill, T. A. Postlethwaite, C.-H. Chen, C. -D. Poon, A. Terzis, A. Chen, J. E. Hutchison, M. R. Clark, G. Wingnall, J. D. Londono, R. Superfine, M. Falvo, C. S. Johnson, Jr., E. T. Samulski and R. W. Murray, *J. Am. Chem. Soc.*, 1995, **117**, 12 537.

13 A. Badia, S. Singh, L. Demers, L. Cuccia, G. R. Brown and R. B. Lennox, *Chem. Eur. J.*, 1996, **3**, 359; A. Badia, L. Cuccia, L. Demers, F. Morin and R. B. Lennox, *J. Am. Chem. Soc.*, 1997, **119**, 268.

CHEMCOMM Communication
www.rsc.org/chemcomm

ITQ-18 a new delaminated stable zeolite

A. Corma,* V. Fornés and U. Díaz

Instituto de Tecnología Química, UPV-CSIC, Universidad Politécnica de Valencia, Avenida de los Naranjos s/n., 46022 Valencia, Spain. E-mail: acorma@itq.upv.es

Received (in Cambridge, UK) 26th September 2001, Accepted 7th November 2001
First published as an Advance Article on the web 30th November 2001

A new delaminated zeolitic material ITQ-18 has been obtained by expanding and exfoliating a laminar precursor of NU-6 (2); while NU-6 (2) has an N_2 surface area of 35 $m^2\ g^{-1}$ and contains bridging hydroxy groups which are in accessible to pyridine, the ITQ-18 sample prepared has an a external surface area of 588 $m^2\ g^{-1}$ with all bridging hydroxy groups being acidic and accessible to pyridine.

One of the most interesting features of zeolites as catalysts is the control of selectivity due to the regular dimensions of the pores and cavities of the structure that introduces the well known shape selectivity effects. However, there are a large number of potential applications that involve the conversion of molecules with a kinetic diameter much larger than the pore dimensions of current zeolites. Thus, in catalytic reactions such as, for instance, hydrocracking of vacuum gas-oil or waxes, the pores of the zeolite catalysts introduce an undesirable shape selectivity effect that directs towards naphtha and gases instead of to diesel and lubes that would be the preferred product. In the field of fine chemicals, products much bulkier than reactants are formed and, in some cases, they remain occluded in the zeolite, blocking the pores and deactivating the catalyst. In the cases described above one can minimize the diffusion limitations by increasing the ratio of the external to the internal surface of the catalyst. This can be done with zeolites by synthesizing small crystallites[1] in which the number of external active sites accessible to large molecules is increased and the activity for the above mentioned reactions is enhanced.[2] Advances have been made in the last decade to produce zeolite crystals of < 10 nm size[3,4] but, up to now, this has been achieved only in a limited number of structures and, in most cases, the yields of the synthesis is low.

A second option for reacting large molecules would involve the preparation of mesoporous molecular sieves, with pore diameters in the range 3–10 nm, which allow the diffusion of bulky reactants and products in and out of the pores. A certain success has been attained for acid and redox catalysis by working with MS-14 materials of which MCM-41 is an example. However, these materials do not show short–range order and, consequently, from the point of view of the stability and catalytic behaviour, they are closer to amorphous than to zeolitic materials. More specifically, the MCM-41 aluminosilicates prepared for acid catalysis show similar catalytic behaviour to amorphous silica-alumina owing to the weak Brönsted acidities generated.[5]

It would be thus of fundamental and practical interest to synthesize zeolitic materials with strong acid sites, allowing the access of large molecules with fast desorption and diffusion of the products to the gas stream. These types of materials should combine the good thermal and hydrothermal stability of zeolites with active sites of zeolitic nature easily accessible to reactants. With these objectives in mind we have developed a series of zeolitic materials the preparation of which involves the delamination of lamellar precursors of zeolites. By this preparation procedure one can obtain, at the limit, single crystalline sheets of zeolitic nature in where all the catalytic active sites are accessible through the external surface.[6] In this way, two new materials ITQ-2[7] and ITQ-6[8] have so far been obtained from lamellar precursors of MCM-22 and ferrierite structures, respectively. These materials showed external surface areas above 600 $m^2\ g^{-1}$ with strong acid sites of zeolitic nature that were active for catalysing reactions[9] for which the corresponding zeolites were strongly limited by the pore dimensions.

Here we report on a new delaminated material denoted ITQ-18 the structure of which is still unknown but which presents a very large external surfaces area with accessible Brönsted acid sites of zeolitic nature.

It has been reported[10] that the synthesis of Nu-6(2) zeolite occurred by calcination of a lamellar precursor [Nu-6(1)], that could also be pillared.[11] The structure of Nu-6(2) is still unknown but the BET area of this zeolite is 79 $m^2\ g^{-1}$ indicating that either the diameter of the pores is very small or the channels are partially blocked, making this zeolite of no use for practical applications. However, if the structure could be delaminated, then the active sites would be made accessible to reactants making this zeolite useful as a catalyst.

The lamellar precursor Nu-6(1) was synthesized as follows: (a) 1.82 g of 4,4′-bipyridine (Fluka, 98% purity) were dissolved in 10.08 g of ethanol (J.T.Baker) to give solution A; (b) 20.06 g

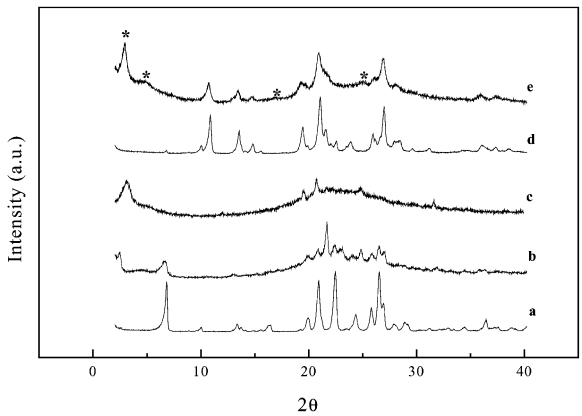

Fig. 1 X-Ray diffraction patterns of (a) as synthesized Nu-6(1), (b) expanded material ($CTMA^+$), (c) expanded material ($DTMA^+$), (d) collapsed material [Nu-6(2)] and (e) ITQ-18.

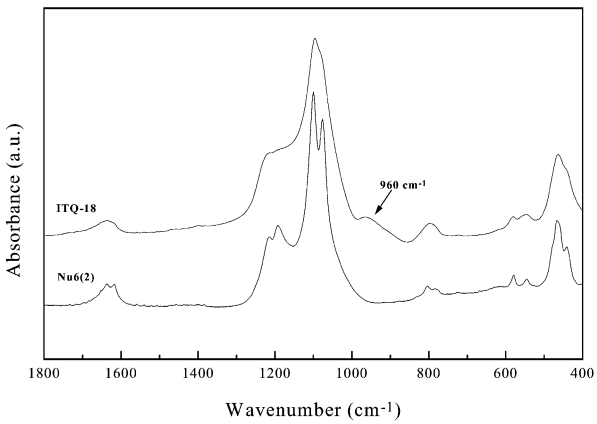

Fig. 2 IR spectra of Nu-6(2) and ITQ-18 in the framework range.

 DOI: 10.1039/b108777k

Table 1 Textural characteristics

Sample	S_{BET}/m² g⁻¹	S_{MIC}/m² g⁻¹	S_{EXT}/m² g⁻¹	V_{TOT}/cm³ g⁻¹	V_{MIC}/cm³ g⁻¹	V_{BJH}/cm³ g⁻¹
Nu-6(2)	79	44	35	0.1116	0.0220	0.0232
ITQ-18	611	23	588	0.5818	0.0120	0.4147

of sodium silicate (Merck, 8.02% Na_2O, 24.92% SiO_2, 67.05% H_2O) were diluted with 13.38 g of MiliQ deionized water to give solution B; (c) 0.62 g of aluminium sulfate [Merck, 51.34% $Al_2(SO_4)_3$, 48.66% H_2O] and 1.52 g of sulfuric acid (Ridel den Häggen, 98% purity) were dissolved in 22.78 g of MiliQ deionized water to give solution C. Then solution B was stirred into solution A followed by solution C. The mixture was reacted in a stirred stainless steel autoclave for 3 days at 135 °C. The resulting product was filtered off and washed three times with distilled water.

Before drying, the lamellar precursor was expanded using a quaternary alkylammonium hydroxide at pH = 12. The X-ray diffraction pattern of the starting material as well as those of the expanded materials are given in Fig. 1 (a), (b) and (c). It can be seen that cetyltrimethylammonium ($CTMA^+$) was incorporated between the layers giving a new diffraction peak at 2θ = 2.3°corresponding to a basal spacing of the swelled zeolite of *ca*. 4.0 nm [Fig. 1(b)]. Since the basal spacing of the collapsed material [Nu-6(2)] is 0.84 nm [Fig. 1(d)] we could assume that the individual sheets of the zeolite should be *ca*. 0.8–0.9 nm thick and, if this is so, then the interlaminar space of the expanded material should be 3.0 nm which roughly corresponds to two layers of CTMAOH. When this molecule was used as swelling agent, not all layers were expanded as can be deduced from the peak appearing at 2θ = 6.5° in Fig. 1(b). However, when decyltrimethylammonium ($DTMA^+$) cation was exchanged all the peaks associated with the non-expanded material disappeared and the basal spacing of the swollen zeolite was 2.85 nm indicating that the $DTMA^+$ has intercalated all the layers [Fig. 1(c)].

The expanded material was then washed thoroughly with water and a suspension with an excess of water was sonicated (50 W, 40 KHz) for 1 h until delamination of the zeolite occured. Finally, calcination at 853 K gave ITQ-18 the XRD pattern of which is shown in Fig. 1(e).

From the results presented so far, and taking into account the fact that the structure of Nu-6 zeolite is unknown and the expected poor quality of XRD spectra of a delaminated material,[6] it is necessary to confirm the delaminated character of ITQ-18 from other physicochemical properties.

Assuming that ITQ-18 is formed mainly by individual sheets of Nu6 zeolite, this should present a high number of terminal silanol groups. Thus, the ^{29}Si NMR spectrum should show an evident increase of the Q^3/Q^4 ratio corresponding to Si(3SiOH) and Si(4Si) units, respectively. This was indeed observed and also confirmed by IR spectroscopy. Fig. 2, which compares the spectra of ITQ-18 and Nu6(2) in the framework region, shows a large increase of the band at 960 cm^{-1} ascribed to terminal $\equiv SiO^-$ groups, formed upon delamination. It is noted that the ITQ-18 retains the IR bands at 540 and 580 cm^{-1} characteristic of the zeolitic structure, which is consistent with the presence of single sheets in which short range order is retained.

As an important consequence of delamination one should expect a very large increase of external surface area accompanied by a strong decrease in microporosity. Indeed, N_2 isotherms show (see Table 1) that while the external surface area of the zeolite Nu6(2) prepared here is only 35 $m^2\ g^{-1}$, that of the delaminated ITQ-18 material is 588 $m^2\ g^{-1}$, which is about 16 times larger. Meanwhile, the microporosity of ITQ-18 is practically negligible.

Summarizing, we can conclude that all the results from physicochemical characterization are in accord with the assumed structure of ITQ-18 being formed by individual sheets of zeolite.

In order to obtain acid catalysts, the precursor Nu6(1) was synthesized in the form of aluminosilicate with Si/Al ratio of 45.

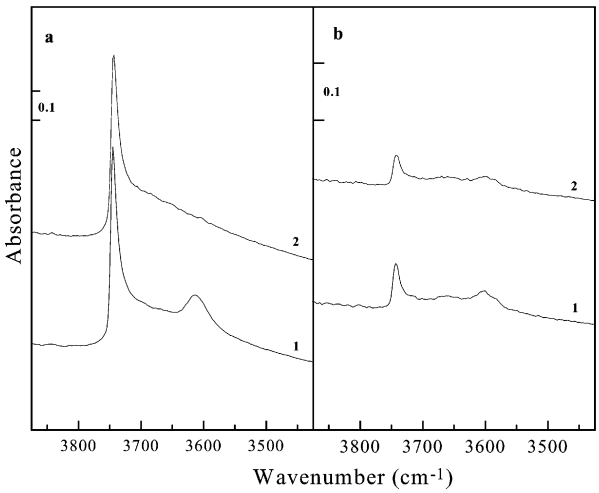

Fig. 3 IR spectra in the OH range for (a) ITQ-18 and (b) Nu-6, before (1) and after (2) pyridine adsorption.

The ^{27}Al MAS NMR spectrum (spectrum not shown) shows the presence of Al^{IV} indicating that, indeed, aluminium was incorporated into the framework of the precursor. After delamination and calcination Al remains in the framework leading to Brönsted acid sites, and the IR spectra in the hydroxy region (Fig. 3) shows a band at 3610 cm^{-1} in both ITQ-18 [Fig.3 (a1)] and, Nu6(2) [Fig.3 (b1)] which corresponds to bridging hydroxy groups that should be acidic. To confirm this assumption pyridine was adsorbed on both materials and it was found that while a negligible amount of the bridging OH groups in Nu6(2) [Fig. 3(b2)] interacted with the probe molecule, confirming the inaccessibility of the micropores of this zeolite, all bridging OH groups in ITQ-18 are accessible to pyridine [Fig. 3(a2)]. In summary, by performing the delamination of a laminar precursor of the Nu-6(2) zeolite, ITQ-18 was obtained which is stable upon calcination, has a very large external surface area, and has an substantial quantity of strong Brönsted acid sites all of which are accessible to pyridine. We should expect ITQ-18 to be active for carrying out acid catalysed reactions.

Financial support by the Spanish MAT2000-1392 is gratefully acknowledged while U. D. thanks the M.E.C. for a doctoral fellowship.

Notes and references

1 P. E. A. de Mor, T. P. M. Beelen and R. A. van Santen, *Microporous Mater.*, 1997, **9**, 117.
2 A. Chica and A. Corma, *J. Catal.*, 1999, **187**, 167.
3 J. A. Martens, J. W. Thybaut, G. B. Marin, P. A. Baron and P. A. Jacobs, *J. Catal.*, 2001, **202**, 324.
4 B. J. Schoeman, J. Sterte and J. E. Otterstedt, *J. Chem. Soc., Chem. Commun.*, 1993, 994.
5 A. Corma, M. S. Grande, V. González-Alfaro and A. V. Orchilles, *J. Catal.*, 1996, **159**, 375.
6 A. Corma, V. Fornés S. B. C. Pergher, Th. L. Maesen and J. G. Buglass, *Nature*, 1998, **396**, 353.
7 A. Corma, U. Díaz, V. Fornés, J. M. Guil, J. Martínez-Triguero and E. J. Creyghton, *J. Catál.*, 2000, **191**, 218.
8 A. Corma, U. Díaz, M. E. Domine and V. Fornés, *Angew. Chem., Int. Ed.*, 2000, **39**, 1499.
9 A. Corma, V. Fornés, J. M. Guil, S. B. C. Pergher, Th. L. Maesen and J. G. Buglass, *Microporous Mesoporous Mater.*, 2000, **38**, 301.
10 T. V. Whittam, *US Pat.*, 4 397 825, 1983.
11 C. T. Kresge and W. J. Roth, *US Pat.*, 5 266 541, 1993.

CHEMCOMM Communication
www.rsc.org/chemcomm

Solventothermal synthesis and X-ray crystal structures of two nickel complexes with novel alkoxy-substituted phthalocyanine ligands†

Christopher D. Molek,[a] Jason A. Halfen,[b] Jocelyn C. Loe[a] and Robert W. McGaff*[a]

[a] *University of Wisconsin-La Crosse, Department of Chemistry, 1725 State Street, La Crosse, WI, USA, 54601. E-mail: mcgaff.robe@uwlax.edu*

[b] *University of Wisconsin-Eau Claire, Department of Chemistry, 105 Garfield Avenue, Eau Claire, WI, USA, 54702-4004. E-mail: halfenja@uwec.edu*

Received (in Purdue, IN, USA) 17th October 2001, Accepted 7th November 2001
First published as an Advance Article on the web 30th November 2001

Solventothermal reactions of nickel acetate tetrahydrate with 1,2-dicyanobenzene in methanol and ethanol yield novel complexes in which nickel atoms are coordinated by modified phthalocyanine ligands with inner rings bearing methoxy and ethoxy substituents, respectively.

Phthalocyanine compounds and related derivatives have long defined an area of great interest, owing in large part to technological applications deriving from their unique optical, electronic, photochemical, and magnetic properties.[1] Although a large number of metal–phthalocyanine complexes have been synthesized and studied, reports of substituted phthalocyanines that have been fully structurally characterized by X-ray methods have remained relatively scarce.[2–14] To our knowledge, only four examples of structurally characterized phthalocyanine complexes in which the inner ring of the ligand has been modified from the parent phthalocyanine have been reported.[3,6,7,12]

We now report the syntheses and X-ray crystal structures of two new nickel phthalocyanine derivatives in which the ligands have been modified by incorporation of alkoxy groups into the inner ring. The syntheses of these products have been accomplished through adaptation of a standard metal–phthalocyanine synthetic procedure that involves reaction of a metal source with phthalodinitrile (1,2-dicyanobenzene) or a derivative thereof. Specifically, we have carried out reactions of nickel acetate tetrahydrate and 1,2-dicyanobenzene in alcohols under very mild solventothermal conditions, resulting in moderate yields of red-orange block-shaped crystals. The reaction in methanol for 6.5 days at 70 °C affords a 36% yield (based upon starting nickel acetate tetrahydrate) of {14, 28-$(CH_3O)_2$Pc}Ni·CH_3OH **1**.† Reaction in ethanol for four days at 90 °C results in a 27% yield (based upon starting nickel acetate tetrahydrate) of {14, 28-$(CH_3CH_2O)_2$Pc}Ni **2**.† These reactions are represented in Scheme 1. In both cases, byproducts include unmodified PcNi, identified on the basis of its IR spectrum, and other unidentified materials. Compound **1** is sparingly soluble in methanol and soluble in toluene, while **2** is very sparingly soluble in ethanol, and moderately soluble in toluene.

Attempts to increase the yield of **1** or **2** by either running the reaction at a higher temperature or for a longer period of time result instead in the formation of increased amounts of the unmodified phthalocyaninato nickel complex. We have observed that the heating of authentic samples of **1** or **2** under conditions similar to those at which they are synthesized (70 °C for **1** and 90 °C for **2**) for periods of time similar to those employed in their syntheses results in partial decomposition of the modified complexes to the blue unmodified complex. This suggests to us that that the formation of the unmodified complex during the syntheses of **1** and **2** probably occurs *via* decomposition of the modified complexes, rather than by a separate competing reaction pathway. Based upon this result, and upon the separate observation that no reaction is apparent upon heating of unsubstituted (phthalocyaninato)nickel(II) in methanol or ethanol at temperatures equivalent to or in excess of those employed in the synthesis of **1** and **2**, we conclude that modification of the phthalocyanine ligands in these species occurs as they form, rather than *following* the formation of an unsubstituted phthalocyanine. The observation that both **1** and **2** can be isolated and then partially converted to unmodified phthalocyaninato nickel(II) amounts to the first definitive structural characterization of isolable intermediates in the preparative reaction of the unmodified complex in the presence of alcohol solvent. The mechanism(s) of this process have been an important issue in the literature for several decades.[15] Studies aimed at determining the time and temperature required for complete conversion of **1** and **2** to unmodified phthalocyaninato nickel(II) are ongoing.

$$Ni(CH_3COO)_2{\cdot}4H_2O + 1,2\text{-}(CN)_2C_6H_4 \xrightarrow{ROH} 14,\ 28\text{-}(RO)_2PcNi + \text{byproducts}$$

1: R = CH_3, 70 °C reaction temp.

2: R = CH_3CH_2, 90 °C reaction temp.

Scheme 1

Compounds **1** and **2** are isostructural and crystallize as large red–orange triclinic blocks.‡ The salient feature in the molecular structures of both **1** and **2** is the presence of alkoxy groups on the 14 and 28 positions on the phthalocyanine macrocycles. As a result, two sp^3-hybridized carbon atoms are present in the ligands and the planarity seen in unmodified Pc is removed. These compounds are the first characterized examples with this structural motif. Fig. 1 shows the crystallographic numbering system employed for both compounds. Thermal ellipsoid plots of **1** and **2** are shown in Figs. 2 and 3, respectively. Fig. 2 shows a 'top view' of **1**, while Fig. 3 is a 'side view' of **2**, highlighting the saddle shape of the ligand.

The saddle shape seen in both modified Pc ligands is more pronounced in **2**, almost certainly owing to the increased steric

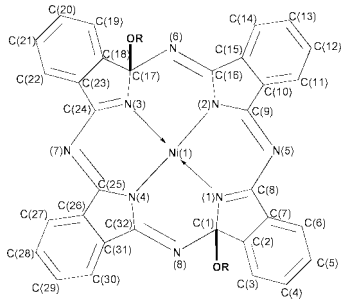

Fig. 1 Line drawing showing the crystallographic numbering system used in **1** and **2** and the positions of the alkoxy groups in both compounds.

† Electronic supplementary information (ESI) available: synthesis and spectroscopic characterization of **1** and **2**. See http://www.rsc.org/suppdata/cc/b1/b109481p/

 DOI: 10.1039/b109481p

bulk of the ethoxy group. We are unsure of the reason **1** and **2** adopt this structure instead of other possibilities that would also serve to accommodate the two alkoxy groups and sp^3-hybridized carbon atoms of the macrocycle. Syntheses of a series of similar compounds and determination of their structures will likely help to answer this question. It is conceivable that other structural motifs may be seen in analogues of **1** and **2**.

The outer rings of the ligands in **1** and **2** show no remarkable features other than the aforementioned overall deviation of the entire ligand from planarity. The bond lengths and angles around the alkoxy-substituted carbon atoms in **1** and **2** are as would be expected for single bonds and sp^3 hybridization of these atoms. All other carbon and nitrogen atoms in **1** and **2**, excepting those in the alkoxy groups, exhibit bond lengths and angles indicative of conjugated double bonds and sp^2 hybridization. The nickel atoms in both **1** and **2** are coordinated in a nearly square planar fashion by four nitrogen atoms. In both cases, two of the Ni–N bonds, on opposite sides of the Ni atom, are longer than the other two Ni–N bonds. In the crystal structure of **1**, one methanol solvate donates a hydrogen bond to a peripheral nitrogen atom in each molecule of the complex, while **2** is free of solvation.

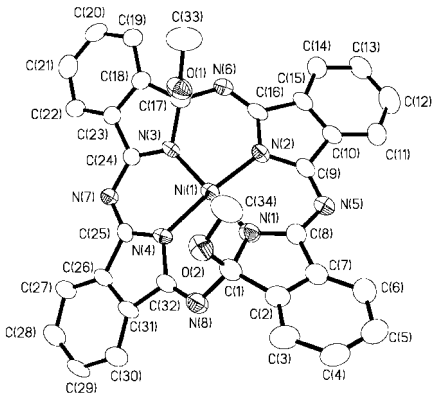

Fig. 2 The crystallographically determined structure, excluding hydrogen atoms and solvated methanol, for **1**. Ellipsoids are drawn at the 50% probability level. Selected bond lengths (Å) and angles (°): Ni(1)–N(1) 1.845(4), Ni(1)–N(2) 1.867(4), Ni(1)–N(3) 1.836(4), Ni(1)–N(4) 1.862(4), C(1)–O(2) 1.418(7), C(1)–C(2) 1.518(8), C(1)–N(8) 1.466(7), C(1)–N(1) 1.472(7), C(17)–O(1) 1.426(7), C(17)–C(18) 1.507(8), C(17)–N(3) 1.479(7), C(17)–N(6) 1.444(7), N(1)–C(8) 1.307(7), N(3)–C(24) 1.309(6); N(1)–Ni(1)–N(2) 89.9(2), N(2)–Ni(1)–N(3) 90.8(2), N(3)–Ni(1)–N(4) 90.5(2), N(4)–Ni(1)–N(1) 90.4(2), C(2)–C(1)–N(8) 112.1(5), C(2)–C(1)–N(1) 103.2(5), N(1)–C(1)–N(8) 112.6(5), N(1)–C(1)–O(2) 111.1(5), C(2)–C(1)–O(2) 114.3(5), N(8)–C(1)–O(2) 103.8(4), N(3)–C(17)–C(18) 103.2(4), N(6)–C(17)–C(18) 112.9(4), N(6)–C(17)–N(3) 114.5(4), O(1)–C(17)–C(18) 114.2(4), O(1)–C(17)–N(3) 102.6(4), O(1)–C(17)–N(6) 109.1(4).

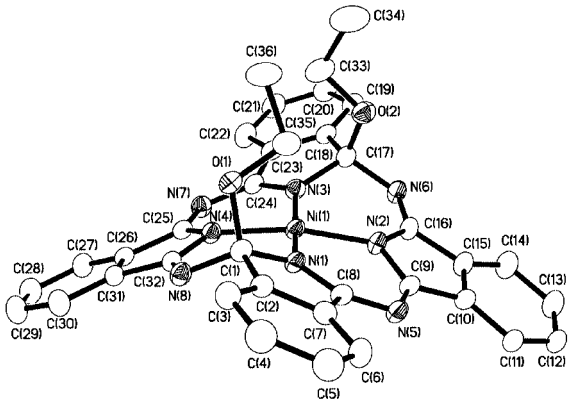

Fig. 3 The crystallographically determined structure, excluding hydrogen atoms, for **2**. Ellipsoids are drawn at the 35% probability level. Selected bond lengths (Å) and angles (°): Ni(1)–N(1) 1.831(4), Ni(1)–N(2) 1.854(4), Ni(1)–N(3) 1.838(4), Ni(1)–N(4) 1.862(4), C(1)–O(1) 1.425(5), C(1)–C(2) 1.517(6), C(1)–N(8) 1.449(6), C(1)–N(1) 1.469(6), C(17)–O(2) 1.414(6), C(17)–C(18) 1.519(6), C(17)–N(3) 1.478(6), C(17)–N(6) 1.452(6), N(1)–C(8) 1.323(6), N(3)–C(24) 1.306(6), N(1)–Ni(1)–N(2) 90.5(2), N(2)–Ni(1)–N(3) 90.8(2), N(3)–Ni(1)–N(4) 90.2(2), N(4)–Ni(1)–N(1) 90.3(2), C(2)–C(1)–N(8) 112.3(4), C(2)–C(1)–N(1) 103.2(4), N(1)–C(1)–N(8) 113.5(4), N(1)–C(1)–O(1) 110.7(4), C(2)–C(1)–O(1) 113.7(4), N(8)–C(1)–O(1) 103.8(3), N(3)–C(17)–C(18) 103.0(4), N(6)–C(17)–C(18) 111.8(4), N(6)–C(17)–N(3) 113.1(4), O(2)–C(17)–C(18) 113.6(4), O(2)–C(17)–N(3) 111.8(4), O(2)–C(17)–N(6) 103.8(4).

It appears that the reaction conditions employed in the synthesis of **1** and **2** are general for primary alcohols, and they lead to the formation of large single crystals that will be amenable to conductivity and optical studies. We believe that this method of synthesis will lead to the discovery of several new phthalocyanine compounds, containing different metals and bearing different alkoxy groups on their ligands.

Acknowledgement is made to the donors of The Petroleum Research Fund, administered by the ACS, for partial support of this research. We further acknowledge the Faculty Research Committee and the College of Science and Allied Health at the University of Wisconsin-La Crosse for additional support.

Notes and references

‡ *Crystal data*: for **1**: M = 665.35, triclinic, space group $P\bar{1}$, a = 7.160(2), b = 12.853(3), c = 16.936(3) Å, α = 93.33(2), β = 99.98(2), γ = 105.28(4)°, V = 1471.9(6) Å^3, Z = 2, μ(Mo-Kα) = 0.712 mm^{-1}, T = 293(2) K. The structure, refined on F^2, converged for 5620 reflections (5170 unique, R_{int} = 0.0892) to give $R1$ = 0.0558 and $wR2$ = 0.1295 for all reflections for which $I > 2\sigma(I)$ and goodness-of-fit = 1.000.

For **2**: M = 661.36, triclinic, space group = $P\bar{1}$, a = 7.950(2), b = 13.080(4), c = 15.395(5) Å, α = 109.12(3), β = 97.99(3), γ = 94.14(3)°, V = 1486.0(8) Å^3, Z = 2, μ(Mo-Kα) = 0.703 mm^{-1}, T = 293(2) K. The structure, refined on F^2, converged for 5587 reflections (5199 unique, R_{int} = 0.1106) to give $R1$ = 0.0509 and $wR2$ = 0.1285 for all reflections for which $I > 2\sigma(I)$ and goodness-of-fit = 1.018.

CCDC reference numbers 174008 and 174009.

See http://www.rsc.org/suppdata/cc/b1/b109481p/ for crystallographic data in CIF or other electronic format.

1 (*a*) N. B. McKeown, *Phthalocyanine Materials: Synthesis, Structure and Function*, Cambridge University Press, Cambridge, 1998 and references therein; (*b*) H. Schultz, H. Lehmann, M. Rein and M. Hanack, *Struct. Bonding (Berlin)*, 1990, **74**, 41 and references therein; (*c*) *Phthalocyanines Properties and Applications*, ed. C. C. Leznoff and A. B. P. Lever, VCH, Cambridge, 1989 and references therein; (*d*) *Phthalocyanines Properties and Applications*, ed. C. C. Leznoff and A. B. P. Lever, VCH, Cambridge, 1993, vol. 2 and references therein; (*e*) *Phthalocyanines Properties and Applications*, ed. C. C. Leznoff and A. B. P. Lever, VCH, Cambridge, 1993, vol. 3 and references therein; (*f*) *Phthalocyanines Properties and Applications*, ed. C. C. Leznoff and A. B. P. Lever, VCH, Cambridge, 1996, vol. 4 and references therein.

2 K. Yase, N. Yasuoka, T. Kobayashi and N. Uyeda, *Acta Crystallogr., Sect. C*, 1988, **44**, 514.

3 C. Ercolani, A. M. Paoletti, G. Pennesi, G. Rossi, A. Chiesi-Villa and C. Rizzoli, *J. Chem. Soc., Dalton Trans.*, 1990, 1971.

4 D. Chabach, M. Lachkar, A. De Cian, J. Fischer and R. Weiss, *New J. Chem.*, 1992, **16**, 431.

5 M. J. Chen, J. W. Rathke and J. C. Huffman, *Organometallics*, 1993, **12**, 4673.

6 J. Janezak and R. Kubiak, *Acta Crystallogr., Sect. C*, 1995, **51**, 2039.

7 J. Janczak and R. Kubiak, *Acta Chem. Scand.*, 1995, **49**, 871.

8 M. J. Chen, L. Nuñez, J. W. Rathke and R. D. Rogers, *Organometallics*, 1996, **15**, 2338.

9 K. Morishige and K. Araki, *J. Chem. Soc., Dalton Trans.*, 1996, 4303.

10 K. Kasuga, M. Kawashima, K. Asano, T. Sugimori, K. Abe, T. Kikkawa and T. Fujiwara, *Chem. Lett.*, 1996, 867.

11 M. Ruf, A. M. Lawrence, B. C. Noll and C. G. Pierpont, *Inorg. Chem.*, 1998, **37**, 1992.

12 M. P. Donzello, C. Ercolani, A. Chiesi-Villa and C. Rizzoli, *Inorg. Chem.*, 1998, **37**, 1347.

13 L. S. Beall, N. S. Mani, A. J. P. White, D. J. Williams, A. G. M. Barrett and B. M. Hoffman, *J. Org. Chem.*, 1998, **63**, 5806.

14 I. Chambrier, M. J. Cook and P. T. Wood, *J. Chem. Soc., Chem. Commun.*, 2000, 2133.

15 For example, see: (*a*) T. J. Hurley, M. A. Robinson and S. I. Trotz, *Inorg. Chem.*, 1967, **6**, 389; (*b*) C. H. Yang and C. Chang, *J. Chem. Soc., Dalton Trans.*, 1982, 2539.

CHEMCOMM Communication
www.rsc.org/chemcomm

β,β′-Fused metallocenoporphyrins†

Hong J. H. Wang, Laurent Jaquinod, Daniel J. Nurco, M. Graça H. Vicente and Kevin M. Smith*‡

Department of Chemistry, University of California, Davis, California 95616, USA

Received (in Corvallis, OR, USA) 28th August 2001, Accepted 22nd October 2001
First published as an Advance Article on the web 4th December 2001

The syntheses of a β,β′-fused ruthenocenoporphyrin (9) and a ferrocenoporphyrin dimer (11) are described.

Molecular systems incorporating porphyrins and metallocenes have great potential as catalysts, chemical sensors, and in porphyrin-assisted electron-transfer processes.[1,2] In recent years, molecules containing both porphyrin and ferrocene fragments have emerged as candidates for self-assembled monolayers in light energy conversion systems.[3] In most of these cases, the metallocene fragment is linked to the porphyrin *meso*- or β-positions through various spacers,[2–4] or directly to a central metal ion.[5] Direct linkages through a single C–C bond at the *meso*-positions have been reported[6] and it has also been shown that metalloporphyrins can form η^5-pyrrolyl–π-metal complexes with ruthenocyl moieties.[7] Our goal was to synthesize metallocenoporphyrins fused through the porphyrin β-positions, in order to enhance intramolecular electronic interactions in these systems.

In order to incorporate a five-membered ring (precursor of Cp^-) onto the porphyrin periphery, we investigated novel functionalizations of readily available 2-nitro-tetraarylporphyrins.[8] The remarkable ability of the nitro group to activate tetraarylporphyrins towards [3 + 2] cycloaddition reactions and its propensity to subsequently act as a leaving group was demonstrated by our synthesis of pyrroloporphyrins.[9] We now report two novel β,β′-fused metallocenoporphyrins (**9** and **11**) prepared *via* a key palladium(0)-catalyzed [3 + 2] cycloaddition reaction, previously applied to 1-nitronaphthalene.[10]

Using strict air-free conditions, nickel(II) 2-nitroporphyrins **1** and **2**[11] were treated with 2-[(trimethylsilyl)methyl]-2-propen-1-yl acetate for two days at 90 °C in the presence of an *in situ* prepared palladium(0) catalyst, to form nitrochlorins **3** and **4**, respectively (as shown by the appearance of an intense Q absorption band at 602 nm). Further heating of the reaction mixture at 100 °C for two days gave, upon elimination of nitrous acid, porphyrins **5** and **6** in 80–88% yields. While the cycloaddition reaction took place smoothly also on the copper complexes, the corresponding zinc(II) complexes required harsher reaction conditions and gave low yields (5%) of the β,β′-fused cyclopentenylporphyrins. Acid-catalyzed double bond migration on **5** and **6** afforded, respectively, porphyrins **7** and **8**. Addition of LDA to a solution of **8** in THF caused a color change from red to green which strongly suggested that two of the porphyrin π-electrons are delocalized into the aromatic

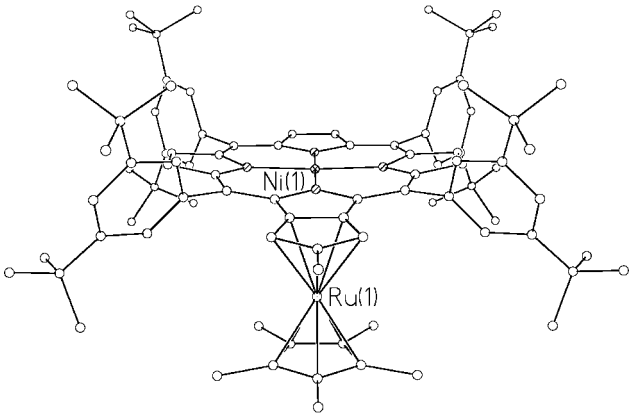

Fig. 1 The molecular structure of **9**; hydrogens have been omitted for clarity.

† Electronic supplementary information (ESI) available: molecular structure of **10**. See http://www.rsc.org/suppdata/cc/b1/b107732e/

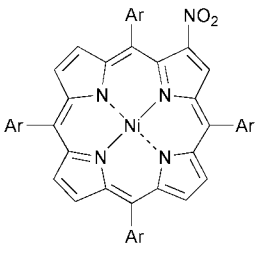

1: Ar = Ph
2: Ar = (3,5-di-Bu^t)Ph

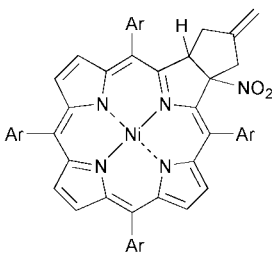

3: Ar = Ph
4: Ar = (3,5-di-Bu^t)Ph

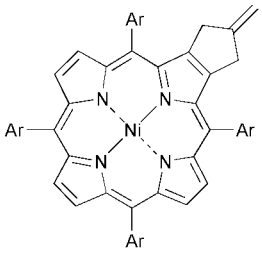

5: Ar = Ph
6: Ar = (3,5-di-Bu^t)Ph

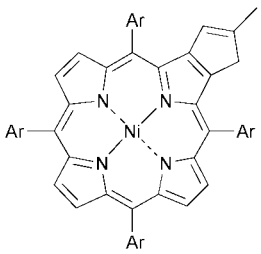

7: Ar = Ph
8: Ar = (3,5-di-Bu^t)Ph

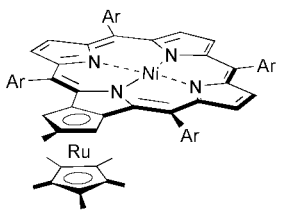

9

Ar = (3,5-di-Bu^t)Ph

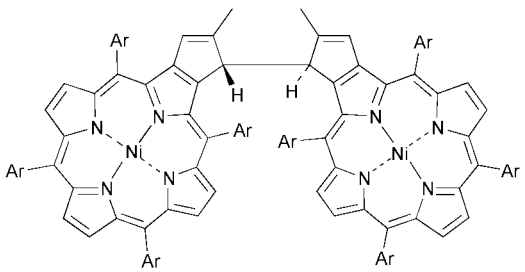

10: Ar = (3,5-di-Bu^t)Ph

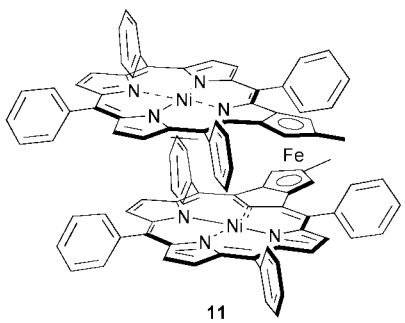

11

 DOI: 10.1039/b107732e

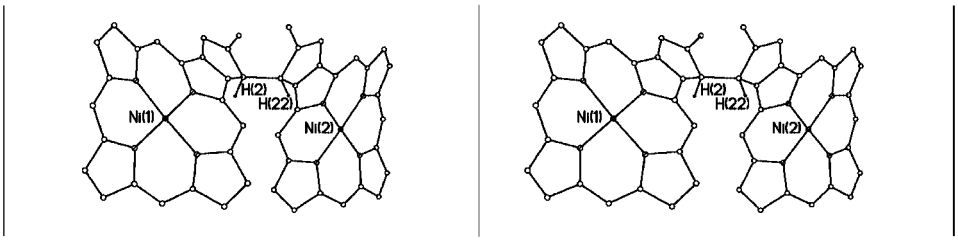

Fig. 2 The molecular structure of **10** in stereoview; 3,5-di-tert-butylphenyl rings and hydrogens, except for those on the bridging carbons, have been omitted for clarity.

system of the newly formed cyclopentadienide anion. Deprotonated **8** reacted with Cp^*RuCl_2 at room temperature for 2–5 days to give air-stable ruthenocenoporphyrin **9** in 25% yield.[12] The formation of **9** was confirmed by LDI–ToF mass spectrometry (m/z = 1408.0) and by ^{1}H NMR spectroscopy (which showed a characteristic singlet at 3.90 ppm corresponding to the fused cyclopentadienide protons).

The molecular structure of **9** was determined by X-ray crystallography (Fig. 1).§ The porphyrin macrocycle was lightly saddled[13] with a MDPMP (macrocyclic atom mean deviation from the porphyrin mean plane) of 0.108 Å. The Ni–N bond lengths averaged 1.965[9] Å, which is longer than in most reported nickel(II) porphyrin crystal structures.[14] The ruthenocenyl rings were aligned in an eclipsed orientation, as is typically observed for this moiety.[14] A porphyrin dimer (**10**) was also isolated (in 15% yield) along with ruthenocenoporphyrin **9** and its structure confirmed by X-ray crystallography (Fig. 2).¶ The use of a ruthenium(III) complex may account for the oxidative dimerization leading to the formation of **10**. Similar dimerizations using $FeCl_3$ as the oxidant have been reported for substituted cyclopentadienides.[15] Both macrocycles in dimer **10** displayed saddle/ruffle hybrid non-planar distortions,[13] had MDPMPs of 0.375 and 0.315 Å, and average Ni–N bond lengths of 1.915[13] and 1.913[6] Å.

Deprotonation of **8** at 0 °C using LDA followed by addition of $FeCl_2$ did not produce the desired bisporphyrinatoferrocene, probably due to the bulkiness of the *meso*-substituents. However under the same conditions, **7** produced the air-stable bisporphyrinatoferrocene **11**[16] in 30% yield. While the UV–visible spectrum of **9** displayed a split Soret band and relatively intense Q bands, that of **11** showed a broad Soret band and no well-defined Q bands. Using variable temperature ^{1}H NMR spectroscopy, two distinct conformational processes could be observed for **11**, arising from hindered adjacent *meso*-phenyls and ferrocene rotations. The β- and cyclopentadienide protons of **11** were found upfield-shifted by 0.5–1 ppm relative to those of **9**. The methyl protons on the fused cyclopentadienide ring of **11** appeared at 1.82 ppm, while the methyl protons on the Cp* ring of ruthenocene **9** gave a singlet at 0.91 ppm. This suggests a partial overlap of the two porphyrin macrocycles with staggered *meso*-phenyl rings.

This work was supported by grant CHE-99-04076 from the US National Science Foundation and grant HL-22252 from the US National Institutes of Health.

Notes and references

‡ Present address: Department of Chemistry, Louisiana State University, Baton Rouge, LA 70803. E-mail: kmsmith@lsu.edu

§ Crystals of **9** were grown from MeOH–THF–H_2O [$C_{90}H_{110}N_4Ni$-Ru·2(THF), FW = 1551.8]. The selected crystal (0.40 × 0.28 × 0.16 mm) was monoclinic, space group $P2_1/m$, with cell dimensions a = 9.3626(5), b = 30.748(2), c = 14.5245(8) Å, β = 99.7930(10)°, V = 4120.5(4) Å^3, and Z = 2. Data were collected with ω-scans on a Bruker SMART 1000 diffractometer with a sealed tube source [λ(Mo-Kα) = 0.71073 Å] at 90(2) K. Diffraction data were collected to 2θ = 63° affording 56880 total reflections. A 2θ cutoff of 55° was applied to give 46122 total, 9601 unique, and 7078 observed ($>2\sigma(I)$) reflections [R_{int} = 0.0898, T_{min} = 0.837, T_{max} = 0.930, ρ_{calc} = 1.251 gcm^{-3}, μ = 0.464 mm^{-1}]. An empirical absorption correction was applied [SADABS 2.0 (Sheldrick, 2000)]. The structure was solved by the Patterson method and refined based on F^2 using all data by full matrix least-squares methods with 492 parameters (Bruker SHELXS-97, SHELXL-97). Hydrogen atom positions were refined with riding models. Final R factors were $R1$ = 0.0773 (observed data) and $wR2$ = 0.192 (all data). CCDC 165704.

¶ Crystals of **10** were grown from MeOH–toluene [$C_{160}H_{190}N_8Ni_2$·2(toluene), FW = 2527.0]. The selected crystal (0.30 × 0.20 × 0.08 mm) was monoclinic, space group $P2_1/c$, with cell dimensions a = 26.7781(15), b = 15.9648(8), c = 36.499(2) Å, β = 101.885(3)°, V = 15269.2(14) Å^3, and Z = 4. Diffraction data were collected and absorption corrected as for **9** (215487 total reflections for 2θ = 63°). A 2θ cutoff of 50° was applied to give 28066 total, 26858 unique, and 13378 observed ($>2\sigma(I)$) reflections [R_{int} = 0.169, T_{min} = 0.916, T_{max} = 0.976, ρ_{calc} = 1.101 gcm^{-3}, μ = 0.299 mm^{-1}]. The structure was solved by direct methods and refined as for **9** with 1685 parameters. Hydrogen atom positions were refined with riding models. Final R factors were $R1$ = 0.0839 (observed data) and $wR2$ = 0.270 (all data). CCDC 165703. See http://www.rsc.org/suppdata/cc/b1/b107732e/ for crystallographic files in .cif or other electronic format.

1 (*a*) A. C. Benniston, *Chem. Soc. Rev.*, 1996, **25**, 427; (*b*) C. D. Hall, G. J. Kirkovits, N. K. Diedovic, T. K. U. Truong and J. R. H. Tucker, *Pure Appl. Chem.*, 1998, **70**, 2359.

2 (*a*) H. Imahori, H. Yamada, Y. Nishimura, I. Yamazaki and Y. Sakata, *J. Phys. Chem. B*, 2000, **104**, 2099; (*b*) M. Fujitsuka, O. Ito, H. Imahori, K. Yamada, H. Yamada and Y. Sakata, *Chem. Lett.*, 1999, 721; (*c*) M. Yanagida, T. Kanai, X. Zhang, T. Kondo and K. Uosaki, *Bull. Chem. Soc. Jpn.*, 1998, **71**, 2555.

3 (*a*) A. K. Burrell, W. M. Campbell, D. L. Officer, S. M. Scott, K. C. Gordon and M. R. McDonald, *J. Chem. Soc., Dalton Trans.*, 1999, 3349; (*b*) R. W. Wagner, P. A. Brown, T. E. Johnson and J. S. Lindsey, *J. Chem. Soc., Chem. Commun.*, 1991, 1463; (*c*) H. Imahori, H. Yamada, S. Ozawa, K. Ushida and Y. Sakata, *Chem. Commun.*, 1999, 1165; (*d*) H. Imahori, H. Norieda, H. Yamada, Y. Nishimura, I. Yamazaki, Y. Sakata and S. Fukuzumi, *J. Am. Chem. Soc.*, 2001, **123**, 100.

4 (*a*) S. W. Rhee, Y. H. Na, Y. Do and J. Kim, *Inorg. Chim. Acta*, 2000, **309**, 49; (*b*) S. W. Rhee, B. B. Park, Y. Do and J. Kim, *Polyhedron*, 2000, **19**, 1961.

5 G. B. Maiya, J.-M. Barbe and K. M. Kadish, *Inorg. Chem.*, 1989, **28**, 2524.

6 N. M. Loim, N. V. Abramova and V. I. Sokolov, *Mendeleev Commun.*, 1996, 46.

7 K. K. Dailey, G. P. A. Yap, A. L. Rheingold and T. B. Rauchfuss, *Angew. Chem., Int. Ed. Engl.*, 1996, **35**, 1833.

8 L. Jaquinod, in *The Porphyrin Handbook*, ed. K. M. Kadish, K. M. Smith and R. Guilard, Academic Press, Boston, MA, 2000, Vol. 1, p 201.

9 L. Jaquinod, C. Gros, M. M. Olmstead, M. Antolovich and K. M. Smith, *Chem. Commun.*, 1996, 1475.

10 C. W. Holzapfel and T. L. van der Merwe, *Tetrahedron Lett.*, 1996, **37**, 2307.

11 (*a*) M. M. Catalano, M. J. Crossley, M. M. Harding and L. G. King, *J. Chem. Soc., Chem. Commun.*, 1984, 1535; (*b*) K. M. Shea, L. Jaquinod and K. M. Smith, *J. Org. Chem.*, 1998, **63**, 7013.

12 **9**: UV/Vis (THF): λ_{max} 412 nm (ε, 103,000), 450 (77,000), 534 (18,100), 576 (16,100), 640 (18,500). ^{1}H NMR ($CDCl_3$): δ 8.57 (d, 2H), 8.47 (s, 2H), 8.48 (d, 2H), 7.81 (m, 8H), 7.67 (t, 2H), 7.64 (t, 2H), 3.90 (s, 2H), 1.75 (s, 3H), 1.45 (s, 72H), 0.91 (s, 15H); MS (LDI-ToF), *m/z* 1408.0.

13 W. Jentzen, X.-Z. Song and J. A. Shelnutt, *J. Phys. Chem. B*, 1997, **101**, 1684.

14 3D Search and Research Using the Cambridge Structural Database (April 2001 release), F. H. Allen and O. Kennard, *Chemical Design Automation News*, 1993, **8**, (1), 31.

15 J. Okuda, E. Herdtweck and E. M. Zeller, *Chem. Ber.*, 1991, **124**, 1575.

16 **11**: UV/Vis (THF): λ_{max} 416 nm (ε, 170,000), 530 (broad). No well-defined Q bands. ^{1}H NMR ($CDCl_3$): δ 8.40 (s, 4H), 8.01 (d, 4H), 7.44 (d, 4H), 7.84 (d, 16H), 7.70 (m, 24H), 3.01 (s, 4H), 1.82 (s, 6H); MS (LDI-ToF), *m/z* 1499.9.

CHEMCOMM Communication
www.rsc.org/chemcomm

Tandem ring-closing metathesis reaction with a ruthenium catalyst containing a N-heterocyclic ligand

Tae-Lim Choi and Robert H. Grubbs*

Arnold and Mabel Beckman Laboratories of Chemical Synthesis, Division of Chemistry and Chemical Engineering, California Institute of Technology, Pasadena, California 91125, USA. E-mail: rhg@its.caltech.edu

Received (in Cambridge, UK) 12th September 2001, Accepted 29th October 2001
First published as an Advance Article on the web 23rd November 2001

The highly active catalyst 2 was used in tandem RCM to make molecules with various ring systems containing α,β-unsaturated carbonyl compounds.

Tandem cyclization reactions build up molecular complexity rapidly from relatively simple starting substrates.[1] Complicated molecules were synthesized in a single step by carbanion,[2] carbocation,[3] free radical,[4] and Pd coupling reaction[5] whose novelty and efficiency were demonstrated by total syntheses of many natural products. Olefin metathesis has become a useful reaction in organic synthesis,[6] and our group recently demonstrated the viability of tandem ring closing metathesis reactions using catalyst **1**.[7] Unfortunately, catalyst **1** could not incorporate more synthetically valuable functionalized olefins such as α,β-unsaturated carbonyl compounds. However, with the development of the more active catalyst **2**,[8] containing a N-heterocyclic ligand, functionalized olefins could participate in RCM and cross metathesis reactions.[9] Herein, we report tandem RCM reactions by using catalyst **2**, to make synthetically useful α,β-unsaturated lactones and enones.

Various substrates containing different olefin arrays were examined for the tandem cyclization and were found to give moderate to excellent yields (Table 1). Entries 1 through 4 demonstrate the viability of tandem ring-opening/ring-closing

Table 1 Tandem RCM to install functionalized olefins[a]

Entry	Substrate	Concentration	Product	Yield
1	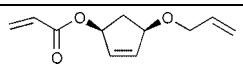	0.05 M	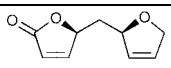	**3**: 81%
2	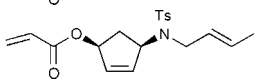	0.05 M	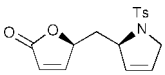	**4**: 89%
3	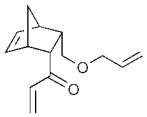	0.005 M	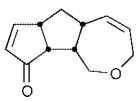	**5**: 45%
4	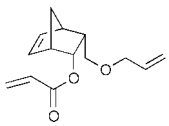	0.005 M	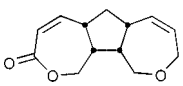	**6**: 47%
5	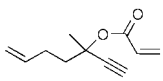	0.03 M	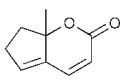	**7**: 95%
6	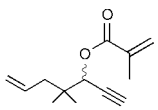	0.03 M	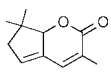	**8**: 86%
7	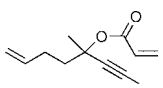	0.03 M	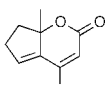	**9**: 72%
8	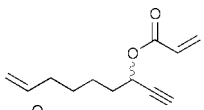	0.015 M	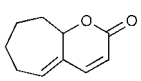	**10**: 68%
9	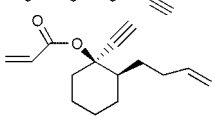	0.03 M	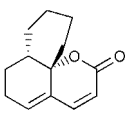	**11**: 100%
10	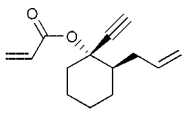	0.06 M	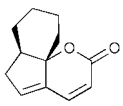	**12**: 74%

[a] 5 mol% catalyst **2** at 40 °C in CH_2Cl_2 for 6–12 h.

 DOI: 10.1039/b108306f

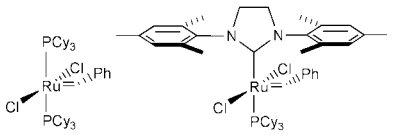

1 2

metathesis. In the case of entries 1 and 2, catalyst **2** reacts with more reactive terminal olefin and the resulting alkylidene opens the 5-membered ring. The sequence of tandem events is completed by ring closing onto the α,β-unsaturated carbonyl olefin (Scheme 1). Fused tricyclic compounds were also synthesized from the highly strained norbonene moiety, but the yields were lower due to competing polymerization (entries 3 and 4).

Another variant of tandem RCM is demonstrated by enyne tandem ring closing metathesis to form fused bicyclic ring systems (entries 5 to 10). In these cases, catalyst **2** also reacts with the terminal olefins preferentially and undergoes rapid intermolecular enyne metathesis to form the first ring, then reacts with the α,β-unsaturated carbonyl olefin to close the final ring (Scheme 2). The fact that 7-membered lactone **A** is never observed, implies that during the first RCM event, the newly formed alkylidene **B** exclusively reacts with acetylenes over acrylates. The more challenging trisubstituted α,β-unsaturated carbonyl olefins were also successfully cyclized (entries 6 and 7). However, an attempt to make a tetrasubstituted α,β-unsaturated carbonyl olefin afforded less than 10% yield of the bicycle with the remainder being monocyclized product. This suggests that disubstituted carbene is formed just as in entry 7, but preferentially reacts with the terminal olefins of the starting molecule over the sterically and electronically demanding α-disubstitued α,β-unsaturated carbonyl olefin. 7,6-Fused bicyclic compounds are available in moderate yield by this method, (entry 8). Lastly, tandem RCM to make 6,5,6- and 6,6,6-fused tricyclic compounds are shown in entries 9 and 10 which demonstrates that this method has potential applications in the synthesis of complex natural products.

The highly active catalyst **2** was used in tandem RCM to make molecules with various ring system. The ability to incorporate α,β-unsaturated carbonyl olefins makes the tandem RCM synthetically more valuable since further manipulations are possible.

The authors would like to thank the NIH for generous support of this research, and Dr M. Scholl, Dr C. W. Lee, Dr S. D. Goldberg, Dr F. D. Toste and A.K. Chatterjee for helpful discussions.

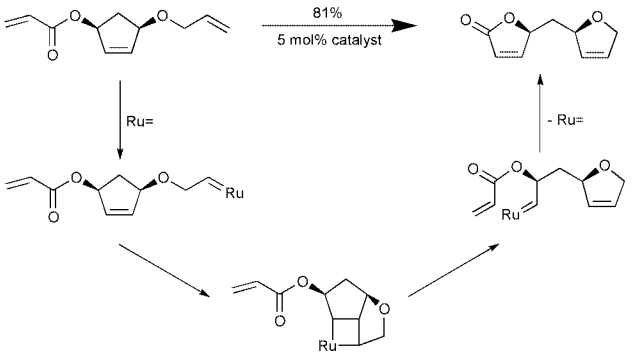

Scheme 1 Ring-opening/Ring-closing tandem RCM.

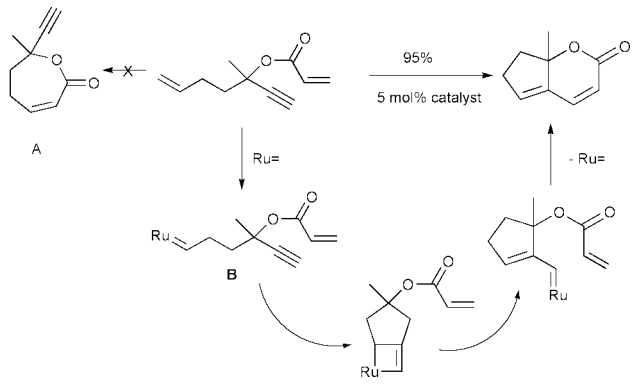

Scheme 2 Eyn-tandem RCM.

Notes and references

1 L. F. Teitze, *Chem. Rev.*, 1996, **96**, 115; T. Hudlickly, *Chem. Rev.*, 1996, **96**, 3; T.-L. Ho, *Tandem Reactions in Organic Synthesis*, Wiley-Interscience, New York, 1992.
2 M. Ihara, K. Makita, Y. Tokunaga and F. Fukumoto, *J. Org. Chem.*, 1994, **59**, 6008.
3 W. S. Johnson, K. Wiedhaup, S. F. Brady and G. L. Olson, *J. Am. Chem. Soc.*, 1974, **96**, 3979.
4 T. Takahashi, W. Katouda, Y. Sakamoto, S. Tomida and H. Yamada, *Tetrahedron Lett.*, 1995, **36**, 2273.
5 Y. Zhang, G. Wu, G. Angel and E. Negishi, *J. Am. Chem. Soc.*, 1990, **112**, 8590; B. M. Trost and Y. Shi, *J. Am. Chem. Soc.*, 1993, **115**, 9421.
6 For recent reviews on organic applications, see: R. H. Grubbs, S. J. Miller and G. C. Fu, *Acc. Chem. Res.*, 1995, **28**, 446; M. Schuster and S. Blechert, *Angew. Chem.*, 1997, **109**, 2124; M. Schuster and S. Blechert, *Angew. Chem., Int. Ed. Engl.*, 1997, **36**, 2067; R. H. Grubbs and S. Chang, *Tetrahedron*, 1998, **54**, 4413; S. K. Armstrong, *J. Chem. Soc., Perkin Trans. 1*, 1998, 371; S. Blechert, *Pure Appl. Chem.*, 1999, **71**, 1393; A. Furstner, *Angew. Chem., Int. Ed. Engl.*, 2000, **39**, 3013.
7 S. H. Kim, N. B. Bowden and R. H. Grubbs, *J. Am. Chem. Soc.*, 1994, **116**, 10801; S. H. Kim, W. J. Zuercher, N. B. Bowden and R. H. Grubbs, *J. Org. Chem.*, 1996, **61**, 1073; W. J. Zuercher, M. Hashimoto and R. H. Grubbs, *J. Am. Chem. Soc.*, 1996, **118**, 6634; W. J. Zuercher, M. Scholl and R. H. Grubbs, *J. Org. Chem.*, 1998, **63**, 4291.
8 M. Scholl, S. Ding, C. W. Lee and R. H. Grubbs, *Org. Lett.*, 1999, **1**, 953.
9 A. K. Chatterjee and R. H. Grubbs, *Org. Lett.*, 1999, **1**, 1751; A. K. Chatterjee, J. P. Morgan, M. Scholl and R. H. Grubbs, *J. Am. Chem. Soc.*, 2000, **122**, 3783; T.-L. Choi, A. K. Chatterjee and R. H. Grubbs, *Angew. Chem.*, 2001, **113**, 1317; T.-L. Choi, A. K. Chatterjee and R. H. Grubbs, *Angew. Chem., Int. Ed. Engl.*, 2001, **40**, 1277; A. K. Chatterjee, T.-L. Choi and R. H. Grubbs, *Synlett*, 2001, 1034; T.-L. Choi, C. W. Lee, A. K. Chatterjee and R. H. Grubbs, *J. Am. Chem. Soc.*, 2001, **123**, 10417.

CHEMCOMM
Communication
www.rsc.org/chemcomm

Efficient mass transfer from an acoustically oscillated gas bubble

Peter R. Birkin,*[a] Yvonne E. Watson[a] and Timothy G. Leighton[b]

[a] *Chemistry Department, University of Southampton, Highfield, Southampton, UK. E-mail: prb2@soton.ac.uk*
[b] *Institute of Sound and Vibration Research, University of Southampton, Highfield, Southampton, UK. E-mail: tgl@isvr.soton.ac.uk*

Received (in Cambridge, UK) 22nd August 2001, Accepted 7th November 2001
First published as an Advance Article on the web 6th December 2001

Efficient mass transfer enhancements as the result of acoustically oscillated gas bubbles are detected using a microelectrode positioned at variable distances from the gas/liquid interface.

The enhancement in mass transfer as the result of bubble motion is extremely important in many industrial scale electrochemical processes.[1] It is thought to be the result of a number of different mechanisms associated with electrochemical bubble growth, detachment and motion under buoyancy forces away from the solid/liquid interface of an electrode.[2] These mechanisms have been investigated by a number of authors. The work by Whitney and Tobias is particularly noteworthy.[3] These authors studied bubble motion using arrays of microelectrodes produced through photolithographic processing. The individual contribution of single bubbles could be detected from a generator microelectrode. However, in all of these studies the enhancement in mass transfer has involved the motion of bubbles under buoyancy forces alone.

Bubbles are also known to be extremely active acoustically, with the sound of running water (*e.g.* in a small waterfall) largely attributed to bubble entrapment. The subsequent bubble pulsation gives the characteristic 'noise', which is observed.[4] In turn gas bubbles within a liquid interact strongly with incident sound waves. If the sound wave is of the correct frequency and pressure amplitude, then a number of different oscillations of a bubble can be induced. These fall broadly into two classes: a breathing mode (or 'pulsation') where the whole bubble expands and contracts with spherical symmetry about the bubble centre; and a second class which lack spherical symmetry. The shape oscillations called Faraday waves[5] are members of this second class. In the steady state the breathing mode occurs at the frequency of the driving sound field, but in contrast Faraday waves occur at half this frequency. Whilst a breathing mode is always excited, generation of Faraday waves requires the driving field to exceed a threshold amplitude.[6] Both the breathing mode and surface waves move the liquid phase of the media to a greater or lesser extent. Fig. 1 shows a photograph of a gas bubble driven into oscillation by irradiation with sound. The distortions in the surface of the bubble can be clearly seen.

However, the contribution to mass transfer of these modes within the liquid phase has not been reported. Here a microelectrode is used to characterise the mass transfer enhancements produced by an oscillating gas bubble. Microelectrodes were chosen for a number of reasons. These included their ability to operate under steady state conditions, their relatively fast response time and their size.[7,8] In the experiments reported here a microelectrode was positioned close to the gas/liquid interface of an air bubble trapped by buoyancy forces under a solid surface. The liquid phase consists of an aqueous solution[9] of 5 mmol dm^{-3} $[Fe(CN)_6]^{-3}$ in 0.2 mol dm^{-3} $Sr(NO_3)_2$. The microelectrode was positioned close to the gas/liquid interface using an X, Y, Z micrometer and stage. The position of the microelectrode with respect to the gas/liquid interface was verified by monitoring the steady state current recorded in the absence of bubble oscillation. When the electrode (a 25 μm diameter Pt microdisc) was < 125 μm away from the nearest point on the stationary bubble wall, the presence of the gas/liquid interface could be detected as a reduction in the steady state current recorded at the microelectrode.[10–12] This was due to hindered diffusion (negative feedback) as a result of the blocking nature of the gas/liquid interface under the conditions stated. Irradiation of the bubble with sound of the appropriate frequency and amplitude results in oscillation of the bubble surface. This oscillation can be electrochemically detected by the microelectrode positioned close to the gas/liquid interface. The motion of the bubble wall will be detected as an enhancement in mass transfer to the microelectrode as a result of the forced convection of the liquid produced by the oscillation of the bubble wall. Fig. 2 shows the enhancement in mass transfer detected as a function of distance away from the gas/liquid interface. In this case, the bubble was driven into oscillation at a pressure sufficient to generate surface waves on the gas/liquid interface. This was observed in two ways. First, the presence of surface waves on the bubble wall was observed optically as a 'shimmer'. Second, when the microelectrode was positioned close to the bubble wall (*ca.* 5–10 μm) the motion of the bubble wall can be resolved electrochemically. This is shown as an insert on Fig. 2. The insert shows the current and pressure† time traces for a bubble driven to oscillate with surface motion. This clearly shows that the current time trace has a component at $0.5f$ (where f represents the drive frequency, in this case 1.46 kHz). This is characteristic of Faraday waves on the surface of the bubble wall, and is confirmed by the photograph of a bubble under similar conditions shown in Fig. 1. Fig. 2 shows that within the first *ca.* 100 μm, the mass transfer enhancement remains approximately constant. Fig. 2 also shows that the current falls as the distance between the microelectrode and the gas/liquid interface of the bubble increases. However, the perturbation in

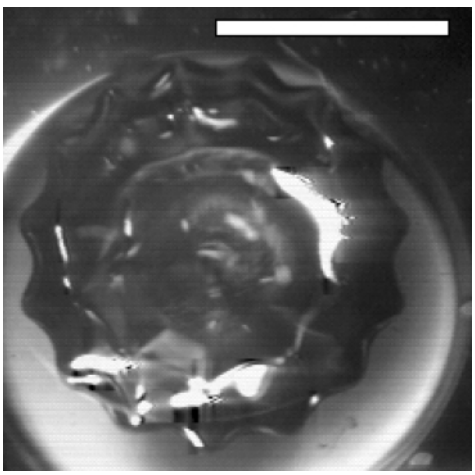

Fig. 1 Photograph taken from below a tethered bubble held by buoyancy forces on the end of a glass rod. The scale bar represents 3 mm. The surface waves can be clearly seen around the perimeter of the gas/liquid interface.

 DOI: 10.1039/b107616g

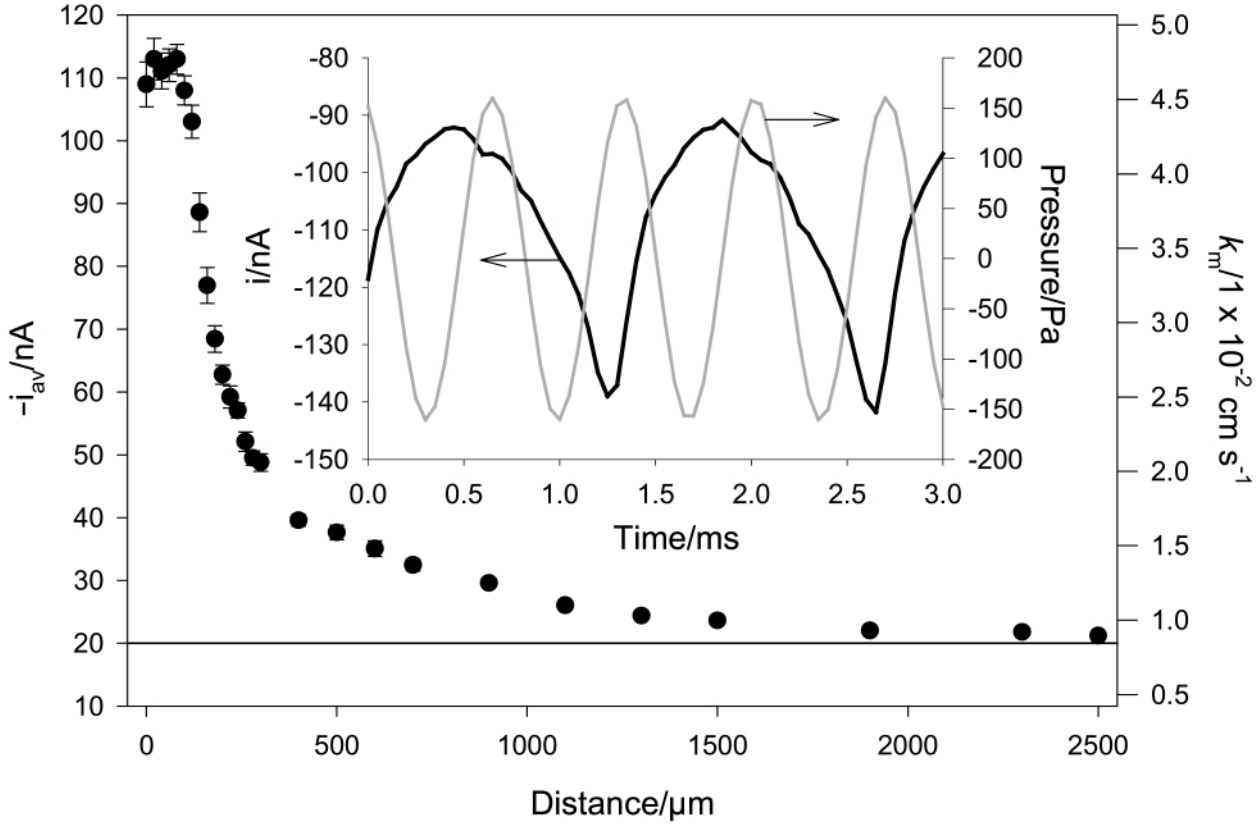

Fig. 2 Plot showing the average current (●) and associated mass transfer coefficient for a single air bubble driven into oscillation by a sound field operating at 1.46 kHz. The solution contained 5 mmol dm^{-3} $[Fe(CN)_6]^{3-}$ in 0.2 mol dm^{-3} $Sr(NO_3)_2$. The error bars show the 95% confidence interval. The insert shows the oscillation in the current (solid line) and pressure† (faint line) as a function of time employing high temporal resolution equipment. The experiment was performed at *ca.* 20–23 °C under aerobic conditions. The solid horizontal line represents the steady state current or mass transfer coefficient for the microelectrode in a stagnant solution.

the mass transfer coefficient can be detected at extended distances away form the gas/liquid interface. A significant enhancement in the time averaged steady state mass transfer to the microelectrode was observed up to distances of *ca.* 2500 μm. This is particularly significant considering that the mass transfer coefficient of the 25 μm diameter platinum microelectrode is already high in stagnant solution (0.008 cm s^{-1}). It is interesting to note that the enhancement in mass transfer as a result of the bubble motion exceeds this value (up to 0.0477 cm s^{-1}) but is brought about by a relatively small pressure amplitude (< 100 Pa). This is a significant point as it clearly demonstrates that enhancing the mass transfer of material to an electrode in this manner would be a significantly more efficient way when compared to the employment of ultrasound to induce cavitation and other high energy phenomena.

Previous studies have shown that ultrasound can enhance mass transfer significantly.[13–15] However, the magnitude of the pressure field required to achieve inertial (transient) cavitation is considerably high. As an example, to generate cavitation in water under standard conditions requires a pressure amplitude in excess of *ca.* 1 atmosphere (101 000 Pa).[4] This is a factor of 1000 higher than the pressures (and in turn a factor of 10^6 in intensity) employed here. Clearly the generation of mass transfer enhancements using acoustically oscillated bubbles, rather than inertial cavitation, would be significantly more efficient. This increase in efficiency is due to the differing mechanisms responsible for the forced convection enhancements observed. The process of inertial cavitation requires that small (*e.g.* of order micron radius) bubbles expand against atmospheric pressure and surface tension forces to a critical radius, before collapsing. However, exciting a large bubble (*e.g.* mm radius) at resonance takes advantage of their exceptionally good acoustic coupling.[4] In turn, the pressure amplitude required to generate surface waves in this case is small, but the enhancement in forced convection is relatively large. As an example, mass transfer coefficients reported from cavitation are on the order[13–15] of 0.1–1 cm s^{-1}. The mass transfer coefficient recorded here is only a factor of 10 less, while the applied pressure is a factor of 1000 less. This is because the excitation of a surface wave does not require a large overall volume change of the bubble, compared to the generation of inertial cavitation.

Notes and references

† Note that the absolute pressure will not be the same as that shown in the insert of Fig. 2 as the presence of the oscillating bubble will alter the measured pressure. The absolute pressure can only be measured when the bubble has been removed from the glass support.

1 M. D. Fouad and G. H. Sedahmed, *Electrochim. Acta*, 1972, **17**, 665.
2 L. J. J. Jenson and E. Berendretch, *Electrochim. Acta*, 1979, **24**, 693.
3 G. M. Whitney and C. W. Tobias, *AIChE J.*, 1988, **34**, 1981.
4 T. G. Leighton, *The Acoustic Bubble*, Academic Press Limited, London, 1994.
5 M. Faraday, *Philos. Trans. R. Soc. London*, 1831, **121**, 319.
6 A. O. Maksimov and T. G. Leighton, *Acta Acustica,*, 2001, **87**, 322.
7 G. Denuault, *Chem Ind. (London)*, 1996, **18**, 678.
8 D. Pletcher, *Microelectrodes: Theory and Application*, ed. M. I. Montenegro, M. A. Queiros and J. L. Daschbach, Kluwer Academic Publishers, Dordrecht, 1990.
9 C. Beriet and D. Pletcher, *J. Electroanal. Chem.*, 1993, **361**, 93.
10 A. J. Bard, F. R. F. Fan, O. Lev and J. Kwak, *Anal. Chem.*, 1989, **61**, 132.
11 J. Kwak and A. J. Bard, *Anal. Chem.*, 1989, **61**, 1221.
12 J. L. Amphlett and G. Denuault, *J. Phys. Chem. B*, 1998, **102**, 9946.
13 P. R. Birkin and S. S. Martinez, *J. Electroanal. Chem.*, 1996, **416**, 127; P. R. Birkin and S. S. Martinez, *J. Chem. Soc., Chem. Commun.*, 1995, 1807.
14 C. R. S. Hagan and L. A. Coury, *Anal. Chem.*, 1994, **66**, 399; H. Zhang and L. A. Coury, *Anal. Chem.*, 1993, **65**, 1552.
15 R. G. Compton, J. C. Eklund and S. D. Page, *J. Appl. Electrochem.*, 1996, **26**, 775; R. G. Compton, J. C. Eklund, S. D. Page and T. O. Rebbitt, *J. Chem. Soc., Dalton Trans.*, 1995, 38.

CHEMCOMM Communication
www.rsc.org/chemcomm

Novel highly symmetrical cube-shaped cation with 16-nitrogen donors

Zhang Bing-guang,[a] Mo Hong,[b] Duan Chun-ying,*[b] He Cheng,[c] Meng Qing-jin,[b] Wang Zhe-ming[c] and Yan Chun-hua[c]

[a] *Department of Chemistry, Wuhan University, Wuhan, P. R. China and State Key Laboratory of Coordination Chemistry, Nanjing University, Nanjing, 210093, P. R. China*
[b] *Coordination Chemistry Institute and State Key Laboratory of Coordination Chemistry, Nanjing University, Nanjing, 210093, P. R. China. E-mail: duancy@nju.edu.cn*
[c] *State Key Laboratory of Rare Earth Materials Chemistry and Applications of Peking University, College of Chemistry and Molecular Engineering, Peking University, Beijing, 100871, P. R. China*

Received (in Cambridge, UK) 9th October 2001, Accepted 6th November 2001
First published as an Advance Article on the web 4th December 2001

A novel highly symmetrical cube-shaped trication $[C_{36}H_{75}N_{16}]^{3+}$ with 16-nitrogen donors is achieved *via* self-assembly in which two water molecules were clathrated within the cavity of the framework.

Highly symmetrical cage-like molecules containing macrocyclic skeleton have always been fascinating targets for synthetic chemists and play an important role in host–guest chemistry.[1] Such frameworks possess cavities capable of entrapping atomic and/or molecular sized guest and have applications of chemistry, biology and materials sciences.[2,3] It has also been postulated that the interior of cage-like molecules can be considered to provide a new phase of matter in which it becomes possible to stabilize reactive intermediates and to observe new forms of stereoisomer.[4] However, for cavities tailored around spherical or globular targets, positioning of binding sites requires the controlled formation of a number of covalent bonds in long, often impractical multi-step syntheses.[5] As an alternative, self-assembly, a special type of synthetic procedure in which several reactions between several reagents occur in one experimental operation to yield the final covalent structure, was used to construct smaller, simpler fragments with enough molecular information to spontaneously reassemble into the desired cavity.[6]

In this paper, we introduce a large spherical cube-shaped host moleculear cation $[H_3L]^{3+}$ (L = $C_{36}H_{72}N_{16}$) (Scheme 1), by way of a self-assembly process in which there appears to be two molecular guests, in the form of two water molecules, within the cavity of the framework. Compound **L** has a T_d-symmetric urotropin-like structure and also somewhat resembles structurally Lehn's sophisticated tricyclic cryptand[7] known as the 'soccer ball molecule' on account of its spherical three-dimensional skeleton. Whereas most of the tricyclic tetraamines such as hexaethylenetetramine[8] and related large tricyclic and cage-like compounds reported by Takemura[9] and Lehn were synthesized by low-yield, long and multi-step methods, compound **L** like that of urotropin forms easily upon mixing of tris(2-ethylamino)amine and formalin† ESI-MS (electrospray ionization mass spectroscopy) in water–methanol solution (in the presence of $HClO_4$) and reveals the presence of a main peak at *m/z* 593, corresponding to the most abundant ion $\{[H_6\mathbf{L}\subset(H_2O)_2][H_2O][ClO_4]_4\}^{2+}$ and confirming the existence of self-assembled cage.

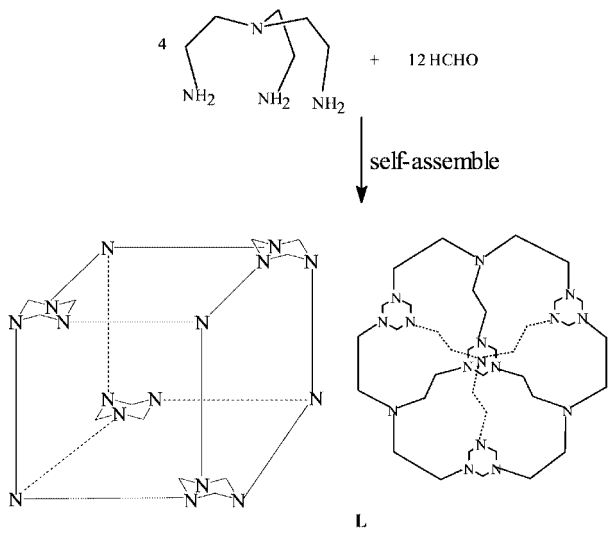

Scheme 1

The most definitive proof for the formation of the T_d-symmetric cage comes from the X-ray crystallographic analysis.‡ One protonated cubed-shaped trication, two guest water molecules as well as three perchlorate anions were found in an asymmetric unit. The cage is slightly deformed from expected T_d symmetry (Fig. 1) with four bridge head nitrogen atoms of tris(2-aminoethyl)amine [N(1), N(11), N(12), and N(13)] and four six-membered $[N(CH_2)]_3$ rings occupying the vertex positions, and the twelve CH_2CH_2 chains along the edges. In addition to its chemical interest, such a host has aesthetic appeal. The edge of the cubic cage is *ca.* 4.3 Å in length (from the head nitrogen atom to the center of the six-membered ring). Among the sixteen nitrogen atoms, three of them, N(2), N(6) and N(13) are protonated with the hydrogen atoms oriented towards the inside of cavity (*endo*), four of them, one from each of the $[N(CH_2)]_3$ six-membered rings, respectively N(7), N(8),

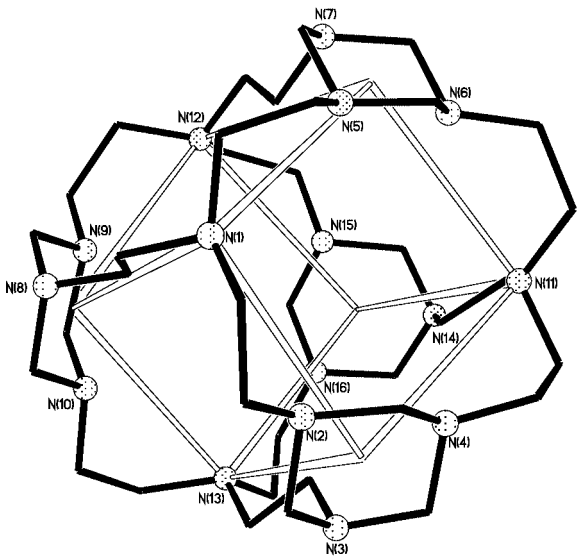

Fig. 1 Molecular structure of the host, showing the T_d-symmetric hexahedral cage. The four bridge head nitrogen atoms of tris(2-aminoethyl)amine and the centers of the six-membered $[N(CH_2)]_3$ rings occupy the vertex positions with the twelve CH_2CH_2 chains forming the edges.

 DOI: 10.1039/b109206p

N(3) and N(14), are *exo* with the lone pairs pointing away from the cavity, whereas the others are oriented towards the inside of the cavity. The twelve *endo* nitrogen bridgeheads delineate the intramolecular cavity. The distances from the center (M) of the cavity to the *endo* nitrogen atoms are in the range of 3.66–3.91 Å, with an average M–N distance of about 3.88 Å. Considering the thickness of each face of the cage, the outer space volume is *ca.* 200 Å^3, while the inner space is just about 50 Å^3. This cavity should be able to form complexes with neutral molecules and anions of appropriate size.

The most interesting structural feature is that there are two water molecules within the cavity of the framework (Fig. 2). The two water molecules lie in the pseudo C_4 axis, which reduces the symmetry of the hexahedral host from T_d to S_4, the O···O separation is *ca.* 2.80 Å with O(1W)–H(1WB)···O(2W) *ca.* 167°, indicating strong H-bonding. An even greater dispersion is observed for the N···O distance range of the twelve *endo* nitrogen atoms from 2.82 to 3.22 Å, with an average N···O separation of about 3.0 Å. These separations are comparable to those found for the N···O hydrogen bonds present in the crystal structure of the NH_4^+ complexes of macrotetrolide antibiotics (2.83–2.93 Å),[10] 18-crown-6 (2.86–2.88 Å),[11] and some H_3O^+ complexes of nitrogen-containing crypts,[12] indicating potential hydrogen bonding between the nitrogen atoms of the host and the included water molecules. Since the host is a protonated ion, and the angles of N(5)–H(5C)···O(1W), N(11)–H(11C)···O(1W) and N(13)–(H13C)···O(2W) are 149°, 175° and 173°, respectively, it is suggested that the host participates in N–H···O hydrogen bonding with the included water molecules. The angles of O(1W)–H(1WA)···N(2), O(2W)–H(2WA)···N(15) and O(2W)–H(2WB)···N(9) are 178°, 167° and 166°, indicating typical O–H···N hydrogen bonding of the water molecules and substantial contact with the host. From the description mentioned above concerning the nature of the hydrogen bonding in the cavity, it is reasonable to speculate that the water molecules may serve as templates; such phenomena involving molecules as templates is not well-established.

Metal template condensation reactions of formaldehyde and amines provide simple, elective, and inexpensive routes to the macrocyclic complexes that have been studied;[13] however, no water molecule or neutral molecule template condensation reactions of formaldehyde and amines have been postulated. In our synthesis of the cryptand, a substantial and aesthetically appealing structure is assembled with modest efficiency from trivial building blocks and eighteen components just using HCHO and tris(2-aminoethyl)amine as starting materials and water molecule as template. This kind of self-assembly is quite interesting for the large cage with high symmetry and falls very nicely into the category of self-assembly and supramolecular chemistry. The hexahedral host reported here is exciting and will be of interest to a wide audience.

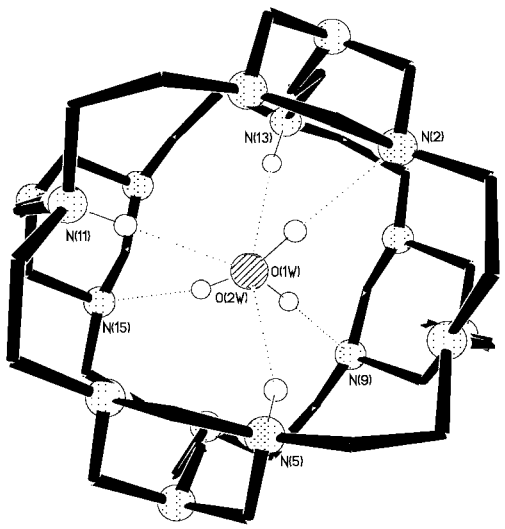

Fig. 2 Perspective view of the host–water complex, showing potential hydrogen bonds. Selected N···O separations (Å). O(1W)···N(2), 2.996(6); O(1W)···N(5), 2.841(6); O(1W)···N(11), 2.994(6); O(2W)···N(9), 2.808(6); O(2W)···N(13), 3.116(6); O(2W)···N(15), 2.958(6).

This work was supported by the National Natural Science Foundation of China.

Notes and references

† *Preparations*. To 100 mL stirred acetonitrile containing perchloric acid (0.5 mL) and sodium acetate (1.2 g, 15 mmol), tris(2-aminoethyl)amine (1.46 g, 10 mmol) in 200 ml dichloromethane and HCHO (2.5 g, 36%, 30 mmol) in 200 ml acetontrile were added drop-wise, respectively. After finishing the addition, the solution was stirred for 4 h and allowed to stand for one week. White solid formed and was removed by filtration, the filtrate was allowed to stand for another week and then the precipitate formed was filtered off and washed with water (3 × 20 mL) and acetone (3 × 30 mL), respectively. Yield 0.35 g (15%) of the compound $[H_3\mathbf{L}\subset(H_2O)_2][ClO_4]_3$. Anal. calcd. for $(C_{36}H_{75}N_{16})(H_2O)_2(ClO_4)_3$: C, 40.6; H, 7.5; N, 21.0; Found: C, 40.4; H, 7.5; N, 20.6%. Pale-yellow crystals suitable for X-ray structure analysis were collected directly.

‡ *Crystal data*. Monoclinic, $P2_1$, molecular formula, $C_{36}H_{75}N_{16}(ClO_4)_3(H_2O)_2$, formula weight, 1066.50, pale-yellow, 0.40 × 0.30 × 0.30 mm, a = 11.483(2), b = 16.512(3), c = 13.051(3) Å, β = 94.82(3)°, V = 2465.8(9) Å^3, Z = 2, T = 293 K, D_c = 1.436 g cm^{-3}. Intensity data were collected on an Enraf-Nonius CCD system. 49970 reflections measured of which 11638 (R_{int} = 0.053) were independent reflection and all were included in the refinement. The structure was solved by direct methods. The oxygen atoms of the perchlorate anions were refined disordered. Non-hydrogen atoms were refined anisotropically, hydrogen atoms attached to the water oxygen atoms and protonated nitrogen atoms were found from difference fourier map, other hydrogen atoms were positioned in their calculated positions. All hydrogen atoms were refined using riding model. Computations were carried on a PC-586 computer using SHELXTL-PC program package. For 705 parameters based on 5921 observed reflections [$I > 2\sigma(I)$] gave the final refined circle R = 0.074, $wR2$ = 0.190 (for all data). CCDC 161379. See http://www.rsc.org/suppdata/cc/b1/b109206p/ for crystallographic files in .cif or other electronic format.

1 D. J. Cram and M. J. Cram, in *Container Molecules and Their Guests: Monographs in Supramolecular Chemistry*, ed. J. F. Stoddart, The Royal Society of Chemistry, Cambridge, 1994; B. Dietrich, P. Viout and J. M. Lehn, *Macrocyclic Chemistry: Aspects of Organic and Inorganic Supramolecular Chemistry*, VCH, Weinheim, 1993.

2 F. Diederich, *Nature*, 1994, **369**, 199–207; R. W. Sallfrank, *Nature*, 1996, **383**, 124–125.

3 M. M. Conn and J. Rebek Jr., *Chem. Rev.*, 1997, **97**, 1647–1668; C. Branden and J. Tooze, *Introduction to Protein Structure*, Garland, New York, 1991, pp. 161–177.

4 D. J. Cram, M. E. Tanner and R. Thomas, *Angew. Chem., Int. Ed. Engl.*, 1991, **30**, 1024–1027; P. Timmerman, W. Verboom, F. C. J. M. Veggel, J. P. M. V. Duynhoven and D. N. Reinhoudt, *Angew. Chem., Int Ed. Engl.*, 1994, **33**, 2345–2348.

5 L. R. MacGillivray and J. L. Atwood, *Angew. Chem., Int. Ed.*, 1999, **38**, 1018–1023; J. D. Mendoza, *Chem. Eur. J.*, 1998, **4**, 1373–1377.

6 D. Philp and J. F. Stoddart, *Angew. Chem., Int. Ed. Engl.*, 1996, **35**, 1154–1196; J. Rebek Jr., *Acc. Chem. Res.*, 1999, **32**, 278–286.

7 E. Graf and J. M. Lehn, *J. Am. Chem. Soc.*, 1975, **97**, 5022–5024; E. Graf, J. P. Kintzinger, J. M. Lehn and J. LeMoigne, *J. Am. Chem. Soc.*, 1982, **104**, 1672–1678.

8 J. Springborg, B. Nielsen, C. E. Olsen and I. Søtofte, *J. Chem. Soc., Perkin Trans. 2*, 1999, 2701–2706; Y. Miyahara, Y. Tanaka, K. Aminmoto, T. Akazawa, T. Sakuragi, H. Kobayshi, K. Kubota, M. Suenage, H. Koyama and T. Inazu, *Angew. Chem., Int. Ed.*, 1999, **38**, 956–959.

9 H. Takemura, T. Shinmyozu and T. Inazu, *J. Am. Chem. Soc.*, 1991, 1323–1331; H. Takemura, K. Otsuka, N. Kon, M. Yasutake, T. Shinmyozu and T. Inazu, *Tetrahedtron Lett.*, 1999, **40**, 5561–5564.

10 K. Neupert-Laves and M. Dobler, *Helv. Chim. Acta*, 1976, **59**, 614–623; Y. Nawata, T. Sakamaki and Y. Titaka, *Acta Crystallogr., Sect. B*, 1977, **33**, 1201–1207.

11 O. Nagano, A. Kobayashi and Y. SasaKi, *Bull. Chem. Soc. Jpn.*, 1978, **51**, 790–793.

12 C. J. Feng, Q. H. Luo, C. Y. Duan, M. C. Sheng and Y. J. Liu, *J. Chem. Soc., Dalton Trans.*, 1998, 1377–1380.

13 M. P. Suh, *Advanced Inorganic Chemistry*, ed. A. G. Sykes, Academic Press, New York, 1997, vol. 44, pp. 93–146; M. P. Suh, M. Y. Han, J. L. Lee, K. S. Min and C. Hyeon, *J. Am. Chem. Soc.*, 1998, **120**, 3819–3820.

CHEMCOMM Communication
www.rsc.org/chemcomm

Reactions of quadruply chelated silyl– and germyl–molybdenum hydrido complexes with carboxylic acids and carbon dioxide: a first example of carbon dioxide fixation utilizing the *trans* effect of a silyl ligand

Makoto Minato, Da-Yang Zhou, Ken-ichiro Sumiura, Ryo Hirabayashi, Yoshitaka Yamaguchi and Takashi Ito*

Department of Materials Chemistry, Graduate School of Engineering, Yokohama National University, 79-5 Tokiwadai, Hodogaya-ku, Yokohama, Japan 240-8501. E-mail: t-ito@ynu.ac.jp

Received (in Cambridge, UK) 30th August 2001, Accepted 7th November 2001
First published as an Advance Article on the web 4th December 2001

The reaction of molybdenum complexes [MoH_3{E(Ph)[$Ph_2PCH_2CH_2P(Ph)C_6H_4$-*o*]$_2$}] (E = Si or Ge) with carboxylic acids gave carboxylato complexes where the carboxylato ligand coordinates to the metal in a unidentate mode; the formato complex was found to be an effective catalyst for carbon dioxide fixation.

Since the first preparation of the transition-metal silyl derivative, $CpFe(CO)_2SiMe_3$ (Cp = η^5-C_5H_5), by Wilkinson and coworkers in 1956,[1] numerous relevant examples have been reported.[2] We previously reported the unexpected formation of a novel molybdenum–silyl complex, [MoH_3{Si(Ph)-[$Ph_2PCH_2CH_2P(Ph)C_6H_4$-*o*]$_2$}] **1a**, which is obtained by the thermal reaction of [MoH_4(dppe)$_2$] **2**, (dppe = $Ph_2PCH_2CH_2PPh_2$) with $PhSiH_3$ and possesses an unusual quadruply chelated ligand.[3] Recently this methodology has been extended to the reaction of **2** with $PhGeH_3$, which is a higher homologue of $PhSiH_3$, and have obtained the same type of complex **1b** having a Mo–Ge bond.[4] Complexes in which two metal atoms of very different character are held in close proximity seem to offer fascinating opportunities to achieve novel types of reaction. We have studied the reactivity of these complexes and a series of new complexes with this quinquidentate ligand has been synthesized from **1**. For example, **1a** reacted with a dialkyl malonate or gaseous dioxygen to afford an η^1-*O*-enolato type complex or a peroxo type η^2-O_2 complex **3**, respectively.[5,6] Herein we report the synthesis and some reactions of dihydrido(carboxylato)molybdenum complexes.

Treatment of **1** with two equiv. of carboxylic acids such as formic acid, acetic acid or benzoic acid in THF at room temperature readily led to the formation of monocarboxylato molybdenum complexes (**4**, E = Si; **5**, E = Ge) in good yields (70–90%, Scheme 1).† In these reactions, the evolution of hydrogen gas was qualitatively confirmed by GLC analysis. In the ^{1}H NMR spectra of the complexes **4**, hydrido signals appeared at around δ −7.9 as a triplet of triplets corresponding to an A_2K_2X spin system. The ^{31}P{H} NMR spectra of complexes **4** contain two resonances at around δ 87 (br d, J_{PP} 122 Hz) and 58 (br d, J_{PP} 122 Hz) in a 1 : 1 ratio. The presence of only two resonances indicates that the molecule **4** has an effective mirror plane which contains the Mo–Si bond. The IR spectra of complexes **4** showed ν(Mo–H) at 1816–1819 cm^{-1} and two ν(OCO) stretching vibrations (asym and sym) at 1609–1618 cm^{-1} and 1326–1360 cm^{-1}, respectively. The fairly large values of $\Delta\nu$ [$\nu(OCO)_{asym}-\nu(OCO)_{sym}$] ranging from 248 to 272 cm^{-1} suggest that the carboxylato ligands in the complexes coordinate to the metal in a unidentate fashion as shown in Scheme 1.[7] The molybdenum–germyl complexes **5** have very similar IR and NMR spectra to **4**, implying that **4** and **5** are isostructural.

The basic features of the structure of these complexes deduced from the spectra were fully confirmed by single crystal X-ray diffraction on **4b**. A view of the molecule is shown in Fig. 1 with selected bond distances and angles.[8] As expected from the IR and NMR results, this complex contains a quinquidentate P_2SiP_2 ligand and a unidentate acetato ligand occupying the axial site. The structure can be compared with that of the above-mentioned peroxo complex, [MoH{Si(Ph)[Ph_2-$PCH_2CH_2P(Ph)C_6H_4$-*o*]$_2$}(η^2-O_2)] **3**.[5] The Mo–Si distance of

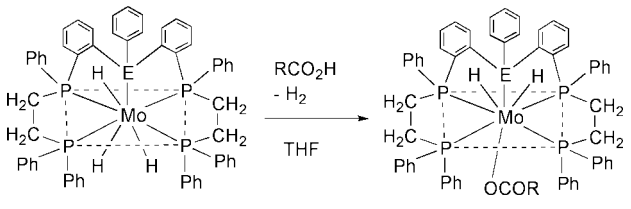

1a (E = Si)
1b (E = Ge)

4a (E = Si, R = H)
4b (E = Si, R = CH_3)
4c (E = Si, R = Ph)
5a (E = Ge, R = H)
5b (E = Ge, R = CH_3)
5c (E = Ge, R = Ph)

Scheme 1

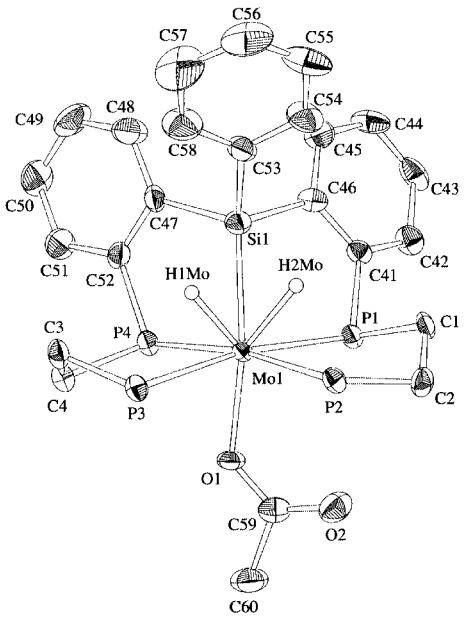

Fig. 1 Thermal ellipsoid plot (30% probability level) for **4b**. Selected bond lengths (Å) and angles (°): Mo1–Si1 2.515(2), Mo1–P1 2.485(2), Mo1–P2 2.507(2), Mo1–P3 2.496(2), Mo1–P4 2.466(2), Si1–C47 1.887(7), Mo1–O1 2.174(5); P1–Mo1–P2 80.31(6), P2–Mo1–P3 96.32(6), Si1–Mo1–O1 143.7(1).

 DOI: 10.1039/b107837m

2.515(2) Å in **4b** is slightly shorter than that of 2.554(5) Å in **3**. On the other hand, the mean Mo–P distance of 2.489 Å in **4b** is a little longer than that found in **3** (2.462 Å).

The parent complex **2** is known to react with carboxylic acids or allyl carboxylates to give cationic and neutral carboxylato complexes, respectively, where the carboxylato ligand coordinates to the metal in a bidentate mode.[9,10] The unusual unidentate coordination of acetate of **4b** may be ascribed to the stability of the P_2SiP_2 coordination.

A toluene solution of complex **1a** was allowed to react under CO_2 pressure (17 atm) at room temperature and **4a** was isolated in 82% yield from the reaction mixture (Scheme 2). Interestingly, **4a** reverted to **1a** quantitatively with accompanying evolution of one mol of CO_2, when warmed in benzene. The reversible insertion reaction of CO_2 into the Mo–H bond under mild conditions is an outstanding feature exhibited by complex **1a** since the parent complex **2** does not react with CO_2 at room temperature although irradiation of a benzene solution of **2** under CO_2 atmosphere yielded a chelated formato-*O,O'* complex.[11] We thought that the high reactivity of **1a** is due to the strong *trans*-influence of the Si fragment since it has been pointed out that the R_3Si group has a strong σ-donor ability and may labilize the ligand in the position *trans* to it.[12] Yet, to date there have been few reports concerning the influence of silyl ligands on the reactivity of transition-metal complexes.[13]

Subsequently, we explored the catalytic activity of **1a** towards carbon dioxide fixation [eqn. (1)]. A toluene solution of

$$HNMe_2 \xrightarrow[PhMe\ \ 110\ °C]{CO_2/H_2,\ \ cat.\ \ \mathbf{1a}\ or\ \mathbf{4a}} HCONMe_2 \qquad (1)$$

complex **1a** was allowed to react under CO_2/H_2 (25/35 atm) pressure in the presence of dimethylamine at 110 °C affording 115 equivalents of *N,N*-dimethylformamide with respect to the complex. In this process, formato complex **4a** was also found to be an efficient catalyst. Presumably, the first step in the catalytic cycle using **1a** may be the formation of **4a**. Neither **2** nor **1b** catalyzed this process suggesting both the Mo–Si linkage and the P_2SiP_2 girdle in **1a** play an important role.

Catalytic carbon dioxide fixation has attracted considerable interest. Most of the reported studies deal with iridium, palladium and ruthenium complexes[14] and reports of catalysis using Group 6 metals are rare.[15] To our knowledge, complex **1a** is the first molybdenum compound which can catalyze the transformation of carbon dioxide into dialkylformamide effectively.

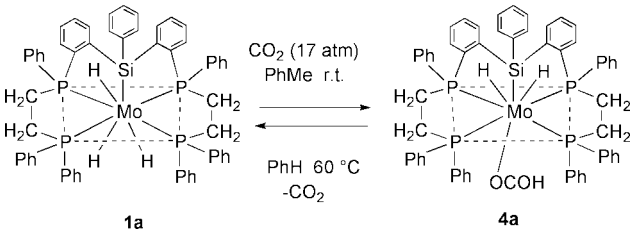

1a **4a**

Scheme 2

This work was supported by a Grant-in-Aid for Scientific Research (B) No. 10450340 and a Grant-in-Aid for Scientific Research on Priority Areas (No. 11120217) from the Ministry of Education, Science, Sports and Culture of Japan.

Notes and references

† *Typical procedure* for the preparation of **4b**: to a solution of **1a** (0.268 g, 26.8 mmol) in dry THF (20 mL) was added acetic acid (0.03 mL) under argon. The resultant solution was stirred for 3 h at ambient temperature. After removal of the solvent under reduced pressure, the residue was washed with diethyl ether and hexane. Recrystallization from THF–hexane gave **4b** (0.255g, 90%). Complex **4b**: ^{1}H NMR (benzene-d_6, 25 °C, 270 MHz): δ −7.96 (tt, *J* 43.3, 17.2 Hz, 2H, Mo–*H*), 1.23 (s, 3H, C*H*$_3$CO) 2.0–3.0 (br m, 8H, PC*H*$_2$); ^{31}P{^{1}H} NMR (benzene-d_6, 109.4 MHz): δ 87.7 (br d, *J* 122 Hz), 59.1 (br d, *J* 122 Hz); Satisfactory elemental analysis data are so far not available, possibly due to the presence of silicon in the molecule.

1 T. S. Piper, D. Lemal and G. Wilkinson, *Naturwissenschaften*, 1956, **43**, 129.
2 J. Y. Corey and J. B. Wilking, *Chem. Rev.*, 1999, **99**, 175.
3 D.-Y. Zhou, M. Minato, T. Ito and M. Yamasaki, *Chem. Lett.*, 1997, 1017.
4 M. Minato, R. Hirabayashi, T. Matsumoto, Y. Yamaguchi and T. Ito, *Chem. Lett.*, 2001, 960.
5 D.-Y. Zhou, L.-B. Zhang, M. Minato, T. Ito and K. Osakada, *Chem. Lett.*, 1998, 187.
6 T. Ito, K. Shimada, T. Ono, M. Minato and Y. Yamaguchi, *J. Organomet. Chem.*, 2000, **611**, 308.
7 K. Nakamoto, *Infrared and Raman Spectra of Inorganic and Coordination Compounds*, Wiley, NY, 3rd edn, 1978, p. 232.
8 *Crystal data* for **4b**: yellow prism; 0.30 × 0.10 × 0.10 mm; $C_{60}H_{56}O_2P_4MoSi{\cdot}C_4H_8O{\cdot}H_2O$, *M* = 1147.14; monoclinic, space group $P2_1/c$(no. 14); *a* = 23.858(1), *b* = 12.1098(3), *c* = 19.5279(7) Å, β = 90.027(1)°, *V* = 5641.9(3) Å^3, *Z* = 4; D_c = 1.350 g cm^{-3}; Rigaku RAXIS-II imaging plate area detector; 298 K; Mo-Kα radiation (λ = 0.71069 Å); μ(Mo-Kα) = 4.15 cm^{-1}; *R* = 0.051. R_w = 0.080 for 5376 unique reflections [$I > 5.00\sigma(I)$]. CCDC reference number 172503. See http://www.rsc.org/suppdata/cc/b1/b107837m/ for crystallographic data in CIF or other electronic format.
9 T. Ito, A. Takahashi and S. Tamura, *Bull. Chem. Soc. Jpn.*, 1986, **59**, 3489.
10 T. Ito, T. Matsubara and Y. Yamashita, *J. Chem. Soc., Dalton Trans.*, 1990, 2407.
11 T. Ito and T. Matsubara, *J. Chem. Soc., Dalton Trans.*, 1988, 2241.
12 J. P. Collman, L. S. Hegedus, J. R. Norton and R. G. Finke, *Principles and Applications of Organo-transition Metal Chemistry*, University Science Books, Mill Valley, CA, 1987, p. 243.
13 H. Tobita, K. Hasegawa, J. J. G. Minglana, L.-S. Luh, M. Okazaki and H. Ogino, *Organometallics*, 1999, **18**, 2058.
14 P. G. Jessop, T. Ikariya and R. Noyori, *Chem. Rev.*, 1995, **95**, 259.
15 D. J. Darensbourg and C. Ovalles, *J. Am. Chem. Soc.*, 1987, **109**, 3330.

CHEMCOMM Communication
www.rsc.org/chemcomm

Intramolecular aromatic 1,5-hydrogen transfer in preparation of oxacyclic naphthalic anhydride *via* unusual Pschorr cyclisation

Xuhong Qian,* Jingnan Cui and Rong Zhang

State Key Laboratory of Fine Chemicals, Dalian University of Technology, Dalian 116012, China

Received (in Cambridge, UK) 20th September 2001, Accepted 1st November 2001
First published as an Advance Article on the web 23rd November 2001

Unusual Pschorr cyclisation *via* naphthyl radical-induced intramolecular aromatic 1,5-hydrogen transfer using the corresponding diazonium salts as starting materials gave five- and six-membered oxacyclic-fused naphthalic anhydride isomers.

Pschorr cyclisation has been widely used in the preparation of polycyclic compounds[1] for over a century.[2] Many applications of this reaction can be found in the pharmaceutical and dye industries. Normally, the reaction was accomplished in a three-step mechanism, namely, the diazotization of an *o*-amino group to a diazonium salt; the dediazoniation of the diazonium salt to a radical intermediate; and the closing of the ring. The rearrangements *via* radical-induced aromatic hydrogen migration to produce isomers are rarely found in Pschorr cyclisation because aromatic compounds are usually poor hydrogen donors. In contrast, radical-induced hydrogen migration is commonly seen when the migrating hydrogen originates from an aliphatic carbon or from a heteroatom.[3,4] After a century of diazonium chemistry, phenyl radical-induced aromatic 1,5-hydrogen migration of the benzophenone derivatives was the only example of such isomerization through Pschorr cyclisation (giving two five-membered ring isomers) and Sandmeyer reaction.[5,6] Despite the lack of reports for similar isomerizations, it has been speculated that aromatic 1,5-hydrogen transfer might be a general phenomenon in aromatic radical transformations. Recently, we found five- and six-membered oxacyclic isomers during preparation of benzoxanthene derivatives used as fluorescent probes. We report herein the naphthyl radical-induced aromatic 1,5-hydrogen transfer in Pschorr cyclisation of the corresponding diazonium salts.

The diazonium salts **1** and **2** were prepared from 4-bromo-1,8-naphthalic anhydride according to the procedure published earlier[7] and all intermediates were characterized by ^{1}H-NMR, MS, IR and elemental analysis.

Pschorr cyclisation of **1** initiated by $CuSO_4$, CuO, or ferrocene produced two isomeric fluorescent compounds **3** and **4** in over 9 : 1 ratio (Table 1, entry 1–3). The most plausible explanation for the 9 : 1 ratio of the isomers is that the initially formed radical **A** rearranged itself to radical **B** by 1,5-hydrogen transfer and that these two radicals in some equilibrium were then converted to the products **3** and **4** (Scheme 1). It has been demonstrated that Pschorr cyclisation and Sandmeyer iododediazoniation of benzophenone derivatives gave cyclized isomers in nearly equal amounts and some iodonized isomers, respectively.[5] However, in our case, the ratio of the cyclized isomers was far from 1 : 1 and the iodonized isomers were hardly found. The iododediazoniation of diazonium salts **1** and **2** gave only iodonized compounds **5** and **6**, respectively (entry 6 and 7). It seems that the 1,5-hydrogen transfer rate between **A** and **B** is slower than that between benzophenone radicals according to the literature.[5] Under similar reaction conditions to entry 1, diazonium salt **2** gave also **3** and **4** in the ratio of 7 : 93 (entry 5). This suggests that radical **B** could be also rearranged into radical **A** and the rate of formation of **B** from **A** is faster than that of **A** from **B.** This indicates that radical **B** is more stable than radical **A**. Even so, the structure of major product and the ratio of isomers still mainly depended on the starting compounds, as the rate of cyclisation to five- and six-membered rings is obviously faster than that of hydrogen transfer. Beyond what we expected, the mode of radical generation had obvious effects on hydrogen transfer, as various initiation methods

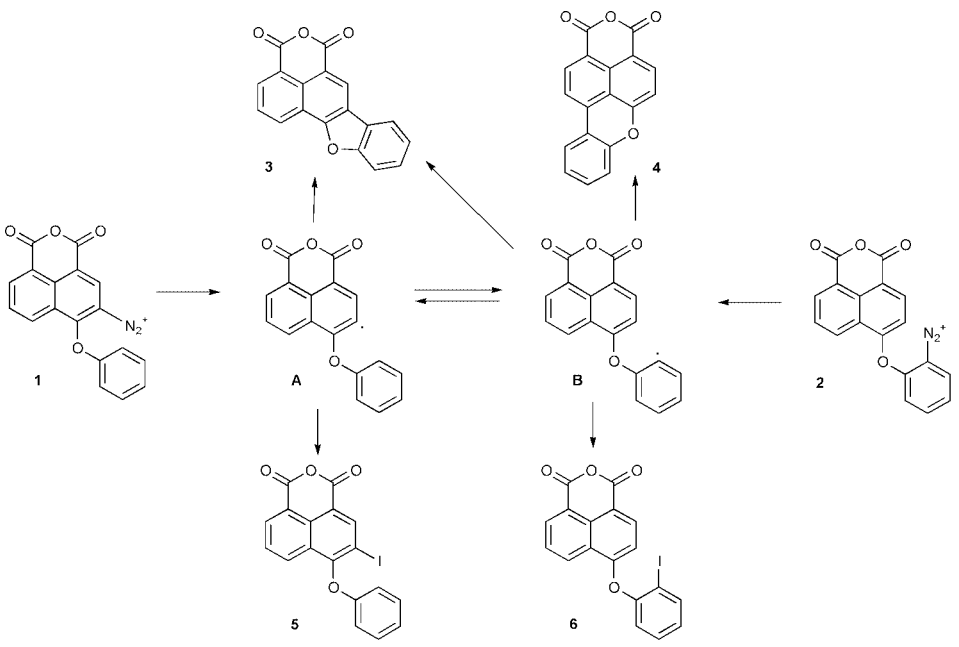

Scheme 1

 DOI: 10.1039/b108874m

Table 1 Pschorr cyclisation and Sandmeyer iododediazoniation of diazonium salts

Entry	Substrate	Reaction	Products	Ratio[a]	Yield[b] (%)
1	**1**	$CuSO_4$, AcOH, H_2O, reflux	**3**:**4**	90:10	90[c]
2	**1**	Ferrocene, acetone, rt	**3**:**4**	94:6	75[c]
3	**1**	CuO, H_2SO_4, rt	**3**:**4**	92:8	80[c]
4	**1**	$CuSO_4$, AcOH, rt	**3**:**4**	83:17	85[c]
5	**2**	$CuSO_4$, AcOH, H_2O, reflux	**3**:**4**	7:93	86[c]
6	**1**	KI, I_2, H_2O, rt	**5**		73
7	**2**	KI, I_2, H_2O, rt	**6**		88

[a] The ratio was determined by HPLC/MS (Hypersil DDS2 column, H_2O + MeOH + AcOH eluent, retention time: **3**, 32 min, **4**, 29 min).[b] The yield was based on the corresponding amino compounds.[c] The yield was obtained in **3** + **4** mixture.

produced a different ratio of isomers (entries 1–4). It suggests that the rate of 1,5-hydrogen transfer between **A** and **B** is sensitive to the environment and can be enhanced (the ratio of **3** and **4** is 83:17) under the conditions of entry 4. This is different from the case of benzophenone derivatives,[5] where solvent showed no effect on the rate of hydrogen transfer.

Molecular modeling using Pcmodel 6.0 showed some differences in their conformations between these 4-phenoxynaphthalic anhydride radicals and the benzophenone radicals, although they were in an aromatic conjugated system. Two aromatic rings next to ether O atom for radicals **A** and **B** were not in the same plane, while for the benzophenone radicals, the carbonyl and two aromatic rings were in the same plane. These conformational differences can be used to explain their differences in the efficiency of radical-induced 1,5-hydrogen transfer, the ratio of isomers, and the solvent effects.

In conclusion, our investigation not only provided the first example of isomerization *via* naphthyl radical-induced aromatic 1,5-hydrogen transfer in naphthalene derivatives during Pschorr cyclisation, but also implied that radical induced-aromatic hydrogen transfer possibly was more common than previously thought in many other aromatic free radical reactions.

Financial support by National Natural Science Foundation of China and The Ministry of Education of China is greatly appreciated.

Notes and references

1 P. H. Leake, *Chem. Rev.*, 1956, **56**, 27; A. J. Floyd, S. F. Dyke and S. E. Word, *Chem. Rev.*, 1976, **76**, 532–535; W. Williams, X. Sun and D. Jebaratnam, *J. Org. Chem.*, 1997, **62**, 4364–4369; J. March, *Advanced Organic Chemistry*, 4th edn., p. 714–715; R. A. Abramovitch, *Adv. Free Radical Chem.*, 1966, **2**, 87.
2 R. Pschorr, *Chem. Ber.*, 1896, **29**, 496.
3 A. L. Beckwith and K. U. Ingold, in *Rearrangements in Ground and Excited States*, ed. P. de Mayo, Academic Press, New York, 1980, **vol. 1**, p. 251.
4 D. P. Curran, K. V. Somayajulu and H. Yu, *Tetrahedron Lett.*, 1992, **33**, 2295.
5 S. Karady, N. L. Abramsom, U.-H. Dolling, A. W. Douglas, G. J. McManemin and B. Marcune, *J. Am. Chem. Soc.*, 1995, **117**, 5425–5426; S. A. Chandler, P. Hanson, A. B. Taylor, P. H. Walton and A. W. Timms, *J. Chem. Soc., Perkin Trans. 2.*, 2001, **2**, 214.
6 D. F. DeTar and D. Relyea, *J. Am. Chem. Soc.*, 1956, **78**, 4302.
7 X. Qian and S. Ren, *J. Chem. Eng, Data*, 1988, **33**, 528–529; W. Yao, X. Qian and Q. Hu, *Tetrahedron Lett.*, 2000, **41**, 7711–7715.

CHEMCOMM Communication
www.rsc.org/chemcomm

Direct detection of the bound sodium ions in self-assembled 5′-GMP gels: a solid-state ^{23}Na NMR approach†

Gang Wu* and Alan Wong

Department of Chemistry, Queen's University, Kingston, Ontario, Canada K7L 3N6. E-mail: gangwu@chem.queensu.ca; Fax: +1-613-533-6669

Received (in Corvallis, OR, USA) 10th August 2001, Accepted 31st October 2001
First published as an Advance Article on the web 4th December 2001

We report an unambiguous solid-state ^{23}Na NMR characterization of the surface and channel sodium ions in self-assembled guanosine-5′-monophosphate (5′-GMP) gels.

Guanosine-5′-monophosphate (5′-GMP) is known to form viscous gels in the presence of alkali metal ions in water.[1] Early X-ray fiber diffraction studies[2,3] have established that the 5′-GMP gel structure consists of a tetrameric arrangement of guanine bases (known as the G-quartet) that are stacked on top of one another forming a right-handed helix with 30° rotation and 3.4 Å advance between adjacent G-quartets; see Scheme 1. Although the presence of alkali metal ions is essential for 5′-GMP gel formation, little is known about the location and stoichiometry of metal ions in this class of self-assembled gel systems. Recently, single crystal X-ray studies revealed that the K^+ and Na^+ ions are located between two G-quartets in $d(G_4T_4G_4)$ and $d(TG_4T)$.[4,5] The mode of ion binding in 5′-GMP gels may be similar to that found in the G-rich DNA sequences, but direct detection of alkali metal ions in 5′-GMP gels has not been reported. It should be noted that solution alkali metal NMR has been used to study the self-association of 5′-GMP;[6] however, the traditional alkali metal NMR method cannot yield site-specific information due to rapid ion exchange in solutions.[7] Recent advances in solid-state NMR methodology in dealing with half-integer quadrupolar nuclei have offered new possibilities for alkali metal NMR to be used as a probe to ion binding in biomolecular systems.[8] For example, Rovnyak *et al.*[9] successfully observed solid-state ^{23}Na NMR signals from the Na^+ ions bound to a DNA quadruplex, $[d(TG_4T)]_4$. However, our recent ^{23}Na NMR results for Na-ionophore complexes[10] did not support the spectral assignment for $[d(TG_4T)]_4$. In this study we apply ^{23}Na magic-angle spinning (MAS) and multiple quantum magic-angle spinning (MQMAS)[11] techniques to various types of 5′-GMP gels and report an unambiguous assignment for the surface and channel Na^+ ions bound to G-quadruplex systems.

Fig. 1A shows the ^{23}Na MAS NMR spectrum of a 5′-GMP gel sample prepared by adding 1.7 mL of 4.0 M NaCl (aq.) to a solution of 320 mg hydrated Na_2(5′-GMP) in 3.4 mL water at rt. In this study, this sample will be referred to as the Na gel sample (**1**). As seen in Fig. 1A, three peaks are observed. The sharp peak centered at $\delta = 7$ ppm is attributed to the presence of excessive NaCl salt in the gel sample. This was confirmed by the fact that this peak can be readily removed by gentle washing the gel sample with 2-methylpentane-2,4-diol (MPD) aqueous solution (40% V/V). The broad signal at $\delta = -1$ ppm is assigned to the Na^+ ions bound to the phosphate groups and water molecules (denoted as the surface Na^+ ions in this study). The weak signal centered at $\delta = -19$ ppm is assigned to the Na^+ ions residing inside the G-quartet channel (denoted as the channel Na^+ ions). The assignment for the channel Na^+ ions is supported by our recent observation that the ^{23}Na NMR signal from Na(Nonactin)SCN appears at $\delta = -16$ ppm.[10] In this complex, the Na^+ ion is coordinated by 8 oxygen atoms from the nonactin molecule,[12] in a cubic fashion very similar to that between two G-quartets.

To confirm the above spectral assignment, we prepared two additional 5′-GMP gel samples. The Cs–Na gel sample (**2**) was prepared by adding 1.0 mL of 3.5 M CsCl (aq.) to an aqueous

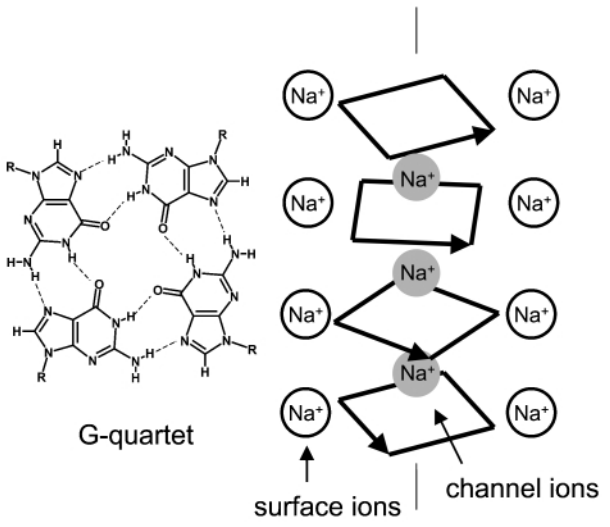

Scheme 1

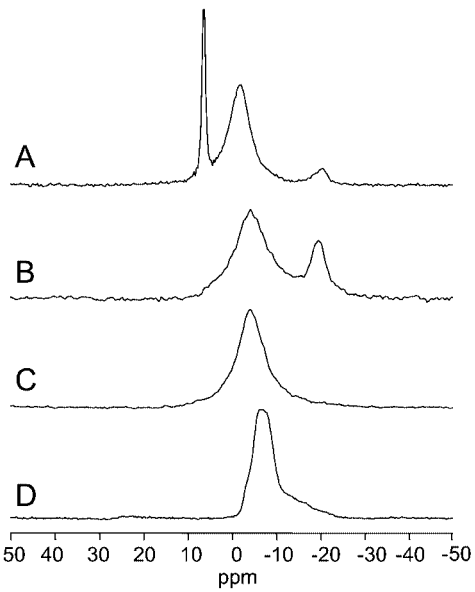

Fig. 1 Solid-state ^{23}Na MAS spectra of 5′-GMP samples. (A) Na gel sample, **1**. (B) Cs–Na gel sample, **2**. (C) K–Na gel sample, **3**. (D) Polycrystalline Na_2(5′-GMP)·$7H_2O$, **4**. All NMR spectra were recorded on a Bruker Avance-500 spectrometer operating at 500.13 and 132.29 MHz for ^{1}H and ^{23}Na nuclei, respectively. The sample spinning frequency was 8000 ± 2 Hz. The RF field strength at the ^{23}Na frequency was approximately 90 kHz.

† Electronic supplementary information (ESI) available: ^{31}P CPMAS spectra of Na gel, Cs–Na gel and Na_2(5′-GMP)·$7H_2O$. See http://www.rsc.org/suppdata/cc/b1/b107353m/

 DOI: 10.1039/b107353m

solution containing 175 mg of Na_2(5′-GMP), followed by recrystallization three times from 40% (V/V) MPD–H_2O. The K–Na gel (**3**) was prepared using KCl (aq.) in a similar procedure as that for **2**. As seen in Fig. 1B, the signal intensity for the surface Na^+ ions is significantly reduced for the Cs–Na gel compared with that for the Na gel sample. This suggests that the Cs^+ ions do not enter the central cavity formed by stacking G-quartets but replace partially the surface Na^+ ions. The observation of a signal at −19 ppm in Fig. 1B indicates that the G-quartet structures are intact in the Cs–Na gel. On the other hand, K^+ ions are preferred over Na^+ ions to occupy at the sites between the G-quartets. Consequently, for the K–Na gel sample, the ^{23}Na NMR signal associated with the channel Na^+ ions disappears completely in Fig. 1C. To make further comparison, we also obtained solid-state ^{23}Na NMR spectra for a polycrystalline sample of Na_2(5′-GMP)·$7H_2O$ (**4**). Because the Na^+ ions in the crystal lattice of **4** are hexacoordinate,[13] the main features of the ^{23}Na MAS spectrum (Fig. 1D) appear between −2 and −10 ppm.

In contrast to the aforementioned low-resolution 1D MAS spectra, the 2D ^{23}Na MQMAS spectra shown in Fig. 2 exhibit significantly improved resolution. For the Na gel sample, the 2D spectrum reveals the presence of two groups of signals originating from the channel Na^+ ions. Careful examination indicates that one of the two spectral regions (labeled as Na2) is severely tilted from the horizontal axis, as illustrated in Fig. 2A. The tilting is a consequence of a distribution of chemical shifts and quadrupole coupling constants, often resulting from the presence of multiple Na^+ sites. From Fig. 2A, the following parameters can be estimated for the Na gel sample: surface Na^+ ions, $C_Q = e^2q_{zz}Q/h \approx 1.6$ MHz, $\eta = (q_{xx} - q_{yy})/q_{zz} \approx 1$, $\delta \approx 3$ ppm; channel Na^+ ions, $C_Q \approx 1.1$ MHz, $\eta \approx 1$, $\delta \approx -18$ ppm. Similarly, the signal for the channel Na^+ ions in the Cs–Na gel sample (Fig. 2B) is also tilted, but does not show resolved signals. This can be explained by a lower ordering of the helices in the Cs–Na gel sample. To further confirm the ordering of helices in gel samples, we obtained ^{31}P CP/MAS NMR spectra (see ESI†). The ^{31}P CP/MAS spectrum of the Na gel exhibits two sharp peaks at 5.0 and 3.8 ppm each with a line width of 200 Hz. On the contrary, the ^{31}P spectrum of the Cs–Na gel shows only a very broad peak at 5.0 ppm of a line width of more than 1000 Hz. The lack of ordering in the Cs–Na gel sample is also reflected from the ^{23}Na MQMAS signal for surface Na^+ ions.

By combining 1D MAS and 2D MQMAS data, we were able to obtain the following parameters for each of the four Na sites in Na_2(5′-GMP)·$7H_2O$: Na1, $C_Q = 1.30$ MHz, $\eta_Q = 0.7$, $\delta = -4.5$ ppm; Na2, $C_Q = 1.85$ MHz, $\eta_Q = 0.5$, $\delta = -2.0$ ppm; Na3, $C_Q = 1.85$ MHz, $\eta_Q = 0.6$, $\delta = -2.0$ ppm; Na4, $C_Q = 2.30$ MHz, $\eta_Q = 0.7$, $\delta = -5.5$ ppm. Based on a simple correlation between C_Q and ion-binding geometry, tentative assignments were made as follows. Na1 can be assigned to the Na site with 4 water molecules and two hydroxy groups from the ribose groups. Na2 and Na3 correspond to the two fully hydrated Na sites. Na4 is due to the site that is coordinated to four water molecules and two N7 nitrogen atoms from the pyrimidine moieties.

Finally, we should point out that the solid-state ^{23}Na NMR spectra for 5′-GMP gels are very similar to those reported for $[d(TG_4T)]_4$.[9] Based on the evidence presented in this study, we conclude that the previous ^{23}Na NMR spectral assignment for $[d(TG_4T)]_4$ was erroneous. In particular, the ^{23}Na NMR signal at 6.8 ppm was incorrectly assigned to channel-bound Na^+ ions. We believe that solid-state ^{23}Na NMR will be a useful technique for detecting Na^+ ions in other metal-directed self-assembly systems as well as in nucleic acids.

G. W. thanks NSERC of Canada for research grants, Queen's University for a Chancellor's Research Award (2000-05) and the Ontario Government for a Premier's Research Excellence Award (2000-05). A. W. thanks Queen's University for an R. S. McLaughlin Fellowship (2000-02). We are also grateful to Chris Freure for assistance at the early stage of this work.

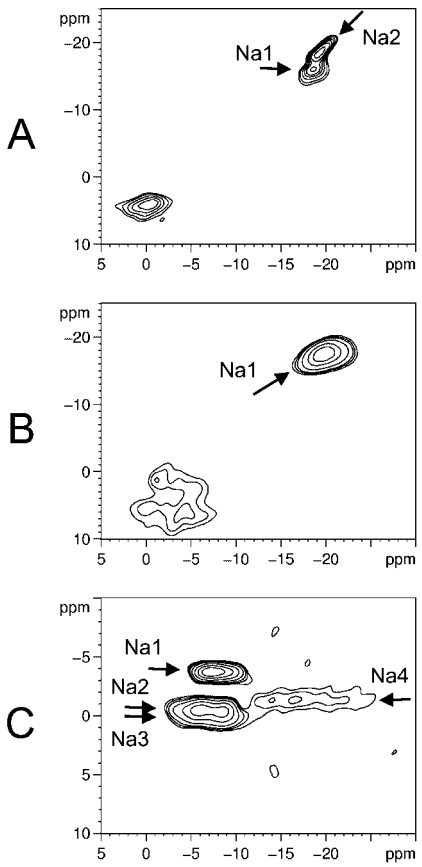

Fig. 2 Contour plot of 2D sheared ^{23}Na MQMAS spectra. (A) Na gel sample, **1** and (B) Cs–Na gel sample, **2**. (C) Polycrystalline Na_2(5'-GMP)·$7H_2O$, **4**. In (A) and (B), 480 scans were collected for each of the 60 t_1 increments with a recycle delay of 1 s. The sample spinning frequency was 5000 ± 2 Hz. In (C), 48 scans were collected for each of the 128 t_1 increments with a recycle time of 2 s. The sample spinning frequency was 8000 ± 2 Hz.

Notes and references

1 See reviews: W. Guschlbauer, J.-F. Chantot and D. Thiele, *J. Biomol. Struct. Dyn.*, 1990, **8**, 491; G. Gottarelli, G. P. Spada and A. Garbesi, *Comprehensive Supramolecular Chemistry*, vol. 9, ed. J.-M. Lehn, J. L. Atwood, D. D. MacNicol, J. A. D. Davies, F. Vögtle, J.-P. Sauvage and M. W. Hosseini, Pergamon, Oxford, UK, 1996, pp. 483–506.
2 M. Gellert, M. N. Lipsett and D. R. Davies, *Proc. Nat. Acad. Sci. USA*, 1962, **48**, 2013.
3 S. B. Zimmerman, *J. Mol. Biol.*, 1976, **106**, 663.
4 C. Kang, X. Zhang, R. Ratliff, R. Moyzis and A. Rich, *Nature (London)*, 1992, **356**, 126.
5 G. Laughlan, A. I. H. Murchie, D. G. Norman, M. H. Moore, P. C. E. Moody, D. M. J. Lilley and B. Luisi, *Science (Washington, D.C.)*, 1994, **265**, 520; K. Phillips, Z. Dauter, A. I. H. Murchie, D. M. J. Lilley and B. Luisi, *J. Mol. Biol.*, 1997, **273**, 171.
6 C. Detellier, A. Paris and P. Laszlo, *C. R. Acad. Sci. Paris Ser. D*, 1978, **286**, 781; M. Borzo, C. Detellier, P. Laszlo and A. Paris, *J. Am. Chem. Soc.*, 1980, **102**, 1124; C. Detellier and P. Laszlo, *J. Am. Chem. Soc.*, 1980, **102**, 1135; A. Delville and C. Detellier and P. Laszlo, *J. Magn. Reson.*, 1979, **34**, 301.
7 H. Deng and W. H. Braunlin, *J. Mol. Biol.*, 1996, **255**, 476.
8 G. Wu, *Biochem. Cell Biol.*, 1998, **76**, 429.
9 D. Rovnyak, M. Buldas, G. Wu, N. V. Hud, J. Feigon and R. G. Griffin, *J. Am. Chem. Soc.*, 2000, **122**, 11 423.
10 A. Wong and G. Wu, *J. Phys. Chem. A*, 2000, **104**, 11 844.
11 L. Frydman and J. S. Harwood, *J. Am. Chem. Soc.*, 1995, **117**, 5367.
12 M. Dobler and R. P. Phizackerley, *Helv. Chim. Acta*, 1974, **57**, 664.
13 S. K. Katti, T. P. Seshadri and M. A. Viswamitra, *Acta Crystallogr., Sect. B: Struct. Sci.*, 1981, **B37**, 1825; C. L. Barnes and S. W. Hawkinson, *Acta Crystallogr., Sect. B: Struct. Sci.*, 1982, **B38**, 812.

CHEMCOMM
Communication
www.rsc.org/chemcomm

De novo design of a five-stranded β-sheet anchoring a metal-ion binding site

Janani Venkatraman,[a] G. A. Naganagowda,[b] R. Sudha[a] and Padmanabhan Balaram*[a]

[a] *Molecular Biophysics Unit, Indian Institute of Science, Bangalore-560012, India. E-mail: pb@mbu.iisc.ernet.in; Fax: 91 80 3600683/91 80 3600535; Tel: 91 80 3602741*
[b] *Sophisticated Instrumentation Facility, Indian Institute of Science, Bangalore-560012, India*

Received (in Cambridge, UK) 5th September 2001, Accepted 1st November 2001
First published as an Advance Article on the web 23rd November 2001

A five-stranded β-sheet bearing two histidine residues as part of a metal-binding site has been designed, synthesised and characterised using NMR and electrospray ionization mass spectrometry techniques.

Construction of well-defined structural elements such as isolated helices,[1,2] helical bundles,[3,4] β-turns and hairpins,[5,6] mixed α/β structures[7] and β-sheets[6,8] have employed common design principles such as (a) incorporation of residues with appropriate secondary structural propensities,[1] (b) utilisation of sequence motifs observed in protein three-dimensional structures as structural templates[4,9] or (c) nucleation of specific conformations by sterically constrained non-protein amino acids.[5,10] Indeed, the use of both normal as well as unusual amino acids that nucleate turns with requisite stereochemistry (type I′ and type II′) have been responsible for the successful design of β-hairpins and small sheets that are stable in aqueous[6,8,11] and organic solvents.[5,12] Attempts at the construction of large multistranded sheets as precursors for the rational design of β-sandwiches and β-barrels have been plagued by problems of solubility and difficulty in characterising the designed structures.[13]

We demonstrate in this communication, the construction of a five stranded β-sheet, whose stable, extended backbone can be further utilised as a template onto which a metal-binding site can be grafted.† The designed 34-residue peptide, **B5** [RGIKV^{D}PGETNT^{D}PSVQF**H**TI^{D}PGYKTL**H**E^{D}PARIVLK], has four ^{D}Pro-Xxx segments designed to nucleate type II′/I′ β-turns (Fig. 1). β-branched residues such as Val/Ile/Thr, which are known to promote β-sheet conformation have been appropriately positioned in the strands. A large number of positively charged residues (Arg/Lys) have been included in the designed sequence to enhance solubility and discourage aggregation.

The design of metal binding sites has often stressed the His_xCys_x motif as appropriate ligands for the chelation of transition metals.[14] We have chosen to position two histidine residues (His 17 and His 26) on adjacent (third and fourth) strands of the five-stranded β-sheet towards the construction of a minimal metal-binding motif. Folding of the **B5** peptide sequence into the target structure would bring the two His residues into the required structural juxtaposition for metal-ion chelation. In addition, the Glu8-His17 pair may also serve as a metal binding site. Tridentate coordination involving Glu8, His17 and His26 is impossible if the constraints of the β-sheet are maintained.

The structure of the **B5** peptide was characterized in detail using high-resolution NMR techniques in methanol, as CD studies indicated the peptide to be poorly structured in water. TOCSY and NOESY experiments permitted complete sequence-specific assignments for **B5**. Spectra derived from NOESY experiments revealed various features consistent with β-sheet structure, such as significantly more intense $C_i^{\alpha}HN_{i+1}H$ ($d_{\alpha N}$) NOEs as compared to the corresponding intraresidue $N_iHC_i^{\alpha}H$ ($d_{N\alpha}$) NOEs. The folding of **B5** into β-sheet conformation with the desired strand registry was corroborated by the presence of several key, long-range NH/NH NOEs and medium intensity, cross-strand $C^{\alpha}H$/ $C^{\alpha}H$ NOEs (Fig. 1, 2) between residues E8/H17, N10/Q15, F16/L25, T18/K23 and H26/I31. The observation of sequential d_{NN} NOEs between residues G7/E8, S13/V14, G21/Y22 and A29/R30 served to confirm the position of the turns. H/D exchange experiments

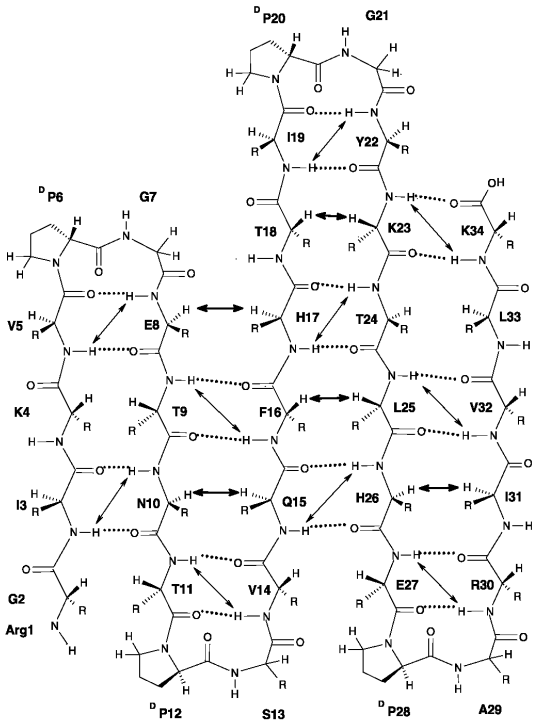

Fig. 1 Schematic representation of the target structure for B5. Important long range NOEs observed are indicated by arrows (darker arrows denote medium NOEs and lighter arrows represent weak NOEs).

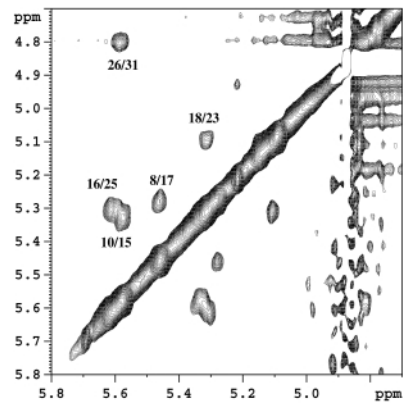

Fig. 2 Partial expansion of the NOESY spectrum of **B5** in CD_3OD at 300 K, indicating long range $C^{\alpha}H$/ $C^{\alpha}H$ NOEs.

 DOI: 10.1039/b107883f

performed on the **B5** peptide in CD_3OD revealed the presence of some slow exchanging amide protons corresponding to residues involved in hydrogen bonding in the β-strands (I3, V5, T9, T11, V14, F16, I19, Y22, T24, R30 and V32).

Structure calculations were performed using DYANA[15] and a total of 228 distance constraints (114 upper and 114 lower), derived from 90 NOEs and H/D experiments. A superposition of ten best structures is shown in Fig. 3a, with a mean RMSD of 1.04 Å for all back bone atoms. Fig. 3b is a ribbon diagram of the mean structure for **B5**, illustrating probable orientations of His17 and His26, the components of the designed metal binding site.

The ability of the peptide to bind a single nickel ion between the two imidazole groups of His17 and His26 was demonstrated by electrospray ionization mass spectrometry (ESIMS) in methanol. Fig. 4 is the ESI mass spectrum of the free peptide and **B5** bound to Ni^{2+}. The mass of the free peptide as revealed by ESIMS is 3785 (Calc. mass = 3785.4). The mass observed for **B5** treated with nickel acetate is 3842, which corresponds to the mass of the peptide + the average mass of Ni^{2+} − 2 [3785.4 + 58.5 − 2; the two most abundant isotopes of nickel are of mass 57.94 (68%) and 59.93 (26.2%)]. The observation of the complex [peptide + Ni^{2+} − 2H] demonstrates simultaneous interaction of the metal ion with two deprotonated imidazole groups. It should be noted that under our conditions of electrospray, coordinated solvent molecules are stripped off the metal ion. Also, attempts to detect sandwich complexes containing a ratio of 2[peptide] : 1 Ni^{2+} were unsuccessful.

Similar results were observed in experiments done with Zn^{2+} ions (data not shown). It is worthy of remark that **B5** has yet another group capable of chelating metal ions, namely Glu8.[16] Indeed, the Glu8/His17 pair could function as a metal ion binding site in a manner analogous to the His17/His26 pair, yielding the observed mass in ESIMS experiments. But **B5** has an overall positive charge of +5 [2 His, 3 Lys, 2 Arg, 1 free amino terminus, 2 Glu and 1 free carboxy terminus], which is reflected in the charge state distribution observed in the ESI mass spectrum of the free peptide (Fig. 4, top); where the +5 charge state is the most abundant. Chelation of a metal ion (M^{2+}) contributes two positive charges to the peptide–metal ion complex, and should have resulted in a shift in the charge envelope of the complex (Fig. 4, bottom). The continued observation of the +5 charge state as the most abundant suggests that two negative charges have been *acquired* by the complex. This is consistent with the loss of two protons by the imidazole groups of His17 and His26 (resulting in two negative charges), rendering the charge of the [His_2-M^{2+}] moiety zero, and maintaining the overall charge of the complex at +5. Involvement of one His and one Glu residue in metal binding would have resulted in the creation of only one new negative charge; in this case the charge state distribution might be expected to be different, with the +6 state being most abundant. CD spectra of peptide–metal complexes closely resembled the parent spectrum, suggesting no major conformational change on metal ion binding, supporting the existence of a preformed template and further indicating the absence of tridentate coordination.

The present design strategy has successfully resulted in the characterisation of a five-stranded β-sheet capable of metal ion coordination. In principle, a metal ion template can be used to assemble individual β-sheet structures to form β-sandwiches and closed β-barrels.

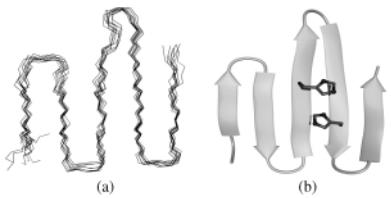

Fig. 3 (a) Superposition of 10 best structures of **B5** obtained from NMR restraints. (b) Ribbon diagram of mean structure illustrating the position of His17 and His26 (side chain positions modeled).

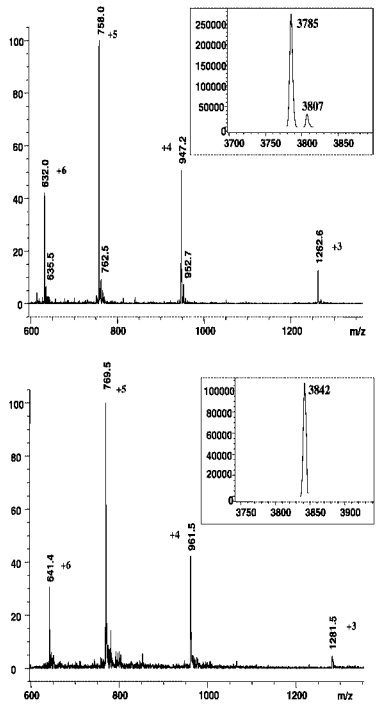

Fig. 4 ESI mass spectra of **B5** (top) and its metallated (Ni^{2+}) form (bottom) illustrating the various charged states observed. Insets show the mass of the two peptide species after deconvolution. Mass spectra were recorded with methanol as the eluting solvent.

Notes and references

† The B5 peptide was synthesised by standard solid-phase methods using Fmoc chemistry and purified by reverse phase HPLC (C18, 10μ) on acetonitrile–water–0.1% TFA gradients. The peptide was characterised by electrospray mass spectrometry and complete NMR analysis on a Bruker 500 MHz spectrometer. Mass spectrometric experiments were carried out on a Hewlett Packard series 1100MSD mass spectrometer.

1 C. A. Rohl and R. L. Baldwin, *Methods Enzymol.*, 1998, **295**, 1.
2 N. R. Kallenbach and Y. Gong, *Bioorg. Med. Chem.*, 1999, **7**, 143.
3 S. T. R. Walsh, H. Cheng, J. W. Bryson, H. Roder and W. F. DeGrado, *Proc. Natl. Acad. Sci. USA*, 1999, **96**, 5486; C. Micklatcher and J. Chmielewski, *Curr. Opin. Struct. Biol.*, 1999, **3**, 724.
4 R. B. Hill, D. P. Raleigh, A. Lombardi and W. F. DeGrado, *Acc. Chem. Res.*, 2000, **33**, 745.
5 P. Balaram, *J. Pept. Res.*, 1999, **54**, 195; S. Gellman, *Curr. Opin. Struct. Biol.*, 1998, **2**, 717.
6 F. Blanco, M. Ramirez-Alvarado and L. Serrano, *Curr. Opin. Struct. Biol.*, 1999, **8**, 107.
7 M. D. Struthers, R. P. Cheng and B. Imperiali, *Science*, 1996, **271**, 342; I. L. Karle, C. Das and P. Balaram, *Proc. Natl. Acad. Sci. USA*, 2000, **97**, 3034; A. R. Mezo, J. J. Ottesen and B. Imperiali, *J. Am. Chem. Soc.*, 2001, **123**, 1002.
8 E. Lacroix, T. Kortemme, M. Lopez de la Paz and L. Serrano, *Curr. Opin. Struct. Biol.*, 1999, **9**, 487.
9 B. I. Dahiyat and S. L. Mayo, *Science*, 1997, **278**, 82.
10 R. Kaul and P. Balaram, *Bioorg. Med. Chem.*, 1999, **7**, 105.
11 T. Kortemme, M. Ramirez-Alvarado and L. Serrano, *Science*, 1998, **281**, 253.
12 C. Das, S. Raghothama and P. Balaram, *J. Am. Chem. Soc.*, 1998, **120**, 5812; C. Das, S. Raghothama and P. Balaram, *Chem. Commun.*, 1999, 967.
13 J. S. Richardson, D. C. Richardson, N. B. Tweedy, K. M. Gernert, T. P. Quinn, M. H. Hecht, B. W. Erickson, Y. Yan, R. D. McClain, M. E. Donlan and M. C. Surles, *Biophys. J.*, 1992, **63**, 1185; Y. E Yan and B. W. Erickson, *Protein Sci.*, 1994, **3**, 1069; T. P. Quinn, N. B. Tweedy, R. W. Williams, J. S. Richardson and D. C. Richardson, *Proc. Natl. Acad. Sci. USA*, 1994, **91**, 8747.
14 M. Klemba, K. H. Gardner, S. Marino, N. D. Clarke and L. Regan, *Nat. Struct. Biol.*, 1995, **2**, 368; Y. Lu and J. S. Valentine, *Curr. Opin. Struct. Biol.*, 1997, **7**, 495.
15 P. Guntert, C. Mumenthaler and K. Wüthrich, *J. Mol. Biol.*, 1997, **273**, 283.
16 J. P. Glusker, *Adv. Protein Chem.*, 1991, **42**, 1.

CHEMCOMM Communication
www.rsc.org/chemcomm

Fast and high conversion phase-transfer synthesis exploiting the liquid–liquid interface formed in a microchannel chip

Hideaki Hisamoto,[a] Takumi Saito,[a] Manabu Tokeshi,[b] Akihide Hibara[a] and Takehiko Kitamori[ab]

[a] *Department of Applied Chemistry, Graduate School of Engineering, The University of Tokyo, 7-3-1 Hongo, Bunkyo-ku, Tokyo 113-8656, Japan. E-mail: hisamoto@appchem.t.u-tokyo.ac.jp; Fax: +81-3-5841-6039; Tel: +81-3-5841-7233*

[b] *Integrated Chemistry Project, Kanagawa Academy of Science and Technology, Sakado, Takatsu-ku, Kawasaki, Kanagawa 213-0012, Japan. E-mail: tokeshi@pop12.odn.ne.jp; Fax: +81-44-819-2092; Tel: +81-44-819-2037*

Received (in Cambridge, UK) 20th July 2001, Accepted 6th November 2001
First published as an Advance Article on the web 4th December 2001

The large specific interfacial areas and short molecular diffusion distances provided by glass microchips play important roles not only for effective phase-transfer synthetic reaction, but also for avoiding an undesirable side reaction.

Recent microchip technology has opened various application fields in chemistry.[1] In particular, applications in analytical chemistry, called 'Micro Total Analysis Systems (μ-TAS)', have been established as one of the largest research fields.[2] On the other hand, growing interest has also focused on applications in synthetic organic chemistry.[3]

As we have pointed out elsewhere, a liquid microspace such as a microchannel or microwell fabricated on a glass microchip provides interesting characteristics such as short molecular diffusion distance, large specific interfacial area (liquid–liquid or liquid–solid), and small heat capacity, all of which can be expected to promote highly effective chemical reactions in the microchip. By exploiting these characteristics, we have demonstrated general chemical reactions.[4]

The microfabricated device also allows us to exploit characteristics of microfluidics such as formation of laminar multi-phase flow. Laminar flow formed by the same solvents (*e.g.* aq.–aq., or org.–org. two phases) has been exploited for analytical purposes and fabrication purposes such as position-selective etching.[5,6] On the other hand, we have been focusing on the laminar flow formed by different solvents such as aqueous–organic multi phase flow.[7] When the organic and aqueous phases were introduced through the two inlets of the microchannel by syringe pumps, a stable liquid–liquid interface formed as seen in the photographs of Fig. 1. In this case, a large specific interfacial area could be obtained without any stirring. By exploiting the large specific interfacial area provided by organic and aqueous phases, demonstration of a fast and high conversion synthesis involving phase transfer should be possible. In addition, stable two-phase flow also allows us easy separation of two phases inside the microchannel under continuous flow conditions by splitting the reaction channel into two channels at its end. We have already succeeded in phase separation inside the microchannel in analytical applications.[8] Thus we chose the phase transfer reaction as the model synthetic reaction to be demonstrated under two-phase laminar flow.

Recent research related to organic synthesis using a microspace has been reported in the field of microreactors.[9] However, no paper has emphasized the liquid–liquid interface as the novel reaction field although it has a possibility to realize both efficient synthesis and phase separation.

In order to realize our concept in an actual experiment, we carried out a preliminary investigation of a phase transfer diazocoupling reaction as one simple example (Fig. 2). Diazocoupling reactions in microchips have been successfully demonstrated for synthesizing small amounts of azobenzene for the purpose of combinatorial synthesis.[10] In contrast, our system based on continuous multiphase flow is expected to synthesize large amounts of chemicals with high conversion. In our case, rapid phase transfer of starting material and the produced chemical species across the liquid–liquid interface play important roles to realize both the fast chemical reaction and isolation of the produced chemical species.

Here we compare the reaction efficiency of microscale and macroscale reaction conditions. The microscale reaction was performed by introducing ethyl acetate containing 5-methylresorcinol (10^{-3} M) and an aqueous phase containing 4-nitrobenzene diazonium tetrafluoroborate (10^{-4} M) through the two-inlets of the microchip under continuous flow conditions. Volume flow rates of organic and aqueous phases were fixed at 10 μl min^{-1} each. In this case, linear flow rate was estimated to be 1.3 cm s^{-1}. When the organic phase made contact with the aqueous phase, distribution of the resorcinol derivative started in the latter phase, and then, it reacted with the diazonium salt. The resulting main product was electrically neutral and it was re-distributed into the organic phase. In the case of macroscale reactions, 10 ml each of the reagent solutions (organic and aqueous solutions) were poured into a glass vessel (3.5 cm diameter) and stirred. In this case, stirring conditions were varied to evaluate the effect of mixing and specific interfacial area on reaction time and conversion. The experimental conditions are shown in Fig. 3. Letting the reaction mixture stand without stirring gave a long molecular diffusion distance and a small specific interfacial area. The weak stirring

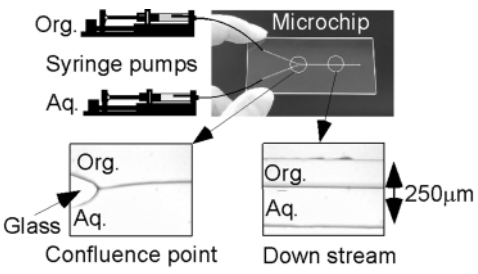

Fig. 1 Photographs showing glass microchip and liquid–liquid interface formed inside the microchannel.

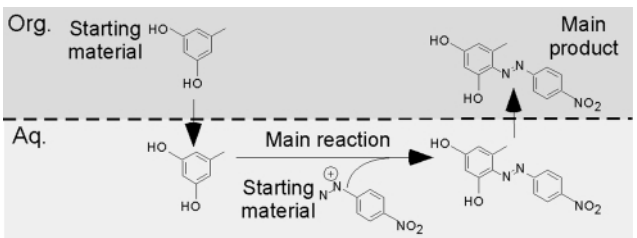

Fig. 2 Phase transfer diazocoupling reaction.

 DOI: 10.1039/b106494k

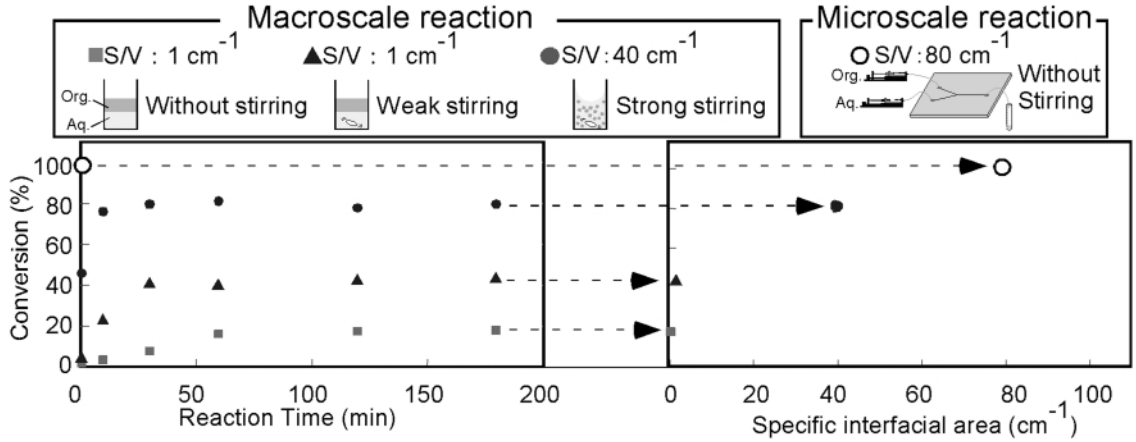

Fig. 3 Reaction conditions and results obtained with phase transfer diazocoupling reaction under microscale and macroscale conditions.

conditions provided effective molecular diffusion conditions, but almost the same specific interfacial area as that without stirring. The strong stirring conditions provided the most effective reaction conditions.

For all the experimental conditions, conversion of the diazonium salt was evaluated by standard reversed phase HPLC using an ODS column. In this case, methanol was used as an eluent at a flow rate of 1 ml min^{-1}. For the microscale reaction, simple introduction of organic and aqueous phases into the microchannel provided a stable liquid–liquid interface, and the specific interfacial area had a larger value than those of the strong stirring and no stirring conditions for the macroscale reaction. In our experimental conditions, the specific interfacial area (surface to volume ratio: S/V) provided by a microchannel 250 μm wide, 100 μm deep and 3 cm in length was calculated to be 80 cm^{-1}.[11]

Fig. 3 also shows reaction profiles and specific interfacial area dependence of conversion for the reaction conditions. For macroscale conditions, increasing the stirring speed gave a fast and high conversion as expected. However, concerning the microscale condition, conversion was higher than for any macroscale conditions studied in this work, although the residence time of starting matrices in the microchannel was only 2.3 seconds. Under macroscale reaction conditions, insoluble precipitate species of a side product were visually observed, the amount of which depended on the mixing conditions (without stirring > weak stirring > strong stirring). In contrast, the microscale reaction conditions gave no precipitate species and the conversion was close to 100%.

For the diazocoupling reaction, an undesirable side reaction of main product and a second diazonium salt to form a bisazo product is known.[12] Thus in our case, the large specific interfacial area and short molecular diffusion distance played important roles in removing the main product from the aqueous phase to the organic phase, which allowed the undesirable side reaction to be avoided. In other words, the microchip condition provided a novel methodology for avoiding a side reaction in a phase transfer synthesis.

Although the amount of starting material of 5-methylresorcinol was in excess compared to that of the diazonium salt, so that the organic phase still included residual material, a conversion of close to 100% was successfully achieved.

This is the first use of the novel synthetic methodology using a microchip, which provides fast and high conversion organic synthesis using the stable liquid–liquid interface formed in the microchannel. The large specific interfacial area and short molecular diffusion distance play important roles not only for effective phase transfer of starting material and produced chemical species, but also for avoiding an undesirable side reaction.

Recent advances in microchip technology have expanded not only for analytical or fabrication purposes but also for proteomics or understanding fundamental fluidic processes. Among them, we have focused on the characteristics provided by a liquid microspace and microfluidics, and demonstrated an attractive application example of microchip technology to synthetic chemistry.

This work was partially supported by Grants for Scientific Research from the Ministry of Education, Science, and Culture, Japan.

Notes and references

1 M. Freemantle, *Chemical and Engineering News*, 1999, **February 22**, 27.
2 *Proceedings of the μTAS'2000 Symposium*, ed. A. van den Berg, W. Olthuis and P. Bergveld, 2000.
3 M. C. Mitchell, V. Spikmans, A. Manz and A. J. de Mello, *J. Chem. Soc., Perkin Trans. 1*, 2001, 514.
4 K. Sato, M. Tokeshi, T. Kitamori and T. Sawada, *Anal. Sci.*, 1999, **15**, 641; M. Tokeshi, T. Minagawa and T. Kitamori, *Anal. Chem.*, 2000, **72**, 1711; H. Hisamoto, T. Horiuchi, M. Tokeshi, A. Hibara and T. Kitamori, *Anal. Chem.*, 2001, **73**, 1382; K. Sato, M. Tokeshi, H. Kimura and T. Kitamori, *Anal. Chem.*, 2001, **73**, 1213; Y. Tanaka, M. N. Slyadonev, A. Hibara, M. Tokeshi and T. Kitamori, *J. Chromatogr. A*, 2000, **894**, 45.
5 A. E. Kamholz, B. H. Weigl, B. A. Finlayson and P. Yager, *Anal. Chem.*, 1999, **71**, 5340.
6 P. J. A. Kenis, R. F. Ismagilov, S. Takayama, G. M. Whitesides, S. Li and H. S. White, *Acc. Chem. Res.*, 2000, **33**, 841.
7 A. Hibara, M. Tokeshi, K. Uchiyama, H. Hisamoto and T. Kitamori, *Anal. Sci.*, 2001, **17**, 89.
8 M. Tokeshi, T. Minagawa, K. Uchiyama, A. Hibara, K. Sato, H. Hisamoto and T. Kitamori, submitted for publication.
9 *Microreactors: New Technology for Modern Chemistry*, ed. W. Ehrfeld, V. Hessel and H. Lowe, John Wiley & Sons, 2000; K. F. Jensen, *Chem. Eng. Sci.*, 2001, **56**, 293; V. Skelton, G. M. Greenway, S. J. Haswell, P. Styring, D. O. Morgan, B. Warrington and S. Y. F. Wong, *Analyst*, 2001, **126**, 7.
10 H. Salimi-Moosavi, T. Tang and D. J. Harrison, *J. Am. Chem. Soc.*, 1997, **119**, 8716.
11 Specific interfacial area was defined by the ratio of interfacial area and volume of organic phase. For strong stirring conditions, specific interfacial area was estimated from the mean diameter of the liquid droplets formed (700 to 800 μm).
12 For the diazocoupling reaction with resorcinol and 4-nitrobenzene diazonium, see *Rodd's Chemistry of Carbon Compounds*, ed. S. Coffey, Elsevier Scientific Publishing Company, New York, 1973, Vol. III, Part C, p. 136, and references cited therein.

CHEMCOMM Communication
www.rsc.org/chemcomm

Complete reversal of enantioselectivity of an enzyme-catalyzed reaction by directed evolution

Dongxing Zha,[a] Stephanie Wilensek,[a] Markus Hermes,[a] Karl-Erich-Jaeger[b] and Manfred T. Reetz*[a]

[a] *Max-Planck-Institut für Kohlenforschung, D-45470 Mülheim/Ruhr, Germany. E-mail: reetz@mpi-muelheim.mpg.de; Fax: +49 208 306 2985*
[b] *Ruhr-Universität Bochum, Lehrstuhl der Mikroorganismen, D-44780 Bochum, Germany*

Received (in Cambridge, UK) 30th October 2001, Accepted 15th November 2001
First published as an Advance Article on the web 6th December 2001

The combination of error prone PCR at high mutation rate and DNA shuffling can be used to invert the direction of enantioselectivity of a lipase-catalyzed hydrolytic kinetic resolution involving a chiral ester.

We have previously demonstrated that the methods of directed evolution[1–3] can be applied successfully in the quest to create enantioselective enzymes for use in organic chemistry.[4,5] The basic strategy involves repeating cycles of gene-mutagenesis and expression coupled with high-throughput screening for enantioselectivity. Specifically, the wild-type lipase from *Pseudomonas aeruginosa*, which catalyzes the hydrolytic kinetic resolution of ester **1** with slight preference for the *S*-acid **2** (selectivity factor $E = 1.1$), was converted into an enzyme-

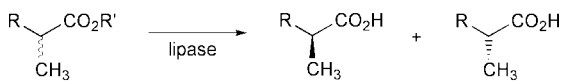

1 R = n-C_8H_{17}, R' = p-NO_2-C_6H_4 — *S*-**2** — *R*-**2**

variant showing high *S*-preference.[4] The selectivity factor *E*, which reflects the relative reaction rate of the two enantiomers, turned out to be 26. This was accomplished by four cycles of random mutagenesis using error prone polymerase chain reaction (epPCR) at low mutation rate corresponding to an average of one amino acid substitution per enzyme molecule, followed by saturation mutagenesis at sensitive positions (hot spots) in the protein. The wild-type lipase consists of 285 amino acids, a number that needs to be considered when calculating the theoretical protein sequence space.[6] By modifying the so-called combinatorial multiple cassette mutagenesis as originally described by Stemmer,[7] enantioselectivity was recently doubled ($E = 51$).[8] We now show that the *direction* of enantioselectivity can be reversed completely by a combination of high error rate epPCR and DNA shuffling.[3] Previously we observed only a small degree of inversion of enantioselectivity on the basis of epPCR alone.[5] Recently Arnold used epPCR and saturation mutagenesis to convert a D-selective hydantoinase into an L-selective variant (ee = 20%).[9] No other cases of reversal of enantioselectivity by directed evolution have been reported to date.

The original library of enzyme variants produced by applying epPCR at low mutation rate to the wild-type gene of the lipase from *Pseudomona aeruginosa* contained only *S*-selective enzymes.[4,5] We therefore carried out the same experiment at a relatively high mutation rate corresponding to about 2–3 amino acid substitutions per enzyme molecule.[6] Upon screening an enzyme library of 15 000 clones,[10] several *S*-selective variants were identified,[8] but also two *R*-selective enzymes 18F9 and 12G12, characterized by a single mutation (V232I) and four mutations (S112P, S147N, T150A and T226A), respectively. The *E*-values were found to be 2.0 and 1.1, respectively. In addition, enzyme 47E6 (with D113G, I142T, S218L and S268N) was identified, showing no preference for either of the two enantiomers ($E = 1.0$).

Gene 18F9 served as the basis for another cycle of epPCR under otherwise identical conditions. As a result of screening 5000 clones, *R*-selective enzyme-variants 18F9E1 (with M16L, A34T and V232I) and OE7 (with V55A, P86L, D113G and V232I) were discovered, displaying *E*-values of 3.7 and 3.0, respectively. In a similar third cycle of epPCR using gene OE7, enzyme-variant 3B6 (with V55A, P86L, D113G, V232I, S237T and Q275L) was generated, resulting in even higher *R*-selectivity ($E = 7.0$). However, further rounds of epPCR-based mutagenesis failed to produce positive results.

Although DNA shuffling has been shown to be effective in the alteration of such functional properties of enzymes as stability and activity,[3] these efforts did not include the evolution of enantioselectivity.[11] In an initial attempt we shuffled genes 18F9, 12G12 and 47E6, hoping that possible non-productive mutations would be eliminated. However, this turned out not to be the case, because no improvements were detected. Consequently, we increased the size of the gene pool and subjected genes 12G12, 47E6, 18F9, 3B6 and OE7 to DNA shuffling. Although no shift to significantly higher enantioselectivity resulted, three *R*-selective enzyme-variants of comparable enantioselectivity were in fact found, namely 14A5 (with V55A, P86L, D113G, S147N, T150A, V232I, S237T and Q275L), 11C8 (with V55A, P86L, A102V, D113G, V232I and S237T) and 16A7 (with V55A, P86L, S71G, D113G, V232I, S237T and S268C), the *E*-values amounting to 6.7, 6.5 and 7.0, respectively.

Since initial attempts to apply saturation mutagenesis at selected hot spots failed to increase enantioselectivity markedly, we reconsidered DNA shuffling. Hoping to increase diversity, gene 18F9E1, which we had generated earlier but neglected to utilize in further experiments, was shuffled with gene 14A5. Upon inspecting a library of 5000 clones, several *R*-selective variants were found, the best one 1G10 (with M16L, A34T, P86L, D113G, S147N, T150A, V232I and S237T) displaying a selectivity factor of $E = 20$ in the model reaction.

By comparing the mutations present in 18F9E1 and 14A5 with those of the new variant 1G10, it becomes clear that mutations V55A and Q275L have been eliminated by the process of DNA shuffling. Obviously, these two mutations exert a negative effect, which means that in the present case DNA shuffling plays the role of 'correcting' non-productive mutational changes brought about earlier. New mutations were not introduced. Finally, a single round of epPCR on top of this (using gene 1G10 at high mutation rate) resulted in yet another substantial improvement, enantioselectivity in favor of *R*-**2** reaching $E = 30$. In this case the enzyme (15B10) has 11 amino acid substitutions (M16L, A34T, P86L, T87S, V94A, D113G, S147N, T150A, L208H, V232I and S237T). Relative to variant 1G10 three new mutations (T87S, V94A and L208H) have been introduced.

It appears that the evolution of pronounced *R*-selectivity requires greater structural change than in the case of *S*-

 DOI: 10.1039/b109913m

selectivity, which seems to be reflected in the comparatively high number of amino acid exchanges. It is also interesting to note that the amino acid substitutions described herein occur at positions which are quite different from the hot spots that were uncovered in the case of the *S*-selective counterparts.[4,5] Although we do not yet have crystallographic data of any of the *S*- or *R*-selective mutants, the X-ray structural analysis of the wild-type lipase from *Pseudomonas aeruginosa* was recently reported by Dijkstra.[12] Of the 11 mutations that we have identified in the *R*-selective enzyme 15B10, some are near the active site, while others occur at remote positions (Fig. 1). It is likely that the enzyme folds in a slightly different way.[4b]

In summary, we have shown that the appropriate combination of epPCR at high error rate and DNA shuffling can be used to invert the enantioselectivity of an enzyme-catalyzed reaction to a synthetically useful level. Accordingly, the generation of *S*-selective (E = 51) and *R*-selective (E = 30) enzymes is possible on an optional basis. The appropriate evolutionary pressure is exerted in each case by screening for the desired enantiomer (*S* or *R*). Whereas knowledge of the structure of the enzyme or of its mechanism of action is not required, a limited amount of navigation in protein sequence space is necessary. In doing so less than a total of 45000 clones were screened.[10] Work is in progress to illuminate the source of *S*- and *R*-selectivity.

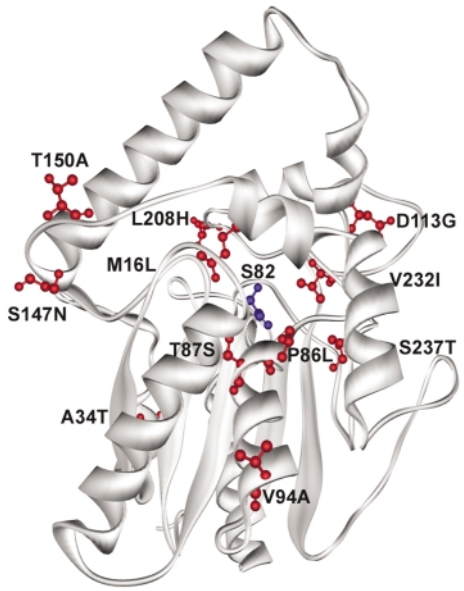

Fig. 1 Structure[12] of the wild-type lipase from *Pseudomonas aeruginosa* showing the active site S82 and the 11 mutations of variant 15B10.

We are also applying DNA shuffling[3] as a tool in the *in vitro* evolution of other enantioselective enzymes for application in synthetic organic chemistry.

Notes and references

1 D. W. Leung, E. Chen and D. V. Goeddel, *Technique (Philadelphia)*, 1989, **1**, 11–15; R. C. Cadwell and G. F. Joyce, *PCR Methods Appl.*, 1994, **3**, S136–S140; B. Steipe, in *Combinatorial Chemistry in Biology*, ed. M. Famulok, E.-L. Winnacker and C.-H. Wong, Springer, Berlin, 1999, vol. 243, pp. 55–86; J. D. Sutherland, *Curr. Opin. Chem. Biol.*, 2000, **4**, 263–269.

2 F. H. Arnold, *Acc. Chem. Res.*, 1998, **31**, 125; F. H. Arnold, *Nature (London)*, 2001, **409**, 253–257.

3 W. P. C. Stemmer, *Nature (London)*, 1994, **370**, 389–391; A. Crameri, S.-A. Raillard, E. Bermudez and W. P. C. Stemmer, *Nature (London)*, 1998, **391**, 288–291.

4 (*a*) M. T. Reetz, A. Zonta, K. Schimossek, K. Liebeton and K.-E. Jaeger, *Angew. Chem.*, 1997, **109**, 2961–2963; *Angew. Chem., Int. Ed. Engl.*, 1997, **36**, 2830–2832; (*b*) K. Liebeton, A. Zonta, K. Schimossek, M. Nardini, D. Lang, B. W. Dijkstra, M. T. Reetz and K. E. Jaeger, *Chem. Biol.*, 2000, **7**, 709–718.

5 (*a*) M. T. Reetz and K. E. Jaeger, *Chem. Eur. J.*, 2000, **6**, 407–412; (*b*) M. T. Reetz, *Pure Appl. Chem.*, 2000, **72**, 1615–1622.

6 The number (N) of theoretically possible lipase-variants can be calculated on the basis of the algorithm $N = 19^{M} \cdot 285!/[(285 - M)! \cdot M!]$, where M = number of exchanged amino acids per enzyme molecule.[5a] Thus, for $M = 1$: $N = 5415$ variants; $M = 2$: $N \cong 15$ million variants; $M = 3$: $N \cong 52$ billion variants. It is likely that in the vast majority of cases these variants will not catalyze the desired reaction at all.

7 A. Crameri and W. P. C. Stemmer, *BioTechniques*, 1995, **18**, 194–196.

8 M. T. Reetz, S. Wilensek, D. Zha and K.-E. Jaeger, *Angew. Chem.*, 2001, **113**, 3701–3703; *Angew. Chem., Int. Ed.*, 2001, **40**, 3589–3591.

9 O. May, P. T. Nguyen and F. H. Arnold, *Nature Biotechnol.*, 2000, **18**, 317–320.

10 (*a*) The original UV/Vis-based screening system[4a] was used to identify hits. In all cases these enzyme mutants were then studied using the racemic substrate (**1**) in separate experiments, analysis being carried out by conventional chiral GC. The *p*-nitro phenol ester **1** was employed in all cases because the hydrolysis product (*p*-nitrophenol) is easily detected UV/Vis-spectroscopically. The disadvantage is that the ester is activated and therefore undergoes a non-catalyzed background reaction to a small extent. This has been considered when reporting *E*-values higher than 20; (*b*) review of high-throughput screening systems: M. T. Reetz, *Angew. Chem.*, 2001, **113**, 292–320; *Angew. Chem., Int. Ed.*, 2001, **40**, 284–310.

11 C.-H. Wong *et al.* applied DNA shuffling in order to evolve an aldolase which catalyzes the aldol reaction of a certain aldehyde not accepted by the wild-type enzyme, enantioselectivity remaining complete: (*a*) S. Fong, T. D. Machajewski, C. C. Mak and C.-H. Wong, *Chem. Biol.*, 2000, **7**, 873–883; (*b*) K. M. Koeller and C.-H. Wong, *Nature (London)*, 2001, **409**, 232–240.

12 M. Nardini, D. A. Lang, K. Liebeton, K.-E. Jaeger and B. W. Dijkstra, *J. Biol. Chem.*, 2000, **275**, 31219–31225.

CHEMCOMM Communication
www.rsc.org/chemcomm

Studies of a nickel-based single molecule magnet: resonant quantum tunnelling in an $S = 12$ molecule†

Cyril Cadiou,[a] Mark Murrie,[d] Carley Paulsen,[b] Vincent Villar,[b] Wolfgang Wernsdorfer[c] and Richard E. P. Winpenny*[a]

[a] *Department of Chemistry, The University of Manchester, Oxford Road, Manchester, UK M13 9PL. E-mail: richard.winpenny@man.ac.uk*
[b] *CRTBT, CNRS, 25 Avenue des Martyrs BP 166, 38042 Grenoble Cedex 9, France*
[c] *Laboratoire Louis Neél, CNRS, 25 Avenue des Martyrs BP 166, 38042 Grenoble Cedex 9, France*
[d] *Department of Chemistry, The University of Edinburgh, West Mains Road, Edinburgh, UK EH9 3JJ*

Received (in Cambridge, UK) 15th August 2001, Accepted 8th November 2001
First published as an Advance Article on the web 28th November 2001

A cyclic dodecanuclear nickel complex is the first single molecule magnet based on nickel(II) centres; the material is also the highest spin molecule to show resonant quantum tunnelling of magnetisation.

It is eight years since the first report of 'single molecule magnetism',[1] *i.e.* the observation that some complexes with high spin ground states show hysteresis in magnetisation *vs.* field. This phenomenon is of great interest, as it offers the promise of enormous technological advances—the storage of magnetic information in individual molecules—and has allowed studies of fundamental processes such as quantum tunnelling.[2] The latter observation has also led some to propose that single molecule magnets (SMMs) could be used in quantum computing.[3]

The original SMMs were a family of dodecanuclear mixed-valent manganese cages, and since that time other SMMs have been reported. The majority have featured manganese[4] or iron,[5] with one report of a vanadium-based SMM.[6] Here we report the first nickel SMM, and a preliminary account of low temperature studies of its magnetic behaviour.

$[Ni_{12}(chp)_{12}(O_2CMe)_{12}(H_2O)_6(THF)_6]$ **1** (chp = 6-chloro-2-pyridonate)[7] is cyclic, containing twelve Ni(II) centres bridged by pyridonate and acetate ligands (Fig. 1). It has crystallographic S_6 symmetry and all rings within the structure pack parallel to each other, and perpendicular to the crystallographic *c*-axis in the space group $R\bar{3}c$.

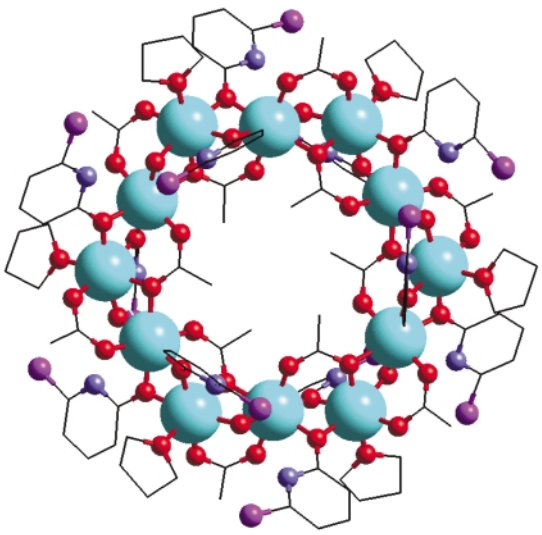

Fig. 1 The structure of **1** (Ni, light blue; O, red; N, blue; Cl, purple; C, black).

Isothermal magnetisation studies on powdered samples‡ at 150 mK saturates at 25.5 μ_B, which confirms a $S = 12$ ground state and gives a *g*-value of 2.13. The curve can be fitted with these parameters and a D/k-value of −0.07 K (D = axial zero-field splitting parameter, k = the Boltzmann constant). When measurements are performed on single crystals with the field parallel to the *c*-axis, hysteresis is seen in magnetisation *vs.* field measurements at sweep rates of 0.035 T s^{-1}, and at temperatures of 0.4 K and lower (Fig. 2: note: M_s, was measured at 1.4 T, *i.e.* a much higher field than shown in Fig. 2). The hysteresis becomes more pronounced as the temperature is lowered and, at 0.2 K and colder, steps become resolved due to resonant quantum tunnelling of magnetisation. These steps, which are most clear at 0.1 and 0.04 K and occur at *ca.* 0, ±0.047 and ±0.094 T (Fig. 2), are due to sudden loss of magnetisation as m_s levels within the $S = 12$ spin ground state manifold come into resonance with m_s levels on the other side of the energy barrier, which allows tunnelling of the magnetisation through this barrier. The levels cross when $\mu_o H_z = nD/g\mu_B$ (where n = an integer). Here the field between two resonances is 0.047 T and $g = 2.13$, therefore we can calculated $D/k = -0.067$ K. The energy barrier for reorientation of magnetisation is given by $E_a = DS^2$, therefore here $E_a/k = 9.6$ K.

Studies of magnetic susceptibility‡ in an alternating field show the frequency (υ) dependent peak in the out-of-phase susceptibility (χ''), characteristic of SMMs (Fig. 3, inset). The maximum moves from *ca.* 0.25 K at 0.001 Hz to *ca.* 0.55 K at the fastest frequency (511 Hz). An Arrhenius treatment of this data gives a second measurement of the energy barrier for reorientation of magnetisation, which is the slope for ln τ *vs.* $1/T$ ($\tau = 1/2\pi\upsilon$), and is found to be between 9 and 10 K, which is in good agreement with resonant tunnelling.

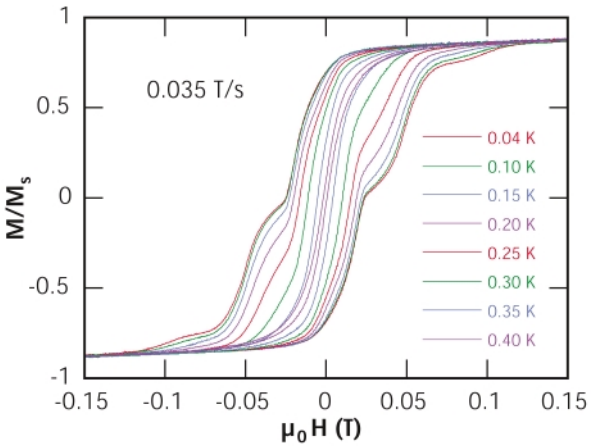

Fig. 2 Magnetisation against field for **1**, showing steps due to tunnelling.

† Electronic supplementary information (ESI) available: saturation magnetisation at 150 mK; $1/\chi'$ *vs.* T. See http://www.rsc.org/suppdata/cc/b1/b108894g/

 DOI: 10.1039/b108894g

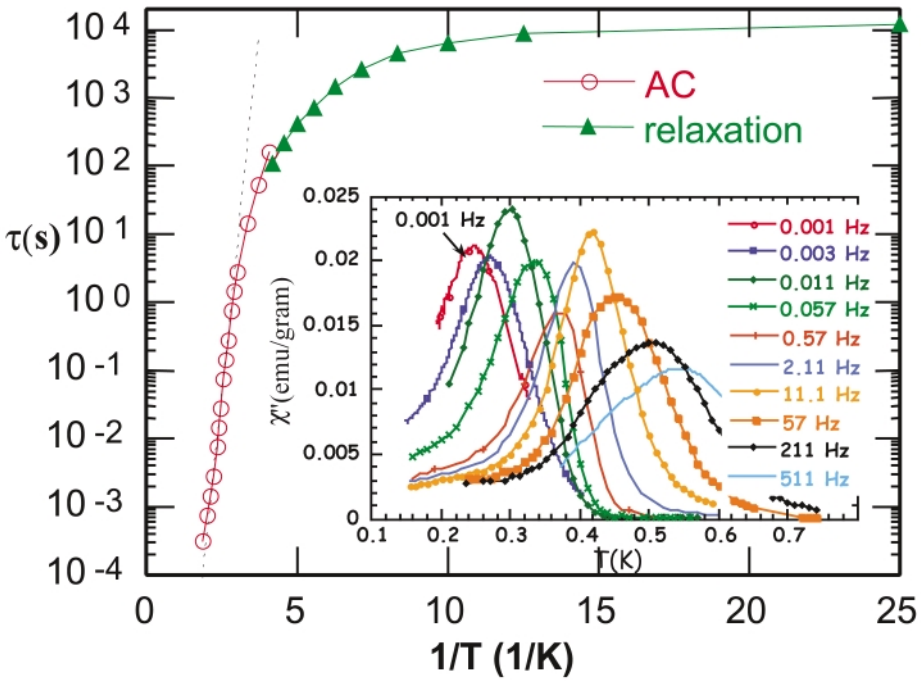

Fig. 3 Main: τ *vs.* $1/T$ measured from ac susceptibility (red circles) or relaxation (green triangles); inset: χ'' of **1** *vs.* T at 10 frequencies.

The exact value for E_a is imprecise, as below 0.2 K saturation is seen similar to that observed in other SMMs. This is because the relaxation rate no longer follows the Arrhenius law as non-thermal pathways become important. Relaxation measurements at below 0.2 K confirm the onset of saturation (Fig. 3).

An unexpected observation is that a plot of $1/\chi'$ *vs.* T from 0.4 to 1.2 K gives a straight line, and extrapolation gives a Weiss constant of +0.25 K, indicating ferromagnetic interactions. At below 1.2 K the cage is predominantly in an $S = 12$ state, therefore *intramolecular* interactions are less important, which implies the positive intercept is due to *intermolecular* exchange. The shortest Ni···Ni contact in **1** between Ni centres in different rings is 10.7 Å, while the distance between ring-centroids is 16.9 Å. This separation and absence of a pathway disfavour an explanation based on super-exchange. Dipolar exchange would give approximately the correct magnitude for this interaction,[10] but would not account for the interaction being ferromagnetic. While intermolecular dipolar exchange has been mentioned in studies of clusters,[9,11] it is neglected in the majority of cases.

Resonant tunnelling of the magnetisation has been observed in molecules where $S = 10$ or lower,[2,5,12] but never in molecules with spin ground states as high as that found for **1**. In other very high spin cages that show slow relaxation of magnetisation, *e.g.* $\{Fe_{19}\}$ cages,[13] intermolecular interactions quench tunnelling effects. The observation of tunnelling in **1** is surprising given both the small anisotropy, approximately one-tenth of that found in $\{Mn_{12}\}$ SMMs,[1] and the evidence of significant coupling between molecules of **1**. These preliminary results require many further experiments for full understanding. Given the apparent value of the intermolecular exchange we may be near a ferromagnetic phase transition. The magnitude of χ'' has an anomalous frequency dependence, which requires further study.

This work was supported by the EPSRC and a TMR network on 'Molecules as Nanomagnets' (HPRN-CT-1999-0012).

Notes and references

‡ Low temperature magnetic properties were measured using a low temperature–high field SQUID magnetometer developed at the CRTBT-CNRS in Grenoble, and on an array of micro-SQUIDS developed at the LLN-CNRS in Grenoble: details in refs. 8 and 9, respectively.

1 R. Sessoli, H.-L. Tsai, A. R. Schake, S. Wang, J. B. Vincent, K. Folting, D. Gatteschi, G. Christou and D. N. Hendrickson, *J. Am. Chem. Soc.*, 1993, **115**, 1804; R. Sessoli, D. Gatteschi, A. Caneschi and M. A. Novak, *Nature*, 1993, **365**, 141.

2 M. A. Novak and R. Sessoli, in *Quantum Tunneling of Magnetization-QTM'94, Vol. 301 of NATO ASI Series E: Applied Sciences*, ed. L. Gunther and B. Barbara, Kluwer Academic Publishers, London, 1995, p 171.; J. R. Friedman, M. P. Sarachik, J. Tejada and R. Ziolo, *Phys. Rev. Lett.*, 1996, **76**, 3830; L. Thomas, F. Lionti, R. Ballou, D. Gatteschi, R. Sessoli and B. Barbara, *Nature*, 1996, **383**, 145.

3 M. N. Leuenberger and D. Loss, *Nature*, 2001, **410**, 789.

4 M. W. Wemple, D. M. Adams, K. S. Hagen, K. Folting, D. N. Hendrickson and G. Christou, *J. Chem. Soc., Chem. Commun.*, 1995, 1591; E. K. Brechin, J. Yoo, M. Nakano, J. C. Huffman, D. N. Hendrickson and G. Christou, *Chem. Commun.*, 1999, 783; A. L. Barra, A. Caneschi, D. Gatteschi, D. P. Goldberg and R. Sessoli, *J. Solid State Chem.*, 1999, **145**, 484; H. Andres, R. Basler, H.-U. Güdel, G. Aromi, G. Christou, H. Büttner and B. Ruffle, *J. Am. Chem. Soc.*, 2000, **122**, 12469.

5 D. Gatteschi, R. Sessoli and A. Cornia, *Chem. Commun.*, 2000, 725 and references therein.

6 Z. Sun, C. M. Grant, S. L. Castro, D. N. Hendrickson and G. Christou, *Chem. Commun.*, 1998, 721.

7 A. J. Blake, C. M. Grant, S. Parsons, J. M. Rawson and R. E. P. Winpenny, *J. Chem. Soc., Chem. Commun.*, 1994, 2363.

8 F. M. Romero, R. Ziessel, M. Bonnet, Y. Pontillon, E. Ressouche, J. Schweizer, B. Delley, A. Grand and Andre C. Paulsen, *J. Am. Chem. Soc.*, 2000, **122**, 1298.

9 W. Wernsdorfer, T. Ohm, C. Sangregorio, R. Sessoli, D. Mailly and C. Paulsen, *Phys. Rev. Lett.*, 1999, **82**, 3903.

10 Using the mean field approximation, $E_{dip}/k = \mu_o(g\mu_B S)^2/4\pi Vk$, where V is the molar volume. For **1**: $g = 2.13$, $S = 12$ and $V = 4.7525 \times 10^{-27}$ m^3, therefore $E_{dip}/k = 0.086$ K.

11 T. Ohm, C. Sangregorio and C. Paulsen, *Eur. Phys. J. B*, 1998, **6**, 195; T. Ohm, C. Sangregorio and C. Paulsen, *J. Low Temp. Phys.*, 1998, **113**, 1141.

12 C. Sangregorio, T. Ohm, R. Sessoli, D. Mailly and C. Paulsen, *Phys. Rev. Lett.*, 1999, **82**, 3903; S. M. J. Aubin, N. R. Dilley, L. Pardi, J. Krzystek, M. W. Wemple, L.- C. Brunel, M. B. Maple, G. Christou and D. N. Hendrickson, *J. Am. Chem. Soc.*, 1998, **120**, 4991.

13 J. C. Goodwin, R. Sessoli, D. Gatteschi, W. Wernsdorfer, A. K. Powell and S. L. Heath, *J. Chem. Soc., Dalton Trans.*, 2000, 1835.

CHEMCOMM Communication
www.rsc.org/chemcomm

The enantioselective generation of bridgehead enolates

Alexander J. Blake,[a] Gerard M. P. Giblin,[b] Douglas T. Kirk,[a] Nigel S. Simpkins*[a] and Claire Wilson[a]

[a] *School of Chemistry, The University of Nottingham, University Park, Nottingham, UK NG7 2RD. E-mail: Nigel.Simpkins@Nottingham.ac.uk; Fax: +44(0) 115 951 3564; Tel: +44(0) 115 951 3533*
[b] *GlaxoSmithKline, Medicines Research Centre, Gunnels Wood Road, Stevenage, Hertfordshire, UK SG1 2NY*

Received (in Cambridge, UK) 3rd October 2001, Accepted 12th November 2001
First published as an Advance Article on the web 6th December 2001

The generation and silylation of bridgehead enolates has been accomplished in high enantiomeric excess using a chiral lithium amide base.

The anti-Bredt nature of bridgehead enolates (more accurately described as α-keto carbanions) derived from ketones having small bridges is expected to make their generation difficult or impossible.[1,2] However in certain cases reactive α-keto carbanions have been formed at bridgehead positions, despite the lack of true enolate character. In these situations the intermediate anion appears highly reactive and displays chemistry that is difficult to control. An example is the metallation of (−)-camphenilone **1** with lithium tetramethylpiperidide (LiTMP).[3] Even in the presence of *in situ* trapping agents, such as Me_3SiCl, the presumed intermediate **2** could not be intercepted and only the aldol product **3** was obtained (Scheme 1).†

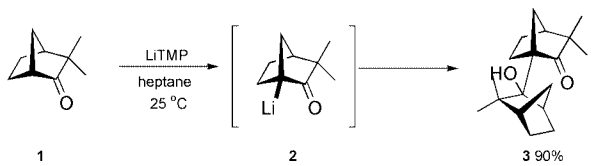

Scheme 1

Feldman and coworkers reported that bicyclo[4.2.1]nona-2,4,7-trien-9-one **4** exhibited a similar tendency towards self-addition when treated with potassium hexamethyldisilazide (KHMDS), to give aldol product **5** in 23% yield (Scheme 2).[4]

As part of our programme of research aimed at exploring the applications of chiral lithium amide bases we became interested in the types of bridgehead enolate presumed to be intermediates in the above Schemes. Herein we describe our preliminary investigations in this area, which show that chiral lithium amide bases allow unprecedented enantioselective access to the products of bridgehead substitution in compounds such as **4**.

Initial studies with ketone **4** demonstrated that external quench protocols were ineffective in trapping the carbanion, leading only to the addition product **5**, albeit in an improved yield of 66%. Instead we turned our attention to deprotonation under *in situ* quench conditions with LDA–LiCl in the presence of Me_3SiCl, a method which we have employed in the past with success.[5] Thus addition of ketone **4** to an excess of LDA–LiCl in the presence of Me_3SiCl (method A, see later) at −105 °C led to the formation of an inseperable mixture of *bis* silylated ketones **6** and **7** in a 4 : 1 ratio and in a combined yield of 63% (Scheme 3).

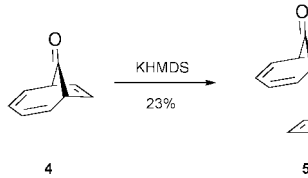

Scheme 2

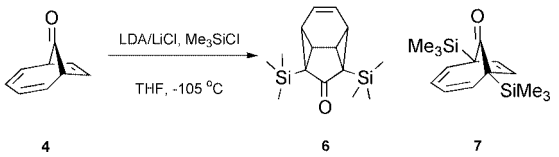

Scheme 3

The formation of the tetracyclic ketone **6** was unexpected and was confirmed following a single crystal X-ray structure determination.‡ This product is the result of double bridgehead substitution followed by a transannular Diels–Alder reaction, the latter process being precedented for this system.[6] We observed no partially silylated ketones corresponding to **6**, which points to its formation purely *via* **7**. An alternative mechanism involving anion initiated cycloaddition of **4** followed by bis-silylation appears to be ruled out following further experiments described below.

By changing the mode of deprotonation to addition of the base to a mixture of ketone and Me_3SiCl (inverse addition) we hoped to minimise formation of the unwanted bis-silyl compounds **6** and **7**. Selected results using this method (method B) are highlighted in Table 1, along with comparison data using method A. We discovered that upon addition of LDA–LiCl to a solution of ketone **4** and Me_3SiCl at −105 °C, the mono silylated ketone **8** was obtained in 38% yield, accompanied by a mixture of **6** and **7** in 17% yield (entry 2).

Next we attempted the asymmetric deprotonation of **4** by employing chiral base (*R*,*R*)-**9**.[7] By using the inverse addition protocol with (*R*,*R*)-**9** at −105 °C we obtained mono silylated ketone (−)-**8** in 76% yield and with an excellent ee of >96% in addition to bis silylated ketones **6/7** in 23% yield (entry 3).§ Conducting the reaction at −78 °C led to a lower yield and slightly lower enantiomeric excess (entry 4). The absolute configuration of (−)-**8** was determined by single crystal X-ray structure determination (Fig. 1).¶

Table 1 Bridgehead deprotonation of ketone **4** in the presence of Me_3SiCl under *in situ* quench conditions

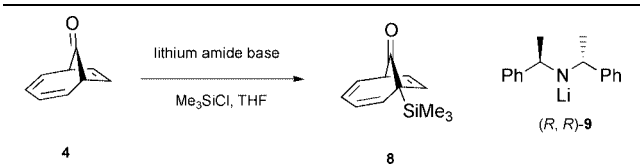

Entry	Lithium amide base	*T*/°C	Method[a]	Yield of **6/7** (%)	Yield of **8** (%)	Ee of **8** (%)
1	LDA/LiCl	−105	A	39	0	—
2	LDA/LiCl	−105	B	17	38	—
3	(*R*,*R*)-**9**/LiCl	−105	B	23	76	>96
4	(*R*,*R*)-**9**/LiCl	−78	B	12	46	92

[a] A—ketone–Me_3SiCl added to base. B—base added to ketone–Me_3SiCl.

 DOI: 10.1039/b108986m

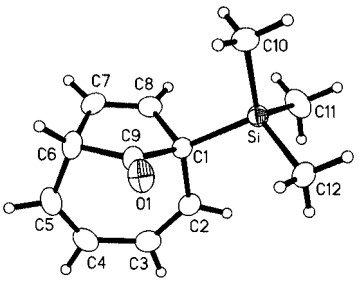

Fig. 1 X-Ray structure of (−)-**8**. Displacement ellipsoids are drawn at the 50% probability level.

We found no trace of a cyclised isomer of **8** corresponding to **6**, and attempts to induce the internal cycloaddition of **8** by heating led only to decomposition. It therefore appears that disilylation of **4** facilitates the cyclisation to give **6**.

The remarkable and unprecedented asymmetric substitution of ketone **4** prompted us to examine similar bridgehead metallations with the saturated ketone **10**, available from **4** by hydrogenation. Treatment of a mixture of ketone **10** and Me_3SiCl with (*R*,*R*)-**9** gave (−)-**11** in 53% yield and 92% optical purity (Scheme 4). The stereochemical configuration and optical purity were assigned by correlation with our earlier results, following hydrogenation of (−)-**8** to give (−)-**11**.

Unfortunately the *in situ* quench approach is incompatible with most electrophiles and we found that inclusion of electrophiles such as methyl iodide, allyl bromide and benzaldehyde gave none of the desired products. However, indirect access to products having alternative types of substituent was found to be possible by fluoride mediated silyl exchange reactions of (−)-**8**, using tetrabutylammonium triphenyldifluorosilicate (TBAT), Table 2.[8]

We expect that substitution occurs without erosion of enantiomeric purity, although this has only been established for entry 5 so far.

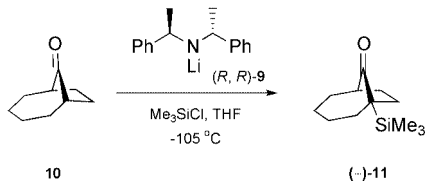

Scheme 4

Table 2 TBAT mediated silyl exchange in the presence of electrophiles

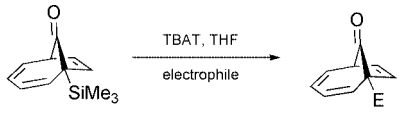

(-)-**8**

Entry	Electrophile, E	Yield (%)
1	MeI	42
2	AllylBr	29
3	BnBr	28
4	c-hexylCHO[a]	78
5	PhCHO[b]	72

[a] Obtained with diastereoisomeric ratio (dr) 4:1 [b] Obtained with dr 3:2.

Similarly, treatment of (−)-**11** in the presence of PhCHO with TBAT in refluxing THF gave the aldol product as a mixture of diastereoisomers (3:2) in 93% yield.

The remarkable enantioselective substitution of ketones **4** and **10** described above may pave the way for successful bridgehead metallation of many other types of bridged carbonyl compounds. Efforts to determine the scope of this chemistry are underway.

We are grateful to the University of Nottingham and GlaxoSmithKline for support of D. T. K. under the CASE scheme.

Notes and references

† Our efforts to control the metallation of **1** were unsuccessful leading only to aldol product **3**.

‡ *Crystal data* for compound **6**. $C_{15}H_{24}OSi_2$, M = 276.52, orthorhombic, a = 12.4355(7), b = 13.6661(8), c = 9.8989(6) Å, U = 1682.3(2) Å^3, T = 150 K, space group $Pna2_1$, Z = 4, μ(Mo-Kα) = 0.200 mm^{-1}, 10738 reflections measured, 3797 unique (R_{int} = 0.042) which were used in all calculations. The final $wR(F)$ = 0.0353, $wR(F^2)$ = 0.0820 (all data). Flack parameter refined to −0.04(9).

§ *Preparation of* (−)-**8** (Method B): A solution of chiral lithium amide base **9** (3.05 mmol), cooled to *ca.* −105 °C (internal temperature) was added dropwise *via* cannula, over 45 min, to a solution of ketone **4** (396 mg, 3 mmol) and Me_3SiCl (1.2 ml, 9 mmol) in THF (30 ml), maintained at that temperature. The resulting solution was allowed to warm slowly to rt over 3 h, quenched with saturated aqueous NH_4Cl (20 ml), and worked up in the usual way.

Purification by flash column chromatography on silica gel (4% Et_2O in light petroleum 40–60 °C as eluent) gave the title compound **8** as a white solid (464 mg, 76%); $[\alpha]_D^{26}$ −182 (*c* 0.99 in $CHCl_3$) mp 87–89 °C. ($C_{12}H_{16}OSi$: Calc: C, 70.55; H, 7.90. Found: C, 70.52; H, 7.79%). δ_H(400 MHz, $CDCl_3$) 0.15 (s, 9H), 3.14 (dd, *J* 2, 7.5 Hz, 1H), 5.62–5.66 (m, 2H), 5.69–5.71 (dd, *J* 2.3, 6.8 Hz, 1H), 5.84–5.97 (m, 3H). δ_C(125 MHz, $CDCl_3$) −3.7 (Me_3Si), 51.6 (C), 54.6 (CH), 122.2 (=CH), 124.6 (=CH), 125.7 (=CH), 127.0 (=CH), 129.3 (=CH), 130.5 (=CH), 218.3 (C=O). HRMS (EI) $C_{12}H_{16}OSi$ requires 204.097. Found 204.0984 (25%), 73.0474 (100, $SiMe_3$). Enantiomeric excess values were established by HPLC (UV detection at 205 and 215 nm) using hexane as eluent and a Chiralcel OD column.

¶ *Crystal data* for compound **8**. $C_{12}H_{16}OSi$, M = 204.34, monoclinic, a = 6.1568(6), b = 7.4191(7), c = 12.9873(12) Å, β = 101.996(2)°, U = 580.3(2) Å^3, T = 150 K, space group $P2_1$, Z = 2, μ(Mo-Kα) = 0.169 mm^{-1}, 4890 reflections measured, 2562 unique (R_{int} = 0.023). The final $wR(F)$ = 0.0276, $wR(F^2)$ = 0.0719 (2552 data). Flack parameter refined to 0.00(8). CCDC 172469 and 172470. See http://www.rsc.org/suppdata/cc/b1/b108986m/ for crystallographic data in CIF or other electronic format.

1 K. J. Shea, *Tetrahedron*, 1980, **36**, 1683; P. M. Warner, *Chem. Rev.*, 1989, **89**, 1067.

2 Previous synthetic use of bridgehead enolates is largely limited to compounds with longer bridges, see for example: P. A. Wender and T. P. Mucciaro, *J. Am. Chem. Soc.*, 1992, **114**, 5878; K. J. Shea, S. L. Gwaltney, II and S. T. Sakata, *J. Org. Chem.*, 1996, **61**, 7438; P. Magnus, D. Parry, T. Iliadis, S. A. Eisenbeis and R. A. Fairhurst, *J. Chem. Soc., Chem. Commun.*, 1994, 1543; M. Yamaura, T. Nakayama, H. Hashimoto, C. Shin and J. Yoshimura, *J. Org. Chem.*, 1988, **53**, 6035.

3 C. S. Shiner, A. H. Berks and A. M. Fisher, *J. Am. Chem. Soc.*, 1988, **110**, 957. See also: U. P. Spitz and P. E. Eaton, *Angew. Chem., Int. Ed.*, 1994, **33**, 2220.

4 K. S. Feldman, J. H. Come, B. J. Kosmider, P. M. Smith, D. P. Rotella and M.-J. Wu, *J. Org. Chem.*, 1983, **48**, 141.

5 Addition of LiCl can have a dramatic effect on rates of metallation, see for example: D. A. Price, N. S. Simpkins, A. M. MacLeod and A. P. Wyatt, *Tetrahedron Lett.*, 1994, **35**, 6159; B. J. Bunn, N. S. Simpkins, Z. Spavold and M. J. Crimmin, *J. Chem. Soc., Perkin Trans. 1*, 1993, 3113.

6 R. D. Miller and D. L. Dolce, *Tetrahedron Lett.*, 1977, 3329.

7 For a review, see: P. O'Brien, *J. Chem. Soc., Perkin Trans. 1*, 1998, 1439.

8 A. S. Pilcher and P. DeShong, *J. Org. Chem.*, 1996, **61**, 6901.

CHEMCOMM Communication
www.rsc.org/chemcomm

Synthesis of tailored bimodal mesoporous materials with independent control of the dual pore size distribution

Jihong Sun, Zhiping Shan, Thomas Maschmeyer, Jacob A. Moulijn and Marc-Olivier Coppens*

Department of Chemical Technology, Delft University of Technology, Julianalaan 136 2628 BL, Delft, The Netherlands. E-mail: M.O.Coppens@tnw.tudelft.nl

Received (in Cambridge, UK) 1st October 2001, Accepted 6th November 2001
First published as an Advance Article on the web 21st November 2001

A new synthesis method is presented to prepare multi-structured porous materials through a fully chemical route that allows control of the smaller and larger mesopore sizes independently.

A well-defined pore size distribution at various scales is desirable for a variety of applications.[1] Experiments and simulations have shown that a hierarchical combination of independently controlled, well-connected smaller and larger mesopores[2] reduces transport limitations in catalysis, resulting in higher activities and better controlled selectivities.[3]

Since the first reported syntheses of MCM-41, there has been intense research activity in designing and synthesizing structured mesoporous solids with controlled pore sizes.[4] Recently, using a variety of techniques, *physical* templating methods were proposed to create large meso- or macropores.[5] However, scale-up of these approaches may not be easy or cheap, prompting for the development of alternative *chemical* templating methods by which larger mesopores (≥10 nm) could be produced in a controlled way.

Here, we present such a method by means of which particles of a primary mesoporous material, *e.g.* MCM-41, are cross-linked using triblock copolymer assemblies as templating agents to form a material with a secondary bimodal pore distribution. By varying the synthesis conditions in the second step, it is possible to synthesize a broad class of such hierarchically structured silicas (Table 1).

In the first step tetraethylorthosilicate, the template cetyltrimethylammonium bromide (CTAB), water and ammonia were mixed at room temperature in a ratio of 1:0.2:160:1.5. This 'primary product' was filtered off and repeatedly washed with distilled water. After drying and calcination, the structure of the 'primary product' was confirmed by XRD (Fig. 1) and nitrogen adsorption, as MCM-41.[6] Its isotherm (sample 1) is consistent with a narrow pore size distribution around 2.6 nm (Fig. 2), as expected for MCM-41.† In the second step, prior to drying, part of the filtered 'primary product' was immersed in a basic (pH ~ 10) 5 wt% solution of a tri-block copolymer surfactant (*e.g.*, P-123) in a solvent (*e.g.*, ethanol). After aging the gel for 2 d in an autoclave at 100 °C, the 'secondary product' was filtered off, repeatedly washed with distilled water, dried at 120 °C for 3 h and calcined at 500 °C for 6 h in air. The formation of novel structures within the secondary product can be deduced from the N_2 adsorption–desorption isotherms of the calcined samples.

The isotherms of all secondary products (samples 2–8), exhibit two inflections (Fig. 2). The first of these (a flat hysteresis loop at $0.4 < P/P_0 < 0.55$) is shifted to a higher relative pressure compared to that of the primary product, and corresponds to a mean pore size of around 3.0–3.3 nm. Meanwhile, the XRD patterns of the secondary products show that the order of the pores has decreased somewhat, while the (100) peak is slightly shifted to lower angles (corresponding to a *d*-spacing of ~4.2 nm), due to the small primary pore size increase (Fig. 1). This results from solvent penetration in the second step into the hydrophobic core of the liquid crystalline template formed by CTAB.[7] The second inflection (a type IV-A hysteresis loop at $0.8 < P/P_0 < 0.98$) indicates the presence of a significant amount of secondary mesopores, with a synthesis dependent pore size distribution at scales >10 nm (Fig. 2 and

Table 1 Texture properties of the samples

Sample	SF[a]	Solvent	d^b/nm Prim.	d^b/nm Sec.	PV[c]/cm^3 g^{-1}	SA[d]/m^2 g^{-1}
1			2.6		0.7	1100
2		Ethanol	3.1	16	1.8	1070
3	P-123[e]	Ethanol	3.3	25	2.6	960
4	P-123	Benzene	5.4	16	2.8	980
5	P-123	Water	3.2	54	2.8	950
6	L-61[f]	Ethanol	3.3	36	3.5	990
7	P-64[g]	Ethanol	3.0	25	2.9	990
8	F-68[h]	Ethanol	3.1	22	2.4	1020

[a] Surfactant. [b] Mean pore diameter. Calculated on the basis of the BJH model for the desorption branch of nitrogen adsorption isotherms. [c] Pore volume. [d] Surface area. [e] $HO(CH_2CH_2O)_{20}(CH_2CH_2CH_2O)_{70}(CH_2CH_2O)_{20}H$. [f] $HO(CH_2CH_2O)_2(CH_2CH_2CH_2O)_{31}(CH_2CH_2O)_2H$. [g] $HO(CH_2CH_2O)_{13}(CH_2CH_2CH_2O)_{30}(CH_2CH_2O)_{13}H$. [h] $HO(CH_2CH_2O)_{76}(CH_2CH_2CH_2O)_{29}(CH_2CH_2O)_{76}H$.

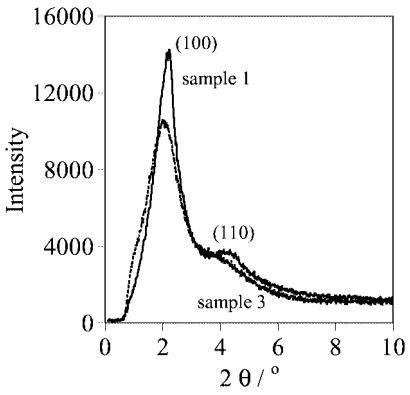

Fig. 1 XRD patterns of samples 1 and 3.

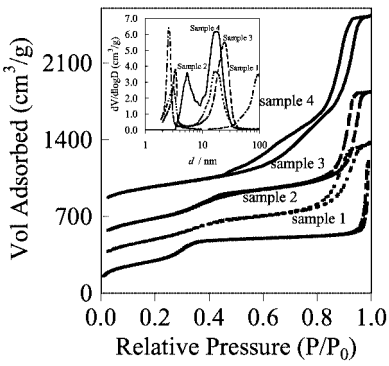

Fig. 2 Nitrogen adsorption–desorption isotherms of the samples (inset: corresponding pore size distributions). Subsequent isotherms are offset by 200 cm^3 g^{-1}.

 DOI: 10.1039/b108860b

Table 1). The shape of this hysteresis loop is quite different in its width from the secondary loop of the primary product in the same region and suggests tubular pores instead of interparticle, textural mesoporosity.[8] At the low surfactant concentrations used here, the micelles do not form a liquid crystal phase, but disordered spherical to flexible rod- or worm-like micelles.[9]

During the initial stage of the secondary product synthesis, the primary MCM-41 gel particles are still soft and deformable; surface silanol groups exposed to the micelles form hydrogen bonds with their hydrophilic heads, while silanol groups of adjoining particles condense around the micelles at the higher temperatures in the autoclave. This view is supported by an examination of ^{29}Si magic-angle spinning nuclear magnetic resonance (MAS-NMR) spectra of the secondary materials which show for, *e.g.*, sample 3, three broad peaks at 91 (Q^2), 101 (Q^3) and 109 ppm (Q^4). The ratio of the peak areas is $Q^2:Q^3:Q^4 = 0.03:0.34:1$, whereas for the primary material (sample 1) it is 0.2 : 0.46 : 1. This suggests that the secondary materials are somewhat more condensed as would be expected as a result of covalent cross-linking.[10]

The conditions during the first step are kept constant, resulting in primary gel particles that are reproducibly within the same size range ~20 nm and the pore size distribution of which centers around 3.1 nm. Mainly by using different solvent and/or surfactant compositions during the second synthesis step, the pore size distribution of the secondary material can be controlled without appreciably modifying the pore size distribution of the primary product.

Two experiments show the role P-123 plays during the formation of secondary product. In a "blank" experiment (not using any micelle-forming P-123 in the second synthesis step, sample 2) a secondary product was obtained, the isotherm of which is consistent with a pore size of 16 nm with a 10 nm width, indicating textural mesoporosity. In a second experiment, using non-polar benzene instead of ethanol as solvent with 5 wt% P-123 (sample 4), the peak of the primary product pore size distribution shifts from 3 to 5.4 nm, because benzene is able to considerably swell CTAB aggregates/micelles located inside the primary product pores. The average secondary pore size is the same as that when no P-123 is used (*i.e.* 16 nm with a width of 10 nm). Benzene, being a better organic solvent than ethanol, dissolves P-123 completely without leading to micelle formation,[11] thus resulting in the same secondary pore size as obtained in the absence of copolymer (sample 2). Therefore, only in the presence of P-123 and under conditions where it can form micelles do we observe mesopores larger than 20 nm (*viz.* Table 1) of tubular type. The secondary pore size of sample 1 (>100 nm) is even larger due to textural interparticle meso/macroporosity.

These data are consistent with our postulate that the two pore systems are formed in independent processes. The mechanism for the formation of MCM-41 is well established,[4a,6] but for the generation of the larger mesopores in the secondary product, it is suggested that in ethanol the surfactants form micelles around which the soft particles of the primary product cross-link by condensation of the surface hydroxy groups of adjoining particles. This is schematically shown in Fig. 3. The size of the micelles, and, therefore, of the so-generated larger secondary pores, depends on the synthesis conditions [*e.g.*, surfactant composition (compare samples 6, 7 and 8), solvent polarity (compare samples 4, 3 and 5), and amount of surfactant]. A similar route to fabricate nanotubes has recently been reported.[12]

Transmission electron microscopy (TEM) images are also consistent with a bimodal pore system, showing regions of less ordered, worm-like, small mesopore channels with a diameter of 3 nm, as well as tubular, rounded, large mesopores with a diameter around 40 nm for, *e.g.*, sample 6, consistent with the

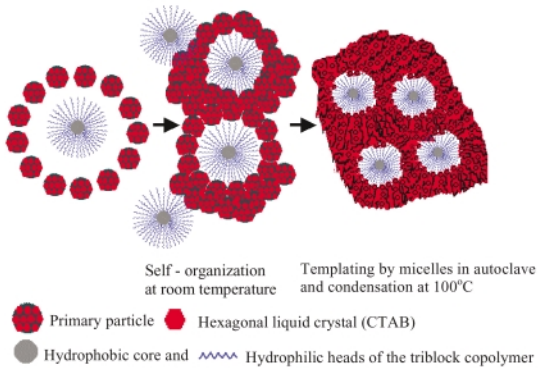

Fig. 3 Schematic representation of bimodal pore formation in the second step.

N_2 adsorption results. It should be noted that the contrast obtainable for amorphous siliceous materials is always inferior to that of ordered materials. Scanning electron microscopy (SEM) images show a smoother morphology for the secondary product compared to the particulate morphology of the primary product.

The method presented here provides a general means to synthesize multi-structured materials with a controlled pore structure over a range of scales. An efficient, hierarchical "road network" can, thus, be designed in a purely chemical way, leading to the desirable structure for a particular application.

We thank Dr P. J. Kooyman for the TEM and P. Boeser for measurement of the adsorption isotherms.

Notes and references

† The typical sharp increase at high pressure is due to inter-particle macroporosity. Also, the XRD pattern is typical for a hexagonally ordered MCM-41, with a *d*-spacing of 3.9 nm for the (100) peak.

1 P. D. Yang, T. Deng, D. Y. Zhao, J. L. Feng, D. Pine, B. F. Chmelka, G. M. Whitesides and G. D. Stucky, *Science*, 1998, **282**, 2244.
2 T. R. Pauly, Y. Liu, T. J. Pinnavaia, S. J. L. Billinge and T. P. Rieker, *J. Am. Chem. Soc.*, 1999, **121**, 8835; S. T. Wong, H. P. Lin and C. Y. Mou, *Appl. Catal., A: Gen.*, 2000, **198**, 103.
3 M.-O. Coppens and G. F. Froment, *Fractals*, 1997, **5**, 493.
4 (*a*) C. T. Kresge, M. E. Leonowicz, W. J. Roth, J. C. Vartuli and J. S. Beck, *Nature*, 1992, **359**, 710; (*b*) A. Corma, Q. Kan, M. T. Navarro, J. Perez-Pariente and F. Rey, *Chem. Mater.*, 1997, **9**, 2123; (*c*) D. Khushalani, A. Kuperman, G. A. Ozin, K. Tanaka, J. Garces, M. M. Olken and N. Coombs, *Adv. Mater.*, 1995, **7**, 842.
5 B. T. Holland, C. F. Blanford and A. Stein, *Science*, 1998, **281**, 538; A. Imhof and D. J. Pine, *Nature*, 1997, **389**, 948; O. D. Velev, T. A. Jede, R. F. Lobo and A. M. Lenhoff, *Nature*, 1997, **389**, 447; L. M. Huang, Z. B. Wang, J. B. Sun, L. Miao, Q. Z. Li, Y. S. Yan and D. Y. Zhao, *J. Am. Chem. Soc.*, 2000, **122**, 3530; C. J. H. Jacobsen, C. Madsen, J. Houzvicka, I. Schmidt and A. Carlsson, *J. Am. Chem. Soc.*, 2000, **122**, 7116.
6 J. S. Beck, J. C. Vartuli, W. J. Roth, M. E. Leonowice, C. T. Kresge, K. D. Schmitt, C. T.-W. Chu, D. H. Olson, E. W. Sheppard, S. B. McCullen, J. B. Higgins and J. L. Schlenker, *J. Am. Chem. Soc.*, 1992, **114**, 10834.
7 J. H. Sun, J. A. Moulijn, J. C. Jansen, Th. Maschmeyer and M.-O. Coppens, *Adv. Mater.*, 2001, **13**, 327.
8 S. J. Gregg and K. S. W. Sing, *Adsorption, Surface Area and Porosity*, Academic Press, London, 2nd edn., 1982.
9 S. A. Bagshaw, E. Prouaet and T. J. Pinnavaia, *Science*, 1995, **269**, 1242; P. Alexandridis and K. Andersson, *J. Phys. Chem. B*, 1997, **101**, 8103; J. P. Zhao, S. G. Wang, Y. J. Gong, D. Wu and Y. H. Sun, *Chem. J. Chin. Univ.*, 2000, **21**, 1797.
10 L. L. Hench and J. K. West, *Chem. Rev.*, 1990, **90**, 33.
11 P. Alexandridis and L. Yang, *Macromolecules*, 2000, **33**, 5574.
12 J. Raez, R. Barjovanu, J. A. Massey, M. A. Winnik and I. Manners, *Angew. Chem., Int. Ed.*, 2000, **39**, 3862.

CHEMCOMM Communication
www.rsc.org/chemcomm

Supramolecular encapsulation of hexaaquo metal ions by second sphere coordination

Sean A. Dalrymple, Masood Parvez and George K. H. Shimizu*

Department of Chemistry, University of Calgary, 2500 University Drive N.W., Calgary, Alberta T2N 1N4, Canada. E-mail: gshimizu@ucalgary.ca

Received (in Columbia, IN, USA) 28th September 2001, Accepted 7th November 2001
First published as an Advance Article on the web 27th November 2001

Two trianions of 1,3,5-tris(sulfomethyl)benzene each form six hydrogen bonds to the water molecules of octahedral $[M(H_2O)_6]^{3+}$ cations to completely encapsulate the metal complexes *via* second sphere coordination.

In general, second sphere coordination refers to any intermolecular interactions with the ligands directly bound to a metal center, *i.e.* the primary coordination sphere. These interactions are typically weak but can have significant effects on the physical properties of the complex. A number of excellent reviews of second sphere complexes, in general, have recently appeared,[1] as well as more specific examinations of second sphere coordination effects on stability and solubility,[2] transport properties,[3] and even effects on relaxivity of Gd^{3+} ions for MRI applications.[4] Second sphere coordination is also of major importance in biological systems, owing to the ubiquitous nature of transition metal ions and the fact that most of these centers experience at least partial hydration.[5] Several examples exist of second sphere complexes with aquo[6] and ammine[7] coordination compounds, however, the second sphere interactions are only with a fraction of the primary coordination sphere. Herein, we present the complete encapsulation of hexaaquo metal ions *via* twelve hydrogen bonds to a second sphere comprised of two trisulfonated ligands. TGA data show the enhanced stability of the primary hydration sphere. Significantly, this phenomenon appears to be general for trivalent hexaaquo metal cations.

$Fe(NO_3)_3$ was complexed to the sodium salt of the trianion of 1,3,5-tris(sulfomethyl)benzene, Na_3L,[8] in an aqueous solution. Diffusion of methanol into this solution yielded yellow crystals of $\{Fe(H_2O)_6\}[Fe(H_2O)_6(L)_2]\cdot 6MeOH$ **1**, suitable for an X-ray analysis.† The structure is highly symmetrical with an asymmetric unit consisting of one-third of a molecule of L, one methanol molecule, one-sixth of each Fe center and two water molecules, one coordinated to each Fe. The crystal structure shows two types of hexaaquo Fe^{3+} centers in the complex. The first center is completely encapsulated by two molecules of L through twelve hydrogen bonds, six to each molecule of L (Fig. 1a) forming an overall trianionic complex. The methylsulfonate groups on each molecule of L adopt a *cis-cis-cis* orientation (*i.e.* they are all on the same side of the benzene core) and cap one of the triangular faces of the octahedral hexaaquo Fe1 center. All six water molecules of Fe1 are crystallographically equivalent (Fe1–O1 1.996(2) Å). Both H atoms of the coordinated water molecule form hydrogen bonds to two sulfonate oxygen atoms from two different sulfonate groups (O1···O4 2.632(2) Å, O1···O5 2.639(2) Å). Thus, each triangular triaquo face of the Fe complex is staggered with respect to the 1,3,5-substitution pattern of L (Fig. 1b).

The hexaaquo Fe2 center is not encapsulated by L but rather is interspersed between the trianionic second sphere complexes in an efficient charge-compensating manner. It also contains only a single crystallographic type of water molecule (Fe2–O2 1.986(2) Å). Down the *c*-axis, the second sphere complexes alternate in a column with the 'naked' hexaaquo Fe2 centers. Separating these two moieties is a layer of three MeOH molecules. This packing is shown in Fig. 2. There are H-bonds between the coordinated water molecules on Fe2 and O3, the sulfonate oxygen atom not involved in H-bonding to the water molecules of Fe1 (O2···O3 2.644(3) Å). The methanol molecule is also involved in hydrogen bonding to the water molecule coordinated to Fe2 (O6···O2 2.563(3) Å) as well as to one of the sulfonate oxygen atoms already forming a H-bond to the water coordinated to Fe1 (O6···O5 2.769(3) Å). Adjacent columns along the *c*-axis are offset by 7.954(2) Å, corresponding to a third the length of the *c*-axis. Thus, a fourth column added to Fig. 2 would align laterally with the first.

Single crystals were also obtained from separate aqueous complexations of Na_3L with $CrCl_3\cdot 6H_2O$ and $AlCl_3\cdot 6H_2O$, again *via* a methanol diffusion, and these were found to be isostructural with complex **1**.[9] Thermogravimetric analyses (TGA) were performed on all three complexes and similar

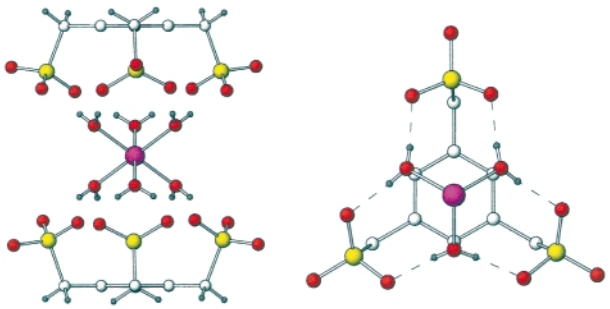

Fig. 1 Two views of the trianionic second sphere moiety of complex **1**. (a) Left, showing the doubly capping mode of L with $[Fe(H_2O)_6]^{3+}$. (b) Right, showing the six hydrogen bonds formed between L and the triangular triaquo faces of $Fe(H_2O)_6]^{3+}$.

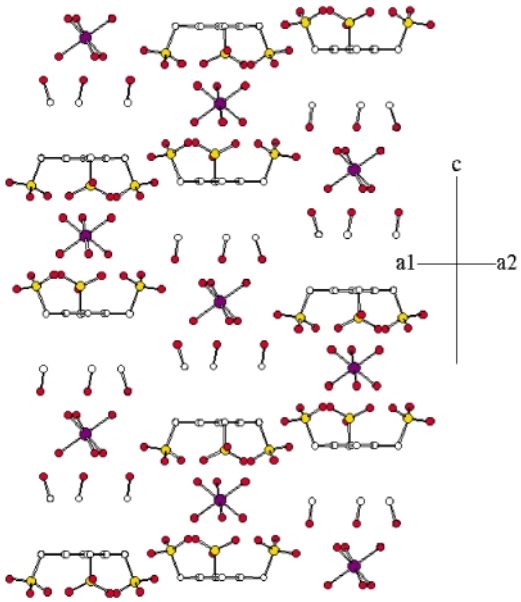

Fig. 2 View of **1** perpendicular to the *c*-axis, showing the offset column arrangement along the *c*-axis and the placement of the MeOH molecules.

 DOI: 10.1039/b110129n

trends were observed in the mass losses.[10] Specifically for **1**, loss of the guest MeOH molecules was rapid, beginning at room temperature to ~110 °C (15.57% calc., 15.88% obs.). This merges with a second mass loss of six water molecules (8.75% calc., 8.95% obs.) up to ~160 °C. Continuing, to ~265 °C, six water molecules (8.75% calc., 8.99% obs.) are lost to fully desolvate the complex. The final mass loss, above 300 °C, corresponds to decomposition of L. The TGA data of all three complexes are shown in Fig. 3 for comparison.

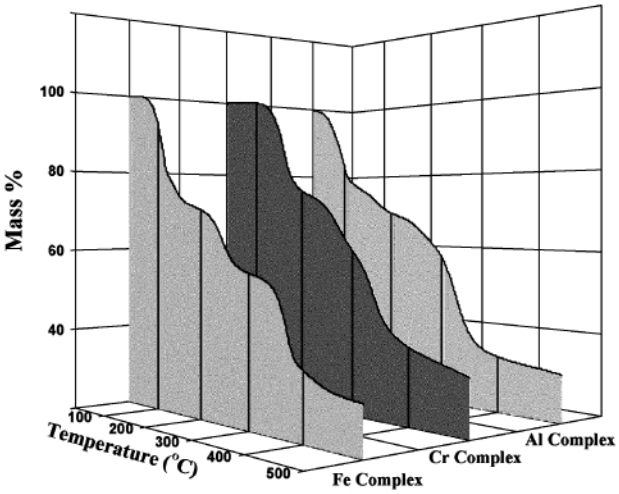

Fig. 3 Thermogravimetric analyses (TGA) of the isostructural $[(M(H_2O)_6)[M(H_2O)_6(L)_2]\cdot 6MeOH$ family of second sphere complexes, where M = Fe^{3+}, Cr^{3+} and Al^{3+}.

Typically, aquo ions in transition metal complexes are lost at temperatures below 150 °C.[11] This correlates very well with the first loss of water observed in **1**, to be assigned to the 'naked' metal cation. The temperature of the second mass loss then shows that the aquo ligands of the encapsulated metal center have been stabilized by >100 °C through the secondary coordination sphere, a very significant value given that only weak interactions are involved.

Notably, isolation of complexes of L with divalent hexaaquo metal cations was not as facile as isolation of their trivalent counterparts. This is not unexpected as, for an analogous encapsulated 2:1 ligand to metal complex, there would only be two-thirds of the positive charge within the capsule to attract the two anionic ligands. As an illustration, a competitive crystallization was performed where equimolar amounts of Na_3L, $Fe(NO_3)_2$ and $Zn(NO_3)_2$ were combined in aqueous solution. Diffusion of methanol into this mixture afforded only yellow crystals of **1**, as confirmed by a partial X-ray data collection. All the Zn^{2+} ions remained in solution.

Sulfonate anions are typically regarded as weakly coordinating ligands.[12] Indeed, most examples of transition metal sulfonate complexes prepared in aqueous media show partial to complete hydration of the metal center.[13,14] While the current results are in keeping with this trend, they also show that, with a sufficient degree of preorganization, sulfonate anions may still have a pronounced effect on the metal center. In addition to showing the stabilization possible with second sphere coordination, in a more general sense, the present study illustrates one of the hallmark principles of supramolecular chemistry,[15] that is, the effects of cooperative binding between multiple weak interactions in a preorganized fashion. Ongoing work concerns elucidating the structural features of the divalent hexaaquo complexes with L as well as hexaammine complexes.

We thank NSERC of Canada and the University of Calgary for financial support of this research.

Notes and references

† *Crystal data* for $[(Fe(H_2O)_6)[Fe(H_2O)_6(L)_2]\cdot 6MeOH$, **1**: $C_{24}H_{66}Fe_2O_{36}S_6$, M = 441.58, trigonal, space group $R\bar{3}h$, $a = b$ = 13.979(2) , c = 23.869(3) Å, $\alpha = \beta$ = 90, γ = 120°, V = 4039.4(8) Å^3, Z = 12, D_c = 1.523 g cm^{-3}, μ(Mo-Kα) = 0.866 mm^{-1}, crystal size 0.50 × 0.42 × 0.22 mm. Data for **1** were collected on a Rigaku AFC6S diffractometer using the ω–2θ scan mode ($3 < 2\theta < 50.1°$) and solved using the teXsan software program.. A total of 1743 reflections were processed of which 1597 were unique and considered significant with $I_{net} > 2.0\sigma(I_{net})$. Final residuals for $I_{net} > 2.0\sigma(I_{net})$ were R = 0.0276 and R_w = 0.0726 (GoF = 1.057) for 120 parameters. CCDC reference number 174132. See http://www.rsc.org/suppdata/cc/b1/b110129n/ for crystallographic data in CIF or other electronic format.

1 S. J. Loeb, in *Comprehensive Supramolecular Chemistry*, ed. J. L. Atwood, J. E. D. Davies, D. D. MacNicol and F. Vögtle, Elsevier Science, New York, 1996, vol. 1, p. 733F. M. Raymo and J. F. Stoddart, *Chem. Ber.*, 1996, **129**, 981.

2 K. Zamaraev, *New. J. Chem.*, 1994, **18**, 3.

3 A. L. Crumbliss, I. Batinic-Haberle and I. Spasojevic, *Pure Appl. Chem.*, 1996, **68**, 1225.

4 M. Botta, *Eur. J. Inorg. Chem.*, 2000, 399.

5 D. R. Williams, *The Metals of Life: the Solution Chemistry of Metal Ions in Biological Systems*, Van Nostrand Reinhold, London, 1971.

6 P. G. Eller and R. A. Penneman, *Inorg. Chem.*, 1976, **15**, 2439; G. Bombieri, G. de Paoli and A. Immirzi, *Inorg. Chim. Acta*, 1976, **18**, L23; P. D. Beer, M. G. B. Drew and M. J. Ogden, *J. Chem. Soc., Dalton Trans.*, 1997, 1489; P. C. Junk and J. L. Atwood, *J. Organomet. Chem.*, 1998, **565**, 179; M. M. Amini, A. L. Rheingold, R. W. Taylor and J. J. Zuckerman, *J. Am. Chem. Soc.*, 1984, **106**, 7289; J. Jarrin, F. Dawans, F. Robert and Y. Jeannin, *Polyhedron*, 1982, **1**, 409; A. Knöchel, J. Kopf, J. Oehler and G. Rudolph, *Inorg. Nucl. Chem. Lett.*, 1978, **14**, 61; T. B. Vance Jr., E. M. Holt, C. G. Pierpont and S. L. Holt, *Acta Crystallogr., Sect. B*, 1980, **36**, 153; R. D. Rogers and L. K. Kurihara, *Inorg. Chim. Acta*, 1987, **130**, 131.

7 H. M. Colquhoun, D. F. Lewis, J. F. Stoddart and D. J. Williams, *J. Chem. Soc., Dalton Trans.*, 1983, 607; H. M. Colquhoun, J. F. Stoddart and D. J. Williams, *Angew. Chem., Int. Ed. Engl.*, 1981, **20**, 1051; B. R. Cameron, S. S. Corrent and S. J. Loeb, *Angew. Chem., Int. Ed. Engl.*, 1995, **34**, 2689; J. E. Kickham and S. J. Loeb, *Inorg. Chem.*, 1995, **36**, 5656; I. Ando, M. Higashi, K. Ujimoto and H. Kurihara, *Inorg. Chim. Acta*, 1999, **282**, 247.

8 L is a new compound and was prepared *via* reaction of α,α′,α″-tribromomesitylene with Na_2SO_3.

9 Unit cell parameters for $[(Cr(H_2O)_6)[Cr(H_2O)_6(L)_2]\cdot 6MeOH$, trigonal, space group $R\bar{3}h$, $a = b$ = 13.936(1) , c = 23.701(3) Å, $\alpha = \beta$ = 90, γ = 120°, V = 3986.2(7) Å^3. Unit cell parameters for $[(Al(H_2O)_6)[Al(H_2O)_6(L)_2]\cdot 6MeOH$, trigonal, space group $R\bar{3}h$, $a = b$ = 13.904(2) , c = 23.799(4) Å, $\alpha = \beta$ = 90, γ = 120°, V = 3984.7(8) Å^3.

10 TGA measurements were performed on a Netzsch STA449C Simultaneous Thermal Analyzer under N_2 at a scan rate of 5 °C min^{-1}.

11 A. W. Apblett, L. A. Cubano, G. D. Georgieva and J. T. Mague, *Chem. Mater.*, 1996, **8**, 650; A. Maleki, R. Gajerski, S. Labus, B. Prochowska-Klisch and K. T. Wojciechowski, *J. Therm. Anal. Calorim.*, 2000, **60**, 17; H. Langfelderova, *J. Therm. Anal.*, 1994, **41**, 955; S. B. Kanungo and S. K. Mishra, *J. Therm. Anal.*, 1997, **48**, 385; M. Maneva and P. Kovandjiev, *J. Therm. Anal.*, 1993, **39**, 1347.

12 G. A. Lawrance, *Chem. Rev.*, 1986, **86**, 17.

13 C. P. Johnson, J. L. Atwood, J. W. Steed, C. B. Bauer and R. D. Rogers, *Inorg. Chem.*, 1996, **35**, 2602; A. J. Shubnell, E. J. Kosnic and P. J. Squattrito, *Inorg. Chim. Acta*, 1994, **216**, 101; E. J. Kosnic, E. L. McClymont, R. A. Hodder and P. J. Squattrito, *Inorg. Chim. Acta*, 1992, **201**, 143; M. A. Leopard, P. J. Squattrito and S. N. Dubey, *Acta Crystallogr., Sect C*, 1999, **55**, 35; B. J. Gunderman, S. N. Dubey and P. J. Squattrito, *Acta. Crystallogr. Sect. C*, 1997, **53**, 17.

14 An exception are Ag sulfonates: G. Smith, B. A. Cloutt, D. E. Lynch, K. A. Byriel and C. H. L. Kennard, *Inorg. Chem.*, 1998, **37**, 3236; G. K. H. Shimizu, G. D. Enright, C. I. Ratcliffe, G. S. Rego, J. L. Reid and J. A. Ripmeester, *Chem. Mater.*, 1998, **10**, 3282; G. K. H. Shimizu, G. D. Enright, C. I. Ratcliffe, K. F. Preston, J. L. Reid and J. A. Ripmeester, *Chem. Commun.*, 1999, 1485.

15 J.-M. Lehn, *Supramolecular Chemistry, Concepts and Perspectives*, VCH, Weinheim, 1995.

CHEMCOMM
Communication
www.rsc.org/chemcomm

Three unique coordination geometries involving 1,2-dimethoxy-4,5-bis(2-pyridylethynyl)benzene

Jeffrey E. Fiscus,[a] Sandra Shotwell,[a] Ralph C. Layland,[b] Mark D. Smith,[a] Hans-Conrad zur Loye*[a] and Uwe H. F. Bunz*[a]

[a] *Department of Chemistry and Biochemistry, The University of South Carolina, Columbia, South Carolina 29208, USA. E-mail: zurloye@sc.edu; bunz@mail.chem.sc.edu*
[b] *Division of Biological and Physical Sciences, Lander University, Greenwood, South Carolina, USA*

Received (in Columbia, MO, USA) 14th September 2001, Accepted 30th October 2001
First published as an Advance Article on the web 3rd December 2001

Reaction of the new ligand 1,2-dimethoxy-4,5-bis(2-pyridylethynyl)benzene with different metal centers under similar reaction conditions led to three distinct structure formation processes: molecular ring closure, dimerization, and polymer formation.

In synthetic, covalent organic chemistry the notion of conformers, oligomers and polymers are distinctly separated and irreconcilable. In supramolecular synthesis on the other hand this conception is less stringent. The utilized building blocks and the variety of binding forces that hold supramolecular assemblies together by arranging organic modules in the solid state makes the border of the very notions of conformers, cycles, and polymers more permeable. Here we wish to demonstrate that one organic module 1,2-dimethoxy-4,5-bis(2-pyridylethynyl)benzene **1**[1] can form a supramolecular cycle, a dimer and polymer utilizing different inorganic connectors $Cu(OAc)_2$, $CoCl_2$ and $[Rh(OAc)_2]_2$.

Single crystals suitable for X-ray diffraction† of Cu(**1**)$(OAc)_2{\cdot}CH_3OH$ **2** were obtained by layering a methanol solution (1 mL) of $Cu(OAc)_2{\cdot}H_2O$ (2.0 mg, 0.01 mmol) over a dichloromethane solution (1 mL) of **1** (6.7 mg, 0.02 mmol), with a layer of pure methanol separating them (20% yield). Crystals of $[Co(\mathbf{1})Cl_2]_2$ **3** were prepared similarly, substituting $CoCl_2{\cdot}6H_2O$ for $Cu(OAc)_2{\cdot}H_2O$ and ethanol for methanol (68% yield).‡ Crystals of *catena*-poly{$[Rh(OAc)_2]_2\mathbf{1}{\cdot}CH_2Cl_2$} **4** were prepared similarly to **2** except that $[Rh(OAc)_2]_2$ was substituted for $Cu(OAc)_2{\cdot}H_2O$ (maintaining the ligand to metal ratio) and ethanol was substituted for methanol (40% yield). These three systems each form a distinctly different structure and between them, demonstrate the importance of the free rotation of the pyridyl rings around the carbon–carbon bonds for facilitating the formation of the three structure types.

Compound **2** demonstrates the preference of Cu^{2+} for square planar coordination with copper positioned snugly between the two pyridyl rings. The resulting N–Cu–N (Cu–N 2.01 Å, N–Cu–N 172.98°) bonds close an eleven membered, triangular ring (Fig. 1), which is nearly identical to the structures reported by Bosch and Barnes for 1,2-bis(2-pyridylethynyl)benzene.[2] The square planar coordination of copper is completed by two *trans* oxygens from separate acetate groups.

Compound **3** contains Co^{2+}, which is found in typical tetrahedral coordination.[3] This tetrahedral preference, apparently, cannot be conveniently satisfied through a ring closure that would require a rotation of the pyridyl rings away from the 180° angle found in the copper complex. The result of such a rotation would be an elongated Co–N bond. Instead, the pyridyl rings rotate away from each other by 128° and bind to separate cobalt atoms with bond lengths of 2.03 Å, which is typical for Co–N bonds. The tetrahedral coordination in each case is completed by two chlorine atoms. The overall structure (Fig. 2) consists of two molecules of **1** bridging two cobalt atoms. An inversion center is located in the middle of the dimer.

The polymeric structure of **4** (Fig. 3) results from the linear coordination preference of $[Rh(OAc)_2]_2$. The structure consists

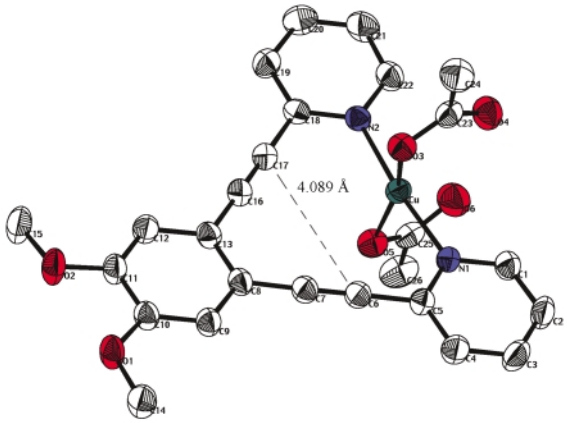

Fig. 1 A single molecule of **2**. The hydrogen atoms and methanol group have been omitted for clarity.

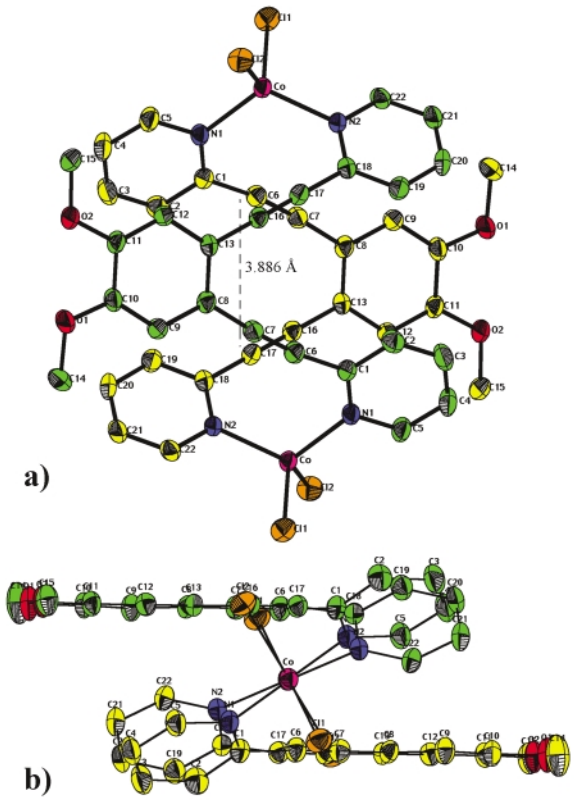

Fig. 2 Hydrogen atoms have been omitted for clarity. (a) a view of **3** from above showing the tetrahedral coordination of cobalt; (b) a view of **3** from the side showing the opposing orientations of **1** and the rotation of the pyridyl rings.

 DOI: 10.1039/b109849g

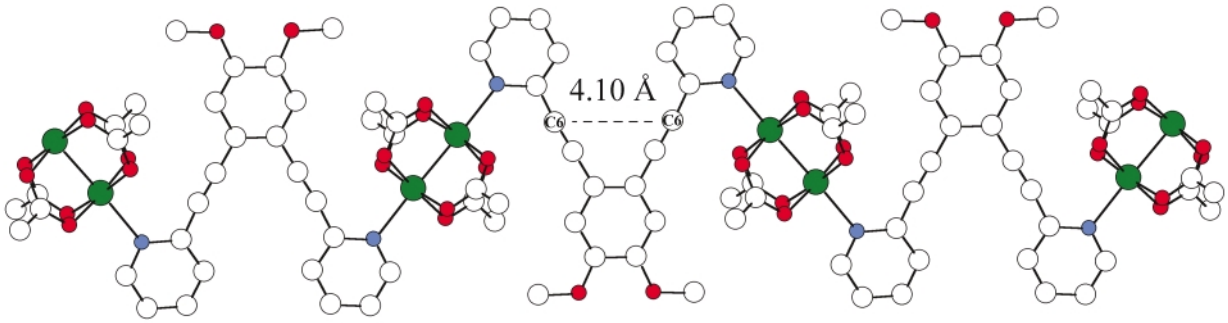

Fig. 3 A view of **4** showing the connectivity of **1** and the rhodium dimer. Hydrogens have been omitted for clarity.

of two acetate-bridged rhodium atoms that connect to the pyridyl rings of two separate molecules of **1** and mimics a conjugated organic polymer. The rhodium is six-coordinate with four equatorial oxygens from the acetate groups, one axial rhodium from the other half of the dimer and one nitrogen belonging to the pyridyl group on the ligand.

Tetrakis(carboxylato)rhodium compounds were first discovered in 1960,[4] but it was not until 1981 that the first polymeric species containing such a rhodium dimer was synthesized.[5] A survey of the CSD indicates that **1** is the largest ligand yet used in such a polymeric species. The polymeric structure is charge balanced, eliminating the need for counter ions competing for binding sites. This leads to higher site symmetry and makes such rhodium dimers attractive building blocks for coordination polymers.[6] Because of its length, the dirhodium moiety cannot fit between the pyridyl rings and achieve ring closure, as in **2**, despite the favorable linear arrangement of the binding sites. Consequently, the pyridyl rings rotate outward by 180° to form a polymer chain with the rhodium dimer bridging adjacent ligands in a zig-zag fashion. This polymer is a supramolecular analogue of the hitherto unknown *ortho*-PPE[7] and as such is a fascinating structure. The Rh–N distance within the polymer is 2.25 Å, typical for Rh–N bonds in such systems.[5,8–10]

One interesting aspect of these structures are the carbon–carbon separations between the alkyne groups on the ligand **1** which, if close enough, could potentially be crosslinked in a Bergman reaction.[11] In **2**, the closed ring conformation results in a C6···C17 separation of 4.089 Å. This is almost the same as the C6···C6 distance of 4.100 Å in **4**, which should represent an unstrained system. By comparison, in **3**, the C6···C17 distance within the same molecule of **1** is 3.886 Å, while the alkyl groups on separate ligands are only 3.548 Å apart (within the range for π–π interactions). This suggests that the copper cation fits between the pyridyl rings without inducing any strain, while in **3**, the dimer formation strains the ligand, bending the pyridyl ligands towards one another, which effects a shorter C6···C17 distance.

These three structures demonstrate the diversity, which can be achieved using **1** that is made possible by the ability of the ligand to distort itself to the preferred coordination environment of the metal center. While one may expect a slight bending of the pyridylethynyl legs either towards or away from each other, these three structures show that rotation of the pyridyl ring around the ethynyl linkage seems more favorable.

Financial support was provided in part by the National Science Foundation through Grants DMR:9873570 and CHE:9814118 and in part by the South Carolina Commission on Higher Education through Grant CHE:R00-U25. The Bruker CCD Single Crystal Diffractometer was purchased using funds provided by the NSF Instrumentation for Materials Research Program through Grant DMR:9975623.

Notes and references

† *Synthesis* of the ligand **1**: under nitrogen, 1,2-dimethoxy-4,5-diiodobenzene (2.00 g, 5.28 mmol),[12] 2-ethynylpyridine (1.09 g, 10.6 mmol),[13] $(Ph_3P)_2PdCl_2$ (50 mg, 71 μmol), CuI (50 mg, 263 μmol) and piperidine (15 mL) are placed in a Schlenk flask and stirred for 24 h at ambient temperature. Aqueous workup followed by chromatography with EtOAc–hexanes (1:9) furnishes the ligand in 22% yield (395 mg) as a colorless powder (mp 154 °C). Spectroscopic data: IR, ν/cm^{-1} 2200 (m), 1590 (w), 1570 (s), 1550 (w), 1510 (s), 1460 (m), 1450 (m), 1435 (w), 1425 (w) 1415 (w), 1360 (s) . ^{1}H NMR (CD_3CN), δ 3.90 (s, 6H, OCH_3), 7.24 (s, 2H, aryl-H), 7.38 (ddd, 2H, pyridyl-H), 7.77 (dt, 2H, pyridyl-H), 7.82 (td, 2H, pyridyl-H), 8.65 (d, 2H, pyridyl-H). ^{13}C NMR ($CDCl_3$), δ 150.28, 149.812, 143.83, 136.38, 127.54, 122.92, 118.65, 114.67, 91.94, 88. 33, 56.34. MS EI, *m*/*z* 340 (100%, M^+), 341 (25%, M^+), 342 (5%, M^+), 325 ($M^+ - CH_3$, 15%,) 309 ($M^+ - OCH_3$, 4%), 263 (M^+ − pyridine, 97%).

‡ *Crystal data* for **2**: $C_{27}H_{26}CuN_2O_7$, M = 554.04, triclinic, space group $P\bar{1}$, a = 8.2357(4), b = 12.5088(6), c = 13.3128(6) Å, α = 78.3000(10)°, β = 72.1170(10)°, γ = 76.6810(10)°, U = 1257.12(10) Å^3, T = 293(2) K, Z = 2, λ = 0.71073 Å, 11656 reflections measured, 5144 unique (R_{int} = 0.0199) which were used in all calculations. $R1$ = 0.0374 and $wR2$ = 0.0922. For **3**: $C_{44}H_{32}Cl_4Co_2N_4O_4$, M = 940.40, monoclinic, space group $P2_1/n$, a = 8.5272(6), b = 18.3653(13), c = 13.3493(9) Å, β = 103.574(2)°, U = 2032.2(2) Å^3, T = 190(2) K, Z = 2, λ = 0.71073 Å, 13541 reflections measured, 4156 unique (R_{int} = 0.0347) which were used in all calculations. $R1$ = 0.0504 and $wR2$ = 0.1107. For **4**: $C_{31}H_{30}Cl_2N_2O_{10}Rh_2$, M = 867.29, monoclinic, space group $C2/c$, a = 21.5985(13), b = 20.2480(12), c = 8.0207(5) Å, β = 103.2650(10)°, U = 3414.1(4) Å^3, T = 190(2) K, Z = 4, λ = 0.71073 Å, 15208 reflections measured, 3504 unique (R_{int} = 0.0545) which were used in all calculations. $R1$ = 0.0613 and $wR2$ = 0.1222. CCDC reference numbers 173558–173560. See http://www.rsc.org/suppdata/cc/b1/b109849g/ for crystallographic data in CIF or other electronic format.

1 S. Shotwell and U. H. F. Bunz, manuscript in preparation.
2 E. Bosch and C. L. Barnes, *Inorg. Chem.*, 2001, **40**, 3097.
3 N. N. Greenwood and A. Earnshaw, *Chemistry of the Elements*, Reed Educational and Professional Publishing, Oxford, 2nd edn., p. 1129.
4 I. I. Chernyaev, E. V. Shenderetskaya and A. A. Karyaguba, *Russ. J. Inorg. Chem.*, 1960, **5**, 559.
5 F. A. Cotton and T. R. Felthouse, *Inorg. Chem.*, 1981, **20**, 600.
6 F. A. Cotton, C. Lin and C. A. Murillo, *Acc. Chem. Res.*, 2001, in press.
7 R. H. Grubbs and D. Kratz, *Chem. Ber.*, 1993, **126**, 149.
8 T. Niu, J. Lu, G. Crisci and A. J. Jacobson, *Polyhedron*, 1998, **17**, 4079.
9 H. Kitamura, T. Ozawa, K. Jitsukawa, H. Masuda, Y. Aoyama and H. Einaga, *Inorg. Chem.*, 2000, **39**, 3294.
10 F. A. Cotton and T. R. Felthouse, *Inorg. Chem.*, 1981, **20**, 584.
11 R. G. Bergman, *Acc. Chem. Res.*, 1973, **6**, 25; T. Chandra, J. C. Huffman and J. M. Zaleski, *Inorg. Chem. Commun.*, 2001, **4**, 434.
12 J. D. Kinder and W. J. Youngs, *Organometallics*, 1996, **15**, 460.
13 D. E. Ames, D. Bull and C. Takundwa, *Synthesis*, 1981, 364.

CHEMCOMM
Communication
www.rsc.org/chemcomm

Stacked molecular triangles: self-assembly using coordination chemistry and hydrogen bonding

Zengquan Qin, Michael C. Jennings and Richard J. Puddephatt*

Department of Chemistry, University of Western Ontario, London, Canada N6A 5B7. E-mail: pudd@uwo.ca

Received (in Cambridge, UK) 26th October 2001, Accepted 14th November 2001
First published as an Advance Article on the web 6th December 2001

The combination of the *cis*-blocked platinum(II) unit (bu_2-bipy)Pt^{2+} with the unsymmetrical *bis*(pyridine) ligand 4-$NC_5H_4C(=O)NH$-4-C_5H_4N gives the molecular triangle complex $[\{Pt(bu_2bipy)(\mu\text{-}4\text{-}NC_5H_4C(=O)NH\text{-}4\text{-}C_5H_4N)\}_3]^{6+}$, which forms stacked pairs in the solid state through intertriangle NH···OC hydrogen bonds and Pt···OC secondary bonds.

There has been much interest in molecular triangles, assembled through coordination chemistry, some of which stack to form materials, A, with nanometre sized channels.[1] However, the stacking has usually been unpredictable, and so the discovery of stacked triangles in these systems has often been serendipitous.[1,2] On the other hand, cyclic oligopeptides have amide groups oriented perpendicular to the ring and they stack in a predictable way through inter-ring NH···OC hydrogen bonding, to give dimers, B, that model protein β-sheet structures or to give 'protein nanotubes'.[3]

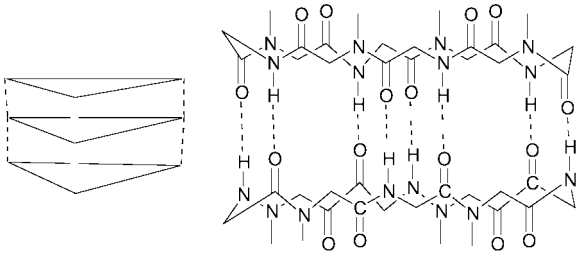

A B

The inorganic molecular triangles have often been prepared using roughly linear, symmetrical bis(pyridine) bridging ligands in combination with a *cis* oriented palladium(II) or platinum(II) unit. Typically, there are no functional groups perpendicular to the triangle to provide orientation through secondary bonding effects,[1,2] and the nature of the stacking, when determined, is often controlled by anion or solvent effects that are difficult to predict. This paper reports a new molecular triangle complex in which a roughly linear bis(pyridine) ligand 4-$NC_5H_4C(=O)NH$-4-C_5H_4N, **1**, is designed to have amide groups between the pyridyl donors[4] that can control the intertriangle stacking.

The reaction of the ligand **1**[4] with $[Pd(bu_2bipy)(thf)_2][BF_4]_2$ or $[Pt(bu_2bipy)(O_3SCF_3)_2]$, bu_2bipy = 4,4′-di-*tert*-butyl-2,2′-bipyridine, occurred by 3 + 3 self-assembly to give the complexes $[M_3(bu_2bipy)_3(\mu\text{-}\mathbf{1})_3]X_6$ (**2a**, M = Pd, X = BF_4; **2b**, M = Pt, X = CF_3SO_3) which were isolated as colorless solids.† These complexes had similar NMR spectra, suggesting similar structures, but the NMR spectra were deceptively simple and did not define the nuclearity of the complexes or the molecular symmetry. The trimeric structure of **2b** was established by an X-ray structure determination (Fig. 1).‡

The cation $[Pt_3(bu_2bipy)_3(\mu\text{-}\mathbf{1})_3]^{6+}$ forms a triangular triplatinum unit with each pair of platinum atoms bridged by a slightly bowed ligand **1**. There are two potential isomers with an unsymmetrical ligand such as **1**, containing NHC_5H_4N (py^a) and $C(O)C_5H_4N$ (py^b) pyridyl donors. The more symmetrical

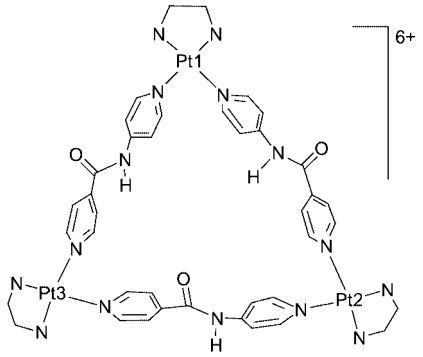

2b

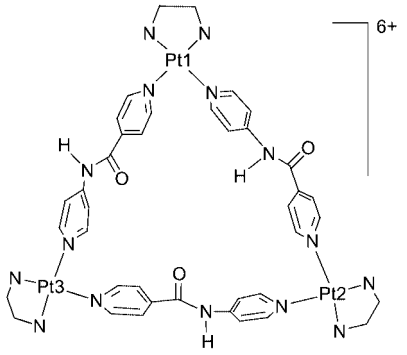

2b′

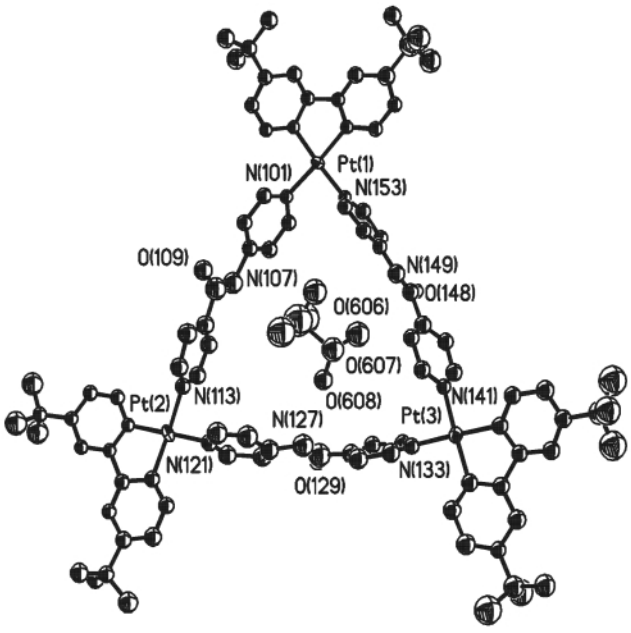

Fig. 1 A view of the cation **2b** with encapsulated triflate anion.

 DOI: 10.1039/b109784a

isomer has symmetry C_{3h}, when each platinum has Pt(py^a)(py^b) coordination, and the less symmetrical isomer has symmetry C_s, when the three platinum atoms have Pt(py^a)$_2$, Pt(py^b)$_2$ and Pt(py^a)(py^b) coordination (assumes free rotation of ligands **1** to give maximum possible symmetry). Complex **2b** has the less symmetrical structure (roughly C_s) with Pt(3), Pt(1) and Pt(2) having Pt(py^a)$_2$, Pt(py^b)$_2$ and Pt(py^a)(py^b) coordination, respectively (Fig. 1). The three Pt atoms form an approximately equilateral triangle with Pt···Pt distances of 13.1 Å, and the three PtN_4 coordination planes are roughly coplanar. However, each pyridyl group of the three bis(pyridyl) ligands is oriented out of the molecular plane so that a large interior cavity is formed. One of the triflate anions is encapsulated in the center of this cavity (Fig. 1). There are relatively short contacts N(127)···O(608) 3.13 and N(149)···O(606) 3.19 Å but the orientation is not appropriate for hydrogen bonding and it is likely that this simply represents a close fit of the triflate ion in the cavity.

The amide groups are oriented roughly perpendicular to the molecular triangle and an interesting supramolecular association occurs between pairs of triangular cations, that are separated by about 5.1 Å and related by a centre of symmetry, as illustrated in Fig. 2. The association occurs primarily through pairwise intertriangle NH···O=C hydrogen bonding between amide groups, with N(107)···O(148A) = N(107A)···O(148) = 2.92 Å. These attractions are supported by two long C=O···Pt contacts with O(129)···Pt(1A) = O(129A)···Pt(1) = 3.36 Å, that probably represent weak electrostatic attractions. The NH groups that are not involved in intertriangle hydrogen bonding take part in hydrogen bonding either with a triflate anion [N(149)···O(206) 2.81 Å] or with a water molecule [N(127)···O(801) 2.90 Å]. The carbonyl groups C(128)O(129) and C(108)O(109) are not involved in hydrogen bonding. The 'dimer of trimer' cations contain two triflate ions in their cavities (Fig. 1) and are surrounded by further disordered triflate ions, as well as by water and acetone solvate molecules. However, there is no further intercation bridging between adjacent 'dimers of trimers'.

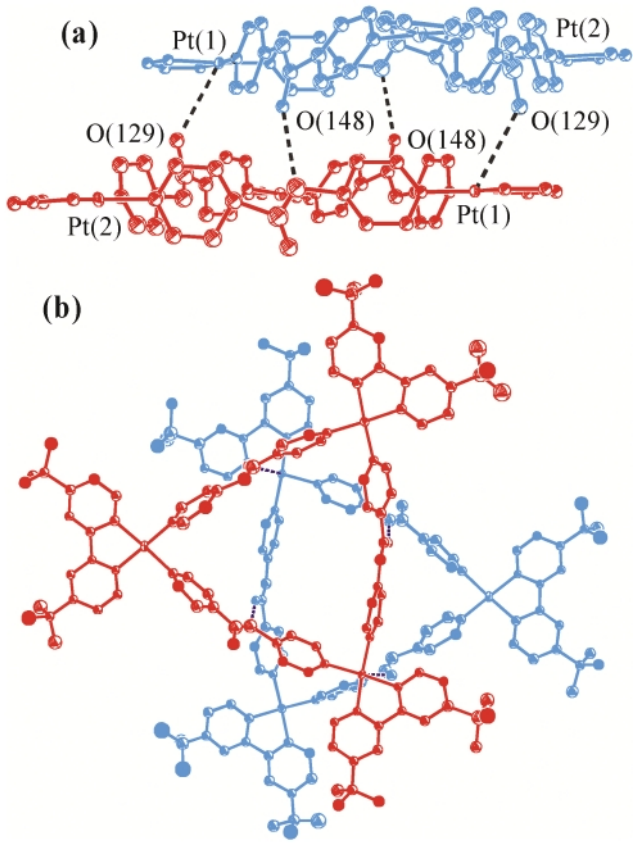

Fig. 2 Side (a) and top (b) views of the dimer of triangles formed *via* hydrogen bonding and weak C=O···Pt interactions between units of **2b**. The triflate anions are omitted for clarity and in (a) only the core atoms of the bu$_2$bipy ligands are shown.

The packing motif is thus different from that of a related triangular hexacation in which all triangles are separated by the same distance and connected by a channel of counter ions and water molecules.[2d] It is possible that the unsymmetrical ring structure found in the structure of **2b** is favored over the more symmetrical one, **2b′**, as a result of the favorable supramolecular association since there is no obvious reason why it would be favored for a simple ring structure. Indeed it should be noted that there is no direct proof that triangles, rather than the more common squares, are present in the solution phase. The complex cation **2b** appears to be the first example of a cyclic coordination compound that forms a dimer architecture similar to that formed by cyclic peptides, and it suggests that the biomimetic approach to organization of molecular triangles and other macrocyclic structures has considerable promise.[3]

We thank the NSERC (Canada) for financial support. R. J. P. thanks the Government of Canada for a Canada Research Chair.

Notes and references

† [{(bu$_2$bipy)Pt(μ-NC$_5$H$_4$-4-CONH-4-C$_5$H$_4$N)}$_3$](CF$_3$SO$_3$)$_6$ **2b**. To a solution of *N*-(pyridin-4-yl)isonicotinamide (0.020 g, 0.100 mmol) in THF (10 mL) was added a filtered solution of [(bu$_2$bipy)Pt(OTf)$_2$] generated *in situ* from [(bu$_2$bipy)PtCl$_2$] (0.053 g, 0.100 mmol) and AgOTf (0.052 g, 0.200 mmol) in CH_2Cl_2–THF (10/10 mL). The white precipitate was collected by filtration, washed with diethyl ether and dried under vacuo. Yield: 68%. Anal. Calc. for $C_{93}H_{99}F_{18}N_{15}O_{21}Pt_3S_6.3H_2O$: C, 38.04; H, 3.60; N, 7.15. Found: C, 38.08; H, 3.30; N, 6.84. ^{1}H NMR (acetone-d$_6$): δ 11.0 (s, 1H, CONH); 9.60 (s, 2H, H^{2,6}); 9.25 (s, 2H, H$^{2',6'}$); 8.82 (s, 2H, H$^{6,6'}$ bu$_2$bipy); 7.65–8.30 (m, 8H, H$^{3,5,3'5'}$ + H$^{3,5,3',5'}$ bu$_2$bipy); 1.45 (s, 18H, Bu). The spectrum was very similar at −80 °C; mp 242 °C.

‡ *Crystal data* for **2b**. $Me_2CO{\cdot}3H_2O$: $C_{96}H_{105}F_{18}N_{15}O_{25}Pt_3S_6$, M = 2988.58, Nonius Kappa-CCD diffractometer, T = 200(2) K, λ = 0.71073 Å, space group $P\bar{1}$, a = 15.2398(9), b = 18.154(1), c = 23.461(1) Å, α = 79.115(3), β = 84.232(3), γ = 77.554(3)°, V = 6212.2(6) Å^3, Z = 2, D_c = 1.598 g cm^{-3}, μ = 3.567 mm^{-1}, $F(000)$ = 2956, reflection collected 43817, unique reflns 15006, $R1$ = 0.0960, $wR2$ = 0.2620 [$I > 2\sigma(I)$]. The cation was well-defined but there was much disorder of the anions and solvent molecules, leading to large residuals. Only the platinum atom and two anions were refined anisotropically. CCDC reference number 173466. See http://www.rsc.org/suppdata/cc/b1/b109784a/ for crystallographic data in CIF or other electronic format.

1 Recent reviews: (*a*) M. Fujita, K. Umemoto, M. Yoshizawa, N. Fujita, T. Kusukawa and K. Biradha, *Chem. Commun.*, 2001, 509; (*b*) B. J. Holliday and C. A. Mirkin, *Angew. Chem., Int. Ed.*, 2001, **40**, 2022; (*c*) S. Leininger, B. Olenyuk and P. J. Stang, *Chem. Rev.*, 2000, **100**, 853; (*d*) F. A. Cotton, C. Lin and C. A. Murillo, *Acc. Chem. Res.*, 2001, in press.

2 (*a*) F. A. Cotton, C. Lin and C. A. Murillo, *Inorg. Chem.*, 2001, **40**, 575; (*b*) A. Sautter, D. G. Schmid, G. Jung and F. Wurthner, *J. Am. Chem. Soc.*, 2001, **123**, 5424; (*c*) R.-D. Schnebeck, E. Freisinger, F. Glahe and B. Lippert, *J. Am. Chem. Soc.*, 2000, **122**, 1381; (*d*) R.-D. Schnebeck, E. Freisinger and B. Lippert, *Chem. Commun.*, 1999, 675; (*e*) J. Hall, S. J. Loeb, G. K. H. Shimizu and G. P. A. Yap, *Angew. Chem., Int. Ed.*, 1998, **37**, 121.

3 (*a*) J. D. Hartgerink, T. D. Clark and M. R. Ghadiri, *Chem. Eur. J.*, 1998, **4**, 1367; (*b*) M. R. Ghadiri, K. Kobayashi, J. R. Granja, R. K. Chadha and D. E. McRee, *Angew. Chem., Int. Ed. Engl.*, 1995, **34**, 93.

4 (*a*) T. S. Gardner, E. Wenis and J. Lee, *J. Org. Chem.*, 1954, **19**, 753; (*b*) M. Kondo, T. Okubo, A. Asami, S.-I. Noro, T. Yoshitomi, S. Kitagawa, T. Ishii, H. Mazsuzaka and K. Seki, *Angew. Chem., Int. Ed.*, 1999, **38**, 140; (*c*) M. Kondo, A. Asami, H.-C. Chang and S. Kitagawa, *Cryst. Eng.*, 1999, **2**, 115.

CHEMCOMM Communication
www.rsc.org/chemcomm

Ditopic azathioether macrocycles as hosts for transition metal salts†

Jason B. Love, Joanna M. Vere, Mark W. Glenny, Alexander J. Blake and Martin Schröder*

School of Chemistry, The University of Nottingham, University Park, Nottingham, UK NG7 2RD. E-mail: m.schroder@nottingham.ac.uk

Received (in Cambridge, UK) 17th October 2001, Accepted 14th November 2001
First published as an Advance Article on the web 6th December 2001

The synthesis and complexation of two heteroditopic lariat azathioether macrocycles L^1 and L^2 incorporating acylurea functionalised pendant arms are described; L^1 and L^2 are capable of simultaneously binding both the cationic and anionic moieties of a metal salt as confirmed by the structures of $[PdCl_2(L^1)]$, $[CuCl(L^2)]_2CuCl_4$ and $[Ag(NO_3)(L^2)]$ and by ^1H NMR studies in solution on $[Ag(NO_3)(L^2)]$.

Interest in the design and synthesis of heteroditopic receptors that can simultaneously bind both cationic and anionic moieties of a metal salt stems from the anticipation that such compounds may act as potent ionophores for the selective extraction and transport of base, toxic and/or precious metal salts from process streams.[1–3] A common approach has been to combine cation complexing agents such as crown O-ethers and calixarenes with proven anion receptors,[1–6] facilitating the tandem complexation of Group 1 halides, pseudo-halides and hydrogen phosphates. However, this choice of cation receptor precludes the *simultaneous* complexation of softer transition metal salts. Indeed, general ditopic receptors for transiton metal salts are exceedingly rare,[7,8] Thioether crowns represent powerful ligands for binding transition metal cations, even under low pH conditions where aza ligands are simply protonated and are no longer able to function as cation receptors.[9] We report herein definitive structural evidence for three systems that show simultaneous cation and anion binding.

Reaction of $PdCl_2$ with the new lariat azathiocrown L^1 in boiling MeCN results in the formation of **1** as a yellow powder (Scheme 1).†‡ Binding of Cl^- in solution by NMR methods could not be probed since **1** is soluble only in protic solvents where H-exchange occurs. The structure of **1**§ confirms the Pd(II) centre ligated in a square-planar geometry to the four S-donors resulting in an overall 'chair' conformation of the ligand. A Pd···Cl contact of 3.364(2) Å is observed at both axial sites of the Pd(II) ion and is indicative of weak electrostatic interactions between these centres. However, when viewing the extended molecular structure of **1**, it becomes apparent that the inner urea N atom N(2) is involved in H-bonding to the Cl^- anion of a second, approximately perpendicular molecule [N(2)···Cl(AA) 3.332(5) Å] (Fig. 1). The outer urea N atom N(3) is found to be H-bonding to the acyl oxygen O(1) of the same arm [N(3)···O(1) 2.689(7) Å] so constricting the librational freedom of the anion host. As expected, the symmetry-related equivalent N(2A) is H-bonded to the Cl^- ClD of a third $[PdCl_2(L^1)]$ molecule [N(2A)···ClD 3.331(5) Å] resulting in supramolecular aggregation *via* a zigzag chain. It is therefore apparent that ligand L^1 is capable of binding not only the Pd^{II} cation within the macrocyclic sulfur array, but also the associated Cl^- anions by concerted intermolecular H-bonding and metal–anion electrostatic interactions with the pendant arm.

The reaction between $CuCl_2$ and L^2 in MeOH (Scheme 1) affords dark green **2**.†‡ The molecular structure of **2** (Fig. 2)§ confirms that the asymmetric unit comprises two $[CuCl(L^2)]^+$ cations and a $[CuCl_4]^{2-}$ dianion. In each cation, the Cu(II) centre is coordinated octahedrally with the inner acyl oxygen of the pendant arm occupying an equatorial site.[10] The cations are organized such that the pendant arms assume a 'parallel' arrangement to each other; this position is presumably dictated by the presence of the $[CuCl_4]^{2-}$ anion, which is H-bonded to the inner urea N–H of each arm [N(2)···Cl(6) 3.29(2), N(5)···Cl(5) 3.27(2) Å]. The observed distorted tetrahedral geometry of $[CuCl_4]^{2-}$ is typical for this dianion.[11] As with L^1, the monobrachial azathioether L^2 is therefore able to simultaneously bind cationic and anionic halo-metal fragments; this system formally represents a methodology for the extraction and transport of $CuCl_2$.

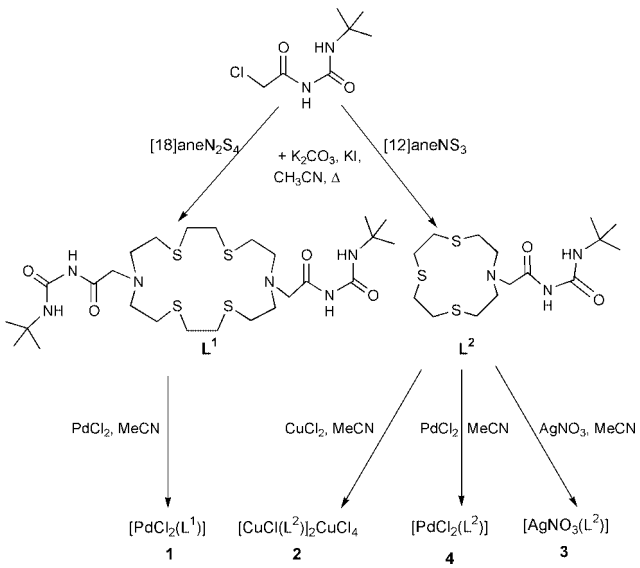

Scheme 1 Synthesis and complexation reactions of the heteroditopic ligands L^1 and L^2.

† Electronic supplementary information (ESI) available: full experimental details. See http://www.rsc.org/suppdata/cc/b1/b109486f/

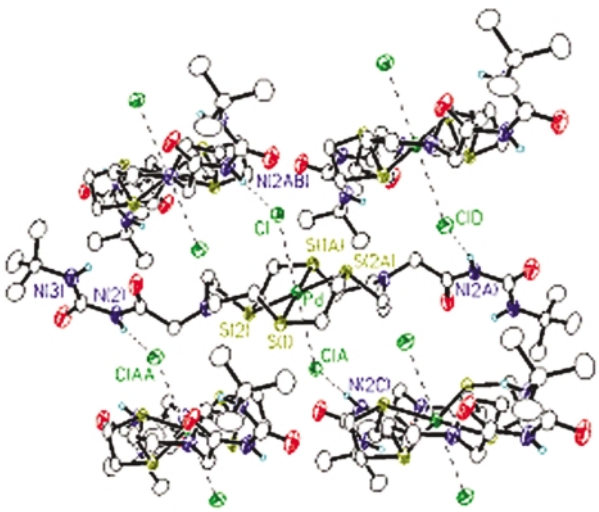

Fig. 1 View of structure of $[PdCl_2(L^1)]$.

 DOI: 10.1039/b109486f

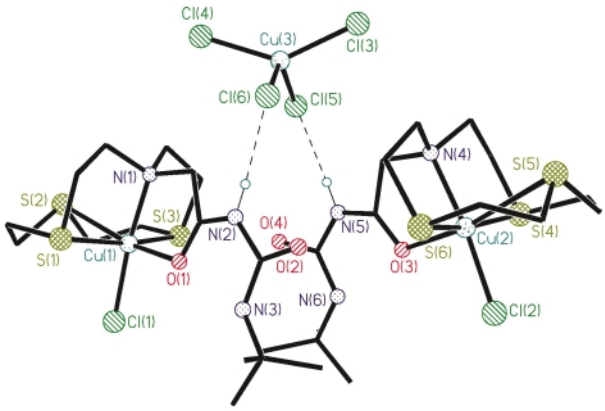

Fig. 2 View of structure of $[CuCl(L^2)]_2CuCl_4$.

Neither **1** or **2** allow for NMR studies on solution complexation. However, the reaction between $AgNO_3$ and L^2 yields $[Ag(NO)_3(L^2)]$, **3**,†‡ which is soluble in CD_3CN. The solid state structure of **3**§ confirms that the Ag(I) cation is complexed by the azathiocrown with the anion receptor arm extending radially (Fig. 3). Inspection of the extended structure reveals a bond between Ag(I) and a S-donor of a second cation [Ag–S(4A) 2.496(2) Å], so completing a five-coordinate, square pyramidal geometry at Ag(I) and affording an overall two-dimensional step-polymeric motif. Although displaying two-fold rotational disorder, the NO_3^- anion is clearly H-bonded to the pendant arm *via* the urea N(15), interacting in varying degrees with O(2), O(2′) and O(1) [N(15)–O(2) 3.27(3), N(15)–O(2′) 2.50(2), N(15)–O(1) 3.43(3) Å].

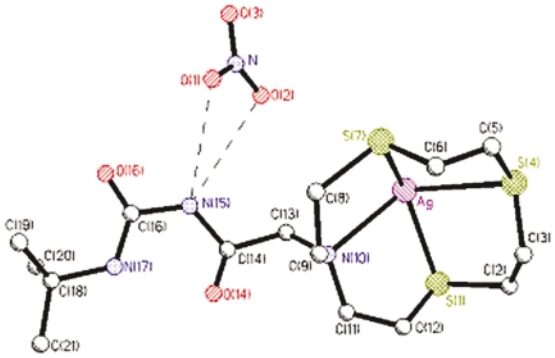

Fig. 3 View of structure of $[Ag(NO_3)(L^2)]$.

Addition of $AgNO_3$ to a solution of L^2 in MeCN leads initially to an upfield shift for the N(15)–H proton from δ_H 9.01 in L^2 to 8.65 on addition of 0.4 equivalents of $AgNO_3$. This upfield shift reflects the breaking of the internal H-bonding in free L^2 (confirmed by structural studies) on complexation to Ag(I) (Scheme 2). On further addition of $AgNO_3$, this resonance shows the expected downfield shift to δ_H 8.85 for **3** reflecting H-bonding of the acylurea arm to the nitrate anion as confirmed by the crystal structure of **3**. Addition of $[^nBu_4N][NO_3]$ to **3** leads

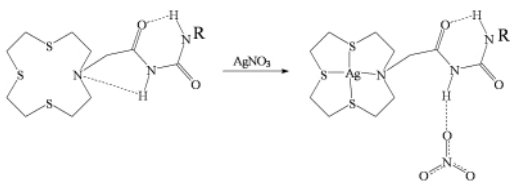

Scheme 2 Cleavage of internal H-bonding in L^2 on binding to $AgNO_3$.

to further downfield shifts for the N(15)–H resonance (to δ_H 9.39, 9.55 and 9.65 on addition of 1, 2 and 3 equivalents of $^nBu_4NNO_3$, respectively) consistent with anion binding in solution. Significantly, addition of $[^nBu_4N][NO_3]$ to L^2 does not shift the N(15)–H resonance; therefore, anion binding to L^2 can only occur once cation binding within the macrocyclic cavity and concomitant cleavage of the internal H-bonding takes place, thus affording an element of cooperativity to this system. Compound **4** has also been prepared and characterised.†‡

In conclusion, we have confirmed that the combination of thioether macrocycles with functionalised acylurea lariat arms affords heteroditopic receptors that have a wide applicability for the complexation of transition metal salts. These results have important implications for the extraction and transport of transition metal salts, especially at low pH where thioether crowns can still function as avid metal cation receptors.

This work was supported by the EPSRC (UK) and Avecia plc.

Notes and references

‡ For **1**: Anal. Found: C, 38.70; H, 5.77; N, 9.92. $C_{26}H_{50}Cl_2N_6O_4PdS_4$ requires: C, 38.30; H, 6.25; N, 10.32%; ^{1}H NMR (CD_3OD): δ_H 8.40 (br s, 1H, NH), 3.9–3.0 (br m's, 28H, macrocycle H/ CH_2), 1.37 (s, 18H, Bu^t); MS (FAB, +ve NBA matrix): *m/z* 744 ($M^+ - 2Cl$ 100%). For **2**: Anal. Found: C, 30.74; H, 4.95; N, 7.58. $C_{30}H_{58}Cl_6Cu_3N_6O_4S_6$ requires: C, 30.99; H, 5.03; N, 7.23%; MS (FAB, +ve NBA matrix): *m/z* 477 {$[CuCl(L^2)]^+$ 45}, 442 {$[Cu(L^2)]^+$ 50%}. For **3**: Anal. Found: C, 33.17; H, 5.39; N, 10.64. $C_{15}H_{29}AgN_4O_5S_3$ requires: C, 32.79; H, 5.32; N, 10.20%; ^{1}H NMR (CD_3CN): δ_H 8.85 (brs, 1H, NH), 8.08 (br s, 1H, NH), 3.40 (s, 2H, CH_2), 2.85 (br m's, 16H, macrocyclic CH_2's), 1.35 (s, 9H, CMe_3); MS (FAB, +ve NBA matrix): *m/z* 488 ($M^+ - NO_3$, 100%); IR (KBr disc): ν/cm^{-1} 3449 (vbr, m), 3299 (br, m), 1712 (s), 1348 (vs). For **4**: Anal. Found: C, 32.71; H, 4.97; N, 8.00. $C_{15}H_{29}Cl_2N_3O_2PdS_3$ requires: C, 32.35; H, 5.25; N, 7.54%. ^{1}H NMR (CD_3OD): δ_H 4.2–3.2 (br m's, 18H, macrocycle H/ CH_2), 1.38 (s, 9H, Bu^t). ^{1}H NMR (CD_3CN): δ_H 8.30 (br s, 1H, NH), 8.15 (br s, 1H, NH), 3.70–2.80 (m's, 18H, macrocyclic H), 1.36 (s, 9H, Bu^t). MS (FAB, +ve NBA matrix): *m/z* 522 ($M^+ - Cl$, 65), 484 ($M^+ - 2Cl$, 70%).

§ CCDC reference numbers 134350–134352. See http://www.rsc.org/suppdata/cc/b1/b109486f/ for crystallographic data in CIF or other electronic format.

1 For recent overview on anion binding, see: P. D. Beer and P. A. Gale, *Angew. Chem., Int. Ed.*, 2001, **40**, 486.

2 J. E. Redman, P. D. Beer, S. W. Dent and M. G. B. Drew, *Chem. Commun.*, 1998, 231; P. D. Beer and S. W. Dent, *Chem. Commun.*, 1998, 825.

3 D. M. Rudkevich, Z. Brzozka, M. Palys, H. C. Visser, W. Verboom and D. N. Reinhoudt, *Angew. Chem., Int. Ed. Engl.*, 1993, **33**, 467; D. M. Rudkevich, J. D. Mercer-Chalmers, W. Verboom, R. Ungaro, F. de Jong and D. N. Reinhoudt, *J. Am. Chem. Soc.*, 1995, **117**, 6124.

4 E. A. Arafa, K. I. Kinnear and J. C. Lockhart, *J. Chem. Soc., Chem. Commun.*, 1992, 61.

5 M. T. Reetz, C. M. Niemeyer and K. Harms, *Angew. Chem., Int. Ed. Engl.*, 1991, **30**, 1472; M. T. Reetz, C. M. Niemeyer and K. Harms, *Angew. Chem., Int. Ed. Engl.*, 1991, **30**, 1474. See also ref. 6 for an energy minimised structure of a metal salt complex.

6 D. M. Rudkevich, A. N. Shivanayuk, Z. Brzozka, W. Verboom and D. N. Reinhoudt, *Angew. Chem., Int. Ed. Engl.*, 1995, **34**, 2124.

7 P. D. Beer, P. K. Hopkins and J. D. McKinney, *Chem. Commun.*, 1999, 1253.

8 D. J. White, N. Laing, H. Miller, S. Parsons, S. Coles and P. A. Tasker, *Chem. Commun.*, 1999, 2077; S. Ghosh, M. Mukherjee, A. K. Mukherjee, S. Mohanta and M. Helliwell, *Acta Crystallogr., Sect C.*, 1993, **50**, 1204.

9 A. J. Blake and M. Schröder, *Adv. Inorg. Chem.*, 1990, **35**, 1 and references therein; T. F. Baumann, J. G. Reynolds and G. A. Fox, *Chem. Commun.*, 1998, 1637.

10 For example of an acyl-O to M interaction see: T. Okuno, S. Ohba and Y. Nishida, *Polyhedron*, 1997, **16**, 3765.

11 K. E. Halvorson, C. Patterson and R. D. Willet, *Acta Crystallogr., Sect. B*, 1990, **46**, 508 and references therein.

CHEMCOMM
Communication
www.rsc.org/chemcomm

Host-guest binding of simple cavitands in water

Xuan Gui and John C. Sherman*

Department of Chemistry, 2036 Main Mall, University of British Columbia, Vancouver, BC, Canada V6T 1Z1. E-mail: sherman@chem.ubc.ca

Received (in Columbia, MO, USA) 16th May 2001, Accepted 1st November 2001
First published as an Advance Article on the web 4th December 2001

Simple water soluble cavitands were prepared and the thermodynamics of their binding with neutral guests in water is reported.

Host–guest chemistry has had an interesting history regarding studies in aqueous *versus* organic solvents. In the prehistoric era, BC (before crowns), there was complexation of apolar molecules by cyclodextrins in water; the main driving force for binding was the hydrophobic effect. With the emergence of crowns, cryptands, spherands, and their relatives, the guests became ions, and water was avoided to reduce the competition of hydration of the ions. As chemists became more bold and host designs became more sophisticated, binding of apolar molecules in organic solvents was explored, as pioneered by Cram using the newly created cavitands as hosts.[1] Soon after, Diederich reported his seminal work on the use of cyclophanes to bind apolar guests in solvents ranging from water to CCl_4.[2] Interest has continued in binding of apolar molecules in water,[3] but cavitands have only occasionally been used in such studies. Deshayes has reported the thermodynamics of complexation of neutral molecules in water using a hemicarcerand-like cage host composed of two cavitands.[4] Rebek has fashioned cavitands with deep cavities and has reported complexation studies in aqueous media.[5] Deep cavity cavitands have been used to extract pollutants from wastewater.[6] Positive charges have been incorporated into the upper rim of cavitands[7,8] and binding of polar (mostly anionic) guests has been reported in water.[8] Yet binding of apolar molecules in water by simple cavitands (*i.e.*, with underivatized rims) has received little attention. Here we report the incorporation of water solubilizing groups into the feet of simple cavitands, which allows the exploration of the intrinsic binding affinity of the cavitand moiety in water without the interfering effect of charges or other groups in the rims. The thermodynamic values obtained suggest, as in Diederich's case, that binding is enthalpy driven, which is somewhat at odds with the simple hydrophobic effect.

We recently reported the incorporation of phosphate groups into the feet of cavitands in the synthesis of de novo proteins.[9] Starting from cavitand **1**,[9] the synthesis of water soluble cavitand **2** was accomplished in a similar manner, as shown in Scheme 1.[10] Binding studies using cavitand **2** and a variety of guests were performed using the common methods for systems whose binding constants are in the 10–10^3 range and undergo fast exchange on the ^{1}H NMR timescale: solutions with fixed guest concentrations and varying host concentrations in D_2O (50 mM $(NH_4)_2CO_3$, pD = 9.4) were prepared, ^{1}H NMR spectra were obtained, and the chemical shift of the guest protons was recorded.[11] Job plots of these data gave an indication of 1 : 1 binding stoichiometry, and linear plots of the binding isotherms were generated for verification of stoichiometry.[12] For guests that bound in a 1 : 1 stoichiometry, Benesi–Hildebrand plots were generated to give an initial estimation of binding constants and Δ_{max} ($\delta_{complex} - \delta_{free}$).[12] Non-linear regression of these data gave the final K_a and Δ_{max},[12] which are reported in Table 1. Guests that did not show evidence for binding include methanol, ethanol, *t*-butanol, phenol, THF, pyrrole, and *N*-methylpyridinium iodide. Guests that bind to **2**, but do not yield 1 : 1 binding stoichiometry include dichloromethane and dimethyl carbonate. Enthalpies and entropies for complexation between cavitand **2** and the three best guests were generated *via* van't Hoff plots;[13] the ensuing results are given in Table 2.

The Δ_{max} values can indicate the binding geometry of the complexes. For example, the large Δ_{max} for the acetyl methyl of ethyl acetate suggests that it is bound deeply within the shielding region of the cavitand. Its methylene is clearly further from the cavity. The alkyl methyl group is closer to the cavity than the methylene. At first this may seem impossible, but it is clear that different binding modes are possible. For ethyl acetate, the predominant binding mode is acetyl methyl in the cavity, yet the alkyl methyl can also bind in the cavity, but only a small percent of the time: whereas the obtained association constants represent the sum of the association constants for all

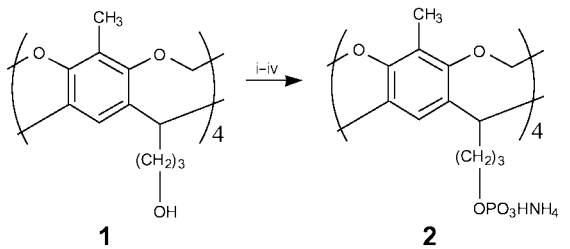

1 **2**

Scheme 1 (i) Diphenyl-*N*,*N*-diethylphosphoramidite, tetrazole, THF, rt; (ii) 30% H_2O_2, −78 °C, 65%. (iii) H_2/Pd/C, rt, 86%. (iv) 0.1 M $(NH_4)_2CO_3$, 100%.

Table 1 Δ_{max} and K_a for cavitand **2** with guests

Guest	Proton	Δ_{max}	K_a (M^{-1})
$(CH_3)_2CO$	$-CH_3$	2.25 ± 0.10	19 ± 1
CH_3CN	$-CH_3$	3.00 ± 0.18	42 ± 3
Toluene	$-H_p$	1.06 ± 0.05	32 ± 2
	$-H_m$	0.91 ± 0.14	26 ± 4
	$-H_o$	0.93 ± 0.08	36 ± 4
	$-CH_3$	2.65 ± 0.23	30 ± 3
Benzene	ArH	0.58 ± 0.12	55 ± 16
$CHCl_3$	–CH	1.07 ± 0.02	120 ± 4
$CH_3CH_2CO_2CH_3$ a b c	$-H_a$	2.11 ± 0.11	64 ± 5
	$-H_b$	1.22 ± 0.04	94 ± 4
	$-H_c$	3.45 ± 0.05	210 ± 6
$CH_3CO_2CH_2CH_3$ a b c	$-H_a$	3.52 ± 0.04	230 ± 8
	$-H_b$	0.74 ± 0.01	180 ± 14
	$-H_c$	0.93 ± 0.01	170 ± 6
$CH_3CO_2CH_3$ a b	$-H_a$	2.19 ± 0.03	270 ± 21
	$-H_b$	2.01 ± 0.02	270 ± 19

Table 2 Thermodynamic values for cavitand **2**·guest at 298K

Guest	$\Delta G°$ kcal mol^{-1}	$\Delta H°$ kcal mol^{-1}	$\Delta S°$ cal mol^{-1} K	$T\Delta S°$ kcal mol^{-1}
$CH_3CO_2CH_3$	−3.4	−5.2 ± 0.1	−6.2 ± 0.2	−1.8
$CH_3CO_2CH_2CH_3$	−3.2	−4.2 ± 0.2	−3.4 ± 0.9	−1.0
$CH_3CH_2CO_2CH_3$	−3.1	−5.1 ± 0.3	−6.6 ± 1.1	−2.1

 DOI: 10.1039/b106586f

binding modes, the Δ_{max} for a particular proton is the weighted average of the Δ_{max} for this proton in different binding modes.[14]

As has been observed even in the very early binding studies of cavitands in organic solvents, the cavity is complementary to and has an affinity for methyl groups.[15] This is consistent with work on carceplexes and hemicarceplexes, which often show high $\Delta\delta$ for methyl groups.[16] As the present system is in water, additional factors come into play such as removing apolar groups from the hydration sphere.[17] Guests such as phenol, pyrrole, and THF are well solvated by water and do not contain methyl groups; thus they do not bind at all to cavitand **2** in water. Methanol, ethanol, *t*-butanol, and *N*-methyl pyridinium iodide contain methyl groups, but they are too hydrophilic for cavitand **2** to compete with water. Acetonitrile has an electropositive methyl group, but it is also well solvated by water, so it binds weakly. Toluene is far too big to fit completely in the cavity, but it can fit its methyl group in and bury some of its hydrophobic bulk. However, binding of toluene is weak, as much of the apolar molecule must remain in water. The esters are all good binders, as they can readily provide electron deficient methyl groups for the cavity. Note that methyl propionate binds predominantly OMe into the cavity, and ethyl acetate binds predominantly acetyl methyl into the π-electron-rich cavity. In each case the more electron poor methyl dictates the preferred binding mode. Methyl acetate appears to bind with each methyl group equally strongly into the cavity (Δ_{max} = 2.19 and 2.01 ppm; since these are weighted averages of the two binding modes, the methyls likely stick well into the cavity in each mode).

The thermodynamic measurements reveal that binding of neutral guests to simple cavitands in water is enthalpy driven. The common hydrophobic effect, where water is freed up to go into the bulk, is normally entropically favored. Our case is like Diederich's[2] and others'[4,18] where the entropic release of water may indeed be at play, but the overall combination of factors renders complexation entropically unfavored. Somewhat unexpected is that the guest (ethyl acetate) that appears to have the greatest modal preference (it prefers to bind acetyl methyl into the cavity) has the least unfavorable entropy of binding. Clearly the entropic factors, both the costly (*e.g.*, reduction in molecularity and conformational freedom) and the empowering (*e.g.*, freeing up water), are complex.[18] Water is nevertheless required for binding.[17] Just as in Diederich's case, a simple way to view this is that the freeing up of water to bulk is necessary to sufficiently reduce the entropic costs of complexation to see binding. Another way to put this is the obvious general situation in any type of complexation: to observe binding, the solvent must be a very poor competitor for the cavity.

We thank NSERC of Canada for financial support.

Notes and references

1 J. R. Moran, S. Karbach and D. J. Cram, *J. Am. Chem. Soc.*, 1982, **104**, 5826.

2 F. Diederich, *Angew. Chem., Int. Ed. Engl.*, 1988, **27**, 362.

3 K. Odashima, A. Itai, Y. Iitaka and K. Koga, *J. Am. Chem. Soc.*, 1980, **102**, 2504; D. Stauffer, R. Barrans and D. Dougherty, *J. Org. Chem.*, 1990, **55**, 2762; S. Ngola, P. Kearney, S. Mecozzi, K. Russell and D. Dougherty, *J. Am. Chem. Soc.*, 1999, **121**, 1192; J. Canceill, L. Lacombe and A. Collet, *J. Chem. Soc., Chem. Commun.*, 1987, 219; L. Zhang, A. Macias, T. Lu, J. I. Gordon, G. W. Gokel and A. E. Kaifer, *J. Chem. Soc., Chem. Commun.*, 1993, 1017; H.-J. Schneider, D. Güttes and U. Schneider, *J. Am. Chem. Soc.*, 1988, **110**, 6449; O. Manabe, K. Asakura and T. Nishi, *Chem. Lett.*, 1990, 1219; J. Huuskonen, J. E. H. Buston, N. D. Scotchmer and H. L. Anderson, *New J. Chem.*, 1999, **23**, 1245.

4 E. L. Piatnitski, R. A. Flowers II and K. Deshayes, *Chem. Eur. J.*, 2000, **6**, 999; See also: O. D. Fox, J. F.-Y. Leung, J. M. Hunter, N. K. Dalley and R. G. Harrison, *Inorg. Chem.*, 2000, **39**, 783.

5 A. R. Renslo, D. M. Rudkevich and J. Rebek, Jr., *J. Am. Chem. Soc.*, 1997, **119**, 9911; T. Haino, D. M. Rudkevich, A. Shivanyuk, K. Rissanen and J. Rebek, Jr., *Chem. Eur. J.*, 2000, **6**, 3797.

6 E. Dalcanale, G. Costantini and P. Soncini, *J. Inclusion Phenom., Mol. Recognit. Chem.*, 1992, **13**, 87.

7 J. R. Fraser, B. Borecka, J. Trotter and J. C. Sherman, *J. Org. Chem.*, 1995, **60**, 1207; B. C. Gibb, A. S. Mezo and J. C. Sherman, *Tetrahedron Lett.*, 1995, **36**, 7587.

8 M. H. B. G. Gansey, F. K. Bakker, M. C. Feiters, H. P. M. Geurts, V. Verboom and D. Reinhoudt, *Tetrahedron Lett.*, 1998, **39**, 5447; D.-R. Ahn, T. W. Kim and J.-I. Hong, *Tetrahedron Lett.*, 1999, **40**, 6045.

9 A. R. Mezo and J. C. Sherman, *J. Org. Chem.*, 1998, **63**, 6824; A. R. Mezo and J. C. Sherman, *J. Am. Chem. Soc.*, 1999, **121**, 8983.

10 All new compounds (the tetraphosphate ester, the tetraphosphoric acid, and **2**) gave the expected ^{1}H NMR and MS data.

11 ^{1}H NMR spectra of cavitand **2** in D_2O showed no changes over a range of 0.5–10 mM.

12 K. A. Connors, *Binding Constants*, John Wiley & Sons, 1987, and references therein; M. T. Bowser and D. D. Y. Chen, *J. Phys. Chem. A*, 1998, **102**, 8063; M. T. Bowser and D. D. Y. Chen, *J. Phys. Chem. A*, 1999, **103**, 197; L. Fielding, *Tetrahedron*, 2000, **56**, 6151; See also X. M. Gui, Thesis, University of British Columbia, 2000.

13 The temperature range was kept small (283–307 K) to obtain good association constants (to keep the % bound in the 20–80% range) and to legitimize the assumption of temperature independence of enthaply and entropy. For methyl propionate, H_c was used for K_a determinations; for ethyl acetate, H_a was used (see Table 1 and note 14). Temperature was determined from methanol or ethylene glycol thermometers: see J. Sandström, *Dynamic NMR Spectroscopy*, Academic Press, Inc., London, New York, 1982; C. Ammann, P. Meier and A. E. Merbach, *J. Magn. Reson.*, 1982, **46**, 319-312; See also http://bmrl.med.uiuc.edu:8080/~dmorris/nmrt_ref.html. The HOD peak was referenced using a calibration curve against ethyl acetate: see H. E. Gottlieb, V. Kotlyar and A. Nudelman, *J. Org. Chem.*, 1997, **62**, 7512.

14 K. A. Connors, *Chem. Rev.*, 1997, **97**,1325; L. Liu and Q.-X. Guo, *J. Phys. Chem. B*, 1999, **103**, 3461. Generation of K_a from different protons for methyl acetate and toluene give the same values for K_a. But values range for ethyl acetate (170–230 M^{-1}) and for methyl propionate (60–210 M^{-1}). It is not unusual to find artificially lower K_as from protons that are more solvent exposed, as is observed in these cases. See: H. Stamm, W. Lamberty and J. Stafe, *J. Am. Chem. Soc.*, 1980, **102**, 1529; V. Rüdiger and H.-J. Schneider, *Chem. Eur. J.*, 2000, **6**, 3771.

15 D. J. Cram, K. D. Stewart, I. Goldberg and K. N. Trueblood, *J. Am. Chem. Soc.*, 1985, **107**, 2574; J. A. Tucker, C. B. Knobler, K. N. Trueblood and D. J. Cram, *J. Am. Chem. Soc.*, 1989, **111**, 3688.

16 A. Jasat and J. C. Sherman, *Chem. Rev.*, 1999, **99**, 931.

17 Water is indeed needed to see binding, as no binding was observed between the best guest, methyl acetate, and the following guest/solvent combinations: cavitand **1** in CD_3OD, the tetraphosphate ester derived cavitand in $CDCl_3$, the tetraphosphoric acid derived cavitand in CD_3OD.

18 A. Marmus, *J. Am. Chem. Soc.*, 2000, **122**, 2120.

CHEMCOMM Communication
www.rsc.org/chemcomm

On the relative magnitudes of *cis* and *trans* influences in metal complexes

Kirsty M. Anderson and A. Guy Orpen

School of Chemistry, University of Bristol, Bristol, UK BS8 1TS. E-mail: guy.orpen@bristol.ac.uk

Received (in Cambridge, UK) 19th September 2001, Accepted 31st October 2001
First published as an Advance Article on the web 4th December 2001

***Cis* and *trans* influences are of similar magnitude in octahedral complexes of Sn^{IV} and Sb^{V} while the *trans* influence is dominant in square planar Pt^{II} (d^8) and d^6-ML_6 cases.**

The concept of *trans* influence, and the related *trans* effect are central to modern molecular inorganic chemistry.[1,2] The *trans* influence, also termed the structural *trans* effect,[3] concerns the ability of a ligand to weaken (and lengthen) the bond *trans* to it in preference to those that are *cis*. Much of the best evidence for this ground-state structural phenomenon and the kinetic *trans* effect is drawn from Pt^{II} chemistry[4] although a substantial literature exists for octahedral transition metal chemistry[5] as recently discussed by Coe and Glenwright.[3] *Trans* influence is also of importance in p-block metal chemistry and some notable examples are cited in refs. 6–9. Theoretical and computational treatments of *trans* influence include the work of Burdett and Albright, Mingos and others.[10,11] While the evidence for *trans* influence in the d-block and especially for d^6 and d^8 metals is well established, the question arises as to its generality. Here we present evidence that at least in p block metal chemistry, *cis* influence can be of similar magnitude to *trans* influence. Further, we offer a qualitative model affording understanding of the relative magnitudes of *cis* and *trans* influences in various electronic circumstances.

Coe and Glenwright[3] pointed out that the mutual effect of ligands is important in determining the extent of *trans* influence and notes that the electron configuration of the metal can also be significant (see pp. 22 and 38 in ref. 3). Indeed in tin(IV) chemistry, Aslanov and coworkers have observed an inverse *trans* influence (see ref. 9 and work cited therein). Here we study the consequences of metal electron configuration by comparing the behaviour of d- and p-block metals with formal valence electron configurations $d^n s^k$ (n = 0, 6, 8, 10; k = 0 and n = 10, k = 0, 2). We approach this problem by seeking appropriate crystal structure data. In a square planar or octahedral complex of the types shown in Scheme 1 we study the effect of a probe ligand L attached to a ML'_n (n = 3 or 5; L′ = L_c = L_t = Cl, CO or NH_3) fragment on the metal–ligand bond lengths *trans* and *cis* to it. Since the *cis* and *trans* ligands are identical, if the *trans* influence is dominant the M–L_t length should change as the M–L bond varies while the M–L_c distance (or its average $<$M–$L_c$$>$) should be relatively invariant. Put in quantitative terms, we can identify three alternative patterns of correlation between M–L_t and $<$M–$L_c$$>$: (i) if the *cis* influence is zero and *trans* influence is completely dominant there should be no correlation (nor would there be if *trans* influence were zero and *cis* influence were not); (ii) if *cis* and *trans* influences are equal then M–L_t should equal $<$M–$L_c$$>$ within experimental uncertainty; (iii) between these extreme cases intermediate degrees of correlation would be expected. In this paper we use three measures of this correlation: the Pearson correlation coefficient (R), the regression line formula and, more crudely, the ratio, S, between the ranges in *trans* and *cis* bond lengths.† We note that R^2 indicates the presence of correlation rather than covariance and so gives no direct information on the relative magnitudes of *cis* and *trans* influence, and S is inevitably not a robust statistic since it depends on extreme values. Therefore the regression line gradient (m in $y = mx + c$, where y = $<$M–$L_c$$>$ and x = M–L_t) is perhaps the more helpful statistic in distinguishing between cases (i), (ii) and (iii). Ideally in case (i) $m \approx 0$, for (ii) $m \approx 1.0$ and for (iii) $0 << m << 1$.

Data were taken from the Cambridge Structural Database[11] for square planar and octahedral metal complexes of the forms: $[Pt^{II}Cl_3L]$, $[W^0(CO)_5L]$, $[Co^{III}(NH_3)_5L]$, $[Te^{IV}Cl_5L]$, $[Bi^{III}Cl_5L]$, $[Sn^{IV}Cl_5L]$, $[Sb^{V}Cl_5L]$ and $[W^{VI}Cl_5L]$ (L = two-electron donor ligand).† The variation of the metal–ligand distances and derived statistics (R^2, m, c, S) are summarised in Table 1. Fig. 1 shows plots of the *trans* length (M–L_t) *vs.* the mean *cis* length ($<$M–$L_c$$>$) for the cases (a) $[Pt^{II}Cl_3L]$, (b) $[W^0(CO)_5L]$, (c) $[Te^{IV}Cl_5L]$, (d) $[Sb^{V}Cl_5L]$ and (e) $[W^{VI}Cl_5L]$.

These plots [Fig. 1(a)–(e)] and the data in Table 1 show varying forms of correlation which depend on the electron configuration of the metal. The d^8 case [Pt^{II}, Fig. 1(a)] has a larger variation in *trans* distance than *cis* (by a factor, S, of 2.4), and shows a corresponding low value of m (0.18). The d^6 cases {$[W^0(CO)_5L]$, Fig. 1(b), and $[Co^{III}(NH_3)_5L]$} are similar to each other (*m ca.* 0.12, S = 2.2–3.1) and to the d^8 case, showing, if anything, slightly more dominance of *trans* influence. The $d^{10}s^2$ cases {$[Te^{IV}Cl_5L]$, Fig. 1(c) $[Bi^{III}Cl_5L]$} show almost perfectly dominant *trans* influence[7] with values of m close to

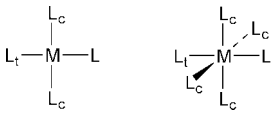

Scheme 1

Table 1 Bond length data and derived statistics

System	Structures/ fragments	Range of M–L_t/Å	Range of M–L_c/Å	R^2	Regression line† $y = mx + c$	S
$Pt^{II}Cl_3L$	67/73	2.262–2.389	2.276–2.333	0.204	0.183x + 1.875	2.40
$W^0(CO)_5L$	322/372	1.836–2.088	1.963–2.075	0.082	0.134x + 1.768	2.25
$Co^{III}(NH_3)_5L$	28/35	1.940–2.105	1.947–2.001	0.092	0.113x + 1.743	3.0
$Sn^{IV}Cl_5L$	57/57	2.355–2.488	2.383–2.492	0.404	0.444x + 1.342	1.35
$Sb^{V}Cl_5L$	112/141	2.271–2.437	2.291–2.411	0.432	0.453x + 1.290	1.38
$W^{VI}Cl_5L$	13/17	2.299–2.493	2.288–2.358	0.580	0.273x + 1.665	2.78
$Te^{IV}Cl_5L$	21/22	2.390–2.560	2.521–2.543	0.017	−0.013x + 2.563	7.8
$Bi^{III}Cl_5L$	15/20	2.533–3.007	2.686–2.757	0.023	−0.021x + 2.764	6.8

 DOI: 10.1039/b108517b

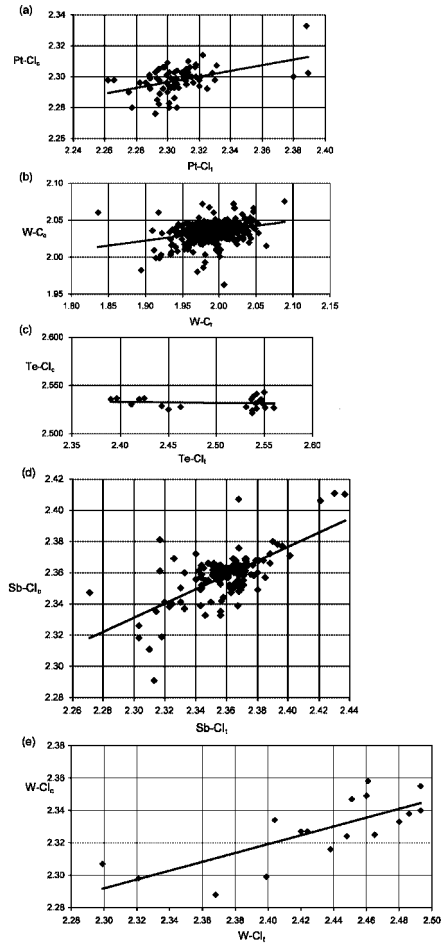

Fig. 1 Scatterplots of M–L_t *vs.* <M–L_c> bond lengths (Å) for (a) [$Pt^{II}Cl_3L$], (b) [$W^0(CO)_5L$], (c) [$Te^{IV}Cl_5L$], (d) [Sb^VCl_5L] and (e) [$W^{VI}Cl_5L$] complexes from the CSD.[11] Regression lines are shown (see Table 1).

zero and large *S* (*ca.* 7). In marked contrast, the $d^{10}s^0$ cases {[$Sn^{IV}Cl_5L$] and [Sb^VCl_5L], Fig.1 (d)} show higher values of *m* (*ca.* 0.45) and smaller ratio of variation in *trans* and *cis* distances (*S* = 1.2–1.4). Finally the d^0 case {[$W^{VI}Cl_5L$], Fig. 1(e)} shows intermediate behaviour with *m* = 0.27 and *S* = 2.8.

Thus in all cases there is some lengthening of *cis* bond lengths as the *trans* bond is lengthened (except for the $d^{10}s^2$ cases for which the *cis* bond lengths are essentially invariant). In none of these cases is there convincing evidence for *cis* bonds being *strengthened* (and shortened) as *trans* bonds are weakened, as some versions of *trans* influence theory would predict (see discussion in refs. 3 and 10). In their theory of *trans* influence[10] Burdett and Albright indicated that more than one effect may be at work (including competition between ligands for the same metal orbital and polarisation of metal–ligand bond orbitals by low-lying empty orbitals). While this is probably the case, on the basis of our observations we can advance a qualitative orbital model as to relative magnitudes of the *trans* and *cis* influences in d- and p-block metals for differing metal electron configurations. Large *cis* influence [*i.e.* type (ii) behaviour, as seen in the $d^{10}s^0$ cases] implies the importance of a non-directional (s) valence orbital at the metal regardless of which mechanism[10] of *trans* influence is at work. The participation of the s orbital requires that *trans* and *cis* ligands feel equally the (σ bonding) effects of perturbation of the M–L bond. Complete absence of *cis* influence [type (i) behaviour] implies there is no s (or d) orbital involvement with *trans* influence being transmitted through a p orbital which can not overlap with *cis* ligand σ donor orbitals. Intermediate cases may be taken to imply some d (or s) orbital involvement at the metal.

To first order we can then identify three patterns of orbital occupancy and the *cis* and *trans* influence behaviour that

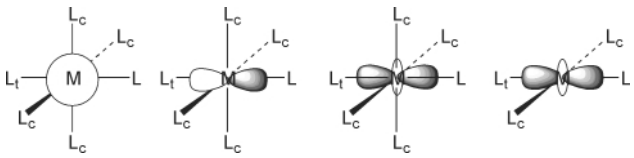

Scheme 2

follows: (a) if the M–L bond contains substantial M s orbital character, *cis* influence is relatively large [see (a) in Scheme 2] as in the $d^{10}s^0$ cases; (b) if the M–L bond has substantial M p orbital character but no s or d character [see Scheme 2(b)] as in the $d^{10}s^2$ cases, *trans* influence is high and *cis* influence is near zero and is shut down by virtue of the s and d orbitals being occupied; (c) if the M–L bond has substantial M d and relatively little M s orbital character [see Scheme 2 (c) and (d)] as in the d^8, d^6 and d^0 cases, then the *cis* influence is small compared to the *trans* influence but not zero, and their relative magnitudes may depend on electron configuration.

This model implicitly omits treatment of π effects which must be significant at least for the carbonyl species. A more complete model would also provide (semi-)quantitative estimates of the relative importance of p *vs.* s or d orbital contributions to the M–L bond or perhaps to the LUMO of the fragment to which L is bound. Development of such a model and its computational testing is in hand.

In summary, the classic *trans*-influence model based on Pt^{II} chemistry is to be used with some caution. While it works well for much of d-block chemistry, in some areas of the periodic table (notably the $d^{10}s^0$ chemistry of Sb^V, Sn^{IV} *etc.*) it does not hold well, and in others (d^0 chemistry) it applies but less powerfully than is often assumed.

We thank Jeremy Harvey for useful discussions and the University of Bristol for financial support (K. M. A.).

Notes and references

† Good quality data {$R < 0.07$ and < 0.05 for $[W^0(CO)_5L]$ species, no errors} were retrieved from the CSD using CCDC software.[12] Ligands L included both neutral and anionic species. Oxidation states and coordination geometries were checked and ambiguous cases eliminated. The mean M–L bond length *cis* to the L ligand (<M–L_c>), the M–L_t and M–L bond lengths were recorded for each appropriate fragment in the structures retrieved. Regression lines were computed with x = M–L_t, y = <M–L_c>. When L = L_c (= L_t), *e.g.* as in $[PtCl_4]^{2-}$, L and L_t were defined by taking the longest bond as M–L. The uncertainties in the individual bond lengths used in this work may be assumed to be on the order of 0.01 Å (see ref. 13).

1 C. E. Housecroft and A. G. Sharpe, *Inorganic Chemistry*, Pearson Educational, Harlow, 2001, p. 574.
2 N. N. Greenwood and A. Earnshaw, *Chemistry of the Elements*, Butterworth Heinemann, Oxford, 2nd edn., 1997, pp. 1164–1165.
3 B. J. Coe and S. J. Glenwright, *Coord. Chem. Rev.*, 2000, **203**, 5.
4 T. G. Appleton, H. C. Clark and L. E. Manzer, *Coord. Chem. Rev.*, 1973, **10**, 335; T. G. Appleton, J. R. Hall and S. F. Ralph, *Inorg. Chem.*, 1985, **24**, 4685; see, also: M. H. Johansson, Å. Oskarsson, K. Lövqvist, F. Kiriakidou and P. Kapoor, *Acta Crystallogr., Sect. C*, 2001, **57**, 1053 and references therein.
5 E. M. Shustorovich, M. A. Porai-Koshits and Yu. A. Buslaev, *Coord. Chem. Rev.*, 1975, **17**, 1.
6 J. T. Leman and A. R. Barron, *Organometallics*, 1989, **8**, 1828.
7 O. Knop, S. C. Choi and D. C. Hamilton, *Can. J. Chem.*, 1992, **70**, 2574.
8 M. Beuter, U. Kolb, A. Zickgraf, E. Brau, M. Bletz and M. Drager, *Polyhedron*, 1997, **16**, 4005.
9 K. A. Paseshnitchenko, L. A. Aslanov, A. V. Jatsenko and S. V. Medvedev, *J. Organomet. Chem.*, 1985, **287**, 187.
10 J. K. Burdett and T. A. Albright, *Inorg. Chem.*, 1979, **18**, 2112.
11 P. D. Lyne and D. M. P. Mingos, *J. Organomet. Chem.*, 1994, **478**, 141; P. D. Lyne and D. M. P. Mingos, *J. Chem. Soc., Dalton Trans.*, 1995, 1635; R. J. Deeth, *J. Chem. Soc., Dalton Trans.*, 1993, 3711; N. Kaltsoyannis and P. Mountford, *J. Chem. Soc., Dalton Trans.*, 1999, 781.
12 F. H. Allen and O. Kennard, *Chem. Des. Autom. News*, 1993, **8**, 1; F. H. Allen and O. Kennard, *Chem. Des. Atom. News*, 1993, **8**, 31.
13 A. G. Orpen and M. J. Quayle, *J. Chem. Soc., Dalton Trans.*, 2001, 1601.

CHEMCOMM
Communication
www.rsc.org/chemcomm

Parallel kinetic resolution of racemic amines using 3-*N*,*N*-diacylaminoquinazolin-4(3*H*)-ones

Abdullah G. Al-Sehemi, Robert S. Atkinson and Christopher K. Meades

Department of Chemistry, Leicester University, Leicester, UK LE1 7RH

Received (in Cambridge, UK) 11th October 2001, Accepted 9th November 2001
First published as an Advance Article on the web 4th December 2001

The two pseudoenantiotopic *N*-acyl groups of enantiopure 3-[*N*-(3-*m*-acetoxyphenylpropanoyl)-*N*-(3-phenylpropanoyl)amine]-2-isopropylquinazolin-4(3*H*)-one 7 each react with a different enantiomer of 2-methylpiperidine giving rise to efficient parallel kinetic resolution (ee > 95%).

In a normal kinetic resolution (KR) the enantiopure reagent reacts preferentially with one enantiomer of the racemic substrate. Under conditions of stoichiometry (2 eq. amine: 1 eq. reagent) this enantiopreference of the reagent must accommodate the diminishing concentration of the more reactive to the less reactive enantiomer as the reaction proceeds. Although high ees are possible under these conditions using enzymes[1] or chemzymes,[2] more often in practice the substrate is used in excess and only the derivatised enantiomer is isolated.

Vedejs has shown that different enantiomers of a racemic substrate can each be reacted at the same rate with pseudoenantiomeric reagents, designed to allow separation of the two derivatised products (parallel kinetic resolution, PKR).[3] The ees of both these derivatives (88% and 95%) are raised because the concentrations of both unreacted enantiomers decline at the same rate throughout the reaction.

We have shown previously that 3-*N*,*N*-diacylaminoquinazolinones (DAQs) *e.g.* **1** bearing a chiral centre and different *N*-acyl groups are separable into diastereoisomers because the N–N bond is a chiral axis.[4] DAQ[1] **1** (Scheme 1) was obtained by reaction of 3-*N*-benzoylamino-quinazolinone (MAQ[1]) **4** with 2-methylpropanoyl chloride–pyridine and the oily and crystalline diastereoisomers separated by chromatography.[5]

Both these enantiopure diastereoisomers of DAQ **1** react chemospecifically with 2-methylpiperidine to give the *N*-benzoylamide **3**; both also react enantioselectively with this amine even under conditions of stoichiometry (1 eq. DAQ: 2 eq. amine). Since the oily and crystalline diastereoisomers differ in configuration at their N–N axis and produce (*R*)-amide **3** (95% ee) and (*S*)-amide **3** (82% ee), respectively, it is the configuration of the N–N axis which controls the sense of enantioselectivity.

The corresponding DAQ[1] **5** was obtained completely diastereoselectively by reaction of MAQ[1] **4** with acetyl chloride–pyridine.† 2-Methylpiperidine reacts with DAQ[1] **5** at both the benzoyl and acetyl groups (ratio 2.5 : 1); from the high ee of the (*S*)-**3** amide and from the low specific rotation of the unreacted 2-methylpiperidine recovered, it appeared that the two amine enantiomers were each reacting preferentially with different *N*-acyl groups[6] *i.e.* the two *N*-acyl groups in DAQ[1] **5** were playing the rôle of the two pseudoenantiomeric reagents in a PKR (see above).[3]

To maximise the opportunity for PKR to be obtained in these amine acylations, we elected to use enantiopure DAQ[1] **7** which contains the N–N axis as the only chiral element. The isoenergetic transition states (TSs) in which each amine enantiomer reacts with its respective pseudoenantiotopic *N*–acyl group can be represented as in Scheme 2(a) and (b).

Although the sites occupied by S, M and L (small, medium, large) groups of the amine are arbitrarily assigned, Scheme 2 incorporates the expected *exo*/*endo*⇌*endo*/*exo* conformational equilibrium for the imide moiety of DAQ[1] **7**[4] and our conclusion is that attack of the amine takes place on the face of the *exo*-oriented imide carbonyl group *syn* to the quinazolinone carbonyl group (*exo*:*cis* to Q).[7] Clearly it is important for the success of the PKR that the ratio of these two imide conformations present is 1 : 1 and remains so throughout the reaction.

The synthesis of DAQ[1] **7** as a single enantiomer was accomplished as in Scheme 3.

DAQ[2] **6** is chemospecifically attacked by amines at the cinnamoyl carbonyl group.‡ After two kinetic resolutions using (*R*)-2-methylpiperidine (2 eq. DAQ: 1 eq. amine), the recovered DAQ[2] **6** had $[\alpha]_D$ 102 (c = 1, CH_2Cl_2) and showed a single peak on a Chiralcel column under conditions where racemic material showed two peaks. Catalytic hydrogenation gave a sample of DAQ **7** of unknown configuration $[\alpha]_D$ 1 (c = 1.0) but believed to be enantiopure.

Reaction of DAQ[2] **7** (1 eq.) with racemic 2-methylpiperidine (1 eq.) was carried out at 5 °C for 48 h. Separation of the crude amide **8** and MAQ[2] **9** which both contain the phenyl ring from their *m*-acetoxyphenyl ring-containing analogues **10** and **11** (Scheme 4) was accomplished by chromatography.

Efficient separation of the amides **8** and **10** from each of their respective MAQ[2]s was then accomplished by trituration with

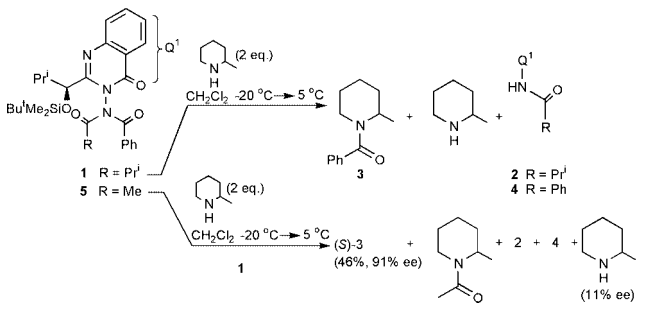

Scheme 1

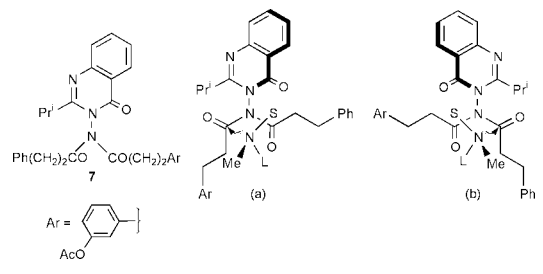

Scheme 2

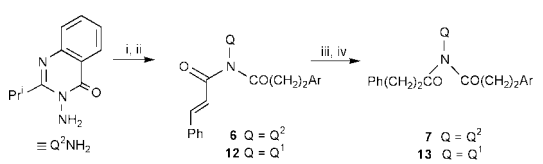

Scheme 3 *Reagents and conditions*: i, PhCH=CHCOCl, pyr. (81%); ii, *m*-acetoxyphenylpropanoylchloride, CH_2Cl_2, pyr. DMF (40%); iii, **6** (2 eq.), (*R*)-2-methylpiperidine (1 eq.), −15 °C, 24 h (KR); repeat; iv, Pd/C, H_2, EtOAc (90%).

 DOI: 10.1039/b109297a

light petroleum taking advantage of the insolubility of the crystalline MAQ[2]s **9** and **11**. The enantiopurities of amides **8** and **10** recovered by this means were indishinguishable, based on their optical rotations, from authentic samples prepared from enantiopure (*R*)- and (*S*)-2-methylpiperidine respectively and their ees are therefore >95%.

The importance of maintaining strict pseudoenantiotopicity for the two DAQ *N*-acyl groups for PKR was shown using DAQ[1] **13**, prepared by a route analogous to that in Scheme 3 except that the two diastereoisomers of DAQ[1] **12** were separated by chromatography and one of them was hydrogenated to DAQ[1] **13** (Scheme 3).

Reaction of DAQ[1] **13** (1 eq.) with racemic 2-methylpiperidine (1 eq.) proceeded at significantly different rates on the two *N*-acyl groups. After 36 h at 5 °C, the reaction was worked up and after chromatography, amide **10** was obtained in 60% yield§ with a rotation again indistinguishable from a sample prepared by acylation of enantiopure (*S*)-2-methylpiperidine with the appropriate acid chloride. Less than 10% of (impure) amide **8** was isolated in this chromatography.

Not only are the two *N*-acyl groups of DAQ[1] **13** pseudodiastereotopic but the *exo*/*endo*⇌*endo*/*exo* ratio can no longer be assumed to be 1:1 and both these factors lead presumably cooperatively to KR rather than PKR. The dual enantiocomplementarity present in these reactions—the preference for reaction of each of the amine enantiomers with their respective pseudoenantiotopic *N*-acyl group—will carry over to the reactions of enantiopure DAQs in which the *N*-acyl groups are pseudodiastereotopic (as in DAQ[1] **13**) or heterotopic (as in DAQ[1] **5**) and greatly affect the chemoselectivity of attack on the two *N*-acyl groups.¶

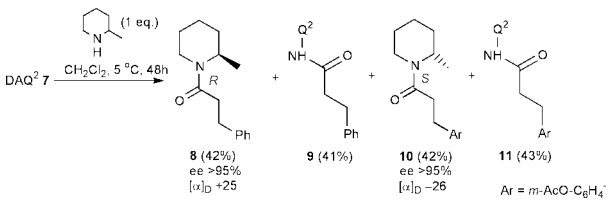

Scheme 4

The advantage of reagents such as DAQ **7** for PKR is that their design will be easier than that of pseudoenantiomeric reagents for which identity of reaction rates must be arrived at by empirical means.

We thank the EPSRC and the Ministry of Education (Saudi Arabia) for funding.

Notes and references

† The relative configuration of DAQ[1] **5** corresponds to that of the crystalline diastereoisomer of DAQ[1] **1** from comparison of their X-ray crystal structures (see ref. 6).

‡ From its relatively easy racemisation, DAQ[2] **6** is believed to have an *exo*/*exo* conformation for its imide as for DAQ[1]s **1** and **5** (see ref. 6).

§ Yield based on only 50% of the amine used reacting and on unreacted DAQ[2] **13** (28%) recovered.

¶ Not surprisingly, similar results to those using DAQ[1] **13** are obtained with the analogous DAQ[1] having both *N*-acyl groups as 3-phenylpropanoyl (for which separation of diastereoisomers is not required). The crude amide recovered in this case was of 60% ee; attack on the two diastereotopic *N*-acyl groups in this case delivers enantiomeric products.

1 C. H. Wang and G. M. Whitesides, *Enzymes in Synthetic Organic Chemistry*, Pergamon Press, Oxford, 1994.
2 For references to non-enzymic enantioselective acylation of alcohols, see A. C. Spivey, T. Fekner and S. E. Spey, *J. Org. Chem.*, 2000, **65**, 3154 and refs. therein.
3 C. Vedejs and X. Chen, *J. Am. Chem. Soc.*, 1997, **119**, 2584.
4 A. G. Al-Sehemi, R. S. Atkinson, J. Fawcett and D. R. Russell, *J. Chem. Soc., Perkin Trans. 1*, 2000, 4413.
5 A. G. Al-Sehemi, R. S. Atkinson, J. Fawcett and D. R. Russell, *Tetrahedron Lett.*, 2000, **41**, 2239.
6 A. G. Al-Sehemi, R. S. Atkinson and J. Fawcett, *J. Chem. Soc., Perkin Trans. 1*, submitted for publication.
7 R. S. Atkinson, E. Barker and M. J. Sutcliffe, *Chem. Commun.*, 1996, 1051; A. G. Al-Sehemi and R. S. Atkinson, unpublished results.

CHEMCOMM
Communication
www.rsc.org/chemcomm

Oxo-deficient dioxylene complexes of Mo(VI) containing 3,6-di-*tert*-butylcatechol

Cai-Ming Liu,†[a] Per Restorp,[a] Ebbe Nordlander*[a] and Cortlandt G. Pierpont*[b]

[a] *Inorganic Chemistry 1, Center for Chemistry and Chemical Engineering, Lund University, P.O. Box 124, Lund SE-221 00, Sweden. E-mail: Ebbe.Nordlander@inorg.lu.se*

[b] *Department of Chemistry and Biochemistry, University of Colorado, Boulder, Colorado, USA. E-mail: Pierpont@Colorado.edu*

Received (in Purdue, IN, USA) 10th September 2001, Accepted 6th November 2001
First published as an Advance Article on the web 4th December 2001

Strong σ and π donation from the oxygen atoms of 3,6-di-*tert*-butylcatechol contributes to the formation of an oxomolybdenum(VI) complex with an unusually basic oxo ligand.

Metal-catalyzed oxidation reactions that formally involve transfer of an oxygen atom occur as important industrial and biological processes. Molybdenum is the metal at the active site of the oxotransferase enzymes,[1] and it has been used in the commercial production of propylene oxide by the Halcon or Oxirane processes.[2] Both processes are thought to involve oxo transfer from an oxomolybdenum(VI) center, and coligand bonding effects are important in destabilizing strongly bound terminal oxo ligands. The *cis*-dioxomolybdenum(VI) structural unit is one of the earliest and most common features of molybdenum(VI) coordination chemistry. Complexes of Mo(VI) that contain a single oxo, or are without oxo ligands, are unusual and are considered to be oxo deficient. Coligands that are strong **σ** and π donors give oxo-deficient complexes, and ligands of this type appear coordinated to the catalytic molybdenum centers. For the oxotransferase enzymes this is an enedithiolate ligand.[1] The Mo(VI) ions associated with commercial oxidation reactions are thought to contain alkoxo ligands, and transfer of an alkyl hydroperoxide proton to the basic metal oxo ligand initiates oxygen transfer to the olefin substrate.[2]

The coordination chemistry of Mo(VI) with catecholate ligands has shown an interesting dependence upon ligand substituents. The tetrachlorocatecholate (Cl_4cat) ligand reacts with $Mo(CO)_6$ to give dimeric $[Mo^{VI}(Cl_4cat)_3]_2$.[3] Reduction of the dimer in the presence of an oxygen atom donor leads to the $[cis\text{-}Mo^{VI}O_2(Cl_4cat)_2]^{2-}$ dianion. Several other $[cis\text{-}Mo^{VI}O_2(cat)_2]^{2-}$ dianions have been reported with unsubstituted and tethered catecholate ligands.[4] However, the coordination chemistry of molybdenum complexes prepared with catecholate ligands containing electron-releasing *tert*-butyl substituents appears to favor formation of oxo-deficient molybdenum(VI) species. The reaction between 3,5-di-*tert*-butyl-1,2-benzoquinone (3,5-dbbq) and $Mo(CO)_6$ has been observed to form $[Mo(3,5\text{-dbcat})_3]$ as the initial product.[5] Further reaction with trace quantities of dioxygen led to the air-stable $[MoO(3,5\text{-dbcat})_2]_2$ dimer.[6] Structural characterization on the dimer showed that adjacent metal centers were linked by bridging catecholate oxygens (**I**).

Recent work with 3,6-dbbq has shown that *tert*-butyl groups at ring sites adjacent to both oxygen atoms block bridging of the type found for $[MoO(3,5\text{-dbcat})_2]_2$.[7] The reaction between $Mo(CO)_6$ and 3,6-dbbq has been used to form the oxomolybdenum(VI) product $[MoO(3,6\text{-dbcat})_2]$ in dilute solution. Condensation of $[MoO(3,6\text{-dbcat})_2]$ monomers in concentrated solution leads to formation of the chiral tetramer $[Mo(\mu\text{-}O)(3,6\text{-dbcat})_2]_4$‡ shown in Fig. 1. Each Mo center of the square is of the same chirality, ΛΛΛΛ or ΔΔΔΔ, resulting

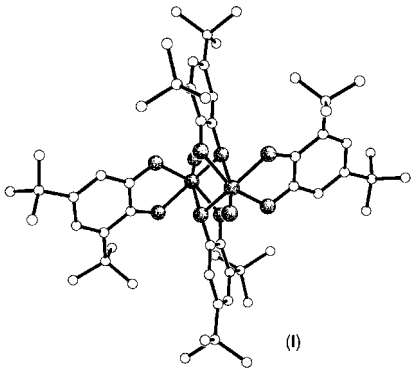

in right- and left-handed four-membered rings alternating in the crystal structure.§ In this respect, the tetramer stands as a unique example of chiral self-assembly.[4a,8] Along edges, the Mo–O lengths are short (1.8761(4) Å), but of values that are typical for bridging oxo ligands. Corner O–Mo–O bond angles of 93.5(2)° and edge Mo–O–Mo angles of 176.5(2)° show that the Mo_4O_4 core of the tetramer closely resembles a regular square.

Freshly prepared solutions of $[MoO(3,6\text{-dbcat})_2]$ react immediately at room temperature with weak donor ligands (*e.g.* dmso, pyridine *N*-oxide, $OAsPh_3$) to give monomeric $[MoO(3,6\text{-dbcat})_2(L)]$ products. Addition reactions to the tetramer occur more slowly or require elevated temperatures.

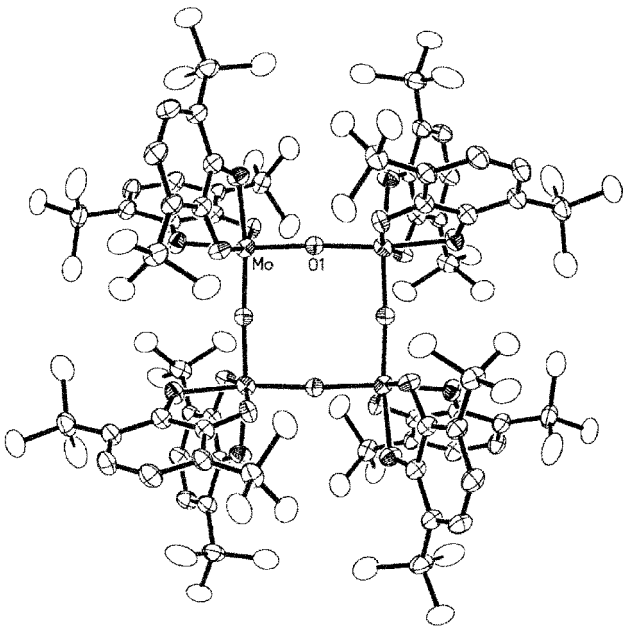

Fig. 1 View of the chiral square ΛΛΛΛ-$[Mo(\mu\text{-}O)(3,6\text{-dbcat})_2]_4$. Selected bond distances (Å) and angles (°) Mo–O^{Oxo} 1.8761(4) Å; Mo–O^{Cat} 1.929(3), 1.993 (3); C–O^{Cat} 1.347(5), 1.344(5); O^{oxo}–Mo–O^{Oxo} 93.5(2); Mo–O^{Oxo}–Mo 176.5(2).

† Present address: Organic Solids Laboratory, Center for Molecular Science, Institute of Chemistry, Chinese Academy of Sciences, Beijing 100080, P. R. China.

 DOI: 10.1039/b108220e

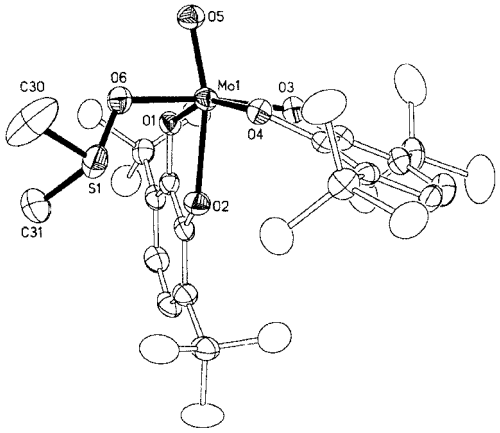

Fig. 2 View of *cis*-MoO(3,6-dbcat)$_2$(dmso). Selected bond distances (Å) and angles (°): Mo–O^{Oxo} 1.690(5); Mo–O^{DMSO} 2.092 (5); O^{Oxo}–Mo–O^{DMSO} 88.1(3).

DMSO has been added to [MoO(3,6-dbcat)$_2$] to give a complex that might potentially be relevant to the chemistry of DMSO reductase.[9] ^{1}H NMR spectra recorded on the product of DMSO addition (in $CDCl_3$) show sharp single resonances for ring and *tert*-butyl protons of the 3,6-dbcat ligands at 6.58 and 1.22 ppm and a resonance for the coordinated dmso ligand at 2.93 ppm.¶ Crystallographic characterization of [MoO(dmso)(3,6-dbcat)$_2$], shown in Fig. 2, has revealed that DMSO addition occurs at a site *cis* to the oxo ligand.§ Consequently, the room-temperature NMR spectrum results from rapid ligand site exchange. Spectra obtained at −98 °C are consistent with the low-symmetry structure found in the solid state. At this temperature four ring proton resonances appear (6.62, 6.59, 6.54 and 6.45 ppm), and *tert*-butyl resonances appear at 0.99, 0.83 ppm, with two overlapped resonances at 1.29 ppm. Proton resonances for the dmso ligand appear at 3.05 and 2.81 ppm showing that rotation about the dmso Mo–O bond is resolved. Room-temperature spectra recorded on solutions of [MoO(dmso)(3,6-dbcat)$_2$] containing additional DMSO show sharp separate resonances for free and complexed dmso molecules indicating that site exchange is either non-dissociative or dissociative by a process that is slow on the NMR time scale. Structural characterization on the pyridine *N*-oxide and triphenylarsine oxide addition products has also provided *cis* addition products pointing to a preference for *cis* coordination by these oxo-donor substrate molecules.[10]

The unusual basicity of the oxo ligand of [MoO(3,6-dbcat)$_2$] results in an apparent dehydration reaction upon treatment with alcohols. In toluene solutions containing isopropyl alcohol, the purple *cis*-diisopropoxide complex, [*cis*-Mo(3,6-dbcat)$_2$-(Pr^{i}O)$_2$],‖ is formed with elimination of water. This reaction normally would be expected to proceed in the reverse direction. Structural characterization of this product has shown that the inner coordination geometry of the Mo (Fig. 3) is similar to that of the tetramer.§ In this case the Mo–O length to the isopropoxide ligands is slightly shorter (1.848(1) Å) than lengths to the bridging oxo ligands. Catecholate substituent effects have been shown to be important in defining charge distribution within complexes containing redox-active metal ions.[11] For the complexes of molybdenum(VI), substituents are responsible for marked differences in the reactivity of co-ordinated oxo coligands.

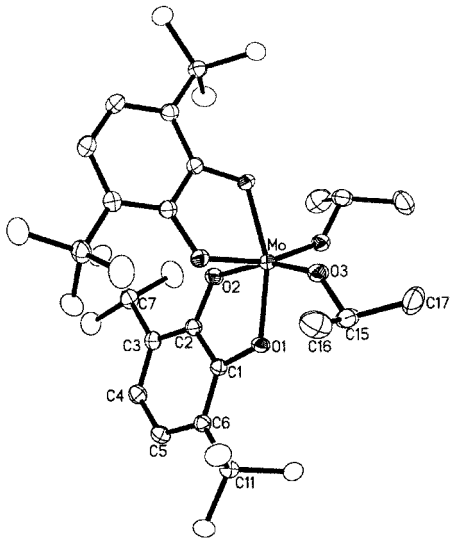

Fig. 3 View of *cis*-Mo(3,6-dbcat)$_2$(OPr^i)$_2$. Selected bond distances (Å): Mo–O^{Cat} 1.955(1), 1.968(1); Mo–O$^{O-Pr^i}$ 1.848(1).

Research at Lund University was supported by the Swedish Natural Science Research Council (NFR). Research at the University of Colorado was supported by the National Science Foundation. C. G. P. would like to thank The Swedish Foundation for International Cooperation in Research and Higher Education (STINT) for a research fellowship.

Notes and references

‡ [MoO(3,6-dbcat)$_2$]$_4$: ^{1}H NMR (300 MHz, C_6D_6, ppm): 6.493 (2, H$_{ring}$), 1.290 (9, H$_{Bu}$), 1.206 (9, H$_{Bu}$); UV–VIS (C_6H_6, λ_{max}/nm): 280 (ε = 16.6 × 10^3 M^{-1} cm^{-1}), 320 (14.3 × 10^3 M^{-1} cm^{-1}), 470 (sh), 625 (14.1 × 10^3 M^{-1} cm^{-1}); IR (KBr, cm^{-1}): 1728 (m), 1626 (w), 1581 (m), 1482 (w), 1461 (m), 1360 (m), 1338 (m), 1261 (s), 1200 (m), 1096 (s), 1024 (s), 990 (w), 948 (m), 802 (s), 757 (s); FAB$^+$-MS *m/z*: 2210 (M$^+$), 554 [MoO(3,6-dbcat)$_2$$^+$].

§ *Crystal data*: for [MoO(3,6-dbcat)$_2$]$_4$: tetragonal, *P*4/*nnc*, *a* = 22.568(2), *c* = 13.0099(12) Å, *V* = 6626.1(9) Å^3, *Z* = 16, *R*(*F*) = 0.058, $R_w(F^2)$ = 0.188. For MoO(3,6-dbcat)$_2$(dmso): triclinic, P$\bar{1}$, *a* = 12.2701(5), *b* = 16.7146(7), *c* = 18.4327(6) Å, α = 92.217(1), β = 90.072(1), γ = 93.114(1)°, *V* = 3771.9(3) Å^3, *Z* = 4, *R*(*F*) = 0.065, $R_w(F^2)$ = 0.188.

For Mo(3,6-dbcat)$_2$(OPr^i)$_2$: monoclinic, *C*2/*c*, *a* = 11.1595(2), *b* = 29.0306(6), *c* = 11.8944(2) Å, β = 116.703(1)°, *V* = 3442.4(1) Å^3, *Z* = 4, *R*(*F*) = 0.032, $R_w(F^2)$ = 0.087. CCDC reference numbers 173929–173931. See http://www.rsc.org/suppdata/cc/b1/b108220e/ for crystallographic data in CIF or other electronic format.

¶ MoO(3,6-dbcat)$_2$(dmso): ^{1}H NMR (300 MHz, $CDCl_3$, 18 °C, ppm): 6.58 (4, H$_{ring}$), 2.925 (6, H$_{DMSO}$), 1.215 (36, H$_{Bu}$); ^{1}H NMR (300 MHz, CD_2Cl_2, −98 °C, ppm): 6.62 (1, H$_{ring}$), 6.59 (1, H$_{ring}$), 6.54 (1, H$_{ring}$), 6.45 (1, H$_{ring}$), 3.05 (3, H$_{DMSO}$), 2.81 (3, H$_{DMSO}$), 1.29 (18, H$_{Bu}$), 0.99 (9, H$_{Bu}$),).83 (9, H$_{Bu}$); UV–VIS ($CHCl_3$, λ_{max}/nm): 275 (15.8 × 10^3 M^{-1} cm^{-1}), 456 (6.5 × 10^3), 625 (sh); IR (KBr, cm^{-1}): 1630 (m), 1575 (m), 1482 (m), 1467 (w), 1392 (m), 1358 (m), 1273 (w), 1241 (w), 1200 (s), 1179 (w), 1125 (m), 1028 (s), 984 (s), 952 (m), 925 (s), 812 (w), 802 (w), 716 (s); FAB$^+$-MS: *m/z* 632(M$^+$), 554 [MoO(3,6-dbcat)$_2$$^+$].

‖ Mo(3,6-dbcat)$_2$(OPr^i)$_2$: ^{1}H NMR (300 MHz, $CDCl_3$, ppm): 6.59 (2, H$_{ring}$), 5.733 (1, H$_{iPrO}$), 1.474 (9, H$_{Bu}$), 1.454 (9, H$_{Bu}$), 1.199 (6, H$_{iPrO}$). UV–VIS ($CHCl_3$, λ_{max}/nm): 273 (17.9 × 10^3 M^{-1} cm^{-1}), 443 (8.52 × 10^3), 616 (6.33 × 10^3); IR (KBr, cm^{-1}): 1591 (w), 1487 (m), 1441 (w), 1385 (s), 1357 (m), 1331 (w),1316 (m), 1287 (w), 1202 (w), 1165 (w), 1127 (w), 1109 (s), 1100 (s), 1031 (w), 977 (vs), 964 (vs), 856 (2), 814 (m), 807 (m), 705 (s); FAB$^+$-MS: *m/z* 656 (M$^+$), 554 [MoO(3,6-dbcat)$_2$$^+$].

1 R. S. Pilato and E. I. Steifel, in *Bioinorganic Catalysis*, ed. J. Reedijk and E. Bouwman, Marcel Dekker, Inc., New York, 1999, pp. 81–152.
2 R. A. Sheldon, in *Applied Homogeneous Catalysis with Organometallic Compounds*, ed. B. Cornils, and W. A. Hermann, VCH Publishers, Weinheim, 1996, pp. 411–424.
3 (*a*) C. G. Pierpont and H. H. Downs, *J. Am. Chem. Soc.*, 1975, **97**, 2123; (*b*) L. A. deLearie and C. G. Pierpont, *Inorg. Chem.*, 1988, **27**, 3842.
4 (*a*) A.-K. Duhme, S. C. Davies and D. L. Hughes, *Inorg. Chem.*, 1998, **37**, 5380; (*b*) A.-K. Duhme, Z. Dauter, R. C. Hider and S. Pohl, *Inorg. Chem.*, 1996, **35**, 3059; (*c*) W. P. Griffith, H. I. S. Nogueira, B. C. Parkin, R. N. Sheppard, A. J. P. White and D. J. Williams, *J. Chem. Soc., Dalton Trans.*, 1995, 1775; (*d*) V. V. Tkachev and L. O. Atovmyan, *Coord. Chem. (USSR)*, 1975, **1**, 845.
5 M. E. Cass and C. G. Pierpont, *Inorg. Chem.*, 1986, **25**, 122.
6 R. M. Buchanan and C. G. Pierpont, *Inorg. Chem.*, 1979, **18**, 1616.
7 C. W. Lange, B. J. Conklin and C. G. Pierpont, *Inorg. Chem,*, 1994, **33**, 1276.
8 (*a*) M. Ziegler, J. J. Miranda, U. N. Andersen, D. W. Johnson, J. A. Leary and K. N. Raymond, *Angew. Chem., Int. Ed.*, 2001, **40**, 733; (*b*) S. Leininger, B. Olenyuk and P. J. Stang, *Chem. Rev.*, 2000, **100**, 853.
9 B. S. Lim, J. P. Donahue and R. H. Holm, *Inorg. Chem.*, 2000, **39**, 263.
10 C.-M. Liu, P. Restorp, E. Nordlander and C. G. Pierpont, manuscript in preparation.
11 C. G. Pierpont, *Coord. Chem. Rev.*, 2001, **216–217**, 99.

CHEMCOMM Communication
www.rsc.org/chemcomm

Nickel-catalysed hydroarylation of alkynes using arylboron compounds: selective synthesis of multisubstituted arylalkenes and aryldienes

Eiji Shirakawa,* Go Takahashi, Teruhisa Tsuchimoto and Yusuke Kawakami

Graduate School of Materials Science, Japan Advanced Institute of Science and Technology, Asahidai, Tatsunokuchi, Ishikawa 923-1292, Japan. E-mail: shira@jaist.ac.jp

Received (in Cambridge, UK) 3rd September 2001, Accepted 8th November 2001
First published as an Advance Article on the web 5th December 2001

Bis(1,5-cyclooctadiene)nickel was found to be an effective catalyst for the addition of the aryl group of arylboron compounds to alkynes in the presence of a proton source, which gives various multisubstituted alkenylarenes or dienylarenes selectively.

Recently much attention has been paid to synthesis of arylalkenes using transition metal catalysts. The reported methods, however, have the following drawbacks. The Heck reaction, one of the most popular reactions leading to arylalkenes, is not so effective for synthesis of multisubstituted arylethenes because multisubstituted ethenes are usually reluctant to participate in the reaction.[1] The addition of a carbon–hydrogen bond of arenes to internal alkynes in the presence of a transition metal catalyst[2] or an acid catalyst,[3] which is an excellent route for multisubstituted arylethenes from the standpoint of atom economy, can be utilized only for rather electron-rich arenes, where the control of the regiochemistry on arenes, in particular monosubstituted benzenes, is difficult. The similar drawbacks hold true also for the transition metal-catalysed oxidative coupling of arenes with alkenes.[4] The nickel-catalysed reaction of arylmagnesium compounds with alkynes gives arylethenes only in low yields, being incompatible with labile functional groups.[5] Furthermore, there has been no convenient way to synthesize aryldienes from alkynes. Herein we report that a nickel complex catalyses the addition of the aryl group of arylboron compounds to alkynes in the presence of a proton source to give hydroarylation products of alkynes, where multisubstituted arylethenes or 1-aryl-1,3-butadienes can be selectively obtained by properly choosing an arylboron compound, a ligand and a proton source.[6]

We first examined the reaction of 2-phenyl-1,3,2-dioxaborinane (**1a**) with 4-octyne (**2a**) in the presence of 5 mol% of bis(1,5-cyclooctadiene)nickel, $Ni(cod)_2$, in dibutyl ether and found that a certain amount of a hydroarylation product of the alkyne, (*E*)-4-phenyl-4-octene (**3a**), was produced (Scheme 1). We considered that the generation of **3a** could occur as shown in Cycle A of Scheme 2. Thus, oxidative addition of the carbon–boron bond of **1a** to the nickel(0) complex followed by insertion of **2a** to the carbon–nickel bond of resulting complex **5** gives alkenylnickel **6**. A small amount of water in the reaction media reacts with complex **6** to afford, through σ-bond metathesis as shown in **7**, Ni–H complex **8**, which undergoes reductive elimination, providing hydroarylation product **3a** and regenerating the nickel(0) complex. Consequently, we expected that addition of a stoichiometric amount of water as a proton source would increase the yield of **3a**, accelerating the σ-bond metathesis. The reaction in the presence of 1 mol amount of water actually proceeded at 80 °C for 5 h to give a 80:20 mixture of **3a** and (4*Z*,6*E*)-4-phenyl-5,6-dipropyl-4,6-decadiene (**4a**) in 98% yield (entry 1 of Table 1).[7] Dimerization–hydroarylation product **4a** should be produced by insertion of another molecule of **4a** into the carbon–nickel bond of **6** to give complex **9**, followed by σ-bond metathesis and reductive elimination (Cycle B in Scheme 2). The reaction was applied to other arylboronates, giving 1:1 adducts as major products (Table 1). The reaction with *p*- or *m*-methoxyphenylboronate proceeded in a similar manner to **1a**, whereas the substitution at an *ortho* position lowered the yield (entries 2–4). An electron-withdrawing substituent decreased the selectivity for **3** over **4** (entry 5). Diphenylethyne also participated in the reaction with **1a** to give a 1:1 adduct exclusively.

Triphenylborane (**11**) as an arylboron compound in combination with triphenylphosphine ligand was also found effective, giving a 264% yield of addition products, where all of the phenyl groups on the boron atom were transferred to alkyne

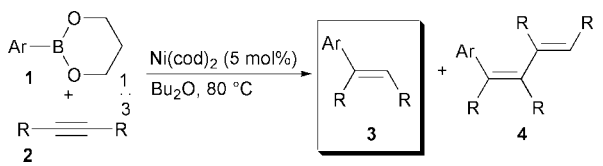

Scheme 1

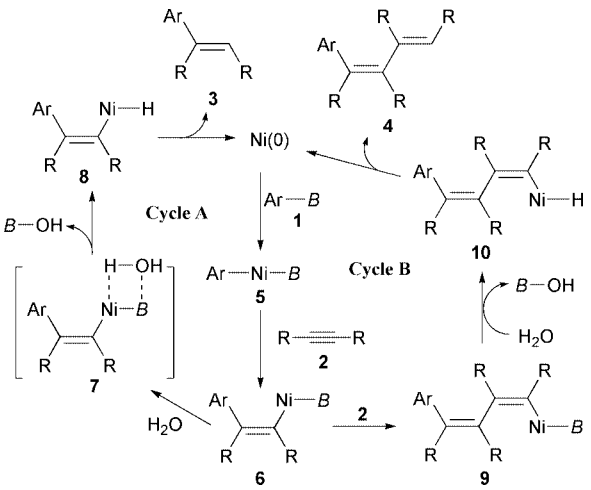

Scheme 2

Table 1 Nickel-catalysed hydroarylation of alkynes with 2-aryl-1,3,2-dioxaborinanes[a]

Entry	Ar	R	Time (h)	Yield (%)[b]	**3**:**4**
1	Ph	Pr	5	98[c]	80:20[c]
2	4-MeO-C_6H_4	Pr	5	70	79:21
3	3-MeO-C_6H_4	Pr	24	62	87:13
4	2-MeO-C_6H_4	Pr	24	31	85:15
5	4-CF_3-C_6H_4	Pr	5	54	54:46
6	Ph	Ph	24	44	>99:1

[a] The reaction was carried out in dibutyl ether (0.34 mL) at 80 °C using a 2-aryl-1,3,2-dioxaborinane (0.25 mmol), an alkyne (0.75 mmol), H_2O (0.25 mmol) and $Ni(cod)_2$ (1.3 μmol). [b] Isolated yield based on 2-aryl-1,3,2-dioxaborinane. [c] Determined by GC.

 DOI: 10.1039/b107866f

carbons (Scheme 3). Use of 1,1′-bis(diphenylphosphino)ferrocene (DPPF) as a ligand in conjunction with phenol as a proton source increased the selectivity of **3a**.

One of the most striking features in the nickel-catalysed hydroarylation of alkynes is the selective formation of 1:2 adducts between an aryl group and an alkyne, brought about by the introduction of arylboronic acids into the reaction. Thus, treatment of arylboronic acids and alkynes with H_2O in the presence of 10 mol% of $Ni(cod)_2$–PPh_3 (1:4) provided 1:2 adducts **4** selectively (Scheme 4). Various aryl- and heteroarylboronic acids can participate in the reaction to give aryl- and heteroaryldienes as major products (Table 2).[8] Phenylboronic

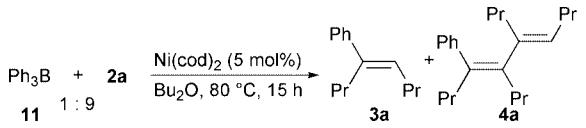

ligand	proton source	GC yield	**3a**:**4a**
PPh_3 (10 mol%)	H_2O (3.0 equiv)	264%	51:49
DPPF (5 mol%)	PhOH (3.0 equiv)	240%	91:9

Scheme 3

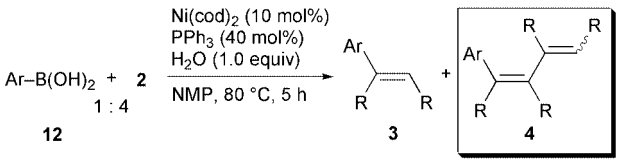

Scheme 4

Table 2 Nickel-catalysed reaction of alkynes with arylboronic acids[a]

Entry	Ar	R	Yield (%)[b]	**3**:**4**
1	Ph	Pr	77	<1:99
2	4-MeO-C_6H_4	Pr	78	8:92
3	2-naphthyl	Pr	73	16:84
4	3-NH_2-C_6H_4	Pr	61	13:87
5	3-thiophenyl	Pr	55	19:81
6[c]	Ph	Ph	72	58:42

[a] The reaction was carried out in NMP (0.34 mL) at 80 °C using an arylboronic acid (0.25 mmol), an alkyne (1.0 mmol), H_2O (0.25 mmol), $Ni(cod)_2$ (2.6 μmol), and PPh_3 (10 μmol). [b] Isolated yield based on arylboronic acid. [c] The reaction was carried out for 24 h.

acid reacted also with diphenylethyne, albeit the selectivity for **4** decreased. To the best of our knowledge, this is the first example of the transition metal-catalysed dimerization–hydroarylation of alkynes.

In conclusion, we have demonstrated that the nickel-catalysed hydroarylation of alkynes provides arylalkenes or aryldienes selectively. Studies on details of the mechanism as well as application of the reaction to other substrates are in progress.

Notes and references

1 (*a*) R. F. Heck, in *Comprehensive Organic Synthesis*, ed. B. M. Trost, I. Fleming and M. F. Semmelhack, Pergamon Press, New York, 1991, vol. 4, ch. 4.3, p. 833; (*b*) A. de Meijere and F. E. Meyer, *Angew. Chem., Int. Ed. Engl.*, 1994, **33**, 2379; (*c*) S. Bräse and A. de Meijere, in *Metal-Catalyzed Cross-Coupling Reactions*, ed. F. Diederich and P. J. Stang, Wiley-VCH, Weinheim, 1998, ch. 3, p. 99.

2 (*a*) C. Jia, D. Piao, J. Oyamada, W. Lu, T. Kitamura and Y. Fujiwara, *Science*, 2000, **287**, 1992; (*b*) C. Jia, W. Lu, J. Oyamada, T. Kitamura, K. Matsuda, M. Irie and Y. Fujiwara, *J. Am. Chem. Soc.*, 2000, **122**, 7252.

3 (*a*) G. Sartori, F. Bigi, A. Pastorio, C. Porta, A. Arienti, R. Maggi, N. Moretti and G. Gnappi, *Tetrahedron Lett.*, 1995, **36**, 9177; (*b*) T. Tsuchimoto, T. Maeda, E. Shirakawa and Y. Kawakami, *Chem. Commun.*, 2000, 1573.

4 (*a*) J. Tsuji and H. Nagashima, *Tetrahedron*, 1984, **40**, 2699; (*b*) C. Jia, W. Lu, T. Kitamura and Y. Fujiwara, *Org. Lett.*, 1999, **1**, 2097; (*c*) H. Weissman, X. Song and D. Milstein, *J. Am. Chem. Soc.*, 2001, **123**, 337.

5 J. G. Duboudin and B. Jousseaume, *J. Organomet. Chem.*, 1978, **162**, 209.

6 We have already reported that nickel complexes are effective catalysts for the addition of organostannanes to alkynes, 1,3-dienes and 1,2-dienes. (*a*) E. Shirakawa, K. Yamasaki, H. Yoshida and T. Hiyama, *J. Am. Chem. Soc.*, 1999, **121**, 10221; (*b*) E. Shirakawa, Y. Nakao, H. Yoshida and T. Hiyama, *J. Am. Chem. Soc.*, 2000, **122**, 9030; (*c*) E. Shirakawa, Y. Nakao and T. Hiyama, *Chem. Commun.*, 2001, 263; (*d*) E. Shirakawa, Y. Yamamoto, Y. Nakao, T. Tsuchimoto and T. Hiyama, *Chem. Commun.*, 2001, 1926.

7 We did not pursue the isolated yield of **3a** because the amount would be diminished during purification with silica gel chromatography. Only 82% of **3a** was recovered after the exposure of pure **3a** to a silica gel column.

8 All the dimerization–hydroarylation products **4** in Table 2 consist of stereoisomers. The ratio of stereoisomers ranges from 2:1 to >9:1. For example, the reaction of phenylboronic acid with **2a** (entry 1 of Table 2) gave a 70:30 mixture of (4*Z*,6*E*)-4-phenyl-5,6-dipropyl-4,6-decadiene (**4a**) and the (4*Z*,6*Z*)-isomer, where configuration of the isomers was determined by NOE in ^{1}H NMR.

CHEMCOMM
Communication
www.rsc.org/chemcomm

Resolving multiple ^{27}Al sites in $AlVO_4$ by ^{27}Al MAS NMR spectroscopy at 21.15 Tesla

Ulla Gro Nielsen, Jørgen Skibsted and Hans J. Jakobsen*

Instrument Centre for Solid-State NMR Spectroscopy, Department of Chemistry, University of Aarhus, Langelandsgade 140, DK-8000 Aarhus, Denmark. E-mail: ulla@chem.au.dk; jskib@chem.au.dk; hja@chem.au.dk

Received (in Cambridge, UK) 5th October 2001, Accepted 14th November 2001
First published as an Advance Article on the web 4th December 2001

A high-resolution 21.15 Tesla magnet (900 MHz for ^{1}H NMR) along with a home-built CP/MAS NMR probe is employed to succesfully resolve three different ^{27}Al resonances in $AlVO_4$, allowing a precise determination of their quadrupole coupling parameters and isotropic chemical shifts.

The recent technological advancement with the successful construction of a persistent high-resolution superconducting 21.15 T magnet at Oxford Instruments, UK will greatly assist solving one of the most challenging problems encountered in solid-state magic-angle spinning (MAS) NMR studies of half-integer quadrupolar nuclei. This originates from the second-order quadrupolar line-broadening which may give rise to severe overlap of heavily broadened resonances for the central transitions in case of multiple sites. Obviously, this can significantly hamper the characterization and assignment of the resonances for the individual sites. These difficulties may be overcome by performing MAS NMR experiments at the highest possible magnetic field (or at several magnetic field strengths), thereby taking advantage of the inverse proportionality of the second-order quadrupole interaction with the magnetic field and also of the increase in chemical shift dispersion.[1–7] Other techniques aiming at resolving overlapping resonances for half-integer quadrupolar nuclei include the methods of dynamic-angle spinning (DAS),[8,9] double rotation (DOR),[8,10] and multiple-quantum (MQ) MAS[11] NMR spectroscopy. In this communication we demonstrate that the intriguing problem of fully understanding and analyzing ^{27}Al MAS NMR spectra of $AlVO_4$, recorded at several intermediate magnetic field strengths, is most easily achieved from a ^{27}Al MAS NMR spectrum recorded at 21.15 T using a home-built 4 mm 900 MHz CP/MAS NMR probe.[12] This ^{27}Al MAS NMR spectrum represents one of the first solid-state NMR spectra recorded on the 21.15 T Oxford magnet.

^{27}Al MAS NMR spectra of the central transition for $AlVO_4$, a model compound for V_2O_5/Al_2O_3-based heterogeneous catalysts, obtained at the moderate magnetic field strengths of 7.05 and 9.39 T are illustrated in Fig. 1(a) and (b). Both spectra are dominated by a quite narrow peak (resonance position $\delta \approx -10$ ppm) superimposed on a broader resonance constituting two or more overlapping ^{27}Al quadrupolar lineshapes. Clearly a straightforward analysis of these spectra in terms of quadrupole coupling parameters (C_Q, η_Q) and isotropic chemical shifts (δ_{iso}) is not possible except for the narrow resonance ($\delta \approx -10$ ppm). Along with the manifold of spinning sidebands (ssbs) for the satellite transitions (not shown) of this resonance, the ^{27}Al spectrum for the narrow peak, *i.e.* the Al(1) site, can be fully analyzed. At 14.09 T the spectrum in Fig. 1(c) shows that one second-order quadrupolar broadened resonance separates out (in the region 5–30 ppm) from the other resonances, while the narrow peak at $\delta \approx -10$ ppm remains superimposed on a somewhat narrower second (*i.e.* number two) quadrupolar broadened resonance, however, almost fully hidden by maximum overlap with the narrow peak. ^{27}Al MAS NMR spectra recorded at 14.09 T have actually been used to determine precise values for C_Q, η_Q and δ_{iso} by analysis of the manifold of ssbs originating from the satellite transitions for the narrow

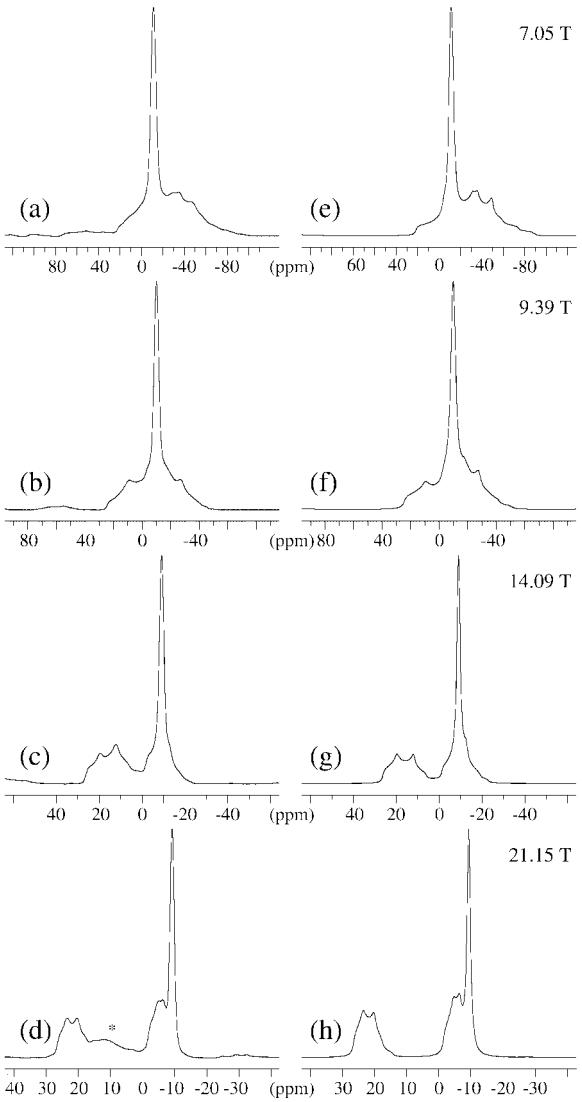

Fig. 1 Experimental ^{27}Al MAS NMR spectra of $AlVO_4$ recorded at (a) 7.05 T (78.1 MHz), (b) 9.39 T (104.2 MHz), (c) 14.09 T (156.3 MHz), and (d) 21.15 T (234.5 MHz) on Varian INOVA-300, -400, -600, and -900 NMR spectrometers, respectively, using home-built 4- and 5-mm CP/MAS NMR probes. The asterisk (*) in spectrum (d) indicate a broad impurity resonance. All experiments employed single-pulse excitation (0.5 μs pulse width, $\gamma B_1/2\pi \approx 55$ kHz), spinning speeds in the range 12–15 kHz, and exact magic-angle setting. Simulated ^{27}Al MAS NMR spectra for $AlVO_4$ are shown on the right-hand side of the experimental spectra, *i.e.* for 7.05 T (e), 9.39 T (f), 14.09 T (g), and 21.15 T (h) using the ^{27}Al NMR parameters (Table 1) determined from the 21.15 and 14.09 T spectra (see text). All spectra are expanded to the same width on a Hz scale.

 DOI: 10.1039/b109042a

peak (Al(1) site) using the STARS program.[13] Furthermore, quite precise values have also been determined from lineshape analysis for the second-order quadrupolar lineshape (Al(3) site) shifted to the region δ 5–30 ppm in the 14.09 T spectrum of Fig. 1(c). We should note that the increased resolution and shift of resonances in Fig. 1(c) are related to the reduced effects of the second-order quadrupolar interaction combined with the increase in chemical shift dispersion. A further and dramatic increase in the spectral resolution is observed when recording the ^{27}Al MAS NMR spectrum at 21.15 T as illustrated in Fig. 1(d). At this magnetic field strength the two ^{27}Al resonances, Al(1) and Al(2), which overlap heavily in the region at $\delta \approx -10$ ppm in the 14.09 T spectrum of Fig. 1(c), become almost completely resolved. Furthermore, for the present sample the spectrum in Fig. 1(d) clearly discloses the presence of a broad ^{27}Al impurity resonance (indicated by an asterisk at $\delta \approx 10$ ppm) from an octahedral ^{27}Al impurity not easily discernible in the lower field spectra. The appearance of this Al impurity (most likely amorphous) came as somewhat of a surprise since no such impurity for the present sample could be detected by powder XRD. Anyway, the 21.15 T spectrum in Fig. 1(d) allows a straightforward lineshape analysis of the two second-order broadened resonances, Al(2) and Al(3), clearly resolved from the narrow Al(1) resonance and the impurity peak, respectively. The resulting C_Q, η_Q and δ_{iso} parameters for these two resonances, along with the Al(1) data derived from a 14.09 T spectrum of the satellite transitions, are considered the optimized parameters for the three Al sites observed for $AlVO_4$ and are summarized in Table 1. The data in Table 1 are used for simulations of the ^{27}Al MAS NMR spectra obtained at the four magnetic field strengths in Fig. 1 and are shown in the right-hand column next to the experimental spectra (Fig. 1(e)–(h)). Excellent agreements are observed between the experimental and simulated spectra for all magnetic field strengths. The minor intensity differences between parts of the experimental and simulated spectra at 7.05, 9.39, and 14.09 T can be ascribed to distortions caused by the broad impurity resonance at $\delta \approx 10$ ppm.

Considering the fact that the crystal structure of $AlVO_4$ is unknown, the present 21.15 T ^{27}Al MAS NMR results (Table 1) for $AlVO_4$ show the presence of two octahedral Al sites (Al(1) and Al(2)) with quite different quadrupole coupling parameters and one penta-coordinated Al site (Al(3)) in the asymmetric unit of its crystal structure.

In conclusion, ^{27}Al MAS NMR at 21.15 T successfully resolves three ^{27}Al sites in $AlVO_4$, allowing a straightforward analysis and characterization of these sites. As an additional benefit, an impurity, unknown to be present beforehand and slightly distorting the spectral intensities at lower magnetic fields, is also resolved at 21.15 T. MQMAS NMR[11] combined with high magnetic fields may be considered an alternative approach to achieve spectral separation of multiple ^{27}Al sites as recently demonstrated in the characterization of USY zeolites.[14] We should note that generally high spinning speeds may be required at 21.15 T because of the increase in chemical shift dispersion. To keep the first-order ssbs outside the ^{27}Al chemical shift range ($\approx$100 ppm) spinning speeds of about 23 kHz is needed, however, such speeds are easily obtained using small rotors. It is also of interest to point out that at the magnetic field of 21.15 T and employing a spinning speed of 50 kHz, recently achieved by Samoson *et al.*,[15] an undistorted ^{27}Al MAS NMR spectrum of the central transition for a single ^{27}Al site with C_Q as large as 26–30 MHz may be obtained (*i.e.* $C_Q(1+\eta_Q/6) \leqslant 30.2$ MHz).[7]

Table 1 ^{27}Al quadrupole coupling parameters (C_Q, η_Q) and isotropic chemical shifts (δ_{iso}) for $AlVO_4$

	C_Q[a]/MHz	η_Q[b]	δ_{iso}[c]/ppm
Al(1)	1.64 ± 0.10	0.30 ± 0.04	−8.9 ± 0.5
Al(2)	5.88 ± 0.10	0.58 ± 0.03	−1.1 ± 1.0
Al(3)	6.73 ± 0.10	0.42 ± 0.02	27.2 ± 0.6

[a] $C_Q = eQV_{zz}/h$. [b] $\eta_Q = (V_{yy} - V_{xx})/V_{zz}$ [c] Isotropic chemical shifts are relative to a 1 M solution of $AlCl_3$.

Claus J. H. Jacobsen, Haldor Topsøe A/S, Denmark kindly provided the $AlVO_4$ sample. Varian Inc. and Oxford Instruments are acknowledged for access to the 900 MHz NMR Facility at Oxford Instruments, Eynsham, UK. The use of the facilities at the Instrument Centre for Solid-State NMR Spectroscopy, University of Arhus, sponsored by the Danish Natural Science Research Council, the Danish Technical Science Research Council, Teknologistyrelsen, Carlsbergfondet, and Direktør Ib Henriksen Fond are acknowledged. J. S. thanks the Danish Natural Science Research Council for financial support (J. No. 0001237).

Notes and references

1 A. Nolle, *Z. Phys.*, 1977, **280**, 231.
2 D. Müller, W. Gessner, H.-J. Behrens and G. Scheler, *Chem. Phys. Lett.*, 1981, **79**, 59.
3 A. Samoson, E. Kundla and E. Lippmaa, *J. Magn. Reson.*, 1982, **49**, 350.
4 E. Oldfield, S. Schramm, M. D. Meadows, K. A. Smith, R. A. Kinsey and J. Ackerman, *J. Am. Chem. Soc.*, 1982, **104**, 919.
5 L. B. Alemany and G. W. Kirker, *J. Am. Chem. Soc.*, 1986, **108**, 6158.
6 B. F. Chmelka, K. T. Mueller, A. Pines, J. Stebbins, Y. Wu and J. W. Zwanziger, *Nature*, 1989, **339**, 42.
7 J. Skibsted, H. Bildsøe and H. J. Jakobsen, *J. Magn. Reson.*, 1991, **92**, 669.
8 A. Llor and J. Virlet, *Chem. Phys. Lett.*, 1988, **152**, 248.
9 K. T. Muller, B. Q. Sun, G. C. Chingas, J. W. Zwanziger, T. Terao and A. Pines, *J. Magn. Reson.*, 1990, **86**, 470.
10 A. Samoson, E. Lippmaa and A. Pines, *Mol. Phys.*, 1988, **65**, 1013.
11 L. Frydman and J. S. Harwood, *J. Am. Chem. Soc.*, 1995, **117**, 5367.
12 H. J. Jakobsen, P. Daugaard, E. Hald, D. Rice, E. Kupce and P. D. Ellis, *J. Magn. Reson.*, submitted.
13 J. Skibsted, N. C. Nielsen, H. Bildsøe and H. J. Jakobsen, *J. Magn. Reson.*, 1991, **95**, 88. STARS is available as a part of the Varian VNMR software.
14 C. A. Fyfe, J. L. Bretherton and L. Y. Lam, *Chem. Commun.*, 2000, 1575.
15 A. Samoson, T. Turhem and Z. Gan, *Solid State Nucl. Magn. Reson.*, 2001, in press, (doi: 10.1006/ssnmr.2001.0037); A. Samoson, *NATO ARW, Magnetic Resonance in Colloid and Interface Science*, St. Petersburg, Russia, June 2001.

CHEMCOMM Communication
www.rsc.org/chemcomm

Chiral recognition by single bilayered phosphatidylcholine vesicles using [5]thiaheterohelicene as a probe

Hiroko Nakagawa, Yuuki Kobori, Maiko Yoshida and Koh-ichi Yamada*

Faculty of Pharmaceutical Sciences, Josai University, Keyakidai, Sakado, Saitama 350-0295, Japan. E-mail: kyama@josai.ac.jp; Fax: +81 49 271 7714; Tel: +81 49 271 7686

Received (in Cambridge, UK) 10th October 2001, Accepted 8th November 2001
First published as an Advance Article on the web 4th December 2001

Incorporated into chiral phosphatidylcholine (PC) vesicles, [5]thiaheterohelicene with a labile helix that functioned as a probe, developed induced CD absorptions which manifested alterations in Cotton effects and intensities by chirality of PC applied, temperature variations, and coexistence of cholesterol or its 5α-epimer.

Phosphatidylcholine (PC) molecules[1] possess a chiral center at the position of the sn-2 carbon of the glycerol backbone. An ethanol solution of monomeric D-DPPC (*R* configuration) shows a positive Cotton effect around 220 nm, whereas an aqueous solution of aggregated D-DPPC demonstrates the opposite Cotton effect around 225 nm due to the formation of vesicles.[2] Achiral 1,6-diphenylhexa-1,3,5-triene (DPH) embedded in the D-DPPC vesicles, induces chirality to develop weak CD absorptions, due to anisotropic circumstances.[2] This induced CD, however, disappears above 40 °C and the conformation of DPH is not disclosed. This paper describes chiral recognition of single bilayered PC vesicles using 2-hydroxymethylthieno[3,2-*e*:4,5-*e*′]di[1]benzothiophene (5HM) as a probe. Although 5HM has a helical shape arising

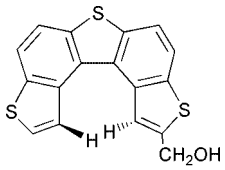

P-5HM

from steric repulsion between the terminal hydrogen atoms in the molecule,[3] the helix of 5HM readily undergoes inversion in a solution because of the weakness of the repulsion, causing a rapid racemizarion. However, in chiral environments such as micelles,[4] crystal fields[5] and several species of serum albumin,[6] 5HM develops induced CD because of a shift in the equilibrium between right-handed (P) and left-handed (M) enantiomers, either of which can easily be determined by the sign of the Cotton effect of the CD absorptions. Furthermore, the induced CD of 5HM is fairly intense and appears in the longer wavelength region, characteristic of its widely conjugated aromatic chromophore.

Incorporation of water-insoluble 5HM into the PC vesicles[7] yielded transparent solutions which manifested intense CD absorptions. Fig. 1 shows the CD spectra of 5HM embedded in the D-DPPC (Fig. 1c) and L-DPPC (Fig. 1f) vesicles together with the spectra of an ethanol solution of monomeric D-DPPC (Fig. 1a) and an aqueous solution of aggregated D-DPPC (Fig. 1b). Characteristic bands of 5HM in the vesicles were observed in the range of 250–380 nm. The Cotton effects of these bands were opposite for the L- and D-DPPC vesicles, presumably because of the influence of the reversed twisting of the bilayers on each other. This fact implies that for both vesicles the equilibrium of 5HM was displaced between the P and M enantiomers in the opposite directions to each other. Comparison of Fig. 1c and f with the CD spectra of 5HM in BSA and chiral micelles clearly indicates that racemic 5HM was converted into a P e.e. in the D-DPPC vesicles and into an M e.e. in the L-DPPC vesicles. From the value of the apparent molecular ellipticity, the extent of the P e.e. in the D-DPPC vesicles was estimated to be approximately 6%. Furthermore, an ethanol solution of D-DPPC containing the same concentrations of 5HM demonstrated no induced CD absorptions.

With a rise in temperature, the UV spectra of 5HM in the L-DPPC vesicles displayed obvious hypsochromic shifts at the absorption maximum near 350 nm with the isosbestic points at 286.2 and 302.8 nm (Fig. 2a). This phenomenon can be explained by the assumption that the elevation of temperature brought about an increase in the fluidity of the vesicles along with an increase in the mobility of the 5HM molecules. The plots of the absorbance of that peak against temperature showed the maximum around 40 °C (Fig. 3a), corresponding to the main phase transition temperature (*T*c) of 41.5 °C, as determined by the DSC method.[8] This trend in the temperature dependence of the absorbance was found for other PCs (DMPC, DSPC and DOPC), and this method is thought to be useful for predicting the *T*c of vesicles.[9] On the other hand, the intensities of the induced CD decreased rapidly with a rise in temperature (Fig. 2b). This decrease may be attributed to the increasing fluidity of the vesicles, which reduced the fixation of the mobile helixes (P and M) of the 5HM molecules. In contrast to the case of DPH, it is intriguing that the induced CD of 5HM did not disappear over 40 °C, but merely weakened. The plots of temperature dependence of the CD intensities demonstrated a discontinuous

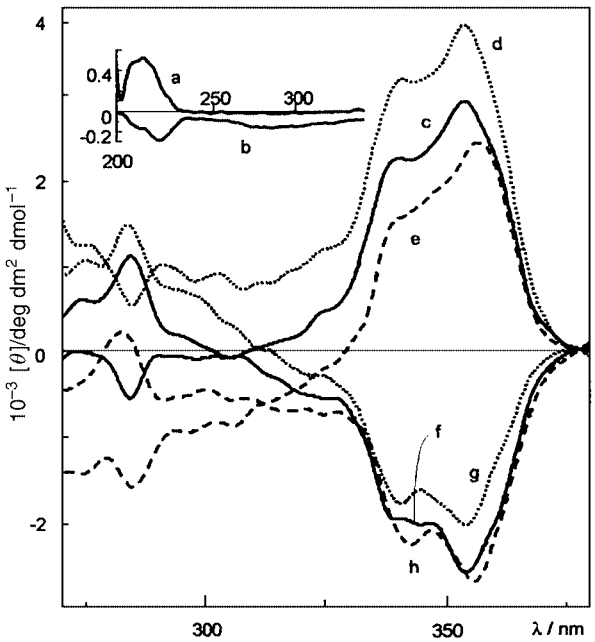

Fig. 1 CD spectra of D-DPPC: (a) in ethanol and (b) in water, CD spectra of 5HM in D-DPPC vesicles: (c) no additives, (d) with Cho and (e) Epi, and CD spectra of 5HM in L-DPPC vesicles: (f) no additives, (g) with Cho and (h) Epi. [D- or L-DPPC] = 5×10^{-4} M, [5HM] = 9×10^{-5} M, [Cho] = [Epi] = 4×10^{-5} M.

 DOI: 10.1039/b109062c

line with two flection points (Fig. 3b). The higher point on the line was at approximately 40 °C which was coincident with the value of the *T*c obtained from the maximum of the absorbance plots. The meaning of the lower point is entirely obscure, but it might be correlated to the pretransition of the bilayered phase. In any event, it is evident that the 5HM in the chiral vesicles provides information on not only chiral recognition, but also on the phase transition of the vesicles.

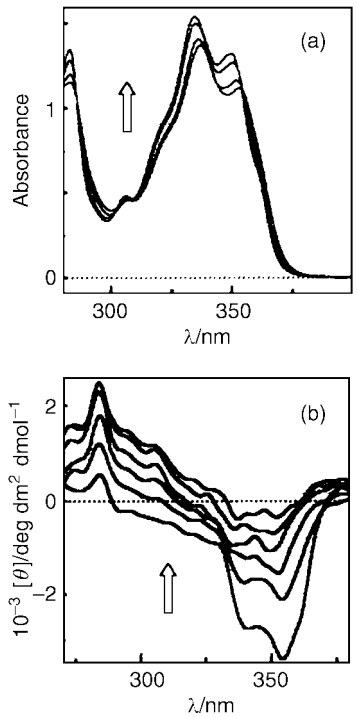

Fig. 2 Temperature dependence of 5HM in L-DPPC vesicles at 5 to 70 °C: (a) UV spectra and (b) CD spectra. [D- or L-DPPC] = 5×10^{-4} M and [5HM] = 9×10^{-5} M.

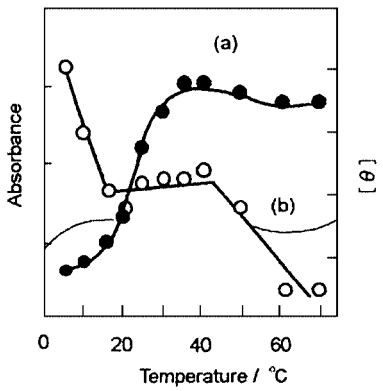

Fig. 3 Plots of temperature dependence of 5HM in L-DPPC vesicles: (a) absorbance at the peak around 350 nm (left axis) and (b) molecular ellipticity ($[\theta]_{284} - [\theta]_{354}$) (right axis).

Next, we examined the effect of the coexistence of cholesterol (Cho) and its epimeric isomer, 5α-epicholesterol (Epi), on the chiral recognition of the DPPC vesicles. Fig. 1c–h exhibits the induced CD spectra of 5HM in the L- and D-DPPC vesicles containing Cho or Epi with 0.44 times concentration of 5HM at 10 °C. In the D-DPPC vesicles, the absorptional intensity around 350 nm increased with the addition of Cho, while the addition of Epi reduced its intensity in comparison to the case with no additives. In marked contrast, the situation was the inverse of the L-DPPC vesicles: Cho reduced the intensity, while Epi slightly enhanced it. These effects suggest that the configuration of the hydroxy groups of Cho and Epi played an important role in the chiral recognition of the DPPC vesicles. Regarding the Cho molecules in the L-PC vesicles, it has been reported that the hydroxy groups exist in the vicinity of the ester carbonyl groups of the PC molecules without hydrogen bonds with the surroundings, and the hydrophobic portions are juxtaposed to the alkyl chains of the PC molecules.[10] Thus, Cho perturbs the orientation of the PC molecules in the gel phase under a temperature of *T*c. These facts may lead to the explanation that the presence of Cho brought about the reduction of the CD intensity in the L-DPPC vesicles because of the decrease in fixation of the 5HM helixes. On the other hand, Epi only slightly affected the increase in the CD intensity. In D-DPPC vesicles, the situations for Cho and Epi seem to be chiroptically opposite to the case in L-DPPC vesicles. These observations imply that the inverse functions of Cho and Epi in the vesicles were revealed by the application of 5HM from the standpoint of chiroptical properties.

Notes and references

1 The following abbreviations are used for phospholipids: DMPC, dimyristoyl phosphatidylcholine; DPPC, dipalmitoyl phosphatidylcholine; DSPC, distealoyl phosphatidylcholine; DOPC, dioleoyl phosphatidylcholine.

2 P. Walde, E. Blöchliger and K. Morigaki, *Langmuir*, 1999, **15**, 2346; P. Walde and E. Blöchliger, *Langmuir*, 1997, **13**, 1668.

3 H. Nakagawa, K. Yamada, H. Kawazura and H. Miyamae, *Acta Crystallogr.*, 1984, **C40**, 1039.

4 K. Yamada, Y. Kobori and H. Nakagawa, *Chem. Commun.*, 2000, 97; H. Nakagawa, K. Gomi and K. Yamada, *Enantiomer*, 1998, **3**, 175.

5 H. Nakagawa, K. Yamada and H. Kawazura, *J. Chem. Soc., Chem. Commun.*, 1989, 1378.

6 K. Yamada, R. Ishii, H. Nakagawa and H. Kawazura, *J. Chem. Soc., Chem. Commun.*, 1994, 1521; K. Yamada, R. Ishii, H. Nakagawa and H. Kawazura, *Chem. Pharm. Bull.*, 1997, **45**(5), 936; K. Yamada, R. Ishii, H. Nakagawa and H. Kawazura, *Tetrahedron: Asymmetry*, 1996, **7**(3), 737.

7 All the PC single bilayered vesicles were prepared by injection methods. S. Batzri and E. D. Korn, *Biochem. Biophys. Acta*, 1973, **298**, 1015; J. M. H. Kremer, M. W. J. v. d. Esker, C. Pathmamanoharan and P. H. Wiersema, *Biochemistry*, 1977, **16**(17), 3932.

8 A. Blume, *Biochemistry*, 1983, **22**, 5436.

9 M. P. Veiga, J. L. R. Arrondo, F. M. Goñi, A. Alonso and D. Marsh, *Biochemistry*, 2001, **40**, 2614.

10 D. L. Worcester and N. P. Franks, *J. Mol. Biol.*, 1976, **100**, 359; S. F. Bush, R. G. Adams and I. W. Levin, *Biochemistry*, 1980, **19**, 4429; M. Cortijo, A. Alonso, J. C. Gomez-Fernandez and D. Chapman, *J. Mol. Biol.*, 1982, **157**, 597.

CHEMCOMM Communication
www.rsc.org/chemcomm

Determination of the absolute configurations of α-amino esters from the ^{19}F NMR chemical shifts of their CFTA amide diastereomers

Tomoya Fujiwara,[a] Kenji Omata,[a] Kuninobu Kabuto,*[a] Chizuko Kabuto,[a] Tamiko Takahashi,[b] Masaru Segawa[b] and Yoshio Takeuchi*[b]

[a] *Department of Chemistry, Graduate School of Science, Tohoku University, Aoba-ku, Aramaki, Sendai 980-8578, Japan. E-mail: kabuto@funorg.chem.tohoku.ac.jp*
[b] *Faculty of Pharmaceutical Sciences, Toyama Medical & Pharmaceutical University, Sugitani 2630, Toyama 930-0194, Japan*

Received (in Cambridge, UK) 28th September 2001, Accepted 30th October 2001
First published as an Advance Article on the web 26th November 2001

The CFTA method has proved to be useful for assigning absolute configuration of α-amino esters by ^{19}F NMR.

One of the most convenient and reliable methods for determination of both absolute configuration and enantiomeric excess (ee) of chiral molecules is ^{1}H NMR analyses of the diastereomers formed by reaction of these molecules with chiral derivatizing agents (CDAs).[1] Among various CDAs developed so far, fluorine-containing CDAs have the advantage of allowing ^{19}F NMR to be used as an additional analytical tool.[2] The greater chemical shift differences of ^{19}F signals compared to ^{1}H signals and the simplicity of ^{19}F NMR spectra add greatly to the value of this approach.[3] However, there have been no reliable methods reported for assigning absolute configuration by ^{19}F NMR that are based on a theoretical and predictable explanation of the source of chemical shift differences.[4]

We previously reported the synthesis of α-cyano-α-fluoro-*p*-tolylacetic acid (CFTA). This reagent proved to be an excellent CDA for determination of ee by ^{19}F NMR[5] and for determination of absolute configuration by ^{1}H NMR.[6] As part of our continuing study of the CFTA agent we now report a consistent relationship between the ^{19}F NMR chemical shifts (δ_F) of diastereomeric CFTA amides of α-amino esters and their absolute configurations. Molecular orbital calculations were used to estimate the conformational equilibria of the similar α-cyano-α-fluorophenylacetic acid (CFPA)[3] amides and these equilibria were used to develop a correlation model based on the chemical shift nonequivalence in the ^{1}H NMR of CFTA amides.

We examined a series of CFTA amides of common α-amino esters (**1**–**13**) to obtain the chemical shift differences ($\Delta\delta_F$) between the diastereomers. The ^{19}F NMR spectrum of the CFTA amide of Gly-OMe (**14**) was used as reference (Table 1).[7] The fluorine signals of (*R*,*S*)-isomers (δ_{RS}) always resonated at 2 to 6 ppm higher field compared to those of the corresponding (*S*,*S*) isomers (δ_{SS}), thus giving consistently minus $\Delta\delta_F$ values. For comparison, $\Delta\delta_F$ values for MTPA[8] amides of the same α-amino esters were also examined. These also gave consistently minus $\Delta\delta_F$ signs, although the magnitudes were considerably smaller than those observed for CFTA amides.

The large $\Delta\delta_F$ values and the consistent relationship between the signs and absolute configurations for diastereomeric CFTA amides combine to make the CFTA amide method very reliable for assigning absolute configuration of α-amino esters using ^{19}F NMR.

The $\Delta\delta_F$ values for diastereomeric CFTA amides can be attributed to different biases in the conformational equilibria between the *ap* and the *sp* conformers shown in Fig. 1, as was previously discussed for the CFTA esters.[6] In the former, the F–C_α bond is *anti-periplanar* (*ap*) to the C = O bond, while in the latter, this bond is *syn-periplanar* (*sp*), respectively. The presence of these two conformers in each CFTA amide diastereomer was supported by molecular orbital calculations on the ground state geometry and energies using the quite similar molecules (*R*,*S*)-**15** and (*S*,*S*)-**15**, *i.e.*, two diastereomeric CFPA amides of Val-OMe.[9] The calculations predicted the preference of the *ap* conformer over the *sp* conformer in accord with the conformation deduced from the sense of

Table 1 ^{19}F chemical shifts of diastereomeric CFTA and MTPA amides[a]

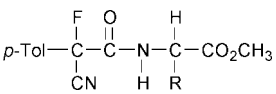

CFTA amide

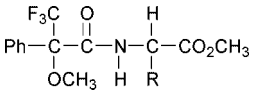

MTPA amide

R	Compound	$\delta_{RS\ (or\ SR)}$/ppm	$\delta_{SS\ (or\ RR)}$/ppm	$\Delta\delta_F$[b]/ppm	$\Delta\delta_F$[b]/ppm
-Me	**1**	−143.163	−140.729	−2.434	−0.386
-Et	**2**	−143.839	−140.843	−2.996	−0.369
-^{i}Pr	**3**	−144.578	−140.948	−3.630	−0.327
-^{t}Bu	**4**	−145.750	−141.676	−4.074	−0.171
-^{i}Bu	**5**	−143.761	−140.061	−3.700	−0.373
-CH(OBn)CH_3	**6**	−144.633	−138.670	−5.963	−0.379
-$CH_2CH_2SCH_3$	**7**	−145.146	−141.151	−3.995	−0.363
-$CH_2CO_2CH_3$	**8**	−143.763	−140.842	−2.921	−0.407
-CH_2CO_2Bn	**9**	−143.344	−140.824	−2.520	−0.325
-$CH_2CH_2CO_2$Et	**10**	−144.771	−140.507	−4.264	−0.389
-$CH_2CH_2CH_2CH_2$NHZ	**11**[c]	−144.398	−140.267	−4.131	−0.449
-Bn	**12**	−145.004	−141.424	−3.580	−0.033
-(3-Indolylmethyl)	**13**	−144.798	−140.398	−4.400	−0.044
-H	**14**	(−142.152)[d]			

[a] Chemical shifts in $CDCl_3$ were determined at 254 MHz for **1**, **3**, **7**, **8**, **12** and at 376 MHz for others. $CFCl_3$ was used as an internal standard.[b] $\delta_{RS\ (or\ SR)} - \delta_{SS\ (or\ RR)}$.[c] Benzyl ester was used.[d] Chemical shift of the racemic CFTA amide.

 DOI: 10.1039/b108842d

chemical shift nonequivalence of the protons in the R and the ester groups between the (*R*,*S*)- and (*S*,*S*)-CFTA diastereomers **1**–**13**.[10]

In the fast equilibrium between *ap* and *sp* conformers for each CFTA amide, the observed δ_F value must be a weighted mean of the chemical shift for each conformer on their populations. Calculation of the δ_F values for (*R*,*S*)-**15** and (*S*,*S*)-**15** predicted that the resonance of the *ap* conformer occurs at higher field than the resonance of the *sp* conformer.[11] The predicted chemical shift differences between *ap* and *sp* conformers (~ 18 ppm) for both diastereomers were considerably greater than that between the diastereomeric two *ap* conformers (~ 1.7 ppm) or the diastereomeric two *sp* conformers (~ 1.5 ppm). From this, we conclude that the observed higher field resonance of the (*R,S*)-CFTA isomer compared to the (*S,S*)-isomer is attributable to a larger population of the *ap* conformer in the (*R,S*)-isomer compared to the population of this conformer in the (*S,S*)-isomer. In addition, these conformational preferences appear to hold for all the diastereomeric amides **1**–**13**.[12] These conformational preferences can be explained by invoking attractive interactions between the eclipsed tolyl and R groups in the (*R*,*S*)-CFTA amide structures. The same interactions would be possible in the *sp* conformer of (*S*,*S*)-amides, but in this case these interactions would increase the population of the *sp* conformer, and hence would shift the ^{19}F signal to lower field.

In order to confirm the presence of attractive interactions, we compared the δ_F values for both (*R*,*S*)- and (*S*,*S*)-diastereomers of **1**–**13** with the δ_F value of racemic **14** (−142.152 ppm), wherein comparable attractive interactions are absent. The signs of the chemical shift differences ($\Delta\delta_F^{Rel}$) of **1**–**13** relative to **14**, *i.e.*, δ_{RS} − (−142.152) for the (*R*,*S*)-isomers and δ_{SS} − (−142.152) for the (*S*,*S*)-isomers, were found to be consistently minus for the (*R*,*S*)-isomers and plus for the (*S*,*S*)-isomers. These results suggest that the *ap* conformer is more populated in the (*R*,*S*)-isomers and less populated in the (*S*,*S*)-isomers, when compared with that of **14**. This strongly supports the presence of attractive interactions proposed above for the amides **1**–**13**.

It should be noted that the regularity observed for the sign of $\Delta\delta_F^{Rel}$ values necessarily provides a simple method for assigning absolute stereochemistry of α-amino esters by using either one of the two CFTA diastereomers. Further investigations to extend the applications and reliability of the CFTA method based on both ^1H and ^{19}F NMR are currently underway.

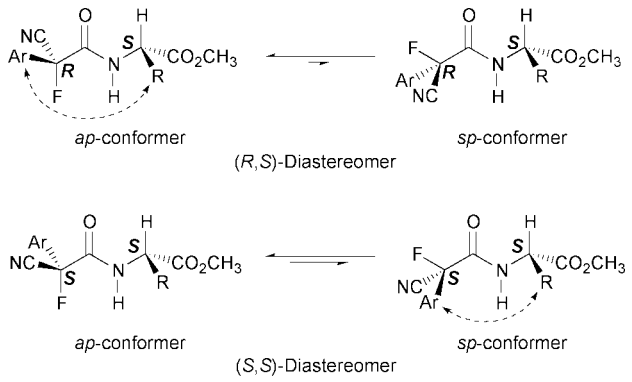

Fig. 1 Conformational equilibria of CFPA (Ar = Ph) and CFTA (Ar = *p*-Tol) amides.

This work was supported by a Grants-in Aid for Scientific Research from the Ministry of Education, Science, Sports and Culture, Japan and by a grant from The Mitsubishi Foundation.

Notes and references

1 T. Kubota, M. Tsuda and J. Kobayashi, *Org. Lett.*, 2001, **3**, 1363; A. Morohashi, M. Satake, H. Nagai, Y. Oshima and T. Yasumoto, *Tetrahedron*, 2000, **56**, 8995; L. C. Chang, D. Chávez, L. L. Song, N. R. Farnsworth, J. M. Pezzuto and D. Kinghorn, *Org. Lett.*, 2000, **2**, 515; M. Murata, S. Matsuoka, N. Matsumori, G. K. Paul and K. Tachibana, *J. Am. Chem. Soc.*, 1999, **121**, 870; see also: I. Ohtani, T. Kusumi, Y. Kashman and H. Kakisawa, *J. Am. Chem. Soc.*, 1991, **113**, 4092; B. M. Trost, J. L Belletire, S. Godleski, P. G. McDougal and J. M. Balkovec, *J. Org. Chem.*, 1986, **51**, 2370; J. M. Seco, Sh. Latypov, E. Quiñoá and R. Riguera, *Tetrahedron Lett.*, 1994, **35**, 2921 and references cited therein.

2 Y. Takeuchi and T. Takahashi, in *Enantiocontrolled Synthesis of Fluoro-organic Compounds*, ed. V. A. Soloshonok, Wiley, Chichester, 1999, p. 497; D. Parker, *Chem. Rev.*, 1991, **91**, 1441; R. Rothchild, *Enantiomer*, 2000, **5**, 457.

3 Y. Takeuchi, N. Itoh, T. Satoh, T. Koizumi and K. Yamaguchi, *J. Org. Chem.*, 1993, **58**, 1812 and references cited therein.

4 In some limited cases, good correlation has been observed between ^{19}F chemical shifts and absolute configurations. G. R. Sullivan, J. A. Dale and H. S. Mosher, *J. Org. Chem.*, 1973, **38**, 2143; M. Apparu, Y. B. Tiba, P-M. Leo, S. Hamman and C. Coulombeau, *Tetrahedron: Asymmetry*, 2000, **11**, 2885.

5 Y. Takeuchi, M. Konishi, H. Hori, T. Takahashi, T. Kometani and K. L. Kirk, *Chem. Commun.*, 1998, 365; Y. Takeuchi, M. Konishi, H. Hori, T. Takahashi and K. L. Kirk, *Enantiomer*, 1999, **4**, 339.

6 T. Takahashi, A. Fukushima, Y. Tanaka, Y. Takeuchi, K. Kabuto and C. Kabuto, *Chem. Commun.*, 2000, 788.

7 The (*R*,*S*)-amides derived from (*R*)-CFTA and (*S*)-amino esters are designated as *RS* and the (*S*,*S*)-amides derived from (*S*)-CFTA and (*S*)-amino esters are designated as *SS*. $\Delta\delta_F = \delta_{RS \text{ or } SR} - \delta_{SS \text{ or } RR}$.

8 J. A. Dale, D. L. Dull and H. S. Mosher, *J. Org. Chem.*, 1969, **34**, 2543.

9 The ground state geometry and energies of (*R*,*S*)-**15** and (*S*,*S*)-**15** were calculated by AM1 method using MOPAC 2000 program to give the *ap* and the *sp* conformers shown in Fig. 1 (Ar = Ph, R = *i*-Pr). The structures of these conformers were optimized by *ab initio* calculation (RHF/6-31+G(d), GAUSSIAN 98 program). The energy differences $\Delta E_{sp\text{-}ap}$ by the *ab initio* calculation are as follows. (*R*,*S*)-**15**: 3.60 kcal mol^{-1} ; (*S*,*S*)-**15**: 2.89 kcal mol^{-1}.

10 The ^1H signals due to the R groups in the (*R*,*S*)-isomers consistently appeared at higher field than those due to the corresponding (*S*,*S*)-isomers, while the signals due to the ester group in the (*R*,*S*)-isomers resonated at lower field than those due to the (*S*,*S*)-isomers. Details will be published elsewhere.

11 The ^{19}F chemical shifts of the two conformers in each diastereomeric CFPA amide **15** were calculated using GAUSSIAN 98 program on the structures optimized by RHF/6-31+G(d). δ_F (ppm. $CFCl_3$ as an internal standard): (*R*,*S*)-**15**, *ap* −148.35; *sp* −130.45. (*S*,*S*)-**15**, *ap* −146.70; *sp* −128.97.

12 The larger $\Delta E_{sp\text{-}ap}$ value (3.60 kcal mol^{-1}) in the (*R*,*S*)-**15** obtained by the *ab initio* calculation compared to that (2.89 kcal mol^{-1}) in the (*S*,*S*)-**15** is qualitatively consistent with this consideration. A similar discussion was conducted regarding the ^{19}F chemical shift non-equivalence in the case of diastereomeric CFTA esters (ref. 6). See also: S. K. Latypov, N. F. Galiullina, A. V. Aganov, V. E. Kataev and R. Riguera, *Tetrahedron*, 2001, **57**, 2231.

CHEMCOMM Communication
www.rsc.org/chemcomm

Synthesis of a gable bis-porphyrin linked with a bicyclo[2.2.2]octadiene ring and its conversion into a conjugated planar bis-porphyrin

Satoshi Ito,[a] Ken-ichi Nakamoto,[a] Hidemitsu Uno,*[b] Takashi Murashima[a] and Noboru Ono*[a]

[a] *Department of Chemistry, Faculty of Science, Ehime University, Matsuyama, 790-8577, Japan*
E-mail: ononbr@dpc.ehime-u.ac.jp
[b] *Advanced Instrumentation Center for Chemical Analysis, Ehime University, Matsuyama, 790-8577, Japan*

Received (in Cambridge, UK) 17th September 2001, Accepted 14th November 2001
First published as an Advance Article on the web 4th December 2001

A soluble porphyrin dimer linked with bicyclo[2.2.2]octadiene was converted in to insoluble conjugated porphyrin dimer by heating at 200 °C, this provides a new strategy for the process control of conjugated porphyrins.

†The preparation of well defined arrays of porphyrins is a popular area of research, not only for its possible application to the elucidation of natural photosynthesis mechanism, but also for functional molecular devices, *e.g.* molecular scale wires, switches and catalysis for the direct four-electron reduction of oxygen to water.[1] Porphyrins can be directly connected with covalent bonds or assembled with hydrogen bonds or transition metals. Porphyrin dimers or oligomers with no significant π-overlap between the neighboring porphyrins were first studied, and highly conjugated porphyrin dimers or oligomers have attracted much interest in recent years. For example, gable porphyrins developed by Tabushi *et al.*[2] contain clefts for molecular recognition. *Meso–meso* linked porphyrin dimers developed by Osuka *et al.*,[3] where the porphyrins lie approximately orthogonal to each other, exhibit strong electronic communication in their excited states to provide a useful basic structure for molecular photonic wires. On the other hand, the group of Arnold has developed conjugated porphyrin dimers, where porphyrins are linked with conjugated triple bonds.[4] The groups of Crossley and Smith have reported further enhanced conjugated porphyrins, namely, edge-fused porphyrin oligomers.[5] The groups of Osuka and Sugiura have reported conversions of non-conjugated β-*meso* linked porphyrin dimers into conjugated fused porphyrin dimers *via* oxidation.[6] The unusual electronic behavior of such porphyrin arrays due to strong ground state conjugation makes them attractive candidates for real molecular wires. Although conjugated porphyrin oligomers constitute an active area of research, only a few structural types have been explored.[4–6] Here we present a new strategy for preparing a conjugated porphyrin dimer **6** from a non-conjugated porphyrin dimer **5**. This new method is based on the retro-Diels–Alder reaction. In previous papers we reported that soluble porphyrins fused with bicyclo[2.2.2]octadiene were converted into insoluble benzoporphyrins *via* the retro-Diels–Alder reaction by heating at 200 °C.[7] As the thermal process does not require any reagents or purification steps, it is ideal for the preparation of conjugated porphyrins.

Dipyrrole **2** linked by bicyclo[2.2.2]octadiene was prepared from ethyl 4,7-dihydro-4,7-ethano-2*H*-isoindole-2-carboxylate **1** in four steps as already reported.[8] De-ethoxycarbonylation of **2** with KOH in ethylene glycol at 170 °C gave **3**. Bis-porphyrin **5** fused with bicyclo[2.2.2]octadiene was prepared by the 3 + 1 approach.[9] The reaction of 2.0 equivalents of tripyrranedicarbaldehyde **4** with 1.0 equivalent of dipyrrole **3**, followed by oxidation with dichlorodicyano-*p*-benzoquinone (DDQ) and metallation with $Zn(OAc)_2$ gave Zn-**5** in 13% overall yield. The requisite tripyrrane dicarbaldehyde **4** was prepared by the reaction of 3,4-diethylpyrrole with 2.0 equivalents of benzyl 5-acetoxymethyl-4-butyl-3-methyl-1*H*-pyrrole-2-carboxylate in AcOH–EtOH, followed by debenzylation and formylation with methyl orthoformate and CF_3CO_2H.

The retro-Diels–Alder reaction of Zn-**5** was carried out by heating at 200 °C under vacuum (10 mm Hg) for 2 h to give a planar bisporphyrin Zn-**6** in quantitative yield (Scheme 1). As this conversion proceeds very cleanly, pure Zn-**6** (estimated by NMR) was isolated without purification. As mentioned in previous papers,[7] porphyrins fused with bicyclo[2.2.2]octadiene rings are generally soluble in organic solvents, where π–π-stacking is inhibited. Planar porphyrins formed *via* the retro-Diels–Alder reaction are insoluble due to the strong π–π-stacking. This retro-Diels–Alder process provides a powerful strategy for the fabrication of electronic devices from π-extended compounds. Expensive and tedious vacuum deposition techniques for the preparation of electronic devices from insoluble materials are exempted by using soluble precursors.

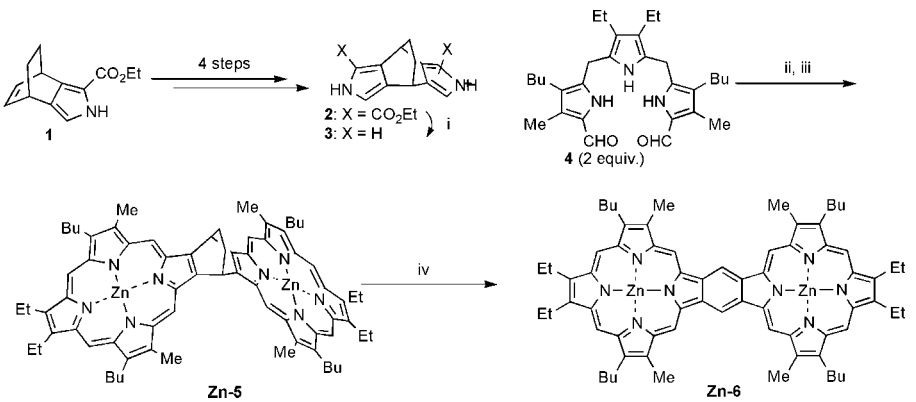

Scheme 1 *Reagents and conditions*: i, KOH, $HO(CH_2)_2OH$, 170 °C, 2 h; ii, $CHCl_3$, TFA, Et_3N, DDQ, iii, $CHCl_3$, $Zn(OAc)_2{\cdot}2H_2O$, iv, 200 °C, 2 h.

 DOI: 10.1039/b108391k

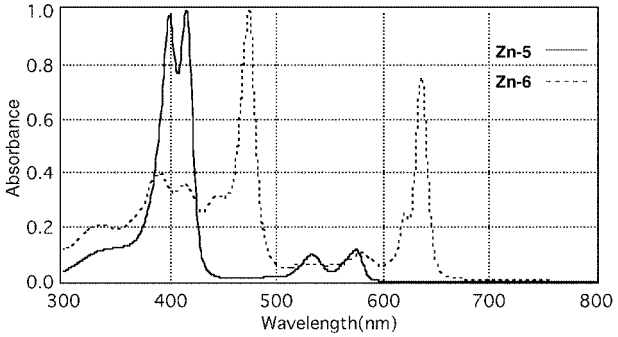

Fig. 1 UV–VIS spectra of bisporphyrins Zn-**5** and Zn-**6**.

As bis-porphyrin **5** is soluble in organic solvents, various metals are also easily introduced into **5** by the reaction with metal salts in organic solvents. Subsequent heating of such metal complexes of **5** gives the metal complexes of **6**, which are difficult to prepare by the reaction of **6** with metal salts. Zn-**5** is soluble in various organic solvents, such as toluene or $CHCl_3$ whereas Zn-**6** is insoluble in toluene or $CHCl_3$.

Absorption spectra of bis-porphyrins Zn-**5** and Zn-**6** were measured in $CHCl_3$ or 5% pyridine–$CHCl_3$, respectively (Fig. 1). The splitting of Soret band (400, 415 nm) was observed in Zn-**5**. The exciton splitting energy in the Soret band is similar to those for the reported gable porphyrins of Tabushi *et al.*.[2] Thus, the dihedral angle and the distance between porphyrins in **5** are estimated to be similar to those of Tabushi's gable porphyrins. As the bicyclo[2.2.2]octane ring is a more rigid spacer than phenylene, porphyrin rings in Zn-**5** are fixed more rigidly than those of other systems. Bis-porphyrin Zn-**5** may be useful as a host for various compounds such as fullerene. In fact, the absorption spectra of Zn-**5** is gradually changed to a broad Soret band at 400 nm by addition of a solution of fullerene, and the splitting of Soret band disappears. Absorption spectra after heating Zn-**5** at 200 °C are shown in Fig. 1. The new absorption spectra can be assigned to be those of Zn-**6**. The red-shift of absorption spectra and the intense Q band are typical for conjugated porphyrin dimers.[5,6] Mass spectra of Zn-**5** and Zn-**6** are identical, since ethylene is eliminated during ionization of Zn-**5**. NMR data support the structure of Zn-**6**.

In conclusion, we have succeeded in the preparation of novel bis-porphyrins **5** and **6**, where the two porphyrin rings are fixed at angles of 120 and 180°, respectively. They provide new models to evaluate intramolecular interaction (singlet or triplet energy transfer or electron transfer) of porphyrin dimers in the excited states or in ground states.[1,4,10]

The work was supported by Grant-in-aid for Scientific Research from the Ministry of Education, Science, Sports and Culture, Japan.

Notes and references

† *Selected data*: for **4**: δ_H ($CDCl_3$) 0.90 (6 H, t, *J* 6.84), 0.93 (6 H, t, *J* 7.32), 1.35 (4 H, m), 2.21 (6 H, s), 2.35–2.45 (8 H, m), 3.82 (6 H, s), 8.8 (1 H, br s), 9.19 (2 H, s), 9.9 (2H, br s); δ_C ($CDCl_3$) 16.5, 17.7, 22.6, 22.7, 23.5, 32.9, 120.5, 121.6, 123.2, 127.9, 132.9, 138.3, 175.3. Calc. for $C_{30}H_{43}N_3O_2$: C, 75.43; H, 9.07; N, 8.80. Found: C, 75.28; H, 9.00; N, 8.58. For Zn-**5**: purple–red powder, mp > 200 °C (decomp.); δ_H ($CDCl_3$) 1.10 (6 H, t, *J* 7.32), 1.73 (4 H, m), 1.84 (6H, t, *J* 7.32), 2.28 (4 H, m), 2.88 (4 H, m), 3.93 (6 H, s), 4.0–4.1 (8 H, m), 7.88 (2 H, m), 10.01 (2 H, s), 10.83 (2 H, s); δ_C ($CDCl_3$) 12.2, 14.2, 18.5, 19.8, 23.1, 26.3, 31.8, 35.4, 36.5, 97.1, 98.6, 136.6, 141.5, 142.1, 142.3, 147.5, 148.3, 148.5, 151; λ_{max} ($CHCl_3$)/nm [relative intensity]: 399 [0.98], 415 [1.00], 533 [0.10], 575 [0.11]; *m/z* (FAB) 1162 ($M^+ - C_2H_4$). For Zn-**6**: green powder, mp > 250 °C, δ_H ($CDCl_3$–C_5D_5N) 1.19 (12 H, t, *J* 7.32), 1.85 (8 H, m), 1.96 (12 H, t, *J* 7.32), 2.37 (8 H, m), 3.97 (12 H, s), 4.12–4.22 (16 H, m), 10.15 (4 H, s), 10.99 (4 H, s), 11.48 (2 H, s); λ_{max} (5% pyridine–$CHCl_3$)/nm [relative intensity]: 334 [0.21], 391 [0.39], 414 [0.35], 445 [0.31], 474 [1.00], 579 [0.11], 620 [0.25], 636 [0.75] .

1 Some recent reviews: N. Aratani and A. Osuka, *Bull. Chem. Soc. Jpn.*, 2001, **74**, 1361; M. Graca, H. Vicente, L. Jaquinond and K. M. Smith, *Chem. Commun.*, 1999, 1771; A. K. Burrell and D. J. Officer, *Synlett*, 1998, 1297; J. P. Collman, P. S. Wagenknechet and J. E. Hutchinson, *Angew. Chem., Int. Ed. Engl.*, 1994, **33**, 1537; D. P. Arnold, *Synlett.*, 2001, 296.

2 I. Tabushi and T. Sasaki, *J. Am. Chem. Soc.*, 1983, **105**, 2694; I. Tabushi and S. Kugimiya, *J. Am. Chem. Soc.*, 1986, **108**, 6926; H. Meier, Y. Kobuke and S. Kugimiya, *J. Chem. Soc., Chem. Commun.*, 1989, 923.

3 A. Osuka and H. Simidzu, *Angew. Chem., Int. Ed. Engl.*, 1997, **36**, 135; Y. H. Kim, D. H. Jeong, D. Kim, S. C. Jeoung, H. S. Cho, S. K. Kim, N. Aratani and A. Osuka, *J. Am. Chem. Soc.*, 2001, **123**, 76.

4 H. L. Anderson, *Chem. Commun.*, 1999, 2323 and references therein.

5 M. J. Crossley, L. J. Govenlock and J. K. Praskar, *Chem. Commun.*, 1995, 2379; L. Jaquinod, O. Siri, R. G. Khoury, M. M. Olmstead and K. M. Smith, *Chem. Commun.*, 1998, 1261; M. G. H. Vincente, M. T. Cancilla, C. B. Lebrilla and K. M. Smith, *Chem. Commun.*, 1998, 2355.

6 K. Sugiura, T. Matsumoto, S. Ohkouchi, Y. Naitoh, T. Kawai, Y. Takai, K. Ushiroda and Y. Sakata, *Chem. Commun.*, 1999, 1957; A. Tsuda, A. Nakano, H. Furuta, H. Yamochi and A. Osuka, *Angew. Chem., Int. Ed.*, 2000, **39**, 558.

7 S. Ito, T. Murashima, H. Uno and N. Ono, *Chem. Commun.*, 1998, 1661; S. Ito, N. Ochi, H. Uno, T. Murashima and N. Ono, *Chem. Commun.*, 2000, 893.

8 H. Uno, S. Ito, M. Wada, H. Watanabe, M. Nagai, A. Hayashi, T. Murashima and N. Ono, *J. Chem. Soc., Perkin Trans. 1*, 2000, 4347 and references therein.

9 A. Bondif and M. Momenteau, *J. Chem. Soc., Chem. Commun.*, 1994, 2096; J. L. Sessler, J. W. Genge, A. Urbach and P. Sanson, *Synlett*, 1996, 187; T. D. Lash, *Chem. Eur. J.*, 1996, **2**, 1197 and references therein.

10 K. Ishii, N. Kobayashi, Y. Higashi, T. Osa, D. Lelievre, J. Simons and S. Yamaguchi, *Chem. Commun.*, 1999, 969; J. Andreasson, J. Kajanus, J. Martensson and B. Albinsson, *J. Am. Chem. Soc.*, 2000, **122**, 9844; J. J. Piet, P. N. Taylor, H. L. Anderson, A. Osuka and J. M. Warman, *J. Am. Chem. Soc.*, 2000, **122**, 1749.

CHEMCOMM Communication
www.rsc.org/chemcomm

Asymmetric routes in the reaction of cyclic ketene ortho ester with aldehydes involving the use of chiral Lewis acid

Chan-Mo Yu,* Jae-Young Lee, Kwangwoo Chun, In-Kyung Choi and Suk-Ku Kang

Department of Chemistry and BK-21 School of Molecular Science, Sungkyunkwan University, Suwon 440-746, Korea. E-mail: cmyu@chem.skku.ac.kr

Received (in Cambridge, UK) 16th August 2001, Accepted 6th November 2001
First published as an Advance Article on the web 26th November 2001

Enantio- and diastereoselective synthesis of *threo* 2 and *erythro* 3 was accomplished by the conversion of 1 with aldehydes promoted by chiral borane 10; enantioselctivities range from 45–95% ee, while diastereoselectivities vary from 4.3–49 : 1 with 8 different aldehydes.

The availability of efficient synthetic methods for achieving absolute stereocontrol *via* a catalytic process in the construction of acyclic systems is of considerable current interest in synthetic chemistry.[1] During the past decades, substantial progress has been made, and as a result, many enantioselective synthetic routes have been extensively explored.[2] Nonetheless, only a few methods exist to establish all stereoisomers selectively, despite their plentiful synthetic potential.[3] Recently we have disclosed novel synthetic methods for the synthesis of both diastereomers **2** and **3** in high levels of stereoselectivity from the ketene ortho ester **1** with an aldehyde mediated by a Lewis acid catalyst (Scheme 1). This highly stereocontrolled transformation for the synthesis of **2** involves the diastereoselective generation of a carbon–carbon bond to form **4** and introduction of ester functionality from hydrolysis of the ortho ester intermediate **4**.[4] A reversal of diastereoselectivity to obtain **3** was realized by an epimerization of intermediate **4** under basic conditions.[5]

The general feature of this transformation is the synthesis of highly functionalized compounds from simple starting materials in high diastereoselectivity. The characteristic feature of this chemical transformation process has encouraged us to carry out further investigation concerning absolute stereoselection to establish all four stereoisomers. This research led to the discovery of efficient enantioselective routes in forming *threo* **2** and *erythro* **3** with high levels of diastereoselectivity and moderate to excellent enantioselectivity. In the course of this study, the absolute configuration of the major component was unambiguously established by comparison with a synthetic sample.

From the mechanistic perspective, major functions for the stereoselectivity are immediately discernable in the catalytic process. Although the exact mechanistic aspects of this transformation have not been rigorously elucidated, the following pathway could be a probable stereochemical route on the basis of product population. We reasoned that if **5** could be a stereochemical model, then it might be possible to control facial selectivity by a chiral catalyst in a predictable fashion. Preliminary investigations for the stereochemical transformation of **1** with aldehyde indicated that the conversion to the corresponding **2** could not be satisfied with a variety of chiral Lewis acids including BINOL–Ti(IV), and bisoxazoline complexes with Cu, Sc, Zn mainly due to a lack of reactivity.[6] However, bisoxazoline–$Sn(OTf)_2$ complex **6**[7] and chiral borane **7**[8] could be a chiral promoter for the enantioselective conversion. Initial attempts to convert **1** to **2** with benzaldehyde in the presence of **6** (20 mol%) at −20 °C in CH_2Cl_2 were met with limited success, providing moderate enantioselectivity with poor diastereoselectivity (47% yield, 76% ee, 2 : 1 dr). A survey of modifications of ligands provided no significant advantages in terms of reactivity and stereoselectivity. On the other hand, reaction of **1** with benzaldehyde in the presence of **7** occurred readily at −78 °C; this chiral Lewis acid was generally superior and chosen for systematic studies.

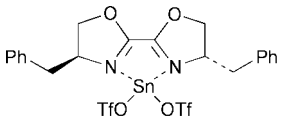

6

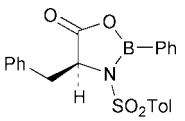

7

Reaction of **1** (R′ = Et) with benzaldehyde in the presence of 20 mol% of **7** for 24 h afforded **2** and **3** in 57% isolated yield in a ratio of 72 : 28 with 77% ee. The lack of diastereoselectivity was attributed to acidic media in the reaction mixture causing epimerization of reaction intermediate **4** for long reaction times. Thus, diastereoselectivity was enhanced by the use of 1 eq. of **7** within 2 h, providing 78% yield in 91 : 9 dr with 83% ee (−78 °C for 2 h in CH_2Cl_2). After surveying numerous modifications of *N*-sulfonylamino acids, the remarkable observation has been made that the use of **10** as a chiral promoter led to the best results in terms of chemical yields and stereoselectivities (PhCHO, 95% yield, **2**:**3** = 97 : 3, 93% ee): (a) chiral Lewis acid **10** was prepared from the reaction of **8** with **9**[9] at 23 °C for 2 h;[10] (Scheme 2) (b) reaction at −78 °C for 30 min in CH_2Cl_2 were the optimal conditions, while with longer reaction times, especially more than 2 h, diminished diastereoselectivity was observed; (c) R^1 = Et in **1** was generally superior to others such as Me and Pr^i in terms of chemical availability and efficacy. It is worthy of note that efficient recovery of the chiral ligand **8** was made after work up procedure.

Under optimal conditions, the reaction was performed by the addition of **1** (R^1 = Et) to a solution of benzaldehyde and **10** in CH_2Cl_2 at −78 °C. After stirring for 30 min, the reaction mixture was quenched with 2 N aqueous HCl followed by work up and silica gel chromatography to afford *threo* **2a** with *erythro* **3a** in a ratio of 97 : 3 as judged by 500 MHz ^{1}H NMR of crude products. With the notion that this protocol might lead to a general and efficient method for the synthesis of multifunctional

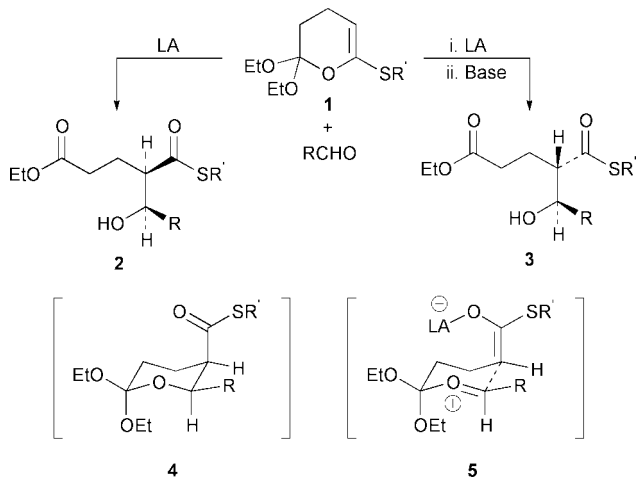

Scheme 1

 DOI: 10.1039/b107454g

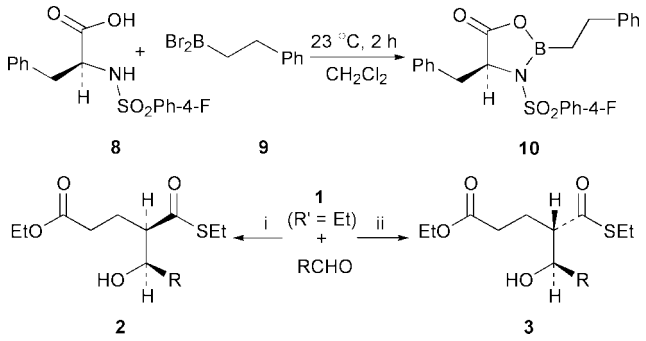

Scheme 2 *Reagents and conditions*: i, **10**, −78 °C, 30 min, CH_2Cl_2; ii, **10**, −78 °C , 2 h, CH_2Cl_2, then DBU, pyridine, −78 °C–23 °C, 24 h.

substances, we set out to determine the scope of reaction with various aldehydes. Indeed, the method is successful with a variety of aldehydes and affords products of high diastereomeric purity with moderate to good enantioselectivies as summarized in Table 1. The ee values were determined by 500 MHz ^{1}H NMR of the corresponding (+)-MTPA ester and/or HPLC or GC analysis using a chiral column as indicated in Table 1.

Table 1 Diastereo- and enantioselective synthesis of **2**[a]

Entry	RCHO	Product	dr (**2**:**3**)[b]	Ee (%)[c]	Yield (%)[d]
1	Ph	**a**	97:3	93	95
2	4-Br-Ph	**b**	95:5	95	88
3	CH_3	**c**	92:8	91	78
4	$PhCH_2$	**d**	95:5	88	77
5	$PhCH_2CH_2$	**e**	94:4	90	83
6	C_6H_{13}	**f**	92:8	84	77
7	PhCH=CH	**g**	81:19	74	79
8	Me_2CH	**h**	88:12	45	61

[a] Reactions were carried out in CH_2Cl_2 at −78 °C for 30 min.[b] Diastereomeric ratio was determined by the analysis of 500 MHz ^{1}H NMR spectra of crude products (all entries) and by GC analysis using HP^{-1} (Hewlett-Packard, cross linked methyl siloxane, 25 m × 0.32 mm × 0.52 μm, entries 3, 4, 6, 8).[c] Ees were determined by preparation of (+)-MTPA ester derivatives, analysis by 500 MHz ^{1}H NMR spectra (entries 1,2,3,4,8) and by HPLC analysis using chiral column (Chiracel OD-H, 3–5% Pr^{i}OH in hexanes, entries 1,2,5,7) and by GC (FID, Chiral Dex-30, G-TA, gamma-cyclodextrin Trifluoroacetyl, 30 m × 0.32 mm, entries 3,6,8).[d] Yields refer to isolated and purified products.

With our research scope of the asymmetric synthesis of *threo* **2**, we turned our attention next to examine possibility of this approach for a reversal of diastereoselectivity.[5] Under optimal conditions, the reaction was performed by addition of **1** to **10** and benzaldehyde in CH_2Cl_2 at −78 °C. After 2 h at −78 °C, freshly distilled pyridine (20 eq.) and DBU (10 eq.) was added during which time a white precipitate was formed. After stirring for 30 min at −78 °C, the cooling bath was removed and the temperature was allowed to rise to 23 °C for 24 h.† After cooling to 0 °C, the reaction mixture was quenched with 2 N aqueous HCl in EtOH followed by work up and silica gel chromatography to afford *erythro* **3a** along with *threo* **2a** in a ratio of 95:5 as judged by 500 MHz NMR of crude products with virtually identical enantiomeric purity compared to that of **2a** in Table 1. In addition, parallel experiments were performed with a variety of aldehydes and the results are summarized in Table 2.

Absolute configuration of **3a** was unambiguously established by a comparison of synthetic samples as illustrated in Fig. 1.‡

In summary, this paper describes methodologies for the enantioselective and diastereoselective synthesis of **2** and **3** in a general and efficient way as a result of the present investigation because of the simplicity of the reaction and the ready availability and efficient recovery of the chiral ligand, and also, absolute configurations of products were unambiguously confirmed by the experiments.

Table 2 Diastereo- and enantioselective synthesis of **3**[a]

Entry	RCHO	Product	dr (**3**:**2**)	Ee (%)	Yield (%)
1	Ph	**a**	95:5	92	88
2	4-Br-Ph	**b**	96:4	95	73
3	CH_3	**c**	91:9	90	75
4	$PhCH_2$	**d**	94:6	86	81
5	$PhCH_2CH_2$	**e**	98:2	91	88
6	C_6H_{13}	**f**	95:5	81	74
7	PhCH=CH	**g**	91:9	71	68
8	Me_2CH	**h**	93:7	48	53

[a] Conditions for analysis of diastereo- and enatioselectivities were identical with Table 1.

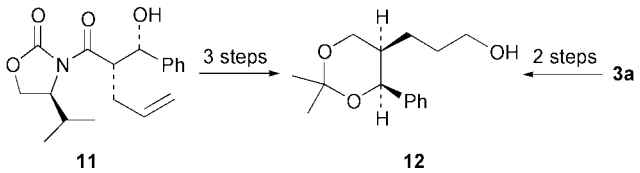

Fig. 1 Determination of absolute configuration.

Generous financial support by grants from the Center for Molecular Design and Synthesis (CMDS: KOSEF SRC) at KAIST and the Ministry of Science and Technology through the National Research Laboratory program is gratefully acknowledged.

Notes and references

† It is important to report that the higher temperature especially over 50 °C for the epimerization of intermediate **4** resulted in seriously diminished chemical yields.

‡ Evans aldol product **11** (9:1 dr)[11] was converted to **12** by 3 steps [i, $LiAlH_4$, −78 °C–0 °C, THF; ii, $MeC(OMe)_2Me$, *p*TsOH (5 mol%), CH_2Cl_2; iii, 9-BBN, 0–23 °C THF, then NaOH, H_2O, 40% overall]. Compound **3a** was also transformed to **12** [i, $LiAlH_4$, −78 °C–0 °C, THF; iii, $MeC(OMe)_2Me$, *p*TsOH (5 mol%), CH_2Cl_2, 67% overall]. Both synthetic **12** from **11** and **3a** has not only the same specific rotation sign but also the identical NMR spectra of (+)-MTPA ester derivatives.

1 For general discussions, see: (*a*) A. H. Hoveyda, D. A. Evans and G. C. Fu, *Chem. Rev.*, 1993, **93**, 1307; (*b*) D. J. Ager and M. B. East, *Asymmetric Synthetic Methodology*, CRC Press, New York, 1996.
2 For examples, see: (*a*) *Catalytic Asymmetric Synthesis*, ed. I. Ojima, Wiley-VCH, New York, 2000; (*b*) *Comprehensive Asymmetric Catalysis I–III*, eds. E. N. Jacobsen, A. Pfaltz and H. Yamamoto, Springer-Verlag, Berlin, 1999; (*c*) *Lewis Acids in Organic Synthesis Vol. 1, 2*, ed. H. Yamamoto, Wiley-VCH, Weinheim, 2000.
3 For examples, the aldol processes, see: (*a*) R. Mahrwald, *Chem. Rev.*, 1999, **99**, 1095–1120; (*b*) S. G. Nelson, *Tetrahedron: Asymmetry*, 1998, **9**, 357–389.
4 (*a*) C.-M. Yu, H.-S. Choi, J.-K. Lee and S.-K. Yoon, *J. Org. Chem.*, 1997, **62**, 6687–6689; (*b*) C.-M. Yu, W.-H. Jung, H.-S. Choi, J. Lee and J.-K. Lee, *Tetrahedron Lett.*, 1995, **36**, 8255–8258.
5 C.-M. Yu, J. Lee, K. Chun, J. Lee and Y. Lee, *J. Chem. Soc., Perkin Trans 1*, 2000, 3622–3626.
6 General discussion, see: J. Seyden-Penne, *Chiral Auxiliaries and Ligands in Asymmetric Synthesis*, John Wiley & Sons, New York, 1995.
7 Reviews, see: (*a*) A. K. Ghosh, P. Mathinanan and J. Cappiello, *Tetrahedron: Asymmetry*, 1998, **9**, 1–45; (*b*) A. Pfaltz, *Acc. Chem. Res.*, 1993, **26**, 339–345.
8 K. Ishihara and H. Yanamoto, in *Advances in Catalytic Process*, ed. M. P. Doyle, JAI, Greenwich, 1995, pp. 29–59.
9 Compound **9** was prepared according to the established procedure and used for next operation without further purification, see: H. C. Brown, N. Ravindran and S. U. Kulkarni, *J. Org. Chem.*, 1980, **45**, 384–389.
10 M. Kinugasa, T. Harada, T. Egusa, K. Fujita and A. Oku, *Bull. Chem. Soc. Jpn.*, 1996, **69**, 3639–3650.
11 D. A. Evans, J. Bartroli and T. L. Shih, *J. Am. Chem. Soc.*, 1981, **103**, 2127–2128.

CHEMCOMM Communication
www.rsc.org/chemcomm

Kinetic resolution of amino alcohol derivatives with a chiral nucleophilic catalyst: access to enantiopure cyclic *cis*-amino alcohols†

Takeo Kawabata,* Kensaku Yamamoto, Yashima Momose, Hiroshi Yoshida, Yoshie Nagaoka and Kaoru Fuji

Institute for Chemical Research, Kyoto University, Uji, Kyoto 611-0011, Japan.
E-mail: kawabata@scl.kyoto-u.ac.jp

Received (in Cambridge, UK) 27th September 2001, Accepted 1st November 2001
First published as an Advance Article on the web 27th November 2001

Acylative kinetic resolution of racemic cyclic *cis*-amino alcohol derivatives with a chiral nucleophilic catalyst proceeds enantioselectively (s = 10–21) at ambient temperature to give enantiopure recovered materials, and the % conversion of the acylation can be readily controlled by the amount of acid anhydride.

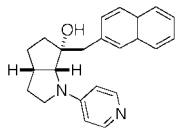

1

β-Amino alcohol functionality is found in many biologically active compounds and is therefore considered an important pharmacophore.[1] The asymmetric synthesis of β-amino alcohols has been extensively studied.[2] Kinetic resolution[3] is another method of choice, and the enzymatic[4,5] and non-enzymatic[6,7] kinetic resolution of racemic amino alcohol derivatives has been reported. Since the theoretical maximum yield is only 50%, kinetic resolution is worthwhile when it is possible to prepare compounds with extremely high enantiomeric purity, which would otherwise be unattainable by asymmetric synthesis. To obtain enantiopure compounds by the kinetic resolution of racemates, high selectivity factor[3] (s) as well as control of the % conversion of the reaction are indispensable. We report here the preparation of nearly enantiopure (≥99% ee) cyclic *cis*-amino alcohol derivatives *via* acylative kinetic resolution with a chiral nucleophilic catalyst. Practically useful levels of enantioselectivity (s = 10–21) were observed in reactions at ambient temperature and the % conversion was readily controlled by the amount of the acylating agent.

Kinetic resolution *via* enantioselective acylation of racemic alcohols by artificial organic molecules has been a focus of current synthetic attention.[6,8,9] We have shown that chiral nucleophilic catalyst **1** could effectively catalyze the acylative kinetic resolution of racemic diol derivatives.[10] Since acylation of an amino group of amino alcohols readily takes place in the absence of catalyst,[11] the amino group was protected and the effect of the protective group on kinetic resolution was examined (Table 1). *Racemic*-**2** with typical carbamate-protective groups such as Boc and Cbz was resolved with moderate enantioselectivity (s = 4.0–4.5) *via* acylation with **1** (entries 1 and 2). However, **2** with amide-protective groups showed better selectivity (s = 8.7–>13, entries 3–5). Enantiomers of a substrate with a *p*-(dimethylamino)benzoyl group were again[10] found to be most effectively differentiated by **1** (s = >13, entry 5). The effects of the acylating agents on the efficiency of kinetic resolution were re-investigated with the *racemic*-**2** (P=COC_6H_4-*p*-NMe_2) under the conditions similar to those in Table 1. The selected results are as follows: Ac_2O (s = 12), (*i*-$PrCO)_2O$ (s = 17), (*t*-$BuCO)_2O$ (s = 6.2), Bz_2O (s = 6.5), *i*-PrCO-OC_6F_5 (s = 17), (2-MeO-$C_6H_4CO)_2O$ (s = 14), (2,4,6-F_3-$C_6H_2CO)_2O$ (s = 19). Among commercial acid anhydrides, isobutyric anhydride gave the highest selectivity, as previously observed.[10] Although the use of the corresponding pentafluorophenyl ester gave selectivity comparable to that with isobutyric anhydride, it was much less effective in kinetic resolution due to its low reactivity (25% conversion after 2 days). 2,4,6-Trifluorobenzoic anhydride gave the highest selectivity, however, we decided to use isobutyric anhydride for further investigation due to its ready availability.

The results of the kinetic resolution of several cyclic amino alcohol derivatives **2a**–**6** are shown in Table 2. Treatment of *racemic*-**2a** with 60 mol% of isobutyric anhydride in the presence of 5 mol% of **1** at 20 °C led to the recovery of (1*R*, 2*S*)-**2a** in 93% ee at 58% conversion (entry 1). Enantiopure **2a** was obtained with a minimum loss of chemical yield by increasing the amount of acid anhydride to 65 mol% (entry 2). Even with 0.5 mol% of the catalyst (catalyst–substrate = 0.9 mg : 131 mg), the acid anhydride was almost completely consumed within 24 h and enantiopure **2a** was recovered (entry 4). Addition of a stoichiometric amount of collidine does not affect the efficiency

† Electronic supplementary information (ESI) available: experimental details. See http://www.rsc.org/suppdata/cc/b1/b108753c/

Table 1 Effects of protective group P on the kinetic resolution of *racemic*-**2** with **1**

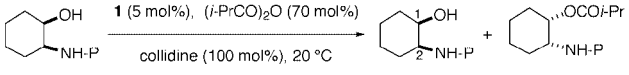

racemic-**2** **2** **3**

Entry	P	Solvent	Reaction time/h	Conversion[a] (%)	Ee of recovered **2** (%)	Ee of **3** (%)	S[b]
1	CO_2t-Bu	$CHCl_3$	24	69	72[c]	33	4.0
2	CO_2CH_2Ph	CH_2Cl_2	5	68[d]	76[c]	—	4.5
3	$COCH_3$	CH_2Cl_2	20	69	96	43	8.7
4	COPh	CH_2Cl_2	20	70	98	42	9.4
5	COC_6H_4-*p*-NMe_2	$CHCl_3$	20	68	>99[c]	47	>13

[a] Conversion was determined by the following equation; conversion (%) = ee (recovered **2**)/ee (recovered **2**) + ee (**3**).[b] S = k (fast-reacting enantiomer)/k (slow-reacting enantiomer), see ref. 3.[c] Absolute congfiguration is (1*R*, 2*S*).[d] Conversion was determined from the ratio of **3** to recovered **2**.

 DOI: 10.1039/b108753c

Table 2 Kinetic resolution of racemic amino alcohol derivatives **2a–6** with **1**[a]

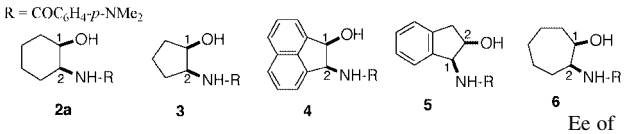

Entry	Substrate	**1**/mol%	$(i\text{-PrCO})_2O$/mol%	Reaction time/h	Conversion[b] (%)	Ee of recovered substrate[c] (%)	Ee of acylated product (%)	*S*
1	**2a**	5	60	9	58	93	68	17 (54)[h]
2[d]	**2a**	5	65	44	63	> 99	59	> 18
3	**2a**	5	70	9	68	> 99	48	> 14
4	**2a**	0.5	70	24	66	> 99	52	> 15
5[e]	**2a**	5	70	9	67	> 99	48	> 14
6[e]	**2a**	0.5	70	24	60	89	59	11
7	**3**	5	70	9	69	> 99	44	> 12
8[f]	**4**	5	60	24	59	97	67	21
9[f]	**4**	5	70	24	68	> 99	46	> 13
10[g]	**5**	5	70	3	64	99	56	17
11	**6**	5	70	9	69	97	46	10
12	**6**	5	75	9	73	99	37	10

[a] A 0.17 M solution of substrate (0.5 mmol) in $CHCl_3$ was treated with isobutyric anhydride at 20 °C in the presence of a catalytic amount of **1** and 100 mol% of collidine, unless otherwise stated.[b] See footnote *a* in Table 1.[c] Absolute configuration of **2a**, **3**, **4**, and **6** is (1*R*, 2*S*) in each case and that of **5** is (1*S*, 2*R*).[d] Run in 0.05 M solution of substrate.[e] Run in the absence of collidine[f] Run in 0.03 M solution of substrate.[g] Run in CH_2Cl_2.[h] *S* value of the kinetic resolution at −40 °C with 0.01 M solution of substrate.

of the kinetic resolution with 5 mol% of **1** (entries 3 *vs.* 5), while it does affect the efficiency with 0.5 mol% of **1** (entries 4 *vs.* 6). Enantiopure amino alcohol derivatives **3–6** were also recovered at 64–73% conversion by similar treatment of the racemates (*s* = 10–21, entries, 7, 9, 10, and 12). In each case, an alcohol with *S* configuration preferentially underwent acylation. The amide-protective group of (1*S*, 2*R*)-**5** was removed by treatment with 6 M HCl to give (1*S*, 2*R*)-1-aminoindan-2-ol (68% yield), which is the key component of the orally active HIV protease inhibitor indinavir.[12,13] In these acylations with **1**, the % conversion could be simply controlled by the amount of acid anhydride so that enantiopure compounds were readily obtained without careful monitoring of the progress of the reaction. This is in contrast to enzymatic acylative kinetic resolution where excess acylating agent is used.[5,14] Even in the case of non-enzymatic acylative kinetic resolution, acylating agents are not always consumed completely within a reasonable reaction time.[9]

The protocol for kinetic resolution was applied to acyclic amino alcohol derivatives. Acylation of an *anti*-amino alcohol derivative, *racemic*-**7**, under the standard conditions (Table 2, footnote *a*) gave recovered **7** with 93% ee at 70% conversion (*s* = 7.1), while the corresponding *syn*-derivative **8** showed negligible selectivity (*s* = 1.0). Kinetic resolution of **9** with a primary hydroxy group progressed with a selectivity factor of 6.8. Another *syn*-amino alcohol derivative **10** (taxol side-chain) was poorly resolved with **1** (28% ee at 71% conversion, *s* = 1.6). Thus, the relative configuration of the β-hydroxyamine critically affects the enantioselectivity of the kinetic resolution promoted by **1**.

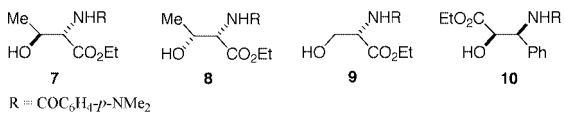

In summary, acylative kinetic resolution of several cyclic *cis*-amino alcohol derivatives with **1** proceeds enantioselectively at ambient temperature to give enantiopure unreacted materials under proper control of the % conversion of the acylation. Complete consumption of acid anhydrides at low catalyst loading indicates that **1** has high catalytic activity. Kinetic and mechanistic investigations are now under way.

This work was supported by a Grant-in-Aid for Scientific Research on Priority Areas (No. 706 : Dynamic Control of Stereochemistry) from the Ministry of Education (Monbusho), Japan.

Notes and references

1 For a recent example: Z. M. Szulc, Y. A. Hannun and A. Bielawska, *Tetrahedron Lett.*, 2000, **41**, 7821.
2 For a representative example: G. Li, H. H. Angert and K. B. Sharpless, *Angew. Chem,. Int. Ed. Engl.*, 1996, **35**, 2813.
3 H. B. Kagan and J. C. Fiaud, *Top. Stereochem.*, 1988, **18**, 249.
4 For a recent example of enzymatic de-acylative kinetic resolution: G. Sekar, R. M. Kamble and V. K. Singh, *Tetrahedron: Asymmetry*, 1999, **10**, 3663.
5 For a recent example of enzymatic acylative kinetic resolution:A. Luna, A. Maestro, C. Astorga and V. Gotor, *Tetrahedron Asymmetry*, 1999, **10**, 1969.
6 For a example of non-enzymatic acylative kinetic resolution: E. R. Jarvo, G. T. Copeland, N. Papaioannou, P. J. Bonitatebus, Jr. and S. J. Miller, *J. Am. Chem. Soc.*, 1999, **121**, 11638.
7 For an oxidative kinetic resolution of β-hydroxyamines: S. Miyano, L. D.-L. Lu, S. M. Viti and K. B. Sharpless, *J. Org. Chem.*, 1985, **50**, 4350.
8 For a leading reference of catalytic asymmetric acylation of alcohols: J. Ichikawa, M. Asamin and T. Mukaiyama, *Chem. Lett.*, 1984, 949.
9 E. Vedejs, O. Daugulis and S. T. Diver, *J. Org. Chem.*, 1996, **61**, 430; J. C. Ruble, H. A. Latham and G. C. Fu, *J. Am. Chem. Soc.*, 1997, **119**, 1492; S. J. Miller, G. T. Copeland, N. Papaioannou, T. E. Horstmann and E. M. Ruel, *J. Am. Chem. Soc.*, 1998, **120**, 1629; E. Vedejs and O. Daugulis, *J. Am. Chem. Soc.*, 1999, **121**, 5813; B. Tao, J. C. Ruble, D. A. Hoic and G. C. Fu, *J. Am. Chem. Soc.*, 1999, **121**, 5091; T. Sano, K. Imai, K. Ohashi and T. Oriyama, *Chem. Lett.*, 1999, 265; A. C. Spivey, T. Fekner and S. E. Spey, *J. Org. Chem.*, 2000, **65**, 3154; G. Naraku, N. Shimamoto, T. Hanamoto and J. Inanaga, *Enantiomer*, 2000, **5**, 135; A. C. Spivey, A. Maddaford, D. P. Leese and A. J. Redgrave, *J. Chem. Soc., Perkin Trans. 1*, 2001, 1785.
10 T. Kawabata, M. Nagato, K. Takasu and K. Fuji, *J. Am. Chem. Soc.*, 1997, **119**, 3169.
11 A pioneering work for catalytic enantioselective acylation of amines was reported recently: S. Arai, S. Bellemin-Laponnaz and G. C. Fu, *Angew. Chem., Int. Ed.*, 2001, **40**, 234.
12 I. W. Davies, C. H. Senanayake, L. Castoguay, R. D. Larsen, T. R. Verhoeven and P. J. Reider, *Tetrahedron Lett.*, 1995, **36**, 7619.
13 For the synthesis and utilities of *cis*-1-aminoindan-2-ol: A. K. Ghosh, S. Fidanze and C. H. Senanayake, *Synthesis*, 1998, 937.
14 For a review: C.-H. Wong, *Chemtracts: Org. Chem.*, 1990, **3**, 91.

CHEMCOMM Communication
www.rsc.org/chemcomm

Chiral phosphite–phosphoroamidites: a new class of ligand for asymmetric catalytic hydrogenation

Montserrat Diéguez,* Aurora Ruiz and Carmen Claver

Departament de Química Física i Inorgànica, Universitat Rovira i Virgili, Pl. Imperial Tarraco 1, 43005 Tarragona, Spain. E-mail: dieguez@quimica.urv.es; Fax: 34 977559563; Tel: 34 977558046

Received (in Cambridge, UK) 5th October 2001, Accepted 9th November 2001
First published as an Advance Article on the web 6th December 2001

A series of novel phosphite–phosphoroamidite ligands, derived from readily available D-xylose, has been used for the first time in the asymmetric Rh-catalyzed hydrogenation of a series of α,β-unsaturated carboxylic acid derivatives with excellent enantioselectivity (ee up to > 99%).

Many chiral phosphorus compounds have been synthesized as ligands for enantioselective metal-catalyzed hydrogenation.[1] Most of them are homodonor ligands, mainly diphosphines[1,2] and diphosphinites.[3] However, the combination of different functionalities in a ligand has already proved beneficial in enantiodiscrimination.[4] In this context, we have recently reported the successful application of mixed phosphine–phosphite ligands in asymmetric hydrogenation.[5]

In the last few years, a group of less electron-rich phosphorus compounds—phosphite[6] and phosphoroamidite[7] ligands—have also demonstrated their potential utility in asymmetric hydrogenation. Therefore we here report the development of a new class of chiral phosphite–phosphoroamidite ligands (**1–4**), which have the advantages of both types of ligands for asymmetric hydrogenation (Fig. 1). These ligands are derived from natural D-xylose so they also have the advantages of carbohydrates, such as availability at low price and facile modular construction, which makes tedious optical resolution procedures unnecessary and facilitates regio- and stereoselective introduction of different functionalities.[8] To the best of our knowledge this is the first example of phosphite–phosphoroamidite ligands applied to hydrogenation.[9]

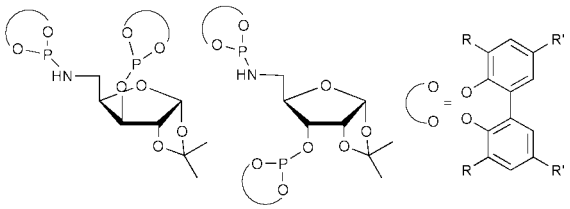

Fig. 1 Phosphite–phosphoroamidite ligands **1–4**.

Ligands **1–4**[10] incorporate a chiral furanoside backbone, which determines their underlying structure, and one amino group at the C5 position. The amino furanosides **5**[11] (Scheme 1) serve as basic frameworks to which several phosphoric acid biphenol esters **6**[12] are attached.

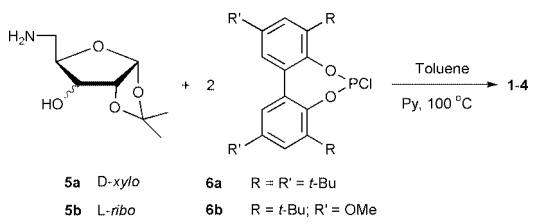

Scheme 1 Synthesis of ligands **1–4**.

The modular nature of these sugar ligands allows a facile systematic variation in the configuration of the stereocenter at carbon atom C-3 at the ligand bridge and in the biphenyl substituents, so the optimum configuration for maximum stereoselectivity can be determined. Thus, we investigated how the different groups attached to the *para* positions of the bisphenol moieties affected enantioselectivity using ligands **1** and **2**, which have the same configuration on the carbon atom C-3. We also investigated the influence of the stereogenic carbonatom C-3 by comparing diastereomeric ligands **3** and **4** with ligands **1** and **2**, which have the opposite configuration at C-3 and the same substituents in the biphenyl moieties.

In the first set of experiments, we used the rhodium-catalyzed hydrogenation of **7** to scope the potential of ligands **1–4**. The reaction proceeded smoothly at room temperature. The catalysts were prepared *in situ* by adding the corresponding phosphite–phosphoroamidite ligands to $[Rh(cod)_2]BF_4$ as a catalyst precursor.[13] The results are given in Table 1.

Interestingly, both enantioselectivity and activity notably improved when the hydrogen pressure was raised from 1 bar to 2.5 bar (entry 1 *vs.* 2). However, further increasing the hydrogen pressure had a positive effect on the activity, while the enantioselectivity remained the same (entries 3 and 5). This contrasts with the decrease in enantioselectivity usually observed with bidentate ligands when the hydrogen pressure is raised.[1a,7a,14] This allowed us to perform the reaction at lower catalyst concentration without loss in enantioselectivity and good activity (entry 6).

The addition of one fold excess of ligand did not affect the outcome of the reaction (entry 4). An increase in enantioselectivity (> 99%, entry 7) combined with good activity was found by lowering the reaction temperature. There were no changes in the enantioselectivities over time, which indicates that no decomposition of the catalyst took place.

Table 1 Asymmetric hydrogenation of **7** with $[Rh(cod)_2]BF_4$/**1–4**[a]

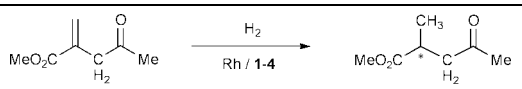

7 **8**

Entry	Ligand	P_{H2}/bar	% Conv. (*t*/h)[b]	% ee[c]
1	**1**	1	100 (20)	65 (*R*)
2	**1**	2.5	45 (8)	97 (*R*)
3	**1**	5	100 (8)	96 (*R*)
4[d]	**1**	5	100 (8)	96 (*R*)
5	**1**	30	100 (1.5)	97 (*R*)
6[e]	**1**	30	100 (10)	97 (*R*)
7[f]	**1**	30	100 (12)	> 99 (*R*)
8	**2**	5	86 (8)	86 (*R*)
9	**3**	5	46 (8)	34 (*R*)
10	**4**	5	40 (8)	30 (*R*)

[a] $[Rh(cod)_2]BF_4$ = 0.01 mmol. Ligand/Rh = 1.1. Substrate/Rh = 100. CH_2Cl_2 = 6 mL. *T* = 25 °C. [b] % Conversion measured by GC. [c] % Enantiomeric excess measured by GC using a Chiraldex G-TA column. [d] Ligand/Rh = 2. [e] Substrate/Rh = 1000. [f] At 5 °C.

 DOI: 10.1039/b109043g

The rest of the ligands were compared under 'standard' conditions *i.e.* dichloromethane as a solvent, 5 bar of hydrogen pressure, a ligand-to-rhodium ratio of 1 and at room temperature. Using ligand **2**, with methoxy groups instead of the *tert*-butyl groups in *para* positions of the biphenol moieties, resulted in slightly lower activity and enantioselectivity (entry 3 *vs.* 8). Ligands **3** and **4** whose configuration of carbon atom C-3 is opposite to those of ligands **1** and **2**, respectively, produced a lower reaction rate and enantioselectivity (entry 3 and 8 *vs.* 9 and 10).

The results clearly show that the enantiomeric excesses and activities depend strongly on the absolute configuration of the C3 stereocenter of the carbohydrate backbone and the substituents in the biphenyl moities. Therefore, enantioselectivities and activities were best using ligand **1** with a *S* configuration at C-3 and *tert*-butyl groups in the *ortho*- and *para*-positions of the biphenyl moieties.

We subsequently applied these new highly efficient phosphite–phosphoroamidite ligands **1**–**4** in the Rh-catalyzed hydrogenation of other benchmark dehydroaminoacid derivatives (Table 2). The results followed the same trend as for substrate **7**. The absolute configuration of the hydrogenated products **10** and **12** is opposite that of the hydrogenated product **8**, but they have the same spatial arrangement.[15] The catalyst precursor with ligand **1** produced the highest enantiomeric excess (98%, entries 5 and 10).

It is remarkable that these phosphite–phosphoroamidite ligands showed a much higher degree of enantioselectivity and higher reaction rates than their corresponding diphosphite analogues under similar reaction conditions (entries 1–4 *vs.* 11 and 12).[13,16]

In summary, we have described the first application of phosphite–phosphoroamite ligands in the asymmetric hydrogenation reaction. These ligands can be easily prepared in a few steps from commercial D-(+)-xylose as an inexpensive natural chiral source. Regarding both good activity and the excellent enantioselectivity (up to >99% ee) obtained in simple unoptimised asymmetric hydrogenation of a series of α,β-unsaturated carboxylic acid derivatives, we feel that a promising new class of ligands—the phosphite–phosphoroamidite—has been disclosed for enantioselective Rh-catalyzed asymmetric hydrogenation. Moreover, because of the modular construction of these phosphite–phosphoroamidite ligands,

Table 2 Asymmetric hydrogenation of methyl *N*-acetylaminoacrylate **9** and methyl (*Z*)-*N*-acetylaminocinnamate **11** with $[Rh(cod)_2]BF_4$/**1**–**4**[a]

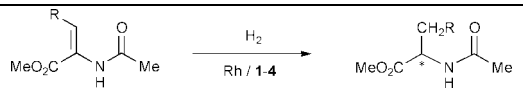

9 R = H
11 R = Ph

10 R = H
12 R = Ph

Entry	Substrate	Ligand	P_{H_2}/bar	% Conv. (*t*/h)[b]	% ee[c]
1	**9**	**1**	5	100 (8)	92 (*S*)
2	**9**	**2**	5	71 (8)	82 (*S*)
3	**9**	**3**	5	46 (8)	15 (*S*)
4	**9**	**4**	5	33 (8)	12 (*S*)
5[d]	**9**	**1**	30	100 (12)	98 (*S*)
6	**10**	**1**	5	77 (8)	94 (*S*)
7	**10**	**2**	5	53 (8)	85 (*S*)
8	**10**	**3**	5	29 (8)	18 (*S*)
9	**10**	**4**	5	35 (8)	17 (*S*)
10[d]	**10**	**1**	30	72 (12)	98 (*S*)
11	**9**	**13**	5	94 (20)	33 (*S*)
12	**9**	**14**	5	56 (20)	4 (*R*)

[a] $[Rh(cod)_2]BF_4$ = 0.01 mmol. Ligand/Rh = 1.1. Substrate/Rh = 100. CH_2Cl_2 = 6 mL. T = 25 °C. [b] % Conversion measured by GC. [c] % ee measured by GC using a Permabond L-Chirasil-Val column. [d] At 5 °C.

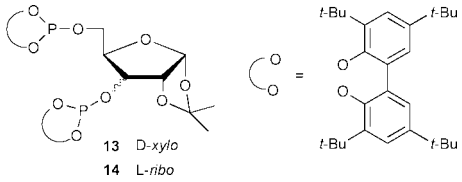

further structural diversity is easy to achieve, so enantioselectivity and catalyst performance can be maximized for each new substrate as required. Studies of this kind, as well as mechanistic studies, are currently under way.

We thank the Spanish Ministerio de Educación, Cultura y Deporte and the Generalitat de Catalunya (CIRIT) for their financial support (PB97-0407-CO5-01).

Notes and references

1 (*a*) R. Noyori, *Asymmetric Catalysis in Organic Synthesis*, Wiley, New York, 1994; (*b*) *Catalytic Asymmetric Synthesis*, ed. I. Ojima, Wiley, New York, 2000; (*c*) *Comprehensive Asymmetric Catalysis*, ed. E. N. Jacobsen, A. Pfaltz and H. Yamamoto, Springer, Berlin, 1999, vol. 1; (*d*) H. Brunner and W. Zettlmeier, *Handbook of Enantioselective Catalysis*, VCH, Weinheim, 1993.

2 (*a*) U. Nettekoven, P. C. J. Kamer, P. W. N. M. van Leeuwen, M. Widhalm, A. L. Speck and M. Lutz, *J. Org. Chem.*, 1999, **64**, 3996; (*b*) U. Barens, M. J. Burk, A. Gerlach and W. Hems, *Angew. Chem., Int. Ed.*, 2000, **39**, 1981.

3 (*a*) A. S. C. Chan, W. Hu, C.-C. Pai and C.-P. Lau, *J. Am. Chem. Soc.*, 1997, **119**, 9570; (*b*) T. A. Ayers and T. V. RajanBabu, *Process Chem. Pharm. Ind.*, 1999, 327; (*c*) R. Selke, *J. Organomet. Chem.*, 1989, **370**, 249.

4 K. Inoguhi, S. Sakuraba and K. Achiwa, *Synlett*, 1992, 169.

5 O. Pàmies, M. Diéguez, G. Net, A. Ruiz and C. Claver, *Chem. Commun.*, 2000, 2383.

6 (*a*) M. T. Reetz and T. Neugebauer, *Angew. Chem., Int. Ed.*, 1999, **38**, 179; (*b*) M. T. Reetz and G. Mehler, *Angew. Chem., Int. Ed.*, 2000, **39**, 3889.

7 (*a*) M. van den Berg, A. J. Minnaard, E. P. Schudde, J. van Esch, A. H. M. de Vries, J. G. de Vries and B. L. Feringa, *J. Am. Chem. Soc.*, 2000, **122**, 11 539; (*b*) G. Franciò, F. Faraone and W. Leitner, *Angew. Chem., Int. Ed.*, 2000, **39**, 1428; (*c*) O. Huttenloch, J. Spieler and H. Waldmann, *Chem. Eur. J.*, 2000, **6**, 671.

8 M. Diéguez, O. Pàmies, A. Ruiz, S. Castillón and C. Claver, *Chem. Eur. J.*, 2001, **7**, 3086.

9 A few phosphite–phosphoroamidite ligands have been described and applied to asymmetric hydroformylation with moderate results, see for instance: S. Naili, I. Suisse, A. Mortreux, F. Agbossou-Niedercron and G. Nowogrocki, *J. Organomet. Chem.*, 2001, **628**, 122 and references cited therein.

10 The new ligands **1**–**4** were synthesized very efficiently in one step by treatment of the corresponding aminoalcohols **5**, easily prepared on large scale from readily available D-(+)-xylose, with two equivalents of the desired *in situ* formed phosphorochloridites **6** in the presence of pyridine. Selected NMR data. **1**: δ_P ($CDCl_3$) 144.8 (br s), 145.1 (s). **2**: δ_P ($CDCl_3$) 144.0 (s), 145.9 (s). **3**: δ_P ($CDCl_3$) 143.2 (s), 150.2 (s). **4**: δ_P ($CDCl_3$) 143.5 (s), 149.3 (s).

11 (*a*) D. F. Ewing, G. Goethals, G. Mackenzie, P. Martin, G. Ronco, L. Vanbaelinghem and P. Villa, *J. Carbohydr. Chem.*, 1999, **18**, 441; (*b*) D. F. Ewing, G. Goethals, G. Mackenzie, P. Martin, G. Ronco, L. Vanbaelinghem and P. Villa, *Carbohydr. Res.*, 1999, **321**, 190.

12 G. J. H. Buisman, P. C. J. Kamer and P. W. N. M. van Leeuwen, *Tetrahedron: Asymmetry*, 1993, **4**, 1625.

13 For general hydrogenation procedure see: O. Pàmies, G. Net, A. Ruiz and C. Claver, *Eur. J. Inorg. Chem.*, 2000, 1287.

14 (*a*) A. Pfaltz and J. M. Brown, *Houben-Weyl Methods of Organic Chemisty*, ed. G. Helchem, R. W. Hoffmann, J. Mulzer and E. Schaumann, Thieme, Stuttgart, 1995, vol. E21, D.2.5.1.2; (*b*) X. Zhang, *Enantiomer.*, 1999, **4**, 541; (*c*) M. J. Burk and F. Bienewald, *Transition Metals For Organic Synthesis*, ed. M. Beller and C. Bolm, Wiley-VCH, Weinheim, 1998, vol. 2; ch. 1.1.2.

15 R. S. Cahn, C. K. Ingold and V. Prelog, *Angew. Chem., Int. Ed. Engl.*, 1966, **5**, 385.

16 O. Pàmies, G. Net, A. Ruiz and C. Claver, *Tetrahedron: Asymmetry*, 2000, **11**, 1097.

CHEMCOMM
Communication
www.rsc.org/chemcomm

Palladium catalyzed arylation of malonate accompanying *in situ* dealkoxycarbonylation

Yoshinori Kondo,* Kiyofumi Inamoto, Masanobu Uchiyama and Takao Sakamoto

Graduate School of Pharmaceutical Sciences, Tohoku University, Aobayama, Aoba-ku, Sendai 980-8578, Japan. E-mail: ykondo@mail.pharm.tohoku.ac.jp

Received (in Cambridge, UK) 18th October 2001, Accepted 7th November 2001
First published as an Advance Article on the web 6th December 2001

One-pot conversion of aryl halides into aryl acetates was achieved by the palladium catalyzed arylation of malonate accompanying *in situ* dealkoxycarbonylation of aryl malonates using Cs_2CO_3 as a base and as a catalyst.

Introduction of an sp^3 carbon side chain into an aromatic ring is one of the important process in organic synthesis and many works have been done using palladium catalyzed reactions.[1] Various approaches have been studied for the synthesis of aryl acetates using coupling reactions[2–4] and very recently significant progress has been made for direct introduction of an acetic acid ester moiety into aromatic rings using palladium catalyzed reactions.[5] On the other hand, introduction of active methylenes into aromatic rings has also been an important subject[6] and Hartwig *et al*. recently succeeded in the arylation of malonate, however a strong base such as NaO^{t}Bu has been used.[7] In connection with our recent studies on chemoselective transformation of functionalized aromatic compounds,[8] we became interested in the introduction of an acetic acid moiety under mild reaction conditions using a weaker base. During the course of our recent studies on the coupling reaction of aryl halides with diethyl malonate, it was found that diethyl phenylmalonate undergoes a dealkoxycarbonylation reaction in the presence of a weak inorganic base. Namely, when we carried out the cross coupling reaction of iodobenzene with diethyl malonate in the presence of $Pd_2(dba)_3$, ^{t}Bu$_3$P using Cs_2CO_3 as a base in dimethoxyethane at 80 °C for 68 h, diethyl phenylmalonate was obtained in 71% yield together with the dealkoxycarbonylated product, ethyl phenylacetate in 11% yield (Scheme 1).

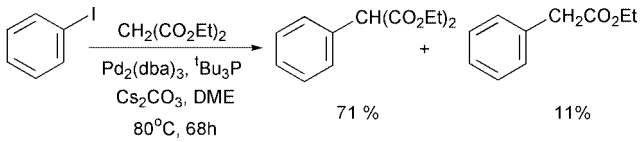

Scheme 1

We focused our interest in this interesting dealkoxycarbonylation and diethyl phenylmalonate was treated with various bases in dimethoxyethane at elevated temperatures. As shown in Table 1, Cs_2CO_3 was found to be the most effective catalyst for the decarbonylative conversion. In order to complete the dealkoxycarbonylation during the cross coupling reaction, the reaction of iodobenzene with diethyl malonate was carried out at an elevated temperature such as 120 °C using 10 equiv. of Cs_2CO_3 for 65 h, and ethyl phenylacetate was obtained in 87% yield exclusively. Similarly, iodoanisole was reacted with the malonate under the same reaction conditions, and 4-methoxyphenyl acetate was obtained in 70% yield. Ethyl 4-iodobenzoate was also successfully reacted with the malonate under the same reaction conditions, and the coupling–dealkoxycarbonylation proceeded smoothly to give the aryl acetate in 61% yield without forming any side reaction products. Aryl bromides were also employed as substrates for this process. The reaction of bromobenzene and 3-bromopyridine gave the corresponding aryl acetates in 78% and 75% yields respectively (Table 2).

Table 1

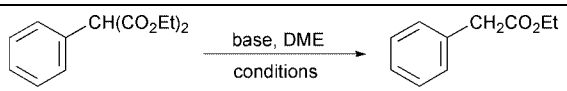

Base	Conditions	Yield (%)
Cs_2CO_3	80 °C, 66 h	15 (78)[a]
Cs_2CO_3	120 °C, 70 h	83 (3)[a]
K_2CO_3	120 °C, 67 h	62 (8)[a]
NaH	120 °C, 70 h	0 (99)[a]

[a] Recovery yields in parentheses.

Table 2

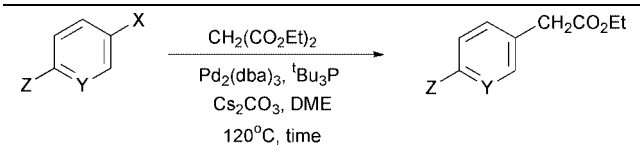

X	Y	Z	Time/h	Yield (%)
I	CH	H	65	87
I	CH	OMe	74	70
I	CH	COOEt	76	61
Br	CH	H	70	78
Br	N	H	45	75

A simple and chemoselective introduction of an acetic acid moiety was accomplished by using the present Pd coupling–dealkoxycarbonylation process and further applications of this method for the facile functionalization of biologically active molecules are underway.

This work was partly supported by the Grant-in Aid for Scientific Research (No. 12672047 and No. 12557198) from the Ministry of Education, Culture, Sports, Science, and Technology, Japan.

Notes and references

1 R. F. Heck, *Palladium Reagents in Organic Synthesis*, New York, Academic Press, 1985; J. Tsuji, *Palladium Reagents and Catalysts*, Chichester, John Wiley & Sons Ltd., 1995.
2 J. F. Fauvarque and A. Justand, *J. Organomet. Chem.*, 1979, **177**, 273; F. Orsini, F. Pelizzoni and L. M. Vallarino, *J. Organomet. Chem.*, 1989, **367**, 375.
3 C. Carfagna, A. Musco, G. Sallese, R. Santi and T. Fiorani, *J. Org. Chem.*, 1991, **56**, 261; R. Galarini, A. Musco, R. Pontellini and R. Santi, *J. Mol. Catal.*, 1992, **72**, L11; F. Agnelli and G. A. Sulikowski, *Tetrahedron Lett.*, 1998, **39**, 8807; T. Sakamoto, Y. Kondo, K. Masumoto and H. Yamanaka, *J. Chem. Soc., Perkin Trans. 1*, 1994, 235; T. Sakamoto, Y. Kondo, K. Masumoto and H. Yamanaka, *Heterocycles*, 1993, **39**, 8807.
4 M. Kosugi, I. Hagiwara, T. Sumiya and T. Migita, *Bull. Chem. Soc. Jpn.*, 1984, **57**, 242.

 DOI: 10.1039/b109418a

5 W. A. Moradi and S. L. Buchwald, *J. Am. Chem. Soc.*, 2001, **123**, 7996; S. Lee, N. A. Beare and J. F. Hartwig, *J. Am. Chem. Soc.*, 2001, **123**, 8410.
6 M. Uno, K. Seto and S. Takahashi, *J. Chem. Soc., Chem. Commun.*, 1984, 932.
7 M. Kawatsura and J. F. Hartwig, *J. Am. Chem. Soc.*, 1999, **121**, 1473.
8 Y. Kondo, N. Takazawa, C. Yamazaki and T. Sakamoto, *J. Org. Chem.*, 1994, **59**, 4717; Y. Kondo, T. Matsudaira, J. Sato, N. Murata and T. Sakamoto, *Angew. Chem., Int. Ed. Engl.*, 1996, **35**, 736; Y. Kondo, M. Shilai, M. Uchiyama and T. Sakamoto, *J. Am. Chem. Soc.*, 1999, **121**, 3539; Y. Kondo, M. Asai, T. Miura, M. Uchiyama and T. Sakamoto, *Org. Lett.*, 2001, **3**, 13.

CHEMCOMM Communication
www.rsc.org/chemcomm

Amplification of the reactivity difference between two methylene groups of cyclodextrins *via* a cap

De-Qi Yuan,* Tomonobu Yamada and Kahee Fujita*

Faculty of Pharmaceutical Sciences, Nagasaki University, 1-14 Bunkyo-machi, Nagasaki 852-8521, Japan. E-mail: deqiyuan@net.nagasaki-u.ac.jp; fujita@net.nagasaki-u.ac.jp; Fax: +81-95-846 5736; Tel: +81-95-846 5736

Received (in Cambridge, UK) 17th September 2001, Accepted 14th November 2001
First published as an Advance Article on the web 6th December 2001

A novel concept has been established for making hetero-disubstituted cyclodextrin derivatives. Upon treatment with imidazole, 6^A,6^B-mesitylenedisulfonyl-capped β-cyclodextrin 1 demonstrated a reactivity about 10 times higher at the 6^B position than at the 6^A position, leading to the selective formation of hetero-disubstituted cyclodextrins 3.

Cyclodextrin derivatives bearing two different sorts of functional groups turn out to be interesting candidates in developing artificial receptors and enzyme-like catalysts.[1] The hetero-bifunctional CDs were not only postulated to effect a three-point recognition of asymmetric species,[2] but also demonstrated to have strong asymmetric induction in catalyzing the chemical transformations such as transamination reactions.[3] However, these hetero-bifunctional CDs are very difficult to access.[4] The routine method includes stepwise substitution of 6^A,6^B-diiodo-β-CD with different nucleophiles.[3] An alternative method included the sulfonylation of mono-substituted CDs.[5] In either case, the reaction is rather a random one and subjected to the competition of over-substitution, giving a mixture of hetero-disubstituted regio-isomers in a comparable ratio together with over-substituted products and starting materials. The separation of desired products is an extremely tedious task, and several reports used the isomeric mixtures in binding and catalysis without separating them from each other.[6]

In principle, as soon as β-CD is modified, the C_7 symmetry is destroyed and all the seven glucose residues become different from each other unless they are all equally modified. That is, a bifunctional β-CD would show different reactivity at its two modified positions. However, this difference is usually trivial as it is observed in the reactions of 6^A,6^B-diiodo-β-CD and can hardly be applied in the selective hetero-bifunctionalization. We reason that any two methylene groups of β-CD, when bridged together by a rigid cap, would have a somewhat fixed conformation since their rotation around the C5–C6 single bond would be greatly confined. If the cap can serve as leaving group in a S_N2 reaction, it may provide a possibility to protect one of the capped methylene residues from the attack of the nucleophile while leaving the other easily accessible to the nucleophile (Scheme 1), that is, to amplify the difference in reactivity between those two modified positions. Herein we describe that the mesitylenedisulfonyl-capped β-CD indeed undergoes a selective ring-opening reaction, and directs imidazole to the 6^B position, offering a promising method to access the hetero-bifunctional CDs.

Mesitylenedisulfonyl chloride was reacted with β-CD in dry pyridine affording the capped CD in *ca.* 20% yield. The capped positions were determined to be 6^A and 6^B by converting the capped CD to bis(phenylthio) species followed by HPLC comparison with authentic samples prepared according to a literature method.[7] The two sulfonated glucosides of **1** are found to be magnetically very different from each other. The geminal protons of one sulfonated methylene group resonate at the magnetic field *ca*. 0.4 ppm higher than those of the other one,[8] implying that the benzene ring is located closer to and thus exercises a stronger shielding effect on one of the two modified methylene residues. This shielded methylene group seems to correspond to glucoside A since the other modified unit demonstrated *ca*. 0.5 ppm upfield shift for its H1, indicating that this H1 is likely to be situated somewhere within the region of ring current effect of the cap, close to the shielded methylene protons.

On treatment with imidazole in DMF, **1** undergoes a ring-opening reaction leading to the formation of two hetero-disubstituted CDs which were isolated in 4% and 42% yields, respectively. FAB-MS and NMR spectra show that the two products are regio-isomers containing one imidazolyl group and one mesitylene residue.[9] The result clearly demonstrates that the mesitylene cap does significantly amplify the difference in reactivity between the 6^A and 6^B positions. We also noted that as long as the cap is opened, *i.e.* one sulfonate group is displaced, another sulfonate group becomes much more resistant to the attack of a second molecule of imidazole and therefore remains unaffected till the complete conversion of the starting material (Scheme 2).

In order to find out whether 6^A or 6^B is more accessible to imidazole, we need to clarify the regio-chemistry of the products. NMR spectra afforded important information. In the ^{1}H NMR (in D_2O, CH_3CN as internal standard: δ = 1.98 ppm) spectrum of the minor product, one of the unmodified methylene groups was observed at 2.94 and 3.19 ppm, the sulfonated one at 4.48 ppm, the imidazole-bearing one at 4.36 and 4.21 ppm, and the other methylene groups in the normal range of 3.65–3.85 ppm. It is documented in literature that an imidazole group attached to a methylene carbon of CDs exercises a strong shielding effect on the subunit linked to the anomeric carbon of the 6-imidazolyl glucoside while it does not significantly influence the one on the other side.[10] The upfield shifted unmodified methylene group can be therefore assigned to that of the sugar clockwise to the 6-imidazolyl glucoside (view from the secondary side), *i.e.* the minor product has the structure of compound **2**, and the major product should be compound **3**. In agreement with this assignment, the major

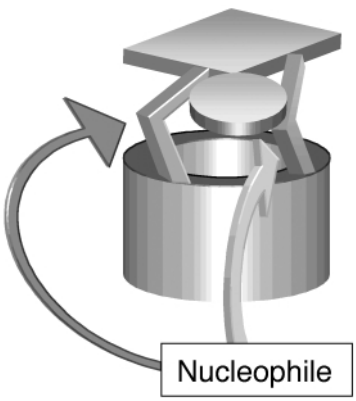

Scheme 1 Illustration for a possible control of reaction selectivity in hetero-bifuctionalization by a suitable cap.

 DOI: 10.1039/b108416j

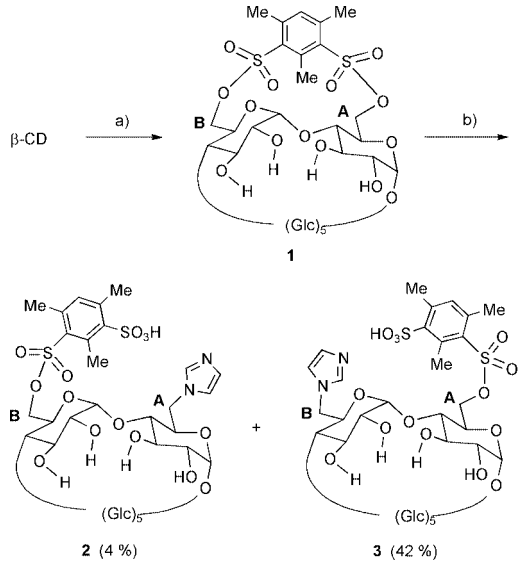

Scheme 2 Synthesis and selective ring-opening of the mesitylenedisulfonyl-capped β-CD. a) Mesitylenedisulfonyl chloride–dry pyridine, 40 °C, 2.5 h; b) imidazole–DMF, 80 °C, 3 h.

product demonstrated no significant upfield shifts for any unmodified methylene groups, whereas the sulfonated methylene group was observed at 3.93 and 3.83 ppm, about 0.5 ppm upfield shifted to that of the minor product.

The above structural assignment was confirmed by enzyme degradation of **3** followed by MS fragmentation analysis of the degradation product (Scheme 3). The sulfonate group of **3** was replaced by $PhCH_2S$ and the resulting compound **4** was

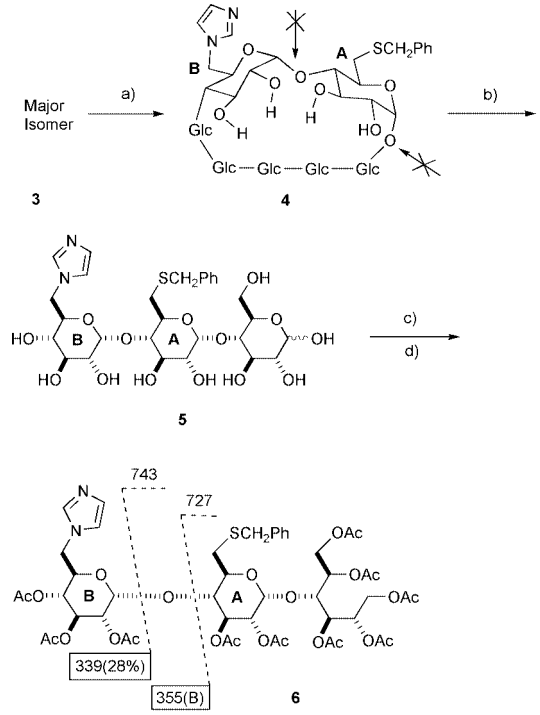

Scheme 3 Enzymatic transformation of **3** incorporated with MS fragmentation analysis. The data denote the mass units expected from the fragmentation between the two modified sugar residues and the enclosed ones were actually observed in the EI-MS spectrum. a) $PhCH_2SH$–Cs_2CO_3–DMF; b) *Taka amylase A*–10% DMSO-phosphate buffer; c) $NaBH_4$–80% ethanol; d) acetic anhydride.

degradated to maltotriose **5** by *Taka amylase A*,[11] an α-amylase that catalyzes the hydrolysis of the α-1,4-glucoside bond of unmodified α-1,4-glucans but usually leaves that of the modified ones unaffected. The sugar sequence of the maltotriose was analysed by MS after it was subjected to further reduction and per-acetylation. As depicted in Scheme 3, the EI MS of **6** demonstrated strong peaks at *m/z* 355 (base peak) and 339 (28%) which correspond to the fragmentation between the two modified glucoside residues of **6**, whereas the fragments at *m/z* 395 (or 687) and 411 (or 671) expected for the alternative arrangement of Im and $PhCH_2S$ groups were not observed.

In conclusion, the present research postulated to amplify the difference in reactivity between the two modified methylene groups of β-CD by a rigid cap; and proved it practicable by taking mesitylenedisulfonyl capped β-CD as an example, offering a promising approach to access the hetero-bifunctional CDs.

Notes and references

1 W. B. Motherwell, M. J. Bingham and Y. Six, *Tetrahedron*, 2001, **57**, 4663; R. Breslow and S. D. Dong, *Chem. Rev.*, 1998, **98**, 1997. In this paper, the sugar units of β-CD derivatives are labeled counterclockwise A, B,…, G, respectively, on view from the secondary hydroxyl side.

2 For recent reviews on the molecular recognition of CDs and their derivatives, see: E. Rizzarelli and G. Vecchio, *Coord. Chem. Rev.*, 1999, **188**, 343; M. V. Rekharsky and Y. Inoue, *Chem. Rev.*, 1998, **98**, 1875.

3 E. Fasella, S. D. Dong and R. Breslow, *Bioorg. Med. Chem.*, 1999, **7**, 709; I. Tabushi, Y. Kuroda, M. Yamada, H. Higashimura and R. Breslow, *J. Am. Chem. Soc.*, 1985, **107**, 5545.

4 For a recent review on the modification of CDs, see: A. R. Khan, P. Forgo, K. J. Stine and V. T. D'Souza, *Chem. Rev.*, 1998, **98**, 1977.

5 K. Fujita, H. Yamamura, Y. Egashira and T. Imoto, *Tetrahedron Lett.*, 1992, **33**, 3511; K. Fujita, H. Yamamura and T. Imoto, *Tetrahedron Lett.*, 1991, **32**, 6737.

6 F. Hamada, M. Narita, K. Kinoshita, A. Makabe and T. Osa, *J. Chem. Soc., Perkin Trans. 2*, 2001, 388–394; S. D. Steven and R. Breslow, *Tetrahedron Lett.*, 1998, **39**, 9343.

7 K. Fujita, A. Matsunaga and T. Imoto, *Tetrahedron Lett.*, 1984, **25**, 5533.

8 *Preparation of capped β-CD* **1**: β-CD (dried overnight *in vacuo* at 100 °C, 3.5 g) was dissolved in dry pyridine (200 ml). The resultant solution was refluxed for a few minutes and the solvent was distilled off until the boiling point of the distillate reached 113 °C. The solution was allowed to cool down to rt and molecular sieves (30 g) were then added in. After the mixture was stirred at rt for a few hours, mesitylenedisulfonyl chloride (1.1 g) was added and the reaction was continued for 2.5 h at 40 °C. Thereafter, the molecular sieves was filtered and the solvent was rota-evaporated. Chromatography of the residue on a reversed-phase Lobar column (RP-18, size C, with a gradient elution from 30% to 65% *aq.* CH_3OH) afforded the capped β-CD **1** (810 mg, 19%). In the ^1H-^{13}C COSY spectrum of **1** (DMSO-d_6, TMS *int.*), one of the sulfonated glucosides was observed at δ 4.58–71.9 and 4.10–71.9 for H6–C6, 3.76–69.8 for H5–C5, 3.22–82.1 for H4–C4, ~3.6–(71.9 to 73.2) for H3–C3, 3.17–71.4 for H2–C2 and 4.40–101.0 ppm for H1–C1 correlation. The other one was observed at δ 4.14–69.9 and 3.84–69.9 for H6–C6, 3.89–69.3 for H5–C5, ~3.25–(81.0 to 81.9) for H4–C4, ~3.65–(71.9 to 73.2) for H3–C3, (3.25 to 3.4)–(71.9 to 72.4) for H2–C2, (4.82 to 4.95)–(101.3 to 102.2) ppm for H1–C1 correlation.

9 *Reaction of* **1** *with imidazole:* Compound **1** (0.5 g, 0.36 mmol) and imidazole (0.5 g, 7.1 mmol) were dissolved in DMF (2 mL) and the solution was stirred at 85 °C for 3 h. The CD species were precipitated with acetone, collected by filtration and applied to chromatography on a reversed-phase Lobar column (RP-18, size C). Elution of the column with 20% *aq.* CH_3OH afforded products **2** and **3** in 4% (elutes faster) and 42% (elutes slower) yields, respectively.

10 D.-Q. Yuan, K. Koga, M. Yamaguchi and K. Fujita, *Chem. Commun.*, 1996, 1943; V. Cucinotta, F. D'Alessandro, G. Impellizzeri and G. Vecchio, *J. Chem. Soc., Chem. Commun.*, 1992, 1743.

11 K. Fujita, A. Matsunaga, Y. Ikeda and T. Imoto, *Tetrahedron Lett.*, 1985, **26**, 6439; K. Fujita, T. Tahara, S. Nagamura, T. Imoto and T. Koga, *J. Org. Chem.*, 1987, **52**, 63.

CHEMCOMM
Communication
www.rsc.org/chemcomm

Inductively coupled plasma mass spectrometry to identify protein drug targets from whole cell systems†

Claire S. Allardyce,[a] Paul J. Dyson,*[a] Fadi R. Abou-Shakra,[b] Heather Birtwistle[b] and Jonathan Coffey[b]

[a] *Department of Chemistry, The University of York, Heslington, York, UK YO10 5DD. E-mail: pjd14@york.ac.uk*
[b] *Micromass UK Ltd, Atlas Park, Simonsway, Manchester, UK M22 5PP*

Received (in Cambridge, UK) 19th September 2001, Accepted 14th November 2001
First published as an Advance Article on the web 7th December 2001

Proteins from cisplatin treated bacterial cells were partially separated by 1D polyacrylamide gel electrophoresis and analysed by laser ablation inductively coupled plasma mass spectrometry; using peptide fingerprinting methods central to proteomics, the band containing the highest levels of platinum was found to contain outer membrane protein A, which may be involved in cisplatin uptake.

The highly successful anticancer drug cisplatin was originally observed to prevent the division of *E. coli* cells,[1] and subsequently, it was found that cisplatin forms adducts with DNA, which inhibit protein synthesis and DNA replication.[2] The interaction between DNA and cisplatin has been structurally and kinetically characterised[3] whereas the ways in which cisplatin interacts with other biomolecules are less well understood. Cisplatin binding to proteins in the cell membrane is observed to be favoured over binding to the phospholipids,[4] resulting in alterations to the structure and properties of the membrane, such as permeability.[5] Membrane permeability can affect the toxicity of the compound, with reduced uptake and accelerated efflux mechanisms being involved in some mechanisms of cisplatin resistance in cancer cell lines.[6] A map of cisplatin metabolism in the cell, in which the key proteins involved in the mechanisms of uptake and drug resistance are identified, would be invaluable in order to understand the features that make cisplatin such an effective anticancer drug, and ultimately facilitate the design of improved anticancer therapies.

With current methods, including proteomics, identifying metal–protein complexes from whole cell systems is a mammoth task that depends on detecting subtle differences in, for example, the migration of the metal–protein species during gel electrophoresis. However, it has been shown that it is possible to rapidly detect metal–protein complexes immobilised in gels by laser ablation ICP-MS.[7] In this communication we extend this approach by combining the laser ablation ICP-MS analysis of protein gels with peptide fingerprinting methods, which are routinely applied in proteomics to identify proteins of interest, to enable metal-bound proteins from whole cell extracts to be rapidly identified.

The proteins from *E. coli* cells, which had been incubated with cisplatin, were partially separated by non-reducing gel electrophoresis.[8] The gel lanes were then analysed by laser ablation inductively coupled plasma mass spectrometry (ICP-MS)[9] and the *m/z* of platinum was detected across the gel (see Fig. 1) that were not observed in the control. The distribution of platinum through the gel was not proportional to the distribution of protein, estimated from a densitometry scan of the gel, suggesting platinum has, to some extent, specific protein targets within the cell. The band with the highest ICP-MS response for the *m/z* of platinum relative to the amount of protein present was selected for peptide fingerprinting by electrospray mass spectrometry. The band was excised from the gel, digested with trypsin and the resultant peptides extracted and analysed by electrospray mass spectrometry and MS/MS, typical of proteomics methods.[10] The masses and sequences of these peptides were combined to produce a peptide fingerprint that indicated a single protein was present in the gel fragment and allowed *ca.* 23% of the total protein sequence[11] to be mapped, unambiguously identifying the protein as Outer Membrane Protein A (OmpA).

OmpA is a ubiquitous, porin-like protein[12] that transverses the outer membrane[13] acting as an ion channel with a low permeability to allow the slow penetration of small solutes.[14] These solutes could include cisplatin, as, although the crystal structure implies that the centre of the β-barrel that traverses the membrane would not carry an ion, there are three flexible extracellular loops that may be involved in a conformational change to allow ion uptake.[15] In addition to its porin function, OmpA is involved in the maintenance of cell shape,[16] hence the cisplatin–OmpA interaction could explain the altered membrane permeability and structure of bacterial membranes after incubation with cisplatin.

OmpA has clinical interest as it is involved in bacterial induced toxicity[17,18] and the mechanism of *E. coli* infectivity, in particular the invasion of macrovascular cells enabling the bacteria to cross the blood brain barrier.[19] OmpA is also secreted into the plasma in a complex with two other proteins, peptidoglycan associated protein and murein lipoprotein, by Gram negative bacteria incubated in human serum, and this complex is bound by immunoglobulin G.[18] Thus, further characterisation of the OmpA–cisplatin interaction may provide

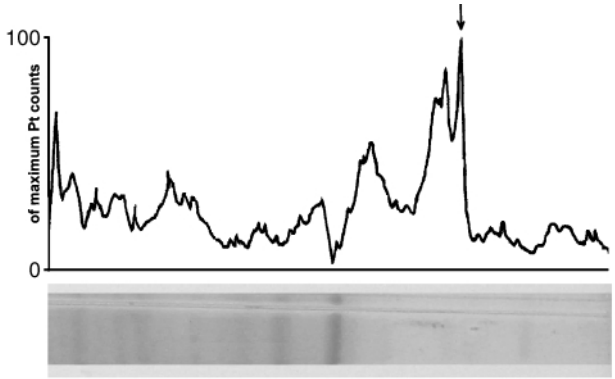

Fig. 1 Non-reducing polyacrylamide gel electrophoresis results for the separation of SDS-denatured proteins from whole bacterial cells after incubation with cisplatin; (top) the ICP-MS trace showing the amount of platinum as a percentage of the maximum reading (6.19×10^4 counts) with distance along the gel and (bottom) a photograph of the gel aligned with the ICP-MS trace. The arrow indicates the region with highest ICP-MS response for the *m/z* for platinum, which was used to identify the gel bands for further analysis.

† Electronic supplementary information (ESI) available: full details of laser ablation ICP-MS and QTOF operating conditions, further experimental details for peptide separation and peptide sequencing maps for OmpA. See http://www.rsc.org/suppdata/cc/b1/b108418f/

 DOI: 10.1039/b108418f

a foundation for drug design against bacterial infections, such as bacterial meningitis.

We are currently conducting further experiments to elucidate the role of OmpA in the uptake and mechanism of cisplatin cytotoxicity. For example, identifying other proteins containing high amounts of platinum immobilised in other areas of the gel to provide a more detailed list of the proteins that are involved in these first stages of the cisplatin interaction with bacterial cells and exploring the effect of incubation time on the cisplatin–protein interactions.

The combination of ICP-MS and protein fingerprinting methods enables proteins tagged with specific elements or isotopes to be rapidly identified. We have also started to use the technique to investigate a new potential ruthenium anticancer drug[20] that shows more specific binding to proteins than cisplatin and these studies will be reported in due course. Furthermore, it may even be possible to extend the technique from cells grown in culture to biopsy material providing a powerful tool for investigating drug metabolism *in vivo*. This combined ICP-MS-protein fingerprinting approach overcomes some of the current limitations of proteomics methods for the investigation of interactions of proteins with small molecules, giving information regarding metal loading of proteins in diseased states as well as identifying drug targets, enabling the rapid characterisation of the molecular basis of disease and therapy.

Notes and references

1 B. Rosenberg, L. Van Camp and T. Krigas, *Nature*, 1965, **205**, 698.
2 E. R. Jamieson and G. J. Lippard, *Chem. Rev.*, 1999, **99**, 2467.
3 J. Reedijk, *Chem. Rev.*, 1999, **99**, 2499.
4 M. Maccarrone, W. F. Nieuwenhuizen, H. F. J. Dullens, M. V. Catni, G. Melino, G. A. Veldink, J. F. G. Vliegenthart and A. F. Agro, *Eur. J. Biochem.*, 1996, **241**, 297.
5 K. Wang, J. F. Lu and R. C. Li, *Coord. Chem. Rev.*, 1996, **151**, 53.
6 B. Salles, P. Calsou, K. Bouayadik and H. Vinial, *Toxicology*, 1994, **93**, 235.
7 J. L. Neilsen, A. Abildtrup, J. Christensen, P. Watson, A. Cox and C. W. McLeod, *Spectrochim. Acta B*, 1998, **53**, 339.
8 Suspensions of *Eschericia coli* JM109 (Promega, USA) in nutrient broth were incubated for 30 min at 37 °C with and without 10 mM cisplatin. The cells were pelleted by centrifugation and resuspended in distilled water (500 μl) before sonication. The cell debris was pelleted by centrifugation and the proteins in the supernatant fractions were separated by non-reducing SDS gel electrophoresis in a 10% polyacrylamide gel and visualised with coomassie brilliant blue G stain (Sigma). The gels were dried in cellulose membranes and analysed by ICP-MS.
9 The non-reducing SDS gel lanes of the unmodified and cisplatin-incubated *E. coli* cells were placed on a Cetac LSX-200 Laser Ablation System (Cetac Technologies), which was coupled to a Micromass Platform ICP Life-MS (Micromass UK Ltd). The laser and Platform ICP-MS can detect platinum at concentrations below 1 ppb under the conditions specified in the ESI.† The gels were ablated using the laser and the resulting plasma analysed for the platinum isotopes using the Platform ICP.
10 R. Aebersold and D. R. Goodlet, *Chem. Rev.*, 2000, **101**, 269.
11 The protein band containing the highest amount of platinum relative to coomassie blue staining was excised from the gel. This in-gel protein sample was automatically processed and trypsin (Promega, USA) digested using a Micromass MassPREP station as described in the ESI.† The resultant peptides were desalted and separated on a C18 column (see ESI†) and directed into the Z-spray source of a Micromass Q-TOF2 mass spectrometer operated in the positive ion mode. All data were processed automatically by means of ProteinLynx software; protein identification was achieved by analysis with ProteinLynx Global Server version 1.0 by matching both the peptide masses and sequences of the digested proteins.
12 A. Pautsch and G. E. Schulz, *Nat. Struct. Biol.*, 1998, **5**, 1013.
13 M. Klose, A. Storiko, Y. D. Stierhof, I. Hinderennach, B. Mutschler and U. Henning, *J. Biol. Chem.*, 1993, **268**, 25 664.
14 N. Saint, C. El Hamel, E. Dé and G. Molle, *FEMS Microbiol. Lett.*, 2000, **190**, 261.
15 A. Arora, D. Rinehart, G. Szabo and L. K. Tamm, *J. Biol. Chem.*, 2000, **275**, 1594.
16 N. Saint, C. El Hamel, E. Dé and G. Molle, *FEMS Microbiol. Lett.*, 2000, **190**, 261; I. Sonntag, H. Schwarz, Y. Hirota and U. Henning, *J. Bacteriol.*, 1978, **136**, 280.
17 J. Hellman, P. M. Loiselle, M. M. Tehan, J. E. Allaire, L. A. Boyle, J. T. Kurnick, D. M. Andres, K. S. Kim and H. S. Warren, *Infect. Immun.*, 2000, **68**, 2566.
18 J. Hellman, E. M. Zanaot, P. M. Loiselle, S. F. Amato, K. M. Black, Y. M. Ge, J. T. Kurnick and H. S. Warren, *J. Infect. Dis.*, 1997, **176**, 1260.
19 N. V. Prasadarao, C. A. Wass, J. N. Weiser, M. E. Stins, S. H. Huang and K. S. Kim, *Infect. Immum.*, 1996, **64**, 146.
20 C. S. Allardyce, P. J. Dyson, D. J. Ellis and S. L. Heath, *Chem. Commun.*, 2001, 1396.

CHEMCOMM Communication
www.rsc.org/chemcomm

Sodium sulfate supported synthesis of cationic cyclophanes using microwaves

Perumal Rajakumar* and Venghatraghavan Murali

Department of Organic Chemistry, University of Madras, Guindy Campus, Chennai 600 025, Tamil Nadu, India. E-mail: perumalrajakumar@hotmail.com

Received (in Corvallis, OR, USA) 3rd October 2001, Accepted 1st November 2001
First published as an Advance Article on the web 6th December 2001

A facile microwave-assisted synthesis of a series of cationic cyclophanes, *viz.* benzimidazolophanes 3a–3f, benzotriazolophanes 3g–3j, through efficient double quaternization of the corresponding precyclophanes 1a–1j with appropriate dibromides 2a–2d in solid phase medium, is described.

Cyclophanes with a heterocyclic ring system possesses a favorable binding site for metal ions[1] and hence can have promising properties[2] as molecular hosts. *m*-Terphenyl based benzimidazolophanes[3] and benzotriazolophanes[4] have been reported from our laboratory. The dicationic benzimidazolophanes **3a–3f** and benzotriazolophanes **3g–3j** could be a potential precursor for the synthesis of [2]catenanes.† In view of the emerging importance of the cationic cyclophanes **3a–3j**, attention has been focused on rapid synthesis of such cyclophanes using sodium sulfate as the solid support under microwave irradiation.

An expeditious solvent-free route to the synthesis of ionic liquids, 1-alkyl-3-methylimidazolium (AMIM) halides, under microwave conditions was reported by Varma *et al.*[5] Recently, solvent free synthesis of metallophthalocyanines under microwave irradiation has been reported by Villemin *et al.*[6] However adopting such solvent free conditions for the synthesis of cyclophanes based on benzimidazole and benzotriazole leads to polymerization. It is well known that for such macrocyclization a high dilution technique is essential. The use of a large excess of conventional volatile solvents like benzene or ethanol for macrocyclization[7] is of ecological and economic concern. Though use of various solid supports like SiO_2, Al_2O_3, Na_2SO_4 for microwave assisted reactions are known,[8] such conditions are seldom used for the synthesis of cyclophanes. Hence we report herewith microwave assisted macrocyclization with solid supports like SiO_2, Al_2O_3 and Na_2SO_4 through a high dilution technique.

For the current investigation we have used a recently introduced (Kenstar, India) modified household microwave oven which has the provision of a wave reflector system for even and uniform heating and a dual wave emission system for rapid heating. The microwave oven was also equipped with a temperature monitoring system with variable Watt power, which helps to control the microwave power to a desirable level.

Cationic cyclophanes **3a–3j** have poor solubility in common organic solvents and hence desorption of the cyclophane from the solid support, like silica or alumina, could not be achieved. Reaction of precyclophanes **1a–1j**[3,4] with the corresponding *m*-terphenyl dibromide **2a–2d**[7] under microwave irradiation condition for 15 min using Na_2SO_4 as solid support afforded the cyclophanes **3a–3j** as shown in Scheme 1.

The cyclophanes thus obtained were characterized by ^1H NMR and ^{13}C NMR as reported earlier from our laboratory.[3,4] The following tabular column shows a comparison of yield and reaction time by the conventional method *viz.* refluxing with CH_3CN for 5 d and microwave assisted synthesis.

From Table 1, it is evident that microwave assisted reactions resulted in a comparable yield of cyclophanes **3a–3j** with that of the conventional method. Benzimidazolophanes were obtained

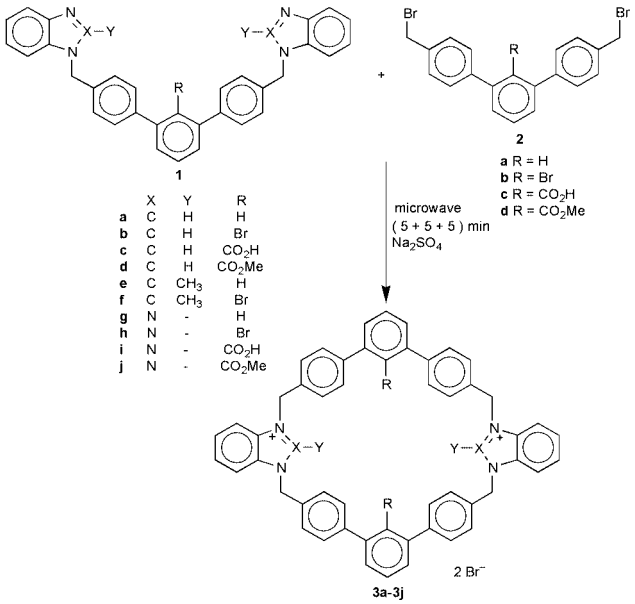

Scheme 1

in moderate yield but benzotriazolophanes were obtained in relatively lower yields, which is probably due to the decomposing nature of benzotriazole under microwave conditions. However, the method that we report here is definitely superior to the existing conventional method.[3,4] The reaction time is dramatically decreased from 5 d to 15 min. The solid support *viz.* Na_2SO_4 used for high dilution purposes can be easily removed by washing with water. Scaling up of the reaction is feasible, as it needs only less expensive and non-polluting Na_2SO_4.

In order to test the role of thermal catalysation during the course of the reaction, the precyclophane **1a** and the dibromide **2a** were adsorbed on Na_2SO_4 solid support and the reaction mixture was thermolysed under identical conditions. The

Table 1 Comparison of yields of cyclophane by microwave method over conventional method

	Conventional method[3,4]		Microwave method	
Cyclophane **3**	Yield (%)	Reaction time	Yield (%)	Reaction time
a	70	5 d	60	15 min
b	60	5 d	54	14 min
c	50	5 d	40	15 min
d	45	5 d	42	13 min
e	50	5 d	45	14 min
f	55	5 d	40	13 min
g	60	5 d	40	15 min
h	57	5 d	35	13 min
i	40	5 d	30	14 min
j	43	5 d	34	15 min

 DOI: 10.1039/b109003h

microwave oven indicated the temperatures as 50 °C, 60 °C and 70 °C after 5, 10 and 15 min respectively. Hence the reaction mixture was thermolysed from 50 °C to 70 °C during a time interval of 15 min. Starting materials were recovered which clearly indicated the microwave protocol and hence necessitates the use of microwaves for macrocyclization.

In conclusion, a solid phase mediated microwave assisted protocol has been developed for the synthesis of various cationic cyclophanes **3a–3j**. The use of a water-soluble solid support (Na_2SO_4) for microwave-assisted reactions would gain popularity in the area of synthesis of supramolecules.

V. M. thanks C.S.I.R., New Delhi for financial assistance and the authors thank UGC-SAP for financial assistance to the department.

Notes and references

† *General procedure for the synthesis of cyclophanes* **3a–3j**: The precyclophanes (10 mmol) **1a–1j** and the corresponding dibromides **2a–2d** (10 mmol) were dissolved in DCM, Na_2SO_4 (5 g) was added to the reaction mixture and a slurry was obtained after stirring for 15 min. DCM was then evaporated under vacuo to give a residue. The adsorbed reagents were then placed in a thick corning glass bowl and subjected to microwave irradiation at 400 W for 15 min with a time interval of 5 min. The reaction mixture was then cooled and washed with water (100 mL), then filtered. The residue thus obtained was washed again with chloroform (100 mL) to remove unreacted organic impurities and the residue was dried to afford the cyclophanes **3a–3j**. The organic impurities are found to be mainly the unreacted precyclophanes and the dibromides.

1 N. Nishino, R. N. Wagner and J. N. Lindsey, *J. Org. Chem.*, 1996, **61**, 7534–7544.
2 P. C. Heillier, J. S. Bradshaw, J. J. Young, X. X. Zhang and R. M. Izatt, *J. Org. Chem.*, 1996, **61**, 7270–7275.
3 P. Rajakumar and M. Srisailas, *Tetrahedron Lett.*, 1997, **38**, 5323–5326.
4 P. Rajakumar and V. Murali, *Tetrahedron*, 2000, **56**, 7995–7999.
5 R. S. Varma and V. V. Namboodiri, *Chem. Commun.*, 2001, 643–644.
6 D. Villemin, M. Hammadi, M. Hachemi and N. Bar, *Fifth International Electronic Conference on Synthetic Organic Chemistry (ECSOC-5), http://www.mdpi.org/ecsoc-5.htm*, 1–30 September 2001 (C0046).
7 A. Kannan, P. Rajakumar, V. Kabaleeswaran and S. S. Rajan, *J. Org. Chem.*, 1996, **61**, 5090.
8 A. Vass, J. Dudas and R. S. Varma, *Tetrahedron Lett.*, 1999, **40**, 4951–4954; T. Patonay, R. S. Varma, A. Vass, A. Levai and J. Dudas, *Tetrahedron Lett.*, 2001, **42**, 1403–1406; A. Vass, J. Dujas, J. Toth and R. S. Varma, *Tetrahedron Lett.*, 2001, **42**, 5347–5349.

CHEMCOMM Communication
www.rsc.org/chemcomm

Catalytic asymmetric epoxidation of aliphatic enones using tartrate-derived magnesium alkoxides†

Olivier Jacques,[a] Sarah J. Richards[b] and Richard F. W. Jackson*[ab]

[a] *Department of Chemistry, Dainton Building, University of Sheffield, Brook Hill, Sheffield, UK S3 7HF. E-mail: r.f.w.jackson@shef.ac.uk*

[b] *Department of Chemistry, Bedson Building, The University of Newcastle, Newcastle upon Tyne, UK NE1 7RU*

Received (in Cambridge, UK) 18th October 2001, Accepted 9th November 2001
First published as an Advance Article on the web 27th November 2001

Simple aliphatic enones can be converted into the corresponding epoxides in 71–93% ee using *tert*-butylhydroperoxide in the presence of a catalyst derived from dibutylmagnesium and di-*tert*-butyl tartrate.

The asymmetric epoxidation of electron-deficient alkenes, especially enones, is currently the focus of much activity, and advances in this area have been recently reviewed.[1] As this review makes clear, while there are many effective methods for the asymmetric epoxidation of enones bearing aryl-substituents **1** (R^1 and/or R^2 = Ar),[2–6] it appears at present that the only method which is generally applicable to the epoxidation of easily enolisable purely aliphatic enones involves the use of the La–BINOL catalysts developed by Shibasaki.[7] Recent optimisation of this system by the addition of $Ph_3As{=}O$ has resulted in an effective catalytic system using 5 mol% of the La–BINOL complex,[8] with good yields and enantiomeric excesses up to 99%, although 95% ee is a more typical outcome.

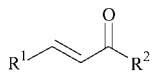

1

We reported earlier that simple chalcone derivatives **1** (R^1 and R^2 = Ar) could be converted into the corresponding epoxides with good to excellent ee using a much less expensive catalyst, prepared from diethyl tartrate and dibutylmagnesium.[9] However, this system was not especially effective for the epoxidation of aliphatic enones, resulting in very poor conversions, although with promising ees around 80%. In this communication, we report how we have been able to modify our original procedure so that it is effective for the asymmetric epoxidation of simple aliphatic enones with high ee.‡

As a model system, we investigated the epoxidation of non-3-en-2-one **1b**. Our first breakthrough came when we established that the addition of 4 Å molecular sieves allowed reasonable conversion into the corresponding epoxide **2b** (Scheme 1). As a further modification, we established that it was possible to prepare the presumed catalyst precursor **3**, simply by addition of L-(+)-diethyl tartrate to a solution of dibutylmagnesium in heptane, followed by removal of the solvent and drying. Characterisation of this amorphous material confirmed that it possessed the molecular composition expected for an oligomer of the species **3**, and the IR spectrum revealed the presence of two carbonyl bands (1741 and 1689 cm^{-1}), clearly indicative of at least one ester group coordinating to the magnesium in a way that is very reminiscent of the analogous titanium–tartrate complex characterised by Sharpless.[10] The material was insoluble in all solvents tested, and it was therefore not possible to obtain an NMR spectrum.

This amorphous material proved to be an effective catalyst for the epoxidation of aliphatic enones using *tert*-butyl

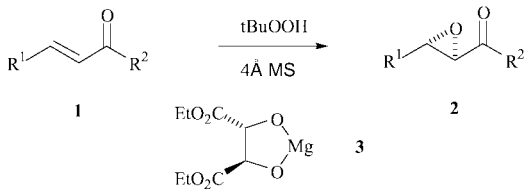

Scheme 1 Asymmetric epoxidation of aliphatic enones using preformed catalyst **3**.

Table 2 Asymmetric epoxidation of non-3-en-2-one **1b** using dialkyl tartrate esters

R	Conversion (%)[a]	Ee (%)[a]
Me	6	63
C_2H_5	21–31	80–85
Bn	23	85
c-$C_{12}H_{23}$	88	90–93
c-C_5H_9	80	92–93
c-C_6H_{11}	70	92
t-Bu	**96**	**93–95**

[a] Conversions and ee values were measured using chiral phase GC

Table 1 Asymmetric epoxidation of aliphatic enones **1** using preformed catalyst **3**

Enone	R^1	R^2	Time/h	Epoxide	Conversion[a] (yield, %)	Ee (%)[a]
1a	C_4H_9	CH_3	120	**2a**	89% (54)	75
1b	C_5H_{11}	CH_3	120	**2b**	81% (54)	79
1b	C_5H_{11}	CH_3	24[b]	**2b**	82% (nd)	82
1c	C_6H_{13}	CH_3	120	**2c**	86% (52)	71
1d	CH_3	Et	144	**2d**	94% (40)	67
1e	3,5-Di-Br-C_6H_3	CH_3	72	**2e**	88% (47)	65

[a] Conversions and ee values were measured using chiral phase HPLC or GC. Conditions are provided in the ESI.† Isolated yields refer to homogeneous material purified by flash chromatography.[b] After an initial 10 mol% of the catalyst **3**, additional portions were added after 4 h (5 mol%) and after a further 4 h (10 mol%).

† Electronic supplementary information (ESI) available: conditions for enantiomeric purity determination for epoxyketones derived by di-*tert*-butyl tartrate mediated epoxidation. See http://www.rsc.org/suppdata/cc/b1/b109421a/

 DOI: 10.1039/b109421a

Table 3 Asymmetric epoxidation of aliphatic enones **1** using di-*tert*-butyl tartrate as ligand

Enone	R^1	R^2	Time/h	Epoxide	Conversion[a] (yield, %)	Ee (%)[a]
1a	C_4H_9	CH_3	24	**2a**	92% (53)	91
1b	C_5H_{11}	CH_3	24	**2b**	96% (59)	93
1c	C_6H_{13}	CH_3	24	**2c**	92% (63)	92
1d	CH_3	Et	24	*ent*-**2d**	95% (67)	71[b]
1e	3,5-Di-Br-C_6H_3	CH_3	24	**2e**	Nd (62)	81

[a] Conversions and ee values were measured using chiral phase HPLC or GC. Conditions are provided in the supplementary material. Isolated yields refer to homogeneous material purified by flash chromatography.[b] L-(−)-di-*tert*-butyl tartrate was used.

hydroperoxide in the presence of 4 Å molecular sieves. The only drawback was that the conversion to epoxide, whilst initially fast, rapidly slowed down, presumably as a result of catalyst inactivation. However, good conversions could be achieved by portionwise addition of further solid catalyst **3** (total of 25 mol%), which was a straightforward solution to the problem. Addition of 25 mol% catalyst initially resulted in very poor conversion. Although in our early experiments we added the catalyst **3** over a period of 3–5 d, it subsequently became clear that the additional catalyst could be added much more quickly, and good conversions could be achieved by addition of a total of 25 mol% catalyst over a period of 24 h. Our results are summarised in Table 1.

While these results were encouraging, the enantiomeric excesses that we obtained were lower than those obtained by Shibasaki. Although in our initial screening of ligands for the epoxidation of chalcone derivatives we had identified diethyl tartrate as the optimum choice, the most profitable approach to the optimisation of our catalyst now appeared to be a re-appraisal of other related ligands under the new optimised conditions for epoxidation of aliphatic enones. We therefore screened a series of tartrate esters, in which the catalyst was simply prepared *in situ*.

Thus, *tert*-butyl hydroperoxide was dried over 4 Å molecular sieves, Bu_2Mg was then added, followed by addition of the ligand and finally non-3-en-2-one. These conditions were very closely related to our original conditions for the epoxidation of chalcone derivatives, with the use of 4 Å molecular sieves as the only significant alteration to this earlier procedure. Our results are reported in Table 2, and two striking features are evident. Firstly the use of tartrate esters derived from secondary or tertiary alcohols gave much higher conversions with only 10 mol% catalyst, and secondly the observed ee's were now over 90%.

From these results, the optimum ligand appears to be commercially available di-*tert*-butyl tartrate, but the more easily prepared and cheaper dicycloalkyl tartrates all give good results. Use of L-(+)-di-*tert*-butyl tartrate for the epoxidation of a range of other aliphatic enones resulted in equally good results for the long chain aliphatic enones, Scheme 2, although the challenging substrate **1d** still falls short of a usable level of enantiomeric excess. Our results are reported in Table 3.

The higher enantiomeric excesses obtained using the bulkier ester derivatives may be rationalised on simple steric grounds, but the apparently higher catalytic activity of the corresponding magnesium tartrate derivatives of these bulkier tartrate esters is not so immediately explained. The most probable explanation is that the magnesium catalysts formed from the bulkier tartrate esters are simply less prone to hydrolysis, and hence to inactivation.

The magnesium tartrate system appears to offer the prospect of an alternative to the excellent La–BINOL system in which

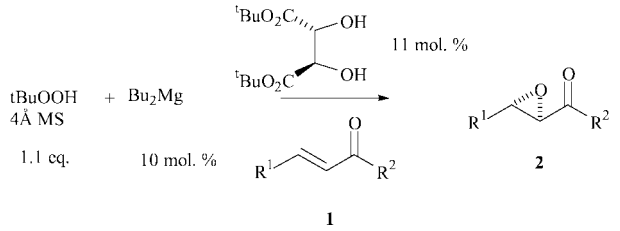

Scheme 2 Asymmetric epoxidation of aliphatic enones using *in situ* generated catalyst.

although the amount of catalyst required is higher (typically 10 mol% for the Mg system, compared with 1–5 mol.% for the La–BINOL system), the cost of the catalyst precursors is several orders of magnitude less.

We thank EPSRC for the award of a research grant (GR/M13633), Rhodia Chirex for studentship support (SJR), and Professor A. McKillop and Dr S. Bone (formerly Rhodia Chirex) for helpful discussions.

Notes and references

‡ **General procedure for the asymmetric epoxidation of aliphatic enones using di-*tert*-butyl tartrate:** *tert*-butyl hydroperoxide (3.7 M in toluene, 1.1 mmol, 1.1 eq.) was dried over activated powdered 4 Å molecular sieves (200 mg, activated for 4 h at 200 °C) for 2 h. Bu_2Mg (1 M in heptane, 0.1 mmol, 0.1 eq.) was added. After stirring for 30 min, L-(+)-di-*tert*-butyl tartrate (0.11 mmol, 0.11 equiv.) was added. After an additional period of 30 min stirring, the aliphatic enone (1 mmol) was added, and the mixture was stirred for 24 h. The conversion and enantiomeric excess were checked either by chiral phase GC or HPLC. We have observed that best results are obtained with solutions of *tert*-butyl hydroperoxide that have been stored over 4 Å molecular sieves for an extended period.

1 M. J. Porter and J. Skidmore, *Chem. Commun.*, 2000, 1215.
2 D. Enders, J. Zhu and G. Raabe, *Angew. Chem., Int. Ed. Engl.*, 1996, **35**, 1725; D. Enders, J. Q. Zhu and L. Kramps, *Liebigs Ann.-Recl.*, 1997, 1101.
3 B. Lygo and P. G. Wainwright, *Tetrahedron*, 1999, **55**, 6289.
4 E. J. Corey and F.-Y. Zhang, *Org. Lett.*, 1999, **1**, 1287.
5 R. W. Flood, T. P. Geller, S. A. Petty, S. M. Roberts, J. Skidmore and M. Volk, *Org. Lett.*, 2001, **3**, 683, and references therein.
6 Z.-X. Wang, S. M. Miller, O. P. Anderson and Y. Shi, *J. Org. Chem.*, 1999, **64**, 6443.
7 M. Bougauchi, S. Watanabe, T. Arai, H. Sasai and M. Shibasaki, *J. Am. Chem. Soc.*, 1997, **119**, 2329.
8 T. Nemoto, T. Ohshima, K. Yamaguchi and M. Shibasaki, *J. Am. Chem. Soc.*, 2001, **123**, 2725.
9 C. L. Elston, R. F. W. Jackson, S. J. F. MacDonald and P. J. Murray, *Angew. Chem., Int. Ed. Engl.*, 1997, **36**, 410.
10 M. G. Finn and K. B. Sharpless, *J. Am. Chem. Soc.*, 1991, **113**, 113.

CHEMCOMM
Communication
www.rsc.org/chemcomm

1,2,9,10,17,18,25,26,27,28,35,36,37,38,39,40-Hexadecasila[2_8](1,2,4,5)-cyclo-phane and its open-chain homologs

Soichiro Kyushin, Tsukasa Kitahara, Ryoji Tanaka, Masanori Takeda, Takeshi Matsumoto and Hideyuki Matsumoto*

Department of Applied Chemistry, Faculty of Engineering, Gunma University, Kiryu, Gunma 376-8515, Japan. E-mail: matumoto@chem.gunma-u.ac.jp; Fax: +81-277-30-1291; Tel: +81-277-30-1290

Received (in Cambridge, UK) 29th August 2001, Accepted 6th November 2001
First published as an Advance Article on the web 6th December 2001

The metathesis of the Si–Si bonds of benzo[1,2:4,5]-bis(1,1,2,2-tetramethyl-1,2-disilacyclobut-3-ene) with $Pd(PPh_3)_4$ gave 1,2,9,10,17,18,25,26,27,28,35,36,37,38,39,40-hexadecasila[2_8](1,2,4,5)cyclophane and its open-chain homologs, in which the σ–π conjugation is extended all over the molecule.

The chemistry of cyclophanes with three or more benzene rings has been studied extensively from the viewpoint of conformational analysis and the formation of inclusion compounds.[1] For example, [2_3](1,4)cyclophane (π-prismand)[2–4] and [2_6](1,2,4,5)cyclophane (deltaphane)[3] have been reported to be effective complexing agents with silver ion. The construction of silicon-bridged cyclophanes seems interesting because the silicon bridges would affect the electron states and the structures of cyclophanes.[5,6] Recently we reported the first synthesis of benzo[1,2:4,5]bis(1,1,2,2-tetraisopropyl-1,2-disilacyclobut-3-ene) (**1**)[7] as part of our study on organosilanes with aromatic rings.[8] We report herein that the methyl analog of **1** can serve as a precursor of 1,2,9,10,17,18,25,26,27,28,35,36,37,38,39,40-hexadecasila-[2_8](1,2,4,5)cyclophane (**9**). We also describe the structures and properties of **9** and its open-chain homologs.

Benzo[1,2:4,5]bis(1,1,2,2-tetramethyl-1,2-disilacyclobut-3-ene) (**4**) was prepared according to the same procedure for **1**:[7] the chlorination of **2**[9] and the intramolecular coupling of the

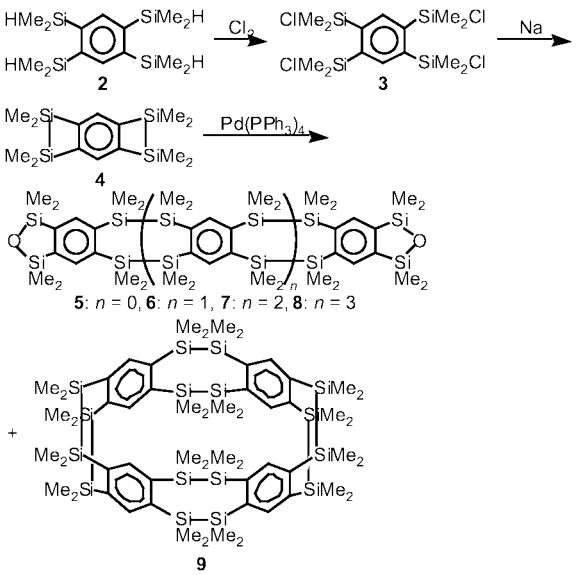

resulting chlorosilane **3** with sodium gave **4**. The intermolecular coupling products such as **5**–**9** were not formed under the conditions used. As the Si–Si bonds of **4** are easily oxidized in the air, **4** was immediately used in the next step without isolation. The metathesis of the Si–Si bonds of **4** with $Pd(PPh_3)_4$[10] gave linear oligomers **5**–**8** and a cyclic oligomer **9** together with a large amount of polymers at room temperature (Fig. 1).† The metathesis of **1** with $Pd(PPh_3)_4$ did not take place at 150 °C because of the steric hindrance of the isopropyl groups.

The structures of the linear oligomers **5**–**8** were determined by spectroscopic data. For example, ^{1}H, ^{13}C and ^{29}Si NMR spectra of the trimer **6** show the presence of three kinds of silicon atoms, three kinds of methyl groups, five kinds of benzene carbons and two kinds of benzene protons. In each oligomer, the terminal Si–Si bonds are oxidized to give Si–O–Si bonds in the air.

The cyclophane **9** was obtained as colorless crystals which is highly insoluble in most organic solvents. The structure of **9** was determined by X-ray crystallography (Fig. 2).‡ This molecule has a rhombic structure consisting of four planar 1,2,4,5-tetrasilylbenzene moieties. The distance between two opposite benzene rings is 7.3 Å. The crystals were obtained by recrystallization from a toluene solution, but no solvent molecule is included in the cavity. The four benzene rings are tilted alternately upward and downward from the cavity. The C(sp^2)–Si–Si–C(sp^2) moieties adopt nearly gauche conformations with the average torsion angle of 54.8°.

The UV spectra of **5**–**7** and **9** are shown in Fig. 3. As the number of repeating units increases, the absorption shifts to the longer wavelength region, and the extinction coefficient becomes far larger than the value expected from the number of repeating units. No significant difference was observed between the linear tetramer **7** and the cyclic tetramer **9**. The bathochromic shift and the increment of extinction coefficients are explained by the σ–π conjugation:[11] π orbitals of a benzene ring are conjugated with four Si–Si σ orbitals, and the four Si–Si σ orbitals are conjugated with the π orbitals of the adjacent benzene rings. Therefore, these compounds are unique systems, in which the σ–π conjugation is extended all over the molecule. Further experiments into the properties of these potentially intriguing compounds are currently under investigation.

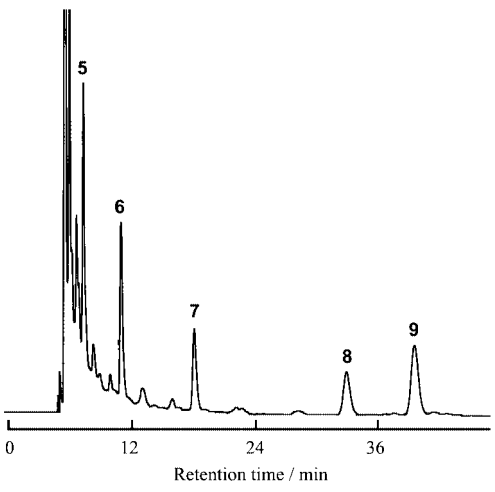

Fig. 1 HPLC analysis of **5**–**9** (ODS, methanol–THF (7:3)).

 DOI: 10.1039/b107706f

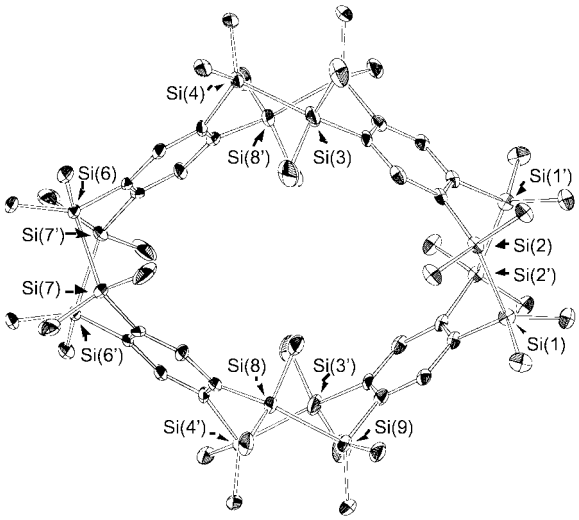

Fig. 2 Molecular structure of **9**. The molecule lies about a 2-fold crystallographic axis. The Si(4) atom and two methyl groups on it are disordered, and only the major positions with the occupancy of 0.815 are shown for clarity. Hydrogen atoms are omitted for clarity. Thermal ellipsoids are drawn at the 30% probability level. Selected bond lengths (Å): Si(1)–Si(2) 2.389(3), Si(3)–Si(4) 2.426(4), Si(6)–Si(7) 2.367(3), Si(8)–Si(9) 2.379(3).

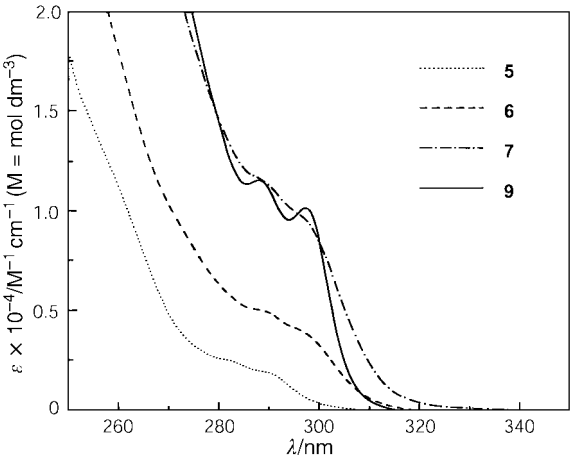

Fig. 3 UV spectra of **5**–**7** in diethyl ether and **9** in THF at room temperature.

This work was supported in part by Grants-in-Aid for Scientific Research from the Japan Society for the Promotion of Science.

Notes and references

† Chlorine was bubbled into a solution of **2** (1.00 g, 3.22 mmol) in carbon tetrachloride (4 ml) at room temperature. When **2** was completely converted into **3**, the solvent was removed under reduced pressure. Compound **3** was obtained almost quantitatively. A solution of **3** in toluene (8 ml) was added dropwise to a refluxing mixture of sodium (1.74 g, 75.7 mmol) and toluene (30 ml), and the reaction mixture was refluxed for 12 h to give **4**. After the solvent was removed under reduced pressure, $Pd(PPh_3)_4$ (0.570 g, 0.493 mmol) and benzene (30 ml) were added to **4**, and the mixture was stirred for 3 h at room temperature. Insoluble materials were removed by filtration and centrifugation. The solvent was evaporated, and the residue was separated by HPLC (ODS, methanol–THF (6 : 4)) to give **5** (8.5 mg, 0.8% from **2**), **6** (6.2 mg, 0.6%), **7** (5.3 mg, 0.5%), **8** (2.5 mg, 0.2%) and **9** (0.9 mg, 0.1%).

3: ^{1}H NMR (C_6D_6) δ 0.66 (s, 24H), 8.51 (s, 2H); ^{13}C NMR (C_6D_6) δ 4.8, 141.8, 143.1; ^{29}Si NMR (C_6D_6) δ −13.0; MS *m/z* (%) 446 (M^+($^{35}Cl_4$), 1), 433 ($^{35}Cl_3{}^{37}Cl$, 100), 93 (37), 73 (29).

4: MS *m/z* (%) 306 (M^+, 22), 291 (100), 73 (34). This compound is characterized by converting into benzo[1,2:4,5]bis(1,1,3,3-tetramethyl-2-oxa-1,3-disilacyclopent-4-ene)[9] in the air.

5: ^{1}H NMR (C_6D_6) δ 0.27 (s, 24H), 0.55 (s, 24H), 7.98 (s, 4H); ^{13}C NMR (C_6D_6) δ 1.0, 1.1, 136.8, 146.0, 147.9; ^{29}Si NMR (C_6D_6) δ −19.0, 14.9; IR (KBr, cm^{-1}) 2920, 1240, 1120, 940, 780; MS *m/z* (%) 644 (M^+, 3), 513 (44), 116 (100), 73 (53); UV (λ_{max} in Et_2O) 283 nm (sh, ε 2400), 291 nm (sh, ε 1800).

6: ^{1}H NMR (C_6D_6) δ 0.28 (s, 24H), 0.47 (s, 24H), 0.49 (s, 24H), 7.948 (s, 4H), 7.953 (s, 2H); ^{13}C NMR (C_6D_6) δ 0.8, 1.01, 1.02, 136.8, 140.2, 144.4, 146.2, 147.8; ^{29}Si NMR (C_6D_6) δ −19.2, −18.8, 14.9; IR (KBr, cm^{-1}) 2950, 1240, 1130, 930, 780; MS *m/z* (%) 950 (M^+, 3), 819 (70), 731 (30), 116 (100), 73 (52); UV (λ_{max} in Et_2O) 289 nm (sh, ε 5000), 299 nm (sh, ε 3500).

7: ^{1}H NMR (C_6D_6) δ 0.28 (s, 24H), 0.42 (s, 24H), 0.47 (s, 24H), 0.49 (s, 24H), 7.94 (s, 4H), 7.95 (s, 4H); ^{13}C NMR (C_6D_6) δ 0.7, 0.8, 1.0, 136.8, 140.2, 144.4, 144.6, 146.3, 147.9; ^{29}Si NMR (C_6D_6) δ −19.2, −18.9, −18.8, 14.7; IR (KBr, cm^{-1}) 2960, 1250, 1140, 930, 790; MS *m/z* (%) 1256 (M^+, 5), 1126 (100), 116 (92); UV (λ_{max} in Et_2O) 289 nm (sh, ε 11500), 299 nm (sh, ε 9000).

8: ^{1}H NMR (C_6D_6) δ 0.28 (s, 24H), 0.42 (s, 48H), 0.47 (s, 24H), 0.49 (s, 24H), 7.92 (s, 2H), 7.93 (s, 4H), 7.95 (s, 4H); ^{13}C NMR (C_6D_6) δ 0.7, 0.8, 1.0, 136.8, 140.2, 142.7, 144.3, 144.5, 144.6, 146.3, 147.9; ^{29}Si NMR (C_6D_6) δ −19.2, −18.9, −18.8, 14.7; MS *m/z* (%) 1563 (M^+, 1), 1433 (92), 116 (100).

9: ^{1}H NMR (C_6D_6) δ 0.44 (s, 48H), 0.47 (s, 48H), 7.81 (s, 8H); ^{13}C NMR (C_6D_6) δ −0.5, 2.1, 139.9, 143.9; ^{29}Si NMR (C_6D_6) δ −18.7; IR (KBr, cm^{-1}) 2920, 2850, 1260, 1170, 800; FD-MS *m/z* (%) 1227 (MH^++2, 100), 1225 (MH^+, 72); UV (λ_{max} in THF) 288 nm (ε 11600), 297 nm (ε 10200).

‡ *Crystal data* for **9**: $C_{56}H_{104}Si_{16}$, F_w = 1226.79, monoclinic, space group *C*2/*c*, *a* = 10.317(2), *b* = 48.495(5), *c* = 15.523(3) Å, β = 105.28(2)°, *V* = 7492(2) Å^3, *T* = 93 K, *Z* = 4, D_c = 1.088 g cm^{-3}, *R* = 0.077, R_w = 0.094 (w = $1/\sigma^2(F_o)$) for 3643 observed reflections. CCDC 171906. See http://www.rsc.org/suppdata/cc/b1/b107706f/ for crystallographic data in CIF or other electronic format.

1 F. Vögtle, *Cyclophane Chemistry: Synthesis, Structures and Reactions*, Wiley, Chichester, 1993.
2 J.-L. Pierre, P. Baret, P. Chautemps and M. Armand, *J. Am. Chem. Soc.*, 1981, **103**, 2986.
3 H. C. Kang, A. W. Hanson, B. Eaton and V. Boekelheide, *J. Am. Chem. Soc.*, 1985, **107**, 1979.
4 P. Saarenketo, R. Suontamo, T. Jödicke and K. Rissanen, *Organometallics*, 2000, **19**, 2346.
5 H. Sakurai, S. Hoshi, A. Kamiya, A. Hosomi and C. Kabuto, *Chem. Lett.*, 1986, 1781; A. Sekiguchi, T. Yatabe, C. Kabuto and H. Sakurai, *Angew. Chem., Int. Ed. Engl.*, 1989, **28**, 757.
6 M. Yoshida, M. Goto and F. Nakanishi, *Organometallics*, 1999, **18**, 1465.
7 S. Kyushin, T. Kitahara and H. Matsumoto, *Chem. Lett.*, 1998, 471.
8 S. Kyushin, Y. Izumi, S. Tsunakawa and H. Matsumoto, *Chem. Lett.*, 1992, 1393; S. Kyushin, M. Ikarugi, S. Tsunakawa, Y. Izumi, M. Miyake, M. Sato, H. Matsumoto and M. Goto, *J. Organomet. Chem.*, 1994, **473**, 19; S. Kyushin, M. Ikarugi, K. Takatsuna, M. Goto and H. Matsumoto, *J. Organomet. Chem.*, 1996, **510**, 121; S. Kyushin, M. Ikarugi, M. Goto, H. Hiratsuka and H. Matsumoto, *Organometallics*, 1996, **15**, 1067; S. Kyushin, T. Shinnai, T. Kubota and H. Matsumoto, *Organometallics*, 1997, **16**, 3800.
9 W. Fink, *Helv. Chim. Acta*, 1974, **57**, 1010.
10 T. Kusukawa, Y. Kabe, B. Nestler and W. Ando, *Organometallics*, 1995, **14**, 2556.
11 C. G. Pitt, R. N. Carey and E. C. Toren, Jr., *J. Am. Chem. Soc.*, 1972, **94**, 3806; H. Sakurai, S. Tasaka and M. Kira, *J. Am. Chem. Soc.*, 1972, **94**, 9285.

CHEMCOMM
Communication
www.rsc.org/chemcomm

A new route for the synthesis of open-framework metal phosphates using organophosphates

S. Neeraj,[a] P. M. Forster,[a] C. N. R. Rao*[ab] and A. K. Cheetham*[a]

[a] *Materials Research Laboratory, University of California, Santa Barbara, CA 93106, USA. E-mail: cheetham@mrl.ucsb.edu*

[b] *Jawaharlal Nehru Center for Advanced Scientific Research, Jakkur Bangalore 560064, India*

Received (in Columbia, MO, USA) 3rd August 2001, Accepted 9th October 2001
First published as an Advance Article on the web 6th December 2001

Use of tributylphosphate, an organophosphate, as the phosphorus source in place of phosphoric acid, has enabled the synthesis of several new open-framework zinc(II) and cobalt(II) phosphates, under solvothermal conditions.

Amongst the many inorganic open-framework structures known to-date, the metal phosphates constitute a large family.[1,2] The synthesis of these compounds is generally carried out under hydrothermal conditions by taking a metal salt and phosphoric acid in the presence of an organic amine, which may act as a template or structure-directing agent. Other strategies include the use of amine phosphates.[3] We have examined whether the use of an organic phosphorus source in place of H_3PO_4 would provide a new way to synthesize these fascinating compounds. This is of interest because the formation of open-framework structures is kinetically controlled and can be highly sensitive to the reaction conditions. In addition, the use of an organic source of phosphorus enables one to employ non-aqueous media for the synthesis. We have carried out several reactions of metal ions with tributylphosphate, both in alcohol and aqueous media, and obtained several open-framework cobalt, zinc and iron phosphates possessing different architectures. In this communication we report this new route for the synthesis of open-framework phosphates.

In a typical synthesis, zinc(II) chloride was dissolved in a butan-2-ol–water mixture. Tributylphosphate was added to the solution followed by an organic amine under constant stirring. The homogenized gel was sealed in a Parr autoclave and heated at 180 °C for 60 h. With different amines (*N*-(2-aminoethyl)-1,3-propanediamine in **I**, 4-(aminomethyl)piperidine in **II** and piperazine in **III**) the reactions yielded three-dimensional phosphates of the following compositions: $[C_5N_3H_{18}]$-$[Zn_3(HPO_4)_3(PO_4)]$ **I**, $[C_4N_2H_{14}]_4[Zn_5(PO_4)_4]_4{\cdot}5H_2O$, **II** and $[C_4N_2H_{12}][Zn_2(PO_4)(H_2PO_4)_2]$ **III**. While **I** and **II**, which possess channels are new, **III** has been reported in the literature.[3]

The structure of **I** is based on a three-dimensional network involving ZnO_4, PO_4 and HPO_4 tetrahedra with all the zinc atoms being linked to P atoms *via* oxygen. There are no Zn–O–Zn linkages present in the structure, hence no three-ring features are observed. The structure of **I** is built up of a stack of parallel layers linked by the corner-shared (CS) 4-ring chains embedded in the interlayer space (Fig. 1a). The layer in turn is made up of zigzag ladders consisting of 8-ring apertures as shown in Fig. 1b. The oxygens of the phosphate of the CS chains link on either side to the zinc tetrahedra of the layers. Such linkages between layers and CS chains result in 16-ring apertures along the *c*-axis, into which the terminal hydroxy groups project.

The framework of **II** is built up from layers and 4-ring ladders. The layers are made up of three types of chains (**A**, **B** and **C**) as can be visualized in Fig. 1c. The phosphate tetrahedra on the chains of type **A** and **B** add on to another set of ZnO_4 tetrahedra to form the 'tubule' like feature, whereas the phosphate tetrahedra common to these chains and the oxygens of the newly added ZnO_4 tetrahedra connect to the oxygens of the 4-ring ladder to form the three-dimensional architecture with 12- and 6-ring channels along the *a*-axis (Fig. 1d). The protonated amine molecule (4-(aminomethyl)piperidine decomposes to give 1,4-diaminobutane) sits in the cavities and interacts with the framework *via* hydrogen bonding.

For the synthesis of cobalt(II) phosphates, a known amount of $CoCl_2{\cdot}6H_2O$ was dissolved in butan-2-ol and tributyl phosphate added to the solution under stirring. The amine (piperazine in **IV**, **V** and diethylentriamine in **VI**) was added after a few minutes and the mixture stirred until it became homogeneous. The gels were sealed in Parr autoclaves at 180 °C for 60 h. By

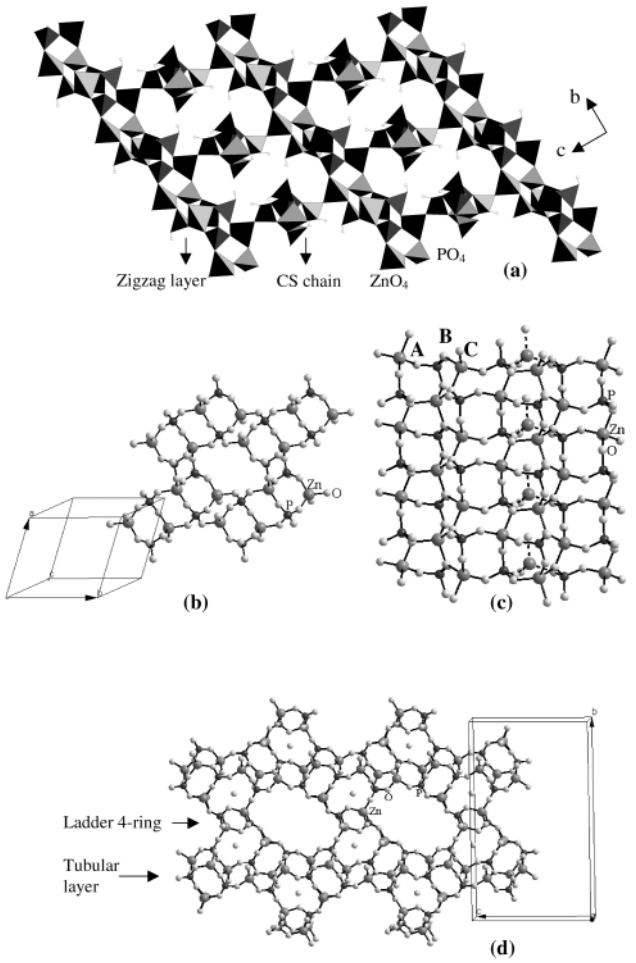

Fig. 1 (a) Polyhedral view of **I**, showing the 16-membered channels along the *a*-axis. Also marked are the CS chain and the layer forming the 16-ring channels and the pendant hydroxy groups protruding into the cavity. (b) A section of **I** showing the zigzag layer containing 8-ring apertures. (c) A section of **II** showing the layer formed of chains **A**, **B** and **C**. Also shown by dotted lines is the ZnO_4 tetrahedron connecting to the oxygen atoms of the phosphate groups of chains (type **A** and **B**) to form the tubule. (d) Ball and stick view of 6- and 12-ring cavities of **II** along the *a*-axis.

 DOI: 10.1039/b107898b

such reactions, we obtained three new open-framework cobalt phosphates $[C_4N_2H_{11}][Co_2(PO_4)(H_2PO_4)_2]$ **IV**, $[C_4N_2H_{12}][Co_2(PO_4)_2]$ **V** and $[C_6N_4H_{22}][Co_7(PO_4)_6]$ **VI**. Of these, **IV** and **VI** possess three-dimensional frameworks and **V** has a layered architecture. Although these cobalt phosphate are new, their zinc phosphate analogues are known in the literature.[3–5] We have also synthesized a known mixed valence iron phosphate[6] by this route.

Framework **IV** is isostructural with the zinc phosphate **III** and has a three-dimensional structure built up of infinite CS chains containing 4-rings running perpendicular to each other and connected at various junctions.[3] Four such junctions form a 16-membered clover-shaped aperture, with the pendant hydroxyl groups from the phosphorus projecting in the cavities. The protonated piperazinium cations occupy the 4-ring windows (Fig. 2a). Framework **V** has a layered topology made up of 3- and 4-membered rings formed by vertex linkage between CoO_4 and PO_4 tetrahedral units. The anionic layer is built up of two kinds of chains, **D** and **E**, made from 3- and 4-rings (Fig. 2b). The presence of a 3-ring chain results in a step-like feature in the layer due to the strain involved in accommodating it and also gives rise to an infinite one-dimensional Co–O–Co chain.

Compound **VI** possesses a three-dimensional architecture and is made of CoO_6, CoO_4 and PO_4 polyhedra, which connect to give rise to a Co_7O_6 cluster. The cobalt octahedron is surrounded by six cobalt tetrahedra to form the Co_7 cluster. Such clusters are linked *via* six PO_4 tetrahedra to other clusters to form the structure. The clusters are arranged in such a manner that each cluster is displaced by half the length of the *c*-axis from its neighbour, forming a honeycomb layer. The next layer of clusters is identical to the first but is displaced along the *a*-axis by half the unit cell so that the honeycomb channels are capped. This type of three-dimensional AB type stacking results in the formation of 8-membered channels at an angle to the *c*-axis (Fig. 2c).

The various structures obtained by using tributylphosphate as the phosphorylating agent confirm that we have found a new route for the formation of open-framework phosphates. The use of the phosphate ester enables us to carry out the reactions under non-aqueous conditions and to isolate new framework structures. It may be noted that pure open-framework Co(II) phosphates have been considered difficult to prepare. The use of the phosphate ester influences the release of phosphate ions in the solution, thereby affecting the course of the reaction and the products formed. The method can be readily extended to phosphonates, carboxylates and other systems.

We thank Unilever plc for their generous support of this work.

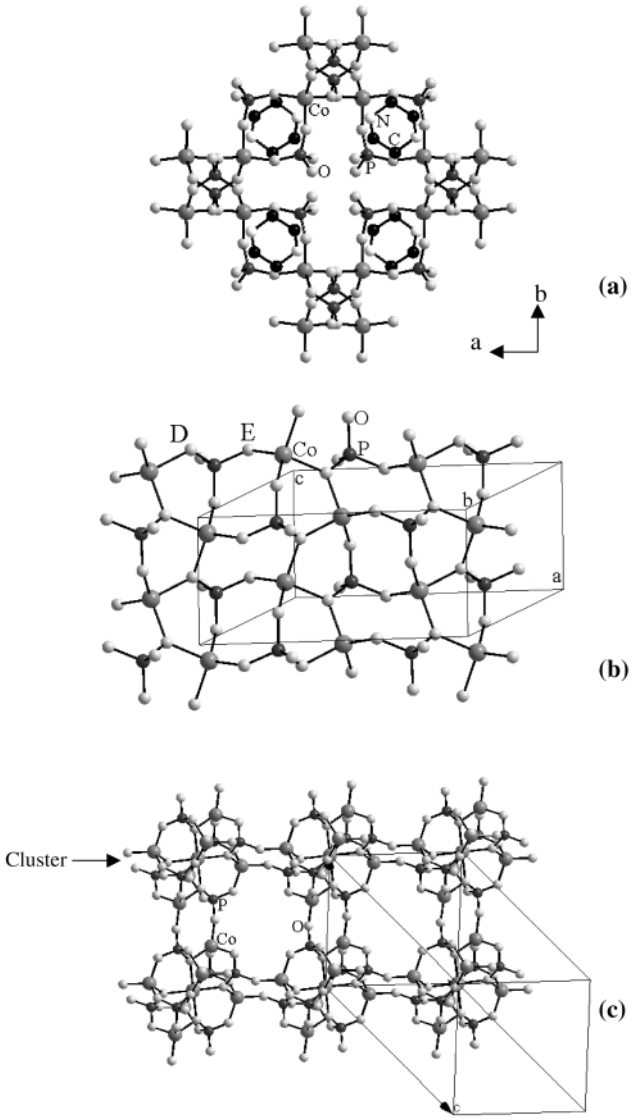

Fig. 2 (a) Structure of **IV** showing clover-shaped 16-ring channels. Also seen are the piperazinium molecules in the 4-ring windows. (b) Structure of **V** showing a single layer. Note the presence of two types of chains **D** and **E** and the infinite Co–O–Co chains. (d) Structure of **VI** showing the 8-membered channels at an angle to the *c*-axis formed by the linkage of Co_7O_6 clusters.

Notes and references

1 A. K. Cheetham, T. Loiseau and G. Férey, *Angew. Chem., Int. Ed. Engl.*, 1999, **38**, 3268.
2 W. H. Meier and D. H. Olson, *Atlas of Zeolite Structure Types*, Butterworth-Heinemann, London, 1992.
3 C. N. R. Rao, S. Natarajan and S. Neeraj, *J. Am. Chem. Soc.*, 2000, **122**, 2810.
4 A. Choudhury, S. Natarajan, S. Neeraj and C. N. R. Rao, *J. Mater. Chem.*, 2001, **11**, 1537.
5 A. A. Ayi, A. Choudhury, S. Natarajan, S. Neeraj and C. N. R. Rao, *J. Mater. Chem.*, 2001, **11**, 1181.
6 V. Zima, K. H Lii, N. Nguyen and A. Ducouret, *Chem. Mater.*, 1998, **10**, 1914.
7 Single crystal X-ray data was collected using a Siemens SMART-CCD diffractometer equipped with a normal focus, 2.4 kW sealed tube X-ray source (Mo-Kα radiation, λ = 0.71073 Å) operating at 45 kV and 40 mA. A hemisphere of intensity data was collected at room temperature in 1321 frames with ω scans (width 0.30° and exposure time of 10–20 s per frame). The structure was solved by direct methods using SHELX-97 and difference Fourier syntheses. Full matrix least-squares refinement against $|F^2|$ was carried out using the SHELXTL-PLUS package of programs. *Unit cell parameters*: for **I**: space group $P\bar{1}$ (no. 2), a = 8.4408(13), b = 9.2630(16), c = 13.8427(20) Å, α = 81.119(15), β = 83.643(12), γ = 72.647(11)°, R = 0.037. For **II**: space group $P2_1/n$ (no. 14), a = 5.1601(6), b = 25.0748(31), c = 14.9860(19) Å, β = 92.610(2)°, R = 0.046. For **IV**: space group $C2/c$ (no. 15), a = 13.4441(49), b = 12.8745(41), c = 8.2243(23) Å, β = 94.640(22)°, R = 0.047. For **V**: space group $P\bar{1}$ (no. 2), a = 5.1534(7), b = 10.7578(13), c = 10.8329(14) Å, α = 66.381(2), β = 89.058(2), γ = 81.674(2)°, R = 0.054. For **VI**: space group $R\bar{3}$ (no. 148), a = 13.4892(18), b = 13.4892(18), c = 14.9839(30) Å, γ = 120°, R = 0.066.

CCDC reference numbers 168260–168264 for **I**, **II**, **IV**, **V** and **VI** respectively.

See http://www.rsc.org/suppdata/cc/b1/b107898b/ for crystallographic data in CIF or other electronic format.

CHEMCOMM Communication
www.rsc.org/chemcomm

Visible light-activated nanosized doped-TiO_2 photocatalysts

A. Fuerte, M. D. Hernández-Alonso, A. J. Maira, A. Martínez-Arias, M. Fernández-García,* J. C. Conesa and J. Soria

Instituto de Catálisis y Petroleoquímica (CSIC), Campus Cantoblanco, 28049-Madrid, Spain. E-mail: m.fernandez@icp.csic.es

Received (in Cambridge, UK) 15th August 2001, Accepted 13th November 2001
First published as an Advance Article on the web 6th December 2001

The report shows that highly doped anatase-like binary mixed oxides constitute a route to improve the performance of nanosized titania photocatalysts under sunlight excitation.

Photocatalytic destruction of organic pollutants in the presence of TiO_2 appears to be a viable decontamination process of widespread application, no matter the state (gas or liquid) or chemical nature of the process target.[1] However, its technological application seems limited for several reasons, among which the most restrictive one is the need to use an ultraviolet (UV) excitation source. The efficient use of sunlight may then appear as an appealing challenge for developing the future generation of photocatalytic materials working with non-polluting energy sources.

In order to explore the photocatalytic behavior of highly doped anatase-like binary mixed oxide systems, we have tried to synthesize substitutional mixed oxides including typical acceptors (like Cr, Ni), donors (like V or Mn), cations with both properties (like Fe) or with intrinsic photocatalytic properties (like Ce, Mo or W), up to a total of 9 different metals. For a random distribution of substitutional acceptor/donor of charge dopants, a gaussian-like density of states appears at the lower/upper part of the conduction/valence band.[2] The corresponding density of states is directly proportional to the dopant concentration, thus giving a clear tool to manage visible light absorption. Nevertheless, a high doping concentration may have detrimental effects because the photocatalytic rate constant typically decreases with a growing level of dopant.[3]

A microemulsion preparation method was used as it facilitates, as much as possible, the homogeneity of chemical composition at a nanoscale level as well as the production of particles with a narrow size distribution.[4] Ti(IV) isopropoxide was added to an inverse emulsion containing an aqueous solution (0.5 M) of precursors salts dispersed in *n*-heptane using Triton X-100 (Aldrich) as surfactant and hexanol as co-surfactant. The resulting mixture was stirred for 24 h, centrifuged, decanted, rinsed with methanol and calcined at 723 K for 2 h.

In Table 1, we report the materials synthesized; in the best cases, up to *ca.* 25 at.% is successfully introduced in the titania structure. Fe, Mn, Ni and Ce-containing mixed oxides have small (maximum) dopant concentrations, expected at least in the first case. The microemulsion method is able to obtain mixed oxides with surface area in the 35–145 $m^2\ g^{-1}$ interval with (primary) particle size ranging from 5 to 13 nm. X-Ray diffraction (data not shown) and Raman spectroscopy (see below) of the systems give evidence that all samples have an anatase-type structure, except the Ti–Cr case, where XRD allows us to roughly estimate a 55:45 anatase:rutile mixture. The absence of well-developed, bulk-like dopant-atom single oxide phases was confirmed using both techniques.

Photocatalytic activities of the highly doped Ti–M mixed oxides in the gas phase toluene mineralization are presented in Table 2. The photocatalytic reactor was made of two concentric Pyrex tubes. The catalyst (100 mg) was coated onto the central section (150 mm) of the inner tube (16 mm o.d.). The reacting mixture (100 ml min^{-1}) was prepared by injecting toluene (*ca.* 1000 ppmv) into a wet oxygen flow before entering the photoreactor. After flowing the mixture for 1 h in the dark (control test), four fluorescent day-light lamps (6W, Sylvania F6W/D, irradiation range 360–750 nm, UV content of 3%) were switched on. Gas composition outlet was analyzed using an on-line gas chromatograph equipped with a capillary column and an electron ionization detector. Toluene photo-oxidation was chosen to test activity as it is a large component of environmental aromatic hydrocarbons and is thought to be an important constituent of anthropogenic emissions in urban atmospheres. In addition, its photo-oxidation is a demanding reaction. Included in Table 2 is the activity of some single oxides prepared by microemulsion and the commercial (anatase + rutile) P25 (Degussa) material. Samples with Fe, Mn, Ni and Ce are not active and were not included in the table.

Among the catalysts tested, those containing W appear to have the highest activity although with a moderate selectivity to benzaldehyde, somewhat paralleling the selectivity of the pure WO_3 oxide. The Ti–W, Ti–Mo and Ti–Nb series present activity while Ti–V and Ti–Cr series do not display detectable photocatalytic activity. It is important to note that these samples

Table 1 Main characterization results of Ti–M mixed oxides

Sample	M atom content (%)[a]	$S_{BET}/m^2\ g^{-1}$	Anatase crystal size/nm[b]
TiO_2	—	106	$8_{.5}$
Ti–V	18	33	13
Ti–Cr	16	100	8
Ti–Nb	20/10	42/125	9/11
Ti–Mo	26/12	77/144	6/7
Ti–W	19/14	122/108	$5/7_{.5}$
Ti–Mn	3	76	11
Ti–Fe	6	90	9
Ti–Ni	3	85	10
Ti–Ce	7	127	9

[a] Measured by AA/ICP. [b] Measured by XRD/TEM.

Table 2 Reaction rate and selectivity of catalysts for gas-phase toluene photo-mineralization with sun light-type radiation

Catalyst[a]	10^{10} Rate/ mol $s^{-1}\ m^{-2}$	10^{8} Rate/ mol $s^{-1}\ g^{-1}$	Selectivity (%)[b]
TiO_2	1.0	1.0	5
TiO_2 P25	0.6_5	0.3_5	14
WO_3	4.6	0.1	100
MoO_3		Not active	
Nb_2O_5		Not active	
W 19	3.3	4.0	13
W 14	1.7	1.9	16
Mo 26	1.9	1.4	5
Mo 12	1.0	1.4	4
Nb 20	0.4	0.2	25
Nb 10	0.4	0.5	18

[a] Ti–M samples are described by the dopant-atom content. [b] To benzaldehyde (other detectable products; CO_2).

 DOI: 10.1039/b107314a

always display lower activity than the home-made titania reference if UV rather than visible light is used. It should be also mentioned that the WO_3 oxide is active although its small surface area leads to a very low reaction rate per gram.

UV-visible spectra suggest that V and Cr containing samples do not present a simple band gap as occurs with titania (Fig. 1). In the visible region of the spectrum, V displays d–d charge localized transitions (for V^{5+}/V^{4+} in the 400–600/600–800 nm region)[5] while Cr has several (O to Cr) charge transfer bands.[6] The electronic modifications induced in the anatase-like oxides with respect to titania evidence the main reason for the failure of the Ti–V and Ti–Cr catalysts. On the other hand, it can be noted that, in agreement with a previous report,[7] the decrease of the V content of the mixed oxide yields active materials when the dopant-atom is below 6 at.% (data not shown).

Samples containing maximum quantities of Nb, Mo and W display (Fig. 1) UV-visible spectra typical of semiconductor materials with estimated band gap absorption onset at 395, 465 and 420 nm, which can be compared with the *ca.* 380 nm characteristic of our nanosized titania specimen. These active samples, as well as the home-made titania reference, have particle sizes in the 5 to 9 nm range, where only moderate size dependency of activity is expected.[8] Comparison with titania references (Table 2) suggests that our samples present up to a four-fold increase with respect to nanosized titania samples, having an activity enhancement with the level of doping for W and a less concentration-dependent behavior for Mo and Nb.

Raman analysis of these three series may allow us to rationalize these results. The spectra of pre-reaction (calcined) materials with varying Ti–M atomic ratios are shown in Fig. 2.

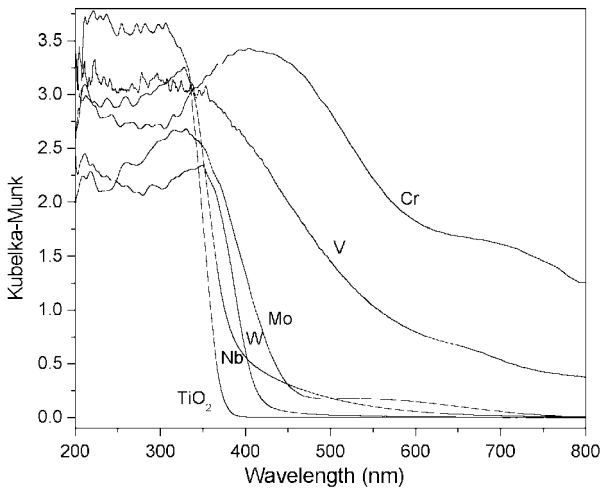

Fig. 1 UV-visible reflectance spectra of Ti–M samples with the highest dopant-atom content.

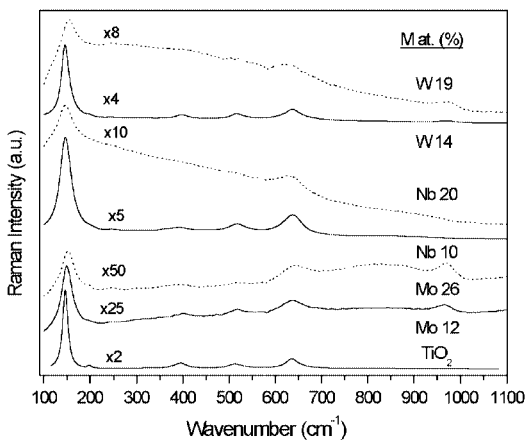

Fig. 2 Raman spectra of Ti–W, Ti–Mo and Ti–Nb specimens.

The analysis of Raman bands suggests that all active materials having a 20–25 at.% level of doping have a surface partially covered by hetero-atom moieties; bands at 975 cm^{-1} for W[9] and 971 cm^{-1} for Mo[10] correspond to W=O and Mo=O bond stretchings, while the 636 cm^{-1} frequency band has a contribution from a Nb–O–Nb deformation.[11] A broad band appears on the Mo spectra in the 690–935 cm^{-1} range.[10,11] All the mentioned bands are characteristic of surface MO_x entities supported on titania, without having any evidence of bulk single oxide formation,[9–11] in agreement with XRD. However, W and Nb materials with lower (*ca.* 10–15 at.%) dopant-atom quantities hardly display discernible Raman bands associated with (single) hetero-atom moieties, while the Mo specimen shows less distorted (frequency/intensity) anatase bands and a decreased intensity for bands ascribed to surface Mo species (Fig. 2), both facts in agreement with the presence of a decreasing amount of Mo species on the titania surface.[10]

The comparison of characterization results with catalytic behavior under solar-type (Table 2) and UV lights suggests that highly doped materials with anatase structure can have significant activity in VOCs elimination under visible light excitation. However, the percentage of hetero-atom present in the catalyst seems to have little relevance for Mo and Nb systems and a significant importance in the case of W. For W, the presence of dopant-atom ad-species on the surface may have catalytic consequences; however, a catalyst produced by deposition of a 4 wt.% WO_x on the anatase synthesized by a two-step microemulsion method displays null activity enhancement over the parent, home-made TiO_2 reference.

It therefore appears that, apart from the impurity derived change in the absorption threshold energy, dependence on the dopant-atom nature seems to have a strong correlation with the main d-electron configuration, as has been already observed by others using UV light.[12–15] In the case of solar light, our study indicates that the heavier elements of group VI are the best dopants for yielding efficient photocatalytic degradation of toluene using highly doped titania samples. This behavior contrasts with that observed for low dopant level samples under UV excitation, which present activity for group V and VI dopant-atoms.[1]

The authors thank the 'Ayuntamiento de Coslada' for partial support of this work.

Notes and references

1 M. R. Hoffmann, S. T. Martin, W. Choi and D. W. Bahnemann, *Chem. Rev.*, 1995, **95**, 69–96.
2 M. M. Cohen, *Introduction to the theory of semiconductors*, Gordon, Amsterdam, 2nd edn. 1999, p. 173.
3 J. Moser, M. Gratzel and R. Galley, *Helv. Chim. Acta*, 1987, **70**, 1056–1062.
4 M.-J. Schwuger, K. Stickdorn and R. Schomacker, *Chem. Rev.*, 1995, **95**, 849–864.
5 Z. Zhao, Y. Yamada, Y. Teng, A. Ueda, K. Nakagawa and T. Kobayashi, *J. Catal.*, 2000, **190**, 215–227.
6 M. Anpo and M. Che, *Adv. Catal.*, 2000, **44**, 119–257.
7 H. Yamasita, Y. Ichihashi, M. Takeuchi, S. Kishiguchi and M. Anpo, *J. Synchrotron Radiat.*, 1999, **6**, 451–453.
8 A. J. Maira, K. L. Yeung, J. Soria, J. M. Coronado, C. Belver, C. Y. Lee and V. Augugliaro, *Appl. Catal.*, 2001, **29**, 327–336.
9 A. Gutierrez-Alejandre, J. Ramírez and G. Busca, *Langmuir*, 1998, **14**, 630–639.
10 I. E. Wachs, *Catal. Today*, 1996, **27**, 437–455.
11 L. J. Burcham, J. Datka and I. E. Wachs, *J. Phys. Chem. B*, 1999, **103**, 6015–6024.
12 T. Nishikawa, Y. Shinohara, T. Nakajima, M. Fujita and S. Mishima, *Chem. Lett.*, 1999, 1133.
13 W. Choi, A. Termin and M. R. Hoffman, *Angew. Chem., Int. Ed. Engl.*, 1994, **33**, 1091–1092.
14 M. E. Zorn, D. T. Tompkins, W. A. Zeltner and M. A. Anderson, *Appl. Catal. B*, 1999, **23**, 1–8.
15 J. G. Highfield and P. Pichat, *New J. Chem.*, 1989, **13**, 61–66.

CHEMCOMM
Communication
www.rsc.org/chemcomm

Remarkable organophosphorus cage compounds from the reaction of cobaltocene and the triphosphole $P_3C_2Bu^t_2CH(SiMe_3)_2$: crystal and molecular structures of $[Co(\eta^5\text{-}C_5H_5)(\eta^4\text{-}C_4H_4CHCHP_6C_4Bu^t_4)]$ and $P_6C_4Bu^t_4CH(SiMe_3)$

Peter B. Hitchcock, John F. Nixon* and Nurgün Sakarya Büyükkidan†

School of Chemistry, Physics and Environmental Science, University of Sussex, Brighton, Sussex, UK BN1 9QJ. E-mail: E-mail J.Nixon@sussex.ac.uk

Received (in Cambridge, UK) 7th September 2001, Accepted 16th November 2001
First published as an Advance Article on the web 6th December 2001

The novel cage compounds $[Co(\eta^5\text{-}C_5H_5)(\eta^4\text{-}C_4H_4CHCHP_6C_4Bu^t_4)]$ and $P_6C_4Bu^t_4CH(SiMe_3)$ are formed from the reaction between cobaltocene and the triphosphole $P_3C_2Bu^t_2CH(SiMe_3)_2$.

Organophosphorus cage compounds are of considerable current interest and synthetic routes usually involve cyclooligomerisation of phospha-alkynes (sometimes metal mediated) or coupling of polyphospholyl anions.[1–4] Recently we described a series of cages containing an additional heteroatom $P_6C_4Bu^t_4E$ **1** (E = S, Se, Te and GeI_2). The chalcogen containing compounds were obtained by an unprecedented reaction involving the facile specific insertion reaction into a P–P bond of the hexaphospha-prismane, $P_6C_4Bu^t_4$.[5,6]

We and others,[7] in unpublished work, have noted that in alkylation reactions of the $P_3C_2Bu^t_2$ anion with $BrCH(SiMe_3)_2$ which afforded the first known 1,2,4-triphosphole, $P_3C_2Bu^t_2CH(SiMe_3)_2$ **2**[8] on occasions also gave two isomeric

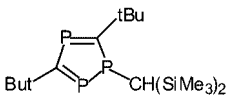

2

organophosphorus cage compounds, $P_6C_4Bu^t_4CHSiMe_3$, albeit in low yield. Since a light-induced radical coupling reaction (with partial elimination of the $CH(SiMe_3)$ side-chain), might be responsible, we have studied the reaction between **2** and the stable organometallic radical cobaltocene.

Thus, treatment of $[Co(\eta^5\text{-}C_5H_5)_2]$ with the triphosphole $P_3C_2Bu^t_2CH(SiMe_3)_2$ **2** in refluxing toluene for 4 h, afforded an approximately equimolar mixture of two novel organophosphorus cage compounds; (i) the colourless $P_6C_4Bu^t_4CH(SiMe_3)$ **3** (6.4%) and (ii) the remarkable red 18e diamagnetic cobalt(I)

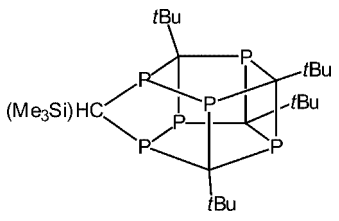

3

complex $[Co(\eta^5\text{-}C_5H_5)(\eta^4\text{-}C_4H_4CHCHP_6C_4Bu^t_4)]$ **4** (5.8%). Both compounds exhibited parent ions in their mass spectra‡ and were fully structurally characterised by single crystal X-ray diffraction methods.§ (Figs. 1 and 2). The organosilanes which are lost from the triphosphole side-chain during the reaction,

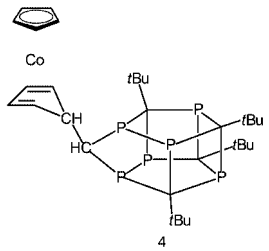

4

(most likely a $CH(SiMe_3)_3/Si_2Me_6$ mixture), were not isolated.

Compound **3** exhibits the expected $^{31}P\{^1H\}$ NMR spectrum,‡ consisting of six distinct resonances whose chemical shifts are all typical for saturated phosphorus atoms in cage structures. Of special structural significance are the signals at 197.5 and 178.8 ppm, which both show only small further P–P couplings, and can be easily assigned to the two cage phosphorus atoms which are bonded solely to carbon, whereas the other four resonances, each involving large doublet patterns, ($^1J_{P(1)P(2)}$ 238.1 and $^1J_{P(4)P(5)}$ 226.5 Hz) arise from the two sets of phosphorus atoms directly bonded to each other.

The molecular structure of **3**, (Fig. 1), represents an addition to the $P_6C_4Bu^t_4E$ family of cages, being derived from the hexaphosphapentaprismane $P_6C_4Bu^t_4$ by a $CHSiMe_3$ bridge linking the two five-membered $P_3C_2Bu^t_2$ rings. The C–C, C–P and P–P bond lengths in **3** all lie in the expected single bond range.

The cobalt complex **4**, which is also a $P_6C_4Bu^t_4E$ cage family member, shows a similar pattern of lines in its $^{31}P\{^1H\}$ NMR spectrum to **3**. It clearly results from the conversion of one of the

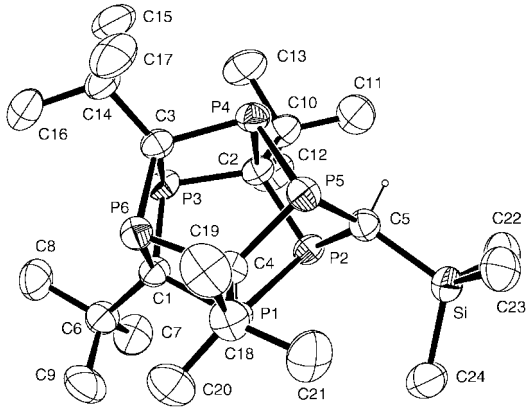

Fig. 1 Molecular structure of **3** Selected bond lengths (Å): P(1)–C(1) 1.8735(17), P(1)–C(4) 1.9078(16), P(1)–P(2) 2.1913(6), P(2)–C(5) 1.8600(17), P(2)–C(2) 1.8675(17), P(3)–C(1) 1.8807(17), P(3)–C(2) 1.8871(18), P(3)–C(3) 1.9029(16), P(4)–C(3) 1.8716(18), P(4)–C(2) 1.9107(16), P(4)–P(5) 2.2042(6), P(5)–C(5) 1.8707(17), P(5)–C(4) 1.8761(17), P(6)–C(3) 1.8724(18), P(6)–C(4) 1.8930(18), P(6)–C(1) 1.9014(16).

† Present address: Department of Chemistry, Faculty of Arts and Science, Gaziosmanpaa University, Tokat, Turkey.

 DOI: 10.1039/b108125j

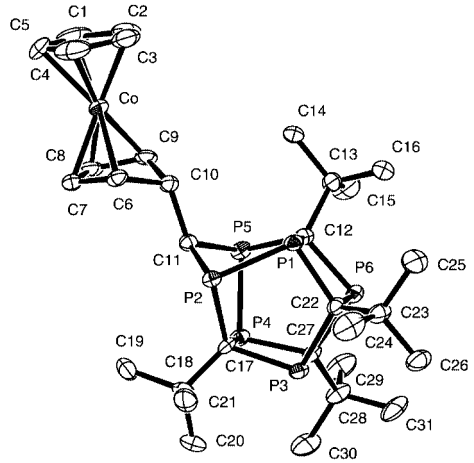

Fig. 2 Molecular structure of **4** Selected bond lengths (Å): Co–C(1) 2.063(6), Co–C(2) 2.041(6), Co–C(3) 2.052(7), Co–C(4) 2.036(7), Co–C(5) 2.072(6), Co–C(6) 2.038(6), Co–C(7) 1.963(5), Co–C(8) 1.949(6), Co–C(9) 2.016(5), P(1)–C(12) 1.897(6), P(1)–C(22) 1.870(5), P(1)–P(2) 2.188(2), P(2)–C(11) 1.857(5), P(2)–C(17) 1.858(5), P(3)–C(22) 1.876(5), P(3)–C(17) 1.893(5), P(3)–C(27) 1.893(5), P(4)–C(27) 1.865(5), P(4)–C(17) 1.897(5), P(4)–P(5) 2.185(2), P(5)–C(12) 1.861(5), P(5)–C(11) 1.882(5), P(6)–C(27) 1.867(6), P(6)–C(12) 1.890(5) P(6)–C(22) 1.897(5), C(8)–C(9) 1.405(8), C(7)–C(8) 1.414(8), C(6)–C(7) 1.423(8) C(10)–C(11) 1.550(7).

original η^5-ligated C_5H_5 rings of cobaltocene into an η^4-bonded C_4H_4CH–fragment of a substituted cyclopentadiene ring, linked to the newly generated $P_6C_4Bu^t{}_4CH$-cage fragment. The overall geometry of the organophosphorus cage in **4**, (Fig. 2), is little different from that observed in **3**, and the bent (C_4H_4CH)–ring fragment and the very similar C(6)–C(7)–C(8)–C(9) bond distances (averaging 1.412(8) Å) suggest electron delocalisation within the η^4-cyclopentadiene–cobalt moeity.

We thank the British Council for financial support (to N. S. and J. F. N.) for part of this work.

Notes and references

‡ **3**: $^{31}P\{^1H\}$ NMR (161.97 MHz, $CDCl_3$, 25 °C) (numbering scheme as in crystal structure) δ 197.5 (P(6), m, $^2J_{P(6)P(5)}$ 30.3, $^2J_{P(6)P(4)}$ 23.0, $^2J_{P(6)P(1)}$ 11.6 Hz), δ 178.8 (P(3), m, $^2J_{P(3)P(2)}$ 26.0, $^2J_{P(3)P(1)}$ 20.9, $^2J_{P(3)P(5)}$ 8.8 Hz), 149.7 (P(4), dm, $^1J_{P(4)P(5)}$ 226.5, $^2J_{P(4)P(6)}$ 23.0, $^2J_{P(4)P(2)}$ 19.3, $^2J_{P(4)P(3)}$ 8.6 Hz), 140.5 (P(1), dm, $^1J_{P(1)P(2)}$ 238.1, $^2J_{P(1)P(3)}$ 20.9, $^2J_{P(1)P(6)}$ 11.6 Hz), 123.0 (P(5), dm, $^1J_{P(5)P(4)}$ 226.5, $^2J_{P(5)P(6)}$ 30.3, $^2J_{P(5)P(2)}$ = 19.3, $^2J_{P(5)P(3)}$ 8.6 Hz), 119.0 (P(2), dm, $^1J_{P(2)P(1)}$ 238.1, $^2J_{P(2)P(3)}$ 26.0, $^2J_{P(2)P(5)}$ = 19.3, $^2J_{P(2)P(6)}$ 8.2 Hz). ^1H NMR (400.13 MHz, $CDCl_3$): δ 1.62 (m, CH), 1.27 (s, 9H, Bu^t), 1.23 (s, 9H, Bu^t), 1.17 (s, 9H, Bu^t), 1.16 (s, 9H, Bu^t), 0.26 (s, 9H, $SiMe_3$). $^{13}C\{^1H\}$ NMR (100.61 MHz, $CDCl_3$, 25 °C): δ 41.5 (s, Bu^t), 41.1 (s, 2(Bu^t)), 40.6 (s, Bu^t), 37.1 (m, *C*Bu^t), 35.1 (m, *C*Bu^t), 30.3 (m, *C*Bu^t), 29.0 (m, *C*Bu^t), 26.7 (m, *C*$SiMe_3$), 1.1 (s, Me).

EI-MS: *m/z* 548 $[P_6C_4Bu^t{}_4CHSiMe_3]^+$, 491 $[P_6C_4Bu^t{}_3CHSiMe_3]^+$, 169 $[CBu^t]^+$, 73 $[SiMe_3]^+$.

4: $^{31}P\{^1H\}$ NMR (161.97 MHz, $CDCl_3$, 25 °C) (numbering scheme as in crystal structure): δ 200.0 (P(3), $^2J_{P(3)P(1)}$ 30.3, $^2J_{P(3)P(5)}$ 7.9, $^2J_{P(3)P(2)}$ 25.0 Hz), 191.1 (P(6), $^2J_{P(6)P(4)}$ 35.4, $^2J_{P(6)P(5)}$ 22.7, $^2J_{P(6)P(2)}$ 7.6 Hz), 149.0 (P(1), $^1J_{P(1)P(2)}$ 242.6, $^2J_{P(1)P(3)}$ 30.3 Hz), 137.5 (P(4), $^1J_{P(4)P(5)}$ 236.2, $^2J_{P(4)P(6)}$ 35.4 Hz), 108.2 (P(5), $^1J_{P(5)P(4)}$ 236.2, $^2J_{P(5)P(6)}$ 22.7, $^2J_{P(5)P(2)}$ 19.3, $^2J_{P(5)P(3)}$ 7.9 Hz), 105.1 (P(2), $^1J_{P(2)P(1)}$ 242.6, $^2J_{P(2)P(3)}$ 25.0, $^2J_{P(2)P(5)}$ 16.3, $^2J_{P(2)P(6)}$ 7.6 Hz).

EI-MS: *m/z* 664 $[CoC_5H_5C_4H_4CHCHP_6C_4Bu^t{}_4CHSiMe_3]^+$, 540 $[C_4H_4CHCHP_6C_4Bu^t{}_4CHSiMe_3]^+$, 476 $[P_6C_5Bu^t{}_4H_2]^+$, 419 $[P_6C_4Bu^t{}_3CH_2]^+$, 355 $[P_4C_5Bu^t{}_3]^+$, 281 $[P_2C_4Bu^t{}_3]^+$, 69 $[CBu^t]^+$.

§ *Crystal data*: for **3**: $C_{24}H_{46}P_6Si$, M = 548.52, triclinic, space group $P\bar{1}$ (no. 2), a = 10.2274(2), b = 12.3429(4), c = 12.7112(4) Å, α = 100.210(2), β = 97.134(2), γ = 102.000(2)°, V = 1522.92(7) Å^3, T = 293(2) K, Z = 2, D_c 1.20 Mg m^{-3}, μ = 0.40 mm^{-1}, λ = 0.71073 Å, $F(000)$ = 588, crystal size 0.2 × 0.2 × 0.1 mm, 18033 measured reflections, 7193 independent reflections (R_{int} = 0.0311), 5978 reflections with $I > 2\sigma(I)$. Final indices $R1$ = 0.036, $wR2$ = 0.091 for $I > 2\sigma(I)$; $R1$ = 0.047, $wR2$ = 0.098 for all data, Data collection: Nonius Kappa CCD Refinement using SHELXL-97. Program package WinGX.

For **4**: $C_{31}H_{47}CoP_6$, M = 664.44, monoclinic, space group $P2_1/c$ (no. 14), a = 9.634(3), b = 32.706(7), c = 10.510(2) Å, β = 98.16(2)°, V = 3278.1(14) Å^3, T = 173(2) K, Z = 4, D_c 1.35 Mg m^{-3}, μ = 0.84 mm^{-1}, λ = 0.71073 Å, $F(000)$ = 1400, crystal size 0.3 × 0.3 × 0.1 mm^3, 6120 measured reflections, 5769 independent reflections (R_{int} = 0.0377), 3897 reflections with $I > 2\sigma(I)$, Final indices $R1$ = 0.056, $wR2$ = 0.119 for $I > 2\sigma(I)$, $R1$ = 0.102, $wR2$ = 0.155 for all data, Data collection: Enraf Nonius CAD4 Structure solution SHELXS-86. Refinement using SHELXL-93.

CCDC reference numbers 172126 and 172127. See http://www.rsc.org/suppdata/cc/b1/b108125j/ for crystallographic data in CIF or other electronic format.

1 (*a*) R. Streubel, *Angew. Chem., Int. Ed. Engl.*, 1995, **34**, 436 and references therein; (*b*) A. Mack and M. Regitz, in *Carbocyclic and Heterocyclic Cage Compounds and Their Building Blocks*, ed. K. K. Laali, J. A. I. Press, Stamford, CT, USA, 1999, p. 199; (*c*) J. F. Nixon, in *Carbocyclic and Heterocyclic Cage Compounds and Their Building Blocks*, ed. K. K. Laali, J. A. I. Press, Stamford, CT, USA, 1999, p. 257; (*d*) B. Geissler, S. Barth, U. Bergsträsser, M. Slany, J. Durkin, P. B. Hitchcock, M. Hofmann, P. Binger, J. F. Nixon, P. von R. Schleyer and M. Regitz, *Angew. Chem., Int. Ed. Engl.*, 1995, **34**, 484; (*e*) V. Caliman, P. B. Hitchcock, J. F. Nixon, M. Hofmann and P. von R. Schleyer, *Angew. Chem., Int. Ed. Engl.*, 1994, **33**, 2202; (*f*) B. Geissler, T. Wettling, S. Barth, P. Binger and M. Regitz, *Synthesis*, 1994, 1337; (*g*) F. Tabellion, A. Nachbauer, S. Leininger, C. Peters, F. Preuss and M. Regitz, *Angew. Chem., Int. Ed. Engl.*, 1998, **37**, 1233.

2 (*a*) L. Weber, *Adv. Organomet. Chem.*, 1997, **41**, 1; (*b*) K. B. Dillon, F. Mathey and J. F. Nixon, *Phosphorus: The Carbon Copy*, J. Wiley, Chichester, 1998, ch. 4.

3 T. Wettling, J. Schneider, O. Wagner, C. G. Kreiter and M. Regitz, *Angew. Chem., Int. Ed. Eng.*, 1989, **28**, 1013; R. Bartsch, P. B. Hitchcock and J. F. Nixon, *J. Organomet. Chem.*, 1989, **375**, C31.

4 (*a*) B. Breit, Ph.D Thesis, University of Kaiserslautern, Germany, 1992; (*b*) M. Regitz, A. Hoffmann and U. Bergsträsser, in *Modern Acetylene Chemistry*, ed. P. J. Stang and F. Diederich, VCH Weinheim, 1995, p. 173; (*c*) M. M. Al-Ktaifani, W. Bauer, U. Bergsträsser, B. Breit, M. D. Francis, F. W. Heinemann, P. B. Hitchcock, A. Mack, J. F. Nixon, H. Pritzkow, M. Regitz, M. Zeller and U. Zenneck, *Chem. Eur. J.*, in press.

5 A. G. Avent, F. G. N. Cloke, M. D. Francis, P. B. Hitchcock and J. F. Nixon, *Chem. Commun.*, 2000, 879.

6 M. M. Al-Ktaifani, D. P. Chapman, M. D. Francis, P. B. Hitchcock, J. F. Nixon and L. Nyulászi, *Angew. Chem., Intl. Ed.*, 2001, **40**, 3974.

7 M. H. Araujo, V. Caliman, E. E. Castellano, A. C. Doriguetto, J. Ellena, P. B. Hitchcock and D. A. Rajão, *J. Braz. Chem.*, submitted.

8 V. Caliman, P. B. Hitchcock and J. F. Nixon, *J. Chem. Soc., Chem. Commun.*, 1995, 1661.

CHEMCOMM
Communication
www.rsc.org/chemcomm

$(TTF)_2[TTF(CO_2H)_2(CO_2)_2]$: a wholly TTF material containing TTF radical cations and TTF derived anions

Nicolas Mercier,* Michel Giffard, Guillaume Pilet, Magali Allain, Piétrick Hudhomme, Gilles Mabon, Eric Levillain, Alain Gorgues and Amédée Riou

Ingénierie Moléculaire et Matériaux Organiques, UMR-CNRS 6501, 2 Bd Lavoisier, 49045 Angers, France. E-mail: nicolas.mercier@univ-angers.fr; Fax: 33.(2).41.73.54.05; Tel: 33.(2).41.73.50.83

Received (in Cambridge, UK) 2nd October 2001, Accepted 8th November 2001
First published as an Advance Article on the web 6th December 2001

Electrooxidation of tetrathiafulvalene (TTF) carried out in the presence of $(Bu_4N)_2TTF(CO_2H)_2(CO_2)_2$ as supporting electrolyte affords wholly TTF organic materials in which TTF cations are associated with $TTF(CO_2H)_2(CO_2^-)_2$ as counteranions.

The electronic properties of radical cation salts of the TTF series strongly depend on the way in which donor π-orbitals overlap in the solid state.[1] This is the consequence of the crystal packing which is itself the result of several intermolecular interactions involving both donors and anions such as hydrogen bonds or van der Waals dispersion forces. In this context, the design of organic anions which can be easily chemically tuned is becoming a main trend.[2] We recently focused on anions derived from carboxylic acids which display a variety of shapes and symmetries and are also likely to build polymeric anionic networks by hydrogen bonds.[3]

We now report the synthesis and characterizations of TTF salts based on the $TTF(CO_2H)_2(CO_2^-)_2$ dianion. The synthesis of a π-donor TTF bearing an anionic group has been previously investigated in order to further form upon electrooxidation the corresponding neutral zwitterionic π-radical.[4] In contrast, our approach consists here of using the tetrabutylammonium salt $2Bu_4N^+,TTF(CO_2H)_2(CO_2^-)_2$ (**1**)† (synthesized from $TTF(CO_2H)_4$[5] and $(Bu_4N)OH$ as starting materials) as supporting electrolyte in the electrooxidation of a donor (TTF itself for example) more easily oxidisable than the TTF core of the anion.

From cyclic voltammetry (Fig. 1), it appears that, as expected from the electron withdrawing character of carboxylic acid groups, the first oxidation potential of $TTF(CO_2H)_4$ (0.57 V *vs.* Ag/AgCl) is clearly greater compared to that of TTF (0.38 V *vs.* Ag/AgCl). The transformation of two $-CO_2H$ groups in two $-CO_2^-$ carboxylate groups, leading to salt (**1**), induces a lowering of the first oxidation potential of 0.09 V (0.48 V *vs.* Ag/AgCl) which nevertheless remains greater than that of TTF.

This result outlines, *a priori*, that only the oxidation of TTF must occur in electrocrystallization experiments when $(Bu_4N)_2TTF(CO_2H)_2(CO_2)_2$ is used as supporting electrolyte, $TTF(CO_2H)_2(CO_2^-)_2$ acting only as a counterion. The electrocrystallization experiments were carried out typically as follows: 20 mL of solution of (**1**) (0.02 mol.L^{-1} in a 90 : 10 CH_2Cl_2–EtOH mixture) were charged in a H-shaped cell, 15 mg of TTF were introduced in the anodic arm and a constant current (I = 2 μA) was applied for twenty days. This led to black single crystals that were formulated as $(TTF)_2[TTF(CO_2H)_2(CO_2)_2]$ (**2**) thanks to their X-ray crystal structure.

Compound (**2**) crystallizes in the centrosymmetrical triclinic space group. The asymmetric unit consists of one $TTF^{\cdot+}$ radical cation and half $TTF(CO_2H)_2(CO_2^-)_2$ anion. This anion is centrosymmetric and fully planar and its nature is unambiguously deduced from the analysis of the bond lengths which appear very close at hand from those encountered in starting salt (**1**); furthermore, a symmetrical intramolecular hydrogen bond situation, also previously described in hydrogenomaleate anion,[6] is observed for both salts (Fig. 2). This shows that TTF cores of $TTF(CO_2H)_2(CO_2^-)_2$ anions remain neutral. As a consequence, all unsubstituted TTF molecules are at the +I oxidation state, which is in good accordance with the observed bond lenghts (*e.g.* an increase of the central C···C bond together with a lowering of the S···C bonds, compared to neutral unsubstituted TTF molecules[7]).

In the crystal structure, TTF units of the anions and $TTF^{\cdot+}$ radical cations are piled up in stacks with the alternance $TTF^{\cdot+}/TTF^{\cdot+}/TTF(CO_2H)_2(CO_2^-)_2$. These stacks, shifted one from each other, form β-type like sheets, giving rise to six relative situations between molecules (numbers 1–6 in Fig. 3). In the stacks, a bond over cycle overlap occurs between the TTF core of the anion and a $TTF^{\cdot+}$ radical cation (interaction 1). However, no S···S distance lower than the sum of van der Waals radii of two sulfur atoms is observed. On the contrary, the strong interaction 4 between two $TTF^{\cdot+}$ species, where a bond over bond overlap situation and four short S···S distances (d = 3.388(5) Å and d = 3.405(5) Å) are present, leads to well defined $(TTF^{\cdot+})_2$ dimers. With regard to adjacent interactions, a

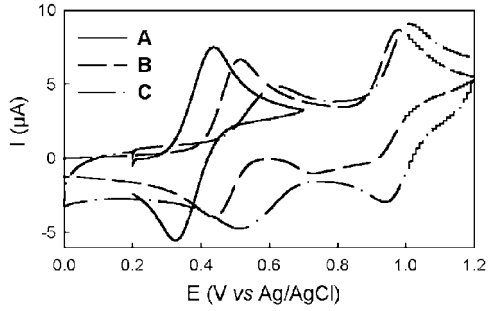

Fig. 1 Cyclic voltammograms of TTF (**A**), $(Bu_4N)_2TTF(CO_2H)_2(CO_2)_2$ (the second wave is not reversible) (**B**) and $TTF(CO_2H)_4$ (**C**) (solvent: acetonitrile; supporting electrolyte: Bu_4NPF_6; v = 0.5 V s^{-1}; reference: Ag/AgCl).

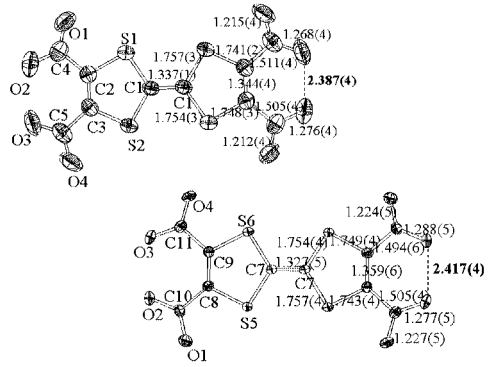

Fig. 2 Ortep views with the numbering scheme and bond lengths (in Å) of $TTF(CO_2H)_2(CO_2^-)_2$ anion in (**1**) (top) and (**2**) (bottom)**.** Bold values are related to O···H···O hydrogen bond lengths; hydrogen atoms have not been located. Ellipsoids are drawn at 50% probability.

 DOI: 10.1039/b108888b

few S···S contacts are also encountered, implying in particular two $TTF^{\cdot+}$ cations (d = 3.537(4) Å and d = 3.560(6) Å for situation 6; d = 3.586(5) Å and d = 3.661(5) Å for situations 2 and 3, respectively).

Of particular interest also are the interactions between neighbouring sheets in the plane denoted A in Fig. 3, where C–H···O interactions are involved (Fig. 4). Such bonds implying hydrogen atoms, either from TTF core in salts based on EDT–$TTFCONH_2$[8] or from ethylene groups of BEDT–TTF molecules,[2b,9] play an important role in the packing of organic conducting salts and consequently in the electronic collective properties.

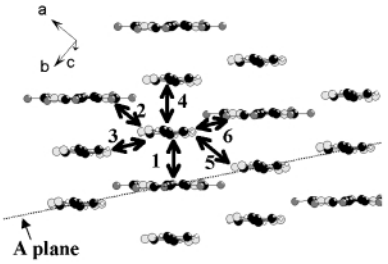

Fig. 3 β-Type like sheet in $(TTF)_2[TTF(CO_2H)_2(CO_2)_2]$ (**2**), including both $TTF^{\cdot+}$ radical cations and $TTF(CO_2H)_2(CO_2^-)_2$ anions.

The original structural feature is that, in a way, the anionic sheets do not exist, allowing a connection of the β-type sheets formed by the TTF units *via* rather strong C–H···O type hydrogen bonds (H(4)···O(4) 2.260(3) Å; H(1)···O(2) 2.356(3) Å).[10] A hydrogen bond network, also including intra-sheet C–H···O interactions (H(1)···O(1); H(3)···O(4)), thus appears (Fig. 4) with cyclic motifs as the one showed in Fig. 4, denoted $R_2^4(8)$ in Etter's notation.[11]

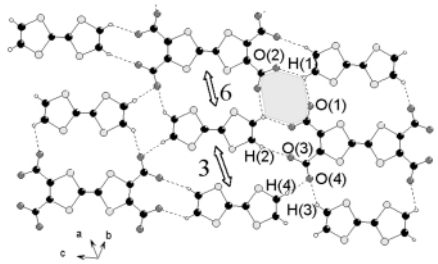

Fig. 4 C–H···O hydrogen bonds network in a A type plane of (**2**). Bond distances (in Å) : H(4)···O(4) 2.260(3); H(1)···O(2) 2.356(3); H(2)···O(3) 2.508(3); H(1)···O(1) 2.544(3); H(3)···O(4) 2.599(3).

As expected from structural considerations discussed above, (**2**) exhibits a $(TTF^{\cdot+})_2$ dimer absorption band[12] at λ = 750 nm (Fig. 5), and a semiconducting behaviour (E_a = 0.10 eV) with

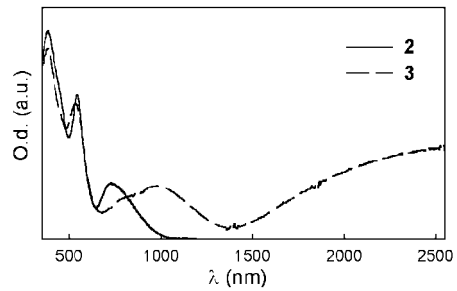

Fig. 5 Optical spectra of $(TTF)_2[TTF(CO_2H)_2(CO_2)_2]$ (**2**) and $(TTF)_3[TTF(CO_2H)_2(CO_2)_2]$ (**3**).

a weak room temperature conductivity ($\sigma = 10^{-5}$ S cm^{-1}). A mixed valence situation would *a priori* lead to a better conductivity. In fact, this situation is encountered in another compound (**3**), a dark brown powder obtained as a minor product in some of the electrocrystallization experiments: (**3**) presents a broad mixed valence absorption band[12] around 2500 nm (Fig. 5). Moreover, from EDX microanalysis,[13] (**3**) can be tentatively formulated as $(TTF)_3[TTF(CO_2H)_2(CO_2)_2]$, *i.e.* the association of two $TTF^{\cdot+}$ cations and one neutral TTF molecule with one $TTF(CO_2H)_2(CO_2^-)_2$ anion. Efforts are under way to obtain single crystals of (**3**).

In conclusion, we have succeeded in the synthesis of wholly TTF salts. This unprecedented concept where TTF-derived anions are incorporated in the donor slabs due to the inter-affinity of the TTF cores, suppressing the classical anion layers, can be extended to various mono, di and polycarboxylic acids derived from TTF. Studies on these promising full organic materials are in progress.

Notes and references

† *Crystal data* for **1** : $C_{42}H_{74}N_2O_8S_4$, M = 863.3, triclinic, a = 9.442(2), b = 10.209(1), c = 12.792(2) Å, α = 96.77(1), β = 98.63(1), γ = 97.72(1), V = 1196.0(7) Å^3, space group P-1, Z = 1, calculated density 1.2 ($\lambda_{MoK\alpha}$ = 0.71069). 4195 reflections collected in the 2.5–25° θ range, 253 parameters from 2778 reflections with $I/\sigma(I) > 3$ converged to R = 0.046, R_W = 0.070. CCDC 172112.

Crystal data for **2** : $C_{22}H_{10}O_8S_{12}$, M = 786.9, triclinic, a = 8.143(1), b = 8.203(1), c = 10.519(2) Å, α = 85.04(1), β = 82.87(1), γ = 84.00(1), V = 691.5(3) Å^3, space group P-1, Z = 1, calculated density 1.89 ($\lambda_{MoK\alpha}$ = 0.71069). 2622 reflections collected in the 2.5–25° θ range, 190 parameters from 1604 reflections with $I/\sigma(I) > 3$ converged to R = 0.036, R_W = 0.054. CCDC 172113. See http://www.rsc.org/suppdata/cc/b1/b108888b/ for crystallographic data in CIF or other electronic format.

1 (*a*) J. M. Williams, J. R. Ferraro, R. J. Thorn, K. D. Carlson, U. Geiser, H. H. Wang, A. M. Kini and M. H. Whangbo, *Organic Superconductors*, Prentice Hall, Englewood Cliffs, 1992; (*b*) J. P. Farges, *Organic conductors. Fundamentals and applications*, Marcel Dekker Inc., New York, 1994.

2 (*a*) I. Olejniczak, B. R. Jones, Z. Zhu, J. Dong, J. L. Musfeldt, J. A. Schlueter, U. Geiser, E. Morales, P. G. Nixon, R. W. Winter and G. L. Gard, *Chem. Mater.*, 2000, **11**, 3160; (*b*) B. H. Ward, J. A. Schlueter, U. Geiser, H. H. Wang, E. Morales. J. P. Parakka, S. Y. Thomas, J. M. Williams, P. G. Nixon, R. W. Winter, G. L. Gard, H. J. Koo and M. H. Whangbo, *Chem. Mater.*, 2000, **12**, 343.

3 M. Giffard, A. Riou, G. Mabon, N. Mercier, P. Molinié and T. P. Nguyen, *J. Mater. Chem.*, 1999, **9**, 851.

4 A. Dolbecq, M. Fourmigué, F. C. Krebs, P. Batail, E. Canadell, R. Clérac and C. Coulon, *Chem. Eur. J.*, 1996, **10**, 1275.

5 C. U. Pittman, Jr., M. Narita and Y. F. Liang, *J. Org. Chem.*, 1976, **41**, 2855.

6 J. E. Barry, M. Finkelstein and S. D. Ross, *J. Org. Chem.*, 1982, **47**, 64.

7 R. C. Teitelbaum, T. J. Marks and C. K. Johnson, *J. Am. Chem. Soc.*, 1980, **102**, 2986.

8 (*a*) K. Heuzé, M. Fourmigué, P. Batail, E. Canadell and P. A. Auban-Senzier, *Chem. Eur. J.*, 1999, **10**, 2971; (*b*) K. Heuzé, C. Mézière, M. Fourmigué, P. Batail, C. Coulon, E. Canadell, P. Auban-Senzier and D. Jérome, *Chem. Mater.*, 2000, **12**, 1898.

9 M. H. Whangbo, D. Jung, J. Ren, M. Evain, J. J. Novoa, F. Mota, S. Alvares, J. M. Williams, M. Beno, A. M. Kini, H. H. Wang and J. R. Ferraro, in *The Physics and Chemistry of Organic Superconductors*, ed. G. Saito and S. Kagoshima, Springer, Berlin, 1990, **51**, 262.

10 Hydrogen atoms of $TTF^{\cdot+}$ cations have been fixed at calculated positions with respect to the sp^2 carbon atom hybridization.

11 M. C. Etter and J. C. MacDonald, *Acta Cryst.*, 1990, **B46**, 256.

12 J. B. Torrance, B. A. Scott and F. B. Kaufman, *Solid. State Commun.*, 1975, **17**, 1369.

13 Single crystals EDX microanalysis (SEM) gives the following average S and O atomic ratios (theoretical values appear in brackets) (**2**) S 60.91 (60), O 39.04 (40); (**3**) S 67.96 (66.7), O 32.04 (33.3).

CHEMCOMM Communication
www.rsc.org/chemcomm

A new method to recover the nanoparticles from reverse micelles: recovery of ZnS nanoparticles synthesized in reverse micelles by compressed CO_2

Jianling Zhang, Buxing Han,* Juncheng Liu, Xiaogang Zhang, Zhimin Liu and Jun He

Center for Molecular Science, Institute of Chemistry, Chinese Academy of Sciences, Beijing 100080, China. E-mail: Hanbx@pplas.icas.ac.cn

Received (in Cambridge, UK) 26th October 2001, Accepted 15th November 2001
First published as an Advance Article on the web 6th December 2001

Zinc sulfide nanoparitcles synthesized in AOT reverse micelles can be recovered by compressed CO_2; more dispersed and uniform nanoparticles can be obtained.

Surfactants can form reverse micelles in non-polar solvents under suitable conditions. Water is readily solubilized in the polar core, forming a so-called water pool. The use of micellar water droplets as a novel environment for nanoparticle synthesis has attracted much attention due to its potential advantages compared with the traditional nanoparticle synthesis methods.[1–5] Since the reaction is restricted in the water core, the diameter of the obtained product particles can be controlled by the size of the water core which is related to the water-to-surfactant ratio (w). Recovery of the particles from the reverse micelles is one of the main steps in this method, and some techniques have been used to recover the particles, such as super-rate centrifugation and filtration. In these methods surfactant is usually precipitated together with the nanoparticles. It is often an exhaustive procedure to remove the surfactant completely and the obtained product particles are always embeded in the surfactant.[6] Ideally the synthesized nanoparticles should be precipitated while the surfactant should remain in the solution.

It is known that a compressed gas can dissolve in an organic solvent and change its properties.[7] The properties of the solvent can be tuned continuously by the pressure of the gas because the solubility of the gas is a function of the pressure. Generally, the properties of a reverse micellar solution vary with the property of the solvent. Thus, the product nanoparticles in reverse micelles may be recovered by dissolving a gas into the solution at suitable conditions. In this work, we used compressed CO_2 to recover the ZnS nanoparticles synthesized in reverse micelles. To our knowledge, similar work has not been reported in the literature, although compressed CO_2 has been used in extraction and fractionation, fine particle generation and recrystallization.[8–11]

In this work isooctane was used as the solvent in which the surfactant AOT can form reverse micelles.† The micellar solution was expanded after CO_2 is dissolved. The volume expansion coefficient $\alpha = (V-V_0)/V_0$ (V_0 and V are the volumes of the solution before and after adding CO_2) and cloud point pressure (P_c) at which AOT begins to precipitate were required for our experiments. These parameters were determined in this work by using the apparatus reported previously.[12]

Na_2S and $ZnSO_4$ can be solubilized in the water pool of the reverse micelles. The synthesis of ZnS nanoparticles in the reverse micelles was similar to that reported by other authors.[13]‡ ZnS particles were formed rapidly in the reverse micelles due to the high rate of the droplet-exchange process.[14]

The existence and concentration of ZnS nanoparticles in the reverse micelles at different CO_2 pressures can be studied by UV spectroscopy.[13]§ The temperature-controlled high-pressure sample cell used was the same as that used previously.[15] As examples, Fig. 1 shows the UV spectra of reverse micellar solutions (w = 15) containing ZnS and Na_2SO_4 at 308.15 K and different CO_2 pressures. For each experiment, the UV cell contained 0.28 mg ZnS and 0.039 g AOT, and the cell was full of solution after expansion with CO_2. Thus, the concentration of ZnS and AOT in the solution are 0.16 mg mL^{-1} and 50 mmol L^{-1} if precipitation does not occur. The absorbances at 271 nm and 220 nm are attributed to ZnS nanoparticles and AOT, respectively.[13] The absorbance of ZnS decreases with increasing pressure, which indicates precipitation of ZnS particles. Our experiments using CO_2-free solutions showed that the absorbance at 271 nm increased linearly with the concentration of ZnS in the concentration range 0–0.5 mg mL^{-1}. Thus, the precipitation percentage of ZnS can be calculated from the absorbance. Fig. 2 shows the dependence of the precipitation percentage of ZnS (P_{ZnS}%) with CO_2 pressure under different conditions. Fig. 2 illustrates that more ZnS particles are precipitated at higher pressures, and less ZnS particles are precipitated at lower w. About 93% ZnS particles can be precipitated at 5.50 MPa for w 15. However, the precipitation of AOT is not considerable at this pressure, as can be seen from Fig. 1. This was further confirmed by an experiment using an optical high-pressure autoclave,[12] which indicated that the

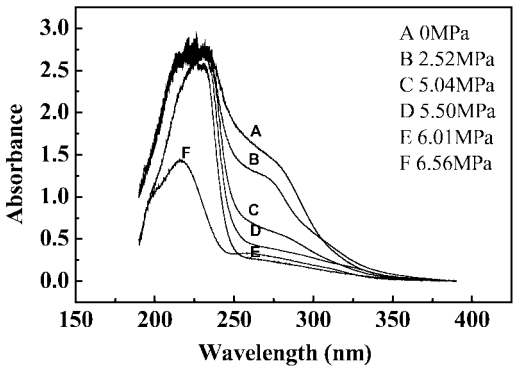

Fig. 1 UV spectra of ZnS in reverse micelles (w = 15, [AOT] = 50 mmol L^{-1}) at 308.15 K and different pressures.

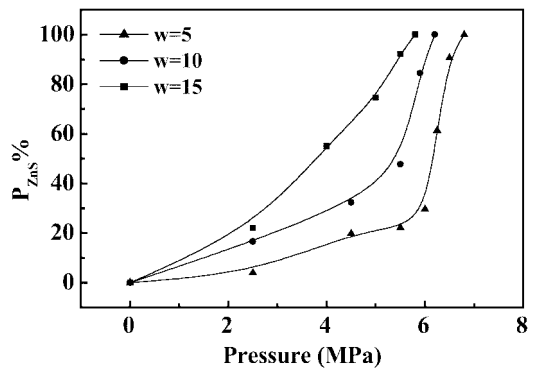

Fig. 2 Precipitation percentage of ZnS (P_{ZnS}%) from reverse micelles ([AOT] = 50 mmol L^{-1}) at 308.15 K.

 DOI: 10.1039/b109802k

cloud point pressure at which AOT begins to precipitate was 5.61 MPa.

On the basis of the investigation above, we could select suitable conditions to prepare and recover ZnS nanoparticles using a larger stainless steel cell of volume 32.60 mL containing a stirrer.¶ To obtain the largest recovery of ZnS without precipitation of AOT, we selected w = 15, and recovered the ZnS from the reverse micelles at 5.50 MPa. The particle size of ZnS was determined by transmission electron microscopy (TEM),‖ and photographs are shown in Fig. 3(a) and (b). The mean particle sizes are of the order of 3–8 nm (stiring rate = 100 rpm) and 1–3 nm (stiring rate = 400 rpm), respectively. The considerable effect of stirring rate on the particle size is due to the enhanced degree of molecular mobility at higher stirring rates. In order to study the effects of operating conditions *i.e.* the value of w, concentration of the surfactant, pressure and temperature on the particle size and size distribution, the particles were also prepared and recovered under other conditions; all the photographs show that small and dispersed particles can be obtained by this method.

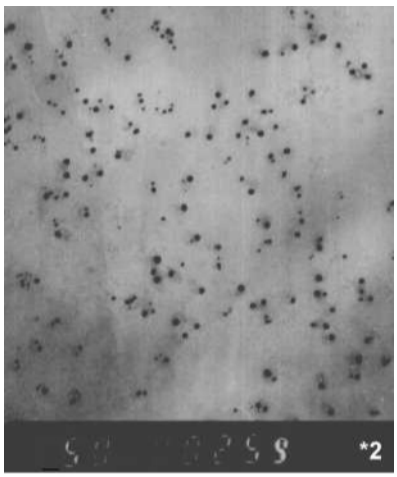

(a)

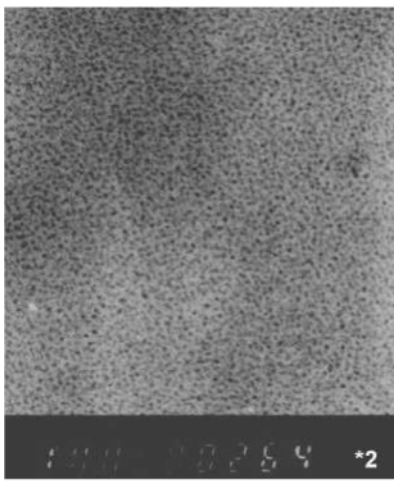

(b)

Fig. 3 TEM photographs of ZnS particles obtained from reverse micelles ([AOT] = 50 mmol L^{-1}, w = 15, [Na_2S] = [$ZnSO_4$] = 8.14 mmol L^{-1}) at 308.15 K and 5.50 MPa; (a) with a stirring rate of 100 rpm, magnification 100 K (1 mm = 10 nm) and (b) with a stirring rate of 400 rpm, magnification 200 K (1 mm = 5 nm).

This work is supported by the National Natural Science Foundation of China (20133030), Ministry of Science and Technology of China (G20000781), and UK/China R & D Project. We are very grateful to Professor Martyn Poliakoff and Mr Adam O'Neil for their valuable suggestions and advice.

Notes and references

† *Materials*: CO_2 (>99.995% purity) was provided by Beijing Analytical Instrument Factory. The surfactant AOT was obtained from Sigma with a purity of 99%. The isooctane, Na_2S, $ZnSO_4$ and $BaCl_2$ supplied by Beijing Chemical Plant were all A. R. grade. Double distilled water was used.

‡ *Typical experimental procedure* for synthesis of ZnS particles in reverse micelles: two micellar solutions containing, respectively, Na_2S and $ZnSO_4$ at the same molar concentration were mixed at constant temperature. The concentration of AOT, w (molar ratio of water to AOT), and the volume of the two solutions were also the same.

§ *Typical experimental procedure* for UV spectra: a spectrophotometer (Model TU-1201, Beijing General Instrument Company) was used to monitor the precipitation of ZnS particles in the reverse micelles at different CO_2 pressures. The path length and the inner volume of the cell are 1.32 cm and 1.74 cm^3, respectively. In a typical experiment, a predetermined amount of micellar solution containing ZnS was loaded into the sample cell. CO_2 was charged until the desired pressure was reached and the system was stabilized at this pressure. The UV spectrum was recorded after equilibrium was reached.

¶ *Typical experimental procedure* for recovery of ZnS particles from reverse micelles: ZnS particles synthesized in the reverse micellar solution were precipitated by CO_2 and deposited at the bottom of the cell. Then CO_2 and the solution were released. IR and a $BaCl_2$ titration experiment indicated that Na_2SO_4 precipitated together with ZnS. Thus, the precipitated sample was washed with water to remove the Na_2SO_4 and then dried in vacuum at 308.15 K for 4 h.

‖ The maximum resolution of the Hitachi H-600A electron microscope was 0.5 nm. A drop of a dispersed solution of particles in ethanol was placed onto a carbon-coated copper grid. After evaporation of the solvent under vacuum electron micrographs were recorded.

1 I. Lisiecki and M. P. Pileni, *J. Phys. Chem.*, 1995, **99**, 5077.
2 U. Natarajan, K. Handique, A. Mehra, J. R. Bellare and K. C. Khilar, *Langmuir*, 1996, **12**, 2670.
3 M. P. Pileni, I. Lisiecki, L. Motte, C. Petit, J. Cieron, N. Moumen and P. Lixon, *Progr Colloid Polym Sci.*, 1993, **93**, 1.
4 M. P. Pileni, *J. Phys. Chem.*, 1993, **97**, 6961.
5 C. Petit and M. P. Pileni, *J. Phys. Chem.*, 1988, **92**, 2282.
6 M. L. Steigerwald, A. P. Alivisatos, J. M. Gibson, T. D. Harris, R. Kortan, A. J. Muller, A. M. Thayer, T. M. Duncan, D. C. Douglass and L. E. Brus, *J. Am. Chem. Soc.*, 1988, **110**, 3046.
7 C. A. Eckert, B. L. Knutson and P. G. Debenedetti, *Nature*, 1996, **383**, 313.
8 D. J. Dixon, G. luna-Barcenas and K. P. Johnston, *Polymer*, 1994, **35**, 3998.
9 E. Reverchon, *J. Supercrit. Fluids*, 1999, **15**, 1.
10 P. M. Gallagher, M. P. Coffey and V. J. Krukonis, *J. Supercrit. Fluids*, 1992, **5**, 130.
11 K. J. Heater and D. L. Tomasko, *J. Supercrit. Fluids*, 1998, **14**, 55.
12 D. Li and B. X. Han, *Macromolecules*, 2000, **33**, 4555.
13 P. Calandra, M. Goffedi and V. T. Liveri, *Colloids Surf.*, 1999, **160**, 9.
14 P. D. I. Fletcher, A. M. Howe and B. H. Robinson, *J. Chem. Soc., Faraday Trans.*, 1991, **I83**, 301.
15 J. Lu, B. X. Han and H. K. Yan, *Ber. Bunsen-Ges. Phys. Chem.*, 1998, **102**, 695.

CHEMCOMM
Communication
www.rsc.org/chemcomm

Salt effect in the synthesis of mesoporous silica templated by non-ionic block copolymers

Chengzhong Yu,[a] Bozhi Tian,[a] Jie Fan,[a] Galen D. Stucky*[b] and Dongyuan Zhao*[a]

[a] *Department of Chemistry, Fudan University, Shanghai, 200433, P. R. China. E-mail: dyzhao@fudan.edu.cn*

[b] *Department of Chemistry and Biochemistry, University of California, Santa Barbara, CA 93106, USA. E-mail: stucky@chem.ucsb.edu*

Received (in Purdue, IN, USA) 24th August 2001, Accepted 12th October 2001
First published as an Advance Article on the web 6th December 2001

The use of inorganic salts during the synthesis of mesoporous materials with block copolymers can dramatically widen the syntheses domain (in temperature, surfactant concentration, *etc.*) and broaden the range of surfactants that can be utilized to produce highly ordered mesostructures.

Mesoporous materials with controlled morphology have potential uses in catalysis, separation, chromatography and large molecular release systems.[1] Recently, highly ordered mesoporous silica SBA-15[2] synthesized by commercial amphiphilic block copolymer surfactants has attracted much attention.[3–5] It is noteworthy that in all the reported synthesis methods for SBA-15 the temperature is optimally controlled at 35–40 °C in order to obtain high ordering of the mesostructures. Moreover, compared to the large number of available block copolymers, only a fraction of these surfactants has been utilized to produce highly ordered mesostructures.

Inorganic salts have been used to control the morphology and porosity of SBA materials.[6] In non-ionic surfactant templating systems, the effect of ionic strength has also been studied.[7,8] Generally, specific interactions are emphasized in these reports, which lead to better order either in mesostructure or morphology.

In this communication we report the synthesis of highly ordered mesoporous silica materials through the use of inorganic salts at low temperatures. The salt effect described here dramatically increases the range of the synthesis parameters that can be used to obtain highly ordered mesostructures as well as the number of block copolymer surfactants that can be used.

Two block copolymers, P123 and B20-5000,[9] are used as the structure-directing agents. The syntheses were carried out according to previous reports,[2,10] except that different amounts of inorganic salts were used at controlled temperatures. In a typical synthesis, 2.0 g of P123 and 8.8 g of potassium chloride were dissolved in 60 mL of 2.0 M HCl at 15 °C. To this solution, 4.2 g tetraethyl orthosilicate (TEOS) were added under vigorous stirring. The final reactant molar composition was 0.02 P123 : 6 KCl : 6 HCl : 166 H_2O : 1 TEOS. After stirring at the same temperature for 1 day, the mixture was transferred into an autoclave and heated at 100 °C for another 24 h. The solid products were collected by filtration and dried at room temperature in air. The resulting powders were calcined at 550 °C for 4 h to remove the templates.

Powder X-ray diffraction (XRD) patterns of as-synthesized and calcined SBA-15 synthesized with P123 and 2 M KCl at 15 °C are shown in Fig. 1(a). Both patterns show well-resolved XRD peaks, which can be assigned to the (100), (110) and (200) reflections of the 2-D hexagonal space group (*p6mm*). The cell parameters are 11.9 and 9.1 nm for as-synthesized and calcined SBA-15 synthesized with salt at 15 °C, respectively. The nitrogen sorption isotherm of the calcined sample is type IV with type H_1 hysteresis loops typical of mesoporous materials with 1-D cylindrical channels (Fig. 2). SBA-15 synthesized at 15 °C has a pore size of 5.9 nm (calculated from both the adsorption and desorption branch by BdB model[11]), a BET surface area of 610 $m^2\ g^{-1}$ and a pore volume of 0.83 $cm^3\ g^{-1}$. These data are similar to those from previous reports.[2,6] The relatively smaller cell parameter and pore size can be attributed to the salt effect (see discussion below). Transmission electron microscopy (TEM) studies have further corroborated the highly ordered hexagonal structures (data not shown).

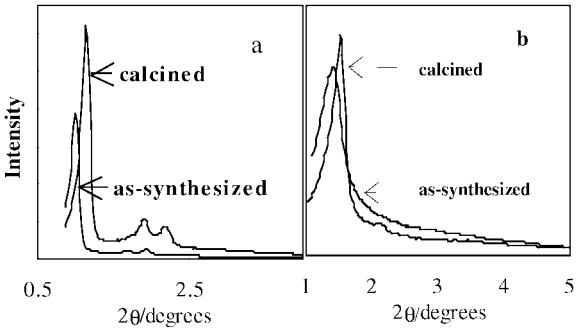

Fig. 1 XRD patterns of as-synthesized and calcined mesoporous silica prepared using (a) P123 at 15 °C with 2.0 M KCl and (b) B20-5000 at 40 °C with 1.0 M KCl. X-Ray data were collected with a Cu-Kα radiation source using a Scintag X_2 diffractometer.

This is the first report that highly ordered mesoporous SBA material can be synthesized at low temperature. By using the same reactants at 15 °C but without salt, no precipitation can be obtained. This is believed to be related to the specific nature of PEO and PPO segments in water. Both PEO and PPO are more

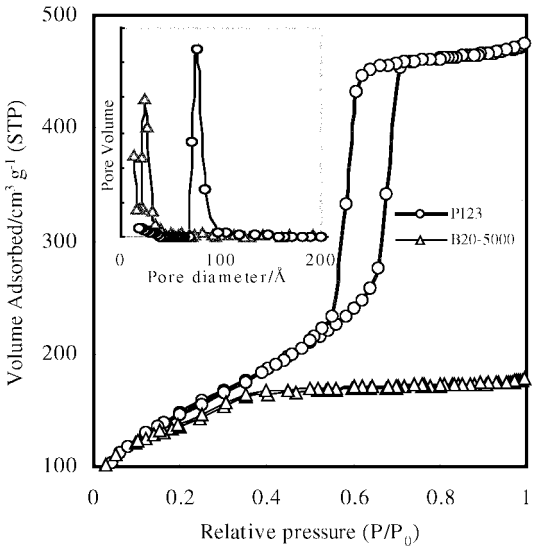

Fig. 2 Nitrogen adsorption–desorption isotherm plots and pore size distribution curve (inset) of calcined mesoporous silica synthesized by P123 and B20-5000 with inorganic salts. N_2 adsorption measurements were performed at 77 K using a Micromeritics ASAP2000 analyzer.

 DOI: 10.1039/b107640j

soluble in water at low temperatures, thus the hydrophilicity/hydrophobicity volume ratio is greater than at high temperature.[12] The formation of the ordered mesostructure precipitate is dependent on the the free energy of formation of the solid mesostructured phase and the free energy of the interface interactions of the silica species and solvent as well as the free energy of organization of the block copolymer as it associates with the species in solution. For the latter contribution, it is interesting to note that at 17 °C the critical micelle concentration (CMC) of P123 is 4.5 wt%,[13] while in a typical synthesis condition of SBA-15 the concentration of P123 in starting reactants is ~3.0 wt%. The decreasing ability to obtain composite phase separation at low temperature parallels the CMC dependence on temperature, making it a useful approximation to the collective free energies of interaction of all the inorganic, solvent, and organic species in solution. Increasing temperature is a convenient method to decrease the CMC by increasing the hydrophobicity of PEO blocks and reducing the hydrophilicity of PPO blocks. On the other hand, the addition of inorganic salts has the same effect as an increase in temperature.[14] For example, the CMC and critical micelle temperature (CMT) of Pluronic P65[15] and F127[16] show a marked decrease in the presence of added sodium chloride. This salt effect also lowers the thermodynamic radius of micelles,[14] and this is in accordance with the decrease in cell parameter and pore size decreasing observed in our experiments. The successful synthesis of highly ordered SBA-15 at low temperature confirms that using inorganic salts is an alternative to increasing temperatures.

The synthesis temperature of highly ordered SBA-15 can be lowered to 10 °C when the concentration of KCl is 2.5 M. On the other hand, at relatively higher temperatures such as 38 °C, the concentration of P123 in starting reactants can be lowered to 1 wt% with 1 M KCl. Other inorganic salts such as NaCl, Na_2SO_4 and K_2SO_4 can also be used to synthesize highly ordered SBA-15 at low temperatures.

It might be argued that during the synthesis of SBA-15 materials, using relatively high temperature is much more convenient than using high concentration of inorganic salts. However this is not necessarily the case, as evident in the uses of the salt effect in the synthesis with another block copolymer B20-5000. It is reported that only disordered mesoporous silica can be obtained with this block copolymer, even at high temperature.[17] By using 1 M KCl at 40 °C, a well-ordered cubic silica structure can be synthesized with a molar reactant composition of 0.01 B20-5000 : 3 KCl : 1.5 HCl : 167 H_2O : 1 TEOS. XRD patterns of as-synthesized material show the first peak at 2θ = 1.36; after calcination at least two peaks are observed (2θ = 1.51, 2.09, Fig. 1(b)). Combined with TEM results, these peaks can be indexed to the (110), (200) reflections of an I type cubic structure. The cell parameters are 9.2 and 8.3 nm for as-synthesized and calcined sample, respectively. TEM images (Fig. 3) also confirm this cubic structure, the cell parameter of calcined sample measured from TEM is 8.0 nm, in good accordance with XRD results. The nitrogen sorption isotherm of the calcined sample is type IV with a slight hysteresis (Fig. 2). The calcined cubic silica structure synthesized by B20-5000 at 40 °C with 1.0 M KCl has a small pore size of 2.4 nm (calculated by the BJH model), a BET surface area of 485 $m^2\ g^{-1}$ and a pore volume of 0.28 $cm^3\ g^{-1}$. We have synthesized large cubic silica mesostructures SBA-16[10] and FDU-1[18] and, in view of the large headgroup ratio of B20-5000, we propose that this cubic structure is similar to that of SBA-16.[10]

In general, the use of inorganic salts in the synthesis of mesoporous materials can give highly ordered structures under very mild conditions. The salt effect provides an alternative and sometimes a required methodology for the synthesis of highly ordered mesoporous materials with certain surfactants that have high CMC values, or in syntheses for which a high temperature is not favored. Using this method, other highly ordered mesoporous materials have been obtained using B40-2500, F98, F108 and F127 as templates. Detailed work will be reported in the future.

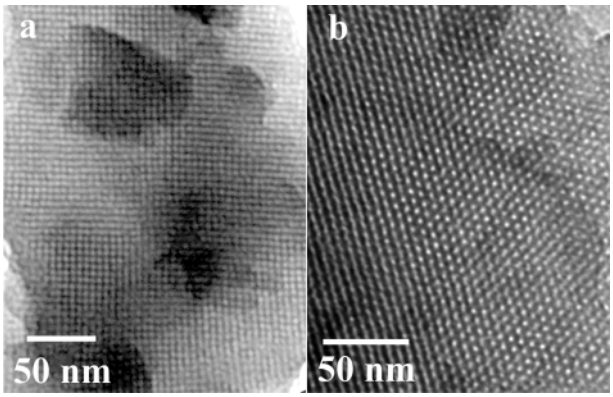

Fig. 3 TEM (JOEL 2000, 200 keV) images of cubic mesoporous silica structure synthesized by B20-5000 at 40 °C with 1 M KCl recorded along (a) the [100] zone axis and (b) the [111] zone axis.

This work was supported by the National Science Foundations of China (Grant No. 29925309 and 29873012), the China Ministry of Education, Shanghai Science Foundation (00JC14014), State Key Basic Res. Prog. (G2000048001), the National Science Foundation of the United States (Grant DMR 96-34396) and the MRL Program of the National Science Foundation (Award DMR 00-80034). C. Y. thanks Professor Colin Booth for useful discussions.

Notes and references

1 J. Y. Ying, C. P. Mehnert and M. S. Wong, *Angew. Chem., Int. Ed.*, 1999, **38**, 56.
2 D. Zhao, J. Feng, Q. Huo, N. Melosh, G. H. Fredrickson, B. F. Chmelka and G. D. Stucky, *Science*, 1998, **279**, 548.
3 M. H. Huang, A. Choudrey and P. D. Yang, *Chem. Commun.*, 2000, 1063.
4 Y. J. Han, G. D. Stucky and A. Butler, *J. Am. Chem. Soc.*, 1999, **121**, 9897.
5 S. Jun, S. H. Joo, R. Ryoo, M. Kruk, M. Jaroniec, Z. Liu, T. Ohsuna and O. Terasaki, *J. Am. Chem. Soc.*, 2000, **122**, 10712.
6 D. Zhao, J. Sun, Q. Li and G. D. Stucky, *Chem. Mater.*, 2000, **12**, 275; P. Schmidt-Winkel, P. Yang, D. I. Margolese, B. F. Chmelka and G. D. Stucky, *Adv. Mater.*, 1999, **11**, 303; D. Zhao, P. Yang, B. F. Chmelka and G. D. Stucky, *Chem. Mater.*, 1999, **11**, 1174.
7 W. Zhang, B. Glomski, T. R. Pauly and T. J. Pinnavaia, *Chem. Commun.*, 1999, 1803; E. Prouzet, F. Cot, G. Nabias, A. Larbot, P. Kooyman and T. J. Pinnavaia, *Chem. Mater.*, 1999, **11**, 1498.
8 S. A. Bagshaw, *J. Mater. Chem.*, 2001, **11**, 831.
9 P123 ($EO_{20}PO_{70}EO_{20}$, MW 5800) is a gift from BASF, B20-5000 ($EO_{43}BO_{14}EO_{43}$, MW 5000) is a gift from the Dow Chemical Company, where EO is poly(ethylene oxide), PO is poly(propylene oxide) and BO is poly(butylene oxide).
10 D. Zhao, Q. Huo, J. Feng, B. F. Chmelka and G. D. Stucky, *J. Am. Chem. Soc.*, 1998, **120**, 6024; Y. Sakamoto, M. Kaneda, O. Terasaki, D. Zhao, J. Kim, G. D. Stucky, H. Shin and R. Ryoo, *Nature*, 2000, **408**, 449.
11 W. Luckens Jr., P. Schmidt-Winkel, D. Zhao, J. Feng and G. D. Stucky, *Langmuir*, 1999, **15**, 5403.
12 K. Mortensen and J. S. Pedersen, *Macromolecules*, 1994, **27**, 4145.
13 G. Wanka, H. Hoffmann and W. Ulbricht, *Macromolecules*, 1994, **27**, 4145.
14 C. Booth and D. Attwood, *Macromol. Rapid Commun.*, 2000, **21**, 501.
15 N. J. Jain, A. George and P. Bahadur, *Colloids Surf. A.*,1999, **157**, 275.
16 P. R. Desai, N. J. Jain, R. K. Sharma and P. Bahadur, *Colloids Surf. A.*, 2001, **178**, 57.
17 Y. A. I. Abu-Lebdeh, P. M. Budd and V. M. Nace, *J. Mater. Chem.*, 1998, **8**, 1839.
18 C. Yu, Y. Yu and D. Zhao, *Chem. Commun.*, 2000, 575; C. Yu, Y. Yu, L. Miao and D. Zhao, *Microporous Mesoporous Mater.*, 2001, **44–45**, 65.

CHEMCOMM
Communication
www.rsc.org/chemcomm

From new tricyclic bisaminal derivatives to *trans-N,N′*-disubstituted cyclams

Raphaël Tripier, Jean-Marie Lagrange, Enrique Espinosa, Franck Denat and Roger Guilard*

Laboratoire d'Ingénierie Moléculaire pour la Séparation et les Applications des Gaz, LIMSAG UMR 5633, Faculté des Sciences Gabriel, 6, Bd Gabriel, 21100 Dijon, France.
E-mail: limsag@u-bourgogne.fr

Received (in Cambridge, UK) 11th October 2001, Accepted 9th November 2001
First published as an Advance Article on the web 7th December 2001

The reactivity of cyclam towards different aldehydes is discussed and the new tricyclic bisaminal derivatives thus obtained are characterized by X-ray crystallography; a new synthesis of *trans*-dibenzylcyclam is also reported.

The design and the synthesis of tetraazacycloalkane derivatives have been the subject of growing interest during the past years owing to the ability of such macrocycles to coordinate various metal cations.[1] Among them, cyclam (1,4,8,11-tetraazacyclotetradecane) has been extensively studied. The presence of four secondary amine functions allows unlimited derivatisation of the macrocycle. However, the selective *N*-functionalisation of cyclic polyamines is not obvious and still represents a challenge.[2] For example, the reaction of cyclam with two equivalents of an alkyl or aryl halide yields a mixture of mono-, di-, tri- and even tetrasubstituted macrocycles. Moreover, in the cyclam series, three *N,N′*-disubstituted isomers exist, depending on the relative positions of the pendant arms, *i.e.* two different *cis*-disubstituted derivatives and the [1,8] isomer also called *trans*-disubstituted cyclam. The *trans*-disubstituted cyclams are of special interest since they can lead to hexacoordinated complexes when the substituents are coordinating arms. *trans-N,N′*-diprotected cyclams are also convenient precursors for the synthesis of three-dimensional systems such as cyclam based cryptands.[3] In order to overcome the tedious work-up necessary to isolate the aimed isomer, we have used the *trans* 'autoprotected' cyclam 1,4,8,11-tetraazacyclotetradecane-5,12-dione for the synthesis of several macropolycycles.[4] However, the substituents which can be introduced on the two remaining amine functions are limited to those surviving the conditions required for the reduction of the amide groups. We have recently reported powerful syntheses of *trans*-disubstituted cyclams involving a tricyclic intermediate obtained by refluxing cyclam with a 30% NaOH solution in dichloromethane.[5,6] This bisaminal cyclam can also be obtained by action of aqueous formaldehyde on cyclam.[7,8]

In this paper, we describe the reactivity of cyclam with various aldehydes. The formaldehyde reacts readily at room temperature and yields the most stable macrotricycle **1** containing two six-membered rings (Scheme 1). Surprisingly, no reaction is observed using benzaldehyde instead of formaldehyde under the same conditions. However, refluxing cyclam

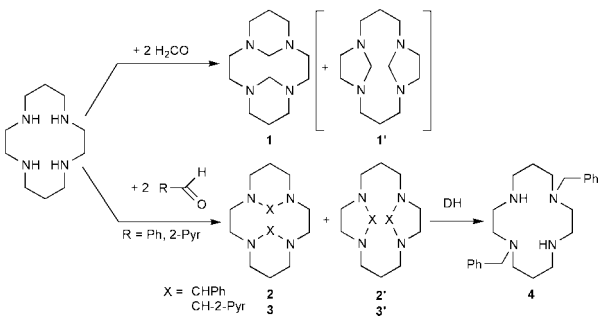

Scheme 1

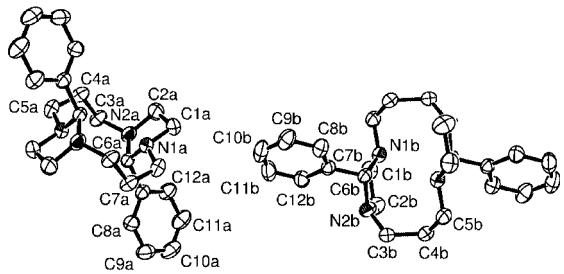

Fig. 1 ORTEP[14] view of **2′**. Ellipsoids are at the 50% probability level. Two half molecules belong to the asymmetric unit.

with three equivalents of benzaldehyde in THF over one week, gives the unexpected bisaminal derivative **2′** containing two five-membered rings as the major product while **2** is the minor derivative.† The two isomers **2** and **2′** are obtained in a 1 : 2 ratio as determined from the ^{1}H NMR spectrum. In these conditions, 2-pyridinecarboxaldehyde (R = 2-Pyr) gives mainly the compound **3**. From these results, it clearly appears that the formation and the structure of the bisaminal compounds are strongly dependent on the nature of the aldehyde as well as on the reaction conditions. We have studied the influence of temperature on the reactivity of cyclam towards 2-pyridinecarboxaldehyde. Ethanol has been chosen as a solvent and the reaction time has been fixed at 24 h. The relative amount of **3** increases with temperature from 50% at 0 °C up to 90% in refluxing ethanol, showing that the macrotricycle containing two six-membered rings is logically the thermodynamic product, while the kinetic product is the isomer containing two five-membered rings **3′**. Consequently, with formaldehyde, which is the most reactive aldehyde among the three tested ones, the compound **1′** should be observable at low temperature. Indeed, cooling down the reaction of cyclam with formaldehyde to −20 °C gives the isomer **1′** in 30% yield, as evidenced by NMR. Compound **1′** readily isomerises into **1** when increasing the temperature. A comparable behaviour of the product of the reaction of glyoxal with triethylenediamine has been observed.[9]

The macrotricycles 15,16-diphenyl-1,5,8,12-tetraazatricyclo[10,2,1,1^{5,8}]hexadecane **2′** and 15,16-dipyridin-2-yl-1,4,8,11-tetraazatricyclo[9,3,1,1^{4,8}]hexadecane **3** have been fully characterized by spectroscopic methods, including 2D NMR experiments, and satisfactory elemental analyses have been obtained. The structures of **2′** and **3** have been established unequivocally by single-crystal X-ray analyses (Figs. 1 and 2).‡ These compounds crystallise with two half molecules belonging to their respective asymmetric unit. In both structures, the two aminal bridges naturally adopt a *trans* conformation. The structure of **3**, in which the two hexahydropyrimidine six-membered rings are in a chair conformation, can be compared to those of **1** or protonated forms of **1** which have been previously reported.[5,7,10] In the solid state, **3** adopts a eq,ax-eq,ax-[2323] conformation like **1**.[8] For steric reasons, the pyridine moieties are in axial positions while the hydrogen atom on each of the two aminal units is equatorial to the six-membered ring.

 DOI: 10.1039/b109199a

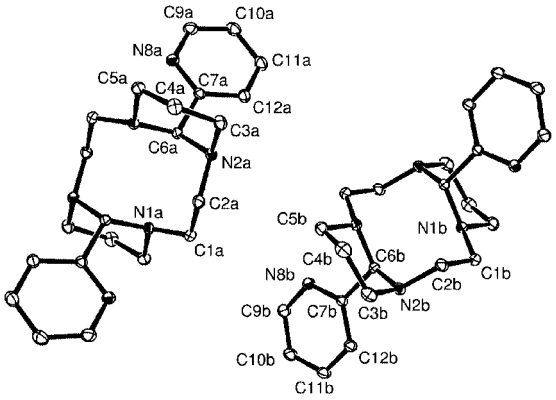

Fig. 2 ORTEP[14] view of **3**. Ellipsoids are at the 50% probability level. Two half molecules belong to the asymmetric unit.

Table 1 Selected ^{1}H and ^{13}C NMR chemical shifts[a]

		δ N–C*H*R–N		
Compound	R	ax	eq	δ N–*C*–N
1	H	2.90[b]	5.45[b]	68.4
1′		n.d.[c]	n.d[c]	88.8
2	Ph	—	6.23	71.9
2′		—	5.23	83.3
3	2-Pyr	—	6.29	72.5
3′		—	5.12	84.4

[a] $CDCl_3$ solvent. [b] Ref. 8. [c] Not determined.

However, the equatorial aminal hydrogen atom is sterically compressed with the lone pair of one nitrogen atom belonging to the other six-membered ring, as discussed previously for compound **1**.[8] The distance between these two atoms in **3** is similar to that reported for **1** (2.26 Å). Consequently, the chemical shift of the equatorial hydrogen atom at rt in $CDCl_3$ is remarkably high (δ = 6.29 ppm) (Table 1). The two phenyl groups in **2′** are also in axial positions and the hydrogen atoms are equatorial to the five-membered rings. The distance between the equatorial hydrogen atom and the closest nitrogen atom is higher than in **3** (2.37 Å) and the equatorial aminal protons in **2′** resonate as a singlet at higher field (δ = 5.23 ppm). It is noteworthy that unlike the protons, the aminal carbon atoms are more deshielded in **2′** and **3′** than in **2** and **3**. To our knowledge, the structure of **2′** gives the first crystallographic evidence of the formation of a cyclam derivative containing two imidazolidine five-membered rings.

Bisaminal derivatives of cyclam are known as convenient precursors for the synthesis of disubstituted cyclams. Indeed, quaternization of two non-adjacent nitrogen atoms of the 1,4,8,11-tetraazatricyclo[9,3,1,1^{4,8}]hexadecane **1** with a suitable alkylating reagent, followed by cleavage of the two aminal bridges with a 3 M NaOH aqueous solution, yields the aimed *trans*-difunctionalised cyclam.[5,6] In particular, Kaden has shown that reductive cleavage of the bisaminal **1** with Raney-Ni in liquid NH_3 yields a mixture of *trans* and *cis* dimethylcyclam.[11] We have studied the reduction of the new bisaminal cyclams with $NaBH_4$. For instance, the treatment of the crude mixture of the isomers **2** and **2′** with a large excess of $NaBH_4$ in refluxing EtOH, gives the *trans*-dibenzylcyclam **4** in 38% yield. Thus, the 1,8-dibenzylcyclam is obtained in a reasonable overall yield (31%). This *trans* diprotected cyclam might be used as a precursor for various *trans* difunctionalised cyclams, since many functional groups can survive the mild conditions required for the removal of the benzyl moieties. This approach represents an alternative route to the known methods.[2]

The results reported herein show how the cyclic structure of cyclam might confer to this tetraamine a peculiar behaviour towards different aldehydes. For the first time, cyclam bisaminal type compounds containing *a priori* unfavourable five-membered imidazolidine rings have been obtained. In order to further study the effects governing the formation of the bisaminal derivatives, and also to extend the scope of this reaction to the preparation of new ligands, the reactivity of other aldehydes towards cyclam is now under investigation.

Notes and references

† *Experimental procedure* for 15,16-diphenyl-1,5,8,12-tetraazatricyclo-[10,2,1,1^{5,8}]hexadecane **2′**: A solution of 7.95 g (75 mmol) of benzaldehyde and 5 g (25 mmol) of cyclam in 250 ml of refluxing THF was heated under reflux for one week. After cooling at rt, the mixture was filtered and the filtrate was evaporated. The residue was washed with petroleum ether to give 7.72 g (82%) of the mixture of **2** and **2′** in a 1 : 2 ratio. The two isomers might be separated by precipitation of **2** in acetonitrile and **2′** has been finally purified by recrystallization in a EtOH–Et_2O (5 : 100) mixture. δ_H 1.82 (q, 4H), 2.82 (m, 4H), 2.96 (m, 4H), 3.14 (m, 8H), 5.23 (s, 2H), 7.2–7.3 (m, 10H); δ_C 27.2, 51.2, 54.2, 83.3, 127.0, 127.3, 128.2. (calc. for $C_{24}H_{32}N_4$. C, 76.54; H, 8.57; N, 14.89. Found: C, 76.21; H, 8.32; N, 14.70%).

‡ X-Ray suitable crystals of **2′** and **3** were grown from a EtOH–Et_2O (5 : 100) mixture and pure EtOH respectively. In both cases the structure was solved using direct methods[12] and refined by full matrix least-squares on F^2.[13]

Crystal data for $C_{24}H_{32}N_4$ **2′**: M = 376.54, monoclinic, a = 16.1230(3), b = 8.6830(1), c = 16.7890(3), β = 118.3191(7)°, U = 2069.10(6) Å^3, T = 293(2) K, space group $P2_1/a$, Z = 4, μ(Mo-Kα) = 0.072 mm^{-1}, 12112 reflections measured, 6062 unique (R_{int} = 0.0440) which were used in all calculations. The final agreement factors were $R(F^2)$ = 0.0774 and $wR(F^2)$ = 0.1343 (all data). CCDC 172390.

Crystal data for $C_{22}H_{30}N_6$ **3**: M = 378.52, monoclinic, a = 12.3990(2), b = 12.8130(2), c = 12.5250(2) Å, β = 96.3540(7)°, U = 1977.60(5) Å^3, T = 110(2) K, space group $P2_1/c$, Z = 4, μ(Mo-Kα) = 0.079 mm^{-1}, 27316 reflections measured, 11105 unique (R_{int} = 0.0280) which were used in all calculations. The final agreement factors were $R(F^2)$ = 0.0588 and $wR(F^2)$ = 0.1260 (all data). CCDC 172391. See http://www.rsc.org/suppdata/cc/b1/b109199a/ for crystallographic data in CIF or other electronic format.

1 See for example: J. S. Bradshaw, K. E. Krakowiak and R. M. Izatt, *Aza-crown Macrocycles*, ed. E. C. Taylor, John Wiley & Son, New York, 1993; R. M. Izatt, K. Pawlak, J. S. Bradshaw and R. L. Bruening, *Chem. Rev.*, 1995, **95**, 2529; A. E. Martell and R. D. Hancock, *Metal Complexes in Aqueous Solutions*, Plenum Press, New York, 1996.

2 F. Denat, S. Brandès and R. Guilard, *Synlett*, 2000, 561 and references therein.

3 B. Boitrel, B. Andrioletti, M. Lachkar and R. Guilard, *Tetrahedron Lett.*, 1995, **36**, 4995; B. Andrioletti, B. Boitrel and R. Guilard, *C. R. Acad. Sc., Sér. II*, 1996, 859.

4 S. Brandès, F. Denat, S. Lacour, F. Rabiet, F. Barbette, P. Pullumbi and R. Guilard, *Eur. J. Org. Chem.*, 1998, 2349; F. Denat, S. Lacour, S. Brandès and R. Guilard, *Tetrahedron Lett.*, 1997, **38**, 4417.

5 G. Royal, V. Dahaoui-Gindrey, S. Dahaoui, A. Tabard, R. Guilard, P. Pullumbi and C. Lecomte, *Eur. J. Org. Chem.*, 1998, 1971.

6 C. Bucher, G. Royal, J.-M. Barbe and R. Guilard, *Tetrahedron Lett.*, 1999, **40**, 2315.

7 E. J. Gabe, Y. Le Page, L. Prasad and G. R. Weisman, *Acta Crystallogr., Sect. B: Struct. Sci.*, 1982, **B38**, 2752.

8 R. W. Alder, E. Heilbronner, E. Honegger, A. B. McEwen, R. E. Moss, E. Olefirowicz, P. A. Petillo, R. B. Sessions, G. R. Weisman, J. M. White and Z.-Z. Yang, *J. Am. Chem. Soc.*, 1993, **115**, 6580.

9 G. Hervé, H. Bernard, N. Le Bris, M. Le Baccon, J. J. Yaouanc and H. Handel, *Tetrahedron Lett.*, 1999, **40**, 2517.

10 R. W. Alder, T. M. G. Carniero, R. W. Mowlam, A. G. Orpen, P. A. Petillo, D. J. Vachon, G. R. Weisman and J. M. White, *J. Chem. Soc., Perkin Trans. 2*, 1999, 589.

11 A. Comparone and T. A. Kaden, *Helv. Chim. Acta*, 1998, **81**, 1765.

12 SIR97 program. A. Altomare, M. C. Burla, M. Camalli, G. L. Cascarano, C. Giacovazzo, A. Guagliardi, A. G. G. Moliterni, G. Polidori and R. Spagna, *J. Appl. Crystallogr.*, 1999, **32**, 115.

13 SHELXL97 program. G. M. Sheldrick, SHELXL97. Program for the Refinement of Crystal Structures. University of Göttingen, Göttingen, Germany, 1997.

14 ORTEP-3 for Windows. L. J. Farrugia, *J. Appl. Crystallogr.*, 1997, **30**, 565.

CHEMCOMM Communication
www.rsc.org/chemcomm

Formation of different framework structured dimeric dianions formed from the reduction of 2,4,6-tricyano-1,3,5-triazine and 1,3,5-tricyanobenzene†

Rico E. Del Sesto, Atta M. Arif and Joel S. Miller*

Department of Chemistry, University of Utah, 315 S. 1400 E. RM 2124, Salt Lake City, Utah, 84112-0850, USA. E-mail: jsmiller@chemistry.utah.edu

Received (in Corvallis, OR, USA) 11th September 2001, Accepted 15th October 2001
First published as an Advance Article on the web 28th November 2001

Reduction of 2,4,6-tricyano-1,3,5-triazine (1) and 1,3,5-tricyanobenzene (2) leads to dianionic dimers with long, ~ 1.57 Å, central C–C bonds. In contrast to 1, which dimerizes at the nitrile substituted carbon, 2 has a different motif as it dimerizes at the hydrogen substituted carbon.

Polynitrile substituted organic molecules are strong electron acceptors that have enabled the development of molecule-based conductors[1] and magnets.[2] For the latter, reduced radical-anionic nitriles can coordinate to metal centers to build covalently bonded extended structures in 1-, 2-, and 3-D.[2] New, reduced polynitrile acceptors may lead to new structure types and new properties. The 2,4,6-tricyano-1,3,5-triazine (**1**) and 1,3,5-tricyanobenzene (**2**) polynitriles have not received much attention. Their D_{3h} symmetry presents the opportunity for building extended 2- and 3-D network structures. Furthermore, upon reduction the radical anion may lead to new magnetic materials, including interesting ferrimagnetic and spin-frustrated systems if all three nitriles (or triazine nitrogens) coordinate to a spin-bearing metal center.

A previous attempt to form $\mathbf{1}^{\cdot-}$ by reduction with sodium and potassium led to the speculation that $\mathbf{3}^{\cdot-}$ was formed through rearrangement of the radical anion $\mathbf{1}^{\cdot-}$[5] based upon the ^{14}N splitting in the EPR spectra suggesting a set of 4 equivalent nitrogens and a second set of two equivalent nitrogens, which is consistent with $\mathbf{3}^{\cdot-}$ and not $\mathbf{1}^{\cdot-}$. Expecting that $\mathbf{3}^{\cdot-}$ was unlikely based upon mechanistic considerations, we sought $\mathbf{1}^{\cdot-}$ or its ensuing species *via* electron transfer reactions under milder reduction conditions.

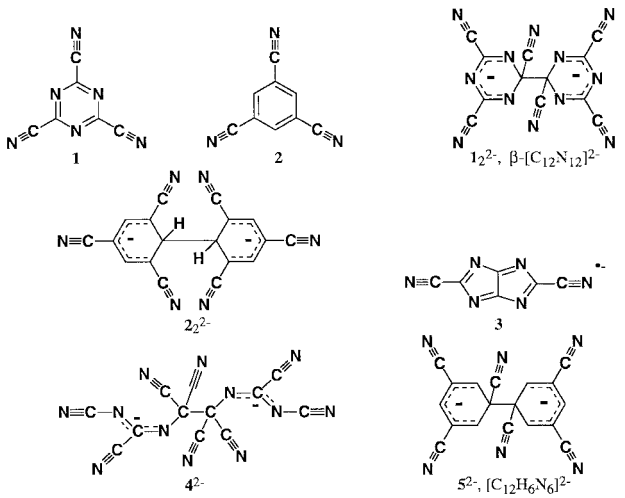

The electrochemistry of **1** shows a cathodic peak at −0.39 V, which shows no reversibility at scan rates from 5–2000 mV s^{-1}. Additionally, an irreversible anodic oxidation is seen at +0.70 V, but appears only after the first pass through the reduction.

† Dedicated to Michael Hanack on the occasion of the 70th birthday.

Unable to isolate any species *via* electrochemical methods, **1** was reacted with the strong electron donor $Cr^o(1,3,5\text{-}C_6H_3Me_3)_2$, $Cr(Mes)_2$, [$E^\circ_{1/2}$ = −0.92 V vs. SCE],[4] which led to the formation of $[Cr(Mes)_2]_2\mathbf{1}_2$‡ composition, whose structure§ consists of the σ-dimer of $\mathbf{1}^{\cdot-}$, β-$[C_{12}N_{12}]^{2-}$, $\mathbf{1}_2^{2-}$ (Fig. 1). This is an isomer of {(1,1,2,2-tetracyano-1,2-ethanediyl)bis[imino-(cyanomethylene)]}bis[cyanamide] ion(2−) $\mathbf{4}^{2-}$, α-$[C_{12}N_{12}]^{2-}$, a linear form of $[C_{12}N_{12}]^{2-}$ previously reported.[5] The central C39–C40 bond of $\mathbf{1}_2^{2-}$ is 1.57 Å. Albeit slightly longer than a typical C–C σ bond it is in excellent agreement with 1.58 Å observed for the central C–C bond in α-$[C_{12}N_{12}]^{2-}$.[5] Examples of bond lengths within the ring are 1.463 Å for C39–N2, 1.467 Å for C39–N3, 1.285 Å for C37–N3, 1.348 Å for C37–N1, 1.350 Å for C38–N1, and 1.289 Å for C38–N2. The longer bond lengths to C39/C40 and shorter bonds to N3/N5 indicate that the anionic charge is localized on the outer half of the ring. However, the rings maintain their planarity, and the ring bond angles around central C′s (C39 and C40) range from 106 to 118.5° indicating that they still maintain some sp^2 character. The two rings are twisted 67° about the C39–C40 bond, as defined by the C45–C39–C40–C46 torsion angle.

The $\upsilon_{C\equiv N}$ absorptions in **1**° are at 2302w, 2276m, 2255s cm^{-1}, but occur only as a very weak peak at ~2245 cm^{-1} in $\mathbf{1}_2^{2-}$. The ring C=N aromatic stretch occurs at ~1520 cm^{-1} for **1**° that increases to ~1590 cm^{-1} upon reduction and dimerization. The minimal change in the $\upsilon_{C\equiv N}$ frequency and 70 cm^{-1} shift in the $\upsilon_{C=N}$ also indicate that the anionic charge is localized within the ring.

EPR studies of $\{[Cr(mes)_2]^+\}_2[\mathbf{1}]_2^{2-}$ show only an absorption at g = 1.990, characteristic of bis(aryl)chromium(I) cations, *e.g.* g = 1.9859 for $[Cr^I(C_6H_6)_2]^{\cdot+}$.[6] The temperature dependence of the magnetic susceptibility, χ, shows typical Curie-Weiss behavior, $\chi \propto (T - \theta)^{-1}$, with an effective

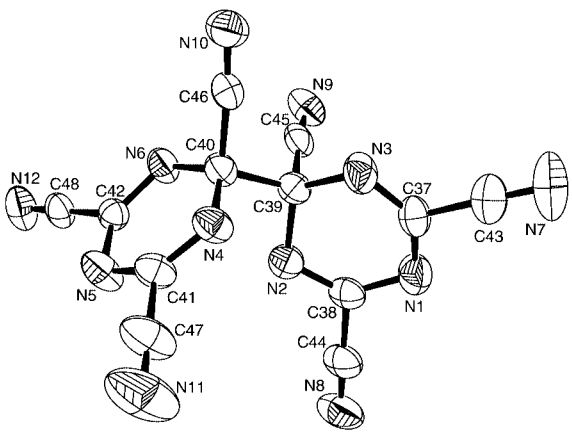

Fig. 1 ORTEP drawing (50%) of, $\mathbf{1}_2^{2-}$ in $\{[Cr(mes)_2]^+\}_2\mathbf{1}_2^{2-}$. Bond lengths are 1.463(3) Å for C39–N2, 1.467(3) Å for C39–N3, 1.285(3) Å for C37–N3, 1.348(3) Å for C37–N1, 1.350(3) Å for C38–N1, and 1.289(3) Å for C38–N2.

 DOI: 10.1039/b108297n

moment of 2.40 μ_B between 20 and 300 K, and a θ value of −8 K. This is consistent with two independent S = 1/2 spins arising from the two Cr^I centers per formula unit, with a *g*-value of 1.990, which would have the expected room temperature effective moment of 2.43 μ_B.

The previously reported electrochemical reduction of 1,3,5-triazine results in this same dimerization[7] producing the C–C σ-dimer, $[C_6H_6N_6]^{2-}$, which could be isolated after proton abstraction from an aqueous solution, and characterized by NMR.

Similar irreversible electrochemical behavior was reported for **2**,[8] which exhibits an irreversible reduction at −1.35 V *vs.* SCE in MeCN, and an anodic irreversible oxidation at −0.03 V.[8] It was speculated that **2** was reduced to the dianion, $\mathbf{2}^{2-}$, which then reacts with a second **2**° to form $\mathbf{5}^{2-}$, which would be isostructural with the previously discussed $\mathbf{1}_2{}^{2-}$.

However, reduction of **2** with $Co^{II}Cp^*_2$¶ (Cp* = pentamethylcyclopentadienide), [$E^\circ_{1/2}$ = −1.47 V],[4] led to the isolation of $[Co^{III}Cp^*_2]\mathbf{2}$, whose crystal structure‖ reveals the formation of the σ-dimer of $\mathbf{2}^{\cdot-}$ involving the *unsubstituted* ring carbons, $[C_{18}H_6N_6]^{2-}$, $\mathbf{2}_2{}^{2-}$ (Fig. 2), with the central C50–C50′ distance at 1.56 Å, comparable to $\mathbf{1}_2{}^{2-}$. The C50 carbons are sp^3 hybridized with all bond angles averaging 109.4°. Bond lengths within the benzene rings are C50–C51 1.509 Å, C51–C52 1.362 Å, C52–C53 1.424 Å, C53–C54 1.405 Å, C54–C55 1.364 Å, and C55–C50 1.523 Å.

Dimerization of $\mathbf{1}^{\cdot-}$ occurs at the substituted ring-C rather than at the ring-N, most likely due to formation of the more energetically stable C–C bond (*ca.* 200 kJ mol^{-1}) with respect to an N–N bond.[9] However, $\mathbf{2}^{\cdot-}$ dimerizes at the unsubstituted ring carbon, analogous to the radical cation of tris(dimethylamino)benzene, which also forms dimers at the unsubstituted carbon.[10] Studies of the reaction of the $\mathbf{2}^{\cdot-}$, *via* photoinduced electron transfer (*in situ* production of $\mathbf{2}^{\cdot-}$), with benzyl[11] and alkyl[12] neutral radicals yielded major products of the benzyl/alkyl substituted **1** at the unsubstituted carbon as well. In both cases, the reactivity of $\mathbf{2}^{\cdot-}$ at the unsubstituted carbon was attributed to the spin density being highest at those carbons, hence dimerization of the radical anion at these carbons as well. This behavior is similar to that of the 1,3,5-tripyrrolidinobenzene, which also dimerizes upon reduction at the unsubstituted carbon.[13]

The $\{[Co^{III}Cp^*_2]^+\}_2\mathbf{2}_2{}^{2-}$ is EPR silent at room temperature, and is diamagnetic at 20 and 300 K consistent with S = 0 Co^{III} and S = 0 dimerized organic radicals.

Analogous to the $\mathbf{1}_2{}^{2-}$ and $\mathbf{2}_2{}^{2-}$, similar types of σ-dimers have been reported for TCNE[14] and TCNQ[15] radical anions. In both cases, the σ-bond can undergo hemolytic cleavage by thermolysis yielding the original individual radical anions.[14–16]

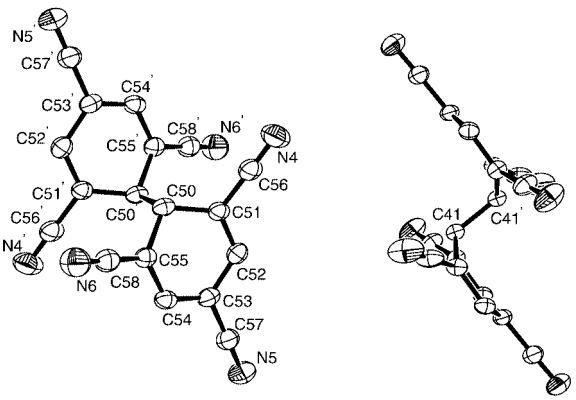

Fig. 2 ORTEP drawing (50%) of $\mathbf{2}_2{}^{2-}$ in $\{[Co^{III}Cp^*_2]^+\}_2\mathbf{2}_2{}^{2-}$. Bond lengths within the benzene rings are C50–C51 1.509(4), C51–C52 1.362(4), C52–C53 1.424(4), C53–C54 1.405(4), C54–C55 1.364(3), and C55–C50 1.523(3) Å.

The isolated electron transfer complexes suggest that the formation of a stable radical anion of $\mathbf{1}^{\cdot-}$ and $\mathbf{2}^{\cdot-}$ is not favorable, as they undergo dimerization to produce the closed-shell dianions, $\mathbf{1}_2{}^{2-}$ and $\mathbf{2}_2{}^{2-}$, respectively. Although $\mathbf{1}^{\cdot-}$ was not isolated, these results suggest that some type of molecular rearrangement or reaction, possibly through an intermediate similar to the isolated $\mathbf{1}_2{}^{2-}$, is responsible for the unexpected EPR signal seen in the reduction of **1** by Carrington and coworkers.[3]

The authors gratefully acknowledge the support from the NSF (Grant No. CHE9320478) and the DOE (Grant No. DE FG 03-93ER45504).

Notes and references

‡ $\{[Cr(mes)_2]^+\}_2[\mathbf{1}]_2{}^{2-}$ was prepared from the reaction of Cr(mes)2 and **1**. υ_{max} (Nujol)/cm^{-1} 2250vw, 159vs, 1327vs, 1150w, 1127w, 910w, 514d.

§ *Crystal data* for $\{[Cr(mes)_2]^+\}_2[\mathbf{1}]_2{}^{2-}\cdot$2MeCN: $C_{50}H_{51}Cr_2N_{13}$, *M* = 938.042, triclinic, space group $P\bar{1}$, *a* = 13.2998(4), *b* = 13.3683(3), *c* = 15.7869(4) Å, α = 65.2084(16)°, β = 79.8988(17)°, γ = 76.4268(16)°, *V* = 2467.55(11) Å^3, *Z* = 2, ρ_{calc} = 1.263 Mg m^{-3}, absorption coefficient 0.488 mm^{-1}, *F* (000) = 980, reflections collected 16356, independent reflections 10914 [*R*(int) = 0.0313], GOF = 1.018, *R* = 0.0504, wR_2 = 0.1129. CCDC 163649.

¶ $\{[Co^{III}Cp^*_2]^+\}_2\mathbf{2}_2{}^{2-}$ was prepared from the reaction of $Co^{II}Cp^*_2$ with **2**. υ_{max} (Nujol)/cm^{-1} 2166s, 2160s, 1582s, 1499s, 1359m, 1310m, 1103m, 1023m, 877m, 632w.

‖ *Crystal data* for $\{[Co^{III}Cp^*_2]^+\}_2\mathbf{2}_2{}^{2-}\cdot$2MeCN: $C_{60}H_{69}Co_2N_7$, *M* = 1006.13, triclinic, space group $P\bar{1}$, *a* = 12.4960(3), *b* = 15.2636(4), *c* = 16.2297(4) Å, α = 76.7828(14)°, β = 67.4061(12)°, γ = 70.5232(12)°, *V* = 2467.55(11) Å^3, *Z* = 2, ρ_{calc} = 1.248 Mg m^{-3}, absorption coefficient 0.664 mm^{-1}, *F*(000) = 1064, reflections collected 18947, independent reflections 12130 [*R*(int) = 0.0344], GOF = 1.020, *R* = 0.0505, wR_2 = 0.1008. In the unit cell there are two halves ($C_9H_3N_3{}^-$) of the **2** dimers asymmetrically oriented within the cell. In this case, C50 and C41 are in the unit cell, and C50′ and C41′ are visualized by expansion of the asymmetric unit (Fig. 2). CCDC 163650.

See http://www.rsc.org/suppdata/cc/b1/b108297n/ for crystallographic data in CIF or other electronic format.

1 *e.g.*, J. R. Ferraro and J. M. Williams, *Introduction to synthetic electrical conductors*, Academic Press, Orlando, 1987.
2 (*a*) V. I. Ovcharenko and R. Z. Sagdeev, *Russ. Chem. Rev.*, 1999, **68**, 345; (*b*) J. S. Miller and A. J. Epstein, *Angew. Chem., Int. Ed. Engl.*, 1994, **33**, 385.
3 A. Carrington, H. C. Longuet-Higgins and P. F. Todd, *Mol. Phys.*, 1965, **9**, 211.
4 M. D. Ward, *Electroanal. Chem.*, 1989, **6**, 181.
5 W. E. Buschmann, A. M. Arif and J. S. Miller, *J. Chem. Soc., Chem. Commun.*, 1995, 2343; J. L. Manson, W. E. Buschmann and J. S. Miller, *Inorg. Chem.*, 2001, **40**, 1926.
6 C. Elschenbroich, E. Bilger, J. Koch and J. Weber, *J. Am. Chem. Soc.*, 1984, **106**, 4297.
7 H.-S. Chien and M. M. Labes, *J. Electrochem. Soc.: Electrochem. Sci. Tech.*, 1986, **133**, 2509.
8 M. Sertel, A. Yildiz, R. Gambert and H. Baumgärtel, *Electrochim. Acta.*, 1986, **31**, 1287.
9 Bond energies based on average bond dissociation energies, *e.g.* T. H. Lowry and K. S. Richardson, *Mechanism and Theory in Organic Chemistry*, 3rd ed., Harper Collins Publishers, New York, 1987, pp 161–162.
10 H. J. Keller, R. Niebl, G. Renner, D. von der Ruhr and D. Schweitzer, *Z. Naturforsch.*, 1988, **43b**, 265.
11 M. Ohashi, N. Aoyagi and S. Yamada, *J. Chem. Soc., Perk. Trans 1*, 1990, 1335.
12 M. Mella, N. d′Alessandro, M. Freccero and A. Albini, *J. Chem. Soc., Perk. Trans 2*, 1993, 515.
13 F. Effenberger, K.-E. Mack, R. Niess, F. Reisinger, A. Steinbach, W.-D. Stohrer, J. J. Stezowski, I. Rommel and A. Maier, *J. Org. Chem.*, 1988, **53**, 4379; J. Heinze, C. Willmann and P. Bäuerle, *Angew. Chem., Int. Ed.*, 2001, **40**, 2861.
14 J. Zhang, L. M. Liable-Sands, A. L. Rheingold, R. E. Del Sesto, D. C. Gordon, B. M. Burkhart and J. S. Miller, *Chem. Commun.*, 1998, 1385.
15 H. Zhao, R. A. Heinz, K. R. Dunbar and R. D. Rogers, *J. Am. Chem. Soc.*, 1996, **118**, 12844; S. Mikami, K-i. Sugiura and J. S. Sakata, *Chem. Lett.*, 1999, 413.
16 H. Zhao, R. A. Heintz, X. Ouyang, K. R. Dunbar, C. F. Campana and R. D. Rogers, *Chem. Mater.*, 1999, **11**, 736.

CHEMCOMM Communication
www.rsc.org/chemcomm

A novel and economical route to (±)-horsfiline using an aryl iodoazide tandem radical cyclisation strategy

Dimitrios Lizos, Régis Tripoli and John A. Murphy*

Department of Pure and Applied Chemistry, University of Strathclyde, 295 Cathedral Street, Glasgow, UK G1 1XL. E-mail: john.murphy@strath.ac.uk; Fax: +44 141 548 4822; Tel: +44 141 548 2389

Received (in Cambridge, UK) 24th September 2001, Accepted 23rd October 2001
First published as an Advance Article on the web 29th November 2001

(±)-Horsfiline has been synthesised using a tandem radical cyclisation as the key step.

The spiropyrrolidinyloxindole nucleus is found in a number of natural products of diverse origin. However, despite their attraction as synthetic targets, the biological profile of these compounds was not exciting—until recently. The recent discovery of more members of this family such as spirotryprostatin A (**1**) and spirotryprostatin B (**2**) caused an increased interest, because they showed *mild* activity as cell-cycle inhibitors,[1] since cell-cycle inhibition frequently equates with *in vitro* anti-cancer activity. However, the crucial discovery was in 1999, when Danishefsky *et al.* showed[2] that unnatural analogues (**3**–**5**), synthesised in the laboratory, were truly potent inhibitors of at least one human breast cancer cell line [more than four orders of magnitude more powerful than spirotryprostatin A itself].

With this as background, we set ourselves the task of finding a new and flexible approach to the synthesis of the spiropyrrolidinyloxindole nucleus, and now present our route, which features a tandem radical cyclisation approach as the key step, in the synthesis of one member of the natural spiropyrrolidinyloxindoles, horsfiline (**6**). Horsfiline[3] has been synthesised by a number of research groups[4–9] using diverse methodologies; the synthesis of Jones and Wilkinson[4] deserves particular mention here since it also used a radical cyclisation approach, although very different from our own. Specifically, our approach features the aryl iodoazide[10] tandem radical cyclisation strategy, which we have recently used to prepare the complex alkaloid, (±)-aspidospermidine.[11]

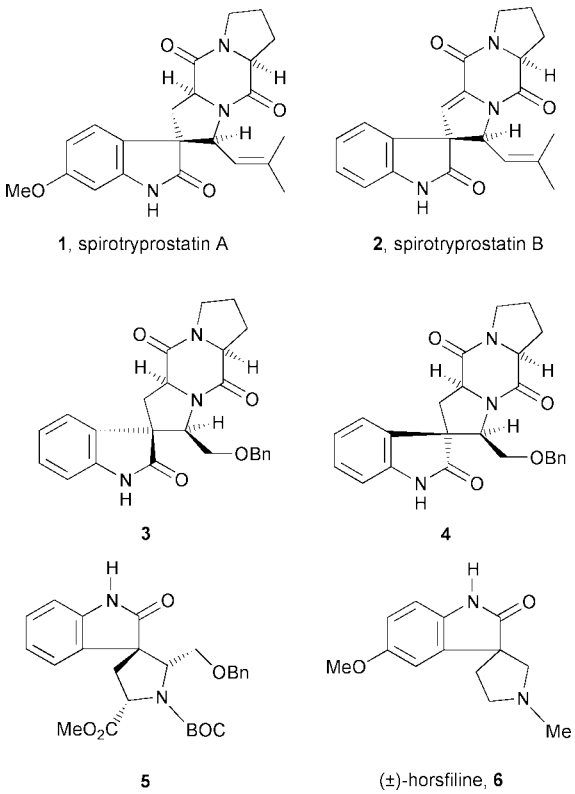

1, spirotryprostatin A **2**, spirotryprostatin B

3 **4**

5 (±)-horsfiline, **6**

Scheme 1

The starting materials for our synthesis are the commercially available and economical compounds, itaconic acid and *p*-anisidine. Double deprotonation of *t*Boc-protected *p*-anisidine **7** (prepared in 91% yield from *p*-anisidine) with *t*-BuLi and reaction with 1,2-diiodoethane afforded the iodide **8** (86%).[12] Deprotection of the *t*-Boc group (89%) and reductive amination with benzaldehyde yielded the required *N*-benzyl derivative **10** (95%). Meanwhile, selective esterification of itaconic acid[13] (82%) and then conversion to the acid chloride **11**, was followed by coupling to the amine **10**, affording amide **12** in 94% yield from the mono-acid. The plan was now to convert this compound to the corresponding azide **18**. Direct reduction of **12** with DIBAL-H yielded alcohol **13**; however, this appeared to be contaminated by, and was inseparable from, the methyl derivative **14** that would result from conjugate addition of DIBAL-H at the α,β-unsaturated amide group. This complication was avoided by protecting the alkene in **12** by conjugate addition of thiophenol. The resulting sulfide **16** (96%) was then reduced to afford the alcohol **17** (55%). [Unexpectedly, this reaction also produced a small amount of amine **15**.] Oxidation of the sulfide and thermal elimination of the resulting sulfoxide yielded the desired alcohol **13** (72%), which was smoothly converted to the azide **18** (68%) with diphenylphosphoryl azide.[14] Cyclisation with tris(trimethylsilyl)silane (TTMSS) followed by *in situ* methylation afforded[15] the tricycle **20** (60% over 2 steps). Finally, this was debenzylated[7,9] to afford horsfiline **6** (87%).

This simple approach to horsfiline illustrates that the aryl iodoazide tandem radical cyclisation strategy[11] is a powerful methodology for accessing the important spiropyrrolidinyloxindole nucleus.

We thank the EPSRC Mass Spectrometry Service Centre, Swansea, for mass spectra, the University of Strathclyde for University studentships (D. L. and R. T.) and the Royal Society for a Leverhulme Senior Research Fellowship (JAM).

Notes and references

1 A. H. Osada, C.-B. Cui, R. Onose and F. Hanaoka, *Bioorg. Med. Chem.*, 1997, **5**, 193.
2 S. Edmondson, S. J. Danishefsky, L. Sepp-Lorenzino and N. Rosen, *J. Am. Chem. Soc.*, 1999, **121**, 2147.
3 A. Jossang, P. Jossang, H. A. Hadi, T. Sévenet and B. Bodo, *J. Org. Chem.*, 1991, **56**, 6527.
4 K. Jones and J. Wilkinson, *J. Chem. Soc., Chem. Commun.*, 1992, 1767.
5 C. Pellegrini, C. Strässler, M. Weber and H.-J. Borschberg, *Tetrahedron: Asymmetry*, 1994, **5**, 1979.
6 S.-I. Bascop, J. Sapi, J.-Y. Laronze and J. Levy, *Heterocycles*, 1994, **38**, 725.
7 C. Fischer, C. Meyers and E. M. Carreira, *Helv. Chim. Acta*, 2000, **83**, 1175.
8 G. Palmisano, R. Annunziata, G. Papeo and M. Sisti, *Tetrahedron: Asymmetry*, 1996, **7**, 1.

 DOI: 10.1039/b108622g

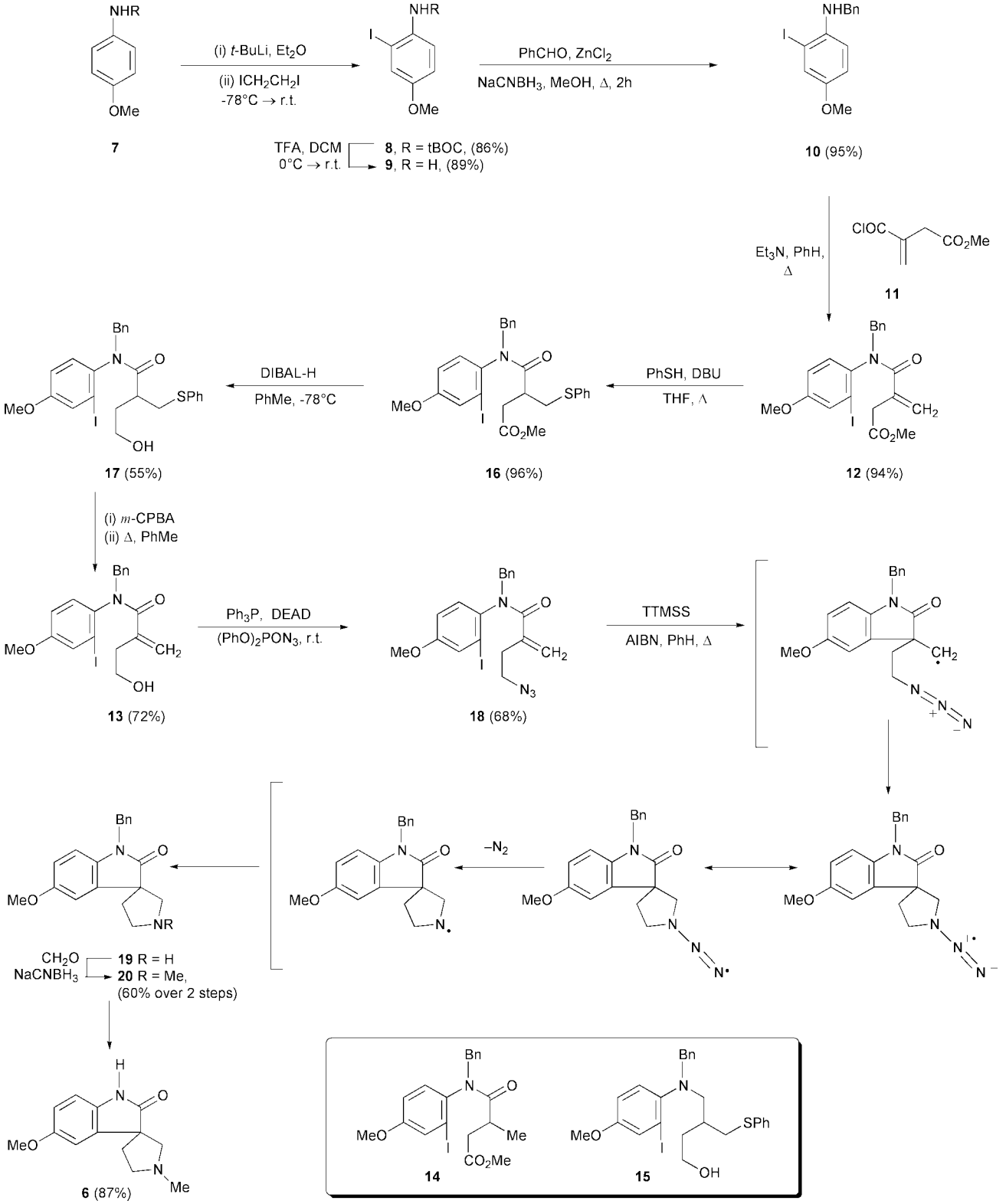

Scheme 2

9 G. Lakshmaiah, T. Kawabata, M. Shang and K. Fuji, *J. Org. Chem.*, 1999, **64**, 1699.

10 For key work on aliphatic iodoazides, see S. Kim, G. H. Joe and J. Do, *J. Am. Chem. Soc.*, 1994, **116**, 5521.

11 (*a*) M. Kizil, B. Patro, O. Callaghan, J. A. Murphy, M. B. Hursthouse and D. Hibbs, *J. Org. Chem.*, 1999, **64**, 7856; (*b*) M. Kizil and J. A. Murphy, *J. Chem. Soc., Chem. Commun.*, 1995, 1409; (*c*) B. Patro and J. A. Murphy, *Org. Lett.*, 2000, **2**, 3599.

12 Y. Kondo, S. Kojima and T. Sakamoto, *J. Org. Chem.*, 1997, **62**, 6507.

13 B. R. Baker, R. E. Schaub and J. H. Williams, *J. Org. Chem.*, 1952, **17**, 116.

14 W. H. Pearson, S. C. Bergmeier and J. P. Williams, *J. Org. Chem.*, 1992, **57**, 3977.

15 Intriguingly, no 6-*endo* product has been isolated from this cyclisation. [See: K. Jones, S. A. Brunton and R. Gosain, *Tetrahedron Lett.*, 1999, **40**, 8935;].

CHEMCOMM Communication
www.rsc.org/chemcomm

$(silox)_3RePMe_3$ (silox = $^tBu_3SiO$) is carbonylated to the double insertion product $(silox)(Me_3P)\{cis\text{-}(CO)_2\}Re\{trans\text{-}(CO_2Si^tBu_3)_2\}$

Adam S. Veige, Peter T. Wolczanski* and Emil B. Lobkovsky

Cornell University, Baker Laboratory, Department of Chemistry & Chemical Biology, Ithaca, New York, USA 14853. E-mail: ptw2@cornell.edu

Received (in Purdue, IN, USA) 30th August 2001, Accepted 6th November 2001
First published as an Advance Article on the web 6th December 2001

A rare example of the migratory insertion of a O-bound ligand, OSi^tBu_3, to a carbonyl occurred in the carbonylation of $(silox)_3RePMe_3$ to afford the double insertion product $(silox)(Me_3P)\{cis\text{-}(CO)_2\}Re\{trans\text{-}(CO_2Si^tBu_3)_2\}$.

Investigations of low coordinate, low valent monomeric and dimeric early transtion metal complexes have been aided by the use of the bulky ancillary siloxide ligand, $^tBu_3SiO$ (silox).[1,2] During nearly 20 years of study, in only one case has silox directly participated in the observed chemistry, shuttling from one tungsten to the other in the conversion of $[(silox)_2W(CO)]_2$ to $(silox)_3WW(silox)(CO)_2$.[3] During the course of carbonylating a rhenium siloxide derivative, evidence of two formal CO insertions into Re–OSi^tBu_3 bonds was obtained. The insertion of CO into any metal–heteroatom bond is unusual, and the modest number of L_nMCO_2R isolated,[4–10] observed,[11] or inferred[12,13] from carbonylation reactions are mostly late transition metal compounds;[4–11] double insertions have not been discovered.

Reduction of $(silox)_3ReCl_2$ **1**[14] by Na/Hg in neat PMe_3 afforded $(silox)_3RePMe_3$ **2** in 57% yield upon crystallization from hexanes [eqn. (1)]. Green **2** is diamagnetic, as expected for

$$(silox)_3ReCl_2 \xrightarrow[-2\ NaCl]{Na/Hg,\ PMe_3} (silox)_3RePMe_3 \qquad (1)$$
1 **2**

a C_{3v} (e^4, $^1A_1$) molecule, and exhibited resonances at δ 1.22 and 1.38 (J_{PH} 10.4 Hz) in its ^1H NMR spectrum corresponding to the silox and PMe_3 protons, respectively.†

As shown in Scheme 1, within 10 min carbonylation of $(silox)_3RePMe_3$ **2** generated free PMe_3 and a mixture of silox–carbonyl complexes, $(silox)_3Re(CO)_x$. One strong IR absorption at 1851 cm^{-1} was observed accompanied by several weaker absorptions at 2018, 1932, 1881 and 1807 cm^{-1}; all shift to 1805 cm^{-1}, and 1960, 1891, 1836 and 1770 cm^{-1} when ^{13}CO was employed. Crystallization from hexanes afforded dark green $(silox)_3ReCO$ **3**, [ν(CO) 1851 cm^{-1}, $^{13}C\{^1H\}$ NMR, δ 195.37] in 79% yield. An X-ray crystal structure determination of **3** confirmed its C_{3v}, monocarbonyl structure (Fig. 1), but the data quality only permitted isotropic refinement.‡ Normal

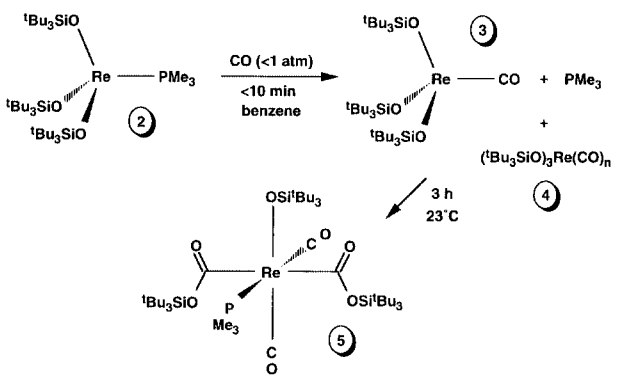

Scheme 1

distances [d(ReO) = 1.852(14) Å (av.), d(SiO) = 1.676(10) Å (av.), d(ReC) = 1.842(17) Å, d(CO) = 1.21(2) Å] are observed, but the angles [$\angle$(O–Re–O) = 117.2(15)° (av.), $\angle$(O–Re–C) = 99.7(29)° (av.)] reflect a distortion toward trigonal monopyramidal (tmp) coordination from tetrahedral. While intersilox repulsions are the probable cause, there is also a subtle electronic advantage to the tmp geometry derived from π-bonding. The remaining IR bands in the original mixture are considered to belong to the carbonyls of $(silox)_3Re(CO)_n$ **4** (n > 1). It is probable that **3** and free CO are in equilibrium with **4**, since a single broad resonance is observed for the silox ligand in the ^1H NMR spectrum of the mixture, and $(silox)_3Re^{13}CO$ (**3**-^{13}C) rapidly exchanges with CO.

Continued monitoring of the solution containing $(silox)_3RePMe_3$ **2** and CO revealed the growth of a new compound **5** at the expense of $(silox)_3ReCO$ **3** and $(silox)_3Re(CO)_n$ **4**. A 2:1 ratio (δ 1.29: δ 1.41) of siloxides was determined by ^1H NMR spectroscopy, and a new PMe_3 resonance was observed at δ 1.22 (J_{PH} 9.2 Hz). Interestingly, the IR spectrum of **5** revealed three CO absorptions at 2024, 1935 and 1631 cm^{-1}. Clearly a type of acyl was present in **5**, and the higher terminal CO frequencies indicated significant competition for π-electron density on Re. The $^{13}C\{^1H\}$ NMR spectrum of **5** corroborated the inequivalent siloxides, and revealed three additional resonances at δ 183.85 (J_{PC} 4.6 Hz), 188.45 (J_{PC} 100.7 Hz) and 198.80 (J_{PC} 8.3 Hz). The large J_{PC} and low frequency CO absorption forced consideration of a phosphaacyl, –$COPMe_3$, but a search of the Cambridge Crystallographic Database revealed no analogous compounds, and it seemed unlikely that carbonyls on a *tris*-silox rhenium(III) fragment would be sufficiently electrophilic to incur formation of a zwitterionic phosphaacyl complex. In addition, the $^{31}P\{^1H\}$ NMR spectrum of **5** revealed a δ −5.58 resonance consistent with a Re–PMe_3 bond.

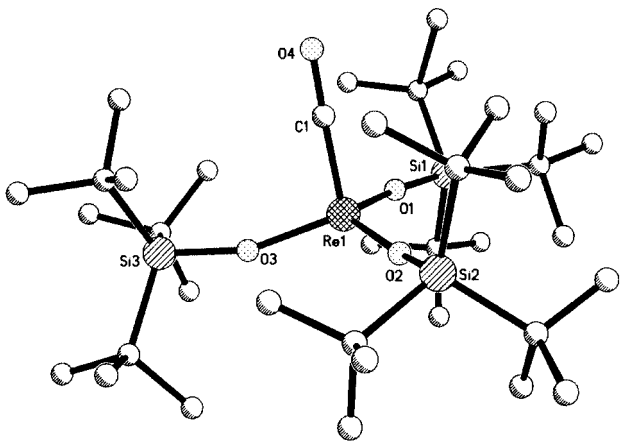

Fig. 1 Molecular view of $(silox)_3ReCO$ **3**. Selected (see text) interatomic distances (Å) and angles (°): Re–O1 1.844(10), Re–O2 1.844(9), Re–O3 1.868(8), Si1–O1 1.669(10), Si2–O2 1.687(9), Si3–O3 1.671(9); O1–Re–C1 96.5(6), O2–Re–C1 102.2(6), O3–Re–C1 100.3(6), O1–Re–O2 116.1(4), O2–Re–O3 116.7(4), O1–Re–O3 118.9(4), Re–C1–O4 178.1(15), Re–O1–Si1 172.8(6), Re–O2–Si2 162.6(6), Re–O3–Si3 161.4(6).

 DOI: 10.1039/b107884b

Since the J_{PC} 100 Hz could be assigned to a large *trans*-P–Re–^{13}CO coupling, a CO insertion to form a siloxy–acyl ligand, $CO_2Si^tBu_3$, was considered. An X-ray structural study of (silox)(Me_3P){*cis*-$(CO)_2$}Re{*trans*-$(CO_2Si^tBu_3)_2$} **5** corroborated this possibility, and proved fully consistent with the spectral data.†‡ As Fig. 2 reveals, **5** possesses *trans*-siloxyacyl ligands and *cis*-CO ligands, one *trans* to a PMe_3 and one *trans* to the remaining siloxide. The environment is pseudo-octahedral, with ∠(O3–Re–CO) = 94.6(3), 171.5(3)°, ∠(OC–Re–CO) = 93.7(3)°, ∠(P–Re–CO) = 84.8(2), 176.8(2)°, and ∠(P–Re–O3 = 86.9(2)°. The silacarboxylates are tipped away from the bulky siloxide [∠(O3–Re–C3) = 104.0(2)°, ∠(O3–Re–C16) = 107.9(2), ∠(C3–Re–C1) = 76.0(2)°, ∠(C16–Re–C1) = 74.8(3)°] and PMe3 [∠(P–Re–C3) = 101.2(2)°, ∠(P–Re–C16) = 95.7(2)°, ∠(C3–Re–C2) = 81.1(3)°, ∠(C16–Re–C2) = 81.2(2)°] ligands. From the perspective of covalent radii, the rhenium–silacarboxylate distances are somewhat long [d(Re–C_{ac}) = 2.077(6), 2.078(5) Å], belying the acyl CO stretch that suggests significant π-back-bonding into this unique ligand.

The remaining distances are rather normal, although the d(Re–O) of 2.032(5) Å is long when compared to systems that favor O(pπ)→M(dπ) interactions.[1–3,14] Clearly the d^4 rhenium mitigates the usual strong π-donor tendencies of the siloxide. Taking the Re–O_3 bond as the z axis, and Re–P in the xz plane, it is likely that d_{xy} and d_{xz} are filled, leaving d_{yz} as the lone receptor orbital for π-donation from the siloxide. Sterics must also play a role in limiting the interaction, as the bulk of the silox is clearly tipped away [∠(Re–O3–Si3) = 157.4(3)°] from the PMe_3 and into the space above the acyl oxygens and a carbonyl. Back-bonding into the silacarboxylates and CO by the filled d_{xy}, and into the two carbonyls by d_{xz}, provides the competition for electron density that renders the CO stretches relatively high. When exposed to ^{13}CO, the CO opposite the PMe_3 ligand was identified as the most labile.

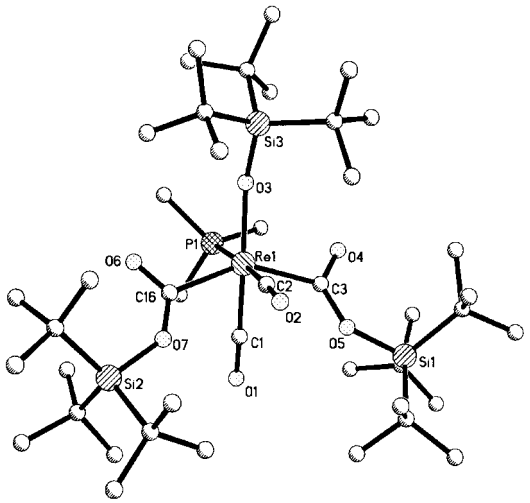

Fig. 2 Molecular view of (silox)(Me_3P){*cis*-$(CO)_2$}Re{*trans*-$(CO_2Si^tBu_3)_2$} **5**. Selected (see text) interatomic distances (Å) and angles (°): Re–C1 1.934(11), Re–C2 1.965(10), Re–P 2.486(3), Si1–O5 1.698(4), Si2–O7 1.691(4), Si3–O3 1.637(5), C1–O1 1.150(9), C2–O2 1.141(8), C3–O4 1.215(7), C3–O5 1.339(9), C16–O6 1.214(8), C16–O7 1.314(8); C3–Re–C16 144.5(3), Re–C3–O4 108.8(5), Re–C16–O6 111.2(4), Re–C3–O5 125.4(4), Re–C16–O7 123.7(4), C3–O5–Si1 134.1(3), C16–O7–Si2 137.3(4).

Presumably the weakening of D(M–OR) in moving to the late metals enables CO insertion to be favorable, because there is no kinetic reasoning that suggests it is intrinsically slow. Consistent with the thermodynamic reasoning is the observation of H(silox) loss from (silox)$_3$RePMe$_3$ **2** upon hydrogenation. The mechanism of CO insertion, whether internal[4–7] or external[9,11] [*i.e.* L_n(silox)Re + CO → {L_nReCO}$^+$[OSi^tBu_3]$^-$ → L_nRe-$CO_2Si^tBu_3$], is currently unknown, but it is likely that the unfavorable sterics of a (silox)$_3$Re$(CO)_x(PMe_3)_y$ ($x + y$ = 2–4) carbonyl derivative would favor insertion to relieve strain about the Re core.

The US National Science Foundation is gratefully acknowledged for financial support.

Notes and references

† *Selected analytical data*: **2**: NMR (C_6D_6), δ_H 1.22 (81 H, s, ^{t}Bu), 1.38 (9 H, d, PMe_3, J_{PH} 10.4 Hz); δ_C 25.32 (*C*Me$_3$), 31.84 [C(*C*H$_3$)$_3$], 56.85 [d, P(CH$_3$)$_3$, J_{PC} 36.7 Hz]; Anal. Calc. for $C_{39}H_{90}O_3Si_3PRe$: C, 51.6, H, 10.0. Found: C, 50.1; H, 9.4% (EA consistently low in carbon). **3**: NMR (C_6D_6), δ_H 1.24 (81 H, s, ^{t}Bu); δ_C 23.81 (*C*Me$_3$), 31.00 [C(*C*H$_3$)$_3$], 195.37 (CO); Anal. calc. for $C_{37}H_{81}O_4Si_3Re$: C, 51.6, H, 9.5%. Found: C, 49.6; H, 9.5% (EA consistently low in carbon). **5**: NMR (C_6D_6), δ_H 1.22 (9 H, d, PMe_3, J_{PH} 9.2 Hz), 1.29 (54 H, s, ^{t}Bu), 1.41 (27 H, s, ^{t}Bu); δ_C 13.47 [d, P(CH$_3$)$_3$, J_{PC} 27.5 Hz], 23.75 (CO_2Si*C*), 23.94 (ReOSiC), 29.84 [CO_2SiC(*C*H$_3$)$_3$], 31.53 [ReOSiC(*C*H$_3$)$_3$], 183.85 (d, CO_2Si, J_{PC} 4.6 Hz), 188.45 (d, CO, J_{PC} 100.7 Hz), 198.80 (d, CO, J_{PC} = 8.3 Hz); δ_P −5.58 (ref. H_3PO_4); IR (Nujol, cm^{-1}) 2024 (vs), 1935 (s), 1631 (s); Anal. Calc. for $C_{43}H_{90}O_7Si_3PRe$: C, 50.6, H, 8.9. Found: C, 50.6; H, 8.9%.

‡ *Crystallographic data*: **3**: $C_{37}H_{81}O_4Si_3Re$, M = 860.49, monoclinic, $P2_1/n$, a = 8.7010(17), b = 21.072(4), c = 24.334(5) Å, β = 93.89(3)°, U = 4451.3(15) Å^3, T = 173(2) K, Z = 4, μ(synchrotron, λ = 0.90000 Å) = 2.843 mm^{-1}, 5400 (R_{int} = 0.0639) independent reflections, R_1 (2σ) = 0.0896. **5**: $C_{43}H_{90}O_7Si_3PRe$, M = 1010.63, triclinic, $P\bar{1}$, a = 13.2908(7), b = 13.4716(8), c = 17.7266(9) Å, α = 96.464(2), β = 104.696(2), γ = 116.971(1)°, U = 2639.1(2) Å^3, T = 173(2) K, Z = 2, μ(Mo-Kα) = 2.442 mm^{-1}, 6387 (R_{int} = 0.0274) independent reflections, R_1 (2σ) = 0.0495.

CCDC reference numbers 173800 and 173801. See http://www.rsc.org/suppdata/cc/b1/b107884b/ for crystallographic data in CIF or other electronic format.

1 P. T. Wolczanski, *Polyhedron*, 1995, **14**, 3335–3362.
2 A. S. Veige, L. M. Slaughter, P. T. Wolczanski, N. Matsunaga, S. A. Decker and T. R. Cundari, *J. Am. Chem. Soc.*, 2001, **123**, 6419–6420 and references therein.
3 R. L. Miller, Ph.D. Thesis, Cornell University, 1993; A.-R. Mayol, Ph. D. Thesis, Cornell University, 1999.
4 H. E. Bryndza, *Organometallics,* 1985, **4**, 1686–1687.
5 K. Osakada, Y.-J. Kim and A. Yamamoto, *J. Organomet. Chem.*, 1990, **382**, 303–317.
6 S. K. Mandal, D. M. Ho, Douglas and M. Orchin, *Inorg. Chem.*, 1991, **30**, 2244–2248.
7 G. D. Smith, B. E. Hanson, J. S. Merola and F. J. Walter, *Organometallics*, 1993, **12**, 568–570.
8 D. W. Dockter, P. E. Fanwick and C. P. Kubiak, *J. Am. Chem. Soc.*, 1996, **118**, 4846–4852
9 W. M. Rees, M. R. Churchill, J. C. Fettinger and J. D. Atwood, *Organometallics*, 1985, **4**, 2179–2185.
10 K. Khumtaveeporn and H. Alper, *Acc. Chem. Res.*, 1995, **28**, 414–422, 520 and references therein.
11 A. M. Gull, J. M. Blatnak and C. P. Kubiak, *J. Organomet. Chem.*, 1999, **577**, 31–37.
12 B. P. Buffin, A. M. Arif and T. G. Richmond, *J. Chem. Soc., Chem. Commun.*, 1993, 1432–1434.
13 P. Kundel and H. Berke, *J. Organomet. Chem.*, 1988, **339**, 103-110.
14 R. E. Douthwaite, P. T. Wolczanski and E. Merschrod, *Chem. Commun.*, 1998, 2591–2592.

CHEMCOMM Communication
www.rsc.org/chemcomm

Do π-dimers of tetrathiafulvalene cation radicals really exist at room temperature?†

Vladimir Khodorkovsky,*[a] Lev Shapiro,[a] Pnina Krief,[a] Alex Shames,[b] Gilles Mabon,[c] Alain Gorgues[c] and Michel Giffard[c]

[a] *Department of Chemistry, Ben-Gurion University of the Negev, Beer Sheva 84105, Israel. E-mail: hodor@bgumail.bgu.ac.il*
[b] *Department of Physics, Ben-Gurion University of the Negev, Beer Sheva 84105, Israel*
[c] *Ingénierie Moléculaire et Matériaux Organiques, CNRS UMR 6501, University of Angers, 2 Bd Lavoisier, F-49045 Angers, France*

Received (in Cambridge, UK) 5th June 2001, Accepted 14th November 2001
First published as an Advance Article on the web 6th December 2001

The longest wave absorption band of the tetramethylthiotetrathiafulvalene cation radical, which is usually interpreted as a π-dimer band, is shown to be the intrinsic cation radical absorption, all studied cation radicals in solution at room temperature exist as paramagnetic monomers and only tetrathiafulvelene and tetramethyltetrathiafulvalene cation radicals undergo π-dimerization at low temperatures.

Currently, the alleged ability of stoichiometric cation-radical salts derived from tetrathio substituted tetrathiafulvalene (TTF) to form π-dimers at room temperature is widely viewed as a proof of the presence of significant intramolecular interactions between the oxidized TTF moieties within a number of supramolecular structures.[1–3] Although NIR absorption bands of a number of tetrachalcogeno TTF cation radicals were ascribed to intrinsic absorptions,[4] the band at *ca*. 850 nm observed in solutions of tetramethylthiotetrathiafulvalene (TMT-TTF) cation radicals is interpreted as the 'π-dimer signature' and, moreover, it has even been claimed that in solution, cation radicals exist only in dimerized diamagnetic form.[5] Here we present the results of our studies unequivocally demonstrating that the above interpretation, based exclusively on analogies is doubtful and that the cation radicals derived from TTF, tetramethyl TTF (TMTTF), TMT-TTF and bis(ethyleneditio) TTF (ET) exist in monomeric paramagnetic form, at least at room temperature.

Formation of π-dimers from ion radicals can easily be monitored by appearance of a new long-wave absorption band (red-shifted from the longest-wave absorption band of the ion-radical) and deviation of the EPR signal intensity from the Curie Law with eventual disappearance of the EPR signal. For TTF derivatives, appearance of a long-wave band in the absorption spectrum of 3,9(10)-dimethyldibenzo $TTF^{\cdot+}$ upon increasing the concentration or decreasing the temperature in acetonitrile, was interpreted as formation of π-dimers.[6] However, no dimerization has been observed for the cation radicals of TTF itself and dibenzo TTF in acetonitrile when cooled to the point when crystallization occurred. The complete change in absorption spectra for $TTF^{\cdot+}$ in ethanol was observed only at 225 K (10^{-3} M solution)[7] and 77 K (10^{-5} M solution)[8] and, although no EPR studies have been made in this case, the interpretation was confirmed by comparison with the solid state spectra. At room temperature, no dimers in 10^{-3} M solutions of $TTF^{\cdot+}$ were present.[8] The above examples of two derivatives differing only by the presence of two methyl groups, dibenzo $TTF^{\cdot+}$ (which does not undergo dimerization) and 3,9(10)-dimethyldibenzo $TTF^{\cdot+}$ (which dimerizes at temperatures close to the room temperature) show that the ability of cation radicals to form π-dimers can depend on quite minor structural changes and, probably, reflects the propensity of a cation radical to form dimers in the solid state.

Unfortunately in the case of $TMT\text{-}TTF^{\cdot+}$, an obviously erroneous absorption spectrum has been reported in the paper describing its first synthesis: 461 nm was given as a longest wave absorption maximum.[9] This paper and the misleading analogy with $TTF^{+\cdot}$, became a source of numerous misinterpretations,[1–3,5,10] whereas the later paper with the correct data[11] (850 nm) remained unnoticed.

The non-stoichiometric salts of TTF are usually less soluble than the stoichiometric ones and often precipitate upon chemical or electrochemical oxidation of the TTF derivatives, a fact that makes the isolation of the pure stoichiometric salts difficult. Recently, we developed an efficient and convenient synthetic procedure for preparation of TTF derived cation radicals involving oxidation by iodobenzene diacetate and a strong acid.[12] This enabled us to reinvestigate the spectroscopic solution behavior of TTF derived cation radicals.

Let us first consider the electronic absorption spectra. UV/Vis/NIR spectra recorded at room temperature for solutions of cation radicals in acetonitrile, methylene chloride and ethanol at various concentrations (10^{-3}–10^{-5} M) in the range of 250–2000 nm are in accord with the published data.[4a,6,7,8,11] Interestingly, the spectra are practically concentration and counter-anion independent (Cl, BF_4, tosylate and CF_3SO_3 anions have been checked so far) and only small shifts of absorption maxima (about 2–5 nm) have been observed in acetonitrile, methylene chloride and ethanol, whereas the general shape of absorption bands remains virtually the same. All spectra are also temperature independent within the experimental error. Considerable bathochromic shifts of the longest-wave absorption bands are observed in the series $TTF^{\cdot+}$, $TMTTF^{\cdot+}$, $TMT\text{-}TTF^{\cdot+}$, $ET^{\cdot+}$ (Table 1). This phenomenon is predictable: an energy change diagram showed that even a single alkylthio substituent attached to the TTF moiety interacts

Table 1 Calculated (TD B3LYP/6-31G**//HF/6-31G**) and experimental longest wave absorption maxima for the cation radicals of TTF, TMTTF, TMT-TTF and ET

Cation radical	Calculated λ_{max}/nm (oscillator strength)	Calculated λ_{max} (nm) (oscillator strength)[a]	Experimental λ_{max}/nm (ε)[b]
$TTF^{\cdot+}$	509 (0.070)	556 (0.05)	580 (4,200)
$(TTF_2)^{2+}$	753 (0.280)	—	714 (EtOH)[7]
$TMTTF^{\cdot+}$	567 (0.123)	—	652 (7,400)
$MeSTTF^{\cdot+}$	729 (0.083)	—	785[13]
$TMT\text{-}TTF^{\cdot+}$	711 (0.043)	—	843 (9,700)
$ET^{\cdot+}$	956 (0.185)	867 (0.28)	954 (10,500)

[a] From ref. 4*a*, calculated by the LNDO/S PERTCI method using the experimental geometry (TTF) and HF/6-31G** geometry (ET). [b] In acetonitrile, room temperature.

† Electronic supplementary information (ESI) available: electronic absorption and EPR spectra. See http://www.rsc.org/suppdata/cc/b1/b104934h/

 DOI: 10.1039/b104934h

mostly with the HOMO^{-1} and not with the HOMO[14] (in the LCBO-MO approximation) and, since the long wave absorption band of TTF cation radical is mainly a HOMO–SOMO transition, *a strong bathochromic shift* for the alkylthio substituted TTF cation radicals is anticipated. This simplified consideration is fully confirmed by higher-level calculations.[15] Geometries of the cation radicals have been optimized on the Hartree–Fock level using the 6-31G** basis set, which has been shown to reproduce the experimental geometry of ET$^{\cdot+}$ within 0.02 Å error.[16] We found that the geometries of other derivatives are reproduced at this level within the same error, whereas the DFT method gave poor results. Noteworthy, geometry optimization of $(TTF_2)^{2+}$ gave the energy minimum at the distance of 3.5 Å between the planes of the slightly distorted TTF molecules, *i.e.*, close to the experimental in solid state, whereas optimization failed for $(TMT\text{-}TTF_2)^{2+}$. The absorption spectra (Table 1) have been calculated using time-dependent density functional theory (TDDFT), which has been demonstrated to afford accurate predictions for neutral molecules and radicals‡ (see ref. 17 and refs. therein). The low energy absorption of methylthio TTF$^{+\cdot}$ (MeSTTF$^{+\cdot}$) is predicted at 729 nm in a reasonable agreement with the experimental value of 785 nm for the dihydrothieno-fused analog.[13] Noteworthy, this band was also ascribed to the π-dimer solely on the grounds of concentration dependence that might stem from any other kind of intermolecular interaction rather than from π-dimerization, as soon as no temperature/concentration anomalies of the EPR signal and appearance of the new π-dimer absorption bands were reported.

Concentrated solutions ($>10^{-3}$ M) of the cation radicals exhibit features of aggregation (intensities of additional absorption bands are *counteranion and concentration dependent*). Spectroscopic features of such solutions will be discussed elsewhere.

Although the theoretical considerations and UV/VIS/NIR spectroscopy results discussed above mean that the probability of cation radical dimerization at room temperature is very small, the direct proof can only be provided by EPR measurements at different temperatures. Our experiments show that all studied cation radicals exhibit strong EPR signals (1 spin per molecule within *ca*. 30% of the experimental error) at room temperature in concentrated (*ca*. 5×10^{-4}) solutions in acetonitrile and ethanol. The *g*-factors of 2.0080, 2.0078 and 2.0075 were found for the cation radicals of TTF, TMT-TTF and ET, correspondingly, in ethanol at 300 K.§ The coupling constant of ^{33}S (0.380 mT, 4S) determined for TMT-TTF$^{\cdot+}$ is close to the value (0.370)[18] found for ET$^{\cdot+}$.

The temperature dependence of the EPR signals was studied for the TTF and TMT-TTF cation radicals in ethanol. The intensity of the EPR signal from TTF$^{\cdot+}$ obeyed the Curie Law up to 265 K and disappearance of the signal at 220 K together with the reported changes in absorption[7] can be safely interpreted as proof for the formation of π-dimers (Fig. 1). Essentially the same trend was observed in methylene chloride and acetonitrile, although the lower solubility in the former and relatively high melting point of the latter make these solvents less suitable.

Owing to a sharper dependence of TMT-TTF$^{\cdot+}$ solubility on temperature, this salt crystallized out of the solution (10^{-4} M) already at *ca*. 280 K, however, above this temperature the Curie Law was obeyed. In more dilute solution (10^{-5} M), crystallization occurred at *ca*. 230 K and at 190 K the signal was still present (Fig. 1). Crystallization of TMT-TTF$^{\cdot+}$ during measurements is also confirmed by the strong temperature hysteresis that was practically absent in the case of TTF$^{\cdot+}$. No other signals in the region of $g \sim 2$ and $g \sim 4$ were detected.

In conclusion, we find that all studied cation radicals in solution at room temperature exist as paramagnetic monomers. The assertion is based on electronic absorption spectra, which are concentration independent in a wide range of concentrations and the presence of a strong EPR signal. The EPR measurements at different temperatures confirm formation of π-dimers for TTF$^{\cdot+}$ below 265 K. No dimerization for TMT-TTF$^{\cdot+}$ was observed up to crystallization at 280 K and 230 K, depending on the concentration. In this case, the paramagnetic monomers were present even at 190 K. Although π-dimerization could be favored in linked analogs,[1–3,5] the reported spectral features fully correspond to those expected for the free cation radicals.

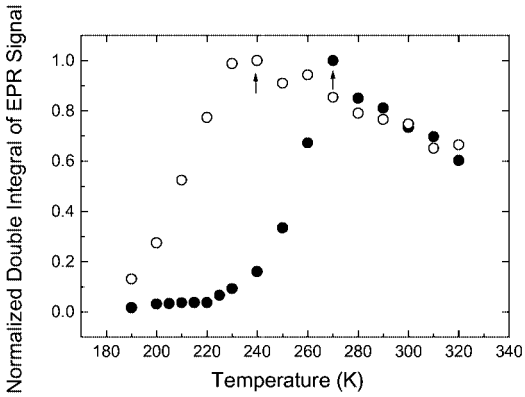

Fig. 1 Temperature dependence of normalized double integral intensity of the EPR signal for TTF$^{\cdot+}$ (closed circles) and TMT-TTF$^{\cdot+}$ (open circles) in ethanol. Arrows point out the beginning of the Curie Law region.

The authors thank the Ministry of Science, Israel, for partial financial support.

Notes and references

‡ Similar results were published after the manuscript was submitted: R. Andreu, J. Garin and J. Orduna, *Tetrahedron*, 2001, **57**, 7883.
§ For TTF$^{\cdot+}$ and ET$^{\cdot+}$ *g*-factors of 2.0081 and 2.0074 were determined in methylene chloride at 233 K[18] and rt.[13]

1 M. B. Nielsen, C. Lomholt and J. Becher, *Chem. Soc. Rev.*, 2000, **29**, 153.
2 M. R. Bryce, W. Devonport, L. M. Goldenberg and C. Wang, *Chem. Commun.*, 1998, 945; C. A. Christensen, L. M. Goldenberg, M. R. Bryce and J. Becher, *Chem. Commun.*, 1998, 509; C. A. Christensen, M. R. Bryce, A. S. Batsanov and J. Becher, *Chem. Commun.*, 2000, 331.
3 F. Le Derf, E. Levillain, G. Trippé, A. Gorgues, M. Sallé, R.-M. Sebastian, A.-M. Caminade and J.-P. Majoral, *Angew. Chem., Int. Ed.*, 2001, **40**, 224.
4 (*a*) K. Zimmer, B. Goedicke, M. Hoppmeier, H. Meyer and A. Schweig, *Chem. Phys.*, 1999, **248**, 263; (*b*) S. Horiuchi, H. Yamochi, G. Saito, K. Sakaguchi and M. Kusunoki, *J. Am. Chem. Soc.*, 1996, **118**, 8604.
5 H. Spangaard, J. Prehn, M. B. Nielsen, E. Levillain, M. Allain and J. Becher, *J. Am. Chem. Soc.*, 2000, **122**, 9486.
6 S. Hünig, G. Kießlich, H. Quast and D. Scheutzow, *Liebigs Ann. Chem.*, 1973, 310.
7 J. B. Torrance, B. A. Scott, B. Welber, F. B. Kaufman and P. E. Seiden, *Phys. Rev. B*, 1979, **19**, 730.
8 R. Bozio, I. Zanon, A. Girlando and C. Pecile, *J. Chem. Phys.*, 1979, **71**, 2282.
9 P. R. Moses and J. Q. Chambers, *J. Am. Chem. Soc.*, 1974, **96**, 945.
10 M. E. Kozlov, Y. Tanaka, M. Tokumoto and T. Tani, *Chem. Phys. Lett.*, 1994, **223**, 318; M. E. Kozlov, Y. Tanaka, M. Tokumoto and T. Tani, *Synth. Met.*, 1995, **70**, 987.
11 Y. N. Kreicberga and O. Y. Neilands, *Zh. Org. Khim.*, 1985, **21**, 2009.
12 M. Giffard, G. Mabon, E. Leclair, N. Mercier, M. Allain, A. Gorgues, P. Molinié, O. Neilands, P. Krief and V. Khodorkovsky, *J. Am. Chem. Soc.*, 2001, **123**, 3852.
13 E. Ribera, J. Veciana, E. Molins, I. Mata, K. Wurst and C. Rovira, *Eur. J. Org. Chem.*, 2000, 2867.
14 V. Khodorkovsky, A. Edzina and O. Neilands, *J. Mol. Electronics*, 1989, **5**, 33.
15 M. J. Frisch *et al.*, *Gaussian 98*, Revision A.7, Gaussian, Inc., Pittsburgh, PA, 1998.
16 E. Demiralp and W. A. Goddard, III, *J. Phys. Chem.*, 1994, **98**, 9781.
17 S. Hirata and M. Head-Gordon, *Chem. Phys. Lett.*, 1999, **302**, 375; D. Sundholm, *Chem. Phys. Lett.*, 2000, **317**, 545.
18 L. Cavara, F. Gerson, D. O. Cowan and K. Lerstrup, *Helv. Chim. Acta.*, 1986, **69**, 141.

CHEMCOMM
Communication
www.rsc.org/chemcomm

Evaluation of the relative importance of Ti–Cl···H–N hydrogen bonds and supramolecular interactions between perfluorophenyl rings in the crystal structures of $[Ti(NR)Cl_2(NHMe_2)_2]$ (R = ^{i}Pr, C_6H_5 or C_6F_5)†

Nico Adams, Andrew R. Cowley, Stuart R. Dubberley, Andrew J. Sealey, Michael E. G. Skinner and Philip Mountford*

Inorganic Chemistry Laboratory, University of Oxford, South Parks Road, Oxford, UK OX1 3QR. E-mail: philip.mountford@chemistry.oxford.ac.uk

Received (in Cambridge, UK) 10th October 2001, Accepted 14th November 2001
First published as an Advance Article on the web 6th December 2001

The three closely-related compounds $[Ti(N^iPr)Cl_2(NHMe_2)_2]$ 1, $[Ti(NC_6H_5)Cl_2(NHMe_2)_2]$ 2 and $[Ti(NC_6F_5)Cl_2(NHMe_2)_2]$ 3 all crystallize in the space group *C*2/*c* with the titanium atoms lying on two-fold axes at (0, *y*, 1/4); in compounds 1 and 2 the molecules are linked in one-dimensional infinite chains by intermolecular Ti–Cl···H–N hydrogen bonds along the direction of the crystallographic *c* axis, whereas in 3 offset face-to-face interactions between the C_6F_5 rings break down the hydrogen bonded chains.

The importance of non-covalent interactions between hydrogen-substituted arene rings in supramolecular chemistry is now well-recognised.[1] Arene–perfluoroarene interactions represent a special case and are, for instance, responsible for the 24 °C melting point of the 1:1 benzene–perfluorobenzene complex (while those of neat benzene and perfluorobenzene are 5.5 and 4 °C, respectively).[2] Such mixed arene–perfluoroarene interactions have recently attracted renewed attention in a range of supramolecular contexts.[3] More recently, reports of the possible importance of supramolecular interactions between pairs of perfluoroarene rings in organic and inorganic/organometallic contexts have appeared.[4] Hunter and Sanders were the first to propose a simple model for the interpretation of intermolecular π-interactions between aromatic molecules.[5] Also recently, Dance and coworkers[6] reported density funtional calculations on the gas-phase dimers $(C_6H_6)_2$ and $(C_6F_6)_2$ and concluded that (i) intermolecular interactions between perfluorinated aromatic rings are slightly *more attractive* than those of the hydro analogues (due mainly to an increased van der Waals component); (ii) calculated intermolecular potentials for offset face-to-face (*off*) interactions between pairs of C_6F_6 rings are twice as favourable as edge-to-face or vertex-to-face interactions; and that (iii) there are no major differences between the supramolecular embraces adopted by poly-phenyl and poly-fluorophenyl systems. Despite these recent, promising indicators of such supramolecular interactions, no clear-cut, 'head-to-head' study has been reported showing the relative importance of fluoroarene–fluoroarene interactions in comparison with possible arene–arene or other (*e.g.* hydrogen bonded) supramolecular motifs. Here we report the molecular and supramolecular structures of a series of closely related compounds that further demonstrate the importance of fluoroarene–fluoroarene interactions in crystal engineering.

As part of our research programme in transition metal imido chemistry[7] we found that the reaction of a very wide range of primary amines RNH_2 (R = alkyl or aryl) with $[TiCl_2(NMe_2)_2]$ in benzene leads to the highly air- and moisture-sensitive imido-bis(dimethylamino) titanium complexes $[Ti(NR)Cl_2(NHMe_2)_2]$ in good to excellent yields.[8] In this communication we focus on the molecular and supramolecular structures of three of these compounds, namely where R = ^{i}Pr **1**, C_6H_5 **2** or C_6F_5 **3**.†‡ The solid state molecular structures are fully consistent with the solution ^{1}H and ^{13}C-{^{1}H} NMR and solid state IR (Nujol mull) spectra given as ESI.†

The molecular structures of $[Ti(NR)Cl_2(NHMe_2)_2]$ (R = ^{i}Pr **1**, C_6H_5 **2** or C_6F_5 **3**) are presented in Fig. 1.‡ All adopt approximately trigonal bipyramidal geometries (equatorial NR and Cl groups) with linear or near-linear Ti=N–R linkages; the intramolecular distances and angles in **1**–**3** are unexceptional in comparison with other titanium imido complexes.[9] Hydrogens were placed in calculated positions (N–H 0.87 Å, C–H 1.00 Å). The structures are approximately isomorphous, with all three compounds crystallizing in the space group *C*2/*c* and the Ti atoms lying on crystallograhpic two-fold axes (passing through the Ti=N bond) at (0, *y*, 1/4) or a symmetry-equivalent position. While the molecular structures of **1**, **2** and **3** are very similar, their supramolecular structures differ significantly.

Molecules of $[Ti(NiPr)Cl_2(NHMe_2)_2]$ **1** form hydrogen bonded chains in the solid state as shown in Fig. 2(a). Hydrogen bonds form between the N–H groups of $NHMe_2$ ligands and Ti–Cl group hydrogen bond acceptors on neighbouring titanium complexes, and propagate in the direction of the crystallographic *c* axis. The Ti–Cl···H–N contacts of 2.51 Å may within error be considered 'short' according to Brammer and Orpen's classification[10] based on a detailed analysis of crystallographic data.[9] Moving on to the phenylimido system $[Ti(NC_6H_5)Cl_2(NHMe_2)_2]$ **2** [Fig. 2(b)] we encouter the same hydrogen-bonded supramolecular arrangement with experimentally comparable Ti–Cl···H–N contacts of 2.46 Å and Cl···H–N angles (158° in **2** *vs.* 160° in **1**). There are single C–H_{arene}···C pairwise contacts (C–H···C = 3.17 Å) between rings of one hydrogen-bonded chain of **2** and the neighbouring one. However, these are considered to be secondary consequences of the favoured Ti–Cl···H–N hydrogen bonded arrangement established for **1** (where no arene–arene interactions are possible). The *a* [16.913(1) *vs.* 16.260(1) Å] and *c* [12.044(1) *vs.* 11.935(1)] unit cell lengths for **1** and **2** are fairly similar while the *b* unit cell dimensions of 9.101(1) and 10.303(1) Å,

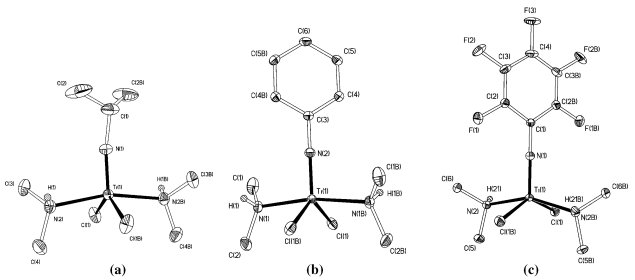

Fig. 1 Structures of $[Ti(NR)Cl_2(NHMe_2)_2]$ [(a) R = ^{i}Pr **1**; (b) R = C_6H_5 **2** and (c) R = C_6F_5 **3**]. C-bound H atoms omitted; displacement ellipoids drawn at the 25% probablility level; H atoms drawn as spheres of arbitrary radius.

† Electronic supplementary information (ESI) available: characterisation and crystal data for compounds **1**–**3**. See http://www.rsc.org/suppdata/cc/b1/b109251k/

 DOI: 10.1039/b109251k

respectively, show the greatest difference (being the direction in which the larger imido substitutent, ^{i}Pr *vs.* C_6H_5, is oriented).

Turning now to the perfluorophenylimido complex $[Ti(NC_6F_5)Cl_2(NHMe_2)_2]$ **3** [Fig. 3(a)] we see immediately that the unit cell has considerably distorted to disrupt the hydrogen bonded chain and arrange the neighbouring perfluorophenyl rings in a close, offset face-to-face (*off*) arrangement. The Ti–Cl···H–N distances of 2.93 Å (associated C···H–N angles = 136°) may now be classified[10] as 'long', and are approximately equal to the sum of the van der Waals radii for H (1.2 Å) and Cl (1.75 Å).[11] The solid state (Nujol mull) IR spectra of **1**, **2** and **3** feature $NHMe_2$ ligand ν(N–H) stretches of 3228, 3220 and 3275 cm^{-1}, respectively, consistent with the variations in Cl···H–N interactions determined by X-ray diffraction. While the unit cell *a* length [15.696(3) Å] in **3** is comparable to those in **1** and **2** (unsurpringly since it is perpendicular to the direction of propagation of the (formerly) hydrogen-bonded chain), there is a substantial expansion in the *b* direction [unit cell length = 15.569(1) Å] and a concomitant large contraction in the *c* unit cell length [6.7371(9) Å]. The separation between neighbouring titanium centres is *c*/2 = 3.365 Å which is just slightly larger than the interplanar separation of 3.23 Å between neighbouring C_6F_5 rings.

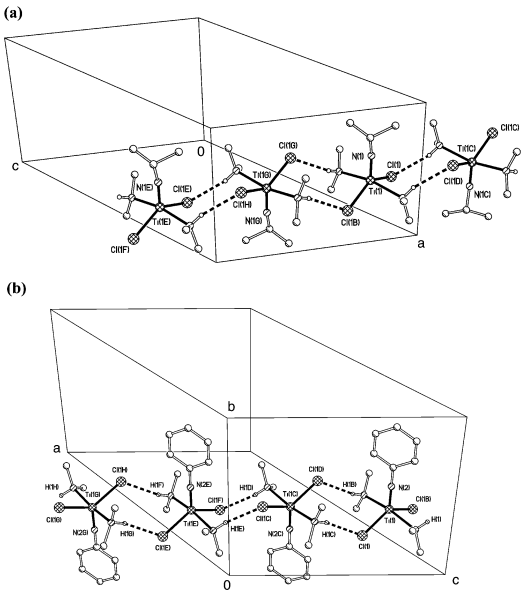

Fig. 2 Portion of the hydrogen-bonded chains of $[Ti(NR)Cl_2(NHMe_2)_2]$ [(a) R = ^{i}Pr **1**; (b) R = C_6H_5 **2**] with carbon-bound H atoms omitted and other atoms drawn as spheres of arbitrary radius.

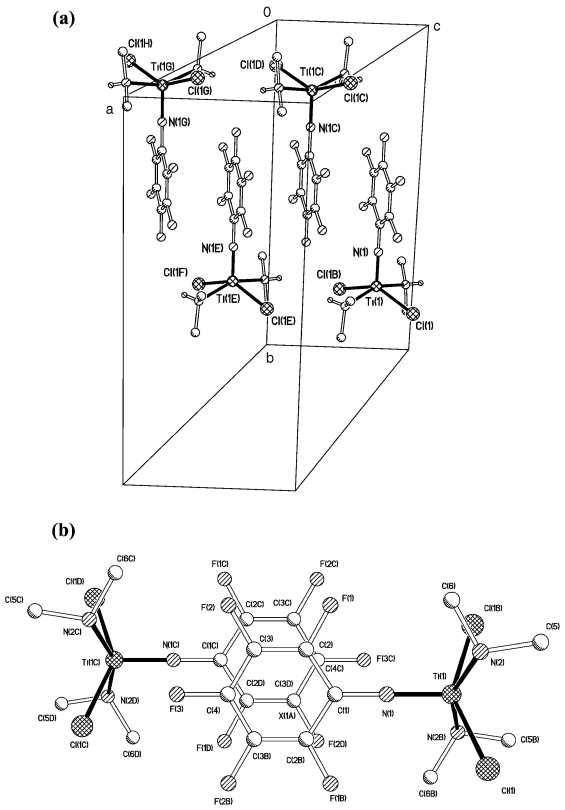

Fig. 3 (a) Portion of the π-stacked chains of $[Ti(NC_6F_5)Cl_2(NHMe_2)_2]$ **3** with carbon-bound H atoms omitted. Intermolecular Ti–Cl···H–N distances = 2.93 Å and Cl···H–N angle = 136°. (b) Relationship between the C_6F_5 groups bonded to N(1) and N(1C). Projected strictly onto the {C(1),C(2),C(3),C(4),C(2B),C(3B)} least-squares plane. Separation between C_6F_5 planes = 3.23 Å.

Fig. 3(b) shows in projection the *off* arrangement of two adjacent C_6F_5 rings. Each of the rings shown is involved in four close contacts to the neighbouring ring, namely two with C···C 3.264(3) Å and two with F···C 3.256(4) Å. In the π-stacked motif in crystals of **3** this gives each ring eight contacts in total (four with each of its two neigbours). The C···C and C···F contacts can be favourably compared to Dance and coworkers' calculated values of 3.19 and 3.14 Å, respectively, for gas-phase *off*-$(C_6F_6)_2$ (being the most stable supramolecular arrangement for this dimer).[6]

In summary, the crystal structures of the three compounds **1**–**3**, when taken together, provide further evidence for the comparatively strong driving force of supramolecular $C_6F_5\cdots C_6F_5$ π-stacking interactions in the solid state. Such interactions appear to be at least as strong as other, well-documented examples such as M–Cl···H–N–M hydrogen bonding.[10] We are continuing to investigate the supramolecular and crystal engineering roles of these types of interactions between C_6F_5 rings for both imido and non-imido systems.

This work was supported by the EPSRC, DSM Research and Millenium Pharmaceuticals Ltd. We thank Professor Ian Dance for disclosing some additional computational results.

Notes and references

‡ CCDC reference numbers 172499–172501. See http://www.rsc.org/suppdata/cc/b1/b109251k/ for crystallographic data in CIF or other electronic format.

1 G. R. Desiraju, *Crystal Engineering: The Design of Organic Solids*, Elsevier, New York, 1989; *The Crystal as a Supramolecular Entity*, ed. G. R. Desiraju, John Wiley, New York, 1996; C. A. Hunter, K. R. Lawson, J. Perkins and C. J. Urch, *J. Chem. Soc., Perkin Trans. 2*, 2001, 651.

2 C. R. Patrick and G. S. Prosser, *Nature*, 1960, **187**, 1021.

3 C. Dai, P. Nguyen, T. B. Marder, A. J. Scott, W. Clegg and C. Viney, *Chem. Commun.*, 1999, 2493; C. J. Aspley, C. Boxwell, M. L. Buil, C. L. Higgitt, C. Long and R. N. Perutz, *Chem. Commun.*, 1999, 1027; W. J. Feast, P. W. Lövenich, H. Puschmann and C. Taliani, *Chem. Commun.*, 2001, 505; G. W. Coates, A. R. Dunn, L. M. Henling, J. W. Ziller, E. B. Lobkovsky and R. H. Grubbs, *J. Am. Chem. Soc.*, 1998, **120**, 3641; H. Adams, J.-L. J. Blanco, G. Chessari, C. A. Hunter, C. M. R. Low, J. M. Sanderson and J. M. Vinter, *Chem. Eur. J.*, 2001, **7**, 3494.

4 M. L. Renak, G. P. Bartholomew, S. Wang, P. J. Ricatto, R. J. Lachicotte and G. C. Bazan, *J. Am. Chem. Soc.*, 1999, **121**, 7787; M. D. Blanchard, R. P. Hughes, T. E. Concolino and A. R. Rheingold, *Chem. Mater.*, 2000, **12**, 1604; M. P. Thornberry, C. Slebodnick, P. A. Deck and F. R. Fronczek, *Organometallics*, 2000, **19**, 5352; P. A. Deck, M. J. Lane, J. L. Montgomery, C. Slebodnick and F. R. Fronczek, *Organometallics*, 2000, **19**, 1013.

5 C. A. Hunter and J. K. M. Sanders, *J. Am. Chem. Soc.*, 1990, **112**, 5525.

6 S. Lorenzo, G. R. Lewis and I. Dance, *New J. Chem.*, 2000, **24**, 295.

7 See for example: S. A. Lawrence, M. E. G. Skinner, J. C. Green and P. Mountford, *Chem. Commun.*, 2001, 705.

8 N. Adams, S. R. Dubberley, A. J. Sealey and P. Mountford, unpublished results.

9 D. A. Fletcher, R. F. McMeeking and D. Parkin, *The United Kingdom Chemical Database Service in J. Chem. Inf. Comput. Sci.*, 1996, **36**, 746; F. H. Allen and O. Kennard, *Chem. Des. Autom. News*, 1993, **8**, 1; F. H. Allen and O. Kennard, *Chem. Des. Autom. News*, 1993, **8**, 31.

10 G. Aullón, D. Bellamy, L. Brammer, E. A. Bruton and A. G. Orpen, *Chem. Commun.*, 1998, 653.

11 A. J. Bondi, *J. Chem. Phys.*, 1974, **68**, 441.

CHEMCOMM Communication
www.rsc.org/chemcomm

Pseudoxazolones, a new class of inhibitors for cysteine proteinases: inhibition of hepatitis A virus and human rhinovirus 3C proteinases

Yeeman K. Ramtohul,[a] Nathaniel I. Martin,[a] Lara Silkin,[a] Michael N. G. James‡[b] and John C. Vederas*†[a]

[a] *Department of Chemistry, University of Alberta, Edmonton, Alberta, Canada T6G 2G2. E-mail: john.vederas@ualberta.ca; Fax: +1 (780) 492 8231; Tel: +1 (780) 492 5475*
[b] *Department of Biochemistry, University of Alberta, Edmonton, Alberta, Canada T6G 2H7. E-mail: michael.james@ualberta.ca; Fax: +1 (780) 492 0886; Tel: +1 (780) 492 4550*

Received (in Cambridge, UK) 9th October 2001, Accepted 14th November 2001
First published as an Advance Article on the web 6th December 2001

Monophenyl and diphenyl pseudoxazolone derivatives of glycine and alanine were prepared and found to be time-dependent inhibitors of hepatitis A virus (HAV) 3C and human rhinovirus (HRV) 3C proteinases with IC_{50} values in the micromolar range.

Cysteine proteinases have attracted much attention as therapeutic targets because of their implication in many diseases such as osteoporosis, Alzheimer's, and arthritis.[1] As part of our ongoing effort on the inhibition of hepatitis A virus (HAV) and human rhinovirus (HRV) 3C cysteine proteinases, we have explored pseudoxazolones as a new motif for inhibition of these enzymes.

HAV causes an acute infection of the liver whereas HRV is the major causative agent for the common cold in humans.[2] Like other picornaviruses, the HAV and HRV genome consists of a small positive strand RNA, which upon translation produces a single polyprotein precursor. This polyprotein undergoes multiple proteolytic cleavages by the 2A and/or 3C proteinases to produce the structural and nonstructural viral components.[3] In HAV, these cleavages are mediated solely by the 3C enzyme, a cysteine proteinase present in all picornaviruses.[4] Crystal structures of HAV 3C[5] and HRV 3C[6] have revealed that these enzymes are distinct from the papain cysteine proteinases and have folds that closely resemble the chymotrypsin serine proteinases.

Several potent inhibitors of HAV 3C and HRV 3C proteinases have been reported by our group[7] and by others.[8] The ability of pseudoxazolones to react with thiols at the imine[9] position suggests that these compounds can be used to inhibit thiol containing enzymes (Fig. 1). We first explored the diphenyl pseudoxazolone analogue of glycine **1** and alanine **2**. These compounds are readily prepared using a modified literature procedure.[10] Condensation of glycine **3** or alanine **4** with 2-chloro-2,2-diphenylacetyl chloride (Scheme 1) gives the corresponding halo adducts, which upon reaction with acetic anhydride–pyridine or DCC undergo cyclization followed by elimination of HCl to afford the desired compounds **1** and **2**. Testing of these compounds against HAV 3C C24S mutant§ indicates that **1** is a time dependent inhibitor with an IC_{50} of 33 μM (Table 1). However, the alanine derivative **2** was found to be less active with an IC_{50} >100 μM, possibly because the methyl group in **2** offers some steric interaction to the nucleophilic thiol of the enzyme. Our next approach was to prepare the monophenyl pseudoxazolone analogues of glycine **5a**,**b** and alanine **6a**,**b**. These compounds can be synthesised as depicted in Scheme 2.[10b,c] Although these pseudoxazolones have previously been reported as a mixture of *E* and *Z* isomers, we were able to separate each isomer by flash column chromatography for full characterisation. The *E* and *Z* configurations were assigned based on the proton (^{1}H) chemical shift of the olefinic hydrogen. The *E* isomer has its olefinic proton

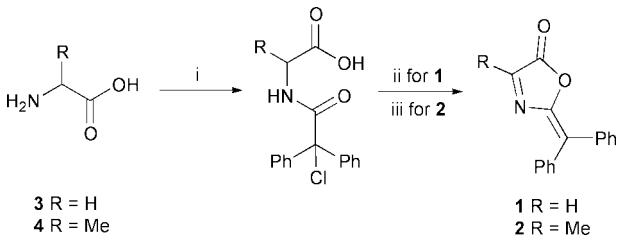

Scheme 1 *Reagents and conditions*: (i) 2-chloro-2,2-diphenylacetyl chloride, propylene oxide, ethyl acetate, Δ (ii) DCC, propylene oxide, CH_3CN, 80% over 2 steps. (iii) Ac_2O, pyridine, 68% over 2 steps.

Table 1 Inhibition data for HAV 3C and HRV 3C proteinases

Compound	HAV 3C IC_{50} (μM)[a]	HRV 3C IC_{50} (μM)[b]
1	33	38
2	>100	>100
5a	6	16
5b	4	17
6a	26	43
6b	>100	>100

[a] *Fluorometric assay conditions*: 0.1 μM HAV 3C, 10 μM Dabcyl-GLRTQSFS-Edans, 2 mM EDTA, 0.1 mg/mL BSA, 100 mM KH_2PO_4–K_2HPO_4, 1% DMF, pH 7.5, 5 min pre-incubation of the enzyme with inhibitor. [b] *Continuous UV assay conditions*: 0.4 μM HRV 3C, 250 μM EALFQ-pNA, 50 mM HEPES, 150 mM NaCl, 1 mM EDTA, 1% DMF, pH 7.5, 5 min pre-incubation of the enzyme with inhibitor.

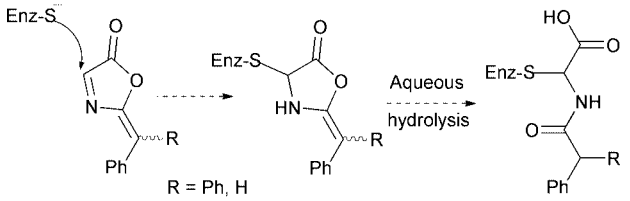

Fig. 1 Possible mode of inactivation by cysteine proteinase.

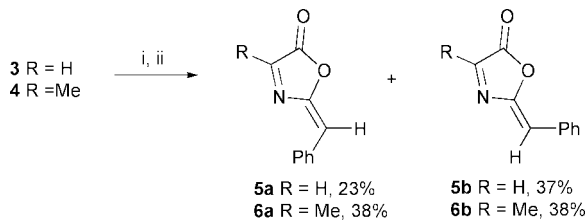

Scheme 2 *Reagents and conditions*: (i) DL-2-chloro-2-phenylacetyl chloride, NaOH, H_2O, 0–5 °C; (ii) Ac_2O, pyridine, the yields reported are over two steps.

† Canada Research Chair in Bioorganic and Medicinal Chemistry.
‡ Canada Research Chair in Protein Structure and Function.

 DOI: 10.1039/b109095j

aligned with the oxazolone ring oxygen and is more deshielded (Fig. 2) compared to the *Z* isomer which is aligned with the imine nitrogen. These observations were further supported by two X-ray crystal structures of **5b** and **6a**¶ (Fig. 3). Although interconversion of the *E* and *Z* double bond is possible, this was not observed for the monophenyl pseudoxazolones. Assay of **5a** and **5b** against HAV 3C proteinase gives time dependent inhibition with IC_{50} of 6 μM and 4 μM, respectively. However, compounds **6a** and **6b** display different levels of inhibition. The *E* isomer **6a** is a time dependent inhibitor with an IC_{50} of 26 μM. However, the *Z* isomer **6b** displays weaker inhibition, with an IC_{50} > 100 μM, indicating that the enzyme has a selectivity for the *E* over the *Z* isomer when there is substitution at the imine carbon. Other derivatives with different substitution at the imine position (data not shown) display the same type of behaviour. This is possibly due to some unfavourable electronic interaction of the phenyl group of **6b** in the active site of the enzyme.

Assays of these pseudoxazolones against HRV 3C proteinase (Table 1) also show the same pattern of inhibition as that observed for the HAV 3C enzyme. Although the inhibition levels are weaker for the HRV 3C proteinase, it should be noted that the amount of enzyme used in the HRV assay (0.4 μM) is more than that for HAV (0.1 μM) because of the limitations of the UV assay used for the former.

In summary, we have shown that pseudoxazolones are potent inhibitors of HAV and HRV 3C enzymes with micromolar IC_{50} values in the range. Although the monophenyl pseudoxazolones of glycine **5a** and **5b** show comparable inhibition, this is not the case with the alanine derivatives, indicating that the enzymes have selectivity for the *E* **6a** over the *Z* isomer **6b**. X-Ray crystal structures of **5b** and **6a** have helped to assign the geometrical configuration of the monophenyl pseudoxazolone analogues. The inhibition data and mass spectrometry suggest that the enzyme forms a covalent bond with the inhibitors. Further mechanistic studies involving ^{13}C labelled analogues and pseudoxazolones with other substitution patterns are in progress. The use of pseudoxazolones for inhibition of other cysteine proteinases is also being explored.

We thank Drs Bruce Malcolm (Schering Plough), Ernst Bergmann and Craig Garen (Biochemistry Department, University of Alberta) for enzyme preparation and helpful suggestions. We are grateful to Dr Robert McDonald for crystallographic analyses. These investigations were supported by the Natural Sciences and Engineering Research Council of Canada (scholarship to N. I. M.; summer studentship to L. S.) and the Alberta Heritage Foundation for Medical Research (scholarship to Y. K. R.).

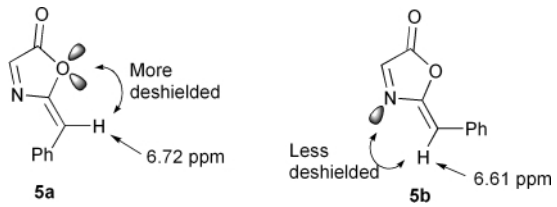

Fig. 2 ^1H Chemical shift of the glycine pseudoxazolone olefinic proton in acetone-d_6 (300 MHz).

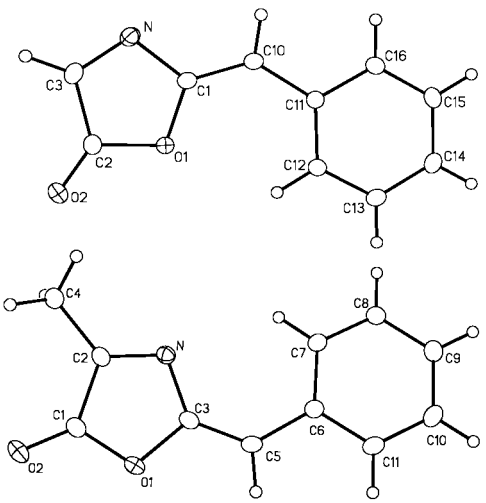

Fig. 3 Crystal structure of **5b** (top) and **6a** (bottom).

Notes and references

§ Enzyme inhibition studies for HAV 3C employed a recombinant C24S mutant in which a non-catalytic external cysteine (Cys24) was replaced by serine and which displays catalytic properties indistinguishable from the wild type enzyme. For an ideal peptide substrate mimicking the 2B/2C junction of the large precursor polyprotein with glutamine preferred at the P_1 residue: the k_{cat} of this enzyme is about 1.8 s^{-1} with a K_m of 2.1 mM at pH 7.5.[4] HRV 3C assays used the 3C proteinase from serotype 14.[7a]

¶ *Crystal data* for **5b**: $C_{10}H_7NO_2$: M = 173.17, triclinic, a = 5.5390(6), b = 7.2645(8), c = 10.4291(11) Å, α = 83.673(2), β = 83.789(2), γ = 80.624(8)°, U = 409.77(8) Å^3, T = 193 K, space group $P\bar{1}$ (No. 2), Z = 2, μ(Mo-Kα) = 0.100 mm^{-1}, 2179 reflections measured, 1641 unique (R_{int} = 0.0164) which were used in all least square calculations, $R_1(F)$ = 0.0374 (for 1365 reflections with $F_o^2 \geq 2\sigma(F_o^2)$), $wR_2(F^2)$ = 0.1037 (for all unique relections).

Crystal data for **6a**: $C_{11}H_9NO_2$: M = 187.19, triclinic, a = 6.0008(8), b = 7.2370(11), c = 10.9282(16) Å, α = 95.403(2), β = 101.029(3), γ = 102.046(3)°, U = 451.10(11) Å^3, T = 193 K, space group $P\bar{1}$ (No. 2), Z = 2, μ(Mo-Kα) = 0.096 mm^{-1}, 2409 reflections measured, 1827 unique (R_{int} = 0.0422) which were used in all least square calculations, $R_1(F)$ = 0.0449 (for 1207 reflections with $F_o^2 \geq 2\sigma(F_o^2)$), $wR(F^2)$ = 0.1113 for all unique relections).

CCDC 172532 and 172533. See http://www.rsc.org/suppdata/cc/b1/b109095j/ for crystallographic data in CIF or other electronic format.

1 For reviews on cysteine proteinases and their inhibitors, see: H.-H. Otto and T. Schirmeister, *Chem. Rev.*, 1997, **97**, 133–171; (*b*) D. Leung, G. Abbenante and D. P. Fairlie, *J. Med. Chem.*, 2000, **43**, 305–341; (*c*) see also the Symposium-in-Print on cysteine protease inhibitors: S. K. Thompson, *Bioorg. Med. Chem.*, 1999, **7**, 571.

2 F. B. Hollinger and J. R. Ticehurst, in *Fields Virology*, ed. B. N. Fields, D. M. Knipe, P. M. Howley, R. M. Channock, J. L. Melnick, T. P. Monath, B. E. Roizmann and S. E. Strauss, Lippincott-Raven Publishers, Philadelphia, 1996.

3 E. M. Bergmann and M. N. G. James, in *Proteases as Targets for Therapy*, ed. K. Von der Helm and B. Korant, Springer, Heiderlberg, 1999.

4 B. A. Malcolm, *Protein Sci.*, 1995, **4**, 1439–1445 and references therein.

5 (*a*) E. M. Bergmann, S. C. Mosimann, M. M. Chernaia, B. A. Malcolm and M. N. G. James, *J. Virol.*, 1997, **71**, 2436–2448; (*b*) for crystal structure of HAV 3C with *N*-iodoacetyl-Val-Phe-NH_2, see: E. M. Bergmann, M. M. Cherney, J. McKendrick, S. Frormann, C. Luo, B. A. Malcolm, J. C. Vederas and M. N. G. James, *Virology*, 1999, **265**, 153–163.

6 D. A. Matthews, W. W. Smith, R. A. Ferre, B. Condon, G. Budahazi, W. Sisson, J. E. Villafranca, C. A. Janson, H. E. McElroy, C. L. Gribskov and S. Worland, *Cell*, 1994, **77**, 761–771.

7 (*a*) R. D. Hill and J. C. Vederas, *J. Org. Chem.*, 1999, **64**, 9538–9546; (*b*) M. S. Lall, C. Karvellas and J. C. Vederas, *Org. Lett.*, 1999, **1**, 803–806; (*c*) B. A. Malcolm, C. Lowe, S. Shechosky, R. T. McKay, C. C. Yang, V. J. Shah, R. J. Simon, J. C. Vederas and D. V. Santi, *Biochemistry*, 1995, **34**, 8172–8174 and references therein.

8 (*a*) S. H. Reich, T. Johnson, M. B. Wallace, S. E. Kephart, S. A. Fuhrman, S. T. Worland, D. A. Matthews T. F. Hendrickson, F. Chan, J. Meadow III, R. A. Ferre, E. L. Brown, D. M. Delisle, A. K. Patick, S. L. Binford and C. E. Ford, *J. Med. Chem.*, 2000, **43**, 1670–1683 and references therein; (*b*) S. Venkatraman, J. Kong, S. Nimkar, Q. M. Wang, J. Aubé and R. P. Hanzlik, *Bioorg. Med. Chem. Lett.*, 1999, **9**, 577–580 and references therein.

9 (*a*) A. Kaneda and R. Sudo, *Bull. Chem. Soc. Jpn.*, 1970, **43**, 2159–2161; (*b*) I. L. Knunyants, O. V. Kil'disheva, M. P. Krasuskaya, M. G. Lin'kova, V. V. Shokina, Z. V. Benevolenskaya and L. P. Rasteikene, *Bull. Acad. Sci. USSR, Div. Chem. Sci. (Engl. Trans.)*, 1959, 1702–1710.

10 (*a*) Y. Iwakura, F. Toda, M. Kosugi and Y. Torii, *J. Org. Chem.*, 1971, **36**, 3990–3992; (*b*) J. A. King and F. H. McMillan, *J. Am. Chem. Soc.*, 1950, **72**, 833–836; (*c*) J. W. Cornforth, in *The Chemistry of Penicillin*, ed. H. T. Clarke, J. R. Johnson and R. Robinson, Princeton University Press, Princeton, NJ, 1949, pp. 688, 739, 793.

CHEMCOMM Communication
www.rsc.org/chemcomm

A stable, high relaxivity, diaqua gadolinium complex that suppresses anion and protein binding†

Dimitri Messeri,[a] Mark P. Lowe,[a] David Parker*[a] and Mauro Botta[b]

[a] *Department of Chemistry, University of Durham, South Road, Durham, UK DH1 3LE. E-mail: david.parker@durham.ac.uk*

[b] *Dipartimento di Scienze e Tecnologie Avanzate, Università del Piemonte Orientale, "Amedeo Avogadro" Corso Borsalino 54, 15100, Alessandria, Italy*

Received (in Cambridge, UK) 12th September 2001, Accepted 14th November 2001
First published as an Advance Article on the web 6th December 2001

The high relaxivity of $[GdaDO3A]^{3-}$ (r_{1p} = 12.3 mM^{-1} s^{-1}, 20 MHz, 298 K, τ_m = 30 ns) in water is maintained in serum solution because the binding of protein and endogeneous anions, *e.g.* HCO_3^-/CO_3^{2-} is suppressed by electrostatic repulsion.

All of the gadolinium complexes used currently as contrast agents in magnetic resonance imaging are mono-aqua species.[1,2] Complexes which possess two bound water molecules have not been used despite the large increase in relaxivity expected from the enhanced paramagnetic contribution, (r_{1p} in eqn. (1), where c is complex concentration, q is the number of

$$r_{1p} = \frac{cq}{55.6}\left[\frac{1}{T_{1m} + \tau_m}\right] \quad (1)$$

inner sphere waters, τ_m is the water exchange lifetime and T_{1m} is the longitudinal water proton relaxation time). The failure to develop such q = 2 systems has arisen for several different reasons. They may possess insufficient kinetic or thermodynamic stability with respect to acid or cation mediated dissociation to allow their safe use *in vivo*.[1–3] In other cases the complexes tend to bind endogeneous anions in serum—such as phosphate, carbonate or lactate—displacing one or both of the inner sphere waters in the ternary complexes and lowering the relaxivity.[4] Occasionally the water exchange lifetime, τ_m is rather long, limiting the relaxivity. Finally, in the presence of a protein such as serum albumin, aided by the interaction of, for example, side chain carboxylates in Glu or Asp residues, the inner sphere waters again may be displaced.[5] Thus although several promising q = 2 gadolinium complexes have been defined,[6] none has been shown to overcome simultaneously each of these constraints.

The complex [GdDO3MA] has been shown to possess sufficiently high stability[7] to allow its safe use *in vivo*. Using this as a starting point, we have examined the behaviour of the derivatives $[GdgDO3A]^{3-}$ **2** and $[GdaDO3A]^{3-}$ **3**, based on the hypothesis that their anionic side chains would inhibit the encounter with negatively charge species. For purposes of comparison, we have contrasted their behaviour to the related series of tetra-substituted complexes **4a**–**c**, derived from the archetypal lanthanide ligand, DOTA (DOTA = 1,4,7,10-tetraazacyclododecane tetraacetate).

The ligands and their Eu and Gd complexes were prepared as stereoisomeric mixtures by reported methods[8] and gave satisfactory ^1H NMR and high resolution ESMS data. The number of bound water molecules in aqueous solution at pH 7 was measured for the series of Eu complexes (Table 1), and revealed that $[EuaDO3A]^{3-}$ possessed two bound waters, whereas in $[EugDO3A]^{3-}$ the Eu ion only bound one. The form of their europium emission spectra also differed significantly in the hypersensitive ΔJ = 2 and 4 manifolds and in the observation of only two distinct transitions in the ΔJ = 1 region for $[EugDO3A]^{3-}$, and three for $[EuaDO3A]^{3-}$. The total emission spectrum of the latter closely resembled that of [EuDO3A]. Emission spectra were also examined in the presence of a simulated extracellular ionic background (30 mM $NaHCO_3$, 100 mM NaCl, 0.9 mM KH_2PO_4, 2.3 mM/0.13 mM potassium lactate/citrate), and in the presence of each anion separately—over the pH range 3.5–10.5. Spectra obtained† revealed that carbonate was bound preferentially in each case. However, the onset of this effect shifted from around pH 7.5 for [Eu-

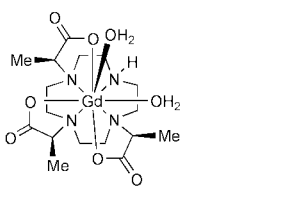

1 [GdDO3MA]

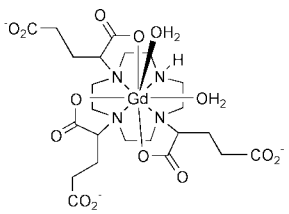

2 $[GdgDO3A]^{3-}$

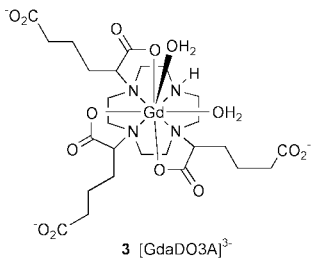

3 $[GdaDO3A]^{3-}$

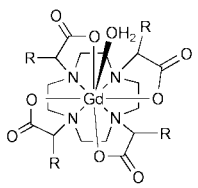

4 a R = H , [GdDOTA]$^-$
b R = $(CH_2)_2CO_2^-$, $[GdgDOTA]^{5-}$
c R = $(CH_2)_3CO_2^-$, $[GdaDOTA]^{5-}$

Table 1 Selected relaxivity data, hydration numbers and correlation times for gadolinium complexes (298 K, 20 MHz)

Complex	r_{1p}[a]/mM^{-1} s^{-1}	τ_m/ns	τ_r/ns	q[b] (±0.2)
$[GdaDO3A]^{3-}$	12.3 (13.8)	30	130	2.2
$[GdgDO3A]^{3-}$	5.4 (6.2)	230	130	1.2
[GdDO3A][d]	6.0	160	66	1.8
$[GdaDOTA]^{3-}$	7.6 (8.9)	200	154	1.0
(*RRRR*)-$[GdgDOTA]^{3-}$	7.3 (9.0)	68[c]	116	1.1
$[GdDOTA]^-$	4.2	224	73	1.0

[a] Values in parenthesis refer to relaxivities in water (pH 7.2) at 65.3 MHz and 293 K. [b] Derived from measurements in H_2O and D_2O of the radiative rate constants for depopulation of the Ln excited state in the corresponding Eu complex[9] (295 K, pH 7.2, I = 0.1 M NaCl, λ_{ex} = 397 nm). [c] Mean τ_m values of 140 and 270 ns were measured for the *RRRS* and *RSRS* isomers containing more of the slower exchanging square antiprismatic isomer.[8] [d] For (*RRR*)-[GdDO3MA], a relaxivity of 4.4 mM^{-1} s^{-1} (20 MHz, 313 K) was reported,[7] with q^{Tb} = 1.4.

† Electronic supplementary information (ESI) available: pH dependence of europium emission spectra, stability screening details and relaxivity/pH plots for selected Gd complexes. See http://www.rsc.org/suppdata/cc/b1/b108294a/

 DOI: 10.1039/b108294a

aDO3A]$^{3-}$ to *ca.* pH 8 for [EugDO3A]$^{3-}$. Taken together, these luminescence studies suggested that intramolecular (seven-ring) carboxylate ligation occurred for [EugDO3A]$^{3-}$, displacing one of the bound waters and slightly suppressing competitive carbonate binding at higher pH (Scheme 1). Different behaviour was exhibited by [EuaDO3A]$^{3-}$, which remained a diaqua species at ambient pH; presumably eight-ring chelate formation is too strained.

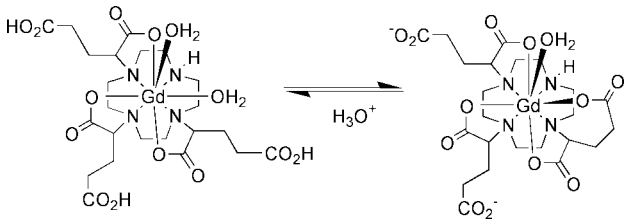

Scheme 1

Relaxivity measurements were made for each complex as a function of pH and magnetic field (NMRD profile). Data are collated in Table 1, together with measurements of water-exchange lifetimes, τ_m, using VT-^{17}O NMR methods[1,2] and estimates of rotational correlation times, τ_r, derived from iterative fitting of NMRD profiles. Most striking is the high relaxivity and the short water exchange lifetime of [GdaDO3A]$^{3-}$, in comparison to both [GdgDO3A]$^{3-}$ (q = 1, long τ_m) and [GdDO3A] (q = 1.8 but rather long τ_m and shorter τ_r). The comparative NMRD profiles (298 K) highlight these differences (Fig. 1). The fast water exchange rate (τ_m = 30 ns, 298 K) for [GdaDO3A]$^{3-}$ is intriguing; it may be a consequence of the structuring effect of the pendant carboxylate groups on the nature of the second sphere of hydration.

The pH dependence of relaxivity for [GdaDO3A]$^{3-}$ was examined at 65.3 MHz in serum and in a simulated extracellular anionic background. At high pH, carbonate ions chelate to the lanthanide centre displacing both water molecules. Limiting maximal relaxivity values were reached at pH 7.3 and 7.0 in the anionic (r_{1p} = 10.1 mM^{-1} s^{-1}, 293 K) and serum (12.3 mM^{-1} s^{-1}) backgrounds respectively, consistent with the pH-dependence of Eu emission intensity discussed above. Polyanionic lanthanide complexes are susceptible to proton and cation-mediated dissociation pathways.[3b,10,11]

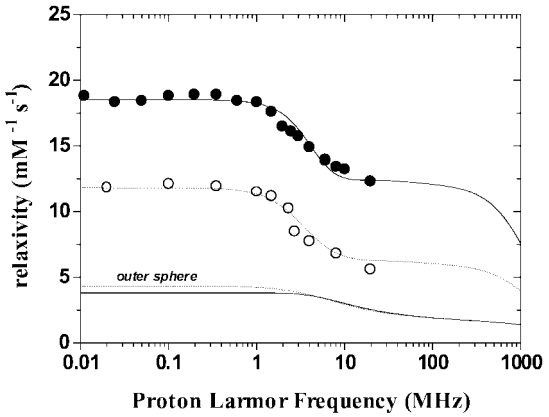

Fig. 1 NMRD profiles for [GdaDO3A]$^{3-}$ (●) and [GdgDO3a]$^{3-}$ (○) (298 K). Best fitting parameters included Δ^2 = 2.75 (3.14) × 10^{-19} s^{-1}, and τ_r = 130 (130) ps.

A useful empirical method assessing kinetic and equilibrium lability has been reported recently. Relaxivity measurements (pH 7 phosphate buffer) are taken as a function of time (0 →125 h) in the presence of endogeneous cations (*e.g.* Zn^{2+}) that may promote dissociation of the free Gd^{3+} ion, which is then trapped as its insoluble phosphate,[12] reducing the observed relaxivity. In this empirical 'screen', [GdaDO3A]$^{3-}$ was ten times more kinetically inert than [GdDTPA]$^{2-}$ (Magnevist) which has been used clinically since 1988.

In summary, [GdaDO3A]$^{2-}$ is the first q = 2 complex that has been shown to be suitable as the basis of an MRI contrast agent. The fast water exchange rate, and minimisation of anion/protein binding suggests it may be a particularly attractive candidate as the basis for higher MW conjugates as needed in MR angiography studies, for example.[1,2]

This work was supported by the EPSRC and Guerbet s.a. (Paris) and was carried out under the EC COST Action D-18, 'Lanthanide Chemistry for Diagnosis and Therapy'.

Notes and references

1 P. Caravan, J. Ellison, T. J. McMurry and R. B. Lauffer, *Chem. Rev.*, 1999, **99**, 2293.
2 *The Chemistry of Contrast Agents in Medical Magnetic Resonance Imaging*, ed. A. E. Merbach and E. Toth, Wiley, New York, 2001.
3 (*a*) K. P. Pulukkody, T. J. Norman, D. Parker, L. Royle and C. J. Broan, *J. Chem. Soc., Perkin Trans. 2*, 1993, 605; (*b*) L. Sarka, L. Burai and E. Brucher, *Chem. Eur. J.*, 2000, **6**, 719.
4 (*a*) J. I. Bruce, R. S. Dickins, L. J. Govenlock, T. Gunnlangsson, S. Lopinski, M. P. Lowe, D. Parker, J. J. B. Perry, S. Aime and M. Botta, *J. Am. Chem. Soc.*, 2000, **122**, 9674; (*b*) L. Burai, R. Kiraly, E. Toth and E. Brucher, *Magn. Reson. Imaging*, 1997, **38**, 146.
5 S. Aime, E. Gianolio, E. Terrono, R. Pagliarin, G. B. Giovenzana, M. P. Lowe, M. Sisti, D. Parker and M. Botta, *J. Biol. Inorg. Chem.*, 2000, **5**, 488.
6 (*a*) S. Aime, M. Botta, S. Geninatti Crich, G. Giovenzana, R. Pagliarin, M. Sisti and E. Terreno, *Magn. Reson. Chem.*, 1998, **36**, S200; (*b*) S. Aime, M. Botta, L. Frullano, S. Geninatti Crich, G. Giovenzana, R. Pagliarin, G. Palmisano, F. R. Sirtori and M. Sisti, *J. Med. Chem.*, 2000, **43**, 4017; (*c*) S. Hajela, M. Botta, S. Giraudo, J. Xu, K. N. Raymond and S. Aime, *J. Am. Chem. Soc.*, 2000, **122**, 11 228; (*d*) Y. Bretonniere, M. Mazzanti, F. A. Dunand, A. E. Merbach and J. Recant, *Chem. Commun.*, 2001, 621; (*e*) S. M. Cohen, J. Xu, E. Radkov, K. N. Raymond, M. Botta, A. Barge and S. Aime, *Inorg. Chem.*, 2000, **39**, 5747.
7 S. I. Kang, R. S. Ranganathan, J. E. Emswiler, K. Kumar, J. Z. Gougoutas, M. F. Malley and M. F. Tweedle, *Inorg. Chem.*, 1993, **32**, 2912.
8 M. Woods, S. Aime, M. Botta, J. A. K. Howard, J. M. Moloney, M. Navet, D. Parker, M. Port and O. Rousseaux, *J. Am. Chem. Soc.*, 2000, **122**, 9781.
9 A. Beeby, I. M. Clarkson, R. S. Dickins, S. Faulkner, D. Parker, L. Royle, A. S. de Sousa, J. A. G. Williams and M. Woods, *J. Chem. Soc., Perkin Trans. 2*, 1999, 493.
10 P. Wedeking, K. Kumar and M. F. Tweedle, *Magn. Reson, Imaging*, 1992, **10**, 641.
11 A. Harrison, C. A. Walker, K. A. Pereira, D. Parker, L. Royle, K. Pulukkody and T. J. Norman, *Magn. Reson. Imaging*, 1993, **11**, 761.
12 S. Laurent, L. Van der Elst, F. Copoix and R. N. Muller, *Investigative Radiol*, 2001, **36**, 115.

CHEMCOMM Communication
www.rsc.org/chemcomm

NMR observation of a new lignin structure, a spiro-dienone†

Liming Zhang* and Göran Gellerstedt

Department of Pulp and Paper Chemistry and Technology KTH, Royal Institute of Technology, SE-100 44 Stockholm, Sweden

Received (in Cambridge, UK) 13th September 2001, Accepted 14th November 2001
First published as an Advance Article on the web 6th December 2001

A spiro-dienone structure (β-1/α-O-α) has been observed as one of the important structures present in spruce and aspen lignins, with abundance as high as 3% in spruce lignin.

Lignin macromolecules consist of phenylpropanoid units that are linked to each other by various types of ether and carbon–carbon bonds. Opinions on the occurrence and frequency of the β-1 linkage in lignin have been quite divergent among wood chemists. The abundance of the β-1 structure has been estimated to range from 1% to 15% in spruce lignin,[1–3] depending on the analytical method applied. The β-1 structure has been observed to be one of the major type of lignin inter-unit linkages by studies using mild hydrolysis[4,5] and thioacidolysis.[6] On the other hand, efforts to detect the β-1 structure in milled wood lignin (MWL) by using ^{1}H NMR,[1] 2D HMQC NMR[7,8] or ozonation[2] have not been very successful, suggesting that this structure might only be a minor constituent in milled wood lignin.

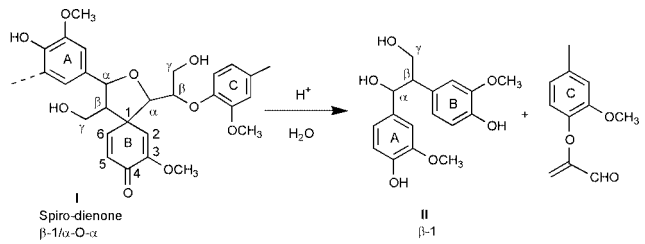

Scheme 1

To explain the discrepancies in the applied analytical methods, it has been suggested that a precursor of the β-1 structure, a dienone structure (**I** in Scheme 1) might be present in native lignin.[9] On acid hydrolysis, the dienone structure would be converted to the β-1 structure (**II** in Scheme 1).

There have been several reports in the literature showing supporting evidence for the presence of such a precursor in lignin. We have observed previously that mild acid hydrolysis of spruce wood meal, pre-methylated with diazomethane, resulted in the release of lignin β-1 dimers predominantly carrying a free phenolic hydroxy group on ring B.[6] This observation suggested that the ring B originally was present in the form of a dienone structure. More evidence supporting the existence of the dienone structures in lignin includes the recent isolation of the sesquineolignan woorenol,[10] the synthesis of spirocyclohexadienone structure by radical coupling of lignin-like model compounds[11] and the isolation of an isochroman structure among the lignin degradation products after a DFRC treatment[12] as well as some 3D NMR evidence.[13] In the present communication, we present direct observations of the spiro-dienone structures of type **I** in spruce and aspen MWLs by NMR techniques.

Two spruce MWL samples and one aspen MWL were prepared. One of the spruce lignin samples (MWL1) was prepared from freshly cut spruce wood by milling with steel-balls for 3 days.[14] The other spruce lignin sample (MWL2) was prepared from an aged spruce wood log by milling with porcelain balls for 14 days.[15] The spiro-dienone structure was

† Electronic supplementary information (ESI) available: ^{13}C, QUAT, HMBC and HSQC NMR spectra. See http://www.rsc.org/suppdata/cc/b1/b108285j/

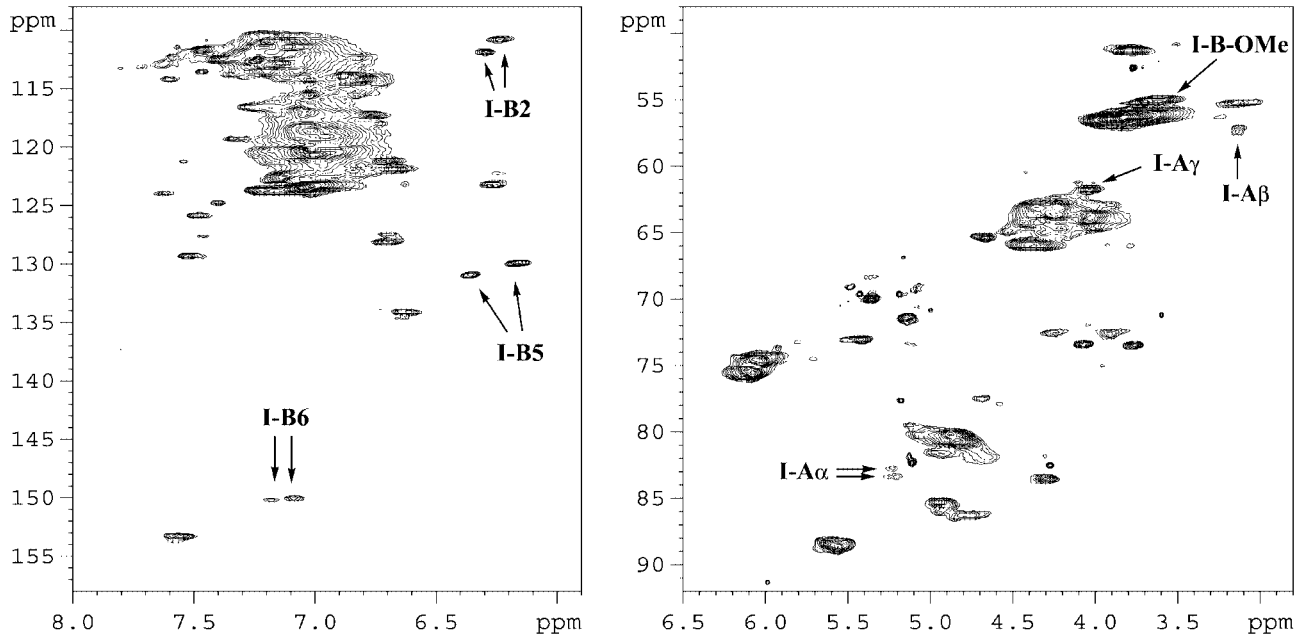

Fig. 1 Signals for the spiro-dienone structure (β-1/α-O-α) were observed and assigned in the HSQC spectrum of an acetylated spruce milled wood lignin (MWL1 acetate in acetone-d_6).

 DOI: 10.1039/b108285j

observed in both spruce and aspen lignins using NMR analyses. In the quantitative ^{13}C NMR spectrum, the signal at 180.7 ppm was assigned to the carbonyl group at position B4. According to the quantitative ^{13}C NMR analyses, the abundance of the dienone structure was estimated to be more than 3% in MWL1, 1.5% in MWL2 and about 1.8% in the aspen lignin.

In the HSQC spectra (Fig. 1) of the two acetylated spruce lignin samples, signals for Aα, Aβ, Aγ, B2, B5, B6 and B-OCH_3 were assigned. The quaternary carbon B1 was observed at 55.5 ppm by a QUAT spectrum. The connections between Aα, Aβ and Aγ and those between B5 and B6 were observed by HSQC-TOCSY experiments. The long-range connections between H-B5/C-B1, H-B5/C-B3, H-B2/C-B4, H-B2/C-B6 and H-B6/C-B4 were established by HMBC experiment.

According to the HSQC spectrum (Fig. 1), there are two isomeric forms of the spiro-dienone structure (**I**) in MWL1. In MWL2, on the other hand, only one of the isomers could be observed. Furthermore, the MWL1 sample contained only a tiny amount of the β-1 structure (**II**) whereas MWL2 had a high content of the β-1 structure (**II**) in the *erythro* conformation. The signal for the α-CH of the *threo* form of the β-1 structure (**II**) appears at 76.6/6.02 ppm, whereas the same signal for the *erythro* β-1 structure (**II**) appears at 75.8/6.13 ppm, very close to the predominant signal for the α-CH of the β-O-4 structures (75.4/6.11 ppm). Possibly, one of the spiro-dienone isomers was less stable and was converted to the *erythro* β-1 structure (**II**) either during storage of the wood or during the extended period of milling. In aspen milled wood lignin, the content of **I** was also found to be higher than the β-1 structure (**II**) according to the intensity of their respective NMR signals. Therefore, the spiro-dienone structure **I** can actually be the predominant form of the β-1 structures present in both soft- and hardwood native lignins.

Notes and references

1 K. Lundquist, *J. Wood Chem. Technol.*, 1987, **7**(2), 179.
2 N. Habu, Y. Matsumoto, A. Ishizu and J. Nakano, *Holzforschung*, 1990, **44**, 67–71.
3 Y. Z. Lai and K. V. Sarkanen, in *Lignins: Isolation and structural studies*, ed. K. V. Sarkanen, and C. H. Ludwig, Wiley Interscience, New York, 1971, p. 228.
4 V. H. Nimz, *Holzforschung*, 1966, **20**, 105.
5 G. Gellerstedt and L. Zhang, *Nordic Pulp Pap. Res. J.*, 1991, **3**(6), 13.
6 C. Lapierre, B. Pollet and B. Monties, *Phytochemistry*, 1991, **30**(2), 659.
7 R. M. Ede, J. Ralph, K. M. Torr and B. S. W. Dawson, *Holzforschung*, 1996, **50**, 161.
8 I. Kilpeläinen, J. Sipilä, G. Brunow, K. Lundquist and R. M. Ede, *J. Agric. Food Chem.*, 1994, **42**, 2790.
9 G. Brunow and K. Lundquist, *Holzforshung*, 1991, **45**, 37–40.
10 K. Yoshikawa, H. Kinoshita and S. Arihara, *J. Nat. Prod.*, 1997, **60**, 511.
11 H. Setälä, A. Pajunen, P. Rummakko, J. Sipilä and G. Brunow, *J. Chem. Soc., Perkin Trans.*, 1999, **1**, 461.
12 J. Peng, F. Lu and J. Ralph, *Phytochemistry*, 1999, **50**, 659.
13 E. Ämmälahti, G. Brunow, M. Bardet, D. Robert and I. Kilpeläinen, *J. Agric. Food Chem.*, 1998, **46**, 5113.
14 A. Björkman, *svensk Papperstidn.*, 1956, **59**, 477.
15 H. H. Brownell, *Tappi*, 1965, **48**(9), 513.

CHEMCOMM Communication
www.rsc.org/chemcomm

Greatly improved activity in ruthenium catalysed butanone synthesis

Robert C. van der Drift,[a] Wilhelmus P. Mul,[b] Elisabeth Bouwman*[a] and Eite Drent[a]

[a] *Leiden Institute of Chemistry, Gorlaeus Laboratories, Leiden University, P.O. Box 9502, 2300 RA Leiden, The Netherlands. E-mail: bouwman@chem.leidenuniv.nl; Fax: +31 71 5274451; Tel: +31 71 5274550*

[b] *Shell International Chemicals BV, Shell Research and Technology Centre Amsterdam, Badhuisweg 3, 1031 CM Amsterdam, The Netherlands*

Received (in Cambridge, UK) 17th September 2001, Accepted 15th November 2001
First published as an Advance Article on the web 6th December 2001

***In situ* mixing of ruthenium trichloride with one equivalent of 1,10-phenanthroline yields a highly active catalyst for synthesis of butanone from buta-1,3-diene.**

Butanone is an industrial solvent, nowadays produced on a Mton scale per year.[1] It is presently prepared from butenes in a three-step process according to eqn. (1).[2] The use of large

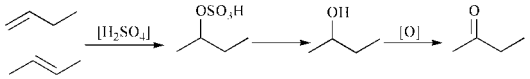

(1)

quantities of concentrated sulfuric acid, which need to be reconcentrated after the second step, make this process in principle less desirable from an environmental and an economical point of view. Therefore, new synthetic strategies have been developed in recent years.

Butadiene is readily obtained from naphtha cracker C_4-streams and its two double bonds make it susceptible towards electrophilic addition. Routes to butanal using butadiene *via* addition of amines[3] or alcohols,[4] followed by isomerisation of the allylic double bond and hydrolysis, have been patented. Acid-catalysed hydration of butadiene gives rise to two regioisomeric alcohols [eqn. (2)], but-3-en-2-ol and but-2-en-1-ol, in

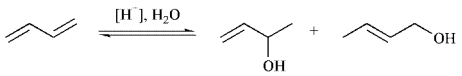

(2)

an equilibrium that lies heavily on the left-hand side. The former alcohol can be isomerised to butanone [eqn. (3)].[5] In a one-pot

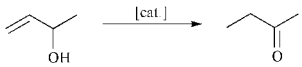

(3)

synthesis, the thermodynamically favourable formation of butanone avoids an extensive (and thus costly) butadiene recycle. Unfortunately, almost all catalysts capable of allylic alcohol isomerisation are strongly poisoned by butadiene.

In the early 1990s, the synthesis of butanone from butadiene catalysed by a mixture of $[Ru(acac)_3]$ (Hacac = pentane-2,4-dione), 1,10-phenanthroline (phen) and a Brønsted acid in water was published.[6] However, the reported cumulative turn over number (TON) of 1200 in 32 h is not sufficiently high to be economically interesting. The limited TON is due to catalyst deactivation *via* two pathways: ligand redistribution and metal reduction, which result in inactive $[Ru(phen)_2(S)_2]^{2+}$ (S = solvent) and $[Ru(phen)_3]^{2+}$ species [eqn. (4)].[6,7] Yet, despite

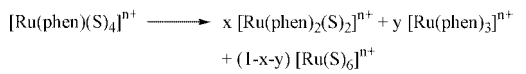

(4)

considerable effort,[8] until now no catalyst was found to be more active.

Strongly coordinating anions like chlorides were originally thought[6] to hamper catalysis by blocking vital coordination sites. In fact, $[RuCl_3{\cdot}xH_2O]$ in combination with two equivalents of 2,2′-bipyridine (bpy) gave only low activity. However, during the course of our studies,[7] it was found that the presence of chloride ions in some cases had a promoting effect. Here, we report the reinvestigation of $RuCl_3$ as catalyst precursor in the synthesis of butanone from butadiene.

The results of *in situ* experiments for the direct conversion of butadiene to butanone are shown in Table 1.† The blank experiments shown in entries 1 and 2 confirm the need for both ruthenium and phenanthroline. Especially the amount of ligand is crucial. Whereas $RuCl_3$ with two equivalents of phen (entry 5) gives only moderate activity that is comparable to previous results (entry 3), $RuCl_3$ with one equivalent phen is by far superior as is shown in entry 4. This result demonstrates clearly that with a chloride-containing precursor high activity can be obtained, contrary to earlier ideas. Mixed with one equivalent of bipyridine, $RuCl_3$ is only as active as $Ru(acac)_3$ with one phen (entry 6).

Not only are initial rates higher, the $RuCl_3$–phen system surpasses the $Ru(acac)_3$–phen system if TONs are considered as well. After a mere two hours, 1400 turnovers can be attained. Importantly, the $RuCl_3$–phen system is exceedingly selective. The most important side products in this reaction are the Diels–Alder dimer of butadiene (vinyl cyclohexene) and butenes together with methyl vinyl ketone, but their formation can be reduced to less than 1% with a suitably low initial butadiene loading of the autoclave. Thus, high TONs can be reached with a minimum amount of side products. This is demonstrated by an experiment in which the amount of butadiene is fed into the autoclave in two consecutive portions. A cumulative TON of 2750 in less than 10 h was obtained. It is to be foreseen that an even higher TON can be reached, since no serious catalyst deactivation occurred over the two runs.

The unexpected high activity of the $RuCl_3$–phen system may be explained by the role the chloride anion plays in preventing the ligand redistribution reaction shown in eqn. (4). Its strong coordination may prevent extensive formation of inactive bis- and tris-phenanthroline complexes, thereby increasing the

Table 1 Synthesis of butanone from butadiene, catalysed by *in situ* generated ruthenium complexes[a]

Entry	Catalyst precursor[b]	TOF/h^{-1}[c]	k/h^{-1}[d]
1	—	0	0
2	$RuCl_3$	2.5[e]	N.d.[f]
3	$Ru(acac)_3$ + 1 eq. phen	230	0.11
4	$RuCl_3$ + 1 eq. phen	960	0.67
5	$RuCl_3$ + 2 eq. phen	230	0.19
6	$RuCl_3$ + 1 eq. bpy	250	0.22
7	$RuCl_3$ + 1 eq. phen + 3 eq. AgOTs	34[e]	0.64
8	$RuCl_3$ + 1 eq. phen[g]	700	0.41

[a] Reactions were performed in a 250 ml Hastelloy C autoclave at 145 °C for 10 h. Substrate: 10 ml butadiene. Acid: 3.5 mmol toluene-*p*-sulfonic acid (HOTs). Solvent: diglyme–water 70 : 30. [b] 0.09 mmol of metal complex was mixed *in situ* with the appropriate amount of ligand. [c] Initial turn over frequency (TOF) calculated with first order rate equations. Turnovers are determined with GLC. Selectivity to butanone: >95%. [d] Determined by fitting first order curves to autoclave pressure *vs.* time plots. [e] Average value over 10 h. [f] N.d. = not determined. [g] Acid: 1.75 mmol HCl

 DOI: 10.1039/b108328g

concentration of catalytically active mono-phenanthroline ruthenium complexes. To verify this hypothesis, several samples taken during the reaction were analysed with mass spectrometry (MS). In the early stages of the reaction, Ru(III)- and Ru(II)-complexes with one phenanthroline, such as $[Ru(phen)Cl_2]^+$ and $[Ru(phen)(S)Cl]^+$ are dominant. This is the first time that ruthenium complexes containing only one phenanthroline ligand could be identified in this reaction.[6] Two other species are present in minor amounts: $[Ru(phen)_2Cl_2]^+$ and its Ru(II) analogue. Most noteworthy is the complete absence of complexes with three phenanthroline ligands. During the reaction, mono-phenanthroline complexes are converted to complexes with two phenanthroline ligands, but *not* with three. At the end of the 10 h reaction, complexes with only one phenanthroline ligand can still be detected. These results from MS prove that chloride ions indeed coordinate strongly to the ruthenium centre and prevent the formation of $[Ru(phen)_3]^{n+}$. In the $Ru(acac)_3$–phen system, between 20 and 40% of the ruthenium was present as $[Ru(phen)_3]^{2+}$.[6]

The present $RuCl_3$–phen system is much more sensitive to the ligand to metal ratio than the $Ru(acac)_3$–phen system. When two equivalents of phenanthroline are added to $RuCl_3$, the strong chloride coordination becomes a problem. $[Ru(phen)_2Cl_2]^+$ is formed instantly and chloride dissociation is slow.[9] With $Ru(acac)_3$, initial dissociation of acac is rate limiting and the influence of phenanthroline concentration is therefore much smaller.

The greater basicity and flexibility of bipyridine compared to phenanthroline render its coordination more reversible and this in turn makes ligand redistribution more prominent. Hence, the lower activity of $RuCl_3$ with one equivalent bpy can be explained by the increased formation of $[Ru(bpy)_2Cl_2]^+$, which is confirmed with MS on a spent catalyst.

Complete removal of chloride ions by silver(I) salts, replacing them with the non-coordinating anions toluene-*p*-sulfonate or trifluoromethane sulfonate, makes the catalyst much less stable. After an induction period, the reaction starts with a comparable rate ($k = 0.64\ h^{-1}$; Table 1, entry 7), but a TON of only 340 is reached after 10 h. These results underline the role of the chloride ion. Removal of chlorides increases ligand redistribution considerably, thereby reducing catalyst lifetime and overall product yield. On the other hand, increasing the chloride concentration by addition of NaCl or using HCl instead of toluene-*p*-sulfonic acid (Table 1, entry 8), decreases reaction rate and TON only slightly. This evidently shows that the hitherto found low activity of $RuCl_3$–phen systems was due to the amount of ligand and not to the presence of coordinating chloride anions.

In conclusion, an improved catalyst system has been found for direct synthesis of butanone from butadiene. $RuCl_3$ *in situ* combined with one equivalent of phenanthroline catalyses this conversion with an initial TOF of 960 h^{-1} and a cumulative TON of at least 2750 after 10 h. This superior result compared to previously reported systems emphasises the need for catalysts that prevent ligand redistribution. The possible use of relatively cheap $RuCl_3$ and HCl brings an industrial process for the direct synthesis of butanone from butadiene within reach. Future studies are aimed at further minimising ligand redistribution, optimisation of the reaction conditions as well as addressing the intriguing question on the valency of Ru in the active complex under butadiene hydration conditions and better understanding of deactivation reactions.

This research was supported by the Technology Foundation STW, applied science division of NWO and the technology programme of the Ministry of Economic Affairs. The authors are indebted to Mr W. W. Jager (SRTCA, The Netherlands) for his skilful technical assistance and to Dr W. J. L. Genuit (SRTCA, The Netherlands) for recording the mass spectra. Dr J. G. de Vries (DSM, The Netherlands) and Mr W. G. Reman (SRTCA, The Netherlands) are thanked for stimulating discussions.

Notes and references

† In a typical experiment, a high-pressure autoclave was filled with 0.09 mmol $[RuCl_3{\cdot}xH_2O]$, the appropriate amount of ligand and 3.5 mmol acid (for the acid-catalysed hydration of butadiene as shown in eqn. (2)). After addition of the diglyme–water (70:30) solvent mixture, the autoclave was closed and purged three times with dinitrogen. Next, buta-1,3-diene was added (10 ml) and the autoclave was heated to 145 °C. After 10 h, the autoclave was cooled to room temperature and the contents were analysed with GLC.

1 *Kirk-Othmer Encyclopedia of Chemical Technology*, 4th Edition, ed. J. I. Kroschwitz Wiley Interscience, New York, 1998.
2 *Ullmann's Encyclopedia of Industrial Chemistry*, 6th Edition, Electronic Release, ed. A. Eckerle, Wiley-VCH, Weinheim, 2000.
3 J. Kanand, M. Roper, R. Paciello and A. Thome, *U.S. Patent No. 5892125*, 1999 (to BASF).
4 J. Kanand, R. Paciello and M. Roper, *U.S. Patent No. 6166265*, 2000 (to BASF).
5 For examples of allylic alcohol isomerisation see: ref 8; G. F. Emerson and R. Pettit, *J. Am. Chem. Soc.*, 1962, **84**, 4591; D. Baudry, M. Ephritikhine and H. Felkin, *Nouv. J. Chim.*, 1978, **2**, 355; K. Tani, *Pure Appl. Chem.*, 1985, **57**, 1845; S. H. Bergens and B. Bosnich, *J. Am. Chem. Soc.*, 1991, **113**, 958; B. M. Trost and R. J. Kulawiec, *J. Am. Chem. Soc.*, 1993, **115**, 2027; J.-E. Bäckvall and U. Andreasson, *Tetrahedron Lett.*, 1993, **34**, 5459; D. V. McGrath and R. H. Grubbs, *Organometallics*, 1994, **13**, 224.
6 E. Drent, *Eur. Patent No. 457387*, 1991 (to Shell); F. Stunnenberg, F. G. M. Niele and E. Drent, *Inorg. Chim. Acta*, 1994, **222**, 225.
7 R. C. van der Drift, J. W. Sprengers, E. Bouwman, W. P. Mul, H. Kooijman, A. L. Spek and E. Drent, manuscript in preparation.
8 R. C. van der Drift, M. Vailati, E. Bouwman and E. Drent, *J. Mol. Catal. A: Chem.*, 2000, **159**, 163.
9 R. G. Wilkins, *Kinetics and Mechanism of Reactions of Transition Metal Complexes*, 2nd edn, VCH, Weinheim, 1991, 400.

CHEMCOMM
Communication
www.rsc.org/chemcomm

Regioselective mononitration of aromatic compounds by zeolite/dinitrogen tetroxide/air in a solvent-free system

Keith Smith,* Saeed Almeer and Christelle Peters

Centre for Clean Chemistry, Department of Chemistry, University of Wales Swansea, Swansea, UK SA2 8PP. E-mail: k.smith@swansea.ac.uk

Received (in Cambridge, UK) 2nd October 2001, Accepted 22nd October 2001
First published as an Advance Article on the web 28th November 2001

Nitration of aromatic compounds using a zeolite catalyst and a combination of dinitrogen tetroxide and air in a sealed system leads to high yields and *para*-selectivities in a clean, solvent-free process.

Electrophilic aromatic substitution reactions are of considerable importance in the production of fine chemicals. However, many traditional processes suffer serious disadvantages, including low selectivity for the desired product and the requirement for large quantities of mineral or Lewis acids as activators. Such acids cause corrosion and generate large volumes of spent reagents. Major efforts are therefore being made to develop processes with lower environmental impact.

Inorganic solids offer significant benefits by providing effective catalysis and, in some cases, enhanced selectivity.[1] For example, in our own research we have utilised zeolites to enhance the *para*-selectivity in chlorination,[2] bromination,[3] acylation[4] and methanesulfonylation[5] reactions of simple aromatic substrates. In addition, such solids are easily recycled.

Aromatic nitration is particularly important since nitro compounds are versatile feedstocks for a range of industrial products, including pharmaceuticals, agrochemicals, dyestuffs, and explosives. Traditional nitration with a mixture of nitric and sulfuric acids[6] is notoriously unselective for nitration of substituted compounds, and disposal of the spent liquors presents a serious environmental concern.[7] Consequently, several alternative methods for aromatic nitrations have been developed.[8–15]

At present, the best combination of high yield, high *para*-selectivity and low solvent use is nitric acid, zeolite HBEA (Hβ) and acetic anhydride (for moderately active aromatics)[12] or trifluoroacetic anhydride (for deactivated aromatics).[13] Even these systems, however, produce carboxylic acid as by-product.

An alternative approach to clean nitration, pioneered by Suzuki *et al.*, involves dinitrogen tetroxide and ozone,[16] or dinitrogen tetroxide with oxygen and a catalyst.[17] The use of oxygen rather than ozone was appealing and we demonstrated that use of zeolite Hß as catalyst provided improved *para*-selectivity and easier catalyst recovery.[18] However, the method still employed a large excess of dinitrogen tetroxide, a halogenated solvent, cooling and a reaction time of two days. Therefore, we continue to study the reaction in order to find ways of overcoming the remaining disadvantages. A recent publication from Suzuki *et al.* reveals that his group is also trying to perfect this zeolite-catalysed approach,[19] and we now therefore disclose our own further findings.

Our initial objective was to improve our previous procedure[18] by avoiding the need for cooling, decreasing the excess of dinitrogen tetroxide used and eliminating the solvent. These features were dictated by the volatility of dinitrogen tetroxide (bp 21 °C). Simply using an autoclave pressurised to 200 psi with oxygen allowed a reaction with the desirable features to proceed quickly and in high yield. Furthermore, when oxygen was replaced by air the reaction was still efficient. With air it required about 12 h to go to completion, still quicker than under the previous conditions.[18] By contrast, when the pressurising gas was nitrogen, virtually no nitration occurred, demonstrating the involvement of oxygen in the reaction.

It was not known whether the by-product was water, nitric acid or a mixture of the two. Eqn. (1) (n = 0–6) covers the various possible stoichiometries.

$$24\ \mathrm{ArH} + (12 + 2n)\ \mathrm{N_2O_4} + (6 + n)\ \mathrm{O_2} = 24\ \mathrm{ArNO_2} + 4n\ \mathrm{HNO_3} + (12 - 2n)\ \mathrm{H_2O} \quad (1)$$

A series of reactions involving different proportions of chlorobenzene to dinitrogen tetroxide was allowed to react to completion (2 days). The results suggested that 3 mol of ArH react with 2 mol of N_2O_4 to give 3 mol of nitro product and 1 mol of HNO_3 (eqn. (2), *i.e.* n = 2 in eqn. (1)).

$$3\ \mathrm{ArH} + 2\ \mathrm{N_2O_4} + \mathrm{O_2} = 3\ \mathrm{ArNO_2} + \mathrm{HNO_3} + \mathrm{H_2O} \quad (2)$$

Various zeolites, with different pore structures, counter-cations and Si:Al ratios, were examined under the new conditions. All zeolites tested catalysed the reaction and provided a modest increase in *para*-selectivity compared to reaction in the absence of catalyst. Zeolite Hß was somewhat faster and gave greater *para*-selectivity than the others, but the differences were not major.

Zeolite Hß was tested with a range of other substrates (Table 1). All substrates tested gave good yields of nitration products, with modest increases in the amounts of *para*-isomer in comparison with traditional methods. The relative reactivities did not appear to be consistent with a normal electrophilic aromatic substitution mechanism.

In an attempt to obtain further information about the system, we investigated the simple adsorption of N_2O_4 on zeolite Hß as a function of temperature. The amount adsorbed dropped steadily as the temperature was increased, but there was still some adsorption even at 80 °C and the amount adsorbed at 20 °C was in the region of 1.53 mmol N_2O_4 per gram of zeolite. By employing excess zeolite we were able to conduct a reaction in ordinary glassware at 20 °C and near-atmospheric pressure, which enabled direct observation of the reaction mixture. Adsorption of N_2O_4 alone onto the zeolite imparted a pale brown hue to the solid. However, when benzene was allowed into the system, the colour of the adsorbed material immediately became much darker. Following admission of oxygen the reaction proceeded slowly to give nitrated product.

We speculate that the dark colour is indicative of an adsorbed intermediate formed by interaction of the substrate with N_2O_4,

Table 1 Nitration of various substrates with N_2O_4, zeolite Hβ and air[a]

Substrate	Yield[b] (%)	*p/o* ratio
Toluene	76	0.9
Benzene	97	—
Fluorobenzene	95	10.1
Chlorobenzene	97	5.6
Bromobenzene	90	4.2

[a] Reactions were carried out with zeolite (3.0 g), substrate (33.0 mmol), and N_2O_4 (1.4 ml, *ca.* 23 mmol), under 200 psi air pressure at room temperature.[b] Calculated by quantitative GC.

 DOI: 10.1039/b108952h

and that its conversion into product requires another reactive species to be formed more slowly between oxygen and the excess N_2O_4. The relative reactivities of different substrates and the small differences observed between the catalytic activities of proton and sodium forms of the same zeolites do not seem to be in line with an acid-catalysed electrophilic substitution reaction under these conditions. We therefore suspect that the reaction is radical in nature. Scheme 1 gives a tentative mechanism that is consistent with the stoichiometry. A similar overall result would be produced if NO_2 radicals were to abstract the first hydrogen atoms and the HNO_2 produced were then to react with oxygen to give $HOONO_2$. However, in that event nitration would be expected in the absence of oxygen.

In previous reports of nitrations of aromatic compounds using dinitrogen tetroxide and zeolites in the absence of solvent, the reactions have been conducted at elevated temperatures in the gas phase.[20,21] It was assumed that the stoichiometry was as shown in eqn. (3) (*c.f.* eqn. (1) with $n = 0$). If that were correct, it is likely that some of the product was formed by the action of nitric acid on the substrate at the elevated temperatures. Therefore, the reactions were likely to be complex and conclusions about the mechanisms based on the overall results need to be treated with caution.

$$4\ ArH + 2\ N_2O_4 + O_2 = 4\ ArNO_2 + 2\ H_2O \qquad (3)$$

In the recent work of the Suzuki group, superior selectivities for production of *para*-isomers were achieved at low conversion using H-ZSM-5 as the zeolite and the substrate as its own solvent in the liquid phase.[19] In the present work we have shown how it is possible to carry out the reaction to give high yields, with modest *para*-selectivities, without solvent, with only the stoichiometric quantity of dinitrogen tetroxide, using air instead of oxygen, and under mild conditions (ambient temperature and a modest pressure). Under these conditions the reaction is rather slow, but simply raising the temperature to 30–40 °C in the sealed system can reduce the required reaction period dramatically. Therefore, only two remaining obstacles prevent this reaction from fulfilling all the desired criteria. One is the relatively low *para*-selectivity (though already better than for traditional methods). The other is the production of a modest amount of nitric acid as by-product, which can deactivate the zeolite by adsorption or reaction, limits the efficiency of usage of the dinitrogen tetroxide feed and could lead to plant corrosion. We continue to search for ways to overcome these remaining disadvantages.

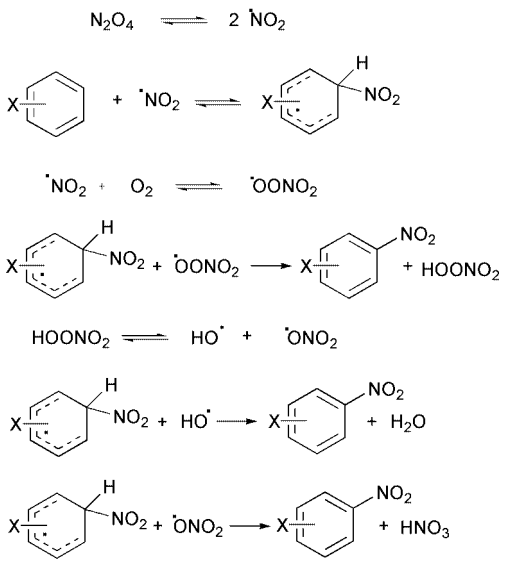

Scheme 1 A speculative mechanism for the reaction. Any or all of the steps involving reaction of the substrate–NO_2 adduct with another radical could proceed by either of two mechanisms: (i) direct hydrogen atom abstraction; or (ii) electron abstraction to give a Wheland intermediate and an anion, followed by proton abstraction from the Wheland intermediate by the anion. Whether the zeolite would play an active part in catalysing any of the processes or merely assist through stabilisation of intermediates by adsorption is an open question.

The reaction of chlorobenzene illustrates the general procedure for the nitration process. The zeolite (3 g) was placed in a 450 ml autoclave, followed by chlorobenzene (3.71 g, 33 mmol). Liquid dinitrogen tetroxide (*ca.* 1.4 ml, *ca.* 23 mmol) was added quickly to the mixture, the autoclave was sealed and pressurised to 200 psi with air, and the mixture was stirred at room temperature for 14 h. The autoclave was then opened and the product was extracted with dichloromethane (200 ml). The extract was washed with water (50 ml), dried ($MgSO_4$) and concentrated under reduced pressure to give the product, which was analysed by GC (hexadecane was added as internal standard).

We thank Zeolyst International for gifts of zeolites and S. A. thanks the Government of Qatar for a studentship.

Notes and references

1 M. Butters, in *Solid Supports and Catalysts in Organic Synthesis*, ed. K. Smith, Ellis Horwood, Chichester, 1992, pp. 130–170 J. M. Thomas and W. J. Thomas, *Principles and Practice of Heterogeneous Catalysis*, VCH, Weinheim, 1997 J. H. Clark, *Catalysis of Organic Reactions Using Supported Inorganic Reagents*, VCH, New York, 1994 *Introduction to Zeolite Science and Practice*, ed. H. Van Bekkum, E. M. Flanigan and J. C. Jansen, *Stud. Surf. Sci. Catal.*, 1991, vol. 58.

2 K. Smith, M. Butters, W. E. Paget, D. Goubet, E. Fromentin and B. Nay, *Green Chem.*, 1999, **1**, 83.

3 K. Smith, P. He and A. Taylor, *Green Chem.*, 1999, **1**, 35.

4 K. Smith, Z. Zhenhua and P. K. G. Hodgson, *J. Mol. Catal. A*, 1998, **134**, 121.

5 K. Smith, G. M. Ewart and K. R. Randles, *J. Chem. Soc., Perkin Trans. 1*, 1997, 1085.

6 G. A. Olah, R. Malhotra and S. C. Narang, *Nitration: Methods and Mechanisms*, VCH, New York, 1989 K. Schofield, *Aromatic Nitration*, Cambridge University Press, Cambridge, 1980.

7 E. R Ward, *Chem. Br.*, 1979, **15**, 297.

8 K. Smith and K. Fry, *Tetrahedron Lett.*, 1989, 5333.

9 R. P. Claridge, N. L. Lancaster, R. W. Millar, R. B. Moodie and J. P. B. Sandall, *J. Chem. Soc., Perkin Trans. 2*, 1999, 1815.

10 T. J. Kwok, K. Jayasuriya, R. Damavarapu and B. W. Brodman, *J. Org. Chem.*, 1994, **59**, 4939.

11 J. M. Bakka, *U.K. Pat. Appl.*, 7827172, 1979B. M. Choudary, M. Sateesh, M. L. Kantam, K. K. Rao, K. V. R. Prasad, K. V. Raghavan and J. A. R. P. Sarma, *Chem. Commun.*, 2000, 25; D. Vassena, A. Kogelbaner and R. Prins, *Catal. Today*, 2000, 275.

12 K. Smith, A. Musson and G. A. DeBoos, *J. Org. Chem.*, 1998, **63**, 8448.

13 K. Smith, T. Gibbins, R. W. Millar and R. P. Claridge, *J. Chem. Soc., Perkin Trans. 1*, 2000, 2753.

14 F. J. Waller, A. G. M. Barrett, D. C. Braddock and D. Ramprasad, *Chem. Commun.*, 1997, 613.

15 M. Dove, B. Manz, J. Montgomery, G. Pattenden and S. Wood, *J. Chem. Soc., Perkin Trans. 1*, 1998, 1589.

16 H. Suzuki and T. Mori, *J. Chem. Soc., Perkin Trans. 2*, 1994, 479.

17 H. Suzuki, S. Yonezawa, N. Nonoyama and T. Mori, *J. Chem. Soc., Perkin Trans. 1*, 1996, 2385.

18 K. Smith, S. Almeer and S. J. Black, *Chem. Commun.*, 2000, 1571.

19 X. Peng, H. Suzuki and C. Lu, *Tetrahedron Lett.*, 2001, **42**, 4357.

20 A. Germain, T. Akouz and F. Figueras, *Appl. Catal. A: Gen.*, 1996, **136**, 57.

21 N. F. Salakhutdinov, K. G. Ione, E. A. Kobzar and L. V. Malysheva, *Russ. J. Org. Chem.*, 1993, **29**, 457.

Typeset and printed by Black Bear Press Limited, Cambridge, England